Phase behaviours and conductivity study of water/CPC/alkan-1-ol (C_4 and C_5)/1-hexane water/oil microemulsions with reference to their structure and related thermodynamics

S.P. Moulik, Wanda M. Aylward, and R. Palepu

Abstract: The microemulsion forming systems of water/cetylpyridinium chloride/butan-1-ol/*n*-hexane, and water/cetylpyridinium chloride/pentan-1-ol/*n*-hexane have been studied with respect to their phase behaviours and percolation of conductance to derive information on their droplet physicochemical characteristics (dimension, interfacial area and composition, and number density). This was carried out at different water contents at specific ratios of surfactant and cosurfactant and at various temperatures. From the information collected, the energetics of the transfer of the alkanol (butan-1-ol and pentan-1-ol) from the continuous oil-phase to the interfacial region (the interphase) have been estimated. At the conductance percolation threshold, the droplets cluster or associate, can be considered to form a pseudophase similar to surfactants forming micelles. Based on this concept, the energetics of the clustering process have been evaluated, and the results are discussed in comparison with other recently studied systems.

Key words: energetics of clustering, percolation, phase diagrams, microemulsions and thermodynamics of transfer.

Résumé : Afin de pouvoir déduire des informations sur les caractéristiques physicochimiques de leurs gouttelettes (dimension, surface et composition interfaciales et nombre de densité), on a déterminé les comportements des phases et la percolation de la conductance des systèmes eau/chlorure de cétylpyridinium/butan-1-ol/hexane et eau/chlorure de cétylpyridinium/pentan-1-ol/hexane qui forment des microémulsions. Cette étude a été effectuée à diverses teneurs en eau, à des rapports spécifiques d'agent de surface et de cosurfactant et à diverses températures. À partir des informations recueillies, on a évalué les énergies de transfert des alcools (butan-1-ol et pentan-1-ol) de la phase huileuse continue à la région interfaciale (interphase). Au seuil de percolation de la conductance, on peut considérer que les agrégats de gouttelettes forment une pseudophase semblable à celles des agents de surface qui forment des micelles. En se basant sur ce concept, on a évalué les énergies associées au processus de formation d'agrégats et on discute des résultats par comparaison avec d'autres systèmes étudiés récemment.

Mots clés : énergies impliquées dans la formation d'agrégats, percolation, diagrammes de phase, microémulsions et thermodynamique de transfert.

[Traduit par la Rédaction]

Introduction

Nanodispersions of water in oil or oil in water can be achieved by proper choice of surfactant and cosurfactant, and their combined addition at appropriate concentrations. When these dispersions are transparent, isotropic, thermodynamically stable and easily formed, they are called microemulsions (1, 2). The water/oil microemulsions can be considered as swollen reverse micelles having a distinct water pool in the core. Microemulsions have attracted the attention of scientists and technologists for their potential uses and applications in the forms of solvents, reaction media, liquid membranes, enhanced oil recovery fluids, media for nanoparticle synthesis, pharmaceutical and cosmetic preparations, etc., (3–8). The study of microemulsions in relation to the conditions of their formation, stability and structure is, therefore, of much current interest to both theoretical and experimental scientists.

For the determination of the internal structure and dynamics and the associated thermodynamics of microemulsions, nuclear magnetic resonance (NMR), small angle neutron scattering (SANS), dynamic light scattering (DLS), small angle X-ray diffraction (SAXRD), time resolved fluorescence quenching (TRFQ), dielectric relaxation, ultrasonic absorption, conductance, viscosity, positron annihilation technique, and calorimetric methods are mostly used (3). In recent years, the conductance method has been successfully, but infrequently, used on microemulsion systems, prepared with ionic surfactants, to elucidate their structural parameters and energetics of structural transitions with reference to both

Received May 19, 2000. Published on the NRC Research Press Web site on December 20, 2000.

S.P. Moulik,[1,2] W.M. Aylward, and R. Palepu.[2] Department of Chemistry, St. Francis Xavier University, Antigonish, NS B2G 2W5, Canada.

[1]Visiting James Chair Research Professor, on leave from: Center for Surface Science, Department of Chemistry Judavpur University, Calcutta - 700032, India.

[2]Authors to whom correspondence may be addressed. SPM: e-mail: spmcssju@cal2.vsnl.net.in; RP: Telephone: (902) 867-3886. Fax: (902) 867-2414. e-mail: rpalepu@stfx.ca

 DOI: 10.1139/cjc-79-1-1 © 2001 NRC Canada

volume induced and temperature induced percolation of conductance (9–16). The conductance of microemulsions is related to the effective medium theory that deals with the conductance of mixed systems of conductors and insulators and can be as well described by appropriate scaling equations. This area has received only limited investigations for water/oil microemulsions in which amphiphile-coated, dispersed, nano water droplets are the conductors and the oil is the insulator.

With this backdrop, we have made a detailed investigation of water/cetylpyridinium chloride/alkan-1-ol (butanol and pentanol)/*n*-hexane, water/oil microemulsion systems at several surfactant/cosurfactant mass ratios and temperatures. The pseudoternary phase diagram of the systems have been constructed. The volume induced percolation results have been analyzed to get the structural information of the droplets. The energetics of droplet association have been evaluated from the temperature effect on the process. The choice of the surfactant cetylpyridinium chloride (CPC) was made because it has a better water solubilization capability compared to cationic surfactants with quaternary ammonium head groups of equal chain length (17).

Experimental section

Materials

Cetylpyridinium chloride (CPC), butan-1-ol, pentan-1-ol, and *n*-hexane were obtained from Sigma–Aldrich. The alkanols were >99% pure. All materials were used as received except the CPC which was recrystallized from an acetone–ethanol mixture. Triply distilled quality water was used for making all solutions.

All measurements were performed in a thermostated water bath of accuracy ±0.01 K.

Method

For the construction of the phase diagrams, CPC/alkanol at a constant mass ratio (1:1) was mixed in different compositions in set *one* with water, and in set *two* with *n*-hexane. Each of the samples in the first set was titrated with *n*-hexane under constant stirring condition at 298 K until it became just cloudy. The same procedure was followed for the second set using water as the titer. The composition of each sample at the point of clouding was recorded and expressed in mass %. The data were then plotted using triangular coordinates to produce a boundary demarcating the biphasic and the monophasic zones comprising both oil/water and water/oil formulations. Several compositions falling well within the turbid region were selected, the components mixed, stirred, and kept overnight. It was visually observed that for all the combinations, there appeared only two phases, one rich in oil and the other rich in water. The occurrence of more than two phases was not observed.

The conductance measurements were taken with a YSI model 32 conductometer, U.S.A. using a cell with a 1.01 cm^{-1} cell constant. A jacketed beaker and an adjustable water bath were used to control and maintain temperature.

In the actual measurements, three surfactant/cosurfactant mass ratios (σ), 0.25, 0.33, and 0.50 were used in the study. A mixture of known masses of CPC, alkanol, and *n*-hexane was placed in the jacketed beaker with the conductivity cell and the temperature was set to a desired value. The initial value of conductance was recorded and water was then successively added to the beaker, with constant stirring. The conductance was recorded at each addition when it stabilized after temperature equilibration. The measurements were continued until a significant rise in conductance followed by a levelling off tendency was observed. The same measurement procedure was followed for different surfactant/cosurfactant/oil compositions and at different temperatures. The observations with successive addition of water to surfactant/cosurfactant/oil systems at a constant temperature is called volume-induced percolation of conductance. In the temperature-induced percolation study, the conductance of a microemulsion sample at a fixed composition was measured with increasing temperature until a rapid rise in the conductance was observed. The conductance measurement was made after careful equilibration of the system at each temperature. Similar sets of measurements were taken on samples of different compositions.

Theoretical background

Conductance method for structure elucidation

For microemulsions, structure elucidation i.e., determination of droplet dimension, interfacial area, and interfacial composition dependency on system composition and temperature, is important. The method of conductance is an indirect but potential method to obtain this information. The basic principle of the method and the related relations are briefly presented below. We are herein concerned with volume-induced percolation of conductance (10–13). The analysis is based on the effective medium theory (EMT) of conductance on binary inclusions (conductors and insulators) (18–20) and has been used very limitedly on microemulsion systems (10–12). It is a potential method and its efficacy has been established in the recent past (10–12). It is used in this study to derive interfacial information, droplet dimensions, and the thermodynamics of cosurfactant transfer.

In the EMT, the conductance equation of Böttcher (19) for a percolating system of isolated spherical dispersion has the following form,

$$[1] \qquad \frac{k - k_c}{k_d - k_c} = \frac{3k}{k_d + 2k}\,\phi_d$$

where k, k_c, and k_d are the conductances of the solution, the continuous medium, and the disperse phase, respectively, and ϕ_d is the volume fraction of the latter. In water/oil microemulsion, the continuous oil-phase is essentially nonconducting (insulator type) and hence $k_c = 0$, so that eq. [1] takes the form

$$[2] \qquad k = 1.5\,k_d(\phi_d - 0.333)$$

From the plot of k vs. ϕ_d or ($\phi_d - 0.333$), the k_d value can be evaluated.

This equation has been used for water/oil microemulsion systems to derive structural information. One basic condition that needs to be fulfilled is the dispersed entities should be of spherical form. Nonspherical dispersions and dispersions forming distinct aggregates should not obey the Böttcher's conductance equation. The EMTDD of Granqvist and Hunderi (21) can be applied to these systems. In that case, a

© 2001 NRC Canada

nonlinear plot between k and ϕ_d with an intercept on the axis at $\phi_d < 0.333$ would be obtained.

The analysis on the conductance of a microemulsion in the light of the EMT for spherical dispersions and EMTDD for chain and cluster forming dispersions has been recently presented and discussed (12). For low conducting water/oil microemulsions produced with different surfactants and oils, spherical dimensions of the droplets at low and even high concentrations have been reported. This has been mentioned and discussed by us (22). In line with this, we herein also consider spherical identities of the droplets for the present percolating systems, and eq. [2] was used to derive the desired information on the water/CPC/alkan-1-ol (C_4 and C_5)/*n*-hexane systems.

It is important to note that to use eq. [2], the volume fraction of the dispersion needs to be known. This is different from the volume fraction of water, for the associated surfactant and cosurfactant molecules become a part of the dispersion. Therefore, unless the proper value of ϕ_d is used, the k vs. ϕ_d plot or k vs. ($\phi_d - 0.333$) plot would not show 0.333 or 0 as the intercept on the x-axis to be in agreement with eq. [2]. Defining the average ratio of cosurfactant and surfactant in the droplet interfacial region (henceforth to be called the interphase) as the structure factor (r) and considering it to be invariable at a constant surfactant /cosurfactant ratio (σ), and independent of the weight fraction of water for a constant temperature in the microemulsion, it can be presented as

$$[3] \qquad r = \frac{N_{cs}}{N_s}$$

where N_{cs} and N_s are the number of cosurfactant and surfactant molecules in the interphase, respectively. At a constant temperature, a fixed concentration of surfactant and of cosurfactant (producing a constant surfactant/cosurfactant ratio), and an unchanging oil content, the effective head group areas, provided by the amphiphle molecules, determine the number and size of the dispersed water droplets. With changing amounts of water, the size and number of droplets adjust to maintain a constant effective interfacial area. The change in the number of amphiphile molecules in the interphase due to solubility requirements is considered to be minor. The aqueous solubilities of the alkanols used in this study are known to be low as well. Thus, for a particular system at a constant temperature, the distribution of the alkanol between the water, interphase, and oil remains essentially constant. The constancy of the structure factor (r) follows from the above and is supported by the good linear plots between k_d and ϕ_d calculated according to eq. [4]. By the principle of mass balance, the effective volume fraction of the disperse phase (10, 11) is given by the relation,

$$[4] \qquad \phi_d = \frac{\rho_t}{\rho_d}\left[W_s\left(1 + r\frac{M_{cs}}{M_s}\right) + W'_{cs} + W_w\right]$$

where ρ_t and ρ_d are the densities of the total solution and the disperse phase respectively; W_s, W'_{cs} and W_w are the mass fractions of surfactant, cosurfactant in the aqueous phase and the water, respectively, and the M_{cs} and M_s are the molar masses of the cosurfactant and the surfactant respectively. W'_{cs} has a contribution when the cosurfactant has appreciable water solubility; here, butan-1-ol has a contribution whereas pentan-1-ol contributes negligibly due to its poor aqueous solubility, and for it $W'_{cs} = 0$.

To obtain the effective ϕ_d, a correct value of r is required to be used in eq. [4]. The following procedure can be followed for a practical solution to obtain r. Several reasonable values of r can be assumed, and for each r, ϕ_d values are calculated for the different levels of water addition in the conductance experiment. These ϕ_d values are then used in eq. [2] to produce plots of k and ($\phi_d - 0.333$) to obtain an intercept on the x-axis. These intercepts are then plotted against the r values, and the r corresponding to the zero intercept is obtained from the plot which is the required structure factor (r) for the studied system.

The radius of the droplet (R_w) and the effective droplet number per unit volume of solution (N_e) are then obtained from the relations (11)

$$[5] \qquad R_w = \frac{3[M_s + rM_{cs} + \{(W_w + W'_{cs})/W_s\}M_s]}{N\rho_d(a_s + ra_{cs})}$$

and

$$[6] \qquad N_e = \frac{3\phi_d}{4\pi R_w^3}$$

where the new terms N, a_s and a_{cs} are Avogadro's number, the cross sectional areas of the surfactant and of the cosurfactant, respectively.

The effective volume of a microemulsion droplet (υ) is given by the relation (11)

$$[7] \qquad \upsilon = \left(\frac{4}{3}\right)\pi R_w^3 + \frac{A_s M_s}{\rho_s N} + \frac{A_{cs} M_{cs}}{\rho_{cs} N}$$

where the new terms A_s and A_{cs} represent the aggregation number of the surfactant and the cosurfactant molecules per droplet, respectively. A_{cs} can be obtained in terms of r and A_s using eq. [3].

The effective radius of the droplets (radius including the length of the interphase) can then be obtained from the relation

$$[8] \qquad R_e = \left(\frac{3\upsilon}{4\pi}\right)^{1/3}$$

The surface area of the droplets per unit volume can be estimated from the relation

$$[9] \qquad A_t = 4\pi R_w^2 N_e$$

Thermodynamics of cosurfactant transfer from oil to the interphase

The structure factor (r) relates the concentration of the cosurfactant in the interphase in terms of the surfactant. The cosurfactant remains distributed between the interphase and the oil phase, apart from the fraction that remains soluble in the aqueous pool satisfying the solubility requirement. From the knowledge of r and the concentrations of the surfactant and cosurfactant in the experimental solution, the standard Gibbs free energy of transfer of cosurfactant from the oil

© 2001 NRC Canada

phase to the interphase in the unitary scale can be estimated from the relation,

$$[10] \quad \Delta G_t^\circ = -RT \ln \frac{n_{cs}^i/(n_{cs}^i + n_s^i)}{n_{cs}^o/(n_{cs}^o + n_o)} = -RT \ln \frac{X_{cs}^i}{X_{cs}^o}$$

where X_{cs}^i and X_{cs}^o are the mol fractions of the cosurfactant in the interphase and oil phase respectively; n_s^i and n_{cs}^i are the number of mol of surfactant and cosurfactant, respectively, in the interphase; n_{cs}^o is the number of mol of cosurfactant in the oil phase; and n_o is the number of mol of oil in the sample. Normally, the thermodynamic distribution constants are obtained from the activities of the components distributed between the phases. However, estimation of the interfacial and bulk activities of the amphiphiles in the present context is complex and, since the species in question have comparable molecular architectures, mol fraction concentration terms can be substituted. Thus, we have used mol fractions in place of activities in our calculations. As a consequence, the subsequently calculated transfer parameters are not derived using a completely rigorous thermodynamic approach; they are good estimations, but they are not exact.

The first derivative of the ΔG_t° with respect to temperature gives the standard entropy of transfer (ΔS_t°) and the corresponding enthalpy of transfer (ΔH_t°) is obtained from the Gibbs–Helmholtz equation.

Thermodynamics of droplet association or clustering

In the process of percolation, the droplets assemble and ion-transfer takes place either by the mechanism of "hopping" or by "transient fusion and mass transfer" or by both (3). In this process, the overall geometry of the droplets is considered to remain more or less unaltered, except that they are physically close to facilitate efficient ion transfer. In the volume-induced percolation, at a sufficient level of water addition, bigger sized droplets promote easier transfer of materials (ions) producing a large change in conductance. The droplets must grow to the right size for this phenomenon to start, often to a radius of 0.5–1.0 nm. In the temperature percolation process, droplet motion increases with temperature, and at some threshold temperature, depending on concentration, they come sufficiently close to exchange or transfer mass (ions) resulting in a rapid increase in the conductance. The process occurs efficiently at a [water]/[amphiphile] mol ratio approximately in the range of 15–35.

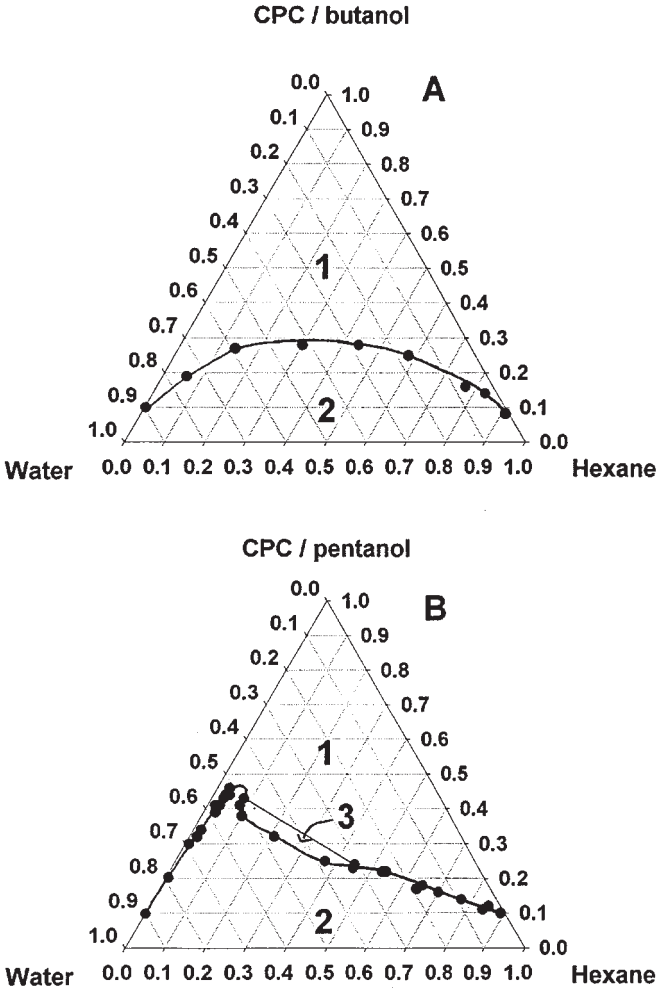
At the percolation threshold, it is convenient to assume that the droplets are in close contact in the form of clusters but maintaining their individual spherical geometry. This is the onset of a pseudophase (14, 16) as envisaged in micelles forming from the association of surfactant monomers.

The standard Gibbs energy change for the clustering process can be obtained from the relation (14, 15).

$$[11] \quad \Delta G_{cl}^\circ = RT \ln X_d$$

where X_d is the mol fraction of the droplets in the microemulsion at the point of the percolation threshold. This equation is comparable with the standard Gibbs energy of micellization ($\Delta G_m^\circ = RT \ln X_{CMC}$) where X_{CMC} is the mol fraction concentration of the surfactant at the critical micellar concentration (CMC). The X_d can be computed from the following equation

Fig. 1. Pseudoternary phase diagrams for the studied microemulsion systems at σ = 0.50 at 298 K. (*a*) water/CPC–butanol/*n*-hexane system; (*b*) water/CPC–pentanol/*n*-hexane system. Regions 1, 2, and 3 represent mono-, bi- and clear-gel phase, respectively.



$$[12] \quad X_d = \frac{N_e}{N_e + n_0' N}$$

where the new term n_0' is the number of mol of oil per unit volume of the microemulsion solution.

The other thermodynamic parameters, standard entropy and enthalpy changes of clustering, then follow from the first derivative of ΔG_{cl}° with respect to temperature and the Gibbs–Helmholtz equation.

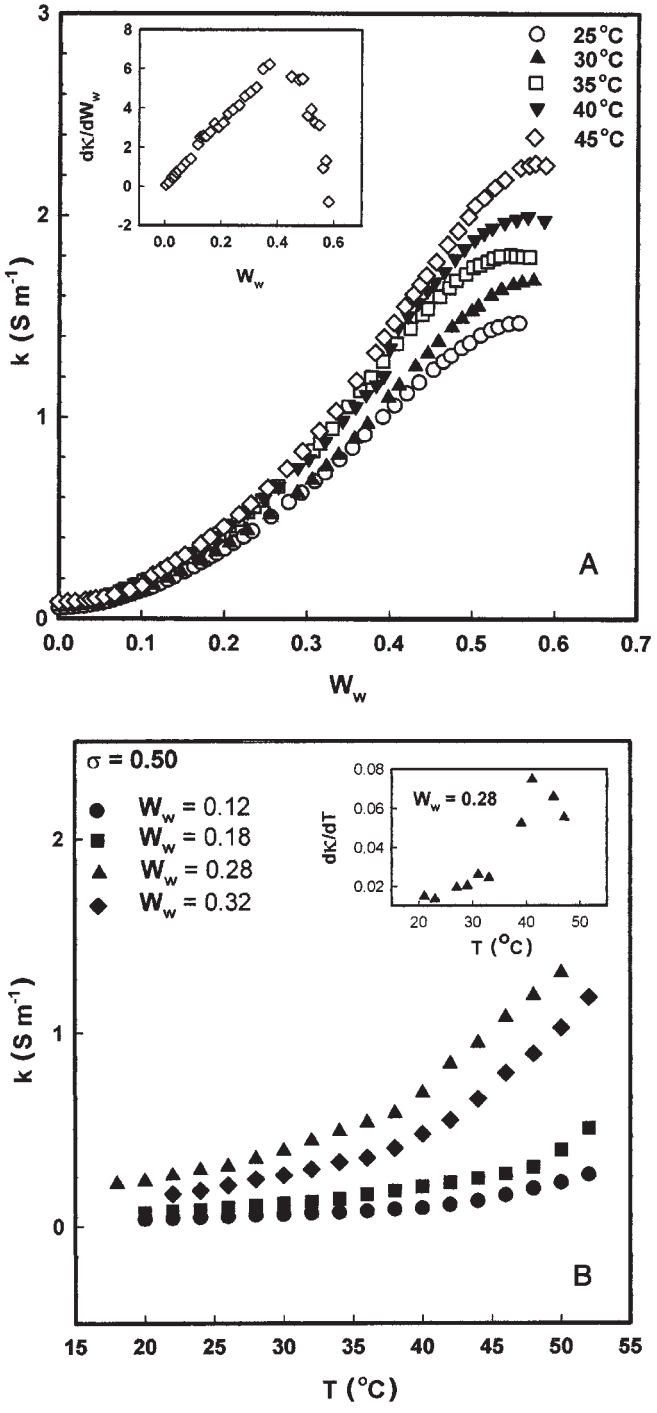
Results

Phase diagrams

The phase behaviours observed at 298 K for the water/CPC/ butan-1-ol/*n*-hexane system and water/CPC/pentan-1-ol/*n*-hexane system at CPC–alkanol mass ratio 1:1 are presented in Fig. 1 as pseudoternary phase diagrams. It is observed that the diagram for butan-1-ol is symmetric, and at the maximum point on the boundary 30% (by mass) of the CPC–butanol mixture dissolves 35% of each of water and hexane. This supports the observation (17), that surfactants such as pyridinium salts are better microemulsion forming

© 2001 NRC Canada

Fig. 2. (*a*) $k - W_w$ profiles for water/CPC–butanol/*n*-hexane system at amphiphile:oil ratio 11:9 at different temperatures at $\sigma = 0.50$. The first derivative plot at 45°C is shown in the inset. W_w at transition = 0.371; (*b*) $k - T$ profiles for the water/CPC–pentanol/*n*-hexane system at different weight fractions (W_w) of water at $\sigma = 0.50$. Mass % compositions as water/CPC–pentanol/*n*-hexane: ● 12:52.8:35.2, ■ 18:49.2:32.8, ▲ 28:43.2:28.8, ◆ 32:40.8:27.2. The first derivative plot is shown in the inset at $W_w = 0.28$ with percolation transition at $T = 41$°C.



agents for alkanol–alkane systems than the quaternary ammonium representatives (better water solubilizer). The phase diagram for pentan-1-ol as the co-surfactant (Fig. 1*b*) is different and unsymmetric compared to that of butan-1-ol. The phase boundary course is almost triangular in shape; the shortest arm of the triangle extends up almost along the base line of the oil. From the apex to half-way down towards the right, there is a clear gel region identified by the loss of flow. At 30% CPC–pentan-1-ol, nearly 40% of oil and 30% of water make a low viscous microemulsion solution. The composition of the vertical apex is 48:47:5, water/CPC–pentanol/hexane. The difference in the phase behaviour between the two systems is considered to arise from the difference in the aqueous solubility of butan-1-ol and pentan-1-ol. The former is much more soluble (1.061 *m*) than the latter (0.255 *m*) at 298 K, and homogenization leading to better microemulsion formation is easier. The better performance of butan-1-ol does not comply with the mixing model of Bansal et al. (23) which proposes that for a stable water/oil microemulsion, the sum of the chain lengths of the cosurfactant and the oil must be comparable to the chain length of the surfactant. Using this rationale, butan-1-ol is shorter than pentan-1-ol by one unit of the chain length and is expected to be less efficient than the latter. Similar inconsistencies in this mixing model have been reported in the past (11).

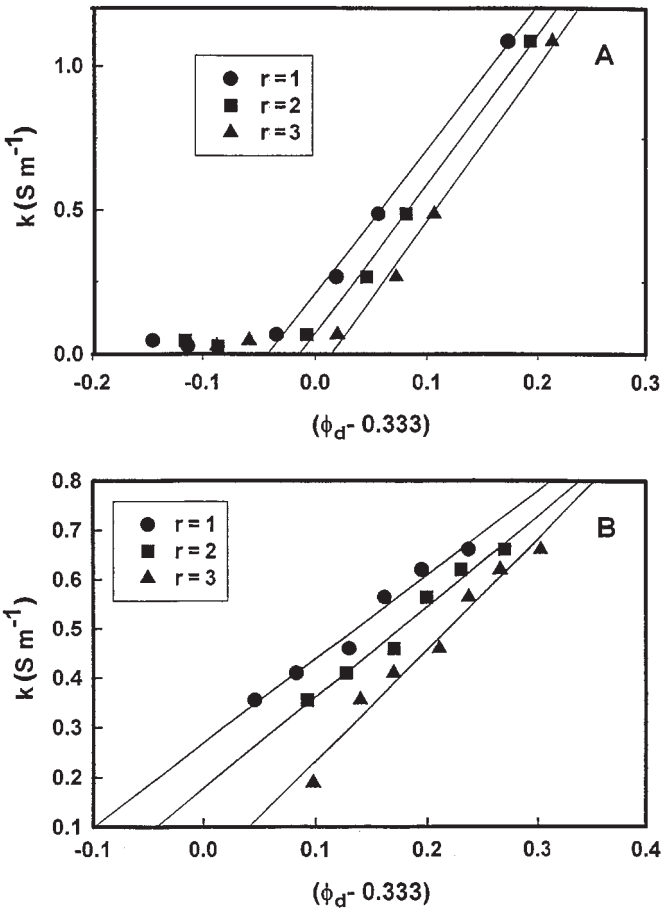
Conductance percolation (r) and k_d.

In Fig. 2*a*, a graphical representation of conductance percolation for the water/CPC/butan-1-ol/*n*-hexane system with $\sigma = 0.50$ weight ratio of surfactant:cosurfactant at five different temperatures is presented. The curves are sigmoidal in nature, and the conductance at all W_w increases systematically with temperature like an electrolyte solution. A first derivative plot of conductance with respect to W_w is shown in the inset at 45°C to demonstrate the transition point at $W_w = 0.371$. At higher temperature, droplets rapidly associate at lower W_w due to their increased kinetic motion. This results in an efficient transfer of ions among themselves resulting in a rapid rise in conductance. The temperature percolation at $\sigma = 0.50$ for four different W_w for the water/CPC/pentan-1-ol/*n*-hexane system is illustrated in Fig. 2*b*. The efficiency of the process for $W_w \geq 0.28$ can be inferred from the figure. The transition temperature for percolation can be obtained from the first derivative plot between k and T (see inset). It is observed that the transition temperature decreases with increasing W_w. Larger droplets associate at relatively lower temperature to exhibit conductance enhancement by the rapid ion-transfer mechanism as suggested above.

In light of eqs. [2]–[4], the representative plots of k and $[\phi_d - 0.333]$ are exhibited in Fig. 3, for the two types of percolating systems studied at $\sigma = 0.50$. In the percolation region, the plots are fairly linear and the least-squares method has been used for obtaining the intercepts on the x-axis for different r values. The plot between the intercept and the r has been observed to be linear (not shown here) with a correlation coefficient of 0.9995 from which the r value with the zero intercept has been obtained. The k_d value has been obtained from the slope of the k vs. $[\phi_d - 0.333]$ plot corresponding to the correct value of r. The r and k_d values obtained at different temperatures and σ values for the percolating systems studied are presented in Table 1. It is observed that at a constant temperature, r decreases with σ and k_d increases. For the system with butan-1-ol, both r and k_d

© 2001 NRC Canada

Fig. 3. (*a*) $k - [\phi_d - 0.333]$ profiles for water/CPC–butanol/*n*-hexane system at 298 K according to eq. [2] for three *r* values 1, 2, and 3; (*b*) $k - [\phi_d - 0.333]$ profiles for the water/CPC–pentanol/*n*-hexane system at 298 K according to eq. [2] for three *r* values 1, 2, and 3.



increase with temperature with a minor deviation; whereas for the pentan-1-ol system, *r* decreases and k_d increases with temperature without any deviation. The microemulsion system with pentan-1-ol is more systematic in conductance behaviour than with butan-1-ol. In the past (11) an inverse relation between the k_d and *r* has been observed which is also observed in this study. At a constant temperature (298 K), a linear trend between k_d and *r* is illustrated in Fig. 4; the two alkanols constitute two lines, pentan-1-ol follows the lower course. The *r* and k_d values obtained in this study are higher than that for the systems studied earlier (11) with CTAB, SDS, and AOT. It appears that individual systems have their specific characteristics of *r* and k_d. It is reasonable to state that a higher value of *r* corresponds to a higher proportion of cosurfactant in the interfacial region to lower the conductance of the disperse phase.

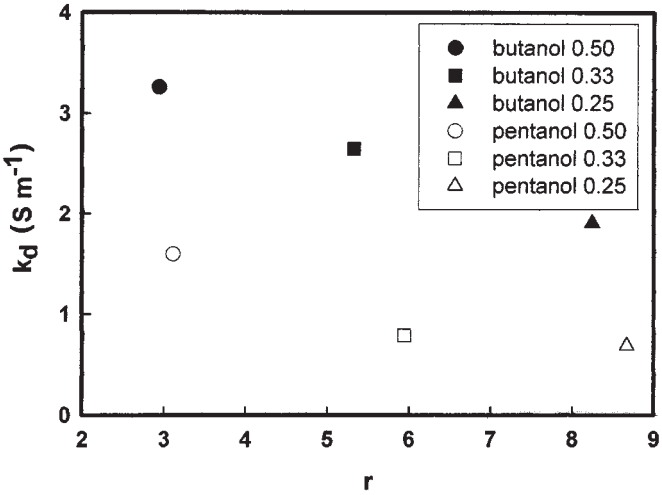
Droplet dimension, number density, and surface aggregation

The structure and related parameters of the two percolating systems studied are presented in Tables 2 and 3 at σ = 0.50 for different weight fractions of water (W_w) and temperature. The results in the tables indicate that the conductance method is suitable to obtain different structural parameters

Table 1. Conductance of the disperse phase (k_d) and the structural parameter (*r*) for the systems studied under conditions of different σ and temperature.

System	Temperature (K)	*r*	k_d (S m^{-1})
		Butan-1-ol	
Hexane–CPC (σ = 0.50)	298	2.94	3.26
Hexane–CPC (σ = 0.50)	303	3.07	4.13
Hexane–CPC (σ = 0.50)	308	3.25	3.84
Hexane–CPC (σ = 0.50)	313	3.49	3.83
Hexane–CPC (σ = 0.50)	318	3.40	4.55
Hexane–CPC (σ = 0.33)	298	5.32	2.65
Hexane–CPC (σ = 0.25)	298	8.24	1.91
		Pentan-1-ol	
Hexane–CPC (σ = 0.50)	298	3.11	1.60
Hexane–CPC (σ = 0.50)	303	3.13	1.86
Hexane–CPC (σ = 0.50)	308	3.03	2.32
Hexane–CPC (σ = 0.50)	313	3.00	3.00
Hexane–CPC (σ = 0.50)	318	2.83	3.88
Hexane–CPC (σ = 0.33)	298	5.94	0.79
Hexane–CPC (σ = 0.33)	303	5.79	1.00
Hexane–CPC (σ = 0.33)	308	5.53	1.33
Hexane–CPC (σ = 0.33)	313	5.34	1.76
Hexane–CPC (σ = 0.33)	318	5.15	2.34
Hexane–CPC (σ = 0.25)	298	8.67	0.69
Hexane–CPC (σ = 0.25)	303	8.70	0.83
Hexane–CPC (σ = 0.25)	308	8.70	1.02
Hexane–CPC (σ = 0.25)	313	8.56	1.30
Hexane–CPC (σ = 0.25)	318	8.37	1.76

Fig. 4. The correlation between k_d and *r* for the studied systems at 298 K at different σ. Closed and open symbols for butan-1-ol and pentan-1-ol as cosurfactants, respectively.



of water/oil microemulsion. The trends of the parameters with W_w and *T* are readily revealed. At a comparable condition (e.g., W_w = 0.05), the droplet dimension (R_w) for the system with butan-1-ol is lower, droplet surface area per mL of solution (A_t) is higher, number density (N_e) is higher, and the aggregation number (A_{cs}) is higher compared to that for pentan-1-ol. With respect to temperature, the parameters vary oppositely between the two systems. For butan-1-ol (Table 2), $R_w(R_e)$ increases with temperature, A_t decreases,

© 2001 NRC Canada

Table 2. Structural parameters[a, b] of water/CPC–butanol/hexane microemulsion system at σ = 0.50 and at different weight fractions of water and temperature.

Structural parameter	Temperature (K)				
	298	303	308	313	318
W_w = 0.05					
R_w (R_e) (nm)	2.64 (3.52)	2.65 (3.53)	2.65 (3.53)	2.66 (3.53)	2.68 (3.54)
$A_t \times 10^8$ (m^2 m^{-3})	4.64	4.64	4.56	4.5	4.35
$N_e \times 10^{23}$ (m^{-3})	53.06	52.6	51.61	50.68	48.36
A_{cs} (A_s)	259 (84)	262 (84)	261 (86)	262 (87)	258 (91)
W_w = 0.10					
R_w (R_e) (nm)	2.93 (3.76)	2.94 (3.76)	2.95 (3.78)	2.96 (3.79)	2.98 (3.83)
$A_t \times 10^8$ (m^2 m^{-3})	4.48	4.48	4.37	4.33	4.22
$N_e \times 10^{23}$ (m^{-3})	41.42	41.11	39.98	39.32	37.68
A_{cs} (A_s)	316 (102)	319 (102)	319 (106)	320 (107)	317 (112)
W_w = 0.17					
R_w (R_e) (nm)	3.40 (4.01)	3.42 (4.03)	3.43 (4.03)	3.44 (4.04)	3.48 (4.07)
$A_t \times 10^8$ (m^2 m^{-3})	4.22	4.19	4.16	4.08	3.93
$N_e \times 10^{23}$ (m^{-3})	29	28.56	28.11	27.44	25.82
A_{cs} (A_s)	416 (134)	419 (134)	419 (139)	422 (141)	426 (150)
W_w = 0.29					
R_w (R_e) (nm)	4.43 (4.82)	4.45 (4.84)	4.47 (4.86)	4.49 (4.87)	4.56 (4.93)
$A_t \times 10^8$ (m^2 m^{-3})	3.72	3.72	3.64	3.61	3.5
$N_e \times 10^{23}$ (m^{-3})	15.06	14.99	14.5	14.24	13.38
A_{cs} (A_s)	680 (219)	684 (219)	688 (227)	693 (231)	696 (246)
W_w = 0.45					
R_w (R_e) (nm)	6.50 (6.69)	6.51 (6.70)	6.57 (6.76)	6.60 (6.79)	6.73 (6.91)
$A_t \times 10^8$ (m^2 m^{-3})	2.96	2.96	2.89	2.87	2.79
$N_e \times 10^{23}$ (m^{-3})	5.58	5.55	5.34	5.25	4.9
A_{cs} (A_s)	1447 (483)	1422 (455)	1435 (474)	1447 (483)	1463 (517)

[a]The cross sectional areas of CPC and butan-1-ol used for calculation are 0.71 and 0.20 nm^2, respectively.
[b]The error limits of R_w (R_e), A_t, N_e, and A_{cs} (A_s) are within ±5, ±6, ±6, and ±8%, respectively.

N_e decreases, and the A_{cs} tends to increase; and for pentan-1-ol (Table 3) except for A_{cs}, a reverse trend is observed with temperature. The A_{cs} values presented in Tables 2 and 3 are all greater than A_s under all conditions. Both $A_{cs} > A_s$ and $A_{cs} < A_s$ have been observed in the previous study (11) working with microemulsions comprising different classes of surfactants, cosurfactants, and oils. The R_e:R_w ratio is on the whole independent of the system composition and temperature. The average value of this ratio obtained in the temperature range of 298–318 K for the butan-1-ol system is 1.180 and that for the pentan-1-ol system is 1.142, giving a combined average of 1.161. This agrees well with our previous report (11), (1.150) and the value of (1.180) reported by Lagourette et al. (24).

The R_w and R_e profiles as a function of W_w at different σ and at 298 K for both the studied microemulsion systems are presented in Fig. 5. It is seen in the figure that both R_w and R_e increase curvilinearly with W_w and the difference between them decreases with increasing σ; for the butan-1-ol system at σ = 0.50, both R_w and R_e almost merge. At higher σ, the size of the waterpool becomes larger and the contribution of the thickness of the interphase is relatively low. The system with pentan-1-ol produces smaller droplets and the contribution of the interphase is still visible at σ = 0.50. Comparable variation in R_w with W_w on the other microemulsion systems was observed in the past (10, 11). In Fig. 6, the number density of the droplets (N_e) are plotted against W_w at different σ values at 298 K. The decline in N_e with W_w is exponential and the value of N_e with butanol is greater than N_e with pentanol in accordance with the R_w relationship between the two alkanols. The N_e values obtained in this study are appreciably higher than those reported earlier (10, 11) with CTAB, SDS, and AOT as surfactants, butan-1-ol and hexylamine as cosurfactants, and using different types of oil.

The A_{cs} and A_s relationship with W_w at different σ values at 298 K (Fig. 7) are also curvilinear; both the parameters increase with W_w and the spread between the two decreases with σ. The cosurfactant, pentan-1-ol gives more spread at each σ compared to butan-1-ol. Such a comparison was not done in our past study but, as mentioned earlier, A_{cs} has been found to be both higher and lower than A_s for a single surfactant:co-surfactant ratio, σ = 0.50 at 293 and 303 K. The more efficient crowding of pentan-1-ol compared to butan-1-ol in the interphase due to its better hydrophobicity (lower aqueous solubility) lowers the interfacial tension more for efficient nanodispersion of water with lower droplet size and increased droplet number. It may be stated here that the dependence of A_t with W_w at different σ values at a constant temperature has been observed to be nearly linear

© 2001 NRC Canada

Table 3. Structural parameters[a, b] of water/CPC–pentanol/hexane microemulsion system at σ = 0.50 and at different weight fractions and temperature.

Structural parameters	Temperature (K)				
	298	303	308	313	318
W_w = 0.05					
R_w (R_e) (nm)	2.95 (3.59)	2.83 (3.58)	2.77 (3.56)	2.75 (3.57)	2.76 (3.57)
$A_t \times 10^8$ (m^2 m^{-3})	1.86	2.97	2.99	3.12	3.03
$N_e \times 10^{23}$ (m^{-3})	24.04	30.15	30.82	32.16	31.39
A_{cs} (A_s)	242 (105)	343 (112)	356 (109)	366 (105)	365 (107)
W_w = 0.15					
R_w (R_e) (nm)	3.97 (4.37)	3.73 (4.22)	3.65 (4.17)	3.60 (4.15)	3.63 (4.16)
$A_t \times 10^8$ (m^2 m^{-3})	0.99	2.87	2.91	2.99	2.94
$N_e \times 10^{23}$ (m^{-3})	12.84	16.58	17.26	18.13	17.65
A_{cs} (A_s)	420 (183)	570 (186)	580 (179)	593 (170)	593 (175)
W_w = 0.20					
R_w (R_e) (nm)	4.57 (5.28)	4.26 (5.13)	4.16 (5.05)	4.10 (4.98)	4.13 (5.03)
$A_t \times 10^8$ (m^2 m^{-3})	0.75	2.88	2.93	3.02	2.95
$N_e \times 10^{23}$ (m^{-3})	9.74	12.76	13.41	14.22	13.69
A_{cs} (A_s)	528 (229)	703 (229)	708 (218)	717 (205)	726 (213)
W_w = 0.25					
R_w (R_e) (nm)	5.28 (5.52)	4.89 (5.19)	4.77 (5.10)	4.69 (5.04)	4.73 (5.07)
110 A_t (m^2 m^{-3})	0.53	2.73	2.77	2.86	2.81
1025 N_e (m^{-3})	6.89	9.19	9.65	10.35	9.95
A_{cs} (A_s)	702 (305)	912 (297)	919 (283)	920 (264)	933 (274)
W_w = 0.41					
R_w (R_e) (nm)	8.32 (9.07)	7.57 (8.48)	7.38 (8.30)	7.22 (8.14)	7.30 (8.23)
111 A_t (m^2 m^{-3})	0.17	2.18	2.22	2.29	2.25
1026 N_e (m^{-3})	2.22	3.05	3.25	3.49	3.36
A_{cs} (A_s)	1745 (759)	2153 (701)	2142 (659)	2142 (614)	2169 (638)

[a]The cross sectional areas of CPC and pentan-1-ol used for the calculations are 0.71 and 0.20 nm^2, respectively.
[b]The error limits of R_w (R_e), A_t, N_e, and A_{cs} (A_s) are within ±5, ±6, ±6, and ±8%, respectively.

with mild curvature here and there in line with our previous study (11).

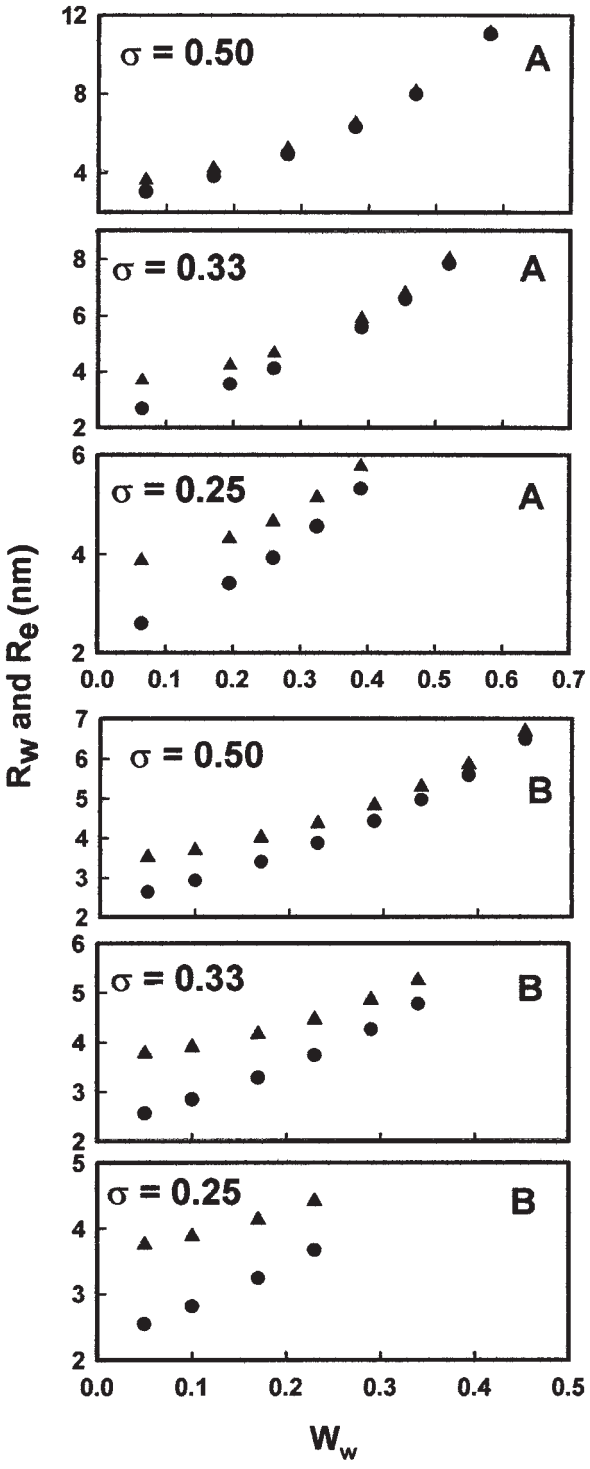
Temperature dependence of structural parameters

In the literature, conflicting results on the dependence of droplet dimension on temperature obtained by different methods are reported. Both decreased and increased droplet size for AOT stabilized water/oil microemulsions in long chain alkanes as oils have been reported from SANS and TRFQ methods (25–27). A change in the droplet dimension of 20–35% (decrease or increase) for a temperature range of 25–35°C has been observed. In the previous report (11) for a 10° rise in temperature we have observed R_w to decrease to the extents of 1, 5, 8, 3, 4, and 8% for CTAB-butanol, SDS-butanol, AOT-butanol, CTAB-hexylamine, SDS-hexylamine, and AOT-hexylamine with 1-heptane as the oil. This, on the whole, agrees with the 20% decrease observed by Rouviere et al. (27) for a temperature increase of 23°. In the present study, for a temperature rise of 20°, we have observed a max decrease of 12% in R_w for the CPC–pentanol case; for the CPC–butanol system, R_w increases instead and maximizes at 4%. These results manifest the differences in the activities of the two alkanols used in this study. The dependence of R_w on temperature for the two systems are presented in Fig. 8 at different W_w and σ values. Small increases and decreases in R_w are observed. More changes in R_w with temperature at higher W_w for the CPC–butanol system (not shown in Fig. 8) have been observed.

The dependence of the aggregation numbers, A_{cs} and A_s (with each droplet in the microemulsion) on temperature is an important aspect of microemulsion stability. For butanol and hexylamine, a max decrease in A_s of 27% and an increase in A_{cs} of 32% have been observed by us for a 10° rise in temperature by the conductance method (11). An increase in the aggregation number of AOT by 50% for a 18° temperature increase has been reported by Lang et al. (26) by the TRFQ method and they have shown an increase of more than 100% for AOT in 1-decane for a temperature rise of 40°. In this study, we have observed a 35% increase in A_{cs} and 16% decrease in A_s for the CPC–pentanol combination, and 2 and 7% increases in A_{cs} and A_s, respectively, for the CPC–butanol pair. The percentage increase in A_{cs} and decrease in A_s observed was also found earlier by us (11) with butan-1-ol as the cosurfactant. For both the studied systems, we find that the total aggregation number A_{scs} ($=A_{cs} + A_s$) within the limits of experimental errors remains virtually independent of temperature. Working at only two temperatures, a decrease in A_{scs} with increasing temperature was

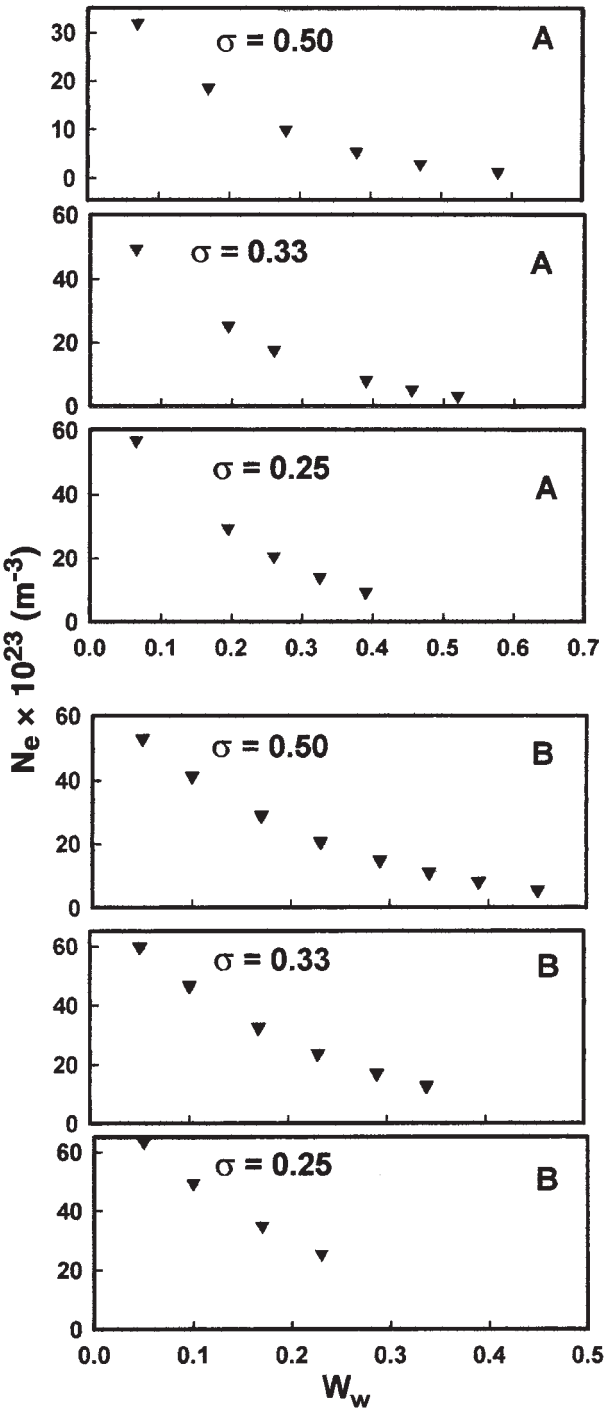
© 2001 NRC Canada

Fig. 5. (*a*) The dependence of R_w and R_e on W_w at 298 K at different σ for the water/CPC–butanol/*n*-hexane system. Symbols: ● R_w, ▲ R_e; (*b*) The dependence of R_w and R_e on W_w at 298 K at different σ for the water/CPC–pentanol/*n*-hexane system. Symbols: ● R_w, ▲ R_e.



revealed earlier (11). Although A_{scs} is relatively constant, the contributions from the two components (A_{cs} and A_s) are self-adjusting to maintain the observed trend in R_w.

Fig. 6. (*a*) The dependence of N_e on W_w at 298 K at different σ for the water/CPC–pentanol/*n*-hexane system; (*b*) The dependence of N_e on W_w at 298 K at different σ for the water/CPC–butanol/*n*-hexane system.



Thermodynamics of transfer of alkanol from the oil to the interphase

The thermodynamic parameters, Gibbs free energy, enthalpy, and entropy of the said transfer process (ΔG_t°, ΔH_t° and ΔS_t°, respectively,) have been obtained from the structure factor *r* and the microemulsion composition following the rationale presented in subsection two of the

© 2001 NRC Canada

Fig. 7. (*a*) The dependence of A_{cs} and A_s on W_w for the water/CPC–butanol/*n*-hexane system at 298 K at different σ. Symbols: ◆ A_{cs}, ■ A_s; (*b*) The dependence of A_{cs} and A_s on W_w for water/CPC–pentanol/*n*-hexane system at 298 K at different σ. Symbols: ◆ A_{cs}, ■ A_s.

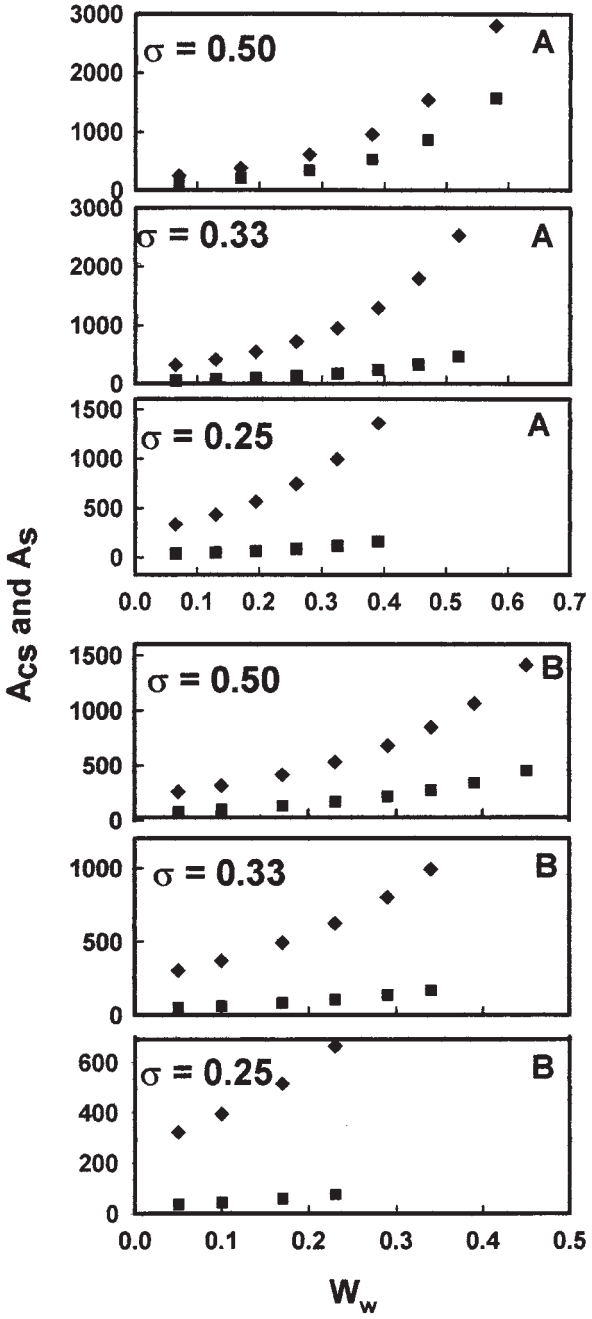
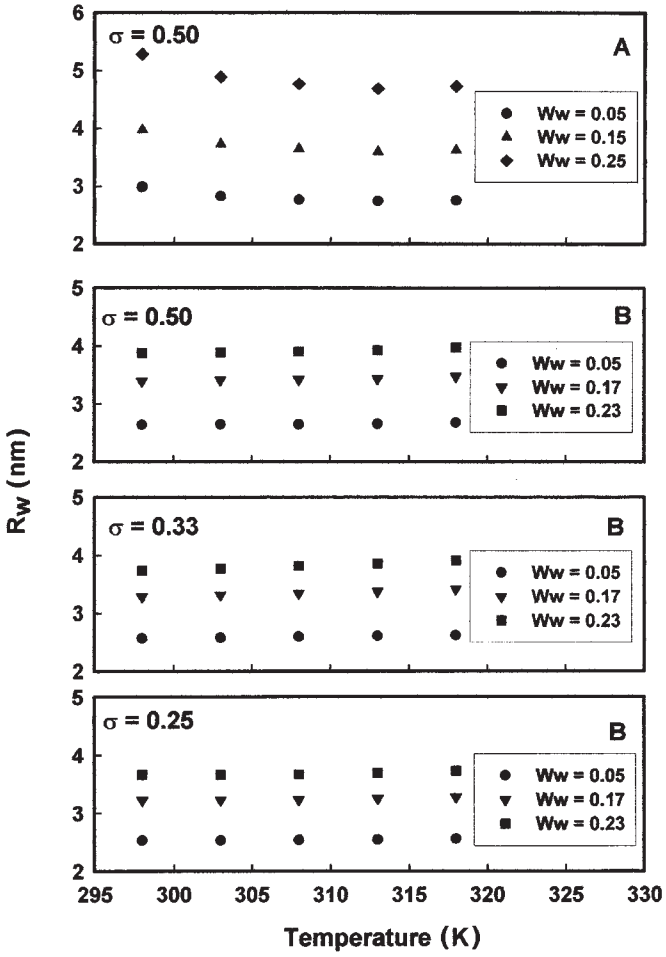


Fig. 8. (*a*) The R_w–temperature profiles for water/CPC–pentanol/*n*-hexane system at σ = 0.50 for different W_w; (*b*) The R_w–temperature profiles for water/CPC–butanol/*n*-hexane system at different σ and W_w.



theoretical background. The results realized for the two microemulsion systems at different σ and temperature values are presented in Table 4. It is observed from the results that ΔG_t° has a mild dependence on both σ and temperature for the system with CPC–butanol. For the other system with CPC–pentanol, the magnitude of ΔG_t° decreases with increasing σ but the temperature dependence is even more mild. On the whole, the transfer process for the second system is slightly more spontaneous than the first. The ΔH_t° values for the second are very small and exothermic, but are endothermic and higher in magnitude for the first. The ΔS_t° are all positive, the second system is less disordered for the transfer process than the first. The exothermic, with a lower ΔS_t°, transfer of pentan-1-ol from the oil to the interphase speaks in favor of an interfacial stabilization which is greater than for the transfer of butan-1-ol.

It may be mentioned here that the magnitudes of the transfer parameters of the alkanols herein obtained are mostly different from those reported by the method of dilution (28, 29). A recent calorimetric method reported that the ΔH_t° and ΔS_t° are both negative (30). These are not in line with the present observations. The ΔG_t° values, however, agree with the earlier findings of Gerbacia and Rosano (31). A comparative study using both the conductivity and the dilution methods under similar experimental conditions would be a worthwhile physicochemical endeavor. This area has been only minimally explored.

Thermodynamics of droplet clustering (association)

On consideration of formation of a pseudophase by the clustering of the droplets at the threshold of conductance percolation (comparable with the formation of micellar pseudophase), the thermodynamics of the said clustering

© 2001 NRC Canada

Table 4. Thermodynamic parameters[a] for the transfer of cosurfactant from the oil-phase to the interphase at 298 K, (45% water).

System	σ	Temperature (K)	r	ΔG_t° (kJ mol^{-1})	ΔH_t° (kJ mol^{-1})	ΔS_t° (J K^{-1} mol^{-1})
H_2O/CPC–butanol/hexane	0.50	298	2.94	–2.03	3.16	17.4
		303	3.07	–2.11		
		308	3.25	–2.21		
		313	3.49	–2.36		
		318	3.40	–2.34		
	0.33	298	5.32	–2.28		
	0.25	298	8.24	–2.50		
H_2O/CPC–pentanol/hexane	0.50	298	3.11	–2.06	–1.26	2.7
		303	3.13	–2.11		
		308	3.03	–2.09		
		313	3.00	–2.10		
		318	2.83	–2.04		
	0.33	298	5.94	–2.48	–0.78	5.6
		303	5.79	–2.47		
		308	5.53	–2.43		
		313	5.34	–2.40		
		318	5.15	–2.38		
	0.25	298	8.67	–2.65	–0.62	6.8
		303	8.70	–2.70		
		308	8.70	–2.74		
		313	8.56	–2.75		
		318	8.37	–2.74		

[a]The error limits of ΔG_t°, ΔH_t°, ΔS_t°, are within ±5, ±7, and ±10%, respectively.

Table 5. Thermodynamic parameters[a] for droplet association for the water/CPC–butanol/hexane and water/CPC–pentanol/hexane systems at different weight fractions at 298 K.

System[b]	W_w	ΔG_{cl}° (kJ mol^{-1})	ΔH_{cl}° (kJ mol^{-1})	ΔS_{cl}° (J K^{-1} mol^{-1})
H_2O/CPC–butanol/hexane (σ = 0.50) (20:44:36)	0.20	–20.0	–11.5	28.5
H_2O/CPC–pentanol/hexane (σ = 0.50) (23:61.6:15.4)	0.23	–15.7	–13.5	7.4
H_2O/CPC–pentanol/hexane (σ = 0.33) (17:66.4:16.6)	0.17	–17.8	–13.7	13.8
H_2O/CPC–pentanol/hexane (σ = 0.25) (10:72:18)	0.10	–15.6	–15.6	0

[a]The error limits of ΔG_{cl}°, ΔH_{cl}°, ΔS_{cl}°, are within ±4, ±6, and ±10%, respectively.
[b]Mass % compositions are given in the parentheses.

(association) process have been evaluated in terms of eqs. [11], [12]. The results for different microemulsion compositions and σ values at 298 K are presented in Table 5. It is observed from the ΔG_{cl}° values that the process of clustering is fairly spontaneous, the CPC–butanol system more so than the CPC–pentanol system. The dependence of ΔG_{cl}° on σ is not systematic. The ΔH_{cl}° values are all reasonably large and negative, and the ΔS_{cl}° values are small and positive; the latter is relatively much larger for the system with butan-1-ol than with pentan-1-ol. The thermodynamics of the clustering of droplets in microemulsion have been recently studied by us (14, 15) and Alexandradis et al. (16) exploiting the method of conductance as herein presented with AOT as the surfactant (which nicely forms microemulsion without a cosurfactant). The ΔH_{cl}° values obtained were all positive, and the corresponding ΔS_{cl}° values were large and positive. The results of this study are at variance with the above with respect to ΔH_{cl}° and ΔS_{cl}°.

It is considered (16) that during clustering, spherical droplets make mutual contacts and become to some extent flattened with absorption of heat (a process that acts against the bending energy that opposes deformation) manifested as the positive enthalpy change. The removal of the solvent molecules between the clustering droplets and the dissimilarities between the free volume of the mobile solvent molecules and the fixed surfactant molecules in the interphase contribute to the positive entropy change. In the present study, the free volume difference between the molecules of hexane (solvent) and the surfactant (CPC) is large, while these differences with butan-1-ol and pentan-1-ol (the cosurfactants) are minor so that the entropy change for the overall process of droplet clustering is also small. It should be also considered that $A_{cs} >> A_s$ (Tables 2 and 3) so that the contributions to ΔS_{cl}° coming from the free volume consideration of the alkanol is much more than from the CPC. It is also seen in Table 5 that ΔS_{cl}° with pentan-1-ol is appreciably lower than ΔS_{cl}° with butan-1-ol although the molecular size difference of the alkanols with *n*-hexane is less for the former than the latter. Since the $+\Delta S_{cl}^\circ$ values are low, the $T\Delta S_{cl}^\circ$ term cannot surpass the $-\Delta G_{cl}^\circ$ in the Gibbs–Helmholtz equation (meant for mutual adjustments among the energetic parameters) to produce a positive enthalpy change for the clustering

© 2001 NRC Canada

process. The association process appears to be a normal one occurring with the release of heat. Thus, although the flattening of the spherical nanodroplets during mutual contact in clustering (as envisioned for the cosurfactant-less microemulsion system with AOT) has been considered to produce positive ΔH_{cl}°, other steric factors may have a significant influence on the process when cosurfactant and oil of comparable size exist in the system. The cosurfactant may even make the interphasial region rigid (3) so that during clustering the interface is mildly or hardly flattened (32) to make the process enthalpy disfavorable. The rigidification of the interface is more with pentan-1-ol than butan-1-ol (33) so that ΔH_{cl}° is more favorable for the latter than the former. The contact between the droplets occur by the interplay of long range van der Waals forces of attraction to essentially become an enthalpy driven process.

The aforesaid analysis of the thermodynamics of the studied clustering process is only tentative. A systematic study using different surfactant–cosurfactant combinations and different types of oil is needed for a pragmatic understanding of the roles of the components in guiding the thermodynamics of the clustering process.

Conclusions

(1) The phase boundary in the ternary phase diagram of the water/CPC/butan-1-ol/*n*-hexane system is symmetric and dome-shaped whereas that of the water/CPC/pentan-1-ol/*n*-hexane system is triangular in shape at 298 K. The latter shows a gel region near the middle.

(2) The above microemulsion forming systems exhibit fair degrees of both volume- and temperature-induced percolations.

(3) The structure factor (r) and the conductance of the disperse phase (k_d) decrease and increase, respectively with the surfactant:cosurfactant mass ratio, σ at a constant temperature. At comparable conditions, r is higher and k_d is lower for pentan-1-ol compared to butan-1-ol as the cosurfactant.

(4) The waterpool diameter of the droplets and the ratio of the interfacial aggregation number (A_{cs}/A_s) are lower and higher with pentan-1-ol than butan-1-ol at comparable conditions. The size of the droplet increases mildly with temperature when butan-1-ol is the cosurfactant and decreases when it is pentan-1-ol.

(5) The free energies of transfer of the alkanols from the oil phase to the interphase (ΔG_t°) are lower than the limited data available in the literature on different systems, except for that of Gerbacia and Rosano (31). The transfer process is entropy-controlled.

(6) The thermodynamics of droplet clustering reported with the combined presence of surfactant and cosurfactant differ with respect to the enthalpy and entropy obtained for systems stabilized with AOT without a cosurfactant. The clustering of the studied system is an enthalpy driven process.

Acknowledgements

RP acknowledges the Operating Research Grant from the Natural Sciences and Engineering Research Council (NSERC) and SPM would like to thank St. F. X. University for the James Chair Visiting Research Professorship. We also would like to thank Mr. Louis Digout for all his technical assistance in the preparation of this manuscript.

References

1. J.H. Schulman, W. Stockenius, and L.M. Prince. J. Phys. Chem. **63**, 1677 (1959).
2. L.M. Prince. *In* Microemulsions. Academic Press, New York. 1977.
3. S.P. Moulik and B.K. Paul. Adv. Colloid Interface Sci. **78**, 99 (1998), and refs. therein.
4. B.K. Paul and S.P. Moulik. J. Dispersion Sci. Technol. **18**, 95 (1997).
5. M. Kahlweit, R. Strey, and R. Schomaker. *In* Reactions in compartmentalized liquids. *Edited by* W. Knoche and R. Schomaker. Springer–Verlag, New York. 1989. p. 1.
6. S. Avramiotis, H. Stamatis, F.N. Kolisis, P. Lianos, and A. Xenakis. Langmuir, **12**, 6320 (1996), and refs. therein.
7. M.P. Pileni. *In* Structure and reactivity in reverse micelles. Elsevier, Amsterdam. 1989.
8. M.P. Pileni. J. Phys. Chem. **97**, 6961 (1993), and refs. therein.
9. J. Sjoblom, R. Lindberg, and S.E. Friberg. Adv. Colloid Interface Sci. **95**, 125 (1996).
10. J. Fang and R. Venable. J. Colloid Interface Sci. **116**, 269 (1987).
11. S.R. Bisal, P.K. Bhattacharya, and S.P. Moulik. J. Phys. Chem. **94**, 350 (1990).
12. S. Pal, S.R. Bisal, and S.P. Moulik. J. Phys. Chem. **96**, 896 (1992).
13. S. Ray, S. Pal, and S.P. Moulik. J. Colloid Interface Sci. **183**, 6 (1996).
14. S. Ray, S.R. Bisal, and S.P. Moulik. J. Chem. Soc. Faraday Trans. 1, 3277 (1993).
15. S.P. Moulik and S. Ray. J. Pure Appl. Chem. **66**, 521 (1994).
16. P. Alexandradis, J.F. Holzwarth, and T.A. Hatton. J. Phys. Chem. **99**, 8222 (1995).
17. R.L. Venable. J. Am. Oil Chem. Soc. **51**, 115 (1985).
18. J.C. Maxwell. *In* Electricity and magnetism. 3rd ed. Oxford University, London. 1982.
19. C.J.F. Böttcher. Recl. Trav. Chim. Pays–Bas, **64**, 47 (1945).
20. D.A.G. Bruggeman. Ann. Phys. **24**, 636 (1935).
21. C.G. Granqvist and O. Hunderi. Phys. Rev. B: Condens. Matter, **37**, 1131 (1976).
22. S.R. Bisal, P.K. Bhattacharya, and S.P. Moulik. J. Phys. Chem. **94**, 4212 (1990).
23. V.K. Bansal, D.O. Shah, and J.P.O'Connell. J. Colloid Interface Sci. **75**, 462 (1980).
24. B. Lagourette, J. Peyrelasse, C. Boned, and M. Clausse. Nature (London), **281**, 60 (1979).
25. C. Toprakcioglu, J.C. Dore, B.H. Robinson, and H. Howe. J. Chem. Soc. Faraday Trans. 1, 80, (1984); J. Chem. Soc. Faraday Trans. 1, 413 (1984).
26. J. Lang, A. Jada, and A. Malliaris. J. Phys. Chem. **92**, 1946 (1988).
27. J.M. Rouviere, A. Court, M. Lindheimer, and B. Brun. J. Chim. Phys. Phys.–Chim. Biol. **76**, 297 (1979).
28. K.S. Birdi. Colloid Polym. Sci. **26**, 628 (1982).
29. H.N. Singh, S. Swarup, R.P. Singh, and S.M. Saleem. Ber. Bunsen–Ges. **87**, 1115 (1983).
30. G. Gu, W. Wang, and H. Yan. J. Therm. Anal. **51**, 115 (1998).
31. W. Gerbacia and H.L. Rosano. J. Colloid Interface Sci. **44**, 242 (1973).
32. R.T. Hamilton, J.F. Billman, and E.W. Kaler. Langmuir, **6**, 2 (1990), and refs. therein.
33. L. Mukhopadhyay, P.K. Bhattacharya, and S.P. Moulik. Colloids Surf. **50**, 295 (1990).

© 2001 NRC Canada

IR Spectroscopy of aqueous alkali halides. Factor analysis

Jean-Joseph Max, Serge de Blois, Alain Veilleux, and Camille Chapados

Abstract: The infrared spectra of ten salts in aqueous solutions were obtained in their solubility range using attenuated total reflection (ATR). The salts are: LiCl, NaCl, KCl, CsCl, $MgCl_2$, NaBr, KBr, NaI, KI, and CsI. The salts, which are completely ionized in water, do not absorb in the IR. Only their interactions with water are observed and analyzed. Factor analysis (FA) applied to the spectra showed that two principal species are present in the solutions: pure water and salt-solvated water. The modifications of the water spectrum are dependent on the nature of the salts, their concentrations and are mainly of first-order. Second-order effects were observed but, being weak, were not investigated. The modifications of the IR-ATR spectrum from pure water to a salt solution are proportional to the modifications of the imaginary part of the refractive index spectrum ($k(\nu)$). This indicates that the anomalous dispersion effects do not interfere with the chemical analysis of the IR-ATR spectra. In every salt studied, the two main species present in the solutions remained stable throughout the salt solubility ranges. Comparison between the IR spectra of the different salts solutions indicates that both anions and cations are in strong interaction with water molecules and are solvated together in stable clusters.

Key words: IR spectroscopy, ATR, liquid, aqueous solutions, factor analysis, principal spectra, LiCl, NaCl, KCl, CsCl, NaBr, KBr, NaI, KI, CsI, $MgCl_2$.

Résumé : Les spectres infrarouges de dix sels en solutions aqueuses dans la gamme de leur solubilité ont été obtenus par réflexion totale atténuée (ATR). Ces sels sont : LiCl, NaCl, KCl, CsCl, $MgCl_2$, NaBr, KBr, NaI, KI et CsI. Les sels qui sont complètement ionisés n'absorbent pas dans l'infrarouge, seules leurs interactions avec l'eau qui en modifie le spectre peuvent être observées et analysées. L'analyse par facteurs (FA) des spectres a montré que deux espèces principales sont présentes dans les solutions: l'eau liquide et l'eau de solvatation du sel. Les modifications du spectre de l'eau dépendent de la nature du sel, de sa concentration et sont principalement du premier ordre. Des effets du second ordre ont été observés, mais compte tenu de leur faible amplitude, ils n'ont pas été pris en compte. Les modifications du spectre IR-ATR de l'eau en présence de sel dans la solution sont proportionnelles aux modifications du spectre de la partie imaginaire de l'indice de réfraction, $k(\nu)$. Ceci démontre que les effets dus à la dispersion anormale sont stables et n'empêchent pas l'analyse chimique directe des spectres IR-ATR, sans la nécessité de passer en spectres $k(\nu)$. Dans chacun des sels étudiés, les deux espèces principales sont stables dans toute la gamme de solubilité. La comparaison des divers spectres d'eau de solvatation indique que les deux ions solubilisés sont en interaction forte avec des molécules d'eau et qu'ils sont solvatés ensemble (par paire) formant avec quelques molécules d'eau des agrégats stables.

Mots clés : spectroscopie IR, ATR, liquide, solutions aqueuses, analyse par facteurs, spectres principaux, LiCl, NaCl, KCl, CsCl, NaBr, KBr, NaI, KI, CsI, $MgCl_2$.

Introduction

In previous papers, we studied at 26.5°C aqueous solutions of NaCl, KCl, and CsCl (1–4) over the solubility range of the salts (as given in ref. 5) by attenuated total reflection infrared spectroscopy (IR-ATR). By applying factor analysis (FA) to the series of spectra, we found that all the spectra for each series could be represented by the sum of two spectra: one for pure water and one for the highest concentration of salt in the series, each spectrum being multiplied by a multiplying factor (MF). Finally, it was found that the MFs were proportional to the salt concentration, indicating that: (*i*) two types of water are present in the solutions; (*ii*) the spectrum of each sample is a linear combination of the spectra of the two types of water; (*iii*) for each type of water, the intensity of aqueous salt solutions follows the Beer–Lambert law. Based on these properties, a simple method of subtracting the water spectra from the IR spectra of aqueous solutions was developed (1, 6).

The spectrum of water is strongly modified when a binary salt, a strong acid, or a strong base is added to it (1–4, 6–10). ATR configuration provides easy sample manipulations and high reproducibility (1–4, 6, 7, 11–17). We previously reported that the modification of the ATR absorbance spectrum

Received October 25, 2000. Published on the NRC Research Press website on December 20, 2000.

J.-J. Max,[1] S. de Blois, A. Veilleux, and C. Chapados.[2] Département de chimie–biologie, Université du Québec à Trois-Rivières, C.P. 500, Trois-Rivières, QC G9A 5H7, Canada.

[1]Current address: Scientech R&D, 247, rue Thibeau, bur. 201, Cap-de-la-Madeleine, QC G8T 6X9, Canada.
[2]Author to whom correspondence may be addressed. Telephone: (819) 376-5052. Fax: (819) 376-5084. e-mail: Camille_Chapados@uqtr.uquebec.ca

 DOI: 10.1139/cjc-79-1-13 © 2001 NRC Canada

of water when a solute is added to the solution is almost proportional to the modification of the spectrum of the imaginary part of the refractive index of water ($k(\nu)$) (2, 4). This property of the ATR spectrum of water is valid only when: (*i*) a substantial difference exists between the refractive index of the crystal and that of the sample; (*ii*) the angle of incidence is higher than the crystal critical angle. The validity remains even when the concentration of water in the solutions is lowered by 35% compared to pure water. When both of these conditions are met, the direct ATR absorbance spectra reflect the chemical changes of the system (2, 4).

In the systems studied, the spectroscopic modifications depended on the species dissolved in water. The species studied — chloride salts (NaCl, KCl, CsCl), a strong acid (HCl), or a strong base (NaOH) — are completely ionized in water and the ions are either nonabsorbing or weakly absorbing compared to water (1–4, 6, 7). The spectroscopic modifications thus reflected the chemical modifications of water (8–10, 18). The changes in the ATR spectrum of water were proportional to the amount of ionic species. In the solutions analyzed, four different types of species of water were identified: pure water, salt-solvated water, HCl- and NaOH-solvated waters. While NaCl-solvated water is very similar to KCl-solvated water, CsCl-solvated water is different. This fact indicates that the cation plays a role in cluster organization. All four types of water remain unchanged in one another's presence except when a reaction occurs. For example, consider the titration of NaOH by HCl which gives NaCl (7). At the outset, pure water and NaOH-solvated water were identified. As the titration proceeded both types of water persisted until neutralization with the formed NaCl-solvated water. After neutralization, the latter was present, at almost constant amounts, with pure water and HCl-solvated water in increasing amounts as HCl was added to the solution. The presence of NaCl did not modify the structure of HCl- or NaOH-solvated waters. From an IR point of view, the ions of each of these species were not solvated separately or independently from their respective counter ions. These results do not support the usual concept of hydration shells of isolated ions (19–21) but are in conformity with previous observations establishing the cooperative action of anions and cations in spectral changes (22).

The groups led by Williams (9, 10) reported experimental values of the optical IR characteristics of aqueous solutions of several binary salts obtained by reflection measurements. Draegert and Williams (10) compared their far-IR results on salt solutions with the results reported by Bernal and Fowler (21) on pure water at different temperatures. The far-IR results on salts solutions were interpreted in terms of structure-makers and structure-breakers produced by solvated ions. The modifications varied with the size and charge of the ions (10). Subsequent results obtained by Rhine et al. (9) in the 5000–350 cm^{-1} region did not support this idea. Rather, they suggested that ion clustering may be a better interpretation of the IR spectra of salt solutions. The results these authors obtained were qualitative due to the low accuracy of the method used and the spectra not being normalized for the number of water molecules. FTIR-ATR sampling is a better method because the path length is fixed, the water bands do not saturate, and the spectra are reproducible.

The purpose of this paper is to obtain the IR-ATR spectra of aqueous solutions at several concentrations up to the solubility limit of several alkali halides (LiCl, NaCl, KCl, CsCl, NaBr, KBr, NaI, KI, and CsI) and one alkaline-earth halide ($MgCl_2$). The latter was added to the alkali series for the purpose of comparison. From the series of spectra we will: (*i*) determine the number of species present in the solutions; (*ii*) obtain the spectra of the species; (*iii*) determine the abundance of the species as a function of the salt concentration; (*iv*) compare the results to detect similarities and dissimilarities on the basis of ion sizes and types of halogens; (*v*) evaluate the optical effects produced by ATR sampling to determine if they prevent the direct chemical analysis of the IR-ATR spectra; (*vi*) evaluate the clustering effects of these salts.

Calculation methods

Factor analysis (FA)

Factor analysis is a method that can sort the principal spectra in series of evolving spectra as a function of one of the system's perturbing parameters such as temperature, pressure, concentration, etc. Within a set of experimental spectra, some spectra may represent pure or almost pure species. In such cases, these spectra can be used as principal spectra for FA (6, 7, 14–17) When the principal spectra can be easily and directly obtained from a set of experimental spectra, FA can be simply performed using a personal computer. Otherwise, a more demanding procedure has to be applied (23). For the salt solutions studied here we used the direct procedure. Each principal spectrum is multiplied by its MF and the results are added. The resulting spectrum is subtracted from the experimental one and the MFs are varied until the difference spectrum is minimized. The best fit is monitored by using the least-squares fit procedure. In the case of aqueous salt solutions, neither principal factor necessary for the procedure is orthogonal to the others since the solution with the highest salt concentration used as the second principal spectrum contains some water organized as in pure water (1–4). However, orthogonality is not required in the FA procedure.

Calculation of sample composition from MFs

The composition of a sample is calculated from the MFs obtained by FA by the method detailed in ref. 4. The concentration of each species present in the solution is obtained by multiplying the MF by the concentration of the corresponding species in the solution used for the principal spectrum. When the principal spectra used in applying FA are not orthogonal, the sample's solvent content is obtained by multiplying the amount of solvent in each solution used for the eigenspectra by its respective MF in the sample and calculating the sum of the values obtained.

Optical effects

Compared to transmission spectra, ATR sampling is known to produce stronger optical effects which modify the spectrum (24–27). These optical effects increase with a decreasing difference between sample and substrate refractive indices, and with a decreasing incidence angle (24, 25, 27). Furthermore, the optical effects are enhanced by the proximity

© 2001 NRC Canada

Table 1. Parameter values of the linear behavior of aqueous salt solutions and characteristics of FA applied to the IR spectra.

Salt	b	c	d	e	f	g	h	i	j	k
	LiCl	NaCl	KCl	CsCl	NaBr	KBr	NaI	KI	CsI	$MgCl_2$
Molar mass (g mol^{-1})	42.394	58.443	74.551	168.358	102.894	119.002	149.89	165.998	259.805	95.211
Variation of the sample density with the salt concentration (c: d = a + bc)										
a (kg L^{-1})	1.0001	1.0001	0.9999	1.0008	1.0002	0.9999	0.9996[a]	0.9992	0.9989	1.0019
b (kg mol^{-1})	0.0216	0.0377	0.0439	0.1239	0.0757	0.0816	0.1090[a]	0.1183	0.2000	0.0693
R^2 [c]	0.9995	0.9994	0.9997	0.9999	0.9999	0.9999	0.9999[a]	1.0000	1.0000	0.9994
Variation of n_D of the sample with the salt concentration (c: $n_D = n_0 + n_1 c$)										
n_0	1.33413	1.33719	1.33353	1.33376	1.33378	1.33374		1.33332		1.33470
n_1(L mol^{-1})	0.00780	0.00888	0.00896	0.01175	0.01289	0.01272	*0.02071*[b]	0.02071	*0.02355*[b]	0.02040
R^2 [c]	0.99933	0.99836	0.99932	0.99929	0.99948	0.99929		0.99995		0.99859
Highest concentration used at 26.5°C (for spectra on Figs. 6 and 7)										
c_{max} (mol L^{-1})	14.16	5.14	4.03	7.15	6.81	4.21	8.19	6.03	3.00	4.29
(g L^{-1})	600	300	300	1200	700	500	1230	1000	400	400
Number of spectra	13	7	7	15	11	11	15	15	17	15
Displacement of ν_2 (cm^{-1})	–4	–2	–2	–4	–8	–5	–20	–16	–4	2
Characteristics of the difference spectra										
Maximum intensity (absolute value in au) of the residue in the ν_2 region[d]										
	0.1	0.02	0.01	0.01	0.03	0.01	0.17	0.06	0.01	0.08
Mean intensity (in au) of the residue[e]										
	0.012	0.004	0.004	0.005	0.004	0.004	0.011	0.008	0.002	0.011

[a]Values taken from the experimental data of the present study.
[b]Values in italic were estimated from the other data (see text).
[c]R^2: quadratic error.
[d]Maximum peak intensity near 1637 cm^{-1} in the residue spectra of the series given for the worst case, that is: the solution where the difference spectrum is the highest (generally at half the maximum of salt concentration).
[e]Value calculated from the residue spectrum (4800–700 cm^{-1}) in the worst case for the series by $\frac{1}{2}\sqrt{\frac{\sum_N (\text{calc.} - \text{exp.})^2}{N-1}}$, where N is the number of data points.

of two strong absorption bands (26). However, as we recently reported, with appropriate ATR sampling the optical effects in the IR spectrum of water are hardly modified when a binary salt is added to the solution. When NaCl, KCl, or CsCl is added to water, the modification of the ATR spectrum is almost proportional to the modification of the $k(\nu)$ spectrum (2, 4).

To evaluate the optical effects in an ATR spectrum, it is necessary to transform it into $k(\nu)$ and $n(\nu)$ spectra. Refractive indices n and k were calculated from the ATR spectra following the method detailed in ref. 2 and used in ref. 4. The value of n was calculated using the Kramers–Krönig transform of k, which was obtained by using an FFT algorithm twice with the proper modifications of the input data parity function. The ATR spectra were recalculated with equations provided in ref. 11 using the substrate and sample complex refractive indices. The excellent fit between experimental and calculated ATR spectra was the validity criterion.

Experimental

Chemicals and solutions

Deionized water was used to prepare the aqueous solutions. Dried salts (24 h at 65°C) of LiCl, NaCl, KCl, CsCl, NaBr, KBr, NaI, KI, CsI, and $MgCl_2$ (all from Aldrich, purity 99%) were used to prepare the aqueous solutions up to their concentration limits. Homogeneous solutions were obtained by weighing the salts in 10 mL volumetric flasks and completing with water. The resulting total mass was measured. The density of the solutions was obtained and compared to the literature data (5, 28).

Density and refractive index of salt solutions

The density of the aqueous solutions as a function of salt concentration c (in mol L^{-1}) of the 10 salts are well approximated by linear relationships. The experimental results obtained by this study are similar to available reported values to within 0.6% (Table 1) (5, 28). The refractive index at the sodium D line (n_D, 17 000 cm^{-1}) (29) as a function of salt concentration of the salt aqueous solutions were obtained from the literature (5) and proven to be well approximated by linear functions with only a negligible second order variation (Table 1).

The value of n_∞ is needed to calculate $k(\nu)$ and $n(\nu)$ (2, 4). We used the n_D values for that purpose. The latter may be considered to be near infinite frequency because it is far from any vibrational and electronic absorption bands (9). The n_D values not available in handbooks were obtained by extrapolation on the basis that, for ions in water, refractivity (n_D) is additive (21). The values are listed in Table 1. The n_D values of 6.03 M KI and 8.19 M NaI obtained using that mode agreed with the literature values (9, 30).

IR measurements

The IR measurements were obtained using a model 510P Nicolet FT-IR spectrometer with a TGS detector. Two KBr windows isolated the measurement chamber from the outside.

© 2001 NRC Canada

The samples were contained in a "Circle cell" (SpectraTech, Inc.) equipped with a ZnSe crystal rod in an ATR configuration (the incident beam is at an angle of 45° with respect to the rod's axis). The spectral range of the ZnSe rod in the spectrophotometer is situated between 6500 and 630 cm^{-1}. The spectra taken at 26.5 ± 0.3°C with a resolution of 4 cm^{-1} were obtained under a flow of nitrogen to ensure a low residue of CO_2 and water vapors in the spectrometer. For the series of NaI, CsCl, CsI, and $MgCl_2$ salt solutions an accumulation of 200 scans were obtained. For the series of LiCl, NaCl, KCl, NaBr, KBr, and KI salt solutions, 20 scans were obtained. The spectrum of pure water and the highest concentrated salt solutions were obtained with an accumulation of 1000 scans from 6500 to 630 cm^{-1}. The cell was carefully washed and dried prior to each measurement. Model 510P is a single-beam spectrometer. A background with the empty cell was taken before the measurement of each sample.

The IR measurements consisted of obtaining the ATR background intensity (R_0) and the ATR sample intensity (R). The R/R_0 ratio produced intensity I for the spectral range studied. Thereafter, the data points {I ($\tilde{\nu}$) vs. $\tilde{\nu}$ (in cm^{-1})} of each spectrum were transferred to a Microsoft Excel spreadsheet program on a personal computer where the numerical treatments were performed. Then intensities I were transformed in absorbance (log (1/I)). A small baseline shift was made to obtain a null mean absorbance in the 4600–4450 cm^{-1} or 6500–6150 cm^{-1} region, depending on the range studied. The reported values of $k(\nu)$ in these regions are approximately 2×10^{-4} and 4×10^{-5} (12), corresponding to 3×10^{-3} and 6×10^{-4} ATR au, respectively. The ATR cell's effective number of reflection (m) as determined by the pure water spectrum and the $k(\nu)$ values from the literature (12) is 6.6.

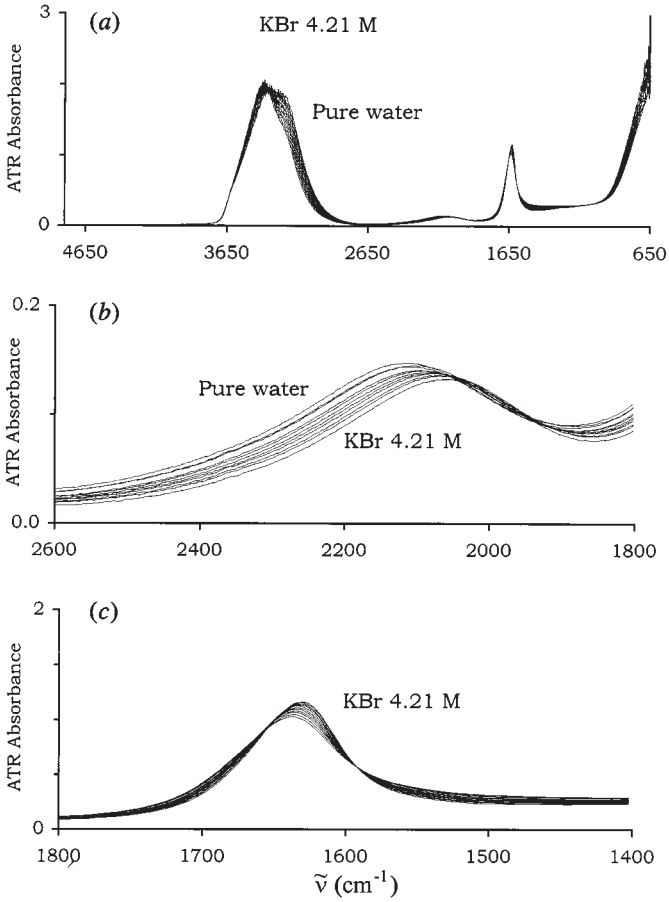
Factor analysis

The principal spectra needed to analyze the series of spectra of aqueous salts were determined from the experimental spectra: pure water and the highest concentrated salt solution. The absorbance of water in the 3450–3150 cm^{-1} region and below 750 cm^{-1} was near saturation, resulting in a noisy signal in these frequency ranges. The region below 700 cm^{-1} was eliminated in the least-squares procedure. The noise in the 3450–3150 cm^{-1} region somewhat reduced the accuracy of FA, but was kept in the minimization procedure. For a few of the salts, minimization produced a sigmoid flexure in certain regions due to a small band displacement.

Transforming ATR spectra into *k* and *n* spectra

The Kramers–Krönig transform is used in the transformation of the ATR spectra into k and n spectra with the use of a FFT algorithm (2, 11). The spectrophotometer supplied 3044 data points from 6500 to 630 cm^{-1}. Data from 0 to 630 cm^{-1} were not available and could not be found in the literature. We used a 8192-point FFT algorithm, thus requiring 4097 experimental data points for the input $k(\nu)$ function (4). The wave number interval between experimental data points was 1.92906 cm^{-1} with which the FFT calculation covered the 0–7900 cm^{-1} region. Values of k in the 6500–7900 and 0–630 cm^{-1} regions were put to 10^{-5}, which incidentally introduced an error below 1000 cm^{-1} (2, 4).

Fig. 1. Experimental IR-ATR absorbance spectra of KBr aq solutions (0–4.21 M). (*a*) Complete spectra; Expanded view of (*b*) 2100 cm^{-1} region; (*c*) HOH deformation region.



Results and discussion

FA applied to the ATR spectra

FA applied to the IR spectra of NaCl, KCl, and CsCl aqueous solutions have been previously reported (1–4). The following provides two examples of FA applied to the IR spectra of salt solutions. KBr was used to illustrate the solutions that behaved like NaCl (NaCl, KCl, NaBr, KBr, and CsI) and NaI for those that behaved differently (LiCl, CsCl, NaI, KI, $MgCl_2$). The FA procedure is the same and was applied to every salt solution presented here.

ATR spectra of aq KBr and NaI solutions

The experimental spectra of the KBr (0–4.21 M) and NaI (0–8.19 M) solutions are presented in Figs. 1 and 2, respectively. Expanded views of the principal regions are shown in Frames (*b*) and (*c*). When KBr and NaI are added to water, the ν_2 band shifts from 1637 to 1632 and 1617 cm^{-1}, respectively, (Figs. 1*c* and 2*c*). The displacement on the ν_2 band of NaI solutions is the greatest displacement observed on all the salts presented here (Table 1). These displacements concur with the data reviewed in ref. 31.

Factor analysis results of the series of ATR spectra

Figures 3 and 4 provide the results of FA applied to the series of experimental spectra of KBr and NaI solutions in

© 2001 NRC Canada

Fig. 2. Experimental IR-ATR absorbance spectra of NaI aqueous solutions (0–8.19 M). (*a*) Complete spectra; Expanded view of (*b*) 2100 cm^{-1} region; (*c*) HOH deformation region.

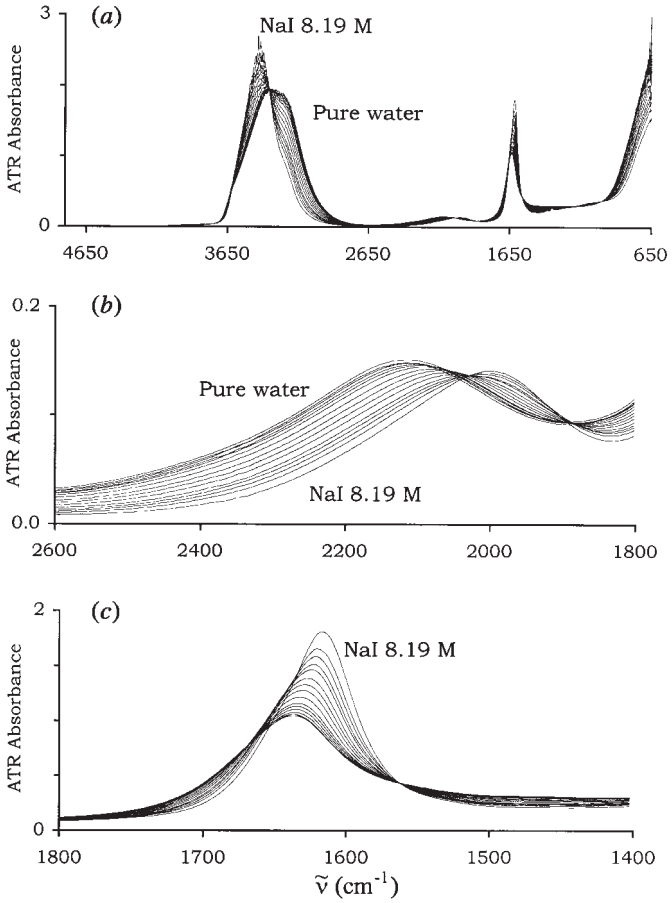
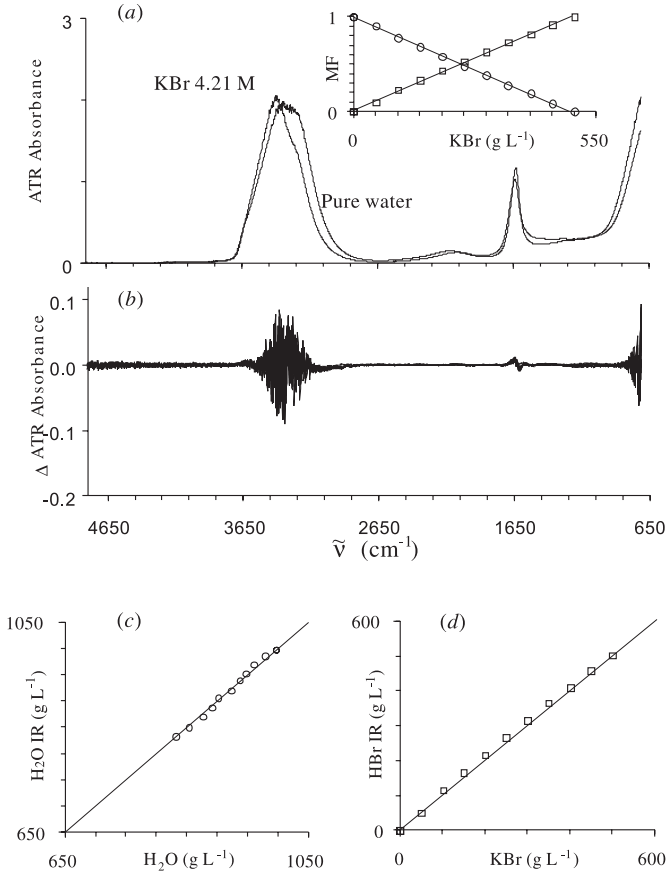


Fig. 3. Result of FA on the KBr aqueous solution spectra. (*a*) Principal spectra used in FA: pure water and 4.21 M KBr. Insert, MFs retrieved; (*b*) Residue spectra. Correlation between the concentration retrieved by IR and that obtained by gravimetry for: (*c*) water; and (*d*) KBr.



Figs. 1 and 2, respectively. The spectra of pure water and those of 4.21 M KBr (Fig. 3*a*) and 8.19 M NaI (Fig. 4*a*) were used as principal spectra in the FA procedure. The linear regressions (full lines in the inserts) of the MFs show that they are nearly proportional to the salt concentration.

The difference between experimental spectra and those retrieved from FA are presented in Figs. 3*b* and 4*b*, respectively. For KBr, compared to the intensity of the experimental spectra (Fig. 1), the residues are less than ±1% at maximum intensity in the strong absorption regions of the KBr solution spectrum and less than ±0.1% in the rest of the spectrum (Fig. 3*b*). For NaI, the residues are less than ±10% at maximum intensity in the ν_2 region of the NaI solution spectrum and less than ±1% in the rest of the spectrum (Fig. 4*b*). The latter percentages apply to the worst situations: the solution containing half the amount of salt of the more concentrated solution. Since the residues for the NaI solutions showed a progression with the salt concentration, we tried unsuccessfully to introduce a third species in the FA procedure. The sigmoid flexure seen in the residue spectra of NaI (Fig. 4*b*), which is due to the displacement of the ν_2 vibration of water, cannot come from the contribution of a stable species and does not result from optical effects (see the section on the optical effects evaluated by the ATR/$k(\nu)$ spectra). We attributed the residue spectra to second-order effects. Of the ten salts studied here, NaI exhibited the strongest second-order effects (Table 1). The residue spectra observed in the KBr solutions (Fig. 3*b*) are typical of what is observed in the other solutions. In Table 1, we report the worst cases in each series, that is the characteristics of the greatest difference spectra (difference between experimental and calculated spectra). The second-order effects are not very strong, even in the worst case. Although neglected in the present study, they are the object of ongoing research.

The two principal factors obtained by FA are sufficient to describe the entire series of KBr and NaI spectra (inserts, Figs. 3*a* and 4*b*). The same FA procedure applied to the rest of the salt solutions gave similar results. We previously obtained similar results for NaCl, KCl, and CsCl aqueous solutions (1–4). This indicates that two types of species of water are present in the samples: pure water and salt-solvated water.

Correlation between IR and gravimetry results

The MFs of Figs. 3*a* and 4*a* (inserts) were transformed into concentrations by the method found in the calculation of sample composition from MFs section. The plots of the concentrations obtained by IR as a function of those obtained by gravimetry are given in Figs. 3*c* and 3*d* for water and KBr, respectively. Those of NaI are given in Figs. 4*c* and 4*d*. The results indicate that all the points are near the solid line, which is the theoretical slope for a perfect one to one correlation. Although well within experimental error, a

© 2001 NRC Canada

Fig. 4. Result of FA on the NaI aqueous solution spectra. (*a*) Principal spectra used in FA: pure water and 8.19 M NaI. Insert, MFs retrieved; (*b*) Residue spectra. Correlation between the concentration retrieved by IR and that obtained by gravimetry for: (*c*) water; and (*d*) NaI.

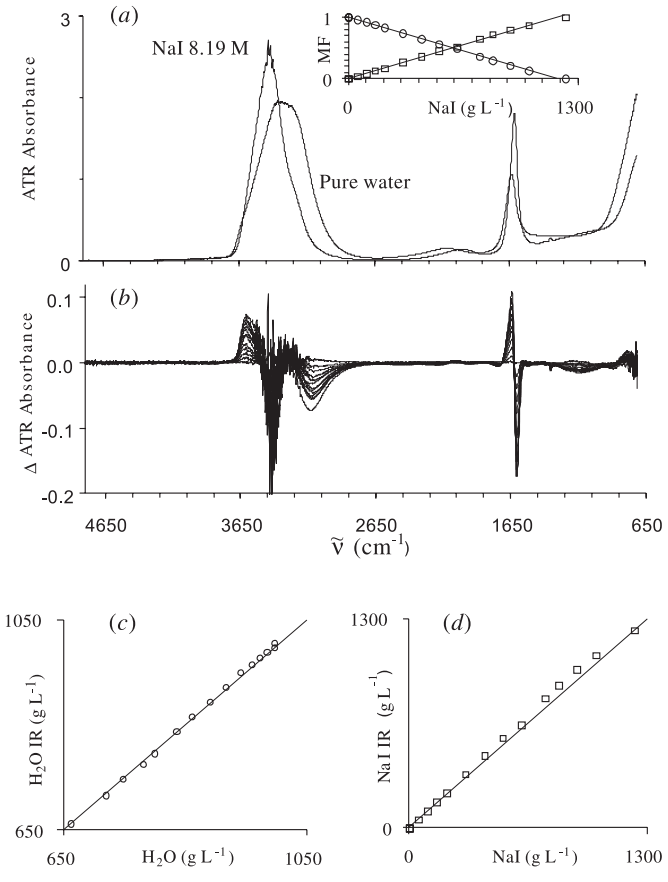
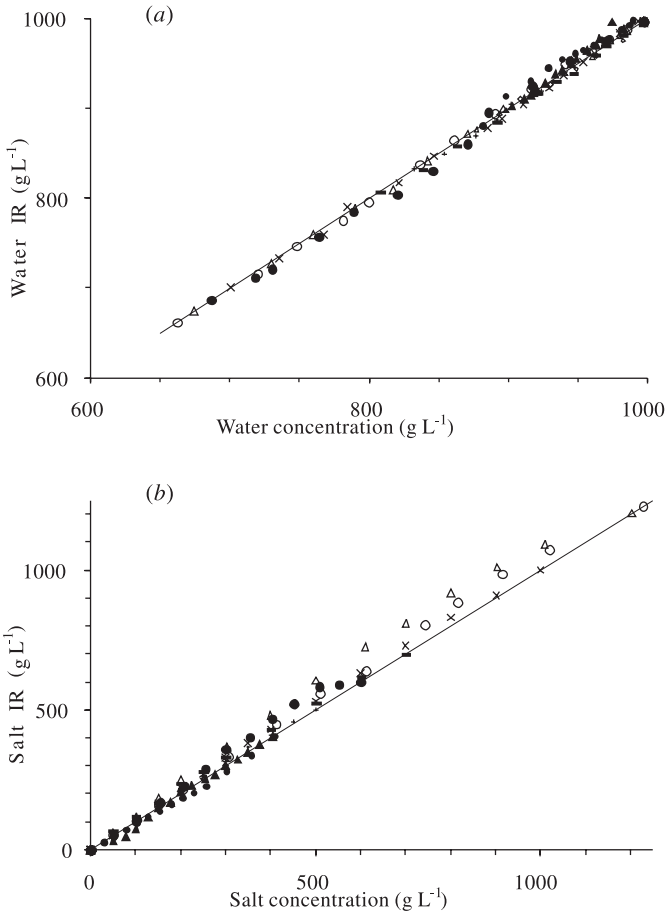


Fig. 5. Correlation between the concentrations retrieved by IR and those obtained by gravimetry for the 10 salts studied: (*a*) water; and (*b*) salt. (O) NaI; (Δ) CsCl; (×) KI; (–) NaBr; (•) LiCl and (▲) CsI. The other salts are not distinguishable.



small deviation from this theoretical one to one correlation which seems statistically significant is observed in Fig. 4*d* for the NaI concentration. This small deviation may stem from second-order effects (1, 4).

The correlation plots between the salt and water concentrations retrieved from the IR spectra and those obtained by gravimetry for all the salts are presented in Fig. 5*a* and 5*b*, respectively. The correlations are very good for the concentrations of both water (Fig. 5*a*) and salt (Fig. 5*b*), although the latter shows small deviations on the CsCl (Δ) and NaI (O) values. These results reinforce the idea that the alkali halides solutions are made up of two types of species, pure water and salt-solvated water, and that these species are stable throughout the entire solubility range, their concentrations depending on the amount of salts in the solutions.

Experimental ATR spectra and optical effects

The IR-ATR spectra are affected by AD, which may cause optical effects that could influence the direct relation between the spectra and the solutions. In particular, the second-order effects that we mentioned previously might have originated from these effects. In this section we address these issues by evaluating the ratio between the ATR and $k(\nu)$ spectra.

The experimental spectra

The experimental IR-ATR spectra of concentrated salt solutions are presented in Fig. 6 for NaCl-like spectra: 5.13 M NaCl, 4.03 M KCl, 6.82 M NaBr, 4.20 M KBr, and 3.00 M CsI. To these spectra we added the water spectrum (trace a). The slight differences observed between these spectra are mostly due to differences in salt concentration and water content.

The spectra which differ from NaCl are presented in Fig. 7 along with the spectrum of water: 14.16 M LiCl, 7.15 M CsCl, 8.19 M NaI, 6.03 M KI, and 4.29 M $MgCl_2$. These spectra not only differ from that of 5.13 M NaCl but are also very different one from the other.

Influence of the optical effects evaluated by the ATR/k(ν) spectra

For pure water and KCl- and CsCl-solvated water, we recently reported that IR-ATR and $k(\nu)$ spectra were related by (4):

$$[1] \qquad \frac{\mathrm{ATR}(\nu)_{\mathrm{solution}}}{k(\nu)_{\mathrm{solution}}} = \left(\frac{n_{\infty\,\mathrm{solution}}}{n_{\infty\,\mathrm{pure\ water}}}\right)^4 \frac{\mathrm{ATR}(\nu)_{\mathrm{pure\ water}}}{k(\nu)_{\mathrm{pure\ water}}}$$

© 2001 NRC Canada

Fig. 6. IR-ATR spectra of aqueous solutions of salts with spectral features similar to those of NaCl: (*a*) pure water; (*c*) 5.14 M NaCl; (*d*) 4.03 M KCl; (*f*) 6.81 M NaBr (g) 4.21 M KBr; and (j) 3.00 M CsI. (*a*) Complete spectra; Expanded view of (*b*) 2100 cm^{-1} region; (*c*) HOH deformation region.

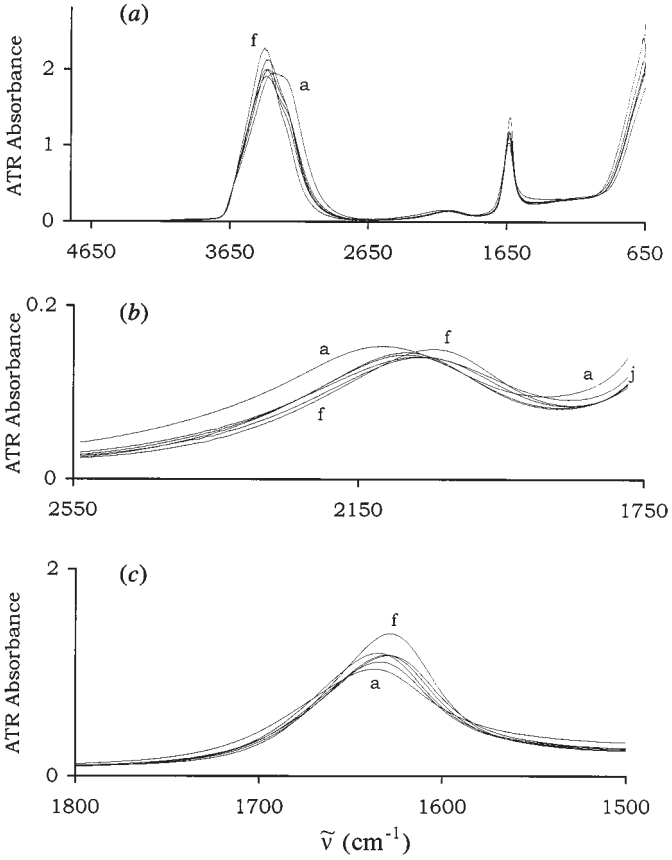
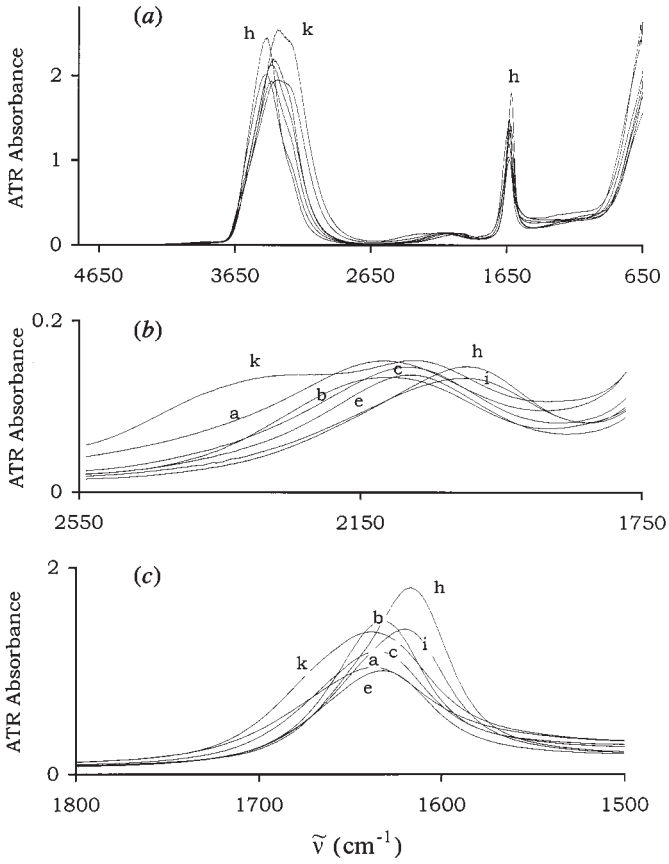


Fig 7. IR-ATR spectra of aqueous solutions of salts with spectral features different from those of NaCl: (*a*) pure water; (*b*) 14.16 M LiCl; (*c*) 5.14 M NaCl (for comparison); (*e*) 7.15 M CsCl; (h) 8.19 M NaI; (*i*) 6.03 M KI; and (k) 4.29 M $MgCl_2$. (*a*) Complete spectra; Expanded view of (*b*) 2100 cm^{-1} region; (*c*) HOH deformation region.

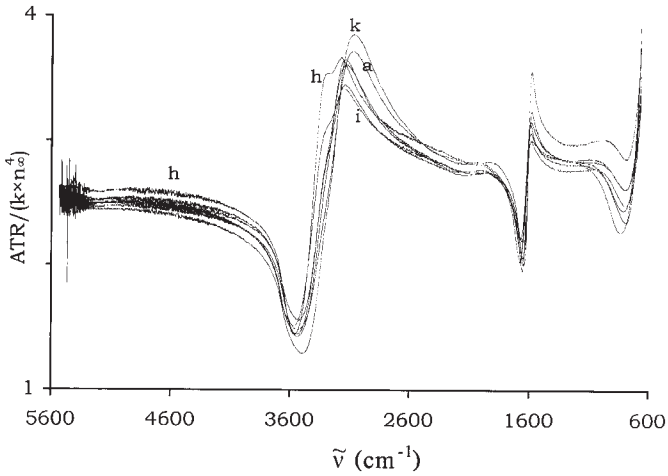


where n_∞ is the refractive index value at infinite wave number (taken as n_D). The correction for the amount of water molecules (1–3) can be omitted because it would be applied to both ATR and *k* spectra and hence is canceled in eq. [1], which is rewritten as follows:

$$[2] \qquad \frac{\mathrm{ATR}(\nu)_{\mathrm{solution}}}{k(\nu)_{\mathrm{solution}}(n_{\infty\,\mathrm{solution}})^4} = \frac{\mathrm{ATR}(\nu)_{\mathrm{pure\ water}}}{k(\nu)_{\mathrm{pure\ water}}(n_{\infty\,\mathrm{pure\ water}})^4}$$

To confirm the validity of eq. [2], the relation of ATR over ($k \times n_\infty^4$) for pure water and for each of the concentrated salt solutions of Fig. 7 were obtained and are presented in Fig. 8. In the latter, only salts that are not NaCl-like are presented because the NaCl-like salts gave overlapping results. The seven curves in Fig. 8 being close together indicates that eq. [2] is valid. The slight variations between the curves as opposed to exact equality are attributed to minor changes in AD effects (4). These results confirm that the modification of the ATR spectrum when a binary salt is added to pure water is proportional to the modification of the imaginary part of the refractive index (*k*) (eq. [1]). Therefore, the optical effects are not responsible for: (*i*) the modification of the ATR spectrum of salt-solvated water compared to that of pure water; (*ii*) the second-order effects observed (Figs. 3*b* and 4*b*).

Fig. 8. Ratios of the IR-ATR spectrum over that of the imaginary part of the refractive index $k(\nu)$ divided by n_∞^4 for the solutions indicated in Fig. 7 (See text, eq. [2]).



© 2001 NRC Canada

Furthermore, the mean value of ATR/($k \times n_\infty^4$) in the 5300 –5450 cm^{-1} region was found to be 2.52 ± 0.09, which can be compared to the square root of the effective number m of reflections in the ATR crystal ($m^{1/2} = 6.6^{1/2} = 2.57$). Work is in progress to substantiate this relation.

Ion pairing in salt-solvated water

The spectrum of NaI is different from that of CsCl (Fig. 7), and both of them are different than that of NaCl. The latter is similar to the spectrum of CsI (Fig. 6). Therefore, no combination of the spectra of NaI and CsCl solutions can give the spectra of NaCl and CsI, which would be the case if the ions were solvated independently. This result does not support previous interpretations that considered monoatomic ions to be solvated independently (8–10, 19, 32–35). Rather, it strengthens our previous interpretation that each pair of ions (monoatomic ions) are bound together, solvated by a fixed number of water molecules to form a cluster (1–4, 7). FA results show that the spectra of aqueous salt solutions are linear combinations of two principal spectra, one for pure water and one for salt-solvated water (refs. 1–4 and present work). Therefore, the clusters made up of one set of salt ions and a fixed number of water molecules are stable throughout the solubility range of these salts. The clusters behave as strongly bound units where the cations and anions are close together in each cluster (3, 4). The differences observed in the spectra (Fig. 7) are the manifestation of the differences in the strong interaction between the ion pairs and water. These conclusions shed new light onto the water solvation process and may be useful for the interpretation of neutron scattering experiments on aqueous solutions (32, 33). Work is in progress which will determine the hydration numbers from the IR spectra.

$MgCl_2$ solutions

The spectrum of 4.29 M $MgCl_2$, an alkaline–earth chloride salt (Fig. 7k) is very different from all other alkaline chloride salts presented in Fig. 7. The intensity of the OH stretching band's low-frequency wing is greatly increased, contrary to the others. This cannot be attributed to the Mg^{2+} solvated ion alone, because the spectrum reported for 7.7 M $Mg(NO_3)_2$ does not exhibit a low-frequency wing as intense as for $MgCl_2$ (36). Therefore, the comparison between the spectrum of aqueous $MgCl_2$ and that of aqueous $Mg(NO_3)_2$ is additional evidence of ion pairing in aqueous solution.

Conclusion

Using adequate ATR sampling, the changes in the ATR spectrum of water are proportional to the changes in its k spectrum. This proves unambiguously that the optical effects do not vary much and that the IR-ATR technique is highly reliable for quantitative chemical analysis of aqueous solutions made directly from the experimental IR-ATR spectra. The elimination of the optical effects is only needed to extract exact optical characteristics of samples.

Factor analysis showed that the IR spectra of aqueous binary salt solutions, and one ternary salt solution, are proportional to the salt concentration. For all the salts studied, two main types of species of water were obtained: pure water and salt-solvated waters. These types of water are stable in the whole solubility range of the salt. These results are added proof of ion pair clustering in water (3, 4, 9). When an alkali halide salt and $MgCl_2$ is dissolved in water, it forms clusters with a finite number of water molecules per ion pair. These clusters are stable throughout the solubility range of the salt. Second-order effects and the behavior of other alkaline earth halides besides $MgCl_2$ are the objects of ongoing research.

References

1. J.-J. Max, M. Trudel, and C. Chapados. Appl. Spectrosc. **52**, 234 (1998).
2. J.-J. Max and C. Chapados. Appl. Spectrosc. **53**, 1045 (1999).
3. J.-J. Max and C. Chapados. Appl. Spectrosc. **53**, 1601 (1999).
4. J.-J. Max and C. Chapados. J. Chem. Phys. **113**, 6803 (2000).
5. C. Weast. Handbook of chemistry and physics. 57th ed. CRC Press, Cleveland. 1977.
6. J.-J. Max and C. Chapados. Appl. Spectrosc. **52**, 963 (1998).
7. J.-J. Max and C. Chapados. Can. J. Chem. **78**, 64 (2000).
8. G. Zundel. The hydrogen bond, recent developments in theory and experiments. *Edited by* P. Schuster, G. Zundel, and C. Sandorfy. North Holland Pub. Co., Amsterdam. Chap. 15. 1976.
9. P. Rhine, D. Williams, G.M. Hale, and M.R. Querry. J. Phys. Chem. **78**, 238 (1974).
10. D.A. Draegert and D. Williams. J. Chem. Phys. **48**, 401 (1968).
11. J.E. Bertie, M.K. Ahmed, and H.H. Eysel. J. Phys. Chem. **93**, 2210 (1989).
12. J.E. Bertie and Z. Lan. Appl. Spectrosc. **50**, 1047 (1996).
13. K. Rahmelow and W. Hübner. Appl. Spectrosc. **51**, 160 (1997).
14. J.-J. Max, G. Bérubé, M. Trudel, S. Groleau, and C. Chapados. Langmuir, **14**, 5051 (1998).
15. J. Baril, J.-J. Max, and C. Chapados. Can. J. Chem. **78**, 490 (2000).
16. J.-J. Max, C. Ménichelli, and C. Chapados. J. Phys. Chem. **104**, 2845 (2000).
17. J.-J. Max, M. Trudel, and C. Chapados. Appl. Spectrosc. **52**, 226 (1998).
18. M.R. Querry, R.C. Waring, E. Holland, G.M. Hale, and W. Nijm. J. Opt. Soc. Am. **62**, 849 (1972).
19. D. Bratko, L. Blum, and D.Q. Wei. *In* Interactions of water in ionic and nonionic hydrates. *Edited by* H. Kleeberg. Springer–Verlag, Berlin. 1987. p. 27; H. Kleeberg. *In* Interactions of water in ionic and nonionic hydrates. *Edited by* H. Kleeberg. Springer–Verlag, Berlin. 1987. p. 89.
20. B. Douglas, D.H. McDaniel, and J.J. Alexander. Concepts and models of inorganic chemistry. 2nd ed. John Wiley & Sons, Inc. New York. 1982.
21. J.D. Bernal and R.H. Fowler. J. Phys. Chem. **1**, 515 (1933).
22. D.W James and R.L. Frost. J. Chem. Soc. Faraday Trans. 1, **74,** 583 (1978).
23. C. Chapados and M. Trudel. Biophys. Chem. **47**, 267, (1993).
24. B. Crawford, T.G. Goplen, and D. Swanson. Advances in infrared and Raman spectroscopy. *Edited by* R.J.H. Clark and R.E. Hester. Heyden, London. Chap. 2. 1978, and refs. therein.
25. M. Milosevic, N.J. Harrick, and S.L. Berets. Appl. Spectrosc. **45**, 126 (1991).
26. J.B. Huang and M.W. Urban. Appl. Spectrosc. **46**, 1014 (1992).
27. M. Hancer, R.P. Sperline, and J.D. Miller. Appl. Spectrosc. **54**, 138 **(**2000).
28. N.A. Lange. Handbook of chemistry. 9th ed. Handbook Publisher, Inc., Sandusky, OH. 1956.

© 2001 NRC Canada

29. D.E. Gray. American Institute of Physics handbook. 3rd ed. McGraw Hill, New York. 1972. pp. 6–106.
30. G.A. Miller. J. Chem. Eng. Data, **21**, 188 (1976).
31. R.E. Verrall. Water, a comprehensive treatise. *Edited by* F. Franks. Plenum Press, New York. Chap. 15. 1973.
32. S. Cummings, J.E. Enderby, G.W. Neilson, J.R. Newsome, R.A. Howe, W.S. Howells, and A.K. Soper. Nature (London), **287**, 714 (1980).
33. D.H. Powell, G.W. Neilson, and J.E. Enderby. J. Phys. Condens. Matter, **5**, 5723 (1993).
34. G.V. Yukhnevich, E.G. Tarakanova, V.D. Maiorov, and N.B. Librovitch. J. Mol. Struct. **265**, 237 (1992).
35. P.-A. Bergström, J. Lindgren, M. Read, and M. Sandström. J. Phys. Chem. **95**, 7650 (1991).
36. D.E. Irish. Structure of water and aqueous solutions. *Edited by* W.A.P. Luck. Verlag Chemie, Weinheim. Chap. III.4. 1974.

© 2001 NRC Canada

Theoretical study on the influence of H_2O for the 1,2-hydrogen shift from hydrogen peroxide (H_2O_2) to water oxide (O-OH_2)

Toshiya Okajima

Abstract: Theoretical calculation was performed to study the solvent effect for the 1,2-hydrogen shift from hydrogen peroxide (H_2O_2) (**1**) to water oxide (O-OH_2) (**2**). Stationary points including transition structures (TSs) were optimized with no geometrical constraint at Becke3LYP/6–311++G** level. All stationary points were tested by frequency analysis and IRC calculation. The activation energies ($\Delta E^{\neq}$) and heats of reaction (ΔH_0) were evaluated at Becke3LYP/6–311++G**//Becke3LYP/6–311++G** level of theory. The following points were clarified: (*i*) inclusion of polarization function (*) and diffusion function (+) for calculation hardly affected the energetic of the reaction; (*ii*) judging from the change of $\Delta E^{\neq}$ and ΔH_0 values, the reaction is predicted to be accelerated by the increase of involving H_2O; (*iii*) proton-relaying mechanism considerably reduced $\Delta E^{\neq}$ values; (*iv*) the endothermicity became monotonically small as the number of solvating H_2O molecules increased. The calculation suggests that the formation of water oxide (O-OH_2) (**2**) from H_2O_2 (**1**) is promoted by a proton-relaying pathway in protic media (such as H_2O).

Key words: theoretical calculation, ab initio, transition structure, 1,2-hydrogen shift, water oxide.

Résumé : On a effectué des calculs théoriques pour étudier l'effet de solvant sur le déplacement 1,2 d'hydrogène à partir du peroxyde d'hydrogène (H_2O_2) (**1**) ver l'oxyde d'eau (O-OH_2) (**2**). On a optimisé les points stationnaires, y compris les structures de transition (ST), en n'imposant aucune contrainte géométrique au niveau Becke3LY/6-311++G**. Tous les points stationnaires ont été vérifiés par l'analyse de fréquence et par des calculs IRC. On a évalué les énergies d'activation ($\Delta E^{\neq}$) et les chaleurs de réaction (ΔH_0) au niveau Becke3LYP/6-311++G**//Becke3LYP/6-311++G** de la théorie. On a clarifié les points suivants: (*i*) l'inclusion, dans les calculs, de la fonction de polarisation (*) et de la fonction de diffusion (+) n'influence pratiquement pas les énergies de la réaction ; (*ii*) en se basant sur les changements dans les valeurs de $\Delta E^{\neq}$ et de ΔH_0, on peut prédire que la réaction est accélérée par l'augmentation de l'eau impliquée; (*iii*) le mécanisme impliquant un relais du proton réduit les valeurs de $\Delta E^{\neq}$ et de ΔH_0 de façon considérable; (*iv*) le caractère endothermique devient faible et monotonique avec l'augmentation du nombre de molécules d'eau de solvatation. Les calculs suggèrent que, dans des milieux protiques (tels que l'eau), la formation d'oxyde d'eau (O-OH_2) (**2**) à partir de H_2O_2 (**1**) est facilitée par une voie impliquant un relais de proton.

Mots clés : calculs théoriques, ab initio, structure de transition, déplacement d'hydrogène 1,2, oxyde d'eau.

[Traduit par la Rédaction]

Introduction

The oxygen atom transfer involving oxygen–oxygen σ bond cleavage (oxo transfer) (1–6) is known to be one of the most important oxidation pathways. Water oxide (O-OH_2) (**2**), which is produced from hydrogen peroxide (H_2O_2) (**1**) by a 1,2-hydrogen shift (see Table 1), is predicted to decompose to H_2O and atomic oxygen [O] easily, and therefore, to be a powerful oxidant (7–9). However, high activation barriers for the conversion of **1** into **2** have been reported (10–13). On the other hand, the studies strongly supporting the involvement of **2** in the oxidation pathway by **1** have also been reported (14–16). Shaefer and co-workers (14, 15) reported the activation energy for this isomerization of **1** into **2** is only 3.3 kcal mol^{-1}. Furthermore, Bach and co-workers (2, 3, 7) and Bach and Andres (12) reported that the coordination of H_2O molecules to **2** drastically raises the oxidizing ability of it. Based on these theoretical works, the author has investigated the role of H_2O involving in this 1,2-type hydrogen shift from the mechanistic point of view. The study is also expected to clarify the role of **2** in the oxidation of biomolecules existing in a hydrophilic environment, such as the living body. In this report, the proton-relaying mechanism involving coordinating H_2O for 1,2-hydrogen shift from **1** to **2**, in which solvating $n$$H_2O$ molecule(s) (n = 0–3) was implicated in, was especially focused on (Scheme 1).

Received July 9, 2000. Published on the NRC Research Press website on December 21, 2000.

T. Okajima.[1] Department of Chemistry, Faculty of Culture and Education, Saga University, Honjo 1, Saga City, Saga 840 Japan.

[1]Telephone: (81) 952-28-8320. Fax: (81) 952-28-8219. e-mail: okajimat@cc.saga-u.ac.jp

Method

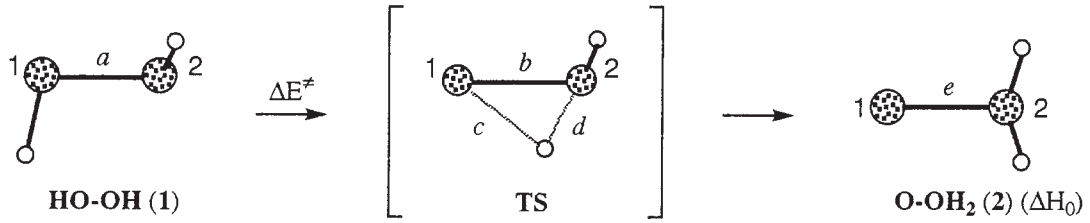
Theoretical calculation was performed using the GAUSSIAN 98 programs (17). Geometries of all stationary points including TSs were optimized utilizing gradient method without any geometrical constraint at the

 DOI:10.1139/cjc-79-1-22 © 2001 NRC Canada

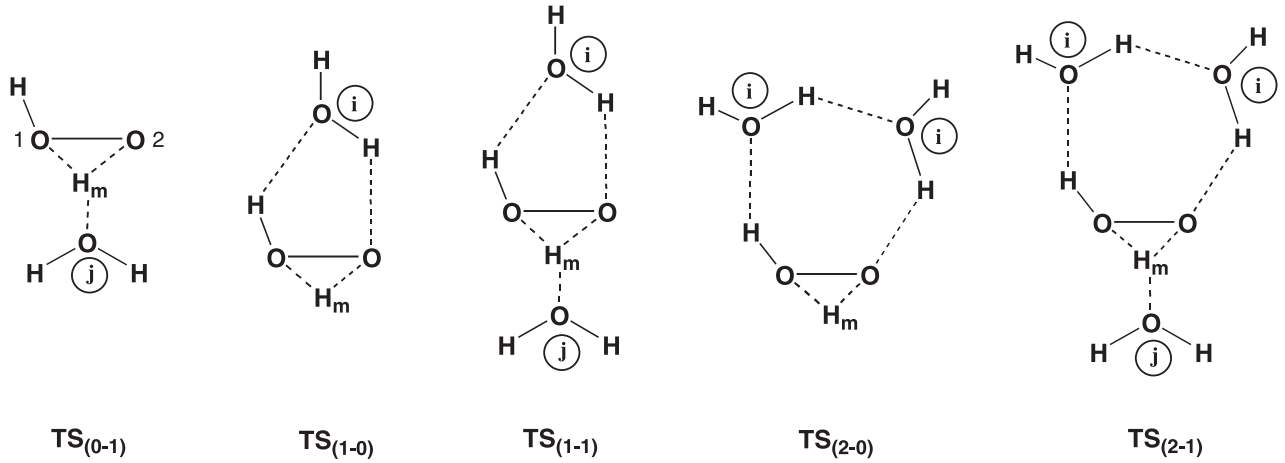
Table 1. The geometrical parameters of the critical stationary points including transition structures for the 1,2-hydrogen shift of H_2O_2 (**1**) leading to water oxide (O-OH_2) (**2**).

	a	*b*	*c*	*d*	*e*	$\Delta E^{\neq}$ (kcal mol^{-1})	ΔH_0 (kcal mol^{-1})
//RHF/6-311++G	1.437[a]	1.658	1.167	1.160	1.680	+57.8	+23.2
//RHF/6-311G**	1.385	1.595	1.179	1.080	1.606	+60.8	+40.4
//RHF/6-311++G**	1.384	1.589	1.182	1.084	1.593	+61.1	+39.5
//MP2/6-311++G	1.557	1.656	1.374	1.084	1.588	+56.6	+41.9
//MP2/6-311G**	1.446	1.570	1.432	1.008	1.505	+59.4	+53.6
//MP2/6-311++G**	1.450	1.564	1.408	1.021	1.498	+58.9	+41.3
//Becke3LYP/6-311++G	1.521	1.700	1.339	1.100	1.610	+49.7	+37.5
//Becke3LYP/6-311G**	1.454	1.635	1.405	1.027	1.560	+53.2	+48.2
//Becke3LYP/6-311++G**	1.454	1.630	1.365	1.044	1.553	+52.9	+45.6

Note: Atomic distances are in angstroms (Å). $\Delta E^{\neq} = E(\mathbf{TS}) - E(\mathbf{1})$ and $\Delta H_0 = E(\mathbf{1}) - E(\mathbf{2})$.

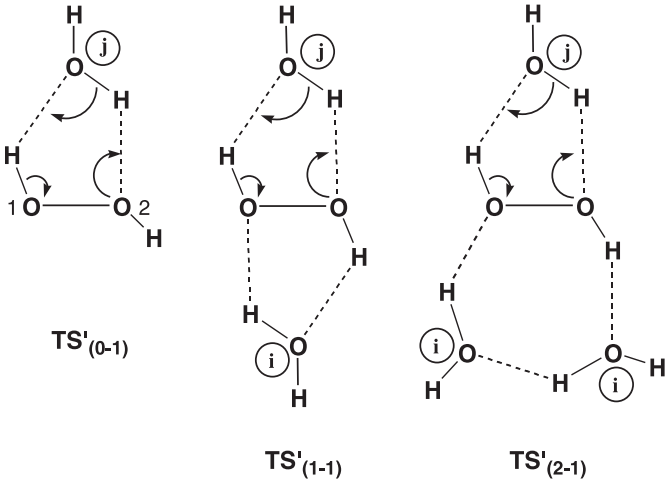


Scheme 1.



Becke3LYP/6–311++G** level (18). Activation energies ($\Delta E^{\neq}$) and heats of reaction (ΔH_0) were evaluated at the Becke3LYP/6–311++G**//Becke3LYP/6–311++G** level. For stationary points, an energy min and max point (TS) were characterized by the correct number of negative eigenvalues of its Hessian matrix, that is, the former and the latter have zero and a single imaginary frequency, respectively. The atomic disposition in the TS are collected in Scheme 1 (in these TSs one hydrogen atom on O^2 in **2** is supplied from *H*-O^1 in **1**) and in Schemes 2 and 3 (proton-relaying mechanism, in which one hydrogen atom in **2** is delivered from the hydrogen bonding H_2O molecule). For two or more H_2O solvating systems, some coordinating modes to the substrate are possible. For example, when two H_2O molecules are involved in the reaction, two types of solvating mode (such as $H_2O_{2(2-0)}$ shown in Fig. 1 and $H_2O_{2(1-1)}$ in Fig. 2 are possible. The TSs expressed by the symbol with a prime mark (′), such as "**TS′**," are proton-relaying TSs. The

Scheme 2.



© 2001 NRC Canada

Scheme 3.

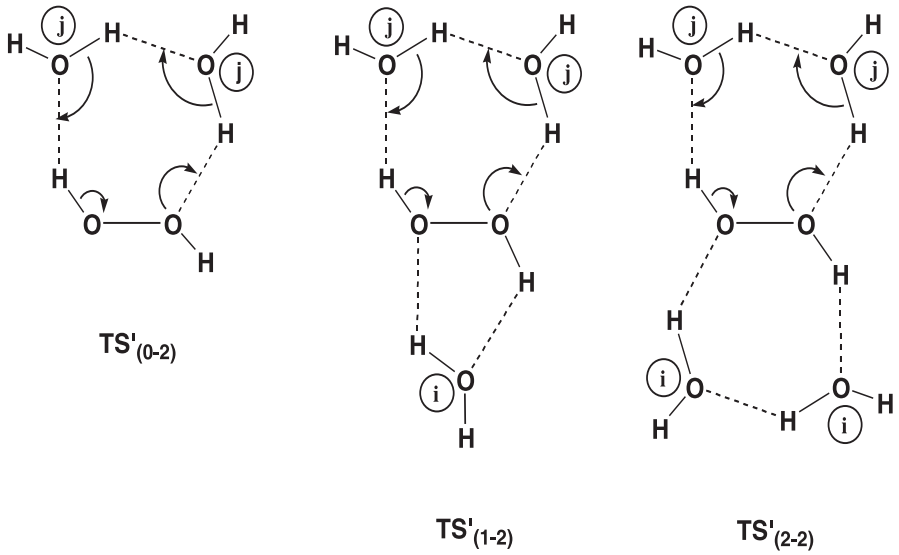
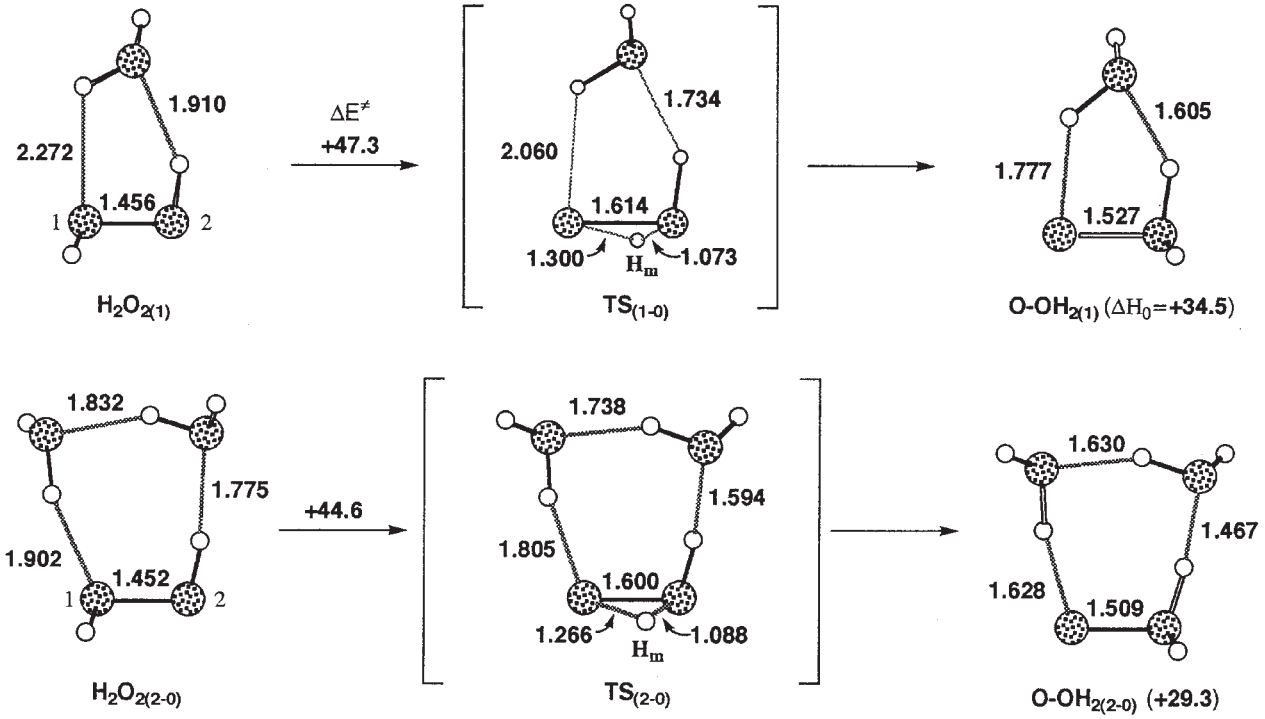


Fig. 1. The critical geometries including $\mathbf{TS}_{(i-0)}$ (i = 1, 2) and geometrical parameters optimized at Becke3LYP/6–311++G** for the 1,2-hydrogen migration between hydrogen peroxide (**1**) and water oxide (**2**). Atomic distances are in angstroms (Å). The energy differences (Becke3LYP/6–311++G**// Becke3LYP/6–311++G**) are in kcal mol^{-1}. $\Delta E^{\neq} = E(\mathrm{TS}) - E(H_2O_2)$ and $\Delta H_0 = E(\mathrm{O\text{-}OH_2}) - E(H_2O_2)$.



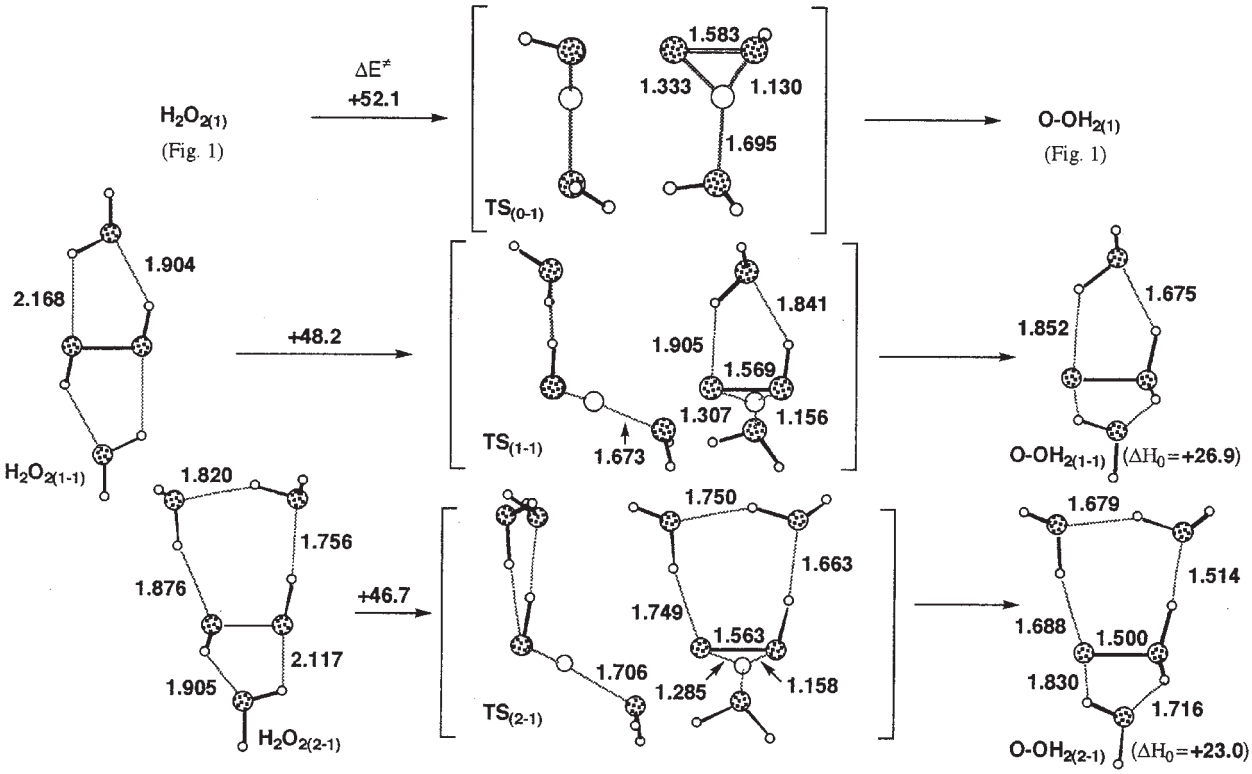
characters "*i*" and "*j*" in the symbols $X_{(i-j)}$ (X = H_2O_2, TS(′), and O-OH_2) seen in the schemes and figures, mean that all H_2O molecules involved in the reaction ($(H_2O)_{i+j}$) are divided into two groups of H_2O clusters, which are marked by i ($(H_2O)_i$) and by j ($(H_2O)_j$), respectively, as shown in Schemes 1–3. These two groups of H_2O molecules coordinate to the substrate from different directions with respect to the O^1—O^2 bond. One group indicated by $(H_2O)_j$ involves in the coordination to H_m in **TS** and in the proton-relay in **TS′**, respectively. The other groups of H_2O ($(H_2O)_i$) appear to play an simple role to the reaction, in which the hydrogen bonding network between $(H_2O)_i$ and the substrate is maintained all through the reaction.

Results and discussion

Table 1 collects the activation energies ($\Delta E^{\neq}$) and heats of reaction (ΔH_0) for the 1,2-hydrogen shift from (HO-OH) (**1**) to water oxide (O-OH_2) (**2**) (Scheme 1) under the consideration of polarization function (marked with an asterisk (*)) and of diffusion function (+). Judging from the critical geometrical parameters of the TSs (*b*, *c*, and *d* in Scheme 1),

© 2001 NRC Canada

Fig. 2. The critical geometries including $\mathbf{TS}_{(i-1)}$ (i = 0–2) and geometrical parameters (Å) optimized at Becke3LYP/6–311++G** for the 1,2-hydrogen migration between **1** and **2**. A single H_2O coordinates to migrating hydrogen atom (H_m). The side view of each TS is also shown. Energies at Becke3LYP/6–311++G**//Becke3LYP/6–311++G** are in kcal mol^{-1}. $\Delta E^{\neq} = E(\mathrm{TS}) - E(H_2O_2)$ and $\Delta H_0 = E(\mathrm{O\text{-}OH_2}) - E(H_2O_2)$.



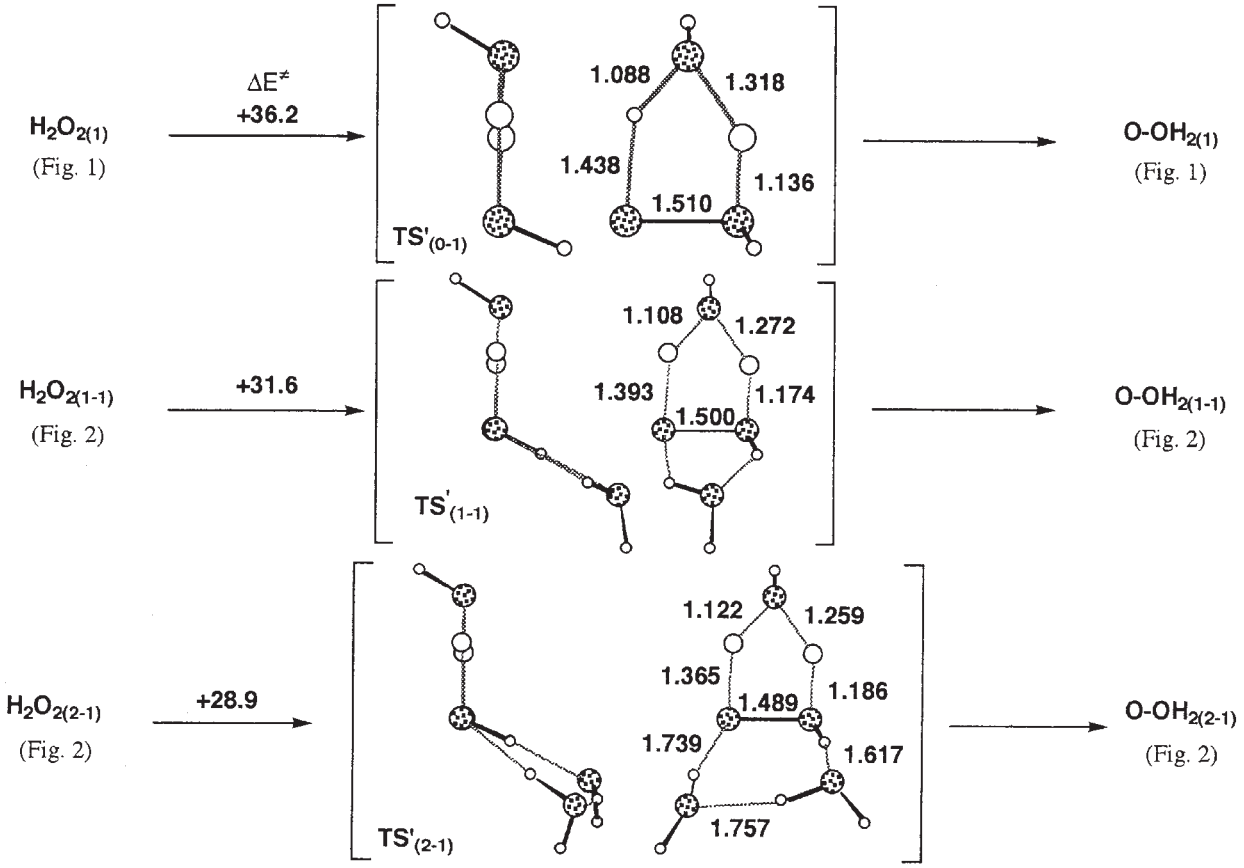
the TSs optimized at the MP2 and Becke3LYP level of theory are very late (atomic distances for breaking $O^1\cdots H$ ranges in 1.3–1.4 Å and those for forming $O^2\cdots H$ in 1.0–1.1 Å) and the RHF structures are rather faster than those optimized at the above mentioned two levels (the atomic distances of breaking $O^1\cdots H_m$ and forming $O^2\cdots H_m$ both range in 1.1–1.2 Å at RHF level). The O^1—O^2 bond lengths in **2** are quite longer than those in **1**, which implies the easy cleavage of the O—O bond of **2** to give water (H_2O) and atomic oxygen [O], and consequently, the strong oxidizing ability of **2**. $\Delta E^{\neq}$ values of the reaction are very high and the reaction is generally quite endothermic and these critical values were not changed very much by considering polarization and diffusion functions for calculation. Consequently, high $\Delta E^{\neq}$ and ΔH_0 values were calculated at all levels of calculation considered here, strongly indicating that the parent reaction from **1** to **2** is fundamentally difficult to proceed under no assistance of H_2O solvent (2).

Figure 1 shows the Becke3LYP/6–311++G** TSs ($\mathbf{TS}_{(i-0)}$, i = 1,2) and some critical geometrical parameters for the 1,2-hydrogen shift from **1** to **2**. In these two TSs, solvating H_2O molecule(s) do not get involved with migrating hydrogen (H_m) directly and coordinate(s) to the substrate from the opposite direction to H_m with respect to the O^1—O^2 bond. In other words, in this path one hydrogen atom (H_m) on **1**, to which none of H_2O coordinates, migrates and all coordinating H_2O plays a simple role as the hydrogen bonding species to the substrate. The breaking $O^1\cdots H$ and forming $O^2\cdots H$ bond lengths became shorter and longer (1.300 and 1.073 Å for $\mathbf{TS}_{(1-0)}$ and 1.266 and 1.088 for $\mathbf{TS}_{(2-0)}$, as compared with those (1.365 and 1.044 Å) for the parent reaction shown in Fig. 1 at Becke3LYP/6–311++G**, respectively, indicating that TSs became early by involving H_2O in the reaction. The H_2O molecules indicated by i (i = 1,2) coordinated to the H_2O_2 moiety ($H_2O_{2(1)}$ and $H_2O_{2(2-0)}$) stay almost on the same position until reaching the product ($\mathrm{O\text{-}OH_{2(1)}}$ and $\mathrm{O\text{-}OH_{2(2-0)}}$, respectively). The $\Delta E^{\neq}$ values calculated at Becke3LYP/6–311++G**//Becke3LYP/6–311++G** (+47.3 and +44.6 kcal mol^{-1} for $\mathbf{TS}_{(1-0)}$ and $\mathbf{TS}_{(2-0)}$, respectively) are considerably smaller than that (+52.9) for the parent reaction. Heats of reaction (ΔH_0) (+34.5 kcal mol^{-1} for $\mathbf{TS}_{(1-0)}$ and +29.3 for $\mathbf{TS}_{(2-0)}$) also became smaller than that (+ 45.6). Moreover, as the coordinating H_2O molecules increase the activation energy and the endothermicity of the reaction became small. Nevertheless, the calculation still predicts the large activation energy and endothermicity for the 1,2-hydrogen shift.

Figure 2 shows the Becke3LYP/6–311++G** TSs for the 1,2-hydrogen shift from **1** to **2** under the consideration of H_2O coordination to migrating hydrogen (H_m). A single H_2O coordinates to H_m (j = 1) and the solvating H_2O is considered to be up to two molecules (i = 0 ($\mathbf{TS}_{(0-1)}$, i = 1 ($\mathbf{TS}_{(1-1)}$), and i = 2 ($\mathbf{TS}_{(2-1)}$)). In $\mathbf{TS}_{(2-1)}$, two of the three coordinating H_2O molecules ($(H_2O)_i$) construct the hydrogen bonding network linking H^2 and O^1 terminals and stays on almost the same position throughout the migration reaction. The other one H_2O molecule coordinates to migrating H_m. As well as the TSs ($\mathbf{TS}_{(1-0)}$ and $\mathbf{TS}_{(2-0)}$) shown in Fig. 1, these three

© 2001 NRC Canada

Fig. 3. The TS geometries including $\mathbf{TS'}_{(i-1)}$ (i = 0, 2) and geometrical parameters (Å) optimized at Becke3LYP/6–311++G** for the 1,2-hydrogen migration between **1** and **2**. The schematic representation for these three TSs are shown in Chart 2. In these three TSs, a single H_2O involves directly in proton-relay between **1** and **2**. The side view of each TS is also shown. Energies at Becke3LYP/6–311++G**//Becke3LYP/6–311++G** are in kcal mol^{-1}. $\Delta E^{\neq} = E(\mathrm{TS}) - E(H_2O_2)$ and $\Delta H_0 = E(\mathrm{O\text{-}OH_2}) - E(H_2O_2)$.

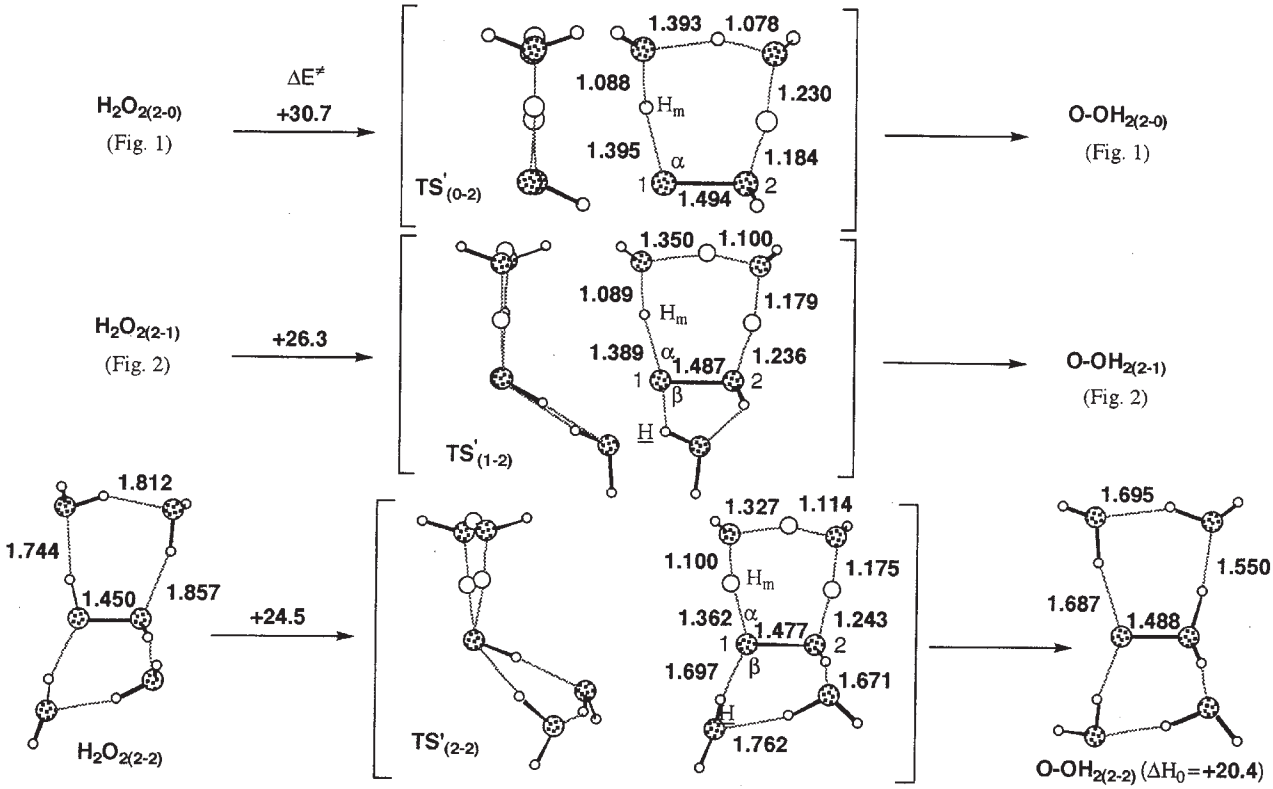


TSs are also earlier than the TS for the reaction of parent **1**. For example, the breaking $O^1\cdots H_m$ and the forming $O^2\cdots H_m$ bond length changes from 1.365, *1.044* (Fig. 1), to 1.300, *1.073* ($\mathbf{TS}_{(1-0)}$), 1.266, *1.088* ($\mathbf{TS}_{(1-0)}$), 1.333, *1.130* ($\mathbf{TS}_{(0-1)}$), 1.307, *1.156* ($\mathbf{TS}_{(1-1)}$), and 1.285, *1.158* ($\mathbf{TS}_{(2-1)}$). In this path, the hydrogen atom (H_m), which is coordinated by a single H_2O, migrates and one hydrogen bond between O^1 and ***H***-OH in **1** is broken and new $O^2\cdots$***H***-OH hydrogen bond is formed in **2**. During the migration, the H_2O molecule rotates around the pivotal migrating hydrogen (H_m). The $\Delta E^{\neq}$s are +52.1 ($\mathbf{TS}_{(0-1)}$), +48.2 ($\mathbf{TS}_{(1-1)}$), and +46.7 kcal mol^{-1} ($\mathbf{TS}_{(2-1)}$), which values are almost the same with the corresponding $\Delta E^{\neq}$s for the TSs having no coordinating H_2O on H_m (+47.3 ($\mathbf{TS}_{(1-0)}$) and +44.6 kcal mol^{-1} ($\mathbf{TS}_{(2-0)}$)), respectively, indicating that the direct coordination of H_2O to H_m has little effect to accelerate the hydrogen migration.

Figures 3 and 4 present Becke3LYP/6–311++G** TSs for the proton-relaying mechanism for the 1,2-hydrogen shift from **1** to **2** involving H_2O molecules. All these TSs are the ones corresponding to the concerted proton-relaying mechanism having single TS on the energy potential surface connecting **1** with **2**. The $\Delta E^{\neq}$ values calculated at Becke3LYP/6–311++G**//Becke3LYP/6–311++G** are in the range +24 ~ +36 kcal mol^{-1}, which are drastically smaller than those (+44 ~ +52) for the pathways proceeding through three-membered TSs (1,2-shift), as shown in Figs. 1 and 2. Focusing on the role of $(H_2O)_i$, hydrogen bonding $(H_2O)_i$ appears to play a simple role in the reaction, however, $\Delta E^{\neq}$ values became monotonically small as the number of $(H_2O)_i$ increases. Considering the fact that atomic disposition in hydrogen bonding $(H_2O)_i$ appears to be maintained on almost the same position all through the reaction, and the fact that there exists little steric congestion between $(H_2O)_i$ and the other parts of the species, the accelerating effect by coordinating $(H_2O)_i$ is considered to be mainly attributing to electronic factors, reducing the fluctuation of the charge on O^1 and O^2 as the reaction proceeds, rather than steric factors. Next, the role of $(H_2O)_j$ in a series of **TS′** was considered. It is plausible that the leaving ability (namely, ability to be eliminated by H_2O) of ***H*** in ***H***O^1-OH is enhanced because of the stabilizing effect of the negative charge growing on O^1 by H_2O coordinating to it. In this case, the leaving and the attacking direction of the proton to O^1 is clearly important. The direct 1,2-hydrogen shift (such as **TS** in Scheme 1 and $\mathbf{TS}_{(i-0)}$ in Fig. 1 suffers severe steric strain because of the proceedings through three-membered ring TSs, which clearly results in the increase of activation energy, and therefore, lowering the reactivity. In proton-relaying $\mathbf{TS'}_{(i-2)}$ (i = 0–2), bond angles of O^2-O^1-H_m designated by α and O^2-O^1-***H***(-OH) by β in Fig. 4 are 104.3° for $\mathbf{TS'}_{(0-2)}$, 107.4, 101.0 for $\mathbf{TS'}_{(1-2)}$, and 105.0, 108.4 for $\mathbf{TS'}_{(2-2)}$, respectively,

© 2001 NRC Canada

Fig. 4. The critical geometries including $\mathbf{TS'}_{(i-2)}$ (i = 0–2) and geometrical parameters (Å) optimized at Becke3LYP/6–311++G** for the 1,2-hydrogen migration between **1** and **2**. The schematic representation for these three TSs are shown in Scheme 3. In these three TSs, two H_2O involves directly in proton-relay between **1** and **2**. The side view of each TS is also shown. Energies at Becke3LYP/6–311++G**//Becke3LYP/6–311++G** are in kcal mol^{-1}. $\Delta E^{\neq} = E(\mathrm{TS}) - E(H_2O_2)$ and $\Delta H_0 = E(\mathrm{O\text{-}OH_2}) - E(H_2O_2)$.



indicating that leaving of $\mathbf{H}^1(\text{-}O^1)$ and H_2O coordination to O^1 occurs at almost ideal angles so as to maintain favorable interaction with lone pairs spread out around O^1. The least $\Delta E^{\neq}$ value (+24.5 kcal mol^{-1}) and the smallest endothermicity (ΔH_0 = +20.4) could be obtained as the reaction path proceeding through $\mathbf{TS'}_{(2-2)}$. These values suggest that the1,2-hydrogen shift from **1** to **2** could be clearly promoted when the assistance of H_2O solvent works effectively.

Finally, Fig. 5 presents Becke3LYP/6–311+G** optimized geometries of H_2O_2 and O-OH_2 having three H_2O molecules ($\mathbf{H_2O_2}_{(3-0)}$ and $\mathbf{O\text{-}OH_2}_{(3-0)}$). Both geometries have a nine-membered hydrogen bonding network linking three H_2O and the substrate. It is also likely that the conversion between H_2O_2 and O-OH_2 proceeds through successive proton transfer along these solvating H_2O molecules. Unfortunately, concerted TSs, in which proton transfer occurs along linking three H_2O could not be located. Considering the larger energy difference between $\mathbf{H_2O_2}_{(3-0)}$ and $\mathbf{O\text{-}OH_2}_{(3-0)}$ (+27.2 kcal mol^{-1}) than that (+20.4) for $\mathbf{TS'}_{(2-2)}$, it is concluded that the proton-relaying mechanism under the involvement of *two* hydrogen bonding H_2O molecules ($\mathbf{TS'}_{(2-2)}$, in this study) is the most favorable pathway.

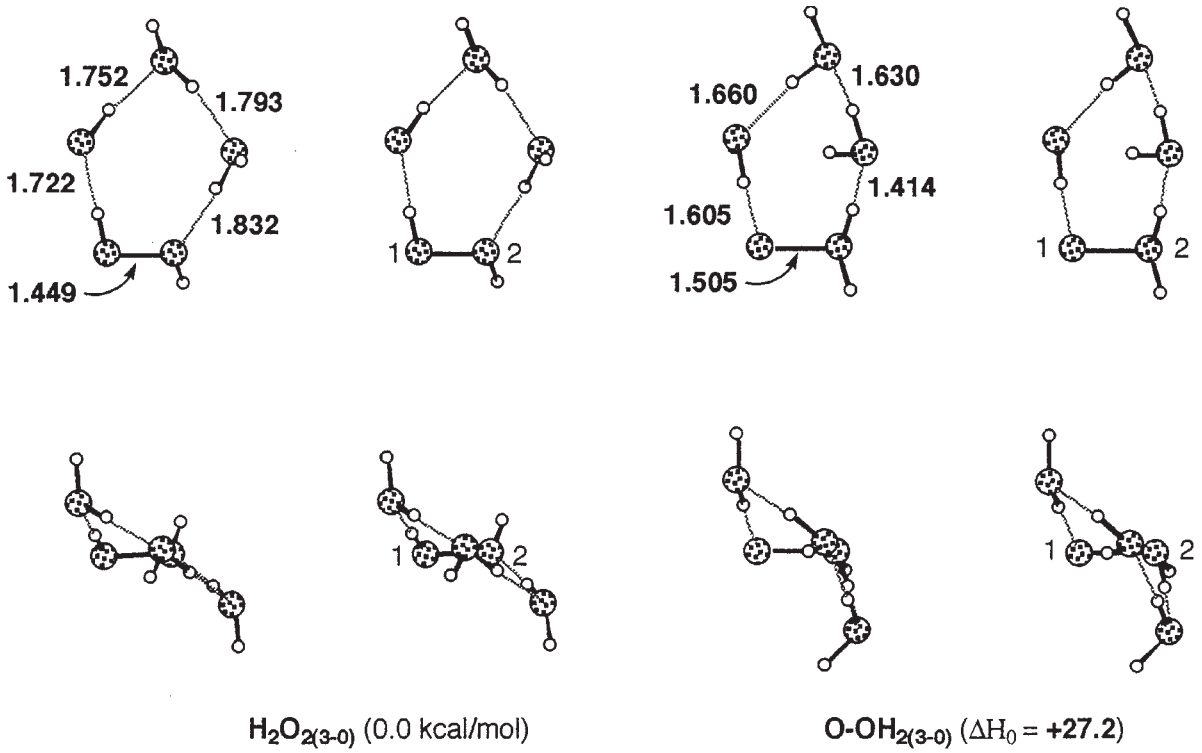
Summary

Theoretical calculation was performed to study the solvent effect for the 1,2-hydrogen shift from hydrogen peroxide (H_2O_2) (**1**) to water oxide (O-OH_2) (**2**) by considering up to four H_2O molecules as the solvent. Geometries including transition structures (TSs) were located by using density functional theory (DFT) at the Becke3LYP/6–311++G** level of theory. Energies were calculated at Becke3LYP/6–311++G** based on the Becke3LYP/6–311++G** geometries. The calculations clarified the following points: (*i*) the inclusion of polarization (*) and diffusion functions for calculation (+) hardly affected the geometries and the energetic of the 1,2-hydrogen shift from **1** to **2**; (*ii*) the involvement of protic solvent to the reaction considerably reduced the activation energies ($\Delta E^{\neq}$) and endothermicity; (*iii*) the activation energy and the endothermicity were considerably reduced as the number of involving H_2O increases, suggesting that the 1,2-hydrogen shift is able to be promoted in the protic media, such as H_2O; (*iv*) the proton-relaying mechanism (the reaction pathway proceeding through **TS′**s) is considered to be the most plausible one for the formation of **2** from **1** in H_2O.

Water oxide (**2**) is a candidate to become a powerful oxidant. However, the activation energy ($\Delta E^{\neq}$) and the endothermicity of the conversion of **1** into **2** are still large to exist for **2** in potential concentration as oxygen donor even in protic media (in H_2O). However, these calculational results could clarify the importance of proton-relaying pathway as the lowering factor of $\Delta E^{\neq}$ for the isomerization of **1** to **2**. Considering this result with Schaefer's works (14, 15) to clarify low activation energy for this isomerization evaluated at high level calculations and with Bach's (2, 3, 7, 8)

© 2001 NRC Canada

Fig. 5. The Becke3LYP/6–311++G** optimized geometries of $\mathbf{H_2O_{2(3-0)}}$ and $\mathbf{O\text{-}OH_{2(3-0)}}$ and Becke3LYP/6–311++G** energy difference between **1** and **2** having three H_2O molecules. Plus sign of the energy means that 1,2-hydrogen migration from **1** to **2** is endothemic ($\Delta H_0 = E(\text{O-OH}_2) - E(\text{H}_2\text{O}_2)$).



works to clarify the role of the coordination of H_2O to raise the oxidizing ability of **2** together, it is suggested that oxidizing species **2** is short-lived but viable and plays an unmarked role for the oxidation of various (bio)molecules especially existing in hydrophilic environments. Considering the unstability of **2**, toxicity of **2** is serious but might be definite, for instance when **2** is just formed in the close proximity to sensitive biomolecules to the oxidants. This situation is quite similar to the behavior of a hydroxyl radical (·OH) that is the strongest activated oxygen and has a very short lifetime.

References

1. D. Cremer and C.W. Bock. J. Am. Chem. Soc. **108**, 3375 (1986).
2. R.D. Bach, J.J.W. McDouall, A.L. Owensby, and H.B. Schlegel. J. Am. Chem. Soc. **112**, 7064 (1990).
3. R.D. Bach, A.L. Owensby, C. Gonzalez, H.B. Schlegel, and J.J.W. McDouall. J. Am. Chem. Soc. **113**, 6001 (1991).
4. R.D. Bach, A.L. Owensby, J.L. Andres, and H.B. Schlegel. J. Am. Chem. Soc. **113**, 7031 (1991).
5. R.D. Bach, A.L. Owensby, C. Gonzalez, and H.B. Shlegel. J. Am. Chem. Soc. **113**, 2338 (1991).
6. R.D. Bach, J.L. Andres, A.L. Owensby, H.B. Schlegel, and J.J.W. McDouall. J. Am. Chem. Soc. **114**, 7207 (1992).
7. R.D. Bach, J.J.W. MacDouall, A.L. Owensby, and H.B. Schlegel. J. Am. Chem. Soc. **112**, 7065 (1990).
8. R.D. Bach, M.-D. Su, and H.B. Schlegel. J. Am. Chem. Soc. **116**, 5379 (1994).
9. R.D. Bach and M.-D. Su. J. Am. Chem. Soc. **116**, 5392 (1994).
10. H.F. Schaefer, III. Acc. Chem. Res. **12**, 288 (1979).
11. J.A. Pople, K. Raghavachari, M.J. Frisch, J.S. Binkley, and P.v.R. Schleyer. J. Am. Chem. Soc. **105**, 6389 (1983).
12. R.D. Bach and J.L. Andres. J. Org. Chem. **57**, 613 (1992).
13. I.I. Moiseev. J. Mol. Catal. **127**, 1 (1997).
14. C. Meredith, T.P. Hamilton, and H.F. Schaefer, III. J. Phys. Chem. **96**, 9250 (1992).
15. H.H. Huang, Y. Xie, and H.F. Schaefer, III. J. Phys. Chem. **100**, 6076 (1996).
16. D. Schroder, C.A. Schalley, N. Goldberg, J. Hrusak, and H. Schwarz. Chem. Eur. J. **2**, 1235 (1996).
17. M.J. Frisch, G.W. Trucks, H.B. Schlegel, G.E. Scuseria, M.A. Robb, J.R. Cheeseman, V.G. Zakrzewski, J.A. Montgomery, Jr., R.E. Stratmann, J.C. Burant, S. Dapprich, J.M. Millam, A.D. Daniels, K.N. Kudin, M.C. Strain, O. Farkas, J. Tomasi, V. Barone, M. Cossi, R. Cammi, B. Mennucci, C. Pomelli, C. Adamo, S. Clifford, J. Ochterski, G.A. Petersson, P.Y. Ayala, Q. Cui, K. Morokuma, D.K. Malick, A.D. Rabuck, K. Raghavachari, J.B. Foresman, J. Cioslowski, J.V. Ortiz, B.B. Stefanov, G. Liu, A. Liashenko, P. Piskorz, I. Komaromi, R. Gomperts, R.L. Martin, D.J. Fox, T. Keith, M.A. Al-Laham, C.Y. Peng, A. Nanayakkara, C. Gonzalez, M. Challacombe, P.M.W. Gill, B. Johnson, W. Chen, M.W. Wong, J.L. Andres, C. Gonzalez, M. Head-Gordon, E.S. Replogle, and J.A. Pople. Gaussian 98, Revision A.4. Gaussian, Inc., Pittsburgh, Pa. 1998.
18. A.D. Becke. J. Chem. Phys. **98**, 5648 (1993).

© 2001 NRC Canada

New chaotic behavior and its effective control in Belousov–Zhabotinsky reaction

Yan-Ni Li, Hao Song, Zun-Sheng Cai, Lan Chen, Zhe Hou, Qing-Li Wei, Ben-Xiang Wu, and Xue-Zhuang Zhao

Abstract: A new "spiral-in-to-spiral-out" mixed-mode type chaos of the Belousov–Zhabotinsky (BZ) reaction in a continuous flow stirred tank reactor (CSTR) is observed. We discussed its evolution and characterization in detail. We controlled the new chaos into steady periodic behavior by two control methods: (*i*) a self-adaptive delayed feedback controlling scheme; and (*ii*) a linear self-interacting feedback controlling scheme.

Key words: BZ-CSTR reaction, chaos, control.

Résumé : On a observé un nouveau type de chaos « spirale-interne-spirale-externe » à mode mixte pour la réaction de Belousov–Zhabotinsky (BZ) dans une cuve de réaction avec agitation et à écoulement continue. On discute en détail de son évolution et de sa caractérisation. On a fait appel à deux méthodes pour contrôler le nouveau chaos en comportement périodique régulier: (*i*) un schéma de contrôle impliquant une rétroaction retardée auto-adaptable et (*ii*) un schéma de contrôle à rétroaction linéaire auto-interdépendante.

Mots clés : réaction BZ-CSTR, chaos, contrôle.

[Traduit par la Rédaction]

Introduction

There are various nonlinear chemical dynamic behaviors in the Belousov–Zhabotinsky (BZ) reaction system, such as multi-stability (1), simple period oscillation (2), quasi-period oscillation (3), mix-mode oscillation (4), and chaos (5). Also, several routes to chaos have been found in the BZ system, such as by the period-doubling bifurcation (6), quasi-period bifurcation (3), intermittent bifurcation (7, 8), and complex bifurcation (9) (such as the interaction of a local subcritical Hopf bifurcation with a global homoclinic bifurcation). Here, we show new spiral-in-to-spiral-out mixed-mode type chaos and its evolution from P1 at the experimental conditions. Also, the four-variable Montanator model (10) has been used for modeling this new phenomenon.

In addition, the control of chaos has received increasing attention. Because chaos is very sensitive to initial conditions, people thought that chaos could not be controlled at first. Over the past few years, however, great progress has been made in developing techniques for control of chaos. Out of the methods which were mostly proposed by physicists (11–16), here we have successfully applied two schemes to control the chaos in this chemical reaction.

Received January 4, 2000. Published on the NRC Research Press Web site on January 24, 2001.

Y.-N. Li, H. Song, Z.-S. Cai[1], L. Chen, Z. Hou, Q.-L. Wei, B.-X. Wu, and X.-Z. Zhao. Department of Chemistry, Nankai University, Tianjin, China, 300071.

[1]Author to whom correspondence may be addressed. Telephone: 022-23509201. e-mail: caizunsh@nankai.edu.cn

Experimental

Experimental method

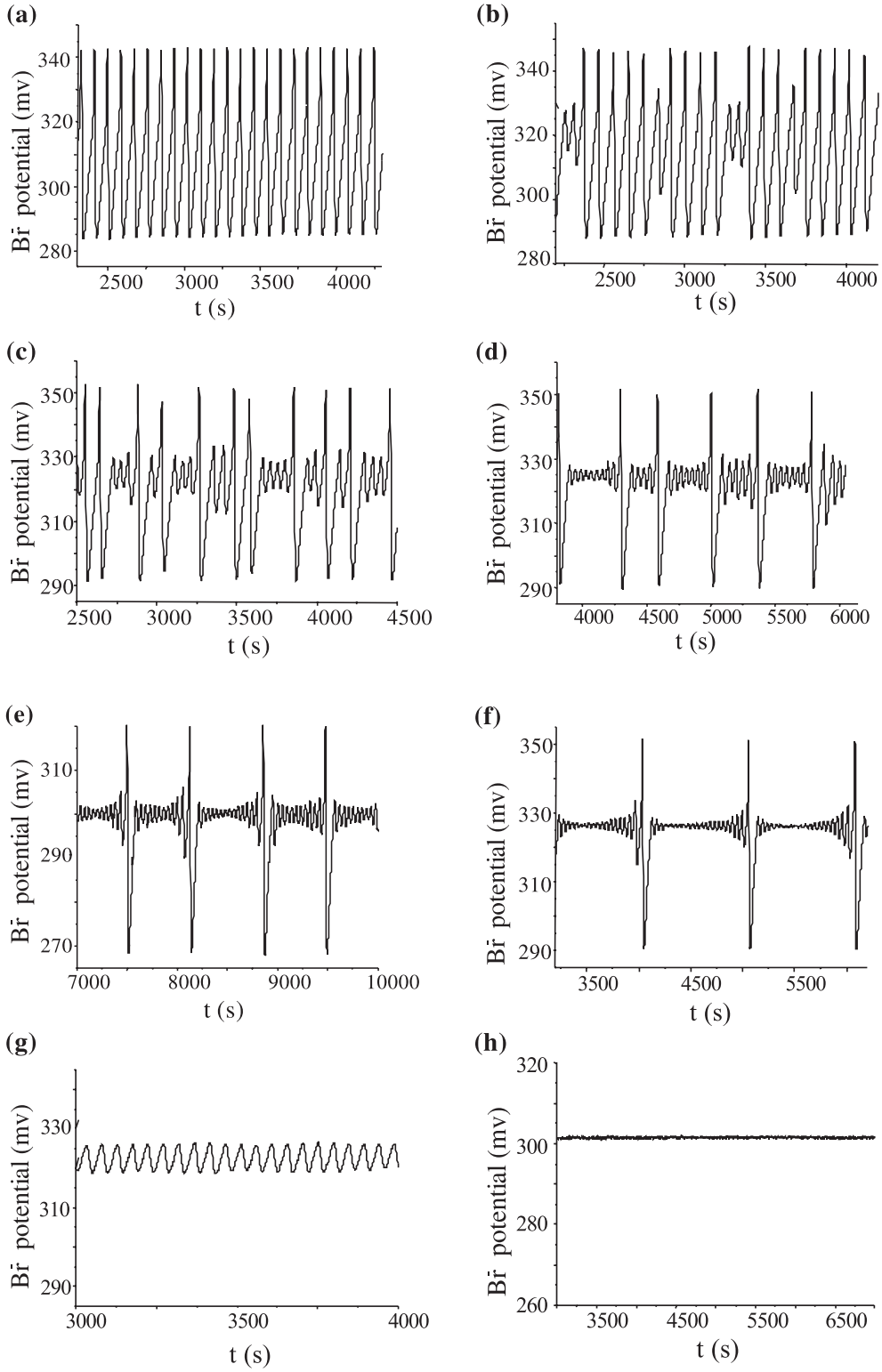
Reaction was carried out in a continuously stirred tank reactor (volume 12.5 mL, stirring rate 1200 rpm). The temperature we used is 28.0 ± 0.1°C, which is different from the temperature of 41°C which gives the quasi-period bifurcation (3). Reagents were fed with separate solutions of malonic acid (MA), sodium bromate (BrO_3^-), and cerous sulphate (Ce^{3+}); the later two solutions are acidified with sulphuric acid (H^+). These three solutions are delivered by a peristaltic pump at a flow regulated on-line by a computer. Although the peristaltic pump generates an oscillating flow while the syringe pump does not, there are no effects in the position of the bifurcation points of the BZ system (10). After mixing, [MA] = 0.25 mol L^{-1}, [BrO_3^-] = 0.1 mol L^{-1}, [Ce^{3+}] = 8.6 × 10^{-4} mol L^{-1}, [H^+] = 0.30 mol L^{-1}. The potential of a bromide-ion-selective electrode was monitored, collected, and stored with 1 Hz, after averaging 10 consecutive measurements at 0.1 s intervals.

Dynamical behavior evolution

The experimental results are summarized in Fig. 1. In brief, at the indicated reaction solution and temperature conditions, when the flow is high, the reaction shows P1 oscillation with large amplitude (Fig. 1*a*). By decreasing the flow, the time series of the normal P1 oscillation is occasionally interrupted by several small amplitude oscillations, and the ratio of the number of small to large oscillations increases with the further decreasing of flow (Fig. 1*b*, 1*c*, and 1*d*). Chaotic behavior is possibly in the making, because at least for Fig. 1*d* we get its Lyapunov exponent (17) to be 0.005 bits s^{-1}. At this point, a slight decreasing of the flow

 DOI: 10.1139/cjc-79-1-29 © 2001 NRC Canada

Fig. 1. Evolution process of experimental new chaos time series. From (*a*)–(*h*), the flow for each solution is 0.12, 0.115, 0.09, 0.07, 0.055, 0.05, 0.04, and 0.03 mL min^{-1}, respectively.



leads to a transition to the spiral-in-to-spiral-out chaos (Fig. 1*e* and 1*f*). Upon further lowering of the flow, this chaos gives way to small amplitude oscillation behavior (Fig. 1*g*). After a further decreasing of the flow, the system crosses a Hopf bifurcation and settles into an equilibrium state (Fig. 1*h*).

Characterization of the new chaos

Analysis of the time series (Fig. 1*e*) provides evidence for the assignment of chaos. The Lyapunov exponent is evaluated, and is 0.0032 bits $s^{-1} > 0$, so that it maybe a chaotic behavior. Phase space (Fig. 2*a*) is reconstructed by time-delay

© 2001 NRC Canada

method (18). The obtained attractor is then further studied, and found that the object in the Poincare Surface of Section (PSS) (Fig. 2*b*) is a smooth linear manifold rather than random distributed points. Also, the one-dimension return map (Fig. 2*c*) constructed from the PSS is an object with order structure, rather than random distributed points. So we have further evidence of the existence of chaos. Seen from the time series (Fig. 1*e*), the differences in amplitudes between large and small oscillations are distinctive. The amplitude of small oscillation changes with time, first decreasing, then increasing. Moreover, the number of the small oscillations between two large amplitude oscillations is not always the same. This indicates that the chaos we obtain is the type of spiral-in-to-spiral-out.

Model simulation

We use the four-variable Montanator model (see Table 1) at about the same conditions as in the experiment to describe the spiral-in-to-spiral-out feature of the time series. The corresponding differential equations are as follows:

[1]
$$\frac{d[Br^-]}{dt} = -k_{D1}[H^+][Br^-][HBrO_2] - k_{D2}[BrO_3^-][H^+]^2[Br^-] + k_{D7}[Ce(IV)][BrMA] + k_{D8}[MA\cdot]_{QSS}[BrMA] + k_f([Br^-]_{mf} - [Br^-])$$

$$\frac{d[HBrO_2]}{dt} = -k_{D1}[H^+][Br^-][HBrO_2] + k_{D2}[BrO_3^-][H^+]^2[Br^-] - 2k_{D3}[HBrO_2]^2 + 0.5k_{D4}[H^+]([Ce]_{tot} - [Ce(IV)])[BrO_2\cdot]_{est} - 0.5k_{D5}[HBr0_2][Ce(IV)] + k_f([HBrO_2]_{mf} - [HBrO_2])$$

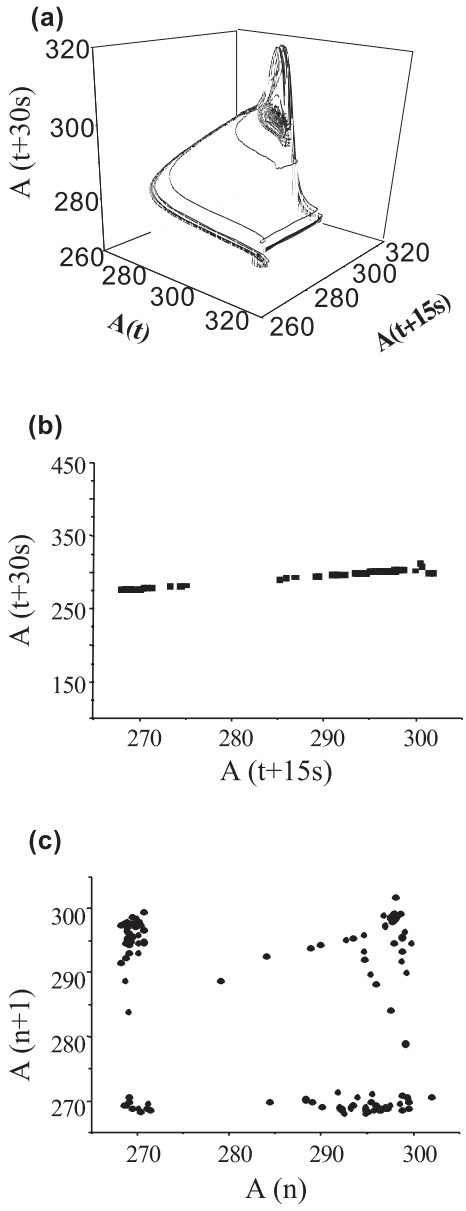
$$\frac{d[Ce(IV)]}{dt} = k_{D4}[H^+]([Ce]_{tot} - [Ce(IV)])[BrO_2\cdot]_{est} - k_{D5}[HBrO_2][Ce(IV)] - k_{D6}[MA][Ce(IV)] - k_{D7}[Ce(IV)][BrMA] + k_f([Ce(IV)]_{mf} - [Ce(IV)])$$

$$\frac{d[BrMA]}{dt} = 2k_{D1}[H^+][Br^-][HBrO_2] + k_{D2}[BrO_3^-][H^+]^2[Br^-] + k_{D3}[HBrO_2]^2 - k_{D7}[Ce(IV)][BrMA] - k_{D8}[MA\cdot]_{QSS}[BrMA] + k_f([BrMA]_{mf} - [BrMA])$$

where

$$[MA\cdot] = \frac{\{-k_{A15}[BrMA] + \{(k_{A15}[BrMa])^2 + 8k_{A13}k_{A18}[MA][Ce^{4+}]\}^{0.5}\}}{4k_{A18}}$$

Fig. 2. Dynamic analysis of the time series of Fig. 1*e*. (*a*) The reconstructed attractor using the time delay method; (*b*) PSS at plane of (t + 15 s) and (t + 30 s) containing the center of the attractor; (*c*) one-dimensional return map constructed from the PSS.



$$[BrO_2\cdot]_{est} = [BrO_2\cdot]_{EQ} = \left(\frac{k_{A7}[HBrO_2]}{k_{A8}}\right)^{0.5}$$

and

k_{A15} = 2.4 × 10^4 L mol^{-1} s^{-1}

k_{A13} = 0.3 L mol^{-1} s^{-1}

k_{A18} = 3.0 × 10^9 L mol^{-1} s^{-1}

k_{A7} = 0.858 s^{-1}

k_{A8} = 4.2 × 10^7 L mol^{-1} s^{-1}

© 2001 NRC Canada

Table 1. Four-variable Montanator model of BZ-CSTR reaction.

Reaction steps	Rate constant
D1: $Br^- + HBrO_2 + \{H^+\} \rightarrow 2BrMA^a$	$k_{D1} = 2.0 \times 10^6\ M^{-2}\ s^{-1}$
D2: $Br^- + \{BrO_3^-\} + \{2H^+\} \rightarrow BrMA + HBrO_2$	$k_{D2} = 2.0\ M^{-3}\ s^{-1}$
D3: $2HBrO_2 \rightarrow BrMA$	$k_{D3} = 3.0 \times 10^3\ M^{-1}\ s^{-1}$
D4: $0.5HBrO_2 + \{BrO_3^-\} + \{H^+\} \rightarrow HBrO_2 + Ce(IV)$	$k_{D4} = 6.2 \times 10^4\ M^{-2}\ s^{-1}$
D5: $HBrO_2 + Ce(IV) \rightarrow 0.5HBrO_2$	$k_{D5} = 7.0 \times 10^3\ M^{-1}\ s^{-1}$
D6: $Ce(IV) + \{MA^b\} \rightarrow$	$k_{D6} = 0.3\ M^{-1}\ s^{-1}$
D7: $BrMA + Ce(IV) \rightarrow Br^-$	$k_{D7} = 30.0\ M^{-1}\ s^{-1}$
D8: $BrMA \rightarrow Br^-$	$k_{D8} = 2.4 \times 10^4\ M^{-1}\ s^{-1}$

[a] $BrMA = BrCH(COOH)_2$.
[b] $MA = CH_2(COOH)_2$.

where subscript "mf" refers to mixed-feed concentration of that component, which is assumed to be zero in the model. The reagent concentrations are: $[BrO_3^-] = 0.10$ mol L^{-1}, $[H^+] = 0.32$ mol L^{-1}, $[MA] = 0.25$ mol L^{-1}, $[Ce^{3+}] = 8.6 \times 10^{-4}$ mol L^{-1}. We use the Gear algorithm (19) to integrate the differential equations. The initial values for the four variables are: $[Br^-]_0 = 2.8260 \times 10^{-6}$ mol L^{-1}, $[HBrO_2]_0 = 2.8420 \times 10^{-5}$ mol L^{-1}, $[Ce(IV)]_0 = 1.1405 \times 10^{-5}$ mol L^{-1}, $[BrMA]_0 = 1.27154 \times 10^{-3}$ mol L^{-1}). Through the numerical study, we also obtained the corresponding evolution process (bifurcation diagram). In addition, we characterize the time series of Fig. 3*a*. The results of characterization (Fig. 3*b*–3*d*) seem to qualitatively agree with the experimental results (Fig. 2), and the Lyapunov exponent calculated is 0.0028 bits s^{-1}, which is also comparable with the experimental value. However, the major difference between the experiment and the model is that there are several periodic windows in the model bifurcation diagram (not shown), but it cannot be seen in experiment evolution investigation (Fig. 1).

Chaos controlling

After discovering the new type of chaos, whether it can be controlled is an open question we were faced with. The following section of the paper is concerned with the control of this new chaotic behavior.

By self-adapted delay feedback controlling scheme

The delay feedback controlling scheme was proposed by Pyragas (20) in 1992. The method deals with a chaotic system that can be presented by a set of ordinary differential equations:

$$[2] \qquad dy/dt = P(y, x) + F(t, p)$$
$$dx/dt = Q(y, x)$$

Variable $y(t)$ can be measured as a system output, while vector x describes the remaining variables of the system that are not available or not of interest for observation. $F(t, p)$ denotes an external perturbation (or controlling rule) on system parameter p, and $F(t, p) = k[y(t - \tau) - y(t)]$ (k is the adjustable parameter). Therefore the difference between the delayed output signal $y(t - \tau)$ and the output signal itself $y(t)$ is used as a control signal. This feedback performs the function of self-control. When the delay time (τ) coincides with the period of the UPO (unstable periodic orbit) which is embedded in the strange attractor, the perturbation vanishes and the chaotic dynamic system is driven to the desired UPO. This method does not require any priori dynamic analysis of the chaotic system and has been applied to the BZ reaction (21) and PO reaction (22). Since the choice of τ is particularly difficult, Pyragas and co-workers (14) modified this scheme in 1995 and proposed the self-adapted delay feedback controlling scheme. Here $\tau_n = t^{(n)}_{max} - t^{(n-k)}_{max}$, where $t^{(n)}_{max}$ defines the moment the nth maximum appears in the output. The period-k UPO can be stabilized by choosing τ_n equal to the interval between k neighbor maxima of the output signal and varying it by computer automatically at each kth maximum. Using this method to control ordinary chemical chaos, we have successfully obtained P1, P2, P3, P4 periodic oscillation (23). The following are the controlling the new chaos with this method.

In the experiment, the controlling rule for the system parameter k_f is constructed as:

$$[3] \qquad k_f = k_f^0 + C\{E(Br^-)_{t-\tau} - E(Br^-)_t\}$$
$$\tau = (t^{(n)}_{max} - t^{(n-k)}_{max})k = \text{integer}$$

where k_f (mL min^{-1}) is the flow of the BZ-CSTR system, $k_f^0 = 0.055$ mL min^{-1} (which is in the chaotic regime), C is an adjustable parameter which reflects the feedback strength. The output signal is the concentration of Br^-($E(Br^-)$) which is monitored by a bromide-ion-selective electrode. τ is the delay time. As τ is changed automatically according to a simple algorithm by computer during the experiment, we need only to adjust C manually so as to regulate the flow k_f to bring the chaotic dynamic behavior onto the UPOs embedded in the strange attractor. Because of the behavior of the new type of chaos (See discussion and conclusion), we only obtained P1 oscillation. The result is shown in Fig. 4*a*.

By linear self-interacting feedback controlling scheme

This method was proposed by Chen et al. (15) in 1994. The main idea is to regulate the self-interacting parameter (the adjustable parameter) by the system output signal itself. Because of the adopting of a linear coupling between the output signal and the system parameter, this method is called the linear self-interacting feedback controlling scheme.

In the experiment, the controlling rule for the system parameter k_f is constructed as follows:

$$[4] \qquad k_f = k_f^0\{1 + C(E(Br^-)_t)\} + R$$

where C is the manually adjustable parameter, which reflects the self-interacting strength. R is a regulator, which may be set specifically for each experiment. In practice, both C and R are adjusted manually to bring the chaos onto UPO, and at

© 2001 NRC Canada

Fig. 3. The results of modeling (k_f = 6.4 × 10^{-4} s^{-1}). (*a*) The time series of chaotic behavior; (*b*) the reconstructed attractor using the time delay method; (*c*) PSS at plane of (*t* + 15 s) and (*t* + 30 s) containing the center of the attractor; (*d*) one-dimensional return map constructed from the PSS.

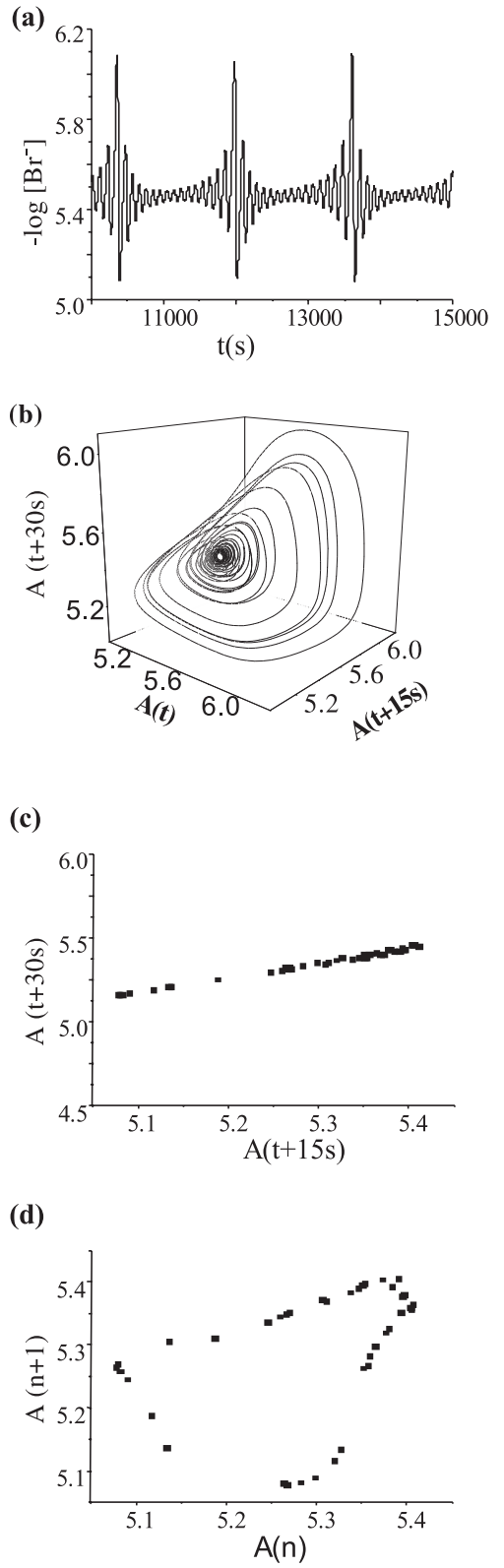
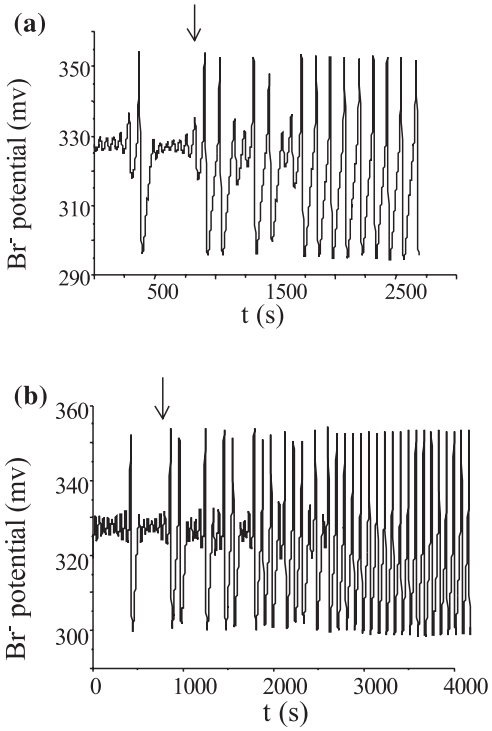


Fig. 4. The results of controlling the new chaotic behavior. Experimental conditions are the same as Fig. 1(*e*). The arrow indicates the time when the control perturbation is switched on. (*a*) Control results by using the self-adapted delay feedback controlling scheme (C = –0.1 mL mV^{-1} min^{-1}); (*b*) control results by using the linear self-interacting feedback controlling scheme (C= –0.10 mV^{-1}, R = 2.275 mL min^{-1}).

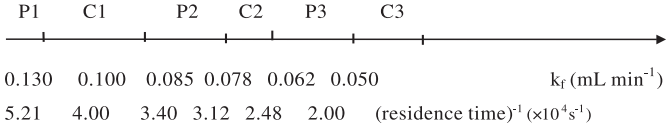


the same time guarantee the pump operating in a proper flow range to ensure the system in its chaotic behavior regime. The others are the same as above. Applying this method, we obtain several periodic oscillations from the ordinary BZ-CSTR chaos effectively (23, 24). For the new chaos, the result is shown in Fig. 4*b*.

Discussion and conclusion

We may assume that the new chaos that we obtained maybe the result of one of the following two types of the coupling of three bifurcations. Either by the coupling of subcritical Hopf bifurcation, supercritical Hopf bifurcation, and homoclinic bifurcation, or by the coupling of local divergent unstable foci, local convergent stable foci, and homoclinic bifurcation, but further work is needed.

In our experiment, applying two methods to control the new chaotic behavior, we get P1 oscillation only. The results do not seem not as good as those while operating on the ordinary chaos. However, thinking from the evolution process, it can be understood: for ordinary chaos in the BZ system, we have obtained the following bifurcation series (22):



© 2001 NRC Canada

It essentially coincides with the one in ref. 25. In such bifurcation series, every chaotic regime is sandwiched by two periodic orbits, which naturally become the dominating UPOs embedded in the strange attractor of the chaos between them. Therefore, the two UPOs that are adjacent with the chaotic regime can be controlled onto easily. However, concerning the new chaos, the evolution process is through the route by decreasing the number of large amplitude oscillations and increasing the number of small amplitude oscillations. During the process, regular behaviors of P*n* oscillations are not emerged. Only at the higher flow, there exists the P1 oscillation as mentioned before. Accordingly, it is the certain results that stable P1 oscillation can be obtained easily.

Acknowledgements

This work is supported by the National Natural Science Foundation of China (Grant no. 29573109).

References

1. P. Gray and S.K. Scott. J. Phys. Chem. **87**, 1835 (1983).
2. M. Orban, P. De Kepper, and I.R. Epstein. J. Am. Chem. Soc. **104**, 2657 (1982).
3. F. Argoul, A. Arneodo, P. Richetti, and J.C. Roux. J. Chem. Phys. **86**, 3325 (1987).
4. V. Petsov, S.K. Scott, and K. Showalter. J. Chem. Phys. **97**, 6191 (1992).
5. R.A. Schmitz, K.R. Graziani, and J.L. Hudson. J. Chem. Phys. **76**, 3040 (1977).
6. K.G. Coffman, W.D. McCormick, Z. Noszticzius, R.H. Simoyi, and H.L. Swinney. J. Chem. Phys. **86**, 119 (1987).
7. Y. Pomeau, J.C. Roux, and A. Rossi. J. Phys. Lett. **A2**, L271 (1981).
8. N. Kreisberg, W.D. McCormick, and H.L. Swinney. Physica D, **50**, 463 (1991).
9. F. Argoul, A. Arneodo, and P. Richetti. Phys. Lett. A, **120**, 269 (1987).
10. L. Gyorgyi, R.J. Field, Z. Noszticzius, W.D. McCormick, and H.L. Swinney. J. Phys. Chem. **96**, 1228 (1992).
11. E. Ott, C. Grebogi, and J.A. Yorke. Phys. Rev. Lett. **64**, 1196 (1990).
12. T. Shinbrot, C. Grebogi, E. Ott, and J.A. Yorke. Nature (London), **363**, 411 (1993).
13. V. Petrov, V. Gaspar, J. Masere, and K. Showalter. Nature (London), **361**, 240 (1993).
14. A. Kittel, J. Parisi, and K. Pyragas. Phys. Lett. A. **198**, 433 (1995).
15. C.C. Chen, C.H. Tsai, and C.C. Fu. Phys. Lett. A, **194**, 265 (1994).
16. P. Richetti and A. Arneodo. Phys. Lett. A, **109**, 359 (1985).
17. A. Wolf, J.B. Swift, H.L. Swinney, and J. Vastano. Physica D, **16**, 285 (1985).
18. R. Mane. *In* Dynamical systems and turbulence, Warwick, 1980. *Edited by* D. Rand and L.S. Yong. Lecture Notes in Mathematics. Springer Press, Berlin. 1981.
19. L.F. Shampine and C.W. Gear. S. Am. Rev. **21**, 1 (1979).
20. K. Pyragas. Phys. Lett. A, **170**, 421 (1992).
21. F.W. Schneider, R. Blittersdorf, A. Forster, T. Hauck, D. Lebender, and J. Muller. J. Phys. Chem. **97**, 12244 (1993).
22. A. Lekebusch, A. Forster, and F.W. Schneider. J. Phys. Chem. **99**, 681 (1995).
23. H. Song, Y.-N. Li, L. Chen, Z.-S. Cai, Y.-J. Li, Z. Hou, B.-X. Wu, and X.-Z. Zhao. Acta Chim. Sin. Chin. Ed. **57**, 1047 (1999).
24. H. Song, Y.-N. Li, L. Chen, Z.-S. Cai, Y.-J. Li, Z. Hou, X.-Z. Zhao. Phys. Chem. Chem. Phys. **1**, 813 (1999).
25. J.S. Turner, J.C. Roux, W.D. McCormick, and H.L. Swinney. Phys. Lett. A, **85**, 9 (1981).

© 2001 NRC Canada

Synthesis of new substituted dihydroheptalene derivatives: SiO_2- and base-catalyzed rearrangement of dimethyl *trans*-3,8-dihydroheptalene-3,8-dicarboxylate

Nurullah Saraçoğlu, Abdullah Menzek, Armağan Kınal, and Metin Balci

Abstract: Dimethyl *trans*-3,8-dihydroheptalene-3,8-dicarboxylate (*trans*-**3**) isomerizes to dimethyl *cis*-3,8-dihydroheptalene-3,8-dicarboxylate (*cis*-**3**) upon treatment with SiO_2. On the other hand, base-catalyzed reaction of *trans*-**3** undergoes a direct 1,3-intramolecular proton shift to give **6** at room temperature in 5 min. Prolonged reaction time formed isomers **7** and **8** in a ratio of 4:1. AM1 calculations indicate that the isomer **8**, which is formed as minor product, has a lower heat of formation (–99.34 kcal mol^{-1}) than that of the major isomer **7** (–92.05 kcal mol^{-1}). However, when a similar reaction was performed at 100°C, the thermodynamically more stable isomer **8** was formed as the major product. Furthermore, cycloaddition reactions of these new dihydroheptalene derivatives **6** and **7** with different dienophiles have been studied. The mechanism has been discussed.

Key words: dihydroheptalene, cycloaddition, 1,3-hydrogen shift, cycloheptatriene–norcaradiene equilibrium.

Résumé : Le *trans*-3,8-dihydroheptalène-3,8-dicarboxylate de diméthyle (*trans*-**3**) s'isomérise en *cis*-3,8-dihydroheptalène-3,8-dicarboxylate de diméthyle (*cis*-**3**) par traitement avec du SiO_2. Par ailleurs, dans une réaction catalysée par les bases, le *trans*-**3** subit un transfert 1,3-intramoléculaire de proton qui, à la température ambiante, conduit directement au produit **6** en cinq minutes. Si le temps de réaction est prolongé, les isomères **7** et **8** se forment dans un rapport de 4:1. Des calculs AM1 indiquent que la chaleur de formation (–99,34 kcal mol^{-1}) l'isomère **8**, qui se forme comme produit mineur, est inférieure à celle (–92,05 kcal mol^{-1}) de l'isomère majeur. Toutefois, lorsqu'on effectue la même réaction à 100°C, il y a formation prédominante de l'isomère **8** qui est thermodynamiquement le plus stable. De plus, on a étudié les réactions de cycloaddition de ces nouveaux dérivés dihydroheptalènes **6** et **7** avec divers diénophiles. On discute du mécanisme.

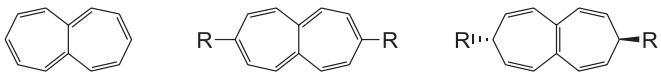
Mots clés : dihydroheptalène, cycloaddition, déplacement 1,3 d'hydrogène, équilibre cycloheptatriène–norcaradiène.

[Traduit par la Rédaction]

Introduction

Heptalene **1** (1), which has been for a long time the subject of theoretical studies, was synthesized by Dauben and Bertelli (2) in 1961. However, it remained poorly accessible. Later Vogel et al. (3) have developed different elegant methods leading to the synthesis of heptalene **1** and its derivatives **2**. In recent years we have been concerned with the synthesis of *trans*-**3** (3*c*, 4*a*), which is dihydroheptalene derivative, in connection with our work on the synthesis of the pyramidalized double bonds (4).

Dihydroheptalene derivative *trans*-**3** consists of two fused cycloheptatriene units where the ester groups have *trans* configuration. We were interested in the isomerization of one ester group in *trans*-**3** to obtain the corresponding isomer *cis*-**3**. In this paper, we describe the SiO_2- and base-catalyzed reactions of *trans*-**3** and the cycloaddition reactions of the newly formed dihydroheptalene derivatives.



1 **2** *trans*-**3**

R = $COOCH_3$

Received September 5, 2000. Published on the NRC Research Press Web site on January 3, 2001.

N. Saraçoğlu and A. Menzek. Department of Chemistry, Atatürk University, 25240 Erzurum, Turkey.
A. Kınal and M. Balci.[1] Department of Chemistry, Middle East Technical University, 06531 Ankara, Turkey.

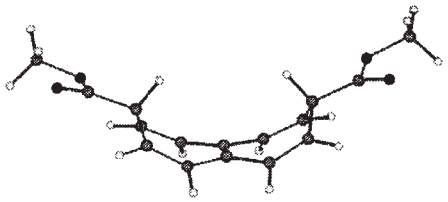
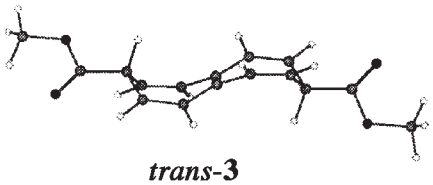
[1]Author to whom correspondence may be addressed. Telephone: (90) 312 210 5140. Fax: (90) 312 210 1280. e-mail: mbalci@metu.edu.tr

Results and discussions

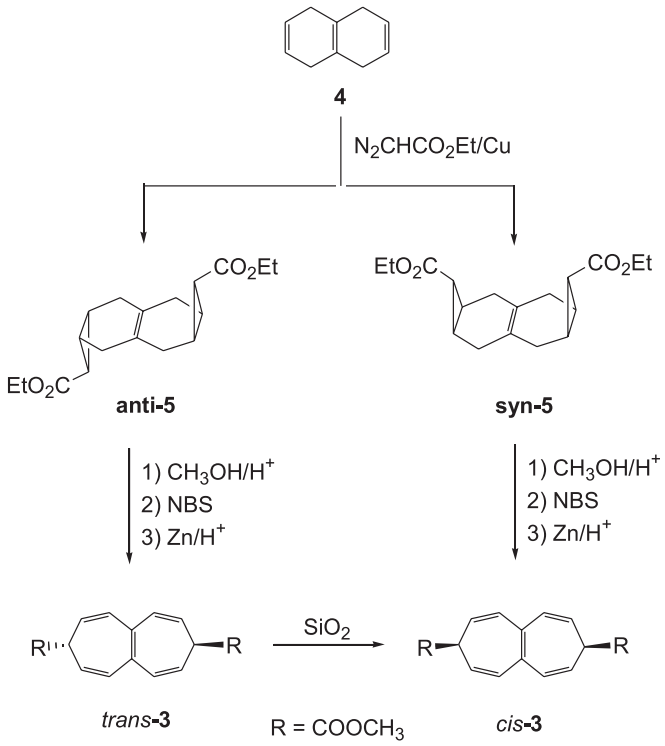
trans-**3** *and cis*-**3** have been synthesized by addition of excess ethyl diazoacetate to isotetraline **4** to deliver bis-adducts *anti*-**5** (3*c*, 4*a*) and *syn*-**5** (4*c*) in 18 and 28% yields, respectively. Transesterification and NBS-bromination followed by Zn-AcOH elimination resulted in the formation of *trans*-**3** and *cis*-**3** (Scheme 1).

 DOI: 10.1139/cjc-79-1-35 © 2001 NRC Canada

Table 1. Optimized geometries and energies of *cis*- and *trans*-**3**.

Structures	AM1 relative energy (kcal mol^{-1})	HF relative energy (kcal mol^{-1})	DFT relative energy (kcal mol^{-1})
 *cis*-**3**	0.0	0.0	0.0
 *trans*-**3**	0.502	1.602	2.621

Scheme 1.



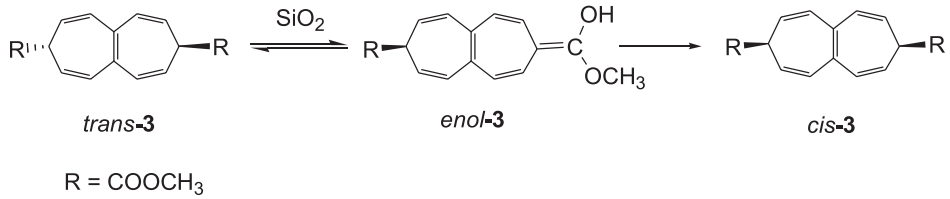
We have noticed that *trans*-**3** was isomerized partly to *cis*-**3** during column chromatography on silica gel. For that reason, *trans*-**3** was refluxed with silica gel in $CHCl_3$. After four days *trans*-**3** was completely rearranged to *cis*-**3** in yield of 61%, no other isomer being detected (Scheme 2). *cis*-**3** was characterized by its 200 MHz ^{1}H NMR spectrum. Its six-line ^{13}C NMR spectrum is particularly informative. Furthermore, structural assignment to compounds *trans*-**3** and *cis*-**3** has been supported by the formation of the cycloaddition products and their X-ray analysis (4). It is very interesting that *trans*-**3** isomerized completely to *cis*-**3**. In this isomerization, silica gel presumably acts as an adsorbent, since silica gel has numerous hydroxyl groups (Si-OH). Hydrogen bonding formed between these hydroxyl groups and the polar carbonyl group of *trans*-**3** seems to play an important role, in forming enol-**3**, which later converts to the thermodynamically more stable isomer *cis*-**3**.

To understand the driving force of this isomerization, firstly, optimized geometry and energies of all conformers were calculated in semiempirical method (AM1 (5)) by using HyperChem 5.01 for Windows. Then, they were optimized by using Hartree–Fock (HF) (6) and Density Functional Theory (DFT) (7) methods of the Gaussian 98 package program (8). The stable geometries of the conformers optimized by the AM1 method were used as input for the HF method calculation. For the DFT optimization method, the optimized geometries of the HF method were used as the input. As basis set, we employed the minimal basis set (STO-3G (9)) for both HF and DFT calculations. Results of these calculations show clearly that the *cis*-**3** isomer has a lower heat of formation than the *trans*-**3** isomer, which indicates that the *cis*-**3** isomer is thermodynamically the most stable one (Table 1).

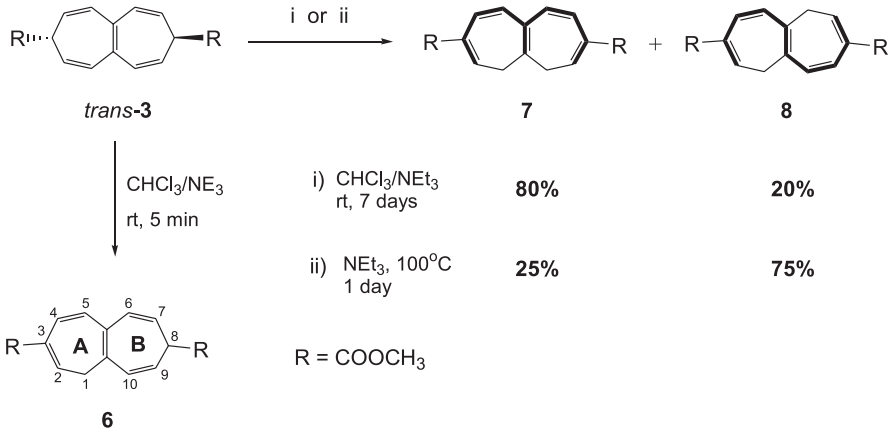
Later, the base-catalyzed intramolecular proton transfer in cycloheptatriene units of *trans*-**3** has been investigated. *trans*-**3** was first treated with a catalytic amount of a proton-donating base, triethylamine in chloroform at room temperature. After 5 min, **6** was formed almost in quantitative yield. The structure of **6** was assigned by ^{1}H and ^{13}C NMR spectra. The most conspicuous features in the ^{1}H NMR spectra of

© 2001 NRC Canada

Scheme 2.



Scheme 3.



this new dihydroheptalene derivative **6** are three distinct AB-systems, which correspond to six olefinic protons. The olefinic proton H_2 resonates as triplet. ^{13}C NMR spectrum with 16 lines is also in agreement with the unsymmetrical structure.

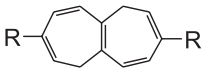
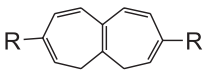
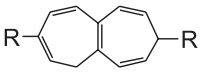
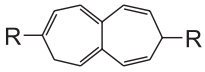
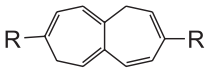
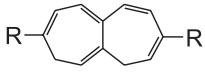
Base-catalyzed reaction of *trans*-**3** undergoes a direct 1,3-intramolecular proton shift. Takahashi et al. (10) have also observed a direct 1,3-proton shift in cycloheptatriene derivatives, the shift proceeding through a 1,3-hydrogen bond-bridged carbanion that is a transition state rather than an intermediate. The mechanism has been supported by MNDO calculations.

The treatment of *trans*-**3** with triethylamine in $CHCl_3$ for seven days afforded a mixture of two isomerization products (**7** (80%) and **8** (20%)) in accord with the usual 1,3-hydrogen transfer in cycloheptatriene derivatives. Attempted separation of this isomeric mixture by column chromatography failed. However, dihydroheptalene derivative **7** was isolated from the reaction mixture by fractional crystallization. The correct structural assignment of **7** was made especially by analysis of ^{13}C NMR. On the basis of the ^1H NMR data and splitting pattern one cannot distinguish between those isomers. A nine-line ^{13}C NMR is in agreement with the structure **7**. However, the isomer **8** gave an eight-line ^{13}C NMR spectrum as expected.

First, *trans*-**3** undergoes a 1,3-hydrogen shift to give **6**. The next hydrogen shift can take place only in the other cycloheptatriene unit (**B**), since the acidity of the methylenic protons in the ring **A** decreased. In the second cycloheptatriene system (**B**) a new 1,3-hydrogen shift can take place in two different directions due to the unsymmetrical structure of **6** providing **7** and **8**.

AM1 calculations indicate that the isomer **8**, which is formed as minor product, has a lower heat of formation (–99.34 kcal mol^{-1}, a fully conjugated system) than the major isomer **7** (–92.05 kcal mol^{-1}) which is cross-conjugated (Table 2). We assume that the activation energy leading to the thermodynamically most stable isomer **8** must be higher than that of **7**. To clarify the course of the migration, we have optimized the geometry of the transition states by the

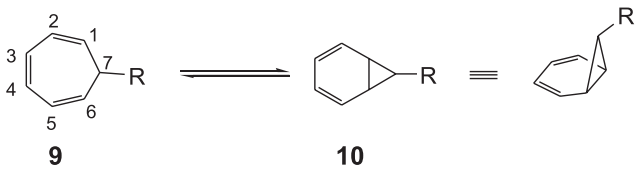
Table 2. ΔH_f values of some isomeric dihydroheptalene derivatives calculated by the AM1 method (in kcal mol^{-1}).

Structure	ΔH_f
	- 99.34
	- 92.05
	- 91.48
	- 88.03
	- 87.80
	- 87.18

Note: R = $COOCH_3$

© 2001 NRC Canada

Scheme 4.



QST2 method in Gaussian 94 (11) and calculated the activation energies for the formation of **7** and **8** (in the absence of the base) starting from the isomer **6**. We found, that the activation barrier for the formation of **7** (E_a = 52.6 kcal mol^{-1}) is much lower than that for the formation of **8** (E_a = 92.6 kcal mol^{-1}).

This assumption was confirmed nicely by carrying out the base-catalyzed reaction at the elevated temperature. The treatment of *trans*-**3** with triethylamine for one day at 100°C afforded again the same isomeric mixture of **7** (25%) and **8** (75%), however in reversed yields. We conclude that the kinetically controlled product **7** is formed at lower temperatures, whereas at higher temperature the thermodynamically more stable isomer **8** is formed as the major product.

We reported that the cycloheptatriene units in *trans*-**3** and *cis*-**3** undergo easily cycloaddition reactions with dienophiles, such as benzyne, dimethyl acetylenedicarboxylate (DMAD), singlet oxygen ($^1O_2$), and *N*-phenyltriazolinedione (PTAD) to form adducts derived from norcaradiene which is in equilibrium with cycloheptatriene (12). The equilibrium for the symmetry-allowed valence isomerization of cycloheptatriene and norcaradiene has been demonstrated. Electron-accepting substituents, such as CHO, COOR, CN, etc., at C-7 tend to shift the equilibrium to the norcaradiene (**10**) side (Scheme 4) (13).

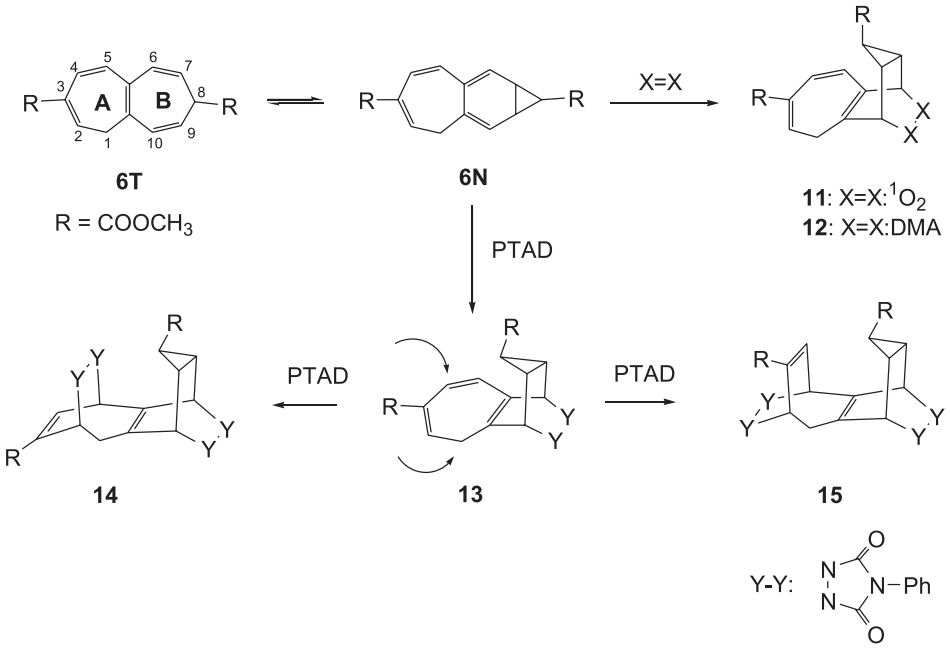
To investigate chemical behavior of cycloheptatriene units in **6** and **7**, they were reacted with some dienophiles. The reactions of (**6T** ⇆ **6N**) consisting of two different cycloheptatriene (CHT) rings with singlet oxygen and DMAD and gave only isolated NOR-adducts **11** and **12**, respectively. Careful examination of the ^{1}H and ^{13}C NMR spectra of the products showed exclusive formation of the norcaradiene adducts where the **B** ring in **6** was involved. Since **6T** is in equilibrium with its valence isomer **6N**, two types of norcaradiene adducts (*exo* and *endo*) are possible. We have revealed the presence of only the *exo* isomers **11** and **12** on the basis of the measured coupling constants at the cyclopropane ring. These results show that cycloheptatriene ring **B** bearing an ester group at C-8 carbon atom is more reactive (forms more norcaradiene isomer) than the cycloheptatriene unit **A** (Scheme 5). This is an expected result. In both cases we observe a strong regio- and stereoselectivity.

Furthermore, it was interesting to examine the behavior of the cycloheptatriene unit **A**. For this reason we have studied the cycloaddition reactions of **6** with 2 mol of triazolinedione (PTAD). Reaction of **6** with PTAD gave two bis-adducts **14** and **15** in a ratio of 1:1. The second mol of PTAD added exclusively to the cycloheptatriene unit.

The cycloheptatriene equilibrates with its valence isomer and forms norcaradiene. In the case of **7** the formation of the norcaradiene isomer is not favored because of the position of the ester group. The ester group can stabilize the norcaradiene structure much better if it is directly attached to an sp^3-carbon atom, which is not the case in **7**. Additionally, the formation of the norcaradiene structure **7N** will cause more strain in the molecule. To test the reactivity of this system, we have treated **7** with singlet oxygen and obtained NOR-product **16** and CHT-product **17** in ratio of 66 and 26%, respectively.

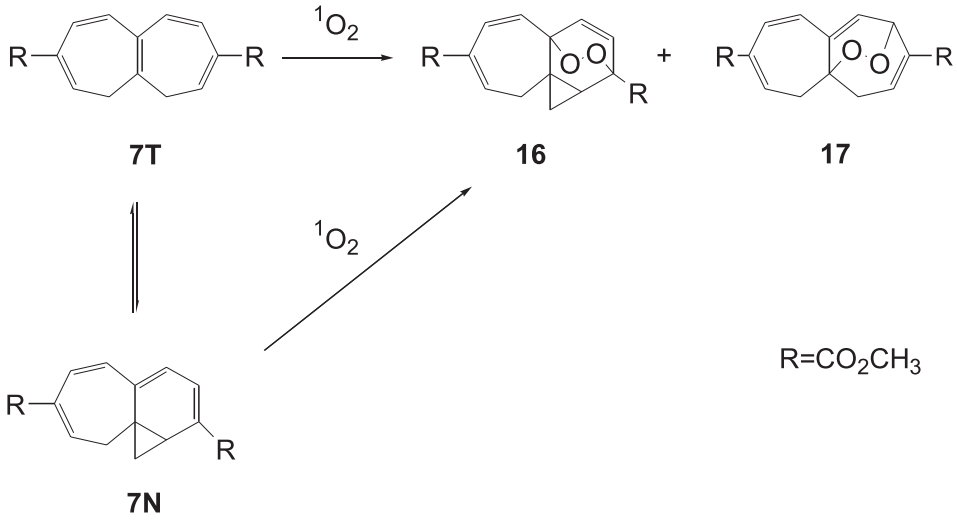
It is remarkable that the NOR-product **16** is formed as the major product. Clearly singlet oxygen intervenes in the cycloheptatriene–norcaradiene equilibrium in **7**. This is not surprising since kinetic studies confirm that the dienophilic reactivity of singlet oxygen toward [2 + 4]-cycloadditon is

Scheme 5.



© 2001 NRC Canada

Scheme 6.



enormous (14). We assume that the dynamic equilibrium in **7** is still on the side of the cycloheptatriene valence isomer. However, the activation barrier for the cycloaddition of singlet oxygen to cycloheptatriene unit in **7** must be significantly higher than the activation barrier for the **7T** ⇆ **7N** valance isomerization which in turn must be higher than the activation barrier for the cycloaddition of singlet oxygen to **7N** to give the adduct **16**. This is not surprising since the planar diene moiety in norcaradiene **7N** should be considerably more reactive towards dienophiles than the twisted diene moiety in cycloheptatriene **7T**.

General

All solvents were dried and distilled by standard procedures. Melting points were determined using a capillary melting point apparatus (Thomas–Hoover) and are uncorrected. IR spectra were obtained from KBr pellets or solution in 0.1 mm cells on an IR recording spectrophotometer. ^{1}H NMR spectra were recorded on a Varian 200 MHz spectrometer and are reported in δ units with TMS as internal standard. All column chromatography was carried out using Merck on silica gel (60-mesh).

Experimental

Dimethyl *cis*-3,8-dihydroheptalene-3,8-dicarboxylate (*cis*-3)

To a solution of *trans*-**3** (1088 mg, 4 mmol) in 70 mL of $CHCl_3$ was added 6.0 g of thin-layer silica gel (741-Kieselgel 60 $HF_{254+366}$). The reaction mixture was refluxed for four days and cooled to room temperature. The reaction mixture was filtered and washed with ethyl acetate. The combined organic solvents were evaporated, and the residue was purified by crystallization from ether, giving *cis*-**3** (660 mg, 61%, pale yellow crystals, mp 114–116°C). IR (KBr, cm^{-1}): 3000, 2950, 2820, 1735, 1615, 1433, 1300, 1205, 1170, 1040, 975, 915, 810, 720. ^{1}H NMR (200 MHz, $CDCl_3$) δ: 6.32 (d, *J* = 9.9 Hz, 4H), 5.81 (dd, *J* = 9.9, 5.6 Hz, 4H), 3.80 (s, 3H), 2.53 (t, *J* = 5.6 Hz, 2H). ^{13}C NMR (50 MHz, $CDCl_3$) δ: 173.51, 139.97, 129.40, 124.40, 52.83, 44.55. Anal. calcd. for $C_{16}H_{16}O_4$: C 70.58, H 5.92; found: C 70.39, H 5.81.

Dimethyl 1,8-dihydroheptalene-3,8-dicarboxylate (6)

A mixture of *trans*-**3** (272 mg, 1 mmol) and NEt_3 (3 drops) in 15 mL of $CHCl_3$ was stirred at room temperature during 5 min and the mixture was diluted by adding 35 mL of $CHCl_3$. The organic phase was washed with a solution of HCl (2 × 20 mL, 5%) and then washed with water (2 × 40 mL), and dried over $MgSO_4$. The residue was purified by crystallization from ether, giving **6** (250 mg, 92%, mp 85–86°C). IR (KBr, cm^{-1}): 2980, 2930, 2830, 1740, 1700, 1610, 1430, 1300, 1250, 1170, 1050, 970. ^{1}H NMR (200 MHz, $CDCl_3$) δ: 6.97 (bd, A part of AB system, *J* = 11.7 Hz, 1H), 6.88 (d, B part of AB system, *J* = 11.7 Hz, 1H), 6.65 (bt, *J* = 7.3 Hz, 1H), 6.27 (d, A part of AB system, *J* = 9.8 Hz, 1H), 6.24 (d, A part of AX system, *J* = 9.7 Hz, 1H), 5.77 (dd, B part of AB system, *J* = 9.8, 5.7 Hz, 1H), 5.50 (dd, X part of AX system, *J* = 9.7, 5.7 Hz, 1H), 3.72 (s, 6H), 3.03 (dd, A part of AB system, *J* = 11.8, 7.3, 1H), 2.37 (bt, *J* = 5.7 Hz, 1H), 2.80 (dd, X part of AX system, *J* = 11.8, 7.3 Hz, 1H). ^{13}C NMR (50 MHz, $CDCl_3$) δ: 173.49, 167.10, 137.82, 135.65, 133.78, 133.04, 130.36, 129.14, 127.21, 126.81, 123.75, 120.01, 52.76, 52.39, 44.87, 35.72. Anal. calcd. for $C_{16}H_{16}O_4$: C 70.58, H 5.92; found: C 70.45, H 5.96.

The reaction of *trans*-3 with NEt_3 for seven days: dimethyl 1,10-dihydroheptalene-3,8-dicarboxylate (7) and dimethyl 1,6-dihydroheptalene-3,8-dicarboxylate (8)

A solution of *trans*-**3** (272 mg, 1 mmol) and five drops NEt_3 in 15 mL of $CHCl_3$ was stirred at room temperature for seven days. To the reaction mixture was then added $CHCl_3$ (35 mL). The organic layer washed with a solution of HCl (2 × 20 mL, 5%) and then washed with water (2 × 40 mL), and dried over $MgSO_4$. The ^{1}H NMR spectrum showed that the reaction mixture consisted of a mixture of **7** (80%) and **8** (20%). The crystallization of this mixture from ether gave (**7**) (mp 142–143 °C). IR (KBr, cm^{-1}): 3000, 2960, 2920, 1700, 1610, 1420, 1340. ^{1}H NMR (200 MHz, $CDCl_3$) δ: 7.10 (d, A part of AB system, *J* = 11.6 Hz, 2H), 6.90 (d, B part of AB system, *J* = 11.6 Hz, 2H), 6.64 (t, *J* = 7.6 Hz, 2

© 2001 NRC Canada

H), 3.78 (s, 6H), 2.52 (d, J = 7.6 Hz, 4H). ^{13}C NMR (50 MHz, $CDCl_3$) δ: 167.37, 133.33, 132.51, 129.77, 129.61, 126.81, 116.43, 52.46, 35.59. Anal. calcd. for $C_{16}H_{16}O_4$: C 70.58, H 5.92; found: C 70.69, H 5.67. (**8**): ^{1}H NMR (200 MHz, $CDCl_3$) δ: 7.08 (d, A part of AB system, J = 11.4 Hz, 2H), 6.70 (d, B part of AB system, J = 11.4 Hz, 2H), 6.47 (t, J = 7.7 Hz, 2 H), 3.72 (s, 6H), 2.57 (d, J = 7.7 Hz, 4H). ^{13}C NMR (50 MHz, $CDCl_3$) δ: 166.60, 133.14, 131.77, 130.36, 129.32, 126.86, 51.86, 33.11.

The reaction of *trans*-3 with NEt_3 at 100°C

A solution of *trans*-**3** (210 mg, 0.77 mmol) and 1.7 g of NEt_3 was heated at 100°C. After 24 h, the reaction mixture was cooled to room temperature. The residue was dissolved in $CHCl_3$ (75 mL) and washed with a solution of HCl (3 × 30 mL, 10%) and then washed with water (2 × 40 mL), and dried over $MgSO_4$. The solvent was removed under reduced pressure. According to the NMR spectrum, the reaction mixture consisted of a mixture of **7** (25%) and **8** (75%).

Photoxygenation of 6: dimethyl *cis*-13,14-dioxatetracyclo[7.3.2.0^{2,8}.0^{10,12}] tetradeca-2(8),3,5-triene-5,11-dicarboxylate (11)

To a stirred solution of **6** (272 mg, 1 mmol) in 30 mL of CCl_4 was added 10 mg of tetraphenyl porpyrine (TPP). The resulting mixture was irradiated with a projection lamp (50 W) while oxygen passed through solution and the mixture was stirred for 1.5 h. The solvent was removed by evaporation. Chromatography of the residue on a silica gel column eluting with $CHCl_3$–*n*-hexane (50 mL, 20:80) and $CHCl_3$ (200 mL) gave the cycloadduct **11** (250 mg, 83%, mp 89–90°C, crystallized from $CHCl_3$–ether). IR (KBr, cm^{-1}): 3000, 2940, 1720, 1705, 1430, 1260, 1160, 1075, 1050. ^{1}H NMR (200 MHz, $CDCl_3$) δ: 7.19 (bd, A part of AX system, J = 11.4 Hz, 1H), 6.60 (d, X part of AX system, J = 11.4 Hz, 1H), 6.54 (t, J = 7.1 Hz, 1 H), 5.09 (bd, J = 4.3 Hz, 1H), 3.80 (s, 3H), 3.62 (s, 3H), 2.73 (dd, A part of AB system, J = 13.4, 7.1 Hz, 1H), 2.51 (dd, B part of AB system, J = 13.4, 7.1 Hz, 1H), 2.19 (m, 2H), 0.62 (t, J = 3.1 Hz, 1H). ^{13}C NMR (50 MHz, $CDCl_3$) δ: 171.83, 166.94, 132.21, 131.23, 130.39, 129.85, 128.94, 124.77, 77.77, 76.37, 52.70, 52.54, 30.06, 21.55, 15.89, 15.19. Anal. calcd. for $C_{16}H_{16}O_6$: C 63.13, H 5.30; found: C 62.94, H 5.19.

The cycloaddition of 6 with DMAD: tetramethyl *exo*-tetracyclo[7.3.2.0^{2,8}.0^{10,12}] tetradeca-2(8),3,5,13-tetraene-5,11,13,14-dicarboxylate (12)

A mixture of **6** (200 mg, 0.74 mmol) and DMAD (130 mg, 0.91 mmol) in 4 mL of $CHCl_3$ was placed into a glass tube, the tube was sealed and heated at 70–80°C. After 13 days, the mixture was cooled to room temperature. The solvent was roto-evaporated, the residue was submitted to column chromatography on silica gel eluting with $CHCl_3$–*n*-hexane (100 mL, 10:90) and cycloadduct **12** was obtained (190 mg, 62%, as pale-yellow liquid). IR (liquid, cm^{-1}): 3000, 2940, 1715, 1625, 1430, 1270, 1120, 1060, 940, 900. ^{1}H NMR (200 MHz, $CDCl_3$) δ: 6.94 (bd, A part of AB system, J = 11.3 Hz, 1H), 6.56 (d, B part of AB system, J = 11.3 Hz, 1H), 6.37 (t, J = 7.5 Hz, 1 H), 4.22 (bd, J = 3.8 Hz, 1H), 4.10 (bd, J = 3.9 Hz, 1H), 3.77 (s, 3H), 3.76 (s, 3H), 3.75 (s, 3H), 3.56 (s, 3H), 2.50 (dd, A part of AB system, J = 13.2, 7.5 Hz, 1H), 2.47 (dd, B part of AB system, J = 13.2, 7.5 Hz, 1H), 2.16–2.02 (m, 2H), 1.14 (t, J = 2.8 Hz, 1H). ^{13}C NMR (50 MHz, $CDCl_3$) δ: 171.49, 167.21, 166.43, 166.39, 147.44, 147.36, 135.63, 130.74, 130.07, 128.98, 127.89, 127.44, 52.86, 52.82, 52.51, 52.26, 47.62, 44.95, 31.36, 30.79, 28.42, 27.88. Anal. calcd. for $C_{22}H_{22}O_8$: C 63.76, H 5.35; found: C 63.94, H 5.22.

The cycloaddition of 6 with 2 mol of PTAD

A solution of **6** (170 mg, 0.63 mmol) and PTAD (300 mg, 1.7 mmol) in 15 mL of $CHCl_3$ was stirred at room temperature for 17 h. The solvent was removed in vacuum and chromatography of the residue on silica gel eluting with $CHCl_3$ (100 mL) gave a mixture of **14** (50%) and **15** (50%). Crystallization of the mixture from CH_2Cl_2–*n*-hexane gave **14** as white crystals (180 mg) and then recrystallization of the residue from CH_2Cl_2–ether gave **15** as white crystals (168 mg).

14: (mp 248–249°C). IR (KBr, cm^{-1}): 3106, 2953, 1780, 1741, 1720, 1642, 1523, 1446, 1421, 1242, 1165, 1038, 936. ^{1}H NMR (200 MHz, $CDCl_3$) δ: 7.55–7.24 (m, 11H), 5.67 (m, 1H), 5.35 (d, J = 4.8 Hz, 1H), 5.26 (d, J = 13.5 Hz, 1H), 4.97 (d, J = 4.7 Hz, 1H), 3.71 (s, 3H), 3.70 (s, 3H), 3.06 (dd, A part of AB system, J = 19.8, 4.4 Hz, 1H), 2.56 (dd, B part of AB system, J = 19.8, 2.5 Hz, 1H), 2.35–2.19 (m, 2H), 1.35 (t, J = 3.0 Hz, 1H). ^{13}C NMR (50 MHz, $CDCl_3$) δ: 172.08, 164.68, 159.96, 159.48, 154.38, 153.95, 141.26, 134.87, 133.18, 132.63, 131.93, 131.24, 131.16, 131.13, 130.83, 130.72, 130.50, 127.46, 59.79, 58.92, 54.69, 54.35, 52.90, 51.80, 37.05, 25.25, 18.29, 17.43. Anal. calcd. for $C_{32}H_{26}N_6O_8$: C 61.73, H 4.21, N 13.50; found: C 61.49, H 4.09, N 13.21.

15: (mp 176–177°C). IR (KBr, cm^{-1}): 3106, 2978, 1804, 1727, 1676, 1523, 1421, 1344, 1242, 1140, 1038, 961, 936. ^{1}H NMR (200 MHz, $CDCl_3$) δ: 7.48 (d, J = 6.6 Hz, 1H), 7.43–7.21 (m, 10H), 5.58 (m, 1H), 5.46 (d, J = 4.8 Hz, 1H), 5.30 (d, J = 6.6 Hz, 1H), 5.00 (d, J = 4.8 Hz, 1H), 3.83 (s, 3H), 3.69 (s, 3H), 2.92 (dd, A part of AB system, J = 19.5, 4.4 Hz, 1H), 2.75 (dd, B part of AB system, J = 19.5, 2.5 Hz, 1H), 2.32–2.15 (m, 2H), 1.16 (t, J = 3.0 Hz, 1H). ^{13}C NMR (50 MHz, $CDCl_3$) δ: 172.13, 165.02, 159.99, 159.81, 154.51, 152.54, 141.23, 135.49, 133.07, 132.93, 132.88, 131.24, 131.00, 130.58, 130.31, 129.47, 127.32, 127.15, 60.46, 58.98, 54.84, 54.39, 52.63, 52.08, 37.37, 25.08, 18.87, 17.63. Anal. calcd. for $C_{32}H_{26}N_6O_8$: C 61.73, H 4.21, N 13.50; found: C 61.39, H 4.12, N 13.34.

The photooxygenation of 7: dimethyl 11,12-dioxatetracyclo[8.2.2.0^{1,7}.0^{7,9}]tetra-deca-2,4,13-triene-3,10-dicarboxylate (16) and dimethyl (1*S*(*R*),9*S*(*R*))-13,14-dioxatri-cyclo[7.3.2.0^{1,7}]tetradeca-3,5,7,10-tetraene-4,10-dicarboxylate (17)

To a solution of **7** (284 mg, 1.04 mmol) in 50 mL of CCl_4 was added 10 mg of tetraphenyl porpyrine (TPP). The resulting mixture was irradiated with a projection lamp (50 W) while oxygen passed through the solution and the mixture was stirred for 2 h. The solvent was evaporated in vacuum. According to the NMR spectrum, the reaction mixture consisted of **7** (8%), **16** (66%), and **17** (26%). Recrystallization of the crude product from $CHCl_3$–ether gave NOR adduct **16** (70 mg), mp 86–87°C. IR (KBr, cm^{-1}): 3095, 3085, 2995,

© 2001 NRC Canada

2940, 2880, 1730, 1710, 1435, 1255, 1130, 1105, 1050, 965. ^{1}H NMR (200 MHz, $CDCl_3$) δ: 7.40 (dd, *J* = 8.8, 4.9 Hz, 1H), 6.74 (bd, A part of AX system, *J* = 12.6 Hz, 1H), 6.38 (bd, A part of AB system, *J* = 8.4, 1H), 6.12 (bd, B part of AB system, *J* = 8.4 Hz, 1H), 5.90 (bd, X part of AX system, *J* = 12.6 Hz, 1H), 3.87 (s, 3H), 3.78 (s, 3H), 3.15 (dd, A part of AX system, *J* = 15.0, 4.9 Hz, 1H), 1.83 (dd, X part of AX system, *J* = 15.0, 8.8 Hz, 1H), 1.66–1.59 (m, 1H), 0.46–0.34 (m, 2H). ^{13}C NMR (50 MHz, $CDCl_3$) δ: 168.52, 166.99, 145.44, 132.34, 130.03, 129.16, 128.78, 127.09, 83.97, 82.05, 53.67, 52.67, 30.99, 20.93, 17.78, 12.17. Anal. calcd. for $C_{16}H_{16}O_6$: C 63.13, H 5.30; found: C 62.85, H 5.18.

Chromatography of the residue on florosil eluting with ethyl acetate – *n*-hexane (5:95) gave the cycloadduct **17** (30 mg, oil). ^{1}H NMR (200 MHz, $CDCl_3$) δ: 7.09 (t, *J* = 7.9 Hz, 1H), 6.83 (td, *J* = 4.0, 1.2 Hz, 1H), 6.64 (d, *J* = 7.4 Hz, 1H), 6.51 (bs, 2H), 5.67 (dd, *J* = 7.4, 1.2 Hz, 1H), 3.79 (s, 3H), 3.76 (s, 3H), 2.73 (dd, A part of AB system, *J* = 20.3, 4.0 Hz, 1H), 2.57 (d, *J* = 7.9 Hz, 2H), 2.56 (dd, B part of AB system, *J* = 20.3, 4.4 Hz, 1H). ^{13}C NMR (50 MHz, $CDCl_3$) δ: 166.72, 165.82, 140.89, 139.37, 135.43, 135.35, 132.96, 131.88, 130.15, 123.89, 83.08, 72.51, 52.73 (2C), 39.26, 36.57. Anal. calcd. for $C_{16}H_{16}O_6$: C 63.13, H 5.30; found: C 63.38, H 5.15.

Acknowledgments

The authors are indebted to the Departments of Chemistry (Middle East Technical University and Atatürk University) for financial support of this work.

References

1. K. Hafner. Pure Appl. Chem. **28**, 153 (1971); (*b*) L.A. Paquette. Isr. J. Chem. **20**, 233 (1980).
2. H.J. Dauben, Jr. and A. Bertelli. J. Am. Chem. Soc. **83**, 4659 (1961).
3. (*a*) E. Vogel, H. Königshofen, J. Wassen, K. Müllen, and J.F.M. Oth. Angew.Chem. **86**, 777 (1974); Angew. Chem. Int. Ed. Engl. **13**, 732 (1974); (*b*) E. Vogel and J. Ippen. Angew. Chem. **86**, 779 (1974); Angew. Chem. Int. Ed. Engl. **13**, 734 (1974); (*c*) E. Vogel and F. Hogrefe. Angew. Chem. **86**, 779 (1974); Angew. Chem. Int. Ed. Engl. **13**, 735 (1974).
4. (*a*) A. Menzek, M. Krawiec, W.H. Watson, and M. Balci. J. Org. Chem. **56**, 6755 (1991); (*b*) A. Menzek and M. Balci. M. Aust. J. Chem. **46**, 1613 (1993); (*c*) A. Menzek, N. Saraçoğlu, M. Krawiec, W.H. Watson, and M. Balci. J. Org. Chem. **60**, 829 (1995); (*d*) M. Balci, S.A. Bourne, A. Menzek, N. Saraçoğlu, and W.H.J. Watson. J. Chem. Crystallogr. **25**, 107 (1995); (*e*) N. Saraçoğlu, A. Menzek, Þ. Sayan, U. Salzner, and M. Balci. J. Org. Chem. **64**, 6670 (1999).
5. M.J.S. Dewar, E.G. Zoebish, E.F. Healy, and J.J.P. Stewart. J. Am. Chem. Soc. **107**, 3902 (1985).
6. (*a*) C.C.J. Roothan. Rev. Mod. Phys. **23**, 69 (1951); (*b*) J.A. Pople and R.K. Nesbet. J. Chem. Phys. **22**, 571 (1959); (*c*) R. McWeeny and G. Dierksen. J. Chem. Phys. **49**, 4852 (1968).
7. (*a*) C. Lee, W. Yang, and R.G. Par. Phys. Rev. B: Condens. Matter, **37**, 785 (1988); (*b*) A.D. Becke. J. Chem. Phys. **98**, 5648 (1993).
8. M.J. Frisch, G.W. Trucks, H.B. Schlegel, G.E. Scuseria, M.A. Robb, J.R Cheeseman, V.G. Zakrzewski, J.A. Montgomery, Jr., R.E. Stratmann, J.C. Burant, S. Dapprich, J.M. Millam, A.D. Daniels, K.N. Kudin, M.C. Strain, O. Farkas, J. Tomasi, V. Barone, M. Cossi, R. Cammi, B. Mennucci, C. Pomelli, C. Adamo, S. Clifford, J. Ochterski, G.A. Petersson, P.Y. Ayala, Q. Cui, K. Morokuma, D.K. Malick, A.D. Rabuck, K. Raghavachari, J.B. Foresman, J. Cioslowski, J.V. Ortiz, A.G. Baboul, B.B. Stefanov, G. Liu, A. Liashenko, P. Piskorz, I. Komaromi, R. Gomperts, R.L. Martin, D.J. Fox, T. Keith, M.A. Al-Laham, C.Y. Peng, A. Nanayakkara, M. Challacombe, P.M.W. Gill, B. Johnson, W. Chen, M.W. Wong, J.L. Andres, C. Gonzalez, M. Head-Gordon, E.S. Replogle, and J.A. Pople. Gaussian 98, Revision A.8. Gaussian, Inc., Pittsburgh, Pa. 1998.
9. W.J. Hehre, R.F. Stewart, and J.A. Pople. J. Chem. Phys. **51**, 2657 (1969).
10. K. Takahashi, T. Suzuki, H. Toda, K. Takase, S. Koseki, and T. Nakajima. J. Org. Chem. **52**, 2666 (1987).
11. C. Peng and H.B. Schlegel. Isr. J. Chem. **33**, 449 (1993).
12. M. Balci. Turk. J. Chem. **16**, 42 (1992).
13. (*a*) R. Hoffmann. Tetrahedron Lett. 2907 (1970); (*b*) H. Günther. Tetrahedron Lett. 5173 (1970).
14. (*a*) A.A. Gorman, G. Lovering, and M.A.J. Rodgers. J. Am. Chem. Soc. **101**, 3050 (1979); (*b*) W. Adam, M. Balci, and B. Pietrzak. J. Am. Chem. Soc. **101**, 6285 (1979); (*c*) W. Adam, F. Adamsky, F.G. Klärner, E.M. Peters, K. Peters, H. Rebollo, W. Rüngeler, and H.G. von Schnering. Chem. Ber. **116**, 1848 (1983).

© 2001 NRC Canada

Thermodynamic of metal complexation of the macrocyclic antibiotic rifampicin

I. Shehatta, I. Kenawy, A.H. Askalany, and Ayman A. Hassan

Abstract: The acid–base and complexation equilibria of rifampicin with H^+, Mn^{2+}, Co^{2+}, Ni^{2+}, Cu^{2+}, Zn^{2+}, Cd^{2+}, Hg^{2+}, and Pb^{2+} were studied by means of potentiometry. The stoichiometric equilibrium constants were determined in 50% (v/v) methanol–water medium at different temperatures and constant ionic strength (0.05 M KCl). It was established that rifampicin has two proton-binding sites. The distribution diagram of the corresponding ionic species as a function of pH is given and indicated that rifampicin exists predominantly in the zwitterionic form at pH ≤ 5. The thermodynamic parameters of protonation and complexation were derived and discussed. The formation of the complexes is spontaneous, more favourable at lower temperatures, entropically unfavourable, and an enthalpy-driven process. The order of the changes in Gibbs energy and enthalpy accompanying the complexation was found to be $Mn^{2+} < Co^{2+} < Ni^{2+} < Cu^{2+} > Pb^{2+} > Zn^{2+} > Cd^{2+} > Hg^{2+}$ in accordance with the well-known sequence of Irving and Williams. The transition series contraction energy (E_r(Mn–Zn)), and the ligand field stabilization energy (δH) were calculated from the enthalpy changes.

Key words: rifampicin, thermodynamics, potentiometry, and complexation.

Résumé : Faisant appel à la potentiométrie, on a étudié les équilibres acide–base et de complexation de la rifampicine avec H^+, Mn^{2+}, Co^{2+}, Ni^{2+}, Cu^{2+}, Zn^{2+}, Cd^{2+}, Hg^{2+} et Pb^{2+}. Les constantes d'équilibre stoechiométriques ont été déterminées dans un mélange méthanol–eau à 50 % (v/v), à diverses températures et à force ionique constante (0,05 M KCl). On a établi que la rifampicine possède deux sites de liaison. On a déterminé le diagramme de distribution des espèces ioniques correspondantes en fonction du pH; il indique que, à des pH ≤ 5, la rifampicine existe principalement sous la forme zwitterionique. On a dérivé les paramètres thermodynamiques de la protonation et de la complexation et on les discute. La formation des complexes est spontanée, plus favorable à faibles températures, défavorable d'un point de vue entropique et le processus est favorisé par l'enthalpie. On a trouvé que le changement dans l'énergie de Gibbs et dans l'enthalpie qui accompagnent la complexation est dans l'ordre $Mn^{2+} < Co^{2+} < Ni^{2+} < Cu^{2+} > Pb^{2+} > Zn^{2+} > Cd^{2+} > Hg^{2+}$, en accord avec la séquence bien connue d'Irving et Williams. À partir des changements d'enthalpie, on a calculé l'énergie de contraction de la série de transition (E_r(Mn–Zn)) ainsi que l'énergie de stabilisation du champ de ligand (δH).

Mots clés : rifampicine, thermodynamique, potentiométrie, complexation.

[Traduit par la Rédaction]

Introduction

Rifamycins are macrocyclic antibiotics. They belong to a class of molecules known as ansamycins. Rifamycins are unique among antibiotics in that they have a characteristic ansa structure, i.e., a ring structure or chromophore spanned by an aliphatic chain. Rifamycins differ from one another in the type and the substituent on their naphthohydroquinone ring. Rifampicin is one of the most semisynthetic compounds of the ansamycin group. Rifampicin is the drug of choice for chemoprophylaxis of meningococcal diseases and meningitis. It shows promise in the treatment of certain non-mycobacterial diseases when combined with β-lactam antibiotic or vancomycin. Furthermore, it has a rapid bactericidal effect on mycobacterium lepra and is used in leprosy.

The role of transition metal ions in the mechanism action of antibacterial drugs was reported (1). Moreover, when a therapeutically affective dose of antibacterial drug is administrated, the balance between the metal ions in vivo and their ligand environment can be considerably altered. This may have an influence on the activity of the drug against bacteria. Also, rifampicin–Pt complexes (2) were useful as antibiotic agents. They have stronger bactericidal effect (against *Staphylococcus aureus* 209p) and less toxicity than rifampicin, and show good H_2O-solubility. Thus, capsules were formulated containing rifampicin–Pt complex. Therefore, to enhance understanding of drug–metal interaction, and in continuation of our previous work (3–7), it is important to assess the reaction between rifampicin and a number of transition-metal ions. These metal ions may be present in the biological systems, or may be taken by an accident.

Received January 13, 2000. Published on the NRC Research Press Web site on January 12, 2001.

I. Shehatta,[1] I. Kenawy, A.H. Askalany, and A.A. Hassan. Chemistry Department, Faculty of Science, Mansoura University, Mansoura, Egypt.

[1]Author to whom correspondence may be addressed. Presently at: Chemistry Department, Faculty of Science, United Arab Emirates University, 17551–Al-Ain, United Arab Emirates. Telephone: 009713 7064218. Fax: 009713 7671291. e-mail: I.Shehatta@uaeu.ac.ae

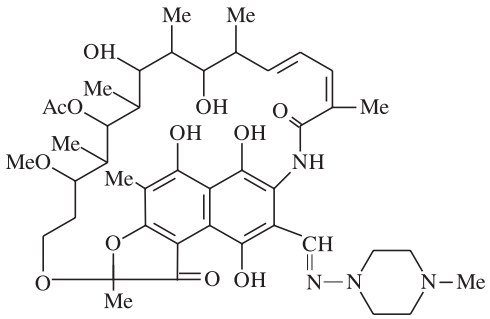
 DOI: 10.1139/cjc-79-1-42 © 2001 NRC Canada

In this paper, we report the determination of the stability constants by pH-metric method for rifampicin complexes of H^+, Mn^{2+}, Co^{2+}, Ni^{2+}, Cu^{2+}, Zn^{2+}, Cd^{2+}, Hg^{2+}, and Pb^{2+} at different temperatures. The thermodynamic functions for these systems were also calculated and correlated with the well-known properties of metal ions. This is done to observe how the different metal environments could affect the affinity of the drug for metal ion.

Experimental

Reagent and materials

Rifampicin (Structure 1) was obtained from El-Nasr Pharmaceutical Chemical Co., Egypt and used without any further purification. Other materials of analytical reagent grade were used, and supplied from different companies. Methanol was purified as described by Lund and Bjerrum (8). The metal salts were provided by BDH as nitrates. All solutions of metal ions were prepared using deionized water and standardized complexometrically by EDTA (9) using suitable indicators. Carbonate-free sodium hydroxide was prepared and standardized potentiometrically with potassium hydrogen phthalate solution.



Structure 1

Apparatus and procedure

Potentiometric measurements were performed using a Metrohm E536 potentiograph equipped with a 665 DOSIMAT (Metrohm, Herisau, Switzerland). The combined glass electrode was standardized before, and checked after each titration with buffer solutions produced by FISHER (New Jersey, U.S.A.). The electrode system was calibrated in terms of hydrogen ion concentrations instead of activities. Thus, all constants determined in this work are concentration constants. All titrations were carried out at 30, 35, and 40°C. This was adjusted to ±0.05°C by circulating water from an ultrathermostat (Köttermann 4130, Germany) through the annular space of a double-walled Pyrex titration cell of 100 mL capacity. Sodium hydroxide was added from the Dosimat and the content of the titration vessel was stirred magnetically. The following solution mixtures (A–C) were prepared and titrated potentiometrically with standard 0.02 M NaOH at constant ionic strength (0.05 M KCl) in 50% (v/v) methanol–water mixture:

(A) 2.5 mL (10^{-2} M) HCl + 2.5 mL (1 M) KCl
= 0.5 mM acid

(B) Solution (A) + 5 mL (5×10^{-3} M) drug
= 0.5 mM drug

(C) Solution (B) + 5 mL (1×10^{-3} M) metal ion
= 0.1 mM metal

All the above solution mixtures were made up to 50 mL with appropriate volumes of methanol and double-distilled water to keep at the 50% (v/v) methanol–water ratio. An Irving and Rossotti (10) pH titration technique was used to determine the protonation constants of rifampicin and formation constants of its complexes. Triplicate titrations have been performed for each system.

All calculations were performed using a computer program based on unweighted linear least-square fits. Moreover, the stability constants have been determined in the low pH region. Thus, the formation of hydroxy complexes could be neglected.

The pH readings were corrected, using the Van Uitert–Hass equation (11):

$$[1] \qquad -\log [H^+] = B + \log U_H^\circ - \log\left(\frac{1}{\gamma_\pm}\right)$$

The values of the correction factor ($\log U_H^\circ$) were obtained experimentally (12) and those of the mean activity coefficients ($\gamma_\pm$) were computed according to the equation given by Harned and Owen (13) assuming the activity coefficients are the same on both molal and molar scales.

$$[2] \qquad \log\left(\frac{1}{\gamma_\pm}\right) = \frac{\left[\dfrac{[Z_1 Z_2]1.29\times10^6\sqrt{2\mu}}{(\varepsilon T)^{3/2}}\right]}{\left[1+\dfrac{3556a^\circ\sqrt{2\mu}}{(\varepsilon T)^{1/2}}\right]}$$

where μ is the ionic strength (0.05 M), T is the absolute temperature (303.15, 308.15, or 313.15 K), Z_1 and Z_2 are the charges of ions in solution at equilibrium, $a°$ is the mean ionic diameter in Å (taken as 6 Å (14)) and ε is the dielectric constant of the medium. The values of $\log U_H^\circ$ were found to be –0.148, –0.153, and –0.157 at 303.5, 308.15, and 313.15 K, respectively, in agreement with the literature values (15).

Results and discussion

Proton–rifampicin system

The ionization constants (Table 1) for rifampicin were determined potentiometrically using the Irving–Rossotti technique (10) at different temperatures in 50% methanol–water mixture. The titrations were carried out at constant ionic strength (0.05 M KCl). The free acid (0.5 mM) and its mixture with rifampicin (0.5 mM) were titrated against carbonate-free sodium hydroxide (20 mM) solution and represented in Fig. 1.

The average number of protons attached per ligand ($\bar{n}_A$) was calculated (10) at different pH values, and was used to calculate the proton association constants of rifampicin applying different computational methods (16). The maximum $\bar{n}_A$ value is found to be ≈ 2 indicating that the investigated

© 2001 NRC Canada

Table 1. The stability constants[a] of metal ions – rifampicin complexes in 50% (v/v) methanol–water mixture, 0.05 M KCl, and at different temperatures.

Cation	Half-method						Least-squares method						Average values					
	303.15 K		308.15 K		313.15 K		303.15 K		308.15 K		313.15 K		303.15 K		308.15 K		313.15 K	
	log K_1	log K_2	log K_1	log K_2	log K_1	log K_2	log K_1	log K_2	log K_1	log K_2	log K_1	log K_2	log K_1	log K_2	log K_1	log K_2	log K_1	log K_2
H^+	10.97[b]	7.04[c]	10.85[b]	6.92[c]	10.73[b]	6.85[c]	—	7.02	—	6.96	—	6.89	10.97	7.03	10.85	6.94	10.73	6.87
Mn^{2+}	6.68	5.19	6.51	5.08	6.45	4.99	6.71	5.22	6.61	5.12	6.42	5.01	6.70	5.21	6.56	5.10	6.43	5.00
Co^{2+}	6.94	5.40	6.84	5.30	6.70	5.18	7.09	5.44	6.90	5.31	6.78	5.22	7.02	5.42	6.87	5.31	6.74	5.20
Ni^{2+}	7.48	5.63	7.34	5.47	7.15	5.34	7.59	5.56	7.42	5.51	7.35	5.42	7.54	5.60	7.38	5.49	7.28	5.38
Cu^{2+}	8.94	6.60	8.78	6.45	8.60	6.31	8.98	6.60	8.80	6.48	8.66	6.37	8.96	6.60	8.79	6.47	8.63	6.34
Zn^{2+}	7.80	6.34	7.67	6.21	7.49	6.11	7.89	6.34	7.74	6.22	7.61	6.08	7.85	6.34	7.71	6.22	7.55	6.10
Cd^{2+}	7.00	5.33	6.81	5.22	6.68	5.13	6.95	5.39	6.85	5.28	6.69	5.15	6.98	5.36	6.83	5.25	6.70	5.14
Hg^{2+}	6.42	4.71	6.31	4.59	6.15	4.51	6.42	4.73	6.28	4.65	6.19	4.53	6.42	4.72	6.30	4.62	6.17	4.52
Pb^{2+}	8.38	6.57	8.24	6.43	8.06	6.29	8.42	6.55	8.24	6.43	8.13	6.31	8.40	6.56	8.24	6.43	8.10	6.30

[a] log K_1 ± (0.03–0.07), log K_2 ± (0.04–0.10).
[b] pK_2.
[c] pK_1.

drug has two dissociable protons. The first proton ionization is assigned to the peprazine group, in good agreement with that previously reported (17), while the other is assigned to the hydroxyl group at C-4. Since the initial pH reading in the drug titration curve was around 3.3, the ionization constant of rifampicin related to the hydroxyl at C-8 (pK_a = 1.7) (17) could not be calculated under the present experimental conditions.

The first association constant was calculated using the half- $\bar{n}_A$ values (16), i.e., at $\bar{n}_A$ = 1.5 from the $\bar{n}_A$–pH curve. This value is confirmed by least-quares method (16) by plotting log $(\bar{n}_A - 1)/(2 - \bar{n}_A)$ vs. pH. While the second association constant is evaluated by the midpoint method (16) using the following equation: log K_1K_2 = 2 pH (at $\bar{n}_A$ = 1)

Metal–rifampicin system

The stepwise formation constants of some divalent metal ions (Mn^{2+}, Co^{2+}, Ni^{2+}, Cu^{2+}, Zn^{2+}, Cd^{2+}, Hg^{2+}, and Pb^{2+}) with rifampicin were calculated potentiometrically at different temperatures (303.15, 308.15, and 313.15 K), constant ionic strength (0.05 M KCl), and in 50% (v/v) methanol–water mixture.

An inspection of the titration curves shown in Fig.1, reveals that the metal–drug titration curves lie below and well separated from the drug titration one. This indicates that the complexation processes occurred with the liberation of hydrogen ions.

Values of $\bar{n}$ and pL are calculated (where $\bar{n}$ is the average number of ligand attached per metal ion and pL is the free ligand exponent). All metal ions form 1:1 and 1:2 (M:L) ratios in solution with rifampicin as gathered from $\bar{n}$, where $\bar{n}$ values extend between 0 and 2.

The stoichiometric stability constants (log K_1 and log K_2) are evaluated using the two well-known methods, namely: (*i*) the half-method (16) in which the formation curves are drawn between $\bar{n}$ and pL and the constants are evaluated at $\bar{n}$ = 0.5 and 1.5, respectively; and (*ii*) the least-squares method (16) using the equation:

$$[3] \qquad \frac{\bar{n}}{(1-\bar{n})[L^-]} = \frac{(2-\bar{n})[L^-]}{1-\bar{n}} K_1K_2 + K_1$$

The stability constant values (Table 1) calculated by the two different methods are in good agreement with each other.

Effect of the ionic strength of the medium on the stability of the complexes

In an attempt to know the possible effects of chloride complexation with the metals, the variation of log *K* values of rifampicin–Cu^{2+} complexes, as a representative example, with the ionic strength of the medium was investigated at 308.15 K in 50% (v/v) methanol–water mixture. The salt concentration have been chosen in the range where extended Debye–Hückel theory is suitable to be applied. Although the values of p*K* and log *K* decrease with increasing ionic strength of the medium (Table 2) in accordance with the Debye–Hückel equation (18), the values obtained in 0.05 M KCl are close to those calculated in absence of the salt.

© 2001 NRC Canada

Fig. 1. Potentiometric titration curves for rifampicin with various metal ions at 303 K.

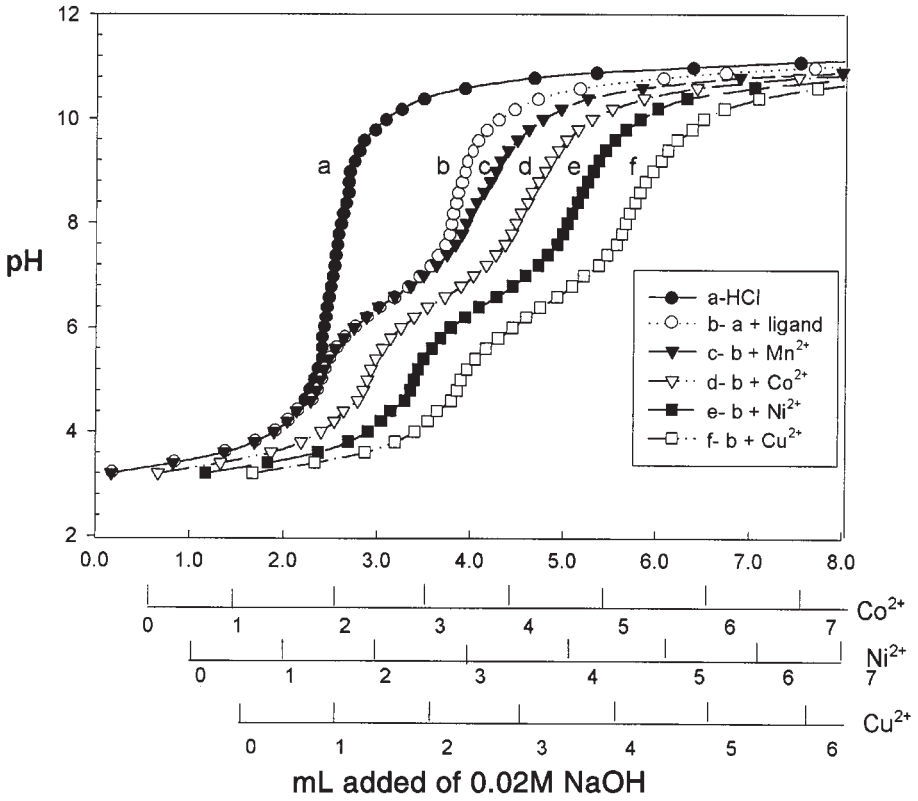


Table 2. Acid ionization constants for rifampicin, and stability constants for its Cu^{2+} complexes, in different concentrations of KCl and 50% (v/v) methanol–water mixture at 308.15 K.

Concentration of KCl (M)	Ionization constants		Stability constants	
	pK_1	pK_2	log K_1	log K_2
0.20	7.07	11.01	8.92	6.60
0.10	6.99	10.91	8.85	6.52
0.05	6.94	10.85	8.79	6.47
0.00[a]	6.81	10.69	8.66	6.34

[a]These values were obtained by linear regression of pK or log K vs. $[KCl]^{1/2}$.

Distribution curves

Fractional compositions of the drugs are necessary to understand stability and transportation models in the gastrointestinal and biological membrane (19). Such transportation depends on the ionization degree of the drugs and their lipid solubility. These terms are dependent upon the pH of the absorptive medium and pK_a values of the drugs (20). In general, the absorption is pH-dependent when the pK_a values of acids are between 2.5 and 7.5. In contrast, for acids with pK_a > 7.5, the absorption is pH-independent (21). Therefore, rifampicin absorption in the intestinal tract is transported by the pH-dependent mechanism.

Rifampicin can exist in three possible forms: as an acidic cation (H_3L^+), uncharged form (H_2L^0) (in equilibrium with its zwitterionic form $H_2L^{\pm}$), and two anionic forms (HL^-) and (L^{2-}), depending on the given pH. At low pH, both the piperazinyl and hydroxyl groups are protonated. At high pH, neither is protonated. At each pH, the fractions of zwitterionic ($H_2L^{\pm}$), and the anionic species (HL^- and L^{2-}) can be calculated (22) and represented in Fig. 2. In solution, $H_2L^{\pm}$ and L^{2-} species approach the total concentration of rifampicin at low (≤5) and high (≥12) pH values, respectively. While HL^- species reach a maximum in the isoelectric pH (pI = [pK_1 + pK_2]/2 = 9). The pH regions where two curves overlap correspond to the pK_a value. Also, the distribution curves (Fig. 2) for metal ions – rifampicin complexes permit us to follow up the stepwise complex formation and to detect at which pH value the different species are formed and facilitate the calculation of the stability constants of ML and ML_2.

Effect of temperature and thermodynamic parameters

The effect of temperature on both stepwise protonation constants of rifampicin and the stability constants of its complexes with Mn^{2+}, Co^{2+}, Ni^{2+}, Cu^{2+}, Pb^{2+}, Zn^{2+}, Cd^{2+}, and Hg^{2+} was investigated. The corresponding thermodynamic functions (ΔG, ΔH, and ΔS) were evaluated using the following relationships:

$$[4] \quad \Delta G = -2.303RT \log K = \Delta H - T\Delta S$$

$$[5] \quad \mathrm{d} \log K/\mathrm{d}(1/T) = \Delta H/2.303R$$

$$[6] \quad \Delta S = (\Delta H - \Delta G)/T$$

From the stability constants (Table 1) and the thermodynamic functions (Table 3) the following conclusions can be obtained: (*i*) pK_a values decrease with increasing temperature, i.e., the acidity of the drug increases with increasing temperature. However, the stepwise stability constants

© 2001 NRC Canada

Fig. 2. Concentration distribution curves as a function of pH for rifampicin and the complexes formed in the Cu(II)–rifampicin system at 303 K.

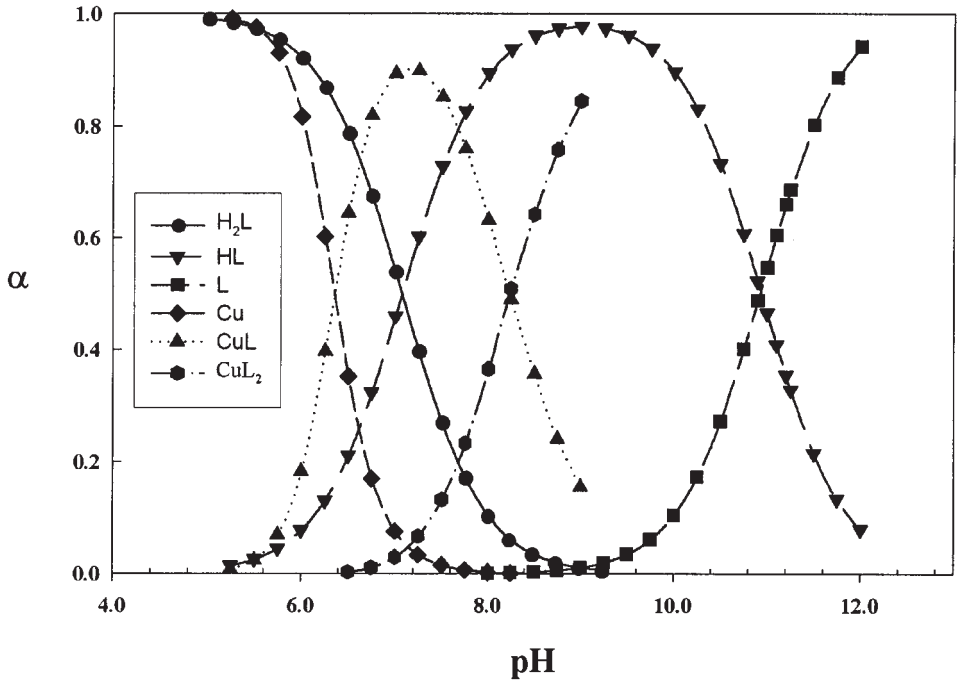


Table 3. Thermodynamic parameters[a] of metal ion – rifampicin complexes in 50% (v/v) methanol–water mixture and 0.05 M KCl at different temperatures.

Cation	Gibbs energy change (kJ mol^{-1})						Enthalpy change 303.15–313.15K (kJ/mol)		Entropy change at 303.15 K (kJ/mol)	
	303.15 K		308.15 K		313.15 K					
	$-\Delta G_1$	$-\Delta G_2$	$-\Delta G_1$	$-\Delta G_2$	$-\Delta G_1$	$-\Delta G_2$	$-\Delta H_1$	$-\Delta H_2$	$-T\Delta S_1$	$-T\Delta S_2$
H+	–63.68	–40.81	–64.08	–40.95	–64.34	–41.19	–43.70	–29.27	19.98	11.54
Mn^{2+}	38.86	30.24	38.71	30.09	38.55	29.95	48.26	39.03	9.40	8.79
Co^{2+}	40.78	31.46	40.54	31.30	40.41	31.15	50.11	40.86	9.33	9.40
Ni^{2+}	43.77	32.56	43.60	32.39	43.47	32.26	51.92	41.65	8.15	9.09
Cu^{2+}	52.03	38.31	51.86	38.17	51.72	38.04	60.80	46.49	8.77	8.18
Zn^{2+}	45.59	36.80	45.43	36.67	45.27	36.52	54.67	45.29	9.08	8.49
Cd^{2+}	40.49	31.11	40.33	30.98	40.17	30.82	50.19	39.91	9.70	8.80
Hg^{2+}	37.31	27.40	37.14	27.26	37.00	27.10	46.39	36.50	9.08	8.10
Pb^{2+}	48.77	38.08	48.62	37.94	48.48	37.77	57.25	47.48	8.48	9.40

[a]ΔG_1 ± (0.17–0.41), ΔG_2 ± (0.23–0.58), ΔH_1 ± (0.24–1.00), ΔH_2 ± (0.41–1.82), $T\Delta S_1$ ± (0.31–0.81), $T\Delta S_2$ ± (0.43–1.78) kJ mol^{-1}.

decrease with an increase of temperature indicating that the complexation process is more favourable at lower temperatures; (*ii*) ΔG values for the dissociation of rifampicin are positive, i.e., the dissociation processes are nonspontaneous while for the metal–ligand, all ΔG values are negative, indicating the spontaneous character of chelation; (*iii*) the positive values of ΔH indicate that the dissociation processes are endothermic in nature and enhance with the rise of temperature. But the chelation processes are exothermic as gathered from the negative ΔH values, supporting that the complexation reactions are more favourable at lower temperatures; (*iv*) the positive values of ΔS for protonation are owing to the increasing disorder as a result of the solvation process. For dibasic acids, like rifampicin, protonation is accompanied by large positive entropy changes. The large increase in entropy on protonation is a result of the release of solvent molecules from the solvation sheath of the interacting species. Also, the complexation processes are entropically unfavourable, as indicated from the negative ΔS values of the complexation. Such negative entropies can be attributed to the extensive solvation of metal chelates in the aqueous–methanol medium, as a result of the exposure of the polar nitrogen, oxygen, and metal ion of the chelate to the solvent molecule (23). The high negative enthalpy and entropy changes are in good agreement with that obtained for similar naphthohydroquinone moieties (24–27).

It is apparent that the complexation of rifampicin with the investigated metal ions in 50% (v/v) methanol–aqueous solution

© 2001 NRC Canada

Fig. 3. Variation of $-\Delta G_1$ (●), $-\Delta H_1$ (○), and $T\Delta S_1$ (▼) for rifampicin complexes with the reciprocal of the radius of the divalent metal ions.

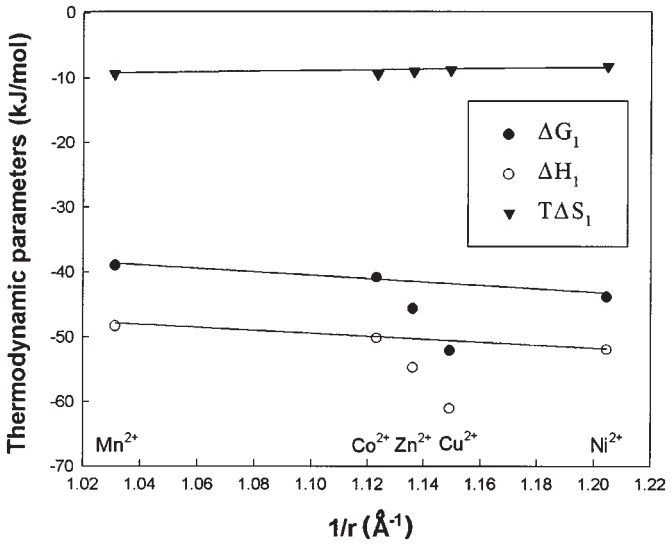
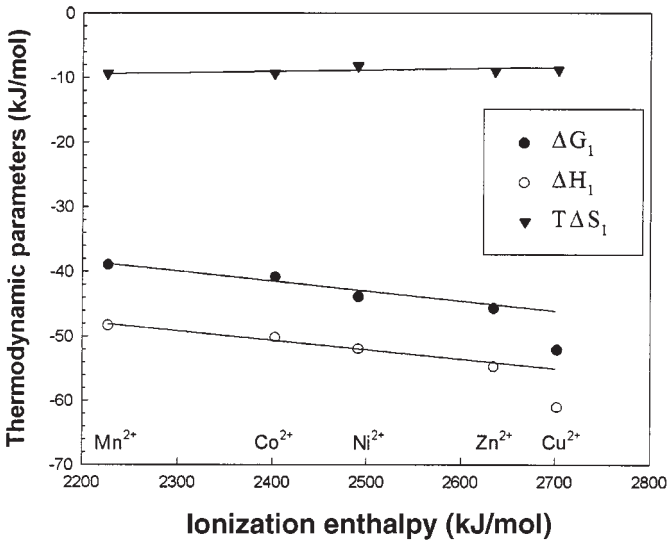


Fig. 4. Variation of $-\Delta G_1$ (●), $-\Delta H_1$ (○), and $T\Delta S_1$ (▼) for rifampicin complexes with the ionization enthalpy of the divalent metal ions.

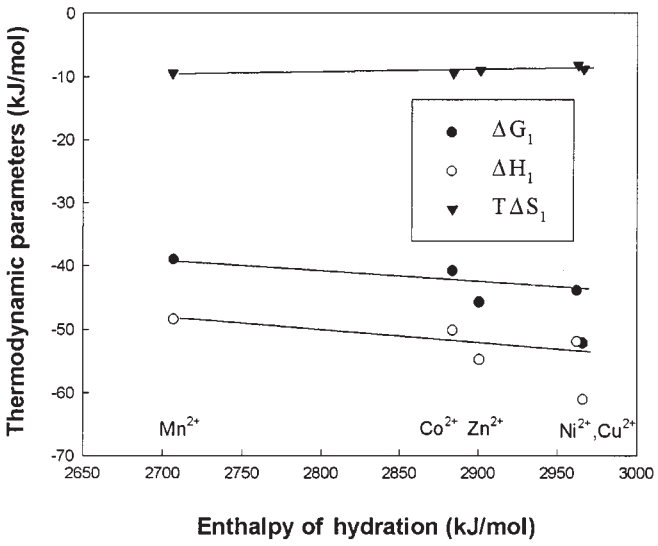


appears to be an enthalpy driven process. This is because both ΔH and ΔS are negative values; (*v*) the correlations of pK_a or log K values vs. $1/T$ are linear, suggesting that ΔC_p^o values for the dissociation and complexation processes are zero over the studied temperature range (303.15–313.15 K).

Factors affecting the stability of metal–rifampicin complexes

In an attempt to know how the different metal environments could affect the affinity of rifampicin for metal ion, it is necessary to correlate the thermodynamic parameters with the characteristic properties of the metal ions. Such study could help us to understand the role of metal ions in the mechanism of action of the drug.

Fig. 5. Variation of $-\Delta G_1$ (●), $-\Delta H_1$ (○), and $T\Delta S_1$ (▼) for rifampicin complexes with the enthalpy of hydration of the divalent metal ions.



The ΔG and ΔH values for rifampicin complexes with Mn^{2+}, Co^{2+}, Ni^{2+}, Cu^{2+}, Pb^{2+}, Zn^{2+}, Cd^{2+}, and Hg^{2+} are correlated with the reciprocal of the metal ionic radius (Fig. 3), the total ionization enthalpy (Fig. 4) at 298 K for the process $M(g) \rightarrow M^{2+}(g) + 2e$, and the enthalpy of hydration (ΔH_H) (Fig. 5). The latter correlation reveals that most of the rifampicin complexes are similar in size and geometry of the coordination sphere to the corresponding aquo ions (28). Similar correlations are also obtained for zinc group (Zn^{2+}, Cd^{2+}, and Hg^{2+} ions) complexes of rifampicin.

The relatively small constant $-T\Delta S$ values ($T\Delta S_1 = -8.88 \pm 0.58$ kJ mol^{-1}) coupled with large values of ΔH support that the transition-metal complexes of rifampicin are stabilized by enthalpy changes.

The $-\Delta G$ and $-\Delta H$ values for rifampicin complexation with the investigated divalent metal ions follow the order:

$$Mn^{2+} < Co^{2+} < Ni^{2+} < Cu^{2+} > Pb^{2+} > Zn^{2+} > Cd^{2+} > Hg^{2+}$$

which is in agreement with the well-known sequence of Irving–Williams (29). This is in line with the fact that the greater the electron acceptor ability of a metal, the stronger will be the complexes that it forms, hence the more $-\Delta G$ and $-\Delta H$ values. In general, it is noted that the ΔG and ΔH values of Cu^{2+} complex do not fall in a straight line and deviates when those values for the metal chelates are plotted against the respective properties of the divalent metal ions. Because of the Jahn–Teller effect (30), Cu^{2+} complex will gain some extra stabilization due to the tetragonal distortion of the octahedral symmetry in its complexes. Also, the complete 3*d*-orbital of Zn^{2+} leads to decrease its ionic radius therefore it gains more stabilization and deviates from the straight lines when ΔG and ΔH values of the metal chelates are plotted vs. the properties of metal ions. The values of log K_1 are greater than those of log K_2 and the difference is

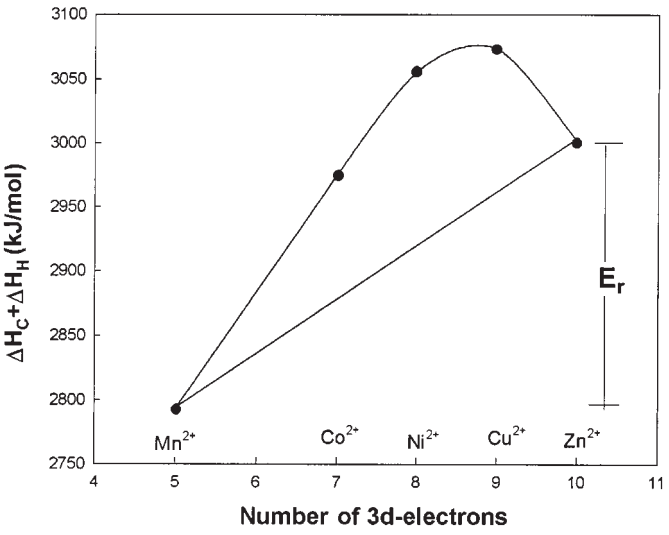
© 2001 NRC Canada

Table 4. The ligand field stabilization energy (δH) for 3*d*-divalent metal ion complexes of rifampicin.

Cations	$-\Delta H_H$[a]	$-\Delta H°$ [a, b]	$-\Delta H_L$[a, c]	$((n-5)/5)E_r$	$-\delta H$[a]
Mn^{2+}	2706.25	87.29	2793.54	—	—
Co^{2+}	2884.19	90.97	2975.16	83.02	98.59
Ni^{2+}	2962.81	93.57	3056.38	124.54	138.29
Cu^{2+}	2966.53	107.29	3073.82	166.06	114.22
Zn^{2+}	2901.15	99.96	3001.11	207.57	—

[a] In kJ mol^{-1}.
[b] $\Delta H° = \Delta H°_1 + \Delta H°_2$.
[c] $\Delta H_L = \Delta H_H + \Delta H°$.

Fig. 6. Values of ($\Delta H_C + \Delta H_H$) for rifampicin complexes of Mn^{2+}, Co^{2+}, Ni^{2+}, Cu^{2+}, and Zn^{2+} plotted against the number of 3*d* electrons.



usually positive (1.4–3.6 log units). This may be attributed to vacant sites of the metal ion are more freely available for the binding of the first ligand than the second. The large ($\log K_1 - \log K_2$) obtained, implies that in these systems not only the statistical effect, which gives $\log K_1 - \log K_2 = 0.68$ units, is considered but also the electrostatic effect and steric hindrance, due to the addition of the second chelating group, are significant. Furthermore, the second ligand (at least in part) may be bound to the central metal ion through a number of its donor groups less than of the first (31).

The effect of inner orbital splitting on the thermodynamic properties of the transition-metal rifampicin complexes

The presence of ligand gives more stability to the metal ion, except those with d^0, d^5, and d^{10} electronic configuration. The extra stabilization known by the ligand field stabilization energy (δH) which arises from the splitting of *d*-orbital and can be determined from the enthalpy change of complexation (32) using the following equation:

$$[7] \quad \delta H(M^{2+}) = \Delta H°(Mn^{2+}) - \left\{\frac{(n-5)}{5}\right\}E_r - \Delta H°(M^{2+}) + \Delta H_H(Mn^{2+}) - \Delta H_H(M^{2+})$$

where *n* is the number of the 3*d*-electrons, E_r is the transition series contraction energy, and $\Delta H°$ and ΔH_H are the complexation and hydration enthalpies, respectively. A plot of ($\Delta H_H + \Delta H°$) of rifampicin complexes as a function of the 3*d*-electrons is a humped curve (Fig. 6) rising to a maximum of about 160 kJ mol^{-1} above the line joining ($\Delta H_H + \Delta H°$) values for Mn^{2+} and Zn^{2+} complexes. The E_r ($Mn^{2+} - Zn^{2+}$) value was found to be 207.57 kJ mol^{-1}. The ligand field stabilization energy (Table 4) follows the order: $Co^{2+} < Ni^{2+} > Cu^{2+}$, which is in agreement with the ligand field theory.

References

1. G. Mendoza Diaz, R. Perez Alonso, and R. Moreno Esparza. J. Inorg. Biochem. 64, 207 (1996).
2. S. Yamabe. Jpn. Kokai Tokkyo Koho JP 0<|>193<|>590; Chem. Abs. 111, 219307z (1989).
3. I.S. Shehatta. Z. Phys. Chem. Bd. 187, 109 (1994).
4. I.S. Shehatta and A.A. El-Bindary. Thermochim. Acta, 237, 357 (1994).
5. A.A. El-Bindary and I.S. Shehatta. Monatsh. Chem. 125, 841 (1994).
6. A.A. El-Bindary, I.S. Shehatta, and E.M. Mabrouk. Monatsh. Chem. 125, 373 (1994).
7. I.S. Shehatta, A.A. El-Bindary, and E.M. Mabrouk. Monatsh. Chem. 126, 852 (1995).
8. H. Lund and J. Bjerrum. Ber. Dtsch. Chem. Ges. 64, 210 (1931).
9. R. Pribil. In Analytical application of EDTA and related compounds. 1st ed. Pergamon Press, Oxford. 1972. p. 72.
10. H. Irving and H.S. Rossotti. J. Chem. Soc. 2904 (1954).
11. L.G. Van Uitert and G.G. Hass. J. Am. Chem. Soc. 75, 451 (1953).
12. J.P. Shukla and S.G. Tandon. J. Electroanal. Chem. 35, 423 (1972).
13. H.S. Harned and B.B. Owen. In The physical chemistry of electrolytic solution. 3rd ed. Reinhold, New York. 1967. pp. 716.
14. R.M. Izatt, G.G. Hass, B.P. Block, and W.C. Fernelius. J. Phys. Chem. 58, 1133 (1954).
15. A. Avdeef, J.E.A. Comer, and S.J. Thomson. Anal. Chem. 65, 42 (1993).
16. H. Irving and H.S. Rossotti. J. Chem. Soc. 3397 (1953).
17. M. Neumann and A. Esanu. Drugs Exp. Clin. Res. 19, 385 (1988).
18. J.T. Edsall and J. Wyman. In Biophysical chemistry. Vol. 1. Academic Press, New York. 1958. pp. 442
19. T. Yamana and A. Tsuji. J. Pharm. Sci. 65, 1563 (1976).
20. J.G. Prieto, L. Santos, J.P. Barrio, and M.L. Alonso. J. Pharm. Sci. 76, 596 (1987).

© 2001 NRC Canada

21. M. Rowland, In Clinical pharmacokinetics concept and application. Lee and Febiger, Philadelphia. 1980. pp. 20.
22. R.J. Sturgeon and S.G. Schulman. J. Pharm. Sci. 66, 959 (1977).
23. W.D. Johnston and H. Frieser. Anal. Chim. Acta, 11, 20 (1954).
24. S. Arora, H.L. Kalra, S.N. Duby, and D.M. Puri. Acta Ceinc. Indica, 4, 16 (1978).
25. T.R. Harkins and H. Fresier. J. Phys. Chem. 63, 309 (1959).
26. S.C. Dhupar, K.C. Srivastava, and S.K. Banerji. J. Indian Chem. Soc. 20, 19 (1973).
27. S.C. Dhupar, K.C. Srivastava, and S.K. Banerji. J. Inst. Chem.i (India), 44, 206 (1972).
28. S. Murakami and Y. Yoshino. J. Inorg. Nucl. Chem. 43, 2070 (1981).
29. H.M. Irving and R.J.P. Williamas. J. Chem. Soc. 3192 (1953).
30. D. Drago. In An introduction to ligand field theory. Methuen, London. 1968.
31. F. Basolo and R.K. Murmann. J. Am. Chem. Soc. 76, 523 (1954).
32. P. George and D.S. McClure. In Progress in inorganic chemistry. Vol. 1. Interscience, New York. 1959. pp. 381

© 2001 NRC Canada

Excess properties for acetophenone + butanols at 298.15 K

Roque Riggio, Juan F. Ramos, and Hector E. Martinez

Abstract: Densities, viscosities, and refractive indexes of binary systems acetophenone + *n*-butanol, + *sec*-butanol, and + 2-methyl-1-propanol have been measured at 298.15 K and atmospheric pressure, over the whole composition range. The excess values of molar volume, viscosity, Gibbs free energy of activation of viscous flow, and internal pressure were calculated from experimental measurements. Based on the variations of the excess functions with composition, conclusions about the molecular interactions in these kinds of mixtures were obtained.

Key words: excess properties, binary mixtures, butanols, acetophenone.

Résumé : Opérant à 298,15 K et à la pression ambiante, on a mesuré les viscosités et les indices de réfraction des systèmes binaires acetofenone + *n*-butanol, + *sec*-butanol et + 2-méthylpropan-1-ol, sur I'ensemble des compositions. Utilisant les données expérimentales, on a calculé les valeurs en excès du volume molaire, de la viscosité, de I'énergie libre d'activation de Gibbs de l'écoulement visqueux et de la pression interne. Sur la base des variations des fonctions d'excès avec la composition, on a tiré des conclusions concernant les interactions moléculaires de ces divers mélanges.

Mots clés : propriétés en excès, mélanges binaires, butanols, acetofenone.

Introduction

To investigate the effects of molecular structure of alcohol isomers on excess molar volumes and viscosity deviations, a series of density, refractive index and viscosity measurements were conducted in our laboratory.

In previous works, we studied several binary liquid solutions of alcohols with different kinds of ketones (1–5). In this contribution, we report the following excess properties: molar volumes (V^E), viscosity (η^E), molar free energy of activation of viscous flow (G^{*E}), and internal pressures (P_i^E), for the mixtures: acetophenone (APH) + *n*-butanol (BuOH), + *sec*-butanol (2-BuOH), and + 2-methyl-1-propanol (I-BuOH), which were calculated from the density, viscosity, and refractive index measured.

Experimental

Components were supplied by Merck–Darmstadt (A.R. grade). All species were dried with anhyd K_2CO_3 and fractionally distilled under a flow of nitrogen. The middle fractions were stored over 3 Å molecular sieve and acetophenone over 4 Å molecular sieve.

Received July 16, 1999. Published on the NRC Research Press Web site on January 24, 2001.

R. Riggio[1] and H.E. Martinez. Facultad de Ciencias Naturales, Universidad Nacional de Salta, Buenos Aires 177.4400. Salta, República Argentina.
J.F. Ramos. Facultad de Ciencias Exactas, Universidad Nacional de Salta, Buenos Aires 177.4400. Salta, República Argentina.

[1]Author to whom correspondence may be addressed. Telephone: (54)(0387)(4255360). e-mail: jramos@unsa.edu.ar

All solutions were prepared by weight using an H11 Mettler balance and were stored in air-tight stoppered bottles.

Density

Densities (ρ) were determined with an Anton Paar DMA46 density meter with a built-in thermostat, and were calibrated with air and doubly distilled water. The accuracy was estimated to be ±0.1 kg m^{-3}.

Viscosity

Viscosities (η) were measured with a Cannon–Fenske viscometer, which was calibrated with doubly distilled water and benzene. The accuracy was estimated to be ±0.5%.

Refractive index

Refractive indexes (n_D) of pure components, as well as mixtures (sodium D line), were measured with a Jena dipping refractometer with an accuracy of ±0.00002. For the viscosity and refractive index, a thermostatic water bath, whose temperature was controlled to ±0.01°C, was used.

The composition of mixture samples was checked frequently by gas chromatography after measurements; the variation was found to be minimal.

Results

In Table 1, we report the experimental physical properties of the pure liquids, along with some literature values for comparison purposes.

The excess functions of the binary systems can be represented by a Redlich–Kister type equation:

$$[1] \qquad X^E = x_i x_j \sum_{k=0}^{n} a_k (2x_i - 1)^k$$

 DOI: 10.1139/cjc-79-1-50 © 2001 NRC Canada

Table 1. Experimental physical properties of the pure liquids at 298.15 K (25).

Component	ρ (kg m^{-3})		η (mPa s^{-1})		n_D	
	Exp.	Lit. (ref.)	Exp.	Lit. (ref.)	Exp.	Lit. (ref.)
APH	1023.4	1023.82 (25)	1.67	1.642 (25)	1.5315	1.5322 (26)
BuOH	805.7	806.0 (25)	2.58	—	1.3974	1.3973 (25)
2-BuOH	802.4	802.6 (25)	3.03	—	1.3950	1.3950 (25)
I-BuOH	798.2	797.8 (25)	3.38	—	1.3938	1.3939 (25)

Note: Abbreviations used: exp. experimental value, lit. literature value, ref. reference.

Table 2. Coefficients a_k from eq. [1] and standard deviations for the binary systems at 298.15 K.

Systems		a_0	a_1	a_2	σ_y
APH + BuOH	ρ	0.0578	–0.0063	0.0029	0.0
	η	–2.13	1.15	–0.91	7.1×10^{-3}
	n_D	0.0407	–0.0036	0.0024	1.1×10^{-4}
APH + 2-BuOH	ρ	0.0514	–0.0062	–0.0003	0.0
	η	–3.09	2.59	–1.72	1.1×10^{-2}
	n_D	0.0397	–0.0030	–0.0002	1.5×10^{-4}
APH + I-BuOH	ρ	0.0568	–0.0065	–0.0006	0.0
	η	–3.38	2.90	–2.08	9.0×10^{-3}
	n_D	0.0372	–0.0037	0.0029	4.4×10^{-5}

Notes: Units for density ρ, kg m^{-3}; for viscosity η, mPa s^{-1}.

where X^E represents any of the properties V^E, η^E, G^{*E}, P_i^E; x_i and x_j are the mol fractions of components i and j, respectively; and a_k denotes the polynomial coefficients. In each case, the optimum number of coefficients was ascertained from an examination of the variation of the standard error of the estimate with n

$$[2] \qquad \sigma = \left[\sum \frac{(X^E_{obs} - X^E_{cal})^2}{n_{obs} - n} \right]^{1/2}$$

where n_{obs} is the number of measurements.

Table 2 shows the values of the coefficients a_k as well as their standard deviation, calculated by the method of least-squares (6).

The excess functions are defined by the following equations, previously used by several authors (7–11):

$$[3] \qquad V^E = V - (X_1 V_1 + X_2 V_2)$$

$$[4] \qquad \eta^E = \eta - (X_1 \eta_1 + X_2 \eta_2)$$

$$[5] \qquad G^{*E} = RT\,[\ln \eta V - (X_1 \ln \eta_1 V_1 + X_2 \ln \eta_2 V_2)]$$

$$[6] \qquad P_i^E = \frac{2^{1/6} RT}{2^{1/6} V - d \mathrm{N}^{1/3} V^{2/3}} - \left(X_1 \frac{2^{1/6} RT}{2^{1/6} V_1 - d_1 \mathrm{N}^{1/3} V_1^{2/3}} + X_2 \frac{2^{1/6} RT}{2^{1/6} V_2 - d_2 \mathrm{N}^{1/3} V_2^{2/3}} \right)$$

where V and η are the molar volumes and the viscosities of the mixtures; V_1, V_2, η_1, and η_2 are the molar volumes and viscosities of the pure components, respectively.

The excess internal pressures (P_i^E) of the liquid mixture were obtained (12) by the equation

$$[7] \qquad P_i^E = P_i - (x_1 P_{i1} + x_2 P_{i2})$$

where P_i, P_{i1}, P_{i2} are the internal pressures of the mixtures and the pure components, respectively, which can be obtained from the Buchler–Hirschfelder–Curtis equation of state (13):

$$[8] \qquad P_i = \frac{2^{1/6} RT}{2^{1/6} V - d \mathrm{N}^{1/3} V^{1/3}}$$

where N is Avogadro's number and d the molecular diameter of the mixture or the pure components, calculated by the equation (14)

$$[9] \qquad d = 2 \left(\frac{n_D^2 - 1}{n_D^2 + 2} V \frac{3}{4 \Pi \mathrm{N}} \right)^{1/3}$$

where n_D are the refractive indexes of the mixtures or the pure components.

The values of the coefficients a_k for the excess functions of the binary systems and their standard deviation, which were calculated by the method of least squares, are shown in Table 3.

Discussion

It is well known that when mixing a highly associated alcohol with a different polar solvent, certain phenomena occur (15–17). Firstly, breaking of the alcohol's associations due to hydrogen bonding takes place. Secondly, specific interactions appear in the mixtures, such as new hydrogen bonds, dispersion forces, keto–enol tautomerism, and steric freedom (18). For the particular systems studied in this contribution, these effects have been identified through analyses of the following excess properties: molar volume, viscosity, free energy of viscous flow, and internal pressure.

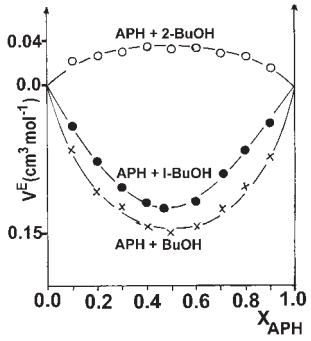
Figure 1 shows excess molar volumes against composition. From the isothermal curves at 298.15 K, the sterically

© 2001 NRC Canada

Table 3. Coefficients a_k from eq. [1] and standard deviation for the binary systems at 298.15 K.

Systems	Coefficients	V^E (m^3 mol^{-1} × 10^6)	η^E (mPa s^{-1})	G^{*E} (J mol^{-1})	P_i^E (kbar)
APH + BuOH	a_o	–0.5613	–1.935	–2567.05	0.0385
	a_1	–0.0191	1.124	878.68	–0.0006
	a_2	–0.2529	–0.930	–618.56	0.0006
	σ_v	5 × 10^{-3}	7 × 10^{-3}	0.67	1 × 10^{-4}
APH + 2-BuOH	a_o	0.1501	–2.686	–3468.51	0.0324
	a_1	–0.0111	2.545	2103.57	–0.0042
	a_2	0.1186	–1.712	–830.12	–0.0009
	σ_v	2 × 10^{-3}	1 × 10^{-2}	0.96	2 × 10^{-4}
APH + I-BuOH	a_o	–0.4816	–3.385	–3431.17	0.0355
	a_1	0.0405	2.896	2034.28	–0.0062
	a_2	0.1414	–2.076	–966.15	0.0030
	σ_y	2 × 10^{-3}	9 × 10^{-3}	0.23	5 × 10^{-5}

Fig. 1. Excess molar volumes of the systems at 298.15 K.



hindered effects on the excess molar volumes can be clearly noticed.

It can also be seen that the isothermal curve at 298.15 K is positive for the APH + 2-BuOH system, meanwhile, for the APH + BuOH and APH + I-BuOH systems, the isothermal curves are negative over the whole composition range. From these observations, we can conclude that for these systems the structure of the alcohol is broken when the mixture is formed. It appears that alcohols with OH-groups located at the very end of the molecular chain are more suitable to forming hydrogen bonds with acetophenone. Consequently, their excess molar volumes are lower than those for other binary systems, at near equimolar conditions. For the mixture containing secondary butanol (2-BuOH), there exists a slight possibility of geometric ordering due to the OH position. Meanwhile, for the APH + BuOH system and, to a lesser extent, for the APH + I-BuOH system, both containing primary alcohols, we believe that a compensating effect produces a negative contribution to the V^E values (19, 20).

The observed behaviour differences between the BuOH and I-BuOH mixtures, and the 2-BuOH mixture can be attributed to the higher steric freedom of the primary alcohols to form intermolecular association complexes through hydrogen bonds between the OH of the alcohol and the keto form to the ketone (21).

For the I-BuOH mixture, the lower V^E negative values are probably due to the steric effect of the α-methyl group and the small keto–enol–OH associates formed.

Fig. 2. Excess viscosities of the systems at 298.15 K.

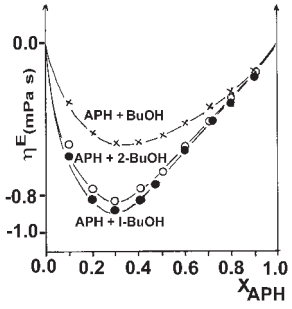


Fig. 3. Excess molar free energies of viscous flow activation by the systems at 298.15 K.

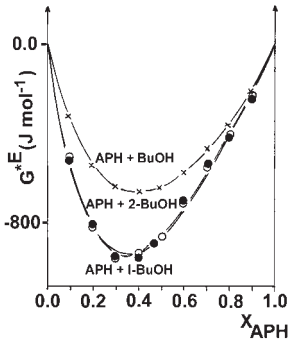


Figure 2 presents excess viscosities of the systems against composition at 298.15 K.

It is observed that all mixtures present negative excess viscosity values, whose decreasing order is the following:

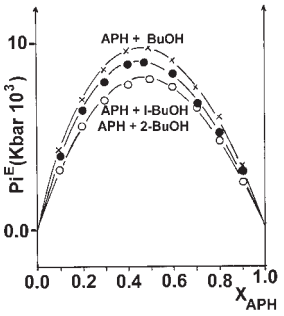
APH + I-BuOH < APH + 2-BuOH < APH + BuOH

According to the above order, negative deviations occur when dispersion forces are preponderant (22). This is in full agreement with the conclusions reached for the V^E behaviour.

Figure 3 shows the dependence of the calculated G^{*E} values upon composition.

© 2001 NRC Canada

Fig. 4. Excess molar internal pressures by the systems at 298.15 K.



Increasing negative deviations with composition can be observed in the order:

$$\text{APH + 2-BuOH} < \text{APH + I-BuOH} < \text{APH + BuOH}$$

It is well known that the strength of molecular interactions increases as G^{*E} decreases. In particular, for the above systems, interactions decrease according to the given order, which is in full agreement with our previous conclusions.

On the other hand, Fig. 4 shows excess internal pressure vs. composition.

We can observe positive P_i^E deviations for all systems studied. For those mixtures showing positive deviations, the attraction forces are greater than the repulsion forces. We know that, in these conditions, acetophenone is present partially in enol form (23), although in tiny quantities (24) and, so, it could be expected that the addition of different alcohols to acetophenone would cause keto–enol interactions, preferably with keto form. Thus, our results may be in good agreement with those expected through predictions reported in the literature.

Acknowledgments

This work was supported by INENCO–CONICET–UNSa, República Argentina.

References

1. R. Riggio, J.F. Ramos, M. Hernandez Ubeda, and J.A. Espindola. Can. J. Chem. **59**, 3305 (1981).
2. H.N. Solimo, R. Riggio, and H.E. Martinez. J. Solution Chem. **15**, 283 (1986).
3. R. Riggio, M. Hernandez Ubeda, J.F. Ramos, and H.E. Martinez. J. Chem. Eng. Data, **25**, 318 (1980).
4. R. Riggio, H.E. Martinez, J.A. Espindola, and J.F. Ramos. J. Chem. Eng. Data, **29**, 11 (1984).
5. R. Riggio, H. Martinez, and N.Z. de Salas. Can. J. Chem. **70**, 2859 (1992).
6. O. Redlich and A.T. Kister. Ind. Eng. Chem. **40**, 345 (1948)
7. R.P. Singh and C.P. Sinha. J. Chem. Eng. Data, **30**, 470 (1985).
8. P. Cea, C. Lafuente, H. Artigas, F.M. Royo, and J. Urieta. Can. J. Chem. **72**, 1921 (1993).
9. A.M. Blanco, J. Ortega, B. Garcia, and J.M. Leal. Thermochim. Acta, **222**, 127 (1993).
10. B.P. Shukla, S.N. Dubey, and H.K. Rai. Z. Phys. Chem. (Leipzig), **268**, 142 (1987).
11. J.M. Smith, H.C. Van Ness, M.M. Abbot. Introducción a la Termodinámica en Ingeniería Química. 5th ed. McGraw-Hill. 1997.
12. J.D. Pandey, N. Pant, and B.R. Chaturvedi. Chem. Scr. **18**, 224 (1981).
13. J.O. Hirschfelder, C.F. Curtis, and R.B. Bird. Molecular theory of gases and liquids. John Wiley & Sons, New York. 1954.
14. S. Glasstone. Tratado de Química Física. Ediciones Aguilar, Madrid. 1970.
15. H.C. Van Ness, J. Van Winkle, H.H. Richtol, and H.E. Hollinger. J. Phys. Chem. **71**, 1483 (1967).
16. G.C. Pimentel and A.L. McClellan. The hydrogen bond. W.H. Freeman and Co., San Francisco. 1960.
17. P. Huyskens. J. Mol. Struct. **100**, 403 (1983).
18. J.E. House. Trans. Ill. State. Acad. Sci. 123 (1966).
19. D.E.G. Jones, I.A. Weeks, S.C. Anand, R.W. Wetmore, and G.C. Benson. J. Chem. Eng. Data, **17**, 501 (1972).
20. G.C. Benson and O. Kiyohara. J. Chem. Eng. Data, **21**, 362 (1976).
21. F. Ratkovics and M. Lazio-Parragi. Fluid Phase Equilib. **17**, 97 (1984).
22. R.J. Fort and W.R. Moore. Trans. Faraday Soc. **62**, 1112 (1966).
23. R.D. Dunlap and R.L. Scott. J. Phys. Chem. **66**, 631 (1962).
24. J.E. Dubois, M. El-Alastoi, and J. Toullec. J. Am. Chem. Soc. **103**, 5393 (1981).
25. J.A. Riddick and W.B. Bunger. Organic solvents. Vol. II. 3rd ed. Wiley-lnterscience, New York. 1970. p. 151, 152, 154, and 249.
26. D.D. Perrin, W.L.F. Armarego, and D.R. Perrin. Purification of laboratory chemical. 2nd ed. Pergamon Press, New York. 1980.

© 2001 NRC Canada

Structure and redox kinetics of nickel(II) tetraazamacrocycles containing pendant carboxylate groups

Robert Ivor Haines, Dean Reginald Hutchings, Rhonda Jane Lucas, and David Miller

Abstract: The nickel(II) complex of the deprotonated pendant-arm macrocycle 5,12-dimethyl-7,14-diphenyl-1,4,8,11-tetraazacyclotetradecane-4,11-diacetate $(L^2)^{2-}$ has been structurally characterized by X-ray crystallography. The Ni(II)L^2 complex crystallizes in the monoclinic system, space group $P2_1/c$, with a = 12.981(8), b = 16.474(6), c = 14.262(7) Å and β = 98.81(4)°. The complex shows a distorted *cis*-geometry about the metal centre, the macrocyclic ligand being folded about a N-Ni-N axis, with the pendant arms coordinated *cis* to one another. The Ni(II)L^1 (where $(L^1)^{2-}$ is *meso*-5,5,7,12,12,14-hexamethyl-1,4,8,11-tetraazacyclotetradecane-4,11-diacetate) and Ni(II)L^2 complexes undergo reversible one-electron oxidation, with redox potentials of 0.717 and 0.766 V (vs. S.H.E.), respectively. Chemical oxidation of the complexes by peroxodisulfate obey overall second-order rate laws. Enthalpies and entropies of activation for Ni(II)L^1 are 38 ± 3 kJ mol^{-1} and –106 ± 9 J K^{-1} mol^{-1}; and for Ni(II)L^2 the corresponding values are 41 ± 5 kJ mol^{-1} and –126 ± 15 J K^{-1} mol^{-1}. Outer-sphere oxidation of Ni(II)L^1 by bis-(triazacyclononane)nickel(III) ($[Ni(III)(tacn)_2]^{3+}$) has been studied, and a self-exchange rate constant for the $[Ni(II)L^1]^{0/+}$ system has been estimated at 55 mol^{-1} dm^3 s^{-1}.

Key words: peroxodisulfate, nickel(II), dicarboxylato-pendant arm macrocycles, bis-(triazacyclononane)nickel(III), self-exchange rate.

Résumé : Faisant appel à la diffraction des rayons X, on a déterminé la structure du complexe de nickel(II) du macrocycle à chaîne latérale déprotoné 5,12-diméthyl-7,14-diphényl-1,4,8,11-tétraazacyclotétradécane-4,11-diacétate $(L^2)^{2-}$. Le complexe Ni(II)L^2 cristallise dans le système monoclinique, groupe d'espace $P2_1/c$, avec a = 12,981(8), b = 16,474(6) et c = 14,262(7) Å et β = 98,81(4)°. Le complexe présente une géométrie *cis* déformée autour de l'atome central neutre, le ligand macrocyclique étant replié autour d'un axe N-Ni-N, avec les chaînes latérales coordinées de façon *cis* l'une par rapport à l'autre. Les complexes de Ni(II)L^1 (dans lequel $(L^1)^{2-}$ est le *méso*-5,5,7,12,12,14-hexaméthyl-1,4,8,11-tétraazacyclotétradécane-4,11-diacétate) et le Ni(II)L^2 subissent chacun une oxydation réversible impliquant un électron et les potentiels redox sont respectivement de 0,717 et de 0,766 V (vs. S.H.E.). L'oxydation chimique des complexes par le peroxodisulfate se fait globalement en fonction des lois de vitesse du deuxième ordre. Les enthalpies et les entropies d'activation sont respectivement de 38 ± 3 kJ mol^{-1} et –106 ± 9 J K^{-1} mol^{-1} pour le Ni(II)L^1 et de 41 ± 5 kJ mol^{-1} et –126 ± 15 J K^{-1} mol^{-1} pour le Ni(II)L^2. On a aussi étudié l'oxydation du Ni(II)L^1 dans la couche externe par le bis(triazacyclononane)nickel(III) ($[Ni(III)(tach)_2]^{3+}$) et on a évalué la constante de vitesse d'autoéchange du système $[Ni(II)L^1]^{0/+}$, qui est de 55 mol^{-1} dm^3 s^{-1}.

Mots clés : peroxodisulfate, nickel(II), macrocycles à chaînes latérales dicarboxylato, bis(triazacyclononane)nickel(III), vitesse d'autoéchange.

[Traduit par la Rédaction]

Introduction

There is significant interest in the synthesis and properties of transition-metal polyazamacrocycles bearing pendant arms, particularly those having arms attached at the nitrogen atoms of the macrocycles (1). Some of these appendages, if they contain ligating atoms, can coordinate to the central metal ion. Most such functionalized macrocycles are often prepared by elaborate multistep procedures, with synthesis of partially functionalized macrocycles being more difficult than fully functionalized ones (2, 3). More recently, a "one-pot" method for producing polyazamacrocycles with appended cyclodextrins has been reported (4). Such complexes find application in ion-selectivity (5), electrocatalysis (6), and tumor-targetting (7). Pendant-arm macrocyclic complexes, because of their thermodynamic stability and ex-

Received November 5, 1999. Published on the NRC Research Press Web site on January 22, 2001.

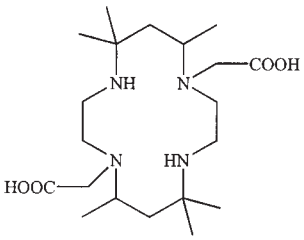
R.I. Haines[1], D.R. Hutchings, and R.J. Lucas. Chemistry Department, University of Prince Edward Island, 550 University Avenue, Charlottetown, PE C1A 4P3, Canada.
D. Miller. Chemistry Department, Memorial University of Newfoundland, St. John's, NF A1B 3X7, Canada.

[1]Author to whom correspondence may be addressed. Telephone: (902) 566-0698. Fax: (902) 566-0632. e-mail: rhaines@upei.ca

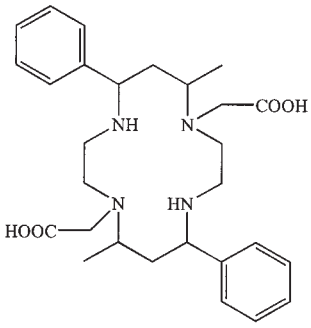
 DOI: 10.1139/cjc-79-1-54 © 2001 NRC Canada

tremely slow acid-dependent dissociation, have important radioimmunotherapeutic value (8, 9). While many studies examine the properties of amino-, nitro-, and pyridyl-arms, the majority involve carboxylate pendant arms (10).

The ability of polyazamacrocycles to stabilize transition-metal ions in unusual oxidation states has been well known for many years (11). We are interested in the redox behaviour of transition-metal macrocycles that contain pendant carboxylate arms, since these appendages coordinate to the central metal ion and may provide an inner-sphere pathway for electron transfer to, or from, other metal centres. Such behaviour has application, for example, in reductive dissolution of iron(III)-bearing ferrites, which constitute corrosion films found in industrial boilers and nuclear reactors (12). The present work reports the kinetics of oxidation of the nickel(II) complexes of two deprotonated carboxylato-pendant arm macrocycles (*meso*-5,5,7,12,12,14-hexamethyl-1,4,8,11-tetraazacyclotetradecane-4,11-diacetate $(L^1)^{2-}$) and (5,12-dimethyl-7,14-diphenyl-1,4,8,11-tetraazacyclotetradecane-4,11-diacetate $(L^2)^{2-}$) to the nickel(III) forms, by peroxodisulfate anion, $S_2O_8^{2-}$. Oxidation of the Ni(II)L^1 complex by the bis-(triazacyclononane)nickel(III) cation $[Ni(tacn)_2]^{3+}$ has also been studied. The X-ray crystal structure of Ni(II)L^2, which has not been reported in the literature, is also described.



L^1H_2



L^2H_2

Experimental

Materials

AnalaR grade potassium peroxodisulphate (BDH) was first washed several times with distilled water, then recrystallized four times from cold water, rinsed with ice water, and dried over P_4O_{10} in vacuo. This procedure was found necessary to obtain reproducible, clean kinetics. All other reagents and solvents were of AnalaR grade and were used without further purification. All solutions were prepared using double-distilled, deionized water.

Synthesis of ligands and complexes

1,4,7-Triazacyclononane (tacn), and its nickel(II) perchlorate complex were synthesized by a modified literature method (13). The functionalized macrocycles *meso*-5,5,7,12,12,14-hexamethyl-1,4,8,11-tetraazacyclotetradecane-1,7-diacetic acid (L^1H_2) and 5,12-dimethyl-7,14-diphenyl-1,4,8,11-tetraazacyclotetradecane-4,11-diacetic acid, (L^2H_2) were prepared according to the literature (14–16). The nickel(II) complex of the deprotonated macrocycle Ni(II)L^1 was prepared by the literature method as the hydrobromide monohydrate (15) and recrystallized from aqueous ethanol prior to use. Yield 70%. IR (KBr cm^{-1}): 3396 (OH), 3124 (NH), 1623 (COO^-). Anal. calcd. for $NiC_{20}H_{41}N_4O_5Br$ (monohydrate): C 43.19, H 7.45, N 10.10; found: C 43.38, H 7.57, N 10.34.

The Ni(II)L^2 complex (isolated as the dihydrate), was prepared as follows: to 250 mg (0.500 mmol) of L^2H_2 dissolved in 20 mL of water was added 238 mg (1.00 mmol) of $NiCl_2 \cdot 6H_2O$. The pH was adjusted to pH 5 with 0.1 mol dm^{-3} NaOH and the mixture was heated to reflux for 24 h. The solution was concentrated to approximately 5 mL and violet crystals precipitated. The crystals were collected, washed with cold water, and air dried to give 177 mg (43%) of product. IR (KBr cm^{-1}): 3448 (OH), 3232 (NH), 1604 (COO^-). Anal. calcd. for $NiC_{28}H_{42}N_4O_6$ (dihydrate): C 57.06, H 7.18, N 9.51; found: C 57.20, H 7.21, N 9.72.

X-ray crystallography

Violet crystals of Ni(II)L^2 suitable for structure determination were obtained from water–ethanol using the vapour diffusion method. The data were collected at a temperature of 26 ± 1°C on a Rigaku AFC6S diffractometer (MoK_α radiation, graphite monochromator) in the ω-2Θ scan mode to 2Θ = 50.1°. Lorentz and polarization corrections were applied. The structure was solved by direct methods (17) using the teXsan crystallographic software package (18). Refined parameters were calculated using anisotropic thermal parameters for nonhydrogen atoms and isotropic factors for all hydrogen atoms. A summary of crystal data is given in Table 1. Atomic positional parameters are given in Table 2 and selected bond lengths and angles are given in Table 3. The full description of the structurally determined thermal parameters, hydrogen atom positional parameters, and a full listing of bond distances and angles have been deposited as supplementary data.[2]

Cyclic voltammetry

Cyclic voltammograms of Ni(II)L^1 and Ni(II)L^2 were measured using a Princeton Applied Research model 482 fast-scanning electrochemical apparatus, in aq 0.10 M trifluoromethanesulphonic acid, under an argon atmosphere. A 1 mm diameter Pt disk working electrode, a platinum wire counter electrode, and a Ag/AgCl (sat. KCl) reference electrode were used.

Kinetics

All kinetics were performed under pseudo-first-order conditions, using an excess of oxidant. Due to the low solubility of the neutral complexes in water, all kinetics were performed

[2] Supplementary material may be purchased from the Depository of Unpublished Data, Document Delivery, CISTI, National Research Council Canada, Ottawa, ON K1A 0S2, Canada (http://www.nrc.ca/cisti/irm/unpub_e.shtml for information on ordering electronically). Hydrogen atom positional parameters and bond distances and angles reported in this paper have been deposited with the Cambridge Crystallographic Data Centre. Copies of the data can be obtained, free of charge, on application to the Director, CCDC, 12 Union Road, Cambridge CB2 1Ez, U.K. (Fax: 44-1223-336033 or e-mail: deposit@ccdc.cam.ac.uk).

© 2001 NRC Canada

Table 1. X-ray crystallographic data for Ni(II)$L^2 \cdot 2H_2O$.

Empirical formula	$C_{28}H_{42}N_4O_6Ni$
Crystal colour, habit	purple, irregular
Formula weight	589.36 g mol^{-1}
Crystal *S*ystem	monoclinic
Space group	$P2_1/c$
a (Å)	12.981(8)
b (Å)	16.474(6)
c (Å)	14.262(7)
β	98.81(4)°
V	3014(5) $Å^3$
ρ_{calc}	1.299 g cm^{-3}
Z value	4
Absorption coefficient (μ)	6.88 cm^{-1}
F_{000}	1256
Reflections collected	5797
Reflections with $I > 2.00\sigma(I)$	3839
Goodness of fit	2.66
R^a	0.056
$R_W{}^b$	0.052

$^aR = \Sigma\ ||F_o| - |F_c||/\Sigma\ |F_o|$.
$^bR_W = [(\Sigma w(|F_o| - |F_c|)^2/\Sigma wF_o^2)]^{1/2}$.

in 20% by volume aqueous ethanol. Because of the relatively low solubility of potassium peroxodisulfate, particularly in binary aqueous mixtures, the concentration range possible using that oxidant was limited. The concentration of the nickel(II) complexes used in all experiments was 5.00×10^{-6} mol dm^{-3}. For the peroxodisulfate experiments, absorbance changes with time were measured using 1 cm path length quartz cells in the thermostatted cell compartment of a Beckman DU-65 recording spectrophotometer. Data were collected using Beckman Datacapture software on an EmPac 386 microcomputer. Ionic strength was kept constant at 0.300 mol dm^{-3} for all kinetic runs, using potassium sulfate. Absorbance measurements were made at 350 nm.

The oxidation kinetics using $[Ni(tacn)_2]^{3+}$ were carried out at a constant ionic strength of 0.100 M, using $NaClO_4$–$HClO_4$. Kinetic measurements were made using a Tritech Dynamics Instruments stopped-flow spectrometer, using a Bausch & Lomb light source and monochromator. The apparatus was thermostatted to ±0.05°C, using a Haake circulating water bath. All solutions were prepared with distilled, deionized water. First-order rate constants (k_{obs}) were calculated from the slopes of linear regression plots of ln ($A_\infty - A_t$) vs. time. Reported values of k_{obs} are the means of at least three measurements. For any given set of conditions, repetitive measurements gave observed rate constant values invariant within 1%.

Stock solutions of $[Ni(tacn)_2]^{3+}$ were prepared freshly in situ for each set of kinetic runs, by oxidation of the nickel(II) form with a stoichiometric deficiency of Co^{3+}(aq).

Results

Structure of Ni(II)L^2

The nickel complex Ni(II)L^2 was found to be only sparingly soluble in pure water and pure ethanol, but was soluble in binary mixtures of these solvents. The complex formed from the ligand L^2H_2 and nickel(II) chloride is a neutral species, containing the deprotonated ligand in a *cis*-configuration. The crystal structure was found to have two waters of crystallization in the lattice. These waters occur in channels between the complexes and are strongly hydrogen bonded with each other, but not to either the nitrogens or the oxygens of the macrocyclic ligand. Both pendant carboxylate arms are coordinated to the central nickel(II) ion, in a slightly distorted octahedral arrangement. An ORTEP diagram of the complex is shown in Fig. 1. All Ni—O and Ni—N bond lengths are very similar (Table 3), close to 2.080 Å.

Table 2. Atomic positional parameters and *B*(eq) values for Ni(II)$L^2 \cdot 2H_2O$.

Atom	*x*	*y*	*z*	*B*(eq)
Ni(1)	0.75914(6)	0.22878(5)	0.22054(5)	2.61(3)
O(1)	0.6731(3)	0.2686(3)	0.0946(3)	3.5(2)
O(2)	0.8693(3)	0.1936(2)	0.1355(3)	3.4(2)
O(3)	0.7119(3)	0.3446(3)	–0.0251(3)	4.2(2)
O(4)	0.8958(3)	0.0960(3)	0.0340(3)	4.6(2)
N(1)	0.6490(3)	0.2611(3)	0.3070(3)	2.8(2)
N(2)	0.7066(4)	0.1104(3)	0.1952(3)	2.8(2)
N(3)	0.8559(4)	0.1844(3)	0.3397(3)	2.9(2)
N(4)	0.8031(4)	0.3502(3)	0.2268(3)	2.8(2)
C(1)	0.5421(4)	0.2402(4)	0.2612(4)	3.1(3)
C(2)	0.5354(5)	0.1473(4)	0.2521(5)	3.7(3)
C(3)	0.5893(5)	0.1048(4)	0.1779(4)	3.4(3)
C(4)	0.7576(5)	0.0641(4)	0.2791(4)	3.2(3)
C(5)	0.8662(5)	0.0970(4)	0.3164(4)	3.4(3)
C(6)	0.9527(5)	0.2330(4)	0.3762(4)	3.5(3)
C(7)	0.9764(4)	0.2980(4)	0.3060(4)	3.5(3)
C(8)	0.9015(5)	0.3690(4)	0.2934(4)	3.3(3)
C(9)	0.7122(5)	0.3932(4)	0.2560(4)	3.4(3)
C(10)	0.6699(5)	0.3477(4)	0.3338(4)	3.5(3)
C(11)	0.4558(5)	0.2712(4)	0.3140(5)	3.6(3)
C(12)	0.3643(5)	0.3025(4)	0.2643(5)	4.3(3)
C(13)	0.2837(5)	0.3269(5)	0.3120(6)	5.4(4)
C(14)	0.2928(6)	0.3229(5)	0.4081(6)	5.4(4)
C(15)	0.3837(6)	0.2930(5)	0.4584(5)	5.5(4)
C(16)	0.4652(5)	0.2666(5)	0.4121(5)	4.8(4)
C(17)	0.5497(5)	0.0178(4)	0.1650(6)	5.3(4)
C(18)	0.7490(5)	0.0831(4)	0.1101(4)	3.6(3)
C(19)	0.8465(5)	0.1281(4)	0.0928(4)	3.3(3)
C(20)	1.0465(5)	0.1826(4)	0.4144(6)	4.5(4)
C(21)	1.1107(6)	0.1515(5)	0.3581(7)	6.0(4)
C(22)	1.1997(7)	0.1050(6)	0.3971(9)	7.8(6)
C(23)	1.2146(9)	0.0944(7)	0.491(1)	9.8(8)
C(24)	1.151(1)	0.127(1)	0.553(1)	12(1)
C(25)	1.0675(7)	0.1702(6)	0.5113(6)	7.7(5)
C(26)	1.9554(5)	0.4468(4)	0.2690(5)	4.8(4)
C(27)	1.8103(5)	0.3680(4)	0.1264(4)	3.4(3)
C(28)	1.7249(5)	0.3238(4)	0.0611(4)	3.4(3)

Electrochemistry

Figure 2(*a*) and (*b*) show the cyclic voltammograms for Ni(II)L^1 and Ni(II)L^2, measured at various scan rates (50–200 mV s^{-1}), between 0 and 1.0 V (vs. S.H.E.). It is clear that the complexes undergo clean, reversible one-electron

© 2001 NRC Canada

Table 3. Selected bond distances (Å) and angles (°) for $Ni(II)L^2 \cdot 2H_2O$.

Bond	Distance	Bonds	Angle
Ni(1)—O(1)	2.072(4)	O(1)-Ni(1)-O(2)	84.9(2)
Ni(1)—O(2)	2.093(4)	O(1)-Ni(1)-N(1)	96.0(2)
Ni(1)—N(1)	2.094(5)	O(1)-Ni(1)-N(2)	91.6(2)
Ni(1)—N(2)	2.080(5)	O(1)-Ni(1)-N(3)	174.6(2)
Ni(1)—N(3)	2.084(5)	O(1)-Ni(1)-N(4)	80.8(2)
Ni(1)—N(4)	2.078(5)	O(2)-Ni(1)-N(1)	178.6(2)
		O(2)-Ni(1)-N(2)	82.8(2)
		O(2)-Ni(1)-N(3)	89.7(2)
		O(2)-Ni(1)-N(4)	94.8(2)
		N(1)-Ni(1)-N(2)	96.0(2)
		N(1)-Ni(1)-N(3)	89.4(2)
		N(1)-Ni(1)-N(4)	86.5(2)
		N(2)-Ni(1)-N(3)	87.3(2)
		N(2)-Ni(1)-N(4)	172.2(2)
		N(3)-Ni(1)-N(4)	100.1(2)

oxidations to the nickel(III) forms. The values of $E°$ for $Ni(II)L^1$ and $Ni(II)L^2$, respectively, are 0.717 V and 0.766 V (vs. S.H.E.) with peak separations of 64 ± 4 mV. The anodic and cathodic peak separations were independent of scan rate. The purity of these voltammograms, for both complexes, suggests that there is little change in geometry, and certainly no change in coordination, on oxidation. This is in keeping with the known tetragonally distorted octahedral coordination of nickel(III) macrocycles (11), and the known structures of the nickel(II) forms, as six-coordinate, high-spin d^8 systems. Addition of sulfate to the solution in the cyclic voltammetry experiments had no effect on redox potential or peak separation, indicating that the anion does not coordinate to either the oxidized or reduced form of the complex.

Kinetics

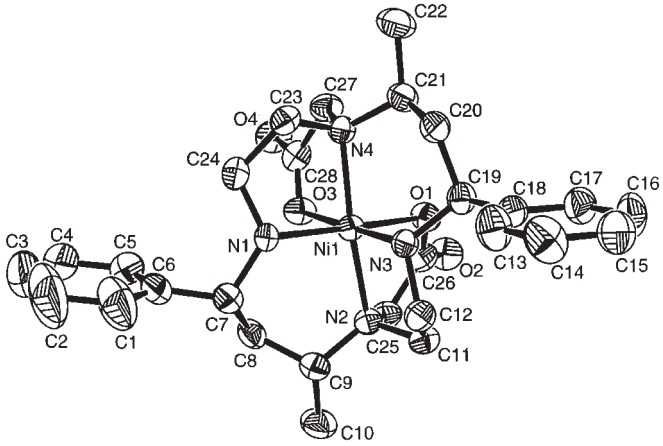
(a) Oxidation by $[Ni(tacn)_2]^{3+}$

The $Ni(II)L^1$ complex was oxidized by $[Ni(tacn)_2]^{3+}$ on the stopped-flow timescale. The reaction was found by spectrophotometric titration to have a 1:1 stoichiometry, and to obey a simple second-order rate law,

$$[1] \qquad \text{rate} = +d[Ni(III)L^1]/dt = k_1[Ni(tacn)_2{}^{3+}][Ni(II)L^1]$$

The reaction was found to be independent of acid over a range of added $[H^+]$ of 0–0.10 mol dm^{-3}. While this is quite a limited range, the ionic strength of the reaction solutions was 0.1 mol dm^{-3}, limiting the upper acid concentration. Separate experiments have shown that there are no spectral changes in solutions of $Ni(II)L^1$ in acid concentrations up to 0.50 mol dm^{-3}, suggesting no protonation–deprotonation equilibria are extant in these media. Hence, a lack of rate dependence on $[H^+]$ is not unexpected. The kinetic data are presented in Table 4. The activation enthalpy and entropy, calculated using the Eyring equation, were found to be 34 ± 4 kJ mol^{-1} and –63 ± 12 J K^{-1} mol^{-1}, respectively.

Fig. 1. ORTEP diagram of the $Ni(II)L^2$ molecule.



(b) Oxidation by $S_2O_8^{2-}$

The $Ni(II)L^1$ and $Ni(II)L^2$ complexes were oxidized smoothly to the tervalent state in 20% by volume aqueous ethanol. The ionic strength was maintained at 0.30 mol dm^{-3} using potassium sulfate. No acid dependence was examined, since the peroxodisulfate ion is known to protonate above $[H^+]$ = 0.01 mol dm^{-3} (19). Figure 3 shows the UV–vis spectral change during the oxidation of $Ni(II)L^1$. The strong peak at 300 nm (ε = 8000 mol^{-1} dm^3 cm^{-1}), with a shoulder at 400 nm (ε = 6000 mol^{-1} dm^3 cm^{-1}) is characteristic of nickel(III) polyazamacrocycles. An isosbestic point at 226 nm indicates that there is no build-up of intermediates during the oxidation. Excellent first-order kinetics were observed over at least five half-lives for the appearance of the nickel(III) products. Addition of the radical scavenger allyl acetate had no effect on the reaction rates. This gives further support for the lack of participation of sulfate radicals in the kinetics of the reactions. The overall reactions corresponds to:

$$[2] \qquad 2\ [Ni(II)L] + S_2O_8^{2-} \rightarrow 2\ [Ni(III)L]^+ + 2\ SO_4^{2-}$$

Tables 5 and 6 list the observed first-order rate constants for oxidation of the $Ni(II)L^1$ and $Ni(II)L^2$ complexes as a function of temperature and $S_2O_8^{2-}$ concentration. Figure 4 illustrates the linear dependence of k_{obs} on $S_2O_8^{2-}$ concentration for oxidation of the $Ni(II)L^1$ complex at several temperatures, showing the reaction to obey an overall second-order rate law. Eyring plots of the temperature-dependent data yielded $\Delta H^{\ddagger}$ = 38 ± 3 kJ mol^{-1}, $\Delta S^{\ddagger}$ = –106 ± 9 J K^{-1} mol^{-1} for $Ni(II)L^1$; and $\Delta H^{\ddagger}$ = 41 ± 5 kJ mol–1, $\Delta S^{\ddagger}$ = –126 ± 15 J K^{-1} mol^{-1} for $Ni(II)L^2$.

Discussion

Structures

A number of X-ray structures of transition-metals complexed by pendant-arm macrocycles similar to L^1 and L^2 are known. Xu et al. (15) have reported the structure of a *cis*-form of NiL^1. In that complex the Ni—N bonds were shorter (2.072, 2.073 Å) for the tertiary nitrogens than the secondary ones (2.091, 2.107 Å). The Ni—O bonds were quite different from each other (2.199, 2.065 Å). On inspection of the geometry about the metal centre, it may be surmised

© 2001 NRC Canada

Fig. 2. (*a*) Cyclic voltammogram of Ni(II)L^1 in 0.10 mol dm^{-3} triflic acid. Scan rates are: (*a*) 50; (*b*) 100; (*c*) 150; and (*d*) 200 mV s^{-1}; (*b*) Cyclic voltammogram of Ni(II)L^2 in 0.10 mol dm^{-3} triflic acid. Scan rates are: (*a*) 50; (*b*) 100; (*c*) 150; and (*d*) 200 mV s^{-1}.

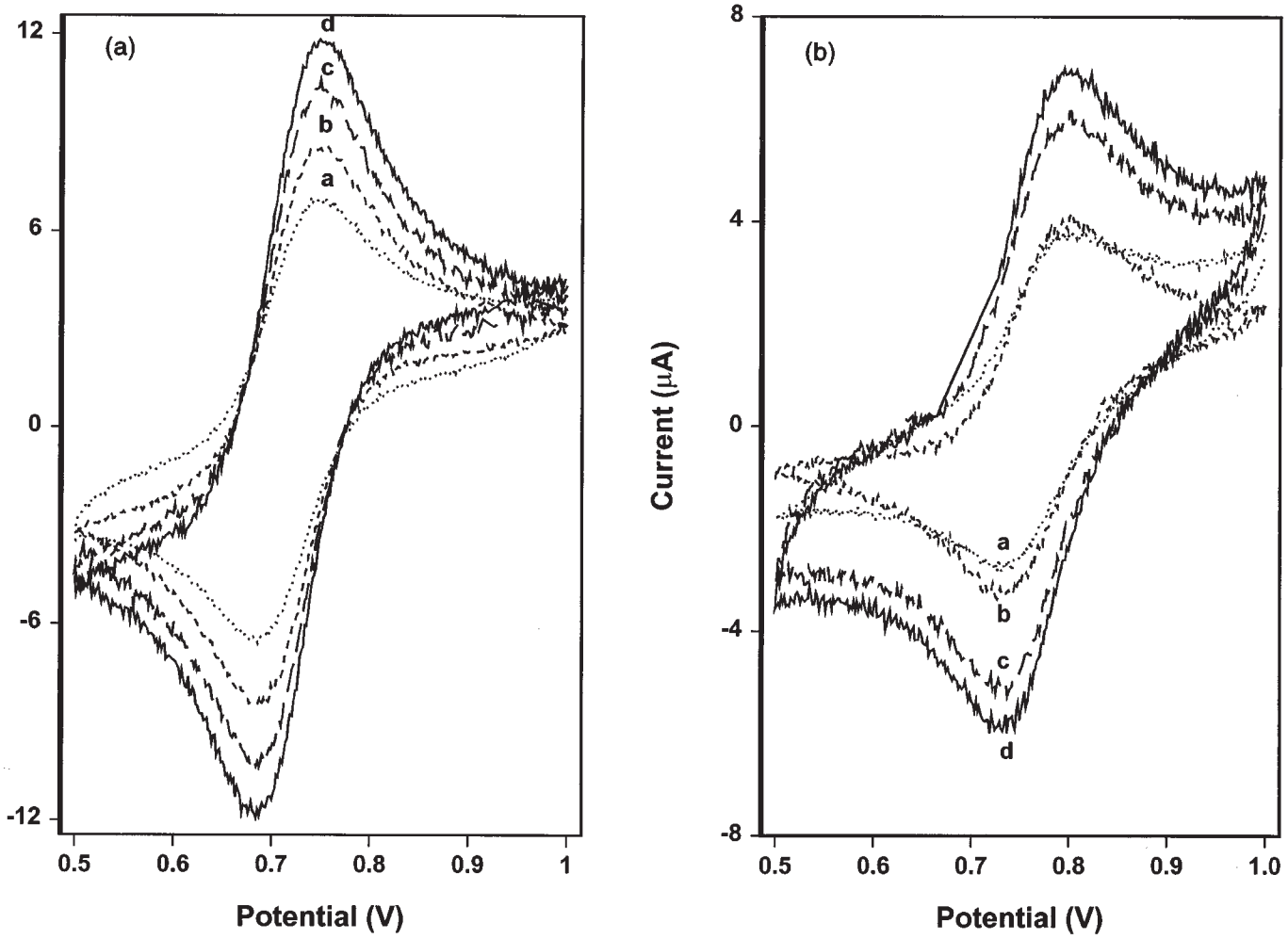


Table 4. Second-order rate constants (k_1 (mol^{-1} dm^3 s^{-1})) for the oxidation of Ni(II)L^1 by $[Ni(tacn)_2]^{3+}$ in 0.10 mol dm^{-3} sodium perchlorate, as a function of temperature.

	k_{obs} (s^{-1})				
Temperature (K)	290.1	294.6	298.0	301.2	304.6
$[Ni(tacn)_2]^{3+} \times 10^3$ (mol dm^{-3})					
0.50	1.25	1.66	1.95	2.03	2.46
	1.22[a]				
	1.24[b]				
0.75	1.89	2.36	2.63	2.76	2.88
1.00	2.37	3.24	3.63	3.83	4.31
	2.38[a]				
	2.41[b]				
1.25	3.00	4.37	4.66	4.93	5.75
1.50	3.42	4.86	5.75	6.27	7.67
	3.39[a]				
	3.44[b]				
k_1 (mol^{-1} dm^3 s^{-1})	2300	3330	3780	4090	4920
+/–	70	120	106	160	390

[a]$[H^+]$ = 0.05 mol dm^{-3}.
[b]$[H^+]$ = 0.10 mol dm^{-3}.

© 2001 NRC Canada

Fig. 3. UV–vis spectra of Ni(II)L^1 (1.13×10^{-4} mol dm^{-3}) and $S_2O_8^{2-}$ (4.96×10^{-3} mol dm^{-3}) in water at 21°C; (*a*) before mixing; and (*b* – *j*) after mixing at 20 s intervals.

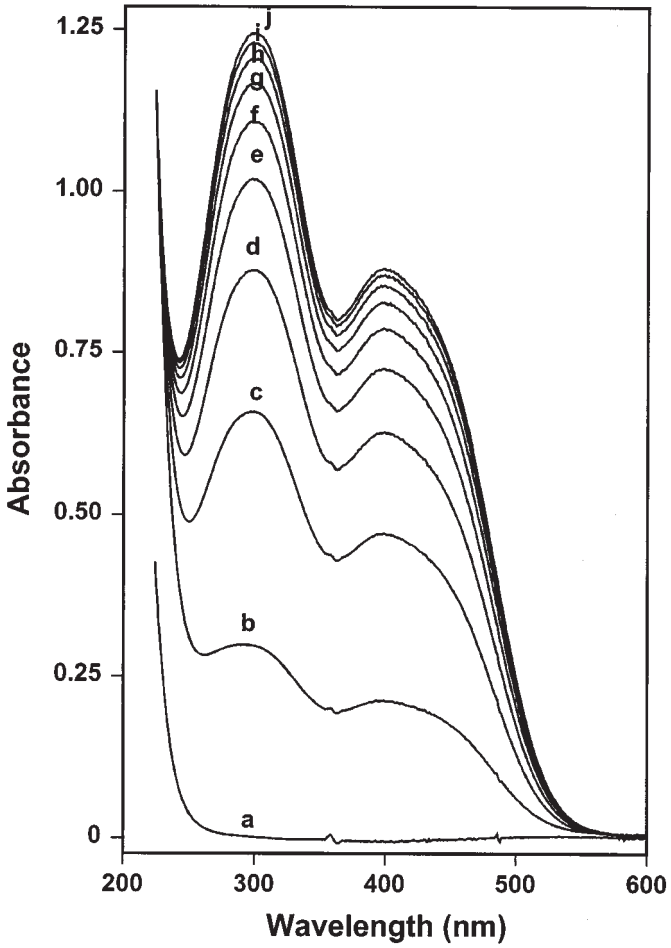


Fig. 4. Dependence of the pseudo-first-order rate constants (k_{obs}) on $S_2O_8^{2-}$ concentration for oxidation of Ni(II)L^1 at several temperatures.

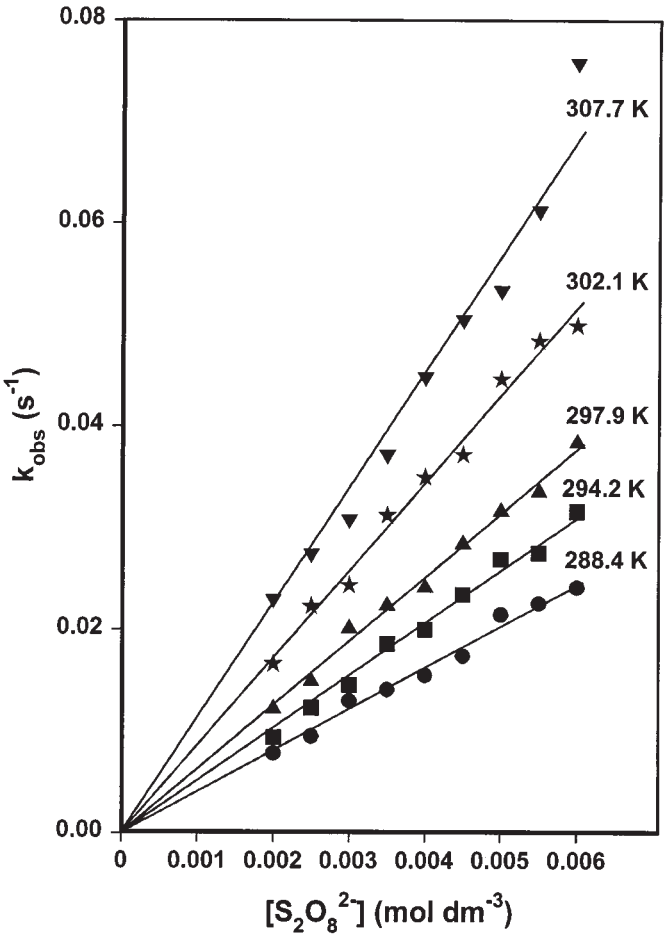


Table 5. Observed first-order rate constants (k_{obs} (s^{-1})) for the oxidation of Ni(II)L^1 as a function of $[S_2O_8^{2-}]$ and temperature (ionic strength = 0.30 mol dm^{-3}).

	$k_{obs} \times 10^2$ (s^{-1})				
Temperature (K)	288.4	294.2	297.9	302.1	307.7
$[S_2O_8^{2-}] \times 10^3$ (mol dm^{-3})					
2.00	0.785	0.938	1.22	1.66	2.30
2.50	0.952	1.23	1.49	2.23	2.75
3.00	1.30	1.45	2.01	2.44	3.09
3.50	1.41	1.86	2.24	3.13	3.72
4.00	1.55	2.00	2.42	3.50	4.48
4.50	1.74	2.35	2.85	3.72	5.05
5.00	2.15	2.70	3.17	4.46	5.34
5.50	2.26	2.76	3.36	4.84	6.12
6.00	2.42	3.17	3.84	4.99	7.58
k_7 (mol^{-1} dm^3 s^{-1})	2.06	2.66	3.16	4.30	5.9
+/–	0.07	0.07	0.107	0.12	0.3

that this difference is in part due to strain in the macrocycle on coordination to the metal. For example, the N-Ni-O angles, that would be 180° for a perfectly octahedral centre, are in fact 176.78° and 163.06°. For the *cis*-NiL^2 structure presented in the present paper, the metal—ligand bond lengths are all remarkably close to one another. For example, the two Ni—O lengths are 2.072 Å and 2.093 Å; the Ni—N lengths are 2.094, 2.078, and 2.084 Å. Also, there is

© 2001 NRC Canada

Table 6. Observed first-order rate constants (k_{obs} (s^{-1})) for the oxidation of Ni(II)L^2 as a function of $[S_2O_8^{2-}]$ and temperature (ionic strength = 0.30 mol dm^{-3}).

	$k_{obs} \times 10^2$ (s^{-1})				
Temperature (K)	292.7	296.2	299.5	302.8	309.8
10^3 $[S_2O_8^{2-}]$ (mol dm^{-3})					
2.00	3.03	3.51	4.78	5.29	7.52
2.50	3.52	4.00	5.58	6.72	9.52
3.00	4.09	4.72	6.95	7.61	11.2
3.50	5.02	5.98	8.52	9.30	12.6
4.00	6.16	6.55	9.18	10.7	14.4
4.50	6.35	7.25	10.4	11.3	17.1
5.00	7.12	8.10	12.1	13.2	19.0
5.50		9.12	13.0	14.5	
6.00		9.85	14.1	15.5	
k_7 (mol^{-1} dm^3 s^{-1})	0.0720	0.0805	0.119	0.130	0.188
+/–	0.0025	0.0020	0.003	0.003	0.004

much less distortion from octahedral geometry, evidenced by the equatorial O-Ni-N angles of 178.6° and 174.6°.

Xu et al. (20) have also reported the structure of macrocycle and the aquanickel(II) complex of a mono-carboxylato-analogue of L^1. That complex takes up a *trans*-III configuration, with four nitrogens in a square plane and the carboxylato- and aqua-ligands in axial positions. In that case the Ni—N bonds were all similar (2.097, 2.093, 2.070, and 2.103 Å), and the Ni—O length (for the carboxylato-arm) was 2.065 Å, with only minor deviations from octahedral geometry. The mean Ni(II)—N bond length for octahedral NiN_6 moieties has been reported (21) to be 2.081 ± 0.026 Å. Hence, the bond lengths reported here for Ni(II)L^2 are not unusual.

The Ni(II)L^1 complex used for kinetic studies in this work has a *trans*-III conformation (22), similar to[3] $[CoL^1]^+$ and the Cu(II)L^2 complexes (15). Based on the electrochemical behaviour of Ni(II)L^1 and Ni(II)L^2, it is assumed that no major structural rearrangements occur on oxidation, and the nickel(III) forms of the two complexes are likely still *cis*- and *trans*-, respectively.

The possible structures and isomers of 14-membered hexamethyl tetraazamacrocycles have been thoroughly described in the past (22, 23). According to Curtis (22), *meso*-macrocycles form metal complexes in the *trans*-III configuration, i.e., the four nitrogen donor atoms are in a square planar arrangement, and the backbone of the macrocycle is in an overall chair conformation. Racemic forms of the macrocycle take up the *cis*-V conformation. Examples of complexes of L^1 and L^2, whose structures agree with Curtis' theory include the C-*meso*-[Cu(II)L^2] (*trans*-III) (16) and rac-[Ni(II)L^1] (*cis*-V). A seeming contradiction is the reported (24) rac-[Cu(II)L^1] complex, that has the *trans*-III configuration. Closer examination of the structure in that paper, however, reveals that the macrocycle was mislabelled, and is actually the *meso* form. In this work, we find that the rac-[Ni(II)L^2] occurs as the *cis*-V configuration, in agreement with Curtis' theory.

Redox mechanisms

$[Ni(tacn)_2]^{3+}$ is well known as an outer-sphere oxidant (25), whose redox reactions do not display acid dependence, unless the reductant undergoes protonation–deprotonation. Hence, this is a useful oxidant to probe the mechanism of electron-transfer from the nickel(II) pendant-arm macrocycles that are the focus of this study. The observed second-order rate law is expected for a system where both reactants are coordinatively saturated, in both oxidized and reduced forms. The measured activation parameters are typical of outer-sphere redox. Because the nickel(II) complexes are high-spin, six-coordinate and hence paramagnetic, and the nickel(III) form is necessarily paramagnetic (d^7), it is not possible to measure the self-exchange rates for the Ni(II)L^1 and Ni(II)L^2 complexes by the usual NMR (26) or EPR methods (27). However, we have been able to estimate the self-exchange rates, using Marcus Theory (28).

For an outer-sphere electron-transfer mechanism, the rate constant for the cross-reaction (k_{12}) is related to the rate constants for the self-exchange rates of the components (k_{11} and k_{22}) and the equilibrium constant K_{12} by the expression $k_{12} = (k_{11}\ k_{22}\ K_{12} f_{12})^{1/2} w_{12}$, where

$$\ln f_{12} = \frac{\left[\ln K_{12} + \left(\frac{w_{12} - w_{21}}{RT}\right)\right]^2}{4\left[\ln\left(\frac{k_{11}k_{22}}{A_{11}A_{22}}\right) + \left(\frac{w_{11} - w_{22}}{RT}\right)\right]}$$

$$w'_{12} = \exp\left[\left(\frac{-w_{12} + w_{21} - w_{11} - w_{22}}{2RT}\right)\right]$$

$$wij = \frac{Z_i Z_j\ e^2}{D_s \sigma_{ij}(1 + \beta\sigma_{ij}(\mu^{1/2}))}$$

$$A_{ij} = \frac{4\pi N \sigma^2 \upsilon b \gamma r}{1000_{ij}}$$

[3] R.I. Haines and R.J. Lucas. Unpublished observations.

© 2001 NRC Canada

w_{ij} is the work required to bring the ions i and j (with charges Z_i and Z_j, respectively) to the separation distance σ_{ij}. This distance is assumed to be equal to the sum of the radii of the ions i and j, β ($= 8\pi Ne^2/1000D_s kT)^{1/2}$, υb is the nuclear frequency that destroys an activated complex configuration, and γr is the thickness of the reaction layer (~0.8 Å); D_s is the dielectric constant of the medium. In the present reaction, where Ni(II)L^1 is neutral, the work terms will be negligible, so w'_{12} becomes unity. Hence, the cross-reaction rate constant may be estimated from the simplified Marcus relationship:

$$k_{12} = (k_{11}\ k_{22}\ K_{12}\ f_{12})^{1/2}$$

where, for small values of K_{12}, the term f is usually assumed to be unity (29). The value of k_{22}, the self-exchange rate for $[Ni(tacn)_2]^{3+}$, has been determined to be 6×10^3 s^{-1} (13). From the electrode potentials of Ni(II)L^1 and $[Ni(tacn)_2]^{2+}$, the K_{12} value is calculated to be 43. Using these values and the experimental value for the cross-reaction rate (k_{12}), the self-exchange rate for $[NiL^1]^{0/+}$ is calculated to be 55 mol^{-1} dm^3 s^{-1} (using $k_{11} = (k_{12}^2/k_{22}\ K_{22})$). For negligible work terms (vide supra) the value of f_{12} is estimated to be 1.13, using the expression $\ln f_{12} = (\ln K_{12})^2/4\ln(k_{11}k_{22})$. This has negligible effect on the estimate of k_{11}. The value for k_{11} is low compared to six-coordinate nickel(II/III) systems, containing the ligands tacn, 2,2′-bipyridyl (bipy), and 1,10-phenanthroline (phen), and their substituted derivatives (31). The self-exchange rates for these complexes have been estimated as 1500 mol^{-1} dm^3 s^{-1} for LL = bipy and phen (30). The self-exchange rate for $[Ni(cyclam)]^{2+/3+}$ has also been measured at 2000 mol^{-1} dm^3 s^{-1} (31). The value for $[NiL^1]^{0/+}$ estimated here is one to two orders of magnitude lower than other nickel systems. Such variations in self-exchange rates for metal complexes with different ligands has been considered reasonable (32). One significant difference between the complex in this study and those literature cases mentioned above is that the $[NiL^1]^{0/+}$ system contains a negatively charged ligand. Interestingly, the self-exchange rate for a nickel complex containing a deprotonated tripeptide has been estimated at 450 mol^{-1} dm^3 s^{-1} (33), which is much closer to that for $[NiL^1]^{0/+}$. We have assumed the reaction to be adiabatic, where the transmission coefficient (κ_{12}) is unity. Any nonadiabatic behaviour ($\kappa_{12} < 1$) would result in a higher calculated value of the self-exchange rate.

We have examined the kinetics of oxidation of both Ni(II)L^1 and Ni(II)L^2 complexes to their Ni(III) forms using peroxodisulfate. The general mechanism for oxidation of transition-metal complexes by the peroxodisulfate anion is well known (34). Reduction of peroxodisulfate characteristically proceeds via rate-determining fission of the peroxo-bond, a step that may be assisted by the presence of a metal ion. The general mechanism for oxidation of cationic nickel(II) macrocycles (35) by the peroxodisulfate anion is:

$$[3] \qquad [Ni(II)L]^{2+} + S_2O_8^{2-} \overset{K_{ip}}{\rightleftharpoons} \{Ni(II)L^{2+}, S_2O_8^{2-}\}$$

ion-pair

$$[4] \qquad \{Ni(II)L^{2+}, S_2O_8^{2-}\} \overset{k_4}{\rightarrow} [Ni(III)L]^{3+} + SO_4^{-} + SO_4^{2-}$$

$$[5] \qquad [Ni(II)L]^{2+} + SO_4^{-} \overset{\text{fast}}{\rightarrow} [Ni(III)L]^{3+} + SO_4^{2-}$$

For oxidation of nickel(II) complexes of neutral square planar macrocycles, the nickel(III) product is known to coordinate sulfate ion, forming the $[Ni(III)L(SO_4)]^+$ cation (36). In the present study, there are no vacant coordination sites at the metal, precluding the possibility of formation of a sulfato-adduct. The rate law derived from the above scheme is

$$[6] \qquad \text{Rate} = 2k_{obs}[Ni(II)L]_{tot} = \frac{2k_4K_{ip}[S_2O_8^{2-}][Ni(II)L]_{tot}}{1 + K_{ip}[S_2O_8^{2-}]}$$

Since the nickel(II) complexes are neutral there is expected to be little or no ion-pairing due to electrostatic effects. Under these conditions, the rate law simplifies to:

$$[7] \qquad \text{Rate} = 2k_7[Ni(II)L][S_2O_8^{2-}]$$

where $k_7 = k_4K_{ip}$. Tables 5 and 6 include values of the second-order rate constants for the two complexes, which differ by a factor of ca. 30 at similar temperatures. This may be attributable to differences in redox potentials, since Ni(II)L^1 is oxidized faster than Ni(II)L^2, and its redox potential is lower by 50 mV.

The activation parameters are very similar to one another, and follow the trend in activation parameters for oxidation of a wide range of transition-metal complexes by peroxodisulfate (35, 37–40), indicating a similar rate-determining step. This is primarily an outer-sphere electron transfer from the nickel(II) macrocycle to the oxidant, with concomitant peroxo-bond fissure. In this mechanism, electron transfer from the nickel complex will generate a positive charge on the neutral reductant, with concomitant increase in negative charge on the oxidant. The latter undergoes peroxo-bond elongation, forming a $^{-}O_3SO—SO_4^{2-}$ moiety in the transition-state, resulting in an increased charge separation. This will lead to increased electrostriction, resulting in a negative entropy. This prediction is supported by the experimentally determined activation entropy. An inner-sphere pathway, with electron transfer via the coordinated carboxylate arms, is not likely, since the oxidant is anionic and would not form a bridge. This is supported by the electrochemical experiments, which showed that the integrity of the six-coordinate environment about the nickel is unaffected by the presence of sulfate. Application of Marcus Theory is not feasible for peroxodisulfate oxidations since, while the oxidant's redox potential is very large (2.01 V) (41), predicting a very high reaction rate, the rates are actually slow, due to the dominant role played by peroxo-bond fissure in the process.

Complexes of L^1 and L^2 provide redox active systems where there is the facility for inner-sphere electron transfer to cationic oxidants, via a potentially bridging carboxylate pendant arm. Current studies in our laboratory are focussed on exploring the redox properties of these complexes with cationic oxidants, with application as inner-sphere reducing agents, for reductive dissolution of transition-metal oxides. Preliminary results on the oxidation of Fe^{II}(aq) and iodide ion by a mono-carboxylato-analogue of the $[Ni(III)L^1]^+$

© 2001 NRC Canada

cation shows evidence of a bridged bimetallic product of the type Ni(II)-L-Fe(III). This work is ongoing, and will be the subject of a future paper.

Acknowledgments

We are grateful to the Natural Sciences and Engineering Research Council of Canada (NSERC) for financial support, and to UPEI for a Senate Committee on Research University Grant. The electrochemical apparatus was purchased through a Canada Foundation for Innovation (CFI)/Atlantic Canada Opportunities Agency (ACOA) grant. We are indebted to the Levesque Foundation for matching funds.

References

1. P.V. Bernhardt and G.L. Lawrance. Coord. Chem. Rev. **104**, 297 (1990).
2. X.H. Bu, D.A. An, Y.T. Chen, M. Shionoya, and E. Kimura. J. Chem. Soc. Dalton Trans. 2289 (1995).
3. P.J. Davies, M.R. Taylor, K.D. Wainwright, P. Harriot, and P.A. Duckworth. Inorg. Chim. Acta, **246**, 1 (1996).
4. F. Charbonnier, T. Humbert, and A. Marsura. Tetrahedron Lett. **39**, 3481 (1998).
5. E. Kimura, T. Koike, and M. Takahashi. J. Chem. Soc. Chem. Commun. 385 (1985).
6. J.-P. Collin and J.-P. Sauvage. J. Chem. Soc. Chem. Commun. 1075 (1987).
7. H.-L. Li, W.C. Anderson, J.Q. Chambers, and D.T. Hobbs. Inorg. Chem. **28**, 863 (1989).
8. J.P.L. Cox, K.J. Jankowski, R. Kataky, D. Parker, N.R.A. Beeley, B.A. Boyce, M.A.W. Eaton, K. Miller, A.T. Millian, A. Harrison, and C. Walker. J. Chem. Soc. Chem. Commun. 797 (1989).
9. J.R. Morphy, D. Parker, R. Kataky, A. Harrison, M.A.W. Eaton, A. Millian, A. Phipps, and C. Walker. J. Chem. Soc. Chem. Commun. 792 (1989).
10. A.D. Sherry, R.D. Brown, C. Geralds, S.H. Koenig, K.T. Kuan, and M. Spiller. Inorg. Chem. **28**, 620 (1989).
11. R.I. Haines and A. McAuley. Coord. Chem. Rev. **39**, 77 (1981).
12. R.A. Speranzini, P.A. Burchart, and K.A. Kanhai. Mater. Perform. **28**, 67 (1989); E. Tachikawa, M. Hoshi, and C. Sagawa. Nucl. Technol. **65**, 138 (1984).
13. A. McAuley, P.R. Norman, and O. Olubuyide. Inorg. Chem. **23**, 1938 (1984); A. McAuley, P.R. Norman, and O. Olubuyide. J. Chem. Soc. Dalton Trans. 1501 (1984).
14. M. Tait, D.H. Busch, and N.F. Curtis. Inorg. Synth. Vol. 18. *Edited by* B. Douglas. Wiley Interscience, New York. 1978. p. 4; p. 10.
15. J. Xu, S. Ni, and Y. Lin. Inorg. Chim. Acta, **111**, 61 (1986).
16. L. Chen, L. Thompson, J. Bridson, J. Xu, S. Ni, and R. Guo. Can. J. Chem. **71**, 1805 (1993).
17. C.J. Gilmore. J. Appl. Crystallogr. **17**, 42 (1984); G. Admirial, G. Beurskens, W.P. Bosman, R. de Gelder, R. Israel, and J.M.M. Smits. The DIRDIF-94 Program System, Technical Report, Crystallographic Laboratory, University of Nijmegen, Netherlands.
18. teXsan for Windows: Crystal Structure Analysis Package. Molecular Structure Corporation. 1997.
19. S.S. Gupta and Y.K. Gupta. Inorg. Chem. **20**, 454 (1981).
20. J. Xu, S. Ni, and Y. Lin. Inorg. Chem. **27**, 4651 (1988).
21. A. McAuley, T. Palmer, and T.W. Whitcombe. Can. J. Chem. **71**, 1792 (1993).
22. N.F. Curtis. Coord. Chem. Rev. **3**, 3 (1968).
23. B. Bosnich, C.K. Poon, and M.L. Tobe. Inorg. Chem. **4**, 1102 (1965).
24. V.K. Belsky, N.R. Streltsova, E.N. Kuzmina, and A.Y. Nazarenko. Polyhedron, **12**, 831 (1993).
25. A.G. Lappin and A. McAuley. Adv. Inorg. Chem. **32**, 241 (1988).
26. P.V. Bernhardt, L. Helm, A. Ludi, and A.E. Merbach. J. Am. Chem. Soc. **107**, 312 (1985).
27. N.B. Lewis, C.D. Coryell, and J.W. Irvine. J. Chem. Soc. 386 (1949).
28. R.A. Marcus. Annu. Rev. Phys. Chem. **15**, 155 (1964); N. Sutin. Prog. Inorg. Chem. **30**, 441 (1983); R.A. Marcus and N. Sutin. Biochim. Biophys. Acta, **811**, 265 (1985).
29. R.B. Jordan. *In* Reaction mechanisms of inorganic and organometallic systems. 2nd ed. *Edited by* P.C. Ford. Oxford University Press, New York. 1998. p. 200.
30. D.H. Macartney and N. Sutin. Inorg. Chem. **22**, 3530 (1983).
31. A.McAuley, D.H. Macartney, and T. Oswald. J. Chem. Soc. Chem. Commun. 274 (1982).
32. D. Astruc. *In* Electron transfer and radical processes in transition-metal chemistry. Wiley–VCH, New York. 1995. p. 20.
33. J.-F. Wang, K. Kumar, and D.W. Margerum. Inorg. Chem. **28**, 3481 (1989).
34. M.L. Tobe and J. Burgess. *In* Inorganic reaction mechanisms. Addison Wesley Longman Limited, New York . 1999. Chap. 9. p. 481, and refs. therein.
35. R.I. Haines and S. Northcott. Can. J. Chem. **70**, 2785 (1992); R.I. Haines, L. Butt, M.K. Park, and D. Wheeler. Can. J. Chem. **71**, 976 (1993).
36. E.S. Gore and D.H. Busch. Inorg. Chem. **12**, 1 (1973).
37. J. Burgess and R.H. Prince. J. Chem. Soc. A, 1772 (1966).
38. V. Holba, O. Grancicova, and P. Paulenova. Transition Met. Chem. (London), **12**, 121 (1987).
39. O. Volarova, J. Benko, and I. Matejekova. Coll. Czech. Chem. Commun. **51**, 1049 (1986).
40. P. Banerjee and P.M. Pujari. Z. Anorg. Allgm. Chem. **473**, 224 (1981).
41. D.A. House. Chem. Rev. **62**, 185 (1962).

© 2001 NRC Canada

The photochemistry of the 4-cyanobenzoic acid esters of *trans*- and *cis*-2-phenylcyclohexanol

J.A. Pincock, S. Rifai, and R. Stefanova

Abstract: Irradiation of *trans*-2-phenylcyclohexyl 4-cyanobenzoate (**4**) in methanol results in formation of the 1-phenylcyclohexene and 4-cyanobenzoic acid as the major products. The mechanism proposed for this example of the Norrish Type II-like reaction, normally inefficient for the π,π* state of esters, begins with intramolecular electron transfer in the excited singlet state. The next step, intramolecular proton transfer, is highly exergonic as a result of the increased acidity of the benzylic hydrogen of the radical cation and the increased basicity of the carbonyl oxygen of the radical anion. The final step is cleavage of the 1,4-biradical. This mechanism is proposed on the basis of product studies, absorption spectra, fluorescence spectra, oxidation and reduction potentials, and nanosecond laser flash photolysis spectra. The stereochemical requirements for the process have also been examined using solution NMR, the X-ray structure, and MM3 calculations. The stereoisomer, *cis*-2-phenylcyclohexyl 4-cyanobenzoate (**5**), undergoes *cis* to *trans* isomerization before photofragmentation. Photolysis of the *cis* isomer in methanol–OD demonstrated that the *cis* to *trans* isomerization occurred by inversion at C1.

Key words : Norrish Type II, aromatic esters, intramolecular electron transfer.

Résumé : Les produits majeurs qui se forment lors de l'irradiation du 4-cyanobenzoate de *trans*-2-phénylcyclohexyle (**4**) dans du méthanol sont le 1-phénylcyclohexène et l'acide 4-cyanobenzoïque. Le mécanisme proposé pour cet exemple de réaction de Norrish type II, normalement inefficace pour l'état π,π* des esters, débute par un transfert intramoléculaire d'électron dans l'état singulet excité. L'étape suivant, un transfert intramoléculaire de proton, est fortement exergonique en raison de l'augmentation de l'acidité de l'hydrogène benzylique du cation radical et d'une augmentation de la basicité de l'oxygène du carbonyle de l'anion radical. La dernière étape est un clivage du biradical-1,4. Ce mécanisme est proposé sur la base de l'étude des produits, des spectres d'absorption et de fluorescence, des potentiels d'oxydation et de réduction et des spectres de photolyse éclair au laser à nanoseconde. On a aussi examiné les exigences stéréochimiques du processus à l'aide de la RMN en solution, de la diffraction des rayons-X et de calculs MM3. Le stéréoisomère 4-cyanobenzoate du *cis*-phénylcyclohexyle (**5**) subit une isomérisation *cis* à *trans* avant la photofragmentation. La photolyse de l'isomère *cis* dans du méthanol–OD permet de démontrer que l'isomérisation *cis* à *trans* se produit par une inversion du C1.

Mots clés : Norrish Type II, esters aromatiques, transfert d'électron intramoléculaire.

[Traduit par la Rédaction]

Introduction

Recently, we have shown that the Norrish Type II-like[2] reaction, normally inefficient for the π,π* state of aromatic esters, proceeds readily if electron transfer in the excited state is favourable (1). Thus, 2-arylethyl 4-cyanobenzoates (**1a**–**c**) fragment on irradiation at 254 nm in either acetonitrile or methanol to give the styrene (**2a**–**c**) and 4-cyanobenzoic acid as the primary photoproducts (Scheme 1). The mechanism proposed proceeds through exergonic intramolecular electron transfer in the excited singlet state with the aryl ring being the donor and the aromatic ester the acceptor. Since the radical cation now has increased acidity and the radical anion increased basicity, proton transfer is now also exergonic. The 1,4-diradical (**3**), in parallel with the critical intermediate in the Norrish Type II reaction of aromatic ketones, then fragments into the two products. Thus, facile hydrogen atom transfer occurs by consecutive electron and proton transfer.

We now describe[3] the photochemistry of *trans*- and *cis*-2-phenylcyclohexyl 4-cyanobenzoate, (**4** and **5**), respectively, using the stereochemistry of these substrates as a probe to clarify the above mechanism. In addition, nanosecond laser

Received July 28, 2000. Published on the NRC Research Press Web site on January 18, 2001.

J.A. Pincock,[1] S. Rifai, and R. Stefanova. Department of Chemistry, Dalhousie University, Halifax, NS B3H 4J3, Canada.

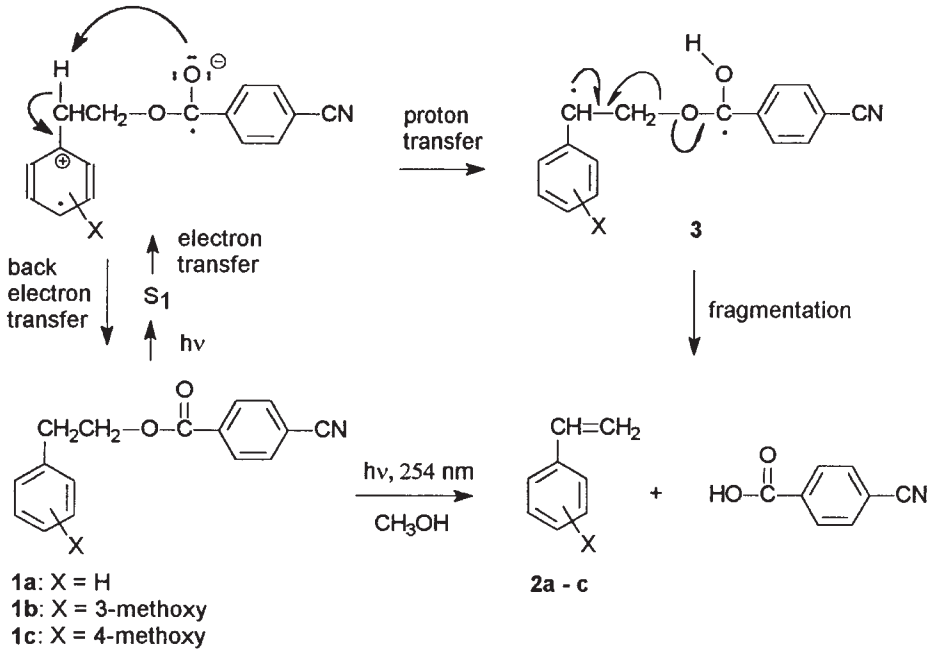
[1]Author to whom correspondence may be addressed. Telephone: (902) 494-3324. Fax: (902) 494-1310. e-mail: PINCOCK@CHEM1.CHEM.DAL.CA

[2]Type II-like was suggested by a referee on the basis of the fact that the proposed mechanism is quite different from the classic one for ketones.

[3]Parts of this work have been presented at the 10th Annual Symposium of the National Science Foundation Center for Photoinduced Charge Transfer, University of Rochester, Rochester, New York, July 1999 and published in the conference proceedings, World Scientific, Singapore, 2000, pp. 27–38.

 DOI: 10.1139/cjc-79-1-63 © 2001 NRC Canada

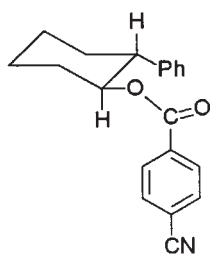
Scheme 1. Mechanism for the Norrish Type II reaction of aryl methyl esters induced by intramolecular electron transfer.

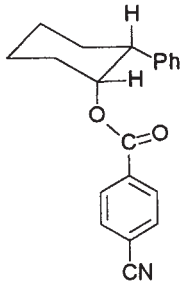


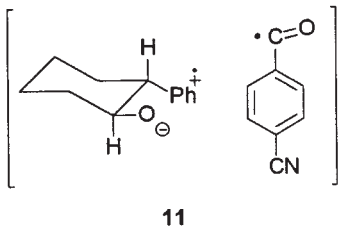
flash photolysis (LFP) results for both the cyclic (**4**) and acyclic (**1**) arylethyl esters will be described.

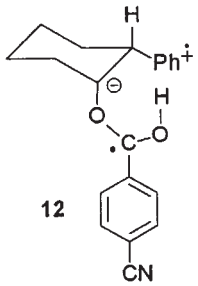
Results and discussion

Compounds **4** and **5** were synthesized from the corresponding alcohols (Aldrich) by condensation with 4-cyanobenzoic acid. In solution, the ^{1}H NMR spectra in $CDCl_3$ demonstrated that the phenyl group was equatorial for both compounds by observation of the axial–axial coupling (11.5 Hz) to two vicinal hydrogens for the hydrogen on the phenyl-substituted carbon in the *trans* isomer but only one (10.7 Hz) in the *cis*. The ester functionality is therefore equatorial in **4** but axial in **5**. X-ray structures of the two confirmed this observation for the solid state (Figs. 1 and 2).[4]









The UV spectra of these compounds indicated that there was essentially no interaction between these chromophores in the ground state. This was demonstrated by comparing an additive spectrum of toluene plus methyl 4-cyanobenzoate with *trans*-2-phenylcyclohexyl 4-cyanobenzoate (**4**), which has the same two chromophores. There is only a minor interaction between the two chromophores in the sense that the intensity of some vibrational modes are altered but there is no evidence for charge transfer absorption at longer wavelengths. The spectra for the *cis* isomer **5** were essentially the same.

In contrast to the absorption spectra, the fluorescence spectra of **4** and **5** are very much weaker than the model compound, toluene. The quantum yield of fluorescence at 280 nm for both is at least a factor of 1000 lower than that for toluene, suggesting intramolecular electron transfer quenching of the excited state. However, this observation cannot be interpreted easily because the 4-cyanobenzoate chromophore has a much higher extinction coefficient than the benzene ring and it does not fluoresce. For instance, the relative absorbance of the two is 7.9:1 at 267 nm, the excitation wavelength used for the fluorescence spectra. Therefore only about 11% of the light is absorbed by the emitting chromophore. Moreover, this emission at 280 nm will be reabsorbed by the 4-cyanobenzoate chromophore.

[4] Crystallographic data has been deposited as supplementary material and may be purchased from: The Depository of Unpublished Data, Document Delivery, CISTI, National Research Council Canada, Ottawa, ON K1A 0S2, Canada (for information on ordering electronically http:\\www.nrc.ca/cisti/irm/unpub_e.shtml). Details of data collection, structure analysis and refinement, and tables of interatomic distances and bond angles have also been deposited with the Cambridge Crystallographic Data Centre and can be obtained on request from: The Director, CCDC, 12 Union Road, Cambridge, CB2 1EZ, U.K. (Fax: 44-1223-336033 or e-mail: deposit@ccdc.cam.ac.uk).

© 2001 NRC Canada

Fig. 1. X-ray crystal structures of **4**.

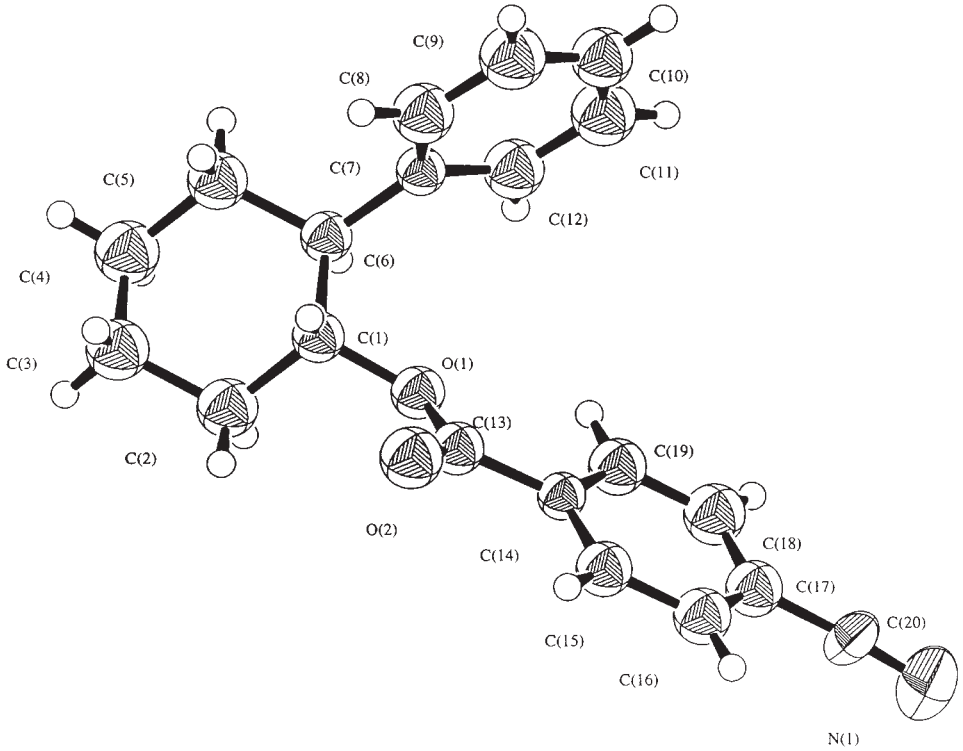
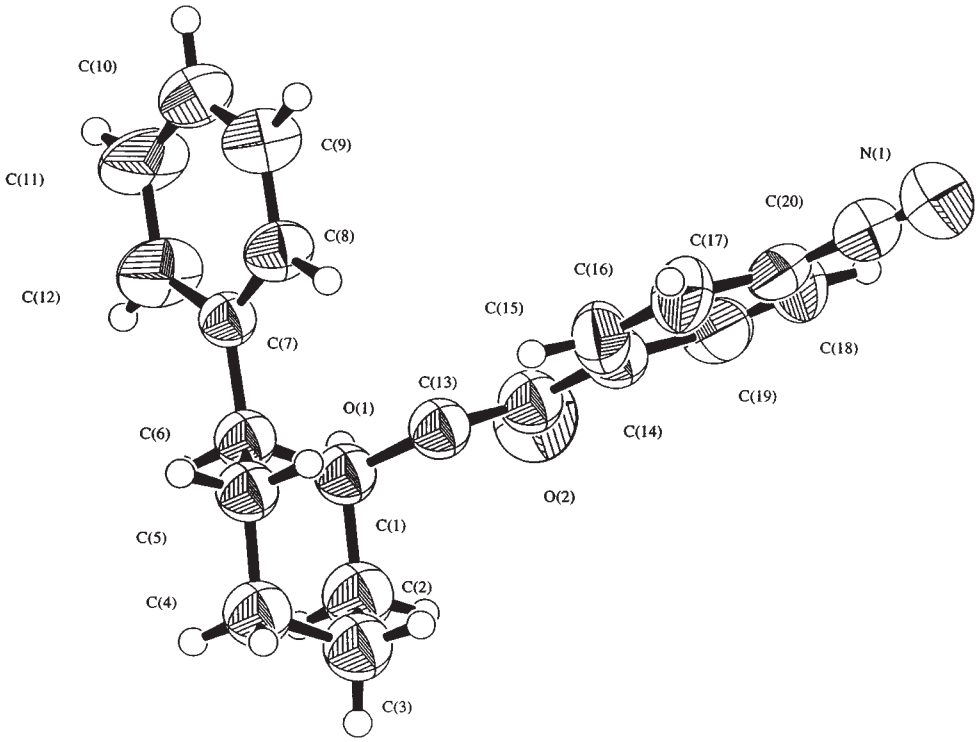


Fig. 2. X-ray crystal structures of **5**.



Since intramolecular electron transfer could not be demonstrated by flourescence quenching, redox potentials along with the Weller equation, eq. [1],[5] were used (2). The oxidation potential of the phenyl fragment of **4** and **5** was estimated at 2.4 V (vs. SCE), the value for toluene (3). The reduction potential of the 4-cyanobenzoate moiety was

[5] Equation [1*a*] is the general equation, eq. [1*b*] to calculate ΔG_{et} in units of kcal mol^{-1} with the electrode potentials in V, the wavelength of excitation in nm, and the distance of separation of the ions in Å.

© 2001 NRC Canada

[1a] $\Delta G_{et} = (E_{ox} - E_{red}) - \Delta E_{o,o} - (NQ_1Q_2) / 4\pi\varepsilon_o\varepsilon r$

[1b] $\Delta G_{et}\,(\text{kcal/mol}) = 23.06(E_{ox} - E_{red}) - \frac{2.86 \times 10^{-4}}{\lambda\,(\text{nm})} - \frac{3.33 \times 10^{2}}{\varepsilon r\,(\text{Å})}$

estimated at 1.66 V (vs. SCE) on the basis of measured values (1) for the acyclic cases (**1a**–**c**). This value also agrees well with a value for methyl 4-cyanobenzoate (4) equal to 1.97 V (vs. $Ag/AgNO_3$) which can be corrected (5) to 1.67 V (vs. SCE). The singlet excitation energy (98.2 kcal mol^{-1}) was estimated from the first vibrational band in the absorption spectrum at 291 nm because the fluorescence emission was too weak to obtain a reliable (0,0) crossing. Using eq. [1], ΔG_{et} equals –4.8 kcal mol^{-1}, ignoring the Coulombic term (which will make the value more negative) because the distance (*r*) between the two charges is not certain. From the X-ray structures the centre-to-centre distance of the aromatic rings is 5.75 Å in **4** (the *trans* isomer) and 6.15 Å in **5** (the *cis* isomer) leading to values of the Coulombic term of –1.8 and –1.6 kcal mol^{-1}, respectively, using a value for the dielectric constant of methanol of 32.7 (6). However, molecular models indicate that these two rings can approach each other face-to-face to distances approaching contact for either of the isomers. The Coulombic term would now be –2.9 kcal mol^{-1} assuming a centre-to-centre distance of 3.5 Å, as estimated for the π-stacking distance in benzene itself (7). These geometries will be discussed further below.

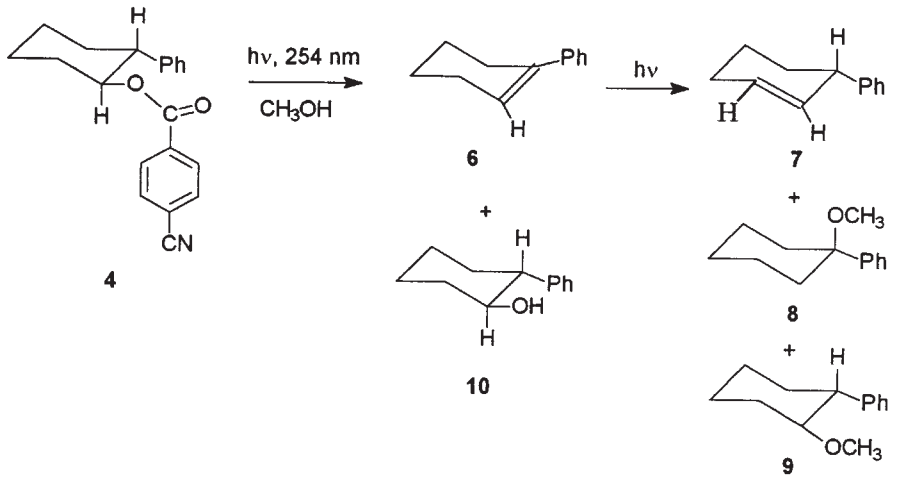
Photolysis of the *trans* isomer (**4**), in methanol (6.0 mM, 254 nm, N_2 purged, 25°C) resulted in a mixture of photoproducts **6**–**10** (eq. [2]) along with 4-cyanobenzoic acid and methyl 4-cyanobenzoate. To our surprise, the major expected product, 1-phenylcyclohexene (**6**), was observed in less than 1% yield even at very low conversions of **4**. That this was the major primary photoproduct was easily demonstrated by addition of 10 mol% of **6** to the reaction before photolysis began. Monitoring by GC indicated that the added **6** was converted to **7**, **8**, and **9**, before **4** began to disappear. This rapid secondary photochemistry of **6** is a result of the fact that **6** has a more strongly absorbing chromophore than the starting ester **4**. The ratio of (**7** + **8** + **9**):**10**, which reflects the ratio of the initial formation of **6**:**10**, was 3:1. The secondary products, **7**:**8**:**9**, were formed in the ratio of 52:34:14.

As expected, and as observed previously for the acyclic cases (**1**), the secondary photolysis of **6** is of three major types: (*i*) deconjugation to 3-phenylcyclohexene (**7**) by electron transfer sensitized formation of the radical cation as previously observed by Arnold and Mines (8) (the cyanobenzoate starting material or photoproducts are presumably the electron acceptor); (*ii*) photochemical *cis* to *trans* isomerization of **6** followed by Markovnikov addition of methanol to form **8** as discussed by Cozens et al. (9); (*iii*) electron transfer sensitized anti-Markovnikov addition of methanol to form **9**-*cis* and **9**-*trans* also as previously reported by Arnold and Shigemitsu (10).

The formation of the major primary photoproduct is consistent with our previously proposed mechanism (Scheme 1) of exergonic intramolecular electron transfer from the aryl ring to the 4-cyanobenzoate group followed by exergonic intramolecular photon transfer to form a 1,4-biradical which then cleaves to form **6**. In fact, photolysis of **4** in acetonitrile also lead to slow formation of **7**, again resulting from deconjugation of **6** by secondary photochemistry. The X-ray structure for the *trans* isomer (**4**) shown in Fig. 1, presents two stereochemical problems for this mechanism. First, the carbon—hydrogen bond at the benzylic carbon (C6—H)[6] has poor overlap with the SOMO of the radical cation of the aryl ring as a consequence of the almost parallel orientation of the π-orbitals of that equatorial group; the estimated dihedral angle (C=C-C6-H) is 13° in the solid. Arnold and coworkers (11) have previously shown that aryl methyl hydrogens in this orientation are not particularly acidic in the corresponding radical cations. Second, the carbonyl oxygen of the ester is remote from that hydrogen. Therefore, formation of 1-phenylcyclohexene by intramolecular hydrogen atom transfer should not be facile from this geometry.

In order to gain a better understanding of the conformation of **4** and **5** in solution, molecular mechanics calculations (MM3) were performed (Figs. 3 and 4). Three minima were obtained for rotation about the cyclohexyl carbon to ester oxygen single bond of **4** and two were found for **5**. For both compounds, these minima were very similar in energy indicating rather flat rotational surfaces. For the *trans* isomer, **4a** is the minimum, but only 0.5 kcal mol^{-1} lower than a structure that is essentially identical to the X-ray one. In addition,

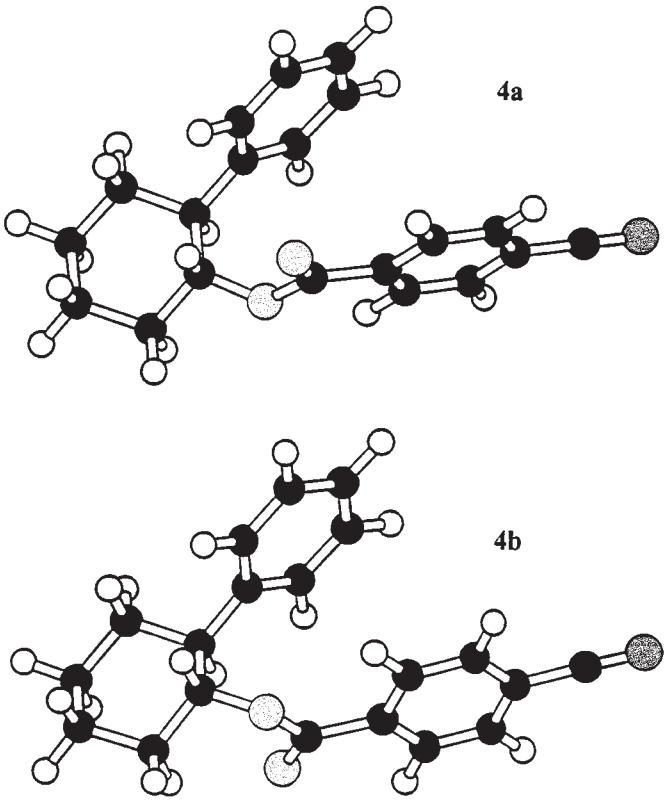
[2]



[6] Carbon atom numbering follows that of the X-ray strucures in Figs. 1 and 2.

© 2001 NRC Canada

Fig. 3. MM3 minimized geometries **4a** and **4b** with the phenyl group equatorial in both.

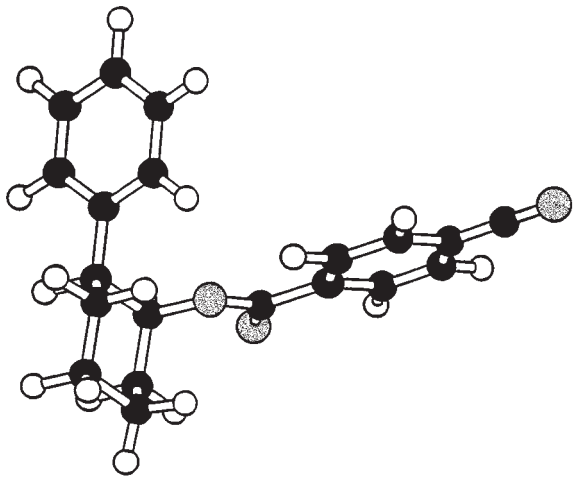


4b only 0.9 kcal mol^{-1} above the minimum, provides an ideal conformation for intramolecular abstraction of the aryl methyl hydrogen. Our conclusion for the mechanism of formation of 1-phenylcyclohexene is, therefore, that proton transfer occurs in the intramolecular radical ion pair created from S_1 of **4**. The formation of this radical ion pair by through-bond electron transfer is favoured by overlap of the π-system of the aryl methyl ring through the C6—C1 σ bond and then to the π-system of the cyanobenzoate moiety. The rotation from **4a** to **4b** may be aided by electrostatic attraction between the two aromatic rings ("harpooning") (12). Another possibility is that the population of the conformer **4b** is high enough to allow efficient reaction to occur. The activation energy for proton transfer is then lowered by the beginning of the rotation in the transition state of the aryl methyl ring as it approaches the geometry required for conjugation with the developing radical center at C6.

The other primary photoproduct for the photolysis of **4** is *trans*-2-phenylcyclohexanol (**10**). The fact that the original stereochemistry of the ester is maintained in this alcohol product suggests ester acyl C—O bond cleavage in the photochemical step. As has been observed previously (13), this reactivity is characteristic of the radical anions of esters, provided that the alkyl group does not form a stabilized radical. In the latter case, alkyl C—O bond cleavage occurs. The sequence of steps that converts the geminate pair **11** to **10** and methyl 4-cyanobenzoate is not known but may proceed by electron transfer to form the acylium cation and the alkoxide anion which are then trapped by methanol.

In order to strengthen these mechanistic arguments, nanosecond LFP experiments have been performed in methanol using a Nd:YAG laser with 266 nm excitation. For **1c**, **4**, and **5** strong transient absorbances at 300 nm were observed (Fig. 5 for **1c** and **4**) with very similar first order decays for **1c** (1.1×10^5 s^{-1}) and **4** (1.2×10^5 s^{-1}) but somewhat faster for **5** (7.7×10^5 s^{-1}). The same transient was observed for methyl 4-cyanobenzoate ($k_d = 1.4 \times 10^5$ s^{-1}) indicating that these species are not derived from the second chromophore in either **1c** or **4**. This absorbance was assigned to the triplet state of the cyanobenzoate chromophore on the basis of the observation that it was quenched by oxygen and by 2,3-dimethyl-1,3-butadiene. Stern–Volmer rate constants for the diene quenching of this transient derived from **1c** and methyl 4-cyanobenzoate were equal to 7.1×10^9 M^{-1} s^{-1} and 1.4×10^{10} M^{-1} s^{-1}, respectively, comparable to the estimated diffusional limit in methanol, 1.2×10^{10} M^{-1} s^{-1} (14).

Fig. 4. MM3 minimized geometry for **5**.



The radical anions of aromatic esters have been generated previously both by pulse radiolysis and photoinduced electron transfer using triethylamine as the donor (13). For instance, 266 nm excitation of ethyl benzoate in ethanol containing 0.1 M triethylamine gave a transient with maxima at 310 and 445 nm. It decayed with second order kinetics indicating that back electron transfer to the radical cation of triethylamine was the dominant pathway for its disappearance. We have also generated the radical anions of methyl 4-cyanobenzoate (**1c** and **4)** using 0.1 M triethylamine. A typical transient spectrum is shown for **4** in Fig. 6. The maxima have shifted to longer wavelength (360 and 490 nm) as a consequence of the nitrile group. The rate constant for first-order decay (inset) in methanol is 8.6×10^5 s^{-1}. We see no evidence for this signal on irradiation of any of the esters in the absence of the added donor, triethylamine.

Our conclusion from these LFP results is that the triplet state of methyl 4-cyanobenzoate is formed in the normal way by intersystem crossing from the singlet state. However, for the bichromophoric esters (**1c** and **4**) intramolecular electron transfer to form the radical ion pair from the excited singlet state is likely too fast to allow efficient intersystem crossing to the triplet state. As discussed above, this suggestion cannot be proven because intamolecular fluorescence quenching cannot be quantitatively monitored. However, the electron transfer is exergonic which normally guarantees that it will be rapid. Therefore, there must be competition in the

© 2001 NRC Canada

Fig. 5. Transient absorbance observed from **1c** and **4** after 266 nm excitation in methanol. Decay traces show first-order fits at 300 nm.

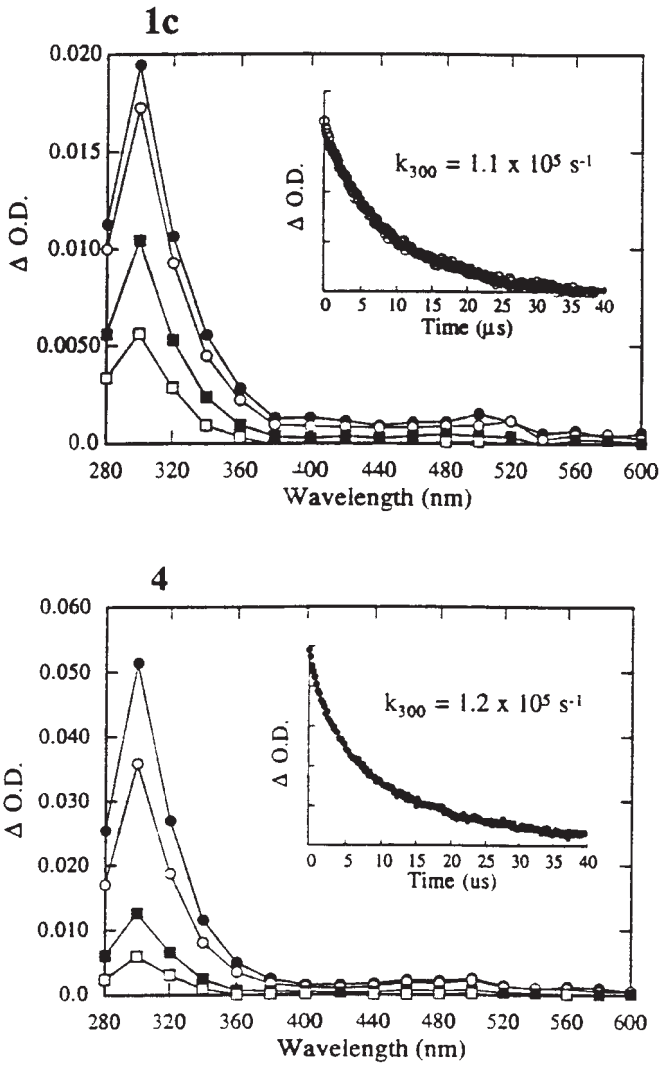
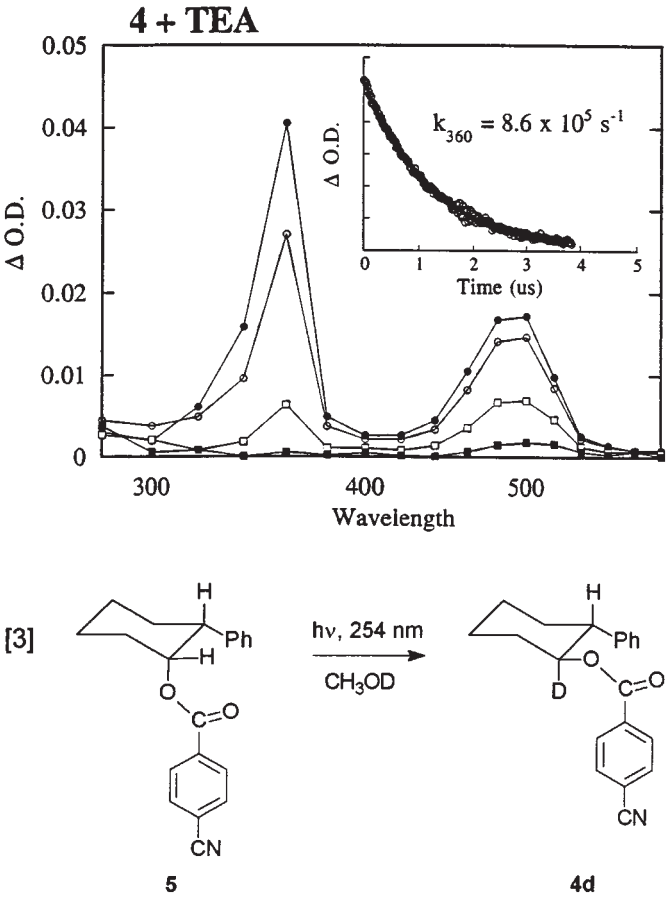


Fig. 6. Transient absorbance observed for **4b** + 0.1 M triethylamine after 266 nm excitation in methanol. Decay traces show first-order fit at 360 nm.



radical ion pair between proton transfer that leads to products and back electron transfer to form the triplet state. Back electron transfer to form triplet states has been observed previously in cases where it is energetically feasible (4, 15). This process is certainly possible for these esters because the excited singlet state, localized on the 4-cyanobenzoate chromophore, is at 98 kcal mol^{-1} and the radical ion pair at approximately 93 kcal mol^{-1} for **4** and 76 kcal mol^{-1} for **1c** (1). The excited triplet state of methyl 4-cyanobenzoate is at 72 kcal mol^{-1} (16) so that back electron transfer resulting in triplet state formation is highly exothermic for **1c** and slightly for **4**.

Finally, as expected on the basis of the X-ray structure (Fig. 2) and MM3 calculations (Fig. 4) for the *cis* isomer **5**, proton transfer in the intramolecular radical ion pair should be geometrically inhibited. In confirmation of this, photolysis of **5** resulted only in photoisomerization to the *trans* isomer **4** (eq. [3]) which then underwent the photochemistry described above. There are three likely mechanisms for this *cis* to *trans* isomerization process: (*i*) C—H bond cleavage at the ester carbon C1; (*ii*) C—H bond cleavage at the benzylic carbon C6; (*iii*) C1—C6 bond cleavage. Pathways 2 and 3 have been observed previously for the radical cations of phenyl substituted alkanes with oxygen substitution at the adjacent carbon (11); pathway 2 is preferred when the SOMO of the phenyl group has good overlap with the C—H bond and pathway 3 when the overlap occurs with the C—C bond. However, irradiation of the *cis* isomer **5** in methanol–OD resulted in formation of the *trans* isomer (**4d**) eq. [3] with deuterium incorporation at C1, that is, pathway 1, above. The fact that deuterium was being incorporated at C1 was initially determined by GC-MS. The molecular ions for these esters are very weak, but an ion corresponding to 1-phenylcyclohexene (*m*/*z* of 156) resulting from McLafferty fragmentation by loss of 4-cyanobenzoic acid, is quite strong. In the *trans* ester **4**, the ratio of *m*/*z* 158:159 = 5.7. After irradiation of the *cis* ester **5** in methanol–OD until the ratio of *trans*:*cis* was 23:77, the *trans* ester now had *m*/*z* 158:159 = 0.40 indicating a large increase in the deuterium content and an increased intensity for the M + 1 peak at 159. The mass spectral fragmentation requires abstraction of a hydrogen from C6, so the deuterium is most likely incorporated at C1. This was confirmed by ^{1}H NMR spectra of this mixture which indicated only the appearance of a signal for *trans* H6 at δ 2.8 but not H1 at δ 5.2. Moreover, the signal for H6 now showed only one large coupling constant to the

© 2001 NRC Canada

anti-hydrogen at C5 but not to the one at C1, which was now deuterium. A possible mechanism for isomerization and exchange is therefore abstraction of the hydrogen at C1 by the radical anion of the 4-cyanobenzoate group. This five-membered cyclic process leading to a distonic radical anion may be favoured by the bringing together of the two aromatic rings in the exciplex so that the ester carbonyl group is close to the C1 hydrogen. The mechanistic details of this exchange are not known but a species like **12** may rationalize the deuterium incorporation from methanol–OD and the *cis* to *trans* isomerization.

Experimental

1-Phenylcyclohexene, 1-phenylcyclohexanol, *trans*-2-phenylcyclohexanol and *cis*-2-phenylcyclohexanol were obtained from Aldrich. Authentic samples of 1-methoxy-1-phenylcyclohexane, *trans*- and *cis*-1-methoxy-2-phenylcyclohexane (**10**) were prepared by reaction of the alcohols with NaH in DMSO (dimethyl sulphoxide) followed by CH_3I. 3-Phenylcyclohexene was prepared by photochemical deconjugation of 1-phenylchclohexene as described previously (8).

Preparation of esters

The esters were prepared by the condensation of the corresponding alcohol (Aldrich) with 4-cyanobenzoic acid (Aldrich) using DCC in dichloromethane and DMAP as the catalyst as described by Neises and Steglich (17).

trans-*2-Phenylcyclohexyl 4-cyanobenzoate (**4**)*: mp 62–64°C (from dichloromethane–hexanes, 46% yield). GC-MS: *m/z* (%): 159 (12), 158 (100, 1-phenylcyclohexene), 143 (21), 131 (12), 130 (80), 129 (22), 115 (13) 102 (47), 91 (98), 75 (10). UV (CH_3OH) λ_{max} (ε): 239 nm (19 600 M^{-1} cm^{-1}), 282 (1470), 290 (1259). ^1H NMR (250 MHz, $CDCl_3$) δ: 7.86 (d, *J* = 8.4 Hz, 2H), 7.60 (d, *J* = 8.4 Hz, 2H), 7.2 (m, 3H), 7.25–7.10 (m, 3H), 5.19 (dt, *J* = 4.6, 10.5 Hz, 1H), 2.83 (dt, *J* = 3.8, 11.5 Hz, 1H), 2.28 (m, 1H), 2.05–1.77 (m, 3H), 1.75–1.30 (m, 4H). ^{13}C NMR ($CDCl_3$) δ: 164.2, 142.8, 134.4, 132.0, 129.8, 128.4, 127.4, 126.6, 118.0, 115.9, 78.0, 49.9, 33.7, 32.2, 25.8, 24.8. HR-MS calcd. for $C_{20}H_{19}NO_2$: 305.1416; found: 305.1421. X-Ray structure (Fig. 1).

cis-*2-Phenylcyclohexyl 4-cyanobenzoate (**5**)*: mp 92–94°C (from dichloromethane–hexane, 41% yield). GC-MS *m/z* (%): 158 (68, 1-phenylcyclohexene), 157 (12) 130 (60), 129 (14), 102 (37), 91 (100). UV (CH_3OH) λ_{max} (ε): 239 nm (22 100 M^{-1} cm^{-1}), 282 (1630), 290 (1340). ^1H NMR (250 MHz, $CDCl_3$) δ: 8.02 (d, *J* = 8.6 Hz, 2H), 7.71 (d, *J* = 8.6 Hz, 2H), 7.26–7.16 (m, 5H), 5.45 (bs, 1H), 2.93 (m, 2H), 2.4–2.1 (m, 2H), 2.02–1.50 (m, 6H). ^{13}C NMR ($CDCl_3$) δ: 163.9, 142.7, 134.6, 132.1, 129.8, 128.2, 127.5, 126.5, 118.0, 116.1, 75.1, 46.5, 30.7, 26.0, 25.8, 20.3. HR-MS calcd. for $C_{20}H_{19}NO_2$: 305.1416; found: 305.1405. X-Ray structure (Fig. 2).

Photolysis

In a typical reaction, 100 mg of **4** in 100 mL of HPLC grade methanol was irradiated in a quartz tube in a Rayonet reactor with 254 nm low-pressure mercury lamps while being purged with nitrogen. The reaction was thermostated at 25°C with an immersion circulating water tube. The reactions were monitored by GC on a 30 m × 0.25 mm J & W DB 200 column using helium as carrier gas (split) and temperature programming (60°C for 1 min, 15°C min^{-1} to 180°C, 180°C for 7 min). Standard samples of the products were used to monitor their appearance. Dark samples were checked for ground-state reactions but none were observed over the short times required for photolysis and analysis.

Laser flash photolysis

The nanosecond laser flash photolysis system at Dalhousie is of standard design using, as excitation source, the fourth harmonic from a Continuum Nd:Yag NY-61 laser (266 nm, ≤8 ns per pulse, ≤15 mJ per pulse).

X-Ray crystallographic analyses were performed on a AFC5R diffractometer with graphite monochromated Mo-K_α radiation and a rotating anode generator.

Acknowledgments

We thank Natural Sciences and Engineering Research Council of Canada (NSERC) for financial support for this work. We also thank Professor T.S. Cameron of the X-Ray Crystallography Center at Dalhousie University for the crystal structures and T. B. Grindley of the Department of Chemistry, Dalhousie University for the MM3 calculations.

References

1. D.P. DeCosta, A.K. Bennett, and J.A. Pincock. J. Am. Chem. Soc. **121**, 3785 (1999).
2. D. Rehm and A. Weller. Isr. J. Chem. **8**, 259 (1970).
3. L. Eberson. Electron transfer reactions in organic chemistry. Springer–Verlag, Berlin. 1987, p. 44.
4. J. Kawakami and M. Iwamura. J. Phys. Org. Chem. **7**, 31 (1994).
5. D.D.M. Wayner. CRC handbook of organic photochemistry. Vol II. *Edited by* J.C. Scaiano. CRC Press, Boca Raton, Florida. 1989. Chpt. 18.
6. S.L. Murov, I. Carmichael, and G.L. Hug. Handbook of photochemistry. 2nd ed. Marcel Dekker, New York. 1993. p. 286.
7. C.A. Hunter and J.K.M. Saunders. J. Am. Chem. Soc. **112**, 5525 (1990).
8. D.R. Arnold and S.A. Mines. Can. J. Chem. **67**, 689 (1989).
9. F.L. Cozens, R.A. McClelland, and S. Steenken. J. Am. Chem. Soc. **115**, 5050 (1993).
10. D.R. Arnold and Y. Shigemitsu. J. Chem. Soc. Chem. Comm. 407 (1975).
11. A.L. Perrott, H.J.P. de Lijser, and D.R. Arnold. Can. J. Chem. **75**, 384 (1997), and refs. therein.
12. J.W. Verhoeven. Pure Appl. Chem. **62**, 1585 (1990), and ref. therein.
13. J. Masnovi. J. Am. Chem. Soc. **111**, 9081 (1989).
14. S.L. Murov, I. Carmichael, and G.L. Hug. Handbook of photochemistry. 2nd ed. Marcel Dekker, New York. 1993. p. 208.
15. H.D. Roth and M.L. Schilling. J. Am. Chem. Soc. **102**, 4303 (1979).
16. D.R. Arnold, J.R. Bolton, and J.A. Pederson. J. Am. Chem. Soc. **94**, 2872 (1972).
17. B. Neises and W. Steglich. Angew. Chem. Int. Ed. Engl. **7**, 522 (1978).

© 2001 NRC Canada

Thermodynamics of triaryltin chloride adduct complexes

Mozaffar Asadi and Khosrow Aein Jamshid

Abstract: The stability constants and the thermodynamic data were measured spectrophotometerically for 1:1 adduct formation of triaryltin chlorides, where aryl groups are *p*-chlorophenyl, phenyl, *p*-, *m*-, and *o*-tolyl, as Lewis acids, with chloride and bromide ions, as Lewis bases, in 50% v/v ethanol–water solvent. The stability constants and the thermodynamic parameters trend, confirmed the following softness trend of tin(IV) in the triaryltin chlorides:

$$(p\text{-}, m\text{-}, o\text{-tolyl})_3SnCl > (\text{phenyl})_3SnCl > (p\text{-chlorophenyl})_3SnCl$$

Key words: tin(IV) complexes, thermodynamic parameters, mixed solvent, adduct formation.

Résumé : Opérant dans des solutions aqueuses d'éthanol à 50 % v/v et faisant appel à la spectroscopie, on a mesuré les constantes de stabilité et les données thermodynamiques pour la formation de l'adduit 1:1 de chlorures de triarylétain (dans lesquels les groupes aryles sont *p*-chlorophényle, phényle, *p*-, *m*- et *o*-tolyle) agissant comme acides de Lewis avec les ions chlorure et bromure agissant comme bases de Lewis. Les constantes de stabilité et la tendance des paramètres thermodynamiques permet de confirmer la tendance suivante dans la mollesse de l'étain(IV) dans les chlorures de triarylétain:

$$(p\text{-}, m\text{- et } o\text{-tolyl})_3SnCl > (\text{phényl})_3SnCl > (p\text{-chlorophényl})_3SnCl$$

Mots clés : complexes d'étain(IV), paramètres thermodynamiques, solvant mixte, formation d'adduit.

[Traduit par la Rédaction]

Introduction

During the last decades there has been considerable interest in the behaviour of organotin halides as Lewis acids. While the tetraorganotin compounds show no evidence of Lewis acidity, the tin(IV) halides are strong Lewis acids which can produce 1:1 and 1:2 adducts in the presence of Lewis bases. The organotin halides R_nSnX_{4-n} are intermediate in Lewis acidity and found between R_4Sn and SnX_4. Generally the acidity is increased when the proportion of the halide is increased.

Recent studies have shown that mono-halides produce predominantly 1:1 adducts in solution with various monodentate bases such as TPPO, DMSO, and DMA (1), while di- and trihalides form a mixture of 1:1 and 1:2 adducts. The 1:1 adducts have been shown, by X-ray diffraction, to have trigonal bipyramid structures with the organo groups lying in the equatorial positions and the 1:2 adducts to have octahedral structures (2).

Received June 25, 2000. Published on the NRC Research Press Web site on January 24, 2001.

M. Asadi[1] and K.A. Jamshid. Chemistry Department, College of Sciences, Shiraz University, Shiraz 71545, I.R. Iran.

[1]Author to whom correspondence may be addressed. Telephone: 0098 71 24829. Fax: (071)20027. e-mail: asadi@chem.susc.ac.ir

The thermodynamic data have been reported for 40 organotin compounds with Lewis bases in benzene solution at 30°C by means of calorimetric titration. It was shown that adduct stabilities enhance with increasing chloride substitution and in the order: Bu < Me < Ph (3).

Holecek et al. (4) have determined the stability constants and the thermodynamic parameters of complex formation of tri-*n*-butyl-, tribenzyl- and triphenyltin(IV) chlorides with pyridine, DMSO, and HMPA. Their studies showed that the stability of the complexes increases in the *R*-substituent series: *n*-butyl < benzyl < phenyl, and in the donor series: pyridine < DMSO < HMPA.

Fujiwara et al. (5) have investigated the reaction between Me_2SnCl_2 with DMF, DMSO, HMPA, and PINO. They have found that with DMF and DMSO (1:1), and HMPA and PINO (1:2) complexes have been formed in solution. The stability constants and $-\Delta H°$ values for these donors are depicted as following the order: DMSO > DMF and PINO > HMPA. The stability constants and $\Delta H°$ values for 1:2 complexes are larger than the 1:1 complexes.

In the present study, the stability constants and the thermodynamic parameters of complex formation of tri-*p*-chlorophenyl, triphenyl, tri-*p*-, tri-*m*- and tri-*o*-tolyltin(IV) chlorides with chloride and bromide bases in 50% v/v ethanol–water solvent have been obtained by using ultraviolet (UV) spectrophotometry in a effort to study the softness property of these triaryltin chlorides. The stability constants were recorded at 35, 45, 55, and 65°C spectrophotometrically

 DOI: 10.1139/cjc-79-1-70 © 2001 NRC Canada

by using Ketelaar's equation and the thermodynamic parameters were obtained by using the van't Hoff equation.

Experimental

Materials

Tetraphenyltin, *p*-bromotoluene, *m*-bromotoluene, *o*-bromotoluene, *p*-bromochlorophenyl, and all solvents were purchased from Merck and Fluka. Solvents that were used in the preparation of Grignard reagents were dried and distilled; all other materials were used without further purification. For the spectroscopy measurements pure NaCl, NaBr, and extra pure ethanol were used as obtained from Merck.

Instrumental

All of the scanning UV spectra were recorded by Philips PU 8750 spectrophotometer.

Synthesis of organotin compounds

The reaction of tintetrachloride with Grignard reagents gives the tetraaryltin compounds:

$$4RMgX + SnCl_4 \rightarrow R_4Sn + 4MgClX$$

The various triaryltin chlorides (Ar_3SnCl) were prepared in a similar manner to Kocheshkov et al. (6) and Stern and Becker (7) in which the tetraaryltin and tintetrachloride in the appropriate proportions are heated together and refluxed for a few hours at 200–210°C to give:

$$3R_4Sn + SnCl_4 \rightarrow 4R_3SnCl$$

The solid triaryltin chlorides were recrystallized from ethanol. The recorded melting point (7), UV (8) and ^{1}H NMR (9) spectra are in agreement with the literature reported values.

Preparation of solutions

The adduct complexes were obtained from the reaction of triaryltin chlorides with donors, according to the following reaction:

$$R_3SnCl + X^- \overset{\text{ethanol}-\text{water } 50\%}{\underset{X^- = Cl^-,\ Br^-}{\rightleftharpoons}} R_3SnClX^-$$

The solutions for spectroscopy measurements were prepared by dissolving 5×10^{-5} M of triaryltin chloride and 0.01–0.09 M of NaCl or NaBr, respectively, in 50% v/v ethanol–water. The triaryltin chloride concentration was kept constant in all solutions, while the donor concentrations varied with a coefficient of 20–200-fold of the acceptor for NaCl and NaBr, respectively. Solutions containing only donor species show no significant absorption.

The solution provided was allowed to stand at 35, 45, 55, and 65°C for 19, 10, 5, and 3 h, respectively. Ultimately, the solution was transferred into the thermostated cell compartment of the instrument, which was kept at constant temperature (±0.1°C) by circulating water, and absorption measurements were carried out at several fixed wavelengths. Scanning from 200 up to 350 nm using the PU-8750 spectrophotometer was performed at selected wavelengths. These wavelengths are listed for each system in Table 1. The fixed wavelengths which were chosen in the region that showed absorbance by the solutions. These absorptions varied with respect to wavelengths of the pure substrate alone. The adducts formed, and the Lewis acceptors show absorption in the same region, while donors show little or no absorption at all. The effect of ionic strength variations of the medium on the stability constants were found to be slight. All the syntheses and solutions preparation were carried out in a fume cupboard, because of to the toxicity of tin compounds.

Table 1. Wavelengths of Ar_3SnCl compounds.

Ar_3SnCl	λ_{nm} ($Ar_3SnClBr^-$)	λ_{nm} ($Ar_3SnCl_2^-$)
(p-Cl-C_6H_4)$_3$SnCl	226–232	226–230
(C_6H_5)$_3$SnCl	224–227	224–228
(p-CH_3-C_6H_4)$_3$SnCl	229–232	228–232
(m-CH_3-C_6H_4)$_3$SnCl	228–232	227–233
(o-CH_3-C_6H_4)$_3$SnCl	228–232	227–233

Results and discussion

The equilibrium constants of the various aryltin chloride complexes studied were calculated by using Ketelaar's (10) equation:

$$[1] \qquad \frac{C_A^\circ C_D^\circ}{A - A_A^\circ - A_D^\circ} = \frac{1}{\varepsilon_C - \varepsilon_A - \varepsilon_D} \times \left[\frac{1}{K} + (C_A^\circ + C_D^\circ)\right]$$

where C_A° and C_D° are the initial concentrations of the acceptor and the donor, respectively; A is the optical density of the solution including the acceptor and the donor, A_A° and A_D° are the optical densities of the pure acceptor and the pure donor in the solution of concentration C_A° and C_D°; ε_C, ε_A, and ε_D are the molar extinction coefficients of the complex, the acceptor, and the donor, respectively. K is the stability constant of the formed complex and the cell optical path length is 1 cm. A plot of $(C_A^\circ\ C_D^\circ)/(A - A_A^\circ - A_D^\circ)$ vs. $(C_A^\circ + C_D^\circ)$ should produce a straight line if only a 1:1 complex is formed, while a mixture of 1:1 and 1:2 or only 1:2 complex in a system would lead to a curve. The stability constants were calculated from the ratio of the slope to the intercept by least-square method using the Excel version 5 computer software. The variation of the stability constant values, particularly for the bromide ion, with the wavelength has led us to use the average value of K for a given system.

The thermodynamic parameters of the studied aryltin chloride complexes were calculated by use of the well known, van't Hoff equation.

$$[2] \qquad \ln K = \frac{-\Delta H^\circ}{RT} + \frac{\Delta S^\circ}{R}$$

where K is the stability constant, R is the gas constant and T is the temperature in degrees Kelvin. While, the thermodynamic parameters of the aryltin chloride complexes were obtained from the linear plots of ln K vs. 1/T. The values of ΔH° and ΔS° were obtained from the slope and the intercept, respectively, by using the Excel version 5 computer program.

The stability constants and the thermodynamic parameters data are collected in Tables 2, 3, 4. The mean of stability constants are given for the 1:1 adducts formation. The

© 2001 NRC Canada

Table 2. The stability constants, K (L mol^{-1}), for Ar_3SnCl with Cl^-, Br^- in 50% v/v ethanol–water solvent.

Ar_3SnCl	65°C	55°C	45°C	35°C
$Ar_3SnCl_2^-$				
p-Chlorophenyl	93.32 ± 3.68[a]	82.00 ± 2.41[b]	76.10 ± 3.01	66.22 ± 2.64
Phenyl	81.73 ± 2.41	73.41 ± 1.91	62.87 ± 2.36	53.76 ± 1.76
p-Tolyl	71.06 ± 2.27	59.37 ± 0.78	50.49 ± 3.08	43.45 ± 1.83
m-Tolyl	68.75 ± 4.90	56.38 ± 1.93	49.47 ± 1.43	41.85 ± 2.31
o-Tolyl	57.40 ± 4.61	49.73 ± 1.16	41.47 ± 0.90	35.32 ± 1.31
$Ar_3SnClBr^-$				
p-Chlorophenyl	131.16 ± 5.42[c]	123.27 ± 5.42	108.55 ± 1.53	96.39 ± 2.21
Phenyl	110.45 ± 1.40	96.85 ± 2.22[d]	86.46 ± 1.17	70.78 ± 2.41
p-Tolyl	104.01 ± 1.40	89.91 ± 3.50[d]	69.46 ± 1.21	57.27 ± 2.86
m-Tolyl	99.23 ± 2.19	84.59 ± 1.34	71.97 ± 2.57	54.86 ± 3.15
o-Tolyl	78.28 ± 3.51	71.30 ± 2.35	59.84 ± 3.48	47.79 ± 1.02

[a]At 61°C.
[b]At 51°C.
[c]At 66°C.
[d]At 54°C.

Table 3. $\Delta G°$ (kJ mol^{-1}) values for Ar_3SnCl with Cl^-, Br^- in 50% v/v ethanol–water solvent.

Ar_3SnCl	65°C	55°C	45°C	35°C
$Ar_3SnCl_2^-$				
p-Chlorophenyl	–12.81 ± 3.67[a]	–11.84 ± 2.37[b]	–11.45 ± 2.91	–10.80 ± 2.49
Phenyl	–12.41 ± 2.30	–11.68 ± 0.68	–10.95 ± 2.97	–10.22 ± 1.55
p-Tolyl	–11.95 ± 2.30	–11.18 ± 0.68	–10.40 ± 2.97	–9.63 ± 1.55
m-Tolyl	–11.84 ± 4.47	–11.08 ± 1.79	–10.31 ± 0.95	–9.55 ± 2.14
o-Tolyl	–11.39 ± 4.29	–10.64 ± 0.40	–9.88 ± 0.28	–9.12 ± 0.69
$Ar_3SnClBr^-$				
p-Chlorophenyl	–13.55 ± 4.69[c]	–13.12 ± 4.09	–12.41 ± 1.12	–11.70 ± 2.03
Phenyl	–13.26 ± 0.94	–12.42 ± 3.41[d]	–11.73 ± 0.50	–10.96 ± 2.69
p-Tolyl	–13.12 ± 0.94	–12.11 ± 3.41[d]	–11.28 ± 0.50	–10.37 ± 2.69
m-Tolyl	–12.95 ± 2.20	–12.16 ± 0.80	–11.20 ± 2.49	–10.32 ± 2.94
o-Tolyl	–12.34 ± 3.53	–11.55 ± 2.33	–10.76 ± 3.30	–9.97 ± 0.05

[a]At 61°C.
[b]At 51°C.
[c]At 66°C.
[d]At 54°C.

formation of 1:1 adducts for triorganotin halides was supported by previous works (11, 12). Previous studies have also showed that triaryltin chlorides form 1:1 adducts with monodentate donors (13).

In the present studies of triaryltin chlorides, efforts were made to provide a quantitative measurement of the behaviour of tin in our compounds. In some of them, in addition to the resonance and electronegative inductive effects of substituted phenyl rings, steric interactions effect may also contribute to the stability constants of these compounds when chloride and bromide ions are used as Lewis bases. The experimental data are explained as follows:

The acceptor property of tin

In some of these aryltin chlorides, in addition to the resonance and electronegative inductive effects of the substituted phenyl rings, steric effects may also contribute to the stability constants of these compounds. The electron-withdrawing or electron-releasing property of substituent groups on a phenyl ring, in the substituted phenyltin chlorides, can influence the softness property of the corresponding central tin atom with respect to the triphenyltin chloride through *d—p* bonding. The presence of a Cl^- electron-withdrawing group causes the $Cl\text{-}C_6H_4^-$ to become a harder ligand than the $C_6H_5^-$ group. Therefore, the tin atom in $(p\text{-}Cl\text{-}C_6H_4)_3SnCl$ has more acceptor property than $(C_6H_5)_3SnCl$, and forms a more stable complex with the donors. Since the electron releasing group, CH_3, on the phenyl rings increases the electron releasing character of phenyl groups to the central tin atom (via induction, resonance, or both), the $(p\text{-}CH_3\text{-}C_6H_4)_3SnCl$ compound has less acceptor properties than $(C_6H_5)_3SnCl$ and hence, forms a less stable complex with the donors. On the basis of what has been described above, the following sequence can be proposed for the soft acid property of triaryltin chlorides which is confirmed with $\Delta G°$ (35°C) and K_{av} (35°C) values of the acceptors with Br^-:

$$(p\text{-}Cl\text{-}C_6H_4)_3SnCl < (C_6H_5)_3SnCl < (p\text{-}CH_3\text{-}C_6H_4)_3SnCl$$

$\Delta G°$ (kJ mol^{-1}) –11.70 : –10.96 : –10.37

K_{av} (M) 96.39 : 70.78 : 57.27

© 2001 NRC Canada

Table 4. $\Delta H°$ and $\Delta S°$ values for Ar_3SnCl with Cl^-, Br^- in 50% v/v ethanol–water solvent.

Ar_3SnCl	$\Delta S°$ (J K^{-1} mol^{-1})	$\Delta H°$ (kJ mol^{-1})
$Ar_3SnCl_2^-$		
p-Chlorophenyl	64.90 ± 2.38	9.20 ± 0.77
Phenyl	72.92 ± 2.51	12.25 ± 0.81
p-Tolyl	77.23 ± 3.29	14.16 ± 1.06
m-Tolyl	76.45 ± 4.55	14.01 ± 1.47
o-Tolyl	75.67 ± 1.79	14.19 ± 0.58
$Ar_3SnClBr^-$		
p-Chlorophenyl	71.23 ± 1.04	10.25 ± 0.33
Phenyl	76.78 ± 4.80	12.70 ± 1.55
p-Tolyl	91.62 ± 7.82	17.86 ± 2.52
m-Tolyl	87.60 ± 6.71	16.67 ± 2.17
o-Tolyl	79.10 ± 7.55	14.41 ± 2.44

In the case of $(p\text{-}CH_3C_6H_4)_3SnCl$, $(m\text{-}CH_3C_6H_4)_3SnCl$, and $(o\text{-}CH_3C_6H_4)_3SnCl$, the existence of a methyl electron-releasing group caused the increasing extent of charge transfer, as the result of hyperconjugation and inductive effects, from the π-orbitals of the benzene ring to the *d*-orbitals of the tin atom. Therefore these compounds have less acceptor properties than $(C_6H_5)_3SnCl$ and form less stable complexes with donors. But according to steric effects, the stability of complexes decreases with increases in steric effects. On the basis of what has been described above the following sequence can be proposed for the complex formation of triaryltin chlorides which is confirmed by $\Delta G°$ (35°C) and K_{av} (35°C) values of the acceptor with Br^-:

$$(p\text{-}CH_3\text{-}C_6H_4)_3SnCl > (m\text{-}CH_3\text{-}C_6H_4)_3SnCl > (o\text{-}CH_3\text{-}C_6H_4)_3SnCl$$

$\Delta G°$ (kJ mol^{-1}) –10.37 : –10.32 : –9.97

K_{av} (M) 57.27 : 54.86 : 47.79

Effect of donors

In this work we have two donors (Cl^-) and (Br^-). In Pearson's classification, (14) Cl^- is a hard base and Br^- is a borderline base. According to Pearson's rules (14) soft acids such as triaryltin chlorides form more a stable complex with the softer base, Br^-. As far as the Sn-Cl hydrolysis is concerned, no experimental evidence is accessible. It is believed that in solutions of the substrates in the presence of high concentrations of Cl^- or Br^- ions (≥10-fold in excess to the substrate) the hydrolysis is so slow that it does not intervene in the experiments. This is probably attributed to the lower absolute hardness (η) of Cl^- and Br^- with respect to H_2O (15, 16). On the basis of this description the following sequence was confirmed by $\Delta G°$ (35°C) and K_{av} (35°C) values for the interaction of $(C_6H_5)_3SnCl$ with Cl^- and Br^-:

$$(C_6H_5)_3SnCl\text{-}Br^- > (C_6H_5)_3SnCl\text{-}Cl^-$$

$\Delta G°$ (kJ mol^{-1}) –10.96 : –10.22

K_{av} (M) 70.78 : 53.76

Effect of solvent

In this work we have used 50% v/v ethanol–water solvent, which is a hard solvent. According to Ahrland (17), a hard solvent binds strongly with hard acceptors and donors. On the other hand this solvent forms weak bonds with soft acceptors and donors. The formation of a complex requires that the bonds between solvent molecules with the acceptor and the donor have to be broken. Therefore, complex formation with the softer donor, Br^-, is preferred. This is confirmed by $-\Delta G°$ (35°C) values of $(C_6H_5)_3SnCl$ with Cl^- and Br^- shown above.

The $\Delta H°$ value and its sign is dependent on two factors: one of these factors is the solvation effect; the other one is the heat of the formation of the complexes (17). The solvation effect for triaryltin chlorides is not important due to the neutrality of these compounds. Since the donor in our series of compounds is constant, the solvation effect is also constant. In the case of $(p\text{-}Cl\text{-}C_6H_4)_3SnCl$, $(C_6H_5)_3SnCl$, and $(p\text{-}CH_3\text{-}C_6H_4)_3SnCl$, the $\Delta H°$ values are predominantly governed by the heat of formation and the solubility of the complexes. Their values increase with increasing softness of the compounds. This is confirmed by the following $\Delta H°$ values of triaryltin chlorides with Br^-:

$$(p\text{-}Cl\text{-}C_6H_4)_3SnCl < (C_6H_5)_3SnCl < (p\text{-}CH_3\text{-}C_6H_4)_3SnCl$$

$\Delta H°$ (kJ mol^{-1}) 10.25 : 12.70 : 17.86

In the case of $(p\text{-}CH_3\text{-}C_6H_4)_3SnCl$, $(m\text{-}CH_3\text{-}C_6H_4)_3SnCl$, and $(o\text{-}CH_3\text{-}C_6H_4)_3SnCl$, according to the first and second factors and also the solubility of the complexes, the $\Delta H°$ values decrease with increasing solubility of the complexes. This is confirmed by the following $\Delta H°$ values of triaryltin chlorides with Br^-:

$$(p\text{-}CH_3\text{-}C_6H_4)_3SnCl > (m\text{-}CH_3\text{-}C_6H_4)_3SnCl > (o\text{-}CH_3\text{-}C_6H_4)_3SnCl$$

$\Delta H°$ (kJ mol^{-1}) 17.86 : 16.67 : 14.41

The K_{av} and $\Delta H°$ values signify that the complex formation between the acceptors and the Br^- ion is preferred, $\Delta H°$ values of the complexes with Br^- are higher than ones with Cl^-. This is confirmed by the following $\Delta H°$ values of triphenyltin chloride with Cl^- and Br^- ions:

$$(C_6H_5)_3SnCl\text{-}Br^- > (C_6H_5)_3SnCl\text{-}Cl^-$$

$\Delta H°$ (kJ mol^{-1}) 12.70 : 12.25

The $\Delta S°$ value and its sign is also dependent on two factors: one of these factors is the difference in the number of particles of the initial substances and the product complexes; the other one is the liberation of solvent molecules from the solvation shells (17). With respect to the first factor, the net entropy change is great and has a positive sign. The solvation effect and, therefore, the liberation of solvent molecules from the solvation shells for triaryltin chlorides is not an important factor, due to the neutrality of these compounds. Since the donor in our series is constant, the solvation effect is constant too. From the above description and also from

© 2001 NRC Canada

the solubility of the complexes, the following order of $\Delta S°$ values for aryltin complexes is confirmed:

$$(p\text{-Cl-}C_6H_4)_3SnCl < (C_6H_5)_3SnCl < (p\text{-}CH_3\text{-}C_6H_4)_3SnCl$$

$\Delta S°$ (J K^{-1} mol^{-1}) 71.23 : 76.78 : 91.62

$$(p\text{-}CH_3\text{-}C_6H_4)_3SnCl > (m\text{-}CH_3\text{-}C_6H_4)_3SnCl > (o\text{-}CH_3\text{-}C_6H_4)_3SnCl$$

$\Delta S°$ (J K^{-1} mol^{-1}) 91.62 : 87.60 : 79.10

As a matter of fact the complex formation between the acceptors and the Br^- ion is more favourable and due to the second factor, $\Delta S°$ values of the complexes with Br^- are higher than with Cl^-. This is confirmed by the following $\Delta S°$ values for $(C_6H_5)_3SnCl$ with Cl^- and Br^- ions:

$$(C_6H_5)_3SnCl\text{-}Br^- > (C_6H_5)_3SnCl\text{-}Cl^-$$

$\Delta S°$ (J K^{-1} mol^{-1}) 76.78 : 72.92

Conclusions

In this work efforts were made to provide a quantitative measure of the softness character of tin(IV) in some triaryltin chlorides, such as tri-*p*-, -*m*-, -*o*-tolyl, triphenyl, and tri-*p*-chlorophenyltin chlorides, through adduct formation with Cl^- and Br^- ions in 50% v/v ethanol–water. The stability constants and the thermodynamic parameters obtained spectrophotometrically have shown the following softness trend of R_3SnCl:

R = *p*-, *m*-, *o*-tolyl > phenyl > *p*-chlorophenyl

Acknowledgments

We are grateful to Shiraz University Research Council for their financial support.

References

1. M. Suzuki. Organometallics, **9**, 3047 (1990).
2. R. Hulme. J. Chem. Soc. 1524 (1963).
3. Y. Farhangi and D.P. Graddon. J. Organomet. Chem. **87**, 67 (1975).
4. J. Holecek, A. Lycka. Polyhedron, **6**, 1037 (1987).
5. H. Fujiwara, F. Sakai, and Y. Sasaki. Bull. Chem. Soc. Jpn. **58**, 1471 (1985).
6. K.A. Kocheshkov, M.M. Nad, and A.P. Alexandrov. Ber. Bunsen-Ges. **67**, 1348 (1934).
7. A. Stern and E.I. Becker. J. Org. Chem. **29**, 3224 (1964).
8. V.S. Griffiths and G.A.W. Derwish. J. Mol. Spectrosc. **3**, 165 (1959).
9. G. Eng and C.R. Dillard. Inorg. Chim. Acta, **31**, 228 (1978).
10. J.A.A. Ketelaar. Recl. Trav. Chim. Pays-Bas, **71**, 1104 (1952).
11. A.C. Sav, L.A. Carpino, and R.R. Holmes. J. Organomet. Chem. **197**, 181 (1980).
12. V.G. Kumer Das, L.K. Mum, and S.G. Blunden. J. Organomet. Chem. **334**, 307 (1987).
13. P.G. Harrison, K. Molloy, R. Philips, P.J. Smith, and A.J. Crowe. J. Organomet. Chem. **160**, 421 (1978).
14. R.G. Pearson. Science (Washington, D.C.), **151**, 172 (1966).
15. D. Dakternieks. J. Organomet. Chem. **476**, 33 (1994).
16. R.B. Jordan. Reaction mechanisms of inorganic and organometallic systems. Oxford University Press, New York. 1991. p. 47, 48.
17. S. Ahrland. Helv. Chim. Acta, **50**, 306 (1967).

© 2001 NRC Canada

Precipitation from alkaline aqueous aluminosilicate solutions

Michael R. North, M. Alejandra Fleischer, and Thomas W. Swaddle

Abstract: The longevity of metastable, highly alkaline Na and K aluminosilicate solutions has been examined over a wide range of Si/Al concentration ratios R ($0.04 \leq R \leq 20$) at 24°C and, in selected cases, at 50 and 75°C. In general, the longest solution lifetimes (t_{ppt}) (several weeks) were found at 24°C and for the highest alkalinities and (or) large R, but long t_{ppt} were also found for $R = 1.0$ at the lower alkalinities. Solution lifetimes generally shortened when the temperature was raised, but the opposite effect was observed with the smaller Al concentrations when $2 \leq R \leq 6$. These results are interpreted in terms of the requirement for ≡Si-OH groups for precipitate growth by condensation and of the relatively high solubility (few nuclei for gel growth) of the aluminosilicate solutes when $R = 1.0$.

Key Words: aluminosilicates, precipitation kinetics, aluminates, aqueous silicates, gelation, Bayer process, zeolite synthesis.

Résumé : Opérant à 24°C (et quelquefois à 50 et à 75°C) et à des rapports (R) de concentration de Si/Al allant de (0,04 à 20), on a déterminé la longévité de solutions métastables et fortement alcalines d'aluminosilicates de Na et de K. En général, les temps de vie en solution les plus longs, t_{ppt} (qui peuvent aller jusqu'à plusieurs semaines), sont observés à 24°C, avec les alcalinités les plus élevées et/ou des valeurs de R élevées; toutefois, aux alcalinités plus faibles, on a aussi observé des valeurs élevées de t_{ppt} lorsque $R = 1,0$. Une augmentation de la température a comme effet de raccourcir les temps de vie en solution; on a toutefois observé l'effet contraire à des concentrations plus faibles d'aluminium quand la valeur de R se situe entre 2 et 6. On interprète ces résultats en fonction de la taille des groupes ≡Si-OH sur la croissance du précipité par condensation et en fonction de la solubilité relativement élevée (peu de noyaux pour la croissance du gel) des solutés aluminosilicates quand $R = 1,0$.

Mots clés : aluminosilicates, cinétique de la précipitation, aluminates, silicates aqueux, gélation, processus de Bayer, synthèse de zéolites.

[Traduit par la Rédaction]

Introduction

Although aluminosilicates are generally very insoluble in water, metastable alkaline aluminosilicate solutions can be involved in many industrial processes (1); for example, in the Bayer process for refining bauxite for aluminum production (2, 3), scale formation in kraft papermaking (4), the setting of Portland cements (5), the exploitation of oil sands by steam injection (6), and the hydrothermal synthesis of zeolites (7–9). The mixing of alkaline aluminate and silicate solutions in particular concentrations typically brings about the formation of aluminosilicate gels (or, less commonly, granular precipitates) which, upon heating in contact with the supernatant solution, are converted to solid zeolites or related materials such as cancrinite (9). Gelation or precipitation may, however, be delayed for long periods depending upon the Al and Si concentrations, the pH, the temperature, and the nature of the cation(s) (10–13), with obvious implications for the carryover of Si in the Bayer process or aluminosilicate scaling. Like the parent aluminosilicate solutions, zeolites are themselves metastable, so that the solution-mediated synthesis of a particular zeolite is largely a matter of kinetic control, involving both the precipitation rate and the rates of silicate or aluminate exchange in the silicate and aluminosilicate solute species (14, 15).

Knowledge of the longevity of aluminosilicate solutions is therefore of intrinsic value, but has been of special interest to us as a prerequisite for study of the speciation and substitution kinetics of aqueous aluminosilicates by ^{29}Si or ^{27}Al NMR spectroscopy (1, 14, 15) for which the prepared solutions must remain stable over the often lengthy spectral accumulation times. For meaningful kinetic studies, it is necessary to limit the number of Si-containing solute species. This can be achieved by maintaining very high alkalinities and (or) elevated temperatures (1). The precipitation studies of Dent Glasser and Harvey (10–12) covered ambient-temperature cases in which the total alkali concentrations ranged up to 5 mol L^{-1} and the $[Si^{IV}]/[Al^{III}]$ ratio R varied from 1 to 8. We report here precipitation time measurements at 24°C for Na and K aluminosilicate solutions over extended ranges of pH with R values ranging from 0.04 to 20, and, in a few cases, at moderately elevated temperatures. These simple experiments involved noting the approximate time (t_{ppt})

Received August 8, 2000. Published on the NRC Research Press Web site on January 22, 2001.

M.R. North, M.A. Fleischer, and T.W. Swaddle.[1]
Department of Chemistry, University of Calgary, Calgary, AB T2N 1N4, Canada.

[1]Author to whom correspondence may be addressed.
Telephone: (403) 220-5358. Fax: (403) 284-1372.
e-mail: swaddle@ucalgary.ca

 DOI: 10.1139/cjc-79-1-75 © 2001 NRC Canada

elapsed between mixing aluminate and silicate solutions and the first visible signs (if any) of gel or precipitate formation. No detailed kinetic analysis was intended; nevertheless, some useful generalizations emerged.

Experimental

All solutions were handled in polyethylene or Teflon™-FEP containers. Amorphous silica was prepared by dropwise hydrolysis of freshly distilled silicon tetrachloride (Fisher Scientific, technical grade) in water. The resultant gel was dried, crushed, washed with water, and oven dried at 250°C. Sodium and potassium hydroxides (BDH assured ACS reagent grade) and high-purity aluminum (Spex) were used as received. Stock NaOH and KOH solutions were prepared by dissolving the hydroxide pellets in freshly degassed deionized water and standardized by titration with potassium hydrogen phthalate. Stock silicate and aluminate solutions were prepared by dissolving silica or aluminum in portions of the stock hydroxide solutions. The use of glassware, which can dissolve in and contaminate highly alkaline media, was strictly avoided.

Test solutions were prepared in Teflon™ tubes by mixing a weighed amount of silicate stock solution with a prepared aluminate solution, the alkalinity of which had been adjusted by mixing with a known amount of stock NaOH or KOH solution. Solution compositions are definitively expressed in terms of the initial concentrations of M_2O (M = K or Na), SiO_2, and Al_2O_3 in mol kg^{-1} of H_2O, the latter including H from all sources to avoid ambiguities arising from the unknown degrees of deprotonation of the hydroxosilicate species. Following mixing, the aluminosilicate solutions were shaken vigorously and sealed. Precipitation times (t_{ppt}) to the visible formation of either a granular precipitate or a gel were then noted with the solution samples either standing on the bench (24.0 ± 1.5°C) or immersed in a thermostat bath (50.0 or 75.0 ± 0.1°C).

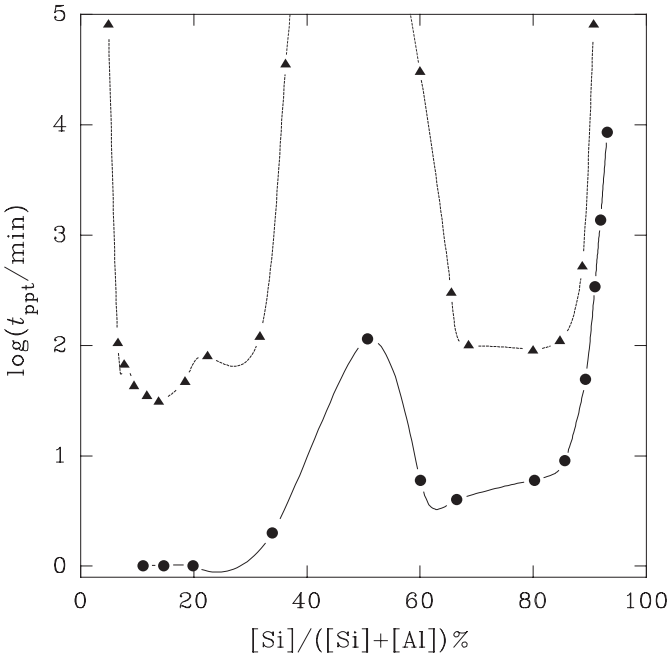
In some cases, the order of mixing the aluminate and silicate solutions was found to affect the measured t_{ppt}. The longer t_{ppt} were always obtained when the dominant reactant (silicate or aluminate) was added to the other, followed by thorough mixing. In the experiments described below, all solutions for which $R \geq 1.0$ were therefore prepared by adding the silicate solutions to the aluminate solutions, and vice versa for $R < 1.0$.

The Si-dominant side of each series was examined by preparing stock solutions of a fixed initial $[M_2O]$ and then performing a series of experiments at a constant $[Al_2O_3]$ while varying the [Si]/[Al] ratio R by varying $[SiO_2]$. In a similar fashion, the Al dominant side was explored by maintaining a constant $[SiO_2]$ while varying $[Al_2O_3]$. Alkali concentrations of 1, 3, 5, and 9 mol kg^{-1} K_2O, and 1, 3, 5, and 7 mol kg^{-1} Na_2O, were examined at room temperature at various concentrations of silicate and aluminate. A few experiments were also performed at 50 and 75°C with 5 mol kg^{-1} K_2O, and at 50°C with 5 mol kg^{-1} Na_2O.

Results and discussion

In general, the sodium solutions produced finely grained precipitates except at the lowest alkalinity studied ($[Na_2O]$ = 1.0 mol kg^{-1}) with $R \geq 1$, when massive gels were rapidly precipitated. The potassium solutions, however, gave gels except when $R > 6$. As the formation of identifiable crystalline products is known to require incubation at elevated temperatures (9, 12), no attempt was made to characterize the apparently amorphous precipitates formed at the relatively low temperatures of these experiments. Somewhat higher alkalinities were accessible with K^+ as the cation ($[K_2O]$ up to 9 mol kg^{-1}) than with Na^+ ($[Na_2O]$ up to 7 mol kg^{-1}). The salient features of the results are presented in Figs. 1–4, in which samples that formed permanent precipitates within the mixing time are arbitrarily given a precipitation time of 1 min.

Fig. 1. Dependence of log t_{ppt} on mol% Si for K^+ solutions with $[K_2O]$ = 3 mol kg^{-1} (●, solid curve) and 5 mol kg^{-1} (▲, dotted curve). For [Si]/([Al] + [Si]) ≤ 50%, [Si] = 0.1 mol kg^{-1}; for [Si]/([Al] + [Si]) ≥ 50%, [Al] = 0.1 mol kg^{-1}. Samples with 40–53 mol% Si at $[K_2O]$ = 5 mol kg^{-1} did not gel in 4 weeks at 24°C.



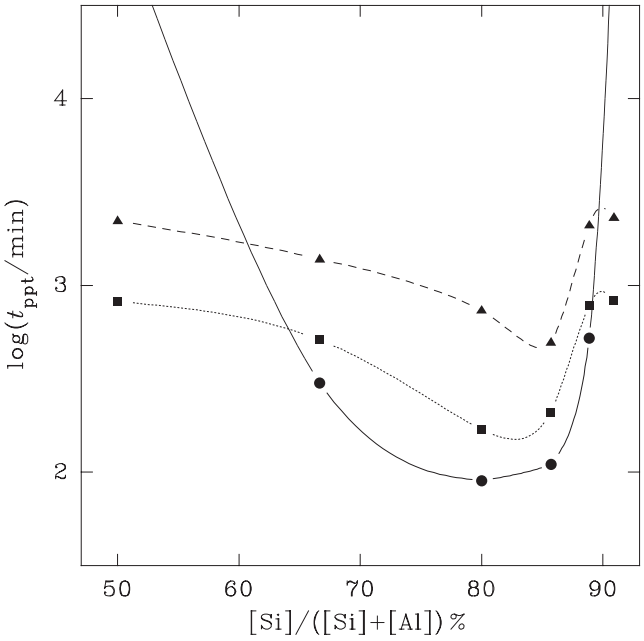
Potassium Solutions

Effect of alkalinity

It was generally found that t_{ppt} increased with increasing alkalinity. Silicate concentrations ranged from 0.1 to 4.0 mol kg^{-1} and $[Al_2O_3]$ from 0.05 to 1.0 mol kg^{-1} (i.e., [Al] from 0.1 to 2.0 mol kg^{-1}) and, at any particular [Si]/[Al] ratio R, t_{ppt} generally increased when the concentration of K_2O was increased (see, for example, the samples with R = 1 in Table 1). Dent Glasser and Harvey (10) noted that, although t_{ppt} for potassium aluminosilicate solutions with $1 \leq R \leq 3$ lengthened with increasing $[K_2O]$, t_{ppt} for samples with higher R and $[K_2O]$ up to 2.5 mol L^{-1} actually decreased with increasing alkalinity. This effect was also observed in the present study, but, at very high alkalinity (5 mol kg^{-1} K_2O or greater), t_{ppt} increased again, as can be seen in Table 1 for samples with R = 4 and 6.

© 2001 NRC Canada

Fig. 2. Dependence of log t_{ppt} on mol% Si and temperature for K^+ solutions with $[K_2O]$ = 5 and $[Al_2O_3]$ = 0.05 mol kg^{-1} at: (●, solid curve) 24°C; (▲, dashed curve) 50°C; (■, dotted curve) 75°C. Samples with 50 or ≥91 mol% Si did not gel in 4 weeks at 24°C.



Effect of [Si]/[Al] ratio

The variation of R at fixed concentrations of K_2O and either constant silicate or constant aluminate concentration had a pronounced effect on t_{ppt}, as shown in Fig. 1. Precipitation times passed through a local maximum for samples with R = 1.0, with the shortest t_{ppt} occurring at R = 0.25 and 4.0, that is, at 20 and 80 mol% Si, respectively, relative to mol (Si + Al). The nature of the precipitate was also found to vary with the R; solutions with more than ca. 85 mol% Si gave granular precipitates which settled out, whereas those of lower Si content tended to form gels, including cases where Al was dominant.

Figure 1 also shows that t_{ppt} increased on increasing $[K_2O]$ from 3 to 5 mol kg^{-1}. In accordance with this trend, gelation was faster at 1 mol kg^{-1} K_2O, whereas at 9 mol kg^{-1} K_2O no gelation was observed in over a month. Measurements with 9 mol kg^{-1} K_2O were restricted to the Si dominant side because stock aluminate solutions with $[Al_2O_3]$ > 0.3 mol kg^{-1} formed a white precipitate (presumably a potassium aluminate) during dissolution of the aluminum.

Although the Si-dominant side of Fig. 1 covers a wider range of $[K_2O]$ than the experiments of Dent Glasser and Harvey (10), trends in t_{ppt} when R was increased at a fixed $[K_2O]$ were similar. It was found that solutions with R > 10 and $[K_2O]$ > 3 mol kg^{-1} were indefinitely stable against gelation. In one instance in which $[K_2O]$ = 5, $[Al_2O_3]$ = 0.23, and R = 10, initial mixing gave immediate precipitation, but subsequent sonication of the sample for 1 h produced a solution which was indefinitely stable. At $[K_2O]$ = 3, however, it was found necessary to go to R = 19 to form an indefinitely stable solution.

It should be noted that although $[K_2O]$ does not change with R, the overall alkalinity does since as R increases the concentration of silicate increases, and therefore total alkalinity decreases.

Fig. 3. Dependence of log t_{ppt} on mol% Si for Na^+ solutions with $[Na_2O]$ = 1.0 mol kg^{-1} (●, solid curve), 3.0 mol kg^{-1} (△, short-dashed curve), 5.0 mol kg^{-1}(▼, long-dashed curve), and 7.0 mol kg^{-1}(□, dotted curve). For [Si]/([Al] + [Si]) ≤ 50%, [Si] = 0.05 mol kg^{-1}; for [Si]/([Al] + [Si]) ≥ 50%, [Al] = $2[Al_2O_3]$ = 0.05 mol kg^{-1}.

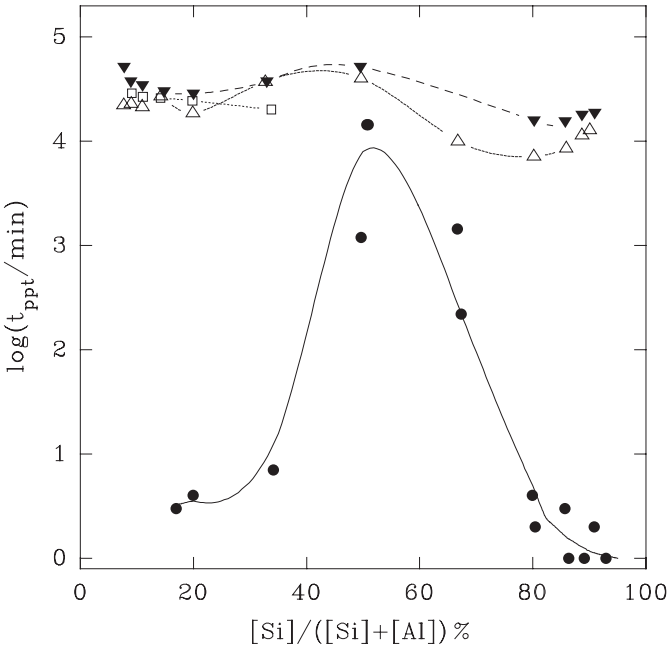
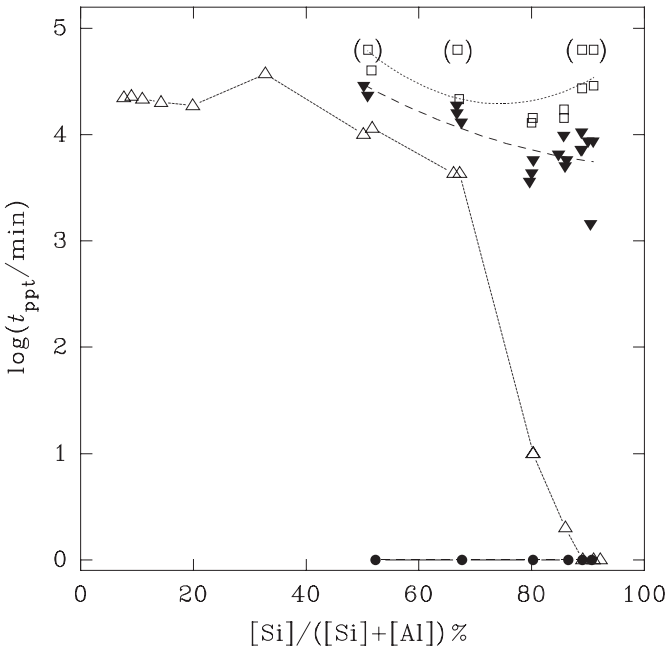


Fig. 4. Dependence of log t_{ppt} on mol% Si for Na^+ solutions as in Fig. 3, but with [Al] doubled. For [Si]/([Al] + [Si]) ≤ 50%, [Si] = 0.1 mol kg^{-1}; for [Si]/([Al] + [Si]) ≥ 50%, [Al] = $2[Al_2O_3]$ = 0.10 mol kg^{-1}. Legend as in Fig. 3. Symbols in parenthesis indicate that no precipitate was formed in 4 weeks.



© 2001 NRC Canada

Table 1. Precipitation times for K^+ solutions with $[Al_2O_3]$ = 0.05 mol kg^{-1}.

$[K_2O]$ (mol kg^{-1})	t_{ppt} (min) at: R = 1	R = 4	R = 6
1.0	2	7	120
3.0	122	6	9
5.0	> 4 × 10^4 [a]	90	110
9.0	> 4 × 10^4 [a]	> 4 × 10^4 [a]	> 4 × 10^4 [a]

[a]No precipitation in one month.

Effect of absolute concentration of silicate and aluminate

In most cases, increasing the absolute concentrations of total silicate and aluminate for a fixed R and K_2O concentration caused t_{gel} to decrease. This effect is shown in Table 2 for samples with R = 1.0.

It was noted above that, when [Si] and the Si/Al ratio were low, increasing the alkalinity retarded gelation. Table 2 shows that t_{gel} decreased as the absolute concentrations of Al and Si increased for any given concentration of K_2O, but, because the concentration of free alkali must also have decreased, it is unclear whether the shortened gelation times were due to the increasing [Al] and [Si] or to the decrease in alkalinity. By the same token, the "unexpected" behaviour noted by Dent Glasser and Harvey (10) for K^+ solutions with high Si:Al ratios, where t_{ppt} can, in some cases, be increased by decreasing the alkalinity, is also suggested by measurements at 5 mol kg^{-1} K_2O; thus, t_{ppt} for samples with $R \approx 8$ increased from ca. 9 h at $[Al_2O_3]$ = 0.05 mol kg^{-1} ($[SiO_2]$ = 0.8 mol kg^{-1}) to 96 h at $[Al_2O_3]$ = 0.1 mol kg^{-1} ($[SiO_2]$ = 1.6 mol kg^{-1}).

Effect of temperature

The effect of increasing the temperature on t_{ppt} was examined for a series of samples with [Si] > [Al] at $[K_2O]$ = 5 mol kg^{-1}. It was expected that gelation times would decrease with increasing temperature because of faster nucleation or gel growth kinetics, and this was certainly found to be the case at $[Al_2O_3]$ = 0.1 mol kg^{-1}, as shown in Table 3. Similarly, at the lower $[Al_2O_3]$ of 0.05 mol kg^{-1}, solutions with R = 1 and 10 that would have remained clear for over a month at 24°C formed precipitates in a few hours at 50 and 75°C. Surprisingly, however, for $2 \leq R \leq 6$ with $[Al_2O_3]$ = 0.05 mol kg^{-1}, t_{ppt} was shorter at 24°C than at 50°C; at 75°C, t_{ppt} was again longer than at room temperature, but still significantly shorter than at 50°C. These results are summarized in Fig. 2. The solids formed in these cases were of a granular nature rather than the usual gels.

Sodium solutions

The behavior of sodium solutions was broadly similar to that of their potassium analogues, but some significant differences were noted. Comparison of Figs. 1 and 3 shows that sodium aluminosilicate solutions with relatively low [Al] or [Si] (0.05 mol kg^{-1}) and alkalinity ($[Na_2O]$ = 1.0 mol kg^{-1}), exhibited an anomalous longevity for $R \approx 1$, like that of their potassium counterparts with higher concentrations. This phenomenon was much less evident, however, when $[Na_2O]$ was increased to 3.0 mol kg^{-1} or higher, in which case t_{ppt} remained fairly constant at around 2–3 weeks over a wide range of R and alkalinity. Indeed, the reproducibility of t_{ppt} at high alkalinities, evident in Fig. 3, is an encouraging measure of the validity of the simple experimental approach.

Table 2. Precipitation times for sample of varying concentrations of aluminate and silicate at a constant [Si]/[Al] ratio R of 1.0.

$[K_2O]$ (mol kg^{-1})	t_{ppt} (min) for $[Al_2O_3]$ (mol kg^{-1}) = 0.05	0.10	0.15	0.20	0.25
1.0	2	0*	0*	0*	0*
3.0	122	0	0*	0*	0*
5.0	> 4 ×10^4	21	5	0*	0*
9.0	> 4 ×10^4	> 4 ×10^4	> 4 ×10^4	3.5 × 10^4	100

*Inferred from results at lower concentrations.

Table 3. Temperature dependence of precipitation times (t_{ppt}) for $[K_2O]$ = 5.0 mol kg^{-1} and $[Al_2O_3]$ = 0.1 mol kg^{-1}.

temp (°C)	t_{ppt} (min) at: R = 1	R = 2	R = 4	R = 6
24	21	11	27	120
50	6	4	4	8

When [Al] was increased to 0.10 mol kg^{-1} on the Si-dominant side (Fig. 4), precipitation of massive gels occurred promptly on mixing at the lowest alkalinity studied ($[Na_2O]$ = 1.0 mol kg^{-1}) for all R values ≥1, and on a time scale of minutes at moderate alkalinity ($[Na_2O]$ = 3.0 mol kg^{-1}) for $R \geq 4$, but, at higher alkalinities, the solutions were consistently long lived (several days to longer than four weeks). In particular, the conspicuous minima in t_{ppt} noted for K^+ solutions of comparable concentrations of alkali and reactants (Fig. 1) were much diminished or arguably absent (Fig. 4). For Na^+ solutions with R = 1, t_{ppt} was short when the alkalinity was low and [Al] was high.

Conclusions

In general, long solution lifetimes are favored by high $[Na_2O]$ or $[K_2O]$. This is attributable to the reduced numbers of ≡Si-OH functions in monomeric or oligomeric silicate ions as the alkalinity is increased, since the formation of a gel or precipitate via condensation reaction [1] requires the availability of ≡Si-OH groups (which are subject to deprotonation at high alkalinity) as well as ≡Al-OH (which are not) (15).

[1] ≡Al-OH + HO-Si≡ → ≡Al-O-Si≡ + H_2O

Reaction [1] also leads to the expectation that the precipitation process will be at least first order in each of [Si] and [Al], so that long solution lifetimes should be expected for high alkalinities and low reactant concentrations. This is borne out by the data of Table 1. Gelation times generally decreased with increasing absolute concentrations of silicate and aluminate. It is difficult, however, to distinguish the effect of increasing [Si] or [Al], as such, from that of the concomitant decrease in alkalinity because formation of silicate and aluminate ions from SiO_2 and Al_2O_3, respectively consumes OH^- (by an indefinite amount, in the former case).

© 2001 NRC Canada

We have shown elsewhere (15) that silicate and aluminosilicate ring or cage structures are much less reactive in condensation processes in solution than their small acyclic analogues. This is due partly to steric constraints, and partly to the reduced number of ≡Si-OH functions available in cyclic silicate anions. The long lifetimes of solutions with high [Si] (>5, right-hand side of Fig. 1) and hence high concentrations of cyclic oligomers (16, 17) can be understood on this basis. For Na^+ solutions, a similar but less pronounced effect can be discerned in Figs. 3 and 4. Solutions with very low [Al] can also be expected to be long lived, as the precipitation process can be viewed as the result of the insertion of Al into an extended silicate structure that would otherwise be soluble. According to Loewenstein's rule (18), Al—O—Al links are avoided in solid aluminosilicates, and presumably this will limit the ready formation of aluminosilicate precipitates to solutions where $R \geq 1.0$. The left-hand half of Fig. 4 is consistent with this expectation, as is the extreme left of Fig. 1.

It is less obvious, however, why there should be a local maximum in solution lifetimes at $R = 1$ for K^+ solutions (Fig. 1) and, at least at low alkalinity and low [Al], for Na^+ solutions also (Fig. 3, cf. Fig. 4). Probably, for $R \approx 1$, most of the Al and Si are present as the ions $(HO)_3AlOSiO_n(OH)_{(3-n)}^{(n+1)^-}$ (n = 1–3), which seem to be capable of existing in stable solution in substantial concentrations at high pH. Significantly, the precipitates that eventually formed from either K^+ or Na^+ aluminosilicate solutions at $R = 1.0$ were granular rather than gel-like, and further growth was slow, consistent with the view that $(HO)_3AlOSiO_n(OH)_{(3-n)}^{(n+1)^-}$ ions, though probably the major vehicles of growth of aluminosilicate precipitates (15), are themselves quite soluble indefinitely in NaOH or KOH media and provide few nuclei for gel growth.

For the most part, increasing the temperature resulted in faster precipitation from both Na^+ and K^+ aluminosilicate solutions. However, the gelation times of the less concentrated aluminosilicate solutions (i.e., $[Al_2O_3] = 0.05$ mol kg^{-1} with $2 \leq R \leq 6$) increased when the temperature was raised to 50°C, but decreased again when the temperature was increased further to 75°C (Fig. 2). Because of the interdependence of the several variables, a definitive assessment of the effect of temperature on t_{ppt} is probably not feasible, but it may be that the anomalous behaviour of the K^+ solutions containing less Al resulted from a reduction in the numbers of gel nuclei at 50°C because of increased solubility, hence retarding precipitation. The "unexpected" behavior of certain K^+ solutions first noted by Dent Glasser and Harvey (10; see above) may similarly have originated in a trade-off between numbers of nuclei and growth rates. The absence of parallel effects for Na^+ solutions is consistent with solubility as the cause of these phenomena. At the higher temperature of 75°C, the increased rate of gel growth may compensate for the reduction in numbers of nuclei and, thus, gelation times begin to decrease again. In any event, these observations imply that aluminosilicates may persist long enough in solution at high temperature and alkalinities to cause significant Si carryover in the Bayer process and to cause scaling in various industrial applications.

Acknowledgments

We thank Dr. E. Vallazza for some preliminary investigations, and the Natural Sciences and Engineering Research Council of Canada for financial support.

References

1. T.W. Swaddle, J. Salerno, and P.A. Tregloan. Chem. Soc. Rev. **23**, 319 (1994).
2. K. Zheng, R. St.C. Smart, J. Addai-Mensah, and A. Gerson. J. Chem. Eng. Data, **43**, 312 (1998).
3. F. King. Aluminium and its alloys. Wiley, Chichester. 1987. pp. 39–44.
4. H.A. Gasteiger, W.J. Frederick, and R.C. Streisel. Ind. Eng. Chem. Res. **31**, 1183 (1992).
5. P. Faucon, A. Delagrave, J.C. Petit, C. Richet, J.M. Marchand, and H. Zanni. J. Phys. Chem. B, **103**, 7796 (1999).
6. P.R. Tremaine, E.E. Isaacs, and J.A. Boon. Chem. Can. 29 (April 1983).
7. H. Kessler. *In* Solid state supramolecular chemistry. *Edited by* G. Alberti and T. Bein. Elsevier, Tarrytown, New York. 1996. pp. 425–464.
8. S.L. Burkett and M.E. Davis. *In* Solid state supramolecular chemistry. *Edited by* G. Alberti and T. Bein. Elsevier, Tarrytown, New York. 1996. pp. 465–483.
9. R.M. Barrer. Hydrothermal chemistry of zeolites. Academic Press, New York. 1982.
10. L.S. Dent Glasser and G. Harvey. J. Chem. Soc. Chem. Commun. 664 (1984).
11. L.S. Dent Glasser and G. Harvey. J. Chem. Soc. Chem. Commun. 1250 (1984).
12. G. Harvey and L.S. Dent Glasser. *In* Zeolite synthesis. *Edited by* M.L. Occelli and H.E. Robson. ACS Symposium Series 398, American Chemical Society, Washington, D.C. 1989. pp. 49–65.
13. E. Vallazza and T.W. Swaddle. Unpublished observations.
14. E. Vallazza, A.D. Bain, and T.W. Swaddle. Can. J. Chem. **76**, 183 (1998).
15. M.R. North and T.W. Swaddle. Inorg. Chem. **39**, 2661 (2000).
16. S.D. Kinrade and T.W. Swaddle. Inorg. Chem. **27**, 4253 (1988).
17. R.K. Harris, E.K.F. Bahlmann, K. Metcalfe, and E.G. Smith. Magn. Reson. Chem. **31**, 743 (1993).
18. W. Loewenstein. Am. Mineral. **39**, 92 (1954).

© 2001 NRC Canada

Excess electrons in aqueous glasses and crystalline ice

Hugh A. Gillis and Terence I. Quickenden

Abstract: Experimental studies of excess electrons in aqueous glasses and crystalline ice are reviewed. Emphasis is placed on studies of the two main optical absorption bands, the well known visible band, which is similar to that of the solvated electron in water, and the IR band which has $\lambda_{max} \geq 2950$ nm. Under some circumstances partial conversion of the IR-absorbing species to the visible-absorbing species has been observed. Evidence indicates that the two species are due to electrons trapped in distinctly different physical environments. Two mechanisms have been proposed for the formation of the visible-absorbing electron in crystalline ice, one involving naturally occurring vacancies and the other radiation produced vacancies. Studies of the UV and visible luminescence emitted when ice at low temperature is irradiated are summarized, and the mechanisms suggested for its production are discussed briefly. The studies on excess electrons in aqueous solids seem to the authors to be highly relevant to the more recent studies of electron solvation in water which are done on a much shorter time-scale. These latter studies are reviewed briefly with the aim of elucidating the relevance.

Key words: visible-absorbing electrons, IR-absorbing electrons, irradiation of aqueous glasses, irradiation of crystalline ice, electron solvation in water.

Résumé : On présente une revue des études expérimentales sur les électrons en excès dans des verres aqueux et dans de la glace cristalline. On met l'emphase sur les études des deux principales bandes d'absorption optique, la bande visible bien connue, qui est semblable à celle de l'électron solvaté dans l'eau et la bande infrarouge dont le $\lambda_{max} \geq$ 2950 nm. Dans certaines circonstances, on peut observer une conversion partielle des espèces qui absorbent dans l'infrarouge en espèces qui absorbent dans le visible. Les données indiquent que les deux espèces sont dues à des électrons piégés dans des environnements physiques différents. Deux mécanismes ont été proposés pour la formation de l'électron absorbant dans le visible dans la glace cristalline; l'une implique les vides qui existent normalement et l'autre ceux qui sont produits par des rayonnements. On présente un résumé des études faites sur la luminescence ultraviolette et visible émise quand on irradie de la glace à basse température et on discute brièvement des mécanismes suggérés pour sa production. Pour les auteurs, il semble que les études sur les électrons en excès dans des solides aqueux sont très pertinentes aux études plus récentes sur la solvatation des électrons dans l'eau qui s'effectue à une échelle de temps beaucoup plus courte. On passe brièvement ces dernières études en revue dans le but d'élucider leur pertinence.

Mots clés : électrons absorbant dans le visible, électrons absorbant dans l'infrarouge, irradiation de verres aqueux, irradiation de la glace cristalline, solvatation des électrons dans l'eau.

[Traduit par la Rédaction]

Introduction

Ever since the solvated electron was identified as the chemical species responsible for the blue colour of solutions of sodium in liquid ammonia (1), it has aroused great interest. This interest is due not only to its important role in radiation chemistry, photochemistry, and electrochemistry, but also because it is a very useful probe of solvent environment and solvation dynamics. The electron can be solvated in solid and liquid water, and in a wide variety of organic liquids and solids such as hydrocarbons, ethers, and alcohols.

Many studies of the solvated electron have been concerned with the dynamics of its formation, i.e., with the processes that take place between the injection of a quasi-free electron into a liquid or solid and the appearance of the comparatively stable solvated electron. The first time-resolved optical absorption studies of electron solvation were conducted in alcohols. Nanosecond pulse radiolysis studies of liquid and glassy alcohols at low temperatures showed an initial absorption in the IR due to trapped electrons (2). Subsequently, the absorption peak shifts continuously to the final spectrum with a peak in the 500–800 nm range; this shift is a reflection of the continuous adjustment of the solvent surrounding the electron to its presence. However, a stepwise mechanism is possible, particularly because the first-order decay observed in the IR corresponds quite well with

Received June 23, 2000. Published on the NRC Research Press Web site on January 24, 2001.

H.A. Gillis[1] and T.I. Quickenden. Department of Chemistry, The University of Western Australia, Nedlands WA 6907, Australia.

[1]Author to whom correspondence may be addressed. Permanent address: St. Francis Xavier University, Antigonish, NS B2G 2W5, Canada. Telephone: (902) 867-2124. Fax: (902) 867-2177. e-mail: hgillis@stfx.ca

 DOI: 10.1139/cjc-79-1-80 © 2001 NRC Canada

the absorption build-up at 550 nm for cold liquid *n*-propyl alcohol (2). A hybrid model has been proposed for electron solvation in methanol at room temperature (3); this involves two electron-solvent configuration states (a weakly bound and a strongly bound one) both of which relax via a continuous shift and between which there is a stepwise transfer.

This review is concerned primarily with excess electrons trapped in aqueous glasses and crystalline ice. These electrons do not show the dramatic shift of a single peak as seen in alcohols; however, they give two well separated absorption bands, and under some circumstances, weakly bound electrons are converted to strongly bound electrons. In the review emphasis is placed on evidence which indicates that the bands are due to electrons trapped in distinctly different environments, and on results which tell us something about those environments. Many of the papers reviewed reported optical absorption studies, but relevant studies of reactions of quasi-free electrons in ice followed by conductivity are also reviewed briefly, as is work on the luminescence emitted when aqueous glasses and ice are irradiated. Much of the work reviewed was done 20–25 years ago, though some has been reported in the past five years. In the opinion of the authors, this work is highly relevant to the current intense activity on the dynamics of the solvation of the electron in water, although it has been largely ignored in papers on this subject. The formation kinetics of the hydrated electron is covered briefly in this review with the aim of elucidating the relevance.

Aqueous glasses

In this section we emphasize the electron absorption band in the IR which is found in some aqueous glasses. The electron that gives the visible absorption band is very similar to the hydrated electron. From the dependence of the ratio of intensities of the two bands on the water content of glasses it was concluded that the IR band is due to an electron trapped in free water (not coordinated to ions or organic molecules), whereas the visible band is trapped in an environment of coordinated water. The two types of electron decay by different mechanisms, and decay of the IR-absorbing species in some glasses is accompanied by growth of the visible-absorbing species.

Visible band

It was first reported in 1962 that γ-irradiated aqueous NaOH glasses at 77 K give an optical absorption with λ_{max} near 585 nm (4, 5); subsequent work showed that the absorption was due to a trapped electron. In this review this species will be referred to as e^-_{vis}. Early work on it has been extensively reviewed (6).

Several published reports show that there is structure in the e^-_{vis} band. Pulse radiolysis studies of several aqueous glasses at ~76 K show that the band is considerably broader and has λ_{max} at longer wavelengths at short times ($<10^{-6}$ s) than at long times or in γ-irradiation experiments (7–9). This broadening is due to increased absorption on the red side of the band. As time elapses absorption at $\lambda > 575$ nm decays while absorption at $\lambda < 575$ nm remains constant or increases, and these changes account for the narrower and blue-shifted spectrum seen in γ-irradiation.

Substructure in the equilibrated e^-_{vis} band (after decay of the red wing) in aq BeF_2 glasses is seen in photobleaching experiments (10). A green band (λ_{max} 530–590 nm) seems to be bleached homogeneously, whereas the red side of the equilibrated e^-_{vis} band seems to bleach inhomogeneously as if it arises from electrons with a range of ground state energies.

Rice et al. (11) have shown that comparison of the photoconductivity spectra of trapped electrons with their optical absorption spectra leads to information about the nature of the optical transitions involved in the absorption band. Some aqueous glasses such as 10 M NaOH show a similar wavelength dependence of photoconductivity and optical absorption spectra for e^-_{vis} which implies the dominance of bound–continuum transitions. For other systems, such as 10 M LiCl, the photoconductivity spectra are somewhat blue-shifted from the absorption spectra; this indicates dominance of bound–bound transitions in the main part of the spectrum and dominance of bound–continuum transitions in the high-energy tail. Nguyen and Walker (12) made a careful measurement of the percentage of bound–continuum character in the optical transition at 694 nm for e^-_{vis} in aq 9.5 M LiCl glass at 77 K and found it to be (3.7 ± 1.8)%. Therefore, about 96% of the transition probability at this wavelength must be to bound excited states. This measurement took account of the number of photoreleased electrons which are retrapped and of those electrons which are bleached by indirect secondary processes.

Detailed geometric information on e^-_{vis} in aqueous glasses has come from various types of electron magnetic resonance studies (13, 14). The electron is shown to be surrounded by six approximately equivalent water molecules, with one OH of each molecule oriented towards the electron. The water molecules are thought to be in an octahedral arrangement. This geometry was originally established for an aq 10 M NaOH glass, but later work showed the same structure for e^-_{vis} in a matrix with less than 10^{-3} M NaOH formed by codepositing sodium atoms and water vapour. Thus the geometric structure proposed does not seem to require the presence of a high concentration of ions.

IR band

Blandamer et al. (15) produced e^-_{vis} by γ-irradiation of an aqueous alkali–metal hydroxide glass at 77 K, bleached it with visible light so that the band with λ_{max} at ~590 nm disappeared and found a new, broad absorption edge, strong in the near-IR and red parts of the spectrum and tailing into the visible. Kevan et al. (16) reported that for γ-irradiation of 10 M NaOH glasses at 77 K to doses greater than 10 Mrad, the trapped electron absorption at 585 nm decreases and a broad band grows in the near-IR with a maximum at approximately 1000 nm. The IR band was attributed to the dielectron; two electrons trapped in the same vacancy. A γ-irradiated mixture of ethylene glycol and water (50:50 by volume) at temperatures ≤30 K showed increasing absorption from 1200 nm out to at least 2000 nm, in addition to the well-known peak in the visible (17). Transient absorption at 1152 nm was produced by photoexcitation of the visible-absorbing trapped electron in some aqueous glasses with a ruby laser pulse (18). In 1976, Buxton et al. (9) reported finding an IR absorption band with a maximum beyond

© 2001 NRC Canada

Fig. 1. Absorption spectra observed at 76 K and 100 ns after the start of a 40 ns pulse in: (*A*) 50:50 v/v ethylene glycol/D_2O glass; (*B*) 9.5 M LiCl glass; and (*C*) 2.5 or 4.0 $MgCl_2$ glass. Spectrum *A* has been displaced upwards by 0.5 unit. From ref. 9.

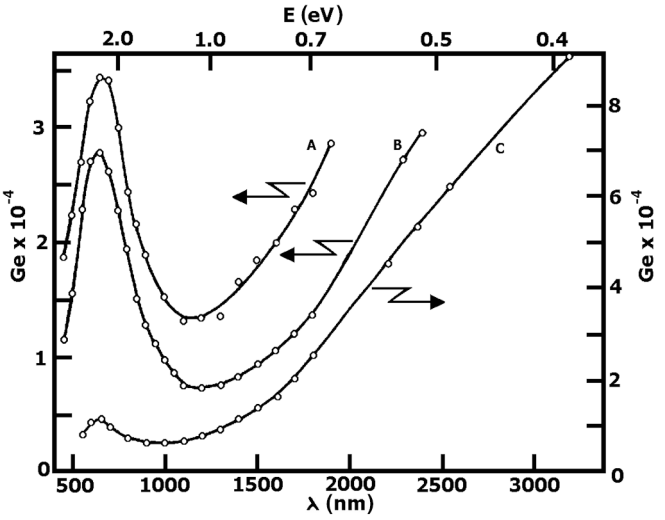
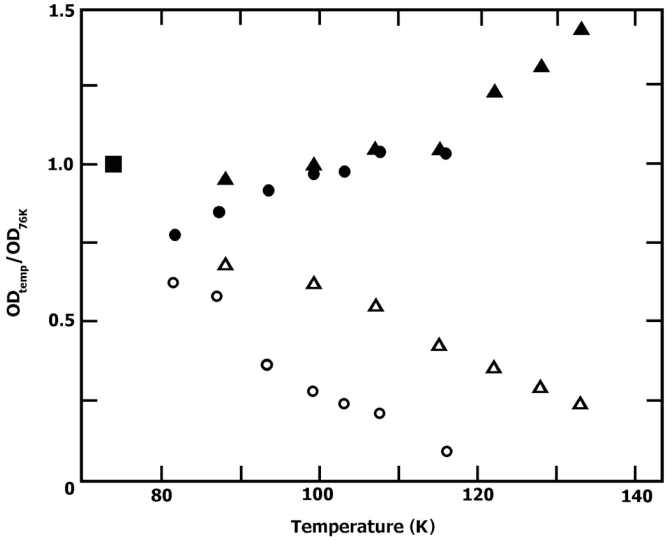


Fig. 2. Effect of temperature on the relative initial intensities of the visible and IR bands: LiCl, 2360 nm (○); LiCl, 650 nm (●); $MgCl_2$, 2360 nm (△); $MgCl_2$, 650 nm (▲); and one point common to all (■). From ref. 9.



3200 nm in the pulse radiolysis of D_2O glasses of ethylene glycol, $MgCl_2$, and LiCl, as well as the trapped electron band with a maximum around 650 nm. Because of the effects of electron scavengers on the IR band, they assigned it also to a trapped electron which they referred to as e^-_{ir}. We shall use the same nomenclature in this article. Absorbance per krad (1 rad = 10^{-2} Gy) at 2360 nm was found to be the same for 5 and 0.5 krad pulses, which strongly suggests that the band is not due to a dielectron. Later, e^-_{ir} was found also in H_2O glasses (19), but the species has been studied mainly in deuterated systems because of their greater transparency in the 1200–3200 nm range. Matrix absorption bands in this region in H_2O arising from overtones and combinations of the fundamental vibrational modes are shifted to higher wavelengths by deuterium substitution.

The absorption spectra observed in three aqueous glasses at about 73 K are shown in Fig. 1. The band due to e^-_{vis} and the partial band attributed to e^-_{ir} are quite distinct although they overlap in the 800–1300 nm region. The effects of temperature, electron scavengers, and glass composition on the two bands are different, and the bands decay at different rates (9). These facts indicate that the spectra refer to different species, and also permit the resolution of the bands in the overlap region.

The resolved IR band closely fits a Lorentzian function on the high energy side (9), and in this respect is similar to spectra observed by Jou and Dorfman (20) for solvated electrons in several ethers. The Lorentzian fit predicts λ_{max} to be 3600 nm for $MgCl_2$ glasses. For *tert*-butanol–D_2O glasses, for which 2500 nm was the highest wavelength at which measurements could be made, a similar Lorentzian fit gives λ = 4350 nm (21). The difference between these two extrapolated values of λ_{max} may not be significant.

Other aqueous glasses in which the IR band was found, in addition to the LiCl, $MgCl_2$, ethylene glycol, and *tert*-butanol glasses already indicated, are BeF_2 and LiBr (10), alkaline glasses (NaOD, KOD, RbOD, and CsOD) at 6 K but not at 76 K (22), $CaCl_2$ (23), and probably a 26.5 mol% H_2O–ethanol glass at 6 K (24). Aqueous glasses at 6 K in which an IR band was looked for and not found are: K_2CO_3, NaO_2CH, $NaClO_4$, $Mg(CH_3CO_2)_2$, and $Mg(ClO_4)_2$ (9). It is not known why the IR band is found in some glasses and not in others; however, Nguyen and Walker (25) concluded that e^-_{ir} is destroyed, or its formation is inhibited, by many of the solutes which are commonly used to make aqueous glasses. They came to this conclusion after studying mixed-solute glasses, specifically using $MgCl_2$ glasses with $CaCl_2$, $Mg(ClO_4)_2$, or ethylene glycol added as a second solute.

The decay of the IR band in ethylene glycol, LiCl, and $MgCl_2$ glasses at 76 K was independent of λ for λ > 1400 nm (9), but of course the decay of the red edge of the band or even of the maximum of the band was not measured.

The photoconductivity spectrum of e^-_{ir} is significantly blue-shifted from its absorption spectrum (11). This implies that e^-_{ir} has bound–bound transitions dominating in the region of the extrapolated optical absorption maximum, and bound–continuum transitions dominating in the high-energy tail of the spectrum (11).

Effects of temperature and scavengers on e^-_{vis} and e^-_{ir}

The effects of increasing the temperature of LiCl and $MgCl_2$ glasses on the intensities of the visible and IR absorption bands are shown in Fig. 2. The IR band steadily decreases in intensity while the visible band remains practically constant up to 120 K and then increases. Part of the decrease in intensity of the IR band is due to faster decay at higher temperatures, which results in more decay before the first measurement at about 100 ns. However, in the $MgCl_2$ glass this effect was negligible up to 114 K.

Buxton et al. (9) found that CrO_4^{2-} or acetone decreased the initial intensities of both e^-_{ir} and e^-_{vis} bands in aq LiCl, $MgCl_2$, and ethylene glycol glasses at 76 K, but the fractional decrease was always greater for e^-_{ir}. They found the addition of HCl to LiCl and $MgCl_2$ glasses scarcely affected

© 2001 NRC Canada

the intensity of either band. The addition of Ag^+ to an aqueous ethylene glycol glass decreased the initial intensities of the e^-_{vis} and e^-_{ir} bands, and a band due to Ag° was produced. In steady-state experiments Rice et al. (11) used nitrate as an electron scavenger for trapped electrons in aqueous 10 M LiCl glasses at 4.2 K, and found that the e^-_{ir} band was reduced much more markedly than the e^-_{vis} band. If electron scavengers merely intercepted quasi-free electrons before they became trapped in deep or shallow traps, their effect on the initial yields of e^-_{ir} and e^-_{vis} would be the same. A possible explanation of the greater reduction in e^-_{ir} yields is the formation of encounter pairs in which the electrons are trapped within the reaction volume of the scavenger and react before detection; the effect is expected to be much more important for shallowly trapped electrons then for deeply trapped ones (9).

Extinction coefficient for e^-_{ir}

The extinction coefficient for e^-_{ir} was determined from the experiments with Ag^+ in a 50:50 aqueous ethylene glycol glass (9). Measurements of the yields of Ag° and its extinction coefficient, and of the decrease in initial yields of e^-_{ir} and e^-_{vis}, and the known extinction coefficient of e^-_{vis} led to a calculated $\varepsilon_{1400} = (5.7 \pm 0.8) \times 10^3\ M^{-1}\ cm^{-1}$ which is convertible into $\varepsilon_{1800} = (1.08 \pm 0.15) \times 10^4\ M^{-1}\ cm^{-1}$. A similar procedure for estimating the extinction coefficient for e^-_{ir} from the irradiation of a 45:55 ethylene glycol–D_2O matrix with 0.01 M sodium salicylate at 6 K gave $\varepsilon_{1800} = (1.3 \pm 0.3) \times 10^4\ M^{-1}\ cm^{-1}$ (26). Another determination came from the photoionization of tryptophan in a 9.5 M LiCl–D_2O glass at 76 K, and it gave $\varepsilon_{1800} = 1.3 \times 10^4\ M^{-1}\ cm^{-1}$ (27). It is reassuring that similar extinction coefficients were found for e^-_{ir} for different glasses and temperatures.

Dependence of $G(e^-_{ir})/G(e^-_{vis})$ on glass composition

For aq LiCl (28), ethylene glycol (26), and BeF_2 glasses (10) at 76 K, increasing the concentration of the nonaqueous component decreases the ratio $G(e^-_{ir})/G(e^-_{vis})$ and to a good approximation does not change the sum $(G(e^-_{ir}) + G(e^-_{vis}))$. The same is true for ethylene glycol glasses at 6 K (26). For D_2O–KOD glasses irradiated at 6 K, the effect of increasing D_2O content is also to increase $G(e^-_{ir})$ and decrease $G(e^-_{vis})$ (22). This trend is not followed by aqueous *tert*-butanol glasses at 72 K, nor at 6 K (21). However, in the latter glasses e^-_{vis} is produced in very small yields even at 72 K, and possibly some of the absorption attributed to e^-_{ir} is due instead to electrons trapped in a glassy *tert*-butanol environment (21).

Studies by NMR techniques of the structure of LiCl glasses indicate that they consist of $(Li{\cdot}4H_2O)^+Cl^-$ units, with water in excess of that required to form $(Li{\cdot}4H_2O)^+$ existing as clusters of free water (not coordinated to ions) packed interstitially between the $(Li{\cdot}4H_2O)^+$ units, and probably amorphous rather than ice-like (29). The simple model proposed was that e^-_{ir} is an electron trapped in free water and e^-_{vis} is an electron trapped in $LiCl{\cdot}4D_2O$ structures, and that these preexisting trapping sites are in competition for quasi-free electrons which would otherwise recombine with geminate positive holes (28). A plot of $G(e^-_{ir})/G(e^-_{vis})$ against [free D_2O]/[$LiCl{\cdot}D_2O$] gives a straight line as expected from this model. This model should apply also to BeF_2 and ethylene glycol glasses.

Yields of e^-_{vis} and e^-_{ir} were measured in LiCl glasses at temperatures between 6 K and 72 K (21, 23, 27, 30, 31). If the model described above were strictly true, yields of the two species would not change much in this temperature range since the ratio of concentrations of the two kinds of traps would not be expected to change in these rigid matrices. However, as the temperature is decreased from 72 K the yields of e^-_{vis} decrease modestly, $(G(e^-_{ir}) + G(e^-_{vis}))$ increases modestly, and yields of e^-_{ir} increase dramatically, especially for the glasses with the highest concentrations of LiCl, that is, those with the lowest yields of e^-_{ir} at 76 K. Most of the results can be explained by adding to the model the assumption that there is an activation energy for electron trapping by deep traps which is slightly larger (perhaps 50–100 cal mol^{-1} larger (1 cal = 4.1868 J)) than any activation energy for trapping by shallow traps or for geminate reaction by quasi-free electrons with holes. This activation energy difference would have no effect at 76 K so that at this temperature the yields of e^-_{vis} and e^-_{ir} would simply reflect the relative numbers of deep and shallow traps available, but of course would have a large effect at 6 K.

Similar effects are seen when the temperature of aqueous ethylene glycol glasses is decreased from 72 to 6 K, i.e., $G(e^-_{ir})$ increases, $G(e^-_{vis})$ decreases, and $(G(e^-_{ir}) + G(e^-_{vis}))$ increases (26).

Bartczak et al. (32) have proposed a model to explain qualitatively the yields of e^-_{ir} and e^-_{vis} in aqueous ionic glasses. This model is based on the lattice theory of concentrated ionic solutions which assumes that the ions form distorted lattices and water molecules fill up empty regions in the lattices. Bartczak et al. (32) suggest that e^-_{ir} is an electron trapped at a cation in the distorted lattice. Because of the repulsive effects of the nearest neighbouring anions this trap is very shallow or even has no bonding level. The trap depth decreases with increased salt concentration, which explains the effects described above of salt concentration on $G(e^-_{ir})$. The model also gives a shallower trap for Na^+ than for Li^+, and no trap at all for K^+ glasses at 72 K, though e^-_{ir} has been seen in K^+ glasses at 6 K. Also, traps in Ca^{2+} glasses are predicted not to be bonding, as contrasted to traps in Mg^{2+} glasses. Measured yields of e^-_{ir} in $MgCl_2$ glasses at 80 K are much larger than for $CaCl_2$ glasses at the same temperature and concentration (23). This model is only applicable to e^-_{ir} in ionic aqueous glasses, and does not deal with this species in aqueous ethylene glycol, *tert*-butanol, or other alcohol glasses, nor with e^-_{ir} in crystalline ice.

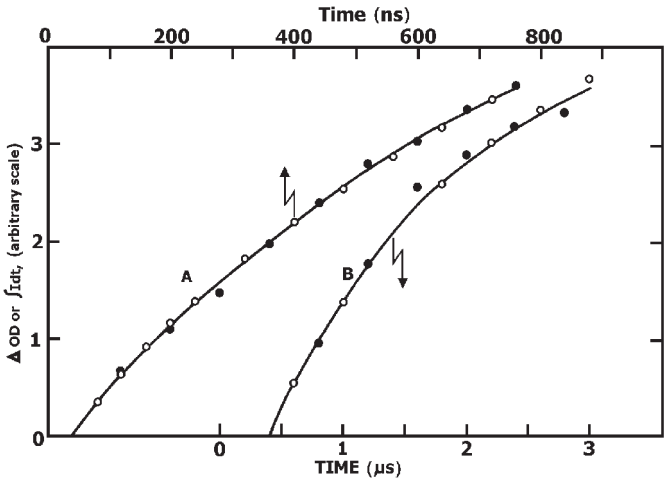
According to the model of Bartczak et al. (32), electrons can also be trapped at anion vacancies; these are deep traps and the electron in one of these traps is e^-_{vis}. Just as for cationic traps, when the nearest neighbours are Li^+ the traps are deeper than when they are Na^+, but the difference is now negligible by comparison with the total trapping energy. This picture of e^-_{vis} seems to be incompatible with the geometric description of e^-_{vis} deduced by Kevan (13, 33) and Kevan and co-workers (14), that is given earlier in this article, that is, that the electron has six water molecules as nearest neighbours.

Decay reactions of e^-_{vis} and e^-_{ir}

In LiCl glasses at 76 K over a wide range of LiCl concentrations, e^-_{vis} decays after 100 ns almost entirely by reaction

© 2001 NRC Canada

Fig. 3. Comparison of the change with time in: IR absorption (–ΔOD (●)) measured at 2350 nm, and integrated emission intensity; $\int I dt$ (○), measured at 425 nm after a 40 ns pulse in 2.5 M $MgCl_2$ glass at: 76 K (*A*); and 102 K (*B*). From ref. 9.



with Cl_2^-, both in the absence of light and during photobleaching (34). Reaction with Cl_2^- is not an important reaction for e_{ir}^- in these glasses.

Pulse radiolysis of LiCl and $MgCl_2$ glasses at 72 K results in light emission which persists after the pulse (9). The spectrum of the emission was found to have a maximum at about 410 nm. The reciprocal of the emission intensity is approximately linear in time. In Fig. 3 the change in optical density due in e_{ir}^- over a given period of time is compared to the integrated intensity of emitted light over the same period of time. The two correspond very closely after a normalization of the ordinate scale, and this correspondence was found to hold for both LiCl and $MgCl_2$ glasses, regardless of temperature. The correlation holds also in the presence of electron scavengers, even though in the case of $MgCl_2$ glasses e_{ir}^- decays more rapidly in the presence of these scavengers. No postpulse emission was detected at temperatures at which the IR band was absent, nor was it observed when 1 M acetone was added to a $MgCl_2$ glass to eliminate the IR band.

The correlation suggests that electron-hole recombination is mainly responsible for the decay of e_{ir}^-, and that recombination is the rate-determining step in the emission process, that is, that the emitting excited state is relatively short-lived (about 20 ns (12)). Tachiya and Mozumder (35) developed a model for geminate-ion recombination by tunnelling. For an exponential distribution of distances between reactants which give a short-lived luminescing product giving light intensity (*I*) in media in which the electron mobility is low, they derived the approximate relationship:

$$[1] \qquad I = k_1 t^{-1}$$

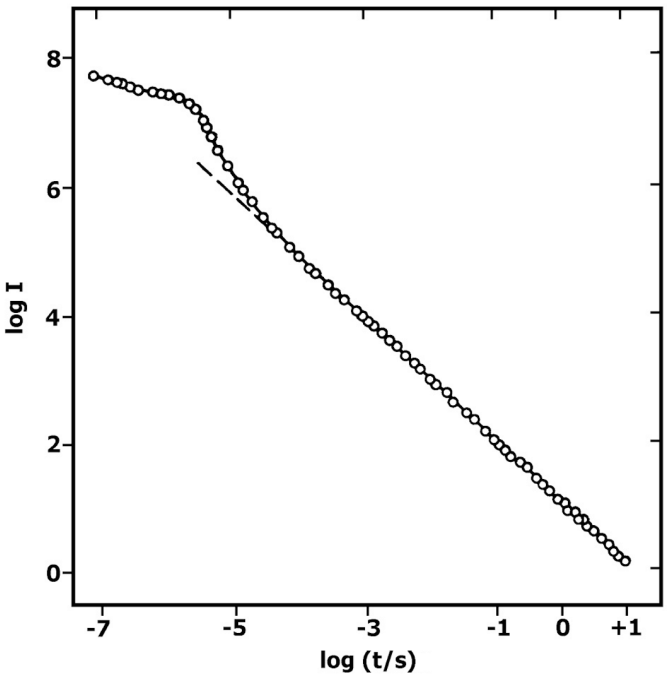
If *I* is also given by

$$[2] \qquad I = k_2 \frac{d}{dt}[e_{ir}^-]$$

it follows that

$$[3] \qquad [e_{ir}^-] = -k_3 \log t + \text{constant}$$

Fig. 4. Light emission at 450 nm from laser excitation of γ-irradiated 9.5 M LiCl glass at 77 K, plotted as the logarithm of the luminescence intensity (in arbitrary units) against the logarithm of time after the laser pulse. From ref. 37.



Buxton et al. (9) found eq. [1] was followed in their experiments, and that $[e_{ir}^-]$ was approximately linear with the logarithm of time over two and a half decades, in accordance with eq. [3].

Wypych and Kroh (36) similarly found good correlations between the change in optical density due to e_{ir}^- and the integrated intensity of emission for LiCl glasses at 6 K, 50 K, and 110 K, for $MgCl_2$ glasses at 6 K and 50 K, and for $CaCl_2$ glasses at 6 K; however, they found the integrated emission intensity correlates better with the change in optical density of e_{vis}^- for $CaCl_2$ glasses at 50 K and 110 K. It is worth noting that for $CaCl_2$ glasses $G(e_{ir}^-)$ is very low and $G(e_{vis}^-)$ is high at 110 K, and even at 50 K the ratio $G(e_{ir}^-)/G(e_{vis}^-)$ is much smaller for $CaCl_2$ glass than for the other two glasses.

When samples of trapped electrons in 9.5 M LiCl and 3.1 M $MgCl_2$ aqueous glasses were bleached by single pulses of 694 nm light from a Q-switched ruby laser, e_{ir}^- was produced and luminescence with λ_{max} around 410 nm was observed (37). The luminescence intensity was measured over eight decades of time (100 ns to 10 s) following the laser pulse. Over much of this period the intensity was inversely proportional to time, just as it was in the pulse radiolysis experiments with these glasses. The interpretation of the experiments is summarized as follows:

$$[4] \qquad e_{vis}^- \xrightarrow{h\gamma} e_{ir}^- \xrightarrow{R} R^{-*} \longrightarrow R^- + h\gamma(\sim 410 \text{ nm})$$

It has been suggested that the reaction centre R of eq. [4] is OH, so that the emission seen would then be fluorescence from excited hydroxide ions (9).

© 2001 NRC Canada

A plot of the logarithm of luminescence intensity (in arbitrary units) from a 9.5 M LiCl glass at 73 K against the logarithm of time after the laser pulse is shown as Fig. 4. Corrections were made for emission from a blank. The bulge for the period 10^{-7}–10^{-5} s after the pulse, corresponding to extra luminescence, is thought to arise from additional, laser-induced fluorescent processes. The straight-line part of the curve has a slope of –0.95, so that eq. [1] is obeyed quite well over six orders of magnitude in time.

Crystalline ice

In this section evidence is reviewed which indicates that e^-_{vis} in crystalline ice is an electron in a lattice vacancy, which is present at significant equilibrium concentration for $T \geq -30$°C or is produced by irradiation. The IR band may be due to electrons trapped in natural cavities that exist in perfect crystals of ice. The rates of decay of e^-_{vis} and e^-_{ir} are affected differently by changes in initial concentration, doping with NH_4F, preirradiation, and temperature, and these observations lead to suggestions for the decay reactions of both species. There is very little direct evidence for the transition $e^-_{ir} \rightarrow e^-_{vis}$ in ice, but the present authors interpret delayed formation of e^-_{vis} after irradiation of ice at –5°C as being due to this reaction.

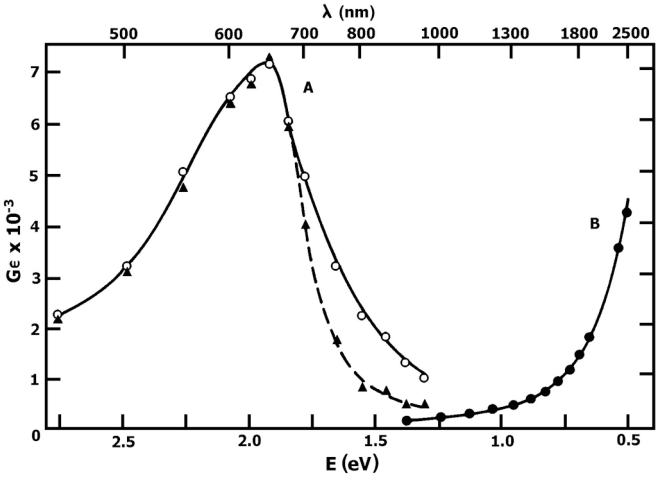
Introduction

The absorption spectrum of electrons produced by pulse radiolysis of crystalline ice at 200, 235, and 263 K was first reported by Shubin et al. (38), who found a λ_{max} similar to that of the solvated electron in water. A short time later a similar trapped electron spectrum in γ-irradiated ice at 77 K was reported by Eiben and Taub (39) and the spectrum in pulse-irradiated ice at various temperatures was reported by Taub and Eiben (40) and Nilsson et al. (41). The half-width of the peak is smaller in ice than in water (41). Taub and Eiben (40) found that the absorption maximum for ice shifts towards the blue with decreasing temperature, and that on a plot of λ_{max} against temperature for both ice and water, the solid-phase line intercepts the liquid-phase line near the freezing point. The absence of a discontinuity indicates strongly that the electron in ice and the electron in water are the same species.

In the early studies the yields of the trapped electron in pulse-irradiated ice were found to decrease markedly with decrease in temperature from –5 to –40°C, but only slowly thereafter (40, 41). Pulse lengths in these experiments were in the range 0.4–200 μs. The *G* (trapped electron) for γ-irradiated ice at 77 K was only about 2×10^{-4}, and a rough pulse experiment at this temperature gave an approximately three-fold larger yield (40). The *G* at –5°C was estimated as 0.3 as a lower limit (40), and at –10°C as 0.3 (41).

Kawabata et al. (42) reported on a pulse radiolysis study of crystalline D_2O ice at 123 K. They found, in addition to the visible band with a peak around 630 nm due to trapped electrons, a broad IR absorption with a peak at 1000 nm which they ascribed to electrons in a shallow trap. Ice doped with 10^{-2} M NH_4F gave higher yields and slower decays for both bands. Absorbance in the visible band increased by about 10% in the first 0.4 ms after the pulse, while the IR absorption was decaying. At longer times the visible band also showed some decay.

Fig. 5. Absorption spectra at 76 K in crystalline D_2O ice. For the visible band (*A*), points were measured at the end of a 30 ns pulse. Points ▲ refer to measurements made 400 ns after the start of the pulse and multiplied by 1.90. For the IR band (*B*), the line is a Lorentzian curve fitted to the experimental points ●, which refer to the end of a 30 ns pulse and were obtained by a short extrapolation from 100 ns. Points for both bands between 1.0 and 1.5 eV have been corrected for contributions from the other band (see text). From ref. 44.



e^-_{vis} and e^-_{ir}

Buxton et al. (43, 44) in a pulse radiolysis study of crystalline D_2O ice over a range of temperatures, found an intense IR absorption band with $\lambda > 2350$ nm, in addition to the well known visible absorption band of the trapped electron. These bands seemed to be similar in some respects to the bands they found in aqueous glasses, so they referred to them also as e^-_{vis} and e^-_{ir}. This convention will also be used in this article.

Absorption spectra for irradiated D_2O ice are shown in Fig. 5. The low-energy side of the e^-_{vis} band decays much faster than the band as a whole. The band-width at half-height is 0.75 and 0.67 eV at 30 ns and 400 ns, respectively. The band-width following γ-irradiation is about 0.58 eV, so further narrowing occurs after 400 ns. The spectrum of irradiated NH_4F-doped (~4×10^{-3} M) crystalline D_2O was found to be very similar to that shown in Fig. 5 but for the doped sample the lifetime of the IR band is much longer than that of the visible band. This permits resolution of the spectrum into two bands, and the points shown in Fig. 5 for both bands at energies between 1.0 and 1.5 eV were obtained in this way.

The experimental points for the e^-_{ir} band fit a Lorentzian function very well; the best fit, shown by the line for band B in Fig. 5, predicts $\lambda_{max} = 2950$ nm. As indicated above, the Lorentzian fit for the e^-_{ir} band for a $MgCl_2$ glass at 76 K gives a predicted λ_{max} of 3600 nm, but this difference may not be experimentally significant. At 151 K the e^-_{ir} band has the same shape as band B of Fig. 5. The visible band at the end of the pulse at 151 K is intermediate between the 30 ns

© 2001 NRC Canada

and 400 ns points of band A in Fig. 5, as expected because of the faster decay of the red edge at the higher temperature.

Effects of dose/pulse and solutes for ice at 76 K

$G\varepsilon$ for both bands was constant within experimental error (±10%) for a variation of dose/pulse at a constant pulse width. The range of dose/pulse was a factor of 8.1 for measurements of e^-_{vis} (45) and 4.5 for measurements of e^-_{ir} (44).

The yields of e^-_{vis} changed little when ice was doped with NH_4F, but those of e^-_{ir} increased strongly with concentration of NH_4F and the decay rate decreased markedly, as indicated in Fig. 6. For a crystal doped with 6.7×10^{-4} M NH_4F, the decay of e^-_{ir} had a half-life of about 25 ms. The effect of accumulated dose on yields of the two types of electrons in pure ice was small, but a previous irradiation of 180 krad doubled the yield of e^-_{ir} for a sample doped with 1.5×10^{-2} M NH_4F and had only a small effect on e^-_{vis} yields.

Decay kinetics for e^-_{vis} and e^-_{ir}

The decay of e^-_{vis} in pure D_2O ice at 76 K does not obey simple first- or second-order kinetics. However, a plot of $OD/(OD)_0$ (where OD_0 is OD at mid-pulse, obtained by extrapolation) against time gives the same curve for a four-fold variation of initial concentration. This strongly suggests that e^-_{vis} decays by reaction with a geminate partner. By contrast, the half-life for decay of e^-_{ir} depends strongly on dose, and therefore, on initial concentration. Figure 6 shows that for previously unirradiated samples at 76 K, the initial decay follows second-order kinetics although deviations from second-order occur at later times. More significantly, the initial slopes for the second-order plots are the same within experimental error for a four-fold variation in initial concentrations. This means that e^-_{ir} and its reaction partner are homogeneously distributed. At higher temperatures (up to 149 K) the half-life for decay of e^-_{ir} still depends strongly on the dose per pulse, though it seems the concentration of e^-_{ir} is always lower than that of its reaction partner (45).

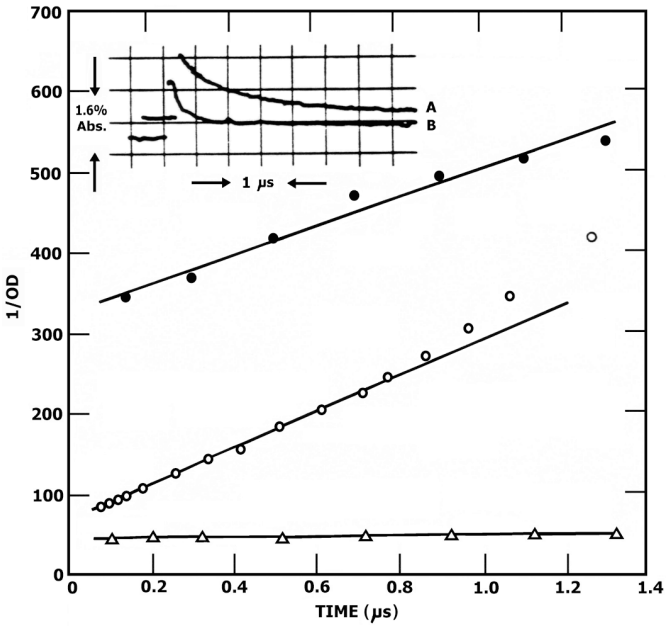
The most likely decay reaction of e^-_{ir} which accounts for homogeneous second-order kinetics in previously unirradiated pure ice is neutralization by D_2O^+:

$$[5] \qquad e^-_{ir} + D_2O^+ \rightarrow D_2O \text{ or } D + OD + \square$$

where $\square$ is a vacancy. This requires that e^-_{qf}, the quasi-free electron which is the precursor of e^-_{ir}, is trapped sufficiently far from the site of ionization that e^-_{ir} has a homogeneous distribution with respect to D_2O^+. In view of the high mobility of e^-_{qf}, this requirement is probably met.

The long life-time of e^-_{ir} ($t_{1/2} \cong 25$ ms) in NH_4F-doped crystals at 73 K implies that it has a low mobility; a mobile e^-_{ir} would be expected to react quickly with trapped OD radicals, for example. However, the second-order rate constant at 73 K is calculated as 4×10^{12} M^{-1} s^{-1} from the straight line for pure ice of Fig. 6 and an estimated extinction coefficient for e^-_{ir} at 2350 nm (see below) (44). This rate constant corresponds to a sum of mobilities of e^-_{ir} and its reaction partner of 1.1×10^{-2} cm^2 V^{-1} s^{-1} (44), which seems reasonable for D_2O^+ moving by a resonant charge transfer process. The mobility of D_3O^+ has been measured as only 1×10^{-3} cm^2 V^{-1} s^{-1} at 95 K and should be rather similar at 73 K (46), so e^-_{ir} is probably not decaying by reaction with D_3O^+.

Fig. 6. Decay of absorption at 2350 nm in crystalline D_2O at 76 K, without additives (○) and (●), and doped with 9.6×10^{-4} M NH_4F (△). All three curves are for the first pulse for a sample. Inset: *A*, oscilloscope trace of absorption at 2350 nm for a previously unirradiated crystal without additives at 76 K; *B*, oscilloscope trace of absorption at 2350 nm for a pure crystal that had received an accumulated dose of 100 krads. From ref. 44.



In ice at a nominal temperature of 6 K (the heat input from the pulse increases the temperature momentarily to an observed 13 K), e^-_{ir} undergoes geminate decay, probably by a tunnelling mechanism (47). Two explanations may be offered for the difference from the second-order decay at 73 K and higher temperatures: (*i*) the Onsager radius, that is, the distance from a charged particle at which the Coulombic energy is equal to kT, is much greater at 6 K than at 73 K; and (*ii*) the rate of geminate recombination might be much slower at 6 K so that we observe geminate electrons that would have disappeared before the shortest observation time at 73 K. In keeping with these ideas, for previously unirradiated samples $G(e^-_{ir})$ is estimated to almost triple when the temperature is lowered from 73 to 6 K.

Preirradiation of crystalline D_2O at a nominal 6 K results in a large increase in $G(e^-_{ir})$, as seen in Fig. 7 (47). This effect may be annealed by heating; Fig. 7 shows the decrease of the preirradiation effect brought about by annealing to two temperatures. The effect was completely eliminated by heating to 120 K. It was proposed that the effect of accumulated dose on ice at 6 K is due to the buildup of products which can trap mobile D_2O^+, the most significant of which is probably the D atom which can react as follows:

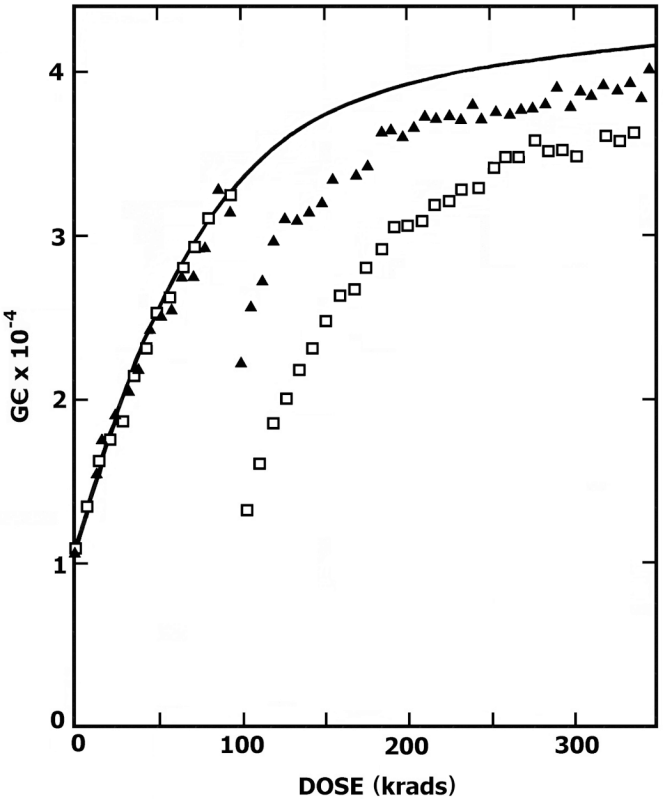
$$[6] \qquad D + D_2O^+ \rightarrow D_3O^+$$

Reaction [6] would compete with a very rapid recombination of the quasi-free electron (e^-_{qf}) with the geminate positive ion

$$[7] \qquad e^-_{qf} + D_2O^+ \rightarrow D_2O^*$$

© 2001 NRC Canada

Fig. 7. *G*ε per pulse as a function of previous dose for pure crystalline D_2O at 6 K, measured at 2350 nm 100 ns after the start of a 40 ns pulse. ▲, sample heated to 12.5 K after 95 krads; □, sample heated to 100 K after 95 krads. Solid curve is a line drawn through the points for a sample with no heating. From ref. 47.



and hence favour the trapping of e^-_{qf}:

[8] e^-_{qf} + ir-trap → e^-_{ir}

Trapped hydrogen atoms in irradiated ice have been found to react over a large temperature range; some react slowly at 60 K whereas others react rapidly at 15 K (48); however, no hydrogen atoms are stabilized at 73 K, so it was proposed that product OD radicals can undergo a reaction similar to rxn. [6]:

[9] $OD + D_2O^+ \rightarrow D_3O^+_2$

This would account for the necessity to heat ice to a temperature at which OD radicals become mobile, about 110 K, to restore a crystal to its original condition.

Nature of trap for e^-_{vis}

The results on the visible band absorption can be interpreted on the basis that it is due to electrons trapped in vacancies in the crystal lattice, but there are two distinctly different origins of these vacancies. At 76 K these vacancies do not exist before a crystal has been irradiated, as indicated by the following calculation. The equilibrium concentration of vacancies at any temperature may be calculated from the Boltzmann equation if the energy required to form a vacancy is known. Estimates of this quantity are 0.3–0.4 eV from the rate of self-diffusion in ice (49) and 0.28 ± 0.07 eV from an investigation of the annealing behavior of γ-irradiated ice by positron annihilation techniques (50). As a crystal is cooled down, a temperature will be reached at which vacancies become frozen in, that is, equilibrium is no longer attained. Radiation-produced vacancies become mobile and disappear in the region of 100–120 K (50, 51) and therefore they must be at equilibrium concentrations at higher temperatures. The maximum concentration of vacancies in unirradiated ice at 76 K is that calculated for 120 K by assuming the heat of formation is 0.3 eV, and that concentration is about 1.3×10^{-11} M. For a pulse typical of those used to obtain the data of Fig. 5, the concentration of e^-_{vis} at the end of the pulse was about 2×10^{-6} M, so the concentration of preexisting vacancies at 76 K is not high enough to account for the results.

Irradiation of ice produces vacancies (50, 52). The following mechanism was proposed as the origin of e^-_{vis} at low temperature (44):

[10] $2D_2O \rightarrow (2D_2O^+ + 2\ e^-_{qf})$

[11] $(2D_2O^+ + 2e^-_{qf}) \rightarrow (D + OD + D_2O^+ + e^-_{qf} + \square)$

[12] $(e^-_{qf} + \square) \rightarrow e^-_{vis}$

Here parentheses around reactants are intended to indicate that the reaction takes place in a spur. Reaction [11] is a neutralization reaction that produces the vacancy, and rxn. [12] is the trapping of a quasi-free electron in the same spur. $G(e^-_{vis})$ in D_2O ice around 76 K was reported as ~0.4 (44) and ~0.6 (53); the latter determination was done with a shorter pulse (6 ns) and is presumably better. These yields mean that 10–15% of e^-_{qf} become e^-_{vis}. This seems plausible for the mechanism proposed since the percentage of spurs containing two or more ion pairs in which the successive rxns. [11] and [12] would occur is expected to be rather low.

The narrowing of the visible absorption band with time, as seen in Fig. 5, is easily explained in terms of a vacancy model. If one water molecule is removed from the tetrahedral structure of ice and an electron occupies this vacancy, then protons from only two of the four water molecules in the first shell point towards the electron. Calculations of the optical transition energy for an electron in a vacancy in ice agree with experiment only if two of the molecules at the corners of the tetrahedron can rotate so that four O—H bonds point to the center, and by assuming also that the OH bond length and the H-O-H angles can change from their values in the perfect crystal (54). Therefore, the narrowing of the visible band seen in Fig. 5 is likely a reflection of the orientation of the OD dipoles and (or) a preferential decay of the less stably trapped electrons.

e^-_{vis} and e^-_{ir} in H_2O ice

Both e^-_{vis} and e^-_{ir} are seen in H_2O ice at temperatures of 6 and 73 K (19). The biggest isotope effect seen is in the lifetime of e^-_{vis}. In D_2O ice around 77 K, $t_{1/2}$ for e^-_{vis} is about 120 ns, and in H_2O ice at the same temperature it is 8 ns (53). Several pieces of evidence indicate that the decay occurs in a spur. The decay reaction is not a reaction with OH; it may be migration of H_3O^+ to e^-_{vis} followed by reaction (53). At 6 K in D_2O ice $t_{1/2}$ for e^-_{vis} decay is about 5 μs (53) and in H_2O ice it is ≤75 ns (19). Thus, the ratio of half-lives

© 2001 NRC Canada

is very high at about 15 around 77 K and ≥67 at 6 K. The fast decay of e^-_{vis} at temperatures around 77 K, especially in H_2O ice, accounts for the very low yields of e^-_{vis} seen in early pulse experiments on ice which used 0.4–200 μs pulses.

e^-_{vis} at temperatures near 273 K

At these higher temperatures e^-_{vis} no longer decays predominantly by geminate recombination as it does at lower temperatures. Rather, the initial half-life for decay depends strongly on the dose in the pulse. A strong dependence of yield of e^-_{vis} in crystalline D_2O at temperatures between 244 and 273 K on dose per pulse has been found (45, 55). This suggests that the precursor of e^-_{vis}, that is, the quasi-free electron e^-_{qf}, undergoes a competition between dropping into a trap such as a vacancy (□) to form e^-_{vis}, or reaction with a radiation product which we designate as X:

[13] $e^-_{qf} + \square \rightarrow e^-_{vis}$

[14] $e^-_{qf} + X \rightarrow$ no e^-_{vis}

It follows that

$$[15] \quad \frac{1}{G(e^-_{vis})} = \frac{1}{G(e^-_{qf})} + \frac{k_{14}[X]}{G(e^-_{qf})\,k_{13}[\square]}$$

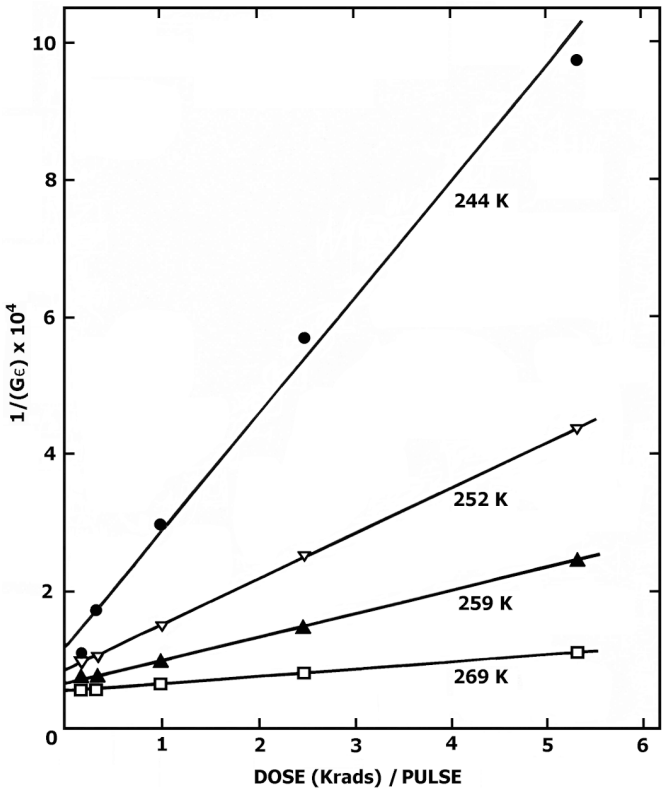
For [X] = a*i*, where *i* is the current during the pulse and a is a proportionality constant

$$[16] \quad \frac{1}{G(e^-_{vis})} = \frac{1}{G(e^-_{qf})} + \frac{k_{14}ai}{G(e^-_{qf})\,k_{13}[\square]}$$

Equation [16] indicates that a plot of $1/G(e^-_{vis})$ or $1/G(e^-_{vis})\varepsilon$ against *i* or dose per pulse for constant pulse length should be a straight line, and Fig. 8 shows that in fact for 40 ns reasonably linear plots are obtained for temperatures between 244 and 269 K. A plot of log (intercept/slope) for the plots of Fig. 8 against $1/T$ gives a reasonably straight line, from the slope of which the Arrhenius parameter *E* was calculated as 0.46 eV. This *E* should be close to the heat of formation of a vacancy, and agrees reasonably with literature values for this quantity (45).

Warman and co-workers (56, 57) irradiated H_2O ice with 25 ps electron pulses and found an absorbing species produced immediately in the pulse, which they designated as species X. They also found the e^-_{vis} absorption spectrum which grew in over a few hundred ps at –5°C. The spectrum of species X is similar to that of e^-_{vis} except that it shows relatively greater absorption on the red side of λ_{max}. Its yield ($G\varepsilon_{660} \cong 9 \times 10^3$) at –5°C is approximately the same as that reported at 80 K (53). Species X is most likely the same as e^-_{vis} seen at 73 K. Warman et al. (57) measured $k = 1.2 \times 10^9\ s^{-1}$ for the decay of this species at 245 K (this rate constant means that species X could not have been seen in the nanosecond pulse radiolysis experiments of Buxton et al. (44)). Combination of this rate constant with $t_{1/2} = 8$ ns (53) for e^-_{vis} in H_2O ice at 80 K gives an activation energy of 27 meV, which is not greatly different from that of 20 meV measured by Kawabata et al. (53) between 80 and 100 K. The similar yields for species X at –5°C and e^-_{vis} near 80 K at first seems surprising in view of the report by Buxton et al. (44) that the yield of e^-_{vis} in D_2O decreases as temperature is increased from 73 to 200 K; however, the apparent decrease is likely due to the limited response time of detection. The measurements for $t_{1/2}$ of e^-_{vis} in D_2O ice by Kawabata et al. (53) of 120 ns at 80 K and 76 ns at 100 K suggest that the yields measured by Buxton et al. (44) at temperatures above 73 K were not initial yields.

Fig. 8. Reciprocals of yields of e^-_{vis} in pure crystalline D_2O, measured at 650 nm, as a function of dose per pulse at different temperatures. The pulse length was 40 ns. From ref. 45.



Warman et al. (57) suggested that species X or low-temperature e^-_{vis} seen by them and Buxton et al. (44) might be an exciton state rather than e^-_{vis}. However, Kawabata et al. (53) found that the decay of e^-_{vis} at 80 K follows Hummel's (58) empirical equation for decay by geminate ion recombination in a spur, and they reported other pieces of evidence which indicate that decay occurs in a spur. We believe that the weight of evidence strongly suggests that species X (which is the same as the low-temperature e^-_{vis}) and e^-_{vis} which grows in over a few hundred picoseconds in ice near 0°C are essentially the same species, though they are produced by different mechanisms, and this species is very similar to the hydrated electron.

Warman et al. (57) found that the build-up of visible absorption could be described by the following reaction scheme:

[17] $H_2O \rightarrow e^-, H_3O^+, X$

[18] $e^- + H_3O^+ \xrightarrow{k_R} H_2O + H$

[19] $e^- + T \xrightarrow{k_T N_T} e^-_T$

© 2001 NRC Canada

[20] $e_T^- \xrightarrow{k_{rel}} e_{sol}^-$

[21] $X \xrightarrow{k_X}$ products

Reaction [19] is the reaction of a quasi-free electron with a naturally occurring trap, and reaction [20] is that of a trapped electron to give a solvated (hydrated) electron. The values of k_R and $k_T N_T$ were determined from conductivity measurements (see below) and, as indicated above, k_X was found to be 1.2×10^9 s^{-1}. The growth curves in the temperature range –5 to –30°C were fitted to give $G\varepsilon$ and k_{rel}. The values found for $G\varepsilon$ are in good agreement with those reported by Nilsson and Pagsberg (55) and Gillis et al. (45), and k_{rel} was found to be 2.2×10^9 s^{-1} at –5°C. The absolute magnitude of k_{rel} is much larger than would be expected on the basis of the bulk dielectric relaxation time for fixed charge.

By doping ice with NH_4F, Warman et al. (57) were able to observe clearly the initial decrease in absorption at λ_{max} of 660 nm followed by growth of absorption due to rxn. [20] (e_{sol}^- is e_{vis}^- in our terminology). This separation of the timescales of decay and growth is good evidence that species X is not a direct precursor of e_{vis}^-. It is unfortunate that these authors did not extend their wavelength range beyond 1000 nm, to attempt the measure the spectrum of e_T^-. Presumably they could not do so because of the low intensity at higher wavelengths of the Cerenkov light which they used for measurements. The species e_T^- is unrelaxed and might have a spectrum similar to that of e_{ir}^-.

Nature of site for e_{ir}^- in ice

Buxton et al. (44) suggested that the IR band in crystalline ice is due to electrons trapped in natural cavities that exist in perfect crystals. In crystals of ordinary ice (ice I_h), molecules form sheets of crinkled six-membered rings normal to the *c* axis. Rings from two adjacent sheets form dodecahedral cavities that are joined together along the *c* axis to form long shafts. It was suggested that electrons trapped in these cavities give rise to the IR band. Before e_{ir}^- had been observed in aqueous solids, Nilsson (59) carried out calculations on this ice-cavity model to see if agreement could be found with the optical transition energy of e_{vis}^-. He found agreement was reasonable if it was assumed that the dipoles of the first coordination shell have time to line up with the electric field during the lifetime of e_{ir}^-. The dipole relaxation times would have to be much less than the dielectric relaxation time of ice which is about 1 ms at –40°C and decreases with temperature (60). Without this assumption the calculated optical transition in the Nilsson treatment is at about 800 nm for ice at –10°C, which of course is at a much higher energy than the extrapolated experimental λ_{max} of 2950 nm.

Kevan (61) calculated an optical absorption peak for the polaron in ice at ~77 K in the 3100–2100 nm region, which agrees nicely with the extrapolated experimental λ_{max}. Julienne and Gary (62) also carried out calculations based on the polaron model. If the dipolar medium molecules are unable to orient themselves with respect to the charge, the optical absorption maxima are calculated to be 2300, 2100, and 1800 nm for cavity sizes of 3.0, 2.5, and 2.0 A°, respectively (62).

We conclude that the polaron model leads to a calculated λ_{max} for e_{ir}^- in reasonable agreement with experiment.

Decay kinetics of quasi-free electrons in ice as followed by conductivity

The decay kinetics of the highly mobile quasi-free electrons formed by nanosecond pulse radiolysis of crystalline ice were studied from –10 to –190°C by using the microwave conductivity method (63). In the temperature range $0°C > T > -40°C$ the lifetime of the quasi-free electron is comparable to the response time of detection, but accurate kinetic data were obtained by using a long (50 ns) pulse and fitting the data in the pulse. Reactions [18] and [19] were the main reactions included in the fitting, but a slight complication arose because of a small conductivity signal that decays over a relatively long period ($t_{1/2} \cong 50$ ns); this signal was attributed to mobile protons and was incorporated into the kinetic fits. The values of $k_T N_T$ obtained in this way should be quite reliable. Arrhenius plots of $k_T N_T$ obtained in this way show a linear dependence above about –70°C for both H_2O and D_2O ice with an activation energy of 0.55 ± 0.05 eV (64).

Warman et al. (63) consider that the trap of eq. [19] is a combination of a D defect and a vacancy, called a dressed vacancy. They point out that in view of the large repulsive force between neighbouring H atoms in a lattice D defect, quite a large fraction of D defects might be expected to reside at vacancy positions where the stress is released.

In the temperature range $-80°C > T > -140°C$, the first half-life of the conductivity signal is inversely proportional to the total dose in the pulse, which indicates that electron decay in this range is mainly by reaction with a product or products which are also formed in the pulse (63). The dominance of this reaction should be even greater for the pulses of much higher dose that were used in the optical absorption studies. However, the conductivity results would seem to be compatible with the small yields of e_{ir}^- found in this temperature range.

The decay rate of quasi-free electrons increases as the temperature is lowered from –140°C. Warman et al. (63) suggest that in the temperature range $-140°C > T > -190°C$ mobile electrons are localized at a trapping site from which they are readily emitted thermally

[22] $S + e^- \leftrightarrow S^-$

Luminescence from ice

UV and visible luminescences are emitted when ice at low temperature is exposed to ionizing radiation. The intensity of the luminescence at some wavelengths from ice at 88 K increases with successive pulses of electrons and reaches a plateau level (65). Studies (66) of such dose accumulation effects have allowed separation of the luminescence into three bands. For H_2O ice at 88 K these bands have the following luminescence yields (G_p) in photons/100 eV: the 280–340 nm band, $G_p = 2 \times 10^{-7}$; the 320–600 nm band, with $\lambda_{max} \cong 385$ nm, $G_p = 1 \times 10^{-5}$ after 50 krad of irradiation but rising to a plateau value of 2×10^{-4} after a total of 1.2–1.5 Mrad; the 500–600 nm band, $G_p = 1 \times 10^{-5}$. The intensities of the 280–340 nm and 500–600 nm bands to a

© 2001 NRC Canada

good approximation are independent of dose in the range 0.50–1.5 Mrad (65, 66).

Decay of the 385 nm luminescence was analyzed into a long-lived first-order component ($t_{1/2}$ = 690 ns for H_2O and 1820 ns for D_2O) and a superimposed short-lived decay which obeys second-order kinetics (67). The ratio of the first-order rate constants, $k(H_2O)/k(D_2O)$ was 2.7 ± 0.3, which agrees with the ratio (2.7) of the mobilities of protons and deuterons in their respective ices in one report (68), though a later report by the same authors gives a smaller ratio of $2 > M(H^+)/M(D^+) \geq 1.3$ (69). Studies of the effect of temperature on the 385 nm luminescence band showed that from 79 to 101 K, the luminescence intensity did not change greatly with temperature (70); however, the intensity fell sharply between 101 and 117 K, which parallels the behaviour of trapped OH (71). The mechanism suggested for the 385 nm luminescence at 88 K is (70):

[23] $H_2O \rightarrow H + OH + H_2O^+ + OH^- + e^-$

[24] $OH \rightarrow OH_t$

[25] $OH_t + e^- \rightarrow OH^-$

[26] $OH^- + H^+ \rightarrow H_2O^* (C^1B_1)$

[27] $H_2O^* (C^1B_1) \rightarrow H_2O (A^1B_1) + h\nu$

As the position of the 385 nm luminescence peak does not change when the early second-order luminescence is followed by the long-lived, first-order emission, it can be concluded that both the early and late emissions arise from the same excited species. The short-lived 385 nm decay may, however, proceed by a different mechanism which does not produce H_2O in the C^1B_1 state. Alternatively, it may proceed by the same mechanism, OH^- again reacting with H^+, but at a different type of location where the $[OH^-]/[H^+]$ ratio is closer to unity.

Emission from irradiated ice has also been studied over the lower temperature range 8–77 K (72). It was found that the emission intensity at 77 and 40 K has a max around 380 nm (very similar to the λ_{max} from the earlier work (65, 66) on ice at 88 K) while the luminescences from ice at 20 and 8 K both show maxima around 330 nm. The emission intensity at 8 K is about 40 times higher than at 77 K. The 330 nm emission at 8 K increases with increasing accumulated dose, as does the peak around 385 nm at 88 K (66). This indicates that trapped irradiation products are implicated in the origin of these peaks. The accumulated dose effect on the 8 K emission is not eliminated by warming to 40 K, but is wiped out by warming to 77 K. The following mechanism is proposed by Miyazaki et al. (72):

[28] $H_2O \rightarrow H_2O_t^+ + e_t^-$

[29] $H_2O_t^+ + e_t^- \rightarrow H_2O^*$

[30] $H_2O^* \rightarrow OH^* (A^2\Sigma^+) + H$

It is concluded by Miyazaki et al. (73) that the trapped electron in rxn. [29] is e_{ir}^-. They chose this mechanism partly because of the effects on luminescence of adding NaOH, HCl, or C_2H_5OH to the water from which ice samples were grown (73). However, these solutes are rather insoluble in ice and the first two form clusters in ice (74), so their effective concentration in the ice samples may have been extremely low. The conclusion was based also on an approximate correspondence between the emission lifetimes and the lifetimes of e_{ir}^-. The correspondence has to be approximate because the emission kinetics are approximately first-order after an initial faster decay, whereas e_{ir}^- decay seems to be geminate and follows a tunnelling mechanism (47).

Further studies are necessary to confirm this or another mechanism, and to provide reasons why the mechanism for production of luminescence should change between 40 and 20 K.

Electron solvation in water

Over the past 25 years many reports have been published of experimental, theoretical, and simulation studies of the solvation kinetics of electrons in water and other polar liquids. In alcohols the time dependence of the spectroscopic changes which accompany the solvation process correlate well with the monomeric dielectric relaxation time of the alcohol (75), and these times are of the order of 10–50 ps. The molecular relaxation time in water is less than 1 ps, and direct observation of the solvation process was only possible after lasers with pulse lengths less than 1 ps became available. Studies of electron solvation in water have been summarized recently by Pépin et al. (76).

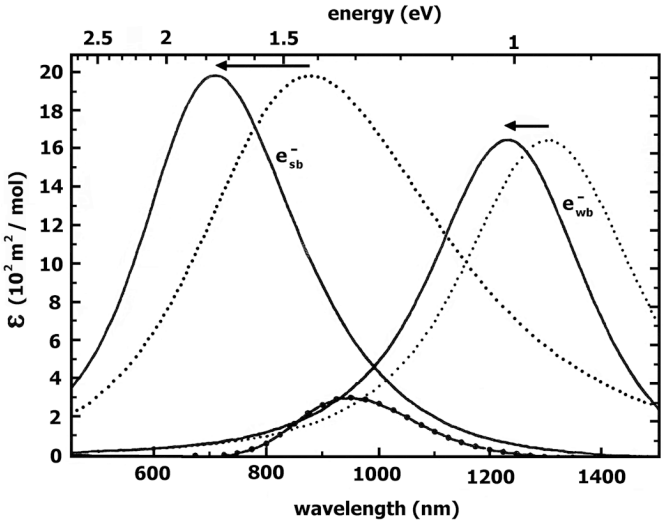
Recent experimental studies on electron solvation in pure water or aqueous salt solutions have been of two types: (*i*) photoionization via two- or multi-photon absorption, followed by a variably delayed probe pulse at a selected wavelength which monitors the induced changes in transmission; and (*ii*) three-pulse experiments: the first preparation pulse generates solvated electrons, which after an equilibration time of typically 1–4 ns are excited by a second pulse to upper states, and a probe pulse monitors changes as in (*i*).

According to Pépin et al. (76), it is generally agreed that a large number of trap states are available to quasi-free electrons in polar media. At very short times the quasi-free electron is trapped to form a weakly-bound species (e_{wb}^-) which absorbs chiefly in the IR. This species undergoes a stepwise transition to a strongly bound species (e_{sb}^-) that absorbs in the visible and which relaxes to become the well-known hydrated electron at long times. Some authors consider the weakly bound species (e_{wb}^-) to be the *p*-like excited states of the hydrated electron (77, 78). Some of the matters on which the various studies disagree are: (*i*) the existence of a direct solvation channel which allows the quasi-free electron to go to the e_{sb}^- state without passing through the e_{wb}^- state; (*ii*) the existence of another species absorbing in the IR due to transient encounter pairs; and (*iii*) the role played by solvent relaxation in the spectral evolution of the absorbing species.

Pépin et al. (76) studied electron solvation in liquid D_2O by the two-pulse method at 20 different wavelengths in the 450–1450 nm range. On the basis of the following picture they were able to get good fits to kinetic traces at all wavelengths: (*i*) trapping starting 0.15 ps after the passage of the excitation pulse's maximum intensity; (*ii*) a stepwise transition with a characteristic time of 0.4 ps between the major species e_{wb}^- and e_{sb}^-; (*iii*) a blue shift of the spectra of both e_{wb}^- and e_{sb}^-, concomitant with the stepwise transition and with a characteristic time of 0.5 ps; (*iv*) magnitudes of

© 2001 NRC Canada

Fig. 9. Molar extinction coefficients ε (SI units are used: 1 m^2 mol^{-1} = 10 M^{-1} cm^{-1}) of the various species that are included in the fit of the observed solvation kinetics of electrons in pure liquid D_2O. The dotted lines represent the spectra of e^-_{wb} and e^-_{sb} before any continuous shift has occurred. The solid lines represent the spectra in the long-time limit, that is, when the continuous shift is completed. The arrows indicate the amplitude of the blue shifts. One should note that, on the energy scale, the widths of the spectra remain constant. From ref. 76.



the blue shifts of e^-_{wb} and e^-_{sb} of 0.06 and 0.34 eV, respectively; (*v*) a probability of direct trapping into the e^-_{sb} configuration of 0.34; and (*vi*) a weak source of absorption in the near-IR (800–1100 nm) with a characteristic decay time of 2.0 ps. The spectra of e^-_{wb}, e^-_{sb}, and the near-IR component are shown in Fig. 9.

The above analysis of electron solvation in liquid D_2O is similar to an analysis of electron solvation in methanol at room temperature by the same authors (3), except that in the latter case the characteristic relaxation times were much greater. These authors (79) used a similar model to reanalyze three-pulse experiments in water (80) and alcohols of various chain lengths (81) and found that the general features of the results could be explained in terms of their hybrid model, by using the kinetic and spectral parameters they found in their own two-pulse experiments (3, 76). However, there are several parameters that are fitted in the model of Pépin et al. (76), and likely other models and parameters would also explain the results. Certainly other authors have used different models and parameters to explain their own results. For example, the two-pulse experiments of Eisenthal and co-workers (82) were interpreted on the basis of a two-state model, but the upper state (referred to as the "wet electron" and considered likely to be a *p*-like excited state) was found to have a broad maximum near 900 nm. Assel et al. (83) consider on the basis of their experiments that the wet electron discussed by Eisenthal and co-workers (82) is really a ground state electron in a hot solvent cavity. Assel et al. (84) reported very recently on three-pulse experiments with pure water; they find the first intermediate (e^-_{wb} in the terminology of Pépin et al. (76)) has λ_{max} = 1000 nm. Similarly, Hertwig et al. (85) on the basis of their two-pulse experiments consider that their initial (~350 fs) spectrum, the maximum of which is red-shifted by about 0.5 eV with respect to that of the thermally relaxed spectrum, is due to hot solvated electrons. They find no evidence for transient electronically excited states of solvated electrons.

Recently Pastina et al. (86) measured hydrogen yields following γ-radiolysis of aqueous solutions with a variety of scavengers of the hydrated electron and its precursor. They concluded that a common precursor is responsible for both molecular hydrogen and the hydrated electron. The mechanism for producing molecular hydrogen is unknown, but a suggestion is the capture of the precursor by water to give the molecular anion, which then either gives molecular hydrogen directly, or decomposes to give a hydride anion which reacts with water to produce molecular hydrogen (86). Presumably the precursor to the hydrated electron considered by Pastina et al. (86) is the same as the e^-_{wb} discussed by Pépin et al. (76); however, the analysis by Pépin et al. (76) assumes that all e^-_{wb} becomes e^-_{sb}, except for the small fraction that undergoes geminate recombination, and the extinction coefficients of Fig. 9 are calculated on this assumption.

Connection between electron solvation in water and in aqueous solids

Very shortly after injection of electrons into water, two major species seem to be present: a weakly bound species e^-_{wb} (sometimes considered to be the *p*-state of the solvated electron) which absorbs mainly in the near-IR, and a strongly bound species (e^-_{sb}) which absorbs in the visible. Some researchers consider that there is another, less important species which also absorbs in the near-IR. A first-order transition $e^-_{wb} \rightarrow e^-_{sb}$ occurs, as well as concomitant blue shifts of both species. The magnitude of the blue shift is greater for e^-_{sb} than for e^-_{wb}, and e^-_{sb} becomes the hydrated electron at long times. A study of hydrogen yields from the γ-radiolysis of aqueous solutions suggests that the precursor of the hydrated electron is also a precursor of molecular hydrogen.

After injection of an electron into ice or some aqueous solids, again two major species are produced: the very weakly bound e^-_{ir}, and the strongly bound e^-_{vis} which at long times is essentially the same as the hydrated electron. The traps for the two species seem to be physically different; therefore, e^-_{ir} does not appear to be an excited state of the hydrated electron. At short times e^-_{vis} undergoes a blue shift, which is much smaller than the blue shift of e^-_{sb} in water. Evidence is strong that the transition $e^-_{ir} \rightarrow e^-_{vis}$ occurs in some glasses under some circumstances, but in crystalline ice the transition has only been observed directly once, at 4 K. It is likely that the transition is slow in aqueous solids, such that reaction of e^-_{ir} with other radiation-produced species is sometimes faster, or such that decay of e^-_{vis} with other radiation-produced species is sometimes faster than its production by the transition.

In both water and aqueous solids there is a direct channel for the transition from quasi-free electrons to the strongly bound state (e^-_{sb} or e^-_{vis}) without going through the weakly bound state, e^-_{wb} or e^-_{ir}.

Thus there are strong similarities between e^-_{ir} and e^-_{wb} and we suggest they are essentially the same species, although

© 2001 NRC Canada

the absorption spectrum of e^-_{wb} is significantly blue-shifted as compared to e^-_{ir}.

Acknowledgement

HAG gratefully acknowledges the support of a Gledden Visiting Senior Fellowship for the period of his stay at the University of Western Australia, July–December 1999.

References

1. C.A. Kraus. J. Am. Chem. Soc. **30**, 1323 (1908).
2. J.H. Baxendale and P. Wardman. J. Chem. Soc. Faraday Trans. 1, **69**, 584 (1973).
3. C. Pépin, T. Goulet, D. Houde, and J.-P. Gerin. J. Phys. Chem. **98**, 7009 (1994).
4. D. Schulte-Frohlinde and K. Eiben. Z. Naturforsch. **17a**, 445 (1962).
5. J. Jortner and B. Scharf. J. Chem. Phys. **37**, 2506 (1962).
6. M. Ogasawara. *In* Excess electrons in dielectric media. *Edited by* C. Ferradini and J.-P. Jay-Gerin. CRC Press, Boca Raton, Fla. 1991. Chap. 9.
7. G.V. Buxton, F.C.R. Cattell, and F.S. Dainton. Trans. Faraday Soc. **67**, 687 (1971).
8. G.V. Buxton and K.G. Kemsley. J. Chem. Soc. Faraday Trans. 1, **71**, 568 (1975).
9. G.V. Buxton, H.A. Gillis, and N.V. Klassen. Can. J. Chem. **54**, 367 (1976).
10. T.Q. Nguyen, D.C. Walker, and H.A. Gillis. J. Chem. Phys. **69**, 1038 (1978).
11. S.A. Rice, G. Dolivo, and L. Kevan. J. Chem. Phys. **68**, 4864 (1978).
12. T.Q. Nguyen and D.C. Walker. J. Chem. Phys. **67**, 2399 (1977).
13. L. Kevan. J. Phys. Chem. **84**, 1232 (1980).
14. S. Schlick, P.A. Narayana, and L. Kevan. J. Chem. Phys. **64**, 3153 (1976).
15. M.J. Blandamer, L. Shields, and M.C.R. Symons. J. Chem. Soc. 3513 (1964).
16. L. Kevan, D.R. Renneke, and R.J. Friauf. Solid State Commun. **6**, 469 (1968).
17. H. Hase, M. Noda, and T. Higashimura. J. Chem. Phys. **54**, 2975 (1971).
18. R. May and D.C. Walker. Chem. Phys. Lett. **30**,69 (1975).
19. G.J. Trudel, H.A. Gillis, N.V. Klassen, and G.G. Teather. Can. J. Chem. **59**, 1235 (1981).
20. F.Y. Jou and L.M. Dorfman. J. Chem. Phys. **58**, 4715 (1973).
21. J. Cygler, N.V. Klassen, and G.G. Teather. Radiat. Phys. Chem. **27**, 47 (1986).
22. G.V. Buxton, M. Medley, G.A. Salmon, P.J. Baugh, R. Catterall, and P.B. Williams. J. Chem. Soc. Faraday Trans. 1, **81**, 3067 (1985).
23. M. Wpych and J. Kroh. Bull. Pol. Acad. Sci. Chem. **40**, 155 (1992).
24. G.V. Buxton, G.A. Salmon, C. Stradowski, and J. Kroh. Radiat. Phys. Chem. **17**, 361 (1981).
25. T.Q. Nguyen and D.C. Walker. J. Chem. Soc. Faraday Trans. 1, **73**, 1958 (1977).
26. Z. Wu, N.V. Klassen, H.A. Gillis, and G.G. Teather. Can. J. Chem. **61**, 189 (1983).
27. N.V. Klassen, G.G. Teather, and F. Kieffer. Can. J. Chem. **57**, 1488 (1979).
28. H.A. Gillis, G.G. Teather, and G.V. Buxton. Can. J. Chem. **56**, 1889 (1978).
29. J.C. Baianu, N. Boden, D. Lightowlers, and M. Mortimer. Chem. Phys. Lett. **54**, 169 (1978).
30. G.V. Buxton, K. Kawabata, and G.A. Salmon. Chem. Phys. Lett. **60**, 48 (1978).
31. J.W. Van Leeuwen, M.G.J. Heijman, and H. Nauta. Radiat. Phys. Chem. **17**, 367 (1981).
32. W.M. Bartczak, M. Hilczer, and J. Kroh. Radiat. Phys. Chem. **17**, 431 (1981).
33. L. Kevan. Acc. Chem. Res. **14**, 138 (1981).
34. N.V. Klassen, R.J. Adams. G.G. Teather, and C.K. Ross. J. Phys. Chem. **84**, 3609 (1980).
35. M. Tachiya and A. Mozumder. Chem. Phys. Lett. **34**, 77 (1975).
36. M. Wypych and J. Kroh. Radiat. Phys. Chem. **4**, 393 (1994).
37. H.A. Gillis and D.C. Walker. J. Chem. Phys. **65**, 4590 (1976).
38. V.N. Shubin, V.A. Zhigunov, V.I. Zolotarevsky, and P.I. Dolin. Nature (London), **212**, 1002 (1966).
39. K. Eiben and I.A. Taub. Nature (London), **216**, 782 (1967).
40. I.A. Taub and K. Eiben. J. Chem. Phys. **49**, 2499 (1968).
41. G. Nilsson, H.C. Christensen, J. Fenger, P. Pagsberg, and S.O. Nielsen. Adv. Chem. Ser. **81**, 71 (1968).
42. K. Kawabata, H. Hori, and S. Okabe. Chem. Phys. Lett. **14**, 223 (1972).
43. G.V. Buxton, H.A. Gillis, and N.V. Klassen. Chem. Phys. Lett. **32**, 533 (1975).
44. G.V. Buxton, H.A. Gillis, and N.V. Klassen. Can. J. Chem. **55**, 2385 (1977).
45. H.A. Gillis, G.G. Teather, and C.K. Ross. J. Phys. Chem. **84**, 1248 (1980).
46. U. Eckener, D. Helmreich, and H. Engelhardt. *In* Physics and chemistry of ice. *Edited by* E. Whalley, S.J. Jones, and L.W. Gold. Royal Society of Canada, Ottawa. 1973.
47. Z. Wu, H.A. Gillis, N.V. Klassen, and G.G. Teather. J. Chem. Phys. **78**, 2449 (1983).
48. J.M. Fluornoy, L.H. Baum, and S. Siegel. J. Chem. Phys. **36**, 2229 (1962).
49. O.E. Mogensen and M. Eldrup. Phys. Lett. A, **60**, 325 (1977).
50. M. Eldrup. J. Chem. Phys. **64**, 5283 (1976).
51. K. Kawabata. J. Chem. Phys. **65**, 2235 (1976).
52. P.N.T. Unwin and J. Muguruma. Phys. Status Solidi A, **14**, 207 (1972).
53. K. Kawabata, Y. Nagata, S. Okabe, N. Kimura, K. Tsumori, M. Kawanishi, G.V. Buxton, and G.A. Salmon. J. Chem. Phys. **77**, 3884 (1982).
54. M. Natori and T. Watanabe. J. Phys. Soc. Jpn. **21**, 1573 (1966).
55. G. Nilsson and P. Pagsberg. Chem. Phys. Lett. **74**, 119 (1980).
56. J.M. Warman and C.D. Jonah. Chem. Phys. Lett. **79**, 43 (1981).
57. J.M. Warman, M. Kunst, and C.D. Jonah. J. Phys. Chem. **87**, 4292 (1983).
58. A. Hummel. J. Chem. Phys. **49**, 4840 (1968).
59. G. Nilsson. J. Chem. Phys. **56**, 3427 (1972).
60. S.R. Gough and D.W. Davidson. J. Chem. Phys. **52**, 5442 (1970).
61. L. Kevan. *In* Progress in solid state chemistry. Vol. 2. *Edited by* H. Reiss. Pergamon Press, Oxford. 1965. Chap. 9.
62. P.S. Julienne and L.P. Gary. Mol. Cryst. **5**, 135 (1968).
63. J.M. Warman, M.P. de Haas, and J.B. Verberne. J. Phys. Chem. **84**, 1240 (1980).
64. M.P. de Haas, M. Kunst, J.M. Warman, and J.B. Verberne. J. Phys. Chem. **87**, 4089 (1983).
65. T.I. Quickenden, S.M. Trotman, and D.F. Sangster. J. Chem. Phys. **77**, 3790 (1982).
66. T.I. Quickenden, S.M. Trotman, and D.F. Sangster. Radiat. Res. **101**, 407 (1985).

© 2001 NRC Canada

67. C.F. Vernon, A.J. Matich, T.I. Quickenden, and D.F. Sangster. J. Phys. Chem. **95**, 7313 (1991).
68. M. Kunst and J.M. Warman. Nature (London), **288**, 465 (1980).
69. M. Kunst and J.M. Warman. J. Phys. Chem. **87**, 4093 (1983).
70. T.I. Quickenden, A.J. Matich, M.G. Bakker, C.G. Freeman, and D.F. Sangster. J. Chem. Phys. **95**, 8843 (1991).
71. A. Plonka, E. Szajdzinska-Pietek, and J. Kroh. Radiat. Phys. Chem. **23**, 583 (1984).
72. T. Miyazaki, Y. Kamiya, K. Fueki, and M. Yasui. J. Phys. Chem. **96**, 9558 (1992).
73. T. Miyazaki, S. Nagasaka, Y. Kamiya, and K. Tanimura. J. Phys. Chem. **97**, 10715 (1993).
74. P.V. Hobbs. Ice physics. Clarendon, Oxford. 1974.
75. G.A. Kenney-Wallace and C.D. Jonah. J. Phys. Chem. **86**, 2572 (1982).
76. C. Pépin, T. Goulet, D. Houde, and J.-P. Jay-Gerin, J. Phys. Chem. A, **101**, 4351 (1997).
77. C. Silva, P.K. Walhout, K. Yokoyama, and P.F. Barbara. Phys. Rev. Lett. **80**, 1086 (1988).
78. B.J. Schwartz and P.J. Rossky. J. Chem. Phys. **101**, 6917 (1994).
79. T. Goulet, C. Pépin, D. Houde, and J.-P. Jay-Gerin. Radiat. Phys. Chem. **54**, 441 (1999).
80. Y. Kimura, J.C. Alfano, P.K. Walhout, and P.F. Barbara. J. Phys. Chem. **98**, 3450 (1994).
81. P.K. Walhout, J.C. Alfano, Y. Kimura, C. Silva, P.J. Reid, and P.F. Barbara. Chem. Phys. Lett. **232**, 135 (1995).
82. H. Lu, F.H. Long, and K.B. Eisenthal. J. Opt. Soc. Am. B, **7**, 1511 (1990).
83. M. Assel, R. Laenen, and A. Laubereau. J. Chem. Phys. **111**, 6869 (1999).
84. M. Assel, R. Laenen, and A. Laubereau. Chem. Phys. Lett. **317**, 13 (2000).
85. A. Hertwig, H. Hippler, and A.N. Unterreiner. J. Phys. Condens. Matter, **12**, A165 (2000).
86. B. Pastina, J.A LaVerne, and S.M. Pimblott. J. Phys. Chem. A, **103**, 5841 (1999).

© 2001 NRC Canada

Scope and limitations in the use of *N*-(PhF)serine-derived cyclic sulfamidates for amino acid synthesis

Lan Wei and William D. Lubell

Abstract: Ring-opening of *N*-(PhF)serine-derived cyclic sulfamidate **17** was achieved with different nucleophiles (β-keto esters, β-keto ketones, dimethyl malonate, nitroethane, sodium azide, imidazole, and potassium thiocyanate) to prepare a variety of amino acid analogs. Two different pathways for ring opening of **17** were elucidated: direct nucleophilic displacement, as well as β-elimination followed by Michael addition. Furthermore, β-keto ester and β-keto ketone products **18k**, **18m**, and **18i** were converted to prolines and pyrazole amino acids.

Key words: glutamate, amino acid, cyclic sulfamidate, proline.

Résumé : L'ouverture des sulfamidates cycliques dérivés de la serine a été explorée avec différents nucléophiles (β-céto esters, 1,3-dicétones, diméthyle de malonate, nitroéthane, azidure de sodium, imidazole et thiocyanate de potassium) pour préparer une variété d'analogues d'acides aminés. Deux voies différentes ont été proposées pour l'ouverture du cycle à cinq membres du sulfamidate **17**: le déplacement nucléophile et l'élimination β suivie de l'addition de Michael. De plus, les β-céto ester **18k**, **18m** et 1,3-dicétone **18i** ont été respectivement convertis en prolines et en acides aminés pyrazoyle.

Mots clés : glutamate, acide aminé, sulfamidate cyclique, proline.

Introduction

Serine-derived cyclic sulfamidates have served in syntheses of a series of amino acid analogs (Fig. 1) (1–3). For example, β-substituted alanines **1**–**11** have been prepared by ring opening of sulfamidate with oxygen, nitrogen, sulfur, and fluorine nucleophiles (1–3). Aspartate analogs **12** and **13** have also been prepared by nucleophilic opening of sulfamidate with a cyanide ion (1, 3). Moreover, γ-acyl pyroglutamate **14** was furnished on treatment of sulfamidate with diethyl malonate (1). These examples demonstrate that serine-derived cyclic sulfamidates are versatile chiral building blocks with complementary reactivity to related β-alanine cation equivalents such as serine-derived β-lactones (4, 5) and aziridines (6, 7).

Interested in harnessing its power to construct peptide mimics and glutamate receptor ligands, we have explored the reactivity of cyclic-sulfamidate **17** derived from *N*-(PhF)serine methyl ester (Scheme 1), because of the proven effectiveness of the PhF protecting group for preserving configurational integrity during manipulations of α-amino carbonyl compounds (PhF = 9-(9-phenylfluorenyl)) (8, 9). Sulfamidate **17** reacted with a series of heteroatomic as well as carbon nucleophiles to provide the desired amino acid analogs; however, careful examination of the configurational integrity of these products revealed that racemization occurred during reactions of **17** with carbon nucleophiles (10). Although enantiopure serine has often been employed as starting material, to the best of our knowledge, the enantiomeric purity of the products from ring opening of its cyclic sulfamidates had been previously reported in only two examples (2). Pyrazole **7** and piperidine **8** were checked for racemization after conversion to diastereomeric amides using, respectively, (*R*)-α-methoxy-α-trifluoromethylphenylacetyl chloride and (–)-menthyl chloroformate. A comparison of the diastereomeric amides with material prepared from racemic serine using proton nuclear magnetic resonance (^{1}H NMR) spectroscopy led the authors to conclude that "no apparent racemization occurred in the course of both the ring opening and the hydrolysis" reactions involved in the preparation of **7** and **8**. This claim contrasted with our discovery of racemization in the reactions of sulfamidate **17** with carbon nucleophiles and provoked a detailed investigation of the enantiomeric purity of the various products from nucleophilic ring opening of sulfamidate **17**.

In reactions with different nucleophiles, sulfamidate **17** was found to undergo additions via two different mechanisms. In the case of weakly basic (conjugate acid $pK_a \leq 7$) nucleophiles, direct nucleophilic displacement occurred to provide enantiopure (>97% ee) β-substituted alanines. On the other hand, carbon nucleophiles, such as the enolates of 1,3-dicarbonyl compounds, added to sulfamidate **17** by a mechanism featuring β-elimination to provide a

Received June 30, 2000. Published on the NRC Research Press Web site on January 24, 2001.

L. Wei and W.D. Lubell.[1] Département de chimie, Université de Montréal, C.P. 6128, Succursale Centre Ville, Montréal, QC H3C 3J7, Canada.

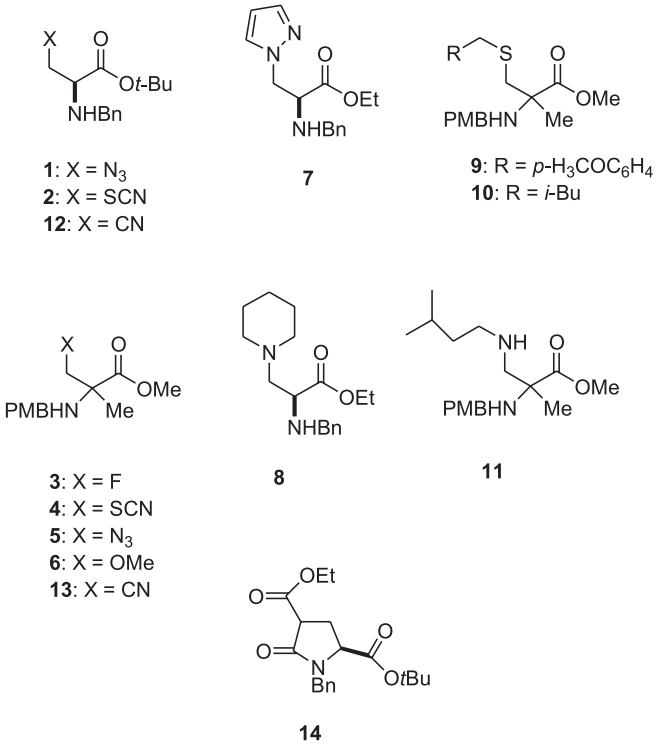
[1]Author to whom correspondence may be addressed. Telephone: (514) 343-7339. Fax: (514) 343-7586. e-mail: Lubell@chimie.umontreal.ca

 DOI: 10.1139/cjc-79-1-94 © 2001 NRC Canada

Table 1. ^{1}H NMR signal assignments of sulfamidites (2*R*)- and (2*S*)-**16**, and sulfamidate **17**.

Position	(2*R*)-**16**	(2*S*)-**16**	**17**
	δ_H [int. mult, *J* (Hz)]	δ_H [int. mult, *J* (Hz)]	δ_H [int. mult, *J* (Hz)]
4	3.51 (1H, dd, 1.4, 7.1)	3.37 (1H, t, 7.9)	3.64 (1H, dd, 4.0, 8.1)
5β	4.41 (1H, dd, 1.4, 9.4)	4.32 (1H, t, 7.9)	4.38 (1H, dd, 4.0, 8.7)
5α	4.75 (1H, dd, 7.1, 9.4)	4.95 (1H, t, 7.9)	4.02 (1H, dd, 8.1, 8.7)
MeO	3.42 (3H, s)	3.57 (3H, s)	3.69 (3H, s)
PhF	7.17–8.17 (13H, m)	7.19–7.77 (13H, m)	7.19–8.22 (13H, m)

Fig. 1. Representative amino acids prepared by ring-opening of serine-derived cyclic sulfamidates.



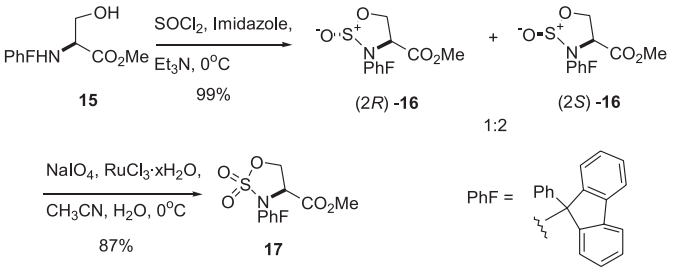
dehydroalanine intermediate that underwent subsequent Michael addition and afforded racemic product. In addition, several nucleophiles were found that caused β-elimination, yet failed to react with the dehydroalanine intermediate in a conjugate addition. This spectrum of reactivity and the utility of the addition products have been evaluated to better define the scope and limitations of *N*-(PhF)serine-derived sulfamidate **17** as a chiral educt for amino acid synthesis.

Results and discussion

Synthesis of cyclic sulfamidate 17

Sulfamidate derivatives of β-amino alcohols permit protection of the nitrogen moiety and conversion of the hydroxyl group into a leaving group. The most direct approach for their construction has been the reaction of the respective β-amino alcohol with sulfuryl chloride; however, this process has usually led to the corresponding aziridines, presumably due to ring closure of the corresponding -OSO_2Cl intermediate (11–13). Because of the difficulties encountered when using sulfuryl chloride, most cyclic sulfamidates have been prepared by oxidation of the corresponding sulfamidites (1–3, 11–22). Following this protocol, (4*S*)-methyl 2,2-dioxo-3-PhF-1,2,3-oxathiazolidine-4-carboxylate (**17**) was synthesized initially by treating *N*-(PhF)serine methyl ester **15** (23) with thionyl chloride, triethylamine, and imidazole in dichloromethane to furnish quantitatively a 1:2 mixture of diastereoisomeric sulfamidites **16** (Scheme 1). Cyclic sulfamidate **17** was then prepared by subsequent oxidation of sulfamidites **16** with sodium periodate and catalytic ruthenium trichloride in acetonitrile and water at 0°C.

Scheme 1. Synthesis of cyclic sulfamidate **17**.

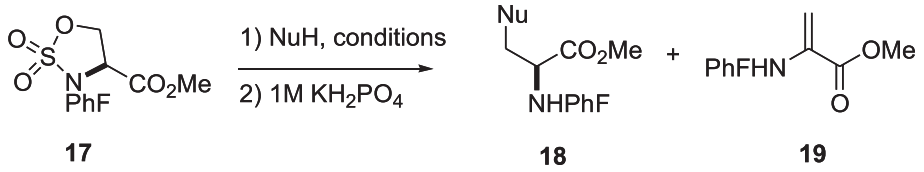


Diastereoisomers (2*R*)-**16** and (2*S*)-**16** could be separated by chromatography and independently converted into five-membered sulfamidate **17**. The assignment of the configuration at sulfur for the diastereoisomers (2*R*)-**16** and (2*S*)-**16** was initially attempted by comparisons of their ^{1}H NMR spectra with that of their oxidation product sulfamidate **17** (Table 1), as well as with spectral data for other cyclic sulfamidites (24). Comparing the spectra of **16** and **17**, we concluded that the (2*R*)-sulfamidite ((2*R*)-**16**), would exhibit similar steric as well as anisotropic effects as sulfamidate **17** (25, 26). For example, in the spectra of (2*R*)-**16** and **17**, the C-4 proton appeared as a doublet of doublets as the result of steric interactions between the exocyclic oxygen atom on sulfur and the PhF group, which twisted the five-membered ring such that significantly different dihedral angles existed between the C-4 and C-5 protons. In contrast, the C-4 proton in (2*S*)-**16** appeared as a triplet indicative of a conformation with similar dihedral angles between the C-4 proton and each of the C-5 protons. The magnetic anisotropy of the S—O bond (26) shifted downfield the resonances of proximal PhF protons as well as the C-4 proton in the spectra of (2*R*)-**16** and **17** relative to the respective signals in the spectrum of (2*S*)-**16**.

The configurational assignments for **16**, which were made based on the ^{1}H NMR chemical shift and coupling constant

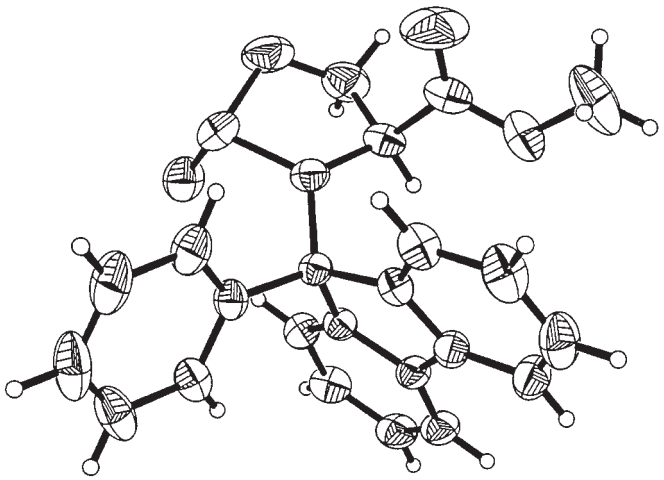
© 2001 NRC Canada

Scheme 2. Ring opening of cyclic sulfamidate **17**.



17 **18** **19**

Fig. 2. ORTEP view of (2*R*,4*S*)-methyl 2-oxo-3-(PhF)-1,2,3-oxathiazolidine-4-carboxylate ((2*R*)-**16**).[2]



values, were confirmed by X-ray crystallographic analysis of (2*R*)-**16** (Fig. 2). Single-crystal X-ray analysis showed that the dihedral angle between the C-4 proton and the C-5α proton was 25.4°, and the dihedral angle between the C-4 proton and the C-5β proton was 82.6°. The crystal structure of (2*R*)-**16** exhibits a conformation in which the α-proton and the α-acid carbonyl are nearly coplanar (159.5°). Since α-deprotonation from the coplanar geometry is stereoelectronically less favoured than from an orthogonal geometry, this arrangement has been suggested to contribute to the configurational stability of PhF amino carbonyl compounds (27, 28).

Ring opening of five-membered cyclic sulfamidate 17

With cyclic sulfamidate **17** in hand, we next examined nucleophilic ring opening using different nucleophiles (Scheme 2, Table 2). Cyclic sulfamidate **17** reacted with heteroatomic nucleophiles to provide products from both nucleophilic displacement at C-5 and proton abstraction at C-4. For example, KSCN, NaN_3, and imidazole, all opened regioselectively the sulfamidate ring to afford, respectively, thioether **18d**, azide **18e**, and imidazole **18f**. Other nucleophiles, such as TBAF, MeONa, diethyl amine, and piperidine, gave mainly dehydroalanine **19** and recovered starting material as observed by NMR spectral analysis of the crude product after aqueous work-up.

Ring opening of sulfamidate **17** was also examined using *C*-nucleophiles including β-keto esters, β-keto ketones, dimethyl malonate, and nitroethane. Treatment of sulfamidate **17** with a premixed solution containing 400 mol% of either β-keto ester, β-keto ketone, or dimethyl malonate and 220 mol% of sodium hydride in DME, followed by heating at 60°C caused ring opening to form the polar sulfamic acid intermediate. Hydrolysis of the reaction mixture with 1 M KH_2PO_4 furnished the desired amino acid derivatives **18i**–**o** after chromatography (Table 2). Since β-keto ester **18k** and β-keto ketone **18i** were difficult to separate from methyl acetoacetate and 2,4-pentanedione, respectively, the crude material was used without purification in the next step towards the preparation of heterocyclic amino acids. Nitroethane reacted with **17** using similar conditions to provide γ-nitro-α-amino pentanoate **18o** in 52% yield as a 10:1 mixture of diastereomers.

β-Keto esters **18k** and **18m** were next converted, respectively, to 5-methylproline **23** and δ-keto α-amino ester **20m**, an intermediate in the synthesis of 5-*tert*-butylproline (29) (Scheme 3). Their respective δ-oxo-α-*N*-(PhF)amino acids were first obtained from hydrolysis and decarboxylation of β-keto esters **18k** and **18m** with sodium hydroxide in ethanol heated at a reflux. Esterification with iodomethane and potassium carbonate in acetonitrile provided methyl 5-oxo-2-[*N*-(PhF)amino]hexanoate (**20k**) and methyl 6,6-dimethyl-5-oxo-2-[*N*-(PhF)amino]heptanoate (**20m**) in 71% and 52% overall yields, respectively, from **17**. Hydrogenation of δ-oxoheptanoate with palladium-on-carbon and di-*tert*-butyl dicarbonate in methanol proceeded by cleavage of the PhF protection, *N*-acylation, imine formation, and hydrogenation of the imine intermediate on the face opposite the methyl ester to furnish *N*-(BOC)-5-methylproline methyl ester (**21**) as the *cis*-diastereomer. Hydrolysis of methyl ester *cis*-**21** with potassium trimethylsilanolate in Et_2O furnished *cis*-*N*-(BOC)-5-methylproline (*cis*-**22**) in 96% yield. In addition, removal of the BOC protecting group with trifluoroacetic acid in dichloromethane provided *cis*-5-methylproline **23** (30, 31).

The utility of β-keto ketone **18i** was illustrated by its conversion to pyrazole amino acid **26** (Scheme 3). Methyl 2-[*N*-(PhF)amino]-3-(3,5-dimethyl-2*H*-pyrazol-4-yl)propanoate (**24**) was initially prepared by treatment of β-keto ketone **18i** with

[2] The structure of (2*R*)-**16** was solved at l'Université de Montréal X-ray facility using direct methods (SHELXS 96) and refined with SHELXL 96: $C_{23}H_{19}NO_4S$, Mr = 405.452, orthorhombic, colourless crystal, space group $P2_12_12_1$, unit cell dimensions (Å) a = 9.5587(2), b = 9.7736(2), c = 21.0498(4), volume of unit cell (Å^3) 1966.53(7), Z = 4, R_1 = 0.0659 for $F^2 > 2\sigma(F^2)$, wR_2 = 0.1613 for all data; GOF = 1.048. The author has deposited the atomic coordinates for the structure of (2*R*)-**16** with the Cambridge Crystallographic Data Centre. The coordinates can be obtained, free of charge, on application to the Director, CCDC, 12 Union Road, Cambridge, CB2 1EZ, U.K. (Fax: 44-1223-336033 or e-mail: deposit@ccdc.cam.ac.uk). Supplementary material may be purchased from the Depository of Unpublished Data Document Delivery, CISTI, National Research Council Canada, Ottawa, ON, K1A OS2, Canada. For information on ordering electronically (http://www.nrc.ca/cisti/irm/unpub_e.shtml).

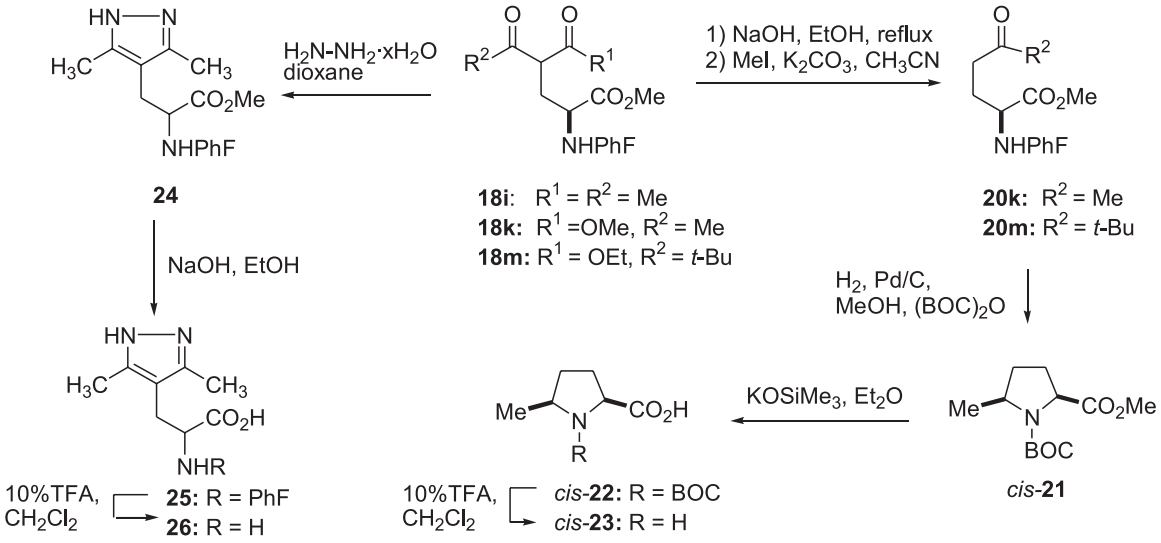
© 2001 NRC Canada

Table 2. Treatment of cyclic sulfamidate **17** with nucleophiles.

Entry	Nucleophilic source	Base	Solvent	Time (h)	Temp (°C)	**18**[a] (% yield)	$[\alpha]_D^{20}$	**19**[c] (% yield)
a	TBAF		DME	18	rt	—		40
b	Et_2NH		DME	18	rt	—		<10
	Et_2NH		MeCN	48	rt	—		50
	Et_2NH		DMF	18	rt	—		100
c	piperidine		MeCN	48	rt	—		30
d	KSCN		DME	48	rt	64	–287°	—
	KSCN		DMF	36	rt	72	–287°	—
e	NaN_3		DME	72	rt	50	–294°	—
	NaN_3		MeCN	72	rt	82	–294°	—
	NaN_3		DMF	1	rt	90	–294°	—
f	imidazole		DME	18	80	85	–241°	—
g	$CH_3(CH_2)_2SH$		DMF	36	rt	—		—
	$CH_3(CH_2)_2SH$	NaH	DMF	36	rt	—		10
h	MeONa		DME	0.5	rt	—		100
i	$MeCOCH_2COMe$	NaH	DME	18	60	66[b]		[d]
j	$PhCOCH_2COMe$	NaH	DME	18	60	45		—
k	$MeCOCH_2CO_2Me$	K_2CO_3	DMF	72	rt	—		100
	$MeCOCH_2CO_2Me$	K_2CO_3	THF	72	rt	30[b]		[d]
	$MeCOCH_2CO_2Me$	Cs_2CO_3	THF	90	rt	—		100
	$MeCOCH_2CO_2Me$	K_3PO_4	DME	18	rt	43[b]		[d]
	$MeCOCH_2CO_2Me$	NaH	THF	6	60	51[b]		—
	$MeCOCH_2CO_2Me$	NaH	DME	4	60	67[b]		—
	$MeCOCH_2CO_2Me$	NaH	DME	18	60	86[b]		—
l	$EtCOCH_2CO_2Et$	NaH	DME	18	60	82		—
m	*t*-$BuCOCH_2CO_2Et$	NaH	DME	18	60	63		—
n	$MeCO_2CH_2CO_2Me$	NaH	DME	18	60	65[b]	–4.3°	—
o	$CH_3CH_2NO_2$	NaH	DME	18	60	52		—

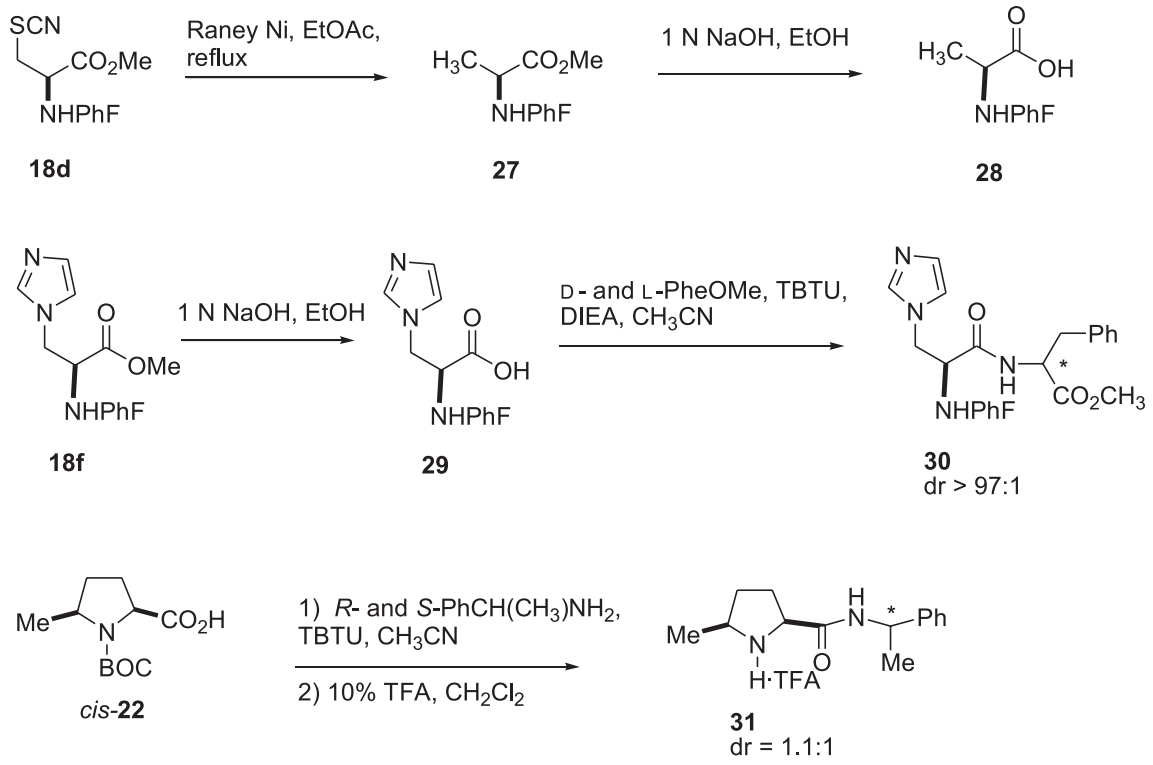
[a]Isolated yield.
[b]Calculated yield from an isolated mixture of **18** and β-dicarbonyl starting material.
[c]Determined by ^{1}H NMR spectroscopy.
[d]Observed by TLC.

Scheme 3. Synthesis of 5-alkylproline **23** and amino-3-(3,5-dimethyl-1*H*-pyrazol-4-yl) propionic acid **26**.



© 2001 NRC Canada

Fig. 3. Evaluation of enantiomeric purity of amino acids **28**, **29**, and *cis*-**22**.



hydrazine hydrate. Hydrolysis of methyl ester **24** with 1 N NaOH in EtOH then furnished 2-[*N*-(PhF)amino]-3-(3,5-dimethyl-1*H*-pyrazol-4-yl)propionic acid (**25**) as a solid after chromatography. Removal of the PhF group was cleanly accomplished by heating **25** with trifluoroacetic acid in dichloromethane at a reflux for 18 h and furnished **26** in 88% yield.

Enantiomeric purity

Enantiomeric purity was evaluated for two products by conversion to diastereomeric derivatives and analysis of the isomeric signals in their ^{1}H NMR spectra. In the case of (2*S*)-*N*-PhF-*S*-cyanocysteine methyl ester (**18d**), conversion to *N*-PhF-L-alanine (**28**) and comparison of its specific rotation with the literature value was used to estimate purity. Cleavage of the S—C bond with Raney nickel in EtOAc at reflux for 6 h gave *N*-PhF-L-alanine methyl ester (**27**). Hydrolysis of *N*-PhF-L-alanine methyl ester (**27**) with 1 N NaOH in ethanol for 1 h gave *N*-PhF-L-alanine (**28**) in 74% overall yield from **18d** (Fig. 3). The specific rotation of *N*-PhF-L-alanine (**28**) and comparison with its literature value (9) ($[\alpha]_D^{20}$ 150° (*c* 0.2, $CHCl_3$), lit. (9) $[[\alpha]_D^{20}$ 163° (*c* 1, $CHCl_3$)) demonstrated that the material from sulfamidate opening was significantly enriched with one enantiomer.

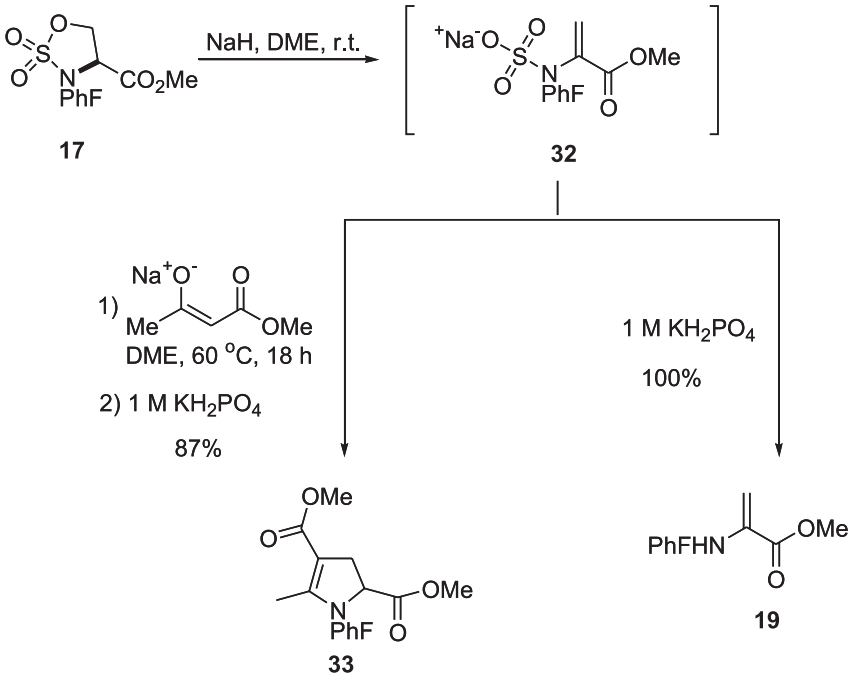
The enantiomeric purity of (2*S*)-methyl 3-(1-imidazol)-2-[*N*-(PhF)amino]propionate (**18f**) was determined after conversion to diastereomeric amides **30**, and subsequent spectral analysis. (2*S*)-3-(1-Imidazol)-2-[*N*-(PhF)amino]propionic acid (**29**) was first synthesized by ester hydrolysis in 86% yield using 1 N NaOH in EtOH. Acid **29** was coupled to L- and D-phenylalanine methyl ester in MeCN with TBTU and DIEA, respectively, at room temperature. Measurement of the methyl ester singlets at 3.71 and 3.76 ppm in $CDCl_3$ by 400 MHz ^{1}H NMR spectroscopy demonstrated **30** to be of >97% diastereomeric excess. Hence, (2*S*)-methyl 3-(1-imidazol)-2-[*N*-(PhF)amino]propionate (**18f**) is presumed to be of >97% enantiomeric purity. We consider, therefore, that no racemization occurred during nucleophilic substitution on cyclic sulfamidate **17** with imidazole nor with potassium thiocyanate nor with azide ion as nucleophiles.

The enantiomeric purity of *cis*-*N*-(BOC)-5-methylproline (*cis*-**22**) was studied after conversion to diastereomeric α-methylbenzylamides **31** by coupling, respectively, to *R*- and *S*-α-methylbenzylamine in MeCN with TBTU followed by removal of the BOC group with 10% TFA in CH_2Cl_2 (Fig. 3). In the ^{1}H NMR spectra of α-methylbenzylamides **31**, the diastereomeric methyl doublets were resolved and came at 1.50 and 1.49 ppm, as well as at 1.46 and 1.42 ppm. Integration of these doublets indicated that **31** was of only 10% diastereomeric excess.

In contrast to the amino acid syntheses using less basic nucleophiles, racemization had evidently occurred during the preparation of *cis*-*N*-(BOC)-5-methylproline **22**. The source of the loss of configurational integrity was narrowed down to the ring opening step after measurement of the specific rotation of δ-keto α-amino ester **20m**, which showed a considerable drop in optical purity ($[\alpha]_D^{20}$ –1.2° (*c* 0.8, $CHCl_3$), lit. (29) $[\alpha]_D^{20}$ –137.7° (*c* 1, MeOH)). Because hydrolysis and decarboxylation of β-keto ester **18m**, prepared from a route featuring acylation of *N*-(PhF)glutamate γ-methyl ester (32), produced enantiopure **20m** ($[\alpha]_D^{20}$ –139° (*c* 0.8, MeOH)), we considered that racemization occurred prior to or during the nucleophilic addition to cyclic sulfamidate **17** and not at the hydrolysis and decarboxylation steps.

© 2001 NRC Canada

Scheme 4. Michael addition of methyl acetoacetate enolate to dehydroalanine sulfamic acid **33**.



Low specific rotation values were also recorded for δ-keto α-amino ester **20k** ($[\alpha]_D^{20}$ –4.8° (*c* 0.15, $CHCl_3$)), pyrazole amino acid **25** ($[\alpha]_D^{20}$ –9.5° (*c* 0.2, MeOH)), and malonate **18i** ($[\alpha]_D^{20}$–4.3° (*c* 0.1, $CHCl_3$)). Because of the characteristically high specific rotations of *N*-(PhF)-α-amino carboxylates (9, 23, 27–29, 32, 33), racemization may be inferred to have occurred in these cases.

Dehydroalanine **19** was formed on ring opening of cyclic sulfamidate **17** by β-elimination induced with a variety of nucleophiles (Table 2). Postulating that the presumed dehydroalanine intermediate **32** could serve as a Michael acceptor for the formation of racemic β-keto ester, we treated sulfamidate **17** with 200 mol% of sodium hydride in DME to induce elimination (Scheme 4). A premixed solution of methyl acetoacetate (300 mol%) and NaH (400 mol%) in DME was then added to the reaction mixture which was heated at 60°C for 18 h. Hydrolysis of the polar sulfamic acid intermediate with 1 M KH_2PO_4 furnished (5*RS*)-methyl *N*-PhF-2-methyl-3-(methyloxy)carbonyl-Δ^2-pyrroline (**33**) in 87% yield. Previously, pyrroline **33** was encountered in the direct ring opening of sulfamidate **17** with the preformed enolate of methyl acetoacetate when the hot reaction mixture was quenched with 1 M KH_2PO_4. Its formation can be avoided by cooling the reaction mixture to room temperature prior to hydrolysis of the sulfamic acid; however, we elected to form pyrroline **33** in the present sequence because it was easier to characterize. Formation of **33** demonstrated that dehydroalanine **19** could serve as a prochiral intermediate for the formation of racemized amino acid product. To verify if sulfamidate racemized prior to ring opening, aliquots were taken at different time intervals from the reaction mixture containing **17** and the preformed enolate of methyl acetoacetate in DME at 60°C. No loss of configurational integrity of sulfamidate **17** was detected after 1 and 2 h of reaction as ascertained by measurement of its specific rotation after isolation by chromatography. Hence, α-deprotonation triggers β-elimination prior to reprotonation and racemization of **17**.

A mechanism that may explain the cause of racemization involves the nucleophile acting as base and removing the α-proton to trigger ring opening with elimination. A second nucleophile may then attack **32** to furnish β-keto ester by a Michael addition (Scheme 5). On the other hand, because (2*S*)-methyl 4-(1-imidazol)-2-[*N*-(PhF)amino]propionate (**18f**) was shown to be of >97% enantiomeric purity, ring opening of cyclic sulfamidate **17** with less basic nucleophiles should involve only nucleophilic displacement.

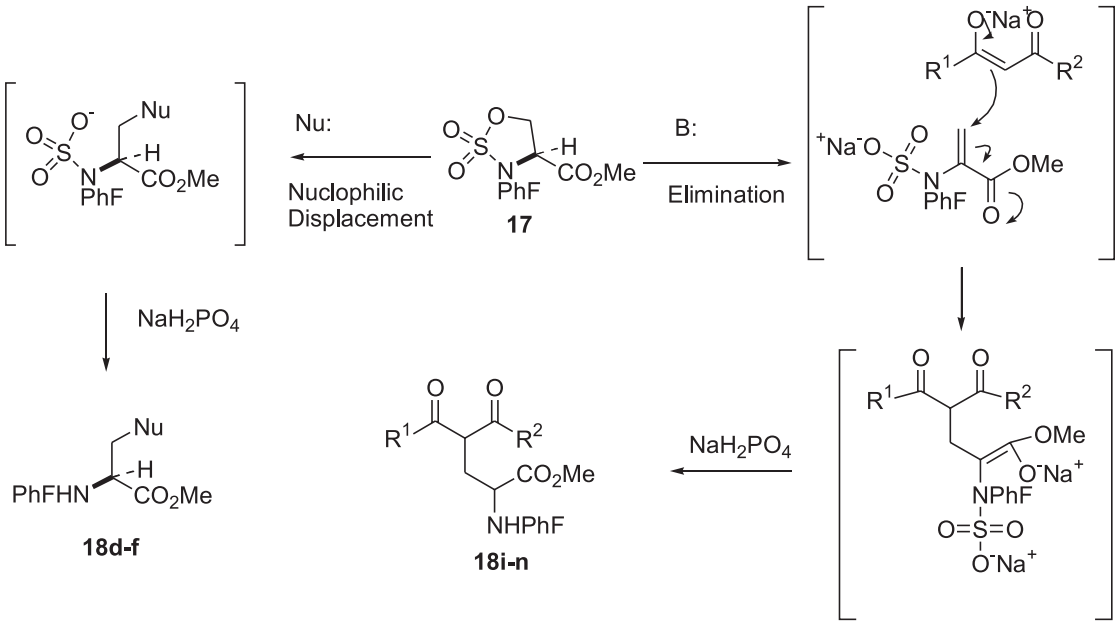
The formation of *N*-(PhF)dehydroalanine **19** by β-elimination on sulfamidate **17** is remarkable in light of a previous report in which the PhF group was found to completely suppress elimination during Mitsunobu reactions on the alcohol of *N*-(PhF)serine methyl ester **15** (34). The related β-*N*-(PhF)enamino ester has previously been reported; however, removal of the α-proton was not required for its formation via base induced rearrangement of dimethyl *N*-(PhF)-3,4-didehydroglutamate (33). In the X-ray crystal structure of cyclic sulfamidite **16**, the α-proton and β-hydroxyl group from serine are constrained in a nearly coplanar geometry within the five-membered ring. Most likely, sulfamidate **17** adopts a similar geometry that can favour orbital overlap facilitating β-elimination. Finally, pyroglutamate **14** should also be considered to be of suspect enantiomeric purity, because dehydoalanine product was encountered in its synthesis using sulfamidate derived from *N*-(Bn)serine *tert*-butyl ester (1).

Conclusion

Five-membered cyclic sulfamidate **17** was synthesized from serine in good yield. Ring opening of five-membered cyclic sulfamidate was achieved using a variety of nucleophiles

© 2001 NRC Canada

Scheme 5. Proposed mechanisms for the ring opening of sulfamidate **17.**



including β-keto esters, β-keto ketones, dimethyl malonate, nitroethane, sodium azide, imidazole, and potassium thiocyanate. A careful analysis of the enantiomeric purity of the products from ring opening of five-member cyclic sulfamidate **17** was performed using optical measurements as well as conversion of particular products to diastereomeric derivatives that were analyzed by NMR spectroscopy. Direct nucleophilic displacement and β-elimination followed by Michael addition were both found to be favoured mechanisms for the additions of different nucleophiles to **23**, which formed enantiopure and racemic amino acid product, respectively. Verification of product enantiomeric purity is thus essential when using serine-derived cyclic sulfamidates as chiral educts for amino acid synthesis.

Supporting information available: ^{1}H and ^{13}C NMR spectra for key compounds.[2]

Experimental section

General

Unless otherwise noted, all reactions were run under nitrogen atmosphere and distilled solvents were transferred by syringe. Tetrahydrofuran (THF) and ether were distilled from sodium–benzophenone immediately before use; 1,1,1,3,3,3-hexamethyldisilazane (HMDS) and CH_2Cl_2 were distilled from CaH_2; Et_3N was distilled from BaO. Final reaction mixture solutions were dried over Na_2SO_4. Chromatography was on 230–400 mesh silica gel; thin layer chromatography (TLC) on aluminum-backed silica plates. Melting points are uncorrected. Mass spectral data, HRMS (EI and FAB), were obtained by the Université de Montréal Mass Spectroscopy facility. ^{1}H NMR (300 and 400 MHz) and ^{13}C NMR (75 and 100 MHz) spectra were recorded in $CDCl_3$. Chemical shifts are reported in ppm (δ units) downfield of internal tetramethylsilane ($(CH_3)_4Si$). Coupling constants are given in Hz. Chemical shifts for aromatic PhF carbons are not reported.

*(2*R*,4*S*)-Methyl 2-oxo-3-(PhF)-1,2,3-oxathiazolidine-4-carboxylate ((2*R*)-**16**) and (2*S*,4*S*)-methyl 2-oxo-3-(PhF)-1,2,3-oxathiazolidine-4-carboxylate ((2*S*)-**16**)*

A solution of *N*-PhF-L-serine methyl ester ((*S*)-**15**, 3.57 g, 10 mmol, prepared according to ref. 23) in 150 mL of dichloromethane was cooled to 0°C, treated with imidazole (2.7 g, 40 mmol) followed by triethylamine (2.8 mL, 20 mmol), stirred for 10 min, then treated with thionyl chloride (0.8 mL, 11 mmol). After stirring an additional 45 min, water (100 mL) was added and the phases were separated. The aqueous phase was extracted with dichloromethane (3 × 50 mL) and the combined organic fractions were washed with water (2 × 50 mL), dried, filtered, and evaporated. The residue was normally used without purification in the next reaction. Purification of the residue by chromatography on silica gel with an eluant of 20–30% EtOAc in hexane provided 4 g (99%) of a 1:2 mixture of diastereomers ((2*R*)-**16** and (2*S*)-**16**). First to elute was (2*R*)-**16**: mp 83–84°C. $[\alpha]_D^{20}$ 121° (*c* 0.14, $CHCl_3$). TLC: R_f = 0.54 (30% EtOAc in hexanes). ^{1}H NMR δ: 3.42 (s, 3H), 3.51 (dd, 1H, *J* = 1.4, 7.1), 4.41 (dd, 1H, *J* = 1.4, 9.4), 4.75 (dd, 1H, *J* = 7.1, 9.4), 7.17–8.17 (m, 13H). ^{13}C NMR δ: 52.1, 59.0, 72.2, 75.2, 171.4. HRMS calcd. for $C_{23}H_{20}O_4NS$ (MH^+): 406.1113; found: 406.1130. Next to elute was (2*S*)-**16**: mp 71–72°C. $[\alpha]_D^{20}$ 243° (*c* 0.38, $CHCl_3$). TLC: R_f = 0.37 (30% EtOAc in hexanes). ^{1}H NMR δ: 3.37 (t, 1H, *J* = 7.9), 3.57 (s, 3H), 4.32 (t, 1H, *J* = 7.9), 4.95 (t, 1H, *J* = 7.9), 7.19–7.77 (m, 13H). ^{13}C NMR δ: 52.5, 61.3, 73.5, 76.2, 170.3. HRMS calcd. for $C_{23}H_{19}O_4NS$ (M^+): 405.1035; found: 405.1046.

*(4S)-Methyl 2,2-dioxo-3-PhF-1,2,3-oxathiazolidine-4-carboxylate (**17**)*

A solution of 2-oxo-1,2,3-oxathiazolidine **16** (1.25 g, 3.1 mmol) in 100 mL of acetonitrile was cooled to 0°C, treated with ruthenium(III) chloride monohydrate (10 mg) followed by sodium periodate (1.28 g, 6 mmol), stirred 10 min, and quenched with water (100 mL). After stirring for 4 h, the reaction mixture was diluted with ether

© 2001 NRC Canada

(100 mL) and the phases were separated. The aqueous phase was extracted with ether (3 × 60 mL). The combined organic fractions were washed with saturated aqueous sodium bicarbonate (100 mL) and brine (50 mL), dried, filtered, and evaporated to a residue that was purified by chromatography on silica gel with an eluant of 10–20% EtOAc in hexane. Evaporation of the collected fractions provided 1.14 g (87%) of **17**: mp 155–156°C. $[\alpha]_D^{20}$ 244° (*c* 0.1, $CHCl_3$). ^{1}H NMR δ: 3.64 (dd, 1H, *J* = 4.0, 8.2), 3.69 (s, 3H), 4.02 (dd, 1H, *J* = 8.2, 8.7), 4.38 (dd, 1H, *J* = 4.0, 8.7), 7.19–8.22 (m, 13H). ^{13}C NMR δ: 52.9, 58.8, 66.8, 77.9, 169.2. HRMS calcd. for $C_{23}H_{19}O_5NS$ (M^+): 421.0984; found: 421.0997.

*(2*S*)-*N*-*PhF*-*S*-cyanocysteine methyl ester (**18d**)*

A solution of (4*S*)-methyl 2,2-dioxo-3-PhF-1,2,3-oxathiazolidine-4-carboxylate (**17**, 48 mg, 0.12 mmol) in 5 mL of DMF was treated with potassium thiocynate 35 mg (0.36 mmol), stirred at room temperature for 36 h, poured into 1 M KH_2PO_4 (20 mL), and extracted with EtOAc (3 × 20 mL). The combined organic phase was washed with brine (20 mL), dried, filtered, and evaporated to a residue that was chromatographed on silica gel eluting with a gradient of 15–20% EtOAc in hexane. Concentration of the collected fractions provided 34.8 mg (72%) of **18d**: mp 149–150°C. $[\alpha]_D^{20}$ –287° (*c* 0.4, $CHCl_3$). ^{1}H NMR δ: 2.88 (dd, 1H, *J* = 4.7, 12.6,), 3.02 (dd, 1H, *J* = 4.7, 5.8), 3.13 (dd, 1H, *J* = 5.8, 12.6), 3.44 (brs, 1H), 3.48 (s, 3H), 7.23–7.75 (m, 13H). ^{13}C NMR δ: 39.5, 52.6, 54.9, 72.8, 112.8, 172.6. HRMS calcd. for $C_{24}H_{21}O_2SN_2$ (MH^+): 401.1324; found: 401.1339.

*(2*S*)-*N*-*(PhF)-3-azido-alanine methyl ester (**18e**)*

A solution of (4*S*)-methyl 2,2-dioxo-3-PhF-1,2,3-oxathiazolidine-4-carboxylate (**17**, 49 mg, 0.12 mmol) in 5 mL of DMF was treated with sodium azide (24 mg, 0.37 mmol), stirred at room temperature for 1 h, poured into 1 M KH_2PO_4 (20 mL), and extracted with EtOAc (2 × 10 mL). The combined organic phase was washed with brine (10 mL), dried, filtered, and evaporated to a residue that was chromatographed on silica gel eluting with a gradient of 10–20% EtOAc in hexane. Concentration of the collected fractions provided 40.3 mg (90%) of **18e** as a thick clear oil. $[\alpha]_D^{20}$ –294° (*c* 0.12, $CHCl_3$). ^{1}H NMR δ: 2.85 (dd, 1H, *J* = 4.7, 5.3), 3.07 (dd, 1H, *J* = 4.7, 12.3), 3.18 (dd, 1H, *J* = 5.3, 12.3), 3.42 (s, 3H), 7.21–7.73 (m, 13H). ^{13}C NMR δ: 52.2, 54.5, 56.4, 73.0, 173.6. HRMS calcd. for $C_{23}H_{21}O_2N_4$ (MH^+): 385.1664; found: 385.1677.

*(2*S*)-Methyl 3-(1-imidazol)-2-[*N*-(PhF)amino]propionate (**18f**)*

A solution of (4*S*)-methyl 2,2-dioxo-3-PhF-1,2,3-oxathiazolidine-4-carboxylate (**17**, 100 mg, 0.24 mmol) in 15 mL of DME was treated with imidazole (49 mg, 0.72 mmol), heated at 80°C for 18 h, poured into 1 M KH_2PO_4 (30 mL), and extracted with EtOAc (3 × 20 mL). The combined organic phase was washed with brine (20 mL), dried, filtered, and evaporated to a residue that was chromatographed on silica gel eluting with a gradient of 5–10% MeOH in EtOAc. Concentration of the collected fractions provided 83.2 mg (85%) of **18f**: mp 146–147°C. $[\alpha]_D^{20}$ –241° (*c* 0.1, $CHCl_3$). MS (*m*/*z*): 410.2 (M + 1), 307.1, 289.1, 257.1, 241.1, 154.1. ^{1}H NMR δ: 2.85 (m, 1H), 3.16 (brs, 1H), 3.35 (s, 3H), 3.83 (dd, 1H, *J* = 4.9, 14.0), 3.94 (dd, 1H, *J* = 6.7, 14.0), 7.01–7.72 (m, 16H). ^{13}C NMR δ: 50.8, 52.3, 56.7, 72.9, 119.7, 128.4, 137.5, 173.4.

General procedure for ring opening of cyclic sulfamidate 17 with β-keto esters, β-keto ketones, and dimethyl malonate

A solution of sodium hydride (prewashed with hexane, 60 wt% in oil, 85 mg, 2.1 mmol) in DME (15 mL) was treated with the respective β-keto ester, β-keto ketone, or dimethyl malonate (3.6 mmol), stirred for 10 min, treated with (4*S*)-methyl 2,2-dioxo-3-PhF-1,2,3-oxathiazolidine-4-carboxylate (**17**, 380 mg, 0.9 mmol), heated at 60°C for 18 h, cooled to room temperature, and poured into 1 M NaH_2PO_4 (50 mL). The mixture was extracted with EtOAc (3 × 50 mL). The combined organic phases were washed with brine (2 × 30 mL), dried, filtered, and evaporated to a residue.

*Methyl 5-oxo-4-(methylcarbonyl)-2-[*N*-(PhF)amino]hexanoate (**18i**)*

Methyl 5-oxo-4-(methylcarbonyl)-2-[*N*-(PhF)amino]hexanoate (**18i**) was prepared from 2,4-pentanedione and used directly in next step. HRMS calcd. for $C_{28}H_{28}O_4N$ (MH^+): 442.2018; found: 442.2033.

*Methyl 5-oxo-4-(phenylcarbonyl)-2-[*N*-(PhF)amino]hexanoate (**18j**)*

Methyl 5-oxo-4-(phenylcarbonyl)-2-[*N*-(PhF)amino]hexanoate (**18j**) was prepared from 1-benzoyl acetone and isolated by chromatography on silica gel eluting with a gradient of 10–20% EtOAc in hexane as a 1.1:1 mixture of diastereomers in 45% yield. ^{1}H NMR δ: 2.00 (s, 3H), 2.07 (m, 4H), 2.17 (s, 3H), 2.58 (m, 2H), 3.26 (s, 3H), 3.28 (s, 3H), 4.78 (t, 1H, *J* = 6.0), 4.83 (dd, 1H, *J* = 4.8, 7.4), 6.70–8.26 (m, 36H). ^{13}C NMR δ: 28.0, 28.7, 33.0, 33.2, 51.69, 51.73, 53.8, 54.5, 59.1, 59.3, 72.7, 72.8, 176.0 (2C), 195.0, 196.1, 202.9, 203.6. HRMS calcd. for $C_{33}H_{30}O_4N$ (MH^+): 504.2175; found: 504.2153.

*Methyl 5-oxo-4-(methyloxycarbonyl)-2-[*N*-(PhF)amino]hexanoate (**18k**)*

Methyl 5-oxo-4-(methyloxycarbonyl)-2-[*N*-(PhF)amino]hexanoate (**18k**) was prepared from methyl acetoacetate and used directly in next step. HRMS calcd. for $C_{28}H_{28}O_5N$ (MH^+): 458.1968; found: 458.1982.

*Methyl 5-oxo-4-(ethyloxycarbonyl)-2-[*N*-(PhF)amino]heptanoate (**18l**)*

Methyl 5-oxo-4-(ethyloxycarbonyl)-2-[*N*-(PhF)amino]heptanoate (**18l**) was prepared from ethyl propionylacetate and isolated as an inseparable 1.1:1 mixture of diastereomers by chromatography on silica gel eluting with a gradient of 10–20% EtOAc in hexane in 82% yield. ^{1}H NMR δ: 0.98 (t, 3H, *J* = 7.2), 1.11 (t, 3H, *J* = 7.2), 1.19 (t, 3H, *J* = 7.2), 1.28 (t, 3H, *J* = 7.2), 1.91–1.99 (m, 4H), 2.32–2.39 (m, 2H), 2.52–2.68 (m, 4H), 3.24 (s, 3H), 3.25 (s, 3H), 3.67 (t, 1H, *J* = 6.4), 3.89–4.10 (m, 3H), 4.23 (dd, 2H, *J* = 7.2, 14.1), 7.14–7.70 (m, 26H). ^{13}C NMR δ: 7.35, 7.59, 13.8, 13.9, 32.5, 32.7, 35.1, 35.3, 51.3, 51.6, 53.6, 54.1, 54.9, 55.6, 61.1, 61.4, 72.6, 72.7, 169.0, 169.7, 175.9, 176.0, 204.6, 205.5. HRMS calcd. for $C_{30}H_{31}O_5NNa$ (M^+ + Na): 508.2100; found: 508.2116.

© 2001 NRC Canada

*Methyl 6,6-dimethyl-5-oxo-4-(ethyloxycarbonyl)-2-[*N*-(PhF)amino]heptanoate (**18m**)*

Methyl 6,6-dimethyl-5-oxo-4-(ethyloxycarbonyl)-2-[*N*-(PhF)amino]heptanoate (**18m**) was prepared from ethyl pivaloylacetate and isolated as an 1:1 mixture of diastereomers by chromatography on silica gel eluting with a gradient of 10–20% EtOAc in hexane in 63% yield. ^{1}H NMR δ: 1.10 (s, 9H), 1.13 (t, 3H, *J* = 7.1), 1.27 (t, 3H, *J* = 7.1), 1.31 (s, 9H), 1.48 (m, 1H), 1.58 (m, 1H), 2.03 (m, 1H), 2.33 (m, 1H), 2.60 (m, 2H), 3.26 (s, 6H), 3.81–3.98 (m, 3H), 4.24 (q, 2H, *J* = 7.1), 4.45 (dd, 1H, *J* = 2.4, 10.4), 7.14–7.71 (m, 26H). ^{13}C NMR δ: 13.7, 14.0, 26.0, 26.2, 33.5, 34.4, 45.3, 45.6, 47.9, 49.8, 51.5, 51.7, 53.6, 54.6, 60.8, 61.2, 72.6, 72.8, 168.9, 169.5, 175.4, 176.5, 209.9, 210.5. HRMS calcd. for $C_{32}H_{35}O_5NNa$ (M^+ + Na): 536.2413; found: 536.2392.

*4-(Methyloxycarbonyl)-2-[*N*-(PhF)]glutamate dimethyl ester (**18n**)*

4-(Methyloxycarbonyl)-2-[*N*-(PhF)]glutamate dimethyl ester (**18n**) was prepared from dimethyl malonate and isolated as a 1:1 mixture of diastereomers by chromatography on silica gel eluting with a gradient of 10–20% EtOAc in hexane in 65% yield. ^{1}H NMR δ: 2.03 (m, 2H), 2.61 (dd, 1H, *J* = 4.7, 8.9), 3.20 (s, 3H), 3.36 (s, 3H), 3.57 (s, 3H), 3.73 (m, 1H), 7.11–7.67 (m, 13H). ^{13}C NMR δ: 33.3, 48.3, 51.5, 52.3, 52.5, 53.7, 72.6, 166.8, 169.0, 169.8. HRMS calcd. for $C_{28}H_{27}O_6NNa$ (M^+ + Na): 496.1736; found: 496.1728.

*Methyl 4-nitro-2-[*N*-(PhF)amino]pentanoate (**18o**)*

A solution of sodium hydride (prewashed with hexane, 60 wt% in oil, 40 mg, 1 mmol) in DME (12 mL) was treated with nitroethane (0.2 mL, 2.8 mmol), stirred at 60°C for 3 h, treated with (4*S*)-methyl 2,2-dioxo-3-PhF-1,2,3-oxathiazolidine-4-carboxylate (**17**, 100 mg, 0.24 mmol), heated at 60°C for 36 h, cooled to room temperature, and poured into 1 M NaH_2PO_4 (30 mL). The mixture was extracted with EtOAc (3 × 30 mL), and the combined organic phases were washed with brine (2 × 30 mL), dried, filtered, and evaporated. Purification of the residue by chromatography on silica gel with an eluant of 0–20% EtOAc in hexane provided 52 mg (52%) of a 10:1 mixture of diastereomers **18o**. The spectra data for the major isomer was as follows. ^{1}H NMR δ: 1.51 (d, 3H, *J* = 6.9), 1.73 (ddd, 1H, *J* = 3.4, 9.4, 14.8), 2.16 (ddd, 1H, *J* = 4.2, 9.1, 14.8), 2.64 (dd, 1H, *J* = 3.4, 9.1), 3.25 (s, 3H), 4.92 (m, 1H), 7.15–7.71 (m, 13H). ^{13}C NMR δ: 20.3, 39.1, 51.8, 52.6, 72.6, 79.4, 175.6. HRMS calcd. for $C_{25}H_{25}O_4N_2$ (MH^+): 417.1814; found: 417.1826.

*Methyl 5-oxo-2-[*N*-(PhF)amino]hexanoate (**20k**)*

Crude methyl 5-oxo-4-(methyloxycarbonyl)-2-[*N*-(PhF)amino]hexanoate (**18k**) was dissolved in EtOH (10 mL), treated with 1 N NaOH (10 mL), and heated at a reflux for 5 h. The mixture was cooled to room temperature and adjusted to pH 5 using 10% HCl. The solution was extracted with EtOAc (3 × 30 mL) and the combined organic phases were washed with brine (30 mL), dried, filtered, and evaporated to a residue that was dissolved in acetonitrile (20 mL), treated with K_2CO_3 (300 mg, 2.2 mmol) and iodomethane (0.3 mL, 4.8 mmol), and stirred at room temperature for 18 h. Brine (50 mL) was added to the reaction mixture, which was extracted with EtOAc (3 × 30 mL). The organic phases were combined, washed with 0.65 M sodium thiosulfate (50 mL) and brine (50 mL), dried, filtered, and evaporated to a residue that was purified by chromatography on silica gel using a gradient of 10–20% EtOAc in hexane. Evaporation of the collected fractions gave 259 mg (71% overall from **17**) of **20k**. ^{1}H NMR δ: 1.71 (m, 2H), 2.11 (s, 3H), 2.45–2.61 (m, 3H), 3.29 (s, 3H), 7.18–7.73 (m, 13H). ^{13}C NMR δ: 28.6, 29.8, 39.6, 51.5, 54.6, 72.8, 176.3, 207.8. HRMS calcd. for $C_{26}H_{26}O_3N$ (MH^+): 400.1913; found: 400.1905.

cis-N-*(BOC)-5-methylproline methyl ester (*cis-***21***)*

A solution of methyl 5-oxo-2-[*N*-(PhF)amino]hexanoate (**20k**, 400 mg, 1 mmol) and di-*tert*-butyldicarbonate (670 mg, 3 mmol) in MeOH (50 mL) was placed into a hydrogenation vessel and treated with palladium-on-carbon (10 wt%, 65 mg). The vessel was filled, vented and filled three times with hydrogen, and the mixture was stirred under 4 atm of hydrogen for 48 h. The mixture was filtered on Celite™ and washed with MeOH (50 mL). The combined organic phase was evaporated to a residue that was purified by chromatography on silica gel using a gradient of 10–15% EtOAc in hexane. Evaporation of the collected fractions gave 225 mg (92%) of *cis*-**21** as an oil. ^{1}H NMR δ (showed a mixture of carbamate isomers): 1.24 (d, 6H, *J* = 6.2), 1.38 (s, 9H), 1.42 (s, 9H), 1.58 (m, 2H), 1.97 (m, 4H), 2.14 (m, 2H), 3.68 (s, 6H), 3.86 (m, 1H), 3.98 (m, 1H), 4.16 (m, 1H), 4.27 (m, 1H). ^{13}C NMR δ (showed a mixture of carbamate isomers): 19.7, 20.5, 28.3, 28.7, 31.6, 32.4, 51.9, 53.9, 59.7, 60.0, 79.5, 158.2, 159.0, 173.0, 173.9. HRMS calcd. for $C_{12}H_{22}O_4N$ (MH^+): 244.1549; found: 244.1556.

cis-N-*(BOC)-5-methylproline (*cis-***22***)*

Methyl ester **21** (110 mg, 0.45 mmol) was dissolved in 10 mL of Et_2O, treated with $KOSi(Me)_3$ (70 mg, 0.55 mmol) and stirred for 18 h at room temperature. The reaction mixture was extracted with water (5 × 20 mL), and the aqueous phases were combined, acidified with acetic acid to pH 2, saturated with NaCl, and extracted with EtOAc (3 × 30 mL). The organic phases were combined, dried, filtered, and evaporated to give 99.4 mg (0.43 mmol, 96%) of *cis*-**22**. ^{1}H NMR (CD_3OD) δ (showed a mixture of carbamate isomers): 1.27 (d, 3H, *J* = 6.2), 1.42 (brs, 9H), 1.65 (m, 1H), 2.02 (m, 2H), 2.23 (m, 1H), 3.96 (m, 1H), 4.18 (m, 1H). ^{13}C NMR (CD_3OD) δ (showed a mixture of carbamate isomers): 20.1, 20.9, 28.6, 28.8, 29.3, 29.8, 32.7, 33.4, 49.6, 49.8, 55.4, 55.7, 61.2, 61.5, 81.2, 81.3, 155.4, 155.8, 176.6, 176.8. HRMS calcd. for $C_{11}H_{20}O_4N$ (MH^+): 230.1392; found: 230.1385.

Enantiomeric purity of cis-N-*(BOC)-5-methylproline (*cis-***22***)*

A room-temperature solution of *cis-N*-(BOC)-5-methylproline (*cis*-**22**, 20 mg, 0.09 mmol) and either (*R*) or (*S*)-α-methylbenzylamine (28 μL, 0.22 mmol) in 1 mL of acetonitrile was treated with benzotriazol-1-yl-1,1,3,3-tetramethyluronium tetrafluoroborate (30 mg, 0.09 mmol) and stirred for 2 h when TLC showed complete disappearance of the starting acid. Brine (2 mL) was added to the reaction mixture, which was then extracted with EtOAc (2 ×

© 2001 NRC Canada

3 mL). The combined organic phase was extracted with 2 N HCl (2 × 2 mL) and $NaHCO_3$ (2 × 2 mL), washed with H_2O (2 × 2 mL) and brine, dried, filtered, and evaporated to a residue that was dissolved in CH_2Cl_2 (5 mL), treated with 0.5 mL TFA, and stirred at room temperature for 1 h. The solution was concentrated, dried, and directly examined by ^{1}H NMR spectroscopy. When (*S*)- and (*R*)-α-methylbenzylamine of 99% diastereomeric purity were used, respectively, the same mixture of diastereomers were obtained. Examination of the methyl doublets at 1.50, 1.49, 1.46, and 1.42 ppm in the ^{1}H NMR spectra in $CDCl_3$ demonstrated **31** to be of 1.1:1 mixture of diastereomers. Hence, *cis*-**22** is presumed to be of 10% enantiomeric excess.

5-Methylproline N′-α-*methyl-benzylamide trifloroacetate (**31**)*

^{1}H NMR (CD_3OD) δ: 1.42 (d, 3H, *J* = 6.6), 1.46 (d, 3H, *J* = 6.6), 1.49 (d, 3H, *J* = 7.0), 1.50 (d, 3H, *J* = 7.0), 1.60 (m, 1H), 1.73 (m, 1H), 2.04 (m, 1H), 2.19 (m, 3H), 2.42 (m, 2H), 3.74 (m, 2H), 4.31 (m, 2H), 5.04 (m, 2H), 7.22–7.37 (m, 10H).

*Methyl [*N*-(PhF)amino]-3-(3,5-dimethyl-2*H*-pyrazol-4-yl)propanoate (**24**)*

Crude methyl 5-oxo-4-(methylcarbonyl)-2-[*N*-(PhF)amino]hexanoate (**18i**) was dissolved in dioxane (10 mL), treated with hydrazine hydrate (60 μL, 1.7 mmol), stirred for 1.5 h, and poured into 1 M NaH_2PO_4 (30 mL). The mixture was extracted with EtOAc (3 × 20 mL), and the combined organic phase was washed with brine (2 × 30 mL), dried, filtered, and evaporated. The residue was normally used without purification in the next reaction. Purification of the residue by chromatography on silica gel with an eluant of 20–30% EtOAc in hexane provided 169 mg (43% overall from **17**) of **24**. ^{1}H NMR δ: 1.99 (s, 6H), 2.50 (m, 2H), 2.58 (m, 1H), 3.22 (s, 3H), 6.73–7.69 (m, 13H). ^{13}C NMR δ: 10.5, 28.8, 51.4, 56.0, 72.9, 111.1, 142.8, 176.6. HRMS calcd. for $C_{28}H_{28}O_2N_3$ (MH^+): 438.2181; found: 438.2189.

*2-*N*-(PhF)Amino-3-(3,5-dimethyl-1*H*-pyrazol-4-yl)propionic acid (**25**)*

Crude methyl [*N*-(PhF)amino]-3-(3,5-dimethyl-2*H*-pyrazol-4-yl)propanoate (**24**) was dissolved in EtOH (5 mL), treated with 1 N NaOH (5 mL), heated at 60°C for 3 h, cooled to room temperature, and then poured into 1 M NaH_2PO_4 (50 mL). The mixture was extracted with EtOAc (2 × 30 mL). The combined organic phases were extracted with 1 N NaOH (2 × 30 mL), the aqueous phase was combined, acidified with citric acid to pH 2, and extracted with EtOAc (2 × 30 mL). The organic phases were combined, dried, filtered, and evaporated to a residue that was purified by chromatography on silica gel with a gradient of 10–20% MeOH in EtOAc as eluant. Evaporation of the collected fractions gave 143 mg (37% over all from **17**) of **25**. ^{1}H NMR (CD_3OD) δ: 1.95 (s, 6H), 2.50–2.54 (m, 3H), 6.61–7.72 (m, 13H). ^{13}C NMR (CD_3OD) δ: 10.5, 29.9, 57.7, 74.3, 112.6, 144.1, 179.1. HRMS calcd. for $C_{27}H_{26}N_3O_2$ (MH^+): 424.2025; found: 424.2043.

*Amino-3-(3,5-dimethyl-1*H*-pyrazol-4-yl)propionic acid (**26**)*

2-[*N*-(PhF)Amino]-3-(3,5-dimethyl-1*H*-pyrazol-4-yl)propionic acid (**25**, 143 mg, 0.34 mmol) was dissolved in 10 mL of CH_2Cl_2, treated with 2 mL of CF_3CO_2H, and heated at a reflux for 18 h. The volatiles were evaporated, and the residue was treated with 10 mL of H_2O and filtered. The aqueous solution was washed with hexanes (2 × 20 mL), and then evaporated to a solid 55 mg (88%) of **26**. ^{1}H NMR (CD_3OD) δ: 2.39 (s, 6H), 3.07 (dd, 1H, *J* = 7.2, 15.3), 3.19 (dd, 1H, *J* = 7.2, 15.3), 4.13 (t, 1H, *J* = 7.2). ^{13}C NMR (CD_3OD) δ: 9.7, 24.6, 53.4, 113.2, 146.1, 170.9. HRMS calcd. for $C_8H_{14}N_3O_2$ (MH^+): 184.1086; found: 184.1090.

*(2*S*)-*N*-PhF-Alanine methyl ester (**27**)*

(2*S*)-*N*-(PhF)-*S*-Cyanocysteine methyl ester (**18d**, 35 mg, 0.09 mmol) was dissolved in EtOAc (10 mL) and treated with Raney nickel (50% slurry in water, ≈ 200 mg). The mixture was heated at a reflux for 6 h, cooled to room temperature, and filtered through Celite™ to remove the catalyst. The filtrate was concentrated. The residue was used without purification in the next reaction. ^{1}H NMR δ: 1.14 (d, 3H, *J* = 7.0), 2.79 (dd, 1H, *J* = 7.0, 14.1), 3.31 (s, 3H), 7.17–7.73 (m, 13H).

*(2*S*)-*N*-PhF-Alanine (**28**)*

Crude (2*S*)-*N*-PhF-alanine methyl ester (**27**) was dissolved in ethanol (5 mL), treated with 1 N NaOH (5 mL), and heated at 75°C for 1 h. The mixture was cooled to room temperature, poured into 1 M KH_2PO_4 (20 mL), and extracted with EtOAc (3 × 20 mL). The combined organic phase was washed with brine (2 × 10 mL), dried, filtered, and evaporated to a residue. Purification of the residue by chromatography on silica gel with an eluant of 60–70% EtOAc in hexane provided 22 mg (74% overall from **18d**) of **28**. $[\alpha]_D^{20}$ 150° (*c* 0.2, $CHCl_3$), lit. (9) $[\alpha]_D^{20}$ 163° (*c* 1, $CHCl_3$). ^{1}H NMR δ: 1.13 (d, 3H, *J* = 7.2), 2.71 (q, 1H, *J* = 7.2), 7.18–7.75 (m, 13H). ^{13}C NMR δ: 19.7, 52.2, 73.0, 175.9.

*(2*S*)-3-(1-Imidazol)-2-[*N*-(PhF)amino]propionic acid (**29**)*

Ester hydrolysis was performed on **18f** (83 mg, 0.2 mmol) using the same conditions described for the preparation of **28** and provided 69 mg (86%) of **29**: mp 156–157°C. $[\alpha]_D^{20}$ –149° (*c* 0.42, $CHCl_3$). ^{1}H NMR δ: 2.97 (t, 1H, *J* = 4.1), 3.94 (dd, 1H, *J* = 4.1, 13.6), 4.23 (dd, 1H, *J* = 4.1, 13.6), 7.18–7.70 (m, 15H), 8.86 (brs, 1H). ^{13}C NMR δ: 52.7, 56.4, 73.2, 119.4, 122.1, 135.6, 172.7. HRMS calcd. for $C_{25}H_{21}O_2N_3$ (M^+): 395.1634; found: 395.1644.

*Enantiomeric purity of (2*S*)-3-(1-imidazol)-2-[*N*-(PhF)amino]propionic acid (**29**)*

A solution of **29** (10 mg, 0.025 mmol) in acetonitrile (1 mL) was treated with D- or L- phenylalanine methyl ester hydrochloride (11 mg, 0.05 mmol), TBTU (16 mg, 0.05 mmol), and diisopropylethylamine (35 μL, 0.20 mmol) at room temperature. After stirring for 1 h, the solution was diluted with ethyl acetate (5 mL), washed with water (2 × 5 mL) and brine (5 mL), dried, and concentrated in vacuo to a crude oil, which was directly examined by ^{1}H NMR spectroscopy. The limits of detection were determined by measuring the diastereomeric methyl ester singlets at 3.71 and 3.76 ppm in $CDCl_3$ in the 400 MHz ^{1}H NMR spectra. Purification by chromatography using a gradient of 5–10%

© 2001 NRC Canada

methanol in EtOAc as eluant gave dipeptides having the following spectra.

*(2*S*)-3-(1-Imidazol)-2-[*N*-(PhF)amino]propionyl-*D*-phenylalanine methyl ester (2′*R*) (**30**)*

^{1}H NMR δ: 2.73 (m, 1H), 2.97 (dd, 1H, *J* = 8.1, 14.1), 3.16 (dd, 1H, *J* = 5.3, 14.1), 3.49 (dd, 1H, *J* = 4.1, 14.6), 3.76 (s, 3H), 4.09 (m, 1H), 4.49 (m, 1H), 7.01–7.68 (m, 21H).

*(2*S*)-3-(1-Imidazol)-2-[*N*-(PhF)amino]propionyl-*L*-phenylalanine methyl ester (2′*S*) (**30**)*

^{1}H NMR δ: 2.80 (m, 1H), 2.88 (dd, 1H, *J* = 6.0, 13.7), 3.11 (dd, 1H, *J* = 5.3, 13.7), 3.56 (dd, 1H, *J* = 4.3, 13.9), 3.71 (s, 3H), 4.21 (m, 1H), 4.73 (m, 1H), 6.80–7.72 (m, 21H).

*Methyl 1-*N*-PhF-2-methyl-3-[(methyloxy)carbonyl]-*Δ^2*-pyrroline (**33**)*

A solution of (4*S*)-methyl 2,2-dioxo-3-PhF-1,2,3-oxathiazolidine-4-carboxylate (**17**, 60 mg, 0.14 mmol) in 8 mL of DME was treated with NaH (40 mg, 1 mmol), stirred at room temperature for 30 min. A 0.5 mL aliquot was taken, poured into 1 M KH_2PO_4, and extracted with EtOAc (2 × 10 mL). The combined organic fractions were concentrated, dried on vacuum, and examined directly by ^{1}H NMR spectroscopy, which showed complete conversion to dehydroalanine **19**. ^{1}H NMR δ: 3.76 (s, 3H), 4.63 (brs, 1H), 5.62 (brs, 1H), 7.20–7.74 (m, 13H)). In a separate flask, a solution of methyl acetoacetate (50 μL, 0.46 mmol) in 3 mL of DME was treated with NaH (25 mg, 0.6 mmol) and stirred at room temperature for 1 h. The enolate solution was then added to the remaining solution of dehydroalanine, stirred at a reflux for 18h, poured into 40 mL of 1 M KH_2PO_4, and extracted with EtOAc (3 × 30 mL). The combined organic phases were washed with brine (2 × 30 mL), dried, filtered, and evaporated to a residue that was chromatographed on silica gel eluting with a gradient of 10–15% EtOAc in hexane. Concentrated of the collected fractions provided 49.6 mg (87%) of **33**. ^{1}H NMR δ: 2.08 (s, 3H), 2.48 (dd, 1H, *J* = 6.8, 12.8), 2.82 (t, 1H, *J* = 12.8), 3.47 (dd, 1H, *J* = 6.8, 12.8), 3.48 (s, 3H), 3.61 (s, 3H), 7.12–7.77 (m, 13H). ^{13}C NMR δ: 13.4, 33.8, 50.8, 52.2, 61.9, 103.5, 161.9, 166.7, 174.7, 174.8. HRMS calcd. for $C_{28}H_{26}O_4N$ (MH^+): 440.1862; found: 440.1870.

Acknowledgment

This research was supported in part by the Natural Sciences and Engineering Research Council of Canada (NSERC) and the Ministère de l'Éducation du Québec. The crystal structure analysis of compound (2*R*)-**16** was performed by Francine Bélanger-Gariépy at l'Université de Montréal X-ray crystallography facility.

References

1. J.E. Baldwin, A.C. Spivey, and C.J. Schofield. Tetrahedron: Asymmetry, **1**, 881 (1990).
2. B.M. Kim and S.M. So. Tetrahedron Lett. **39**, 5381 (1998).
3. L.T. Boulton, H.T. Stock, J. Raphy, and D.C. Horwell. J. Chem. Soc. Perkin Trans. 1, 1421 (1999).
4. S.V. Pansare and J.C. Vederas. J. Org. Chem. **54**, 2311 (1989), and refs. 2*a–d* cited within.
5. S.V. Pansare, G. Huyer, L.D. Arnold, and J.C. Vederas. Org. Synth. **70**, 1 (1992).
6. L. Dubois, A. Mehta, E. Tourette, and R.H. Dodd. J. Org. Chem. **59**, 434 (1994), and refs. 1–13 cited within.
7. B. Hofmann, P. Dauban, J.P. Biron, P. Potier, and R.H. Dodd. Heterocycles, **46**, 473 (1997).
8. B.D. Christie and H. Rapoport. J. Org. Chem. **50**, 1239 (1985).
9. W.D. Lubell and H. Rapoport. J. Am. Chem. Soc. **109**, 236 (1987).
10. L. Wei and W.D. Lubell. Org. Lett. **2**, 2595 (2000).
11. D. Alker, K.J. Doyle, L.M. Harwood, and A. McGregor. Tetrahedron: Asymmetry, **1**, 877 (1990).
12. M. Pilkington and J.D. Wallis. J. Chem. Soc. Chem. Commun. 1857 (1993).
13. H.S.H. Gautun, T. Bergan, and P.H.J. Carlsen. Acta Chim. Scand. **53**, 446 (1999).
14. G.J. White and M.E. Garst. J. Org. Chem. **56**, 3178 (1991).
15. H.S.H. Gautun and P.H.J. Carlsen. Tetrahedron: Asymmetry, **6**, 1667 (1995).
16. (*a*) B. Aguilera, A. Fernandez-Mayoralas, and C. Jaramillo. Tetrahedron, **53**, 5863 (1997); (*b*) B. Aguilera and A. Fernandez-Mayoralas. J. Org. Chem. **63**, 270 (1998).
17. K.K. Andersen and M. Kociolek. J. Org. Chem. **60**, 2003 (1995).
18. M.E. Van Dort, Y.W. Jung, P.S. Sherman, M.R. Kilbourn, and D.M. Wieland. J. Med. Chem. **38**, 810 (1995).
19. M. Okuda and K. Tomioka. Tetrahedron Lett. **35**, 4585 (1994).
20. D. Ok, M.H. Fisher, M.J. Wyvratt, and P.T. Meinke. Tetrahedron Lett. **40**, 3831 (1999).
21. B. Aguilera and A. Fernandez-Mayoralas. Chem. Commun. 127 (1996).
22. T.A. Lyle, C.A. Mafill, and S.M. Pizenberger. J. Am. Chem. Soc. **109**, 7890 (1987).
23. W.D. Lubell and H. Rapoport. J. Org. Chem. **54**, 3824 (1989).
24. G. Lowe and M.A. Reed. Tetrahedron: Asymmetry, **1**, 885 (1990).
25. B.B. Lohray. Synthesis, 1035 (1992).
26. J.A. Deyrup and C.L. Moyer. J. Org. Chem. **34**, 175 (1969).
27. M. Atfani and W.D. Lubell. J. Org. Chem. **60**, 3184 (1995).
28. J.M. Huphrey, R.J. Bridges, J.A. Hart, and A.R. Chamberlin. J. Org. Chem. **59**, 2467 (1994).
29. E. Beausoleil, B. L'Archevêque, L. Bélec, M. Atfani, and W.D. Lubell. J. Org. Chem. **61**, 9447 (1996).
30. H. Li, T. Sakamoto, and Y. Kikugawa. Tetrahedron Lett. **38**, 6677 (1997).
31. T.L. Ho, B. Gopalan, J.J. Nestor Jr. J. Org. Chem. **51,** 2405 (1986).
32. H.H. Ibrahim and W.D. Lubell. J. Org. Chem. **58**, 6438 (1993).
33. M.M. Paz and J. Sardina. J. Org. Chem. **58**, 6990 (1993).
34. R.J. Cherney and L. Wang. J. Org. Chem. **61**, 2544 (1996).

© 2001 NRC Canada

Solvation of a water molecule in cyclohexane and water

Giuseppe Graziano

Abstract: Reliable values for the thermodynamic functions associated with the solvation of a water molecule in its own liquid phase and in cyclohexane, at 25°C, are obtained using experimental data from different investigations. They are successfully rationalized by means of a general theory of solvation. The standard Gibbs energy change is given by the balance of two contrasting terms: the work to create a cavity in the solvent suitable to host the water molecule; and the work to turn on the water–solvent interactions. It proves that the work of cavity creation is largely overwhelmed by the formation of two H-bonds in liquid water, whereas it is almost exactly counterbalanced by the establishment of van der Waals interactions in liquid cyclohexane.

Key words: water, cavity creation, H-bonds, van der Waals interactions.

Résumé : En se basant sur des données expérimentales obtenues au cours d'études diverses, on a déterminé des valeurs fiables pour les fonctions thermodynamiques associées à la solvatation d'une molécule d'eau dans sa propre phase liquide ainsi que dans le cyclohexane, à 25°C. On peut les rationaliser facilement à l'aide d'une théorie générale de solvatation. Le changement d'énergie standard de Gibbs est donné par l'équilibre entre deux termes en opposition: le travail nécessaire pour créer une cavité dans le solvant approprié pour servir d'hôte à la molécule d'eau et le travail pour déclencher les interactions eau–solvant. Ce changement démontre que le travail de création de la cavité est très assujetti à la formation de deux liaisons hydrogènes dans l'eau liquide alors que, dans le cyclohexane liquide, elle est pratiquement exactement contrebalancée par la création d'interactions de van der Waals.

Mots clés : eau, création d'une cavité, liaisons hydrogènes, interactions de van der Waals.

[Traduit par la Rédaction]

Introduction

Currently there is great interest in solvation processes in view of the pivotal role played by the solvent medium in the stabilization of the native structure of biological macromolecules, and in the kinetics and thermodynamics of chemical and biochemical reactions (1–3). To avoid dangerous ambiguities, however, the meaning of the term solvation has to be precisely defined. We adopt the general definition proposed by Ben-Naim (4): solvation refers to the transfer of a solute molecule from a fixed position in the ideal gas-phase to a fixed position in the liquid phase, at constant temperature and pressure. The corresponding standard thermodynamic quantities, referred to the molar concentration scale, do not contain the effects of the difference in density between the two phases, and account solely for the solute–solvent coupling work; they are denoted by a superscript filled circle.

The solvation of nonpolar, polar, and charged species in water has been largely and deeply investigated, both experimentally and theoretically (5–8), because water is, by far, the most important and widely used solvent. However, it would be interesting to compare the solvation of a water molecule in its own liquid phase and in a standard nonpolar solvent such as cyclohexane. The solvation of water in nonpolar media merits attention in its own right (9), and for its implication in several molecular recognition phenomena (10), and in the transport mechanism of water across biological membranes (11).

By combining the data compiled by Ben-Naim and Marcus (12), and the detailed solubility measurements by Wolfenden and Radzicka (13), it is possible to determine the Ben-Naim standard enthalpy, entropy and Gibbs energy changes, at 25°C, associated with the following processes: (*i*) solvation of a water molecule in liquid water ($H_2O(g) \rightarrow H_2O(l)$); (*ii*) solvation of a water molecule in liquid cyclohexane ($H_2O(g) \rightarrow H_2O(chx)$); (*iii*) transfer of a water molecule from liquid water to liquid cyclohexane ($H_2O(l) \rightarrow H_2O(chx)$). The determined values are collected in Table 1.

The process $H_2O(g) \rightarrow H_2O(l)$ is spontaneous because the Gibbs energy change is large and negative ($\Delta G^{\bullet} = -26.3$ kJ mol^{-1}) and is enthalpy-driven since $\Delta H^{\bullet} = -41.7$ kJ mol^{-1} and $\Delta S^{\bullet} = -51.7$ J K^{-1}mol^{-1}. For the process $H_2O(g) \rightarrow H_2O(chx)$, $\Delta G^{\bullet}$ amounts to –0.2 kJ mol^{-1}, indicating that for a water molecule it is practically the same to stay in the gas-phase or to dissolve in liquid cyclohexane. This is an important result, as stressed by Wolfenden and Radzicka (13), who proposed a qualitative explanation without, however, performing a complete theoretical analysis. It should be

Received October 3, 2000. Published on the NRC Research Press Web site on February 9, 2001.

G. Graziano.[1] Dipartimento di Chimica, Università di Napoli "Federico II," Complesso Universitario di Monte S.Angelo, Via Cinthia – 80126 Napoli, Italy, and Facoltà di Scienze, Università del Sannio, Via Porta'Arsa, 11 – 82100 Benevento, Italy (e-mail: graziano@chemistry.unina.it and graziano@unisannio.it).

 DOI: 10.1139/cjc-79-2-105 © 2001 NRC Canada

Table 1. Ben-Naim standard enthalpy, entropy, and Gibbs energy changes, at 25°C, associated with the following processes: (*i*) solvation of a water molecule in liquid water ($H_2O(g) \rightarrow H_2O(l)$); (*ii*) solvation of a water molecule in liquid cyclohexane, ($H_2O(g) \rightarrow H_2O(chx)$); (*iii*) transfer of a water molecule from liquid water to liquid cyclohexane, ($H_2O(l) \rightarrow H_2O(chx)$). The values are obtained by combining the data reported in refs. 12 and 13.

	$\Delta H^\bullet$ (kJ mol^{-1})	$\Delta S^\bullet$ (J K^{-1} mol^{-1})	$\Delta G^\bullet$ (kJ mol^{-1})
$H_2O(g) \rightarrow H_2O(l)$	–41.7	–51.7	–26.3
$H_2O(g) \rightarrow H_2O(chx)$	–5.9	–19.1	–0.2
$H_2O(l) \rightarrow H_2O(chx)$	35.8	32.6	26.1

underscored that both solvation processes are exothermic and lead to an entropy decrease, but the changes are significantly larger in magnitude in the case of liquid water.

For the process $H_2O(l) \rightarrow H_2O(chx)$, $\Delta G^\bullet$, $\Delta H^\bullet$, and $\Delta S^\bullet$ are all large and positive, indicating that the transfer is not spontaneous, as expected, and it is dominated by enthalpic effects. A water molecule strongly prefers to stay in liquid water rather than in liquid cyclohexane.

It would be desirable to rationalize the experimental data within a unified approach; this is exactly the aim of the present work.

Results and discussion

For a solvation process, the following equation has general validity (14–17):

$$[1] \qquad \Delta G^\bullet = \Delta G_c + E_a$$

ΔG_c is the work of cavity creation, involving the exclusion of solvent molecules from the region of space that has to be occupied by the solute molecule; it is a positive quantity that contrasts solvation. E_a is a negative quantity and represents the solute–solvent energetic interactions. We would like to show that this equation works well also for the solvation thermodynamics of a molecule like water.

Reliable estimates of ΔG_c in any solvent can be obtained by means of scaled particle theory (SPT) (14, 18). In SPT calculations, we assume that both water and cyclohexane molecules are spherical, with a hard-sphere diameter of 2.80 Å and 5.63 Å (19), respectively. The value selected for water is physically sound, because it is close to the location of the first max in the oxygen–oxygen radial distribution function of water, as determined from X-ray and neutron scattering measurements (20). In addition, the actual densities of water and cyclohexane are used in SPT calculations (at room temperature the volume packing density is 0.383 for water and 0.517 for cyclohexane). For the creation of a cavity of 2.80 Å diameter at 25°C, the following values are obtained: ΔG_c = 14.7 kJ mol^{-1} in water, and 10.9 kJ mol^{-1} in cyclohexane. The value of ΔG_c in water is significantly larger than that in cyclohexane due to the small size of water molecules. This geometrical feature amplifies the excluded volume effect upon solute insertion into liquid water with respect to all other solvents (15, 16, 21).

The SPT value of ΔG_c in cyclohexane appears to be accurate because SPT works well for nonpolar liquids owing to its fundamental assumptions (18). Also the SPT estimate of ΔG_c in liquid water appears to be accurate because Monte Carlo and molecular dynamics computer simulations (22), using both the test particle insertion method and perturbation approaches, resulted in ΔG_c values of about 15 kJ mol^{-1} for a cavity of 2.80 Å diameter at 25°C. The latter investigations used sophisticated water models with explicit information on H-bonds, whereas SPT completely neglects orientational order and H-bonds. As a consequence, the fact that the estimates of ΔG_c in liquid water are so close is a strong indication that the work of cavity creation does not depend on the existence of H-bonds, when the solvent density is fixed (23).

For the evaluation of E_a we have to consider that: (*i*) a water molecule entering liquid water forms an average of two H-bonds with the surrounding water molecules (i.e., in liquid water, assuming an ideal tetrahedral coordination, each water molecule is engaged in four H-bonds; each H-bond, however, is shared between two molecules, so that the net number of H-bonds a water molecule forms is two); (*ii*) a water molecule entering liquid cyclohexane cannot form H-bonds and establishes solely van der Waals interactions with the surrounding cyclohexane molecules.

For the first case, Pauling (24), with simple arguments, determined that the average effective strength of a H-bond in water $< \varepsilon(\text{H-bond}) > = -21$ kJ mol^{-1}, so that $E_a = -42$ kJ mol^{-1} for a water molecule in its own liquid phase. The latter value is in satisfactory agreement with theoretical results, as can be verified by looking at the figures of the intermolecular energy for a set of widely used models of liquid water, quoted in the second line of Table III in ref. 25. Actually, Pauling's estimate of $< \varepsilon(\text{H-bond}) >$ can be derived in a slightly more rigorous way, as it is shown below. According to the Landolt-Börnstein tables (26), the enthalpy of liquid water at 25°C amounts to –34.1 kJ mol^{-1}. For a liquid phase, the enthalpy can be equated to the internal energy, which is the sum of kinetic and potential energies. As a first approximation, the potential energy of liquid water can be considered equal to the average effective strength of two H-bonds per molecule, while, at room temperature, the kinetic energy contains both translational and rotational contributions. In the reliable assumption that liquid water can be treated by classical statistical mechanics, each translational and rotational degree of freedom contributes (1/2)*RT* to the kinetic energy, so that:

$$[2] \qquad H \approx U = (3/2)RT + (3/2)RT + 2 < \varepsilon(\text{H-bond}) >$$

where *H* and *U* are the enthalpy and internal energy per molecule, respectively, of liquid water, and *R* is the gas constant. Performing the calculations, one readily obtains $< \varepsilon(\text{H-bond}) > = -20.8$ kJ mol^{-1} at 25°C, and $E_a = -41.6$ kJ mol^{-1} for a water molecule in its own liquid phase.

Alternatively, following the proposal by Walrafen et al. (27), one can imagine that, for each hydrogen atom of a water molecule, there is a general energetic contribution independent of the orientations of neighboring molecules ($E_a(g)$) and a specific contribution orientation-dependent ($E_a(s)$). $E_a(g)$ arises from dipole–dipole, dispersive and dipole-induced dipole interactions among neighboring water molecules and is always turned on and favorable. Adopting the

© 2001 NRC Canada

procedure devised by Walrafen et al. (27), $E_a(g) = -13.0$ kJ per mol of hydrogen atoms. $E_a(s)$ is related to the formation of a specific H-bond interaction between two water molecules correctly oriented. According to theoretical calculations and simulations (28), a two-state mechanism can be assumed for each H-bond, and so for $E_a(s)$, it is turned on or turned off, depending on the relative orientation of the two water molecules (i.e., the energy distribution is discrete and bimodal). As a consequence, for each temperature, there is a fraction of H-bonds broken (f_b) and a fraction intact ($1 - f_b$). According to the Muller's model (29), $E_a(s) = -9.8$ kJ per mol of hydrogen atoms and $f_b = 0.205$ at 25°C. Therefore, $E_a = 2(-13.0) + 2(0.795)(-9.8) = -41.6$ kJ mol^{-1} for a water molecule in its own liquid phase. It is pleasing that the obtained estimates are very close.

In the second case, the van der Waals interactions of a water molecule in liquid cyclohexane consist solely of dispersive and dipole-induced dipole contributions. We assumed that the latter contribution, arising from the interaction of water dipole with the polarizable cyclohexane molecules, can be absorbed into the parameterization of the dispersive contribution. This assumption is reasonable because both terms depend on the inverse sixth power of distance (30), and is usually employed in molecular mechanics force fields (31). We performed calculations using Pierotti's formula (14), which employs the Lennard–Jones potential and considers the radial distribution function of solvent molecules to be unit around the central solute molecule. The dipole-induced dipole contribution is taken into account by increasing the ε/k value of water, where ε is the well-depth in the Lennard–Jones potential and k is the Boltzmann constant. We used $\varepsilon/k = 573$ K for cyclohexane, as determined by Wilhelm and Battino (19), and $\varepsilon/k = 145$ K for water. The latter is larger than the customary values of about 80 K, but is in the middle of the values for argon (125 K) and krypton (169 K) (14, 16). In this respect, it is worth noting that the dipole-induced dipole contribution should be substantial in view of the large values of both the dipole moment of water and the polarizability of cyclohexane. The selected ε/k values lead to $E_a = -11.1$ kJ mol^{-1} for a water molecule in liquid cyclohexane.

This estimate illustrates that there is no phobia of a water molecule for nonpolar solvents: the energetic interactions are attractive. Actually, E_a is even larger and negative for a water molecule in *n*-heptane or benzene, because, at 25°C, $\Delta G^\bullet = -1.3$ kJ mol^{-1} for the solvation of water into *n*-heptane, and $\Delta G^\bullet = -7.3$ kJ mol^{-1} for the solvation of water into benzene (13). In particular, since the SPT estimate for a cavity of 2.80 Å diameter in benzene, at 25°C, is $\Delta G_c = 11.7$ kJ mol^{-1}, the water-benzene interaction energy should be $E_a = \Delta G^\bullet - \Delta G_c = -7.3 - 11.7 = -19.0$ kJ mol^{-1}, which is a large negative quantity.

The fundamental point is that for both the solvation processes the sum $\Delta G_c + E_a$ closely corresponds to the experimental $\Delta G^\bullet$ values. For $H_2O(g) \rightarrow H_2O(l)$, $\Delta G_c + E_a = 14.7 - 41.6 = -26.9$ kJ mol^{-1}, while for $H_2O(g) \rightarrow H_2O(chx)$, $\Delta G_c + E_a = 10.9 - 11.1 = -0.2$ kJ mol^{-1}. This is a confirmation of the general validity of eq. [1], and has to be widely recognized. In liquid cyclohexane the work of cavity creation is practically balanced by the van der Waals interaction energy, whereas in liquid water the energy gain for the formation of two H-bonds largely counterbalances the work of cavity creation. It is worth noting that the same equation works equally well for the solvation of a water molecule in its own liquid phase and in cyclohexane, as well as for the solvation of a cyclohexane molecule in its own liquid phase and in water (32).

For the transfer $H_2O(l) \rightarrow H_2O(chx)$, it results $\Delta\Delta G_c + \Delta E_a = -3.8 + 30.5 = 26.7$ kJ mol^{-1}, in fair agreement with the experimental value. Clearly, the loss of two H-bonds dominates the transfer energetics, largely overwhelming the difference in the work of cavity creation and the establishment of van der Waals interactions in liquid cyclohexane.

We turn now to the enthalpy and entropy changes; for a solvation process they are given by the following general relations (33, 34):

$$[3] \qquad \Delta H^\bullet = E_a + \Delta H_r$$

$$[4] \qquad \Delta S^\bullet = \Delta S_x + \Delta S_{nx}$$

ΔH_r is the enthalpy contribution due to solvent reorganization upon solute insertion; ΔS_x is the entropy contribution owing to the excluded volume effect associated with cavity creation, and is calculated as $\Delta S_x = -\Delta G_c/T$ (i.e., ΔG_c is a purely entropic quantity (35), being a direct measure of the probability that a certain region of space is devoid of solvent molecules); ΔS_{nx} is the nonexcluded volume entropy contribution.

For $H_2O(g) \rightarrow H_2O(l)$, $E_a = -41.6$ kJ mol^{-1}, close to $\Delta H^\bullet$, so that ΔH_r is negligible; $\Delta S_x = -49.3$ J K^{-1}mol^{-1}, close to $\Delta S^\bullet$, so that ΔS_{nx} is vanishingly small (see Table 1). This means that there is very little reorganization of the water H-bonded network upon insertion of a water molecule. Such a result is the expected one, in view of the well-established plasticity of the H-bonded network of liquid water (6, 36).

For $H_2O(g) \rightarrow H_2O(chx)$, $E_a = -11.1$ kJ mol^{-1} and $\Delta H_r = \Delta H^\bullet - E_a = 5.2$ kJ mol^{-1}; $\Delta S_x = -36.6$ J K^{-1} mol^{-1} and $\Delta S_{nx} = \Delta S^\bullet - \Delta S_x = 17.5$ J K^{-1}mol^{-1}. Therefore, the insertion of a water molecule in liquid cyclohexane causes a significant structural reorganization, affording positive contributions to both the enthalpy and entropy changes. Such contributions, however, cancel each other in the Gibbs energy balance because enthalpy-entropy compensation holds for the solvent structural reorganization (37).

A last point merits attention. The analysis shows that the negative entropy changes associated with both solvation processes are not caused by a poorly defined ordering of solvent molecules around the inserted solute. The physical cause of such negative values is the excluded volume effect upon solute insertion, which leads to a significant reduction in the configuration space accessible to solvent molecules. This mechanism is operative in all liquids because they are a condensed state of the matter, and each molecule possesses a finite volume.

In conclusion, the present work indicates that a unified theoretical approach is able to rationalize the solvation thermodynamics of water as well as noble gases, hydrocarbons and aliphatic alcohols (15, 16, 32–34). It is simply necessary to recognize that: (*i*) energy has to be spent to create a cavity in the solvent suitable to host the solute molecule; (*ii*) energy is gained by turning on the solute–solvent interactions, which may consist of H-bonds, as well as van der Waals

© 2001 NRC Canada

interactions. The balance of these two opposing contributions governs the solvation thermodynamics of every noncharged solute.

Acknowledgements

Work supported by a P.R.I.N. grant from the Italian Ministry for University, and Scientific and Technological Research (M.U.R.S.T., Rome).

References

1. W. Blokzijl and J.B.F.N. Engberts. Angew. Chem. Int. Ed. Engl. **32**, 1545 (1993).
2. R. Wolfenden. Science (Washington, D.C.), **222**, 1087 (1983); R.U. Lemieux. Acc. Chem. Res. **29**, 373 (1996); P. Buchwald. Perspect. Drug Discovery Des. **19**, 19 (2000).
3. Faraday Discuss. **103**, whole issue (1996).
4. A. Ben-Naim. Solvation thermodynamics. Plenum Press, New York. 1987.
5. D.R. Biggerstaff, D.E. White, and R.H. Wood. J. Phys. Chem. **89**, 4378 (1985); H. Naghibi, S.F. Dec, and S.J. Gill. J. Phys. Chem. **91**, 245 (1987); D. Krause and B.B. Benson. J. Sol. Chem. **18**, 823 (1989); G.I. Makhatadze and P.L. Privalov. J. Mol. Biol. **213**, 375 (1990).
6. J.L. Finney, A.K. Soper, and J.Z. Turner. Pure Appl. Chem. **65**, 2521 (1993); J.L. Finney and A.K. Soper. Chem. Soc. Rev. **23**, 1 (1994); K.S. Sidhu, J.M. Goodfellow, and J.Z. Turner. J. Chem. Phys. **110**, 7943 (1999).
7. A. Filipponi, D.T. Bowron, C. Lobban, and J.L. Finney. Phys. Rev. Lett. **79**, 1293 (1997); D.T. Bowron, A. Filipponi, C. Lobban, and J.L. Finney. Chem. Phys. Lett. **293**, 33 (1998); D.T. Bowron, A. Filipponi, M.A. Roberts, and J.L. Finney. Phys. Rev. Lett. **81**, 4164 (1998).
8. H.A. Yu and M. Karplus. J. Chem. Phys. **89**, 2366 (1988); B. Guillot and Y. Guissani. J. Chem. Phys. **99**, 8075 (1993); A. Wallqvist and B.J. Berne. J. Phys. Chem. **99**, 2893 (1995).
9. T. Tassaing, Y. Danten, M. Besnard, E. Zoidis, J. Yarwood, Y. Guissani, and B. Guillot. Mol. Phys. **84**, 769 (1995); Y. Danten, T. Tassaing, and M. Besnard. J. Phys. Chem. A **104**, 9415 (2000).
10. E.W. Chung, D.A. Henriques, D. Renzoni, M. Zvelebil, J.M. Bradshaw, G. Waksman, C.V. Robinson, and J.E. Ladbury. Structure, **6**, 1141 (1998).
11. A. Finkelstein. Water transport through lipid bilayers, pores, and plasma membranes. Wiley-Interscience, New York. 1987. p. 94.
12. A. Ben-Naim and Y. Marcus. J. Chem. Phys. **81**, 2016 (1984).
13. R. Wolfenden and A. Radzicka. Science (Washington, D.C.), **265**, 936 (1994).
14. R.A. Pierotti. J. Phys. Chem. **67**, 1840 (1963); J. Phys. Chem. **69**, 281 (1965); Chem. Rev. **76**, 717 (1976).
15. B. Lee. Biopolymers, **24**, 813 (1985); Biopolymers, **31**, 993 (1991).
16. G. Graziano. Can. J. Chem. **76**, 437 (1998); J. Chem. Soc. Faraday Trans. **94**, 3345 (1998); Phys. Chem. Chem. Phys. **1**, 3567 (1999).
17. L.R. Pratt and D. Chandler. J. Chem. Phys. **67**, 3683 (1977); S. Garde, A.E. Garcia, L.R. Pratt, and G. Hummer. Biophys. Chem. **78**, 21 (1999).
18. H. Reiss. Adv. Chem. Phys. **9**, 1 (1966).
19. E. Wilhelm and R. Battino. J. Chem. Phys. **55**, 4012 (1971).
20. A.H. Narten and H.A. Levy. Science (Washington, D.C.), **165**, 447 (1969); A.K. Soper and M.G. Phillips. Chem. Phys. **107**, 47 (1986).
21. M. Lucas. J. Phys. Chem. **80**, 359 (1976); L.E.S. de Souza and D. Ben-Amotz. J. Chem. Phys. **101**, 9858 (1994); A. Wallqvist and D.G. Covell. Biophys. J. **71**, 600 (1996).
22. T.C. Beutler, D.R. Beguelin, and W.F. van Gunsteren. J. Chem. Phys. **102**, 3787 (1995); G. Hummer, S. Garde, A.E. Garcia, A. Pohorille, and L.R. Pratt. Proc. Natl. Acad. Sci. U.S.A. **93**, 8951 (1996); P.E. Smith. J. Phys. Chem. B **103**, 525 (1999); I. Tomas-Oliveira and S.J. Wodak. J. Chem. Phys. **111**, 8576 (1999).
23. B. Madan and B. Lee. Biophys. Chem. **51**, 279 (1994); M. Ikeguchi, S. Shimizu, S. Nakamura, and K. Shimizu. J. Phys. Chem. B **102**, 5891 (1998).
24. L. Pauling. The nature of the chemical bond. 3rd ed. Cornell University Press, Ithaca, New York. 1960. p. 468.
25. W.L. Jorgensen, J. Chandrasekhar, J.D. Madura, R.W. Impey, and M.L. Klein. J. Chem. Phys. **79**, 926 (1983).
26. Landolt-Börnstein Tables. 4. Teil, II. Band, Springer–Verlag, Berlin. 1961. p. 412.
27. G.E. Walrafen, M.R. Fisher, M.S. Hokmabadi, and W.H. Yang. J. Chem. Phys. **85**, 6970 (1986).
28. K.A.T. Silverstein, A.D.J. Haymet, and K.A. Dill. J. Chem. Phys. **111**, 8000 (1999); J. Am. Chem. Soc. **122**, 8037 (2000).
29. N. Muller. J. Sol. Chem. **17**, 661 (1988); Acc. Chem. Res. **23**, 23 (1990).
30. F. London. Trans. Faraday Soc. **33**, 8 (1937).
31. S.J. Weiner, P.A. Kollman, D.A. Case, U.C. Singh, C. Ghio, G. Alagona, S. Profeta, and P. Weiner. J. Am. Chem. Soc. **106**, 765 (1984).
32. G. Graziano. Can. J. Chem. **78**, 1233 (2000).
33. B. Lee and G. Graziano. J. Am. Chem. Soc. **118**, 5163 (1996).
34. G. Graziano. Phys. Chem. Chem. Phys. **1**, 1877 (1999); Biophys. Chem. **82**, 69 (1999).
35. B. Lee. J. Chem. Phys. **83**, 2421 (1985); G. Graziano. J. Phys. Soc. Jpn. **69**, 1566 (2000).
36. R.D. Mountain and D. Thirumalai. Proc. Natl. Acad. Sci. U.S.A. **95**, 8436 (1998).
37. B. Lee. Biophys. Chem. **51**, 271 (1994).
38. N. Morel-Desrosiers and J.P. Morel. Can. J. Chem. **59**, 1 (1981).

Appendix

It should be noted that both ΔG_c and E_a are not directly measurable quantities; only their sum can be tested against experimental ΔG^* values. This basic fact cannot be circumvented or eluded. Estimates of ΔG_c and E_a are calculated using ad hoc assumptions that cannot be considered valid in general (this statement is entirely true also with regard to computer simulations). The validity and reliability of the assumptions have to be verified by comparing the calculated sum $\Delta G_c + E_a$ with experimental ΔG^* data.

In principle, SPT enables the calculation of the work to create a spherical cavity in a solvent without making use of any adjustable parameter (18). However, SPT results depend significantly upon the value of the hard-sphere diameter selected for the solute and solvent molecules (38). For instance, we can select σ = 2.75 Å for H_2O molecules. It results: ΔG_c = 10.6 kJ mol^{-1} and 13.2 kJ mol^{-1} to create a cavity of 2.75 Å diameter at 25°C in liquid cyclohexane and

© 2001 NRC Canada

liquid water, respectively; and E_a = –10.9 kJ mol^{-1} in cyclohexane, using the same parameters reported in the text. The insertion of these estimates in eq. [1] leads to a slightly worse agreement with experimetal data. For $H_2O(g) \rightarrow H_2O(chx)$, $\Delta G_c + E_a = 10.6 - 10.9 = -0.3$ kJ mol^{-1} compared to $\Delta G^{\bullet} = -0.2$ kJ mol^{-1}; for $H_2O(g) \rightarrow H_2O(l)$, $\Delta G_c + E_a = 13.2 - 41.6 = -28.4$ kJ mol^{-1} compared to $\Delta G^{\bullet} = -26.3$ kJ mol^{-1}. Clearly, a very small reduction in the σ value of H_2O molecules has a little effect on the ΔG_c estimate in liquid cyclohexane, but an appreciable effect on the ΔG_c estimate in liquid water.

The sensitivity of SPT should not be a problem if the molecular diameters could be accurately determined. This is feasible for spherical or nearly spherical molecules, but there is no reliable recipe to assign the hard-sphere diameter to nonspherical molecules. From a physicochemical point of view, the best procedure is to use as hard-sphere diameter the distance value at which occurs the first maximum in the radial distribution function for the center-of-mass of the molecules of the selected liquid, as determined by X-ray and (or) neutron scattering measurements (i.e., the oxygen–oxygen radial distribution function for water, and the ring center-ring center radial distribution function for benzene). This is the procedure adopted in the present work. The following point, however, merits attention.

A water molecule should have two sizes depending on the interactions in which it is involved (23). When it is H-bonded to other water molecules σ = 2.80 Å, as revealed by the location of the first peak in the oxygen–oxygen radial distribution function of liquid water. When it is not H-bonded to neighbor molecules σ = 3.17 Å, that is the van der Waals diameter of an oxygen atom. As a consequence, the latter value of σ should be the correct one for a water molecule dissolved in liquid cyclohexane. Using the same parameters reported in the text, except σ = 3.17 Å for H_2O, it proves that: ΔG_c = 12.9 kJ mol^{-1} and E_a = –12.6 kJ mol^{-1} in liquid cyclohexane at 25°C. The latter estimates differ from those reported in the text, but, unequivocally confirm the practically complete cancellation of ΔG_c and E_a contributions for the $H_2O(g) \rightarrow H_2O(chx)$ process, in agreement with experimental data.

It is evident that all the above concerns and calculations do not detract anything from the qualitative general validity of our approach and derived conclusions.

© 2001 NRC Canada

Epoxide of a ketene acetal. The first 2,2-dialkoxyoxirane to be isolated

Małgorzata Dawid, Paul C. Venneri, and John Warkentin

Abstract: Dimethoxycarbene, generated at 110°C in benzene by thermolysis of 2,2-dimethoxy-5,5-dimethyl-Δ^3-1,3,4-oxadiazoline, reacted with cyclohexanone to afford 2,2-dimethoxyspiro[2.5]-1-oxaoctane. It is the first oxirane of a ketene acetal that could be isolated and characterized by ^{1}H NMR-, ^{13}C NMR-, and IR spectroscopy. The identical oxirane might be expected from conrotatory cyclization of the appropriate carbonyl ylide. That ylide was generated under identical conditions by thermolysis of an oxadiazoline precursor (3,4-diaza-2,2-dimethoxy-1-oxaspiro[4.5]dec-3-ene) (**14**). The ylide could either cyclize or fragment to dimethoxycarbene and cyclohexanone. Addition of 4-*tert*-butylcyclohexanone, to trap dimethoxycarbene in competition with the cyclohexanone generated from **14** and, to leave the ylide closure pathway as the only route to the oxirane, showed that the carbonyl ylide does cyclize. However, fragmentation of the carbonyl ylide is relatively fast compared to its cyclization and most of it fragments to dimethoxycarbene and cyclohexanone. Oxirane formation from the carbene and ketone is probably either a concerted cycloaddition or it occurs in two steps, by nucleophilic attack at the carbonyl carbon to form the C—C bond first, prior to ring closure. If the carbene is bonded first to O of the carbonyl group, as it is in the carbonyl ylide, subsequent formation of the C—C bond is too slow, relative to fragmentation of the ylide, to afford the oxirane ring efficiently.

Key words: carbonyl ylide, dialkoxyoxirane, dimethoxycarbene, oxadiazoline, oxirane.

Résumé : Le diméthoxycarbène, généré à 110°C dans le benzène par thermolyse de la 2,2-diméthoxy-5,5-diméthyl-Δ^3-1,3,4-oxadiazoline, réagit avec la cyclohexanone pour conduire à la formation du 2,2-diméthoxyspiro[2,5]-1-oxooctane. Il s'agit du premier oxirane d'un acétal de cétène à être isolé et caractérisé par RMN du ^{1}H et du ^{13}C et par spectroscopie IR. On pourrait s'attendre à la formation d'un oxirane identique par cyclisation conrotatoire de l'ylure de carbonyle approprié. On a généré l'ylure dans des conditions identiques par thermolyse d'un précurseur oxadiazoline, le 3,4-diaza-2,2-diméthoxy-1-oxospiro[4,5]déc-3-ène (**14**). Cet ylure peut donner lieu soit à une cyclisation ou à une fragmentation en diméthoxycarbène et cyclohexanone. L'addition de 4-*tert*-butylcyclohexanone, pour piéger le diméthoxycarbène en compétition avec la cyclohexanone générée à partir du composé **14** et pour s'assurer que la voie réactionnelle impliquant une fermeture de l'ylure est la seule voie disponible à l'oxirane, a permis de démontrer que l'ylure de carbonyle se cyclise. Toutefois, la fragmentation de l'ylure de carbonyle est relativement rapide par rapport à sa cyclisation et elle conduit à la formation de fragments diméthoxycarbène et cyclohexanone. La formation de l'oxirane à partir du carbène et de la cétone se produit probablement par le biais d'une cycloaddition concertée ou en deux étapes, par une attaque nucléophile sur le carbone du carbonyle conduisant en premier lieu à la formation d'une liaison C—C avant la fermeture du cycle. Si le carbène commençait par se lier à l'oxygène du carbonyle, comme c'est le cas dans l'ylure de carbonyle, la formation subséquente de la liaison C—C est trop lente, en comparaison avec la fragmentation de l'ylure, pour conduire de façon efficace à la formation du cycle oxirane.

Mots clés : ylure de carbonyle, dialkoxyoxirane, diméthoxycarbène, oxadiazoline, oxirane.

[Traduit par la Rédaction]

Introduction

2,2-Dialkoxy-, 2-alkoxy-2-aryloxy-, 2,2-diaryloxy- and analogous trioxy- or tetraoxyoxiranes have never been isolated. 2,2-Dialkoxyoxiranes may also be viewed as strained orthoformates or as carbonyl-group-protected α-lactones. While oxiranes are well-known (1) and easily prepared with a variety of substituents, α-lactones are generally too unstable to be isolated unless they have electron-withdrawing groups at C2 (2). Presumably ring strain in the ground state, and carboxylate-like stabilization of the transition state, drives the ring opening, and destabilization of the positive end of the dipole is required to make α-lactones persistent (Scheme 1).

2,2-Dialkoxyoxiranes could, in principle, undergo thermal conrotatory ring opening to a carbonyl ylide (3) or else the alkoxy groups might cause cleavage of a different bond, with the cationic entity delocalized (Scheme 2). The latter process had been suggested earlier by Kopecky et al. (4). They, and Hoffmann and Schneider (5), studied the ozonolysis

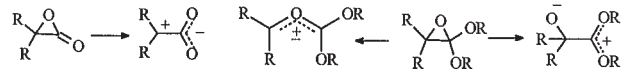
Received August 1, 2000. Published on the NRC Research Press Web site on February 9, 2001.

M. Dawid, P.C. Venneri, and J. Warkentin.[1] Department of Chemistry, McMaster University, Hamilton, ON L8S 4M1, Canada.

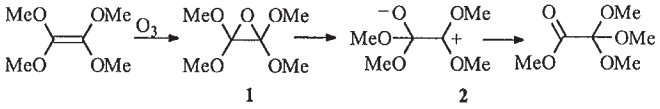
[1]Corresponding author (e-mail: warkent@mcmaster.ca).

 DOI: 10.1139/cjc-79-2-110 © 2001 NRC Canada

Scheme 1.

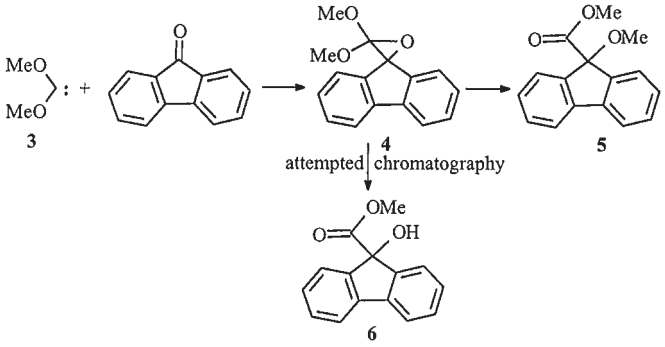


Scheme 2.



(The ozonide and other intermediates are not shown)

Scheme 3.



of tetramethoxyethylene, which gave methyl trimethoxyacetate.

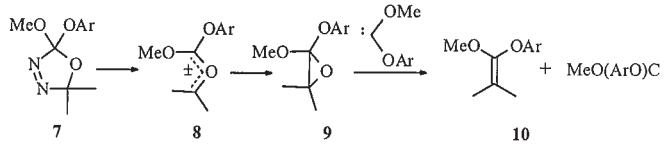
The ester appeared to be derived from opening of oxirane **1** to a dipolar intermediate (**2**) that rearranged (Scheme 2) (4). An oxirane intermediate (**4**) was indicated in another case by the fact that dimethoxycarbene (**3**), generated at 110°C in the presence of fluorenone, afforded **5** (Scheme 3) (6). Although **4** could not be isolated, because it was converted into **6** during chromatography, it was possible to glean the ^{13}C NMR spectrum of **4** from the spectrum of a mixture (6). Moreover, Couture et al. (7) inferred the intermediacy of 2-methoxy-2-aryloxy oxiranes (**9**) on a path from oxadiazolines **7** to ketene acetals **10** (Scheme 4) although such intermediates were not actually observed.

We now report the isolation, spectroscopic characterization, and hydrolysis of the first 2,2-dialkoxyoxirane (**13**) that could be isolated. It was obtained by the thermolysis of oxadiazoline **11** in the presence of cyclohexanone. Thermolysis of **11** generates dimethoxycarbene (**3**) by sequential loss of N_2 and acetone (8), and the carbene reacted with the ketone in a [2 + 1] cycloaddition, either directly or via intermediate **12**. With the oxirane in hand, we were able to assess whether or not it can also arise from thermolysis of oxadiazoline **14**, via cyclization of the corresponding carbonyl ylide (**15**) under the same conditions (Scheme 5).

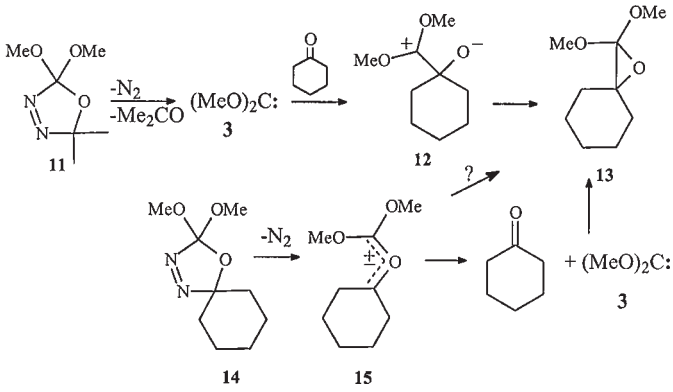
Results and discussion

Thermolysis of 2,2-dimethoxy-5,5-dimethyl-Δ^3-1,3,4-oxadiazoline **11** (8, 9) in the presence of cyclohexanone gave a mixture from which **13** was isolated by means of gas chromatography, in ca. 12% yield. The crude reaction mixture did not appear to contain the product of ring expansion

Scheme 4.



Scheme 5.



(2,2-dimethoxycycloheptanone) which we would have recognized and isolated, based on experience with ring expansion of cycloalkanones with dimethoxycarbene. The products of ring expansion of cyclobutanones and cyclopropanones were readily isolated and identified (10).

Reasonable mechanisms for the formation of **13** from **14** are in Scheme 5, which includes successive fragmentation of oxadiazoline **14** to carbonyl ylide **15** (7, 11), which could close directly (the question mark in Scheme 5) or fragment to form cyclohexanone and dimethoxycarbene (**3**). Dimethoxycarbene could then attack cyclohexanone to afford **13**. To answer the mechanistic question the known reaction between dimethoxycarbene and cyclohexanone (above) was suppressed by including 4-*tert*-butylcyclohexanone (**16**), to act as a competitor to any cyclohexanone formed from **15**. Any **13** formed at a high concentration of **16** would have to be attributed to cyclization of **15**, if the yield of **13** were to become independent of the concentration of **16** at higher values of [**16**].

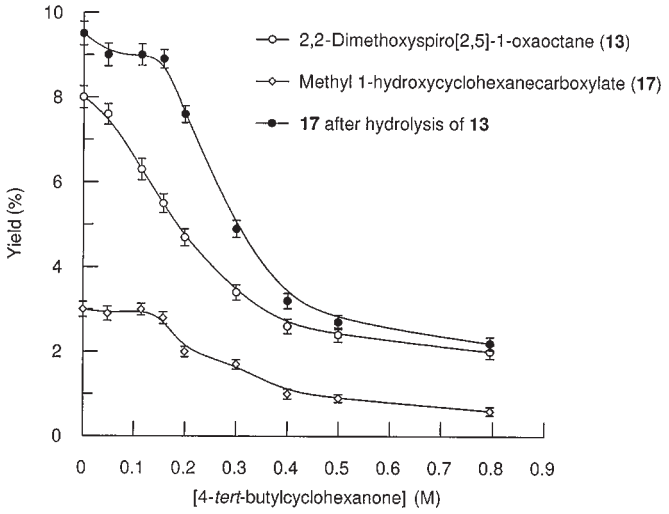
The results show that the yield of **13** drops as the concentration of **16** is increased, from an initial value near 10% to a limiting value that is near 2% (Fig. 1). Thus, most of the **13** arises from attack of dimethoxycarbene on cyclohexanone (both formed by fragmentation of **15**) rather than from cyclization of **15**. In other words, **15** cyclizes slowly at 110°C compared to the rate at which it fragments to **3** and cyclohexanone, and it is primarily these products that then react to afford **13** in the absence of **16** (Scheme 5).

We assume that **16** actually captures dimethoxycarbene to form the diastereomeric *tert*-butyl analogues of **13**, but separation of those product from the reaction mixture was not attempted.

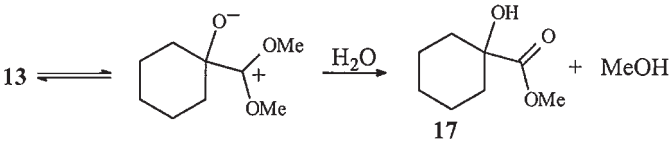
Attempts to isolate **13** by either column or radial chromatography on silica led invariably to the α-hydroxy ester (**17**) (Scheme 6). Isolation of **13** by means of gas chromatography, but not by chromatography on silica, implies that hydrolysis normally destroys such compounds. Deliberate

© 2001 NRC Canada

Fig. 1. Yields of **13** and **17**, from thermolysis of **14**, as a function of the concentration of 4-*tert*-butylcyclohexanone (M), and yields of **17** after hydrolysis of **13**. The error bars are standard deviations from five injections into the GC.



Scheme 6.



hydrolysis of **13**, dissolved in C_6D_6 in an NMR tube, by addition of a drop of water and a drop of trifluoroacetic acid also afforded **17**. Water alone, added to a solution of **13** in benzene, also caused hydrolysis but the reaction took two days. The instability of **13** in the presence of water is not surprising. Opening of the oxirane ring in a polar environment is probably fast and unidirectional (Scheme 6), even without acid catalysis, because of the *gem* dialkoxy substituents, as Kopecky et al. (4) had surmised.

We suspect that analogous dialkoxyoxiranes may, in general, be intermediates when dialkoxycarbenes attack ketones, and that some of them are more labile than **13** at the temperature (100–110°C) that is commonly used for fragmentation of the oxadiazoline source of **3**. Subtle differences in the ground state stabilities of a dialkoxyoxirane (such as **13**) and in the barriers to ring expanded products, or to carbene and ketone starting materials, could determine whether or not an analogue of **13** accumulates sufficiently for its detection and potential isolation. At this time we do not know whether the cyclohexyl ring of **13** is critical or whether there will be other dialkoxyoxiranes that are stable enough to be isolated.

Experimental

Synthesis of 11

Compound **11** was prepared according to published procedures (8, 12).

Thermolysis of 11 and isolation of 13

In a sealed tube, a degassed solution of **11** (0.100 g, 0.625 mmol) in benzene (5 g) containing cyclohexanone at 0.22 M concentration (0.123 g, 1.25 mmol) was heated with an oil bath at 110°C for 24 h. The solution was concentrated in vacuo and the concentrate was subjected to semipreparative gas chromatography on a 6′ × ¼″ glass column packed with OV-17. The column temperature was initially at 60°C for 3 min and it was then raised at 5° min^{-1} to 200°C. 2,2-Dimethoxyspiro[2.5]1-oxaoctane (**13**) was isolated in ca. 12% yield as a clear liquid. IR (CCl_4) cm^{-1}: 2990–2850, 1450. ^{1}H NMR (200 MHz, C_6D_6) δ: 1.52–1.89 (m, 10H), 3.25 (s, 6H). ^{13}C NMR (50 MHz, C_6D_6) δ: 21.7, 26.4, 32.1, 51.4, 77.9, 113.3. EI-MS *m*/*z* (rel. intensity): 173 ($M^{\cdot+}$ + 1, 9), 141 (4), 105 (100), 81 (12), 59 (14).

Hydrolysis of 13 to methyl 1-hydroxycyclohexanecarboxylate (17)

Addition of water and catalytic trifluoroacetic acid to a solution of **13** gave **17** (13) as a clear liquid. IR (CCl_4) cm^{-1}: 3542 (br), 2900–2850, 1730. ^{1}H NMR (200 MHz, C_6D_6) δ: 1.35–1.80 (m, 10H), 3.23 (s, 3H), 3.70 (s, br, 1H). ^{13}C NMR (50 MHz, C_6D_6) δ: 21.5, 25.6, 35.1, 52.0, 73.7, 177.7. EI-MS *m*/*z* (rel. intensity): 99 ($M^{\cdot+}$-CO_2Me, 21), 84 (38), 75 (4), 49 (100). Failure to generate a significant molecular ion signal, because of loss of the CO_2R fragment, is a characteristic of α-hydroxy esters and their hydroxyl-group derivatives (14).

Preparation of authentic methyl 1-hydroxycyclohexanecarboxylate (17)

The hydroxyester was prepared according to a procedure from the literature (15).

Preparation of 3,4-diaza-2,2-dimethoxy-1-oxaspiro[3,4]dec-3-ene (14)

Compound **14** was prepared by oxidative cyclization of the methoxycarbonyl hydrazone of cyclohexanone using lead tetraacetate as described previously for analogues (8). To a stirred, ice-cooled solution of lead(IV) acetate (31.92 g) in anhyd MeOH (75 mL) under dry N_2 was added, by drops, a solution of the methoxycarbonylhydrazone of cyclohexanone (10.19 g) in MeOH (75 mL). When addition of the hydrazone solution was complete, the ice bath was removed and the mixture was stirred for 4 h as the temperature rose to that of the room. Aqueous NaOH (10%, 30 mL) was added and stirring was continued for 45 min. About one-third of the MeOH was removed with a rotary evaporator before CH_2Cl_2 (25 mL) was added for extraction with a separatory funnel. After three more extractions with CH_2Cl_2 the combined extract was washed three times with 5% $NaHCO_3$. The organic layer was dried over $CaCl_2$ and, after evaporation of the solvent, the crude product was purified by column chromatography (hexane/ethyl acetate, 24:1) to afford **14** as a clear liquid, in 66% yield. ^{1}H NMR (200 MHz, $CDCl_3$) δ: 1.50 – 2.04 (m, 10H), 3.47 (s, 6H). ^{13}C NMR (50.3 MHz, $CDCl_3$) δ: 22.7, 24.6, 33.5 (CH_2 groups), 51.7 (CH_3), 120.9 (C5), 136.1 (C2). EI-MS *m*/*z*: (mol. ion not observed), 169 $[M\text{-}OMe]^{\cdot+}$, 113, 91, 90, 81, 67, 59 (100%), 41.

© 2001 NRC Canada

Thermolysis of 14 with added 4-*tert*-butylcyclohexanone

Samples of 1 mL of solutions containing **14** (0.1 M) and 4-*tert*-butylcyclohexanone (0.05, 0.10, 0.15, 0.20, 0.30, 0.40, 0.50, and 0.80 M) in dry benzene were sealed into thermolysis tubes and heated with an oil bath at 110°C for 72 h. The crude mixtures were analysed by GC–FID (megabore capillary column, DB-1, 0.53 mm × 30 m) with 1,4-dimethoxybenzene as internal standard. For analysis of **17**, which was always present (presumably from adventious water), the GC was calibrated with the authentic ester. Hydrolysis after the analysis gave a solution that no longer contained **13**. That solution was then analysed for **17**. As Fig. 1 shows, the sum of the yields of **13** and **17** before hydrolysis are in good agreement with the yield of **17** after hydrolysis.

Acknowledgements

The authors gratefully acknowledge an NSERC grant-in-aid, from which this work was financed, and an NSERC Postgraduate Scholarship to P.C.V.

References

1. M. Bartok and K. L. Lang. Small ring heterocycles. Part 3. *In* Heterocyclic Compounds. Vol. 42. *Edited by* A. Hassner. Wiley, New York. 1985. pp. 1–196.
2. (*a*) W. Adam, J.-C. Liu, and O. Rodriguez. J. Org. Chem. **38**, 2269 (1973); (*b*) P.L Coe, A. Sellars, J.C. Tatlow, G. Whittaker, and H.C. Fielding. J. Chem. Soc. Chem. Commun. 362 (1982).
3. Y. Yamaguchi, H.F. Schaefer III, and I.L. Alberts. J. Am. Chem. Soc. **115**, 5790 (1993), and refs. therein.
4. K.R. Kopecky, J. Molina, and R. Rico. Can. J. Chem. **66**, 2234 (1988).
5. R.W. Hoffmann and J. Schneider. Chem. Ber. **100**, 3698 (1967).
6. D.L. Pole and J. Warkentin. J. Org. Chem. **62**, 4065 (1997).
7. P. Couture, M. El-Saidi, and J. Warkentin. Can. J. Chem. **75**, 326 (1997).
8. M. El-Saidi, K. Kassam, D.L. Pole, T. Tadey, and J. Warkentin. J. Am. Chem. Soc. **114**, 8751 (1992).
9. K. Kassam, D.L. Pole, M. El-Saidi, and J. Warkentin. J. Am. Chem. Soc. **116**, 1161 (1994).
10. P.C. Venneri and J. Warkentin. Can. J. Chem. **78**, 1194 (2000).
11. P. Sharma and J. Warkentin. Tetrahedron Lett. **36**, 7591 (1995).
12. A. de Meijere, S.I. Kozhushkov, D.S. Yufit, R. Boese, T. Haumann, D.L. Pole, P.K. Sharma, and J. Warkentin. Liebigs Ann. 601 (1996).
13. (*a*) W.D. Woessner. Chem. Lett. 43 (1976); (*b*) P.M. Booth, C.M.J. Fox, and S.V. Ley. J. Chem. Soc. Perkin Trans. 1, 121 (1987).
14. V. Roussis and D.F. Wiener. J. Org. Chem. **54**, 627 (1989).
15. J. Leon, W.F. Barthel, and S.A. Hall. J. Org. Chem. **19**, 490 (1954).

© 2001 NRC Canada

Photochemical preparation of cyclopropanes from cyclobutanones

Jailall Ramnauth and Edward Lee-Ruff

Abstract: A general method for the preparation of cyclopropanes is reported. Triplet-photosensitized reactions of a series of cyclobutanones give cyclopropanes as the major product. Part 1 describes the synthesis of substituted cyclobutanones used in this study. In Part 2, the photo-reactions of cyclobutanones are reported. Triplet-sensitized reactions of cyclobutanones using acetone as a sensitizer give cyclopropanes as the major non-polar products. The extent of photodecarbonylation seems to be dependent on α-substitution. Electron-donating groups promote decarbonylation while electron-withdrawing groups favour cycloelimination.

Key words: photodecarbonylation, cyclobutanones, cyclopropanes, triplet-sensitization.

Résumé : On décrit une méthode générale de préparation des cyclopropanes. Les réactions photosensibilisées de triplets d'une série de cyclobutanones conduisent à des cyclopropanes comme produits majeurs. Dans la première partie, on décrit la synthèse des cyclobutanones substituées utilisées dans cette étude. Dans la deuxième partie, on décrit les photoréactions des cyclobutanones. Les réactions sensibilisées de triplets de cyclobutanones utilisant de l'acétone comme sensibilisateur conduisent à la formation de cyclopropanes comme produits non polaires principaux. Le degré de photodécarbonylation semble dépendre de la substitution en α. Les groupes électrodonneurs favorisent la décarbonylation alors que les groupes électroattracteurs favorisent la cycloélimination.

Mots clés : photodécarbonylation, cyclobutanones, cyclopropanes, sensibilisation triplet.

[Traduit par la Rédaction]

Introduction

Small ring compounds have become more than just a curiosity to chemists. In particular, cyclopropane-containing compounds have played an important role in organic synthesis (1). In contrast to simple alkanes and cycloalkanes, such as cyclopentane and cyclohexane, cyclopropanes participate in a variety of reactions under mild conditions. This increased reactivity of cyclopropanes has been attributed to the deformation of bond angles from normal values as well as torsional effects. Cyclopropane derivatives are also known to constitute the basic framework of biologically active compounds present in animals, plants, and microorganisms, or to be generated as intermediates in primary and secondary metabolic processes (2).

A variety of methods are available for the synthesis of cyclopropanes, but only a few of these have been reported from ring-contraction reactions of cyclobutane derivatives (3). In conjunction with our work on the synthesis and photochemistry of cyclobutanones (4, 5), we are interested in the photodecarbonylation of cyclobutanones as a potential route to cyclopropanes. Preliminary studies have indicated that cyclopropane formation is dominant from a triplet-excited cyclobutanone (6). The triplet-sensitized photochemistry of cyclobutanones appears to take a completely different course of events compared to its singlet state chemistry and is an area that has been relatively unexplored. The impetus for this work is the increasing availability of cyclobutanones in both chiral and achiral forms (7). With three centres amenable to functionalization, cyclobutanones could be valuable precursors to substituted cyclopropanes.

In this paper, we report the synthesis and triplet-photosensitized reactions of a series of substituted cyclobutanones to assess substitution patterns towards photodecarbonylation.

Received August 14, 2000. Published on the NRC Research Press Web site on February 16, 2001.

J. Ramnauth and E. Lee-Ruff.[1] Department of Chemistry, York University, Toronto, ON M3J 1P3, Canada.

[1]Corresponding author (telephone: (416) 736–5443; fax: (416) 736–5936. e-mail: leeruff@yorku.ca).

Results and discussion

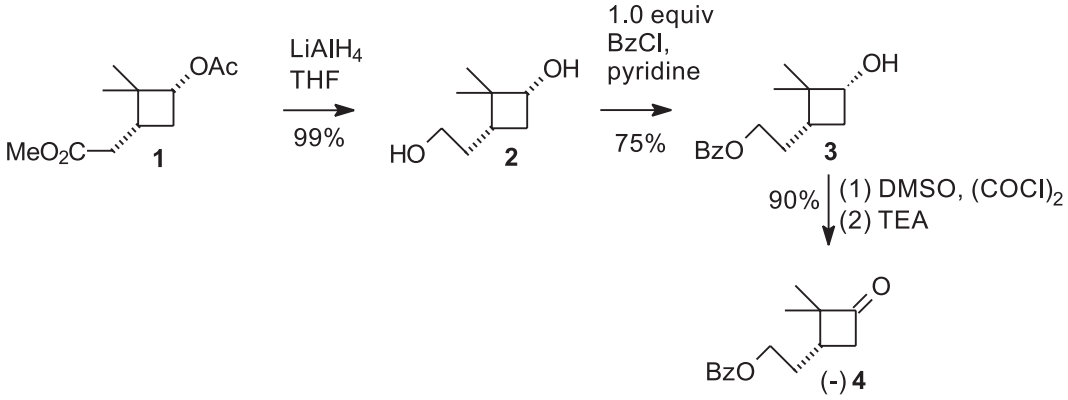
Synthesis of cyclobutanones

The optically active cyclobutanone **((–)-4**) was prepared from the cyclobutane diester (**1**), which was obtained from *cis*-pinonic acid of 92% optical purity (8). The latter compound is an oxidation product of the naturally occurring (+)-α-pinene. The synthesis of (–)-**4** was carried out according to Scheme 1. The diester (**1**) was reduced with $LiAlH_4$ to the diol (**2**) in quantitative yield. This crude diol was then monoprotected with 1.0 equiv of benzoyl chloride at 0°C to hydroxy benzoate (**3**) in 75% yield. This alcohol was then oxidized under Swern conditions to give cyclobutanone ((–)-**4**) in 90% yield after flash column chromatography. The structure of (–)- **4** was ascertained from its spectral and analytical data.

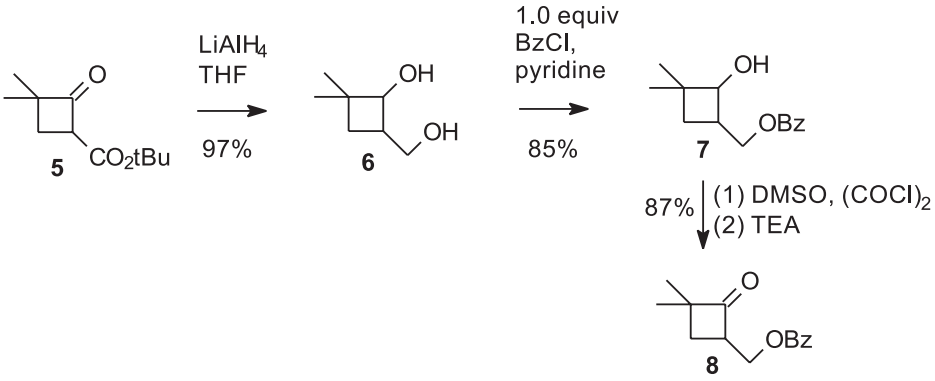
The racemic 2,2,4-trisubstituted cyclobutanone (**5**) was synthesized according to a literature procedure; the key step

 DOI: 10.1139/cjc-79-2-114 © 2001 NRC Canada

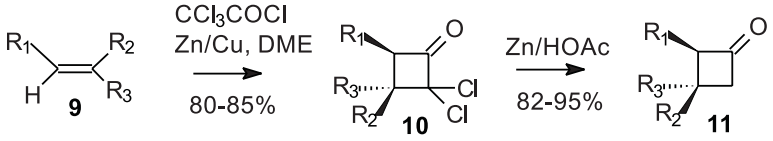
Scheme 1.



Scheme 2.



Scheme 3.



9 a $R_1=R_2=H$, $R_3=CH_2OBz$	**10 a**	**11 a**
9 b $R_1=R_2=H$, $R_3=CH_2CH_2OBz$	**10 b**	**11 b**
9 c $R_1=CH_2OBz$, $R_2=R_3=CH_3$,	**10 c**	**11 c**
9 d $R_1=CH_3$, $R_2=CH_3$, $R_3=CH_2OBz$	**10 d**	**11 d**
9 e $R_1=CH_3$, $R_2=CH_2OBz$, $R_3=CH_3$	**10 e**	**11 e**

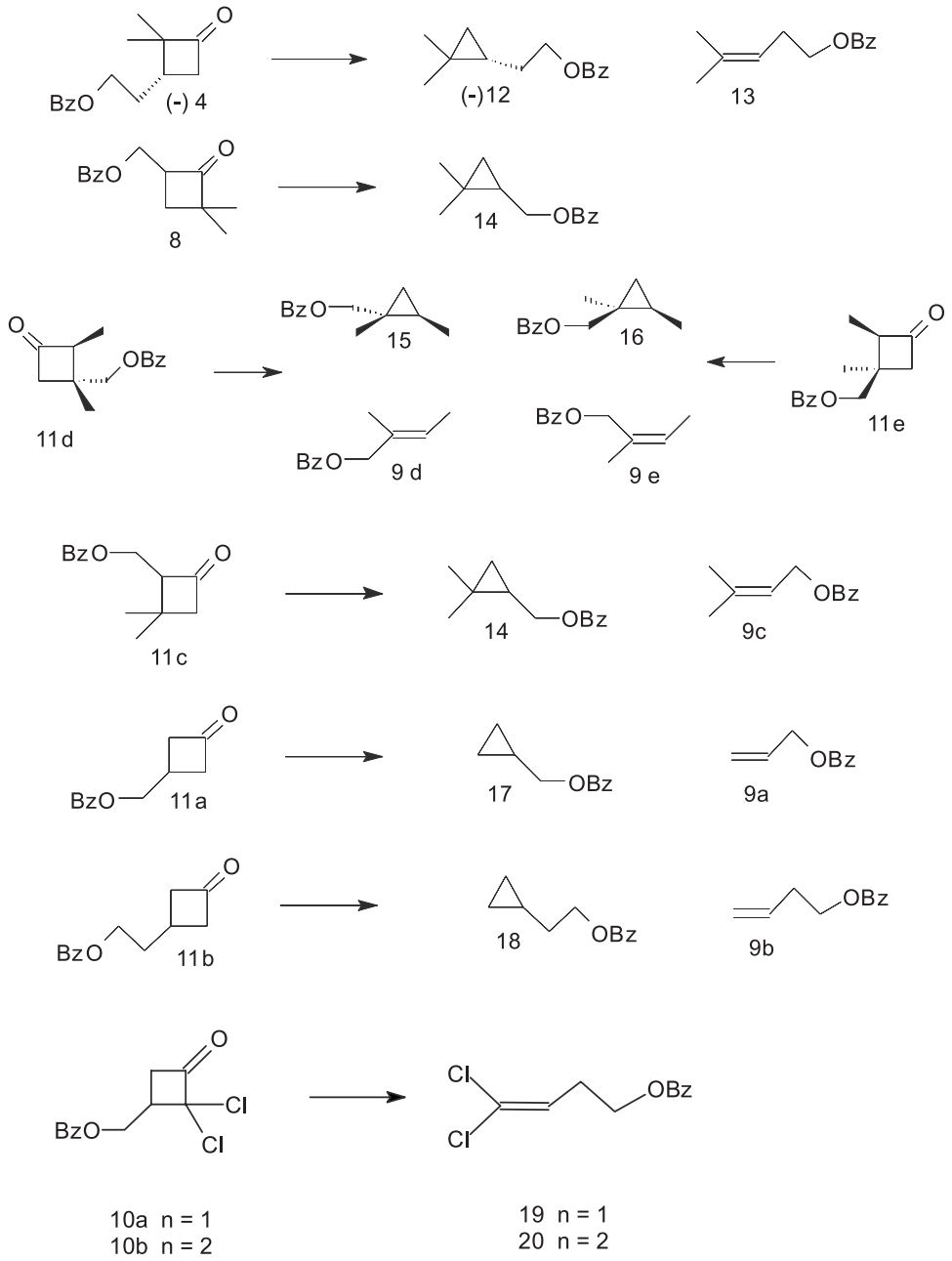
involved a [2 + 2] cycloaddition of *t*-butyl acrylate to *N*,*N*-dimethylisobutenylamine (9). This compound was then converted to cyclobutanone **8** according to Scheme 2. The synthesis of **8** involved the reduction of **5** to diol **6** in quantitative yield followed by protection of its primary hydroxyl group with 1 equiv of benzoyl chloride at –20°C in a yield of 85%. This alcohol was then oxidized under Swern conditions to give the targeted compound **8** in a yield of 87%. The structure of this ketone was confirmed by spectral and analytical data.

Cyclobutanone derivatives (**11a**–**e**) were prepared according to Scheme 3. The olefins (**9a**–**e**) were prepared by esterification of the corresponding alcohol with benzoyl chloride in pyridine in yields ranging from 90–95%. These olefins were then treated with dichloroketene (generated in situ from activated zinc with trichloroacetyl chloride) in the presence of DME (10) to give the cycloadducts (**10a**–**e**) in yields of 80–85%. In all cases, only one regio- and (or) stereoisomer was obtained as determined by ^1H and ^{13}C NMR. The regioisomer of the dichloroketene adduct **10c** was also ascertained by X-ray crystallography (11).

These dichlorocyclobutanones were dechlorinated with zinc powder in acetic acid to give cyclobutanones (**11a**–**e**) in high yields ranging from 85–95%. The structures of all cyclobutanones were confirmed by spectral and analytical data. Cyclobutanone **11a** showed 9 peaks in the ^{13}C NMR spectrum and a symmetrical pattern for the cyclobutyl protons in the ^1H NMR spectrum. A similar analysis was made for **11b** to confirm its regioisomeric structure. The structures of the regioisomers **11c** and **11d** were confirmed by 2-D ^1H COSY experiments. The splitting patterns in the ^1H NMR spectra were consistent with the assigned structures. The

© 2001 NRC Canada

Scheme 4.



stereochemistry of **11d** and **11e** was assigned based on the starting olefins. Also, ^{13}C and ^{1}H NMR data showed that there is no interconversion of the two isomers under the acidic conditions used in the dechlorination reaction.

Photolyses of cyclobutanones

Photolyses were performed using a medium-pressure mercury arc lamp with a Pyrex filter. Photolyses were conducted in acetone for the triplet sensitized reactions while comparative non-sensitized irradiations were carried out in THF. The samples were thoroughly degassed with argon prior to irradiation. The samples were photolyzed for 4 h and the crude photolysis products were purified by chromatography. Conversions were on average >90%. In cases where mixtures of olefins and cyclopropanes were obtained, relative yields were determined by ^{1}H NMR or HPLC analysis.

The products derived from the photolysis of the different substituted cyclobutanones are illustrated in Scheme 4. The yields for the photolyses in acetone are tabulated (Table 1). For photoreactions in THF, the major products were the olefins for all of the cyclobutanones except for cyclobutanone **8**. For this cyclobutanone, an intractable polymeric mixture was obtained. This suggests that the initial photoproducts were not stable under these conditions leading to oligomerization.

The structures of all photoproducts were assigned based on spectral and analytical data. It is evident from the results that under triplet-sensitized conditions cyclopropanes are the

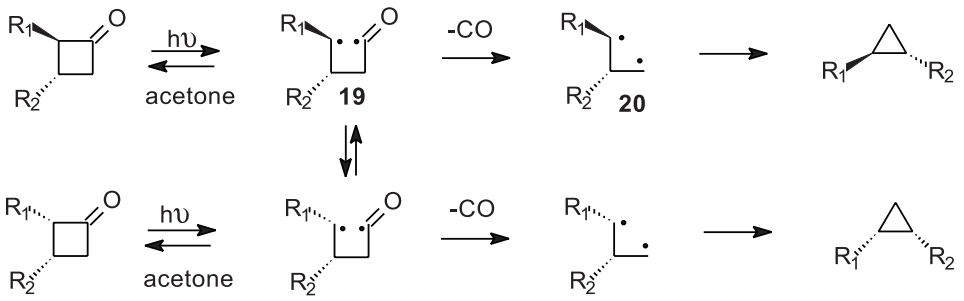
© 2001 NRC Canada

Table 1. Yields of photoproducts for photoreactions of cyclobutanones in acetone.

Cyclobutanone	Products		Ratio of cyclopropane:olefin
	Cyclopropane	Olefin	
(–)-4	**(–)-12** (72 %)	**13** (trace)	1:0
8	**14** (85%)	not detected	1:0
10a		**19** (65%)[a]	0:1
10b		**20** (58%)[a]	0:1
11a	**17** (81%)	**9a** (6%)	13.5:1
11b	**18** (78%)	**9b** (6%)	13:1
11c	**14** (64%)	**9c** (10%)	6.4:1
11d, 11e	**15** (41%), **16** (27%)	**11d** (2%), **11e** (2%)	17:1

[a]Ref. 12.

Scheme 5.



major products while olefins are the major products under non-sensitized conditions. The photodecarbonylation reaction seems to be quite general.

It is apparent that the extent of photodecarbonylation is dependent on the α-substituent. We compared the ratio of cyclopropane to olefin to look at the efficiency of the decarbonylation pathway with varying substituents (Table 1). The results indicate that electron-donating groups promote decarbonylation. (–)-Cyclobutanone **4** with two electron-donating methyl groups at the α-position gave cyclopropane **12** as the only product. The lowest ratio of cyclopropane to olefin was obtained for cyclobutanone **11c** which has a weak electron-withdrawing benzoyloxymethyl group at the α-position. In the extreme case, with α,α-dichlorocyclobutanones **10a** and **10b**, cycloelimination to give 1,1-dichloroalkene is the only reaction (12).

The stereoisomeric cyclobutanones **11d** and **11e** provide examples of cyclobutanones with methyl substituents at the α-position. But more importantly, they provide a stereochemical probe for epimerization in the photodecarbonylation reaction. Under triplet-sensitized conditions these two cyclobutanones gave similar product distributions as determined by ^{1}H NMR analyses. It was surprising to see that the products showed no memory effect of the starting cyclobutanone stereochemistry unlike the photochemical ring-expansion under non-sensitized conditions (5).

In general, the extent of epimerization at the α-carbon in the decarbonylation of cyclobutanones will depend on the lifetimes of the intermediate acyl-alkyl diradical **19** and the 1,3-diradical **20** (Scheme 5). A thermodynamic equilibration of these intermediates would give an epimeric mixture of cyclopropanes. After 1 h of irradiation under triplet-sensitized conditions, analysis of the unreacted cyclobutanones **11d** and **11e** showed that about 10% of the other epimer was formed. It is likely that the decarbonylation products undergo equilibration at the 1,4-diradical stage. This stereochemical scrambling of starting materials does not occur under non-sensitized conditions. This indicates the presence of a stereochemically labile triplet 1,4-acyl-alkyl diradical intermediate under the triplet-sensitized conditions. The triplet 1,3-diradical formed after decarbonylation would be expected to undergo rapid epimerization relative to ring closure which would also allow for equilibration of the final products.

The cyclopropane photoproducts are photochemically inert under the acetone sensitized conditions, e.g., irradiation of **16** for 4 h showed no epimerization with complete recovery eliminating the possibility for stereochemical equilibration at the cyclopropane stage.

Conclusion

It has been shown that triplet-sensitized reactions of cyclobutanones, using acetone as a sensitizer, gave cyclopropanes as the major non-polar products. Under non-sensitized conditions, the photochemistry of cyclobutanones gave mostly cycloelimination products. The extent of photodecarbonylation seems to be dependent on the nature of the α-substituents. Electron-donating groups promote decarbonylation while electron-withdrawing groups favour cycloelimination. The triplet-sensitized photoreactions of *E*-3-benzoyloxymethyl-2,3-dimethylcyclobutanone (**11d**) and *Z*-3-benzoyloxymethyl-2,3-dimethylcyclobutanone (**11e**), a pair of epimeric cyclobutanones, gave a similar product distribution. The distribution of products does not show any memory effect of the starting ketone stereochemistry. In both

© 2001 NRC Canada

cases, the major product was *E*-1-benzoyloxymethyl-1,2-dimethylcyclopropane, along with its stereoisomer and minor elimination products. It is evident from these results that the photodecarbonylation reaction is not stereoselective and bond rotation in the diradical intermediates occurs faster than ring closure. Since the cyclobutanones are prepared from [2 + 2] cycloadditions of alkenes and ketene or ketene equivalents, this two step process represents an alternate route for cyclopropanations under neutral conditions which could find many applications. The reaction can also be a potential route to sterically congested cyclopropanes.

Experimental

Melting points (mp) were determined on a Reichert melting point apparatus and were uncorrected. NMR spectra were recorded on a Bruker ARX 400 (400 MHz) spectrometer in $CDCl_3$ containing 1% TMS unless otherwise noted. Chemical shifts are quoted in delta (δ) values in parts per million (ppm) downfield from TMS (δ = 0). Mass spectra (MS) were recorded at 70 eV electron impact mode on a Kratos profile mass spectrometer. Optical rotations were measured using a Perkin–Elmer 241 polarimeter at 22°C. Fourier transform infrared spectra (FT-IR) were recorded on a Pye Unicam SP3–200 spectrometer as thin films or KBr pellets. HPLC analysis was performed on a Waters M6000A instrument with a Lamda-Max model 481 LC detector using UV detection (254 nm), a Hewlett–Packard integrator, and a Spherisorb Silica analytical column from Sigma–Aldrich. Elemental analyses were performed by Guelph Chemical Laboratories Ltd.

Photolyses were carried out using a Hanovia 450 W medium-pressure mercury arc lamp in a water-cooled quartz immersion well. Pyrex tubes containing the samples were strapped around this well and the assembly immersed in an ice water bath. The samples were purged with argon for 30 min prior to irradiation. All solvents used in these reactions were dried and distilled.

Analytical thin layer chromatography (TLC) was performed on commercially prepared silica gel 60F 254 plastic sheets (E. Merck & Co.). Preparative TLC was performed on Aldrich silica gel 60F 254 precoated glass plates. For column chromatography, Silicycle silica gel (flash chromatography grade, 20–45 μm) was used.

Synthesis of (–)-3-[2-(benzoyloxy)ethyl]-2,2-dimethylcyclobutanone (4)

To a stirred suspension of $LiAlH_4$ (2.5 g, 65.2 mmol) in dry Et_2O (100 mL) at 0°C under argon was added **1** (8) (7.0 g, 32.6 mmol) in 60 mL dry Et_2O dropwise over a period of 30 min. The reaction mixture was then heated to reflux for 4 h. After cooling in an ice-water bath the following were added dropwise in sequence: (*i*) 2.4 mL H_2O in 7.6 mL THF; (*ii*) 2.4 mL 15% aq. NaOH; and, (*iii*) 7.2 mL H_2O. The resulting mixture was stirred at ambient temperature for an additional 30 min after which it was filtered and washed with Et_2O (3 × 100 mL). The ether extracts were combined and dried over anhyd Na_2SO_4 and concentrated to give 4.7 g (99.7%) of **2**. This crude diol was dissolved in dry pyridine (50 mL) and cooled to 0°C. To this solution was added dropwise benzoyl chloride (4.4 g, 31.3 mmol, 0.95 equiv) in dry pyridine (20 mL) over a period of 30 min. The reaction was kept at this temperature for 4 h and then allowed to warm to room temperature. After this time, the reaction mixture was concentrated and diluted with CH_2Cl_2 (300 mL). The organic phase was washed with H_2O (3 × 50 mL), 1% HCl (3 × 50 mL), sat. aq $NaHCO_3$ (3 × 50 mL), H_2O (2 × 50 mL) and dried over Na_2SO_4. Evaporation of the solvent, followed by flash silica gel chromatography (6:1, hexane:ethyl acetate), gave 5.8 g (75%) of **3**. MS *m/z*: 249 (M + 1). FT-IR (neat) cm^{-1}: 3410, 1719. ^1H NMR ($CDCl_3$) δ: 8.04–7.42 (m, 5H), 4.29–4.22 (m, 2H), 3.75–3.70 (m, 1H), 2.39–2.14 (m, 1H), 1.88–1.50 (m, 5H), 1.09 (s, 3H), 0.99 (s, 3H). ^{13}C NMR ($CDCl_3$) δ: 166.7, 133.0, 130.3, 129.6, 128.4, 74.1, 64.1, 43.9, 34.5, 34.4, 29.1, 28.1, 15.2. The crude product was used for the next step.

A solution of oxalyl chloride (1.25 mL, 15 mmol) in dry CH_2Cl_2 (60 mL) was cooled to –60°C with constant stirring under argon. To this mixture, DMSO (2.0 g, 25 mmol) in dry CH_2Cl_2 (12 mL) was added over a 5 min period. After an additional 10 min of stirring, **3** (2.5 g, 10.1 mmol) in CH_2Cl_2 (25 mL) was added over a 5 min period. After 15 min, TEA (7.0 mL) was added over a 5 min period, and the resulting mixture was allowed to warm to room temperature. The reaction mixture was treated with H_2O (30 mL) and stirred for 10 min to separate the two layers. The organic layer was separated and the aqueous layer was extracted with CH_2Cl_2 (2 × 50 mL). The combined organic extract was washed with 2% HCl (2 × 50 mL), H_2O (50 mL), sat. aq $NaHCO_3$ (50 mL), sat. aq NaCl (50 mL), and dried over $MgSO_4$. Purification by flash silica gel chromatography (6.25:1, hexane:ethyl acetate) gave 2.2 g (90%) of the title compound as a colourless oil. $[\alpha]_D^{22}$ = –23.0° ($CHCl_3$, *c* 1.5). MS *m/z*: 246. FT-IR (neat) cm^{-1}: 1777.1, 1718.3. ^1H NMR ($CDCl_3$) δ: 8.05–7.27 (m, 5H), 4.40–4.36 (m, 2H), 3.21 (dd, *J* = 8.9, 8.7 Hz, 1H), 2.84 (dd, *J* = 7.7, 9.9 Hz, 1H), 2.23–2.10 (m, 2H), 1.93–1.85 (m, 1H), 1.22 (s, 3H), 1.15 (s, 3H). ^{13}C NMR ($CDCl_3$) δ: 214.3, 166.6, 133.1, 130.1, 129.6, 128.5, 63.9, 61.1, 48.6, 33.6, 29.9, 23.4, 17.3. Anal. calcd. for $C_{15}H_{18}O_3$: C 73.14, H 7.37; found: C 72.94, H 7.76.

Synthesis of (±)-2-benzoyloxymethyl-4,4-dimethylcyclobutanone (8)

The keto-ester **5** (9) was reduced according to the procedure described for the reduction of diester **1** to give compound **6** (mixture of isomers) in a yield of 98%. ^1H NMR of major isomer δ: 4.06 (d, *J* = 7.3 Hz, 1H), 3.86 (t, *J* = 10.9 Hz, 1H), 3.74 (dd, *J* = 4.2, 6.8 Hz, 1H), 3.20 (br s, 1H), 3.05 (br s, 1H), 1.62–1.54 (m, 2H), 1.11 (s, 3H), 1.06 (s, 3H). ^{13}C NMR ($CDCl_3$) of major isomer δ: 76.4, 63.2, 37.9, 35.4, 32.3, 28.8, 22.3. This crude diol was used in the next step without further purification. The hydroxy ester **7** was prepared in 85% yield by a slightly modified procedure as described for the preparation of **3**. This reaction was conducted at –20°C instead of 0°C. ^1H NMR ($CDCl_3$) of major isomer δ: 8.04–7.26 (m, 5H), 4.73 (dd, *J* = 1.7, 9.8, Hz, 1H), 4.18 (dd, *J* = 4.8, 6.6 Hz, 1H), 3.97–3.95 (m, 1H), 2.84 (d, *J* = 3.5 Hz, 1H), 2.77–2.73 (m, 1H), 1.76–1.73 (m, 1H), 1.68–1.61 (m, 1H), 1.14 (s, 3H), 1.08 (s, 3H). This compound was oxidized under Swern conditions as before to give **8** as a colourless oil in a yield of 87% after flash silica

© 2001 NRC Canada

gel chromatography (4:1, hexane:ethyl acetate). MS *m/z*: 233 (M + 1). FT-IR (neat) cm^{-1}: 1772.6, 1718.5. ^1H NMR ($CDCl_3$) δ: 7.99–7.38 (m, 5H), 4.49 (d, *J* = 4.9 Hz, 2H), 3.78–3.73 (m, 1H), 2.08 (t, *J* = 11.0 Hz, 1H), 1.86 (dd, *J* = 3.2, 8.3 Hz, 1H), 1.24 (s, 3H), 1.18 (s, 3H). ^{13}C NMR ($CDCl_3$) δ: 214.2, 166.4, 133.1, 129.9, 129.6, 128.4, 62.0, 58.3, 54.2, 30.3, 23.5, 21.7. Anal. calcd. for $C_{14}H_{16}O_3$: C 72.39, H 6.95; found: C 72.25, H 7.07.

General procedure for the preparation of dichlorocyclobutanones 10a–e

A two-neck round-bottom flask, equipped with a magnetic stirrer, dropping funnel, and argon inlet was charged with activated zinc (4 equiv) and the olefin (1 equiv) in anhyd ether (2 mL $mmol^{-1}$ of olefin). To this vigorously stirred suspension was added dropwise a mixture of trichloroacetyl chloride (2 equiv), 1,2-dimethoxyethane (DME) (2 equiv), and anhyd ether (1 mL $mmol^{-1}$) over a period of about 30 min. This mixture was stirred overnight at room temperature. After this time, hexane was added (~50 mL) and the suspension stirred for 5 min to precipitate the zinc salts. The solution was then decanted and treated sequentially with H_2O (100 mL), sat. aq $NaHCO_3$ (3 × 100 mL), sat. aq NaCl (100 mL), and dried over Na_2SO_4. The syntheses of compounds **10a** and **10b** have been reported previously (12).

*4-Benzoyloxymethyl-2,2-dichloro-3,3-dimethylcyclobutanone (**10c**)*

Prepared from olefin **9 c** in 82% yield. The crude product was recrystallized from hexane to give creamish coloured crystals, mp 61–62°C. FT-IR (KBr) cm^{-1}: 1801, 1716. ^1H NMR ($CDCl_3$) δ: 8.02–7.44 (m, 5H), 4.62 (dd, *J* = 5.0, 6.8 Hz, 1H), 4.46 (dd, *J* = 3.1, 8.7 Hz, 1H), 3.94 (dd, *J* = 3.2, 5.6 Hz, 1H), 1.58 (s, 3H), 1.36 (s, 3H). ^{13}C NMR ($CDCl_3$) δ: 192.3, 166.0, 133.4, 129.6, 129.4, 128.6, 91.9, 62.6, 59.0, 45.1, 24.5, 21.1. Anal. calcd. for $C_{14}H_{14}Cl_2O_3$: C 55.85, H 4.69; found: C 56.00, H 4.81.

E-*3-Benzoyloxymethyl-2,2-dichloro-3,4-dimethylcyclobutanone (**10d**)*

Prepared in 81% yield from olefin **9d**. The crude product was passed through a short plug of silica gel to give a white solid, mp 99–100°C. FT-IR (neat) cm^{-1}: 1800, 1726. ^1H NMR ($CDCl_3$) δ: 8.26–7.65 (m, 5H), 4.87 (d, *J* = 11.6 Hz, 1H) 4.81 (d, *J* = 11.6 Hz, 1H), 3.93 (q, *J* = 7.1 Hz, 1H), 1.55 (s, 3H), 1.39 (d, *J* = 7.0 Hz, 3H). ^{13}C NMR ($CDCl_3$) δ: 194.9, 166.0, 133.4, 129.7, 129.5, 128.6, 90.2, 68.5, 56.0, 47.4, 16.9, 8.6. Anal. calcd. for $C_{14}H_{14}Cl_2O_3$: C 55.85, H 4.69; found: C 55.80, H 4.83.

Z-*3-Benzoyloxymethyl-2,2-dichloro-3,4-dimethylcyclobutanone (**10e**)*

Prepared in 81% yield from olefin **9e**. The crude product was passed through a short plug of silica gel to give a viscous yellow oil which solidified on standing at –10°C overnight, mp 75–76°C. FT-IR (neat) cm^{-1}: 1800, 1726. ^1H NMR ($CDCl_3$) δ: 8.03–7.52 (m, 5H), 4.63 (d, *J* = 11.9 Hz, 1H) 4.51(d, *J* = 11.9 Hz, 1H), 3.71 (q, *J* = 7.5 Hz, 1H), 1.65 (s, 3H), 1.37 (d, *J* = 7.0 Hz, 3H). ^{13}C NMR ($CDCl_3$) δ: 194.9, 166.0, 133.4, 129.7, 129.5, 128.6, 90.2, 68.5, 56.0, 47.4, 16.9, 8.6. Anal. calcd. for $C_{14}H_{14}Cl_2O_3$: C 55.85, H 4.69; found: C 55.81, H 4.66.

General procedure for the dechlorination of cyclobutanones 11a–e

A one-neck round-bottom flask was charged with zinc powder (5 equiv) and glacial acetic acid (1.5 mL/equiv). To this vigorously stirred suspension was slowly added the dichlorocyclobutanone (1 equiv) in glacial acetic acid (1 mL/equiv). After addition, the mixture was heated to 60°C for 30 min. The reaction mixture was cooled, diluted with anhyd ether (100 mL) and then filtered. The filtrate was then treated with sat. aq $NaHCO_3$ (5 × 100 mL), sat. aq NaCl (1 × 100 mL), and dried over Na_2SO_4. In general, the crude products contained very little impurity and were purified using a short plug of silica gel with 4:1 (hexane:ethyl acetate). Compounds **11c**–**e** were purified by flash silica gel chromatography, using methylene chloride as the eluent.

*3-Benzoyloxymethylcyclobutanone (**11a**)*

Prepared in 95% yield from compound **10a**. FT-IR (neat) cm^{-1}: 1787, 1719. ^1H NMR ($CDCl_3$) δ: 8.04–7.26 (m, 5H), 4.50 (d, *J* = 6.1 Hz, 2H), 3.29–3.21 (m, 2H), 3.04–2.89 (m, 3H). ^{13}C NMR ($CDCl_3$) δ: 205.9, 166.4, 133.2, 129.8, 129.6, 128.5, 67.2, 50.1, 23.0. Anal. calcd. for $C_{12}H_{12}O_3$: C 70.58, H 5.92; found: C 70.65, H 5.76.

*3-[2-(Benzoyloxy)ethyl]cyclobutanone (**11b**)*

Prepared in 93% yield from **10b**. FT-IR (neat) cm^{-1}: 1786, 1718. ^1H NMR ($CDCl_3$) δ: 8.04–7.43 (m, 5H), 4.40 (t, *J* = 6.1 Hz, 2H), 3.28–3.20 (m, 2H), 2.86–2.79 (m, 2H), 2.60–2.56 (m, 1H), 2.12–2.07 (m, 2H). ^{13}C NMR ($CDCl_3$) δ: 207.2, 166.5, 133.1, 130.1, 129.5, 128.4, 63.7, 52.7, 35.0, 21.4. Anal. calcd. for $C_{13}H_{14}O_3$: C 71.55, H 6.47; found: C 71.73, H 6.37.

*2-Benzoyloxymethyl-3,3-dimethylcyclobutanone (**11c**)*

Prepared in 95% yield from compound **10c**. FT-IR (neat) cm^{-1}: 1779, 1720. ^1H NMR ($CDCl_3$) δ: 8.02–7.42 (m, 5H), 4.54 (dd, *J* = 4.9, 6.8 Hz, 1H), 4.45 (dd, *J* = 3.0, 8.8 Hz, 1H), 2.97–2.91 (m, 1H), 2.70 (dd, *J* = 2.5, 14.5 Hz, 1H), 2.66 (dd, *J* = 1.3, 16.1 Hz, 1H), 1.49 (s, 3H), 1.29 (s, 3H). ^{13}C NMR ($CDCl_3$) δ: 205.5, 166.2, 133.1, 129.9, 129.6, 128.5, 66.2, 59.9, 58.5, 30.0, 29.6, 22.8. Anal. calcd. for $C_{14}H_{16}O_3$: C 72.39, H 6.95; found: C 72.34, H 6.84.

E-*3-Benzoyloxymethyl-2,3-dimethylcyclobutanone (**11d**)*

Prepared in 85% yield from **10d**. FT-IR (neat) cm^{-1}: 1780, 1720. ^1H NMR ($CDCl_3$) δ: 8.04–7.44 (m, 5H), 4.42 (s, 2H), 3.32 (m, 1H), 3.16 (d, *J* = 19.6 Hz, 1H), 2.59 (d, *J* = 16.8 Hz, 1H), 1.24 (s, 3H), 1.09 (d, J = 7.5 Hz, 3H). ^{13}C NMR ($CDCl_3$) δ: 208.6, 166.4, 133.3, 129.8, 129.6, 128.6, 58.9, 54.0, 32.5, 18.2, 8.5. Anal. calcd. for $C_{14}H_{16}O_3$: C 72.39, H 6.95; found: C 72.34, H 7.24.

Z-*3-Benzoyloxymethyl-2,3-dimethylcyclobutanone (**11e**)*

Prepared in 87% yield from **10e**. FT-IR (neat): 1780, 1720 cm^{-1}. ^1H NMR ($CDCl_3$) δ: 8.06–7.50 (m, 5H), 4.43 (dd, *J* = 11.7, 15.8 Hz, 2H), 3.23–3.21 (m, 1H), 3.00 (s, 2H), 1.57 (s, 3H), 1.23 (d, *J* = 7.0 Hz, 3H). ^{13}C NMR ($CDCl_3$) δ: 208.5, 166.2, 133.2, 129.7, 129.6, 128.6, 68.2, 62.1, 53.9,

© 2001 NRC Canada

32.9, 24.5, 8.3. Anal. calcd. for $C_{14}H_{16}O_3$: C 72.39, H 6.95; found: C 72.36, H 6.79.

*(–)-Cyclopropane (**12**)*

Prepared in 72% yield from (–)-cyclobutanone **4**. $[\alpha]_D^{22}$ = –12.1° ($CHCl_3$, *c* 0.7). MS *m*/*z*: 218 (M^+). ^{1}H NMR ($CDCl_3$) δ: 8.07–7.42 (m, 5H), 4.39–4.36 (t, *J* = 6.9 Hz, 2H), 1.88–1.83 (m, 1H), 1.73–1.67 (m, 1H), 1.08 (s, 3H), 1.05 (s, 3H), 0.60–0.59 (m, 1H), 0.47–0.44 (m, 1H), 0.00 (t, *J* = 4.7 Hz, 1H). ^{13}C NMR ($CDCl_3$) δ: 166.7, 132.8, 130.6, 129.6, 128.3, 65.5, 29.1, 27.4, 21.2, 20.0, 19.5, 15.3. Anal. calcd. for $C_{14}H_{18}O_2$: C 77.03, H 8.31; found: C 76.84, H 8.55.

*Olefin (**13**)*

^{1}H NMR ($CDCl_3$) δ: 8.05–7.42 (m, 5H), 5.20–5.18 (m, 1H), 4.29 (t, *J* = 7.0 Hz, 2H), 2.46–2.49 (m, 2H), 1.72 (s, 3H), 1.66 (s, 3H).

*1-Benzoyloxymethyl-2,2-dimethylcyclopropane (**14**)*

Prepared in 85% yield from cyclobutanone **8**. ^{1}H NMR ($CDCl_3$) δ: 8.09–7.45 (m, 5H), 4.52 (dd, *J* = 4.9, 6.9 Hz, 1H), 4.17 (dd, *J* = 2.8, 8.7 Hz, 1H), 1.18 (s, 3H), 1.13 (s, 3H), 1.10–1.09 (m, 1H), 0.62 (dd, *J* = 4.1, 4.5 Hz, 1H), 0.31 (t, *J* = 4.9 Hz, 1H). ^{13}C NMR ($CDCl_3$) δ: 166.8, 132.8, 130.6, 129.6, 128.3, 66.7, 27.1, 22.6, 20.1, 18.8, 16.4. Anal. calcd. for $C_{13}H_{16}O_2$: C 76.43, H 7.89; found: C 76.16, H 8.17.

Acknowledgments

We would like to thank the Natural Sciences and Engineering Research Council of Canada (NSERC) for financial support.

References

1. H.N.C. Wong, M.-Y. Hon, C.-W. Tse, Y.-C. Yip, J. Tanko, and T. Hudlicky. Chem. Rev. **89**, 165 (1989).
2. J. Salaun and M.S. Baird. Curr. Med. Chem. **2**, 511 (1995).
3. J. Salaun. Chem. Rev. **89**, 1247 (1989).
4. E. Lee-Ruff, F.-D. Xi, and J.H. Qie. J. Org. Chem. **61**, 1547 (1996).
5. E. Lee-Ruff, W.Q. Wan, and J.L. Jiang. J. Org. Chem. **59**, 2114 (1994).
6. J. Ramnauth and E. Lee-Ruff. Can. J. Chem. **75**, 518 (1997).
7. E. Lee-Ruff. *In* Methods in organic chemistry. Vol. E17. *Edited by* A. De Meijere. Houben-Weyl, G. Thieme Verlag, Stuttgart. Chap. 1.3.4.3. 1997. p. 179.
8. M. Karpf and C. Djerassi. J. Am. Chem. Soc. **103**, 302 (1981).
9. W.C. Agosta and D.K. Herron. J. Org. Chem. **34**, 2782 (1969).
10. B.D. Johnston, E. Czyzewska, and A.C. Oehlschlager. J. Org. Chem. **52**, 3693 (1987).
11. E. Lee-Ruff and J. Ramnauth. Acta Cryst. Section C, **54**, IUC9800029 (1998).
12. J. Ramnauth and E. Lee-Ruff. Can. J. Chem. **77**, 1245 (1999).

© 2001 NRC Canada

Gaussian basis sets for the atoms from K through Xe

R. Centoducatte, E.V.R. de Castro, and F.E. Jorge

Abstract: An improved generator coordinate Hartree–Fock (IGCHF) method is used to generate Gaussian basis sets for the atoms from K (Z = 19) through Xe (Z = 54). The Griffin–Hill–Wheeler–HF equations are integrated using the integral discretization technique. The ground state HF total energies obtained by us are compared with those calculated with the original GCHF method and with other approaches reported in the literature. The largest difference between our energy values and the corresponding ones computed with a numerical HF method is equal to 6.003 mhartree for Kr (Z = 36).

Key words: improved generator coordinate Hartree–Fock method, Gaussian basis sets, total energies.

Résumé : On a utilisé une méthode de Hartree–Fock avec générateur de coordonnées amélioré (IGCHF) pour générer des ensembles de base gaussiens pour les atomes allant de K (Z = 19) à Xe (Z = 54). On a intégré les équations de Griffin–Hill–Wheeler–HF en faisant appel à une technique de discrétisation intégrale. Les énergies totales de HF que l'on a obtenues pour l'état fondamental sont comparées à celles calculées par la méthode de GCHF originale et avec celles obtenues par d'autres approches rapportées dans la littérature. La plus grande différence entre les valeurs d'énergies que l'on a obtenues et celles obtenues par des calculs à l'aide d'une méthode de HF numérique est égale à 6,003 mhartree pour le Kr (Z = 36).

Mots clés : méthode de Hartree–Fock avec générateur de coordonnées amélioré, ensembles de base gaussiens, énergies totales.

[Traduit par la Rédaction]

Introduction

Hartree–Fock (HF) wave functions for atoms and atomic ions can be constructed numerically (1). However, practical convenience dictates a very frequent use of Roothaan–HF (RHF) wave functions (2) in which the radial parts of the atomic orbitals are algebraically approximated by expansion in a set of basis functions such as Slater-type functions (STFs) or Gaussian-type functions (GTFs). The majority of contemporary molecular quantum chemical calculations use basis sets composed of GTFs. There are good reviews and compendia (3–6) of GTF basis sets either in uncontracted or contracted form.

In 1986, Mohallem et al. (7) developed the generator coordinate HF (GCHF) method and applied this methodology in the generation of universal basis sets (UBSs) of STFs and GTFs (8,9). In the last three years, Jorge and co-workers (10–14) have used with success the GCHF method in the generation of UBSs and of adapted Gaussian basis sets for light and heavy atoms.

Received October 19, 2000. Published on the NRC Research Press Web site on February 16, 2001.

R. Centoducatte and F.E. Jorge.[1] Departamento de Física, Universidade Federal do Espírito Santo, 29060-900 Vitória, ES, Brazil.
E.V.R. de Castro. Departamento de Química, Universidade Federal do Espírito Santo, 29060-900 Vitória, ES, Brazil.

[1]Corresponding author (e-mail: jorge@cce.ufes.br).

Recently, Jorge and de Castro (15) developed an improved GCHF (IGCHF) method that was used to generate accurate Gaussian basis sets (GBSs) for the first-row atoms (15) and second-row atoms and atomic ions (16). From these basis sets (15,16) we have generated contracted GBSs which were used to calculate various physical and chemical properties of first- (17) and second-row (18) diatomic molecules.

In this work, we report GBSs for the third- and fourth-row atoms in their ground state generated with the IGCHF method (15). Our total energy results are compared with the corresponding values obtained with the original GCHF method (7), with the fully optimized basis sets (19) of STFs and with a numerical HF (NHF) (20) approach.

Improved generator coordinate Hartree–Fock method

The GCHF method (7) has been used to describe the electronic structure of atoms and molecules. This model describes the one-electron functions as an integral transform

$$[1] \qquad \psi_i(1) = \int \phi_i(1,\alpha)\, f_i(\alpha)\, d\alpha \qquad i = 1, \ldots, n$$

where the ϕ_i are the generator functions (in this work are GTFs), the f_i are the weight functions, and α is the generator coordinate. The application of eq. [1] to calculate expectation values using Slater determinant leads to the Griffin–Hill–Wheeler–HF (GHWHF) eqs. (7). These are a set of integral equations of the form

 DOI: 10.1139/cjc-79-2-121 © 2001 NRC Canada

$$[2] \qquad \int [F(\alpha,\beta) - \varepsilon_i S(\alpha, B)] f_i(\beta) d\beta = 0 \qquad i-1,\ldots,n$$

where the ε_i are the HF eigenvalues, and the Fock ($F(\alpha, \beta)$) and overlap ($S(\alpha, \beta)$) kernels are defined in ref. 7. An analytic solution of eq. [2] for multieletronic systems is not possible and, thus, it is integrated numerically through a technique called integral discretization (ID) (21). This technique is implemented through a relabelling of the generator coordinate space, i.e.,

$$[3] \qquad \Omega = \ln\alpha / A \qquad A > 1$$

where A is a scaling parameter determined numerically. The new generator coordinate space (Ω) is discretized for each *s*, *p*, *d*, and *f* symmetry in an equally spaced mesh $\{\Omega_i\}$ so that:

$$[4] \qquad \Omega_k = \Omega_{\min} + (k-1)\Delta\Omega \qquad k = 1,\ldots,N$$

In eq. [4] N corresponds to the number of discretization points defining the basis set size, $\Omega_{\min}$ is the initial point, and $\Delta\Omega$ an increment. Thus, the original GCHF method (7) corresponds to the use of only one arithmetic sequence (eq. [4]) of equally spaced points $\{\Omega_i\}$ to generate single-optimized GBSs (SOGBSs).

Recently, Jorge and de Castro (15) have introduced a simple modification in the GCHF method that produces improvements in the HF atomic energy values without adding more functions (GTFs in our case); this procedure has been named as IGCHF method. In this new approach (15) the new generator coordinate space, Ω, is discretized for each *s*, *p*, *d*, and *f* symmetry in three independent arithmetic sequences,

$$[5] \qquad \Omega_k = \begin{cases} \Omega_{\min} + (k-1)\Delta\Omega & k = 1,\ldots,j \\ \Omega'_{\min} + (k-1)\Delta\Omega' & k = j+1,\ldots,M \\ \Omega''_{\min} + (k-1)\Delta\Omega'' & k = M+1,\ldots,N \end{cases}$$

For a given value of N, the number of parameters now to be optimized for each symmetry when we use eq. [5] is three times that of the original GCHF method (see eq. [4]). In ref. 15, we named the GBSs generated through the eqs. [3] and [5] as triple-optimized GBSs (TOGBSs).

We call attention to the fact that when eq. [5] is used there is no longer an equally spaced mesh $\{\Omega_i\}$, because now there are three arithmetic sequences to generate the basis function exponents for each symmetry.

Results and discussion

We have used an IGCHF method (15) presented in the last section to calculate the total energies for the atoms from K (Z = 19) through Xe (Z = 54). Throughout the calculations the scaling parameter value A (see eq. [3]) is equal to 6.0. All calculations were carried out using a modified version of the ATOMSCF program (22). For each atom studied here, the optimization process of each approach (GCHF and IGCHF) is repeated until the total energy value is stabilized within 10 significant figures.

Table 1 displays the ground state HF total energies (in hartree) computed with the SOGBSs and TOGBSs, and with a NHF (20) approach. For the GCHF (7) and IGCHF (15) methods, we choose GTF basis sets of the same size (see the fifth column of Table 1) with the purposes to compare the energy values. From this table, we can notice that, for all atoms studied here, our results are always more stable than those computed with the SOGBSs, and that the largest improvement in the energy is 2.755 mhartree for In. Beside this, the errors in the energy values computed with our TOGBSs relatively to the NHF limits, are always smaller than 6.004 mhartree.

The good performance of the TOGBSs is attributed to the IGCHF (15) method, because since we have now three independent arithmetic sequences for each *s*, *p*, *d*, … symmetry (see eq. [5]), it is possible to describe independently the inner, intermediate and outer electrons of a given symmetry. On the other hand, the SOGBSs generated with the original GCHF method (7) have only one arithmetic sequence (see eq. [4]) to describe these three different regions of each atomic symmetry. It is important to mention here that for the *d* symmetry of all third- and fourth-row atoms we have used the same set of exponents of the SOGBSs, because there are no large exponents for this symmetry, that is, the electrons of the *d* orbitals are far from the nucleus. Thus, for these atoms we have optimized, with the IGCHF method (15), only the GTF exponents of *s* and *p* symmetries.

The widely used RHF wave functions of Clementi and Roetti (23) for the atoms from He through Xe were improved by reoptimization (19) of the STF exponents. For the third-row and Te and I atoms the energies computed with our TOGBSs are larger than those obtained with fully optimized basis sets of STFs (19), whereas for the atoms from Rb through Sb and for Xe, the opposite occurs.

Conclusions

We have constructed accurate GBSs with the IGCHF method (15) for the third- and fourth-row atoms. These wave functions are appropriated to be used in HF atomic and molecular calculations of physical and chemical properties.

Our total energies are closer to the NH*F* values (20) than the corresponding values calculated with the original GCHF method (7) using GBSs of same size. For the atoms from Rb through Xe (except for Te and I) the present results are better than those calculated with the fully optimized basis sets (19) of STFs. The total energy errors do not exceed 6.003 mhartree.

An application of the TOGBSs generated in this work in calculations of some properties of third- and fourth-row diatomic molecules is in progress. Full details about the wave functions reported here are available upon request to the e-mail address: jorge@cce.ufes.br.

Acknowledgments

The authors are very grateful to the financial support by CNPq (Brazilian Agency).

References

1. C. Froese-Fischer. The Hartree–Fock method for atoms. Wiley, New York. 1977.
2. C.C.J. Roothaan. Rev. Mod. Phys. **23**, 69 (1951).
3. R. Ahlrichs and P.R. Taylor. J. Chem. Phys. **78**, 315 (1981).
4. S. Huzinaga. Comput. Phys. Rep. **2**, 279 (1985).
5. E.R. Davidson and D. Feller. Chem. Rev. **86**, 681 (1986).

© 2001 NRC Canada

Table 1. Ground state HF total energies in hartree (sign reversed) for the atoms from K (Z = 19) through Xe (Z = 54).

Z	Atom	Configuration	State	GBS size	SOGBS[a] (as calculated in this work)	TOGBS[b] (this work)	NHF [c]
19	K	[Ar]4*s*(1)	^{2}S	20*s*13*p*	599.1634498	599.1637621	599.1647865
20	Ca	[Ar]4*s*(2)	^{1}S	21*s*13*p*	676.7572344	676.7574308	676.7581857
21	Sc	[Ar]4*s*(2)3*d*(1)	^{2}D	20*s*13*p*10*d*	759.7341836	759.7344920	759.7357178
22	Ti	[Ar]4*s*(2)3*d*(2)	^{3}F	20*s*13*p*10*d*	848.4042367	848.4045829	848.4059967
23	V	[Ar]4*s*(2)3d(3)	^{4}F	20*s*13*p*10*d*	942.8823196	942.8827138	942.8843374
24	Cr	[Ar]4*s*(1)3*d*(5)	^{7}S	20*s*13*p*10*d*	1043.353979	1043.354417	1043.356376
25	Mn	[Ar]4*s*(2)3*d*(5)	^{6}S	20*s*13*p*10*d*	1149.863619	1149.864140	1149.866251
26	Fe	[Ar]4*s*(2)3*d*(6)	^{5}D	20*s*13*p*10*d*	1262.440683	1262.441281	1262.443665
27	Co	[Ar]4*s*(2)3*d*(7)	^{4}F	20*s*13*p*10*d*	1381.411190	1381.411892	1381.414553
28	Ni	[Ar]4*s*(2)3*d*(8)	^{3}F	20*s*13*p*10*d*	1506.867139	1506.867924	1506.870908
29	Cu	[Ar]4*s*(1)3*d*(10)	^{2}S	20*s*13*p*10*d*	1638.959169	1638.959737	1638.963742
30	Zn	[Ar]4*s*(2)3*d*(10)	^{1}S	20*s*13*p*10*d*	1777.843481	1777.844486	1777.848116
31	Ga	[Ar]4*s*(2)3*d*(10)4*p*(1)	^{2}P	22*s*13*p*10*d*	1923.255079	1923.255897	1923.261009
32	Ge	[Ar]4*s*(2)3*d*(10)4*p*(2)	^{3}P	22*s*14*p*9*d*	2075.353405	2075.353937	2075.359733
33	As	[Ar]4*s*(2)3*d*(10)4*p*(3)	^{4}S	22*s*14*p*9*d*	2234.232429	2234.233196	2234.238654
34	Se	[Ar]4*s*(2)3*d*(10)4*p*(4)	^{3}P	22*s*14*p*9*d*	2399.861092	2399.861947	2399.867611
35	Br	[Ar]4*s*(2)3*d*(10)4*p*(5)	^{2}P	22*s*14*p*9*d*	2572.434622	2572.435361	2572.441332
36	Kr	[Ar]3*s*(2)3*d*(10)4*p*(6)	^{1}S	22*s*14*p*9*d*	2752.048102	2752.048974	2752.054977
37	Rb	[Kr]5*s*(1)	^{2}S	22*s*16*p*11*d*	2938.352546	2938.354572	2938.357453
38	Sr	[Kr]5*s*(2)	^{1}S	23*s*16*p*11*d*	3131.542302	3131.543184	3131.545686
39	Y	[Kr]5*s*(2)4*d*(1)	^{2}D	24*s*16*p*12*d*	3331.680503	3331.681381	3331.684169
40	Zr	[Kr]5*s*(2)4*d*(2)	^{3}F	24*s*16*p*13*d*	3538.992004	3538.992932	3538.995064
41	Nb	[Kr]5*s*(1)4*d*(4)	^{6}D	23*s*16*p*13*d*	3753.593465	3753.594463	3753.597727
42	Mo	[Kr]5*s*(1)4*d*(5)	^{7}S	23*s*16*p*13*d*	3975.545002	3975.545938	3975.549499
43	Tc	[Kr]5*s*(2)4*d*(5)	^{6}S	26*s*16*p*13*d*	4204.786484	4204.786870	4204.788736
44	Ru	[Kr]5*s*(1)4*d*(7)	^{5}F	25*s*16*p*13*d*	4441.536271	4441.536892	4441.539487
45	Rh	[Kr]5*s*(1)4*d*(8)	^{4}F	25*s*17*p*14*d*	4685.878637	4685.879442	4685.881703
46	Pd	[Kr]4*d*(10)	^{1}S	24*s*17*p*13*d*	4937.918470	4937.918880	4937.921023
47	Ag	[Kr]5*s*(1)4*d*(10)	^{2}S	25*s*17*p*13*d*	5197.695075	5197.695718	5197.698472
48	Cd	[Kr]5*s*(2)4*d*(10)	^{1}S	25*s*16*p*14*d*	5465.129785	5465.130626	5465.133141
49	In	[Kr]5*s*(2)4*d*(10)5*p*(1)	^{2}P	25*s*17*p*14*d*	5740.161728	5740.164483	5740.169154
50	Sn	[Kr]5*s*(2)4*d*(10)5*p*(2)	^{3}P	25*s*18*p*13*d*	6022.926898	6022.927864	6022.931694
51	Sb	[Kr]5*s*(2)4*d*(10)5*p*(3)	^{4}S	25*s*18*p*13*d*	6313.480742	6313.481591	6313.485319
52	Te	[Kr]5*s*(2)4*d*(10)5*p*(4)	^{3}P	24*s*18*p*13*d*	6611.778554	6611.779850	6611.784058
53	I	[Kr]5*s*(2)4*d*(10)5*p*(5)	^{2}P	25*s*18*p*13*d*	6917.976264	6917.977047	6917.980895
54	Xe	[Kr]5*s*(2)4*d*(10)5*p*(6)	^{1}S	26*s*18*p*13*d*	7232.134224	7232.135150	7232.138363

[a]HF total energies obtained by using single-optimized Gaussian basis set (SOGBS).
[b]HF total energies obtained by using our triple-optimized Gaussian basis set (TOGBS).
[c]Numerical HF (NHF) total energies for K to Xe obtained from ref. 20.

6. S. Wilson. Adv. Chem. Phys. **67**, 439 (1987).
7. J.R. Mohallem, R.M. Dreizler, and M. Trsic. Int. J. Quantum Chem. Symp. **20**, 45 (1986).
8. J.R. Mohallem and M. Trsic. J. Chem. Phys. **86**, 5043 (1986).
9. H.F.M. da Costa, M. Trsic, and J.R. Mohallem. Mol. Phys. **62**, 91 (1987).
10. F.E. Jorge, E.V.R. de Castro, and A.B.F. da Silva. J. Comp. Chem. **216**, 317 (1997).
11. E.V.R. de Castro and F.E. Jorge. J. Chem. Phys. **108**, 5225 (1998).
12. F.E. Jorge, P.R. Librelon, and A. Canal Neto. J. Comput. Chem. **19**, 858 (1998).
13. F.E. Jorge and E.P. Muniz. Int. J. Quantum Chem. **71**, 307 (1999).
14. F.E. Jorge and M.L. Franco. Chem. Phys. **253**, 21 (2000).
15. F.E. Jorge and E.V.R. de Castro. Chem. Phys. Lett. **302**, 454 (1999).
16. E.V.R. de Castro, F.E. Jorge, and J.C. Pinheiro. Chem. Phys. **243**, 1 (1999).
17. J.C. Pinheiro, F.E. Jorge, and E.V.R. de Castro. J. Mol. Struct: THEOCHEM **491**, 81 (1999).
18. J.C. Pinheiro, F.E. Jorge, and E.V.R. de Castro. Int. J. Quantum Chem. **78**, 15 (2000).
19. T. Koga, H. Tatewaki, and A.J. Thakkar. Phys. Rev. A: At. Mol. Opt. Phys. **47**, 4510 (1993).
20. T. Koga, S. Watanabe, K. Kanayama, R. Yasuda, and A.J. Thakkar. J. Chem. Phys. **103**, 3000 (1995).
21. J.R. Mohallem. Z. Phys. D: At. Mol. Clusters, **3**, 339 (1986).
22. S.J. Chakravorty, G. Corongiu, J.R. Flores, V. Sonnad, E. Clementi, V. Carravetta, and I. Cacelli. Modern techniques in computational chemistry: MOTECC-89. *Edited by* E. Clementi. ESCOM, Leiden, 1989.
23. E. Clementi and C. Roetti. At. Data Nucl. Data Tables **14**, 177 (1974).

© 2001 NRC Canada

Possible structures for H-Cu-CH_3 molecules

Martyn C.R. Symons and Raymond E. March

Abstract: EPR spectra for H-Cu-CH_3 molecules in glasses at 77 K show ^{63}Cu hyperfine splitting that accords with a $d^1_{x^2-y^2}$ orbital for the semi-occupied molecular orbital (SOMO) rather than a $d^1_{z^2}$ SOMO. The *g*-values also strongly imply a $d^1_{x^2-y^2}$ configuration. The estimated spin densities on the H- and -CH_3 ligands are small. It is argued that the molecule must be strongly bent in order to favour this SOMO and that this bending may be induced by weak solvation.

Key words : H-Cu-CH_3, EPR spectra, molecular structure, hyperfine splitting.

Résumé : Les spectres RPE de molécules de H-Cu-CH_3 dans des solides à l'état vitreux, à 77 K, présentent des dédoublements hyperfins du ^{63}Cu qui sont plutôt en accord avec la présence d'une orbitale $d^1_{x^2-y^2}$ moléculaire semi-occupée (OMSO) que d'une OMSO $d^1_{z^2}$. Les valeurs de *g* impliquent aussi fortement une configuration $d^1_{x^2-y^2}$. Les évaluations des densités de spin sur les ligands H- et CH_3- indiquent que celles-ci sont faibles. On suggère que, pour favoriser une telle OMSO, la molécule doit être fortement déformée et que cette déformation pourrait être induite par une faible solvatation.

Mots clés : H-Cu-CH_3, spectre RPE, structure moléculaire, dédoublement hyperfin.

[Traduit par la Rédaction]

Introduction

Most Cu^{II} complexes have four strongly bonded ligands arranged, commonly, in a square planar configuration with two weakly bonded axial ligands. A few such complexes, especially in constrained protein ligand structures, tend towards structures with four nearly tetrahedral ligands such as in the blue copper proteins. In contrast, Cu^{I} complexes are bonded normally to four tetrahedrally bonded ligands where the bonding is sp^3 hybridized on copper to a first approximation. Hence, it seemed of interest to study the EPR spectrum of the unusual copper derivative H-Cu-CH_3. When the ligands are considered as H^- and CH_3^-, this complex can be regarded as a Cu^{II} complex.

Experimental

The photochemical reaction of methane with copper atoms isolated in a matrix was reported originally by Billings et al. (1). Ozin et al. (2) identified H-Cu-CH_3 from a narrow-band photolysis study of the Cu/CH_4 system. A detailed study of the formation and photochemistry of $HCuCH_3$ was reported by Parnis et al. (3). The best results were obtained using dilute solutions (ca. 0.1 M) in methyltetrahydrofuran at 77 K. EPR spectra were measured at 77 K using a Varian E109 X-band spectrometer. Microwave powers were in the 1–5 mW range. Modulation frequencies were ca. 100 kHz. The spectra were the same within these ranges.

Received May 22, 2000. Published on the NRC Research Press Web site on February 27, 2001.

M.C.R. Symons. De Montfort University, Leicester, LE19 BH, UK.
R.E. March.[1] Department of Chemistry, Trent University, Peterborough, ON K9J 7B8, Canada.

[1]Corresponding author (telephone: (705) 748-1361; fax: (705) 748-1625; e-mail: rmarch@trentu.ca).

Results and discussion

A typical EPR spectrum is shown in Fig. 1; the data taken from this spectrum are listed in Table 1. Both the ^{63}Cu hyperfine splitting and the *g*-values are typical of a $d^1_{x^2-y^2}$ semi-occupied molecular orbital (SOMO). Hence, perhaps surprisingly, the complex must be strongly bent, rather than linear, since a $d^1_{z^2}$ configuration is ruled out by the data. Before discussing the reasons for our choice of the $d^1_{x^2-y^2}$ SOMO, we considered the structures of related species, specifically, the $PbCH_3^{\bullet 2+}$ centre (4), $AgH^{\bullet +}$(5), and the recently discovered $HHgCH_3^{\bullet +}$ radical cation (6). The $PbCHCH_3^{\bullet 2+}$ centre was formed by exposing $Pb^{2+}(CH_3CO_2^-)_2$ to ionizing radiation at 77 K. The centre was identified by its EPR spectrum (4). The data extracted from the EPR spectrum of the centre are included in Table 1. They show that a monomethyl centre Pb-CH_3^{2+} was formed. It was suggested that this centre was formed by electron loss from acetate ions, to give CH_3CO_2• radicals, which readily lose CO_2 to give CH_3• radicals. These radicals then added to the relatively weakly coordinated lead cations to yield the $(Pb\text{-}CH_3)^{2+}$ centre.

The ^{207}Pb hyperfine coupling ($A_{//}$ = 1928 G; $A_{\perp}$ = 1700 G) (G = 10^{-4} T) shows that the 6*s*-orbital character is very large (≈25%), whilst the purely anisotropic hyperfine coupling due to population of the outer 6*p*-orbital gives a population of ≈43%. Hence, the spin-density on Pb is ≈ 68%. These values, determined in the usual way (7), are very approximate but always give good qualitative structures.

At first glance, the spin-density on the protons of the –CH_3 group, as gauged from the isotropic proton hyperfine couplings, is very high, since the splitting compared to methyl radicals is ≈ 23%. However, •CH_3 radicals are planar,

 DOI: 10.1139/cjc-79-2-124 © 2001 NRC Canada

Fig. 1. A typical first derivative, X-band EPR spectrum for a dilute solution of $HCuCH_3$ in methyltetrahydrofuran, obtained after exposure to ^{60}Co γ-rays at 77 K and partial annealing to remove signals from the solvent. The spectra were calibrated using a Mn^{2+} probe (not shown). The EPR data taken therefrom are listed in Table 1.

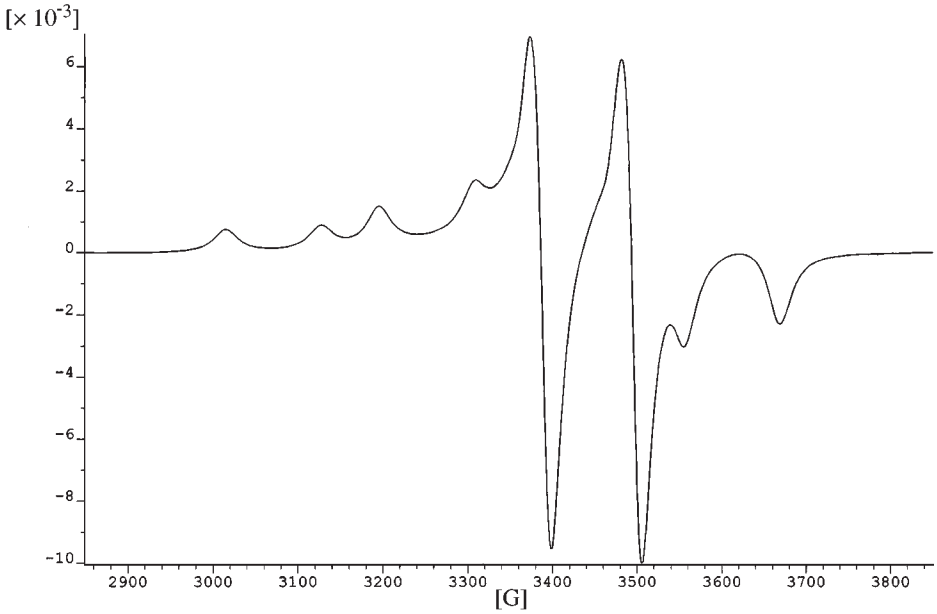


Table 1. Some of the EPR parameters for H-Cu-CH_3 and related compounds.

		Hyperfine couplings/G^a			*g*-values		
Centre	Nucleus	$A_=$	$A_\perp$	A_{iso}	$g_=$	$g_\perp$	Ref.
$HCuCH_3$	$^1H(H)$	112	104	106.7	2.085	2.037	*b*
	$^1H(CH_3)$	—	—	≤6			
	^{63}Cu	180	≈0	60			
$PbCH_3^{2+}$	^{207}Pb	1928	1700	1776	1.953	1.988	5
	^1H	24	20	21.3			
$CH_3HgH^{\bullet+}$(*a*)	$^1H(CH_3)$	—	—	15	2.0025	1.985	6
	$^1H(H)$	—	—	10			
(*b*)	$^1H(H)$	—	—	462	2.0025	1.975	

[a] $G = 10^{-4}$ T.
[b] This work.

whereas in Pb-CH_3 the –CH_3 group should be pyramidal. As a •CH_3 radical starts to become pyramidal, the originally negative coupling caused by spin polarisation of the C-H σ-electrons passes through zero and becomes positive because direct delocalization onto the protons becomes allowed. Hence, in this case, with a considerable share of the bonding electrons, the groups must be strongly pyramidal with quite large spin-density on the carbon, by difference, this is ≈32%.

The $AgH^{\bullet+}$ radical centres are similar. They were first formed by irradiating aqueous sulphuric acid glasses containing silver perchlorate. The ejected electrons added to Ag^+ to give Ag• atoms that have very well defined EPR features. On annealing, the trapped hydrogen atoms reacted with Ag^+ to give $AgH^{\bullet+}$. A range of other diatomic σ^*-radicals have also been prepared (8).

We have also studied the $(Ag_2H)^{\bullet 2+}$ radical formed similarly on annealing in concentrated sulphuric acid (9). In contrast with $HCuCH_3^{\bullet 2+}$, these radicals were clearly linear, with high spin-density on all three atoms. This condition arises because there are now two extra electrons with the result that the *d*-manifold is full. Now the two ligands can avoid each other using the outer 6*s* orbital on silver, with some contributions from the 6*p* and $5d_z^2$ orbitals.

Another radical that has been studied recently is H-Hg-$CH_3^{\bullet+}$ (6). This centre, together with $(CD_3)_2Hg^{\bullet+}$, $(C_2H_5)_2Hg^{\bullet+}$ and $(C_2H_5)_2Cd^{\bullet+}$ (10), were prepared by exposing very dilute solutions of the parent compound in freon ($CFCl_3$) to ionizing radiation at 77 K. Under these conditions, it is well established that only electron-loss processes occur (11, 12). Only the H-Hg-$CH_3^{\bullet+}$ radical-cations are considered here, and the data are given in Table 1. Two distinct centres were detected at 77 K. One had a very large ^1H hyperfine splitting (462 G) and there was nothing detectable from the methyl protons. The other had a very small proton coupling to the hydride ligand but a relatively large coupling to the methyl protons (15 G). No coupling to ^{199}Hg or to ^{201}Hg could be detected. These results have been interpreted in terms of two alternative limiting structures. For (*a*), it is

© 2001 NRC Canada

suggested as $(H\bullet\text{---}HgCH_3)^+$ while for (*b*), it is suggested as $(H\text{-}Hg\text{---}\bullet CH_3)^+$, with the positive charge primarily on mercury.

As suggested above, the limiting structure for the copper derivative is $(H–Cu^{2+}–CH_3^-)$ with a bond angle of ≈90°, and a high spin-density in the $d^1_{x^2-y^2}$ orbital. The explanation appears to lie in the relative electron affinities of Cu^{2+} and Hg^{3+} (that is, for $H–Hg^{3+}–CH_3^-$). For this species, the electron affinity of the Hg^{3+} cation is, relatively, very high. This condition is due, in part, to the 3+ charge and, in part, to the large *d*–*s* gap for mercury. Hence, electron loss occurs primarily from the ligands since the electron affinities of hydrogen and carbon (*sp* hybridized) are comparable. There is no clear preference for $(C_2H_5)_2Cd^{\bullet+}$ radical cations, the two ethyl groups are equivalent, both with high spin-densities (10) and typical *g*-values. It is concluded that the $H\text{-}Hg\text{-}CH_3^{\bullet+}$ radical-cation can exist in two stable forms, one being close to H• and the other close to $\bullet CH_3$. Indeed, both these radicals were also detected in high yields. This situation is very rare. Another example, is that of the $SnH_4^{\bullet+}$ radical cation (13). Again, at 77 K, two alternative structures were detected. In one case, a σ^* type of species $(H\text{-}\bullet SnH_3)^+$ was found. However, in the other, bond angles had changed as for $CH_4^{\bullet+}$, with two strongly coupled protons and two very weakly coupled protons.

There remains the problem as to why the $d^1_{x^2-y^2}$ configuration is favoured for $HCuCH_3$ over the near linear $d^1_{z^2}$ configuration. It is suggested tentatively that this configuration arises because of weak coordination of solvent molecules in the two positions.

Conclusions

We conclude that the $H\text{-}Cu\text{-}CH_3$ molecule does not have a linear structure with a $d^1_{z^2}$ ground state. This suggests that the molecule is strongly bent such that the $d^1_{x^2-y^2}$ structure is favoured. We suggest tentatively that this bent structure occurs, at least in part, because of the coordination of two solvent molecules along the *x*- and *y*-axes.

Acknowledgement

Some of this work was carried out at Leicester University by project students.

References

1. W.E. Billings, M.M. Konarski, R.H. Hauge, and J.L. Margrave. J. Am. Chem. Soc. **102**, 7393 (1980).
2. G.A. Ozin, D.F. McIntosh, S.A. Mitchell, and J. Garcia-Prieto. J. Am. Chem. Soc. **103**, 1574 (1981).
3. J.M. Parnis, S.A. Mitchell, J. Garcia-Prieto, and G.A. Ozin. J. Am. Chem. Soc. **107**, 8169 (1985).
4. R.J. Booth, H.C. Starki, and M.C.R. Symons. J. Chem. Soc. Faraday Trans. **68**, 1688 (1972).
5. R.S. Eachus and M.C.R. Symons. J. Chem. Soc. 1336 (1970).
6. M.J. Almond, A. Ragabah, D.A. Rice, L.A. Sheridan, P.J. Craig, G. Stojak, and M.C.R. Symons. J. Chem. Soc. Faraday Trans. **90**, 3153 (1994).
7. M.C.R. Symons. ESR spectroscopy: chemical and biochemical aspects. Van Nostrand Reinholt, London. 1978.
8. R.S. Eachus and M.C.R. Symons. J. Chem. Soc. 3080 (1970).
9. R.S. Eachus and M.C.R. Symons. J. Chem. Soc. 1329 (1970).
10. A. Hasegawa, J. Rideout, and M.C.R. Symons. J. Chem. Soc. Dalton Trans. 637 (1990).
11. M. Shiotani. Magn. Reson. Rev. **12**, 333 (1987).
12. M.C.R. Symons. Chem. Soc. Rev. 393 (1984).
13. A. Hasegawa, S. Kaminaka, M. Hayashi, M.C.R. Symons, and J. Rideout. J. Chem. Soc. Dalton Trans. 1667 (1984).

© 2001 NRC Canada

Potassium borohydride reducing route to phase-pure nanocrystalline InSb at low temperature

Jun Lu, Yi Xie, Xuchuan Jiang, Wei He, Ping Yan, and Yitai Qian

Abstract: The phase-pure III–V binary antimonide (InSb) was first prepared through a novel solution route at a temperature of 200°C:

$$2InCl_3 + 6KBH_4 + 2Sb \xrightarrow{en} 2InSb + 6KCl + 6BH_3 + 3H_2\uparrow$$

Mean crystallite dimensions of 40 nm were determined from X-ray powder diffraction. Transmission electron microscopy images showed that the spherical grains with a diameter of 40–60 nm and the rodlike grains with a size of 120 × 1500 nm coexisted in the same product. The reaction proceeds with indium as the intermediate and a solution–liquid–solid mechanism is proposed for the one-dimensional growth.

Key words: indium antimonide, nanorod, phase-pure, solvothermal, solution–liquid–solid mechanism.

Résumé : On a réalisé la première préparation de l'antimoniure binaire III–V en phase pure en opérant à 200°C et en faisant appel à une nouvelle voie de synthèse en solution

$$2InCl_3 + 6KBH_4 + 2Sb \xrightarrow{en} 2InSb + 6KCl + 6BH_3 + 3H_2\uparrow$$

Sur la base du diagramme de poudre de la diffraction des rayons X, on a déterminé que les dimensions moyennes de la cristallite sont de 40 nm. Les images obtenues par microscopie électronique de transmission montrent que, dans le même produit, des grains sphériques d'un diamètre de 40 à 60 nm coexistent avec des grains en forme de tiges mesurant 120 × 1500 nm. La réaction implique la formation d'indium comme intermédiaire et on propose un mécanisme solution–liquide–solide pour la croissance unidirectionnelle.

Mots clés : antimoniure d'indium, nanotige, phase pure, solvothermique, mécanisme solution–liquide–solide.

[Traduit par la Rédaction]

Introduction

The discovery of markedly different properties from the bulk materials and the promise of exploiting these properties for making devices has led to widespread research activity in the field of nanocrystalline materials for both scientific and technological applications (1). Among these nanocrystalline materials, the III–V (13–15) group of compound semiconductors are well-known electronic and optoelectronic materials (2). Compared with II–VI semiconductors, the III–V conductors have a greater degree of covalent bonding, a decreased ionic lattice and larger excition diameters (the excition diameter in GaAs is 190 Å, compared with 60 Å for CdS) (3). For this reason, quantum size effects on the optical spectra have been predicted to be more pronounced in the III–V class of materials than in the II–VI group (4). To date, the majority of work has been focused on II–VI materials (5), while III–V semiconductors, including an important direct band gap semiconductor (InSb) have been studied relatively little due to the numerous difficulties encountered in their preparations.

The present zeal for new routes to the III–V compound semiconductors is motivated by several goals such as safe precursors and low reaction temperatures (6). Several new strategies have emerged in the last decade (for a recent review see ref. 7) including, dehalosilylation and related reactions (8), metathesis reactions (9), metal organic precursors' alcoholysis (10), and pyrolysis of single-source precursors that incorporate the elements of a compound in a single molecule (11). Although these methods are very useful and mild in comparison with traditional solid-state reactions (usually above 1000°C), they still require relatively high processing or post-treatment temperatures (200–500°C) to obtain fully crystallized products. Very recently, a solution–liquid–solid (SLS) mechanism was developed to grow well-crystallized III–V semiconductor fibers at much lower temperatures (111–203°C for InP; 203°C for InAs and GaAs) (12). The SLS is closely analogous to the well known vapor–liquid–solid (VLS) mechanism (13), where whisker crystals are grown from flux droplets that are fed from the vapor phase rather than the solution phase.

To our knowledge, no phase-pure antimonide has been obtained using the above methods, while elemental antimony has often coexisted in the final products (9*a*, 14). There may

Received August 8, 2000. Published on the NRC Research Press Web site on March 8, 2001.

J. Lu, Y. Xie[1], X. Jiang, W. He, P. Yan, and Y. Qian. Structure Research Laboratory and Laboratory of Nanochemistry & Nanomaterials, University of Science & Technology of China, Hefei, Anhui 230026, P. R. China.

[1]Corresponding author (e-mail: yxie@ustc.edu.cn).

 DOI: 10.1139/cjc-79-2-127 © 2001 NRC Canada

be two reasons why preparing phase-pure antimonides are so difficult. One is that the formation of SbH_3 and the metal organic precursors of antimony is more difficult than As and P. The other is that the relatively strong metallicity of elemental antimony is not favoring the formation of antimonides. The development of a synthetic method for preparing phase-pure antimonides, especially III–V antimonides, is an ultimate challenge for material scientists. In this paper, we describe a novel route to phase-pure InSb nanocrystals at temperatures as low as 200°C.

KBH_4 and its derivatives have been used to prepare finely divided powders of metals and alloys by reducing the metal salts in an organic solvent, such as THF and hydrocarbons (15). We have extended it to prepare nanocrystals of MSe (M = Cd) (16) at room temperature, and InP (17) and InAs (18) at 160°C. In this paper, we successfully produced phase-pure InSb nanocrystals via exploiting the potassium borohydride reducing route at relatively low temperature as follows:

$$[1]\qquad 2InCl_3 + 6KBH_4 + 2Sb \xrightarrow{en} 2InSb + 6KCl + 6BH_3 + 3H_2\uparrow$$

Experimental section

All reagents were of analytical grade or better, and the indium chloride was purified by mixing it in thionyl chloride ($SOCl_2$) at reflux for 45 min before being used. Reactions were carried out in a Teflon-lined autoclave. A mixture of ethylenediamine (40 mL), Sb (0.609 g, 5 mmol), $InCl_3$ (4.428 g, 20 mmol), and KBH_4 (3.228 g, 60 mmol) were added to a 50 mL flask. The mixture was ultrasonically mixed for 4 h before being transferred into a Teflon-lined autoclave. The autoclave was kept at 100, 120, 160, or 200°C for 36 h and then cooled to room temperature. The products were filtered off, washed with absolute alcohol, HCl (1 M), and distilled water, then dried in a vacuum at room temperature for 4 h.

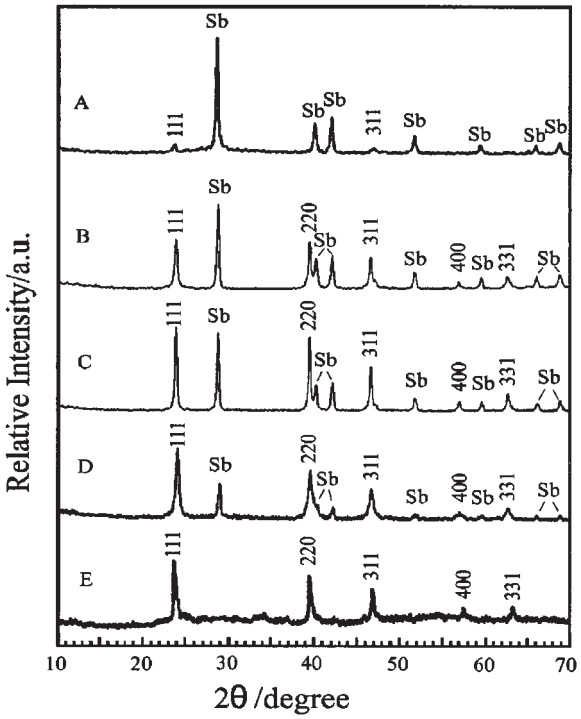
Powder X-ray diffraction (XRD) patterns were performed on a Japan Rigaku D/Max γA rotating anode X-ray diffractometer with Ni-filtered Cu Kα radiation (λ = 1.54178 Å). Transmission electron microscopy (TEM) measurements were made on a Hitachi H-800 transmission electron microscope with an accelerating voltage of 200 kV. Samples were deposited from ethanol solutions of the products onto thin amorphous carbon films supported by copper grids.

Purity and composition of the product were detected by X-ray photoelectron spectra (XPS) on an ECSALab MKII instrument with Mg Kα radiation as the exciting source. The binding energies obtained in the XPS analysis were corrected by referencing the C 1 s peak to 284.60 eV.

Results and discussion

The reaction of $InCl_3$, antimony (molar ratio: $InCl_3/Sb = 4$), and potassium borohydride at 200°C in ethylenediamine resulted in a black precipitate, which was washed with HCl (1 M) (here, HCl was used to dissolve the excessive indium reduced by KBH_4) and dried. The XRD pattern (Fig. 1*e*) of the sample agrees with the bulk InSb reflections, indicating the same cubic blende lattice structure

Fig. 1. XRD patterns of the products with the molar ratio of $InCl_3/Sb = 4$ after 1 M HCl treatment at: (*a*) room temp. (*b*) 100°C, (*c*) 120°C, (*d*) 160°C, (*e*) 200°C.



(19). Average crystallite sizes are about 40 nm, as estimated by the Scherrer equation.

The molar ratios of the reactants ($InCl_3/Sb$) and the temperature played important roles in preparing a phase-pure product. In our experiments we found that if the molar ratio of $InCl_3/Sb$ was lower than 4, no phase-pure InSb was obtained, even if the temperature was raised to 300°C. When the molar ratio of $InCl_3/Sb$ was as high as 4, the yield of InSb increased, while the antimony content decreased with the temperature, as seen over the range of 100–200°C (Fig. 1*b*–*e*). Moreover, the reaction did not initiate at all at room temperature. These facts led us to believe the chemical pathway is as follows:

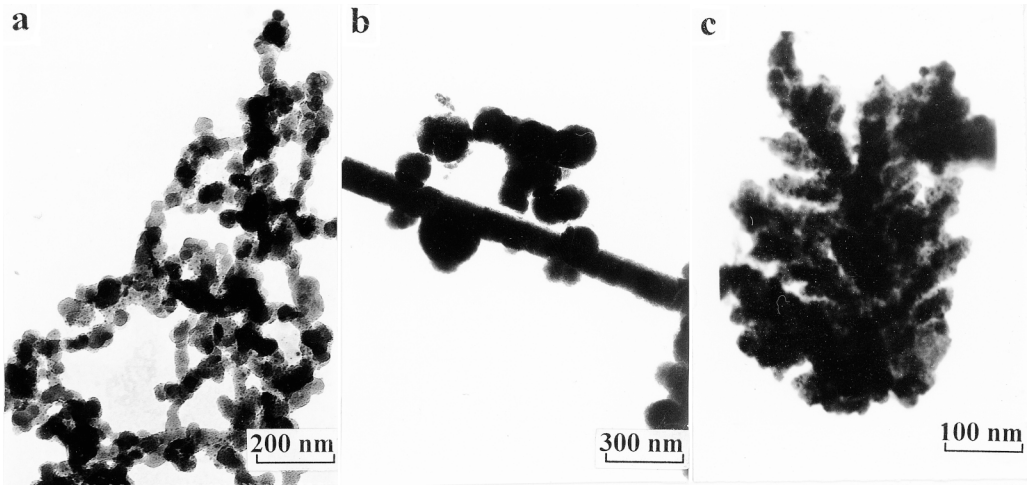
$$[2]\qquad 2InCl_3 + 6KBH_4 + 2Sb \longrightarrow 2In + 6KCl + BH_3 + 3H_2\uparrow$$

$$[3]\qquad 2In + 2Sb \longrightarrow 2InSb$$

All of the above facts can be rationalized as follows: it is very difficult to obtain phase-pure InSb due to the relatively strong metallicity of elemental antimony, whilst the atmosphere of rich indium is benefited by the formation of phase-pure InSb. To prepare phase-pure InSb, the molar ratio of $InCl_3/Sb$ should be as high as 4. On the other hand, the first step cannot take place at room temperature. When the reaction temperature was as low as 100°C, the freshly formed indium only reacted with antimony to a very small extent, however, when the temperature is raised to 160°C, which is above the melting point of indium (mp = 156.4°C), the reaction is almost complete and only trace amounts of antimony

© 2001 NRC Canada

Fig. 2. TEM images for InSb nanocrystals prepared at 200°C with the reactant molar ratio ($InCl_3$/Sb = 4).



coexisted in the product. When the temperature is raised to 200°C, the reaction is complete and phase-pure InSb is obtained, which is confirmed by XRD patterns (Fig. 1*e*). These results indicate that the reaction temperature plays a very important role for the synthesis of phase-pure InSb when the ratio of $InCl_3$/Sb is as high as 4.

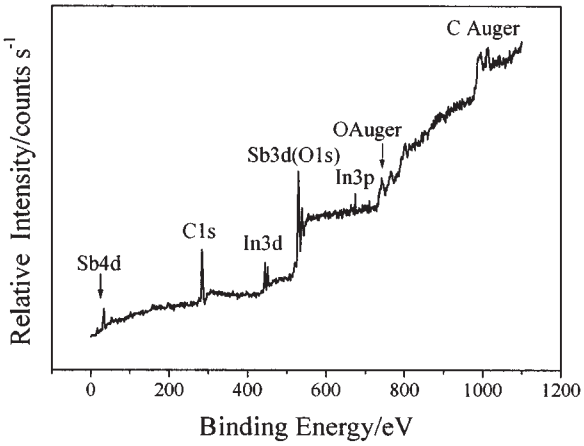
Transmission electron microscopy images for sample D (molar ratio: $InCl_3$/Sb = 4, prepared at 200°C) are shown in Fig. 2. The spherical particles (Fig. 2*a*) with the average diameter of about 50 nm are obtained. A nanorod (120 × 1500 nm) is also clearly seen from the same sample (Fig. 2*b*). More careful observation showed that the nanorod itself is composed of small particles. Another interesting feature is that the products have a crystalline growth extinction of dendritic crystals (Fig. 2*c*). The dendritic structure is a fractal object, which had been proved by Nittmann and Stanley (20). The ratio of In:Sb in the final product is 1.058:1 as measured by energy-dispersion X-ray (EDX) analysis.

According to the melting point of indium (156.4°C), the reaction can be regarded as a two-stage process, one is where the range of temperature is 100 to ~156.4°C, the other is 156.4 to ~200°C. Among the three well-known whisker-growth mechanisms, i.e., VLS, vapor–solid (VS), and SLS, the formation of InSb nanorods in our reaction is most similar to the SLS mechanism under the second-stage conditions. Such a system, which includes liquid indium and an organic solvent, is favorable for the formation of rodlike InSb particles. Otherwise, the formation of the product cannot be explained by the SLS mechanism. Although the reaction occurs, no rodlike products were obtained below 120°C, which provides a strong evidence for the SLS mechanism. We considered that the spherical particles of the product (Fig. 2*a*) formed at the first stage of the reaction process, and the rodlike particles (Fig. 2*b*) formed at the second stage, which further confirmed the proposed SLS mechanism.

As to the crystalline growth extinction of dendritic crystal (Fig. 2*c*), we cannot explain it at present, but we are conducting more experiments to investigate this.

Ethylenediamine also played a key role in the formation of InSb nanocrystals. Experiments show that it can disperse antimony powder and readily dissolve KBH_4, thereby increasing the surface area of reactants and promoting the reaction at relatively low temperatures. When benzene was used as the solvent, the reaction did not take place, presumably due to the poor solubility of KBH_4 in benzene.

Fig. 3. XPS survey spectrum for InSb nanocrystals prepared at 200°C.



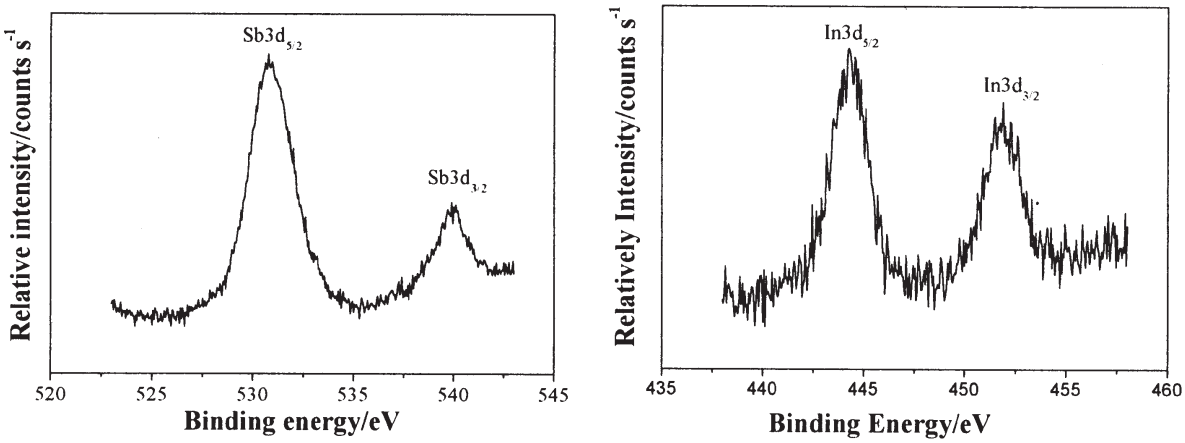
X-ray photoelectron spectroscopy has been used to measure the elemental composition of the nanocrystals. A survey spectrum is shown in Fig. 3. The survey indicates the presence of In and Sb, as well as C and O (from reference absorbed gaseous molecules). There are no peaks for Cl or N (from starting material) in the survey spectrum.

Higher resolution spectra were also taken of the In3*d* and Sb3*d* regions (Fig. 4). The binding energy is 444.7 eV for In3$d_{5/2}$ and 539.95 eV for Sb3$d_{5/2}$, which is in agreement with the literature (21).

Peak areas of these high-resolution scans were measured and used to calculate the In:Sb ratio for the nanocrystals. Quantification of the peaks gives a ratio of In:Sb of 1.075:1, which closely agrees with the formula of InSb. As a result of our EDX and XPS analyses, we conclude that the nanocrystals are close to stoichiometric InSb.

© 2001 NRC Canada

Fig. 4. High-resolution XPS scans of the In3*d* and Sb3*d* cores.



Conclusion

In summary, phase-pure III–V binary antimonide, InSb, was prepared through a new solution route. Nanocrystalline InSb was successfully synthesized via a novel solvothermal reaction of $InCl_3$ with antimony and KBH_4 in ethylenediamine at a temperature of 200°C for 36 h. The reaction proceeds through a metallic indium intermediate, and an SLS mechanism is proposed for the one-dimensional growth. By choosing a suitable system, it is reasonable to expect that this safe mild route can be extended to the preparation of other metal antimonides.

Acknowledgment

Financial support from both the Chinese National Foundation of Natural Research and Outstanding Youth Fund is gratefully acknowledged.

References

1. (*a*) G.D. Stucky and J.E. MacDougall. Science (Washington, D.C.), **247**, 669 (1990); (*b*) M.A. Reed. Science (Washington, D.C.), **262**, 195 (1993); (*c*) A.P. Alivisatos. Science (Washington, D.C.), **271**, 933 (1996).
2. (*a*) S.M. Sze. Physics of semiconductor devices. 2nd ed. John Wiley and Sons, New York. 1981; (*b*) B.G. Streetman. Solid state electronic devices. 3rd ed. Prentice Hall, Englewood Cliffs, N.J. 1990; (*c*) C.R.M. Grovenor. Microelectronic materials. Adam Hilger, Philadelphia, Pa. 1989.
3. M.A. Olshavsky, A.N. Goldstein, and A.P. Alivisatos. J. Am. Chem. Soc. **112**, 9439 (1990).
4. L.E. Brus. J. Chem. Phys. **79**, 5566 (1983).
5. (*a*) M.L. Sreigerwald and L.E. Brus. Acc. Chem. Res. **23**, 183 (1990); (*b*) J.J. Shiang, A.N. Goldstein, and A.P. Alivisatos. J. Chem. Phys. **92**, 3232 (1990); (*c*) A.P. Alivisatos, T.D. Harris, P.J. Carroll, M.L. Sreigerwald, and L.E. Brus. J. Chem. Phys. **90**, 3463 (1989); (*d*) L.E. Brus. J. Phys. Chem. **90**, 2555 (1986); (*e*) C.B. Murray, D.J. Norris, and M.G. Bawendi. J. Am. Chem. Soc. **115**, 8706 (1993); (*f*) J.E.B. Katari, V.L. Colvin, and A.P. Alivisatos. J. Phys. Chem. **98**, 4109 (1994).
6. W.E. Buhro. Polyhedron, **13**, 1131 (1994).
7. R.L. Wells and W.L. Galdfelter. J. Cluster Sci. **8**, 2 (1997).
8. (*a*) R.L. Wells, S.R. Aubuchon, S.S. Kher, M.S. Lube, and P.S. White. Chem. Mater. **7**, 793 (1995); (*b*) H. Uchida, T. Matsunaga, H. Yoneyama, T. Sakata, H. Mori, and T. Sasaki. Chem. Mater. **5**, 716 (1993).
9. (*a*) R.E. Treece, G.S. Macala, L. Rao, T. Franke, H. Eckert, and R.B. Kaner. Inorg. Chem. **32**, 2745 (1993); (*b*) S.S. Kher and R.L. Wells. Chem. Mater. **6**, 2056 (1994); (*c*) Y. Xie, Y. Qian, W. Wang, S. Zhang, and Y. Zhang. Science (Washington, D.C.), **272**, 1926 (1996).
10. (*a*) E.K. Byrne, T. Douglas, and K.H. Theopold. Mater. Res. Soc. Symp. Proc. **131**, 59 (1989); (*b*) T. Douglas and K.H. Theopold. Inorg. Chem. **30**, 594 (1991).
11. (*a*) A.H. Cowley and R.A. Jones. Angew. Chem. Int. Ed. Engl. **28**, 1208 (1989); (*b*) M. Green and P. O'Brien. J. Chem. Soc. Chem. Commun. 2459 (1998).
12. (*a*) T.J. Trentler, K.M. Hickman, S.C. Goel, A.M. Viano, P.C. Gibbons, and W.E. Buhro. Science (Washington, D.C.), **270**, 1791 (1995); (*b*) T.J. Trentler, S.C. Goel, K.M. Hickman, A.M. Viano, M.Y. Chiang, A.M. Beatty, P.C. Gibbons, and W.E. Buhro. J. Am. Chem. Soc. **119**, 2172 (1997).
13. R.S. Wagner. *In* Whisker technology. *Edited by* A.P. Levitt. Wiley, New York. 1970. Chap. 3.
14. (*a*) I.P. Parkin. Chem. Soc. Rev. 199 (1996); (*b*) R.A. Baldwin, E.E. Foos, and R.L. Wells. Mater. Res. Bull. **32**, 159 (1997).
15. H. Bönnemann, W. Brijous, and T. Joussen. Angew. Chem. Int. Ed. Engl. **29**, 273 (1990).
16. W. Wang, Y. Geng, P. Yan, F. Liu, Y. Xie, and Y. Qian. J. Am. Chem. Soc. **121**, 4062 (1999).
17. P. Yan, Y. Xie, W. Wang, F. Liu, and Y. Qian. J. Mater. Chem. **9**, 1831 (1999).
18. P. Yan, Y. Xie, J. Lu, W. Wang, and Y. Qian. Chem. Mater. **11**, 2619 (1999).
19. Joint Committee on Powder Diffraction Standards (JCPDS), File No. 6-208.
20. J. Nittmann and H.E. Stanley. Nature (London), **321**, 663 (1986).
21. C.D. Wagner, W.W. Riggs, L.E. Davis, J.F. Moulder, and G.E. Muilenberg. Handbook of X-ray photoelectron spectroscopy. Perkin-Elmer Corporation, Physical Electronics Division. Printed in U.S.A. 1979.

© 2001 NRC Canada

A spectrophotometric study of Fe(II)-chloride complexes in aqueous solutions from 10 to 100°C

Renhai Zhao and Pujing Pan

Abstract: The absorption spectra of Fe(II)-chloride solutions were measured in both the UV (ultraviolet) and near-IR (near infrared) regions at temperatures ranging from 10 to 100°C with chloride concentrations from 0.1 to 16 mol kg^{-1}. The stability constants of all Fe(II)-chloride complexes were derived from the spectra using a non-negative nonlinear least-squares computer program (SQUAD). Earlier work on this system reported in the literature was rigorously reassessed. The activity coefficients of the ionic species were calculated using both the Pitzer model and the Helgeson model. The results obtained with UV and near-IR spectra and with different activity coefficient calculation models are in general agreement. Other useful thermodynamic data, including the Gibbs energies, enthalpies, and entropies for complex formation, were also obtained. It was found that the Fe(II)-chloride complexes gradually undergo a configuration transformation from octahedral to tetrahedral coordination as the temperature and (or) chloride concentration increases. This coordination change is of significant importance to the nuclear reactors, as the presence of the tetrahedral complex can increase the solubility of iron in steam generator crevices.

Key words: Fe(II)-chloride complexes, stability constants, solution thermodynamics, spectrophotometry, reactor chemistry.

Résumé : Opérant à des températures allant de 10 à 100°C, à des concentrations de chlorure allant de 0,1 à 16 mol/kg, on a mesuré les spectres d'absorption UV (ultraviolet) et proche infrarouge (proche-IR) de solutions de chlorure de Fe(II). Sur la base des spectres obtenus et faisant appel à un programme informatique des moindres carrés non linéaires non négatifs, on a évalué les constantes de stabilité de tous les complexes de chlorure de Fe(II). On a réévalué d'une façon rigoureuse un travail antérieur sur ce système rapporté dans la littérature. On a calculé les coefficients d'activité des espèces ioniques à l'aide du modèle de Pitzer et du modèle dHelgeson. Les résultats obtenus à l'aide des spectres UV et proche infrarouge et avec différents modèles de calcul des coefficients d'activité sont généralement en bon accord. On a aussi évalué d'autres données thermodynamiques utiles, y compris les énergies de Gibbs, les enthalpies et les entropies de formation des complexes. On a trouvé que l'augmentation de température et/ou de concentration en chlorure provoque une transformation graduelle des complexes de Fe(II) alors que la configuration passe d'une coordination octaédrique à tétraédrique. Ce changement de coordination revêt une importance significative dans les réacteurs nucléaires puisque la présence du complexe tétraédrique peut augmenter la solubilité du fer dans les crevasses des générateurs de vapeur d'eau.

Mots clés : complexes de chlorure de Fe(II), constantes de stabilité, thermodynamique de solutions, spectrophotométrie, chimie des réacteurs.

[Traduit par la Rédaction]

Introduction

Water is used as the heat transfer medium in nuclear steam generators. Its corrosiveness depends on a number of parameters, including pH, E_h, temperature, and the impurities it contains such as chloride, sulfate, and carbonate ions. The complex formation due to the presence of these impurities is important in stabilizing dissolved metal ions and, therefore, can enhance the solubility of metals by a few orders of magnitude. In tight crevices and deep sludge piles, solutes may be concentrated by a factor as high as 10^4 due to differential evaporation. The chloride concentration predicted for such an environment was in the range of 1–15 *m* (mol kg^{-1}). Typically, the stability of a metal complex in aqueous solutions increases with an increase in temperature. Much of the CANDU® steam generator and feedtrain are made of carbon steel. Corrosion products from carbon steel would, therefore, predominate in the secondary system. The most abundant anionic impurity usually observed in the steam generator system is chloride. Concentration of the dissolved impurities, in the presence of iron oxides from carbon steel corrosion, may be expected to lead to the formation of concentrated chloride solutions and complexes of iron ions with chloride. This study focuses on the stability of

Received April 14, 2000. Accepted December 13, 2000. Published on the NRC Research Press Web site on March 12, 2001.

R. Zhao[1] and P. Pan.[2] Reactor Chemistry Branch, Atomic Energy of Canada Ltd., Chalk River Laboratories, Chalk River, ON K0J 1J0, Canada.

[1]Present address: Industrial Organization and Finance Division, Statistics Canada, Ottawa, ON K1A 0T6, Canada.
[2]Corresponding author (present address: Radiation Protection Bureau, Health Canada, 775 Brookfield Road, Ottawa, ON K1A 1C1, Canada. e-mail: Pujing_Pan@hc-sc.gc.ca).

 DOI: 10.1139/cjc-79-2-131 © 2001 NRC Canada

Fe(II)-chloride complexes. The resulting information is considered to be of importance in understanding and predicting steam generator chemistry, particularly in crevices.

Because the Fe(II)-chloride complexes are very weak and it is difficult to avoid fast oxidation of Fe(II) in the presence of trace oxygen, few studies on Fe(II)-chloride complexation in aqueous solutions have been reported. There is a large scatter in the early values of stability constants of Fe(II)-chloride complexes. One important reason for this scatter is that indirect studies through solubility measurements (1, 2), kinetic measurements (3, 4), complexation with organics (5), and isocoulombic estimation methods (6) were used for stability constant determination. In spectrophotometric studies (7, 8) the spectral measurements were usually limited to a limited range of wavelengths (cf. ref. 9 for a more thorough review of the literature on Fe(II)-chloride complexes).

The most recent spectrophotometric study on stability constants of Fe(II)-chloride complexes was carried out by Heinrich and Seward (10), in aqueous solutions from 25 to 200°C with chloride concentration from 0.01 to 3.4 *m*. The tetrahedral complexes, however, were neglected in their work. Previous work (11, 12) has clearly demonstrated that Fe(II)-chloride complexes undergo a configuration transformation from octahedron to tetrahedron at high temperatures (near or above 100°C) and (or) high chloride concentrations. The complex configuration change is also apparent from the measured spectra of Heinrich and Seward (10). The neglect of tetrahedral complexes in Heinrich and Seward (10) could have caused appreciable errors in the final fitted stability constants.

Recently, Palmer and Hyde (13) investigated the formation of the monochloroiron(II) complex in aqueous solutions using potentiometry, from 125 to 295°C at I = 1.0 *m*. The formation of tetrahedral Fe(II)-chloride complexes in the solutions was also completely neglected over the entire temperature range in this work.

The present study was designed to obtain reliable stability constants of Fe(II)-chloride complexes in aqueous solution, by means of improved experimental and computational techniques.

Experimental

Chemicals used in this work were mainly from Aldrich Chemicals (Fe(II)-chloride tetrahydrate 99.995%; deuterium oxide 99.9 at.% D; deuterium chloride 37 wt.%, 99.5 at.% D; platinum black, 10 μm powder; iron powder 99.99+%). They were used as received without further purification. Doubly distilled and deionized water (resistivity > 13.0 × 10^6 Ω cm) was used for preparing solutions. Crystals of NaCl or LiCl were heated at 150°C for over 2 h to remove moisture before they were added into solutions for adjusting chloride concentrations.

Each solution was prepared immediately before use and all sample weighing and transfer were performed in a glove box purged with nitrogen gas. The solution preparation system was slightly pressurized (<6 psig, 1 psi = 6894.757 Pa) with hydrogen gas to generate a reducing atmosphere and facilitate sample loading. Thus, solutions were in a closed system throughout the entire preparation process. About 0.01 g of platinum black was added before the solution was purged with hydrogen. The solution was gently heated to about 50°C for about 30 min to allow complete reduction of Fe(III) to Fe(II) under hydrogen atmosphere (5 psig). The cell was purged with hydrogen and the solution and platinum black were then loaded into the cell at the same time. About 20% of total cell volume was allowed for liquid expansion upon heating.

A total of 15 solutions were made for each wavelength region (UV or near-IR) for spectral measurements. For the UV region, solutions (about 0.10 *m* Fe(II)) were made by dissolving hydrated $FeCl_2$ directly in water, with no HCl added, because there is little hydrolysis of Fe(II) ions in neutral solutions over the temperatures covered in this study (less than 0.001% at 25°C (14)). NaCl was then added to make solutions of 0.2–5.8 *m* chloride.

In the near infrared (near-IR) region, water interferes severely with the Fe(II) bands of interest. Fe(II) solutions were prepared using D_2O and DCl so that the upper limit of the useful wavelength was extended from about 1350 nm (7407 cm^{-1}) to about 1850 nm (5405 cm^{-1}) with 10 mm pathlength, and the whole *d–d* transition band of the Fe(II) octahedral complexes could be observed. Pure iron powder was dissolved in a mixture of DCl and D_2O, and the calculated amount of D_2O was added to make a Fe(II) stock solution of 0.5031 *m*. The desired chloride concentration (1.15–5.43 *m)* for each solution used was achieved by adding the calculated amount of NaCl.

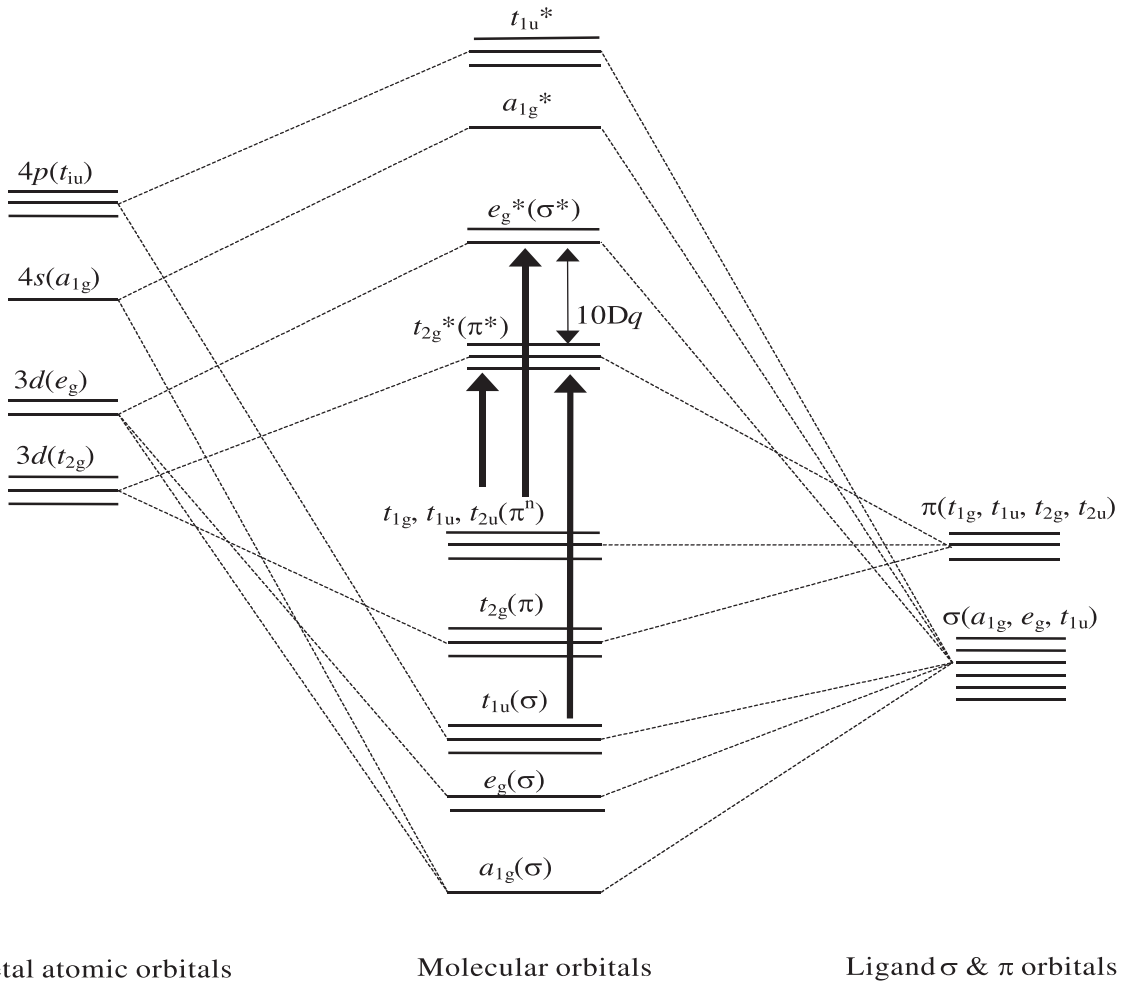
The solutions used for investigating the configuration transformation from octahedral to tetrahedral complexes in both regions were prepared by adding LiCl to obtain much higher chloride concentrations (7.68–16.28 *m*). The corresponding blank solutions that contained the same chloride concentrations and no Fe(II) ions were prepared in the same way as the sample solutions.

In neutral to slightly acidic aqueous solutions, the Fe(III) species have two absorption bands in the UV region centered at 49 505 and 33 898 cm^{-1}, respectively. Our measured spectra with different Fe(III) solutions show that the Fe(III) band at 33 898 cm^{-1}, which is somewhat remote from the Fe(II) band at 41 667 cm^{-1}, is about 105 times stronger than the Fe(II) band at 41 667 cm^{-1}. Therefore, any trace amount of Fe(III) species in solution should be easily detected based on spectral scans in the UV region (27 778–33 898 cm^{-1}). Solutions were checked before and after experiments and showed a flat background absorption in this region, indicating that Fe(III) contamination was undetectable. Fe(III) species used in this work, have no absorption bands in the near-IR region.

A UV-vis near-IR spectrophotometer (Cary 5E, Varian) was employed for absorption spectral measurement in the regions from 27 778 to 57 143 cm^{-1} (UV) and from 5263 to 16 667 cm^{-1} (near-IR). The instrument is equipped with a 6 × 6 thermostatic cell-holder mounted on a sample transport accessory. The cell-holder block with solutions can be cooled down to –10°C and heated up to 100°C in 2 to 3 min with an accuracy of ±0.3°C, and the temperature gradient between the block and the solution was less than 0.5°C. A spectrophotometric cell (NSG Precision Cells Inc.) with a nominal 10 mm pathlength was connected with a solution preparation system through Teflon tubing and valves which have near zero oxygen permeability to prevent oxygen ingression. The same cell was used for the measurements of

© 2001 NRC Canada

Fig. 1. Schematic molecular orbital diagram for octahedrally coordinated Fe(II)-chloride complexes. The d → d transition is shown as a light double arrow and possible charge transfer transitions are shown as heavy arrows. This diagram and Fig. 2 were constructed based on refs. 10, 13, and 15.



both Fe(II) and blank solutions to eliminate variations in pathlength and absorbance by the cell. An oxygen remover (Oxiclear from Aldrich Chemical Co.) was connected to the hydrogen cylinder to reduce oxygen to below 50 ppb.[3]

In the UV region, all spectra were collected at 10 cm^{-1} intervals with a scan rate of 1500 cm^{-1}/min, from 28 000 to 57 100 cm^{-1}. In the near-IR region, all spectra were collected at 0.25 nm intervals with a scan rate of 90 nm/min, from 600 to 1900 nm (16 667 to 5263 cm^{-1}). The spectral bandwidth (SBW) was set to 1.5 nm and the slit was fully open. All solutions, including the blank solutions, were run using a double beam mode with water (UV region) or heavy water (near-IR region) as the reference material. The absorptions due to solvent and chloride were then eliminated by subtraction.

The spectra were collected in the same order for each solution, starting from 25°C, then from 100 to 80, 60, 40, 25, and 10°C sequentially. A comparison of the two spectra measured at 25°C would indicate if there was a concentration change of solution after heating it up to 100°C. The chloride concentration for each solution at each temperature was corrected individually. Typically, a correction factor of 0.5–1.5% was applied to the solution concentrations after heating, assuming that the concentration changes arose from differential water evaporation only.

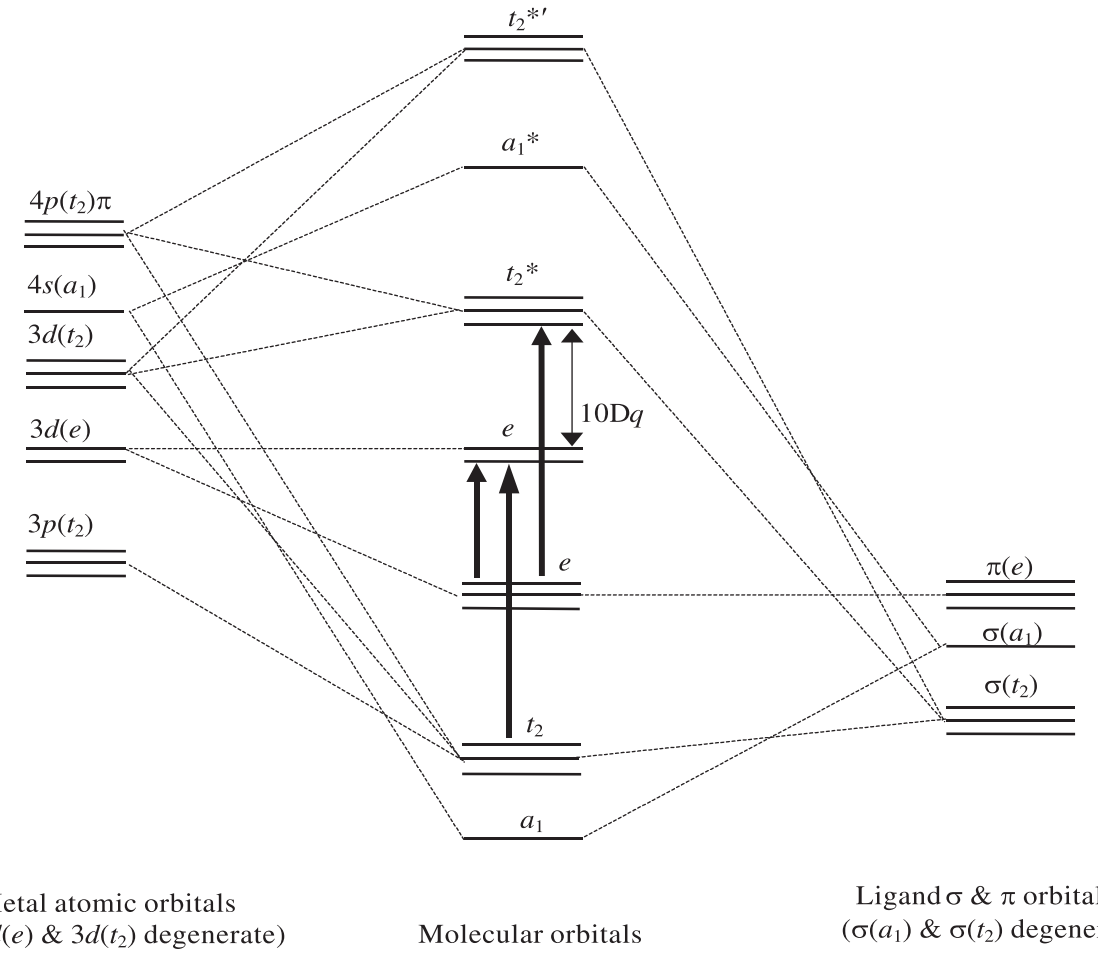
Coordination chemistry of Fe(II)

Transition metal chemistry is largely governed by its *d*-electron configuration. With a d^6 configuration, Fe(II) has the greatest possible ligand field stabilization energies (LFSE) in octahedrally (O_h) coordinated strong (low spin) ligand fields. Even in weak (high spin) ligand fields, octahedral Fe(II) complexes are still favored in terms of 10Dq[4] decrease. However, tetrahedral (T_d) complexes are often favored at higher temperatures and (or) higher chloride concentrations because of the vibrational stretching of the metal–ligand bond and steric requirements. Schematic molecular orbital energy levels for Fe(II) octahedral and tetrahedral complexes are shown in Figs. 1 and 2 (cf. refs. 11, 15, 16). For both octahedral and tetrahedral Fe(II) complexes, the spin-allowed *d–d* transitions, being orbitally forbidden and weak, occur in the near-IR region. Other

[3] More experimental details can be found in ref. 9.
[4] For a definition of 10Dq, see ref. 17.

© 2001 NRC Canada

Fig. 2. Schematic molecular orbital diagram for tetrahedrally coordinated Fe(II)-chloride complexes. The d → d transition is shown as a light double arrow and possible charge transfer transitions are shown as heavy arrows.



transitions, both spin and Laporte allowed charge transfers, are intense and occur in the UV region. All these transitions are closely related to the strength of the applied ligand field (10Dq).[4]

The spin allowed $d \rightarrow d$ transition for a Fe(II) ion in an octahedral ligand field ($t_{2g} \rightarrow e_g$) is at about 10 000 cm^{-1} with a maximum molar extinction coefficient (ε_{max}) ~1.1 L mol^{-1} cm^{-1} (17). This transition corresponds directly to the 10Dq for a d^6 ion in an O_h field (17). Because of tetragonal distortion of O_h symmetry when non-equivalent ligands surround the metal ion, or Jahn–Teller distortion in the case of six equivalent ligands (H_2O), either a split band with two components or a broad and asymmetric band may be observed for this transition (18). The separation of Jahn–Teller distorted splitting is about 2300 cm^{-1}, varying with temperature (12, 18).

At room temperature, Fe(II) ion, resembling other first-row transition metal ions, exists as the hexaaquo complex in dilute aqueous solutions (11). Water is replaced stepwise by Cl^- as the chloride concentration or temperature increases. Correspondingly, a tetragonal splitting will gradually become dominant over the Jahn–Teller effect. The 10Dq of these mixed ligand complexes (e.g., 9000 cm^{-1} for the monochloroiron(II) complex) will be slightly less than that of the hexaaquo ion because Cl^- ion is a weaker ligand compared to H_2O in the spectrochemical series (17). The 10Dq of a complex also decreases (red shift) with an increase of temperature because the vibrational stretching of the metal–ligand bond increases and ligand field strength decreases accordingly at higher temperatures. Strictly speaking, the conversion from hexaaquo to chloroaquo complexes changes the O_h symmetry (removal of center of symmetry) and relaxes orbital forbiddenness of the $d \rightarrow d$ transition, and therefore, the ligand field band is more intense (12).

When temperature or chloride concentration is sufficiently high, the distorted octahedral structure of Fe(II) complexes may undergo a coordination change to a tetrahedral geometry (T_d). A tetrahedral Fe(II) complex will also exhibit only one spin-allowed transition, $e \rightarrow t_2$, at about 4/9 the energy of the $t_{2g} \rightarrow e_g$ transition in an O_h field with the same ligands (17). It was suggested that this band should lie near 4160 cm^{-1} (12) and was 10–100 times stronger than that of a similar octahedral complex because it is partially orbitally allowed because of d–p mixing in T_d coordination (17).

In octahedrally coordinated Fe(II) complexes, there are potentially four charge transfer transitions $u \rightarrow g$ for two groups of orbitals: t_{1g}, t_{2u}, t_{1u}, t_{2g} (π orbitals) and t_{1u}, e_g, a_{1g} (σ orbitals). Therefore, four bands might occur from t_{1u}, t_{2u} (π), and t_{1u}(σ) to e and t. Three of them have been clearly observed for $FeCl_2$ solid crystal at 10 K (19, 20).

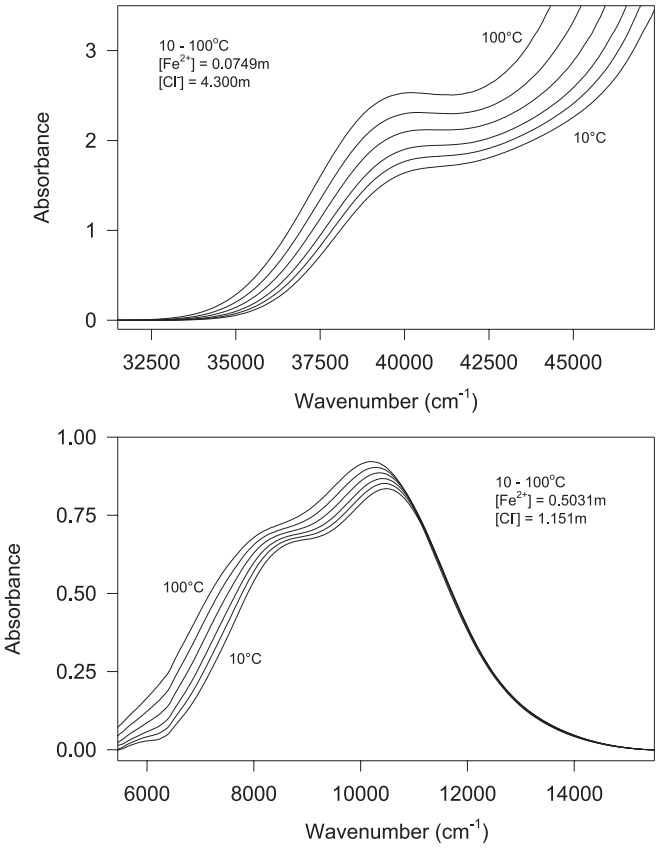
© 2001 NRC Canada

In our experiments, the absorption spectra of aqueous solutions of Fe(II)-chloride show unresolved bands around 40 000–45 000 cm^{-1} and a stronger band around 50 000 cm^{-1}. Unlike the spectra of solid crystals, these bands have severe overlapping with solvent absorption. They might be assigned to the transitions: t_{1u}, $t_{2u}(\pi) \rightarrow t_{2g}^*$, $t_{1u}(\sigma) \rightarrow t_{2g}^*$, and t_{1u}, $t_{2u}(\pi) \rightarrow e_g^*$, as shown in Fig. 1.

As in the case of octahedral complexes, tetrahedral complexes have three possible charge transfer transitions (Fig. 2): $t_2(\sigma) \rightarrow e$ (Fe 3*d*), *e* (Cl lone pair π) $\rightarrow e$ (Fe 3*d*), and *e* (Cl lone pair π) $\rightarrow t_2$* (16). At least two of those transitions were observed in our spectra under the current experimental conditions (centered around 37 000 and 44 000 cm^{-1}).

Several studies on the ligation number for Fe(II)-chloride complexes indicate that $Fe(H_2O)_6^{2+}$ was present predominantly in aqueous solution at 25°C even at chloride concentrations up to 8 *m* (21, 22), and that the maximum ligation number is 2 at temperatures ranging from 25 to 90°C (11). However, Vogel Koplitz et al. (12) studied the Fe(II)-chloride complexes spectrophotometrically with chloride concentrations ranging from 1 to 11 *m* and at temperatures from 25 to 82°C, and found that octahedral complexes with chloride ligation numbers up to 4 were present over this range, as determined by principal factor analysis and from the rule of average environment. At higher temperatures and (or) chloride concentrations, the formation of some tetrahedral complexes, possibly $FeCl_4^{2-}$, was also reported by the authors (12). Most of the other work on Fe(II)-chloride complexes in aqueous solution (e.g., refs. 6, 13) was based on the assumption that only the monochloroiron(II) complex was present in solution and, therefore, only the first stability constant was obtained.

Fig. 3. Absorption spectra of 0.07491 *m* $FeCl_2$ in 4.300 *m* NaCl aqueous solution in the UV region (top), and 0.5031 *m* Fe(II) in aqueous solution with 1.151 *m* chloride (bottom) in the near-IR region at 10, 25, 40, 60, 80, and 100°C (from bottom to top).



Spectra

Each spectrum was five-point-smoothed, 261 points selected at 50 cm^{-1} (UV) and 4.5 nm (near-IR) intervals, and formatted into the input data set for SQUAD (a FORTRAN program originally written by Leggett and co-workers (23–26)). At each temperature, the input data set for SQUAD consists of 15 spectra with 3915 data points in total, covering a spectral range from 34 000 to 47 000 cm^{-1} (UV) or from 5484 to 15 302 cm^{-1} (near-IR) with slight variations because absorbance bands shift with temperature. Some representative spectra, with constant chloride concentration at varied temperature, are shown in Fig. 3.

The equilibria between Fe^{2+}(aq) and chloride ions in aqueous solution can be generalized as:

$$[1] \qquad Fe(H_2O)_6^{2+} + nCl^- \rightleftharpoons Fe(H_2O)_{6-n}Cl_n^{2-n} + nH_2O$$

$$[2] \qquad Fe(H_2O)_6^{2+} + mCl^- \rightleftharpoons Fe(H_2O)_{4-m}Cl_m^{2-m} + (m+2)H_2O$$

where the coordination numbers of chloride are $0 \le n \le 6$ and $0 \le m \le 4$. The activity of water under our experimental conditions is nearly constant and was considered unity. According to Susak and Crerar (11), the chloride ligation number of Fe(II) octahedral complexes is less than or equal to 2 ($n \le 2$ in eq. [1]). It was shown (12) that the stoichiometry of Fe(II) tetrahedral complex appeared to be $FeCl_4^{2-}$. These observations were confirmed in this work, and are consistent with those on the cobalt(II) chloride system (27). Therefore, eqs. [1] and [2] may be combined and simplified to:

$$[3] \qquad Fe^{2+} + nCl^- \rightleftharpoons FeCl_n^{2-n}$$

with $n = 4$ referring to the tetrahedral complex. Then the stability constant β for a Fe(II)-chloride complex may be written as:

$$[4] \qquad \beta_n = \frac{[FeCl_n^{2-n}]\gamma_n}{[Fe^{2+}]\gamma_{Fe^{2+}}[Cl^-]^n\gamma_{Cl^-}^n}$$

where the square brackets [ ] represent molalities (mol kg^{-1}) and γ is the individual ion activity coefficient. Sodium chloride is essentially dissociated in aqueous solutions at temperatures up to 150°C (28) and, therefore, the NaCl concentrations in the solutions were not corrected in this work.

Beer's law states that at a given wavelength

$$[5] \qquad A = \sum_n (FeCl_n^{2-n})\varepsilon_n l$$

where *A* and ε are absorbance and molar absorptivity, respectively, at a given wavelength, *l* is the path length, round brackets () denote molar concentration (mol L^{-1}). Combining eqs. [4] and [5] yields:

$$[6] \qquad A = \sum_n \beta_n Y_n [Fe^{2+}][Cl^-]^n \varepsilon \gamma_{Fe^{2+}} \gamma_{Cl^-}^n \gamma_n^{-1} l$$

© 2001 NRC Canada

where Y_n is a factor to convert the concentration of the *n*th complex from molality (mol kg^{-1}) to molarity (mol L^{-1}), and can be calculated using the following equation:

$$[7] \qquad Y_n = \frac{1000d}{1000 + m_1W_1 + m_2W_2 + \ldots}$$

where m_1, m_2, W_1, and W_2 are the molalities and formula weights of solutes 1 and 2 in solution, respectively, d is the solution density.

Because of the lack of data, the same eq. [7] was also used to convert molalities to molarities for heavy water solutions with the following relationship assumed:

$$[8] \qquad \frac{d_H}{d_H^\circ} = \frac{d_L}{d_L^\circ}$$

where d_H, d_L, d_H°, and d_L° are the densities of D_2O solution, H_2O solution, pure D_2O and pure H_2O, respectively.

Thus, given sufficient absorbance values A, the βs and molar absorptivities for various Fe(II) species can be obtained from eq. [6] using numerical methods.

The nonlinear least-squares program SQUAD searches for the combination of apparent formation constants (activity coefficients were not considered) and molar absorptivities which best describe the supplied total concentrations of metal and ligand, and data of absorbance. The program was modified in this work to be used in a PC environment with activity coefficient calculations incorporated in an iterative process so that true thermodynamic stability constants could be obtained.

It is noted that no isosbestic point is present in any of the spectra measured (Fig. 3); therefore, there were more than two major species present in the system when either the temperature or ligand concentration changed. However, if more than two octahedral complexes were assumed or the tetrahedral complex was included, no meaningful convergence could be achieved with our data using SQUAD. We conclude that the concentrations of the octahedral complexes with chloro coordination number >2, if any, are insignificant and below detection in most of the solutions (tetrahedral complex will be discussed later). Extensive work on cobalt(II) chloride complexes suggests that, over a wide range of temperature and chloride concentration, the ligation does not exceed 4 and that $CoCl(H_2O)_5^+$ and $CoCl_2(H_2O)_4^0$ are the major complexes in most cases (27, 29, 30).

For all Fe(II) containing species, the absorption bands in the near-IR region due to *d–d* transitions are relatively weak compared to the charge transfer bands in the UV region. Therefore, results obtained with the near-IR spectra are intended to serve as cross-checks for those obtained with the UV spectra.

Activity coefficients

The ionic interaction model of Pitzer (31) is one of the most widely used methods for electrolyte activity calculations. But, few Pitzer parameters are currently available for complexed species. For the purpose of comparison, a semi-empirical method by Helgeson et al. (32) was also used in this work. A comparison of the data obtained independently using the two different methods with relevant discussions follows.

Pitzer model

Pitzer and co-workers (31, 33, 34) developed a theoretical model for electrolyte solutions by combining the Debye–Hückel equation with additional terms in the form of virial coefficients. This model has successfully provided an alternate formulation of statistical mechanics for a number of multicomponent solution systems (35, 36).

The Pitzer equations for the natural logarithms of the activity coefficients of cations (M) and anions (X) are given as (31):

$$[9] \qquad \ln\gamma_M = z_M^2F + \sum_a m_a(2B_{Ma} + ZC_{Ma}) + \sum_c m_c(2\Phi_{Mc} + \sum_a m_a\psi_{Mca}) + \sum_{a<a'}\sum m_a m_{a'}\psi_{Maa'} + z_M\sum_c\sum_a m_c m_a C_{ca} + 2\sum_n m_n\lambda_{nM} + \ldots$$

$$[10] \qquad \ln\gamma_X = z_X^2F + \sum_c m_c(2B_{cX} + ZC_{cX}) + \sum_a m_a(2\Phi_{Xa} + \sum_c m_c\psi_{cXa}) + \sum_{c<c'}\sum_a m_c m_{c'a}\psi_{cc'X} + |z_X|\sum_c\sum_a m_c m_a C_{ca} + 2\sum_n m_n\lambda_{nM} + \ldots$$

where

$$[11] \qquad F = f^\gamma + \sum_c\sum_a m_c m_a B'_{ca} + \sum_{c<c'}\sum m_c m_{c'}\Phi'_{cc'} + \sum_{a<a'}\sum m_a m_{a'}\Phi'_{aa'}$$

$$[12] \qquad f^\gamma = -A_\phi\left[\frac{I^{1/2}}{1+bI^{1/2}} + \frac{2}{b}\ln(1+b\sqrt{I})\right]$$

$$[13] \qquad Z = \sum_i m_i|z_i|$$

A_ϕ is the Debye–Hückel limiting law constant and taken from Archer and Wang (37), b is a universal parameter with the value of 1.2 $kg^{1/2}$ $mol^{-1/2}$, I is the ionic strength, m_i and z_i are the molality and charge of species i, respectively, B and C are adjustable parameters derived from experimental data of single salt solutions, Φ is related to short range interactions between like charged ions and long range electrical forces due to unsymmetrical mixing where the charges on c and c' (or a and a') differ, Φ′ is the ionic strength derivative of Φ, ψ accounts for the short range interactions between one ion of one sign and two dissimilar ions of opposite sign, λ represents the short range interactions between neutral solute species and charged ions, and subscripts c and a represent cations and anions and the sums are over the various cations c, c' or over the anions a, a'.

The parameters C_{MX} are related to the tabulated parameters derived from data on aqueous single salt systems

$$[14] \qquad C_{MX} = \frac{C^\Phi_{MX}}{2\sqrt{z_M z_X}}$$

All coefficients B_{MX} in the Pitzer equations are expressed as functions of ionic strength I

$$[15] \qquad B_{MX} = \beta^{(0)}_{MX} + \beta^{(1)}_{MX}g(\alpha I^{1/2})$$

$$[16] \qquad B'_{MX} = [\beta^{(1)}_{MX}g'(\alpha I^{1/2})]/I$$

where

© 2001 NRC Canada

$$[17] \quad g(x) = \frac{2[1-(1+x)e^{-x}]}{x^2}$$

$$[18] \quad g'(x) = \frac{-2\left[1-\left(1+x+\frac{x^2}{2}\right)e^{-x}\right]}{x^2}$$

and α has the value of 2.0 $kg^{1/2}$ $mol^{-1/2}$ for the most common salts.

The Pitzer model has the advantage of being able to account for all the possible interactions between all pairs and triplets of solute species that may exist in those multicomponent solutions. However, the higher order terms involving interactions between ions of like sign and an unsymmetrical mixing (Φ), interactions between one ion of one sign and two dissimilar ions of opposite sign (Ψ), and interactions between ions and neutrals (λ) are usually trivial, and were ignored in this work.

As shown in eqs. [14]–[16], the B_{MX} and C_{MX} functions incorporate ion interaction parameters, i.e., Pitzer parameters $\beta^{(0)}_{MX}$, $\beta^{(1)}_{MX}$, C^{Φ}_{MX}, which are specific to the particular salt MX, representing short-range interactions specific to the interacting ions M^{z+} and X^{z-} in solution. Therefore, the single salt parameters $\beta^{(0)}_{MX}$, $\beta^{(1)}_{MX}$, and C^{Φ}_{MX} for all the solutes are required to calculate the activity coefficients of ionic species using the Pitzer equations.

The Pitzer parameters for NaCl (Na^+-Cl^-) were from Pitzer (38), the values for the other solutes are discussed as follows.

$FeCl_2$ (Fe^{2+}-Cl^-): The Pitzer parameters for $FeCl_2$ (Fe^{2+}-Cl^-) at 25°C were taken from Pitzer (31), but no data are available at other temperatures. However, temperature derivatives of the Pitzer parameters are available for $CoCl_2$ (39). Based on the fact that all the Pitzer parameters for $CoCl_2$ are very similar to those for $FeCl_2$ at 25°C, it was reasonable to use the temperature derivatives for $CoCl_2$ to calculate the Pitzer parameters for $FeCl_2$ at temperatures other than 25°C. The increments calculated from temperature derivatives were then added to the corresponding values of Pitzer parameters for $FeCl_2$ at 25°C (9).

$FeCl_2$ ($FeCl^+$-Cl^-): The Pitzer parameters for this system are not available at any temperature. It is noted that many physical parameters including crystal and ionic radii, effective electrostatic radius, and Born constants are very close for the two metal ions Fe(II) and Cu(II) (16, 32). Thus, as a good approximation, the Pitzer parameters ($\beta^{(0)}$ = 0.0651, $\beta^{(1)}$ = 0.554, and C^{ϕ} = 0.0244) for the ion-pair $CuCl^+$-Cl^- (36) could be used as initial values in SQUAD for the $FeCl^+$-Cl^- ion pair.

Assuming only the monochloro complex in solution, eq. [4] can be rearranged to

$$[19] \quad \ln\beta_1 - \ln K^* + \ln\gamma_{Fe^{2+}} = \ln\gamma_{FeCl^+} - \ln\gamma_{Cl^-}$$

where K^* is the concentration quotient. Substituting $\ln\gamma_{Cl^-}$ in eq. [19] with eqs. [9] and [10] and consolidating all terms without $\beta^{(0)}_{FeCl^+,Cl^-}$, $\beta^{(1)}_{FeCl^+,Cl^-}$, and $C^{\Phi}_{FeCl^+,Cl^-}$ into an *f*-term yields:

$$[20] \quad \ln\beta_1 - \ln K^* + \ln\gamma_{Fe^{2+}} + f(m_{Cl^-}, m_{Fe^{2+}}, m_{FeCl^+}) = \beta^{(0)}_{FeCl^+,Cl^-} 2(m_{Cl^-} - m_{FeCl^+})$$

$$[21] \quad \ln\beta_1 - \ln K^* + \ln\gamma_{Fe^{2+}} + f'(m_{Cl^-}, m_{Fe^{2+}}, m_{FeCl^+}) = \beta^{(1)}_{FeCl^+,Cl^-} 2(m_{Cl^-} - m_{FeCl^+})g$$

$$[22] \quad \ln\beta_1 - \ln K^* + \ln\gamma_{Fe^{2+}} + f''(m_{Cl^-}, m_{Fe^{2+}}, m_{FeCl^+}) = C^{\Phi}_{FeCl^+,Cl^-} 2(m_{Cl^-} - m_{FeCl^+})Z$$

In eqs. [20]–[22], the left-hand side terms are known, and the Pitzer parameters $\beta^{(0)}_{FeCl^+,Cl^-}$, $\beta^{(1)}_{FeCl^+,Cl^-}$, and $C^{\Phi}_{FeCl^+,Cl^-}$ can be calculated in an iterative process (9). In a given cycle, one parameter was calculated at a time with the other two fixed, and the calculated data were then used as input values for the next round of calculations.

Helgeson model

In the Debye–Hückel equation, the charging process, omitting all the direct effects of short range forces, is used as an approximation to obtain thermodynamic properties. Adding the effects of the short range forces to the Debye–Hückel equation, Helgeson (28) presented extended equations that were used to describe the electrolyte behavior for the relatively minor species in aqueous solutions with a high chloride concentration. The equation of Helgeson et al. (32) gives a close approximation of individual ion activity coefficients over a wide range of chloride concentration, temperature, and pressure (9).

Results and discussion

Complex configuration transition

Although the amount of tetrahedral complex is insignificant in the solutions used for SQUAD analysis, it can be important or even dominant at around 100°C with higher chloride concentrations, such as those found in steam generator crevices under lay-up or shutdown conditions. Therefore, the tetrahedral Fe(II)-chloride complex cannot be ignored and has to be investigated even at relatively low temperatures (<100°C). In our study the absorbance of the tetrachloroiron(II) complex ($FeCl_4^{2-}$) was observed in solutions with high chloride concentrations, in both the UV and near-IR regions.

Near-IR region

The *d–d* transition of a Fe(II)-chloride tetrahedral complex is expected to appear in the near-IR region centered at around 4160 cm^{-1}, with molar absorptivities 10–100 times greater than those of octahedral complexes (17). Even with heavy water and DCl, only the tail of this band was observed in the region from 5405 to 6250 cm^{-1}. This tail becomes more pronounced as the chloride concentration or temperature increases (Fig. 4). In Fig. 4, the intensities of the band centered near 10 000 cm^{-1} (which is primarily due to the octahedral complexes) decrease while those centered near 4160 cm^{-1} (of which only the tail is visible and which are primarily due to the tetrahedral complex) increase as the temperature or chloride concentration increases. This indicates that the amount of the tetrahedral complex increases at the expense of the octahedral complexes.

© 2001 NRC Canada

Fig. 4. Top: near–IR absorption spectra of 0.02445 *m* Fe(II) in 8.742 *m* chloride (added as LiCl and DCl) aqueous solution at 10, 25, 40, 60, 80, and 100°C (from bottom to top at 6000 cm^{-1}); Bottom: near–IR absorption spectra of Fe(II)-chloride solutions at 100°C. Solution concentrations are (from bottom to top at 6000 cm^{-1}): 1.51, 5.43, 8.74, 10.04, 12.49, and 15.26 *m*.

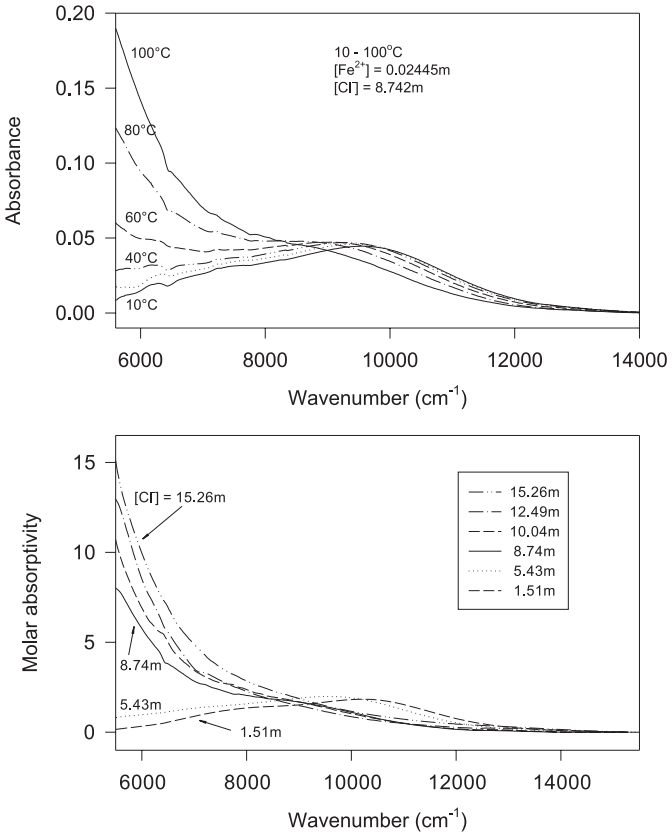
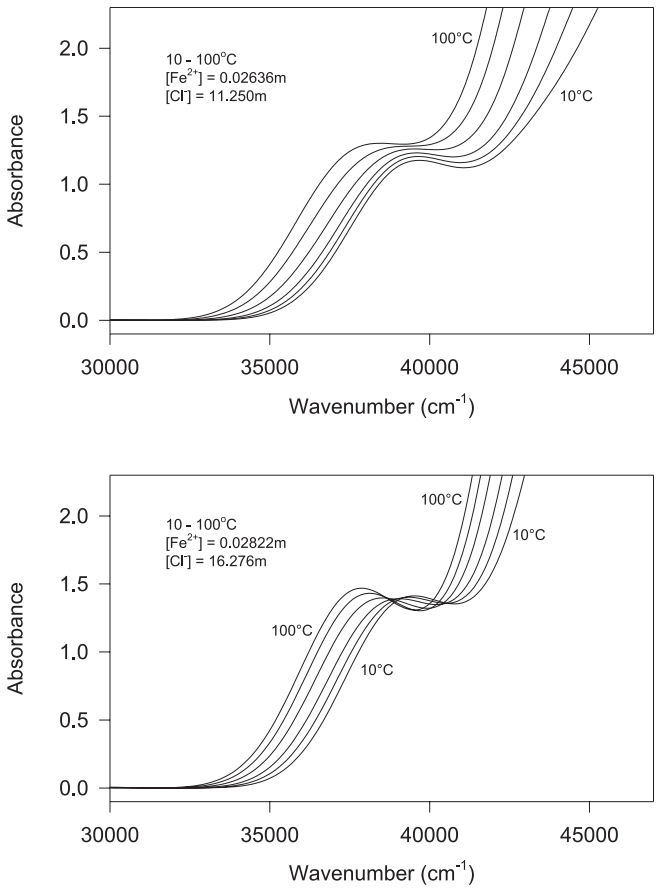


Fig. 5. Variation of absorption spectra with temperature (10, 25, 40, 60, 80, and 100°C, from bottom to top) for 0.02636 *m* $FeCl_2$ in 11.250 *m* total chloride (added as LiCl) (top graph), and for 0.02822 *m* $FeCl_2$ in 16.276 *m* total chloride (bottom graph), in the UV region. Note that the band due to tetrahedral complex (37 500 cm^{-1}) increases at the expense of the octahedral complex band (39 500 cm^{-1}) as temperature increases.



UV region

It was expected that the charge transfer bands for tetrahedrally coordinated Fe(II)-chloride complexes would appear in the UV region. Figure 5 shows the absorption spectra for 0.027 *m* $FeCl_2$ in solutions of varying total chloride concentrations and at various temperatures from 10 to 100°C. It demonstrates that the band at 39 500 cm^{-1} at a low total chloride concentration and low temperature decreases, and a new band at 37 500 cm^{-1} increases with an increase of chloride concentration and (or) temperature.

The band at 37 500 cm^{-1} was assigned to one of the charge transfers of the tetrahedral Fe(II)-chloride complex, because for the solutions whose UV spectra show a well-defined band at 37 500 cm^{-1}, the near-IR spectra show clearly that the tetrahedral complex is predominant in the solutions.

As can be seen from Figs. 4 and 5, octahedral and tetrahedral Fe(II)-chloride complexes coexist in solutions over a wide range of temperature and chloride concentration. In Fig. 6, however, the tetrahedral band at about 37 500 cm^{-1} remains in the same position over a chloride concentration range approximately from 12.46 to 16.28 *m*, with the molar absorptivities little changed. The unsaturated shoulder portion of a strong band at high wavenumbers (cutoff at about 42 000 cm^{-1} in Fig. 6) shows a similar characteristic; there is little further red shift with an increase of chloride concentration from 12.46 to 16.28 *m*. These observations suggest that: (*i*) the tetrahedral complex becomes predominant when the chloride concentration and (or) the temperature are sufficiently high; (*ii*) the band at high wavenumbers can be attributed to the tetrahedral complex; and (*iii*) there is probably only one tetrahedral complex in solution. Following Vogel Koplitz et al. (12), we assume that the only tetrahedral Fe(II)-chloride complex in solution is $FeCl_4^{2-}$. This assumption is consistent with the work by Pan and Susak (27) on Co(II)-chloride complexes.

For this equilibrium

$$[23] \quad Fe(H_2O)_6^{2+} + 4Cl^- \rightleftharpoons FeCl_4^{2-} + 6H_2O$$

we have

$$[24] \quad K_T = \frac{[FeCl_4^{2-}]}{[Fe^{2+}][Cl^-]^4} \frac{\gamma_{FeCl_4^{2-}}}{\gamma_{Fe^{2+}}\gamma_{Cl^-}^4}$$

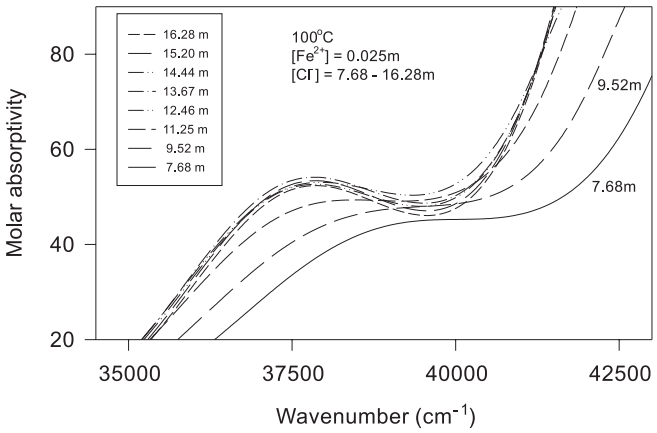
© 2001 NRC Canada

Table 1. Summary of Fe(II)-chloride complex stability constants refined in SQUAD.

	Helgeson model		Pitzer model			
T (°C)	log β_1 /UV[a]	log β_2 /UV[a]	log β_1 /UV[a]	log β_2 /UV[a]	log β_1 /near–IR[b]	log β_2 /near–IR[b]
10	–0.566	–2.06	–0.730	–2.27	–0.575	—
25	–0.307	–1.72	–0.425	–1.75	–0.506	—
40	–0.074	–1.57	–0.326	–1.56	–0.395	—
60	0.031	–1.27	–0.001	–1.23	0.002	—
80	0.247	–0.923	0.219	–1.01	0.195	—
100	0.544	–0.408	0.473	–0.616	0.521	–1.03

Note: In this table and elsewhere in this work, the stability constants β_1, β_2, and β_4 correspond to the species: $FeCl^+$, $FeCl^0_2$, and $FeCl^{2-}_4$.
[a]Values obtained using the UV spectra.
[b]Values obtained using the near-IR spectra.

Fig. 6. Absorption spectra of about 0.025 *m* $FeCl_2$ aqueous solutions with chloride concentrations from 7.68 to 16.28 *m* (added as LiCl) at 100°C in the UV region. Chloride concentrations for the discernible three spectra at the bottom are 7.68, 9.52, and 11.25 *m*.



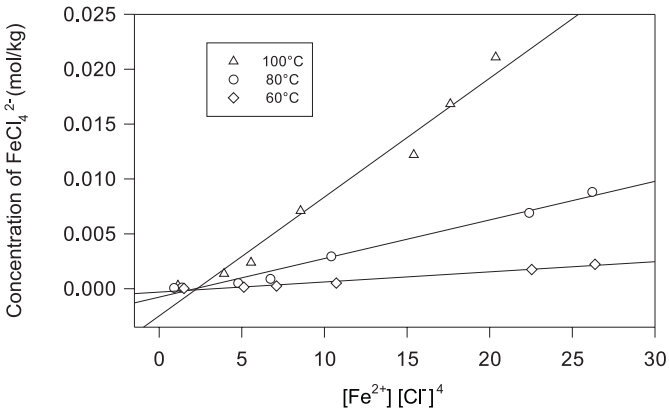
$$[25] \quad [FeCl_4^{2-}] = K_T[Fe^{2+}][Cl^-]^4 \frac{\gamma_{Fe^{2+}}\gamma^4_{Cl^-}}{\gamma_{FeCl_4^{2-}}}$$

where K_T is the equilibrium constant for the configuration transition reaction (H_2O activity was assumed unity). Using the approximation method of Vogel Koplitz et al. (12), the fraction of tetrahedral complex in a solution can be estimated. Because $\gamma_{Fe^{2+}}$ and $\gamma_{FeCl_4^{2-}}$ largely cancel out and γ_{Cl^-} does not deviate appreciably from unity over a large concentration range (40), as a further approximation, the activity term on the right hand side of eq. [25] was taken as unity. The plots of $[FeCl_4^{2-}]$ as a function of $[Fe^{2+}][Cl^-]^4$ show straight lines at 60, 80, and 100°C (Fig. 7). The linear relationship is a convincing evidence that equilibrium [25] is adequate for describing the octahedral–tetrahedral complex transformation in solutions. The equilibrium constant of eq. [24] is obtained from the slopes in Fig. 7 as 9.23×10^{-4} at 60°C, 3.51×10^{-4} at 80°C, and 1.08×10^{-3} at 100°C.

Stability constants

The stability constants for the octahedrally coordinated complexes refined in SQUAD with activity coefficients calculated using the Helgeson and Pitzer models, are listed in Table 1. No convergence could be achieved using the near-IR spectra with the Helgeson model. Generally, better results with smaller standard deviations were obtained using the UV spectra, regardless of the activity calculation model used. These stability constants are averaged and listed in Table 2 as the accepted values.

Fig. 7. Concentration of the tetrahedral complex $FeCl_4^{2-}$ against $[Fe^{2+}][Cl^-]^4$ at 60, 80, and 100°C. Solutions with chloride concentrations greater than 2.2 *m* were used for the plot.



Our determined value of β_1 at 25°C (0.394) falls in the middle range of literature values (9). Our data are also compared with the other two high-temperature studies of Fe(II)-chloride complexes in Table 3. As stated by Palmer and Hyde (13), their reported values for β_1 are in very good agreement with those of Heinrich and Seward (10). Whereas the β_1 values determined in this work differ appreciably from these two earlier works (Table 3). However, this and previous work (11, 12) clearly demonstrate that tetrahedrally coordinated chloro-Fe(II) complexes are present in significant amounts at or near room temperatures at sufficiently high chloride concentrations, and that they are predominant at elevated temperatures (near and above 100°C) even at moderately low chloride concentrations. Obviously, the tetrachloroiron(II) complex cannot be ignored in Heinrich and Seward's work (10), given that their experimental conditions ranged from 25 to 200°C and 0.01 to 3.4 *m* chloride concentration. Even though the chloride concentrations are relatively low (<0.11 *m*) in the solutions of Palmer and Hyde (13), at temperatures near 300°C the tetrachloroiron(II) complex can be important (9). Besides, because very acidic solutions (0.01 to 3.4 *m* HCl) were used by Heinrich and Seward (10), substantial water molecules would exist in the form of H_3O^+, and this could change water's properties as a ligand and affect the coordinating ability of the chloride ions

© 2001 NRC Canada

Table 2. Cumulative and stepwise stability constants of Fe(II)-chloride complexes.[a]

Temp (°C)	log β_1	log β_2	log β_4	ln K_1	ln K_2	ln K_T[b]
10	–0.648 ± 0.082	–2.16 ± 0.10	—	–1.42	–3.53	—
25	–0.366 ± 0.059	–1.74 ± 0.02	—	–0.933	–3.07	—
40	–0.200 ± 0.13	–1.56 ± 0.01	—	–0.557	–3.04	—
60	0.015 ± 0.016	–1.25 ± 0.02	–4.1	0.0247	–2.91	–9.4
80	0.233 ± 0.014	–0.967 ± 0.044	–3.5	0.508	–2.73	–8.1
100	0.509 ± 0.035	–0.512 ± 0.10	–2.9	1.18	–2.33	–6.7

[a]Errors quoted are standard deviations from two or three values listed in Table 1.
[b]Defined in eq. [24].

Table 3. Comparison of stability constant (log β_1) for the first Fe(II)-chloride complex.

T (°C)	Heinrich & Seward (10)	Palmer & Hyde (13)	This work
25	–0.16	–0.125	–0.366
50	–0.022	–0.026	–0.079[a]
100	0.215	0.266	0.509

[a]Average of values at 40 and 60°C, as in Table 2.

accordingly. Finally, real systems encountered in industrial applications are not well represented by either the Fe(II)-H_2O-HCl (10) or the diluted Fe(II)-H_2O-NaCl (13) system.

Complexation thermodynamics

Thermodynamic parameters $\Delta_r G°$, $\Delta_r H°$, and $\Delta_r S°$ for the complexation reactions between Fe(II) and Cl^- can be obtained from the temperature dependence of the stability constants. The free energy change for a reaction can be calculated using

$$[26] \quad \Delta_r G° = -RT \ln K$$

where K is the equilibrium constant (Table 2) for one of the following equilibria

$$[27] \quad Fe^{2+} + Cl^- \rightleftharpoons FeCl^+$$

$$[28] \quad FeCl^+ + Cl^- \rightleftharpoons FeCl_2^0$$

$$[29] \quad Fe^{2+} + 4Cl^- \rightleftharpoons FeCl_4^{2-}$$

Because the present experiments cover a relatively small range of temperature (10–100°C), $\Delta_r H°$ and $\Delta_r S°$ were assumed constant, so that

$$[30] \quad \ln K = \frac{\Delta_r S°}{R} - \frac{\Delta_r H°}{RT}$$

Both $\Delta_r H°$ and $\Delta_r S°$ can be derived from a linear fit of ln K against $1/T$ as shown in Fig. 8. The fitted results are tabulated in Table 4.

Both of our obtained enthalpy and entropy changes for the first Fe(II)-chloride complex formation are positive and larger than those reported previously (10, 13). In fact, all the entropy and enthalpy values obtained for Fe(II)-chloride complex formations as listed in Table 4 are positive, indicating that these complex formations are more like hard–hard interactions. The obtained data also indicate that replacement of water by chloride in the complexes is endothermic, and the driving force for complex formation is the overall increase of entropy through releasing water molecules into the bulk solution.

Fig. 8. Plot of ln K against $1/T$ for Fe(II)-chloride complex formations.

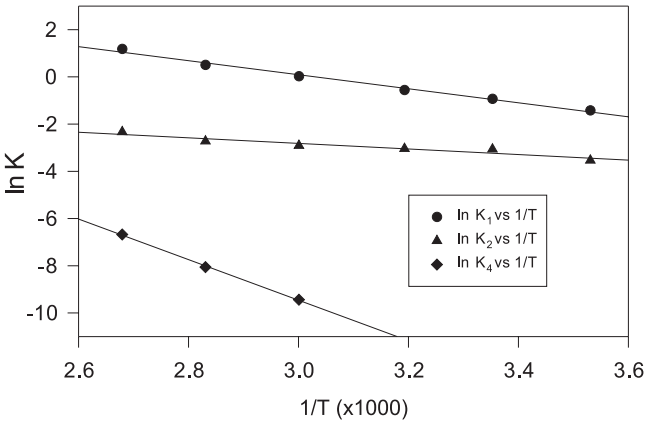


Table 4. Thermodynamic parameters for Fe(II)-chloride complex formations

T (°C)	10	25	40	60	80	100
$\Delta_r G_1°$ (kJ mol^{-1})	3.35	2.31	1.45	–0.068	–1.49	–3.67
$\Delta_r G_2°$ (kJ mol^{-1})	8.32	7.59	7.91	8.06	8.00	7.24
$\Delta_r G_4°$ (kJ mol^{-1})	—	—	—	26.2	23.7	20.7

Reaction	$\Delta_r H°$ (kJ mol^{-1})	$\Delta_r S°$ (J mol^{-1} K^{-1})
1	24.7 ± 1.2	75.0 ± 3.6
2	9.9 ± 1.5	6.1 ± 4.7
4	71.4 ± 2.5	136 ± 7

Note: Subscripts/reactions 1, 2, 4 refer to reactions [27], [28], and [29] in the text, respectively.

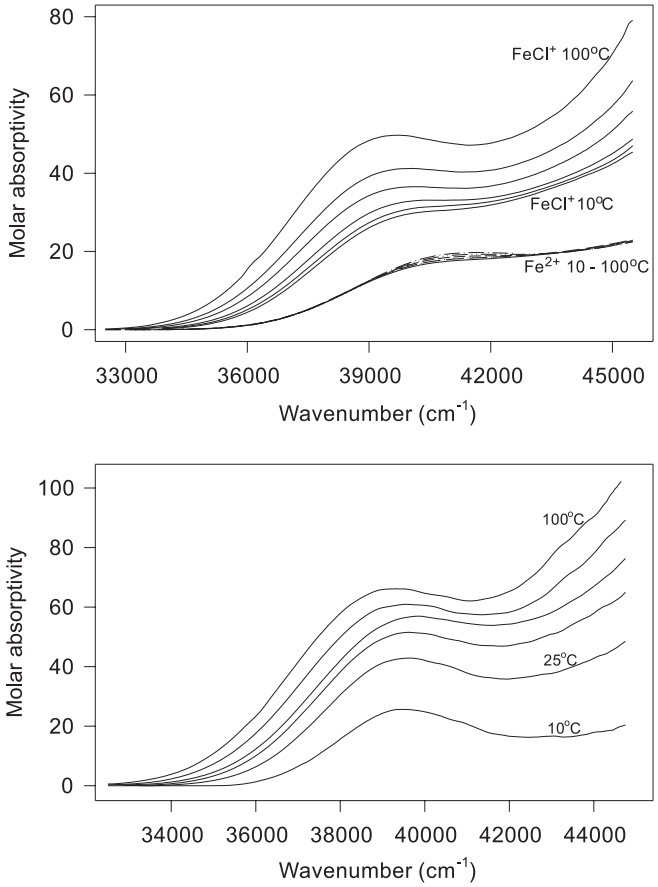
The tetrachloroiron(II) complex is relatively weak with a large positive enthalpy and hence energetically not favored with respect to octahedral complexes at room temperatures. The configuration transition from octahedrally to tetrahedrally coordinated complexes is, therefore, driven by an entropy increase and thus favored at higher temperatures, in addition to being favored stoichiometrically by an increase of chloride concentration.

Molar absorptivities and complex distributions

Increased molecular vibrations and rotations at elevated temperature relax ligand fields, resulting in a decrease in 10Dq. This is shown by the slight band shifts towards lower energies at higher temperatures observed in Figs. 9 and 10

© 2001 NRC Canada

Fig. 9. Molar absorptivities of Fe^{2+}(aq) and $FeCl^+$ (top graph) and $FeCl_2^0$ (bottom graph) at 10, 25, 40, 60, 80, and 100°C (from bottom to top) in the UV region, derived from SQUAD refinements.



for Fe(II)-chloride complexes in both the UV and near-IR regions. These stronger molecular vibrations and rotations at higher temperatures can partially remove the center of symmetry of an O_h coordination, and the Laporte selection rule is partially overcome to yield stronger absorptivities for Laporte forbidden bands. These absorptivities increase with increase of temperature as shown in Figs. 9 and 10 for Fe(II)-chloride species.

As water molecules in $Fe(H_2O)_6^{2+}$ are replaced stepwise by chloride ions, the absorption bands of $FeCl^+$ and $FeCl_2^0$ become more intense at a given temperature (Figs. 9 and 10) because of the removal of center of symmetry of the complexes. The absorption bands of the complexes $FeCl^+$ and $FeCl_2^0$ also shift to lower wavenumbers at a given temperature, indicating that replacement of H_2O by Cl^- decreases the octahedrally coordinated ligand field strength. This observation was expected because Cl^- is a weaker ligand than H_2O. It is noted that at higher temperatures (near 100°C), molar absorptivities in the region from 5556 to 7142 cm^{-1} for $FeCl^+$ increase greatly with temperature (Fig. 10), erratically deviating from the trend shown at lower temperatures. This is due to the formation of the tetrahedral complex. To minimize this problem, spectra with chloride concentrations higher than 4.45 *m* (tetrahedral complex >4.5% for [Cl^-] >4.45 *m* at 100°C) were removed from the data set for SQUAD at 100°C.

Fig. 10. Molar absorptivities of Fe^{2+}(aq) and $FeCl^+$ at 10, 25, 40, 60, 80, and 100°C (from bottom to top) in the near-IR region, derived from SQUAD refinements.

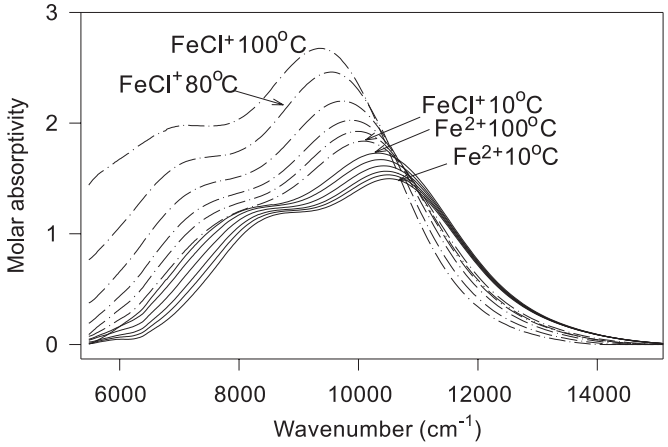
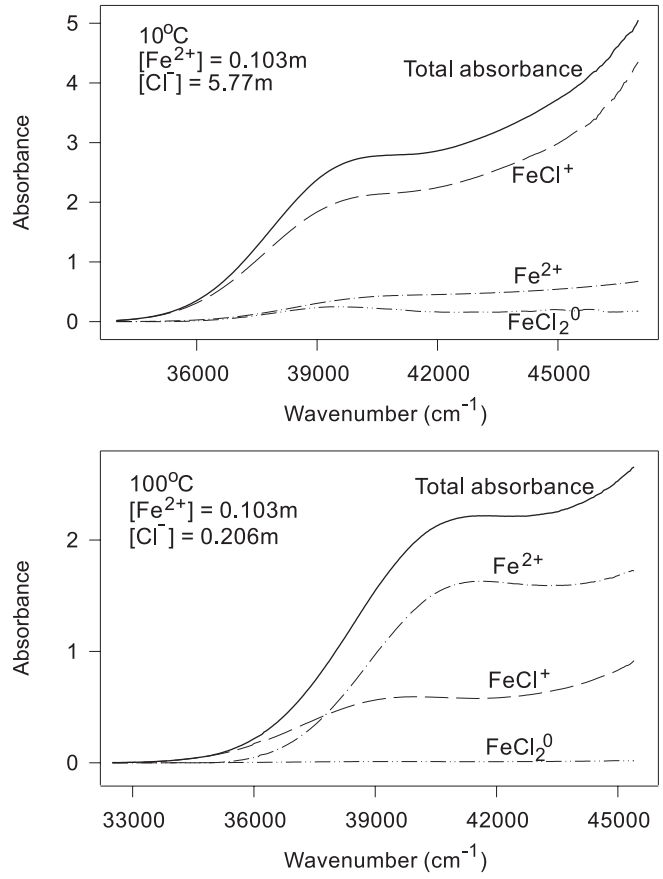


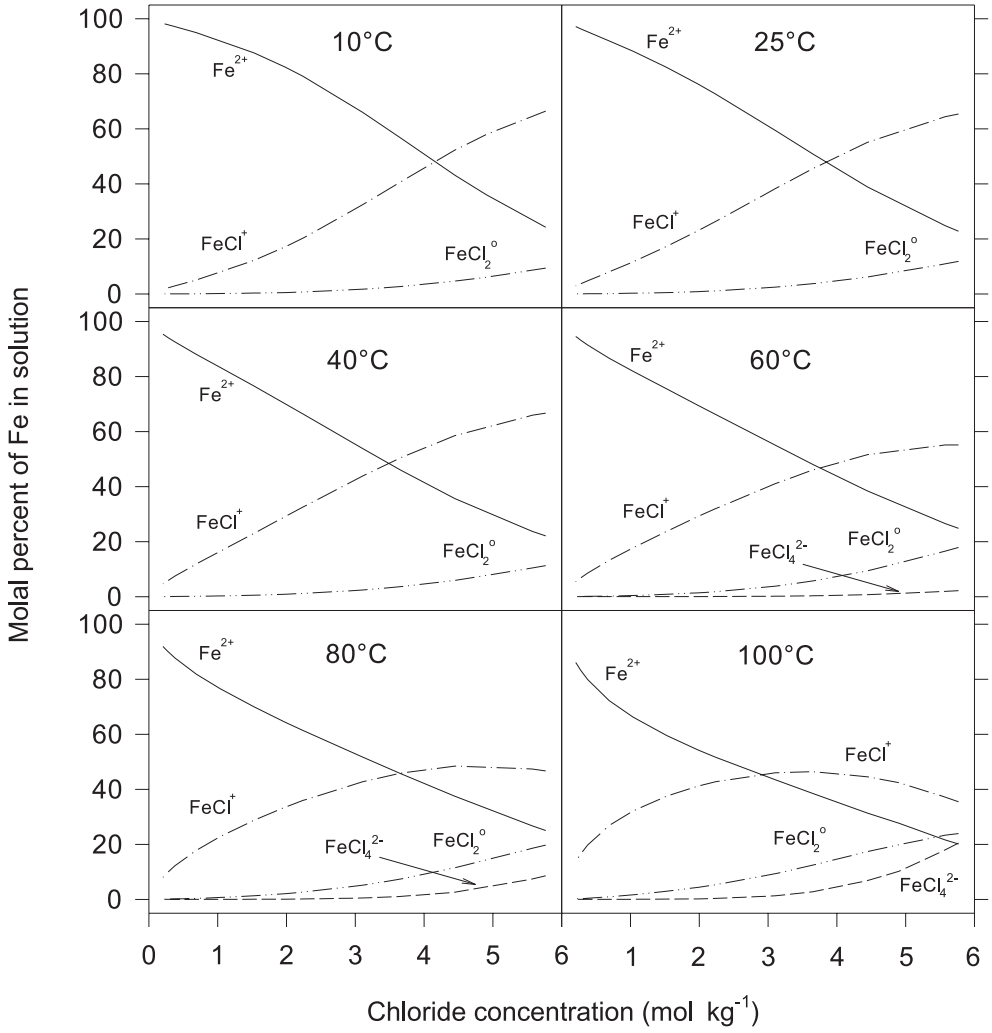
Fig. 11. Total absorbance and contributions from the individual Fe(II) species in high chloride solution at 10°C (top) and in low chloride solution at 100°C (bottom), derived from SQUAD refinements.



When the molar absorptivities and stability constant of each Fe(II) complex are derived from SQUAD at a specific temperature, the absorbance and concentration of the species can be easily calculated for a solution of known Fe(II) and chloride concentrations. Representative absorption spectra with the specific contributions of each Fe(II) containing species, are shown in Fig. 11 at temperatures of 10 and

© 2001 NRC Canada

Fig. 12. Percentage molal contribution of Fe^{2+}(aq), $FeCl^{+}$, $FeCl_2^0$, and $FeCl_4^{2-}$ in aqueous solution as a function of total chloride concentration at 10, 25, 40, 60, 80, and 100°C, derived from SQUAD refinements in the UV region.



100°C. Not surprisingly, the absorption band of free Fe(II) ion dominates the absorption spectra of solutions with low Fe(II) concentrations and at low temperatures. When chloride concentration or temperature gets sufficiently high, the absorption bands of complexes $FeCl^+$ and $FeCl_2^0$ contribute more to the observed spectra (Fig. 11).

In Fig. 12, the percentages of all Fe(II) species are plotted as a function of total chloride concentration in solution at 10, 25, 40, 60, 80, and 100°C. It is noted that the free Fe^{2+}(aq) ion predominates in solutions from 10 to 100°C with chloride concentration less than 3 *m*. The monochloroiron(II) complex, $FeCl^+$, becomes important in solutions with chloride concentrations greater than 1.0 *m*. The dichloroiron(II) complex, $FeCl_2^0$, is always a minor species in solutions (<20%), and the tetrachloroiron(II) complex becomes important only at 100°C and when the chloride concentration exceeds 4 *m* (Fig. 12).

Applications to steam generator systems

To quantitatively assess the effect of hydrolysis and chloro-complex formation on the extent of dissolution of Fe(II) iron, a log [Cl^-] vs. pH diagram depicting the predominance of Fe(II) species at 25 and 100°C was constructed (Fig. 13). The hydrolysis constants of Fe(II) have been reported by several groups (14, 41, 42); the most recent values by Ziemniak et al. (14) were used in this work.

Figure 13 shows that at 25°C in solutions with low chloride concentrations (<1.0 *m*), the free Fe(II) ion (Fe^{2+}(aq)) is predominant over a wide pH range. Only when pH > 9 does the first hydrolyzed Fe(II) species, $FeOH^+$, become predominant. At low temperatures, the higher order hydrolyzed Fe(II) species are relatively unimportant. However, at higher temperatures (near 100°C), the free ion is predominant over a much narrower range of pH, while the second hydrolyzed species ($Fe(OH)_2^0$) becomes more important. At 100°C, the predominance region of the first hydrolysis species ($Fe(OH)^+$) shrinks considerably and the third hydrolysis species ($Fe(OH)_2^0$) gains some importance.

At 25°C, the monochloroiron(II) complex ($FeCl^+$) does not dominate over the free Fe(II) ion until the chloride concentration approaches 2.5 *m*. At 100°C, $FeCl^+$ becomes predominant at chloride concentrations below 0.5 *m*. As the temperature further increases, the Fe(II)-chloride complexes are expected to be even more important.

In steam generators, dissolved impurities can concentrate in crevices and other local areas with restricted coolant flow

© 2001 NRC Canada

Fig. 13. Log [Cl^-] against pH diagrams showing predominance of Fe(II) species at 25°C (top) and 100°C (bottom). The boundaries represent conditions where two species are equal in molar concentrations. Data for chloride species were determined in this work, while those for hydrolyzed species were from Ziemniak et al. (14). The same data were also used for Fig. 14.

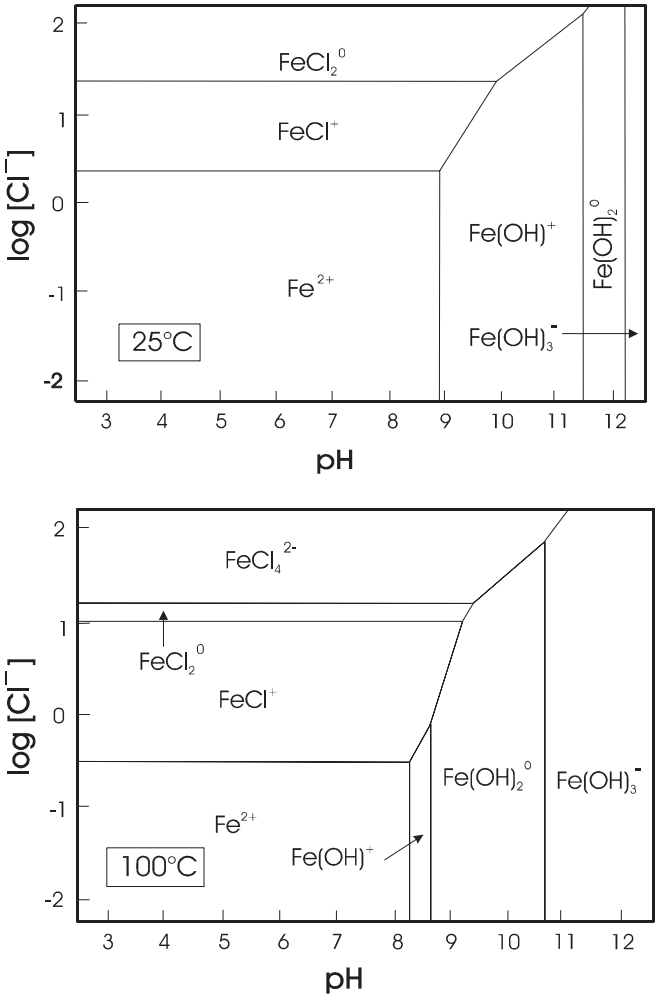
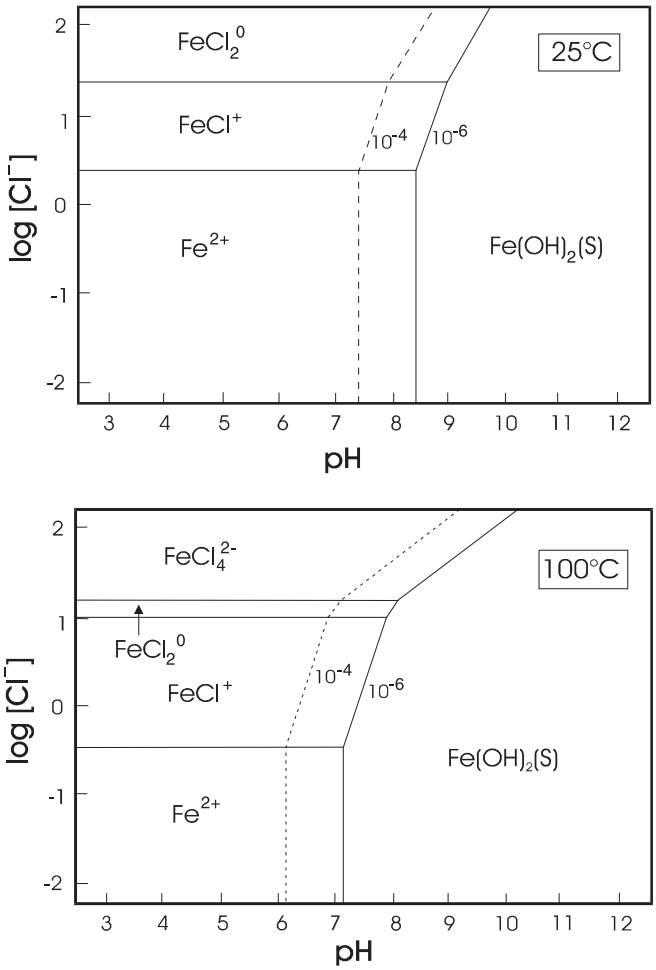


Fig. 14. Diagrams showing the solubility of $Fe(OH)_2$(s) as a function of pH and log [Cl^-] at 25°C (top) and 100°C (bottom). Solid lines between aqueous species and the solid are the 10^{-6} *m* (56 ppb Fe) contours, and the dashed lines are 10^{-4} *m* (5.6 ppm Fe) contours. The boundaries between aqueous species represent conditions where two species are equal in molar concentrations.



because of differential evaporation of water. This hideout process may generate a highly concentrated corrosive solution next to the heat transfer surface. Laboratory tests show that the high temperature pH values of the crevice solutions were slightly higher than or near the neutral point (pH 4–9), and the chloride concentrations were predicted to be in the range of 1–15 *m*. Under such conditions, it is obvious that the monochloroiron(II) complex is the predominant dissolved form of iron at or near 100°C (Fig. 13).

During reactor lay-up or shutdown, local boiling in areas of restricted flow will stop because of the temperature decrease along the heat transfer interface, and the "hidden" impurities will return back to the bulk system. This process may increase the concentrations of chloride and other anions substantially in the bulk water in some local areas; the predominant Fe(II) species in water may change from the free ion to the monochloroiron(II) complex ($FeCl^+$) and result in increased corrosion of the secondary heat transfer system due to complex formation (Fig. 13). However, it should be pointed out that this scenario does not appear to be supported by the station chemistry data. Even with the hideout return, the bulky secondary system is likely still sufficiently clean to prevent significant Fe(II)-chloride complex from forming.

Recently, Ziemniak et al. (14) showed that over a temperature range of 20–80°C, magnetite solubility was independent of the dissolved hydrogen level. They suggested that magnetite solubility behavior at low temperatures up to 83°C is controlled by a surface layer of hydrous Fe(II) oxide at a dissolved hydrogen concentration of 234 μ*m*; at a hydrogen partial pressure of 1 atm (1 atm = 101 325 Pa), this hydrous Fe(II) oxide is stable up to 116°C.

Assuming $Fe(OH)_2$(s) to be the controlling solid phase in steam generator systems at temperatures of 25–100°C, we plot Fe(II) solubilities as a function of chloride concentration and pH in Fig. 14. Comparing the two diagrams in Fig. 14, it is noticed that an increase in temperature from 25 to 100°C will actually moderately decrease the level of dissolved Fe(II) in solution over a wide range of pH and chloride concentration. For example, assuming dissolved chloride to be 5.0 *m* in solution and pH (at 25°C) to be 9.0,

© 2001 NRC Canada

the dissolved Fe(II) concentrations at 25 and 100°C are calculated to be 8.8 ppb and 0.36 ppb, respectively. However, if the chloride concentration gets sufficiently high so that the tetrachloroiron(II) complex becomes predominant, the formation of the tetrachloroiron(II) complex will greatly increase the solubility of Fe(II) hydroxide (Fig. 14). At 100°C and a pH of 8.0, an increase in chloride concentration from 0.0 *m* to 17.0 *m* will enhance the dissolved Fe(II) in solution from 0.89 to 93 ppb. Such a high chloride concentration is rare even at extreme conditions in crevices; it is used in the calculation to illustrate that when the tetrachloroiron(II) complex does form, its enhancement effect to iron dissolution is substantial. Such an enhancement effect is less of an issue at low temperatures (<100°C), but will be much more pronounced at higher temperatures, where the tetrachloroiron(II) complex forms at much lower chloride concentrations. It should be pointed out that these discussions are based on the assumption that the system is in chemical equilibrium. In reality, there may not be sufficient time for chemical equilibrium to be attained, and kinetics may play a vital role in the generator systems.

Conclusions

The stability constants of all Fe(II)-chloride complexes were derived from the measured UV and near-IR absorption spectra using a non-negative nonlinear least-squares computer program (SQUAD), with the activity coefficients of the ionic species calculated using both the Pitzer model and the Helgeson model. The results obtained with UV and near-IR spectra and with different activity coefficient calculation models are generally in good agreement. It was found that the Fe(II)-chloride complexes gradually undergo a configuration transformation from octahedral to tetrahedral coordination when the temperature and (or) chloride concentration increase. This coordination change is governed by mass balance, and driven by an increase in entropy.

At steam generator crevice conditions, the presence of high concentration of chloride ion will enhance the corrosion of carbon steel and other Fe-bearing alloys by forming Fe(II)-chloride complexes. The occurrence and predominance of the tetrachloroiron(II) complex at higher temperatures and chloride concentrations will further enhance the solubility of iron in steam generator systems. Further work at temperatures up to 300°C is required to fully assess the effect of Fe(II)-chloride complex formation on the corrosion of carbon steel and other Fe-bearing alloys under steam generator conditions, and is presently in progress.

Acknowledgments

We thank B.J. Balakrishnan and R.J. Lemire of AECL for their valuable comments and discussions. The work was partly funded by the AECL Underlying Chemistry Program.

References

1. D.A. Crerar and H.L. Barnes. Econ. Geol. **71**, 722 (1976).
2. D.A. Crerar, N.J. Susak, and M. Borcsik. Geochim. Cosmochim. Acta, **42**, 1427 (1978).
3. C.F. Wells and M.A. Salam. Trans. Faraday Soc. **63**, 620 (1967).
4. H. Po and N. Sutin. Inorg. Chem. **7**, 621 (1968).
5. S. Raman. J. Inorg. Nucl. Chem. **38**, 1741 (1976).
6. J.R. Ruaya. Geochim. Cosmochim. Acta, **52**, 1983 (1988).
7. K.G. Ashurst. The thermodynamics of the formation of chlorocomplexes of iron (III), cobalt (II), iron (II), manganese (II) and copper (II) in perchlorate medium. Natl. Inst. Metallurgy, Johannesburg, Report no. 1820 (1976).
8. L. Vincze, B. Kraut, and S. Papp. Inorg. Chim. Acta, **85**, 89 (1984).
9. R. Zhao. Ph.D. Thesis, University of Regina. 1997.
10. C.A. Heinrich and T.M. Seward. Geochim. Cosmochim. Acta, **54**, 2207 (1990).
11. N.J. Susak and D.A. Crerar. Geochim. Cosmochim. Acta, **49**, 555 (1985).
12. L. Vogel Koplitz, D.S. McClure, and D.A. Crerar. Inorg. Chem. **26**, 308 (1987).
13. D.A. Palmer and K.E. Hyde. Geochim. Cosmochim. Acta, **57**, 1393 (1993).
14. S.E. Ziemniak, M.E. Jones, and K.E.S. Combs. J. Solution Chem. **24**, 837 (1995).
15. K.E. Johnson and J.R. Dickinson. *In* Advances in molten salt chemistry. *Edited by* J. Braunstein, G. Mamantou, and G.P. Smith. Plenum Press, New York. 1973. pp. 83–192.
16. J.E. Huheey. Inorganic Chemistry. 3rd ed., Harper & Row Publishers, New York. 1983.
17. B.N. Figgis. Introduction to ligand fields. John Wiley & Sons, New York. 1966.
18. G. Winter. Aust. J. Chem. **21**, 2859 (1968).
19. J. Simonetti and D.S. McClure. J. Chem. Phys. **71**, 793 (1979).
20. S. Hirako and R. Onaka. J. Phys. Soc. Jpn. **47**, 1255 (1982).
21. H. Kanno and J. Hiraishi. J. Raman Spectrosc. **12**, 224 (1982).
22. M.J. Apted, G.A. Waychunas, and G.E. Brown. Geochim. Cosmochim. Acta, **49**, 2081 (1985).
23. D.J. Leggett. Anal. Chem. **49**, 276 (1977).
24. D.J. Leggett. Talanta, **30**, 579 (1983).
25. D.J. Leggett, S.L. Kelly, L.R. Shiue, Y.T. Wu, D. Chang, and K.M. Kadish. Talanta, **30**, 579 (1983).
26. D.J. Leggett. Computational methods for the determination of formation constants. CRC Press, Boston. 1985.
27. P. Pan and N.J. Susak. Geochim. Cosmochim. Acta, **53**, 327 (1989).
28. H.C. Helgeson. Am. J. Sci. **267**, 729 (1969).
29. A.S. Skibsted and J. Bjerrum. Acta Chem. Scand. A. **32**, 429 (1978).
30. T.W. Swaddle and L. Fabes. Can. J. Chem. **58**, 1418 (1980).
31. K.S. Pitzer. *In* Activity coefficients in electrolyte solutions. 2nd ed. *Edited by* K.S. Pitzer. CRC Press, Boston. 1991. pp. 75–153.
32. H.C. Helgeson, D.H. Kirkham, and G.C. Flowers. Am. J. Sci. **281**, 1249 (1981).
33. K.S. Pitzer. J. Phys. Chem. **77**, 268 (1973).
34. K.S. Pitzer and J.J. Kim. J. Am. Chem. Soc. **96**, 5701 (1974).
35. S.L. Clegg and M. Whitfield. *In* Activity coefficients in electrolyte solutions. 2nd ed. *Edited by* K.S. Pitzer. CRC Press, Boston. 1991. pp. 279–434.
36. H.H. Haung. J. Solution Chem. **18**, 1069 (1989).
37. D.G. Archer and P. Wang. J. Phys. Chem. Ref. Data, **19**, 371 (1990).
38. K.S. Pitzer. Acc. Chem. Res. **10**, 371 (1977).
39. D.R. Schreiber, J. Huebner, S. Rahmani, and F.J. Millero. J. Solution. Chem. **22**, 201 (1993).
40. P. Pan. Ph.D. Thesis, University of New Brunswick. 1989.
41. F.H. Sweeton and C.F. Baes. J. Chem. Thermodyn. **2**, 479 (1970).
42. P.R. Tremaine and J.C. LeBlanc. J. Solution Chem. **9**, 415 (1980).

© 2001 NRC Canada

Intervalence transfer in a new benzotriazolate bridged ruthenium–iron complex

Reginaldo C. Rocha and Henrique E. Toma

Abstract: The unsymmetrical dinuclear ruthenium–iron complexes $[(NH_3)_5Ru–bta–Fe(CN)_5]^n$ (where bta = benzotriazolate; n = –2, –1, 0) were prepared as solid sodium salts from $[Ru^{II}(NH_3)_5(bta)]^+$ or $[Ru^{III}(NH_3)_5(bta)]^{2+}$ and $[Fe^{II}(CN)_5(H_2O)]^{3–}$ and characterized in aqueous solution by means of electrochemical and spectroelectrochemical methods. UV-vis, near-infrared, IR, and cyclic and differential pulse voltammetry data suggest that the related mixed valent species belong to a valence trapped formulation, featuring localized Ru(III) and Fe(II) oxidation states. In spite of the class II categorization in the Robin and Day scheme, this system shows a remarkable metal–metal electronic coupling, as deduced from an intense, low-energy, and very broad intervalence band in the near-IR region. In addition, the mixed valence state displays enhanced stabilization in relation to the isovalent state. The intervalence transfer properties are discussed on the basis of Hush's theory.

Key words: ammineruthenium complexes, cyanoiron complexes, mixed valence, intervalence, benzotriazole, benzotriazolate.

Résumé : En faisant réagir $[Ru(II)(NH_3)_5(bta)]^+$ ou $[Ru(III)(NH_3)_5(bta)]^{2+}$ avec $[Fe(II)(CN)_5(H_2O)]^{3–}$, on a obtenu les complexes dinucléaires, non symétriques, de ruthénium–fer $[(NH_3)_5Ru\text{-}bta\text{-}Fe(CN)_5]^n$ (dans lesquels bta = benzotriazolate; n = –2, –1, 0) et on les a caractérisés par des méthodes électrochimiques et spectroélectrochimiques. Les spectres UV-vis, IR et proche IR et les données de voltampérométrie pulsée différentielle suggère que l'espèce apparentée à valences mixtes appartient à une formulation piégée de valence typique caractérisée par des états d'oxydation localisés pour le Ru(III) et le Fe(II). En dépit d'une caractérisation comme classe II dans le schéma de Robin et Day, ce système présente un couplage électronique métal-métal remarquable sur la base d'une bande d'intervalence intense, de faible énergie et très large dans la région du proche infrarouge. De plus, son état de valence mixte présente une grande stabilisation par rapport aux états isovalents. On discute des propriétés de transfert intervalence en se basant sur la théorie de Hush.

Mots clés : complexes ammineruthénium, complexe cyanofer, valence mixte, intervalence, benzotriazole, benzotriazolate.

[Traduit par la Rédaction]

Introduction

Dinuclear mixed valency complexes (1) have been extensively studied (2–4) due to their importance as simple models for inter and (or) intramolecular electron transfer related processes (5–9). One approach, in order to verify the electronic coupling parameters in such systems as a function of their donor-acceptor configuration, can be performed by conveniently choosing the nature of the metal and (or) ancillary ligands of each moiety, i.e., by designing unsymmetrical systems. This is one of the reasons why an enormous variety of synthetic heteronuclear bi, tri, and polymetallic complexes have been reported in the literature (1–4, 10–33).

Dinuclear complexes based on the Ru^{III}/Ru^{II} (2, 3, 14, 34) and (or) Fe^{III}/Fe^{II} (2, 35–39) couples have played a central role in the study of mixed valence chemistry because of their rich and versatile redox chemistry, in association with their d^5/d^6 configuration. They also present favorable kinetic properties and are thermodynamically stable. The similarity between the pentacyanoferrate(II)/(III) and pentaammineruthenium(II)/(III) moieties (35), has been exploited in the study of the mixed valence chemistry of the neutral heterodinuclear $(NH_3)_5Ru^{III}(pz)Fe^{II}(CN)_5$ complex (where pz = pyrazine) (40, 41).

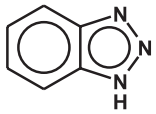
Aromatic *N*-heterocycles, on the other hand, have proven to be suitable ligands and bridging groups in coordination chemistry (42–44). The triazole derivatives, for instance, have been largely studied in ruthenium and osmium chemistry of discrete compounds or supermolecules (19, 45–52). In particular, benzotriazole (btaH) which is a *N*-heterocyclic species exhibiting three vicinal coordinating N-atoms for the formation of mono and dinuclear complexes with transition metal ions. In addition, btaH has been employed as an efficient corrosion inhibitor for copper and its alloys (53) and provides an interesting model species in bioinorganic chemistry. Nevertheless, except for an investigation on the linkage isomerism in $[Fe^{II,III}(CN)_5]^{3–/2–}$ (54) and $[Ru^{II,III}(NH_3)_5]^{2+/3+}$ (55) complexes, the coordination chemistry of benzotriazole with first- or second-row transition metals has not been readily explored up to the present time.

Received July 17, 2000. Published on the NRC Research Press Web site on March 9, 2001.

R.C. Rocha and H.E. Toma.[1] Instituto de Química, Universidade de São Paulo, Caixa Postal 26077, CEP 05513–970, São Paulo, SP, Brazil.

[1]Corresponding author (telephone: +55-11-38183887; fax: +55-11-38155579; e-mail address: henetoma@iq.usp.br).

 DOI: 10.1139/cjc-79-2-145 © 2001 NRC Canada



benzotriazole
(**btaH**)

In order to improve the understanding of electronic interactions and intervalence transfer in benzotriazole ruthenium-ammine and iron-cyano complexes, we carried out a detailed investigation on the novel unsymmetrical dinuclear species $[(NH_3)_5Ru(bta)Fe(CN)_5]^n$ (n = –2, –1, or 0 for the fully reduced [II,II], mixed valent [III,II], and isovalent oxidized [III,III] species, respectively). Analogous to the pyrazine derivative (40), the mixed valent molecule exhibited the $Ru^{III}Fe^{II}$ oxidation states for its individual acceptor–donor metal centers, whose formulation was based on electrochemical and spectroscopic investigations for the starting mononuclear and dinuclear complexes. To our surprise, this species showed an unusually strong metal–metal electronic communication, through the benzotriazolate bridging ligand, in comparison with other similar complexes in the $[(NH_3)_5Ru(L)Fe(CN)_5]^n$ series (e.g., L = pyrazine (40, 41), 4,4′-bipyridine (41), cyanide (56), 1,2-bis(4-pyridyl)ethane (57), pyridinecarboxamido (58), imidazolate (59), 4- and 3-cyanopyridine (60), and 4,4′-dipyridylamine (61)). However, analysis of the intervalence band parameters, in light of the Hush formalism (62–64) and the Robin–Day classification (2, 3, 65), revealed that the $[(NH_3)_5Ru^{III}(bta)Fe^{II}(CN)_5]^-$ complex possesses localized charges and is categorized as a valence trapped class II system.

Experimental

Syntheses and preparation of compounds

Starting materials

$[Ru(NH_3)_6]Cl_3$ (Johnson Matthey; recrystallized), $Na_2[Fe(CN)_5(NO)]\cdot 2H_2O$ (J.T.Baker). All other chemicals and organic solvents employed in the syntheses were analytical reagent grade (Aldrich, J.T.Baker, Merck, or Sigma) and were used without further purification. High purity, deoxygenated water was used through out the experiments. Deionized water was obtained by passing distilled water through a Nanopure (Barnstead) purification system.

btaH/bta⁻ ligands

Benzotriazole (btaH) was purchased from Aldrich and recrystallized from ethanol/water. The lithium benzotriazolate [Li(bta)] salt was prepared by mixing equimolar amounts of btaH and lithium hydroxide, followed by slow evaporation to dryness at room temperature. The UV spectra of the neutral ligand and its corresponding deprotonated anion, in aqueous solutions, gave absorption bands as follows λ (nm) (ε (mol^{-1} dm^3 cm^{-1})): btaH, 257 (4560), 274 (3800, sh); bta^-, 273 (6990). The pK_a values, to be used in this work, for the benzotriazole free ligand were extracted from literature (66): 1.17 ($btaH_2^+$/btaH) and 8.38 ± 0.03 (btaH/bta^-).

$[Ru(NH_3)_5Cl]Cl_2$

The preparation of pentaammine(chloro)ruthenium(III) chloride was based on the classical literature procedure (67).

$Na_3[Fe(CN)_5(NH_3)]\cdot 3H_2O$

The sodium amminepentacyanoferrate(II) complex was prepared as previously described (68). Anal. calcd. for $C_5H_9N_6O_3FeNa_3$ (MW = 326.0): C 18.42, H 2.78, N 25.78; found: C 18.25, H 2.93, N 25.92.

$[Ru^{II}(NH_3)_5(btaH)](PF_6)_2\cdot 3H_2O$

$[Ru(NH_3)_5Cl]Cl_2$ (58.6 mg, 0.2 mmol) was dissolved in water (5 mL) and reduced for 30 min with zinc amalgam, under an argon atmosphere. Then the solution was transferred by syringe techniques or via Teflon® tubing to a recipient containing benzotriazole (238.2 mg, 2.0 mmol). The orange solution was treated with concentrated solution of ammonium hexafluorophosphate (5 mL) yielding a yellow precipitate. The solid product was collected on a filter, washed with a small volume of ethanol and dried in vacuum in the presence of anhyd calcium chloride. Yield: 85–90%. Anal. calcd. for $C_6H_{26}F_{12}N_8O_3P_2Ru$ (MW = 649.3): C 11.10, H 4.04, N 17.26; found: C 10.95, H 4.11, N 17.04.

$[Ru^{III}(NH_3)_5(btaH)](PF_6)_3\cdot 2H_2O$

The yellow $[Ru(NH_3)_5(btaH)](PF_6)_2$ solid (prepared as described above) was redissolved in water and completely oxidized by passing a flow of O_2 gas through the solution. The reddish product was isolated from the slow evaporation of a concentrated solution with excess of NH_4PF_6. Anal. calcd. for $C_6H_{24}F_{18}N_8O_2P_3Ru$ (MW = 776.3): C 9.28, H 3.12, N 14.43; found: C 9.39, H 3.24, N 14.47.

$Na_3[Fe^{II}(CN)_5(btaH)]\cdot 3H_2O$

The mononuclear iron complex was prepared similarly to the published procedure (54). $Na_3[Fe(CN)_5(NH_3)]\cdot 3H_2O$ (326.0 mg, 1.0 mmol) was added to a deoxygenated H_2O/ethanol (3:1) solution (20 mL) containing benzotriazole (178.7 mg, 1.5 mmol). After ~20 min, the yellow mixture was evaporated under vacuum to a volume of 3–5 mL. Then, cold acetone (15 mL) was dripped on the solution. The solid was collected by filtration, washed with a mixture acetone/ethanol (2:1) and dried under vacuum in the presence of anhyd calcium chloride. Yield: 80–85%. Anal. calcd. for $C_{11}H_{11}N_8O_3FeNa_3$ (MW = 428.1): C 30.86, H 2.59, N 26.18; found: C 30.93, H 2.66, N 26.13.

$Na_2[(NH_3)_5Ru^{II}(bta)Fe^{II}(CN)_5]\cdot 4H_2O$

The fully reduced dinuclear compound was obtained by adding $Na_3[Fe(CN)_5(NH_3)]\cdot 3H_2O$ (65.6 mg, 0.20 mmol) to 5.0 mL of an argon saturated, neutral solution of $[Ru(NH_3)_5(btaH)](PF_6)_2\cdot 3H_2O$ (129.6 mg, 0.20 mmol). The initially pale yellow mixture became immediately orange colored. After 30 min, cold deaerated ethanol/acetone (1:3) (20 mL) was added to the mixture and a dark yellow precipitate was formed. The solid was filtered off, washed with a cold ethanol/acetone (1:3) mixture and dried under vacuum over anhyd calcium chloride. Yield: 80–90%. Anal. calcd. for $C_{11}H_{27}N_{13}O_4FeNa_2Ru$ (MW = 608.3): C 21.72, H 4.47, N 29.93; found: C 21.65, H 4.64, N 29.96.

© 2001 NRC Canada

Alternatively, this dinuclear complex was freshly prepared and characterized in aqueous solution by means of spectroscopic and electrochemical methods, as described below.[2,3]

Cyclic voltammetry: In the electrochemical measurements the complex solution was obtained by adding $Na_3[Fe(CN)_5(NH_3)]\cdot 3H_2O$ (8.2 mg, 0.025 mmol) to 5.0 mL of a deaerated 0.05 mol dm^{-3} acetate buffer solution (pH 4.7) containing $[Ru(NH_3)_5(btaH)](PF_6)_2\cdot 3H_2O$ (16.2 mg, 0.025 mmol). Then, the pH of the mixture was adjusted to 8.8–9.0 through the controlled addition of 3.0 mol dm^{-3} sodium hydroxide solution.

Spectroelectrochemistry: In the spectroelectrochemical measurements, the complex was also prepared according to the above procedure. However, it used $Na_3[Fe(CN)_5(NH_3)]\cdot 3H_2O$ (18.4 mg, 0.050 mmol) and $[Ru(NH_3)_5(btaH)](PF_6)_3\cdot 3H_2O$ (32.5 mg, 0.050 mmol) instead. In order to avoid/minimize the electronic absorption by water in the near-IR region of the spectra, D_2O was employed as solvent.

Sodium trifluoroacetate (NaTFA) and potassium nitrate (both 0.25 mol dm^{-3}) were employed as supporting electrolytes in the cyclic voltammetry and spectroelectrochemical measurements, respectively.

$Na[(NH_3)_5Ru^{III}(bta)Fe^{II}(CN)_5]\cdot 5H_2O$ [4]

The mixed valent dinuclear complex was prepared by two different methods: (*a*) by mixing equimolar amounts (0.20 mmol) of $Na_3[Fe^{II}(CN)_5(NH_3)]\cdot 3H_2O$ and $[Ru^{III}(NH_3)_5(btaH)](PF_6)_3\cdot 2H_2O$ in neutral aqueous solutions, under argon; (*b*) by treating a solution of $Na_2[(NH_3)_5Ru^{II}(bta)Fe^{II}(CN)_5]\cdot 4H_2O$ with 1 equiv of sodium peroxydisulfate. In both cases, further handling of the brownish product was carried out in the same way as for the reduced complex. Yield: 85–90%. Anal. calcd. for $C_{11}H_{29}N_{13}O_5FeNaRu$ (MW = 603.3): C 21.90, H 4.84, N 30.18; found: C 21.99, H 5.02, N 30.20.

$(NH_3)_5Ru^{III}(bta)Fe^{III}(CN)_5\cdot 6H_2O$ [4]

The fully oxidized neutral compound was obtained by adding excess (about 3 equiv) of $Na_2S_2O_8$ to the $Na[(NH_3)_5Ru^{III}(bta)Fe^{II}(CN)_5]\cdot 5H_2O$ complex (0.2 mmol) in water (5 mL). After reacting, the resulting violet solution was cooled to 0°C and left in the ice bath for 30 min. Then, the precipitate was handled as before. Yield: 75–80%. Anal. calcd. for $C_{11}H_{31}N_{13}O_6FeRu$ (MW = 598.4): C 22.08, H 5.22, N 30.43; found: C 21.95, H 5.40, N 30.33.

Instrumentation and methods

The electronic spectra in the ultraviolet–visible (UV–vis) and near-infrared (near-IR) regions were recorded on a Hewlett-Packard model 8453 diode-array spectrophotometer (1 cm or 0.025 cm quartz cells) and on a Guided-Wave model 260 fiber-optics instrument (adjustable optical path length; measured by reflectance), respectively.

Cyclic and differential pulse voltammetry measurements were carried out by using a Princeton Applied Research–PAR model 283 potentiostat (from EG&G Instruments, Inc.). A conventional three-electrode arrangement was employed in the measurements; it consists of a glassy carbon working electrode, a Luggin capillary with Ag/AgCl (KCl 1.0 mol dm^{-3}) reference electrode ($E°$ = 0.222 V vs. SHE), and a platinum wire as the auxiliary electrode, in aqueous solutions containing sodium trifluoroacetate (NaTFA) or potassium nitrate (0.10 or 0.25 mol dm^{-3}) as supporting electrolyte. All solutions were thoroughly degassed with argon prior to beginning the experiments, and before each measurement the solutions were purged with argon gas. Working electrodes were polished by using alumina paste (Struers). All potential values in this paper are uncorrected for junction potentials and given in V vs. standard hydrogen electrode (SHE).

Spectroelectrochemical measurements in the UV–vis region were carried out with a Princeton Applied Research–PAR model 173 potentiostat or a model 366 bi-potentiostat in parallel with the diode-array spectrophotometer. A three-electrode system was designed for a rectangular quartz cell of 0.025 cm internal optical path length (69). A gold minigrid was used as a transparent working electrode, in the presence of a small Ag/AgCl reference electrode and a platinum auxiliary electrode. The cell was located directly in the spectrophotometer, and the absorption change was monitored during the electrolysis.

Spectroelectrochemistry measurements in the near-IR region were performed by using a fiber-optic probe for in situ measurements in a specially designed quartz, flat bottom electrochemical cell, as used in earlier works (70, 71). In this case, the fiber-optic probe was placed perpendicular to the mirror surface of the platinum electrode, which was kept approximately 0.020 cm from the bottom, providing a constant optical pathlength. This cell was then filled with the D_2O solution.

The vibrational spectra of the solid dinuclear compounds in KBr pellets were measured with a Shimadzu model 8300 Fourier Transform infrared (FT-IR) spectrophotometer.

The pK_a evaluations were made by means of electrochemical measurements as a function of pH. A cell was specially designed in order to combine simultaneous pH measurements with cyclic voltammetry. pH measurements were carried out with a MD21 digital pH meter from Digimed Ltd. Calibration of the pH meter was performed using pH 4.00, 7.00 and 10.00 commercial standard buffers, at 25°C.

Elemental analyses were conducted by Analytical Center Laboratory of the Instituto de Química, Universidade de São Paulo.

Molecular mechanics calculations were performed by using the MM+ module, a modified MM2 force field (72) within the HyperChem 5.1 program (Hypercube, Inc., Gainesville, Florida, U.S.A., 1999). Geometry optimizations were carried out with a gradient of 1×10^{-5} kcal $Å^{-1}$ mol^{-1}

[2] The freshly prepared solutions from either the isolated solid or directly from the mixture of the starting mononuclear complexes show identical cyclic voltammograms and electronic spectra.

[3] All prolong-time measurements involving the photo-sensitive $[Fe(CN)_5]^{2-/3-}$ derivatives were run in the absence of light. This procedure avoids further substitution processes involving the cyanide ligands.

[4] This oxidized complex was also generated by electrolysis (vide infra). In both chemical and electrochemical synthetical procedures, the same electronic spectrum was obtained, as well as cyclic voltammogram for their corresponding solutions of the complex.

© 2001 NRC Canada

Table 1. Comparison of pK_a, electrochemical and spectroscopic parameters for the starting and the mononuclear complexes.

Compound	pK_a [a] (ref.)	$E_{1/2}$ (V) [b] (ref.)	LMCT (nm) (ref.)	MLCT (nm) (ref.)
$[Fe^{III}(CN)_5(NH_3)]^{2-}$	—	0.33 (73)	372 (800)[c] (74) 394 (700)[d] (74)	—
$[Fe^{II}(CN)_5(NH_3)]^{3-}$	—	0.33 (73)	—	230 (1×10^4; sh)[e] (75) 398 (450)[f] (75)
$[Fe^{III}(CN)_5(H_2O)]^{2-}$	—	0.39 (76)	340 (750)[c] (76) 394 (750)[d] (76)	—
$[Fe^{II}(CN)_5(H_2O)]^{3-}$	—	0.39 (76)	—	442 (640)[f] (76)
$[Ru^{III}(NH_3)_5(H_2O)]^{3+}$	4.2 (77)	0.066 (78)	268 (760) (79)	—
$[Ru^{II}(NH_3)_5(H_2O)]^{2+}$	10.7 (77)	0.066 (78)	—	295 (1830)
$[Ru^{III}(NH_3)_5(Cl)]^{2+}$	—	–0.042 (78)	328 (1860) (79)	—
$[Ru^{II}(NH_3)_5(Cl)]^{+}$	—	–0.042 (78)	—	270 (900) (80)
$[Ru^{III}(NH_3)_5(btaH)]^{3+}$	4.3 [g]	0.210	337 (660)[h] 448 (360)[i]	—
$[Ru^{III}(NH_3)_5(bta)]^{2+}$	—	0.025	315 (3650 sh)[h] 467 (2060)[i]	—
$[Ru^{II}(NH_3)_5(btaH)]^{2+}$	8.3 [g]	0.210	—	410 (11310)
$[Ru^{II}(NH_3)_5(bta)]^{+}$	—	0.025	—	389 (7760)
$[Fe^{III}(CN)_5(btaH)]^{2-}$	6.3 [g]	0.420	365 (1170)[d] 396 (875 sh)[h] 487 (1020)[i]	—
$[Fe^{III}(CN)_5(bta)]^{3-}$	—	0.215	365 (990)[d] 392 (840 sh)[h] 582 (2180)[i]	—
$[Fe^{II}(CN)_5(btaH)]^{3-}$	9.6 [g]	0.420	—	388 (4440)
$[Fe^{II}(CN)_5(bta)]^{4-}$	—	0.215	—	350 (2100)

[a]The pK_a value for the neutral benzotriazole free ligand is 8.38 (ref. 66).
[b]Potential vs. SHE.
[c]$(NH_3)\sigma\rightarrow d_\pi(Fe^{III})$ transition.
[d]$(CN^-)\pi\rightarrow d_\pi(Fe^{III})$ transition; refs 59, 88, and 89.
[e]$(Fe^{II})d_\pi\rightarrow\pi^*(CN^-)$ transition.
[f]*d–d* transition.
[g]Electrochemically determined, in this work, by measuring potentials as a function of pH.
[h](L)$\pi_1\rightarrow d_\pi(M^{III})$ transition; where π_1 is the most external occupied π level of the benzotriazolate ligand.
[i](L)$\pi_2\rightarrow d_\pi(M^{III})$ transition.

as a convergence criterion, in a conjugate gradient algorithm. The calculations were processed on a PC Windows platform with a Pentium III microprocessor.

Results and discussion

Mononuclear complexes

In spite of our emphasis on the mixed valent complex, we found it necessary to characterize some aspects of the mononuclear species in order to understand the properties of the dinuclear complexes. Although their properties are partially reported elsewhere (54, 55), the relevant data are summarized in Table 1 along with, for comparison purposes only, the data concerning the starting materials (73–80).

Dinuclear complexes $[(NH_3)_5Ru(bta)Fe(CN)_5]^n$ (n = –2, –1, or 0)

In aqueous solution, the amminepentacyanoferrate(II) ion ($[Fe(CN)_5(NH_3)]^{3-}$) undergoes substitution of NH_3 to form the corresponding aquacomplex, $[Fe(CN)_5(H_2O)]^{3-}$ (81) which, in turn, readily reacts with *N*-heterocyclic ligands (36). The reaction of $[Ru^{II}(NH_3)_5(bta)]^+$ and $[Fe^{II}(CN)_5(NH_3)]^{3-}$ (equimolar ratio) in aqueous solution at pH ~ 9.0, under an argon atmosphere, produced an orange color complex, analogous to the one isolated in the solid form (the reaction of oxidized $[Ru^{III}(NH_3)_5(bta)]^{2+}$ and reduced $[Fe^{II}(CN)_5(NH_3)]^{3-}$ species was also followed at pH 6.0, generating a brownish product; see Experimental section). It is worthy to note that, at the experimental pH, deprotonation of the monocoordinated benzotriazole takes place (Table 1), making binding of this species to the cyanoiron(II) unit (from the $[Fe(CN)_5(H_2O)]^{3-}$ ion) possible.

The cyclic and differential pulse voltammograms of this new species exhibit two well-defined reduction processes at E_1 = 0.390 V and E_2 = –0.090 V vs. SHE (Fig. 1), providing the first piece of evidence for the formation of the new unsymmetrical dinuclear complex, $[(NH_3)_5Ru(bta)Fe(CN)_5]^{2-}$. Another important indication of its existence is the presence of a strong electronic absorption band in the NIR region after the addition of 1 equiv of a chemical oxidant (i.e., peroxydisulfate), which is consistent with the generation of the mixed valent species, $[(NH_3)_5Ru^{III}(bta)Fe^{II}(CN)_5]^-$. The formulation of the Ru(III) and Fe(II) oxidation states was initially based on comparison of the reduction potentials, E_1 and E_2, of the Fe^{III}/Fe^{II} and Ru^{III}/Ru^{II} redox couples, respectively, in the starting mononuclear complexes (Table 1). This

© 2001 NRC Canada

Fig. 1. Cyclic voltammograms (*a*) and differential pulse voltammogram (*b*) of the $[(NH_3)_5Ru(bta)Fe(CN)_5]^-$ complex in an aqueous solution (C = 5.0 × 10^{-3} mol dm^{-3}; I = NaTFA 0.25 mol dm^{-3}; pH 6.5). (DPV working conditions: pulse height = 0.025 V; pulse width = 0.005 s; scan rate = 100 mV s^{-1}; step/droptime = 0.020 s).

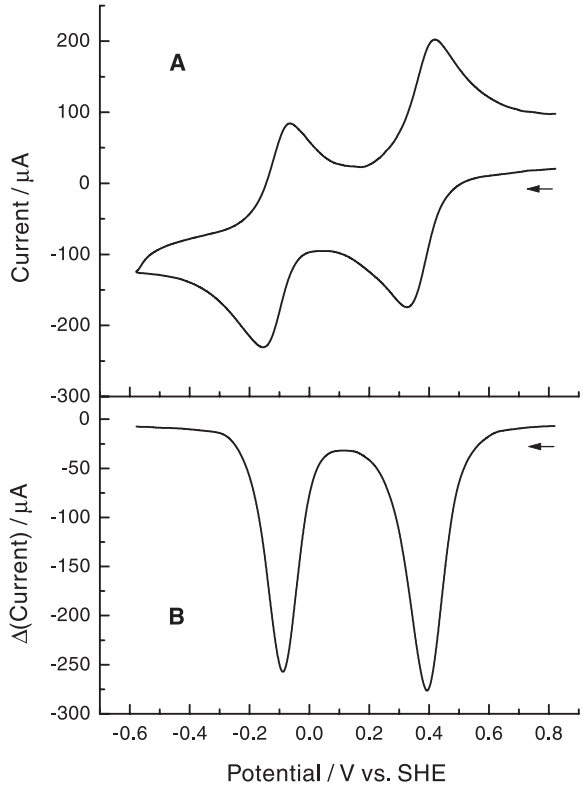
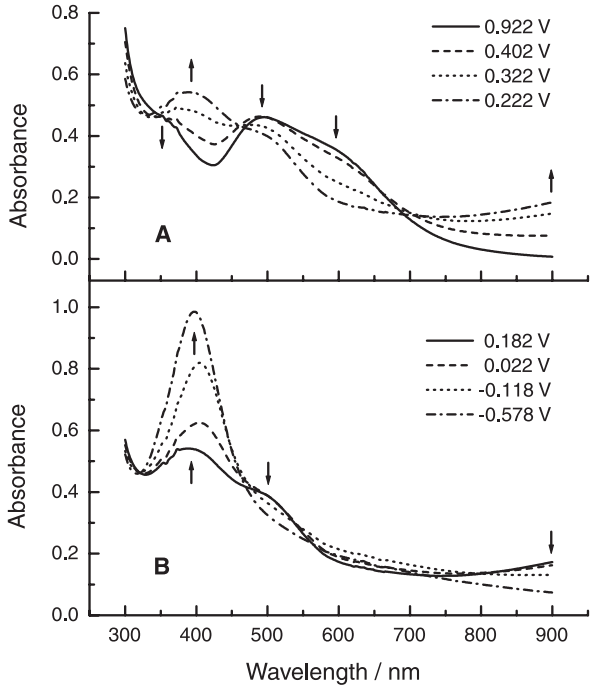


Fig. 2. Electronic spectra of the $[(NH_3)_5Ru(bta)Fe(CN)_5]^n$ complexes (n = –2, –1, 0) under application of potentials (C = 5.0 × 10^{-3} mol dm^{-3}; l = 0.025 cm; I = NaTFA 0.25 mol dm^{-3}; pH 6.5; applied potentials vs. SHE are indicated in the figure).



type of assignment must take into account an important feature of Fe–L–Ru related complexes, since their oxidation states can be formulated as Fe^{II}–Ru^{III} (as is the case in the majority of the literature examples (40, 41, 56–59, 61)), Fe^{III}–Ru^{II} (60), or even a mixture of both electronic isomers (60). In order to give support for the preliminary assignment simply from their potentials analysis, infrared spectra (see below) and UV–vis spectroelectrochemical (Fig. 2) measurements were carried out.

As reported before (40), comparison among the infrared spectra of the three dinuclear complexes (reduced isovalent [II,II], oxidized isovalent [III,III], and mixed valent [II,III] species) shows that they are nearly the same, except for the CN^- and NH_3 absorption bands. It is known (82) that the frequencies associated with the vibrations of the CN^- and NH_3 groups depend on the nature and charge of the metal ions to which they are coordinated. The symmetric deformation and rocking vibrational modes of the coordinated NH_3 group occur at frequencies which usually increase with the oxidation state and electronegativity of the central ion in the complex (83, 84). For ruthenium hexaammines in the II and III oxidation states, they appear at 1220 and 769 cm^{-1} (85) and 1316–1362 and 788 cm^{-1} (86), respectively. Therefore, the observed shifts from 1263 cm^{-1} ($\delta_{NH_3(sym)}$; strong) and 754 cm^{-1} (ρ_{NH_3}; medium) in the totally reduced (II,II) complex to 1308 cm^{-1} (s) and 795 cm^{-1} (m) in the mixed valent (II,III) complex are indicative of the oxidation of the ruthenium(II) center. This hypothesis is corroborated by the fact that practically no changes were observed in these bands from the mixed valent to the completely oxidized (III,III) species (1315 cm^{-1} (s) and 804 cm^{-1} (m)).

The cyanide stretching frequency (ν_{CN}), however, is seen at 2055 cm^{-1} (s) for both the (II,II) and (II,III) species and is diagnostic of cyanoferrate(II) complexes (82, 87). In the case of cyanoiron(III) complexes the cyanide stretching frequency is usually observed in the 2100–2150 cm^{-1} region, which is in accordance with the absorption for the fully oxidized [III,III] species (2117 cm^{-1} (s) and 2161 cm^{-1} (m)). These results, therefore, agree with a valence trapped system in which the oxidized acceptor center is mainly localized on the ruthenium ammine moiety.

The UV–vis electronic spectra of the oxidized isovalent complex (Ru^{III}-bta-Fe^{III}) (generated at potentials higher than 0.4 V; Fig. 2*a*) show two absorption bands at 495 nm (3700 mol^{-1} dm^3 cm^{-1}) and 590 nm (sh; 2800 mol^{-1} dm^3 cm^{-1}). These bands were assigned to the ligand-to-metal charge transfer (LMCT) transitions involving the ruthenium and iron centers, i.e., $\{bta^-\}\pi \rightarrow d_\pi\{Ru^{III}(NH_3)_5\}$ and $\{bta^-\}\pi \rightarrow d_\pi\{Fe^{III}(CN)_5\}$. The analogous bands for the mononuclear complexes occur at 467 nm (2060 mol^{-1} dm^3 cm^{-1}) and 582 nm (2180 mol^{-1} dm^3 cm^{-1}), respectively (Table 1). The fact that the LMCT transition to Fe(III) appears at lower energy with respect to the one centered on Ru(III) is consistent with the stronger oxidizing ability of iron. A shoulder is also seen around 360 nm and can be tentatively assigned to a $(CN^-) \rightarrow d_\pi(Fe^{III})$ LMCT transition (59, 88, 89).

When the mixed valent species (Ru^{III}-bta-Fe^{II}) is electrolytically produced by applying potentials between E_1 and E_2 (Fig. 1), two bands can be seen in the spectra (Figs. 2*a* and

© 2001 NRC Canada

Table 2. Some electrochemical, spectroscopic, and mixed valence parameters for a series of unsymmetrical $[(NH_3)_5Ru^{III}–L_b–Fe^{II}(CN)_5]^n$ dinuclear complexes.

L_b	$E_{1/2}(1)$ [a] (V) [c]	$E_{1/2}(2)$ [b] (V) [c]	$\Delta E_{1/2}$ [d] (V)	K_c [d]	λ_{max} (nm)	ε_{max} (mol^{-1} dm^3 cm^{-1})	$\Delta\nu_{1/2}$ (exp) (cm^{-1})	$\Delta\nu_{1/2}$ (calc) (cm^{-1})	H_{ab} (cm^{-1})	α^2 ($\times 10^3$)	Ref.
1	0.72	0.49	0.23	7.7×10^3	1650	1550	4300	3700	600	9.8	41
2	0.64	0.31	0.33	3.8×10^5	—	—	—	—	—	—	41
3	—	—	—	—	1020	3000	—	4900	1500	22	56
4	0.44	0.29	0.15	3.4×10^2	—	—	—	—	—	—	57
5	—	—	—	—	645	570	5100	5100	480	9.5	58
6	0.30	–0.20	0.50	2.8×10^8	979	962	5000	4100	756	5.4	59
7[e]	0.66 [b]	0.50 [a]	0.16	5.0×10^2	938	850	3900	4900	410	1.5	60
8[e]	0.60 [b]	0.53 [a]	~0.07	~15	—	—	—	—	—	—	60
9	0.44	0.17	0.27	3.9×10^4	725	600	5400	5400	500	1.3	61
10	0.390	–0.090	0.480	1.30×10^8	1210	3900	6500	4370	1675	41	This work

Note: The bridging ligand (L_b) is given in the Table as: **1** = pyrazine; **2** = 4,4′-bipyridine, **3** = cyanide, **4** = 1,2-bis(4-pyridyl)ethane, **5** = pyridinecarboxamido, **6** = imidazolate, **7** = 4-cyanopyridine, **8** = 3-cyanopyridine, **9** = 4,4′-dipyridilamine, and **10** = benzotriazolate.

[a]Refers to the iron(III/II) couple.

[b]Refers to the ruthenium(III/II) couple.

[c]Potential vs. SHE.

[d]Unsymmetrical system; the redox separation and the corresponding global ΔG_c does not reflect the stabilization by electron delocalization, since there is an intrinsic $\Delta E_{1/2}$ between the redox potentials associated to the non-equivalent ammineruthenium and cyanoiron moieties (see details in the text).

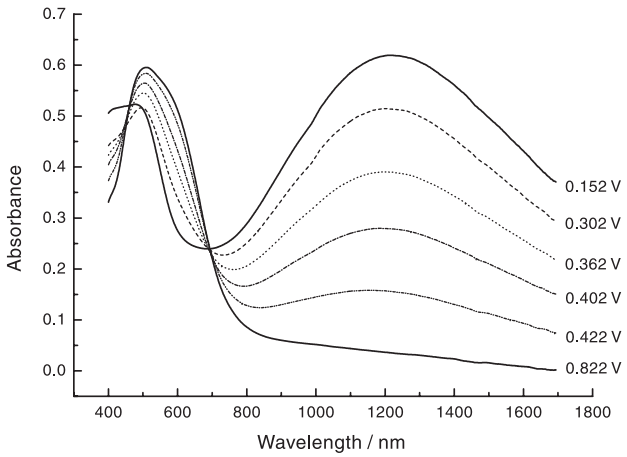
[e]The oxidation states for the mixed valent complex were proposed according to the Ru^{II}–Fe^{III} formulation.

2*b*): one around 500 nm, which refers to the already mentioned LMCT involving the $\{Ru^{III}(NH_3)_5\}$ moiety; and a new one that appears at 390 nm (4300 mol^{-1} dm^3 cm^{-1}), corresponding to the metal-to-ligand charge transfer (MLCT) transition on the iron unit, $\{Fe^{II}(CN)_5\}d_\pi \rightarrow \pi^*\{bta^-\}$. In the mononuclear cyanoiron complex, an analogous band was observed at 350 nm (2100 mol^{-1} dm^3 cm^{-1}) and 388 nm (4440 mol^{-1} dm^3 cm^{-1}) for the deprotonated and protonated species, respectively, reflecting the π-acceptor effect of the ruthenium(III) moiety to the iron(II) π-donor center in the mixed valent dinuclear complex. This comparison suggests that the hydrogen ion (H^+) and the $[Ru^{III}(NH_3)_5]^{3+}$ fragment exert similar electronic effects when bound to the benzotriazolate ligand in $[Fe^{II}(CN)_5(bta)]^{4-}$, since the MLCT energy in the mixed valent Ru^{III}-Fe^{II} species and the reduction potential for the Ru^{III}-$Fe^{III/II}$ couple are close to those observed in the protonated $[Fe(CN)_5(btaH)]^{3-}$ monomer (Table 1).

With potentials below 0 V vs. SHE, the completely reduced species Ru^{II}-bta-Fe^{II} is generated and the spectra (Fig. 2*b*) show only an intense (7800 mol^{-1} dm^3 cm^{-1}) and broad band around 400 nm. In light of the corresponding bands in the mononuclear species at 389 and 350 nm, this envelope consists of both $Ru^{II} \rightarrow bta^-$ and $Fe^{II} \rightarrow bta^-$ MLCT transitions (Table 1).[5]

Based on the above discussion, the alternative formulation (Ru^{II}-Fe^{III}) can be ruled out, and the complex can be unambiguously identified as having the $[(NH_3)_5Ru^{III}(bta)Fe^{II}(CN)_5]^-$ configuration. In order to investigate the intervalence transfer (IT) related processes for this mixed valent species, a spectroelectrochemical study in the vis–near-IR region was performed (Fig. 3). The results confirm that the intense (ε = 3900 ± 200 mol^{-1} dm^3 cm^{-1})[6] and broad ($\Delta\nu_{1/2}$ = 6500 cm^{-1})[7] band at 1210 nm (or 8265 cm^{-1}) only occurs when the system is submitted to a potential between 0.4 and –0.1 V (Figs. 1 and 3, Table 2). The maximum absorption intensity is reached when the applied potential approaches 0.15 V vs. SHE (Fig. 3), which is the middle point between the two

Fig. 3. Spectroelectrochemistry of the dinuclear complex $[(NH_3)_5Ru(bta)Fe(CN)_5]^{n-}$ in a D_2O solution (C = 1.0 × 10^{-2} mol dm^{-3}; l = 0.016 ± 0.001 cm; I = KNO_3 0.25 mol dm^{-3}; pD 6.0; applied potentials vs. SHE are indicated in the figure).



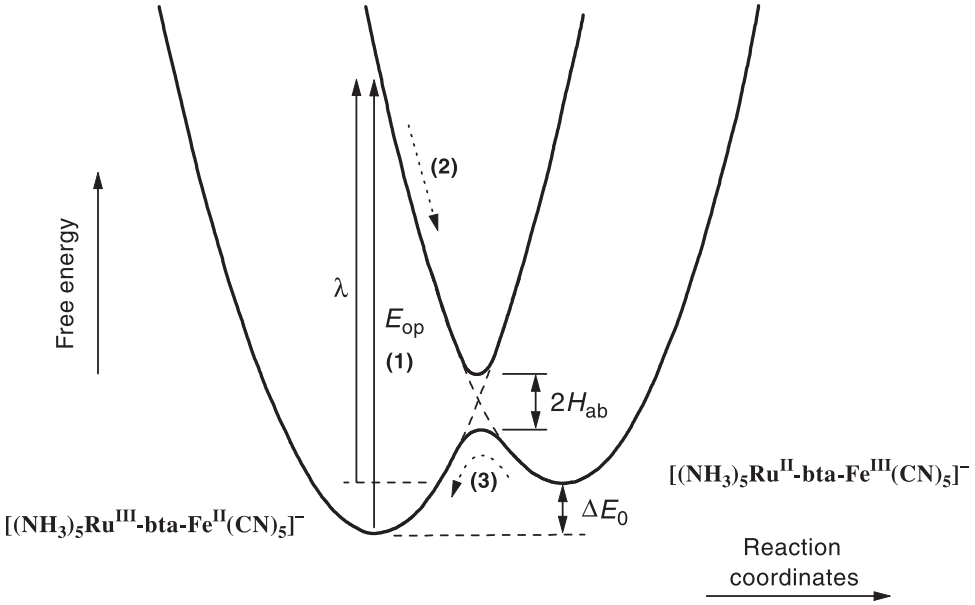
[5]In the spectroelectrochemical measurements, all species were practically 100% recovered.

[6]This uncertainty comes from the experimental error associated to the optical pathlength, which is not known and has to be indirectly determined through a standardized solution; see *Experimental* section for details on the employed reflectance apparatus.

[7]The near–IR absorption band was deconvoluted from the CT bands in the visible region by assuming that the IT transition results in a single symmetrical Gaussian band (spectrum in cm^{-1}) and no change in the vis-bands' profiles. Such deconvolution methods have already been discussed in details elsewhere (90).

© 2001 NRC Canada

Scheme 1.



reversible wave couples shown in the cyclic voltammograms (Fig. 1). Potential values above or below this point show that the absorptivity gradually decreases until the band completely disappears at the positive (>0.5 V) and negative (< – 0.2 V) extremes of the range. At these extremes the oxidized and reduced isovalent species should be fully generated (Fig. 1).[5]

The behavior described above clearly reveals the presence of an oxidized (acceptor) and another reduced (donor) site in the E_1 to E_2 range, whose observed low-energy band is consistent with a metal-metal charge transfer (MMCT) and is characteristic of mixed valence complexes (1–9). Therefore the two redox pairs established by the electrochemical data may be ascribed as follows:

[1*a*] $(NH_3)_5Ru^{III}-bta-Fe^{III}(CN)_5 \overset{E_1 = 0.390V}{\rightleftharpoons} [(NH_3)_5Ru^{III}-bta-Fe^{II}(CN)_5]^-$

[1*b*] $[(NH_3)_5Ru^{III}-bta-Fe^{III}(CN)_5]^- \overset{E_2 = -0.090V}{\rightleftharpoons} [(NH_3)_5Ru^{II}-bta-Fe^{II}(CN)_5]^{2-}$

In addition, the band at 1210 nm originates from the intervalence transition from the donor {$(CN)_5Fe^{II}$–} to the acceptor {–$Ru^{III}(NH_3)_5$} unit, as shown in eq. [2]:

[2] $[(NH_3)_5Ru^{III}(d\pi_3^1)-bta-(d\pi_3^2)Fe^{II}(CN)_5]^- \xrightarrow{h\nu} [(NH_3)_5Ru^{II}(d\pi_3^2)-bta-(d\pi_3^1)Fe^{III}(CN)_5]^-$

where $d\pi_3$ is the highest $d\pi$ energy level among the three nearly degenerated t_{2g}-type metal orbitals.

In a subsequent step an inverse electron transfer (ET) process, following a thermal path (eq. [3]), should take place (see representation in the diagram of Scheme 1) since the system is unsymmetrical and, at the equilibrium state, there is a driving force, ΔE_0, favoring the thermodynamically stable electronic isomer, $[(NH_3)_5Ru^{III}(bta)Fe^{II}(CN)_5]^-$.

[3] $[(NH_3)_5Ru^{II}(d\pi_3^2)-bta-(d\pi_3^1)Fe^{III}(CN)_5]^- \xrightarrow{\Delta, k_{th}} [(NH_3)_5Ru^{III}(d\pi_3^1)-bta-(d\pi_3^2)Fe^{II}(CN)_5]^-$

In Hush's model (2–9, 62–64), configurational-coordinate energy diagrams (or simply potential energy diagrams) have been used as a powerful tool (91) for describing light-induced electron transfer reactions, as shown in Scheme 1 for the unsymmetrical $[(NH_3)_5Ru(bta)Fe(CN)_5]^-$ ion. Thus, the energy of the IT transition (E_{op}) for this type of systems will equal the sum of λ, the reorganizational energy (i.e., Franck-Condon energy), and the ΔE_0 (where ΔE_0 is the difference in internal energy between the thermally equilibrated ion Ru^{III}-bta-Fe^{II} and its higher-energy redox isomer Ru^{II}-bta-Fe^{III}, which is the product of optical ET after having undergone vibrational and rotational relaxation). The meaning and magnitude of H_{ab}, the resonance energy between the reagent and product states at the curves intersection, will be explored below.

The thermodynamic stability of the mixed valent complex relative to the isovalent species can be estimated (92–94) from the comproportionation constant (K_c) associated with the equilibrium in eq. [4].

[4] $(NH_3)_5Ru^{III}-bta-Fe^{III}(CN)_5 + [(NH_3)_5Ru^{II}-bta-Fe^{II}(CN)_5]^{2-} \Downarrow K_c$

$2[(NH_3)_5Ru^{III}-bta-Fe^{II}(CN)_5]^-$

By assuming that $\Delta G_c = -RT\ln(K_c) = -nF(\Delta E_{1/2})$ for the comproportionation reaction, then K_c can be calculated (92, 93) based on the potential separation, where $\Delta E_{1/2} = |E_1 - E_2| =$ 480 mV. For $\Delta E_{1/2}$ given in mV, at 298 K, the expression for K_c becomes eq. [5].

© 2001 NRC Canada

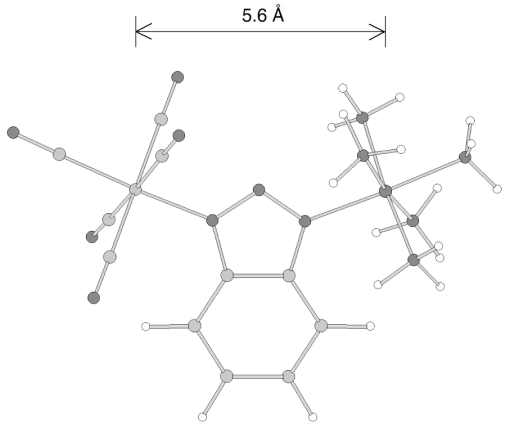
$$[5] \qquad K_c = \frac{[Ru^{III}Fe^{II}]^2}{[Ru^{III}Fe^{III}][Ru^{II}Fe^{II}]} = \exp\left(\frac{\Delta E_{1/2}}{25.69\ mV}\right)$$

The calculated value of K_c for this system was 1.30×10^8, giving a ΔG_c value of –11.1 kcal mol^{-1} (3870 cm^{-1}) (Table 2).[8] In spite of the high magnitude of the comproportionation constant, which is typical of complexes with relatively strong electronic coupling, it is important to remember that the system is not symmetric and there is an intrinsic ΔE associated with the difference of formal reduction potentials of the starting moieties ($E_{1/2}$ values for $[Ru(NH_3)_5(bta)]^{2+}$ and $[Fe(CN)_5(bta)]^{3-}$ are 0.025 and 0.215 V vs. SHE, respectively, in such a way that $\Delta E_{(mono)}$ = 190 mV). Thus the magnitude of ΔG_c is not totally related to the stabilization of the complex by electron delocalization at the mixed valence state (95–97).

In fact, the $\Delta E_{(mono)}$ value could be taken as rough approximation of ΔE_0,[9] which, in this case, would be near 0.19 eV (~1530 cm^{-1}) and refers to an approximation of $\Delta G°$ (2, 3), the driving force of the thermodynamically favorable ET reaction (see eq. [5] and Scheme 1), i.e., the released energy in the back electron transfer reaction $[(NH_3)_5Ru^{II}(bta)Fe^{III}(CN)_5]^- \rightarrow [(NH_3)_5Ru^{III}(bta)Fe^{II}(CN)_5]^-$. In addition, the Franck-Condon principle imposes that the optical (light-induced) intramolecular ET reaction occurs with $E_{op} = \nu_{max} = \lambda + \Delta E_0$ (2–9). Hence, within the limitation of this approach,[9] the reorganization energy (λ) was estimated as 6735 cm^{-1}, from the thermodynamic barrier (ΔE_0) and the IT absorption energy (ν_{max}).

Although some efforts have been made to determine the isolated contribution of delocalization energy in unsymmetrical systems (97–99), no theoretical treatment including a normalization of $\Delta E_{1/2}$ ($E_2 - E_1$ in the dinuclear species) as a function of the intrinsic difference of potential ($\delta(\Delta E)$) for the distinct starting moieties is known. As an approximation, however, in order to compare with the results from symmetrical mixed valence systems, $\Delta E_{(mono)}$ should be subtracted from $\Delta E_{1/2}$ (i.e., 480 – 190 mV), yielding an effective stabilization of 290 mV (from the monomers to the dimer). This resulting stabilization (referred here as $\Delta G'_c$) would contribute 2340 cm^{-1} to the comproportionation energy. Even so, it is important to recognize that this energy is a sum of, at least (97), four terms (2, 3, 95, 96): $\Delta G_{en} + \Delta G_{el} + \Delta G_s + \Delta G_d$, where ΔG_{en} is an entropic factor which reflects the statistical distribution of eq. [4] (evaluated as 1/2RT ln 1/4); ΔG_{el} is an electrostatic factor arising from the repulsion of the two charged metal centers joined by the bridge; ΔG_s is the synergistic factor, arising from the stabilization by charge transfer and outer-sphere donor effects; and ΔG_d (delocalization or resonance factor), is the stabilization energy component originating from the electron delocalization. For weakly coupled systems, the magnitude of ΔG_d can be estimated by $\Delta G_d = H_{ab}^2/\lambda$ (2, 3), from the Franck-Condon energy (λ) and the mixed valence resonance stabilization energy (H_{ab}) which can be extracted from the IT band parameters (see sections below).

Fig. 4. Molecular structure of the $[(NH_3)_5Ru(bta)Fe(CN)_5]^-$ complex, calculated by molecular mechanics geometry optimization.



In the bta-system, the calculated value of ΔG_d is 417 cm^{-1}. Considering that ΔG_d is generally ~ 1% (<20 mV) of H_{ab} in most class II reported cases (2–4), the obtained value (~25%) reflects a significant delocalization in this complex, even though it represents only about 50 mV of 340 mV corresponding to $\Delta G'_c$. This also means that the most of the comproportionation stabilization in the mixed valent dinuclear complex comes from the combined $(Fe^{II})d_\pi \rightarrow \pi_L^*$ and $\pi_L \rightarrow d_\pi(Ru^{III})$ charge-transfer and electrostatic effects.

Molecular structure

The molecular structure of the unsymmetrical dinuclear $[(NH_3)_5Ru(bta)Fe(CN)_5]^-$ complex, based on MM+ molecular mechanics geometry optimization calculations, is illustrated in Fig. 4. The two metal ions and the bridging ligand are located in the same plane, exhibiting a metal-metal distance of 5.6 Å.

In previous work involving the symmetrical $[\{Ru(edta)\}_2\text{-}\mu\text{–}L]^{4-}$ complexes (L = benzotriazolate or benzimidazolate) (70), we proposed that their contrasting IT properties could be partially explained by the fluxional coordination mode of the benzotriazolate one (54, 55, 100). Theoretical calculations revealed, however, that {Ru(edta)} terminal units offer a special situation where a steric vacancy (101) makes the metal-metal approximation through the benzotriazolate feasible to an intermediate binding position where the Ru–Ru distance should be shorter than the one resulting from the conventional N1–N3 coordination. On the other hand, in this system, this type of behavior is not expected due to the more sterically hindered structure associated with the rather larger pentacyano and pentaammine moieties. Thus, the unsymmetrical benzotriazolate derivative will have a metal–metal separation very close to that observed for the symmetrical

[8] The dimer investigated herein has sufficiently large $\Delta E_{1/2}$ value that corrections for comproportionation to the observed extinction coefficients (95, 96) were ignored.

[9] ΔE_0 has usually been obtained from the reduction potentials of model compounds or directly from $\Delta E_{1/2}$, the difference between the (III,III) and (III,II) reduction potentials of the dimer itself (where the electronic coupling is negligible). However, the latter method suffers from the fact that synergistic effects, stabilization of M(II) by M(III), electron delocalization, etc., cannot be appropriately assessed. In this way, it seems that, although the method adopted here does not provide an accurrate value of ΔE_0, it is more realistic for the type of investigated system than others.

© 2001 NRC Canada

benzimidazolate one, where the fluxional mechanism does not take place. Consequently, one can consider the ruthenium-iron distance as being slightly shorter than the one calculated for the edge-to-edge model, $[(NH_3)_5Ru\text{-}N1\text{-}bta\text{-}N3\text{-}Fe(CN)_5]^-$, i.e., 5.6 Å, whose value will be used as the ET ratio in the electronic coupling evaluation (see next section).

Intervalence transfer properties

It is interesting to note that the IT band for this mixed valent complex is much broader and stronger than the ones observed previously for the symmetrical diruthenium species (70). These intensities are reflected in the oscillator strength ($f_{os} = 0.117 \pm 0.005$) and in the transition dipole moment ($\mu = 1.14 \pm 0.03$) related to this heterodinuclear complex, which were given by eqs. [6] and [7] (102–105).

$$[6] \qquad f_{os} = 4.61\times10^{-9}\,(\varepsilon_{max})\,(\Delta\bar{\nu}_{1/2})$$

$$[7] \qquad \mu = [\,f_{os}/(1.08\times10^{-5}\,(\bar{\nu}_{max}))]^{1/2}$$

Three classes of systems may be distinguished depending on the magnitude of the interaction between the donor–acceptor sites (65). Using the Mulliken formalism (106, 107), Hush showed that the electronic coupling element and the extent of electron delocalization in the mixed valence species can be estimated from the IT band parameters (62–64). However, according to this model, the theory applies only for class II systems (65), where the electronic interaction is weak or moderately strong and can be treated as a discrete perturbation. Hence, a criterion for evaluating or classifying the degree of electronic coupling is given by the Hush model (2–4, 62–64), through the calculation of the spectral half-bandwidth $\Delta\nu_{1/2}$ for the IT band, by using the eq. [8]:

$$[8a] \qquad \Delta\bar{\nu}_{1/2} = [16\,(\ln 2)\,RT(E_{op} - \Delta E_0)]^{1/2}$$

$$\Downarrow$$

$$[8b] \qquad \Delta\bar{\nu}_{1/2} = [2310\,(E_{op} - \Delta E_0)]^{1/2} \quad \text{(at 298K)}$$

where the calculated $\Delta\nu_{1/2}$ value corresponds to the limiting value for a class II mixed valence complex. The experimental values below this limiting $\Delta\nu_{1/2}$ value are typical of systems exhibiting substantial electronic coupling between the metal centers, as is the case for valence delocalized complexes (class III).

The theoretical value of $\Delta\nu_{1/2}$ for the $[(NH_3)_5Ru(bta)Fe(CN)_5]^-$ complex is 4060 cm^{-1}. As a consequence of the estimated values being much lower than the observed one (6500 cm^{-1}), it was confirmed that this system can be properly described as a localized class II mixed valence model, in terms of the Robin and Day categorization (2–4, 65). Application of eqs. [9] and [10] for evaluation of electronic coupling matrix element and delocalization from the IT parameters (2–9, 62–64) may, therefore, appropriately provides the magnitude of the interaction between the metal centers.

$$[9] \qquad H_{ab} = 2.05\times10^{-2}\left(\frac{(\varepsilon_{max})(\Delta\bar{\nu}_{1/2})\,(\bar{\nu}_{max})}{d^2}\right)^{1/2}$$

$$[10] \qquad \alpha = \frac{H_{ab}}{E_{op}}$$

The energy of the optical absorption ($\nu_{max} = E_{op}$), its molar absorptivity (ε_{max}), and the corresponding bandwidth at half-height ($\Delta\nu_{1/2}$) values for the IT band of the mixed valent species, $[(NH_3)_5Ru^{III}(bta)Fe^{II}(CN)_5]^-$, are 8265 cm^{-1}, 3900 mol^{-1} dm^3 cm^{-1}, and 6500 cm^{-1}, respectively. The electron transfer distance (d) is usually taken to be the intermetallic separation (2–9) and it was extracted to be 5.6 Å from molecular geometry optimizations (see *Molecular calculations* above or *Experimental* section for computational details).

The H_{ab} and α^2 parameters for electronic coupling energy and ground state electron delocalization degree were calculated to be 1675 cm^{-1} and 0.041, respectively. Even though this benzotriazolate species contains an "nonlinear" bridging ligand, to our surprise, their magnitude is superior to the pyrazine-analogue (40, 41), and reflects the efficient metal-metal communication through the apparently more conductive bta-bridge. As in this case the fluxional mobility in the benzotriazolate should not be significant, the unexpected differences in intervalence properties between the pyrazine and benzotriazolate unsymmetrical systems are better interpreted in terms of π-electronic character of the bridging ligand, which in turn dictates the superexchange mechanism (8, 9). While benzotriazole acts as either a slight π-acceptor or a weak donor ligand (relatively electron rich), pyrazine behaves as a strong π-acceptor ligand (electron poor), such that the hole-transfer and electron-transfer mechanisms (108), respectively, should take place in their corresponding pentaammineruthenium(III)-pentacyanoferrate(II) dinuclear complexes. Therefore, since the cyanoiron(II) fragment also behaves as a partial π-donor unit (since it is stabilized through π-backdonation) and the pentaammineruthenium(III) as a π-acceptor (Lewis acid) group in the mixed valent species, the benzotriazolate π-levels approach, in energy, the metal $d\pi$ orbitals, and consequently, can better distribute–communicate the extra charge from iron to ruthenium. By extrapolation of this reasoning, it would seem obvious that ligands with strong σ,π-donor character should promote an enhanced intermetallic coupling. Interestingly, the imidazolate derivative of the type $[(NH_3)_5Ru^{III}\text{–}L\text{–}Fe^{II}(CN)_5]^-$ (59), shows about half of the resonance energy involved in the benzotriazolate system reported herein (it should be pointed out that imidazolate and benzotriazolate bridges have actually almost the same metal-to-metal electron transfer distance). If the same superexchange mechanism is operating in both systems, then some other characteristic is making the latter special, as we have observed before (70, 109).

Conclusions

From the discussion, one can conclude that the features of the $[(NH_3)_5Ru^{III}(bta)Fe^{II}(CN)_5]^-$ species are quite remarkable for this type of mixed valence complex, where these results approach those previously reported for class III systems

© 2001 NRC Canada

(2, 3) even though their electronic charges are valence trapped. A more illustrative comparison is provided by the analogous dinuclear complexes of the series $[(NH_3)_5Ru(L)Fe(CN)_5]^n$ that have emerged in recent years (L = pyrazine (40, 41), 4,4′-bipyridine (41), cyanide (56), 1,2-bis(4-pyridyl)ethane (57), pyridinecarboxamido (58), imidazolate (59), 3- and 4-cyanopyridine (60), and 4,4′-dipyridilamine (61)), for which the mixed valence and comproportionation properties (Table 2) are rather modest as compared to the observed ones in this communication. Indeed, these literature examples possess H_{ab} values up to ~750 cm^{-1} (59) while the one for the benzotriazole derivative is higher than 1600 cm^{-1}. The unusual interaction observed in this study is even more exceptional when one takes into account the non-linearity of the bridging ligand employed in this work, as many symmetrical or unsymmetrical examples of dimers comprehend μ-symmetrical and linear bridges of similar structural dimensions (2–4).

A favorable aspect for the relatively strong metal-metal electronic coupling, as well as for the high stability of the electronic (or redox) isomer formulated as Ru^{III}-Fe^{II} is the existence of the (donor bridging ligand) $\pi \rightarrow d_\pi$ (acceptor Ru^{III} ion) charge-transfer interaction, which is reinforced by the π-donor ability of the $[Fe^{II}(CN)_5]^{3-}$ moiety. This statement is supported by the fact that the redox potential at the ruthenium center is more negative in the dinuclear complex (– 0.090 V) than in the protonated $[Ru^{III/II}(NH_3)_5(btaH)]^{3+/2+}$ (0.210 V), or even in the deprotonated $[Ru^{III/II}(NH_3)_5(bta)]^{2+/+}$ (0.025 V) monomers. From the same reasoning, this unidirectional π-conjugation can eventually decrease the stability of some isovalent Ru^{II}-Fe^{II} species with strong π-donor ligands (59), where the π-donor effect takes place on both the ruthenium(II) and the iron(II) units, but in the opposite direction. Conversely, in the fully oxidized state (Ru^{III}-Fe^{III}) the acceptor $M^{III}X_5$ moieties compete for the poor π-donor ability of the benzotrizolate bridge.

Although benzotriazole is not typically a strong σ,π-donor ligand, as it is the case of imidazole (59) and its derivatives (110), the facts observed herein corroborate the hypothesis of benzotriazolate acts primarily as a donor (relative to the acceptor property) bridge. The Fe^{III}/Fe^{II} couple in the benzotriazolate complexes, for instance, have lower potentials than $[Fe^{III/II}(CN)_5(H_2O)]^{2-/3-}$ (Table 1), which indicates the weak π-acceptor ability of this ligand.

The superexchange mechanism operating in the charge conduction through the bridges is better rationalized, in the present example, by hole-transfer rather than electron-transfer. The electron-transfer mechanism is well established in pyrazine or pyridine derivatives with low-energy π* orbitals, but, as demonstrated in this study, this is not the case for benzotriazolate. On the contrary, hole-transfer is favored by the energy match between the metal d_π and the populated π ligand levels.

Acknowledgements

The support from John Simon Guggenheim Memorial Foundation, and the Brazilian agencies FAPESP and CNPq is gratefully acknowledged.

References

1. Mixed-valence compounds: theory and applications in chemistry, physics, geology, and biology. *Edited by* D.B. Brown. Proceedings of the NATO Advanced Study Institute, D. Reidel, Dordrecht, Holland. 1980.
2. C. Creutz. Prog. Inorg. Chem. **30**, 1 (1983).
3. R.J. Crutchley. Adv. Inorg. Chem. **41**, 273 (1994).
4. M.D. Ward. Chem. Soc. Rev. **24**, 121 (1995).
5. T.J. Meyer. Acc. Chem. Res. **11**, 94 (1978).
6. M.D. Newton and N. Sutin. Ann. Rev. Phys. Chem. **35**, 437 (1984).
7. M.D. Newton. Chem. Rev. **91**, 767 (1991).
8. Electron transfer in inorganic, organic, and biological systems. Advances in chemistry series (228). *Edited by* J.R. Bolton, N. Mataga, and G. McLendon. American Chemical Society, Washington, D.C. 1991.
9. Electron transfer reactions: inorganic, organometallic, and biological applications. Advances in chemistry series (253). *Edited by* S.S. Isied. American Chemical Society, Washington, D.C. 1997.
10. D. Chatterjee, H.C. Bajaj, and A. Das. Inorg. Chem. **32**, 4049 (1993).
11. E.H. Cutin and N.E. Katz. Polyhedron, **12**, 955 (1993).
12. L.A.A. Deoliveira, L. Dellaciana, and A. Haim. Inorg. Chim. Acta, **225**, 129 (1994).
13. K. Kalyanasundaram and M.K. Nazeeruddin. Inorg. Chim. Acta, **226**, 213 (1994).
14. V. Balzani, A. Juris, M. Venturi, S. Campagna, and S. Serroni. Chem. Rev. **96**, 759 (1996); and refs. therein.
15. M. Frank, M. Nieger, F. Vogtle, P. Belser, A. Von Zelewsky, L. De Cola, V. Balzani, F. Barigelletti, and L. Flamigni. Inorg. Chim. Acta, **242**, 281 (1996).
16. W.M. Laidlaw and R.G. Denning. Inorg. Chim. Acta, **248**, 51 (1996).
17. Y. Wu, B.W. Pfennig, S.L. Sharp, D.R. Ludwig, C.J. Warren, E.P. Vicenzi, and A.B. Bocarsly. Coord. Chem. Rev. **159**, 245 (1997).
18. F.R. Keene. Coord. Chem. Rev. **166**, 121 (1997).
19. R. Hage, H.E.B. Lempers, J.G. Haasnoot, J. Reedijk, F.M. Weldon, and J.G. Vos. Inorg. Chem. **36**, 3139 (1997).
20. M. Milkevitch, B.W. Shirley, and K.J. Brewer. Inorg. Chim. Acta, **264**, 249 (1997).
21. L.C. Sun, H. Berglund, R. Davydov, T. Norrby, L. Hammarstrom, P. Korall, A. Borje, C. Philouze, K. Berg, A. Tran, M. Andersson, G. Stenhagen, J. Martensson, M. Almgren, S. Styring, and B. Akermark. J. Am. Chem. Soc. **119**, 6996 (1997).
22. M.D. Ward, C.M. White, F. Barigelletti, N. Armaroli, G. Calogero, and L. Flamigni. Coord. Chem. Rev. **171**, 481 (1998).
23. L. De Cola and P. Belser. Coord. Chem. Rev. **177**, 301 (1998).
24. R. Ziessel, M. Hissler, A. El-Ghayoury, and A. Harriman. Coord. Chem. Rev. **180**, 1251 (1998).
25. J.P. Collin, P. Gavina, V. Heitz, and J.P. Sauvage. Eur. J. Inorg. Chem. 1 (1998).
26. W. Paw, W.B. Connick, and R. Eisenberg. Inorg. Chem. **37**, 3919 (1998).
27. C.A. Bignozzi, R. Argazzi, G.F. Strouse, and J.R. Schoonover. Inorg. Chim. Acta, **276**, 380 (1998).
28. T.J. Rutherford and F.R. Keene. J. Chem. Soc. Dalton Trans. 1155 (1998).
29. W.T. Wong. J. Chem. Soc. Dalton Trans. 1253 (1998).
30. K.L. Bushell, S.M. Couchman, J.C. Jeffery, L.H. Rees, and M.D. Ward. J. Chem. Soc. Dalton Trans. 3397 (1998).

© 2001 NRC Canada

31. M. Venturi, A. Credi, and V. Balzani. Coord. Chem. Rev. **186**, 233 (1999).
32. A.D. Shukla, B. Whittle, H.C. Bajaj, A. Das, and M.D. Ward. Inorg. Chim. Acta, **285**, 89 (1999).
33. D. Chatterjee. Polyhedron, **18**, 1767 (1999).
34. E.A. Seddon and K.R. Seddon. *In* The chemistry of ruthenium. *Edited by* R.J.H. Clark. Elsevier Science, Amsterdam. 1984.
35. H.E. Toma and J.M. Malin. Inorg. Chem. **12**, 1039 (1973).
36. H.E. Toma and J.M. Malin. Inorg. Chem. **12**, 2080 (1973).
37. C.M. Elliott, D.L. Derr, S. Ferrere, M.D. Newton, and Y.P. Liu. J. Am. Chem. Soc. **118**, 5221 (1996).
38. A. Haim. *In* Electron transfer reactions: inorganic, organometallic, and biological applications. Advances in chemistry series (253). *Edited by* S.S. Isied. American Chemical Society, Washington, D.C. 1997. p. 239.
39. M. Glockle and W. Kaim. Angew. Chem. Int. Ed. **38**, 3072 (1999).
40. H.E. Toma and P.S. Santos. Can. J. Chem. **55**, 3549 (1977).
41. A. Yeh and A. Haim. J. Am. Chem. Soc. **107**, 369 (1985).
42. J. Reedijk. *In* Comprehensive coordination chemistry. Vol. 2. *Edited by* G. Wilkinson, R.D. Gillard, and J.A. McCleverty. Pergamon Press, Oxford. 1987.
43. E.C. Constable and P.J. Steel. Coord. Chem. Rev. **93**, 205 (1989).
44. P.J. Steel. Coord. Chem. Rev. **106**, 227 (1990).
45. C. Long and J.G. Vos. Inorg. Chim. Acta, **89**, 125 (1984).
46. R. Hage, A.H.J. Dijkhuis, J.G. Haasnoot, R. Prins, J. Reedijk, B.E. Buchanan, and J.G. Vos. Inorg. Chem. **27**, 2185 (1988).
47. F. Barigelletti, L. De Cola, V. Balzani, R. Hage, J.G. Haasnoot, J. Reedijk, and J.G. Vos. Inorg. Chem. **28**, 4344 (1989).
48. R. Hage, J.G. Haasnoot, H.A. Nieuwenhuis, J. Reedijk, D.J.A. Deridder, and J.G. Vos. J. Am. Chem. Soc. **112**, 9245 (1990).
49. R. Hage, J.G. Haasnoot, J. Reedijk, R.Y. Wang, and J.G. Vos. Inorg. Chem. **30**, 3263 (1991).
50. S. Serroni, S. Campagna, G. Denti, T.E. Keyes, and J.G. Vos. Inorg. Chem. **35**, 4513 (1996).
51. E. Muller, M.K. Nazeeruddin, M. Gratzel, K. Kalyanasundaram, and J.C. Prome. New J. Chem. **20**, 759 (1996).
52. A.C. Lees, B. Evrard, T.E. Keyes, J.G. Vos, C.J. Kleverlaan, M. Alebbi, and C.A. Bignozzi. Eur. J. Inorg. Chem. 2309 (1999).
53. R. Walker. J. Chem. Ed. **57**, 789 (1980).
54. H.E. Toma, E. Giesbrecht, and R.L.E. Rojas. Can. J. Chem. **61**, 2520 (1983).
55. H.E. Toma, E. Giesbrecht, and R.L.E. Rojas. J. Chem. Soc. Dalton Trans. 2469 (1985).
56. A. Burewicz and A. Haim. Inorg. Chem. **27**, 1611 (1988).
57. J.A. Olabe and A. Haim. Inorg. Chem. **28**, 3277 (1989).
58. H.Y. Huang, W.J. Cheng, C.C. Yang, and A. Yeh. Inorg. Chem. **30**, 1862 (1991).
59. A.P. Parise, L.M. Baraldo, and J.A. Olabe. Inorg. Chem. **35**, 5080 (1996).
60. A.E. Almaraz, L.A. Gentil, L.M. Baraldo, and J.A. Olabe. Inorg. Chem. **35**, 7718 (1996).
61. C.-L. Lin, K. Hung, A. Yeh, H.-T. Tsen, and C.-C. Su. Inorg. Chem. **38**, 411 (1999).
62. N.S. Hush. Prog. Inorg. Chem. **8**, 391 (1967).
63. N.S. Hush. Electrochim. Acta, **13**, 1005 (1968).
64. N.S. Hush. Coord. Chem. Rev. **64**, 135 (1985).
65. M.B. Robin and P. Day. Adv. Inorg. Chem. Radiochem. **10**, 247 (1967).
66. L.D. Hansen, B.D. West, E.J. Baca, and C.L. Blank. J. Am. Chem. Soc. **90**, 6588 (1968).
67. L.H. Vogt, J.L. Katz, and S.E. Wiberly. Inorg. Chem. **4**, 1157 (1965).
68. G. Brauer. Handbook of preparative inorganic chemistry. 2nd ed. Vol. 2. Academic Press, New York. 1965. p. 1511.
69. H.E. Toma and C. Cipriano. J. Electroanal. Chem. **263**, 313 (1989).
70. R.C. Rocha, K. Araki, and H.E. Toma. Inorg. Chim. Acta, **285**, 197 (1999).
71. F.N. Rein and H.E. Toma. Polyhedron, **17**, 1439 (1998).
72. N.L. Allinger. J. Am. Chem. Soc. **99**, 8127 (1977).
73. R. Stasiw and R.G. Wilkins. Inorg. Chem. **8**, 157 (1969).
74. R. Gale and A.J. McCaffery. J. Chem. Soc. Dalton Trans. 1344 (1973).
75. H.E. Toma, J.M. Martins, and E. Giesbrecht. J. Chem. Soc. Dalton Trans. 1610 (1978).
76. H.E. Toma. Inorg. Chim. Acta, **15**, 205 (1975).
77. P.C. Ford. Coord. Chem. Rev. **5**, 75 (1970).
78. H.S. Lim, D.J. Barclay, and F.C. Anson. Inorg. Chem. **11**, 1460 (1972).
79. J.A. Stritar and H. Taube. Inorg. Chem. **8**, 2281 (1969).
80. J.H. Baxendale, M.A.J. Rodgers, and M.D. Ward. J. Chem. Soc. A, 1246 (1970).
81. H.E. Toma and J.M. Malin. Inorg. Chem. **13**, 1772 (1974).
82. K. Nakamoto. Infrared spectra of inorganic and coordination compounds. 2nd ed. Wiley-Interscience, New York. 1970.
83. J.K. Wilmshurst. Can. J. Chem. **38**, 467 (1960).
84. L. Sacconi, A. Sabatini, and P. Gans. Inorg. Chem. **3**, 1772 (1964).
85. M.B. Fairey and R.J. Irving. Spectrochim. Acta, **22**, 359 (1966).
86. A.D. Allen and C.V. Senoff. Can. J. Chem. **45**, 1337 (1967).
87. E.F. Herington and W. Kynaston. J. Chem. Soc. 3555 (1955).
88. N.E. Katz, C. Creutz, and N. Sutin. Inorg. Chem. **27**, 1687 (1988).
89. E.H. Cutin and N.E. Katz. Polyhedron, **10**, 653 (1991).
90. M.L. Naklicki and R.J. Crutchley. Inorg. Chim. Acta, **225**, 123 (1994).
91. N.A. Lewis. J. Chem. Ed. **57**, 478 (1980).
92. D.E. Richardson and H. Taube. Inorg. Chem. **20**, 1278 (1981).
93. D.E. Richardson and H. Taube. Coord. Chem. Rev. **60**, 107 (1984).
94. W. Kaim and V. Kasack. Inorg. Chem. **29**, 4696 (1990).
95. J.E. Sutton, P.M. Sutton, and H. Taube. Inorg. Chem. **18**, 1017 (1979).
96. J.E. Sutton and H. Taube. Inorg. Chem. **20**, 3125 (1981).
97. F. Salaymeh, S. Berhane, R. Yusof, R. de la Rosa, E.Y. Fung, R. Matamoros, K.W. Lau, Q. Zheng, E.M. Kober, and J.C. Curtis. Inorg. Chem. **32**, 3895 (1993).
98. J.C. Curtis, B.P. Sullivan, and T.J. Meyer. Inorg. Chem. **22**, 224 (1983).
99. G.A. Neyhart, J.T. Hupp, J.C. Curtis, C.J. Timpson, and T.J. Meyer. J. Am. Chem. Soc. **118**, 3724 (1996).
100. R.C. Rocha, K. Araki, and H.E. Toma. Transition Met. Chem. 23, 13 (1998).
101. T. Matsubara and C. Creutz. Inorg. Chem. **19**, 1956 (1979).
102. A.B.P. Lever. Inorganic electronic spectroscopy. 2nd ed. Elsevier, Amsterdam. 1985.
103. C. Creutz, M.D. Newton, and N. Sutin. J. Photochem. Photobiol. A: Chem. **82**, 47 (1994).
104. R.J. Cave and M.D. Newton. Chem. Phys. Lett. **249**, 15 (1996).
105. Y.-G.K. Shin, B.S. Brunschwig, C. Creutz, and N. Sutin. J. Phys. Chem. **100**, 8157 (1996).
106. R.S. Mulliken. J. Am. Chem. Soc. **64**, 811 (1952).
107. R.S. Mulliken and W.B. Person. Molecular complexes. Wiley, New York. 1969.
108. G. Giuffrida and S. Campagna. Coord. Chem. Rev. **135/136**, 517 (1994).

© 2001 NRC Canada

109. R.C. Rocha and H.E. Toma. Inorg. Chim. Acta. **310**, 65 (2000).

110. M. Haga, T. Ano, K. Kano, and S. Yamabe. Inorg. Chem. **30**, 3843 (1991).

© 2001 NRC Canada

Catalytic pathways in the ethanolysis of fenitrothion, an organophosphorothioate pesticide. A dichotomy in the behaviour of crown/cryptand cation complexing agents[1]

Vimal K. Balakrishnan, Julian M. Dust, Gary W. vanLoon, and Erwin Buncel

Abstract: The rates of displacement of 3-methyl-4-nitrophenoxide ion from the pesticide, fenitrothion, by alkali metal ethoxides in anhydrous ethanol were followed spectrophotometrically. Through product analysis experiments, which included ^{31}P NMR and GC-MS, as well as spectrophotometric analysis, three reaction pathways were identified: nucleophilic attack at the phosphorus centre, attack at the aliphatic carbon, and a minor S_NAr route (≤7%). Furthermore, a consecutive process was found to occur on the product of attack at the phosphorus centre. For purposes of kinetic treatment, the processes at the aliphatic and aromatic carbon were combined (i.e., the minor S_NAr pathway was neglected), and the observed reaction rate constants were dissected into rate coefficients for nucleophilic attack at phosphorus and at aliphatic carbon. Attack at phosphorus was found to be catalyzed by the alkali metal ethoxides in the order KOEt > NaOEt > LiOEt. Catalysis arises from alkali metal ethoxide aggregates in the base solutions used (0–1.8 M); treatment of the system as a mixture of free ethoxide, ion-paired metal ethoxide, and metal ethoxide dimers resulted in a good fit with the kinetic data. An unexpected dichotomy in the kinetic behaviour of complexing agents (e.g., DC-18-crown-6, [2.2.2]cryptand) indicated that the dimers are more reactive than free ethoxide anions, which are in turn more reactive than ion-paired metal ethoxide. The observed relative order of reactivity is explained in the context of the Eisenman theory in which the free energy of association of the metal ion with the rate-determining transition state is largely determined by the solvent reorganization parameter. In contrast with displacement at the phosphorus centre, attack at the aliphatic carbon was not found to be catalyzed by alkali metals. In this case, the free ethoxide anion was more reactive than either the ion-paired metal ethoxide or the dimeric aggregate. The differing effects of alkali metals on the two pathways is ascribed largely to the leaving group pK_a. For carbon attack, the pK_a value estimated for demethyl fenitrothion, 2.15, is sufficiently low that metal ions are not required to stabilize the rate-determining transition state. In contrast, for phosphorus attack, 3-methyl-4-nitrophenoxide, with a pK_a of 7.15, requires stabilization by metal ion interactions. Hence, alkali metal ions catalyze attack at phosphorus, but not attack at the carbon centres.

Key words: organophosphorothioate, pesticide, fenitrothion, ethanolysis, alkali metal ethoxide, ion-pair reactivity, dimers, catalysis, competitive pathways.

Résumé : Faisant appel à la spectrophotométrie, on a déterminé les vitesses de déplacement de l'ion 3-méthyl-4-nitrophénolate à partir du pesticide, fénitrothion, sous l'influence d'éthylates de métaux alcalins, dans l'éthanol anhydre. Sur la base d'analyses des produits qui ont impliqué la RMN du ^{31}P et la SM–CG ainsi que des analyses spectrophotométriques, on a pu identifier trois voies réactionnelles: une attaque nucléophile sur le centre phosphoré, une attaque au niveau du carbone aliphatique et une voie S_NAr mineure (inférieure à 7%). De plus, on a observé que le produit résultant d'une attaque au niveau du phosphore donne lieu à un processus consécutif. Pour les besoins du traitement cinétique, on a combiné les processus au niveau des atomes de carbone aliphatique et aromatique (c'est-à-dire que l'on néglige la voie S_NAr mineure) et on a disséqué les constantes de vitesse réactionnelles observées en coefficients d'attaque nucléophile au niveau du carbone aliphatique et du phosphore. On a trouvé que l'attaque au niveau du phosphore est catalysée par les éthylates de métaux alcalins dans l'ordre KOEt > NaOEt > LiOEt. Dans les solutions basiques utilisées (0–1,8 M), la catalyse provient d'agrégats d'éthylate du métal alcalin; si l'on traite le système comme un mélange d'éthylate libre, d'éthylate formant une paire d'ions avec le métal et de dimères d'éthylate métallique, on obtient un bon ajustement avec les données cinétiques. Une dichotomie inattendue dans le comportement des

Received October 26, 2000. Published on the NRC Research Press Web site on March 16, 2001.

V.K. Balakrishnan, G.W. vanLoon, and Erwin Buncel.[2] Department of Chemistry, Queen's University, Kingston, ON K7L 3N6, Canada.
J.M. Dust. Departments of Chemistry and Environmental Science, Sir Wilfred Grenfell College, Corner Brook, NF A2H 6P9, Canada.

[1]Part 4 in a series on "Mechanisms of abiotic degradation and soil–water interactions of pesticides and other hydrophobic organic compounds." For previous papers in this series, see ref. 1.
[2]Corresponding author (e-mail: buncele@chem.queensu.ca; fax: (613) 533-6669).

 DOI: 10.1139/cjc-79-2-157 © 2001 NRC Canada

agents complexants (par exemple, le cryptand-[2.2.2], DC-18-couronne-6) indique que les dimères sont plus réactifs que les anions éthylates libres qui, de leur côté, sont plus réactifs que l'éthylate métallique sous la forme de paire d'ions. On explique l'ordre de réactivité relative observé en faisant appel à la théorie d'Eisenman selon laquelle l'énergie libre d'association de l'ion métallique avec l'état de transition de l'étape cinétiquement déterminante est déterminée principalement par le paramètre de réorganisation du solvant. Par opposition avec la réaction de déplacement au centre phosphoré, on a trouvé que l'attaque au niveau du carbone aliphatique n'est pas catalysée par les métaux alcalins. Dans ce cas, l'anion éthylate libre est plus réactif que l'éthylate métallique sous la forme de paire d'ions ou sous la forme d'agrégat dimère. Les effets différents des métaux alcalins sur les deux voies réactionnelles sont attribués en grande partie au pK_a du groupe partant. Dans le cas de l'attaque sur l'atome de carbone, la valeur du pK_a estimée pour le desméthylfénitrothion, 2,15, est tellement base qu'il n'est pas nécessaire de faire intervenir des ions métalliques pour stabiliser l'étape cinétiquement déterminante de l'état de transition. Par ailleurs, pour l'attaque au niveau du phosphore, la stabilisation par des interactions avec l'ion métallique est nécessaire pour le 3-méthyl-4-nitrophénolate dont le pK_a est de 7,15. En conséquence, les ions des métaux alcalins catalysent l'attaque au niveau du phosphore, mais pas l'attaque au niveau des centres carbonés.

Mots clés : organophosphorothioate, pesticide, fénitrothion, éthanolyse, éthylate de métal alcalin, réactivité de la paire d'ions, dimères, catalyse, voies réactionnelles en compétition.

[Traduit par la Rédaction]

Introduction

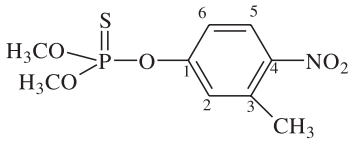
Due to their biological and environmental importance, the degradation of organophosphorus compounds has been studied extensively over the past several decades (1–5). In addition to investigations of the pathways and mechanisms of degradation, research has highlighted the role played by metal ions and surfaces in the abiotic degradation process (6).

From a mechanistic viewpoint, organophosphorus esters are known to undergo a variety of degradation processes. For a phosphorus phenolate ester containing both alkyl and aryl substituents, three decomposition pathways can be envisaged: attack at phosphorus, resulting in P—OAr cleavage; attack at the aliphatic carbon with C—O cleavage; and attack on the aromatic moiety with Ar—O cleavage (2–4).

In aqueous reactions with weakly nucleophilic phenolate ions, Kirby and Younas (4*a*) have shown that aryl methylphosphate anion ($(^{-}O)(MeO)P(O)$-OAr) reacts at the phosphorus and aromatic centres at approximately equal rates, and that C—O bond fission was not significant. In the case of tetrabenzylpyrophosphate ($(PhCH_2O)_2(O)P$-O-$P(O)(OCH_2Ph)_2$), reaction with *n*-propoxide ion occurred competitively at both the phosphorus centre and the aliphatic carbon. In reactions with hydroxide anion, phosphate esters are found to undergo only P—OAr cleavage via an S_N2 (P) mechanism (3). In their studies on the reaction of a series of phosphinate esters with alkali metal ethoxides, Buncel and co-workers (7–11) found that reaction occurred exclusively at the phosphorus centre of the P=O compounds investigated.

The present work represents a continuation of the previous studies conducted in this laboratory on nucleophilic substitution at phosphorus and sulfur centres and catalysis–inhibition by alkali metal ethoxides in ethanol (7–11). The studies showed that for the phosphorus-based esters, alkali metal ions were uniformly catalytic, with reactivities following the order: LiOEt > NaOEt > KOEt > CsOEt > EtO^{-}. However, with sulfonate esters, the reactivities were in the order: CsOEt > KOEt > NaOEt > $^{-}$OEt > LiOEt, with LiOEt acting as an inhibitor.

As an extension of the studies with a variety of P=O and O=S=O compounds, it was deemed logical to proceed to P=S compounds, which comprise the majority of organophosphorus pesticides in use today. Specifically, the compound studied is fenitrothion (*O*,*O*-dimethyl-*O*-(3-methyl-4-nitro)phenylphosphorothioate (**1**), a broad-spectrum insecticide used extensively throughout the world for the control of agricultural and forest pests (12). In Canada, its main application, since 1969, is in the control of the spruce budworm in the forests of the Atlantic provinces (13).



1

In the present paper, kinetic data are described for displacement not only at the P=S centre, but also for reaction via two other competitive pathways of fenitrothion ethanolysis (S_N2 (C) and S_NAr). Alkali metal ethoxides were found to catalyze reaction at phosphorus, but not at the aliphatic or aromatic carbon centres.

Results and discussion

Reaction pathways

The reaction of fenitrothion with alkali metal ethoxides in ethanol was studied spectrophotometrically by following, over time, the formation of 3-methyl-4-nitrophenoxide, the product of attack at the phosphorus centre. It was soon noted, however, that the absorbance at infinite time of the aryloxide product (A_{inf}) was lower than that predicted when the reaction occurred solely via nucleophilic displacement at phosphorus. The expected A_{inf} value at 398 nm, given an initial fenitrothion concentration of 7.72×10^{-5} M and a cuvette pathlength of 1 cm, was 1.45; the observed A_{inf} values ranged over 0.68–1.39 (see Table S1 of the supplementary

© 2001 NRC Canada

Table 1. Distribution of starting material and products at various times of reaction, as determined by ^{31}P NMR and GC-MS product analysis experiments on the reaction of 0.02 M fenitrothion with 0.898 M KOEt at room temperature.

Time (min)	% fenitrothion	% S_N2 (P) products	% S_N2 (C) products	% S_NAr products	% consecutive pathway
0	100	0	0	0	0
30	69.6	12.0	17.8	0.6	0
45	53.7	25.9	18.7	1.7	0
60	46.1	30.4	21.6	1.9	0
90	34.2	30.6	30.9	4.3	0
120	21.1	36.9	38.0	4.0	0
240	4.3	56.1	35.5	4.1	0
1 320	0	49.7	43.4	6.9	0
4 320	0	35.6	43.2	4.5	16.7
7 200	0	24.6	41.5	5.8	28.1
10 080	0	23.0	39.9	5.1	32.0
14 400	0	9.3	41.2	6.7	42.8
15 840	0	9.1	39.5	6.3	45.1
25 680	0	0	44.8	5.4	49.8

data).[3] The data show that, in general, the observed A_{inf} values increase in tandem with increasing $[MOEt]_o$.

The significant deviation of A_{inf} values from the expected value suggested the intervention of alternative reaction pathways, leading to additional products. Two likely possibilities were an S_N2 process involving nucleophilic attack at the aliphatic methoxy carbon and an S_NAr process in which ethoxide attacked at the C-1 position of the electron-deficient aromatic moiety.

Further evidence on this aspect was obtained through ^{31}P NMR and GC-MS experiments. The degradation of a 0.020 M solution of fenitrothion in 0.898 M KOEt was followed via ^{31}P NMR over a period of 18 days. The initial reading showed a single peak at 67 ppm, corresponding to the chemical shift of **1**. As the reaction proceeded, two product peaks were observed: the first, at 72.6 ppm, was attributed to *O*-ethyl-*O*,*O*-dimethylphosphorothioate (**5**), the product of attack at the phosphorus centre, and the second, at 54.9 ppm, demethyl fenitrothion (**2**) from competitive nucleophilic attack at the methoxy carbon. These three peaks were monitored until no fenitrothion remained (ca. 6 h) at which point only the products were monitored.

Over the next 17 days, it was found that a consecutive reaction occurred involving **5**, which was seen to gradually disappear, while a new peak appeared at 58.6 ppm and was identified as dimethylphosphorothioic acid (**3**). The concentration of **2** remained constant throughout this interval. While **3** appears to be largely formed as a product of the consecutive reaction of **5** with KOEt, it is also possible that some amount of **3** may arise from a competitive S_NAr process occurring on **1**. Moreover, a consecutive reaction between **2** and KOEt could also give rise to **4**.

Unfortunately, the sensitivity of the ^{31}P NMR experiments was insufficient to conclusively determine whether or not S_NAr products were formed; if they were formed, the product concentration was below that observable using ^{31}P NMR. To determine whether or not an S_NAr process occurs, and if so, whether it occurs as a competitive or consecutive reaction, another product analysis experiment was undertaken using GC-MS.

The underlying principle of this experiment was that if **4** could be detected, the existence of an S_NAr pathway would be confirmed. Furthermore, given that **2** was found to be stable to KOEt (within the detection limits of NMR) for 17 days, following the disappearance of **1**, any consecutive process would be slow. Therefore, if **4** were to be detected while **1** was still in solution then the S_NAr process would indeed be competitive.

The results of this experiment are presented in Table 1. Importantly, the presence of **4** is detected within 30 min of initiation of the reaction, at which time **1** remains present in the reaction mixture. After 6 h, when **1** had disappeared from solution, the concentrations of both **2** and **4** remain almost constant, proving that **4** does not arise from a consecutive process on **2**. Therefore, fenitrothion is clearly subject to a competitive S_NAr process. Hence, it can be unambiguously concluded that the ethanolysis of fenitrothion entails a minor ($\leq$7%) S_NAr route taking place at the C-1 position of the aromatic ring. Furthermore, a slow consecutive process occurs on the phosphorus product of the S_N2 (P) pathway. The reaction processes are summarized in Scheme 1.

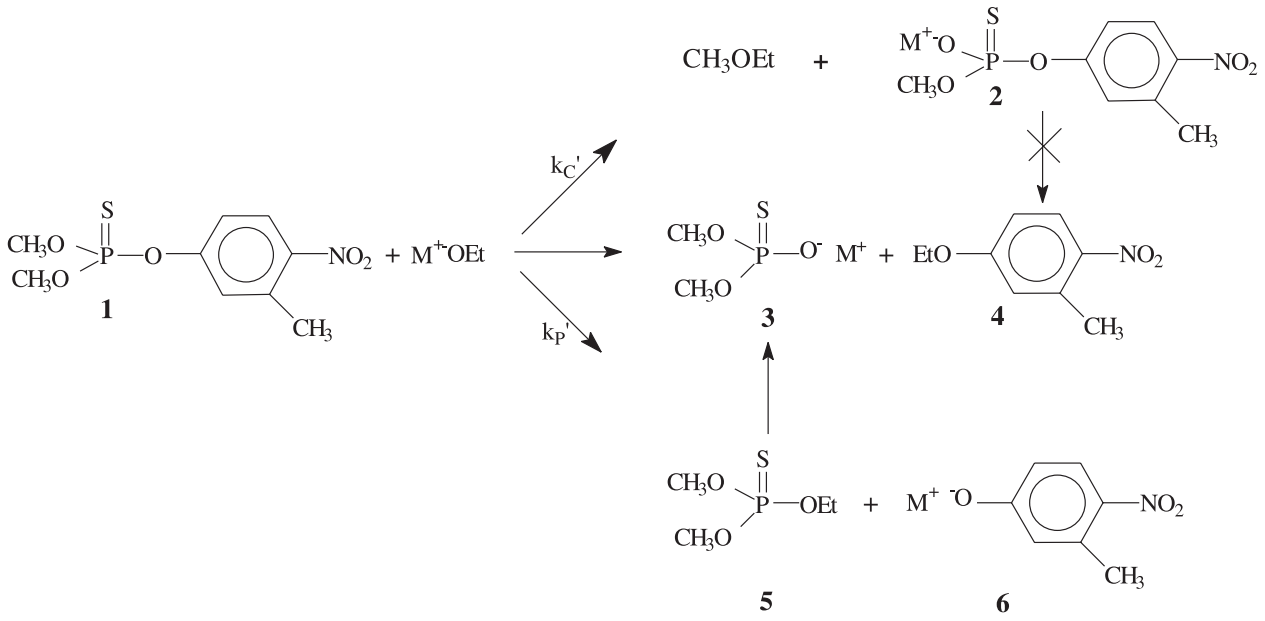
As the products of the S_NAr process accounted for not more than 7% of reaction (as determined by GC-MS), for the purposes of kinetic treatment the contribution of the S_NAr process to the overall rate is deemed to be essentially negligible, and for the sake of simplicity the kinetics are treated in terms of competitive processes arising from the S_N2 (C) and S_N2 (P) pathways. Thus the observed rate constants are dissected into an observed rate of attack at phosphorus (k'_P) and an observed rate of attack at the aliphatic carbon (k'_C), according to eqs. [1] and [2]:

$$[1] \qquad k_{obs} = k'_P + k'_C$$

[3] Tables of absorbances and rate constants (Tables S1–S3) and the derivation of eq. [4] (Appendix) have been deposited as supplementary material and may be purchased from: The Depository of Unpublished Data, Document Delivery, CISTI, National Research Council Canada, Ottawa, Canada, K1A 0S2. For information on obtaining material electronically go to http://www.nrc.ca/cisti/irm/unpub_e.shtml.

© 2001 NRC Canada

Scheme 1.



[2] $$\frac{k'_P}{k'_C} = \frac{[\mathbf{6}]}{[\mathbf{2}]}$$

The concentration of 3-methyl-4-nitrophenoxide ion (**6**) was determined directly from spectrophotometric measurements, while the concentration of **2** was determined by subtracting $[\mathbf{6}]_{inf}$ from $[\mathbf{1}]_o$.

The S_N2 (P) process: catalytic pathways revealed by a dichotomy in the behaviour of complexing agents

Phenomenology

To investigate the effect of aggregation of alkali metal ethoxides on the degradation processes, experiments were conducted with different concentrations of LiOEt, NaOEt, and KOEt (Table 2). While the concentration ranges that could be studied depended on the respective solubilities of the given alkali metal ethoxide in anhyd ethanol, it is evident that the effect of increasing [MOEt] is most pronounced with $M^+ = K^+$, and least pronounced where $M^+ = Li^+$.

It can be seen from the plots of k'_P vs. $[MOEt]_o$ (Fig. 1*a*, and expanded plot in Fig. 1*b*) that the apparent reactivity of these nucleophiles towards fenitrothion increases in the order LiOEt < NaOEt < KOEt (although the difference in reactivity between NaOEt and KOEt is not readily distinguished until higher concentrations are used). Note that, while reaction of fenitrothion with LiOEt yielded a linear plot of k'_P vs. $[LiOEt]_o$, *upward curvature* is seen in similar plots of k'_P vs. [NaOEt] and [KOEt], respectively. This upward curvature is more pronounced with KOEt than with NaOEt.

In previous studies investigating metal ion catalysis of reactions of phosphinate and sulfonate compounds with ethoxide ion in ethanol at 25°C (7–11), such upward curvature was attributed to the higher reactivity of the metal ethoxide ion pair compared with the free ethoxide anion. In such a scenario, the addition of macrocyclic complexing agents to the reaction system should result in a decrease in the rate of reaction at phosphorus. However, as can be seen in Fig. 2, at low concentrations of MOEt the addition of crown/cryptand complexing agents resulted in an *increase* in

Table 2. Pseudo-first-order rate constants (k_{obs}) for the reaction of fenitrothion with LiOEt, NaOEt, and KOEt in EtOH at 25°C.

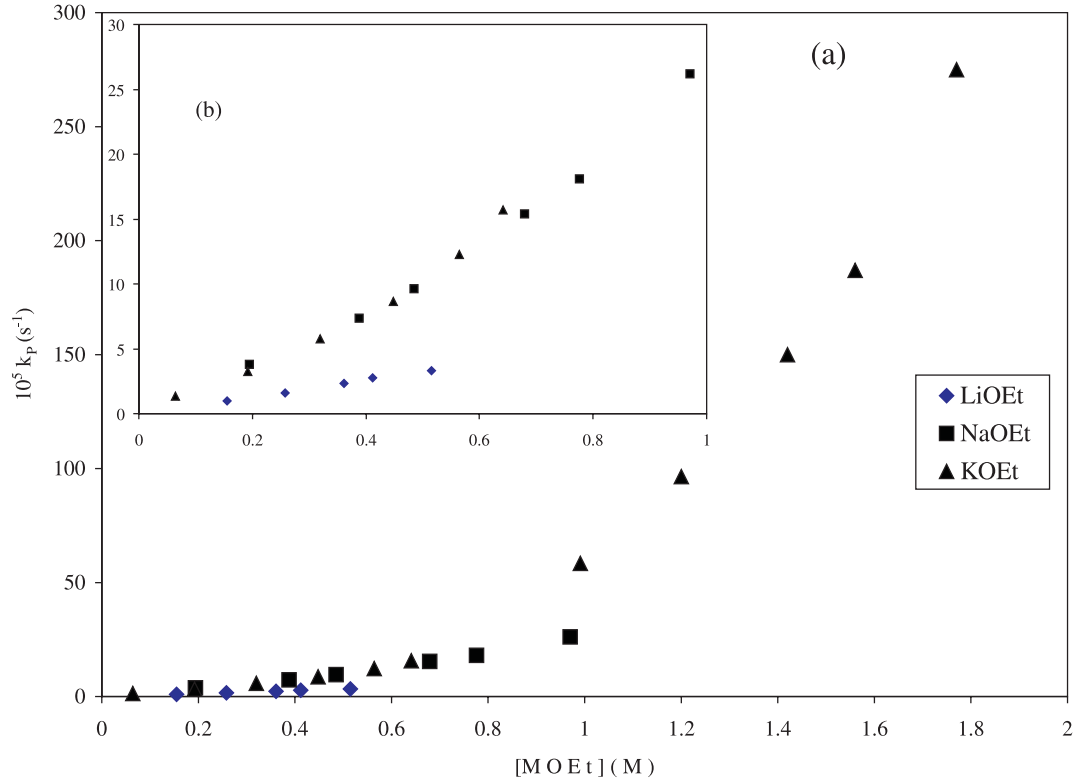
$[MOEt]_o$	$10^5 k_{obs}$ (s^{-1})	$10^5 k_P'$ (s^{-1})	$10^5 k_c'$ (s^{-1})
M = Li			
0.155	2.05 ± 0.07	0.96 ± 0.05	1.09 ± 0.05
0.258	3.24 ± 0.16	1.57 ± 0.10	1.67 ± 0.10
0.361	4.67 ± 0.13	2.32 ± 0.10	2.35 ± 0.10
0.412	5.49 ± 0.18	2.79 ± 0.13	2.70 ± 0.13
0.515	6.57 ± 0.19	3.32 ± 0.14	3.25 ± 0.14
M = Na			
0.194	6.14 ± 1.00	3.79 ± 0.66	2.35 ± 0.66
0.388	11.1 ± 1.05	7.36 ± 0.77	3.74 ± 0.77
0.485	14.1 ± 1.21	9.63 ± 0.92	4.47 ± 0.92
0.679	21.1 ± 1.10	15.4 ± 0.94	5.70 ± 0.94
0.776	24.8 ± 1.79	18.1 ± 1.44	6.70 ± 1.44
0.97	33.3 ± 1.84	26.2 ± 1.67	7.10 ± 1.67
M = K			
0.0641	2.11 ± 0.21	1.32 ± 0.07	0.79 ± 0.07
0.192	4.91 ± 0.23	3.25 ± 0.09	1.66 ± 0.09
0.320	8.52 ± 0.09	5.77 ± 0.06	2.75 ± 0.06
0.448	11.9 ± 0.08	8.62 ± 0.07	3.28 ± 0.07
0.564	16.4 ± 1.48	12.3 ± 0.60	4.10 ± 0.60
0.641	20.4 ± 0.59	15.7 ± 0.30	4.70 ± 0.30
0.991	68.3 ± 1.36	58.4 ± 1.63	9.90 ± 1.63
1.20	106 ± 1.06	96.5 ± 1.70	9.50 ± 1.70
1.42	158 ± 2.37	150 ± 1.70	8.00 ± 1.70
1.56	195 ± 3.46	187 ± 2.30	8.00 ± 2.30
1.77	287 ± 6.61	275 ± 4.20	12.0 ± 4.20

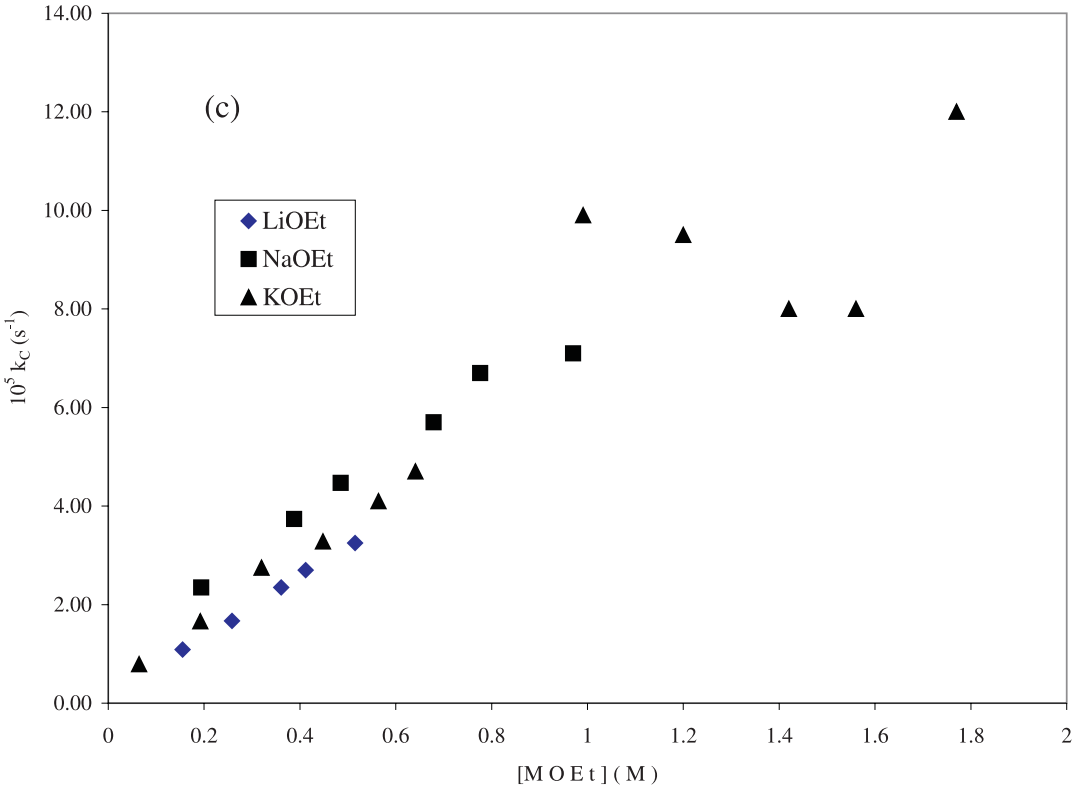
Note: The k_{obs} values have been dissected as shown in eqs. [1] and [2].[a]

[a]The error in k_{obs} values represents the standard deviation about the mean (obtained from replicate runs). The error in k_P' and k_c' arises from propagation of the error about the mean with the error in the infinity absorbance values used in the dissection of k_{obs}.

© 2001 NRC Canada

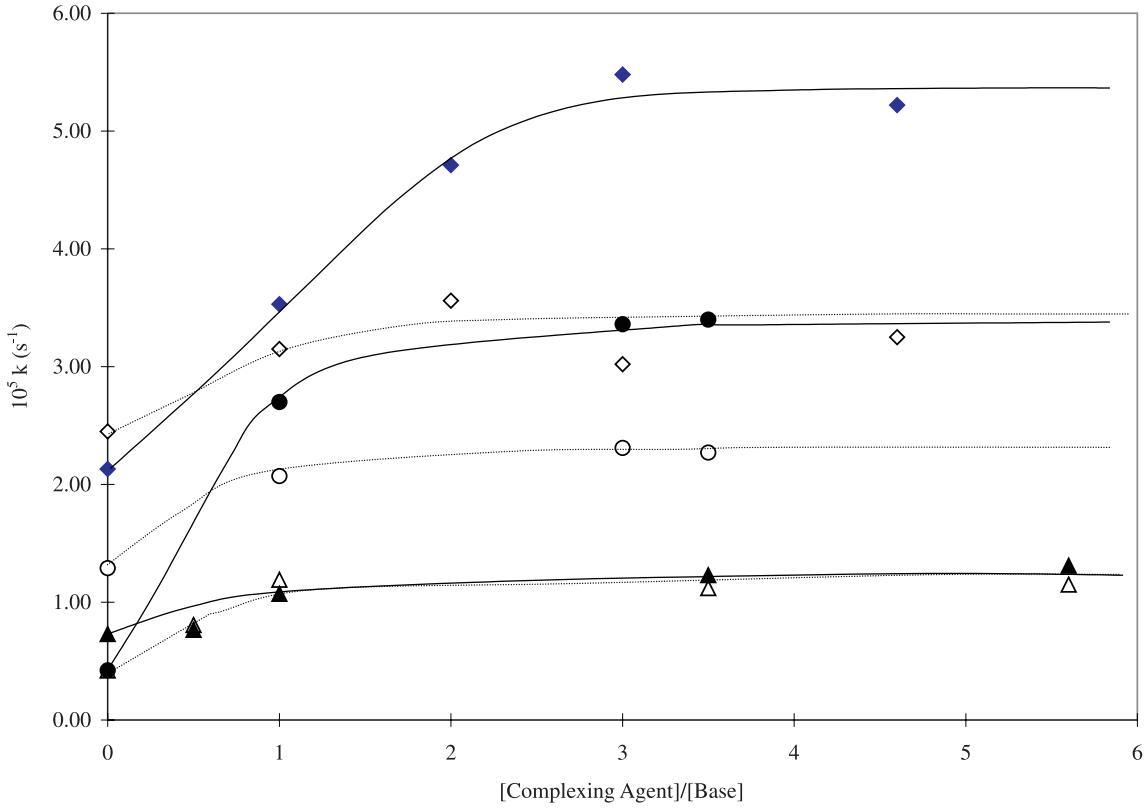
Fig. 1. (*a*) Graphs showing the effect of [MOEt] (0–2 M) on the ethanolysis of fenitrothion in anhyd ethanol at 25°C. Pseudo-first-order rate constants are for attack at phosphorus. (*b*) Expanded plot of the effect of [MOEt] (0–1 M) on the ethanolysis of fenitrothion in anhyd ethanol at 25°C. Pseudo-first-order rate constants are for attack at phosphorus. (*c*) Effect of [MOEt] (0–2 M) on the ethanolysis of fenitrothion in anhyd ethanol at 25°C. Pseudo-first-order rate constants are for attack at the aliphatic carbon.





© 2001 NRC Canada

Fig. 2. The effect of complexing agents on the reaction of fenitrothion with alkali metal ethoxides at 25°C. For attack at the phosphorus centre: ◆ 0.179 M KOEt in the presence of 18-C-6; ▲ 0.0535 M KOEt and [2.2.2] cryptand; ● 0.119 M LiOEt and [2.1.1] cryptand. The analogous open symbols (◇, △, ○) represent the observed rate of attack at the carbon centre under the same conditions.



the rate of attack at the phosphorus centre (Table S2, supplementary data). Thus, at low $[MOEt]_o$ free ethoxide is found to be *more reactive* than the metal ethoxide ion pair. Since the relative amount of free ethoxide decreases with increasing $[MOEt]_o$, the addition of complexing agents had a greater effect in the more concentrated MOEt solutions, where they allowed for the release of a proportionately larger quantity of free ethoxide. The low solubility of the complexing agents limited these experiments to situations where the initial concentration of MOEt used was below the level at which upward curvature is seen in Fig. 1. To accommodate both the low solubility of the complexing agents and the need to work at concentrations of KOEt where curvature was present, these experiments were repeated at 50°C (Table S3, supplementary data).[3]

Figure 3 shows the effect of KOEt on attack at phosphorus and at the aliphatic carbon at 50°C. At this temperature, note that for the trace representing attack at phosphorus, upward curvature begins at approximately 0.6 M KOEt (in contrast with the onset of curvature at 25°C, which occurs at about 0.3 M). Figure 4 depicts the effect of the macrocyclic complexing agent, dicyclohexyl-18-crown-6 (DC-18-C-6) on the ethanolysis reaction at 50°C in both 0.404 and 0.898 M KOEt. At 0.404 M KOEt, where the plot of k'_P vs. [KOEt] is essentially linear, the addition of DC-18-C-6 results in a *rate enhancement*, prior to the attainment of a plateau. The behaviour is similar to that observed at low concentrations of KOEt at 25°C. On the other hand, when the concentration of KOEt was increased to 0.898 M, the addition of DC-18-C-6 resulted in a *decreased rate* of attack at phosphorus (Fig. 4).

For the displacement reaction at the phosphorus centre, the fact that upward curvature in plots of k'_P vs. [MOEt] becomes apparent only at high [MOEt] (Fig. 3, at 50°C), coupled with the rate decrease observed upon addition of DC-18-C-6 (to sequester K^+ ions) to the reaction of fenitrothion with 0.898 M KOEt (Fig. 4), suggests that at high $[KOEt]_o$ an aggregative species of alkali metal ethoxide acts to catalyze the reaction. However, as noted above, addition of the same complexing agent to a lower concentration of KOEt (0.404 M) reacting with fenitrothion resulted in a rate increase, consistent with the results presented in Fig. 2 (using low concentrations of MOEt at 25°C).

The upward curvature observed in the plot showing rate dependence on alkali metal ethoxide concentration prompted an evaluation of the rate data using the H_M and J_E basicity functions (14, 15). The H_M scale refers to the basicity of alkali metal methoxide ions in methanol, at 25°C, and was developed using various weak acid indicators (e.g., 2-*tert*-butyl substituted phenols and 2,6-di-*tert*-butyl substituted phenols). On the other hand, Gold and Toullec's J_E scale was developed from equilibrium measurements of Meisenheimer adduct formation between 2,4-dinitrophenetole and alkali metal ethoxides in ethanol, at 25°C. Typically, when the enhanced basicity of the medium is responsible for increased reaction rates, a linear relationship between the acidity function and rate is observed. Under ideal circumstances, the

© 2001 NRC Canada

Fig. 3. Graph showing the dependence of rate constant on [KOEt] for the ethanolysis of fenitrothion at 50°C. Pseudo-first-order rate constants are shown for attack at both the phosphorus (k'_P) and aliphatic carbon (k'_c) centres.

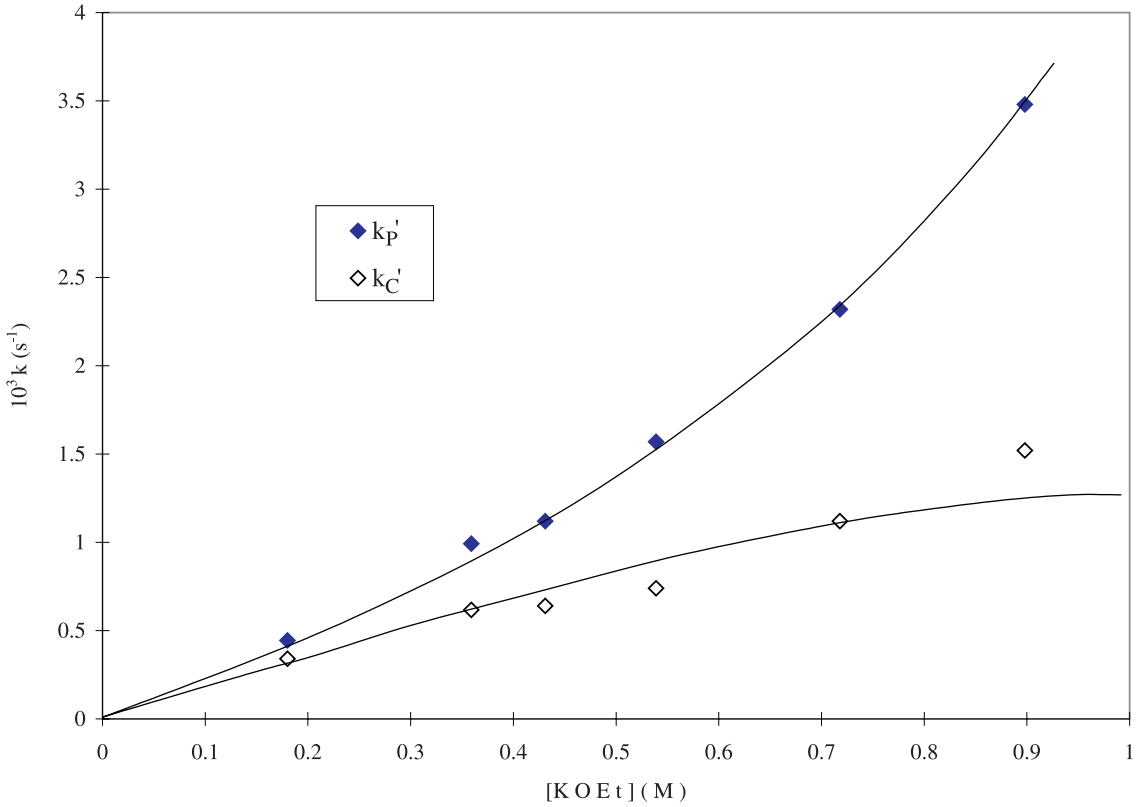
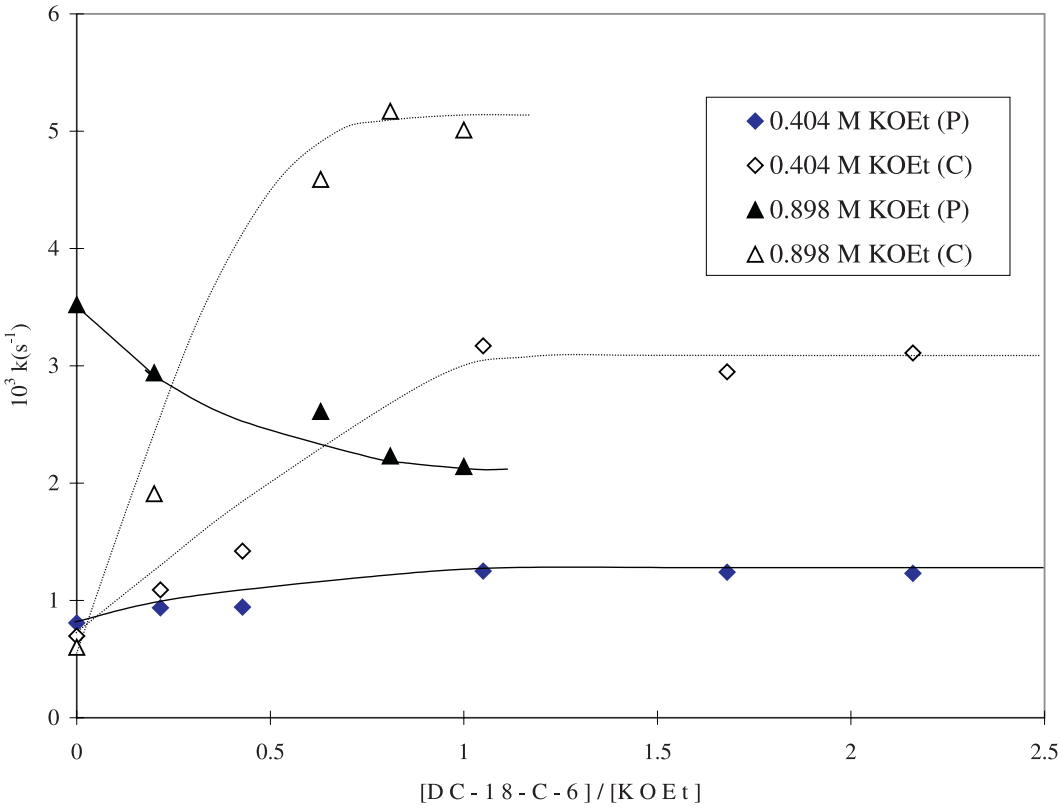


Fig. 4. Effect of DC-18-C-6 on the degradation of fenitrothion in KOEt at 50°C, for attack at both phosphorus (k'_P) and aliphatic carbon (k'_c).



© 2001 NRC Canada

plots would not only be linear, but would have a slope of unity. However, there have been circumstances reported where the relationship was *linear with a nonunity slope* (14). In such cases, it was determined that the assumption that solvent activity remained constant was incorrect, and so solvent activity was corrected for, thus giving a unit slope. In the present study, plots of H_M and J_E vs. rate took the form of a gentle S-shaped curve, with initial slope 0.45 and a final slope of 0.58. From the overall nonlinearity of the plot, it was concluded that no correlation existed between the rate data reported here and either acidity function.

In summary, on the basis of the kinetic data described above for the complexing agents, we propose that the mechanism of ethanolysis involves the reactivity of three species of alkali metal ethoxides: free ethoxide, ion-paired alkali metal ethoxide, and a metal ethoxide aggregate present in equilibrium. In the following sections, the nature, reactivity, and role of the aggregate in the reaction under study will be carefully examined.

Catalysis by alkali metal alkoxide aggregates

A variety of studies have shown that alkali metal alkoxides not only form ion pairs in solution but also are able to organize themselves into higher order aggregates (16–24). Dinnebier et al. (16*a*) reported on powder diffraction studies of alkali metal phenoxides in which a hexameric structure was assigned for C_6H_5OK, while Chisholm et al. (17) likewise showed the single-crystal X-ray structure of $LiOCMe_2Ph$ to be consistent with hexameric structures. In addition, using cryoscopy they showed that lithium *tert*-butoxide had a degree of aggregation of 6 in benzene. Generally, the smaller alkali metal *tert*-alkoxides form higher order aggregates than do larger alkali metals (K, Rb, Cs), which tend to adopt a tetrameric structure in benzene solution (18). Jackman and Rakiewicz (19), too, have documented cases of aggregate formation in solutions of lithium 2,6-dimethylphenolate and its isomer, lithium 3,5-dimethylphenolate (20), in THF, dioxolane, and diethyl ether. The former was found to exist as a dimer, whereas the latter formed tetrameric species.

The existence of these aggregates in solution cannot be regarded as inconsequential, as studies have shown that these clusters can be the primary reactants responsible for controlling reactivity (21–24). DePue and Collum (21) investigated the *N*-alkylation of lithium diphenylamide with *n*-butyl bromide in THF–hydrocarbon mixtures and found that the reaction could be explained in terms of catalysis by lithium diphenylamide monomers, in equilibrium with less reactive dimers. Furthermore, evidence of reaction involving free ions was inferred from the existence of a competitive elimination pathway which produced 1-butene. More recently, Streitwieser and co-workers (22, 23) investigated the alkylation of the cesium and lithium enolates of *p*-phenylisobutyrophenone in THF and found that the cesium enolate consisted of a mixture of monomeric, dimeric, and tetrameric species in THF solution, with monomers being most reactive. The lithium enolates, meanwhile, were found to exist in monomeric and tetrameric forms, again with monomers making the largest contribution to rate, even in situations where the tetramer was the predominant species. Although the preceding studies generally found monomeric forms to be more reactive than higher order aggregates, the recent study by Gagne and co-workers (24) of the ester metathesis reaction between *tert*-butyl acetate and various methyl esters in hexane showed that alkali metal *tert*-butoxides possessing a higher degree of aggregation (i.e., hexamers) can be more reactive than their less aggregated counterparts (i.e., tetramers).

It is critical to note that these previous kinetic studies involving aggregated alkali metal alkoxides have generally been performed in nonpolar, aprotic solvents. How then can these studies be applied to the behaviour of alkali metal ethoxides in ethanol?

The speciation of the alkali metal ethoxide in solution spans the general continuum given in eq. [3] (25, 26).

$$[3]\quad \underset{\text{(Free ions)}}{M^+ + {}^-OEt} \rightleftharpoons \underset{\text{(SSIP)}}{M^+ \,//\, {}^-OEt} \rightleftharpoons \underset{\text{(CIP)}}{(M^+\,{}^-OEt)} \rightleftharpoons \underset{\text{(Dimer)}}{(M^+\,{}^-OEt{:}\,M^+\,{}^-OEt)} \rightleftharpoons \underset{\text{(Higher order aggregate)}}{(M^+\,{}^-OEt)_n}$$

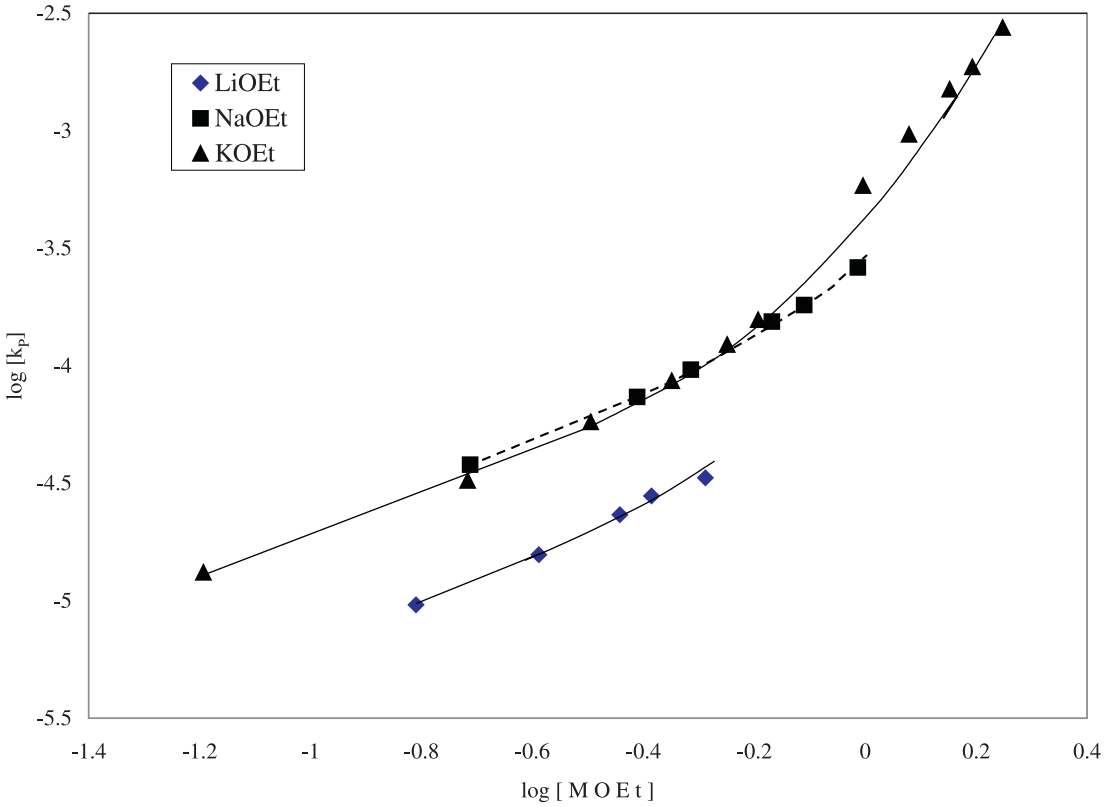
The position of the equilibrium in this continuum is significantly affected by the ability of the solvent to support charge separation. Aprotic donor solvents such as THF might reasonably be expected to better solvate cationic species than aprotic, nondonor, nonpolar solvents such as hexane. Consequently, it is not surprising that aggregates of higher order (i.e., hexamers (24)) are present in hexane than are normally found in THF (in which dimeric and tetrameric aggregates predominate (19–23)). Extending this rationale to polar, protic solvents such as ethanol, the ability to support charge separation is enhanced via hydrogen-bonding interactions, leading to the reasonable expectation that charge separated, rather than highly aggregated, species will be favoured and that the maximum aggregate size will be lower than in nonpolar, aprotic solvents.

It has been suggested that in *dilute* alkali metal ethoxide solutions in ethanol, contact (or solvent separated) ion pairs are the dominant associated species (25, 26). However, as the total base concentration increases, the equilibrium depicted in eq. [3] shifts to the right (i.e., towards higher order aggregates). Conversely, an increase in temperature results in a leftward shift in the aforementioned equilibrium, towards free ethoxide. In ethanol, at concentrations of less than 0.3 M, at 25°C, the two alkali ethoxide species present in solution are considered to be free ions and monomeric alkali metal ion pairs (SSIP and CIP).

Consequently, in the low-concentration range of MOEt used in this study, the main species in solution are known to be free ions in equilibrium with ion-paired alkali metal ethoxide. However, as $[MOEt]_o$ is increased, higher order aggregates would be expected to form. Plots of log k'_P vs. log $[MOEt]_o$ can be used to provide evidence of this type of behaviour (24). Upon examination of these plots (Fig. 5), one observes that the slope is generally near unity when $[MOEt]_o < 0.45$ M. However, above this concentration the plots begin to exhibit curvature, with LiOEt reaching a final slope of 1.3, NaOEt attaining a value 1.7, and KOEt achieving a slope of 3.1. Once again, it should be noted that the

© 2001 NRC Canada

Fig. 5. Graph showing the variation of reaction order with MOEt concentration in order to detect the participation of alkali metal ethoxide aggregates in the ethanolysis of fenitrothion.



lower solubilities of both LiOEt and NaOEt precluded their use at higher concentrations (as were used with KOEt), where one expects that the slopes of the curves would continue to increase in the same manner as that observed with KOEt.

The non-unity orders in MOEt may be explained in terms of the equilibrium between the reacting species depicted in eq. [3]. If one of the kinetically active species is present in a smaller concentration than another, a perturbation in the log–log plot ensues (24). Gagne and co-workers (24) used such an argument in rationalizing the nonunity slope of log–log plots of the ester metathesis reaction, concluding that in hexane, NaO-*t*-Bu exists predominantly as a tetramer in equilibrium with a more reactive hexamer. Applying a similar argument to the system under study here, it appears reasonable that the upward curvature seen in the high-concentration region of plots of log k'_P vs. log $[MOEt]_o$ can be attributed to the formation of alkali metal ethoxide clusters that are more reactive than either the free ethoxide or ion-paired metal ethoxide. If the dimers depicted in eq. [3] are taken to be the said species of clustered alkali metal ethoxide, the overall reaction order would approach 4.0, a point worth bearing in mind in the subsequent discussion.

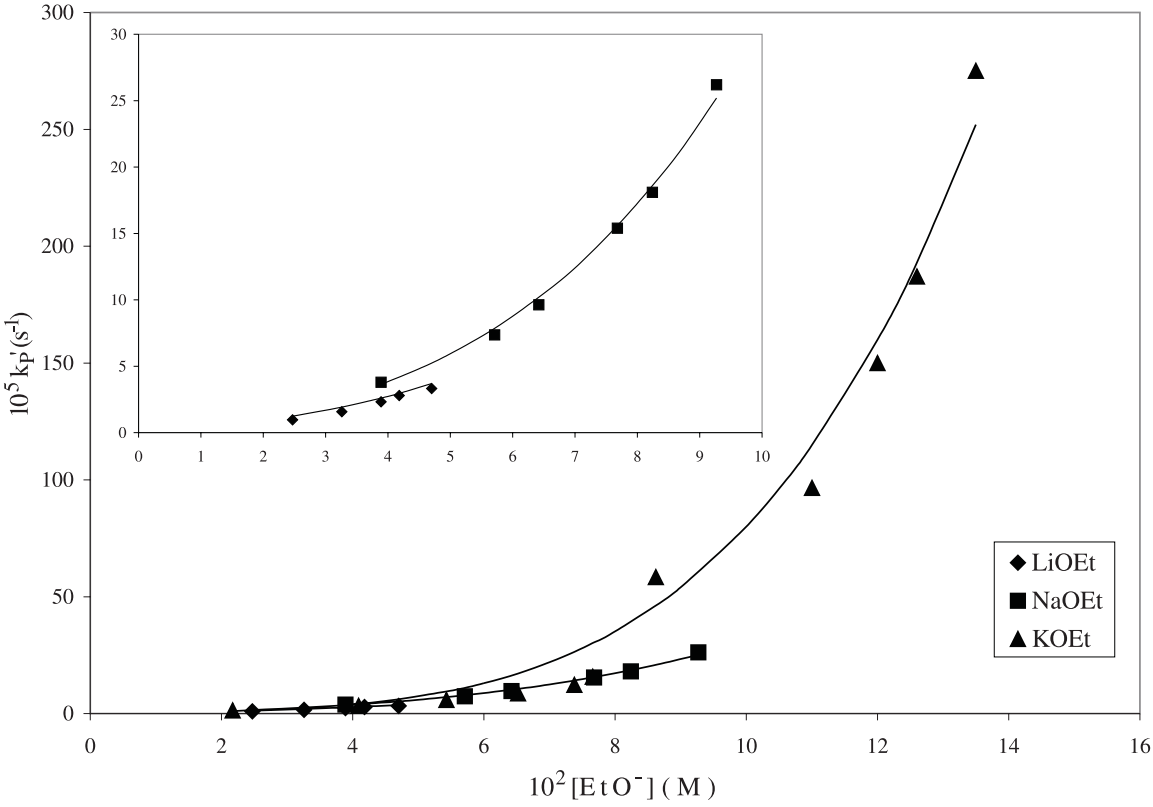
The significance of the behavioural dichotomy of crown/cryptand complexing agents

To further investigate the hypothesis that the formation of reactive alkali metal ethoxide aggregates was responsible for catalyzing fenitrothion ethanolysis, varying concentrations of the macrocyclic complexing agent DC-18-C-6 were added to the reaction of fenitrothion and KOEt, where [KOEt] was high enough that curvature was present in Fig. 3. As stated earlier, this required performing the experiment at 50°C in order to be able to add sufficiently high concentrations of DC-18-C-6. It should be noted that at 50°C, curvature is observed in plots of k'_P vs. $[KOEt]_o$ only when $[KOEt]_o$ > 0.6 M (Fig. 3). This observation is itself consistent with the idea that alkali metal ethoxide aggregates play a role in the reaction, since an increase in temperature would shift the equilibrium away from aggregate formation (26). When the 50°C experiment was performed at 0.404 M KOEt (where plots of k'_P vs. $[KOEt]_o$ are not curved), it was found that the addition of increasing amounts of DC-18-C-6 resulted in a *rate increase* for attack at phosphorus, up to a maximum rate at which a plateau resulted. However, at 50°C and 0.898 M KOEt (where curvature is present), addition of increasing amounts of DC-18-C-6 resulted in a *decreased rate* of attack at the phosphorus centre, once again, culminating in a plateau. *These findings confirm the existence of two regimes of reactivity: a low-concentration regime where free ethoxide anions are more reactive than ion-paired metal ethoxide, and a high-concentration regime where free ethoxide anions are less reactive than are the alkali metal ethoxide clusters.*

Considering that polar, protic solvents are better able to support charge separation than nonpolar, aprotic solvents and that aggregation numbers in alcoholic solutions tend to decrease with decreasing alkyl chain length (26), taken together with the fact that the plot of log k'_P vs. log $[KOEt]_o$

© 2001 NRC Canada

Fig. 6. The fit of the data to eq. [4] for reaction at the phosphorus centre (k'_P) of fenitrothion with MOEt. The inset omits overlapping data from KOEt, leaving only the data for LiOEt and NaOEt.



(Fig. 5) shows a reaction order greater than 3, we suggest that the two regimes of reactivity are as follows. At low concentrations of MOEt, the metal ethoxide is largely present as ion-paired ethoxide in equilibrium with free ethoxide (25, 26), but as the concentration of MOEt increases, the contribution of alkali metal ethoxide dimers to the rate of ethanolysis becomes significant. Based on the dichotomy in the behaviour of the complexing agents, the following relationships hold in terms of reactivity: $k^P_{dim} > k^P_{EtO^-} > k^P_{MOEt}$.

Thus, the reaction of fenitrothion with MOEt is depicted in Scheme 2, where k'_P is expressed as:

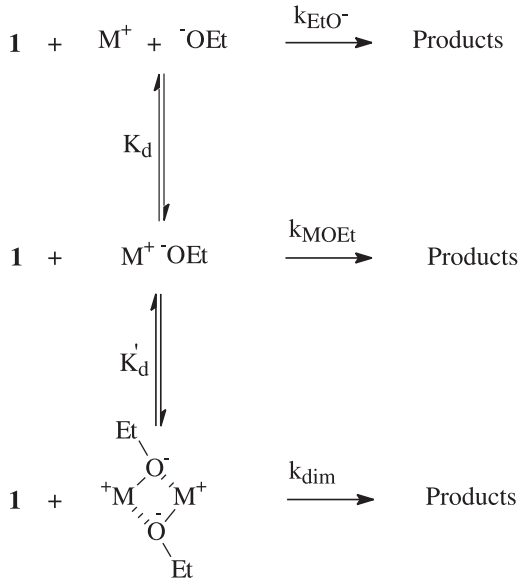
$$[4] \qquad k'_P = \frac{k^P_{dim}}{K'_d K_d}[EtO^-]^4_{eq} + \frac{k^P_{MOEt}}{K_d}[EtO^-]^2_{eq} + k^P_{EtO^-}[EtO^-]_{eq}$$

A full derivation of eq. [4] is given in the Appendix, supplementary data.[3] The fit of the data (using GraphPad Prism, a nonlinear least-squares-fitting program) to eq. [4] is shown in Fig. 6. For both LiOEt and NaOEt, the fits are good with correlation coefficients (R^2) of 0.987 and 0.995, respectively, while for KOEt also a reasonable fit (R^2 = 0.981) was obtained.

The terms in eq. [4] are as follows:

K_d represents the dissociation constant for ion-paired metal ethoxide in ethanol at 25°C and is available from the literature (27).

Scheme 2.



K'_d represents the dissociation constant for the alkali metal ethoxide dimer, and k^P_{dim} denotes the reactivity of the dimer for attack at the phosphorus centre of fenitrothion. The ratio k^P_{dim}/K'_d was obtained using GraphPad Prism. For KOEt, $k^P_{dim}/K'_d = 7.94 \times 10^{-2}$ M^{-2} s^{-1}; for NaOEt, 1.31×10^{-2} M^{-2} s^{-1}; and for LiOEt, 5.00×10^{-3} M^{-2} s^{-1}.

k^P_{MOEt} is defined as the reactivity of ion-paired metal ethoxide towards attack at the phosphorus centre. With

© 2001 NRC Canada

Table 3. Percentage contribution of the metal ethoxide dimer, ion-paired metal ethoxide, and free ethoxide to the observed rate of ethanolysis at phosphorus (k_P'), for LiOEt, NaOEt, and KOEt.

[MOEt] (M)	10^2[EtO$^-$] (M)	$10^5 k_P'$ (s^{-1}) (expt)	$10^5 k_P'$ (s^{-1}) (calcd)	Dimer (rate %)	Ion-paired (rate %)	Free EtO$^-$ (rate %)
M = Li						
0.155	2.47	0.96 ± 0.05	1.24	3.2	41.8	55.0
0.258	3.26	1.57 ± 0.10	1.92	6.2	47.0	46.8
0.361	3.89	2.32 ± 0.10	2.60	9.3	49.4	41.3
0.412	4.18	2.79 ± 0.13	2.96	10.9	40.1	39.0
0.515	4.70	3.32 ± 0.14	3.69	14.0	50.8	35.1
0.641	5.27	NA[a]	4.63	17.6	50.9	31.4
0.991	6.61	NA[a]	7.56	26.8	49.1	24.1
1.20	7.29	NA[a]	9.52	31.4	47.4	21.1
1.42	7.45	NA[a]	10.0	32.5	47.0	20.5
1.56	8.34	NA[a]	13.3	38.4	44.3	17.3
1.77	0.891	NA[a]	15.9	42.0	42.5	15.5
M = Na						
0.194	3.89	3.79 ± 0.66	3.63	8.4	62.0	29.6
0.388	5.71	7.36 ± 0.77	7.85	18.1	61.8	20.1
0.485	6.42	9.63 ± 0.92	10.2	22.3	60.3	17.4
0.679	7.68	15.4 ± 0.9	15.6	29.9	56.5	13.6
0.776	8.24	18.1 ± 1.4	18.6	33.2	54.5	12.3
0.970	9.27	26.2 ± 1.7	25.2	39.1	50.7	10.1
1.20	10.36	NA[a]	34.6	45.2	56.5	8.3
1.42	11.32	NA[a]	43.9	49.6	43.3	7.1
1.56	11.89	NA[a]	51.2	52.4	41.2	6.4
1.77	12.69	NA[a]	62.3	55.9	38.5	5.6
M = K						
0.064	2.17	1.32 ± 0.07	1.04	15.4	26.5	58.1
0.192	4.09	3.25 ± 0.09	4.10	48.8	23.7	27.5
0.320	5.43	5.77 ± 0.06	9.43	65.9	18.2	15.9
0.448	6.52	8.62 ± 0.07	17.1	75.2	14.3	10.5
0.564	7.38	12.3 ± 0.6	26.4	80.3	12.0	7.7
0.641	7.66	15.7 ± 0.3	30.2	81.7	11.3	7.0
0.991	8.62	58.4 ± 1.6	46.2	85.5	9.4	5.1
1.20	11.0	96.5 ± 1.7	115	91.2	6.1	2.7
1.42	12.0	150 ± 1.7	160	92.7	5.2	2.1
1.56	12.6	187 ± 2.3	193	93.4	4.8	1.8
1.77	13.5	275 ± 4.2	252	94.3	4.2	1.5

Note: The values are calculated based on the fit obtained to eq. [4], and the calculated values are compared to the k_P' values determined experimentally at 25°C.

[a]Due to the low solubilities (at 25°C) of LiOEt and NaOEt, experiments could not be run at these concentrations. However, theoretical values were obtained by calculation from eq. [4].

KOEt, it was determined from the various experiments involving complexing agents as being 6.45×10^{-5} M^{-1} s^{-1}. This was done by first determining the value for $k^P_{EtO^-}$ (as outlined below), and since dimers are not present at the low $[KOEt]_o$ at which $k^P_{EtO^-}$ was determined, the first term on the right-hand side of eq. [4] becomes negligible. Using the value for k^P_{obs} obtained in the absence of complexing agent, the resulting simplified version of eq. [4] was solved for k^P_{MOEt}. In the case of NaOEt and LiOEt, this parameter was determined using GraphPad Prism. For NaOEt, k^P_{MOEt} was 1.46×10^{-4} M^{-1} s^{-1}, while for LiOEt a value of 4.01×10^{-5} M^{-1} s^{-1} was obtained.

$k^P_{EtO^-}$, the reactivity of free ethoxide anion towards the phosphorus centre, was experimentally determined from the complexing agent studies to be 2.76×10^{-4} M^{-1} s^{-1}. This was done by dividing the rate constant (k_P') at the plateau observed in Fig. 2 by $[MOEt]_o$. The concentration of free ethoxide at equilibrium is given as $[EtO^-]_{eq}$ in eq. [4].

Although differences in solubility limited the range over which LiOEt and NaOEt could be used in comparison with KOEt, the theoretical curves for both metals are calculated to cover the same range as covered using KOEt (Table 3).

It is seen from Table 3 that for all three metal ethoxide systems, the reactivity proceeds in the order: dimer > free ethoxide ion > ion-paired metal ethoxide, with dimerized KOEt being more reactive than dimerized NaOEt, which is in turn more reactive than dimerized LiOEt. The contribution made by each species to the observed rate of nucleophilic displacement at phosphorus is itemized in Table 3. It is readily apparent from the Table that at lower concentrations of MOEt, the putative contribution of the alkali metal ethoxide dimer is much less than that of the free

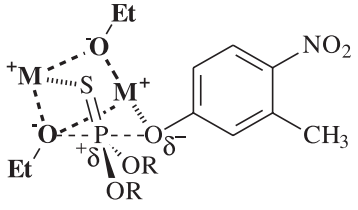
© 2001 NRC Canada

ethoxide or ion-paired metal ethoxide. However, at higher concentrations of MOEt, the contribution of the dimer to the overall rate becomes much more significant, which in the case of LiOEt causes the *relative* contribution of ion-paired metal ethoxide to decrease from an apparent maximum.

Further evidence of metal ion involvement in accelerating fenitrothion ethanolysis was found by carrying out reactions in the presence of additional K^+ ions, in the form of an unreactive salt, potassium acetate (Table 4). In this case, there was an *increase in the rate of attack at phosphorus*. We suggest then that the addition of KOAc shifts the equilibrium towards the more reactive dimer, resulting in the observed rate increase. The nature of the aggregate itself is unclear at this time, given that not only are pure KOEt dimers possible but so too are mixed dimers involving both KOEt and KOAc (19, 20). Regardless of the nature of the dimer, it is certain that ethoxide (not acetate) acts as the nucleophilic species, since a mixture of fenitrothion and KOAc (such that the total K^+ concentration used was equivalent to that at the highest ratio of [KOAc]/[KOEt] reported in Table 4) did not result in any reaction over 7 days. In fact, since the pK_a of acetic acid in ethanol is 10.32 (28) and the autoprotolysis constant for ethanol (at 25°C) is 3×10^{-20} (29), the equilibrium constant for the reaction of acetate with ethanol is calculated to be 1.5×10^{-10}. Therefore, the expected concentration of ethoxide would be 1.58×10^{-5} M, giving an estimated rate constant of 4.35×10^{-9} s^{-1} (i.e., a half-life of approximately 5 years)!

Structure of the fenitrothion-dimeric metal ethoxide transition state

The greater reactivity of the alkali metal ethoxide dimers can be rationalized upon consideration of structure **7**, depicting the transition state (TS) for the reaction of fenitrothion with the MOEt dimer species. Although structure **7** depicts a TS for a concerted S_N2 (P) process (2), it should be noted that previous studies on similar phosphorus-centred systems have found that reaction can occur as a two-stage process, via a penta-coordinate intermediate, with nucleophilic attack being rate-determining (8). However, as both scenarios have identical rate laws, structure **7** was chosen for simplicity. In this structure, the dimer plays several roles which contribute to stabilization of the incipient negative charge of the transition state. First, alkali metal interaction with the aryl oxygen neutralizes the developing charge on the leaving group, thus enhancing its nucleofugality. Second, alkali metal can bind to the polarizable sulfur atom, leading to increased electrophilicity at the phosphorus centre. Finally, the transition state depicted in structure **7** allows one metal ethoxide ion pair in the dimer to align the ethoxide of the other pair in the best orientation for backside nucleophilic attack.



7

Table 4. Pseudo-first-order rate constants for the reaction of fenitrothion with 0.025 M KOEt in the presence of added KOAc, at 25°C. k_{obs} are dissected as shown in eqs. [1] and [2].

[KOAc]/[KOEt]	$10^6 k_{obs}$ (s^{-1})	$10^6 k'_P$ (s^{-1})	$10^6 k'_C$ (s^{-1})
0	8.30	4.37	3.93
2.32	8.30	5.22	3.08
4.20	8.80	5.92	2.88
6.96	10.3	7.32	2.98
8.82	12.2	9.17	3.03
11.2	13.8	11.3	2.50

The multiple points of attachment afforded by the dimers are not available with either the singly ion-paired metal ethoxide or the free ethoxide anion, and thus the dimer is more reactive than both. The finding that free ethoxide is more reactive than ion-paired metal ethoxide is consistent with conventional wisdom, which suggests that in nucleophilic displacement reactions, the free (dissociated) nucleophile should be more reactive than an ion-paired species. Note, however, that such is not always the case, as previous studies using phosphorus- and sulfur-centred esters (7–11) have found. Ion-paired alkali metal ethoxide in fact served to catalyze the ethanolysis reaction. We will return to the contrast between catalysis in P=O systems and P=S systems later in this discussion.

Selectivities of alkali metal ethoxides (Eisenman theory)

An explanation for the relative ordering in metal reactivities arises from Eisenman theory, which was originally posited to explain alkali metal ion selectivity patterns for ion-exchange resins and glass electrodes (30). According to Eisenman, two competing factors govern the nature of cation interactions with a fixed anionic species. The first is the attractive electrostatic interaction, which is the energy gained when ions of opposite charge approach one another. The second factor is the free energy expended to rearrange the solvent molecules around the ions to allow for close approach (or contact) of the two ionic species. The free energy involved in the latter would be closely related to the standard free energy of hydration for the ions involved. Therefore, the free energy required for the displacement of cation 2 by cation 1 ($\Delta G^\circ_{1/2}$) on a fixed anion grouping can be expressed as

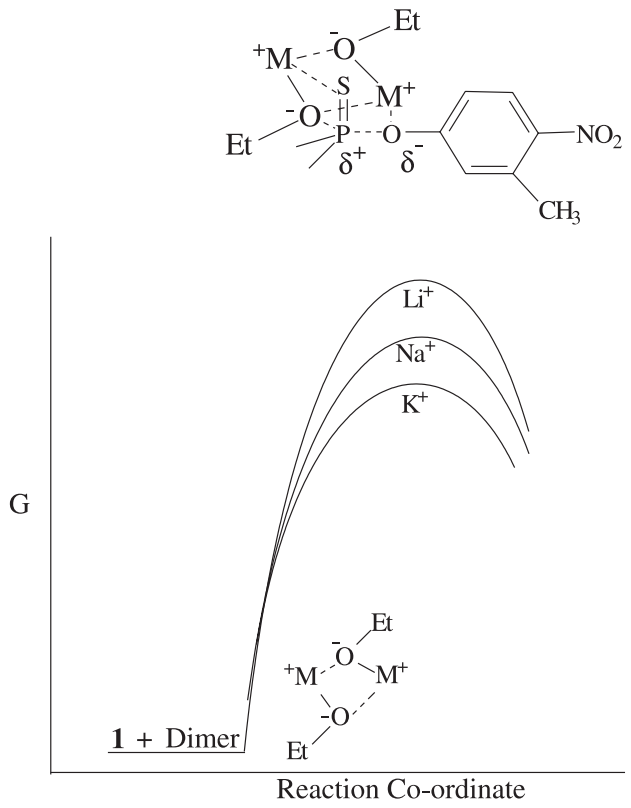
$$[5] \qquad \Delta G^\circ_{1/2} = \left(\frac{e^2}{r_A + r_2} - \frac{e^2}{r_A + r_1} \right) - (\Delta G_2 - \Delta G_1)$$

where r_A is the radius of the anion, r_1 and r_2 are the ionic radii of cations 1 and 2, respectively, ΔG_1 and ΔG_2 are the solvation energies of the cations, and e is the electronic charge. If $\Delta G^\circ_{1/2}$ has a negative value, the anion exhibits selectivity towards cation 1, and conversely, a positive value for $\Delta G^\circ_{1/2}$ results in selectivity towards cation 2.

Consider now a case where r_A is large (i.e., low field strength anion or an anion with delocalized charge). In such a scenario, the first bracketed term in eq. [5] will be small, and $\Delta G^\circ_{1/2}$ will be determined by the solvation energy term of eq. [5]. Hence, one expects the selectivity to decrease in the order $K^+ > Na^+ > Li^+$. However, for high electric field

© 2001 NRC Canada

Fig. 7. Free energy reaction profile for the reaction at the phosphorus centre of fenitrothion with MOEt dimers, with the relative ordering of both the ground state and transition state energies being determined using Eisenmann theory. Note that the transition state structure has a more dispersed negative charge than present in the ground state, which accounts for the reversal of the transition state stabilities.



strength anions (i.e., r_A is small and charge is localized) electrostatic attraction overcomes cation solvation and selectivity proceeds as $Li^+ > Na^+ > K^+$, as predicted by Coulomb's law. As the electric field strength of the anion is varied between these extremes, intermediate selectivity sequences are observed. Although originally designed for predicting anion interactions with ion-exchange resins, Buncel and co-workers (11) showed that the principles of Eisenman theory could be applied to chemical kinetics. In their study, the reaction of a variety of phosphinate and sulfonate esters (PO and SO_2 centres) with alkali metal ethoxides was described. It was found that the sequences for the transition states for reaction with the phosphinates were all located at the high electric field strength end of the spectrum, while the sulfonate esters exhibited selectivities at the opposite extreme.

Returning once again to structure **7**, a comparison of the transition states based on Eisenman theory predicts the following. In the transition state, a negative charge is delocalized amongst the dimeric nucleophile, sulfur, and leaving group oxygen. Consequently, Eisenman theory predicts that the transition state stabilization depicted in Fig. 7 proceeds as: KOEt > NaOEt > LiOEt, and therefore, the rate of reaction at the phosphorus centre of fenitrothion with dimerized alkali metal ethoxides should proceed in the observed order, i.e., KOEt > NaOEt > LiOEt.

A comparison of P=S and P=O systems

Previous studies (7–11) have found that singly ion-paired metal ethoxide species are more reactive than the free ethoxide anion with respect to attack at P=O centres. However, in this work we report that the opposite holds true at the P=S centre of fenitrothion, indicating that ion-paired alkali metal ethoxide is *less* associated with the transition state in the P=S system than in the P=O system.

A possible explanation of this reversal arises from Hard–Soft Acid Base (HSAB) theory (31). According to this theory, Li^+, Na^+, and K^+ ions are classified as "hard". In the P=O system, the $P^+–O^-$ canonical form makes a significant contribution to the overall hybrid. Consequently, the P centre bears significant positive charge and would be considered hard, while the corresponding negative charge on the oxygen renders the oxygen hard as well. Since ethoxide anion is also deemed hard, it would have a favourable interaction with the formally positive phosphorus atom. Furthermore, the hard metal cation would preferentially associate with the hard phosphoryl oxygen. In the case of EtO^- alone, there is only the hard–hard interaction with the P centre, and thus the ion-paired metal ethoxide has more favourable interactions with the P=O centre than does free ethoxide alone.

However, in the P=S system, the comparable $P^+–S^-$ form would not be expected to contribute as significantly; there would be good *p–p* overlap between P and S bonding orbitals. As a π-bonded moiety, P=S would be more polarizable than P=O, and the less electronegative sulfur, therefore, would be considered "soft". The P centre, by contrast, is bonded to three attached oxygen substituents that effectively withdraw electron density from the P centre so that it remains hard, although arguably less hard than the P site of the comparable P=O system. Consequently, the interaction of the ethoxide anion (hard) with the phosphorus atom remains favoured, but the interaction between alkali metal cation and the sulfur atom is not. Therefore, ion-paired metal ethoxide is predicted to be *less* reactive than free ethoxide at a P=S centre, exactly as was observed here.

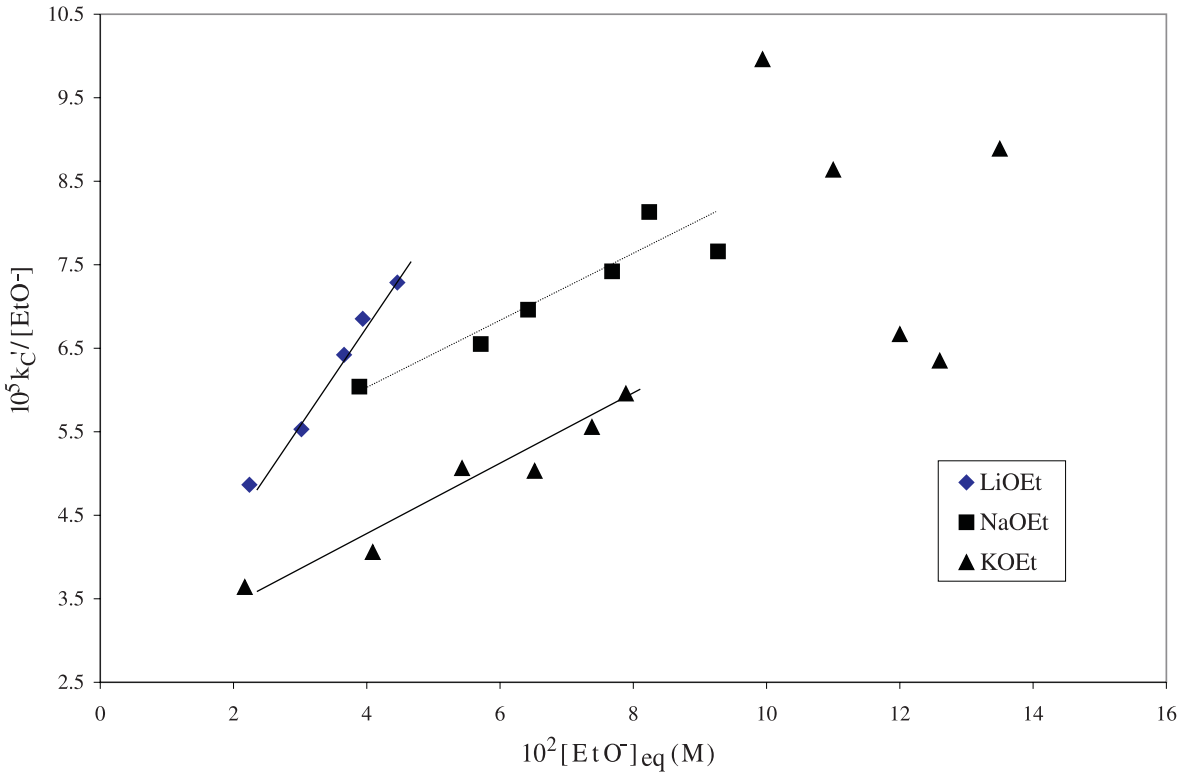
The S_N2 (C) process

In their studies of the reaction between methyl 2,4-dinitrophenyl phosphate monoanion and a variety of weakly nucleophilic phenolates, Kirby and Younas (4*a*) found all three reaction pathways (S_N2 (C), S_N2 (P), and S_NAr) to be operative. In contrast to what is reported here, Kirby reported that the S_N2 (C) pathway was not significant in comparison to the S_N2 (P) and S_NAr processes. However, in their studies using 2-(substituted phenyl)-2-oxo-1,3,2-dioxaphosphorinans, Kirby and Khan found that reaction proceeded exclusively via cleavage of the P—OAr bond (4*b*). Thus, it may be that the S_NAr process observed with methyl 2,4-dinitrophenyl phosphate monoanion was a consequence of electrostatic repulsion between the nucleophile and the phosphorus centre that would reduce reactivity at P, coupled with an aromatic ring which was activated towards S_NAr reaction by the presence of two nitro groups.

In the case of fenitrothion, since there is only one electron-withdrawing nitro group on the aromatic ring, the ring-carbon

© 2001 NRC Canada

Fig. 8. The fit of the data for the S_N2 (C) reaction of fenitrothion with LiOEt, NaOEt, and KOEt to eq. [7].



is unlikely to be sufficiently electron deficient to favour an S_NAr reaction (32). Consequently, the S_NAr process on fenitrothion becomes a minor reaction pathway.

On the other hand, reaction at the aliphatic methoxy carbon was observed by Greenhalgh et al. (5*b*) in fenitrothion hydrolysis under acidic conditions. Under alkaline conditions, Me—O bond fission was not observed.

The observed rate behaviour for S_N2(C) displacement reactions at the aliphatic centre of fenitrothion (Figs. 1*c* and 3) shows no evidence of metal ion catalysis with any of the nucleophiles used. In fact, the plots of k_c' vs. $[MOEt]_o$ exhibit, within experimental error, downward curvature. It should be noted that the error bars are larger at higher $[MOEt]_o$, owing mainly to uncertainty in the concentration of **2**, which was determined by subtracting the measured concentration of **6** (the product of attack at phosphorus) from the initial fenitrothion concentration. For example, when $[KOEt]_o$ = 1.56 M, the measured absorbance for the phenoxide product was 1.39 ± 0.01. For the reaction to proceed exclusively by attack at phosphorus, the expected infinity absorbance is 1.45. The difference, then, is due to products arising from the S_N2(C) pathway, and accounts for 0.06 ± 0.01 absorbance units, a relative uncertainty of ca. 17%. With this level of uncertainty in some of the data points, one might be tempted to state that plots of k_c' vs. $[MOEt]_o$ are, within error, linear. In principle, a linear second-order plot would suggest that all forms of the nucleophile (i.e., free ethoxide, ion-paired metal ethoxide, and dimers) are equally reactive, contradicting the observed findings from the addition of complexing agents (Figs. 2 and 4), which showed that for attack at the aliphatic centre, *free ethoxide is more reactive* than either ion-paired or dimerized alkali metal ethoxide.

The suggested downward curvature in Figs. 1*c* and 3 is not unprecedented. For other S_N2 reactions at carbon, downward curvature in a second-order plot has been shown to indicate that dissociated anions are more reactive than are ion-paired anions (33, 34), exactly as is observed in this study. The addition of KOAc to the reaction of fenitrothion with 0.025 M KOEt (Table 4), which results in a right-ward shift of the equilibrium depicted in Scheme 3, confirms this finding, as evidenced by the corresponding decrease in the values for k_c'.

For reaction at the aliphatic centre, Scheme 2 continues to apply except that where the reactivity order for reaction at phosphorus was dimers > free ethoxide > ion-paired metal ethoxide, as discussed above, the S_N2(C) reaction proceeds in the order: free ethoxide > dimers, ion-paired metal ethoxide (with no distinction possible between the reactivities of these latter two species). The experimental data should fit eq. [6] (derived in the same manner as eq. [4]):

$$[6] \qquad \frac{k_c'}{[EtO^-]_{eq}} = \frac{k_{dim}^C}{K_d' K_d}[EtO^-]_{eq}^3 + \frac{k_{MOEt}^C}{K_d}[EtO^-]_{eq} + k_{EtO^-}^C$$

where k_{dim}^C is the rate of reaction due to dimerized metal ethoxide, and K_d' is the dissociation constant of said dimers. Since k_{dim}^C is less than $k_{EtO^-}^C$, and the values for $[EtO^-]^3$ are much smaller than those for $[EtO^-]$, the first term on the

© 2001 NRC Canada

right-hand side of eq. [6] is treated here as being negligible, and eq. [6] reduces to a convenient linear equation, eq. [7].

$$[7] \qquad \frac{k'_c}{[EtO^-]_{eq}} = \frac{k^C_{MOEt}}{K_d}[EtO^-]_{eq} + k^C_{EtO^-}$$

The essentially linear fit of the data to eq. [7] is shown in Fig. 8.

The average $k^C_{EtO^-}$ value obtained from the plots is 3.18×10^{-4} M^{-1} s^{-1}, whereas the experimentally determined $k^C_{EtO^-}$ value is $(2.39 \pm 0.53) \times 10^{-4}$ M^{-1} s^{-1}. Given that the experimentally determined value for k^C_{EtO-} was obtained at low $[MOEt]_o$ (i.e., where the relative error in the final absorbance measurements was smaller than at the higher $[MOEt]_o$ included in the fitting to eq. [7]), it can be stated that the theoretical and experimental $k^C_{EtO^-}$ values are largely in agreement.

Leaving group pK_a values can largely explain why no metal ion catalysis is observed for the $S_N2(C)$ process yet is observed for attack at phosphorus. For metal ion catalysis to be observed, the metal ion (either as an ion pair with ethoxide or as a dimer) must participate in stabilizing the rate-determining transition state. For the $S_N2(C)$ pathway, the estimated pK_a of demethyl fenitrothion of 2.15 (based on the pK_a of H_3PO_4 (35)) is sufficiently low that metal ions are not required to stabilize the rate-determining transition state, whereas the conjugate acid of the aryl oxide leaving group for the reaction at phosphorus has a pK_a of 7.15, and can thus be stabilized by metal ion interactions.

The fact that higher MOEt concentrations favour attack at phosphorus further suggests that the geometry of the dimer (as shown in **7**) is better suited for attack at the phosphorus centre rather than the aliphatic carbon. A significant part of the catalytic role of the dimer thus appears to be the ability to orient the nucleophile towards nucleophilic attack, a function the dimer cannot perform for the $S_N2(C)$ degradation pathway.

Experimental

Materials

Anhydrous ethanol was obtained by refluxing absolute ethanol with magnesium turnings in the presence of iodine followed by distillation. Solutions of potassium or sodium ethoxide were prepared by dissolving clean potassium or sodium metal (Aldrich) in anhyd ethanol at 0°C, under nitrogen. Lithium ethoxide solutions were prepared in a similar manner by dissolving lithium hydride (Alfa–Aesar) in dry ethanol. If required, the ethoxide solutions were filtered at the end of the reaction in the glove box under nitrogen to remove any insoluble materials. The concentration of base was determined by titration with anhyd potassium hydrogen phthalate (KHP, VWR). All other chemicals were purchased from Aldrich unless otherwise indicated.

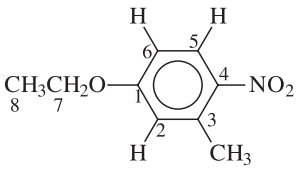
The macrocyclic complexing agents that were purchased from Aldrich were dicyclohexyl-18-crown-6 (DC-18-C-6), 18-C-6, [2.2.2] cryptand, and [2.1.1] cryptand. Potassium acetate (KOAc) was purchased from VWR. All were used without further purification.

The fenitrothion (96.7%) used in this study was a gift from Sumitomo Chemicals (Japan) and was purified as follows. Fenitrothion was loaded directly onto the head of a column (34 × 5 cm) of silica gel (wet-packed with hexane) and eluted using successive volumes of hexane (800 mL, discarded) and toluene (1600 mL). The toluene fraction was collected in a round-bottom flask and the solvent removed under reduced pressure, at a temperature not greater than 40°C in order to avoid the possible isomerization of fenitrothion (36, 37). The purity of the product was verified by both GC-MS and NMR (13).

Synthesis of authentic standards

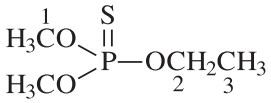
3-Methyl-4-nitro-ethoxybenzene

To 5-fluoro-2-nitrotoluene (0.500 g, 3.22×10^{-3} mol) was added DABCO (1,4-diazabicyclo[2.2.2]octane, 1.1 equiv) and KOEt (0.896 M, 1.1 equiv) in anhyd ethanol (95 mL), and the solution was allowed to stir overnight in a nitrogen dry box. Iced 20% v/v HCl (200 mL) was added, and the cloudy solution was reduced by rotary evaporation at which point the flask was left in a refrigerator overnight. The crystals were then filtered, recrystallized from water, and dried in an Abderhalden drying pistol, yield 20%: mp 54–54.3°C (lit. (38): 53–55°C). EI-MS (solvent: chloroform) *m/z*: 181.2. ^{1}H NMR (400 MHz, $CDCl_3$) δ: 1.43 (t, $^3J_{H7–H8}$ = 7.00 Hz, 3H, C*H*$_3$CH$_2$O-), 2.61 (s, 3H, 3-C*H*$_3$ aryl ring), 4.09 (q, $^3J_{H8–H7}$ = 7.00 Hz, 2H, CH$_3$C*H*$_2$O-), 6.78 (m, 2H, *H*-2, -6), 8.06 (dd, $^3J_{H6–H5}$ = 8.60, $^4J_{H2–H5}$ = 2.68 Hz, 1H, *H*-5).



O-Ethyl-O,O-dimethylphosphorothioate

To *O,O*-dimethylthiophosphoryl chloride (3.966 g, 0.0247 mol) was added KOEt (0.898 M, 1.1 equiv) in anhyd ethanol (47 mL), and the solution was allowed to stir overnight. The precipitate (KCl) was removed by filtering the mixture through a bed of celite, and the remaining ethanol was removed under reduced pressure without the application of heat. The resulting pale yellow oil was purified by flash chromatography using 4:1 diethyl ether : chloroform as eluent. The final product was a pale yellow oil. EI-MS (solvent: chloroform) *m/z*: 170.0. ^{1}H NMR (400 MHz, $CDCl_3$) δ: 1.33 (td, $^3J_{H2–H3}$ = 9.20, $^4J_{P–H}$ = 0.40 Hz, 3H, C*H*$_3$CH$_2$O-), 3.74 (d, C*H*$_3$O-, $^3J_{P–H}$ = 9.00 Hz, 6H), 4.13 (qd, $^3J_{H3–H2}$ = 9.20, $^3J_{P–H}$ = 1.80 Hz, 2H, CH$_3$C*H*$_2$O-). ^{13}C NMR (400 MHz, $CDCl_3$) δ: 16.19 (C-3), 54.76 (C-1), 64.85 (C-2). ^{31}P NMR (400 MHz, DMSO-d_6, relative to 85% H_3PO_4) δ: 72.78.

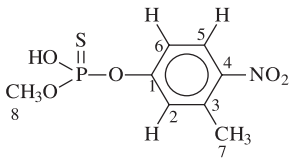


Demethyl fenitrothion

Following the procedure of Chambers and Matthews (39), fenitrothion (1.3227 g, 4.77×10^{-3} mol, Sumitomo Chemicals) was added to KBr (0.596 g, 1.05 equiv) in methanol (25 mL), and the solution was brought to reflux for 20 h, with stirring,

© 2001 NRC Canada

while argon was passed through the solution to ensure that the methyl bromide byproduct was removed (thus preventing *S*-methylation of demethyl fenitrothion). The methanol was then removed under reduced pressure at which point the residual fenitrothion was dissolved in diethyl ether, and the demethyl fenitrothion salt was extracted into water. The water was acidified using an excess of HCl, and another extraction with diethyl ether was performed. The diethyl ether was then removed under reduced pressure, yielding a pale yellow oil. GC-MS(EI) (solvent: $CDCl_3$; using GC parameters outlined below) *m*/*z*: 263 (GC peak at 20.65 min). ^{1}H NMR (300 MHz, $CDCl_3$) δ: 2.63 (s, 3H, aryl-C*H*$_3$), 3.92 (d, $^3J_{P-H}$ = 14.1 Hz, 3H, C*H*$_3$O-), 6.15 (s, 2H, -O*H*), 7.21 (d, $^3J_{H5-H6}$ = 9.0 Hz, 2H, *H*-2,-6), 8.05 (d, $^3J_{H6-H5}$ = 9.0 Hz, 1H, *H*-5,). ^{13}C NMR (300 MHz, $CDCl_3$) δ: 21.2 (C-7), 55.5 (C-8), 119.6, 125.1, 127.1 (C-2,5,6), 136.8, 146.2, 153.9 (C-1,3,4). ^{31}P NMR (300 MHz, DMSO-d_6, relative to 85% H_3PO_4) δ: 54.8, 16.4 (impurity, ~12%).



Kinetic measurements

General

Duplicate kinetic runs by UV–vis spectrophotometry were followed using either a Varian CARY3, a Hewlett–Packard 8452A, or Perkin–Elmer λ-5 spectrophotometer. The instruments were equipped with thermostatted cell-holders, and the temperature inside the 10 mm quartz cuvette was maintained at 25.0°C. All reactions were carried out under pseudo-first-order conditions in which the concentration of base was at least 100 times greater than the initial substrate concentration. All solutions were transferred from the round-bottom flasks to the quartz cuvettes, under nitrogen, using gas-tight syringes.

The reactions were followed by one of two methods. The first method involved using the HP8452A spectrophotometer for repeat scanning between 200 and 650 nm. This provided information pertaining to the rate of product appearance and substrate disappearance. The second method involved monitoring the appearance of product at a fixed wavelength, corresponding to the maximum absorption of the product (λ_{max}), as determined by the first method. In the case of fenitrothion degradation in basic ethanol, λ_{max} for the 3-methyl-4-nitrophenoxide ion was found to be 398 nm.

In general, each reaction was followed for 3 half lives, and the infinity absorbance value (A_{inf}) was taken after 10 half lives. Pseudo-first-order rate constants, k_{obs}, were determined from linear plots of log ($A_{inf} - A_t$) versus time, where A_t is the absorbance value at time *t*. Specifically, the slope of the plot was equal to $2.303k_{obs}$.

Product analysis experiments

Two types of product analysis experiments were performed.

The first method involved the use of ^{31}P NMR, in a pseudo-first-order kinetic experiment. An NMR sample was prepared such that it contained 0.898 M KOEt and 0.02 M fenitrothion, in anhyd ethanol. A sealed capillary tube containing DMSO-d_6 was placed into the NMR sample tube as signal lock, and spectra were acquired on a 300 MHz Bruker NMR instrument every 15 min for the first 15 h of reaction, and then obtained periodically over the next 17 days in order to monitor possible consecutive reactions. By comparisons with both authentic standards and literature values, the peaks observed throughout this reaction were determined to be those for **1** (67.0 ppm), **5** (72.6 ppm), and **2** (54.9 ppm). **3** (58.6 ppm) was identified from the available literature value (40).

The second method of product analysis involved the use of GC-MS. As described above, a reaction was initiated between 0.898 M KOEt and 0.02 M fenitrothion in anhyd ethanol. A 0.1 mL aliquot of the reaction mixture was removed at various time intervals. To this aliquot was added 1.14 equiv of HCl, which quenched the reaction, and the quenched aliquot was then extracted with $CHCl_3$ (2 × 1 mL). The $CHCl_3$ extract was dried over $MgSO_4$, transferred to a vial, and stored in a refrigerator until analysis by GC-MS was performed, using a Fisons 8000 gas chromatography instrument equipped with a MD800 mass spectrometer. The GC was equipped with a DB-5 capillary column and used helium as the carrier gas at a flowrate of 6 psig. At the start of the injection, the oven temperature was set to 85°C for 3 min and ramped at a rate of 10°C/min until reaching 215°C. Particular attention was paid to the peak for 3-methyl-4-nitro-ethoxybenzene, which was quantitated by comparison to the GC-MS results of the authentic compound.

Acknowledgements

This research was supported by the Natural Sciences and Engineering Research Council of Canada (G. vL. and E.B.) and by the Principal's Research Fund of Sir Wilfred Grenfell College (J.M.D.). The authors are grateful to B.G. Cox (Zeneca, U.K.), R. Kluger (University of Toronto), and S. Hoz (Bar-Ilan University, Israel) for helpful discussions.

References

1. (*a*) M.T. Annandale, G.W. vanLoon, and E. Buncel. Can. J. Chem. **76**, 873 (1998); (*b*) R. Sha'ato, E. Buncel, D.G. Gamble, and G.W. vanLoon. Can. J. Soil. Sci. **80**, 301 (2000); (*c*) J.E. Omakor, I. Onyido, G.W. vanLoon, and E. Buncel. J. Chem. Soc. Perkin Trans. 2, 324 (2001).
2. (*a*) J.R. Cox, Jr., and O.B. Ramsay. Chem. Rev. **64**, 317 (1964); (*b*) R.F. Hudson. Structure and mechanism in organophosphorus chemistry. Academic Press, London. 1965; (*c*) A.J. Kirby and S.G. Warren. The organic chemistry of phosphorus. Elsevier, Amsterdam. 1967; (*d*) A.N. Pudovik. Chemistry of organophosphorus compounds. MIR Publishers, Moscow. 1989.
3. (*a*) N. Bourne and A. Williams. J. Am. Chem. Soc. **106**, 7591 (1984); (*b*) N. Bourne, E. Chrystiuk, A.M. Davis, and A. Williams. J. Am. Chem. Soc. **110**, 1890 (1988); (*c*) S.A. Ba-Saif, A.M. Davis, and A. Williams. J. Org. Chem. **54**, 5483 (1989); (*d*) S.A. Ba-Saif, M.A. Warring, and A. Williams. J. Am.

© 2001 NRC Canada

Chem. Soc. **112**, 8115 (1990); (*e*) A. Williams. Adv. Phys. Org. Chem. **27**, 1 (1992).
4. (*a*) A.J. Kirby and M. Younas. J. Chem. Soc. B, 1165 (1970); (*b*) A.J. Kirby and S.A. Khan. J. Chem. Soc. B, 1172 (1970).
5. (*a*) J. Toullec and M. Moukawim. Chem. Commun. 221 (1996); (*b*) R. Greenhalgh, K.L. Dhawan, P. Weinberger. J. Agric. Food Chem. **28**, 102 (1980).
6. (*a*) R. Breslow. Adv. Enzymol. Relat. Areas Mol. Biol. **58**, 1 (1986); (*b*) M.J. Young and J. Chin. J. Am. Chem. Soc. **117**, 10577 (1995); (*c*) A. Torrents and A.T. Stone. Soil Sci. Soc. Am. **58**, 738 (1994).
7. R. Nagelkerke, M.J. Pregel, E.J. Dunn, G.R.J. Thatcher, and E. Buncel. Org. React. **29**, 11 (1995).
8. (*a*) E.J. Dunn and E. Buncel. Can. J. Chem. **67**, 1440 (1989); (*b*) E.J. Dunn, R.Y. Moir, E. Buncel, J.G. Purdon, and R.A.B. Bannard. Can. J. Chem. **68**, 1837 (1990).
9. M.J. Pregel and E. Buncel. J. Chem. Soc. Perkin Trans. 2, 307 (1991).
10. M.J. Pregel, E.J. Dunn, and E. Buncel. J. Am. Chem. Soc. **113**, 3545 (1991).
11. M.J. Pregel, E.J. Dunn, R. Nagelkerke, G.R.J. Thatcher, and E. Buncel. Chem. Soc. Rev. 449 (1995).
12. C. Tomlin. The pesticide manual. 10th ed. Royal Society of Chemistry, London. 1994.
13. Fenitrothion: the effects of its use on environmental quality and its chemistry. Associate Committee on Scientific Criteria for Environmental Quality. National Research Council Canada Publication 14104 (1975).
14. (*a*) C.H. Rochester. Acidity functions. Academic Press, London. 1970; (*b*) F. Peure and R. Schaal. Bull. Soc. Chim. Fr. 2636 (1963); (*c*) R. Schaal and F. Peure. Compt. Rend. Ser. C, **260**, 4020 (1963); (*d*) F. Terrier and R. Schaal. Compt. Rend. Ser. C, **264**, 465 (1967).
15. V. Gold and J. Toullec. J. Chem. Soc. Perkin Trans. 2, 596 (1979).
16. (*a*) R.E. Dinnebier, M. Pink, J. Sieler, and P.W. Stephens. Inorg. Chem. **36**, 3398 (1997); (*b*) J.R. Jones. Trans. Faraday Soc. **64**, 440 (1968).
17. M.H. Chisholm, S.R. Drake, A.A. Naini, and W.E. Streib. Polyhedron, **10**, 805 (1991).
18. M.H. Chisholm, S.R. Drake, A.A. Naini, and W.E. Streib. Polyhedron, **10**, 337 (1991).
19. L.M. Jackman and E.F. Rakiewicz. J. Am. Chem. Soc. **113**, 1202 (1991).
20. L.M. Jackman, E.F. Rakiewicz, and A.J. Benesi. J. Am. Chem. Soc. **113**, 4101 (1991).
21. J.S. DePue and D.B. Collum. J. Am. Chem. Soc. **110**, 5524 (1988).
22. A. Streitwieser, Jr., J.A. Krom, K.V. Kilway, and A. Abbotto. J. Am. Chem. Soc. **120**, 10801 (1998).
23. A. Abbotto, S.S-W. Leung, A. Streitwieser, Jr., and K.V. Kilway. J. Am. Chem. Soc. **120**, 10807 (1998).
24. M.G. Stanton, C.B. Allen, R. Kissling, A.L. Lincoln, and M.R. Gagne. J. Am. Chem. Soc. **120**, 5981 (1998).
25. V. Pechanec, O. Kocian, and J. Zavada. Coll. Czech. Chem. Commun. **47**, 3405 (1982).
26. K.J. Msayib and C.I.F. Watt. Chem. Soc. Rev. 237 (1992).
27. J. Barthel, G. Bader, and M. Raach-Lenz. Z. Phys. Chem. (Munich), **84**, 10 (1973).
28. E. Grunwald and B.J. Berkowitz. J. Am. Chem. Soc. **73**, 4939 (1951).
29. H.A. Laitinen. Chemical analysis. McGraw–Hill Book Co., Toronto. 1960.
30. D. Reichenberg. *In* Ion exchange. Vol. 1. *Edited by* J.A. Marinsky. M. Dekker, New York. 1966. Chap. 7.
31. (*a*) R.G. Pearson. Surv. Prog. Chem. **5**, 1 (1969); (*b*) R.G. Pearson. Inorg. Chem. **27**, 734 (1988).
32. (*a*) F. Terrier. Nucleophilic aromatic displacement. The effect of the Nitro Group. VCH Publisher, New York. 1991; (*b*) E. Buncel, J.M. Dust, and F. Terrier. Chem. Rev. **95**, 2261 (1995).
33. P. Jones, P. Harrison, and L. Wynne-Jones. J. Chem. Soc. Perkin Trans. 2, 1679 (1979).
34. N.N. Lichten and K.N. Rao. J. Am. Chem. Soc. **83**, 2417 (1961).
35. D.A. Skoog, D.M. West, and F.J. Holler. Fundamentals of analytical chemistry. 5th ed. Saunders Publishing, London. 1988.
36. M. Eto, L.C. Tan, Y. Oshima, and K. Takehara. Agric. Biol. Chem. **32**, 656 (1968).
37. R.D. O'Brien. Toxic phosphorus esters. Academic Press, New York. 1960.
38. M. Ozaki. J. Soc. Org. Synth. Chem. Jpn. **13**, 80 (1955).
39. J. Chambers and W.A. Matthews. Bull. Environ. Contam. Toxicol. **18**, 326 (1977).
40. J.C. Tebby. Handbook of phosphorus-31 nuclear magnetic resonance data. CRC Press, Boca Raton. 1991.

© 2001 NRC Canada

Two-photon absorption of styryl-quinolinium, -pyridinium, and -barbituric acid derivatives, and intramolecular charge transfer

XiaoMei Wang, Chun Wang, WenTao Yu, YuFang Zhou, Xian Zhao, Qi Fang, and MinHua Jiang

Abstract: A series of new chromophores, styryl-parent end-capped with various donors, and with barbituric acid, methyl-pyridinium, and methyl-quinolinium as the acceptors, have been synthesized and characterized by element analysis or X-ray diffraction. Using the *Z*-scan system, their two-photon absorption (TPA) cross-section values (δ) have been determined under excitation with 10 Hz, and 1064 nm, 35 ps mode-locked Nd:YAG laser pulse in DMF with d_0 = 0.05 M. The effective δ value is as high as 10.9×10^{-48} cm^4 s per photon for *trans*-4-(4′-*N*,*N*-diphenyl amino) styryl-*N*-methyl quinolinium iodide (DPASQI). The δ value increases from barbituric acid- to pyridinium- to quinolinium-derivatives apparently due to the increase in both the conjugated degree and planarity; however, when the acceptor is fixed, the δ value increases from dialkyl amino groups to diphenyl amino groups even though the latter is a weaker donor than the dialkyl amino groups. Theoretical calculations confirm that the increased distortion from planarity for the barbituric acid derivative makes its δ value decrease. The relatively large δ value for quinolinium- or pyridinium-derivatives originates from larger intramolecular charge transfer, which can be characterized by the difference of dipole moment ($\Delta\mu_{ge}$) between the S_0 and S_1, and the transition dipole moment ($M_{ee'}$) between S_1 and S_2.

Key words: two-photon absorption, intramolecular charge transfer, styryl-quinolinium, styryl-pyridinium, styryl-barbituric acid.

Résumé : On a synthétisé une série de nouveaux chromophores, un styryle de base recouvert de divers donneurs et des accepteurs comme l'acide barbiturique et les ions méthylpyridinium et méthylquinoléinium et on les a caractérisés par analyse élémentaire ou diffraction des rayons X. Faisant appel à un système à balayage Z et opérant dans le DMF avec d_0 0,05 M, une excitation de 10-Hz et une pulsation laser Nd:YAG de 35 ps en mode bloqué, on a déterminé les valeurs, δ, des sections efficaces de leur absorption de deux photons. Dans le cas de l'iodure du *trans*-4-((4′-*N*,*N*-diphénylamino) styryl-*N*-méthylquinoléinium (« DPASQI »), la valeur δ effective s'élève jusqu'à $10{,}9 \times 10^{-48}$ cm^4 s/photon. Par ailleurs, la valeur de δ augmente en passant de l'acide barbiturique, puis aux dérivés pyridinium et quinoléinium; il semble que cette situation résulte d'une augmentation tant du degré de conjugaison que de la planarité. De plus, lorsque l'accepteur est fixé, la valeur de δ augmente des groupes dialkylamino aux groupes diphénylamino même si ces derniers sont des donneurs plus faibles que les groupes dialkylamino. Des calculs théoriques confirment que, dans le cas de l'acide barbiturique, l'augmentation de la distorsion par rapport à la planarité provoque une diminution de la valeur de δ. La valeur relativement élevée de δ pour les dérivés quinolinéinium et pyridinium trouverait son origine dans un important transfert de charge intramoléculaire qui peut être caractérisé par la différence du moment dipolaire ($\Delta\mu_{ge}$) entre S_0 et S_1 et la transition du moment dipolaire ($M_{ee'}$) entre S_1 et S_2.

Mots clés : absorption à deux photons, transfert de charge intramoléculaire, styryl-quinoléinium, styryl-pyridinium, styryl-acide barbiturique.

[Traduit par la Rédaction]

Introduction

Organic conjugated chromophores with a large two-photon absorption (TPA) cross-section emerge as very attractive elements for use in a number of optical applications such as optical data storage, up-converted lasing, and optical power limiting (1–10). Numerous organic compounds have been investigated experimentally and theoretically in order to understand the structure–property relationship of materials with large TPA cross-sections (11–17). Some general structural parameters for increasing the molecular TPA cross-section values (δ) have gradually been drawn in several laboratories (11–15). For example: (*i*) increasing the donor and acceptor strength; (*ii*) changing the character of the conjugated bridge; (*iii*) increasing the planarity of the chromophores; and (*iv*) extending the conjugated length. The results of theoreti-

Received June 19, 2000. Published on the NRC Research Press Web site on March 14, 2001.

X.M. Wang, C. Wang, W.T. Yu, Y.F. Zhou, X. Zhao, Q. Fang, and M.H. Jiang.[1] State Key Laboratory of Crystal Materials, Shandong University Jinan, 250100 China.

[1]Corresponding author (e-mail: mhjiang@sdu.edu.cn).

 DOI: 10.1139/cjc-79-2-174 © 2001 NRC Canada

Table 1. Optical properties and calculated structural parameters for all chromophores.

Chromophore	$\theta^{d/o\ a}$	$\Delta\mu_{ge}$ (debye)	$M_{ee'}$ (debye)	β (cm GW^{-1})	δ ($\times 10^{-48}$) cm^4 s photon^{-1}
HMASBA	70	0.7	—	0.60	3.9
PSPI	Planar	3.4	8.5	0.91	5.7
DEASPI	Planar	8.1	8.2	1.09	6.8
HEASPI	Planar	8.2	8.6	1.12	7.0
DPASPI	Planar	11.8	9.8	1.42	8.8
HMASQI	Planar	10.6	—	1.41	8.8
DPASQI	Planar	12.1	—	1.75	10.9

[a]The dihedral angle between two rings of the backbone.

Table 2. Crystallographic data for DPASPI and HMASQI.

	DPASPI	HMASQI
Formula	$C_{26}H_{23}IN_2$	$C_{21}H_{23}IN_2O$
MW	490.36	446.31
T (K)	293	293
System	Orthorhombic	Monoclinic
Space group	*Pbca*	$P2_1/n$
a, b, c (Å)	10.5638(14), 11.1909(19), 37.255(4)	10.0512(11), 16.2879(12), 12.3328(8)
α, β, γ (°)	90	90, 102.307(6), 90
V (Å^3)	4404.2(11)	1972.6(3)
Z	8	4
D calcd. (g cm^{-1})	1.479	1.503
Absorption coefficient (mm^{-1})	1.468	1.634
F (000)	1968	896
Crystal size (mm)	0.20 × 0.28 × 0.25	0.35 × 0.30 × 0.20
θ range (deg)	2.2–25.0	2.10–26.00
Index range	$-12 \le h \le 1$, $-13 \le k \le 1$, $-44 \le l \le 1$	$-1 \le h \le 12$, $-1 \le k \le 20$, $-15 \le l \le 15$
Refl. collected	4906	4906
Independent refl.	3847 [R (int) = 0.064]	3882 [R (int) = 0.0230]
Max and min transmission	0.301 and 0.202	0.689 and 0.561
Final R indices [$I > 2\sigma(I)$]	R_1 = 0.0776, wR_2 = 0.2372	R_1 = 0.0358, wR_2 = 0.0824
R indices	R_1 = 0.1409, wR_2 = 0.2372	R_1 = 0.0558, wR_2 = 0.0939
Largest diff. peak and hole (e Å^{-3})	1.79 and –1.11	0.5809 and – 0.499
GoF on F^2	0.93	1.066
Data/restraint/parameters	3847 / 0 / 262	3882 / 0 / 226

cal studies further reveal that the TPA δ value is related to the imaginary part of the third-order polarizability (16),

$$[1] \qquad \delta(\omega) = \frac{4\pi h\omega^2}{n^2 c^2} L^4 \,\mathrm{Im}\ \gamma(-\omega;\omega,\omega,-\omega)$$

where h is Planck's constant, n is the index of refraction of the medium, L is a local field factor (equal to 1 for vacuum), and c or ω is the speed of light or the frequency of light. When the frequency (ω) is left out of consideration, the third-order polarizability (γ) can be expressed as eq. [2] (17–18),

$$[2] \qquad \gamma_{xxxx} = 24\frac{M_{ge}^2}{E_{ge}^2}\left[\frac{\Delta\mu^2{}_{ge}}{E_{ge}} + \sum_{e'}\frac{M_{ee}^2}{E_{ge'}} - \frac{M_{ge}^2}{E_{ge}}\right]$$

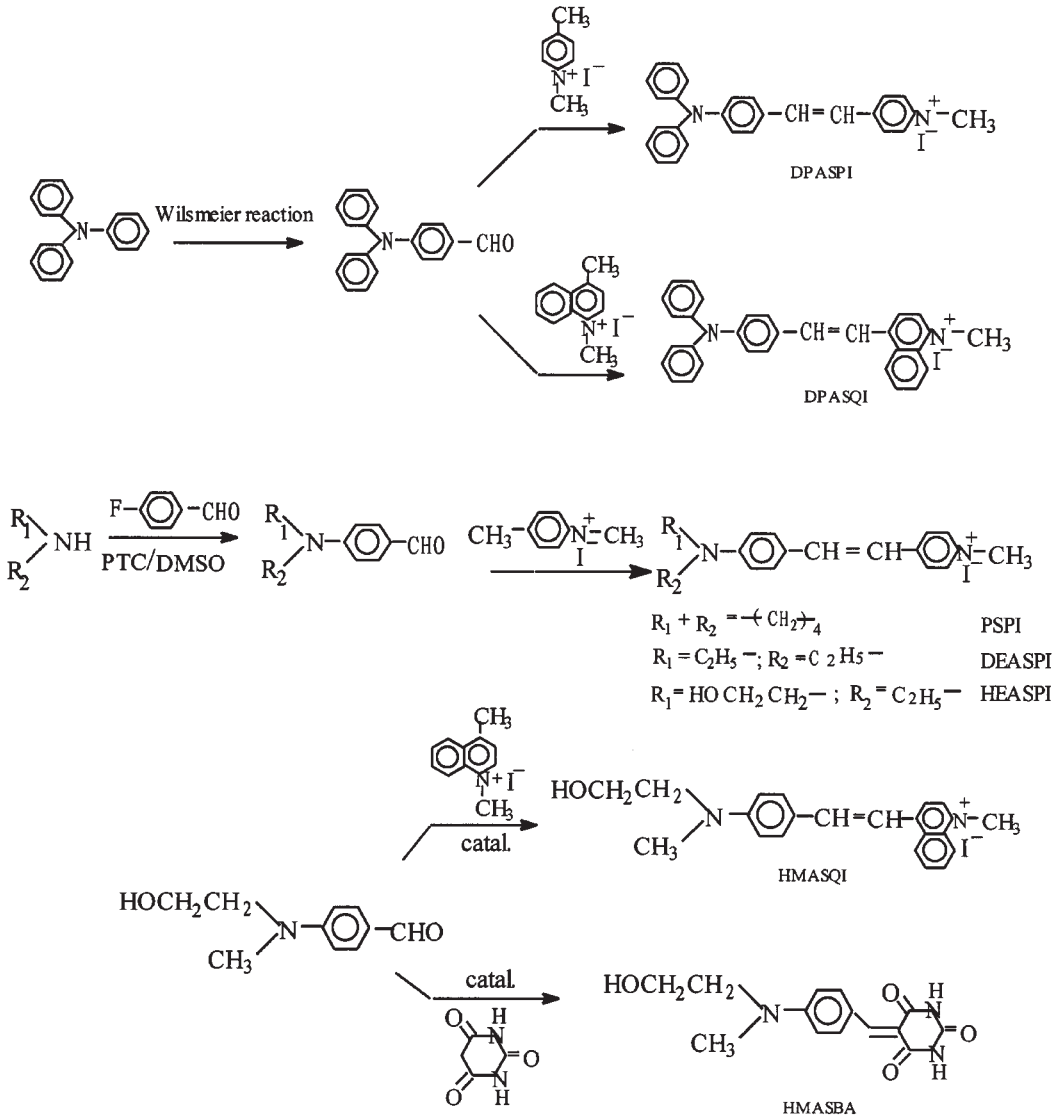
where $\Delta\mu_{ge}$ is the difference of dipole moment between the ground state (S_0) and the first excited state (S_1); M_{ge} or $M_{ee'}$ is the transition dipole moment between S_0 and S_1 or between the two lowest excited states, that is, S_1 and S_2, and E_{ge} or $E_{ge'}$ is the difference between ground and excited state energy or between the two excited states. The first two terms in eq. [2] make a positive contribution to the TPA process (17).

It is evident that the TPA δ value is dependent not only on the difference between the ground- and excited-state dipole moment but also the transition dipole moment between two excited states. It is rational to deduce that materials with large $\Delta\mu_{ge}$ and $M_{ee'}$ must have exhibited high δ values due to stronger intramolecular charge transfer.

Based on this idea, we calculated structural parameters, such as $\Delta\mu_{ge}$ and $M_{ee'}$, for π-donor–acceptor compounds. One of the better candidate groups for generating a larger intramolecular charge shift is the substituted styryl-pyridinium cations. Other promising candidates are the substituted styryl-quinolinium cations. These kinds of salts possess the fused aromatic heterocyclic ring that may improve π-electron delocalization and result in better TPA properties. In addition the structural parameters for the barbituric acid derivative have also been calculated to examine the influence planarity and conjugated length upon TPA property. The calculation results are shown in Table 1.

© 2001 NRC Canada

Scheme 1.



methyl-pyridinium and further to methyl-quinolinium moiety, and also by varying the donor strengths in the order of: dialkylamino group > diphenylamino group. On the basis of correlated quantum-chemical calculation and experimental measurement results, we further demonstrate that large $\Delta\mu_{ge}$ and $M_{ee'}$ can result in large intramolecular charge transfers, which have contributed to enhance the two-photon absorption cross-section.

Experimental

Synthesis

The decomposition temperatures were measured on a Perkin–Elmer TGS-2 thermogravimetric analyzer at a rate of 20°C min^{-1} under nitrogen atmosphere. Element analyses were performed on a Perkin 2400. Mass spectra were recorded with an HP5989 apparatus. NMR spectra were determined on FX-90Q NMR spectrometer (TMS as standard).

Synthesis of donor and acceptor components

4-Pyrrolidinyl benzaldehyde, 4-(*N*,*N*-diethyl amino)benzaldehyde, 4-(*N*,*N*-diphenyl amino)benzaldehyde, 4-(*N*-hydroxyethyl-*N*-ethyl amino)benzaldehyde and 4-(*N*-hydroxyethyl-*N*-methyl amino)benzaldehyde were synthesized according to ref. 11.

4-Methyl-*N*-methylquilinonium iodide was synthesized by the reaction of lepidine (4.3 g, 30 mmol) and methyl iodide (4.4 g, 31 mmol) in ethanol (30 mL) at reflux temperature for 2 h. After cooling, the solution was filtered and recrystallized in ethanol. Yellow needle crystals were obtained with yield 80%.

Synthesis of chromophores

Chromophores were synthesized by the Knoevenagel condensation reaction of the appropriate substituted benzaldehyde and the acceptor components such as 4-methyl-*N*-methylpyridinium iodide and 4-methyl-*N*-methylquinolinium iodide with a catalytic amount of piperidine. For example, a mixture of equal molar 4-(*N*,*N*-diphenyl amino)benzaldehyde (3.5 g, 13 mmol) and 4-methyl-*N*-methylquinolinium iodide (3.7 g, 13 mmol) were stirred in ethanol (20 mL) at reflux temperature overnight in the presence of 4–5 drops piperdine. After cooling, the crude product of DPASQI

© 2001 NRC Canada

Table 3. Selected bond lengths (Å) and angles (°) for HMASQI.

N(1)—C(10)	1.331(5)	C(2)—C(3)	1.406(6)	C(9)—C(10)	1.372(6)
N(1)—C(2)	1.381(5)	C(3)—C(4)	1.355(6)	C(11)—C(123)	1.352(5)
N(1)—C(1)	1.475(5)	C(4)—C(5)	1.402(7)	C(12)—C(13)	1.442(5)
N(2)—C(16)	1.353(5)	C(5)—C(6)	1.367(6)	C(13)—C(18)	1.395(5)
N(2)—C(21)	1.464(6)	C(6)—C(7)	1.414(5)	C(13)—C(14)	1.403(5)
N(2)—C(19)	1.480(6)	C(7)—C(8)	1.448(5)	C(14)—C(15)	1.362(6)
O(1)—C(20)	1.465(6)	C(8)—C(9)	1.386(5)	C(15)—C(16)	1.408(6)
C(2)—C(7)	1.413(5)	C(8)—C(11)	1.436(5)	C(16)—C(17)	1.405(6)
C(17)—C(18)	1.379(6)	C(19)—C(20)	1.460(7)		
C(2)-N(1)-C(10)	120.5(3)	C(3)-C(4)-C(5)	120.4(4)	C(19)-C(20)-O(1)	105.4(4)
C(10)-N(1)-C(1)	118.9(4)	C(6)-C(5)-C(4)	120.1(4)	C(12)-C(11)-C(8)	124.9(4)
C(2)-N(1)-C(1)	120.6(3)	C(5)-C(6)-C(7)	121.4(4)	C(11)-C(12)-C(13)	126.4(4)
C(16)-N(2)-C(21)	121.6(4)	C(2)-C(7)-C(6)	117.3(4)	C(18)-C(13)-C(14)	115.9(4)
C(16)-N(2)-C(19)	121.9(4)	C(2)-C(7)-C(8)	120.3(3)	C(18)-C(13)-C(12)	123.6(3)
C(21)-N(2)-C(19)	115.6(4)	C(6)-C(7)-C(8)	122.4(4)	C(14)-C(13)- C(12)	120.4(4)
N(1)-C(2)-C(3)	120.4(4)	C(9)-C(8)-C(11)	122.9(4)	C(15)-C(14)-C(13)	122.0(4)
N(1)-C(2)-C(7)	119.2(3)	C(9)-C(8)-C(7)	115.9(3)	C(14)-C(15)-C(16)	122.3(4)
C(3)-C(2)-C(7)	120.4(4)	C(11)-C(8)-C(7)	121.3(3)	N(2)-C(16)-C(17)	120.5(4)
C(4)-C(3)-C(2)	120.4(4)	C(10)-C(9)-C(8)	121.9(4)	N(2)-C(16)-C(15)	123.5(4)
C(18)-C(17)-(16)	121.1(4)	N(1)-C(10)-C(9)	122.3(4)	C(17)-C(16)-C(15)	116.0(4)
C(17)-C(16)-(13)	122.6(4)	N(1)-C(10)-C(9)	122.3(4)	C(20)-C(19)-N(2)	109.9(4)

(*trans*-4-[(4′-*N*,*N*-diphenyl amino) styryl]-*N*-methyl quinolinium iodide) was filtered then purified by column chromatography on silica gel using acetone–ethanol (1:1) as the eluent. Needle deep-rose crystals were obtained after evaporation with a yield of 55% and the decomposition temperature (*T*d) = 254.87°C. Element analysis: Anal. calcd.: C 66.67, H 4.66, N 5.18; found: C 66.03, H 4.59, N 5.12.

trans-4-[(4′-*N*-Hydroxyethyl-*N*-methyl amino) styryl]-*N*′-methyl quinolinium iodide (HMASQI) was synthesized by the same method. Purified by column chromatography on silica gel using acetonitrile–water (1:1) as the eluent. Strip-like purple crystals were obtained after evaporation. Yield 60% and *T*d = 278.11°C. Element analysis: Anal. calcd.: C 56.51, H 5.19, N 6.28; found: C 56.48, H 5.13, N 6.38. (See Table 3 for bond lengths and angles).

Using the same method mentioned above, we synthesized the chromophores of pyridinium derivatives.

trans-*4-[4′-(*N,N-*Diphenylamino) styryl]*-N-*methyl pyridinium iodide (DPASPI)*: The crude product was purified by column chromatography on silica gel using ethane–chloroform (1:1) as the eluent. Yield 82% and *T*d = 260.2°C. Element analysis: Anal. calcd.: C 63.68, H 4.73, N 5.71; found: C 63.63, H 4.85, N 5.67. See Table 4 for bond lengths and angles.

trans-*4-(4′-Pyrrolidinyl styryl)*-N-*methyl pyridinium iodide (PSPI)*: The crude product was purified by column chromatography on silica gel with ethanol as the eluent. Yield 82% and *T*d = 260.6°C. Element analysis: Anal. calcd.: C 55.11, H 5.35, N 7.14; found: C 55.0, H 4.84, N 7.59.

trans-*4-[4′-(*N,N-*Diethylamino) styryl]*-N-*methyl pyridinium iodide (DEASPI)*: Purified by column chromatography on silica gel with ethanol as the eluent. Yield 84% and *T*d = 264.7°C. Element analysis: Anal. calcd.: C 54.84, H 5.88, N 7.10; found: C 54.34, H 5.46, N 6.98.

trans-*4-[4′-(*N-*Hydroxyethyl*-N-*ethyl) amino)styryl]*-N-*methyl pyridinium iodide (HEASPI)*: Purified by column chromatography on silica gel with ethanol as the eluent. Yield 85% and *T*d = 286.7°C. Element analysis: Anal. calcd.: C 52.69, H 5.69, N 6.83; found: C 52.43, H 5.21, N 6.45.

*5-(4-*N-*Hydroxyethyl*-N-*methylamino tyryl) barbituric acid (HMASBA)*: A mixture of equal molar 4-(*N*-hydroxyethyl-*N*-methyl amino) benzaldehyde (3.58 g, 20 mmol) and barbituric acid (2.56 g, 20 mmol) was refluxed in the presence of Et_3N (3.2 g, 32 mmol) in water–ethanol (15:15 mL) until a clear solution was obtained. The reaction was kept at reflux for an additional 2 h, then the solvent was removed by evaporation. After 2–3 days the resulting precipitate was washed several times with water and acetone, then dried. Red microcrystals with a yield of 80% and *T*d = 245.49°C were obtained. MS *m*/*z*: 289 (M^+), 258, 120. ^{1}H NMR δ: 10.73 (d, *J* = 11.46 Hz, 2H), 8.24 (d, *J* = 8.6 Hz, 2H), 7.98 (s, 1H), 6.68 (q, *J* = 8.6 Hz, 2H), 4.71 (1H, s), 3.53 (4H, s), 3.07 (3H, s). Element analysis: Anal. calcd.: C 58.12, H 5.23, N 14.53; found: C 57.64, H 4.85, N 14.38.

Crystal structure determination

Crystal data and other information on structure determination are given in Tables 2–4. X-ray diffraction data were made on a Bruker P4 four-cycle diffractometer and graphite-monochromated Mo Kα radiation was used (λ = 0.71073 Å). The structures were solved by direct method and refined by full-matrix least-squares on F^2. The refinement was on F^2 of reflections with $F_0 \geq 4\sigma(F_0)$ to minimize $\Sigma w(|F_0| - |F_c|)^2$. Anisotropic displacement parameters were refined for all nonhydrogen atoms, and isotropic hydrogen atoms were constrained to ride on their parent carbon atoms with fixed bond lengths and idealized bond angles.

Linear optical property

The λ_{max} values for all chromophores in DMF with d_0 = 1.00×10^{-5} M have been measured with a Hitachi U-3500

© 2001 NRC Canada

Table 4. Selected bond lengths (Å) and angles (°) for DPASPI.

C(1)—N(1)	1.481(16)	C(7)—C(8)	1.277(17)	C(17)—C(18)	1.360(17)
C(2)—N(1)	1.355(13)	C(8)—C(9)	1.427(16)	C(18)—C(19)	1.379(16)
C(6)—N(1)	1.320(15)	C(9)—C(14)	1.372(16)	C(19)—C(20)	1.362(16)
N(2)—C(12)	1.424(13)	C(9)—C(10)	1.431(16)	C(21)—C(22)	1.393(15)
N(2)—C(15)	1.416(13)	C(10)—C(11)	1.359(16)	C(21)—C(26)	1.387(60)
N(2)—C(21)	1.416(13)	C(11)—C(12)	1.381(15)	C(22)—C(23)	1.372(16)
C(2)—C(3)	1.359(16)	C(12)—C(13)	1.393(15)	C(23)—C(24)	1.404(19)
C(3)—C(4)	1.353(17)	C(13)—C(14)	1.375(16)	C(24)—C(25)	1.341(18)
C(4)—C(5)	1.412(19)	C(15)—C(16)	1.358(15)	C(25)—C(26)	1.359(16)
C(4)—C(7)	1.524(17)	C(15)—C(20)	1.425(15)		
C(5)—C(6)	1.388(17)	C(16)—C(17)	1.377(16)		
C(1)-N(1)-C(2)	117.6(9)	C(8)-C(9)-C(10)	126.2(10)	C(17)-C(18)-(19)	118.7(11)
C(1)-N(1)-C(6)	123.4(9)	C(8)-C(9)-C(14)	118.2(10)	C(18)-C(19)-(20)	122.8(11)
C(2)-N(1)-C(6)	118.8(8)	C(10)-C(9)-C(14)	115.6(10)	C(15)-C(20)-(19)	117.5(10)
C(12)-N(2)-C(15)	119.9(8)	C(9)-C(10)-C(11)	120.9(11)	N(2)-C(21)-(22)	121.1(10)
C(12)-N(2)-C(21)	116.8(8)	C(10)-C(11)-C(12)	122.0(10)	N(2)-C(21)-(26)	121.3(9)
C(15)-N(2)-C(21)	122.6(8)	N(2)-C(12)-C(11)	123.5(9)	C(22)-C(21)-(26)	117.5(10)
N(1)-C(2)-C(3)	121.6(8)	N(2)-C(12)-C(13)	118.5(9)	C(21)-C(22)-(23)	121.9(11)
C(2)-C(3)-C(4)	121.9(11)	C(11)-C(12)-C(13)	118.1(10)	C(22)-C(23)-(24)	117.8(11)
C(3)-C(4)-C(5)	116.3(11)	C(12)-C(13)-C(14)	119.6(10)	C(23)-C(24)-(25)	120.9(12)
C(3)-C(4)-C(7)	118.7(11)	C(9)-C(14)-C(13)	123.7(11)	C(24)-C(25)-(26)	120.8(11)
C(5)-C(4)-C(7)	125.0(11)	N(2)-C(15)-C(16)	121.7(9)	C(21)-C(26)-(25)	121.1(10)
C(4)-C(5)-C(6)	119.8(11)	N(2)-C(15)-C(20)	119.0(9)	C(16)-C(17)-(18)	120.4(10)
N(1)-C(6)-C(5)	121.6(11)	C(16)-C(15)-C(20)	119.2(10)	C(15)-C(16)-(17)	121.3(10)
C(4)-C(7)-C(8)	124.5(12)	C(7)-C(8)-C(9)	123.7(12)		

Linear optical property

The λ_{max} values for all chromophores in DMF with d_0 = 1.00×10^{-5} M have been measured with a Hitachi U-3500 recording spectrophotometer from quartz curettes of 1 cm path.

Measurement of the two-photon absorption cross section (δ value)

The *Z*-scan system with an open aperture ($S = 1$), which is insensitive to the nonlinear refraction, can be used to measure the nonlinear absorption cross-section. Such *Z*-scan traces with open apertures are expected to be symmetrical with respect to the focus ($Z = 0$), where they have a minimum transmittance (e.g., multiphoton absorption) or a maximum transmittance (e.g., saturation of absorption). In fact, the nonlinear absorption coefficient (β) that is due to TPA can be easily calculated from the transmittance curves.

For a temporally Gaussian pulse, the normalized energy transmittance can be given as (19),

$$[3] \qquad T(z, S = 1) = \frac{1}{\sqrt{\pi}\, q_0(z,0)} \int_{-\infty}^{+\infty} \ln (1 + q_0)(z,0) e^{-\tau^2} \mathrm{d}\tau$$

where $q_0(z,t) = \beta I_0 L_{\mathrm{eff}} / (1 + z^2/z_0^2)$. When there is no linear absorption, $L_{eff} = L$. L is the sample thickness, z_0 and $\pm z$ are the position of focus point and the range of scanning, respectively, and I_0 is the peak irradiance.

For $| q_0 | 1$, the transmittance (T) can be expressed in terms of the peak irradiance in a summation form more suitable for numerical evaluation,

$$[4] \qquad T(z, S = 1) = \sum_{m=0}^{\infty} \frac{[-q_0(z,0)]^m}{(m+1)^{3/2}} = \sum_{m} \frac{\beta I_0 L / (1 + z^2/z_0^2)}{(m+1)^{3/2}}$$

Thus, once an open-aperture *Z*-Scan ($S = 1$) is performed, the TPA coefficient β can be unambiguously deduced and if the concentration d_0 (in units of mol L^{-1}) of the solution is known, the molecular TPA cross section δ (in units of cm^4 s per photon) can be determined by using the following relationship,

$$[5] \qquad h\nu\beta = \delta N_0 = h\nu\delta N_A d_0 \times 10^{-3}$$

where $h\nu$ is the energy of the incident photon. N_A is Avogadro's constant.

We have accomplished TPA cross-section measurement for all chromophores with the sample thickness of 2 mm and a relatively high concentration of $d_0 = 0.05$ M, using a focussed 35 ps, 1064 nm mode-locked Nd:YAG laser. Using the above equations, we can get the TPA coefficient (β) and TPA δ value, which are presented in Table 1. The final measured results of all samples are given in Table 1 with an experimental uncertainty of ±15%. The typical open aperture *Z*-scan curves are shown in Fig. 1, which depicts the open-aperture trace at peak irradiance $I_0 = 3.64$ GW cm^{-2}.

Calculation of the structures

Charge density distribution in both ground and excited states, the difference between the ground and excited state dipole moment ($\Delta\mu_{ge}$), the transition dipole moment between two lowest states ($M_{ee'}$), and the dihedral angle between two rings of the backbone ($\theta^{d/0}$) were all calculated with the PM3 and ZINDO semiempirical methods.

© 2001 NRC Canada

Fig. 1. Normalized *Z*-scan transmittance of: (*a*) DPASQI and (*b*) HMASQI, measured using ps pulses at λ = 1064 nm with I_0 = 3.64 GW cm^{-2}.

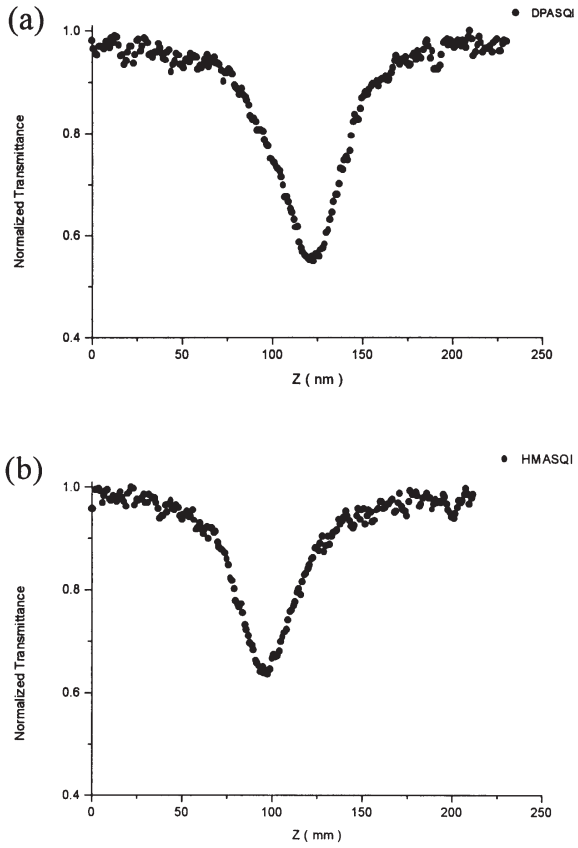
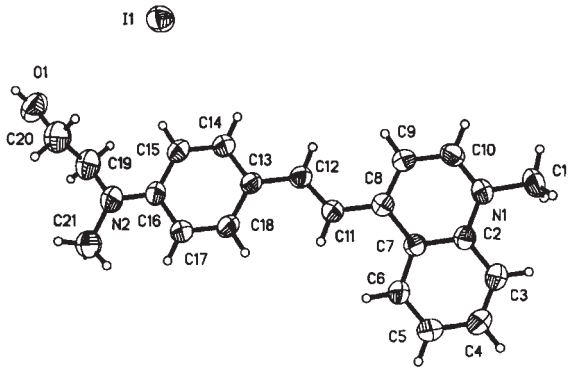


Fig. 2. Molecular structure of HMASQI.



monoclinic crystal system of the centrosymmetric space group $P2_1/n$ with the unit cell parameters of a = 10.0512(11) Å, b = 16.2879(12) Å, c = 12.3328(8) Å, β = 102.307(6)°. Bond lengths of C8—11, C11—12, and C12—13 are 1.436(5), 1.352(5), and 1.442(5) Å, respectively owing to strong π-electron conjugation between the substituted phenyl ring and quinolinium ring. Bond angles of ∠C6-7-8, ∠C2-7-8, ∠N1-C2-C3, and ∠N1-C2-C7 are 122.4(4)°, 120.3(3)°, 120.4(4)°, and 119.2(3)°, respectively, which shows that the quinolinium ring possesses excellent planarity. The packing diagram shows that HMASQI molecules stack to form a layer-like structure along the *b*-axis. The donor-end of one

Fig. 3. Packing diagram of HMASQI.

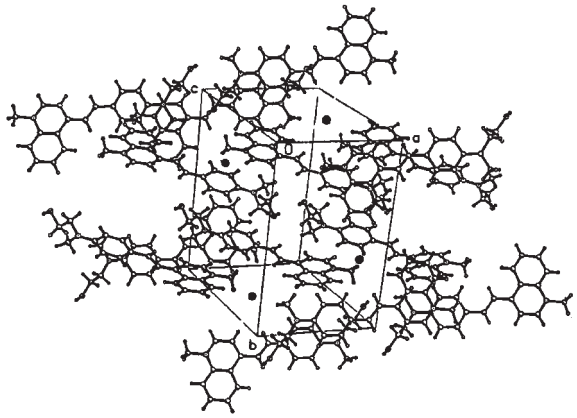
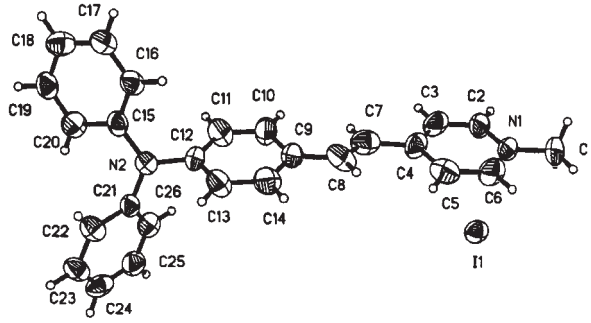


Fig. 4. Molecular structure of DPASPI.



molecule is overlapped with the acceptor-end of the other molecule along the *a*-axis. The anions (I^-) fill in the space among the cations.

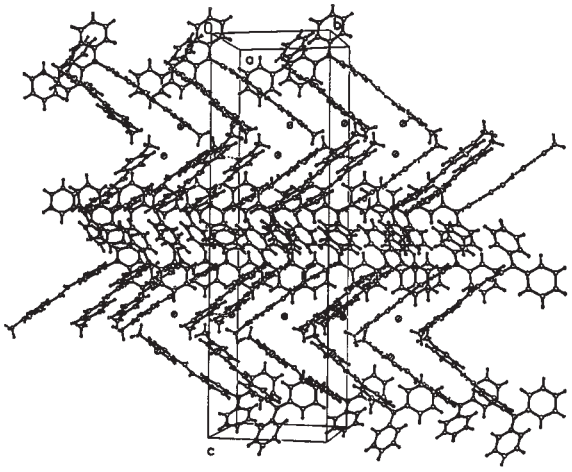
The structures of DPASPI are shown in Figs. 4 and 5. This crystal belongs to the orthorhombic crystal system of centrosymmetric space group *Pbca* with eight molecules in the unit cell. The two phenyl rings of the backbone are almost in the identical plane with the dihedral angle of 3.6°, while the other two phenyl rings on the donor-end deviate from this plane. From the packing diagram of DPASPI (shown in Fig. 5), one can see that the donor groups overlap, or stagger, each other while the acceptor-ends align face to face with the definite degree. Along the *c*-axis, the donor- and acceptor-groups present chain-like channels among the space filling in the anions.

Two-photon absorption and intramolecular charge transfer

Linear absorption for all chromophores is shown in Fig. 6. The influences from the quartz liquid cell and the solvent DMF have been subtracted. One can see that maximum absorption bands are 463 nm for the barbituric acid derivative and 458 ~ 482 nm for the pyridinium derivatives. Upon replacing the acceptor group with a larger conjugated fragment (*N*-methyl-quinolinium) one can observe a bathochromic shift of the long-wave absorption band to 514 ~ 554 nm. This suggests that the electronic interactions between the donor and acceptor groups induce the spectral shift to lower energy in the order of: quilidinium derivatives > pyridinium derivatives > barbituric acid derivatives.

© 2001 NRC Canada

Fig. 5. Packing diagram of DPASPI.

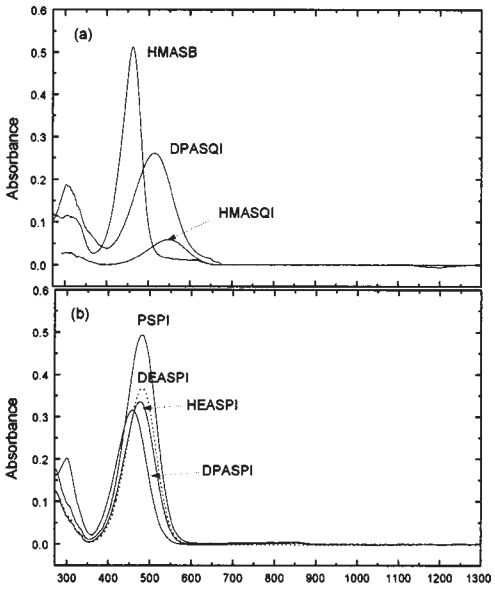


It must be noted that there is no linear absorption for all chromophores in the region from ~700 to ~1300 nm. So pumped by a 1064 nm laser pulse, the linear absorption can be excluded because two-photon excitation via virtual intermediate state can proceed, consistent with the fact that the nonlinear absorption occurs at a frequency in the region of one-photon transparency. It should be stressed that valid structure–property relationships can only be ascertained for those molecules that have their two-photon absorption peak at approximately the same wavelength. If the two-photon absorption peak shifts greatly from the wavelength that is away from the experimental wavelength of 1064 nm, then the comparison of absolute cross-sections is misleading. From Fig. 6, one can see that the maximum absorption wavelengths of all chromophores do not deviate too much. It is for this reason that the structure–property relationships deduced from the experimental data in this work are valid at 1064 nm.

Two-photon absorption cross-sections measured in DMF for the newly synthesized chromophores are summarized in Table 1. From Table 1, one can see that when the acceptor is fixed to the *N*-methyl pyridinium moiety, while the donor strength decreases, the δ values increase from 5.7×10^{-48} cm^4 s per photon for PSPI, to 7.0×10^{-48} cm^4 s per photon for HEASPI, to 8.8×10^{-48} cm^4 s per photon for DPASPI. This suggests that the δ value is not always proportional to the donor strength. Similar results can be observed in quinolinium moiety. When acceptor is fixed to *N*-methyl quinolinium moiety, with the decrease in donor strength, the two-photon absorption cross-section values change from 8.8×10^{-48} cm^4 s per photon for HMASQI to 10.9×10^{-48} cm^4 s per photon for DPASQI.

It is clear that with the acceptor structural factor changing from barbituric acid to pyridinium and further to quinolinium, δ values are gradually enhanced, in the range of $3.8 \times 10^{-48} \sim 10.9 \times 10^{-48}$ cm^4 s per photon. The barbituric acid derivative exhibits a relatively small cross-section, which can be explained as the molecular planarity seems to be critical in enhancing TPA cross-section values. Calculation shows that the dihedral angle between the benzene ring and the barbituric acid (70° for HMASBA) distorts the planarity and reduces the conjugated length, which is a disadvantage with respect to intramolecular charge transfer.

Fig. 6. Vis-IR absorption spectra of all chromophores in DMF with $d_0 = 1.00 \times 10^{-5}$ M.



Replacing barbituric acid by a pyridinium or a quinolinium fragment, greatly decreases the dihedral angle between two aromatic rings so as to be negligible. Consequently, a relatively large value for the cross-section was obtained.

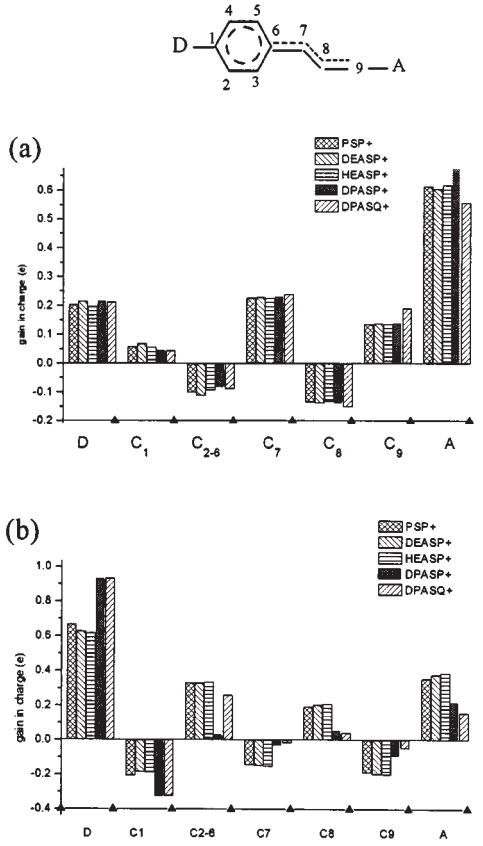
In a comparison of these newly synthesized compounds with some other chromophores recently reported (13, 20), we found that the δ value of 10.9×10^{-48} cm^4 s per photon for DPASQI is remarkable considering the limited conjugation length. For example, the TPA δ value for DPASQI is nearly same as that of 6-(4-pyridyl)-*N*,*N*-diphenyl-2-naphthylamine ($\delta = 12.9 \times 10^{-48}$ cm^4 s per photon) (13), but almost twice that of the nitro-containing fluorescent derivative ($\delta = 6.5 \times 10^{-48}$ cm^4 s per photon) (20). The difference of their TPA cross-section resulting from the variation of both the acceptor group and the character of the conjugated bridge shows that the quinolinium ring is a good acceptor group and that the TPA δ value can be significantly enhanced if a better planar moiety (as a conjugated bridge) is inserted in a donor-quinolinium ring pair. Since the quinolinium ring possesses better planarity, as confirmed by the crystallographic data of HEASQI mentioned above, this characteristic has to contribute to the intramolecular charge transfer that can be measured by such structural parameters as $\Delta\mu_{ge}$ and $M_{ee'}$ or the change of charge distribution on each atom between the ground and the excited state.

The structural parameters calculated by the PM3 and ZINDO methods are presented in Table 1. From this table, one can conclude that the chromophores with large $\Delta\mu_{ge}$ and $M_{ee'}$ values possess relatively high δ value. For example, $M_{ee'}$ values in pyridinium derivatives change in the order of $DPASP^+ > HEASP^+ \sim PSP^+ \sim DEASP^+$, while $\Delta\mu_{ge}$ values change in the order of $DPASP^+ > HEASP^+ \sim DEASP^+ >> PSP^+$. The measured δ values, with the order of DPASPI > HEASPI ~ DEASPI > PSPI, confirmed that the experimental results are in agreement with the calculation.

Charge density (e) distribution for part of the chromophore cations in the ground state (shown in Fig. 7(*a*)), and in the

© 2001 NRC Canada

Fig. 7. Histogram of the π-charge distribution (e) in the: (*a*) ground state and (*b*) in the excited state, for part of the chromophores.



excited state (shown in Fig. 7(*b*)), are plotted in histogram form. One can see that in the ground state there is no alternation of charge density distribution. For example, the charge densities over D (donor) and atom C1 are both positive, and the charge densities over A (acceptor) and atom C9 are both positive too. Once in the excited state, the great charge redistribution occurs, accompanying with the significant charge positive–negative alternation, where the positive charge increases on the donor-end (D), and in the meantime, decreases on the acceptor-end (A). For example, one can see that in the ground state, the charge distribution of the $DPASP^+$ cation is in such a way: Q_D = +0.21 e and Q_A = +0.83 e; while in the excited state, Q_D = +0.93 e and Q_A = +021 e, indicating a large charge redistribution on the two-terminals occurs. It is interesting to note that such a π-charge transfer degree is consistent with the $\Delta\mu_{ge}$ and $M_{ee'}$ values and also in accordance with the enhancement of δ value. So DPASPI exhibits relatively large δ values among pyridinium derivatives because of its larger $\Delta\mu_{ge}$ (11.8 debye) and $M_{ee'}$ (9.8 debye) values. HMASBA exhibits smaller δ value because of its small change of dipole moment (0.8 debye). Its charge distribution is also small: Q_{ami} = +0.04 e, Q_{bar} = –0.27 e in the ground state, and Q_{ami} = +0.25 e, Q_{bar} = –0.28 e in the excited state, which shows that only a weak charge transfer between the ground and the excited state has occurred.

Conclusions

A series of new chromophores, styryl-parent end-capped with various substituted amino groups as donors, and barbituric acid, methyl-pyridinium, and methyl-quinolinium as the acceptors, has been synthesized and characterized by element analysis or X-ray diffraction.

We confirm both theoretically and experimentally that the TPA cross-section is strongly influenced by intramolecular charge transfer, which is characterized by the difference between the ground and excited state dipole moment ($\Delta\mu_{ge}$) and the transition dipole moment between the excited states ($M_{ee'}$) or the change of charge distribution on each atom between ground and excited state. Based on above point of view, the structure–property relationships of two-photon absorption (TPA) property can be interpreted reasonably, which can provide some useful information for molecular design with large TPA cross-sections.

The barbituric acid derivative possesses a relatively small TPA cross-section value due to its being heavily distorted from planarity and short conjugated length, which hinders intramolecular charge transfer. In contrast to this, quinolinium derivatives exhibit relatively large TPA cross-section due to its excellent planarity.

Both the *N*,*N*-diphenylamino group and the quinolinium ring are effective groups for enhancing TPA cross-sections, although the *N*,*N*-diphenylamino group is not a strong donor in comparison with the *N*,*N*-diakylamino group. Quantum chemical calculation shows that when the *N*,*N*-diphenylamino group and the quinolinium ring are matched, a relatively large charge transfer is produced ($\Delta\mu_{ge}$ = 12.1 debye), which confirms that TPA cross-section is not proportional to electron-donating strength, but dominated by intramolecular charge transfer.

Acknowledgments

This work was supported by a grant for State program of China. The authors are grateful to Prof. Sun Zhenrong and Prof. Ding Liangen in the Department of Physics, Normal University of East China for their help to measure the two-photon absorption cross-sections for all chromophores.

References

1. B.H. Cumpston, S.P. Ananthavel, and S. Barlow. Nature (London), **3,** 1041 (1999).
2. D.A. Parthenopoulos and P.M. Rentzepis. J. Appl. Phys. **68**, 5814 (1990).
3. D.A. Parthenopoulos and P.M. Rentzepis. Science (Washington, D.C.), **245**, 843 (1989).
4. J.E. Ehrlich, X.L. Wu, and I.Y.S. Lee. Opt. Lett. **22**, 1843 (1997).
5. G.S. He, R. Gvishi, P.N. Prasad, and B.A. Reinhardt. Opt. Commun. **117**, 133 (1995).
6. G.S. He, R. Signorini, and P.N. Prasad. Appl. Opt. **37**, 5720 (1998).
7. J.D. Bhawalkar, G.S. He, and P.N. Prasad. Rep. Prog. Phys. **59**, 1052 (1996).
8. G.S. He, L. Yuan, and Y.P. Cui, M. Li, and P.N. Prasad. J. Appl. Phys. **81**, 2529 (1997).

© 2001 NRC Canada

9. G.S. He, K.S. Kim, L.X. Yuan, N. Cheng, and P.N. Prasad. Appl. Phys. Lett. **71**, 1619 (1997).
10. G.S. He, J.D. Bhawalkar, C.F, Zhao, C.K. Park, and P.N. Prasad. Appl. Phys. Lett. **68**, 3549 (1996).
11. C.F. Zhao, G.S. He, J.D. Bhawalkar, C.K. Park, and P.N. Prasad. Chem. Mater. **7**, 1979 (1995).
12. C.F. Zhao, C.K. Park, and P.N. Prasad. Chem. Mater. **7**, 1237 (1995).
13. B.A. Reinhardt, L.L. Brott, S.J. Clarson, A.G. Dillard, and J.C. Bhatt. Chem. Mater. **10**, 1863 (1998).
14. G.S. He, L.X. Yuan, N. Cheng, and P.N. Prasad. J. Opt. Soc. Am. B, **14**, 1079 (1997).
15. C.W. Spangler. J. Mater. Chem. **9**, 2013 (1999).
16. M. Albota, D. Beljonne, J.L. Bras, J.E. Ehrlich, J.Y. Fu, A.A. Heikal, and S.E. Hess. Science (Washington, D.C.), **281**, 11 (1998).
17. F. Meyers, S.R. Marder, B.M. Pierce, and J.L. Brédas. J. Am. Chem. Soc. **116**, 10 703 (1994).
18. T. Kogej, D. Beljonne, F. Meyyers, J.W. Perry, S.R. Marder, and J.L. Brédas. Chem. Phys. Lett. **298**, 1 (1998).
19. S.B. Mansoor, A.A. Said, T.H. Wei, D.J. Hagan, and E.W.V. Stryland. IEEE J. Quantum Electron. **26,** 760 (1990).
20. K.D. Belfield, D.J. Hagan, E.W.V. Stryland, K.J. Schafer, and R.A. Negres. Org. Lett. **1**, 10 (1999).

© 2001 NRC Canada

Novel polyfluoroalkylated pyrazoles from 2-polyfluoroacylcycloalkanones and hydrazines: syntheses and unequivocal molecular structure assignment

D.V. Sevenard, O.G. Khomutov, M.I. Kodess, K.I. Pashkevich, I. Loop, E. Lork, and G.-V. Röschenthaler

Abstract: The reaction between 2-trifluoroacetylcycloalkanones and methylhydrazine or phenylhydrazine exclusively yields 3-CF_3-pyrazoles. When the chain length of the polyfluorinated substituent in $R^FC(O)$ group increases, 5-R^F-pyrazoles are isolated. The reaction of 2-trifluoroacetylcyclohexanone with 2-hydrazinopyradine gives 5-hydroxypyrazoline, an intermediate in the formation of 5-CF_3-pyrazoles. The regiochemistry of the condensation is probably controlled by the nucleophilicity of the terminal nitrogen in the mono substituted hydrazines and by the steric requirements of the R^F group in the 1,3-diketones. Polymethylene chain containing pyrazoles obtained from the 1,3-diketones in question and hydrazine prefer the 3-R^F tautomeric form, irrespective of carbocyclic ring size and polyfluoroalkyl group chain length.

Key words: polyfluorinated 1,3-diketones, hydrazines, isomeric pyrazoles, molecular structure.

Résumé : Les 2-trifluoroacétylcyclohexanones réagissent de façon avec la méthyl- ou la phénylhydrazine pour donner exclusivement des 3-CF_3-pyrazoles. Une augmentation de la longueur de la chaîne du substituant polyfluoré du groupe $R^FC(O)$ conduit à une augmentation de la quantité de 5-R^F-pyrazoles produite. La réaction de la 2-trifluoroacétylcyclohexanone avec la 2-hydrazinopyradine conduit à la formation de la 5-hydroxypyrazoline, un intermédiaire dans la formation des 5-CF_3-pyrazoles. La régiochimie de la condensation est contrôlée par le caractère nucléophile de l'azote terminal des hydrazines monosubstituées et les facteurs stériques du groupe R^F dans les 1,3-dicétones. Les pyrazoles comportant une chaîne polyméthylène obtenus à partir des 1,3-dicétones en question et de l'hydrazine favorisent la forme tautomère du 3-R^F, quelle que soit la grandeur du cycle carboné et de la longueur de la chaîne du groupe polyfluoroalkyle.

Mots clés : 1,3-dicétones polyfluorées, hydrazines, pyrazoles isomères, structure moléculaire.

[Traduit par la Rédaction]

Introduction

Pyrazoles, a class of compounds with biological activity (1–9), are available from the reaction of hydrazines with 1,3-diketones. In the case of unsymmetrical 1,3-diketones and mono substituted hydrazines, the formation of regioisomeric pyrazoles is possible (Scheme 1).

A regiospecific pathway has been discussed (4–8, 10) for reactions involving 2-acylcycloalkanones, but only the 4,5-polymethylene (5, 8, 10) or the 3,4-polymethylene structure (4, 6, 7) have been reported. A mixture of regioisomers has also been found (11, 12). Introducing polyfluorinated groups into 1,3-diketones substantially increases the steric and electronic inequivalence of the electrophilic centers, allowing an unequivocal course of the reaction to obtain only *one* of the two possible pyrazoles, e.g., as in the case of mono (het)aryl substituted hydrazines (9, 13–19). Nevertheless, both regioisomeric products have also been mentioned (7, 19, 20). If the hydrochloride salt of arylhydrazine is used, the reaction is regioselective, while for the respective free arylhydrazine, a mixture of isomers has been obtained (21). In the case of methylhydrazine, no regiospecificity has been observed (16, 22).

For hydrazines with acyl-, (thio)carbamoyl-, and some hetaryl-substituents, the reaction pathway is different. In the case of the non-fluorinated substrate, pyrazoles not only are obtained (23), but also a variety of intermediates. For example, mono- or bis-hydrazones (23, 24) and 2-pyrazolines (23–25), while with polyfluorinated 1,3-diketones, mostly 5-hydroxy-2-pyrazolines are formed (3, 26–30). Their molecular structures have been determined by X-ray diffraction (26, 27) and ^{13}C NMR spectroscopic studies (28, 29). On the

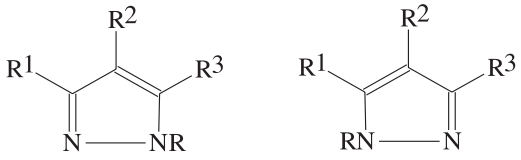
Received September 15, 2000. Accepted December 12, 2000. Published on the NRC Research Press Web site on March 16, 2001.

D.V. Sevenard, **I. Loop**, **E. Lork**, **and G.-V. Röschenthaler.**[1] Institute of Inorganic & Physical Chemistry, University of Bremen, Leobener Strasse, 28334 Bremen, Germany.
O.G. Khomutov, **M.I. Kodess**, **and K.I. Pashkevich**. Institute of Organic Synthesis, Ural Branch of the Russian Academy of Sciences, 20 ul. S. Kovalevskoi, 620219 Ekaterinburg, Russian Federation.

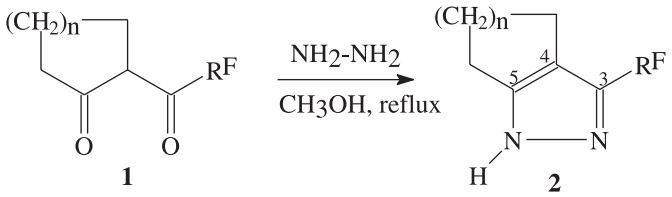
[1]Corresponding author (telephone: +49-421-218-2493; fax: +49-421-218-4267; e-mail: gvr@chemie.uni-bremen.de).

 DOI: 10.1139/cjc-79-2-183 © 2001 NRC Canada

Scheme 1.



Scheme 2.



	n	R^F
a	1	CF_3
b	1	C_4F_9
c	2	CF_3
d	2	CF_2CF_2H
e	2	C_4F_9

basis of the NMR data, the isomeric structure of some 5-hydroxy-3-pyrazolines reported (16) was, in our opinion, assigned ambiguously.

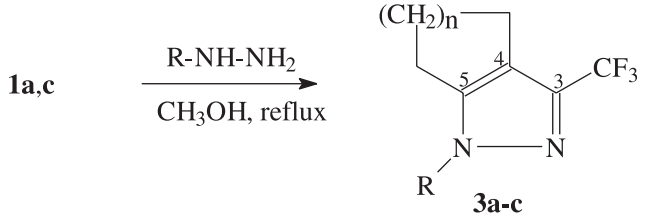
The question still remains: what is the structure of the pyrazoles synthesized from polyfluoralkyl 1,3-diketones and hydrazine (3, 13, 16, 20, 31) or from the dehydration of the 5-hydroxy-5-R^F-pyrazolines, which were isolated in some cases (3, 20, 32) and can exist in two tautomeric forms (Scheme 1, R = H) (33, 34)? Here we investigate the reaction of 2-polyfluoroacylcycloalkanones with hydrazine, and its mono-substituted derivatives, to unambiguously determine the structures of the new products.

Results and discussion

The reaction of 1,3-diketones (**1a**–**e**) and hydrazine furnish solid pyrazoles (**2a**–**e**) (Scheme 2) as the only products, which exist in only one tautomeric form at 25°C in $CDCl_3$ according to the ^1H, ^{13}C, and ^{31}P NMR data (one set of signals, Tables 1 and 2). A possible fast 1*H*–2*H* equilibrium, on the NMR time scale, (33) is unlikely, since the temperature-dependent ^{13}C NMR spectra of compound **2c** (Table 3) taken at 25, –10, and –50°C show no significant difference of the respective δ_C values, e.g., 0.01 ppm/°C for carbon-bearing CF_3 groups and 0.0005 ppm/°C for carbon C5 (similar deviations, where no tautomeric equilibria are in effect, were found, cf. ref. 35).

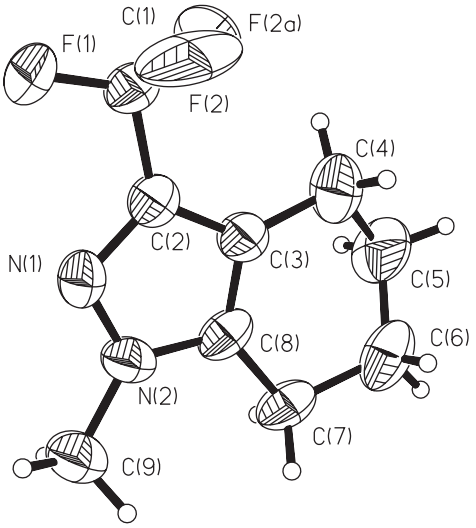
Heating, in methanol, (also in benzene for **3c**) the reaction between trifluoromethyl substituted 1,3-diketones (**1a**,**c**) and methylhydrazine or phenylhydrazine yields regiospecifically 3-trifluormethylpirazoles (**3a**–**c**) (Scheme 3), where the NH_2 moiety attacks the trifluoroacetyl group followed by subsequent heterocyclization.

Scheme 3.



3	n	R
a	2	CH_3
b	1	C_6H_5
c	2	C_6H_5

Fig. 1. Molecular structure of compound **3a** (for clarity, the disordering is not depicted).



Analysis of the X-ray crystal structure reveals the unit cell of compounds **3a** and **3b** to contain two molecules (four for **3c**). Supplementary material for **3a**–**c** has been deposited.[2] The molecular structures of **3a**–**c** (Figs. 1–3, Table 4) are characterized by a planar pyrazolic ring featuring a pentagon with angles between 104.1° and 112.6°. The fused cyclohexene ring in **3c** displays a twist conformation, with C5 being 27.8 pm above and with C6 being 47.5 pm below the plane (C4-C3-C8-C7). The methyl and CF_3 groups of **3a** are in the pyrazol plane. Both are slightly disordered, forming two positions from rotations around the C—C and C—N bonds, respectively. The tetramethylene moiety is creating the two possible twist conformations by disordering in a 1:1 ratio. Atoms C4, C3, C8, and C7 are located on the crystallographic mirror plane, whereas C5 and C6 lie 45.4 pm above and 31.0 pm below the plane, respectively. The

[2] Supplementary material may be purchased from the Depository of Unpublished Data, Document Delivery, CISTI, National Research Council Canada, Ottawa, ON K1A 0S2, Canada. For information on obtaining material electronically go to http://www.nrc.ca/cisti/irm/unpub_e.shtml. Tables of atomic coordinates for the structure(s) reported in this paper have been deposited with the Cambridge Crystallographic Data Centre. Copies of the data can be obtained, free of charge, on application to the Director, CCDC, 12 Union Road, Cambridge CB2 1EZ, U.K. (Fax: 44-1223-336033 or e-mail: deposit@ccdc.cam.ac.uk).

© 2001 NRC Canada

Table 1. ^{1}H and ^{19}F NMR data of compounds **2**, **3**, and **5**.

	^{1}H NMR δ (*J* in Hz)			^{19}F NMR δ (*J* in Hz) [^{19}F{^{1}H} NMR]
	$(CH_2)_{n+2}$	R^F	R	
2a	2.57–2.83 (m, 6H)	—	13.0 (br s, 1H)	–62.52 (s)
2b	2.49–2.64 (m, 2H), 2.68–2.83 (m, 4H)	—	12.7 (br s, 1H)	–127.18 (m, 2F, CF_2), –124.77 (m, 2F, CF_2), –111.55 (t, $^{4}J_{F-F}$ = 12.9, 2F, CF_2), –82.26 (t, $^{4}J_{F-F}$ = 9.5, 3F, CF_3)
2c	1.75–1.86 (m, 4H), 2.61–2.67 (m, 4H)	—	12.6 (br s, 1H)	–62.41 (t, $^{5}J_{F-H}$ = 0.9) [–62.41[a] (s)]
2d	1.68–1.83 (m, 4H), 2.53–2.66 (m, 4H)	6.00 (tt, $^{2}J_{H-F}$ = 53.6, $^{3}J_{H-F}$ = 3.7, 1H)	11.9 (br s, 1H)	–136.86 (dt, $^{2}J_{F-H}$ = 53.4, $^{3}J_{F-F}$ = 6.9, 2F), –114.58 (m, 2F)
2e	1.69–1.81 (m, 4H), 2.48–2.64 (m, 4H)	—	9.8 (br s, 1H)	—
2f	1.26 (s, 4H), 1.78–1.92 (m, 4H)	6.08 (tt, $^{2}J_{H-F}$ = 52.2, $^{3}J_{H-F}$ = 5.7, 1H)	11.6 (br s, 1H)	—
3a	1.70–1.88 (m, 4H), 2.50–2.65 (m, 4H)	—	(*a*) 3.76 (q, $^{6}J_{H-F}$ = 0.6, 3H), (*b*) 3.76[b] (s, 3H)	–62.60 m[c] [–62.60[c,d] (t, $^{5}J_{F-H}$ = 0.9)]
3b	1.67–1.96 (m, 2H), 2.54–2.77 (m, 4H)	—	6.51–7.25 (m, 5H)	–62.87 (s)
3c	1.75–1.90 (m, 4H), 2.63–2.77 (m, 4H)	—	7.37–7.55 (m, 5H)	–62.82 (t, $^{5}J_{F-H}$ = 0.9) [–62.82[a] (s)]
3d	1.75–1.91 (m, 4H), 2.7 (br s, 4H)	6.25 (tt, $^{2}J_{H-F}$ = 53.5, $^{3}J_{H-F}$ = 4.8, 1H)	7.32–7.48 (m, 5H)	–138.01 (dt, $^{2}J_{F-H}$ = 53.4, $^{3}J_{F-F}$ = 8.6, 2F), –114.83 (m, 2F)
3e	1.59–1.87 (m, 4H), 2.42–2.80 (m, 4H)	—	(*a*) 3.77 (t, $^{6}J_{H-F} \approx 0.7$), (*b*) 3.77[e] (s, 3H)	–127.90 (s, 2F, CF_2), –111.68 (q, $^{4}J_{F-F}$ = 9.8, 2F, CF_2), –81.36 (t, 3F, CF_3)
5a	1.79–1.94 (m, 4H), 2.70–2.80 (m, 4H)	—	7.44 (s, 5H)	–57.09 (s)
5b	1.71–1.95 (m, 4H), 2.64–2.85 (m, 4H)	5.63 (tt, $^{2}J_{H-F}$ = 53.8, $^{3}J_{H-F}$ = 3.4, 1H)	7.42 (m, 5H)	–135.97 (dt, $^{2}J_{F-H}$ = 53.6, $^{3}J_{F-F}$ = 7.0, 2F), –109.7 (br s, 2F)
5c	1.59–1.87 (m, 4H), 2.42–2.80 (m, 4H)	—	(*a*) 3.90 (m, 3H), (*b*) 3.90[e] (t[f], 3H), (*c*) 3.90[g] (t[f], 3H)	–127.53 (s, 2F, CF_2), –110.06 (q, $^{4}J_{F-F}$ = 9.8, 2F, CF_2), –81.36 (t, 3F, CF_3)
5d	1.73–1.93 (m, 4H), 2.67–2.80 (m, 4H)	—	7.33–7.46 (m, 5H)	–127.44 (m, 2F, CF_2), –123.11 (m, 2F, CF_2), –106.56 (t, $^{4}J_{F-F}$ = 12.9, 2F, CF_2), –82.26 (t, $^{4}J_{F-F}$ = 9.5, 3F, CF_3)
5e	1.71–1.95 (m, 4H), 2.65–2.85 (m, 4H)	—	7.4 (br s, 5H)	–127.59 (m, 2F, CF_2), –123.40 (m, 2F, CF_2), –124.2 (br s, 2F, CF_2), –122.27 (t, 2F, CF_2, $^{4}J_{F-F}$ = 12.1), –106.45 (t, 2F, CF_2, $^{4}J_{F-F}$ = 13.8), –82.29 (t, 3F, CF_3, $^{4}J_{F-F}$ = 9.5)

[a]Irradiating CH_2 protons.
[b]Irradiating CF_3 fluorines.
[c]In DMSO-d_6.
[d]Irradiating CH_3 protons.
[e]Irradiating the α-CF_2 group.
[f]Broad signal.
[g]Irradiating the β-CF_2 group.

second conformer with C5′ and C6′ was generated by applying the symmetry operation.

In the ^{1}H and ^{19}F NMR spectra of compound **3a** (see Table 1), a surprising $^{6}J_{H-F}$ coupling was observed between

© 2001 NRC Canada

Table 2. ^{13}C NMR (J in Hz) of compounds **2**, **3**, and **5**.

	C3[a]	C4[a]	C5[a]	$(CH_2)_{n+2}$[a]	R^F	R^a
2a	135.48 (q, $^2J_{C-F}$ = 38.2)	125.12 (q, $^3J_{C-F}$ = 1.8)	152.92	22.62, 23.83, 30.93	121.89 (q, $^1J_{C-F}$ = 268.1)	—
2b	133.72 (t, $^2J_{C-F}$ = 26.1)	126.37–127.39 (m)	153.36 (m)	22.94, 23.76, 30.68	103.12–127.71 (m)	—
3a	137.95 (q, $^2J_{C-F}$ = 36.6)	114.99 (q, $^3J_{C-F}$ = 1.5)	140.14	19.98, 21.26, 22.14, 22.36	122.17 (q, $^1J_{C-F}$ = 268.5)	35.92
3b	137.02 (q, $^2J_{C-F}$ = 38.6)	127.54 (q, $^3J_{C-F}$ = 1.9)	150.30	22.60, 26.53, 30.87	121.62 (q, $^1J_{C-F}$ = 268.6)	119.90, 126.94, 129.39, 139.70
3c	140.11 (q, $^2J_{C-F}$ = 36.9)	116.19 (q, $^3J_{C-F}$ = 1.2)	140.39	20.10, 22.29, 22.56, 23.47	122.15 (q, $^1J_{C-F}$ = 269.2)	123.80, 127.86, 129.17, 139.15
3d	140.38 (t, $^2J_{C-F}$ = 29.7)	117.33	139.04	20.30, 22.25, 22.45, 23.43	110.01 ($^1J_{C-F}$ = 250.5, $^2J_{C-F}$ = 36.1), 113.72 (tt, $1J_{C-F}$ = 244.8, $^2J_{C-F}$ = 27.0)	123.60, 123.73, 129.13, 140.31
3e	136.25 (t, $^2J_{C-F} \approx 28$)	116.89 (t, $^3J_{C-F}$ = 2.2)	140.26	20.34 (m), 21.34, 22.11, 22.45	104.5–125.7 (m)	36.02
2c	138.89 (q, $^2J_{C-F}$ = 36.6)	114.23 (q, $^3J_{C-F}$ = 1.5)	141.51	19.70, 20.80, 22.12, 22.53	122.27 (q, $^1J_{C-F}$ = 268.8)	—
2d	138.81 (t, $^2J_{C-F}$ = 29.6)	115.39	141.28	20.03, 20.82, 22.09, 22.66	110.17 (tt, $^1J_{C-F}$ = 250.8, $^2J_{C-F}$ = 39.3), 114.02 (tt, $^1J_{C-F}$ = 245.3, $^2J_{C-F}$ = 28.1)	—
2e	137.18 (t, $^2J_{C-F}$ = 28.1)	115.70 (t, $^3J_{C-F}$ = 1.7)	140.91	20.03 (m), 20.80, 21.99, 22.62	103.2–124.7 (m)	—
5a	150.54	120.06 (q, $^3J_{C-F}$ = 1.6)	128.34 (q, $^2J_{C-F}$ = 37.8)	21.25 (q, $^4J_{C-F}$ = 1.4), 23.17 (q, $^5J_{C-F}$ = 0.8), 23.20, 23.69	121.23 (q, $^1J_{C-F}$ = 269.6)	126.22 (q, $^5J_{C-F}$ = 1.1), 129.21, 129.36, 140.19
5b	150.15	120.36	127.85 (t, $^2J_{C-F}$ = 30.2)	20.93, 22.72, 22.86, 23.24	109.51 (tt, $^1J_{C-F}$ = 253.0, $^2J_{C-F}$ = 40.5) [b]	127.20, 128.72, 129.13, 140.14
5c	148.7 (br s)	120.75 (t, $^3J_{C-F}$ = 2.2)	[b]	20.7 (br s), 22.11, 22.77, 23.01	104.5–125.7 (m)	38.7 (m)
5d	150.60 (t, $^4J_{C-F}$ = 1.1)	121.90 (t, $^3J_{C-F}$ = 2.1)	126.80 (tt, $^2J_{C-F}$ = 29.8, $^3J_{C-F}$ = 1.1)	21.35 (m), 23.16, 23.2 (br s), 23.66	103.28–121.28 (m)	127.80 (m), 128.94, 129.57, 140.69
5e	150.57	121.9 (br s)	126.87 (t, $^2J_{C-F}$ = 29.6)	21.3 (br s), 23.13, 23.20, 23.65	102.28–127.09 (m)	127.8 (br s), 128.90, 129.54, 140.71
[c]	150.9	118.3	132.4 (t, $^2J_{C-F}$ = 28)	20.1, 22.6, 22.7, 23.1	109.1 (td, $^1J_{C-F}$ = 235, $^5J_{C-F}$ = 3.3)	104.8 (d, $^2J_{C-F}$ = 24), 111.7 (dd, $^2J_{C-F}$ = 23), 123.6 (dd, $^2J_{C-F}$ = 12), 130.1 (d), 157.0 (dd, $^1J_{C-F}$ = 254), 162.6 (dd, $^1J_{C-F}$ = 254)
[d]	150.9	119.3	129.2 (q, $^2J_{C-F}$ = 38)	20.4, 22.4, 22.5, 23.1	120.3 (q, $^1J_{C-F}$ = 270)	104.7 (d, $^2J_{C-F}$ = 24), 111.3 (dd, $^2J_{C-F}$ = 23), 123.8 (dd, $^2J_{C-F}$ = 13), 130.4 (d), 158.1 (dd, $^1J_{C-F}$ = 254), 163.1 (dd, $^1J_{C-F}$ = 254)

[a]All signals are singlets unless indicated otherwise.
[b]Signal not found.
[c]3-Difluoromethyl-4,5,6,7-tetrahydro-2-(2,4-difluorophenyl)-2*H*-indazole (11).
[d]3-Trifluoromethyl-4,5,6,7-tetrahydro-2-(2,4-difluorophenyl)-2*H*-indazole (11).

© 2001 NRC Canada

Table 3. ^{13}C NMR (J in Hz) data of compound **2c** at different temperatures.

T (°C)	C3[a], ($^2J_{C-F}$)	C4[a], ($^3J_{C-F}$)	C5[b]	$(CH_2)_{n+2}$[b]	CF_3[a], ($^2J_{C-F}$)
25	138.89 (36.6)	114.23 (1.6)	141.51	19.70, 20.80, 22.12, 22.53	122.27 (268.8)
–10	138.52 (36.4)	114.13 (1.6)	141.50	19.58, 20.67, 21.99, 22.39	122.16 (268.8)
–50	138.11 (36.4)	113.99 (1.8)	141.47	19.38, 20.51, 21.79, 22.18	121.97 (268.8)

[a]All signals are quartets.
[b]All signals are singlets.

Table 4. The selected bond lengths (pm) and angles (°) of compounds **3a–c**.

3a		**3b**		**3c**	
N(1)—N(2)	132.5(5)	N(1)—N(2)	136.4(2)	N(1)—N(2)	135.5(2)
N(1)—C(2)	134.9(6)	N(1)—C(8)	142.6(2)	N(1)—C(9)	142.5(2)
N(2)—C(9)	143.2(6)	N(2)—C(1)	133.3(3)	N(2)—C(1)	133.2(2)
C(1)—C(2)	149.8(6)	C(1)—C(7)	148.8(3)	C(1)—C(2)	148.0(3)
N(1)-N(2)-C(8)	112.0(3)	N(2)-N(1)-C(6)	110.49(15)	N(2)-N(1)-C(8)	111.84(14)
N(1)-N(2)-C(9)	120.6(4)	N(2)-N(1)-C(8)	118.69(16)	N(2)-N(1)-C(9)	119.20(13)
N(2)-N(1)-C(2)	104.3(3)	C(1)-N(2)-N(1)	104.87(16)	C(1)-N(2)-N(1)	104.10(14)
N(1)-C(2)-C(3)	111.4(4)	N(2)-C(1)-C(2)	112.06(17)	N(2)-C(1)-C(3)	112.64(16)
N(1)-C(2)-C(1)	121.4(4)	N(2)-C(1)-C(7)	118.48(18)	N(2)-C(1)-C(2)	118.36(16)

Fig. 2. Molecular structure of compound **3b**.

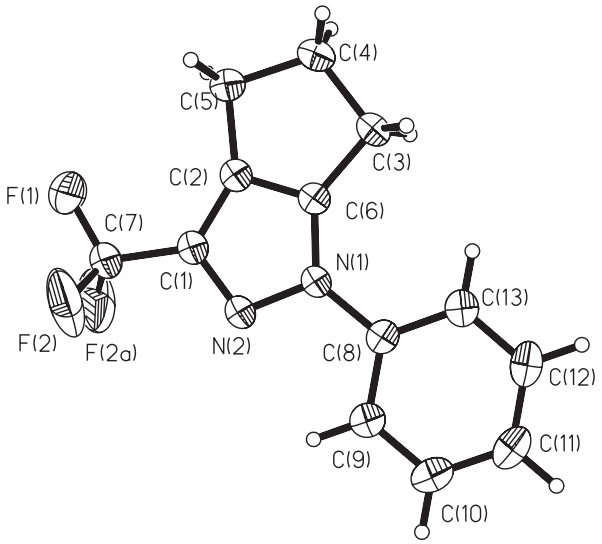
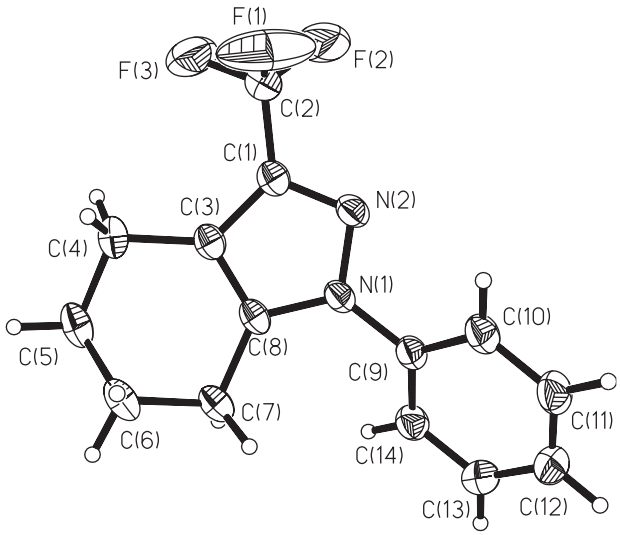


Fig. 3. Molecular structure of compound **3c**.



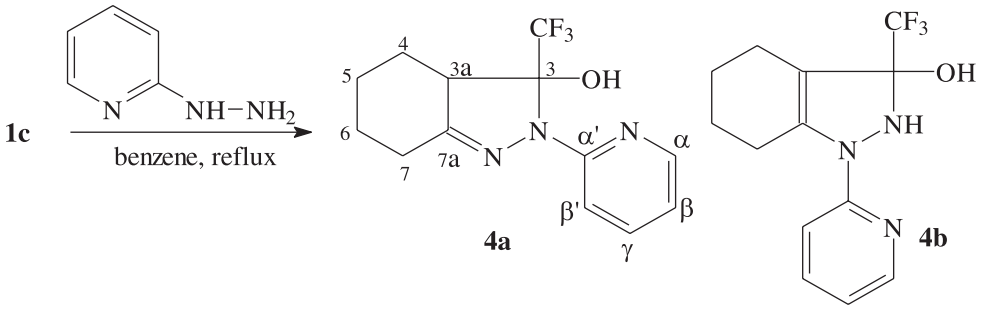
the CH_3 and CF_3 group. In a $^1H\{^{19}F\}$ NMR experiment, the quartet for the CH_3 at 3.76 ppm ($^6J_{H-F}$ = 0.6 Hz) was transformed into a singlet, while the CF_3 multiplet, at –62.60 ppm in the ^{19}F NMR spectrum, was transformed into a triplet (with CH_2 protons, $^5J_{F-H}$ = 0.9 Hz) by irradiating the CH_3 resonance.

When 2-hydrazinopyridine was used instead of phenylhydrazine, the reaction pathway changed. Molecule **1c** furnished, as in the case of (thio)semicarbazides (27, 28), the 2-*R*-indazole derivative **4a** (Scheme 4) as indicated by the two chiral carbon atom signals (97:3) in the ^{19}F NMR spectrum, representing the two possible diastereomers. The ^{13}C NMR data (δ_c (C^3) = 92.36, $^2J_{C-F}$ = 32.3 Hz, which indicates sp^3-hybridization), supports the proposed structure (see also refs. 36–38). The constitutional isomer **4b**, assigned to similar compounds (16, 39), could be ruled out because of the presence of a resonance representing the methylidyne proton at δ_H = 3.15 (dd, $^3J_{H-H}$ = 10.7, 6.3 Hz).

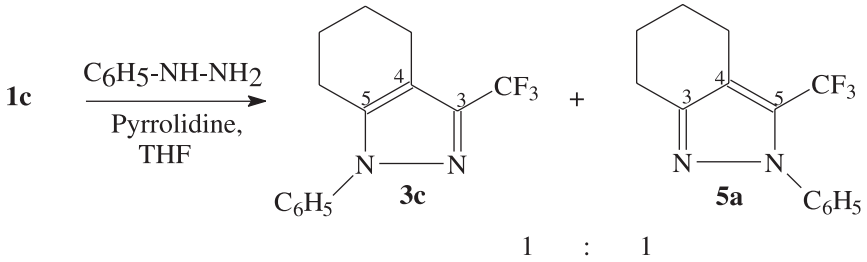
Two pyrazoles with a vicinal arrangement between R^F and a 2,4-difluorophenyl group were obtained from condensation of the 1,3-diketones and hydrazine in the presence of equimolar amounts of pyrrolidine, giving 5-hydroxypyrazolines, which were subsequently dehydrated (11). According to ref. 38, a semi-aminal is formed in the first step, which is a product of the addition of the pyrrolidine nitrogen to the polyfluoroacyl group (cf. ref. 40) and then a reaction with phenylhydrazine proceeds. However, 1,3-diketones and amines form ammonium salts at ambient temperatures, which produce β-aminoenones upon heating (41). The semi-aminals described in ref. 38 are probably pyrrolidinium salts. Obviously, the synthetic procedure of the aforementioned pyrazoles is based on the variation of the relative

© 2001 NRC Canada

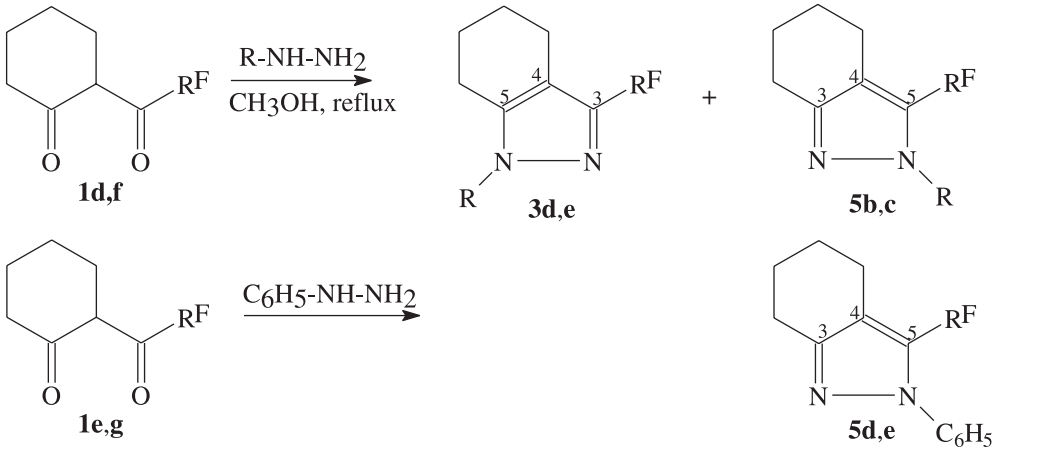
Scheme 4.



Scheme 5.



Scheme 6.



1	R^F
d	CF_2CF_2H
e	C_4F_9
f	C_3F_7
g	C_6F_{13}

3	R^F	R
d	CF_2CF_2H	C_6H_5
e	C_3F_7	CH_3

5	R^F	R
b	CF_2CF_2H	C_6H_5
c	C_3F_7	CH_3
d	C_4F_9	
e	C_6F_{13}	

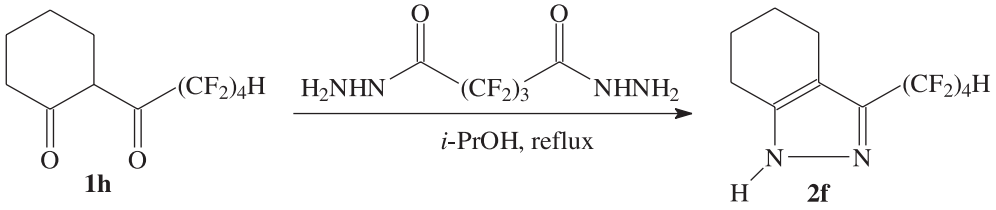
reactivity of the 1,3-diketone electrophilic centers by in situ generation of the respective β-aminoenones (11). Applying the same conditions for the reaction of **1c** with phenylhydrazine, an isomeric mixture of pyrazoles **3c** and **5a** (1:1) was found (Scheme 5), which could be separated by column chromatography. The formation of hydroxypyrazoline intermediate was not observed, the relative stability was probably controlled not only by the presence of a polyfluoroalkyl substituent (42) but also by the presence of a hydrogen-bridge acceptor as in the case of **4a**, where the OH proton probably interacted with the pyridine nitrogen atom, as confirmed by IR absorption in the 3000–3400 cm^{-1} region.

In the ^{13}C NMR spectrum of compound **5a**, a quartet (J = 1.1 Hz) appeared in one of the phenyl carbon signals, presumably due to a "through-space" coupling of the *ortho*-carbon nuclei with the CF_3 group fluorine nuclei, as also seen in ref. 11.

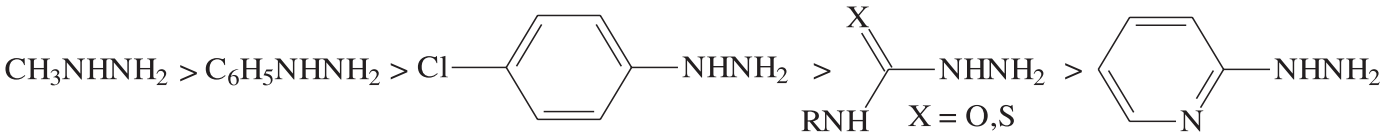
Increasing the chain length of the polyfluoroalkyl moiety R^F in the 1,3-diketone changed the direction of the non-catalyzed reaction with methylhydrazine and phenylhydrazine. For **1a**, **c** (R^F = CF_3), 3-trifluoromethylpyrazoles

© 2001 NRC Canada

Scheme 7.



Scheme 8.



were obtained exclusively; for **1d** (R^F = CF_2CF_2H) and **1f** (R^F = C_3F_7), a mixture of the isomeric pyrazoles, **3d**, **5b** (5:6) and **3e**, **5c** (5:2) (as determined by comparing NMR integral intensities of the reaction mixtures), were obtained, respectively (Scheme 6). For **1e**, **g** (R^F = C_4F_9, C_6F_{13}), only 2-indazole derivates **5d**, **e** were found, where the NH_2 group attacked the cyclohexanone keto carbon. Like **3a**, compounds **3e** and **5c** are featuring CH_3-CF_2 through-bond coupling. For **3e**, a broad triplet was observed with $^6J_{H-F} \approx$ 0.7 Hz ($\Delta\nu_{1/2} \approx$ 2.0 Hz); for **5c**, a broad multiplet ($\Delta\nu_{1/2}$ = 3.6 Hz) was observed due to $^5J_{H-F}$ and $^7J_{H-F}$ coupling with the $CF_2CF_2CF_3$ system, as confirmed by $^1H\{^{19}F\}$ NMR experiments (see Table 1).

The pyrazoles **2c**–**e**, **3d**, **e**, and **3a**, **c** investigated by X-ray diffraction show similar ^{13}C NMR features (Table 2), but differ significantly from the spectrum of the 5-CF_3-pyrazole **5a**. This prompted us to assume a 3-CF_3-structure for cyclohexane ring containing compounds **2c**–**e**, **3d**, **e**. The same argument applies for the trimethylene substituted pyrazoles **2a**, **b** for which ^{13}C NMR data (Table 2) are comparable with those of compound **3b** (see its molecular structure, Fig. 2). The similarity of ^{13}C NMR spectra of compounds **5b**–**e** with those of pyrazoles **5a** and compounds mentioned in ref. 11 led us to propose a 5-CF_3-pyrazole structure.

When 1,3-diketone **1h** was reacted with perfluoroglutaric dihydrazide in a 2:1 ratio, surprisingly the *N*-H pyrazole **2f** (Scheme 7) was obtained, indicating hydrolytical cleavage.

The reactions of asymmetric binucleophiles with trifluoroacetyl group containing bielectrophiles mentioned above can be qualitatively characterized as acid–base interactions according to the Pearson concept (43, 44). The decrease in hardness of the terminal nitrogen in the binucleophiles from left to right (see Scheme 8) alters the position of the NH_2 attack. The NH_2-group of the first two hydrazines interacts with the harder electrophilic center, namely in the $CF_3C(O)$ group, the last two compounds interact with the softer keto carbon in the cycloalkane ring. Compound 4-chlorophenylhydrazine furnished a mixture of the two possible pyrazoles (7).

When 1,3-diketones with longer polyfluoroalkyl substituents were treated, the attack of the NH_2 group was probably controlled by steric factors (45); as in the case of R^F = CF_2CF_2H and C_3F_7,where a mixture of isomers was found. In the case of R^F = C_4F_9, C_6F_{13}, only 5-R^F-pyrazoles were obtained, where the NH_2 group interacted with the cyclohexane keto carbon.

Our results show that structural assignment based solely on whether spin–spin couplings between the substituents at pyrazole are observed or absent would lead to erroneous conclusions. Following the arguments in ref. 16, compound **3a** should have the 2-CH_3-indazole structure because of the spin–spin interaction between the CH_3 and CF_3. This could subsequently let one assume the wrong geometry of compounds **2c**–**e**, **3c**–**e**, since they have similar ^{13}C NMR parameters. Therefore, it appears as if the trimethylene and tetramethylene substituted compounds **3b** and **3a**, **c**–**e** were derivatives of the isomeric pyrazole, although the ^{13}C shift difference of the respective nuclei reflect probably only the ring strain difference of the corresponding bicyclic systems.

There is one case where the structures of 5-CF_3 pyrazoles and their 3-CF_3 isomers, which were obtained as well, were unequivocally assigned based on chemical transformations and NMR data (18, 19, 29, 30, 32). The ^{13}C NMR signals of CF_3-C^3 were found at ca. δ_C = 145, and of CF_3-C^5 at δ_C = 133. However, this rule is not general and cannot be applied for the CF_3 substituted pyrazoles in this work, where for CF_3-C^3 δ_C = 137.95 (**3a**), 137.02 (**3b**), 140.11 (**3c**), and for CF_3-C^5 δ_C = 128.34 (**5a**) have been observed. The ^{19}F NMR shift values found for CF_3 group containing pyrazoles (29, 32), δ_F (3-CF_3) ≈ –62 and δ_F (5-CF_3) ≈ –58, applies also for **2a**, **c**, **3a**–**c**, **5a** (see Table 1) but only for $CDCl_3$ solutions. This has to be taken into account for ref. 32 where ^{19}F NMR data from a solution of *N*-H pyrazoles in a DMSO-d_6–$CDCl_3$–CF_3COOH mixture were used for the structure determination. In this case, the ^{13}C NMR parameters indicate the CF_3 group at C^3 with δ_C (C^3) = 141.61, whereas the ^{19}F NMR data (δ_F = –57.35) correspond to the 5-CF_3-pyrazole.

Obviously, the δ_F value for the difluoromethylene group connected with the pyrazole ring is also indicative for the structural assignment. In the ^{13}C NMR data of 3-CF_2CF_2H isomer **3d** the respective signal was observed at δ_F = –114.8; in case of 5-CF_2CF_2H isomer **5b**, δ_F = –109.7 (solvent $CDCl_3$). These findings correspond to the δ_F value of compound **2d** (δ_F = –114.6, nitrogen is not substituted), where a

© 2001 NRC Canada

Table 5. MS (*m*/*z*, %) data of compounds **2**, **3**, and **5**.

2b	326 (M^+, 18), 307 ($[M - F]^+$, 3), 157 ($[M - C_3F_7]^+$, 18), 107 ($[M - C_4F_9]^+$, 8), 69 (CF_3^+, 3) and other fragments
2c	190 (M^+, 50), 194 ($[M - N_2]^+$, 100), 121 ($[M - CF_3]^+$, 20), 69 (CF_3^+, 6) and other fragments
2d	222 (M^+, 60), 194 ($[M - N_2]^+$, 100), 171 ($[M - CF_2H]^+$, 36), 143 ($[M - N_2 - CF_2H]^+$, 44), 121 ($[M - CF_2CF_2H]^+$, 26) and other fragments
3b	252 (M^+, 100), 233 ($[M - F]^+$, 10), 183 ($[M - CF_3]^+$, 24), 77 ($C_6H_5^+$, 46) and other fragments
3c	266 (M^+, 100), 247 ($[M - F]^+$, 10), 197 ($[M^+ - CF_3]^+$, 18), 77 ($C_6H_5^+$, 62) and other fragments
3d	298 (M^+, 100), 270 ($[M - N_2]^+$, 50), 247 ($[M - CF_2H]^+$, 35), 197 ($[M - CF_2CF_2H]^+$, 20), 77 ($C_6H_5^+$, 55) and other fragments
5a	266 (M^+, 100), 197 ($[M - CF_3]^+$, 30) and other fragments
5b	298 (M^+, 100), 270 ($[M - N_2]^+$, 30), 247 ($[M - CF_2H]^+$, 22), 197 ($[M - CF_2CF_2H]^+$, 68), 77 ($C_6H_5^+$, 55), 51 (CF_2H^+, 14) and other fragments
5d	416 (M^+, 100), 397 ($[M - F]^+$, 10), 247 ($[M - C_3F_7]^+$, 31), 197 ($[M - C_4F_9]^+$, 32), 77 ($C_6H_5^+$, 35) and other fragments
5e	516 (M^+, 100), 247 ($[M - C_5F_{11}]^+$, 42), 197 ($[M - C_6F_{13}]^+$, 36), 77 ($C_6H_5^+$, 26) and other fragments

3-R^F structure is assumed due to the ^{13}C NMR data. From the literature and this work, the following typical ^{19}F and ^{13}C NMR data for the 3-R^F- or 5-R^F geometry of the polyfluoroalkyl group substituted pyrazoles could be defined (as reference structures compounds whose geometry unequivocally were determined by X-ray diffraction or by specific chemical reactions were taken).

3-R^F isomer

(1) δ_F (CF_3) = ca. –62, for pyrazoles from the respective linear (29, 37, 38) and carbocyclic 1,3-diketones;
(2) δ_F (CF_2CF_2H) = ca. –115, for pyrazoles from carbocyclic 1,3-diketones;
(3) δ_C (C^3) and δ_C (C^5) are similar: δ_C = 136–141, for pyrazoles with any R^F from cyclohexane containing 1,3-diketones; and δ_C = 140–145, for pyrazoles with R^F = CF_3 from linear 1,3-diketones (18, 19, 29, 30);
(4) δ_C (C^3) = ca. 135 and δ_C (C^5) = ca. 152, for pyrazoles from 2-trifluoracetylcyclopentanone.

5-R^F isomer

(1) δ_F (CF_3) = ca. –58, for pyrazoles from the respective linear (29, 32, 38) and carbocyclic 1,3-diketones;
(2) δ_F (CF_2CF_2H) = ca. –110, for pyrazoles from carbocyclic 1,3-diketones;
(3) δ_C (C^3) = ca. 150, δ_C (C^5) = ca. 130, for pyrazoles from 2-polyfluoroacylcyclohexanones; δ_C (C^3) = ca. 149, δ_C (C^5) = 133, for pyrazoles from linear 1,3-diketones (19, 29, 30).

Experimental

Mass spectra (EI, 70 eV) were carried out on a MAT 8200 spectrometer (Table 5). IR spectra were recorded on a Specord-75 IR spectrophotometer as suspensions in nujol. NMR spectra were recorded in deuterochloroform solutions on a Tesla BS-587A instrument operating at 80.1 MHz (^1H, standard: TMS), 20.1 MHz (^{13}C, standard: TMS), and 75.3 MHz (^{19}F, standard: CCl_3F) and on a Bruker DPX-200 spectrometer operating at 200.1 MHz (^1H), 50.3 MHz (^{13}C), and 188.3 MHz (^{19}F). Double resonance experiments $^1H\{^{19}F\}$ and $^{19}F\{^1H\}$ were performed on a Tesla 587A supplied with a specially designed decoupler unit operating on ^{19}F frequency (46). Chromatography was performed with a silica gel column (normal phase, MATREX, Grace GmbH). 2-Polyfluoroacylcycloalkanones **1a** (47), **c** (11, 47), **f**, **g** (48), **d**, **e** (49), **h** (50) were synthesized by a Claisen-type condensation of cyclopentanone or cyclohexanone and alkylpolyfluoroacylates in the presence of lithium hydride in dried benzene (49).

2-Perfluoropentanoylcyclopentanone (1b)

To a stirred suspension of sodium methoxide (3.2 g, 60 mmol) in diethyl ether (100 mL) was added dropwise the mixture of cyclopentanone (4.8 g, 58 mmol) and methyl perfluoropentanoate (16.0 g, 58 mmol). The mixture was stirred for 24 h at room temp, then quenched by the addition of 10% H_2SO_4 (60 mL). The organic layer was separated and the water phase additionally extracted with diethyl ether (2 × 20 mL) and the combined extracts were dried over $MgSO_4$. The solvent was evaporated and the crude product distilled at reduced pressure with Vigreaux column to yield 13.5 g (71%) of a colorless liquid: bp 52°C (0.5 torr). ^1H NMR (major enol-tautomer) δ: 1.91–2.06 (m, 2H, CH_2), 2.47–2.56 (m, 2H, CH_2), 2.74–2.84 (m, 2H, CH_2), 13.0 (br s, 1H, O*H*). MS *m*/*z* (%): 330 (M^+, 18), 169 ($C_3F_7^+$, 3), 119 ($C_2F_5^+$, 3), 111 ($[M - C_4F_9]^+$, 100) and other fragments. HRMS *m*/*z* calcd. for $C_{10}H_7F_9O_2$: 330.0302; found: 330.0300.

General procedure for preparing compounds 2a–e, 3a–c, 5d, e (for 2d, 3c: method A)

A mixture of **1** (10 mmol) and hydrazine (10 mmol) (for **2**: 80% hydrazine hydrate (1.2 g, 30 mmol) in methanol (20 mL) (for **5e**: in 20 mL ethanol) was heated at reflux for 4 h (for **2b**: 10 h, for **2c**: 5 h, for **3a**: 6h), cooled to ambient temp, and diluted with water (100 mL). For **2a**–**e**, the mixture was extracted with $CHCl_3$ (3 × 10 mL). The combined extracts were dried with $MgSO_4$. After removal of the solvent, the solid residue was recrystallized (Table 6) to afford **2a**, **c**–**e** as colorless crystals (**2b**: pale yellow crystals). For **3a**, the precipitated solid was dried and recrystallized (Table 6) to afford product as colorless crystals. For **3b**, **c**, **5d**,

© 2001 NRC Canada

Table 6. Yield, melting point, and elemental analysis (HRMS) data for compounds **2**, **3**, and **5**.

	Compound	Yield (%)	mp (°C) (solvent)	Molecular formula	Found/calcd (%) C	H	F	N
2a	3-Trifluoromethyl-5,6-dihydro-1,4-*H*-cyclopenta-[*d*]-pyrazole	58	132–133 (hexane)	$C_7H_7F_3N_2$	47.62/47.73	4.11/4.00	32.22/32.36	15.73/15.91
2b	3-Perfluorobutyl-5,6-dihydro-1,4-*H*-cyclopenta-[*d*]-pyrazole	82	67–68 (perfluoro-1,1-dimethylcyclohexane)	HRMS *m*/*z* calcd. for $C_{10}H_7F_9N_2$: 326.0465; found: 326.0463.				
2c	3-Trifluoromethyl-4,5,6,7-tetrahydro-1*H*-indazole	63	120–121 (perfluoro-1,1-dimethylcyclohexane)	$C_8H_9F_3N_2$	50.54/50.53	4.97/4.77	29.42/29.97	14.80/14.73
2d	4,5,6,7-Tetrahydro-3-(1,1,2,2-tetrafluoroethyl)-1*H*-indazole	(*a*) 60, (*b*) 76	108–111 (perfluoro-1, 1-dimethylcyclohexane)	$C_9H_{10}F_4N_2$	48.74/48.65	4.63/4.54	34.18/34.20	12.53/12.61
2e	3-Perfluorobutyl-4,5,6,7-tetrahydro-1*H*-indazole	83	116.5 (hexane)	$C_{11}H_9F_9N_2$	38.66/38.83	2.63/2.67	50.12/50.26	8.39/8.24
2f	4,5,6,7-Tetrahydro-3-(1,1,2,2,3,3,4,4-octafluorobutyl)-1*H*-indazole	16	83–84 (petrol. ether)	$C_{11}H_{10}F_8N_2$	41.29/41.01	3.06/3.13	47.03/47.17	8.78/8.70
3a	3-Trifluoromethyl-4,5,6,7-tetrahydro-1-methyl-1*H*-indazole	93	49 (petrol. ether)	$C_9H_{11}F_3N_2$	52.99/52.94	5.31/5.43	27.50/27.91	13.48/13.72
3b	3-Trifluoromethyl-5,6-dihydro-1-phenyl-1,4-*H*-cyclopenta-[*d*]-pyrazole	35	77.0–77.5 (perfluoro-1,1-dimethylcyclohexane)	$C_{13}H_{11}F_3N_2$	61.53/61.90	4.42/4.40	22.73/22.60	11.28/11.11
3c	3-Trifluoromethyl-4,5,6,7-tetrahydro-1-phenyl-1*H*-indazole	(*a*) 51, (*b*) 21	68–71 (ethanol)	$C_{14}H_{13}F_3N_2$	63.43/63.15	4.96/4.92	21.34/21.40	10.66/10.52
3d	4,5,6,7-Tetrahydro-3-(1,1,2,2-tetrafluoroethyl)-1-phenyl-1*H*-indazole	5	Oil	HRMS *m*/*z* calcd. for $C_{15}H_{14}F_4N_2$: 298.1093; found: 298.1099.				
3e	3-Perfluoropropyl-4,5,6,7-tetrahydro-1-methyl-1*H*-indazole	52 (spectr.)	Oil	$C_{11}H_{11}F_7N_2$	43.24/43.43	3.72/3.64	43.62/43.71	9.36/9.21
5a	3-Trifluoromethyl-4,5,6,7-tetrahydro-2-phenyl-2*H*-indazole	6	Oil	HRMS *m*/*z* calcd. for $C_{14}H_{13}F_3N_2$: 266.1031; found: 266.1040.				
5b	4,5,6,7-Tetrahydro-3-(1,1,2,2-tetrafluoroethyl)-2-phenyl-2*H*-indazole	3	Oil	HRMS *m*/*z* calcd. for $C_{15}H_{14}F_4N_2$: 298.1093; found: 298.1097.				
5c	3-Perfluoropropyl-4,5,6,7-tetrahydro-2-methyl-2*H*-indazole	21 (spectr.)	Oil	$C_{11}H_{11}F_7N_2$	43.24/43.43	3.72/3.64	43.62/43.71	9.36/9.21
5d	3-Perfluorobutyl-4,5,6,7-tetrahydro-2-phenyl-2*H*-indazole	22	68.0–68.5 (perfluoro-1,1-dimethylcyclohexane)	$C_{17}H_{13}F_9N_2$	48.73/49.04	3.29/31.5	41.42/41.08	6.81/6.73
5e	3-Perfluorohexyl-4,5,6,7-tetrahydro-2-phenyl-2*H*-indazole	30	60–61 (hexane)	$C_{19}H_{13}F_{13}N_2$	44.28/44.20	2.64/2.54	47.83/47.84	5.45/5.43

© 2001 NRC Canada

Table 7. Details of X-ray crystal structure data, measurement of intensities, and data processing of X-ray investigation of compounds **3a–c**.

	3a	**3b**	**3c**
Formula	$C_9H_{11}F_3N_2$	$C_{13}H_{11}F_3N_2$	$C_{14}H_{13}F_3N_2$
MW	204.20	252.24	266.26
Crystal size (mm)	0.7 × 0.4 × 0.4	0.8 × 0.7 × 0.7	0.8 × 0.7 × 0.5
Crystal system	monoclinic	monoclinic	orthorhombic
Space group	$P2_1/m$	$P2_1/m$	$P2_12_12_1$
a (pm)	834.0(3)	794.00(10)	804.30(10)
b (pm)	739.90(10)	705.70(10)	850.40(10)
c (pm)	851.0(2)	1095.2(2)	1806.5(4)
α (°)	90	90	90
β (°)	115.46	109.79	90
γ (°)	90	90	90
V (nm^3)	0.4741(2)	0.57743(15)	1.2356(3)
Z	2	2	4
D_x (Mg m^{-3})	1.430	1.451	1.431
μ (Mo Kα) (mm^{-1})	0.128	0.121	0.117
2θ range (°)	2.65–24.99	2.73–27.50	2.65–27.51
F(000)	212	260	552
Index range	h –8 → 1	h –10 → 10	h –10 → 10
	k –8 → 8	k –9 → 9	k –11 → 11
	l –10 → 10	l –13 → 14	l –23 → 23
Reflections collected	1918	5025	10766
Independent reflections	863 (R_{int} = 0.0313)	1435 (R_{int} = 0.0303)	2837 (R_{int} = 0.0564)
Completeness to θ_{max} (%)	95.6	99.9	99.8
Data/restraints/parameter	863/0/105	1435/0/109	2837/0/175
GoF on F^2	1.054	1.069	1.045
$R[F^2 > 2\sigma(F^2)]$	0.0790	0.0515	0.0421
$wR(F^2)$	0.2296	0.1382	0.1169
Extinction coefficient	0.03(2)	0.079(12)	0.007(3)
Largest difference peak and hole (e Å^{-3})	0.856 and –0.307	0.431 and –0.307	0.421 and –0.262
Absolute structure parameter	—	—	–1.2(11)

and **e**, the reaction mixture was extracted with $CHCl_3$ (3 × 10 mL). The combined extracts were dried using $MgSO_4$. After removal of the solvent, the residue was purified by column chromatography ($CHCl_3$) and recrystallized (Table 6) to give **3b**, **c**, and **5e** as colorless crystals (**5d**: yellow crystals).

Preparation of 2d (method B)

A mixture of **1d** (3.0 g, 13 mmol), hydrazine dihydrochloride (1.4 g, 13 mmol), and triethylamine (2.7 g, 27 mmol) in methanol (30 mL) was heated at reflux for 4 h. The cooled mixture was diluted with water (100 mL). Mixture was extracted with $CHCl_3$ (3 × 10 mL). The combined extracts were dried with $MgSO_4$; removal of the solvent gave a solid residue which was recrystallized (Table 6).

Preparation of 3c (method B)

A mixture of **1c** (1.0 g, 5 mmol) and phenylhydrazine (0.6 g, 5 mmol) in benzene (20 mL) was heated at reflux for 4 h. After removal of the solvent, the residue was purified by column chromatography ($CHCl_3$) and recrystallized (Table 6).

Reaction of 1d with phenylhydrazine

A mixture of **1d** (1.4 g, 6 mmol) and phenylhydrazine (0.7 g, 6 mmol) in methanol (15 mL) was heated at reflux for 4 h. The cooled mixture was diluted with water (100 mL). Mixture was extracted with $CHCl_3$ (3 × 10 mL). The combined extracts were dried with $MgSO_4$. After removal of the solvent, the residue was purified by chromatography ($CHCl_3$:*n*-pentane) to yield **3d** (higher R_f, 0.1 g, yellow oil) and **5b** (lower R_f, 0.05 g, colorless oil) (Table 6).

Reaction of 1f with methylhydrazine

A mixture of **1f** (4.9 g, 17 mmol) and methylhydrazine (0.8 g, 17 mmol) in methanol (30 mL) was heated to reflux for 4 h. After removal of the solvent, the residue was purified by column chromatography ($CHCl_3$) to yield a mixture of **3e** and **5c** as a colorless oil (Table 6).

Reaction of 1c with phenylhydrazine in the presence of pyrrolidine

To a solution of **1c** (2.0 g, 10 mmol) in THF (10 mL) was added pyrrolidine (0.7 g, 10 mmol) followed by separation using 1.0 g molecular sieves (3 Å). After stirring at 0°C for 30 min, a solution of phenylhydrazine (1.1 g, 10 mmol) in THF (5 mL) was added, and the mixture was allowed to warm slowly to room temp for 12 h. The mixture was diluted with water (100 mL) and extracted with $CHCl_3$ (3 × 10 mL). The combined extracts were dried with $MgSO_4$ and concentrated to 5 mL, followed by flash chromatography

© 2001 NRC Canada

Table 8. Atomic coordinates (× 10^4) and equivalent isotropic displacement parameters ($pm^2 \times 10^{-1}$) for **3a**.

	x	*y*	*z*	U_{eq}
F(1)	9293(5)	2790(30)	4384(5)	113(6)
F(2)	9996(17)	980(20)	2971(17)	112(5)
F(2A)	10309(19)	1270(30)	2730(20)	117(6)
N(1)	5975(5)	2500	1888(5)	50(1)
N(2)	4571(5)	2500	358(5)	50(1)
C(8)	5053(6)	2500	–1024(5)	50(1)
C(3)	6816(6)	2500	–335(6)	52(1)
C(7)	3742(6)	2500	–2859(6)	57(1)
C(1)	9244(6)	2500	2872(5)	54(1)
C(9)	2812(7)	2500	256(7)	64(2)
C(2)	7374(6)	2500	1486(5)	50(1)
C(4)	7770(9)	2500	–1446(7)	74(2)
C(6)	4824(12)	2081(12)	–3911(8)	75(4)
C(5)	6543(12)	3113(13)	–3312(9)	83(3)

Note: U_{eq} is defined as one third of the trace of the orthogonalized U_{ij} tensor.

Table 9. Atomic coordinates (× 10^4) and equivalent isotropic displacement parameters ($pm^2 \times 10^{-1}$) for **3b**.

	x	*y*	*z*	U_{eq}
N(1)	6030(2)	2500	282(2)	30(1)
N(2)	6708(2)	2500	–708(2)	35(1)
C(1)	5277(3)	2500	–1786(2)	34(1)
C(2)	3677(3)	2500	–1516(2)	32(1)
C(3)	2687(3)	2500	328(2)	36(1)
C(4)	1039(3)	2500	–941(2)	44(1)
C(5)	1676(3)	2500	–2136(2)	37(1)
C(6)	4202(2)	2500	–196(2)	30(1)
C(7)	5561(3)	2500	–3060(2)	44(1)
C(8)	7243(3)	2500	1584(2)	32(1)
C(9)	9076(3)	2500	1807(2)	39(1)
C(10)	10265(3)	2500	3070(2)	47(1)
C(11)	9649(4)	2500	4104(2)	53(1)
C(12)	7827(4)	2500	3875(2)	57(1)
C(13)	6612(3)	2500	2616(2)	44(1)
F(1)	4047(2)	2500	–4030(2)	94(1)
F(2)	6478(2)	1015(2)	–3219(1)	90(1)

Note: U_{eq} is defined as one third of the trace of the orthogonalized U_{ij} tensor.

using $CHCl_3$ to give 0.5 g of mixture of **3c**, **5a** (1:1, from ^1H and ^{19}F NMR data) as yellow oil. **5a** was isolated by column chromatography ($CHCl_3$:*n*-hexane, 1:3, lower R_f) as yellow oil (0.15 g, Table 6).

3-Trifluoromethyl-3,3a,4,5,6,7-hexahydro-3-hydroxy-2-(pyridin-2-yl)-2*H*-indazole (4a)

A mixture of **1c** (0.6 g, 3 mmol) and 2-hydrazinopyridine (0.3 g, 3 mmol) in benzene (20 mL) was heated at reflux for 4 h. Removal of the solvent gave a residue which was purified by column chromatography ($CHCl_3$) and recrystallized to yield **4a** as colorless crystals (0.2 g, 23 %): mp 76.5–77°C (perfluoro-1,1-dimethylcyclohexane). IR (ν, cm^{-1}): 1555, 1585 (C = N, Py), 3000–3400 (OH). ^1H NMR δ: 1.34–2.81 (m, 8H, 4CH_2), 3.15 (dd, $^3J_{H-H}$ = 10.7, 6.3 Hz, 1H, C*H*), 6.76 (ddd, $^3J_{\beta-\alpha}$ = 5.2 Hz, $^3J_{\beta-\gamma}$ = 6.6 Hz, $^3J_{\beta-\beta'}$ = 1.5 Hz, 1H, β-*H*), 7.30 (dd, $^3J_{\beta'-\gamma}$ = 8.4 Hz, 1H, β′-*H*), 7.59 (ddd, $^3J_{\gamma-\alpha}$ = 1.8 Hz, 1H, γ-*H*), 8.03 (dd, 1H, α-*H*), 8.74 (s, 1H, O*H*). ^{19}F NMR δ: –77.86, –82.79 (s, ratio of integral intensities 3:97). ^{13}C NMR δ: 23.95, 25.50, 26.29, 27.65 (s, $C^{4,5,6,7}$), 53.13 (s, C^{3a}), 92.36 (q, C^3, $^2J_{C-F}$ = 32.3 Hz), 112.21, 115.85, 138.18, 145.15, 157.16 (five s, Py-ring), 124.30 (q, CF_3, $^1J_{C-F}$ = 287.5 Hz), 157.50 (s, C^{7a}). Anal. calcd for $C_{13}H_{14}F_3N_3O$: C 54.73, H 4.95, F 19.98, N 14.73; found: C 54.49, H 4.98, F 19.54, N 14.93.

Table 10. Atomic coordinates (× 10^4) and equivalent isotropic displacement parameters ($pm^2 \times 10^{-1}$) for **3c**.

	x	*y*	*z*	U_{eq}
F(1)	3615(2)	9597(3)	2375(1)	86(1)
F(2)	5655(3)	8515(3)	1869(1)	113(1)
F(3)	5706(3)	10916(3)	2093(1)	107(1)
N(1)	3992(2)	10825(2)	–2(1)	28(1)
N(2)	4946(2)	10818(2)	617(1)	30(1)
C(1)	4010(2)	10089(2)	1119(1)	30(1)
C(2)	4731(3)	9789(3)	1860(1)	39(1)
C(3)	2465(2)	9610(2)	834(1)	29(1)
C(4)	1051(2)	8694(2)	1166(1)	35(1)
C(5)	–437(2)	8679(3)	634(1)	40(1)
C(6)	102(2)	8430(2)	–169(1)	37(1)
C(7)	1168(2)	9794(2)	–446(1)	33(1)
C(8)	2498(2)	10099(2)	112(1)	27(1)
C(9)	4696(2)	11345(2)	–683(1)	28(1)
C(10)	6354(2)	10973(2)	–830(1)	34(1)
C(11)	7030(3)	11416(3)	–1504(1)	41(1)
C(12)	6087(3)	12211(3)	–2019(1)	43(1)
C(13)	4457(3)	12592(3)	–1860(1)	39(1)
C(14)	3744(2)	12169(2)	–1187(1)	33(1)

Note: U_{eq} is defined as one third of the trace of the orthogonalized U_{ij} tensor.

4,5,6,7-Tetrahydro-3-(1,1,2,2,3,3,4,4-octafluorobutyl)-1*H*-indazole (2f)

A mixture of **1h** (1.0 g, 3 mmol) and perfluoroglutaric dihydrazide (0.4 g, 1.5 mmol) in 2-propanol (15 mL) was heated at reflux for 12 h. The cooled mixture was diluted with water (50 mL) and extracted with $CHCl_3$ (3 × 10 mL). The combined extracts were dried with $MgSO_4$. Removal of the solvent gave a residue which was purified by column chromatography ($CHCl_3$) and recrystallized, affording **2f** (0.15 g) as colorless crystals (Table 6).

X-ray crystal structure parameters

The X-ray structure studies of compounds **3a–c** were performed at –100°C on a Siemens P4 diffractometer with low-temperature device LT2, using graphite-monochromated Mo Kα radiation (λ = 71.073 pm). Full-matrix least-squares refinement has been carried out with the SHELX-97 program system (51). Details of crystal data, measurement of intensities, and data processing are summarized in Table 7. Atomic coordinates are summarized in Tables 8–10. All structures were solved by direct methods. All non-hydrogen atoms were refined anisotropically, and the positions of the hydrogen atoms were calculated as a riding model. The

© 2001 NRC Canada

weighting schemes where $w^{-1} = \sigma^2(F_o)^2 + (0.1560P)^2 + 0.3680P$ (**3a**); where $w^{-1} = \sigma^2(F_o)^2 + (0.0698P)^2 + 0.2304P$ (**3b**); $w^{-1} = \sigma^2 (F_o)^2 + (0.0621P)^2 + 0.3798P$ (**3c**) where $P = (F_o^2 + 2F_c^2)/3$. Single crystals were crystallized from hexane: colorless prisms (**3a**) and plates (**3b**, **c**).

Acknowledgements

We gratefully acknowledge financial support of the Deutsche Forschungsgemeinschaft (Grant 436 RUS 113/445/0) and generous gifts of chemicals from Dr. Karl-Heinz Hellberg, Solvay Fluor und Derivate GmbH, Hannover, Germany. Inge Erxleben, Dr. Peter Schulze, and Dr. Thomas Dülcks, Institute of Organic Chemistry, University of Bremen, are thanked for recording mass spectra, and Dr. Lyudmila N. Bazhenova and co-workers, Institute for Organic Synthesis, Ural Branch of the Russian Academy of Sciences, Ekaterinburg (Russian Federation), for carrying out elemental analyses.

References

1. H.A. Wagner. U.S. Patent no. 3200128 (1965); Chem. Abs. **63**, 13272 (1965).
2. T. Nishiwaki. Bull. Chem. Soc. Jpn. **42**, 3024 (1969).
3. H.V. Secor and J.F. DeBardeleben. J. Med. Chem. **14**, 997 (1971).
4. J.J. Ozol, E.E. Liepinsh, and G.J. Dubur. Khim. Geterotiskl. Soedin. **11**, 1545 (1975).
5. J. Bourdais and J.M.A. Peyroux. Ger. Offen. N 2630015 (1977); Chem. Abs. **87**, p5969d (1977).
6. Sumimoto Chemical Co, Ltd. Jpn. Kokai Tokkyo Koho JP 61, 78768 (1986); Chem. Abs. **106**, 5024c (1987).
7. J.W. Lyga, R.M. Patera, M.J. Plummer, B.P. Halling, and D.A. Yuhas. Pestic. Sci. **42**, 29 (1994).
8. K. Niigata, T. Marujama, S. Hayashibe, H. Shikama, T. Takasu, M. Umeda, and E. Hirasaki. Jpn. Kokai Tokyo Koho JP 06, 298737 (1995); Chem. Abs. **122**, 133181n (1995).
9. S.R. Bertenshaw, J.J. Talley, D.J. Rogier, M.J. Graneto, C.M. Koboldt, and Y. Zhang. Bioorg. Med. Chem. Lett. **6**, 2827 (1996).
10. B. Eistert and R. Wessendorf. Chem. Ber. **84**, 2590 (1961).
11. J.W. Lyga, R.N. Henrie, G.A. Meier, R.W. Creekmore, and R.M. Patera. Magn. Reson. Chem. **31**, 323 (1993).
12. R. Jacquer and G. Maury. Bull. Soc. Chim. Fr. **1**, 316 (1967).
13. Kh.-O. Kim, G.A. Tolstikov, and V.S. Bazalitskaya. J. Gen. Chem. U.S.S.R. **40**, 455 (1970).
14. K.I. Pashkevich, V.I. Saloutin, A.N. Fomin, V.V. Berenblit, V.S. Plashkin, and I. Ya. Postovskiy. Zh. Vses. Khim. O-va. **26**, 105 (1981).
15. A.D. Sinegibskaya, K.I. Pashkevich, V.I. Saloutin, N.A. Klyuev, and E. Kh. Dank. Khim. Geterotiskl. Soedin. **4**, 555 (1978).
16. A. Umada, T. Okano, and S. Eguchi. Synthesis, 1457 (1994).
17. K.C. Joshi, R. Jain, A. Dandia, and K. Sharma. J. Heterocycl. Chem. **25**, 1641 (1988).
18. S.P. Singh, S. Sehgal, L.S. Tarar, and S.N. Dhawan. Indian J. Chem. Sect. B, **29**, 310 (1990).
19. S.P. Singh, D. Kumar, D. Savita, and M.D. Threadgill. Indian J. Chem. Sect. B, **31**, 233 (1992).
20. J.L. Peglion, R.E. Pastor, and A.R. Cambon. Bull. Soc. Chim. Fr. **5**–**6**, 309 (1980).
21. T.D. Penning, J.J. Talley, S.R. Bertenshaw, J.S. Carter, P.W. Collins, S. Docter, M.J. Graneto, L.F. Lee, J.W. Malecha, J.M. Miyashiro, R.S. Rogers, D.J. Rogier, S.S. Yu, G.D. Anderson, E.G. Burton, J.N. Cogburn, S.A. Gregory, C.M. Koboldt, W.E. Perkins, K. Seibert, A.W. Veenhuizen, Y.Y. Zhang, and P.C. Isakson. J. Med. Chem. **40**, 1347 (1997).
22. S.I. Selivanov, R.A. Bogatkin, and B.A. Ershov. Zh. Org. Khim. **18**, 909 (1982).
23. K.N. Zelenin, O.V. Solod, and A.B. Tomchin. Zh. Obshch. Khim. **57**, 584 (1987).
24. J. Castells and R. Roser. An R. Soc. Esp. Fis. Quim. Ser. B 62, **4**–**5**, 409 (1966); **4**–**5**, Chem. Abs. **65**, 20117b (1966).
25. K.N. Zelenin, A.B. Tomchin, O.V. Solod, and M. Yu. Malov. Khim. Geterotiskl. Soedin. **1**, 128 (1986).
26. S.I. Yakimovich, I.V. Zerova, K.N. Zelenin, V.V. Alexeev, and A.R. Tugusheva. Zh. Org. Khim. **33**, 418 (1997).
27. K.I. Pashkevich, D.V. Sevenard, and O.G. Khomutov. Russ. Chem. Bull. **48**, 359 (1999).
28. K.I. Pashkevich, O.G. Khomutov, and D.V. Sevenard. Zh. Org. Khim. **36**, 1180 (2000).
29. S.P. Singh, J.K. Kapoor, D. Kumar, and M.D. Threadgill. J. Fluorine Chem. **83**, 73 (1997).
30. S.P. Singh, D. Kumar, and J.K. Kapoor. J. Chem. Res. Synop. 163 (1993).
31. J.P. Bouillon, C. Ates, Z. Janousek, and H.G. Viehe. Tetrahedron Lett. **34**, 5075 (1993).
32. S.P. Singh, D. Kumar, B.G. Jones, and M.D. Threadgill. J. Fluorine Chem. **94**, 199 (1999).
33. J.K. Williams. J. Org. Chem. **29**, 1377 (1964).
34. J. Catalan, J.C. del Valle, R.M. Claramunt, M.D. Santa Maria, V. Bobosik, R. Mocelo, and J. Elguero. J. Org. Chem. **60**, 3427 (1995).
35. P.E. Hansen, S.N. Ibsen, T. Kristensen, and S. Bolvig. Magn. Reson. Chem. **32**, 399 (1994).
36. P.N. Kondrat'ev, Z.E. Skryabina, V.I. Saloutin, and L.M. Khalilov. Zh. Org. Khim. **28**, 1380 (1992).
37. J.-P. Bouillon, A.-M. Frisque-Hesbain, Z. Janousek, and H.G. Viehe. Heterocycles, **40**, 661 (1995).
38. J.W. Lyga and R.M. Patera. J. Heterocycl. Chem. **27**, 919 (1990).
39. Ya.V. Burgart, A.S. Fokin, O.G. Kuzueva, O.N. Chupakhin, and V.I. Saloutin. J. Fluorine Chem. **92**, 101 (1998).
40. A. Gazit and Z. Rappoport. J. Chem. Soc. Perkin Trans. 1, 2863 (1984).
41. V.I. Filyakova, V.G. Ratner, N.S. Karpenko, and K.I. Pashkevich. Izv. Ros. Akad. Nauk Ser. Khim. **9**, 2278 (1996).
42. K.I. Pashkevich, V.I. Saloutin, and I. Ya. Postovskiy. Usp. Khim. **50**, 325 (1981).
43. R.D. Chambers, A.R. Edwards, A. Batsanov, and J.A.K. Howard. J. Fluorine Chem. **88**, 95 (1998).
44. R.J. Pearson. Usp. Khim. **40**, 7 (1971); **40**, 1259 (1971).
45. V.V. Chapurkin. Zh. Org. Khim. **32**, 44 (1996).
46. M.I. Kodess, V.Z. Shaburov, and S.N. Frolov. Instrum. Exp. Tech. **42**, 379 (1999).
47. J.D. Park, H.A. Brown, and J.R. Lacher. J. Am. Chem. Soc. **75**, 4753 (1953).
48. H. Trabelsi and A. Cambon. Synthesis, 315 (1992).
49. K.I. Pashkevich, O.G. Khomutov, and D.V. Sevenard. Zh. Org. Khim. **34**, 1798 (1998) (Russ. J. Org. Chem. **34**, 1727 (1998)).
50. D.V. Sevenard, O.G. Khomutov, O.V. Koryakova, V.V. Sattarova, M.I. Kodess, J. Stelten, I. Loop, E. Lork, K.I. Pashkevich, and G.-V. Röschenthaler. Synthesis, 1738 (2000).
51. G.M. Sheldrick. SHELX-97. Program for crystal structure determination. University of Göttingen, Germany. 1997.

© 2001 NRC Canada

Synthesis, X-ray crystal structure, and solid-state ^{13}C NMR study of tris(9-crown-3)triphenylene

Gerald W. Buchanan, Majid F. Rastegar, and Glenn P.A. Yap

Abstract: Benzo-9-crown-3 ether trimerizes in the presence of $FeCl_3$ and aqueous H_2SO_4 to produce tris(9-crown-3)triphenylene in 25.4% yield. This compound crystallizes in the monoclinic $P2_1/c$ space group: a = 13.759(2) Å, b = 13.318(2) Å, c = 13.399(2) Å, β = 96.883(2)°, with Z = 4. The three 9-crown-3 ether units of the trimer possess different geometries and there is substantial deviation from coplanarity in the three aromatic rings. ^{13}C NMR chemical shifts in the solid state are consistent with this lack of symmetry and are discussed in terms of the X-ray crystal-structure data.

Key words: crown ether, trimerization, stereochemistry.

Résumé : Dans l'acide sulfurique aqueux ou en présence de $FeCl_3$, l'éther benzo-9-couronne-3 se trimérise pour conduire à la formation du tris(9-couronne-3)triphénylène avec un rendement de 25,4 %. Ce composé cristallise dans le système monoclinique, groupe d'espace $P2_1/c$, avec a = 13,759(2) Å, b = 13,318(2) Å et c = 13,399(2) Å, β = 96,883(2)° et Z = 4. Les trois unités d'éthers 9-couronne-3 du trimère possèdent des géométries différentes et les trois noyaux aromatiques sont loin d'être coplanaires. Les déplacements chimiques en RMN du ^{13}C à l'état solide sont en accord avec ce manque de symétrie et on en discute en fonction des données structurales obtenues par diffraction des rayons X.

Mots clés : éther couronne, trimérisation, stéréochimie.

[Traduit par la Rédaction]

Introduction

Hexaalkoxy-substituted triphenylenes show liquid-crystal properties if the side chains are of sufficient length. Hence, these molecules are important models for discotic liquid crystals (1, 2). Recently, a procedure for preparing 2,3,6,7,10,11-hexamethoxytriphenylene in near-quantitative yield was reported (3) using oxidative trimerization of 1,2-methoxybenzene. Herein, we report the application of this method to the synthesis of a novel tris(9-crown-3)triphenylene.

Received August 25, 2000. Published on the NRC Research Press website on March 16, 2001.

G.W. Buchanan[1] and M.F. Rastegar. Ottawa–Carleton Chemistry Institute, Department of Chemistry, Carleton University, Ottawa, ON K1S 5B6, Canada.
G.P.A. Yap. Ottawa–Carleton Chemistry Institute, Department of Chemistry, University of Ottawa, Ottawa, ON K1A 6N5, Canada.

[1]Corresponding author (e-mail: gwbuchan@ccs.carleton.ca; telephone: (613) 520–3841; fax: (613) 520–3749).

[2]Supplementary material may be purchased from the Depository of Unpublished Data, Document Delivery, CISTI, National Research Council Canada, Ottawa, ON K1A OS2, Canada. For information on obtaining material electronically go to http://www.nrc.ca.cisti/irm/unpub_e.shtml. Supplementary material referred to in this paper have also been deposited with the Cambridge Crystallographic Data Centre. Copies of the data can be obtained, free of charge, on application to the Director, CCDC, 12 Union Road, Cambridge CB2 IEZ, U.K. (fax: 44-1223-336033 or e-mail: deposit @ccdc.cam.ac.uk).

The X-ray crystal structure has been determined, and a comparison of the solution and solid-phase ^{13}C NMR spectra is included. The observed multiplicity in the ^{13}C NMR spectrum clearly shows the lack of any symmetry elements in the crystal structure. The chemical shifts in the solid state are discussed in light of the X-ray crystal structure data.

Results and discussion

The synthesis, NMR spectra, and X-ray crystal structure of benzo-9-crown-3 ether (**1**) have been reported previously (4). In the presence of $FeCl_3$ and H_2SO_4, **1** trimerizes in 25.4% yield to the triphenylene system (**2**) depicted in Fig. 1.

Figure 2 shows the ORTEP diagram for **2**, while the solid-state ^{13}C NMR spectra are shown in Fig. 3. Table 1 contains atomic bond lengths and angles. Torsion angles involving non-hydrogen atoms are collected in Table 2, while the crystallographic data are presented in Table 3. Atomic coordinates and equivalent isotropic displacement factors are in Table 4. Anisotropic temperature factors are available as supplementary data.[2]

X-ray crystal structure

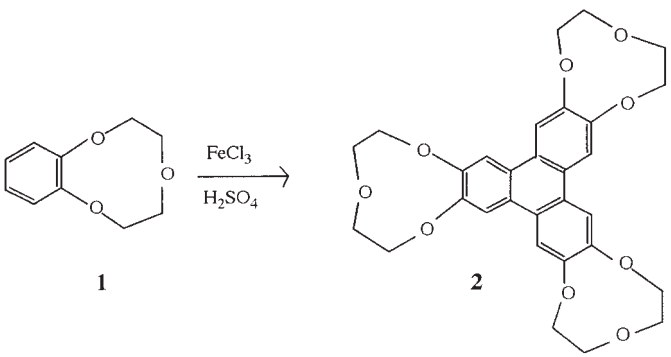
In discussing the conformations of the three nine-membered rings of **2**, it is useful to compare these with the torsion angles for the parent benzo-9-crown-3 system (**1**). Also, when viewing the ORTEP plot of **2** (Fig. 2), it is clear that there is a "northern" ring (i.e., C3–C8), an "eastern" ring (i.e., C13–C18), and a "western" ring (i.e., C23–C28). A comparison of torsion angles is presented in Table 5, and it is evident that the three nine-membered rings of **2** have

 DOI: 10.1139/cjc-79-2-195 © 2001 NRC Canada

Table 1. Selected bond lengths and angles.

(*a*) Selected atomic bond lengths (Å).					
O1—C3	1.378(3)	O1—C4	1.427(3)	O2—C6	1.414(3)
O2—C5	1.420(4)	O3—C8	1.395(3)	O3—C7	1.433(3)
O4—C13	1.375(3)	O4—C14	1.437(3)	O5—C15	1.420(4)
O5—C16	1.432(3)	O6—C18	1.384(3)	O6—C17	1.444(3)
O7—C23	1.379(3)	O7—C24	1.435(3)	O8—C25	1.429(3)
O8—C26	1.434(3)	O9—C28	1.371(3)	O9—C27	1.426(3)
C1—C10	1.402(3)	C1—C30	1.474(3)	C4—C5	1.504(4)
C6—C7	1.496(4)	C10—C11	1.471(3)	C11—C20	1.417(3)
C14—C15	1.506(4)	C16—C17	1.482(4)	C20—C21	1.460(3)
C21—C30	1.413(3)	C24—C25	1.499(4)	C26—C27	1.499(4)
(*b*) Selected atomic bond angles (°).					
C3-O1-C4	116.4(2)	C6-O2-C5	115.8(2)		
C8-O3-C7	114.7(2)	C13-O4-C14	124.9(2)		
C15-O5-C16	114.1(2)	C18-O6-C17	115.8(2)		
C23-O7-C24	116.9(2)	C25-O8-C26	114.1(2)		
C28-O9-C27	124.7(2)	C10-C1-C30	119.5(2)		
C2-C1-C30	121.9(2)	O1-C3-C2	121.8(2)		
O1-C3-C8	118.5(2)	O1-C4-C5	109.3(2)		
O2-C5-C4	110.1(2)	O2-C6-C7	111.1(2)		
O3-C7-C6	113.0(2)	C9-C8-O3	119.6(2)		
C3-C8-O3	120.5(2)	C1-C10-C11	120.5(2)		
C9-C10-C11	121.1(2)	C12-C11-C10	121.5(2)		
C20-C11-C10	119.2(2)	O4-C13-C12	114.0(2)		
O4-C13-C18	128.1(2)	O4-C14-C15	112.8(2)		
O5-C15-C14	114.5(2)	O5-C16-C17	109.8(2)		
O6-C17-C16	109.7(2)	C19-C18-O6	119.5(2)		
O6-C18-C13	121.2(2)	C19-C20-C21	123.1(2)		
C11-C20-C21	119.9(2)	C22-C21-C20	122.1(2)		
C30-C21-C20	120.1(2)	C22-C23-O7	120.3(2)		
O7-C23-C28	120.1(2)	O7-C24-C25	110.7(2)		
O8-C25-C24	110.4(2)	O8-C26-C27	114.9(2)		
O9-C27-C26	116.0(2)	O9-C28-C29	113.8(2)		
O9-C28-C23	127.0(2)	C29-C30-C1	121.2(2)		
C21-C30-C1	119.6(2)				

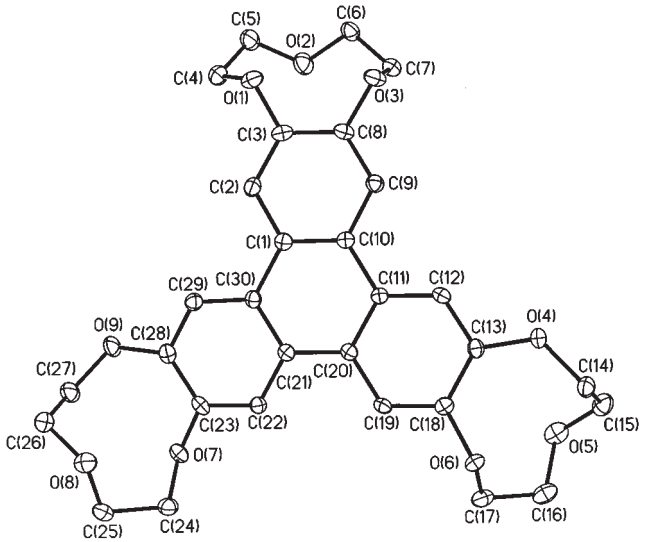
Fig. 1. Synthetic scheme for **2**.



substantially different geometries and that the structure lacks any element of symmetry. Interestingly, the "eastern" nine-membered (C13–C18) ring has a conformation that is essentially identical to that of **1**, with the torsion angles differing on the average by only approximately 4°.

Another feature of note in the geometry of **2** is the non-planarity observed in the region containing the four fused

Fig. 2. ORTEP diagram of **2**.



© 2001 NRC Canada

Table 2. Selected torsion angles (°).

C30-C1-C2-C3	173.9(2)	C4-O1-C3-C2	–60.0(3)
C4-O1-C3-C8	121.9(3)	C1-C2-C3-O1	–177.1(2)
C3-O1-C4-C5	–102.9(3)	C6-O2-C5-C4	–110.5(3)
O1-C4-C5-O2	56.3(3)	C5-O2-C6-C7	128.3(3)
C8-O3-C7-C6	95.3(3)	O2-C6-C7-O3	–77.4(3)
O1-C3-C8-C9	174.0(2)	O1-C3-C8-O3	–4.5(4)
C2-C3-C8-O3	177.3(2)	C7-O3-C8-C9	88.0(3)
C7-O3-C8-C3	–93.5(2)	O3-C8-C9-C10	–178.9(2)
C30-C1-C10-C9	172.5(2)	C2-C1-C10-C11	173.3(2)
C30-C1-C10-C11	–9.0(3)	C8-C9-C10-C11	–176.4(2)
C1-C10-C11-C12	–170.6(2)	C9-C10-C11-C12	7.9(3)
C1-C10-C11-C20	6.5(3)	C9-C10-C11-C20	–175.0(2)
C10-C11-C12-C13	176.3(2)	C14-O4-C13-C12	–173.0(4)
C14-O4-C13-C18	8.4(4)	C11-C12-C13-O4	180.0(2)
C1-C12-C13-C18	–1.3(4)	C13-O4-C14-C15	81.7(3)
C16-O5-C15-C14	–71.7(3)	O4-C14-C15-O5	–67.6(3)
C15-O5-C16-C17	114.8(3)	C18-O6-C17-C16	103.6(2)
O5-C16-C17-O6	–63.0(3)	C17-O6-C18-C19	71.9(3)
C17-O6-C18-C13	–111.3(3)	O4-C13-C18-C19	–179.3(2)
O4-C13-C18-O6	4.0(4)	C12-C13-C18-O6	–174.5(2)
O6-C18-C19-C20	175.6(2)	C18-C19-C20-C21	–179.2(2)
C10-C11-C20-C19	–175.4(2)	C12-C11-C20-C21	–179.8(2)
C10-C11-C20-C21	3.1(3)	C19-C20-C21-C22	–13.8(4)
C11-C12-C21-C22	167.8(2)	C19-C20-C21-C30	168.2(2)
C11-C20-C21-C30	–10.1(3)	C20-C21-C22-C23	179.3(2)
C21-C22-C23-O7	171.4(2)	C24-O7-C23-C22	70.3(3)
C24-O7-C23-C28	–116.1(3)	C23-O7-C24-C25	95.9(3)
C26-O8-C25-C24	114.1(2)	O7-C24-C25-O8	–60.8(3)
C25-O8-C26-C27	–63.4(3)	C28-O9-C27-C26	65.8(4)
O8-C26-C27-O9	–73.3(3)	C27-O9-C28-C29	–159.6(3)
C27-O9-C28-C23	25.9(4)	C22-C23-C28-O9	178.2(2)
O7-C23-C28-O9	4.5(4)	O7-C23-C28-C29	–169.7(2)
O9-C28-C29-C30	–175.6(2)	C28-C29-C30-C1	171.9(2)
C20-C21-C30-C29	–176.0(2)	C22-C21-C30-C1	–170.4(2)
C20-C21-C30-C1	7.6(3)	C10-C1-C30-C29	–174.4(2)
C2-C1-C30-C29	3.3(4)	C10-C1-C30-C21	1.9(3)
C2-C1-C30-C21	179.5(2)		

aromatic rings. The most pronounced effect is in the C19-C20-C21-C22 region where the torsion angle is –13.8(4)°. The C9-C10-C11-C12 torsion angle is 7.9(3)°, while the smallest deviation from planarity occurs in the C2-C1-C30-C29 region, with a torsion angle of 3.3(4)°.

Finally, it is of interest to observe that there are two aromatic C—O—C bonds that have a remarkably large bond angles. Specifically, the C13-O4-C14 angle is 124.9(2)° and the C28-O9-C27 angle is 124.7(2)°. These values are approximately 10° larger than the values for the other four units of this type in **2** and most likely arise from intermolecular crystal-packing influences. Consistent with these large bond angles are the relatively short O4—C13 and O9—C28 bond lengths (Table 1*a*), which suggest substantial double bond character in these units.

^{13}C NMR Spectra

The solution ^{13}C spectrum ($CDCl_3$ solvent) contains only five resonances, as expected from the three-fold symmetry element present in the planar depiction of **2**, which arises from sufficiently rapid conformational interconversions at room temperature. The aromatic C-O appears at 158.9 ppm. In contrast, the solid-state ^{13}C cross-polarized magic angle spinning (CPMAS) NMR spectrum shown in Fig. 3*a* shows six resolved resonances for the aromatic carbons bearing oxygen, with the chemical shifts ranging from 151.1 to 156.5 ppm. This is consistent with the observed lack of symmetry in the crystal structure. One can tentatively assign these resonances to specific carbons of solid **2**, from an examination of the C—O bond lengths (Table 1). The underlying tenet here is that the shortest C—O bond will have the most double-bond character and hence be the most deshielded (i.e., highest δ_c value). Thus, we assign the most deshielded resonance at 156.5 ppm to C28, since the O9—C28 bond length is the shortest (1.371(3) Å). The O4—C13 bond is 1.375(3) Å, and thus, the line at 155.0 ppm is attributed to C13. The O1—C3 bond length is 1.378(3) Å and the O7—C23 bond is 1.379(3) Å, so the lines at 153.4 and 152.6 ppm, respectively, can be associated with these carbons. Finally, the O6—C18 bond is 1.384(3) Å long, and the O3—C8 is the longest bond at 1.395(3) Å. Thus, the resonances at 151.6 and 151.1 ppm are attributed to these carbons, respectively. The uncertainty of 0.003 Å in the experimental measurements of bond lengths must be noted, hence some interchange of assignments for C—O bonds whose lengths differ by < 0.006 Å may be possible.

The six quaternary carbons of the central ring of **2** (i.e., C1, C10, C11, C20, C21, and C30) are clearly evident in the dipolar dephased (DPD) version of the ^{13}C CPMAS NMR spectrum (Fig. 3*b*). Due to peak overlap, rather than the six resonances, there are four peaks in the ratio of 1:2:2:1 at

Table 3. Crystallographic data for tris(9-crown-3)triphenylene (**2**).

Chemical formula	$C_{30}H_{30}O_9$
Formula weight (g mol^{-1})	534.54
Temperature (K)	293(2)
Crystal system	monoclinic
Space group	$P2_1/c$
a (Å)	13.759(2)
b (Å)	13.318(2)
c (Å)	13.399(2)
β (°)	96.883(2)
V (Å^3)	2437.6(6)
Z (molecules per unit cell)	4
ρ (calcd.) (g cm^{-3})	1.457
Crystal dimensions (mm)	0.1 × 0.1 × 0.1
Radiation (Å)	Mo Kα, 0.71073
Octants measured	*h*(–18 to 17), *k*(0 to 17), *l*(0 to 17)
θ range (°)	1.49 to 28.68
No. of unique reflections	6090
No. of reflections measured	18 805
No. of reflections with $I > 2\sigma(I)$	5753
R_1 ($I > 2\sigma(I)$)	0.0639
R_1 (all data)	0.1253
wR_2 (all data)	0.1543
wR_2 ($I > 2\sigma(I)$)	0.1343
GoF	1.034
Largest diff. peak and hole (eÅ^{-3})	0.463, –0.270

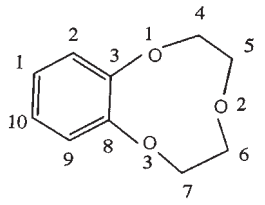
© 2001 NRC Canada

Table 4. Atomic coordinates ($\times 10^4$) and equivalent isotropic displacement parameters (Å^2 $\times 10^3$).

	x	y	z	U_{eq}
O1	6 479(2)	–22(1)	3 389(1)	40(1)
O2	7 986(2)	–1270(1)	2 964(2)	45(1)
O3	8 284(2)	890(1)	3 693(1)	35(1)
O4	10 086(1)	2559(1)	8 413(1)	32(1)
O5	11 123(1)	1339(1)	10 125(1)	41(1)
O6	9 161(1)	1940(1)	10 218(1)	26(1)
O7	5 627(1)	–2004(1)	9 486(1)	31(1)
O8	3 740(1)	–1097(1)	9 250(1)	37(1)
O9	4 577(1)	–2188(1)	7 465(1)	38(1)
C1	6 897(2)	–3(2)	6 172(2)	25(1)
C2	6 469(2)	–190(2)	5 179(2)	31(1)
C3	6 913(2)	119(2)	4 360(2)	30(1)
C4	6 276(2)	–1036(2)	3 087(2)	44(1)
C5	7 032(2)	–1384(2)	2 440(2)	46(1)
C6	8 572(2)	–516(2)	2 595(2)	36(1)
C7	8 984(2)	175(2)	3 420(2)	35(1)
C8	7 804(2)	609(2)	4 510(2)	28(1)
C9	8 209(2)	843(2)	5 464(2)	27(1)
C10	7 762(2)	561(2)	6 318(2)	23(1)
C11	8 178(2)	869(2)	7 334(2)	22(1)
C12	8 949(2)	1544(2)	7 487(2)	24(1)
C13	9 323(2)	1895(2)	8 427(2)	24(1)
C14	10 669(2)	2947(2)	9 290(2)	33(1)
C15	11 465(2)	2234(2)	9 708(2)	41(1)
C16	10 732(2)	1483(2)	11 058(2)	39(1)
C17	9 671(2)	1250(2)	10 929(2)	34(1)
C18	8 881(2)	1558(2)	9 266(2)	24(1)
C19	8 127(2)	878(2)	9 123(2)	23(1)
C20	7 751(2)	504(2)	8 175(2)	22(1)
C21	6 941(2)	–210(2)	8 027(2)	22(1)
C22	6 612(2)	–739(2)	8 835(2)	25(1)
C23	5 842(2)	–1405(2)	8 701(2)	26(1)
C24	5 227(2)	–1513(2)	10 298(2)	34(1)
C25	4 132(2)	–1579(2)	10 163(2)	34(1)
C26	3 262(2)	–1765(2)	8 508(2)	38(1)
C27	3 914(2)	–2542(2)	8 126(2)	40(1)
C28	5 338(2)	–1542(2)	7 735(2)	28(1)
C29	5 669(2)	–1050(2)	6 932(2)	28(1)
C30	6 480(2)	–414(2)	7 049(2)	24(1)

Note: U_{eq} is defined as one-third of the trace of the orthogonalized U_{ij} tensor.

Table 5. Comparison of nine-membered ring torsion angles (°) in **1** (4) with those in **2**.



1

Network	**1**	C3-C8 (**2**)	C13-C18 (**2**)	C23-C28 (**2**)
C7-O3-C8-C3	–10.5	–93.5	8.4	–116.1
C7-O3-C8-C9	170.3	88.0	–173.0	70.3
C4-O1-C3-C2	79.9	–60.0	71.9	–159.6
C4-O1-C3-C8	–105.5	121.9	–111.2	25.9
O2-C6-C7-O3	–63.3	56.3	–63.0	–60.8
O1-C4-C5-O2	–66.7	–77.4	–67.6	–73.3
C8-O3-C7-C6	98.7	95.3	103.6	95.9
C6-O2-C5-C4	108.7	–110.5	114.8	114.1

124.5, 125.2, 126.2, and 127.6 ppm. In solution a single peak is observed for these carbons at 125.9 ppm.

For the aromatic CHs (i.e., C2, C9, C12, C19, C22, and C29), a single peak at 116.2 ppm is seen in solution. In contrast, the solid-phase spectrum shows six resonances with a range of chemical shifts from 112.1 to 121.3 ppm. Again, this multiplicity in the solid-state spectrum is consistent with the lack of symmetry in the crystal structure. There are several factors contributing to the observed solid-state chemical shift differences for these carbons. Our analysis of these factors will concentrate on differences in two torsion angles for networks involving these carbons as terminal atoms (Table 6). For example, for the C2 site, the C2-C1-C30-C29 angle is 3.3(4)°, while the C2-C3-O1-C4 angle is 60.0(3)°. For C29, a common angle of 3.3° occurs for the C29-C30-C1-C2 network, but the C29-C28-O9-C27 angle is 159.6(3)°. Thus, a substantial chemical shift difference is expected between C2 and C29. Indeed, the angular dependence of the isotropic ^{13}C NMR shielding tensor for anisole has been calculated (5), and using these calculations as a model, one would anticipate that C29 would be shielded by approximately 4 ppm relative to C2.

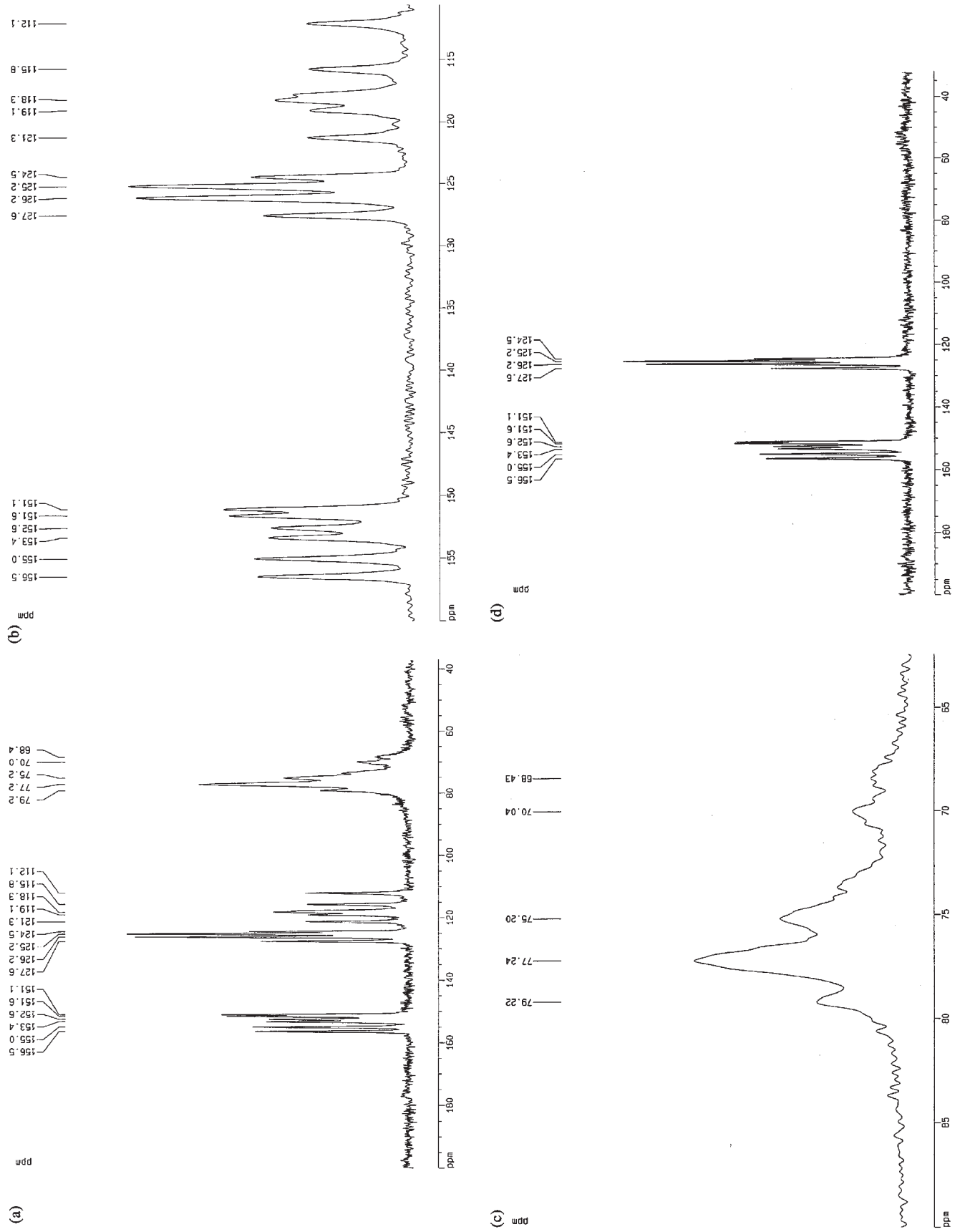
The other factor that is expected to influence the ^{13}C shieldings for the aromatic CH of **2** is the degree of planarity that exists between the adjacent aromatic rings. Any deviations from planarity will reduce the steric interactions and lead to deshielding effects. Thus, there will be enhanced shielding contributions to C2 and C29 from this effect (θ = 3.3(4)°) relative to C9 and C12 (θ = 7.9(3)°), and in turn, relative to C19 and C22 (θ = 13.8(4)°). Taking both factors into account for each of the six carbons, one can arrive at a predicted order of shielding as follows: C29 > C12, C2 > C9 > C19, C22.

For the aliphatic carbons of **2**, the chemical shift range in the solid-state ^{13}C NMR spectrum is approximately 9 ppm, with five clearly resolved lines in the approximate ratio of 1:1:3:5:2 (from high to low field). In solution there are just two lines at 72.0 and 73.7 ppm. For solid **1**, the range is approximately 8 ppm. Although it is expected that torsional effects will play a part in determining the chemical shifts of the 12 unique aliphatic carbons of **2**, it is difficult to make any unambiguous assignments. However, if one uses the angular dependence of the ^{13}C shifts of anisole as a model and examines the torsion angles in **2**, one would predict that C7 would be the most deshielded aliphatic carbon of **2** and that C14 would be the most shielded.

The central carbons C5, C6, C15, C16, C25, and C26 (i.e., those most remote from the aromatic rings) are likely to have similar chemical shifts and probably give rise to the largest peak around 77 ppm in the solid phase spectrum.

© 2001 NRC Canada

Fig. 3. (*a*) 50.3 MHz ^{13}C CPMAS NMR spectrum of **2**; (*b*) aromatic region of ^{13}C CPMAS NMR spectrum of **2**; (*c*) aliphatic region of ^{13}C CPMAS NMR spectrum of **2**; and (*d*) dipolar dephased ^{13}C CPMAS NMR spectrum of **2**.



© 2001 NRC Canada

Table 6. Torsion angles influencing ^{13}C shieldings for CH sites of **2**.

Network	Torsion angle (°)
C2-C1-C30-C29	3.3(4)
C2-C3-O1-C4	–60.0(3)
C9-C10-C11-C12	7.9(3)
C9-C8-O3-C7	88.0(3)
C12-C11-C10-C9	7.9(3)
C12-C13-O4-C14	–173.0(4)
C19-C20-C21-C22	–13.8(4)
C19-C18-O6-C17	71.9(3)
C22-CC21-C20-C19	–13.8(4)
C22-C23-O7-C24	70.3(3)
C29-C30-C1-C2	3.3(4)
C29-C28-O9-C27	–159.6(3)

The dipolar dephased version of the ^{13}C CPMAS NMR spectrum is shown in Fig. 3*d* where the resonances for all the carbons bearing hydrogen have disappeared. This is normal behaviour and indicates that there is no large-amplitude molecular motion in the crown ether portions of **2**. This is in contrast to the case for some larger macrocyclic systems, such as complexes of 12-crown-4, 15-crown-5, and 18-crown-6, where substantial residual intensity has been observed in the dipolar dephased solid-state ^{13}C NMR spectra due to at least partial motion averaging of the dipolar C-H interactions (6).

Experimental

Materials

Synthesis of **2** was carried out as follows. A 1 L double-necked round-bottom flask was fitted with a dropping funnel and a condenser. The flask had a gas outlet tube going into a dilute NaOH solution. To a mixture of $FeCl_3$ (48.7 g, 0.3 mol), CH_2Cl_2 (400 mL) and concentrated H_2SO_4 (1 mL) in this flask was added **1** (17.9 g, 0.1 mol) in CH_2Cl_2 (100 mL), dropwise with vigorous stirring. The mixture was brought to reflux for 24 h. Then methanol (150 mL) was added, and the mixture was brought to reflux for another 3 h. After cooling, CH_2Cl_2 (300 mL) was added to the mixture and washed with distilled water (3 × 300 mL). The combined organic layers were dried over anhyd Na_2SO_4, and the solvent was removed by rotary evaporation to yield 16.0 g of a black oil. ^1H NMR indicated that this was a mixture of **1** and **2** in a ratio of ca. 3:1.

The black oil was boiled in hexane (3 × 400 mL) to produce a deep-brown precipitate. This solid was collected by filtration and washed further with boiling hexane (200 mL) to yield a dark-brown powder. Final purification was carried out via flash column chromatography on silica gel, with 1:1 acetone:petroleum ether as eluent. The resulting light-brown solid was dissolved in a minimum quantity of absolute ethanol and boiled with activated charcoal. Upon cooling of the light-yellow filtrate, colourless needles of **3** were obtained. Total yield was 4.5 g (25.4%) (mp 264–266°C). ^{13}C NMR (400 MHz, $CDCl_3$) δ: 72.0, 74.7, 116.2, 125.9, 151.1.

^{13}C NMR spectra

The solution ^{13}C NMR spectra were recorded at 100.6 MHz using a Bruker AMX-400 instrument with complete ^1H noise decoupling. An Aspect 3000 processing controller was employed, and all standard microprograms used are in the Bruker software library.

The solid phase ^{13}C NMR spectra were recorded at 50.3 MHz using a Bruker ASX-200 solid-state NMR spectrometer equipped with a Bruker 7 mm triple resonance probe. The magic angle was set accurately using the ^{79}Br resonance of KBr and maximizing the number of rotational echoes in the FID. Magic angle spinning rates were approximately 5 kHz. ^1H 90° pulses were 3.5–3.8 μs with contact times of 1 s. Chemical shifts were referenced to the ^{13}C resonance of $Si(Si(CH_3)_3)_4$, which has a chemical shift of 3.7 ppm relative to TMS. Dipolar dephased spectra were obtained via interruption of the ^1H decoupling for 40 μs immediately following the cross-polarization pulse.

X-ray crystallographic studies and structure refinement

Suitable crystals were selected and mounted on thin glass fibres using viscous oil. Data were collected on a Bruker AX SMART 1k CCD diffractometer using 0.3° scans at 0, 90, and 180°. Unit cell parameters were determined from 60 data frames collected at different sections of the Ewald sphere. Semi-empirical absorption corrections based on equivalent reflections were applied (7).

Unit cell parameters and systematic absences in the diffraction data are consistent with the space group $P2_1/c$. The structure was solved by direct methods, completed with difference Fourier syntheses and refined with full-matrix least-squares procedures based on F^2. All non-hydrogen atoms were refined with anisotropic displacement parameters and hydrogen atoms were treated as idealized contributions. All scattering factors and anomalous dispersion factors are contained in the SHEXTL 5.1 program library.

References

1. A.M. Levelut. J. Chim. Phys. **80**, 149 (1983).
2. S. Chandrasekhar and G.S. Ranganath. Rep. Prog. Phys. **53**, 57 (1990).
3. H. Naarmann, M. Hanack, and R. Mattmer. Synthesis, 477 (1994).
4. G.W. Buchanan, A.B. Driega, A. Moghimi,C. Bensimon, R.A. Kirby, and T.D. Bouman. Can. J. Chem. **71**, 1983 (1993).
5. C.M. Carter, J.C. Facelli, D.W. Alderman, D.M. Grant, N.K. Dalley, and B.K. Wilson. J. Chem. Soc. Faraday Trans. 1, 84, 3673 (1988).
6. G.W. Buchanan. Prog. Nucl. Magn. Reson. Spectrosc. **34**, 327 (1999).
7. R. Blessing. Acta Crystallogr. Sect. A, **A51**, 33 (1995).

© 2001 NRC Canada

Factors limiting oxygen delignification of kraft pulp

Leonid G. Akim, Jorge Luiz Colodette, and Dimitris S. Argyropoulos

Abstract: Softwood kraft pulp was subjected to a laboratory one- and three-stage oxygen delignification process. Pulp and liquor samples were collected at different stages of the process with particular attention being paid to the early and late stages. A novel residual lignin isolation method extracted about 65% of the oxidized residual lignins at a purity exceeding 90%. Using this methodology coupled to quantitative ^{31}P NMR, ^{13}C NMR, 2D heteronuclear (HMQC) NMR spectroscopic and analytical pyrolysis techniques allowed a thorough characterization of the residual and solubilized lignin fractions at the various stages of the process. Our conclusions do not point to a single factor as being responsible for the limits confronting oxygen delignification. Amongst the major factors impeding the effectiveness of oxygen delignification are: (*i*) the accumulation of relatively inert 5,5′ biphenyl structures originally present in kraft lignin from dibenzodioxocin ring opening reactions; and (*ii*) the accumulation of considerably less reactive *p*-hydroxyphenyl structures. Detailed quantitative information was obtained and discussed in relation to the presence and role of these unreactive phenolic fractions on the residual oxidized lignins. As such we arrived at important conclusions as to why and how these structures remain and accumulate on the fiber. In addition, issues related to the profiles of the total phenolic hydroxyl content of the residual lignins and the remaining arylglycerol β-*O*-4 structures are discussed.

Key words: analytical pyrolysis, biphenyl structures, HMQC, NMR, oxidation mechanism, oxygen delignification, *p*-hydroxyphenyl moieties, quantitative ^{13}C NMR, quantitative ^{31}P NMR, residual lignin, solubilized lignin, total phenolic hydroxyls.

Résumé : De la pâte au sulfate (pâte kraft) provenant de bois résineux a été soumise en laboratoire à un processus de délignification par l'oxygène, à une ou trois étapes. Les échantillons de pâte et de liqueurs ont été recueillies à différents stades du processus, en portant une attention particulière aux stades du début et de la fin. Une nouvelle méthode d'isoler la lignine résiduelle a permis d'extraire environ 65 % des lignines résiduelles oxydées, avec un degré de pureté supérieur à 90 %. Faisant appel à cette technologie couplée à des techniques spectroscopiques [RMN du ^{31}P, RMN du ^{13}C, RMN hétéronucléaire en deux dimensions (« HMQC »)] ou d'analyses pyrolytiques, il a été possible de faire une caractérisation complète des fractions de lignines résiduelles et solubilisées, à divers stades du processus. Nos résultats ne permettent pas d'attribuer à un seul facteur les limites auxquelles on doit faire face lors de la délignification par l'oxygène. Parmi les facteurs qui limitent l'efficacité de la délignification par l'oxygène, les plus importants sont: (*i*) l'accumulation de structures 5,5′ biphényles relativement inertes qui sont originalement présentes dans la lignine de la pâte kraft et qui proviennent de réactions d'ouverture de cycles des dibenzodioxocines et; (*ii*) l'accumulation de structures *p*-hydroxyphényles qui sont beaucoup moins réactives. On a obtenu des informations quantitatives détaillées et on en discute en termes de la présence et du rôle de ces fractions phénoliques non réactives sur les lignines oxydées résiduelles. Sur cette base, on est arrivé à d'importantes conclusions sur le pourquoi et comment ces structures se maintiennent et s'accumulent sur la fibre. De plus, on discute des questions apparentées aux profils en contenu en hydroxyles phénoliques totaux des lignines résiduelles et en structures β-*O*-4-arylglycérol résiduelles.

Mots clés : pyrolyse analytique, structures biphényles, HMQC, RMN, mécanisme d'oxydationm délignification par l'oxygène, portions *p*-hydroxyphényles, RMN du ^{13}C quantitative, RMN du ^{31}P quantitative, lignine résiduelle, lignine solubilisée, hydroxyles phénoliques totaux.

[Traduit par la Rédaction]

Introduction

Regulatory and economic pressures have driven the pulp and paper industry to implement new delignification and bleaching practices. A major transition is the partial replacement of chlorine or chlorine dioxide delignification stages with oxygen delignification. The environmental, technical and economic benefits of oxygen delignification include lower chemical requirements in subsequent bleaching sequences, higher brightness with equivalent amount of chemicals, lower rejects and lower water consumption and subsequent effluent discharge due to the greater recycling potential of

Received September 21, 2000. Published on the NRC Research Press Web site on March 12, 2001.

L.G. Akim, J.L. Colodette, and D.S. Argyropoulos.[1] Department of Chemistry, Pulp and Paper Research Centre, McGill University, 3420 University St., Montreal, QC H3A 2A7, Canada.

[1]Corresponding author (e-mail: dargyr@po-box.mcgill.ca).

 DOI: 10.1139/cjc-79-2-201 © 2001 NRC Canada

oxygen stage effluents (1, 2). The effectiveness of an oxygen delignification stage is however limited to 50% delignification. Beyond this level, severe cellulose degradation takes place, resulting in the deterioration of pulp viscosity and strength characteristics (3, 4). This selectivity issue is a drawback of oxygen delignification.

A number of approaches aimed at extending oxygen delignification have been proposed and implemented in the industry. Double stage oxygen delignification has shown some potential (5, 6). However, even under idealized laboratory conditions, the effectiveness of double stage oxygen delignification with thorough interstage washing failed to exceed 70% delignification (7). Chirat and Lachenal (8) in their study of multistage oxygen delignification showed that a significant fraction of the residual lignin remains within the pulp even after four stages of oxygen delignification.

Finding ways to obtain lower kappa numbers, using oxygen delignification would curtail the expensive chemicals needed in subsequent bleaching stages. However, achieving a viable "extended" oxygen delignification process is more likely if the mechanisms responsible for limiting the process are better understood. During the past decade a number of studies have addressed lignin oxidation with molecular oxygen under alkaline conditions. The early efforts centered on elucidating the reaction mechanism of oxygen delignification using lignin model compound under homogeneous reaction conditions (9, 10). Moieties bearing free phenolic hydroxyls groups exhibited a higher reactivity toward oxidation than their etherified counterparts (11–13). Based on the accumulated data Gierer (14) proposed a reaction mechanism which involves the phenolate anions, formed under the alkaline conditions of the process, being converted into phenoxy radicals followed by the formation of hydroperoxides and the eventual degradation of aromatic rings to muconic acids.

Further developments in this area have been associated with structural studies of residual lignin isolated from oxygen delignified pulp using either acidolysis (15, 16) or enzymatic digestion (17). In the early papers of this series, Gellerstedt et al. (15) reported that the residual lignin, in an oxygen-delignified pulp "has few remaining phenolic hydroxyl groups." However, ensuing efforts by Sun and Argyropoulos (18) and Johansson et al. (19) did not confirm such a drastic depletion.

Aromatic condensation reactions have also been thought to decrease the reactivity of lignin moieties toward oxygen delignification (20, 21). The reactivity of various condensed units present in kraft pulp were explored using degradation techniques. Condensed structures such as diphenylmethane and biphenyls were found to be resistant during oxygen delignification and were held responsible for the slow phase of oxygen delignification (20). The phenylcoumaran structures were pronounced to be the least stable amongst the resistant condensed moieties (20). The reactivity of the condensed structures within residual kraft lignin under oxygen delignification conditions was recently evaluated in detail (21). Even under homogeneous oxidative conditions with no mass transfer limitations operated, the 5,5′ biphenyl condensed structures were found to be fairly stable toward the oxidation.

Despite the many research efforts the question of which structures are responsible for activation and which are responsible for lignin deactivation during oxygen delignification still remains unanswered. Our continuing efforts to address this question are now focused at systematically examining the residual lignins within an oxygen delignified fiber. To do this a newly developed residual lignin isolation method which provided residual lignin in high yield was coupled with a systematic sampling of delignified pulp and spent liquor at different stages of oxygen delignification. The isolated residual and solubilized lignins were then subjected to detailed spectroscopic analyses. This approach allowed a systematic assessment of the structural changes occurring within the lignin during the oxidation process. To strengthen our conclusions and augment our data, lignins isolated from a multistage treatment were also examined.

Experimental

Oxygen delignification

Black spruce softwood (*Picea mariana*) kraft pulp of kappa no. 29.9 was chelated with DTPA for 30 min at 50°C and thoroughly washed before the oxygen delignification process.

A custom-made 2.5 L kettle reactor was used for oxygen delignification. The reactor was equipped with a central shaft and impellers for effective pulp mixing at medium consistencies. An elaborate computer interface provides a precise control of all major process parameters and of any desired process scenarios.

In all experiments the amount of pulp used in the oxygen delignification stage (oven-dry basis) at a consistency of 10%, an oxygen pressure of 0.68 MPa, and at 90°C was 50 g. At the beginning of each experiment the NaOH charge was 2.5% (on oven-dry pulp). A 1% charge (on oven-dry pulp) of $MgSO_4$ was also added at this time to ensure optimum stabilization of the carbohydrates. The pulp was mixed with the chemicals and placed in the preheated reactor. After reaching 90°C, oxygen pressure was applied. At the end of the desired reaction time the pressure was released, the reactor opened, and the pulp was discharged and filtered. The spent liquor was collected and the pulp was washed thoroughly with de-ionized water. For the second and third stages the washed pulp was remixed with the same amount of fresh chemicals and loaded into the preheated reactor using the same procedure and conditions described above. Kappa no., viscosity, and Klason lignin contents of the pulps were measured according to the PAPTAC standard methods (22).

Homogeneous oxidation of spent liquor

The spent liquor from a 20-min oxygen delignification stage was collected, filtered without dilution, and placed in a glass-lined 1 L Parr reactor. To avoid metal ion contamination all interior parts of the reactor were coated with Teflon®. The system was then heated to 90°C and an oxygen pressure of 0.68 MPa was applied upon reaching temperature. The time of oxidation at temperature and pressure was 60 min with continuous mixing. After the treatment, the solubilized lignin was isolated according to the procedure

© 2001 NRC Canada

Table 1. Oxygen delignification data characterizing the pulp at single and multiple oxygen stages and the residual lignins isolated.

Total delignification time (min)	Kappa no. (Klason + UV lignin content (%))	Viscosity (mPa s)	Residual lignin yield (%)	Lignin elemental analysis data (%)			
				C	H	N	OCH_3
One-stage oxygen delignification							
0 (initial pulp)	30.0 (4.3)	42.0	68	60.0	5.7	0.71	11.6
10	23.2 (3.6)	37.0	56	59.7	5.8	1.00	12.1
20	20.6 (3.0)	35.0	61	60.4	5.9	1.33	9.8
50	17.0 (2.4)	32.0	52	61.2	6.3	1.40	8.8
80	15.2 (2.1)	30.0	69	58.4	5.6	1.66	8.8
160	14.7 (1.8)	28.3	65	58.1	5.6	1.84	9.0
Multistage oxygen delignification							
60 (20 + 20 + 20)[a]	13.4 (1.4)	28.5	69	54.5	5.5	2.64	—
160 (20 + 20 + 120)[b]	12.5 (1.1)	26.6	62	55.7	5.5	1.95	—

[a]Three-stage 60 min delignificaiton comprised of three 20-min individual stages.
[b]Three-stage 160 min delignification comprised of two 20-min and one 120-min individual stages.

described in ref. 27, ensuring that the yields of lignin recovery were near quantitative.

Lignin isolation

Solubilized lignins were precipitated from the spent liquor by acidification with 1 M solution of HCl to pH 1.5. The precipitated lignin was then centrifuged, washed repetitively with acidified water (pH 2.0), and freeze-dried.

The residual lignins were isolated using a method recently developed in our laboratory (23). The method initially requires a mild enzymatic hydrolysis step with cellulase. The solubilized lignin was then precipitated by acidification and combined with the undissolved residue remaining after the enzymatic treatment. This mixture was then subjected to a very mild acidolytic treatment (0.05 M of HCl solution in dioxane–water (85:15) mixture). The lignin-containing solution was acidified with 1 M HCl to pH 2.0, the precipitated lignin was then centrifuged, repetitively washed with 0.01 M HCl, and freeze-dried. At the end of the isolation procedure the lignin was extracted with dichloromethane to remove accumulated extractives. The yield of the extracted lignin ranged from 55 to 70% (Table 1). The protein contamination was calculated based on the nitrogen content (Table 1) and further calculations of functional groups content within the residual lignin were made taking this into account. Elemental and methoxyl analyses were carried out by the Schwarzkopf Microanalytical Laboratories, Woodside, New York.

Oxidation of lignin model compounds

Two lignin model compounds were oxidized: 4-methylphenol (*p*-cresol) and 2-methoxy-4-methylphenol. Both compounds were purchased from Aldrich and used without purification. In preparation for the oxidation process, *p*-cresol (0.54 g, 0.005 mol) and 2-methoxy-4-methylphenol (0.69 g, 0.005 mol) were dissolved in 0.625 M NaOH (250 mL). The mixture was then placed in a glass-lined Parr reactor and oxidized at an oxygen pressure of 0.68 MPa at 90°C for 60 min with continuous agitation. After the treatment an internal standard (3,4-dimethylphenol) (0.154 g, 0.001 mol) was added, the mixture was acidified with 2 M HCl to pH 2.0 and repetitively extracted with ethylacetate. The combined extracts were then dried over $MgSO_4$ and quantitatively analyzed using a Hewlett–Packard HP 5890A gas chromatograph, equipped with a DB 5 30 m × 0.25 mm packed silica capillary column (film thickness 0.25 μm) and a flame ionization detector. The injection port temperature was 280°C and the oven temperature was raised from 70°C to 200°C with a gradient of 15°C min^{-1}.

NMR spectroscopy

Quantitative ^{31}P NMR spectra of the lignins were acquired using a Varian Unity 500 spectrometer operating at 202.3 MHz according to the method described by Granata and Argyropoulos (24). Prior to the analysis the lignin was phosphitylated with 2-chloro-4,4,5,5-tetramethyl-1,3,2-dioxaphospholane and cholesterol was employed as an internal standard. An inverse gated decoupling sequence was employed with a pulse width of 90° and a relaxation delay between pulses of 5 s. About 300 transients were acquired to ensure high signal–noise ratio. For each lignin sample at least two spectra were recorded to ensure reproducibility with low standard error. The spectra were integrated and the amounts of the different functional groups were calculated as described elsewhere (24).

Quantitative ^{13}C NMR spectra of the lignins were acquired on a Varian Unity 500 NMR spectrometer operating at 125.7 MHz with an inverse gated decoupling sequence using a newly developed acquisition protocol described by Zia et al. (25). The weighed amount of lignin (400–450 mg) was placed into a 10 mm (o.d.) NMR tube and dissolved in DMSO-d_6 (2.7 mL). A measured amount of 1,3,5-trioxane (30–35 mg) was added as an internal standard and $Cr(acac)_3$ (2 mg) was added as a relaxation agent. The sweep width of the spectra was 59 970 Hz, the pulse width was 14.1 μs, and the relaxation delay was 12.5 s. For each spectrum about 7000–8000 scans were accumulated. The resulting spectra were integrated and the integrals compared with those of the internal standard as described elsewhere (25).

One-bond ^{13}C–^{1}H heteronuclear quantum coherence (HMQC) correlation spectra were recorded using a Varian Unity 500 NMR spectrometer with a 5 mm inverse geometry probe. To record the spectra 100 mg of lignin was dissolved in 0.7 mL of DMSO-d_6 in a 5 mm (o.d.) sample tube. The

© 2001 NRC Canada

spectra were acquired using 170 scans over 256 increments of 2 K data points over 10 ppm in F2 (^{1}H) and 140 ppm in F1 (^{13}C). To suppress the ^{1}H–^{13}C magnetization, a BIRD presaturaration sequence was used. The polarization transfer delay between ^{1}H and ^{13}C was set to 140 Hz and the relaxation delay was 0.8 s. After processing with F1 zero filling, $\pi/2$ shifted squared sinebell apodization and Fourier transformation were applied. The resulting matrix was 1024(F2) × 1024(F1) real points.

Analytical pyrolysis (Py-GC-MS)

The isolated residual lignin sample (0.5 mg) was placed into the pyrolysis chamber of a pyroprobe 2000 (Chemical Data System) and purged with helium through the chamber for 10 s prior to pyrolysis to minimize oxidation. The interface starting temperature was 250°C. The temperature was then increased at a rate of 20°C ms^{-1} to 550°C, and it was held at this temperature for 10 s. The GC-MS analyses were carried out on a Hewlett–Packard 5972 mass spectrometer interfaced to a Hewlett–Packard HP 5890A gas chromatograph equipped with a DB-5 30 m × 0.25 mm packed silica capillary column with a film thickness of 0.25 μm. The column temperature was held at 70°C for 4 min and it was then increased by 4°C min^{-1} to 280°C. The pyrolysis products were identified by their mass spectra fragmentation pattern. The relative content of *p*-hydroxyphenyl structures was calculated as a ratio of peak area assigned to these structures, to the total peak area.

Results and discussion

The lignin content in the oxygen-delignified pulp and the elemental analysis of the isolated residual and spent liquor lignins are shown in Table 1. The pulp and spent liquors were sampled at different intervals within a 160-min first stage delignification and at the end of a 60-min (3 × 20) three-stage and also a 120-min (2 × 20 and 1 × 120) three-stage process. During this effort the residual lignin was isolated using a mild enzymatic hydrolysis protocol, followed by a mild acidolytic treatment (23). In this novel isolation procedure the primary cellulolytic treatment digests most of the carbohydrates thus exposing the residual lignin and the mild acidolytic treatment ensures minimum secondary condensation reactions. This method supplies an excellent yield of residual lignins even for heavily oxidized pulps, i.e., an oxygen-delignified pulp after three stages (about 62 to 63%, Table 1). More details of the procedure and detailed lignin analyses and purity data have been described by Argyropoulos et al. (23). This represents a major improvement over previous reports that implied that conventional methods of enzymatic hydrolysis could not provide an acceptable yield for such heavily oxidized pulps (26).

The isolated lignins were studied using a broad range of NMR spectroscopic techniques, namely quantitative ^{31}P NMR, ^{13}C NMR, and 2D heteronuclear (HMQC) NMR spectroscopy. Quantitative information on the different types of functional groups in the lignins was collected and analyzed to follow the changes occurring within the kraft pulp lignin during multistage oxygen delignification.

The kappa no. measured after various time intervals of the oxygen delignification shows that after 50–60 min of oxidation the delignification had significantly slowed. Attempts to use a multistage approach only marginally reduced the lignin content (to kappa no. 12.5) (representing about 60% delignification). As anticipated, the introduction of the multistage approach showed no significant improvement in the effectiveness of oxygen delignification, in agreement with various large scale industrial operations (7). Recent claims by industry suppliers in relation to extending these limits, most likely, rest with lignin leaching effects at the second stage and not on actual degradation by oxygen (6).

The role of phenolic hydroxyl groups

Most early efforts attempted to unravel the mechanism of oxygen delignification using lignin model compounds (9, 10). These studies suggested that the reactivity of the phenylpropane units bearing free phenolic hydroxyl groups far surpassed that of non-phenolic structures. To this effect Gierer (14) regards the role of free phenolic units as the centers of radical formation. Consequently, amongst all the lignin functional groups we focused our attention on the free phenolic hydroxyl groups because of the evidence pointing to their important role in the chemistry of oxygen delignification.

In two earlier accounts the extreme depletion of phenolic groups during oxygen delignification has been cited as the factor responsible for the limits of the process (15, 16). Chirat et al. (26) and Johansson and Ljunggren (12) however, reported that the decrease of the amount of free phenolic hydroxyls is significant but even after extensive multistage delignification there is still an abundance of such groups within the lignin. In addition, our earlier research on oxidation of isolated residual kraft lignin (27), pointed out that even under extreme and idealized oxidation conditions (140°C, 80 min, homogeneous solution, and thorough mixing) about 50% of the initial amount of the total phenolic OH remained within the lignin structure. Our data was also later supplemented and supported by that of Moe and Ragauskas (28) who showed free phenolic hydroxyl content within residual kraft lignin decreased by only about 30–40% after oxygen delignification.

The amount of phenolic hydroxyls present in the residual lignin of oxidized kraft pulp was determined by quantitative ^{31}P NMR spectroscopy (Table 2). The residual lignins isolated from the delignified pulps show a rapid depletion of the total free phenolic hydroxyl units during the initial 10 min of oxygen delignification from 1.87 to 1.42 mmol g^{-1}, which represents a 24% decline. Then after 50 min of treatment, the amount of the phenolic hydroxyl units was seen to stabilize at approximately 60% and did not further decrease (Fig. 1). Application of three stages of delignification with thorough interstage washing did not result in any significant additional decrease of the phenolic hydroxyl level (Table 2). More specifically, even after two 20-min stages and a third 120-min stage the amount of phenolic units within the residual lignin was 1.21 mmol g^{-1}. This figure is marginally lower than the corresponding amount within the residual lignin from the pulp delignified in a single 160-min stage (1.31 mmol g^{-1}).

While it is very likely that the decrease of phenolic OH units is a consequence of lignin oxidation reactions, our data indicates that factors other than the lack of phenolic OH

© 2001 NRC Canada

Table 2. Phenolic group content (mmol g^{-1}) in lignins isolated from pulp and spent liquor after oxygen deliginification as determined by quantitative ^{31}P NMR spectroscopy.

Time of treatment (min)	Non-condensed guaiacyl units[a]	Total condensed units[b]	5,5′ Condensed units[c]	*p*-Hydroxy-phenyl units[d]	Total free phenolic units
Solubilized lignins in spent liquor					
10	0.85	1.05	0.57	Not detected	1.90
20	0.65	0.87	0.47	—	1.52
50	0.56	0.81	0.44	—	1.37
80	0.49	0.80	0.43	—	1.29
80 (20 + 60)[e]	0.41	0.76	0.55	—	1.17
160	0.38	0.72	0.46	—	1.10
20 + 20 + 20[f]	0.40	0.77	0.51	—	1.17
20 + 20 + 120[f]	0.25	0.58	0.37	—	0.83
Residual lignins in pulp					
0	0.87	0.96	0.44	0.04	1.87
10	0.63	0.69	0.34	0.10	1.42
20	0.55	0.77	0.38	0.12	1.44
50	0.42	0.70	0.37	0.15	1.27
80	0.44	0.75	0.42	0.15	1.34
160	0.44	0.72	0.49	0.15	1.31
20 + 20 + 20[f]	0.48	0.75	0.46	0.18	1.41
20 + 20 + 120[f]	0.34	0.73	0.44	0.14	1.21

[a]140.0–138.5 ppm area.
[b]144.0–140.1 ppm area.
[c]141.6–140.1 ppm area.
[d]138.4–137.5 ppm area.
[e]After 20 min of treatment the liquor was extracted without dilution and further oxidized in a Parr reactor (90°C, 100 psi of oxygen) for 60 min.
[f]Three stage delignification with interstage washing (see footnote of Table 1).

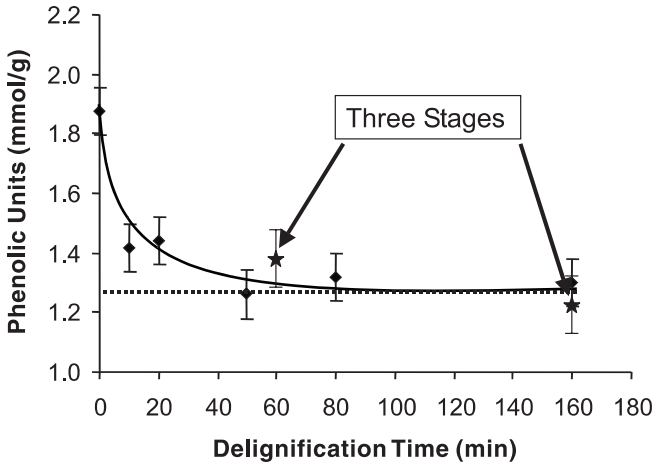
groups cause the oxygen delignification to reach a ceiling. Our continuing efforts to locate these factors prompted further investigation of the structural features of isolated residual lignins.

The role of condensation reactions

In earlier work we demonstrated that under homogeneous oxidative conditions the rate of elimination of condensed phenolic units in residual kraft lignin was slower than the rate of elimination of uncondensed guaiacyl phenolic units (21). Amongst the condensed structures, 5,5′ biphenolic structures showed the highest resistance. They decreased in the initial phase of oxidation but after about 40 min of treatment their content did not further decrease. This resulted in a significant accumulation of the condensed hydroxyl content within the oxidized residual lignin (21). The origin of 5,5′ biphenolic moieties in kraft lignin are the eight-membered dibenzodioxocins ring structures recently discovered by Brunow and co-workers (29). Recent work in our laboratory has shown that they constitute about 10% of the phenyl propane units in lignin, or about 10 such rings are present per 100 phenyl propane units (30, 31). Dibenzodioxocins, under kraft pulping conditions open quantitatively to release large amounts of 5,5′ biphenolic moieties, making the presence of these units abundant in residual kraft lignin (31).

Consequently, we paid particular attention to the behavior of the condensed phenolic structures, and more specifically on the development of 5,5′ biphenyl structures within the residual lignins as a function of intensity of oxygen delignification. Within the solubilized lignins the condensed

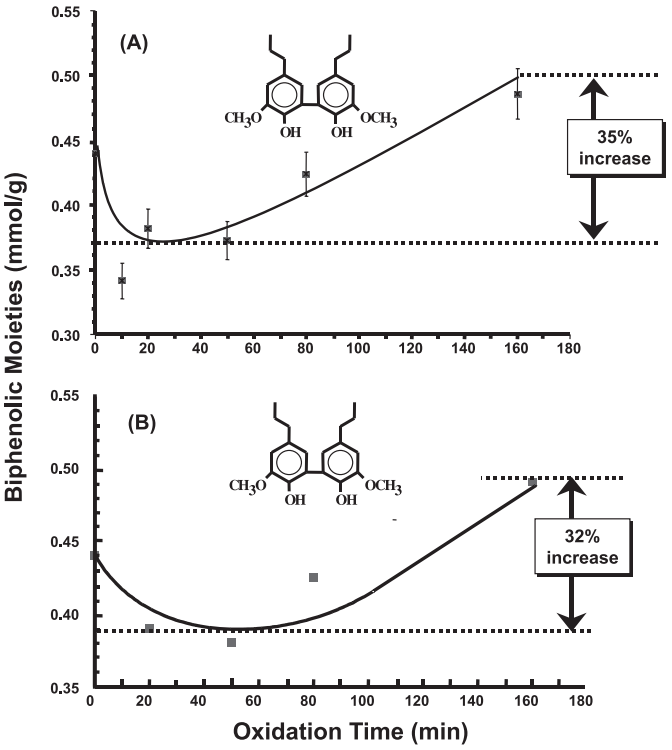
Fig. 1. Total phenolic hydroxyl group content measured in isolated residual lignin at various intervals along an oxygen delignification process.



phenolic OH content was found to decrease by about 25–30% during the initial stages of delignification (20 min) and then remained essentially constant (Table 2). In the residual lignins, however, the 5,5′ biphenolic condensed structures were found to decrease from 0.44 to 0.38 mmol g^{-1} during the early phases of oxygen delignification, and then started to build up again to a value of 0.49 mmol g^{-1} level (Fig. 2*a*). However, when the liquor coexisting with the pulp was replaced in a series of multistage experiments, the content of

© 2001 NRC Canada

Fig. 2. 5,5′-Biphenyl moieties present within the residual lignin at various points along a conventional oxygen delignification process. The upper plot (2*a*) shows the data derived from quantitative ^{31}P NMR of analyses of the lignins, while the lower plot (2*b*) shows the data for the same moieties derived from quantitative ^{13}C NMR analyses.



5,5′ biphenyls did not increase. Even after a prolonged three-stage delignification the level of 5,5′ hydroxyls remained at 0.44 mmol g^{-1}, which is lower than the 0.49 mmol g^{-1} level reached in the corresponding one-stage oxygen delignification (Table 2).

In an effort to further support our measurements of 5,5′ biphenolic structures we measured them using an independent method. For this purpose we developed a quantitative ^{13}C NMR protocol (25) (using an internal standard) and as such we were able to measure the precise amounts of 5,5′ etherified and non-etherified biphenyl moieties and their development within residual oxidized lignins as a function of the extent of oxidation. The data of Fig. 2*b* confirmed that the content of non-etherified 5,5′ biphenyl structures after 80 min increased over the overall time scale of the oxidation. In addition, the etherified 5,5′ structures were also seen to increase (Table 4, see C3 in the last column). The inert nature of such moieties under oxygen delignification conditions could be held responsible for this enrichment.

Our observations so far correlate well with earlier experiments attempting to understand the mechanism of oxygen delignification, using isolated residual kraft lignin oxidized under homogeneous conditions (21, 27). These accounts coupled with the present findings support the idea that the etherified and even non-etherified 5,5′ biphenolic structures are unreactive under oxygen delignification conditions. The accumulation of these groups during oxygen delignification could be another factor imposing limits to the process while the role of lignin–carbohydrate linkages still remains unclear.

Table 3. Relative content of *p*-hydroxyphenyl moieties present in the products of analytical pyrolysis of oxidized residual lignins (%), as determined by oxygen delignification.

Time of oxidation (min)	Relative content of *p*-hydroxyphenyl (%)
0	2.3
20	2.5
50	3.4
80	3.5
160	4.0

The observed increase of 5,5′ biphenyl hydroxyls could be attributed to secondary condensation reactions. Such reactions, which are likely to occur between phenoxy radicals forming on the mobile solubilized fraction and the radicals forming on immobilized residual lignin could generate new 5,5′ condensed structures. Earlier efforts in our laboratory have demonstrated and quantified that these coupling reactions occur with catechol and 3-methoxy-4-hydroxy toluene (32). These compounds were shown to produce significant quantities of 5,5′ related products under oxidative conditions.

In an effort to further support and substantiate this rationalization we carried out the following series of experiments, schematically represented in Fig. 3.

After 20 min of pulp oxidation in the medium-consistency oxygen delignificaton reactor, the extracted liquor was quantitatively collected and further oxidized for an additional 60 min (without dilution) in a Parr reactor (see Fig. 3). After the oxidation, the lignin was recovered quantitatively and subjected to detailed analyses (Table 2). The amount of 5,5′ condensed phenolic units formed by this liquor treatment in the absence of fiber were found to be 0.55 mmol g^{-1}. This figure was found to be 22% higher than experiments where the fiber was present throughout the oxidation for a total treatment time of 80 min (Table 2).

It is thus reasonable to assume that phenols liberated from the lignocellulosic matrix could form highly mobile and reactive radicals which may recombine with similar moieties present on the fiber. This process could lead to the formation of new 5,5′ unreactive biphenolic moieties present on the fibre, explaining the ^{31}P and ^{13}C NMR data of Fig. 2 and Table 3, respectively.

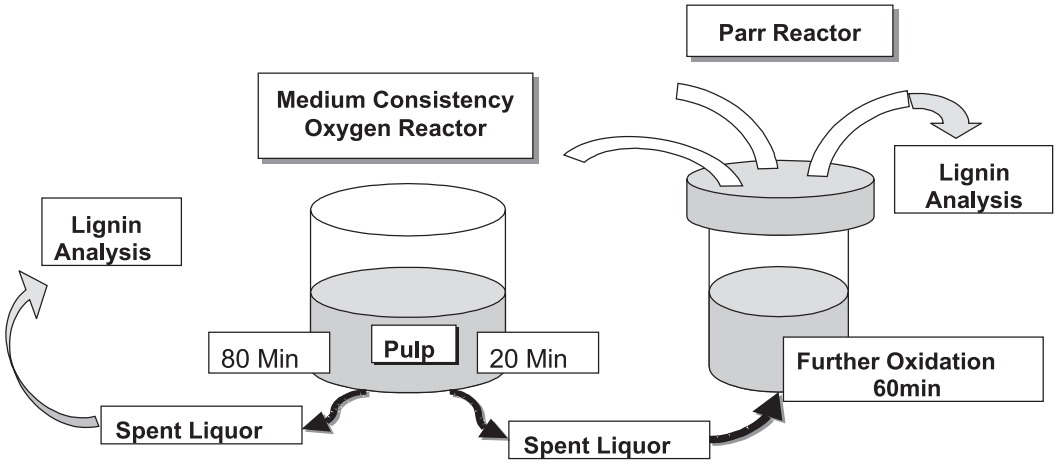
Noncondensed phenolic hydroxyls

Other functional groups that require attention are the noncondensed phenolic hydroxyls. Studies with lignin model compounds (12, 33) and residual lignin have shown that under oxygen delignification conditions such moieties are much more reactive than biphenyl structures (20).

The noncondensed guaiacyl units in the solubilized lignins decreased monotonically from 0.85 (at 10 min) to 0.25 mmol g^{-1}, as the delignification time was extended and the oxidation intensified (Table 2). However, the changes that occurred to the noncondensed phenolic moieties were different within the residual lignin. As delignification proceeded, the guaiacyl phenolic hydroxyl content in the residual

© 2001 NRC Canada

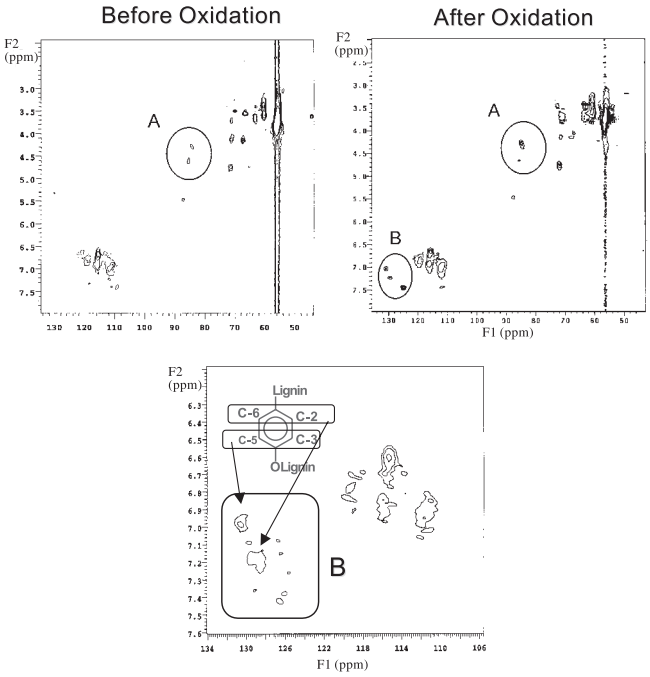
Fig. 3. A schematic showing the series of experiments carried out aimed at confirming the occurrence of 5,5′ linkages between mobile phenoxy radicals and immobilized residual fibre lignin.



lignin also decreased but in a different fashion (Table 2). During the initial rapid phase of delignification the level of noncondensed phenols within the residual lignin was reduced by about 50%. This level was then maintained throughout the rest of the process irrespective of the intensity of oxidation. Only after a series of prolonged delignification stages, one may observe a decrease of these moieties to about 40% of the initial level.

Based on these data it is clear that noncondensed units bearing free phenolic hydroxyls possess excellent reactivity under oxygen delignification conditions. However, the fact that the delignification stops well in advance from the total depletion of these units casts a reasonable doubt to the claim that their depletion is responsible for the ceiling of oxygen delignification.

Fig. 4. HMQC spectra and specific signal assignments for residual lignin isolated from a pulp before and after 80 min of oxygen delignification. Where: (*a*) 4-hydroxy-3-methoxyphenol correlations and (*b*) *p*-hydroxyphenyl correlations.



Accumulation of *p*-hydroxyphenyl units

A comparison of the HMQC (one-bond ^{13}C–^{1}H correlation technique, which displays the signals of carbon atoms directly linked to protons) NMR spectra of the initial residual lignin and the sample isolated after 80 min of delignification (Fig. 4) revealed that a new group of signals appeared in the spectra of the oxidized lignin. These signals appear in the downfield region assigned to aromatic nuclei (Fig. 4, region B) characteristic of *p*-hydroxyphenyl structures (34) while region A is characteristic of guaiacyl correlations. In the spectrum of residual kraft lignin (Fig. 4) before oxidation the *p*-hydroxyphenyl signals are below the detection limit and could not be identified.

To further confirm and quantify the presence of these structures within the residual lignin we examined the quantitative ^{31}P NMR spectra of the isolated residual lignins. The *p*-hydroxyphenyl OH gives rise to a well-resolved peak at 137.8 ppm in the spectra of the oxidized lignin (35). As such their amount within the residual lignin was quantified and was shown to progressively increase by more than three-fold during oxygen delignification (from 0.04 mmol g^{-1} at 0 min to 0.15 mmol g^{-1} at 160 min (Table 2, Fig. 5)). When the content of these structures was calculated on a per g of pulp basis it was found that their content remained essentially constant throughout the delignification process. This clearly indicates that these units accumulate and do not form during oxygen delignification.

A series of isolated residual lignin samples was subjected to further analyses using a combination of analytical pyrolysis coupled to a gas chromatographic and a mass spectroscopic detector (Py-GC-MS). The results in Table 4 show that the relative content of p-hydroxyphenyl units within the pyrolysis products increased with increasing delignification time.

It is a known fact that softwood lignin contains small amounts of *p*-hydroxyphenyl units. Estimates for their abundancy vary from 5% (*Picea abies* (36)) to 13% (*Pinus taeda* (37)). If *p*-hydroxyphenyl units survive oxygen

© 2001 NRC Canada

Table 4. Quantitative structural information for residual oxidized lignins obtained by ^{13}C NMR spectroscopy (mmol g^{-1}).

Spectral range (ppm)	Assignment	Delignification time (min)				
		0	20	80	160	80[b]
154.8–150.2	C3 in G[a] (5–5′etherified)	0.67	0.73	0.83	0.88	0.92
154.8–140.1	C3,4 in all G; C4 in H[a]	9.25	7.31	6.92	6.94	7.32
140.1–122.6	C1 in G; C5 in G(5-condensed); C2,6 in H	8.69	6.46	6.73	7.04	8.36
122.6–105.1	C2,5,6 in G; C3,5 in H	9.67	7.21	6.84	6.63	7.69
154.8–105.1	Total Aromatic	27.6	20.1	20.5	20.6	23.4
89.2–67.3	Cα + Cβ in β-*O*-4[c]	1.25	1.15	1.20	1.07	—[d]
64.2–58.4	(-CH_2OH)	0.88	0.91	0.73	0.63	—[d]
58.2–54.2	OCH_3 (calculated in % weight)	4.05 (12.5)	3.62 (11.2)	3.10 (9.6)	2.80 (8.6)	3.04 (9.4)
—	OCH_3 (elemental analysis data)	11.7	9.8	8.8		—

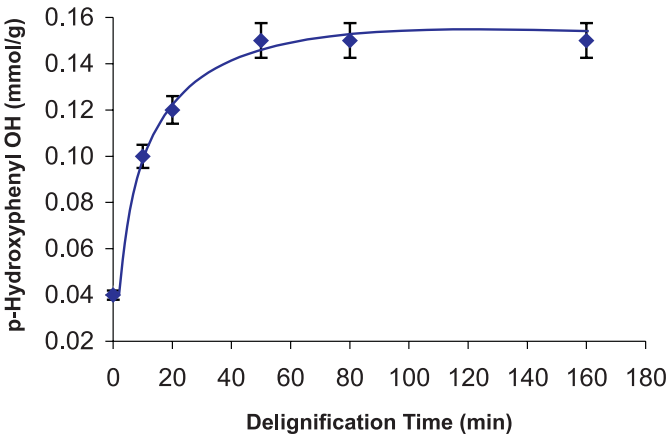
[a]G = guaiacyl units, H = *p*-hydroxyphenyl units.

[b]Solubilized lignin after 80 min of the delignification.

[c]Sum of the amount of Cα and Cβ atoms was divided by two to show the amount of β-*O*-4 units.

[d]Data are not reliable due to carbohydrate contamination.

Fig. 5. *p*-Hydroxyphenyl OH content in the residual lignin at various points along a conventional oxygen delignification process.



delignification, or at least undergo only limited degradation compared to the guaiacyl units, such moieties may accumulate within the residual lignin. Additional support of this contention arises from literature accounts claiming the accumulation of *p*-hydroxyphenyl units during the process of oxidative delignification with peroxyacids or laccase-mediator systems (38, 39).

Since three independent analytical techniques corroborate the presence and accumulation of such units within the oxygen delignified pulp, this represents convincing evidence for their presence and role in the process. Unfortunately, however there are no literature accounts of directly comparing the oxidative reactivity of *p*-hydroxyphenyl structures with their guaiacyl counterparts. To address this issue we designed a set of experiments where two model compounds, namely: 4-hydroxy toluene and its guaiacyl counterpart (3-methoxy-4-hydroxy toluene) were oxidized under conditions resembling those of oxygen delignification. The products of the oxidation were then quantified by gas chromatography. It was found that 45% of 4-hydroxy toluene remained unreacted while only 12% of the guaiacyl phenol remained in the reaction mixture. This experiment demonstrated the higher stability of *p*-hydroxyphenyl moieties under oxygen delignification conditions. This provides additional evidence that their accumulation contributes to impairing the rate of the process as oxidation intensifies. Since considerably higher amounts of *p*-hydroxyphenyl units exist in hardwood than in softwood, the accumulation of such units could be even more pronounced during oxygen delignification of hardwood pulps. This may, in part, explain the tendency of hardwood pulps to be more difficult than softwood pulps to delignify with oxygen (4).

Other lignin structural changes

The quantitative ^{13}C NMR spectra of the residual lignins isolated from the pulp at different oxidation times are shown in Fig. 6.

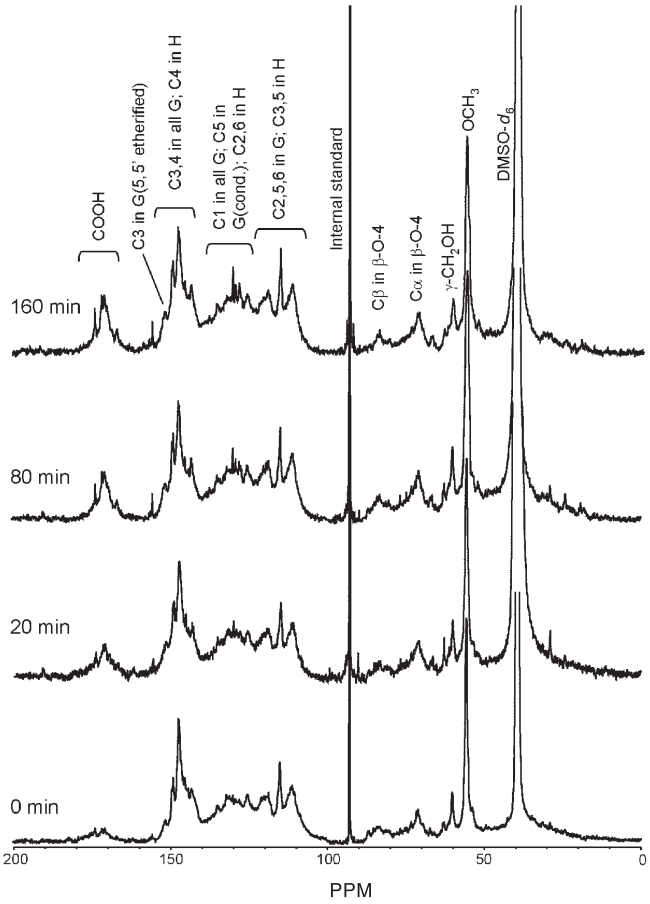
Notably, these spectra were similar to those of an oxidized residual lignin recently published by Gellerstedt et al. (40). The only visible difference is the peak at 171.8 ppm assigned to carboxylic carbon atoms. This peak significantly increases as the time of delignification increases. This increase correlates well with the amount of protein contaminants present in the residual lignins and could be attributed to signals of amidic carbonyl group present in proteins. A group of signals due to *p*-hydroxyphenyl structures and probably signals from olefinic carbons at 130.2–129.3 ppm, also progressively increased in size as the oxidation intensified.

A comparison of the ^{13}C spectra of Fig. 6 brings to light that all the changes in the residual lignin structure are of a quantitative rather than qualitative character. In this respect, our quantitative ^{13}C NMR acquisition conditions significantly facilitated the extraction of information and the comparison of the spectra.

There are a number of reports demonstrating that residual β-*O*-4 structures present within kraft lignin are stable under oxygen delignification conditions (13, 28, 40). The signal area between 89.2–67.3 ppm was assigned to Cα and Cβ signals of the atoms involved in β-*O*-4 bonds based on our HMQC spectra and previous accounts (41). The data supplied by quantification of these areas showed that the abundancy of these moieties does not change during the initial 80 min of oxidation (Table 4), i.e., it remained at about 1.20 mmol g^{-1}. This amount decreased to 1.07 mmol g^{-1} when the total oxygen delignification time reached 160 min.

© 2001 NRC Canada

Fig. 6. Quantitative ^{13}C NMR spectra of residual lignins at various points along a conventional oxygen delignification process.



Under extensive oxygen delignification conditions the oxidative degradation of aliphatic side-chains may also become pronounced. This is confirmed by the amount of the γ-CH_2OH groups which significantly decreased during the process (Table 4). A possible mechanism operating could be that of a reverse aldol condensation reaction causing γ-carbon elimination.

The methoxyl content of all residual oxidized lignins gradually decreased during oxygen delignification ranging from 4.1 to 2.8 mmol g^{-1} (Table 4). The difference between the two extreme values is about 32%. This data correlate well with published accounts (16) and our elemental analyses data (Table 1) and can be rationalized on the basis of demethoxylation reactions occurring prior to aromatic ring cleavage (11, 27).

To further assess the differences between the solubilized and residual kraft lignins the quantitative ^{13}C NMR spectra of lignins isolated after 80 min of oxygen delignification were compared. Unfortunately, minor carbohydrate contaminants within the sample of the solubilized lignin prevented a reliable quantification of the aliphatic region. However, data obtained by quantification of the aromatic region (Table 4) revealed that at the same stage of oxygen delignification, (23.4 and 20.5 mmol g^{-1}, respectively) the solubilized lignin was of higher aromaticity compared to its residual lignin counterpart.

Conclusions

A number of factors are responsible for imposing limits usually encountered in oxygen delignification. While phenolic hydroxyl groups are reactive under oxygen delignification conditions their presence is not essential for continuing reactivity at latter stages of the process. 5,5′ Biphenyl structures are relatively inert toward oxidation and accumulate within the residual lignin. Radical coupling reactions are also likely to occur between phenoxy guaiacyl radicals in the liquor and on the fiber, resulting in the formation of 5,5′ structures. Considerably less reactive *p*-hydroxyphenyl structures were also observed to accumulate within the residual lignin. However, the nature of the linkage of the remaining lignin moieties to the fiber still remains unclear. The likelihood of lignin–carbohydrate linkages being formed during oxygen delignification, anchoring lignin moieties on the fibre is currently under investigation in our laboratory.

Acknowledgments

The authors would like to express their gratitude to Mr. Ernst Palus and Mr. Tibor Kristof for their assistance with residual lignin isolation and pulp analyses. In addition, Dr. Anna-Stiina Jaaskelainen also deserves our gratitude for carrying out the Py-GC-MS analyses, Mr. Yujun Sun for participating in a number of valuable discussions, and Mrs. Barbara van Lierop for reviewing the manuscript.

References

1. T.J. McDonough. Tappi J. **78**, 55 (1995).
2. L. Olin and A. Teder. Tappi J. **62**, 43 (1979).
3. V. Masura. Cellul Chem. Technol. **27**, 201 (1993).
4. T.J. McDonough. *In* Pulp bleaching. Principles and practice. *Edited by* C.W. Dence and D.W. Reeve. Tappi, Atlanta. 1996. pp. 213–239.
5. P. Liias, T. Merikallio, and T. Metsa-Rauma. *In* Proceedings of the International Pulp Bleaching Conference. Helsinki, Finland. 1998. pp. 269–274.
6. M. Bokström and S. Nordén. Extended oxygen delignification. *In* Proceedings of the International Pulp Bleaching Conference. Vol. 1. Helsinki, Finland. 1998. pp. 23–31.
7. R.W. Allison and S.W. Wrathall. *In* Proceedings of the International Pulp Bleaching Conference. Vol. 1. Helsinki, Finland. 1998. pp. 41–48.
8. C. Chirat and D. Lachenal. Limits of oxygen delignification. *In* Proceedings of the Tappi Pulping Conference. Vol. 1. Montreal, QC, Canada. 1998. pp. 619–704.
9. K. Kratzl, P. Claus, W. Lonsky, and J.S. Gratzl. Wood Sci. Technol. **8**, 35 (1974).
10. K. Kratzl, J. Gratzl, and P. Claus. Adv. Chem. Ser. **59**, 157 (1966).
11. S.J. Ljunggren. J. Pulp Paper Sci. **12**, 54 (1986).
12. E. Johansson and S.J. Ljunggren. J. Wood Chem. Technol. **14**, 507 (1994).
13. S. Ljunggren, G. Gellerstedt, and M. Petersson. Chemical aspects of the degradation of lignin during oxygen bleaching. *In* Proceedings of the 6th International Symposium on Wood and

© 2001 NRC Canada

Pulping Chemistry. Vol. 1. Melbourne, Australia. 1991. pp. 229–235.
14. J. Gierer. Holzforsch. **51,** 34 (1997).
15. G. Gellerstedt, K. Gustafsson, and E.L. Lindfors. Nordic Pulp Pap Res. J. **1**, 14 (1986).
16. G. Gellerstedt, and L. Heuts. J. Pulp Pap. Sci. **23**, 335 (1997).
17. B. Hortling, T. Tamminen, P. Tikka, and J. Sundquist. Structures of the residual lignins of modified kraft pulps compared with conventional and oxygen-bleached kraft pulps. *In* Proceedings of the 7th International Symposium on Wood and Pulping Chemistry. Vol. 1. Beijing, China. 1993. pp. 313–317.
18. Y. Sun and D.S. Argyropoulos. J. Pulp Pap. Sci. **21**, 185 (1995).
19. E. Johansson, I.D. Suckling, and R.M. Ede. Effect of O and OO delignification on the structure of residual lignin from *Pinus radiata* pulp. *In* Proceedings of the 9th International Symposium on Wood and Pulping Chemistry. Vol. 1. Montreal, QC, Canada. 1997. pp. J1–1.
20. Y.-Z. Lai, M. Funaoka, and H.-T. Holzforsch. **48**, 355 (1994).
21. D.S. Argyropoulos and Y. Liu. J. Pulp Pap. Sci. **26**, 107 (2000).
22. PAPTAC Standards Methods: G.18, G.24P, G.8/G.9 PAPTAC (2000).
23. D.S. Argyropoulos, E. Palus, and Y. Sun. Isolation of residual kraft lignin in high yield and purity. Submitted for publication.
24. A. Granata and D.S. Argyropoulos. J. Agric. Food Chem. **43**, 1538 (1995).
25. S. Zia, L.G. Akim, and D.S. Argyropoulos. Quantitative ^{13}C NMR of lignins with internal standards. Submitted for publication.
26. C. Chirat, D. Cardoba-Barrau, and D. Lachenal. Effect of oxygen on residual lignin: ways to improve lignin removal. *In* Proceedings of the 10th International Symposium on Wood and Pulping Chemistry. Vol. 1. Yokohama, Japan. 1999. pp. 238–241.
27. F. Asgari and D.S. Argyropoulos. Can. J. Chem. **76**, 1606 (1998).
28. S.T. Moe and A.J. Ragauskas. Holzforschung, **53**(4), 416 (1999).
29. P. Karhunen, P. Rummakko, J. Sipila, G. Brunow, and I. Kilpelainen. Tetrahedron Lett. **36** (1995).
30. D.S. Argyropoulos, L. Akim, and B. Ahvazi. Salient reactions in lignin during pulping and bleaching. Proceedings of the Tappi Pulping Conference, Boston, Mass. Nov. 6–8, 2000. Vol. 143. Paper 54-1.
31. S.I. Tohmura and D.S. Argyropoulos. Determination of arylglycerol-β-aryl ethers and other linkages in native and technical lignins. J. Agric. Food Chem. **49**, 155e2 (2000).
32. Y. Sun, M. Fenster, A. Yu, R.M. Berry, and D.S. Argyropoulos. Can. J. Chem. **77**, 667 (1999).
33. S. Ljunggren and E. Johansson. Nordic Pulp Pap. Res. J. **5**, 148 (1990).
34. D. Robert, D. Piersantelli, L. Jouanin, V. Ferret, B. Pollet, and C. Lapierre. ^{13}C NMR spectroscopy of lignins from transgenic poplars deficient in *O*-methytransferase and cinnamyl alcohol dehydrogenase. *In* Proceedings of the 10th International Symposium on Wood and Pulping Chemistry, Yokohama, Japan, 1999. Vol. III, pp. 18–21.
35. C. Crestini and D.S. Argyropoulos. J. Agric. Food Chem. **45**, 1212 (1997).
36. M. Erickson, S. Larsson, and G.E. Miksche. Acta Chem. Scan. **27**, 1675 (1973).
37. W.G. Glasser and H.R. Glasser. Pap. Puu, **63**(2), 71 (1981).
38. K. Poppius-Levlin, T. Tamminen, K. Rajanen, and A.-S. Jääskeläinen. Suitability of laccase/mediator systems for hardwood kraft pulp delignification. *In* Proceedings of the 10th International Symposium on Wood and Pulping Chemistry, Yokohama, Japan, 1999, Vol. 1, pp. 556–561.
39. T. Tamminen, T. Elder, W. Wang, and K. Poppius-Levlin. Proceedings of the 7th International Conference On Biotechnology in the Pulp and Paper Industry, Vancouver, Canada, 1998, Vol. A, pp. A107–110.
40. G. Gellerstedt, L. Heuts, and D.J. Robert. J. Pulp Pap. Sci. **25**, 111 (1999).
41. J. Ralph, J.M. Marita, S.A. Ralph, R.D. Hatfield, F Lu, R.M. Ede, J. Peng, S. Quideau, R.F. Helm, J.H. Grabber, H. Kim, G. Jimenez-Monteon, Y. Zhang, H.-J.G. Jung, L.L. Landucci, J.J. MacKay, R.R. Sederoff, C. Chapple, and A.M. Boudet. *In* Advances in lignocellulosics Characterization. *Edited by* D.S. Argyropoulos. Tappi Press, Atlanta. 1999. pp. 55–108.

© 2001 NRC Canada

Classical analysis of intermolecular potentials for Ar–CO_2 rotational collisions[1]

J.C. Belchior, J.P. Braga, and N.H.T. Lemes

Abstract: Classical trajectory calculations have been performed for four potential energy functions to describe Ar–CO_2 collisions. A comparison is given between classical cross sections calculated using the two most recent potential surfaces and two older intermolecular potential surfaces based on the electron gas model. The two-dimensional atom ellipsoid model has also been applied for the study of multiple collisions. The model was able to predict such a phenomenon in agreement with quantum scattering results previously published for an ab initio potential surface in the region of very low collision energy. On the other hand, the two older potentials showed multiple collision effects at very high energies. The comparison of the cross sections showed some deviations from the experimental data. By introducing two parameters, a modified surface is proposed by changing the most recent intermolecular potential. In this case the agreement with experimental measurements and theoretical scattering cross sections was considerably improved. It is concluded that global potential surfaces for describing Ar–CO_2 interaction are not well established. To achieve the requirement of reproducing all properties of this system, the present work suggests that one needs further experimental and theoretical investigations.

Key words: classical trajectories, dynamics, cross sections, Ar–CO_2 collisions, potentials.

Résumé : Afin de décrire les collisions Ar–CO_2, on a effectué des calculs de trajectoire classique pour quatre fonctions d'énergie potentielle. On présente une comparaison des sections efficaces classiques calculées d'une part à l'aide les surfaces de potentiel les plus récentes et d'autre part avec deux surfaces de potentiel intermoléculaire plus anciennes basées sur le modèle du gaz électronique. On a aussi appliqué le modèle de l'atome bidimensionnel ellipsoïdal à l'étude des collisions multiples. Le modèle a pu prédire un tel phénomène en accord avec des résultats de diffusion quantique publiés antérieurement pour une surface de potentiel ab initio dans la région de très faible énergie de collision. Par ailleurs, les deux potentiels les plus vieux ne permettent de mettre en évidence les effets de collisions multiples qu'aux énergies très élevées. La comparaison des sections efficaces met en évidence des déviations par rapport aux données expérimentales. En introduisant deux paramètres, on propose une surface modifiée résultant du changement du potentiel intermoléculaire le plus récent. Dans ce cas, l'accord entre les mesures expérimentales et les sections efficaces de diffusion théoriques est grandement amélioré. On conclut que les surfaces de potentiel global permettant de décrire l'interaction Ar–CO_2 n'est pas bien établie. Afin d'atteindre les conditions requises pour reproduire toutes les propriétés de ce système, il découle de notre travail que de nouvelles études expérimentales et théoriques sont nécessaires.

Mots clés : trajectoires classiques, dynamique, sections efficaces, collisions Ar–CO_2, potentiels.

[Traduit par la Rédaction]

Introduction

During the past few years, considerable attention has been focused on the study of the Ar–CO_2 system, as has been discussed in refs. 1 and 2. However, the Ar–CO_2 intermolecular interaction has not yet been fully understood (1), since according to Roche et al. (3) "the only potential that gives a satisfactory account of the line-broadening coefficients is the modified electron gas potential of Preston and Pack" (4), while this same potential provides very poor agreement with van der Waals spectra. The disagreement with the van der Waals spectra suggests that the long-range forces can be improved.

Several types of experimental data are available for the Ar–CO_2 interaction, all measured with a high degree of accuracy (5). Second virial coefficients were obtained for Ar–CO_2 mixtures, and for several temperatures, comparisons with the experimental results of Lichtenthaler and Schafer (6) and of Cottrell et al. (7) show satisfactory agreement. However, for dynamic studies, generally the most informative data from which details of the intermolecular potential can be deduced are obtained from crossed molecular beam experiments. Usually such measurements allow for the extraction of information about the anisotropy of the interaction (8). For the Ar–CO_2 interaction, crossed molecular beam scattering data were obtained by Kalinin et al. (9) and by Loesch (10).

In particular, the experimental measurements of Loesch, which are based on high-resolution molecular beam techniques, have provided state-to-state rotational total cross sections for three collision energies, namely 0.069, 0.11, and 0.19 eV. Classical trajectory calculations were also performed (10) for a simple model potential, and qualitative agreement with the experimental results (i.e., the cross sections) was found. As indicated by Loesch, the state-to-state rotational cross sections are very sensitive to the anisotropy of the repulsive interaction, in particular, and satisfactory agreement was found for a speci-

Received February 14, 2000.
Published on the NRC Research Press Web site on March 16, 2001.

J.C. Belchior[2] and J.P. Braga. Departamento de Quimica – ICEx, Universidad Federal de Minas Gerais, Pampulha, (31.270-901) Belo Horizonte, MG – Brazil.
N.H.T. Lemes. Universidade Vale do rio Verde, Av. Castelo Branco 82, (37.410-000) Três Corações, MG – Brazil.

[1]Work supported by the Conselho Nacional de Desenvolvimento Científico e Technológico (CNPq) and the Fundaçâo de Amparo à Pesquisa do Estado de Minas Cerais (FAPEMIG), Brazil.

[2]Corresponding author (e-mail: belchior@dedalus.lcc.ufmg.br).

 DOI: 10-1139/cjc-79-2-211 © 2001 NRC Canada

fied geometric anisotropy. Simultaneously and independently, Parker et al. (11) proposed an intermolecular potential energy function based on an electron gas model that included correlation, Coulomb, and exchange contributions to the interaction energy. A full potential surface was obtained with contributions of both short- and long-range terms. Use of this potential surface for the calculation of the second virial coefficients gave rise to reasonable agreement between the calculated and experimental values. As has been pointed out in ref. 1, this surface, referred to hereafter as surface 1, was the first realistic potential with both short- and long-range components available for the study of $Ar-CO_2$ collisions. Later, Preston and Pack (4) considered another potential surface, obtained by modifying the long-range van der Waals interaction. This potential surface is referred to hereafter as surface 2. Classical trajectory (~30 000) calculations have been performed for both potentials, and in general, acceptable agreement has been found with the experimental measurements of Loesch (10). Small deviations were observed between the calculated and experimental values for differential cross sections corresponding to small Δj transitions. However, as indicated by Preston and Pack (4), such disagreement would be possible since the angular distribution for low Δj values could be unreliable. They noted that surface 1, which gave satisfactory agreement with the experiments, was the most reliable potential and was preferable for studying $Ar-CO_2$ rotational collisions.

Very recently, an ab initio intermolecular potential was obtained using the Møller–Plesset perturbation theory with a large basis set (12), and the data were fitted using procedures recommended by Buckingham et al. (13). This potential has qualitative features of the anisotropy that are comparable to the exchange-quadrupole model of Cooper and Hutson (14). Later, extensive classical and quantum scattering calculations were carried out (2) using this potential energy function. It was pointed out by ter Horst and Jameson that orbital resonances are to be expected for low total energy; this was confirmed on the basis of quantum and classical trajectory calculations. However, no comparison with experimental state-to-state differential or total rotational cross sections was performed, and therefore it appears that such effects have not been fully analysed. This will be discussed in more detail in the present work in light of the two-dimensional atom ellipsoid model.

In an independent study, Roche et al. (3) have utilized nine different $Ar-CO_2$ potential energy functions available in the literature to carry out quantum scattering calculations and to test the ability of these potentials to reproduce the spectra of such a system. Both IOS (15, 16) and CS (16) approximations were used to calculate the pressure-broadening cross sections, but none of the nine potentials gave a satisfactory account of the spectroscopic properties analysed. The goal of Hutson et al. (1) was to obtain an intermolecular potential capable of providing a quantitative potential which was able to reproduce a wide range of the spectrum. Their new potential energy function is based on a nonlinear least-squares method of fitting to both high-resolution van der Waals spectra and second virial coefficients. The new surface was able to reproduce the spectra of the $Ar-CO_2$ interaction with high accuracy, and the relative average error for almost all properties compared was found to be very small. As pointed out by Preston and Pack (4) a correct intermolecular potential would be intermediate to the two potentials used in refs. 4 and 11. This was an important conclusion of Hutson et al. (1), i.e., "...the shape of the repulsive wall in the electron gas potentials is actually quite good and our value for the depth of the minimum at $\theta = 90^o$ is between surface 1 and surface 2." As previously quoted (1), these two surfaces (1 and 2) have a poor representation of the attractive wall, while other fitted potentials (17, 18) provide better representation in the attractive region but provide unsatisfactory representations of the repulsive wall.

The ab initio potential energy function of Marshall et al. (12) was used to study $Ar-CO_2$ collisions and extensive classical and quantum calculations were carried out, but no state-to-state rotational total cross sections were evaluated. Virial coefficients were calculated for several potential energy surfaces, and a comparison with the experimental data for several temperatures was done. Moreover, transport properties were calculated, and an extensive comparison of several types of spectroscopic data was carried out for all available $Ar-CO_2$ potentials. However, it was concluded (2) that "...the ab-initio surface fitted by Marshall et al. (12) provided a disappointing representation of the potential."

Most of the studies of the $Ar-CO_2$ system have been carried out for spectroscopic or thermodynamic phenomena. Very recently, Roche et al. (19) carried out an accurate analysis of the potential surface proposed in ref. 1. They tested the potential for reproducing collisional properties such as line-broadening cross sections. However, even with several intermolecular potentials available, the important features for understanding the $Ar-CO_2$ interaction without also considering cross sections may be still unsatisfactory. We have also very recently used surface 4 for analysing scattering cross sections; these studies have suggested new experiments for new fitting procedures in order to calculate accurate potential energy functions (20).

The present study analyses the two oldest potentials (1 and 2) and the two latest surfaces (3 and 4). A full comparison of classical trajectory calculations for these surfaces and the new ab initio potential (surface 3) will be carried out with the experimental state-to-state rotational total cross sections of Loesch (10). Moreover, the two-dimensional (2D) atom-ellipsoid model (21) will be used to analyse the importance of multiple collisions. Finally, calculations based on the latest surface of Hutson et al. (1), surface 4, will be compared with the experimental state-to-state rotational total cross sections of Loesch (10) and also with the results obtained using the other three surfaces.

The intermolecular potentials

Although several intermolecular potentials have been proposed to study $Ar-CO_2$ collisions, the present work considers only four of them. The surface of Parker et al. (11), surface 1, is written as

$$[1] \qquad V(r,\gamma) = \sum_{n=0,2,\ldots} V_n(r) P_n(\cos\gamma)$$

$$= v^{HF}(r,\gamma) + v^{COR}(r,\gamma)$$

©2001 NRC Canada

Table 1. Parameters of surfaces 1 and 2 (values in atomic units).

$n \rightarrow$	0	2	4	6	8	10
$A_{n1}^{(1)}$	22.4247	63.5744	99.1128	318.652	332.826	435.837
A_{n2}	−0.716288	−0.811806	−1.17577	−1.88135	−2.14596	−2.44616
A_{n3}	−0.0869136	−0.0753131	−0.0477138	0.0	0.0	0.0
$B_{n1}^{(1)}$	0.599056	0.207391	0.0523497	0.0374991	0.0137376	0.108283
B_{n2}	−0.650479	−0.620877	−0.735340	−1.05547	−1.03942	−2.04765
B_{n3}	−0.0320299	−0.0310717	−0.0296750	−0.0182219	−0.0494781	0.0
r_n	6.32925	6.90026	6.96450	∞	∞	∞
$C_6(n)$	114.5	26.6	0.0	0.0	0.0	0.0
$C_8(n)$	2380	2080	410	0.0	0.0	0.0
$A_{n1}^{(2)}$	29.0852	82.4571	128.551	318.652	332.826	435.837
$B_{n1}^{(2)}$	0.599056	0.207391	0.0523497	0.0374991	0.0137376	1.08283

in which v^{HF} and v^{COR} are the short- and long-range contributions, each with a corresponding Legendre expansion. Surfaces 1 and 2 differ mainly in the long-range terms. The functional form for the short-range component is common, and is written as

$$[2] \qquad v_n^{\mathrm{HF}}(r) = A_{n1}^{(1)} \exp(A_{n2} r + A_{n3} r^2)$$

with the $A_{n1}^{(1)}$, A_{n2}, and A_{n3} values provided in Table 1 ($A_{n1}^{(1)}$ is replaced by $A_{n1}^{(2)}$ for surface 2). For surface 1 the long-range terms are given by

$$[3] \qquad v_n^{\mathrm{COR}}(r) = -B_{n1}^{(1)} \exp(B_{n2} r + B_{n3} r^2) \qquad r \le r_n$$

$$v_n^{\mathrm{COR}}(r) = -C_6(n) r^{-6} - C_8(n) r^{-8} \qquad r > r_n$$

with r_n, $B_{n1}^{(1)}$, B_{n2}, B_{n3}, $C_6(n)$, and $C_8(n)$ all given in Table 1. Surface 2, which is more anisotropic than surface 1, has a different exponential prefactor $B_{n1}^{(2)}$ for $r \le r_n$, and has the form

$$[4] \qquad v_n^{\mathrm{COR}}(r) = -(B_{n1}^{(2)} - B_{n1}^{(1)}) \exp(B_{n2} r + B_{n3} r^2) - C_6(n) r^{-6} - C_8(n) r^{-8}$$

for $r > r_n$ with the parameters also given in Table 1.

The ab initio surface of Marshall et al. (12) (surface 3) can be summarized as a sum of several terms, short-range energy (v_{sr}), the dispersion energy (v_{disp}), and the induction energy (v_{ind}). The complete intermolecular potential is written as

$$[5] \qquad V(r, \gamma) = v_{\mathrm{sr}} + v_{\mathrm{disp}} + v_{\mathrm{ind}}$$

where

$$[6] \qquad v_{sr}(r, \gamma) = A \exp\{-\beta(\gamma)[r - r_{ref}(\gamma)]\}$$

with both $\beta(\gamma)$ and $r_{\mathrm{ref}}(\gamma)$ expanded in Legendre series as

$$[7] \qquad \beta(\gamma) = \sum \beta_L P_L(\cos\gamma)$$

Table 2. Parameters for surface 3 (values are in atomic units).

v_{sr}	v_{ind}	v_{disp}
A = 4.35889E+01	$C_{8,0}^{\mathrm{ind}}$=202.945	$C_{6,0}^{\mathrm{disp}}$=186.178
$r_{\mathrm{ref},0}$=1.49681	$C_{8,2}^{\mathrm{ind}}$=231.937	$C_{6,2}^{\mathrm{disp}}$=106.532
$r_{\mathrm{ref},2}$=1.35945	$C_{8,4}^{\mathrm{ind}}$=173.953	$C_{8,0}^{\mathrm{disp}}$=0.0
$r_{\mathrm{ref},4}$=0.103711	$C_{10,0}^{\mathrm{ind}}$=4257.40	$C_{8,2}^{\mathrm{disp}}$=0.0
$r_{\mathrm{ref},6}$=-0.232085	$C_{10,2}^{\mathrm{ind}}$=2359.70	$C_{8,4}^{\mathrm{disp}}$=0.0
$r_{\mathrm{ref},8}$=0.1741	$C_{10,4}^{\mathrm{ind}}$=2356.01	$C_{10,0}^{\mathrm{disp}}$=293258
β_0=1.85782	$C_{10,6}^{\mathrm{ind}}$=6.86952	$C_{10,2}^{disp}$=528639
β_2=0.0209364		$C_{10,4}^{\mathrm{disp}}$=0.0
β_4=0.101625		$C_{10,6}^{\mathrm{disp}}$=0.0
β_6=-0.0964734		
β_8=0.0698541		

Note: Multiply the dispersion coefficients by 1.012 (see table VI of this ref. 12 for more details).

$$r_{\mathrm{ref}}(\gamma) = \sum r_{\mathrm{ref}_L} P_L(\cos\gamma)$$

The dispersion energy is also represented as a Legendre expansion,

$$[8] \qquad v_{\mathrm{disp}}(r, \gamma) = -\sum_{n=6}^{\mathrm{even}} \sum_{L=0}^{n-4} \frac{D_n(\beta(\gamma), r) C_{n,L}^{\mathrm{disp}} P_L(\cos\gamma)}{r^n}$$

with

$$[9] \qquad D_n(\beta, r) = 1 - \mathrm{e}^{-\beta r} \sum_{k=0}^{n} \frac{[\beta r]^k}{k!}$$

Finally, the induction energy contribution is written as

$$[10] \qquad v_{\mathrm{ind}}(r, \gamma) = -\sum_{n=8}^{\mathrm{even}} \sum_{L=0}^{n-4} \frac{C_{n,L}^{\mathrm{ind}} P_L(\cos\gamma)}{r^n}$$

The parameters in eqs. [6]–[10] are found in Table 2.

The latest surface available for $Ar-CO_2$ collision is that proposed by Hutson et al. (1) by fitting a wide range of spectroscopic data. Actually, they have proposed two slightly different potential energy functions, but as later pointed out (1), the difference between these potentials is not particularly significant.

©2001 NRC Canada

Table 3. Parameters of surface 4 (values in atomic units).

A_{iL}	β_{iL}	C_{in}^{L}
32.27581	2.03171	50.5
11.85757	1.79571	1593
−9.41362	2.09529	61580
32.36857	2.12256	13.635
−3.40252	1.87293	430.2
−1.68672	2.18922	16630
−1.91165	1.96196	
1.10092	1.98533	

Therefore, only the surface referred to in ref. 1 as the "single repulsion" potential has been considered here. It is a site–site potential, which can be written in the form (surface 4)

$$[11] \quad V(r,\gamma) = \sum_{i=1}^{3}\left[\sum_{L} S_{iL}(r_i)P_L(\cos\gamma_i) - \sum_{n=6,8,10}\sum_{L=0,2,4} C_{in}^{L}P_L(\cos\gamma_i)r_i^{-n}D(r_i)\right]$$

in which i is summed over the three sites on the CO_2 molecule, $S_{iL}(r_i)$ is given by

$$[12] \quad S_{iL}(r_i) = A_{iL}\exp[-\beta_{iL}(r_i - r_{\text{ref}})]$$

where r_{ref} was fixed to $7.0a_0$ and the damping function , $D(r_i)$, is given by

$$[13] \quad D_i(r_i) = \begin{cases} 1 & \text{for } i \geq r_i^d \\ \exp[-0.4((r_i^d/r_i)-1)^2] & \text{for } r_i < r_i^d \end{cases}$$

where r^d is equal to $12.85a_0$. The parameters of this surface are given in Table 3. More details of the parameters of surface 1, 2, 3, and 4 may be found in refs. 4, 12, and 1.

The key equations for classical trajectory calculations

The classical trajectory method is well detailed elsewhere (22), and therefore it will be only summarized here. The Hamiltonian of an atom-linear molecule system can be written as

$$[14] \quad H = \frac{1}{2\mu}\left[P_X^2 + P_Y^2 + P_Z^2\right] + \frac{1}{2I}\left[P_\theta^2 + \frac{P_\phi^2}{\sin^2\theta}\right] + V(r,\cos\gamma)$$

in which μ is the reduced mass of the system; I is the moment of inertia of the linear molecule; P_X, P_Y, and P_Z are the components of the linear momentum of the incoming atom; P_θ and P_ϕ are the components of the angular momentum of the molecule; θ and ϕ are describing the orientation of the molecule; and $V(r,\gamma)$ is the intermolecular potential. The relative angle γ is given by

$$[15] \quad \cos\gamma = \frac{(X_A\sin\theta\cos\phi + Y_A\sin\theta\sin\phi + Z_A\cos\theta)}{r}$$

where X_A, Y_A, and Z_A are the coordinates of the incoming atom. Following the usual procedure, the set of 10 coupled equations given in ref. 22 can be obtained, and by defining a set of initial conditions the Runge–Kutta method can be used to integrate the classical coupled equations. The total energy was conserved to better than eight digits. Scattering cross sections $\sigma_{jj'}$ can be calculated using the Monte Carlo statistical method as

$$[16] \quad \sigma_{jj'} = \pi b_{\max}^2 P_{jj'}$$

in which $P_{jj'}$ is the transition probability. The latter has been calculated by boxing the calculated final rotational angular momentum. In the present case it has been truncated to the next even final j, i.e., for values smaller than an odd integer number this is truncated to the smallest even value otherwise to the next greatest even value.

Table 4. The dynamical parameters used in the classical trajectory calculations (40 000 trajectories performed for all surfaces).

Surfaces	$r_{\max}$ (Å)	$b_{\max}$ (Å)
Surface 1 (Parker et al. (11))	30	15
Surface 2 (Preston and Pack (4))	30	15
Surface 3 (Marshall et al. (12))	18	15
Surface 4 (Hutson et al. (1))	18	15

The maximum impact parameter, $b_{\max}$, was chosen as described in Table 4, and each one was selected randomly from the distribution $b = b_{\max}(\xi)^{1/2}$, where ξ is a random number ranging between 0 and 1. The angles, θ and ϕ were also generated randomly between 0 and π and 0 and 2π, respectively.

Results and discussion

Ellipsoid model

The two-dimensional (2D) atom-ellipsoid model is well detailed elsewhere (21), and the theory will not be described here. The analysis based on such a model can give qualitative information concerning the anisotropy of a particular system (23). In the present analysis, two sets of calculations will be carried out for each potential described in section 2 by considering firstly the repulsive component of a surface and then the full potential surface.

Resonance effects were recently analysed by ter Horst and Jameson (2), using the ab initio potential of Marshall et al. (12), namely surface 3. However, although comparisons of classical trajectory and close coupling calculations were made, no direct comparison was made with state-to-state scattering cross sections for any of the energies used by Loesch (10). Moreover, most of the analyses in ref. 2 were carried out based on comparisons with second virial coefficient data, spectroscopic constants, and transport properties. As was pointed out in ref. 2,

©2001 NRC Canada

potential 1 can reproduce most of those experimental data, and surface 2 shows good agreement for some but not for all data: as stated by ter Horst and Jameson (2), "the only surface that gave a satisfactory account of the line broadening coefficients was surface 2." It is interesting that in ref. 2 the collision energy used for analysing the resonances was 40 cm^{-1} (4.96 meV). Such an energy is too low to provide any comparison with the experiments of Loesch (10), for which the lowest energy is 69 meV.

According to ref. 24 the occurrence of multiple rotational collisions can be determined by a comparison between $\epsilon \equiv \mu/I$ and ϵ_c, which is evaluated from

[17] $$\epsilon_c = \frac{\beta - \alpha}{(A-B)\left[2B(\sqrt{2A-B} - \sqrt{A}) + (A-B)(\beta-\alpha)\right]}$$

with

[18] $$\beta = \pi - \cos^{-1}\left(\frac{A-B}{A}\right)$$

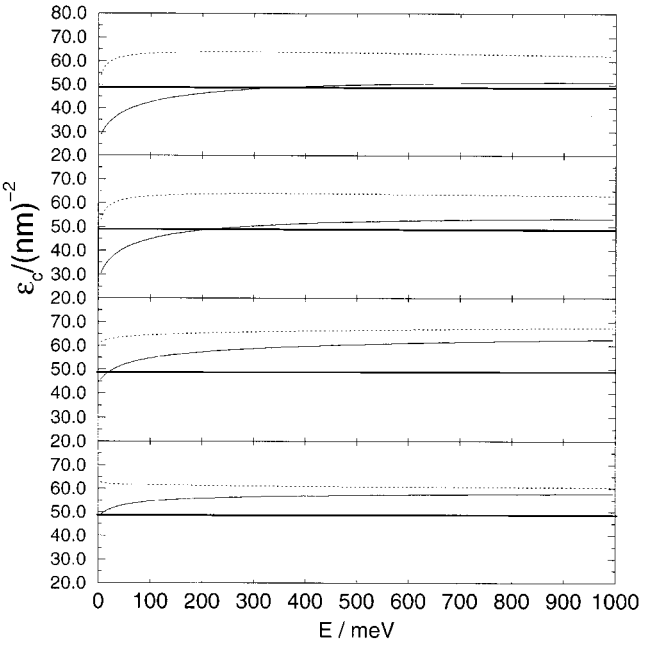
[19] $$\alpha = \frac{1}{2}\cos^{-1}\left(\frac{A-B}{A+B}\right)$$

and the parameters A and B are defined by $A = r$ when $V(r, 0) - E = 0$ and $B = r$ when $V(r, \pi/2) - E = 0$, where E is the collision energy. If ϵ_c is smaller than ϵ, then multiple collisions will be present. Figure 1 shows ϵ_c as a function of the collision energy for the potentials described in section 2. The contributions of the repulsive component and the full surface are illustrated separately. The repulsive component of surfaces 1, 2, and 3 are almost the same, as can be seen from comparisons between the dotted curves in this figure. Notice that for the first three surfaces ϵ_c increases with collision energy and becomes constant at high energies, while surface 4 shows a different behaviour, especially for very low collision energy. This indicates that multiple-collision effects can be associated with long-range forces. In addition, according to this model, surface 3 gives rise to multiple-collision effects only for collision energies below 20 meV, while for surfaces 1 and 2 such effects can be expected for much higher collision energies of order 200 meV. This may explain the analysis of resonances in ref. 2 where the collision energy used was 40 cm^{-1} (4.96 meV) in concordance with the conclusions of this effect stated there. It appears that the 2D model has failed in the case of surface 4, as it predicts the complete absence of multiple collisions.

Classical trajectory analysis

Classical trajectory calculations have been performed using the potentials of Parker and co-workers (surface 1), Preston and Pack (surface 2), Marshall et al. (surface 3) and Hutson and collaborators (surface 4). Although Preston and Pack have also carried out classical trajectories, the present calculations provide additional details for their surfaces by splitting out the short- and long-range contributions and comparing the classical results with those obtained using more recent potential

Fig. 1. From the top, ϵ_c (multiple collision effects) as a function of the collision energy E for surfaces 1, 2, 3, and 4. The thicker solid lines correspond to the value of ϵ, while the dotted curves show ϵ_c corresponding to the repulsive components of the surfaces and the solid curves show ϵ_c for the full surfaces.



energy functions (surfaces 3 and 4). The analyses of all present calculations are predicted upon treating the experimental measurements of Loesch (10) as the exact results.

Each intermolecular potential comparison made with the experimental results of Loesch is based upon 40 000 classical trajectory calculations carried out with the CO_2 molecule initially in rotational state $j_i = 6$. The classical cross sections calculated using the two oldest potentials are compared with the results obtained using the two latest surfaces for the Ar−CO_2 interaction. The collision energies 0.069, 0.11, and 0.19 eV are those used for the experimental measurements of Loesch (10). Figure 2 shows the results for surfaces 1 and 2 (the two oldest) and surface 4 (ref. 1), while Fig. 3 compares the calculations for surfaces 3 and 4. In both Figs. 2 and 3, only the short-range forces have been taken into account. In Fig. 4 the classical trajectory calculations for the three energies used are compared considering the whole intermolecular potentials.

Figure 2 shows the state-to-state rotational total cross sections. The repulsive intermolecular potentials 1 and 2 are very similar, with slight differences only in the values of the parameter $A_{n1}^{(1)}$ of eq. [2]. Hence, the cross sections in Fig. 2 are almost the same, but as can be seen, small differences do exist. For example, at collision energy 0.069 eV, the cross sections calculated using surface 2 rise up slightly for $j' = 22$, while for surface 1 this is not observed. The greatest difference can be observed at energy 0.19 eV for j' between 30 and 40. As can be seen in this figure, the experimental data are in reasonable agreement with the theoretical results, as has been found previously for surfaces 1 and 2. These surfaces are better for the lowest collision energy and become worse as the energy increases. The repulsive component of surface 4 provides better

©2001 NRC Canada

Fig. 2. State-to-state rotational cross sections for repulsive potentials (surfaces 1, 2, and 4). The experimental results of Loesch (10) are shown by the filled squares and the cross sections calculated for surface 4, illustrated by the thick lines, have also been included for comparison.

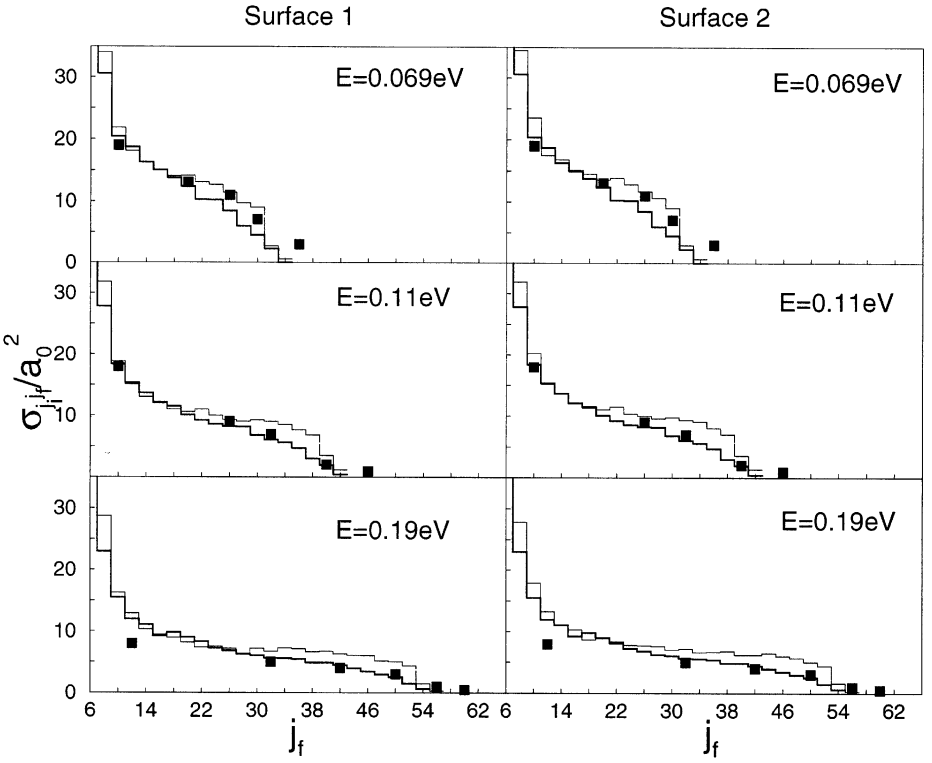
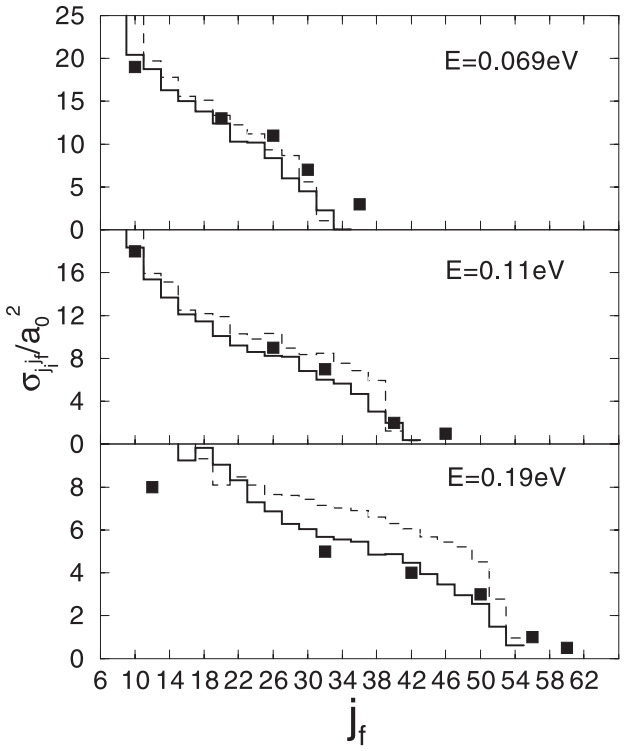


Fig. 3. Comparison of state-to-state rotational cross sections for surface 3 (dashed lines), surface 4 (solid lines), and the experimental data (filled squares).

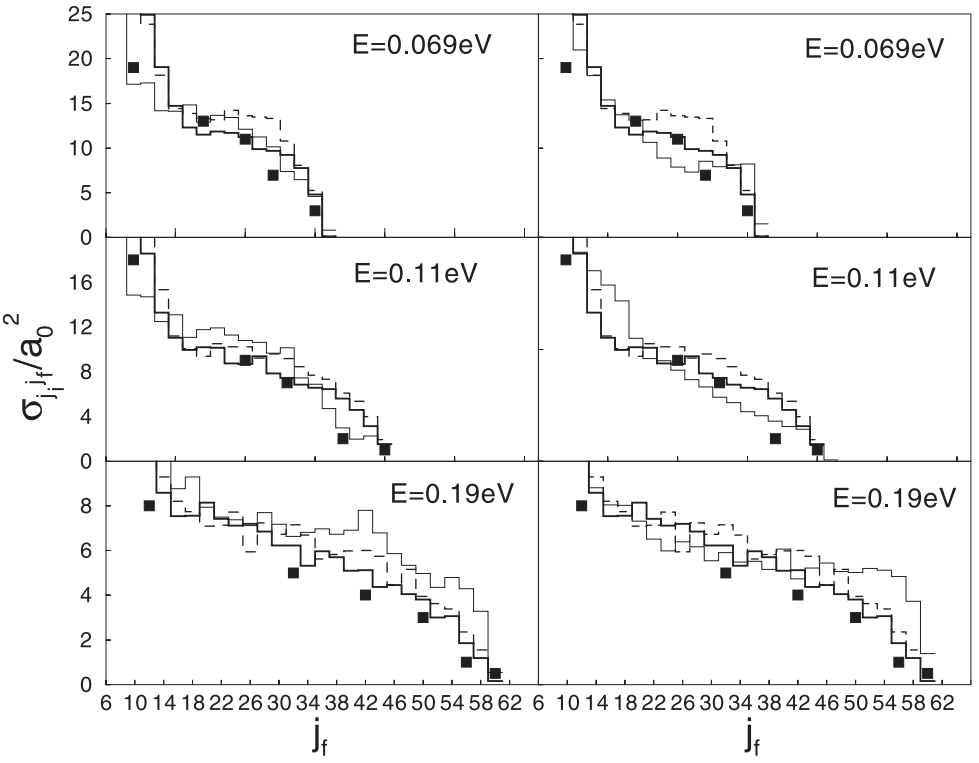


results for the two higher energies, and it does not deviate much from the experimental data, even at the lowest energy.

In general, a full potential contains components of short- and long-range forces. In this case, if there is no charge involved, the core of the particles will contribute to the repulsive term of the potential, while the attractive component, due to the dispersion and induction energies, will mainly contribute to the tail of the surface. If one models the interaction considering only repulsive forces, the tail will certainly be present but it will describe only how the interaction goes to zero. These two quantities are important for increasing or decreasing the rotational transition probability. An analysis of the tail of the potential when only repulsive forces are involved was previously investigated for rotational collisions through quantum mechanics (25). When attractive forces are present the tail of the potential will have two contributions: one from the repulsive component and the other from the attractive term. The results compared in Fig. 2 were calculated by considering only repulsive forces, and hence the tail of these surfaces will only be due to the repulsive component. When no attractive forces are involved only contributions due to the core are present. At lower collision energy the tail may be more important than at higher energies. As can be observed, the results in this figure show that surfaces 1 and 2 provide better agreement with almost all the experimental data at low energies, while surface 4 provides good agreement for small Δj transitions. As the collision energy increases, there is better agreement between the results obtained using surface 4. This is more evident at 0.11 eV collision energy. A unique deviation is observed for the latest transition, i.e., at $j' = 46$, which

©2001 NRC Canada

Fig. 4. Comparison of experimental (filled squares) and calculated state-to-state rotational cross sections for full potentials. Thin solid lines, surface 1 (left panels), surface 2 (right panels); dashed lines, surface 3; thick solid line, surface 4.



may be attributed to the absence of the long-range component of the surfaces. At the highest collision energy, the agreement is improved for surface 4, while it is much worse for surfaces 1 and 2. A small deviation is also observed at $j' = 12$, which is unexpected since the other small transitions are in good agreement when only the repulsive term of the potential is included. Therefore, the analysis considering only the short-range contribution by comparing surfaces 1 and 2 and surface 4, shows that the core contribution of the repulsive force of surface 4 is accurate for low collision energy and even better for higher collision energies where, as expected, the core contribution increases. Although there is some satisfactory agreement with the experimental results of Loesch (10), the short-range contribution of surface 4 may be improved further, especially its tail, for low collision energies.

The cross sections calculated using surfaces 3 and 4 are compared (also only short-range contributions) in Fig. 3. The results for the highest $\Delta j'$s are not reproduced when only the contribution of repulsive potentials is taken into account. Although both surfaces show deviations at the lowest collision energy, especially for high Δj transitions, the agreement improves as the energy increases. As can be seen, the ab initio potential of Marshall et al. (12) (surface 3) fares better than surface 4 for the lowest collision energy, especially for high Δj's. The surface of Hutson and co-workers gives much better agreement with experiment at higher energies (0.11 and 0.19 eV) and for almost all rotational transitions. In particular, at 0.11 eV (the middle figure), there is no deviation at all for any of the results. It seems that the tail of the short-range component of surface 3 is better than that of surface 4, while the core of the latter is better than that of surface 3. In summary, the results shown in Figs. 2 and 3 may provide sufficient information to confirm that the short-range contribution, either of surface 3 or surface 4, may sufficiently explain the Ar−CO_2 repulsive interaction with surface 4 showing better agreement than surface 3.

Figure 4 compares the state-to-state cross sections for all surfaces (see Table 1) considering the full intermolecular potential, i.e., the contributions of both short- and long-range forces. On the whole, some improvements are observed in the agreement between the calculated and experimental cross sections. For example, at the lowest energy (top figure) surfaces 1 and 2 provide better agreement for the highest j' compared to the same cross section in Fig. 2. On the other hand, the cross section for $j' = 30$ (surface 1) has decreased in intensity, while at $j' = 24$ (surface 2) it has increased. At 0.11 eV, both surfaces 1 and 2 show improved agreement when compared to Fig. 2. However, at the highest collision energy the level of agreement is worse when the long-range contribution is taken into account. For surface 3 not only was there no marked improvement in agreement found when the long-range term was included, but also the level of agreement was decidedly worse at all collision energies. At low collision energies, especially, one should expect an improvement on the level of agreement, and the fact that this was not seen suggests that the attractive component of surface 3 may be incorrect. This confirms the conclusion in ref. 2 that this ab initio potential "provides a disappointing representation of the potential energy surface." For surface 4 there is improved agreement for the σ_{6-34} cross section at 0.069 eV, but the level of agreement worsens for other cross sections: for example, the cross section for $j' = 18$ is now worse than the result shown in

©2001 NRC Canada

Fig. 5. State-to-state rotational cross sections for experimental data (filled squares), surface 4 (solid line), and modified surface 4 (dot-dashed line) at the collision energy of 0.069 eV.

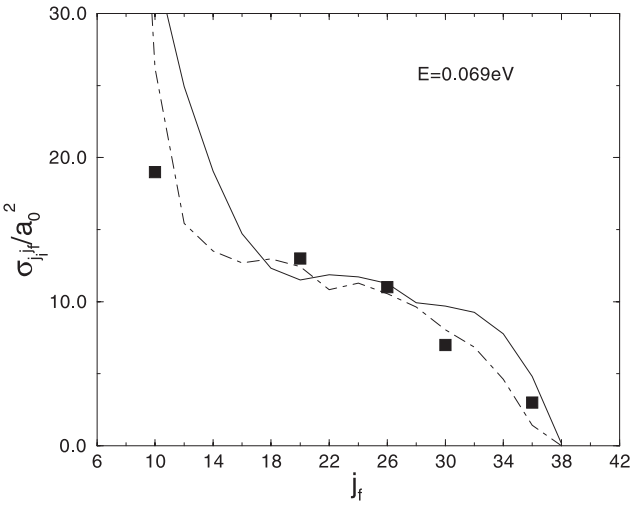


Fig. 6. State-to-state rotational cross sections for experimental data (filled squares), surface 4 (solid line), and modified surface 4 (dot-dashed line) at the collision energy of 0.19 eV.

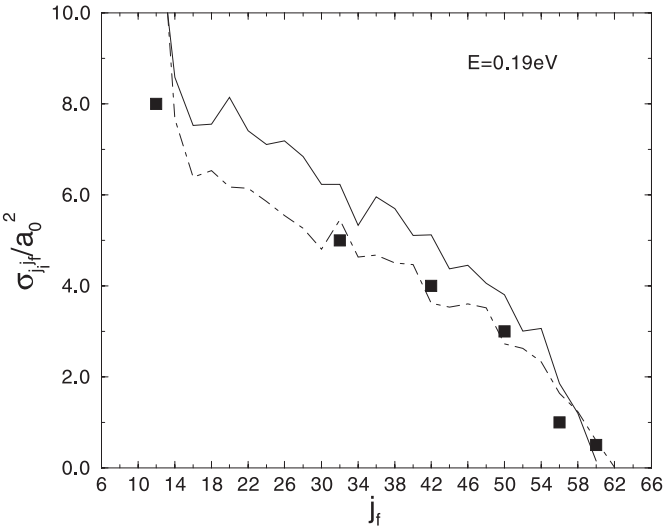


Fig. 2, as is also the case for $j' = 20$, $j' = 28$, and $j' = 30$. For each of these transitions the deviations between the calculated and experimental values are larger. Thus, the expectation that the level of agreement between the calculated and experimental results should be improved when the long-range component is taken into account has not been observed, and it appears that the long-range contribution of surface 4 is too strong. This is clearly observed for the three highest transitions, i.e., $j' = 26$, $j' = 30$, and $j' = 36$ at $E = 0.069$ eV. The values calculated for these cross sections using surface 4 lie below the experimental results in Fig. 2 while, in Fig. 4, the calculated cross sections calculated using the full surface 4 lie above the experimental cross sections. This suggests that better agreement might be achieved if the long-range component of surface 4 was to be modified.

For 0.11 eV, the calculated results are in good agreement with experimental with only one deviation, i.e., for $j' = 38$. The calculated value for this cross section was drastically reduced with the inclusion of the long-range component of the potential. While it appears again that the long-range contribution is too strong, it is less so than was observed for the collision energy 0.069 eV. For collision energy 0.19 eV an upwards shift is observed for all cross sections, but with the results remaining close to the experimental data of Loesch. Comparison of the cross sections for this energy in Figs. 2 and 4 indicates that the results using only the repulsive component of the potential were actually much better, with almost all calculated transitions in quantitative agreement with the experimental data. Inclusion of the long-range component in the calculations at the other two collision energies also gives worse comparisons. However, as stated in ref. 19, "no further work on improving the potentials at present" may be necessary, referring to surface 4. What is important to point out is that such a surface, obtained by fitting high-resolution spectroscopic data, seems to be the best surface available for reproducing a wide range of experimental data. This should also hold for scattering cross section data, but the results shown in Fig. 4 may indicate that the surface should be modified in order to obtain accurate state-to-state rotational cross sections as well, especially at higher collision energies.

We propose a modification of the surface of ref. 1 by introducing two additional parameters, specifically a short-range and a long-range parameter, in order to provide a surface that incorporates state-to-state rotational cross section data. A trial and error procedure discussed previously (26) has been applied to obtain values for these two parameters. Although we have not found a general surface with the present modification, much better agreement has been achieved for the rotational cross sections.

For analysing the agreement between the calculated scattering cross sections and the experimental data, surface 4 was chosen to be slightly modified, as described above. Although any modification of it may not be correct, especially if the attractive component of it is also changed, this modification may show that a simple modification of the fitting procedure of this surface may provide a global potential energy surface for completely describing the Ar–CO_2 interaction.

Figures 5 and 6 compare classical trajectory state-to-state rotational total cross sections for collision energies 0.069 and 0.19 eV, respectively. Calculations have been performed using the original surface 4 and a modification of it. As can be seen from Fig. 5, a single parameter introduced into the long-range contribution suffices to improve agreement with the experimental state-to-state rotational cross sections of Loesch (10) at 0.069 eV. The parameter reduces the Hutson et al. (1) long-range contribution by a factor 1.574 in order to produce the agreement shown in the figure: for example, at $j' = 20$ surface 4 (original) gives a calculated cross section of $11.5a_0^2$, while the modified surface 4 gives $12.4a_0^2$, which is in much better agreement with the experimental results. Further, the results obtained using surface 4 (original) show a small minimum in the cross sections between $j' = 18$ and $j' = 22$, whereas the results obtained using the modified surface show a small maximum that provides better agreement with the cross section at $j' = 20$. Moreover, while the cross sections calculated using surface 4 (original) show a broad maximum for $j' > 28$, those

©2001 NRC Canada

calculated using the modified surface 4 lie closer to the experimental measurements of Loesch (10): for example, the cross section calculated using the modified potential 4 is now much closer to the experimental cross section for $j' = 30$ than is that obtained with the original surface 4. As observed in this figure, there is a very good improvement in the potential 4. Therefore, if this single number was enough to provide better agreement, and if the collision energy increases, one might expect a lesser influence of the long-range component, hence a small number should be expected for 0.19 eV collision energy. Moreover, the present analysis seems to show that the short-range component of surface 4 is correct, since it was not modified at low energy.

Figure 6 compares the cross sections at collision energy 0.19 eV using surface 4 (original) and the modified surface 4. A preliminary analysis using only one parameter, as was done to generate the results shown in Fig. 5, did not provide accurate results, and it was deemed necessary to introduce a second parameter to control the short-range component of the interaction. In this case the short-range contribution was increased by 0.274, while the long-range force was reduced by a factor of 1.3. In general, the contribution of the attractive part of the potential decreases with increasing collision energy. However, by comparing the results in Fig. 5 (0.069 eV) and Fig. 6 (0.19 eV), such a behaviour appears to be not observed for the original potential (surface 4): it appears as if the long-range interaction has provided an upwards shift with increasing collision energy.

At this collision energy (0.19 eV), however, a change to the short-range component was also required. This collision energy is about 175% greater than the lowest collision energy (0.069 eV). The latter corresponds to approximately three times greater than the dissociation energy of the surface 4 for the T configuration and even greater at the linear approach. These values are certainly much greater at higher collision energies. Therefore, less influence of the long-range component for the higher energies would be expected. It is observed that there is a very small difference between the two multipliers. It is exactly the difference between the short-range parameter (1.574) used in the case of the results shown in Fig. 5 and the new value, 1.3, i.e., 0.274. The latter was needed to correct the short-range component of surface 4. Therefore, these multipliers show that as of yet there is no global potential energy surface for fully described Ar–CO_2 interaction. Although such a surface can describe several spectroscopic properties.

Normally, either the tail or the core contribution of the repulsive component could be responsible for such a shift. The inclusion of two parameters allowed better agreement to be attained between the experimental measurements of Loesch (10) and the classical trajectory state-to-state cross sections. As can be seen with the modified surface 4, all the classical trajectory results are in quantitative agreement with the experimental data. Moreover, the short-range factor introduced was able to increase the repulsive force, and this has pushed cross sections down, and hence, closer to the experimental results.

Finally, it is important to note that the modified surface has certainly changed the entire long-range contribution and, for the highest collision energy, also the short-range contribution, and as a consequence, the modified surface may no longer be able to reproduce most of the spectroscopic properties. One possibility, given that this modified potential was obtained by fitting to high-resolution experimental state-to-state rotational cross section data measured by Loesch (10), is to calculate spectroscopic properties with a high level of accuracy using the original surface or to perform collision studies using the modified version of the potential. When dealing with Ar−CO_2 rotational collisions at low energies, one can reduce only the long-range contribution by a factor of 1.574 or at high energies, one can use the short-range parameter (0.274) and also the long-range factor (1.3). This shows that the whole surface 4 was changed, and indeed it will not describe spectroscopic data, but it also shows that a simple modification during the fitting procedure may be done in order to improve the agreement with the scattering cross section experiments.

Although surface 4 has been shown to be highly accurate for spectroscopic properties (19), the present work shows that it is not accurate enough to reproduce some of rotational cross sections that are also sensitive to the potential as well as those properties shown in ref. 1. For example, the rainbow positions and the final rotational states of the molecule are drastically affected by the long-range terms of the interaction (27). Hence, a sensitive analysis of the angular distribution of the state-resolved differential cross sections may also contribute to improve the attractive term of the potential. The latter may not be sensible to the transport properties, but it is very sensitive to the repulsive and attractive components of the surface (27). Therefore, for almost all properties the surface of Hutson and co-workers is accurate enough, but it does not provide quantitative reproduction of all Ar−CO_2 rotational cross sections as analysed in the present study.

Concluding remarks

This work has mainly been concerned with analysing two recent potential energy functions (3 and 4) for describing the Ar–CO_2 system. Although a slight modification of the Hutson et al. (10) surface for studying rotational collisions was proposed, it is important to point out that their potential energy function may be the best surface available up to now without any modification for studying spectroscopy properties (19). On the other hand, for cross sections, the actual work has provided a critical analysis of the latest surfaces, with special attention given to the potentials 3 and 4.

The potential of Hutson and co-workers (19) is based on fitting procedures, and very recently a new potential has been calculated by Misquitta et al. (28) based on ab initio methods. Calculations of spectroscopic properties using the latter produced the same level of accuracy in some spectroscopic properties as the potential proposed in ref. 19. Therefore, according to the analysis shown in this paper, it is expected that this new ab initio potential will also produce poor results for rotational cross sections, but this needs to be tested.

Although it has been shown in this contribution that the agreement of scattering cross sections can be improved by introducing two parameters to multiply the short- and long-range components, it is clear that it is not the right suggestion, since the spectroscopic data will also change. This is even more drastically effected if the modification is mainly done in the attractive part of the surface. Nevertheless, the modified potential can better match the experimental measurements, and hence, one can see that it is indeed necessary to carry out further detailed analyses for future fitting procedures for the Ar–CO_2 system.

©2001 NRC Canada

Therefore, the present study may indicate that a new potential energy function could be fitted to match all the available data, i.e., spectroscopy and state-to-state cross sections. Nevertheless, a general surface has not been proposed, and it is clear that other studies are needed. The present paper showed that potential 4 can also be improved to match state-to-state cross sections with only two parameters.

Acknowledgements

We would like to thank Professor Jeremy Hutson and Professor M. Szczęśniak for providing their subroutines to calculate the potential energy functions. We are also in indebted to the unknown referee who pointed out many mistakes in our manuscript.

References

1. J.M. Hutson, A. Ernesti, M.M. Law, C.F. Roche, and R.J. Wheatley. J. Chem. Phys. **105**, 9130 (1996).
2. M.A. ter Horst and C.J. Jameson. J. Chem. Phys. **105**, 6787 (1996).
3. C.F. Roche, A. Ernesti, J.M. Hutson, and A.S. Dickinson. J. Chem. Phys. **104**, 2156 (1996).
4. R.K. Preston and R.T. Pack. J. Chem. Phys. **66**, 2480 (1977).
5. J.M. Steed, T.A. Dixon, and W. Klemperer. J. Chem. Phys. **70**, 4095 (1979).
6. R.N. Lichtenthaler and K. Schafer. Ber. Bunsen-Ges. (Phys. Chem. Chem. Phys.) **73**, 1525 (1969).
7. T.L. Cottrell, R.A. Hamilton, and R.P. Taubinger. Trans. Faraday Soc. **52**, 1530 (1956).
8. L.S. Bontuyan, A.G. Suits, B.J. Whitaker, and P.L. Houston. J. Phys. Chem. **97**, 6342 (1993).
9. A.P. Kalinin, V.N. Khromov, and V.R. Leonas. Mol. Phys. **47**, 811 (1982).
10. H.J. Loesch. Chem. Phys. **18**, 431 (1976).
11. G.A. Parker, R.L. Snow, and R.T. Pack. J. Chem. Phys. **64**, 1668 (1976).
12. P.J. Marshall, M.M. Szczęśniak, J. Sadlej, G. Chalasiński, M.A. ter Horst, and C.J. Jameson. J. Chem. Phys. **104**, 6569 (1996).
13. A.D. Buckingham, P.W. Fowler, and J.M. Hutson. Chem. Rev. **88**, 963 (1988).
14. A.R. Cooper and J.M. Hutson. J. Chem. Phys. **98**, 5337 (1993).
15. R.T. Pack. J. Chem. Phys. **60**, 633 (1974).
16. P. McGuire and D.J. Kouri. J. Chem. Phys. **60**, 2488 (1974).
17. E.J. Bohac, M.D. Marshall, and R.E. Miller. J. Chem. Phys. **97**, 4890 (1992).
18. A.M. Hough and B.J. Howard. J. Chem. Soc. Faraday Trans. **83**, 191 (1987).
19. C.F. Roche, A.S. Dickinson, A. Ernesti, and J.M. Hutson. J. Chem. Phys. **107**, 1824 (1997).
20. J.C. Belchior, N.H.T. Lemes, and J.P. Braga. Chem. Phys. Phys. Chem. **1**, 23 (1999).
21. S.D. Bosanac. Phys. Rev. A: At. Mol. Opt. Phys. **26**, 282 (1982).
22. S. Chapman and S. Green. J. Chem. Phys. **67**, 2317 (1977).
23. J.C. Belchior and J.P. Braga. Chem. Phys. **213**, 303 (1996).
24. S.D. Bosanac. Chem. Phys. Lett. **103**, 484 (1983).
25. J.C. Belchior, J.N. Murrell, and S.D. Bosanac. Mol. Phys. **77**, 727 (1992).
26. J.C. Belchior and J.P. Braga. Chem. Phys. **205**, 401 (1996).
27. J.R. Pliego, Jr., J.C. Belchior, and J.P. Braga. Phys. Rev. A: At. Mol. Opt. Phys. **54**, 2091 (1996).
28. A.J. Misquitta, R. Bukowski, and K. Szalewicz. J. Chem. Phys. **112**, 5308 (2000).

©2001 NRC Canada

Studies on the synthesis and properties of bischelating dioxotetraamine macrocycle, its metal complexes and thermodynamic stability in aqueous solution

Xun-Cheng Su, Zhi-Fen Zhou, Hua-Kuan Lin, Shou-Rong Zhu, Hong-Wei Sun, Guang-Hua Zhao, and Yun-Ti Chen

Abstract: A new route to obtain *C*-functionalized dioxotetraamine, in which two independent chelating groups 8-quinolinol and dioxotetraamine are included, is described. In addition, two trinuclear metal complexes are synthesized and fully characterized. The thermodynamic properties of the ligand and its respective metal complex were investigated by a potentiometric titration method. Coupled with UV spectra, the difference in affinities for copper ion between dioxotetraamine and 8-quinolinol in the new ligand are investigated and the results show that 8-quinolinol is a stronger donor group than the dioxotetraamine macrocycle in an aqueous solution. Over pH 3~11, 8-quinolinol interacts 100% with the copper ions while dioxotetraamine is only partially coordinated.

Key words: macrocycle, dioxotetraamine, 8-quinolinol, copper ion, stability constants.

Résumé : On décrit une nouvelle façon d'obtenir de la dioxotétraaamine *C*-fonctionnalisée dans laquelle on a inclus deux groupes chélatants indépendants, le 8-quinoléinol et la dioxotétraamine. De plus, on a synthétisé et complètement caractérisé deux complexes métalliques trinucléaires. Faisant appel à une méthode de titrages potentiométriques, on a étudié les propriétés thermodynamiques de chaque ligand et celles du complexe métallique correspondant. En se basant sur ces résultats et sur les spectres UV, on a étudié la différence dans les affinités pour l'ion cuivre entre la dioxotétraamine et le 8-quinoléinol dans le nouveau ligand; les résultats montrent que, en solution aqueuse, le 8-quinoléinol est un groupe donneur plus fort que le macrocycle dioxotétraamine. À des pH allant de 3 à environ 11, le 8-quinoléinol interagit à 100% avec l'ion cuivre alors que la dioxotétraamine n'est que partiellement coordiné.

Mots clés : macrocycle, dioxotétraamine, 8-quinoléinol, ion cuivre, constantes de stabilité.

[Traduit par la Rédaction]

Introduction

Macrocyclic polyamines are of great interest in the field of coordination chemistry and have been studied intensively in recent years (1) because they possess cavities capable of providing a favorable environment for transition metal ions. The strength of the ion binding is determined by ion size, macrocyclic cavity size, and ligand conformation (1b). Macrocyclic oxopolyamines are unique metal chelators, and their structure bears the dual features of macrocyclic polyamines and oligopeptides (2). Because of their important biological functions and some unusual properties, oxopolyamines have been extensively studied and their structural features in biological significance are well recognized (2). The two amide groups in macrocyclic dioxotetraamines, for example, are equivalent, but when coordinated to a 3*d* metal ion they can be dissociated successively. Furthermore, dioxotetraamines can stabilize higher states of some transition metals and have been developed as effective oxidants and biomimetic redox catalysts. The functionalization of macrocycles allows us to modify or introduce new properties into a ligand such that: (*i*) it can make the ligand more selective toward a metal ion; (*ii*) it can increase or decrease the thermodynamic stability and the kinetic inertness; (*iii*) it can change the solubility and extractability into an organic phase; or (*iv*) it can covalently attach the macrocycle to a polymeric support or to a protein (3). Functionalization can be achieved using either a carbon or a nitrogen atom of the ring as an attaching point. Generally, the modifications based on such macrocyclicmolecules have been focused on *N*-substituted pendant-arm groups, while the *C*-substituted research is relatively rare (4). The *C*-substituted derivatives have the advantage of not influencing the nature of the heteroatomic donor group and are ideal substituents. 8-Quinolinol is known to be a good chelating ligand and can form stable complexes with most metal ions. Moreover, being a fluorescent active group, the pendent-arm 8-quinolinol can facilitate the modification of macrocyclic hosts for easy detection by methods such as UV or fluorescence spectroscopy

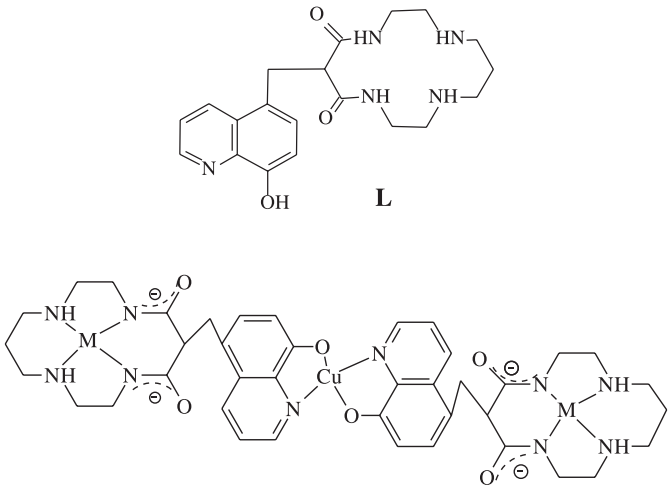
Received August 4, 2000. Published on the NRC Research Press Web site on March 15, 2001.

X.-C. Su, Z.-F. Zhou, H.-K. Lin[1], S.-R. Zhu, H.-W. Sun, G.-H. Zhao, and Y.-T. Chen. Department of Chemistry, Nankai University, Tianjin 300071, P. R. China.

[1]Corresponding author (fax: 0086–022–23502458; e-mail: hklin@nankai.edu.cn).

 DOI: 10.1139/cjc-79-2-221 © 2001 NRC Canada

Fig. 1. The structures of ligand (**L**) and its metal complexes.



(5). Therefore, in this paper we report a simple method to obtain an 8-quinolinol functionalized dioxotetraamine **(L)** (Fig. 1).

At given conditions two trinuclear metal complexes were prepared and fully characterized by FAB-MS, IR and electron paramagnetic resonance (EPR) spectroscopy, and elemental analysis. The stability constants of the ligand complexes with a proton and with copper(II) were studied by means of pH titration, along with UV spectroscopy. The affinity of 8-quninolinol and dioxotetraamine in the new ligand (**L**) to the copper(II) ion was compared and the results show that for Cu^{2+}, 8-quninolinol is a stronger donor group than dioxotetraamine macrocycle, and at 1:1 molar ratio (M:**L**) the former binds 100% to the metal ions while the dioxotetraamines are only partially coordinated.

Experimental

Synthesis

8-Quinolinol and diethyl malonate were purchased from Aldrich and The Chinese Academy of Martial and Medical Science, respectively. All other chemicals were of analytical reagent grade, and were used without further purification. The Fourier-transform IR spectra were taken on a FT-IR 170SX (Nicolet) spectrometer. Elemental analyses were made on a Perkin-Elmer 240C analyzer. MS was conducted on VG ZAB-HS instrument. Proton NMR spectra were recorded on a Bruker AC-P200 spectrometer operating at 200 MHz at 25°C in $CDCl_3$ or DMSO-d_6 solution with tetramethylsilane as the internal reference. Electronic absorption spectra were obtained from a Shimadzu UV-240 spectrophotometer. The compound 5-chloromethyl-8-quinolinol hydrogen chloride was prepared according to literature (6).

5-[(2,2-Bisethoxycarbonyl)ethyl]-8-quinolinol: A mixture of 5-chloromethyl-8-quinolinol hydrogen chloride (1.56 g, 6.8 mmol), diethyl malonate (1.07 g, 8.2 mmol), and anhyd K_2CO_3 (2.35 g, 17 mmol) in dry DMF (30 mL) was stirred at room temperature under a nitrogen atmosphere. After three days, the mixture was filtered, and the residue was thoroughly washed with DMF. The combined organic extracts were concentrated in vacuum to afford a light yellow oil, which was purified by column chromatography over silica gel eluting with EtOAc–C_6H_{12} (1:4) to give **2**, as colorless crystals (yield ≈ 40%), mp 77.5–78.0°C. FT-IR (KBr pellet) cm^{-1}: 3356, 1729 ($\nu_{C=O}$), 1256, 1202. ^1H NMR ($CDCl_3$) δ: 1.12–1.19 (br s, 6H), 3.54–3.68 (m, 3H), 4.07–4.14 (m, 4H), 7.03–8.77 (m, 6H). Anal. calcd. for $C_{18}H_{19}NO_5$: C 64.35, H 5.99, N 4.41; found: C 64.62, H 6.16, N 4.47.

Ligand L: 5-[2,2-bis(ethoxycarbonyl)]ethyl]-8-quinolinol (2.57 g, 8 mmol) was dissolved in absolute ethanol (300 mL) and then an equivalent amount of polyamine was added slowly with constant stirring. The resulting mixture was kept of reflux under N_2 for about two weeks. Then the reaction solution was concentrated to 20 mL and the product was precipitated in the refrigerator. The isolated yellow solid was washed with cold ethanol three times to afford the pure ligand (yield 24%). CI-MS *m*/*z*: 386.3 $[M + 1]^+$. FT-IR (KBr pellet) cm^{-1}: 3340, 2931, 1672 ($\nu_{C=O}$), 1624, 1473. ^1H NMR (DMSO-d_6) δ: 1.50 (m, 2H), 2.49–2.83 (br s, 4H), 3.33–3.60 (br s, 11H), 6.95 (m, 1H), 7.18 (m, 1H), 7.54 (m, 2H), 8.42 (m, 1H), 8.80 (m, 1H). Anal. calcd. for $C_{20}H_{27}N_5O_3 \cdot 0.5H_2O$: C 60.90, H 7.15, N 17.75; found: C 61.12, H 7.45, N 17.55.

Complex 1 ($L_2 \cdot Cu_3$): A solution of $Cu(OOCMe)_2$ (0.136 g, 0.75 mmol) in H_2O (10 mL) was added dropwise over 20 min to the methanol solution of **L** (0.197 g, 0.5 mmol) with constant stirring and the pH was adjusted to pH 6~7 with NaOH. The mixture was stirred for another hour and then concentrated to 10 mL. After cooling the product was filtered off and washed with acetone three times and dried in vacuum (yield 50%). FAB-MS *m*/*z*: 956 $[Cu_3L_2 + H]^+$. FT-IR (KBr pellet) cm^{-1}: 3396, 3243, 1640, 1581 ($\nu_{C=O}$), 1506. UV (ε, mol dm^{-3} cm^{-1}): 5.69×10^3 (400 nm, MeOH), 2.27×10^3 (340 nm, MeOH). Conductivity (Ω^{-1} dm^{-3} cm^{-1}): 3.43 (10^{-3} mol dm^{-3} in DMSO at 25°C). Anal. calcd. for $C_{40}H_{54}N_{10}O_6Cu_3 \cdot 9H_2O$: C 42.99, H 5.91, N 12.54; found: C 42.82, H 5.60, N 12.65.

Complex 2 ($L_2 \cdot Cu \cdot Ni_2$): A solution of $Cu(OOCMe)_2$ (0.045 g, 0.25 mmol) in H_2O (10 mL) was added to the 20 mL methanol solution of **L** (0.195 g, 0.5 mmol) with stirring. After 10 min, $Ni(ClO_4)_6 \cdot 6H_2O$ (0.186 g, 0.5 mmol) in H_2O (10 mL) was added dropwise and then a small amount of NaOH was added. The stirring was continued for 10 h and then pH was adjusted to about 8.0. The resulting solution was concentrated to 10 mL and the product was precipitated. The yellow-green solid was filtered and washed with acetone and dried in vacuum (yield 54%). FAB-MS *m*/*z*: 944 $[CuNi_2L_2 + H]^+$. FT-IR (KBr pellet) cm^{-1}: 3386, 3215, 1640, 1576 ($\nu_{C=O}$), 1556. UV (ε, mol dm^{-3} cm^{-1}): 5.70×10^3 (400 nm, MeOH), 3.29×10^3 (340 nm, MeOH). Conductivity (Ω^{-1} dm^{-3} cm^{-1}): 6.61 (10^{-3} mol dm^{-3} in DMSO at 25°C). Anal. calcd. for $C_{40}H_{54}N_{10}O_6CuNi_2 \cdot 6H_2O$: C 45.59, H 5.74, N 13.29; found: C 45.59, H 5.96, N 13.49.

Potentiometric titrations

Potentiometric equilibrium measurements of the ligands in the absence or presence of Cu(II) ions were carried out with a Beckman pH meter (Model Φ71) equipped with a type 39841 combination electrode. Typical concentrations of

© 2001 NRC Canada

Table 1. Protonation constants of the macrocyclic dioxotetraamines.

	log K_1	log K_2	log K_3	log K_4
L	9.86 ± 0.03	9.35 ± 0.02	5.79 ± 0.05	4.55 ± 0.02
Dioxocyclam[a]	9.67	5.90		

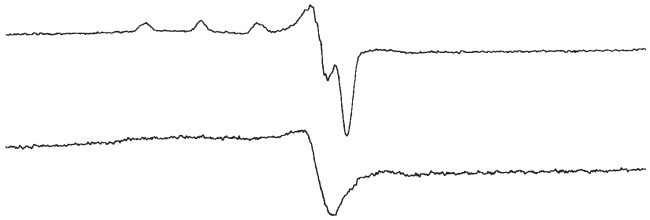
Note: I = 0.10 mol dm^{-3} $NaNO_3$ at 25 ± 0.1°C.
[a]Reference 2*e*.

Table 2. Overall stability constants of metal chelates.

	L
log β_{11-2}	3.97 ± 0.11
log β_{11-1}	13.49 ± 0.07
log β_{110}	18.56 ± 0.10
log β_{112}	27.64 ± 0.05
pH range	2.9~10.3

Note: Molar ratio of **L**:copper ion (1:1).

Fig. 2. EPR spectra of $[CuNi_2L_2]$ (top) and $[Cu_3L_2]$ (bottom). Experimental conditions: 1 mmol dm^{-3} solution in MeOH, T = 110 K (mid range, 3300G; scan range, 2000G; scan time, 100 s).



experimental solutions were 1 × 10^{-3} mol dm^{-3} of ligand with equal molar concentrations of metal ion. The ligand was dissolved in an adequate amount of dilute HNO_3 (about 3 equiv) and then titrated with 0.1 mol dm^{-3} NaOH. Redistilled (in quartzware) H_2O was used for preparing all the solutions. $NaNO_3$ and $Cu(NO_3)_2$ were recrystallized with redistilled H_2O before use. The concentrations of Cu^{2+} in the stock solution were analyzed by EDTA titration methods. The ionic strength was adjusted to 0.1 mol m^{-3} with $NaNO_3$. All titrations were carried out under N_2 at 25°C. Computations of equilibrium constants were made using a program based on the improved TITFIT technique (7). Species-distribution curves were calculated and plotted with the DP program (7). For each system at least two titrations were performed, and each titration contained about 45 experimental points. Table 1 illustrates the protonation constants of the ligand **L**.

Coordinating tendencies of **L** toward aq Cu(II) ions was investigated by means of pH titrations with a standard base solution containing the ligand and $Cu(NO_3)_2$ in equivalent amounts plus excess acid (about 3 equiv). The titration curves were simulated with a computer program and the complex species present at equilibrium were chosen and their equilibrium constants were refined to the best curve fitting. In the following text, each species will be denoted by (p, q, r) where: p is the stoichometric coefficient of the metal in the complex, q that of the ligand, and r that of the hydrogen ions. A negative value of r indicates that the complex has released a proton (for instance, from the amide group of the ligand or from the coordinated H_2O). The stability constants of the ligands with the metal ion (Cu(II)) are listed in Table 2, and titration and distribution curves are shown in Figs. 3 and 4.

Results and discussion

Synthesis of ligand and metal complexes

Starting from 5-chloromethyl-8-quinolinol hydrogen chloride that is easily prepared, the preparation of **L** involves two simple steps and does not require the use of chromatography. In our work, the novel preparation of cyclic dioxotetraamine has a significant advantage in that any desirable substituent can be introduced on the carbon atom of the macrocyclic skeleton. In addition, the size of the macrocycle can be changed easily by judicious choice of the linear tetraamine. Moreover, the 8-quinolinol substituted macrocycle has two independent chelating groups and both can form metal complexes; therefore, the modified macrocycle possesses advantageous properties over the dioxotetraamine in coordination chemistry, especially for the generation of polymeric complexes.

It is known that when dioxotetraamine reacts with a transition metal ion such as Cu^{2+} or Ni^{2+}, each amide group will dissociate a proton in an effort to form more stable complexes (2). The absorption spectra of metal oxinate complexes have been studied extensively (8) and, therefore, the absorption spectra can be used to investigate whether the metal ion is coordinated to 8-quinolinol and if it is chelated to the macrocycle. In our work, the electronic absorption of these metal complexes (λ ~ 400 nm) is characteristic of a copper oxinate complex and it can be concluded that in the two trinuclear complexes each metal ion binds two 8-quinolinol moieties. IR results show that the C=O absorption decreases from 1672 cm^{-1} in the free ligand to 1581 and 1576 cm^{-1} in the complexes $[CuL_2]$ and $[CuNi_2L_2]$, respectively, indicating that the protons dissociate from the amide groups, and the amido nitrogen atoms coordinate to the metal ion. The molar conductivities in DMSO at 25°C for the trinuclear metal complexes **1** and **2** are 3.43 × 10^{-3} and 6.61 × 10^{-3} mol dm^{-3}, respectively, demonstrating that both metal complexes are neutral (9). FAB-MS results (956.2 [**1** + H]$^+$ and 944.2 [**2** + H]$^+$) further establish the formation of the trinuclear metal complexes. The EPR spectra of $[Cu_3L_2]$ and $[CuNi_2L_2]$ are similar, with $[Cu_3L_2]$ exhibiting much broader peaks, indicating a similar coordinating structure of the copper complex (Fig. 2). In methanol glass at 110 K, the EPR spectrum of $[Cu_3L_2]$ is too broad and no characteristic absorption is observed. This probably indicates that there is dipole–dipole coupling between the metal centers in $[Cu_3L_2]$ spectrum, which is different from that of $[CuNi_2L_2]$. These result reveals that the dioxotetraamine macrocyclic groups in metal complexes such as $[Cu_3L_2]$ are not parallel but instead

© 2001 NRC Canada

Fig. 3. Titration curves of ligand (**L**) and its copper(II) complex with base: (*a*) 0.001 mol dm^{-3} **L**, (*b*) 0.001 mol dm^{-3} **L** and 0.001 mol dm^{-3} $Cu(NO_3)_2$. **B**/**L** is the ratio of mol of standard base (**B**) added to the mol of ligand (**L**).

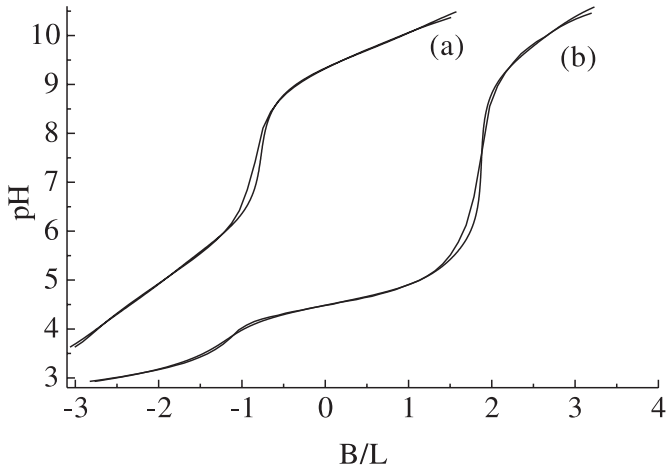
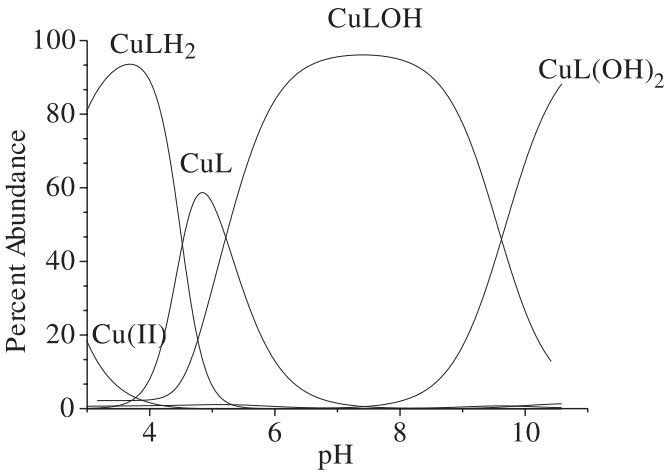


Fig. 4. Species distribution curve for copper(II) complexes of **L** (1:1 molar ratio) as a function of pH in 0.1 mol dm^{-3} $NaNO_3$ solution at 298.15 K.



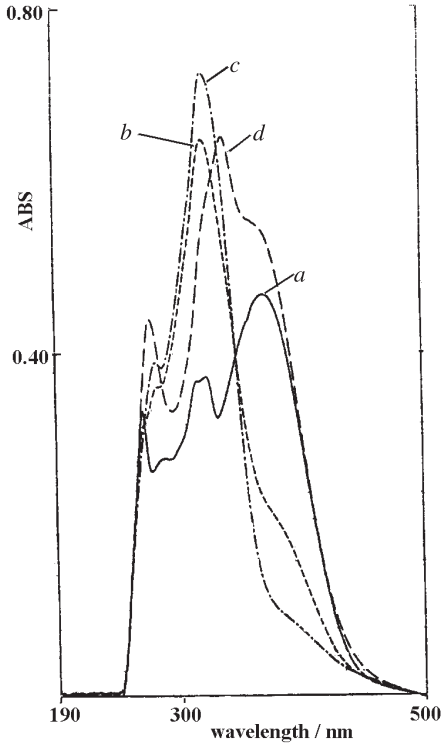
are at an angle and interact with each other through dipole–dipole forces (10).

Thermodynamic properties

The acid-base behavior of the ligand in aq $NaNO_3$ (0.1 mol dm^{-3}) at 25°C has been investigated through pH titration. Figure 3 shows the titration curves of **L** and its copper(II) complex. Figure 4 shows the distribution curves of metal complex species. In the pH range investigated (ca. 3–11), the dioxotetraamine can bind four protons, presumably two at the amine groups and two at the oxygen and nitrogen atoms of 8-quinolinol. The stepwise protonation equilibria constants have been determined and are shown in Table 1. For comparison, log *K* values of the stepwise protonation equilibra of a similar 14 membered macrocycle, dioxocyclam (2*e*), are also reported.

For macrocyclic dioxotetraamine, K_1 is the protonation constant for the phenolate. The value is somewhat lower

Fig. 5. UV–vis absorption spectra (25°C) of **L** (2.975×10^{-4} mol dm^{-3}) at different pH: (*a*) 2.82, (*b*) 4.88, (*c*) 7.29, (*d*) 10.04.

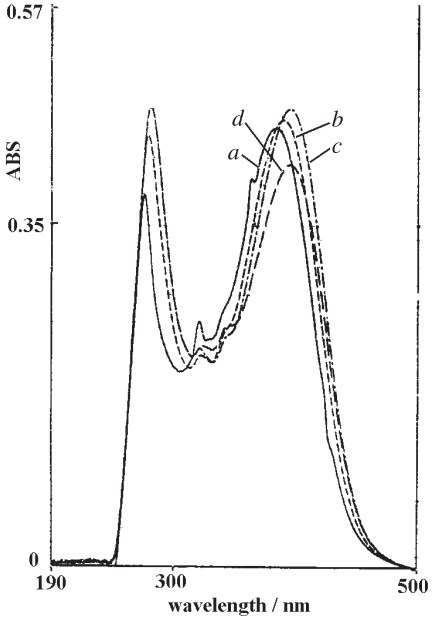


than that of free 8-quinolinol (log K_1 = 11.20) (11), which can be attributed to solvent effects since the free 8-quinolinol is insoluble in water and its protonation constants were determined in 1,4-dioxane–water. K_2 and K_3 are assigned to be the protonation constants of the macrocycle, which are similar to those of dioxocyclam, while K_4 can be attributed to the nitrogen atom of 8-quinolinol.

The incorporation of Cu(II) by the ligand (**L**) in aqueous solution was studied to identify the species formed and to evaluate the complexation constants of these compounds (Fig. 4). In fact, 8-quinolinol and the dioxotetraamine macrocycle are both strong chelating agents for many transition metal ions, especially copper(II), however, the two chelators cannot bind simultaneously to the same metal ion. In other words, if the metal ion lies in the dioxotetraamine cavity, 8-quinolinol can not act as a bidentate ligand and bind to the same metal ion due to the intrinsic strain of **L**. Likewise if 8-quinolinol chelates to a metal ion, the same metal ion can not promote the deprotonation of the dioxotetraamine amide to enter into its cavity. Therefore, if the ligand:metal molar ratio is 1:1, there are two possible modes of coordination: (*i*) 8-hydroxyquinoline is 100% coordinated to the copper ion; (*ii*) dioxotetraamine is incorporating the copper ion. Since the UV absorption of 8-quinolinolato copper complex differs greatly from that of free 8-quinolinol, the complex can be easily detected using UV spectroscopy. Consequently, the UV spectra of free ligand (**L**) and its copper complex were studied by varying the pH. Titrations, monitored by UV–vis spectroscopy, of free ligand (**L**) and its copper complex are shown in Figs. 5 and 6, respectively. The UV–vis absorption of **L** varies with

© 2001 NRC Canada

Fig. 6. UV–vis absorption spectra (25°C) of **L** (2.081×10^{-4} mol dm^{-3}) and Cu(II) (2.081×10^{-4} mol dm^{-3}) at different pH: (*a*) 3.02, (*b*) 4.84, (*c*) 7.50, (*d*) 10.01.



an increase in pH, which implies that the depronation of 8-quinolinol affects the electronic spectrum (Fig. 5). In case of the copper(II) complex, the UV–vis absorption is very similar to that of 8-quinolinol copper complex and exhibits only small changes with an increase in pH (Fig. 6), implying that in a 1:1 (molar ratio) metal complex, 8-quinolinol acts as bidentate group and chelates 100% to the copper ion over pH 3~10. Consequently, the dioxotetraamine can only be partially coordinated, and hence, 8-hydroxyquinoline is a stronger donor group than the dioxotetraamine macrocycle in **L**. And thus, it can be concluded that while titrating 8-quinolinol is 100% coordinated. The pH titrations provide a better tool for indicating the relative affinity of the ligand for H^+ or Cu^{2+}. If the metal's binding affinity to ligand is stronger than that of proton, the protonation constant of the ligand in the metal complex will be smaller than that of free ligand. From Tables 1 and 2, it is evident that the sum of the dioxotetraamine's protonation constants ($\log (\beta_{112}/\beta_{110}) = 9.08$) in the copper complex is much smaller than that of free **L** ($\log (K_2K_3) = 15.14$), implying that the dioxotetraamine behaves as a donor group. As discussed above, the dioxotetraamine actually interacts with copper ion, but the copper ion does not promote the deprotonation of dioxotetraamines's amides to enter into its cavity. Using these results, along with the UV–vis spectra, we can speculate as to the structure of the species at different stages of the pH titration. In the positively charged complex $(CuLH_2)^{3+}$ (112), 8-quinolinol chelates to the copper ion and the dioxotetraamine is doubly protonated. As the pH increases, the protonated amine groups in dioxotetraamine will be deprotonated and interact with Cu through a coordination bond, resulting in the formation of CuL (110) (pH ca. 4.5). When the pH is increased further, CuLOH (11–1) and $CuL(OH)_2$ (11–2) will be formed, which can be attributed to the deprotonation of coordinated water molecules. Notably, the CuLOH, in which OH^{-1} coordinates to copper ion, is very stable over pH 6–8 where metal catalysts play their role most efficiently.

In conclusion, we present a new route to obtain the *C*-functionalized macrocycles that include an 8-quinolinol group as a bidentate pendant arm. The results show that the new ligand can form trinuclear complexes using two independent chelators: 8-quinolinol and dioxotetraamine. 8-Quinolinol is a stronger donor group than dioxotetraamine and at a metal:ligand molar ratio of 1:1, where 8-quinolinol is 100% bound to copper ion while dioxotetraamine is only partially interacting with copper through coordination bonds.

Acknowledgments

This project (29971018) was supported from the National Natural Science Foundation of China, the Nature Science Foundation of Tianjin, and the National Key Laboratory of the Coordination Chemistry, Nanjing University.

References

1. (*a*) A. Bencini, A. Bianchi, P. Paoletti, and P. Paoli. Coord. Chem. Rev. **120**, 51 (1991); (*b*) V.J. Thom, C.C. Fox, and J.C.A. Boeyens. J. Am. Chem. Soc. **106**, 1953 (1984).
2. (*a*) R.W. Hay, M.P. Pujari, and F. McLaren. Inorg. Chem. **23**, 3033 (1984); (*b*) L. Fabbrrizzi, T.A. Kaden, A. Perotti, B. Seghi, and L. Siegfried. Inorg. Chem. **25**, 321 (1986); (*c*) M.B. Inoue, C.A. Villegas, K. Asano, M. Nakamura, M. Inoue, and Q. Fernando. Inorg. Chem. **31**, 2480 (1992); (*d*) H. Sigel and R.B. Martin. Chem. Rev. **82**, 385 (1982); (*e*) S. Zhu, F. Kou, H. Lin, C. Lin, M. Lin, and Y. Chen. Inorg. Chem. **35**, 5851 (1996).
3. P.V. Bernhardt and G.A. Lawarance. Coord. Chem. Rev. **104**, 297 (1990).
4. (*a*) T.A. Kaden. Topics Curr. Chem. **121**, 157 (1984); (*b*) R.W. Hay. Current Topics in Macrocyclic Chemistry in Japan. Hiroshima School of Medicine, Hiroshima, Japan. 1987. p 56.
5. A.V. Bordunov, J.S. Bradshaw, X.X. Zhang, K.N. Dallely, X. Kou, and R.M. Izatt. Inorg. Chem. **35**, 7229 (1996).
6. M. Kolobielski. J. Heterocycl. Chem. **3**, 275 (1966).
7. H.W. Sun. Ph.D.Thesis. Nankai University, Tianjin, China. 1998.
8. K. Sone. J. Am. Chem. Soc. **75**, 5207 (1953).
9. W.J. Geary. Coord. Chem. Rev. **7**, 81 (1971).
10. P.V. Bernhardt and L.A. Jones. Chem. Commun. 665 (1997).
11. R.L. Stevenson and H. Freiser. Anal. Chem. **39**, 1354 (1967).

© 2001 NRC Canada

Formation of heterocyclic arylboronates by thermally induced 1,4-aryl migration in diarylboron chelates of *C*-(1-hydroxyalkyl)nitrones. Crystal and molecular structures of some of the rearrangement products and of one of the educts[1]

Wolfgang Kliegel, Gottfried Lubkowitz, Jens O. Pokriefke, Steven J. Rettig, and James Trotter

Abstract: Synthesis of heterocyclic arylboronates has been carried out by thermally induced rearrangement of diarylboron chelates of *C*-(1-hydroxyalkyl)nitrones. The structures have been determined from spectroscopic data and from X-ray analyses. Thermoanalytical and time-dependent NMR measurements give information on the nature of the isomerization reaction. Crystal data (at 293 K for **2j**, 180 K for the others): **1m**, monoclinic, $P2_1/n$, a = 14.059(3), b = 12.5531(13), c = 14.8531(6) Å, β = 95.8067(12)°, Z = 4; **2j**, triclinic, $\bar{P}1$, a = 10.4729(11), b = 13.5896(11), c = 9.5803(7) Å, α = 104.764(6), β = 103.279(7), γ = 107.278(7)°, Z = 2; **2m**, monoclinic, $P2_1/n$, a = 14.9442(13), b = 11.990(2), c = 16.0613(4) Å, β = 114.0153(7)°, Z = 4; **9**, monoclinic, $P2_1/n$, a = 11.123(2), b = 18.433(3), c = 13.4852(4) Å, β = 108.2075(7)°, Z = 4. The structures were solved by direct methods and refined by full-matrix least-squares procedures to $R(F, I \geq 3\sigma(I))$ = 0.036, 0.052, 0.043, and 0.040, respectively, for AFC6 data for **2j** and CCD data for **1m**, **2m**, and **9**. All four molecules contain six-membered OBONCC rings, with an approximately planar ON=CC segment in the educt **1m** and approximately planar OBOC segments in the rearrangement products. A probable transition state geometry is derived for the isomerization process.

Key words: diarylboron chelates, *C*-(1-hydroxyalkyl)nitrones, heterocyclic arylboronates, organoboron compounds, rearrangement, crystal structures.

Résumé : On a réalisé la synthèse d'arylboronates hétérocycliques par le biais d'un réarrangement induit de façon thermique de chélates diarylbores de *C*-(1-hydroxyalkyl)nitrones. On a déterminé les structures à l'aide de données spectroscopiques et d'analyses de diffractions des rayons X. Des mesures thermoanalytiques et de RMN faites en fonction du temps permettent d'obtenir des informations sur la nature de la réaction d'isomérisation. Données cristallographiques (à 293 K pour **2j** et 180 K pour les autres): **1m**, monoclinique, $P2_1/n$, a = 14,059(3), b = 12,5531(13) et c = 14,8531(6)Å, β = 95,8067(12)°, Z = 4; **2j**, triclinique, $\bar{P}1$, a = 10,4729(11), b = 13,5896(11) et c = 9,5803(7)Å, α = 104,764(6), β = 103,279(7) et γ = 107,278(7)°, Z = 2; **2m**, monoclinique, $P2_1/n$, a = 14,9442(13), b = 11,990(2) et c = 16,0613(4)Å, β = 114,0153(7)°, Z = 4; **9**, monoclinique, $P2_1/n$, a = 11,123(2), b = 18,433(3) et c = 13,4852(4)Å, β = 108,2075(7)°, Z = 4. On a résolu les structures par des méthodes directes et on les a affinées par la méthode des moindres carrés (matrice entière) jusqu'à des valeurs de ($R(F, I \geq 3\sigma(I))$ = 0,036, 0,052, 0,043 et 0,040 respectivement pour les données AFC6 pour **2j** et pour les données CCD pour **1m**, **2m** et **9**. Les quatre molécules comportent des cycles OBONCC à six chaînons pour lesquels l'éduit **1m** comporte un segment ON=CC approximativement planaire et des segments OBOC approximativement planaires dans les produits de réarrangement. On a déduit une géométrie probable de l'état de transition du processus d'isomérisation.

Mots clés : chélates diarylbores, *C*-(1-hydroxyalkyl)nitrones, arylboronates hétérocycliques, composés organiques du bore, réarrangement, structures cristallines.

[Traduit par la Rédaction]

Received October 10, 2000. Published on the NRC Research Press Web site on March 15, 2001.

W. Kliegel, G. Lubkowitz, and J.O. Pokriefke. Institut für Pharmazeutische Chemie der Technischen Universität Braunschweig, Beethovenstrasse 55, 38106 Braunschweig, Germany.
S.J. Rettig and J. Trotter.[2] Department of Chemistry, University of British Columbia, 2036 Main Mall, Vancouver, BC V6T 1Z1, Canada.

[1]Structural studies of organoboron compounds LXXIII. This is the final paper in this collaborative series and is dedicated by W.K. and J.T. to the memory of their dear friend and colleague, Steven J. Rettig, who died on 27 October 1998. Previous paper in this series: ref. 1.

[2]Corresponding author (e-mail: jtrt@xray4.chem.ubc.ca).

 DOI: 10.1139/cjc-79-2-226 © 2001 NRC Canada

Introduction

In previous work (1), we described the synthesis of various diarylboron chelates derived from *N*-alkylnitrones of 2-hydroxycarbaldehydes and 2-hydroxyketones. The six-membered cyclic B,N-betaine structure **1** was postulated from elemental analyses and spectroscopic data of the crystalline compounds. Some of these compounds were very sensitive towards thermal stress and could not be recrystallized from heated solvents; nuclear magnetic resonance (NMR) spectra of solutions of these materials also indicated the presence of some rearrangement products. Other examples of **1**, however, were stable and could be recrystallized even from boiling solvents.

In this work, we describe the results of an investigation of this rearrangement and its products. The supposed molecular structure of educts and products is corroborated by X-ray crystallographic analyses of one of the diarylboron chelates **1** and several of the isomeric arylboronates **2**.

Experimental

General procedures

The synthesis of the compounds **1** was described previously (1), with the exception of **1k** and **1n**, which were obtained as mixtures with the corresponding rearrangement products (see below).[3] All reactions were carried out under normal conditions, without protective gas atmosphere. Melting points (uncorrected): Linström apparatus and Büchi SMP 20. IR: PYE-Unicam SP 3–200, Philips PU 9800 FT-IR Spectrometer, V 3.00, and ATI Mattson Genesis Series FT-IRTM Rev. I. ^{1}H NMR: Varian EM 390 and Bruker AM 400. ^{11}B NMR: Bruker AC 200. Elemental analyses: Carlo Erba CHNO elemental analyzer 1106; boron and chlorine titrimetrically after Schöniger-oxidation with Methrom Potentiograph E 536/Dosimat 655. Differential scanning calorimetry: Perkin Elmer DSC 2 with standard measuring head 319–0006 and Thermal Analysis DATA Station 3600, N_2 gas (1.5 bar; 1 bar = 100 kPa) for rinsing; Seiko DSC 220 with disk station SSC 5200 H; measurement of test samples (3–5 mg) in cold-welded aluminum pots, standard heating rate of 5°C min^{-1}; calibration with In and Sn; diagram: mW (y), temp.°C (x); sample time 0.4 s. Thermo-Gravimetry and Differential Thermoanalysis: Seiko TG/DTA 220 with disk station 5200 H; measurement of test samples (2–3 mg) in open aluminum pots, heating rate of 5°C min^{-1}; calibration with In and Sn; diagram: DTA μV (y_1), TG % mass loss (y_2), temp. °C (x); sample time 0.4 s.

4,6-Dimethyl-2,5-diphenyl-1,3-dioxa-4-aza-2-boracyclohexane (2a)

1a (1) (0.53 g, 2 mmol) is refluxed in 30 mL of toluene for about 10 min until test samples of the solution no longer gave a blue color reaction with diphenylcarbazone, indicating absence of an intact diphenylboron moiety (1, 2).[4] The solvent is distilled off in vacuo, and the remaining colored oil is dissolved in a small amount of ethanol. Upon cooling, down to –18°C, colorless crystals are obtained and recrystallized from absolute ethanol. Yield: 0.31 g (58%) of colorless needles, mp 77–78°C. IR (KBr, cm^{-1}): 1600 (C=C), 1310 (B-O); ^{1}H NMR (90 MHz, $CDCl_3$–TMS) δ: 1.08 (d, J = 7 Hz, C-CH_3), 2.56 (s, N-CH_3), 3.18 (d, J = 9 Hz, N-CH-C), 4.39 (m, O-CH), 7.07–7.31 (m, 8 aromatic H), 7.58–7.73 (m, 2 aromatic H). Anal. calcd. for $C_{16}H_{18}BNO_2$: C 71.94, H 6.79, B 4.05, N 5.24; found: C 71.83, H 6.83, B 4.10, N 5.25.

4-*tert*-Butyl-6-methyl-2,5-diphenyl-1,3-dioxa-4-aza-2-boracyclohexane (2b)

1b (0.31 g, 1 mmol) is reacted as described above for **2a** (about 15 min). Yield: 0.20 g (65%) of colorless needles, mp 122–123°C. IR (KBr, cm^{-1}): 1600 (C=C), 1310 (B-O); ^{1}H NMR (90 MHz, $CDCl_3$–TMS) δ (ppm): 1.02 (d, J = 7 Hz, CH_3C-O), 1.06 (s, C(CH_3)$_3$), 3.66 (d, J = 8 Hz, N-CH), 4.42 (m, O-CH), 7.19–7.42 (m, 8 aromatic H), 7.68–7.88 (m, 2 aromatic H). Anal. calcd. for $C_{19}H_{24}BNO_2$: C 73.80, H 7.82, N 4.53; found: C 73.82, H 7.83, N 4.41.

4-Benzyl-6-methyl-2,5-diphenyl-1,3-dioxa-4-aza-2-boracyclohexane (2c)

1c (0.34 g, 1 mmol) is reacted as described above for **2a** (about 20 min). Yield: 0.22 g (64%) of colorless crystals, mp 119°C. IR (KBr, cm^{-1}): 1600 (C=C), 1308 (B-O); ^{1}H NMR (90 MHz, $CDCl_3$–TMS) δ: 1.09 (d, J = 7 Hz, CH_3C-O), 3.48 (d, J = 9 Hz, O-C-CH), 3.60 (d, J = 14 Hz, N-CH_2), 4.50 (m, O-CH), 7.24–7.43 (m, 13 aromatic H), 7.68–7.74 (m, 2 aromatic H). Anal. calcd. for $C_{22}H_{22}BNO_2$: C 76.99, H 6.46, B 3.15, N 4.08; found: C 77.04, H 6.54, B 3.16, N 4.05.

4-Benzhydryl-6-methyl-2,5-diphenyl-1,3-dioxa-4-aza-2-boracyclohexane (2d)

1d•C_2H_5OH (0.23 g, 0.5 mmol) is reacted as described above for **2a** (about 20 min). Yield: 0.18 g (86%) of colorless crystals, mp 144–145°C. IR (KBr, cm^{-1}): 1600 (C=C), 1310 (B-O). ^{1}H NMR (90 MHz, $CDCl_3$–TMS) δ: 1.02 (d, J = 7 Hz, CH_3C-O), 3.41 (d, J = 8 Hz, O-C-CH), 4.48 (m, O-CH), 5.03 (s, N-CH(aryl)$_2$), 7.10–7.51 (m, 18 aromatic H), 7.58–7.75 (m, 2 aromatic H). Anal. calcd. for $C_{28}H_{26}BNO_2$: C 80.20, H 6.25, N 3.34; found: C 80.30, H 6.27, N 3.43.

4, 5, 6-Trimethyl-2,5-diphenyl-1,3-dioxa-4-aza-2-boracyclohexane (2e)

1e (0.56 g, 2 mmol) is reacted in 10 mL of benzene as described above for **2a**. The oily residue is dissolved in a small amount of ethanol and mixed with a few drops of petroleum ether for crystallization. If necessary, the solution is cooled. Yield: 0.34 g (61%) of colorless crystals, mp 74°C. IR (KBr, cm^{-1}): 1600 (C=C), 1308 (B-O). ^{1}H NMR (90 MHz, $CDCl_3$–TMS), δ: 0.97 (d, J = 7 Hz, CH_3C-O), 1.37 (s, N-C-CH_3), 2.50 (s, N-CH_3), 4.60 (q, J = 7 Hz, O-CH), 7.17–8.10 (m, 10 aromatic H). ^{11}B NMR (64 MHz, $CDCl_3$–Et_2OBF_3) δ: 27.0 ($w_{1/2}$ = 385 Hz). Anal. calcd. for $C_{17}H_{20}BNO_2$: C 72.62, H 7.17, B 3.85, N 4.98; found: C 72.70, H 7.25, B 3.88, N 4.92.

[3] The boron chelate **1l** could not be isolated because of an immediate complete rearrangement to **2l** proceeding under various conditions.
[4] The compounds **2** give a red-violet colored solution upon addition of diphenylcarbazone, indicating the monoarylboron moiety (2*a*).

© 2001 NRC Canada

5,6-Dimethyl-2,5-diphenyl-4-propyl-1,3-dioxa-4-aza-2-boracyclohexane (2f)

1f (0.62 g, 2 mmol) is reacted as described above for **2e**. Yield: 0.51 g (82%) of colorless crystals, mp 62°C. IR (KBr, cm^{-1}): 1599 (C=C), 1307 (B-O). ^1H NMR (90 MHz, $CDCl_3$–TMS) δ: 0.87 (d, J = 7 Hz, CH_3C-O), 0.97 (m, CH_3C-C-N), 1.47 (s, N-C-CH_3), 1.77 (m, C-CH_2-C-N), 2.00–2.87 (m, N-CH_2), 4.60 (q, J = 7 Hz, O-CH), 7.20–8.13 (m, 10 aromatic H). ^{11}B NMR (64 MHz, $CDCl_3$–Et_2OBF_3) δ: 27.1 ($w_{1/2}$ = 428 Hz). Anal. calcd. for $C_{19}H_{24}BNO_2$: C 73.80, H 7.82, B 3.50, N 4.53; found: C 73.76, H 7.92, B 3.51, N 4.69.

4-Isopropyl-5,6-dimethyl-2,5-diphenyl-1,3-dioxa-4-aza-2-boracyclohexane (2g)

1g (0.62 g, 2 mmol) is reacted as described above for **2e**. Yield: 0.38 g (62%) of colorless crystals, mp 131°C. IR (KBr, cm^{-1}): 1598 (C=C), 1305 (B-O). ^1H NMR (90 MHz, $CDCl_3$–TMS) δ: 0.90 (d, J = 7 Hz, CH_3C-O), 1.13 and 1.20 (d and d, J = 7 Hz, $C(CH_3)_2$), 1.47 (s, N-C-CH_3), 2.97 (sept, J = 7 Hz, N-CH), 4.57 (q, J = 7 Hz, O-CH), 7.20–8.10 (m, 10 aromatic H). ^{11}B NMR (64 MHz, $CDCl_3$–Et_2OBF_3) δ: 27.3 ($w_{1/2}$ = 428 Hz). Anal. calcd. for $C_{19}H_{24}BNO_2$: C 73.80, H 7.82, B 3.50, N 4.53; found: C 73.78, H 7.76, B 3.52, N 4.83.

4-Cyclohexyl-5,6-dimethyl-2,5-diphenyl-1,3-dioxa-4-aza-2-boracyclohexane (2h)

1h (1.03 g, 3 mmol) is reacted as described above for **2e**. Yield: 0.63 g (60%) of colorless crystals, mp 122°C. IR (KBr, cm^{-1}): 1599 (C=C), 1308 (B-O). ^1H NMR (90 MHz, $CDCl_3$–TMS) δ: 0.80–2.23 (m, $(CH_2)_5$), 0.90 (d, J = 7 Hz, CH_3C-O), 1.53 (s, N-C-CH3), 2.63 (m, N-CH), 4.60 (q, J = 7 Hz, O-CH), 7.17–8.13 (m, 10 aromatic H). ^{11}B NMR (64 MHz $CDCl_3$–Et_2OBF_3) δ: 27.0 ($w_{1/2}$ = 428 Hz). Anal. calcd. for $C_{22}H_{28}BNO_2$: C 75.65, H 8.08, B 3.10, N 4.01; found: C 75.54, H 8.08, B 3.07, N 3.86.

4-Benzyl-5,6-dimethyl-2,5-diphenyl-1,3-dioxa-4-aza-2-boracyclohexane (2i)

1i (1.07 g, 3 mmol) is reacted in 10 mL of ethanol as described above for **2e**. Crystallization may start during the refluxing or upon cooling of the solution. Yield: 0.47 g (44%) of colorless crystals, mp 135°C. IR (KBr, cm^{-1}): 1598 (C=C), 1304 (B-O); ^1H NMR (90 MHz, $CDCl_3$–TMS) δ: 1.00 (d, J = 7 Hz, CH_3C-O), 1.53 (s, N-C-CH_3), 3.63 (s, N-CH_2), 4.67 (q, J = 7 Hz, O-CH), 7.03–7.87 (m, 15 aromatic H). ^{11}B NMR (64 MHz, $CDCl_3$–Et_2OBF_3) δ: 27.0 ($w_{1/2}$ = 385 Hz). Anal. calcd. for $C_{23}H_{24}BNO_2$: C 77.33, H 6.77, B 3.03, N 3.92; found: C 77.38, H 6.88, B 3.13, N 3.68.

4-Benzhydryl-5,6-dimethyl-2,5-diphenyl-1,3-dioxa-4-aza-2-boracyclohexane (2j)

1j (0.87 g, 2 mmol) is reacted as described above for **2i**. Yield: 0.48 g (56%) of colorless crystals, mp 158°C. IR (KBr, cm^{-1}): 1601 (C=C), 1314 (B-O). ^1H NMR (90 MHz, $CDCl_3$–TMS) δ: 0.90 (d, J = 7 Hz, CH_3C-O), 1.00 (s, N-C-CH_3), 4.80 (q, J = 7 Hz, O-CH), 4.97 (s, N-CH), 7.08–7.93 (m, 20 aromatic H). ^{11}B NMR (64 MHz, $CDCl_3$–Et_2OBF_3) δ (ppm): 26.8 ($w_{1/2}$ = 514 Hz). Anal. calcd. for $C_{29}H_{28}BNO_2$: C 80.38, H 6.51, B 2.49, N 3.23; found: C 80.36, H 6.52, B 2.54, N 3.03.

Single crystals suitable for X-ray analysis were obtained by very slow crystallization from absolute ethanol.

4-Benzhydryl-5,6-dimethyl-2,5-di(4′-methylphenyl)-1,3-dioxa-4-aza-2-boracyclohexane (2k)

3-Hydroxy-2-butanone (0.88 g, 10 mmol) and di(4-methylphenyl)borinic acid (**3**) (2.10 g, 10 mmol) are dissolved in 10 mL of absolute ethanol, if necessary under slight warming. A solution of *N*-benzhydrylhydroxylamine (1.99 g, 10 mmol) in 10 mL of ethanol is added without stirring, after pre-cooling of both solutions. At –18°C crystallization starts spontaneously or after rubbing with a glass stick. The crystals are filtered off and are washed rapidly with a small amount of ethanol and small portions of ether. Yield: 2.63 g (55%) of colorless crystals of **4-benzhydryl-5,6-dimethyl-2,2-di(4′-methylphenyl)-1,3-dioxa-4-azonia-2-borata-4-cyclohexene (1k)**[5]; mp 120°C (rearrangement to **2k**). IR (KBr, cm^{-1}): 1604 (C=N/C=C). ^1H NMR (400 MHz, CD_2Cl_2–TMS, at –17°C), δ: 1.58 (d, J = 7 Hz, O-C-CH_3), 2.14 (s, N=C-CH_3), 2.18 (s, 2 aryl-CH_3), 4.76 (q, J = 7 Hz, O-CH), 6.53 (s, N-CH), 6.56–7.27 (m, 18 aromatic H). ^1H NMR (90 MHz, $CDCl_3$–TMS, at ambient temp.) δ: 0.90 (d, J = 7 Hz, O-C-CH_3, 30% of 3 H), 2.10 (s, N=C-CH_3, 70% of 3 H), 2.27 (s, 2 aryl-CH_3, 30% of 6 H), 2.40 (s, 2 aryl-CH_3, 70% of 6 H), 4.60–4.97 (m, O-CH), 5.00 (s, N-CH, 70% of 1 H), 6.43 (s, N-CH, 30% of 1 H), 6.70–7.83 (m, 18 aromatic H). ^{11}B NMR (64 MHz, $CDCl_3$–Et_2OBF_3, at ambient temp) δ: 5–7 (very weak, broad), 28.0 ($w_{1/2}$ = 590 Hz). Anal. calcd. for $C_{31}H_{32}BNO_2$: C 80.70, H 6.99, B 2.34, N 3.04; found: C 80.65, H 7.27, B 2.34, N 2.96. **1k** (0.92 g, 2 mmol) is reacted as described above for **2i**. Yield: 0.62 g (67%) of colorless crystals, mp 180°C. IR (KBr, cm^{-1}): 1609 (C=C), 1308 (B-O). ^1H NMR (90 MHz, $CDCl_3$–TMS) δ: 0.90 (d, J = 7 Hz, O-C-CH_3), 0.97 (s, N=C-CH_3), 2.40 (s, 2 aryl-CH_3), 4.87 (q, J = 7 Hz, O-CH), 5.07 (s, N-CH), 7.17–7.97 (m, 18 aromatic H). ^{11}B NMR (64 MHz, $CDCl_3$–Et_2OBF_3) δ: 28.0 ($w_{1/2}$ = 520 Hz). Anal. calcd. for $C_{31}H_{32}BNO_2$: C 80.70, H 6.99, B 2.34, N 3.04; found: C 80.64, H 7.04, B 2.35, N 2.92.

4-Benzhydryl-2,5-di(4′-methoxyphenyl)-5,6-dimethyl-1,3-dioxa-4-aza-2-boracyclohexane (2l)

1-Hydroxy-2-butanone (0.88 g, 10 mmol) and di(4-methoxyphenyl)borinic acid (obtained by hydrolysis (3) from the 2-aminoethyl ester (**4**)) (2.42 g, 10 mmol) are dissolved in 10 mL of absolute ethanol, if necessary under slight warming. A solution of *N*-benzhydrylhydroxylamine (1.99 g, 10 mmol) in 10 mL of ethanol is added after pre-cooling of both solutions. After 5 h at –18°C crystals precipitate that do not give the blue color reaction with diphenylcarbazone, which would have indicated an Ar_2B-moiety of the intermediate **1l** (2), but rather a reddish color indicating the complete rearrangement to **2l**. Yield: 2.35 g (48%) of colorless crystals, mp 163°C. IR (KBr, cm^{-1}): 1603

[5] The product gives a blue-colored solution upon the addition of diphenylcarbazone in ethanol, indicating the presence of the chelated diarylborenium (Ar_2B^+) ion (2).

© 2001 NRC Canada

(C=C), 1306 (B-O). ^{1}H NMR (90 MHz, $CDCl_3$–TMS) δ: 0.90 (d, J = 7 Hz, O-C-CH_3), 0.97 (s, N-C-CH_3), 3.77 (s, 2 OCH_3), 2.73 (q, J = 7 Hz, B-O-CH), 4.97 (s, N-CH), 6.53–8.00 (m, 18 aromatic H). ^{11}B NMR (64 MHz, $CDCl_3$–Et_2OBF_3) δ: 27.8 ($w_{1/2}$ = 813 Hz). Anal. calcd. for $C_{31}H_{32}BNO_4$: C 75.46, H 6.54, B 2.19, N 2.84; found: C 75.40, H 6.67, B 2.14, N 2.71.

4-Benzhydryl-2,2-di(4′-chlorophenyl)-5,6-dimethyl-1,3-dioxa-4-azonia-2-borata-4-cyclohexene (1m)

The compound was prepared as described in the preceding paper (1). Single crystals suitable for X-ray analysis were obtained by very slow crystallization from dichloromethane/petroleum ether (bp 30–70°C) using the liquid diffusion method (5).

4-Benzhydryl-2,5-di(4′-chlorophenyl)-5,6-dimethyl-1,3-dioxa-4-aza-2-boracyclohexane (2m)

1m (1.01 g, 2 mmol) is reacted as described above for **2i**. Yield: 0.52 g (52%) of colorless crystals, mp 180°C. IR (KBr, cm^{-1}): 1590 (C=C), 1308 (B-O); ^{1}H NMR (90 MHz, $CDCl_3$–TMS) δ: 0.93 (d, J = 7 Hz, O-C-CH_3), 1.03 (s, N-C-CH_3), 4.77 (q, J = 7 Hz, O-CH), 4.97 (s, N-CH), 7.17–7.90 (m, 18 aromatic H). ^{11}B NMR (64 MHz, $CDCl_3$–Et_2OBF_3)δ: 24.1 ($w_{1/2}$ = 642 Hz). CI-MS (isobutane, 100°C, pos. mode) m/z: 502 (2%, M^+). Anal. calcd. for $C_{29}H_{26}BCl_2NO_2$: C 69.35, H 5.22, B 2.15, Cl 14.12, N 2.79; found: C 69.27, H 5.19, B 2.22, Cl 14.13, N 2.71.

Single crystals suitable for X-ray analysis were obtained by very slow crystallization from absolute ethanol.

5,6-Dimethyl-4-(4′-methylphenyl)-2,5-diphenyl-1,3-dioxa-4-aza-2-boracyclohexane (2n)

3-Hydroxy-2-butanone (0.44 g, 5 mmol) and oxybis(diphenylborane) (0.87 g, 2.5 mmol) are dissolved in 5 mL of absolute ethanol, if necessary under slight warming. A solution of *N*-(4-methylphenyl)hydroxylamine (0.62 g, 5 mmol) in 5 mL of absolute ethanol is added without stirring, after pre-cooling of both solutions. During storage at –18°C, crystals are forming that are separated and washed rapidly with a small amount of cooled ethanol and small portions of ether. Yield: 1.21 g (68%) of colorless crystals containing 95% of **2n** and 5% of the intermediate **1n**; mp 70°C (complete rearrangement to **2n**). IR (KBr, cm^{-1}): 1615 (C=N/C=C). ^{1}H NMR (90 MHz, $CDCl_3$–TMS, at ambient temp.) δ: 1.06 (d, J = 7 Hz, O-C-CH_3, 95% of 3H), 1.43 (s, N-C-CH_3, 95% of 3H), 1.73 (q, J = 7 Hz, O-C-CH_3, 5% of 3H), 1.86 (s, N=C-CH_3, 5% of 3H), 2.23 (s, aryl-CH_3, 95% of 3H), 2.43 (s, aryl-CH_3, 5% of 3H), 5.03 (q, J = 7 Hz, O-CH), 6.63–8.06 (m, 14 aromatic H). ^{11}B NMR (64 MHz, $CDCl_3$–Et_2OBF_3, at ambient temp.) δ: 5–7 (very weak broad signal, partially hidden under the ground signal), 28.0 ($w_{1/2}$ = 420 Hz). Anal. calcd. for $C_{23}H_{24}BNO_2$: C 77.33, H 6.77, B 3.03, N 3.92; found: C 77.24, H 6.86, B 3.13, N 3.75. The mixture **1n**/**2n** is reacted as described above for **2i** to give **2n**. Yield: 0.44 g (64%) of colorless crystals, mp 111°C. IR (KBr, cm^{-1}): 1601 (C=C), 1311 (B-O). ^{1}H NMR (90 MHz, $CDCl_3$–TMS) δ: 1.07 (d, J = 7 Hz, O-C-CH_3), 1.43 (s, N-C-CH_3), 2.23 (s, aryl-CH_3), 5.03 (q, J = 7 Hz, O-CH), 6.63–8.05 (m, 14 aromatic H); ^{11}B NMR (64 MHz, $CDCl_3$–Et_2OBF_3) δ: 28.0 ($w_{1/2}$ = 390 Hz). Anal. calcd. for $C_{23}H_{24}BNO_2$: C 77.33, H 6.77, B 3.03, N 3.92; found: C 77.03, H 6.73, B 3.13, N 3.82.

4-Benzhydryl-5,6-dimethyl-2-(1′-naphthyl)-2-phenyl-1,3-dioxa-4-azonia-2-borata-4-cyclohexene (8) (mixture of diastereomers)

3-Hydroxy-2-butanone (0.88 g, 10 mmol) and *B*-naphthyl-*B*-phenylborinic acid (**6**) (2.32 g, 10 mmol) are dissolved in 10 mL of absolute ethanol. A solution of *N*-benzhydrylhydroxylamine (1.99 g, 10 mmol) in 10 mL of ethanol is added without stirring, after precooling of both solutions. During storage of the mixture at –18°C, crystallization starts spontaneously or after rubbing with a glass stick. The crystals are filtered off and are washed rapidly with a small amount of absolute ethanol and small portions of ether. Yield: 2.89 g (60%) of colorless crystals,[5] mp 130–131°C (rearr.). IR (KBr, cm^{-1}): 1590 (C=N/C=C). ^{1}H NMR (400 MHz, $CDCl_3$–TMS) δ: 1.56 (d, J = 7 Hz, O-C-CH_3, 60% of 3H), 1.57 (d, J = 7 Hz, O-C-CH_3, 40% of 3H), 2.04 (s, N=C-CH_3, 60% of 3H), 2.13 (s, N=C-CH_3, 40% of 3H), 4.55 (q, J = 7 Hz, O-CH, 60% of 1H), 4.81 (q, J = 7 Hz, O-CH, 40% of 1H), 6.59 and 6.60 (s and s, ratio of peak areas 1:1, N-CH, 40% of 1H), 6.99–8.54 (m, 22 aromatic H). ^{11}B NMR (64 MHz, $CDCl_3$–Et_2OBF_3) δ: 8.3 ($w_{1/2}$ = 342 Hz). Anal. calcd. for $C_{33}H_{30}BNO_2$: C 81.99, H 6.25, B 2.24, N 2.90; found: C 81.89, H 6.35, B 2.26, N 2.78.

4-Benzhydryl-5,6-dimethyl-2-(1′-naphthyl)-5-phenyl-1,3-dioxa-4-aza-2-boracyclohexane (9)

8 (0.97 g, 2 mmol) is reacted as described above for **2i**. Yield: 0.43 g (45%) of colorless crystals,[6] mp 181°C. IR (KBr, cm^{-1}): 1599/1574 (C=C), 1304 (B-O). ^{1}H NMR (90 MHz, $CDCl_3$–TMS) δ: 0.97 (d, J = 7 Hz, O-C-CH_3), 1.07 (s, N-C-CH_3), 4.97 (q, J = 7 Hz, O-CH), 5.07 (s, N-CH), 7.03–8.60 (m, 22 aromatic H); ^{11}B NMR (64 MHz, $CDCl_3$–Et_2OBF_3) δ: 27.0 ($w_{1/2}$ = 513 Hz). Anal. calcd. for $C_{33}H_{30}BNO_2$: C 81.99, H 6.25, B 2.24, N 2.90; found: C 82.01, H 6.37, B 2.22, N 2.83.

Single crystals suitable for X-ray analysis were obtained by slow crystallization from dichloromethane/petroleum ether (bp 30–70°C) using the liquid diffusion method (5).

X-ray crystallographic analyses of 2j, 2m, 9, and 1m

Crystallographic data appear in Table 1. The final unit-cell parameters were obtained by least-squares based on 25 reflections (2θ = 90–110°) for **2j**, and 17642, 17505, and 17 642 (2θ = 5–64°) for **2m, 9,** and **1m**, respectively. The data were processed,[7] corrected for Lorentz and polarization effects, and absorption (based on a ψ-scan for **2j**, and analysis of symmetry-equivalent data for the others).

The structures were solved by direct methods, the coordinates of the non-hydrogen atoms being determined from *E*-maps or from subsequent difference Fourier syntheses.

[6] The compound **9** gives a reddish solution upon addition of diphenylcarbazone in ethanol, indicating the monoarylboron moiety (2a).

[7] *teXsan: Crystal structure analysis package*. Unix version 1.7. Molecular Structure Corporation. The Woodlands, Tex., U.S.A. 1995; and *d*TREK: Area Detector Software*. Molecular Structure Corporation, The Woodlands, Tex., U.S.A. 1997.

© 2001 NRC Canada

Table 1. Crystallographic data.

Compound	**1m**[a]	**2j**[b]	**2m**[a]	**9**[a]
Formula	$C_{29}H_{26}BCl_2NO_2$	$C_{29}H_{28}BNO_2$	$C_{29}H_{26}BCl_2NO_2$	$C_{33}H_{30}BNO_2$
MW	502.25	433.36	502.25	483.42
Crystal system	monoclinic	triclinic	monoclinic	monoclinic
Space group	$P2_1/n$	$\bar{P}1$	$P2_1/n$	$P2_1/n$
a (Å)	14.059(3)	10.4729(11)	14.9442(13)	11.123(2)
b (Å)	12.5531(13)	13.5896(11)	11.990(2)	18.433(3)
c (Å)	14.8531(6)	9.5803(7)	16.0613(4)	13.4852(4)
α (°)	90	104.764(6)	90	90
β (°)	95.8067(12)	103.279(7)	114.0153(7)	108.2075(7)
γ (°)	90	107.278(7)	90	90
V (Å^3)	2607.8(5)	1188.1(2)	2628.7(4)	2626.5(5)
Z	4	2	4	4
ρ_{calc} (g cm^{-3})	1.279	1.211	1.269	1.222
F(000)	1048	460	1048	1024
Radiation	Mo	Cu	Mo	Mo
μ (cm^{-1})	2.75	5.81	2.73	0.75
Size (mm)	0.25 × 0.4 × 0.45	0.25 × 0.3 × 0.5	0.2 × 0.25 × 0.45	0.2 × 0.35 × 0.4
Corr. factors	0.83–0.93[c]	0.80–0.87[d]	0.83–0.95[c]	0.80–0.99[c]
φ range	0–190	—	0–190	0–190
ω range	–22 to 18	—	–22 to 18	–22 to 18
Osc. width (°)	0.5	—	0.5	0.5
Images, time (s)	460, 90	—	460, 35	460, 90
$2\theta_{max}$ (°)	56	155	54	55
Total reflections	23908	5119	24412	24416
Unique reflections	6429	4843	5675	6325
R_{merge}	0.056	0.019	0.055	0.083
No. with $I \geq 3\sigma(I)$	2277	3723	2775	2864
No. of variables	316	299	317	454
$R(F)$ ($\geq 3\sigma(I)$)	0.052	0.036	0.043	0.040
$R_w(F^2)$ (all)	0.102	0.031 (F)	0.085	0.077
GoF	1.90	0.85	1.99	1.48
Max Δ/σ	0.001	0.004	0.001	0.006
Residual density (e Å^{-3})	–0.45 to 0.51	–0.12 to 0.13	–0.44 to 0.38	–0.46 to 0.39

[a]Temperature 180 K, Rigaku/ADSC CCD diffractometer, Mo Kα (λ = 0.71069 Å), graphite monochromator, takeoff angle 6.0°, aperture 94.0 × 94.0 mm at a distance of 39.2 mm from the crystal, $\sigma^2(F^2) = (C + B)/\mathrm{Lp}^2$ (C = scan count, B = background count), function minimized $\Sigma w(|F_o^2| - |F_c^2|)^2$, where $w = 1/\sigma^2(F_o^2)$, $R(F) = \Sigma||F_o| - |F_c||/\Sigma|F_o|$, $R_w(F^2) = (\Sigma w(|F_o^2| - |F_c^2|)^2/\Sigma w|F_o^2|^2)^{1/2}$, and gof = $[\Sigma w(|F_o^2| - |F_c^2|)^2/(m - n)]^{1/2}$.

[b]Temperature 294 K, Rigaku/AFC6 diffractometer, Cu Kα (λ = 1.54178 Å), graphite monochromator, takeoff angle 6.0°, aperture 6.0 × 6.0 mm at a distance of 285 mm from the crystal, ω–2θ scan at 32°/min (in ω) (up to 9 scans), scan width (1.10 + 0.20tanθ)°, crystal decay 2.6%, $\sigma^2(F^2) = (C + B)/\mathrm{Lp}^2$ (C = scan count, B = background count), function minimized $\Sigma w(|F_o| - |F_c|)^2$, where $w = 1/\sigma^2(F_o)$, $R(F) = \Sigma||F_o| - |F_c||/\Sigma|F_o|$, $R_w(F) = (\Sigma w(|F_o| - |F_c|)^2/\Sigma w|F_o|^2)^{1/2}$, and gof = $[\Sigma w(|F_o| - |F_c|)^2/(m - n)]^{1/2}$.

[c]Includes crystal decay (if any), absorption, and scaling corrections performed in a single step.

[d]Absorption based on ψ scan.

The non-hydrogen atoms were refined with anisotropic thermal parameters, and the hydrogen atoms were refined with isotropic thermal parameters for **9** and fixed in idealized positions for the others. Corrections for secondary extinction were needed only for **2j** and **2m** (coefficients 2.96(3) and 0.23(1) × 10^{-5}, respectively). Neutral atom scattering factors for all atoms and anomalous dispersion corrections for the non-hydrogen atoms were taken from the *International Tables for X-Ray Crystallography*. Ring torsion angles are listed in Table 2, and selected bond lengths and angles in Table 3. Complete tables of atomic coordinates, bond lengths and angles, hydrogen atom parameters, anisotropic thermal parameters, torsion angles, and intermolecular contacts are included in supplementary material[8] as a Crystallographic Information File (CIF).

Isothermal long-time ^{1}H NMR measurements of 1/2 e, j, k, m, and n

A test sample of **1** (0.05 mmol) was dissolved in ice-cooled CD_2Cl_2, and the ^{1}H NMR spectra (400 MHz) was recorded at the operating temperature of the NMR spectrometer (25°C), repeatedly at fixed time-intervals dependent upon the rate of the rearrangement reaction, which had been determined roughly beforehand. The decrease of concentration of the educt **1** (and the increase of concentration of the rearrangement product **2**) was calculated from the changing peak

[8]Copies of material on deposit may be purchased from the Depository of Unpublished Data, Document Delivery, CISTI, National Research Council Canada, Ottawa, ON K1A 0S2, Canada (http://www.nrc.ca/-cisti/irm/unpub_e.shtml for information on ordering electronically).

© 2001 NRC Canada

Table 2. Torsion angles (deg, σ = 0.2–0.3°) in the six-membered rings.

	1m	2j	2m	9
C-O-B-O	+61.7	–0.1	+6.6	–3.8
O-B-O-N	– 48.3	–15.7	–11.3	–5.5
B-O-N-C	+16.2	+52.6	+42.0	+44.2
O-N-C-C	+6.2	–69.1	–62.6	–68.7
N-C-C-O	+6.3	+52.9	+57.5	+59.0
C-C-O-B	– 42.1	–20.4	–31.4	–25.0

areas of corresponding signals. From the log (conc.% educt) vs. time (min) plots, the rate constants (*k*), the half-life ($t_{1/2}$), and the correlation coefficient (*r*) were calculated by standard methods.

Results and discussion

Synthesis and spectroscopy of 2

The thermally induced rearrangement of the diarylboron chelates **1** to the cycloboronates **2** had been detected as a more-or-less partial process during attempts to recrystallize and during NMR experiments with solutions of **1** (1). Complete transformation to **2** was achieved by refluxing **1** in solvents such as benzene, toluene, or ethanol, while monitoring the progress of the reaction by the color reaction with diphenylcarbazone (2).[4,5] An immediate synthesis of **2** was also possible without the preformation of the diarylboron chelate **1**, if a three-component one-pot reaction of carbonyl compound, the hydroxylamine, and the diarylborinic acid was conducted in a heated solvent. Certain compounds, like **2l**, could be obtained only by this method, because of the high tendency of isomerization of the preceding diarylboron chelate **1l**, which we were not able to isolate even without applying heat. Other chelates, like **1k** or **1n**, were obtained only as mixtures with **2k** and **2n**, respectively. Heating of these mixtures in ethanol resulted in complete rearrangement to **2k** and **2n**, respectively.

The infrared spectra of the crystalline compounds **2** are generally characterized by the disappearance of the N=C vibration, a distinctive mark in most of the spectra of the boron chelates **1** (1). In addition, a strong absorption band between 1304 and 1314 cm^{-1}, which is not present in the spectra of **1**, is conspicuous in the spectra of **2**. This band has been assigned formerly to the B—O stretching vibration of borates and boronates (7).[9] Another striking phenomenon can be observed in comparing the 1600 cm^{-1} region of the spectra of the educt **1** and the rearrangement product **2**, if **1** contains a diphenylboron moiety and no further aromatic ring system, as in **1a**, **1b**, and **1e**–**h**. In these cases, the diphenylboron chelates **1** do not show a considerable or detectable ν_{16}-ring stretching vibration of the *B*-aryl residues, whereas the corresponding isomerization products **2** display distinct ν_{16} bands, typical for mono-substituted benzene derivatives with an increased perturbation of the ring π-system (8). The low intensity of the ν_{16} bands in the diphenylboron compounds **1** might indicate the decreased interaction between the phenyl ring π-system and the tetra-coordinated (sp^3) boron atom. On the other hand, the trivalent phenylboronate moiety of **2** allows an increased interaction between the phenyl ring π-system and the (sp^2) boron atom, thus intensifying the ν_{16} band given by the migrated phenyl residue, now positioned at C5 of the cycloboronate ring.[10]

Table 3. Selected bond lengths and angles.

	1m	2j	2m	9
(A) Bond lengths (Å)				
B—O(N)	1.556(3)	1.368(2)	1.372(3)	1.372(2)
B—O(C)	1.461(3)	1.349(2)	1.360(2)	1.364(2)
B—C	1.599, 1.624(3)	1.552(2)	1.544(3)	1.561(2)
O—N	1.368(2)	1.457(1)	1.452(2)	1.455(1)
N—C (ring)	1.286(2)	1.492(2)	1.495(2)	1.497(2)
O—C	1.399(2)	1.442(2)	1.440(2)	1.447(2)
C—C (ring)	1.502(3)	1.560(2)	1.556(2)	1.554(2)
C—Cl	1.743, 1.749(2)		1.736, 1.740(2)	
(B) Angles (°, σ = 0.1–0.2°)				
O-B-O	106.1	122.7	121.9	121.5
B-O-N	113.8	114.3	117.7	116.8
O-N-C (ring)	123.1	108.8	110.8	108.9
N-C-C (ring)	121.7	102.7	103.7	102.3
C-C-O (ring)	113.2	111.6	111.3	110.1
C-O-B	113.0	121.0	120.1	120.7

In the ^{1}H NMR spectra of **2**, generally all signals of the aliphatic protons of residues R, R^1, and R^2 are shifted to a higher field compared to the corresponding signals of the educts **1**, a consequence of the transformation of the N=C double bond into a N—C single bond ring segment and the deshielding effect caused thereby. The largest change occurs, as expected, in the N=CH methine-proton signal of compounds **1a–d**, which are shifted about 3.4 ppm upfield after the rearrangement to **2a**–**d**.

Additional proof for the isomerization comes from the ^{11}B NMR spectra of some examples of **2**, which display resonance signals between (Et_2OBF_3) = 26 and 28 ppm, indicating the (sp^2) boron atom of the cycloboronate, whereas the ^{11}B signals of the boron chelates **1** range between 3 and 9 ppm (1), typical for tetracoordinate (sp^3) boron nuclei (10).

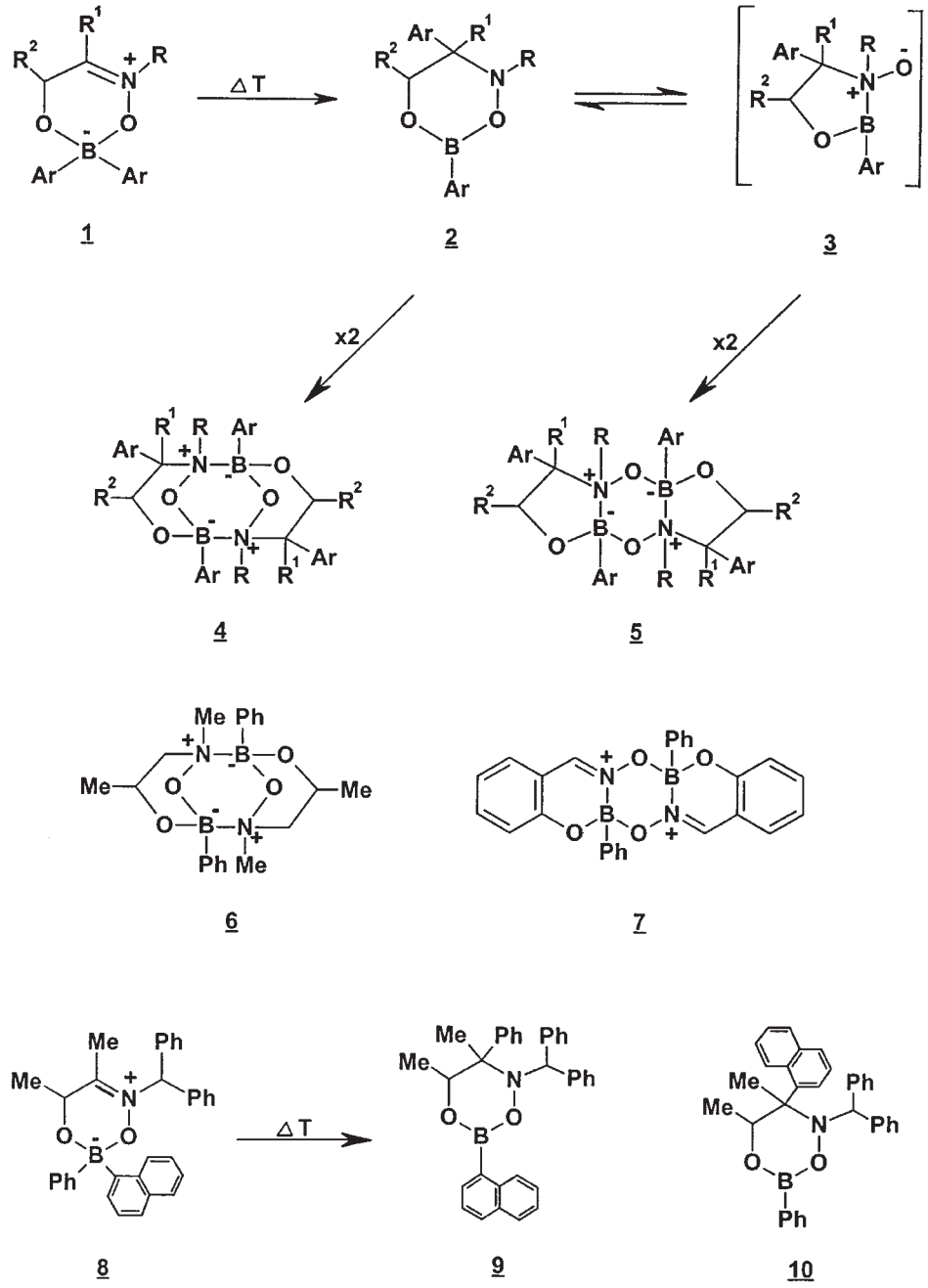
The spectroscopic data, together with the elemental analyses and the red color reaction with diphenylcarbazone,[4] suggest the molecular structure **2** exists, at least in solution, but cannot exclude unambiguously the presence of dimers like **4** or **5** in the solid state. These types of BONBON dimers resemble the BONBON compounds **6** (11) or **7** (12), which have been fully characterized by X-ray crystallographic structure analyses and demonstrate the possibility of the formation of such dimers. An EI mass spectrum of **2m** gave as the highest mass feature the molecular ion of the monomer **2m**, but this observation could result from a complete dissociation of one of the possible dimers, **4** or **5**. However, the

[9] The strength of the band and its stability of position can be ascribed to the partial double bond character of the B—O bond by pp (π)-back donation (7*a*, *b*).

[10] A similar increase of intensity of the ν_{16} ring stretching band had been observed after the thermal rearrangement of another type of diphenylboron chelate having one of the *B*-phenyl ligands transformed into a *B*-phenyloxy ligand (9*a*, *b*).

© 2001 NRC Canada

Scheme 1.



X-ray crystallographic analyses of **2j** and **2m** prove unambiguously the monocyclic arylboronate structure **2** (see below).

Synthesis and spectroscopy of 9

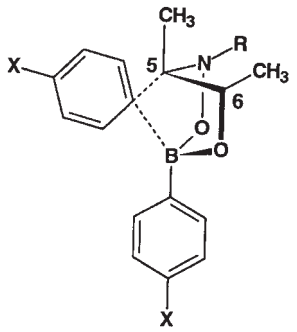
The thermally induced isomerization was not achieved with derivatives of dinaphthylborinic acid. The compounds **1** (Ar = 1-naphthyl) could be recrystallized unchanged even from high boiling solvents (1). To test the different migration tendency of *B*-phenyl and *B*-naphthyl residues, we synthesized compound **8**, a derivative of a "mixed" diarylborinic acid. Compound **8** was obtained as a mixture of stereoisomers. The ^{1}H NMR spectrum of the isolated batch of crystals points to a 3:2 mixture of the two possible racemates, by exhibiting a 3:2 ratio of corresponding peak areas.[11] We did not succeed in separating the diastereomers, the physical properties of which seem to differ only slightly.[12] In the ^{11}B NMR spectrum, for instance, only one broad signal at 8.3 ppm is registered for the tetracoordinate boron nucleus of the obviously present diastereomers. Thus, **8** (as a mixture of stereoisomers) was brought to reflux in ethanol and yielded 45% of a crystalline product which gave the red color-reaction with diphenylcarbazone,[6] and had the elemental analysis and the spectroscopic data of a monoarylboronate **9** or **10**. These data closely resembled those of the cycloboronates **2** in all respects, but did not distinguish between the alternative constitutions, **9** or **10**. An X-ray crystallographic analysis (see below) confirms the molecular

© 2001 NRC Canada

Scheme 2.

		R	R^1	R^2	Ar
1/2	**a**	CH_3	H	CH_3	Ph
	b	$C(CH_3)_3$	H	CH_3	Ph
	c	CH_2Ph	H	CH_3	Ph
	d	$CHPh_2$	H	CH_3	Ph
	e	CH_3	CH_3	CH_3	Ph
	f	n-C_3H_7	CH_3	CH_3	Ph
	g	i-C_3H_7	CH_3	CH_3	Ph
	h	C_6H_{11}	CH_3	CH_3	Ph
	i	CH_2Ph	CH_3	CH_3	Ph
	j	$CHPh_2$	CH_3	CH_3	Ph
	k	$CHPh_2$	CH_3	CH_3	4-$CH_3C_6H_4$
	l	$CHPh_2$	CH_3	CH_3	4-$CH_3OC_6H_4$
	m	$CHPh_2$	CH_3	CH_3	4-ClC_6H_4
	n	4-$CH_3C_6H_4$	CH_3	CH_3	Ph

Scheme 3.



11

structure **9**, demonstrating the expected preferential migration of the phenyl group. This might explain the thermal stability of the dinaphthylboron chelates, on the basis of an impeded migration of the comparatively bulky naphthyl residue.

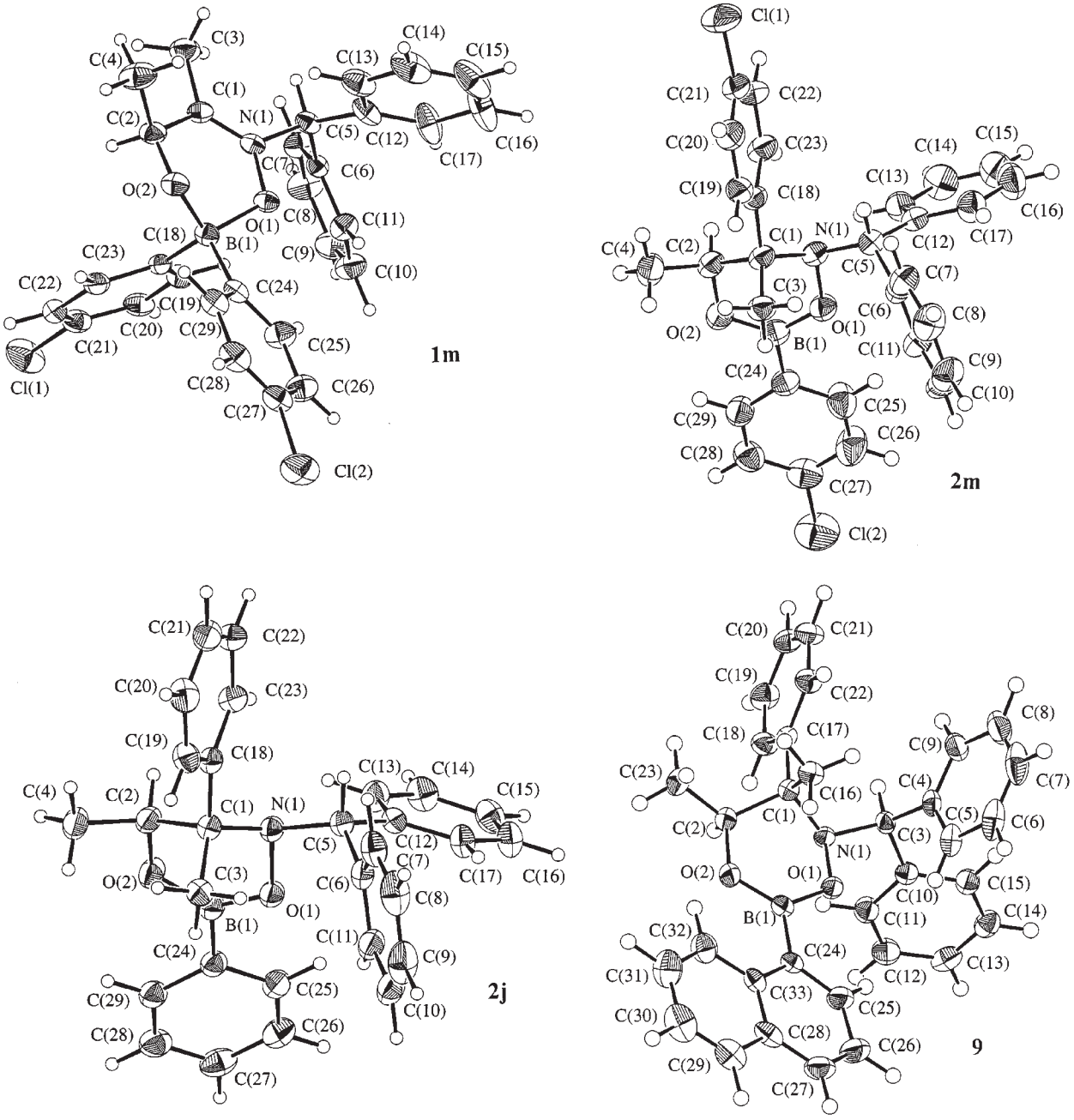
X-ray cyrstal structure analyses of 1m, 2j, 2m, and 9

The X-ray analyses confirm the postulated molecular structures of the rearrangement products **2j**, **2m**, and **9** (Fig. 1), proving the aryl-1,4-migration in each case, with an impediment for migration of the bulkier naphthyl residue. In addition, the structure of **2m** furnishes evidence for the identity of the scission and recombination site of the migrating aryl ring. For direct comparison of the rearrangement product with its educt, an additional analysis was carried out for **1m** that bears 4-chlorophenyl groups, allowing location of the linking position before and after the aryl migration.

The six-membered BONCCO ring of **1m** (Fig. 1) possesses an approximately planar O(1)-N(1)=C(1)-C(2) grouping (dihedral angle = 6.2° (Table 2)), with B displaced by about 0.4 Å from this plane and O(2) displaced by a smaller amount in the opposite direction. The conformation may thus be described as a distorted half-chair (an alternative description is as a distorted envelope, with a roughly planar five-atom section, with B at the flap). The tetrahedral arrangement of the ligands around the boron atom is typical for all diarylboron chelates of bidentate ligands. As expected, the pseudo-axial *B*-aryl bond B(1)—C(18) (1.624 Å) is somewhat longer (by 0.025 Å) than the pseudo-equatorial B(1)—C(24) bond (1.599 Å). The difference between the two O—B bond lengths indicates the better donor quality of the alcoholate ligand, which makes a stronger O—B bond (O(2)—B(1) = 1.461 Å), compared to that of the nitrone ligand with the weaker O—B bond (O(1)—B(1) = 1.556 Å). This (nitrone) O—B bond, however, seems to possess an increased binding strength relative to that of a seven-membered analogous diphenylboron chelate with a (nitrone) O—B distance of 1.593 Å reported previously (1). The mean C—B (1.612 Å) and O—B (1.509 Å) distances with a mean C—B/O—B bond length ratio of 1.068, in the upper range of values estimated for this kind of compound (15), suggest a slightly stronger ligand binding to the diarylboron nucleus in **1m** compared to the seven-membered analog (C—B/O—B ratio of 1.059) (1). The endocyclic C=N double bond

© 2001 NRC Canada

Fig. 1. Views of the molecules of **1m**, **2j**, **2m**, and **9**; 25% (**1m**, **2j**) and 50% (**2m**, **9**) probability ellipsoids are shown for the non-hydrogen atoms.



(C(1)—N(1) = 1.286 Å) and the nitrone N—O bond (N(1)—O(1) = 1.368 Å) are about normal and are in accord with the corresponding bond distances in seven-membered boron chelates with endocyclic nitrone moieties (1, 16). To the best of our knowledge **1m** is the first example of the type **1** boron chelates (1) structurally characterized by an X-ray crystallographic analysis.

The heterocyclic structures of **2j**, **2m**, and **9** contain in each case a trigonal planar sp^2-hybridized boron atom, whcih is typical for six-membered cycloboronates (17, 18). The ring geometry in each molecule is again a half-chair, with an approximately planar OBOC grouping (dihedral angle = 0.1–6.6°, Table 2), with displacement by ca. 0.5 Å on opposite sides of this plane of N and C-5 (C(1) in the ORTEP diagrams, Fig. 1).

Assuming that all of the rearrangement products presented here, **2** and **9**, have an identical BONCCO ring skeleton, they possess the same heterocyclic structure that had been established previously for the reaction products of various 2-(*N*-alkylhydroxylamino)alkanols with arylboronic acids (19), for *N*-unsubstituted analogs of **2** derived from bulky arylboronic acids (18) and also for *N*-acyl derivatives (20). In accordance with the near planarity at the sp^2-hybridized boron atoms in all three compounds, **2j**, **2m**, and **9**, there are

© 2001 NRC Canada

the relatively short O—B bonds (between 1.349 and 1.372 Å, Table 3), indicating the partial double bond character that results from O—B *pp* (π) back donation. In each case, the (C)O—B bond is distinctly shorter (by 0.008–0.019 Å) than the (N)O—B bond, indicating the better *p* (π) donor quality of the alcoholate ligand compared to the hydroxylamine ligand. The increased double bond character of the (C)O—B bonds is also reflected by the interior angles at O(2) and B(1) between 120.1 and 122.7° in all three compounds, whereas the interior angle at O(1) is somewhat compressed (114.3–117.7°), as a result of less double bond character. The B—C(aryl) distance in **2j**, **2m**, and **9** ranges between 1.544 and 1.561 Å, and is typical for many cyclic arylboronates (17, 18). Even though in (sp^2) B—C(aryl) bonds a *pp* (π) interaction seems to play a minor role (17, 18), the aryl rings in **2j**, **2m**, and **9** are not far from coplanar with the OBOC ring portion of the cycloboronate, with rotations of about 20, 1, and 18°, respectively (the exact values depend on which plane or dihedral angle is used to define the rotation). The deviation in **9** from coplanarity between the naphthyl ring and the OBOC plane is presumably due to intramolecular steric reasons, as in mesitylboronates (17, 18); there may be a weak C-H···O interaction (C(32)-H···O(2) in Fig. 1, H···O = 2.29(1) Å). The deviation in **2j** is likely an intermolecular effect.

The comparison of the structural features of the educt **1m** and the product **2m** points out some essential geometrical changes as a consequence of the chemical transformation, which might be generally applicable for the educt/product pair **1**/**2**. The aryl 1,4-migration from the (sp^3) boron atom B(1) to the nitrone carbon atom C(1) converts the short C=N double bond (C(1)—N(1) = 1.286 Å) of the nitrone function in **1m** into a long C—N single bond (C(1)—N(1) = 1.495 Å) of the dialkylhydroxylamine moiety in **2m**.[13] The nitrone reduction is accompanied by the oxidation of the borinic to a boronic acid function, transferring the double bond character of the nitrone bonds into the O-B-O segment of the ring, causing the shortening of the O—B bonds from the mean value of 1.509 Å in **1m** to a mean value of 1.366 Å in **2m**. This change includes the widening of the O-B-O angle from 106.1° in the (sp^3) boron complex **1m** to 121.9° in the trigonal (sp^2) boron compound **2m**. All of the remaining bonds in the BONCCO ring are elongated by 0.05–0.08 Å going from **1m** to **2m**, in particular the N—O bond, which loses its partial double bond character still present in the nitrone function of **1m**. The angles at N(1) in **2m** (106.0–117.6, average 111.5°) indicate tetrahedral geometry at the (sp^3) N atom (lone-pair pseudo-axial); the (sp^2) N atom in **1m** has nearly planar geometry (angles = 110.5–123.1, average, 118.2°). Considering the conformational change of the six-membered ring system, the aryl 1,4-migration results in a displacement of the planar part within the BONCCO ring, by transferring planarity from the ON=CC segment in **1m** to the OBOC segment in **2m**.

In all crystallographically analyzed rearrangement products, **2** and **9**, the vicinal methyl groups at ring positions C5 and C6 are in *cis*-configuration This indicates that, in each case, the migrating aryl residue seems to be that one that is positioned *trans* to the methyl group at C6 in the educt **1** and **8**, respectively. Examination of the ORTEP diagrams (Fig. 1) of the educt/product pair **1m**/**2m** shows that the aryl residue (with C(18)-C(23) and Cl(1)), which is *trans* to 6-CH_3 in the educt **1m** (C(4) in Fig. 1), migrates to C5 (C(1) in Fig. 1), via the supposed transition state **11**, and that consequently the methyl groups at C5 and C6 (C(3) and C(4) in Fig. 1) of the product **2m** are in a *cis*-configuration.

Preliminary thermoanalyses

The melting behaviour of certain specimens of **1** (e.g., **j**, **k**, **m**, and **n**) gave the first hints of a thermally induced transformation reaction: a sudden liquefaction of the substance at temperatures between 70 and 130°C was followed by recrystallization at the same or even higher temperature, until the final melting or decomposition at a still higher temperature.[14] This could be interpreted as a primary exothermic rearrangement reaction of **1** to result in the isomer **2**, which melts and decomposes at further raised temperatures. In those cases, with a melting point of **2** lower than the rearrangement temperature, only a single "liquefaction point" was observed, as to be expected. For **1m** and **2m**, the molecular structure of each was unambiguously established by X-ray crystallography (see above), the rearrangement point was observed at about 130°C, and the melting temperature of the rearrangement product at 180°C. In a differential scanning calorimetry (DSC) experiment, the transformation process showed two peaks, one at 130.5°C representing the exothermic isomerization of the B,*N*-betainic heterocycle **1m** to the energetically favored cycloboronate **2m**, including the negative recrystallization enthalpy,[15] and another at 179.8°C representing the positive fusion enthalpy of **2m** (Fig. 2). Approximately the same reaction progress was registered in a differential thermoanalytical/thermogravimetric (DTA/TG) experiment with **1m**. The DTA-curve showed approximately coinciding peaks, as displayed by the DSC-thermogram, for rearrangement/recrystallization (132.8°C) and fusion (183.3°C), and was in accordance with the TG-curve, indicating mass constancy up to the rearrangement point and no loss of mass during the transformation to **2m**. Rapid mass decrease at the fusion point of **2m** showed the decomposition of the compound (Fig. 2). The DSC data gave an isomerization/ recrystallization enthalpy of $\Delta H_{iso} + \Delta H_{rcr} = -179.3$ J g^{-1} (–90.05 kJ mol^{-1}) and a fusion enthalpy of $\Delta H_{fus} = 47.7$ J g^{-1} (23.96 kJ mol^{-1}) for the solid state transition from **1m** to **2m**. Similar values were gathered from the DSC data of **1**/**2i**–**k** and **8**/**9** (Table 4). In the DSC thermogram of **1j**/**2j** (see supplementary material)[8] the first exothermic reaction peak was split into two separate peaks at 103 and 112°C,

[13]The same type of thermally induced 1,4-shift of one *B*-phenyl group had been observed previously with open-chain nitrone–triphenylborane adducts (21) and with diphenylboron chelates of salicylaldonitrones (16, (*a*) W. Kliegel, D. Nanninga, S.J. Rettig, and J. Trotter. Can. J. Chem. **62**, 845 (1984); (*b*) W. Kliegel, D. Nanninga, and U. Lauterbach. Unpublished results). It represents fundamentally another kind of reductive arylation, like nitrone reductions by organometallic reagents (22).

[14]Similar observations are known for diarylboron chelates that undergo another type of thermal rearrangement (aryl-1,2-migration) (9).

[15]Possibly the rearrangement (liquefaction) and recrystallization might be registered as two separate peaks for chronologically resolved processes by measuring with considerably lower heating rates to those applied in this first experiment (5°C min^{-1}).

© 2001 NRC Canada

Table 4. Thermographic data (DSC) of **1/2(i**, **j**, **k**, and **m)** and **8**/**9**.

	Observed mp of **1**[a] (°C)	Isomerization/ recrystallization temp (DSC) (°C)	Observed mp of **2**[a] (°C)	$\Delta H_{iso} + \Delta H_{rcr}$ (J g^{-1})	ΔH_{fus} (J g^{-1})
1/2i	120	118	135	–227.9	36.4
1/2j	105	103/112	158	–143.3	65.6
1/2k	120	117	180	–200.0	70.4
1/2m	130	130	180	–179.3	47.7
8/9	130	130	181	–173.4	52.7

[a]mp (uncorr.) observed in the Linström apparatus; lit. (1) and this work.

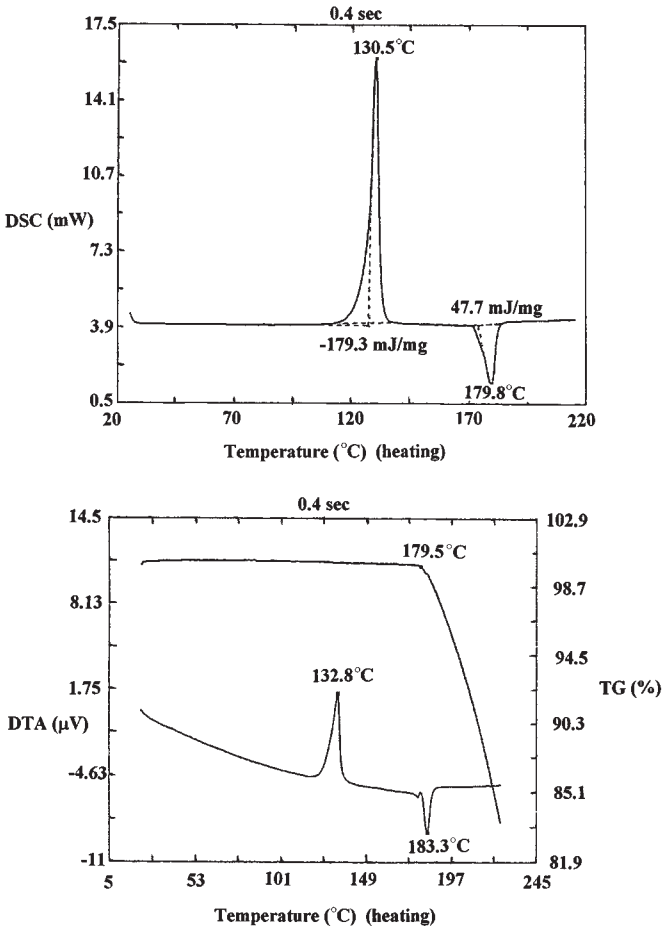
very likely the rearrangement reaction and the recrystallization process. The endothermic fusion peak at 152°C possessed approximately the same peak area as the crystallization peak at 112°C, which would be consistent. A preliminary idea of the thermal behaviour of those compounds **1** that rearrange at temperatures near or above the melting point of **2** was given by the DTA/TG thermogram of **1g**/**2g** (see supplementary material)[8]. In this case, the presence of only one single peak indicated the isomerization reaction at 142°C, and the loss of mass started as this temperature was approached. This should be equivalent to an instantaneous decomposition of the emerging rearrangement product **2g**, the fusion point of which has been found at lower temperatures of about 131°C.

Time-dependent NMR measurements

Since many of the boron compounds **1** isomerize even at room temperature or during the ^{1}H NMR mearsurements (at 25°C) and even ice cold solvents could not prevent partial rearrangement, a low-temperature ^{1}H NMR experiment has been carried out. It demonstrated, however, that the reaction rate from –40°C to 0°C seems to be very slow and that a progressively faster isomerization can be detected at higher temperatures up to 25°C (from the changing ratio of peak areas between educt **1** and product **2** during the increase of temperature). To obtain more specific information on the rate of transformation, the ^{1}H NMR spectra of variously substituted compounds **1** (or **1** containing a portion of already generated isomer **2**) were recorded at 25°C over an extended period of time (several half-life periods). For this purpose, on the one hand, a series of diphenylboron chelates with *N*-methyl- (**1e**), *N*-benzhydryl- (**1j**), and *N*-tolyl-substitution (**1n**), and on the other hand, a series of *N*-benzhydryl derivatives of di(4-chlorophenyl)- (**1m**), diphenyl- (**1j**), and di(4-tolyl)-boron chelates (**1k**) were selected to investigate the influence of the *N*-substitution and of the *B*-aryl residues on the reaction rate. The ^{1}H NMR spectra were recorded, using CD_2Cl_2 as a solvent, with periodic registration of the decrease and increase, respectively, of the signal intensities of **1** and **2**. Suitable, sufficiently separated marker signals for comparison of the peak areas were the quadruplet of the C6 single proton and additionally, in case of the *N*-benzhydryl derivatives, the singlet of the N-CH methine proton.

The concentration vs. time plots (Fig. 3) indicate an influence of both the *N*-substituent R and the *B*-substituent Ar on the rate of isomerization. The linearity of the log (conc. of educt) vs. time plots of **1** indicates a first-order reaction and suggests an intramolecular aryl 1,4-shift, which might include a transition state like **11**, as has been postulated for the

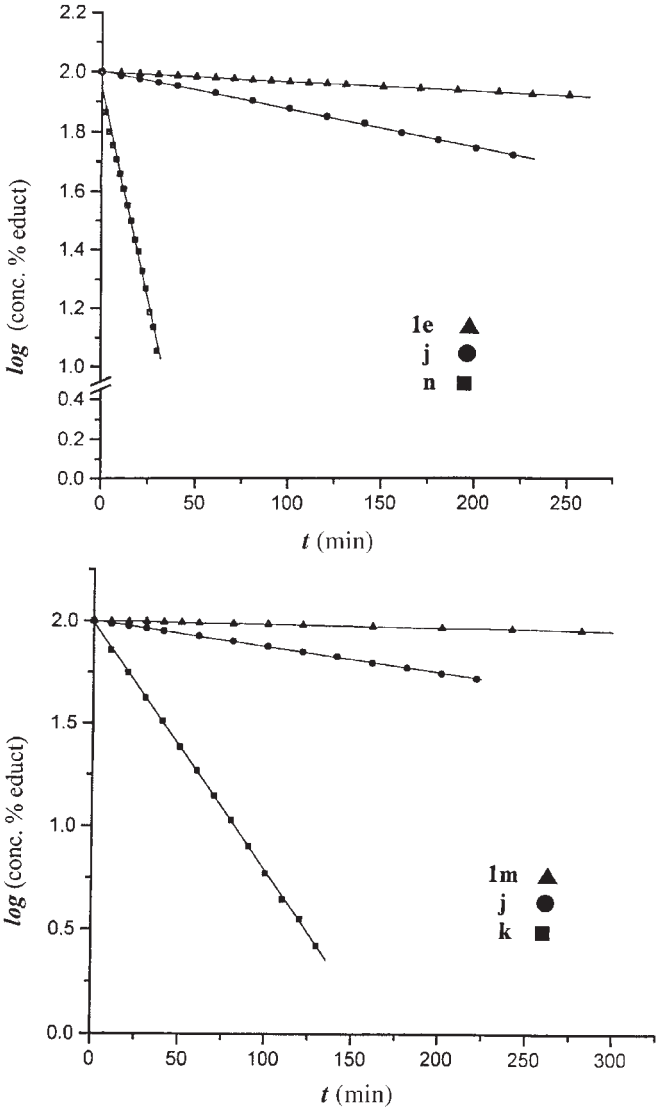
Fig. 2. Differential scanning calorimetry (DSC) and thermogravimetry and differential thermoanalysis (TG/DTA) thermograms of **1/2m**.



1,4-shift in the diarylboron chelates of salicyaldonitrones (16). From the kinetic parameters (Fig. 3, Table 5), it is clearly apparent that the reaction rate is increased by diminishing the electron density at C5 to enable or facilitate the formation of the transition state (**11**) of the aryl migration, in the order *N*-methyl < *N*-benhydryl < *N*-tolyl. Considering the influence of the *B*-aryl residues, the 4-chlorophenyl substiutent is a comparatively poor leaving group, with the order of the rate of migration, 4-chlorophenyl < phenyl < 4-tolyl, indicating the increase of electron density at the leaving position of the aryl ring by inductive effects, which facilitates the formation of the transition state **11** (X = Cl, H, CH_3) and accelerates the rearrangement.

© 2001 NRC Canada

Fig. 3. Isomerization rates of diphenylboron derivatives **1e**, **j**, and **n** and of *N*-benzhydryl derivatives **1m**, **j**, and **k**.



Acknowledgements

We thank the Natural Sciences and Engineering Research Council of Canada and the Fonds der Chemischen Industrie, Frankfurt am Main, Germany, for financial support. We are grateful to the Chemische Institute der Technischen Universität Braunschweig, Braunschweig, Germany, for ^{1}H and ^{11}B NMR and mass spectra, and to the Institute für Pharmazeutische Technologie der Technischen Universität Braunschweig for DSC/DTA/TG measurements.

References

1. W. Kliegel, G. Lubkowitz, J.O. Pokriefke, S.J. Rettig, and J. Trotter. Can. J. Chem. **78**, 1325 (2000).
2. (*a*) R. Neu. Z. Anal. Chem. **176**, 334 (1960); (*b*) B. Friese and F. Umland. Anal. Chim. Acta **96**, 303 (1978).
3. G.E. Coates and J.G. Livingstone. J. Chem. Soc. 4909 (1961).

Table 5. Rate constants (k), half-life values ($t_{1/2}$), and correlation coefficients (r) of the isomerization reaction **1** to **2**.

	$k \times 10^4$ (min^{-1})	$t_{1/2}$ (min)	r
1/2n	666	10.4	–0.9967
1/2k	278	24.9	–0.9999
1/2j	29	237	–0.9997
1/2e	7.4	940	–0.9993
1/2m	3.5	2006	–0.9976

4. T.P. Povlock and W.T. Lippincott. J. Am. Chem. Soc. **80**, 5409 (1958).
5. P.G. Jones. Chem. Ber. **17**, 222 (1981).
6. R.L. Letsinger and N. Remes. J. Am. Chem. Soc. **77**, 2489 (1955).
7. (*a*) R.L. Werner and K.G. O'Brien. Austr. J. Chem. **8**, 355 (1955); **9**, 137 (1956); (*b*) W. Gerrard. The organic chemistry of boron. Acid Press, London. 1961. p. 223; (*c*) H. Steinberg. Organoboron chemistry. Vol. 1. Boron-oxygen and boron-sulfur compounds. Wiley, New York. 1964, p. 871.
8. R. Katritzky and R.D. Topsom. Angew. Chem. **82**, 106 (1970); Angew. Chem. Int. Ed. Engl. **7**, 86 (1970)
9. (*a*) W. Kliegel. Liebigs. Ann. Chem. **763**, 61 (1972); (*b*) W. Kliegel and E. Ahlenstiel. J. Organomet. Chem. **277**, 173 (1984); (*c*) W. Kliegel, S. Sarge, H.K. Cammenga, S.J. Rettig, and J. Trotter. Reactivity of solids. Materials science monographs 28 A & B, p. 725. Amsterdam. 1985; (*d*) E. Ebeling, W. Kliegel, S.J. Rettig, and J. Trotter. Can. J. Chem. **67**, 933 (1989).
10. (*a*) H. Nöth and B. Wrackmeyer. Nuclear magnetic resonace spectroscopy of boron compounds. Springer, Berlin. 1978; (*b*) R. Köster (*Editor*). Houben-Weyl: Organobor-Verbindungen III. Vol. XIII/3c. Thieme, Stuttgart. 1984.
11. W. Kliegel, G. Lubkowitz, S.J. Rettig, and J. Trotter. Can. J. Chem. **70**, 2809 (1992).
12. S.J. Rettig and J. Trotter. Can. J. Chem. **61**, 206 (1983).
13. (*a*) M.S. Korobov, L.E. Nivorozhkin, L.E. Konstantinovsky, and V.I. Minkin. J. Chem. Soc. Chem. Commun. 169 (1982); (*b*) M.S. Korobov, L.E. Nivorozhkin, L.V. Belen'kaya, L.E. Konstantinovsky, and V.I. Minkin. J. Gen. Chem. USSR [Zh. Obshch. Khim.], **52**, 748 (1982); (*c*) M.S. Korobov, G.S. Borodkin, N.I. Borisenko, T.A. Ryskina, L.E. Nivorozhkin, and V.I. Minkin. J. Mol. Struct. (THEOCHEM) **200**, 61 (1989); (*d*) P.V. Ragué Schleyer and E.-U. Würthwein. J. Chem. Soc. Chem. Commun. 1008 (1982).
14. E. Vedejs, R.W. Chapman, S. Lin, M. Müller, and D.R. Powell. J. Am. Chem. Soc. **122**, 3047 (2000); and refs. therein.
15. W.R. Cullen, S.J. Rettig, J. Trotter, and E.B. Wickenheiser. Can. J. Chem. **66**, 2007 (1988).
16. W. Kliegel, U. Lauterbach, S.J. Rettig, and J. Trotter. Can. J. Chem. **65**, 1457 (1987).
17. W. Kliegel, G. Lubkowitz, S.J. Rettig, and J. Trotter. Can. J. Chem. **69**, 234 (1991); and refs. therein.
18. W. Kliegel, G. Lubkowitz, S.J. Rettig, and J. Trotter. Can. J. Chem. **72**, 1154 (1994).
19. W. Kliegel, H. Amt, H. Becker, U. Lauterbach, G. Lubkowitz, S.J. Rettig, and J. Trotter. Can. J. Chem. **72**, 2118 (1994).
20. W. Kliegel, L. Preu, U. Schumacher, S.J. Rettig, and J. Trotter. Can. J. Chem. **70**, 1176 (1992).
21. P. Paetzold and G. Schimmel. Z. Naturforsch. **35b**, 568 (1980).
22. (*a*) R. Bloch. Chem. Rev. **98**, 1407 (1998); (*b*) M. Lombardo and C. Trombini. Synthesis, 759 (2000).

© 2001 NRC Canada

The syntheses of 6-*C*-alkyl derivatives of methyl α-isomaltoside for a study of the mechanism of hydrolysis by amyloglucosidase

Ulrike Spohr, Nghia Le, Chang-Chun Ling, and Raymond U. Lemieux

Abstract: The epimeric (6a*R*)- and (6a*S*)-*C*-alkyl (methyl, ethyl and isopropyl) derivatives of methyl α-isomaltoside (**1**) were synthesized in order to examine the effects of introducing alkyl groups of increasing bulk on the rate of catalysis for the hydrolysis of the interunit α-glycosidic bond by the enzyme amyloglucosidase, EC 3.2.1.3, commonly termed glucoamylase (AMG). It was previously established that methyl (6a*R*)-*C*-methyl α-isomaltoside is hydrolysed about 2 times faster than methyl α-isomaltoside and about 8 times faster than its *S*-isomer. The kinetics for the hydrolyses of the ethyl and isopropyl analogs were also recently published. As was expected from molecular model calculations, all the *R*-epimers are good substrates. A rationale is presented for the catalysis based on conventional mechanistic theories that includes the assistance for the decomposition of the activated complex to products by the presence of a hydrogen bond, which connects the 4a-hydroxyl group to the tryptophane and arginine units. It is proposed that activation of the initially formed complex to the transition state is assisted by the energy released as a result of both of the displacement of perturbed water molecules of hydration at the surfaces of both the polyamphiphilic substrate and the combining site and the establishment of intermolecular hydrogen bonds, i.e., micro-thermodynamics. The dissipation of the heat to the bulk solution is impeded by a shell of aromatic amino acids that surround the combining site. Such shields are known to be located around the combining sites of lectins and carbohydrate specific antibodies and are considered necessary to prevent the disruption of the intermolecular hydrogen bonds, which are of key importance for the stability of the complex. These features together with the exquisite stereoelectronic dispositions of the reacting molecules within the combining site offer a rationalization for the catalysis at ambient temperatures and near neutral pH. The syntheses involved the addition of alkyl Grignard reagents to methyl 6-aldehydo-α-D-glucopyranoside. The addition favoured formation of the *S*-epimers by over 90%. Useful amounts of the active *R*-isomers were obtained by epimerization of the chiral centers using conventional methods. Glycosylation of the resulting alcohols under conditions for bromide-ion catalysis, provided methyl (6a*S*)- and (6a*R*)-*C*-alkyl-hepta-*O*-benzyl-α-isomaltosides. Catalytic hydrogenolysis of the benzyl groups afforded the desired disaccharides. ^{1}H NMR studies established the absolute configurations and provided evidence for conformational preferences.

Key words: amyloglucosidase (AMG), *exo*-anomeric effect, 6-*C*-alkyl-α-D-glucopyranosides and isomaltosides, mechanism of enzyme catalysis.

Résumé : On a réalisé la synthèse des dérivés (6a*R*) et (6a*S*)-*C*-alkyles (méthyle, éthyle et isopropyle) de l'α-isomaltoside de méthyle (**1**) afin d'étudier les effets provoqués par l'introduction de groupements alkyles de plus en plus volumineux sur la catalyse de l'hydrolyse de la liaison glycosidique α par l'enzyme amyloglucosidase, EC 3.2.1.3, que l'on dénomme souvent glucoamylase (AMG). Il a été établi antérieurement que le (6a*R*)-*C*-méthyl-α-isomaltoside de méthyle s'hydrolyse environ deux fois plus rapidement que l'α-isomaltoside de méthyle et environ huit fois plus rapidement que son isomère *S*. Les mesures cinétiques pour les hydrolyses des analogues éthyle et isopropyle ont aussi été publiées récemment. Tel qu'on pouvait s'y attendre sur la base de calculs sur des modèles moléculaires, tous les épimères *R* sont de bons substrats. On propose une rationalisation de la catalyse qui est basée sur la théorie mécanistique conventionnelle mais qui, pour la décomposition du complexe activé en produits, implique une aide apportée par la présence dans le complexe d'une liaison hydrogène reliant le groupe 4a-hydroxyle aux unités de tryptophane et d'arginine qui se trouvent loin du centre réactionnel. Il est suggéré que le passage du complexe qui se forme initialement à état de transition se produit avec l'aide de l'énergie libérée en raison à la fois du déplacement des molécules d'eau d'hydratation perturbées sur les surfaces tant du substrat polyamphiphile que du site qui se combine ainsi ce que celle qui résulte de la création de liaisons hydrogènes intermoléculaires, de la microthermodynamique. On indique qu'il y a eu empêchement à la dispersion de la chaleur vers l'ensemble du milieu réactionnel causé par une sorte de coquille

Received June 16, 2000. Published on the NRC Research Press Web site on March 16, 2001.

U. Spohr[1], N. Le[2], C.-C. Ling, and R.U. Lemieux.[3] Department of Chemistry, The University of Alberta, Edmonton, AB T6G 2G2, Canada.

[1]Corresponding author (e-mail: uspohr@aol.com).
[2]Taken in part from a Ph.D. Thesis, University of Alberta, 1990.
[3]Deceased.

 DOI: 10.1139/cjc-79-2-238 © 2001 NRC Canada

formée d'acides aminés aromatiques qui entoure le site où se produit la combinaison. De tels coquilles ont déjà été observées autour des sites où se produit la combinaison des lectines et des anticorps spécifiques aux hydrates de carbone et ils sont considérés comme nécessaires pour empêcher l'interruption des liaisons hydrogènes d'importance capitale à la stabilité du complexe. Ces caractéristiques ainsi que les dispositions stéréoélectroniques exquises des molécules qui réagissent à l'intérieur du site où se produit la combinaison permettent de rationaliser la catalyse à la température ambiante et à un pH pratiquement neutre. Les synthèses impliquent l'addition des réactifs de Grignard alkylés sur le 6-aldéhydo-α-D-glucopyranoside de méthyle. L'addition conduit à la formation préférentielle (90%) des épimères *S*. On a obtenu des quantités utiles des isomères actifs, *R*, par épimérisation des centres chiraux à l'aide de méthodes conventionnelles. La glycosylation des alcools qui en résultent, dans des conditions de catalyse par l'ion bromure, a permis d'obtenir les (6a*R*) et (6a*S*)-*C*-alkyl-*O*-benzyl-α-isomaltosides de méthyle. L'hydrogénolyse catalytique des groupes benzyles fournit ensuite les disaccharides désirés. Des études de RMN du ^{1}H ont permis de déterminer les configurations absolues et ont permis d'obtenir des données relatives aux préférences conformationnelles.

Mots clés : amyloglucidase (AMG), effet anomère *exo*, α-D-glucopyranosides et isomaltosides 6-*C*-alkylés, mécanisme de catalyse enzymatique.

[Traduit par la Rédaction]

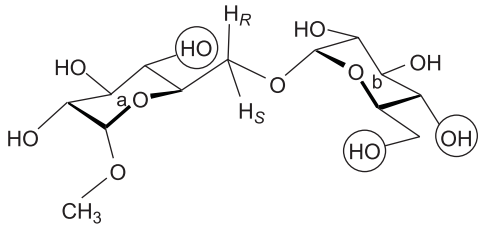
Nomenclature and conventions: The nomenclature follows the general rules of organic chemistry. Thus, the introduction of a methyl group at *C*-6 of methyl α-D-glucopyranoside gives methyl (6*R*)-*C*-methyl-α-D-glucopyranoside not methyl 7-deoxy-β-L-glycero-D-gluco-heptopyranoside. For reasons of clarity and convenience, the so-called "reducing unit" of a disaccharide is termed the *a*-unit. The nonreducing unit is the *b*-unit. The 6a-epimers are given the same compound number but distinguished by their absolute configurations (*R* or *S*). The m, e and i letters that follow the number of a compound are to identify the alkyl substituent: methyl, ethyl or isopropyl, respectively. The rings of glucopyranosides are taken as residing in an essentially rigid $^4C_1$-conformation. The three flexible bonds that link the two glucose units at the 6a-position of an isomaltoside, namely, C-1b-O-6a, O-6a-C-6a and C-6a-C-5a, describe three torsion angles $\phi° =$ O-5b/C-6a, $\psi° =$ C-1b/C-5a, and $\omega° =$ O-6a/O-5a, respectively.

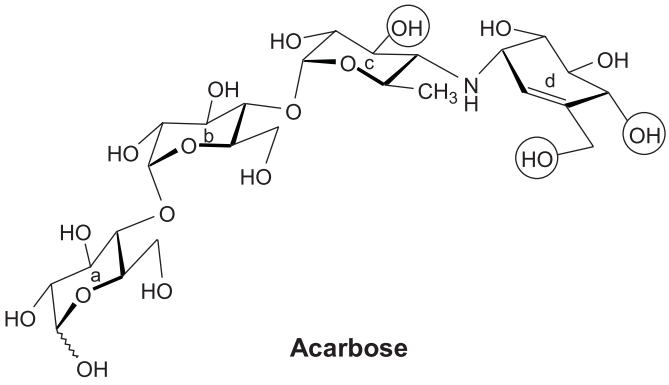
Introduction

The long known (1) industrially important enzyme, amyloglucosidase (EC 3.2.1.3), referred to herein as AMG, is an anomeric-centre inverting exoglycosidase that catalyzes the release of β-D-glucopyranose from the non-reducing end of starch and other related poly- and oligosaccharides (2, 3). AMG catalyzes the hydrolysis of the $1 \rightarrow 4$ linkage of maltose 30–50 times more rapidly than the $1 \rightarrow 6$ linkage of isomaltose. For both substrates three hydroxyl groups were found virtually indispensable, by means of chemical mapping (4, 5), for high enzyme activity. These essential hydroxyl groups circled in Fig. 1 for **1** are located at the 4a, 4b, and 6b positions for both the β- (5) and α- (6) methyl isomaltosides. For methyl β-maltoside these key hydroxyls are located at positions 3a, 4b, and 6b (4). As seen in Table 1, deoxygenation of the 4a-hydroxyl of methyl α-isomaltoside decreases the rate of hydrolysis by about a thousand-fold (6). It is conceivable that the enzyme recognizes the conformation of these substrates that have OH-4a of an isomaltoside (**1**) and OH-3a of a maltoside, which are in similar spatial relationship to the OH-4b and OH-6b of the nonreducing *b*-unit (5).

Chemical mapping (6) of the interaction of methyl α-isomaltoside with AMG proved to be in total agreement with both the kinetic data reported by Bock and co-workers (4, 5)

Fig. 1. The structure of methyl α-isomaltoside that displays the pro-*R* and pro-*S* hydrogen atoms at the *C*-6a position. Acarbose is a strong inhibitor ($\Delta G = -16.3$ kcal mol^{-1}) of the hydrolysis of **1** by the enzyme AMG.





and the X-ray crystal structure of the acarbose–AMG complex (7, 8). Substantially weaker interactions involve the hydroxyl groups at the 3a, 2b, and 3b positions (6). As expected from the X-ray crystal structure of the acarbose–AMG complex the OH-2a (see Table 1) and the aglycon at the 1a position remain in the aqueous phase. The fact that methyl (6a*R*)-*C*-methyl-α-isomaltoside (***R*-2m**) (9) is hydrolyzed 8 times faster than the *S*-epimer (***S*-2m**) suggests, as previously noted (9), that the *C*-methyl group of the *R*-isomer does not impede complex formation. Indeed, Frandsen et al. (10) found that the 6a-*C*-methyl group of ***R*-2m** projects into a surrounding aqueous phase to become hydrophobically associated to the enzyme. In the simulated complex of isomaltoside with AMG (6), it is the pro-*R* hydrogen that

© 2001 NRC Canada

Table 1. The effect of monodeoxygenations and *C*-alkylation on the kinetics for the hydrolysis of methyl α-isomaltoside catalyzed by AMG.

Compound	k_{cat} (s^{-1})	K_m (mM)	k_{cat}/K_m (s^{-1} mM^{-1})	$\Delta\Delta G$ (kcal mol^{-1})
Methyl α-isomaltoside (**1**)[a]	0.88	20.0	4.4×10^{-2}	0
Methyl 2a-deoxy-α-isomaltoside[b]	0.5	19.1	2.6×10^{-2}	0.33
Methyl 4a-deoxy-α-isomaltoside[b]	0.00067	8.8	7.6×10^{-5}	4.02
Methyl 2b-deoxy-α-isomaltoside[b]	0.18	21.2	8.5×10^{-3}	1.04
Methyl (6a*R*)-*C*-methyl-α-isomaltoside[c] (***R*-2m**)	0.68	0.71	9.6×10^{-1}	–1.95
Methyl (6a*S*)-*C*-methyl-α-isomaltoside[c] (***S*-2m**)	1.1	90.0	1.2×10^{-2}	0.82
Methyl (6a*R*)-*C*-ethyl-α-isomaltoside[a] (***R*-2e**)	1.2	3.3	3.6×10^{-1}	–1.33
Methyl (6a*R*)-*C*-isopropyl-α-isomaltoside[a] (***R*-2i**)	0.8	47.0	1.7×10^{-2}	0.56

[a]Data from ref. 10.
[b]Data from ref. 6.
[c]Data from ref. 9.

Table 2. Calculated values for the most energetically favorable conformers of methyl α-isomaltoside and *C*-6a alkylated congeners.

Compound	Conformer[a]	Torsional angles for the 1 → 6 linkages (°)			*E*	$\Delta E_{B\text{-}A}$
		φ	ψ	ω	(kcal mol^{-1})	(kcal mol^{-1})
Methyl α-isomaltoside (**1**)	A	–51	–169	–60	–4.2	
	B	–45	167	163	–0.96	3.3
Methyl (6a*R*)-*C*-methyl-α-isomaltoside (***R*-2m)**	A	–54	89	52	–3.7	
	B	–45	167	163	–1.3	2.4
Methyl.(6a*R*)-*C*-isopropyl-α-isomaltoside (***R*-2i**)	A	–54	70	48	–5.8	
	B	–45	167	163	1.56	7.3

[a]Conformers A are the preferred conformations established by GEGOP calculation. These were found to not be compatible with the combining site of the acarbose–AMG complex. Consequently, the values of the φ, ψ, and ω torsion angles were changed in order to achieve a fit. An acceptable fit could not be achieved keeping the *b*-unit in the chair-conformation. However, a fine fit was obtained on changing the conformation of the *b*-unit to the half-chair conformer. The Δ*E* values refer to the differences in energy that are expected to arise from relaxation of the φ, ψ, and ω torsion angles of the B conformers to those of the A conformers.

projects into the channel of water, which in supports the statement that only the *R*-isomers are good substrates (10). Furthermore, this data suggests that a substantial body of bulk water extends from near the 6a-CH_2 group on the side of the complex that includes the catalytic water molecule. It was on this basis that it had seemed likely that the (6a*R*)-*C*-methyl group of ***R*-2m** could be replaced by bulkier groups and still retain good substrate activity. To test this hypothesis, the ***R*-** and ***S*-2e** (6a-*C*-ethyl) and ***R*-** and ***S*-2i** (6a-*C*-isopropyl) analogs were synthesized and made available to Frandsen et al. (10) for kinetic studies.

We considered that should these compounds (***R*-2e** and ***R*-2i**) prove to be good substrates for AMG that it would also follow that all are accepted into the active site with similar φ, ψ, and ω torsion angles for the inter-unit bonds. It was also thought that the effect of the bulky alkyl groups on the rate of hydrolysis could provide insight to the structure of the transition state since the bulkier groups can be expected to better define the conformational requirements for the inter-unit *C*-5a to *C*-1b linkages.

Discussion

Theoretical discussion

GEGOP calculations (11) were used to estimate the preferred conformations for compounds **1**, ***R*-2m**, and ***R*-2i**. The results are presented in Table 2 as conformers A (see also Fig. 6) and are compared against reference compound methyl α-isomaltoside (**1**). It is seen that the different alkylating groups do not have a large effect on the orientation of the agluconic carbon (*C*-6a) (φ torsion angles range from –51° to –54°). The conformational preferences for the more rigid compounds (***R*-2m** and ***R*-2i**) appear to be similar but are significantly different as compared to the global minimum energy conformation of **1**. This inference is supported by the nuclear Overhauser enhancement (NOE) data presented in Table 3. As expected from the GEGOP calculations (Table 2), saturation of H-1b enhanced the signal for H-6a almost equally for the three 6a-alkylated compounds. The NOE data for the *S*-isomers are also recorded in Table 3, but the *S*-isomers are not further discussed because of their poor performance as substrates for AMG (10).

Prior to a consideration of conformers B, a brief review, for the more salient features of the mechanism for the hydrolysis of an α-D-glucopyranoside by AMG, is useful. An outline is presented in Fig. 2.

The mechanism (Fig. 2) has been established as an acid-base catalyzed reaction. The X-ray crystal structure of the acarbose–AMG complex (7, 8) displays a well situated "catalytic" water molecule for nucleophilic attack at the anomeric centre of the *b*-unit which results in the displacement of the *a*-unit (see Fig. 3). The nucleophilicity of this water molecule is enhanced by the involvement of both of its hydrogen atoms in hydrogen bonds with two oxygen atoms

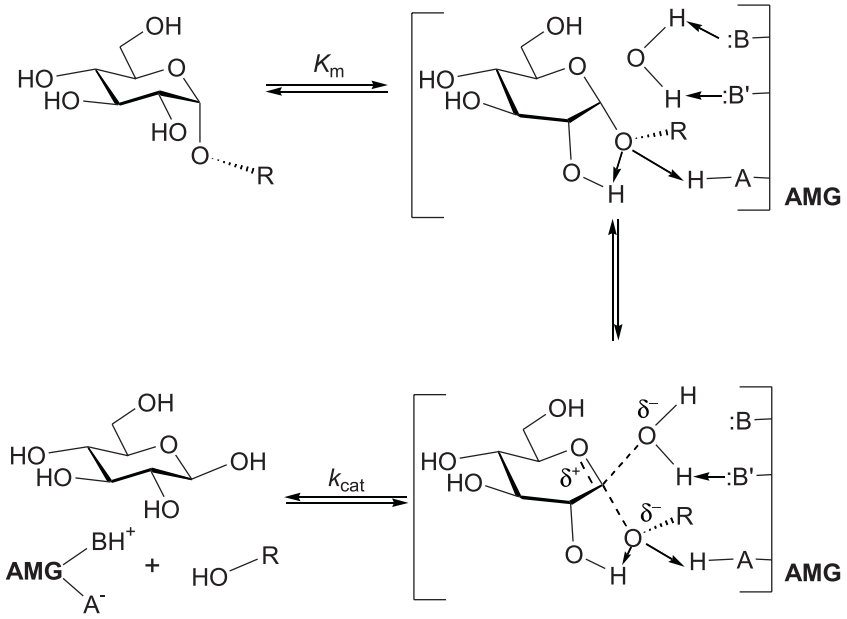
© 2001 NRC Canada

Table 3. NOE of methyl 6-*C*-alkyl-α-isomaltosides (**2m**, **2e**, and **2i**).

Compound	6a-*C*-Substituent	Proton saturated	Proton enhancement (%)			
			H-1b	H-2b	H-6a*R*	H-6a*S*
***R*-2m**	CH_3-	H-1b	—	15.2	—	9.9
***R*-2m**	CH_3-	H-6a	10.8	—	—	—
***R*-2e**	CH_3H_2-	H-1b	—	13.2	—	8.7
***R*-2i**	$(CH_3)_2CH$-	H-1b	—	15.5	—	13.3[a]
***S*-2m**	CH_3-	H-1b	—	9.5	2.4	—
***S*-2e**	CH_3H_2-	H-1b	—	17.1	7.6	—
S-2i	$(CH_3)_2CH$-	H-1b	—	17.7	6.7	—

[a]Signal may contain small contributions from H-4, H-3 signals.

Fig. 2. Schematic of key features in the acid-base catalyzed hydrolysis of an α-D-glucopyranoside by the enzyme amyloglucosidase (AMG). The structural features of **1** that are involved in the formation of the complex are not shown.



(see Fig. 3), one with the carboxylate group of Glu 400 and the other with OH-6b. The OH-6b is also hydrogen bonded to the carboxylate of Asp 55 (7, 8). Experimental evidence in support of this type of delocalization of electron density in conjugated hydrogen bonds was established by Lemieux and Pavia (12) and now termed the "cooperativity effect" (13). These and other interactions expected to be present in the transition state were reviewed in a recent publication (6). The acid catalysis is promoted by proton donation from Glu 179 (Fig. 3), where the acidity of the carboxyl group of Glu 179 is expected to be enhanced by electron donation to a proton on Glu 124 (not shown in Fig. 3). It is to be noted (Table 1) that deoxygenation of OH-2b caused little change in the kinetic parameters. This suggestion that OH-2b is not involved in assisting the leaving of the *a*-unit must take into consideration that 2-deoxyglycosides are much more prone to hydrolysis when the 2-substituent is more electronegative, such as a hydroxyl group. Also, in the case of the 2b-deoxy compound, a water molecule may assist in relaying the electrophilicity of the Arg 305 to the 6a-oxygen atom (6). Certainly, a hydrogen bond between OH-2b and the leaving group can be expected to strengthen as the C-1b—O-6a bond is stretched to achieve the transition state.

The conformation of the valienamine moiety of acarbose (Fig. 1), as previously pointed out (6), provides an acceptable working model for the construction of the transition state where the C-5b, O-5b, C-1b, and C-2b atoms of the *b*-unit are coplanar and the oxygen of the catalytic water molecule, C-1b and the leaving O-6a atoms are colinear. Evidence in support of the structure of the transition state for inversions at anomeric centres was obtained in 1955 (14). The X-ray structure also can serve as a model for the structure of the complex displayed in Fig. 2. Although the mole fraction of the half-chair conformation for the *b*-unit of **1** is undoubtedly very small, its formation once **1** is complexed with AMG must be virtually spontaneous, especially since the active site conforms for the acceptance of acarbose. The B conformers listed in Table 2 are based on this consideration. Accordingly, it is expected that formation of the half-chair conformer will substantially weaken the *endo*- and *exo*-anomeric effects (15) and, thereby, render the anomeric centre more susceptible to nucleophilic attack.

As already mentioned, hydrogen bonding of OH-4a to Trp 178 (assisted by Arg 305) greatly enhances the rate of catalysis. Our attempts to establish these hydrogen bonds using both the *a*- and *b*-units in the $^4C_1$ chair conformation proved

© 2001 NRC Canada

unattractive. However, when the *b*-unit was placed in the half-chair conformation (see Table 2 and Figs. 3 and 6), the same hydrogen-bond networks presented in the acarbose–AMG complex (7, 8) are well established.

As seen in Table 2 the ϕ, ψ, and ω torsion angles for the *b*-unit are the same for each compound. However, large differences in conformational energy are indicated and, therefore, complex formation involving substrate ***R*-2m** should be slightly favored over complexation with **1** and much more than with substrate ***R*-2i**. As seen in Table 1, the kinetically determined K_m values are 20 (**1**), 0.7 (***R*-2m**), and 47 (***R*-2i**). The increase in complexation of AMG with ***R*-2m** as compared to AMG with **1** can be attributed to hydrophobic association of the 6a-C-methyl group with both Trp 120 and Trp 52, as shown in Fig. 4. This hydrophobic association is not present during formation of the **1**–AMG complex. Also, the conformational energy of ***R*-2m** in the complex is expected (Table 2) to be about 0.9 kcal mol^{-1} less than that for substrate **1**. These considerations support an increase in the rate of hydrolysis of ***R*-2m** (10). However, this is not the case for ***R*-2i**. As seen in Table 1, the equilibrium for complex formation (K_m) for ***R*-2i** is much less favorable than it is for ***R*-2m** (K_m = 0.71 for ***R*-2m** vs. 47 for ***R*-2i**). This difference is mainly due to the large conformational strain required to form the ***R*-2i**–AMG complex (Table 2). This resistance to complex formation is undoubtedly strongly moderated by important hydrophobic associations of the two methyl groups of the isopropyl group as is illustrated in Fig. 4*b*. Frandsen et al. (10) employed, in part, this synthetically imposed hydrophobic association in a study of site-specific mutagenic changes in the structure of AMG to conclude that "the versatility of AMG catalysis….emphasizes the significance of hydrophobic interactions in protein-carbohydrate complexation." We suggest that this is not necessarily the case with respect to the classical definition of the driving force for hydrophobic associations which involves the release of ordered water molecules to bulk. The strength of hydrophobic interactions was recently observed in the binding of *N*-acetyllactosamine by the lectin, *Erythrina corallodendron* (16). The X-ray crystal structure of the complex shows a strong association of the H-2, H-4, and H-5 on the α-side of the β-D-galactose unit with the appropriately positioned phenylalanine group. In this regard, although Monte Carlo simulations (17) for the hydration of the β-D-Gal unit of the Lewis b-OMe tetrasaccharide suggest that the formation of a shell of disordered perturbed water molecules extends over the hydrophobic α-side, some ordering of the water molecules cannot be discounted. In either event, the association of complementary surfaces should be energetically favorable in aqueous solution whether ordered or perturbed water molecules are released to bulk.

As seen in Table 2, the *b*-unit of the B conformers are highly strained. We suggest that the relaxation of this conformational strain energy provides the necessary assistance for the stretching of the C-1b—C-6a glycosidic bond and thereby promotes decomposition to the products. This structural feature is key for the catalysis of the hydrogen bonds of OH-4a to Trp 178 and Arg 305. Indeed, as previously noted (10), the k_{cat} values for **1**, ***R*-2m**, ***R*-2e**, and ***R*-2i** are remarkably similar.

Prior to a consideration of hydrophobic forces involved in the binding of **1** by AMG, it is of interest to examine the thermodynamics of the binding of the H-type 2-OMe trisaccharide by the lectin, *Ulex europaeus* (UE-1) (18, 19). The main driving force for binding is enthalpic, ΔH = –29 kcal mol^{-1}, which is countered by a large *decrease* in entropy, $T\Delta S$ = –20.5 kcal mol^{-1} (18). Inspection of the X-ray crystal structure for the UE-I–H-type 2-OMe complex reveals, as seen in Fig. 5, that two hydrophobic interactions are present: one involves Tyr 220 with the C-6 methylene group of the GlcNAc unit and the other involves valine 134 with the *C*-6 methyl group of the α-L-Fuc unit. These interactions, if truly hydrophobic in character, are obviously not compatible with the aforesaid thermodynamic parameters that show a decrease in entropy rather than an increase in entropy as expected for hydrophobic association. The proximity of these groups to the trisaccharide requires the displacement of water. Judging from the thoroughly polyamphiphilic surface (20) of the H-type 2-OMe molecule (19), perturbed water molecules must have been displaced, as in the case of Tyr 220. The interaction of Val 134 with the *C*-6-methyl group of the fucosyl group may result in an increase in entropy from the disordering of water molecules in an endothermic process. However, these contributions, if present, are strongly obscured by the large decreases in both enthalpy and entropy that are expected to arise mainly from the return of perturbed water molecules from both the combining site and the epitope of the trisaccharide to bulk (21, 22). This process has been termed the *hydraphobic* effect.

The binding of **1** with AMG is similar in that along with the establishment of numerous attractive polar interactions one hydrophobic group comes into close contact with disaccharide **1**. As seen in Fig. 4, the only nonpolar contact of less than 2.5 Å (omitting the interactions with the *R*-6a-methyl and *R*-6a-isopropyl groups) is between Trp 317 and H-2b. The presence of this large aromatic amino acid unit in the epitope is expected to contribute to the stability of the complex, since, along with the release of the ordered water molecules at its surface, it is also expected to participate in the release of perturbed water molecules from the polyamphiphilic surface of the substrate (**1**). This is clearly evident from the CPK molecular models displayed in Fig. 6.

The thermodynamic parameters for the hydrolysis of **1** catalyzed by AMG are not known. However, in view of the extensive polyamphiphilic surface of **1** and that of the complementary combining site, it is expected that complexation involves the release of a large number of perturbed water molecules (21). The decrease in enthalpy that is expected to result is amplified by the formation of nine intermolecular hydrogen bonds (see Fig. 3). In view of this large polar contribution and the paucity of hydrophobic interactions, the formation of the complex must result in a substantial (perhaps as great as 60 kcal mol^{-1}) decrease in enthalpy. As will be discussed below, the liberation of this heat is expected, as previously discussed (21), to participate in promoting the complex to the transition state (6) (see Fig. 2).

However, Sigurskjold et al. (23) have determined that the binding of the inhibitor acarbose by AMG is driven by both enthalpic (ΔH = –9.7 kcal mol^{-1}) and entropic ($T\Delta S$ = 6.6 kcal mol^{-1}) values. The increase in entropy is expected to arise from an important hydrophobic contribution. This is

© 2001 NRC Canada

Fig. 3. A display of the intermolecular hydrogen bonds that are formed during the binding of **1** in the half-chair conformation and *C*-6a-alkyl derivatives (R = H, Me, Et, or *i*-Pr) into the site occupied by the *c*- and *d*-units of acarbose.

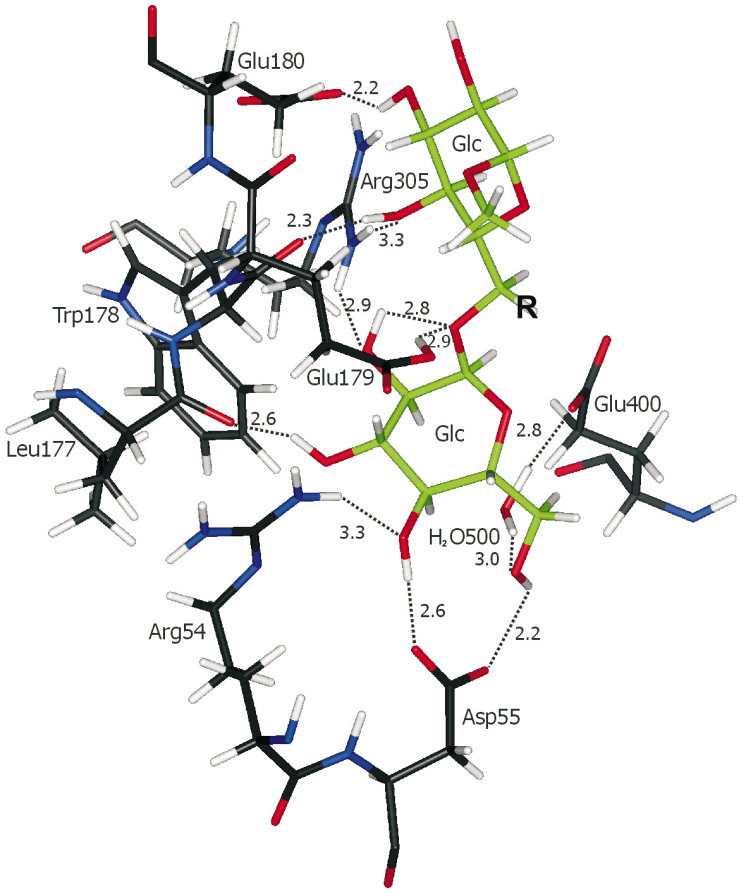
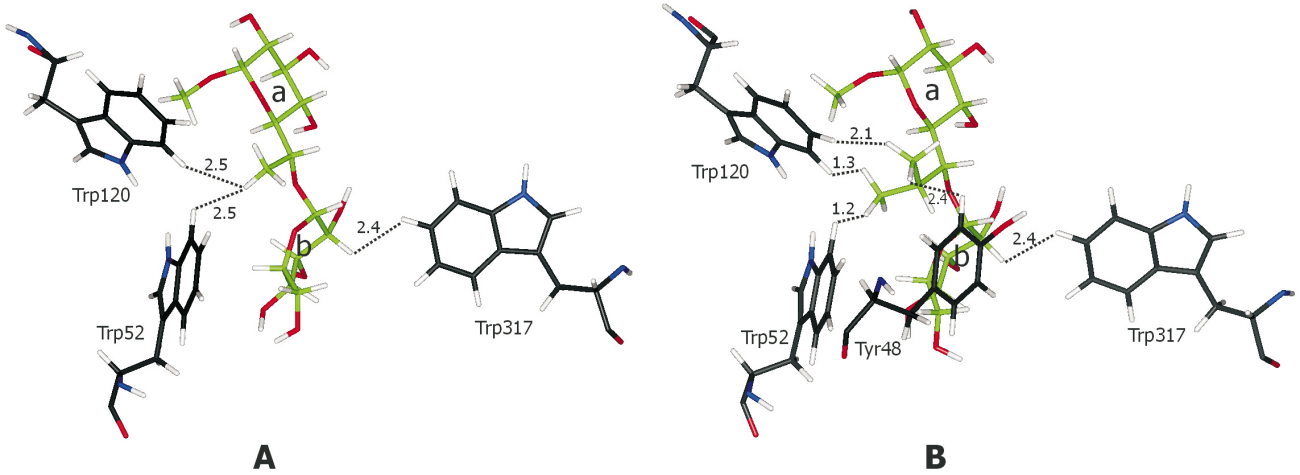


Fig. 4. Display of the near van der Waals' contacts of hydrophobic groups of AMG with nonpolar hydrogen atoms of 6a-alkyl derivatives of **1**. The hydrophobic associations of the methyl group of ***R*-2m** and the isopropyl group of ***R*-2i** are not present in the complex formed with **1**. Consequently, it appears that the only van der Waals contact with **1** involves a hydrogen of Trp 317 that is 2.4 Å away from *H*-2b.



not surprising since the terminal unit of the pseudo-tetrasaccharide (Fig. 1) is a derivative of cyclohexene, which along with the *C*-6a-methyl group of the neighboring 6-deoxy glucose the cyclohexene like unit offers a substantial hydrophobic surface to the aqueous phase (see Fig. 1). The ordered water molecules, along with disordered water molecules hydrogen bonded to the binding site, must be displaced during the binding process. Evidently, the increase in entropy caused by the hydrophobic component dominates the decrease in entropy expected from hydrophobic contributions.

© 2001 NRC Canada

Fig. 5. The structures of the complex of the lectin *Ulex europaeus* (UE-I) and the H-type 2–OMe trisaccharide (α-L-Fuc(1→2)β-D-Gal(1→4)β-D-GlcNAc-OMe) obtained by docking into the combining site of UE-I, which accepts (*R*)-2-methyl-2,4-pentanediol (L.T.J. Delbaere and M. Vandonselaar, private communication). Structure A identifies the key intermolecular hydrogen bonds that are required to established the formation of the complex. Structure B identifies the near van der Waals' contacts established between Tyr 220 and the β-D-GlcNAc and β-D-Gal units and of Val 134 with the α-L-Fuc unit.

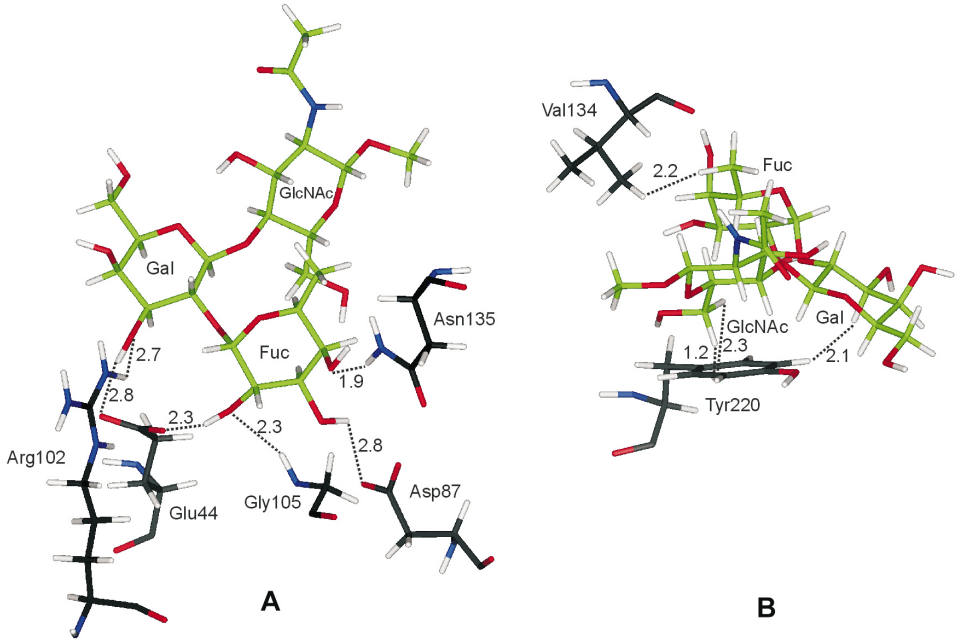
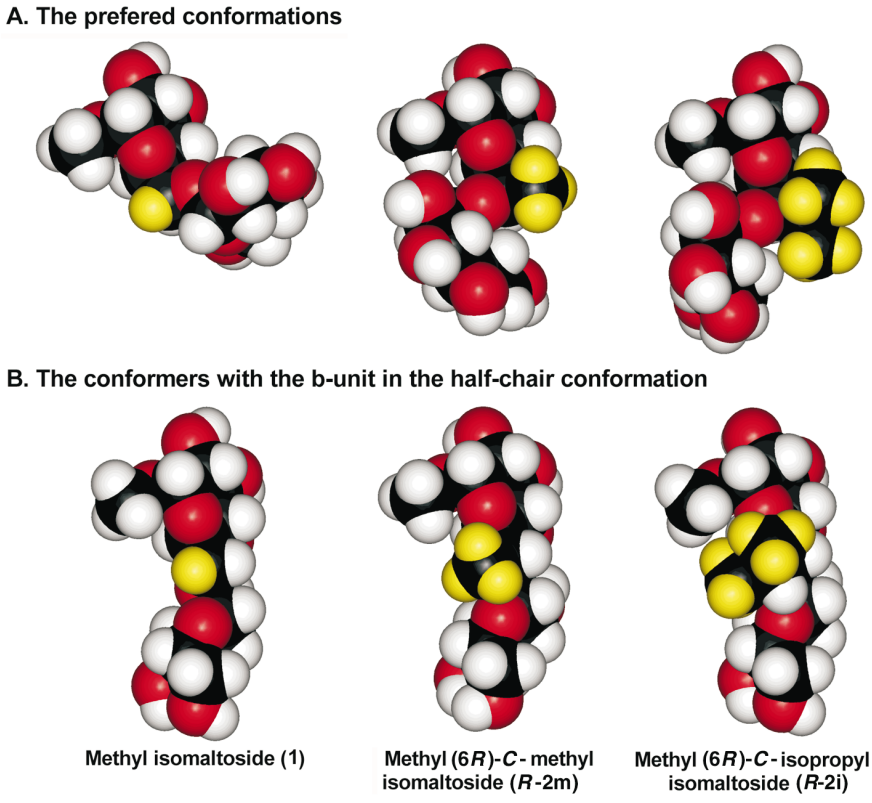


Fig. 6. CPK models based in GEGOP calculations that display the polyamphiphilic surface of substrates **1**, ***R*-2m**, and ***R*-2i**: (*a*) the three preferred conformations in aqueous solution. The pro-*R* hydrogen of **1** is presented in yellow as are the methyl groups of ***R*-2m** and ***R*-2i**. Introduction of the alkyl groups at position 6a results in a similar conformation which is different than that of **1**; (*b*) CPK models representation of the preferred conformation with the *b*-unit in the half-chair conformation with all ***R*-6a** substituents pointing in the same direction. These conformers allow hydrogen bonding between OH-4a and both Trp 178 and Arg 305.



© 2001 NRC Canada

Fig. 7. This graphic is of AMG looking down to the combining site that is occupied by ***R*-2m** (white–hydrogens, green–carbons, and red–oxygen atoms). It is seen that a channel exists for water molecules to access the OH-3a region of the active site. The 6a-methyl group, which remains in the aqueous phase, is visible just below the methoxy group. The yellow atoms belong to aromatic side chains of amino acids that surround the active site, as shown in Fig. 8.

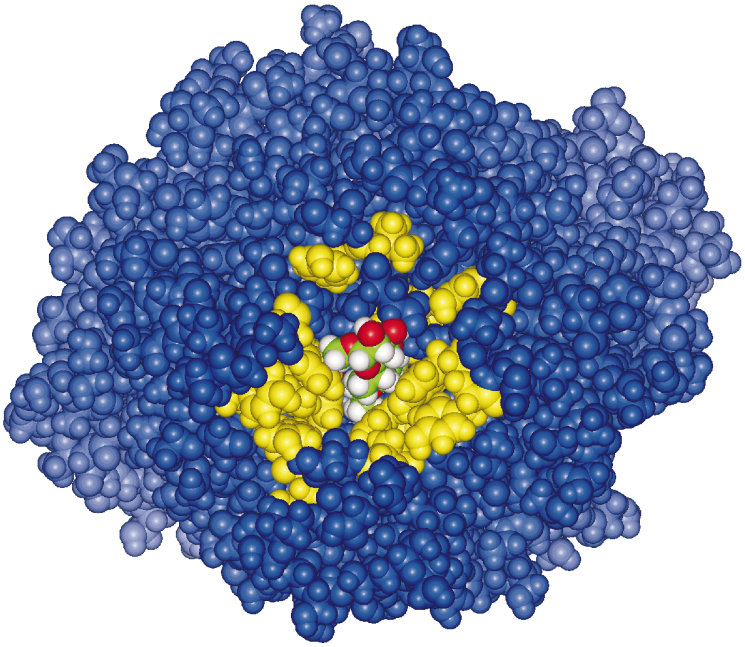
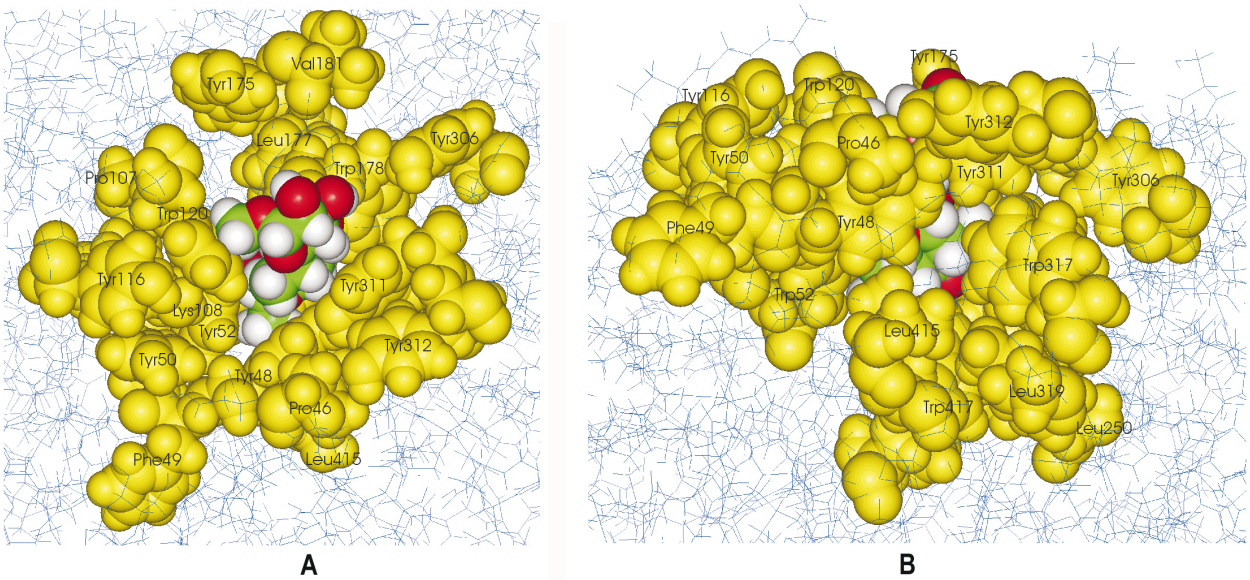


Fig. 8. The aromatic shield that protects the polar interactions (Fig. 2) in the complex from being disrupted by water: (*a*) is a close-up (amino acids are removed for clarity); (*b*) is a side view of the shield of largely nonpolar aromatic groups that is expected to provide thermal insulation of the heat of dehydration to assist achievement of the transition state. The slit in the shield through which a position of the substrate can be viewed does not exist but is occupied by other nonaromatic amino acid residues. The apparent close-packing is not real. However, their proximities are sufficient to provide effective protection of the polar interaction of the complex.

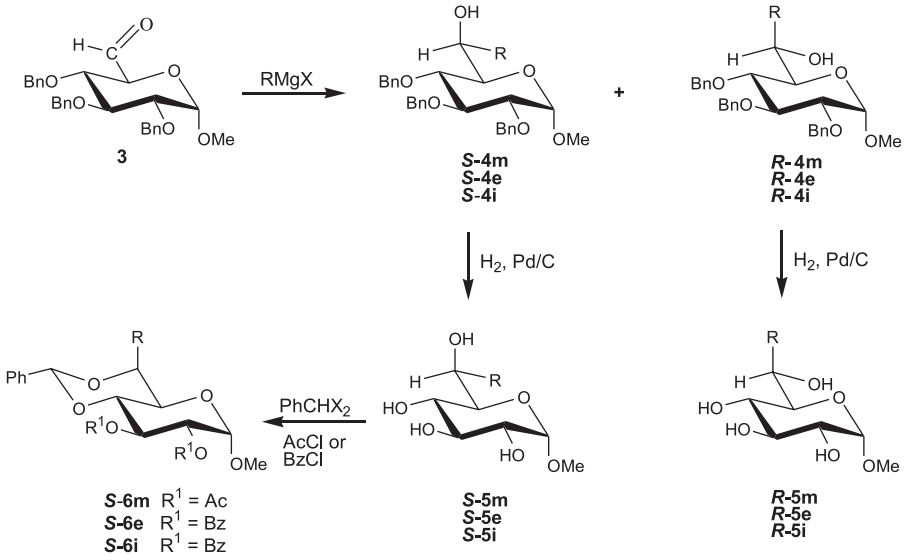


The heat liberated from the latter effect is large enough to cancel the endothermicity of the hydrophobic contribution by 9.7 kcal mol^{-1} and, consequently, the strong exothermicity of the binding of **1** by AMG is supported. Recall that this is the source of heat required to activate the complex to the transition state.

In 1990, Delbaere et al. (24) noted that for the Lewis b–*Griffonia simplicifolia* complex many of the amino acids, except for the diglycine bridge, near the periphery of the polar receptor site have aromatic side chains. These structural features were also observed for antibodies (25) and appear to be necessary for the combining site of all carbohydrate-binding

© 2001 NRC Canada

Scheme 1.



proteins. In general, carbohydrates are held in the cavity mainly by attractive polar interactions in the form of intermolecular hydrogen bonds. Hydrophobic associations are present and important, especially in the case of antibodies (25), but are of minor importance for the binding of oligosaccharides by many lectins. In this regard, the driving force for association is provided by a strong *decrease* in enthalpy and a slight *decrease* in entropy. Clearly, binding occurs in cavities in order to avoid disrupting the association of polar bonds with the bulk water. We suggest that the purpose of the largely aromatic coating surrounding of the polar complex is to provide a strong shield from the bulk water. Not surprisingly, therefore, the active site of the enzyme AMG that binds isomaltose is surrounded by amino acids that contain aromatic side chains (see Fig. 7). These large hydrophobic groups are expected to act as a shield and thus, at high concentrations, prevent water from seeping into the complex. It has been proposed that lower dielectric constants in the binding in a cavity favor the formation of the polar bonds. However, this stabilization of polar bonds must also apply to the water molecules that are displaced by the carbohydrate.

Finally, we propose that the shield of hydrophobic aromatic groups that surround the catalytic site of AMG (see Fig. 8) also serves as thermal insulation to lower the rate of the dissipation of the heat of complex formation (the hydraphobic effect) to bulk. This energy is expected to be the main source of activation for the **1**–AMG complex to the transition state (Fig. 2). This concept of heat being liberated from reacting molecules and being maintained in a suitable submicro-environment to eventually serve as the activation energy for another reaction may be a general feature of enzyme catalysis. This proposal is similar to the energy dissipation in enzyme catalysis proposed by Cramer and Freist (26).

Synthesis

The syntheses of the 6-*C*-alkyl glucosides **4m**, **4e**, and **4i** (Scheme 1) started from the known methyl 6-aldehydo-α-D-glucopyranoside (**3**) (27) that was prepared by oxidation of methyl 2,3,4-tri-*O*-benzyl-α-D-glucopyranoside (28). Molecule **3** was then reacted with the methyl, ethyl and isopropyl Grignard reagents in the usual fashion to yield mixtures of the *R*- and *S*-epimers, namely, the 6-*C*-methyl, 6-*C*-ethyl, and 6-*C*-isopropyl glucosides, (**4m**, **4e**, and **4i**). In agreement with Cram's rule (29), the *S*-isomers were produced in excess. The ratio of the *S*- to *R*-epimers was about 10:1 for **4m** and **4e** and 20:1 for **4i**.

In the case of the methyl Grignard, procedures to prepare ***R*,*S*-4m**, involved converting the crude product into a mixture of 6-*O*-(3,5-dinitrobenzoyl) esters from which the *S*-isomer crystallized and was purified by recrystallization. Zemplen methanolysis then provided the pure ***S*-4m**. The crude products obtained from the ethyl and isopropyl Grignard reagents could be separated by column chromatography into the pure *R*- and *S*-isomers. As will be described below (Schemes 2 and 3) larger amounts of the *R*-isomers, in each case, were obtained by inversion of the C-6 chiral centres of the *S*-compounds.

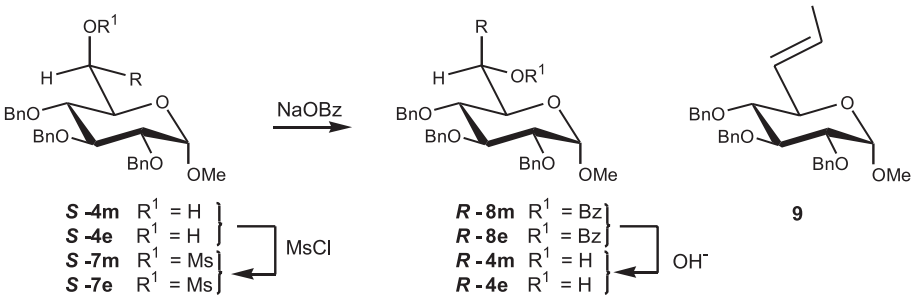
Both the *R*- and *S*-epimers of **4m**, **4e,** and **4i** were debenzylated by catalytic hydrogenolysis to obtain pure preparations of both the *R*- and *S*-*C*-6-epimers, **5m**, **5e**, and **5i (**Scheme 1).

For the configurational assignments, the *S*-isomers, (***S*-5m**, ***S*-5e**, and ***S*-5i**), were converted into the 4,6-*O*-benzylidene derivatives (***S*-6m**, ***S*-6e**, and ***S*-6i**) by reaction with α,α-dibromo- or α,α-dichlorotoluene in pyridine at elevated temperature followed by acylation. The absolute configuration of compound ***S*-6m** was unequivocally established by the NOE's obtained by saturation of the axial C-6 methyl group (see Table 4). The configurations of compounds ***S*-6e** and ***S*-6i** are assigned on the basis that the $J_{5,6}$ coupling constants (reported in Table 4). The coupling constant of 6.0 Hz is too small for coupling of antiperiplanar hydrogen atoms. Furthermore, the value of $J_{5,6}$ of ***S*-6m**, a compound of known configuration, is essentially the same as those for ***S*-6e** and ***S*-6i**, indicates that all three compounds are configurationally related. It is also relevant that these three *S*-compounds were the major products of the Grignard reactions and, therefore, are surely configurationally related.

For the preparation of larger amounts of ***R*-4m** and ***R*-4e** (Scheme 2), mesylated ***S*-7m** and ***S*-7e** were prepared and reacted with sodium benzoate in *N*,*N*-dimethylformamide at

© 2001 NRC Canada

Scheme 2.



Scheme 3.

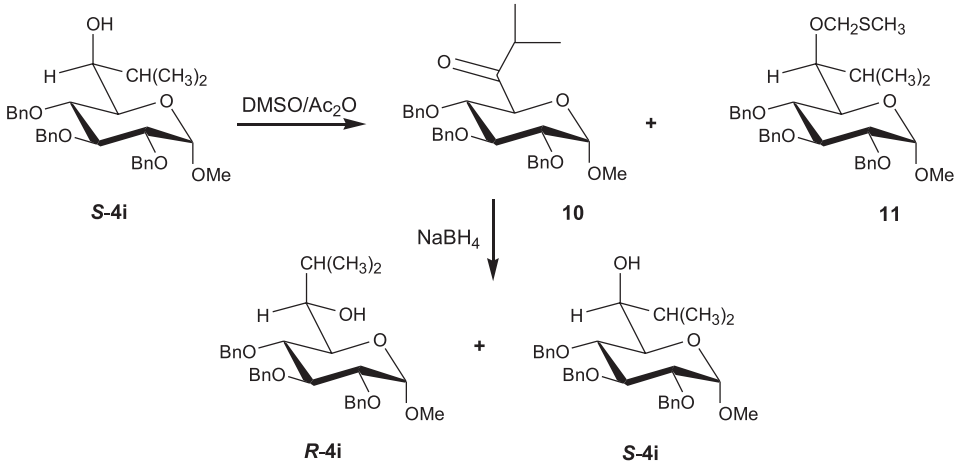


Table 4. ^{1}H NMR chemical shifts (ppm) and coupling constants (Hz) in $CDCl_3$ for the benzylidene derivatives ***S*-6m**[a], ***S*-6e**, and ***S*-6i**.

	***S*-6m**	***S*-6e**	***S*-6i**
H-1 ($J_{1,2}$)	4.93 (3.5)	5.15 (3.5)	5.16 (3.5)
H-2 ($J_{2,3}$)	4.87 (10.0)	5.19 (9.5)	5.21 (9.5)
H-3 ($J_{3,4}$)	5.57 (9.0)	6.04 (9.5)	6.06 (9.5)
H-4 ($J_{4,5}$)	3.91 (10.0)	4.15 (10.0)	4.21 (10.0)
H-5 ($J_{5,6}$)	4.15 (6.0)	4.33 (6.0)	4.43 (5.5)
H-6 ($J_{6,CH_{1,2,3}}$)	4.50 (7.0)	4.25 (3.5,11.0)	3.88 (10.0)
C*H*Ph	5.80	5.78	5.72
CH_3O	3.41	3.43	3.43
CH_3	1.48	1.13 (7.5)	1.15, 1.13 (6.5)
$CH_{(1,2)}$	—	2.18, 1.79	2.62

[a]NOE experiments performed by irradiation of the CH_3-C6 doublet at 1.48 ppm caused enhancements of the *H*-6, *H*-4, and C*H*Ph signals by 6.2%, 2.9%, and 4.1%, respectively.

120°C followed by saponification of the products. Dehydromesylation of ***S*-7e** also resulted in compound **9**. Its *E*-configuration was assigned by the large $J_{5,6}$ coupling constant (14.5 Hz) (30).

The inversion of configuration at *C*-6 of ***S*-4i** (Scheme 3) to obtain ***R*-4i** was achieved by reduction of ketone **10** with sodium borohydride. Ketone **10** was prepared by oxidation of ***S*-4i** with dimethylsulfoxide and acetic anhydride (31). The crude product was mixture of ketone **10** and methylthiomethylene ether **11** (3:2). The borohydride reduction of **10** provided an epimeric mixture of ***R*-4i** and ***S*-4i** (5:1).

Preparation of the α-linked disaccharides ***R*-2m**, ***R*-2e**, and ***R*-2i** is outlined in Scheme 4. Bromide-ion catalyzed glycosylation conditions using 6-*O*-acetyl-2,3,4-tri-*O*-benzyl-α-D-glucopyranosyl bromide (**12**), tetraethylammonium bromide (32) and alcohol ***R*-4m** produced ***R*-14m**. Coupling of tetra-*O*-benzyl-α-D-glucopyranosyl bromide (**13**) with alcohols ***R*-4e** and ***R*-4i** was achieved in the presence of the cupric bromide–*N*,*N*-dimethylformamide complex (33). The protecting groups were removed in the usual manner to yield the desired compounds. The *C*-6a epimeric disaccharides ***S*-2m**, ***S*-2e**, and ***S*-2i** were prepared by similar procedures.

The ^{1}H NMR data for the disaccharides are presented in Table 5. The large ^{1}H coupling constants for $J_{2,3}$, $J_{3,4}$, and $J_{4,5}$ confirm the $^4C_1$-conformations of the pyranose rings. The $J_{5,6}$ coupling constants are ≤2.5 Hz. This suggests that a positive synclinal (+g) relationship exists between H-5a and H-6a, which is in agreement with the calculated ω angles for the two conformers A and B presented in Table 2.

Experimental

General methods

The ^{1}H NMR spectra were measured at 300 MHz and 360 MHz (Bruker AM 300 and WM 360) with tetramethylsilane as internal standard for $CDCl_3$ solutions. Reference standard for D_2O solutions was acetone (2.23 ppm). The ^{13}C NMR spectra were recorded at 75 MHz

© 2001 NRC Canada

Scheme 4.

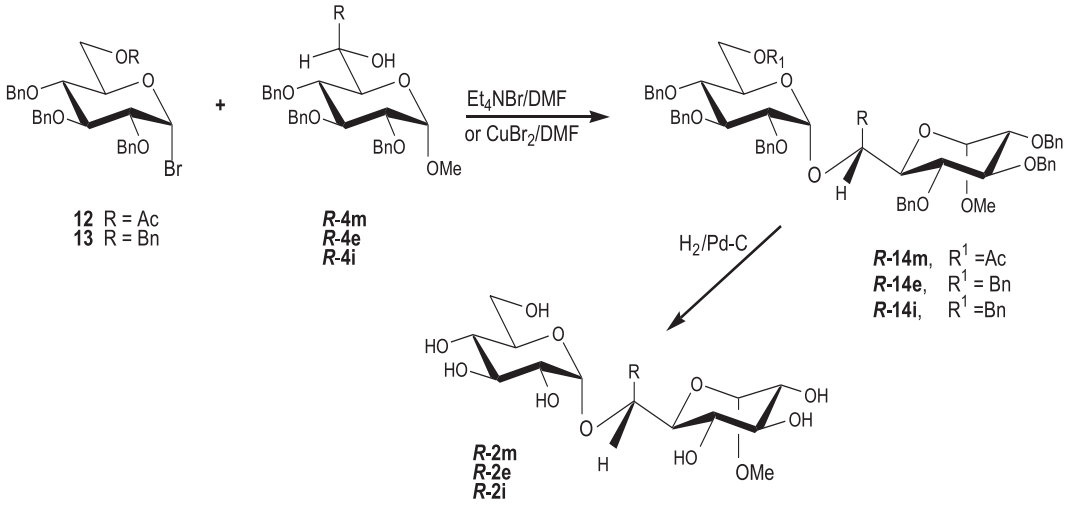


Table 5. ^{1}H NMR chemical shifts (ppm) and coupling constants (Hz) for methyl 6-*C*-methyl, -ethyl-, and -isopropyl-α-isomaltosides[a].

	(6*R*)-*C*-alkyl-isomaltosides			(6*S*)-*C*-alkyl-isomaltosides		
	***R*-2m**	***R*-2e**	***R*-2i**	***S*-2m**	***S*-2e**	***S*-2i**
a-unit						
H-1 ($J_{1,2}$)	4.80 (4.0)	4.78 (3.5)	4.79 (3.5)	4.85 (4.0)	4.84 (3.5)	4.81 (3.5)
H-2 ($J_{2,3}$)	3.57 (9.5)	3.56 (9.5)	3.58	n.a.	3.55 (9.5)	3.51
H-3 ($J_{3,4}$)	3.67 (9.0)	3.66 (9.0)	3.65	n.a.	3.63	3.63 (9.5)
H-4 ($J_{4,5}$)	3.39 (10.5)	3.47 (9.5)	3.68	n.a.	3.57	3.53 (9.5)
H-5 ($J_{5,6}$)	3.83 (2.5)	3.89 (1.5)	3.92 (1.5)	3.64	3.77 (<1)	3.90 (<1)
H-6 ($J_{6,CH}$)	4.17	3.94 (~5)	3.67 (~6.5)	4.28	3.98 (4.5, 9.5)	3.97 (5.5)
$CH_{(2)}$	—	1.71	2.15	—	1.77	2.29
CH_3	1.29 (6.5)	1.02 (7.5)	1.025 (6.5)	1.28 (6.5)	0.94 (7.2)	1.04 (7.5)
CH_3	—	—	1.018 (6.8)	—	—	1.03 (7.5)
CH_3O	3.44	3.44	3.43	3.43	3.45	3.51
b-unit						
H-1 ($J_{1,2}$)	5.07 (3.5)	5.12 (3.5)	5.20 (3.5)	5.09 (3.5)	5.12 (3.5)	5.17 (3.5)
H-2 ($J_{2,3}$)	3.55 (9.5)	3.57 (10.0)	3.56 (9.5)	3.56 (9.5)	3.54 (10.0)	3.57 (9.5)
H-3 ($J_{3,4}$)	3.73 (10.0)	3.74 (9.5)	3.74	3.69	3.70	3.77 (9.0)
H-4 ($J_{4,5}$)	3.41	3.42 (9.5)	3.41 (9.5)	3.43	3.44 (9.5)	3.46 (9.5)
H-5	n.a.	3.82	3.83	n.a.	3.73	3.74
H-6 ($J_{5,6}$)	3.88 (5.0)	3.85–3.78	n.a.	n.a.	n.a.	3.83
H-6′ ($J_{5,6'}$)	3.76 (4.0)	n.a.	n.a.	n.a.	n.a.	3.80

[a]Spectra recorded in D_2O with acetone as internal reference set at 2.23 ppm at 360 MHz.

with dioxane (67.4 ppm) as reference for D_2O solutions and the $CDCl_3$ signal (77.0 ppm) as reference in $CDCl_3$ solutions. Optical rotations were measured at room temperature (23 ± 1°C) in a 1 dm cell on a Perkin–Elmer 241 polarimeter. Thin-layer chromatography was performed on precoated plates of silica gel (60-F254, E. Merck, Darmstadt) and visualized by spraying with 5% sulfuric acid in ethanol followed by heating. For column chromatography, silica gel 60 (230–400 mesh, E. Merck, Darmstadt) and distilled solvents were used. All solvents and reagents were purified and dried according to standard procedures. Melting points are uncorrected.

The molecular modeling was carried out on an SGI Indigo II. A suite of software from Molecular Simulations Inc., San Diego, was used to build and minimize the (6*R*)-*C*-alkylated glucopyranosyl units using AMBER forcefield. The coordinates of these (6*R*)-*C*-alkylated glucopyranosyl units were then exported to the GEGOP program[4] (11) for use in grid searchs, minimizations, and Monte-Carlo simulations.

[4] R. Stuike-Prill and B. Meyer. Geometry of GlycOProteins. Version 2.6. 1992.

© 2001 NRC Canada

Methyl 6-aldehydo-2,3,4-tri-*O*-benzyl-α-D-glucopyranoside (3)

Dried chromium trioxide (25.9 g, 259 mmol) was added to a solution of pyridine (40.9 g, 517 mmol) in dichloromethane (400 mL). The mixture was mechanically stirred at room temperature for 30 min. A solution of methyl 2,3,4-tri-*O*-benzyl-α-D-glucopyranoside (28) (10.0 g, 21.6 mmol) in dichloromethane (22 mL) was rapidly added and the resulting mixture stirred at room temperature for 10 min. The reaction mixture was then decanted and the black tarry precipitate was extracted with ether several times. The combined organic solutions were filtered through a pad of silica gel-G to provide a colorless slightly yellow oily residue which was co-evaporated with toluene (2 × 200 mL) to remove residual pyridine. The oily residue was dried under vacuum overnight before use to give crude **3** (6.94 g, 70%). The relative intensity of the singlet at 9.65 ppm (^{1}H NMR) attributed to H-6 indicated an about 90% content of **3**. $[\alpha]_D$ + 8.2° (*c* 1.0, chloroform), lit. (27) 13.6° (*c* 2.6, chloroform). IR (cm^{-1}): 1741 (CHO). ^{1}H NMR ($CDCl_3$) δ: 9.65 (s, 1H, *H*-6), 7.40–7.10 (m, 15H, 3*Ph*), 5.05–4.50 (m, 7H, 3CH_2Ph, *H*-1), 4.17 (d, $J_{4,5}$ = 10.0 Hz, 1H, *H*-5), 4.08 (dd, $J_{3,4}$ = 9.0 Hz, $J_{2,3}$ = 9.5 Hz, 1H, *H*-3), 3.57 (dd, $J_{3,4}$ = 9.0 Hz, $J_{4,5}$ = 10.0 Hz, 1H, *H*-4), 3.50 (dd, $J_{1,2}$ = 3.5 Hz, $J_{2,3}$ = 9.5 Hz, 1H, *H*-2), 3.38 (s, 3H, CH_3O).

Methyl 2,3,4-tri-*O*-benzyl-(6*S*)-*C*-methyl-α-D-glucopyranoside (*S*-4m)[5]

A solution of the crude aldehyde **3** (6.94 g, 15.0 mmol) in ether (30 mL) was added dropwise to a 0.6 N methylmagnsesium iodide solution in ether (50 mL, 30 mmol) and the reaction mixture was stirred at room temperature for 2 h. The reaction was quenched by the dropwise addition of aq sat. ammonium chloride. The mixture was diluted with water, extracted with ether and the organic solution was dried and evaporated to provide a yellow oil (5.96 g). The ^{1}H NMR spectrum was consistent with the presence of the desired compounds ***S*-4m** and ***R*-4m** in the ratio of about 10:1.

The crude mixture of ***S*-4m** and ***R*-4m** (0.59 g, 1.2 mmol) was reacted in pyridine (10 mL) with 3,5-dinitrobenzoyl chloride (0.51 g, 2.25 mmol) in the presence of a catalytic amount of 4-dimethylaminopyridine (few milligrams). The reaction mixture was stirred at room temperature until analysis by TLC indicated the reaction was completed. The usual work-up provided a yellow residue which crystallized spontaneously and was recrystallized from methanol. The compound characterized as the 6-*O*-(3,5-dinitrobenzoyl) derivative of ***S*-4m**, namely methyl 2,3,4-tri-*O*-benzyl-6-*O*-(3,5-dinitrobenzoyl)-(6S)-*C*-methyl-α-D-glucopyranoside, was obtained in 74% yield (0.612 g), mp 68–70°C. $[\alpha]_D$ + 52.2° (c 0.85, chloroform).

The 6-*O*-(3,5-dinitrobenzoyl) derivative of ***S*-4m** (1.00 g, 1.49 mmol) was dissolved in dioxane (50 mL) followed by the addition of 1 N sodium hydroxide solution (20 mL). After stirring for 1 h, the mixture was diluted with dichloromethane and filtered over a pad of silica gel-G, the organic solution was washed with water, dried and evaporated to give ***S*-4m** (0.69 mg, 97%) as a solid, mp 82–84°C. $[\alpha]_D$ + 26.9° (c 1.0, chloroform). ^{1}H NMR ($CDCl_3$) δ 7.40–7.20 (m, 15H, 3*Ph*), 5.01–4.63 (3ABq, 6H, 3CH_2Ph), 4.58 (d, $J_{1,2}$ = 3.5 Hz, 1H, *H*-1), 4.05 (dq, $J_{5,6}$ = 1.5 Hz, $J_{6,CH3}$ = 6.5 Hz, 1H, *H*-6), 3.99 (dd, $J_{3,4}$ = 9.0 Hz, $J_{2,3}$ = 9.5 Hz, 1H, *H*-3), 3.62 (dd, $J_{4,5}$ = 10.0 Hz, $J_{3,4}$ = 9.0 Hz, 1H, *H*-4), 3.50 (dd, $J_{2,3}$ = 9.5 Hz, $J_{1,2}$ = 3.5 Hz, 1H, *H*-2), 3.42 (dd, $J_{5,6}$ = 1.5 Hz, $J_{4,5}$ = 10.0 Hz, 1H, *H*-5), 3.34 (s, 3H, CH_3O), 1.25 (d, $J_{6,7}$ = 6.5 Hz, 3H, CH_3C-6). Anal. calcd. for $C_{29}H_{34}O_6$: C 72.78, H 7.16; found: C 72.94, H 6.82.

Methyl 2,3,4-tri-*O*-benzyl-(6*S*)-*C*-ethyl-α-D-glucopyranoside (*S*-4e) and -(6*R*)-C-ethyl-α-D-glucopyranoside (*R*- 4e*)*

A solution of crude methyl 6-aldehydo-2,3,4-tri-*O*-benzyl-α-D-glucopyranoside (**3**) (1.6 g, 3.46 mmol) in tetrahydrofuran (20 mL) was transferred slowly into a 0.5 N ethylmagnesium chloride solution in tetrahydrofuran (21 mL, 10.1 mmol) with stirring. After 1 h, the reaction was processed as described for ***S*-4m**. The crude material was applied to a column of silica gel (hexane–ethyl acetate, 5:1, 4:1) to provide in the main fraction the title compound ***S*-4e** (1.043 g, 61%) as a syrup. $[\alpha]_D$ + 12° (c 1.4, chloroform). ^{1}H NMR ($CDCl_3$) δ: 7.38–7.22 (m, 15H, 3*Ph*), 5.01–4.64 (3ABq, 6H, 3CH_2Ph), 4.56 (d, $J_{1,2}$ = 3.5 Hz, 1H, *H*-1), 3.99 (t, $J_{2,3} \sim J_{3,4}$ = 9.0 Hz, 1H, *H*-3), 3.70 (m, *H*-6), 3.66 (t, $J_{3,4} \sim J_{4,5}$ = 9.5 Hz, 1H, *H*-4), 3.53 (br d, $J_{5,6}$ < 1 Hz, 1H, *H*-5), 3.49 (dd, $J_{1,2}$ = 3.5 Hz, $J_{2,3}$ = 9.5 Hz, 1H, *H*-2), 3.35 (s, 3H, CH_3O), 1.67 (m, 1H, CH_2CH$_3$), 1.50 (m, 1H, CH_2CH$_3$), 0.95 (t, *J* = 7.5 Hz, 3H, CH_3CH$_2$). Anal. calcd. for $C_{30}H_{36}O_6$: C 73.15, H 7.37; found: C 73.26, H 7.32. Continued development of the column eluted epimer methyl 2,3,4-tri-*O*-benzyl-(6*R*)-*C*-ethyl-α-D-glucopyranoside (109 mg, 6.4%) as a crystallizing syrup. $[\alpha]_D$ + 35° (*c* 0.4, chloroform). ^{1}H NMR ($CDCl_3$) δ: 7.40–7.20 (m, 15H, 3*Ph*), 5.04–4.61 (3ABq, 6H, 3CH_2Ph), 4.55 (d, $J_{1,2}$ = 3.5 Hz, 1H, *H*-1), 4.02 (t, $J_{2,3} \sim J_{3,4}$ = 9.0 Hz, 1H, *H*-3), 3.70–3.63 (m, 1H, *H*-5, *H*-6), 3.50 (dd, $J_{1,2}$ = 3.5 Hz, $J_{2,3}$ = 9.5 Hz, 1H, *H*-2), 3.49 (t, $J_{3,4} \sim J_{4,5}$ = 9.0 Hz, 1H, *H*-4), 3.38 (s, 3H, CH_3O), 1.54 (m, 1H, CH_2CH$_3$), 1.42 (m, 1H, CH_2CH$_3$), 0.93 (t, *J* = 7.5 Hz, 3H, CH_3CH$_2$). Anal. calcd. for $C_{30}H_{36}O_6$: C 73.15, H 7.37; found: C 72.47, H 7.47.

Methyl 2,3,4-tri-*O*-benzyl-(6*S*)-*C*-isopropyl-α-D-glucopyranoside (*S*-4i) and -(6*R*)-*C*-isopropyl-α-D-glucopyranoside (*R*-4i*)*

Crude aldehyde **3** (2.47 g, 5.34 mmol) in tetrahydrofuran (30 mL) was reacted with isopropylmagnesium chloride as described for the preparation of ***S*-4e** The crude reaction product was purified on a column of silica gel (hexane–ethyl acetate, 5:1 → 3:1) to provide in the first fraction the minor epimer ***R*-4i** (73.8 mg, 2.7%) as a slowly crystallizing syrup. $[\alpha]_D$ + 26.4° (*c* 0.4, chloroform). ^{1}H NMR ($CDCl_3$) δ: 7.40–7.23 (m, 15H, 3*Ph*), 5.06–4.62 (3ABq, 6H, 3CH_2Ph), 4.53 (d, $J_{1,2}$ = 3.5 Hz, 1H, *H*-1), 4.03 (t, $J_{2,3} \sim J_{3,4}$ = 9.5 Hz, 1H, *H*-3), 3.69 (dd, $J_{4,5}$ = 9.5 Hz, $J_{5,6}$ = 6.0 Hz, 1H, H-5), 3.60 (t, $J_{3,4} \sim J_{4,5}$ = 9.0 Hz, 1H, *H*-4), 3.53 (dd, $J_{6,CH}$ = 4.0 Hz, $J_{5,6}$ = 6.0 Hz, 1H, *H*-6), 3.50 (dd, $J_{1,2}$ = 3.6 Hz, $J_{2,3}$ = 9.5 Hz, 1H, *H*-2), 3.40 (s, 3H, CH_3O), 1.96 (m, 1H, C*H*(CH$_3$)$_2$), 0.95 (d, *J* = 7.0 Hz, 3H, CH(CH_3)$_2$), 0.89 (d, *J* = 7.0 Hz, 3H, CH(CH_3)$_2$). Anal. calcd. for $C_{31}H_{38}O_6$: C 73.49, H 7.56; found: C 73.27, H 7.72. Continued development of the

[5] Methyl 2,3,4-tri-*O*-benzyl-7-deoxy-β-L-glycero-D-gluco-heptopyranoside.

© 2001 NRC Canada

column eluted the major epimer ***S*-4i** (1.46 g, 54%) as a syrup. $[\alpha]_D$ + 12.1° (*c* 0.7, chloroform). ^{1}H NMR ($CDCl_3$) δ: 7.40–7.23 (m, 15H, 3Ph), 5.00–4.64 (3ABq, 6H, 3CH_2Ph), 4.55 (d, $J_{1,2}$ = 3.5 Hz, 1H, *H*-1), 3.99 (tX, $J_{2,3}$ = 9.5 Hz, $J_{3,4}$ = 9.0 Hz, 1H, *H*-3), 3.75 (br d, $J_{4,5}$ = 9.5 Hz, $J_{5,6}$ < 1 Hz, 1H, *H*-5), 3.67 (t, $J_{3,4} \sim J_{4,5}$ = 9.0 Hz, 1H, *H*-4), 3.48 (dd, $J_{1,2}$ = 3.5 Hz, $J_{2,3}$ = 9.5 Hz, 1H, *H*-2), 3.38 (s, 3H, CH_3O), 3.33 (br d, $J_{6,CH}$ = 8.5 Hz, 1H, *H*-6), 1.83 (m, 1H, CH(CH_3)$_2$), 1.01 (d, *J* = 7.0 Hz, 3H, (CH_3)$_2$CH), 0.89 (d, *J* = 7.0 Hz, 3H, (CH_3)$_2$CH). Anal. calcd. for $C_{31}H_{38}O_6$: C 73.49, H 7.56; found: C 73.53, H 7.67.

General procedure for the catalytic hydrogenolysis of *O*-benzyl derivatives

A mixture of the benzyl derivative (200 mg, 0.2–0.4 mmol) and 5% palladium-on-carbon (200 mg) in methanol (10–15 mL) was hydrogenated in the hydrogen stream until completion (TLC). The catalyst was removed by filtration and the solvent evaporated. The resultant material was applied to a column of Iatrobeads® (chloroform-methanol-water) followed by gel filtration on a column of Sephadex LH 20 (50% ethanol) to provide the deprotected material.

*Methyl (6*S*)*-C-*methyl*-α-D-*glucopyranoside (***S*-5m**)

Compound ***S*-5m** was prepared from ***S*-4m** in quantitative yield by catalytic hydrogenolysis following the general procedure. The solid material could be recrystallized from 98% ethanol/hexane to give needle like crystals; mp 136–137°C; $[\alpha]_D$ + 150° (*c* 0.2, water). ^{1}H NMR (D_2O) δ: 4.80 (d, $J_{1,2}$ = 3.5 Hz, 1H, *H*-1), 4.16 (dq, $J_{5,6}$ = 1.5 Hz, $J_{6,CH3}$ = 6.5 Hz, 1H, *H*-6), 3.62 (dd, $J_{2,3}$ = 10.0 Hz, $J_{3,4}$ = 9.0 Hz, 1H, *H*-3), 3.55 (dd, $J_{1,2}$ = 3.5 Hz, $J_{2,3}$ = 10.0 Hz, 1H, *H*-2), 3.46 (dd, $J_{4,5}$ = 10.0 Hz, $J_{3,4}$ = 9.0 Hz, 1H, *H*-4), 3.39 (s, 3H, CH_3O), 3.38 (dd, $J_{4,5}$ = 10.0 Hz, $J_{5,6}$ = 1.5 Hz, 1H, *H*-5), 1.29 (d, *J* = 6.5 Hz, 3H, CH_3C-6). ^{13}C NMR (D_2O) δ: 100.24 (C-1), 74.49, 74.41, 72.31, 70.74, 65.26, 55.89 (CH_3O), 19.72 (*C*H_3C-6). Anal. calcd. for $C_8H_{16}O_6$: C 46.15, H 7.75; found: C 46.04, H 7.46.

*Methyl (6*S*)*-C-*ethyl*-α-D-*glucopyranoside (***S*-5e**)

Compound ***S*-5e** was prepared from ***S*-4e** by catalytic hydrogenolysis following the general procedure and obtained as a white solid (89%) after lyophilization of the aq solution. $[\alpha]_D$ + 150° (*c* 0.2, water). ^{1}H NMR (D_2O) δ: 4.80 (d, $J_{1,2}$ = 3.5 Hz, 1H, *H*-1), 3.85 (m, 1H, *H*-6), 3.64 (dd, $J_{2,3}$ = 9.5 Hz, $J_{3,4}$ = 9.0 Hz, 1H, *H*-3), 3.55 (dd, $J_{1,2}$ = 3.5 Hz, $J_{2,3}$ = 9.5 Hz, 1H, *H*-2), 3.53 – 3.50 (m, 2H, *H*-4, *H*-5), 3.41 (s, 3H, CH_3O), 1.64 (m, 2H, CH_2CH$_3$), 0.95 (t, *J* = 7.5 Hz, 3H, CH_3CH$_2$); ^{13}C NMR (D_2O) δ: 100.17 (C-1), 74.27, 72.60, 72.06, 70.47, 70.30, 55.87 (CH_3O), 26.70 (CH_3CH_2), 10.67 (*C*H_3CH$_2$).

*Methyl (*6S*)*-C-*isopropyl*-α-D-*glucopyranoside (***S*-5i**)

Compound ***S*-5i** was prepared from ***S*-4i** by catalytic hydrogenolysis following the general procedure and obtained as a white solid (95%) after lyophilization of its aq solution. $[\alpha]_D$ + 150° (*c* 0.3, water). ^{1}H NMR (D_2O) δ: 4.79 (d, $J_{1,2}$ = 3.5 Hz, 1H, *H*-1), 3.70 (dd, $J_{4,5}$ = 9.5 Hz, $J_{5,6}$ < 1 Hz, 1H, *H*-5), 3.64 (dd, $J_{3,4}$ = 8.5 Hz, $J_{2,3}$ = 9.5 Hz, 1H, *H*-3), 3.56 (dd, $J_{3,4}$ = 8.5 Hz, $J_{4,5}$ = 9.5 Hz, 1H, *H*-4), 3.54 (dd, $J_{1,2}$ = 3.5 Hz, $J_{2,3}$ = 9.5 Hz, 1H, *H*-2), 3.47 (dd, $J_{6,CH}$ = 9.5 Hz, $J_{5,6}$ < 1 Hz, 1H, *H*-6), 3.44 (s, 3H, CH_3O), 1.92 (m, 1H, CH(CH_3)$_2$), 1.01 (d, *J* = 6.5 Hz, 3H, CH(CH_3)$_2$), 0.91 (d, *J* = 6.5 Hz, 3H, CH(CH_3)$_2$). ^{13}C NMR (D_2O) δ: 100.48 (C-1), 74.36, 74.14, 71.99, 71.13, 70.39, 56.50 (CH_3O), 30.61 (*C*H(CH_3)$_2$), 19.84, 19.32 (*C*H_3)$_2$CH).

*Methyl (*6R*)*-C-*methyl*-α-D-*glucopyranoside (***R*-5m**)

Compound ***R*-5m** was prepared from ***R*-4m** in quantitative yield by catalytic hydrogenolysis following the general procedure; mp 135–136°C. $[\alpha]_D$ + 148° (*c* 1.0, water). ^{1}H NMR (D_2O) δ: 4.82 (d, $J_{1,2}$ = 4.0 Hz, 1H, *H*-1), 4.20 (dq, $J_{5,6}$ = 2.5 Hz, $J_{6,CH3}$ = 6.0 Hz, 1H, *H*-6), 3.71 (dd, $J_{4,5}$ = 10.0 Hz, $J_{5,6}$ = 2.5 Hz, 1H, *H*-5), 3.68 (dd, $J_{3,4}$ = 9.0 Hz, $J_{2,3}$ = 10.0 Hz, 1H, *H*-3), 3.58 (dd, $J_{1,2}$ = 4.0 Hz, $J_{2,3}$ = 10.0 Hz, 1H, *H*-2), 3.44 (s, 3H, CH_3O), 3.38 (dd, $J_{3,4}$ = 9.0 Hz, $J_{4,5}$ = 10.0 Hz, 1H, *H*-4), 1.25 (d, *J* = 6.5 Hz, 3H, CH_3C-6). ^{13}C NMR (D_2O) δ: 100.02 (C-1), 74.17, 74,12, 72.07, 71.73, 67.14, 55.76 (*C*H_3O), 15.85 (*C*H_3C-6). Anal. calcd. for $C_8H_{16}O_6$: C 46.15, H 7.75; found: C 45.99, H 7.50.

*Methyl (*6R*)*-C-*ethyl*-α-D-*glucopyranoside (***R*-5e**)

Compound ***R*-5e** was prepared from ***R*-4e** by catalytic hydrogenolysis following the general procedure and obtained as a foam after freeze-drying its aqueous solution (87%). $[\alpha]_D$ + 152° (*c* 0.4, water). ^{1}H NMR (D_2O) δ: 4.78 (d, $J_{1,2}$ = 3.5 Hz, 1H, *H*-1), 3.78 (m, 1H, *H*-6), 3.69 (dd, $J_{4,5}$ = 10.0 Hz, $J_{5,6}$ = 1.5 Hz, 1H, *H*-5), 3.64 (dd, $J_{3,4}$ = 8.5 Hz, $J_{2,3}$ = 9.5 Hz, 1H, *H*-3), 3.54 (dd, $J_{1,2}$ = 3.5 Hz, $J_{2,3}$ = 9.5 Hz, 1H, *H*-2), 3.43 (dd, $J_{3,4}$ = 8.5 Hz, $J_{4,5}$ = 10.0 Hz, 1H, *H*-4), 3.41 (s, 3H, CH_3O), 1.64 (m, 1H, CH_2CH$_3$), 1.53 (m, 1H, CH_2CH$_3$), 0.98 (t, *J* = 7.5 Hz, 3H, CH_3CH$_2$). ^{13}C NMR (D_2O) δ: 100.00 (C-1), 74.26, 74.05, 73.39, 72.01, 71.55, 55.78 (*C*H_3O), 23.94 (*C*H_2CH$_3$), 10.84 (*C*H_3CH$_2$).

*Methyl (*6R*)*-C-*isopropyl*-α-D-*glucopyranoside (***R*-5i**)

Compound ***R*-5i** was prepared from ***R*-4i** by catalytic hydrogenolysis following the general procedure and obtained as a white solid (85%) after lyophilization of its aqueous solution. $[\alpha]_D$ + 123.4° (*c* 0.2, water). ^{1}H NMR (D_2O) δ: 4.78 (d, $J_{1,2}$ = 3.5 Hz, 1H, *H*-1), 3.74 (dd, $J_{4,5}$ = 9.5 Hz, $J_{5,6}$ = 4.0 Hz, 1H, *H*-5), 3.67 (dd, $J_{3,4}$ = 9.0 Hz, $J_{2,3}$ = 9.5 Hz, 1H, *H*-3), 3.58 (dd, $J_{3,4}$ = 9.0 Hz, $J_{4,5}$ = 9.5 Hz, 1H, *H*-4), 3.57 (dd, $J_{6,CH} \sim$ 6.5 Hz, *J* = 40 Hz, 1H, *H*-6), 3.54 (dd, $J_{1,2}$ = 3.5 Hz,$J_{2,3}$ = 9.5 Hz, 1H, *H*-2), 3.42 (s, 3H, CH_3O), 2.04 (m, 1H, CH(CH_3)$_2$), 0.96 (d, *J* = 6.5 Hz, 3H, CH(CH_3)$_2$), 0.95 (d, *J* = 6.5 Hz, 3H, CH(CH_3)$_2$). ^{13}C NMR (D_2O) δ: 100.10 (C-1), 78.63, 74.16, 72.33, 71.86, 71.49, 56.12 (*C*H_3O), 30.11 (*C*H(CH_3)$_2$), 20.09, 17.96 ((*C*H_3)$_2$CH).

Methyl 2,3-di-*O*-acetyl-4,6-*O*-benzylidene-(6*S*)-*C*-methyl-α-D-glucopyranoside (*S*-6m)

A stirred solution of ***S*-5m** (16 mg, 0.053 mmol) and α,α-dibromotoluene (112 mg, 0.45 mmol) in pyridine (15 mL) was heated at reflux for 2 h. The mixture was cooled and then acetic anhydride (3 mL) was added. After 48 h at room temperature, the mixture was poured into ice water followed by extraction with chloroform, washing and drying of the organic solution and evaporation. The resultant product was purified by thin layer chromatography on silica gel (hexane–ethyl acetate, 3:2) to give ***S*-6m** (15 mg, 51%) as a solid, mp 132–134°C. $[\alpha]_D$ + 50.2° (*c* 0.3, chloroform). The ^{1}H NMR

© 2001 NRC Canada

data are reported in Table 4. ^{13}C NMR ($CDCl_3$) δ: 170.48, 169.76 (2CO), 137.40, 128.92, 128.22, 126.24 (Ph), 97.59 (C-1), 94.07 (*C*HPh), 72.74, 71.50, 70.49, 69.66 (C-2, C-3, C-4, C-5), 64.45 (C-6), 55.34 (CH_3O), 20.79, 20.65 ($2CH_3CO$), 11.28 (CH_3C-6). Anal. calcd. for $C_{19}H_{24}O_8$: C 59.99, H 6.36; found: C 59.55, H 6.06.

Methyl 2,3-di-*O*-benzoy-4,6-*O*-benzylidene-(6*S*)-*C*-ethyl-α-D-glucopyranoside (*S*-6e)

A solution of ***S*-5e** (49 mg, 0.22 mmol) and α,α-dichlorotoluene (100 μL, 0.78 mmol) in pyridine (7 mL) was heated at reflux for 4 h. Then more reagent (75 μL, 0.58 mmol) was added and heating was continued for 4.5 h. The mixture was cooled to ice bath temperature and benzoyl chloride (100 μL, 0.86 mmol) was added. After 2 h at this temperature, the mixture was poured into ice water, extracted with dichloromethane, followed by washing of the organic solution with water, drying and evaporation. The resultant material was purified on a column of silica gel (hexane-ethyl acetate, 9:1, 0.05% triethylamine) to provide labile, solid ***S*-6e** (56 mg, 49%) which was not analytically pure and was only characterized by ^{1}H NMR spectroscopy. The ^{1}H NMR data are reported in Table 5.

Methyl 2,3-di-*O*-benzoyl-4,6-*O*-benzylidene-(6*S*)-*C*-isopropylidene-α-D-glucopyranoside (*S*-6i)

***S*-5i** (37 mg, 0.16 mmol) was converted into ***S*-6i (**41 mg, 49%) as described for the preparation of ***S*-6e.** Labile ***S*-6i** contained a minor component (13%) that could not be removed. The ^{1}H NMR data are reported in Table 4.

Methyl 2,3,4-tri-*O*-benzyl-6-*O*-methanesulfonyl-(6*S*)-*C*-methyl-α-D-glucopyranoside (*S*-7m*)*

To a solution of ***S*-4m** (135 mg, 0.28 mmol) in pyridine (5 mL) at 0°C was added methanesulfonyl chloride (87 mg, 0.76 mmol). After 2 h at room temperature, the mixture was poured into ice-water, extracted with dichloromethane and the organic solution washed with saturated aqueous sodium bicarbonate and water, followed by drying and evaporation. Purification of the resultant material on a column of silica gel (toluene–acetone, 6:1) provided mesylate ***S*-7m** (104 mg, 66%) as a syrup. $[\alpha]_D$ + 9.3° (*c* 1.2, chloroform). ^{1}H NMR ($CDCl_3$) δ: 7.40–7.25 (m, 15H, 3*Ph*), 5.32 (dq, J_{6,CH_3} = 6.5 Hz, $J_{6,5}$ = 1.0 Hz, 1H, *H*-6), 5.06–4.62 (m, 7H, $3CH_2$Ph, *H*-1), 4.02 (m, 1H, *H*-5), 3.65–3.53 (m, 3H, *H*-3, *H*-4, *H*-2), 3.36 (s, 3H, CH_3O), 3.04 (s, 3H, CH_3SO_2), 1.53 (d, *J* = XX Hz, 3H, CH_3C-6). ^{13}C NMR ($CDCl_3$) δ: 138.54–127.74 (Ph), 98.26 (C-1), 82.30, 79.71, 77.17, 73.55, 72.38 (C-2, C-3, C-4, C-5, C-6), 75.74, 75.31, 75.00 ($3CH_2$Ph), 55.33 (CH_3O), 39.54 (CH_3SO_2-), 17.73 (CH_3C-6). Anal. calcd. for $C_{30}H_{36}O_8S$: C 64.73, H 6.52, S 5.76; found: C 64.85, H 6.55, S 5.52.

Methyl 2,3,4-tri-*O*-benzyl-(6*S*)-*C*-ethyl-6-*O*-methanesulfonyl-α-D-glucopyranoside (*S*-7e)

***S*-4e** (419 mg, 0.85 mmol) was reacted with methanesulfonyl chloride (100 μL, 1.29 mmol) as described for the preparation of ***S*-7m**. Purification of the resultant material on a column of silica gel (toluene–ethyl acetate, 10:1) provided mesylate ***S*-7e** (439 mg, 90%) as a syrup. $[\alpha]_D$ – 15.2° (*c* 0.4, chloroform). ^{1}H NMR ($CDCl_3$) δ: 7.40–7.20 (m, 15H, 3*Ph*), 5.12 (br t, J_{6,CH_2} = 7.5 Hz, 1H, *H*-6), 5.06–4.63 (3ABq, 6H, $3CH_2$Ph), 4.62 (d, $J_{1,2}$ = 3.5 Hz, 1H, *H*-1), 4.02 (t, $J_{2,3} \sim J_{3,4}$ = 9.5 Hz, 1H, *H*-3), 3.76 (br d, $J_{4,5}$ = 9.5 Hz, 1H, *H*-5), 3.64 (t, $J_{3,4} \sim J_{4,5}$ = 9.5 Hz, 1H, *H*-4), 3.55 (dd, $J_{1,2}$ = 3.5 Hz, $J_{2,3}$ = 9.5 Hz, 1H, *H*-2), 3.38 (s, 3H, CH_3O), 3.07 (s, 3H, CH_3SO_2), 1.94 (m, 2H, CH_2CH_3), 0.99 (t, *J* = 7.5 Hz, 3H, CH_3CH_2). Anal. calcd. for $C_{31}H_{38}O_8S$: C 65.24, H 6.71; found: C 64.86, H 7.03.

Methyl 2,3,4-tri-*O*-benzyl-(6*R*)-*C*-methyl-α-D-glucopyranoside (*R*-4m)

A stirring mixture of mesylate ***S*-7m** (600 mg, 1.08 mmol) and sodium benzoate (1.0 g, 7.0 mmol) in *N*,*N*-dimethylformamide (20 mL) was heated at 120° for 17 h. It was diluted with dichloromethane, filtered and the solution washed with water, dried and evaporated. The resultant material was purified by HPLC (hexane–acetone, 10:1) to give methyl 6-*O*-benzoyl-2,3,4-tri-*O*-benzyl-(6*R*)-*C*-methyl-α-D-glucopyranoside (***R*-8m**) (294 mg, 47%) as a syrup. $[\alpha]_D$ + 9.8° (*c* 1.04, chloroform). ^{1}H NMR ($CDCl_3$) δ: 8.40–7.20 (m, 20H, 3*Ph*, *Bz*), 5.47 (dq, $J_{5,6}$ = 2.0 Hz, J_{6,CH_3} = 7.0 Hz, 1H, *H*-6), 5.03–4.65 (m, 6H, $3CH_2$Ph), 4.64 (d, $J_{1,2}$ = 4.0 Hz, 1H, *H*-1), 4.04 (dd, $J_{2,3}$ = 9.5 Hz, $J_{3,4}$ = 9.0 Hz, 1H, *H*-3), 3.93 (dd, $J_{4,5}$ = 10.0 Hz, $J_{5,6}$ = 2.0 Hz, 1H, *H*-5), 3.52 (dd, $J_{1,2}$ = 4.0 Hz, $J_{2,3}$ = 9.5 Hz, 1H, *H*-2), 3.42 (dd, $J_{3,4}$ = 9.0 Hz, $J_{4,5}$ = 10.0 Hz, 1H, *H*-4), 3.38 (s, 3H, CH_3O), 1.18 (d, *J* = 7.0 Hz, 3H, CH_3C-6). Anal. calcd. for $C_{36}H_{38}O_7$: C 74.20, H 6.57; found: C 74.33, H 6.55.

Benzoate ***R*-8m** (137 mg, 0.24 mmol) was dissolved in dioxane (10 mL) and 1 N sodium hydroxide solution (6 mL) was added. After stirring for 48 h at 60°C, the mixture was diluted with dichloromethane and filtered over a pad of silica gel-G. The dichloromethane solution was washed with water, dried and evaporated to give solidifying ***R*-4m** (80 mg, 71%), mp 89–90°C. $[\alpha]_D$ + 28° (*c* 0.4, chloroform). ^{1}H NMR ($CDCl_3$) δ: 7.34–7.16 (m, 15H, 3*Ph*), 4.98–4.53 (m, 6H, $3CH_2$Ph), 4.50 (d, $J_{1,2}$ = 3.5 Hz, 1H, *H*-1), 3.95 (dd, $J_{2,3}$ = 9.5 Hz, $J_{3,4}$ = 9.0 Hz, 1H, *H*-3), 3.88 (m, 1H, *H*-6), 3.55 (dd, $J_{4,5}$ = 10.0 Hz, $J_{5,6}$ = 4.5 Hz, 1H, *H*-5), 3.43 (dd, $J_{1,2}$ = 3.5 Hz, $J_{2,3}$ = 9.5 Hz, 1H, *H*-2), 3.35 (dd, $J_{3,4}$ = 9.0 Hz, $J_{4,5}$ = 10.0 Hz, 1H, *H*-4), 3.31 (s, 3H, CH_3O), 2.49 (d, $J_{6,OH}$ = 6.0 Hz, 1H, OH), 1.05 (d, J_{6,CH_3} = 6.5 Hz, 3H, CH_3C-6). Anal. calcd. for $C_{29}H_{34}O_6$: C 72.78, H 7.16; found: C 72.81, H 7.07.

Methyl 2,3,4-tri-*O*-benzyl-(6*R*)-*C*-ethyl-α-D-glucopyranoside (*R*-4e)

A stirring mixture of mesylate ***S*-7e** (430 mg, 0.75 mmol) and sodium benzoate (600 mg, 4.16 mmol) in *N*,*N*-dimethylformamide (20 mL) was heated at 120° for 20 h. The solution was diluted with dichloromethane, filtered and the solution washed with water, dried and evaporated. The resultant material (methyl 6-*O*-benzoyl-2,3,4-tri-*O*-benzyl-(6*R*)-*C*-ethyl-α-D-glucopyranoside (***R*-8e**)) and potassium hydroxide (2.5 g) in 90% ethanol (50 mL) was kept at reflux for 3 h. The mixture was neutralized with acetic acid, evaporated, and the remainder taken up in dichloromethane. Washing of the solution with water, drying and evaporation was followed by column chromatography of the crude product on a column of silica gel (hexane–ethyl acetate, 4:1 → 3:1). Evaporation of the first fraction provided (*E*)-methyl

© 2001 NRC Canada

2,3,4-tri-*O*-benzyl-6,7,8-trideoxy-α-D-gluco-oct-6-enopyranoside (**9**) (105 mg, 22%) as a crystallizing syrup. $[\alpha]_D$ + 1.8°, $[\alpha]_{365}$ –33.4° (*c* 0.5, chloroform). ^{1}H NMR ($CDCl_3$) δ: 7.40–7.20 (m, 15H, 3*Ph*), 5.85 (m, 1H, *H*-7), 5.42 (ddd, $J_{6,5}$ = 7.5 Hz, J_{6,CH_3} = 1.5 Hz, $J_{6,7}$ = 14.5 Hz, 1H, *H*-6), 4.98–4.59 (3ABq, 6H, 3CH_2Ph), 4.56 (d, $J_{1,2}$ = 3.5 Hz, 1H, *H*-1), 4.01 (m, 1H, *H*-5), 3.96 (t, $J_{2,3} \sim J_{3,4}$ = 9.5 Hz, 1H, *H*-3), 3.51 (dd, $J_{1,2}$ = 3.5 Hz, $J_{2,3}$ = 9.5 Hz, 1H, *H*-2), 3.37 (s, 3H, CH_3O), 3.23 (t, $J_{3,4} \sim J_{4,5}$ = 9.5 Hz, 1H, *H*-4), 1.73 (m, 3H, CH_3CH=CH). Anal. calcd. for $C_{30}H_{34}O_5$: C 75.92, H 7.22; found: C 76.05, H 7.31. Continued development eluted ***R*-4e** (159 mg, 43%), identical to the minor Grignard product of aldehyde **3**.

Methyl 2,3,4-tri-*O*-benzyl-7,8-dideoxy-7-*C*-methyl-α-D-gluco-octopyranos-6-uloside (10)

A solution of ***S*-4i** (100 mg, 0.20 mmol) in dimethylsulfoxide (1.5 mL) and acetic anhydride (0.75 mL) was kept at room temperature for 15 h. The solution was evaporated and the residue was taken up in dichloromethane, washed with water, and evaporated to dryness. The ^{1}H NMR spectrum indicated a product mixture of ketone **10** and ether **11** in the ratio 1.6:1. Column chromatography on silica gel (toluene–ethyl acetate, 49:1) provided pure ketone **10** (55 mg, 55%) as an oil. However, a crude product mixture was used for the subsequent reduction because of the difficult separation. $[\alpha]_D$ + 6.4° (*c* 0.6, chloroform). IR ($CHCl_3$) cm^{-1}: 1730 (CO). ^{1}H NMR ($CDCl_3$) δ: 7.40–7.15 (m, 15H, 3*Ph*), 5.00–4.50 (3ABq, 6H, 3CH_2Ph), 4.58 (d, $J_{1,2}$ = 3.5 Hz, 1H, *H*-1), 4.35 (d, $J_{4,5}$ = 9.5 Hz, 1H, *H*-5), 4.02 (t, $J_{3,4} \sim J_{2,3}$ = 9.5 Hz, 1H, *H*-3), 3.72 (t, $J_{3,4} \sim J_{4,5}$ = 9.5 Hz, 1H, *H*-4), 3.54 (dd, $J_{1,2}$ = 3.5 Hz, $J_{2,3}$ = 9.5 Hz, 1H, *H*-2), 3.42 (s, 3H, CH_3O), 2.85 (m, 1H, CH(CH_3)$_2$), 1.12 (d, *J* = 6.5 Hz, 3H, CH(CH_3)$_2$), 1.07 (d, *J* = 6.5 Hz, 3H, CH(CH_3)$_2$). Anal. calcd. for $C_{31}H_{36}O_6$: C 73.79, H 7.19; found: C 73.45, H 7.11.

Methyl 2,3,4-tri-*O*-benzyl-(6*R*)-*C*-isopropyl-α-D-glucopyranoside (*R*-4i)

To a solution of crude ketone **10** (0.40 mmol) in methanol (10 mL) was added, with stirring, sodium borohydride (65 mg, 1.72 mmol) at ice bath temperatures. After 30 min, the solution was evaporated, and the residue was taken up in dichloromethane, washed with water, dried, and evaporated. The product mixture was applied to a column of silica gel (hexane–ethyl acetate, 6:1 → 5:1 → 4:1) to provide in the first fraction methyl 2,3,4-tri-*O*-benzyl-(6*S*)-*C*-isopropyl-6-*O*-methylthiomethylene-α-D-glucopyranoside (**11**) (63 mg, 28%). $[\alpha]_D$ + 30° (*c* 0.8, chloroform). ^{1}H NMR ($CDCl_3$) δ: 7.40–7.20 (m, 15H, 3*Ph*), 5.06–4.58 (m, 8H, CH_2S, 3CH_2Ph), 4.65 (d, $J_{1,2}$ = 3.5 Hz, 1H, *H*-1), 4.02 (dd, $J_{2,3}$ = 9.5 Hz, $J_{3,4}$ = 9.0 Hz, 1H, *H*-3), 3.83 (br d, $J_{4,5}$ = 9.5 Hz, 1H, *H*-5), 3.73 (br d, $J_{6,CH}$ = 7.0 Hz, 1H, *H*-6), 3.65 (dd, $J_{3,4}$ = 9.0 Hz, $J_{4,5}$ = 9.5 Hz, 1H, *H*-4), 3.56 (dd, $J_{1,2}$ = 3.5 Hz, $J_{2,3}$ = 9.5 Hz, 1H, *H*-2), 3.43 (s, 3H, CH_3O), 2.20 (br s, 3H, CH_3S), 2.17 (m, 1H, CH(CH_3)$_2$), 1.01 (d, *J* = 6.5 Hz, 3H, CH(CH_3)$_2$), 0.99 (d, *J* = 6.5 Hz, 3H, CH(CH_3)$_2$). Anal. calcd. for $C_{33}H_{42}O_6S$: C 69.94, H 7.47, S 5.66; found: C 69.81, H 7.65, S 5.73. Continued elution afforded *R*-epimer ***R*-4i** (90 mg, 44%) identical to the minor Grignard product of aldehyde **3**. Further development eluted *S*-epimer ***S*-4i** (22 mg, 11%) identical to the major Grignard product of aldehyde **3**.

Methyl 6-*O*-(6-*O*-acetyl-2,3,4-tri-*O*-benzyl-α-D-glucopyranosyl)-2,3,4-tri-*O*-benzyl-(6*R*)-*C*-methyl-α-D-glucopyranoside (*R*-14m)

A solution of 6-*O*-acetyl-2,3,4-tri-O-benzyl-α-D-glucopyranosyl bromide (**12**) (34) (2.1 mmol) in dichloromethane (5 mL) was added to a stirring mixture of ***R*-4m** (500 mg, 1.04 mmol), tetraethylammonium bromide (420 mg, 2.00 mmol), *N*,*N*-dimethylformamide (1 mL) and 4 Å molecular sieves (powdered, 2 g) in dichloromethane (5 mL). The mixture was stirred under nitrogen for several days until completion (TLC), diluted with dichloromethane and filtered. The solution was washed with sat. aq $NaHCO_3$ and water, followed by drying and evaporation. The crude product was applied to a column of silica gel (hexane–ethyl acetate, 4:1) to provide ***R*-14m** (587 mg, 59%). $[\alpha]_D$ + 78.2° (*c* 1.1, chloroform). ^{1}H NMR ($CDCl_3$) δ: 7.40–7.20 (m, 30H, 6*Ph*), 5.00 (d, $J_{1b,2b}$ = 3.5 Hz, 1H, *H*-1b), 4.67 (d, $J_{1a,2a}$ = 3.5 Hz, 1H, *H*-1a), 5.03–4.51 (m, 12H, 6CH_2Ph), 4.27 (dd, $J_{5b,6b}$ = 4.5 Hz, $J_{6b,6b'}$ = 11.5 Hz, 1H, *H*-6b), 4.21 (dd, $J_{5b,6b'}$ = 2.5 Hz, $J_{6b,6b'}$ = 11.5 Hz, 1H, *H*-6b′), 4.08–3.91 (m, 4H, *H*-3a, *H*-3b, *H*-6a, *H*-5b), 3.78 (dd, $J_{5a,6a}$ = 0.5 Hz, $J_{4a,5a}$ = 10.0 Hz, 1H, *H*-5a), 3.57–3.43 (m, 3H, *H*-4a, *H*-4b, *H*-2a), 3.41 (dd, $J_{2b,3b}$ = 9.5 Hz, $J_{1b,2b}$ = 3.5 Hz, 1H, *H*-2b), 3.29 (3, 3H, CH_3O), 1.99 (s, 3H, CH_3CO), 1.16 (d, $J_{6a,CH3}$ = 6.5 Hz, 3H, CH_3C-6a). Anal. calcd. for $C_{58}H_{64}O_{12}$: C 73.09, H 6.77; found: C 73.46, H 6.61.

2,3,4,6-Tetra-*O*-benzyl-α-D-glucopyranosyl bromide (13) (32)

Oxalyl bromide (190 μL, ~1.8 mmol) was added to a stirring solution of 2,3,4,6-tetra-*O*-benzyl-D-glucopyranose (650 mg, 1.20 mmol) in dichloromethane (10 mL) and *N*,*N*-dimethylformamide (0.5 mL, 7.0 mmol). After 20 min at room temperature, the mixture was poured into ice water and the organic solution was washed twice with ice-cold water, dried and evaporated to provide **13** (quant.) as a syrup.

Methyl 2,3,4-tri-*O*-benzyl-(6*R*)-*C*-ethyl-6-*O*-(2,3,4,6-tetra-*O*-benzyl-α-D-glucopyranosyl)-α-D-glucopyranoside (*R*-14e) and -β-D-glucopyranoside

A solution of bromide **13** (1.12 mmol) in 1,2-dichloroethane (4 mL) was transferred into a stirring mixture of ***R*-4e** (159 mg, 0.32 mmol), copper(II) bromide (260 mg, 1.16 mmol), *N*,*N*-dimethylformamide (350 μL, 4.93 mmol) in 1,2-dichloroethane (2 mL) containing powdered 4 Å molecular sieves (1 g). After 44 h, toluene (15 mL) and moist pyridine (7.5 mL) were added. After stirring for 30 min, the mixture was filtered and the solvent evaporated. The resultant material was applied to a column of silica gel (hexane–ethyl acetate, 5:1) to first provide the β-anomer of ***R*-14e** (50 mg, 15%) as a syrup. $[\alpha]_D$ + 26.4° (*c* 0.6, chloroform). ^{1}H NMR ($CDCl_3$) δ: 7.40–7.15 (m, 35H, 7*Ph*), 5.01–4.51 (m, 35H, 7CH_2Ph), 4.60 (d, overlapped, *H*-1a), 4.45 (d, $J_{1b,2b}$ = 7.5 Hz, 1H, *H*-1b), 4.00 (t, $J_{2a,3a} \sim J_{3a,4a}$ = 9.5 Hz, 1H, *H*-3a), 3.48 (dd, $J_{1a,2a}$ = 3.5 Hz, $J_{2a,3a}$ = 9.5 Hz, 1H, *H*-2a), 3.40 (s, overlapped, CH_3O), 1.63 (m, 1H, C$H_2$$CH_3$), 1.40 (m, 1H, C$H_2$$CH_3$), 0.88 (t, *J* = 7.5 Hz, 3H, C$H_3$$CH_2$). Anal. calcd. for $C_{64}H_{70}O_{11}$: C 75.71, H 6.95; found: C 75.40, H 6.91.

© 2001 NRC Canada

Continued elution of the column provided the α-anomer ***R*-14e** (240 mg, 73%) as a syrup. $[\alpha]_D$ + 57° (*c* 1.0, chloroform). ^{1}H NMR ($CDCl_3$) δ: 7.40–7.10 (m, 35H, 7*Ph*), 5.12 (d, $J_{1b,2b}$ = 3.5 Hz, 1H, *H*-1b), 4.97–4.42 (m, 14H, 7CH_2Ph), 4.52 (d, overlapped, $J_{1a,2a}$ = 3.5 Hz, 1H, *H*-1a), 4.01 (t, $J_{2b,3b} \sim J_{3b,4b}$ = 9.5 Hz, 1H, *H*-3b), 3.97 (t, $J_{2a,3a} \sim J_{3a,4a}$ = 9.5 Hz, 1H, *H*-3a), 3.93 (m, 1H, *H*-5b), 3.85 (br d, $J_{4a,5a}$ = 9.5 Hz, $J_{5a,6a}$ < 1 Hz, 1H, *H*-5a), 3.73 (m, 3H, *H*-4a, *H*-6a, *H*-6b), 3.64 (t, $J_{3b,4b} \sim J_{4b,5b}$ = 9.5 Hz, 1H, *H*-4b), 3.60 (dd, $J_{6b,6b'}$ = 11.0 Hz, $J_{6b',5b}$ = 1.5 Hz, 1H, *H*-6b′), 3.53 (dd, $J_{1b,2b'}$ = 3.5 Hz, $J_{2b,3b}$ = 9.5 Hz, 1H, *H*-2b), 3.35 (dd, $J_{1a,2a}$ = 3.5 Hz, $J_{2a,3a}$ = 9.5 Hz, 1H, *H*-2a), 3.32 (s, 3H, CH_3O), 1.61 (m, 2H, CH_2CH$_3$), 0.89 (t, *J* = 7.5 Hz, 3H, *C*H$_3$CH_2). Anal. calcd. for $C_{64}H_{70}O_{11}$: C 75.71, H 6.95; found: C 75.38, H 6.88.

Methyl 2,3,4-tri-*O*-benzyl-(6*R*)-*C*-isopropyl-6-*O*-(2,3,4,6-tetra-*O*-benzyl-α-D-glucopyranosyl)-α-D-glucopyranoside (*R*-14i)

Alcohol ***R*-4i** (150 mg, 0.30 mmol) was reacted with bromide **13** (1.24 mmol) for 6 days as described for the preparation of ***R*-14e**. Column chromatography (hexane–ethyl acetate, 8:1 → 7:1) provided ***R*-14i** (178 mg, 58%) as a thick syrup. $[\alpha]_D$ + 56.4° (*c* 0.3, chloroform). ^{1}H NMR ($CDCl_3$) δ: 7.40–7.10 (m, 35H, 7*Ph*), 5.26 (d, $J_{1b,2b}$ = 3.5 Hz, 1H, *H*-1b), 4.96–4.42 (m, 14H, 7CH_2Ph), 4.52 (d, $J_{1a,2a}$ = 3.5 Hz, 1H, *H*-1a), 4.01 (t, $J_{2b,3b} \sim J_{3b,4b}$ = 9.5 Hz, 1H, *H*-3b), 3.96 (t, overlapped, $J_{2a,3a} \sim J_{3a,4a}$ = 9.5 Hz, 1H, *H*-3a), 3.74, (dd, $J_{6b,6b'}$ = 11.0 Hz, $J_{6b,5b}$ = 3.5 Hz, 1H, *H*-6b), 3.61 (dd, $J_{6b',5b}$ = 1.5 Hz, $J_{6b,6b'}$ = 11.0 Hz, overlapped,1H, *H*-6b′), 3.54 (dd, $J_{1b,2b}$ = 3.5 Hz, $J_{2b,3b}$ = 9.5 Hz, 1H, *H*-2b), 3.51 (d, $J_{6a,CH}$ = 8.5 Hz, 1H, *H*-6a), 3.34 (dd, $J_{1a,2a}$ = 3.5 Hz, $J_{2a,3a}$ = 9.5 Hz, 1H, *H*-2a), 3.32 (s, 3H, CH_3O), 2.08 (m, 1H, C*H*(CH$_3$)$_2$), 0.98 (d, *J* = 6.5 Hz, 3H, CH(CH_3)$_2$), 0.89 (d, *J* = 6.5 Hz, 3H, CH(CH_3)$_2$). Anal. calcd. for $C_{65}H_{72}O_{11}$: C 75.85, H 7.05; found: C 75.78, H 7.27.

Methyl 6-*O*-(6-*O*-acetyl-2,3,4-tri-*O*-benzyl-α-D-glucopyranosyl)-2,3,4-tri-*O*-benzyl-(6*R*)-*C*-methyl-α-D-glucopyranoside (*S*-14m)

Compound ***S*-4m** (100 mg, 0.21 mmol) was reacted with bromide **12** (0.42 mmol) as described for the preparation of ***R*-14m**. Usual processing and chromatography provided ***S*-14m** (101 mg, 51%) $[\alpha]_D$ + 0.5° (*c* 1.06, chloroform). ^{1}H NMR ($CDCl_3$) δ: 7.40–7.20 (m, 30H, 6*Ph*), 5.09 (d, $J_{1b,2b}$ = 3.5 Hz, 1H, *H*-1b), 5.02–4.49 (m, 7H, 3CH_2Ph, *H*-1a), 4.26–4.06 (m, 3H, 2*H*-6b, *H*-1a), 4.06–3.94 (m, 3H, *H*-3b, *H*-3a, *H*-5b), 3.77 (dd, $J_{3a,4a}$ = 9.5 Hz, $J_{4a,5a}$ = 9.0 Hz, 1H, *H*-4a), 3.56 (dq, $J_{5a,6a}$ = 2.0 Hz, $J_{4a,5a}$ = 9.0 Hz, 1H, *H*-5a), 3.56–3.47 (m, 2H, *H*-2a, *H*-2b), 3.46 (dd, $J_{3b,4b}$ = 9.0 Hz, $J_{4b,5b}$ = 10.0 Hz, 1H, *H*-4b), 3.38 (s, 3H, CH_3O), 1.92 (s, 3H, CH_3CO), 1.33 (d, J_{6a,CH_3} = 6.0 Hz, 3H, CH_3C-6a). Anal. calcd. for $C_{57}H_{64}O_{12}$: C 73.09, H 6.77; found: C 72.84, H 6.85.

Methyl 2,3,4-tri-*O*-benzyl-(6*S*)-*C*-ethyl-6-*O*-(2,3,4,6-tetra-*O*-benzyl-α-D-glucopyranosyl)-α-D-glucopyranoside (*S*-14e)

Alcohol ***S*-4e** (170 mg, 0.35 mmol) was reacted with bromide **13** (1.24 mmol) for 4 days as described for the preparation of ***R*-14e**. Column chromatography (hexane–dichloromethane-ethyl acetate, 20:10:1–2) provided ***S*-14e** (243 mg, 69%) as a syrup. $[\alpha]_D$ + 48° (*c* 0.5, chloroform). ^{1}H NMR ($CDCl_3$) δ: 7.35–7.10 (m, 35H, 7*Ph*), 5.02 (d, $J_{1b,2b}$ = 3.5 Hz, 1H, *H*-1b), 4.96–4.43 (m, 14H, 7CH_2Ph), 4.59 (d, $J_{1a,2a}$ = 3.5 Hz, 1H, *H*-1a), 3.98–3.96 (m, 3H, *H*-3b, *H*-5b, *H*-3a), 3.84 (t, $J_{3a,4a} \sim J_{4a,5a}$ = 9.0 Hz, 1H, *H*-4a), 3.81 (br t, overlapped, J_{6a,CH_2} = 7.0 Hz, 1H, *H*-6a), 3.68–3.66 (m, 2H, *H*-5a, *H*-4b), 3.64 (dd, overlapped, $J_{6b,6b'}$ = 11.0 Hz, $J_{6b,5b}$ = 2.5 Hz, 1H, *H*-6b), 3.52–3.51 (m, 2H, *H*-2b, *H*-6b′), 3.45 (dd, $J_{2a,3a}$ = 9.5 Hz, $J_{1a,2a}$ = 3.5 Hz, 1H, *H*-2a), 3.37 (s, 3H, CH_3O), 1.78 (m, 2H, CH$_3$CH_2), 0.94 (t, *J* = 7.5 Hz, 3H, CH_3CH$_2$). Anal. calcd. for $C_{64}H_{70}O_{11}$: C 75.71, H 6.95; found: C 75.52, H 7.08.

Methyl 2,3,4-tri-*O*-benzyl-(6*S*)-*C*-isopropyl-6-*O*-(2,3,4,6-tetra-*O*-benzyl-α-D-glucopyranosyl)-α-D-glucopyranoside (*S*-14i)

Alcohol ***S*-4i** (160 mg, 0.32 mmol) was reacted with bromide **13** (1.29 mmol) for 5 days as described for the preparation of ***R*-14e**. Column chromatography (hexane–ethyl acetate, 6:1, 5:1) provided ***S*-14i** (207 mg, 64%) as a tough syrup. $[\alpha]_D$ + 57.4° (*c* 0.4, chloroform). ^{1}H NMR ($CDCl_3$) δ: 7.35–7.10 (m, 35H, 7Ph), 5.02–4.36 (m, 16H, 7CH_2Ph, *H*-1a, *H*-1b), 4.04 (t, $J_{2b,3b} \sim J_{3b,4b}$ = 9.5 Hz, 1H, *H*-3b), 4.00 (m, overlapped, 1H, *H*-5b), 3.95 (t, $J_{2a,3a} \sim J_{3b,4b}$ = 9.0 Hz, 1H, *H*-4a), 3.90 (t, $J_{3a,4a} \sim J_{4a,5a}$ = 9.0 Hz, 1H, *H*-4a), 3.74 (br d, $J_{5a,6a}$ < 1 Hz, 1H, *H*-5a), 3.68 (t, $J_{3a,4a} \sim J_{4b,5b}$ = 9.0 Hz, 1H, *H*-4b), 3.62 (dd, $J_{6b,6b'}$ = 11.0 Hz, $J_{6b,5b}$ = 2.5 Hz, 1H, *H*-6b), 3.57 (dd, $J_{6b',5b}$ = 1.5 Hz, $J_{6b,6b'}$ = 11.0 Hz, 1H, *H*-6b′), 3.55 (d, $J_{6a,CH}$ = 6.5 Hz, 1H, *H*-6a), 3.51 (dd, $J_{1b,2b}$ = 3.5 Hz, $J_{2b,3b}$ = 9.5 Hz, 1H, *H*-2b), 3.41 (s, 3H, CH_3O), 3.38 (dd, $J_{1a,2a}$ = 3.5 Hz, $J_{2a,3a}$ = 9.0 Hz, 1H, *H*-2a), 2.03 (m, 1H, C*H*(CH$_3$)$_2$), 1.03 (d, 3H, *J* = 6.5 Hz, CH(CH_3)$_2$), 1.00 (d, 3H, *J* = 6.5 Hz, CH(CH_3)$_2$). Anal. calcd. for $C_{65}H_{72}O_{11}$: C 75.85, H 7.05; found: C 75.67, H 7.14.

Methyl 6-*O*-(α-D-glucopyranosyl)-(6*R*)-*C*-methyl-α-D-glucopyranoside (*R*-2m)

To a solution of compound ***R*-14m** (440 mg, 0.46 mmol) in methanol (20 mL) was added a catalytic amount of sodium methoxide. After stirring overnight, it was deionized with Amberlite IRC-50 H^+. Evaporation of the methanol provided methyl 2,3,4-tri-*O*-benzyl-(6*R*)-*C*-methyl-6-*O*-(2,3,4-tri-*O*-benzyl-α-D-glucopyranosyl)-α-D-glucopyranoside (347 mg, 83%) as an oil. $[\alpha]_D$ + 65.2° (*c* 0.34, water). ^{1}H NMR ($CDCl_3$) δ: 7.40–7.20 (m, 30H, 6*Ph*), 5.00 (d, $J_{1b,2b}$ = 4.5 Hz, 1H, *H*-1b), 4.98–4.53 (m, 13H, 6CH_2Ph, *H*-1a), 4.08–3.91 (m, 3H, *H*-3a, *H*-3b, *H*-6a), 3.81–3.67 (m, 4H, *H*-5a, *H*-5b, H$_2$-6b), 3.56–3.37 (m, 4H, *H*-4a, *H*-4b, *H*-2a, *H*-2b), 3.29 (s, 3H, CH_3O), 1.13 (d, $J_{6a,CH3}$ = 6.5 Hz, 3H, CH_3C-6a). Anal. calcd. for $C_{56}H_{62}O_{11}$: C 73.82, H 6.86; found: C 73.23, H 7.23.

The deacetylation product of ***R*-14m**, namely methyl 2,3,4-tri-*O*-benzyl-(6*R*)-*C*-methyl-6-*O*-(2,3,4-tri-*O*-benzyl-α-D-glucopyranosyl)-α-D-glucopyranoside, (247 mg, 0.27 mmol) was debenzylated following the general procedure to give solid ***R*-2m** (80 mg, 80%), mp 231–232°C. $[\alpha]_D$ + 228.1° (*c* 0.43, water). The ^{1}H NMR data are reported in Table 5. ^{13}C NMR (D_2O) δ: 100.13 (C-1a), 97.98 (C-1b), 73.89, 73.73, 73.37, 72.98, 72.02, 71.89, 71.80, 71.48, 70.51, 56.09

© 2001 NRC Canada

(CH_3O), 15.12 (CH_3C-6a). Anal. calcd. for $C_{14}H_{25}O_{11}$: C 45.53, H 6.82; found: C 45.18, H 6.97.

Methyl (6*R*)-*C*-ethyl-6-*O*-(α-D-glucopyranosyl)-α-D-glucopyranoside (*R*-2e)

Compound ***R*-2e** was prepared from ***R*-14e** by catalytic hydrogenolysis following the general procedure and obtained as a white solid (89%) after lyophilization of an aqueous solution. $[\alpha]_D$ + 182.5° (*c* 0.3, water). The ^{1}H NMR data are reported in Table 5. ^{13}C NMR (D_2O) δ: 100.36 (C-1a), 97.01 (C-1b), 78.21, 73.94, 73.73, 73.10, 72.09, 71.89, 71.28, 70.92, 70.47, 61.43 (C-6b), 56.46 (CH_3O), 22.73 (CH_2CH_3), 11.48 (CH_3CH_2).

Methyl 6-*O*-(α-D-glucopyranosyl)-(6*R*)-*C*-isopropyl-α-D-glucopyranoside (*R*-2i)

Compound ***R*-2i** was prepared from ***R*-14i** by catalytic hydrogenolysis following the general procedure and obtained as a white solid (87%) after lyophilization of an aqueous solution. $[\alpha]_D$ + 190.5° (*c* 0.2, water). The ^{1}H NMR data are reported in Table 5. ^{13}C NMR (D_2O) δ: 100.23 (C-1a), 97.86 (C-1b), 82.69, 73.99, 73.64, 73.27, 72.36, 71.88, 71.73, 71.34, 70.47, 61.45 (C-6b), 56.39 (CH_3O), 30.23 ($CH(CH_3)_2$), 20.75, 19.94 ($CH(CH_3)_2$).

Methyl 6-*O*-(α-D-glucopyranosyl)-(6*S*)-*C*-methyl-α-D-glucopyranoside (*S*-2m)

Compound ***S*-14m** (292 mg, 0.31 mmol) was deacetylated as described for ***R*-14m** to provide methyl 2,3,4-tri-*O*-benzyl-(6*S*)-*C*-methyl-6-*O*-(2,3,4-tri-*O*-benzyl-α-D-glucopyranosyl)-α-D-glucopyranoside (269 mg, 96%) as an oil. $[\alpha]_D$ + 47.6° (*c* 2.0, chloroform). ^{1}H NMR ($CDCl_3$) δ: 7.40–7.10 (m, 30H, 6*Ph*), 5.03 (d, $J_{1b,2b}$ = 3.5 Hz, 1H, *H*-1b), 5.01–4.57 (m, 13H, 6CH_2Ph, *H*-1a), 4.32 (dq, $J_{5a,6a}$ = 1.5 Hz, J_{6a,CH_3} = 6.5 Hz, 1H, *H*-6a), 4.01 (dd, $J_{2b,3b}$ = 9.5 Hz, $J_{3b,4b}$ = 9.0 Hz, 1H, *H*-3b), 3.98 (dd, $J_{2a,3a}$ = 9.5 Hz, $J_{3a,4a}$ = 10.0 Hz, 1H, *H*-3a), 3.84–3.72 (m, 2H, *H*-5b, *H*-4a), 3.66–3.49 (m, 5H, 2*H*-6a, *H*-5a, *H*-4b, *H*-2a), 3.46 (dd, $J_{1b,2b}$ = 3.5 Hz, $J_{2b,3b}$ = 9.5 Hz, 1H, *H*-2b), 3.36 (s, 3H, CH_3O), 1.32 (d, J_{6a,CH_3} = 6.5 Hz 3H, CH_3C-6). Anal. calcd. for $C_{56}H_{62}O_{11}$: C 73.82, H 6.86; found: C 73.20, H 6.95.

The deacetylation product of ***S*-14m**, namely methyl 2,3,4-tri-*O*-benzyl-(6*S*)-*C*-methyl-6-*O*-(2,3,4-tri-*O*-benzyl-α-D-glucopyranosyl)-α-D-glucopyranoside, (126 mg, 0.138 mmol) was debenzylated following the general procedure to give crystalline ***S*-2m** (40 mg, 78%), mp 127–128°. $[\alpha]_D$ + 175.3° (*c* 0.3, water). The ^{1}H NMR data are reported in Table 5. ^{13}C NMR (D_2O) δ: 100.03 (C-1a), 95.56 (C-1b), 74.49, 74.15, 73.68, 73.04, 72.25, 71.99, 70.24, 68.50, 61.17, 55.67 (CH_3O), 14.76 (CH_3-6a).

Methyl-(6*S*)-*C*-ethyl-6-*O*-(α-D-glucopyranosyl)-α-D-glucopyranoside (*S*-2e)

Compound ***S*-2e** was prepared from ***S*-14e** by catalytic hydrogenolysis following the general procedure and obtained as a white solid (94%) after lyophilization of an aqueous solution. $[\alpha]_D$ + 198° (*c* 0.2, water). The ^{1}H NMR data are reported in Table 5. ^{13}C NMR (D_2O) δ: 100.31 (C-1a), 96.31 (C-1b), 74.77, 74.47, 73.85. 73.15, 72.37, 72.01, 70.93, 70.29, 70.14, 61.21 (C-6b), 56.38 (CH_3O), 21.67 (CH_2CH_3), 10.02 (CH_3CH_2).

Methyl 6-*O*-(α-D-glucopyranosyl)-(6*S*)-*C*-isopropyl-α-D-glucopyranoside (*S*-2i)

Compound ***S*-2i** was prepared from ***S*-14i** by catalytic hydrogenolysis following the general procedure and obtained as a white solid (98%) after lyophilization of an aqueous solution. $[\alpha]_D$ + 192° (*c* 0.2, water). The ^{1}H NMR data are reported in Table 5. ^{13}C NMR (D_2O) δ: 100.63 (C-1a), 96.52 (C-1b), 76.45, 74.20, 73.70, 73.05, 72.67, 71.90, 70.86, 70.51, 70.33, 61.15 (C-6b), 57.43 (CH_3O), 28.42 ($CH(CH_3)_2$, 19.04, 17.72 ($CHCH_3)_2$).

Acknowledgements

This research was supported by the Pharmaceutical Manufacturers Association of Canada (Prize to R.U.L.) and in part by the Natural Sciences and Engineering Council of Canada. We are deeply grateful to Professor D.R. Bundle for the use of his computer graphic facilities and the collaboration of his Research Associate, Dr. Chang-Chun Ling.

References

1. R.U. Lemieux and U. Spohr. Adv. Carbohydr. Chem. Biochem. **50**, 1 (1994).
2. J.H. Pazur and T. Ando. J. Biol. Chem. **237**, 297 (1962).
3. K. Hiromi, M. Kawai, and S. Ono. J. Biochem. (Tokyo), **59**, 476 (1966).
4. K. Bock and H. Pedersen. Acta Chem. Scand. Ser. B, **41**, 617 (1987).
5. K. Bock, T. Skrydstrup, and S. Refn. J. Carbohydr. Chem. **10**, 969 (1991).
6. R.U. Lemieux, U. Spohr, M. Bach, D.R. Cameron, T.B. Frandsen, B.B. Stoffer, B. Svensson, and M.M. Palcic. Can. J. Chem. **74**, 319 (1996).
7. A.E. Aleshin, L.M. Firsov, and R.B. Honzatko. J. Biol. Chem. **269**, 15 631 (1994).
8. A.E. Aleshin, B. Stoffer, L.M. Firsov, B. Svensson, and R.B. Honzatko. Biochemistry, **35**, 8319 (1996).
9. M.M. Palcic, T. Skrydstrup, K. Bock, N. Le, and R.U. Lemieux. Carbohydr. Res. **250**, 87 (1993).
10. T.P. Frandsen, M.M. Palcic, C. Dupont, and B. Svensson. Carbohydr. Res. **314**, 127 (1998).
11. R. Stuike-Prill and B. Meyer. Eur. J. Biochem. **194**, 903 (1990).
12. R.U. Lemieux and A.A. Pavia. Can. J. Chem. **47**, 4441 (1969).
13. J.E. Del Bene and J.A.J. Pople. J. Chem. Phys. **58**, 3605 (1973).
14. R.U. Lemieux and G. Huber. Can. J. Chem. **33**, 128 (1955).
15. J.P. Praly and R.U. Lemieux. Can. J. Chem. **65**, 213 (1987).
16. R.U. Lemieux, C.-C. Ling, H. Streicher, and N. Sharon. Israel J. Chem, in press (2001).
17. H. Beierbeck, L.T.J. Delbaere, M. Vandonselaar, and R.U. Lemieux. Can. J. Chem. **72**, 463 (1994).
18. O. Hindsgaul, D.P. Khare, M. Bach, and R.U. Lemieux. Can. J. Chem. **63**, 2653 (1985).
19. U. Spohr, E. Paszkiewicz-Hnatiw, N. Morishima, and R.U. Lemieux. Can. J. Chem. **70**, 254 (1992).
20. R.U. Lemieux, L.T.J. Delbaere, H. Beierbeck, and U. Spohr. Involvement of water in host–guest interactions. Ciba Foundation Symposium no. 158. Host–Guest Molecular Interactions: From Chemistry to Biology, July 3–5, 1990. Wiley, Chichester, London, U.K. 1991. pp. 231–248.
21. R.U. Lemieux. Acc. Chem. Res. **29**, 373 (1996).
22. R.U. Lemieux. How proteins recognize and bind oligosaccharides. *In* Carbohydrate antigens, ACS Symposium Series 519.

© 2001 NRC Canada

Edited by Per J. Garegg and Alf A. Lindberg. American Chemical Society, Washington, D.C. 1993.
23. B.W. Sigurskjold, C.R. Berland, and B. Svensson. Biochemistry, **33**, 10191 (1994).
24. L.T.J. Delbaere, M. Vandonselaar, L. Prasad, J.W. Quail, P.V. Nikrad, J.R. Pearlstone, M.R. Carpenter, L.B. Smillie, U. Spohr, and R.U. Lemieux. Can. J. Chem. **68**, 1116 (1990).
25. M. Cygler, D.R. Rose, and D.R. Bundle. Science (Washington, D.C.), **253**, 442 (1991).
26. F. Cramer and W. Freist. Acc. Chem. Res. **20**, 79 (1987).
27. H. Hashimoto, K. Asano, F. Fujii, and J. Yoshimura. Carbohydr. Res. **104**, 87 (1982).
28. A. Liptak, I. Jodal, and P. Nanasi. Carbohydr. Res. **44**, 1 (1975).
29. D.J. Cram and F.A.A. Elhafez. J. Am. Chem. Soc. **74**, 5828 (1952).
30. D.H. Williams and J. Fleming. Spectroscopic methods in organic chemistry. MacGraw-Hill, U.K. 1980.
31. J.D. Albright and L. Goodman. J. Am. Chem. Soc. **87**, 4217 (1965).
32. R.U. Lemieux, K.B. Hendricks, R.V. Stick, and K. James. J. Am. Chem. Soc. **97**, 4056 (1975).
33. O.P. Srivastava, R. Mendez, and A.P. Venot. Abstracts of the XVth International Carbohydrate Symposium. Yokohama, Japan. August 12–17. 1990. p. 84.
34. G. Zemplén, Z. Csürös, and S. Angyal. Chem. Ber. **70**, 1848 (1937).

© 2001 NRC Canada

Réaction compétitive de la substitution homolytique intramoléculaire : décomposition de peroxydes allyliques dans le thioglycolate de méthyle

Marie-Josèphe Bourgeois, Marianne Vialemaringe, Monique Campagnole et Evelyne Montaudon

Résumé : La décomposition des peroxydes allyliques dans le thioglycolate de méthyle conduit toujours à un mélange d'époxyde et de peroxyde adduit. Selon la nature de la chaîne allylique, l'un ou l'autre est formé très majoritairement, sinon exclusivement. C'est le premier exemple où la réaction de transfert d'un atome d'hydrogène peut l'emporter sur la substitution homolytique intramoléculaire. Les facteurs influençant la compétition sont étudiés.

Mots clés : peroxydes allyliques, époxydes, substitution homolytique intramoléculaire, transfert.

Abstract: The decomposition of allylic peroxides in methyl thioglycolate always leads to both epoxide and adduct peroxide. According to the nature of the allylic chain, either epoxide or peroxide is the predominant product, if not the only one. It is the first example where the hydrogen transfer is as fast as the intramolecular homolytic substitution. The influence of different factors upon the competition is studied.

Key words: allylic peroxides, epoxides, intramolecular homolytic substitution, transfer.

Introduction

L'addition radicalaire de substrats Z-H à des peroxydes allyliques, substitués ou non (**1a**), conduit toujours à l'époxypropanation de ces substrats, à l'exclusion de tout produit d'addition (1). Le radical adduit issu de la fixation de Z˙ à la double liaison n'évolue que par substitution homolytique intamoléculaire S_Hi (schéma 1, voie *a*, Z = radical alkyle et X = H).

Tous nos essais en vue d'établir une base de comparaison pour l'évolution de la constante de vitesse de la S_Hi — utilisation de substrats susceptibles de donner facilement une réaction de transfert ou mise en jeu de peroxydes conduisant à des radicaux adduits particulièrement fragiles susceptibles de se réarranger — sont restés vains. Ainsi, lorsque ZX est le tétrachlorure de carbone, la constante de vitesse du transfert de l'atome de chlore est encore insuffisante pour concurrencer la S_Hi; s'il s'agit du bromotrichlorométhane, seule la réaction de transfert est observée (schéma 1, voie *b*, Z = CCl_3 et X = Br) (1). Nous pensions que cette dernière réaction l'emporterait également lorsque le thioglycolate de méthyle, connu pour être un excellent agent de transfert (2, 3) au même titre que le bromotrichlorométhane, est opposé au peroxyde de *t*-butyle et de *trans*-pinocarvéyle, **1g**. Or, il n'en est rien et dans ce cas, seul l'époxyde **2g** est obtenu, ni le transfert d'hydrogène ni éventuellement la β–scission du radical adduit n'étant observés (schéma 2) (4).

Ne pouvant comparer les résultats issus de peroxydes de structures aussi différentes, nous avons opposé au thioglycolate de méthyle le peroxyde d'allyle et de *t*-butyle, **1a**, et des homologues diversement substitués. Le choix de ce substrat, dont la réactivité est analogue à celle des autres thiols, s'explique par la simplicité des signaux qui le caractérisent dans les spectres RMN ^1H et ^{13}C des produits formés. Cette publication décrit les résultats de cette étude.

Reçu le 1 juillet 2000. Publié sur le site Web des Presses scientifiques du CNRC le March 28, 2001.

M.-J. Bourgeois, M. Vialemaringe, M. Campagnole et E. Montaudon.[1] Institut du Pin, Laboratoire de Chimie des Substances Végétales, Université Bordeaux 1, 351 Cours de la Libération, 33405 F-Talence Cédex, France.

[1]Auteur correspondant (tél. : 05 56 84 62 55; téléc. : 05 56 84 64 22; courriel : e.montaudon@ipin.u-bordeaux.fr).

Choix des méthodes et conditions d'étude

Les peroxydes testés sont rassemblés dans le schéma 3.

Les premiers essais sur le peroxyde **1g** montrent que les conditions habituelles (chauffage à 110°C d'un mélange contenant un équivalent de peroxyde, un excès de substrat et 0,1 équivalent de peracétate de *t*-butyle) sont à proscrire : en effet, la décomposition du peroxyde est rapide et brutale. La présence d'un amorceur est inutile, la réaction se produisant même dans l'obscurité; le thioglycolate de méthyle a du reste été additionné avec succès au styrène à 100°C, sans amorçage (5). Le mélange mis en jeu est uniquement constitué du peroxyde et du thiol pris dans le rapport molaire 1/1,05. La réaction est effectuée à différentes températures n'excédant pas 80°C et entraînant des durées de réaction adaptées (voir partie expérimentale).

 DOI: 10.1139/cjc-79-3-257 © 2001 CNRC Canada

Schéma 1.

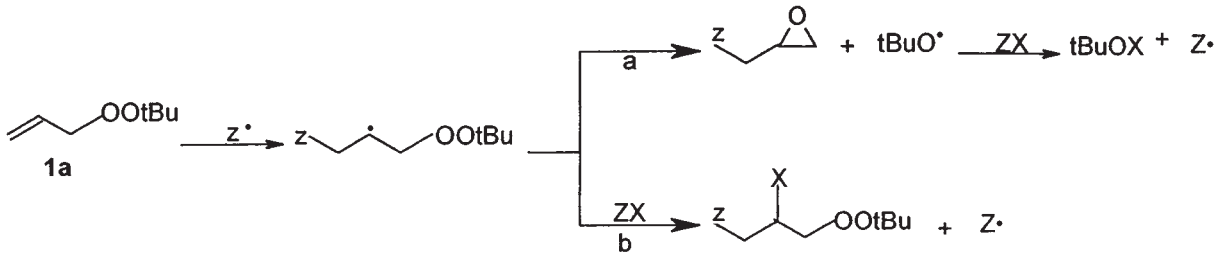


Schéma 2.

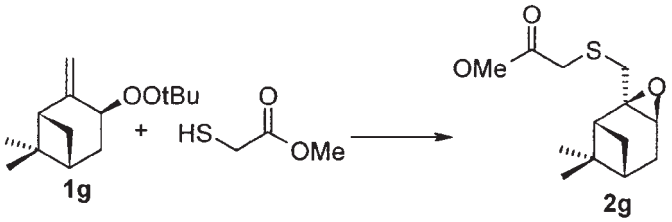
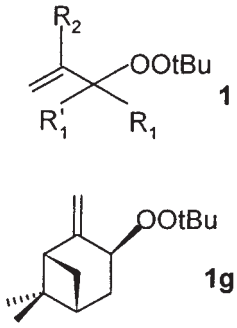
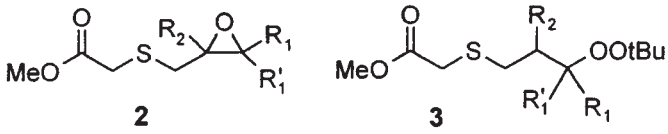


Schéma 3.



	R_1	R'_1	R_2
a	H	H	H
b	Me	H	H
c	H	H	Me
d	Me	Me	H
e	Me	H	Me
f	Me	Me	Me

Schéma 4.



Résultats et discussion

Le tableau 1 regroupe les résultats obtenus : rendements en époxyde **2** et (ou) adduit **3** susceptibles de se former (schéma 4), proportions relatives de l'époxyde par rapport à l'ensemble époxyde–peroxyde adduit. On observe que le taux de transformation des peroxydes est toujours très important, voire même total (74 à 100 %), sauf cas particulier de **1f**.

Proportions relatives époxyde/peroxyde adduit

L'époxyde et le peroxyde adduit sont tous les deux présents, sauf dans le cas du peroxyde de pinocarvéyle, **1g**. Pour les peroxydes linéaires, la proportion d'époxyde (par rapport à l'ensemble époxyde–peroxyde adduit) varie de 4 à 98 %.

Deux configurations sont possibles pour les époxydes **2b** et **2e**. **2b** est effectivement formé sous les formes *cis* et *trans* dans le rapport 15/85 (détermination effectuée par chromatographie en phase gazeuse (CPG) et résonance magnétique nucléaire (RMN)), régi par la stabilité relative des radicaux conformères impliqués dans l'étape de S_Hi (6). L'attribution *cis–trans* est possible grâce à la RMN ^{13}C : dans un cycle époxyde disubstitué en 1, 2, les carbones liés au cycle sont plus blindés lorsque les deux substituants sont en *cis* que lorsqu'ils sont en *trans* (6). **2e** est également présent sous ses deux formes isomères *cis–trans*, relativement aux carbones 4 et 7, dans les proportions 55/45 (évaluation effectuée par RMN).

Le degré de substitution du peroxyde initial, la classe du radical adduit et la température de l'expérience influencent l'orientation de la réaction : (*i*) la présence et l'accumulation de substituants sur le peroxyde initial favorisent la S_Hi : la proportion d'époxyde est maximale pour **f** et **e**, diminue pour **d**, **c** et **b**, et devient très minoritaire pour **a**. Ceci va dans le sens d'une formation plus rapide des petits cycles les plus substitués. (*ii*) La présence de un ou plusieurs substituants sur le site radicalaire initialement formé favorise la S_Hi : pour le même nombre de substituants sur la chaîne alkyle, il se forme plus d'époxyde avec **c** qu'avec **b**; avec **e** qu'avec **d**. Un radical tertiaire conduit plus facilement qu'un radical secondaire à un époxyde de même degré de substitution. (*iii*) L'élévation de la température favorise également la S_Hi. Il est en effet connu que les processus monomoléculaires sont, dans ces conditions, plus accélérés que les processus bimoléculaires.

Stabilité des époxydes

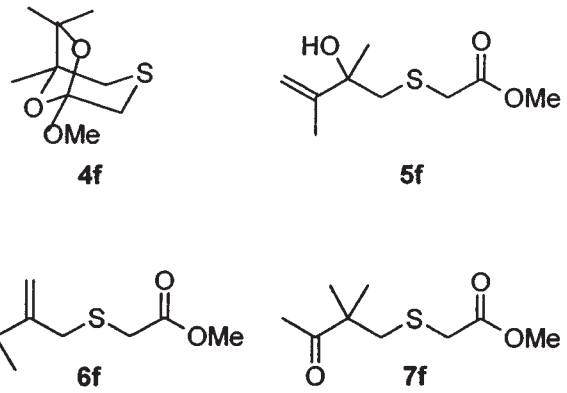
Les résultats obtenus à partir des peroxydes **1d**, **1e**, **1g** et surtout **1f** montrent une chute anormale du rendement en époxydes aux fortes températures : les époxydes tri- et surtout tétra-substitués semblent peu stables dans le milieu. La stabilité de l'époxyde **2f** a été plus particulièrement testée.

Traité à 80°C, le peroxyde **1f** conduit, à côté de l'époxyde **2f** et du peroxyde adduit **3f**, à des composés absents des décompositions réalisées à –10°C, à savoir l'orthoester **4f**, le mélange d'alcools **5f** et **6f** et la cétone **7f** (schéma 5), dans les proportions relatives 28, 60 et 12 %.

Une réaction normalement effectuée à –10°C, puis portée 1 h à 80°C, ne contient plus l'époxyde **2f**, mais les produits secondaires précédents dans les mêmes proportions. L'époxyde **2f** pur n'est pas transformé par un chauffage à 80°C durant 5 h en présence d'un équivalent de RSH; par contre, il disparaît totalement en donnant le mélange précédent dans les mêmes proportions s'il est chauffé à 80°C, soit en présence de 0,1 équivalent de RSH et un équivalent de *t*-butanol durant 5 h, soit en présence de 1 équivalent de

© 2001 CNRC Canada

Schéma 5.



t-butanol durant 15 h. Le *t*-butanol, éventuellement associé au thiol, facilite donc le processus de réarrangement thermique déjà observé à partir de δ,ε-époxycétones et d'acétates de 3,4-époxyalkyle (7).

Comparaison avec le peroxyde de *t*-butyle et de pinocarvéyle, 1g

Le modèle le plus proche de **1g** est le peroxyde **1e** : ils comportent tous les deux un substituant sur un carbone sp^2 et un autre sur le carbone allylique. Si **1e** ne donne que très peu de peroxyde adduit (<5 %), **1g** n'en donne pas du tout. Même avec un rapport molaire thiol/**1g** de 10/1 ou à –10°C (conditions favorisant le transfert), le peroxyde adduit **3g** est toujours absent. On peut estimer que les peroxydes **1e** et **1g** ont un comportement tout à fait analogue, l'encombrement du composé bicyclique rendant encore plus difficile une réaction de transfert déjà défavorisée.

Conclusion

Cette étude de décomposition des peroxydes allyliques dans les thiols nous a permis de trouver la réaction étalon de la substitution homolytique intramoléculaire que nous recherchions. Alors qu'avec tous les agents bons donneurs d'hydrogène par coupure d'une liaison C—H seul l'époxyde se forme, avec les thiols les réactions de transfert et de substitution homolytique intramoléculaire deviennent compétitives. En série peroxyde allylique linéaire, l'époxyde et le peroxyde adduit coexistent toujours. Le pourcentage d'époxyde par rapport au mélange époxyde – peroxyde adduit varie de 4 à 98 %, en fonction de la température, de la substitution de la chaîne allylique initiale et de la classe du site radicalaire. Dans le cas particulier du peroxyde d'allyle et de *t*-butyle, le peroxyde adduit est même obtenu avec le très bon rendement de 80 %. La réactivité du peroxyde de *t*-butyle et de *trans*-pinocarvéyle, qui semblait a priori très surprenante, s'explique donc logiquement en fonction des résultats obtenus en série linéaire.

Partie expérimentale

Techniques utilisées

Les analyses et déterminations de structure ont été réalisées sur les appareils suivants : (*i*) chromatographie en phase gazeuse : chromatographe DELSI DI 200 équipé d'une colonne CP SIL-8 CB (longueur 25 m, diamètre intérieur 0,25 mm, épaisseur du film 0,25 μm). Les dosages ont été effectués par la méthode de l'étalon interne. (*ii*) Spectres de RMN ^{1}H et ^{13}C : appareil Brucker AC 250 fonctionnant à 250 MHz et 62,9 MHz respectivement, en solution dans du chloroforme deutérié; les déplacements chimiques sont en ppm par rapport au tétraméthylsilane. Des expériences 2D de corrélation ont été réalisées quand cela était nécessaire. (*iii*) Spectres de masse : spectromètres éventuellement couplés à un chromatographe en phase gazeuse : FISONS-Instrument type Autospec-EQ en impact électronique (SMIE) (70 eV) ou en ionisation chimique (SM-IC) (NH_3), ou spectromètre à trappe ionique Varian Saturn 4D en impact électronique. Les intensités sont en pourcentage relatif par rapport au pic de base (100 %). Les masses moléculaires exactes sont déterminées, chaque fois que possible, par analyse en haute résolution.

Les purifications sont faites par chromatographie sur gel de silice ou par chromatographie liquide haute performance sur un appareil Millipore Waters Delta Prep 3000 équipé d'une colonne TW PREP-PAK Porasil 15 μm.

Matières premières

Certains peroxydes sont déjà décrits : **1a** et **1c** (8), **1b**, **1d** et **1g** (9). Les peroxydes **1e** et **1f** proviennent de la réaction du trichloroacétimidate de *t*-butyle (10) avec les hydroperoxydes correspondants issus de la photooxygénation du 2-méthyl-but-2-ène et du diméthyl-but-2-ène respectivement (11). Le peroxyde **1e** n'a pu être obtenu pur, il est accompagné de l'isomère **1d**, les hydroperoxydes précurseurs se formant simultanément (dans les proportions 53/47) lors de la photooxygénation; une chromatographie sur silice permet d'enrichir **1e** : rdt = 70 %; pureté = 85 %. Le peroxyde **1f** est obtenu pur : rdt= 85 %.

Peroxyde de 3-méthyl-but-3-èn-2-yle et de t*-butyle (**1e**) (en mélange avec **1d** : 85/15)*

RMN ^{1}H δ : 4,9–4,7 (m, 2H, *H*-4), 4,5–4,2 (m, 1H, *H*-2), 1,6 (s, 3H, Me-3), 1,19 (d, *J* = 13,4 Hz, 3H, Me-2), 1,15 (s, 9H, *t*-Bu). RMN ^{13}C δ : 145,4 (C-3), 111,9 (C-4), 82,7 (C-2), 78,4 (*C*Me$_3$), 26,3 (C*Me*$_3$), 24,4 (Me-3), 17,4 (C-1).

Peroxyde de 2,3-diméthyl-but-3-èn-2-yle et de t*-butyle (**1f**)*

RMN ^{1}H δ: 4,95–4,8 (m, 2H, *H*-4), 1,81 (s, 3H, Me-3), 1,33 (s, 6H, *H*-1, Me-2), 1,25 (s, 9H, *t*-Bu). RMN ^{13}C δ : 149,8 (C-3), 110,3 (C-4), 81,4 (C-2), 78,3 (*C*Me$_3$), 26,6 (C*Me*$_3$), 24,5 (C-1, Me-2), 18,7 (Me-3).

Addition du thioglycolate de méthyle

La décomposition des peroxydes insaturés dans les thiols à 110°C (conditions habituelles pour les autres substrats ZH) étant brutale, la réaction est effectuée à 80°C (1 h), 60°C (2 h), 30°C (18 h) et même à –10°C (4 jours). L'addition d'un amorceur radicalaire est inutile; on peut même procéder dans l'obscurité. Le rapport thiol/peroxyde est de 1,05/1 sauf études préparatives particulières où pour favoriser l'époxyde ou le peroxyde adduit on utilise respectivement les rapports 0,5/1 et 2/1.

© 2001 CNRC Canada

Tableau 1. Décomposition des peroxydes dans le thioglycolate de méthyle.

	Peroxydes **1**	T (°C)[a]	Époxydes **2**[b]	Peroxydes adduits **3**[b]	[**2**]×100/[**2**]+[**3**]
a	R_1 = H	30	3	80	4
	R'_1 = H	60	7	73	9
	R_2 = H	80	8	73	10
b	R_1 = Me	30	15[c]	82	15
	R'_1 = H	60	24[c]	70	26
	R_2 = H	80	39[c]	50	44
c	R_1 = H	30	33	67	33
	R'_1 = H	60	50	50	50
	R_2 = Me	80	62	32	66
d	R_1 = Me	30	42	32	57
	R'_1 = Me	60	67	16	81
	R_2 = H	80	63	15	81
e	R_1 = Me	30	84[d]	5	94
	R'_1 = H	60	92[d]	<2	>98
	R_2 = Me	80	77[d]	<2	>97
f	R_1 = Me	–10	82	10	89
	R'_1 = Me	30	30	4	—
	R_2 = Me	80	5	3	—
g	*t*-butyl et	–10	—	0	100
	trans-pinocarvéyle	30	88	0	100
		60	88	0	100
		80	62	0	100

Nota : Le rapport molaire peroxyde **1**/thiol = 1/1,05.
[a]Quatre jours dans l'obscurité à –10°C; 18 h à 30°C; 2 h à 60°C; 1 h à 80°C.
[b]Dosés par CPG par la méthode de l'étalon interne.
[c]Présent sous deux formes diastéréoisomères *cis*/*trans* : 15/85.
[d]Présent sous deux formes diastéréoisomères *cis*/*trans* (relativement aux carbones 4 et 7) : 55/45.

Études analytiques

Elles sont réalisées à partir de 1,5 mmol de peroxyde. Le mélange est introduit dans un tube à vis placé dans un bain thermorégulé ou dans le congélateur du réfrigérateur pendant le temps voulu. Les produits de réaction sont ensuite dosés en chromatographie en phase gazeuse.

Études préparatives

On opère dans un ballon muni d'un réfrigérant à partir de 10 mmol de peroxyde. Après avoir chassé les produits légers sous le vide de la trompe à eau, on sépare les produits de réaction par HPLC (éluant : éther de pétrole – éther 80/20 ou 70/30).

Étude de la stabilité de l'époxyde 2f

Après avoir réalisé la réaction d'addition du thiol à –10°C, on dose l'époxyde formé puis on porte le mélange réactionnel à 80°C pendant 1 h et on dose en CPG les nouveaux composés. On les isole par chromatographie sur colonne de silice.

Produits de réaction

*5,6-Époxy-3-thiahexanoate de méthyle (**2a**)*

SM-IC : 180 $[M + NH_4]^+$, 163 $[M + H]^+$. Non isolé, détecté par quelques signaux RMN ^{1}H δ : 3,3 (s, 2H, *H*-2), 2,9 (m, 3H, *H*-5,6).

*6-t-Butylperoxy-3-thiahexanoate de méthyle (**3a**)*

SM-IC : 254 $[M + NH_4]^+$. RMN ^{1}H δ : 3,9 (t, *J* = 6 Hz, 2H, *H*-6), 3,7 (s, 3H, OCH_3), 3,2 (s, 2H, *H*-2), 2,7 (t, *J* = 7 Hz, 2H, *H*-4), 2,0–1,7 (m, 2H, *H*-5), 1,2 (s, 9H, *t*-Bu). RMN ^{13}C δ : 170,6 (C-1), 79,6 (*C*Me_3), 79,3 (C-6), 51,9 (OCH_3), 33,0 (C-2), 29,1 (C-4), 27,3 (C-5), 26,1 (Me_3).

*5,6-Époxy-3-thiaheptanoate de méthyle (**2b**)*

Mélange de deux diastéréoisomères. SM-IC : 194 $[M + NH_4]^+$, 177 $[M + H]^+$. RMN ^{1}H δ : 3,62 (s, 3H, OCH_3), 3,22 (s, 2H, *H*-2), 2,9–2,6 (m, 4H, *H*-4, 5, 6), 1,2 (d, *J* = 5 Hz, 3H, *H*-7). RMN ^{13}C (*cis*/*trans*) δ : 170,6 (C-1), 56,0/58,4 (C-5), 52,8/54,4 (C-6), 52,4 (OCH_3), 30,2/33,9 (C-4), 33,4 (C-2) 13,2/17,3 (C-7). M calc. pour $C_7H_{12}O_3S$: 176,0507; tr. 176,0509.

*6-t-Butylperoxy-3-thiaheptanoate de méthyle (**3b**)*

SM-IC : 268 $[M + NH_4]^+$. RMN ^{1}H δ : 4,2–4 (m, 1H, *H*-6), 3,66 (s, 3H, OCH_3), 3,17 (s, 2H, *H*-2), 2,65 (t, *J* = 7 Hz, 2H, *H*-4), 2,0–1,6 (m, 2H, *H*-5), 1,16 (s, 9H, *t*-Bu), 1,13 (d, *J* = 6,3 Hz, 3H, *H*-7). RMN ^{13}C δ : 170,9 (C-1), 79,8 (*C*Me_3), 78,0 (C-6), 52,3 (OCH_3), 34,2 (C-5), 33,4 (C-2), 28,8 (C-4), 26,4 (Me_3), 18,5 (C-7).

*5,6-Époxy-5-méthyl-3-thiahexanoate de méthyle (**2c**)*

SM-IC : 194 $[M + NH_4]^+$, 177 $[M + H]^+$. RMN ^{1}H δ : 3,7 (s, 3H, OCH_3), 3,3 (s, 2H, *H*-2), 2,75 (s, 2H, *H*-4), 2,72 et 2,58 (AB, *J* = 5 Hz, 2H, *H*-6), 1,4 (s, 3H, Me). RMN ^{13}C δ : 170,5 (C-1), 56,1 (C-5), 52,9 (C-6), 52,2 (OCH_3), 38,6

© 2001 CNRC Canada

(C-4), 33,5 (C-2), 19,9 (Me). M calc. pour $C_7H_{12}O_3S$: 176,0507; tr. 176,0509.

*6-*t*-Butylperoxy-5-méthyl-3-thiahexanoate de méthyle (**3c**)*

SM-IC : 268 $[M + NH_4]^+$. RMN ^1H δ : 3,9–3,7 (m, 2H, *H*-6), 3,65 (s, 3H, OCH_3), 3,15 (s, 2H, *H*-2), 2,8–2,3 (m, 2H, *H*-4), 2,1–2,0 (m, 1H, *H*-5), 1,15 (s, 9H, *t*-Bu), 0,95 (d, *J* = 7 Hz, 3H, Me). RMN ^{13}C δ : 170,6 (C-1), 79,9 (CMe_3), 78,2 (C-6), 52,0 (OCH_3), 36,7 (C-4), 33,8 (C-2), 32,2 (C-5), 26,2 (Me_3), 16,4 (Me).

*5,6-Époxy-6-méthyl-3-thiaheptanoate de méthyle (**2d**)*

SM-IC : 208 $[M + NH_4]^+$, 191 $[M + H]^+$. RMN ^1H δ : 3,65 (s, 3H, OCH_3), 3,32 et 3,22 (AB, *J* = 15 Hz, 2H, *H*-2), 2,9 (X de ABX, *J*AX = *J*BX = 5 Hz, 1H, *H*-5), 2,72 et 2,70 (AB de ABX, *J*AB = 14 Hz, 2H, *H*-4), 1,25 et 1,22 (2s, 6H, *H*-7, Me). RMN ^{13}C δ : 170,6 (C-1), 62,9 (C-5), 58,6 (C-6), 52,2 (OCH_3), 33,1 (C-2), 31,2 (C-4), 24,4 (C-7), 18,7 (Me). M calc. pour $C_8H_{14}O_3S$: 190,066 37; tr. 190,066 39.

*6-*t*-Butylperoxy-6-méthyl-3-thiaheptanoate de méthyle (**3d**)*

SM-IC : 282 $[M + NH_4]^+$. RMN ^1H δ : 3,7 (s, 3H, OCH_3), 3,2 (s, 2H, *H*-2), 2,65–2,55 (m, 2H, *H*-4), 1,8–1,7 (m, 2H, *H*-5), 1,13 et 1,12 (2s, 15H, *H*-7, Me, *t*-Bu). RMN ^{13}C δ : 170,9 (C-1), 79,4 (CMe_3), 78,3 (C-6), 52,2 (OCH_3), 38,8 (C-5), 33,4 (C-2), 27,4 (C-4), 26,4 (Me_3), 24,6 (C-7, Me).

*5,6-Époxy-5-méthyl-3-thiaheptanoate de méthyle (**2e**)*

Deux diastéréoisomères (55/45) en mélange avec **2d**. SM-IC : 208 $[M + NH_4]^+$, 191 $[M + H]^+$. RMN ^1H δ : 3,6 (s, 3H, OCH_3), 3,31–3,08 (m, 2H, *H*-2), 2,87–2,54 (m, 3H, *H*-4,6), 1,28–1,14 (m, 6H, *H*-7, Me). RMN ^{13}C (*cis/trans*) δ : 170,6 (C-1), 60,0 (C-5), 58,2/59,7 (C-6), 52,2 (OCH_3), 35,2/40,2 (C-4), 33,5 (C-2), 21,4/15,6 (Me), 13,9/13,8 (C-7).

*6-*t*-Butylperoxy-5-méthyl-3-thiaheptanoate de méthyle (**3e**)*

SM-IC : 282 $[M + NH_4]^+$. RMN ^1H δ : seuls sont indiqués les signaux caractéristiques : 3,66 (s, 3H, OCH_3), 4,03–3,91 (m, 1H, *H*-6). RMN ^{13}C (deux diastéréoisomères) δ : 170,9 (C-1), 81,4/81,0 (C-6), 79,7 (CMe_3), 52,2 (OCH_3), 36,8/36,0 (C-5), 36,4/36,1 (C-4), 33,9/33,8 (C-2), 26,50 (Me_3), 26,57/26,44 (Me), 14,5/14,4 (C-7).

*5,6-Époxy-5,6-diméthyl-3-thiaheptanoate de méthyle (**2f**)*

SM-IC : 222 $[M + NH_4]^+$, 205 $[M + H]^+$. RMN ^1H δ : 3,55 (s, 3H, OCH_3), 3,25 et 3,08 (AB, *J* = 15 Hz, 2H, *H*-2), 2,79–2,55 (AB, *J* = 13 Hz, 2H, *H*-4), 1,26, 1,18 et 1,15 (3s, 9H, *H*-7, Me-5, Me-6). RMN ^{13}C δ : 171,6 (C-1), 63,7 (C-5 ou C-6), 62,2 (C-6 ou C-5), 52,2 (OCH_3), 37,3 (C-4), 33,6 (C-2), 21,1, 20,7 et 18,3 (C-7, Me-5, Me-6). M calc. pour $C_9H_{16}O_3S$: 204,0820; tr. 204,0809.

*6-*t*-Butylperoxy-5,6-diméthyl-3-thiaheptanoate de méthyle (**3f**)*

SM-IC : 296 $[M + NH_4]^+$. RMN ^1H δ : 3,65 (s, 3H, OCH_3), 3,22 et 3,13 (AB, *J* = 14,8 Hz, 2H, *H*-2), 3,04–2,94 (m, 1H, *H*-4), 2,2–2,03 (m, 1H, *H*-4), 2,0–1,8 (m, 1H, *H*-5), 1,13 et 1,01 (2s, 15H, *H*-7, Me-6, *t*-Bu), 0,94 (d, *J* = 6,8 Hz, Me-5). RMN ^{13}C δ : 171,1 (C-1), 82,2 (C-6), 78,3 (CMe_3), 52,2 (OCH_3), 40,1 (C-5), 35,3 (C-4), 33,8 (C-2), 26,5 (Me_3), 23,3 et 20,4 (C-7, Me-6), 14,2 (Me-5).

*1-Méthoxy-5,6,6-triméthyl-7,8-dioxa-3-thiabicyclo[3.2.1]octane (**4f**)*

SM-IC : 222 $[M + NH_4]^+$, 205 $[M + H]^+$. SM-IE *m/z* (%) : 204 ($M^{\bullet+}$, 32), 128 (13), 113 (23), 83 (40), 82 (100), 67 (29), 57 (13), 45 (21), 43 (56), 41 (23). IR (cm^{-1}) : 1114,8 et 1088,1 (C-O-C). RMN ^1H δ : 3,34 (s, 3H, OCH_3), 2,87 et 2,48 (AB, *J* = 12,4 Hz, 2H, *H*-2 ou 4), 2,84 et 2,25 (AB, *J* = 13,5 Hz, 2H, *H*-4 ou 2), 1,53, 1,25 et 1,19 (3s, 9H, Me-5, 2Me-6). RMN ^{13}C δ : 117,5 (C-1), 84,5 (C-5 ou C-6), 82,4 (C-6 ou C-5), 48,8 (OCH_3), 31,5 et 30,9 (C-2, C-4), 26,8, 21,5 et 20,6 (Me-5, 2Me-6). M calc. pour $C_9H_{16}O_3S$: 204,0820; tr. 204,0819.

*5-Hydroxy-5,6-diméthyl-3-thiahept-6-ènoate de méthyle (**5f**) et 6-hydroxy-6-méthyl-5-méthylidényl-3-thiaheptanoate de méthyle (**6f**) en mélange*

SM-IC : 222 $[M + NH_4]^+$, 204 $[M + NH_4\text{-}H_2O]^+$. IR (cm^{-1}) : 3494,0 (OH), 3090,7 (=C-H), 1732,4 (C=O), 1642,0 (C=C). RMN ^1H δ : **5f** : 5,00–4,95 (m, 2H, *H*-7), 3,63 ou 3,63 (s, 3H, OCH_3), 3,12 (s, 2H, *H*-2), 2,99 et 2,64 (AB, *J* = 13,5 Hz, 2H, *H*-4), 1,67 (s, 3H, Me-6), 1,26 (s, 3H, Me-5); **6f** : 5,12 et 4,78 (2s, 2H, CH_2=), 3,63 ou 3,62 (s, 3H, OCH_3), 3,31 (s, 2H, *H*-4), 3,20 (s, 2H, *H*-2), 1,29 (s, 6H, *H*-7, Me-6). RMN ^{13}C δ : 171,3 (C-1), 170,9 (C-1), 150,0 (C_q=), 148,9 (C_q=), 112,9 (CH_2=), 110,9 (CH_2=), 74,6 (COH), 72,8 (COH), 52,5 (CH_3O), 52,4 (CH_3O), 44,2, 34,7, 33,9, 32,2 (C-2, C-4), 29,9 (2Me de **6f**), 26,7 (Me-5 de **5f**), 19,3 (Me-6 de **5f**).

*5,5-Diméthyl-6-oxo-3-thiaheptanoate de méthyle (**7f**)*

SM-IC : 222 $[M + NH_4]^+$: 205 $[M + H]^+$. SM-IE *m/z* (%) : 204($M^{\bullet+}$, 5), 101(34), 99(91), 56(11), 55(21), 45(20), 43(100), 41(12). RMN ^1H δ : 3,67 (s, 3H, OCH_3), 3,17 (s, 2H, *H*-2), 2,79 (s, 2H, *H*-4), 2,10 (s, 3H, *H*-7), 1,16 (s, 6H, 2Me-5). RMN ^{13}C δ : 212,5 (C-6), 170,6 (C-1), 52,4 (OCH_3), 48,8 (C-5), 42,2 (C-2), 35,1 (C-4), 25,4 (C-7), 24,2 (2Me-5). M calc. pour $C_9H_{16}O_3S$: 204,0820; tr. 204,0822.

*4-(7,7-Diméthyl-3-oxatricyclo[4.1.1.$0^{2,4}$] oct-2-yl)-3-thiabutanoate de méthyle (**2g**)*

Décrit dans (4).

Références

1. M.J. Bourgeois, B. Maillard et E. Montaudon. Tetrahedron, **42**, 5309, (1986) et références citées.
2. C. Walling. Free radicals in solution. Wiley, New York. 1957. pp. 257, 319 et références citées.
3. J.A. Claisse, D.I. Davies et L.T. Parfitt. J. Chem. Soc. (C). 258, (1970).
4. M. Vialemaringe, M.J. Bourgeois, M. Campagnole et E. Montaudon. Synthesis, 1607 (1999).
5. R.R. Hiatt et P.D. Bartlett. J. Am. Chem. Soc. **81**, 1149 (1959).
6. X. Lubeigt, F. Flies, M.J. Bourgeois, E. Montaudon et B. Maillard. Can. J. Chem. **69**, 1320 (1991).
7. H.H. Wasserman et E.H. Barber. J. Am. Chem. Soc. **91**, 3674 (1969). J.L. Coke, H.J. Williams et S. Natarajan. J. Org. Chem. **42**, 2380 (1977).
8. J. Moulines, M.J. Bourgeois, M. Campagnole, A.M. Lamidey, B. Maillard et E. Montaudon. Synth. Commun. **20**, 349 (1990).

© 2001 CNRC Canada

9. M.J. Bourgeois, E. Montaudon et B. Maillard. Tetrahedron, **49**, 2477 (1993).
10. A. Armstrong, I. Brackenridge, R.F.W. Jackson et J.M. Kirk. Tetrahedron Lett. **29**, 2483 (1988).
11. W. Adam et A. Griesbeck. Synthesis, 1050 (1986).

© 2001 CNRC Canada

Bis(1-phenyl-1-propyne) complexes of tungsten(II): crystal structures of $[WI_2(CO)(NCR)(\eta^2\text{-}MeC_2Ph)_2]$ (R = Me, Et, or Ph)

Paul K. Baker, Michael G.B. Drew, and Deborah S. Evans

Abstract: Reaction of $[WI_2(CO)_3(NCMe)_2]$ with two equivalents of 1-phenyl-1-propyne (MeC_2Ph) in CH_2Cl_2, and in the absence of light, gave the bis(1-phenyl-1-propyne) complex $[WI_2(CO)(NCMe)(\eta^2\text{-}MeC_2Ph)_2]$ (**1**) in 77% yield. Treatment of equimolar quantities of **1** and NCR (R = Et, *i*-Pr, *t*-Bu, Ph) in CH_2Cl_2 afforded the nitrile-exchanged products, $[WI_2(CO)(NCR)(\eta^2\text{-}MeC_2Ph)_2]$ (**2**–**5**) (R = Et (**2**), *i*-Pr (**3**), *t*-Bu (**4**), Ph (**5**)). Complexes **1**, **2**, and **5** were structurally characterized by X-ray crystallography. All three structures have the same pseudo-octahedral geometry, with the equatorial sites being occupied by *cis* and parallel alkyne groups, which are *trans* to the *cis*-iodo groups. The *trans* carbon monoxide and acetonitrile ligands occupy the axial sites. In structures **1** and **2**, the methyl and phenyl substituents of the 1-phenyl-1-propyne ligands are *cis* to each other, whereas for the bulkier NCPh complex (**5**), the methyl and phenyl groups are *trans* to one another. This is the first time that this arrangement has been observed in the solid state in bis(alkyne) complexes of this type.

Key words: bis(1-phenyl-1-propyne), carbonyl, nitrile, diiodo, tungsten(II), crystal structures.

Résumé : La réaction du $[WI_2(CO)_3(NCMe)_2]$ avec deux équivalents de 1-phénylprop-1-yne (MeC_2Ph), dans le CH_2Cl_2, en absence de lumière, conduit à la formation du complexe bis(1-phénylprop-1-yne) $[WI_2(CO)(NCMe)(\eta^2\text{-}MeC_2Ph)_2]$ (**1**) avec un rendement de 77%. La réaction de quantités équimolaires de **1** et de NCR (R = Et, *i*-Pr, *t*-Bu, Ph) conduit à la formation de produits d'échange avec les nitriles, $[WI_2(CO)(NCR)(\eta^2\text{-}MeC_2Ph)_2]$ (**2**–**5**) (R = Et (**2**), *i*-Pr (**3**), *t*-Bu (**4**), Ph (**5**)). On a déterminé les structures des composés **1**, **2** et **5** par diffraction des rayons X. Les trois structures comportent la même géométrie pseudo-octaédrique dans laquelle les sites équatoriaux sont occupés par des groupes alcynes *cis*- et parallèles qui sont *trans* par rapport aux groupes *cis*-iodo. Le monoxyde de carbone *trans* et les ligands acétonitriles occupent des sites axiaux. Dans les structures des composés **1** et **2**, les groupes méthyle et phényle des ligands 1-phénylprop-1-yne sont *cis* l'un par rapport à l'autre alors que dans le complexe **5** plus encombré, les groupes méthyle et phényle sont *trans* l'un par rapport à l'autre. C'est la première fois qu'un tel arrangement peut être observé à l'état solide dans des complexes bis(alcyne) de ce type.

Mots clés : bis(1-phénylprop-1-yne), carbonyle, nitrile, diiodo, tungstène(II), structures cristallines.

[Traduit par la Rédaction]

Introduction

Over the past 30 years, extensive developments of the chemistry of alkyne complexes of molybdenum(II) and tungsten(II) have been made (1, 2). To date, the majority of the literature work on bis(alkyne) complexes of Mo(II) and W(II) containing halogens and (or) carbonyl ligands has involved symmetrical alkynes such as 2-butyne (3–11), diphenylacetylene (3–5, 7, 8, 11), hexafluoro-1-butyne (6, 12, 13) and 3-hexyne (7, 14). Complexes of the general type $[MXX'(CO)(NCMe)(\eta^2\text{-}RC_2R)_2]$ (3, 8, 10, 14) and $[\{M(\mu\text{-}X)X'(CO)(NCMe)(\eta^2\text{-}RC_2R)\}_2]$ (X = Br or I) (8, 10, 11) have been well-established by Baker and co-workers (2, 3, 8, 10, 11).

Complexes containing unsymmetric alkynes (RC_2R') are less common. Dimeric complexes, such as $[\{M(\mu\text{-}I)I(CO)(NCMe)(\eta^2\text{-}RC_2R')\}_2]$ (M = Mo, W; R = Ph, R′ = Me, CH_2OH; R = Me, R′ = PhS, *p*-TolS) (11), $[\{W(\mu\text{-}I)Br(CO)(NCMe)(\eta^2\text{-}MeC_2Ph)\}_2]$ (10), and $[WBr_2(CO)(\eta^2\text{-}MeC_2Ph)_2]$ (15), and monomeric complexes, including $[WXX'(CO)(NCMe)(\eta^2\text{-}PhC_2Me)_2]$ (8, 10), $[Mo(CO)(\eta^2\text{-}RC_2R')_2(\eta^5\text{-}C_5H_5 \text{ or } C_9H_7)][BF_4]$ (R = H, R′ = Me; R = H, R′= *t*-Bu; R = Me, R′ = Ph) (4), and $[Mo(NCMe)(\eta^2\text{-}RC_2R')_2(\eta^5\text{-}C_5H_5 \text{ or } C_9H_7)][BF_4]$ (R = R′ = Me; R = H, R′ = *t*-Bu; R = H, R′ = *i*-Pr; R = Me, R′ = Ph) (5), have been reported.

In this work, we describe a modified synthesis of $[WI_2(CO)(NCMe)(\eta^2\text{-}MeC_2Ph)_2]$ (**1**) and the nitrile exchange reactions of **1** with NCR to give four new complexes, $[WI_2(CO)(NCR)(\eta^2\text{-}MeC_2Ph)_2]$ (R = Et (**2**), *i*-Pr (**3**), *t*-Bu (**4**), Ph (**5**)). The crystal structures of **1**, **2**, and **5** are also reported, with the structure for complex **5** being the first reported example of bis(unsymmetrical alkyne) complexes of

Received August 8, 2000. Published on the NRC Research Press Web site on April 2, 2001.

P.K. Baker[1] and D.S. Evans. Department of Chemistry, University of Wales, Bangor, Gwynedd, LL57 2UW, UK. **M.G.B. Drew.** Department of Chemistry, University of Reading, Whiteknights, Reading, RG6 6AD, UK.

[1]Corresponding author (e-mail: chs018@bangor.ac.uk; telephone: 01248–382379; fax: 01248–370528).

 DOI: 10.1139/cjc-79-3-263 © 2001 NRC Canada

Table 1. Physical data for the $[WI_2(CO)(NCR)(\eta^2\text{-}MeC_2Ph)_2]$ complexes (**1**–**5**).

Complex	Colour	Yield (%)	Elemental analysis (%)[a] C	H	N
1 $[WI_2(CO)(NCMe)(\eta^2\text{-}MeC_2Ph)_2]$	bright gold	77	34.2 (34.1)	2.4 (2.6)	1.9 (1.9)
2 $[WI_2(CO)(NCEt)(\eta^2\text{-}MeC_2Ph)_2]$	yellow	72	35.1 (35.1)	3.1 (2.8)	1.9 (1.9)
3 $[WI_2(CO)(NC\textit{i}\text{-}Pr)(\eta^2\text{-}MeC_2Ph)_2]$	yellow-gold	74	36.4 (36.0)	2.9 (3.0)	1.9 (1.8)
4 $[WI_2(CO)(NC\textit{t}\text{-}Bu)(\eta^2\text{-}MeC_2Ph)_2]$	yellow-gold	61	37.6 (36.9)	3.3 (3.4)	1.7 (1.8)
5 $[WI_2(CO)(NCPh)(\eta^2\text{-}MeC_2Ph)_2]$	yellow	74	39.4 (39.0)	2.8 (2.6)	2.1 (1.8)

[a]Calculated values in parenthesis.

this type to have *cis* and parallel alkyne ligands with *trans* Me and Ph groups.

Experimental

General procedures

All reagents were purchased from Lancaster Synthesis or Aldrich–Sigma and were used as received. The starting material used in the preparation of **1**, namely $[WI_2(CO)_3(NCMe)_2]$, was prepared according to literature methods (16, 17). Elemental analyses (C, H, N) were determined using a Carlo Erba Elemental Analyser MOD 1108 (using Helium as a carrier gas). IR spectra were obtained using a Perkin–Elmer 1600 FT-IR spectrometer. ^1H and $^{13}C\{^1H\}$ NMR spectra were recorded on a Bruker AC 250 MHz NMR spectrometer and referenced to tetramethylsilane ($SiMe_4$).

Preparation of $[WI_2(CO)(NCMe)(\eta^2\text{-}MeC_2Ph)_2]$ (1)

To a solution of $[WI_2(CO)_3(NCMe)_2]$ (3.007 g, 4.980 mmol) in dichloromethane (30 cm^3), in a foil-covered Schlenk tube, was added 1-phenyl-1-propyne (1.250 mL, 1.160 g, 9.986 mmol) and the solution was stirred for 24 h. Filtration of the resultant gold-brown solution over celite, followed by removal of the solvent in vacuo gave the product $[WI_2(CO)(NCMe)(\eta^2\text{-}MeC_2Ph)_2]$ (**1**) as a bright gold solid. Recrystallization from dichloromethane–diethyl ether solution (2/3 by volume) and cooling to –17°C, gave single yellow crystals suitable for X-ray crystallography. Yield of pure product was 2.836 g (77 %).

Preparation of $[WI_2(CO)(NCPh)(\eta^2\text{-}MeC_2Ph)_2]$ (5)

To a solution of $[WI_2(CO)(NCMe)(\eta^2\text{-}MeC_2Ph)_2]$ (0.540 g, 0.731 mmol) in dichloromethane (30 cm^3) was added benzonitrile (PhCN) (0.080 mL, 0.081 g, 0.781 mmol) and the solution was stirred for 22 h. Filtration of the resultant gold-brown solution over celite, followed by removal of the solvent in vacuo gave the product $[WI_2(CO)(NCPh)(\eta^2\text{-}MeC_2Ph)_2]$ (**5**) as a yellow solid. Recrystallization from dichloromethane–diethyl ether solution (2/3 by volume) and cooling to –17°C, gave single yellow crystals suitable for X-ray crystallography. Yield of pure product was 0.433 g (74 %).

Similar reactions of equimolar quantities of **1** and NCR in CH_2Cl_2 at room temp gave the acetonitrile exchanged products $[WI_2(CO)(NCR)(\eta^2\text{-}MeC_2Ph)_2]$ (R = Et (**2**), *i*-Pr (**3**), and *t*-Bu (**4**)). Complexes **1**–**5** were fully characterized by elemental analysis (C, H, N) (Table 1), IR spectrosopy (Table 2), ^1H NMR spectroscopy (Table 3) and ^{13}C NMR spectroscopy (Table 4).

Table 2. Infrared data[a] for the $[WI_2(CO)(NCR)(\eta^2\text{-}MeC_2Ph)_2]$ complexes (**1**–**5**).

Complex	IR data		
1	2296 (w)	2076 (s, sh)	1594 (w)
2	2294 (w)	2078 (s, sh)	1594 (w)
3	2293 (w)	2074 (s, sh)	1594 (w)
4	2289 (w)	2075 (s, sh)	1594 (m)
5	2274 (m)	2081 (s, sh)	1595 (m)

[a]Run as thin films in chloroform between NaCl plates (s = strong, m = medium, w = weak, sh = sharp).

X-ray crystallographic experimental details for 1, 2, and 5

Crystal data were collected with Mo Kα radiation using the MARresearch Image Plate System. The crystals were positioned at 70 mm from the Image Plate. One hundred frames were measured at 2° intervals with a counting time of 2 min. Data analysis was carried out with the XDS program (18). The structures were solved using direct methods with the SHELXS 86 program (19). Complexes **1** and **2** are isomorphous. The non-hydrogen atoms were refined with aniostropic thermal parameters. The hydrogen atoms were included in geometric positions and given thermal parameters equivalent to 1.2 times those of the atom to which they were attached. Empirical absorption corrections were carried out using the DIFABS program (20). The structures were refined on F^2 using SHELXL (21). Crystal data and structure refinements for **1**, **2**, and **5** are given in Table 5. Bond lengths (Å) and angles (°) for **1**, **2**, and **5** are given in Tables 6 and 7, respectively.

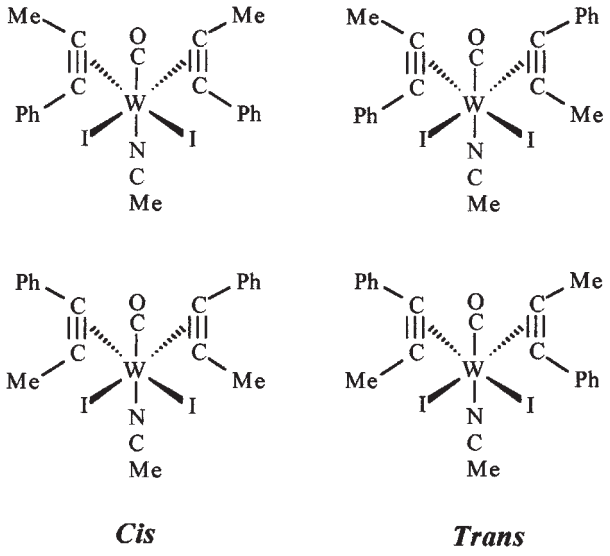
Results and discussion

Modified synthesis, structural characterization, and detailed NMR spectroscopic analysis of the bis(1-phenyl-1-propyne) complex $[WI_2(CO)(NCMe)(\eta^2\text{-}MeC_2Ph)_2]$ (1)

The complex $[WI_2(CO)(NCMe)(\eta^2\text{-}MeC_2Ph)_2]$ (**1**) has been synthesized by a modified procedure to the literature method (8), with both the *cis*- and *trans*-isomers of product **1** being identified by ^1H and $^{13}C\{^1H\}$ NMR spectroscopy. Two equivalents of 1-phenyl-1-propyne were added to a solution of $[WI_2(CO)_3(NCMe)_2]$ in dichloromethane, in a foil-covered Schlenk tube, and the solution was stirred for 24 h at room temperature. Filtration of the resultant gold-brown solution over celite, followed by removal of the solvent in vacuo gave the product $[WI_2(CO)(NCMe)(\eta^2\text{-}MeC_2Ph)_2]$ (**1**) as a bright gold solid. Recrystallization from dichloromethane–diethyl ether solution (2/3 by volume) and cooling

© 2001 NRC Canada

Fig. 1. Representation of the arrangement of substituents on each alkyne ligand to give *cis*- and *trans*-isomers.



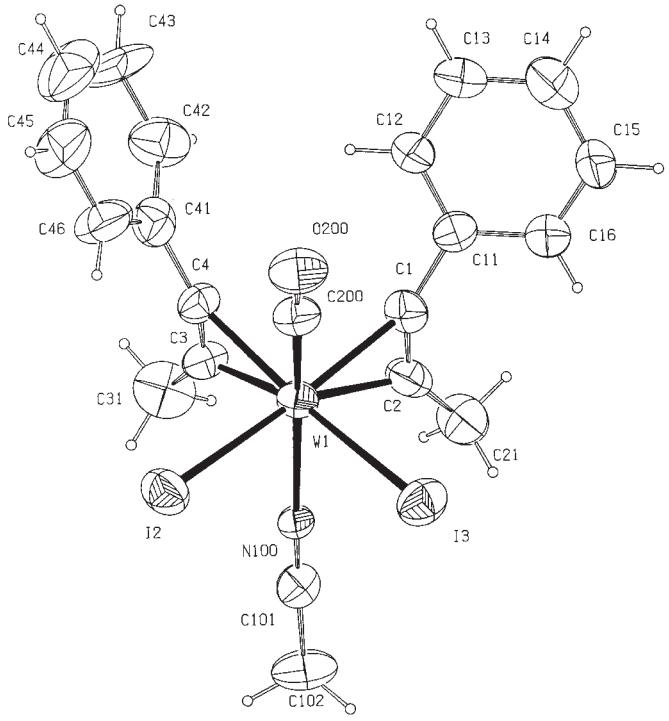
to –17°C, gave single yellow crystals of **1** suitable for X-ray crystallography.

Complex **1** has been fully characterized by elemental analysis (C, H, N), IR spectroscopy, ^{1}H NMR, and ^{13}C{^{1}H} NMR spectroscopy (Tables 1–4). The complex is soluble in chlorinated solvents and acetonitrile, but is insoluble in diethyl ether and hydrocarbon solvents such as hexane. The complex is air stable for up to 15 min and can be stored for up to two months at –17°C with no obvious signs of deterioration. Solutions of **1** showed decomposition within 24 h upon exposure to air.

The IR spectrum for **1** (Table 2) shows a strong carbonyl stretching frequency at 2076 cm^{-1}, a weak acetonitrile stretching band at 2296 cm^{-1}, and a weak alkyne band at 1594 cm^{-1}. The ν(C≡C) stretching band for the coordinated alkyne was found at a lower wavenumber than for uncoordinated alkynes (typically at 2260–2190 cm^{-1} for unsymmetrical alkynes (22)) and can be mainly attributed to the σ–π-donation of the bonding electrons of the alkyne to the tungsten atom and also the back-bonding between anti-bonding π*-orbitals of the alkyne and the filled *d*-orbitals of tungsten. Although two isomers have been observed in solution (see next section), the difference electronically at the metal centre is small and is not expected to affect the IR stretching frequency to any significant degree.

The crystal data obtained for complex **1**, coupled with the proton and carbon NMR data, showed that two isomers were present for the bis(1-phenyl-1-propyne) complex [WI_2(CO)(NCMe)(η^2-MeC_2Ph)$_2$] (**1**). To aid interpretation of data, the isomers were designated *cis* and *trans* with respect to the substituents of the alkyne groups (Fig. 1). Faller and Murray (23) reported similar isomeric forms for cationic bis(alkyne) complexes of the type [Mo(CO)(η^2-HC_2R)$_2$(η^5-C_5H_5)]$^{+}$, where three isomers were possible (C_s symmetry): (*i*) the two R groups can be *trans* to one another; (*ii*) mutually *cis* proximal to the carbonyl; or (*iii*) mutually *cis* distal to the carbonyl. For complex **1**, four isomers are possible

Fig. 2. Crystal structure of [WI_2(CO)(NCMe)(η^2-MeC_2Ph)$_2$] (**1**).



(Fig. 1) however, only the *cis*-isomer with the larger phenyl group proximal to the carbonyl is obtained (Fig. 2).

The ^{1}H NMR spectrum of **1** (Table 3) showed a broad resonance at 7.55–7.22 ppm (m, 20H, *Ph*C_2Me, *cis* and *trans*) and five other resonances found further upfield. The *cis*-isomer displayed resonances at 3.14 ppm (s, 6H, PhC_2*Me*) and 2.25 ppm (s, 3H, NC*Me*), while the *trans*-isomer showed resonances at 3.18 ppm (s, 3H, PhC_2*Me*), 3.10 ppm (s, 3H, PhC_2*Me*), and 2.52 ppm (s, 3H, NC*Me*). Variable temperature ^{1}H NMR studies of single crystals of **1** in CD_2Cl_2 between 0°C and –80°C showed little change in the chemical shifts compared to the spectrum recorded at +25°C, with only a slight broadening and diminution of signal size observed. This suggests that there is no change in the isomer ratio as the temp of the solution is decreased and that neither isomer is preferred at lower temperatures. Single crystals of **1** were dissolved in d_8-toluene and a series of ^{1}H NMR spectra were obtained from +25°C to +100°C. Although broadening of the signals was observed, which suggests that the complex is fluxional, no coalescence temperature could be obtained.

The ^{13}C{^{1}H} NMR spectrum of **1** (Table 4) was assigned for both the *cis*- and *trans*-isomers. The carbonyl signal, the acetonitrile (*C*≡N) resonance, and the signal for the methyl group of the acetonitrile were observed at 203.59, 135.29, and 4.37 ppm, respectively, for the *cis*-isomer and at 202.96, 137.49, and 4.72 ppm, respectively, for the *trans*-isomer, which shows, as expected, only a subtle difference between the two isomers. From the integral ratios of the methyl groups of both the 1-phenyl-1-propyne and acetonitrile ligands, the *cis*- to *trans*-isomer ratio was determined to be approximately 55:45.

The most obvious difference between the two isomers was the number of alkyne contact carbon resonances. The *trans*

© 2001 NRC Canada

Table 3. ^{1}H NMR data[a] for the $[WI_2(CO)(NCR)(\eta^2\text{-}MeC_2Ph)_2]$ complexes (**1**–**5**).

Complex	^{1}H (ppm)
1	7.55–7.22 (m, 20H, CH_3C_2*Ph*, *cis* and *trans*), 3.18 (s, 3H, CH_3C_2Ph, *trans*), 3.14 (s, 6H, CH_3C_2Ph, *cis*), 3.10 (s, 3H, CH_3C_2Ph, *trans*), 2.55 (s, 3H, CH_3CN, *trans*), 2.25 (s, 3H, CH_3CN, *cis*)
2	7.32–6.96 (br m, 20H, CH_3C_2*Ph*, *cis* and *trans*), 2.94 (s, 3H, CH_3C_2Ph, *trans*), 2.91 (s, 6H, CH_3C_2Ph, *cis*), 2.87 (s, 3H, CH_3C_2Ph, *trans*), 2.74 (q, 2H, *J* = 7.6, CH_3CH_2CN, *trans*), 2.47 (q, *J* = 7.6 Hz, 2H, CH_3CH_2CN, *cis*), 1.10 (t, *J* = 7.6 Hz, 3H, CH_3CH_2CN, *trans*), 0.83 (t, *J* = 7.6 Hz, 3H, CH_3CH_2CN, *cis*)
3	7.50–7.25 (m, 20H, CH_3C_2*Ph*, *cis* and *trans*), 3.22 (s, 1H, Me_2CHCN, *trans*), 3.16 (s, 3H, CH_3C_2Ph, *trans*), 3.13 (s, 6H, CH_3C_2Ph, *cis*), 3.08 (s, 3H, CH_3C_2Ph, *trans*), 3.01 (s, 1H, Me_2CHCN, *cis*), 1.41–1.32 (m, 6H, $(CH_3)_2$CHCN, *trans*), 1.12 (d, *J* = 7.1 Hz, 6H, $(CH_3)_2$CHCN, *cis*)
4	7.60–7.20 (m, 20H, CH_3C_2*Ph*, *cis* and *trans*), 3.15 (s, 3H, CH_3C_2Ph, *trans*), 3.10 (s, 6H, CH_3C_2Ph, *cis*), 3.05 (s, 3H, CH_3C_2Ph, *trans*), 1.45 (s, 9H, $(CH_3)_3$CCN, *trans*), 1.20 (s, 3H, $(CH_3)_3$CHCN, *cis*)
5	7.75–7.25 (br m, 30H, *Ph*CN/CH_3C_2*Ph*, *cis* and *trans*), 3.20 (s, 3H, CH_3C_2Ph, *trans*), 3.15 (s, 6H, CH_3C_2Ph, *cis*), 3.10 (s, 3H, CH_3C_2Ph, *trans*)

[a]Spectra recorded in $CDCl_3$ at +25°C, referenced to $SiMe_4$ (s = singlet, d = doublet, t = triplet, q = quartet, m = multiplet, br = broad).

Table 4. ^{13}C NMR data[a] for the $[WI_2(CO)(NCR)(\eta^2\text{-}MeC_2Ph)_2]$ complexes (**1**–**5**).

Complex	^{13}C{^{1}H} (ppm)
1	*cis*: 203.59 (s, *C*≡O), 168.70 (s, CH_3C≡*C*Ph), 162.93 (s, CH_3C≡CPh), 135.29 (s, *C*≡N), 131.47–127.48 (m, CH_3C_2*Ph*), 20.90 (s, *C*H_3C_2Ph), 4.37 (s, *C*H_3CN)
	trans: 202.96 (s, *C*≡O), 175.77 (s, CH_3C≡*C*Ph), 168.56 (s, CH_3C≡*C*Ph), 161.56 (s, CH_3C≡CPh), 160.31 (s, CH_3C≡CPh), 137.49 (s, *C*≡N), 131.47–127.48 (m, CH_3C_2*Ph*), 21.43 (s, *C*H_3C_2Ph), 17.75 (s, *C*H_3C_2Ph), 4.72 (s, *C*H_3CN)
2[b]	*cis*: 203.66 (s, *C*≡O), 168.48 (s, CH_3C≡*C*Ph), 162.77 (s, CH_3C≡CPh), 135.21 (s, *C*≡N), 129.09–127.21 (m, CH_3C_2*Ph*), 20.39 (s, *C*H_3C_2Ph), 12.52 (s, *C*H_2CN), 8.67 (s, *C*H_3CH_2CN)
	trans: 203.30 (s, *C*≡O), 182.40 (s, CH_3C≡*C*Ph), 175.16 (s, CH_3C≡*C*Ph), 168.58 (s, CH_3C≡CPh), 161.46 (s, CH_3C≡CPh), 137.35 (s, *C*≡N), 129.09–127.21 (m, CH_3C_2*Ph*), 20.83 (s, *C*H_3C_2Ph), 16.95 (s, *C*H_3C_2Ph), 12.65 (s, *C*H_2CN), 9.17 (s, *C*H_3CH_2CN)
3	*cis*: 203.51 (s, *C*≡O), 168.69 (s, CH_3C≡*C*Ph), 162.99 (s, CH_3C≡CPh), 135.59 (s, $(CH_3)_2CH$*C*N), 129.33–127.44 (m, CH_3C_2*Ph*), 21.48 (s, $(CH_3)_2$*C*HCN), 20.76 (s, *C*H_3C_2Ph), 18.78 (s, $(CH_3)_2$CHCN)
	trans: 202.76 (s, *C*≡O), 175.18 (s, CH_3C≡*C*Ph), 161.60 (s, CH_3C≡*C*Ph), 160.13 (s, CH_3C≡CPh), 156.36 (s, CH_3C≡CPh), 137.55 (s, $(CH_3)_2CH$*C*N), 129.33–127.44 (m, CH_3C_2*Ph*), 21.64 (s, $(CH_3)_2$*C*HCN), 21.15 (s, *C*H_3C_2Ph), 18.95 (s, $(CH_3)_2$CHCN), 17.33 (s, *C*H_3C_2Ph)
4	*cis*: 203.96 (s, *C*≡O), 168.55 (s, CH_3C≡*C*Ph), 162.65 (s, CH_3C≡CPh), 135.49 (s, *t*-Bu*C*≡N), 129.22–127.34 (m, CH_3C_2*Ph*), 31.47 (s, $(CH_3)_3$*C*CN), 26.74 (s, $(CH_3)_3$CCN), 20.76 (s, *C*H_3C_2Ph)
	trans: 203.27 (s, *C*≡O), 175.13 (s, CH_3C≡*C*Ph), 173.16 (s, CH_3C≡*C*Ph), 161.21 (s, CH_3C≡CPh), 159.70 (s, CH_3C≡CPh), 137.35 (s, *t*-Bu*C*≡N), 129.22–127.34 (m, CH_3C_2*Ph*), 31.74 (s, $(CH_3)_3$*C*CN), 27.20 (s, $(CH_3)_3$CCN), 21.08 (s, *C*H_3C_2Ph), 17.36 (s, *C*H_3C_2Ph)
5	*cis*: 203.39 (s, *C*≡O), 168.43 (s, CH_3C≡*C*Ph), 162.80 (s, CH_3C≡CPh), 133.09–132.14 (m, Ph*C*≡N), 130.05–127.49 (m, CH_3C_2*Ph*), 20.85 (s, *C*H_3C_2Ph)
	trans: 202.59 (s, *C*≡O), 175.37 (s, CH_3C≡*C*Ph), 168.15 (s, CH_3C≡*C*Ph), 161.39 (s, CH_3C≡CPh), 160.13 (s, CH_3C≡CPh), 135.66–134.99 (m, Ph*C*≡N), 130.05–127.49 (m, CH_3C_2*Ph*), 21.22 (s, *C*H_3C_2Ph), 17.48 (s, *C*H_3C_2Ph)

[a]Spectra recorded in $CDCl_3$ at +25°C, referenced to $SiMe_4$ (s = singlet, d = doublet, m = multiplet). [b]Spectrum recorded in $CDCl_3$–d_6-acetone at +25°C, referenced to $SiMe_4$.

© 2001 NRC Canada

Table 5. Crystal data and structure refinement for complexes **1**, **2**, and **5**.

	1	**2**	**5**
Formula	$C_{21}H_{19}I_2NOW$	$C_{22}H_{21}I_2NOW$	$C_{26}H_{21}I_2NOW{\cdot}CH_2Cl_2$
Formula weight	739.05	753.05	886.01
Temp (K)	293(2)	293(2)	293(2)
Wavelength (Å)	0.71073	0.71073	0.71073
Crystal system	monoclinic	monoclinic	monoclinic
Space group	$P2_1/n$	$P2_1/n$	$P2_1/n$
Unit cell dimensions			
a (Å)	7.598(9)	7.699(10)	11.521(21)
b (Å)	13.806(15)	14.051(15)	8.722(10)
c (Å)	21.190(2)	21.784(23)	30.520(3)
β (°)	92.42(1)	91.95(1)	94.17(1)
Volume (Å^3)	2220(4)	2355.2	3059(6)
Z	4	4	4
Calculated density (mg m^{-3})	2.205	2.124	1.924
Absorption coefficient (mm^{-1})	7.991	7.537	5.988
F(000)	1356	1392	1656
θ range for data collection (°)	2.42–25.92	2.37–25.95	2.93–25.81
Index ranges	$0 \le h \le 9$	$0 \le h \le 9$	$-13 \le h \le 12$
	$-16 \le k \le 16$	$-16 \le k \le 16$	$0 \le k \le 10$
	$-25 \le l \le 25$	$-26 \le l \le 26$	$-37 \le l \le 37$
Reflections collected	7152	5842	8553
Unique reflections	3992	3675	5051
R (int)	0.0416	0.0615	0.0511
Data/restraints/parameters	992/0/239	3675/0/248	5051/0/309
GoF on F^2	1.101	1.112	1.147
Final *R* indices [$I > 2\sigma(I)$]	$R_1 = 0.0538$	$R_1 = 0.0665$	$R_1 = 0.0855$
	$wR_2 = 0.1451$	$wR_2 = 0.1933$	$wR_2 = 0.1878$
R indices (all data)	$R_1 = 0.0638$	$R_1 = 0.0888$	$R_1 = 0.1008$
	$wR_2 = 0.1536$	$wR_2 = 0.2266$	$wR_2 = 0.1950$
Largest difference peak and hole (e Å^{-3})	2.681 and –2.101	2.175 and –1.699	2.195 and –3.885

$R_1 = \Sigma S(F_o\text{-}F_c)/\Sigma(F_o)$, $wR_2 = [\Sigma\{w(F_o^2-F_c^2)^2\}/\Sigma\{w(F_o^2)^2\}]^{1/2}$, $w = 1/\sigma^2(F_o^2)$.

Table 6. Selected bond lengths (Å) for complexes **1**, **2**, and **5**.

1		**2**		**5**	
W(1)—C(200)	2.012(10)	W(1)—C(100)	2.043(15)	W(1)—C(100)	2.054(16)
W(1)—C(2)	2.048(10)	W(1)—C(31)	2.076(17)	W(1)—C(11)	2.04(2)
W(1)—C(3)	2.058(10)	W(1)—C(21)	2.074(14)	W(1)—C(41)	2.110(18)
W(1)—C(1)	2.099(9)	W(1)—C(41)	2.125(13)	W(1)—C(31)	2.117(15)
W(1)—C(4)	2.101(9)	W(1)—C(11)	2.118(13)	W(1)—C(21)	2.145(17)
W(1)—N(100)	2.164(8)	W(1)—N(200)	2.169(12)	W(1)—N(200)	2.171(14)
W(1)—I(2)	2.842(2)	W(1)—I(3)	2.8666(12)	W(1)—I(2)	2.872(3)
W(1)—I(3)	2.875(2)	W(1)—I(2)	2.9021(11)	W(1)—I(3)	2.909(3)

complex has four resonances at 175.77 (Ph*C*≡CMe), 168.56 (Ph*C*≡CMe), 161.56 (PhC≡*C*Me), and 160.31 (PhC≡*C*Me) ppm, due to their unequal environments, whereas the *cis*-isomer has only two alkyne contact carbon resonances at 168.70 (2 × Ph*C*≡CMe) and 162.93 (2 × PhC≡*C*Me) ppm. This difference was also supported by the presence of two methyl group signals for the alkynes of the *trans*-isomer (PhC$_2$*Me*) (21.43 and 17.75 ppm) and the presence of only one signal for the equivalent alkynes of the *cis*-isomer (PhC$_2$*Me*) (20.90 ppm). In both cases, the alkynes are donating an average of three electrons each to the tungsten centre, determined from Templeton and Ward's correlation (24) of the number of electrons donated by an alkyne and the alkyne contact carbon chemical shift, which also enables complex **1** to obey the effective atomic number rule.

The solid state structure of **1** was determined by X-ray crystallographic methods (Fig. 2). The formal geometry is eight-coordinate, however, if each alkyne is regarded as occupying one coordination site, the complex can be described as six-coordinate, which is more convenient when considering the local geometry of each ligand. The carbonyl ligand is *trans* to the acetonitrile group, the two alkyne moieties are mutually *cis*, and each alkyne is *trans* to an iodine atom. This arrangement is characteristic of bis(alkyne) complexes

© 2001 NRC Canada

Table 7. Selected bond angles (°) for complexes **1**, **2**, and **5**.

1		**2**		**5**	
C(200)-W(1)-C(2)	111.3(4)	C(100)-W(1)-C(31)	111.8(6)	C(11)-W(1)-C(100)	115.0(7)
C(200)-W(1)-C(3)	111.6(4)	C(100)-W(1)-C(21)	110.5(6)	C(11)-W(1)-C(41)	95.8(7)
C(2)-W(1)-C(3)	95.5(4)	C(31)-W(1)-C(21)	96.5(6)	C(100)-W(1)-C(41)	111.9(7)
C(200)-W(1)-C(1)	76.5(4)	C(100)-W(1)-C(41)	77.4(5)	C(11)-W(1)-C(31)	108.3(7)
C(2)-W(1)-C(1)	35.5(3)	C(31)-W(1)-C(41)	34.4(6)	C(100)-W(1)-C(31)	75.9(7)
C(3)-W(1)-C(1)	102.4(4)	C(21)-W(1)-C(41)	109.1(6)	C(41)-W(1)-C(31)	36.2(6)
C(200)-W(1)-C(4)	76.3(4)	C(100)-W(1)-C(11)	76.2(6)	C(11)-W(1)-C(21)	35.9(6)
C(2)-W(1)-C(4)	108.7(4)	C(31)-W(1)-C(11)	102.3(6)	C(100)-W(1)-C(21)	80.1(7)
C(3)-W(1)-C(4)	35.3(3)	C(21)-W(1)-C(11)	35.3(5)	C(41)-W(1)-C(21)	102.2(6)
C(1)-W(1)-C(4)	94.2(4)	C(41)-W(1)-C(11)	94.1(5)	C(31)-W(1)-C(21)	92.6(7)
C(200)-W(1)-N(100)	161.6(4)	C(100)-W(1)-N(200)	161.4(6)	C(11)-W(1)-N(200)	82.2(6)
C(2)-W(1)-N(100)	79.7(3)	C(31)-W(1)-N(200)	80.4(5)	C(100)-W(1)-N(200)	155.9(6)
C(3)-W(1)-N(100)	80.9(3)	C(21)-W(1)-N(200)	80.8(5)	C(41)-W(1)-N(200)	81.2(6)
C(1)-W(1)-N(100)	115.2(3)	C(41)-W(1)-N(200)	113.8(5)	C(31)-W(1)-N(200)	116.2(7)
C(4)-W(1)-N(100)	115.1(3)	C(11)-W(1)-N(200)	116.1(5)	C(21)-W(1)-N(200)	118(6)
C(200)-W(1)-I(2)	82.3(3)	C(100)-W(1)-I(3)	82.8(4)	C(11)-W(1)-I(2)	88.1(5)
C(2)-W(1)-I(2)	160.4(3)	C(31)-W(1)-I(3)	91.2(4)	C(100)-W(1)-I(2)	81.9(5)
C(3)-W(1)-I(2)	92.1(3)	C(21)-W(1)-I(3)	160.5(4)	C(41)-W(1)-I(2)	162.0(4)
C(1)-W(1)-I(2)	157.6(2)	C(41)-W(1)-I(3)	87.3(4)	C(31)-W(1)-I(2)	156.5(5)
C(4)-W(1)-I(2)	87.7(3)	C(11)-W(1)-I(3)	158.1(4)	C(21)-W(1)-I(2)	91.3(5)
N(100)-W(1)-I(2)	83.7(2)	N(200)-W(1)-I(3)	82.9(3)	N(200)-W(1)-I(2)	81.9(4)
C(200)-W(1)-I(3)	83.0(3)	C(100)-W(1)-I(2)	83.4(4)	C(11)-W(1)-I(2)	162.3(5)
C(2)-W(1)-I(3)	84.4(3)	C(31)-W(1)-I(2)	163.0(4)	C(100)-W(1)-I(3)	79.2(5)
C(3)-W(1)-I(3)	164.1(3)	C(21)-W(1)-I(2)	84.4(4)	C(41)-W(1)-I(3)	87.9(4)
C(1)-W(1)-I(3)	86.8(3)	C(41)-W(1)-I(2)	159.4(4)	C(31)-W(1)-I(3)	84.8(5)
C(4)-W(1)-I(3)	158.4(2)	C(11)-W(1)-I(2)	88.3(4)	C(21)-W(1)-I(3)	159.1(4)
N(100)-W(1)-I(3)	83.5(2)	N(200)-W(1)-I(2)	83.1(3)	N(200)-W(1)-I(2)	81.3(5)
I(2)-W(1)-I(3)	83.45(6)	I(3)-W(1)-I(2)	83.03(4)	I(2)-W(1)-I(3)	83.30(8)

of this type and is comparable to those of $[WI_2(CO)(NCMe)(\eta^2\text{-}RC_2R)_2]$ (R = Me, Ph) (8). The structure of **1** (Fig. 2) shows the opposite arrangement of alkyne ligands to that proposed by Baker and co-workers (8), in which the methyl groups of the 1-phenyl-1-propyne ligand were thought to be *cis* to the carbonyl moiety due to intramolecular effects in the structures of $[WI_2(CO)(NCMe)(\eta^2\text{-}RC_2R)_2]$ (R = Me, Ph) (8). The alkyne and CO ligands are competing for the same π-electron density as the tungsten atom (1), which is why the W—C(CC) bonds nearest the W-CO unit are longer than the W—C(CC) bonds *cis* to the poor π-acceptor NCMe ligand.

The W—I bond lengths for **1** are 2.842(2) and 2.875(2) Å, respectively (Table 6), which are similar to those of analogous complexes $[WI_2(CO)(NCMe)(\eta^2\text{-}MeC_2Me)_2]$ (2.843(1) and 2.859(1) Å) and $[WI_2(CO)(NCMe)(\eta^2\text{-}PhC_2Ph)_2]$ (2.848(1) and 2.862(2) Å) (8). The internal angle for **1** (I(2)-W(1)-I(3)) of 83.45(6)° (Table 7) is comparable with those of $[WI_2(CO)(NCMe)(\eta^2\text{-}MeC_2Me)_2]$ and $[WI_2(CO)(NCMe)(\eta^2\text{-}PhC_2Ph)_2]$ at 83.51(4) and 83.96(4)°, respectively (8). The bond lengths of the two alkyne carbons with the methyl substituents of **1** (W(1)—C(2) and W(1)—C(3)) were found to be 2.048(10) and 2.058(10) Å, respectively, and are slightly longer than the analogous bond lengths for $[WI_2(CO)(NCMe)(\eta^2\text{-}MeC_2Me)_2]$, but comparable to those of $[WI_2(CO)(NCMe)(\eta^2\text{-}PhC_2Ph)_2]$ (8). It has been previously observed (1) that the C≡C bond lengths are insensitive to whether the alkyne ligand is donating 2, 3, or 4 electrons to the metal in these systems.

The alkyne carbons with phenyl substituents were found to have bond lengths to W of 2.099(9) and 2.101(9) Å for W(1)—C(1) and W(1)—C(4), respectively, which are comparable with related carbons of $[WI_2(CO)(NCMe)(\eta^2\text{-}MeC_2Me)_2]$ (2.099(15) and 2.119(15) Å) and $[WI_2(CO)(NCMe)(\eta^2\text{-}PhC_2Ph)_2]$ (2.070(16) and 2.083(15) Å) (8). In complex **1**, the two carbons C(1) and C(4), which are closest to the carbonyl group, have a longer bond than that between C(2) and C(3), which are closer to the nitrile substituent. This difference is probably due to steric effects between the alkyne substituents and the carbonyl group, and is also observed for the 2-butyne and diphenylacetylene analogues (8). The tungsten—carbonyl bond length in **1** (W(1)—C(200)) of 2.012(10) Å compares with that of $[WI_2(CO)(NCMe)(\eta^2\text{-}PhC_2Ph)_2]$ (8) at 2.018(17) Å, rather than $[WI_2(CO)(NCMe)(\eta^2\text{-}MeC_2Me)_2]$ (8) at 1.937(14) Å, which is expected as the immediate environments of the carbonyl carbon (*cis* to alkynes with phenyl substituents) are more alike.

The data for complex **1** is slightly different to that previously reported (8) due to both *cis* and *trans* isomers being identified and the data being assigned by careful comparison with the series of analogues (**2**–**5**). This has enabled a more accurate assignment of data such that individual isomers can be distinguished rather than just the *cis*-isomer, as originally reported (8).

© 2001 NRC Canada

Fig. 3. Crystal structure of $[WI_2(CO)(NCEt)(\eta^2\text{-}MeC_2Ph)_2]$ (**2**).

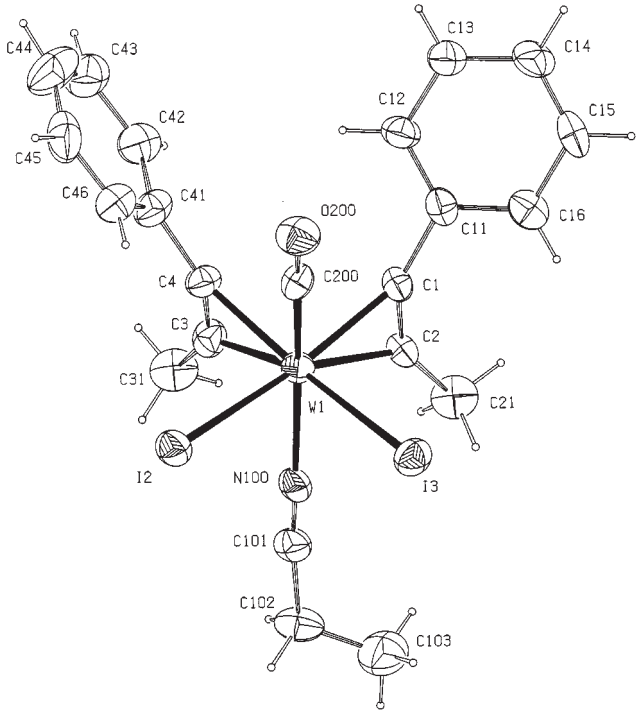
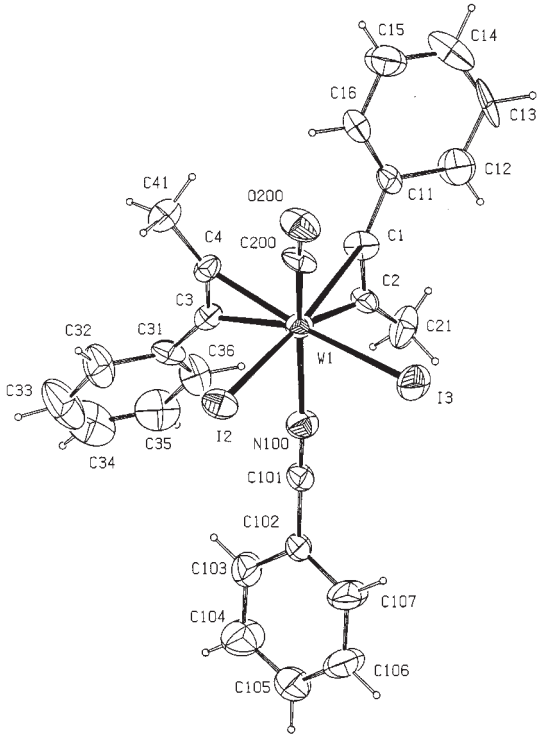


Fig. 4. Crystal structure of $[WI_2(CO)(NCPh)(\eta^2\text{-}MeC_2Ph)_2]$ (**5**).



Preparation and characterization of the nitrile exchanged bis(1-phenyl-1-propyne) complexes $[WI_2(CO)(NCR)(\eta^2\text{-}MeC_2Ph)_2]$ (R = Et, *i*-Pr, *t*-Bu, and Ph) (2–5)

Equimolar quantities of **1** and NCR (R = Et, *i*-Pr, *t*-Bu, Ph) were mixed in CH_2Cl_2 at room temp to give the acetonitrile-exchanged products $[WI_2(CO)(NCR)(\eta^2\text{-}MeC_2Ph)_2]$ (**2**–**5**) in high yield. In all four complexes, complete exchange of the acetonitrile ligand was observed, with no residual peaks attributable to the acetonitrile group detected in any of the spectroscopic data of complexes **2**–**5**. Complete nitrile exchange occurs with the reaction of one equivalent of NCR because acetonitrile is the most labile ligand in the complex and,hence, is completely exchanged. At room temp, the addition of excess NCPh, for example, to **1** for 6 h affords only **1** and NCPh.

Complexes **2**–**5** were fully characterized by elemental analysis (C, H, and N), IR spectroscopy, ^{1}H NMR spectroscopy, and $^{13}C\{^1H\}$ NMR spectroscopy (Tables 1–4). The complexes are soluble in chlorinated solvents and acetonitrile, but insoluble in diethyl ether and hydrocarbon solvents. All four complexes are less stable than **1**, in the solid state, with deterioration apparent in solid samples stored at –17°C for over six weeks.

The IR spectra of complexes **2**–**5** (Table 2) all show a strong carbonyl stretching band between 2081 and 2074 cm^{-1}, a weak nitrile stretching band between 2294 and 2274 cm^{-1}, and a weak alkyne band at either 1594 or 1595 cm^{-1}. The ^{1}H NMR spectra of **2**–**5** (Table 3) show multiplets at around 7.75–6.96 ppm due to the phenyl group of both *cis*- and *trans*-isomers and, in the case of complex **5**, the phenyl moiety of benzonitrile for both isomers. The methyl groups of 1-phenyl-1-propyne and the expected signals for each nitrile substituent were detected as distinct signals for each isomer of **2**–**4** (Table 3). Using integral ratios from the ^{1}H NMR spectra, the *cis*:*trans* isomer ratio for all four complexes (**2**–**5**) was determined to be approximately 55:45, which is similar to the isomer ratio obtained for the acetonitrile complex (**1**). This suggests that there is a common equilibrium of isomeric forms in solution, regardless of which isomer is preferred in the solid state.

The $^{13}C\{^1H\}$ NMR spectra of **2**–**5** (Table 4) were also assigned for both the *cis*- and *trans*-isomers, as described earlier for complex **1**, but with the presence of signals associated with each of the nitrile ligands. For complexes **2**–**5**, the chemical shifts of the alkyne contact carbons show an average of three-electron donation per 1-phenyl-1-propyne to the tungsten centre (24), thus enabling all the complexes to obey the effective atomic number rule.

Complexes **2** and **5** were structurally characterized by X-ray crystallography as the *cis*- and *trans*-isomers, respectively (Figs. 3 and 4) using suitable single crystals grown from dichloromethane–diethyl ether solution (3/8 by volume, cooled to –17°C for 48 h (**2**), 2/3 by volume, cooled to –17°C for 24 h (**5**)). It is probable that the bulky phenyl group of benzonitrile in complex **5** favours the *trans*-isomer in the solid state, with both isomers being detected in solution, as previously described. The molecular structure of **5** contains one molecule of dichloromethane, which was not apparent in subsequent elemental analyses or in ^{1}H or $^{13}C\{^1H\}$ NMR data performed using solid collected from the mother liquor (rather than crystals themselves, as only enough crystals for X-ray crystallography were obtained).

As for **1**, both **2** and **5** are formally eight-coordinate, but can be regarded as six-coordinate by considering each alkyne as occupying one coordination site. For **2**, which is isomorphous with **1**, the carbonyl ligand was found to be *trans* to the propionitrile group, with the two alkyne moieties

© 2001 NRC Canada

mutually *cis* and each alkyne *trans* to one iodine atom, as observed for complex **1**, and the previously described complexes $[WI_2(CO)(NCMe)(\eta^2\text{-}RC_2R)_2]$ (R = Me, Ph) (8).

The W—I bond lengths for **2** (2.8666(12) and 2.9021(11) Å) (Table 6) are slightly longer than those of **1**, and the internal angle (I(2)-W(1)-I(3)) of 83.03(4)° (Table 7) is less than that of **1**. The W—N bond lengths for **1** and **2** of 2.164(8) and 2.169(12) Å, respectively, are comparable, and the bond length between the nitrogen and its adjacent carbon atom (C≡N) were shown to be 1.088(12) Å for **1** and 1.129(19) Å for **2**.

The crystal structures of two similar complexes, $[WI_2(CO)(NC\textit{t}\text{-}Bu)(\eta^2\text{-}MeC_2Me)_2]$ (25) and $[WI_2(CO)(NCPh)(\eta^2\text{-}MeC_2Me)_2]$ (26), have been previously reported. These complexes were obtained from the addition of excess 2-butyne to $[WI_2(CO)_3(NC\textit{t}\text{-}Bu)_2]$ and $[WI_2(CO)_3(NCPh)_2]$, respectively. The nitrile exchange complex $[WI_2(CO)\{NCCH_2(C_3H_4S\text{-}3)\}(\eta^2\text{-}MeC_2Me)_2]$ (27) has also been structurally characterized. The W—N bond lengths for $[WI_2(CO)(NCR)(\eta^2\text{-}MeC_2Me)_2]$ (R = *t*-Bu, Ph, and $NCCH_2(C_3H_4S\text{-}3)$) are 2.175(9), 2.15(2), and 2.13(4) Å, respectively, which are sufficiently similar to conclude that the nature of the R substituent does not affect the length of W—N bond to any significant degree. The crystal structure of **5** shows the *trans* arrangement of alkynes (Fig. 1) and is the first bis(alkyne) tungsten(II) complex of the type $[WI_2(CO)(NCR)(\eta^2\text{-}R'C_2R'')]$ (R = alkyl or aryl group; $R' \neq R''$) to be crystallographically characterized for the *trans*-isomer, which was initially thought to be unfavoured (8). In complex **5**, the carbonyl ligand was found to be *trans* to the benzonitrile group, with the two alkyne moieties mutually *cis*, and each alkyne *trans* to one iodine atom, as observed for complexes **1** and **2** and the literature complexes $[WI_2(CO)(NCMe)(\eta^2\text{-}RC_2R)_2]$ (R = Me, Ph) (8). The major difference between **1**, **2**, and **5** is the position of the alkyne substituents. In **1** and **2**, the two phenyl groups of 1-phenyl-1-propyne are next to one another (*cis*-isomer), whereas in **5** the two phenyl groups are opposite one another (*trans*-isomer).

The crystal structure of the bis(2-butyne) complex $[WI_2(CO)(NCPh)(\eta^2\text{-}MeC_2Me)_2]$ has been reported by Baker and co-workers (26) and, due to the symmetric alkyne, has no isomeric forms as encountered for **1**, **2**, and **5**. The W—I bond lengths for **5** (2.872(3) and 2.909(3) Å) are comparable with those of $[WI_2(CO)(NCPh)(\eta^2\text{-}MeC_2Me)_2]$ (2.8613(13) and 2.8407(13) Å), and the internal angle (I(2)–W(1)–I(3)) of 83.30(8)° is similar to that of $[WI_2(CO)(NCPh)(\eta^2\text{-}MeC_2Me)_2]$ at 83.53(4)°. The W—N bond length (2.171(14) Å) and the bond length between the nitrogen and its adjacent carbon atom (C≡N) (1.12(2) Å) for **5**, are also in good agreement with those of $[WI_2(CO)(NCPh)(\eta^2\text{-}MeC_2Me)_2]$ (W—N = 2.15(2) and C≡N = 1.12(2) Å). These similarities suggest that the different alkynes do not overly affect the other tungsten—ligand bonds in complexes **5** and $[WI_2(CO)(NCPh)(\eta^2\text{-}MeC_2Me)_2]$ (26).

The tungsten—carbon(carbonyl) bond length for **5** (2.054(16) Å) shows that the *trans*-isomer compares well with analogous bond lengths for complexes **1** and **2** (2.012(10) and 2.043(15) Å, respectively). The alkyne carbon—tungsten bond lengths for **5** (2.04(2), 2.117(15) (*Me*), 2.145(17), and 2.110(18) (*Ph*) Å) are all quite similar, with the W—C(R) bond (for R = Me) being shorter than the W—C(R′) bond (for R = Ph), which can explained in terms of the electron withdrawing–donating properties of the different substituents. Despite the fact that **5** is the *trans*-isomer, there is very little difference in the angles subtended at the metal centre compared to the *cis*-forms of **1** and **2**, as is apparent from Table 7. We found no evidence that intermolecular effects, including π-stacking, were a significant factor in the preference of isomer formed.

In the three crystallographically characterized complexes **1**, **2**, and **5**, the average back bend angle (β) (28) was calculated from the R–C≡C and R′–C≡C angles, and all were in the region of 30–40°, as expected (1, 2, 27). The angles were found to be: **1** (36.5 (Me) and 34.2° (Ph)), **2** (35.8 (Me) and 37.0° (Ph)), and **5** (36.4 (Me), 41.0 (Me), 32.9 (Ph), and 34.8° (Ph)).

Acknowledgements

DSE thanks the EPSRC for a studentship. We also thank the EPSRC and the University of Reading for funds for the Image Plate System, and A. W. Johans for his assistance with the crystallographic investigations.

References

1. J.L. Templeton. Adv. Organomet. Chem. **29**, 1 (1989).
2. P.K. Baker. Adv. Organomet. Chem. **40**, 45 (1996).
3. N.G. Aimeloglou, P.K. Baker, M.M. Meehan, and M.G.B. Drew. Polyhedron, **17**, 3455 (1998).
4. M. Bottrill and M. Green. J. Chem. Soc. Dalton Trans. 2365 (1977).
5. S.R. Allen, P.K. Baker, S.G. Barnes, M. Green, L. Trollope, L. Manojlović-Muir, and K.W. Muir. J. Chem. Soc. Dalton Trans. 873 (1981).
6. J.L. Davidson and D.W.A. Sharp. J. Chem. Soc. Dalton Trans. 2531 (1975).
7. J.L. Davidson and G. Vasapollo. J. Chem. Soc. Dalton Trans. 2239 (1985).
8. E.M. Armstrong, P.K. Baker, and M.G.B. Drew. Organometallics, **7**, 319 (1988).
9. J. L. Davidson and G. Vasapollo. J. Chem. Soc. Dalton Trans. 2855 (1988).
10. P.K. Baker, A. Bury, and K.R. Flower. Polyhedron, **8**, 2587 (1989).
11. E.M. Armstrong, P.K. Baker, and S.G. Fraser. J. Chem. Res. (S) 52, (1988); J. Chem. Res. (M) 0410, (1988).
12. J.L. Davidson. J. Organomet. Chem. **419**, 137 (1991).
13. J.L. Davidson, G. Vasapollo, J.C. Millar, and K.W. Muir. J. Chem. Soc. Dalton Trans. 2165 (1987).
14. M. Al-Jahdali, P.K. Baker, and M.G.B. Drew. Z. Naturforsch. **54b**, 171 (1999).
15. J.L. Davidson and G. Vasapollo. Polyhedron, **2**, 305 (1983).
16. P.K. Baker, S.G. Fraser, and E.M. Keys. J. Organomet. Chem. **309**, 319 (1986).
17. P.K. Baker and M.M. Meehan. Inorg. Synth. In Press.
18. W. Kabsch. J. Appl. Crystallogr. **21**, 916 (1988).
19. G.M. Sheldrick. Acta Crystallogr. Sect. A: Fundam. Crystallogr. **A46**, 467 (1990).
20. N. Walker and D. Stuart. Acta Crystallogr. Sect. A: Fundam. Crystallogr. **A39**, 158 (1983).
21. G.M. Sheldrick. SHELXL. Program for crystal structure refinement. University of Göttingen. 1993.

© 2001 NRC Canada

22. R.M. Silverstein, G.C. Bassler and T.C. Morrill. Spectroscopic identification of organic compounds. 5th ed. J. Wiley & Sons, Chichester. 1991.
23. J.W. Faller and H.H. Murray. J. Organomet. Chem. **172**, 171 (1979).
24. J.L. Templeton and B.C. Ward. J. Am. Chem. Soc. **102**, 3288 (1980).
25. P.K. Baker, M.E. Harman, M.B. Hursthouse, A.J. Lavery, K.M.A. Malik, D.J. Muldoon, and A. Shawcross. J. Organomet. Chem. **484**, 169 (1994).
26. M.G.B. Drew, P.K. Baker, D.J. Muldoon, A.J. Lavery, and A. Shawcross. Gazz. Chim. Ital. **126**, 625 (1996).
27. P.K. Baker, M.G.B. Drew, S. Edge, and S.D. Ridyard. J. Organomet. Chem. **409**, 207 (1991).
28. M. Bochmann. Organometallics 2 – complexes with transition metal–carbon π-bonds. Oxford Science Publications, Oxford University Press, Oxford. 1996.

© 2001 NRC Canada

N′-tert-Butyl-*N′*-aroyl-*N*-(alkoxycarbonylmethyl)-*N*-aroylhydrazines, a novel nonsteroidal ecdysone agonist: syntheses, insecticidal activity, conformational, and crystal structure analysis

S. Cao, X. Qian and G. Song

Abstract: Seventeen *N′-tert*-butyl-*N′*-aroyl-*N*-(alkoxycarbonylmethyl)-*N*-aroylhydrazines were synthesized, and their insecticidal activities against armyworm (*Leucania separata* (Walker)) were tested. The conformation and structure of compound **1b** was studied by ^{1}H NMR spectroscopy and X-ray crystallography. The crystal structure belongs to the orthorhombic system and the N—N bond adopts a *gauche* conformation, which was assumed to be the active conformation, with a dihedral angle of 69.9°.

Key words: N′-tert-butyl-*N′*-aroyl-*N*-(alkoxycarbonylmethyl)-*N*-aroylhydrazine, syntheses, insecticidal activity, conformation, crystal structure.

Résumé : On a effectué la synthèse de dix-sept *N′-tert*-butyl-*N′*-aroyl-*N*-(alkoxycarbonylméthyl)-*N*-aroylhydrazines et on a évalué leur activités insecticides contre la légionnaire uniponctuée (*Leucania separata* (Walker)). On a étudié la conformation et la structure du composé **1b** par RMN du ^{1}H et par diffraction des rayons X. La structure cristalline fait partie du système orthorhombique et la liaison N—N adopte une conformation *gauche*, qui devrait être la conformation active, avec un angle dièdre de 69,9°.

Mots clés : *N′-tert*-butyl-*N′*-aroyl-*N*-(alkoxycarbonylméthyl)-*N*-aroylhydrazine, synthèse, activité insecticide, conformation, structure cristalline.

[Traduit par la Rédaction]

Introduction

RH-5849 and RH-5992 are two well-known synthetic nonsteroidal ecdysone agonists mimicking the molting hormone (20-hydroxyecdysone) in larval insects, and exhibiting insecticidal activity by inducing premature and incomplete molting of larvae, but show low toxicity to nontarget species (1–3). Researchers use RH-5849 as a prototype compound and then introduce various substituents on phenyl rings or the nitrogen atoms of the compound to optimize moulting hormone, as well as insecticidal activity (4, 5).

In the course of our studies on diacylhydrazine (6), we were interested in *N*,*N′*-disubstituted diacylhydrazines because, up to now, there was no clear explanation as to why when the hydrogen of the second nitrogen atom of diacylhydrazine was replaced with other groups the compound still retained its activity. In this paper, we introduce a polar group (an ester group to the atom of another nitrogen) in order to enhance the lipophilicity and broaden the spectrum of insecticidal activity of *N-tert*-butyl diacylhydrzide (Fig. 1). The preliminary bioassay tests show that some compounds exhibited good insecticidal activity on armyworm (*Leucania separata* (Walker)). The lowest LC_{50} was 6 ppm.

Received August 7, 2000. Published on the NRC Research Press Web site on Aprl 2, 2001.

S. Cao, X. Qian[1, 2], and G. Song. Institute of Pesticides and Pharmaceuticals, East China University of Science and Technology, Shanghai, 200237, P. R. China.

[1]Corresponding author (telephone: 0086-021-64252945; fax: 0086-021-64251386; e-mail: xhqian@ecust.edu.cn).

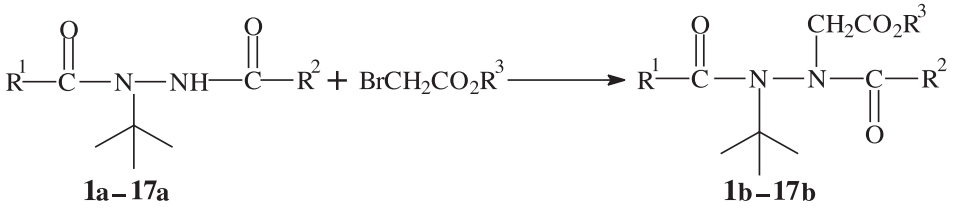
[2]Present address: State Key Laboratory of Fine Chemicals. Dalian University of Technology, Dalian 116012, P. R. China.

Experimental

All chemicals were obtained from Shanghai Chemical Reagent company Ltd. and used without further purification. Infrared spectra were done using a Nicolet 20SX FT-IR instrument. Mass spectra were recorded on a HITACHI M80 mass spectrometer using electron impact (EI) as the ion source and reported as *m*/*z*. Proton NMR spectra were obtained on a Bruker-AC 500 (500 MHz) spectrometer using $CDCl_3$ or DMSO-d_6 as the solvent and were reported in parts per million (δ) downfield from tertramethylsilane (internal reference). The analyses for elemental composition were undertaken with an Italy MOD-1106 analyzer. Isolation and purification were done by column chromatography on silica gel 60 (300–400 mesh). Analytical thin layer chromatography (TLC) was carried out on precoated plates (silica gel 60 F_{254}), and melting points were uncorrected.

 DOI: 10.1139/cjc-79-3-272 © 2001 NRC Canada

Scheme 1.



General synthetic procedures

Synthesis of symmetrical N-tert-*butyl diaroylhydrazines (2a–9a, 11a)*

tert-Butylhydrazine hydrochloride (4.98 g, 4 mmol) was dissolved in methylene chloride (20 mL). To this solution was added 10% aqueous sodium hydroxide (4.8 mL, 12 mmol). A solution of appropriate acid chloride (8 mmol) in methylene chloride was then added at 0–5°C to the rapidly stirring two-phase system. A white precipitate was formed in 4 h. The mixture was filtered and recrystallized from ethanol–water to give the desired compound in good yield, generally in the range of 70–90%.

Synthesis of unsymmetrical N-tert-*butyl diaroylhydrazines (1a, 10a, 12a–17a)*

N-tert-Butyl aroylhydrazine (25 mmol) was stirred vigorously in a two-phase system of methylene chloride (50 mL) and 10% aqueous sodium hydroxide (25 mL, 63 mmol) until all dissolved. To this solution was added a solution of acid chloride (25 mmol) in methylene chloride (25 mL). After 4–6 h at room temp, the solid was removed and washed with water. Recrystallization from ethanol gave the desired compound in high yield (70–90%).

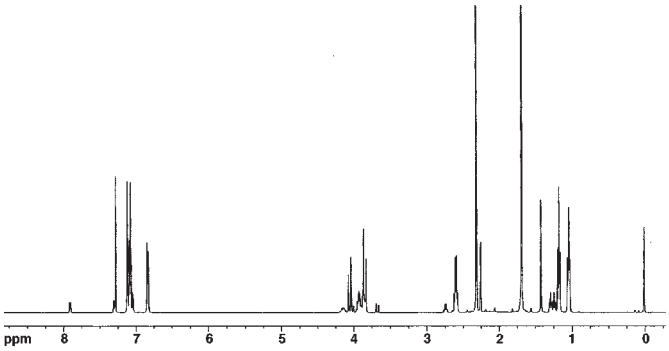
Synthesis of N′-*tert-butyl*-N′-*aroyl*-N-*(alkoxycarbonylmethyl)-N-aroylhydrazines (1b–17b)*

A mixture of *N-tert*-butyl diaroylhydrazine (3 mmol, **1a–17a**), sodium hydride (3.2 mmol, 60% suspension in paraffin oil), and dry DMF (15 mL) was stirred at room temp for 2 h. To the mixture was added ethyl bromoacetate or methyl bromoacetate (3 mmol) and dry DMF (2 mL). The reaction mixture was stirred at 35–40°C for 8–10 h. After cooling the mixture was treated with water (30 mL) and extracted with chloroform (3 × 15 mL). The organic layer was washed with water, dried $MgSO_4$, and concentrated. The residue was chromatographed over a column of silica gel and eluted with petroleum ether–ethyl acetate (2:1) (60–90°C). The title compounds were obtained (Scheme 1). The preparative and spectral data of **1a–17a** and **1b–17b** are listed in Tables 1–4.

Synthesis of N-*(ethoxycarbonylmethyl) dibenzoylhydrazine (18)*

Ethyl hydrazinoacetate hydrochloride ($NH_2NHCH_2CO_2C_2H_5 \cdot HCl$) (0.62 g, 4 mmol) was dissolved in methylene chloride (20 mL). To this solution was added 10% aqueous sodium hydroxide (4.8 mL, 12 mmol). A solution of benzoyl chloride (1.12 g, 8 mmol) in methylene chloride was then added at 0–5°C to the rapidly stirring two-phase system. A white precipitate was formed in 6 h. The mixture was filtered and recrystallized from ethyl acetate. A colourless solid was obtained in a yield of 74%, mp 108–109°C. EI-MS *m/z* (%): 327 ($[M+1]^+$, 19), 309 (78), 253 (19), 122 (28), 105 (46), 77 (100). FT-IR (KBr) (cm^{-1}): 1745, 1680, 1650. ^{1}H NMR ($CDCl_3$) δ: 1.28 (t, J = 7.2 Hz, 3H), 4.20 (t, J = 7.2 Hz, 2H), 4.64 (br s, 2H), 7.27–7.62 (m, 10H), 8.60 (s, NH). Anal. calcd. for $C_{18}H_{18}N_2O_4$: C 66.25, H 5.56, N 8.58; found: C 66.06, H 5.44, N 8.52.

Fig. 1. ^{1}H NMR spectrum of compound **1b**.



Results and discussion

Chemical

When the crude products (**1b–17b**) were purified by column chromatography, *N-tert*-butyl substituted benzamide by-products were also obtained (yield 10–15%), including *N-tert*-butyl benzamide, *N-tert*-butyl-4-fluoro-benzamide, *N-tert*-butyl-4-ethylbenzamide, and *N-tert*-butyl-4-methoxy benzamide (structures were determined by ^{1}H NMR). Reaction at higher temperature (50–60°C) yielded 20–25% of these by-products. When the substituted group attached to the aromatic ring was a strong electron-releasing or -withdrawing group, such as CH_3O- or $-NO_2$, the main product was *N-tert*-butyl substituted benzamide; the desired product was not obtained. The results showed that the N—N bond was easily cleavaged in a NaH–DMF system.

The ^{1}H NMR spectrum (in $CDCl_3$) of **1b** clearly showed that there exist two conformational isomers (Fig. 1). The ratio of isomer **A** (major) to isomer **B** (minor) is approximately 85:15. In the ^{1}H NMR spectrum of **1b**, the signals for most of the protons of minor isomer are shifted downfield as compared to the corresponding signals of the major isomer (**A**), while the signals of $(CH_3)_3$, CH_3Ar, and NCH_2CO_2 are upfield shifted. The geminal hydrogens of NCH_2CO_2 are not magnetically equivalent and, therefore, are coupled with each other (J = 17.9 Hz). Similarly, each line of the methylene hydrogens quartet ($CO_2CH_2CH_3$) is further split to a doublet due to the methylene hydrogens having different magnetic environments. Similar results were observed from the ^{1}H NMR spectra of **2b–17b**. ^{1}H NMR

© 2001 NRC Canada

Table 1. Experimental and ^{1}H NMR data for **1a**–**17a**.

	R^1	R^2	mp (°C) (lit.)	^{1}H NMR (δ) (DMSO-d_6)
1a	C_6H_3(3,5-$(CH_3)_2$)	C_6H_4(4-C_2H_5)	192–193 (194–195)	1.17 (t, *J* = 7.6 Hz, 3H), 1.58 (s, 9H), 2.20 (s, 6H), 2.63 (q, *J* = 7.6 Hz, 2H), 6.90–7.49 (m, 7H), 10.08 (s, NH)
2a	C_6H_5	C_6H_5	173–174 (174–175)	
4a	C_6H_4(4-F)	C_6H_4(4-F)	195–197[a] (196–198)	
5a	C_6H_4(4-CH_3)	C_6H_4(4-CH_3)	218–219[a] (218–220)	
6a	C_6H_4(4-Cl)	C_6H_4(4-Cl)	> 240[a] (> 240)	
7a	C_6H_4(4-Br)	C_6H_4(4-Br)	218–219[a] (219–220)	
8a	C_6H_4(4-C_2H_5)	C_6H_4(4-C_2H_5)	180–181[b] (178)	1.11 (tt, *J* = 7.7 Hz, *J* = 7.7 Hz, 6H), 1.48 (s, 9H), 2.05 (q, *J* = 7.6 Hz, 4H), 7.11–7.42 (m, 8H), 10.53 (s, NH)
9a	C_6H_4(3-CH_3)	C_6H_4(3-CH_3)	150–151[a] (152–153)	
10a	C_6H_4(4-C_2H_5)	C_6H_5	166–167	1.12 (t, *J* = 7.6 Hz, 3H), 1.56 (s, 9H), 2.55 (q, *J* = 7.6 Hz, 2H), 7.02–7.38 (m, 9H), 8.52 (s, NH)
11a	C_6H3(3,5-$(CH_3)_2$)	C_6H_3(3,5-$(CH_3)_2$)	210–211	1.58 (s, 9H), 2.18 (s, 6H), 2.21 (s, 6H) 6.84–7.26 (m, 6H), 8.11 (s, NH)
12a	C_6H_3(3,5-$(CH_3)_2$)	C_6H_5	205–206	1.52 (s, 9H), 2.20 (s, 6H), 6.89–7.42 (m, 8H), 8.20 (s, NH)
13a	C_6H_4(4-C_2H_5)	C_6H_3(3,5-$(CH_3)_2$)	173–174	1.13 (t, *J* = 7.5 Hz, 3H), 1.57 (s, 9H), 2.22 (s, 6H), 2.55 (q, *J* = 7.5 Hz, 2H), 7.08–7.45 (m, 7H), 10.07 (s, NH)
14a	C_6H_5	C_6H_4(4-C_2H_5)	210–211	1.18 (t, *J* = 7.6 Hz, 3H), 1.58 (s, 9H), 2.61 (q, *J* = 7.7 Hz, 2H), 7.07–7.45m (m, 9H), 8.10 (s, NH)
15a	C_6H_4(3-CH_3)	C_6H_4(4-C_2H_5)	136–137	1.15 (t, *J* = 7.5 Hz, 3H), 1.58 (s, 9H), 2.19 (s, 3H), 2.60 (q, *J* = 7.5 Hz, 2H), 7.01–7.37 (m, 8H), 8.56 (s, NH)
17a	C_6H_4(4-CH_3)	C_6H_4(4-C_2H_5)	189–190	1.22 (t, *J* = 7.5 Hz, 3H), 1.60 (s, 9H), 2.28 (s, 3H), 2.64 (q, *J* = 7.6 Hz, 2H), 7.05–7.39 (m, 8H), 8.26 (s, NH)

[a]See ref. 7.
[b]See ref. 8.

Table 2. Experimental and IR data for **1b**–**17b**.

	R^1	R^2	R^3	Yield (%)	mp (°C)	IR (cm^{-1}) (C=O)
1b	C_6H_3(3,5-$(CH_3)_2$)	C_6H_4(4-C_2H_5)	C_2H_5	62	116–117	1740, 1680, 1660
2b	C_6H_5	C_6H_5	C_2H_5	45	84–85	1740, 1690, 1650
3b	C_6H_3(3,5-$(CH_3)_2$)	C_6H_4(4-C_2H_5)	CH_3	50	109–110	1750, 1670, 1640
4b	C_6H_4(4-F)	C_6H_4(4-F)	C_2H_5	40	74–75	1750, 1670, 1660
5b	C_6H_4(4-CH_3)	C_6H_4(4-CH_3)	C_2H_5	65	97–98	1750, 1675, 1630
6b	C_6H_4(4-Cl)	C_6H_4(4-Cl)	C_2H_5	61	95–96	1750, 1680, 1670
7b	C_6H_4(4-Br)	C_6H_4(4-Br)	C_2H_5	63	109–110	1740, 1680, 1640
8b	C_6H_4(4-C_2H_5)	C_6H_4(4-C_2H_5)	C_2H_5	60	100–101	1740, 1670, 1660
9b	C_6H_4(3-CH_3)	C_6H_4(3-CH_3)	C_2H_5	64	91–92	1750, 1680, 1660
10b	C_6H_4(4-C_2H_5)	C_6H_5	C_2H_5	60	102–103	1740, 1690, 1660
11b	C_6H_3(3,5-$(CH_3)_2$)	C_6H_3(3,5-$(CH_3)_2$)	C_2H_5	62	123–124	1750, 1680, 1670
12b	C_6H_3(3,5-$(CH_3)_2$)	C_6H_5	C_2H_5	58	133–134	1760, 1690, 1650
13b	C_6H_4(4-C_2H_5)	C_6H3(3,5-$(CH_3)_2$)	C_2H_5	60	93–94	1765, 1685, 1660
14b	C_6H_5	C_6H_4(4-C_2H_5)	C_2H_5	55	88–89	1760, 1675, 1665
15b	C_6H_4(3-CH_3)	C_6H_4(4-C_2H_5)	C_2H_5	60	98–99	1740, 1660, 1630
16b	C_6H_4(3-CH_3)	C_6H_4(4-C_2H_5)	CH_3	60	102–103	1760, 1670, 1660
17b	C_6H_4(4-CH_3)	C_6H_4(4-C_2H_5)	C_2H_5	63	95–96	1760, 1680, 1670

spectra of **2b**–**17b** reveal that the introduction of an ester group to another nitrogen may cause the molecular rotations around the N—N bond to be "frozen" sufficiently for these differences to be detected.

Biological Activities

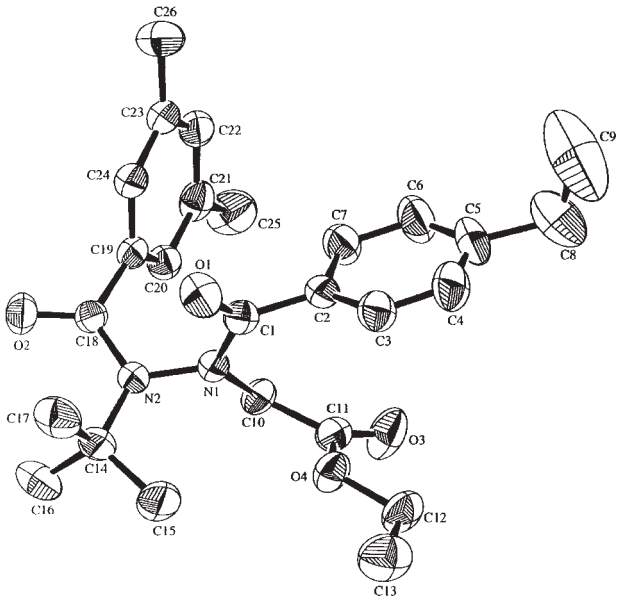
Insecticidal activity was assessed with third-instar larvae of *Leucania separata* (Walker). The method was similar to the procedure described in the literature (11). Compounds were dissolved in DMF, and water was serially diluted to achieve the desired range of concentrations (ppm). For each concentration, 20–40 insects were used and at least six different concentrations were applied in order to calculate LC_{50} values (ppm). Insecticidal activities of the new 10 compounds (**1**–**3b**, **7b**, **13**–**17b**) were shown in Table 5. Of the other eight compounds (**4b**, **5b**, **8**–**12b**, **18b**), the LC_{50}

© 2001 NRC Canada

Table 3. Microanalytical and mass spectral data for **1b**–**17b**.

	Elemental analysis (%) (theor.)			MS (*m*/*z*) (%)
	C	H	N	
1b	70.64 (71.20)	7.81 (7.81)	6.34 (6.39)	439 ([M+1]$^+$, 20), 364 (100), 133 (82), 105 (30)
2b	69.27 (69.09)	6.83 (6.85)	7.21 (7.32)	382 (M$^+$, 13), 308 (100), 105 (15), 77 (6)
3b	70.68 (70.73)	7.64 (7.60)	6.59 (6.60)	425 ([M+1]$^+$, 5), 351 (15), 133 (100), 105 (9)
4b	63.49 (63.15)	5.85 (5.78)	6.68 (6.69)	419 ([M+1]$^+$, 10), 345 (100), 290 (14), 123 (33)
5b	70.10 (70.22)	7.49 (7.36)	6.48 (6.82)	410 (M$^+$, 12), 337 (4), 136 (3), 119 (100)
6b	58.63 (58.54)	5.53 (5.36)	6.50 (6.20)	451 (M$^+$, 7), 394 (6), 141 (100), 111 (78)
7b	48.93 (48.91)	4.43 (4.48)	5.26 (5.19)	541 (M$^+$, 8), 468 (13), 183 (100), 157 (25), 104 (13)
8b	71.58 (71.21)	7.89 (7.81)	6.35 (6.39)	483 (M$^+$, 2), 134 (100), 105 (26), 79 (23)
9b	70.29 (70.22)	7.36 (7.36)	6.72 (6.82)	411 ([M+1]$^+$, 5), 336 (4), 119 (100), 91 (21)
10b	70.22 (70.22)	7.30 (7.36)	6.75 (6.82)	412 ([M+2]$^+$, 6), 337 (73), 134 (100), 105 (87)
11b	71.27 (71.21)	7.88 (7.81)	6.54 (6.39)	439 (M$^+$, 7), 382 (43), 365 (70), 105 (100)
12b	70.41 (70.22)	7.36 (7.36)	6.82 (6.82)	411 (M$^+$, 66), 356 (45), 337 (100), 134 (66)
13b	71.20 (71.21)	7.84 (7.81)	6.46 (6.39)	439 (M$^+$, 10), 365 (86), 134 (82), 105 (100)
14b	70.13 (70.22)	7.36 (7.36)	7.01 (6.82)	411 (M$^+$, 11), 355 (11), 336 (100), 133 (90)
15b	70.76 (70.73)	7.63 (7.60)	6.63 (6.60)	425 (M$^+$, 15), 351 (100), 133 (63), 119 (23)
16b	70.36 (70.22)	7.39 (7.36)	6.85 (6.82)	409 ([M–1]$^+$, 3), 336 (100), 133 (57), 119 (85)
17b	71.13 (70.73)	7.68 (7.60)	6.60 (6.60)	425 (M$^+$, 4), 351 (90), 133 (100), 119 (83), 91 (19)

Fig. 2. X-ray crystal structure of compound **1b**.



values were not determined as they showed no, or attenuated, biological activity at concentrations as high as 500 ppm.

In general, unsymmetrical *N′-tert*-butyl-*N*-(alkoxycarbonylmethyl)-*N′*,*N*-diaroylhydrazines are more active than symmetrical *N′-tert*-butyl-*N*-(alkoxycarbonylmethyl)-*N′*,*N*-diaroylhydrazines, and the activitives of halogen-containing symmetrical compounds are higher than those of non halogen-containing compounds. Comparison of the observed activity values of **1b**, **5b**, **8b**–**15b**, and **17b** with their parent compound (**2b**) showed that the activity of multialkyl-substituted compounds varied drastically, with activity dependent on the type, number, and position of substituents. Although **1b** was found to be one of the most active compounds, exchange of the position of the *tert*-butyl and ester groups (**13b**) resulted in a significant loss of activity. Replacement of the *tert*-butyl group on the hydrazine (**2b**) by a hydrogen atom gave an inactive compound (**18**). These results suggest that the bulky *tert*-butyl group and its position is critical to the activity. This is in agreement with observations of Chan et al. (9) and Hsu et al. (10).

X-ray crystal structure of 1b

Three of the products (**1b, 3b**, and **15b**) showed potent insecticidal activity on armyworm. They were weaker than tebufenozide (RH-5992), but they were more potent than RH-5849. These results are not inconsistent with the literature (10), which suggest that when the hydrogen of the secondary nitrogen atom (NH) was substituted with an unhydrolyzable group the compound tends not to be active.

The X-ray crystal structure of RH-5849 was reported previously by Chan et al. (9), who suggested that the N—N bond in RH-5849 adopts a *gauche* conformation with a dihedral angle of –71.8 or –58.1°, and that this conformation is essential to the activity of the molecule. In order to explain why replacement of the hydrogen on the nitrogen of *N-tert*-butyl diaroylhydrazine by an ester group (or another group) still gave an active compound, we studied the X-ray crystal structure of **1b** (Fig. 2). Different from the two conformations of **1b** observed in a $CDCl_3$ solution (^{1}H NMR of **1b**, see Fig. 1), only one conformation exists in the crystalline state. Structure analysis reveals that the N—N bond in **1b** also adopts a *gauche* conformation. A dihedral angle of 69.9° for C(1)-N(1)-N(2)-C(18) is also observed, but its direction of rotation is opposite to that of RH-5849. Similar to the crystal of RH-5849, the amide bearing the *N*-ester group has an *s-cis* conformation, whereas the amide bearing the *N-tert*-butyl group has an *s-trans* conformation, with the steric bulk of the *tert*-butyl group causing the phenyl group to be directed away from the molecule. The dihedral angle between two phenyl rings is 96.11°, which is much larger, compared to the data of RH-5849 (66.3 or 60.8°), due to the ester group pushing the phenyl ring upward. To further

© 2001 NRC Canada

Table 4. ^{1}H NMR data of **1b**–**17b**.

	% Yield Isomer A (B)	^{1}H NMR (δ) ($CDCl_3$)
1b	85 (15)	A: 1.05 (t, *J* = 7.1 Hz, 3H), 1.18 (t, *J* = 7.6 Hz, 3H), 1.69 (s, 9H), 2.32 (s, 6H), 2.61 (q, *J* = 7.6 Hz, 2H), 3.93 (qq, *J* = 7.1 Hz, *J* = 17.8 Hz, 2H), 3.96 (q, *J* = 17.9 Hz, 2H), 6.83–7.12 (m, 7H) B: 1.25 (t, *J* = 7.1 Hz, 3H), 1.30 (t, *J* = 7.6 Hz, 3H), 1.43 (s, 9H), 2.26 (s, 6H), 2.75 (q, *J* = 7.6 Hz, 2H), 3.85 (q, *J* = 16.5 Hz, 2H), 4.15 (qq, *J* = 7.1 Hz, *J* = 17.9 Hz, 2H), 7.02–7.92 (m, 7H)
2b	85 (15)	A: 1.02 (t, *J* = 7.1 Hz, 3H), 1.69 (s, 9H), 3.84 (qq, *J* = 7.1 Hz, *J* = 17.8 Hz, 2H), 3.97 (q, *J* = 17.7 Hz, 2H), 6.77–7.34 (m, 10H) B: 1.23 (t, *J* = 7.1 Hz, 3H), 1.38 (s, 9H), 3.85 (q, *J* = 16.9 Hz, 2H), 4.16 (qq, *J* = 7.1 Hz, *J* = 17.8 Hz, 2H), 7.82–7.98 (m, 10H)
3b	83 (17)	A: 1.18 (t, *J* = 7.6 Hz, 3H), 1.67 (s, 9H), 2.30 (s, 6H), 2.60 (q, *J* = 7.6 Hz, 2H), 3.44 (s, 3H), 3.95 (q, *J* = 17.8 Hz, 2H), 6.86–7.10 (m, 7H) B: 1.28 (t, *J* = 7.6 Hz, 3H), 1.40 (s, 9H), 2.24 (s, 6H), 2.73 (q, *J* = 7.6 Hz, 2H), 3.66 (s, 3H), 3.85 (q, *J* = 16.5 Hz, 2H), 7.01–7.90 (m, 7H)
4b	83 (17)	A: 1.07 (t, *J* = 7.1 Hz, 3H), 1.67 (s, 9H), 3.90 (qq, *J* = 7.2 Hz, *J* = 17.5 Hz, 2H), 3.95 (q, *J* = 17.0 Hz, 2H), 6.96–7.10 (m, 8H) B: 1.25 (t, *J* = 7.1 Hz, 3H), 1.41 (s, 9H), 3.84 (q, *J* = 16.4 Hz, 2H), 4.23 (qq, *J* = 7.2 Hz, *J* = 17.5 Hz, 2H), 7.04–8.06 (m, 8H)
5b	81 (19)	A: 1.03 (t, *J* = 7.2 Hz, 3H), 1.67 (s, 9H), 2.28 (s, 3H), 2.37 (s, 3H), 3.91 (qq, *J* = 7.2 Hz, *J* = 17.5 Hz, 2H), 3.94 (q, *J* = 17.9 Hz, 2H), 6.76–7.18 (m, 8H) B: 1.25 (t, *J* = 7.2 Hz, 3H), 1.41 (s, 9H), 2.34 (s, 3H), 2.42 (s, 3H), 3.75 (q, *J* = 16.5 Hz, 2H) 4.13 (qq, *J* = 7.2 Hz, *J* = 17.5 Hz, 2H), 7.08–7.40 (m, 8H)
6b	80 (20)	A: 1.04 (t, *J* = 7.1 Hz, 3H), 1.65 (s, 9H), 3.91 (qq, *J* = 7.2 Hz, *J* = 17.5 Hz, 2H), 3.96 (q, *J* = 17.2 Hz, 2H), 6.87–7.15 (m, 8H) B: 1.26 (t, *J* = 7.2 Hz, 3H), 1.43 (s, 9H), 3.86 (q, *J* = 16.5 Hz, 2H), 4.25 (qq, *J* = 7.2 Hz, *J* = 17.5 Hz, 2H), 7.06–7.95 (m, 8H)
7b	89 (11)	A: 1.05 (t, *J* = 7.3 Hz, 3H), 1.64 (s, 9H), 3.86 (qq, *J* = 7.3 Hz, *J* = 17.5 Hz, 2H), 3.97 (q, *J* = 17.3 Hz, 2H), 6.74–7.54 (m, 8H) B: 1.26 (t, *J* = 7.2 Hz, 3H), 1.39 (s, 9H), 3.88 (q, *J* = 16.5 Hz, 2H), 4.11 (qq, *J* = 7.2 Hz, *J* = 17.5 Hz, 2H), 7.31–7.85 (m, 8H)
8b	85 (15)	A: 1.00 (t, *J* = 7.1 Hz, 3H), 1.15 (t, *J* = 7.6 Hz, 3H), 1.25 (t, *J* = 7.6 Hz, 3H), 1.68 (s, 9H), 2.56 (q, *J* = 7.6 Hz, 2H), 2.70 (q, *J* = 7.6 Hz, 2H), 3.87 (qq, *J* = 7.1 Hz, *J* = 17.9 Hz, 2H), 3.98 (q, *J* = 17.9 Hz, 2H), 6.68–7.42 (m, 8H) B: 1.22 (t, *J* = 7.1 Hz, 3H), 1.26 (t, *J* = 7.6 Hz, 3H), 1.34 (t, *J* = 7.6 Hz, 3H), 1.42 (s, 9H), 3.78 (q, *J* = 16.6 Hz, 2H), 4.24 (qq, *J* = 7.1 Hz, *J* = 17.9 Hz, 2H), 7.16–7.98 (m, 8H)
9b	79 (21)	A: 1.03 (t, *J* = 7.2 Hz, 3H), 1.69 (s, 9H), 2.23 (s, 3H), 2.33 (s, 3H), 3.88 (qq, *J* = 7.2 Hz, *J* = 17.9 Hz, 2H), 3.95 (q, *J* = 17.9 Hz, 2H), 6.57–7.16 (m, 8H) B: 1.24 (t, *J* = 7.2 Hz, 3H), 1.39 (s, 9H), 2.24 (s, 3H), 2.34 (s, 3H), 3.97 (q, *J* = 16.4 Hz, 2H) 4.23 (qq, *J* = 7.2 Hz, *J* = 17.9 Hz, 2H), 7.04–7.30 (m, 8H)
10b	90 (10)	A: 1.01 (t, *J* = 7.2 Hz, 3H), 1.25 (t, *J* = 7.6 Hz, 3H), 1.68 (s, 9H), 2.69 (q, *J* = 7.6 Hz, 2H), 3.86 (qq, *J* = 7.2 Hz, *J* = 17.9 Hz, 2H), 3.98 (q, *J* = 18.1 Hz, 2H), 6.73–7.24 (m, 9H) B: 1.24 (t, *J* = 7.2 Hz, 3H), 1.27 (t, *J* = 7.6 Hz, 3H), 1.38 (s, 9H), 2.67 (q, *J* = 7.6 Hz, 2H), 3.85 (q, *J* = 16.5 Hz, 2H), 4.15 (qq, *J* = 7.2 Hz, *J* = 17.0 Hz, 2H), 7.29–7.98 (m, 9H)
11b	88 (12)	A: 1.06 (t, *J* = 7.2 Hz, 3H), 1.68 (s, 9H), 2.19 (s, 6H), 2.31 (s, 6H), 3.90 (qq, *J* = 7.2 Hz, *J* = 16.9 Hz, 2H), 3.92 (q, *J* = 17.9 Hz, 2H), 6.42–7.09 (m, 6H) B: 1.30 (t, *J* = 7.2 Hz, 3H), 1.38 (s, 9H), 2.26 (s, 6H), 2.37 (s, 6H), 3.86 (q, *J* = 16.6 Hz, 2H) 4.17 (qq, *J* = 7.2 Hz, *J* = 16.9 Hz, 2H), 6.99–7.51 (m, 6H)
12b	84 (16)	A: 1.04 (t, *J* = 7.1 Hz, 3H), 1.68 (s, 9H), 2.31 (s, 6H), 3.92 (qq, *J* = 7.2 Hz, *J* = 16.8 Hz, 2H), 3.93 (q, *J* = 16.7 Hz, 2H), 6.87–7.34 (m, 8H) B: 1.24 (t, *J* = 7.1 Hz, 3H), 1.38 (s, 9H), 2.25 (s, 6H), 3.92 (q, *J* = 16.5, Hz, 2H), 4.15 (qq, *J* = 7.2 Hz, *J* = 16.8 Hz, 2H), 7.00–7.93 (m, 8H)
13b	89 (11)	A: 1.03 (t, *J* = 7.3 Hz, 3H), 1.22 (t, *J* = 7.6 Hz, 3H), 1.68 (s, 9H), 2.17 (s, 6H), 2.69 (q, *J* = 7.6 Hz, 2H), 3.85 (q, *J* = 17.3 Hz, 2H), 3.94 (qq, *J* = 7.2 Hz, *J* = 17.8 Hz, 2H), 6.36–7.42 (m, 7H) B: 1.27 (t, *J* = 7.1 Hz, 3H), 1.29 (t, *J* = 7.6 Hz, 3H), 1.40 (s, 9H), 2.36 (s, 6H), 2.65 (q, *J* = 7.6 Hz, 2H), 3.80 (q, *J* = 16.5 Hz, 2H), 4.10 (qq, *J* = 7.3 Hz, *J* = 17.9 Hz, 2H)

© 2001 NRC Canada

Table 4 (*concluded*).

	% Yield Isomer A (B)	^{1}H NMR (δ) ($CDCl_3$)
14b	89 (11)	A: 1.01 (t, *J* = 7.3 Hz, 3H), 1.15 (t, *J* = 7.6 Hz, 3H), 1.68 (s, 9H), 2.55 (q, *J* = 7.3 Hz, 2H), 3.81 (qq, *J* = 7.3 Hz, *J* = 17.9 Hz, 2H), 4.01 (q, *J* = 18.0 Hz, 2H), 6.71–7.49 (m, 9H) B: 1.21 (t, *J* = 7.1 Hz, 3H), 1.27 (t, *J* = 7.6 Hz, 3H), 1.42 (s, 9H), 2.71 (q, *J* = 7.6 Hz, 2H), 3.91 (q, *J* = 16.4 Hz, 2H), 4.20 (qq, *J* = 7.3 Hz, *J* = 17.9 Hz, 2H), 7.27–7.96 (m, 9H)
15b	86 (14)	A: 1.03 (t, *J* = 7.1 Hz, 3H), 1.17 (t, *J* = 7.6 Hz, 3H), 1.68 (s, 9H), 2.34 (s, 3H), 2.57 (q, *J* = 7.6 Hz, 2H), 3.89 (qq, *J* = 7.1 Hz, *J* = 17.9 Hz, 2H), 3.96 (q, *J* = 17.9 Hz, 2H), 6.77–7.31 (m, 8H) B: 1.23 (t, *J* = 7.1 Hz, 3H), 1.27 (t, *J* = 7.6 Hz, 3H), 1.43 (s, 9H), 2.30 (s, 3H), 2.73 (q, *J* = 7.6 Hz, 2H), 3.82 (q, *J* = 16.5 Hz, 2H), 4.14 (qq, *J* = 7.1 Hz, *J* = 17.9 Hz, 2H), 7.24–7.94 (m, 8H)
16b	84 (16)	A: 1.09 (t, *J* = 7.6 Hz, 3H), 1.60 (s, 9H), 2.27 (s, 3H), 2.52 (q, *J* = 7.6 Hz, 2H), 3.35 (s, 3H), 3.90 (q, *J* = 17.8 Hz, 2H), 6.74–7.24 (m, 8H) B: 1.21 (t, *J* = 7.6 Hz, 3H), 1.34 (s, 9H), 2.23 (s, 3H),2.66 (q, *J* = 7.6 Hz, 2H), 3.57 (s, 3H), 3.77 (q, *J* = 16.4 Hz, 2H), 7.21–7.86 (m, 8H)
17b	80 (20)	A: 1.031 (t, *J* = 7.1 Hz, 3H), 1.15 (t, *J* = 7.6 Hz, 3H), 1.66 (s, 9H), 2.37 (s, 3H), 2.57 (q, *J* = 7.6 Hz, 2H), 3.88 (qq, *J* = 7.1 Hz, *J* = 17.9 Hz, 2H), 3.95 (q, *J* = 17.9 Hz, 2H), 6.78–7.39 (m, 8H) B: 1.21 (t, *J* = 7.2 Hz, 3H), 1.26 (t, *J* = 7.6 Hz, 3H), 1.41 (s, 9H), 2.33 (s, 3H), 2.72 (q, *J* = 7.6 Hz, 2H), 3.75 (q, *J* = 16.5 Hz, 2H), 4.10 (qq, *J* = 7.1 Hz, *J* = 17.9 Hz, 2H), 7.12–7.96 (m, 8H)

Table 5. Molting hormonal activity against armyworm.

Compd	LC_{50} (ppm)[a]	Compd	LC_{50} (ppm)
1b	7.58 ± 0.12	**13b**	>50
2b	>50	**14b**	21.87 ± 0.07
3b	6.12 ± 0.10	**15b**	5.13 ± 0.13
6b	>50	**16b**	9.55 ± 0.04
7b	>50	**17b**	34.67 ± 0.09

[a]Values with mean ± standard deviation were taken from three or four experimental runs.

elucidate structural details of **1b**, we studied the conformations and energies of this compound using the PCMODEL method. The energy minimum conformation of **1b** is similar to that obtained from the X-ray crystal structure of **1b**. Therefore, based on the results from X-ray crystal structure analysis and the PCMODEL method, we can suggest that the major conformational isomer in solution may also adopt the *gauche* conformation.

Crystallographic experimental details

Crystal data for **1b** ($C_{26}H_{34}N_2O_4$). MW = 438.57 g mol^{-1}. Recrystallized from ethyl acetate. Orthorhombic space group, *a* = 21.842(3), *b* = 24.375(4), *c* = 9.559(3) Å. *V* = 5089(1) $Å^3$, space group *Pbca* (no. 61), *Z* = 8, D_{calcd} = 1.14 g cm^{-3}, *F*(000) = 1888.00, μ (Mo Kα) = 0.77 cm^{-1}, *T* = 293 K. Of the 5028 unique reflections measured, 1735 [I 2.50σ(I)] were used in refinement. *R* = 0.055, *wR* = 0.059. The experimental data were collected on a Rigaku AFC7R diffractometer using graphite monochromated Mo K α radiation (λ = 0.71069 Å). The structure was solved by direct methods and expanded using Fourier techniques. All calculations were performed using the teXan crystallgraphic software package of Molecular Structure Corporation.

Conclusions

Good insecticidal activities were obtained when the ester group was introduced to the hydrazine linkage. The crystal structure showed that the introduction of the ester group at the second nitrogen may cause the steric repulsion between the ester and the *tert*-butyl group, but the basic conformation (active conformation) is unchanged. These results can give a clear explanation to the fact why many *N′-tert*-butyl-*N*-substituted-N, *N′*-diaroylhydrazines are still active, and have encourage us to pursue the search of new, more effective analogues as promising pesticidal candidate through the modification of the second nitrogen of hydrazine.

Acknowledgements

This study was financially supported by National Natural Science Foundation of China and Shanghai Foundation of Science and Technology.

References

1. K.D. Wing, Science (Washington, D.C.), **241**, 467 (1988).
2. B. Shimizu, Y. Nakagawa, K. Hattori, N. Kurihara, and T. Ueno. Steroids, **62**, 638 (1997).

© 2001 NRC Canada

3. Y. Nakagawa, K. Hattori, B. Shimizu, and M. Akamatsu. Pestic. Sci. **53**, 267 (1998).
4. R.A. Murphy, and A.C.T. Hsu. Eur. Pat. Appl. EP 245950, 1987; Chem. Abstr. **109**: 37 651z (1988).
5. T. Totani, Y. Kato, Y. Yamamoto, T. Watabe, M. Yanagi, and Y. Tsukamoto. JP 08 231 528, 1996; Chem. Abstr. **125**: 328 499y (1996).
6. X.H. Qian. J. Agric. Food Chem. **44**, 1538 (1996).
7. K. Vekataraman, D.P. Wright Jr., and R.A. Herman. USP 4 857 550; Chem. Abstr. **112:** 55 266c (1990).
8. A.K. Mohammed-Ali, T.H. Chan, A.W. Thomas, and G.M. Strunz. Can. J. Chem. **73**, 550 (1995).
9. T.H. Chan, A. ALi, J.F. Britten, A.W. Thomas, G.M. Strunz, and A. Salonius. Can. J. Chem. **68,** 1178 (1990).
10. A.C.T. Hsu, T.T. Fujimoto, and T.S. Dhadialla. Phytochemicals for pest control. ACS Symp. Ser. no. 658. *Edited by*, P.A. Hedin. American Chemical Society, Washington, D.C. 1995. p. 206.
11. G. Smagghe and D. Degheele. Pestic. Sci. **42**, 85 (1994).

© 2001 NRC Canada

Overtone intensities in neopentane and tetramethylsilane

Michael W. P. Petryk and Bryan R. Henry

Abstract: The CH vibrational overtone transitions of vapour phase neopentane-d_0, -d_6, -d_9, and tetramethylsilane (TMS) are investigated via conventional absorbance spectroscopy and intracavity laser photoacoustic spectroscopy (ICL-PAS). The CH stretching overtones of neopentane-d_0 are observed in the energy range $\Delta v_{CH} = 3$–9 (8 400 to 22 000 cm^{-1}) and in the range $\Delta v_{CH} = 3$–8 for the remaining neopentanes and TMS. While we have extended the range of previous studies, our main focus in this work has been on overtone intensities. The oscillator strengths of the neopentane-d_0 overtone transitions are determined directly by conventional absorbance spectroscopy for $\Delta v_{CH} = 3$–6 and via ICL-PAS with methane as an internal standard for $\Delta v_{CH} = 4$–7. The correspondence of measured intensities for the two techniques demonstrates the usefulness of the latter for higher overtone ICL-PAS spectra. The experimentally determined Morse parameters $\widetilde{\omega}$ and $\widetilde{\omega}x$ as well as the harmonically coupled anharmonic oscillator (HCAO) model are used in conjunction with dipole moment functions that are derived from ab initio computations to calculate overtone transition intensities for the neopentanes and TMS.

Key words: local mode, overtone transition, absolute intensity, photoacoustic spectroscopy.

Résumé : Faisant appel à la spectroscopie d'absorbance conventionnelle et à la spectroscopie photoacoustique laser intracavité (SPA-LIC), on a étudié les transitions harmoniques vibrationnelles du CH, en phase vapeur, des néopentanes-d_0, -d_6, -d_9, et du tétraméthylsilane (TMS). Les harmoniques d'élongation du CH du néopentane-d_0 ont été observées sur la plage d'énergie $\Delta v_{CH} = 3$–9 (8,400 à 22,000 cm^{-1}) alors qu'on les observe sur la plage d'énergie $\Delta v_{CH} = 3$–8 pour les autres néopentanes et pour le TMS. Même si on a élargi les connaissances déjà acquises dans des études antérieures, le but principal du présent travail était d'examiner les intensités des harmoniques. On a déterminé les forces de l'oscillateur des transitions harmoniques pour le néopentane-d_0 soit directement par spectroscopie d'absorbance conventionnelle $\Delta v_{CH} = 3$–6 soit par le biais de la (SPA-LIC) $\Delta v_{CH} = 4$–7. La correspondance des intensités mesurées par les deux techniques démontre l'utilité de la dernière pour les harmoniques plus élevées des spectres de SPA-LIC. On a utilisé les paramètres de Morse obtenus expérimentalement, $\widetilde{\omega}$ et $\widetilde{\omega}x$, le modèle de l'oscillateur anharmonique couplé de façon harmonique ainsi que les fonctions de moment dipolaire dérivées de calculs ab initio pour calculer les intensités de la transition harmonique des néopentanes et du TMS.

Mots clés : mode local, transition harmonique, intensité absolue, spectroscopie photoacoustique..

[Traduit par la Rédaction]

Introduction

The vibrational overtone stretching transitions of XH bonds (X = C, N, O, etc.) are dominated by transitions to states whose components have all of the vibrational energy localized within one of a series of equivalent XH oscillators. This apparent localization of energy in a single bond makes the overtone spectra of large molecules appear very simple. In the absence of coupling, one transition peak is observed for each non-equivalent XH bond. Furthermore, the localization of energy in XH oscillators makes overtone spectroscopy an extremely sensitive probe for detecting changes in molecular environment (1, 2) which can manifest themselves as small changes in structural parameters such as bond length (3–5), and conformation (2, 6).

In the absence of very strong coupling we would expect the overtone transitions of neopentane-d_0 ($C(CH_3)_4$), -d_6 ($C(CH_3)_2(CD_3)_2$), and -d_9 ($C(CH_3)(CD_3)_3$) to be simple, with only one transition peak. In fact, the overtone transitions of neopentane have complicated structures and the CH overtone transitions themselves are much broader than those of other $M(CH_3)_4$ homologues (7, 8). This investigation has been undertaken to obtain more accurate, higher energy CH stretching overtone spectra of neopentane-d_0, -d_6, -d_9, and tetramethylsilane (TMS) ($Si(CH_3)_4$) than are currently available as a first step towards determining which factors might contribute to the anomalous profiles of the neopentanes.

Previously, the vibrational overtones of gas (7–11) and liquid (7, 12, 13) phase neopentane-d_0, as well as neopentane-d_6 and -d_9 (10, 11) have been studied with conventional absorption spectroscopy (7, 9–14), Raman spectroscopy (13), and intracavity laser photoacoustic spectroscopy (ICL-PAS) techniques up to seven quanta of stretching excitation (8) in the vapour phase. The overtone spectra of TMS have been studied in the vapour (7, 8, 15, 16) and liquid (7, 17–21) phases with conventional absorption spectroscopy (7, 15), ICL-PAS (8, 16), and piezoelectric detection (18–21) methods at energies of up to seven quanta of CH stretching excitation (8) in the vapour phase.

For CH stretching the off-diagonal coupling terms of the molecular Hamiltonian (represented in a local mode basis) are small compared to the diagonal cubic and quartic terms (22). Furthermore, the differences in magnitude between the energy

September 22, 2000 Published on the NRC Research Press Web site on April 2, 2001.

M.W.P. Petryk and B.R. Henry.[1] Department of Chemistry and Biochemistry, University of Guelph, Guelph, Ontario N1G 2W1, Canada

[1] Corresponding author: (fax: (519) 766-1499); email: henry@chembio.uoguelph.ca).

 DOI: 10-1139/cjc-79-3-279 © 2001 NRC Canada

contributions from the cubic and quartic terms and the off-diagonal coupling terms increase with increasing vibrational excitation. The net result is that the potential of a molecule with a number of anharmonic oscillators is effectively separable, and the molecule can be treated as a collection of diatomic Morse potentials, in which, couplings are taken as perturbations (23). Morse potentials have an advantage over some more generalized functions in that their wave functions can be solved analytically (23). The basis states for a series of XH Morse oscillators can be conveniently written as $|\upsilon_1\rangle|\upsilon_2\rangle, \ldots, |\upsilon_i\rangle, \ldots$ or simply as $|\upsilon_1\upsilon_2 \ldots \upsilon_i \ldots\rangle$,where υ_i is the number of vibrational quanta in the i^{th} XH oscillator. Spectrally "bright" states, i. e., those states which carry intensity from the $\upsilon = 0$ vibrational state, are pure local mode states which are well described by a linear combination of components in which all of the vibrational energy is localized ($|\upsilon 0 \ldots 0\rangle$, $|0\upsilon \ldots 0\rangle$, etc.). The pure local mode wave functions of three coupled, identical XH oscillators of local C_{3v} symmetry arising from the linear combination of these basis states may be denoted as $|\upsilon 00\rangle_{A_1}$ and $|\upsilon 00\rangle_E$. The various symmetrized components for these bright states approach degeneracy with increasing excitation so that symmetry effects are generally not observed for $\Delta v_{CH} \geq 3$. In cases where it is impossible to resolve the nearly degenerate states, it is useful to refer to them collectively as $|\upsilon 00\rangle_{A_1E}$. The local mode description (24–28) has been extended to multi-oscillator systems in the harmonically coupled anharmonic oscillator (HCAO) model (13, 28–30).

Absolute overtone transition intensities can be calculated from the transition dipole moment and vibrational wave functions. The wave functions of the ground and excited vibrational states are calculated from the experimental values of the local mode parameters (23, 28) $\widetilde{\omega}$, $\widetilde{\omega}x$, and γ' (the interoscillator coupling parameter for XH oscillators on the same atom X) within the HCAO model. A dipole moment function (DMF) is derived from ab inito calculations (31–33). The calculated intensities will be compared to measured values that are obtained both photoacoustically and by conventional absorption spectroscopy.

Experimental

Sample preparation

Neopentane-d_0 (Matheson Gas Products, 99.87%) was used without further purification. A gas chromatograph–mass spectrometer analysis revealed that the neopentane-d_0 contained no significant levels of impurities. Both neopentane-d_6 and neopentane-d_9 (Fisher, 99.9+%) were also used without further purification.

NMR grade tetramethylsilane (TMS) was obtained as a liquid (Aldrich, 99.9+%) and was degased by repeated freeze-pump-thaw cycles. Prior to its introduction into a spectrometric gas cell, TMS was dried by passing it through molecular sieves.

Conventional absorbance spectroscopy

A Varian Cary 5e UV–vis–near-IR conventional absorption spectrometer equipped with a gas cell was used to record overtone transitions in the range $\Delta v_{CH} = 3$–6. The spectral resolution of the Cary 5e is wavelength dependent: 0.7 cm^{-1} at 8 300 cm^{-1} ($\Delta v_{CH} = 3$), 1.2 cm^{-1} at 11 000 cm^{-1} ($\Delta v_{CH} = 4$), 1.8 cm^{-1} at 13 400 cm^{-1} ($\Delta v_{CH} = 5$), and 2.5 cm^{-1} at 15 900 cm^{-1} ($\Delta v_{CH} = 6$). The vacuum line and gas cells were evacuated to a pressure of about 10^{-2} torr (1 torr = 133.32 Pa) for at least 4 h prior to introducing the sample into a Wilks variable length gas cell fitted with Melles Griot BK7 Schott glass windows.

Intracavity laser photoacoustic spectroscopy

ICL-PAS is a technique which exploits the photoacoustic effect, i. e., ICL-PAS relies on the thermal generation of sound waves from an absorbing sample exposed to *modulated* incident light. An output coupler is chosen which nearly completely reflects the laser radiation back into the cavity, thereby maximizing intracavity power. The photoacoustic (PA) sample cell is positioned within the laser cavity to take advantage of the higher intracavity power levels and the longer effective path length. Intense laser excitation, combined with the essentially zero background noise of this technique, results in high sensitivity. Extraneous noise is further suppressed by referencing the acoustic detector to the excitation source modulator via a lock-in amplifier.

ICL-PAS has certain shortcomings. In particular, it is difficult to obtain absolute absorption intensities as the dependence of photoacoustic signal strength ($S(\nu)$) on various parameters cannot be easily extended to subtly different experimental conditions. At a frequency (ν), the relationship between the photoacoustic signal strength ($S(\nu)$), the incident light intensity ($I(\nu)$), the absorbance of the sample ($A(\nu)$), and $k(\nu)$ (some unknown component(s) accounting for numerous factors such as coupling gas pressure and temperature, cell dimensions, microphone location and sensitivity) can be expressed as (34, 35)

$$[1] \qquad S(\nu) = k(\nu)I(\nu)A(\nu)$$

Since the factor $k(\nu)$ depends upon so many variables it is impractical to evaluate experimentally for all possible experimental conditions, therefore, PA spectra typically yield only absorption intensities of a chromophore relative to other chromophores within the cell. The inferential assumption here is that $k(\nu)$ is invariant to changes in ν over the narrow range of frequencies encountered during a given spectral scan. This assumption is generally valid as typical ICL-PAS scanning ranges are 100 nm or less owing to instrumental limitations.

Our ICL-PAS setup has been described in detail elsewhere (36–38), and only a brief summary is supplied here. A 20 W Coherent Innova 200 argon ion laser is used to pump a Coherent 599 tunable dye laser or a broadband Coherent 890 Ti:sapphire (Ti:sapph) laser. The pump laser beam is mechanically chopped, and the output signal is referenced to the chopper and amplified, digitized, and exported to a personal computer where it is later normalized to the intracavity power. The Ti:sapph laser has three sets of optics (short wave, mid wave, and long wave) which enable it to scan a region from 9 300 to 14 700 cm^{-1} ($\Delta v_{CH} = 3$–5). By varying the dyes and the optics, the dye laser can access the region from 12 300 to 23 900 cm^{-1} ($\Delta v_{CH} = 5$–9). Tuning is accomplished via birefringent filters, which have resolutions of approximately 0.4 cm^{-1}.

The gas line and PA cell are evacuated to a pressure of 10^{-3} to 10^{-4} torr (1 torr = 133.32 Pa) for at least four hours prior to sample introduction to ensure complete dryness.

©2001 NRC Canada

Table 1. The methane transitions which were used to obtain the absolute intensities of the neopentane-d_0 pure local mode transitions.

Normal mode transition	Energy[a] (cm^{-1})	Oscillator strength[b,c]	Nearest neopentane-d_0 local mode transition[a]
$3\nu_1+\nu_3$	11 250	$(1.92 \pm 0.05) \times 10^{-9}$	$\|400\rangle \leftarrow \|000\rangle$
$4\nu_1+\nu_3$	13 750	$(3.47 \pm 0.03) \times 10^{-10}$	$\|500\rangle \leftarrow \|000\rangle$
$5\nu_1+\nu_3$	16 160	$(6.01 \pm 0.06) \times 10^{-11}$	$\|600\rangle \leftarrow \|000\rangle$
$5\nu_1+\nu_3+(\nu_2$ or $\nu_4)$	17 360	$(4.71 \pm 0.06) \times 10^{-12}$	$\|700\rangle \leftarrow \|000\rangle$

[a] From ref. 40. The four fundamental CH_4 vibrations are the $\nu_1 = 2914\ cm^{-1}$ symmetric stretch, the $\nu_3 = 3020\ cm^{-1}$ asymmetric stretch, and the $\nu_2 = 1526\ cm^{-1}$ and $\nu_4 = 1306\ cm^{-1}$ bending modes.
[b] The conversion factor from intensity (I) expressed in (km amagat cm)$^{-1}$ to dimensionless oscillator strength (f) is $f = I \times 4.204 \times 10^{-13}$ (km amagat cm) (60).
[c] The oscillator strength for the $3\nu_1 + \nu_3$ transition (40) has been divided by 1.4 to account for intensity ascribed to unresolved rovibrational transitions (vide infra).

Absolute Oscillator Strength via ICL-PAS

As noted above, ICL-PAS allows the determination of the relative absorbances of chromophores within a sample, but does not allow *direct* determination of absolute absorbances. In order to obtain absolute absorbances with ICL-PAS, Perry et al. (39) have used the published methane absorbances of Giver (40) to calibrate their PA cell. An intracavity configuration is extremely sensitive to the alignment of the PA cell within the laser cavity. Thus their determination of the oscillator strengths of various deuterated methanes was only approximate.

It would be preferable in an intracavity configuration to employ an internal standard to assuage the limitations imposed by the dependence of intracavity power levels on cell alignment.

Previous determinations of absolute oscillator strengths via ICL-PAS have been carried out by Gutow et al. (41), who determined the absolute absorbances of the $\Delta v_{CH} = 5, 6$ transitions of ethane and ethylene with reference to the published absorption strengths of HD (42). Wong and Moore (43) have used methane as an internal standard to determine the $\Delta v_{CH} = 6$ overtone transition intensities of numerous alkanes, alkenes, and haloalkanes. Manzanares et al. (8) have used methane and ethylene as internal standards to determine the intensities of the $\Delta v_{CH} = 5, 6$ overtones of $M(CH_3)_4$ where M = C, Si, Ge, and Sn.

The choice of methane as an internal standard in the determination of the $\Delta v_{CH} = 4$–7 overtone transition intensities of neopentane (38) is an appropriate one as both molecules have overtone transition energies which are disparate enough that they will not overlap significantly, yet these gases have CH overtone transition energies which are similar enough to allow their overtone transition to be recorded in one continuous scan.

In order to compare the PA intensities of neopentane and methane in an ICL-PAS experiment it is important that both gases be exposed to identical spectral intensities within the laser cavity. Unlike intracavity laser absorption spectroscopy (ICLAS) where some 10^4 modes are active (44), the presence of a birefringent filter in the ICL-PAS laser cavity (vide supra) restricts the number of active modes to approximately fifteen. With only a few closely spaced modes oscillating around the center of the gain line, variations in inversion (and therefore in intensity) will be smeared out owing to the presence of spatially shifted standing wave patterns of these modes (45) within the (homogeneous) laser. The intracavity spectral intensities of modes whose wavelengths correspond to methane rovibrational transitions will not be different from those of neopentane, which is a broad bandwidth absorber.

The tacit assumption which is made when methane is used as an internal standard for neopentane in a phase-sensitive photothermal technique, such as ICL-PAS, is that both gases have similar deactivation efficiencies. Since our phase-sensitive detection scheme locks onto only one signal, mismatched deactivation efficiencies could lead to the loss of signal intensity and subsequent erroneous results.

The deactivation efficiencies of neopentane and methane are expected to be different. Large molecules such as neopentane and benzene undergo rapid and complete intramolecular vibrational energy redistribution (IVR) and, thus, are expected to have efficient vibrational deactivations. On the other hand, small molecules such as methane and methane-d_3 undergo IVR on a much longer time scale and, therefore, should have lower deactivation efficiencies than neopentane. The criterion for being able to use methane as an internal standard for neopentane is that both gases have comparable deactivation efficiencies *on the time scale of our experiment*.

The effect of the different deactivation efficiencies of methane and neopentane on our ICL-PAS system was investigated using phase-sensitive detection. In our laboratory setup, phase-sensitive detection is achieved by referencing the microphone to the mechanical chopper via a lock-in amplifier. The phase angle at which the PA signal is collected can be varied from 0° to 360° in increments of 0.025° relative to the duty cycle of the mechanical chopper. The signal maxima arising from the two different gases will occur at the same phase angle if the deactivation efficiencies of neopentane and methane are equivalent on the time scale of our ICL-PAS experiment.

The ratio of methane and neopentane was chosen to give comparable absorbances by the two gases. The laser was tuned to the excitation frequency of a neopentane overtone maximum and the phase angle was determined for maximum absorption. Similarly, the phase angle at the methane overtone maximum was determined. It was found that the phase difference was less than 3 degrees at each overtone and, thus, any difference in the deactivation efficiencies of the two gases is a negligible source of error in our experiment.

The methane transitions that were used to determine the neopentane-d_0 overtone intensities are listed in Table 1. The

©2001 NRC Canada

Table 2. Scaling factors to convert the areas of methane overtone transitions obtained via deconvolution into integration areas similar to those of Giver.[a]

Δv_{CH}	Scaling factor
4	0.970
5	0.656
6	0.653
7	0.705

[a] See ref. 40

intensities of these transitions were taken from Giver (40). It is important to note that in Giver's work, the rovibrational structure of the methane $3\nu_1+\nu_3$ transition was not resolved. However, our ICL-PAS instrumentation does resolve this structure. The effect of the unresolved rovibrational structure in Giver's work increases the apparent intensity of the $3\nu_1+\nu_3$ transition by 30%. This increase was calculated through a comparison of our resolved spectrum and its associated area with the corresponding area where rotational lines were broadened to produce a spectrum similar in appearance to that of Giver (40). Therefore, we have revised the intensity for the $3\nu_1+\nu_3$ transition in methane in Table 1 by dividing it by a factor of 1.4 (vide infra).

Giver (40) determined the absorption intensities by using the absorption minima between adjacent bands to define the limits of the integration. He made no attempt to correct for the overlap of adjacent bands. Correction factors (see Table 2) had to be determined to enable us to relate the area determined through a deconvolution of a spectrum in our work to the area obtained by a minimum to minimum integration.

Theory and calculations

Local modes of vibration and the HCAO model

The XH stretching overtone spectra can be interpreted within the local mode model of molecular vibration (24, 25). Within this model the XH stretching potential is often described as a Morse potential. The energy eigenvalues of a Morse oscillator can be rearranged to give the frequency ($\tilde{\nu}$) (in cm^{-1}) of an overtone transition from the ground state $\upsilon' = \upsilon \leftarrow \upsilon'' = 0$ in the form (46)

$$[2] \qquad \tilde{\nu} = \upsilon\tilde{\omega} - (\upsilon^2 + \upsilon)\tilde{\omega}x$$

The values of the Morse parameters $\tilde{\omega}$ and $\tilde{\omega}x$ are obtained from a fit of eq. [2]. The eigenstates are obtained within the HCAO model (9, 13, 28–30) in terms of Morse oscillator wave functions with the assumption of harmonic coupling between the CH oscillators (28).

Overtone intensities

Experimental intensities are conveniently expressed in terms of the dimensionless oscillator strength (f) (47). By applying the ideal gas law and using the appropriate physical constants (48) we obtain an expression for f in the form

$$[3] \qquad f = 8.0267 \times 10^{-7}(\text{torr m cm})\frac{1}{p\,l}\int A(\tilde{\nu}_{eg})\mathrm{d}(\tilde{\nu}_{eg})$$

Table 3. Pure local mode transition peak properties of gaseous neopentane-d_0 as observed via ICL-PAS (Δv_{CH} = 4–9) and conventional absorption spectroscopy (Δv_{CH} = 3).

Δv_{CH}	Spectrometer/ laser	Gas pressure (torr)	Energy (cm^{-1})	FWHM (cm^{-1})[a]
3	Cary 5e	187.5	8 410	47
4	Ti:sapph (mw)	11.0 ± 0.3	10 979	58
5	Ti:sapph (sw)	10.0 ± 0.1	13 437	58
6	DCM dye	200.0 ± 0.5	15 755	100
7	Coumarin 6 dye	200.0 ± 0.4	17 966	149
8[b]	Coumarin 102 dye	≈ 450	20 035	170
9[c]	Stilbene 3 dye	≈ 850	21 987	182

[a] The full width at half-maximum of the central peak from the deconvolution.
[b] The spectrum was obtained by coadding two spectra.
[c] The spectrum was obtained by coadding six spectra.

where p is the gas pressure expressed in torr (1 torr = 133.32 Pa), l is the path length expressed in meters, and $A(\tilde{\nu}_{eg})$ is the absorbance as a function of frequency in wavenumbers (cm^{-1}), all at 298 K.

The intensity of a vibrational overtone transition can be calculated from HCAO wave functions and a suitable dipole moment function (DMF). The coupling between the methyl CH oscillators is treated within the HCAO model as pairwise interactions between the i^{th} and j^{th} internal displacement coordinates, which are q_i along CH_i and q_j along CH_j, respectively. Ab initio calculations have been used (31–33, 49, 50) to obtain discrete values for the dipole moment as a function of q_i and q_j. In the present paper, the values of the dipole moment were calculated as the bonds q_1 and q_2 were stretched or compressed about the equilibrium XH bond length r_e by ±30 pm in increments of 10 pm with all other molecular coordinates constant at their equilibrium values. The continuous DMF of two coupled XH oscillators is approximated by a fourth order Taylor series expansion along their internal stretch coordinates q_1 and q_2

$$[4] \qquad \boldsymbol{\mu}(q_1, q_2) = \sum_{i,j=1}^{i+j=4} \boldsymbol{\mu}_{ij} q_1^i q_2^j$$

where $\boldsymbol{\mu}_{ij}$ are the DMF derivatives

$$[5] \qquad \boldsymbol{\mu}_{ij} = \frac{1}{i!j!}\frac{\partial^{i+j}\boldsymbol{\mu}}{\partial q_1^i \partial q_2^j}$$

which were obtained by fitting an interpolating polynomial of degree $n-1$ to n ab inito values of the dipole moment. Terms up to fourth order were retained in eq. [4], including the pairwise mixed derivatives $\partial^2\boldsymbol{\mu}/\partial q_1^1 \partial q_2^1$, $\partial^3\boldsymbol{\mu}/\partial q_1^1 \partial q_2^2$, and $\partial^3\boldsymbol{\mu}/\partial q_1^2 \partial q_2^1$. It is especially important to include terms beyond linear as the second order derivatives $\partial^2\boldsymbol{\mu}/\partial q_1^2$ and $\partial^2\boldsymbol{\mu}/\partial q_2^2$ contribute significantly more intensity to overtone transitions than do the linear terms. As the methyl groups in neopentane and TMS are assumed to have local C_{3v} symmetry, the interactions of q_i or q_j with the remaining CH stretch coordinate q_k is generated by rotating the $\boldsymbol{\mu}(q_1, q_2)$ grid with a similarity transformation.

©2001 NRC Canada

Table 4. Pure local mode transition peak properties of gaseous TMS-d_0 as observed via ICL-PAS ($\Delta v_{CH} = 4$–8) and conventional absorption spectroscopy ($\Delta v_{CH} = 3$).

Δv_{CH}	Spectrometer	Pressure (torr)	Energy[a] (cm^{-1})	FWHM ([a,b])
3	Cary 5e	8.3 ± 1.5	8 426	41
4	Ti-sapph (mw)	11.8 ± 0.4	*10 898*	*54*
			11 013	32
5	Ti-sapph (sw)	15.6 ± 0.1	*13 434*	*32*
			13 506	46
6	DCM dye	70.2 ± 0.1	*15 769*	*39*
			15 819	43
7	Coumarin 6 dye	161.8 ± 0.1	18 014	36
8[c]	Coumarin 102 dye	≈450	20 134	36

Note: Fermi resonances are indicated by two sets of values.
[a]Italicized values are for $|\upsilon - 1, 0, 0\rangle + 2\upsilon_{bend}$.
[b]The full width at half-maximum of the central peak from the deconvolution.
[c]The spectrum was obtained by coadding two spectra.

With the appropriate physical constants (48), the oscillator strength of an overtone transition can be expressed as

$$[6] \qquad f = 4.70175 \times 10^{-7} (\text{cm D}^{-2}) \tilde{\nu}_{eg} |\boldsymbol{\mu_{eg}}|^2$$

where $\tilde{\nu}_{eg}$ is the transition frequency in wavenumbers (cm^{-1}), and $\boldsymbol{\mu_{eg}}$ is the transition dipole moment function in Debye

$$[7] \qquad \boldsymbol{\mu_{eg}} = \langle e|\boldsymbol{\mu}|g\rangle$$

where e and g are the excited and ground state wave functions, respectively, and $\boldsymbol{\mu}$ is the DMF.

Results and discussion

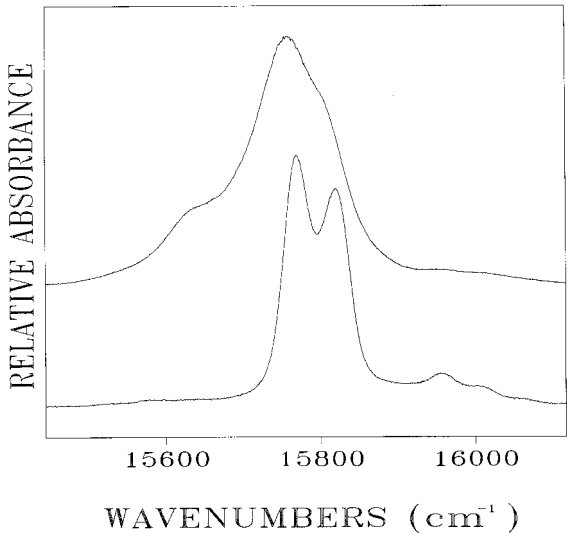
Experimental spectra

Experimental spectra were deconvoluted in SpectraCalc[2] with the least number of peaks required to reasonably reproduce the experimental spectrum. It was found that Lorentzian profiles led to the best deconvolutions for most of the overtone spectra. In cases where more than one Lorentzian was required to deconvolute a vibrational overtone transition, the dominant Lorentzian is chosen to represent the pure local mode transition. In cases where there exist two dominant Lorentzians (which have comparable intensities), the Lorentzian that is chosen to represent the pure local mode transition is the one that gives the most linear Birge–Sponer plot (vide infra). Summaries of the spectrometers (lasers), the sample pressures, the transition energies, and the FWHM values of neopentane-d_0 and TMS are given in Tables 3 and 4.

As we have noted, we have measured the spectra of neopentane-d_0, -d_6, and -d_9. The -d_6 and -d_9 spectra are similar to the -d_0 spectrum, although there are subtle differences that probably arise from coupling between CH stretching local modes and methyl torsion (51). In the present paper, we report local mode parameters and intensities for all three neopentanes. In a future publication we will compare the spectral structure in neopentane-d_0, -d_6, and -d_9.

[2]SpectraCalc is commercially available software from Galactic Industries Corporation.

Fig. 1. The ICL-PAS (DCM dye) $\Delta v_{CH} = 6$ regions of the vapour phase overtone spectra of neopentane (top) and TMS (bottom). Gas pressures were 200.0 and 70.2 torr (1 torr = 133.32 Pa), respectively, at room temperature.



A Fermi resonance (52, 53) is observed in TMS in the range $\Delta v_{CH} = 4$–6 (see Fig. 1). The $|\upsilon - 1, 0, 0\rangle|2\upsilon_b\rangle$ states (where υ_b refers to a CH bending mode) steal intensity from the unresolved $|\upsilon, 0, 0\rangle_{A_1E}$ transitions. Since the $|\upsilon - 1, 0, 0\rangle|2\upsilon_b\rangle$ states are nearly resonant with the $|\upsilon, 0, 0\rangle_{A_1E}$ pure local mode states, the former act as "doorway states" into the vibrational bath which facilitate IVR (11, 54, 55). The $|\upsilon - 1, 0, 0\rangle|2\upsilon_b\rangle$ states do not have any appreciable intrinsic intensity. At $\Delta v_{CH} = 6$ (see Fig. 1 and compare to Fig. 2) the nearly identical intensities of the resonant $|5, 0, 0\rangle|2\upsilon_b\rangle$ and $|6, 0, 0\rangle_{A_1E}$ states indicate a very strong coupling.

In order to measure the $\Delta v_{CH} = 8$ spectra of neopentane-d_0, -d_6, -d_9, and TMS, the dye Coumarin 102 was employed and two spectra were coadded. Gas pressures were approximately 450 torr (1 torr = 133.32 Pa). Asymmetries in the CH stretching overtone transitions of the neopentanes persist.

Poor signal to noise ratios coupled with the short life span of the Stilbene 3 dye made it impractical to study the $\Delta v_{CH} = 9$ transitions of the deuterated neopentanes. Only neopentane-d_0 was recorded in this region. Six spectra were coadded to produce the profile in Fig. 3.

The low intensities of these signals made the detection of neopentane-d_0 overtone transitions above $\Delta v_{CH} = 9$ unattainable.

Local mode parameters

Values of $\widetilde{\omega}$ and $\widetilde{\omega}x$ were obtained from both Birge–Sponer plots and from quadratic fits of the transition energy vs. υ (eq. [2]) for vapour phase neopentane-d_0, -d_6, -d_9, and TMS. Birge–Sponer plots tend to underemphasize the contributions of higher overtone transitions, however, the results obtained via

©2001 NRC Canada

Table 5. Local mode parameters (cm^{-1}) obtained from quadratic fits of the transition energy vs. υ using data in the range $\Delta v_{CH} = 3$–9 for neopentane-d_0, and data in the range $\Delta v_{CH} = 4$–8 for -d_6, -d_9, and TMS.

	Present work		Literature	
	$\widetilde{\omega}$	$\widetilde{\omega}x$	$\widetilde{\omega}$	$\widetilde{\omega}x$
neopentane-d_0	3049 ± 2	60.6 ± 0.3	3038 ± 5[a] 3031[b]	58.7 ± 1.2[a] 57.6[b]
neopentane-d_6	3042 ± 4	59.8 ± 0.6	3040 ± 2[a]	59.1 ± 0.4[a]
neopentane-d_9	3048 ± 5	60.4 ± 0.8	3040.59 ± 0.04[a]	59.07 ± 0.01[a]
TMS	3043 ± 1[c]	58.7 ± 0.2[c]	3049.6[b]	59.4[b]

[a]Taken from (11) where data in the range $\Delta v_{CH} = 2$–5 were used.
[b]Taken from (8) where data in the range $\Delta v_{CH} = 2$–7 were used.
[c]TMS analysis accounts for Fermi resonance at $\Delta v_{CH} = 4$–6.

Fig. 2. The ICL-PAS (Coumarin 6 dye) $\Delta v_{CH} = 7$ regions of the vapour phase overtone spectra of neopentane (top) and TMS (bottom). Gas pressures were 200.0 and 161.8 torr (1 torr = 133.32 Pa), respectively, at room temperature.

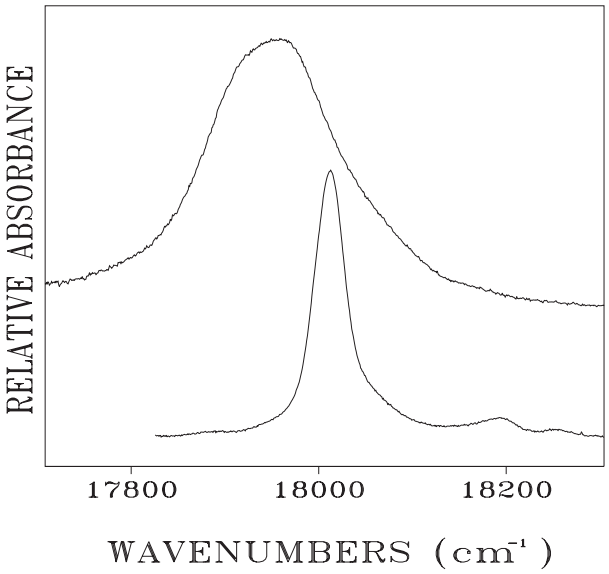
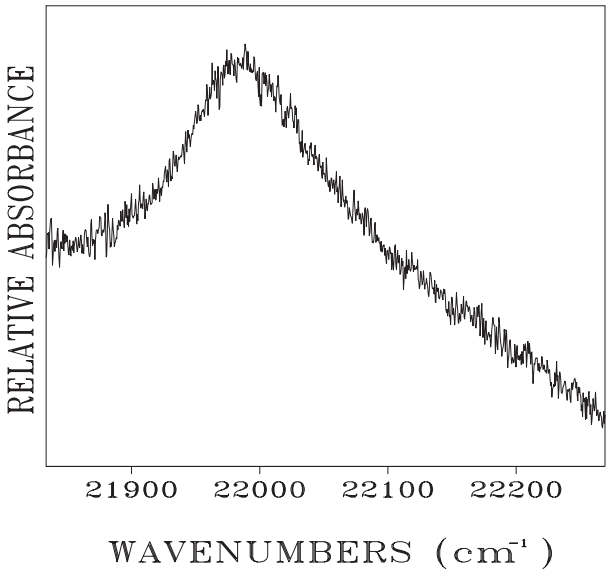


Fig. 3. The ICL-PAS (Stilbene 3 dye) $\Delta v_{CH} = 9$ regions of the vapour phase overtone spectra of neopentane. The spectral region is the sum of six coadded spectra. Gas pressures were approximately 850 torr (1 torr = 133.32 Pa) at room temperature.



both methods are the same within experimental error. Birge–Sponer plots of TMS and the neopentanes were linear, which indicates that in the higher energy regimes ($\Delta v_{CH} \geq 3$) the CH stretching vibrations of the neopentanes and TMS are well described as uncoupled anharmonic Morse oscillators. Those values of $\widetilde{\omega}$ and $\widetilde{\omega}x$ determined via a quadratic fit are compared to literature values in Table 5. Accurate values of local mode frequency ($\widetilde{\omega}$) and anharmonicity ($\widetilde{\omega}x$) have been obtained. Contrary to previous work (7, 8), the $\widetilde{\omega}$ value of TMS was found to be slightly lower than that of neopentane-d_0. The magnitude of the anharmonicity of neopentane-d_0 was found to be larger than that of TMS, in agreement with previously published data (7, 8). The anharmonicities of the neopentanes are identical within experimental error.

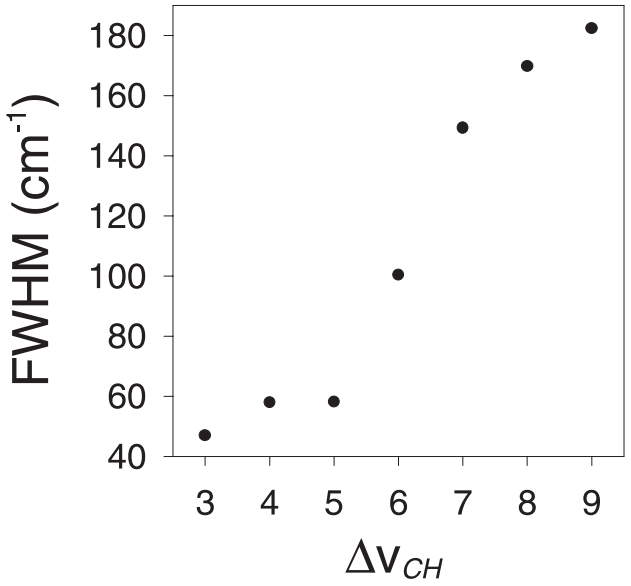
Full width at half-maximum

In agreement with previous work (7), we found that the FWHM values of neopentane are larger than those of TMS. A monotonic increase in the FWHM values of the pure local mode transitions of neopentane-d_0 with increasing excitation can be seen in Table 3 and in Fig. 4. Of particular interest is the fact that the most pronounced increases in the FWHM values of neopentane-d_0 occur in going from $\Delta v_{CH} = 5$ to $\Delta v_{CH} = 6$ and from $\Delta v_{CH} = 6$ to $\Delta v_{CH} = 7$.

The assumption, which is implicit in the interpretation of the overtone spectra of neopentane-d_0 and TMS, is that we are observing a central CH local mode excitation, i. e., we are not simply observing the excitation of several molecular eigenstates which correspond to a global excitation of the molecule. It is assumed that these pure CH local modes are the only "bright" states. To justify our assumption that we are observing bright CH stretching local mode overtones, we refer to the three principles that Sage and Jortner (23) have used to support the concept of XH stretching local modes. The first of these principles is *energetics*; a Morse oscillator adequately describes the $\Delta v_{CH} =$ 2–6 region of aromatic and aliphatic hydrocarbons (56, 57). In

©2001 NRC Canada

Fig. 4. The full-width at half maximum of the pure local mode transitions of neopentane as a function of the number of vibrational quanta.



the present paper we find that a Morse oscillator adequately describes the $\Delta v_{CH} = 3$–9 region of neopentane-d_0 and the $\Delta v_{CH} = 3$–8 regions of neopentane-d_6, -d_9, and TMS. The second principle is that of *relative intensities* in which the intensity of the $\Delta v_{CH} = 6$ CH overtone of C_6H_6 is roughly six times that of C_6D_5H (57). Again, in the present paper it was found that the overtone intensity of neopentane-d_0 is approximately twice that of neopentane-d_6 and four times that of neopentane-d_9 at each overtone. The final principle is *absolute intensities*. The intensity of higher CH vibrational overtones can be approximated by additively equal contributions from all local CH bond modes (17, 51). Our intensity calculations successfully account for the observed absolute intensities (vide infra) and are based on additivity.

Observed overtone transition intensities

Dimensionless oscillator strengths for neopentane-d_0, -d_6, -d_9, and TMS (see Table 6 and Fig. 5) were obtained from spectra that were measured with a conventional Cary 5e spectrometer over the energy ranges indicated in Table 6. Within the Born–Oppenheimer approximation, the intensities of neopentane-d_0, -d_6, and -d_9 are expected to be proportional to the number of CH oscillators in the sample if there are no large changes in the transition frequency $\tilde{\nu}_{eg}$ or in the transition dipole moment function $\boldsymbol{\mu}_{eg}$ (see eq. [6]). The oscillator strength of neopentane-d_0 at any given overtone is twice that of neopentane-d_6 within 5%, reflecting the relative number of CH oscillators in the two molecules. A similar relationship is observed between the oscillator strengths of neopentane-d_0 and neopentane-d_9, where the former is four times more intense than the latter to within 2%. The oscillator strengths of TMS at various overtones were found to be approximately 70% larger than for the corresponding overtones of neopentane-d_0 owing primarily to much larger fourth order derivatives in the DMF, $\boldsymbol{\mu}_{40}$ and $\boldsymbol{\mu}_{04}$ (see eq. [5]).

Fig. 5. The negative logarithms of the absolute oscillator strengths of various overtone transitions in neopentane obtained with a Cary 5e conventional absorbance spectrometer or with ICL-PAS using methane as an internal standard. The gas pressures and temperatures for the conventional absorbance spectrometer are given in Table 6.

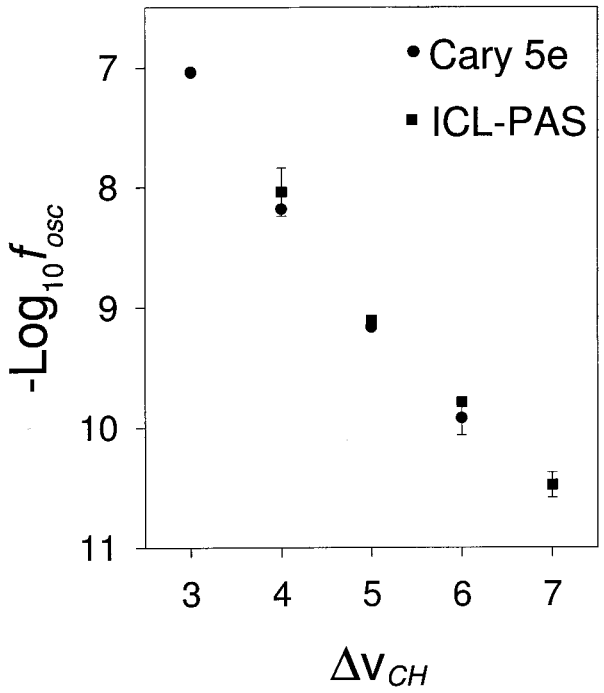
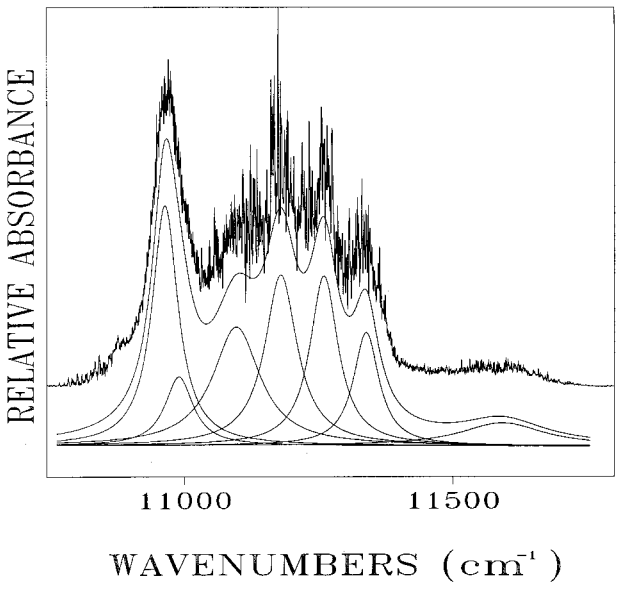


Fig. 6. The Ti:sapph (mw) ICL-PAS $\Delta v_{CH} = 4$ region of the overtone spectrum of a mixture of neopentane and methane. The experimental spectrum (top) has been vertically offset for clarity. The individual Lorentzian functions and the linear base line fit to the experimental spectrum are also shown. The sum of these two curves is also included. The χ^2 value for the fit was 6.062×10^{-8}.



©2001 NRC Canada

Table 6. The oscillator strengths of neopentane-d_0, neopentane-d_6, neopentane-d_9, and TMS obtained with a Cary 5e conventional absorption spectrometer.

	Local mode transition	Pressure (torr (1 torr = 133.32 Pa))	Temperature (°C)	Oscillator strength[a,b]
Neopentane-d_0	$\|200\rangle \leftarrow \|000\rangle$	188	23.5	$(3.9 \pm 0.8) \times 10^{-7}$
	$\|300\rangle \leftarrow \|000\rangle$	188	23.5	$(9.2 \pm 0.9) \times 10^{-8}$
	$\|400\rangle \leftarrow \|000\rangle$	126	22.1	$(6.5 \pm 0.7) \times 10^{-9}$
	$\|500\rangle \leftarrow \|000\rangle$	188	23.8	$(6.8 \pm 1.4) \times 10^{-10}$
	$\|600\rangle \leftarrow \|000\rangle$	525	22.4	$(1.2 \pm 0.4) \times 10^{-10}$
Neopentane-d_6	$\|300\rangle \leftarrow \|000\rangle$	215	21.7	$(4.7 \pm 0.5) \times 10^{-8}$
	$\|400\rangle \leftarrow \|000\rangle$	215	21.6	$(3.4 \pm 0.3) \times 10^{-9}$
	$\|500\rangle \leftarrow \|000\rangle$	215	21.7	$(3.4 \pm 0.7) \times 10^{-10}$
Neopentane-d_9	$\|300\rangle \leftarrow \|000\rangle$	48	21.5	$(2.4 \pm 0.2) \times 10^{-8}$
	$\|400\rangle \leftarrow \|000\rangle$	48	21.5	$(1.7 \pm 0.3) \times 10^{-9}$
TMS	$\|300\rangle \leftarrow \|000\rangle$	8.3	22.5	$(1.4 \pm 0.3) \times 10^{-7}$
	$\|400\rangle \leftarrow \|000\rangle$	8.3	21.8	$(1.4 \pm 0.3) \times 10^{-8}$
	$\|500\rangle \leftarrow \|000\rangle$	8.3	21.9	$(1.4 \pm 0.3) \times 10^{-9}$

[a]Measured intensity of the total band (see text).

[a]Errors represent a "worst case" estimated uncertainty in our deconvolution areas of 20%.

The $\Delta v_{CH} = 4$ region of the ICL-PAS spectrum of a mixture of methane and neopentane-d_0 was obtained with a Ti:sapph laser equipped with mid wave (mw) optics and is presented in Fig. 6. The methane $3\nu_1 + \nu_3$ transition required four Lorentzians while the unresolved neopentane $|400\rangle_{A_1E}$ transitions were approximated by two Lorentzians. The spikes on the neopentane transition correspond well to known water vapour lines while the most intense spikes on the methane transition do not. The methane structure has been attributed to congested rovibrational transitions by Perry et al. (39). The intracavity power levels (which are recorded simultaneously with the PA signal) varied smoothly and showed no evidence of the selective absorption of intensity from modes whose frequencies correspond with methane rovibrational transitions.

The intensity of the unresolved neopentane-d_0 $|400\rangle_{A_1E}$ transitions relative to the methane transition is obtained by dividing the sum of the areas of its deconvoluted peaks by the sum of the areas of the methane deconvoluted peaks. The absolute oscillator strength of the neopentane-d_0 $|400\rangle_{A_1E}$ transitions (see Table 7) was then obtained by factoring in the pressures of the two gases, as well as the known oscillator strength of methane and the scaling factor (which relates Giver's (40) integrated areas to our deconvolution areas, vide supra) for the methane $3\nu_1 + \nu_3$ transition. As we have noted, we have revised Giver's $3\nu_1 + \nu_3$ intensity (see Table 1) by a factor of 1.4 to account for the comparison between resolved and unresolved rotational structure (vide supra). The uncertainty introduced in revising Giver's $3\nu_1+\nu_3$ intensity makes our ICL-PAS value for $\Delta v_{CH} = 4$ more uncertain than the corresponding values for $\Delta v_{CH} = 5$ and 6. In addition to this error, the propagation of experimental errors was approximated by assuming an error in the area of each constituent Lorentzian to be 10%. Other sources of experimental error such as pressure gauge fluctuations were taken into account and found to be negligible.

A Ti:sapph laser equipped with short wave (sw) optics was used to obtain the ICL-PAS spectrum of a mixture of neopentane-d_0 and methane in the $\Delta v_{CH} = 5$ region. Figure 7 shows the rich structure of the methane transition, which is attributed to congested rovibrational transitions. The $4\nu_1 + \nu_3$ transition of methane is deconvoluted as a single Lorentzian while the unresolved $|500\rangle_{A_1E}$ transitions in neopentane-d_0 require four Lorentzians. The combined absolute oscillator strength of neopentane-d_0 in this region is given in Table 7. It was obtained from the pressures and the relative absorbances of the two gases, the known oscillator strength of the methane $4\nu_1+\nu_3$ transition, and the associated scaling factor (vide supra) for this transition. As at $\Delta v_{CH} = 4$, the intracavity power levels varied smoothly and showed no evidence of the selective mode absorption (vide supra).

The absolute oscillator strength of the unresolved $|600\rangle_{A_1E}$ transitions in neopentane-d_0 were arrived at by comparison to the methane $5\nu_1 + \nu_3$ transition. The $\Delta v_{CH} = 6$ region was obtained with a DCM dye laser and is shown, along with its deconvolution, in Fig. 8. Congested rovibrational transitions are again observed in methane. The combined absolute oscillator strength of the neopentane-d_0 $|600\rangle_{A_1E}$ transitions is given in Table 7. This value was obtained in a manner identical to that for the $|500\rangle_{A_1E}$ transitions (vide supra).

The unresolved neopentane $|700\rangle_{A_1E}$ transitions and the $5\nu_1+\nu_3 + (\nu_2$ or $\nu_4)$ transitions of methane were observed with a Rhodamine 110 dye laser and are presented in Fig. 9. Some of the methane structure is caused by congested rovibrational transitions, however, traces of water vapour are also present and absorb in this range. The methane transition is deconvoluted as a single Lorentzian. The combined absolute oscillator strength of the neopentane-d_0 $|700\rangle_{A_1E}$ transitions was obtained in a manner identical to that for the $|500\rangle_{A_1E}$ transitions (vide supra) and is given in Table 7.

The absolute oscillator strengths of neopentane-d_0 which were obtained from ICL-PAS are compared with those from a conventional spectrometer in Table 7. These values are represented graphically in Fig. 5. Aside from the problem at $\Delta v_{CH} = 4$ with the PA value, the most significant source of experimental uncertainty in the oscillator strengths is in the deconvoluted

©2001 NRC Canada

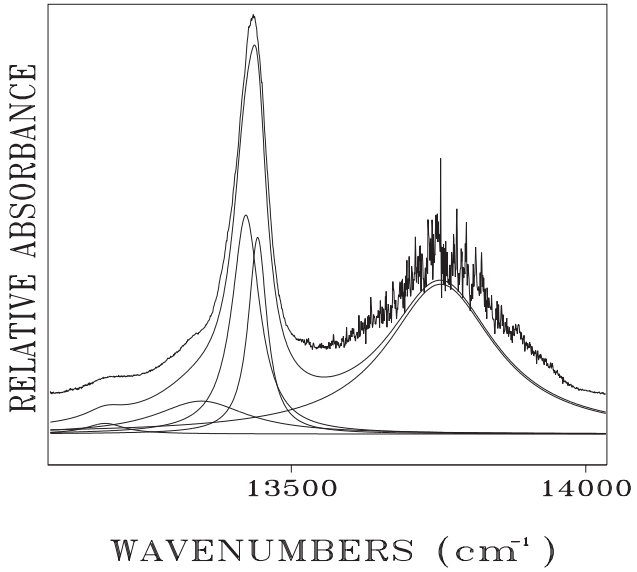
Table 7. A comparison of the oscillator strengths of neopentane-d_0 from a Cary 5e conventional absorbance spectrometer with those from ICL-PAS with methane as an internal standard

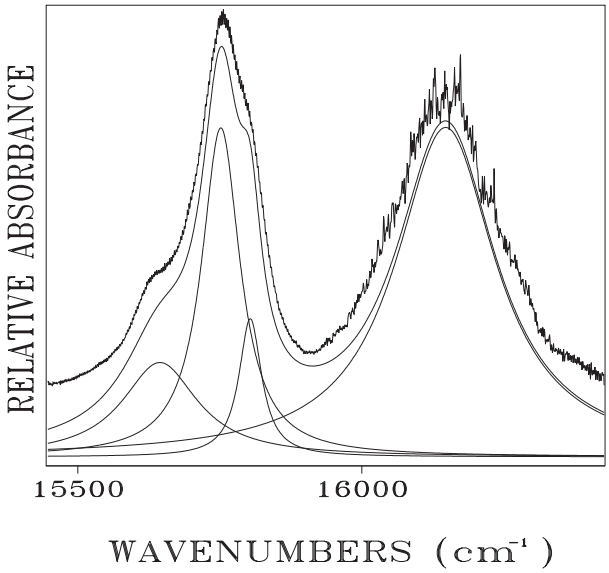
		Oscillator strength		
Δv_{CH}	Laser	ICL-PAS	Literature ICL-PAS	Cary 5e
3	—	—	—	$(9.2 \pm 0.9) \times 10^{-8}$
4	Ti:sapph (mw)	$(9.8 \pm 3.3) \times 10^{-9}$	—	$(6.5 \pm 0.7) \times 10^{-9}$
5	Ti:sapph (sw)	$(7.1 \pm 2.2) \times 10^{-10}$	4.19×10^{-11}[a,b]	$(6.8 \pm 1.4) \times 10^{-10}$
6	Dye (DCM)	$(1.6 \pm 0.5) \times 10^{-10}$	4.63×10^{-12}[a,b]	$(1.2 \pm 0.4) \times 10^{-10}$
7	Dye (R110)	$(3.4 \pm 1.0) \times 10^{-11}$	—	—

[a]Taken from ref. 8.
[b]The conversion factor from absorption cross section, $\sigma(\tilde{\nu})$, expressed in (cm^2 $molecule^{-1}$) to dimensionless oscillator strength (f) is $f = \sigma(\tilde{\nu}) \times 1.1296 \times 10^{12}$ (cm^{-2} molecule) (62).

Fig. 7. The Ti:sapph (sw) ICL-PAS $\Delta v_{CH} = 5$ region of the overtone spectrum of a mixture of neopentane and methane. The experimental spectrum (top) has been vertically offset for clarity. The individual Lorentzian functions and the linear base line fit to the experimental spectrum are also shown, as well as their sum. The χ^2 value for the fit was 2.437×10^{-9}.

Fig. 8. The ICL-PAS (DCM dye) $\Delta v_{CH} = 6$ region of the overtone spectrum of a mixture of neopentane and methane. The experimental spectrum (top) has been vertically offset for clarity. The individual Lorentzian functions and the linear base line fit to the experimental spectrum are also shown, as well as their sum. The χ^2 value for the fit was 7.432×10^{-9}.





peak areas. In the region of the spectrum where the two techniques overlap, i. e., $\Delta v_{CH} = 4$–6, we observe good agreement to within experimental error. This agreement establishes the reliability of the photoacoustic intensity measurements. Moreover, it supports the use of correction factors for the internal standard.

Calculated overtone transition intensities

Previous work (58–60) has shown that electron correlation in the DMF does not play an important role in determining overtone transition intensities for most molecules. We found the same result in this work. Overtone transition intensities that used HCAO vibrational wave functions and ab inito DMFs from dipole moments calculated with levels of theory, which included electron correlation (i. e., MP2, QCISD, etc.), showed no improvement over intensities from DMFs at the Hartree–Fock level. However, unlike the general trend observed in our previous work (58, 59), calculated intensities of neopentane-d_0 did not asymptotically approach experimentally determined overtone intensities from above with the use of progressively larger basis sets. Kjaergaard et al. (59) had previously observed that increasing the basis set size did not always lead to improved agreement between calculated and observed overtone intensities in the case of methane. They postulated that the HCAO model may not adequately describe all the significant coupling modes of methane. The same situation is likely to be true for the neopentanes.

We carried out calculations for a number of ab inito DMFs which combined different levels of theory and basis set size (38) using Gaussian 98 (61). DMFs calculated at both HF and MP2 levels of theory with basis sets which varied in size from 6-31G to 6-311++G(2d,2p) all led to intensities which were in reason-

©2001 NRC Canada

Table 8. Calculated and experimental overtone oscillator strengths of neopentane-d_0.

State	$f\left(\frac{HF}{6-311++G(d,p)}\right)$	f (Experimental)[a]
$\|100\rangle A_1 + E$	1.21×10^{-4}	—
$\|200\rangle A_1 + E$	1.39×10^{-7}	—
$\|110\rangle A_1 + E$	4.65×10^{-7}	—
$\Delta v_{CH} = 2$ total	6.04×10^{-7}	—
$\|300\rangle A_1 + E$	6.58×10^{-8}	—
$\|210\rangle A_1 + 2E + A_2$	1.79×10^{-8}	—
$\Delta v_{CH} = 3$ total	8.38×10^{-8}	$(9.2 \pm 0.9) \times 10^{-8}$
$\|400\rangle A_1 + E$	8.36×10^{-9}	—
$\|310\rangle A_1 + 2E + A_2$	9.97×10^{-10}	—
$\Delta v_{CH} = 4$ total	9.38×10^{-9}	$(6.5 \pm 0.7) \times 10^{-9}$
$\|500\rangle A_1 + E$	1.09×10^{-9}	—
$\|410\rangle A_1 + 2E + A_2$	7.75×10^{-11}	—
$\Delta v_{CH} = 5$ total	1.17×10^{-9}	$(7.1 \pm 2.2) \times 10^{-10}$
$\|600\rangle A_1 + E$	1.62×10^{-10}	—
$\|510\rangle A_1 + 2E + A_2$	7.76×10^{-12}	—
$\Delta v_{CH} = 6$ total	1.70×10^{-10}	$(1.6 \pm 0.5) \times 10^{-10}$
$\|700\rangle A_1 + E$	2.80×10^{-11}	—
$\|610\rangle A_1 + 2E + A_2$	9.68×10^{-13}	—
$\Delta v_{CH} = 7$ total	2.90×10^{-11}	$(3.4 \pm 1.0) \times 10^{-11}$
$\|800\rangle A_1 + E$	5.53×10^{-12}	—
$\|710\rangle A_1 + 2E + A_2$	1.46×10^{-13}	—
$\Delta v_{CH} = 8$ total	5.68×10^{-12}	—
$\|900\rangle A_1 + E$	1.24×10^{-12}	—
$\|810\rangle A_1 + 2E + A_2$	2.57×10^{-14}	—
$\Delta v_{CH} = 9$ total	1.26×10^{-12}	—

[a]Values at $\Delta v_{CH} = 3$–4 are from a Cary 5e conventional absorbance spectrometer while values at $\Delta v_{CH} = 5$–7 are from ICL-PAS with methane as an internal standard.

ably good agreement with experimental neopentane-d_0 intensities in the energy range $\Delta v_{CH} = 3$–7. In order of decreasing correspondence, the best agreements between calculated and experimental neopentane-d_0 intensities in this energy range were realized with DMFs calculated from the following combinations of theory and basis set (see Table 8 and Fig. 10):

HF / 6-311++G(d,p) > HF / 6-311+G(d,p) >

HF / 6-311++G(2d,2p) ≈ MP2 / 6-31G(d,p)

The oscillator strengths of TMS were calculated in a similar manner and these values are compared to experimental intensities in Table 9 and Fig. 11. Once again, the same basis sets at both HF and MP2 levels of theory led to DMFs which gave reasonably good agreement with experimental TMS intensities in the energy range $\Delta v_{CH} = 3$–5.

In decreasing order, the best agreement between calculated and experimental TMS intensities in this energy range were realized with DMFs calculated from the following combinations of theory and basis set:

Fig. 9. The ICL-PAS (R110 dye) $\Delta v_{CH} = 7$ region of the overtone spectrum of a mixture of neopentane and methane. The experimental spectrum (top) has been vertically offset for clarity. The individual Lorentzian functions and the linear base line fit to the experimental spectrum are also shown. The sum of these two curves is also included. The χ^2 value for the fit was 3.181×10^{-10}.

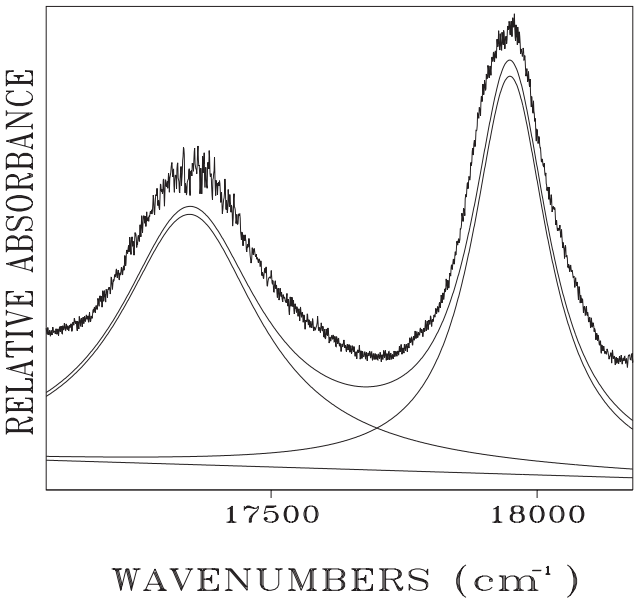
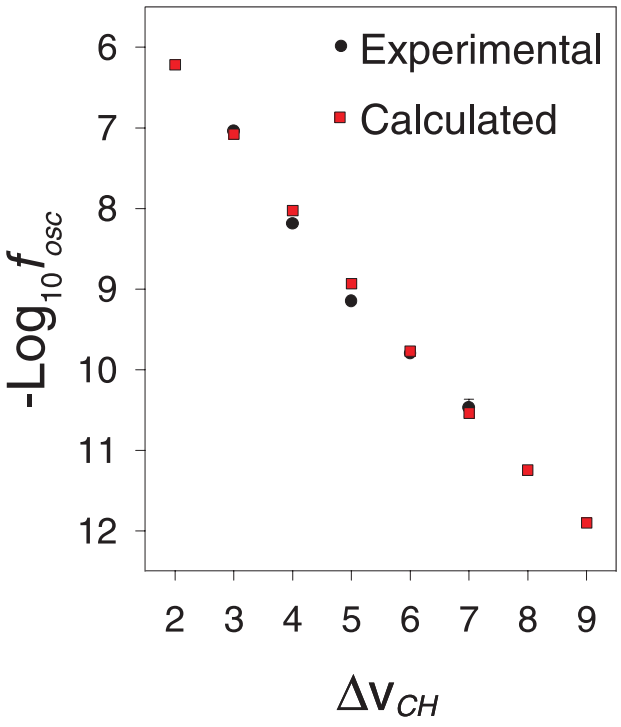
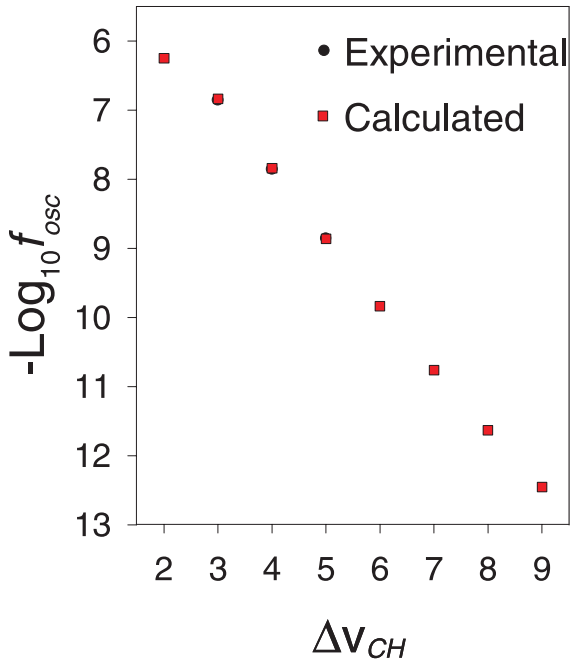


Fig. 10. The negative logarithm of experimental and calculated (HF / 6-311++G(d,p)) oscillator strengths of overtone transitions in neopentane.



©2001 NRC Canada

Fig. 11. The negative logarithm of experimental and calculated (HF / 6-31G(d,p)) oscillator strengths of overtone transitions in TMS.



HF / 6-31G(d,p) > HF / 6-31G ≈ MP2 / 6-31G > MP2 / 6-31G(d,p)

In particular, those levels of theory and basis set which worked well to predict the overtone intensities of neopentane-d_0 also gave good results in TMS.

Conclusions

The vibrational overtone spectrum of gas phase neopentane-d_0 was studied in the energy range 8 400 cm^{-1} ($\Delta v_{CH} = 3$) to 22 000 cm^{-1} ($\Delta v_{CH} = 9$), while the overtone spectra of gas phase neopentane-d_6, -d_9, and vapour phase TMS were studied in the energy range of 8 400 cm^{-1} ($\Delta v_{CH} = 3$) to 20 100 cm^{-1} ($\Delta v_{CH} = 8$). Conventional absorbance spectroscopy was used to access the lower energy overtones ($3 \leq \Delta v_{CH} \leq 6$) while ICL-PAS techniques were used in the higher energy regions ($4 \leq \Delta v_{CH} \leq 9$). Birge–Sponer plots for TMS and the neopentanes were linear across this energy range which indicates that the vibrational CH stretching overtones of the neopentanes and TMS are well described as uncoupled Morse oscillators. A splitting which arises from Fermi resonance was observed in the TMS spectra in the range $\Delta v_{CH} = 3$–6. Asymmetries have been observed in the spectra of neopentane at $\Delta v_{CH} = 4$–8 which indicate a coupling of the unresolved $|\upsilon 00\rangle_{A_1E}$ states to methyl torsion.

ICL-PAS spectroscopy was used with methane as an internal standard to obtain the absolute absorbance intensities of neopentane-d_0 in the energy range $\Delta v_{CH} = 4$–7. Good agreement was realized between these intensities and those obtained via conventional absorbance spectroscopy in the region of $\Delta v_{CH} = 4$–6. This is a useful result since very weak high-energy overtone transitions can only be observed by intracavity laser techniques.

Table 9. Calculated and experimental overtone oscillator strengths of TMS.

State	$f\left(\frac{HF}{6-311++G(d,p)}\right)$	f (Experimental)[a]
$\|100\rangle A_1 + E$	8.10×10^{-5}	—
$\|200\rangle A_1 + E$	3.36×10^{-7}	—
$\|110\rangle A_1 + E$	2.29×10^{-7}	—
$\Delta v_{CH} = 2$ total	5.65×10^{-7}	—
$\|300\rangle A_1 + E$	1.32×10^{-7}	—
$\|210\rangle A_1 + 2E + A_2$	1.40×10^{-8}	—
$\Delta v_{CH} = 3$ total	1.46×10^{-7}	$(1.4 \pm 0.3) \times 10^{-7}$
$\|400\rangle A_1 + E$	1.37×10^{-8}	—
$\|310\rangle A_1 + 2E + A_2$	7.32×10^{-10}	—
$\Delta v_{CH} = 4$ total	1.44×10^{-8}	$(1.4 \pm 0.3) \times 10^{-8}$
$\|500\rangle A_1 + E$	1.33×10^{-9}	—
$\|410\rangle A_1 + 2E + A_2$	4.96×10^{-11}	—
$\Delta v_{CH} = 5$ total	1.38×10^{-9}	$(1.4 \pm 0.3) \times 10^{-9}$
$\|600\rangle A_1 + E$	1.41×10^{-10}	—
$\|510\rangle A_1 + 2E + A_2$	4.23×10^{-12}	—
$\Delta v_{CH} = 6$ total	1.46×10^{-10}	—
$\|700\rangle A_1 + E$	1.69×10^{-11}	—
$\|610\rangle A_1 + 2E + A_2$	4.46×10^{-13}	—
$\Delta v_{CH} = 7$ total	1.73×10^{-11}	—
$\|800\rangle A_1 + E$	2.28×10^{-12}	—
$\|710\rangle A_1 + 2E + A_2$	5.69×10^{-14}	—
$\Delta v_{CH} = 8$ total	2.33×10^{-12}	—
$\|900\rangle A_1 + E$	3.43×10^{-13}	—
$\|810\rangle A_1 + 2E + A_2$	8.56×10^{-15}	—
$\Delta v_{CH} = 9$ total	3.52×10^{-13}	—

[a]Values at $\Delta v_{CH} = 3$–5 are from a Cary 5e conventional absorbance spectrometer.

The absolute overtone intensities of neopentane-d_0 and TMS were accurately predicted by calculations which used the HCAO model and the experimental parameters $\widetilde{\omega}$, $\widetilde{\omega}x$, and γ' to obtain the vibrational wave functions, and ab inito calculations to obtain the DMFs. In the case of neopentane-d_0, the combination of theory and basis set, which gave a DMF that led to the best agreement between observed and calculated overtone intensities in the energy range $\Delta v_{CH} = 3$–7, was HF / 6-311++G(d,p). The best agreement for TMS was achieved with an ab inito DMF calculated at the HF / 6-31G(d,p) level. However, all calculations led to satisfactory agreement with the absolute experimental intensities, despite the fact that the only parameters in the theory were obtained directly from the overtone transition energies.

Acknowledgments

We are grateful to Dr. Richard Smith at McMaster University for the gas chromatograph – mass spectrometer purity analysis

©2001 NRC Canada

of neopentane-d_0. We are also grateful to the Natural Sciences and Engineering Council of Canada for financial support.

References

1. B.R. Henry and M.A. Mohammadi. Chem. Phys. **55**, 385 (1981).
2. B.R. Henry. Acc. Chem. Res. **20**, 429 (1987).
3. B.R. Henry, K.M. Gough, and M.G. Sowa. Int. Rev. Phys. Chem. **5**, 133 (1986).
4. B.R. Henry and D.J. Swanton. J. Mol. Struct. **202**, 193 (1989).
5. H.G. Kjaergaard, R.J. Proos, D.M. Turnbull, and B.R. Henry. J. Phys. Chem. **100**, 19273 (1996).
6. R.L. Swofford, M.E. Long, and A.C. Albrecht. J. Chem. Phys. **65**, 179 (1976).
7. B.R. Henry, M.A. Mohammadi, I. Hanazaki, and R. Nakagaki. J. Phys. Chem. **87**, 4827 (1983).
8. C.Manzanares I, N.L.S. Yamasaki, E. Weitz, and J.T. Knudtson. Chem. Phys. Lett. **117**, 477 (1985).
9. B.R. Henry and M.A. Mohammadi. Chem. Phys. Lett. **75**, 99 (1980).
10. A.W. Tarr and B.R. Henry. Chem. Phys. Lett. **112**, 295 (1984).
11. A.W. Tarr and B.R. Henry. J. Chem. Phys. **84**, 1355 (1986).
12. B.R. Henry and W.R.A. Greenlay. J. Chem. Phys. **72**, 5516 (1980).
13. B.R. Henry, A.W. Tarr, O.S. Mortensen, W.F. Murphy, and D.A.C. Compton. J. Chem. Phys. **79**, 2583 (1983).
14. D.C. McKean. J. Mol. Struct. **113**, 251 (1984).
15. C. Manzanares I. Chem. Phys. Lett. **207**, 159 (1993).
16. R.A. Bernheim, F.W. Lampe, J.F. O'Keefe, and J.R. Qualey III. J. Phys. Chem. **89**, 1087 (1985).
17. M.S. Burberry and A.C. Albrecht. J. Chem. Phys. **71**, 4631 (1979).
18. C.K.N. Patel and A.C. Tam. Chem. Phys. Lett. **62**, 511 (1979).
19. C.K.N. Patel, A.C. Tam, and R.J. Kerl. Nature (London) **286**, 368 (1980).
20. C. Manzanares I. Chem. Phys. Lett. **181**, 51 (1991).
21. C. Manzanares I, J. Peng, and V.M. Blunt. J. Phys. Chem. **96**, 6212 (1992).
22. M.L. Elert, P.R. Stannard, and W.M. Gelbart. J. Chem. Phys. **67**, 5395 (1977).
23. M.L. Sage and J. Jortner. Adv. Chem. Phys. **47**, 293 (1981).
24. R.J. Hayward and B.R. Henry. J. Mol. Spectrosc. **57**, 221 (1975).
25. B.R. Henry. Acc. Chem. Res. **10**, 207 (1977).
26. I.A. Watson, B.R. Henry, and I.G. Ross. Spectrochim. Acta A **37**, 857 (1981).
27. R. Mecke and R. Ziegler. Z. Phys. **101**, 405 (1936).
28. O.S. Mortensen, B.R. Henry, and M.A. Mohammadi. J. Chem. Phys. **75**, 4800 (1981).
29. M.S. Child and T.R. Lawton. Faraday Discuss. Chem. Soc. **71**, 273 (1981).
30. M.S. Child and L. Halonen. Adv. Chem. Phys. **57**, 1 (1984).
31. H.G. Kjaergaard. Ph.D. Thesis. Odense Univerity, Denmark, 1992.
32. O.S. Mortensen, M.K. Ahmed, B.R. Henry, and A.W. Tarr. J. Chem. Phys. **82**, 3903 (1985).
33. A.W. Tarr, D.J. Swanton, and B.R. Henry. J. Chem. Phys. **85**, 3463 (1986).
34. B.J. Schattka, D.M. Turnbull, H.G. Kjaergaard, and B.R. Henry. J. Phys. Chem. **99**, 6327 (1995).
35. B.I. Niefer, H.G. Kjaergaard, and B.R. Henry. J. Chem. Phys. **99**, 5682 (1993).
36. B.R. Henry and M.G. Sowa. Prog. Anal. Spectrosc. **12**, 349 (1989).
37. B.R. Henry, H.G. Kjaergaard, B. Neifer, B.J. Schattka, and D.M. Turnbull. Can. J. Appl. Spectrosc. **38**, 42 (1993).
38. M.W.P. Petryk. Master's Thesis. University of Guelph, Guelph, Ontario, Canada, 1998.
39. J.W. Perry, D.J. Moll, A. Kuppermann, and A.H. Zewail. J. Chem. Phys. **82**, 1195 (1985).
40. L.P. Giver. J. Quant. Spectrosc. Radiat. Transfer, **19**, 311 (1978).
41. J.H. Gutow, J. Davidsson, and R.N. Zare. Chem. Phys. Lett. **185**, 120 (1991).
42. J.T. Trauger and M.E. Mickelson. Icarus, **56**, 176 (1983).
43. J.S. Wong and B. Moore. J. Chem. Phys. **77**, 603 (1982).
44. D. Romanini. *In* Cavity-ringdown spectroscopy: An ultratrace-absorption measurement technique. *Edited by* K.W. Busch and M.A. Busch. American Chemical Society, Washington, DC, USA. 1999. p. 125.
45. O. Svelto. Principles of lasers. 4^{th} ed. Plenum Press, New York, USA. 1998.
46. B.R. Henry. *In* Vibrational spectra and structure. Vol. 10. *Edited by* J.R. Durig. Elsevier Scientific, Amsterdam. 1981. p. 269.
47. P.W. Atkins. Molecular quantum mechanics. 2^{nd} ed. Oxford University Press, Oxford. 1983.
48. E.R. Cohen and B.N. Taylor. J. Res. Natl. Bur. Stand. **92**, 85 (1987).
49. H.G. Kjaergaard, H. Yu, B.J. Schattka, B.R. Henry, and A.W. Tarr. J. Chem. Phys. **93**, 6239 (1990).
50. H.G. Kjaergaard, B.R. Henry, and A.W. Tarr. J. Chem. Phys. **94**, 5844 (1991).
51. M.S. Burberry, J.A. Morrell, A.C. Albrecht, and R.L. Swofford. J. Chem. Phys. **70**, 5522 (1979).
52. B.R. Henry and M.K. Ahmed. J. Phys. Chem. **90**, 1993 (1986).
53. M.G. Sowa, B.R. Henry, and Y. Mizugai. J. Phys. Chem. **97**, 809 (1993).
54. M.G. Sowa and B.R. Henry. J. Chem. Phys. **95**, 3040 (1991).
55. E.L. Sibert III, W.P. Reinhardt, and J.T. Hynes. J. Chem. Phys. **81**, 1115 (1984).
56. R.L. Swofford, M.E. Long, M.S. Burberry, and A.C. Albrecht. J. Chem. Phys. **66**, 664 (1977).
57. R.L. Swofford, M.S. Burberry, J.A. Morrell, and A.C. Albrecht. J. Chem. Phys. **66**, 5245 (1977).
58. H.G. Kjaergaard and B.R. Henry. Mol. Phys. **83**, 1099 (1994).
59. H.G. Kjaergaard, C.D. Daub, and B.R. Henry. Mol. Phys. **90**, 201 (1997).
60. C.D. Daub, B.R. Henry, M.L. Sage, and H.G. Kjaergaard. Can. J. Chem. **77**, 1775 (1999).
61. M.J. Frisch, G.W. Trucks, H.B. Schlegel, G.E. Scuseria, M.A. Robb, J.R. Cheeseman, V.G. Zakrzewski, J.A. Montgomery Jr, R.E. Stratmann, J.C. Burant, S. Dapprich, J.M. Millam, A.D. Daniels, K.N. Kudin, M.C. Strain, O. Farkas, J. Tomasi, V. Barone, M. Cossi, R. Cammi, B. Mennucci, C. Pomelli, C. Adamo, S. Clifford, J. Ochterski, G.A. Petersson, P.Y. Ayala, Q. Cui, K. Morokuma, D.K. Malick, A.D. Rabuck, K. Raghavachari, J.B. Foresman, J. Cioslowski, J.V. Ortiz, B.B. Stefanov, G. Liu, A. Liashenko, P. Piskorz, I. Komaromi, R. Gomperts, R.L. Martin, D.J. Fux, T. Keith, M.A. Al-Laham, C.Y. Peng, A. Nanayakkara, C. Gonzalez, M. Challacombe, P.M.W. Gill, B. Johnson, W. Chen, M.W. Wong, J.L. Andres, C. Gonzalez, M. Head-Gordon, E.S. Replogle, and J.A. Pople. Gaussian 98, Revision A.5. Gaussian Inc., Pittsburgh, PA. 1998.
62. W. Kauzmann. Quantum chemistry. Academic Press, New York. 1957.

©2001 NRC Canada

Synthesis of the diborylated ferrocene 1,1′-bis-(bis-pentafluorophenylboryl)ferrocene and the X-ray structure of its trimethylphosphine adduct

Bryon E. Carpenter, Warren E. Piers, and Robert McDonald

Abstract: The diborylated ferrocene compound 1,1′-Fc[B(C_6F_5)$_2$]$_2$ (**2**) was prepared via a transmetallation reaction involving 1,1′-Fc(HgCl)$_2$ and two equivalents of ClB(C_6F_5)$_2$. Although this reaction is very clean spectroscopically, isolated yields of **2** were never greater than 40% owing to the high solubility of the compound in non-donor solvents. Compound **2** is similar in its properties to the related monoborylated complex FcB(C_6F_5)$_2$ (**1**) reported previously, particularly the UV–vis spectrum, which exhibits an intense charge transfer absorption (λ_{max} = 233 nm, $\varepsilon = 1.64 \times 10^4$) assignable to an $Fe_{dz^2/dx^2-y^2} \rightarrow B_p$ transition. However, **2**, is significantly more Lewis acidic than **1**, reacting with weak donors such as acetonitrile at room temperature, and effecting methide abstraction from Cp_2ZrMe_2 under mild conditions. Complex **2** also forms a bis(trimethylphosphine) adduct (**3**), which was structurally characterized via X-ray crystallography.

Key words: organoboranes, ferrocene derivatives, multidentate Lewis acids.

Résumé : On a préparé le ferrocène diborylé 1,1′-Fc[B(C_6F_5)$_2$]$_2$, **2**, par une réaction de transmétallation impliquant le 1,1′-Fc(HgCl)$_2$ et deux équivalents de ClB(C_6F_5)$_2$. Même si d'un point de vue spectroscopique cette réaction est propre, les rendements en produit **2** isolé n'ont jamais dépassé 40% en raison de la grande solubilité du composé dans les solvants non donneurs. Les propriétés du composé **2** sont semblables à celles du complexe monoborylé apparenté, FcB(C_6F_5)$_2$ (**1**), dont on a rapporté la synthèse antérieurement, particulièrement le spectre UV–vis qui présente une absorption de transfert de charge intense (λ_{max} = 233 nm; $\varepsilon = 1{,}64 \times 10^4$) que l'on peut attribuer à une transition $Fe_{dz^2/dx^2-y^2} \rightarrow B_p$. Toutefois, **2** est beaucoup plus acide que **1**; il réagit à la température ambiante avec les donneurs faibles, tel l'acétonitrile, et il peut effectuer l'enlèvement d'un méthide à partir du Cp_2ZrMe_2 dans des conditions douces. Le complexe **2** forme aussi un adduit bis(tripméthylphosphine), **3**, dont on a caractérisé la structure par diffraction des rayons X.

Mots clés : organoboranes, dérivés du ferrocène, acides de Lewis multidentate.

Introduction

Borylated ferrocenes (1) and perfluoroaryl substituted boranes (2) are two important classes of boron compounds. The former group is of interest for probing fundamental bonding questions (3), and because they act as precursors to unique coordination (4) or covalent (5) ferrocene containing polymeric materials. The latter class has found application as Lewis acid activators for olefin polymerization processes involving single site catalysts (6) and in the arena of organic synthesis (7), due to their superior Lewis acid strength and hydrolytic stability.

Received October 26, 2000. Published on the NRC Research Press Web site on April 7, 2001.

B.E. Carpenter and W.E. Piers[1]. Department of Chemistry, University of Calgary, 2500 University Drive N.W., Calgary, AB T2N 1N4, Canada.
R. McDonald. X-ray Crystallography Laboratory, Department of Chemistry, University of Alberta, Edmonton, AB T6G 2G2, Canada.

[1]Corresponding author (telephone: (403) 220-5746; fax: (403) 289-9488; e-mail: wpiers@ucalgary.ca).

Recently we have explored the chemistry of ferrocenyl derivatives borylated with -B(C_6F_5)$_2$ groups, bringing these two classes of borane compounds together. In a previous paper (8), we described in detail the synthesis and chemistry of the monoborylated ferrocene FcB(C_6F_5)$_2$ (**1**). Here we describe the diborylated complex 1,1′-Fc[B(C_6F_5)$_2$]$_2$ (**2**), which represents a new member in a growing family of highly electrophilic diboranes (9), and contrast its chemistry with that of **1**.

Results and discussion

Whereas the monoborylated ferrocenyl compound Fc[B(C_6F_5)$_2$] (**1**), was readily prepared by direct borylation (8) of ferrocene with HB(C_6F_5)$_2$ (10), reaction of the metallocene with two to three equivalents of the borane did not proceed to a clean diborylated product. Instead, only mixtures of **1** (≈30%) and the target diborylated ferrocene 1,1′-Fc[B(C_6F_5)$_2$]$_2$ (**2**) (≈70%), were produced. Since the solubility properties of these compounds are similar, **2** proved inseparable from the monoborylated **1** via crystallization. The high sensitivity of the Fc—B bond towards proteolysis precluded chromatographic methods for separation.

 DOI: 10.1139/cjc-79-3-291 © 2001 NRC Canada

Therefore, to produce the desired diborane, we turned to a metathetical route utilizing 1,1′-Fc(HgCl)$_2$ (11) and 2 equiv of ClB(C$_6$F$_5$)$_2$ (12) (eq. [1]). This method is also viable for preparing ferrocenyl borane **1**, so to obtain clean samples of **2**, highly pure 1,1′-Fc(HgCl)$_2$ was required. A modified preparation of this compound using 1,1′-FcLi$_2$·TMEDA (13) and HgCl$_2$ fulfilled this need, giving 1,1′-Fc(HgCl)$_2$, which was free from FcHgCl. The reaction shown in eq. [1] proceeds slowly owing to the poor solubility of 1,1′-Fc(HgCl)$_2$, but produces **2** essentially quantitatively, as judged by spectrocopy. However, due to the extreme solubility of **2** in both hexanes and aromatic solvents, isolated yields of analytically pure material were only 25–40% depending on the scale of the reaction.

Complex **2** is intensely maroon colored when dissolved in common non-donor solvents, and is isolated as a waxy solid when crystallized from saturated solutions in hexamethyldisiloxane at –35°C. Although single crystals of **2** are obtainable from Me$_3$SiOSiMe$_3$ solution, severe disorder problems precluded satisfactory refinement of the data set; nonetheless, this experiment was consistent with the connectivity required by **2**.[2] The ^{1}H NMR spectrum shows two signals, a broadened one at 4.39 ppm for the protons α to the boryl group, and a sharper multiplet at 4.75 ppm for the β protons. Cyclic voltammetric measurements on **2** (1 mM in α,α,α-trifluorotoluene with [Bu$_4$N][B(C$_6$F$_5$)$_4$] (100 mM) as supporting electrolyte (14), scan rate = 100 mV s^{-1}) reveals a quasi-reversible one-electron oxidation at +820 mV relative to ferrocene–ferrocenium ($E_{1/2}$ Fc–Fc$^+$ = 0 mV), which is roughly double the potential observed for monoborylated ferrocene (**1**) (+450 mV). The intense color of the compound is similar to that observed for **1** and arises from a charge transfer absorption (λ_{max} = 233 nm, ε = 1.64 × 10^4) assignable to an $Fe_{dz^2/dx^2-y^2} \rightarrow B_p$ transition from the metallocene-based HOMO into the empty *p* orbitals of the boryl groups (3). In our previous paper (8), we argued that the ^{19}F NMR data for monoborylated **1** was consistent with a significant Fe → B interaction since the chemical shift separation between the *meta* and *para* fluorine atoms was midway between that observed for free, unligated boranes and Lewis base adducts of these boranes. A similar phenomenon is observed in **2**, but the difference in the chemical shifts observed for the *meta* and *para* fluorine atoms of the C$_6$F$_5$ rings ($\Delta_{m,p}$) is a measure of the electron density on boron (15); the boron centers in **2** have less electron density ($\Delta_{m,p}$ = 10.7 ppm) than **1** ($\Delta_{m,p}$ = 9.2 ppm). Thus, because the Fe → B interaction is spread over two boryl groups, the individual interactions are attenuated somewhat as the extent of borylation grows (3).

This is also manifested in the compound's behavior as a Lewis acid, in comparison to **1**, since the weaker Fe → B interaction leads to stronger Lewis acidity for the boron centers in **2**. For example, on the Child's scale (16), monoborylated **1** scored a very low value of 0.37 ± 0.03 relative to BBr$_3$ at 1.00. In comparison, diborylated **2** measures a Lewis acidity of 0.70 ± 0.03, which is closer to the value of 0.77 found for B(C$_6$F$_5$)$_3$ itself (17). Furthermore, whereas acetonitrile binds to the boron center in **1** only at low temperatures (reversibly), it complexes to the boron centers in **2** at room temperature, as evidenced by the immediate decolorization of benzene solutions of **2** in the presence of 2 to 3 equiv of the Lewis base. Soon thereafter, a yellow solid precipitates from these solutions. The loss of the deep maroon color is indicative of a disruption of the Fe → B interaction upon complexation of the boron centers by CH$_3$CN. Based on the single set of resonances observed in the ^{19}F NMR spectrum of this yellow solid, it is probably the bis(acetonitrile) adduct of **2**, although it was not fully characterized due to its insolubility.

Exposure of maroon solutions of **2** to a slight excess of the stronger Lewis base PMe$_3$ again led to an immediate decolorization of the solution to a yellow color, from which a precipitate consisting of the bis(trimethylphosphine) adduct (**3**) soon developed (eq. [2]). This compound proved more amenable to analysis, and the ^{1}H and ^{19}F NMR data for **3** are fully consistent with formation of the C_{2v} symmetric bis(phosphine) adduct. The ^{11}B (–13.4 ppm) and ^{31}P (–14.5 ppm) NMR spectral data are similar to those found for **1**·PMe$_3$ and also indicate that the two boryl fragments are related by symmetry. This was confirmed by X-ray analysis of single crystals of **3**; the solid state structure is shown in Fig. 1, along with selected metrical data. Further details on this structure can be found in the Supporting Information.[3] The two -B(C$_6$F$_5$)$_2$·PMe$_3$ moieties are oriented differently with respect to the ferrocenyl core of the molecule. For example, the P(1)-B(1)-C(1)-C(5) torsion angle of –11.1(4)° indicates that the P(1)-B(1) vector lies essentially in the C(1)-C(5) plane. In contrast, the P(2)-B(2)-C(6)-C(10) dihedral angle is 70.8(3)°, such that this P—B bond is oriented nearly perpendicular to the corresponding Cp ring plane. Presumably, these differences are due to packing effects. While the bond angles within these fragments differ somewhat as a consequence, bond distances are

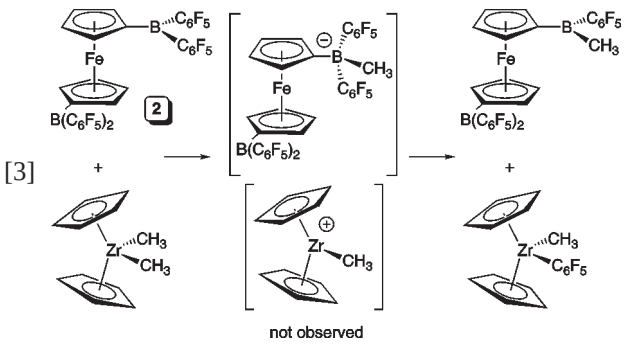
[2] B.E. Carpenter, W.E. Piers, and W. Clegg. Unpublished results.

[3] Supplementary material may be purchased from the Depository of Unpublished Data, Document Delivery, CISTI, National Research Council Canada, Ottawa, ON K1A 0S2, Canada. For information on obtaining material electronically go to http://www.nrc.ca/cisti/irm/unpub_e.shtml. Supplementary material referred to in this paper has also been deposited with the Cambridge Crystallographic Data Centre. Copies of the data can be obtained, free of charge, on application to the Director, CCDC, 12 Union Road, Cambridge CB2 1EZ, U.K. (Fax: 44-1223-336033 or e-mail: deposit@ccdc.cam.ac.uk).

© 2001 NRC Canada

comparable and also similar to those found in the PMe_3 adduct of **1**. The Cp rings in **3** are almost eclipsed with respect to one another, deviating by 12.5° from a fully eclipsed conformation.

The enhanced Lewis acidity of diborane **2** relative to **1** is also shown in its observed reactivity with the metallocene Cp_2ZrMe_2. Perfluoroaryl substituted boranes of various types are capable of abstracting methide anions from metallocenes such as this, a reaction which constitutes an activation of the dialkyl metallocene in olefin polymerization reactions. Thus, it was surprising that monoborylated ferrocene (**1**) underwent absolutely no reaction with the dimethylzirconocene reagent. In contrast, diborylated **2** is observed to undergo a slow reaction with Cp_2ZrMe_2, as indicated in eq. [3]. Although a stable ion pair is not observed,



such a species is likely an intermediate on the way to the observed products, which form after rapid back-transfer of a $-C_6F_5$ group from the putative ion pair $[Cp_2ZrCH_3]^+[\mathbf{2}\cdot CH_3]^-$. Similar back-transfer reactions have been observed in ion pairs formed from boranes of general formula $RB(C_6F_5)_2$ (R = aliphatic group) (18). Although the behavior of this ion pair is not ideal, these observations do indicate that **2** is Lewis acidic enough to effect methide abstraction, unlike monoboryl ferrocene (**1**).

In conclusion, we have prepared a diborylated ferrocene incorporating $-B(C_6F_5)_2$ units in the 1,1′ positions. Although it is not an effective olefin polymerization initiator due to the facile aryl back-transfer reaction, the diborylated compound is demonstrably more Lewis acidic than the monoborylated species due mainly to the weaker Fe → B interactions in the more heavily borylated acid.

Experimental Section

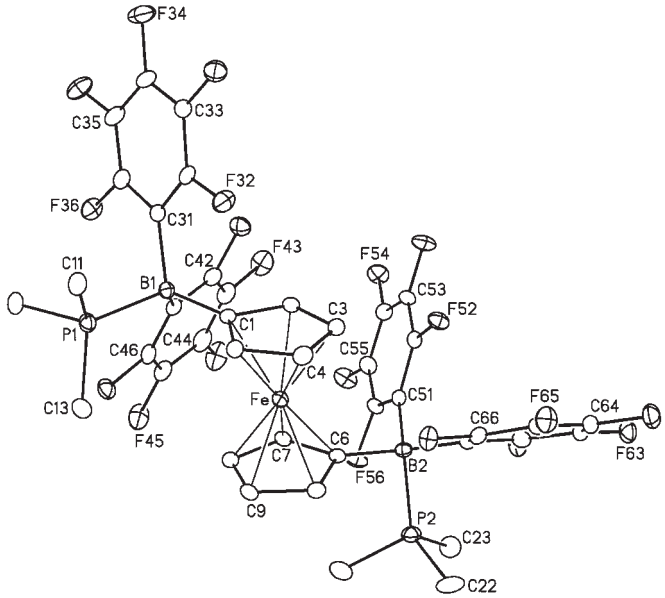
General

General procedures have been described in detail elsewhere (8). Reagents employed were prepared from literature procedures cited in the text.

Modified preparation of 1,1′-Fc(HgCl)$_2$

To a solution of $FcLi_2\cdot$TMEDA (1.60 g, 5.90 mmol) dissolved in THF (50 mL) was added a solution of mercuric chloride (3.53 g, 13.0 mmol, 2.2 equiv) in THF (15 mL) via cannula transfer. The clear orange solution immediately turned chalky orange upon addition of mercuric chloride. The orange suspension was stirred for 24 h under argon. The orange solid was collected by filtration and washed with

Fig. 1. ORTEP diagram of **3**. Selected bond distances (Å): B(1)—C(1) 1.615(5), B(1)—C(31) 1.666(5), B(1)—C(41) 1.639(5), B(1)—P(1) 1.996(4), B(2)—C(6) 1.617(4), B(2)—C(51) 1.645(5), B(2)—C(61) 1.648(4), B(2)—P(2) 2.036(4). Selected bond angles (°): P(1)-B(1)-C(1) 108.3(2), P(1)-B(1)-C(31) 101.4(2), P(1)-B(1)-C(41) 115.7(2), C(1)-B(1)-C(31) 111.8(2), C(1)-B(1)-C(41) 109.4(3), C(31)-B(1)-C(41) 110.1(3), C(2)-C(1)-B(1) 125.3(3), C(5)-C(1)-B(1) 131.2(3), P(2)-B(2)-C(6) 99.39(19), P(2)-B(2)-C(51) 114.2(2), P(2)-B(2)-C(61) 103.0(2), C(6)-B(2)-C(51) 108.1(3), C(6)-B(2)-C(61) 122.0(3), C(51)-B(2)-C(61) 109.8(2), C(7)-C(6)-B(2) 122.9(3), C(10)-C(6)-B(2) 130.7(3).



THF. Removal of the solvent under vacuum afforded an insoluble orange product. Yield 3.23 g (4.90 mmol, 83%). There was no trace of FcHgCl by ^{1}H NMR spectroscopy.

Preparation of 2

1,1-Bis(chloromercuric)ferrocene (1.47 g, 2.24 mmol) and $ClB(C_6F_5)_2$ (1.70 g, 4.48 mmol) were placed into a 100 mL bomb, and dry hexanes (50 mL) were added via vacuum transfer. The vessel was warmed slowly to 60°C in an oil bath and stirred for 72 h. The orange suspension changed to a dark maroon solution with a grey precipitate. The warm product mixture was cannula transferred to a 100 mL flask fitted with a frit assembly, and filtered. The solid was washed with hexanes until the washings were colourless. The solvent was removed under vacuum and the resulting oily maroon solid was recrystallized from a minimum amount of hexamethyldisiloxane at –35°C. Yield: 537 mg (0.605 mmol, 27%). UV (trifluorotoluene) λ_{max} (nm) (ε ($M^{-1}cm^{-1}$)): 233 (1.64×10^4). ^{1}H NMR (C_6D_6) δ: 4.75 (m, (AA'XX') $^3J_{H,H}$ = 1.6 Hz, 4H, H_β), 4.39 (br m, WHM = 5.4 Hz, 4H, H_α). ^{13}C NMR (C_6D_6) δ: 145.7 (d, $^1J_{C,F}$ = 244 Hz), 142.5 (d, $^1J_{C,F}$ = 256 Hz, C_p), 137.8 (d, $^1J_{C,F}$ = 253 Hz), 114.1 (br s, $C_{ipso}(C_6F_5)$), 80.0 (s, C_β), 79.1 (s, C), 75.1 (br s, $C_{ipso}(C_5H_4)$). ^{11}B NMR (d_8-toluene) δ: signal too broad to observe. ^{19}F NMR (C_6D_6) δ: –129.8 (d, 8F, F_o), –150.0 (t, 4F, F_p), –160.7 (dt, 8F, F_m). Anal. calcd. for $C_{34}H_8B_2F_{20}Fe$: C 46.73, H 0.92; found: C 46.35, H 0.61.

© 2001 NRC Canada

Table 1. Summary of data collection and structure refinement details for **3.**

Formula	$C_{40}H_{26}B_2F_{20}FeP_2$
Formula weight (g mol^{-1})	1026.02
Temperature (K)	193
λ (Å)	0.71073
Dimensions (mm^3)	0.22 × 0.20 × 0.04
Crystal system	monoclinic
Space group	$P2_1/c$
a (Å)	11.1605(9)
b (Å)	21.7099(18)
c (Å)	16.7151(12)
β (°)	102.0813(16)
V (Å^3)	3960.3(5)
Z	4
$\rho_{calc.}$ (mg m^{-3})	1.721
μ (mm^{-1})	0.589
Range of transmission factors	0.6284–0.9350
Scan type	φ rotations (0.3°), ω scans (0.3°)
2θ (max) (deg)	52.80
No. of reflections	19 507
Unique reflections	8091
No. of variables	586
Restraints	0
R_1	0.0439
wR_2	0.0890
GoF	0.852
Residual density (e Å^{-3})	–0.324–0.336

Preparation of 3

A solution of **2** (100 mg, 0.114 mmol) in hexanes was cooled to –78°C and a slight excess of trimethylphosphine (0.285 mmol, 2.5 equiv) in a 35.1 cm^3 bulb, was vacuum transferred (150 mm Hg (1 mm Hg = 133.322 Pa)) into the vessel. Upon warming to room temperature, the maroon solution quickly turned colour to a yellow suspension; stirring continued for an additional 60 min. The solvent was removed along with the unreacted PMe_3 under vacuum to afford 107 mg (85%) of a yellow powder. A single crystal was obtained from toluene solution. ^{1}H NMR (d_8-toluene) δ: 4.29 (br m, 4H, *H*), 3.62 (br m, 4H, H_α), 0.41 (d, $^2J_{P,H}$ = 10.6 Hz, 18H, CH_3). ^{13}C NMR (d_8-toluene) δ: 147.9 (d, $^1J_{C,F}$ = 239 Hz), 139.6 (d, $^1J_{C,F}$ = 246 Hz, C_p), 137.6 (d, $^1J_{C,F}$ = 264 Hz), 120.1 (br s, $C_{ipso}(C_6F_5)$), 73.9 (*C*), 72.2 (*C*), 9.1 (d, $^1J_{C,P}$ = 37 Hz, *C*H$_3$), $C_{ipso}(C_5H_4)$ not found. ^{11}B NMR (d_8-toluene) δ: –13.4 (d, WHM = 190 Hz). ^{19}F NMR (d_8-toluene) δ: –127.5 (d, 8F, F_o), –157.3 (t, 4F, F_p), –163.3 (dt, 8F, F_m). ^{31}P NMR (d_8-toluene) δ: –14.5 (br s).

Reaction of 2 with Cp_2ZrMe_2

In the dry box **2** (30 mg, 0.034 mmol, 1.08 equiv) and Cp_2ZrMe_2 (8 mg, 0.032 mmol) were loaded into a dry NMR tube and dissolved in d_8-toluene (ca. 0.5 mL). The NMR tube was flame sealed and shaken. The ^{1}H NMR spectrum was monitored until the reaction was complete (≈6 h). ^{1}H NMR (d_8-toluene) δ: 5.69 (s, 10H, Zr(C_5H_5)), 4.62 (m, J = 1.8 Hz, 2H, H_β for one C_5H_4B ring), 4.52 (m, J = 1.8 Hz, 2H, H_β for one C_5H_4B ring), 4.37 (m, 2H, H_α for one C_5H_4B ring), 4.14 (m, 2H, H_α for one C_5H_4B ring), 0.82 (s, 3H, BCH_3), 0.26 (t, $^2J_{H,F}$ = 4.0 Hz, 3H, ZrCH_3).

X-ray crystallography

Crystals of **3** were coated in Paratone–8277 oil; one of these was mounted on a glass fiber for diffraction measurements. Data were collected using a Bruker P4/RA diffractometer with a SMART 1000 CCD detector[4], using monochromated Mo Kα radiation at –80°C. Data were integrated to a maximum 2θ value of 52.80°, and were corrected for absorption through use of the SADABS procedure[4]. The structure of **3** was solved using the program SHELXS 86 (19), and the structure was refined using full-matrix least-squares methods (SHELXL 93) (20)[5] 2σ (F_o^2) is used only for calculating R_1, and is not relevant to the choice of reflections for refinement. *R*-factors based on F_o^2 are statistically about twice as large as those based on F_o, and *R*-factors based on all data will be even larger.[5] All nonhydrogen atoms were refined anisotropically and all hydrogen atoms were placed in idealized positions as suggested by the sp^2 or sp^3 hybridizations of their attached carbons. Details of crystal data, data collection, and structure refinement have been provided in Table 1.

Acknowledgments

Funding for this work from the Natural Sciences and Engineering Research Council of Canada (NSERC) is gratefully acknowledged. B.E.C and W.E.P thank Professor Scott Hinman (Calgary) for use of his electrochemical equipment and helpful discussions.

References

1. A. Togni and T. Hayashi (Editors). Ferrocenes. VCH, Weinheim. 1995.
2. W.E. Piers and T. Chivers. Chem. Soc. Rev. 345 (1997).
3. A. Appel, F. Jäkle, T. Priermeier, R. Schmid, and M. Wagner. Organometallics, **15**, 1188 (1996).
4. (*a*) F. Jäkle, M. Mattner, T. Priermeier, and M. Wagner. J. Organomet. Chem. **502**, 123 (1995); (*b*) F. Jäkle, T. Priermeier, and M. Wagner. Chem. Ber. **128**, 1163 (1995); (*c*) M. Fontani, F. Peters, W. Scherer, W. Wachter, M. Wagner, and P. Zanello. Eur. J. Inorg. Chem. 1453 (1998).
5. (*a*) F. Jäkle, T. Priermeier, and M. Wagner. J. Chem. Soc. Chem. Commun. 1765 (1995); (*b*) E. Herdtweck, F. Jäkle, and M. Wagner. Organometallics, **16**, 4737 (1997); (*c*) H. Braunschweig, R. Dirk, M. Müller, P. Nguyen, R. Resendes, D.P. Gates, and I. Manners. Angew. Chem. Int. Ed. Engl. **36**, 2338 (1997); (*d*) M.J.G. Lesley, U. Mock, N.C. Norman, A.G. Orpen, C.R. Rice, and J. Starbuck. J. Organomet. Chem. **582**, 116 (1999).

[4] Programs for diffractometer operation, data collection, data reduction, and absorption correction were those supplied by Bruker.

[5] Refinement on F_o^2 for all reflections (all of these having $F_o^2 \geq -3\sigma(F_o^2)$). Weighted *R*-factors (wR_2) and all goodnesses of fit (GoF) S are based on F_o^2; conventional *R*-factors R_1 are based on F_o, with F_o set to zero for negative F_o^2. The observed criterion of $F_o^2 > 2\sigma(F_o^2)$ is used only for calculating R_1, and is not relevant to the choice of reflections for refinement. *R*-factors based on F_o^2 are statistically about twice as large as those based on F_o, and *R*-factors based on all data will be even larger.

© 2001 NRC Canada

6. E.Y.-X. Chen and T.J. Marks. Chem. Rev. **100**, 1391 (2000).
7. K. Ishihara and H. Yamamoto. Eur. J. Org. Chem. 527 (1999).
8. B.E. Carpenter, W.E. Piers, M. Parvez, G.P.A. Yap, and S.J. Rettig. Can. J. Chem. In press.
9. W.E. Piers, G.J. Irvine, and V.C. Williams. Eur. J. Inorg. Chem. 2131 (2000).
10. D.J. Parks, W.E. Piers, and G.P.A. Yap. Organometallics, **17**, 5492 (1998).
11. R.W. Fish and M. Rosenblum. J. Org. Chem. **30**, 1253 (1965).
12. R.D. Chambers and T. Chivers. J. Chem. Soc. 3933 (1965).
13. M.D. Rausch and D.J. Ciappenelli. J. Organomet. Chem. **10**, 127 (1967).
14. R.J. LeSuer and W.E. Gieger. Angew. Chem. Int. Ed. Engl. **39**, 248 (2000).
15. (*a*) A.D. Horton, J. de With, A.J. van der Linden, and H. van de Weg. Organometallics, **15**, 2672 (1996); (*b*) A.D. Horton and J. de With. Organometallics, **16**, 5425 (1997).
16. R.F. Childs, D.L. Mulholland, and A. Nixon. Can. J. Chem. **60**, 801 (1982).
17. L. Luo and T.J. Marks. Top. Catal. **7**, 97 (1999).
18. K. Köhler, W.E. Piers, S. Xin, Y. Feng, A.M. Bravakis, A.P. Jarvis, S. Collins, W. Clegg, G.P.A. Yap, and T.B Marder. Organometallics, **17**, 3557 (1998).
19. G.M. Sheldrick. Acta Crystallogr. Sect A: Fundam. Crystallogr. **A46**, 467 (1990).
20. G.M. Sheldrick. SHELXL 93. Program for crystal structure determination. University of Göttingen, Germany, 1993.

© 2001 NRC Canada

Cobalt-59 chemical shift and quadrupolar tensors of simple octahedral cobalt(III) complexes

Christopher W. Kirby and William P. Power

Abstract: Analysis of the solid-state powder ^{59}Co NMR spectra of ten simple inorganic cobalt(III) complexes at 11.75, and in most cases, 4.7 T have permitted the assignment of specific ligand planes to ranges of values of the observed chemical shift principal components. The relevant chemical shift components were determined from the simulations of the powder line shapes. These simulations also provided the relative orientations of the chemical shift (CS) and electric field gradient (efg) tensors, as well as magnitude and asymmetry of the ^{59}Co quadrupolar coupling. Using symmetry arguments and ab initio calculations, as appropriate or necessary, the orientations of the efg tensors in the molecular frame were deduced. This allowed the determination of the CS tensors in the molecular frame and thus assignment of the ligand planes responsible for the observed values of chemical shifts.

Key words: cobalt, chemical shift, quadrupolar coupling, solid state NMR.

Résumé : L'analyse des spectres RMN du ^{59}Co de poudres à l'état solide de six complexes inorganiques simples du cobalt(III), déterminés à 11,75 T et, dans la plupart des cas à 4,7 T, on permit d'attribuer des plans de ligand spécifique à des plages de valeurs des composants principaux des déplacements chimiques observés. On a déterminé les composantes des déplacements chimiques appropriés en faisant appel à des simulations des formes de raies des poudres. Ces simulations ont aussi permis de déterminer les orientations relatives des tenseurs du déplacement chimique et du gradient du champ électrique ainsi que l'amplitude et l'asymétrie du couplage quadripolaire du ^{59}Co. Utilisant des arguments de symétrie et des calculs ab initio, suivant les cas et les nécessités, on a pu déduire les orientations des tenseurs du gradient du champ électrique dans l'environnement moléculaire. Ceci a permis de déterminer les tenseurs du déplacement chimique dans l'environnement moléculaire et finalement l'attribution des plans de ligand responsables des valeurs observées pour les déplacements chimiques.

Mots clés : cobalt, déplacement chimique, couplage quadripolaire, RMN à l'état solide.

[Traduit par la Rédaction]

Introduction

In the past few years, there has been a renewed interest in ^{59}Co chemical shielding with the advent of computational methods using density functional theory (DFT) to predict shielding in heavy atoms (1–6). Chan and Au-Yeung (5) have reported calculated chemical shielding (CS) tensors of five simple octahedral cobalt(III) complexes. Godbout and Oldfield (6) have also performed a DFT study on six cobalt(III) complexes of which four are the same studied by Chan and Au-Yeung. With the increasing availability and power of these new theoretical methods, more experimental data concerning the magnitude and orientation of the chemical shift and quadrupolar coupling tensors is needed to aid in their improvement and refinement.

The first reports of ^{59}Co CS tensor determinations were provided by single-crystal NMR (7–12). These experiments were carried out at low magnetic fields, and, therefore, the precision of the experiments, in terms of CS data, is low. The first high-field single-crystal ^{59}Co NMR experiment was completed on $Co(acac)_3$ (acac = acetylacetonate) at 9.4 T (13). In this study, the orientations of the CS and electric field gradient (efg) tensors were unambiguously determined as well as the orientation of these tensors in the molecular frame. Chan and Au-Yeung (5) as well as Godbout and Oldfield (6) have calculated the CS tensor for this complex. The span ($\Omega = \delta_{11} - \delta_{33}$) of the shift tensor reported in the single-crystal ^{59}Co NMR study more closely agrees with the computations of Chan and Au-Yeung.

The first report of powder ^{59}Co NMR spectra of highly symmetric cobalt(III) complexes by Eaton et al. (14) appeared before a general theory for powder NMR line shape simulations for quadrupolar nuclei in low symmetry sites was available. This limited their ability to comment quantitatively on the interactions responsible for the observed anisotropic line shapes. Shortly thereafter (in 1990) two groups independently reported techniques for the analysis of powder line shapes of half-integer-spin quadrupolar nuclei ($I = n/2$ where $n = 3$, 5, 7, or 9), which had chemical shielding and quadrupolar tensors that were both non-axially symmetric and non-coincident (15, 16). Since then, the chemical shift and quadrupolar tensors of only three anionic cobalt complexes have been completely determined using this more

Received October 18, 2000. Published on the NRC Research Press Web site on April 3, 2001.

C.W. Kirby[1] and W.P. Power.[2] Department of Chemistry, University of Waterloo, Waterloo, ON N2L 3G1, Canada.

[1]Current address: Department of Chemistry, University of Western, London, ON N6A 5B7, Canada.
[2]Corresponding author (telelphone: (519) 888-4567 ext. 3626; fax: (519) 746-0435; e-mail: william.power@uwaterloo.ca).

 DOI: 10.1139/cjc-79-3-296 © 2001 NRC Canada

general NMR line shape theory (17, 18). Other classes of complexes that have been studied using solid-state powder ^{59}Co NMR include cobalt clusters (19, 20), battery materials (21), and biologically relevant cobalt complexes (22–24). We have also performed a single-crystal ^{59}Co NMR on vitamin B_{12} (25), and our results agree quite closely with those of the powder ^{59}Co NMR study (23).

In this report, we present the ^{59}Co solid-state powder NMR spectra of ten octahedral inorganic cobalt(III) complexes. The CS and efg tensors have been determined, as well as the relative orientations of the two tensors in each complex. Specific ligand planes were assigned to the observed values of the chemical shift principal components, by using the orientation of the two tensors and symmetry arguments or ab initio calculations, to determine the orientation of the efg tensor in the molecular frame. We believe these results will provide important experimental comparison for ongoing efforts aimed at improving theoretical methods for prediction of transition-metal chemical shielding.

Theory

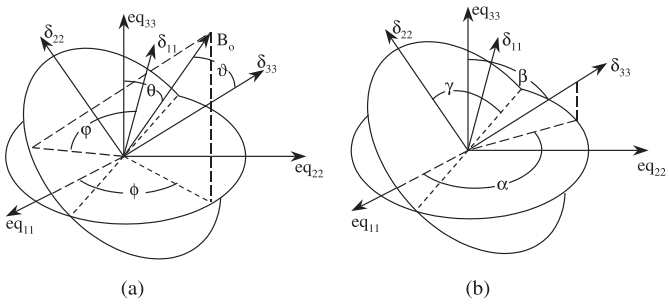
For a quadrupolar nucleus, only the Zeeman, quadrupolar, and chemical shielding interactions need to be considered, and the nuclear-spin Hamiltonian is given as

$$[1] \qquad \hat{H}_T = \hat{H}_Z + \hat{H}_Q + \hat{H}_{CS}$$

There are two situations that arise depending on the strength of the quadrupolar coupling with respect to the Zeeman interaction: first-order (Q_1) or second-order (Q_2) quadrupolar effects. Q_1 is sufficient to describe the response of the quadrupolar nucleus when the quadrupolar interaction is only a first-order perturbation of the Zeeman interaction (similar to all other NMR interactions that are only first order perturbations). If the quadrupolar effects are larger, Q_2 must be considered as well. As a guide for ^{59}Co NMR, at 11.75 T, a χ of 1.5 MHz or greater is required before Q_2 needs to be considered; at 4.7 T, a χ of only 950 kHz necessitates consideration of Q_2. Using the estimates of χ from previous ^{59}Co relaxation studies in solution (26), we observe that all of the complexes described in this study fall into the second-order regime (i.e., Q_2 must be considered) if the solution and solid-state χs are equivalent. Hence, the central $m = +1/2 \leftrightarrow -1/2$ transition should dominate the observed ^{59}Co NMR spectra. If the satellite transitions are observed, Q_2 will shift them but the splitting between any pair of satellite transitions will be determined solely by Q_1.

The theory describing the origin of NMR powder line shapes for quadrupolar nuclei in general crystal sites, has been described in detail elsewhere (15, 16). Figure 1*a* uses the angles θ and ϕ to describe the orientation with respect to the magnetic field (B_o) of the efg tensor, where $|eq_{33}| \geq |eq_{11}| \geq |eq_{22}|$ are the three orthogonal components of this tensor in its principal axis system (PAS). The angles ϑ and φ describe the orientation with respect to B_o of the CS tensor, where $\delta_{11} \geq \delta_{22} \geq \delta_{33}$ are the three principal components of this tensor in its PAS. In general, powder NMR line shapes of the central ($+1/2 \leftrightarrow -1/2$) transition of quadrupolar nuclei with half-integer spin are described by the following equation:

Fig. 1. (*a*) Orientation of the CS and efg tensors with respect to B_o; (*b*) the Euler angles (α, β, and γ) orient the CS tensor in the PAS of the efg tensor.



$$[2] \qquad \nu = \nu_o(\delta_{11} \sin^2 \vartheta \cos^2 \varphi + \delta_{22} \sin^2 \vartheta \sin^2 \varphi + \delta_{33} \cos^2 \vartheta) + \frac{\nu_Q^2\left[I(I+I) - \frac{3}{4}\right]}{6\nu_o}[A(\phi) \cos^4 \theta + B(\phi) \cos^2 \theta + C(\phi)]$$

where

$$[3] \qquad \nu_Q = \frac{3\chi}{2I(2I-1)}$$

I is the nuclear spin quantum number, ν_o is the Larmor frequency, and $\chi = eq_{33}eQ/h$ is the quadrupolar coupling constant, with eq_{33} the largest or so-called "principal" component of the electric field gradient (efg) tensor and eQ the nuclear quadrupole moment,

$$[4] \qquad A(\phi) = -\frac{27}{8} - \frac{9}{4}\eta_Q \cos 2\phi - \frac{3}{8}\eta_Q^2 \cos^2 2\phi$$

$$[5] \qquad B(\phi) = -\frac{30}{8} - \frac{1}{2}\eta_Q^2 + 2\eta_Q \cos 2\phi + \frac{3}{4}\eta_Q^2 \cos^2 2\phi$$

$$[6] \qquad C(\phi) = -\frac{3}{8} - \frac{1}{3}\eta_Q^2 + \frac{1}{4}\eta_Q \cos 2\phi - \frac{3}{8}\eta_Q^2 \cos^2 2\phi$$

and η_Q is the asymmetry of the efg tensor ($\eta_Q = (eq_{22} - eq_{11}) / eq_{33}$). However, it is only possible to obtain the orientations of the tensors with respect to the molecule using single-crystal NMR, a dipolar interaction, or in systems where there is high crystal symmetry (orthorhombic or higher point-symmetry). Therefore, to simulate solid-state ^{59}Co NMR spectra, the relative orientations of the two tensors are described via the Euler angles (α, β, and γ, as seen in Fig. 1*b*) using the following expressions:

$$[7] \qquad \sin \vartheta \cos \varphi = \cos \gamma \cos \beta \cos (\phi - \alpha) + \sin \gamma \sin \theta \sin (\phi - \alpha) - \cos \gamma \sin \beta \cos \theta$$

$$[8] \qquad \sin \vartheta \sin \varphi = -\sin \gamma \cos \beta \sin \theta \cos (\phi - \alpha) + \cos \gamma \sin \theta \sin (\phi - \alpha) + \sin \gamma \sin \beta \cos \theta$$

$$[9] \qquad \cos \vartheta = \sin \beta \sin \theta \cos (\phi - \alpha) + \cos \beta \cos \theta$$

Hence, in general, eight variables are needed to fully describe the interactions responsible for the anisotropic NMR

© 2001 NRC Canada

Table 1. Summary of solid-state ^{59}Co NMR data.

Compound	Synthesis	δ_{11} (ppm)	δ_{22} (ppm)	δ_{33} (ppm)	χ (MHz)	η_Q	Euler angles (°)
$[Co(en)_3]Cl_3$	A[a]	7172 ± 5	7172 ± 5	6939 ± 5	2.99 ± 0.01	0	$\alpha = \beta = \gamma = 0$
trans-$[Co(NH_3)_4(NO_2)_2]NO_3$	B[b]	7240 ± 25	7065 ± 15	6910 ± 25	12.0 ± 0.5	0 ± 0.05	α is arbitrary $\beta = 32 \pm 5$ $\gamma = 57 \pm 5$
cis-$[Co(NH_3)_4(NO_2)_2]NO_3$	B[b]	7445 ± 30	7040 ± 15	7025 ± 25	12 ± 1	0.7 ± 0.1	$0 < \alpha, \gamma < 10$ $\beta = 22 \pm 2$
$[Co(NH_3)_5(NO_2)]Cl_2$	C[c]	7610 ± 20	7545 ± 15	7340 ± 10	11.25 ± 0.25	0.55 ± 0.05	$\alpha = 7 \pm 2$ $\beta = 88 \pm 2$ $\gamma = 7 \pm 2$
$Na_3[Co(NO_2)_6]$	D[d]	7744 ± 5	7565 ± 5	7565 ± 5	8.2 ± 0.1	0	$\alpha = \gamma = 0$ $\beta = 90$
$[Co(NH_3)_5Cl]Cl_2$	D[d]	9450 ± 40	9450 ± 40	7890 ± 40	29 ± 1	$0 < \eta < 0.1$	$0 < \beta < 5$ α, γ are arbitrary
$[Co(NH_3)_5(CO_3)]NO_3 \cdot 1/2H_2O$	D[d]	9805 ± 30	9360 ± 15	7750 ± 25	20 ± 1	0.08 ± 0.03	$0 < \alpha < 15$ $\beta = 1 \pm 1$ $0 < \gamma < 10$
cis-$[Co(NH_3)_4(CO_3)]NO_3$	E[e]						
site 1		10 165 ± 25	9910 ± 15	8860 ± 25	18 ± 1	0.3 ± 0.05	$\alpha = 40 \pm 10$
site 2			9975 ± 15				$\beta = 4 \pm 1$ $\gamma = 30 \pm 10$
Na[Co(edta)]	F[f]	11 870 ± 75	9995 ± 40	9125 ± 50	35 ± 2	0.4 ± 0.1	$0 < \alpha, \gamma < 10$ $\beta = 18 \pm 2$
$Co(acac)_3$	D[d]	13 205 ± 20	12 270 ± 15	12 015 ± 20	5.5 ± 0.5	0.2 ± 0.05	$\alpha = 75 \pm 10$ $\beta = 86 \pm 3$ $\gamma = 15 \pm 3$

[a]See ref. 35.
[b]See ref. 36.
[c]Generously donated by A. J. Carty (National Research Council).
[d]Obtained from Aldrich.
[e]See ref. 37.
[f]See ref. 38.

line shape of a quadrupolar nucleus in the solid-state: the three principal components of the CS tensor, the quadrupolar coupling constant (χ), its asymmetry (η_Q), and the Euler angles relating the fixed orientations of the two tensors in the molecular frame. To establish accurate values for the eight parameters used in describing such a powder NMR line shape, it is normally necessary to obtain spectra at two or more magnetic field strengths.

Experimental

The cobalt(III) complexes were made by standard literature procedures, were commercially available, or were graciously provided by a colleague, as seen in Table 1. All samples were referenced to 1.0 M $K_3[Co(CN)_6]$ (aq). Solid-state ^{59}Co NMR spectra were acquired at 11.75 T on a Bruker AMX-500 NMR spectrometer and at 4.7 T on a Bruker DSX-200 NMR spectrometer where possible (vide infra). Samples were prepared by crushing the sample with a mortar and pestle and packing them into 5 mm NMR tubes. Samples were limited to the central region of the rf coil. At 4.7 T, a spin-echo pulse sequence was used for all spectra. At 11.75 T, a simple one pulse experiment was attempted to obtain all spectra except for Na[Co(edta)] (edta = ethylenediamine tetraacetate), which has a very broad line shape. In some spectra, Lorentzian "tails" were present due to the probe's finite dead time.

Calculations of the ^{59}Co NMR powder line shapes were performed on a Pentium computer using a Windows-based software package[3] that incorporates the POWDER routine (27) with additions for quadrupolar nuclei (15). The values of the three principal components of the chemical shift tensor, the quadrupolar coupling constant, the asymmetry of the efg tensor, and the Euler angles were optimized to maximize the agreement (visually) between the experimental and calculated line shapes of the central transition, with particular emphasis placed on the positions of critical frequencies (peaks and shoulders) in the spectra. Crystal structures were used to determine whether any constraints on the CS or efg tensors were necessary due to nuclear site symmetry.

The orientations of the efg tensors were estimated by consideration of local symmetry arguments or obtained using Gaussian 94 (28) for *cis*-$[Co(NH_3)_4(NO_2)_2]NO_3$ running on a SGI Indigo^2 XL workstation. For this complex, no crystal structure has been published, hence Gaussian 94 was used to obtain an optimized structure of the cation only and the resulting efg tensor. The calculations were performed using the LanL2DZ basis set with Hartree–Fock methods.

[3]WSolids NMR simulation package obtained from K. Eichele and R.E. Wasylishen, Dalhousie University, Halifax, Canada.

© 2001 NRC Canada

Fig. 2. Breakdown of the simulation of $[Co(en)_3]Cl_3$ at 11.75 T.

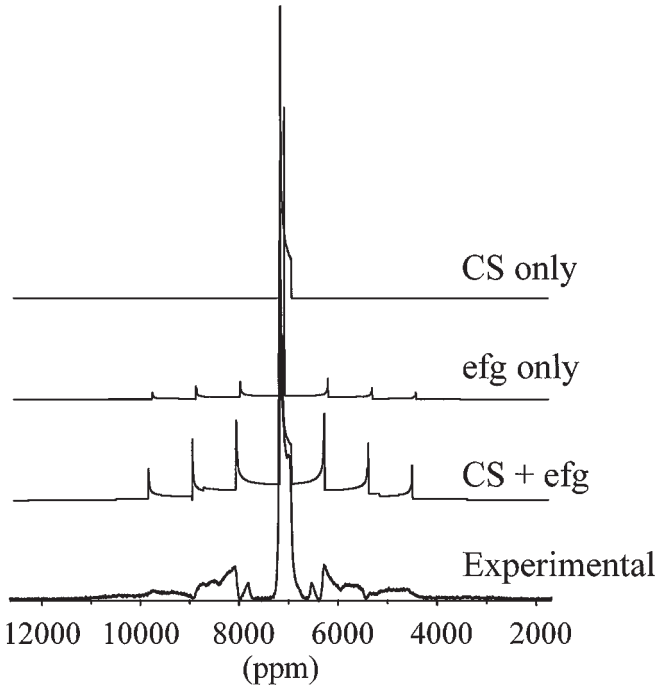
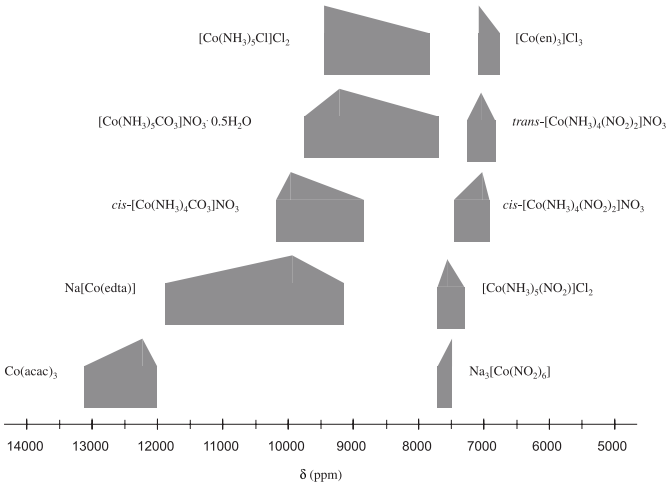


Fig. 3. Chemical shift tensors of ten inorganic cobalt(III) complexes.



Results and Discussion

Simulations of the ^{59}Co NMR spectra were performed for all of the spectra at 11.75 T as well as for the complexes for which spectra were obtained at 4.7 T. The results of the simulations are summarized in Table 1. Any values in Table 1 without "±" indicated are parameters that must be exactly 0 or 90° under crystallographic symmetry constraints.

For most compounds, only the central transition (m = +1/2 ↔ −1/2) was observed due to the large quadrupolar splitting causing the satellites to fall outside the observable spectral window. One example where the satellites as well as the central transition was observed was $[Co(en)_3]Cl_3$ (en = ethylenediamine). The crystal structure of $[Co(en)_3]Cl_3$ (29) indicated that the compound crystallizes in the trigonal space group *P*3*c*1. Therefore, the cobalt CS and efg tensors were required to be both axially symmetric and coincident, placing constraints on the analysis of the spectra of this complex. As seen in Table 1, the CS tensor was axially symmetric with $\delta_{11} = \delta_{22}$ and the principal components of the CS and efg tensors were aligned such that δ_{33} and eq_{33} were coincident (i.e., $\beta = 0$). Figure 2 shows the calculated spectra of this compound at 11.75 T; considering in turn: only the chemical shift tensor, only the efg tensor, the resulting full simulation including both interactions, and the experimental spectrum. The experimental spectrum shows some phase distortion due to the dead time of the probe. It is impossible to refocus all of the central and satellite transitions simultaneously with a single echo sequence. This complex is the only one in this series where all of the satellites are observed because whenever χ was larger and (or) the tensors were not aligned, the central transition dominated the spectrum, and the satellites fell outside the spectral window or became obscured under the central transition.

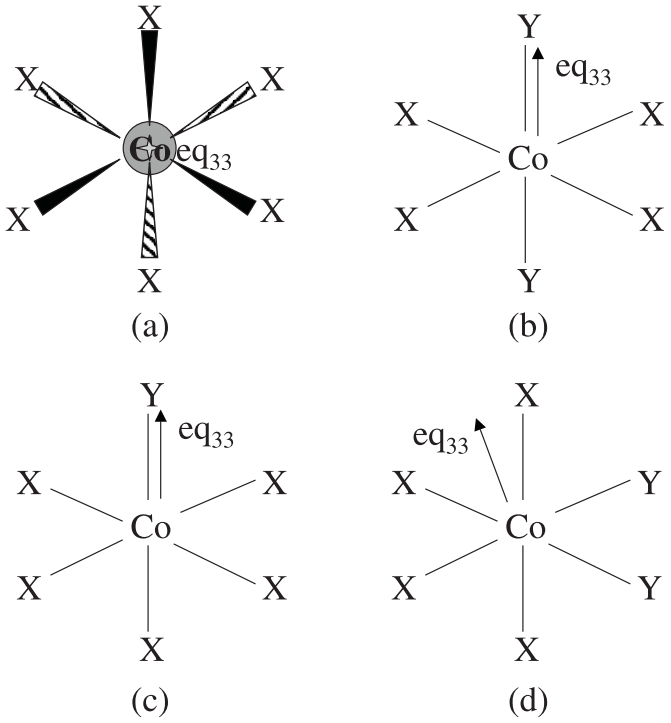
The only other complex that had constraints dictated by its crystal structure was $Na_3[Co(NO_2)_6]$, which crystallizes in the rhombohedral space group $R\bar{3}m$ (30); the cobalt nuclei sit on sites of threefold symmetry. All other complexes studied here did not have any constraints placed on the cobalt sites by their crystallographic symmetry, hence all eight parameters had to be used to obtain suitable simulations of the spectra.

At 4.7 T, the solid-state ^{59}Co NMR spectra of $[Co(NH_3)_5Cl]Cl_2$ and Na[Co(edta)] were difficult to obtain due to the large χs associated with these complexes, therefore, useful spectra were not obtained. A spectrum of *cis*-$[Co(NH_3)_4(NO_2)_2]NO_3$ was not obtained at the lower magnetic field due to the small amount of compound (approximately 5 mg), which was insufficient for sensitivity reasons. Cobalt-59 spectra of the other seven complexes were obtained at both 4.7 and 11.75 T, and the spectra at both fields were used to obtain unambiguous simulations.

Chemical shift tensors are of greatest interest when it is possible to identify trends that are present from similar compounds. Plots of the chemical shift tensors only (i.e., no quadrupolar interaction) of the complexes in this study are shown on the chemical shift scale (with respect to 1.0 M $K_3[Co(CN)_6]$ (aq)) at the bottom of Fig. 3. The magnitudes of the CS components alone are not sufficient; it is also important to consider the orientation of the tensors. Using basic symmetry arguments, as well as results from Gaussian 94 (28), it is possible to predict, or at least suggest, the orientation of the ^{59}Co efg tensors in each complex. Since absolute magnitudes of the efg tensor were not desired, and the orientations are dictated predominantly by local symmetry, the orientations of the efg tensor provided by calculations at this modest level of theory (HF/LANL2DZ) should be instructive nonetheless. These orientations of the efg tensors, in turn,

© 2001 NRC Canada

Fig. 4. The orientation of the principal component of efg tensors in the four classes of compounds in this study: (*a*) CoX_6, (*b*) *trans*-CoX_4Y_2, (*c*) CoX_5Y, and (*d*) *cis*-CoX_4Y_2.



permit the orientation of the CS tensor in the molecular frame to be deduced using the Euler angles.

We will introduce two definitions to simplify the ensuing discussion of chemical shielding tensor orientations and trends: eq_{33} will be called the "principal component" of the efg tensor, and the principal component of the CS tensor that is furthest from δ_{iso} will be termed the "principal director" of the CS tensor. The complexes will be discussed in four basic frameworks: CoX_6, CoX_5Y, *trans*-CoX_4Y_2, and *cis*-CoX_4Y_2. The orientation of the efg tensors of these four types of ligand arrangements is given in Fig. 4, and representative spectra of a complex from each of these categories are displayed in Fig. 5.

CoX_6

This group consists of three complexes: $[Co(en)_3]Cl_3$, $Na_3[Co(NO_2)_6]$, and $Co(acac)_3$. $Na_3[Co(NO_2)_6]$ crystallizes in a rhombohedral space group with the cobalt nucleus at the origin of the rhombohedral cell (30). The principal component of the efg tensor must lie along the threefold axis, and since β was 90°, it lies along δ_{11} (the principal director) with $\delta_{22} = \delta_{33}$. These results agree closely with those obtained previously via powder ^{59}Co NMR (17). $Co(acac)_3$ is similar to $Na_3[Co(NO_2)_6]$ in that the principal component of the efg lies along the normal to one face of the octahedron which is closest to a threefold axis ($Co(acac)_3$ does not have a true threefold axis since it crystallizes in the space group $P2_1/c$) (31). A β value of 86° was found for this complex, which would put the principal component of the efg approximately along δ_{11}. The orientation of the two tensors in this study, as well as the span of the CS tensor, agree quite well with those of a recent single-crystal ^{59}Co study of $Co(acac)_3$ (13). For $[Co(en)_3]Cl_3$, β was 0° and δ_{33} lies along the principal component of the efg tensor. The principal component of the efg would lie along the threefold axis of this molecule that crystallizes in a trigonal space group (29).

CoX_5Y

This group also comprises three complexes: $[Co(NH_3)_5Cl]Cl_2$, $[Co(NH_3)_5CO_3]NO_3{\cdot}2H_2O$, and $[Co(NH_3)_5NO_2]Cl_2$. For the first two of these complexes, β was small (6° or less). Therefore, the unique component of the efg should lie close to δ_{33}. If eq_{33} lies along δ_{33}, δ_{33} would have to be the principal director of the chemical shift tensor. This is observed for both complexes even though the spans vary between the two. In $[Co(NH_3)_5NO_2]Cl_2$, β was 90°, and thus, eq_{33} should lie close to δ_{11}. The principal director in $[Co(NH_3)_3NO_2]Cl_2$ was observed to be δ_{11} in agreement with the observed β value of 90°.

trans-CoX_4Y_2

trans-$[Co(NH_3)_4(NO_2)_2]NO_3$ was unique because it was the only complex in this study with a *trans* arrangement of ligands. The principal component of the efg tensor was expected to lie along a Co—NO_2 bond. Since the Euler angles for this complex were all nonzero and non-90°, the efg and the chemical shift tensors did not have any components that were coincident. The principal director of the chemical shift tensor was observed to be δ_{11}, but in fact, there was not a true principal director in this complex since the chemical shift tensor was far from axial symmetry.

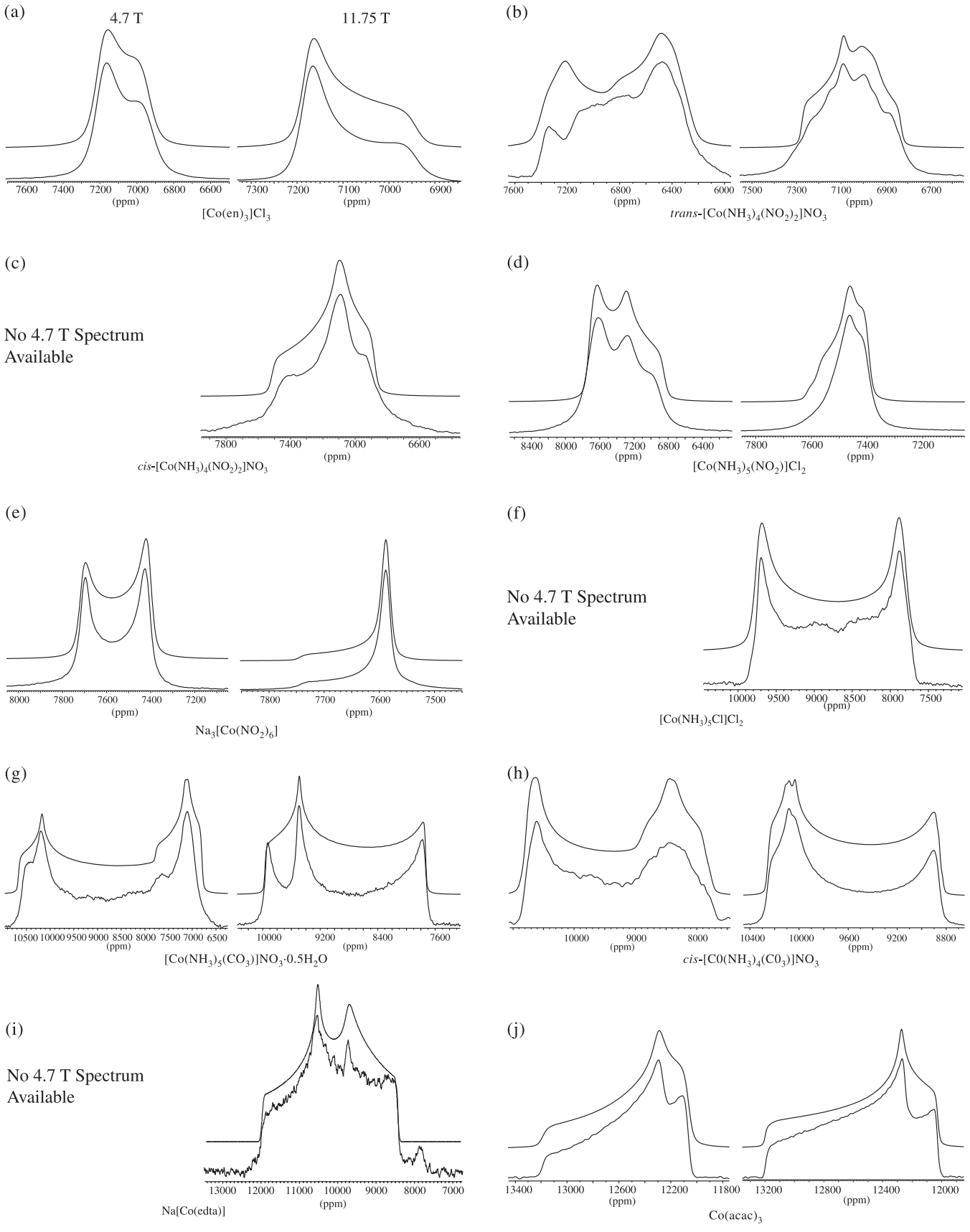
cis-CoX_4Y_2

This last group contained the following complexes: Na[Co(edta)], *cis*-$[Co(NH_3)_4(NO_2)_2]NO_3$, and *cis*-$[Co(NH_3)_4CO_3]NO_3$. From a Gaussian 94 calculation of the efg tensor of *cis*-$[Co(NH_3)_4(NO_2)_2]^+$, the principal component of the efg tensor was predicted to lie close to a Co—NH_3 bond that was perpendicular to the ligand plane containing the two nitro groups, and slightly tilted away from the nitro groups (see Fig. 4). A similar orientation was assumed for the other two complexes, in that the efg lies close to one of the Co—X bonds and perpendicular to the ligand plane containing the two Y groups. The principal director of the chemical shift tensors of Na[Co(edta)] and *cis*-$[Co(NH_3)_4(NO_2)_2]NO_3$ was δ_{11} while it was δ_{33} for *cis*-$[Co(NH_3)_4CO_3]NO_3$. With a β value of 4° for *cis*-$[Co(NH_3)_4CO_3]NO_3$, the principal component of the efg lies close to the principal director of the chemical shift tensor, and may, in fact, lie along a Co—NH_3 bond. In the other two complexes, the principal director of the chemical shift tensor does not lie along the principal component of the efg tensor. For Na[Co(edta)], a similar case to that of *trans*-$[Co(NH_3)_4(NO_2)_2]NO_3$ was observed, in that the chemical shift tensor was not symmetric and there was not a true principal director in the complex. For *cis*-$[Co(NH_3)_4(NO_2)_2]NO_3$ the principal component of the efg was not very different from eq_{11} since η_Q is 0.9. Therefore, the principal component of the efg and the principal director of the chemical shift tensor are not relevant to these two complexes.

In attempting to understand the origin of chemical shift tensors, it is beneficial to determine planes that are responsible for specific magnitudes of the principal components of

© 2001 NRC Canada

Fig. 5. Solid-state ^{59}Co NMR spectra at 4.7 and 11.75 T: (*a*) $[Co(en)_3]Cl_3$, (*b*) *trans*-$[Co(NH_3)_4(NO_2)_2]NO_3$, (*c*) *cis*-$[Co(NH_3)_4(NO_2)_2]NO_3$, (*d*) $[Co(NH_3)_5NO_2]Cl_2$, (*e*) $Na_3[Co(NO_2)_6]$, (*f*) $[Co(NH_3)_5Cl]Cl_2$, (*g*) $[Co(NH_3)_5(CO_3)]NO_3{\cdot}1/2H_2O$, (*h*) *cis*-$[Co(NH_3)_4CO_3]NO_3$, (*i*) Na[Co(edta)], and (*j*) $Co(acac)_3$.



© 2001 NRC Canada

Table 2. Comparison of solid-state and solution ^{59}Co NMR results.

Compound	$\delta_{iso(solution)}$[a] (ppm)	$\delta_{iso(solid)}$ (ppm)	$\chi_{solution}$[a] (MHz)	χ_{solid} (MHz)	Ω (ppm)
$[Co(NH_3)_5(NO_2)]Cl_2$	7565	7498	1.87	12.25	270
$Co(acac)_3$	12 570	12 497	2.88	5.5	1190
trans-$[Co(NH_3)_4(NO_2)_2]NO_3$	7175	7072	4.01	12	330
cis-$[Co(NH_3)_4(NO_2)_2]NO_3$	7227	7170	4.10	12	420
$[Co(NH_3)_5(CO_3)]NO_3 \cdot 1/2H_2O$	9053	8972	7.57	20	2055
cis-$[Co(NH_3)_4(CO_3)]NO_3$	9662	9645–9667	7.81	18	1305
$[Co(NH_3)_5Cl]Cl_2$	8793	8930	9.79	29	1560
Na[Co(edta)]	10 237	10 330	11.1	35	2745

[a]Taken from ref. 26.

the chemical shift tensors. Each principal component of a chemical shift tensor depends on electronic excitations, specifically magnetic-dipole-allowed *d–d* transitions, in the plane perpendicular to its axis. Using the data from this study, the following ligand planes have been determined to give rise to specific values of chemical shifts: (*i*) a four-nitrogen (4-N) plane gives rise to shifts between 6910–7890 ppm, (*ii*) a 3-N 1-O or 3-N 1-Cl plane gives rise to shifts between 8860–9805 ppm, (*iii*) a 2-N 2-O plane gives rise to shifts between 9910–10165 ppm, and (*vi*) a 4-O plane gives rise to shifts between 12030–13185 ppm. The range of the 2-N 2-O plane may be increased as high as 11870 ppm if one assumes that of the chemical shift tensor of Na[Co(edta)] was a result of a 2-N 2-O plane; however, it is not clear that this orientation for the δ_{11} component can be assigned from the results presented in Table 1.

As stated earlier, with DFT calculations now available, experimental data of this quality are needed to aid in the improvement of the calculations. Of the ten complexes studied here, ab initio calculations have been reported for four: $Co(NO_2)_6^{3-}$, $Co(en)_3^{3+}$, $Co(acac)_3$, and *cis*-$Co(NH_3)_4CO_3^+$ (5, 6). The first three of these complexes should be readily calculated because all of the ligands of Co are the same (either six nitrogens or oxygens). Both Chan and Au-Yeung (5) as well as Godbout and Oldfield (6) have calculated the chemical shielding tensors of $Co(acac)_3$. The calculations of the span of the chemical shift tensor by Chan and Au-Yeung agree reasonably well with our experimental CS tensor (approximately 10% too small), while Godbout and Oldfield's is smaller by almost 25%. Both groups have also calculated the shielding tensor of *cis*-$Co(NH_3)_4CO_3^+$, however, they both report spans (Ω) that are greater than those measured experimentally (contrary to both groups predicting smaller spans for the compound) and Godbout and Olfield's calculations are significantly better in this case. This discrepancy may result from the different counterion (Br^-) present in the experimental single-crystal diffraction goemetries (32) used in the calculations and the NO_3^- counterion in the complex characterized experimentally by solid-state NMR here. Godbout and Oldfield have also calculated the tensors of $Co(NO_2)_6^{3-}$ and $Co(en)_3^{3+}$; however, their calculated tensors are not axially symmetric (which they have to be by crystal symmetry) and differ by approximately 200 ppm in both cases (too small for $Co(NO_2)_6^{3-}$ while too large for $Co(en)_3^{3+}$).

A comparison between the solution and solid-state ^{59}Co NMR results is also instructive. The solid-state isotropic chemical shifts (δ_{iso}) can be obtained from the average of the principal components of the chemical shift tensors. Table 2 shows the solution and solid-state NMR δ_{iso}s, χs, and Ωs. From Table 2 one can see that the isotropic chemical shifts in solution and in the solid-state are all within approximately 100 ppm, which is close considering the large chemical shift range for cobalt. There is no trend observed between the isotropic shifts and the χs, but Ω, in general, increases with increasing χ. For convenience in this discussion, we will assume that the values of χ are positive in both solution and solid-state; the only real consequence of this is the assumption that their values will be of *the same sign* in solution and solid, which appears to be reasonable. The solid-state χs are much larger than those measured in solution. This could be due to several factors, including a change in geometry and (or) conformation between solution and solid states, or that the solid-state values in Table 2 are measured directly from a spectrum while the solution values are measured indirectly from the relaxation studies. In fact, the value of $\chi_{solution}$ includes any contribution from asymmetry in the quadrupolar coupling constants, via the term $(1 + \eta_Q^2/3)^2$ in the spin-lattice relaxation expression (26); since η_Q lies in a range from 0 to 1, estimates of χ from solution relaxation data are upper-bound estimates, with the "true" χ up to 13.3% less. In addition, $\chi_{solution}$ is only as good as the correlation time measured, which, in the relaxation studies, was obtained from the carbon T_1s of two complexes since T_1 minima could not be reached due to temperature limitations of the solvent. Another possible origin of the differences between solution and solid-state data is changes in either intramolecular, intermolecular, or both contributions to observed values. Since the isotropic shifts are consistent between solution and solid-state, and chemical shielding is predominantly a local phenomenon, the intramolecular term should be constant between phases. Intermolecular effects could arise from interactions between two (or more) solute molecules, or between a solute molecule and a solvent molecule. Since $\chi_{solution}$ is less than χ_{solid}, one might take this as evidence that the intermolecular χ has a negative sign, but if one uses the arguments of Osten and Jameson (33), one would expect that intermolecular effects would increase as concentration increases, as observed in the ^{59}Co relaxation of Na[Co(edta)] (26). At maximum concentration (a solid) the largest χ is observed, and, therefore, the intermolecular χ is positive between solute molecules. Thus, if there is an influence from the solvent on χ, it must be negative.

© 2001 NRC Canada

Conclusions

Solid-state ^{59}Co NMR spectra of ten simple inorganic cobalt(III) complexes have been obtained at 11.75 and, in most cases, at 4.7 T as well. From the spectra, their ^{59}Co CS and efg tensors have been determined. The isotropic chemical shifts in the solid-state are close to those found in solution considering the large chemical shift range for cobalt. The quadrupolar coupling constants determined from the solid-state spectra were all larger than those determined from the ^{59}Co relaxation studies, but the spans of the CS tensors were, in general, found to increase with increasing quadrupolar coupling constants. Several ligand planes responsible for specific chemical shifts have been determined. The planes are (*i*) 4-N plane gives rise to shifts between 6910–7890 ppm, (*ii*) 3-N 1-O or 3-N 1-Cl plane gives rise to shifts between 8860–9805 ppm, (*iii*) 2-N 2-O plane gives rise to shifts between 9910–10165 ppm (possibly up to 11870 ppm), and (*vi*) 4-O plane gives rise to shifts between 12030–13185 ppm.

Acknowledgments

We thank Dr. Arthur J. Carty (National Research Council of Canada) for his gift of $[Co(NH_3)_5(NO_2)]Cl_2$ and Dr. Patricia Aroca-Ouellette (University of Toronto) for her assistance in using the DSX-200. We are also grateful to the Natural Sciences and Engineering Research Council of Canada (NSERC) for financial assistance in the form of operating and equipment grants.

References

1. J.C.C. Chan and S.C.F. Au-Yeung. Annu. Rep. NMR Spectrosc. **41**, 1 (2000).
2. Y. Ruiz-Morales, G. Schreckenbach, and T. Ziegler. J. Phys. Chem. **101**, 4121 (1997).
3. M. Buhl. Organometallics **16**, 261 (1997).
4. J.C.C. Chan and S.C.F. Au-Yeung. J. Mol. Struct.: THEOCHEM. **393**, 93 (1997).
5. J.C.C. Chan and S.C.F. Au-Yeung. J. Phys. Chem. A, **101**, 3637 (1997).
6. N. Godbout and E. Oldfield. J. Am. Chem. Soc. **119**, 8065 (1997).
7. H.W. Spiess, H. Hass, and H. Hartmann. J. Chem. Phys. **50**, 3057 (1969).
8. H.W. Spiess and R.K. Sheline. J. Chem. Phys. **53**, 3036 (1970).
9. E.S. Mooberry, M. Pupp, J.L. Slater, and R.K. Sheline. J. Chem. Phys. **55**, 3655 (1971).
10. E.S. Mooberry and R.K. Sheline. J. Chem. Phys. **56**, 1852 (1972).
11. E.C. Reynhardt. Can. J. Phys. **52**, 1398 (1974).
12. E.C. Reynhardt. J. Phys. Chem. **7**, 4135 (1974).
13. K. Eichele, J.C.C. Chan, R.E. Wasylishen, and J.F. Britten. J. Phys. Chem. A, **101**, 5423 (1997).
14. D.R. Eaton, R.J. Buist, and B.G. Sayer. Can. J. Chem. **65**, 1332 (1987).
15. W.P. Power, R.E. Wasylishen, S. Mooibroek, B.A. Pettitt, and W. Danchura. J. Phys. Chem. **94**, 591 (1990).
16. J.T. Cheng, J.C. Edward, and P.D. Ellis. J. Phys. Chem. **94**, 553 (1990).
17. S.C. Chung, J.C.C. Chan, S.C.F. Au-Yeung, and X.-P. Xu. J. Phys. Chem. **97**, 12685 (1993).
18. P. Zhou, S.C.F. Au-Yeung, and X.-P. Xu. J. Am. Chem. Soc. **121**, 1030 (1999).
19. J. Hirschinger and P. Granger, J. Rosé. J. Phys. Chem. **96**, 4815 (1992).
20. P. Kempgens, J. Hirschinger, K. Elbayed, J. Raya, P. Granger, and J. Rosé. J. Phys. Chem. **100**, 2045 (1996).
21. P. Ganguly, T.N. Venkatraman, P.R. Rajamohanan, and S. Ganapathy. J. Phys. Chem. B, **101**, 11099 (1997).
22. A. Medek, V. Frydman, and L. Frydman. J. Phys. Chem. B, **101**, 8959 (1997).
23. A. Mekek, V. Frydman, and L. Frydman. Proc. Natl. Acad. Sci. U.S.A. **94**, 14242 (1997).
24. A. Medek, V. Frydman, and L. Frydman. J. Phys. Chem. A, **103**, 4830 (1999).
25. W.P. Power, C.W. Kirby, and N.J. Taylor. J. Am. Chem. Soc. **120**, 9428 (1998).
26. C.W. Kirby, C.M. Puranda, and W.P. Power. J. Phys. Chem. **100**, 14618 (1996).
27. D.W. Alderman, M.S. Solum, and D.M. Grant. J. Chem. Phys. **84**, 3717 (1986).
28. M.J. Frisch, G.W. Trucks, H.B. Schlegel, P.M.W. Gill, B.G. Johnson, M.A. Robb, J.R. Cheeseman, T. Keith, G.A. Petersson, J.A. Montgomery, K. Raghavachari, M.A. Al-Laham, V.G. Zakrzewski, J.V. Ortiz, J.B. Foresman, J. Cioslowski, B.B. Stefanov, A. Nanayakkara, M. Challacombe, C.Y. Peng, P.Y. Ayala, W. Chen, M.W. Wong, J.L. Andres, E.S. Replogle, R. Gomperts, R.L. Martin, D.J. Fox, J.S. Binkley, D.J. Defrees, J. Baker, J.P. Stewart, M. Head-Gordon, C. Gonzalez, and J.A. Pople. GAUSSIAN 94, Rev. D.4. GAUSSIAN, Inc. Pittsburgh, PA. (1995).
29. P.A. Whuler, C. Brouty, P. Spinat, and P. Herpin. Acta Crystallogr. **B31**, 2069 (1975).
30. Y. Okaya, R. Pepinsky, Y. Takeuchi, H. Kiroya, A. Shimada, P. Gallitelli, N. Stemple, and A. Beevers. Acta Crsystallogr. **10**, 798 (1957).
31. G.J. Kruger, E.C. Reynhardt. Acta Crystallogr. **B30**, 822 (1974).
32. G.A. Barclay and B.F. Hoskins. J. Chem. Soc. 586 (1962).
33. H.J. Osten and C.J. Jameson. Mol. Phys. **57**, 553 (1986).
34. J.B. Work and J.P. McReynolds. Inorg. Synth. **2**, 221 (1946).
35. G.B. Kauffman, S.F. Abbott, S.E. Clark, J.M. Gibson, and R.S. Meyers. Inorg. Synth. **18**, 69 (1978).
36. G. Schessinger. Inorg. Synth. **6**, 173 (1960).
37. M. Kimura and I. Miyamoto. Bull. Chem. Soc. Jpn. **67**, 2136 (1994).

© 2001 NRC Canada

The reduction of I_2 by H_2O_2 in aqueous solution

J.M. Ball and J.B. Hnatiw

Abstract: The reduction of I_2 by hydrogen peroxide, a primary water radiolysis product, has been identified as a key reaction that would influence iodine volatility in nuclear reactor accident conditions (1–3). Although there have been a number of studies of the reduction of I_2, there exists a great degree of controversy regarding the intermediates involved, the effect of buffers, and the general rate law (1–9). Because the rates and the mechanism of this reaction are important in predicting the pH dependence of iodine behaviour in reactor containment building after a postulated reactor accident, we have undertaken a kinetic study of I_2 reduction by H_2O_2 in aqueous solution over a pH range of 6–9. The experiments were performed using stopped-flow instrumentation and monitoring the decay of I_3^- spectrophotometrically. The effects of buffer catalysis have been examined by comparison of kinetic data obtained in sodium barbital (5,5-diethylbarbituric acid), disodium citrate, and disodium hydrogen phosphate buffers. The effect of buffers, combined with the complex acid dependence of the rate law, explains many of the discrepancies reported in earlier literature.

Key words: hydrogen peroxide, molecular iodine, kinetics, iodine volatility.

Résumé : On a identifié la réduction de I_2 par le peroxyde d'hydrogène, un produit de radiolyse primaire de l'eau, comme une réaction clé qui pourrait influencer la volatilité de l'iode dans des conditions d'accident d'un réacteur nucléaire (1–3). Même s'il y a déjà eu plusieurs études de la réduction, il y a encore un grand degré de controverse concernant les intermédiaires impliqués, l'effet des tampons et la loi générale de vitesse (1–9). Compte tenu du fait que les vitesses et le mécanisme de cette réaction sont importants pour prédire la relation entre le comportement de l'iode et le pH dans un édifice permettant de contenir un réacteur après un accident de réacteur présumé, on a entrepris une étude cinétique de la réduction du I_2 par H_2O_2, en solution aqueuse, à des pH allant de 6 à 9. On a réalisé les expériences à l'aide d'instruments à flux stoppé et on a suivi la disparition de l'ion I_3^- de façon spectrophotométrique. On a étudié les effets de catalyse par des tampons en faisant une comparaison des données cinétiques obtenues dans des tampons de barbital sodique (acide 5,5-diéthylbarbiturique), de citrate disodique et de phosphate d'hydrogène disodique. L'effet des tampons, combiné à la relation complexe entre le degré d'acidité et la loi de vitesse, permet d'expliquer beaucoup de disparités rapportées dans la littérature antérieure.

Mots clés : peroxyde d'hydrogène; iode moléculaire; cinétique; volatilité de l'iode.

[Traduit par la Rédaction]

Introduction

Iodine species are important in the assessment of the radiological consequences of a nuclear reactor accident because the radiologically toxic ^{131}I is one of the most abundant fission products that would be released from fuel. Iodine also has the potential to form numerous volatile species, which, once airborne in containment, could be released to the atmosphere through containment leakage or during controlled venting.

The reduction of iodine by peroxide in aqueous solutions has been recognized as an important process that would govern iodine volatility in containment after a reactor accident. The reaction has,therefore, been recently investigated as part of a number of reactor safety research programs (1–3). A large body of early literature also exists regarding the iodine–peroxide couple because of its role in the Bray–Liebhafsky oscillatory reactions, which were discovered in 1921 (4–8). Unfortunately, there is no consensus in the literature on a mechanism for the reaction, and in cases where the same general rate law is reported, calculated rate constants vary by two orders of magnitude (5, 6). Moreover, much of the experimental data obtained to date has been in acidic or neutral solutions, conditions which may not be representative of containment in a reactor accident scenario.

Studies of the kinetics of iodine reduction by peroxide in the pH range 2–7 have been performed by Shiraishi et al. (1), Abel (4), and Liebhafsky (5). Abel (4) and Liebhafsky (5) derived general rate laws in which iodine reduction exhibited a $1/[H^+]^2$ dependence, consistent with their proposed reaction scheme in which peroxide, or the peroxodyl anion (HO_2^-) reacts with either the hypoiodite anion (OI^-), or with hypoiodite (HOI).[2]

$$[1] \quad I_2 + H_2O \rightleftharpoons HOI + I^- + H^+$$

$$[2] \quad HOI \rightleftharpoons OI^- + H^+$$

Received February 18, 2000. Published on the NRC Research Press Web site on April 6, 2001.

J.M. Ball[1] and J.B. Hnatiw. AECL, Chalk River Laboratories, Fuel Safety Branch, Chalk River, ON K0J 1J0, Canada.

[1]Corresponding author (telephone: (613) 584-3311 ext. 3874; fax: (613) 584-1220; e-mail: ballj@aecl.ca).

[2]The effect of oxidation of I^- by H_2O_2 ($H_2O_2 + I^- \rightarrow HOI + OH^-$) on the kinetics of reduction of I_2 were accounted for by Liebhafsky, but were negligible in the other studies. In neutral to basic solution, with $[I^-]$ less than 10^{-2} M the reaction is slow, since the rate constant is small (0.012 M^{-1} s^{-1} (1)).

 DOI: 10.1139/cjc-79-3-304 © 2001 NRC Canada

Table 1. Experimental conditions for measurements of the rate of loss of I_3^- from buffered solutions containing I_2, I^-, and H_2O_2[a].

Experiment	Initial $[I^-]$ (M)	Initial $[I_2]$ (M)	$[I_3^-]$[b] (M)	Initial $[H_2O_2]$ (M)	Buffer	Buffer conc. (M)	Temp. (°C)	pH range
1	5×10^{-4}	1×10^{-5}	2.6×10^{-6}	1×10^{-3}	barbital	5×10^{-3}	25	6.5–9
2	5×10^{-4}	1×10^{-5}	2.6×10^{-6}	1×10^{-3}	barbital	2.5×10^{-3}	25	6.5–9
3	5×10^{-4}	1×10^{-5}	2.6×10^{-6}	1×10^{-3}	barbital	7.5×10^{-3}	25	6.5–9
4	5×10^{-4}	1×10^{-5}	2.6×10^{-6}	1×10^{-3}	barbital	1×10^{-2}	25	6.5–9
5	1×10^{-3}	1×10^{-5}	4×10^{-6}	1×10^{-3}	barbital	5×10^{-3}	25	6.5–9
6	2.5×10^{-4}	1×10^{-5}	1.5×10^{-6}	1×10^{-3}	barbital	5×10^{-3}	25	6.5–9
7	5×10^{-4}	1×10^{-5}	2.6×10^{-6}	1×10^{-4}	barbital	1×10^{-2}	25	6.5–9
8	5×10^{-4}	1×10^{-5}	2.6×10^{-6}	5×10^{-3}	barbital	1×10^{-2}	25	6.5–9
9	5×10^{-4}	1×10^{-5}	2.6×10^{-6}	1×10^{-3}	citrate	1×10^{-2}	25	6–7
10	2.5×10^{-4}	1×10^{-5}	1.5×10^{-6}	1×10^{-3}	citrate	1×10^{-2}	25	6–7
11	1×10^{-3}	1×10^{-5}	4×10^{-6}	1×10^{-3}	citrate	1×10^{-2}	25	6–7
12	5×10^{-4}	1×10^{-5}	2.6×10^{-6}	5×10^{-3}	citrate	1×10^{-2}	25	6–7
13	5×10^{-4}	1×10^{-5}	2.6×10^{-6}	1×10^{-3}	citrate	2×10^{-2}	25	6–7
14	5×10^{-4}	1×10^{-5}	2.6×10^{-6}	1×10^{-3}	phosphate	5×10^{-2}	25	6–8.5
15	1×10^{-3}	1×10^{-5}	4×10^{-6}	1×10^{-3}	phosphate	5×10^{-2}	25	6–8.5
16	5×10^{-4}	1×10^{-5}	2.6×10^{-6}	5×10^{-3}	phosphate	5×10^{-2}	25	6–8.5
17	5×10^{-4}	1×10^{-5}	2.6×10^{-6}	1×10^{-3}	phosphate	2×10^{-2}	25	6–8.5
18	5×10^{-4}	1×10^{-5}	2.6×10^{-6}	1×10^{-3}	phosphate	5×10^{-2}	15	6–8.5
19	5×10^{-4}	1×10^{-5}	2.6×10^{-6}	1×10^{-3}	phosphate	5×10^{-2}	35	6–8.5
20	5×10^{-4}	1×10^{-5}	2.6×10^{-6}	1×10^{-3}	phosphate	5×10^{-2}	42	6–8.5

[a]Ionic strength was maintained at 0.2 M with $NaClO_4$.
[b]Calculated from eq. [10] and confirmed spectrophotometrically.

[3] $HOI + HO_2^- \rightarrow I^- + O_2 + H_2O$

[4] $OI^- + H_2O_2 \rightarrow I^- + O_2 + H_2O$

Deviations from the $1/[H^+]^2$ rate law derived from the above equations were reported by Shiraishi et al. (1) who measured the overall rate of the reduction by observing the rate of loss of I_3^- from solutions containing I_2 and I^- at pH 6 to 7. He explained his observation by incorporating rxns. [5]–[7] to the above reaction scheme.

[5] $I_2 + I^- \rightleftharpoons I_3^-$

[6] $I_2 + OH^- \rightleftharpoons I_2OH^- \rightleftharpoons HOI + I^-$

[7] $I_2OH^- + H_2O_2 \rightarrow 2I^- + O_2 + H_3O^+$

In experiments performed at pH 7 and 9, Kessi-Rabia et al. (6) observed that the rate of iodine reduction exhibited a $1/[H^+]$ dependence. His proposed reaction scheme was identical to that reported by Liebhafsky (5) (see rxns. [1]–[5]), but he suggested that the simple inverse dependence upon $[H^+]$ arose as a result of the forward rate of rxn. [1] becoming rate determining at pH 7 and above (i.e., a rapid equilibrium cannot be assumed for the hydrolysis of iodine represented in rxn. [1]).

Preliminary stopped-flow studies performed in our laboratories (9) confirmed that the rate law for the reduction of I_2 by H_2O_2 in the pH range of 6–9 deviates from the $1/[H^+]^2$ relationship reported in refs. 1, 5, and 6. However, the peroxide and buffer dependencies of the rates observed in ref. 9 were not accounted for by the reaction scheme suggested by Kessi-Rabia et al. (7). We, therefore, performed a more complete study of the kinetics of the reduction as a function of acid, peroxide, iodide, and buffer concentration in three buffers to attempt to derive a rate law that describes the reduction over a large range of conditions.

Experimental

Iodine (I_2) (99.999%), sodium hydroxide (99.99%), and dihydrogen sodium phosphate (99.99%) were used as purchased from Aldrich. Sodium iodide (99.99%) was purchased from Aldrich and dried at 100°C overnight prior to use. Sodium citrate (99.99%) was standardized by titration with sodium hydroxide. Sodium perchlorate (99.99%) was standardized by passing a 2 M solution through an ion exchange resin, and titrating the resulting acid. Hydrogen peroxide was purchased as a 30% solution from Mallinkrodt and standardized by titration with potassium permanganate solution. Sodium barbital (97.5%) was purchased from BDH and dried overnight prior to use. All reagents and reaction solutions were diluted in water purified with a Milli-Q reagent grade water system.

Kinetic studies were performed using a Hi-Tech Scientific SF-61MX stopped-flow multi mixing unit and a Hi-Tech Scientific M300 monochromator spectrophotometer. Stock solutions containing I_2 and I^- were prepared, and the desired concentration of the resulting I_3^- solution obtained by dilution with water purged with argon. I_3^- solutions were analyzed spectrophotometrically prior to each use (adsorption 353 nm, $\varepsilon = 27500\ M^{-1}\ cm^{-1}$). They were then placed in one of the stopped-flow solution reservoirs. For every measurement, the I_3^- solution was mixed in the stopped flow apparatus with equal volumes of pH adjusted solutions containing peroxide and buffer, adjusted to 0.2 M ionic strength with sodium perchlorate, and purged with argon. Solution reservoirs drive syringes and observation cells were temperature controlled using a circulating water bath. All solutions were

© 2001 NRC Canada

temperature stabilized to the desired temperature (±0.2°C) prior to each test run.

Reactant concentrations were chosen such that the reaction was pseudo first-order in I_2 (i.e., an excess of H_2O_2 and I^- were used). The decay of I_3^- (which is assumed to be in rapid equilibrium with I_2 and its hydrolysis products (1, 11)) was monitored at various pH values for a given set of conditions by measuring its absorbance at 353 nm using a tungsten light source. Initial concentrations and conditions for each experiment are presented in Table 1.

At each pH, six to twelve repetitive runs using the same solution and operating conditions were averaged and fitted with a built-in fitting function to obtain a first-order decay rate constant (k_{obs}). All of the decay curves obeyed first-order kinetic behaviour up to about three half-lives. The variance of each decay profile with the mean absorbance vs. time plot ranged from about 1–10% of the total absorbance. However the deviation of individual first-order decay rates from the average decay rate was less than 5%.

Results and discussion

Derivation of a rate law

Figure 1 shows the $[H^+]$ dependence of the observed pseudo-first-order rate constant for decay of I_3^- (k_{obs}) from solutions initially containing I_3^- (2.6×10^{-6} M) and H_2O_2 (1×10^{-3} M) buffered with 5×10^{-3} M barbital buffer. A plot of k_{obs} vs. $1/[H^+]^2$ (Fig. 1*a*) demonstrates that the overall rate constant deviates significantly from a $1/[H^+]^2$ dependence. This would not be the case if the reaction schemes, proposed in refs. 1, 5, and 6, were valid. A more convenient plot for extracting kinetic information is shown in Fig. 1*b* where $[H_2O_2]/k_{obs}[H^+]$ is plotted against $[H^+]$. To a first approximation, $1/k_{obs}[H^+]$ varies linearly with $[H^+]$. From Fig. 1*b*, the relationship in eqs. [8] and [9] are evident.

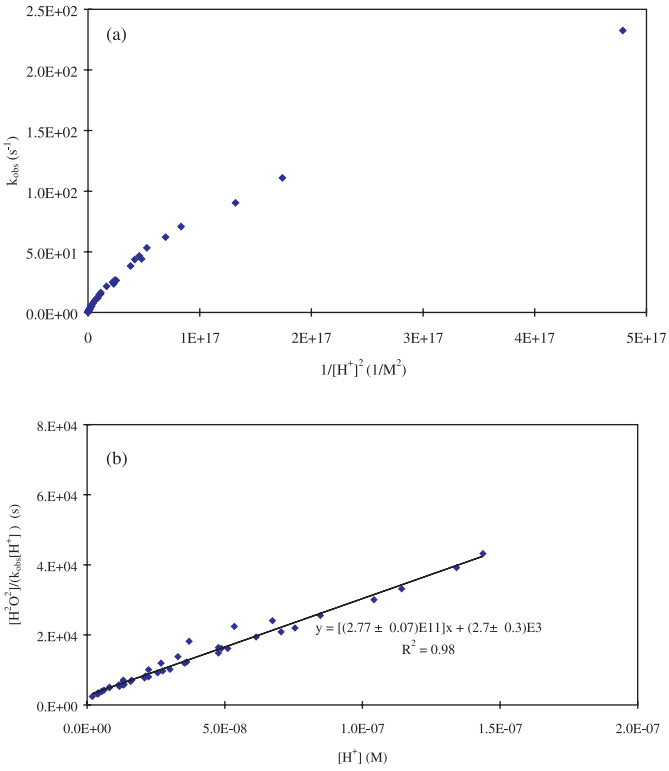
$$[8] \qquad \frac{1}{k_{obs}[H^+]} \propto k'[H^+] + k''$$

$$[9] \qquad \frac{1}{k_{obs}} \propto k'[H^+]^2 + k''[H^+]$$

The effects of the peroxide and the iodide concentrations on the rate of reduction of I_2 by peroxide are shown in Figs. 2 and 3. The dependence of the reduction rate on the concentrations of these species implies that the rate-determining step must have both an iodide and peroxide concentration dependence. The mechanism proposed by Kessi-Rabia et al. (6), in which the forward rate of the iodine hydrolysis equilibrium (rxn. [1]) is the rate-determining step, is, therefore, ruled out as a possible mechanism.

The qualitative behaviour exhibited in Figs. 1–3 can be accounted for by a reaction mechanism analogous to that proposed by Connick (10) for the reduction of Cl_2 by H_2O_2.

Fig. 1. Plots of (*a*) k_{obs} (the psuedo-first-order rate constant for loss of I_3^- from solutions containing H_2O_2) vs. $1/[H^+]$ and (*b*) $[H_2O_2]/k_{obs}[H^+]$ vs. $[H^+]$ for initial concentrations of 1×10^{-5} M I_2, 5×10^{-4} M I^-, 5×10^{-3} M sodium barbital, and 1×10^{-3} M H_2O_2 at 25°C. A linear least-squares fit of the data is shown in (*b*).



The mechanism involves the formation of IO_2H as an intermediate, and could occur by reaction of molecular iodine or one of its hydrolysis products (I_2OH^- or HOI) with peroxide, or perhydroxy radical. For example:

Scheme 1[2]

$$[10] \qquad I_2 + I^- \rightleftharpoons I_3^-$$

$$[11a] \qquad I_2 + OH^- \rightleftharpoons I_2OH^-$$

$$[11b] \qquad I_2OH^- \rightleftharpoons HOI + I^-$$

$$[12] \qquad I_2OH^- + H_2O_2 \rightleftharpoons I^- + IO_2H + H_2O$$

$$[13] \qquad IO_2H + OH^- \rightarrow I^- + H_2O + O_2$$

Alternatively, reaction of the I_2 hydrolysis product (HOI) with H_2O_2 to form the intermediate IO_2H could occur, in which case rxn. [12] would be replaced by:

[2] The direct reaction of I_2 with HO_2^- could also be invoked. In this kinetically equivalent scheme rxns. [11*a*], [11*b*], and [12] in Scheme 1 could be replaced with:

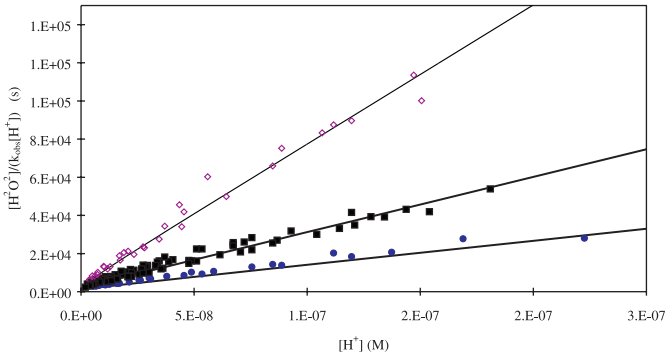
Scheme 1′

$$[11] \qquad H_2O_2 \rightleftharpoons HO_2^- + H^+$$

$$[12] \qquad I_2 + HO_2^- \rightleftharpoons IO_2H + I^-$$

© 2001 NRC Canada

Fig. 2. Iodide concentration dependence of $[H_2O_2]/k_{obs}[H^+]$ vs. $[H^+]$ at 25°C. Initial concentrations used were: 1×10^{-5} M I_2, 5×10^{-3} M sodium barbital, and 1×10^{-3} M H_2O_2 with 2.5×10^{-4} (●), 5×10^{-4} (■), and 1×10^{-3} (◇) M I^-. Unbroken lines represent values calculated using the rate law from Scheme 1 and the rate constants from Table 2.



Scheme 2

[12′] $HOI + H_2O_2 \rightleftharpoons IO_2H + H_2O$

Scheme 2 leads to rate expression that is slightly different from that of Scheme 1 because the concentration of the iodine species (HOI) in the rate-determining step has an iodide dependence due to *both* equilibrium rxns. [10] and [11b].

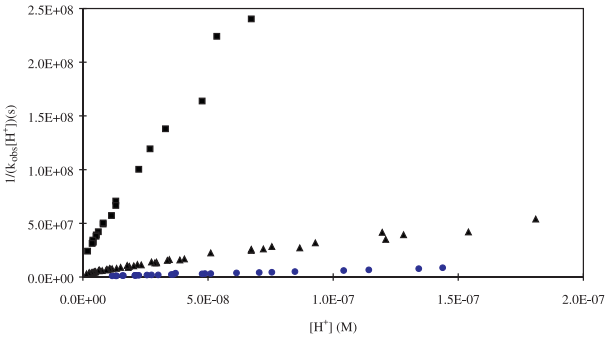
For either Scheme 1 or 2, the overall rate of reduction of I_2 by peroxide ($d[O_2]/dt$) may be expressed as the sum of loss of I_2, I_3^-, I_2OH^-, and HOI from solution. Assuming a rapid equilibrium between I_2, its hydrolysis products (I_2OH^- and HOI), and I_3^- (3), the overall rate can be expressed in terms of the measured rate of loss of I_3^- ($-d[I_3^-]/dt$ or $k_{obs}[I_3^-]$)[3]:

$$[14] \quad \frac{dO_2}{dt} = -k_{13}[IO_2H][OH^-] = \left(1 + \frac{1}{K_{10}[I^-]} + \frac{k_{11a}[OH^-]}{K_{10} - [I^-]} + \frac{K_{11a}K_{11b}[OH^-]}{K_{10}[I^-]^2}\right)\frac{d[I_3^-]}{dt}$$

The values of K_{10} (700 (13)), K_{11a} (2.9×10^4 (11)), and K_{11b} (1.7×10^{-3} (1)) are such that, for the pH range 6–9 and iodide concentrations from 2.5×10^{-4} to 1×10^{-3} M employed in these experiments, the second two terms in brackets on the right side of eq. [14] can be ignored to give:

$$[15] \quad \frac{d[O_2]}{dt} = \left(1 + \frac{1}{K_{10}[I^-]}\right)k_{obs}[I_3^-] = k_{13}[IO_2H][OH^-]$$

Fig. 3. Peroxide concentration dependence of $1/k_{obs}[H^+]$ vs. $[H^+]$ at 25°C. Initial concentrations used were: 1×10^{-5} M I_2, 5×10^{-4} M I^-, and 5×10^{-3} M sodium barbital with 5×10^{-3} (●), 1×10^{-3} (▲), and 1×10^{-4} (■) M H_2O_2.



Assuming the reaction proceeds via Scheme 1, and using a steady state approximation to solve for the concentration of IO_2H leads to the expression:

$$[16] \quad k_{obs} = \frac{K_w^2 K_{11} k_{12} k_{13}}{k_{13}K_w[H^+] + k_{-12}[I^-][H^+]^2}\left(\frac{[H_2O_2]}{1 + K_{10}[I^-]}\right)$$

where K_w is the dissociation constant for water, and K_{11} is either the formation constant for I_2OH^- (K_{11a}, Scheme 1) or the dissociation constant for H_2O_2 (Scheme 1′, footnote 2). The equation may be rearranged to give the plotting form used in Figs. 1–3:

$$[17] \quad \frac{[H_2O_2]}{k_{obs}} = (1 + K_{10}[I^-])\left(\frac{k_{-12}[I^-][H^+]}{K_w^2 K_{11} k_{12} k_{13}} + \frac{1}{k_{12}K_{13}K_w}\right)$$

A plot of $[H_2O_2]/k_{obs}[H^+]$ vs. $[H^+]$ should, therefore, give a straight line with:

$$[18] \quad \text{slope} = \frac{(1 + k_{10}[I^-])(k_{-12}[I^-])}{K_w^2 K_{11} k_{12} k_{13}}$$

$$[19] \quad \text{intercept} = \frac{1 + K_{10}[I^-]}{K_{11}k_{12}K_w}$$

If Scheme 2 is the mechanism, the rate law is :

$$[20] \quad \frac{[H_2O_2]}{k_{obs}[H^+]} = (1 + K_{10}[I^-])\left(\frac{k_{-12}[I^-][H^+]}{K_w^2 K_{11} k_{12} k_{13}} + \frac{[I^-]}{k_{12}K_{10}K_w}\right)$$

where K_{11} is $K_{11a} \times K_{11b}$. A plot of $[H_2O_2]/k_{obs}[H^+]$ vs. $[H^+]$ should give a straight line with

[3] The substitutions used are:

$$-\frac{d[I_2]}{dt} = \frac{1}{K_{10}[I^-]}\frac{d[I_3^-]}{dt},$$

$$\frac{d[I_2OH^-]}{dt} = K_{11a}[OH^-]\frac{d[I_2]}{dt} = \frac{K_{11a}[OH^-]}{K_{10}[I^-]}\frac{d[I_3^-]}{dt}$$

$$\frac{d[HOI]}{dt} = K_{11a}K_{11b}\frac{[OH^-]}{[I^-]}\frac{d[I_2]}{dt} = \frac{K_{11a}K_{11b}[OH^-]}{K_{10}[I^-]^2}\frac{d[I_3^-]_4}{dt}$$

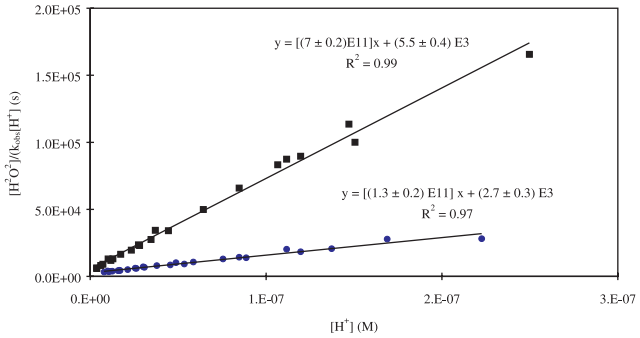
© 2001 NRC Canada

Table 2. Estimated rate constants[a] (using Scheme 1 as a mechanism) for the reduction of I_2 by H_2O_2 in aqueous solution.

Buffer	Barbital	Citrate	Phosphate	ΔE_a (kJ M^{-1})
k_{12} (M^2 s^{-1}) [a]	(2.25 ± 0.27) × 10^6	(2.25 ± 0.27) × 10^6	(2.25 ± 0.27) × 10^6	31 ± 3
k_{-12} (M^2 s^{-1}) [b]	(1 ± 0.4) × 10^7	(1 ± 0.4) × 10^7	(1 ± 0.4) × 10^7	92 ± 10
k_{13} (M^2 s^{-1}) [b]	(2 ± 0.8) × 10^9	(2 ± 0.8) × 10^9	(2 ± 0.8) × 10^9	54 ± 6
k_{23} (M^2 s^{-1})[b]	(3 ± 1) × 10^5	(2 ± 1) × 10^4	(7 ± 2) × 10^4	91 ± 10 (phosphate)[c]

[a]From a linear least-squares fit of all of the data obtained with 2.5 × 10^{-4} and 5 × 10^{-4} M barbital buffer.
[b]Rate constants reported are those that provide a best fit to *all* of the available data. Rate constants obtained from non-linear least-squares fits to individual data sets (i.e., data obtained for a given set of conditions in Table 1) deviated from these values. The deviations are reported in brackets.
[c]From a linear least-squares fit of ln k vs. $1/T$ obtained at various temperatures in phosphate buffer.

Fig. 4. A plot of $[H_2O_2]/k_{obs}[H^+]$ vs. $[H^+]$ for1 × 10^{-5} M I_2, 1 × 10^{-3} M H_2O_2, and 5 × 10^{-3} M barbital buffer with 2.5 × 10^{-4} (●) and 1 × 10^{-3} (■) M I^- at 25°C. Linear least-squares fits to the data are shown.



$$[21] \quad \text{slope} = \frac{(1 + K_{10}[I^-])\, k_{-12}[I^-]}{K_w K_{11} k_{12} k_{13}}$$

$$[22] \quad \text{intercept} = \frac{[I^-] + K_{10}[I^-]^2}{K_{11} k_{12} K_w}$$

One can distinguish between Scheme 1 and 2 by the iodide dependence of the intercept value of plots of $[H_2O_2]/k_{obs}[H^+]$ vs. $[H^+]$. For citrate and phosphate buffer measurements, which used buffer concentrations of 0.01–0.05 M (to provide kinetic data comparable to that obtained in earlier investigations (1, 4, 5)), these plots deviated significantly from linearity at high pH values. The deviation, which arose due to the effect of buffer catalysis (see below), made it difficult to assign an "intercept" value to the experimental data. Fortunately, plots of data obtained using barbital buffer at lower concentrations (0.005 M) did not significantly deviate from linearity, and a linear least-squares fit of the data provided a reasonable estimate of the intercept. The linear least-squares fit of the data in Fig. 4 shows that the intercept values from data obtained using iodide concentrations of 2.5 × 10^{-4} and 1 × 10^{-3} M differ by a factor of about 2 (note that the ratio of the intercept values depends only upon the value used for $[I^-]$). This is much closer to the ratio of the intercept values expected for Scheme 1 (1.45) than for Scheme 2 (5.8). It should also be noted that it was not possible to use Scheme 2 to fit all of the data obtained from the three different buffer types, and various iodide and peroxide concentrations. For this reason, we believe the reaction proceeds via Scheme 1 and (or) the kinetically equivalent Scheme 1′ (footnote 2).

Fig. 5. Barbital buffer concentration dependence of $[H_2O_2]/k_{obs}[H^+]$ vs. $[H^+]$ at 25°C. Initial concentrations were: 5 × 10^{-4} M I^-, 1 × 10^{-5} M I_2, 1 × 10^{-3} M H_2O_2 with 2.5 × 10^{-3} (□) and 1 × 10^{-2} (×) M barbital buffer. Unbroken lines represent values calculated using the rate law from Scheme 1 and the rate constants from Table 2.

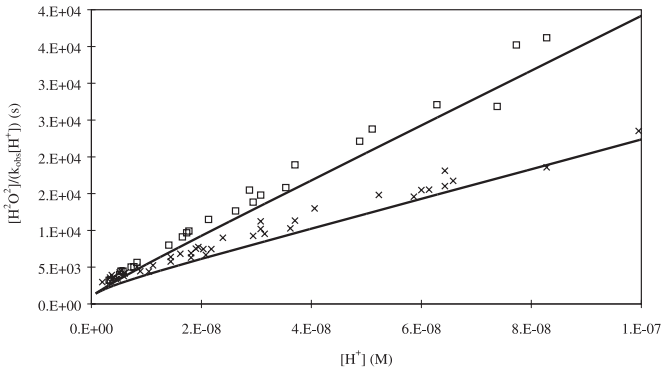


Figure 5 shows the effect of barbital buffer concentration on the rate of disappearance of I_3^- from a solution initially containing I_2 and I^- when mixed with H_2O_2. The plot of $[H_2O_2]/k_{obs}[H^+]$ vs. $[H^+]$, for two buffer concentrations demonstrates that the slope (eq. [18]) is sensitive to buffer concentration, whereas the intercept (eq. [19]) is not. Because the intercept is proportional to $1/K_{11}k_{12}K_w$, the data implies that neither rxn. [11] nor [12] can be participating in the catalysis step. Buffer catalysis by sodium barbital must therefore be due to catalysis of rxn. [13] alone. General base catalysis of the reaction by:

$$[23] \quad IO_2H + B^- \rightarrow I^- + BH + O_2$$

may be accommodated in the rate expression of eq. [16] by substituting:

$$k_{13}K_w = k_{13}K_w + k_{23}K_b[BH]:$$

where K_b is the buffer dissociation constant and B^- and BH are the basic and acidic forms of the buffer, respectively.

When buffer catalysis is included in eq. [17], the formulation for the slope and intercept of plots of $[H_2O_2]/k_{obs}[H^+]$ vs. $[H^+]$ become:

$$[24] \quad \text{slope} = \frac{(1 + K_{10}[I^-])(k_{-12}[I^-])}{K_w K_{11} k_{12}(k_{13}K_w + k_{23}K_b[BH])} = k_{ov}$$

$$[25] \quad \text{intercept} = \frac{1 + K_{10}[I^-]}{K_{11} k_{12} K_w}$$

© 2001 NRC Canada

Fig. 6. A comparison of observed and calculated values of $[H_2O_2]/k_{obs}[H^+]$ vs. $[H^+]$ for phosphate buffer at 25°C. (*a*) Iodide dependence of observed values with initial concentrations of: 5×10^{-2} M phosphate buffer, 1×10^{-5} M I_2, and 1×10^{-3} M H_2O_2 with 5×10^{-4} (●) and 1×10^{-3} (×) M I^-. Unbroken lines represent calculated values. (*b*) Observed values for 2×10^{-2} M phosphate buffer with 1×10^{-5} M I_2, 1×10^{-3} M H_2O_2, and 5×10^{-4} M (■) I^-. The unbroken line represents calculated values.

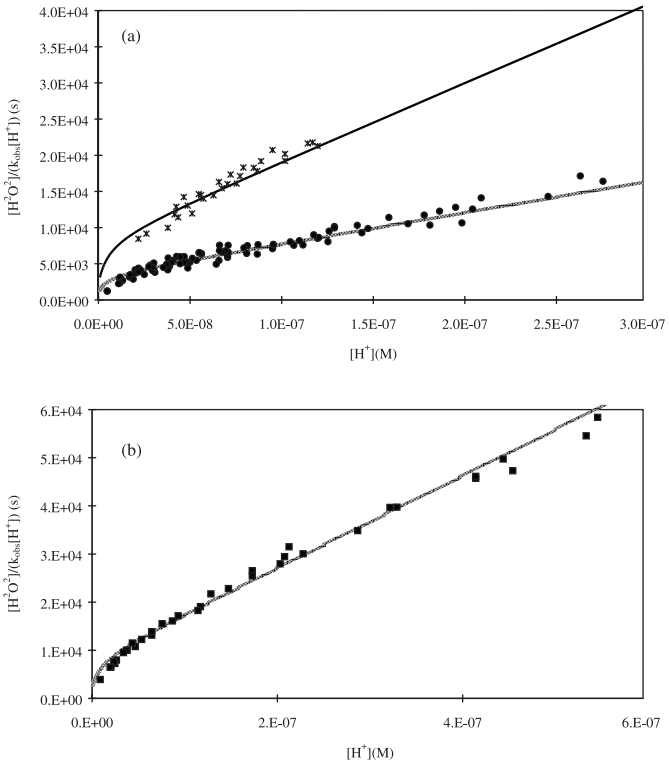
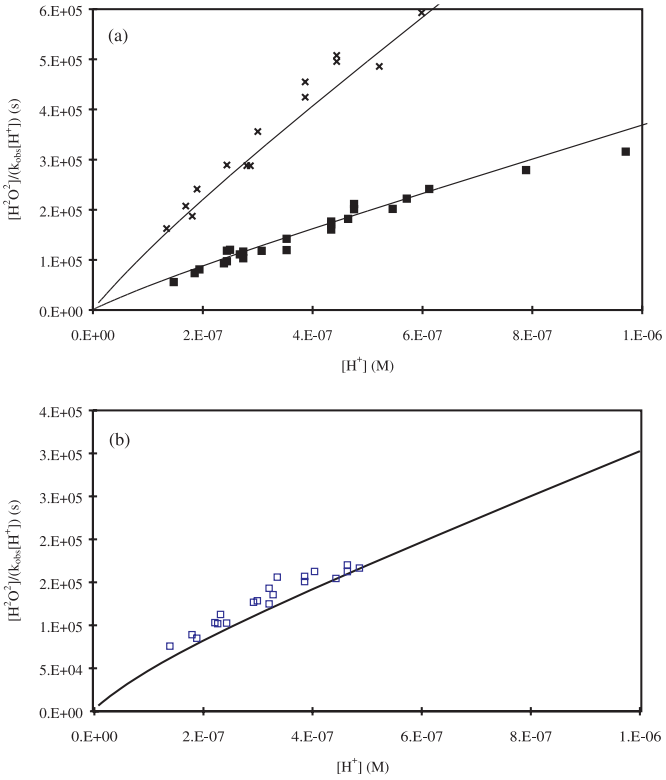


Fig. 7. A comparison of observed and calculated values of $[H_2O_2]/k_{obs}[H^+]$ vs. $[H^+]$ for citrate buffer at 25°C. (*a*) Iodide dependence of observed values with initial concentrations of 1×10^{-2} M citrate buffer, 1×10^{-5} M I_2, and 1×10^{-3} M H_2O_2 with 5×10^{-4} (■) and 1×10^{-3} (×) M I^-. Unbroken lines represent calculated values. (*b*) Observed values for 2×10^{-2} M citrate buffer, 1×10^{-5} M I_2, and 1×10^{-3} M H_2O_2 with 5×10^{-4} M (□) I^-. The unbroken line represents calculated values.



Evaluation of rate constants

Values for k_{12}, k_{-12}, k_{13}, and k_{23} were estimated from the data. Literature values of 700 M^{-1} (13), 2.9×10^4 M^{-1} (11, 12), and 1×10^{-14} (14) were used for K_{10}, K_{11}, and K_w, respectively. An estimate for k_{12} was obtained from the intercept values of linear least-squares fits of $[H_2O_2]/k_{obs}[H^+]$ vs. $[H^+]$ for mixtures of $I_2/I^-/I_3^-$ and H_2O_2 in barbital buffer. Scheme 1 was assumed to be the mechanism. The ratio $k_{-12}/k_{12}k_{13}$ was then estimated by plotting the gradients (eq. [24]) of a series of $[H_2O_2]/k_{obs}[H^+]$ vs. $[H^+]$ plots against barbital buffer concentration (2.5×10^{-3}, 5×10^{-3}, 7.5×10^{-3}, and 1×10^{-2} M) and extrapolating to zero buffer concentration. Individual values for the rate constants k_{-12}, k_{13}, and k_{23} were then estimated by obtaining a best fit to all of the experimentally observed first-order decay rates of $[I_3^-]$ (k_{obs} $[I_3^-]$) using a numerical integration package for solving chemical kinetics.[4] In addition to the reaction set for Scheme 1, reactions describing the dissociation of HOI (1), and the disproportionation of HOI and OI^- (12, 14) were used. Numerical solutions for the concentration of I_2, I_2OH^-, HOI, I_3^-, and IO_2H were obtained, and a first-order decay rate for I_3^- was calculated for various pH values.

The rate constants k_{12}, k_{-12}, and k_{13} determined for barbital buffer were then used to estimate values for k_{23} for citrate and phosphate buffers. Values for individual rate constants are presented in Table 2. Comparisons of calculated (using the rate law for Scheme 1 and the constants in Table 2) vs. experimental plots of $[H_2O_2]/k_{obs}[H^+]$ vs. $[H^+]$ are presented in Figs. 2, 5, 6, and 7 for selected data obtained in barbital, citrate, and phosphate buffers, respectively. Note that the values for the rate constants presented in Table 2 were used in the calculations shown in the figures. These values represent the rate constants that provided a best fit to *all* of the available data. Rate constants obtained by non-linear least-squares optimization of individual data sets deviated from these mean values. This deviation is also indicated in Table 2.

The agreement between calculated and experimental values over a wide range of conditions supports the assignment of the rate law to the mechanism presented in Scheme 1. The assumptions that I_2, its hydrolysis products, and I_3^- are in rapid equilibrium, and that IO_2H can be treated by a steady-state approximation, were also verified by obtaining numerical solutions for k_{obs} using a numerical integration package.[4] The individual decay rate constants obtained by numerical

[4] FACSIMILE – AEA Technologies. Harwell Laboratory, Oxfordshire, UK.

© 2001 NRC Canada

Fig. 8. A plot of ln (slope $H_2O_2/k_{obs}[H^+]$ vs. $[H^+]$) vs. $1/T$ for 1×10^{-5} M I_2, 1×10^{-3} M H_2O_2, 0.05 M phosphate buffer, and 5×10^{-4} (◆) and 1×10^{-3} (■) M I^-. Linear least-squares fits to the data are shown as unbroken lines with the value for the slope in *K*.

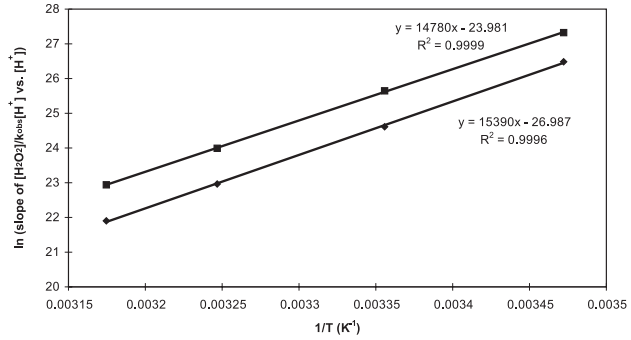
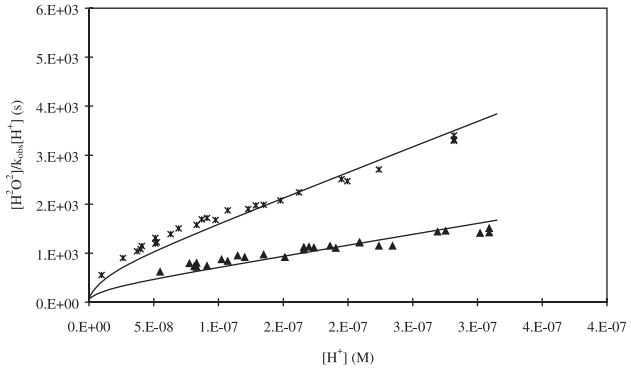


Fig. 9. A comparison of observed and calculated values for $H_2O_2/k_{obs}[H^+]$ vs. $[H^+]$ at 42°C. Initial concentrations were: 1×10^{-5} M I_2, 1×10^{-3} M H_2O_2, 0.05 M phosphate buffer, and 5×10^{-4} (▲) and 1×10^{-3} (×) M I^-. Unbroken line represents calculated values.



solution for each condition differed by less than 10% to those calculated using the steady state approximation.

The temperature dependence of the reduction of I_2 by H_2O_2

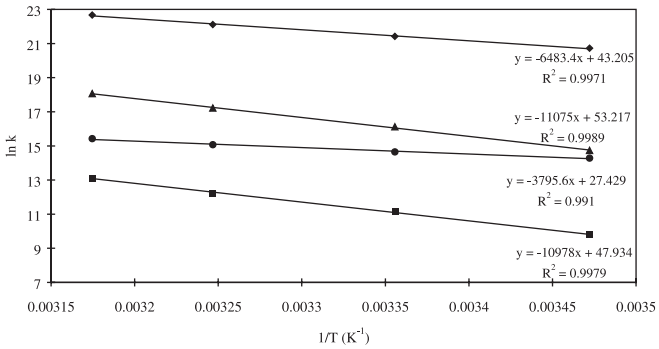
The temperature dependence of the reaction rate constants k_{12}, k_{-12}, k_{13}, and k_{23} were obtained by performing measurements of the rate of loss of I_3^- in peroxide solutions at 15, 25, 35, and 42°C in phosphate buffer. Measurements were obtained using 1×10^{-5} M I_2, 1×10^{-3} M H_2O_2, and 0.05 M phosphate buffer with both 5×10^{-4} and 1×10^{-3} M I^-. Plots of $[H_2O_2]/k_{obs}[H^+]$ vs. $[H^+]$ were generated for each set of conditions. The overall rate constant,

$$k_{ov} = \frac{(1 + K_{10}[I^-])(k_{-12}[I^-])}{K_w K_{11} k_{12}(k_{13}K_w + k_{23}K_b[BH])}$$

was estimated from the slope of these plots. A plot of ln k_{ov} vs. $1/T$, as shown in Fig. 8, gives an estimated activation energy for the overall rate constant of 125 kJ mol^{-1}.

Solutions for eq. [24] were calculated using trial values for k_{-12}, k_{12}, k_{13}, and k_{23}, and using the appropriate values for K_w (14), K_{10} (15), K_{11} (16), and K_b (14) as a function of temperature, with the constraints being that the overall activation energy be approximately 125 kJ mol^{-1}, and that the individual rate constants were consistent with values previously determined from data obtained at 25°C. These solutions were compared with experimental data obtained at 15, 25, 35, and 42°C to obtain a best fit to the data. A comparison of the calculated values of $H_2O_2/k_{obs}[H^+]$ vs. $[H^+]$ to the values observed at 42°C is shown in Fig. 9. The agreement between calculated and observed values is typical. Individual values of k_{12}, k_{-12}, k_{13}, and k_{23} that were selected on the basis of providing the best fit (non-linear least-squares regression analysis) to the data were also found to follow the Arrhenius law (See Fig. 10). Activation energies estimated from linear least-squares fits of ln *k* vs. $1/T$ for the individual rate constants are tabulated in Table 2.

Fig. 10. A plot of ln *k* vs. $1/T$ for individual values of k_{12} (●), k_{-12} (▲), k_{13} (◆), and k_{22} (■) used to obtain a best fit to the data. Linear least-squares' equations used to fit the data to straight lines are indicated.



Conclusions

The kinetic data obtained in these experiments support the formulation of the rate law derived for Scheme 1. It should be noted that this rate law is also consistent with data obtained in earlier investigations. Discrepancies in the rate laws previously reported for this reduction resulted from the different pH conditions (1, 5) or iodide concentrations (7) under which the experiments were performed, whereas variations in reported rates (1, 2, 6) of reaction could be accounted for by the effects of buffer catalysis. Thus, our observed overall rates of reduction of I_2 in phosphate and citrate buffers are similar to those reported by Liebhafsky (5) and Shiraishi et al. (1) under the same conditions. The rate law derived from Scheme 1 is also consistent with the findings of Kessi-Rabia et al. (6). Furthermore, the overall temperature dependence of the iodine hydrolysis–peroxide reduction is similar to that measured by Liebhafsky (16).

Acknowledgements

The authors would like to thank J. C. Wren and N. H. Sagert for helpful discussions and assistance in editing the manuscript, and H. E. Sims for his many contributions in interpreting the data and developing a mechanism. The work reported in this document was funded by the COG (CANDU Owners Group) R&D Program: Working Party 06, Containment Behaviour, WPIR No. 425, 606, and 608 under the

© 2001 NRC Canada

joint participation of Ontario Power Generation, Hydro, Quebec, New Brunswick Power, and AECL.

References

1. H. Shiraishi, H. Okuda, Y. Morinago, and K. Ishigure. *In* Proceedings of the third CSNI workshop on iodine chemistry in reactor safety. *Edited by* K. Ishigure, M. Saeki, K. Soda, and J. Sigimoto. Japan Atomic Energy Research Institute, Tokai-muri, Japan. 1992. p. 152.
2. J.W. Fletcher and O.A. Miller. *In* Proceedings of the specialists workshop on iodine chemistry in reactor safety. *Edited by* A.M. Dean and P.E. Potter. Harwell Report AERE R 11 974, Harwell, United Kingdom. 1986. p. 107.
3. J.C. Wren, N.H. Sagert, and H.E. Sims. *In* Proceedings of the third CSNI workshop on iodine chemistry in reactor safety. *Edited by* K. Ishigure, M. Saeki, K. Soda, and J. Sigimoto. Tokai-muri, Japan. 1992. p. 381.
4. E.Z. Abel. Physik. Chem. **96**, 1 (1920).
5. H.A. Liebhafsky. J. Amer. Chem. Soc. **54**, 3499 (1932).
6. M. Kessi-Rabia, M. Gardes-Albert, R. Julien, and C. Ferradini. J. Chim Phys. Phys. Chim. Biol. **92**, 1104 (1993).
7. J.H. Baxendale. Adv. Catal. **4**, 31 (1952).
8. L. Kolar-Anic and G. Schmitz. J. Chem. Soc. Faraday Trans. **88**, 2364 (1992).
9. J.M. Ball, J.B. Hnatiw, and H. Sims. *In* Proceedings of the fourth CSNI/OECD workshop on the chemistry of iodine in reactor safety. *Edited by* S. Guntay. Wurenlingen, Switzerland. 1997. p. 507.
10. R.E Connick. J. Am Chem. Soc. **69**, 1509 (1946).
11. D.A. Palmer and R. Van Eldik. Inorg. Chem. **25**, 928 (1986).
12. J.C. Wren, J. Paquette, S. Sunder, and B.L. Ford. Can. J. Chem. **64**, 2284 (1986).
13. D.A. Palmer, R.W. Ramette, and R.E., Mesmer. J. Solution Chem. **13**, 673, (1984).
14. Chemical rubber company handbook of chemistry and physics. 43rd *ed*. CRC Publishing Co., Cleveland. 1962. p. 1751.
15. I. Lengeyel, I.R.Epstein, and K. Kustin. Inorg. Chem. **32**, 5880 (1994).
16. H.A. Liebhafsky. Chem. Rev. **17**, 89 (1935).

© 2001 NRC Canada

Cyclopropanation of benzylidenemalononitrile with dialkoxycarbenes and free radical rearrangement of the cyclopropanes

Nadine Merkley, Paul C. Venneri, and John Warkentin

Abstract: Thermolysis of 2-cinnamyloxy-2-methoxy-5,5-dimethyl-Δ^3-1,3,4-oxadiazoline (**1a**) and the analogous 2-benzyloxy-2-methoxy compound (**1b**) at 110°C, in benzene containing benzylidenemalononitrile, afforded products of apparent regiospecific addition of methoxycarbonyl and cinnamyl (or benzyl) radicals to the double bond. When the thermolysis of **1a** was run with added TEMPO, methoxycarbonyl and cinnamyl radicals were captured. Thermolysis of the 2,2-dibenzyloxy analogue (**1c**) in the presence of benzylidenemalononitrile gave an adduct that is formally the product of addition of benzyloxycarbonyl and benzyl radicals to the double bond. In this case, a radical addition mechanism could be ruled out, because the rate constant for decarboxylation of benzyloxycarbonyl radicals is very large. A mechanism that fits all of the results is predominant cyclopropanation of benzylidenemalononitrile by the dialkoxycarbenes derived from the oxadiazolines, in competition with fragmentation of the carbenes to radical pairs. The cyclopropanes so formed then undergo homolytic ring-opening to the appropriate diradicals. Subsequent β-scission of the diradicals to afford radical pairs, and coupling of those pairs, gives the final products. Thus, both carbene and radical chemistry are involved in the overall processes.

Key words: cyclopropane, dialkoxycarbene, β-scission, oxadiazoline, radical.

Résumé : La thermolyse de la 2-cinnamyloxy-2-méthoxy-5,5-diméthyl-Δ^3-1,3,4-oxadiazoline (**1a**) et du composé analogue, 2-benzyloxy-2-méthoxy (**1b**), à 110°C, dans du benzène contenant du benzylidènemalononitrile, conduit à la formation des produits provenant d'une addition apparemment régiospécifique des radicaux méthoxycarbonyles et cinnamyles (ou benzyles) sur la double liaison. Lorsqu'on a effectué la thermolyse de **1a** en présence de TEMPO, les radicaux méthoxycarbonyles et cinnamyles sont piégés. La thermolyse de l'analogue 2,2-dibenzyloxy (**1c**), en présence de benzylidènemalononitrile, conduit à la formation d'un adduit qui est formellement le produit d'addition des radicaux benzyloxycarbonyles et benzyles sur la double liaison. Dans ce cas, on peut éliminer la possibilité d'un mécanisme d'addition radicalaire en raison de la valeur élevée de la constante de vitesse de décarboxylation des radicaux benzyloxycarbonyles. Un mécanisme qui permet d'expliquer tous les résultats implique une cyclopropanation prédominante du benzylidènemalononitrile par les dialkoxycarbènes dérivés des oxadiazolines qui serait en compétition avec la fragmentation des carbènes en paires de radicaux. Les cyclopropanes ainsi formés subissent alors une ouverture de cycle homolytique conduisant aux biradicaux appropriés. Une scission subséquente β des biradicaux fournit des paires de radicaux et le couplage de ces paires conduit aux produits finaux. Ainsi, les processus globaux impliqueraient à la fois de la chimie des radicaux et de celle des carbènes.

Mots clés : cyclopropane, dialkoxycarbène, scission β, oxadiazoline, radical.

[Traduit par la Rédaction]

Introduction

Fragmentations of dialkoxycarbenes to radical pairs in the gas-phase have been known for some time (1, 2), but the analogous homolyses in solution are still relatively new (3–5). Thermolysis of cinnamyloxy(methoxy)- (3), benzyloxy(methoxy)- (4), and dibenzyloxy-oxadiazolines (**1**) (5) in benzene led primarily to formation of the appropriate dioxycarbenes (**3**) through carbonyl ylides (**2**). The carbenes fragmented to corresponding radical pairs (Scheme 1). A minor side reaction of **1** was a dipolar cycloreversion to the carbonate and 2-diazopropane (not shown). Carbene intermediates were trapped with *tert*-butyl alcohol (3–5), and radical intermediates were trapped with TEMPO (3–5). In the absence of TEMPO, the radical pairs (**4** and **5a**) coupled to esters (**6a** and **7)**, whereas **4** and **5b** afforded **6b** (Scheme 2).

Evidence for the sequential formation of carbenes and radicals raised some interesting questions regarding the consequences of generating the carbenes in the presence of an olefinic trap with the potential for reaction with both the carbenes and the radicals. For instance, could the carbenes be trapped fast enough as cyclopropanes, by suitably substituted olefins, to suppress carbene fragmentation to radicals?

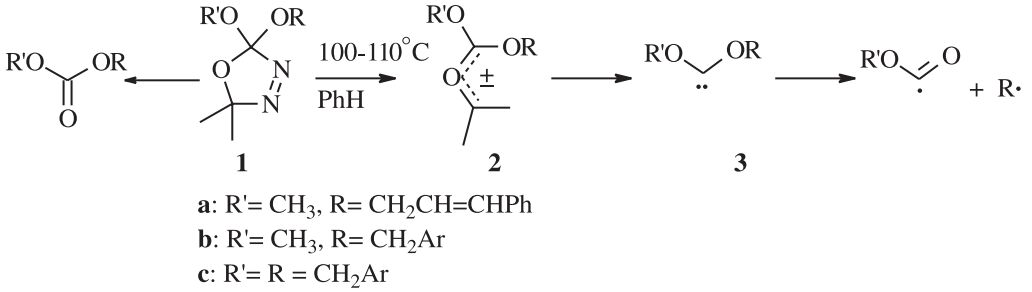
Received October 18, 2000. Published on the NRC Research Press Web site on April 12, 2001.

N. Merkley, P.C. Venneri, and J. Warkentin.[1] Department of Chemistry, McMaster University, Hamilton, ON L8S 4M1, Canada.

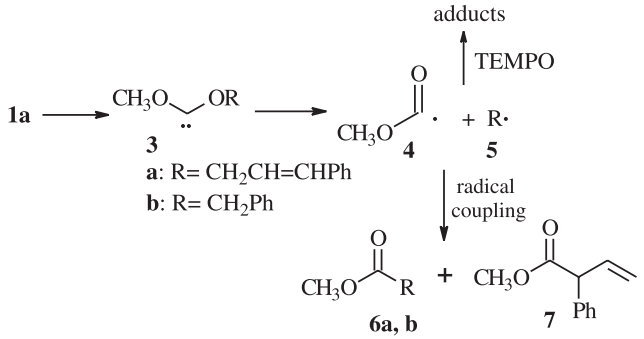
[1]Corresponding author (e-mail: warkent@mcmaster.ca; fax: (905) 522–2509).

 DOI: 10.1139/cjc-79-3-312 © 2001 NRC Canada

Scheme 1.



Scheme 2.



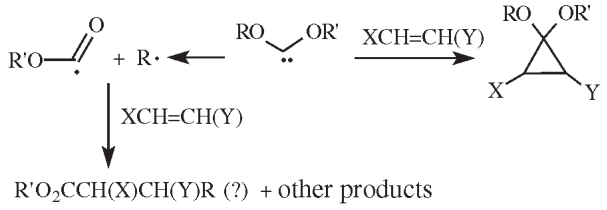
Alternatively, if cyclopropanation were slow enough to make carbene fragmentation predominant, could the very different radicals (e.g., methoxycarbonyl and benzyl) possibly be trapped with some regioselectivity (Scheme 3)?

We now report the thermolysis of **1a**–**c** in the presence of **8**, showing that cyclopropanation of the benzylidenemalononitrile by the first-formed carbene is the fastest reaction (at [**8**] = 0.16–0.20 M) (Scheme 4). Thereafter, radical pairs are indeed involved but they originate primarily from ring-opening of the cyclopropanes and not from fragmentation of the carbenes.

Results and discussion

Thermolysis of 2-cinnamyloxy-2-methoxy oxadiazoline (**1a**) in the presence of benzylidenemalononitrile (**8**) in benzene at 110°C for 24 h afforded products **9a** and **10** in 2:1 ratio in a combined yield of 45**%** (isolated) (Scheme 4). A sequential ylide → carbene → radical-pair mechanism was considered in view of the evidence described above for formation of radical pairs from **1a** (3), although the other three potential products from addition of the radicals to benzylidenemalononitrile were not found. To probe for radical intermediates, a stable free radical (TEMPO) was included with **1a** and **8**. The yields of **9a** and **10** were reduced and new products **11** and **12**, generated from radical-coupling of the methoxycarbonyl and phenylallyl radicals with TEMPO, were obtained (Scheme 4). The alternative product of trapping of the phenylallyl radical by TEMPO was not observed; we assume that it is more sterically hindered, and, therefore, less stable than **12**, and is eventually converted to **12** at 110°C by dissociation–recoupling. The yields of **9a** and **10**, estimated by GC, were depressed about

Scheme 3.



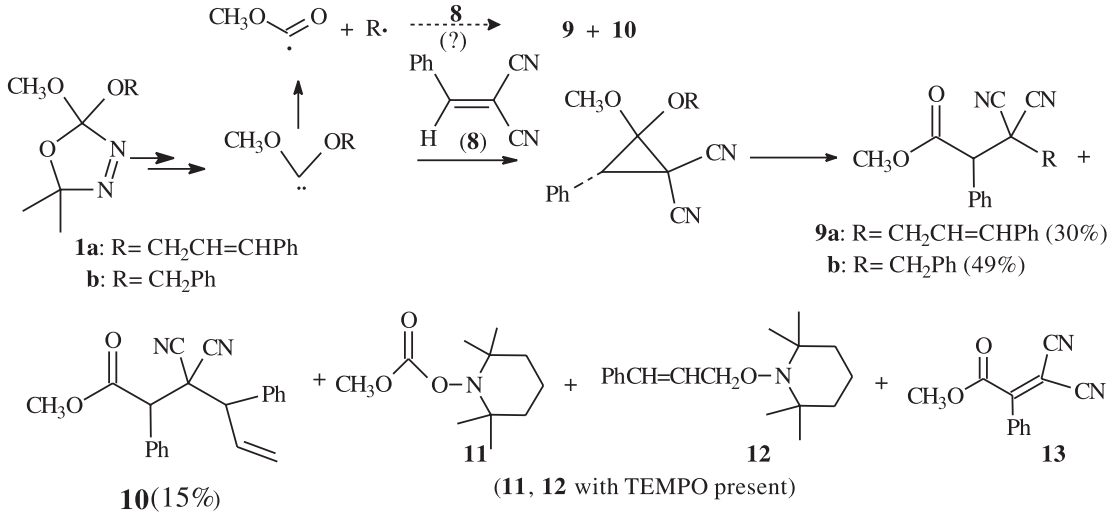
fourfold by TEMPO as would be expected if they had arisen from radicals. The yield of disproportionation product **13**, estimated in the same way, rose about fivefold when TEMPO was present.

These facts can probably be accounted for as follows: TEMPO does not interfere with cyclopropanation by the carbene, but it does scavenge diffusively separated radicals arising from carbene fragmentation. Adducts **11** and **12** are products of such scavenging. Compounds **9a**, **10**, and **13** come primarily from ring-opening of the cyclopropane and subsequent β-scission, with the radical pairs either coupling or disproportionating in the solvent cage, or else diffusing apart (Scheme 5). Again, TEMPO captures the radicals that become free but not radicals from a caged pair. The increased yield of **13** in the presence of TEMPO could be the result of disproportionation between TEMPO and the methyl 1,1-dicyano-2-phenylpropanoyl radical (Scheme 5), which presumably couples reversibly with TEMPO and, therefore, leads to **11** eventually.

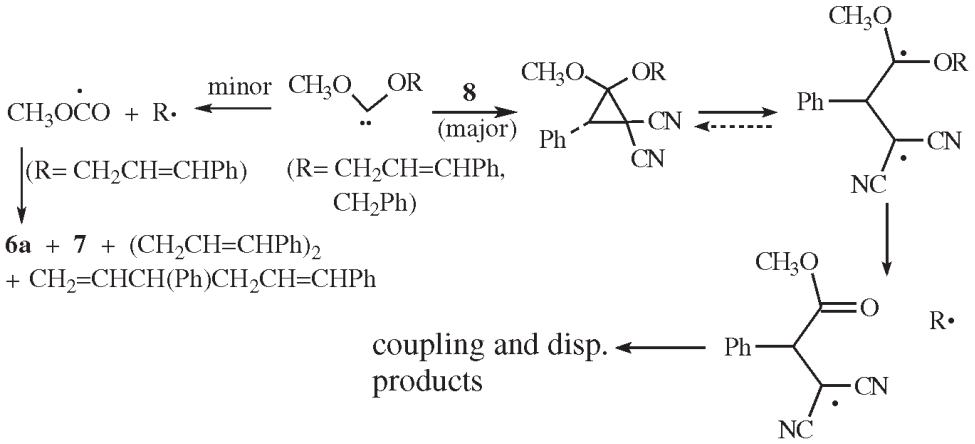
The alternative interpretation that **9a** and **10** of Scheme 4 came from sequential additions of carbene-derived methoxycarbonyl and phenylallyl radicals to **8** must be rejected. It would require that those additions be both regio- and order-selective, the methoxycarbonyl radical adding first (faster) to **8**. Moreover, in the second step, there would have to be a considerable selectivity for the adduct radical to couple with the phenylallyl radical, rather than with the methoxycarbonyl radical. That apparent selectivity, favouring phenylallyl over methoxycarbonyl radicals, is not obviously in keeping with a radical mechanism, because coupling reactions do not have appreciable activation energies, but are, in many cases, essentially diffusion controlled. Moreover, although radical additions of small molecules (XY) to multiple bonds are well-known, they do not involve sequential reactions of X• and Y• with the alkene. Instead, they normally proceed by addition of X• to one atom of the multiple bond, followed by a radical–molecule reaction (chain trans-

© 2001 NRC Canada

Scheme 4.



Scheme 5.



fer by abstraction of Y• from XY) that attaches Y• to the other atom of the former multiple bond, and regenerates X•.

On the other hand, the cyclopropanation mechanism, followed by rearrangement via β-scission of a diradical (Scheme 5), is attractive. Cyclopropane formation from nucleophilic carbenes and **8** is easy to envision, and subsequent rearrangement of the cyclopropane seemed likely, given that 1,1-dialkoxycyclopropanes undergo thermal ring-opening readily (6–8). Such ring-openings of cyclopropanes have generally been described with a heterolytic mechanism (9)[2], presumably because cyclopropanes with vicinal electron withdrawing and donating groups undergo the opening most easily (6, 7, 9[2]). The fact that the formation of **9a** and **10** was suppressed when TEMPO was present with **8**, requires that at least a fraction of **9a** and **10** come from free radicals that are capable of being trapped, and suggests that those compounds arise from homolytic, rather than heterolytic, ring-opening. Homolytic ring-opening of cyclopropanes is a tenable alternative to heterolytic cleavage, for Baldwin (10) has shown that there is a correlation of the rates of thermal enantiomerization of 1,2-disubstituted cyclopropanes with radical stabilization energies.

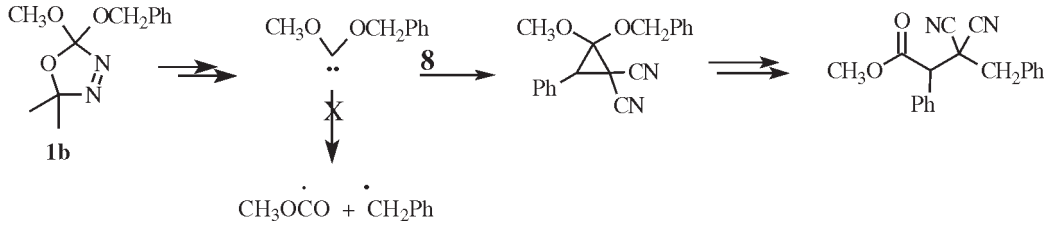
Additional products from the thermolysis of **1a** with **8** (Scheme 5) that were detectable in trace amounts by GC–MS were the esters **6a** and **7** as well as two products with masses appropriate for dimers of phenylallyl radicals. The esters are presumably derived from nonscavengeable caged radical pairs formed from the carbene. Dimers of phenylallyl are not surprising as products from diffusion out of the solvent cage. This result indicates that most, but not all, of the carbene from **1a** is captured by **8** before it can fragment (Scheme 5).

Under the same conditions, different results were obtained with **1b** and **8**. In that case, the ester (methyl phenylacetate) expected from in-cage-coupling of methoxycarbonyl and benzyl radicals was not detected. Failure to find it presumably means that benzyloxy(methoxy)carbene fragments more slowly to a radical pair than cinnamyloxy(methoxy)carbene (Scheme 6). The alternative explanation that the former carbene adds more rapidly to **8**, is less likely.

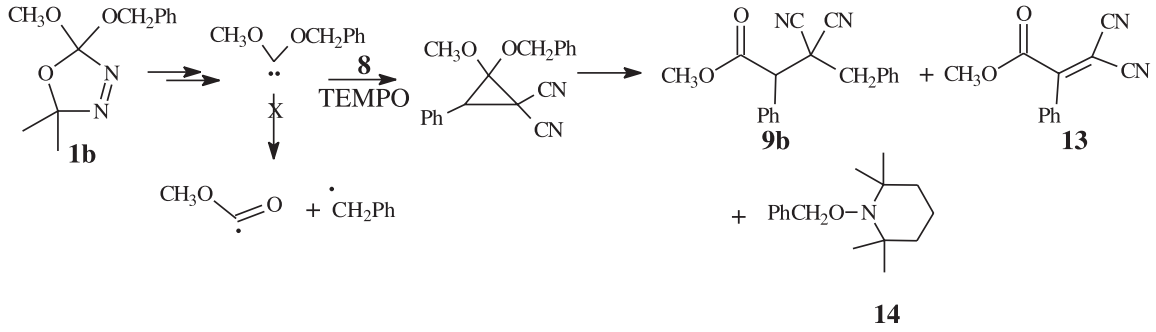
[2] Page 77 in particular.

© 2001 NRC Canada

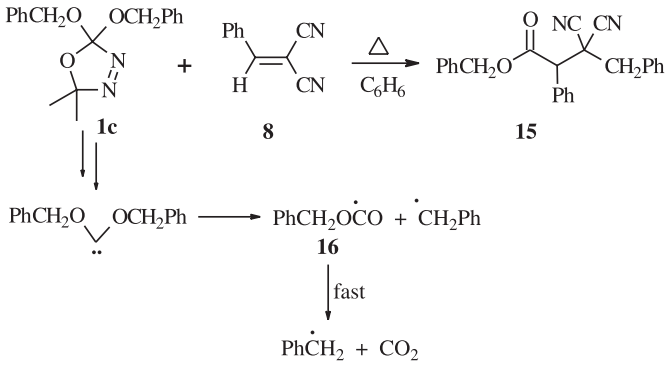
Scheme 6.



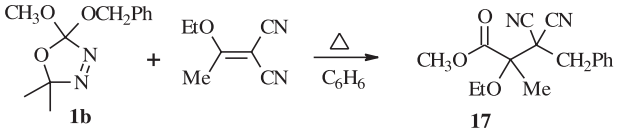
Scheme 7.



Scheme 8.



Scheme 9.



With both **8** and TEMPO present, **1b** afforded disproportionation product **13** and the product of trapping of benzyl radicals with TEMPO (**14**) (Scheme 7). Adduct **12**, from trapping of the methoxycarbonyl radical with TEMPO, was not identified in this case.

Experiments with **1c** and **8** were particularly revealing as confirmation of the cyclopropanation mechanism of Scheme 7. A major product was **15** (Scheme 8), which could not have arisen from addition of benzyloxycarbonyl radicals (**16**) and benzyl radicals to **8,** because **16** decarboxylates very rapidly, with $k_{110°C} \approx 10^9$ s^{-1} (extrapolated from Arrhenius parameters) (11). A carbene mechanism must, therefore, be invoked to account for **15** (Scheme 8), and the use of analogy to assign the same mechanism to the reactions of **1a** and **1b** with **8** seems to be reasonable.

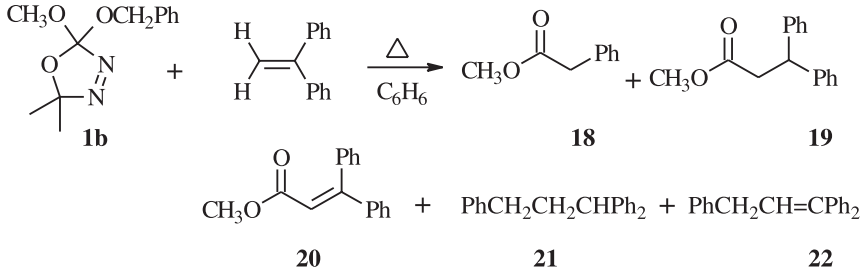
1,1-Diphenylethylene was known to react with dimethoxycarbene to afford the expected cyclopropane in good yield (12), and the same carbene reacted similarly with ethyl cinnamate (12). To look for similar cycloadditions with benzyloxy(methoxy)carbene, thermolyses of **1b** in the presence of 1,1-diphenylethylene, (1-ethoxyethylidene)malononitrile, and both dimethyl and diethyl benzalmalonate were also investigated. (1-Ethoxyethylidene)malononitrile behaved like benzylidenemalononitrile (Scheme 9), although it produced **17** in quite low yield (ca. 17%), but the other alkenes reacted too slowly with benzyloxy(methoxy)carbene to afford cyclopropane intermediates. Instead the carbene fragmented to radicals, and those radicals reacted with the alkenes. For example, a complex mixture of products was obtained from 1,1-diphenylethylene, and not all components were identified. It was possible, by means of GC and with authentic compounds in hand, to identify the major products as **18**–**22** (Scheme 10). Methyl phenylacetate is presumably the result of cage-coupling of the radical pair from benzyloxy(methoxy)carbene. Methyl 3,3-diphenylpropanoate and methyl 3,3-diphenylpropenoate must come from addition of the methoxycarbonyl radical to 1,1-diphenylethylene and subsequent disproportionation. Similarly, 1,1,3-triphenylpropane and 1,1,3-triphenyl-1-propene are derived from addition of benzyl radical to 1,1-diphenylethylene and subsequent disproportionation. The disproportionations could be between both identical and nonidentical radicals, of course. The malonic ester derivatives were investigated in less detail. A major product in each case was methyl phenylacetate (Scheme 11). Analysis by GC–MS showed that products expected from cyclopropanation and subsequent ring-opening were absent. Thus, the geminal nitrile groups of **8** appear to be necessary for fast cyclopropanation by dialkoxycarbenes that fragment to radicals in the absence of a good trapping agent.

Summary

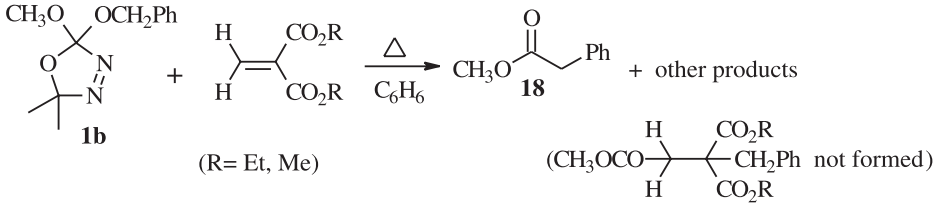
At 110°C benzylidenemalononitrile and 1-ethoxy(ethylidene)malononitrile at ca. 0.16–0.20 M capture benzyl-

© 2001 NRC Canada

Scheme 10.



Scheme 11.



oxy(methoxy)carbene and analogues, in [1 + 2] cycloadditions before they can fragment to radical pairs, such as methoxycarbonyl and benzyl. The resulting cyclopropanes undergo ring-opening, probably reversibly, to diradicals that then undergo β-scission to radical pairs. Such pairs couple (primarily) or disproportionate. Some alkenes lacking the *gem* dicyanoalkenyl functional group (such as 1,1-diphenylethylene) as well as diethyl and dimethyl benzylidenemalonates, are not cyclopropanated fast enough by the carbenes under the same conditions, and they react instead with the radicals from carbene fragmentation.

The sequence involving cyclopropanation could be useful, affording complex products in modest yield in a one-pot reaction. On the other hand, radical pair additions to alkenes that are not cyclopropanated rapidly by dialkoxycarbenes have very little potential utility.

Experimental

General

Chemical shifts for ^{1}H NMR spectra are relative to TMS or $CHCl_3$ (in $CDCl_3$, δ = 7.24) or C_6HD_5 (in C_6D_6, δ = 7.15). Those for ^{13}C NMR spectra are relative to the C_6D_6 triplet (δ = 128.0) or the $CDCl_3$ triplet (δ = 77.0). Mass spectra were recorded with a VGH ZAB-E double focusing instrument or with a Hewlett–Packard MSD GC–MS. Analytical GC work was done with a Varian Vista 600 instrument equipped with a flame ionization detector and a DB1 Megabore capillary column (0.53 mm × 30 m).

Thermolysis of 1a in the presence of 8

A solution of oxadiazoline **1a** (300 mg, 1.15 mmol) and **8** (300 mg, 1.95 mmol) in benzene (10 mL) in a 25 mL thermolysis tube was heated to distill out 2.5 mL of benzene together with adventitious water. The sample was then freed of gases by means of three freeze–pump–thaw cycles before the tube was sealed and heated at 110°C for 21 h. The crude sample was analyzed by GC and GC–MS before it was concentrated and the residue was subjected to flash chromatography on 25 g of basic alumina (Fisher Brockman 1), which had been activated by heating to 120°C for 24 h. The column dimensions were 2 × 15 cm and elution was with 30% ethyl acetate in hexanes. Two major fractions were collected.

*Methyl 3,3-dicyano-2,6-diphenyl-5-hexenoate (**9a**)*

Clear liquid, 30% yield (isolated). EI-MS *m*/*z* (%): 330 $[M]^+$ (1), 299 (1), 271 (1), 154 (6), 150 (59), 117 (100), 115 (49), 91 (41), 77 (24), 59 (14), 51 (8). CI-MS (NH_3) *m*/*z*: 348 $[M + 18]^+$. IR (CCl_4) (cm^{-1}): 1750 (C=O). ^{1}H NMR (500 MHz, C_6D_6) δ: 2.30 (dd, ^2J = 13.9 Hz, ^3J = 7.4 Hz, 1H), 2.40 (dd, ^2J = 13.9 Hz, ^3J = 7.4 Hz, 1H), 3.15 (s, 3H), 3.73 (s, 1H), 6.08 (dt, ^3J = 15.7 Hz, ^3J = 7.4 Hz, 1H), 6.27 (d, ^3J = 15.7 Hz, 1H). ^{13}C NMR (125 MHz, C_6D_6) δ: 39.3, 40.8, 52.2, 55.5, 114.2, 114.6, 118.9, 126.8, 128.3, 128.3, 129.2, 129.5, 129.6, 131.1, 135.9, 138.0, 168.7.

*Methyl 3,3-dicyano-2,4-diphenyl-5-hexenoate (**10**)*

Clear liquid, 15% yield (isolated). CI-MS (NH_3) *m*/*z*: 348 $[M + 18]^+$. ^{1}H NMR (500 MHz, C_6D_6) δ: 3.10 (s, 3H), 3.70 (s, 1H), 4.08 (d, ^3J = 9.0 Hz, 1H), 5.05 (dt, ^3J = 10.2 Hz, ^2J = 1.0 Hz, 1H), 5.12 (dt, ^3J = 16.8 Hz, ^2J = 1.0 Hz, 1H), 6.25 (ddd, ^3J = 16.8 Hz, ^3J = 10.2 Hz, ^3J = 9.0 Hz, 1H), 6.94–7.38 (m, 10H). ^{13}C NMR (125 MHz, C_6D_6) δ: 47.3, 52.3, 54.1, 54.4, 113.9, 114.4, 121.8, 129.0, 129.1, 129.3, 129.4, 129.8, 130.4, 131.8, 133.8, 136.2, 169.0.

Thermolysis of 1a in the presence of 8 and TEMPO

A similar thermolysis, except for omission of the azeotropic distillation and the inclusion of TEMPO (300 mg, 1.92 mmol), gave a solution that was analyzed by GC to reveal small amounts of the esters **9a** and **10**. Chromatography gave, as major products, the adducts of the methoxycarbonyl and the phenylallyl radical with TEMPO (**11** and **12**).

(11)

Clear liquid. EI-MS *m*/*z* (%): 215 $[M]^+$ (2), 200 $[M - 15]^+$ (100), 156 (5), 83 (77), 69 (24), 55 (96), 41 (52). ^{1}H NMR (200 MHz, C_6D_6) δ: 1.09 (s, 6H), 1.25 (s, 6H), 1.08–1.56 (m, 6H), 3.39 (s, 3H). ^{13}C NMR (25 MHz, C_6D_6) δ: 17.2,

© 2001 NRC Canada

20.4, 31.7, 40.0, 54.3, 60.4, 147.0. HRMS: calcd. for $C_{11}H_{21}NO_3$: 215.1521; found: 215.1510.

(12)

Clear liquid. EI-MS *m/z*: 274 $[M + 1]^+$ (11), 156 $[M - 117]^+$ (100), 117 $[M - 156]^+$ (52), 69 (22), 41 (19). ^{1}H NMR (200 MHz, C_6D_6) δ: 1.31 (s, 6H), 1.38 (s, 6H), 1.27–1.59 (m, 6H), 4.60 (d, ^3J = 5.8 Hz, 1H), 4.61 (d, ^3J = 5.8 Hz, 1H), 6.36 (dt, ^3J = 16.0, 5.8 Hz, 1H), 6.69 (d, ^3J = 16.0 Hz, 1H), 7.11–7.34 (m, 5H). ^{13}C NMR (25 MHz, C_6D_6) δ: 17.5, 20.3, 33.3, 40.0, 59.9, 78.5, 126.0, 126.8, 127.6, 128.9, 131.8, 137.6. HRMS: calcd. for $C_{18}H_{27}NO$: 273.2093; found: 273.2081.

In a second run, aimed at finding additional products, a solution of 2-cinnamyloxy-2-methoxy oxadiazoline (**1a)** (106.2 mg, 0.40 mmol), **8** (125.8 mg, 0.82 mmol), and TEMPO (157.0 mg, 1.0 mmol) in benzene (5 mL) was heated as described above. Analysis by GC–MS indicated **9a** and **10** in low yields, as well as **13** (below) and **12**.

Thermolysis of 1b in the presence of 8

A solution of 2-benzyloxy-2-methoxy-5,5-dimethyl-Δ^3-1,3,4-oxadiazoline (**1b**) (106 mg, 0.45 mmol) and benzylidenemalononitrile (**8**) (130 mg, 0.84 mmol) in benzene (5 mL) was sealed into a thermolysis tube (after a freeze–pump–thaw cycle), which was then heated for 24 h at 110°C with an oil bath. The benzene was removed by distillation and the crude residue was chromatographed on silica (Chromatotron, 30% EtOAc–hexanes) to afford **9b**. Methyl phenylacetate was not found.

Methyl 3,3-dicyano-2,4-diphenylbutanoate (9b)

White solid, 49% yield (isolated), mp 127 to 128°C. EI-MS *m/z* (%): 305 $[M + H]^+$ (1), 150 (78), 121 (27), 91 (100), 65 (22). ^{1}H NMR (200 MHz, C_6D_6) δ: 2.77 (d, ^2J = 13.6 Hz, 1H), 2.85 (d, ^2J = 13.6 Hz, 1H), 3.15 (s, 3H), 3.67 (s, 1H), 6.99–7.11 (m, 6H), 7.19–7.23 (m, 2H), 7.30–7.34 (m, 2H). ^{13}C NMR (50 MHz, C_6D_6) δ: 41.59, 42.89, 52.42, 56.03, 114.25, 114.69, 128.29, 128.84, 128.98, 129.39, 129.78, 130.69, 131.52, 132.26, 168.90. HRMS: calcd. for $C_{19}H_{17}N_2O_2$: 305.1290; found: 305.1297.

Thermolysis of 1b in the presence of 8 and TEMPO

A solution of **1b** (112.9 mg, 0.4787 mmol), **8** (113.9 mg, 0.739 mmol), and TEMPO (188.9 mg, 1.21 mmol) in benzene (5 mL) was heated as described above. Separation of the crude product mixture by radial chromatography (Chromatotron, 30% EtOAc–hexanes) gave a fraction containing mostly methyl 3,3-dicyano-2,4-diphenylbutanoate. It was chromatographed again with 100% hexanes as eluent to give methyl 3,3-dicyano-2,4-diphenylbutanoate (**9b**) (37.3 mg, 0.1227 mmol, 26%) and methyl 3,3-dicyano-2-phenylpropenoate (**13**) as a yellow oil (2.7 mg, 0.0125 mmol, 2.6%). EI-MS *m/z* (%): 212 $[M]^+$ (70), 197 (89), 153 (73), 127 (100), 100 (35), 77 (89), 51 (92). ^{1}H NMR (200 MHz, C_6D_6) δ: 3.18 (s, 3H), 6.82–6.86 (m, 5H). HRMS: calcd. for $C_{12}H_8N_2O_2$: 212.0586; found: 212.0583. The product of coupling of benzyl radicals with TEMPO was identified by GC–MS. It had been isolated and characterized previously (4, 13).

Thermolysis of 1c in the presence of 8

A solution of 2,2-dibenzyloxy-5,5-dimethyl-Δ^3-1,3,4-oxadiazoline (5) (**1c**) (102.3 mg, 0.328 mmol) and **8** (106.9 mg, 0.694 mmol) in benzene (5 mL) gave a mixture that was partially separated by radial chromatography (Chromatotron, 30% EtOAc–hexanes). The fractions collected were purified by further chromatography (30% EtOAc–hexanes) to collect a fraction rich in benzyl 3,3-dicyano-2,4-diphenylbutanoate. Rechromatography of that fraction, with 100% hexanes as eluent, gave pure benzyl 3,3-dicyano-2,4-diphenylbutanoate.

Benzyl 3,3-dicyano-2,4-diphenylbutanoate (15)

Yellow oil, 37% yield (isolated). EI-MS *m/z* (%): 381 $[M + H]^+$ (3), 245 (7), 226 (3), 91 (100), 65 (11). ^{1}H NMR (200 MHz, $CDCl_3$) δ: 3.24 (s, 2H), 3.96 (s, 1H), 5.15 (d, ^2J = 12.0 Hz, 1H), 5.31 (d, ^2J = 12.0Hz, 1H), 7.24–7.41 (m, 15H). ^{13}C NMR (50 MHz, $CDCl_3$) δ: 41.57, 42.59, 55.46, 68.05, 113.77, 114.07, 128.61, 128.74, 128.86, 128.93, 129.32, 129.39, 129.83, 130.33, 130.67, 131.42, 134.48, 168.05. HRMS: calcd. for $C_{25}H_{21}N_2O_2$: 381.1603; found 381.1604.

Thermolysis of 1b in the presence of (1-ethoxyethylidene)malononitrile

A solution of **1b** (109.75 mg, 0.465 mmol) and (1-ethoxyethylidene)malononitrile (113.7 mg, 0.836 mmol) in benzene (5 mL) was heated as described above. The crude ester was separated by means of radial chromatography (Chromatotron, 20% EtOAc–hexanes), and it was purified by rechromatography with 100% hexanes as eluent. The regiochemistry of the product was determined by 2D NMR spectroscopy (HMBC). A three-bond correlation was observed between the ^{13}C signal at 172.65 ppm and the methyl proton signal at 2.23 ppm.

Methyl 3,3-dicyano-2-ethoxy-2-methyl-4-phenylbutanoate (17)

Yellow oil, 17% yield (isolated). EI-MS *m/z* (%): 287 $[M + H]^+$ (3), 179 (12), 151 (16), 91 (100). ^{1}H NMR (500 MHz, $CDCl_3$) δ: 1.29 (t, ^3J = 7.0 Hz, 3H), 2.23 (s, 3H), 3.30 (s, 3H), 3.50 (dq, ^2J = 9.6 Hz, ^3J = 7.0 Hz, 1H), 3.55 (dq, ^2J = 9.6 Hz, ^3J = 7.0 Hz, 1H), 4.53 (d, ^2J = 11.7 Hz, 1H), 4.56 (d, ^2J = 11.7 Hz, 1H), 7.31–7.34 (m, 1H), 7.34–7.37 (m, 4H). ^{13}C NMR (125 MHz, $CDCl_3$) δ: 14.62, 19.40, 50.43, 59.29, 65.48, 90.45, 111.38, 112.15, 127.95, 128.39, 128.71, 136.02, 172.65. HRMS: calcd. for $C_{16}H_{19}N_2O_3$: 287.1396; found: 287.1381.

Thermolysis of 1b in the presence of diethyl benzalmalonate

A solution of **1b** (84.7 mg, 0.359 mmol) and diethyl benzalmalonate (0.198 g, 0.798 mmol) in benzene (5 mL) was heated as described above. Analysis by GC–MS indicated that there were many products, methyl phenylacetate was a major one. A component with a mass appropriate for $C_{23}H_{26}O_6$ (formally the adduct of methoxycarbonyl and benzyl radicals with diethyl benzalmalonate) was absent. The reaction mixture was not analyzed further.

© 2001 NRC Canada

Thermolysis of 1b in the presence of dimethyl benzalmalonate

A solution of **1b** (115.6 mg, 0.489 mmol) and dimethyl benzalmalonate (14) (18.06 mg, 0.821 mmol) in benzene (5 mL) was heated as described above. Analysis by GC–MS indicated that there were many products, methyl phenylacetate was a major one. A compound with a mass appropriate for $C_{21}H_{22}O_6$ (formally the adduct of methoxycarbonyl and benzyl radicals with dimethyl benzalmalonate) was absent. The products were not analyzed further.

Thermolysis of 1b in the presence of 1,1-diphenylethylene

A solution of **1b** (100 mg, 0.42 mmol) and 1,1-diphenylethylene (152 mg, 0.84 mmol) in benzene (5 mL) was heated as described above. The crude reaction mixture was analyzed by means of GC with authentic compounds for comparison of retention times. The compounds identified and the approximate relative amounts (as determined by integration of the GC traces), are listed as follows: (*i*) methyl phenylacetate, 3.3 parts; (*ii*) methyl 3,3-diphenylpropanoate (**19**) (15), 1.2 parts; (*iii*) methyl 3,3-diphenylpropenoate (**20**) (16), 1.0 part; (*iv*) 1,1,3-triphenylpropane, 1.2 parts; and (*v*) 1,1,3-triphenylpropene, 1.1 parts.

Synthesis of reference samples

1,1,3-Triphenylpropene (**22**) was synthesized from ethyl hydrocinnamate by analogy to a procedure in the literature (17). 1,1,3-Triphenylpropane (**21**) was synthesized by catalytic hydrogenation of the crude 1,1,3-triphenylpropene. Methyl 3,3-diphenylpropenoate (**20**) (16) and methyl 3,3-diphenylpropanoate (**19**) (15) were isolated together from the appropriate thermolysis experiment and a composite spectrum was obtained that agreed well with the sum of the individual spectra in the literature. The mixture was used for coinjection onto the GC column.

References

1. R.J. Crawford and R. Raap. Proc. Chem. Soc. London, 370 (1963).
2. (*a*) R.W. Hoffmann, R. Hirsch, R. Fleming, and M.T. Reetz. Chem. Ber. **105**, 3532 (1972); (*b*) P.C. Oele and R. Louw. Tetrahedron Lett. **48**, 4941 (1972).
3. P.C. Venneri and J. Warkentin. J. Am. Chem. Soc. **120**, 11182 (1998).
4. N. Merkley, M. El-Saidi, and J. Warkentin. Can. J. Chem. **78**, 356 (2000).
5. N. Merkley and J. Warkentin. Can. J. Chem. **78**, 942 (2000).
6. M.L. Graziano and R. Scarpati. J. Chem. Soc. Perkin Trans. 1, 289 (1985).
7. M.L. Graziano and G. Cimminiello. J. Chem. Res. Synop. 42 (1989).
8. (*a*) M.L. Graziano, M.R. Iesce, and F. Cermola. Synthesis, 1944 (1990); (*b*) H. Tokuyama, M. Isaka, and E.J. Nakamura. J. Am. Chem. Soc. **114**, 5523 (1992).
9. H.-U. Reissig. Top. Curr. Chem. **144**, 73 (1988).
10. J.E. Baldwin. J. Chem. Soc. Chem. Commun. 31 (1988).
11. P.A. Simakov, F.N. Martinez, J.H. Horner, and M. Newcomb. J. Org. Chem. **63**, 1226 (1998).
12. R.W. Hoffmann, W. Lilienblum, and B. Dittrich. Chem. Ber. **107**, 3395 (1974).
13. C.J. Hawker, G.G. Barclay, A. Orellana, J. Dao, and W. Devonport. Macromolecules, **29**, 5245 (1996).
14. C.F.H. Allen and F.W. Spangler. *In* Organic synthesis coll. Vol. III. *Edited by* E.C. Horning. John Wiley and Sons, London. 1955. p. 377.
15. (*a*) M. Bergdahl, E-L. Lindstedt, M. Nilsson, and T. Olsson. Tetrahedron, **44**, 2055 (1988); (*b*) M.T. Rahman and S.L. Saha. J. Organomet. Chem. **199**, 9 (1980).
16. Y. Ishino, M. Mihara, S. Nishihama, and I. Nishiguchi. Bull. Chem. Soc. Jpn. **71**, 2669 (1998).
17. C.F.H. Allen and S. Converse. *In* Organic synthesis coll. Vol. I. *Edited by* H. Gilman. John Wiley and Sons, London. 1941. p. 226.

© 2001 NRC Canada

Diaryloxycarbenes from oxadiazolines

Xiaosong Lu, Darren L. Reid, and John Warkentin

Abstract: Symmetric and unsymmetric 2,2-diaryloxy-5,5-dimethyl-Δ^3-1,3,4-oxadiazolines were synthesized by oxidative cyclization of aryloxycarbonyl hydrazones of acetone with lead tetraacetate and subsequent treatment of the product mixture with a phenol in acidic solution. Thermolysis of the oxadiazolines in benzene solution at 110°C afforded carbonyl ylide intermediates that cyclize, in part, to the corresponding 2,2-diaryloxyoxirane intermediates. The oxiranes, which were not observed, are required to account for the 1,1-diaryloxy-2-methylpropenes (ketene acetals) that were isolated. Most of the carbonyl ylides fragment to acetone and diaryloxycarbenes. The latter form dimers (tetraaryloxyethenes) or they can be trapped with phenols to form orthoformates. Diphenoxycarbene was also trapped with dimethyl acetylenedicarboxylate (DMAD). The method appears to be the first for generating the parent diphenoxycarbene under relatively mild conditions in solution, and the only one to date for generating unsymmetrically substituted diaryloxycarbenes. Minor competing fragmentations of the oxadiazolines to 2-diazopropane and the appropriate diaryl carbonates, were also observed.

Key words: diarylcarbonate, diaryloxycarbene, diaryloxy oxadiazoline, ketene acetal, orthoformate.

Résumé : On a synthétisé des 2,2-diaryloxy-5,5-diméthyl-Δ^3-1,3,4-oxadiazolines symétriques et non-symétriques par cyclisation oxydante d'aryloxycarbonylhydrazones de l'acétone avec du tétraacétate de plomb et par traitement subséquent du mélange réactionnel à l'aide d'un phénol en solution acide. La thermolyse des oxadiazolines, dans le benzène, à 110°C, conduit à la formation d'intermédiaires ylures de carbonyle qui se cyclisent, en partie, pour donner les intermédiaires 2,2-diaryloxyoxiranes correspondants. Les oxiranes, que l'on n'a pas observés, sont nécessaires pour expliquer la formation des 1,1-diaryloxy-2-méthylpropènes (acétals du cétène) qui ont été isolés. La plupart des ylures de carbonyle se fragmentent en acétone et ne diaryloxycarbènes. Ces derniers forment des dimères (tétraaryloxyéthènes) ou on peut les piéger avec des phénols avec lesquels ils conduisent à la formation d'orthoformiates. On a aussi piégé le diphénoxycarbène avec l'acétylènedicarboxylate de diméthyle (ACDM). Il semble que la méthode est la première qui permette de générer le diphénoxycarbène parent dans des conditions relativement douces, en solution, et c'est la première à avoir été utilisée pour générer des diaryloxycarbènes substitués de façon non symétrique. On a aussi observé des fragmentations mineures, des oxadiazolines, en compétition avec la réaction principale, qui conduisent au 2-diazopropane et aux carbonates de diaryle appropriés.

Mots clés : carbonate de diaryle, diaryloxycarbène, diaryloxyoxadiazoline, acétal du cétène, orthoformiate.

[Traduit par la Rédaction]

Introduction

There are now many methods for generating a variety of carbenes in solution for studies of their chemistry (1). They include carbenes with an alkyl, alkoxyl, amino, aryl, halogen, or vinyl substituent, to name only a few (2). Various bis(heteroatom) carbenes have also been generated. The latter, with amino or alkoxyl substituents are distinctly nucleophilic (3). Aryloxy- or diaryloxycarbenes should be comparatively less nucleophilic than alkoxy analogues, because an aryl group competes conjugatively with the carbenic virtual orbital for electron density from the oxygen atom, and because phenyl is inductively electron-withdrawing, relative to alkyl. Their lower (and tunable) nucleophilicity, and the fact that an aryloxy group of aryloxymethoxycarbenes can undergo ipso-substitution (4) during reaction with dimethyl acetylenedicarboxylate (DMAD), suggests that aryloxy- and diaryloxy-carbenes could show other new chemistry.

Unsymmetric diaryloxycarbenes ((ArO)Ar′OC:) remain unreported, although many dialkoxycarbenes and alkoxyphenoxycarbenes have been studied thoroughly. Diphenoxycarbene has been reported several times (5–7). It was generated by treating chlorodiphenoxymethane with a strong base or with silver glycinate, and more recently, by thermolysis of an oxadiazoline (7) (Scheme 1). The former methods for generating the carbene limit the study of the chemistry of diaryloxycarbenes, especially those with different substituents in the two rings, not only because the conditions can lead to competing reactions, but also because the precursors are not readily accessible.

We now report the preparation of seven 2,2-diaryloxy oxadiazolines (**1**) and the thermolysis of the parent

Received October 27, 2000. Published on the NRC Research Press Web site on April 12, 2001.

X. Lu, D.L. Reid, and J. Warkentin.[1] Department of Chemistry, McMaster University, Hamilton, ON L8S 4M1, Canada.

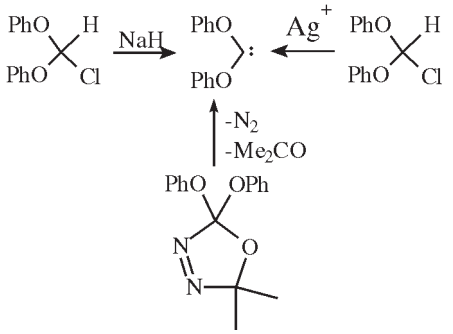
[1]Corresponding author (e-mail: warkent@McMaster.ca; fax: (905) 522-2509).

 DOI: 10.1139/cjc-79-3-319 © 2001 NRC Canada

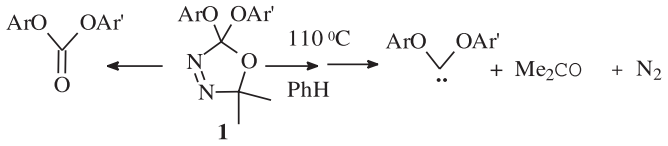
Table 1. Rate constants for thermolysis of diaryloxy oxadiazolines in benzene.

C2 substituents	C_6H_5O, *p*-$MeOC_6H_4O$	C_6H_5O, *p*-MeC_6H_4O	C_6H_5O, C_6H_5O	C_6H_5O, *p*-CNC_6H_4O
$k_{110°C}$ ($\times 10^5$) (s^{-1})	9.3	11.7	11.8	17.9
Relative rate	0.8	1.0	1.0	1.5

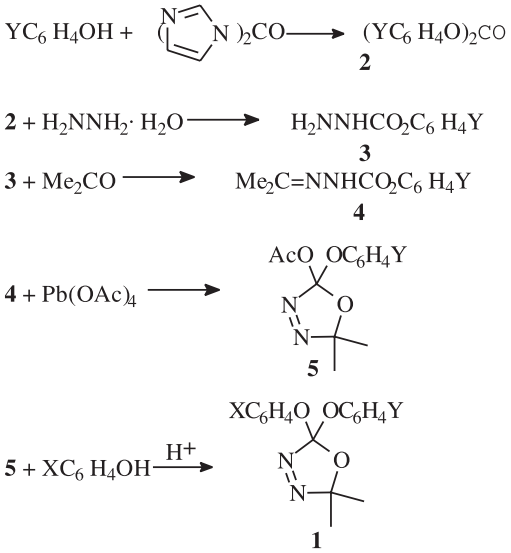
Scheme 1.



Scheme 2.



Scheme 3.



diphenoxy compound, as well as some substituted analogues, in solution at 110°C to generate diaryloxycarbene intermediates (Schemes 2 and 3). Oxadiazolines (**1**) are not more difficult to prepare than corresponding 2-aryloxy-2-methoxy oxadiazolines or 2,2-dialkoxy oxadiazolines, they are thermally stable compounds at room temperature, and they represent the most convenient source of diaryloxycarbenes that is currently available.

Results and discussion

2,2-Diaryloxy-Δ^3-1,3,4-oxadiazolines were prepared from appropriate diaryl carbonates according to Scheme 3. Diphenyl carbonate is commercially available and other carbonates were prepared either from a phenol and 1,1′-carbonyldiimidazole or by transesterification of diphenyl carbonate (not shown). Hydrazinolysis of the diaryl carbonates, in contrast to that of dimethyl carbonate, requires some care to minimize displacement of both aryloxy groups. Condensation of **3** with acetone and subsequent oxidative cyclization (6) to **4** were straightforward, as was the exchange step (8).

Thermolysis of oxadiazoline **1a** in benzene-d_6 occurred with first order kinetics, with $k_{110°C} = 1.17 \times 10^{-4}$ s^{-1}, about tenfold faster than thermolysis of the 2,2-dimethoxy analogue (8). Rate constants for four of the diaryloxy oxadiazolines are gathered in Table 1. It is evident that a *p*-substituent has only a small effect on the rate constant for thermolysis, and both the sense of the effect (*p*-CN, *p*-OMe) and its magnitude fit a mechanism in which 1,3-dipolar cycloreversion to N_2 and a carbonyl ylide is the rate-limiting step (Scheme 4). The preferred sense of the cycloreversion, to place either XC_6H_4O or YC_6H_4O into the *endo* position, is not known. The intermediacy of a carbonyl ylide was also indicated strongly by the formation of a ketene acetal (vide infra).

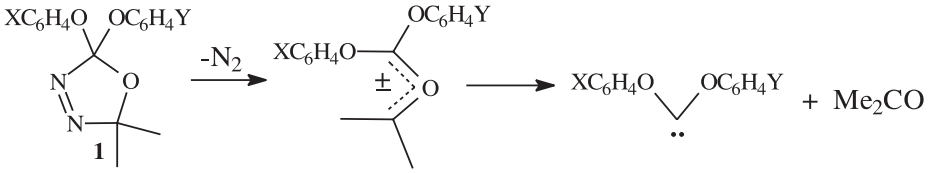
a: X=Y= H; **b**: X= H, Y= *p*-CN; **c**: X= H, Y= p-OMe; **d**: X= H, Y= *p*-Me; **e**: X= *p*-OMe, Y= *p*-CN; **f**: X= *p*-CN, Y= *p*-Me; **g**: X= *o*-OMe, Y= H.

To demonstrate that a carbene is formed upon thermolysis, **1a** was heated in benzene alone or in benzene containing a phenol. From thermolysis of **1a** in the absence of a trapping agent, the carbene dimer tetraphenoxyethene (**6**) was formed in ca. 41% yield, together with **7**–**10** (Scheme 5). Ketene acetal **7** is most likely derived from a carbonyl ylide intermediate (**11**) that closes to oxirane **12** (9). Neither the ylide nor the oxirane arise from attack of the carbene on acetone, as added acetone-d_6 did not result in deuterium incorporation into any of the products. Attack on **12** by carbene **13**, to transfer the oxirane oxygen, leads to **7** and carbonate **8** (Scheme 6). Deoxygenation of oxiranes and desulfurization of thiiranes by carbenes is known (10).

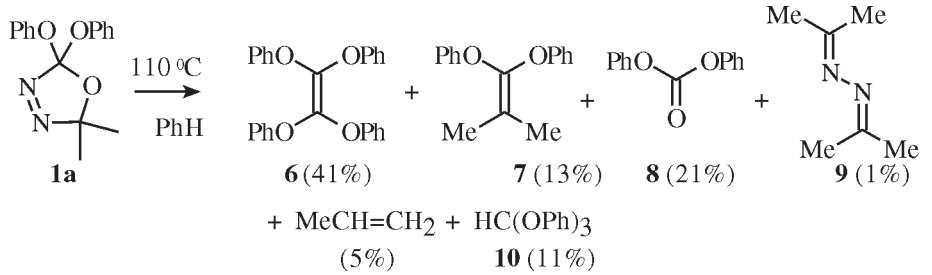
Some of the carbonate is also derived from a competing cycloreversion of **1a** to afford **8** and 2-diazopropane. That process, which would seem to account for the acetone azine (**9**) and propene, must be relatively minor, because of the low total yield of products that are probably derived from 2-diazopropane. In the presence of traces of phenol (presumably derived from reaction of an intermediate or product with adventitious water) 2-diazopropane is expected to be protonated to afford 2-propyl cation–phenoxide ion pairs, which could lead to both propene and isopropyl phenyl ether. The possibility that most of the propene arises from dimethylcarbene, by fragmentation of the carbonyl ylide intermediate to dimethylcarbene and diphenyl carbonate in competition with its fragmentation to diphenoxycarbene and

© 2001 NRC Canada

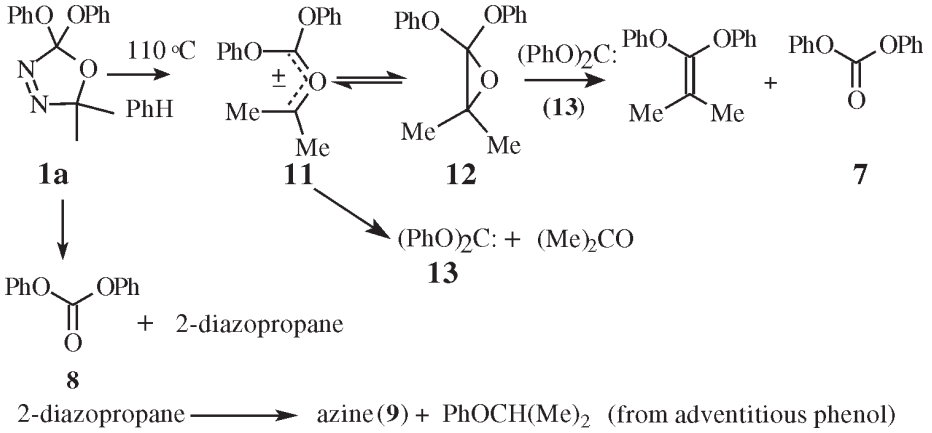
Scheme 4.



Scheme 5.



Scheme 6.



acetone, can be excluded. Although dimethylcarbene would certainly afford propene, the rate constant for 1,2 H-migration is very large (10^7 s^{-1} at room temp) (11) and detection of isopropyl phenyl ether from carbene insertion into phenol at low concentrations of phenol should be difficult. Orthoformate **10** (Scheme 5) is probably derived from the trapping of carbene **13** by phenol. A trace of phenyl formate, detected by GC–MS only, can be attributed to the capture of some of the carbonyl ylide intermediate by water, to generate an intermediate that would lead to phenyl formate (plus acetone and phenol) (Scheme 6). Deliberate addition of water prior to thermolysis of **1a** in benzene did lead to phenyl formate, and other products. Thermolyses of **1c** and **1e** were studied less thoroughly, but the appropriate ketene acetal and the expected carbene dimers were obtained.

Thermolysis of **1a** in benzene with added phenol led to orthoformate (**10**) in 70% yield (Scheme 7). Diphenyl carbonate was a coproduct, and isopropyl phenyl ether (**14**) as well as propene, but not acetone azine, were found. A likely source of **14** is 2-diazopropane, which is expected to react efficiently with phenol in excess to prevent the formation of acetone azine and give **14** instead.

Finally, thermolysis of **1a** in the presence of DMAD gave a product of ipso-aromatic substitution (**15**, Scheme 8), analogous to a product from monoaryloxycarbenes and DMAD (4), as well as bicyclo[1.1.0]butanes **16** and **17**. Those products have been reported in a preliminary communication (7).

Experimental

General methods

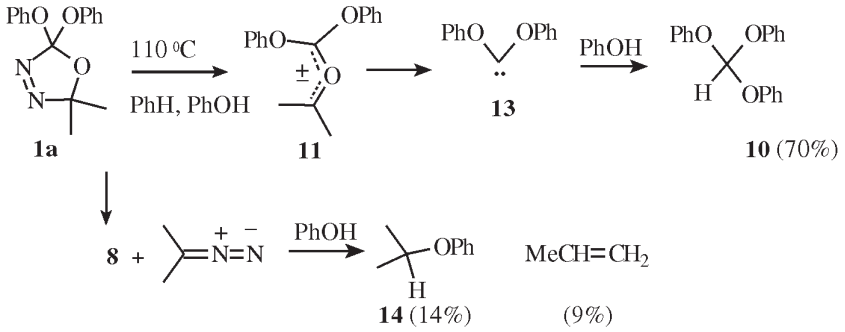
NMR spectra were recorded on a Bruker AC-200 or AC-300 NMR spectrometer. IR spectra were recorded with a Biorad FTS-40 spectrophotometer, with the sample in CCl_4. The IR bands are labeled qualitatively with the symbols br, s, or m for broad, strong, or medium intensities, respectively. Weak bands are omitted. Melting points were recorded on a Thomas–Hoover capillary melting point apparatus, and are uncorrected.

Synthesis of diaryl carbonates

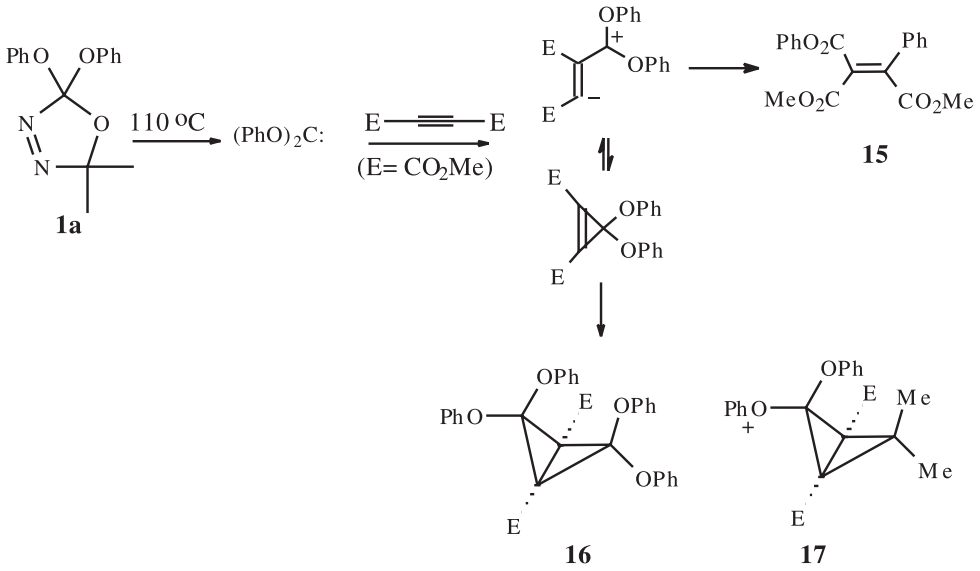
Diphenyl carbonate is commercially available. The other diaryl carbonates were prepared by treating *N*,*N*′-carbonyl diimidazole with a substituted phenol or by *trans*-esterification of diphenyl carbonate.

© 2001 NRC Canada

Scheme 7.



Scheme 8.



Di-p-*cresyl carbonate (**2d**)*

Compound **2d**, mp 113 to 114°C (lit. (12) mp 113°C), was obtained as a white solid (41.8 g, 69%) by refluxing a solution of 53.5 g (0.25 mol) of diphenyl carbonate with *p*-cresol (162 g, 1.5 mol) in toluene (300 mL) containing triethylamine (151.5 g, 1.5 mol). ^{1}H NMR (200 MHz, $CDCl_3$) δ: 2.35 (s, 6H), 7.11–7.25 (m, 8H).

Di-p-*methoxyphenyl carbonate (**2c**)*

Carbonate **2c**, mp 93 to 94°C (lit. (13) mp 95.5–96°C), was prepared in 66% yield by the reaction of *N*,*N*′-carbonyl diimidazole (16.2 g, 0.10 mol) with *p*-methoxy phenol (49.6 g, 0.40 mol). ^{1}H NMR (200 MHz, $CDCl_3$) δ: 3.80 (s, 6H), 6.88–7.20 (m, 8H). ^{13}C NMR (75 MHz, $CDCl_3$) δ: 55.6, 114.5, 121.7, 144.7, 152.8, 157.6.

Aryl hydrazinocarboxylates

A solution of diaryl carbonate and hydrazine hydrate (1.2 equiv) in dichloromethane was stirred for 24 h. After evaporation of all the volatile components, including part of the excess hydrazine hydrate, enough diethyl ether was added to form a clear solution before hexane was added dropwise to crystallize the hydrazide.

Phenyl hydrazinocarboxylate

Mp 104 to 105°C (lit. (14) mp 105 to 106°C), was prepared by reaction of diphenyl carbonate with hydrazine hydrate at 0°C. ^{1}H NMR (200 MHz, $CDCl_3$) δ: 3.88 (s, 2H, NH_2), 6.40 (s, 1H, NH), 7.26 (m, 5H, ArH).

p-*Tolyl hydrazinocarboxylate*

This was obtained in 53% yield by the reaction of 27.5 g (0.114 mol) of di-*p*-tolyl carbonate with hydrazine *mono*-hydrate (6.80 g, 0.136 mol) in CH_2Cl_2 (100 mL). White solid, mp 116 to 117°C (lit. (14) mp 115–117°C). EI-MS *m*/*z*: 166 $[M]^+$ (8), 108 $[MeC_6H_4O]^+$ (100), 91 (8), 77 (16), 65 (7), 51 (9). CI-MS (NH_3) *m*/*z*: 184 $[M+18]^+$ (28), 167 $[M+1]^+$ (100). IR (CCl_4) (cm^{-1}): 3457 (m), 1753 (s), 1549 (m), 1510 (m), 1462 (s), 1255 (m), 1220 (s), 1206 (s), 1024 (m). ^{1}H NMR (200 MHz, $CDCl_3$) δ: 2.33 (s, 3H), 3.86 (s, 2H, NH_2), 6.39 (s, 1H, NH), 6.99–7.26 (m, 4H). ^{13}C NMR (50 MHz) δ: 20.8, 121.0, 129.9, 135.2, 148.5, 157.1.

Other aryl hydrazinocarboxylates were not isolated but were used directly in the next step.

(Phenoxycarbonyl)hydrazone of acetone

Phenyl hydrazinocarboxylate (5.74 g, 37.7 mmol) was stirred with $NaSO_4$ (~6 g) in acetone (150 mL) for 12 h. The

© 2001 NRC Canada

crude reaction mixture was filtered and concentrated to give the (phenoxycarbonyl)hydrazone compound of acetone (6.87 g, 35.7 mmol) in 64% overall yield, as a white solid, mp 125 to 126°C. EI-MS *m/z*: 192 $[M]^+$ (2), 98 $[M\text{-}PhOH]^+$ (30), 94 $[PhOH]^+$ (100), 66 (22), 65 (20), 56 $[N{=}C(CH_3)_2]^+$ (13). CI-MS (NH_3) *m/z*: 210 $[M+NH_4]^+$, 193 $[M+H]^+$. ^1H NMR (200 MHz, $CDCl_3$) δ: 1.84 (s, 3H), 2.06 (s, 3H), 6.79–7.40 (m, 5H), 7.98 (s, 1H, NH). ^{13}C NMR (75 MHz, $CDCl_3$) δ: 16.2, 25.2, 115.4, 121.5, 125.6, 129.3.

p-Cresoxycarbonyl hydrazone of acetone

In an analogous reaction, di-*p*-tolyl carbonate (27.5 g, 0.113 mol) gave 11.4 g (61%) of the *p*-cresoxycarbonyl hydrazone of acetone as a white solid, mp 122–124°C. EI-MS *m/z*: 206 $[M]^+$ (7), 108 $[MeC_6H_4O]^+$ (100), 99 (15), 77 (7), 6 (6), 41 (4). CI-MS (NH_3) *m/z*: 207 $[M+1]^+$ (53). IR (CCl_4) (cm^{-1}): 3250 (m), 2922 (m), 1781 (m), 1735 (m), 1720 (s), 1508 (m), 1491 (m), 1390 (m), 1361 (s), 1253 (m), 1216 (s), 1202 (s), 1018 (m). ^1H NMR (200 MHz, $CDCl_3$) δ: 1.87 (s, 3H), 2.09 (s, 3H), 2.33 (s, 3H), 7.03–7.26 (m, 4H), 7.79 (s, 1H, NH). ^{13}C NMR (75 MHz, $CDCl_3$) δ: 16.2, 20.8, 25.4, 121.2, 129.8, 135.3, 148.5, 152.3.

Other carbonyl hydrazones of acetone were synthesized according to the above procedure.

Oxidation of hydrazones to 2-acetoxy-2-aryloxy oxadiazolines

The general procedure involved dropwise addition, over 1 to 2 h, of a solution of an aryloxycarbonyl hydrazone of acetone (5 g, 0.02 mol) in CH_2Cl_2 (60 mL) under dry nitrogen, to a stirred solution of 1.2 equiv (ca. 10 g) of lead tetraacetate at 0°C. After the addition, the solution was kept in the ice bath for 2 h and then at room temperature overnight. The solution was washed with 10% aq $NaHCO_3$ (4 × 50 mL) and the organic layer was dried with anhyd $MgSO_4$. Filtration and evaporation of the solvent left a yellow oil containing the desired oxadiazoline (about 70%) and an acyclic isomer ($ArOCON{=}NC(OAc)Me_2$, about 30%), estimated by means of integration of the ^1H NMR spectrum. Unlike 2-acetoxy-2-methoxy oxadiazolines, the 2-acetoxy-2-aryloxy oxadiazolines can be isolated by chromatography on SiO_2 (radial or column) with 5% ethyl acetate in hexane as the eluting solvent.

2-Acetoxy-5,5-dimethyl-2-phenoxy-Δ^3-1,3,4-oxadiazoline

To a stirred and ice cooled solution of lead tetraacetate (12.69 g, 28.62 mmol, 1.0 M) in methylene chloride (10 mL) under nitrogen was added (by drops over 20 min) a solution of the (phenoxycarbonyl)hydrazone of acetone (15) (5.0 g, 26.00 mmol, 0.9 M) in methylene chloride (20 mL). The reaction solution, which changed colour from yellow to brown, was stirred for an additional 2 h during which time the ice melted. A small amount of a brown precipitate was observed. Water (~10 mL) and CH_2Cl_2 (~10 mL) were added to the reaction mixture that was then filtered through a pad of Celite. The filtrate was washed with aqueous sodium bicarbonate (5%) until the bubbling stopped and extracted with CH_2Cl_2. Drying over anhyd $MgSO_4$, filtration, and concentration gave 4.48 g of a mixture containing 58% of the oxadiazoline and 42% of $PhOCON{=}NC(OAc)Me_2$. Composite ^1H NMR (200 MHz, $CDCl_3$) δ: 1.35 (s, Me), 1.66 (s, Me), 1.71 (s, Me_2), 2.10 (s, OCOMe of oxadiazoline), 2.02 (s, OCOMe), 7.28 (m).

*2-Acetoxy-5,5-dimethyl-2-phenoxy-Δ^3-1,3,4-oxadiazoline (**5a**)*

The title compound was isolated by chromatography as a pale yellow oil, in 72% yield. ^1H NMR (200 MHz, $CDCl_3$) δ: 1.35 (s, 3H), 1.66 (s, 3H), 2.09 (s, 3H), 7.15–7.31 (m, 5H). ^{13}C NMR (75 MHz, $CDCl_3$) δ: 21.2, 22.6, 23.9, 121.7, 123.4, 125.0, 129.1, 133.1, 151.3, 165.9. (In 2,2-dialkoxy-5,5-dimethyl-Δ^3-1,3,4-oxadiazolines the C5 and C2 signals in the ^{13}C NMR spectrum are near 119 and 137 ppm, respectively) (9).

The other 2-acetoxy-2-aryloxy oxadiazolines were not separated from their acyclic isomers but the crude products from oxidation were used directly for preparation of diaryloxy oxadiazolines.

Synthesis of diaryloxy oxadiazolines (1)

In general, both symmetric and unsymmetric 2,2-diaryloxy oxadiazolines were synthesized by exchanging the acetoxy group of a 2-acetoxy-2-aryloxy oxadiazoline for a second aryloxy group. A solution of a 2-acetoxy-2-aryloxy oxadiazoline (ca. 5 g) and 3 equiv (ca. 7 g) of a substituted phenol in CH_2Cl_2 was acidified with catalytic trifluoroacetic acid. After refluxing for 16 h, the solution was extracted with three 30 mL portions of 10% NaOH to remove excess phenol and to destroy the acyclic acetoxy compound. Separation of the organic layer, drying with anhyd $MgSO_4$, and filtration resulted in a solution of the 2,2-diaryloxy oxadiazoline in CH_2Cl_2. Evaporation of the solvent and purification of the residue by chromatography afforded the oxadiazoline in pure form.

*5,5-Dimethyl-2,2-diphenoxy-Δ^3-1,3,4-oxadiazoline (**1a**)*

The procedure for the synthesis of 5,5-dimethyl-2,2-diphenoxy-Δ^3-1,3,4-oxadiazoline is typical. A 50 mL round-bottom flask was charged with 1.05 g of a mixture of 2-acetoxy-2-phenoxy oxadiazoline (ca. 57%) and its acyclic isomer (ca. 43%), phenol (0.412 g, 4.38 mmol, 0.5 M), a catalytic amount of trifluoroacetic acid (0.06 mL, 0.74 mmol), and CH_2Cl_2 (8.5 mL). The solution was stirred for 24 h at room temperature before aq NaOH (10 mL, 10% w/v) was added and stirring was continued for 3 h. Dichloromethane was added and the organic layer was separated and extracted with water. Drying ($MgSO_4$), filtration, and concentration gave the 2,2-diphenoxy oxadiazoline (**1a**, 51%) as a white solid, mp 59.5–60.5°C. EI-MS *m/z* (%): $[M]^+$ not observed, 215 (11), 191 $[M\text{-}OPh]^+$ (100), 135 (37), 119 (78), 105 (46), 77 $[Ph]^+$ (43). IR (CCl_4) (cm^{-1}): 3071 (m), 3047 (m), 2996 (m), 1785 (s), 1594 (s), 1492 (s), 1459 (m). ^1H NMR (200 MHz, $CDCl_3$) δ: 1.22 (s, 6H), 7.09–7.33 (m, 10H). ^{13}C NMR (50.3 MHz, C_6D_6) δ: 23.5 ($C(CH_3)_2$), 121.5 (C2), 122.1 (C2 or C3 of Ar), 124.9 (C4 of Ar), 129.1 (C3 or C2 of Ar), 136.0 (C5), 151.6 (C1 of Ar).

2-p-*Cyanophenoxy-5,5-dimethyl-2-phenoxy-Δ^3-1,3,4-oxadiazoline (**1b**)*

^1H NMR (200 MHz, $CDCl_3$) δ: 1.26 (s, 3H), 1.46 (s, 3H), 7.14–7.65 (m, 9H). ^{13}C NMR (75 MHz, $CDCl_3$) δ: 23.3, 24.1, 107.8, 118.5, 121.2, 122.1, 122.5, 125.5, 129.3, 133.6, 135.2, 151.0, 155.4.

© 2001 NRC Canada

2-p-*Methoxyphenoxy-5,5-dimethyl-2-phenoxy-*Δ^3*-1,3,4-oxadiazoline (**1c**)*

Pale yellow oil. IR (CCl_4) (cm^{-1}): 3069 (m), 2996 (s), 2938 (s), 2909 (s), 2838 (s), 1837 (m), 1780 (s), 1599 (s), 1511 (s), 1383 (m), 1369 (m), 1296 (m), 989 (m). ^{1}H NMR (200 MHz, $CDCl_3$) δ: 1.17 (s, 3H), 1.21 (s, 3H), 3.73 (s, 3H), 6.76–7.29 (m, 9H). ^{13}C NMR (75 MHz, $CDCl_3$) δ: 23.4, 23.6, 55.4, 113.9, 121.3, 122.0, 123.7, 124.8, 129.1, 136.2, 144.9, 151.7, 156.9.

2-p-*Cresoxy-2-phenoxy-5,5-dimethyl-*Δ^3*-1,3,4-oxadiazoline (**1d**)*

Clear oil. IR (CCl_4) (cm^{-1}): 3039 (m), 2994 (s), 2939 (m), 1780 (m), 1593 (s), 1507 (s), 1494 (s), 1458 (m), 1383 (m), 1369 (m), 1288 (m), 1087 (br), 989 (m). ^{1}H NMR (200 MHz, $CDCl_3$) δ: 1.21 (s, 6H), 2.27 (s, 3H), 7.07–7.29 (m, 9H). ^{13}C NMR (75 MHz, $CDCl_3$) δ: 20.6, 23.5, 121.3, 122.1, 124.8, 129.1, 129.5, 134.5, 136.1, 149.4, 151.8.

2-p-*Cyanophenoxy-2-*p-*methoxyphenoxy-5,5-dimethyl-*Δ^3*-1,3,4-oxadiazoline (**1e**)*

^{1}H NMR (200 MHz, $CDCl_3$) δ: 1.21 (s, 3H), 1.43 (s, 3H), 3.73 (s, 3H), 6.75–7.66 (m, 8H). ^{13}C NMR (75 MHz, $CDCl_3$) δ: 23.0, 23.9, 55.2, 107.5, 113.9, 118.3, 121.0, 122.2, 123.5, 133.4, 135.3, 144.0, 155.4, 157.0.

2-p-*Cresoxy-2-*p-*cyanophenoxy-5,5-dimethyl-*Δ^3*-1,3,4-oxadiazoline (**1f**)*

IR (CCl_4) (cm^{-1}): 3106 (s), 3039 (m), 2996 (m), 2940 (m), 2871 (m), 2232 (s), 1899 (m), 1781 (m), 1606 (s), 1503 (m), 1384 (m), 1370 (m), 1290 (m), 1133 (s), 1019 (m), 989 (m). ^{1}H NMR (200 MHz, $CDCl_3$) δ: 1.24 (s, 3H), 1.43 (s, 3H), 2.26 (s, 3H), 7.04 (s, 4H), 7.43–7.63 (m, 4H, Ar-CN). ^{13}C NMR (50 MHz) δ: 20.4, 23.0, 23.8, 107.5, 118.2, 120.9, 121.8, 122.2, 129.5, 133.3, 134.9, 135.1, 148.5, 155.3.

2-o-*Methoxyphenoxy-2-phenoxy-5,5-dimethyl-*Δ^3*-1,3,4-oxadiazoline (**1g**)*

Pale yellow oil. EI-MS *m*/*z*: 245 $[M\text{-}N{=}N{=}C(CH_3)_2{+}1]^+$ (9), 221 $[M\text{-}OPh]^+$ (38), 191 $[M\text{-}OC_6H_4OMe]^+$ (72), 165 (34), 149 (100), 135 (65), 119 (27), 77 (65). CI-MS (NH_3) *m*/*z*: 332 $[M+18]^+$ (17). ^{1}H NMR (200 MHz, $CDCl_3$) δ: 1.18 (s, 3H), 1.21 (s, 3H), 3.77 (s, 3H), 6.8–7.36 (m, 9H). ^{13}C NMR (75 MHz, $CDCl_3$) δ: 23.1, 23.5, 55.8, 112.5, 120.2, 121.5, 121.6, 121.8, 123.9, 124.6, 126.0, 128.9, 136.3, 140.5, 151.7, 152.5. HRMS: Anal. calcd. for $C_{17}H_{18}N_2O_4Na$: 337.1164; found: 337.1180.

General method for thermolyses

All thermolyses were carried out by immersing the sealed thermolysis tubes containing the samples (ca. 0.2 mol in 10–15 mL of benzene, dried by refluxing over CaH_2) in a constant-temperature oil bath at 110.0 ± 0.2°C for 24 h. Spectroscopic data of pure compounds came from chromatographically isolated products. Radial chromatography, with ethyl acetate in hexanes for elution, was used for small-scale reactions, and column chromatography for larger scale reactions (0.2–1 g of oxadiazoline).

Thermolysis products from 5,5-dimethyl-2,2-diphenoxy-Δ^3**-1,3,4-oxadiazoline in the absence of trapping agents**

5,5-Dimethyl-2,2-diphenoxy-Δ^3-1,3,4-oxadiazoline (**1a**) (0.82 g, 2.88 mmol) was heated at 110°C in benzene (25 mL). The solvent was evaporated and the residue was chromatographed (Chromatotron) to give carbene dimer **6a** (41%), ketene acetal **7** (13%), and diphenyl carbonate (21%). The yields came from a thermolysis experiment carried out in a sealed NMR tube containing *p*-dimethoxybenzene as internal standard. After the thermolysis, the ^{1}H NMR spectrum (300 s relaxation delay) was integrated without opening the tube. The solution was also analysed by GC–FID to estimate the yields of the products.

*Dimer of diphenoxycarbene (**6a**)*

White solid, mp 162 to 163°C (lit. (6) mp 168°C). EI-MS *m*/*z* (%): 396 $[M]^+$ (4), 291 (4), 199 (25), 153 (20), 141 (30) 105 (18), 77 (100), 51 (89). CI-MS (NH_3) *m*/*z* (%): 397 $[M+1]^+$ (2), 199 (100). IR (CCl_4) (cm^{-1}): 1592 (m), 1548 (m), 1491 (s), 1221 (s), 1202 (s), 1163 (m), 1105 (s). ^{1}H NMR (200 MHz, C_6D_6) δ: 6.74–7.28 (m, 10H, Ph). ^{13}C NMR (75 MHz, $CDCl_3$) δ: 116.7, 123.3, 129.5, 137.4, 155.7.

*1,1-Diphenoxy-2-methylpropene (**7a**)*

White solid, mp 41 to 42°C. EI-MS *m*/*z* (%): 141 $[M+1]^+$ (10), 140 $[M]^+$ (33), 147 (10), 119 (100), 91 (50), 77 (45), 41 (37). CI-MS (NH_3) *m*/*z* (%): 241 $[M+1]^+$ (100), 240 $[M]^+$ (33), 119 (100). IR (CCl_4) (cm^{-1}): 3044 (m), 2919 (m), 2861 (m), 1716 (s), 1596 (br), 1491 (br), 1221 (br), 1194 (br), 1164 (s), 1148 (br), 1073 (m). ^{1}H NMR (200 MHz, C_6D_6) δ: 1.75 (s, 6H, Me), 6.96–7.29 (m, 10H, Ph). ^{13}C NMR (75 MHz, $CDCl_3$) δ: 16.5, 105.0, 116.1, 122.4, 129.3, 144.4, 155.8.

Thermolysis products from 2-(4-methoxyphenoxy)-5,5-dimethyl-2-phenoxy-Δ^3**-1,3,4-oxadiazoline (1c) in the absence of trapping agents**

Oxadiazoline (**1c**) (0.67 g, 2.14 mmol) was heated at 110°C in benzene (20 mL). Evaporation of the solvent and radial chromatography of the residue gave carbene dimers (**6c**) (38.5%) as a 1:1 mixture of isomers, ketene acetal (**7c**) (10.9%), and 4-methoxyphenoxy phenoxy carbonate (23%). Yields came from a thermolysis experiment carried out in a sealed NMR tube containing *p*-xylene as internal standard. After the thermolysis, the ^{1}H NMR spectrum (300 s relaxation delay) was integrated without opening the tube.

Dimers of p-*methoxyphenoxy(phenoxy)carbene (**6c**)*

White solid, mp 99–101.5°C. The *E*- and *Z*-isomers, in ca. 1:1 ratio from the ^{1}H NMR spectrum, could not be separated. Composite spectra for two isomers are listed. EI-MS *m*/*z* (%): 457 $[M+1]^+$ (12), 351 (9), 321 (10), 239 (16), 184 (15), 135 (100), 92 (52), 78 (100), 51 (38). CI-MS (NH_3) *m*/*z* (%): 458 $[M+2]^+$ (64), 457 $[M+1]^+$ (10). IR (CCl_4) (cm^{-1}): 3002 (m), 2952 (m), 2836 (m), 1595 (s), 1503 (s), 1466 (m), 1297 (m), 1199 (br), 1102 (s), 1041 (s). ^{1}H NMR (200 MHz, $CDCl_3$) δ: 3.74 (s, 3H), 3.75 (s, 3H), 6.77–7.31 (m, 18H). ^{13}C NMR (75 MHz, $CDCl_3$) δ: 55.6, 114.6, 116.7, 118.0, 123.2, 129.4, 137.7, 149.6, 155.7.

© 2001 NRC Canada

*1-(*p*-Methoxyphenoxy)-1-phenoxy-2-methylpropene (**7c**)*

Clear oil. EI-MS *m/z* (%): 270 $[M]^+$ (45), 149 (100), 119 (85), 91 (68), 77 (60), 41 (40). CI-MS (NH_3) *m/z* (%): 271 $[M+1]^+$ (100). IR (CCl_4) (cm^{-1}): 2916 (m), 1715 (s), 1594 (s), 1550 (m), 1504 (s), 1492 (s), 1465 (m), 1245 (m), 1217 (s), 1192 (s), 1158 (br), 1103 (m), 1043 (m). ^1H NMR (200 MHz, $CDCl_3$) δ: 1.72 (s, 3H), 1.77 (s, 3H), 3.73 (s, 3H), 6.74~7.29 (m, 9H). ^{13}C NMR (75 MHz, $CDCl_3$) δ: 16.5, 55.6, 104.1, 114.4, 116.1, 117.2, 122.3, 129.3, 144.9, 149.6, 155.1, 155.9. HRMS: Anal. calcd. for $C_{17}H_{18}O_3$: 270.1262; found: 270.1256.

p-*Methoxyphenyl phenyl carbonate (15, 16)*

EI-MS *m/z* (%): 244 $[M]^+$ (42), 200 (11), 185 (22), 157 (4), 123 (83), 107 (12), 95 (30), 77 (100), 65 (30), 51 (31). CI-MS (NH_3) *m/z* (%): 262 $[M+18]^+$ (100), 244 $[M]^+$ (82). IR (CCl_4) (cm^{-1}): 3049 (m), 3006 (m), 2955 (m), 2912 (m), 1779 (br), 1596 (s), 1502 (br), 1462 (s), 1442 (m), 1296 (s), 1232 (br), 1178 (br), 1103 (m), 1039 (s), 1009 (s). ^1H NMR (200 MHz, $CDCl_3$) δ: 3.78 (s, 3H), 6.87–7.39 (m, 9H). ^{13}C NMR (75 MHz, $CDCl_3$) δ: 55.6, 114.5, 120.9, 121.7, 126.2, 129.5, 144.6, 151.1, 152.4, 157.6.

Thermolysis products from 2-(*p*-cyanophenoxy)-2-(*p*-methoxyphenoxy)-5,5-dimethyl-Δ^3-1,3,4-oxadiazoline (1e) in the absence of trapping agents

Thermolysis of oxadiazoline (**1e**) (0.48 g, 1.40 mmol) in benzene (20 mL), evaporation of the solvent and radial chromatography of the residue gave carbene dimers (**6e**) as a 1.25:1 mixture of isomers (28%), ketene acetal (**7c**) (12%), and *p*-cyanophenoxy *p*-methoxyphenoxy carbonate (16%).

Dimers of p-*cyanophenoxy(*p-*methoxyphenoxy)carbene*

The spectra are composites of the *E*- and *Z*-isomers (isomer ratio 1.25:1) estimated from the ^1H NMR spectrum. It was not possible to determine which isomer was the major one. EI-MS *m/z* (%): 506 $[M]^+$ (8), 135 (100), 123 (36), 107 (28), 102 (45), 77 (70), 43 (68). CI-MS (NH_3) *m/z* (%): 524 $[M+18]^+$ (3). IR (CCl_4) (cm^{-1}): 2954 (m), 2838, 2232 (m), 1604 (s), 1503 (s), 1296 (m), 1216 (s), 1183 (s), 1168 (m), 1099 (s), 1040 (m). ^1H NMR (200 MHz, $CDCl_3$) δ: 3.76 (s, 3H), 3.77 (s, 2.4H), 6.78–7.64 (m, 14.4H). ^{13}C NMR (75 MHz, $CDCl_3$) δ: 55.6, 107.3, 114.8, 117.2, 117.3, 117.8, 118.0, 118.4, 134.1, 137.2, 148.7, 148.9, 156.2, 158.5, 158.6.

*1-(*p*-Cyanophenoxy)-1-(*p*-methoxyphenoxy)-2-methylpropene (**7e**)*

EI-MS *m/z* (%): 295 $[M]^+$ (28), 149 (100), 124 (34), 116 (22), 77 (15), 41 (61). CI-MS (NH_3) *m/z* (%): 313 $[M+18]^+$ (24), 296 $[M]^+$ (90). IR (CCl_4) (cm^{-1}): 1041 (m), 1136 (m), 1155 (br), 1194 (s), 1232 (s), 1504 (s), 1605 (m), 1717 (m), 2230 (m), 2936 (m). ^1H NMR (200 MHz, $CDCl_3$) δ: 1.70 (s, 3H, Me), 1.78 (s, 3H, Me), 3.75 (s, 3H, OMe), 6.76–7.59 (m, 8H, ArH). ^{13}C NMR (75 MHz, $CDCl_3$) δ: 16.3, 16.4, 55.6, 105.7, 105.8, 114.6, 116.8, 117.0, 118.8, 133.9, 143.9, 149.2, 155.4, 159.2. HRMS: Anal. calcd. for $C_{18}H_{17}NO_3$: 295.1122; found: 295.1153.

p-*Cyanophenyl* p-*methoxyphenyl carbonate*

White solid, mp 103–105°C. EI-MS *m/z* (%): 269 $[M]^+$ (34), 254 (31), 225 (9), 210 (23), 154 (6), 123 (100), 107 (84), 77 (77), 65 (32). CI-MS (NH_3) *m/z* (%): 287 $[M+18]^+$ (48), 269 $[M]^+$ (89), 123 (100). IR (CCl_4) (cm^{-1}): 3004 (m), 2932 (m), 2838 (m), 2232 (m), 1781 (s), 1717 (m), 1605 (s), 1505 (s), 1465 (m), 1296 (m), 1225 (s), 1183 (s), 1041 (m). ^1H NMR (200 MHz, $CDCl_3$) δ: 3.79 (s, 3H, OMe), 6.88–7.72 (m, 8H, Ar). ^{13}C NMR (75 MHz, $CDCl_3$) δ: 55.5, 110.1, 114.5, 117.9, 121.5, 121.9, 133.7, 144.2, 151.4, 153.8, 157.7.

Thermolyses of diphenoxy oxadiazoline in the presence of acetone-d_6

A solution of **1a** (15.2 mg, 0.053 mmol) in benzene-d_6 (0.5 mL) containing acetone-d_6 (36.8 μL, 0.500 mmol) and dimethoxybenzene (internal standard, 7.4 mg, 0.054 mmol) was heated at 110°C for 24 h. Analysis by GC–MS showed that none of the products contained deuterium.

Thermolyses of di(aryloxy) oxadiazolines in the presence of phenols

Oxadiazoline (**1a**) (1 g, 3.50 mmol) was heated at 105°C for 24 h in benzene (25 mL) containing phenol (3.3 g, 35 mmol). The only product that could be isolated was triphenyl orthoformate (mp 73 to 74°C, lit. (17) mp 75°C), as a white solid in 76% yield. EI-MS *m/z* (%): 199 (100), 171 (7), 153 (31), 141 (4), 94 (17), 77 (72), 65 (20), 51 (31). CI-MS (NH_3) *m/z* (%): 199 $[M\text{-}OPh]^+$ (93). IR (CCl_4) (cm^{-1}): 3069 (m), 3046 (m), 1784 (m), 1597 (s), 1491 (s), 1363 (m), 1289 (m), 1228 (s), 1206 (s), 1061 (s), 1028 (m), 997 (m). ^1H NMR (200 MHz, $CDCl_3$) δ: 6.81 (s, 1H, $(PhO)_3CH$), 7.06–7.33 (m, 15H). ^{13}C NMR (75 MHz, $CDCl_3$) δ: 110.9, 118.2, 123.6, 129.6, 153.9.

Thermolyses of diaryloxy oxadiazolines in the presence of *p*-cresol

A solution of oxadiazoline **1a** (1.14 g, 4.02 mmol) in benzene (25 mL) containing *p*-cresol (4.32 g, 40 mmol) was heated at 105°C for 24 h. *p*-Tolyl diphenyl orthoformate was isolated as a white solid, mp 82 to 83°C, in 65% yield. EI-MS *m/z* (%): 213 $[M\text{-}OPh]^+$ (98), 199 $[M\text{-}OC_6H_4OMe]^+$ (100), 167 (16), 153 (21), 108 (16), 91 (46), 77 (85), 55 (40), 51 (28). CI-MS (NH_3) *m/z* (%): 213 $[M\text{-}OPh]^+$ (100), 199 $[M\text{-}OC_6H_4OMe]^+$ (81). IR (CCl_4) (cm^{-1}): 3069 (m), 3043 (m), 2927 (m), 2869 (m), 1596 (s), 1495 (s), 1363 (m), 1288 (m), 1194 (s), 1171 (s), 1032 (s). ^1H NMR (200 MHz, $CDCl_3$) δ: 2.27 (s, 3H), 5.56 (s, 1H, CH), 6.98–7.31 (m, 14H). ^{13}C NMR (75 MHz, $CDCl_3$) δ: 20.5, 111.0, 118.0, 123.4, 129.6, 130.0, 133.0, 151.5, 153.8. By GC–MS it was possible to detect traces of *p*-cresyl isopropyl ether and diphenyl carbonate.

Similarly, a solution of **1b** (0.2 g, 0.65 mmol) and *p*-cresol (0.56 g, 5.18 mmol) in benzene (25 mL) was heated at 105°C for 24 h. *p*- Tolyl *p*-cyanophenyl phenyl orthoformate was isolated as a pale yellow oil, in 84% yield. EI-MS *m/z* (%): 238 $[M\text{-}OPh]^+$ (55), 224 $[M\text{-}OC_6H_4Me]^+$ (88), 213 $[M\text{-}OC_6H_4CN]^+$ (93), 196 (19), 185 (9), 167 (9), 153 (7), 123 (5), 107 (17), 91 (62), 77 (100), 65 (45), 51 (21). CI-MS (NH_3) *m/z* (%): 238 $[M\text{-}OPh]^+$ (37), 224 $[M\text{-}OC_6H_4Me]^+$ (47), 213 $[M\text{-}OC_6H_4CN]^+$ (100). IR (CCl_4) (cm^{-1}): 3067

© 2001 NRC Canada

(m), 3039 (m), 2926 (m), 2231 (m), 1607 (s), 1549 (m), 1508 (s), 1257 (m), 1208 (s), 1172 (s), 1068 (s). ^{1}H NMR (200 MHz, $CDCl_3$) δ: 2.31 (s, 3H), 6.62 (s, 1H, CH), 6.96–7.62 (m, 13H). ^{13}C NMR (75 MHz, $CDCl_3$) δ: 20.6, 106.8, 110.6, 118.1, 118.6, 124.0, 130.0, 130.2, 133.7, 133.9, 151.2, 153.5, 156.9.

In a similar experiment, oxadiazoline **1c** (0.47 g, 1.50 mmol) in benzene (25 mL) containing *p*-cresol (1.29 g, 11.94 mmol) was heated at 105°C for 24 h. The major product was *p*-tolyl *p*-methoxyphenyl phenyl orthoformate, obtained as a pale yellow oil in 70% yield. EI-MS *m*/*z* (%): 243 $[M\text{-}OPh]^+$ (19), 229 $[M\text{-}OC_6H_4Me]^+$ (31), 213 $[M\text{-}OC_6H_4OMe]$ (100), 185 (7), 167 (13), 152 (6), 123 (12), 107 (16), 91 (32), 77 (49), 65 (24), 51 (13). CI-MS (NH_3) *m*/*z* (%): 243 $[M\text{-}OPh]^+$ (40), 229 $[M\text{-}OC_6H_4Me]^+$ (59), 213 $[M\text{-}OC_6H_4OMe]^+$ (100). IR (CCl_4) (cm^{-1}): 3038 (m), 3004 (m), 2953 (m), 2934 (m), 2836 (m), 1592 (m), 1549 (m), 1507 (s), 1463 (m), 1247 (m), 1208 (s), 1070 (s), 1042 (m), 1016 (m). ^{1}H NMR (200 MHz, $CDCl_3$) δ: 2.29 (s, 3H), 3.74 (s, 3H), 6.47 (s, 1H, CH), 6.80–7.32 (m, 13H). ^{13}C NMR (75 MHz, $CDCl_3$) δ: 20.6, 55.5, 111.7, 114.6, 118.1, 120.0, 123.4, 129.5, 130.0, 132.9, 141.6, 147.4, 151.7, 154.0, 155.9.

Thermolysis of 1a in the presence of DMAD

A solution of **1a** (0.49 g, 1.73 mmol) in benzene (8.5 mL) containing DMAD (0.223 g, 1.57 mmol) was heated at 110°C for 24 h. Evaporation of the benzene followed by column chromatography afforded **15** and diphenyl carbonate (32.5%) as well as two new products, **16** and **17**.

*Phenyl (*E*)-2,3-bis(methoxycarbonyl)-3-phenyl propionate (**15**)*

Yield 40%, clear oil. EI-MS *m*/*z* (%): 341 $[M+1]^+$ (8), 309 $[M\text{-}31]^+$ (16), 247 (100), 219 (62), 175 (25), 151 (31), 129 (100), 105 (26), 59 (100). CI-MS (NH_3) *m*/*z* (%): 358 $[M+18]^+$ (100), 341 $[M+1]^+$ (38), 247 (100). IR (CCl_4) (cm^{-1}): 3066 (m), 3034 (m), 3003 (m), 2954 (s), 1761 (br), 1735 (br), 1634 (m), 1593 (s), 1492 (s), 1436 (s), 1323 (s), 1306 (s), 1271 (br), 1230 (br), 1186 (br), 1161 (s), 1068 (s), 1012 (s). ^{1}H NMR (200 MHz, $CDCl_3$) δ: 3.90 (s, 6H, OMe), 6.74–7.55 (m, 10H, Ph). ^{13}C NMR (75 MHz, $CDCl_3$) δ: 53.0, 53.1, 121.0, 126.2, 127.7, 128.9, 129.4, 130.4, 132.8, 148.1, 1050.0, 162.7, 163.0, 167.0. HRMS: Anal. calcd.: 341.1025; found: 341.1026.

*Dimethyl 2,2,4,4-tetraphenoxybicyclo[1.1.0]butane-1,3-dicarboxylate (**16**)*

Yield 8%, oil. EI-MS *m*/*z* (%): 538 $[M]^+$ (4), 445 (11), 341 (3), 219 (5), 105 (17), 77 (100), 51 (39). CI-MS (NH_3) *m*/*z* (%): 539 $[M+1]^+$ (52), 445 (69). IR (CCl_4) (cm^{-1}): 2951 (m), 1734 (s), 1705 (s), 1645 (m), 1591 (s), 1562 (m), 1491 (s), 1436 (m), 1337 (m), 1301 (m), 1273 (m), 1254 (m), 1193 (s), 1163 (s), 1063 (s). ^{1}H NMR (200 MHz, $CDCl_3$) δ: 3.66 (s, 6H, OMe), 6.88–7.25 (m, 20H, OPh). ^{13}C NMR (75 MHz, $CDCl_3$) δ: 51.7, 96.9, 117.0, 119.0, 123.7, 124.4, 129.2, 129.3, 152.8, 154.6, 158.6, 165.9. HRMS: Anal. calcd. for $C_{32}H_{26}O_8$: 538.1628; found: 538.1629.

*Dimethyl 4,4-dimethyl-2,2-diphenoxybicyclo[1.1.0]butane-1,3-dicarboxylate (**17**)*

Yield 4%, oil. EI-MS *m*/*z* (%): 382 $[M]^+$ (25), 351 $[M\text{-}31]^+$ (22), 323 (12), 289 (100), 261 (50), 229 (16), 197 (27), 169 (15), 77 (23), 49 (28). CI-MS (NH_3) *m*/*z* (%): 400 $[M+18]^+$ (10), 382 (4), 351 (100). IR (CCl_4) (cm^{-1}): 2954 (m), 1729 (br), 1593 (m), 1550 (m), 1494 (s), 1439 (m), 1334 (m), 1266 (s), 1206 (s), 1081 (s), 1013 (m). ^{1}H NMR (200 MHz, C_6D_6) δ: 1.35 (s, 3H, Me), 1.65 (s, 3H, Me), 3.29 (s, 6H, OMe), 6.70–7.52 (m, 10H, OPh). ^{13}C NMR (75 MHz, $CDCl_3$) δ: 21.3, 21.8, 42.2, 48.6, 52.0, 117.2, 117.4, 122.4, 123.0, 128.3, 129.1, 129.8, 154.5, 154.8, 164.8. HRMS: Anal. calcd. for $C_{22}H_{22}O_6$: 382.1416; found: 382.1426.

A similar thermolysis with **1a** (1.674 g, 5.90 mmol) and DMAD (0.230 g, 1.60 mmol) in benzene (8.5 mL), gave **16** in 32% yield. Compound **17** was apparently not formed in an appreciable amount; none could be isolated.

Thermolysis rate constants

The rates of decomposition of the oxadiazolines were monitored by ^{1}H NMR spectroscopy at 300 MHz. A sample, typically containing 1.25×10^{-4} mol of an oxadiazoline and 7 mg of *p*-xylene (internal standard) in C_6D_6 (0.5 mL), was degassed and sealed into a medium-walled NMR tube. At appropriate time intervals during thermolysis, the tube was removed from the oil bath and quickly chilled to room temperature to record the ^{1}H NMR spectrum. All oxadiazoline thermolyses were run simultaneously. Linear regression analyses of the data (ln (I / I_0) vs. time, where I and I_0 are the normalized integrals of a given resonance at time t and at time zero, respectively), gave first-order decomposition rate constants from the slopes of the calculated best fits including the origin. Rate constants for thermolysis of four members of the family **1** are in Table 1.

Acknowledgements

The authors gratefully acknowledge financial support from Natural Sciences and Engineering Council of Canada (NSERC), as well as the assistance of Brian Sayer and Dr. Kirk Green with NMR spectroscopy and mass spectrometry, respectively. D.L.R. is also grateful for a Sherman Scholarship.

References

1. M. Regitz. Methoden der crganischen Chemie. Vol. E19b. *Edited by* Thieme. Houben-Weyl, Stuttgart. 1989.
2. (*a*) Advances in carbene chemistry. Vol. 1. *Edited by* U. H. Brinker. JAI Press, Greenwich, CT, U.S.A. 1994; Advances in carbene chemistry. Vol. 2. *Edited by* U. H. Brinker. JAI Press, Stamford, CT, U.S.A. 1998; (*b*) J. Warkentin, J. Chem. Soc. Perkin Trans. 1, 2161 (2000).
3. R.A. Moss. Acc. Chem. Res. **22**, 15 (1989).
4. X. Lu and J. Warkentin. Tetrahedron Lett. **40**, 1483 (1999).
5. J.W. Scheeren, R.J.F.M. Staps, and R.J.F. Nivard. Recl.: J. R. Neth. Chem. Soc. **92**, 11 (1973).
6. H. Scheibler, U. Faass, and B. Hadji-Valassis. J. Prakt. Chem. **279**, 70 (1958).
7. X. Lu and J. Warkentin. Org. Lett. (2000) in press.
8. M. El-Saidi, K. Kassam, D.L. Pole, T. Tadey, and J. Warkentin. J. Am. Chem. Soc. **114**, 8751 (1992).
9. K. Kassam, D.L. Pole, M. El-Saidi, and J. Warkentin. J. Am. Chem. Soc. **116**, 1161 (1994).
10. J.P. Pezacki, P.D. Wood, T.A. Gadosy, J. Lusztyk, and J. Warkentin. J. Am. Chem. Soc. **120**, 8681 (1998).

© 2001 NRC Canada

11. D.A. Modarelli, S. Morgan, and M.S. Platz. J. Am. Chem. Soc. **114**, 7034 (1992).
12. M. Copisarow. J. Chem. Soc. 253 (1929).
13. J.F. Marlier and M.H. O'Leary. J. Am. Chem. Soc. **112**, 5996 (1990).
14. P. Vlasak, P. Parik, J. Klicnar, and J. Mindl. Collect. Czech. Chem. Commun. **63**, 793 (1998).
15. C. Copeland and R.V. Stick. Aust. J. Chem. **37**, 1483 (1984).
16. P. Brown and C. Djerassi. J. Am. Chem. Soc. **89**, 2711 (1967).
17. H. Baines and J.E. Driver. J. Chem. Soc. **125**, 907 (1924).

© 2001 NRC Canada

Investigation of two-component mixed self-assembled monolayers on gold

Zhen Wang, Yan-Li Shi, and Hu-Lin Li

Abstract: Two-component mixed self-assembled monolayers (SAMs) composed of 2-mercapto-5-methyl-1,3,4-oxadiazole (MMO) and 1-dodecanethiol ($C_{12}SH$) in various molar percentages were prepared on gold surfaces by self-assembly. X-ray photoelectron spectroscopy (XPS) and wettability results gave evidence that the coverage of MMO was controlled by the composition of MMO in the assembling solution. The monolayer coverage and apparent rate constant of the redox active probes in solution of different molar ratios of mixed SAMs could be calculated using impedance measurements. The cyclic voltammetry reveals that the probes are selectively passed through the mixed SAMs depending upon their properties.

Key words: self-assembled monolayers (SAMs), X-ray photoelectron spectroscopy (XPS), electrochemistry, electrochemical impedance analysis.

Résumé : On a préparé des monocouches autoassemblées mixtes à deux composants (MAA) de 2-mercapto-5-méthyl-1,3,4-oxadiole (MMO) et de dodécane-1-thiol ($C_{12}SH$), à divers pourcentages molaires, par autoassemblage sur des surfaces d'or. La spectroscopie photoélectronique des rayons X (SPX) et les propriétés de mouillage ont permis d'obtenir des données indiquant que la couverture de MMO est contrôlée par la composition de MMO dans la solution qui conduit à l'assemblage. La couverture de monocouche et les constantes de vitesse apparentes des sondes redox actives en solution de divers rapports molaires de multicouches autoassemblées mixtes peuvent être calculées par des mesures d'impédance. La voltampérométrie cyclique révèlent que, suivant leurs propriétés, les sondes peuvent passer de façon sélective à travers des multicouches autoassemblées mixtes.

Mots clés : monocouches autoassemblées (MSA), spectroscopie photoélectronique des rayons X, électrochimie, analyse d'impédance électrochimique.

[Traduit par la Rédaction]

Introduction

The development of self-assembled monolayers (SAMs) has received particular attention. SAMs prepared from the long chain alkanethiols are well-known examples of two-dimensional ordered structures in which the chains appear to approach the ideal rigid–rod limit of all-trans conformations with a uniform tilt angle (1–3). However, defects will always be present, even for maximum coverage films on atomically flat substrates. Furthermore, a larger number of partially disordered structure phases will arise from homogeneous films of uniform density to heterogeneous films of macroscopic patches of organized adsorbates (4, 5). Recently, controlling surface properties by heterogeneity in monolayer has attracted increasing attention (6–8). Multi-component SAMs derived from the adsorption of organosulfur compounds on gold are useful in fundamental studies of wetting (9, 10), electron transfer (11–13), and also provide elements for the fabrication of molecular-based devices and sensors (14, 15).

Received July 4, 2000. Published on the NRC Research Press Web site on April 9, 2001.

Z. Wang, Y.-L. Shi, and H.-L. Li.[1] Chemistry Department of Lanzhou University, Lanzhou, 730000, P. R. China.

[1]Corresponding author (telephone: +86-931-8912517; fax: +86-931-8912582; e-mail: lihl@lzu.edu.cn).

Two-component SAMs have been widely investigated (12, 16–19). Mixed monolayers that incorporate molecular "gate" sites are developed to obtain monolayers with molecular recognition properties (20–22). However, the factors governing the formation of mixed SAMs are not well understood. It is generally accepted that the long-chain alkanethiols are always preferentially adsorbed compared to short-chain alkanethiols, and that monolayer composition appears to be thermodynamically controlled (17, 23). For example, Chidsey et al. (12) showed that two-component SAMs could be enriched slightly in one component by equilibrating the monolayer in a solution containing the desired component. On the basis of this result, the authors concluded that molecules adsorbed at the defect sites are labile and can exchange with solution phase species, while molecules adsorbed at terraces were stable and did not exchange to any significant extent. Rowe and Creager (24) and Bain and Whitesides (25) have confirmed this founding.

The 1,3,4-oxadiazole compound is one of various very useful materials in modern technology such as the flash counting materials of nucleus physics, neutron physics, and atomic energy physics. In this paper, we introduce the thiol-substituted oxadiazole compound into the self-assembly system to supply a new method to draw the defect into the surface. We characterized the two-component mixed SAMs using X-ray photoelectron spectroscopy (XPS) and impedance measurements. One of these two components, which

 DOI: 10.1139/cjc-79-3-328 © 2001 NRC Canada

we call the framework component, is an *n*-alkanethiol about 25 Å long. The other, much shorter organo-mercaptan (MMO), which we call the template, induces defects within the much longer, kelp-forest-like framework. Two different probe molecules were applied to investigate the monolayer properties in terms of the theory developed by Amatore et al. (26).

Within the context of this theory, monolayers that contain either many closely spaced small defects or a few large defects, give rise to voltammograms that have shapes defined by linear diffusion of a bulk-phase redox species. Monolayers that contain only a few very small defects spaced sufficiently far apart that their diffusion layers do not overlap, give rise to voltammograms that are characterized by radial diffusion.

Experimental

2-Mercapto-5-methyl-1,3,4-oxadiazole (MMO) was synthesized according to literature (27). All other chemicals were analytical reagents and used as received.

X-ray photoelectron spectroscopy (XPS)

XPS measurements were carried out using an Escalab 220iXL system (VG Scientific Inc.) with a monochromatic Mg Kα X-ray source (1284.6 eV). The pressure in the chamber during analysis was approximately 2×10^{-10} torr (1 torr = 133.322 Pa). The binding energies were corrected using the Au ($4f_{2/7}$) peak energy standard. A take-off angle of 50° from the surface was employed. Spectra were recorded with 50 eV pass energy, 1 mm spot, and 300 W electron beam power with an acquisition time of 5 min. The acquisition time used was sufficiently short that sample damage did not affect the spectra significantly.

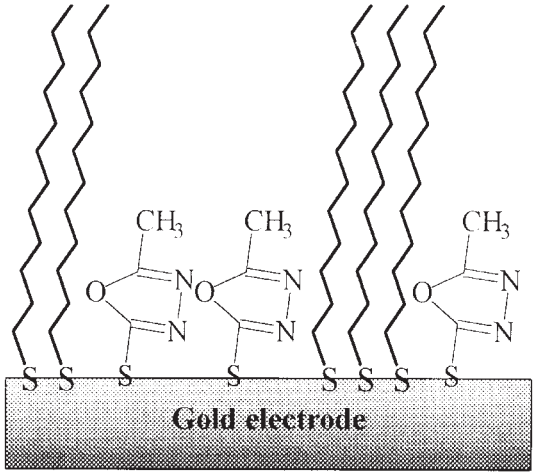
Wettability measurements

Contact angle measurements were performed with a JJC-II contact-angle goniometer under ambient conditions (21–23°C, 50–60% relative humidity) using yellow light to illuminate the liquid droplet. The contact angles were obtained by expanding a droplet from a microsyringe until it advanced smoothly across the surface, and then measured 10–20 s after expansion. At least four results were read for each sample.

Electrochemical measurements

The cyclic voltammograms were carried out with BAS-100B electrochemical analyzer. Electrochemical impedance spectroscopy was performed using CHI Model 660A Electrochemical Workstation. The conventional three-electrode system was used throughout the experiment. All potentials were reported versus a Ag–AgCl (3 mol L^{-1} KCl) reference electrode. A platinum foil was employed as the counter electrode. The working electrode was a bare or SAMs-modified gold-disk electrode (geometric area: 0.03799 cm^2). The gold electrode was cleaned by potential-scanning in H_2SO_4 (0.5 mol L^{-1}) between –200 mV and +1400 mV until a stable cyclic voltammogram was obtained. After the cleaning process, the substrates were rinsed with distilled water and ethanol, then immediately immersed into the assembling solution. Cyclic voltammetry was performed in a solution containing only one oxidation state of the redox couple, such as $Ru(NH_3)_6Cl_3$ (1 mmol L^{-1}) or $K_3Fe(CN)_6$ (1 mmol L^{-1}) in KCl (0.1 mol L^{-1}). The solutions used for impedance measurements always contained equal concentrations of the oxidized and reduced forms of the redox couple, such as 1 mmol L^{-1} $K_3Fe(CN)_6$ and $K_4Fe(CN)_6$ in KCl (0.1 mol L^{-1}), and measurements were conducted in a wide frequency range from 100 kHz to 0.05 Hz. In impedance experiments, the DC applied potential is held at an open circuit potential, and a small amplitude AC potential is applied. All the experiments were carried out at room temperature.

Fig. 1. The schematic diagram of mixed self-assembled monolayers of $C_{12}SH$ and MMO adsorbed on the gold surface.



Substrate preparation

The substrates employed in the XPS and wettability measurements were prepared by evaporating 200 nm gold (99.99%) onto a glass slide (7.5 × 2.5 cm) precoated with chromium (10–15 nm) at the evaporation rate of 0.1 nm s^{-1}. The base pressure was always $<3.5 \times 10^{-6}$ torr (1 torr = 133.322 Pa) and the evaporation pressure $<5.5 \times 10^{-6}$ torr. The gold slides were cleaned in a heated and freshly prepared "piranha solution" (3:1 concentrated H_2SO_4:30% H_2O_2) for 5 min, and then rinsed with distilled water and ethanol (caution: piranha solution reacts violently with organic compounds, and it should be handled with extreme care). SAMs were prepared by immersing clean gold substrate into a series of ethanol solutions (1.0 mmol L^{-1}) containing 1-dodecanethiol ($C_{12}SH$) and MMO with different molar percentages over 24 h to reach a saturated and steady coverage. Afterwards, the substrates were washed with ethanol and dried in N_2 atmosphere prior to characterization. The schematic diagram of mixed self-assembled monolayers of $C_{12}SH$ and MMO adsorbed on the gold surface is shown in Fig. 1.

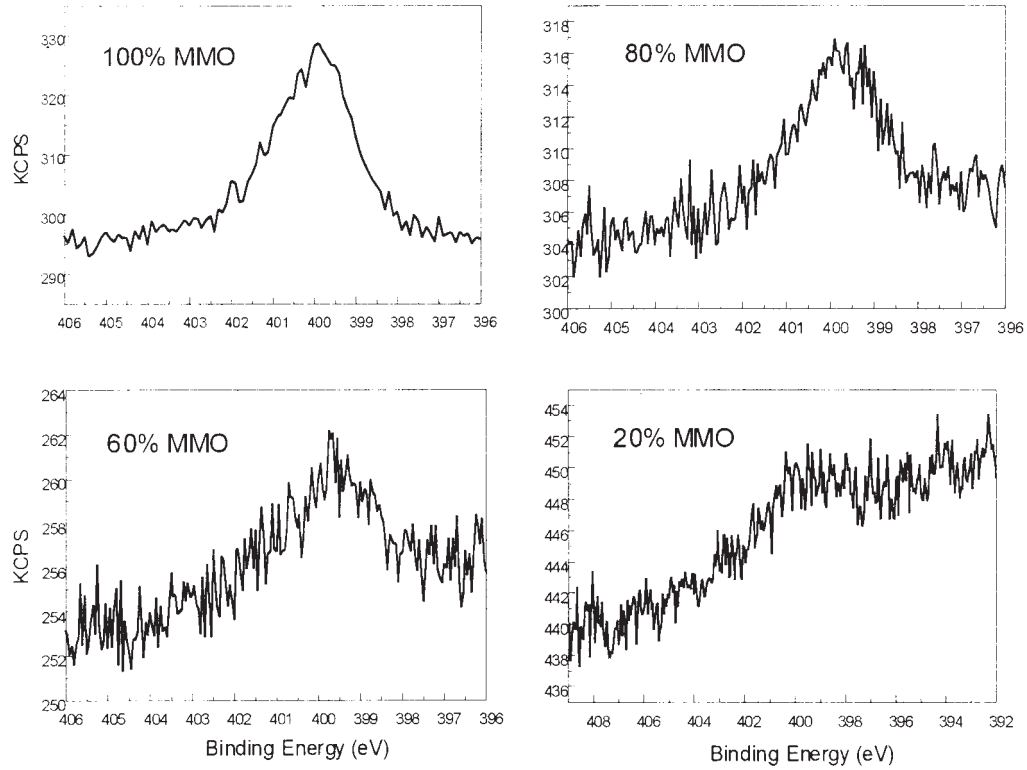
Results and discussion

X-ray photoelectron spectroscopy (XPS)

In an XPS experiment, the samples are exposed to monochromic X-ray radiation and the properties of inner-shell electrons are probed. Figure 2 shows typical XPS spectra of mixed monolayers with different molar percentages in which the N_{1s} region at 399.5 eV is clearly observed (KCPS

© 2001 NRC Canada

Fig. 2. XPS spectra (the N_{1s} region) of SAMs derived from ethanol solutions containing mixtures of $C_{12}SH$ and MMO on gold. The compositions of the assembling solution are illustrated as molar percentage of MMO in solution.



is kilo counts per second). The MMO coverage in SAMs could be directly estimated from the peak area of the N_{1s} region. The N_{1s} peak area increased with increasing MMO ratio in the assembly solution (Fig. 2), indicating that the coverage of MMO could be controlled by the solution composition. According to Whitesides (9), the composition of the relative component of acid-terminated thiol incorporated in the monolayers could be obtained from normalizing the ratio of O_{1s}:S_{2p}. In the SAMs under consideration, for simplicity, we assumed that the part of the SAMs above the sulfur tail group could be represented by a total, and then the S_{2p} counts could be considered to represent the total SAMs coverage. Usually, in the SAMs system, the signal intensity of an element will be represented by the formula:

$$[1] \qquad I = I_0 b \mathrm{e}^{-\mathrm{d}l(\lambda \sin \theta)}$$

where I is the signal intensity observed in the SAMs, I_0 is the signal intensity of the element on the surface, b is a correction factor, l is the depth of the element in the SAMs, λ is the attenuation level of the photo-electron in this system, and θ is the angle between the detector and the surface. But the values of I_0, b, and λ are not obtained in the experiment, and the two nitrogen atoms were present at different depths, so we simplified the ratios of nitrogen to sulphur taking the sensitivity factor into consideration (0.42 and 0.54 for N_{1s} and S_{2p}, respectively):

$$[2] \qquad \frac{N'_{\mathrm{MMO}} \times 0.54}{S'_{\mathrm{MMO}} \times 0.42} = k \frac{N_{\mathrm{MMO}}}{S_{\mathrm{MMO}}}$$

N' and S' represent the relative atomic numbers detected in the XPS, N and S represent the realistic atomic numbers in the MMO molecule, and k is the constant related to the depth of the nitrogen atom. If we consider that the orientation of MMO in the pure MMO SAMs is similar to that in the mixed SAMs, and distribution of sulphur elements changed little, the value of k is constant:

$$[3] \qquad \frac{N'_{\mathrm{Mix}} \times 0.54}{S'_{\mathrm{Mix}} \times 0.42} = k \frac{xN_{\mathrm{MMO}}}{xS_{\mathrm{MMO}} + (1-x)S_{\mathrm{C_{12}SH}}}$$

x is the molar percentage of MMO in the SAMs. For the molar percentages of MMO in the mixed SAMs, the x values obtained from the above two equations are used as the y-axis of Fig. 3.

Wettability

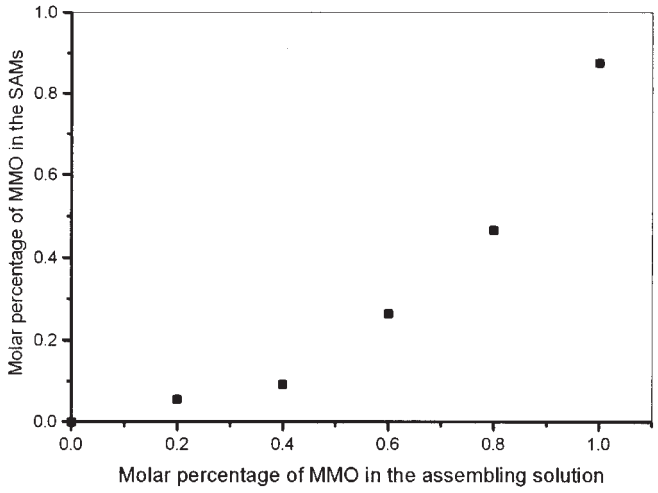
The quality and microscopic structure of the mixed SAMs were also estimated from wetting measurements. Young described the relationship (29) between the free energy of the surface and a unique contact angle, under ideal conditions, for a system in equilibrium as:

$$[4] \qquad \gamma_{\mathrm{LV}} \cos\theta = \gamma_{\mathrm{SV}} - \gamma_{\mathrm{SL}}$$

where θ is the contact angle at the three-phase interface, while γ_{LV}, γ_{SV}, and γ_{SL} are surface-free energies at the liquid-vapor, solid-vapor, and solid-liquid interfaces, respectively. Monolayers containing exposed polar groups and disordered monolayers have much lower contact angles. If the mixed monolayers containing two components are homogeneous, and the two components affect surface wettability

© 2001 NRC Canada

Fig. 3. Plot of the molar percentage of MMO in the SAMs as a function of the molar percentage of MMO in the assembling solution.



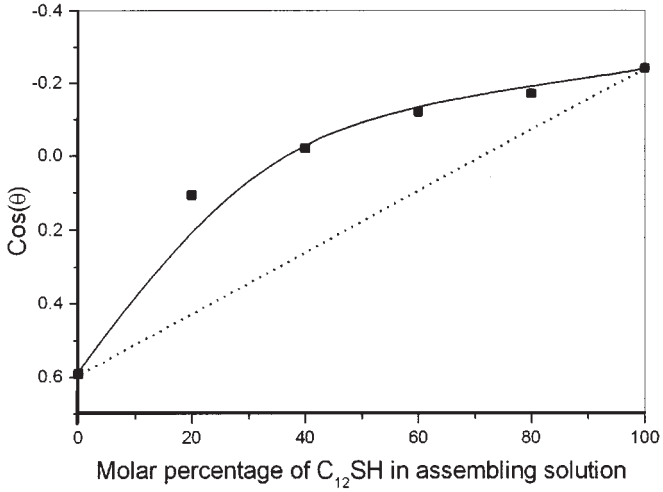
independently, the Cassie equation is appropriate for interpretation of wettability results (30, 31):

$$[5] \qquad \cos\theta = f_1 \cos\theta_1 + f_2 \cos\theta_2$$

where θ is the contact angle of a liquid on the heterogeneous surface, f_1 and f_2 are the fractions of the two types of chemical groups at the surface, and θ_1 and θ_2 are the contact angles of this liquid on the pure homogeneous surfaces of the two function groups, respectively. Consequently, changes in cos θ are linearly dependent on the composition of the surface for an ideal surface (32–39). Hence, the composition and quality of a monolayer are usually checked quickly and easily with this technique.

The cosine of contact angles of pure water on freshly prepared monolayers composed of mixtures of MMO and $C_{12}SH$ are shown as a function of the surface composition. The SAMs become more hydrophobic as the percentage of $C_{12}SH$ in the assembling solution increases because $C_{12}SH$ SAMs are more hydrophobic than MMO SAMs. The obviously nonlinear behavior displayed in Fig. 4 indicate that the wettability of SAMs mixed with $C_{12}SH$ and MMO is highly nonideal. The relation between surface wettability and the surface composition of the mixed SAMs demonstrates the complexity of the interactions at the film–air–probe-liquid three-phase interface. Bain and his colleagues (8, 9, 25) studied the wettability of SAMs mixed with methyl groups and other polar-group-terminated alkanethiols that have similar chain length. They found that the curve of cos θ vs. surface composition usually appeared concave rather than convex. The mixed SAMs considered here are also consistent with a polar component (MMO) and a low surface energy component ($C_{12}SH$). However, in contrast with that observed by Bain, Fig. 4 demonstrates a convex curve, which indicates that the SAMs mixed with MMO and $C_{12}SH$ are more hydrophobic than predicted by Cassie's equation (eq. [5]). The major differences of our system compared to Bain's (25) is that the lengths of the two components studied here are very different, and the $C_{12}SH$ molecule is about two times larger than the MMO molecule.

Fig. 4. The cosines of contact angle (θ) of pure water on SAMs-modified surfaces as a function of the percentage of $C_{12}SH$ in assembling solution. The solid line shows the tendency as a guide, and the dashed line represents an expected linear relationship.



Electrochemical impedance measurements

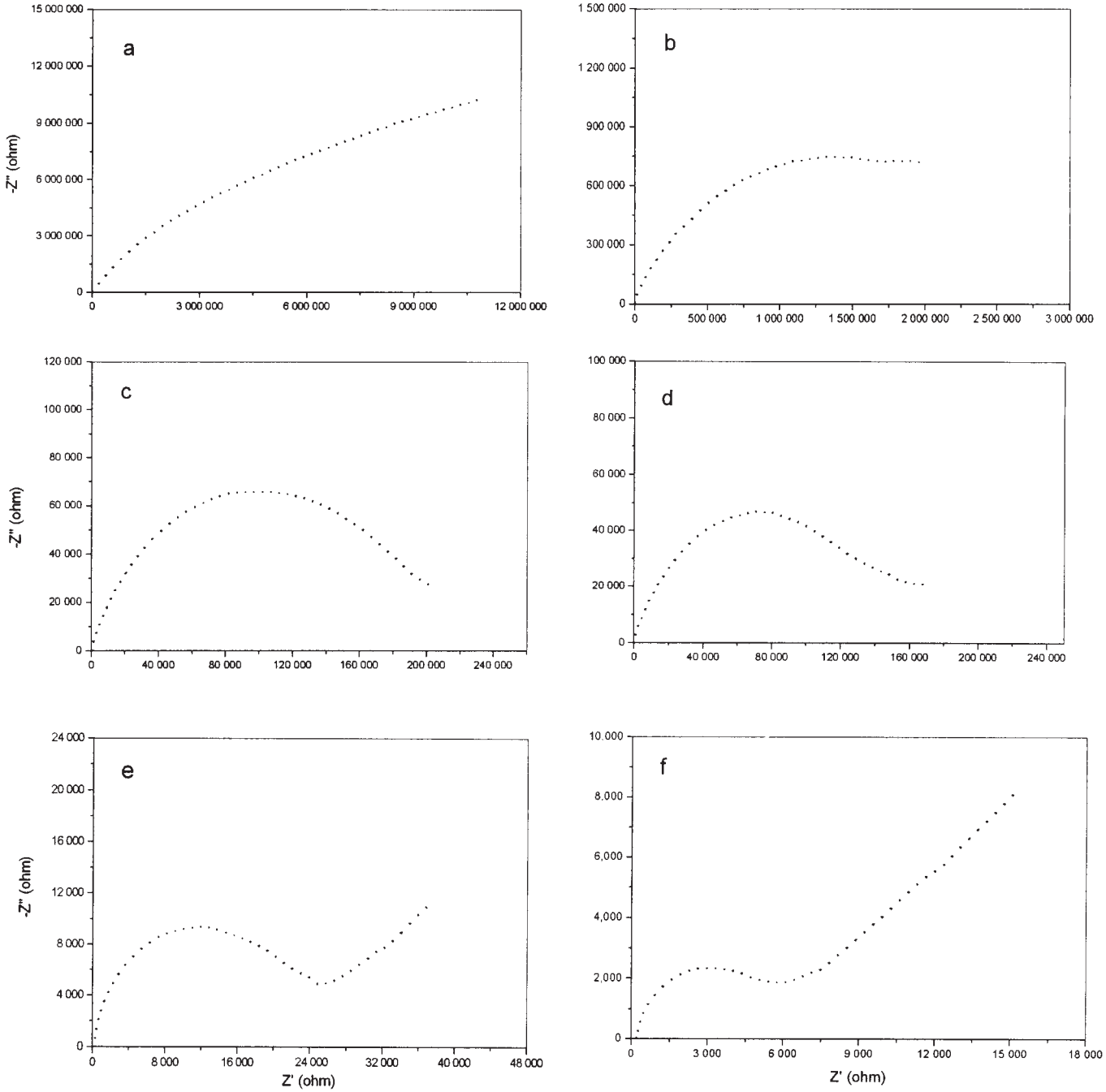
Impedance measurements have been applied successfully to investigate these types of assembled monolayers and electron transfer through the monolayers, as impedance can provide valuable information about the surface coverage of the monolayer and apparent rate constant of the redox-active probes in solution.

In impedance experiments, the DC applied potential is held at an open circuit potential, and a small amplitude of AC potential is applied. The response is often shown in a complex impedance presentation and results are interpreted in terms of an equivalent electrical circuit. According to Randles' equivalent circuit (40), two frequency regions can be distinguished to understand the change in faradic impedance due to the presence of electroactive species at the electrode–SAM–electrolyte interface. In the low frequency region, mass transfer via diffusion has to be taken into account, whereas the microarray behavior of the defect within the passivating monolayer disturb the $\omega^{-1/2}$ depedence of the Warburg impedence (41). The deviation from semi-infinite diffusion is due to the defects in the monolayers, which are far apart from each other. In this type of situation, the overlap of diffusion fields is not achieved and radial diffusion seems to be valid (42). We focused our attention on the more interesting part of the Nyquist plot at the high frequencies, where the electrode reaction is purely kinetically controlled, and the heterogeneous charge transfer resistance (R_{ct}) is expected to increase due to the inhibition of the electron transfer by the monolayer present on the electrode surface (43). From this increase in the charge transfer resistance, one can calculate the approximate fractional coverage of the gold electrode (Γ) (44), assuming that the current is due to the defects within the monolayer:

$$[6] \qquad \Gamma = 1 - \left[\frac{R_{ct}}{R'_{ct}}\right]$$

© 2001 NRC Canada

Fig. 5. The Nyquist plots obtained from SAMs modified with a mixture of $C_{12}SH$ and MMO for 24 h. Molar percentages in solution, with $K_3Fe(CN)_6$ (1 mmol L^{-1}) and $K_4Fe(CN)_6$ (1 mmol L^{-1}) in aq KCl solution (0.1mol L^{-1}): (*a*) 100% $C_{12}SH$, (*b*) 80% $C_{12}SH$, (*c*) 60% $C_{12}SH$, (*d*) 40% $C_{12}SH$, (*e*) 20% $C_{12}SH$, and (*f*) 100% MMO. 100 kHz–50 Hz frequency ranges used.



where R_{ct} indicates the charge transfer resistance of pure gold electrode and R'_{ct} is the corresponding term of the passivated electrode covered by the monolayers containing various molar percentages of $C_{12}SH$ and MMO.

Several Nyquist plots for a gold electrode modified by various molar percentages in solution are shown in Figs. 5*a–f*. Figure 5*a* shows a Nyquist plot obtained from an apparently defect-free $C_{12}SH$ monolayer. The resistance was too large to measure in this experiment. The relative molar percentages of the two components were changed steadily, and the obvious occurances of the different processes are displayed in the other five Nyquist plots (Figs. 5*b–f*). The impedance in Fig. 5*c* is observed to be substantially smaller than in Fig. 5*b*, which is due to the larger amount of defects existing in the mixed monolayers of 5*c* compared to 5*b*. With the increase of the concentration of MMO, the Nyquist plot could be an intermediate system. The Nyquist plot is a semi-circle at high frequencies (kinetic control) and changes to a

© 2001 NRC Canada

Table 1. Different parameters obtained for mixed SAMs on a gold electrode from impedance measurements.

	Molar percentage (C_{12}SH:MMO)				
	8:2	6:4	4:6	2:8	0:10
Charge transfer resistance (R_{ct}) (Ω cm^2)	106 000	7220	5600	911	220
Apparent electrode coverage (Γ) (%)	99.96	99.40	99.20	95.25	80.40
Apparent rate constant of $Fe(CN)_6^{3-}$:$Fe(CN)_6^{4-}$ (k_{app}) (cm s^{-1})	2.5×10^{-6}	4.1×10^{-5}	4.7×10^{-5}	2.9×10^{-4}	1.2×10^{-3}

straight line at low frequencies (diffusion control). It is known that the lower intercept on the Z' axis is at $Z' = R_\Omega$ (R_Ω = solution resistance) and the higher intercept is at $Z' = R_\Omega + R_{ct}$. The frequency that gives the largest -Z″ value on the semi-circle is equal to $1/R_{ct}C_{dl}$ (C_{dl} = double layer capacitance). The rate constant of the $K_3Fe(CN)_6$:$K_4Fe(CN)_6$ ratio could be calculated from the impedance plot of the gold electrode modified with different molar percentages of the two components, since the monolayer behaves as a microelectrode assembly leading to an expected decrease in the rate constant (40). Thus, from eq. [7], for a one-electron first-order reaction with $c_o = c_r = c$ and unit geometric area:

$$[7] \qquad R_{ct} = \frac{RT}{j_0 F}$$

and

$$[8] \qquad j_0 = Fk_{app}c$$

Combination of eqs. [7] and [8] gives

$$[9] \qquad k_{app} = \frac{RT}{F^2 R_{ct} c}$$

Based on these formulas, Nyquist plots, and impedance measurements, different parameters obtained for the mixed SAMs on a gold electrode are shown in Table 1. From the data listed in the table, one can see that the apparent electrode coverage decreased with the increase of molar ratio of MMO because the degree of order and close-packed structure in the MMO monolayer is less than that of the C_{12}SH monolayer. The apparent rate constant of the $Fe(CN)_6^{3-}$–$Fe(CN)_6^{4-}$ couple increased with the increase of molar ratio of MMO in solution. The apparent rate constant of $Fe(CN)_6^{3-}$–$Fe(CN)_6^{4-}$ at a bare gold electrode was taken as 2.6×10^{-2} cm s^{-1} (45, 46). The rate constant of $Fe(CN)_6^{3-}$–$Fe(CN)_6^{4-}$ of pure MMO obtained in the experiments is smaller than 2.6×10^{-2} cm s^{-1}, because the formation of MMO monolayers on the gold surface has the effect of preventing the probe molecule's penetration.

Electrochemical investigation

XPS and wettability results demonstrated that binary composite monolayers have been prepared. The film composition, which was affected by the composition of the assembling solution, changed the film structure dramatically. Next we examined the electrochemical properties of the mixed SAMs using two different probe molecules to access the gold surface.

Electrochemical response of $Ru(NH_3)_6^{3+}$ on SAMs

The cyclic voltammograms shown in Fig. 6 are obtained from an electrode prepared by soaking a gold electrode in ethanol solutions containing various molar percentages of MMO and C_{12}SH. We were able to reproduce the data shown in Fig. 6 four times within 10%. Following modification, the electrode potential was cycled between +300 mV and –500 mV at 100 mV s^{-1} in an aqueous electrolyte solution consisting of $Ru(NH_3)_6Cl_3$ (1 mmol L^{-1}) and KCl (0.1 mol L^{-1}). In the presence of defect sites that have the correct combination of size and interaction energies, the $Ru(NH_3)_6^{3+}$ probe molecule should penetrate the inert frame work and undergo electron exchange with the underlying gold surface. The electron transfer should be facile since the electron-transfer rate constant for $Ru(NH_3)_6^{3+}$ is large (21, 47). If the probe molecules cannot penetrate the monolayer framework, they can only be reduced by electrons that tunnel through the C_{12}SH layer. Since the distance of closest approach of the probe to the electrode surface is approximately the thickness of the monolayer, about 21–25 Å (48, 49), the tunneling current should be small relative to that arising from direct electron transfer at defect sites.

Figure 6*e* shows the results obtained for a nominally defect-free C_{12}SH monolayer surface. The roughly exponential shape of the cyclic voltammogram is consistent with electron tunneling through the film (21, 50–52). The voltammogram shape of Fig. 6*d* arises from radial diffusion of $Ru(NH_3)_6^{3+}$ to small, widely dispersed defect sites (defect sites include the domain formed by the MMO molecules) on the electrode surface. As the concentration of the template molecules in the assembling solution increases relative to the framework, the charging current increases, and there is a clear departure from pure radial to a mixed linear–radial regime. Mixed diffusion behavior is shown in Fig. 6*c*. Figure 6*b* is indistinguishable from that of a bare gold electrode.

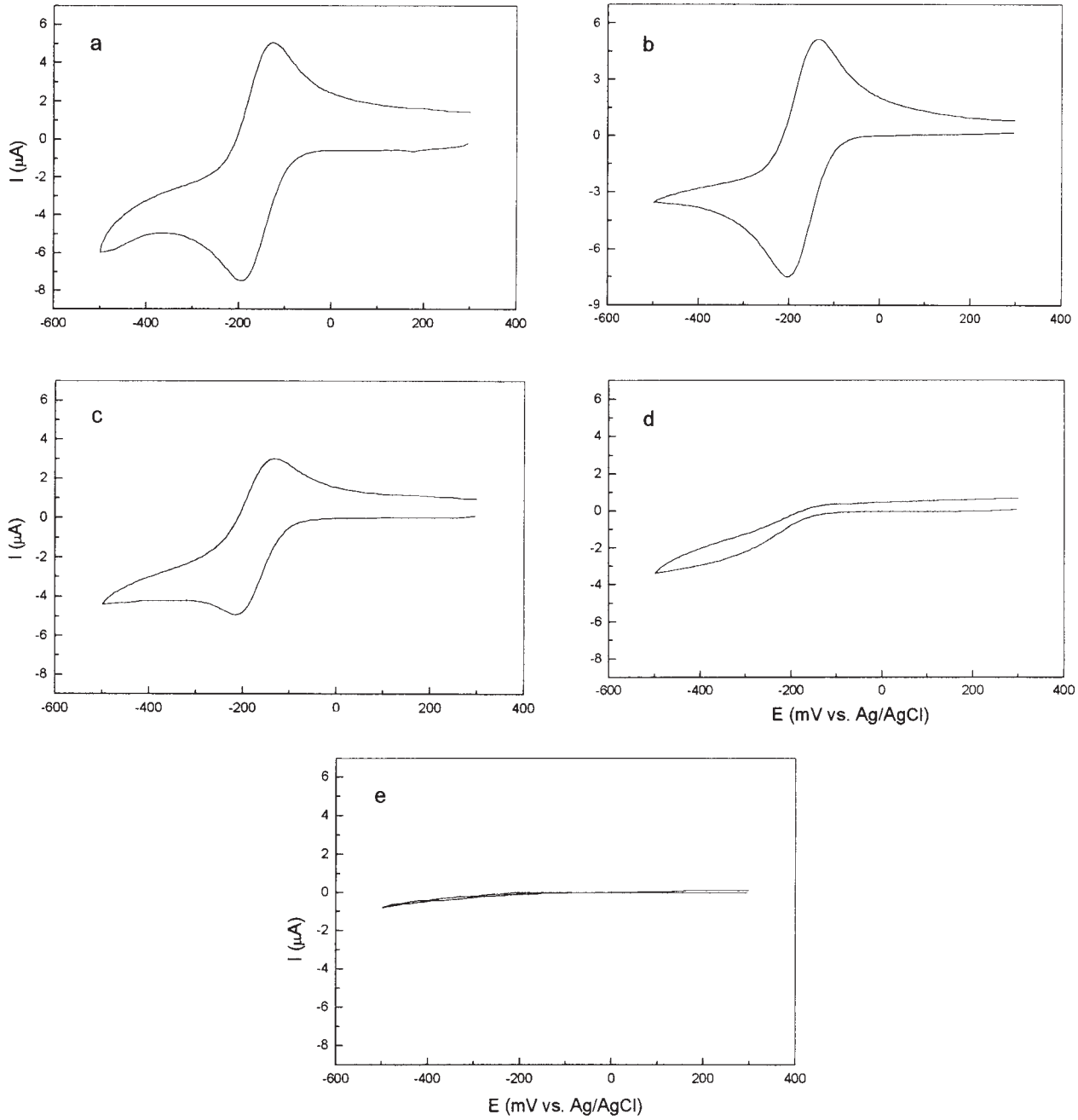
Electrochemical response of $Fe(CN)_6^{3-}$ on SAMs

Figure 7 presents data analogous to that shown in Fig. 6, except that the solution-phase redox-probe molecule is $K_3Fe(CN)_6$. This set of data follows the general trend discussed for $Ru(NH_3)_6^{3+}$. The only difference between the cyclic voltammograms shown in Figs. 6 and 7 is that the transition from radial to linear diffusion occurs at a higher MMO concentration for $Fe(CN)_6^{3-}$ than for $Ru(NH_3)_6^{3+}$. Since the monolayers used to generate Figs. 6 and 7 are the same, and the size of the two probe molecules are approximately the same on the basis of their diffusion coefficients[2], there is

[2] For $Fe(CN)_6^{3-}$: $D = 7.6 \times 10^{-6}$ cm^2 s^{-1}, see D. T. Sawyer and J. L. Roberts Jr. Experimental electrochemistry for chemistry. Wiley, New York. 1974. p. 77; for $Ru(NH_3)_6^{3+}$: $D = 7.1 \times 10^{-6}$ cm^2 s^{-1}, see A.J. Bard, J.A. Crayston, G.P. Kttleson, T.V. Shea, and M.S. Wrighton. Anal. Chem. **58**, 2321 (1986).

© 2001 NRC Canada

Fig. 6. Cyclic voltammetric response of $Ru(NH_3)_6Cl_3$ (1 mmol L^{-1}) on (*a*) bare gold, and mixed SAMs with: (*b*) 90% MMO, (*c*) 80% MMO, (*d*) 70% MMO, and (*e*) 100% $C_{12}SH$ (molar percentage in solution). The supporting electrolyte was KCl solution (0.1 mol L^{-1}), and scan rate was 100 mV s^{-1}.



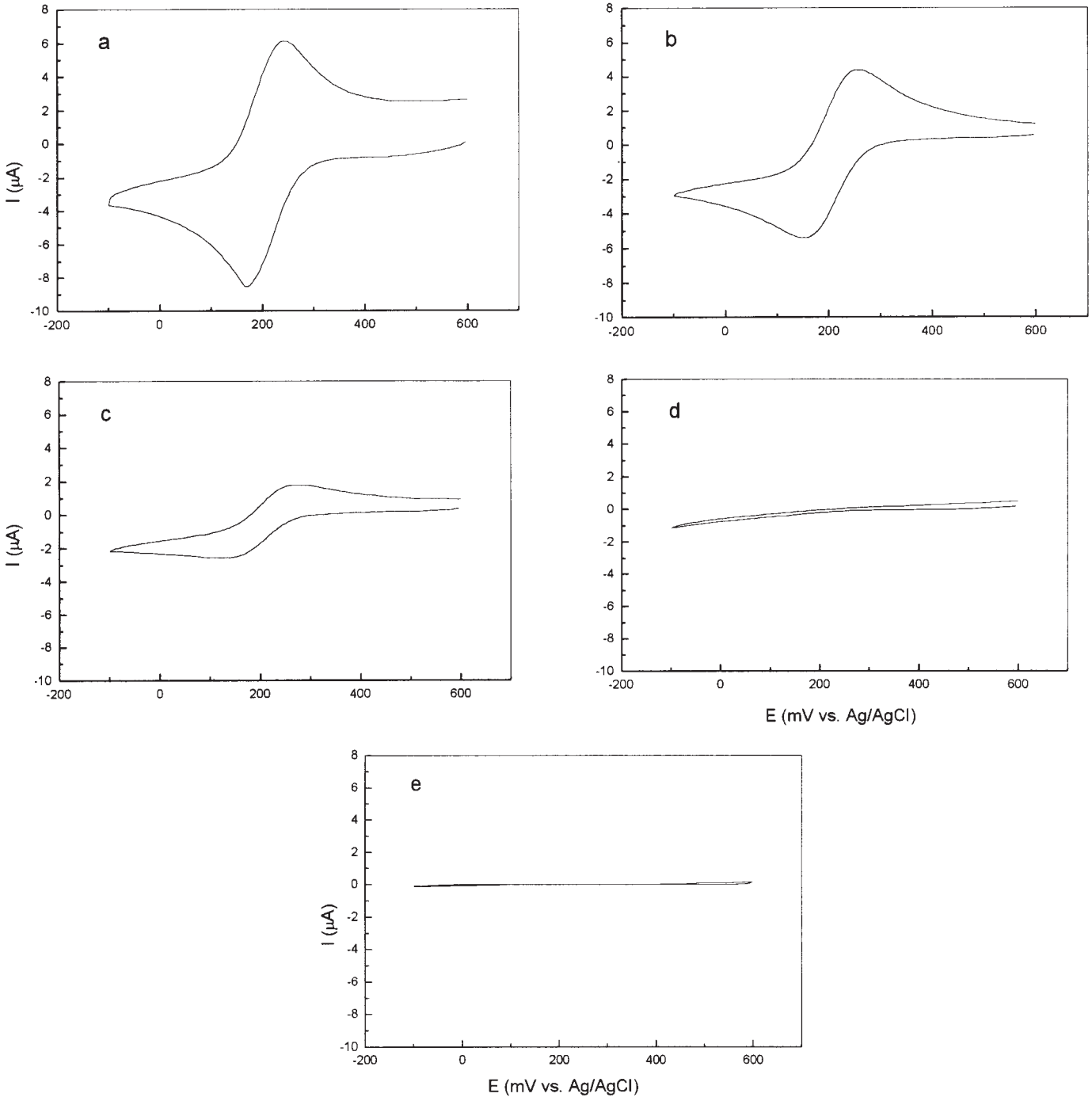
only one possible explanation for this behavior: some of the defect sites that admit $Ru(NH_3)_6^{3+}$ do not admit $Fe(CN)_6^{3-}$. That is, although the total number and average size of the defects are fixed, there are differences in the nature of the intermolecular interactions between the probe molecules and the mercaptan component of short length in this system.

Conclusions

Self-assembled monolayers composed of MMO and $C_{12}SH$ with various molar percentages were prepared and characterized on a gold surface. Our experiments prove that the composition of the mixed monolayers could be controlled by the ratio of MMO and $C_{12}SH$ in the assembling solution. The chemical nature of the template–framework ratio of the assembling solution control the size and chemical properties of the defects. Impedance measurements supply some related parameters, such as apparent electrode coverage and apparent rate constant of the redox couple. When the molar ratio of MMO is 80%, $Ru(NH_3)_6^{3+}$ penetrates the monolayer easily, but $Fe(CN)_6^{3-}$ does not. This phenomenon resulted from the differences in the nature of

© 2001 NRC Canada

Fig. 7. Cyclic voltammetric response of $K_3Fe(CN)_6$ (1 mM) on (*a*) bare gold, and mixed SAMs with: (*b*) 90% MMO, (*c*) 80% MMO, (*d*) 70% MMO, and (*e*) 100% $C_{12}SH$ (molar percentage in solution). The supporting electrolyte was KCl solution (0.1 mol L^{-1}), and scan rate was 100 mV s^{-1}.



the intermolecular interactions between the probe molecules and the mercaptan component of short length in this system.

Acknowledgment

This work was supported by the National Natural Science Foundation of China (grant no. 29 773 018).

References

1. A. Ulman. An introduction to ultrathin oganic film, from Langmuir–Blodgett to self-assembly. Academic Press, San Diego, CA. 1991.
2. L.H. Dubios and R.G. Nuzzo. Annu. Rev. Phys. Chem. **43**, 437 (1992).
3. A. Ulman. Chem. Rev. **96**, 1533 (1996).

© 2001 NRC Canada

4. D.L. Allara, A.N. Parikh, and E. Judge. J. Chem. Phys. **100**, 1761 (1994).
5. N. Collazo and S.A. Rice. Langmuir, **7**, 3144 (1991).
6. S.D. Evans, R. Sharna, and A. Ulman. Langmuir, **7**, 156 (1991).
7. P.E. Labinis, M.A. Fox, J.P. Folkers, and G.M. Whitesides. Langmuir, **7**, 3167 (1991).
8. C.D. Bain and G.M. Whitesides. Science (Washington, D.C.), **240**, 62 (1988).
9. C.D. Bain, J. Evall, and G.M. Whitesides. J. Am. Chem. Soc. **111**, 7155 (1989).
10. P.E. Labinis and G.M. Whitesides. J. Am. Chem. Soc. **114**, 1990 (1992).
11. A. El Kasmi, J.M. Wallace, E.F. Bowden, S.M. Binet, and R.J. Linderman. J. Am. Chem. Soc. **120**, 225 (1998).
12. C.E.D. Chidsey, C.R. Bertozzi, T.M. Putvinski, and A.M. Mujsce. J. Am. Chem. Soc. **112**, 4301 (1990).
13. C.E.D. Chidsey. Science (Washington, D.C.), **251**, 919 (1991).
14. G.K. Rowe and S.E. Creager. Langmuir, **7**, 2307 (1991).
15. K. Motesharei and D.C. Myles. J. Am. Chem. Soc. **120**, 7328 (1998).
16. E.B. Troughton, C.D. Bain, G.M. Whitesides, R.G. Nuzzo, D.L. Allara, and D.L. Porter. Langmuir, **4**, 365 (1988).
17. L.A. Bumm, J.J. Arnold, M.T. Cygan, T.D. Dunbar, T.P. Burgin, L. Jones, D.L. Allara, J.M. Tour, and P.S. Weiss. Science (Washington, D.C.), **271**, 1705 (1996).
18. S.J. Stranick, A.N. Parikh, Y.T. Tao, D.L. Allara, and P.S. Weiss. J. Phys. Chem. **98**, 7636 (1994).
19. D.L. Allara. Biosens. Bioelectron. **10**, 771 (1995).
20. I. Rubinstein, S. Steinberg, Y. Tor, A. Shanzer, and J. Sagiv. Nature (London), **332**, 426 (1988).
21. R. Bilewicz and M. Majda. J. Am. Chem. Soc. **113**, 5464 (1991).
22. O. Chailapakul and R.M. Crooks. Langmuir, **9**, 884 (1993).
23. P.E. Laibinis, R.G. Nuzzo, and G.M. Whitesides. J. Phys. Chem. **96**, 5097 (1992).
24. G.K. Rowe and S.E. Creager. Langmuir, **10**, 1186 (1994).
25. C.D. Bain and G.M. Whitesides. Langmuir, **5**, 1370 (1989).
26. C. Amatore, J.M. Saveant, and D.J. Tessier. J. Electroanal. Chem. **147**, 39 (1983).
27. E. Hoggarth. J. Chem. Soc. 4811 (1952).
28. A.W. Adamson and I. Ling. Adv. Chem. Ser. **43**, 57 (1964).
29. T. Young. Miscellaneous Work. Vol. 1. *Edited by* G. Peakock. Murry, London. 1855. p. 418.
30. A.B.D. Cassie and S. Baxter. Trans Faraday Soc. **40**, 546 (1944).
31. A.B.D. Cassie. Discuss. Faraday Soc. **3**, 11 (1948).
32. C.D. Bain and G.M. Whitesides. J. Am. Chem. Soc. **110**, 5897 (1988).
33. P. Silbernan, L. Leger, D. Ausserre, and J.J. Benattar. Langmuir, **7**, 1647 (1991).
34. S.R. Wasserman, Y.T. Tao, and G.M. Whitesides. Langmuir, **5**, 1074 (1989).
35. J.D. Le Grange, J.L. Markham, and C.R. Kurkjian. Langmuir, **9**, 1749 (1993).
36. R. Maoz and J. Sagiv. J. Colloid Interface. Sci. **100**, 465 (1984).
37. G. Carson and S. Granick. J. Appl. Polym. Sci. **37**, 2767 (1989).
38. C.R. Kessel and S. Granick. Langmuir, **7**, 532 (1991).
39. A. Ulman. Adv. Mater. (Weinheim Ger.) **2**, 573 (1990).
40. M. Sluyters-Rehbach and J.H. Sluyters. *In* Electroanalytical chemistry. Vol. 4. *Edited by* A.J. Bard. Dekker, New York. 1970.
41. H.O. Finklea, D.A. Sinder, J. Fedyk, E. Sabatini, Y. Gaini, and I. Rubinstein. Langmuir, **9**, 3660 (1993).
42. K. Tokuda, T. Gueshi, and H. Matsuda. J. Electroanal. Chem. **102**, 41 (1979).
43. C. Amatore, J.M. Saveant, and D. Tessier. J. Electroanal. Chem. **147**, 39 (1983).
44. E. Sabatini, I. Rubinstein, R. Maoz, and J. Sagiv. J. Electroanal. Chem. **219**, 365 (1987).
45. E. Sabatani, J. Cohen-Boulakia, M. Bruening, and I. Rubinstein. Langmuir, **9**, 2974, (1993).
46. X. Cui, D. Jiang, P. Diao, J. Li, R. Tong, and X. Wang. J. Electroanal. Chem. **470**, 9, (1999).
47. R.M. Penner, M.J. Heben, T.L. Longin, and N.S. Lewis. Science (Washington, D.C.), **250**, 118 (1990).
48. M.D. Porter, T.B. Bright, D.L. Allara, and C.E.D. Chidsey. J. Am. Chem. Soc. **109**, 3559 (1987).
49. C.D. Bain, E.B. Troughton, Y.T. Tao, J. Evall, G.M. Whitesides, and R.G. Nuzzo. J. Am. Chem. Soc. **111**, 321 (1989).
50. C.E.D. Chidsey and D. N. Loiacono. Langmuir, **6**, 682 (1990).
51. C.A. Miller, P. Cuendet, and M. Gratzel. J. Phys. Chem. **95**, 877 (1991).
52. A.M. Becka and C.J. Miller. J. Phys. Chem. **251**, 919 (1992).

© 2001 NRC Canada

Flow injection-chemiluminescent assay for the determination of superoxide dismutase activity

Hong Yeob Choi, Jin Hyang Song, Yong Sung Park, Gabriel Lord, and Dong Ki Park

Abstract: Superoxide dismutase (SOD) activity was measured using a flow injection-chemiluminescent assay (FI-CLA) based on xanthine–xanthine oxidase dependent superoxide ($O_2^{\bullet -}$) formation. The mobile phase consists of 50 mM potassium phosphate buffer (pH 7.4) containing lucigenin (5 μM) and xanthine (0.3 mM). Under optimum conditions, bovine albumin did not affect chemiluminescence at concentrations of 1–1000 μg mL^{-1} and KCN inhibited 100% of the Cu, Zn-SOD activity using 5 μL of a 0.23 mM concentration. The analysis of one sample was done in less than 30 s with a relative standard deviation of ±3.1%. SOD activity in the biological samples was correlated to the amount of exogenously applied SOD. The FI-CLA method reported here appears to be one of the faster and more useful tools used to assay SOD activity.

Key words: superoxide dismutase, flow injection-chemiluminescent assay, superoxide, xanthine oxidase, lucigenin.

Résumé : L'activité de la dismutase du superoxyde (SOD) a été mesurée par chimiluminescence à injection continue (FI-CLA) basée sur la formation de superoxyde ($O_2^{\bullet -}$) par l'oxydase de xanthine. La phase mobile était constituée de 50 mM de phosphate de potassium (solution-tampon de pH 7.4), de lucigénine 5 μM et de xanthine 0.3 mM. Dans des conditions optimales, l'albumine de bovins n'affectait pas la chimiluminescence à des concentrations de 1 jusqu'à 1000 μg mL^{-1} et le KCN inhibait l'activité du SOD-Cu,Zn à 5 μL de solution 0.23 mM. L'analyse d'un échantillon s'effectuait en moins de 30 s avec une déviation standard de ±3.1 %. L'activité du SOD dans les échantillons biologiques a été corrélé à la quantité appliquée exogéniquement au SOD. La méthode FI-CLA mentionée ici s'avère l'une des méthodes les plus rapides et un des outils les plus précieux pour évaluer l'activité du SOD

Mots clés : dismutase du superoxyde, évaluation par chimiluminescence à injection continue, superoxyde, oxydase de xanthine, lucigénine.

[Traduit par la Rédaction]

Introduction

The detection and measurement of superoxide anion ($O_2^{\bullet -}$) flow within cells is of critical importance for investigating the physiological and pathological roles of $O_2^{\bullet -}$. The short-lived and reactive radical ($O_2^{\bullet -}$) can be considered as a nonclassical messenger molecule, i.e., the signal transduction is mediated via its chemical reactivity. Acting on one hand as defense against viral or bacterial attack, it can, on the other hand, cause oxidative damage to proteins, DNA, and lipids.

Superoxide dismutases (SOD) catalyze the dismutation of two molecules of $O_2^{\bullet -}$ into hydrogen peroxide and molecular oxygen (1). It is generally accepted that SOD play a major protective role in living cells and have been widely used as pharmacological tools in the study of pathophysiological mechanisms. Since the discovery of SOD, numerous direct and indirect methods for the activity assay have been developed; many methods for the determination of SOD activity have emerged based on enzymatically or chemically produced superoxide (2–9) and on immunochemistry (10). Amongst these methods, the use of lucigenin-amplified chemiluminescence (CL) (6) has been gaining popularity largely because of its simplicity and sensitivity in usage. However, the validity of lucigenin as a detecting probe has recently been questioned because $O_2^{\bullet -}$ is generated by lucigenin itself in several in vitro enzymatic systems (11, 12). More recently, however, Skatchkov et al. (11) demonstrated that the concentration of lucigenin is a critical parameter affecting the probe's validity, and their spin-trapping studies revealed that lucigenin at 250 μM increased $O_2^{\bullet -}$ production severalfold while 5 μM lucigenin did not stimulate $O_2^{\bullet -}$ production (11, 13). Thus, lucigenin at a concentration of 5 μM is a valid probe for assessing $O_2^{\bullet -}$.

Received June 12, 2000. Published on the NRC Research Press Web site on April 12, 2001.

H.Y. Choi[1], J.H. Song[2], and D.K. Park. Department of Applied Biology and Chemistry, Konkuk University, Seoul, Korea.
Y.S. Park. Kingston Regional Cancer Centre and Department of Oncology, Queen's University, 25 King Street West, Kingston, ON K7L 5P9, Canada.
G. Lord. Department of Chemistry and Chemical Engineering, The Royal Military College of Canada, Kingston, ON K7K 7B4, Canada.

[1]Department of Physiology, Queen's University, Kingston, ON K7L 3N6, Canada.
[2]Corresponding author (telephone: +82(2) 450-3755; e-mail: parks@kkucc.ac.kr).

 DOI: 10.1139/cjc-79-3-337 © 2001 NRC Canada

In this paper, we present a simple and continuous one-step flow injection system based on lucigenin-amplified CL for the assay of SOD activity using a concentration of 5 μM lucigenin. The reaction of lucigenin-derived CL is initiated by interaction between the lucigenin cation radical and xanthine–xanthine oxidase (XOD) derived $O_2^{\bullet -}$ to yield an unstable dioxetane intermediate. The lucigenin dioxetane decomposes to produce two molecules of *N*-methylacridone, one of which is in an electronically excited state, which upon relaxation to the ground state emits a photon (13). The presence of SOD activity is, therefore, determined by a reduction in $O_2^{\bullet -}$ concentration and, hence, reduced CL intensity.

Materials and methods

Materials

Lucigenin (*bis*-*N*-methylacridinium nitrate), xanthine, xanthine oxidase (EC 1.1.3.22, from buttermilk, 0.69 U mg^{-1} protein), superoxide dismutase (EC 1.15.1.1), Cu, Zn-SOD (from bovine erythrocytes, 4000 U mg^{-1} protein), Mn-SOD (from E. coli, 4000 U mg^{-1} protein), catalase (EC 1.11.1.6, from bovine liver, 58 000 U mg^{-1} protein), glutathione reductase (EC 1.6.4.2, from bovine intestinal mucosa, 100 U mg^{-1} protein), bovine albumin, ascorbic acid, potassium phosphate, glutathione, adrenaline, and cysteine were purchased from Sigma Chemical Co. (St. Louis, Mo). Potassium cyanide (KCN) was obtained from Fluka (Buchs, Switzerland) and all other chemicals were reagent grade.

Tissue preparation

Following 24 h of starvation and anesthesia by diethyl ether inhalation, guinea pigs were perfused through the aorta with ice cold 0.9% NaCl until the heart and major organs were visibly blanched. Liver, heart, kidney, lung, and brain were excised, snap-frozen, and stored at –80°C. For the tissue homogenate preparation, frozen tissue was thawed in ice cold 50 mM potassium phosphate buffer (pH 7.4), blotted, weighed, and minced (14). Each tissue was homogenized on ice in a 10 mL volume of the buffer with a Teflon™-homogenizer (Iwaki Co., Japan). Homogenates (10%) were then subjected to three sonication cycles of 30 pulses, on ice, with a 1 min interval between cycles, in a Bransonic sonifier (Branson Co., Shelton, CT). The resultant extract was clarified by centrifugation. The supernatant was diluted 10-fold using 50 mM potassium phosphate buffer (pH 7.4).

Flow injection-chemiluminescent assay

The CL was measured with a spiral flow cell and filter-equipped photon counting spectrophotometer (CLD-110, Tohoku Electronic Industry, Sendai, Japan) connected to a pump (Gilson Model 303) and a sample injection valve (Rheodyne Model 7125, 20 μL). The tubing diameter and length between injector and detector was 0.25 mm ID and 40 cm, respectively. The dispersed light from the grating was simultaneously detected on the photocathode with the image sensor in the range of 300–650 nm. The photons counted in the range of 300–650 nm were computed as total spectral intensity. The mobile phase consisted of 50 mM potassium phosphate buffer (pH 7.4) containing lucigenin (5 μM) and xanthine (0.3 mM); the flow rate was maintained at 1 mL min^{-1} using the pump. In order to measure SOD activity, the mixture of XOD (15 mU, according to manufacture's information) and SOD and (or) test samples were injected. The 15 mU XOD was used as a reference for measurement of changes in CL intensity and the XOD amount could be readily varied by changing the experimental conditions. The injected volumes of XOD, SOD, and test samples used were dependent upon each concentration, and only very small amounts (1–5 μL) were needed. The reduced CL intensities of the mixtures were compared to those of the CL intensities of 15 mU of XOD. SOD activities of test samples were measured based on a standard curve, using a purified SOD preparation (according to manufacture's information). The percentage reduction of CL can be calculated using the equation:

$$[1] \qquad \% \text{ reduction of CL} = [(A - B)/A] \times 100$$

where *A* is the CL intensity generated from the injection of the 15 mU XOD only and *B* is the CL intensity generated from the injection of XOD (15 mU) and SOD and (or) test sample.

Optimization tests

The action of xanthine oxidase on CL intensity was tested. The optimum pH for the xanthine–XOD dependent CL was examined using 50 mM potassium phosphate buffer with a 5.4–8.4 pH range. The effect of temperature was measured in the range of 25–55°C. Bovine albumin was injected in concentrations of 1–1000 μg mL^{-1} in order to test the interference of protein. The inhibition of Cu, Zn-SOD activity was tested by the addition of KCN. Cyanide anion binds Cu, thereby causing the inhibition.

Results

Optimization

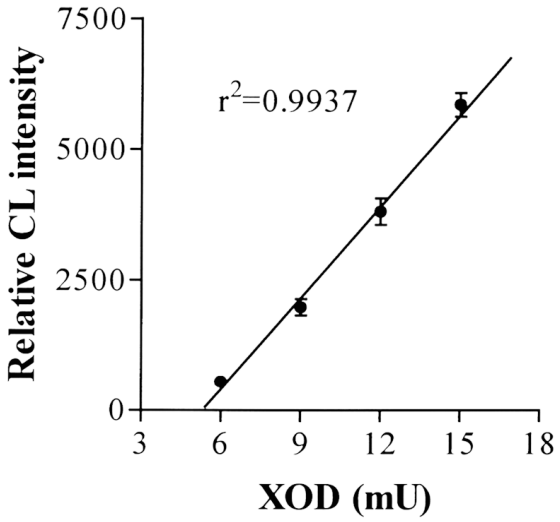
XOD concentrations related directly and linearly to CL intensity (Fig. 1). As shown in Fig. 2, the intensity of the CL signal increased with an increase in the reaction pH and temperature of the detector. For standard assays, suboptimal physiological condition (pH 7.4, 38°C) were chosen to construct a system with which to assess the SOD activity of tissues and cells. Bovine albumin, injected as a mixture of 15 mU XOD and albumin (5 μL), did not affect CL at concentrations of 1–1000 μg mL^{-1}. KCN, injected as a mixture of 15 mU XOD, KCN (5 μL), and 75 mU SOD, inhibited 50 and 100% of Cu, Zn-SOD activity at concentrations of 0.15 and 0.23 mM, respectively.

Calibration curve of standard SOD

By transforming the values of CL intensities into logarithms, it was found that, under optimum conditions, the pure Cu, Zn-SOD linearly inhibited the xanthine–XOD dependent CL. The linear regression equation was $y = 3.8299 - 0.2018x$; the correlation coefficient (r^2) was 0.9931 (Fig. 3). A log-plot (inset of Fig. 3) demonstrates that the reduction was not directly proportionate to Cu, Zn-SOD concentrations, but rather follows an exponential function. A 50% reduction of CL was detected at 18.56 mU of Cu, Zn-SOD against 15 mU XOD. The results of 10 consecutive runs with the mixture of 15 mU XOD and 14.8 mU of Cu,

© 2001 NRC Canada

Fig. 1. Effect of XOD concentration on lucigenin CL induced by xanthine–XOD. All concentrations of XOD were injected using the optimized conditions as described under *Results*. Each point denotes mean ±SD of three determinations.



Zn-SOD showed high analysis speed and reproducibility (Fig. 4). We achieved a relative standard deviation of ±3.1%, and each run was performed in less than 30 s.

SOD activity in tissues and standard addition

To test the applicability and validity of this system to the determination of SOD activity in tissues, tissue samples of guinea pigs were used. The mixture of 15 mU XOD and 5 μL of tissue extracts diluted by 1:10 was injected with or without exogenous SOD. The total SOD activity varied amongst the tissues, with the activity in the liver being much higher than in other tissues. The results of the standard addition experiment show that the degree of reduced CL intensity correlates to the amount of exogenously applied SOD (Table 1).

Specificity evaluation

The present study was done to assess the specificity and sensitivity of the assay. Glutathione, adrenaline, and cysteine, which are well-known natural reductants in tissues, inhibited the CL intensity in a dosage-dependent manner. A 50% reduction of CL was detected using 5 μL of 4.64 mM glutathione, 0.38 mM adrenaline, and 6.44 mM cysteine, respectively. Catalase also showed a dosage-dependent behavior, but it was about 1.3×10^4 times less efficient than SOD; giving a 50% reduction at 237.8 U. Glutathione reductase did not affect the intensity of CL signal with additions up to 300 U. Ascorbic acid, one of the strongest reductants and radical scavengers and a major antioxidative substance against aqueous radicals in the blood (15), demonstrated a different pattern of activity. Ascorbic acid increased the CL at 0.01 and 0.1 mM concentrations, but reduced the CL by 82.3 and 95.4% at 1 and 10 mM, respectively (Fig. 5).

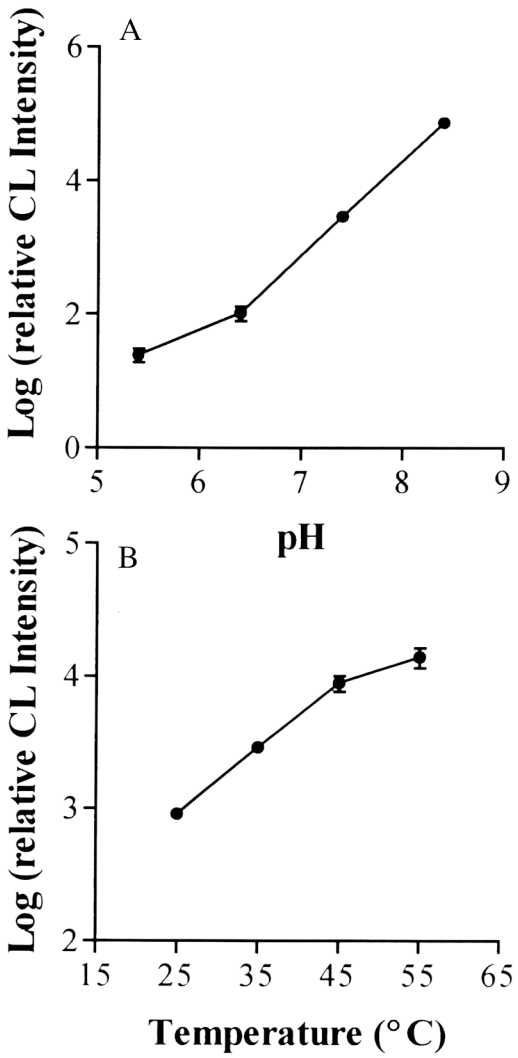
Discussion

Although the CL probe (lucigenin) has been shown to be suitable for detecting $O_2^{\bullet -}$ (6, 16), a more sensitive and useful method is required for application in a wide range of clinical uses. The method must permit a low concentration (5 μM) of lucigenin to be used effectively, while precluding the possible generation of superoxide by lucigenin itself. In these respects, several important advantages over the currently available methods are apparent with the use of the flow injection-chemiluminescent assay (FI-CLA) for CL-based SOD activity utilizing xanthine–XOD dependent $O_2^{\bullet -}$ formation.

First, the instrumentation is simple, and the highly sensitive detector (CLD-110) makes possible the use of small amounts of sample in very small volumes as well as requiring low concentrations of lucigenin. Also, there is no need for incubation steps or the addition of any other reagents for amplifying the lucigenin-enhanced CL.

Second, the dynamic range for detection of SOD activity is adhered to. The concentration of SOD that gives a 50% reduction of CL is often used as an indicator of sensitivity in assay protocols. Our FI-CLA system reaches this level with 18.56 mU of Cu, Zn-SOD against 15 mU XOD. However,

Fig. 2. Effects of (*a*) assay pH and (*b*) temperature on CL responses with the injection of 15 mU XOD. Each point denotes mean ±SD of three determinations. SD bars shown only when they are bigger than the symbol used.



© 2001 NRC Canada

Fig. 3. Inhibition of xanthine–XOD dependent CL by Cu, Zn-SOD. The different concentrations of Cu, Zn-SOD were injected with the mixture of 15 mU XOD. The concentration of SOD: (*a*) 0 mU, (*b*) 15 mU, (*c*) 30 mU, (*d*) 45 mU, and (*e*) 60 mU.

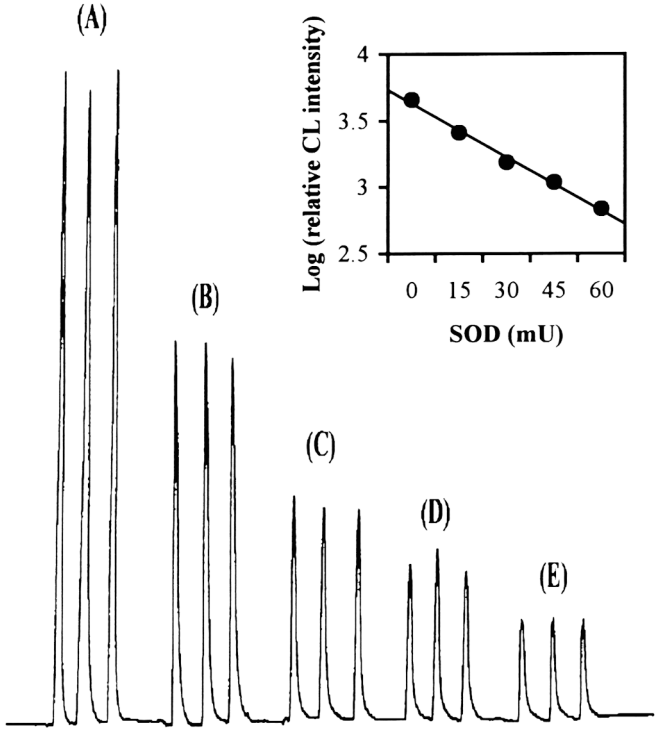
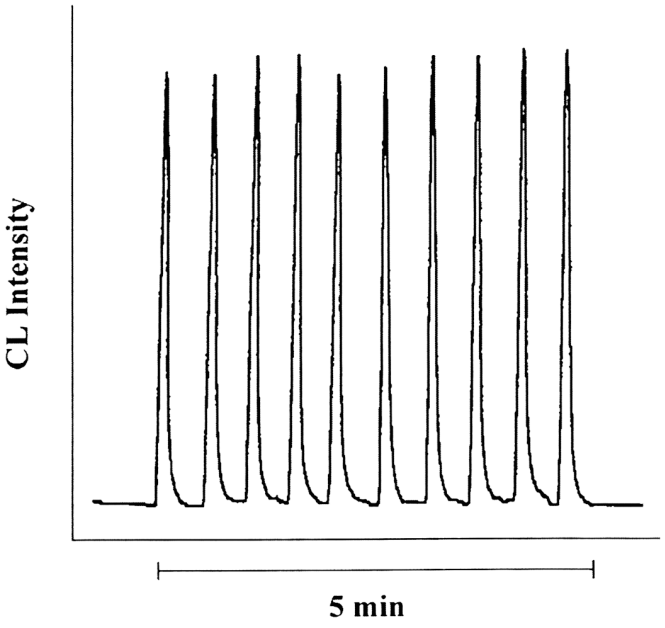


Fig. 4. Ten consecutive runs of the mixture of 15 mU XOD and 14.8 mU of Cu, Zn-SOD.



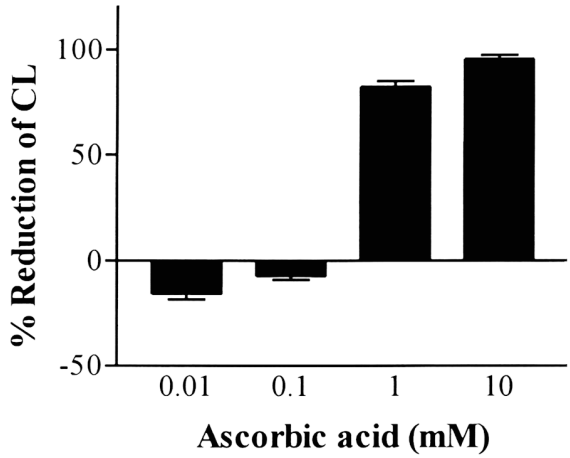
the concentration of SOD to get the 50% reduction of CL can be lowered by reducing the amount of XOD which controls the amount of $O_2^{\bullet -}$ produced. As described in the *Materials* section, the injected amounts of XOD, SOD, and test sample were readily varied in this system.

Table 1. Measurement of SOD activities in tissue extracts.

Tissue	SOD added (ng)	SOD activity[a] (ng 5 μL^{-1} ± 3 SD)
Brain	—	4.35 ± 0.13
	1.0	5.40 ± 0.11
Heart	—	5.46 ± 0.07
	1.0	6.38 ± 0.08
Kidney	—	9.58 ± 0.30
	1.0	10.51 ± 0.33
Lung	—	6.94 ± 0.12
	1.0	7.88 ± 0.25
Liver	—	26.38 ± 0.17
	1.0	27.11 ± 0.11

[a]SOD activity was based on standard curve.

Fig. 5. Changes in inhibition of CL by ascorbic acid concentrations. Each concentration was injected with the mixture of XOD (15 mU) and ascorbic acid (5 μL). Vertical bars denote mean ±SD of three determinations.



Third, a highly reproducible and rapid analysis can be carried out very conveniently by direct injection of the mixture of XOD and SOD and (or) a test sample, allowing a wide clinical application (Fig. 4).

The kinetics of CL are mainly dependent upon pH and temperature (17). Increasing pH through the pH range of 5.4–8.4 and temperature through the range of 22–55°C, increased CL intensity, which did not reach a maximum in our system. The use of suboptimal physiological conditions (pH 7.4, 38°C) has a distinct advantage in the application to biological samples. In fact, physiological pH is the most suitable for optimal activity of Mn-SOD, which is not reliably assayed at the elevated pH values that are required by other sensitive methods (18, 19). The standard curve of Mn-SOD was essentially identical with Cu, Zn-SOD under the same conditions (data not shown).

The exponential behavior of SOD activity agrees well with previous studies (19, 20). SOD that was thermally inactivated at 100°C for 5 min did not affect the intensity of the CL signal (data not shown), proving that no residual loss of CL occurred. KCN is able to completely restore CL by inhibiting Cu, Zn-SOD, proving that CL specifically originated from the superoxide radical (21).

© 2001 NRC Canada

Tissue samples can be readily analysed using this method. SOD activity in tissue homogenates is correlated to the amount of exogenously applied purified SOD (Table 1). However, it must be kept in mind that natural reductants and radical scavengers might also have a role in the activities of the tissue samples, even if their reaction specificity is much lower than that of SOD. Therefore, the activity should be regarded as a total SOD-like activity of a given sample. To avoid all interference by the compounds mentioned above, we recommend that samples be dialyzed against suitable media, or rapidly desalted through a small Sephadex G-25 (coarse) column prior to the assay (22).

Ascorbic acid leads to either positive (reducing CL intensity) or negative (enhancing CL intensity) effects depending on the concentration (Fig. 5). The dual role of ascorbic acid as an anti- and pro-oxidant has been repeatedly documented (23–25). It is assumed that ascorbic acid potentiates the formation of the lucigenin cation radical or $O_2^{\bullet -}$ is generated by the autoxidation of ascorbic acid at low concentrations.

Based on the above data, we conclude that FI-CLA is a simple, rapid, and reliable method for determining SOD activity. In particular, this new system is expected to be applied to a wide range of biochemical and clinical examinations.

References

1. J.M. McCord and I. Fridovich. J. Biol. Chem. **244**, 6049 (1969).
2. C. Beauchamp and I. Fridovich. Anal. Biochem. **44**, 276 (1971).
3. S. Marklund. J. Biol. Chem. **251**, 7504 (1976).
4. Y. Oyanagui. Anal. Biochem. **142**, 290 (1984).
5. B. Corbisier, A. Houbion, and J. Remacle. Anal. Biochem. **164**, 240 (1987).
6. K. Faulkner and I. Fridovich. Free Radic. Biol. Med. **15**, 447 (1993).
7. U. Hiroyuki, M. Susumu, I. Toshinao, and S. Masayoshi. Anal. Biochem. **251**, 206 (1997).
8. P.S. Mikhael, S. Daniel, H. Ulrich, A. Erik, and M. Thomas. Biochem. Biophys. Res. Commun. **248**, 382 (1998).
9. F. Lisdat, B. Ge, E. Ehrentreich-Förster, R. Reszka, and F.W. Scheller. Anal. Chem. **71**, 1359 (1999).
10. T. Porstmann, R. Wietschke, R. Grunow, and S. Jahn. J. Immunol. Methods, **127**, 1 (1990).
11. M.P. Skatchkov, D. Sperling, U. Hink, A. Mulsch, D.G. Harrison, I. Sindermann, T. Meinertz, and T. Munzel. Biochem. Biophys. Res. Commun. **254**, 319 (1999).
12. S.I. Liochev and I. Fridovich. Free Radic. Biol. Med. **25**, 926 (1998).
13. Y. Li, H. Zhu, P. Kuppusamy, V. Roubaud, J.L. Zweier, and M.A. Trush. J. Biol. Chem. **273**, 2015 (1998).
14. R.E. Heikkila, and F. Cabbat. Anal. Biochem. **75**, 356 (1976).
15. I.F.F. Benzie and J.J. Strain. Anal. Biochem. **239**, 70 (1996).
16. J.K. Laihia, C.T. Jansen, and M. Ahotupa. Free Radic. Biol. Med. **14**, 457 (1993).
17. D. Slawinska and J. Slawinski. Anal. Chem. **47**, 2101 (1975).
18. S. Marklund. J. Biol. Chem. **251**, 7504 (1976).
19. F. Paoletti, D. Aldinucci, A. Mocali, and A. Caparrini. Anal. Biochem. **154**, 536 (1986).
20. J.F. Ewing and D.R. Janero. Anal. Biochem. **232**, 243 (1995).
21. B.L. Geller and D.R. Winge. Anal. Biochem. **128**, 86 (1983).
22. L. Flohe and F. Otting. Methods Enzymol. **105**, 93 (1983)
23. D.M. Miller and S.D. Aust. Arch. Biochem. Biophys. **271**, 113 (1989).
24. E. Baysal, S.G. Sullivan, and A. Stern. Int. J. Biochem. **21**, 1109 (1989).
25. G.N. Bijur, M.E. Ariza, C.L. Hitchcock, and M.V. Williams. Environ. Mol. Mutagen. **30**, 339 (1997).

© 2001 NRC Canada

Synthesis and characterization of an homologous series of bis(amido)diazadipnictetidines (Pnict = P, As, Sb, Bi)

Neil Burford, T. Stanley Cameron, Kim-Chung Lam, Daren J. LeBlanc, Charles L.B. Macdonald, Andrew D. Phillips, Arnold L. Rheingold, Laura Stark, and Denise Walsh

Abstract: Spectroscopic and structural features are presented for the first homologous series of diazadipnictetidines, which have the general formula $[DipNPnN(H)Dip]_2$ (Pn = P, As, Sb, Bi; Dip = 2,6-diisopropylphenyl). The compounds are obtained from a general reaction of the corresponding halopnictine with excess LiN(H)Dip, which was previously reported for $[DipNBiN(H)Dip]_2$. However, isolation is improved by the introduction of LiN(H)-*t*-Bu (at the appropriate stoichiometry) following the addition of LiN(H)Dip. The intermediate steric presence of the Dip substituent is suitable to support the heterocatenate framework for all homologues. This is in contrast to the small substituents (e.g. alkyl), which enable both bis- and tris-amination, and the larger substituent (Mes* = tri-*tert*-butylphenyl), which can impose coordinative unsaturation (aminoiminopnictine) for the smaller congeners (P and As).

Key words: phosphorus, arsenic, antimony, bismuth, phosphazanes, phosphetidines, synthesis, structures, spectroscopic characterization.

Résumé : On a déterminé les caractéristiques spectroscopiques et structurales de la première série d'homologues des diazadipnictétidines de formules générales $[DipNPhN(H)Dip]_2$ (Pn = P, As, Sb, Bi; Dip = 2,6-diisopropényllphényle). Les composés ont été obtenus par une réaction générale de l'halopnictine correspondante avec du LiN(H)Dip en excès, telle que rapportée antérieurement pour le $[DipNBiN(H)Dip]_2$. Toutefois, il est plus facile d'isoler les produits si l'on introduit une quantité stoechiométriquement appropriée de LiN(H)-*t*-Bu à la suite de l'addition du LiN(H)Dip. La présence stérique intermédiaire du substituant Dip est appropriée pour supporter le squelette hétérocaténate pour tous les homologues; cette propriété contraste avec celles des petits substituants (par exemple, alkyles) qui permettent de faire aussi bien des bis- que des tris-aminations et avec celle du substituant plus encombrant (Mes* = tri-*tert*-butylphényle) qui peut imposer une insaturation coordinatrice (aminoiminopnictine) aux congénères plus petits (P et As).

Mots clés : phosphore, arsenic, antimoine, bismuth, phosphazane, phosphétidine, synthèse, structure, caractérisation spectroscopique.

[Traduit par la Rédaction]

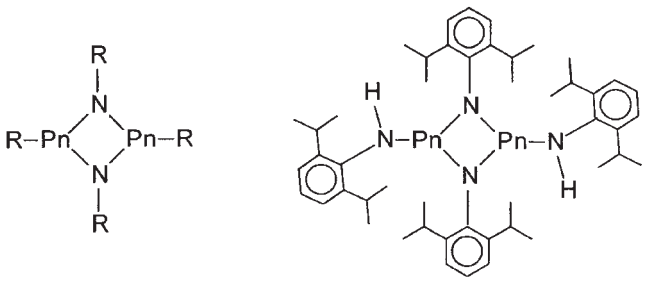
Introduction

Cyclodiphosphazanes (**1P**) (more commonly known as diazadiphosphetidines (1) or cyclo-1,3-diaza-2,4-diphosphabutanes) represent a prominent component of established nitrogen–phosphorus chemistry (2, 3). They are distinguished by the ubiquitous four-membered heterocatenated ring structure, which contrasts the more flexible and varied ring sizes observed for the formally unsaturated phosphazenes (4). Although analogous pnictetidine heterocycles involving the heavier elements of group 15 (P, As, Sb, Bi) have been structurally characterized (5–17), each represents a unique derivative and many involve cage or cluster structures

Received August 30, 2000. Published on the NRC Research Press Web site on April 12, 2001.

N. Buford[1], T.S. Cameron, D.J. LeBlanc, C.L.B. Macdonald, A.D. Phillips, L. Stark, and D. Walsh. Dalhousie University, Department of Chemistry, Halifax, NS B3H 4J3, Canada.
K.-C. Lam and A.L. Rheingold. University of Delaware, Department of Chemistry, Newark, DE 19716, U.S.A.

[1]Corresponding author (telephone: (902) 494-3190; fax: (902) 494-1310; e-mail: Neil.Burford@dal.ca).



1Pn **2Pn**

Pn = P, As, Sb, or Bi

 DOI: 10.1139/cjc-79-3-342 © 2001 NRC Canada

incorporating the pnictetidine moiety, thereby impeding direct structural or spectroscopic comparison. In this context, the structural report for the first unsupported bismetidine derivative (**2Bi**) (18) and the spectroscopic characterization of the arsenic analogue (**2As**) (19) prompted us to exploit the use of the 2,6-diisopropylphenyl (Dip) substituent and extrapolate the synthetic procedures to isolate and characterize the first phosphetidine, arsetidine, stibetidine, and bismetidine (homologous) series (**2Pn**).

Experimental procedures

General

Diethyl ether was obtained from ACP Chemicals Inc., hexane from Van Waters & Rogers, and arsenic(III) chloride from Kodak Chemicals. All other chemicals and reagents were obtained from Aldrich. Sample handling and reactions were performed under oxygen and moisture free conditions (20). *n*-Butyllithium (1.6 M in hexanes) and 2,6-diisopropylaniline ($DipNH_2$) were used as supplied. *tert*-Butylamine was dried at reflux over KOH and CaH_2. Dichloromethane was dried at reflux over CaH_2 and P_4O_{10}. Diethylether and hexane were dried over sodium–benzophenone. Deuterated solvents were dried over CaH_2. PCl_3 and $AsCl_3$ were distilled, and $SbCl_3$ was sublimed in vacuo prior to use. $BiCl_3$ was used as received. Lithium amides were prepared in situ under an atmosphere of nitrogen by adding an equimolar quantity of *n*-BuLi via a septum to a stirred solution (diethyl ether) at room temp of the amine, followed by stirring for at least 8 h. Melting points were obtained on samples sealed in glass capillaries under dry nitrogen using a Fisher–Johns apparatus. FT-IR spectra were recorded as Nujol™ mulls on CsI plates using a Nicolet 510P spectrometer. FT-Raman spectra were recorded on powder samples sealed in 1 mm diameter glass tubes with a laser power of 166 mW using a Bruker RFS-100 spectrometer. Vibrational spectra are presented as wavenumber (cm^{-1}) maxima with ranked intensities for each absorption, the most intense given a ranking of 1. Chemical analyses were performed by Beller Laboratories, Göttingen, Germany. Solution (CD_2Cl_2) ^{31}P and ^{1}H NMR data were recorded at room temp on samples sealed in evacuated Pyrex™ tubes using a Bruker AC-250 spectrometer (working at 250.13 MHz for ^{1}H and 101.26 MHz for ^{31}P). Chemical shifts are reported in ppm relative to external standards (TMS for ^{1}H, 85% aq. H_3PO_4 for ^{31}P). UV–vis spectra were obtained on a Varian Cary 100Bio UV–vis spectrometer at room temp.

Preparative procedures and spectroscopic characterization data

*[DipNPN(H)Dip]$_2$ (**2P**)*

In an evacuated vessel, a solution of LiN(H)Dip (18.5 mmol) was added over a period of ca. 30 min to a stirred solution of PCl_3 (0.84 g, 6.1 mmol) in Et_2O (20–30 mL) to give a bright yellow solution and a white precipitate. After stirring for 2 days the mixture was filtered through a fine fiberglass frit and all volatiles were removed in vacuo to give a yellow oil and pale yellow cube-shaped crystals. The oil was decanted from the crystals, which were washed three times by cold spot back-distillation (20) to afford 0.34 g (0.88 mmol, 14%) of yellow crystals, mp 125–138°C. UV–vis λ_{max} (nm) (ε (M^{-1} cm^{-1})): 230–250, 360 (3000), 430 (600). FT-IR (cm^{-1}) (ranked intensity): 3370 (22), 3057 (23), 1436 (1), 1381 (4), 1327 (5), 1263 (12), 1248 (10), 1242 (15), 1191 (8), 1186 (9), 1105 (17), 1097 (18), 1043 (21), 936 (26), 899 (6), 881 (7), 867 (3), 798 (2), 785 (13), 746 (11), 738 (19), 717 (24), 532 (20), 518 (25), 480 (14), 430 (16). IR-Raman (cm^{-1}) (ranked intensity): 3059 (5), 3021 (9), 2958 (1), 2912 (2), 2865 (3), 1590 (6), 1441 (8), 1269 (4), 1109 (16), 1044 (11), 954 (18), 884 (12), 684 (10), 521 (14), 442 (17), 292 (15), 147 (7), 78 (13). ^{1}H NMR (CD_2Cl_2) δ: 1.03 (d, J = 7 Hz, 24H), 1.27 (d, J = 7 Hz, 24H), 3.10 (sept, J = 7 Hz, 4H), 3.91 (sept, J = 7 Hz, 4H), 5.43 (s, 2H), 6.9–7.3 (m, 12H). ^{31}P NMR (CD_2Cl_2) δ: 118. Anal. calcd. for $C_{24}H_{35}N_2P$: C 75.36, H 9.22, N 7.32; found: C 75.30, H 9.33, N 7.25.

*[DipNAsN(H)Dip]$_2$ (**2As**)*

Under an atmosphere of nitrogen, $AsCl_3$ (0.8 mL, 9.1 mmol) was added to a cooled (0°C) solution of LiN(H)Dip (27 mmol) in Et_2O (50 mL) over a period of 10 min to give an orange solution and a white precipitate. After stirring at room temperature for 2 days, the solution was frozen and the vessel was evacuated. After thawing, LiCl was filtered from the solution and volatiles were slowly removed under static vacuum to leave a red oil, which was dissolved in hexane and filtered. Slow removal of solvent under static vacuum gave a pale yellow crystalline solid with an oil, which was decanted, and the crystals were washed three times by cold spot back-distillation (20) to yield 0.67 g (0.78 mmol, 17 %), mp 166–169°C. UV–vis λ_{max} (nm) (ε (M^{-1} cm^{-1})): 230–250, 323 (1000). FT-IR (cm^{-1}) (ranked intensity): 3398 (19), 3055 (20), 1432 (1), 1383 (7), 1327 (12), 1313 (5), 1254 (21), 1242 (4), 1234 (6), 1186 (3), 1104 (24), 1098 (13), 887 (25), 856 (11), 843 (15), 820 (17), 794 (10), 785 (2), 766 (14), 696 (23), 686 (9), 518 (22), 421 (18), 368 (15). IR-Raman (cm^{-1}) (ranked intensity): 3056 (11), 3020 (18), 2958 (3), 2925 (2), 2865 (9), 1589 (4), 1460 (17), 1433 (13), 1328 (24), 1263 (6), 1249 (1), 1180 (20), 1160 (29), 1108 (15), 1042 (16), 954 (28), 885 (14), 843 (26), 669 (19), 605 (25), 539 (23), 507 (30), 448 (22), 364 (12), 274 (21), 223 (27), 145 (8), 102 (10), 84 (7), 71 (5). ^{1}H NMR (CD_2Cl_2) δ: 1.08 (d, J = 7 Hz, 24H), 1.25 (d, J = 7 Hz, 24H), 2.99 (sept, J = 7 Hz, 4H), 4.02 (sept, J = 7 Hz, 4H), 5.57 (s, 2H), 6.7–7.2 (m, 12H), additional minor signals speculatively assigned to As[N(H)Dip]$_3$. Anal. calcd. for $C_{24}H_{35}N_2As$: C 67.59, H 8.27, N 6.57; found: C 68.06, H 8.01, N 6.45.

*[DipNSbN(H)Dip]$_2$ (**2Sb**)*

Under an atmosphere of nitrogen, a solution of LiN(H)Dip (12 mmol) was added via cannula to a cooled (–78°C) solution of $SbCl_3$ (1.33 g, 5.83 mmol) in Et_2O (20 mL) to give a yellow solution and a white precipitate. After stirring for less than 5 min, a solution of LiN(H)-*t*-Bu (5.9 mmol) was added. The reaction mixture was stirred for 60 min at –78°C and then at room temperature for 4 h. The solution was frozen and the vessel was evacuated. After thawing, the reaction mixture was filtered and the volatile components were removed in vacuo to leave a peach coloured oil, from which a bright yellow powder precipitated on addition of hexane (20 mL). Filtration and slow removal

© 2001 NRC Canada

of the solvent under static vacuum gave yellow cube-shaped crystals, which were spectroscopically identical to the powder, combined yield 1.50 g (54%), mp 197–199°C. UV–vis λ_{max} (nm) (ε (M^{-1} cm^{-1})): 230–250, 395 (3600). FT-IR (cm^{-1}) (ranked intensity): 3381 (17), 3053 (16), 1431 (2), 1383 (10), 1322 (7), 1311 (13), 1259 (6), 1240 (3), 1231 (5), 1190 (4), 1100 (14), 885 (20), 858 (12), 840 (11), 794 (15), 772 (1), 759 (8), 697 (18), 670 (9), 514 (19). IR-Raman (cm^{-1}) (ranked intensity): 3054 (12), 2962 (6), 2912 (3), 2862 (4), 1588 (2), 1468 (17), 1430 (5), 1248 (1), 1103 (16), 1038 (15), 883 (7), 839 (10), 547 (13), 360 (11), 212 (9), 133 (8), 92 (14). ^{1}H NMR (CD_2Cl_2) δ: 0.88 (d, J = 7 Hz, 24H), 1.25 (d, J = 7 Hz, 24H), 2.73 (sept, J = 7 Hz, 4H), 4.30 (sept, J = 7 Hz, 4H), 5.15 (s, 2H), 6.7–7.2 (m, 12H), additional minor signals speculatively assigned to $Sb[N(H)Dip]_3$. Anal. calcd. for $C_{24}H_{35}N_2Sb$: C 60.88, H 7.45, N 5.92; found: C 60.75, H 7.50, N 5.96.

*[DipNBiN(H)Dip]$_2$ (**2Bi**)*

2Bi was prepared by the procedure described for the antimony analogue (**2Sb**) using LiN(H)Dip (9.9 mmol), $BiCl_3$ (1.56 g, 4.95 mmol) suspended in Et_2O (20 mL), and LiN(H)-*t*-Bu (4.9 mmol) for a crystalline yield of 1.35 g (49%) (consistent with previously reported (18): mp 163°C. ^{1}H NMR δ: 0.98 (d, J = 7 Hz, 24H), 1.40 (d, J = 7 Hz, 24H), 2.93 (sept, J = 7 Hz, 4H), 4.54 (sept, J = 7 Hz, 4H), 5.94 (s, 2H), 6.9 (m, 12H)). UV–vis λ_{max} (nm) (ε (M^{-1} cm^{-1})): 230–250, 474 (2000). FT-IR (cm^{-1}) (ranked intensity): 3360 (16), 3043 (15), 1426 (2), 1381 (7), 1327 (14), 1262 (9), 1242 (3), 1221 (6), 1182 (4), 1175 (12), 1097 (13), 846 (10), 832 (8), 767 (1), 752 (5), 505 (11). IR-Raman (cm^{-1}) (ranked intensity): 3044 (12), 2955 (10), 2910 (7), 1587 (2), 1422 (4), 1383 (17), 1243 (1), 1190 (9), 1038 (15), 885 (13), 832 (8), 536 (6), 449 (11), 322 (14), 215 (16), 166 (3), 74 (5).

X-ray crystallography

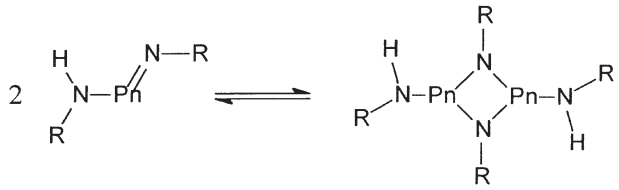
Crystals were obtained as described above and mounted in Pyrex™ capillaries in a drybox, except for **2P**, which was immersed in fluorolube oil and attached to a glass pin and immediately frozen in the cold stream of the diffractometer.

For **2P**, unit cell determination and data collection were performed, with graphite monochromated radiation (Mo Kα, λ = 0.71073 Å) by Φ and ω scans, on a Siemens P4 diffractometer equipped with a Bruker AXS SMART CCD detector (21). Structure solution and refinement were performed with the SHELX-97 (22) and SHELXTL (23) software packages. All nonhydrogen atoms were refined anisotropically, while the hydrogen atoms, which were placed geometrically in idealized positions, were allowed to ride on the heavy atom to which they were bonded with U_{iso} equal to 1.2 U_{eq} of the heavy atom.

For **2As** and **2Sb**, unit cell determination and data collection were performed, with graphite monochromated radiation (Cu Kα, λ = 1.54178 Å) and $\omega - 2\theta$ scans, on a Rigaku AFC5R diffractometer. The data were corrected for Lorentz and polarisation effectsas absorption (psi scans) and a secondary extinction coefficient were refined in each case. Structure solution and refinement were performed with use of the teXsan crystallographic software package (24). The structures were solved by direct methods. All nonhydrogen atoms were refined anisotropically. Hydrogen atoms were included at calculated positions but were not refined (C—H = 0.95 Å). Crystallographic details are summarized in Table 1 and selected bond lengths and angles are presented in Table 2.[2]

Results and discussion

Phosphazanes are readily synthesised by a variety of procedures, the most common being the reaction of an amine with a halophosphine. Although applicable to some arsines (25, 26), amination of the heavier pnictines (As, Sb, Bi) is generally complicated by the weaker and more labile N—Pn bond (as compared to N—P), which results in multiple products. More effective procedures have involved the introduction of lithium amides or silylated amines at the appropriate stoichiometry and in the presence of a base to effect the dehydrohalogenation reaction responsible for dimerization, however, stoichiometric combinations can be unpredictable. For example, the reaction of $BiCl_3$ with 3 equiv of LiN(H)Dip provides the pnictetidine **2Bi** (18), presumably with concomitant formation of 2 equiv of H_2NDip. Contrary to intuitive appreciation of steric factors, the corresponding reaction of $BiCl_3$ with 3 equiv of LiN(H)Mes* (Mes* = 2,4,6-tri-*tert*-butylphenyl, a bulkier substituent) effects quantitative amination to $Bi[N(H)Mes^*]_3$, as it does for $SbCl_3$ (27). In contrast, the reactions of PCl_3 or $AsCl_3$ with 3 equiv of LiN(H)Mes* give the aminoiminopnictines (28), which can be considered as the monomers (**3P** and **3As**) of the pnictetidine dimers (**4P** and **4As**), respectively.



3Pn **4Pn**

The number and variety of known derivatives for **1** indicate that the pnictetidine frame is favorable for all members of group 15, making **1** a key representative of the developing N–Pn chemistry. Comparisons between pnictetidines with different pnictogen centers are currently restricted by the diversity of substitution formats that have been reported. We

[2] Supporting information available: thermal ellipsoid diagrams for each of the structures, tables of crystallographic data, atomic coordinates, isotropic and anisotropic displacement parameters, bond lengths, and angles, and a CIF file for **2P**. Supplementary material may be purchased from the Depository of Unpublished Data, Document Delivery, CISTI, National Research Council Canada, Ottawa, ON K1A 0S2, Canada. For information on obtaining material electronically go to http://www.nrc.ca/cisti/irm/unpub_e.shtml. Crystallographic information has been deposited with the Cambridge Crystallographic Data Centre. Copies of the data can be obtained, free of charge, on application to the Director, CCDC, 12 Union Road, Cambridge CB2 1EZ, U.K. (Fax: 44-1223-336033 or e-mail: deposit@ccdc.cam.ac.uk).

© 2001 NRC Canada

Table 1. Summary of the crystal data, data collection, and refinement conditions for **2P**, **2As**, and **2Sb**.

	2P	**2As**	**2Sb**
Formula	$C_{48}H_{70}N_4P_2$	$C_{48}H_{70}N_4As_2$	$C_{24}H_{35}N_2Sb$
Formula weight	765.02	852.95	473.30
Crystal system	monoclinic	monoclinic	triclinic
Space group	*C*2/c	$P2_1$/c	*P*-1
a (Å)	14.837(6)	11.666(3)	11.104(1)
b (Å)	16.376(7)	23.299(3)	11.779(1)
c (Å)	18.853(8)	18.018(2)	10.292(4)
α (°)	90	90	96.53(2)
β (°)	101.17(3)	98.86(1)	98.64(2)
γ (°)	90	90	115.990(7)
V (Å^3), *Z*	4494(3), 4	4839(1), 4	1171.6(5), 2
D_{calc} (Mg m^{-3})	1.131	1.192	1.342
λ (Å)	0.71073	1.54178	1.54178
μ (mm^{-1}), *F*(000)	0.133, 1664	1.954, 1808	9.370, 488
Crystal size (mm^3)	0.30 × 0.30 × 0.20	0.03 × 0.15 × 0.20	0.08 × 0.32 × 0.18
Crystal color, habit	yellow, block	pale yellow, plate	yellow, block
Diffractometer	Siemens–Bruker CCD	Rigaku AFC5R	Rigaku AFC5R
Scan type	Φ and ω	ω/2θ	ω/2θ
Temperature (K)	253(2)	296(1)	296(1)
Absorption correction	—	ψ-scan	ψ-scan
Transmission factors	0.9739–0.9612	1.000–0.7706	1.000–0.6067
Data collected	3446	8499	4027
Unique data	2757	8065	3804
Observed data, criterion	1819, $I > 2\sigma I$	2785, $I > 3\sigma I$	2695, $I > 3\sigma I$
R_{int}, $2\theta_{max}$ (°)	0.043, 46.02	0.038, 127.1	0.075, 127.2
Refined parameters	252	488	245
Refinement on	F^2	*F*	*F*
R_1, wR_2 (observed data)	0.0516, 0.1029	—	—
R_1,[a] wR_2 (all data)	0.0961, 0.1205	—	—
R,[b] *wR* (observed data)	—	0.045, 0.038	0.045, 0.053
S[c]	1.022	1.69	1.55
Final Δρ map (e Å^{-3})	0.199, –0.189	0.38, –0.54	0.90, –0.88

[a] $R_1 = \Sigma(||F_o| - |F_c||) / \Sigma|F_o|$; $wR_2 = \{\Sigma[w(F_o^2 - F_c^2)^2] / \Sigma[w(F_o^2)^2]\}^{1/2}$.
[b] $R = R_1 = \Sigma(||F_o| - |F_c||) / \Sigma|F_o|$; $wR_2 = \Sigma w(|F_o| - |F_c|)^2 / \Sigma w(F_o^2)]^{1/2}$.
[c] $[\Sigma w(F_o^2 - F_c^2)^2 / (n - p)]^{1/2}$ for **2P** and $S = [\Sigma w(|F_o| - |F_c|)^2 / (n–p)]^{1/2}$ for **2As** and **2Sb**, *n* = number of data and *p* = number of refined parameters.

have now prepared the first homologous series of diaminodiazapnictetidines employing the 2,6-diisopropylphenyl (Dip) substituent, with bis-1,3-(2,6-diisopropylphenyl)-bis-2,4-(2,6-diisopropylphenylamino)-cyclo-1,3-diaza-2,4-di-p- nictabutanes (**2**) being derived from the previously reported arsenic **2As** (19) and bismuth **2Bi** (18) derivatives.

Although the title compounds (**2**) are all likely present in the reaction mixtures of the respective halopnictine with H_2NDip, these compounds have been isolated from reactions of $PnCl_3$ with LiN(H)Dip, thereby generalizing the synthetic approach first employed for **2As** (19) and **2Bi** (18). By using 2 equiv of LiN(H)Dip with $PnCl_3$ followed by the introduction of 1 equiv of LiN(H)-*t*-Bu, which enables in vacuo removal of the by-product (H_2N-*t*-Bu), we have isolated **2Sb** and improved the isolation procedure for **2Bi**. The reactions of $PnCl_3$ with 3 equiv of LiN(H)Dip produce one equiv of H_2NDip (low volatility and viscous oil readily identified, as an impurity, in the ^{1}H NMR spectrum), which is difficult to separate from the reaction mixture and hinders isolation of crystalline samples of **2**.

The four homologues of **2** have been comprehensively characterized. Solution NMR data (^{1}H and ^{31}P) are distinctive and can be interpreted in terms of the substitution pattern of **2**, and the compounds are clearly distinguished by vibrational spectra (IR and Raman). The N—H stretch is obvious (cf. 3397cm^{-1} for **2As**) (19), and a consistent three-band pattern at 1250, 1425, and 1600 cm^{-1}, evident in the Raman spectra, is tentatively assigned to vibrations associated with the Dip substituents. Further assignments are hindered by the complexities associated with the organic substituents. The distinctive colours of the solids **2P** (pale yellow), **2As** (cream), **2Sb** (bright yellow), and **2Bi** (red) are correlated with two weak bands in the visible region of the electronic spectra, which we tentatively assign to $n \rightarrow \pi^*$ transitions. Two additional intense, high-energy bands (230 and 250 nm) are analogous to those observed for the parent amine (H_2NDip) and are assigned to transitions involving the aryl substituents.

Selected solid state structural features for the derivatives of **2** are presented for comparison in Table 2. Representative

© 2001 NRC Canada

Table 2. Selected structural parameters for derivatives of **2**.

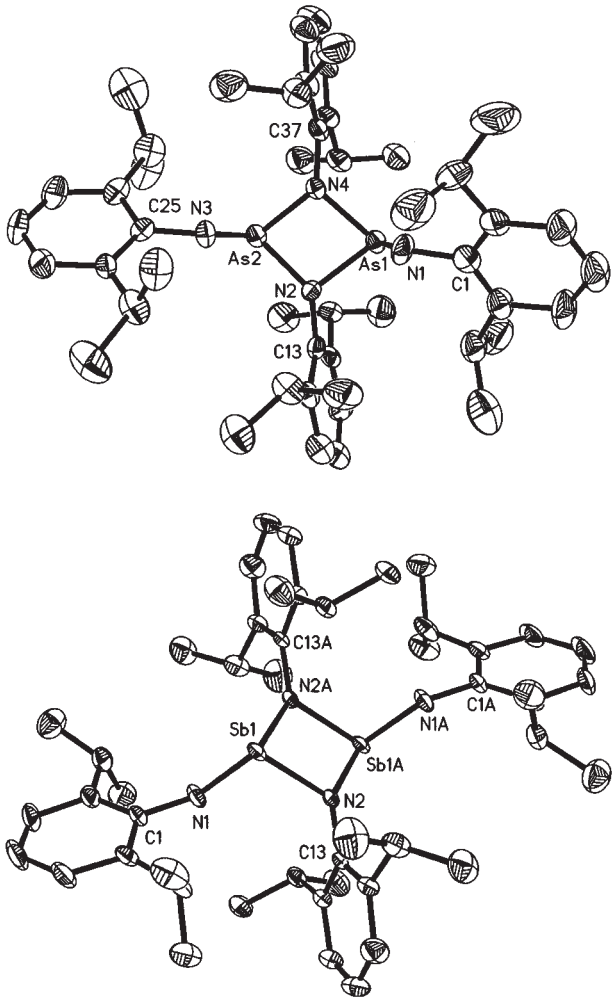
	2P	**2As**	**2Sb**	**2Bi**[18]
Bond lengths (Å)				
Pn1—N1	1.661(3)	1.838(7)	2.032(6)	2.164(4)
Pn1—N2	1.727(3)	1.872(7)	2.064(6)	2.174(5)
Pn1—N2A	1.739(3)	—	2.032(6)	2.158(4)
As1—N4	—	1.888(6)	—	—
As2—N2	—	1.885(7)	—	—
As2—N3	—	1.839(7)	—	—
As2—N4	—	1.878(6)	—	—
Pn1···Pn1A	2.606(2)	—	3.191(1)	3.355(3)
As1···As2	—	—	2.833(1)	—
Bond angles (°)				
N1-Pn1-N2	107.22(14)	101.3(3)	97.3(3)	97.4(2)
N1-Pn1-N2A	105.26(14)	—	99.0(3)	93.0(2)
N1-As1-N4	—	99.7(3)	—	—
N2-Pn1-N2A	80.01(15)		77.7(3)	78.5(2)
N2-As1-N4	—	79.0(3)	—	—
N2-As2-N4	—	78.9(3)	—	—
N3-As2-N2	—	99.3(3)	—	—
N3-As2-N4	—	102.8(3)	—	—
C1-N1-Pn1	126.0(2)	122.9(6)	127.0(6)	125.4(3)
C13-N2-Pn1	128.5(2)	125.4(6)	125.0(4)	125.4(3)
C13-N2-Pn1A	122.0(2)	—	128.8(5)	125.7(3)
C13-N2-As2	—	120.2(5)	—	—
C25-N3-As2	—	127.4(6)	—	—
C37-N4-As1	—	120.5(5)	—	—
C37-N4-As2	—	127.8(5)	—	—
Pn1-N2-Pn1A	97.54(14)	—	102.3(3)	101.5(2)
As1-N2-As2	—	97.9(3)	—	—
As1-N4-As2	—	97.6(3)	—	—
Sum of angles around Pn	292.49	280, 281	274	268.9
Fold angle about Pn-B-Pn vector (°)	154.5(1)	150.4	0	0

views of the molecular structures of **2As** and **2Sb** are shown in Fig. 1. A variety of crystal structures are observed despite the uniform substitution pattern and the essentially symmetric four-membered molecular ring present in all four cases. Isolated samples of **2Sb** and **2Bi** are isostructural involving a *trans*-configuration about the centrosymmetric planar heterocycle. In contrast, **2P** and **2As** have symmetric (*C*2/*c*) and asymmetric ($P2_1/c$) *cis*-configured molecular structures, respectively. Both display substantial folding of the heterocycle (Pn–Pn vector fold angles: P 154.5(1)°, As 150.4(2)°). Within each derivative of **2**, the endocyclic N—Pn bond lengths are essentially indistinguishable. The exocyclic N—Pn bonds are slightly shorter for Pn = P and As, but are identical to the endocyclic bonds when Pn = Sb and Bi. A slight increasing trend in Pn-N-Pn angle and a decreasing trend in N-Pn-N angle in the order P, As, Sb, Bi are evident. The N(*exo*)-P-N(*endo*) angles are anomalously large in comparison with the more routine angles observed for the other derivatives (Pn = As, Sb, and Bi), indicating that steric interactions between the substituents may be partly responsible for the nonplanarity of the heterocycle. Nevertheless, the planarity of the *trans*-configuration and puckering of the *cis*-configurations are consistent with observations for the numerous structural reports for diazadiphosphetidine derivatives (3). The consistency of the four-membered heterocyclic frame, in spite of the substituent steric influences, is possibly responsible for the observed configurational distinctions imposed by the relative atomic sizes of the pnictogen elements.

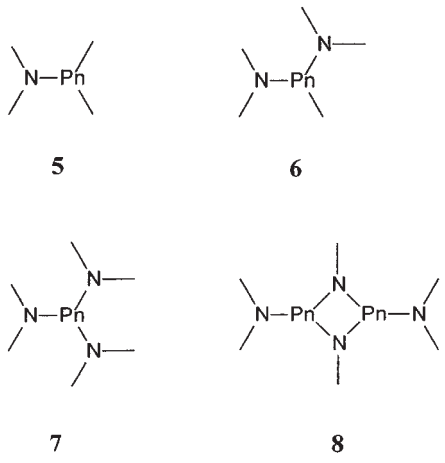
The data presented for compounds **2P**, **2As**, and **2Sb** complement the spectroscopic data previously reported for **2As** (19) and the structural and spectroscopic data for **2Bi** (18) to complete the first homologous series of diazadipnictetidines. We attribute the preferential isolation and general stability of these systems to the intermediate steric influences of the Dip substituent. The degree of amination of a pnictine is understandably limited by the spatial (steric) requirements of both the number of substituents on nitrogen and steric bulk of those substituents. Depending on reaction stoichiometry and conditions, small substituents (e.g., Me, Ph, *t*-Bu) generally enable all three degrees of amination (mono-**5**, bis-**6**, and tris-**7**) of pnictines, as well as oligomeric arrangements resulting from condensation reactions, for which the pnictetidine **1** (or **4**/**8**) is the most obvious product. In the context of the data available for NMes* substitution, the sterically smaller Dip substituent may be expected to allow for trisamination. For Sb and Bi, however, the observations

© 2001 NRC Canada

Fig. 1. Crystallographic views of **2As** (top) and **2Sb** (bottom) with 30% probability displacement ellipsoids. For clarity, hydrogen atoms have been omitted.



reveal that slightly lower steric strain imposed by the Dip substituent (relative to Mes*) favours condensation to the diazadipnictetidine **4** over trisamination.



Conclusions

The intermediate steric presence of the Dip substituent is suitable to support all heterocatenate frameworks for the first homologous series of diazadipnictetidines. The generally applicable synthetic procedure involves the reaction of LiN(H)Dip with the corresponding chloropnictine; isolation is enhanced using an equivalent of LiN(H)-*t*-Bu. Consistent structural features are evident throughout the series except for configurational differences, which may be of minimal energetic significance.

Acknowledgments

We thank the Natural Sciences and Engineering Research Council of Canada (NSERC), the Killam Trust and the Sumner Foundation for funding, the Atlantic Regional Magnetic Resonance Centre and Dr. F. Cozens for the use of instrumentation, Natasha Zwarun for obtaining the UV–vis spectra, and Katherine Robertson for help with processing the crystallographic data for **2As** and **2Sb**.

References

1. F.G. Mann. The heterocyclic derivatives of phoshorus, arsenic, antimony, and bismuth. *Edited by* Weissburger and Taylor. E.C. Wiley, New York. 1970.
2. R. Keat. Top. Curr. Chem. **102**, 89 (1982).
3. L. Stahl. Coord. Chem. Rev. **210**, 203 (2000).
4. C.W. Allen. Coord. Chem. Rev. **130**, 137 (1994).
5. A.J. Edwards, M.A. Beswick, J.R. Galsworthy, M.A. Paver, P.R. Raithby, M.A. Rennie, C.A. Russell, K.L. Verhorevoort, and D.S. Wright. Inorg. Chim. Acta, **248**, 9 (1996).
6. S. Chitsaz, K. Harms, and K. Dehnicke. Z. Anorg. Allg. Chem. **625**, 939 (1999).
7. A. Bashall, M.A. Beswick, C.N. Harmer, A.D. Hopkins, M. McPartlin, M.A. Paver, P.R. Raithby, and D.S. Wright. J. Chem. Soc. Dalton Trans. 1389 (1998).
8. M.A. Beswick, N. Choi, A.D. Hopkins, M. McPartlin, M.A. Paver, and D.S. Wright. Chem. Commun. 261 (1998).
9. R.A. Alton, D. Barr, A.J. Edwards, M.A. Paver, P.R. Raithby, M.A. Rennie, C.A. Russell, and D.S. Wright. J. Chem. Soc. Chem. Commun. 1481 (1994).
10. D. Barr, A.J. Edwards, S. Pullen, M.A. Paver, P.R. Raithby, M.A. Rennie, C.A. Russell, and D.S. Wright. Angew. Chem. Int. Ed. Engl. **33**, 1875 (1994).
11. S.C. James, N.C. Norman, A.G. Orpen, M.J. Quayle, and U. Weckenmann. J. Chem. Soc. Dalton Trans. 4159 (1996).
12. M.A. Beswick, N.L. Cromhout, C.N. Harmer, M.A. Paver, P.R. Raithby, M.A. Rennie, A. Steiner, and D.S. Wright. Inorg. Chem. **36**, 1740 (1997).
13. M. Björgvinsson, H.W. Roesky, F. Pauer, and G.M. Sheldrick. Chem. Ber. **125**, 767 (1992).
14. M. Rhiel, F. Weller, J. Pebler, and K. Dehnicke. Angew. Chem. Int. Ed. Engl. **33**, 569 (1994).
15. A.J. Edwards, M.A. Paver, P.R. Raithby, M.A. Rennie, C.A. Russell, and D.S. Wright. Angew. Chem. Int. Ed. Engl. **33**, 1277 (1994).
16. M.A. Beswick, E.A. Harron, A.D. Hopkins, P.R. Raithby, and D.S. Wright. J. Chem. Soc. Dalton Trans. 107 (1999).
17. A. Bashall, M.A. Beswick, E.A. Harron, A.D. Hopkins, S.J. Kidd, M. McPartlin, P.R. Raithby, A. Steiner, and D.S. Wright. Chem. Commun. 1145 (1999).

© 2001 NRC Canada

18. U. Wirringa, H.W. Roesky, M. Noltemeyer, and H.-G. Schmidt. Inorg. Chem. **33**, 4607 (1994).
19. U. Wirringa, H.W. Roesky, M. Noltemeyer, and H.-G. Schmidt. Angew. Chem. Int. Ed. Engl. **32**, 1628 (1993).
20. N. Burford, J. Müller, and T.M. Parks. J. Chem. Educ. **71**, 807 (1994).
21. SMART area detector dontrol and integration software. Bruker AXS Inc. Madison, Wisconsin. 1998.
22. G.M. Sheldrick. SHELXL 97. University of Göttingen, Göttingen, Germany. 1997.
23. G.M. Sheldrick. SHELXTL 5.03. Siemens Analytical Xray Instruments Inc., Madison, Wisconsin. 1994.
24. teXsan for Windows 1. Molecular Structure Corporation, The Woodlands, Texas. 2000.
25. G.I.L.I.A. Kokorev, V.A. Naumov, Sh.Kh. Badrutdinov, and F.D. Yambushev. Zh. Obshch. Khim. **59**, 1381 (1989).
26. E.V. Avtomonov, K. Megges, X. Li, J. Lorberth, S. Wocaldo, W. Massa, K. Harms, A.V. Churakov, and J.A.K. Howard. J. Organomet. Chem. **544**, 79 (1997).
27. N. Burford, C.L.B. Macdonald, K.N. Robertson, and T.S. Cameron. Inorg. Chem. **35**, 4013 (1996).
28. P.B. Hitchcock, M.F. Lappert, A.K. Rai, and H.D. Williams. J. Chem. Soc. Chem. Commun. 1633 (1986).

© 2001 NRC Canada

2000 Alfred Bader Award Lecture

In the footsteps of Pasteur: asymmetric induction in the photochemistry of crystalline ammonium carboxylate salts

John R. Scheffer

Abstract: This review describes the development of a new, synthetically useful method of asymmetric synthesis in organic photochemistry. Similar in many ways to the Pasteur procedure for resolving racemic carboxylic acids and organic amines, the method relies on the use of crystalline organic salts in which the enantioselectivity of a photochemical reaction of an achiral organic ion (for example, a carboxylate anion) is governed in the solid state by the presence of an optically pure counterion (for example, an optically active ammonium ion). Such optically pure counterions are termed ionic chiral auxiliaries. Salts containing ionic chiral auxiliaries are required to crystallize in chiral space groups, which provide the asymmetric environment necessary for chiral induction. Using this methodology, we have obtained near-quantitative optical yields in a wide variety of photochemical reactions.

Key words: photochemistry, solid state, chiral auxiliaries, asymmetric synthesis, crystal structure–reactivity relationships.

Résumé : Cet article de revue décrit le développement d'une nouvelle méthode, utile, de synthèse asymétrique en photochimie organique. Semblable à plusieurs points de vue à la méthode de Pasteur de dédoubler les acides carboxyliques et les amines organiques racémiques, la méthode est basée sur l'utilisation de sels organiques cristallins dans lesquels l'énantiosélectivité d'une réaction photochimique d'un ion organique achiral (par exemple, un ion carboxylate) est régie à l'état solide par la présence d'un contre-ion optiquement pur (par exemple, un ion ammonium optiquement actif). De tels contre-ions optiquement purs sont dénommés auxiliaires chiraux ioniques. Des sels contenant des auxiliaires chiraux ioniques sont nécessaires pour obtenir une cristallisation dans des groupes spatiaux chiraux qui fournissent l'environnement asymétrique nécessaire à l'induction chirale. À l'aide de cette technologie, nous avons pu obtenir des rendements optiques pratiquement quantitatifs dans un grand nombre de réactions photochimiques.

Mots clés : photochimie, état solide, auxiliaires chiraux, synthèse asymétrique, relations structure cristalline–activité.

[Traduit par la Rédaction]

Introduction

Before embarking on a description of our work dealing with asymmetric synthesis in the crystalline state, a few words are in order concerning the title of this presentation. Without in any way trying to equate our work with that of Pasteur's in terms of significance, there are, nonetheless, some interesting connections. One of these is that several of the ideas presented in this review were developed in 1997 while I was on sabbatical leave at the University of Strasbourg. At the same university, approximately 150 years earlier, Louis Pasteur carried out much of his most famous and important research dealing with the isolation of optically active substances (1), and it was genuinely inspiring to think that one might literally, as well as figuratively, be following in the great man's footsteps. The scientific relationship between Pasteur's work and ours will be presented later in the review.

Received November 20, 2000. Published on the NRC Research Press Web site on April 30, 2001.

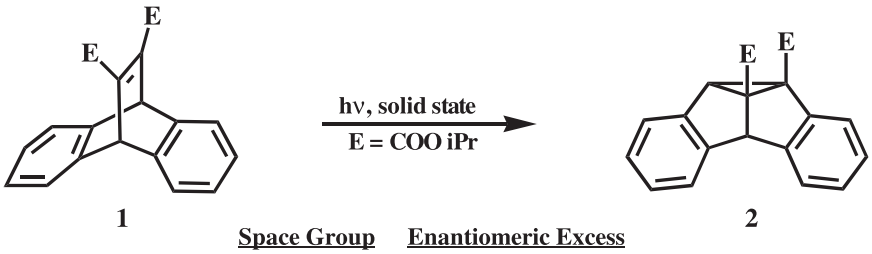
J.R. Scheffer. Department of Chemistry, University of British Columbia, 2036 Main Mall, Vancouver, BC V6T 1Z1, Canada (telephone: (604) 822-3266; fax: (604) 822-2847; e-mail: scheffer@chem.ubc.ca).

Origin of the ionic chiral auxiliary concept

In the mid-1980s, one of my graduate students, Miguel Garcia-Garibay, discovered that the achiral compound diisopropyl 9,10-dihydro-9,10-etheno-anthracene-11,12-dicarboxylate (**1**) spontaneously crystallizes in the chiral space group $P2_12_12_1$, and that irradiation of enantiomorphously pure single crystals of this substance leads to the di-π-methane rearrangement product **2** in near quantitative enantiomeric excess (Scheme 1) (2). The critical importance of a chiral space group to this so-called absolute asymmetric reaction was highlighted by the fact that a dimorph of diester **1** in the achiral space group *Pbca* rearranged in the solid state to give racemic **2**. While absolute asymmetric syntheses had been documented prior to this time for bimolecular solid state reactions ((3) and for the first example of an absolute

 DOI: 10.1139/cjc-79-4-349 © 2001 NRC Canada

Scheme 1.



Space Group	Enantiomeric Excess
$P2_12_12_1$ (chiral)	95%
Pbca (achiral)	0%

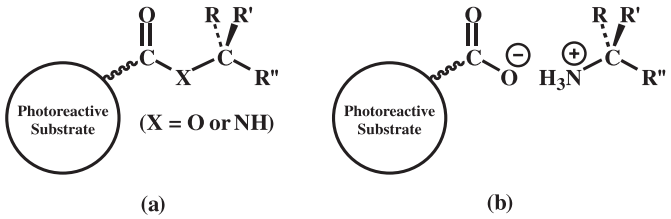
asymmetric synthesis see, ref. 3*a*), this was the first reported example of a *unimolecular* absolute asymmetric photorearrangement.

Encouraged by the high optical yield obtained in this reaction, we set out to devise a more general method by which the crystalline state could be used to achieve asymmetric induction in photochemical reactions. For reviews on asymmetric induction in organic photochemistry, see ref. 4. One problem with absolute asymmetric synthesis as a general method is that the great majority of achiral compounds do *not* crystallize in one of the 65 chiral space groups (of 230 total space groups) that are essential for success (5). For a more recent discussion of space group frequencies see ref. 5*b*. A second major obstacle is that, at present, there is no general understanding of the relationship between molecular structure and crystal structure. In other words, it is virtually impossible to predict when an achiral molecule will crystallize in a chiral space group. It is clear, therefore, that what is needed is a method of *guaranteeing* the presence of a chiral space group, and that absolute asymmetric synthesis, while fascinating and perhaps of relevance to theories of the prebiotic origins of optical activity on earth (6), will never be synthetically useful in the general sense.

How is it possible to guarantee the presence of a chiral space group? The simple answer is to equip the reactant with an optically pure chiral auxiliary. Such compounds are *required* to crystallize in chiral space groups because the molecules of which the lattice is composed cannot pack in mirror-symmetric or centrosymmetric arrangements. Incidentally, for those wondering how achiral molecules can also crystallize in chiral space groups (albeit rarely and unpredictably), a good way to visualize this is to imagine a right or left-handed spiral staircase constructed of achiral building blocks (e.g., bricks).

Two types of chiral auxiliary can be envisaged: covalent and ionic (Fig. 1). In the covalent type (Fig. 1*a*), the optically pure chiral auxiliary is tethered to the achiral reactant by a covalent bond, typical examples being via ester or amide formation between a carboxylic acid and an alcohol or an amine. In contrast, ionic chiral auxiliaries are attached by means of salt bridges between ions (Fig. 1*b*). At the time we began this work (1989) the use of ionic chiral auxiliaries in asymmetric synthesis was unknown, and for this reason we concentrated our efforts in this area. Since then Zhang and Corey (7) have shown that optically active quaternary ammonium ions can be used successfully in enantioselective alkylation, Michael addition, nitroaldol, and epoxidation reactions.

Fig. 1. Covalent (*a*) and ionic (*b*) chiral auxiliaries.

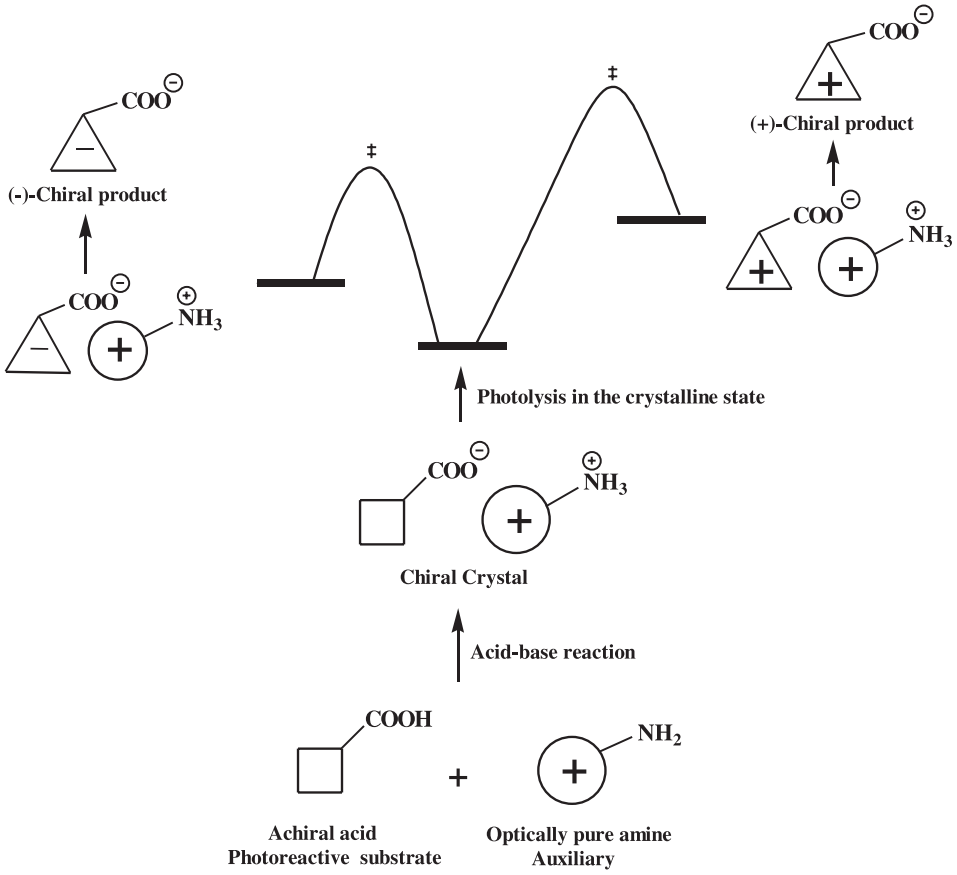


In addition to novelty, there were a number of practical reasons for choosing to work with ionic chiral auxiliaries. Chief among these is the fact that salts tend to have much higher melting points than purely covalent compounds of comparable molecular weight. This is important when conducting reactions in the crystalline state, since salts are less likely to melt as the reaction proceeds and, as a result, higher conversions are possible. Melting, of course, leads to loss of topochemical control of reaction selectivity as the periodic, three-dimensional regularity of the crystal lattice is degraded. We also hoped that, because of their strong lattice forces, ionic compounds might be more prone to undergo single crystal-to-single crystal or topotactic solid state photochemistry. Reactions of this type represent the Holy Grail of solid state chemistry, because they allow the reacting crystal to be monitored by X-ray diffraction throughout the course of the transformation. This is not possible for the great majority of solid state reactions, which are nontopotactic in nature and involve formation of the product in polycrystalline form (8). The beauty of topotactic reactions for asymmetric induction studies is that they permit the absolute configuration of the starting material to be correlated with that of the product through X-ray crystallography of partially reacted crystals. For a review of absolute configuration correlation studies in topotactic as well as nontopotactic solid state photoreactions, see ref. 9. For salts, this works best when the absolute configuration of the chiral auxiliary is known, which is usually the case. We shall see an example of such a study later in the paper.

Another practical advantage of salts for asymmetric induction studies is that they are readily prepared by simple acid-base chemistry, and once the asymmetric induction is complete, the ionic chiral auxiliary can be easily removed, typically by diazomethane workup to form the methyl ester of the carboxylate anion component. Finally, it is important to mention that it is not necessary to work with single crystals in the case of substrates containing ionic or covalent chiral auxiliaries. This is because all crystals in such

© 2001 NRC Canada

Fig. 2. Hypothetical solid-state reaction of the anionic component of a salt of an achiral carboxylic acid with an optically pure amine. In the example shown, formation of the (–)-product is favored kinetically.



materials have the same chirality. As a result, one can photolyze polycrystalline samples weighing dozens or even hundreds of milligrams, an important feature if the method is to become synthetically useful.

Scientific connection with Pasteur

The solid state ionic chiral auxiliary approach to asymmetric synthesis has close parallels to the procedure devised by Pasteur to resolve racemic carboxylic acids. In this procedure, first used in 1853 to resolve racemic tartaric acid (10), the racemic carboxylic acid is treated with an optically pure amine (cinchonicine or quinicine in Pasteur's case) to form a pair of diastereomerically related salts. These are then separated by fractional crystallization, and subsequent acidification of each diastereomerically pure salt regenerates the carboxylic acid in optically pure form.

What we are proposing to do in the ionic chiral auxiliary method is to generate a chiral carboxylic acid in situ by photolysis of an achiral precursor in the presence of an optically pure amine (Fig. 2). Such reactions proceed through ionic transition states that are diastereomerically related, and given a sufficiently large difference in activation energy for a kinetically controlled process, can in principle lead to near-quantitative yields of a single product enantiomer. This method has an advantage over the conventional Pasteur resolution procedure in terms of yield, since the maximum yield of a given enantiomer that can be obtained in the latter case is 50% (and in practice is often considerably less) (11). Furthermore, the ionic chiral auxiliary approach allows either optical antipode of the photoproduct to be prepared by simply changing the configuration of the auxiliary. This is a relatively easy matter these days given the commercial availability of a wide variety of chiral auxiliaries in both enantiomeric forms.

Test reaction requirements

In order to be suitable for testing the solid state ionic chiral auxiliary approach to asymmetric synthesis, photochemical reactions must meet the following requirements: (*i*) the reaction must be one in which an achiral starting material is converted into a chiral photoproduct; high quantum yields are desirable. (*ii*) The reactant must contain an acidic or basic functional group that allows for salt formation with a suitable chiral auxiliary. In nearly all of the systems we have investigated, the reactant contains a carboxylic acid group and the chiral auxiliary is an optically pure amine. The reason for this is that diazomethane workup of the reaction mixture affords the photoproduct as the corresponding methyl ester, which is relatively easy to chromatograph, isolate and analyze for ee. (*iii*) The reactant must crystallize in a conformation favorable for reaction. Hydrogen abstraction reactions, for example, only work in the solid state if the C=O···H distance is of the order of 2.8 ± 0.2 Å (for a discussion of the geometric requirements for intramolecular hydrogen atom transfer in the solid state, see ref. 12). Since most conformationally flexible molecules crystallize in or near

© 2001 NRC Canada

Scheme 2.

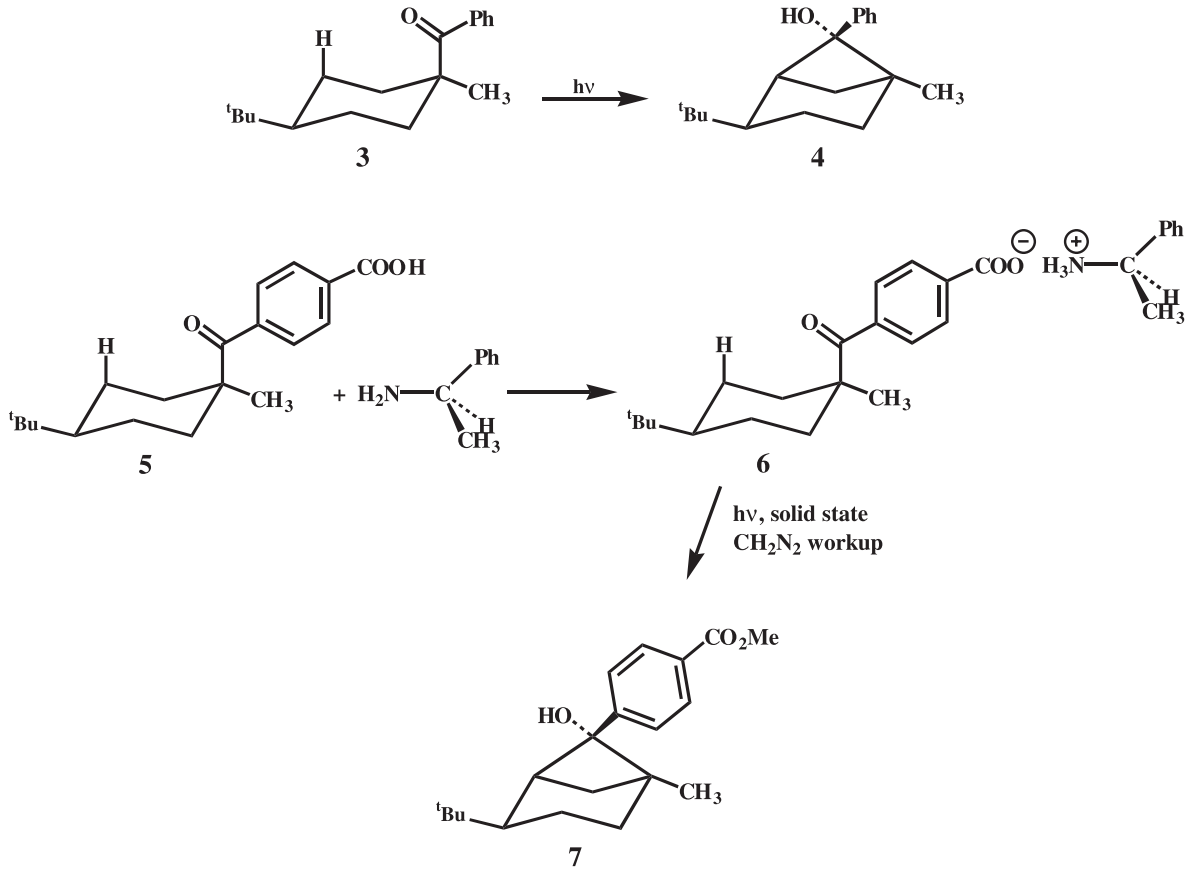


Table 1. Asymmetric induction in the solid state photochemistry of salt **6**.

Irradiation time (min)	Conversion (%)	Enantiomeric excess (%)
5	7	96.9
15	24	96.5
25	66	94.3
45	85	92.1

their lowest energy conformations (13), molecular mechanics calculations give a good indication of the conformation to be found in the solid state.

Examples of the solid state ionic chiral auxiliary method

cis-4-*tert*-Butyl-1-benzoylcyclohexane derivatives

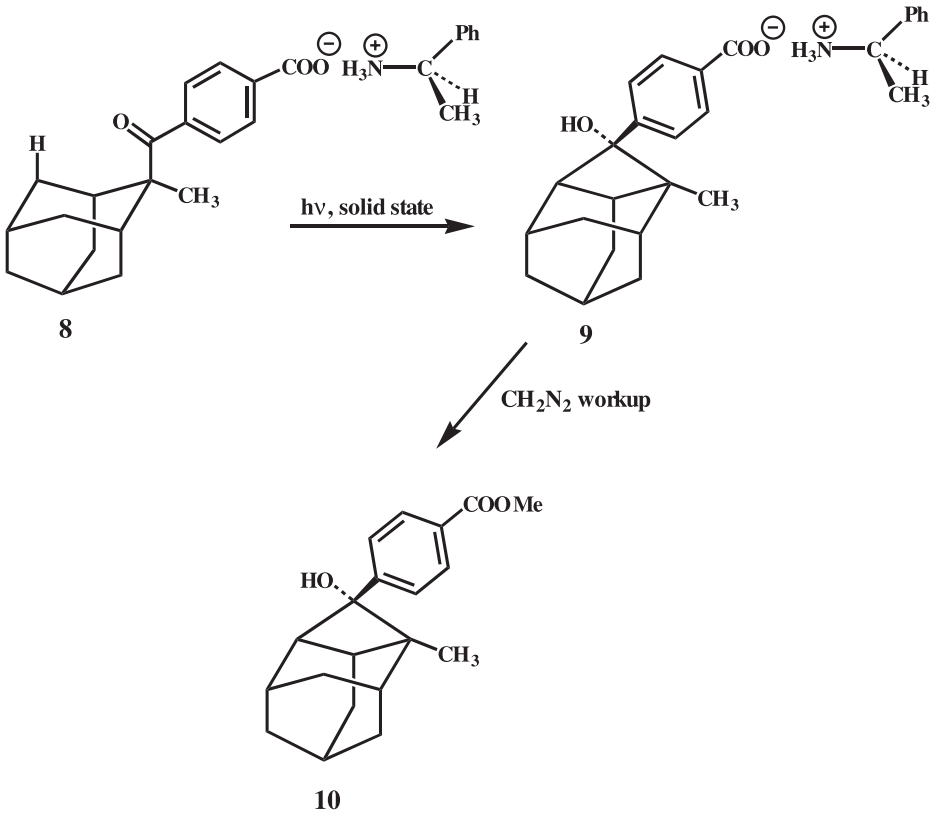
In 1974, Lewis et al. (14) showed that solution phase irradiation of achiral ketone **3** affords excellent yields of the corresponding racemic cyclobutanol **4** (Scheme 2). This reaction, an example of Yang photocyclization (see ref. 15 for examples of Norrish type II photochemistry), seemed ideal for our purposes since it fulfills all the requirements outlined above. In particular, molecular mechanics calculations indicated a feasible hydrogen atom abstraction geometry for the lowest energy conformer, and all that was required was to introduce a carboxylic acid group into compound **3** without disturbing its plane of symmetry; this was readily accomplished through synthesis of the corresponding *p*-carboxylic acid **5** (16).

Treatment of keto-acid **5** with (*R*)-(+)-1-phenylethylamine gave salt **6**, and photolysis of polycrystalline samples of this material followed by diazomethane workup gave (–)-**7** in optical yields as high as 97% (Table 1) (16). As shown in the table, the enantiomeric excess (ee) decreased slightly with increasing conversion, a feature that appears to be general to the method. We attribute this decrease in ee to crystal breakdown resulting from defect sites generated by product molecules that do not fit into the reactant lattice. Despite this, the pleasant fact is that >90% ee is maintained even at conversions as high as 85%. As predicted, use of the enantiomeric chiral auxiliary (*S*)-(–)-1-phenylethylamine gave essentially the identical ee of (+)–**7**. These results clearly indicate the considerable synthetic potential of the ionic chiral auxiliary approach to asymmetric induction. Finally, irradiation of salt **6** in solution was found to afford racemic cyclobutanol **7**, a result that highlights the importance of the crystalline state for asymmetric induction.

Several additional ionic chiral auxiliaries were investigated in the case of keto-acid **5**, and the results are summarized in Table 2. Clearly, not all chiral auxiliaries work equally well, and an important task was to try to understand why some salts give much higher ees than others. We have recently solved this problem and shall address this question later in the review. For now, suffice it to say that for every photochemical reaction that we have studied via the solid

© 2001 NRC Canada

Scheme 3.



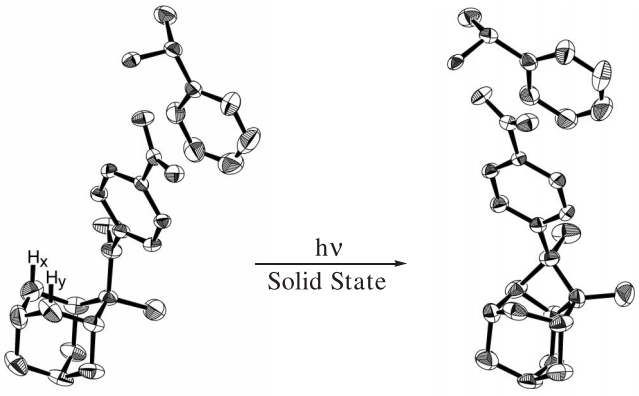
8 9 10

Table 2. The use of other ionic chiral auxiliaries in the solid state photochemistry of keto-acid **5**.

Amine	Conversion (%)	Enantiomeric excess (%)
(+)-Prolinol	31	(–)-08.5
(+)-Pseudoephedrine	18	(+)-97.3
(+)-Arginine	29	(+)-84.6
(–)-Ephedrine	26	(+)-67.3
(–)-Norephedrine	34	(+)-95.8
(–)-Prolinamide	51	(+)-68.2

state ionic chiral auxiliary method, it has always been possible to find at least one and often two or three chiral auxiliaries that give ees of 90% or more. More often than not, for reasons that we do not understand, the 1-phenylethylammonium ion has proven to give the highest ees.

Fig. 3. Molecular structure of the *same crystal* prior to (**8**) and following (**9**) irradiation in the solid state. The hydrogen atoms have been omitted for clarity.



8 9

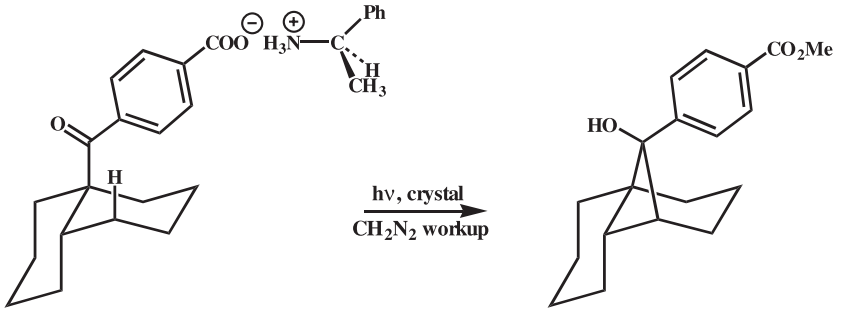
Single crystal-to-single crystal photorearrangement of a 2-benzoyladamantane derivative

As an extension of our work with the *cis*-4-*tert*-butyl-1-benzoylcyclohexane system discussed above, we investigated the solid state photochemistry of a series of 2-benzoyladamantane derivatives (16). During these studies, we noticed that irradiation of crystals of salt **8** (Scheme 3) led to excellent yields of photoproduct salt **9** without any noticeable change in the appearance of the crystals. Treatment of the irradiated crystals with diazomethane afforded methyl ester **10** in ees that varied from a high of 88% ee at 3.5% conversion to 82.4% ee at 82.3% conversion. These results suggested that the conversion of salt **8** into photoproduct salt **9** was a single crystal-to-single crystal (topotactic) process, and this possibility was, therefore, investigated further.

Accordingly, a single crystal of salt **8** was subjected to X-ray diffraction analysis and then photolyzed for a sufficient time (2 h) to convert it quantitatively into salt **9**, whereupon a second data set was collected. Both data sets refined successfully in space group $P2_12_12_1$ to final R values of 4.6 and 4.9%, thus verifying that the solid state photorearrangement is indeed a topotactic process. Figure 3 shows the molecular structures of the salts before and after photolysis. As is

© 2001 NRC Canada

Scheme 4.

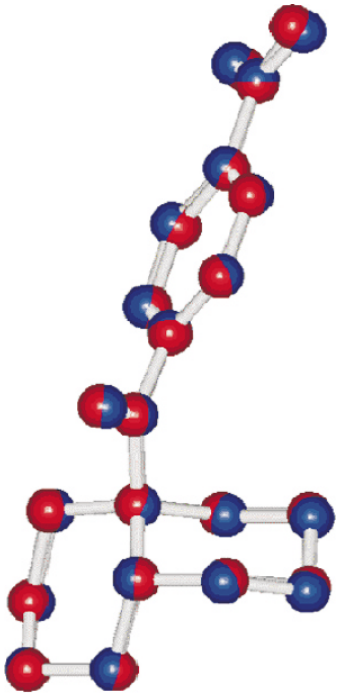


11 **12**

evident, the reactant and product have similar shapes and sizes. This is reflected by a root mean-square error of only 0.53 Å calculated for the overlap of the two structures (17), which is undoubtedly the reason for the single crystal-to-single crystal nature of the reaction, i.e., the photoproduct fits very well into the lattice site of the reactant.

Furthermore, because the absolute configuration of the 1-phenylethylammonium ion is known, the absolute configuration of the anion is established, and this allows us to determine whether γ-hydrogen atom H_X or H_Y was abstracted. The experimental results clearly show that H_X is the reactive hydrogen atom, and this is consistent with its closer proximity (2.60 Å) to the carbonyl oxygen, as compared to H_Y (3.59 Å) (for an example where a difference in C=O···H_γ distance of only 0.27 Å leads to exclusive abstraction of the closer hydrogen in the solid state, see ref. 18). The crystal structures shown in Fig. 3 also reveal the reason for the high diastereoselectivity of the conversion of salt **8** into salt **9**. Following abstraction of H_X, the 1,4-hydroxybiradical intermediate finds itself in a conformation ideally suited for least motion closure to the observed *endo*-aryl photoproduct. Formation of the *exo*-aryl cyclobutanol would require an approximately 180° rotation of the –Ċ(OH)Ar substitutent, a large amplitude motion that is impossible in the crystalline state. The same explanation applies to the diastereoselective conversion of salt **6** into *endo*-aryl cyclobutanol photoproduct **7** (Scheme 2) (16).

Fig. 4. RMS overlay of chiralty-matched conformational enantiomers of salt **11** (cations not shown). The red spheres correspond to one conformational enantiomer, the blue spheres to the other.



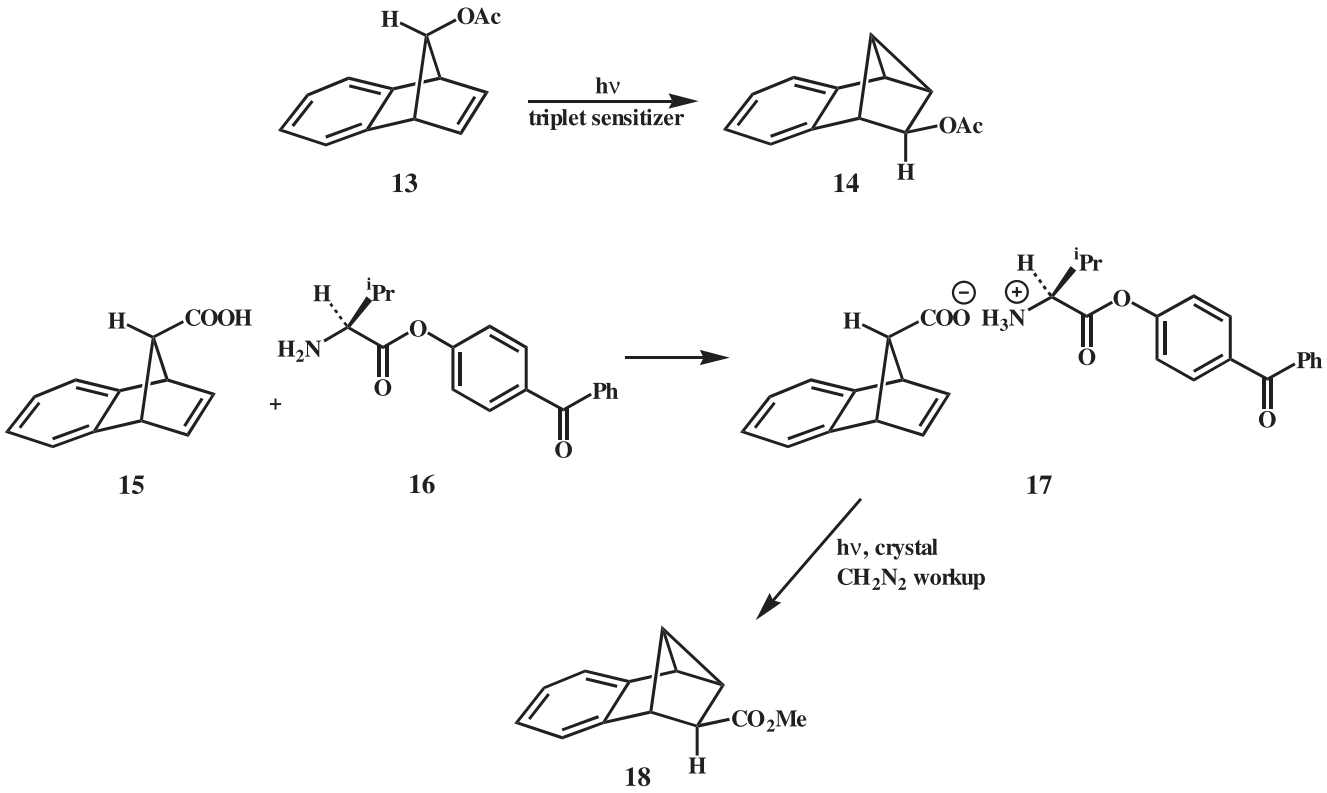
cis-9-Decalyl aryl ketone derivatives

Next we discuss the use of the ionic chiral auxiliary method in the photochemistry of *cis*-9-decalyl aryl ketone derivatives. Consider the example shown in Scheme 4. In a Yang photocyclization reaction (15) that is simultaneously regio-, diastereo-, and enantioselective, irradiation of crystals of salt **11** leads to chiral cyclobutanol **12** with an ee of 98% at 85% conversion (19). Similar results were obtained with the (*R*)-bornyl ammonium salt. As in the cases discussed above, X-ray diffraction studies revealed that the molecular conformation of the reactant is responsible for the remarkable selectivity observed. Salt **11** crystallizes in a conformation that brings the axial γ-hydrogen atom at C4 (shown in Scheme 4) into close proximity with the carbonyl oxygen atom (2.62 Å). Abstraction of this hydrogen leads to a biradical that closes with "retention of configuration" at the carbonyl carbon to afford cyclobutanol **12**. As in the case of salts **6** and **8** discussed above, formation of the alternative diastereomer requires a topochemically forbidden 180° bond rotation of the bulky –Ċ(OH)Ar group, and is, therefore, not observed. Serving once again to highlight the importance of the crystalline state to the success of the ionic chiral auxiliary method, irradiation of salt **11** in solution led to racemic **12**. We have yet to observe a measurable ee in solution for any of our chiral salts.

One of the ionic chiral auxiliaries investigated in the *cis*-decalyl aryl ketone system led to relatively low ees. This was the (1*R*,2*S*)-norephedrine salt, which gave photoproduct **12** in 30% ee at 55% conversion. In this case we were able to obtain an X-ray crystal structure of the starting salt, which allowed us to pinpoint the structural features responsible for the low ees observed. The key feature of this salt, which distinguishes it from those that lead to high ees, is that it crystallizes with equal amounts of two crystallographically independent ion pairs in the asymmetric unit. Remarkably, the two independent photoreactive carboxylate anions were found to exist as near-perfect enantiomers, reaction of which give rise to opposite product enantiomers, thus accounting

© 2001 NRC Canada

Scheme 5.



for the low ees observed. Because the independent enantiomers are conformers of one another, they are termed conformational enantiomers (19). When only one conformational enantiomer of the reactive ion is present in the crystal, as in the 1-phenylethylammonium salt **11**, high ees are observed.

Figure 4 represents the superposition of the two conformational enantiomers of the reactive anion of the norephedrine salt, one as found in the crystal, and the other as its mirror image. As can be seen there is a nearly perfect atom-for-atom overlap of the two structures (root-mean-square error of 0.08 Å). This sort of packing arrangement may turn out to be fairly common. To date, we have identified six other examples in widely different systems, and in every case low but measurable ees are observed (20). This raises the interesting question of why *any* ee is observed at all, since all other factors being equal, irradiation of crystals containing equal amounts of two conformational enantiomers might be expected to lead to racemic photoproducts. We believe the answer lies in the fact that the two conformational enantiomers reside in structurally different reaction cavities, and that one of these cavities allows the reaction to proceed at a slightly faster rate than the other (for an example of a solid state reaction in which two independent molecules in the asymmetric unit react at measurably different rates, see ref. 21). Viewed another way, the conformational enantiomers form diastereomeric salts with the common optically pure amine, and should, therefore, not react at exactly the same rate.

Benzonorbornadiene derivatives

As a final example of the use of the ionic chiral auxiliary method for asymmetric synthesis, we describe our work with benzonorbornadiene derivatives. In solution, such compounds are well known to undergo triplet-sensitized di-π-methane photorearrangement (22) to afford tetracyclic products, a typical example being the conversion of the achiral acetoxy derivative **13** into chiral photoproduct **14** (23) (Scheme 5).

This and similar reactions require the use of triplet energy sensitizers, which leads to problems in the crystalline state because of the difficulty in preparing two component solid solutions of sensitizer and substrate (24). Previous work from our research group has shown that ionic auxiliaries can function as solid state photosensitizers (25), and we, therefore, decided to go one step further and design an ionic auxiliary that could play two roles simultaneously; the first as chiral auxiliary and the second as triplet energy sensitizer. Carboxylic acid **15** (Scheme 5) was chosen as the achiral reactant and amine **16** was synthesized in optically pure form to serve as the chiral photosensitizer (26). These two compounds were combined to afford salt **17**, which was then irradiated in the crystalline state and subsequently treated with diazomethane to form ester **18**. Under conditions of 100% conversion at –20°C, this compound was formed in a gratifying 91% ee, a remarkable result given the fact that salt **17** is not conformationally biased toward formation of one photoproduct enantiomer over the other.

Factors responsible for asymmetric induction

Unlike the majority of ground state reactions involving asymmetric induction, where the chiral agent is intimately associated in the transition state, the role of the ionic chiral

© 2001 NRC Canada

auxiliary in the solid state photochemical reactions described above is simply to ensure that the salts crystallize in chiral space groups. This means that the chiral auxiliary can be attached to any part of the reactive molecule and does not need to be close to the site of reaction. In the case of salts **6**, **8**, and **11**, the role of the ionic chiral auxiliary is to preorganize the reactant anions in a single, homochiral conformation that permits abstraction of only one of two possible enantiotopic hydrogen atoms. Once hydrogen abstraction takes place, the enantioselectivity of the process is determined. Cyclization of the 1,4-hydroxybiradical can occur only at the carbon atom from which the hydrogen was removed, leading to a single enantiomer of each of the two possible diastereomers. In every case studied so far, biradical closure occurs in the solid state with "retention of configuration" at the carbonyl carbon such that only the least-motion diastereomer is formed. Thus, in addition to being enantioselective, these ionic chiral auxiliary-mediated reactions are diastereoselective.

In the case of the di-π-methane photorearrangement of salt **17**, reactant conformation plays little or no role in determining enantioselectivity, since to all intents and purposes, the reactive species is symmetrical except for twisting in the carboxylate group. The first step of the mechanism in this case is vinyl-benzo bridging (22), which can occur in two different ways leading to opposite enantiomers. In such circumstances, it is the shape and size of the solid state "reaction cavity," i.e., the space occupied by a single molecule in a crystal whose walls are composed of the neighboring molecules in the lattice (27), which governs enantioselectivity. Such *environmental* control of enantioselectivity is more difficult to pin down than conformational control. Visual inspection of the packing diagram often provides no obvious clue to reaction selectivity, which is the cumulative result of a large number of small interactions and requires detailed computational analysis. The approach taken is to construct a computationally amenable "mini-lattice" of 50–100 molecules based on the X-ray crystal structure of the reactant. The central molecule in the mini-lattice is then replaced with a transition state analogue and the energy of the resulting ensemble calculated using molecular mechanics. For recent progress in this area, the interested reader is referred to the work of Zimmerman and co-workers (28) as well as that of Houk and co-workers (29). Such calculations were not possible in the case of salt **17** because we were unable to obtain a crystal structure. We were, however, able to utilize this approach to rationalize the enantioselectivity of a different, non-ionic solid state photorearrangement (30).

Epilogue

The focus of this article has been to outline the general principles underlying the use of ionic crystals in bringing about asymmetric induction in photochemical reactions. Owing to space restrictions, the success of the ionic chiral auxiliary approach could be illustrated with only a few examples, and the purpose of this epilogue is to point out that the method has been applied with equal success to several additional systems (31–43). As a result, there seems little doubt that this technique can now be classified as one of the most general and useful methods of asymmetric synthesis in organic photochemistry.

Acknowledgments

Acknowledgment is made to the donors of the Petroleum Research Fund, administered by the American Chemical Society, for partial support of this research. Financial support by the Natural Sciences and Engineering Research Council of Canada (NSERC) is also gratefully acknowledged. I would also like to acknowledge funding by NATO in the form of a Senior Guest Fellowship (1997–98), as well as thank Jean-Marie Lehn, Université Louis Pasteur, Strasbourg, France for hospitality during a sabbatical visit. Finally, I would like to dedicate this paper to the members of my research group, past and present, whose hard work, dedication, and perspicacity were responsible for bringing this project to fruition.

References

1. P. Debré. Louis Pasteur. Johns Hopkins University Press, Baltimore, 1998.
2. (*a*) S.V. Evans, M. Garcia-Garibay, N. Omkaram, J.R. Scheffer, J. Trotter, and F. Wireko. J. Am. Chem. Soc. **108**, 5648 (1986); (*b*) L. Caswell, M.A. Garcia-Garibay, J.R. Scheffer, and J. Trotter. J. Chem. Ed. **70**, 785 (1993).
3. (*a*) K. Penzien and G.M.J. Schmidt. Angew. Chem. Int. Ed. Engl. **8**, 608 (1969); (*b*) M. Vaida, R. Popovitz-Biro, L. Leiserowitz and M. Lahav. *In* Photochemistry in organized and constrained media. *Edited by* V. Ramamurthy. VCH, New York, 1991. Chap. 6.
4. (*a*) H. Rau. Chem. Rev. **83**, 535 (1983); (*b*) Y. Inoue. Chem. Rev. **92**, 741 (1992); (*c*) J.P. Pete. Adv. Photochem. **21**, 135 (1996); (*d*) S.R.L. Everitt and Y. Inoue. *In* Molecular and supramolecular photochemistry. Vol. 3. *Edited by* V. Ramamurthy and K.S. Schanze. Marcel Dekker, New York, 1999. Chap. 2.
5. (*a*) J. Jacques, A. Collet, and S.H. Wilen. Enantiomers, racemates and resolutions. Wiley, New York, 1981; (*b*) C.S. Brock and J.D. Dunitz. Chem. Mater. **6**, 1118 (1994).
6. B.L. Feringa and R.A. van Delden. Angew. Chem. Int. Ed. **38**, 3418 (1999).
7. F.-Y. Zhang and E.J. Corey. Org. Lett. **2**, 1097 (2000) and references cited therein.
8. A.E. Keating and M.A. Garcia-Garibay. *In* Molecular and supramolecular photochemistry. Vol. 2. Marcel Dekker, New York, 1998. Chap. 5.
9. M. Leibovitch, G. Olovvson, J.R. Scheffer, and J. Trotter. Pure Appl. Chem. **69**, 815 (1997).
10. L. Pasteur. C.R. Acad. Sci. **37**, 162 (1853).
11. (*a*) E.L. Eliel and S.H. Wilen. Stereochemistry of organic compounds. Wiley, New York, 1994. Chap. 7; (*b*) A. Collet. Angew. Chem. Int. Ed. **37**, 3239 (1999).
12. H. Ihmels and J.R. Scheffer. Tetrahedron. **55**, 885 (1999).
13. J.D. Dunitz. X-Ray analysis and the structure of organic molecules. Cornell University Press, Ithaca, New York, 1979. p. 312.
14. F.D. Lewis, R.W. Johnson, and D.E. Johnson. J. Am. Chem. Soc. **96**, 6090 (1974).
15. (*a*) N.C. Yang and D.H. Yang. J. Am. Chem. Soc. **80**, 2913 (1958); (*b*) P. Wagner and B-S. Park. *In* Organic photochemistry. Vol. 11. *Edited by* A. Padwa. Marcel Dekker, New York, 1991. Chap. 4.

© 2001 NRC Canada

16. M. Leibovitch, G. Olovsson, J.R. Scheffer, and J. Trotter. J. Am. Chem. Soc. **120**, 12755 (1998).
17. Calculations were performed using the HyperChem/ChemPlus software package (versions 5.11/2.0) and reflect the minimized RMS displacement of the non-hydrogen atoms.
18. A.D. Gudmundsdottir, T.J. Lewis, L.H. Randall, J.R. Scheffer, S.J. Rettig, J. Trotter, and C-H. Wu. J. Am. Chem. Soc. **118**, 6167 (1996).
19. E. Cheung, T. Kang, J.R. Raymond, J.R. Scheffer, and J. Trotter. Tetrahedron Lett. **40**, 8729 (1999).
20. E. Cheung, T. Kang, M.R. Netherton, J.R. Scheffer, and J. Trotter. J. Am. Chem. Soc. **122**, in press.
21. O. Godsi, E. Natan, M. Kapon, U. Peskin, and Y. Eichen. Abstracts of the XVIII IUPAC symposium on photochemistry. Dresden, Germany, July 2000. p. 270.
22. H.E. Zimmerman. *In* Organic photochemistry. Vol. 11. *Edited by* A. Padwa. Marcel Dekker, New York, 1991. Chap.1.
23. J.J. Tufariello and D.W. Rowe. J. Org. Chem. **36**, 2057 (1971).
24. M. Garcia-Garibay, J.R. Scheffer, J. Trotter, and F. Wireko. Tetrahedron Lett. **28**, 1741 (1987).
25. J.N. Gamlin, G. Olovsson, K. Pitchumani, V. Ramamurthy, J.R. Scheffer, and J. Trotter. Tetrahedron Lett. **37**, 6037 (1996).
26. K.M. Janz and J.R. Scheffer. Tetrahedron Lett. **40**, 8725 (1999).
27. (*a*) M.D. Cohen. Angew. Chem. Int. Ed. Engl. **14**, 386 (1975); (*b*) M.D. Cohen. Mol. Cryst. Liq. Cryst. **50**, 1 (1979); (*c*) R.G. Weiss, V. Ramamurthy, and G.S. Hammond. Acc. Chem. Res. **26**, 530 (1993).
28. H.E. Zimmerman, P. Sebek, and Z. Zhu. J. Am. Chem. Soc. **120**, 8549 (1998) and references cited therein.
29. A.E. Keating, S.H. Shin, K.N. Houk, and M.A. Garcia-Garibay. J. Am. Chem. Soc. **119**, 1474 (1997).
30. M.A. Garcia-Garibay, K.N. Houk, A.E. Keating, C.J. Cheer, M. Leibovitch, J.R. Scheffer, and L-C. Wu. Org. Lett. **1**, 1279 (1999).
31. J.R. Scheffer and A.D. Gudmundsdottir. Tetrahedron Lett. **31**, 6807 (1990).
32. A.D. Gudmundsdottir and J.R. Scheffer. J. Photochem. Photobiol. A. **54**, 535 (1991).
33. R. Jones, J.R. Scheffer, J. Trotter, and J. Yang. Tetrahedron Lett. **33**, 5481 (1992).
34. A.D. Gudmundsdottir, J.R. Scheffer, and J. Trotter. Tetrahedron Lett. **35**, 1397 (1994).
35. A.D. Gudmundsdottir, W. Li, J.R. Scheffer, S. Rettig, and J. Trotter. Mol. Cryst. Liq. Cryst. **240**, 81 (1994).
36. H. Koshima, A. Maeda, N. Masuda, T. Matsuura, K. Hirotsu, K. Okada, H. Mizutani, Y. Ito, T.Y. Fu, J.R. Scheffer, and J. Trotter. Tetrahedron Asymmetry, **5**, 1415 (1994).
37. R. Jones, J.R. Scheffer, J. Trotter, and J. Yang. Acta Cryst. **B50**, 601 (1994).
38. E. Cheung, M.R. Netherton, J.R. Scheffer, and J. Trotter. J. Am. Chem. Soc. **121**, 2929 (1999).
39. E. Cheung, K. Rademacher, J.R. Scheffer, and J. Trotter. Tetrahedron Lett. **40**, 8733 (1999).
40. E. Cheung, M.R. Netherton, J.R. Scheffer, and J. Trotter. Tetrahedron Lett. **40**, 8737 (1999).
41. E. Cheung, K. Rademacher, J.R. Scheffer, and J. Trotter. Tetrahedron, **56**, 6739 (2000).
42. E. Cheung, K.C.W. Chong, S. Jayaraman, V. Ramamurthy, J.R. Scheffer, and J. Trotter. Org. Lett. **2**, 2801 (2000).
43. E. Cheung, M.R. Netherton, J.R. Scheffer, J. Trotter, and A. Zenova. Tetrahedron Lett. **41**, 9673 (2000).

© 2001 NRC Canada

Synthesis and spectroscopic properties of benzo- and naphthofuryl-3-hydroxychromones

Andrey S. Klymchenko, Turan Ozturk, Vasyl G. Pivovarenko, and Alexander P. Demchenko

Abstract: With the focus of designing new fluorescent probes, four new 3-hydroxy-chromone derivatives bearing benzofuran and naphthofuran groups were synthesized. They show bathochromic absorption shifts relative to 3-hydroxyflavone with the ability of retention to display the excited-state proton transfer. Disruption of the planarity by the methyl group in the furan ring leads to a decrease of both the extinction coefficient and the contribution of long wavelength absorption band, while molecules without a methyl group showed two distinct absorption bands. Shifts to longer wavelengths are also observed in fluorescent spectra, and the absence of the methyl group results in a dramatic increase of fluorescence quantum yield and lifetime. Of the extended 3-hydroxychromone derivatives, 3-hydroxy-2-naphtho[2,1-*b*]furan-2-yl-chromone has shown comparable, and in some cases better, absorption and fluorescence properties than the 3-hydroxychromones synthesized so far, which make it a highly promising candidate as molecular probe for analytical chemistry, biophysics, and cellular biology.

Key words: benzo- and naphthofuryl-3-hydroxyflavone, synthesis, electronic spectra, fluorescence, excited state proton transfer.

Résumé : Dans le but de développer de nouvelles sondes fluorescentes, on a synthétisé quatre nouveaux dérivés de la 3-hydroxychromone portant des groupes benzofurane et naphtofurane. Par rapport à la 3-hydroxyflavone, ils présentent des déplacements bathochromes d'absorption tout en conservant leur habilité à donner lieu à un transfert de proton dans l'état excité. La présence du groupe méthyle dans le noyau furane conduit à un manque de planéité qui provoque une diminution du coefficient d'extinction ainsi que de la contribution de la bande d'absorption de grande longueur d'onde alors que les molécules sans groupe méthyle présentent deux bandes d'absorption distinctes. On observe aussi des déplacements vers les longueurs d'onde plus élevées dans les spectres de fluorescence et l'absence du groupe méthyle conduit à une augmentation dramatique du rendement quantique de fluorescence et du temps de vie. Parmi les dérivés de la 3-hydroxychromone allongés, il a été démontré que, comparées à celles des 3-hydroxychromones synthétisés jusqu'à maintenant, l'absorption et les propriétés de fluorescence de la 3-hydroxy-2-naphto[2,1-*b*]furan-2-ylchromone sont au moins comparables et, quelquefois meilleures; il s'agit donc d'un candidat plein de promesses comme sonde moléculaire pour la chimie analytique, la biophysique et la biologie cellulaire.

Mots clés : benzo- et naphtofuryl-3-hydroxyflavone, synthèse, spectres électroniques, fluorescence, transfert de proton dans l'état excité.

Introduction

3-Hydroxyflavones (**1a**–**d**) have interesting specific spectroscopic properties, which make them important chromophores for the preparation of new fluorescence probes and molecular sensing devices for applications in analytical chemistry, biophysics, and cellular biology (1, 2). They exhibit dual fluorescence due to excited state intramolecular proton transfer (ESIPT) from the 3-hydroxy moiety to the carbonyl group. The latter is characterized by a significant Stokes shift of about 10 000 cm^{-1} (3). This results in the isomerization of the normal excited form of the flavonol to a phototautomer. These two excited isomers return to the ground state with the emission of photons of different energies separated by 5000–6000 cm^{-1} (60–80 nm). The positions and the ratio of intensities of these two bands exhibit strong dependence on solvent polarity (4) and hydrogen bonding with the solvent molecules (2, 4, 5). These particular features suggest that 3-hydroxyflavones can be effectively used as fluorescence probes to investigate the structure and physical properties of biological membranes such as polarity, hydration, transmembrane potential, and the transformations of their structure under various conditions (6, 7). For example, interdigitated gel phase formation of lipid membrane bilayer in the presence of alcohols (8, 9) can be followed by 3-hydroxyflavone probes (10).

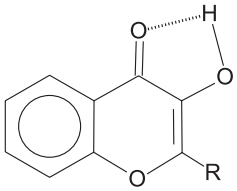
So far, 4-amino derivatives of 3-hydroxyflavone (**1a**–**d**) have been widely investigated as fluorescent membrane probes and fluorescent chelators (11, 12). However, most modifications of the structure were focused on extensions of 3-hydroxyflavone system at the chromone fragment, while extensions of phenyl side have not been extensively explored.

Received November 28, 2000. Published on the NRC Research Press Web site on April 24, 2001.

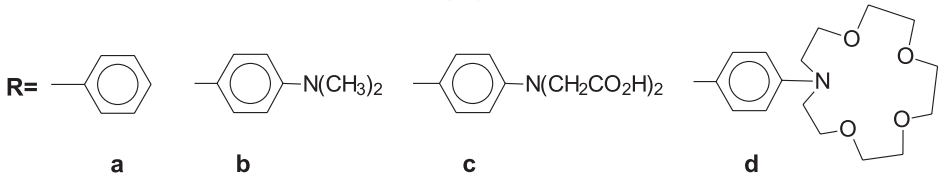
S. Klymchenko, T. Ozturk, and A.P. Demchenko.[1] TUBITAK Marmara Research Center, Gebze-Kocaeli 41470, Turkey.
V.G. Pivovarenko. Kiev Taras Shevchenko University, Department of Chemistry, 252017, Ukraine.

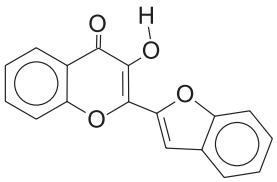
[1]Corresponding author (telephone: (0262) 641-2300 (ext. 4003); fax: (0262) 641-2309; e-mail: dem@rigeb.gov.tr).

 DOI: 10.1139/cjc-79-4-358 © 2001 NRC Canada

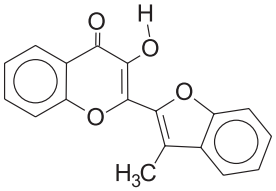


1a-d

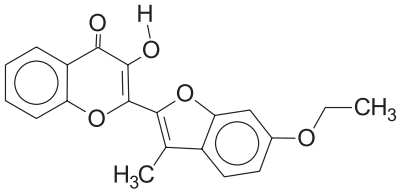




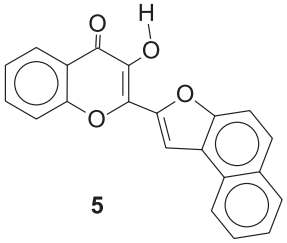
2



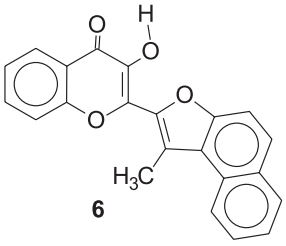
3



4



5



6

To modify and improve the chromophore properties, we have synthesized four new chromones bearing benzofuran (**3** and **4**) and naphtofuran groups (**5** and **6**). It is expected that such systems may display improved fluorescent properties due to the following reasons: (*i*) their conjugation systems are larger than 3-hydroxyflavone, therefore, absorption and emission bands are expected to shift to longer wavelengths; (*ii*) furan oxygen might compete for the 3-hydroxy group's proton, which should increase the sensitivity of the molecule to hydrogen bonding interactions with the surrounding molecules; (*iii*) the presence of methyl group in the furan ring should lead to a decrease of planar structure stability, which is a crucial factor for fluorescence properties; and (*iv*) the furan ring is a π-electron-abundant system, and it is known that an electron donor in position two of the chromone ring increases the transfer of electron density to the carbonyl group in the excited state, which usually leads to the enhancement of the proton transfer and stabilizes the proton transferred tautomeric form. Furthermore, having shifted the absorption and emission bands to longer wavelengths, such heterocyclic systems are expected to serve better in biological systems, since most cells respond poorly to short wavelength excitation (13), and intrinsic cellular pigments interfere with the analysis. Therefore, it is highly desirable to locate the emission peaks in a region where background fluorescence (auto-fluorescence) from cellular pigments is very low. It is, also, well known that longer wavelength light is much less attenuated, and reduced Raleigh and Raman scattering with longer wavelength would yield much lower background signal. Obviously, having extended conjugation systems would be advantagous to reach these goals.

Although all the chromones (**2**–**6**) have shown absorption and fluorescence spectra at longer wavelengths compared with the 3-hydroxyflavone (**1a**), naphthofurylhydroxychromone **5** exhibits superior properties of both higher quantum yields and relatively longer wavelength absorption and fluorescence spectra. These properties make it one of the best fluorescence probe candidates among the 3-hydroxychromones synthesized so far.

Experimental

Melting points were determined on a Kofler hostage microscope melting point apparatus and are uncorrected. Microanalyses were performed with a Carlo Erba 1106 Elemental Analyzer. Proton NMR spectra were recorded at 200 MHz on JEOL PMX 270 MHz spectrometer. Tetramethylsilane (TMS) was used as the internal standard in all NMR spectra run in $CDCl_3$ or DMSO-d_6. Mass spectra were recorded on a Kratos MS-25 mass spectrometer with an ionization potential of 70 eV. All column chromatography were performed on silica gel (Merck, Kieselgel 60H, Art 7736). Absorption spectra were recorded on a Cary 3 Bio-spectrophotometer (Varian) in the concentration range of 10^{-5} M. Fluorescence measurements were recorded on a Quanta Master spectrofluorometer (Photon Technology International). Quantum yields were measured by reference to 3-hydroxyflavone (ϕ_F = 0.046 in acetonitrile, 0.024 in ethanol, 0.29 in toluene). Fluorescence lifetimes with ≈0.5 ns resolution were recorded on Strobe Master time-resolved fluorometer (Photon Technology International), which has nitrogen-filled pulsed lump as a light source (excitation

© 2001 NRC Canada

380 nm) and stroboscopic principle for registration of emission decay curves.

3-Hydroxy-2-(benzo[*b*]furan-2-yl)chromone (**2**) was synthesized using the procedure described elsewhere (15).

3-Hydroxy-2-(3-methylbenzo[*b*]furan-2-yl)chromone (3)

To a solution of 3-methylbenzo[*b*]furan-2-carbaldehyde (**9**) (0.1 g, 0.63 mmol) and 2-hydroxyacetophenone (**7**) (0.085 mL, 0.71 mmol) in ethanol (5 mL) was added 70% potassium hydroxide (0.11 g, 2 mmol) dropwise. The mixture was left stirring at room temp for 24 h, and to the resultant red (*E*)-1-(2-hydroxyphenyl)-3-(3-methylbenzo[*b*]furan-2-yl)-2- propen-1-one (**14**) solution was added 30% hydrogen peroxide (0.5 mL, 4.4 mmol). After stirring for an additional 2 h, the precipitate was filtered, washed with ethanol (5 mL), and crystallized from ethanol to obtain **2** (40 mg, 22%), mp 172°C. EI-MS *m*/*z*: 292.1 (M^+), 275.0, 263.1, 249.0, 235.1, 221.0, 171.0, 144.0, 121.0, 115.0. ^{1}H NMR (200 MHz, $CDCl_3$) δ: 2.58 (s, 3H), 6.90 (s, 1H, H-exchangeable), 7.29–7.78 (m, 7H), 8.28 (dd, *J* = 8.0, 1.3 Hz, 1H). Anal. calcd. for $C_{18}H_{12}O_4$: C 73.97, H 4.14; found: C: 73.75, H: 4.14.

General procedure for synthesis of 1-(2-hydroxyphenyl)-2-propen-1-one derivatives

To a solution of appropriate benzo- or naphtho[*b*]furan-2-carbaldehyde (0.57 mmol) and 2-hydroxyacetophenone (**7**) (0.07 mL, 0.58 mmol) in ethanol (5 mL) was added 70% potassium hydroxide (0.07 g, 1.25 mmol) dropwise, and the mixture was left stirring for 24 h. In the case of the naphtho-derivatives, the mixture was heated in water bath at 50°C for the same time. Then, the mixture was poured into water (20 mL), neutralized with dilute HCl, and the resultant precipitate was filtered and washed with water to yield the product, which is pure enough to use for the next step.

*(*E*)-3-(6-Ethoxy-3-methylbenzo[*b*]furan-2-yl)-1-(2-hydroxyphenyl)-2-propen-1-one (**15**)*

Purified over silica gel column (hexane–ethyl acetate, 5:1), yield 49%, mp 106°C. EI-MS *m*/*z*: 322.1 (M^+), 305.1, 276.1, 265.1, 229.1, 202.1, 189.1, 174.1, 161.0, 147.0, 133.0, 121.0. ^{1}H NMR (200 MHz, $CDCl_3$) δ: 1.48 (t, *J* = 7.1 Hz, 3H), 2.41 (s, 3H), 4.11 (q, *J* = 7.1 Hz, 2H) 6.87–7.05 (m, 4H), 7.41–7.55 (m, 4H), 7.65 (d, *J* = 14.8 Hz, 1H), 7.89 (d, *J* = 14.8 Hz, 1H), 8.00 (dd, *J* = 8.0, 1.1 Hz, 1H), 13.05 (s, 1H, H-exchangeable). Anal. calcd. for $C_{20}H_{18}O_4$: C 74.52, H 5.63; found: C 73.8, H 5.56.

*(*E*)-1-(2-Hydroxyphenyl)-3-naphtho[2,1-*b*]furan-2-yl-2-propen-1-one (**16**)*

Crystallized from acetonitrile, yield 95%, mp 198°C. EI-MS *m*/*z*: 314.1 (M^+), 297.1, 285.1, 257.1, 239.1, 221.0, 194.1, 181.1, 165.1. ^{1}H NMR (200 MHz, $CDCl_3$) δ: 6.99 (d, *J* = 15.9 Hz, 1H), 7.03 (d, *J* = 15.9 Hz, 1H), 7.30–8.18 (m, 10H,), 8.15 (d, *J* = 8.0 Hz, 1H), 12.91 (s, 1H, H-exchangeable). Anal. calcd. for $C_{21}H_{14}O_3$: C 80.24, H 4.49; found: C 80.03, H 4.44.

*(*E*)-1-(2-Hydroxyphenyl)-3-(1-methylnaphto[2,1-*b*]furan-2-yl)-2-propen-1-one (**17**)*

Crystallized from butanol, yield 64%, mp 174°C. EI-MS *m*/*z*: 328.1 (M^+), 310.1, 235.1, 208.1, 195.1, 178.1, 121.0. ^{1}H NMR (200 MHz, $CDCl_3$) δ: 2.83 (s, 3H) 6.98 (d, *J* = 15.9 Hz, 1H), 7.02 (d, *J* = 15.9 Hz, 1H), 7.48–8.07 (m, 9H), 8.40 (d, *J* = 8.1 Hz, 1H), 13.03 (s, 1H, H-exchangeable). Anal. calcd. for $C_{22}H_{16}O_3$: C 80.47, H 4.91; found: C 80.30, H 4.87.

General procedure for synthesis of 3-hydroxychromone derivatives

To a solution of appropriate 1-(2-hydroxyphenyl)-2-propen-1-one derivative (**15**–**17**) (0.22 mmol) in ethanol (5 mL) was added subsequently 70% potassium hydroxide (0.1 g, 1.8 mmol) and 30% hydrogen peroxide (0.4 mL, 3.5 mmol). The mixture was then heated at reflux for 1 h, cooled to room temp, and the precipitate was filtered, washed with water, and crystallized from appropriate solvent.

*2-(6-Ethoxy-3-methylbenzo[*b*]furan-2-yl)-3-hydroxychromone (**4**)*

Crystallized from acetonitrile, yield 31%, mp 186°C. EI-MS *m*/*z*: 336.1 (M^+), 307.1, 265.1, 251.1, 237.1, 223.1, 187.1, 165.1, 160.1, 154.1, 140.1, 131.1, 121.0, 77.0. ^{1}H NMR (200 MHz, $CDCl_3$) δ: 1.46 (t, *J* = 7.1 Hz, 3H), 2.55 (s, 3H), 4.09 (q, *J* = 7.1 Hz, 2H), 6.85 (s, 1H, H- exchangeable), 6.94 (dd, *J* = 8.6, 2.1 Hz, 1H), 7.09 (d, *J* = 2.0 Hz, 1H), 7.39–7.59 (m, 2H), 7.72 (td, *J* = 6.8, 1.4 Hz, 1H), 8.26 (dd, *J* = 8.1, 1.4 Hz, 1H). Anal. calcd. for $C_{20}H_{16}O_5$: C 71.42, H 4.79; found: C 71.38, H 4.73.

*3-Hydroxy-2-naphtho[2,1-*b*]furan-2-yl-chromone (**5**)*

Crystallized from acetic acid, yield 40%, mp 253°C. EI-MS *m*/*z*: 328.1 (M^+), 299.1, 271.1, 215.1, 164.1, 152.1. ^{1}H NMR (200 MHz, DMSO-d_6) δ: 7.47–8.01 (m, 7H), 8.09 (d, *J* = 7.8 Hz, 1H), 8.16 (d, *J* = 7.8 Hz, 1H), 8.30 (s, 1H), 8.43 (d, *J* = 7.8 Hz, 1H), 10.35 (s, 1H, H-exchangeable). Anal. calcd. for $C_{21}H_{12}O_4$: C 76.82, H 3.68; found: C 76.61, H 3.69.

*3-Hydroxy-2-(1-methylnaphtho[2,1-*b*]furan-2-yl)-chromone (**6**)*

Crystallized from acetic acid, yield 31%, mp 187°C. EI-MS *m*/*z*: 342.1 (M^+), 299.1, 285.1, 271.1, 185.1. ^{1}H NMR (200 MHz, DMSO-d_6) δ: 2.77 (s, 3H) 7.47–8.00 (m, 7H), 8.11 (d, *J* = 8.0 Hz, 1H), 8.17 (d, *J* = 8.0 Hz, 1H), 8.52 (d, *J* = 8.2 Hz, 1H), 9.68 (s, 1H, H-exchangeable). Anal. calcd. for $C_{22}H_{14}O_4$: C 77.19, H 4.12; found: C 77.1, H 4.05.

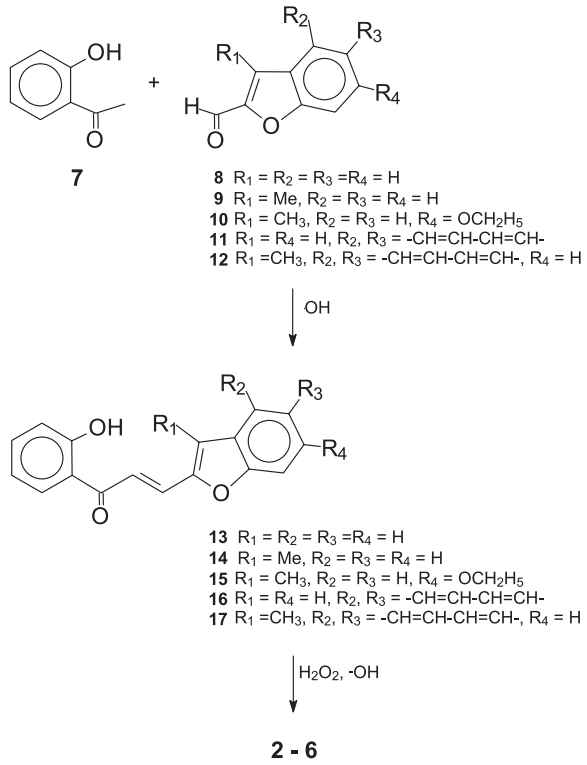
Results and discussion

The syntheses of the target molecules **2**–**6** were carried out by employing the well-established Algar–Flynn–Oyamada reaction (14). Condensation of 2-hydroxyacetophenone (**7**) with the aldehydes **8**–**12**, synthesized as described elsewhere (15–19), in basic solution gave the intermediates **13**–**17**, respectively (Scheme 1). Treatment of these intermediates with hydrogen peroxide in basic ethanol solution led to the formation of 3-hydroxychromones **2**–**6**, respectively.

All the 3-hydroxychromones (**2**–**6**) possess absorption spectra at longer wavelengths compared with 3-hydroxyflavone (**1a**) in various solvents (Fig. 1: acetonitrile (*A*), ethanol (*E*), toluene (*T*)), and of all the 3-hydroxychromones (**2**–**6**), 3-hydroxy-2-naphthofurylchromone (**5**) is found to

© 2001 NRC Canada

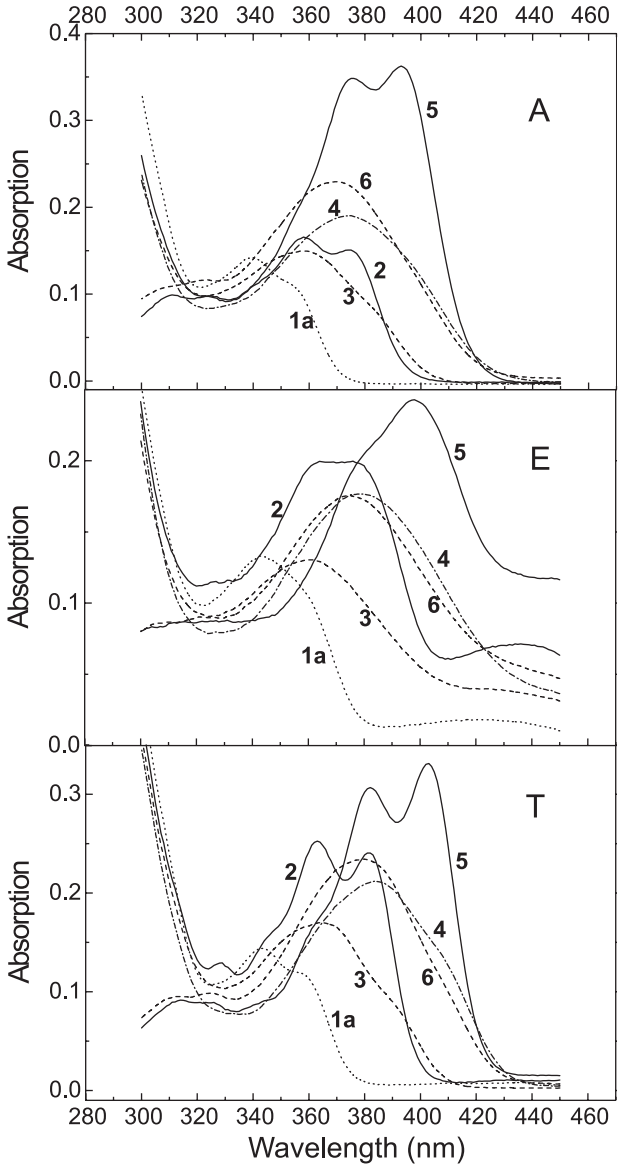
Scheme 1.



have the longest wavelength position of absorption spectrum. This result is related to the extension of the π-conjugation system. The effect of addition of methyl group at C-3 position of the furan ring can be observed as decrease of absorption at long-wavelength part of the spectra. Thus, the absorption spectra of chromones **3**, **4**, and **6** bearing methyl group at C-3 position of the furan ring, show only one absorption band at shorter wavelengths, with a small shoulder at longer wavelengths, while compounds without a methyl group (**2** and **5**) show two distinct absorption bands. One of the possible suggestions for these observed differences could be that the methyl group dramatically effects the hydrogen bonding capabilities of 3-OH group with solvent, but it is unlikely in view of the following reasons. First, this cannot explain the presence of long-wavelength band in absorption spectra of compounds **2** and **5** for all the solvents, including nonpolar toluene. Second, it is in contradiction with observed small differences between absorption spectra of chromones **2** and **5** in toluene and in acetonitrile, where the blue shift is correlated with the increase of polarity (Figs. 1*A* and *T*). The latter means that hydrogen bonding of 3-OH group with acetonitrile is either very weak, even for the case of non-methylated chalcones, or unimportant for energetic profile of the molecules. The critical role of methyl group in absorption of compounds **3**, **4**, and **6** can be explained by a steric factor that may lead to statistical non-planarity between benzo- and naphthofuran and chromone rings, which has been already studied on 2′-, 3′-, and 4′-methyl-3-hydroxyflavones (20). Therefore, it can be suggested that planarity of the chromone molecule is the necessary condition for existence of the long-wavelength band.

In the light of the previous studies (20) we can assume that the absorption at short-wavelength is due to the normal

Fig. 1. Absorption spectra of chromones **1a**, **2**–**6** in different solvents: acetonitrile (*A*); ethanol (*E*); and toluene (*T*).



excitation of 3-hydroxychromone ring, and the long wavelength absorption, as in the case of planar compounds **2** and **5**, is the result of charge transfer from the benzo- and naphthofuran part to the 3-hydroxychromone system. Small long-wavelength absorption shoulders in the spectra of **3**, **4**, and **6** can be explained by less efficient π-electron delocalization between the furan and chromone parts as a result of distortion of the planarity. Non-planarity results not only in a decrease of intensity of the long-wavelength absorption band, but also in a decrease of the extinction coefficient (Table 1), while the introduction of a strong electron donating group, such as ethoxy, to the benzofuryl group (**4**), shifts the absorption band to longer wavelengths in comparison with its analogues (**2** and **3**) (Figs. 1*A*, *E*, and *T*).

Fluorescence spectra of **2**–**6** showed dual fluorescence in all solvents which were used for the absorption measurements (Figs. 2*A*, *E*, and *T*). Dual fluorescent behavior is well explained to be due to the excited state intramolecular proton

© 2001 NRC Canada

Table 1. Spectral properties of chromones **1a**, **2**–**6**.

	Solvent	Absorption wavelength (nm)	Position of long-wavelength peak (nm)	Extinction coefficient ($\times 10^{-5}$) (mol^{-1} cm^{-1})	Fluorescence quantum yield	Lifetime of long-wavelength band (ns)
1a	Acetonitrile	339	525	0.143	0.046	0.94
	Ethanol	343	531.5	0.133	0.024	0.5
	Toluene	343	528	0.144	0.29	2.66
2	Acetonitrile	338	542	0.165	0.177	2.09
	Ethanol	367	544	0.198	0.122	1.41
	Toluene	365	547	0.253	0.396	3.87
3	Acetonitrile	357	565	0.15	0.033	0.68
	Ethanol	361	560	0.131	0.061	0.71
	Toluene	364	572.5	0.171	0.134	2.15
4	Acetonitrile	373	580	0.190	0.0272	≤0.5
	Ethanol	378	—	0.177	0.118	≤0.5
	Toluene	383	586	0.212	0.058	0.71
5	Acetonitrile	376	559	0.348	0.14	1.93
	Ethanol	398	555	0.243	0.22	1.77
	Toluene	403	562.5	0.331	0.371	3.08
6	Acetonitrile	370	576	0.229	0.052	0.83
	Ethanol	375	—	0.176	0.129	≤0.5
	Toluene	379	582	0.234	0.09	0.87

transfer (ESIPT), which is the result of the partial isomerization of the excited normal isomer to a phototautomer. These two forms, then, return to the ground state with the emission of different energies exhibiting two fluorescent bands, at short and long wavelengths for the normal and phototautomer excited forms, respectively.

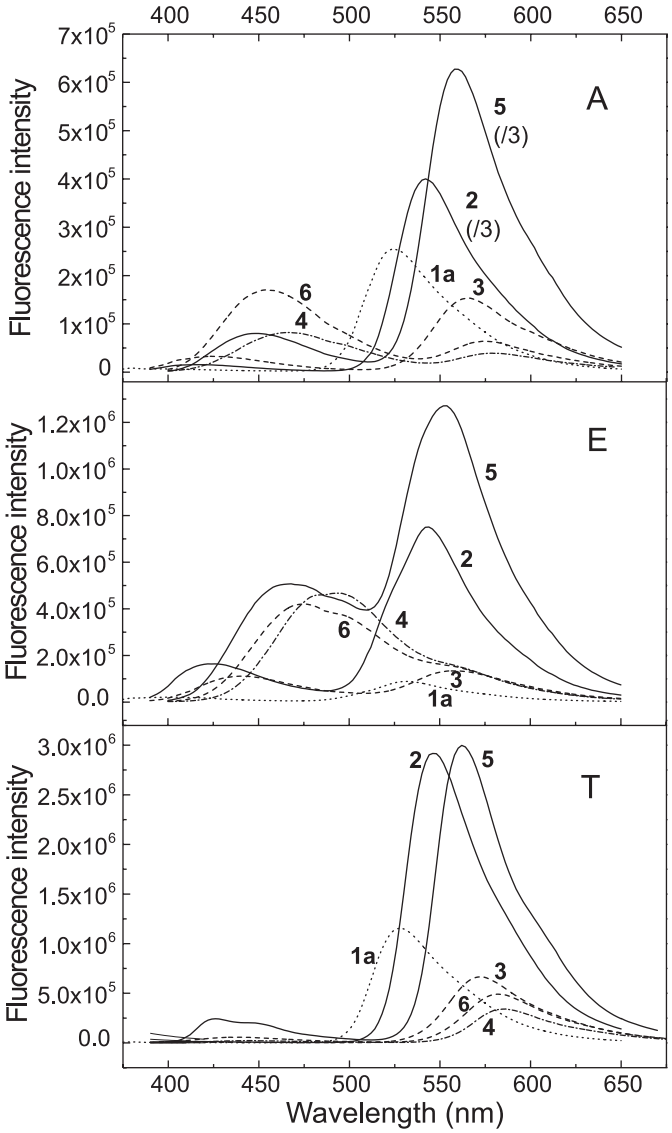
Fluorescent measurements of compounds **2**–**6** indicate that replacement of the phenyl group of 3-hydroxyflavone (**1a**) for longer aromatic systems, such as benzo- or naphthofuryl, leads to a significant red shift (ca. 50 nm) (Table 1). In polar solvents, such as acetonitrile and ethanol, two distinctive fluorescent bands are observed, while only the long-wavelength band is recorded in nonpolar solvent (toluene). The exception is naphthofurylchromone **5**, which showed considerable short-wavelength fluorescence band in both polar and nonpolar solvents. It appears that the strongest among the solvent effects is the change in ratio of intensities of normal excited form emitting at shorter wavelength to phototautomer form emitting at longer wavelength (I_{N^*}/I_{T^*}). This can be explained as the preference of hydrogen bonding of the 3-OH group with the solvent as compared to intramolecular hydrogen bonding of 3-OH with the carbonyl group. However, in acetonitrile this ratio is still very small, especially for the case of non-methylated chromones (**2** and **5**), which supports the above statement based on absorption data that hydrogen bonding of 3-OH group of the chromones with acetonitrile is very weak and does not significantly change the energetic profile of the molecules.

The fluorescence quantum yield of compounds **2** and **5**, was found to be higher than that of 3-hydroxyflavone, and the addition of methyl group in C-3 position decreases the fluorescence quantum yield considerably (Table 1). Furthermore, the effect of methyl group was found to cause an increase in the I_{N^*}/I_{T^*} ratios for compounds **3**, **4**, and **6**. These results correspond to the increased I_{N^*}/I_{T^*} ratio for 3-hydroxyflavone with a methyl group at position 2 of the phenyl ring (20).

It is interesting to note that the molecules with methyl group in furan ring (**3**, **4**, and **6**) demonstrate stronger red shifted (by 22–28 nm, which is 670–880 cm^{-1}) fluorescent bands compared with the corresponding non-methylated derivatives (**2** and **5**) (Table 1). Taking into account that the position of the long-wavelength maximum of 3-hydroxyflavones is not very sensitive to 2- or 3- substituents of the phenyl ring, the fact of the red shift, caused by such a weak electron donor as methyl group, is important and requires further investigation. Since a red shift is observed in both polar and nonpolar solvents arguments regarding the differences in hydrogen bonding between solvent and molecules **2** and **3**, and **5** and **6** do not explain this effect. It could be suggested that the non-planar molecules, with the steric hindrance of the methyl group, relax to a more stable planar excited conformation characterized by lower energies with an emission at longer wavelengths. Red shifts in fluorescence due to flattening of a molecule in an excited state is known for some heterocyclic compounds (21). Since, fluorescence of the phototautomer of 3-hydroxychromones requires a planar conformation between the 2-aryl and chromone rings (20), it is understandable that the red shift, caused by flattening of the non-planar chromones with the methyl group in furan ring **3**, **4**, and **6**, is much stronger for the long-wavelength fluorescence band. For instance, in acetonitrile the long-wavelength band of **3** (compared with **2**) is red shifted by 24 nm (782 cm^{-1}), whereas the short-wavelength band is red shifted by just 6 nm (339 cm^{-1}).

© 2001 NRC Canada

Fig. 2. Fluorescence spectra of chromones **1a**, **2**–**6** in different solvents: acetonitrile (*A*); ethanol (*E*); and toluene (*T*) (excitation for: **1a** (340 nm); **2** and **3** (360 nm); **4**–**6** (390 nm)).



Furthermore, the methyl group causes the decrease of fluorescence lifetime (Table 1) and lowers the fluorescence intensity, which also indicates its dramatic influence on relaxation pathways.

In conclusion, we have synthesized a series of 3-hydroxychromones, which have comparable, and in some respects better, absorption and fluorescence properties than the 3-hydroxychromones synthesized so far. They have comparably higher quantum yield, display absorption and fluorescence at longer wavelengths in different solvents, and some of them have longer fluorescent lifetimes. These properties make benzo- and naphthofuryl-3-hydroxychromones highly promising candidates for fluorescence probes design. Currently, the preparation of membrane probes and fluorescent chalators using the chromophoric systems **2** and **5** are underway, and the results will be published in due course.

Acknowledgements

We are grateful to A. D. Roshal (Institute of Chemistry of Kharkov State University, Kharkov 310077, Ukraine) for lifetime measurements, to V. P. Khilya (Kiev Taras Shevchenko University, Department of Chemistry, 252017, Ukraine) for providing some chemicals, and to TUBITAK Marmara Research Center, Turkey for the financial support.

References

1. P. K. Sengupta, and M. Kasha. Chem. Phys. Lett. **68**, 382 (1979).
2. D. McMorrow and M. Kasha. J. Am. Chem. Soc. **88**, 2235 (1984).
3. B.J. Schvartz, L.A. Peteanu, and C.B. Harris. J. Phys. Chem. **96**, 3591 (1992).
4. T.C. Swiney and F.D. Kelley. J. Chem. Phys. **99**, 211 (1993).
5. G.A. Bruker, T.C. Swinney, and D.F. Kelley. J. Phys. Chem. **95**, 3190 (1991).
6. T.-J. McIntosh, S.A. Simon, J.C. Ellington, and N.A. Porter. Biochemistry, **23**, 4038 (1984).
7. J.L. Slater and C. Huarg. Prog. Lipid. Res. **27**, 325 (1989).
8. L.F. Braganza and D.L. Worcester. Biochemistry, **25**, 2591 (1986).
9. H. Komatsu and E.S. Rowe. Biochemistry, **30**, 2463 (1991).
10. O.P. Bondar, V.G. Pivovarenko, and E.S. Rowe. Biochem. Biophys. Acta, **1369**, 119 (1998).
11. V.G. Pivovarenko, A.V. Tuganova, A.S. Klimchenko, and A.P. Demchenko. Cell. Mol. Bio. Lett. **2**, 355 (1997).
12. A.D. Roshal, A.V. Grigorovich, A.O. Doroshenko, V.G. Pivovarenko, and A.P. Demchenko. J. Phys. Chem. **102**, 5907 (1998).
13. A.D. Williams and F.S. Fay. Am. J. Physiol. **250**, 779 (1986).
14. J. Algar and J. Flynn. Proc. R. Ir. Acad. **B42**, 1 (1934).
15. L.G. Grishko, A.V. Turov, I.A. Potrusaeva, and V.P. Khilya. Ukr. Khim. Zhurn. **49**, 2, 174 (1983).
16. D. Gupta. Chem. Ber. **97**, 3577 (1964); Chem. Abs. **62**, 6449e (1965).
17. T. Abe and T. Shimizu. Nippon Kagaku Kaishi, **87**, 870 (1966); Chem. Abs. **65**, 18 546g (1966).
18. J.N. Chatterjea and S.K. Roy. J. Indian Chem. Soc. **45**, 45 (1968); Chem. Abs. **69**, 43 706B (1968).
19. G. Giovanninetti, L. Garuti, A. Chiarini, and R. Gaggi. Farmaco Ed. Sci. **36**, 94 (1981); Chem. Abs. **94**, 208 625f (1981).
20. A.J.G. Strandjord, D.E. Smith, and P.F. Barbara. J. Phys. Chem. **89**, 11, 236 (1985).
21. A.O. Doroshenko, A.V. Kirichenko, V.G. Mitina, and O.A. Ponomaryov. J. Photochem. Photobiol. A, 15 (1996).

© 2001 NRC Canada

Mechanism of ipso aromatic substitution by reaction of aryloxy(methoxy)carbenes and diaryloxycarbenes with DMAD

Xiaosong Lu and John Warkentin

Abstract: Some aryloxy(methoxy)carbenes and diaryloxycarbenes attack dimethyl acetylenedicarboxylate (DMAD) with aryl group transfer to an alkyne carbon of DMAD. In this study diaryloxycarbenes with different aryl groups that could be transferred competitively, were generated in the presence of DMAD to probe for the mechanism of that ipso aromatic substitution. It was found that a *para* electron-withdrawing substituent, relative to an electron-donating substituent, facilitated migration of an aryl group. Mechanisms in accord with these findings involve initial nucleophilic attack by the carbene at an alkyne carbon of DMAD. That step is followed by either nucleophilic, ipso attack on the aromatic ring or by electron transfer, from the side chain of the aromatic ring into the ring itself.

Key words: aromatic substitution, diaryloxycarbene, DMAD, ipso, nucleophilic.

Résumé : Quelques aryloxy(méthoxy)carbènes et diaryloxycarbènes attaquent l'acétylènedicarboxylate de diméthyle (ACDM) avec un transfert de groupe aryle vers un atome de carbone alcyne du ACDM. Dans le présent travail, dans le but d'étudier le mécanisme de cette réaction de substitution aromatique ipso, on a généré en présence du ACDM des diaryloxycarbènes portant divers groupes aryles qui peuvent être en compétition pour un transfert. On a trouvé que, par opposition à un substituant électrodonneur, un substituant électroaffinitaire facilite la migration d'un groupe aryle. Les mécanismes qui correspondent à ces faits impliquent une attaque nucléophile initiale par le carbène au niveau du carbone de l'alcyne du ACDM. Cette étape est suivie par une attaque nucléophile ipso du noyau aromatique ou par un transfert d'électron à partir de la chaîne latérale du noyau aromatique vers le cycle lui-même.

Mots clés : substitution aromatique, diaryloxycarbène, ACDM, ipso, nucléophile.

[Traduit par la Rédaction]

Introduction

Recently, we (1) reported the results of thermolysis of bis-oxadiazoline **1** in benzene containing dimethyl acetylenedicarboxylate (Scheme 1). The multifunctional product (**2**) must have arisen from a cascade of reactions, including transfer of the aryl ring from oxygen to carbon. Analogous substitution reactions were also observed with a simpler oxadiazoline (**3a**) (1), and with 5,5-dimethyl-2,2-diphenoxy-Δ^3–1,3,4-oxadiazoline (**3b**) (2, 3) (Scheme 2). The only related reaction that we are aware of is that between an aminothiocarbene and diethyl acetylenedicarboxylate, reported by Scherowsky et al. (4) in 1977 (Scheme 3). Although a variety of ipso substitutions on benzene derivatives are known (5), oxy-substituents are not generally among the leaving groups unless there are activating nitro groups in the ring also. It was therefore of interest to try to establish the mechanism of the substitution reactions of Schemes 1 and 2. We now report that competition reactions, with diaryloxycarbenes ((ArO)(Ar′O)C:), gave evidence for preferential transfer of the more electron-deficient aryl group from oxygen to an alkyne carbon atom of DMAD.

Received November 16, 2000. Published on the NRC Research Press Web site on April 27, 2001.

X. Lu and J. Warkentin.[1] Department of Chemistry, McMaster University, Hamilton, ON L8S 4M1, Canada.

[1]Corresponding author (telephone: (905) 525-9140; fax: (905) 522–2509. e-mail: warkent@mcmaster.ca).

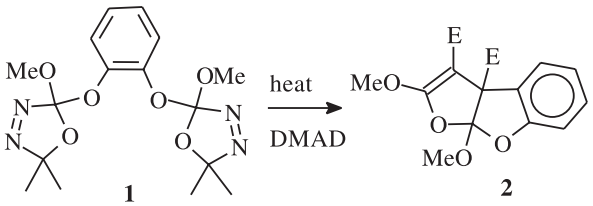
Methods, results, and discussion

The strategy for determining the effect of aryl substituents involved generation of unsymmetric diarylcarbenes (**5**) so as to have internal competition, between the aryl groups in a dipolar (or other) intermediate (**6a**, **7a**), in the step that generates *isomeric* esters (Scheme 4). In all but one case the substituents in the aryl groups were in the *p*-position, and it was assumed that a conformational preference (**6a**, **7a**) would be small at most. It is probably irrelevant because the Curtin–Hammett principle is expected to apply (6). Although intermediates **6a** and **7a** presumably epimerize to **6b** and **7b**, through a small barrier, that too should be irrelevant because intramolecular substitution cannot occur with the ester groups *trans*, as in **6b** and **7b**.

5,5-Dimethyl-2,2-diphenoxy-Δ^3-1,3,4-oxadiazoline (**11**, Ar = Ar′ = Ph), the first 2,2-diaryloxy oxadiazoline (2), was prepared by hydrazinolysis of diphenyl carbonate, subsequent reaction of the hydrazide (**8**) with acetone to afford **9**, oxidative cyclization of **9** to **10** with lead tetraacetate (LTA) in CH_2Cl_2, and acid-catalyzed reaction of **10** with phenol (Scheme 5) (3, 7). Unsymmetric analogues (**11**, one or both aryl groups bearing a substituent) were prepared similarly (3).

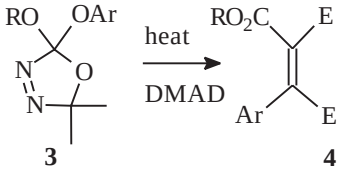
 DOI: 10.1139/cjc-79-4-364 © 2001 NRC Canada

Scheme 1.



(DMAD = dimethyl acetylenedicarboxylate; E = CO_2Me)

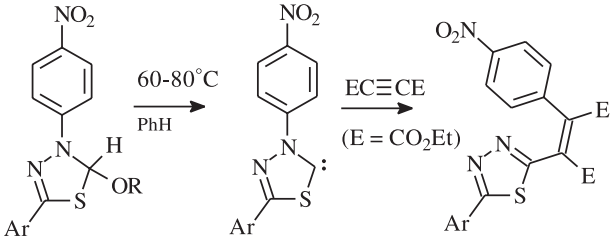
Scheme 2.



(a) R= Me, Ar= *o*-$MeOC_6H_4$; (b) R = Ar = Ph
(DMAD = dimethyl acetylenedicarboxylate;
E = CO_2Me)

Thermolysis of oxadiazolines **11** as benzene solutions containing DMAD, at 110°C in sealed tubes, gave one or both of the isomeric esters (**12**, **13**) in yields (or composite yields) between 28 and 37% (of isolated material) and a diaryl carbonate (**14**) in 25–35% yield (Scheme 6). The esters were separated from other products by means of radial chromatography, which also separated the isomers in the one case that gave both. Assignment of structure followed from the NMR spectra of the products and from the GC–MS patterns. In their EI mass spectra, aryl esters afford base peaks from loss of the fragment ArO in the case of ArOCOC(E)=C(Ar′)E, and from loss of Ar′O in the case of Ar′OCOC(E)=C(Ar)E. It was therefore easy to assign the gross structures of the esters from **11a**–**d** and of the isomeric

Scheme 3.



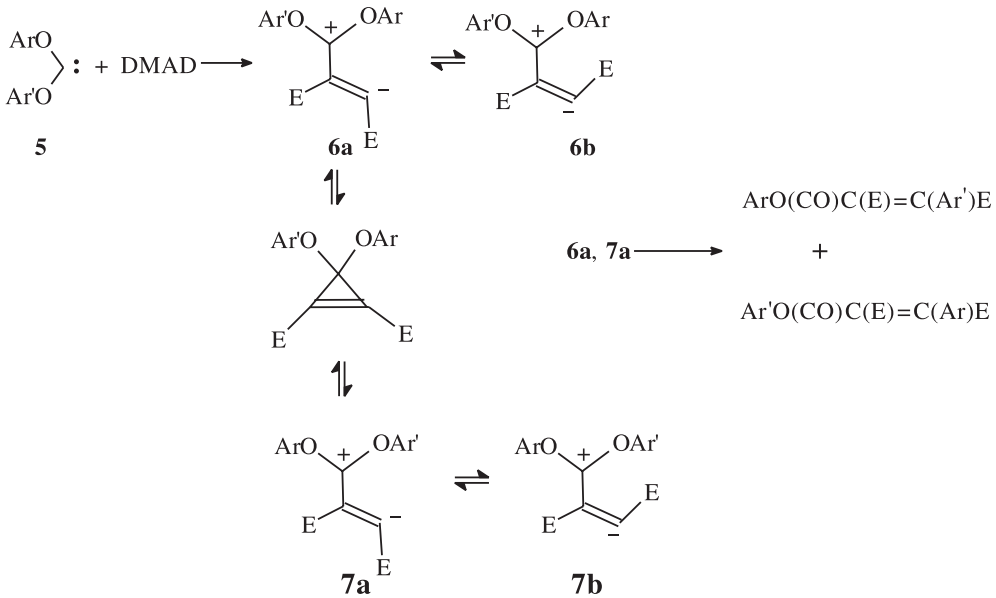
(R = H, Me)

esters from **11e** (Scheme 6). The geometry (ArOCO and CO_2Me groups *trans*) was established for **12a** by single crystal X-ray diffraction and that geometry was assumed for the other triesters **12**, and for **13e**, on the basis of analogy.

The effects of substituents on the ease of ipso substitution, given by the yield ratios (**13**:**12**) rather than by the absolute yields, are in the order *p*-CN >> *o*-MeO > H > Me > *p*-MeO (Table 1).

It is clear from Table 1 that an electron-withdrawing group in the *p*-position increases the migratory aptitude of an aryl group whereas an electron-donating group decreases it. Unfortunately, most substrates gave only one of the two possible esters and it was not possible to construct a Hammett plot and to estimate the value of ρ. However, the sense of the substituent effect is unmistakable, and the effect cannot be small. We suggest that a likely mechanism to account for the migratory aptitudes is that illustrated with Scheme 7, for the case X=H, Y=CN. The steps to the carbene are well-precedented (8), as are the attack of nucleophilic carbenes on DMAD and other alkynes (9–12) and the reversible ring-opening and ring-closing of cyclopropenes and (or) vinylcarbenes (13–16). Moreover, Boger et al. (17) and Boger and Brotherton-Pleiss (18) have reported reactions of an intermediate (a π-delocalized vinylcarbene) analogous to **15** in Scheme 7. We assume that **15** is equilibrated with cyclopropene **16**, in view of the fact that diphenoxy

Scheme 4.



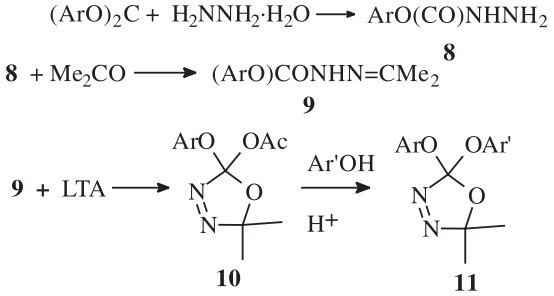
© 2001 NRC Canada

Table 1. Yields (%) of esters (**12**, **13**) and carbonate (**14**) from oxadiazolines (**11**).

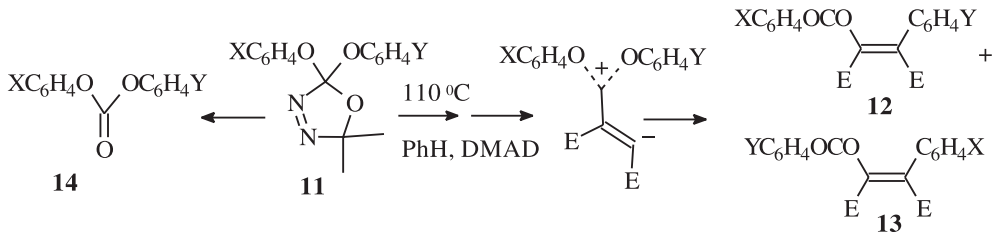
11	12	13	13:12	14
a	37	<2[a]	<0.05	29
b	28	<2[a]	<0.07	26
c	37	<2[a]	<0.05	30
d	38	<2[a]	<0.05	32
e	11	25	2.3	35

[a]Not detected. We did not experience any difficulties with detection of the esters by ^{1}H NMR spectroscopy, and we estimate that the yield of the detected isomer was at least 15-fold greater than that of the isomer that was not detected.

Scheme 5.

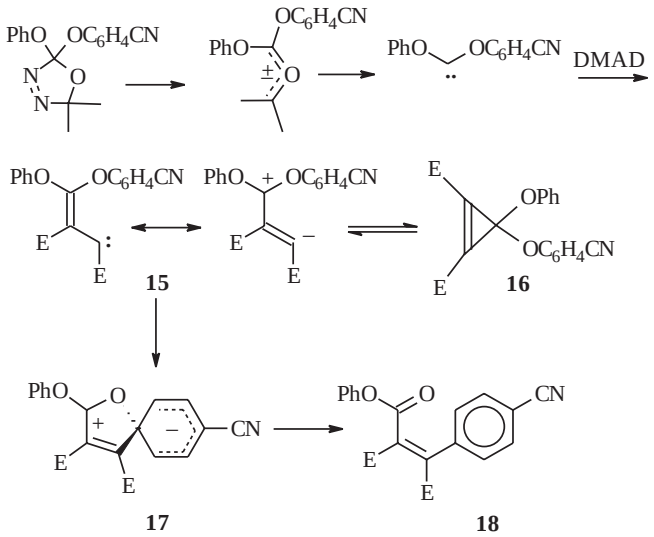


Scheme 6.



(a) X= *p*-OMe, Y= *p*-CN; (b) X= *p*-Me, Y= *p*-CN; (c) X= H, Y= *p*-CN; (d) X= *p* -OMe, Y= H; (e) X= *o*-OMe, Y= H; E = CO_2Me

Scheme 7.

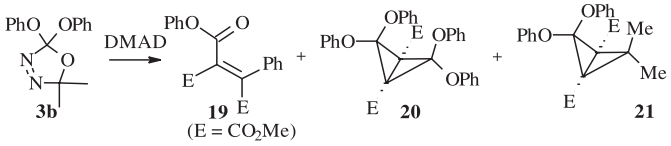


oxadiazoline **3b**, when thermolyzed in the presence of DMAD, affords not only **19** but also **20** and **21** (2) (Scheme 8).

Intermediate **15** also affords **18**, presumably via **17**, which is analogous to the intermediate usually invoked in describing nucleophilic aromatic substitutions (5). Dipolar intermediates in ipso nucleophilic aromatic substitution have been demonstrated many times (19).

A concerted reaction, leading directly from the carbene and DMAD to the product, is unlikely given that aromatic substitutions generally occur through intermediates. However, a more complex stepwise process, involving electron transfer (e.t.) *before* ring closure but leading to the observed

Scheme 8.



result (Scheme 9) cannot be ruled out with confidence. Some intermolecular chemistry of intermediates similar to **15** is thought to involve electron transfer from a π-delocalized vinylcarbene intermediate, and subsequent coupling of a radical cation and radical anion pair (Scheme 10) (20).

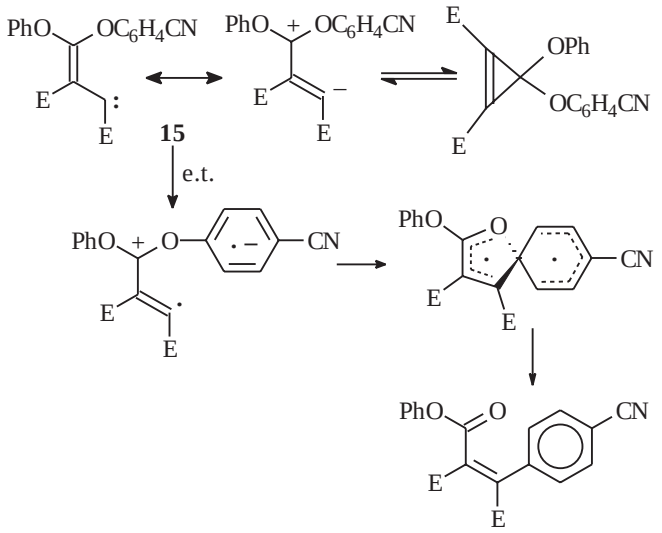
A special interaction must be invoked for the *o*-methoxy substituent, which promoted migration whereas the *p*-methoxy group was not effective. Given that a likely mechanism (Scheme 7) involves a dipolar intermediate, it is logical to propose that the *o*-methoxy group exerts its effect through space, rather than through bonds (Scheme 11). A through-space interaction of the *ortho* methoxy group with the positive center of a dipolar intermediate would help to orient the aryl group for attack, as shown in Scheme 11. Such an involvement would differentiate strongly between the *o*- and *p*-methoxy groups, which presumably have similar conjugative effects.

Summary

Diaryloxycarbenes attack DMAD to afford unsaturated triesters, by attack at the *sp*-carbon and migration of an aryl group from oxygen to the other *sp*-carbon of DMAD. If the aryloxy groups are *para*-substituted, the aryl group that is transferred preferentially is the one that is more

© 2001 NRC Canada

Scheme 9.



electron-deficient. The *ortho*- but not the *para*-methoxy group also promotes migration, presumably by stabilizing an electrophilic site by donation of electron density from the oxygen atom through space. Aryloxymethoxycarbenes (1) probably react with DMAD by an analogous mechanism.

Experimental section

General

NMR spectra were recorded with a Bruker AC-200 or AC-300 NMR spectrometer and IR spectra were obtained with a Biorad FTS-40 spectrophotometer, with the sample in CCl_4. The IR bands are labeled qualitatively with the symbols br, s, and m for broad, strong, and medium intensity bands. Weak bands are not listed. The eluting solvent for radial chromatography was a gradient of ethyl acetate (2.5–10 vol. %) in hexanes. Melting points were obtained with a Thomas Hoover capillary melting point apparatus, and are uncorrected.

Synthesis of diaryl carbonates

Diphenyl carbonate is commercially available. The other diaryl carbonates were prepared as described earlier (3).

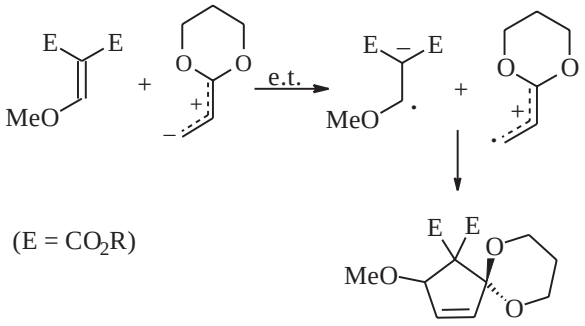
Thermolysis of 11a with DMAD

The procedure described below for thermolysis of **11a** with DMAD is typical.

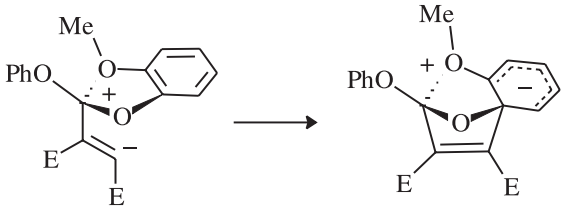
2-(*p*-Cyanophenoxy)-2-(*p*-methoxyphenoxy)-5,5-dimethyl-Δ^3-1,3,4-oxadiazoline (1.03 g, 3.04 mmol) was heated in the presence of DMAD (0.52 g, 3.66 mmol) in 25 mL of benzene (sealed tube) at 110°C for 24 h. Radial chromatography following evaporation of the solvent gave **12a** (37%) and **14a** (29%).

*Triester **12a***: white crystals, mp: 121 to 122°C. EI-MS *m/z* (%): 395 (M, 7), 364 (M – 31, 6), 272 (100), 244 (40), 200 (42), 154 (96), 123 (71), 95 (40), 59 (80). CI-MS (NH_3) *m/z* (%): 413 (M + 18, 19), 396 (M + 1, 17), 272 (100). HRMS *m/z* (%): calcd. for $C_{21}H_{17}NO_7$: 395.1005; found: 395.1026. IR (CCl_4) cm^{-1}: 2955m, 2839m, 2234m, 1746br, 1637m, 1608m, 1505s, 1437m, 1270br, 1232br, 1188br, 1073s, 1038s, 1010s. ^1H NMR (200 MHz, $CDCl_3$) δ: 3.76 (s, 3H, OMe), 3.87 (s, 3H, OMe), 3.92 (s, 3H, OMe), 6.67–6.85 (m, 4H, ArH), 7.58–7.74 (m, 4H, ArH). ^{13}C NMR (75 MHz, $CDCl_3$) δ: 53.3 (2 × OMe), 55.5, 113.9, 114.5, 117.8, 121.4, 128.5, 128.9, 132.4, 137.2, 143.1, 145.2, 157.7, 162.3, 162.4, 165.8.

Scheme 10.



Scheme 11.



The *E*-configuration of **12a** (ArOCO and CO_2Me groups *trans*) was confirmed by means of single crystal X-ray diffraction.

p-*Cyanophenyl* p-*methoxyphenyl carbonate (**14a**)*: white solid, mp: 103–105°C. EI-MS *m/z* (%): 269 (M, 34), 254 (31), 225 (9), 210 (23), 154 (6), 123 (100), 107 (84), 77 (77), 65 (32). CI-MS (NH_3) *m/z* (%): 287 (M + 18, 48), 269 (M, 89), 123 (100). IR (CCl_4) cm^{-1}: 3004m, 2932m, 2838m, 2232m, 1781s, 1717m, 1605s, 1505s, 1465m, 1296m, 1225s, 1183s, 1041m. ^1H NMR (200 MHz, $CDCl_3$) δ: 3.79 (s, 3H, OMe), 6.88–7.72 (m, 8H, ArH). ^{13}C NMR (75 MHz, $CDCl_3$) δ: 55.5, 110.1, 114.5, 117.9, 121.5, 121.9, 133.7, 144.2, 151.4, 153.8, 157.7.

Thermolysis of oxadiazoline (11b) with DMAD

Thermolysis of 2(*p*-cyanophenoxy)-5,5-dimethyl-2(*p*-methylphenoxy)-Δ^3-1,3,4-oxadiazoline in the presence of DMAD gave **12b** (26%) and **14b** (28%).

*Triester **12b***: pale yellow oil. EI-MS *m/z* (%): 348 (M – Me), 272 (M – OC_6H_4Me, 100), 244 (23), 200 (23), 176 (14), 154 (46), 107(8), 77 (23), 59 (32), 51 (9). CI-MS (NH_3) *m/z* (%): 397 (M + 18, 33), 380 (M + 1), 272 (M – OC_6H_4Me, 100). HRMS *m/z* calcd. for $C_{21}H_{17}NO_6$: 379.1056; found: 379.1073. IR (CCl_4) cm^{-1}: 2956m, 2234m, 1746s, 1639m, 1610m, 1507s, 1437s, 1269s, 1229s, 1189s, 1075s, 1010s. ^1H NMR (200 MHz, $CDCl_3$) δ: 2.30 (s, 3H, Me), 3.88 (s, 3H, OMe), 3.92 (s, 3H, OMe), 6.66–7.13 (m, ArH of C_6H_4Me), 7.58–7.73 (m, ArH of C_6H_4CN). ^{13}C NMR (75 MHz, $CDCl_3$) δ: 20.7, 53.3 (2 × OMe), 99.8, 113.9,

© 2001 NRC Canada

117.8, 120.3, 120.6, 128.6, 130.0, 132.4, 136.3, 137.2, 145.2, 147.5, 162.1, 162.4, 165.8.

p-*Cyanophenyl* p-*tolyl carbonate* ***14b***: white solid, mp: 91 to 92°C. EI-MS *m/z* (%): 65 (30), 77 (33), 91 (100), 102 (19), 209 (13), 253 (M^+, 23). CI-MS (NH_3) *m/z* (%): 253 (M + 1, 37), 271 (M + 18, 18). HRMS *m/z* calcd. for $C_{15}H_{11}NO_3$: 253.0739; found: 253.0745. IR (CCl_4) cm^{-1}: 2234m, 1783s, 1604m, 1507s, 1287m, 1229s, 1189s, 1167s, 1018m, 1006m. ^1H NMR ($CDCl_3$) δ: 2.36 (s, 3H, Me), 7.12–7.25 (m, 4H, C_6H_4Me), 7.40–7.73 (m, 4H, C_6H_4CN). ^{13}C NMR (50 MHz) δ: 20.8, 110.3, 117.9, 120.4, 122.0, 130.2, 133.8, 136.4, 148.6, 151.3, 154.0.

Thermolysis of oxadiazoline (11c) with DMAD

Thermolysis of 2(*p*-cyanophenoxy)-5,5-dimethyl-2-phenoxy-Δ^3–1,3,4-oxadiazoline in the presence of DMAD gave **12c** (37%) and **14c** (30%).

Triester ***12c***: pale yellow oil. EI-MS *m/z* (%): 365 (M, 2), 334 (M – OMe, 7), 272 (M – OPh, 100), 244 (17), 200 (13), 176 (8), 154 (14), 77 (9), 59 (37). CI-MS (NH_3) *m/z* (%): 383 (M + 18, 84), 272 (M – OPh, 100). IR (CCl_4) cm^{-1}: 2955m, 2233m, 1742b, 1638m, 1593m, 1550m, 1492s, 1436s, 1307m, 1267b, 1233b, 1189s, 1160m, 1074s, 1010s. ^1H NMR (200 MHz, $CDCl_3$) δ: 3.89 (s, 3H, OMe), 3.93 (s, 3H, OMe), 6.77–7.76 (m, 9H, ArH). ^{13}C NMR (75 MHz, $CDCl_3$) δ: 53.4 (2 × OMe), 114.0, 117.8, 120.7, 126.6, 128.6, 128.7, 129.6, 132.5, 137.1, 145.4, 149.6, 162.0, 165.9.

p-*Cyanophenyl phenyl carbonate* ***(14c)***: white solid, mp: 79 to 80°C. EI-MS *m/z* (%): 239 (M, 33), 195 (22), 167 (28), 140 (5), 121 (13), 102 (21), 77 (100), 65 (35), 49 (30), 43 (76). CI-MS (NH_3) *m/z* (%): 257 (M + 18, 21), 239 (M, 89). IR (CCl_4) cm^{-1}: 2235m, 1782s, 1603m, 1550m, 1507m, 1495m, 1221br, 1186s, 1163s, 1008m. ^1H NMR (200 MHz, $CDCl_3$) δ: 7.26–7.74 (m). ^{13}C NMR (75 MHz, $CDCl_3$) δ: 110.3, 118.0, 120.7, 122.0, 126.7, 130.0, 133.9, 150.7, 151.1, 153.9.

Thermolysis of *p*-methoxyphenoxy phenoxy oxadiazoline (11d) with DMAD

Thermolysis of 2-(*p*-methoxyphenoxy)-2-phenoxy-5,5-dimethyl-Δ^3–1,3,4-oxadiazoline in the presence of DMAD gave **12d** (38%) and **14d** (32%).

Triester ***12d***: light yellow oil. EI-MS *m/z* (%): 370 (M, 2), 339 (M – OMe, 5), 311 (7), 277 (6), 247 (100), 219 (41), 151 (16), 129 (22), 95 (10), 59 (27). CI-MS (NH_3) *m/z* (%): 388 (M + 18, 8), 371 (M + 1, 15), 247 (100). IR (CCl_4) cm^{-1}: 3004m, 2954m, 2839m, 1743br, 1633m, 1505s, 1437m, 1269s, 1232s, 1188s, 1070m, 1039m, 1012m. ^1H NMR (200 MHz, $CDCl_3$) δ: 3.75 (s, 3H, OMe), 3.90 (s, 6H, 2 × OMe), 6.65–7.49 (m, 9H, ArH). ^{13}C NMR (75 MHz, $CDCl_3$) δ: 53.0, 53.1, 55.5, 114.4, 121.7, 126.3, 127.7, 128.9, 130.4, 132.8, 143.4, 148.0, 157.6, 162.7, 163.4, 167.0.

p-*Methoxyphenyl phenyl carbonate* ***(14d)***: light yellow oil. EI-MS *m/z* (%): 245 (M + 1, 21), 244 (M, 100), 200 (15), 185 (32), 157 (11), 124 (60), 123 (46), 95 (25), 77 (95), 65 (30), 41 (24). CI-MS (NH_3) *m/z* (%): 262 (M + 18, 100), 244 (M, 100). IR (CCl_4) cm^{-1}: 3006m, 2956m, 2838m, 1780s, 1596m, 1507s, 1465m, 1442m, 1298m, 1229s, 1182s, 1103m, 1071m, 1041m, 1010m. ^1H NMR (200 MHz, $CDCl_3$) δ: 3.80 (s, 3H, OMe), 6.88–7.44 (m, 9H, ArH). ^{13}C NMR (75 MHz, $CDCl_3$) δ: 55.6, 114.5, 120.9, 121.8, 126.2, 129.5, 144.6, 151.1, 152.4, 157.6.

Thermolysis of oxadiazoline 11e with DMAD

Thermolysis of 2(*o*-methoxyphenoxy)-5,5-dimethyl-2-phenoxy-Δ^3–1,3,4-oxadiazoline in the presence of DMAD gave **12e** (11%) and **13e** (25%) as well as **14e** (35%).

Triester ***12e***: pale yellow oil. EI-MS *m/z* (%): 371 (M + 1, 4), 339 (10), 277 (M – 93, 100), 249 (100), 219 (10), 205 (28), 181 (18), 159 (20), 131 (45), 103 (12), 65 (40). CI-MS (NH_3) *m/z* (%): 388 (M + 18, 34), 371 (M + 1, 40), 277 (M – 93, 100). HRMS *m/z* calcd. for $C_{20}H_{19}O_7$ (M + H): 371.1131; found: 371.1108. IR (CCl_4) cm^{-1}: 3005m, 2954s, 2841m, 1745br, 1592s, 1550br, 1493s, 1461m, 1436m, 1226br, 1162m, 1117m. ^1H NMR (200 MHz, $CDCl_3$) δ: 3.80 (s, 3H, OMe), 3.84 (s, 3H, OMe), 3.90 (s, 3H, OMe), 6.77–7.46 (m, 9H, ArH). ^{13}C NMR (75 MHz, $CDCl_3$) δ: 52.9, 53.0, 55.8, 111.3, 120.8, 121.0, 123.0, 126.1, 129.3, 130.0, 130.1, 131.8, 144.2, 150.1, 156.9, 162.7, 163.9, 166.9.

Triester ***(13e)***: pale yellow oil. EI-MS *m/z* (%): 371 (M + 1, 5), 247 (M – 123, 100), 219 (53), 175 (19), 151 (16), 129 (31), 95 (22), 77 (28), 59 (33). CI-MS (NH_3) *m/z* (%): 388 (M + 18, 38), 371 (M + 1, 12), 247 (M – 123, 100). HRMS *m/z* calcd. for $C_{20}H_{19}O_7$ (M + H): 371.1131; found: 371.1108. IR (CCl_4) cm^{-1}: 2954m, 2841m, 1760m, 1742br, 1633m, 1609m, 1501s, 1436m, 1308m, 1263br, 1232br, 1198br, 1174s, 1110s, 1069m, 1010m. ^1H NMR (200 MHz, $CDCl_3$) δ: 3.74 (s, 3H, OMe), 3.90 (s, 3H, OMe), 3.92 (s, 3H, OMe), 6.63–7.60 (m, 9H, ArH). ^{13}C NMR (75 MHz, $CDCl_3$) δ: 53.0 (2 × OMe), 55.8, 112.6, 120.7, 122.3, 126.1, 127.3, 128.1, 128.7, 130.3, 132.6, 138.9, 148.2, 151.2, 162.5, 163.0, 167.2.

o-*Methoxyphenyl phenyl carbonate* ***(14e)***: white solid, mp: 58 to 59°C. EI-MS *m/z* (%): 244 (M, 100), 200 (28), 185 (10), 151 (20), 124 (20), 95 (33), 77 (84), 65 (37). CI-MS (NH_3) *m/z* (%): 262 (M + 18, 100), 244 (M, 100). IR (CCl_4) cm^{-1}: 2962m, 2841m, 1784s, 1550br, 1503br, 1465m, 1310m, 1233br, 1191s, 1173s, 1113m. ^1H NMR (200 MHz, $CDCl_3$) δ: 3.89 (s, 3H, OMe), 6.92–7.44 (m, 9H, ArH). ^{13}C NMR (75 MHz, $CDCl_3$) δ: 56.0, 112.6, 120.7, 120.9, 122.2, 126.1, 127.3, 129.5, 140.0, 151.0, 151.2, 151.6.

Acknowledgements

The authors gratefully acknowledge the financial support of the Natural Sciences and Engineering Research Council of Canada (NSERC) and the assistance of Mr. Brian Sayer and Dr. Kirk Green with NMR spectroscopy and mass spectrometry.

References

1. X. Lu and J. Warkentin. Tetrahedron Lett. **40**, 1483 (1999).

© 2001 NRC Canada

2. (*a*) X. Lu and J. Warkentin. Org. Lett. **2**, 3501 (2000); (*b*) X. Lu and J. Warkentin. Org. Lett. **3**, 143 (2001).
3. X. Lu, D.L. Reid, and J. Warkentin. Can. J. Chem. **79**, 319 (2001).
4. G. Scherowsky, K. Dünnbier, and G. Höfle. Tetrahedron Lett. **24**, 2095 (1977).
5. E. Buncel, J.M. Dust, and F. Terrier. Chem. Rev. **95**, 2262 (1995).
6. (*a*) D.Y. Curtin. Rec. Chem. Prog. **15**, 111 (1954); (*b*) J.I. Seeman. Chem. Rev. **83**, 83 (1983).
7. M. El-Saidi, K. Kassam, D.L. Pole, T. Tadey, and J. Warkentin. J. Am. Chem. Soc. **114**, 8751 (1992).
8. K. Kassam, D.L. Pole, M. El-Saidi, and J. Warkentin. J. Am. Chem. Soc. **116**, 1161 (1994).
9. P. Couture, M. El-Saidi, and J. Warkentin. Can. J. Chem. **75**, 326 (1997).
10. R.W. Hoffmann, W. Lilienblum, and B. Dittrich. Chem. Ber. **107**, 3395 (1974).
11. K. Kassam and J. Warkentin. J. Org. Chem. **59**, 5071 (1994).
12. K. Kassam, P.C. Venneri, and J. Warkentin. Can. J. Chem. **75**, 1256 (1997).
13. K. Kassam and J. Warkentin. Can. J. Chem. **75**, 120 (1997).
14. J.R. Al Dulayymi, M.S. Baird, L.Rajaram, and W. Clegg. J. Chem. Res. Synop., 344 (1994).
15. J.R. Al Dulaymi, M.S. Baird, H.L. Fitton, and L. Rajaram. J. Chem. Soc. Perkin Trans. 1, 1633 (1994).
16. E. J York, W Dittmar, R. Stevenson, and R.G. Bergman. J. Am. Chem. Soc. **95**, 5680 (1973). 17. D.L. Boger, C.E. Brotherton, and G.I. Georg. Org. Synth. **65**, 32 (1987).
18. D.L Boger and C.E. Brotherton-Pleiss. *In* Advances in cycloaddition. Vol. 2. *Edited by* D.P Curran. JAI Press, Greenwich, CT. 1990. pp.147–216.
19. (*a*) C.F. Bernasconi and F. Terrier. J. Am. Chem. Soc. **97**, 7458 (1975); (*b*) C.F. Bernasconi, C.L. Gehriger, and R.H. de Rossi. J. Am. Chem. Soc. **98**, 8451 (1976); (*c*). J. Sunamoto, H. Kondo, F. Yanase, and H. Okamoto. Bull. Soc. Chim. Jpn. **53**, 1361 (1980); (*d*) V.I. Minken, L.P. Oleckhnovitch, and Y.A. Zhdanov. Acc. Chem. Res. **14**, 210 (1981); (*e*) F. Terrier. Nucleophilic aromatic displacement. VCH, New York. 1991.
20. D. L. Boger and J. Wysocki, Jr. J. Org. Chem. **53**, 3408 (1988).

© 2001 NRC Canada

Determination of the complexation properties of a crosslinked poly(acrylic acid) gel with copper(II), nickel(II), and lead(II) in dilute aqueous solution

Catherine Morlay, Yolande Mouginot, Monique Cromer, and Olivier Vittori

Can. J. Chem. Downloaded from www.nrcresearchpress.com by Renmin University of China on 09/07/12
For personal use only.

Abstract: The possible removal of copper(II), nickel(II), or lead(II) by an insoluble crosslinked poly(acrylic acid) was investigated in dilute aqueous solution. The binding properties of the polymer were examined at pH = 6.0 or 4.0 with an ionic strength of the medium μ = 0.1 or 1.0 M ($NaNO_3$) using differential pulse polarography as an investigation means. The highest complexing capacity of the polyacid was obtained with lead(II) at pH = 6.0 with μ = 0.1 M, 4.8 mmol Pb(II)/g polymer. The conditional stability constants of the complex species formed were determined using the method proposed by Ruzic assuming that only the 1:1 complex species was formed; for lead(II) at pH = 6.0 and μ = 0.1 M, log K' = 5.3 ± 0.2. It appeared that the binding properties of the polymer increased, depending on the metal ion, in the following order: Ni(II) < Cu(II) < Pb(II). The complexing capacity and log K' values decreased with the pH or with an increase of the ionic strength. These results were in agreement with the conclusions of our previous studies of the hydrosoluble linear analogues. Finally, with the insoluble polymer, the log K' values were comparable to those previously obtained with the linear analogue whereas the complexing capacity values expressed in mmol g^{-1} were slightly lower.

Key words: insoluble crosslinked poly(acrylic acid), copper(II), nickel(II), and lead(II) complexation.

Résumé : La possibilité d'éliminer le cuivre(II), le nickel(II) ou le plomb(II) par un acide polyacrylique réticulé insoluble a été étudiée en solution aqueuse diluée. Les propriétés complexantes du polymère ont été examinées à pH 6,0 ou 4,0 et avec une force ionique du milieu μ valant 0,1 ou 1,0 M ($NaNO_3$) en utilisant la polarographie impulsionnelle différentielle. La capacité complexante la plus élevée du polyacide a été obtenue avec le plomb (II) à pH 6,0 et avec μ = 0,1 M, 4,8 mmol Pb (II)/g de polymère. Les constantes de stabilité conditionnelles des espèces complexes formées ont été déterminées à l'aide de la méthode proposée par Ruzic qui suppose la seule formation du complexe 1:1 ; pour le plomb(II) à pH 6,0 et pour μ = 0,1 M, log K' = 5,3 ± 0,2. Il est apparu que les propriétés complexantes du polymère étaient accrues, selon la nature du cation métallique, dans l'ordre suivant : Ni(II) < Cu(II) < Pb(II). Les valeurs de la capacité complexante et de log K' décroissent avec le pH ou avec une augmentation de la force ionique du milieu. Ces résultats sont en accord avec les conclusions de nos précédentes études relatives aux homologues linéaires hydrosolubles. Enfin, les valeurs de log K' obtenues avec le polymère insoluble sont comparables à celles obtenues précédemment avec l'homologue linéaire alors que les valeurs de la capacité complexante, exprimées en mmol g^{-1}, sont légèrement plus faibles.

Mots clés : acide polyacrylique réticulé insoluble, complexation (cuivre(II), nickel(II) et plomb(II)).

Introduction

Some insoluble crosslinked polymers, called superabsorbents, present many industrial applications which are linked to their important water-absorbing capacity (10 to several hundred times their dry weight) (1–3). Although the bulk of the research and development effort has been placed on disposable absorbent products, numerous other applications have been developed (water-retention of soils for agricultural applications, water-absorbing construction materials, electronics and cabling, food packaging, thickeners (2, 3)). Some interesting new applications of superabsorbents are emerging, for example in the cosmetic industry, to develop new sensors or for the controlled release of substances such as pharmaceuticals, pesticides, or fertilizers (3).

In our (4–7) previous studies of metal complexation with linear hydrosoluble poly(acrylic acids) (HPAAs) of high molecular weight, we showed that HPAAs were able to trap different metal ions. There is some literature relative to this field of research but there is a complete lack of data for their insoluble crosslinked analogues, i.e., superabsorbents of a carboxylic nature.

The aim of this work was to study the metal complexation properties of an insoluble crosslinked PAA (Aquakeep® SAP X 50 R superabsorbent) in dilute aqueous solution and to compare these properties with those previously obtained with HPAAs, their linear analogues. The metal ions copper(II),

Received July 7, 1999. Published on the NRC Research Press Web site on April 24, 2001.

C. Morlay[1], Y. Mouginot, M. Cromer, and O. Vittori. Laboratoire d'Electrochimie Analytique – LICAS, Université Claude Bernard Lyon 1, CPE, 43 Bvd du 11 novembre 1918, 69622 Villeurbanne CEDEX, France.

[1]Corresponding author (telephone: (33) 4 72 44 82 63; fax: (33) 4 72 44 84 79; e-mail: morlay@univ-lyon1.fr).

 DOI: 10.1139/cjc-79-4-370 © 2001 NRC Canada

Can. J. Chem. Downloaded from www.nrcresearchpress.com by Renmin University of China on 09/07/12
For personal use only.

nickel(II), and lead(II) are investigated. Copper(II), often mentioned in the literature, constitutes a reference ion that can be used for comparison purposes. Nickel(II) and lead(II) are metal cations representative of highly pollutant substances. The choice of the analytical technique used (differential pulse polarography) as well as the choice of the pH range considered (pH = 4.0–6.0) were justified in a previous paper (6). We also studied the effect of the ionic strength of the medium (μ = 0.1 or 1.0 M) on the binding properties of Aquakeep®.

The previous potentiometric study carried out with Aquakeep® in dilute aqueous solution provided us with fundamental information on the binding properties of the polymer towards copper(II), nickel(II) (8), and lead(II) (9). However, no quantitative estimation of the specific amount of metal ion that can be fixed by the polyacid could be made from these experimental results. Compared to potentiometry, the polarographic approach and the data treatment methods we used allow not only the determination of the stability constants of the complex species formed with Aquakeep® but also the estimation of its complexing capacity at a constant pH value.

The two methods we used to treat the experimental data have been applied by numerous authors to determine the metal-binding capacity of the bulk organic matter of natural waters of different origins (10–13). However, apart from our own previous results, there is no available data relative to the determination of the complexing capacity of PAAs, hydrosoluble or not.

Theory

As previously explained (4), molar concentration has little meaning for polymer compounds. Thus, we shall define for polycarboxylic acids the total content of titratable acid functions of the sample under study (C_A, expressed in equiv L^{-1}). C_A corresponds to the total reactive site (potentially complexing site) concentration of the polymer introduced in the analysis cell as used next for the complexation study.

The binding properties of a given polymer can be described in terms of the saturation of its complexing sites (10, 11). The macromolecule may be considered as the central group which is able to fix a certain number of metal ions. The complexing capacity of the ligand (C') may then be defined as the maximum ability of the molecule to fix a given metal ion. The complexing capacity of Aquakeep® was determined through the titration of the ligand with the metal ion of interest at a fixed pH (10, 11). From the graph of the measured current i (i corresponds to the free metal ion concentration (m)) vs. the total metal ion concentration introduced (C_M), one can estimate the value of C'_{obs}; C'_{obs} corresponds to the value of C_M at which the break in the titration curve occurs. The C'_{obs} value is needed to obtain the saturation of the ligand. Therefore, the value of $C_M - m$ represents the maximum concentration of the metal ion which can be bound to the complexing agent studied. The value of $C_M - m$ corresponds to the horizontal segment between the curves i vs. C_M obtained in the absence and in the presence of the ligand.

The same sets of experimental data were also treated using the method described by Ruzic (14). This method allows the calculation of C' (C'_{calc} throughout our work) and K', the conditional stability constant of the MA (metal–ligand) complex species formed, from the graph of $m/(C_M - m)$ vs. m. All the definitions and assumptions needed for this study have already been described (6).

Table 1. Main characteristics of Aquakeep® SAP X 50 R.

Particle size distribution	<100 μm	<1%
	100–500 μm	50–75%
	500–800 μm	20–40%
	>800 μm	<5%
Density	0.67 ± 0.05 g cm^{-3}	
Residual monomers	<100 ppm	
Residual humidity	5.5 ± 0.2%	
Water retention after 30 min	31 ± 3 g g^{-1}	
Absorption capacity with 0.9% NaCl	57 g g^{-1}	
Gelling time	85 s	

Experimental

Reagents

The poly(acrylic acid) used was Aquakeep® SAP X 50 R superabsorbent, Elf-Atochem Co. (Levallois-Perret, France). All the experiments were carried out using the same batch of polymer which was stored in a polyethylene flask, at room temperature (20°C) and in the dark. It was used without any further treatment. Its main characteristics are presented in Table 1.

The previous potentiometric study of the acid–base properties of Aquakeep® (8) showed that the polymer exhibits both a weak and a very weak acidity (specific values: 6.7 ± 0.1 and 2.1 ± 0.1 mequiv g^{-1}, respectively). The weak acidity of Aquakeep® is characterized by a pK_m^H value of 5.40 ± 0.05. This study also showed that the carboxylic groups accounting for the very weak acidity of Aquakeep® dissociate at pH values above 7.5. This acidity was thus not considered for the study of metal complexation carried out at pH ≤ 6.0.

All the other reagents were of analytical grade. Metal ion stock solutions (0.2 M) were prepared from copper nitrate (Prolabo, France), nickel or lead nitrate (Fluka Chemika, Switzerland), and then standardized using an EDTA disodium salt solution (Merck, Germany). The stock solution of supporting electrolyte ($NaNO_3$ (Fluka Chemika)) was 1 M. All the solutions were prepared with freshly distilled water.

Apparatus and procedure

We used the apparatus described in ref. 6. The instrumental parameters used to perform the differential pulse polarography (DPP) measurements are presented in Table 2.

All the samples were treated in the same way. The measurements were performed at 25.0 ± 0.1°C under a nitrogen atmosphere and with a 50 mL total volume of solution in the analysis cell. The response of the polarographic system in the DPP mode was calibrated (in the absence of polymer) for each of the metal ions, at each of the two pH values. The pH was adjusted at 4.0 or 6.0 ± 0.1 by the addition of microquantities of dilute solutions of nitric acid or sodium hydroxide. It was also calibrated at each of the two ionic

© 2001 NRC Canada

Can. J. Chem. Downloaded from www.nrcresearchpress.com by Renmin University of China on 09/07/12
For personal use only.

Table 2. Instrumental parameters used for DPP measurements.

Drop life time (s)	2
Scan rate (mV s^{-1})	2
Cathodic pulse amplitude (mV)	50
Pulse duration (ms)	48
Potential range scanned (V)	+ 0.2 to –1.5

strengths examined (μ = 0.1 or 1.0 M). The curves *i* vs. C_M were obtained for corrected metal ion final concentrations in the 4×10^{-5} to 8×10^{-4} M range. The responses of the different systems were recorded after the deaeration of the samples by a 5 min nitrogen bubbling. These calibrations were then verified for a few values of C_M before each experiment.

Each experiment of progressive saturation of Aquakeep® was carried out with 10.0 ± 0.1 mg of the polyacid (C_A = 1.34 ± 0.02 mequiv L^{-1}). After a 20 min nitrogen bubbling at the desired values of pH and ionic strength, a blank was systematically recorded. The titration of Aquakeep® was then carried out at pH 6.0 or 4.0 with μ = 0.1 or 1.0 M. The successive 30 µL additions of the metal ion stock solution (C_M in the 1.2×10^{-4} to 1.2×10^{-3} M range, i.e., C_A/C_M in the 1.1–11.2 range) were performed while Aquakeep® was maintained in suspension in the analysis cell by a vigorous stirring (500 rpm). The pH of the medium was continuously verified and corrected if necessary. The reproducibility of both metal ion complexations was determined by carrying out the same experiment twice. Direct current polarograms were recorded, both in the absence and in the presence of Aquakeep®, to check the shape of the polarographic waves.

The complexation of metal ions by Aquakeep® proved not to be a fast phenomenon and preliminary experiments were needed to determine the contact time under stirring required before the polarographic analysis could be performed, that is time to reach the equilibrium state. The study of the complexation rate of Aquakeep® was carried out at pH 6.0 with μ = 0.1 or 1.0 M. Two hundred µL of the metal ion stock solution were added to the Aquakeep® suspension ($C_M = 8 \times 10^{-4}$ M) and the response of the system (corresponding to the free metal ion residual concentration (*m*)) was then recorded at different times. The pH of the medium was continuously checked.

Results and discussion

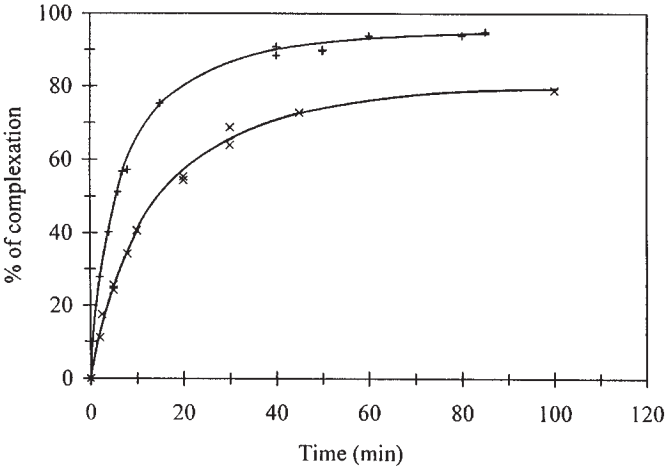
Using the formula proposed by Baes and Mesmer (15) and taking into account the maximum value of C_M examined, we ensured that neither soluble nor insoluble metal hydroxides were significantly formed at any of the pH values considered during the experiments.

The Aquakeep® blanks always presented null or negligible values of *i* at the peak potentials of the different metal ions examined. The response of the polarographic systems investigated was linear over all the metal concentration range considered, in the absence and in the presence of Aquakeep®.

Complexation rate of Aquakeep®

Figure 1 shows the evolution of the complexation yield vs. time for Aquakeep® with lead(II) at pH 6.0 and for μ = 0.1 or 1.0 M. Very similar curves were obtained with the other metal ions examined. From these results, the maximum complexation yields were obtained at μ = 0.1 M for Pb(II) > Cu(II) >> Ni(II) at 95, 90, and 50%, respectively. The complexation of nickel(II) was the most affected by an increase in the ionic strength of the aqueous medium. For nickel(II) there was a 37% decrease in the signal, whereas for copper(II) and lead(II) it was only 13% and 17%, respectively.

Fig. 1. Complexation yield vs. time for Aquakeep® ($C_A = 1.34 \times 10^{-3}$ equiv L^{-1}) with lead(II) at pH 6.0 and μ = 0.1 M (+) or 1.0 M (x).



All the curves reached a plateau but after a 45 min contact time under continuous stirring, the complexation yield was less than 5% below its max value. This stirring time was thus chosen for the following experiments of progressive saturation of Aquakeep® by the different metal ions; it would allow the measurement of *m* at a quasiequilibrium state while avoiding a long time between subsequent additions of the metal ion.

Complexation properties of Aquakeep®

The curves *i* vs. C_M obtained for nickel(II) at pH 6.0 and μ = 0.1 M and for copper(II) at pH 4.0 and μ = 1.0 M, both in the absence or in the presence of Aquakeep®, are shown in Figs. 2 and 3, respectively. The other curves obtained in the presence of Aquakeep® presented very similar shapes. However, for nickel(II) in all experimental conditions examined except the one above, the curves did not present any change in their slope and were very close, if not identical, to the calibration curves (obtained in the absence of Aquakeep®) indicating a very poor complexation. Therefore, no value of C'_{obs} was measurable in this case. The same phenomenon had also been observed previously with HPAAs in the same conditions of pH and ionic strength (6). For copper(II) in the presence of Aquakeep® at pH 4.0 and μ = 0.1 M, the first part of the graph *i* vs. C_M, observed for $C_M < C'_{obs}$, had an anomalous shape. The same phenomenon had been observed previously with HPAAs (6). The value of C'_{obs} estimated in this case was a maximum value.

The values of C'_{obs} and $C_M - m$ (the bound metal concentration) estimated for the different systems Aquakeep®/metal ion are presented in Tables 3 and 4 for pH 4.0 and 6.0,

© 2001 NRC Canada

Can. J. Chem. Downloaded from www.nrcresearchpress.com by Renmin University of China on 09/07/12
For personal use only.

Table 3. Values obtained for the saturation of Aquakeep® with copper(II), nickel(II), or lead(II) at pH 4.0 and for different values of ionic strength (C_A = 1.34 × 10^{-3} equiv L^{-1}).

	C'_{obs} (mmol g^{-1})	$C_M - m$ (mmol g^{-1})	C_M/C_A	$(C_M - m)/C_A$	C'_{obs} (mmol g^{-1})	$C_M - m$ (mmol g^{-1})	C_M/C_A	$(C_M - m)/C_A$
	μ = 0.1 M				μ = 1.0 M			
Cu(II)	≤2.9[a]	2.5	0.86	0.37	2.4	1.5	0.81	0.22
Ni(II)	NM[b]	NM[b]	NM[b]	NM[b]	NM[b]	NM[b]	NM[b]	NM[b]
Pb(II)	3.6	3.2	0.79	0.47	2.6	1.9	0.82	0.28

[a]Maximum estimated value of C'_{obs}.
[b]Value not measurable.

Table 4. Values obtained for the saturation of Aquakeep® with copper(II), nickel(II), or lead(II) at pH 6.0 and for different values of ionic strength (C_A = 1.34 × 10^{-3} equiv L^{-1}).

	C'_{obs} (mmol g^{-1})	$C_M - m$ (mmol g^{-1})	C_M/C_A	$(C_M - m)/C_A$	C'_{obs} (mmol g^{-1})	$C_M - m$ (mmol g^{-1})	C_M/C_A	$(C_M - m)/C_A$
	μ = 0.1 M				μ = 1.0 M			
Cu(II)	4.8	4.7	0.99	0.69	4.2	3.6	0.85	0.54
Ni(II)	2.9	2.3	0.76	0.34	NM[a]	NM[a]	NM[a]	NM[a]
Pb(II)	4.9	4.8	0.85	0.71	4.4	4.1	0.87	0.60

[a]Value not measurable.

Fig. 2. Curves *i* vs. C_M obtained for Aquakeep® (C_A = 1.34 × 10^{-3} equiv L^{-1}) with nickel(II) at pH 6.0 and μ = 0.1 M ((+): in the absence of Aquakeep®; (x): in the presence of Aquakeep®).

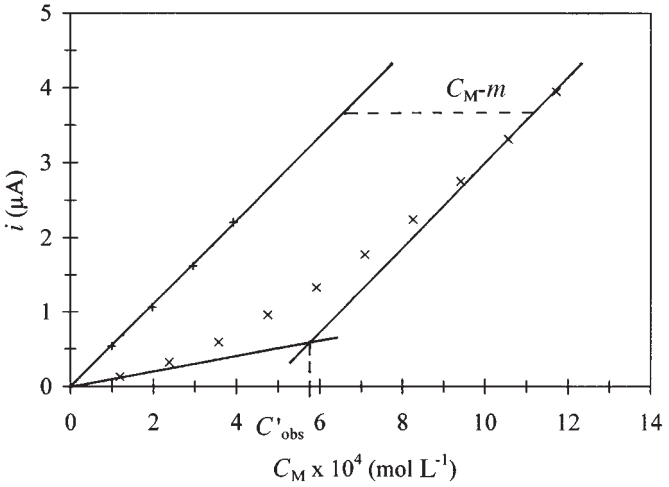
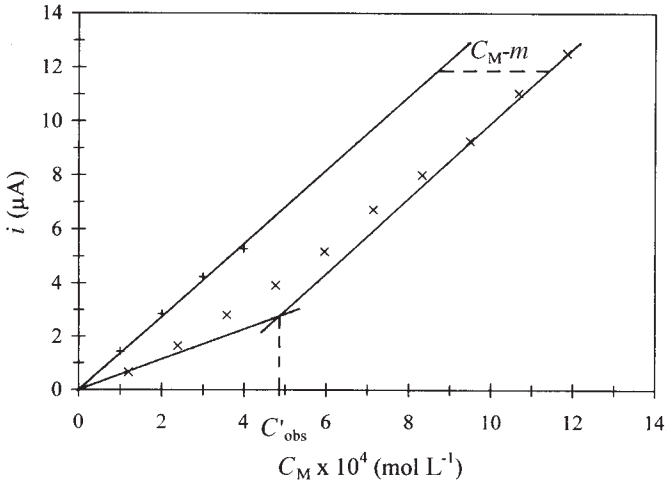


Fig. 3. Curves *i* vs. C_M obtained for Aquakeep® (C_A = 1.34 × 10^{-3} equiv L^{-1}) with copper(II) at pH 4.0 and μ = 1.0 M ((+): in the absence of Aquakeep®; (x): in the presence of Aquakeep®).



respectively. As C'_{obs} and $C_M - m$ are conditional values, which depend on the experimental conditions such as aqueous medium characteristics and especially the amount of Aquakeep® added to the solution, they were expressed in mmol of metal/g of polymer. The values of C_M and $C_M - m$ were calculated at the point where the representation becomes linear again. The experimental error on the values of C'_{obs} and $C_M - m$ was estimated at ± 4 × 10^{-5} M or 0.2 mmol g^{-1}.

The same sets of experimental data were also treated using the method described by Ruzic (14). Figures 4 and 5 show the curves of $m/(C_M - m)$ vs. *m* corresponding to the experimental points obtained in Figs. 2 and 3, respectively. The values of C'_{calc} and log K' were calculated from the slope and intercept of the linear regressions applied to all the experimental points of these graphs. Except for copper(II) at pH 4.0 and μ = 0.1 M, there was good agreement between the experimental points and the plot of the linear regression applied to these points, indicated by a high value of the correlation coefficient (r^2). This showed that the method proposed by Ruzic (14) could be successfully used for the different systems Aquakeep®/metal ion considered here.

Tables 5 and 6 present the values of C'_{calc}, log K', r^2, and *n* (number of observations) obtained for the different systems Aquakeep®/metal ion considered at pH 4.0 and 6.0, respectively. As C'_{calc} and K' are conditional value, C'_{calc} was expressed in mmol of metal/g of polymer. The experimental error on the values of C'_{calc} and log K' was estimated at ± 4 × 10^{-5} M (or 0.2 mmol g^{-1}) and ±0.2, respectively. However, for copper(II) at pH 4.0 and μ = 0.1 M, the dispersion of the experimental points led to a larger uncertainty on the estimation of C'_{calc} and log K'; these values are given in brackets in Table 5.

© 2001 NRC Canada

Table 5. Values of C'_{calc}, log K', n, and r^2 obtained for the different systems Aquakeep®/metal ion at pH 4.0 and for different values of ionic strength ($C_A = 1.34 \times 10^{-3}$ equiv L^{-1}).

	C'_{calc} (mmol g^{-1})	log K'	n	r^2	C'_{calc} (mmol g^{-1})	log K'	n	r^2
	μ = 0.1 M				μ = 1.0 M			
Cu(II)	3.9	3.4	10	0.8213	1.8	3.6	10	0.9925
Ni(II)	NM[a]	NM[a]	—	—	NM[a]	NM[a]	—	—
Pb(II)	3.6	4.2	9	0.9980	2.3	3.8	10	0.9795

[a]Value not measurable.

Table 6. Values of C'_{calc}, log K', n, and r^2 obtained for the different systems Aquakeep®/metal ion at pH 6.0 and for different values of ionic strength ($C_A = 1.34 \times 10^{-3}$ equiv L^{-1}).

	C'_{calc} (mmol g^{-1})	log K'	n	r^2	C'_{calc} (mmol g^{-1})	log K'	n	r^2
	μ = 0.1 M				μ = 1.0 M			
Cu(II)	5.1	4.5	10	0.9855	4.7	3.9	10	0.9951
Ni(II)	2.8	3.9	10	0.9984	NM[a]	NM[a]	—	—
Pb(II)	4.8	5.3	10	0.9992	3.6	4.3	10	0.9920

[a]Value not measurable.

Fig. 4. Curves $m/(C_M - m)$ vs. m obtained for Aquakeep® ($C_A = 1.34 \times 10^{-3}$ equiv L^{-1}) with nickel(II) at pH 6.0 and μ = 0.1M.

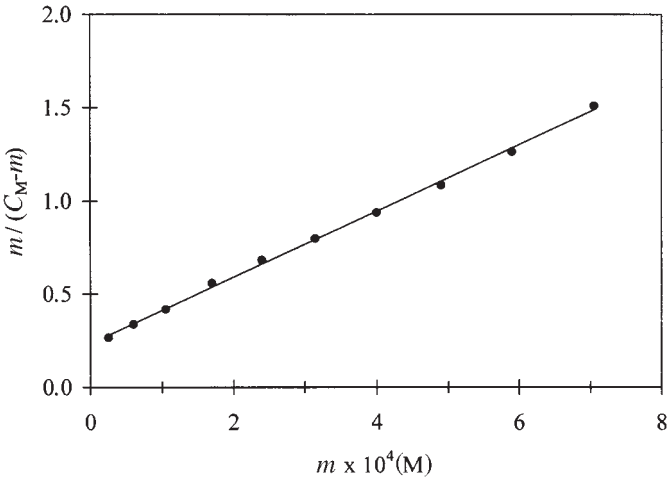
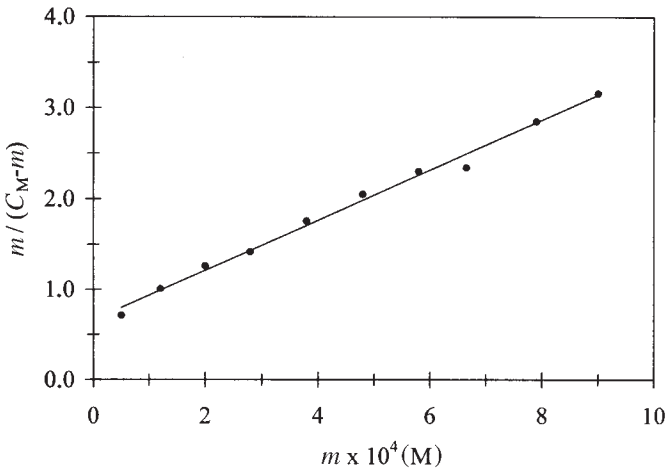


Fig. 5. Curves $m/(C_M - m)$ vs. m obtained for Aquakeep® ($C_A = 1.34 \times 10^{-3}$ equiv L^{-1}) with copper(II) at pH 4.0 and μ = 1.0 M.



If we compare the values of all the parameters estimated during this work, i.e., C'_{obs}, $C_M - m$, C'_{calc}, and log K', we can draw the following conclusions: (*i*) for one metal ion and for given values both of pH and ionic strength of the aqueous medium, the values of C'_{obs}, $C_M - m$, and C'_{calc} are of the same order of magnitude; (*ii*) the four parameters show that lead(II) tends to be more readily bound to Aquakeep® than copper(II) and much more than nickel(II) for the same values of pH and ionic strength; and (*iii*) finally, for all the metal ions examined, each of the four parameters is significantly lowered by a decrease of the pH or by an increase of the ionic strength of the medium. For copper(II) and lead(II) this decrease, as expected, is more pronounced when the two parameters are varied simultaneously.

We also calculated the values of C_M/C_A (metal to ligand concentration ratio) and $(C_M - m)/C_A$ (the occupation rate of the ligand complexing sites) at the point where the saturation of the polyacid with the metal ion was reached (Tables 3 and 4). At pH 6.0 and for μ = 0.1 M, the value of $(C_M - m)/C_A$ was around 70% for copper(II) and lead(II) and it was around half this value for nickel(II). This would indicate that when the ligand is saturated not all the potentially available complexing sites of the polyacid are occupied. In every case, the value of $(C_M - m)/C_A$ decreased with the pH of the medium or with an increase of μ.

Explanations, summarised in a previous paper, on the large influence of pH on the binding properties of polyacids in general (6), observed that the deprotonated form of the reactive sites (i.e., carboxylate groups) is primarily responsible for the binding of metal ions onto polymers of a carboxylic nature (16–19). The pH of the medium influences the binding of metal ions via the change in the degree of dissociation of the polyacid (α_A). A previous potentiometric study of Aquakeep® (8) carried out with μ = 0.1 M allowed the determination of the evolution of α_A vs. pH: α_A = 0.18 and 0.58 for pH = 4.0 and 6.0, respectively.

Can. J. Chem. Downloaded from www.nrcresearchpress.com by Renmin University of China on 09/07/12
For personal use only.

© 2001 NRC Canada

Table 7. $(C_M - m)/C_A$ values obtained with the HPAA ($C_A = 1.0 \times 10^{-3}$ equiv L^{-1}) and with Aquakeep® ($C_A = 1.34 \times 10^{-3}$ equiv L^{-1}) at pH = 6.0 and $\mu = 0.1$ M.

	HPAA		Aquakeep®	
	(mmol mequiv^{-1})	(mg g^{-1})	(mmol mequiv^{-1})	(mg g^{-1})
Cu(II)	0.46	370	0.69	300
Ni(II)	0.19	140	0.34	140
Pb(II)	0.50	1300	0.71	980

All the results obtained with Aquakeep® can be compared with those obtained previously with a linear, hydrosoluble poly(acrylic acid) having a high average molecular weight (3×10^6) (6, 7). The experiments with the HPAA were carried out at pH = 6.0 ± 0.1, with $\mu = 0.1$ M ($NaNO_3$) and using the same analytical procedure. The total content of titratable acid functions in the analysis cell was $C_A = 1.0 \times 10^{-3}$ equiv L^{-1}.

The metal complexation with HPAA was a fast reaction with only a short time before reaching an equilibrium state (about 1 min). The polarographic analysis could be carried out almost immediately. The delay observed with Aquakeep® can be explained by a steric effect of the reticulous structure of the polymer, limiting the accessibility of some of its inner complexing sites. Clearly, for the four parameters considered, the same stability order was found for the complexes formed with HPAA. Nickel(II) was weaker bound to the polymer than copper(II) and lead(II) (this was much more visible on the C' and $C_M - m$ values). The values of log K' are not significantly different between HPAA and Aquakeep® for nickel(II) and lead(II); however, the value of log K' obtained for the system HPAA/copper(II) (log $K' = 5.2 \pm 0.2$) was significantly higher than that determined for the system Aquakeep®/copper(II). The same effect of pH of the medium on the complexing properties (C' and log K' values) was also observed with HPAA (6, 7).

The values of $(C_M - m)/C_A$, when expressed in mmol mequiv^{-1}, are systematically higher with Aquakeep® than those found with HPAA. However, when expressed in mg g^{-1} of polymer, comparable or slightly lower values of $(C_M - m)/C_A$ are found with Aquakeep® (Table 7). For example, for comparable ligand concentrations, Aquakeep® is able to fix a maximum (obtained with lead(II)) of 0.71 mol of metal ion per equiv of complexing sites at pH = 6.0 and $\mu = 0.1$ M, whereas HPAA in the same conditions could only fix a max (also obtained with lead(II)) of 0.50 mol of metal ion per equiv (7). However, still in the same conditions, 1 g HPAA was able to complex 1.30 g lead(II) (7) whereas Aquakeep® only complexed 0.98 g.

We did not find any data in the literature relative to this study of complexing properties of an acrylic acid derivated polymer gel using voltammetric methods. However, we did find work relative to the complexing properties of methacrylic acid derivated polymer gels using potentiometry (20–22). These studies had not been carried out in conditions of saturation of the polymer ligand and therefore their stability constants could not be compared to those we determined. We did not consider studies relative to natural substances or natural waters as the complexing material in this case is not well-defined and not comparable with our studies.

Conclusion

The binding capacity of Aquakeep®, as well as the stability constant of the complex species formed with copper(II), nickel(II), or lead(II) were calculated in dilute aqueous solution. The results obtained with this insoluble crosslinked poly(acrylic acid) (stability order of the complexes formed and the influence of pH and ionic strength of the aqueous medium) were in very good agreement with those we previously obtained from the potentiometric or the polarographic studies of its linear hydrosoluble analogues (4–7). In both cases, the highest values of C' and log K' were obtained with lead(II), at pH 6.0 and $\mu = 0.1$ M. This shows that there is no significant difference in the complexing properties of Aquakeep® and HPAA.

Acknowledgments

We wish to thank the Elf-Atochem Co. who kindly provided the Aquakeep® SAP X 50 R superabsorbent and also Christine Clozel for her expertise in English.

References

1. P.M. Budd. *In* Industrial water soluble polymers. *Edited by* C.A. Finch. The Royal Society of Chemistry, Cambridge. 1996. Chap. 1.
2. K.S. Kazanskii and S.A. Dubrovskii. *In* Polyelectrolytes hydrogels chromatographic materials. *Edited by* S.A. Dubrovskii, A.E. Ivanov, K.S. Kazanskii, N.P. Kuznetsova, V.V. Saburov, G.V. Samsonov and V.P. Zubov. Advances in polymer science 104. Springer–Verlag, Berlin. 1992. Chap. 3.
3. F.L. Buchholz. *In* Modern superabsorbent polymer technology. *Edited by* F.L. Buchholz and A.T. Graham. Wiley, New York. 1998. Chaps. 5 and 7.
4. C. Morlay, M. Cromer, Y. Mouginot, and O. Vittori. Talanta, **45**, 1177 (1998).
5. C. Morlay, M. Cromer, Y. Mouginot, and O. Vittori. Talanta, **48**, 1159 (1999).
6. C. Morlay, M. Cromer, and O. Vittori. Water Res. **34**, 455 (2000).
7. S. Perret, C. Morlay, M. Cromer, and O. Vittori. Water Res. **34**, 3614 (2000).
8. Y. Mouginot, C. Morlay, M. Cromer, and O. Vittori. Anal. Chim. Acta, **407**, 337 (2000).
9. C. Morlay, Y. Maginot, M. Cromer, M. Chatelut, and O. Vittori. Can J. Chem. **78**, 1637 (2000).
10. T.M. Florence. *In* Trace element speciation: analytical methods and problems. *Edited by* G.E. Batley. CRC Press, Inc., Boca Raton, Florida. 1989. Chap. 4.
11. J. Buffle. Complexation reactions in aquatic systems. An analytical approach. *Edited by* Ellis Horwood, Chichester. 1988. Chap. 6.
12. H.W. Nürnberg. *In* Complexation of trace metals in natural waters. *Edited by* C.J.M Kramer and J.C. Duinker. Nijhoff M. & Junk W. Publishers, The Hague. 1984. Part II.
13. B.T. Hart. Environ. Technol. Lett. **2**, 95 (1981).
14. I. Ruzic. Anal. Chim. Acta, **140**, 99 (1982).
15. C.F. Baes and R.E. Mesmer. The hydrolysis of cations. Wiley, New York. 1976. Chaps. 10, 12, and 15.
16. G. Manzini, A. Cesaro, F. Delben, S. Paoletti, and E. Reisenhofer. Bioelectrochem. Bioenerg. **12**, 443 (1984).

© 2001 NRC Canada

Can. J. Chem. Downloaded from www.nrcresearchpress.com by Renmin University of China on 09/07/12
For personal use only.

17. R. Subramanian and P. Natarajan. Indian J. Chem. **24A**, 432 (1985).
18. R.F.M.J. Cleven and H.P. Van Leeuwen. Int. J. Environ. Anal. Chem. **27**, 11 (1986).
19. M.A.G.T. Van den Hoop, F.M.R. Leus, and H.P. Van Leeuwen. Coll. Czech. Chem. Commun. **56**, 96 (1991).
20. W.M. Anspach and J.A. Marinsky. J. Phys. Chem. **79**, 433 (1975).
21. J.A. Marinsky and W.M. Anspach. J. Phys. Chem. **79**, 439 (1975).
22. J.A. Marinsky. J. Phys. Chem. **86**, 3318 (1982).

Can. J. Chem. Downloaded from www.nrcresearchpress.com by Renmin University of China on 09/07/12
For personal use only.

© 2001 NRC Canada

Synthesis and evaluation of novel β-lactam inhibitors of human leukocyte elastase

K.P. Koteva, André M. Cantin, W.A. Neugebauer, and E. Escher

Abstract: A series of β-lactam derivatives were synthesized and tested to determine the structure–activity relationship for inhibition of human leukocyte elastase (HLE), a serine protease involved in several degenerative lung and tissue diseases. The most potent IC_{50} values were obtained with neutral hydrophobic 7α-methoxy cephalosporanic acid derivatives. Tryptophanyl-9-fluorenylmethyl ester and *N*-benzhydryl piperazine derivatives of 7α-methoxy cephalosporanic acid represent two novel HLE inhibitors, with length of action persisting beyond 24 h.

Key words: β-lactams, neutrophil elastase, protease inhibitors, peptides.

Résumé : Une série de dérivés de molécules β-lactames fut synthétisée et analysée afin de déterminer la relation structure-activité en tant qu'inhibiteurs de l'élastase neutrophilique humaine (ENH), une protéase impliquée dans plusieurs maladies pulmonaires et tissulaires. Les valeurs inhibitrices (IC_{50}) les plus puissantes furent obtenues avec des dérivés neutres hydrophobes de l'acide 7α-methoxy cephalosporanique. Les dérivés tryptophanyl-9-fluorenylmethyl ester et *N*-benzhydrylpiperazine de l'acide 7α-methoxy cephalosporanique représentent deux nouveaux inhibiteurs de l'ENH, dont l'effet persiste plus de 24 heures.

Mots clés : β-lactames, élastase neutrophilique, inhibiteurs de protéases, peptides.

Introduction

Elastin is a proteinaceous part of the extracellular matrix, commonly called connective tissue. It gives coherence and elasticity to many tissues, such as lung, yellow tendon, and cartilage of joints. Elastin remodeling is controlled by a fine balance between continuous elastin synthesis and breakdown by neutrophil and tissue elastases. Human leukocyte (neutrophil) elastase (HLE, EC 3.4.21.37) secreted by polymorphonuclear neutrophils (PMN) has been considered over two decades as one of the most interesting therapeutic targets in several lung diseases (1). One of the main functions of HLE is the degradation of structural proteins, such as elastin, fibronectin, and collagen (2). Under normal physiological conditions, the lungs are protected from excessive HLE elastolytic activity by endogenous inhibitors such as α1-protease inhibitor (α1-PI) and α2-macroglobulin (α2-M). However, the rate of elastin (and collagen) degradation is greatly enhanced under a variety of clinical conditions. In particular, pulmonary emphysema, rheumatoid arthritis, acute respiratory distress syndrome (ARDS), and cystic fibrosis (CF) (3–5) are characterized by an excessive destruction of connective tissue of the lung and joints. Neutrophil elastase is believed to participate in this process (6). Although α1-PI is present in the CF-lung, it is inactive in most patients, apparently due to oxidative and proteolytic processes (7, 8). Myeloperoxidase present in CF respiratory secretions converts Cl^- to OCl^- in the presence of hydrogen peroxide, inducing a large oxidant burden in the airways (9, 10). Moreover, bronchial secretions from CF-patients can directly inactivate α1-PI through elastase-mediated proteolysis (11). Therefore, individuals with CF have a functional deficiency of airway α1-PI (11, 12). They are especially susceptible to the early development of lung disease. It is reasonable to expect that a selective inhibitor of HLE might be useful for the treatment of emphysema, rheumatoid arthritis, CF, and other diseases. This provides a rationale for developing such inhibitors of low molecular weight for the evaluation of their efficacy to supplement natural inhibitors in diseases involving HLE (13). Several classes of HLE inhibitors have been reported in the past, including *N*-arylbenzylisothiazolinone 1,1-dioxide (14), fatty acids (15), sulfonyl fluorides (16), 4*H*-3,1-benzoxazin-4-one, 4-chloroquinazolines (17), azapeptide *p*-nitrophenyl esters (18), and cephalosporin derivatives. The discovery that neutral cephalosporins are inhibitors of mammalian serine proteinases led Zimmerman and co-workers (19) to evaluate the activity of clavulanic acid and its benzyl esters as inhibitors of HLE. The free acid, known to inhibit the bacterial β-lactamase, was inactive against HLE, but its benzyl ester had good activity against HLE. This observation prompted several investigators to select a large number of β-lactams for evaluation as inhibitors of HLE and other mammalian serine proteases (20–28).

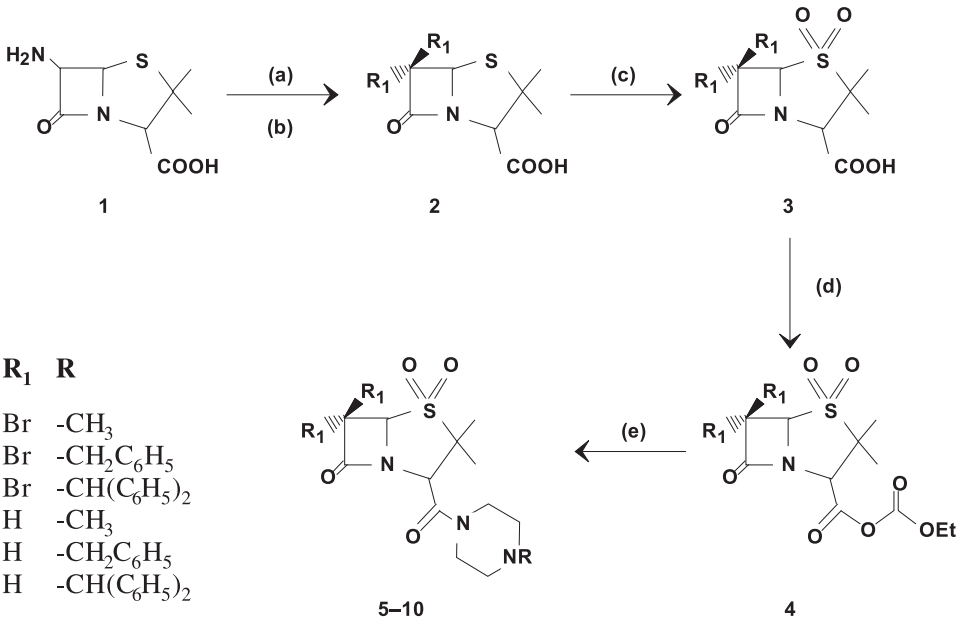
Received September 15, 2000. Published on the NRC Research Press Web site on May 3, 2001.

K.P. Koteva, W.A. Neugebauer, and E. Escher. Department of Pharmacology, Faculty of Medicine, University of Sherbrooke, 3001, 12ème Avenue Nord, Sherbrooke, QC J1E 5N4, Canada.
André M. Cantin.[1] Pulmonary Research Unit, Faculty of Medicine, University of Sherbrooke, 3001, 12ème Avenue Nord, Sherbrooke, QC J1E 5N4, Canada.

[1]Corresponding author (telephone: (819) 346-1110 ext: 14893; fax: (819) 564-5377; e-mail: acanti01@courrier.usherb.ca).

 DOI: 10.1139/cjc-79-4-377 © 2001 NRC Canada

Scheme 1.



	R_1	R
5	Br	$-CH_3$
6	Br	$-CH_2C_6H_5$
7	Br	$-CH(C_6H_5)_2$
8	H	$-CH_3$
9	H	$-CH_2C_6H_5$
10	H	$-CH(C_6H_5)_2$

Reagents: (a) $NaNO_2 \cdot H_2SO_4$; (b) Br_2; (c) $KMnO_4$ / 85% H_3PO_4; (d) EEDQ/DMF; (e) *R*-piperazine

Our objective was to develop a series of novel HLE synthetic inhibitors, including hydrophobic residues covalently linked to β-lactam structures (dibromopenicillanic acid, sulbactam, and 7α-methoxycephalosporin sulfone). Our first approach was to choose three different *N*-substituted piperazines: *N*-methylpiperazine, *N*-benzylpiperazine, and *N*-benzhydrylpiperazine (*N*-Bhpip). They were covalently linked to 6,6-dibromopenicillanic acid-(*S*,*S*)-dioxide (**5**–**7**) and penicillanic acid-(*S*,*S*)-dioxide (sulbactam) (**8**–**10**) (Scheme 1). From this group, *N*-Bhpip was detected as the most potent substituent. Based on the knowledge that *tert*-butyl 7α-methoxycephalosporanate 1,1-dioxide is a potent inhibitor of HNE, we hypothesized that replacing the *tert*-butyl group with hydrophobic amino acids would yield novel potent HNE inhibitors. With a 4-mer combinatorial peptide library, we have shown earlier that hydrophobic amino acids have definite anti-elastase effect (29). The selected amino acids and amino acid esters were covalently linked to 7α-methoxy cephalosporin sulfone (**20**–**31**) and tested for anti-elastase effect.

Experimental

General methods: chemistry

Melting points were measured on a Thomas–Hoover capillary melting point apparatus and were uncorrected. FT-IR spectra were recorded by using PerkinElmer Model 1600 spectrophotometer in chloroform. ^{1}H NMR spectra were recorded on a Bruker 300 spectrophotometer in DMSO-d_6 or $CDCl_3$ referenced to tetramethylsilane as an internal standard at 0.00 ppm. MS spectra were recorded on a high resolution mass spectrophotometer Z AB-IF (electron ionization, 70 eV) and Voyager Biospectrometry Workstation^{TM} based on matrix assisted laser desorption ionization mechanism (MALDI-TOF). Molecular ion peaks for compounds **5**–**10** were obtained. The MS of products **19**–**25**, except product **22**, revealed no molecular ion peak. However, a characteristic homologue $[M]^+$ ion series, subsequently missing – SO_2, – OCH_3, and – $CO\text{-}CH_3COO$, could be assigned. Chromatography generally refers to flash silica gel 60 200–400 mesh (SiliCycle, Quebec, QC, Canada) and TLC plates (Merck Kieselgel 60 F_{254}) with detection using UV or ninhydrine. Thin-layer chromatograms were developed in the following solvent systems: (a) $CHCl_3$:MeOH:AcOH, 95:5:3; (b) BuOH:AcOH:H_2O, 5:2:3; (c) BuOH:pyridine:H_2O, 4:1:1; (d) EtOAc:BuOH:AcOH:H_2O, 2:1:1:1; (e) $CHCl_3$:MeOH:AcOH, 5:3:1; (f) EtOAc:hexane, 8:2; (g) MeOH:$CHCl_3$, 8:2; (h) $CHCl_3$:MeOH, 7:3; or (i) $CHCl_3$:MeOH, 5:5. HPLC wt% analysis was performed on a Waters System 600E Controller at the following conditions: column C18 Bondpack (3.9 × 300 mm), eluent 95:5 (A:B isocratic at 1.0 mL min^{-1}, A = H_2O (0.05% TFA v/v), B = CH_3CN (0.05% TFA v/v)), UV detector at 254 nm. Dimethylformamide (DMF) was distilled over ninhydrine. Dry dichloromethane (DCM) was obtained after filtration over basic alumina. Dicyclohexylcarbodiimide (DCC) was used as 8% solution in DCM. 6,6-Dibromopenicillanic acid-(*S*,*S*)-dioxide was prepared according to refs. 30 and 31. 6-Aminopenicillanic acid (6-APA) and penicillanic acid-(*S*,*S*)-dioxide (sulbactam) were purchased from Sigma-Aldrich (ON, Canada). 7-Aminocephalosporanic acid (7-ACA) was purchased from Fluka (Ronkonkoma, NY). Abbreviations for amino acids follow the recommendations of the IUPAC-IUB Commission on Biochemical Nomenclature (32). Other abbreviations are described as follow: *tert*-butyloxycarbonyl (Boc), 9-fluorenylmethyl ester (OFm), benzyl ester (OBz), *tert*-butyl ester (O-*t*-Bu), *o*-nitrophenyl ester (ONp), 9-aminofluorene (NFm), 7α-methoxycephalosporanic acid 1,1-dioxide (CA).

© 2001 NRC Canada

Synthesis of the compounds 5–10 (Scheme 1)

Method A

To a stirred solution of dibromopenicillanic acid-(*S,S*)-dioxide (0.5 g, 1.2 mmol) in DCM (1 mL) was added DCC (1.5 mL, 0.6 mmol) at 0°C. The reaction mixture was then stirred for 20 min. After the filtration of dicyclohexylurea, the solution was used immediately in the next step. *N*-Methylpiperazine (0.55 g, 6.0 mmol) was added and the reaction was carried out at –5 to 0°C for 2 h. Then ice cold water was added and the mixture was stirred for 15 min. The organic layer was separated and the aqueous phase was extracted three times with DCM. The combined DCM extracts were washed with water, citric acid (10%), and brine. After drying over anhydrous sodium sulfate, the solvent was evaporated off under reduced pressure.

Method B

The synthesis was carried out using the method of mixed anhydrides. For this purpose 1-ethoxycarbonyl-2-ethoxy-1, 2-dihydroquinoline (EEDQ) (33) was used as a coupling reagent. *N*-Benzylpiperazine (0.7 g, 4 mmol) was added to a DMF solution of 6,6-dibromopenicillanic acid-(*S,S*)-dioxide (1.5 g, 4 mmol) followed by EEDQ (1.1 g, 4 mmol). The reaction mixture was then stirred for 48 h at room temp. Then ethyl acetate was added and the organic solution was extracted with water, citric acid (10%), and sodium bicarbonate (1 M). After drying over anhydrous sodium sulfate, the ethyl acetate solution was concentrated under vacuum and purified.

Method C

To a DMF solution of 1-methylpiperazine (0.4 g, 4 mmol), *N*-hydroxybenzotriazole (HOBt) (0.65 g, 4 mmol), 2-(1*H*-benzotriazole-1-yl)-1,1,3,3- tetramethyluronium tetrafluoroborate (TBTU) (1.37 g, 4 mmol), and *N*-methylmorpholine (NMM) (8 mmol) were added, followed by sulbactam (1 g, 4 mmol). The reaction mixture was stirred at room temp for 16 h. Then the mixture was diluted with water (70 mL) and extracted three times with ethyl acetate (100 mL). The organic layer was concentrated under reduced pressure and the isolated product purified.

*(2S)-6,6-Dibromo-3,3-dimethyl-7-oxo-4-thia-1-azabicyclo[3.2.0] heptane-2-(4′-methylpiperazine-4′-yl-1′-amido)-4,4-dioxide (**5**)*: Compound **5** was obtained according to method A and purified by preparative thin layer chromatography. Yield: 28%. EI-MS *m/z* ($C_{13}H_{19}Br_2N_3O_4S$, MW 473.19): 473. FT-IR (cm^{-1}): 3400, 1808, 1753, 1672. ^1H NMR (DMSO-d_6) δ: 3.6 (m, 8H) 2.4 (m, 3H), 1.2 (s, 3H), 1.0 (s, 3H).

*(2S)-6,6-Dibromo-3,3-dimethyl-7-oxo-4-thia-1-azabicyclo[3.2.0] heptane-2-(4′-benzylpiperazine-4′-yl-1′-amido)-4,4-dioxide (**6**)*: The synthesis was carried out using method B. Yield: 30%. EI-MS *m/z* ($C_{19}H_{23}Br_2N_3O_4S$, MW 549.28): 550. FT-IR (cm^{-1}): 1802, 1734, 1649, 1633, 1570. ^1H NMR (DMSO-d_6) δ: 7.60 (m, 5H), 4.72 (t, *J* = 6.1 Hz, 2H), 3.61 (m, 8H), 2.43 (s, 3H), 1.60 (s, 3H), 1.39 (s, 3H).

*(2S)-6,6-Dibromo-3,3-dimethyl-7-oxo-4-thia-1-azabicyclo[3.2.0] heptane-2-(4′-benzhydrylpiperazine-4′-yl-1′-amido)-4,4-dioxide (**7**)*: Compound **7** was obtained using method A. Yield: 45%. EI-MS *m/z* ($C_{25}H_{27}Br_2N_3O_4S$, MW 625.38): 625. FT-IR (cm^{-1}): 2982, 2808, 2760, 1817, 1757, 1690, 1662, 1599, 1551. ^1H NMR (DMSO-d_6) δ: 7.35 (m, 10H), 4.20 (t, *J* = 8.2 Hz, 2H), 3.61 (m, 8H), 2.38 (s, 3H), 1.59 (s, 3H), 1.42 (s, 3H).

*(2S)-3,3-Dimethyl-7-oxo-4-thia-1-azabicyclo[3.2.0]heptane-2-(4′-methylpiperazine-4′-yl-4′-amido)-4,4-dioxide (**8**)*: Compound **8** was obtained according to method C. Yield: 18%. EI-MS *m/z* ($C_{13}H_{21}N_3O_4$ S, MW 315.39): 315. FT-IR (cm^{-1}): 3460, 1790, 1667. ^1H NMR (DMSO-d_6) δ: 3.4–3.8 (m, 8H), 2.4–2.6 (m, 3H), 1.58 (s, 3H), 1.37 (s, 3H).

*(2S)-3,3-Dimethyl-7-oxo-4-thia-1-azabicyclo[3.2.0]heptane-2-(4′-benzylpiperazine-4′-yl-1′-amido)-4,4-dioxide (**9**)*: The synthesis of compound **9** was carried out using method A. Yield: 20%. EI-MS *m/z* ($C_{19}H_{25}N_3O_4S$, MW 391.49): 391. FT-IR (cm^{-1}): 3465, 1789, 1666. ^1H NMR (DMSO-d_6) δ: 7.2–7.4 (m, 5H), 4.88 (s, 1H), 4.73 (s, 1H), 3.4–3.8 (m, 8H), 2.4–2.6 (m, 3H), 1.61 (s, 3H), 1.38 (s, 3H).

*(2S)-3,3-Dimethyl-7-oxo-4-thia-1-azabicyclo[3.2.0]heptane-2-(4′-benzhydrylpiperazine-4′-yl-1′-amido)-4,4-dioxide (**10**)*: Compound **10** was prepared using method C. Yield: 40%. EI-MS *m/z* ($C_{25}H_{29}N_3O_4S$, MW 467.59): 467. FT-IR (cm^{-1}): 3479, 1790, 1681, 1651. ^1H NMR (DMSO-d_6) δ: 7.30 (m, 10H), 4.91 (s, 1H), 4.68 (s, 1H), 3.4–3.8 (m, 8H), 2.4–2.6 (m, 3H), 1.62 (s, 3H), 1.42 (s, 3H).

Chemistry of 7-methoxy cephalosporanic acid-1,1-dioxide *tert*-butyl-7β-aminocephalosporanate (12) (Scheme 2)

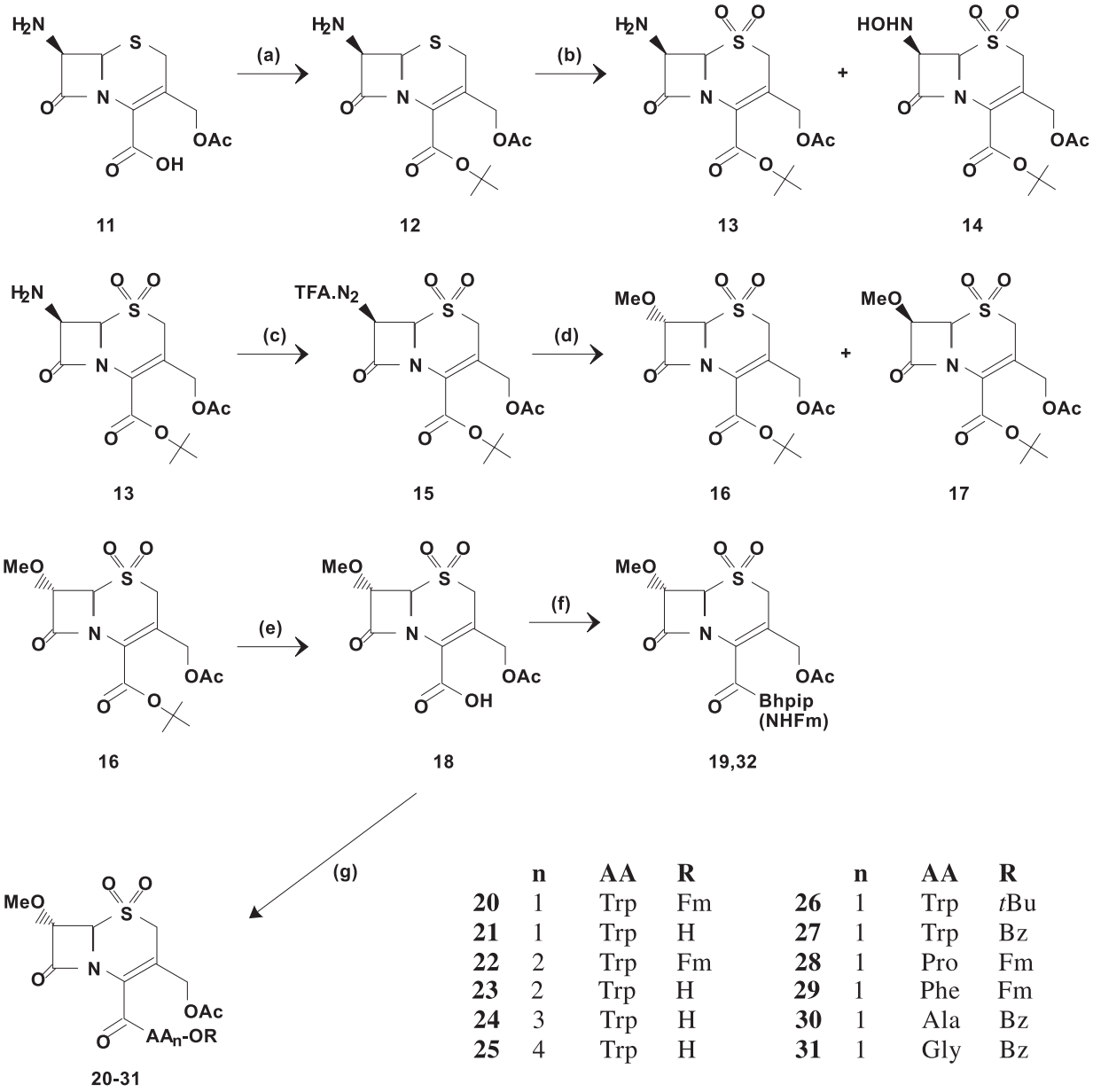
Dry dioxan was freed from peroxides by passage through a column of neutral alumina. To 100 mL of this solvent was added, by turns, ice cooled sulfuric acid (10 mL), 7-ACA (**11**) (10 g, 0.036 mol), and isobutylene (78.8 mL, 0.73 mol). The mixture was sealed in a pressurized bottle, stirred at room temp for 2 h, and then poured into an excess of ice cooled sodium bicarbonate solution (500 mL). Vigorous release of CO_2 occurred. The pH of the aqueous layer was checked during the quenching to maintain a basic pH (pH 8–9) Extraction with ethyl acetate and evaporation of the solvent gave a brown oil residue, which was then purified through a column of silicagel G 60 A (100 g) with chloroform as the eluent. Yield: 41%, mp 110°C. EI-MS *m/z* ($C_{14}H_{20}N_2O_5S$, MW 328.39): 272 [M – $C(CH_3)_3]^+$, 240 [M – $CO\text{-}CH_3COO]^+$. FT-IR (cm^{-1}): 3459, 2975, 1785, 1723, 1526. ^1H NMR ($CDCl_3$) δ: 5.03 (d, *J* = 13.5 Hz, 1H), 4.94 (d, *J* = 5.2 Hz, 1H), 4.79 (d, *J* = 13.5 Hz, 1H), 4.76 (d, *J* = 5.2 Hz, 1H), 3.55 (d, *J* = 18.3 Hz, 1H), 3.35 (d, *J* = 18.3 Hz, 1H), 2.09 (s, 3H), 1.70 (br s, 2H, NH_2), 1.54 (s, 9H).

tert-*Butyl-7β-aminocephalosporanate-1,1-dioxide (**13**)*

In a 250 mL three-necked round-bottomed flask, equipped with a stirrer and device for external cooling–heating was dissolved **12** (5 g, 0.015 mol) in ethyl acetate (100 mL) at 25°C. The solution was stirred quickly while solid sodium tungstate dihydrate (0.5 g, 0.001 mol) and 30% hydrogen peroxide (6.25 mL, 0.061 mol) were added. The temperature of this biphasic mixture was maintained at 20–25°C with cooling for 2 h. The reaction mixture took on a yellow cast due to the

© 2001 NRC Canada

Scheme 2.



	n	AA	R		n	AA	R
20	1	Trp	Fm	**26**	1	Trp	*t*Bu
21	1	Trp	H	**27**	1	Trp	Bz
22	2	Trp	Fm	**28**	1	Pro	Fm
23	2	Trp	H	**29**	1	Phe	Fm
24	3	Trp	H	**30**	1	Ala	Bz
25	4	Trp	H	**31**	1	Gly	Bz

Reagents: (a) isobutylene/H_2SO_4; (b) H_2O_2/Na_2WO_4; (c) isopropylnitrite/TFA/EtOAc;
(d) MeOH/rhodium octanoate dimer / Et_3N; (e) TFA/thioanisol/water;
(f) DCC/HOBT/benzhydrylpiperazine(Bhpip)or 9-N_2H-fluorene; (g) H-$(Trp)_n$-OR (R = Fm or H)

formation of the oxidizing species, sodium pertungstate. After 2 h, an additional amount of 30% hydrogen peroxide (1.25 mL, 0.012 mol) was added. After 18 h, an additional hydrogen peroxide amount was added and the batch was left until completion (21 h). When the reaction was deemed complete (TLC), the mixture was diluted with ethyl acetate (150 mL) and cooled to 10°C. The reaction mixture was well stirred while a solution of sodium sulfite (5 g, 0.037 mol) in water (100 mL) was added slowly to decompose any remaining hydrogen peroxide. After 10 min a test for residual peroxide was performed (starch iodide). The biphasic mixture was further cooled to 5°C, and a cold (5°C) solution of aqueous sodium bicarbonate solution (5%) was added to decompose any oxime by-product (**14**). The reaction mixture was stirred for 10 min at 5°C. Stirring was discontinued until the layers were ready to be separated (30 min). The lower aqueous layer was removed and discarded. The upper ethyl acetate product layer was then washed with saturated sodium chloride solution (100 mL). The organic layer was dried over sodium sulfate (5 g), filtered, and cake washed with ethyl acetate (50 mL). The combined filtrate and liquid phases from washing were concentrated under vacuum to give an oily residue, which was further purified through a silicagel G 60A column, using chloroform–methanol (0 → 50% MeOH). Yield: 18.5%. EI-MS

© 2001 NRC Canada

m/z ($C_{14}H_{20}N_2O_7S$, MW 360.51): 273 [M – SO_2 – $C(CH_3)_3$]$^+$, 196 [M – SO_2 – $COOC(CH_3)_3$]$^+$. FT-IR (cm^{-1}): 3360, 2978, 1798, 1731, 1643, 1359, 1154, 1128. ^1H NMR ($CDCl_3$) δ: 5.12 (d, *J* = 14.0 Hz, 1H), 4.91 (d, *J* = 5.2 Hz, 1H), 4.79 (d, *J* = 14.0 Hz, 1H), 4.76 (d, *J* = 4.9 Hz, 1H), 3.66 (d, *J* = 18.6 Hz, 1H), 2.33 (br s, 2H), 2.09 (s, 3H), 1.54 (s, 9H).

tert-*Butyl-7-diazocephalosporanate-1,1-dioxide (**15**)*

A 500 mL three-necked round-bottomed flask equipped with a mechanical agitator and nitrogen bubbler was charged with **13** (0.5 g, 0.0014 mol) in ethyl acetate (15 mL). A freshly prepared solution of isopropyl nitrite (0.16 g, 20 mmol) in DCM (33) was added to the stirred solution at 15–20°C, followed by a catalytic amount of TFA. The batch temperature rose to 31°C over 15 min and the reaction mixture was stirred for 1 h at this temperature. When the diazotization was complete, the batch was diluted with ethyl acetate and concentrated under reduced pressure at 30°C or less to the previous volume (NB: in isolated form the diazo compound may be explosive, however, previous investigators have suggested that this material may be handled safely as a dilute solution in ethyl acetate. Therefore, it was important that the product did not crystallize near the neck of the flask during concentration. The above flash concentration removed most of the excess unreacted isopropyl nitrite, isopropyl alcohol by-product, and methylene chloride.). Afterwards, the batch was diluted with fresh ethyl acetate and used immediately in the next step.

tert-*Butyl-7α-methoxycephalosporanate-1,1-dioxide (**16**)*

Simultaneously to the preparation of the diazocephalosporanate (**15**), rhodium octanoate dimer (20 mg, 0.02 mmol) was dissolved in methanol (1.7 mL) and diluted with ethyl acetate (13 mL). The solution was let to cool. The mixture from the previous step, containing **15**, was cooled to –5°C and vacuum was purged three times with nitrogen. Before the reaction with the compound **15**, triethylamine (0.05 mL) was added to the catalyst mixture, and the solution was stirred for 5 min. The color changed from blue green to purple, probably due to ligand exchange and (or) complexation of the rhodium octanoate dimer with triethylamine. The catalyst solution was added to the solution of diazocompound for about 1 h. The reaction was carried out in an open flask to eliminate nitrogen gas. After 1 h, the batch was concentrated in vacuo, washed with deionized water, containing sodium chloride and phosphoric acid, and then washed with a solution of 10% sodium chloride. The ethyl acetate layer was dried over anhydrous sodium sulfate and then passed through a bed of silicagel G 60A. The silicagel was then washed with ethyl acetate. The batch and wash were combined and concentrated in vacuo to 40 mL. Hexane (8 mL) was slowly added, the crystallization occurred progressively. The crystallization mixture was further concentrated to 5 mL, diluted with hexane (12 mL) over 4 h, let with stirring 4 h at 25°C, and then for 24 h at 0–5°C. The batch was filtered and cake washed with 6 mL of hexane. The residue was dried completely in vacuo. The major product fraction contained 220 mg (24%) of a white crystalline solid, mp 130 to 131°C (EtOAc–hexane), and was identified as *tert*-butyl-7α-methoxycephalosporanate-1,1-dioxide (**16**) on the basis of its spectral characteristics. EI-MS *m/z* ($C_{15}H_{23}NO_8S$, MW 377.42): 273 [M – $COOC(CH_3)_3$]$^+$, 208 [M – SO_2 – $COOC(CH_3)_3$]$^+$, 180 [M – SO_2 – $COOC(CH_3)_3$ – CO]$^+$, 150 [M – SO_2 – $COOC(CH_3)_3$ – CO – OCH_3]$^+$. FT-IR (cm^{-1}): 2978, 1797, 1723, 1693, 1513, 1369, 1157, 1128. ^1H NMR ($CDCl_3$) δ: 5.20 (d, *J* = 14.1 Hz, 1H), 4.99 (d, *J* = 5.0 Hz, 1H), 4.88 (d, *J* = 12.0 Hz, 1H), 4.34 (d, *J* = 13.2 Hz, 1H), 3.99 (d, *J* = 18.8 Hz, 1H), 3.70 (d, *J* = 18.8 Hz, 1H), 3.60 (s, 3H), 2.10 (s, 3H), 1.55 (s, 9H).

*7α-Methoxycephalosporanic acid-1,1-dioxide (**18**)*

A solution of **16** (50 mg, 0.1 mmol) and thioanisol (0.8 mL) in TFA (4 mL) was stirred at 0°C for 30 min and was then evaporated in vacuo. Two additional aliquots of DCM were added and then evaporated to remove most of the residual TFA. The compound was used directly in the next amidation step.

Synthesis in solution of H-Trp-Trp-Trp-Trp-OH (Boc-Trp-OFm) (34), Boc-strategy (Scheme 3)

9-Fluorenylmethanol (5.07 g, 0.0258 mol) and imidazol (2.35 g, 0.0345 mol) were added to tetrahydrofurane (40 mL). The suspension was stirred at room temp and *t*-Boc-Trp-ONp (**33**) (10 g, 0.23 mol) was added. Stirring was continued for 18 h. The solvent was then removed under reduced pressure. The residue was dissolved in ethyl acetate, and the solution washed with 2% citric acid solution, sodium bicarbonate solution (0.5 N), and water. The ethyl acetate solution was dried over anhydrous sodium sulfate and evaporated to dryness. The compound was purified by flash chromatography silicagel G 60A, using chloroform as an eluent. Yield 80%. R_f^a: 0.55, R_f^b: 0.84, t_R: 13.6 min. EI-MS *m/z* ($C_{30}H_{30}N_2O_4$, MW 482.58): 482, 178, 130. FT-IR (cm^{-1}): 3409, 3328, 3007, 2979, 2930, 1736, 1699, 1664, 1617, 1590.

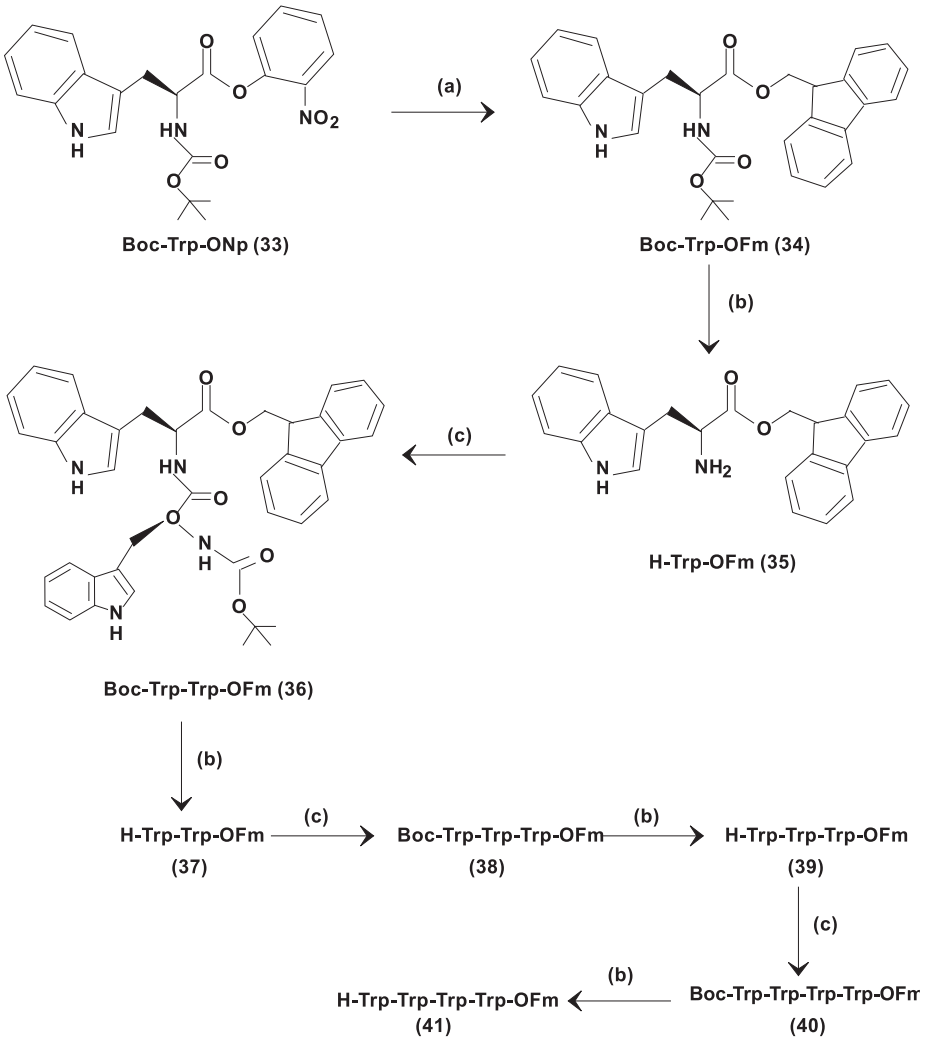
*H-Trp-OFm·HCl (**35**)*: Boc-Trp-OFm (**34**) (2.5g, 5 mmol) was dissolved in ether and HCl gas was passed through the solution until precipitation was observed. The amino acid ester hydrochloride was filtered, washed several times with hexane and dried. Yield 95%, mp 200°C. R_f^a: 0.12, R_f^b: 0.80, t_R: 15.4 min. EI-MS *m/z* ($C_{25}H_{22}N_2O_2$, MW 382.47): 382, 178, 152, 130.

*Boc-Trp-Trp-OFm (**36**)*: To a solution of **35** (0.650 g, 1.5 mmol) and HOBt (0.3 g, 1.9 mmol) in DMF (15 mL) was added NMM (0.2g, 1.9 mmol) followed by **33** (0.8 g, 1.9 mmol). The solution was stirred for 4 h at room temp. A 10-fold excess of water was then added, and the obtained suspension was extracted with ethyl acetate. The organic layer and extracts were combined, washed with 0.1% sodium bicarbonate solution, and evaporated under vacuum. The process was followed by TLC and HPLC. The product was further purified by flash chromatography, using silicagel G 60A and $CHCl_3$–MeOH (0 → 50% MeOH) as the eluent. After the purification step, the obtained compound was 1g (91%), mp 88–90°C. R_f^a: 0.60, R_f^b: 0.83, t_R: 20 min. EI-MS *m/z* ($C_{41}H_{40}N_4O_5$, MW 668.80): 669, 569. FT-IR (cm^{-1}): 3409, 3328, 3007, 2977, 2931, 1736, 1697, 1664, 1617, 1591.

*H-Trp-Trp-OFm·HCl (**37**)*: The deprotection was carried out using the procedure already described for **35**. Yield 78%, mp 164 to 165°C. R_f^a: 0.15, R_f^b: 0.78, t_R: 16.5 min. EI-MS *m/z* ($C_{36}H_{32}N_4O_3$, MW 568.68): 569. FT-IR (cm^{-1}): 3409, 3007, 1736, 1697, 1664, 1516.

© 2001 NRC Canada

Scheme 3.



Reagents: (a) 9-fluorenylmethanol/imidazol/THF; (b) ether/HCl(gas); (c)**26**/HOBt/NMM/DMF

*Boc-Trp-Trp-Trp-OFm (**38**)*: The synthesis was carried out using the method described above for **36**. Yield 90%, mp 93–95°C. R_f^a: 0.64, R_f^b: 0.80, t_R: 21.5 min. EI-MS *m*/*z* ($C_{52}H_{50}N_6O_6$, MW 855.01): 855, 475, 374, 146. FT-IR (cm^{-1}): 3404, 3318, 2928, 1736, 1690, 1663, 1509.

*H-Trp-Trp-Trp-OFm·HCl (**39**)*: The Boc-deprotection was carried out according to the method described above. Yield 70%. R_f^a: 0.04, R_f^b: 0.81, t_R: 17.4 min. EI-MS *m*/*z* ($C_{47}H_{42}N_6O_4$, MW 754.90): 755.

*Boc-Trp-Trp-Trp-Trp-OFm (**40**)*: The reaction was carried out according to the method described above. After 16 h water was added and then the extraction with ethyl acetate was done. After purification, the peptide fractions were pooled together and submitted to TLC, HPLC, and EI-MS analysis. The first and major product was Boc-$(Trp)_4$-OFm (M^+ = 1041, MW 1040), and the second one was *tert*-butylated Boc-$(Trp)_4$-OFm (M^+ = 1097, MW 1096). R_f^a: 0.30, R_f^b: 0.70, t_R: 22 min. EI-MS *m*/*z* ($C_{63}H_{60}N_8O_7$, MW 1041.23): 1040, 941, 740, 569, 474, 375.

Solid phase synthesis of H-Trp-Trp-Trp-Trp-OH, Fmoc-strategy

Synthesis was performed using Fmoc-Trp(Boc)-Wang resin, substitution Fmoc-Trp-(Boc)-OH (0.4 mmol g^{-1}, 2.5 eq), DCC (2.5 eq), and HOBt (5 eq), and NMM as a base. The resin cleavage was carried out with TFA–ethanedithiol–water (95:2.5:2.5) for 1 h at room temp. The following compounds were synthesized:

*H-Trp-Trp-Trp-OH (**39**)*: EI-MS *m*/*z* ($C_{33}H_{35}N_6O_4$, MW 576.66): 577.

*H-Trp-Trp-Trp-Trp-OH (**41**)*: EI-MS *m*/*z* ($C_{44}H_{42}N_8O_5$, MW 762.88): 763.

7α-Methoxycephalosporanic acid-1,1-dioxide derivatives (19–31) (Scheme 2)

*CA-Bhpip (**19**)*

To a solution of **18** (42.5 mg, 0.1 mmol) in DMF (3 mL) was added NMM to pH 8, followed by HOBt (19 mg,

© 2001 NRC Canada

0.1 mmol) and DCC (0.5 mL, 0.1 mmol). The mixture was stirred over 30 min at 0°C. *N*-Bhpip (44 mg, 0.17 mmol) was added and the stirring continued overnight. When the reaction was complete DCM was added, followed by water, and the layers were allowed to separate. The organic layer was washed with citric acid solution (2%), water, and brine. After drying over anhydrous sodium sulfate the solvent was removed under reduced pressure. The compound was then purified by column chromatography on silicagel G60 A using chloroform–methanol (0 → 50% MeOH) as a mobile phase. EI-MS *m/z* ($C_{28}H_{31}N_3O_7S$, MW 553.64): 458 [M – SO_2 – CH_3CO]$^+$, 208 [M – SO_2 – CH_3CO – Bhpip]$^+$. FT-IR (cm^{-1}): 3387, 2936, 1791, 1735, 1682, 1522. ^{1}H NMR ($CDCl_3$) δ: 7.60 (m, 10H), 5.20 (d, *J* = 1.6 Hz, 1H), 4.99 (d, *J* = 14.0 Hz, 1H), 4.88 (d, *J* = 1.6 Hz, 1H), 4.34 (d, *J* = 14.0 Hz, 1H), 3.99 (d, *J* = 19.0 Hz, 1H), 3.4–3.8 (m, 8H), 2.10 (s, 3H).

*CA-Trp-OFm (**20**)*

To a solution of **35** (47 mg, 0. 1mmol), HOBt (19 mg, 0.1 mmol), and TBTU (40 mg, 0.1mmol) in DMF (2 mL) was added NMM to pH 8 followed by **18** (40 mg, 0.1 mmol). The reaction was checked using TLC. After 7 h the reaction was stopped and 10-fold excess of water was added. The solution was then extracted with ethyl acetate. The ethyl acetate layer was dried over anhydrous sodium sulfate and the solvent was removed under reduced pressure. EI-MS *m/z* ($C_{36}H_{33}N_3O_9S$, MW 683.74): 273 [M – CO – Trp-OFm]$^+$, 208 [M – SO_2 – CO – Trp-OFm]$^+$. FT-IR (cm^{-1}): 1797, 1789, 1769, 1745, 1738, 1731, 1713, 1681, 1667, 1573. ^{1}H NMR (DMSO-d_6) δ: 7.2–7.8 (m, 12H), 6.82 (d, *J* = 2.5 Hz, 1H), 5.18 (d, *J* = 1.6 Hz, 1H), 4.80 (s, 2H), 4.67 (d, *J* = 12.8 Hz, 2H), 4.42 (s, 2H), 4.09 (s, 2H), 3.24 (s, 3H), 2.09 (s, 3H).

*CA-Trp-OH (**21**)*: The compound was obtained after deprotection of carboxyl function with 15% piperidine in DMF. EI-MS *m/z* ($C_{22}H_{25}N_3O_9S$, MW 507.52): 369 [M – SO_2 – CH_3CO – OCH_3]$^+$, 183 [M – SO_2 – CH_3CO – OCH_3 – CO – Trp]$^+$. FT-IR (cm^{-1}): 2925, 2854, 1789, 1734, 1714, 1667, 1557, 1519.

*CA-(Trp)$_2$-OFm (**22**)*: The synthesis was carried out according to the method described above. Yield: 31%. EI-MS *m/z* ($C_{47}H_{43}N_5O_{10}S$, MW 869.96): 870. FT-IR (cm^{-1}): 2925, 2854, 1789, 1729, 1714, 1667, 1557, 1519.

*CA-Trp-Trp-OH (**23**)*: Yield 56%. EI-MS *m/z* ($C_{33}H_{33}N_5O_{10}S$, MW 691.72): 413 [M – SO_2 – Trp – OCH_3]$^+$, 199 [M – SO_2 – OCH_3 – CO – Trp]$^+$. FT-IR (cm^{-1}): 2925, 2854, 1789, 1734, 1714, 1667, 1557, 1519.

*CA-(Trp)$_3$-OH (**24**)*: 7α-Methoxycephalosporanic acid-1,1-dioxide (**18**) (37 mg, 0.1 mmol) in DMF was added to peptide-resin (250 mg, 0.4 mmol g^{-1}), followed by DCC (0.65 mL, 0.1 mmol), HOBt (17 mg, 0.1 mmol), and a drop of NMM. The synthesis was carried out overnight. After washing and drying, the resin was cleaved with a mixture of TFA–thioanisol–water (3.5:25:0.25) for 1 h at room temp. The peptide was further precipitated in ice cooled ether (200 mL). The solvent was then evaporated and the product lyophilised (purity 98%, HPLC). EI-MS *m/z* ($C_{44}H_{45}N_7O_{11}S$, MW 879.95): 783 [M – SO_2 – OCH_3]$^+$. FT-IR (cm^{-1}): 1790, 1771, 1742, 1670, 1653, 1637, 1593, 1532, 1510.

*CA-(Trp)$_4$-OH (**25**)*: Yield: 10%. EI-MS *m/z* ($C_{55}H_{55}N_9O_{12}S$, MW 1066.17): 969 [M – SO_2 – OCH_3]$^+$. FT-IR (cm^{-1}): 2926, 2852, 1794, 1774, 1736, 1701, 1666, 1654, 1560, 1523, 1509.

*CA-Trp-O-t-Bu (**26**)*: Yield: 12%. EI-MS *m/z* ($C_{26}H_{31}N_3O_9S$, MW 561.62): 563, 228 [M – CH_3 – $OCOCH_2$ – Trp-O-*t*-Bu]$^+$, 136 [M – CH_3OCOCH_2 – Trp-O-*t*-Bu – SO_2]$^+$. FT-IR (cm^{-1}): 3370, 1787, 1735, 1679, 1508, 1458, 1385, 1157. ^{1}H NMR (DMSO-d_6) δ: 7.18 (m, 4H), 6.80 (d, *J* = 2.5 Hz, 1H), 5.19 (d, *J* = 1.6 Hz, 1H), 4.81 (t, *J* = 6.4 Hz, 1H), 4.75 (s, 2H), 4.40 (d, *J* = 2.5 Hz, 1H), 4.08 (s, 2H), 3.32 (s, 3H), 2.12 (s, 3H), 1.45 (s, 9H).

*CA-Trp-OBz (**27**)*: Yield: 10%. EI-MS *m/z* ($C_{29}H_{29}N_3O_9S$, MW 595.63): 596, 484 [M – OCH_3 – SO_2 – CH_3]$^+$, 277 [M – CO – Trp-OBz]$^+$, 137 [M – CO – Trp-OBz – SO_2 – CH_2OCOCH_3]$^+$. FT-IR (cm^{-1}): 3378, 1795, 1741, 1666, 1571, 1135. ^{1}H NMR (DMSO-d_6) δ: 7.20 (m, 5H), 7.18 (m, 4H), 6.80 (d, *J* = 2.8 Hz, 1H), 5.21 (d, *J* = 1.4 Hz, 1H), 4.81 (t, *J* = 7.1 Hz, 1H), 4.75 (s, 2H), 4.42 (d, *J* = 2.5 Hz, 1H), 4.08 (s, 2H), 3.33 (s, 3H), 2.07 (s, 3H).

*CA-Pro-OFm (**28**)*: Yield: 8%. EI-MS *m/z* ($C_{30}H_{30}N_2O_9S$, MW 594.64): 595, 564 [M – OCH_3]$^+$, 286 [M – Pro-OFm]$^+$. FT-IR (cm^{-1}): 3410, 2960, 1794, 1550. ^{1}H NMR (DMSO-d_6) δ: 7.3–7.8 (m, 8H) 5.21 (d, *J* = 1.4 Hz, 1H), 4.75 (s, 2H), 4.70 (d, *J* = 12.8 Hz, 2H), 4.46 (d, *J* = 15.8 Hz, 1H), 4.21 (t, *J* = 7.0 Hz, 1H), 4.08 (s, 2H), 3.32 (t, *J* = 6.3 Hz, 2H), 3.24 (s, 3H), 2.09 (s, 3H), 1.87 (t, *J* = 7.5 Hz, 2H), 1.60 (m, 2H).

*CA-Phe-OFm (**29**)*: Yield: 10%. EI-MS *m/z* ($C_{34}H_{32}N_2O_9S$, MW 644.70): 645, 614 [M – OCH_3]$^+$. FT-IR (cm^{-1}): 3401, 1790, 1731, 1679, 1391, 1185. ^{1}H NMR (DMSO-d_6) δ: 7.8–7.1 (m, 13H), 5.22 (d, *J* = 1.4 Hz, 1H), 4.81 (t, *J* = 7.5 Hz, 1H), 4.75 (s, 2H), 4.40 (d, *J* = 12.8 Hz, 1H), 4.13 (s, 2H), 3.3 (s, 3H), 2.11 (s, 3H).

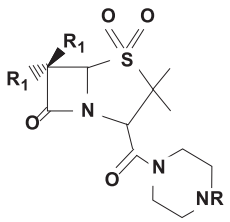
*CA-Ala-OBz (**30**)*: Yield: 12%. EI-MS *m/z* ($C_{20}H_{22}N_2O_9S$, MW 466.47): 466, 407 [M – $COOCH_3$]$^+$, 343 [M – $COOCH_3$ – SO_2]$^+$, 233 [M – $COOCH_3$ – SO_2 – OBz]$^+$, 135 [M – $COOCH_3$ – SO_2 – CO – Ala-OBz]$^+$. FT-IR (cm^{-1}): 3370, 2983, 1786, 1739, 1662, 1384, 1227, 1156. ^{1}H NMR (DMSO-d_6) δ: 7.4–7.6 (m, 5H), 5.22 (d, *J* = 1.2 Hz, 1H), 4.75 (d, *J* = 12.8 Hz, 2H), 4.43 (d, *J* = 12.0 Hz, 1H), 4.07 (d, *J* = 5.8 Hz, 2H), 4.08 (s, 2H), 3.24 (d, *J* = 18.6 Hz, 3H), 2.10 (s, 3H).

*CA-Gly-OBz (**31**)*: Yield: 30%. EI-MS *m/z* ($C_{19}H_{20}N_2O_9S$, MW 452.44): 452, 355 [M – $COOCH_3$ – SO_2]$^+$, 261 [M – $COOCH_3$ – SO_2 – OBz]$^+$, 107 (OBz), 135 [M – $COOCH_3$ – SO_2 – CO – Gly-OBz]$^+$. FT-IR (cm^{-1}): 3408, 1786, 1738, 1710, 1665, 1385, 1134. ^{1}H NMR (DMSO-d_6) δ: 7.4–7.6 (m, 5H), 5.22 (d, *J* = 1.2 Hz, 1H), 4.75 (d, *J* = 12.8 Hz, 2H), 4.4 (d, *J* = 12.8 Hz, 1H), 4.13 (d, *J* = 6.9 Hz, 2H), 4.08 (s, 2H), 3.24 (d, *J* = 18.6 Hz, 3H), 2.10 (s, 3H).

*CA-NFm (**32**)*: Yield: 40%. EI-MS *m/z* ($C_{24}H_{22}N_2O_7S$, MW 482.51): 451 [M – OCH_3]$^+$. FT-IR (cm^{-1}): 3411, 2874, 1788, 1726, 1665, 1368, 1187. ^{1}H NMR (DMSO-d_6) δ: 7.3–7.8 (m, 8H), 5.21 (s, 1H), 4.75 (s, 2H), 4.46 (s, 1H), 4.42 (d, *J* = 12.8 Hz, 1H), 3.35 (s, 3H), 2.01 (s, 3H).

© 2001 NRC Canada

Table 1. Physico-chemical data and anti-elastase activity of penicillin amides **5**–**10**.



	R	R_1	% yield	mp (°C)	t_r (min)	R_f[a]	IC_{50}	Formula
5	CH_3	Br	28	oil	14.7	[b]0.59, [f]0.66	>40	$C_{13}H_{19}Br_2N_3O_4S$
6	$CH_2C_6H_5$	Br	30	oil	10.5	[a]0.09, [f]0.64	inactive	$C_{19}H_{23}Br_2N_3O_4S$
7	$CH(C_6H_5)_2$	Br	45	oil	15.2	[b]0.57, [i]0.66	>40	$C_{25}H_{27}Br_2N_3O_4S$
8	CH_3	H	18	oil	—	[a]0.21, [f]0.48	>40	$C_{13}H_{21}N_3O_4S$
9	$CH_2C_6H_5$	H	20	oil	—	[a]0.15, [f]0.50	inactive	$C_{19}H_{25}N_3O_4S$
10	$CH(C_6H_5)_2$	H	40	oil	—	[a]0.20, [b]0.51	40	$C_{25}H_{29}N_3O_4S$

[a]TLC solvent systems are described in *General methods* section.

Elastase inhibition assay

Neutrophil elastase (HNE) activity was determined with the specific human neutrophil elastase substrate *N*-methoxy-succinyl-alanyl-alanyl-prolyl-valyl-*p*-nitroanilide (MeO-Succ-Ala-Ala-Pro-Val-pNA, Sigma, St. Louis) as described in ref. 12. HNE inhibitory capacity was determined by incubating 20 nM HNE with 0–1 μM inhibitor for 1–24 h at room temp. Residual elastase activity was assayed with MeO-Succ-Ala-Ala-Pro-Val-pNA by measuring the change in absorbance 1 min at 410 nm in a spectrophotometer (model DU7, Beckman Instruments Inc., Montreal, Qc).

Results and discussion

Chemistry

Penicillin derivatives

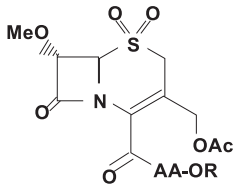
The commercially available 6-APA, (**1**) (Scheme 1) was first converted to 6,6-dibromopenicillanic acid (**2**) using a diazotization–halogenation procedure (30). A high-yield conversion of **1** to **2** was achieved since the diazo intermediate, once formed, was more easily brominated. The biphase of the diazotization–bromination reaction exploited the solubility of bromine and the 6,6-dibromopenicillanic acid intermediate in organic solvents and the solubility of hydrogen bromide in water. Following Scheme 1, **1** was added to a cooled DCM–sulfuric acid mixture, containing sodium nitrite and bromine, and was converted to the desired 6,6-dibromopenicillanic acid (**2**) in high yield (80%). 6,6-Dibromopenicillanic acid (**2**), once formed, was converted in a very high yield (more than 90%) to the corresponding sulfone (**3**) by a potassium permanganate oxidation (31). The synthesis of the final compounds **5**–**10** was achieved using three different methods: (A) method of symmetrical anhydrides, using dicyclohexylcarbodiimide (DCC) as a coupling reagent, (B) method of mixed anhydrides with the use of EEDQ (33) as a coupling reagent, and (C) amidation via HOBt active ester procedure, using the activating agent TBTU or with DCC. The compounds having formula **5**–**10** obtained after synthesis were 93–99% pure as evidenced by HPLC and TLC analysis (Table 1). They were isolated as micro-crystalline solids or oils. FT-IR, EI-MS, and ^{1}H NMR spectroscopy confirmed the structures.

*Synthesis of 7α-methoxy-cephalosporanic acid-1,1-dioxide (**18**) (Scheme 2)*

The synthesis was carried out according to Scheme 2. 7-ACA (**11**) was used as a starting material. It was apparent that any synthesis of **18** must involve two key chemical transformations, i.e., oxidation of 1-sulfide to the corresponding 1-sulfone and conversion of the 7β-amino group to the 7α-methoxy group. For this reason our preparation followed the procedure described by Blackock et al. (34). Following Scheme 2, the carboxylic function of **11** was protected by esterification with isobutylene, using the method of Stedmann (35). Compound **12** was then oxidized to *tert*-butyl-7-aminocephalosporanate-1,1-dioxide (**13**). Direct oxidation of 7-ACA *tert*-butyl ester to the corresponding sulfone caused some unique problems due to the potential for *N*-oxidation of the 7-amino group. As in step one, we believed that protection from *N*-oxidation might come via protonation of the amine prior to the oxidation step. Our initial attempts to oxidize compound **12** using *m*-chloroperoxybenzoic acid (*m*-CPBA) were unsuccessful. However, using sodium tungstate as a catalyst and 30% hydrogen peroxide solution we managed to obtain the sulfone, but in very low yield (18.5%). Some *N*-oxidation occurred to form 20% of a nearly insoluble and crystalline by-product, 7-hydroxyimino sulfone derivative (**14**) of 7-ACA *tert*-butyl ester. Synthesis of *tert*-butyl-7α-methoxycephalosporanate-1,1-dioxide (**16**) was the next step. For the diazotization–methoxylation procedure we followed the method previously described (34). The use of isopropyl nitrite as the diazotizing reagent facilitated the workup, as the by-product (isopropyl alcohol) reaction could be readily removed from the reaction mixture by vacuum replacement concentration. The fast reaction rate of methoxylation ensured a higher insertion yield, but slowing down the rate with a reduced methanol and catalyst charge increased stereoselectivity. For this reason cold (0°C) ethyl acetate solution, containing rhodium octanoate dimer, methanol, and thriethylamine was added slowly over 1 h to the cold solution of the diazocomponent. *tert*-Butyl-7β-methoxy-cephalosporanate (**17**) was also obtained as a by-product.

© 2001 NRC Canada

Table 2. Physico-chemical data and antielastase activity of cephalosporin amides **20**–**31**.



	AA	R	% yield	mp (°C)	R_f[a]	t_R (min)	IC_{50}	Formula
20	Trp	Fm	24	foam	[b]0.65, [c]0.84	8.7	0.8	$C_{36}H_{33}N_3O_9S$
21	Trp	H	42	oil	[a]0.01, [b]0.66	—	>40	$C_{22}H_{25}N_3O_9S$
22	$(Trp)_2$	Fm	37	oil	[a]0.05, [b]0.60	10.0	15	$C_{47}H_{43}N_5O_{10}S$
23	$(Trp)_2$	H	98	oil	[b]0.72, [c]0.80	13.7	>40	$C_{33}H_{33}N_5O_{10}S$
24	$(Trp)_3$	H	31	oil	[a]0.09, [b]0.67	17.9	>40	$C_{44}H_{45}N_7O_{11}S$
25	$(Trp)_4$	H	56	oil	[b]0.95, [c]0.80	18.1	>40	$C_{35}H_{55}N_9O_{12}S$
26	Trp	*t*-Bu	10	oil	[a]0.10, [b]0.60	15.2	<40	$C_{26}H_{31}N_3O_9S$
27	Trp	Bz	10	oil	[a]0.11, [b]0.58	11.4	10	$C_{29}H_{29}N_3O_9S$
28	Pro	Fm	8	oil	[d]0.76, [e]0.41	12.7	>40	$C_{30}H_{30}N_2O_9S$
29	Phe	Fm	10	oil	[a]0.06, [b]0.62	9.6	<40	$C_{34}H_{32}N_2O_9S$
30	Ala	Bz	12	oil	[b]0.07, [h]0.20	10.9	>40	$C_{20}H_{22}N_2O_9S$
31	Gly	Bz	30	oil	[a]0.05, [h]0.17	10.7	<40	$C_{19}H_{20}N_2O_9S$

[a]TLC solvent systems are described in *General methods* section.

The free acid **18** was obtained by cleavage of *tert*-butyl ester group with TFA–thioanisol. Compound **18**, a light yellow oil, was used without isolation in the next amidation step.

Synthesis in solution of H-Trp-Trp-Trp-Trp-OH, Boc-strategy (Scheme 3)

A method for the synthesis of tetra-tryptophanyl-9-fluorenylmethyl ester was developed. From numerous methods proposed for the preparation of amino acids esters, we selected the imidazol-catalyzed transesterification of a commercially available protected amino acid active ester, Boc-Trp-ONp (33). Following Scheme 3, in the first step the *o*-nitrophenylester group was substituted with the 9-fluorenylmethyl ester group using the method of Bednarek and Bodansky (36). The *tert*-butyloxycarbonyl amino protection of **34**, **36**, **38**, and **40** could be cleaved either by TFA or by gaseous HCl as the fluorenylmethyl ester group remains unaffected under these conditions. For the synthesis we chose gaseous HCl Boc-cleavage. The next tryptophanyl residue was then attached using Boc-Trp-ONp ester. The coupling was carried out using HOBt–active ester in situ formation in the presence of NMM as a base. It is interesting to note that the fluorenylmethyl group contributes to the solubility of the protected peptides in organic solvents. Thus, fluorenylmethyl esters might offer some advantages in peptide synthesis, particularly because they are readily removable under mild conditions (15% piperidine in DMF).

Solid phase synthesis of H-Trp-Trp-Trp-Trp-OH, Fmoc-strategy

Synthesis was performed using Fmoc-Trp(Boc)-Wang resin, substitution Fmoc-Trp(Boc)-OH (0.4 mmol g^{-1}, 2.5 eq), DCC (2.5 eq), HOBt (5 eq), and MMM as a base. The cleavage from the resin was carried out with TFA–ethanedithiol–water (95:2.5:2.5) for 1 h at room temp. The final product (**41**) was purified by HPLC.

7α-Methoxycephalosporanic acid derivatives (19–32) (Scheme 2)

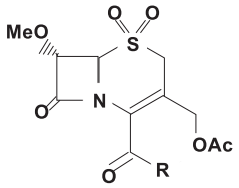
The synthesis of the compounds with the formula **19**–**32** was achieved in low to moderate yield using the method of active esters. The predicted structures were confirmed by FT-IR, NMR, and EI-MS spectroscopy. Physico-chemical data for the compounds from this series are shown in Tables 2 and 3.

In vitro activity

In vitro inhibition of HLE activity by the target compounds is shown in Tables 1, 2, and 3 as nominal IC_{50} values (μM). From the results in Table 1, it can be seen that the compounds prepared on the basis of the penicillin structures (dibromopenicillanic acid and sulbactam) are very poor time-dependant inhibitors of HLE. From this series of compounds, we chose *N*-Bhpip as the most promising substituent and it was determined that compound **19**, on the basis of cephalosporin structures, had a strong anti-elastase effect (IC_{50} = 0.8 μM) (Table 3). Substitution of *N*-Bhpip with 9-aminofluorene gave compound **32**, which exhibited poor anti-elastase activity. Biological data for the compounds with amino acids and amino acid esters covalently linked to the cephalosporin (structures **20**–**31**) are shown in Table 2. Replacement of the *tert*-butyl ester group in **16** with tryptophanyl-9-fluorenylmethyl ester gave compound **20**, possessing the same anti-elastase activity as **19**. The free carboxylic group on **21** gave a diminished anti-elastase effect. The addition of more tryptophanyl residues gave poor HLE inhibitors (**22**–**25**), as demonstrated by the absence of activity in the compound with up to four tryptophanyl residues. Both the tryptophanyl residue and the Fm ester group were found to be essential for anti-HLE activity. Replacement of the Fm ester group in **20** with *t*-Bu (**26**) and benzyl (Bz) (**27**) ester groups gave poor anti-elastase inhibitors. Furthermore, the importance of tryptophanyl was

© 2001 NRC Canada

Table 3. Physico-chemical data and antielastase activity of cephalosporin sulfones.



	R	% yield	mp (°C)	R_f[a]	t_R (min)	IC_{50}	Formula
16	O-*t*-Bu	24	130 to 131	[a]0.53, [f]0.55	—	1.0	$C_{15}H_{23}NO_8S$
19	Bhpip	42	foam	[a]0.15, [b]0.54	10.9	0.8	$C_{28}H_{31}N_3O_7S$
32	NHFm	30	oil	[f]0.29, [g]0.73	—	<40	$C_{24}H_{22}N_2O_7S$

[a]TLC solvent systems are described in *General methods* section.

demonstrated by the substitution of tryptophanyl 9-fluorenylmethyl ester with prolyl-9-fluorenylmethyl ester and phenylalanyl-9-fluorenylmethyl ester yielding compounds **28** and **29**, respectively, with reduced anti-elastase activity. Finally, the substitution of tryptophanyl-9-fluorenylmethyl ester with commercially available alanyl benzyl ester (**30**) and glycyl benzyl ester (**31**) gave the same results.

Conclusion

We have demonstrated that replacement of *t*-butyl ester group in 7α-methoxycephalosporanic acid 1,1-dioxide with tryptophanyl-9-fluorenylmethyl ester (compound **20**) yields a strong HLE inhibitor with a length of action beyond 24 h. Deprotection of the carboxylic function resulted in loss of activity. Replacement of tryptophan with tetra-tryptophan or other amino acids, as well as replacement of tryptophanyl-9-fluorenylmethyl ester with other tryptophanyl-esters led to compounds with diminished anti-elastase effect. However, replacement of tryptophanyl-9-fluorenylmethyl ester with the hydrophobic *N*-Bhpip gave compound **19** having the same inhibitory effect as **20**, both of which are novel HLE inhibitors.

Acknowledgements

This study was supported by a grant from the Canadian Cystic Fibrosis Foundation (CCFF). Dr. Koteva was a fellow of the CCFF and Dr. Escher is holder of a J.C. Edwards chair of cardiovascular research. The authors thank Diane Cloutier for expert technical assistance, Micheline Poulin for excellent secretarial assistance, and Maud Deraët for proof-reading of this contribution.

References

1. S. Suter, U.B. Schaad, P. Roux-Lombard, E. Girardin, G. Grau, and J.M. Dayer. Am. Rev. Respir. Dis. **140**, 1640 (1989).
2. P.M. Starkey and A.J. Barrett. Biochem. J. **155**, 265 (1976).
3. R.G. Crystal. J. Clin. Invest. **85**, 1343 (1990).
4. J. Travis and G.S. Salvesen. Annu. Rev. Biochem. **52**, 655 (1983).
5. E.J. Campbell and M.A. Campbell. J. Cell. Biol. **106**, 667 (1988).
6. E.J. Campbell, R.M. Senior, J.A. McDonald, and D.L. Cox. J. Clin. Invest. **70**, 845 (1982).
7. A.B. Cohen and H.L. James. Am. Rev. Respir. Dis. **126**, 25 (1982).
8. P.M. Henson and R.B. Johnston Jr. J. Clin. Invest. **79**, 669 (1987).
9. J.R. Mohammed, B.S. Mohammed, L.J. Pawluk, D.M. Bucci, N.R. Baker, and W.B. Davis. J. Lab. Clin. Med. **112**, 711 (1988).
10. K.C. Meyer and J. Zimmerman. J. Lab. Clin. Med. **121**, 654 (1993).
11. A. Cantin, G. Bilodeau, and R. Begin. Pediatric Pulmonology **7**, 12 (1989).
12. A.M. Cantin, S. Lafrenaye, and R.O. Begin. Pediatric Pulmonology, **11**, 249 (1991).
13. G.L. Snider. Eur. J. Respir. Med. **146**, 17 (1986).
14. B.M. Ashe, R.L. Clark, H. Jones, and M. Zimmerman. J. Biol. Chem. **256**, 11 603 (1981).
15. B.M. Ashe and M. Zimmerman. Biochem. Biophys. Res. Commun. **75**, 194 (1977).
16. M.O. Lively and J.C. Powers. Biochem. Biophys. Acta, **525**, 171 (1978).
17. T. Teshima, J.C. Griffin, and J.C. Powers. J. Biol. Chem. **257**, 5085 (1982).
18. J.C. Powers, R. Boone, D.L. Carroll, B.F. Gupton, C.M. Kam, N. Nishino, M. Sakamoto, and P.M Tuhy. J. Biol. Chem. **259**, 4288 (1984).
19. J.B. Doherty, B.M. Ashe, L.W. Argenbright, P.L. Barker, R.J. Bonney, G.O Chandler, M.E. Dahlgren, C.P Dorn, P.E. Finke, R.A. Firestone, D. Fletcher, W.K. Hagmann, R. Mumford, L. O'Grady, A.L. Maycock, J.M. Pisno, S.K. Shah, K.R. Thompson, and M. Zimmerman. Nature (London), **322**, 192 (1986).
20. J.B Doherty, B.M. Ashe, P.L. Barker, T.J. Blacklock, J.W. Butcher, G.O. Chandler, M.E. Dahlgren, P. Davies, C.P. Dorn, Jr., P.E. Finke, R.A. Firestone, W.K. Hagmann, T. Halgren, W.B. Knight, A.L. Maycock, M.A. Navia, L. O'Grady, J. Pisano, S.K. Shah, K.R. Thompson, H. Weston, and M. Zimmerman. J. Med. Chem. **33**, 2513 (1990).
21. P.E. Finke, B.M. Ashe, W.B. Knight, A.L. Maycock, M.A. Navia, S.K. Shah, K.R. Thompson, D.J. Underwood, H. Weston, M. Zimmerman, and J.B. Doherty. J. Med. Chem. **33**, 2522 (1990).
22. S.K. Shah, K.A. Brause, G.O. Chandler, P.E. Finke, B.M. Ashe, H. Weston, W.B. Knight, A.L. Maycock, and J.B. Doherty. J. Med. Chem. **33**, 2529 (1990).
23. W.B. Knight, A.L. Maycock, B.G. Green, B.A. Ashe, P. Gale, H. Weston, P.E Finke, W.K. Hagmann, S.K. Shah, and J.B. Doherty. Biochemistry, **31**, 4980 (1992).

© 2001 NRC Canada

24. M. Alpegiani, A. Baici, and P. Bissolino. Eur. J. Med. Chem. **27**, 875 (1992).
25. M. Alpegiani, P. Bissolino, E. Perrone, G. Cassinelli, and G. Franceschi. Tetrahedron Lett. **32**, 6207 (1991).
26. M. Alpegiani, P. Bissolino, and D. Borghi. Bioorg. Med. Chem. Lett. **2**, 1127 (1992).
27. S.N. Maiti, D.E. Woods, and A.M. Cantin. Drugs Future, **23**, 635 (1998).
28. M. Alpegiani, P. Bissolino, R. Corigli, S. Del Nero, E. Perrone, V. Rizzo, N. Sacchi, G. Cassinelli, G. Franceschi, and A. Baici. J. Med. Chem. **37**, 4003 (1994).
29. A. Lavoie, A.M. Cantin, and E. Escher. *In* Pept. Chem. Struct. Biol. Proc. 14th Am. Pept. Symp. *Edited by* P.T. Kaumeya and R.S. Hodges. Mayflower Sci., Kingswinford, U.K. 1996. pp. 297–298.
30. R.A. Volkmann, R.D. Carroll, R.B. Drolet, M.L. Elliott, and B.S. Moore. J. Org. Chem. **77**, 3344 (1982).
31. D.A. Johnson, C.A. Panetta, and P.E. Copper. J. Org. Chem. **28**, 1927 (1963).
32. IUPAC- IUB joint commission on biochemical nomenclature (JCBN). Eur. J. Pharmacol. **163**, 263 (1983).
33. B. Belleau and G. Malek. J. Am. Chem. Soc. **90**, 1651 (1968).
34. T.J. Blackock, J.W. Butcher, P. Sohar, T.R. Lamanec, and J.E. Grabowski. J. Org. Chem. **54**, 3907 (1988).
35. J.R Stedman. J. Med. Chem. **9**, 444 (1966).
36. M.A. Bednarek and M. Bodansky. Int. J. Pept. Protein Res. **21**, 196 (1983).

© 2001 NRC Canada

Excess enthalpies of the ternary mixtures: ethyl *tert*-butylether + *n*-heptane + (*n*-decane or *n*-dodecane) at 298.15 K

Zhaohui Wang, Yoshiteru Horikawa, George C. Benson, and Benjamin C.-Y. Lu

Abstract: Excess molar enthalpies, measured at 298.15 K in a flow microcalorimiter, are reported for the two ternary systems, ethyl *tert*-butylether + *n*-heptane + *n*-decane and ethyl *tert*-butylether + *n*-heptane + *n*-dodecane. Smooth representations of the results were used to construct constant enthalpy contours on Roozeboom diagrams. It is shown that useful estimates of the ternary enthalpies can be obtained from the Liebermann–Fried model using only the physical properties of the components and their binary mixtures.

Key words: excess enthalpies, ternary mixtures, ethyl *tert*-butylether, *n*-alkanes, Liebermann–Fried model.

Résumé : Utilisant un microcalorimètre à écoulement, on a mesuré les enthalpies molaires en excès, à 298,15 K, de deux systèmes ternaires, oxyde d'éthyle et de *tert*-butyle + *n*-heptane + *n*-décane et oxyde d'éthyle et de *tert*-butyle + *n*-heptane + *n*-dodécane. On a utilisé des représentations aplanies des résultats pour construire des contours de constante d'enthalpie sur des diagrammes de Roozeboom. On a démontré que l'on peut obtenir des évaluations utiles des enthalpies ternaires à l'aide du modèle de Liebermann–Fried en n'utilisant que les propriétés physiques des composants et de leurs mélanges binaires.

Mots clés : enthalpies en excès, mélanges ternaires, oxyde d'éthyle et de *tert*-butyle, alcanes linéaires, modèle de Liebermann–Fried.

[Traduit par la Rédaction]

Introduction

In view of the use of ethers as oxygenating agents in gasoline technology, the properties of ether + hydrocarbon systems are of considerable interest. A recent paper (1) from our laboratory described measurements of the excess molar enthalpies of the two ternary mixtures (ethyl *tert*-butylether + *n*-hexane + *n*-heptane and ethyl *tert*-butylether + *n*-hexane + *n*-octane). As a continuation of that investigation, we have made similar measurements for the analogous systems (ethyl *tert*-butylether + *n*-heptane + (either *n*-decane or *n*-dodecane)).

Experimental

Ethyl *tert*-butylether (ETBE), with mol fraction purity exceeding 0.97, was purchased from TCI America. The *n*-heptane (nC7), *n*-decane (nC10), and *n*-dodecane (nC12) were obtained from Sigma-Aldrich. The *n*-alkanes had purities of at least 99 mol%. Apart from partial degassing, all of the component liquids were used without further purification. Their densities, measured at 298.15 K, were 735.39, 680.14, 726.26, and 745.29 kg m^{-3} for ETBE, nC7, nC10, and nC12, respectively. These values are in reasonable agreement with the literature (2–4).

An LKB-Produkter AB (Bramma, Sweden) flow microcalorimeter (Model 10700-1) was used to measure excess molar enthalpies (H^E_m) at 298.150 ± 0.003 K. Details of this equipment and its operation have been described previously (5). The excess molar enthalpies of the ternary mixtures were investigated by measuring the excess molar enthalpies ($H^E_{m,1+23}$) for several pseudo-binary mixtures, in which component 1 (ETBE) was added to binary mixtures of components 2 (nC7) and 3 (either nC10 or nC12), having a fixed mol ratio x_2/x_3. These binaries were prepared by weighing. The excess molar enthalpy ($H^E_{m,123}$) of the ternary mixture was then obtained from the relation:

$$[1] \qquad H^E_{m,123} = H^E_{m,1+23} + (1 - x_1) H^E_{m,23}$$

where $H^E_{m,23}$ is the excess molar enthalpy of the particular binary mixture. Over most of the mol fraction range, the errors in the excess molar enthalpies are estimated to be less than ±0.5%. Errors in the mol fractions of the ternary mixtures are estimated to be less than 5×10^{-4}.

Results and discussion

Excess molar enthalpies ($H^E_{m,ij}$ $(i < j)$) at 298.15 K for four of the five constituent binaries of present interest, have been reported in the literature: ETBE + nC7 (6), ETBE + nC10 and ETBE + nC12 (7), and nC7 + nC12 (8). Table 1 summarizes the present experimental measurements for the binary system nC7 + nC10. The smoothing function:

Received December 1, 2000. Published on the NRC Research Press Web site on April 27, 2001.

Z. Wang, Y. Horikawa, G.C. Benson[1], and B.C.-Y. Lu. Department of Chemical Engineering, University of Ottawa, Ottawa, ON K1N 6N5, Canada.

[1]Corresponding author (telephone: (613) 562–5800 (6118); fax: (613) 562–5172; e-mail: gbenson@eng.uottawa.ca).

 DOI: 10.1139/cjc-79-4-388 © 2001 NRC Canada

Table 1. Experimental excess molar enthalpies $H^{E}_{m,23}$ (J mol^{-1}) at 298.15 K for $x_2CH_3(CH_2)_5CH_3 + (1 - x_2)CH_3(CH_2)_8CH_3$.

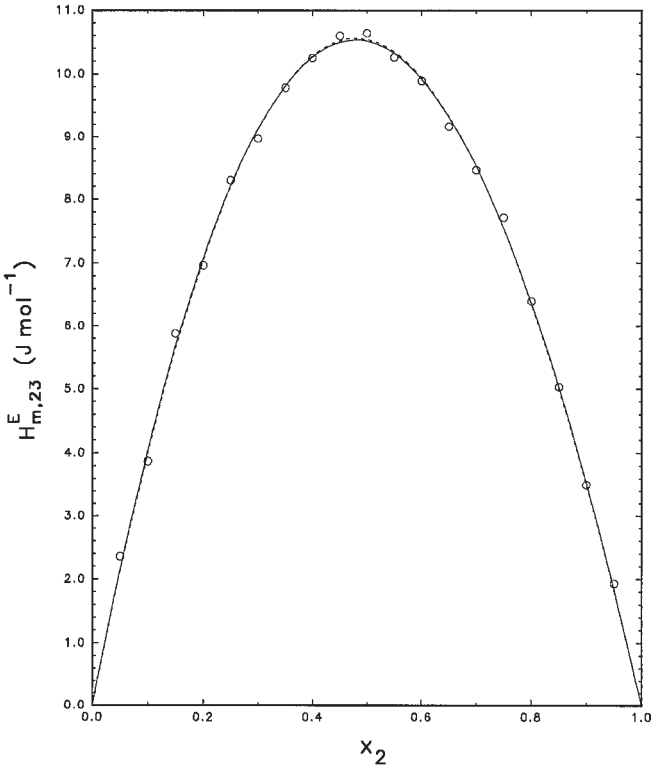
x_2	$H^{E}_{m,23}$	x_2	$H^{E}_{m,23}$	x_2	$H^{E}_{m,23}$	x_2	$H^{E}_{m,23}$	x_2	$H^{E}_{m,23}$
0.0500	2.36	0.2500	8.30	0.4500	10.60	0.6500	9.17	0.8502	5.03
0.1000	3.87	0.2999	8.98	0.4999	10.64	0.7002	8.46	0.9000	3.51
0.1499	5.88	0.3504	9.79	0.5497	10.26	0.7500	7.71	0.9500	1.93
0.2002	6.97	0.4000	10.25	0.6004	9.90	0.8004	6.41	—	—

Table 2. Parameters (h_k) and standard deviations (s) for the representation of $H^{E}_{m,ij}$ at 298.15 K by eq. [2].

Component		Parameters				
i	j	h_1	h_2	h_3	h_4	s
nC7	nC10	42.06	3.55	—	—	0.12
ETBE	nC7[a]	1124.24	12.58	61.80	70.75	0.68
ETBE	nC10[b]	1458.02	–133.95	43.59	—	2.48
ETBE	nC12[b]	1733.01	–211.76	63.62	—	2.10
nC7	nC12[c]	121.20	4.01	–4.07	–3.76	0.10

[a]See ref. 6.
[b]See ref. 7.
[c]See ref. 8.

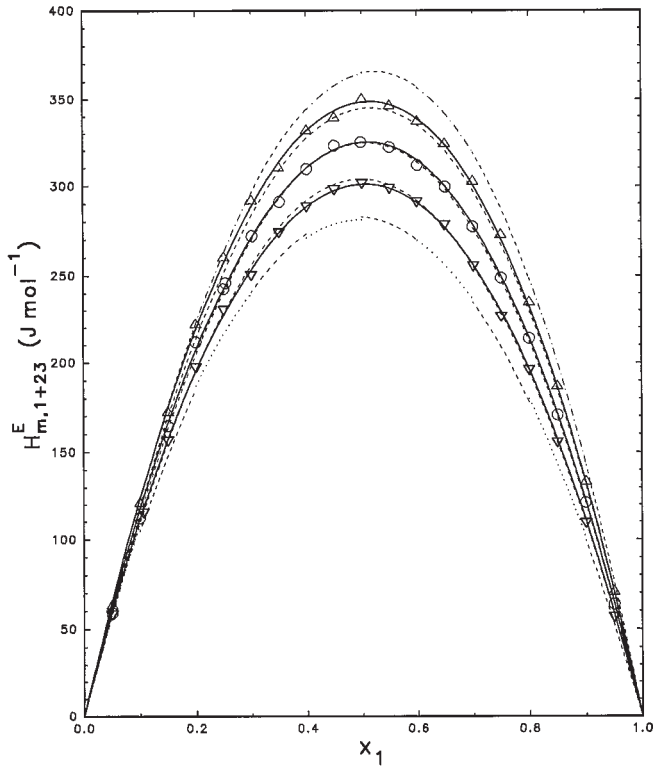
Fig. 1. Excess molar enthalpies ($H^{E}_{m,23}$) (J mol^{-1}) at 298.15 K, for $x_2CH_3(CH_2)_5CH_3 + x_3CH_3(CH_2)_8CH_3$. Experimental results: present work (○). Curves: calculated from the representation of the results by eq. [2] (—); Liebermann–Fried fit (- - -).



$$[2] \qquad H^{E}_{m,ij} = x_i(1-x_i)\sum_{k=1}^{n} h_k(1-2x_i)^{k-1}$$

was fitted to these results by the method of least squares with all points weighted equally. The number of coefficients (n) employed in the fit was selected on the basis of the changes in the values of the standard deviation (s) for increasing values of n (F-test). Values of the coefficients (h_k)

Fig. 2. Excess molar enthalpies ($H^{E}_{m,1+23}$) at 298.15 K, for the addition of ETBE to binary mixtures of nC7 + nC10 to form $x_1CH_3CH_2OC(CH_3)_3 + x_2CH_3(CH_2)_5CH_3 + x_3CH_3(CH_2)_8CH_3$. Experimental results: $x_2/x_3 = 0.3332$ (△); $x_2/x_3 = 1.0002$ (○); $x_2/x_3 = 3.0008$ (▽). Curves: $x_2 = 0$ (·—·—), Wang et al. (7); $x_3 = 0$, (····) Peng et al. (6); calculated from the representation of the results by eqs. [3] and [4], using the ternary term $H^{E}_{m,T}$ given in the footnote of Table 3 (—); estimated from the Liebermann–Fried model (- - - -).



are listed in Table 2, along with those for the representations of the four other binary systems. Also included in Table 1

© 2001 NRC Canada

Table 3. Experimental excess molar enthalpies ($H^E_{m,1+23}$) (J mol^{-1}) at 298.15 K for the addition of ETBE to nC7 + nC10 to form $x_1CH_3CH_2OC(CH_3)_3 + x_2CH_3(CH_2)_5CH_3 + x_3CH_3(CH_2)_8CH_3$, and values of $H^E_{m,123}$ (J mol^{-1}) calculated from eq. [1] using the smooth representation of $H^E_{m,23}$ (J mol^{-1}) by eq. [2].

x_1	$H^E_{m,1+23}$[a]	$H^E_{m,123}$	x_1	$H^E_{m,1+23}$[a]	$H^E_{m,123}$	x_1	$H^E_{m,1+23}$[a]	$H^E_{m,123}$
x_2/x_3 = 0.3332, $H^E_{m,23}$ /(J mol^{-1}) = 11.03								
0.0501	63.38	73.86	0.4002	332.08	338.70	0.6999	302.78	306.09
0.0999	121.11	131.04	0.4500	339.52	345.59	0.7498	272.87	275.63
0.1500	172.38	81.76	0.5002	350.22	355.73	0.8002	234.92	237.12
0.1998	222.16	230.99	0.5499	346.47	351.43	0.8499	186.92	188.58
0.2499	260.29	268.56	0.5999	337.29	341.70	0.9000	133.45	134.55
0.3001	292.13	299.85	0.6496	324.04	327.91	0.9500	70.78	71.33
0.3498	310.49	317.66						
x_2/x_3 = 1.0002, $H^E_{m,23}$ /(J mol^{-1}) = 10.51								
0.0501	59.04	69.03	0.3511	291.32	298.14	0.6999	277.26	280.42
0.0992	112.45	121.92	0.4003	309.73	316.04	0.7500	248.85	251.48
0.1499	164.65	173.59	0.4503	322.97	328.75	0.8000	214.00	216.10
0.2002	211.78	220.19	0.4986	325.01	330.28	0.8501	170.73	172.31
0.2500	242.62	250.51	0.5500	322.05	326.78	0.8999	121.11	122.16
0.2535	246.04	253.89	0.6004	311.77	315.97	0.9500	63.68	64.21
0.3013	272.07	279.42	0.6504	299.72	303.40			
x_2/x_3 = 3.0008, $H^E_{m,23}$/(J mol^{-1}) = 4.74								
0.0499	58.43	62.93	0.4002	288.75	291.59	0.7008	255.56	256.98
0.1059	115.74	119.98	0.4501	298.38	300.99	0.7506	226.64	227.82
0.1498	156.70	160.73	0.5002	301.82	304.19	0.7999	196.26	197.21
0.2000	197.78	201.57	0.5500	299.03	301.16	0.8500	155.76	156.47
0.2501	230.70	234.25	0.5990	291.38	293.28	0.9001	109.62	110.09
0.2997	250.53	253.85	0.6488	278.48	280.14	0.9500	56.83	57.07
0.3501	274.27	277.35						

[a]Ternary term for representation of $H^E_{m,1+23}$ by eqs. [3] and [4]: $H^E_{m,T}$ (J mol^{-1}) = $(x_1x_2x_3/(1 - x_1 + x_2))(456.81 - 484.35x_1 - 661.81x_2)$, s = 2.06.

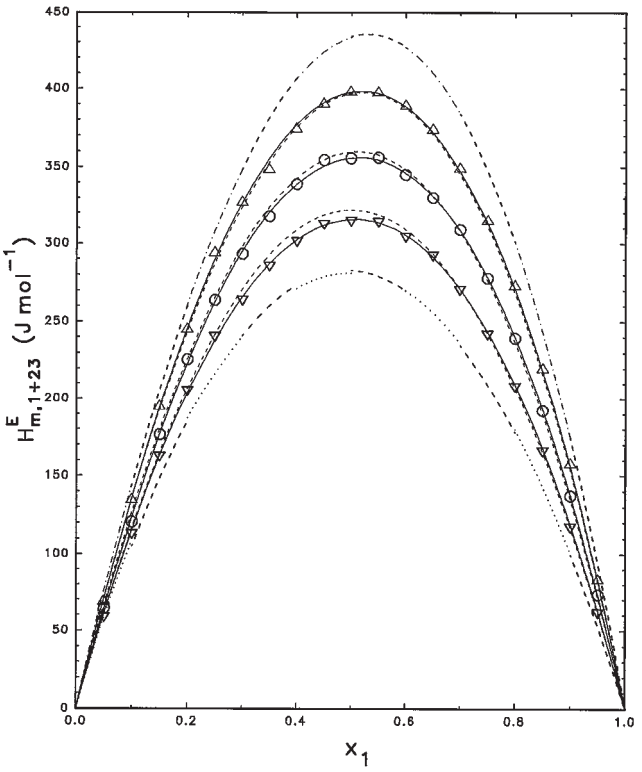


Fig. 3. Excess molar enthalpies ($H^E_{m,1+23}$) at 298.15 K, for the addition of ETBE to binary mixtures of nC7 + nC12 to form $x_1CH_3CH_2OC(CH_3)_3 + x_2CH_3(CH_2)_5CH_3 + x_3CH_3(CH_2)_{10}CH_3$. Experimental results: x_2/x_3 = 0.3335 (△); x_2/x_3 = 0.9999 (○); x_2/x_3 = 3.0029 (▽). Curves: x_2 = 0, (·—·—) Wang et al. (7); x_3 = 0 (····), Peng et al. (6); calculated from the representation of the results by eqs. [3] and [4], using the ternary term $H^E_{m,T}$ given in the footnote of Table 4 (—); estimated from the Liebermann–Fried model (- - - -).

are the values of the standard deviation (s) for each of the representations. Plots of the experimental results in Table 1 and their representation by eq. [2] are presented in Fig. 1.

The experimental results for $H^E_{m,1+23}$ and the corresponding values of $H^E_{m,123}$ are listed in Tables 3 and 4 for the nC10 and nC12 ternary systems, respectively. Plots of $H^E_{m,1+23}$ vs. the mol fraction (x_1) of ETBE are given in Figs. 2 and 3. Also included in these figures are the smooth representations of the excess molar enthalpies of the constituent-binaries, corresponding to the cases x_2 = 0 and x_3 = 0. These were calculated from eq. [2] using the coefficients in Table 2. In all cases, the maximum values of $H^E_{m,1+23}$ and $H^E_{m,123}$ occur near x_1 = 0.5, and for comparable values of x_2/x_3, the maximum is larger for the mixture with nC12. For both systems at constant x_1, the enthalpies decrease as x_2/x_3 increases.

© 2001 NRC Canada

Table 4. Experimental excess molar enthalpies ($H^E_{m,1+23}$) (J mol^{-1}) at 298.15 K for the addition of ETBE to nC7 + nC12 to form $x_1CH_3CH_2OC(CH_3)_3 + x_2CH_3(CH_2)_5CH_3 + x_3CH_3(CH_2)_{10}CH_3$, and values of $H^E_{m,123}$ (J mol^{-1}) calculated from eq. [1] using the smooth representation of $H^E_{m,23}$ (J mol^{-1}) by eq. [2].

x_1	$H^E_{m,1+23}$[a]	$H^E_{m,123}$	x_1	$H^E_{m,1+23}$[a]	$H^E_{m,123}$	x_1	$H^E_{m,1+23}$[a]	$H^E_{m,123}$
x_2/x_3 = 0.3335, $H^E_{m,23}$/(J mol^{-1}) = 22.83								
0.0496	68.87	90.56	0.3992	374.42	388.13	0.6999	349.38	356.23
0.0998	134.65	155.20	0.4496	390.58	403.14	0.7504	314.94	320.64
0.1498	195.06	214.47	0.4991	398.19	409.62	0.7998	273.09	277.66
0.2000	245.27	263.53	0.5498	397.81	408.09	0.8502	220.06	223.48
0.2499	294.28	311.40	0.6003	389.34	398.46	0.9000	157.89	160.17
0.3000	327.35	343.33	0.6501	374.02	382.01	0.9501	83.34	84.48
0.3494	348.53	363.38	—	—	—	—	—	—
x_2/x_3 = 0.9999, $H^E_{m,23}$/(J mol^{-1}) = 30.30								
0.0501	64.16	92.94	0.3997	339.06	357.25	0.7001	308.90	317.99
0.1001	120.37	147.64	0.4501	354.43	371.09	0.7499	277.75	285.33
0.1501	176.49	202.24	0.4995	355.63	370.79	0.7997	239.38	245.45
0.2001	225.83	250.07	0.5501	356.15	369.78	0.8501	192.44	196.98
0.2501	263.67	286.39	0.6001	345.27	357.39	0.9000	137.22	140.25
0.3006	293.18	314.37	0.6500	330.09	340.70	0.9500	73.38	74.90
0.3498	317.55	337.25	—	—	—	—	—	—
x_2/x_3 = 3.0029, $H^E_{m,23}$/(J mol^{-1}) = 22.24								
0.0500	58.80	79.92	0.4002	301.66	315.00	0.6996	270.56	277.24
0.1000	113.19	133.20	0.4500	312.84	325.07	0.7499	242.29	247.85
0.1500	162.74	181.64	0.5001	314.88	326.00	0.7998	208.36	212.81
0.2001	205.51	223.30	0.5503	314.24	324.24	0.8501	166.34	169.67
0.2498	240.80	257.48	0.6004	304.60	313.48	0.9002	117.53	119.75
0.3002	263.99	279.55	0.6502	292.58	300.36	0.9500	61.96	63.07
0.3501	85.78	300.23	—	—	—	—	—	—

[a]Ternary term for representation of $H^E_{m,1+23}$ by eqs. [3] and [4]: $H^E_{m,T}$ (J mol^{-1}) = $x_1x_2x_3(16.07 + 3483.96x_1 - 1654.81x_2 - 8496.55x_1^2 - 244.63x_1x_2 + 1461.44x_2^2 + 5442.69x_1^3)$, s = 1.94.

As in our previous work (1), the values of $H^E_{m,1+23}$ were represented as a sum of binary terms with an added ternary correction:

$$[3] \qquad H^E_{m,1+23} = \left[\frac{x_2}{1-x_1}\right] H^E_{m,12} + \left[\frac{x_3}{1-x_1}\right] H^E_{m,13} + H^E_{m,T}$$

where the values of the $H^E_{m,ij}$ were calculated from the appropriate smoothing functions. The form (which was adopted for the latter contribution):

$$[4] \qquad \frac{H^E_{m,T}}{\text{J mol}^{-1}} = \left[\frac{x_1x_2x_3}{1+b(x_2-x_1)}\right](c_0 + c_1x_1 + c_2x_2 + c_3x_1^2 + c_4x_1x_2 + c_5x_2^2 + c_6x_1^3 + c_7x_1^2x_2 + \ldots)$$

is similar to the form used by Morris et al. (9) but with the possibility of incorporating an extra skewing factor $(1 + b(x_2 - x_1))^{-1}$. Values of b = 1 and b = 0 were used for the nC10 and nC12 systems, respectively. The values of the parameters (c_k) were obtained from least-squares analyses, in which eqs. [3] and [4] were fitted to the experimental $H^E_{m,1+23}$ in Tables 3 and 4. The results of these analyses are given in the footnotes of the tables, where the standard deviations (s) of the representations are also indicated. The solid curves in Figs. 2 and 3 were calculated from these representations.

Table 5. Values of the interaction parameters A_{ij} and A_{ji}, standard deviation (s) (J mol^{-1}), and isobaric thermal expansivity (α_p) (kK^{-1}) at 298.15 K.

Component					α_p	
i	j	A_{ij}	A_{ji}	s	i	j
ETBE	nC7	0.8726	0.9305	2.10	1.401	1.256
ETBE	nC10	0.9596	0.7906	2.43	1.401	1.051
nC7	nC10	1.0218	0.9622	0.13	1.256	1.051
ETBE	nC12	0.9680	0.7418	2.06	1.401	0.960
nC7	nC12	1.0637	0.9008	0.12	1.256	0.960

Equations [1]–[4] were also used to calculate the constant $H^E_{m,123}$ contours plotted on the Roozeboom diagrams in Figs. 4*a* and 5*a*. The general characteristics of these plots are very similar and are comparable to those found in our earlier work (1). All of the contours extend to the edges of the triangle and there is no indication of an extremum lying within the triangle.

Recently, it has been found that the Liebermann–Fried model (10) can be extended to provide estimates of the thermodynamic properties of multicomponent systems using only the properties of the pure components and interaction parameters derived from analyses of the excess enthalpies of their constituent-binaries. This approach was investigated for the present systems. Reference can be made to the work of Wang et al. (1) for the equations used in this application.

© 2001 NRC Canada

Fig. 4. Contours for constant values of $H^{E}_{m,123}$ /(J mol^{-1}) for the system ETBE + nC7 + nC10 at 298.15 K. (*a*) Calculated from the representation of the experimental results by eqs. [1]–[4] with $H^{E}_{m,T}$ from the footnote of Table 3. (*b*) Estimated from the Liebermann–Fried model.

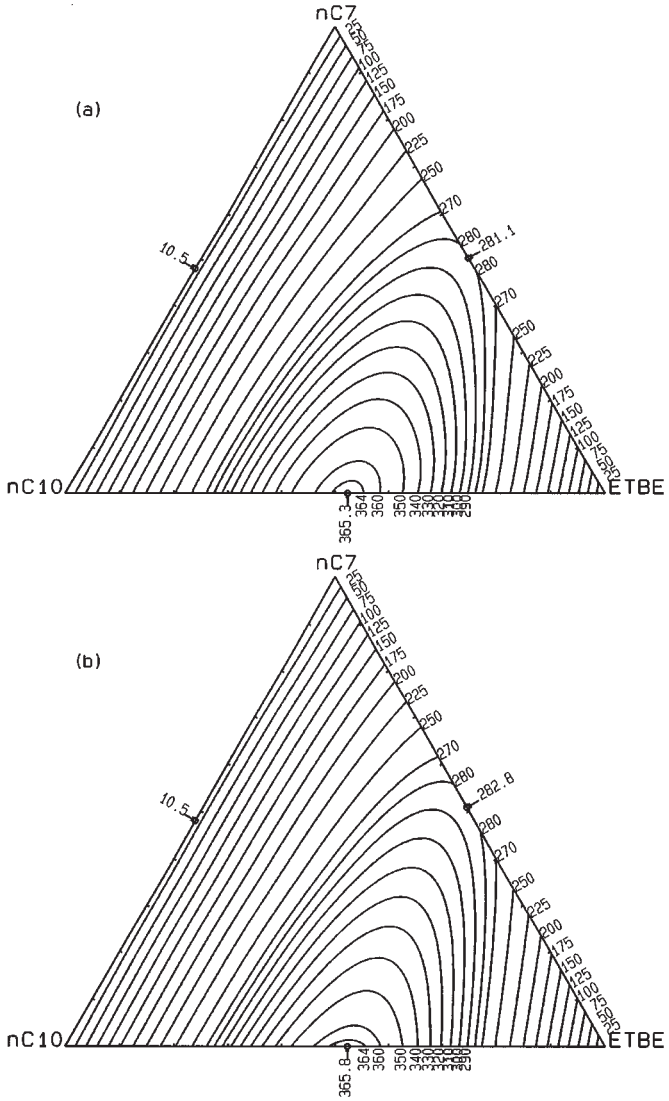
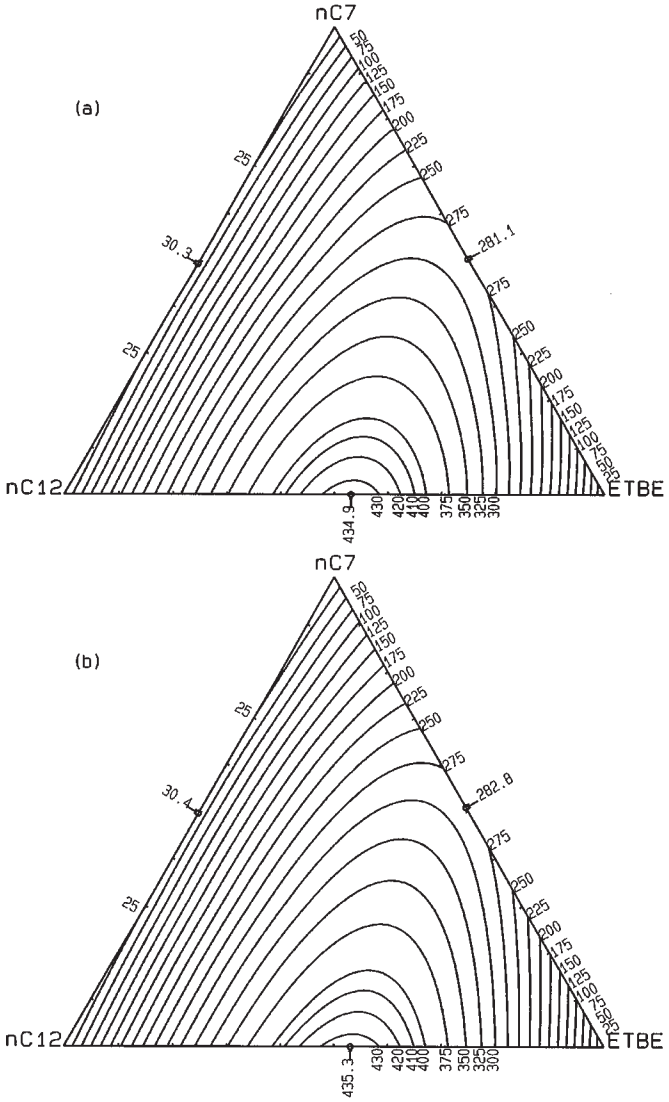


Fig. 5. Contours for constant values of $H^{E}_{m,123}$ /(J mol^{-1}) for the system ETBE + nC7 + nC12 at 298.15 K. (*a*) Calculated from the representation of the experimental results by eqs. [1]–[4] with $H^{E}_{m,T}$ from the footnote of Table 4. (*b*) Estimated from the Liebermann–Fried model.



The Liebermann–Fried interaction parameters (A_{ij} and A_{ji}) for the constituent-binaries are given in Table 5. These values were obtained by fitting the Liebermann–Fried formula for H_{ij} to the primary experimental data for the excess molar enthalpies given in Table 1 and refs. 6–8. Also included in the table are the standard deviations obtained in the fitting process, and values of the isobaric thermal expansivity (α_p) (2, 11), used in evaluating the contributions due to the different sizes of the molcules.

Using the values of the parameters given in Table 5, $H^{E}_{m,1+23}$ and $H^{E}_{m,123}$ were estimated for the present ternary mixtures. The Liebermnn–Fried fits of $H^{E}_{m,ij}$ and the results for $H^{E}_{m,1+23}$ are shown as dashed curves in Figs. 1–3. In general, the fits of $H^{E}_{m,ij}$ are quite good, but there is a tendency to over-estimate the values of $H^{E}_{m,1+23}$. The mean absolute relative deviations of the 58 points for the nC10 system in Table 3 and the 57 points for the nC12 system in Table 4 amount to 1.1% and 1.3%, respectively.

Constant $H^{E}_{m,123}$ contours were also estimated on the basis of the Liebermann–Fried model. For both systems, the overall characteristics of these are quite similar to those derived from the representations of the experimental data by eqs. [1]–[4]. The results of the estimations are shown on the Roozeboom diagrams in Figs. 4*b* and 5*b*. It is clear from a comparison of parts (*a*) and (*b*) in these figures, that for the present type of systems the model provides useful estimates of $H^{E}_{m,123}$ without requiring the direct investigation of the excess enthalpies of any ternary mixtures.

Acknowledgements

The authors are indebted to the Natural Sciences and Engineering Research Council of Canada (NSERC) for financial support of this work.

© 2001 NRC Canada

References

1. Z. Wang, D.-Y. Peng, G.C. Benson, and B.C.-Y. Lu. J. Chem. Thermodyn. In press 10 November 2000.
2. M. Obama, Y. Oodera, N. Kohama, T. Yanase, Y. Saito, and K. Kusano. J. Chem. Eng. Data, **30**, 1 (1985).
3. TRC thermodynamic tables; non-hydrocarbons. Thermodynamics Research Center, The Texas A&M University System, College Station, Tex. 1988. p. a-6090.
4. TRC thermodynamic tables; hydrocarbons. Thermodynamics Research Center, The Texas A&M University System, College Station, Tex. 1988. pp. a-1010 and a-1011.
5. R. Tanaka, P.J. D'Arcy, and G.C. Benson. Thermochim. Acta, **11**, 163 (1975); F. Kimura, G.C. Benson, and C.J. Halpin. Fluid Phase Equilib. **11**, 245 (1983).
6. D.-Y. Peng, Z. Wang, G.C. Benson, and B.C.-Y. Lu. J. Chem. Thermodyn. In press 6 June 2000.
7. Z. Wang, Y. Horikawa, G.C. Benson, and B.C.-Y. Lu. J. Soln. Chem. In press.
8. M.K. Kumaran and G.C. Benson. J. Chem. Thermodyn. **18**, 993 (1986).
9. J.W. Morris, P.J. Mulvey, M.M. Abbott, and H.C. Van Ness. J. Chem. Eng. Data, **20**, 403 (1975).
10. E. Liebermann and V. Fried. Ind. Eng. Chem. Fundam. **11**, 350 (1972); Ind. Eng. Chem. Fundam. **11**, 354 (1972).
11. G.C. Benson, B. Luo, and B.C.-Y. Lu. Can. J. Chem. **66**, 531 (1988).

© 2001 NRC Canada

Demethoxylation and hydroxylation of methoxy- and hydroxybenzoic acids by OH-radicals. Processes of potential importance for food irradiation

Birgit Gaisberger and Sonja Solar

Abstract: The hydroxylation process for methoxy- and hydroxy-benzoic acids (MBA, HBA) induced by γ-radiation is compared. 2-, 3-, and 4-methoxybenzoic acid as well as 3-hydroxybenzoic acid have been irradiated in N_2O and aerated solutions up to 1.5 kGy. The products were analyzed by HPLC. The results for 2- and 4-HBA have been taken from literature data. The $OH^{\bullet}$-adduct distribution is generally the same for the hydroxy- as well as for the methoxy-benzoic acid isomers. With both 4-HBA and 4-MBA more than 65% C3-adducts and about 15% C4-adducts are formed, which could be proved by their reactions with $K_3Fe(CN)_6$. Oxidation of the nonipso-adducts of 3-HBA and 3-MBA results in 84 and 87% of the corresponding phenols. Whereas in N_2O-saturated solutions only part of the $OH^{\bullet}$-radicals leads to substrate decomposition, in the presence of air, the degradation of both kinds of compounds is equivalent to $[OH^{\bullet}]$. The nonipso $OH^{\bullet}$-adducts of the HBAs are converted into 68–77% hydroxylation products. With the MBAs, the hydroxylation process is ≤10%. This is attributed to different decay pathways of the peroxyl radicals, intermediates formed by O_2 addition to the $OH^{\bullet}$-adducts. The hydroxyperoxycyclohexadienyl radicals of the HBAs decay mainly by $HO_2^{\bullet}$ elimination to the corresponding phenols, those of the MBAs decay predominantly by fragmentation of the benzene ring, yielding to nonidentified aliphatic products. The replacement of $-OCH_3$ by -OH is practically not influenced by the presence of oxygen, it increases in the sequence 3-MBA < 4-MBA < 2-MBA. For 2-MBA, yields of more than 15% are obtained. Both processes, hydroxylation as well as demethoxylation, might be of importance for the recognition of radiolytical changes in foodstuff.

Key words: γ-radiolysis, methoxybenzoic acids, hydroxybenzoic acids, phenolic acids, food components, reaction mechanisms, product analysis, HPLC analysis.

Résumé : On a fait une étude comparative des processus d'hydroxylation, induits par un rayonnement γ, des acides méthoxy- et hydroxy-benzoïques (AMB, AHB). On a irradié les acides 2-, 3- et 4-méthoxybenzoïques ainsi que l'acide 3-hydroxybenzoïque en solutions saturées en N_2O et en solutions aérées, jusqu'à 1,5 kGy. On a analysé les produits par CLHP. Les résultats pour les acides 2- et 4-AHB correspondent aux données que l'on peut retrouver dans la littérature. La distribution de l'adduit $OH^{\bullet}$ est généralement la même pour les isomères des acides hydroxy- ainsi que méthoxy-benzoïques. Avec les acides 4-AHB et 4-AMB il se forme dans chaque cas plus de 65% d'adduits C3 et environ 15% d'adduits C4 ce qui a pu être démontré par leurs réactions avec le $K_3Fe(CN)_6$. L'oxydation des adduits non ipso des acides 3-AHB et 3-AMB conduit à la formation de 84 et de 87% des phénols correspondants. Lors des réactions en solutions saturées en N_2O, il n'y a qu'une partie des radicaux $OH^{\bullet}$ qui conduit à une décomposition du substrat; par ailleurs, en présence d'air, la dégradation des deux types de composés est équivalent à la $[OH^{\bullet}]$. Les adduits de $OH^{\bullet}$ non ipso des AHB sont transformés à 68–77% en produits d'hydroxylation. Avec les AMB, le processus d'hydroxylation est ≤ 10%. Ceci est attribué à divers modes de décomposition des radicaux peroxyles qui se forment de façon intermédiaire par l'addition de O_2 aux adduits $OH^{\bullet}$. Les radicaux hydroxyperoxycyclohexadiényles des AHB se décomposent principalement par une élimination de $HO_2^{\bullet}$ conduisant aux phénols correspondants alors que ceux des AMB se décomposent principalement par une fragmentation du noyau benzénique en conduisant à des produits aliphatiques non identifiés. Le remplacement d'un $-OCH_3$ par un -OH n'est pratiquement pas influencé par la présence d'oxygène; il augmente dans la séquence 3-AMB < 4-AMB < 2-AMB. Pour le 2-AMB, on obtient des rendements de plus de 15%. Les deux processus, l'hydroxylation ainsi que la déméthoxylation, peuvent présenter de l'intérêt pour la reconnaissance des changements radiolytiques dans les aliments de nature végétale.

Mots clés : radiolyse γ, acides méthoxybenzoïques, acides hydroxybenzoïques, acides phénoliques, composants alimentaires, mécanismes réactionnels, analyse des produits, analyse par CLHP.

[Traduit par la Rédaction]

Received July 20, 2000. Published on the NRC Research Press Web site on April 30, 2001.

B. Gaisberger and S. Solar.[1] Institute for Theoretical Chemistry and Structural Biology, University of Vienna, Althanstr. 14, A-1090 Vienna, Austria.

[1]Corresponding author (telephone: +43-1-4277-52725; fax: +43-1-4277-52795; e-mail: sonja.solar@univie.ac.at).

 DOI: 10.1139/cjc-79-4-394 © 2001 NRC Canada

Introduction

Hydroxybenzoic acids and their derivatives are ubiquitous in plant material. The phenolic groups of these compounds are often methoxylated or present as glycoside (1–3). Upon irradiation of aqueous aromatic compounds, the main primary process is the electrophilic addition of $OH^{\bullet}$-radicals to activated ring positions, which can eventually result in hydroxylation of the initial material. Such radiolytically formed hydroxylated compounds can be used as markers for irradiated food, as is the case with *o*-tyrosine, originating from phenylalanine in protein rich food (4–7). The detection of hydroxylation products from phenolic acid-food components was proposed in 1989 as a promising chemical method for the detection of irradiation treatment of fruits and vegetables (8, 9), but no marker compounds have been found so far.

For methoxybenzoic acids, it has been reported that upon irradiation in the presence of N_2O and at pH ≤ 3, radical cations and phenoxyl radicals are generated. Radical cations are formed from the nonipso $OH^{\bullet}$-adducts by an acid-catalysed water elimination. The phenoxyl radicals result from methanol elimination from the ipso adduct carrying the methoxyl group (10, 11). The work of these authors concentrated on the detection of these radical intermediates by pulse radiolysis and on the determination of methanol. There are, however, no data concerning the formation of the phenolic products from methoxylated benzoic acids. Upon radiolysis of *ortho*- and *para*-hydroxybenzoic acid, the formation of phenolic products has been found to be the major reaction path (12–15).

This study focuses on a comparison of γ-radiation-induced degradation and hydroxylation processes of benzoic acids with free as well as methoxylated OH-groups, and its importance for the detection of radiation-chemical changes of phenolic components in food of plant origin. Priority was given to the influence of oxygen on the product distribution.

Experimental

Chemicals and preparation of the solutions

All chemicals were of the highest purity commercially available: 4-methoxybenzoic acid (4-MBA) (*p*-anisic acid) (Aldrich, 99%), 3-MBA (*m*-anisic acid) (Aldrich, 99%), 2-MBA (*o*-anisic acid) (Fluka, 99%), 2-hydroxybenzoic acid (2-HBA) (Merck, 98%), 3-HBA and 4-HBA (Merck, 98%), 3,4-dihydroxybenzoic acid (3,4-DHBA) (Aldrich, 97%), 2,3-DHBA (Aldrich, 99%), 2,5-DHBA (Aldrich, 97%), 4-hydroxy-3-methoxybenzoic acid (vanillic acid (VA)) (Aldrich, 97%), 3-hydroxy-4-methoxybenzoic acid (isovanillic acid (iso-VA)) (Sigma, 97%), 2-hydroxy-3-methoxybenzoic acid (3-methoxysalicylic acid (3-MSA)) (Aldrich, 97%), 4-MSA (Aldrich, 97%), 5-MSA (Aldrich, 97%), sodium hydroxide (Fluka, 98%), $K_3Fe(CN)_6$ (Fluka, 98%), and phosphoric acid (Aldrich, 98%). Solutions were made with triple-distilled water. To obtain oxidizing conditions, the solutions were saturated with high purity N_2O or oxygen (5.0, Messer Griessheim) prior to irradiation.

Gamma radiolysis

γ-Radiolysis experiments (Gammacell 220, MDS Nordion International Inc., Kanata, Ontario, Canada) were carried out at a dose rate of 160 Gy min^{-1}, which was determined by Fricke dosimetry using a radiation chemical yield of *G*-value[2] *G* (Fe^{3+}) = 15.6 = 1.617 μmol J^{-1} (16).

Product analysis

Product analysis was carried out by high-performance liquid chromatography (HPLC) using a Hewlett–Packard 1050 chromatograph (column: 125 × 4 mm Spherisorb ODS 2 RP-18 (5 μm), Lichrosorb precolumn, flow rate 1.0 ml min^{-1}) equipped with a multiple wavelength detector. The mobile phase consisted of water (Millipore® filtered) and methanol (Promochem, HPLC grade), the binary gradient was water–methanol 10–35%. (The gradient was 1–5 min: H_2O:CH_3OH = 90:10, 5–10 min: H_2O:CH_3OH = 85:15, 10–20 min: H_2O:CH_3OH = 65:35 per volume). As for 3-HBA the mobile phase was H_2O:CH_3OH = 90:10. The individual compounds were detected by measuring their absorptions at 210, 235, and 255 nm. Concentrations were determined by calibration with standard solutions. The identity of the products was confirmed by comparing the retention time and the UV spectra to that of the corresponding standards. Irradiations were carried out at least in duplicate, the HPLC analyses were reproducible within 10%.

Results and discussion

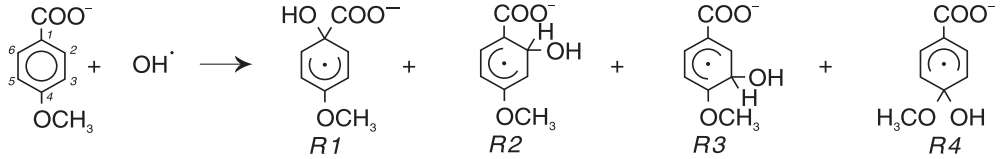
Radiolysis in the presence of N_2O

In the first step of the investigations, the seven products obtained as a consequence of the $OH^{\bullet}$-radical reactions with the isomers of MBA (anisic acids) were studied. These compounds were used as model substrates for derivatives of hydroxybenzoic acids having the phenol group linked with other residues. 3-HBA was investigated for comparison.

Exposure of water or dilute aqueous solutions to γ-radiation leads to the primary species e^-_{aq}, $OH^{\bullet}$, $H^{\bullet}$, H_2, and H_2O_2. In the presence of N_2O, the e^-_{aq} are converted into $OH^{\bullet}$ (eq. [1]), yielding a *G* ($OH^{\bullet}$) = 5.5, which corresponds to a concentration of 0.57 μmol J^{-1}.

[1] $$e^-_{aq} + N_2O \rightarrow OH^{\bullet} + OH^- + N_2$$

By addition of $OH^{\bullet}$ to methoxylated benzoic acids, isomeric methoxyhydroxycyclohexadienyl radicals (demonstrated for 4-MBA in eq. [2]) are formed, which after several

[2] 

[2] *G*-value is the number of molecules reacting per 100 eV of absorbed energy. Conversion into SI-units: a *G*-value of 1 molecule per 100 eV corresponds to a radiation-chemical yield of 0.10364 μmol J^{-1}.

© 2001 NRC Canada

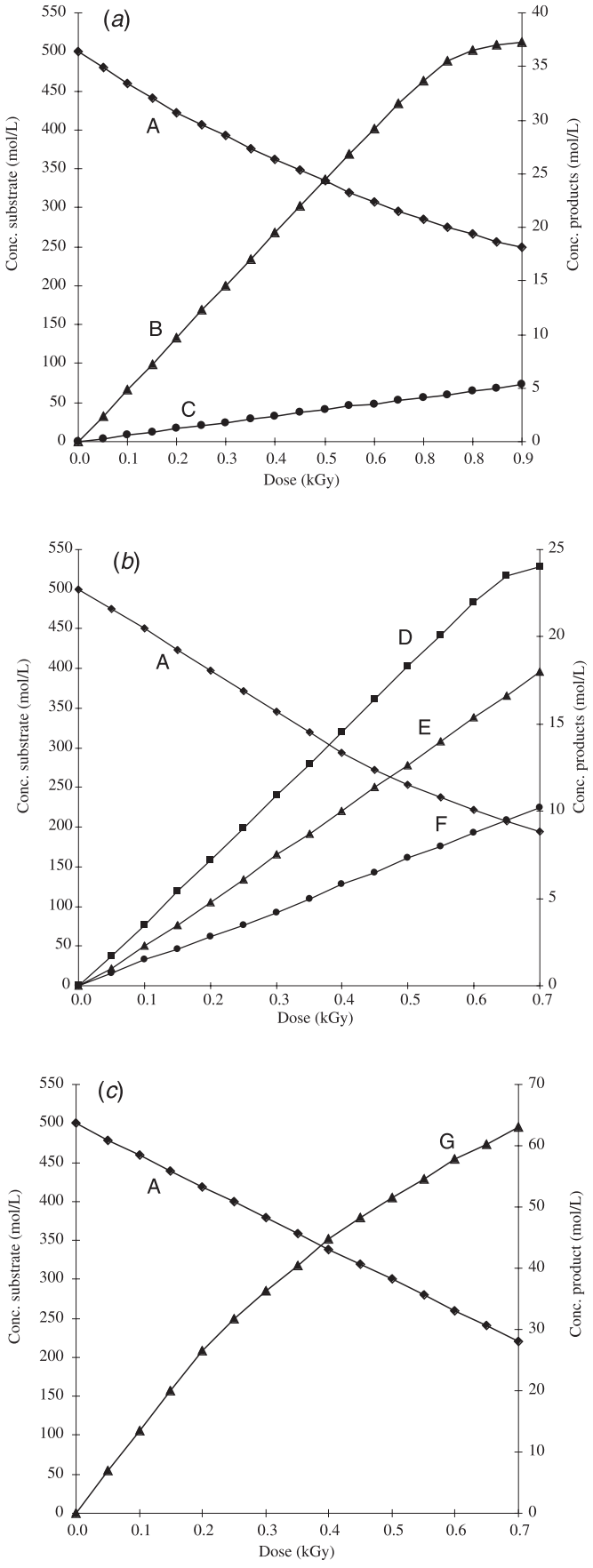


Fig. 1. Concentration–dose dependence curves obtained from irradiated N_2O-saturated aqueous solutions of 5×10^{-4} M of (*a*) 4-MBA, (*b*) 3-MBA, and (*c*) 2-MBA at pH = 8 to 9. List of symbols: (A) decrease of the substrates, (B) formation of iso-VA and 4-HBA, (C) formation of 3,4-DHBA, (D) formation of 3-HBA, (E) formation of VA, (F) formation of 3-MSA, and (G) formation of 2-HBA.

reaction steps, may lead to hydroxylation and oxidative demethoxylation.

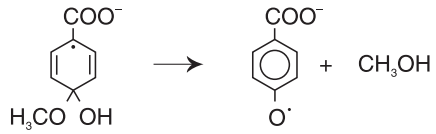
The substrates degradation and product formations obtained on radiolysis of aqueus N_2O-saturated 5×10^{-4} M 2-, 3-, and 4-MBAs (pH 8–9) as a function of dose (50 Gy steps) are presented in Figs. 1*a–c*. The irradiations were carried out up to an absorbed dose that gives rise to about 50% substrate decomposition. Representative chromatograms are given in Figs. 2*a–c*.

Degradation

The initial degradation yields (G_i)[3], are similar for 4-MBA and 2-MBA (G_i = 3.9 and 4.0), which corresponds to about 70% $OH^{\bullet}$-radical consumption, with the *meta*-isomer 91% of the $OH^{\bullet}$-radicals giving rise to decomposition. The linearity of degradation with dose (up to 300 and 400 Gy for 4-MBA and 3-MBA, respectively), and to more than 700 Gy for 2-MBA, is given in Figs. 1*a–c*. The highest dose for a 50% degradation is required for 4-MBA (0.9 kGy). The HBAs are decomposed to a clearly smaller extent: G_i (-2-HBA) = 2.4 and G_i (-4-HBA) = 2.8 (14, 15). For 3-HBA a decomposition yield of G_i (-3-HBA) = 2.1 was obtained, the 50% degradation is at 1.3 kGy (Table 1). The low initial degradation yields of the HBAs indicate the occurrence of reactions leading to a reformation of the substrates.

Product formation

In the case of 4-MBA, two products could be detected by HPLC (Figs. 1*a* and 2*a*): iso-VA resulting from R3, and 4-HBA which has R4 as precursor (the $OH^{\bullet}$-adduct formed by attachment of $OH^{\bullet}$ to the ring carbon carrying the methoxyl group). Such ipso-adducts have been found to decay by acid- and base-catalyzed or uncatalyzed elimination of CH_3OH producing phenoxyl radicals, the rate constant at pH = 7 was found to be $k \approx 5 \times 10^4$ s^{-1} (10, 11). In the case of radical R4 the 4-carboxyphenoxyl radical is formed (eq. [3]).

[3] 

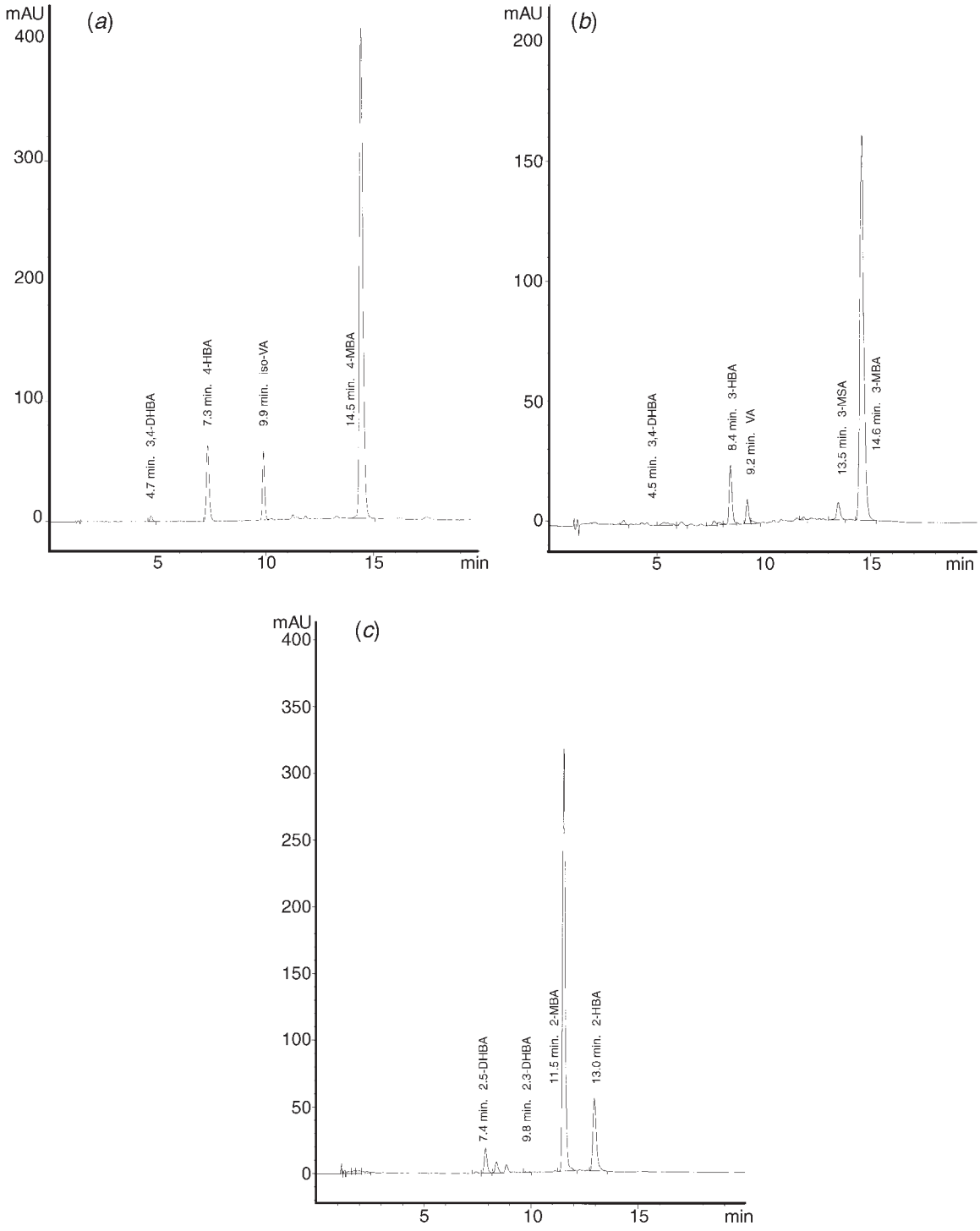
R4

The yield of the demethoxylation product 4-HBA (G_i = 0.5), accounts for about 10% of the total $OH^{\bullet}$-radicals. This is more than twice as much as reported by O'Neill et al. (10), who used methanol determinations for quantification. The product arising from an $OH^{\bullet}$ attack on the *meta*-position of 4-MBA, is only detectable in traces. The finding of hydroxylation products in *ortho*- and *para*-positions, and the lack of products in *meta*-position to the *ortho–para*-directing

[3] Initial *G*-values (G_i) are calculated from the linear part of dose–yield plots before secondary reactions occur.

© 2001 NRC Canada

Fig. 2. Chromatograms of 5×10^{-4} M N_2O-saturated aqueous solutions of (*a*) 4-MBA irradiated with 0.5 kGy at pH = 9.0, 255 nm; (*b*) 3-MBA irradiated with 0.7 kGy at pH = 8.6, 235 nm; (*c*) 2-MBA irradiated with 0.7 kGy at pH = 8.5, 235 nm.



methoxyl group is in line with the electrophilic nature of the $OH^{\bullet}$-radical (17, 18). The production of the hydroxylation product iso-VA is very low (G_i = 0.46, 8.4% of $OH^{\bullet}$). The formation of the secondary product 3,4-DHBA can also be observed (Fig. 1*a*). It results from the reaction of $OH^{\bullet}$ with the primary final substances 4-HBA and iso-VA. In contrast to 4-MBA, the hydroxylation of 4-HBA is quite efficient; 33% of $OH^{\bullet}$ resulted in 3,4-DHBA with G_i = 1.8 (14, 15) (Table 1).

With 2-MBA, the replacement of the -OCH_3-group by -OH is more effective (G_i (2-HBA) = 1.3), it corresponds to more than 20% of $OH^{\bullet}$. This value is nearly five times higher than that found by methanol determinations (10). The yield of the expected hydroxylation products 2-methoxy-3-

© 2001 NRC Canada

Table 1. Initial yields of degradation (G_i), 50% degradation (kGy), and the hydroxylated products (G_i, percentage of $OH^•$) produced by reaction of $OH^•$ with 500 μmol of the isomers MBAs (pH = 8) and HBAs (pH = 6) obtained in N_2O-saturated solutions.

Substrate (500 μmol)	Decomposition		Hydroxylation total		Replacement -OCH_3		Replacement -COO^-	
	G_i	50% degr. (kGy)	G_i	% of $OH^•$	G_i	% of $OH^•$	G_i	% of $OH^•$
2-MBA	4.0	0.6	≈0.4	<7	1.3	23	0	0
3-MBA	5.0	0.5	0.38	6.9	0.35	6.4	0	0
4-MBA	3.9	0.9	0.46	8.4	0.46	8.4	0	0
2-HBA[a]	2.4	1.1	2.0	35	—	—	0.03	0.5
3-HBA	2.1	1.3	1.3	24	—	—	0	0
4-HBA[a]	2.8	0.7	1.8	33	—	—	0.6	11

Note: G ($OH^•$) = 5.5 or 0.57 μmol J^{-1}.
[a]Taken from the literature (14, 15).

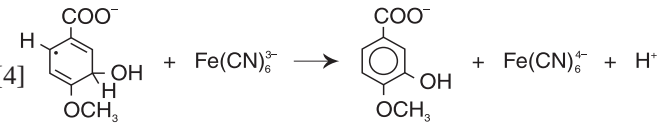
hydroxybenzoic acid and 2-methoxy-5-hydroxybenzoic acid is very low (Figs. 1*c* and 2*c*). Since these compounds were not available for calibration, their yields could only be estimated to approximately $G_i < 0.5$. Comparing this result with the hydroxylation of the corresponding HBA, it is again obvious that in the case of the latter, the hydroxylation process is distinctly higher (Table 1). For salicylic acid, an 83% conversion of the decomposed acid (G_i (-2-HBA) = 2.4) into 2,3- and 2,5-DHBA (G_i = 1.6 and 0.4, respectively), has been reported (13, 14). This selective reaction of $OH^•$ enables the detection of the hydroxylation products of salicylic acid as an indicator for the appearance of $OH^•$ radical in vivo (19).

Irradiation of the *meta*-isomer of anisic acid produces about 6.5% demethoxylation (G_i (3-HBA) = 0.35) and 7% total hydroxylation (G_i (VA) = 0.24 and G_i (3-methoxysalicylic acid) = 0.14) (Figs. 1*b* and 2*b*). The compound 5-methoxysalicylic acid, expected from the $OH^•$ adduct in *para*-position to -OCH_3, could not be detected. Under the conditions used, it has a retention time of 15.5 min. In this time range there is, however, no compound detectable (Fig. 2*b*). Radiolytic products of 3-HBA have been determined in the course of this work. Thirty-eight percent of the $OH^•$-radicals contribute to its degradation (G_i (-3-HBA) = 2.1), the 50% decomposition dose is 1.3 kGy. The hydroxylation products 2,3-, 2,5-, and 3,4-DHBA are formed with G_i = 0.37, 0.43, and 0.52, respectively (Figs. 3*a* and *b*).

The total hydroxylation attributed to substrate degradation is 60%, which is comparable to that of 4-HBA. In contrast to 2- and 4-HBA, no replacement of the carboxyl group is observable. This may be attributed to the *meta*-positioning of the *ortho–para*-directing -OH-group vs. -COO^-, which reduces the probability of $OH^•$-attachment at the carboxyl group.

The yields of degradation, and product formation for the methoxy- and hydroxy-benzoic acids, are summarized in Table 1. Hydroxylation is assigned to the total amount of products resulting from $OH^•$-adducts where $OH^•$ is attached to ring carbons not carrying methoxyl-, hydroxyl-, or carboxyl-groups.

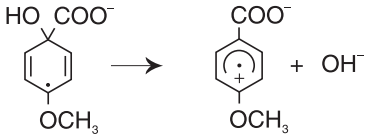
To elucidate whether the pronounced differences in hydroxylation of hydroxy- compared to methoxy-benzoic acids could at least partly be attributable to a different pattern of $OH^•$-radical addition to these substrates, irradiations in the presence of $K_3Fe(CN)_6$ have been performed. $K_3Fe(CN)_6$ and the quinones *p*-benzoquinone and 2-methylbenzoquinone, which have a somewhat lower redox potential, are frequently used to oxidize hydroxycyclohexadienyl radicals, for example, from anisole (17) and phenol (18), to the corresponding phenols. The rate constant for the electron transfer from the isomeric methoxyhydroxycyclohexadienyl radicals of anisole to $K_3Fe(CN)_6$ has been found to be $k(ox)_{o,p} = 2.4 \times 10^9$ M^{-1} s^{-1} for the *ortho*- and *para*-isomer and $k(ox)_m = 2 \times 10^7$ M^{-1} s^{-1} for the *meta*-isomer (17). The distribution of the isomeric hydroxycyclohexadienyl radicals was determined for 4-MBA, 3-MBA, and 3-HBA. For 2-MBA this process could not be carried out because of the lack of

[4] 

hydroxylation products for calibration. The oxidation step is demonstrated for the C3-adduct of 4-MBA (eq. [4]).

The detected oxidation products together with those reported for 4-HBA, obtained by using various quinones as oxidants (12), are summarized in Tables 2*a* and *b*.

The result clearly shows, that the MBAs and HBAs exhibit a similar $OH^•$-adduct distribution. The yields of hydroxylation products primarily formed on the nonipso $OH^•$-adducts are practically the same. 4-MBA and 4-HBA result in 68 and 69% total hydroxylation, respectively, with 3-MBA and 3-HBA 87 and 84% phenolic compounds are produced, respectively, (Tables 2*a* and *b*). For anisole the demethoxylation process has been found to be independent of the presence of an oxidant (17), but it is influenced by pH (11). Radiolysis of 4-MBA without oxidants at pH > 10 showed an increase of 4-HBA formation to 17%, which improves the material balance to about 85%. 4-Methoxyphenol and 3-methoxyphenol, the decarboxylation analogoues to hydroquinone and resorcinol, could not be detected (Tables 2*a* and *b*). Nevertheless, in the case of 4-MBA, the remaining 15% of $OH^•$ presumably adds to the C-1 position; this adduct probably decays by elimination of OH^- forming radical cations (eq. [5]).

[5] 

Since the yields of the nonipso $OH^•$-adducts of methoxy- and hydroxy-benzoic acids are equivalent (Tables 2*a* and *b*),

© 2001 NRC Canada

Table 2*a*. Comparison of the yields of oxidation products from the primary $OH^{\bullet}$-adducts from 4-MBA (500 μmol substrate, 100 μmol $K_3Fe(CN)_6$, N_2O) and 4-HBA (12).

Ring position	4-Methoxybenzoic acid		4-Hydroxybenzoic acid	
	Product	% of $OH^{\bullet}$	Product	% of $OH^{\bullet}$
C1	4-Methoxyphenol	0	Hydroquinone	16
C2	4-MSA	traces	2,4-DHBA	4
C3	iso-VA	68	3,4-DHBA	65
C4	4-HBA	10 (17[a])	4-HBA	15[b]
Total yield		~78 (~85[a])		100
Total hydroxylation[c]		~68		69

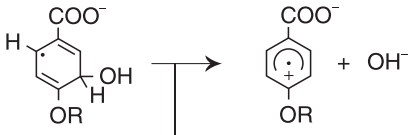
[a]At pH > 10.
[b]Taken from the difference to 100%.
[c]Resulting from the nonipso $OH^{\bullet}$-adducts.

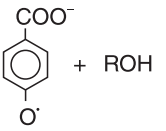
Table 2*b*. Comparison of the yields of oxidation products from the primary $OH^{\bullet}$-adducts from 3-MBA and 3-HBA (500 substrate, 100 μmol $K_3Fe(CN)_6$, N_2O).

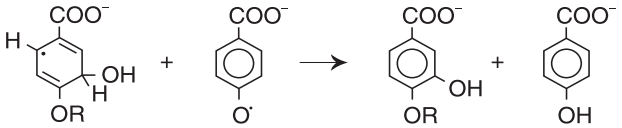
Ring position	3-Methoxybenzoic acid		3-Hydroxybenzoic acid	
	Product	% of $OH^{\bullet}$	Product	% of $OH^{\bullet}$
C1	3-Methoxyphenol	Not detected	Resorcinol	Not detected
C2	3-MSA	29	2,3-DHBA	27
C3	3-HBA	10	3-HBA	16[a]
C4	VA	29	3,4-DHBA	31
C5	3-H-5-MBA[b]	Not detected	3,5-DHBA	Not detected
C6	5-MSA	29	2,5-DHBA	26
Total yield		97		100
Total hydroxylation[c]		87		84

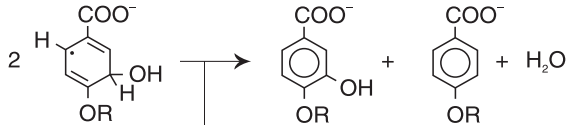
[a]Taken from the difference to 100%.
[b]3-Hydroxy-5-methoxybenzoic acid.
[c]Resulting from the nonipso $OH^{\bullet}$-adducts.

their diverse hydroxylation can be attributed to the different decay pathways of the $OH^{\bullet}$-adducts. Principally, these transients can undergo unimolecular (eqs. [6] and [7]), and bimolecular reactions (eqs. [8], [9], and [10]):

[6] 

[7] 

[8] 

[9] 

[10] dimerisation

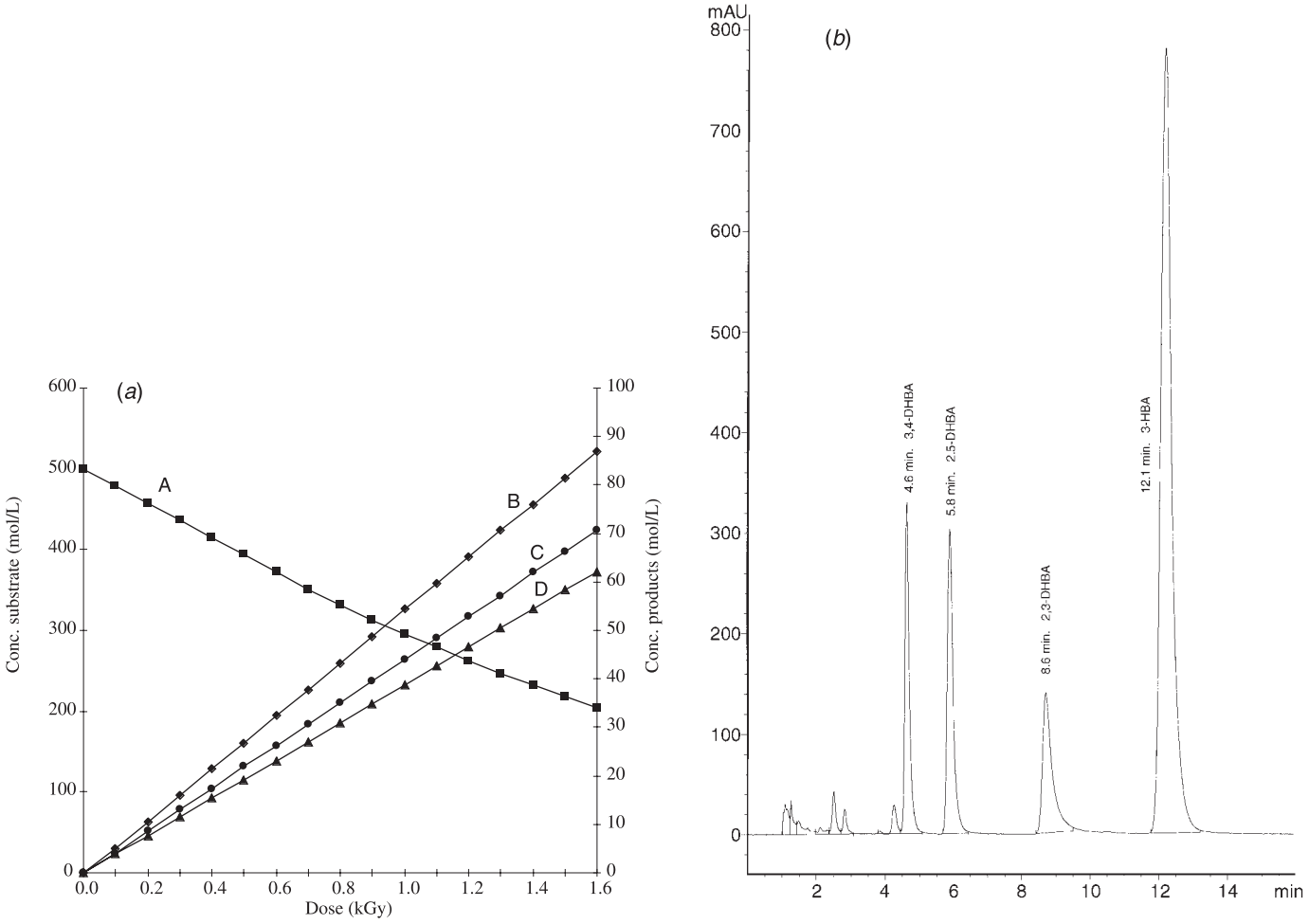
In acid solutions in the case of methoxylated benzoic acids (R = CH_3), the formation of radical cations (eq. [6]), has been found to be the major path. Their production have been followed for di- and tri-methoxylated benzoic acids in the pH range 1–3 using optical and conductometric pulse radiolysis (10). For HBAs (R = H, eq. [7]), an acid- and base-catalyzed water-splitting takes place (12–15). During γ-radiolysis the concentration of radicals is very low, and first-order reactions are likely to proceed faster than second-order ones. Thus the radicals formed initially may be altered by first-order processes (eqs. [6] and [7]), before radical centers are finally removed by second-order dismutation and dimerization (eqs. [8], [9], and [10]). Cross reactions (eq. [8]) between phenoxyl radicals (e.g., resulting from ipso-adducts, eq. [3]) and hydroxycyclohexadienyl radicals, seem quite probable because of the driving force exerted by the different redox potentials. For the MBAs, phenoxyl radical production is restricted to eq. [3]. Therefore hydroxylation- and demethoxylation-products formed via eq. [8], are generated in the same proportion as can be seen for 3- and 4-MBA (>6 and 8% each) (Table 1). In the case of HBAs, besides hydroxylation, the starting compound is regenerated. The latter is reflected in the lower initial degradation yield of the HBAs (Table 1).

Radiolysis in the presence of $SO_4^{-\bullet}$

Degradation rates of 4-MBA initiated by its radical cation have not yet been reported. The generation of $4\text{-MBA}^{+\bullet}$ is achieved by oxidation of 4-MBA with $SO_4^{-\bullet}$ (k_{13} = 3.5 ×

© 2001 NRC Canada

Fig. 3*a*. Concentration–dose dependence curves obtained from irradiated N_2O-saturated aqueous solutions of 5×10^{-4} M 3-HBA at pH = 6.2. List of symbols: (A) decrease of 3-HBA, (B) formation of 3,4-DHBA, (C) formation of 2,5-DHBA, and (D) formation of 2,3-DHBA. **Fig. 3*b*.** Chromatogram at 210 nm of 5×10^{-4} M N_2O-saturated aqueous solution of 3-HBA irradiated with 1.2 kGy at pH = 6.2.



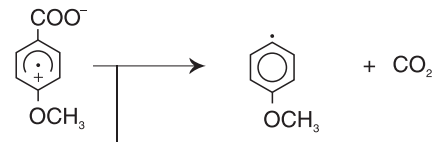
10^9 M^{-1} s^{-1}) (20), which is formed by reduction of $S_2O_8^{2-}$ with e_{aq}^- in air-free solutions ($k_{12} = 1.1 \times 10^{10}$ M^{-1} s^{-1}) (21). The $OH^{\bullet}$-radicals are scavenged by 2-methyl-2-propanol (*t*-BuOH) ($k_{11} = 6 \times 10^8$ M^{-1} s^{-1}) (22) (eqs. [11], [12], and [13]). Concentrations used were 500 μmol 4-MBA, 5 mmol $K_2S_2O_8$, and 100 mmol *t*-BuOH (pH = 6.5, Ar saturation). Since k (e_{aq}^- + 4-MBA) = 2×10^9 M^{-1} s^{-1}) (23) 5 mmol $K_2S_2O_8$ are sufficient to scavenge 98% of the e_{aq}^-.

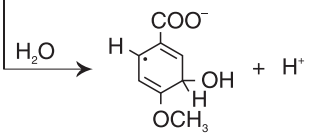
[11] $(CH_3)_3COH + OH^{\bullet} \rightarrow H_2O + (CH_3)_2C^{\bullet}H_2COH$

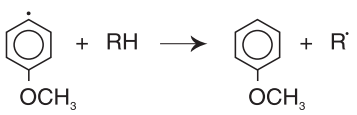
[12] $e_{aq}^- + S_2O_8^{2-} \rightarrow SO_4^{-\bullet} + SO_4^{2-}$

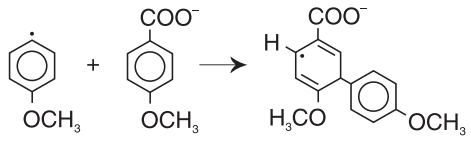
[13] $SO_4^{-\bullet} + \text{4-MBA} \rightarrow \text{4-MBA}^{+\bullet} + SO_4^{2-}$

Radical cations of benzoic acid have been found to decay by decarboxylation, giving rise to phenyl radicals, and (or) by addition of water to hydroxycyclohexadienyl radicals. For benzoate the distribution of these radicals is 70%:30% (24). Phenyl radicals are known to decay by H-abstraction, for example, from donors such as alcohols or by addition to an aromatic system resulting in the formation of substituted cyclohexadienyl radicals. The rate constants for both processes are in the range of 10^6–10^7 M^{-1} s^{-1} (25). The cyclohexadienyl radicals can be oxidized, thus giving stable biphenylic products, which has been demonstrated for halogenated benzoic acids (26). On the basis of these results, the following decay reactions of 4-$MBA^{+\bullet}$ are likely to proceed:

[14] 

[15] 

[16] 

[17] 

© 2001 NRC Canada

Table 3. Initial yields of degradation (G_i), 50% degradation (kGy), and hydroxylated products (G_i, percentage of $OH^•$), obtained by radiolysis of 500 μmol aerated solutions of the isomers of MBAs (pH = 8) and HBAs (pH = 6).

Substrate (500 μmol)	Decomposition		Hydroxylation total		Replacement -OCH_3		Replacement -COO^-	
	G_i	50% (kGy)	G_i	% of $OH^•$	G_i	% of $OH^•$	G_i	% of $OH^•$
2-MBA	2.7	1.1	<0.28	<10	0.46	16.4	0	0
3-MBA	2.8	0.9	0.28	10	0.18	6.4	0	0
4-MBA	2.9	1.1	0.16	5.7	0.32	10.6	0	0
2-HBA[a]	2.6	1.4	1.95	69	—	—	0.45	16
3-HBA	2.7	1.4	2.16	77	—	—	0	0
4-HBA[a]	2.7	1.0	1.9	68	—	—	0.5	18

Note: G ($OH^•$) = 2.8 or 0.29 μmol J^{-1}.
[a]Taken from the literature (14, 15).

If water addition (eq. [15]) is of importance, hydroxylated compounds may be formed after fixing of the hydroxyl moiety on the ring via e.g., eqs. [8] and [9]. Methoxyphenyl radicals (eq. [14]) should result in anisole (eq. [16]), and (or) in various methoxylated biphenyls, having e.g., eq. [17] as precursor. Since such biphenyl compounds were not available as reference substances, their formation could not be confirmed by HPLC.

The degradation rate is rather slow (G_i (-4-MBA) = 0.6), which corresponds to 22% of e^-_{aq}. No hydroxylation products could be detected, demonstrating that water addition to the radical cation (eq. [15]) plays a minor role. Anisole is not produced either, therefore, presumably, biphenyls formed via eq. [17], can be expected to be the major products in the decay process of the radical cations of 4-MBA. Since no radiolytic products were detectable, the concentration vs. dose plot, as well as the HPLC chromatogram, are not presented. The data were of similar quality to those in earlier figures.

Radiolysis in the presence of oxygen

Oxygen is present in plant tissue, and, therefore, its influence on radiolytic product formation has to be taken into account. The substrates have been irradiated in aerated solutions ($[O_2] = 0.25 \times 10^{-3}$ M). In the presence of oxygen, the reducing radicals $H^•$ and e^-_{aq} are scavanged, forming $HO_2^•$ and $O_2^{-•}$:

[18] $H^• + O_2 \rightarrow HO_2^•$ $k = 2.1 \times 10^{10}\ M^{-1}\ s^{-1}$ (20)

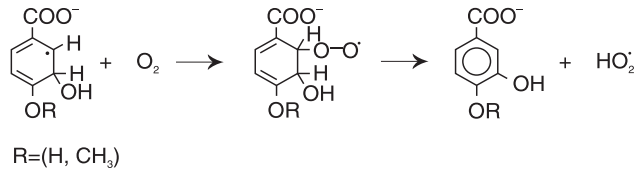
[19] $e^-_{aq} + O_2 \rightarrow O_2^{-•}$ $k = 2.0 \times 10^{10}\ M^{-1}\ s^{-1}$ (20)

[20] $H^+ + O_2^{-•} \leftrightarrows HO_2^•$ pK = 4.8

The rates of reactions of superoxide radicals with organic substances have been found to be rather slow (27), thus $OH^•$-radicals remain the most reactive species. As the main difference to the N_2O conditions, the addition of oxygen to the primarily formed $OH^•$-adducts is to be expected. The peroxyl radicals formed thereby may undergo various decay processes. The most ubiquitous are $HO_2^•$ or $O_2^{-•}$ elimination, especially by those radicals which carry the peroxyl radical function in *ortho*-position to the H-atom to be eliminated (28).

This reaction course is demonstrated on the C3-$OH^•$-adducts of 4-MBA and 4-HBA:

[21]



It was of particular interest whether the presence of oxygen would enhance the formation of hydroxylation products of the MBAs as was the case in the presence of the oxidant $K_3Fe(CN)_6$ and as has been reported for 2- and 4-HBA (14, 15). As a consequence, this would enhance the probability for using hydroxylated products of phenolic acids as markers for irradiation treatment of food-vegetables, as has been suggested previously (8, 9).

Aerated solutions of 500 μmol 2-, 3-, and 4-MBA as well as 3-HBA (pH 8), have been irradiated in 50 Gy steps. The substrate degradation and the concentration of the phenolic products are presented in Figs. 4*a–d* as a function of dose. Characteristic chromatograms are given for 3-MBA and 3-HBA in Figs. 5*a* and *b.*

The initial yields of degradation, phenolic product formation, as well as the 50% decomposition dose for the isomers of MBA and HBA are summarized in Table 3.

Decomposition

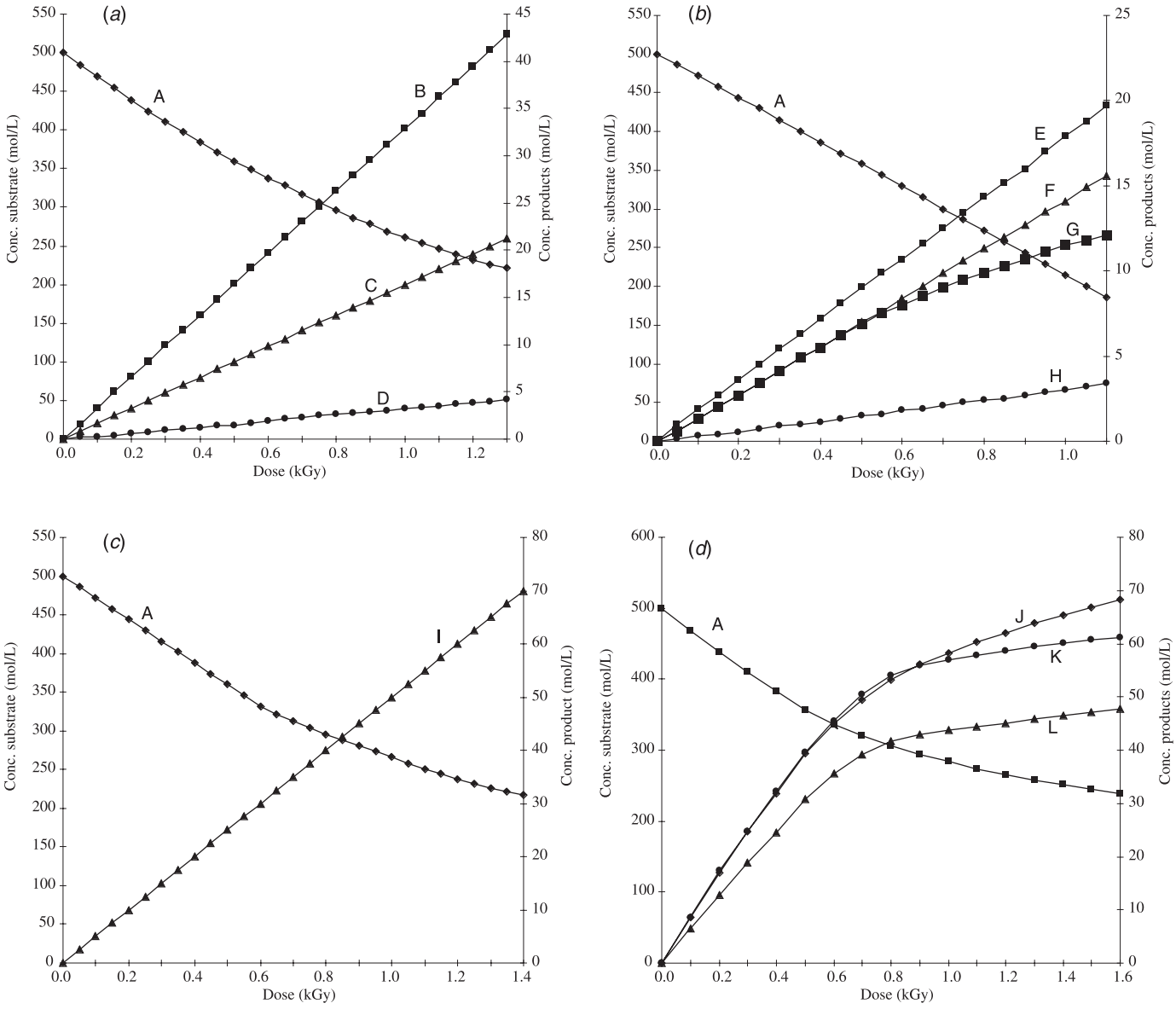
In contrast to the N_2O saturated solutions in the presence of air, no substrate reversion takes place. All $OH^•$-radicals contribute to the degradation of the hydroxy- and methoxybenzoic acids, indicating the addition of O_2 to the $OH^•$-adducts. Their decomposition rates are comparable, a dose of about 1 kGy is required for 50% degradation. 2-HBA and 3-HBA exhibit a somewhat higher radiation resistance; their half-life dose is 1.4 kGy.

Product formation

Upon radiolysis of the HBAs in the presence of air, a considerable amount of phenolic products has been found. For salicylic acid: 2,3-DHBA (G_i = 0.85) and 2,5-DHBA (G_i = 1.1) (13, 14), this corresponds to a conversion of 69% of the $OH^•$-radicals into hydroxylation of the substrate. In the case of 4-HBA, 3,4-DHBA is formed with G_i = 1.9 (i.e., 68% of $OH^•$) (12, 14). 3-HBA yields three hydroxylation products: 2,3-DHBA (G_i = 0.61), 2,5-DHBA (G_i = 0.77), and 3,4-DHBA (G_i = 0.77), in total this amounts to 77% of the $OH^•$-radicals. Whereas the conversion factor of $OH^•$ to

© 2001 NRC Canada

Fig. 4. Concentration–dose dependence curves obtained from irradiated aerated aqueous solutions of 5×10^{-4} M of (*a*) 4-MBA, (*b*) 3-MBA, (*c*) 2-MBA, and (*d*) 3-HBA at pH = 7–9. List of symbols: (A) decrease of the substrates, (B) formation of 4-HBA, (C) formation of iso-VA, (D) formation of 3,4-DHBA, (E) formation of 3-HBA, (F) formation of VA, (G) formation of 3-MSA, (H) formation of 3,4-DHBA, (I) formation of 2-HBA, (J) formation of 3,4-DHBA, (K) formation of 2,5-DHBA, and (L) formation of 2,3-DHBA.



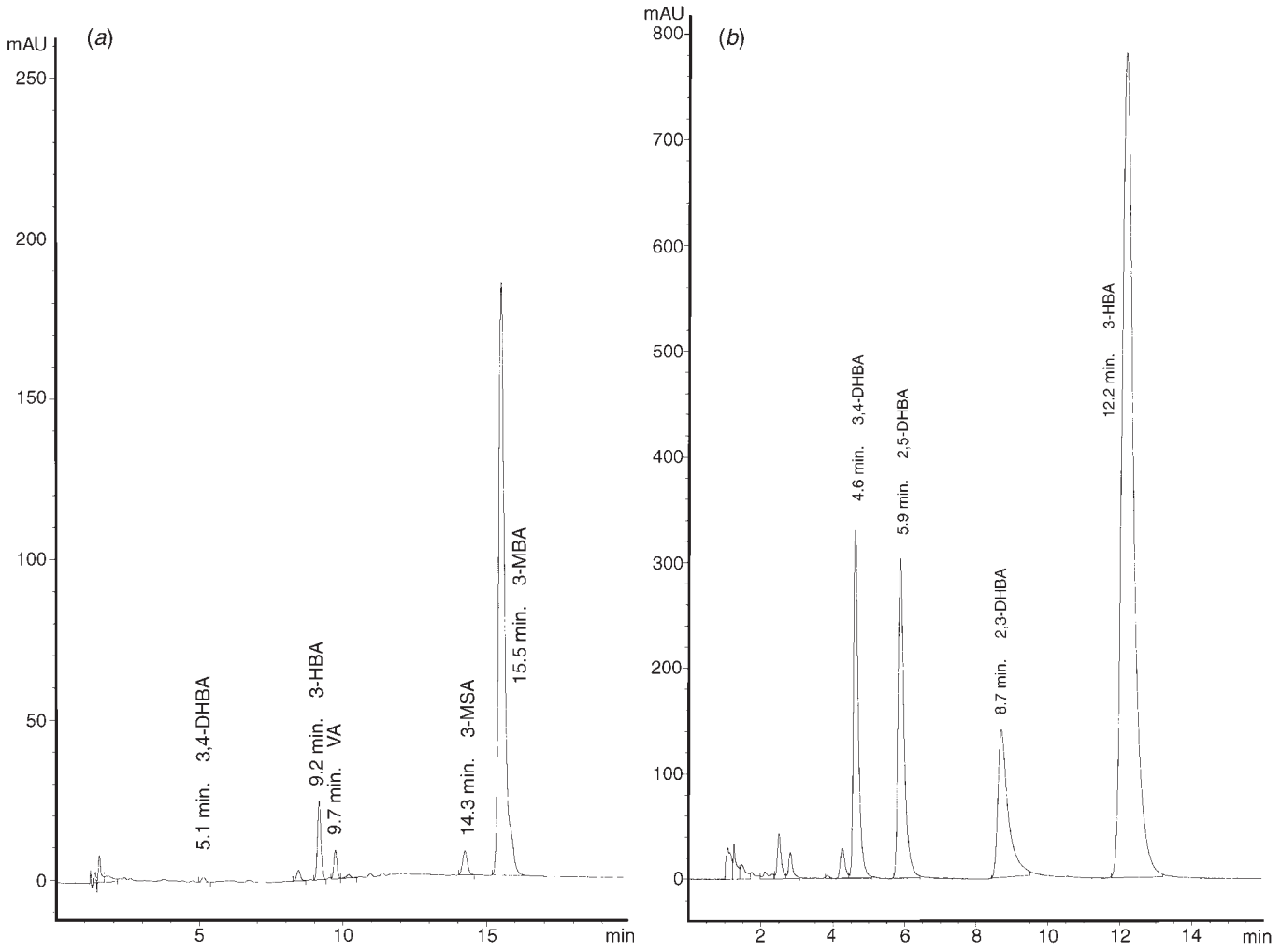
hydroxylation was 0.3 ± 0.06 for the HBAs in N_2O, in aerated solutions its value is 0.75 ± 0.05, which confirms the proceeding of eq. [21] as major reaction pathway at radiolysis of HBAs in aerated solutions.

For the MBAs, the presence of air is not reflected in an enhancement of $OH^{\bullet}$ conversion, either into hydroxylation or into the oxidative replacement of the methoxyl group (Tables 1 and 3). The yields of both product types about 10%, except the demethoxylation of 2-MBA, which is >15%. The hydroxylation product for 4-MBA (iso-vanillic acid) is formed with $G_i = 0.16$. The products expected for 2-MBA, 2-methoxy-3-hydroxybenzoic acid and 2-methoxy-5-hydroxybenzoic acid, which were not available for calibration, could be estimated to be <10% (Fig. 4*c*). From the *meta*-isomer 3-MBA, only two of three possible substances were detectable, VA and 3-MSA with $G_I = 0.14$ each. The product with -OH in *para*-position to the $-OCH_3$ group (5-methoxysalicylic acid), is not formed, as was the case in N_2O-saturated solutions (Table 3). In addition, experiments in oxygen-saturated solutions ($[O_2] = 1.25 \times 10^{-3}$ M) have been carried out. Even a level of oxygen which was five times higher did not influence the yield of the hydroxylation products.

The rate constants of the $OH^{\bullet}$-adducts of the MBAs and HBAs with oxygen are not known, but it can be assumed that they are comparable. For anisole and benzoate this rate constant has been found to be $k = 8 \times 10^8$ M^{-1} s^{-1} and $k = 2 \times 10^8$ M^{-1} s^{-1}, respectively, (28, 29). Thus it can be deduced that the rate constant for oxygen addition to the $OH^{\bullet}$-adducts of the MBAs is sufficiently large to ensure a quantitative

© 2001 NRC Canada

Fig. 5. Chromatograms of 5×10^{-4} M aerated aqueous solutions of (*a*) 3-MBA irradiated with 1.0 kGy at pH = 8.4, 235 nm; (*b*) 3-HBA irradiated with 1.2 kGy at pH = 6.9, 210 nm.



conversion into peroxyl radicals, as is the case with the HBAs. The decay, however, takes different courses. As could be shown for benzene and substituted benzenes, if O_2 instead of $K_3Fe(CN)_6$ is used as oxidant, the conversion of the hydroxycyclohexadienyl radicals into the corresponding phenols is no longer quantitative (29, 30). There are mainly two competitive decay pathways for hydroxycyclohexadienylperoxyl radicals: (*i*) $HO_2^{\bullet}$ elimination leading to phenols, and (*ii*) a formation of *endo*-peroxidic structures, which in turn are converted into peroxyl radicals and subsequently undergo fragmentation (29–31). Apparently fragmentation is the dominant reaction path with the MBAs. This is confirmed by the fact that no aromatic products are detectable by HPLC. Presumably aliphatic aldehydes and acids are the radiolytic products.

The yields for the products resulting from $-OCH_3$ replacement did not change in aerated solutions. This independence of demethoxylation on the presence of an oxidant is in line with the data obtained for anisole (17). The dominant reaction for the ipso-adducts carrying the methoxyl group is a prompt methanol elimination under formation of phenoxyl radicals. Since the decay of the latter is not influenced by the presence of oxygen, the product partition in aerated and N_2O solutions is comparable (Tables 1 and 3).

Conclusions

Although the primarily formed $OH^{\bullet}$-adducts are present in the same concentration for both the hydroxy- and methoxybenzoic acids, their final hydroxylation product yields are distinctly different. Whereas 68–77% of the $OH^{\bullet}$-adducts of the HBAs are converted to hydroxylation products in the presence of air, only about 10% hydroxylation occurs with the $OH^{\bullet}$-adducts of the MBAs. This fact is attributable to different decay pathways of the intermediate peroxyl radical.

The detection of hydroxylation products of phenolic acids has been suggested as a promising method for the identification of irradiated food of plant origin. Free HBAs, in the nonmethoxylated form, will produce sufficient amounts of hydroxylation products. If the OH-groups of phenolic acid derivatives are, however, linked to other residues (e.g., present as ether, ester, or glycoside) the hydroxylation process can expected to be of less significance.

© 2001 NRC Canada

The oxidative replacement of the -OCH_3 by -OH amounts to between 10–20%. Such addition–elimination reactions may be of importance for e.g., the release of glycoside residues. Preliminary radiolysis results from chlorogenic acid (3-(3,4-dihydroxycinnamoyl)quinic acid) showed the formation of caffeic acid (3,4-dihydroxycinnamic acid), indicating the occurrence of this process.

Acknowledgement

The financial support of this work by the Oesterreichische Nationalbank, Jubiläumsfonds, project JFP 6749, is gratefully acknowledged.

References

1. K. Herrmann. Fortschr. Chem. Org. Naturst. **3**, 73 (1978).
2. Römpp Lexikon Lebensmittelchemie. *Edited by* G. Eisenbrand and P. Schreier. G. Thieme Verlag Stuttgart, New York. 1995.
3. H.-D. Belitz and W. Grosch (*Editors*). In Lehrbuch der Lebensmittelchemie. 3rd. ed. Springer-Verlag, Berlin. 1987. p. 494.
4. N. Chuaqui-Offermanns and T.E. McDougall. J. Agric. Food Chem. **39**, 200 (1991).
5. C. Krach, G. Sontag, S. Solar, and N. Getoff. Z. Lebensm. Unter.-Forsch. **A204**, 417 (1997).
6. C. Krach, G. Sontag, and S. Solar. Food Res. Int. **32**, 43 (1999).
7. C.H. McMurray, E.M. Stewart, R. Gray, and J. Pearce (*Editors*). Detection methods for irradiated foods. The Royal Society of Chemistry, Cambridge. 1996. p. 303.
8. M. Grootveld and R. Jain. Radiat. Phys. Chem. **34**, 925 (1989).
9. M. Grootveld and R. Jain. Free Radical Res. Commun. **5**, 271 (1989).
10. P. O'Neill, D. Schulte-Frohlinde, and S. Steenken. J. Chem. Soc. Faraday Discuss. **63**, 141 (1977).
11. S. Steenken and P. O'Neill. J. Phys. Chem. **81**, 505 (1977).
12. R.F. Anderson, K.P. Patel, and M.R.L. Stratford. J. Chem. Soc. Faraday Trans. 1. **83**, 3177 (1987).
13. Z. Maskos, D. Rush, and W.H. Koppenol. Free Radicals Biol. Med. **8**, 153 (1990).
14. F. Swoboda. Msc. Thesis. University of Vienna, Austria. 1996.
15. F. Swoboda and S. Solar. Radiat. Phys. Chem. **56**, 291 (1999).
16. H. Fricke and E.J. Hart. *In* Radiation dosimetry. *Edited by* F.H. Attix, W.C. Roesch, and E. Töchilin. Academic Press, New York. 1966. p.167.
17. S. Steenken and N.V. Raghavan. J. Phys. Chem. **83**, 3101 (1979).
18. N.V. Raghavan and S. Steenken. J. Am. Chem. Soc. **102**, 3495 (1980).
19. M. Grootveld and B. Halliwell. Biochem. J. **237**, 499 (1986).
20. P. Neta, V. Madhavan, H. Zemel, and R.W.Fessenden. J. Am. Chem. Soc. **99**, 163 (1977).
21. P. Neta, R.E. Huie, and A.B. Ross. J. Phys. Chem. Ref. Data. **17**, (1988).
22. G.V. Buxton, C.L. Greenstock, W.P. Helman, and A.B. Ross. J. Phys. Chem. Ref. Data. **17**, (1988).
23. B. Gaisberger. Msc. Thesis. University of Vienna, Austria. 1998.
24. H. Zemel and W. Fessenden. J. Phys. Chem. **82**, 2670 (1978).
25. V. Madhavan, R.H. Schuler, and R.W. Fessenden. J. Am. Chem. Soc. **100**, 888 (1978).
26. I.A. Jankovic, L.R. Josimovic, and S.V. Jovanovic. Radiat. Phys. Chem. **51**, 293 (1998).
27. B.H.J. Bielski, D.E. Cabelli, R.L. Arudi, and A.B. Ross. J. Phys. Chem. Ref. Data. **14**, 1041 (1985).
28. C. von Sonntag and H.-P. Schuchmann. *In* Peroxyl radicals. *Edited by* Z.B. Alfassi. John Wiley & Sons Ltd., Chichester. 1997. p. 173.
29. X. Fang, X.-M. Pan, A. Rahmann, H.-P. Schuchmann, and C. von Sonntag. Chem. Eur. J. **7**, 423 (1995).
30. X.-M. Pan, M.N. Schuchmann, and C. von Sonntag. J. Chem. Soc. Perkin Trans. 2, 289 (1993).
31. G. Merga, H.-P. Schuchmann, M. Rao, and C. von Sonntag. J. Chem. Soc. Perkin Trans. 2, 1097 (1996).

© 2001 NRC Canada

Glutathione radical: Intramolecular H abstraction by the thiyl radical

A. Rauk, D.A. Armstrong, and J. Berges

Abstract: Ab initio computations (B3LYP/6-31G(D)) were used to predict transition structures and energies of activation for intramolecular H atom transfer to a thiyl radical ($RS^{\cdot}$) from the α-C—H bonds of glutathione (**1**) and from the model compounds, *N*-formylcysteinylglycine (**2**) and *N*-(2-thioethanyl)-γ-glutamine (**3**). For each compound, transition structures were located by in vacuo calculations on the neutral non-zwitterionic system. Thermodynamic functions derived at the same level and single point calculations at the B3LYP/6-311+G(3df,2p) level, were used to derive free energies of activation ($\Delta G^{\neq}$) and reaction ($\Delta G°$). For abstraction of the α-C—H (Gly) by the thiyl radical in the gas phase, $\Delta G^{\neq}$ = 134 kJ mol^{-1} if the amide link to Gly is in the more stable (*Z*)-configuration, and $\Delta G^{\neq}$ = 52 kJ mol^{-1} if it is in the less stable (*E*)-configuration. The isomerization of the amide group requires about 95 kJ mol^{-1}. Previous studies had indicated that for intramolecular reaction of the thiyl radical at α-C—H (Cys), $\Delta G^{\neq}$ = 110 kJ mol^{-1}. The lowest energy pathway for intramolecular H-transfer to the thiyl radical is from α-C—H (Gln), $\Delta G^{\neq}$ = 37–42 kJ mol^{-1}, and corresponds rather well with experimental results in solution ($\Delta G^{\neq}$ = 43 kJ mol^{-1}). The calculated free energy change for the equilibrium between thiyl and α-C forms of the glutathione radical is $\Delta G°$ = –54 kJ mol^{-1}. The value estimated from experimental data is $\Delta G°$ = –37 kJ mol^{-1}. The agreement between the energies from theory in the gas phase and experiment in solution suggests that the free energies of solvation of reactant thiyl radical, transition structures for H abstraction, and the product α-C-centred radical, are very similar. The effects of solution were estimated by two continuum models (SCIPCM and COSMO). The SCIPCM model yields results very similar to the gas phase, predicting a modest lowering of the activation free energy. The results from the COSMO method were inconclusive as to whether a rate enhancement or decrease could be expected.

Key words: glutathione, thiyl radical, α-C-radical, hydrogen transfer.

Résumé : On a effectué des calculs ab initio (B3LYP/6-31G(D)) pour prédire les structures de transition et les énergies d'activation pour le transfert intramoléculaire d'un atome H à un radical thiyle ($RS^{\cdot}$) à partir des liaisons α-C—H du glutathion (**1**) et de composés modèles (*N*-formylcystéinylglycine (**2**) et *N*-(2-thioéthanyl)-γ-glutamine (**3**)). Pour chacun des composés, on a localisé les structures de transition par des calculs dans le vide au même niveau et on a utilisé des calculs ponctuels au niveau B3LYP/6-311+G(3df,2p) pour en tirer les énergies libres d'activation ($\Delta G^{\neq}$) et de réaction ($\Delta G°$). Pour l'enlèvement du α-C—H (Gly) par le radical thiyle en phase gazeuse, $\Delta G^{\neq}$ = 134 kJ mol^{-1} si la liaison amide du Gly est dans la configuration la plus stable (*Z*) et $\Delta G^{\neq}$ = 52 kJ mol^{-1} si elle est dans la configuration (*E*) qui est moins stable. L'isomérisation du groupe amide nécessite environ 95 kJ mol^{-1}. Des études antérieures avaient suggéré que pour la réaction intramoléculaire du radical thiyle avec le α-C—H (Cys), $\Delta G^{\neq}$ = 110 kJ mol^{-1}. La voie réactionnelle de plus faible énergie pour le transfert intramoléculaire vers le radical thiyle à partir de α-C—H (Gln), $\Delta G^{\neq}$ = 37–42 kJ mol^{-1}, et cette valeur correspond assez bien avec les résultats expérimentaux en solution, $\Delta G^{\neq}$ = 43 kJ mol^{-1}. La valeur calculée pour le changement d'énergie libre pour l'équilibre entre le thiyle et les formes α-C du radical glutathion est $\Delta G°$ = –37 kJ mol^{-1}. L'accord entre les énergies calculées de façon théorique en phase gazeuse et les valeurs expérimentales en solution suggère qu'il y existe une grande similarité entre les énergies libres de solvatation du radical thiyle qui réagit, des structures de transition pour l'enlèvement de H et du produit à radical centré sur le α-C. On a évalué les effets de solution par deux modèles continus, SCIPCM et COSMO. Le modèle SCIPCM conduit à des résultats qui sont très semblables à ceux obtenus en phase gazeuse et il prédit un faible abaissement de l'énergie libre d'activation. Les résultats obtenus grâce à la méthode COSMO ne permettent pas de conclure si l'on peut s'attendre à une augmentation ou à une diminution de la vitesse de réaction.

Mots clés : glutathion, radical thiyle, radical α-C, transfert d'hydrogène.

[Traduit par la Rédaction]

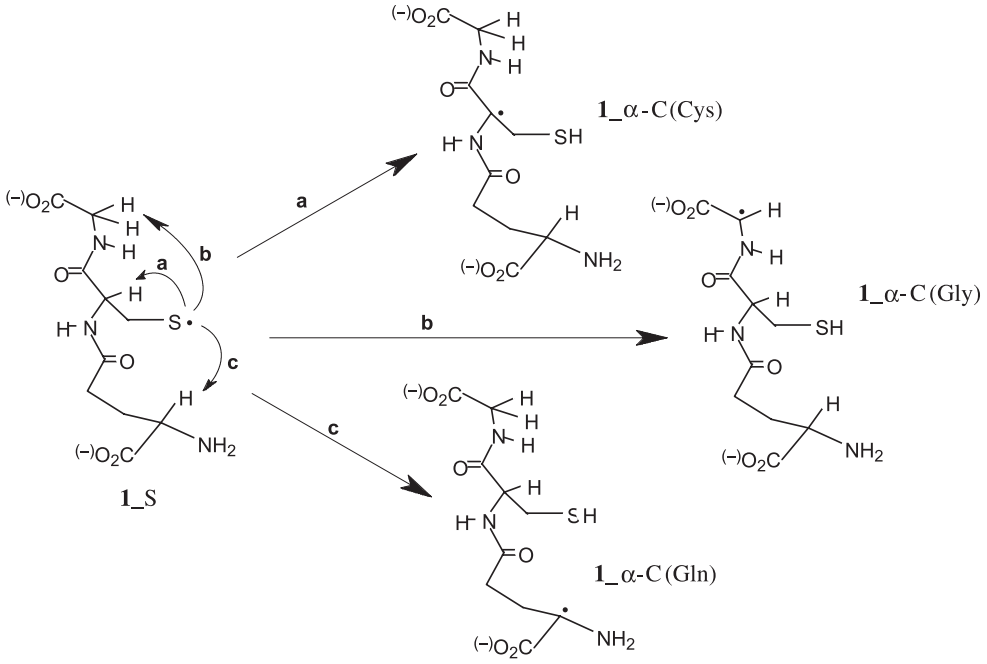
Received December 20, 2000. Published on the NRC Research Press Web site on April 30, 2001.

A. Rauk[1] and D.A. Armstrong. Department of Chemistry, The University of Calgary, Calgary, AB T2N 1N4, Canada.
J. Berges. Laboratoire de Chimie Theorique, Tour 22-23, Case courrier 137, Universite Pierre et Marie Curie, 4, place Jussieu, 75252 Paris CEDEX 05, France.

[1]Corresponding author (telephone: (403) 2220-6247; fax: (403) 289-9488; e-mail: rauk@chem.ucalgary.ca).

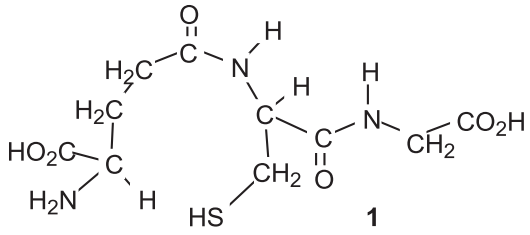
 DOI: 10.1139/cjc-79-4-405 © 2001 NRC Canada

Fig. 1. The three pathways for intramolecular H atom transfer in GSH thiyl radical.



Introduction

Glutathione (γ-glutamylcysteinylglycine, GSH **1**) is a ubiquitous tripeptide which plays a number of vital roles in cell metabolism, including repair of oxidative damage in red blood cells and elsewhere (1). In the central nervous system, as well as being a free radical scavenger, GSH has been suggested to function as redox modulator of ionotropic receptor activity, and possibly as a neurotransmitter (2). Decreased GSH levels have been associated with increased oxidative stress in various neurological disorders, including Lou Gehrig's disease (ALS), Parkinson's disease, and Alzheimer's disease (2).



1

The side group of the cysteine residue reacts rather rapidly with all oxidizing agents, including $OH^{\bullet}$ (3–5), $Br_2^{(-\bullet)}$, and $N_3^{\bullet}$, forming the thiyl radical ($RS^{\bullet}$), which, in experiments involving glutathione, has been shown to abstract a hydrogen atom intramolecularly from the α-carbon centre of the glutamyl residue (6, 7). Indeed it has been concluded that at physiological pH, under conditions of both low GSH and O_2 concentration, where the product $[O_2][GSH]\ 1 \times 10^{-7}$, the intramolecular H-transfer pathway becomes the main controlling route for processing of the initially formed thiyl radical (7).

The cysteine residue is present in most proteins and in a number of them, plays a central active role in oxidation–reduction reactions where free radicals can be involved. In thioredoxin reductase and similar enzymes, cysteines appear in pairs of the type -Cys-X-X-Cys- and reduction is effected through electron transfers which cycle between disulfide and sulfhydryl forms (1, 8). The reactivity and ultimate fate of the thiyl radical of GSH serves as a realistic model for parallel processes which can occur in proteins.

In a more general sense, the site of radical formation causing oxidative damage to proteins is a matter of great interest, since such damage is implicated in numerous pathological disorders (3) and in the process of aging. Oxidation is generally initiated by $OH^{\bullet}$ radicals or other radicals created from enzyme reactions (3, 9–12), or by ultraviolet and ionizing radiation (13). The α-carbon center of amino acid residues is also a major point of direct attack (3, 14, 15).

In previous work (16), we have established the methodology for the accurate determination of α-C—H bond dissociation energies (BDEs). We showed explicitly in the case of glycine, alanine, serine, and threonine residues (17), and the anhydrides of glycine and alanine (18), that the α-C—H BDEs are lower than for RS—H, and therefore could potentially be damaged by thiyl radicals. We (17) also established that some site specificity of such oxidative damage is expected, namely that these residues in disordered or β-sheet (glycine only) regions of the protein may be most readily damaged, but that the α-helical secondary structure confers some protection.

The present work addresses the modes of internal transfer of oxidative damage from the cysteine thiyl radical of GSH. The three potential pathways of H atom abstraction from the α-C-centers (rxn. [1]) are shown in Fig. 1. Experimental observations by pulse-radiolysis–EPR have been interpreted as following path **c**, i.e., H-transfer from the α-C site of the glutamyl moiety (19).

An examination is made of the effects of aqueous solution on the energetics of the H atom transfer pathways using continuum models. For the large molecules considered here, it is not possible to optimize structures in the presence of the

© 2001 NRC Canada

solvent reaction field. Since the initial structures must be optimized in the "gas phase," we have used the neutral species rather than the anionic species, which predominate at the conditions of the experiment (pH above 7), but which yield nonrepresentative self-solvated conformations in vacuum.

Computational details

All ab initio calculations presented here were performed with the Gaussian-94 (G94) and Gaussian-98 (G98) molecular orbital packages (20). The geometry optimizations and frequency calculations were carried out at the B3LYP/6-31G(d) level by the hybrid HF–DFT procedure implemented in the Gaussian molecular orbital packages. The vibrational frequencies were scaled by a factor of 0.98 in considering the zero-point energy (ZPE) (21) and in the calculation of thermodynamic functions (($H^\circ_{298} - H^\circ_0$) and S°_{298}). The latter were calculated in the rigid rotator-harmonic oscillator approximation (22). All internal motions were considered as vibrations. The gas phase partition functions for molecular rotation and translation were considered to be unchanged in solution.

Single point calculations at the B3LYP/6-31G(d,p) level with keyword SCRF=SCIPCM (23), and at the B3LYP/6-311+G(3df,2p) level with keyword SCRF=CPCM (the continuum model, COSMO (24), using Pauling radii (25, 26)) were carried out to evaluate the free energy of solution in water. The implementation (called CPCM in G98) provides an analysis of the total free energy of solvation (ΔG (solv)) in terms of electrostatic and nonelectrostatic contributions (ΔG (es) and ΔG (nes), respectively), while the SCIPCM model as implemented in G94, contains only the electrostatic terms (23, 26).

The energies (E) and ZPE results of B3LYP calculations, and derived "relative" quantities (ΔH°_0, ΔH°_{298}, ΔS°_{298}, and ΔG°_{298}) are collected in Table 1. Relative quantities are relative to the most stable conformer of each species. The quantities in columns 11, 12, and 14 (ΔG (es) and ΔG (nes)) are not relative quantities. ΔG (es) in column 11 is the electrostatic part of the free energy of aqueous solvation (ΔG (solv)) as reported by G98 using SCRF=CPCM and Pauling radii. ΔG (ns) in column 12 is the nonelectrostatic part of ΔG (solv). ΔG (es) in column 14 is taken as the difference between B3LYP energies calculated with and without the presence of the reaction field specified as SCRF=SCIPCM.

The relative enthalpy at 0 K (ΔH°_0 (column 4)), is identified with the relative vibrationally corrected Born–Oppenheimer energy (eq. [1]):

$$[1] \qquad \Delta H^\circ_0 = \Delta E + \Delta ZPE$$

The relative enthalpies at 298 K (ΔH°_{298} (columns 5 and 9)) are calculated according to eq. [2]):

$$[2] \qquad \Delta G^\circ_{298} = \Delta H^\circ_0 + \Delta(H^\circ_{298} - H^\circ_0)$$

The relative gas phase free energies at 298 K (ΔG°_{298} (columns 7 and 10)) are calculated according to eq. [3]), using ΔS°_{298} from column 6:

$$[3] \qquad \Delta G^\circ_{298} = \Delta H^\circ_{298} - 298.15 \times \Delta S^\circ_{298}$$

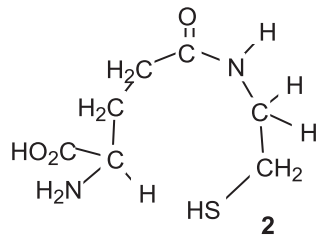
Finally, the relative free energies in aqueous solution (columns 13 and 15) are obtained by adding the relative electrostatic part of ΔG (solv) (ΔG (es) from columns 11 and 14) to the gas phase ΔG°_{298} at the B3LYP/6-311+G(3df,2p)// B3LYP/6-31G(d) level (column 10) (eq. [4]):

$$[4] \qquad \Delta G^\circ_{298}(\text{aq}) = \Delta G^\circ_{298}(\text{g}) + \Delta\Delta G \text{ (es)}$$

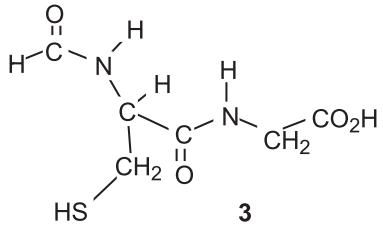
The reasons for using only the electrostatic part of ΔG (solv) from the CPCM calculations are discussed below.

Results and discussion

The parent compound (**1**) and its radical derivatives exist in numerous conformational forms. A full search of the conformational space was not attempted for the parent, nor any of the free radical minima or transition structures. Instead, only fully optimized structures close to the geometry of the TSs for H-transfer and some structures for the parent molecules which should be among the most stable, were considered. The computational details are provided in Table 1. The B3LYP/6-31G(d) structures of representative neutral non-zwitterionic conformers of **1**, and of compounds *N*-formylcysteinylglycine (**2**) and *N*-(2-thioethanyl)-γ-glutamine (**3**), which were chosen as models for the larger GSH system, are shown in Fig. 2.



2



3

As illustrated in Fig. 3, **1** and **2** have two amide linkages (groups *Amide1* and *Amide2*). Subsequent figures show the structures of the S-centred (thiyl) and α-C-centred radicals, and the connecting transition structures (TSs). The labelling is transparent. Thus, the thiyl radical of one of the conformations of (*Z*)-**2** (labelled (*Z*)-**2a**_S) is connected to the α-C-centred radical ((*Z*)-**2a**_α-C) by TS ((*Z*)-**2**_TS) (Fig. 4). The reaction, which corresponds to intramolecular H-transfer from the Gly moiety to the Cys moiety, is discussed below. In the discussion that follows, energy related references are to the relative free energies at 298 K in the gas phase (column 10, Table 1) and in aqueous solution (column 15, Table 1) unless specified otherwise. These are shown in bold in Table 1.

The solution model

We chose two continuum models in an attempt to simulate the effect of solvation on the activation parameters for

© 2001 NRC Canada

Table 1. Total B3LYP *E*nergies (*E*), zero point energies (*ZPE*), and relative[a] energies in the gas phase and in aqueous solution.

	Gas phase									Solution				
SCIPCM[b]	6-31G(d)						6-311+G(3df,2p)						CPCM[c]	
Species	*E* (hartree)	*ZPE* (kJ mol^{-1})	ΔH°_0 (kJ mol^{-1})	ΔH°_{298} (kJ mol^{-1})	ΔS°_{298} (J mol^{-1} K^{-1})	ΔG°_{298} (kJ mol^{-1})	*E* (hartree)	ΔH°_{298} (kJ mol^{-1})	ΔG°_{298} (kJ mol^{-1})	ΔG(es)[d] (kJ mol^{-1})	ΔG(ns)[e] (kJ mol^{-1})	ΔG°_{298}[f] (kJ mol^{-1})	ΔG(es)[g] (kJ mol^{-1})	ΔG°_{298}[f] (kJ mol^{-1})
Parent														
1a	–1405.13684	770.3	5.1	4.2	–7.2	6.4	–1405.56718	2.3	**4.4**	–181.1	39.1	0.0	–85.1	**0.0**
1b	–1405.13847	769.5	0.0	0.0	0.0[h]	0.0	–1405.56807	0.0	**0.0**	–156.4	41.1	20.3	–70.9	**9.8**
1c	–1405.13169	768.4	16.7	16.0	3.2	16.9	–1405.56336	11.5	**10.6**	–172.5	39.0	14.8	–74.8	**16.5**
Radical														
1a_TS	–1404.47675	731.7	82.1	78.9	–23.5	87.0	–1404.90253	84.9	**99.3**	–156.9	36.6	80.7	–74.9	**100.8**
1a_S	–1404.49120	745.7	57.9	57.8	28.2	50.5	–1404.91590	66.6	**65.7**	–159.8	37.9	44.2	–72.7	**69.4**
1a_α-C	–1404.51006	737.1	0.0	0.0	0.0[h]	1.1	–1404.93722	2.3	**9.8**	–117.7	38.5	10.3	–65.8	**20.4**
1b_TS	–1404.47867	729.4	74.8	72.6	–9.6	76.6	–1404.90568	75.4	**85.7**	–130.8	66.2	93.2	–73.6	**88.5**
1b_S	–1404.50052	744.3	32.1	32.0	21.4	26.8	–1404.92389	44.3	**45.4**	—[i]	—[i]	—	–68.2	**53.7**
1b_α-C	–1404.50706	734.2	5.0	6.4	25.2	0.0	–1404.93754	0.0	**0.0**	–138.3	70.3	0.0	–76.5	**0.0**
Parent														
(*Z*)-**2**	–1043.27582	456.2	0.0	0.0	0.0[h]	0.0	–1043.56567	0.0	**0.0**	–116.2	21.9	0.0	–50.3	**0.0**
(*E*)-**2**	–1043.27208	457.3	10.9	10.3	–11.6	13.8	–1043.56220	9.6	**13.1**	–112.4	22.9	16.8	–50.4	**13.0**
2_TS	–1043.24056	453.1	89.6	87.7	–18.8	93.3	–1043.52976	89.4	**95.0**	–116.3	24.8	94.9	–49.2	**96.1**
Radical														
(*Z*)-**2**_TS	–1042.58438	417.1	135.6	132.4	–23.2	139.3	–1042.86915	145.4	**152.3**	–113.7	23.6	145.2	–57.0	**144.9**
(*Z*)-**2a**_S	–1042.63173	432.7	26.6	25.8	0.6	25.6	–1042.91442	44.3	**44.0**	–121.2	21.3	29.5	–57.6	**36.1**
(*Z*)-**2b**_S	–1042.63976	430.8	3.6	3.0	5.9	1.2	–1042.92305	19.8	**18.1**	–115.3	21.6	9.4	–46.2	**21.4**
(*Z*)-**2a**_α-C	–1042.62881	424.0	25.7	25.2	–4.5	26.6	–1042.91696	29.4	**30.7**	–95.3	33.8	42.0	–56.7	**23.5**
(*Z*)-**2b**_α-C	–1042.63825	423.1	0.0	0.0	0.0[h]	0.0	–1042.92796	0.0	**0.0**	–107.6	22.1	0.0	–49.6	**0.0**
(*E*)-**2**_TS	–1042.61105	416.6	65.0	62.2	–28.3	70.6	–1042.89441	78.9	**87.3**	–92.5	31.3	101.4	–44.6	**92.5**
(*E*)-**2**_S	–1042.63452	431.9	18.4	17.6	–2.5	18.3	–1042.91792	34.2	**34.9**	–111.6	21.9	29.9	–47.6	**36.9**
(*E*)-**2**_α-C	–1042.63396	423.0	11.2	11.5	2.4	10.8	–1042.92351	11.9	**11.2**	–104.4	22.7	13.5	–47.7	**13.1**
Parent														
3a	–1008.56486	585.9	0.0	0.0	0.0[h]	0.0	–1008.83858	0.0	**0.0**	–93.4	14.4	2.7	–47.5	**0.0**
3b	–1008.56264	584.1	4.1	5.4	7.6	3.1	–1008.83684	4.1	**1.8**	–97.9	16.5	0.0	–45.6	**3.7**
3c	–1008.55811	583.5	15.4	16.3	12.6	12.6	–1008.83422	10.1	**6.3**	–94.1	16.4	8.3	–44.7	**9.1**
Radical														
3a_TS	–1007.90422	544.2	82.5	79.1	–47.7	93.3	–1008.17607	90.1	**104.3**	–97.3	19.4	87.4	–48.0	**104.4**
3a_S	–1007.92847	560.2	34.6	33.0	–18.8	38.6	–1008.19566	56.7	**61.8**	–79.3	19.8	62.9	–38.8	**71.2**
3a_α-C	–1007.93520	550.4	7.3	7.0	–12.7	10.8	–1008.20992	10.5	**14.3**	–91.5	23.7	3.1	–49.5	**12.9**

© 2001 NRC Canada

Table 1 (*Concluded*).

	Gas phase						Solution					
SCIPCM[b]	6-31G(d)					6-311+G(3df,2p)					CPCM[c]	
Species	*E* (hartree)	*ZPE* (kJ mol^{-1})	ΔH°_0 (kJ mol^{-1})	ΔH°_{298} (kJ mol^{-1})	ΔS°_{298} (J mol^{-1} K^{-1})	ΔG°_{298} (kJ mol^{-1})	*E* (hartree)	ΔH°_{298} (kJ mol^{-1})	ΔG°_{298} (kJ mol^{-1})	ΔG(es)[d] (kJ mol^{-1})	ΔG(ns)[e] (kJ mol^{-1})	ΔG°_{298}[f] (kJ mol^{-1})	ΔG(es)[g] (kJ mol^{-1})	ΔG°_{298}[f] (kJ mol^{-1})
3b_TS	–1007.90837	544.9	72.4	68.4	–55.8	85.0	–1008.17818	84.8	**101.4**	–90.6	18.4	91.1	–47.3	**102.2**
3b_S	–1007.92046	558.7	54.1	52.8	–10.3	55.8	–1008.18826	74.5	**77.5**	–79.1	46.8	78.6	–45.9	**79.6**
3b_α-C	–1007.93768	549.6	0.0	0.0[h]	0.0	0.0	–1008.21372	0.0	**0.0**	–80.3	41.3	0.0	–48.1	**0.0**

[a]Relative to the most stable in each grouping.
[b]6-31G(d,p) basis set.
[c]6-311+G(3df,2p) basis set.
[d]The electrostatic part of the free energy of solution (ΔG (solv)) as reported by G98.
[e]Nonelectrostatic part of ΔG (solv).
[f]Relative free energy on solution, calculated from ΔG(es) (see eq. [4]).
[g]*E* (SCIPCM) – *E* (gas phase) at the B3LYP/6-31G(d,p) level.
[h]S°_{298} (J mol^{-1} K^{-1}): **1b** 705.4, **1a**_α-C 679.2, (*Z*)-2 536.4, (*Z*)-**2b**_α-C 524.4, **3a** 539.9, **3b**_α-C 546.2.
[i]Unable to converge SCRF=CPCM with Pauling radii.

intramolecular H-transfer reaction. Polarizable continuum models (PCM) have been widely used since their introduction in 1981 (27) for the study of chemical processes in solution. These models require the definition of a molecular surface across which the mutual electrostatic response of the solute and solvent can be calculated. For complex molecules, the surface is defined by overlapping spheres, taking cognizance of the physical size of solvent molecules as well (26). The "self-consistant isodensity polarizable continuum model" (SCIPCM) (23), defines the surface as an isodensity contour derived from the molecular wave function in the presence of the solvent reaction field. We also chose the "conductor" PCM method (CPCM) on the basis of favorable results in the literature (25, 28), and opted to use Pauling radii rather than the default UAHF radii since we were dealing with H-transfer TSs (25). As well as the electrostatic part of the solute–solvent interaction calculated by SCIPCM, the CPCM method evaluates the "nonelectrostatic" contribution which originates from formation of the molecular cavity (defined by overlapping spheres) in the solvent. The electrostatic and nonelectrostatic components of the computed free energies of solvation by CPCM, ΔG (es) and ΔG (ns), respectively, for all species are listed separately in columns 11 and 12 of Table 1. The electrostatic terms are derived directly from the SCRF wave function as mapped onto the surface of the cavity occupied by the molecule. The nonelectrostatic terms originate from the shape of the cavity, which may be problematic for large molecules which have concave surfaces and holes. It seems reasonable that isomeric substances should have similar values for ΔG (ns). To within a few kJ mol^{-1}, this is the case for most of the species listed in Table 1. Thus ΔG (ns) for the conformers of each of the parent systems differ by less than 3 kJ mol^{-1}. The radical species for the most part show only slightly wider variation. However, the two successfully converged **1b**_ radicals differ by about 30 kJ mol^{-1} from the structurally similar **1a**_ series and a similar variability is seen in two of the **3b**_ series compared to the **3a**_ group. We have concluded that the extreme variations in ΔG (ns) are not physically reasonable and therefore base our estimates of the differential effects of solvation (namely the data in Column 13 of Table 1) solely on ΔG (es). Where ΔG (ns) is indeed nearly constant, its omission has only a minor effect on the relative free energies in solution. Experimental evidence (29) supports the notion that since parent and radical differ only by a single H atom from a relatively nonpolar C—H bond, the free energy of solution of the parent and the radical should be similar. This approximation would appear to be valid also in the case of GSH and its thiyl- and α-C-centered radicals since both S—H and α-C—H bonds are relatively nonpolar. In short, the differential effects of solvation should not be dramatic and the solution phase relative energies should be similar to the gas phase values. Comparison of the gas phase values and the SCIPCM- and CPCM-derived solution values will provide a basis for the assessment of the applicability of the latter to large polar molecules.

Structures of the parent molecules

The relative free energies (ΔG°_{298}) in the absence and presence of solvation (SCIPCM), of the conformations of

© 2001 NRC Canada

Fig. 2. Optimized conformations of the parent systems. Dipole moments and relative free energies (kJ mol^{-1}) in the gas phase ($\mu_{(g)}$ and $\Delta G°(g)$) and solution ($\mu(aq)$ and $\Delta G°(aq)$).

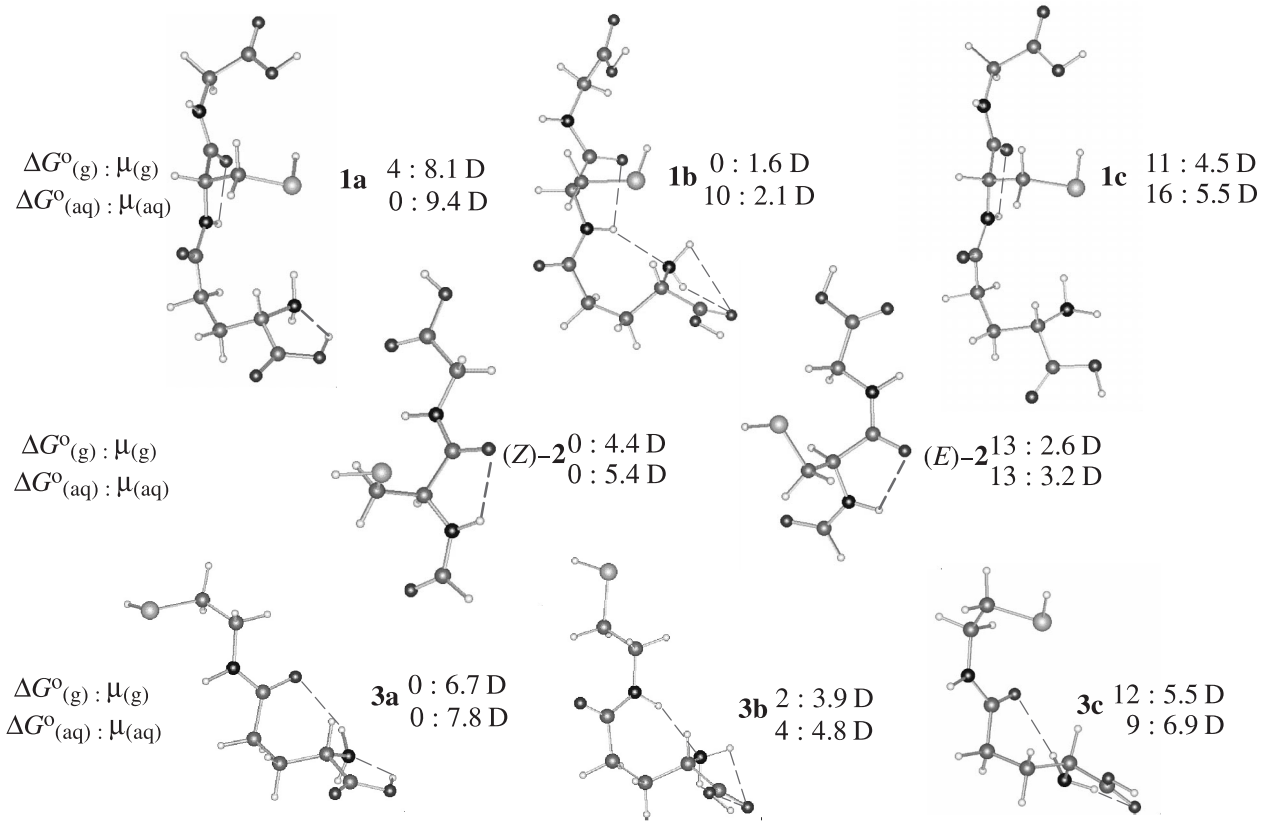
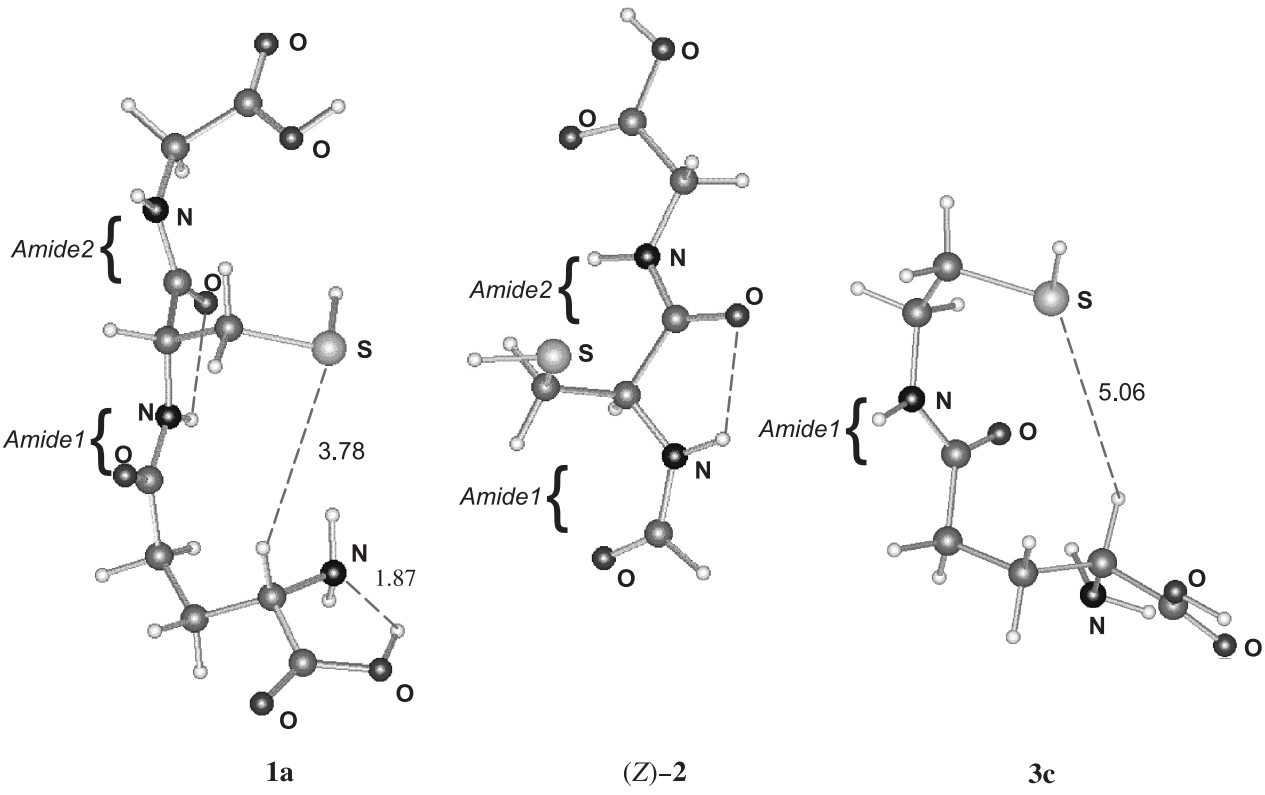
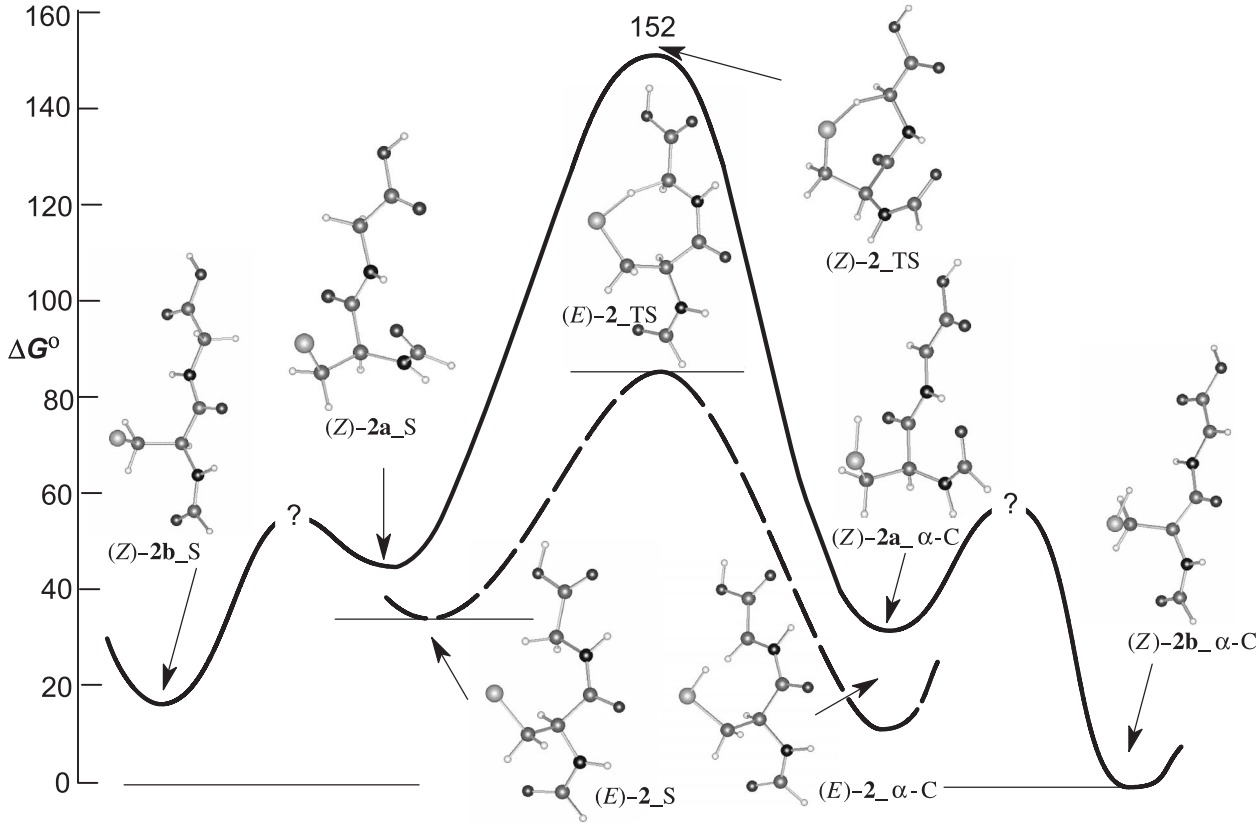


Fig. 3. Selected conformations of GSH **1** and two model systems (*N*-formylcysteinylglycine (**2**) and *N*-(2-thioethanyl)-glutamine (**3**)).



© 2001 NRC Canada

Fig. 4. Free energy (kJ mol^{-1}) profile for intramolecular H abstraction by (*Z*)-**2** and (*E*)-**2** in the gas phase.



the parent molecules considered in this study are given beside the structures in Fig. 2. In **1a**, **1b**, **1c**, and (*Z*)-**2** both *Amide1* and *Amide2* (see Fig. 3) are in their more stable *anti*- (*Z*) configurations and the two are oriented relative to each other so as to be linked by an H-bonding interaction between the N—H bond of *Amide1* and the carbonyl O atom of *Amide2*. This interaction, which exists in the "extended" conformation of the protein backbone, is missing in **3** which lacks the *Amide2* group. An indication of the relative importance of the additional intramolecular H-bonding interactions may be gained by examination of the relative energies of the conformations of **3**. Conformations **3a** and **3b** are similar in energy. **3b** has the amino NH_2 and COOH groups in a bifurcated arrangement, as does the most stable gas phase structure of glycine (30), and an additional H-bond between the amino group and the N—H of *Amide1*. **3a** has the amino NH_2 and COOH groups in an orientation which may be regarded as the precursor to the zwitterionic form which would exist in solution at neutral pH. This form in glycine (in the gas phase) is 6 kJ mol^{-1} less stable than the bifurcated form (30). It has the largest dipole moment. **3a** also has an additional H-bond between the amino NH_2 and the carbonyl O of *Amide1*. **3a** is more stable than **3b** by 2 kJ mol^{-1} in the gas phase and this difference increases to 4 kJ mol^{-1} in solution. Conformation **3c**, in which the amino group only acts as a weak H-bond donor, is substantially less stable in both phases.

Conformation **1a**, which lacks the secondary H-bonding interaction of **3a**, is less stable by 4 kJ mol^{-1} than **1b** in the absence of solvent but is predicted by the SCIPCM (and CPCM) procedure to be the most stable structure in solution, probably due to its large dipole moment (9.4 D). It should be emphasized that of the many conformations of GSH **1**, only extended structures which have the SH group in proximity to the α-C—H of the glutamyl moiety were considered. The corresponding thiyl radical would be poised to directly abstract the α-C H atom, as discussed below.

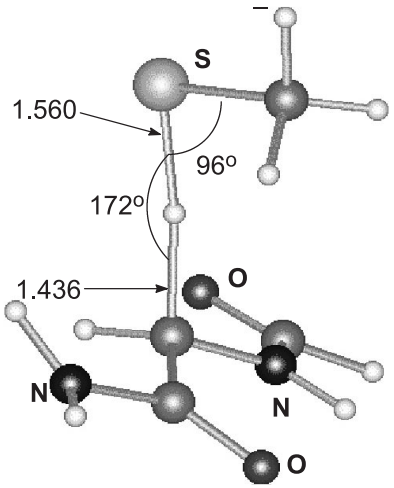
The model system **2** was chosen to examine H-abstraction from the glycine moiety of GSH **1**. Only two structures with the *Amide1–Amide2* interaction noted above were selected, differing by the configuration at *Amide2*. (*E*)-**2**, which has a *cis* transit of the backbone through the amide group, is 13 kJ mol^{-1} less stable than (*Z*)-**2** both in the presence and absence of solvent. A TS for interconversion of (*Z*)-**2** and (*E*)-**2**, **2**_TS (Table 1) was located. The isomerization at *Amide2* is predicted to be hindered by about 95 kJ mol^{-1} relative to (*Z*)-**2**, independent of phase.

α-C—H bond dissociation enthalpies (BDEs)

As a means of assessing the thermodynamic feasibility for the three pathways shown in Fig. 1, the magnitudes of the C—H BDEs for each of the α-C sites are compared to the S—H BDE. Feasibility is evident when BDE α-C—H BDE S—H. The α-C—H bond of the Cys residue is flanked by amide groups. Thus, on the basis of studies on model peptides, α-C—H BDE(Cys) = 346 kJ mol^{-1}, and S—H BDE (Cys) = 366 kJ mol^{-1} (31). Unfortunately, the model peptide studies do not apply directly to the Gly or Gln residues. The Gly residue has an amide linkage through the N atom but a free COOH group. One may expect that the α-C—H BDE (Gly)

© 2001 NRC Canada

Fig. 5. Transition structure for H abstraction by methanethiyl radical from *N*-formylglycinamide **4**.

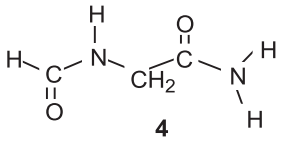


≤ 350 kJ mol^{-1}, the value estimated for a Gly residue in a peptide environment (31), since the COOH group is a better electron acceptor than the CONHR group and would enhance the captodative stabilization (32) of the radical. In the case of the Gln residue, the α-C—H is flanked by an NH_2 group and a neutral COOH group. As for Gly, the α-C—H BDE of Gln may be as much as 20 kJ mol^{-1} lower than the value (334 kJ mol^{-1}) calculated for the Gln residue in a peptide (31). The α-C—H BDE of the Gln residue of GSH has been estimated from experimental data to be no higher than 329 kJ mol^{-1} (7). Here the carboxyl flanking group is ionized and the stabilization would be slightly less effective than for the present calculations.

Approximate bond dissociation enthalpies for the α-C—H bond may be obtained from the present calculations by the isodesmic procedure (31), using the isodesmic partner (glycine) and the most stable structures for the parent systems and the corresponding radicals at the B3LYP/6-31G(d) level of theory. The isodesmic procedure would normally entail an uncertainty of ±10 kJ mol^{-1}. However, the uncertainty is greater in this case because without an exhaustive conformational search, we cannot be sure that the most stable conformers have been located. Using **1b** and **1a**_α-C, a value of 320 kJ mol^{-1} is derived for α-C—H BDE(Gln). Using **3a** and **3b**_α-C, a second estimate of α-C—H BDE(Gln) (313 kJ mol^{-1}) may be derived. These values are consistent with the maximum value of 329 kJ mol^{-1} derived from experiments (7). Using (*Z*)-**2** and (*Z*)-**2b**_α-C, α-C—H BDE(Gly) = 344 kJ mol^{-1}. Similarly, three identical values of 356 kJ mol^{-1} may be derived for the S—H BDE: for **1**, using **1b** and **1b**_S; for **2**, using (*Z*)-**2** and (*Z*)-**2b**_S; and for **3**, using **3a** and **3a**_S. For determination of S—H BDEs, the isodesmic partner is methanethiol. For the isodesmic reactions, the theoretically derived value (331 kJ mol^{-1}) for the BDE(α-C—H) of glycine (16) and the experimental value (360 kJ mol^{-1} for the BDE (S—H) of methanethiol (33), respectively, were used. The calculated BDE (S—H) of GSH **1** is in good agreement with the predicted value (367 kJ mol^{-1}) for Cys model peptide (34). Thus the α-C—H bonds of all three of the residues of GSH **1** involved in the H abstraction pathways in Fig. 1 are weaker than the S—H bond of the Cys residue and in principle, the thiyl radical could abstract an H atom from any of the α-C-sites.

Intermolecular H-transfer

We have previously predicted that the transfer of an α-C—H atom to thiyl in neutral glycine or the model system (*N*-formylglycinamide **4** + methanethiyl radical) entails a free energy of activation of approximately 60 kJ mol^{-1} at 298 K. This value may be taken as the reference for an unconstrained H-transfer of this type. The reaction proceeds via the transition structure shown in Fig. 5 (34). The principal features of the unstrained prerequisite geometry for α-C to S transfer are illustrated here, namely near collinearity of



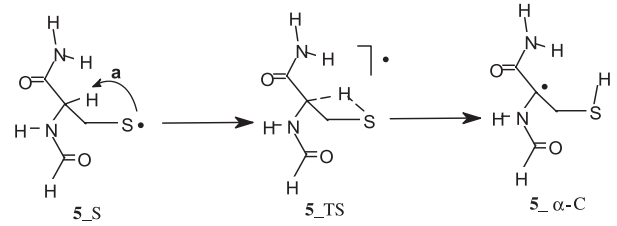
4

the α-C-H-S angle, an approximate angle of 90° at S and a trajectory more or less along the original α-C—H bond.

Intramolecular H-transfer in GSH 1: α-C—H (Cys) to S

The intramolecular α-C to S transfer of an H atom with the Cys residue has previously been examined in the model peptide system (*N*-formylcysteinamide (**5**) (eq. [5])): it is hindered by an enthalpy of activation of 115 kJ mol^{-1} (34). In this case, the cyclic transition state, consisting of only four atoms, cannot achieve the ideal geometry shown in Fig. 5. This value (115 kJ mol^{-1}) should be very similar in GSH **1** itself. We do not examine it further.

[5]

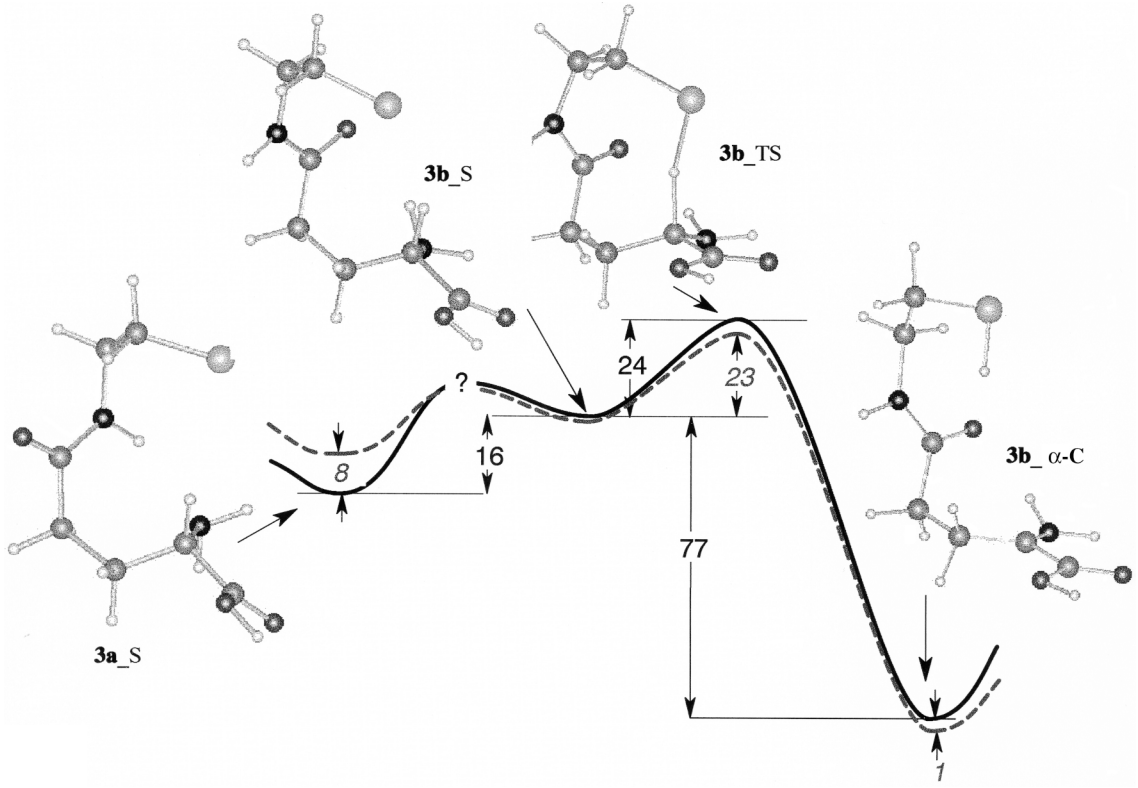


Intramolecular H-transfer in GSH 1 (modelled by 2): α-C—H (Gly) to S

Transfer of H from the α-C of the glycyl moiety would involve a seven-membered ring with an embedded amide group (Amide2, Fig. 3). Because an amide group is quasi-planar, its incorporation into a seven-membered ring would incur severe steric strain if it is in the normal (*Z*)-configuration, but would be relatively strain free if it is in the less favourable (*E*)-configuration (see Fig. 2). We have examined the possibility of H-transfer to thiyl radical from the α-C of the Gly residue using *N*-formylcysteinylglycine **2** as a model compound. Model **2** has both *Amide1* and *Amide2* groups, with *Amide2 endo* to the seven-membered ring of the TS. The structures of the S- and α-C-centered radicals and the TSs are shown in Fig. 4 along with the gas phase free energy profile plotted relative to the most stable structure ((*Z*)-**2b**_α-C). It is immediately clear that H-transfer in the (*Z*) compound is hindered by a very high barrier (134 kJ mol^{-1})

© 2001 NRC Canada

Fig. 6. Free energy (kJ mol^{-1}) profile for intramolecular H abstraction by **3b**_S in the gas phase (solid line, normal numbers) and solution (dashed line, italics).



and entails a 75° distortion from planarity of the *Amide2* group in (*Z*)-**2**_TS. H-transfer from the less stable (*E*) conformer ((*E*)-**2**_S) is hindered by a barrier (52 kJ mol^{-1}) which is actually less than the acyclic case, modelled by reaction of *N*-formylglycinamide (**6**) with methanethiyl radical ($\Delta G^{\neq}$ = 63 kJ mol^{-1} (34)). However, since the parent compound is in the (*Z*) conformation (compare (*Z*)-**2** and (*E*)-**2**, Table 1), the thiyl radical initially formed ((*Z*)-**2**_S) is 69 kJ mol^{-1} below the (*E*)-**2**_TS barrier. Furthermore, conversion of (*Z*)-**2**_S to (*E*)-**2**_S would be hindered by a barrier of about 95 kJ mol^{-1}, as is the case with the parent system. The situation in solution is predicted to be very similar to that shown in Fig. 4.

Intramolecular H-transfer in 3: α-C—H (Gln) to S

The most plausible site of H atom abstraction is the α-C—H site of the Gln residue of GSH **1** as deduced experimentally (6, 7, 19). The TS has a nine-membered ring with sufficient flexibility to readily accommodate the ideal TS requirements shown in Fig. 5. The normal (*Z*) configuration of *Amide1* is readily incorporated into the large ring with minimal distortion. Two orientations of *Amide1* are possible, depending on which face is turned into the ring. These approximately correspond to the **a** and **b** conformations of the parent system **3** (Fig. 2). This reaction was investigated in model system **3**, and in GSH **1**, itself. We discuss first the model system **3**, and conclude with GSH **1**.

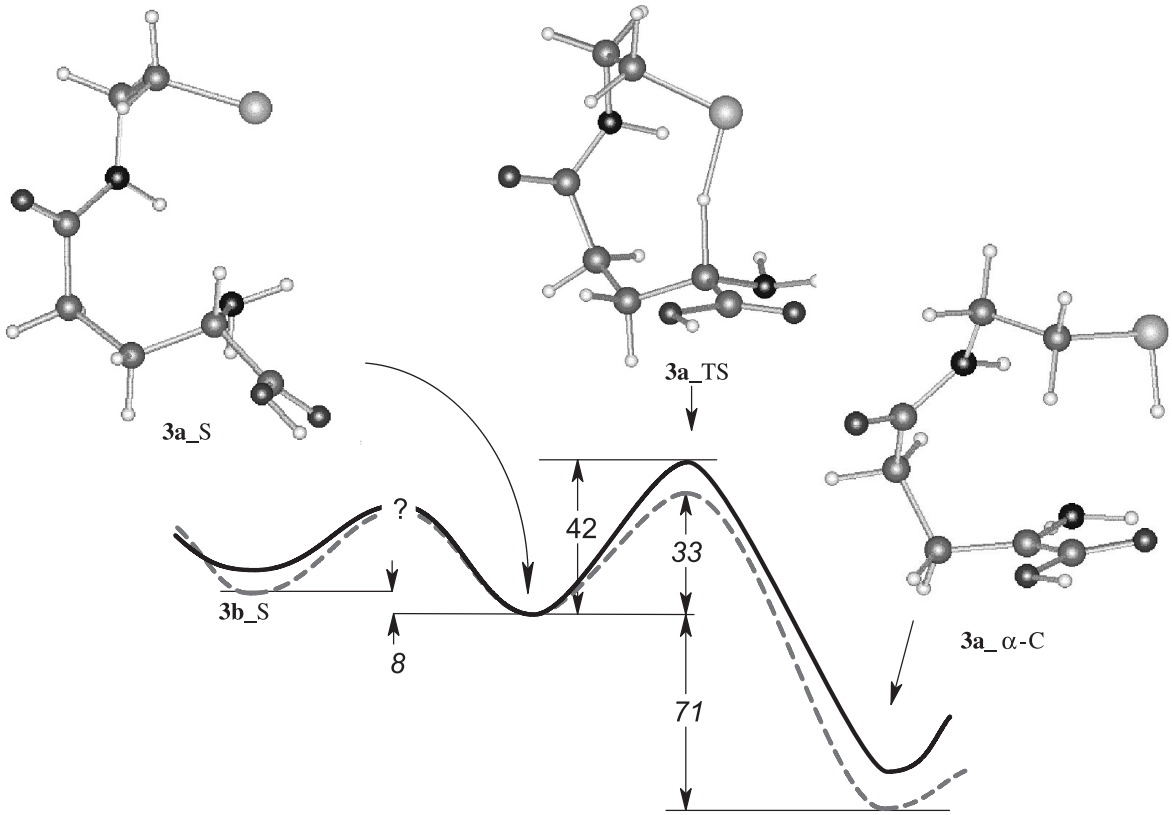
Of the two conformations of the thiyl radical of **3** considered here, **3a**_S is more stable than **3b**_S by 16 kJ mol^{-1} in the absence of solvent and by 8 kJ mol^{-1} in water. The free energy reaction profile of the conversion of **3b**_S to **3b**_α-C via **3b**_TS in the presence and absence of solvent is shown in Fig. 6. The aqueous free energy of activation ($\Delta G^{\neq}$) is only 23 kJ mol^{-1} in water, and 24 kJ mol^{-1} in the gas phase, starting from **3b**_S, the immediate precursor to the TS. From the lower energy conformer (**3a**_S) the values are 31 kJ mol^{-1} and 40 kJ mol^{-1}, respectively. The aqueous profile for the conversion of **3a**_S to **3a**_α-C via **3a**_TS in the presence and absence of solvent is shown in Fig. 7. The free energy of activation ($\Delta G^{\neq}$) is predicted to be 33 kJ mol^{-1} in water and 42 kJ mol^{-1} in the gas phase.

Intramolecular H-transfer in GSH 1: α-C—H (Gln) to S

Two conformations of the thiyl radical of GSH (**1a**_S and **1b**_S) were considered here. The latter (**1b**_S) is predicted to be more stable by 20 kJ mol^{-1} in the absence of solvent and by 16 kJ mol^{-1} in water by the SCIPCM method. It was not possible to converge the SCRF calculations for **1b**_S for any basis set (6-31G(d), 6-31G(d,p), 6-311+G(3df,2p) were attempted) in the model CPCM with Pauling radii. With the 6-31G(d,p) basis set, SCRF=CPCM with the default united atom radii *did* converge, however. At this level, **1a**_S is predicted to lie 13 kJ mol^{-1} above **1b**_S in water. The gas phase reaction profile of the more stable conformer (**1b**_S) is shown in Fig. 8: $\Delta G^{\neq}$ = 40 kJ mol^{-1} and $\Delta G°$ = – 45 kJ mol^{-1}. The exothermicity of the reaction is somewhat greater than that deduced experimentally in water ($\Delta G°$ = –37 kJ mol^{-1}) (7). As shown in Fig. 9, $\Delta G^{\neq}$ for the reaction with the less stable conformers (**1a**_S → [**1a**_TS] → **1a**_α-C) is somewhat lower: $\Delta G^{\neq}$ = 34 kJ mol^{-1} and $\Delta G°$ = –56 kJ mol^{-1} in the gas

© 2001 NRC Canada

Fig. 7. Free energy (kJ mol^{-1}) profile for intramolecular H abstraction by **3a**_S in the gas phase (solid line, normal numbers) and solution (dashed line, italics).



phase, and $\Delta G^{\neq}$ = 31 kJ mol^{-1} and $\Delta G°$ = – 49 kJ mol^{-1} in water. However, **1a**_S is less stable than **1b**_S, yielding an overall greater activation free energy for this pathway.

Effect of solvation

The present solution modelling results with the SCIPCM method (shown in Figs. 6–9) are consistent with a lowering of $\Delta G^{\neq}$ in solution relative to the gas phase. Inspection of the ΔG (es) data for the radicals of **1** and **3** in column 14 of Table 1 reveals that the lowering is due to a small preference for solvation of the TS relative to the thiyl radical. On the other hand, the results for the CPCM method shown in column 13 of Table 1 are inconclusive as to the effect of solvation on the activation free energy. The results for the reaction (**1a**_S → [**1a**_TS] → **1a**_α-C) suggest that solvation may raise the free energy of activation by a small amount (2 kJ mol^{-1}). This is also true for the reaction ((*Z*)-**2a**_S → [(*Z*)-**2a**_TS] → (*Z*)-**2a**_α-C (Table 1)) while for the reaction ((*E*)-**2**_S → [(*E*)-**2**_TS] → (*E*)-**2**_α-C (Table 1)) the barrier is raised by a more substantial amount, 20 kJ mol^{-1}. On the other hand, the results for the model systems (**3a**_S → [**3a**_TS] → **3a**_α-C and **3b**_S → [**3b**_TS] → **3b**_α-C) suggest a lowering of the barrier in water. The reason for such divergent results in such closely related systems is not at all obvious. We must conclude that single point SCRF=CPCM methodology applied to systems of the size considered here cannot distinguish the trends for the effects of solvation.

The most reliable predictors of the free energy changes for the reaction of GSH thiyl radical are the gas phase results shown in Fig. 8. These results ($\Delta G^{\neq}$ = 40 kJ mol^{-1}, $\Delta G°$ = – 45 kJ mol^{-1}) are applicable to solution under the assumption stated above that differential effects of solvation should be small. Direct evaluation of the effect of solvation by the SCIPCM methodology suggest that the free energy of activation should be lower ($\Delta G^{\neq}$ = 35 kJ mol^{-1}) and the exothermicity should be higher ($\Delta G°$ = –54 kJ mol^{-1}).

Entropy of mixing

The data in Table 1 refer to individual components of a complex mixture. Where one conformer dominates the mixture of the reactant (thiyl radical in this case), and one TS is clearly the most stable, the free energy of activation of the reaction may be computed as the difference of the free energies of just these two species. For GSH thiyl radical, one may choose **1b**_S and **1b**_TS and obtain $\Delta G^{\neq}$ = 35 kJ mol^{-1} from the solution phase results (Fig. 8). In the general case, the entropy of a substance composed of a number (n) of components (i) is given by eq. [6]:

$$[6] \qquad S = \Sigma_i^n \chi_i S_i - R\Sigma_i^n \chi_i \ln \chi_i$$

where χ_i and S_i are the mol fraction and entropy, respectively, of conformer i. and R is the gas constant. The last term is the entropy of mixing, which is approximately equal to R ln n in the event that there are n low-energy conformations which are approximately equally populated. For a highly flexible molecule, this may be significant. Consider the case of **1b**_S → [**1b**_TS], shown in Fig. 10. The five single bonds specifically labelled are in the part of the molecule which forms the cyclic TS for thiyl abstraction of the H atom from the Gln moiety. Bonds b_1, b_2, and b_5 are threefold

© 2001 NRC Canada

Fig. 8. Free energy (kJ mol^{-1}) profile for intramolecular H abstraction by **1b**_S in the gas phase (solid line, normal numbers) and solution (dashed line, italics).

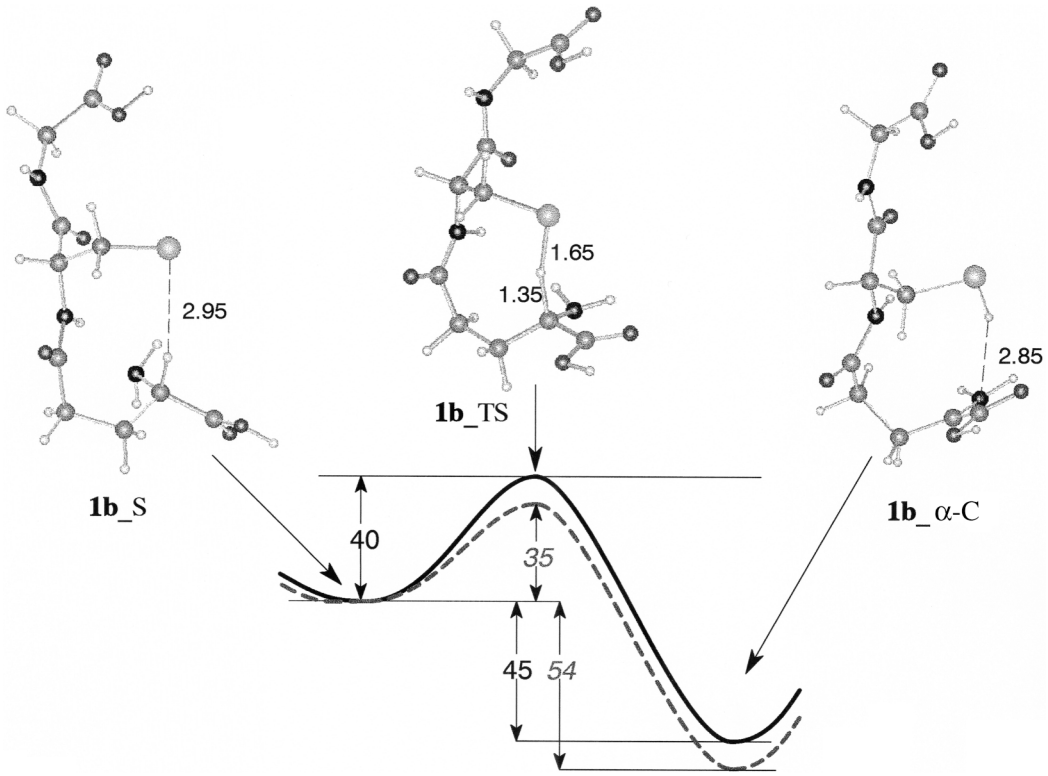
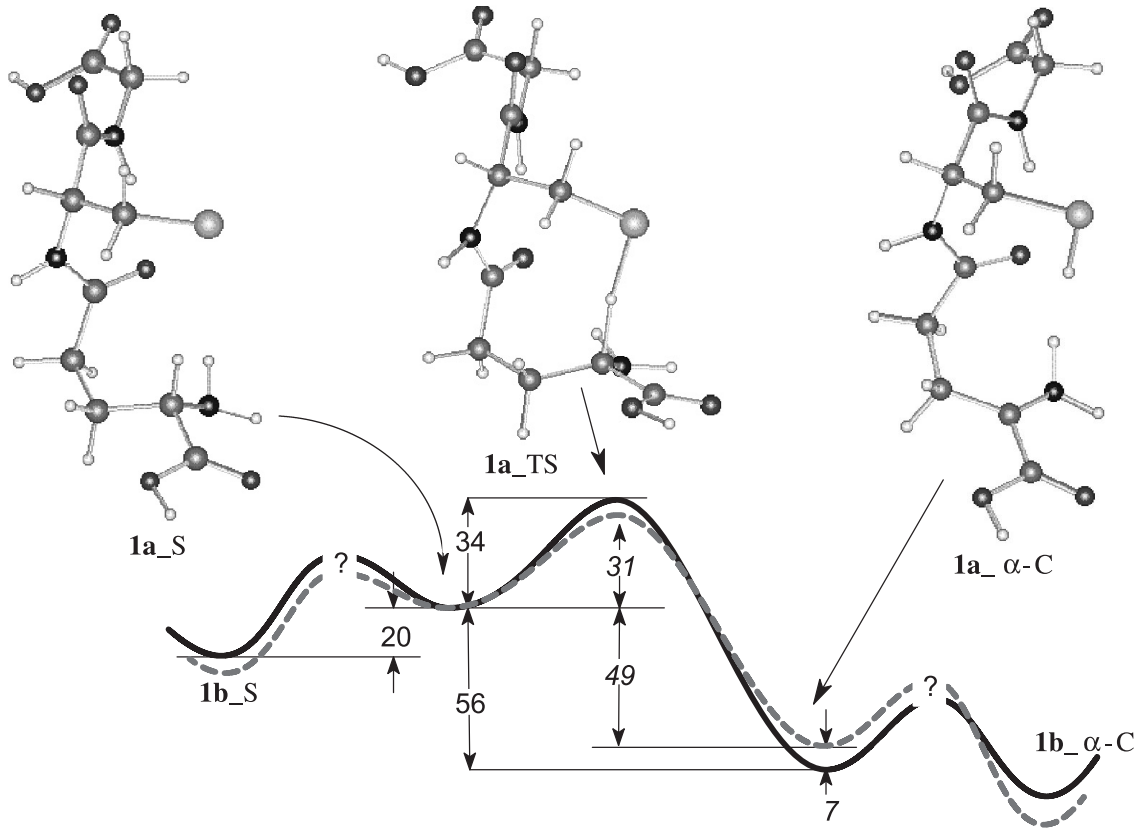
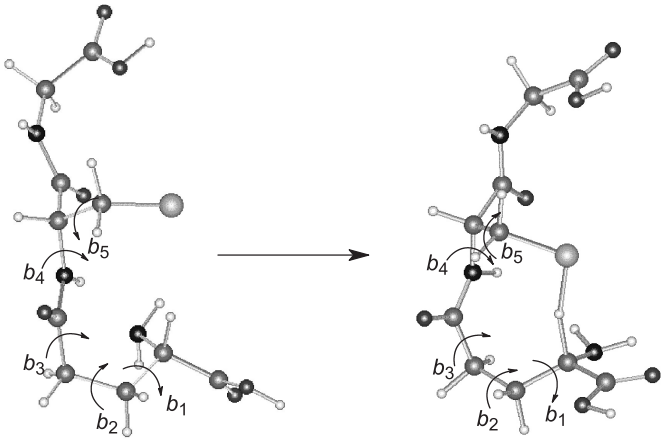


Fig. 9. Free energy (kJ mol^{-1}) profile for intramolecular H abstraction by **1a**_S in the gas phase (solid line, normal numbers) and solution (dashed line, italics).



© 2001 NRC Canada

Fig. 10. Definition of bonds involved in the process, **1b**_S → [**1b**_TS] (see text).



1b_S **1b**_TS

rotors, while b_3 and b_4 are twofold rotors. Independent rotations about these may generate as many as 108 conformations, one of which is **1a**_S, another **1b**_S. These rotational degrees of freedom are affected by the necessity to make a cyclic TS. For instance, rotation about b_3 is accompanied by rotation about b_4, and only certain *gauche* conformations are permitted for the threefold rotors (b_1, b_2, and b_5). The number of conformations available to the TS is reduced to about eight, two of which are **1a**_TS and **1b**_TS. This restriction in the conformational freedom would raise the free energy of activation by $-RT$ (ln 8 – ln 108) = 6.7 kJ mol^{-1} at 298 K, corresponding to an order of magnitude reduction in reaction rate. Even if there were only one other conformation as important as **1b**_S, and if **1b**_TS were the only accessible TS, the increase in the free energy of activation due to the entropy of mixing is almost 2 kJ mol^{-1}. Thus the entropy of mixing would have the effect of raising the free energy of activation into the range 37–42 kJ mol^{-1}.

The rate of H atom transfer

In the case of a unimolecular reaction, the rate constant for the reaction (k_T) is related to the free energy of activation ($\Delta G^{\neq}$) by eq. [7] (35):

$$[7] \qquad k_T = (k_B T/h)\ \exp(-\Delta G^{\neq}/RT)$$

Two independent experimental determinations place the rate of the thiyl to α-C radical transformation in the range 1.5 to 1.8 × 10^5 s^{-1} at 298 K (6, 19). This implies that $\Delta G^{\neq}$ = 43 kJ mol^{-1}. Both experiments were carried out at pH 10, where all acidic groups of GSH (including the Gln amino group) are deprotonated. At this pH, the SH group will also be deprotonated after H-transfer, but that should not affect the barrier height. The present calculations were carried out on the neutral system. Protonation of the Gln carboxyl may have a small effect on the barrier height, but the Gly carboxyl group will be sufficiently removed so as not to perturb the thermochemistry at the thiyl and α-C centres to a significant extent. Indeed, the experimental value is in remarkable agreement with the gas phase value for the lowest energy process ($\Delta G^{\neq}$ = 40 kJ mol^{-1} (Fig. 8)) and with the solution phase value which falls in the same range after inclusion of a contribution from the entropy of mixing. Addition of the free energy contribution from the entropy of mixing will have a lesser effect on the free energy change for the reaction since both reactants and products have similar conformational flexibility.

Conclusions

The bond dissociation enthalpies of the S—H bond and the α-C—H bonds of the three residues of glutathione (GSH), calculated by the method of isodesmic reactions, are (in kJ mol^{-1}): S—H 356, α-C—H (Gly) 344, α-C—H (Cys) 346 (31), α-C—H (Gln) 320. The last value is consistent with expectations based on experiment (7). Calculations on the radicals derived from GSH **1** and two model systems (*N*-formylcysteinylglycine (**2**) and *N*-(2-thioethanyl)-γ-glutamine (**3**)) suggest that the free energy of activation for abstraction of the α-C—H (Gly) by the thiyl radical in the gas phase is hindered by a barrier of 134 kJ mol^{-1} if the amide link to Gly is in the more stable (*Z*)-configuration, but is reduced to 52 kJ mol^{-1}, if it is in the less stable (*E*)-configuration. However, the isomerization of the amide group requires about 95 kJ mol^{-1}. Previous studies had indicated that intramolecular reaction of the thiyl radical at α-C—H (Cys) would encounter a barrier of 110 kJ mol^{-1} (34). The lowest energy pathway for intramolecular H-transfer to thiyl radical is from α-C—H (Gln). The gas phase barrier ($\Delta G^{\neq}$ = 40 kJ mol^{-1}) for the lower energy pathway and the solution phase barrier for the mixture of conformers ($\Delta G^{\neq}$ = 37– 42 kJ mol^{-1}) are in excellent agreement with that expected from the experimentally observed rate of reaction (6, 19) in solution ($\Delta G^{\neq}$ = 43 kJ mol^{-1}). The calculated free energy change ($\Delta G°$ = –54 kJ mol^{-1}) is higher than that estimated from experimental observations of solution equilibria ($\Delta G°$ = –37 kJ mol^{-1}) (7). The good agreement between theory in the gas phase and experiment in solution suggests that the free energies of solvation of reactant thiyl radical, transition structures for H abstraction, and the product α-C-centred radical, are very similar. This has direct support within the SCIPCM model (see ΔG (es) values in column 14 of Table 1). However, attempts to model the effects of solvation using the continuum self-consistent reaction field and the COSMO procedure (SCRF=CPCM) with Pauling radii, were inconclusive even as to whether a rate enhancement or decrease could be expected. This is possibly due to artefacts originating from complex cavities for these large molecules.

Acknowledgements

The financial support of the Natural Sciences and Engineering Council of Canada (NSERC) is gratefully acknowledged. We would also like to thank the Institut du Developement et des Ressources en Informatique Scientifique (IDRIS) (project no. 980946) and the Multimedia Advanced Computational Infrastructure (MACI) for providing computer facilities and technical assistance for this work.

© 2001 NRC Canada

References

1. L.A. Moran, K.G. Scrimgeour, H.R. Horton, R.S. Ochs, and J.D. Rawn. Biochemistry. 2nd ed. Neil Patterson Publ., Prentice Hall, Englewood Cliffs, NJ. 1994.
2. J.S. Bains and C.A. Shaw. Brain Res. Brain Res. Rev. **25**, 335–358 (1997).
3. E.R. Stadman. Ann. Rev. Biochem. **62**, 797 (1993).
4. G.V Buxton, C.L. Greenstock, W.P Helman, and A.B. Ross. J. Phys. Chem. Ref. Data, **17**, 513 (1988).
5. V.A. Sharpatyi. High Energy Chem. **29**, 77 (1995).
6. R. Zhao, J. Lind, G. Merényi, and T.E. Eriksen. J. Am. Chem. Soc. **116**, 12010 (1994).
7. R. Zhao, J. Lind, G. Merényi, and T.E. Eriksen. J. Chem. Soc. Perkin Trans. 2, 569 (1997).
8. N. Takahashi, and T.E. Creighton. Biochemistry, **35**, 8342 (1996).
9. H. Sies. (*Editor*). Oxygen stress. Academic Press, London. 1985.
10. H. Sies. (*Editor*). Oxidative stress–oxidants and anti-oxidants. Academic Press, London. 1991.
11. M.G. Simic, K.A. Taylor, J.F. Ward, and C. von Sonntag. (*Editors*). Oxygen radicals in biology and medicine. Plenum Press, New York. 1988.
12. K.J.A. Davies. (*Editor*). Oxidative damage and repair: chemical, biological, and medical aspects. Pergamon Press, New York. 1991.
13. C. von Sonntag. The chemical basis of radiation biology. Taylor and Francis, London. 1987.
14. (*a*) W.M. Garrison. Curr. Top. Rad. Res. **4**, 43 (1968); (*b*) W.M. Garrison. Rad. Res. Rev. **3**, 305 (1972).
15. O.J. Mieden and C. von Sonntag. Z. Naturforsch. B: Chem. Sci. **44b**, 959 (1989).
16. D.A. Armstrong, D. Yu, and A. Rauk. Can. J. Chem. **74**, 1192 (1996).
17. D.A. Armstrong, A. Rauk, and D. Yu. J. Am. Chem. Soc. **119**, 208 (1997).
18. M. Jonsson, D.D.M. Wayner, D.A. Armstrong, D. Yu, and A. Rauk. J. Chem. Soc. Perkin Trans. 2, 1967 (1998).
19. L. Grierson, K. Hildebrand, and E. Bothe. Int. J. Radiat. Biol. **62**, 265 (1992).
20. (*a*) M.J. Frisch, G.W Trucks, H.B. Schlegel, G.E. Scuseria, M.A. Robb, J.R. Cheeseman, V.G. Zakrzewski, J.A. Montgomery, Jr., R.E. Stratmann, J.C. Burant, S. Dapprich, J.M. Millam, A.D. Daniels, K.N. Kudin, M.C. Strain, O. Farkas, J. Tomasi, V. Barone, M. Cossi, R. Cammi, B. Mennucci, C. Pomelli, C. Adamo, S. Clifford, J. Ochterski, G.A. Petersson, P.Y. Ayala, Q. Cui, K. Morokuma, D.K. Malick, A.D. Rabuck, K. Raghavachari, J.B. Foresman, J. Cioslowski, J.V. Ortiz, A.G. Baboul, B.B. Stefanov, G. Liu, A. Liashenko, P. Piskorz, I. Komaromi, R. Gomperts, R.L. Martin, D.J. Fox, T. Keith, M.A. Al-Laham, C.Y. Peng, A. Nanayakkara, M. Challacombe, P.M.W. Gill, B. Johnson, W. Chen, M.W. Wong, J.L. Andres, C. Gonzalez, M. Head-Gordon, E.S. Replogle, and J.A. Pople. Gaussian 98 (Revision A.7). Gaussian, Inc., Pittsburgh, PA. 1998; (*b*) M.J. Frisch, G.W. Trucks, H.B. Schlegel, P.M.W. Gill, B.G. Johnson, M.A. Robb, J.R. Cheeseman, T. Keith, G.A. Petersson, J.A. Montgomery, K. Raghavachari, M.A. Al-Laham, V.G. Zakrzewski, J.V. Ortiz, J.B. Foresman, C.Y. Peng, P.Y. Ayala, W. Chen, M.W. Wong, J.L. Andres, E.S. Replogle, R. Gomperts, R.L. Martin, D.J. Fox, J.S. Binkley, D.J. Defrees, J. Baker, J.P. Stewart, M. Head-Gordon, C. Gonzalez, and J.A. Pople. Gaussian 94 (Revision B.3). Gaussian, Inc., Pittsburgh, PA. 1995.
21. A.P. Scott and L. Radom. J. Phys. Chem. **100**, 16502 (1996).
22. D.A. McQuarrie. Statistical thermodynamics. Harper & Row, New York. 1973.
23. J.B. Foresman, T.A. Keith, K.B. Wiberg, J. Snoonian, and M.J. Frisch. J. Phys. Chem. **100**, 16098 (1996).
24. (*a*) A. Kamt and G. Schuurmann. J. Chem. Soc. Perkin Trans. 2, 799 (1993); (*b*) J. Andzelm, C. Kolmel, and A. Kamt. J. Chem. Phys. **103**, 9312 (1995).
25. R. Arnaud, C. Adamo, M. Cossi, A. Milet, Y. Vallee, and V. Barone. J. Am. Chem. Soc. **122**, 324 (2000).
26. V. Barone, M. Cossi, and J. Tomasi. J. Phys. Chem. **107**, 3210 (1997).
27. S. Miertus, E. Scrocco, and J. Tomasi. Chem. Phys. **55**, 117 (1981).
28. V. Barone and M. Cossi. J. Phys. Chem. A, **102**, 1995 (1998).
29. (*a*) H. D. Beckhaus and C. Rüchardt. Angew. Chem. Int. Ed. Engl. **26**, 770 (1986); (*b*) J.M. Kanabus-Kaminska, B.C. Gilbert, and D. Griller. J. Am. Chem. Soc. **111**, 3311 (1989), and refs. therein.
30. D. Yu, D.A. Armstrong, and A. Rauk. Can. J. Chem. **70**, 1762 (1992).
31. A. Rauk, D. Yu, J. Taylor, G.V. Shustov, D.A. Block, and D.A. Armstrong. Biochemistry, **38**, 9089 (1999).
32. H.-G. Viehe, Z. Janousek, R. Merényi, And L. Stella. Acc. Chem. Res. **18**, 148 (1985).
33. B. Ruscic and J. Berkowitz. J. Chem. Phys. **97**, 1818 (1992).
34. A. Rauk, D. Yu, and D.A. Armstrong. J. Am. Chem. Soc. **120**, 8848 (1998).
35. R.S. Berry, S.A. Rice, and J. Ross. Physical chemistry. 2nd ed. Oxford University Press, Oxford, U.K. 2000. p. 917.

© 2001 NRC Canada

Incorporation of ^{13}C glucose into nicotinamide in *E. coli* and in *S. cerevisiae*

Ram Nath Gupta, Thomas Hemscheidt, Brian G. Sayer, and Ian D. Spenser

Abstract: The mode of incorporation into nicotinamide of label from ^{13}C-labeled samples of D-glucose, in *Escherichia coli* and *Saccharomyces cerevisiae*, was determined by means of ^{13}C NMR spectroscopy. The results, which confirm and extend early studies with radioactive tracers, permit a definitive choice to be made between alternative biogenetic proposals.

Key words: nicotinic acid, nicotinamide, biosynthesis, glucose incorporation, ^{13}C NMR.

Résumé : Faisant appel à la spectroscopie RMN du ^{13}C, on a déterminé le mode d'incorporation du ^{13}C d'échantillons de D-glucose marqué dans le nicotinamide d'*Escherichia coli* et de *Saccharomyces cerevisiae*. Les résultats, qui confirment et qui étendent la portée d'études antérieures à l'aide de marqueurs radioactifs, permettent de faire un choix définitif entre les diverses propositions biogénétiques.

Mots clés : acide nicotinique, nicotinamide, biosynthèse, incorporation du glucose, RMN du ^{13}C.

[Traduit par la Rédaction]

Introduction

Two major de novo pathways of nicotinic acid biosynthesis are known (for a review see ref. 1). The key intermediate of both routes is quinolinic acid which in the two pathways originates from different precursors.

The first of the pathways to the vitamin to be described is found in mammalian tissues, in molds and fungi, in yeasts under aerobic conditions, and in some higher plants. The primary precursor of this pathway is tryptophan. The steps and the enzymology of this route are well established (for a review see ref. 1).

That another route to the vitamin must exist became probable when it was shown that nicotinic acid in *Escherichia coli* (2) and trigonelline, the methylbetaine of nicotinic acid, in a higher plant (3), were not derived from tryptophan. This second pathway, which would appear to be more widely distributed than the route from tryptophan,[2] is found in prokaryotes in general, e.g., *E. coli* (5), *Mycobacterium tuberculosis* (6) and other bacteria, and also in yeasts under anaerobic conditions (7, 8). This route generates nicotinic acid by condensation of a triose phosphate with a dicarboxylic acid related to aspartic acid. The mechanism whereby these two precursors combine to yield the skeleton of nicotinic acid has not been established.

The first detailed incorporation studies related to this alternative pathway of nicotinic acid biosynthesis were carried out with higher plants.[3] This early work with ^{14}C-labeled substrates established incorporation of label from glycerol, and from dicarboxylic acids related to succinic acid (for summary see ref. 13). It is certain from tracer work with ^{14}C-labeled substrates that glycerol (and hence triose phosphate) supplies C-4, C-5, and C-6 of the ring. Label from [1,3-^{14}C]glycerol was found predominantly, and approximately equally, at C-4 and C-6, whereas label from [2-^{14}C]glycerol entered C-5 of the pyridine ring (13). Label from D-[3-^{14}C]glyceraldehyde entered mainly C-4 (55 ± ?[4]%), with the rest of the radioactivity spread throughout the molecule (14).

The dicarboxylic acid supplies carbon atoms C-2, C-3 of the ring system, and the two carboxylic acid groups of quinolinic acid (and thence of nicotinic acid, after decarboxylation of the carboxyl group at C-2). ^{14}C from [2,3-^{14}C]succinate as well as from [2-^{14}C]acetate labeled C-2 and C-3 of the pyridine ring approximately equally, while label from [1-^{14}C]acetate, [1,4-^{14}C]succinate, as well as from [4-^{14}C]aspartic

Received December 22, 2000. Published on the NRC Research Press Web site on May 3, 2001.

R.N. Gupta, B.G. Sayer, and I.D. Spenser.[1] Department of Chemistry, McMaster University, Hamilton, ON L8S 4M1, Canada.
T. Hemscheidt. Department of Chemistry, University of Hawaii at Manoa, 2545 The Mall, Honolulu, Hawaii 96822.

[1]Corresponding author (telephone: (905) 525-9140 ext. 23245; fax: (905) 522-2509; e-mail: spenser@mcmaster.ca).

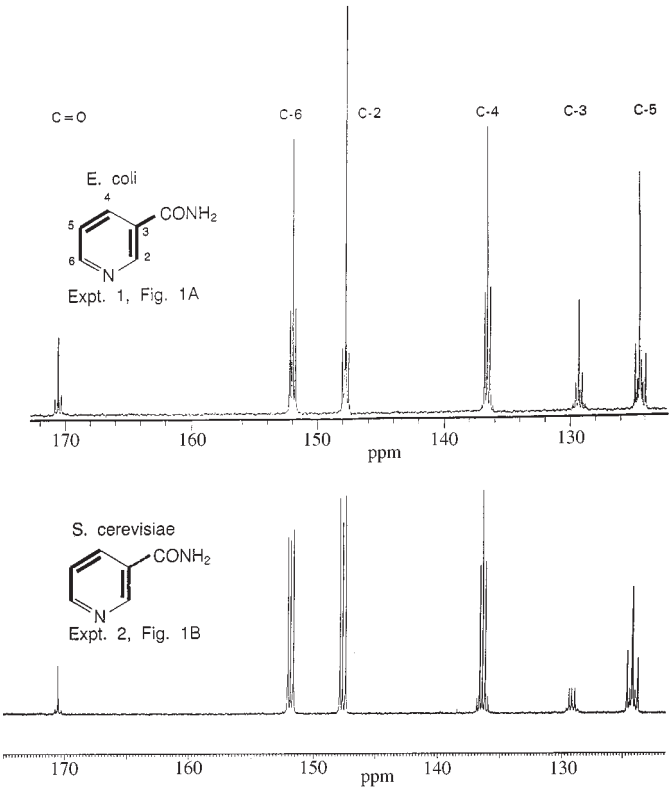
[2]The view that nicotinic acid (niacin) and its congener, nicotinamide, components of NAD and related coenzymes, was universally derived from tryptophan was firmly held until the mid-1950ies. But even today, current textbooks of biochemistry (4), if they refer to niacin biosynthesis at all, persist in stating categorically that the sole route to nicotinic acid starts from tryptophan.

[3]Results, showing the precise distribution of label from ^{14}C-labeled substrates within the pyridine ring of the alkaloids nicotine and anabasine in intact tobacco plants and within ricinine in the castor bean plant, can be extrapolated to the origin of the nicotinic acid ring system, since it has been demonstrated that the intact ring of nicotinic or of quinolinic acid serves as the precursor of the pyridine ring of the tobacco alkaloids (9–11) and of ricinine (12).

[4]Experimental error not reported.

 DOI: 10.1139/cjc-79-4-418 © 2001 NRC Canada

Fig. 1. ^{13}C NMR spectrum of nicotinamide derived from D-[$^{13}C_6$]glucose: (A) from *E. coli* (expt 1); and (B) from *S. cerevisiae* (expt 2).



acid entered solely into the carboxyl carbon of nicotinic acid. It is noteworthy that label from [3-^{14}C]aspartic acid, as well as from [3-^{14}C]malic acid, entered both C-2 (38 ± ?[4]% of the total specific activity of the labeled product) and C-3 (57 ± ?[4], 61 ± ?[4]%), rather than being confined to C-3 (15), as would have been expected if aspartic acid had been incorporated intact.

In *E. coli*, label from [1-^{14}C]glycerol entered C-4 (57 ± ?[4]%) and C-6 (40 ± ?[4]%) of quinolinic acid (16), while label from [1-^{14}C]dihydroxyacetone 1-phosphate entered C-4 exclusively (17). Label from D-[1-^{14}C]glucose (and probably also from D-[6-^{14}C]glucose) was spread over the whole molecule, with preferential entry into C-4 (24 ± ?[4]%) and C-6 (25 ± ?[4]%) whereas label from D-[2-^{14}C]glucose entered C-5 preferentially (78 ± ?[4]%) (16).

All available evidence thus points to the derivation of the ring system of quinolinic acid, and hence of that of nicotinic acid, from a triose plus a compound related to aspartic acid (18).

Two genes, *nadA* and *nadB*, that control the biosynthesis of nicotinic acid in *E. coli* and *S. typhimurium*, have been mapped and expressed (for a review see ref. 19, 20) and the corresponding gene products have been characterized (20, 21). The *nadB* gene product ("B protein"), L-aspartic acid oxidase (EC 1.4.3.16), is present not only in *E. coli* (22) but also in a higher plant (cotton) (23). It catalyzes the dehydrogenation, in the presence of FAD, of L-aspartic acid to yield 2-iminobutanedioic acid (2-iminosuccinic acid, referred to incorrectly as iminoaspartic acid) (24). However, there appears to be some question whether or not in *E. coli* the C-N fragment of aspartic acid is incorporated intact into the vitamin (25). Certainly, 2-iminosuccinic acid is generated also from oxalacetic acid plus ammonium sulfate (24).

The *nadA* gene product ("A protein"), quinolinate synthase (26), catalyzes the condensation of 2-iminosuccinic acid as the source of the fragment N-1,C-2,3,CO_2H of nicotinic acid, with the triose phosphate as the source of the fragment C-4,5,6. Both dihydroxyacetone phosphate and glyceraldehyde phosphate react readily in this condensation reaction. The identification of the former as the actual substrate for the condensation reaction rests on a single experiment with an inhibitor of triose phosphate isomerase (26).

The disposition of the triose on entry into the C_3 unit C-4,5,6 differs in alternative biogenetic proposals.

In a recently published hypothetical biogenetic sequence, the carbon atom of the phosphotriose that bears the phosphate ester group is postulated to yield C-6 of nicotinic acid (27). A similar disposition of the triose phosphate on entry into nicotinic acid had been advanced earlier (21, 28, 29). Alternatively, the phosphate ester carbon atom of the triose was postulated to generate C-4 of the niacin ring system (1, for a review see ref. 11, 14, 22, 30).

We now present results which establish that the latter alternative is the correct one.

Results and discussion

We have employed NMR spectroscopy to examine the mode of incorporation of ^{13}C-labeled D-glucose into nicotinamide in *E. coli* B WG2 (a *pdxH*$^-$ auxotroph) and in *S. cerevisiae* strain ATTC 7752 (IFO 1234). These are the micro-organisms that we had employed in our previous investigations of pyridoxine (31) and thiamin biosynthesis (32).

The ^{13}C NMR method had not hitherto been applied in the study of niacin biosynthesis. To do so, a method of isolation with minimal carrier dilution had to be developed. The method that eventually proved successful, described in the experimental section, was based on the isolation of nicotinamide, a weak base that can be isolated from the cell hydrolysate by solvent extraction and can then be further purified by liquid chromatography. Nicotinamide is quite stable. There is no significant hydrolysis of nicotinamide when it is heated in 0.1 M HCl solution for 1 h. In earlier investigations of niacin biosynthesis with ^{14}C, significant carrier dilution was required when either quinolinic acid or nicotinic acid, amphoteric compounds, were isolated. To test the utility of the method, D-[$^{13}C_6$]glucose was selected as the substrate whose incorporation was examined. Incorporation into nicotinamide of multicarbon units derived from this bond-labeled substrate[5] was indeed observed both in

[5] These experiments cannot differentiate between the two pathways since the distribution of D-[$^{13}C_6$]glucose-derived label within niacin in both pathways is predicted to be identical: In triose–aspartate-derived niacin the C_3 unit C-4,5,6 is generated via a triose while the C_2 unit C-2,3 arises via a dicarboxylic acid that is ultimately also derived via a triose, but can randomize its label by tricarboxylic acid cycling. In the aerobic route to niacin from glucose via tryptophan, a C_3 unit of glucose is incorporated into C-4,5,6 of niacin via erythrose while the C_2 unit C-2,3 arises via phosphoenolpyruvate.

© 2001 NRC Canada

Table 1. ^{13}C NMR spectrum of nicotinamide: chemical shifts and coupling constants.

Chemical shift[a] (ppm)	Carbon atom no.	Coupling constants (±0.5 Hz) ^{13}C-^{13}C	
124.7	C-5	$^1J_{C\text{-}5,C\text{-}4}$	54.4
		$^1J_{C\text{-}5,C\text{-}4} + {}^1J_{C\text{-}5,C\text{-}6}$	108.8
129.2	C-3	$^1J_{C\text{-}3,C\text{-}2}$	58.1
		$^1J_{C\text{-}3,C=O}$	64.0
		$^1J_{C\text{-}3,C\text{-}2} + {}^1J_{C\text{-}3,C=O}$	122.1
136.8	C-4	$^1J_{C\text{-}4,\ C\text{-}5}$	54.4
147.7	C-2	$^1J_{C\text{-}2,C\text{-}3}$	58.1
151.8	C-6	$^1J_{C\text{-}6,C\text{-}5}$	54.4
170.9	C=O	$^1J_{C=O,C\text{-}3}$	64.0

[a]Chemical shift (ppm) relative to dioxane as internal standard (66.6 ppm with respect to TMS at 0 ppm).

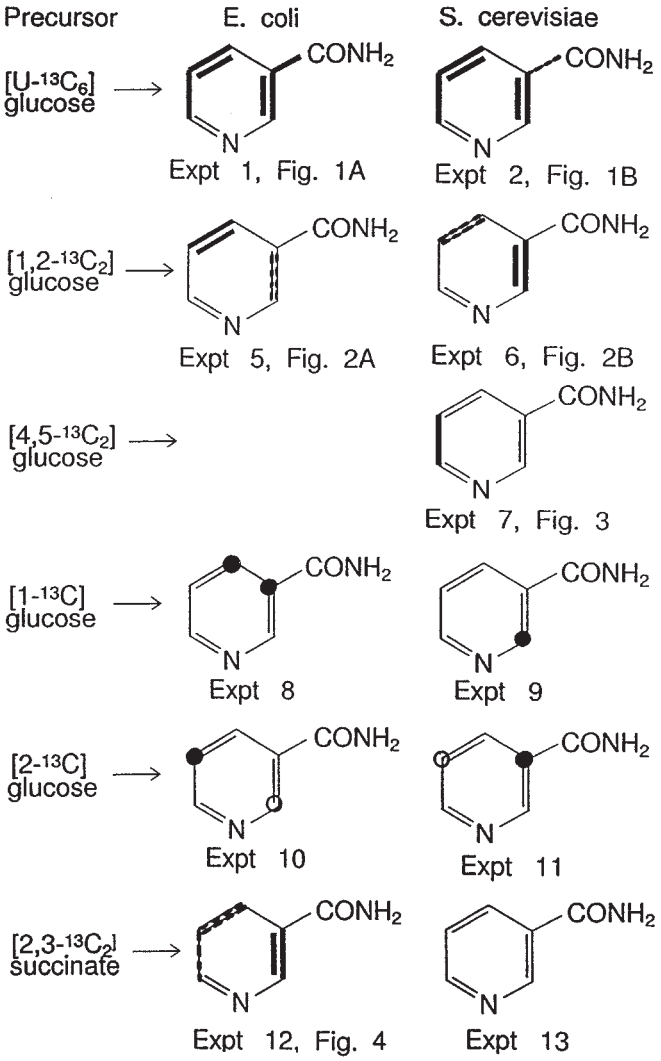
E. coli (expt 1, Fig. 1A) and in yeast (expt 2, Fig. 1B). ^{13}C NMR chemical shifts and coupling constants are summarized in Table 1.

The appearance of multiplets straddling the signals due to C-4 (136.8 ppm, $^1J_{C\text{-}4,\ C\text{-}5}$ = 54.4 Hz), C-5 (124.7 ppm, $^1J_{C\text{-}5,\ C\text{-}4} + {}^1J_{C\text{-}5,\ C\text{-}6}$ = 108.8 Hz), and C-6 (151.8 ppm, $^1J_{C\text{-}6,\ C\text{-}5}$ = 54.4 Hz) and of doublets at the signals due to C-2 (147.7 ppm, $^1J_{C\text{-}2,\ C\text{-}3}$ = 58.1 Hz) and C-3 (129.2 ppm, $^1J_{C\text{-}3,\ C\text{-}2}$ = 58.1 Hz) that were observed in the ^{13}C NMR spectrum of nicotinamide from *E. coli* (expt 1, Fig. 1A) confirmed that a C_3 unit and a C_2 unit derived from D-[$^{13}C_6$]glucose had been incorporated. Some scrambling of label had taken place during the incubation period, as indicated by the presence of a low intensity doublet around the carbonyl signal, showing low level labeling of the $CONH_2$ carbon atom and coupling with C-3 of the ring. The labeling patterns observed in these and subsequent experiments are summarized in Scheme 1.

The fact that ^{13}C incorporation into nicotinamide was detected served to show that the experimental procedure can be employed in the investigation of nicotinamide biosynthesis.

Using this method, an experiment was then carried out to establish the disposition of the triose phosphate upon its entry into the C_3 fragment C-4,5,6 of the pyridine ring of nicotinamide in *E. coli*. The distribution pattern of label from D-[1,2-$^{13}C_2$]glucose (expt 5, Fig. 2A) distinguished among the two possible modes of entry of the triose into the C_3 unit C-4,5,6 of the ring. The spectrum of the nicotinamide sample derived from D-[1,2-^{13}C]glucose (Fig. 2A) shows that the C-5 signal (124.7 ppm, $^1J_{C\text{-}5,\ C\text{-}4}$ = 54.4 Hz) is coupled to the signal due to C-4 (136.8 ppm, $^1J_{C\text{-}5,\ C\text{-}4}$ = 54.4 Hz). As before, low intensity satellites are present at other carbon signals, due to some scrambling of label. Since the signal due to bond-labeling at C-5 (124.7 ppm) shows coupling to only one other carbon, C-4, whereas in the spectrum of D-[$^{13}C_6$]glucose-derived nicotinamide the signal for C-5 had shown coupling to two other carbon atoms ($^1J_{C\text{-}5,\ C\text{-}4} + {}^1J_{C\text{-}5,\ C\text{-}6}$ = 108.8 Hz), this coupling pattern shows that a C_2 unit derived from the precursor was incorporated into C-4,5 of the nicotinamide.

Scheme 1. Observed incorporation of ^{13}C into nicotinamide (see Figs. 1–4).



Upon glycolysis, C-1 and C-2 of glucose give rise, respectively, to the phosphohydroxymethyl carbon and the carbonyl carbon atom of dihydroxyacetone phosphate and then, by triosephosphate isomerization, to the phosphohydroxymethyl carbon atom and the central carbon atom of D-glyceraldehyde phosphate. The incorporation pattern of ^{13}C from D-[1,2-^{13}C]glucose proves that incorporation of the phosphotriose takes place in such a way that C-4, but not C-6, of nicotinamide is derived from the phosphohydroxy carbon atom, as had been proposed by Gholson and coworkers (22) and others (1, 11, 14, 30).

Incorporation of label from D-[$^{13}C_6$]glucose and from D-[1,2-$^{13}C_2$]glucose into the C_2 fragment C-2,3 of nicotinamide in *E. coli* must now be examined. This fragment, together with the carbonyl carbon atom is derived from 2-iminosuccinic acid, the *nadB* gene product (see *Introduction*).

Since aspartic acid and related dicarboxylic acids originate from glucose-derived triose phosphates in several steps, via [$^{13}C_3$]phosphoenolpyruvate and thence by carboxylation to [1,2,3-$^{13}C_3$]oxaloacetate, an intact C_2 unit derived from D-[$^{13}C_6$]glucose was expected to enter C-2,3 of nicotinamide.

© 2001 NRC Canada

Fig. 2. ^{13}C NMR spectrum of nicotinamide derived from D-[1,2-$^{13}C_2$]glucose: (A) from *E. coli* (expt 5); and (B) from *S. cerevisiae* (expt 6).

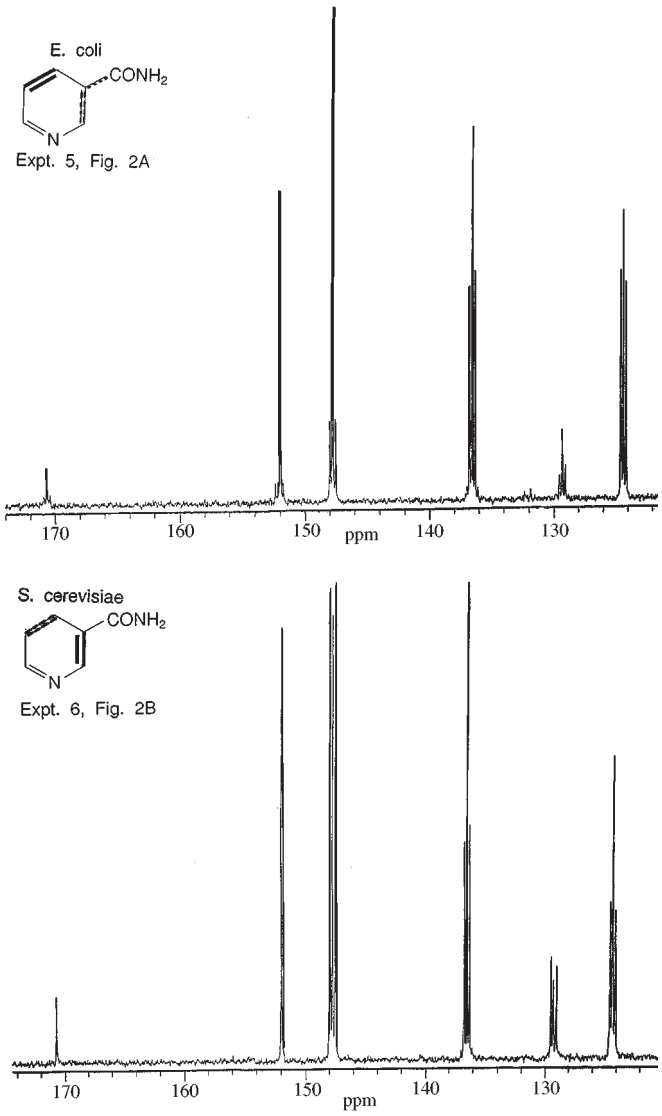


Fig. 3. ^{13}C NMR spectrum of nicotinamide derived from D-[4,5-$^{13}C_2$]glucose (expt 7).

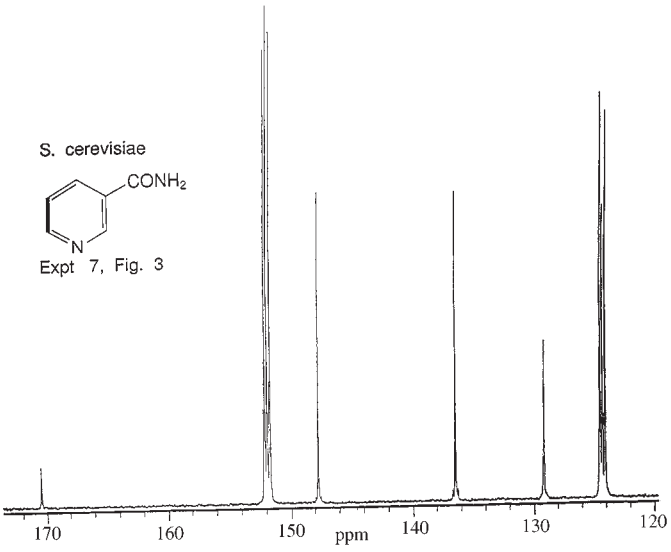
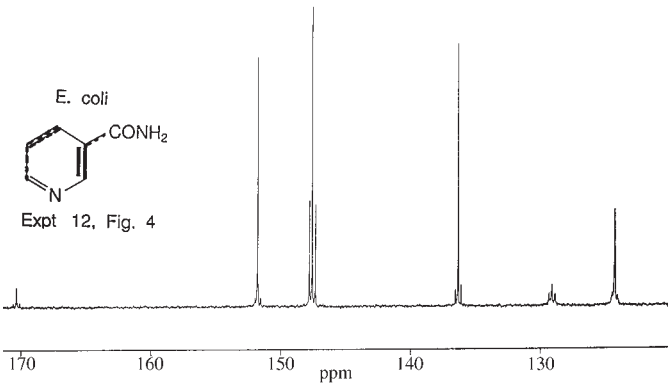


Fig. 4. ^{13}C NMR spectrum of nicotinamide derived from sodium [2,3-$^{13}C_2$]succinate (expt 12).



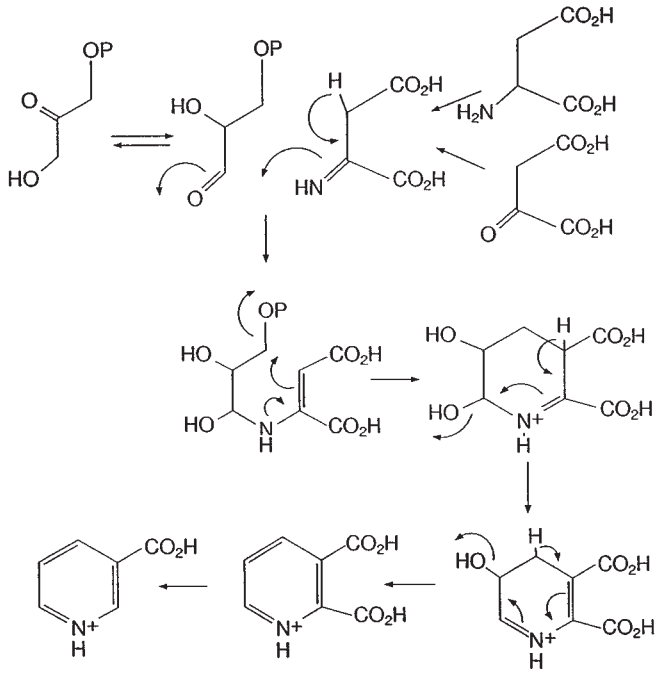
The appearance of doublets at the signals due to C-2 (147.7 ppm, $^1J_{C\text{-}2,\ C\text{-}3}$ = 58.1 Hz) and C-3 (129.2 ppm, $^1J_{C\text{-}3,\ C\text{-}2}$ = 58.1 Hz) (Fig. 1A) showed that this had indeed occurred. Incorporation of label from glucose by this multistep route had presumably taken place via quinolinic acid, followed by decarboxylation, i.e., with loss of the labeled oxaloacetate carboxyl group derived from C-3 of glucose. The low-intensity multiplet around C-3 (129.2 ppm, $^1J_{C\text{-}3,\ C\text{-}2}$ + $^1J_{C\text{-}3,\ C=0}$ = 122.1 Hz), indicating incorporation of an intact C_3 unit into C-2,3,CO, is explicable on the basis of [1,2,3-$^{13}C_3$]oxaloacetate recycling through the tricarboxylic acid cycle to yield [2,3,4-$^{13}C_3$]oxaloacetate, which upon entry into nicotinamide, loses the unlabeled carboxyl group.

Another indication for involvement of an intermediate derived from aspartate was the observation that when incubation with D-[$^{13}C_6$]glucose was carried out in the presence of excess unlabeled aspartic acid (expt 3), incorporation of ^{13}C into the C_2 unit C-2,3 of the ring was lowered, relative to the ^{13}C incorporation into the C_3 unit C-4,5,6. This was shown by the observation that the ratios of the intensities of the doublets C-6:C-2 and C-4:C-2 (5.3 and 5.1, respectively), in the nicotinamide spectrum from the latter incubation, were found to be more than twice as large as the corresponding ratios in the spectrum of the sample obtained from the incubation with glucose alone (expt 1) (C-6:C-2 = 2.1, C-4:C-2 = 2.3). It should be mentioned, parenthetically, that in a similar set of experiments with yeast (expts 4 and 2, respectively), in which nicotinamide showed an incorporation pattern similar to that of the nicotinamide derived from D-[$^{13}C_6$]glucose in *E. coli*, these ratios were unaffected by the presence of aspartic acid. This confirms that in yeast under aerobic conditions the triose–aspartic acid route to nicotinamide is at best of minor importance.

This conclusion is borne out by the results of incorporation experiments with sodium [2,3-$^{13}C_2$]succinate. In *E. coli* (expt 12, Fig. 4) label from this precursor was found in the C_2 unit C-2,3 (C-2: 147.7 ppm, $^1J_{C\text{-}2,\ C\text{-}3}$ = 58.2 Hz; C-3:

© 2001 NRC Canada

Scheme 2. A possible mechanism of the triose phosphate–aspartate pathway of nicotinic acid biosynthesis.

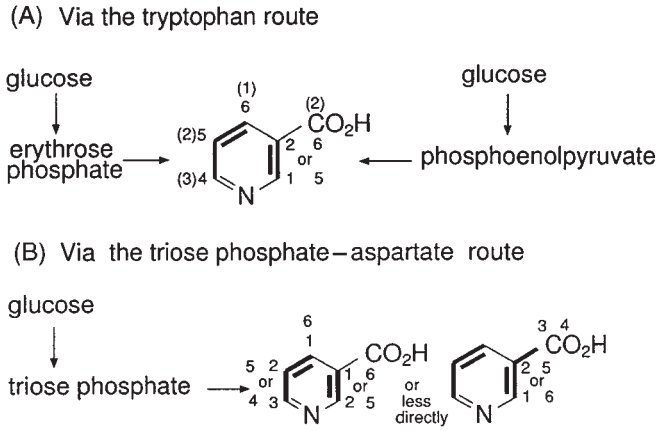


129.2 ppm, $^{1}J_{C\text{-}3,\ C\text{-}2}$ = 58.2 Hz) of nicotinamide.[6] In the spectrum of yeast nicotinamide, from the same precursor (expt 13), incorporation of ^{13}C was not detectable.

A mechanism for the biosynthesis of quinolinic acid (and hence of nicotinic acid), based on the condensation of 2-iminosuccinic acid with dihydroxyacetone phosphate, was advanced by Gholson and co-workers in 1982 (22). In order to arrive at the desired target, quinolinic acid, from these precursors, the proposed mechanism included steps that were equivalent to an isomerization of dihydroxyacetone phosphate into D-glyceraldehyde phosphate. Derivation of quinolinic acid by condensation of 2-iminosuccinic acid with D-glyceraldehyde phosphate rather than with dihydroxyacetone phosphate offers a much simpler path to the product (Scheme 2). It would be desirable to confirm by further experiment that the gene product of *nadA*, quinolinate synthase, is indeed specific for dihydroxyacetone phosphate, as seems to be generally assumed on the basis of a single experimental observation (26), or whether D-glyceraldehyde phosphate serves as the substrate.

As already mentioned,[5] the triose–aspartate route cannot be distinguished from the tryptophan route on the basis of the incorporation pattern of label derived from ^{13}C bond-labeled samples of D-glucose, since the sites of entry of multicarbon units from glucose are similar in the two pathways (Fig. 1). But even though the distribution of the multicarbon fragments is similar, the relative efficiency of entry into the two sites of nicotinamide, C-4,5 and C-2,3, was found to differ: Comparison of the spectra of nicotinamide derived from D-[1,2-$^{13}C_2$]glucose (Fig. 2) shows that in the triose–aspartate-derived *E. coli* sample (expt 5) the triose-derived C_2 unit C-4,5 was much more highly enriched than the aspartate-derived C_2 fragment C-2,3 (Fig. 2A). By contrast, in the tryptophan-derived aerobic *S. cerevisiae* sample (expt 6) the C_2 fragment C-2,3, derived via phosphoenolpyruvate, was much more highly enriched than the erythrose-derived C_2 unit C-4,5 (Fig. 2B). In the case of the samples derived from D-[U-$^{13}C_6$]glucose (Fig. 1) the quantitative difference in the incorporation of multicarbon units was minor. In nicotinamide derived from D-[4,5-$^{13}C_2$]glucose in *S. cerevisiae* (expt 7, Fig. 3) coupling was confined to C-5,6 (Scheme 3A).

Scheme 3. Incorporation of carbon atoms of glucose into nicotinic acid. Solid lines represent incorporation of multicarbon fragments. Numbers refer to the carbon atoms of glucose from which indicated sites within nicotinic acid are derived.



When singly ^{13}C-labeled samples of glucose are used as substrates, differentiation of the two pathways is possible. The distribution of label observed in the nicotinamide obtained in these experiments is shown in Scheme 1.

On the basis of well-established evidence (4) the tryptophan route is predicted to deliver label from D-[1-^{13}C]glucose into C-2 of niacin, while label from D-[2-^{13}C]glucose is predicted to enter C-3 as well as the carbonyl carbon. The triose–aspartate route is expected to deliver C-1 of glucose mainly into C-4 and C-3 of niacin, with some minor amount entering C-2. By contrast, C-2 of glucose is delivered into C-5 and C-2 of niacin, with a minor quantity entering C-3. Niacin generated by the two different pathways should thus be ^{13}C-enriched at different sites (Scheme 3).

To determine which of the nicotinamide carbon atoms of the samples derived from D-[1-^{13}C]- and D-[2-^{13}C]-glucose in *E. coli* (expts 8 and 10) and in *S. cerevisiae* (expts 9 and 11) had been significantly enriched, peak areas of each of the signals in the ^{13}C NMR spectra of these four samples were compared with those of the corresponding signals in a spectrum of a standard nicotinamide sample. The signal areas in the spectra of the ^{13}C-enriched samples were normalized using the signal of C-6 of nicotinamide as a baseline, since, from the experiments with D-[1,2-$^{13}C_2$]glucose, the C-6 signal was known to be unenriched in each case. The signals with maximum enrichment were thus identified. The differences

[6] The additional low level incorporation of C_2 units into C=O,C-3; C-4,5 and C-5,6 shown in Fig. 4 is presumably due to tricarboxylic acid cycle recycling of [2,3-$^{13}C_2$]succinate and due to gluconeogenesis, in the course of the 18 h incubation that was required to reach the desirable cell density in expt 12.

© 2001 NRC Canada

Table 2. Experimental details.

Expt no.	Substrates	mg L^{-1}	No. of incubations	Time (h)	^{13}C NMR spectrum
E. coli B WG2					
1	D-[U-$^{13}C_6$]glucose	100	5 × 1 L	12	Fig. 1A
	D-glucose	900			
3	D-[U-$^{13}C_6$]glucose	100	5 × 1 L	15	
	D-glucose	900			
	L-aspartic acid	300			
5	D-[1,2-$^{13}C_2$]glucose	200	5 × 1 L	15	Fig. 2A
	D-glucose	800			
8	D-[1-^{13}C]glucose	400	5 × 1 L	15	
	D-glucose	600			
10	D-[2-^{13}C]glucose	300	5 × 1 L	12	
12	D-glucose	700			
	Na [2,3-$^{13}C_2$]succinate	200	5 × 1 L	18	Fig. 4
	D-glucose	1000			
S. cerevisiae ATTC 7752 (IFO 1234)					
2	D-[U-$^{13}C_6$]glucose	1000	2 × 1 L	12	Fig. 1B
	D-glucose	4000			
4	D-[U-$^{13}C_6$]glucose	1000	1 L	12	
	D-glucose	4000			
	L-aspartic acid	1500			
6	D-[1,2-$^{13}C_2$]glucose	1000	2 × 1 L	12	Fig. 2B
	D-glucose	4500			
7	D-[4,5-$^{13}C_2$]glucose	500	2 × 1 L	18	Fig. 3
	D-glucose	3500			
9	D-[1-^{13}C]glucose	5000	1 L	12	
11	D-[2-^{13}C]glucose	2000	2 × 1 L	24	
	D-glucose	1500			
13	Na [2,3-$^{13}C_2$]succinate	1000	2 × 1 L	20	
	D-glucose	8000			
	L-threonine	250			
	L-proline	250			
	L-histidine	250			

in the distribution of label from D-[1-^{13}C]- and D-[2-^{13}C]glucose in the samples derived by the triose–aspartate route (*E. coli*) and the tryptophan route (aerobically grown *S. cerevisiae*) are manifest (Scheme 1).

Experimental

^{13}C-labeled compounds

All but one of the ^{13}C-labeled compounds were purchased from Cambridge Isotope Laboratories, Andover, MA. The exception was D-[4,5-$^{13}C_2$]glucose, which was obtained from Isotech Inc., Miamisburg, OH.

Micro-organisms

E. coli B WG2 and *S. cerevisiae* ATTC 7752 (IFO 1234) were cultured and worked up as described earlier (32). *E. coli* cultures grown to a cell density of 1.0 at 620 nm (12–15 h) were found to contain ca. 60–80 μg L^{-1} nicotinamide. Yeast cultures grown to a cell density of 1.6 or greater (12–24 h) contained ca. 300–400 μg L^{-1}. Incubations with labeled compounds in *E. coli* cultures were carried out with 5 × 1 L cultures. Yeast incubations were performed with 1 L or with 2 × 1 L yeast cultures (Table 2).

Isolation of nicotinamide

The cells were harvested by centrifugation (10 min at room temp) and the cells from the multiflask incubations were pooled. The separated cells were suspended in dilute HCl (0.1 M, 10 mL per 1 L batch of cells) and the mixture was autoclaved for 1 h at 121°C. After cooling, acetate buffer (1 M, pH 5.5) was added to adjust the pH of the suspension to pH 4.7.

The suspension was centrifuged for 10 min at room temp. The cell debris was sonicated twice in water (20 mL) and the clear supernatant collected. The pH of the combined supernatant was adjusted (if necessary) with acetate buffer (0.2 M, pH 4.7).

The cell hydrolysate was spiked with 1 mL of an aqueous solution containing 3 mg per mL nicotinamide. The solution was centrifuged if necessary to remove suspended solids. The supernatant was applied to a 80 mm × 10 mm column of Amberlite CG50 (H^+ form) and the drainings were

© 2001 NRC Canada

collected. The column was washed with water (120 mL). The drainings and washings were combined and evaporated at 50°C under vacuum.

The residue was treated with 100 μL portions of a saturated solution of sodium carbonate (total sodium carbonate solution ca. 0.4–0.5 mL), until the pH was 9, followed by dichloromethane (25 mL). After mixing, anhydrous sodium sulfate (5 g) was added and the mixture allowed to stand overnight. The organic layer was separated and filtered through a small column with a filter disc, containing ca. 2 g anhydrous sodium sulfate.

The solid cake was stirred twice with dichloromethane (15 mL), filtered and the combined filtrates evaporated. The residue was dissolved in water (2 mL), treated with 1M HCl (20 μL), and the solution applied to a 500 mg column of SCX (a silica based strong cation exchange resin, Varian, Harbor City, CA), which had been washed in turn with column volumes (ca. 10 mL) of 1M NH_4OH, methanol, 1M HCl, and methanol, followed by a water wash, until the eluate was neutral. All the washings were carried out at a medium flow rate by applying suction. However, the sample was passed through the column at a slow rate by reducing the suction. The column was drained completely by increasing the suction to a maximum. The column was then washed with water (5 mL) and methanol (2.5 mL) at a medium rate and the product was then eluted with a mixture of dichloromethane (20 mL), methanol (2 mL), and concd. NH_4OH (0.2 mL). The elution was carried out by gravity or under mild positive pressure of nitrogen.

The eluate was evaporated to dryness to yield nicotinamide, sufficiently pure for NMR. The recovery and purity of nicotinamide was monitored by liquid chromatography (HPLC) using a Beckman Ultrasphere (5 μm, 25 cm × 4.6 mm) ODS column. The column was eluted with a mobile phase containing formic acid (400 μL), concd. NH_4OH (800 μL), and acetonitrile (15 mL) per L of water, at a flow rate of 1 mL min^{-1}. The peaks were detected at 254 nm. Under these conditions nicotinamide eluted at 13 min. The average recovery of spiked nicotinamide was ca. 90%. When traces of impurities accompanied the nicotinamide sample, it was purified by HPLC, using a Beckman Ultrasphere (5 μm, 25 cm × 10 mm) semipreparative column, using the same mobile phase that was used with the analytical column, at a flow rate of 2.5 mL min^{-1}.

Isolation of nicotinamide from the cell hydrolysate of *S. cerevisiae* was carried out by the same procedure used for the isolation from the *E. coli* cell hydrolysate.

NMR Spectroscopy

NMR spectra were acquired at McMaster and at the University of Hawaii. At McMaster: Bruker DRX 500 spectrometer operating at 11.74 T, using a Bruker 2.5 mm microprobe; pulse width 90° (8 μs); spectral width 28 985.5 Hz; recycle delay 4.6 s; digital resolution 0.88 Hz per data point. At University of Hawaii: GE Omega 500 spectrometer, using a Nalorac 3 mm microtube; pulse width 60°; recycle delay 2 s; 32 k data points. Spectra were 125.776 Hz proton decoupled ^{13}C NMR spectra of nicotinamide in D_2O (100 μL). Approximately 50 000 transients were required to generate the ^{13}C spectra showing satellites.

Acknowledgments

Research grants from the National Institute of General Medical Sciences, US Public Health Service, and from the Natural Sciences and Engineering Research Council of Canada (NSERC) are gratefully acknowledged. We thank Richard M. Pauloski for skilled technical assistance.

References

1. (*a*) J.W. Foster and A.G. Moat. Microbiol. Rev. **44**, 83 (1980); (*b*) A.G. Moat and J.W. Foster. *In* Pyridine nucleotide coenzymes, chemical, biochemical and medical aspects. *Edited by* D. Dolphin, R. Poulson, and O. Avramović. Wiley, New York. 1987. Part B, pp. 1–24.
2. C. Yanofsky. J. Bacteriol. **68**, 577 (1954).
3. E. Leete, L. Marion, and I.D. Spenser. Can. J. Chem. **33**, 405 (1955).
4. (*a*) A.L. Lehninger. Principles of biochemistry. 2nd ed. Worth Publishers, New York. 1993. p. 520; (*b*) D. Voet and J.G. Voet. Biochemistry. 2nd ed. J. Wiley & Sons, New York. 1995. p. 741; (*c*) L. Stryer. Biochemistry. 4th ed. W.H. Freeman, New York. 1995. p. 755; (*d*) R. Montgomery, T.W. Conway, A.A. Spector, and D. Chappell. Biochemistry. 6th ed. Mosby, St. Louis. 1996. p. 264; (*e*) T.M. Devlin. Textbook of biochemistry. 4th ed. Wiley-Liss, New York. 1997. p. 475; (*f*) G.L. Zubay. Biochemistry. 4th ed. Wm. C. Brown, McGraw Hill, Dubuque, IA. 1998. p. 661.
5. (*a*) M.V. Ortega and G.M. Brown. J. Am. Chem. Soc. **81**, 4437 (1959); (*b*) M.V. Ortega and G.M. Brown. J. Biol. Chem. **235**, 2939 (1960).
6. D. Gross, A. Feige, R. Stecher, A. Zureck, and H.-R. Schütte. Z. Naturforsch. **27 b**, 1116 (1965).
7. F. Ahmad and A. G. Moat. J. Biol. Chem. **241**, 775 (1966).
8. H.-D. Heilmann and F. Lingens. Hoppe Seyler's Z. Physiol. Chem. **349**, 231 (1968).
9. E. Leete. Bioorg. Chem. **6**, 273 (1977).
10. K.S. Yang, R.K. Gholson, and G.R. Waller. J. Am. Chem. Soc. **87**, 4184 (1965).
11. E. Leete. *In* Alkaloids: Chem. Biol. Perspect. Vol.1. *Edited by* S.W. Pelletier. J. Wiley & Sons, New York. 1983. pp. 85–152.
12. K.S. Yang and G.R. Waller. Phytochemistry, **4**, 881 (1965).
13. I.D. Spenser. *In* Comprehensive biochemistry. Vol. 20. *Edited by* M. Florkin and E.H. Stotz. Elsevier, Amsterdam. 1968. pp. 275–281.
14. J. Fleeker and R.U. Byerrum. J. Biol. Chem. **242**, 3042 (1967).
15. M. Jackanicz and R.U. Byerrum. J. Biol. Chem. **241**, 1296 (1966).
16. J.L.R. Chandler, R.K. Gholson, and T.A. Scott. Biochim. Biophys. Acta, **222**, 523 (1970).
17. F.D. Wicks, S. Sakakibara, R.H. Gholson, and T.A. Scott. Biochim. Biophys. Acta, **500**, 213 (1977).
18. F.D. Wicks, S. Sakakibara, and R.K. Gholson. J. Bacteriol. **136**, 136 (1978).
19. T. Penfold and J.W. Foster. *In E. coli* and *S. typhimurium*, Cellular and molecular biology. Vol. 1, 2nd ed. ASM Press, Washington, D.C. 1996. pp. 721–730.
20. (*a*) R. Flachmann, N. Kunz, J. Seifert, M. Gütlich, F.-J. Wientjes, A. Läufer, and H.G. Gassen. Eur. J. Biochem. **175**, 221 (1988); (*b*) J. Seifert, N. Kunz, R. Flachmann, A. Läufer, K.-D. Jany, and H.G. Gassen. Biol. Chem. Hoppe-Seyler, **371**, 239 (1990).
21. G.R. Griffith, J.L.R. Chandler, and R.K. Gholson. Eur. J. Biochem. **54**, 239 (1975).

© 2001 NRC Canada

22. S. Nasu, F.D. Wicks, and R.H. Gholson. J. Biol. Chem. **257**, 626 (1982).
23. Y. Hosokawa, E. Mitchell, and R.K. Gholson. Biochem. Biophys. Res. Commun. **111**, 188 (1983).
24. S. Nasu and R.K. Gholson. Biochem. Biophys. Res. Commun. **101**, 533 (1981).
25. (*a*) B.M. Steiner, J.T. Heard, Jr., and G.J. Tritz. J. Bacteriol. **141**, 989 (1980); (*b*) J.T. Heard, Jr., and G. J. Tritz. Biochem. Biophys. Res. Commun. **95**, 1517 (1980); (*c*) J.T. Heard, Jr., B.M. Steiner, and G.J. Tritz. Current Microbiol. **5**, 279 (1981).
26. N. Suzuki, J. Carlson, G. Griffith, and R.K. Gholson. Biochim. Biophys. Acta, **304**, 309 (1973).
27. T.P. Begley, C. Kinsland, S. Taylor, M. Tandon, R. Nicewonger, M. Wu, N. Kelleher, N. Campobasso, and Y. Zhang. Top. Curr. Chem. **195**, 93 (1998).
28. J. Chen and G. J. Tritz. Microbios, **16**, 207 (1976).
29. J.B. Foster and A.G. Moat. J. Bacteriol. **133**, 775 (1978).
30. J. Arditti and J. B. Tarr. Am. J. Bot. **66**, 1105 (1979).
31. R.E. Hill, K. Himmeldirk, I.A. Kennedy, R.M. Pauloski, B.G. Sayer, E. Wolf, and I.D. Spenser. J. Biol. Chem. **271**, 30 426 (1996).
32. K. Himmeldirk, B.G. Sayer, and I.D. Spenser. J. Am. Chem. Soc. **120**, 3581 (1998).

© 2001 NRC Canada

Chelated fluoroboron cations. III. Spectroscopic evidence for ring size and steric limitations to chelate formation by amine chelating donors

J. Stephen Hartman and James A.W. Shoemaker

Abstract: Factors affecting the ability of potentially chelating amine ligands to form chelated fluoroboron cations are explored by ^{19}F and ^{11}B NMR spectroscopy and fast atom bombardment mass spectrometry (FAB-MS). Five-membered chelate rings form much more readily than six-membered. Some potentially chelating ligands give rise to additional fluoroboron species by various redistribution and decomposition reactions.

Key words: chelated fluoroboron cations, ^{19}F NMR, ^{11}B NMR; FAB-MS, *N,N,N′,N′*-tetraethylethylenediamine.

Résumé : Faisant appel à la spectroscopie RMN du ^{19}F et du ^{11}B et la spectrométrie de masse par bombardement avec des atomes rapides, on a étudié les facteurs qui affectent la facilité de former des cations fluoroborés chélatés à partir de ligands aminés pouvant éventuellement donner lieu à de la chélation. Les chélates avec cycles à cinq chaînons se forment beaucoup plus facilement que ceux à six chaînons. Certains des ligands pouvant éventuellement donner lieu à de la chélation conduisent à d'autres espèces fluoroborés impliquant diverses réactions de redistribution et de décomposition.

Mots clés : cations fluoroborés chélatés, RMN du ^{19}F, RMN du ^{11}B, FAB-MS, *N,N,N′,N′*-tétraéthyléthylènediamine.

[Traduit par la Rédaction]

Introduction

We have recently reported the formation of chelated fluoroboron cations $(DD)BF_2^+$ involving substituted ethylenediamine (en) ligands, notably *N,N,N′,N′*-tetramethylethylenediamine (Me_4en) and *N,N,N′,N″,N″*-pentamethyldiethylenetriamine (Me_5dien) (1). There are various possible routes to these species (1, 2): (*i*) displacement of a donor and a heavy halide ion from $py{\cdot}BF_2Cl$ or $ISOX{\cdot}BF_2X$ (X = Cl or Br; py = pyridine; ISOX = isoxazole (a very weak donor));



ISOX

(*ii*) stepwise displacement of py from $(py)_2BF_2^+$; and (*iii*) reaction of the ligand with $Et_2O{\cdot}BF_3$. Routes (*i*) and (*ii*) are effective for *t*-amine chelating ligands such as Me_4en and Me_5dien, while route (*iii*) gives only BF_3 adducts, in which each donor site is coordinated to a separate BF_3 molecule. This is in accord with earlier work in which others had tried and failed to obtain the chelated $(Me_4en)BF_2^+$ by this route (3). However, $Et_2O{\cdot}BF_3$ does react to form chelated fluoroboron cations with some rigid donor molecules such as 1,10-phenanthroline (2, 4), in which the donor sites are geometrically constrained to favour chelation, i.e., there is donor preorganization (5). Most of the few known chelated fluoroboron cations have five-membered chelate rings except for 1,8-bis(dimethylamino)naphthalene (DMAN) (2) which gives rise to a six-membered ring. However boron forms a wide range of five- and six-membered ring chelate compounds (6), and there are even some 7-membered-ring chelate compounds (7). Hence there is no evident reason why fluoroboron chelates should not form with a similarly wide range of ligands.

We now report an extension of our studies of the formation of chelated fluoroboron cations (1, 2) to a wider range of amine chelating ligands, with emphasis on the effects of increased steric hindrance and chelate ring size, using the ligands *N,N,N′,N′*-tetraethylethylenediamine (Et_4en), *N,N,N″,N″*-tetraethyldiethylenetriamine (Et_4dien), di-(2-picolyl)amine (DPA) (8), 1,3-bis(dimethylamino)propane (*N,N,N′,N′*-tetramethylpropylenediamine) (Me_4pn), *N,N,N″,N″*-tetraethyldipropylenetriamine (Et_4dipn), and bis(dimethylamino)methane (*N,N,N′,N′*-tetramethylmethylenediamine) (Me_4mn). Although none of the chelated fluoroboron cations of these ligands have precipitated cleanly as single species as in our previous studies (1, 2), much has been learned about these systems from spectroscopic studies.

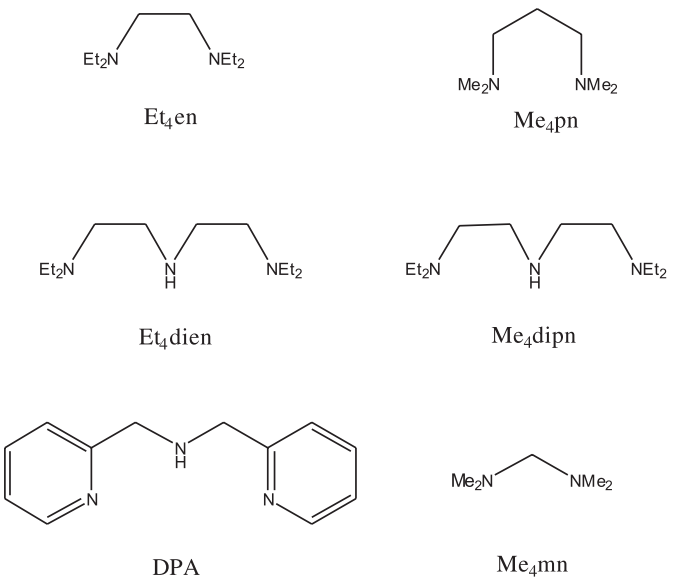
Received July 31, 2000. Published on the NRC Research Press Web site on May 3, 2001.

J.S. Hartman[1] and J.A.W. Shoemaker.[2] Department of Chemistry, Brock University, St. Catharines, ON L2S 3A1, Canada

[1]Corresponding author (telephone: (905) 688-5550; fax: (905) 682-9020; e-mail: shartman@chemiris.labs.brocku.ca).
[2]Present address: Symyx Technologies Inc., 3100 Central Expressway, Santa Clara, CA 95051, U.S.A.

 DOI: 10.1139/cjc-79-4-426 © 2001 NRC Canada

Scheme 1.



Experimental

Materials and methods

Materials were handled with standard inert-atmosphere Schlenk line and glove bag techniques. The chelating ligands, all from Aldrich, were stored over 3 Å Molecular Sieve that had been heated in a muffle furnace at 400°C for more than 3 h and cooled over a period of 0.5 h in a vacuum desiccator, and were used without further purification. Boron trifluoride (Aldrich, 99.5%), boron trifluoride etherate (Aldrich), boron trichloride (Matheson, 99.5%) boron tribromide (Aldrich, 99.9%), isoxazole (ISOX, Aldrich 99%), ammonium hexafluorophosphate (Aldrich, 95+%), and pyridine (Aldrich, 99.5%) were all handled as described previously (1). Acetone (Caledon, HPLC grade), chloroform (Caledon, hydrocarbon stabilized, 99.8%), chloroform-d_1 (Cambridge Isotope Laboratories, 99.8%), and nitromethane (Fisher Scientific) were dried over 3 Å Molecular Sieve, and were used without further purification.

The $py{\cdot}BF_nX_{3-n}$, $ISOX{\cdot}BF_nCl_{3-n}$, and $ISOX{\cdot}BF_nBr_{3-n}$ adduct systems were prepared in Schlenk vessels by methods described previously (9, 10) and handled as described in the previous paper in this series (2). $(py)_2BF_2^+$ was prepared as described previously (2) and precipitated as its PF_6^- salt with ammonium hexafluorophosphate. Subsequent reactions were carried out on 20 mg mL^{-1} solutions of $(py)_2BF_2^+{\cdot}PF_6^-$ in acetone. Reactions of $Et_2O{\cdot}BF_3$ with the chelating donors were carried out by adding neat $Et_2O{\cdot}BF_3$, dissolved in benzene, chloroform, acetone, or diethyl ether, to 1–15 mL of solution containing 20–100 mg of the chelating donor in the same solvent.

Most ^{19}F and ^{11}B NMR spectra were obtained on a Bruker AC-200 4.7 T multinuclear FT-NMR spectrometer operating at 188.31 (^{19}F) and 64.20 MHz (^{11}B), using 5 mm NMR tubes. ^{19}F NMR spectra were obtained with 16K FID's, 16K zero-filling, spectral windows of up to 35 000 Hz, with between 256 and 4096 30° pulses, and a relaxation delay of 1.0 s. The 90° pulse durations were 6.6 (^{19}F) and 17.1 μs (^{11}B). ^{19}F NMR chemical shifts are accurate to ±0.1 ppm and were internally referenced to C_6F_6 as a secondary standard (–162.7 ppm from $CFCl_3$), and are reported in ppm from $CFC1_3$. ^{11}B spectra were obtained with 16K FID's and spectral windows of up to 6400 Hz, and were referenced to external $Et_2O{\cdot}BF_3$. Some ^{19}F and ^{11}B NMR spectra were obtained at 30°C on a Bruker DRX-500 11.7 T multinuclear FT-NMR spectrometer (McMaster University) operating at 470.53 (^{19}F) and 160.46 MHz (^{11}B) using between 40 and 128 30° pulses with 32K FID's. The 90° pulse durations were 7.5 (^{19}F) and 15.0 μs (^{11}B). Spectral windows of 42 016 (^{19}F) and 40 000 Hz (^{11}B) were used. ^{11}B solid state magic angle spinning (MAS) NMR spectra were obtained on a Bruker DPX-300 7.4 T multinuclear FT-NMR spectrometer, as described previously (2), using trimethyl borate as the external standard (chemical shift 18.3 ppm from $Et_2O{\cdot}BF_3$).

Positive ion fast atom bombardment (FAB) mass spectra were obtained on a Concept 1S double beam mass spectrometer, with 8 KV accelerating voltage using Xe collision gas at 7.5 W power. 3-Nitrobenzyl alcohol (NBA) was normally used as the liquid matrix. Data were collected on a Kratos DART data system with SUN Spectrostation 10, using XMACH3 software.

Specific reactions

Et_4en plus $py{\cdot}BF_nCl_{3-n}$

Et_4en displaces py from its BF_3 adduct but does not react with the other py adducts, which is consistent with its high steric hindrance and analogous to the behaviour of Et_3N (9). The displaced py proceeds to form $(py)_2BF_2^+$.

Et_4en plus $ISOX{\cdot}BF_nCl_{3-n}$

Addition of Et_4en to a chloroform solution of the $ISOX{\cdot}BF_nCl_{3-n}$ adducts ($ISOX:BF_3:BCl_3:Et_4en$ = 4:1:3:4 mol equiv) gave rapid displacement of ISOX to form the $Et_4en{\cdot}BF_nCl_{3-n}$ adducts, according to ^{19}F and ^{11}B NMR (Table 1). Upon standing, new NMR signals appeared that arise from the $BF_nCl_{4-n}^-$ anions (11), and ^{19}F 1:1:1:1 quartets at –150.1 and –139.4 ppm that we attribute to chelated $(Et_4en)BF_2^+$ and $(Et_4en)BFCl^+$, respectively. In addition, two overlapping 1:1:1:1 quartets at –159.8 and –159.9 ppm are seen, both with $^1J_{BF}$ = 47 Hz, which appear after different lengths of time in different samples. Positive ion FAB-MS spectra of the chloroform solution, obtained using an NBA matrix, confirm the presence of $(Et_4en)BF_2^+$ (*m*/*z* 221, 100%) and $(Et_4en)BFCl^+$ (*m*/*z* 237, ~2%, with the correct isotope pattern). A further FAB-MS peak that occurs at *m*/*z* 270 (~20%) possibly arises from loss of HF from $(Et_4en)(ISOX)BF_2^+$; it also appears in the FAB-MS spectrum of the Et_4en plus $ISOX{\cdot}BF_nBr_{3-n}$ reaction mixture. This peak gives rise to metastable peaks at 173.2 (11%), 172.2 (13%), 171.2 (72%), 101.1 (5%), 100.1 (100%), and 86.1 (16%).

Et_4en plus $ISOX{\cdot}BF_nBr_{3-n}$

On addition of Et_4en to $ISOX{\cdot}BF_nBr_{3-n}$ a brown solid, insoluble in nitromethane, separates from the orange-brown chloroform solution. The positive ion FAB-MS spectrum of the solid shows the presence of $(Et_4en)BF_2^+$ (*m*/*z* 221, 100%), $(Et_4en)BFBr^+$ (*m*/*z* 281, 15.8%, higher than the

© 2001 NRC Canada

Table 1. ^{11}B and ^{19}F NMR parameters of boron trihalide adducts.

	^{19}F chemical shift (ppm) in		^{11}B chemical shift (ppm) in		$^{1}J_{BF}$ (Hz) in	
	$CDCl_3$	CH_3NO_2	$CDCl_3$	CH_3NO_2	$CDCl_3$	CH_3NO_2
$Et_2O{\cdot}BF_3$	–153.9		0.0			
$Me_4mn{\cdot}BF_3$[a,b]	–162.2		0.1		17	
$Et_4en{\cdot}BF_3$[a]	–151.2		0.1		18	
$Me_4pn{\cdot}BF_3$[a]	–161.2	–159.0	0.1	1.2	16	15
$Me_4mn{\cdot}(BF_3)_2$[a,b]	–160.6		0.3		16	
$Et_4en{\cdot}(BF_3)_2$[a]	–150.3				18	
$Me_4pn{\cdot}(BF_3)_2$[a]	–160.7	–157.2			16	16
$Me_4mn{\cdot}BF_2Cl$	–140.5		4.5		46	
$Et_4en{\cdot}BF_2Cl$	–127.5				44	
$Me_4pn{\cdot}BF_2Cl$	–139.4	–137.5	4.6	5.8	44	43
$Me_4dipn{\cdot}BF_2Cl$	–138.3					
$Me_4mn{\cdot}BFCl_2$	–127.9		7.0		68	
$Et_4en{\cdot}BFCl_2$	–112.5				73	
$Me_4pn{\cdot}BFCl_2$	–128.4	–126.8	8.4	9.5	70	69
$Me_4dipn{\cdot}BFCl_2$	–128.1					
$Me_4mn{\cdot}BCl_3$			7.5			
$Et_4en{\cdot}BCl_3$			9.0			
$Me_4pn{\cdot}BCl_3$			10.1			

[a]Determined from reaction of the base with $Et_2O{\cdot}BF_3$ in diethyl ether:chloroform solution (1:5).
[b] ^{19}F chemical shifts in chloroform are –161.6 and –159.3 ppm for $Me_4mn{\cdot}BF_3$ and $Me_4mn{\cdot}(BF_3)_2$, respectively.

signal intensities previously seen for (*t*-amine)$BFBr^+$ species (1)), and the *m*/*z* 270 species noted above (10.2%), as well as the ion cluster $[(Et_4en{\cdot}H_2)^{2+}{\cdot}Br^-]^+$ (*m*/*z* 253, ~2%).

This is typical of many of the following reactions. Solids often appear due to saturation of the mother liquor by one or more of the reaction products. Typically, FAB-MS and (or) NMR spectroscopy show that these solids consist of mixtures of haloboron cation salts.

Et_4dien plus ISOX·BF_nCl_{3-n}

Excess Et_4dien added to a chloroform solution of the ISOX·BF_nCl_{3-n} adducts (ISOX:BF_3:BCl_3:Et_4en = 4:1:3:4 mol equiv) readily forms (Et_4dien)BF_2^+, as confirmed by positive ion FAB-MS (in NBA matrix) on both the chloroform mother liquor, and on the brown solid generated by removing the chloroform: (Et_4dien)BF_2^+ (*m*/*z* 264, 32.3 and 83.4%, respectively)), ($C_{12}H_{28}N_3$)BF^+ (loss of HF from (Et_4dien)BF_2^+) (*m*/*z* 244, 17.1 and 33.8%), and Et_4dien·H^+ (*m*/*z* 216, 31.0 and 100%). The ^{19}F NMR spectrum of the chloroform solution included two equal-intensity signals at –153.1 and –160.0 ppm, consistent with the nonequivalent BF_2 fluorines expected from (Et_4dien)BF_2^+, in which coordination is by the central nitrogen and one terminal nitrogen (1). There are many additional ^{19}F NMR signals (less than 20% of the total ^{19}F peak intensity) from unknown species, including singlets at –122.3 (broad), –131.2 (broad), and –148.8 ppm, and 1:1:1:1 quartets at –143.4 ($^1J_{BF}$ = 50 Hz), –150.5 ($^1J_{BF}$ = 62 Hz), and –151.8 ppm (probably a quartet, but poorly resolved). The ^{19}F spectrum of the brown solid, dissolved in nitromethane, gave major signals for (Et_4dien)BF_2^+ and a small BF_4^- signal at –150.5 ppm, as well as a broad singlet at –137.3 ppm and a 1:1:1:1 quartet at –131.3 ppm ($^1J_{BF}$ ~ 26 Hz, poorly resolved). The ^{11}B NMR spectrum of the chloroform mother liquor had the (Et_4dien)BF_2^+ signal as 40% of the total peak intensity, BCl_4^- 30%, ISOX·BCl_3 8%, and unknown species (broad signal from 1 to –1 ppm) 22%, but no chlorofluoroborate anion signals were observed.

DPA plus ISOX·BF_nCl_{3-n}

DPA added to a chloroform solution of the ISOX·BF_nCl_{3-n} adducts (ISOX:BF_3:BCl_3:DPA = 4:1:3:4 mol equiv) apparently gives (DPA)BF_2^+, on the basis of positive ion FAB-MS results (in NBA matrix). The yellow chloroform mother liquor and the brown oil, generated by removing the chloroform under vacuum, both gave very low intensity FAB mass spectra, which included peaks arising from DPA·H^+ (*m*/*z* 200, 7.3 and 100%, respectively) and a peak at *m*/*z* 55 (100 and 22%). The brown oil gave an additional peak corresponding to ($C_{12}H_{12}N_3$)BF^+ (*m*/*z* 228, 20%), consistent only with loss of HF from (DPA)BF_2^+. The chloroform solution gives many ^{19}F NMR peaks, including broad singlets at –149.8, –150.9, –153.4, –154.6, and 156.5 ppm, a BF_4^- signal, and a 1:1:1:1 quartet at –147.8 ppm ($^1J_{BF}$ = 52 Hz). The brown oil, dissolved in nitromethane, gives a ^{19}F NMR spectrum with a much larger BF_4^- peak, broad singlets at –138.7, –144.4, –145.2, –153.4, and –155.5 ppm, and a 1:1:1:1 quartet at –151.7 ppm ($^1J_{BF}$ = 42 Hz). A few of these peaks may arise from boron trihalide adducts of DPA.

Me_4pn plus py·BF_nCl_{3-n}

Me_4pn, added in small portions to the py·BF_nCl_{3-n} adducts in chloroform solution, gives a yellow solution. ^{19}F and ^{11}B NMR spectra show that py·BF_3 and py·BF_2Cl react over several hours to give $Me_4pn{\cdot}BF_3$, $(py)_2BF_2^+$, and (py)(Me4en)BF_2^+. py·$BFCl_2$ and py·BCl_3 are much less reactive, although a small amount of $(py)_2BFCl^+$ does form after several hours by attack of py (displaced from its BF_3 adduct) on py·$BFCl_2$. Further reactions occur over several days. FAB mass spectra confirm the presence of (py)(Me_4pn)BF_2^+ (*m*/*z* 258) in solution. Addition of a single large portion of Me_4pn,

© 2001 NRC Canada

instead of several small portions, gives immediate separation of a white foam-like material at the top of the mixture, identified as primarily $Me_4pn \cdot BF_3$ by ^{19}F NMR.

Me_4pn plus $ISOX \cdot BF_nCl_{3-n}$

Addition of Me_4pn to chloroform solutions of $ISOX \cdot BF_nCl_{3-n}$ ($ISOX:BF_3:BCl_3:Me_4pn$ = 2:1:1:2 and 4:1:3:4 mol equiv) gives immediate formation of a red solid at the top, and the colourless solution turns orange. NMR spectra of the solution show the presence of $Me_4pn \cdot BF_3$, $Me_4pn \cdot BFCl_2$, $Me_4pn \cdot BFCl_2$, and $Me_4pn \cdot BCl_3$ (Table 1), with the chlorine-containing species being more abundant in the 4:1:3:4 sample. The red solid gives positive ion FAB-MS spectra showing the presence of $Me_4pn \cdot H^+$ (*m/z* 131, 100%), but no fluoroboron cations. The ^{11}B and ^{19}F NMR spectra of the red solid, dissolved in 3:1 acetone:sulpholane (slightly soluble) or nitromethane (more soluble) indicate the presence of the same species as in the orange solutions, and again there is no indication of the presence of fluoroboron cations.

Me_4pn plus $ISOX \cdot BF_nBr_{3-n}$

Addition of Me_4pn to chloroform solutions of $ISOX \cdot BF_nBr_{3-n}$ ($ISOX:BF_3:BBr_3:Me_4pn$ = 5:2:3:5 and 4:1:3:4 mol equiv) gives immediate precipitation, and only a small amount of $Me_4pn \cdot BF_3$ was detected in the mother liquor by ^{19}F NMR. As with the corresponding Me_4en and Me_5dien systems (1), the precipitates are insoluble in various solvents. After drying, they give FAB mass spectra showing the presence of $Me_4pn \cdot H^+$ (*m/z* 131, 100%) and $[(Me_4pn \cdot H_2)^{2+} \cdot Br^-]^+$ (*m/z* 211, 12%), but there are no signals corresponding to fluoroboron cations. ^{11}B MAS NMR spectra of the precipitates are broad and poorly resolved, with most of the signal intensity in the BF_nBr_{3-n} adduct range (+2 ppm to –10 ppm) and little in the fluoroboron cation range (+10 to +2 ppm) (1).

Me_4dipn plus $ISOX \cdot BF_nCl_{3-n}$

Me_4dipn added to a chloroform solution of the $ISOX \cdot BF_nCl_{3-n}$ adducts ($ISOX:BF_3:BCl_3:Me_4dipn$ = 4:1:3:4 mol equiv) gives an orange solution from which a brown solid gradually precipitates. One sample remained supersaturated and no precipitate appeared until after the ^{19}F NMR spectrum was obtained. This spectrum included two equal-intensity ^{19}F peaks at –164.7 and –170.9 ppm, as well as many singlets: –128.1 (broad), tentatively $Me_4dipn \cdot BFCl_2$; –138.3 (broad), tentatively $Me_4dipn \cdot BF_2Cl$; –158.9, –160.0, and –161.0 ppm (one of which probably arises from $Me_4dipn \cdot BF_3$), and broad peaks at –168.0, –174.3, and –176.4 ppm. Positive ion FAB mass spectra on the chloroform solution and on the brown solid gave only $Me_4dipn \cdot H^+$ (*m/z* 188) and its fragments.

Me_4mn plus $py \cdot BF_nCl_{3-n}$

Me_4mn displaces py from its BF_3 adduct but does not react with the other py adducts. The displaced py proceeds to form $(py)_2BF_2^+$.

Me_4mn plus $ISOX \cdot BF_nCl_{3-n}$

Me_4mn readily displaces ISOX from the $ISOX \cdot BF_nCl_{3-n}$ adducts in chloroform to form the $Me_4mn \cdot BF_nCl_{3-n}$ (*n* = 0–3) adducts, as shown by ^{11}B and ^{19}F NMR (Table 1). A number of further reactions occur on standing, as shown by NMR monitoring and discussed below, but no evidence for the chelated cation could be obtained by FAB mass spectrometry under various conditions, running the reaction solution neat or mixed with the matrix liquids NBA, NOPE, sulpholane, or glycerol, which have been effective in other difficult cases (1,2). The principal FAB-MS peaks correspond to $Me_2NH_2^+$ (*m/z* 46) and $Me_2N{=}CH_2^+$ (*m/z* 58).

Me_4mn plus $ISOX \cdot BF_nBr_{3-n}$

On reacting Me_4mn with $ISOX \cdot BF_nBr_{3-n}$ in chloroform a yellow solid precipatates, which is insoluble in nitromethane. Positive ion FAB-MS of the solid does not indicate the presence of any fluoroboron cations.

Reactions with $Et_2O \cdot BF_3$

Reacting Et_4en, Me_4pn, and Me_4mn with $Et_2O \cdot BF_3$ in chloroform (1:1 mol ratio of base to $Et_2O \cdot BF_3$) gives white precipitates, and the ^{19}F NMR spectra of the supernatant liquids contain 1:1:1:1 quartets arising from the mono- and bis-BF_3 adducts (Table 1), in addition to a small BF_4^- signal. The white precipitates, dissolved in nitromethane, give ^{19}F NMR signals of the mono- and bis-BF_3 adducts. When the bases are reacted with excess $Et_2O \cdot BF_3$ in chloroform (1:2 and 1:3 mol ratios of base to $Et_2O \cdot BF_3$), the supernatant liquid contains only a very small ^{19}F NMR signal of the base$\cdot(BF_3)_2$ adduct, most of which had precipitated, as well as an $Et_2O \cdot BF_3$ signal at –153.9 ppm. These precipitate too consist of the mono- and bis-BF_3 aducts. With Me_4mn an additional fluorine-containing species is present in the supernatant liquid from all three mol ratios of Me_4mn to $Et_2O \cdot BF_3$, giving a small ^{19}F NMR 1:1:1:1 quartet at –157.5 ppm ($^1J_{BF}$ = 20 Hz), which is reasonably consistent with $Me_2NH \cdot BF_3$. FAB mass spectra gives no evidence for fluoroboron cations.

Reactions with $(py)_2BF_2^+$

Of the six ligands in Scheme 1, only Me_4pn and Me_4dipn (2 to 10 molar excess) undergo substitution reactions with $(py)_2BF_2^+$, giving new ^{19}F NMR 1:1:1:1 quartets over several hours that we assign to $(py)(Me_4pn)BF_2^+$ and $(py)(Me_4dipn)BF_2^+$ on the basis of their chemical shifts and $^1J_{BF}$ values (Table 2). The yield of $(py)(Me_4pn)BF_2^+$ increases as the excess of Me_4pn increases, up to about 40% at ambient temperature or 30% at 50°C. Positive ion FAB mass spectra confirm the existence of $(py)(Me_4pn)BF_2^+$, but there is no evidence for chelated $(Me_4pn)BF_2^+$. With Me_4dipn the new ^{19}F NMR quartet is very small, and $(py)(Me_4dipn)BF_2^+$ could not be confirmed by FAB-MS. The larger the excess of Me_4dipn, the smaller the size of this ^{19}F quartet, and it was not detectable in samples that had been allowed to stand at 50°C.

Results

The best-behaved systems are Et_4en, Me_4pn, and Me_4mn, which give clean displacement of ISOX from its BF_nCl_{3-n} and BF_nBr_{3-n} adducts. The other systems, each having an N—H bond, give additional products that are apparently related to loss of hydrogen halide from the reactive N—H and B—Cl or B—Br bonds. The more detailed studies were therefore carried out on Et_4en, Me_4pn, and Me_4mn. None of

© 2001 NRC Canada

Table 2. ^{11}B and ^{19}F NMR parameters of boron trihalide adducts.

	^{19}F chemical shift (ppm) in		^{11}B chemical shift (ppm) in		$^{1}J_{BF}$ (Hz) in	
	$CDCl_3$	Acetone	$CDCl_3$	Acetone	$CDCl_3$	Acetone
(ISOX)(Et_4en)BF_2^+	[a]		0.9		28	
(py)(Me_4pn)BF_2^+	–160.0	–159.7		3.0	29	28
(py)(Me_4dipn)BF_2^+		–159.8				28
(Me_4mn)BF_2^+ [b]	–138.9		3.9		43	
(Et_4en)BF_2^+	–150.1		3.9		35	
(Et_4dien)BF_2^+ [c]	–160.0	–158.5[d]	3.5		34	35[d]
	–153.1	–150.8[d]			34	34[d]
(DPA)BF_2^+ [b]	–154.6	–153.4[d]				
	–156.6	–155.4[d]				
(Me_4dipn)BF_2^+ [b,e]	–164.7				~32	
	–170.9				~32	
(py)(Me_4dipn)$BFCl^+$	–150.1				53	
(Et_4en)$BFCl^+$	–139.4		8.8		62	

[a]Not resolved; overlaps the (Et_4en)BF_2^+ and Et_4en·BF_3 signals.
[b]Tentative assignment.
[c] $^2J_{FF}$ = 61 Hz.
[d]In nitromethane.
[e]Data from only one of several samples, in which precipitation was delayed. $^2J_{FF}$ ~ 61 Hz.

these react with $Et_2O{\cdot}BF_3$ to give fluoroboron cations, but only form the 1:1 and 1:2 BF_3 adducts except for Me_4mn,which forms these plus an additional species, apparently $Me_2NH{\cdot}BF_3$. Me_4pn and Me_4dipn displace only a single py from $py_2BF_2^+$, while none of the other systems can displace even one py.

Five-membered ring chelating ligands

Et_4en and Et_4dien react with the ISOX·BF_nX_{3-n} (n = 0–3) adducts much like the less sterically hindered Me_4en and Me_5dien (1), with rapid displacement of the weakly basic ISOX from its adducts by the chelating base and subsequent closure of the chelate ring by heavy halide ion displacement. A major difference is formation of the tetrahaloborate anions $BFCl_3^-$, $BF_2Cl_2^-$, and especially BCl_4^- as major products, as shown by ^{11}B and ^{19}F NMR (11). The ^{19}F spectrum of a sample, in which insufficient Et_4en is available to displace all of the ISOX from its adducts, shows strong $BFCl_3^-$ and $BF_2Cl_2^-$ signals (Fig. 1), while the ^{11}B spectrum of the same sample has an intense BCl_4^- peak (Fig. 2). This sample had been allowed to stand for a day, and all of the Et_4en·BF_2Cl had reacted to give chelated (Et_4en)BF_2^+ (^{19}F NMR 1:1:1:1 quartet at –151 ppm; its $^1J_{BF}$ value of 35 Hz distinguishes it from Et_4en·BF_3 which has a similar chemical shift but a much smaller $^1J_{BF}$ value of 18 Hz.) Several additional ^{19}F NMR signals, most having low intensity, gain in intensity very slowly over time (Fig. 1). The largest of these, at –159.8 ppm, resembles two overlapping 1:1:1:1 quartets, both with $^1J_{BF}$ = 47 Hz.

^{19}F NMR shows that the potentially tridentate Et_4dien, on addition to a chloroform solution of the ISOX·BF_nCl_{3-n} adducts, forms bidentate (Et_4dien)BF_2^+ with the centre and one terminal nitrogen coordinated to boron. The similarity of the ^{19}F NMR spectrum to that of (Me_5dien)BF_2^+, which we have previously studied in detail (1), is striking. The two equal-intensity ^{19}F peaks, split by $^1J_{BF}$ and $^2J_{FF}$ couplings (Fig. 3), can be assigned to the prochiral and nonequivalent BF_2 fluorines, the nonequivalence arising from chirality of the central nitrogen, as in (Me_5dien)BF_2^+ ($^1J_{BF}$ = 34 Hz and $^2J_{FF}$ = 62 Hz, compared to $^1J_{BF}$ = 33 Hz and $^2J_{FF}$ = 61 Hz for (Me_5dien)BF_2^+ (1)). The parent ion FAB-MS peak at m/z 264 confirms the presence of (Et_4dien)BF_2^+, while the peak at m/z 244 is consistent with loss of HF due to the presence of the reactive N—H proton.

DPA probably reacts with ISOX·BF_nCl_{3-n} to give the desired chelated (DPA)BF_2^+, on the basis of the m/z 228 FAB peak, which corresponds to loss of HF from (DPA)BF_2^+ as seen with (Et_4dien)BF_2^+. However no parent ion peak is detected. This system has low stability and undergoes multiple reactions, and no spin-spin splittings are visible, preventing unambiguous assignments of adduct and cation ^{19}F resonances from among the many signals present. Every sample does give two equal-intensity broad peaks (–154.6 and –156.6 ppm in chloroform; –153.4 and –155.5 ppm in nitromethane), which is consistent with bidentate coordination and nonequivalent fluorines, as seen with Et_4dien and Me_5dien.

Potential six-membered ring chelating ligands

Me_4pn displaces Cl^- from py·BF_2Cl to form the nonchelated (py)(Me_4pn)BF_2^+, but differs from the five-membered ring chelating ligands in that the coordinated Me_4pn does not displace the second pyridine to form the chelate complex. The inability of Me_4pn to undergo chelation allows us to study the conditions for maximization of (py)(DD)BF_2^+ without complications due to further reactions. ^{19}F NMR monitoring of the reaction of Me_4pn with py·BF_nCl_{3-n} (mol ratio of Me_4pn:py:BF_3:BCl_3 = 3:4:2:2) (Fig. 4*a*) shows that Me_4pn displaces py from about 80% of the py·BF_3 within 2.4 h, while only 25% of the py·BF_2Cl has reacted. The py released from py·BF_3 competes effectively with Me_4pn in attacking py·BF_2Cl, so that the predominant fluoroboron cation formed is $(py)_2BF_2^+$ (25% of the total ^{19}F NMR signal intensity, vs. only 5% for (py)(Me_4pn)BF_2^+). The low-steric-hindrance py is evidently a much more

© 2001 NRC Canada

Fig. 1. 470.59 MHz ^{19}F NMR spectra of a $CDCl_3$ solution of ISOX·BF_nCl_{3-n} (ISOX:BF_3:BCl_3 = 4:1:3 mol ratio) to which Et_4en (insufficient to displace all the ISOX) had been added, after standing for: (*a*) one day; and (*b*) 4 days, at ambient temperature.

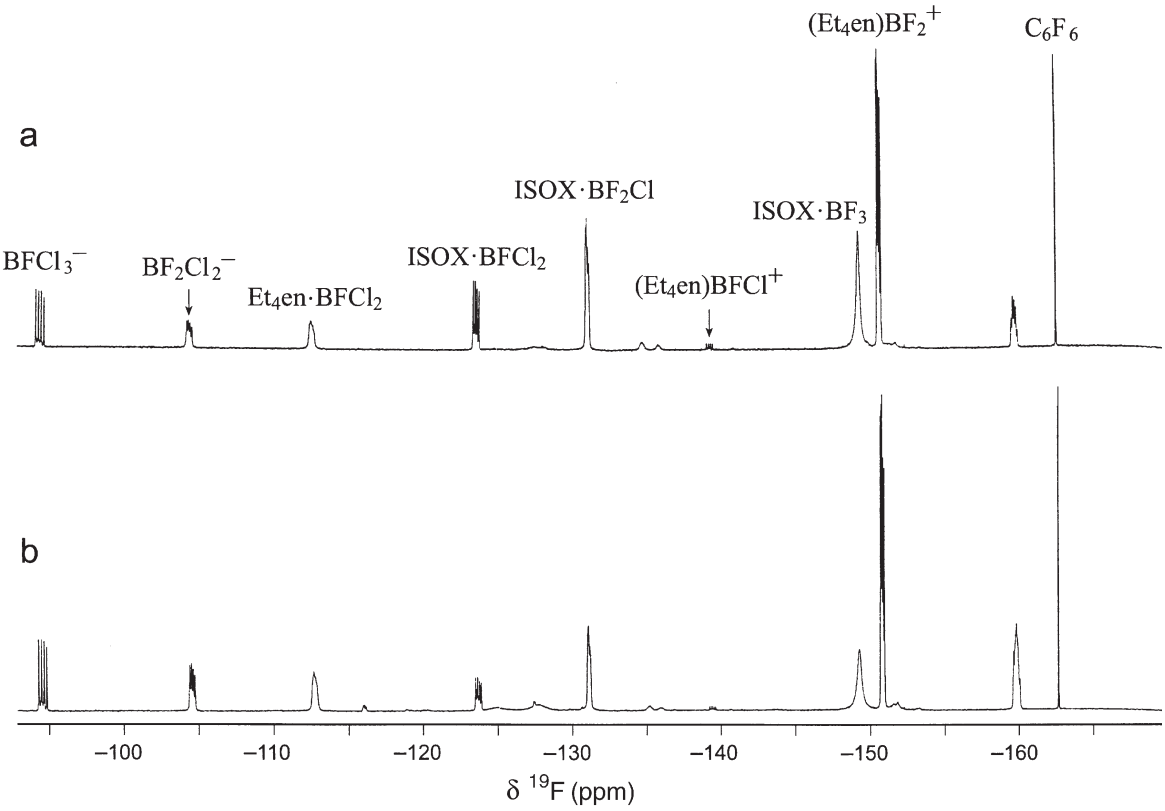
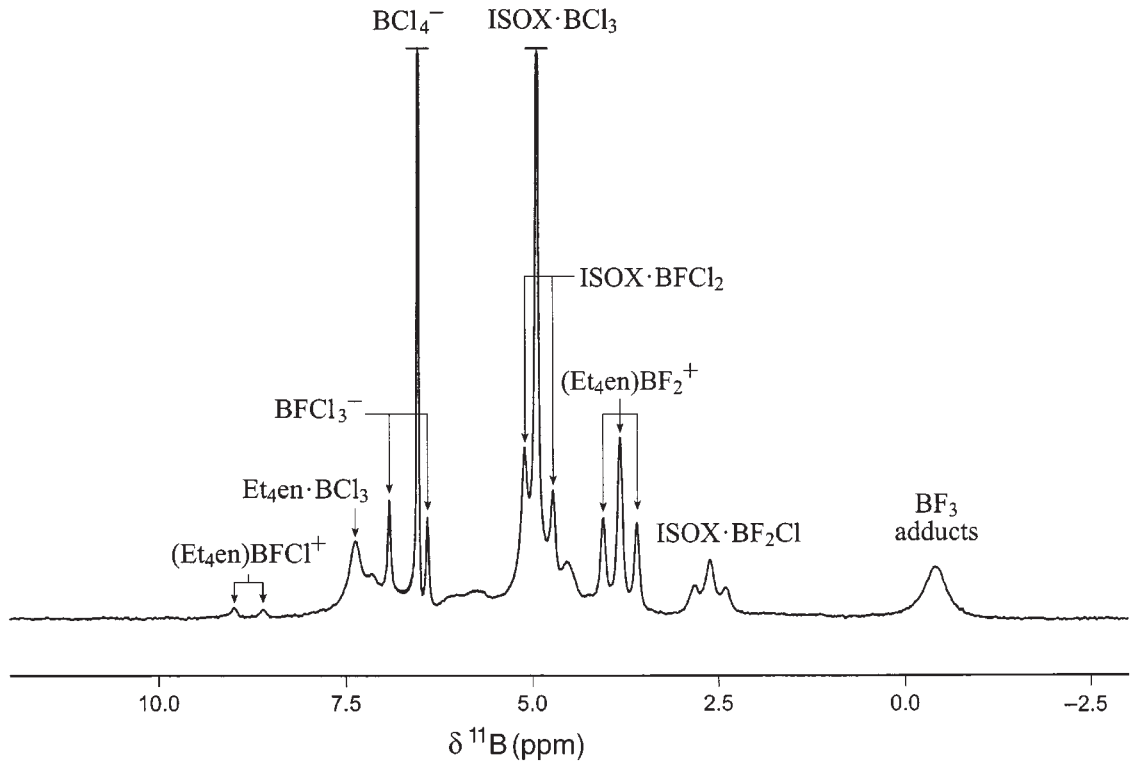
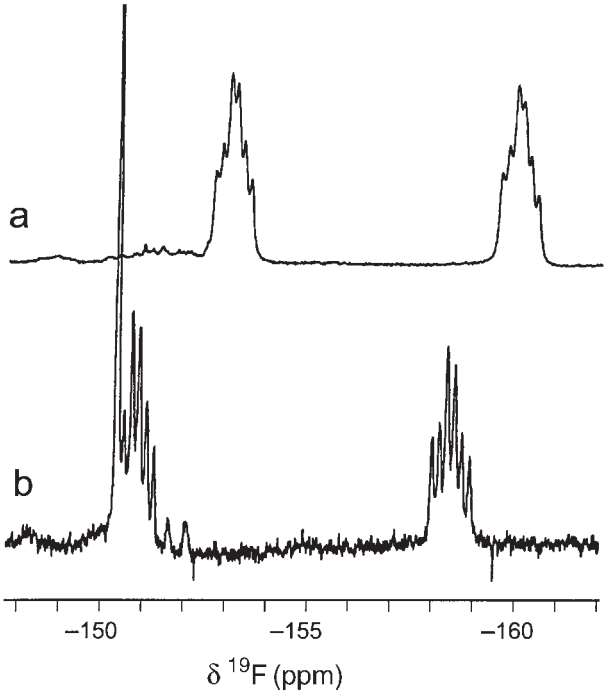


Fig. 2. 160.46 MHz ^{11}B NMR spectrum of the same sample as Fig. 1, after standing for one day at ambient temperature.



© 2001 NRC Canada

Fig. 3. 188.31 MHz ^{19}F NMR spectra (–148 to –162 ppm region only) of a $CDCl_3$ solution of ISOX·BF_nCl_{3-n} (4:1:3 mol ratio) to which Et_4dien had been added (*a*) in chloroform, and (*b*) in nitromethane. The spin-spin splittings, better resolved in nitromethane, are consistent with BF_2 nonequivalence in chelated $(Et_4dien)BF_2^+$.

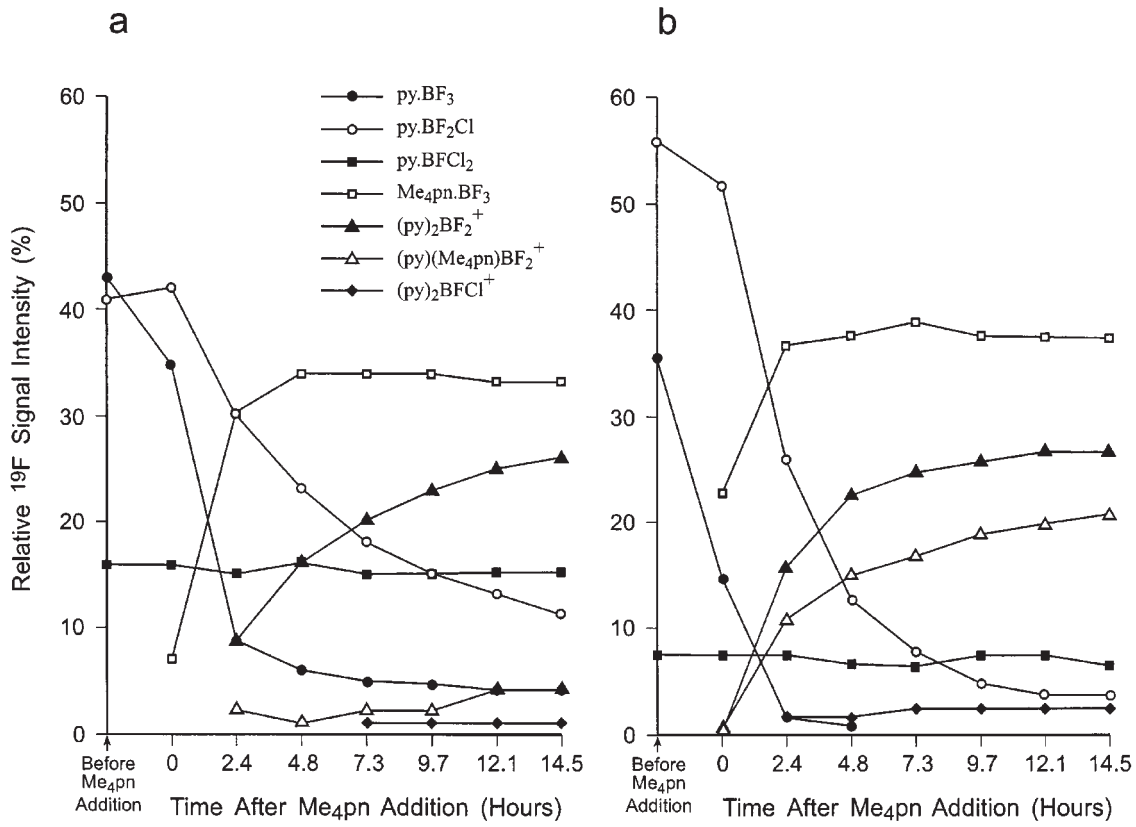


effective nucleophile despite its much lower basicity (pK_b 8.8 compared to $pK_b \approx 4$ for *t*-amines such as Me_4pn).

The formation of $(py)(Me_4pn)BF_2^+$ can be optimized by (*i*) increasing the concentration of Me_4pn so it can compete more effectively with the displaced py, and (*ii*) using a py·BF_nCl_{3-n} solution that is richer in Cl than in F, since this minimizes the amount of py·BF_3 which is the only adduct which readily releases py. A Me_4pn:py:BF_3:BCl_3 mol ratio of 5:5:2:3 optimizes both of these factors to give a much larger $(py)(Me_4pn)BF_2^+$ signal (20% of the total ^{19}F NMR signal intensity), although the $py_2BF_2^+$ signal remains large (Fig. 4*b*).

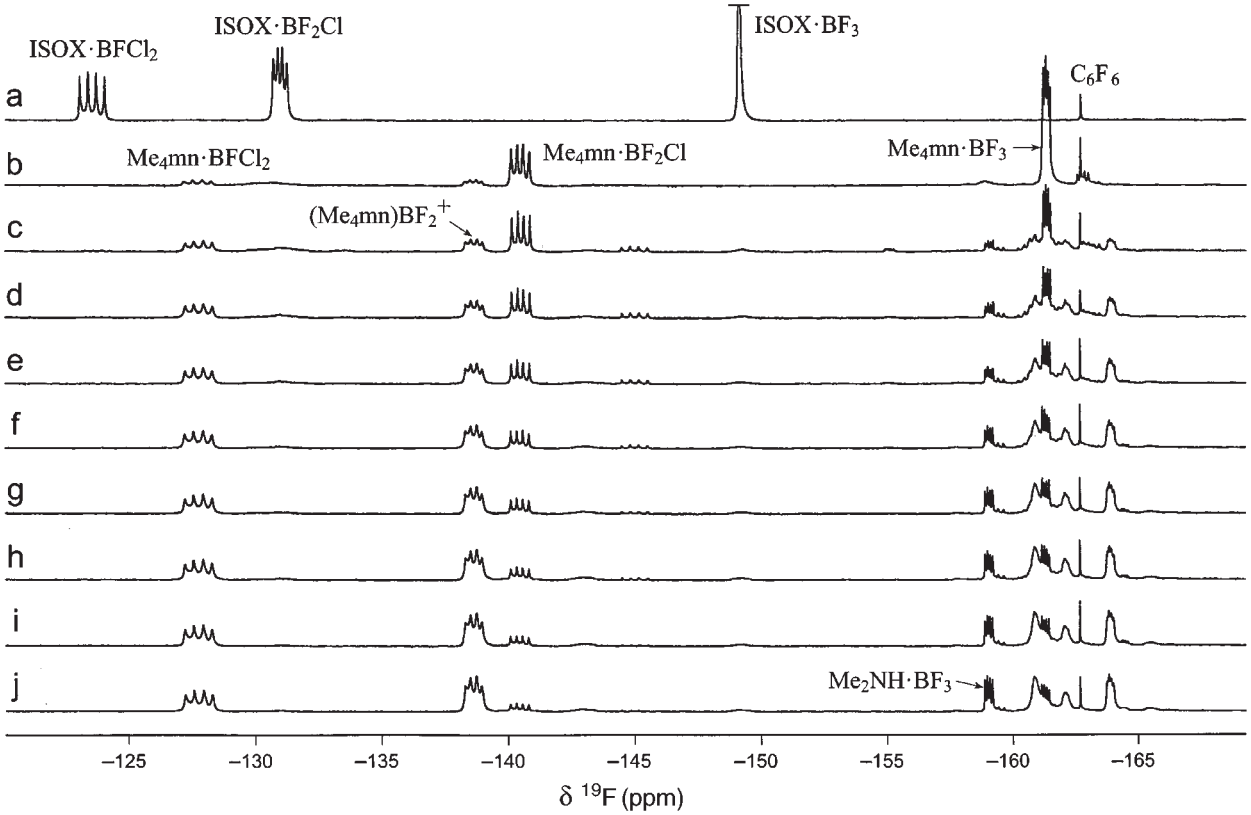
Further reactions occur over several days. Me_4pn very slowly displaces py from py·BF_2Cl to form Me_4pn·BF_2Cl (unusual since most ligands displace Cl^- rather than py from py·BF_2Cl (9, 10, 12)). Me_4pn also reacts very slowly with $(py)_2BF_2^+$ to give more $(py)(Me_4pn)BF_2^+$, and with py·$BFCl_2$ to give primarily $(py)(Me_4pn)BFCl^+$ but also some Me_4pn·$BFCl_2$. Thus the initial reactions of Fig. 4 occur under kinetic control, but the greater basicity of Me_4pn eventually wins out, with more Me_4pn becoming coordinated as the system moves very slowly toward thermodynamic equilibrium. However even on prolonged standing Me_4pn does not displace pyridine from $(py)(Me_4pn)BF_2^+$ or $(py)(Me_4pn)BFCl^+$ to give the bis(Me_4pn) cations, and no chelated $(Me_4pn)BF_2^+$ can be detected even when the concentration of $(py)(Me_4pn)BF_2^+$ is optimized.

Fig. 4. Plots of changes in ^{19}F NMR (188.31 MHz) signal intensity with time in the ambient-temperature reaction of Me_4pn with py·BF_nCl_{3-n}, in chloroform, for samples with Me_4pn:py:BF_3:BCl_3 mol ratios of (*a*) 3:4:2:2 and (*b*) 5:5:2:3. The proportions in the latter sample are optimized for formation of $(py)(Me_4pn)BF_2^+$ (20% of the total ^{19}F intensity compared to 5% in (*a*)).



© 2001 NRC Canada

Fig. 5. 188.31 MHz ^{19}F NMR spectra of: (*a*) a chloroform solution of ISOX·BF_nX_{3-n} (ISOX:BF_3:BX_3 = 4:1:3 mol ratio); (*b*) the same solution a few minutes after addition of sufficient Me_4mn to displace all of the ISOX; (*c*) the same solution as spectrum (*b*) after standing at ambient temperature for 5.4 h; (*d–j*) after further standing at room temperature for successive 5.7-hour intervals, up to a total time of 45.2 h. Small 1:1:1:1 quartets arising from $BFCl_3^-$ and $BF_2Cl_2^-$ are also present at –94.6 and –104.4 ppm, respectively, in spectrum (*b*), and their intensities diminish and disappear over a day.



Me_4pn, like other potentially chelating ligands (1, 2), reacts far more readily with ISOX·BF_nCl_{3-n} and ISOX·BF_nBr_{3-n} than with py·BF_nCl_{3-n}, with ISOX being rapidly displaced to give $Me_4pn·BF_3$, $Me_4pn·BFCl_2$, $Me_4pn·BFCl_2$, and $Me_4pn·BCl_3$. Also the displaced ISOX, unlike py, is too weak a base to compete in forming cations. However, under conditions which readily give the five-membered chelated fluoroboron cations, there is no displacement of chloride to give chelated $(Me_4pn)BF_2^+$ or $(Me_4pn)BFCl^+$. Even on reaction with ISOX·BF_nBr_{3-n} no fluoroboron cations form, despite Br^- displacement being much easier than Cl^- displacement.

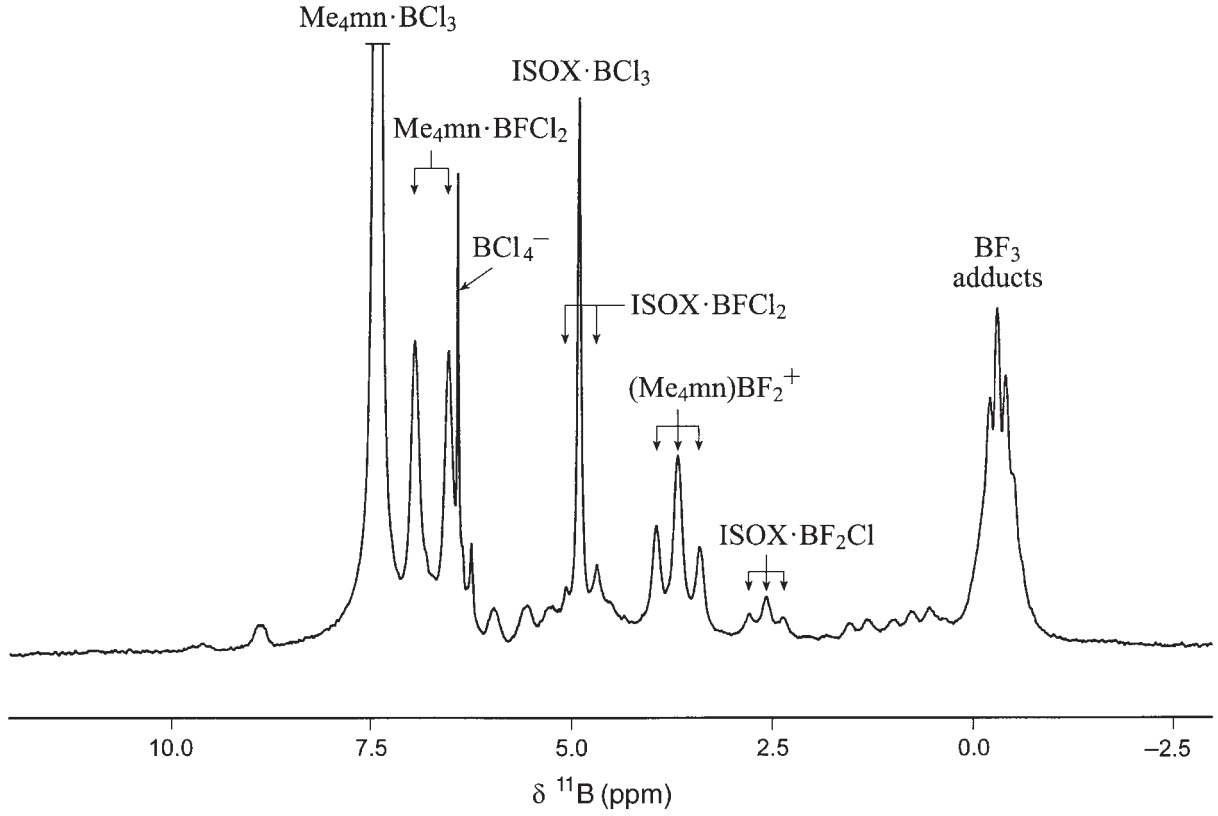
Although rapid decomposition occurs in the Me_4dipn-ISOX·BF_nCl_{3-n} system and there is no FAB-MS evidence for chelated $(Me_4dipn)BF_2^+$, there is convincing ^{19}F NMR evidence. As with Et_4dien and DPA, two equal-intensity ^{19}F NMR peaks appear at high field (–164.7 and –170.9 ppm), consistent with nonequivalent BF_2 fluorines and hence with chelation by the central nitrogen and one end nitrogen in $(Me_4dipn)BF_2^+$. The –164.7 ppm chemical shift value is consistent with a fluorine in a six-membered ring (2), *cis* to a methyl group and a longer hydrocarbon chain on the adjacent nitrogens, while the peak at –170.9 ppm is consistent with a fluorine that is *cis* to a methyl group and to a hydrogen atom on the adjacent nitrogens, since lower steric hindrance causes a shift to higher field. The chemical shift difference of 6.2 ppm is very similar to the difference of 6.9 ppm described above for $(Et_4dien)BF_2^+$ for which the FAB-MS evidence is conclusive, and consistent with the 5.5 ppm difference observed previously in $(Me_5dien)BF_2^+$ (1). The spin-spin splittings, consistent with $^1J_{BF}$ ~ 32 and $^2J_{BF}$ ~ 70 Hz, support this interpretation.

Me_4mn, a possible four-membered ring chelating ligand

^{19}F NMR spectra of a chloroform solution of the ISOX·BF_nCl_{3-n} adducts, before and after the addition of sufficient Me_4mn to displace all of the ISOX, are shown in Fig. 5. Me_4mn rapidly displaces ISOX to form all four of the $Me_4mn·BF_nCl_{3-n}$ adducts (Fig. 5*b*), and many further changes occur over two days (Figs. 5*c* to 5*j*). Also, small ^{19}F NMR 1:1:1:1 quartets at –95.0 and –104.8 ppm arising from $BFCl_3^-$, and $BF_2Cl_2^-$, respectively (11) (off scale in Figs. 5*c–g*), appear shortly after the addition of Me_4mn, and then diminish and disappear over about a day. As is usual in such systems, the $Me_4mn·BF_2Cl$ 1:1:1:1 quartet diminishes in intensity and is replaced by a new quartet at –138.9 ppm ($^1J_{BF}$ = 41 Hz), with the rate of growth of the new quartet matching the rate of shrinkage of $Me_4mn·BF_2Cl$, while the intensity of the $Me_4mn·BFCl_2$ quartet remains essentially unchanged. The loss of the BF_2Cl adduct signal is normally due to Cl^- displacement by a neutral base molecule, so the new quartet normally arises from a difluoroboron cation, and in this case the most plausible product is the chelated cation $(Me_4mn)BF_2^+$. Its ^{19}F chemical shift is consistent with a

© 2001 NRC Canada

Fig. 6. 160.46 MHz ^{11}B NMR spectrum of a $CDCl_3$ solution of ISOX·BF_nCl_{3-n} (ISOX:BF_3:BCl_3 = 4:1:3 mol ratio) to which Me_4mn (insufficient to displace all the ISOX) had been added, after standing for one day.



trend related to ring size: the six-membered (DMAN)BF_2^+ species absorbs at –164.4 ppm (2) and the five-membered (DD)BF_2^+ species absorbs in the –146 to –157 ppm range (1, 2), so a four-membered (DD)BF_2^+ species could well absorb at –138.9 ppm. However, we have not detected a FAB-MS signal corresponding to this ion (or to any other fluoroboron cation), so its identification remains tentative.

The high-field ^{11}B NMR spectrum of a sample to which insufficient Me_4mn had been added to displace all the ISOX, and which had been allowed to stand for a day (Fig. 6), is consistent with Fig. 5 and shows that unmixed-halogen species predominate. By far the largest ^{11}B NMR signal arises from $Me_4mn·BCl_3$. There is also a sharp but low-intensity BCl_4^- signal and a moderately large 1:2:1 triplet corresponding to the –138.9 ppm ^{19}F NMR signal, as well as small mixed-halogen adduct and chlorofluoroborate anion signals, and signals from several unidentified minor species.

However, many additional reactions occur. The $Me_4mn·BF_3$ ^{19}F signal diminishes on standing and many new ^{19}F signals appear, especially in the –158 to –166 ppm region (Figs. 5*c*–*j*). Trace amounts of about 30 unidentified species can be detected over the entire spectral range by high-field (11.7 T) ^{19}F NMR. This complexity is consistent with the expected sensitivity of Me_4mn to traces of acid. Me_4mn is a formaldehyde derivative and can be used as a reagent in the Mannich reaction (13). Protonation gives Me_2NH and $Me_2N{=}CH_2^+$, and Lewis acids should react similarly. These reactions have not been studied in detail but it is noteworthy that the prominent 1:1:1:1 quartet at –159.0 ppm ($^1J_{BF}$ = 18 Hz), which continues to grow over two days, is consistent with the formation of $Me_2NH·BF_3$ (lit. in CH_3CN: ^{19}F chemical shift = –158.8 ppm, $^1J_{BF}$ = 16 Hz; ^{11}B chemical shift = 0.5 ppm (14)). A 1:1:1:1 quartet with similar chemical shift and $^1J_{BF}$ value also appears on reaction of Me_4mn with $Et_2O·BF_3$ and with $py_2BF_2^+$, so $Me_2NH·BF_3$ apparently forms in these systems as well.

Discussion

Factors affecting chelation

While all of the potentially chelating ligands of Scheme 1 rapidly displace ISOX from its adducts, in contrast to slow displacement of pyridine from its BF_nCl_{3-n} adducts (Fig 4), this step is readily followed by chelate formation if the chelate rings are five-membered rather than six-membered. We had anticipated that Et_4en, more hindered than Me_4en and Me_5dien (1), might form the chelate only very slowly or not at all, on the basis of the huge differences in ease of heavy halide ion displacement and fluoroboron cation formation across the series Me_3N, Me_2NEt, $MeNEt_2$, NEt_3 (12). Nevertheless Et_4en readily forms chelated (Et_4en)BF_2^+, (Et_4en)$BFCl^+$, and (Et_4en)$BFBr^+$ from (Et_4en)·BF_2X and (Et_4en)·BFX_2 (X = Cl, Br). In contrast, Me_4pn forms only the $Me_4pn·BF_nX_{3-n}$ adducts, with no subsequent heavy halide ion displacement even on prolonged standing. The BF_2Cl adduct of the potentially four-membered ring chelating ligand Me_4mn, like the potentially five-membered ring chelating ligands, does give rise to a major new species which may be (Me_4mn)BF_2^+. However, the formation of Me_2NH by decomposition of Me_4mn, as described above,

© 2001 NRC Canada

raises additional possibilities for the identity of the new ^{19}F and ^{11}B NMR signals tentatively assigned to $(Me_4mn)BF_2^+$ in Figs. 5 and 6. Further studies of this system would be desirable. We note however that four-membered $(BN)_2$ rings are known to exist as dimers of many $R_2N{=}BX_2$ systems (15), as do four-membered $(BO)_2$ rings, although examples are scarce (16). Hence there is nothing implausible about a four-membered-ring chelated $(Me_4mn)BF_2^+$.

The only clear-cut exception to date to the preference for five- over six-membered fluoroboron cation chelate rings is the formation of the six-membered-ring cation $(DMAN)BF_2^+$ (DMAN = 1,8-bis(dimethylamino)naphthalene) (2), in which there is effective preorganization (5) of the ligand, the two nitrogens being constrained to be close together in the free ligand. In fact, with DMAN no intermediate with only one nitrogen coordinated, analogous to $Me_4pn{\cdot}BF_2Cl$, could be detected (2), due to extreme crowding at the donor sites; DMAN cannot coexist with two fluorines and a heavy halogen about boron. Me_4dipn apparently gives a second case of a fluoroboron cation with a six-membered chelate ring, whose formation is favoured relative to Me_4pn by the decreased steric hindrance of the secondary-amine central nitrogen. However the N—H bond also favours decomposition, so that the presence of $(Me_4dipn)BF_2^+$ could not be confirmed by FAB-MS.

The preference for five- over six-membered fluoroboron chelate rings is unexpected because many six-membered as well as five-membered ring chelate complexes involving boron are known (6). The preference for five-membered ring formation might be a kinetic or a thermodynamic effect. Both entropy and kinetic effects should favour closure of five-membered chelate rings over six-membered, but a molecular modelling approach indicates that, with small atoms such as beryllium(II) and boron(III), enthalpy should favour six-membered chelate rings over five-membered (5, 17). The bite angle of the chelating ligand is of crucial importance in determining the stability of chelate complexes (18). The preference for five- over six-membered ring formation suggests that kinetic rather than thermodynamic effects are predominant. Ready formation of the four-membered fluoroboron cation chelate system ($(Me_4mn)BF_2^+$) would be consistent with this. Molecular modeling studies of the fluoroboron cations would be desirable.

Observation of FAB-MS peaks corresponding to the chelated fluoroboron cation parent ion does not rigorously exclude the possibility that the solution species are actually oligomeric open-chain adducts $(\text{–N—NBF}_2^+\text{–})_n$. However such oligomeric species are more likely to form as the separation of the nitrogen atoms increases, i.e., with Me_4pn rather than with the potentially five-membered ring chelating donors. Since the Me_4pn-containing systems do not give a FAB-MS peak corresponding to the chelated fluoroboron cation parent ion, the possibility is remote that any of the other potentially chelating donors generate their chelated fluoroboron cation parent ion peak from oligomeric open-chain adducts.

Potentially tridentate ligands such as Et_4dien and Me_5dien, when coordinated in a bidentate fashion as in their difluoroboron cations, have the possibility of being fluxional, undergoing rapid dissociation of the coordinated end nitrogen and attachment of the other end nitrogen atom (19). We can exclude this process for $(Et_4dien)BF_2^+$ and $(Me_5dien)BF_2^+$ since it would racemize the cation and collapse the nonequivalent BF_2 fluorine NMR signals, whether the reaction is dissociative or is associative with inversion at boron.

Chlorofluoroborate anion formation and halogen redistribution reactions

Displacement reactions on the $ISOX{\cdot}BF_nCl_{3-n}$ adducts can lead to formation of large amounts of $BF_nCl_{4-n}^-$ ions, provided that the amount of displacing ligand added is sufficient to react with only a fraction of the $ISOX{\cdot}BF_nCl_{3-n}$ adducts, and that Cl^- as well as ISOX is displaced. The chloride ion so generated is a sufficiently strong base to displace ISOX from its adducts to form the chlorofluoroborate anions, which survive indefinitely in solution in the absence of a sufficiently strong base to displace Cl^- and regenerate fluoroboron adducts and cations. This occurs for example when sufficient Et_4en is added to react with only a fraction of the $ISOX{\cdot}BF_nCl_{3-n}$ adducts (Fig. 1). However if an excess of a chelating donor or other strong donor is added to the $ISOX{\cdot}BF_nCl_{3-n}$ system, Cl^- cannot compete effectively with the strong donor in displacing ISOX, and the chlorofluoroborate anions are either undetectable or are formed in only small amounts. Thus we have detected the mixed chlorofluoroborate anions in only a few of our previously studied systems, most notably with the highly hindered DMAN (2).

The same behaviour is not observed on reaction with the $ISOX{\cdot}BF_nBr_{3-n}$ system. There are severe solubility limitations, and even if the $BF_nBr_{4-n}^-$ ions were to form they would not be detectable by ambient-temperature NMR because halogen redistribution among the $BF_nBr_{4-n}^-$ ions is rapid and would collapse their NMR signals (11).

We have previously observed $BF_nCl_{4-n}^-$ formation in some mixed boron trihalide adduct systems that do not involve the ISOX adducts notably with amidines (20) and tetramethylurea (21), which have low steric hindrance, and also to a small extent with 2-(methylthio)-2-thiazoline (10). A different mechanism is required here because there is no weak donor analogous to ISOX that can be easily displaced by Cl^- from its adducts, and we previously suggested a carbene mechanism for $BF_nCl_{4-n}^-$ formation in the amidine systems (20). Although neither amidines nor DMAN, when present alone in solution, are sufficiently basic to displace HCl from chloroform to generate dichlorocarbene, this carbene can be generated from chloroform by anhydrous fluoride ion (22), traces of which might form in our systems. Further work to determine the mechanisms of chlorofluoroborate anion generation in these systems is desirable.

Fluorine and chlorine tend to "unscramble" from mixed chlorofluoroboron species on prolonged standing in many of our systems (20), as is evident from ^{11}B NMR signal intensities, e.g., Figs. 2 and 6. Typically, the mother liquor from the reaction of Et_4dien with $ISOX{\cdot}BF_nCl_{3-n}$ gave ^{11}B NMR signal intensities of 40% for $(Et_4dien)BF_2^+$, 30% for BCl_4^-, 8% for $ISOX{\cdot}BCl_3$, and 22% for a broad hump from 1 to –1 ppm, which apparently arises from various BF species, and little else. However ^{11}B NMR spectra, even at 11.7 T, often give only limited information because the 4-coordinate chloro- and fluoroboron compounds have a very narrow chemical shift range. ^{19}F is a far more sensitive nucleus than ^{11}B and has vastly superior chemical shift dispersion in these

© 2001 NRC Canada

systems, but reliance on ^{19}F can lead to a distorted picture since it cannot detect the non-fluorine-containing boron species which are often major components. Despite its poor resolution, ^{11}B NMR clearly shows how small a fraction of the total boron in equilibrated solutions has both chlorine and fluorine substitutents.

Further reactions

These are highly reactive systems with unexplored chemistry, and there are hints of intriguing new species which merit further study. For example when Et_4en is reacted with either $ISOX{\cdot}BF_nCl_{3-n}$ or $ISOX{\cdot}BF_nBr_{3-n}$, a major ^{19}F NMR signal appears, which resembles two overlapping 1:1:1:1 quartets at –159.8 and –159.9 ppm, both with $^1J_{BF}$ = 47 Hz (Fig 1).

Our attempts to isolate PF_6^- salts of chelated fluoroboron cations, by methods that have been successful with non-chelated fluoroboron cations (9, 10, 12, 20), have not been successful. We have been able to isolate a few chelated fluoroboron cations as their Cl^- and BF_4^- salts in earlier studies (1, 2), but the ligands in the present study have been less favourable. Further work is desirable on isolation of salts of these systems.

Conclusions

A few generalizations are possible. (*i*) Five-membered ring chelated fluoroboron cations form far more readily than six-membered. (*ii*) The presence of an N—H bond greatly increases the rate of decomposition, forming HCl and HBr in the presence of B—Cl and B—Br bonds, and this interferes with the desired reactions. *N*-Methylation of Et_4dien, DPA, and Me_4dipn would be desirable to eliminate this side reaction. (*iii*) The presence of an N—H bond allows facile HF loss in FAB-MS, and this can prevent FAB-MS detection of the parent fluoroboron cation.

These are very reactive systems, with many reactions occurring simultaneously. Success in forming fluoroboron cations is dependent on competition of desirable reactions with undesirable ones, and the relative rates apparently depend on various factors. Despite being more stable than many of the other species present, the fluoroboron cations themselves are prone to hydrolysis and decomposition. We will report elsewhere our studies of the reactions of $py_2BF_2^+$ and related fluoroboron cations.[3]

Acknowledgements

We thank Tim Jones for assistance with the instrumentation, Paul Ragogna for lab assistance, Prof. Alex F. Janzen (University of Manitoba) and Prof. M. F. Richardson (Brock University) for helpful discussions, Dr. Don Hughes and Brian Sayer (McMaster University) for assistance with the 11.7 Tesla NMR instrument, and the Natural Sciences and Engineering Research Council of Canada (NSERC) for meagre financial support.

References

1. J.A.W. Shoemaker and J.S. Hartman. Can. J. Chem. **77**, 1856 (1999).
2. J.S. Hartman and J.A.W. Shoemaker. Polyhedron, **19**, 165 (2000).
3. (*a*) H.C. Brown, B. Singaram, and J.R. Schwier. Inorg. Chem. **18**, 51 (1979); (*b*) H.C. Brown and B. Singaram. Inorg. Chem. **18**, 53 (1979); (*c*) B. Singaram and G.G. Pai. Hetrocycles, **18**, 387 (1982).
4. (*a*) N. Wiberg and J.W. Buchler. Chem. Ber. **96**, 3000 (1963); (*b*) N. Wiberg. and J.W. Buchler. J. Am. Chem. Soc. **85**, 243 (1963); (*c*) N.M.D. Brown and P. Bladon. J. Chem. Soc. A, 526 (1969); (*d*) T. Onak, H. Rosendo, G. Siwapinyoyos, R. Kubo, and L. Liauw. Inorg. Chem. **18**, 2943 (1979); (*e*) K.R. Koch and S. Madelung. Polyhedron, **10**, 2221 (1991); (*f*) D.D. Axtell, A.V. Campbell, P.C. Keller, and J.V. Rund. J. Coord. Chem. **5**, 129 (1976); (*g*) S. Hünig and I. Wehner. Heterocycles, **28**, 359 (1989).
5. (*a*) A.E. Martell, R.D. Hancock, and R.J. Motekaitis. Coord. Chem. Rev. **133**, 39 (1994), especially p. 47; (*b*) P. Comba. Coord. Chem. Rev. **182**, 343 (1999).
6. H. Höpfl, J. Organomet. Chem. **581**, 129 (1999).
7. W. Kliegel, J. Metge, S.J. Rettig, and J. Trotter. Can. J. Chem. **76**, 1082 (1998).
8. G.S. Matouzenko, A. Bousseksou, S. Lecocq, P.J. van Köningsbruggen, M. Perrin, O. Kahn, and A. Collete. Inorg. Chem. **36**, 2975 (1997).
9. M.J. Farquharson and J.S. Hartman. Can. J. Chem. **74**, 1309 (1996).
10. J.S. Hartman, E.I. Ilnicki, J.A.W. Shoemaker, W.R. Szerminski, and Z. Yuan. Can. J. Chem. **76**, 1317 (1998).
11. J.S. Hartman and G.J. Schrobilgen. Inorg. Chem. **11**, 940 (1972).
12. M.J. Farquharson and J.S. Hartman. Can. J. Chem. **67**, 1711 (1989).
13. (*a*) J. March. Advanced organic chemistry. Reactions, mechanisms, and structure. 4th ed. John Wiley and Sons, New York. 1992. pp. 900–902; (*b*) S. J. deSolms. J. Org. Chem. **41**, 2650 (1976); (*c*) E.C. Taylor and Y. Shvo. J. Org. Chem. **33**, 1719 (1968).
14. C. W. Heitsch. Inorg. Chem. **4**, 1019 (1965).
15. (*a*) A.J. Banister and N.N. Greenwood. J. Chem. Soc. 1534 (1965); (*b*) N. Greenwood and J. Walker. J. Chem. Soc. A, 959 (1967).
16. J.M. Burke, M.A. Fox, A.E. Goeta, A.K. Hughes, and T.B. Marder. Chem. Commun. 2217 (2000).
17. (*a*) R.D. Hancock. Progr. Inorg. Chem. **37**, 187 (1989); (*b*) R. D. Hancock. Acc. Chem. Res. **23**, 253 (1990); (*c*) R.D. Hancock. J. Chem. Educ. **69**, 615 (1992).
18. P. Dierkes and P.W.N.M. van Leeuwen. J. Chem. Soc. Dalton Trans. 1519 (1999)
19. (*a*) E.W. Abel, V.S. Dimitrov, N.J. Long, K.G. Orrell, A.G. Osborne, H.M. Pain, V. Sik, M.B. Hursthouse, and M.A. Mazid. J. Chem. Soc. Dalton Trans. 291 (1993); (*b*) P.J. Heard, P.M. King, A.D. Bain, P. Hazendonk, and D.A. Tocher. J. Chem. Soc. Dalton Trans. 4495 (1999); (*c*) P. J. Heard, A.D. Bain, and P. Hazendonk. Can. J. Chem. **77**, 1707 (1999).
20. J.S. Hartman, Z. Yuan, A. Fox, and A. Nguyen. Can. J. Chem. **74**, 2131 (1996).
21. J.S. Hartman and G.J. Schrobilgen. Inorg. Chem. **13**, 874 (1974).
22. J. Hayami, N. Ono, and A. Kaji. Tetrahedron Lett. 1385 (1968).

[3] J.S. Hartman, J.A.W. Shoemaker, A.F. Janzen, P.J. Ragogna, and W.R. Szerminski. paper in preparation.

© 2001 NRC Canada

Application of nonporous polyurethane (PU) membranes and porous PU thin films as sample supports for MALDI-MS of wheat proteins

Mark E. McComb, Richard D. Oleschuk, Art Chow, Hélène Perreault, Ragnar G. Dworschak, Marek Znamirowski, Werner Ens, Kenneth G. Standing, and Ken R. Preston

Abstract: Non-porous polyurethane (PU) membranes and porous PU thin films are used as sample supports for MALDI-TOFMS. Mass spectra obtained are compared with those acquired using metal targets and the crushed matrix method. The compounds characterized are wheat proteins which consist of moderately water-soluble gliadins, and of water-insoluble low molecular weight (LMW) and high molecular weight (HMW) glutenins. Mass spectra obtained using the PU supports are in general of good quality, and this method of sample preparation is the most convenient for sample handling. In the case of gliadins and LMW glutenins, the spectra obtained on PU are comparable with those obtained using metal supports. Isolation of the LMW and HMW wheat proteins characterized in this study requires the use of buffers incompatible with MALDI. Spectra of samples containing buffer components on PU supports are of better quality than those obtained using the crushed matrix method. This effect is attributed to stronger protein binding onto the PU supports, which allows for extensive washing and removal of water soluble buffer components. The PU film, when cast onto a MALDI probe, is porous and flat in topology. The differences in surface characteristics between the PU film and the PU membrane result in slight variations in the mass spectra. The extent of surface charging, observed significantly using 50 μm thick PU membranes, decreases with 25 μm membranes and becomes insignificant with PU thin films. An important advantage of using the PU supports is the possibility of preparing samples on the film or membrane in the field and of analysing them at a later time. This is especially important when samples are susceptible to chemical degradation in solution. These proteins are known to degrade while stored in solution. We have thus incorporated the use of PU membrane–film supports into our routine analysis of these proteins.

Key words: gliadins, glutenins, MALDI, membrane supports, polymeric supports, time-of-flight analysis.

Résumé : On utilise des membranes non poreuses de polyuréthane (PU) et des films minces poreux de PU comme supports échantillons pour la « MALDI-TOFMS ». On a comparé les spectres de masse obtenus par cette méthode avec ceux obtenus en utilisant des cibles métalliques et par la méthode des matrices broyées. Les composés caractérisés sont des protéines de blé formées de gliadines modérément solubles dans l'eau et de gluténines insolubles dans l'eau de faibles poids moléculaires (« LMW ») et de poids moléculaires élevés (« HMW »). En général, les spectres de masse obtenus en utilisant les supports de PU sont de bonne qualité et cette méthode de préparation des échantillons est la plus commode pour le maniement de l'échantillon. Dans le cas des gliadines et des gluténines LMW, les spectres obtenus sur des supports de PU sont comparables à ceux obtenus en utilisant des supports métalliques. L'isolement des protéines de blé de LMW et de HMW caractérisées dans cette étude nécessite l'utilisation de tampons incompatibles avec la MALDI. Les spectres d'échantillons contenant des composants de tampons, réalisés sur des supports de PU, sont de meilleure qualité que ceux obtenus en faisant appel à la méthode de la matrice broyée. Cet effet est attribué à la fixation plus forte de la protéine sur les supports de PU, ce qui permet d'effectuer des meilleurs lavages et l'élimination des composants de tampons solubles dans l'eau. Le film de PU fixé sur une sonde MALDI est poreux et de topologie plane. Les différences dans les caractéristiques de surface entre le film de PU et la membrane de PU conduisent à de légères variations dans les spectres de masse. Le niveau de formation de charge à la surface, qui est relativement élevé lorsqu'on utilise des membranes de PU de 50 μm d'épaisseur, diminue avec les membranes de

Received February 7, 2001. Published on the NRC Research Press Web site on April 30, 2001.

M.E. McComb[1], R.D. Oleschuk[2], A. Chow, and H. Perreault.[3] Department of Chemistry, University of Manitoba, Winnipeg, MB R3T 2N2, Canada.
R.G. Dworschak, M. Znamirowski, W. Ens, and K.G. Standing. Department of Physics, University of Manitoba, Winnipeg, MB R3T 2N2, Canada.
K.R. Preston. Canadian Grain Commission-Grain Research Laboratory, 1403-303 Main St., Winnipeg, MB R3C 3G8, Canada.

[1]Department of Biochemistry, Boston University School of Medicine, Boston, MA 02218-2526, U.S.A.
[2]Department of Chemistry, Queens University, Kingston, ON K7L 3N6, Canada.
[3]Corresponding author (e-mail: perreau@cc.umanitoba.ca; fax: (204) 474-7608).

 DOI: 10.1139/cjc-79-4-437 © 2001 NRC Canada

25 μm et il devient pratiquement nul avec les films minces de PU. Un avantage important d'utiliser des supports de PU est la possibilité de préparer des échantillons sur le film ou la membrane sur le terrain et de les analyser plus tard. Ceci est particulièrement important quand les échantillons sont susceptibles aux dégradations chimiques si ils restent en solution. Il est connu que ces protéines se dégradent lorsqu'on les conserve en solution. On a donc incorporé l'utilisation de supports membrane–film de PU dans l'analyse de routine de ces protéines.

Mots clés : gliadines, gluténines, MALDI, support membranaire, supports polymériques, analyse par temps d'envol.

[Traduit par la Rédaction]

Introduction

Matrix-assisted laser desorption–ionization time-of-flight mass spectrometry (MALDI-TOFMS), first introduced in 1988 by Karas et al., provides a rapid and convenient means for the characterization of proteins and peptides (1). Since its introduction, MALDI-TOFMS has been used for a large number of applications for the characterization of several types of biological molecules (2–6). The method is relatively tolerant of impurities, such as salts and buffers, even at concentrations which hamper other ionization processes such as electrospray ionization (ESI).

Numerous experimental parameters, such as sample preparation, may affect the sensitivity, resolution, and accuracy of measurements. Several methods of sample preparation using different matrices have thus been developed for MALDI-TOFMS applications (7). In spite of the relative tolerances, one main concern is the presence of interfering components such as salts, buffers, and detergents which may result in adduct formation and widening of peaks. Techniques for sample purification prior to MALDI-TOFMS analysis have thus been developed. Many of these are based on traditional separation techniques including dialysis, filtration, and chromatography. Another approach is to purify the sample directly on the surface of the MALDI probe. By incorporating the sample-purification step with the addition of matrix, the time frame of analysis may be reduced and only a minimal amount of sample is required.

Various approaches to on-probe sample-purification based on a common theme have been explored. In all of these a substrate is first deposited onto the surface of the MALDI probe, either by mechanical adhesion to the surface (i.e., polymeric membranes and films), or by covalent attachment to the surface. The substrate possesses a chemical or physical property which allows it to selectively bind the analyte of interest. Once the analyte is bound, it is possible to remove other components from the surface by washing procedures. Addition of the matrix to the probe, in a suitable solvent, releases the bound analyte, which then may cocrystallize with the matrix for analysis by MALDI. This overall approach is easy and cost effective. Moreover, it makes sample preconcentration possible through application of successive sample aliquots to the probe.

Surface enhanced affinity capture (SEAC), introduced by Hutchens and Yip (8), was an early example of sample pretreatment directly on the MALDI probe. The SEAC probe surface was modified with a functional group (agarose) used to selectively bind the analyte of interest. Another similar example involved the use of a small amount of powdered chromatographic packing placed on the MALDI target (9). Also, C-18-derivatized targets have been prepared using self-assembled monolayers of octadecyl mercaptan placed on a gold-coated probe (10).

An alternative technique involves modifying the probe surface by the addition of a polymeric membrane or film which binds to the sample protein and allows washing of buffer components. This approach, based on the use of membranes for automatic protein sequencing, is now used routinely for sample purification and introduction into the mass spectrometer (2, 3, 6). Hydrophobic–ionic interactions between the sample and the film or membrane, allow the selective removal of interfering buffer components. Addition of matrix solution directly onto the surface promotes partitioning of the analyte and salts- or buffer-components between the liquid phase and the surface of the film or membrane. Derivatization and proteolytic digestion may be performed on the surface of the film or membrane. Membranes, which are readily available in large quantities and various sizes, are very convenient for transporting samples from the preparation site to the MALDI-TOFMS laboratory. A number of different polymeric supports have been examined for use with MALDI. An early example by Mock et al. (11) used an electrosprayed surface of nitrocellulose to create a thin film on a gold surface. Since then, a number of other membranes and films have been used. These include nitrocellulose (12–14), polyethylene (15, 16), Nafion (perfluorosulfonated ion exchange membrane) (17), nylon (18), cellulose (14), poly(vinylidene difluoride) (PVDF) (19), polypropylene (16), paraffin wax (20), Teflon® (poly(tetrafluoroethylene)) (21), and polyurethane (22, 23). Recently, there have been reports on the use of nonporous Teflon® surfaces for MALDI, which are now available as commercial targets from Bruker Daltonics, Bremen, Germany (24–26).

Our laboratory was first to introduce the use of nonporous polyurethane (PU) membranes as sample supports for MALDI-TOFMS characterization of peptides and proteins derived from biological samples (22, 23). In our first report on the subject, we focused on the analysis of low molecular weight proteins and peptides. We observed that the nonporous surface of the membrane provided improved mass spectra in comparison with a porous membrane surface, and sample purification could be performed easily, directly on the membrane surface. Additionally, the nonporous membrane surface proved to be useful for on-probe proteolytic digestion and (or) purification of proteins for peptide mass-mapping. We also observed that qualitative aspects of spectra, such as peak shape and peak width, depended on the laser fluence and repetition rate of data acquisition, consistent with electrostatic charging occurring near or on the membrane surface. This motivated our investigation on the use of thinner PU membranes (25 μm thickness) and thin PU films for use as sample supports.

© 2001 NRC Canada

In this paper, we report the use of nonporous PU membranes and porous PU thin films for MALDI-TOFMS, particularly in the analysis of wheat proteins. MALDI-MS has been used to accurately and quickly determine the masses of specific glutenin subunits of wheat (27, 28), and our laboratory has recently characterized gliadins and glutenin subunits by MALDI-MS on metal targets as part of an ongoing collaborative project with the Canadian Grain Commission, Grain Research Laboratory (29). Gliadins have limited solubility in water, and glutenins are insoluble. The wheat gliadins consist of a group of ca. 100 proteins, with a low molecular weight range of 30–40 kDa. The glutenins are large polymeric proteins composed of two groups of subunits: low molecular weight (LMW) (30–40 kDa) and high molecular weight (HMW) (65–90 kDa) subunits. These subunit proteins are heterogeneous and are thought to have some degree of post-translational modification (i.e., glycosylation). The reagents required for their isolation (i.e., 1% DTT, 2 M urea, 0.082 M trisHCl) are not favourable for analysis by MALDI. We discuss the ease of sample preparation, time frame of analysis, and show comparisons between spectra obtained using nonporous membranes, porous thin films, and steel targets. Statistical figures are used for spectral comparisons at different levels e.g., spectrum-to-spectrum reproducibility on the same sample, on different samples from the same batch prepared with a given method, and on samples from the same batch prepared with different methods. These results are meant to demonstrate the overall usefulness and advantages of PU substrates. With this robust approach and its easy sample preparation schemes, PU membranes and films as supports yielded spectra as reproducible as obtained with steel targets and other recently developed nonporous substrates (26).

Experimental

All chemicals used in this study were of reagent grade unless otherwise stated. High performance liquid chromatography (HPLC) grade acetonitrile, dithiothreitol (DTT), and ethanol were from Fisher Scientific (Fair Lawn, NJ). Trifluoroacetic acid (TFA) was from Sigma (St. Louis, MO). HPLC grade deionized water, prepared with a Milli-Q® plus-TOC water purification system (Millipore, Bedford, MA), was employed in all solutions.

PU sample supports

The nonporous ether-type PU membrane (25 μm in thickness (XPR625-FS)), was supplied by Stevens Elastomerics (Northampton, MA). Complete details on the preparation of PU membranes for sample supports are available elsewhere (23). In brief, the PU membrane was rinsed in methanol prior to the addition of sample. After rinsing and matrix application, the membrane was trimmed to the size of the MALDI probe and affixed to it using 3M® Spray Mount adhesive (3M, London, ON). Porous PU thin films were prepared by first dissolving the solid PU membrane in tetrahydrofuran and then depositing ca. 10 μL of the liquid onto the probe surface, spreading it around, and then allowing it to dry.

Scanning electron microscopy

The PU membrane and film were characterized by scanning electron microscopy (SEM). Scanning electron micrographs were obtained on a Cambridge Instruments microscope located in the Department of Geological Sciences, University of Manitoba. Samples prepared on PU membranes and on metallic surfaces were coated with gold and palladium by plasma deposition prior to analysis. Images were recorded with magnifications of 30× and 300×.

Protein extraction

Pure samples of the Biggar wheat variety from the Canada Prairie Spring commercial class were obtained from stocks maintained at the Grain Research Laboratory in Winnipeg, MB, Canada. Wheat samples (25 g) were ground in a UDY cyclone sample mill equipped with a 1 mm sieve. Gliadins were extracted from ground grain (1.0 g) into 70% (v/v) ethanol (6 mL) at room temperature for 60 min. Glutenins were then extracted from the remaining grist with 1% DTT in 100% *n*-propanol (29, 30). The LMW glutenin fraction was extracted by precipitating out the HMW glutenins with the addition of 1% DTT in 50% *n*-propanol to bring the final concentration to ca. 65% *n*-propanol. The HMW glutenin precipitate was washed with 1% DTT in 65% *n*-propanol and then resolubilized in 1% DTT and 2 M urea in buffered (0.082 M trisHCl, pH = 7.0) 50% *n*-propanol (30). Extracts were then centrifuged at 20 000 *g* for 10 min. The extraction procedure is outlined in Fig. 1. Typically, the samples were deposited onto the MALDI targets within one day to minimize sample loss and degradation. Samples on metal targets were analyzed by MALDI-MS within one day while samples on PU surfaces were analyzed within 14 days.

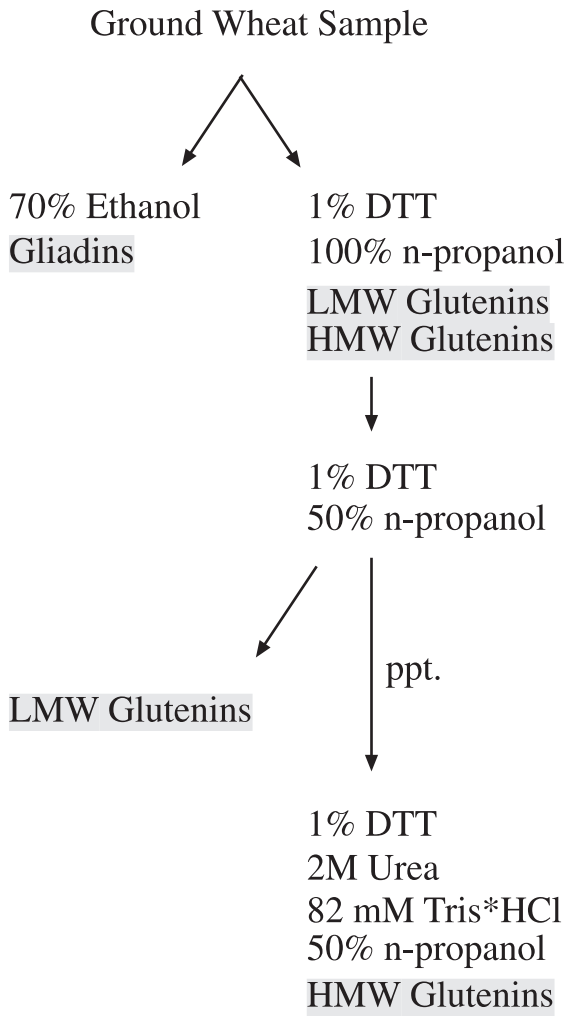
Sample preparation

The stock wheat protein solutions had concentrations varying from 30 to 600 mM. The matrix solution used in all analyses was a saturated solution of 3,5-dimethoxy-4-hydroxycinnamic acid (sinapinic acid) in 0.1% TFA and acetonitrile (2:1 v/v). For samples on steel probes, the crushed matrix method was used (31). A 2 μL aliquot of the matrix solution was first applied to the sample probe, allowed to dry, and then crushed. The stock solution was then mixed (1:10 v/v) with the matrix solution and a few microlitres of the mixture were applied to the crushed spot on the sample probe. When a visible film began to form (ca. 10–60 s), the spot was rinsed with cold deionized water for 10 s and then allowed to dry thoroughly prior to analysis. This process was repeated if necessary to deposit enough protein onto the surface of the probe to acquire MALDI mass spectra.

Samples were prepared on PU substrates by first depositing 2 μL of the protein solution onto the film or membrane surfaces. After the samples were completely dried, 2 μL of methanol were added to enhance protein sorption onto PU. For sample preparation without a washing step, 2 μL of the saturated matrix solution were added and allowed to dry prior to analysis. For preparation with a washing step, 25 μL of deionized water were deposited on the surface of each sample and allowed to stand for 1 min to solubilize as much material as possible. This large droplet was then removed with a pipette. This step was repeated once more to ensure

© 2001 NRC Canada

Fig. 1. Extraction procedure for wheat gliadins and glutenins (27).



that the protein samples were as free from water soluble material as possible. The matrix was added just prior to analysis.

Matrix assisted laser desorption–ionization

Positive-ion mass spectra were obtained in the linear mode on a MALDI-TOF mass spectrometer built in-house (32). A nitrogen laser (VSL 337 ND, Laser Science Inc., Cambridge, MA, U.S.A.) was used with intensity set just above threshold. For some of the gliadin and LMW glutenin subunits, a two-grid delayed extraction system (33) was employed, with a 25 kV DC accelerating potential on the probe and first grid, and a 3 kV pulse applied to the probe 1.2 μs after the laser pulse. The 3 kV pulse was supplied by a high voltage switch (Behlke, Frankfurt, Germany). For the HMW glutenin fraction, DC extraction was employed with the target and first grid potentials of 30 kV and 18 kV, respectively. Following desorption and acceleration, ions drifted through a field-free region of 1.2 m in which the nominal pressure was 3×10^{-7} torr (1 torr = 133.322 Pa). The ions were detected with microchannel plates and the signal was recorded with a LeCroy 9350AM 500 MHz digital oscilloscope from which the spectra were summed by a UMAX Supermac C600 computer. Approximately 150–200 shots were accumulated per spectrum on samples prepared on the steel targets while ca. 50 shots were sufficient for samples on PU supports. The gliadin- and LMW-glutenin-subunit spectra were calibrated externally with carbonic anhydrase (29021 Da), while the HMW-glutenin-subunit spectra were calibrated externally with human transferrin (79549 Da). Improved mass accuracy would have been possible with internal calibration, however the emphasis in this work was on the examination and evaluation of PU films and membranes for sample analysis.

Results and discussion

Characterization of polyurethane films and membranes

Membranes and films have different advantages when used as sample supports for MALDI analysis of proteins. While films may be directly deposited onto the surface of the MALDI target, membranes must be attached, usually with an adhesive, which introduces an additional step into the analytical scheme. Because films are thin, the possibility of surface charging is reduced or eliminated. One distinct advantage of membranes is that the sample may be applied prior to affixing the membrane onto the probe surface. This allows samples to be collected directly on the surface of the membrane outside the MALDI laboratory. A number of different polymeric film and membrane supports are available, thus a specific type may be chosen for a selected class of analyte.

For preparation of PU thin films, some PU membrane material was dissolved in THF, cast onto the surface of the MALDI probe and allowed to dry under ambient conditions. Fig. 2 compares SEM images taken on the 25 μm thick PU membrane (*a* and *b*), and the PU film (*c* and *d*). The surface topology of both the membrane and film was flat, unlike the uneven rough surfaces typical of other membranes examined previously (15). Unexpectedly, the surface of the PU film was porous as shown in Figs. 2*c* and *d*. Porosity is introduced when the film dries on the probe after casting. The extent of porosity varies with rate of drying and solvent volatility, among other parameters. The pore sizes ranged from ca. 1 μm to 8 μm in diameter, with most pores being in the 2–3 μm range. The film was less than 1 μm thick, i.e., thinner than ca. 1 μm as calculated from the amount of material deposited and the surface area of the probe.

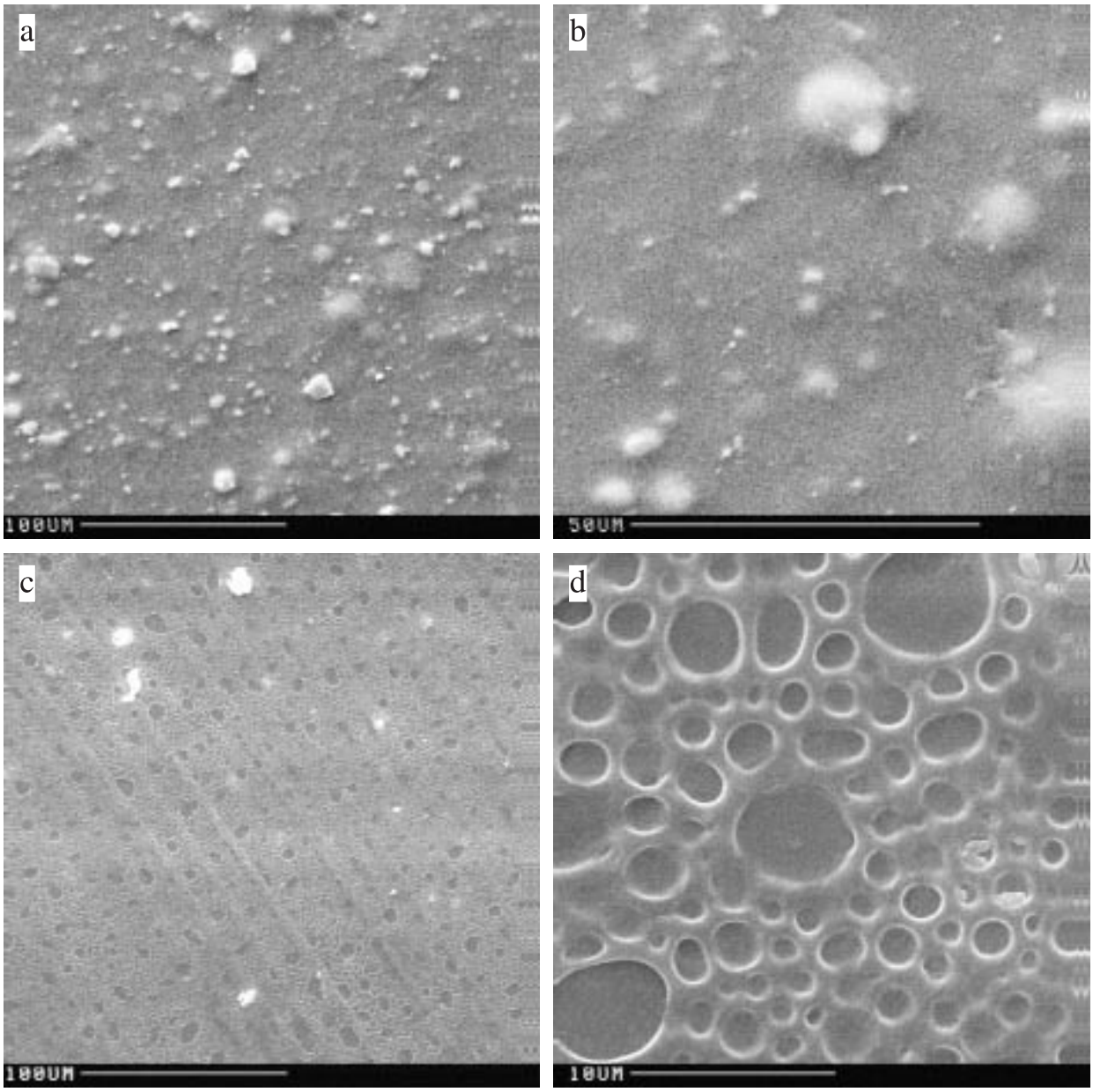
In general, thinner conductive surfaces (e.g., metal targets) or porous surfaces, such as PU films, reduce the time frame of static discharge of an insulating surface on a MALDI target. However, porous surfaces result in greater extent of analyte adsorption away from the surface, thus making it unavailable for laser desorption or resulting in a spread in the flight-time measurements (22). Nonporous flat surfaces allow a maximal extent of protein sorption at the surface, yielding better MALDI signals and better resolution than porous surfaces. An ideal substrate material would be a PU thin film with flat topology, either nonporous or with very small pores (e.g., <1 μm).

Charging

MALDI spectra of bovine insulin were obtained using PU membranes and thin films and compared qualitatively with those obtained using steel targets. With the laser intensity set just above threshold, all three surfaces produced similar

© 2001 NRC Canada

Fig. 2. Scanning electron micrographs taken at different magnifications: (*a*) PU membrane 30×; (*b*) PU membrane 300×; (*c*) PU film 30×; and (*d*) PU film 300×.

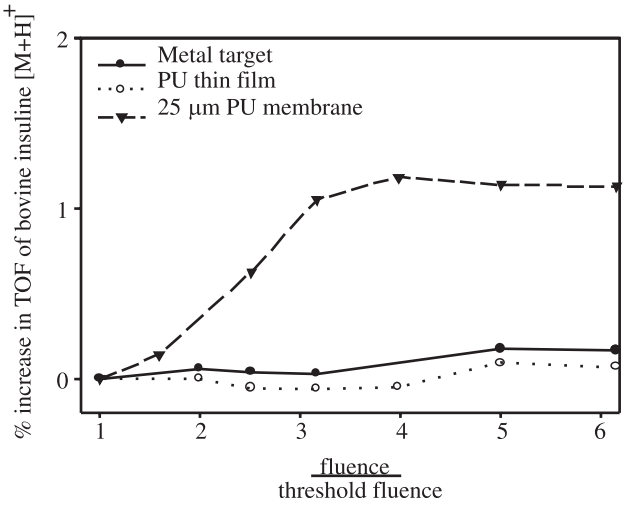


spectra in terms of resolution and mass accuracy, which were typical of the instrument (32) (see overlap of first data point of each set in Fig. 3, and two sample spectra, bottom of Fig. 4). Comparisons between spectra of myoglobin and bovine insulin obtained using PU membranes and steel targets had shown the same trends (22). Charging of the membrane, sometimes observed in MALDI (18), occurred with the 25 μm and 50 μm thick PU membranes at laser intensities two to three times above threshold using a laser pulse rate of ca. 2 Hz on the laser (22). Charging was not observed with the PU thin films, nor with the steel targets. We attributed this to the thinness and surface porosity of the film, which would be expected to facilitate dispersal of static charge. To overcome the charging observed with the membrane, it was necessary to reduce the pulse rate of the laser to ca. 0.5 Hz to allow dispersal of the static charge. Figure 4 shows the effect of charging on the spectrum of bovine insulin on a PU film. All six spectra result from summing 50 shots, and were acquired at a shot frequency of 1 Hz using 35 pmol of bovine insulin in sinapinic acid matrix. The film thickness was ca. 1 μm. The laser intensity was decreased from Spectrum 1 to Spectrum 6. The variation in time-of-flight was of the order of only ca. 0.1%.

Qualitative measurements of the charging observed are shown in Fig. 3. The time-of-flight of bovine insulin $[M+H]^+$ ions was measured as a function of laser intensity on the three surfaces employed. With the 25 μm PU membrane, the time-of-flight increased by nearly 1.5% at higher laser intensity, relative to the value measured at threshold. Spectra obtained using the PU film were less influenced by the laser intensity, and charging occurred only at maximum intensity. Spectra obtained using the steel target were not

© 2001 NRC Canada

Fig. 3. Influence of laser intensity on the time-of-flight of bovine insulin $[M+H]^+$ ions: comparison of sample supports.

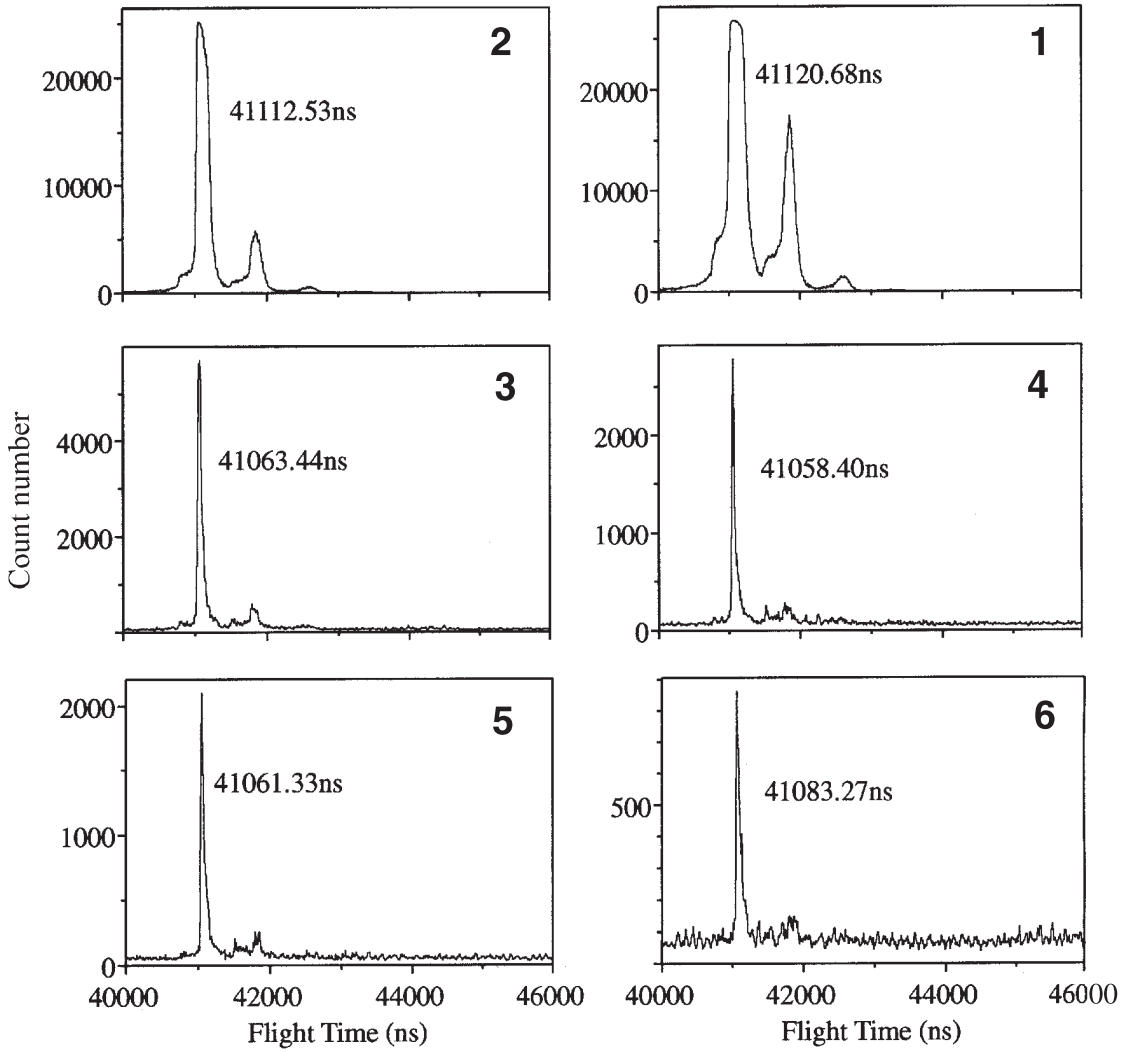


influenced. It is noted that the maximum laser fluence used was about six times above threshold, and would not normally be used in MALDI analysis.

Proteins from wheat

Our laboratory has recently characterized some wheat gliadins and LMW- and HMW-glutenin subunits on metal targets by MALDI-MS (29). The spectra obtained on wheat gliadins in the 70% ethanol fraction (see *Experimental*) were in general of good quality, informative, and relatively easy to acquire. This was not the case for the spectra of LMW and HMW wheat glutenins. Extraction of the glutenin proteins requires buffers that are incompatible with the usual MALDI protocol. Using the crushed matrix method, successive applications of protein were necessary, followed by washing, to obtain informative spectra. With this method, a spectrum was not obtained for every target, even for samples from the same preparation on separate targets. For example, for HMW glutenins, only two significant spectra were obtained out of numerous attempts. PU films and membranes as supports produced informative spectra for every target prepared, and were thus more reliable than metal targets. Addition of

Fig. 4. MALDI-TOF mass spectra of bovine insulin on a 1 μm-thick PU film, with increasing laser intensity from Spectrum 6 (just above threshold) to Spectrum 1, showing that charging causes a time-of-flight shift of only ca. 0.1% on film surfaces.



© 2001 NRC Canada

Fig. 5. MALDI-TOF mass spectra of gliadins: (*a*) metal target; (*b*) PU membrane; (*c*) PU film. Spectra in *b* and *c* were acquired without sample washing. Peaks marked with an asterisk were used for statistical analysis.

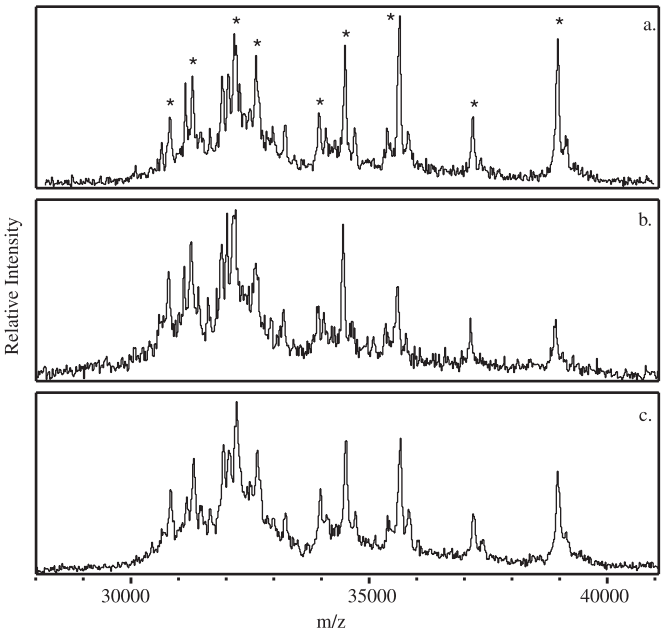
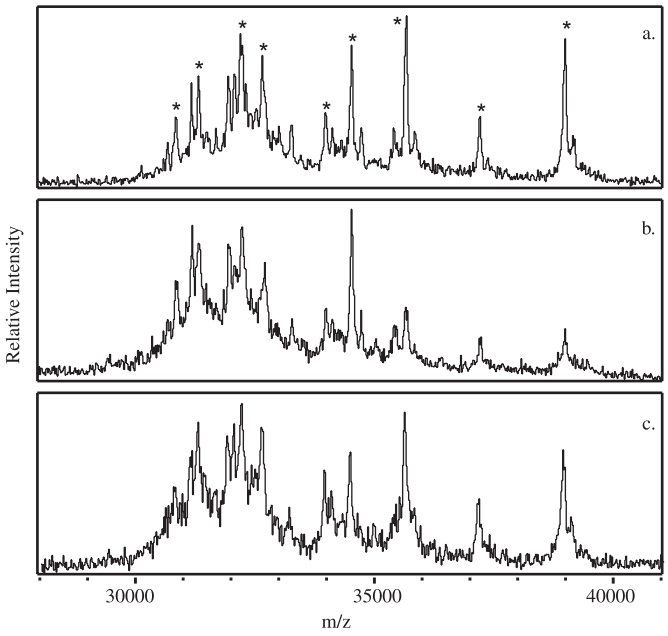


Fig. 6. MALDI-TOF mass spectra of gliadins: (*a*) metal target; (*b*) PU membrane; (*c*) PU film. All spectra were acquired with sample washing, for comparison. Peaks marked with an asterisk were used for statistical analysis.



methanol as an organic modifier appeared to enhance the extent of analyte binding by partitioning salts away from the surface and favoring interactions of the surface with hydrophobic peptides and proteins.

Stability and time-reproducibility considerations

It was important to consider the elapsed time between sample extraction and MALDI analysis. The general trend observed in our laboratory is that dried protein samples, when placed onto the PU surfaces, are stable for up to several weeks prior to analysis by MALDI-TOFMS. In the specific case of the wheat proteins, several samples of each class of protein were analyzed in replicate, without observing any detrimental effects from up to 14 days of storage. In essence there was no observable change in their mass spectra, and reproducibility was as good as for spectra acquired the same day (see discussion on sample-to-sample reproducibility below).

More importantly, we observed that glutenins were not stable in solution and necessitated to be deposited on substrates within one day following extraction. Once on PU substrates, these proteins could be analyzed by MALDI without detectable spectral deterioration, again within 14 days. Solution instability is a serious limitation in a laboratory without a dedicated MALDI instrument, and necessitates immediate use of solution methods for analysis. Prolongation of the possible analysis time frame to up to two weeks following extraction therefore constitutes a real advantage of using our method. For both glutenins and gliadins, no samples were analyzed past two weeks of storage. It is however generally accepted that once deposited on polymer substrates, dried protein samples can be stored for prolonged periods of time.

Gliadins

To demonstrate that the membrane surfaces did not adversely contribute to the mass spectra of the wheat samples, initial spectra were obtained without the use of the washing protocol. Figure 5 shows MALDI mass spectra of wheat gliadins obtained using the different sample supports, without washing. All three types of targets employed produced similar spectra. These results are not surprising as this fraction of wheat proteins did not necessitate the use of involatile buffer components during extraction and thus resulted in relatively clean samples. For comparison, Fig. 6 shows spectra of the same class of proteins prepared on a metal target and PU supports while incorporating sample washing.

In an attempt to determine the best sample preparation method for MALDI-MS of gliadins, standard deviations on heights of peaks indicated in Figs. 5 and 6 with asterisks were calculated for each sample. At least three MALDI spectra were used for each calculation, and each spectrum was the sum of 50–150 shots obtained over the entire surface of the target. Ideally the whole spectrum should be used for comparison, however, this would not necessarily be more useful, unless a specific low-concentration substance was targeted. We have already demonstrated that peak areas provide for better statistical treatment of data on the PU surfaces (34). Here, due to peak overlap of the many proteins within the gliadin sample, it was not possible to adequately calculate peak areas. For relatively clean samples, the standard deviations of peak heights obtained with the crushed matrix method were lower than those obtained with PU supports. This is in agreement with the higher standard deviations observed with the dried droplet method of crystallization compared with fast crystallization (35). The

© 2001 NRC Canada

Table 1. Reproducibility in peak intensities for spectra obtained on samples using each of the sample preparation methods.

Sample preparation method[b]	Range of % standard deviation in (*n*) replicate sample measurements[a]		
	Gliadins: 9 peaks	LMW glutenin: 8 peaks	HMW glutenin: 4 peaks
Metal target	1.7906–10.5804 (3)	—	—
PU-neat	1.2109–17.7627 (4)	—	—
Film-neat	6.6964–20.7079 (3)	—	—
Metal target	1.7906–10.5804 (3)	1.0857–28.2738 (3)	6.9718–25.2637 (2)[c]
PU-wash	4.2591–21.5920 (5)	2.2794–20.2353 (3)	4.7230–18.8722 (5)
Film-wash	2.9293–38.6338 (4)	7.8881–21.1377 (4)	1.7378–40.6924 (4)

[a]% SD: range based on the number of peaks in each class of spectra (9, 8, and 4 peaks, respectively), for (*n*) replicate measurements. Peaks are indicated with asterisks in Figs. 5–8.

[b]PU-neat and film-neat: the sample was mixed with matrix and placed directly on the surface of the PU membrane or PU film. Identical method to sample preparation on metal targets as there was no washing involved. PU-wash and film-wash: washing protocol used (see *Experimental*).

[c]For the HMW gliadins prepared on PU, only two spectra were obtained even after repeated attempts.

Table 2. Comparison of mean reproducibility of spectra obtained on gliadin samples prepared using different methods.

Sample preparation method	Correlation of mean peak intensities[a]				
	Metal target	PU-neat	Film-neat	PU-wash	Film-wash
Metal target	—	—	—	—	—
PU-neat	0.8901	—	—	—	—
Film-neat	0.5287	0.8383	—	—	—
PU-wash	0.6737	0.8826	0.9065	—	—
Film-wash	0.4284	0.7512	0.9097	0.9762	—

[a]Peaks as per Table 1 and Figs. 5–8.

results, presented in part of Table 1 (Gliadins column), indicate that for this class of wheat proteins, washing has a negative effect on reproducibility, while changing substrates has a consistent effect of decreasing the extent of reproducibility in the order metal > PU > film. The negative effect of washing may be expected, because the gliadin samples were clean to begin with, moderately water soluble, and thus not entirely compatible with the hydrophobic surfaces of PU membranes and films. It is possible that some of the sample was removed from the membrane surface during the washing step. For comparing spectral reproducibility for samples of the same class, prepared using the same method but on different consecutive samples and analyzed on different days (within 2 weeks), statistical correlations were used, and found to be greater then 90% for gliadins, indicating a relatively reproducible sample preparation method. A statistical comparison was also made between spectra prepared using the different methods. The results are shown in Table 2 for gliadins. These indicate that both the physical nature of the surface and the chemical interaction of the sample with the surface influence spectral features. In terms of surface influence, PU-wash spectra (see definition of abbreviated terms at the foot of Table 1) correlate well with those obtained using PU-neat. Also, film-wash spectra correlate well with film-neat results. PU-neat substrates have a surface topology similar to that of metal targets, and a high correlation is observed between spectra acquired using these two methods. There is also correlation dependence on washing or nonwashing of the sample, e.g., PU-wash spectra correlate well with film-wash results.

The overall pattern of relative intensities for the protein ions was different for PU and steel sample substrates. This may be due to a difference in protein affinity between the PU and the crushed matrix on the steel probe, as the degree of surface hydrophobicity will influence the extent of protein and peptide binding. Different degrees of sorption would thus result in the release of variable amounts of protein during the washing and matrix application steps. These findings are similar to results obtained in our laboratory for comparison of PU and steel supports for peptide mixtures (22, 23). Walker et al. (19) have made similar observations with the use of polymeric supports for protein analysis. They suggested that some protein is removed during washing and not all of it may be released from the polymer surface after applying the matrix solution.

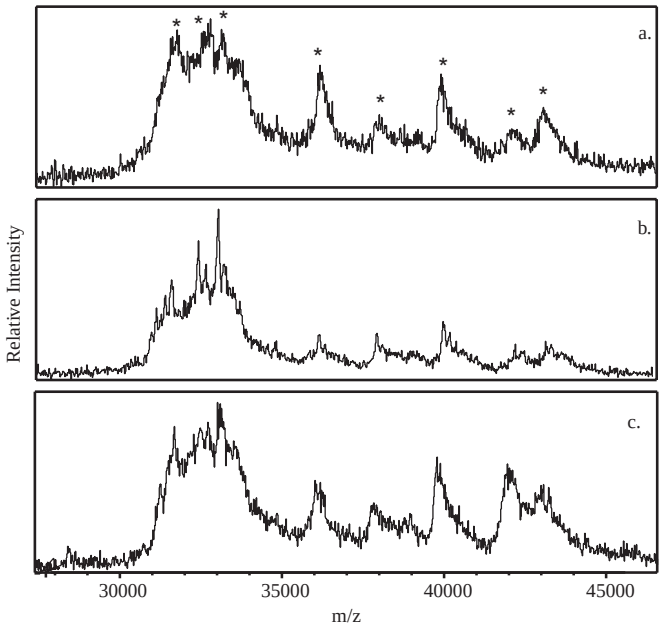
Low molecular weight glutenins

The benefit of using PU substrates is more apparent in the analysis of the LMW glutenins as shown in Fig. 7. For these proteins, it was not possible to record spectra using the steel targets without washing, possibly due to the presence of 1% DTT and other components required for their extraction. Spectra were more easily obtained using the PU supports, which yielded better signal uniformity and shot-to-shot reproducibility than metal targets. The washed samples on film and membrane also yielded better signal-to-noise ratios than unwashed samples. Spectra could be obtained from the entire surface of samples prepared on PU supports, while samples prepared on the steel targets required rastering of the target to find useful ionization sites. Between 150–200 shots were required to obtain spectra on the steel targets compared with ca. 50 shots with PU supports. The spectra of best quality were obtained on PU membranes, with better definition of the 30 000–33 000 *m*/*z* range due, presumably, to removal of buffer components, which resulted in broadened peaks in the other samples.

An indication of the extent of reproducibility on single samples of this class of proteins is given in the central

© 2001 NRC Canada

Fig. 7. MALDI-TOF mass spectra of LMW glutenins: (*a*) metal target; (*b*) PU membrane; (*c*) PU film. All spectra were acquired with sample washing. Peaks marked with an asterisk were used for statistical analysis.



column of Table 1. Eight peaks were used to obtain standard deviations. These results show no significant improvement owing to PU substrates compared with metal surfaces, although they are transparent to the fact that many metal targets needed to be prepared to produce only a few spectra, while most PU targets produced informative data. Table 1 shows that reproducibility in peak heights obtained on film surfaces was slightly worse than on membranes, which in turn produced spectra as reproducible as, or more reproducible, than metal targets.

Sample-to-sample reproducibility with LMW glutenins on separate targets, same sample preparation method, and different day of analysis (within 2 weeks), resulted in correlations of ca. 90% in peak heights. There were slight variations in peak heights when using different supports. These results are shown in Table 3. These correlations appear to depend on both surface chemistry and topology, similar to results obtained with the gliadin proteins. These factors have been known to affect the formation of matrix crystals. Following this idea, PU-wash spectra correlate well with film-wash data, showing similar surface chemistry. Metal spectra correlate well with PU-wash spectra, both surfaces being nonporous. Differences in the surface morphology of the film vs. membrane may contribute to some of the variations observed. The PU surface composition depends on the method of fabrication (e.g., casting, extrusion) and on the type of contact surface during casting of the polymer (36). Changing the proportions of hard (crystalline) and soft (amorphous) segments at the polymer surface leads to different protein sorption characteristics (37). In this application, casting the PU onto the MALDI probe may alter the surface composition of the polymer, leading to different affinities for the different wheat proteins present. In addition, as the membrane is nonporous, the surface area available for protein

Table 3. Comparison of mean reproducibility of spectra obtained on LMW glutenin samples prepared using different methods.[a]

Sample preparation method	Correlation of mean peak intensities[b]		
	Metal target	PU-wash	Film-wash
Metal target	—	—	—
PU-wash	0.09317	—	—
Film-wash	0.8257	0.9307	—

[a]Useful spectra were not obtained on unwashed samples on metal or PU supports.
[b]Peaks as per Table 1 and Figs. 5–8.

binding would be expected to be greater than that of the film, which would influence the amount of protein available for analysis by MALDI. With nonporous surfaces, all the sample is likely to remain on the top and easily accessible to the UV laser.

High molecular weight glutenins

Results from the analysis of the HMW glutenin fraction are shown in Fig. 8. The quality of the spectra at first glance is similar for the three washed substrates. However, use of the PU membrane resulted in less noise in the mass spectra and both PU surfaces yielded good signals with fewer laser shots. Spectra were not obtained on any target without washing. With metal targets, only two useful spectra were obtained even after numerous attempts. When using the PU surfaces, useful spectra could be obtained on nearly every sample. More concentrated buffer components are present in the HMW fraction (1% DTT and 2 M urea in buffered 0.082 M trisHCL (pH = 7.0), see Fig. 1) than in the LMW glutenin and gliadin samples. Removal of buffers was necessary to generate spectra. The far right column of Table 1 shows ranges of standard deviations obtained for spectra recorded on single samples using four peaks (marked with asterisks in Fig. 8). These results are similar to those obtained with LMW glutenins. In general, spectra obtained on films were less reproducible in terms of peak heights than those acquired using PU membranes, which tended to be more reproducible than metal target data.

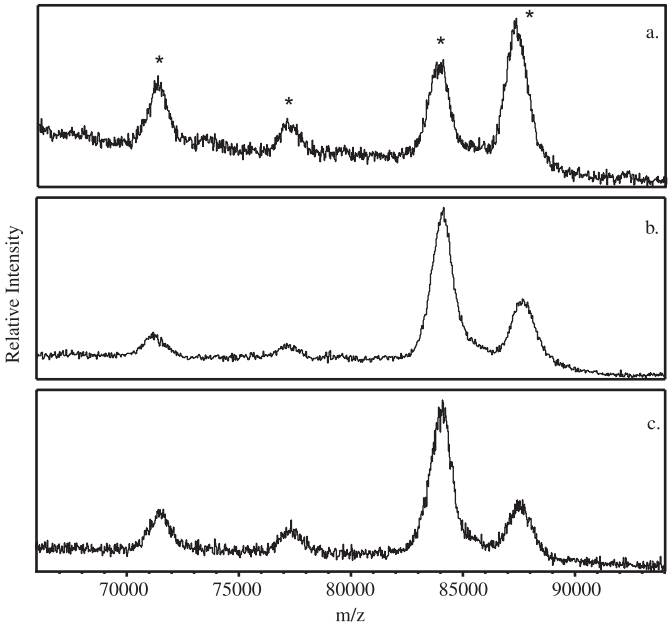
Sample-to-sample reproducibility with HMW glutenins on separate targets, same sample preparation method, and different days of analysis (within two weeks), resulted in correlations of ca. 90% in peak heights, with the exception of metal surfaces with only two spectra obtained. The best sample-to-sample spectral reproducibility with separate targets was obtained using the PU membrane, which gave correlations greater then 90% on peak heights.

There were significant variations in peak heights with PU supports vs. metal targets, as indicated in Table 4. In this case, the affinity of the PU surface for proteins played a significant role in controlling relative signals. The best correlations appear to result from similarities in the surface chemistry of PU film and membrane surfaces: PU-wash spectra correlate well with film-wash spectra. Because of different extents of interaction between analytes and substrate, relative intensities differed for spectra acquired on PU supports vs. metal, thus yielding low correlations.

This class of compounds was the most difficult to analyse in terms of probability of obtaining informative spectra on a given sample. When using the metal targets, several attempts

© 2001 NRC Canada

Fig. 8. MALDI-TOF mass spectra of HMW glutenins: (*a*) metal target; (*b*) PU membrane; (*c*) PU film. All spectra were acquired with sample washing. Peaks marked with an asterisk were used for statistical analysis.



were required for each sample and a large number of shots were required to obtain acceptable signal-to-noise ratios. It was also necessary to acquire spectra within a very short time frame once the samples were extracted, due to degradation in solution. Overall, PU supports allowed a significant increase in throughput. The samples, once applied to the PU supports, were stable for several days prior to analysis, allowing sufficient time for shipping if required. Once prepared, the bulk of the samples prepared on PU surfaces would easily yield informative MALDI spectra.

Conclusions

Comparing the two PU systems, the signals were slightly better with analysis on the nonporous PU membrane. This was attributed to an increase in surface area available for protein sorption on the membrane compared to the film, and differences in surface morphology. More noticeable was the difference between the relative intensities of the protein ion signals measured using the steel targets and the PU supports. Nevertheless, each spectrum contained the same information (*m*/*z*) regardless of the support used. We are currently investigating various factors that are believed to affect the type and extent of protein sorption that occurs onto PU membranes.

For gliadins, there was no improvement by using PU supports vs. traditional MALDI sample preparation methods. Gliadin samples were initially clean, and these proteins are relatively hydrophilic. On the other hand, there was no disadvantage in using PU supports. The main advantage of the PU supports for these proteins was the convenience of sample handling.

The washing procedures significantly improved the signal-to-noise ratios in the mass spectra, particularly for the

Table 4. Comparison of mean reproducibility of spectra obtained on HMW glutenin samples prepared using different methods.[a]

Sample preparation method	Correlation of mean peak intensities[b]		
	Metal target	PU-wash	Film-wash
Metal target	—	—	—
PU-wash	0.1904	—	—
Film-wash	0.096	0.9995	—

[a]Useful spectra were not obtained on unwashed samples on metal or PU supports.
[b]Peaks as per Table 1 and Figs. 5–8.

LMW- and HMW-glutenin samples. Use of the PU supports allowed more vigorous sample washing due to the stronger interaction of the proteins with the PU surfaces compared with matrix and steel targets. Advantages of PU supports, which are not obvious from the spectra shown in this paper, are ease of sample manipulation, and ease of obtaining and storing samples prior to analysis. Once the wheat protein sample is placed onto the membrane or film, it is stable for at least two weeks prior to analysis. This was not the case with liquid samples of wheat proteins, which degraded rapidly during storage. The PU membranes were particularly useful as one large piece of membrane could be used to collect several samples outside of the laboratory and then store them prior to analysis. Spectra were obtained with greater ease and equivalent reproducibility on the PU supports, in particular the PU membrane, thus increasing the confidence that samples, once acquired, would yield informative spectra. Based on this work, we have incorporated the use of the PU supports for the routine analysis of the LMW- and HMW-wheat-glutenin proteins.

Acknowledgments

We thank the members of the Time of Flight laboratory for helpful discussion. We thank Natural Sciences and Engineering Research Council of Canada (NSERC) for financial support and the University of Manitoba for a Graduate Fellowship awarded to M.E. McComb.

References

1. M. Karas, D. Bachmann, U. Bahr, and F. Hillenkamp. Int. J. Mass Spectrom. Ion Processes, **60**, 53 (1987).
2. M.M. Vestling and C. Fenselau. Mass Spectrom. Rev. **14**, 169 (1995).
3. K. Strupat, C. Eckerskorn, M. Karas, and F. Hillenkamp. *In* Mass Spectrometry in the biological sciences. *Edited by* A.L. Burlingame and S.A. Carr. Humanan Press, Totowa, NJ. 1996. p. 203.
4. M. Karas, U. Bahr, and U. Giessman. Mass Spectrom. Rev. **10**, 335 (1991).
5. F. Hillenkamp and M. Karas. Methods. Enzymol. **193**, 280 (1990).
6. E.J. Zaluzec, D.A. Gage, and J. Throck-Watson. Protein Expression Purif. **6**, 109 (1995).
7. M. Kussmann, E. Nordhoff, H. Rahbek-Nielsen, S. Haebel, M. Rossel-Larsen, L. Jakobsen, J. Gobom, E. Mirgorodskaya, A. Kroll-Kristensen, L. Palm, and P. Roepstorff. J. Mass Spectrom. **32**, 593 (1997).

© 2001 NRC Canada

8. T.W. Hutchens and T. Yip. Rapid Commun. Mass Spectrom. **7**, 576 (1993).
9. J.C. Rouse and J.E. Vath. Anal. Biochem. **238**, 82 (1996).
10. A.H. Brockman, B.S. Dodd, and R. Orlando. Anal. Chem. **69**, 4716 (1997).
11. K.K. Mock, C.W. Sutton, and J.S. Cotrell. Rapid. Commun. Mass Spectrom. **6**, 233 (1992).
12. J. Bai, M.G. Qian, Y. Liu, X. Liang, and D.M. Lubman. Anal. Chem. **67**, 1705 (1995).
13. L.M. Preston, K.K. Murray, and D.H. Russell. Biol. Mass Spectrom. **22**, 544 (1993).
14. H. Zhang and R.M. Caprioli. J. Mass Spectrom. **31**, 690 (1996).
15. J.A. Blackledge and A.J. Alexander. Anal. Chem. **67**, 843 (1995).
16. T.A. Worrall, R.J. Cotter, and A.S. Woods. Anal. Chem. **70**, 750 (1998).
17. J. Bai, Y. Liu, T.C. Cain, and D.M. Lubman. Anal. Chem. **66**, 3423 (1994).
18. E.J. Zaluzec, D.A. Gage, and J. Throck-Watson. J. Am. Soc. Mass Spectrom. **5**, 230 (1994).
19. A.K. Walker, Y. Wu, R.B. Timmons, and G.R. Kinsel. Anal. Chem. **71**, 268 (1999).
20. K.C. Hung and H. Rashidzadeh. Anal. Chem. **70**, 3088 (1998).
21. K.C. Hung, H. Ding, and B. Guo. Anal. Chem. **71**, 518 (1999).
22. M.E. McComb, R.D. Oleschuk, D.M. Manley, L.J. Donald, A. Chow, J.D.J. O'Neil, W.E. Ens, K.G. Standing, and H. Perreault. Rapid Commun. Mass Spectrom. **11**, 1716 (1997).
23. M.E. McComb, R.D. Oleschuk, A. Chow, W. Ens, K.G. Standing, M. Smith, and H. Perreault. Anal. Chem. **70**, 5142 (1998).
24. J. Gobom, H. Eickhoff, M. Horn, T. Przewieslik, C. Luebbert, H. Lehrach, and E. Nordhoff. Proc. 48th ASMS Conf. Mass Spectrom. Allied Topics, WPH 297 (2000).
25. E. Nordhoff, J. Gobom, M. Mueller, K.D. Kloppel, H. Eickhoff, H. Lehrach, and M. Shuerenberg. Proc. 48th ASMS Conf. Mass Spectrom. Allied Topics, TOC 3:00 (2000).
26. M. Shuerenberg, C. Luebbert, H. Eickhoff, M. Kalkum, H. Lehrach, and E. Nordhoff. Anal. Chem. **72**, 3436 (2000).
27. D.R. Hichman, P. Roepstorff, P.R. Shewry, and A.S. Tatham. J. Cereal Sci. **22**, 99 (1995).
28. E. Mendez, E. Camafeita, J.S. Sebastian, I. Valle, J. Solis, F.J. Mayer-Posner, D. Suckau, C. Marfisi, and F. Soriano. J. Mass Spectrom. Rapid Commun. Mass Spectrom. S123 (1995).
29. R.G. Dworschak, W. Ens, K.G. Standing, K.R. Preston, B.A. Marchylo, M.J. Nightingale, S.G. Stevenson, and D.W. Hatcher. J. Mass Spectrom. **33**, 429 (1998).
30. B.A. Marchylo, J.E. Kruger, and D.W. Hatcher. J. Cereal Sci. **9**, 113 (1989).
31. F. Xiang and R.C. Beavis. Rapid. Commun. Mass Spectrom. **8**, 199 (1994).
32. X. Tang, R.C. Beavis, W. Ens, F. Lafortune, B. Schueler, and K.G. Standing. Int. J. Mass Spec. Ion Processes. **85**, 43 (1988).
33. R.S. Brown and J. Lennon. Anal. Chem. **67**, 1998 (1995).
34. R.D. Oleschuk, M.E. McComb, A. Chow, W. Ens, K.G. Standing, H. Perreault, Y. Marois, and M. King. Biomaterials, **21**, 1701 (2000).
35. R.W. Garden and J.V. Sweedler. Anal. Chem. **72**, 30 (2000).
36. S.L. Goodman, S.R. Simmons, S.L. Cooper, and R.M. Albrecht. Trans. Soc. Biomaterials, **15**, 201 (1989).
37. M.D. Lelah, L.K. Lambrecht, B. Young, and S.L. Cooper. J. Biomed. Mater. Res. **17**, 1 (1983).

© 2001 NRC Canada

Tautomerization tendencies of 2-acetylcycloalkanones, 2-acetyl-1,3-cycloalkanediones, and cyclic β-keto esters of five- and six-membered rings

Antonio Rojas, Alfonso Perez-Encabo, Ignacio Herraiz-Sierra, and Carlos A. Blanco

Abstract: NMR and kinetics studies of the tautomeric equilibrium of 2-acetylcycloalkanones, 2-acetyl-1,3-cycloalkanediones, and methyl 2-oxocycloalkanecarboxylates of five- and six-membered rings have been carried out. By comparing ^{1}H NMR and ^{13}C NMR spectra recorded in D_2O–$DOCD_3$ and $CDCl_3$, with those results derived using a bromination kinetic procedure in dilute aqueous solution, information concerning tautomeric interconversion is provided. Some discussions considering ionisation equilibria and rate constants involved have also been considered. Solvent and concentration effects on keto–enol equilibria have also been discussed.

Key words: 2-acetylcycloalkanones, 2-acetyl-1,3-cycloalkanediones, methyl 2-oxocycloalkanecarboxylates, equilibrium, tautomerization, ionization.

Résumé : On a effectué des études RMN et cinétiques sur l'équilibre tautomère de 2-acétylcycloalcanones, de 2-acétylcycloalcane-1,3-diones et de 2-oxocycloalcanecarboxylates de méthyle de composés à cinq et à six chaînons. En comparant les spectres RMN du ^{1}H et du ^{13}C enregistrés dans le D_2O–$DOCD_3$ et $CDCl_3$ avec ceux obtenus à l'aide de la méthode cinétique de bromation dans des solutions aqueuses diluées, on en a tiré des informations relatives à l'interconversion tautomérique. On présente aussi quelques discussions relatives à l'équilibre d'ionisation et aux constantes de vitesse. On discute aussi des effets de solvant et de concentration sur l'équilibre cétoénolique.

Mots clés : 2-acétylcycloalcanones, 2-acétylcycloalcane-1,3-diones, 2-oxocycloalcanecarboxylates de méthyle, équilibre, tautomérisation, ionisation.

[Traduit par la Rédaction]

Introduction

Structure reactivity effects are important guidelines in the elucidation and interpretation of complexation mechanisms, since the structure of ligands can indeed affect their ligand equilibria (1) (tautomerization, ionization) as well as complexation processes.

Acyclic 1,3-dicarbonylic compounds having already been studied (1), our attention has now been focused on alicyclic ligands with different functionalities: 2-acetylcycloalkanones, 2-acetyl-1,3-cycloalkanediones, and cyclic β-keto esters. These structures present a common feature, the possibility of assuming *endo*-cyclic and *exo*-cyclic enol forms.

2-Acetylcycloalkanones, which are suitable substrates for metal chelation, have become quite useful, both with regard to current health issues (2) (intermediate in preparation of HIV inhibitors) and other industrial applications (3) (inhibitor for metal corrosion).

It is well known that 2-acetylcycloalkanones form enol isomers and that the extent of enolization is controlled mainly by the strong intramolecular hydrogen bond formed, apart from the concentration, solvents, and temperature (4). The relative stabilities of the two enol forms are strongly influenced by the ring size and it is accepted that the five-membered ring systems favour an *exo*-cyclic enol, whereas six-, seven-, and eight-membered ring systems favour an *endo*-cyclic enol.

The β,δ-tricarbonyl compounds are the higher analogues of the dicarbonyl compounds and can take triketo-, monoenol-, and bisenol-forms in their tautomeric equilibrium. Accordingly, they can behave as bidentate or terdentate ligands to form metal chelate complexes. The investigation of these keto-monoenol and -dienol equilibria has shown that the bisenol content of the heptane-2,4,6-trione increases with decrease in the polarity of the solvent used and a high percentage of the triketo-form was found in solvents of high

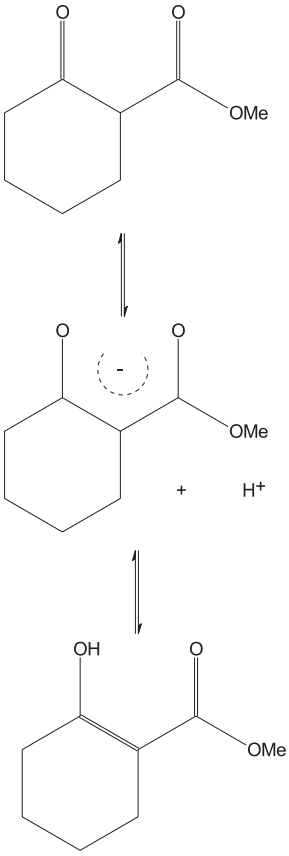
Received September 11, 2000. Published on the NRC Research Press Web site on May 3, 2001.

A. Rojas. Departamento de Química Física, Facultad de Ciencias, Universidad de Valladolid, 47005 Valladolid, Spain.
A. Perez-Encabo and I. Herraiz-Sierra. Departamento de Química Orgánica, Facultad de Ciencias, Universidad de Valladolid, 47005 Valladolid, Spain.
C.A. Blanco.[1] Departamento Ingenieria Agricola y Forestal, E.T.S. Ingeniarias Agrarias, Universidad de Valladolid, 34071 Palencia, Spain.

[1]Corresponding author (fax: 34-79-712099; e-mail: cblanco@iaf.uva.es).

 DOI: 10.1139/cjc-79-4-448 © 2001 NRC Canada

Scheme 1.



dielectric constant (5). 2-Acetyl-1,3-cycloalkanediones, are symmetrical cyclic β,β′-triketones, which present only one acidic protonizable hydrogen and subsequently can not form polynuclear coordination compounds with metal ions.

In order to understand the factors that affect the ligand chemical behaviour, in this contribution we extended the work to structurally similar *cyclic* β-*keto esters*, which exhibit also the phenomenon of keto–enol tautomerism and may present similar *endo*-cyclic as well as *exo*-cyclic enol forms (6, 7) (Scheme 1). In fact, these β-keto esters behave as bidentate ligands, and are able to form coordination compounds similar to those of the β-diketones with metal ions such as Mn(II), Fe(III), Co(II), Ni(II), Cu(II) and La(III), Ce(III) and Pr(III) (8, 9).

Furthermore, alkyl esters of 2-oxocycloalkanecarboxylic acids are receiving considerable attention, not only from the viewpoints of synthesis (10–13), reactivity (14–16), spectroscopic behaviour (17), but also because of their pharmacological and therapeutic properties, which make them useful lead compounds for the development of safer antiepileptic drugs (18) or derivatives with antiinflammatory effects (19).

Because of the lack of tautomerization studies of 2-acetylcycloalkanediones and β-keto esters, we now report a comparative study of equilibria on structurally similar 2-acetylcycloalkanones, 2-acetyl-1,3-cycloalkanediones, and methyl 2-oxocycloalkanecarboxylates. Five- and six-membered ring derivatives have been the major focus of our studies since the relative stabilities of the *endo*- and *exo*-cyclic enol form are strongly influenced by the ring size, and it has been found (7, 20) that the tendency is inverted from five- to six-membered ring systems.

Since these ligands are so important in aqueous complexation, the equilibria study is focused on diluted aqueous solutions although for sake of comparison, chloroform will also be used for comparison with a solvent of relatively low polarity. To our knowledge, this is the first work where an NMR tautomeric study concerning this kind of ligands in dilute aqueous solution has been reported.

Experimental

2-Acetylcyclopentanone, (Hacpt, H being the enolic hydrogen atom), 2-acetylcyclohexanone (Hacx), 2-acetyl-1,3-cyclopentanedione (Hacpd), 2-acetyl-1,3-cyclohexanedione (Hacxd), and methyl 2-oxocyclopentanecarboxylate (Hmcp) were obtained from Aldrich; methyl 2-oxocyclohexanecarboxylate (Hmcx), was purchased from Fluka, all of them reagent grade. All were purified by distillation under reduced pressure, except 2-acetyl-1,3-cyclopentanedione (Hacpd) which was purified by recrystallization. Stock solutions were standardized by titration with standard sodium hydroxide.

The source of hydrogen ions was perchloric acid (Merck). Unless otherwise indicated, all materials (D_2O, $DOCD_3$, etc.), were of analytical reagent grade, and were used without further purification.

pH measurements were made using a CRISON 2002 pH meter calibrated to read hydrogen ion concentration directly by titrating solutions of perchloric acid with standard sodium hydroxide solutions.

UV–vis spectra were recorded on a Hitachi U-3OOO spectrophotometer. A Spectronic 1201 UV–vis spectrophotometer which includes a kinetic resident program, was used to follow the kinetic runs.

^1H NMR and ^{13}C NMR spectra were recorded on a BRUKER AC-300. They were taken at 300 and 75 MHz, respectively, in D_2O–$DOCD_3$ and $CDCl_3$. The chemical shifts were given in ppm relative to TMS.

Results and discussion

Equilibria may be analysed on the basis of the speed with which equilibrium is attained and considering the final equilibrium concentrations (equilibrium constant). Both aspects of the equilibrium (speed of attainment and position) are important for a proper understanding of tautomeric equilibrium and subsequent ligand behaviour in chelation reactions in solution.

The position of the keto–enol equilibrium can be modified by several effects, one of the most important being the medium in terms of solvent polarity. Thus, in this work we have tried to avoid effects other than solvent but simultaneously focusing attention on solvent concentration ratios.

Since, interconversion between *endo*- and *exo*-cyclic enol tautomers is very fast these compounds exist as equilibrium mixtures of the keto and enol forms, and the tautomerism exhibited by the ligand (HL) is usually represented as in eq. [1]:

© 2001 NRC Canada

Fig. 1. ^{13}C NMR spectrum of methyl 2-oxocyclopentanecarboxylate.

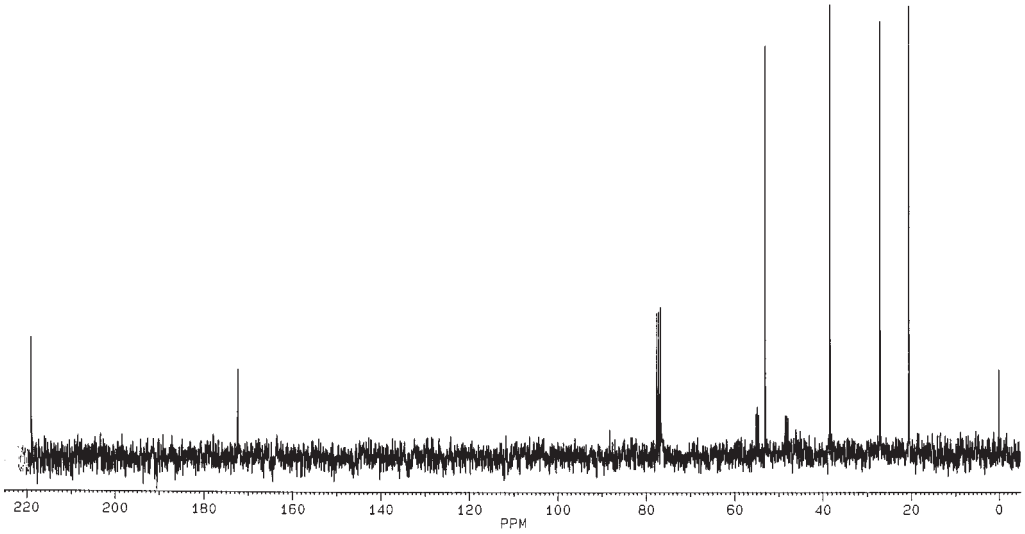


Table 1. ^1H NMR chemical shifts (δ (ppm)) of -CH_3 protons of keto and enol tautomers.

		Keto-form		Enol-form	
Compound	Medium	$COCH_3$	CO_2CH_3	$COCH_3$	CO_2CH
	$CDCl_3$	2.3	–	1.9	–
	D_2O	2.1	–	1.8	–
	$CDCl_3$	–	–	2.5	–
	D_2O	–	–	3.1	–
	$CDCl_3$	–	3.7	–	–
	D_2O	–	3.5	–	–
	$CDCl_3$	–	–	2.1	–
	D_2O	2.1	–	1.9	–
	$CDCl_3$	–	–	2.6	–
	D_2O	–	–	2.2	–
	$CDCl_3$	–	3.8	–	3.7
	D_2O	–	3.7	–	3.6

Note: In $CDCl_3$ medium δ (ppm) is given using TMS as internal reference. When D_2O was used, chemical shifts were measured with respect to the residual water signal at δ = 4.64 ppm.

$$[1] \quad HK \underset{k_k}{\overset{k_e}{\rightleftharpoons}} HE$$

where k_e is the rate of enolization, k_k the rate of ketonization, and HK and HE represent the keto and enol tautomers, respectively.

The advantages of NMR techniques in studies of tautomeric phenomena have been demonstrated (7, 21–23). In the keto–enol equilibria, in which the tautomers are only partially interconverted at room temperature, the proton and carbon signals of individual isomers (e.g., Fig. 1) may be easily distinguishable, which allows the calculation of the keto–enol ratio in the medium.

Since a major factor that cannot be overlooked is the medium effects in the tautomerization equlilibria, solvents consisting of a mixture of D_2O–$DOCD_3$ and $CDCl_3$ were utilized. Chemical shifts of both tautomers are included in Table 1 and Table 2.

Table 2. ^{13}C NMR chemical shifts (δ (ppm)) of carbonyl group in D_2O–CD_3OD.

	Keto-form		Enol-form		
Compound	CO	CO_2	CO	Csp_2	$COHsp_2$
	–	–	223;214	–	–
	–	–	206	117	184
	219	173	–	–	–
	–	–	205	112	186
	–	–	204;206	116	186
	220	176	–	103	179

Note: δ from TMS as external reference in $CDCl_3$.

In order to study the concentration effects over the tautomeric equilibria several NMR spectra were registered in the 0.002–0.2 mol dm^{-3} concentration range (Table 3). All keto–enol ratios are summarised in Table 3.

To allow us also to check the accuracy of the tautomeric equilibrium measurement in dilute aqueous solution, in addition to the mentioned NMR study, a kinetic procedure was also carried out.

The keto–enol interconversion in 2-acetyclcycloalkanones has been investigated by using a spectrophotometric method to measure the rate at which bromine is added (24) from which the ratio [HE]/[HK] which is equal to the quotient between enolization and ketonization rate constants may be easily determined. The enol tautomer reacts instantly with the bromine. To maintain equilibrium some of the keto

© 2001 NRC Canada

Table 3. Enol fraction (y), ionization rate constants (k_e and k_d), and ionization constant (pK_a).

								
NMR	y	$DCCl_3$ [HL]= 0.2 mol dm^{-3}	0.50	1.0	——	1.0	1.0	0.70
		$D_2O/DOCD_3$ [HL]= 0.2 mol dm^{-3}	0.30	1.0	——	0.85	1.0	0.25
		$D_2O/DOCD_3$ [HL]= 2×10^{-3} mol dm^{-3}	0.17	1.0	——	0.30	1.0	0.08
Bromination		$H_2O/HOCH_3$ [HL]= 2×10^{-3} mol dm^{-3}	0.16	1.0	0.05	0.29	1.0	0.02
	k_e/s^{-1}	$H_2O/HOCH_3$ [HL]= 2×10^{-3} mol dm^{-3}	0.118	——	8.30×10^{-3}	5.90×10^{-4}	——	1×10^{-2}
	k_d/s^{-1}	$H_2O/HOCH_3$ [HL]= 2×10^{-3} mol dm^{-3}	2.97×10^{3}	6.41×10^{5}	3.01×10^{1}	6.38	5.99×10^{4}	4.74×10^{1}
Semiempirical	y	AM1-SM2	0.40	1.0	0.04	0.90	1.0	0.12
	y_{exo}	AM1-SM2	0.24	0.43	0.00	0.00	0.00	0.00
	y_{endo}	AM1-SM2	0.16	0.57	0.04	0.90	1.0	0.12
Spectrophotometric	pK_a	$H_2O/HOCH_3$ [HL]=2×10^{-5} mol dm^{-3}	7.8	4.7	10.3	10.2	5.70	10.5

tautomer converts to the enol tautomer which then reacts with bromine. Hence, the rate of enolization parallels the rate of bromination, which will reach a limiting rate given by eq. [2]

$$[2] \qquad -d[Br_2]/dt = -d[HK]/dt = k_e[HK]$$

In this situation, the concentration of HK is given by eq. [3], where A is the absorbance due to bromine at any time t at the observation wavelength (452 nm), l is the path length, ε is the absorption coefficient of bromine at 452 nm, $[HL]_0$ and $[Br_2]_0$ are the total concentrations of 2-acetyclcycloalkanone (enol plus keto-forms) and bromine respectively at time zero.

$$[3] \qquad [HK] = A/\varepsilon l + [HL]_0 - [Br_2]_0$$

Substitution from eq. [3] into eq. [2] followed by integration gives eq. [4], where C is a constant,

$$[4] \qquad -\ln (A/\varepsilon l + [HL]_0 - [Br_2]_0) = k_e t + C$$

In eq. [4] the term in the parenthesis corresponds to the keto-tautomer concentration. A plot of the left-hand side of eq. [4] vs. time gives a straight line of slope k_e. Since k_e/k_k = [HE]/[HK] and [HL] = [HE] + [HK], the intercept values obtained in these plots were used to determine the enol fraction (y = [HE]/[HL]) allowing determination of ketonization rate constants k_k.

A small volume (100–200μl) of bromine stock solution was added to 2.5–3.0 mL of a previously standardized ligand solution placed in the thermostatted cell compartment of the spectrophotometer. The diketone concentrations in the cell ranged from 7.47×10^{-4} mol dm^{-3} to 2.45×10^{-3} mol dm^{-3} whereas bromine concentrations ranged from 7.88×10^{-4} mol dm^{-3} to 2.37×10^{-3} mol dm^{-3}. Changes in absorption at 452 nm were recorded at 0.5 s intervals. Each bromine solution contained 1×10^{-3} mol dm^{-3} NaBr in order to suppress hydrolysis of bromine.

Since the presence of OH^- might promote the interconversion between keto and enol tautomers catalytically, bromitation experiments have been carried out in acidic medium (0.1–0.001 mol dm^{-3}). It was shown that the H^+ concentrations had little or no effect on the tautomeric equilibrium.

The ketonization rate constant (k_k) was determined from graphical consideration (25) over the first-order bromination equation as indicated above, and secondly from acid treatment of a solution of 2-acetyclcycloalkanones in sodium hydroxide medium. In this latter case, the value of k_k was determined by reacting a solution of the diketone which had been adjusted to a pH of approximately 11 with sodium hydroxide and which contained the compound almost exclusively as enolate ion, with excess perchloric acid. The enolate ion is rapidly protonated and the subsequent readjustment of the equilibrium to the equilibrium concentrations of keto and enol tautomers was monitored spectrophotometrically at 290 nm. A first-order plot of these absorbance changes gives ($k_e + k_k$) from which k_k can be calculated. From this information and a consideration of the total concentration of reacting bromine, enol fraction values (y) have been determined.

The above mentioned halogenation procedure has been carried out for 2-acetyl-1,3-cycloalkanediones. In this case when bromine and triketone are in equimolecular conditions

© 2001 NRC Canada

all the bromine reacts instantaneously. These results suggest that the mentioned triketones are present only in monoenol form. When the bromine concentration is higher than the triketone, the subsequent rate of bromination is governed by the rate of a second enol formation in the previously monobrominated molecule. In fact, addition of a second bromine molecule results from the possibility of internal proton transfer arrangement within the molecule since the first brominated molecule still remains a β-dicarbonyl system.

Finally, although β-keto esters present different functionality than 2-acetylcycloalkanones, they can conventionally be regarded as compounds with a similar tautomeric equilibrium (7) for which a similar bromination procedure has been extended.

The ionization equilibrium, apart from its importance for predicting both stability constants (26) and decomplexation rate contants (27) of a wide range of 1,3-dicarbonylic monochelates, is also closely related to the tautomeric equilibrium analysed.

In fact, the enolization of 1,3-dicarbonylic compounds does not proceed by direct transfer of a proton from carbon to oxygen. Instead, the enolate ion is formed as an intermediate and eq. [5] is a more complete description of the actual mechanism.

$$[5] \quad HK \underset{k_b}{\overset{k_a}{\rightleftharpoons}} H^+ + E^- \underset{k_d}{\overset{k_c}{\rightleftharpoons}} HE$$

In eq. [5], $k_{c\ kb}$ k_d k_a and k_c is diffusion-controlled (28) (≈3 × 10^{10} dm^3 mol^{-1} s^{-1}).

Moreover, the equilibrium constants for ionization may be partitioned as follows:

$$[6] \quad HL \overset{k_{HL}}{\rightleftharpoons} H^+ + E^-$$

In eq. [6] HL represents the carbonylic molecule and E^- the enolate ion (common product of the ionization of either keto or enol tautomers). This overall dissociation constant (K_{HL}) can be partitioned between the equilibrium constant K_{HE} and K_{HK}, the dissociation constants of the enol and keto tautomers respectively, eq. [7] and [8],

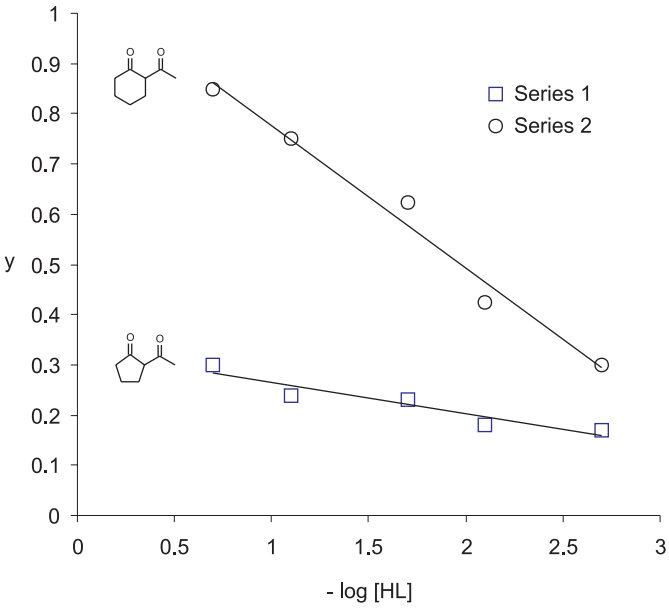
$$[7] \quad HK \overset{k_{HK}}{\rightleftharpoons} H^+ + E^-$$

$$[8] \quad HE \overset{k_{HE}}{\rightleftharpoons} H^+ + E^-$$

These constants can be related through the equation: $1/K_{HL} = 1/K_{HE} + 1/K_{HK}$. Taking into account that $K_{HE}/K_{HK} = [HE]/[HK]$, values of $K_{HE} = K_{HL}/y$ may be similarly calculated. Thus, in terms of the ionization scheme, $k_e = k_a$ and $k_k = K_{HE}k_b$ and the values of k_d may be calculated from the known values of K_{HE} and k_c, assuming that the k_c pathway is diffusion-controlled.

K_{HL} values were determined potentiometrically by titrating solutions of the mentioned carbonylic compounds having concentrations in the range 1.0×10^{-3} to 1.0×10^{-2} mol dm^{-3} with standard sodium hydroxide solutions in a double-walled titration cell under an atmosphere of nitrogen gas. Data treatment was carried out using the program SUPERQUAD (29). Since compounds of this class readily undergo hydrolysis or cleavage in alkaline solution, for the less acidic ligands it was thought desirable to check these results by the method of parallel straights (30) through spectrophotometric measurements. Standard buffer solutions were prepared in a pH range close to the *pK* of the ligand (6). The wavelengths were selected at regular intervals around the absorption max of the ligand associated with the $\pi \rightarrow \pi^*$ transition. The averaged p*K* of the ligands at 25°C are shown in Table 3.

Fig. 2. Enol fraction dependence on the 2-acetylcycloalkanone concentrations.



A first analysis of results in Table 3 shows a very good agreement between halogenation and NMR results when the solvent and ligand concentrations are similar.

In this case, the reaction medium plays a decisive role in the observed equilibrium position. These results also reveal the predomination of the less polar tautomer in nonpolar solvents and the more polar tautomer in polar solvents. It has been also verified that high D_2O concentrations shifted the equilibrium to the keto tautomeric form (Fig. 2). Thus concentration effects might be interpreted as an increase in medium polarity.

One important feature which emerges from Table 3 is that regardless of the solvent utilized, the keto-form in β-keto esters and the enol form in β,β′-triketones are the most stable.

In 2- acetylcycloalkanones, tautomer content has been determined from the integration of the methyl group signal on ^{1}H NMR (Table 1). Methyl groups in the enol tautomer appear upfield relative to the same methyl group in keto-form. In the ^{13}C NMR spectra, keto- and enol-forms can also be distinguished (Table 2).

These compounds show that the percentage of enol tautomer, especially the nature of the enol form, depends on ring size. Although the content of enol tautomer depends strongly on the solvent used (Table 1), five-membered ring systems

© 2001 NRC Canada

favours an *exo*-enol tautomer, while in six-membered rings systems the *endo*-enol form is the predominant. On dissolution in solvents of low polarity, the percentage of the less polar *cis*-enolic form increases and on the other hand, polar solvents displace the equilibrium towards the polar diketo-form.

Thus, in chloroform the enol tautomer is predominant and even in the case of Hacx the keto tautomer was undetected. On the other hand, in deuterium oxide the keto tautomer is predominant and its percentage depends on the carbonylic compound concentration (Fig. 2). This can be explained in terms of the solvation of the carbonyl groups by the polar solvent molecules, thus increasing the relative stability of the diketo-form (31, 32).

Analysis of ^{1}H and ^{13}C NMR spectra of β,β′-triketones indicated that the monoenol form was present in both solvents while the triketo-form was undetected. ^{1}H-NMR spectra shows a single signal for methyl group and in the ^{13}C NMR two carbonyl signals appear as well as an alkene group signal.

In β-keto esters, the percentage of enolic forms was determined from the integration of the methoxy signal (CH_3O) of keto and enol tautomers on the ^{1}H NMR (Table 1). The methyl signal in the enol tautomer is displaced towards high fields. This was confirmed by ^{13}C NMR (Table 2) where the enol form shows an alkene group, with two signals (δ = 180, 110 ppm).

The degree of enolization of cyclic keto esters seems to depend on ring size. Thus five-membered keto esters are completely in keto-form in chloroform and deuterium oxide. Six-membered keto esters show that keto-ester-form is prevalent but the enol content increases with the concentration of keto ester, as with Hacpt (Fig. 2).

All of this leads us to deduce that when an *endo*-enol form is close to a quasiaromatic H-bonded (7) system it increases the enol content. Therefore, in six-membered rings where "olefinic strain" (33) is less there is a higher enol content.

The ionization rate constants, are important not only per se but also due to their importance in establishing complexation mechanisms. In order to obtain an idea about ionization equlilibria, rate constants of ionization processes (k_a and k_d) have been determined (Table 3). The results obtained indicate that the rate constants for ionization of the keto and enol tautomers of Hacx are about three orders of magnitude less than the homologous five-membered rings. Considering both p*K* and ionization rate values, it can be assumed that ionisation in Hacpt is energetically and kinetically advantageous.

When comparing ionization rates of Hacx with other six-membered derivative compound rates (Hacxd and Hmcx) the former is at least one order of magnitude less than the next smallest value.

It can also be observed that the substitution of a carbonyl group in a second α-position at the acetyl group changes acidity of the ligand strongly (the K_{HL} of triketones is larger than the K_{HL} of its homologous diketones). There are two important effects that can influence a compound's acidity, the inductive effect and the resonance effect, although in the case of bulky molecules the steric effect may also be considered. Unfortunately, in most molecules, several effects are working simultaneously and it becomes extremely difficult and complex to interpret the observed differences in acidity or basicity in terms of a single structural feature. In this case the stabilisation of the anion as we go from dicarbonylic compounds to β,β′-tricarbonylic compounds, may be interpreted not only by three carbonylic groups over the same tertiary carbon through inductive and resonance effects, but also by intramolecular hydrogen bonding.

Since enolization equilibria and intermolecular proton transfer reactions in these ligands are particularly attractive even from a theoretical point of view (34), several parameters have been calculated at different semiempirical computational levels. AM1 calculations (35) have been performed with the Spartan Plus program.

Once the structures have been fully optimized, AM1-SM2 results reveal the predomination of the *exo*-cyclic enol form in Hacpt and the *endo*-cyclic enol form Hacx (Table 3). The relative stabilities of the two enol forms in 2-acetylcycloalkanones are influenced by the ring size, since five-membered ring systems favour an *exo*-cyclic enol, whereas six favour an *endo*-cyclic enol (36). The results observed in 2-acetylcyclopentanone (0.24 *exo*, 0.20 *endo*) might be explained on the basis of steric factors (37), and torsional and angle bending strains (38) which can cause deviations from the expected behaviour.

In the case of β,β′-triketones, these theoretical calculations which show that the triketo content is negligible are in good agreement with the data available from the mentioned kinetic and NMR methods.

Agreement between experiments and predictions is also very good when analysing β-keto ester results. In these compounds, only a really undetectable amount of the enol form (y = 0.04) is calculated for Hmcp and a slightly higher amount in the Hmcx (y = 0.12) as is the case. Furthermore, the *endo*-enolic form predicted is also in agreement with literature predictions (7, 20) which corroborate the semiempirical results obtained.

Acknowledgement

The authors acknowledge financial support by the Consejería de Educación y Cultura de la Junta de Castilla y Leon and the Fondo Social Europeo.

We wish to express our thanks to Isabel Caballero for his kind cooperation in the work which is included in this article.

References

1. J. Toullec. *In* The chemistry of enols. *Edited by* Z. Rappoport. John Wiley, Chichester. 1990.Chap. 6.
2. J.M. Hoffman Jr., C.S. Rooney, W.S. Saari, J.S. Wai, T.M. Williams, D.L. Bamberger, and J.H. Jones. Eur. Pat. Appl. E.P. 462 800. 1991.
3. H. German. U.S. Patent **4**, 324 676. 1982.
4. N. Cir and L.W. Reeves. Can. J. Chem. **43**, 3057 (1965).
5. U. Casellato, P.A. Vigato, and M. Vidali. Coord. Chem. Rev. **23**, 31 (1977).
6. C.A. Blanco and A. Rojas. J. Phys. Org. Chem. **13**, 97 (2000).
7. K.R. Kallury, U.J. Krull, and M. Thomson. J. Org. Chem. **53**, 1320 (1988).

© 2001 NRC Canada

8. M.A. Bañares, A. Angoso, J.L. Manzano, B. Macías, and V. Rives. Spectosc. Lett. **17**, 197 (1984).
9. M.A. Bañares, A. Angoso, J.L. Manzano, E. Rodriguez, and M.T. Blasco. Inorg. Chim. Acta, **139**, 135 (1987).
10. E. Piers and R.W. Friesen. J. Org. Chem. **51**, 3405 (1986).
11. R.W. Carling and A.B. Holmes. J. Chem. Soc. Chem. Commun. 565 (1986).
12. L.A. Paquette and D.T. Belmont. J. Org. Chem. **50**, 4102 (1985).
13. M. Botta, S. Castelli, and A. Gambacorta. Tetrahedron, **41**, 2913 (1985).
14. D. Gravel and M. Labelle. Can. J. Chem. **63**, 1874 (1985).
15. M. Kobayashi, K. Umemura, N. Watanabe, and H. Matsuyama. Chem. Lett. 1067 (1985).
16. G. Pattenden and G.M. Robertson. Tetrahedron Lett. **27**, 399 (1986).
17. A.I. Kol'tsov and G.M. Kheifets. Russ. Chem. Rev. **40**, 773 (1971).
18. J. Palaty and F.S. Abbott. J. Med. Chem. **38**, 3398 (1995).
19. M. Inoue, K. Hashimoto, T. Kuwahara, Y. Sugimoto, T. Uesako, and T. Funato. PCT Int. Appl. WO 9 218 504 (Cl. C07D487/04) 29 Oct. 1992) JP.
20. K.A.K. Ebraheem, S.T. Hamdi, and M.N. Khalaf. Can. J. Spectrosc. **26**, 225 (1981).
21. M. Bassetti, G. Cerichelli, and B Floris. Gazz. Chim. Ital. **116**, 579 (1986).
22. (*a*) S.J. Rhoads. J. Org. Chem. **31**, 171 (1966); (*b*) P.S. Steyn and P.L. Wessels. Tetrahedron Lett. **47**, 4707 (1978).
23. S. Forsen and M. Nilsson. The chemistry of the carbonyl group. Vol 2. *Edited by* J. Zabicky. Interscience, London. 1970. p. 157 and refs. cited therein.
24. (*a*) C. Blanco and M.J. Hynes. J. Chim. Phys. **86**, 1989 (1989); (*b*) Inorg. Chim. Acta, **173**, 115 (1990).
25. M.L. Moyá, A. Rodriguez, F. Sanchez, C. Blanco, and M.J. Hynes. Int. J. Chem. Kinet. **24**, 359 (1992).
26. C.A. Blanco. J. Chem. Soc. Perkin Trans. 2, **12**, 2741 (1998).
27. C.A. Blanco. New J. Chem. **19**, 99 (1995).
28. M. Eigen and L.C. Maeyer. *In* Technique of organic chemistry. Vol VIII. Part II. *Edited by* S.L. Friess, E.S. Lewis and A. Weissberger. Interscience, New York. 1963.
29. P. Gans, A. Sabatini, and A. Vacca. J. Chem. Soc. Dalton Trans. 1195 (1985).
30. P. Maroni and J.P. Calmon. Bull. Soc. Chim. Fr. 519 (1964).
31. M.T. Rogers and J.L. Burdett. Can. J. Chem. **43**, 1516 (1965).
32. G. Allen and R.A. Dwek. J. Chem. Soc. 161 (1966).
33. M. Kobayashi, K. Umemura, N. Watanabe, and H. Matsuyama. Chem. Lett. 1067 (1985).
34. D. Lee, C.K. Kim, B.S. Lee, I. Lee, and B.C. Lee. J. Comput. Chem. **18**, 56 (1997).
35. M.J.S Dewar, E.G Zoebisch, E.F Heady, and J.J.P. Stewart. J. Am. Chem. Soc. **107**, 3902 (1985).
36. (*a*) H.C. Brown, H.J. Brewster, and H. Shechter. J. Am. Chem. Soc. **76**, 467 (1954); (*b*) H.C. Brown. J. Org. Chem. **22**, 439 (1957).
37. R.D. Campbell and H.M. Gilow. J. Am. Chem. Soc. **84**, 1440 (1962).
38. E.W. Garbisch, Jr. J. Am. Chem. Soc. **87**, 505 (1965).

© 2001 NRC Canada

Potentiometric titration study of two novel polydenate ligands and investigations of their complexes

Dengke Cao, Hua-Kuan Lin, Zhi-Fen Zhou, Shou-Rong Zhu, Xun-Cheng Su, and Yun-Ti Chen

Abstract: Two novel linear polyamine ligands, *N*,*N*′-bis-(2-(*N*″-2-hydroxyl-5-bromobenzyl)aminoethyl) malondiamide (**L_1**) and *N*,*N*′-bis-(3-(*N*″-2-hydroxyl-5-bromobenzyl)aminopropyl) malondiamide (**L_2**), have been synthesized and fully characterized by elemental analysis (^{1}H NMR and IR spectroscopy) (Fig. 1). The binding ability of ligands **L_1** and **L_2** to metal ions such as Cu(II), Zn(II), Co(II), Mn(II), Mg(II), and Ca(II) has been investigated by the potentiometric method in 1,4-dioxane–water (v/v = 15:100) and KNO_3 (0.1 mol dm^{-3}) at 25.0°C. In view of the linear structures of **L_1** and **L_2**, binuclear metal complexes can be formed in solution by controlling Cu(II)-5-substituted *o*-phenanthroline (Rphen, R = CH_3, H, Cl, NO_2):**L** to a 2:1 molar ratio, whereas the mononuclear metal complexes form at molar ratio M(II):**L** of 1:1, where M(II) is Cu(II), Zn(II), Co(II), Mn(II), Mg(II), and Ca(II). The stability constants of metal complexes have been determined and further discussed. In addition, two manganic complexes have been synthesized and IR and electronic spectra showed their coordination nature.

Key words: linear polyamine ligand, 5-substituted *o*-phenanthroline, mononuclear and binuclear metal complex, stability, spectrum.

Résumé : On a réalisé la synthèse de deux nouveaux ligands polyamines linéaires, *N*,*N*′-bis-(2-*N*″-2-hydroxy-5-bromobenzyl)aminoéthyl)malondiamide (**L_1**) et *N*,*N*′-bis-(3-*N*″-2-hydroxy-5-bromobenzyl)aminopropyl)malondiamide (**L_2**) et on en a fait la caractérisation complète par analyses élémentaires, RMN du ^{1}H et par IR. Faisant appel à des mesures potentiométriques et opérant dans un mélange 1,4-dioxane–eau, à 25°C, dans des solutions contenant 0,1 mol dm^{-3} de KNO_3, on a étudié les possibilités de fixation des ligands **L_1** et **L_2** aux ions métalliques Cu(II), Zn(II), Co(II), Mn(II), Mg(II) et Ca(II). Compte tenu des structures linéaires des ligands **L_1** et **L_2**, il existe une possibilité de former des complexes métalliques binucléaires en solution si on contrôle le rapport molaire entre le sel de Cu(II) de l'*o*-phénanthroline substituée en position 5 (Rphen; R = CH_3, H, Cl, NO_2)/**L** (2:1) alors qu'il se forme des complexes métalliques mononucléaires lorsque le rapport molaire (M(II):**L**) est de 1:1 (M(II) = Cu(II), Zn(II), Co(II), Mn(II), Mg(II) et Ca(II)). On a déterminé et on discute des constantes de stabilité des complexes métalliques. De plus, on a synthétisé deux complexes manganiques et, sur la base de leurs spectres IR et électroniques, on en a déduit la nature de leur coordination.

Mots clés : ligand polyamine linéaire, *o*-phénanthroline substituée en position 5, complexes métalliques mononucléaires et binucléaires, stabilité, spectre.

[Traduit par la Rédaction]

Introduction

In recent years, the research of polynuclear metal complexes has increased dramatically due to the introduction of appropriate ligands such as linear polyamine that is able to form mononuclear or binuclear metal complexes by controlling the reaction conditions. Dominguez-Vera et al. (1) reported the ligand *N*,*N*′-bis(3-aminopropyl) oxamidate (oxpn), the mononuclear [Cu(cis-oxpn)], and the binuclear $[Cu_2(trans\text{-}oxpn)]^{2+}$ species were prepared by controlling pH and the Cu(II):oxpn molar ratio. Additionally, the synthesis of manganic complexes has been a subject of considerable importance, because manganic ions serves various important roles in biological systems (2), and to date, many metal enzymes containing manganic ions have been found (3).

In this paper, we report an attempt at preparing some novel ligands and metal complexes. Two novel linear ligands shown in Fig. 1, *N*,*N*′-bis-(2-(*N*″-2-hydroxyl-5-bromobenzyl)aminoethyl) malondiamide (**L_1**) and *N*,*N*′-bis-(3-(*N*″-2-hydroxyl-5-bromobenzyl)aminopropyl) malondiamide (**L_2**) have been synthesized and characterized. The potentiometric method has been used to investigate the formation of mononuclear and binuclear complexes in solution. The Mn**L_1** and Mn**L_2** complexes have been prepared and characterized by elemental analyses (IR and UV spectroscopy).

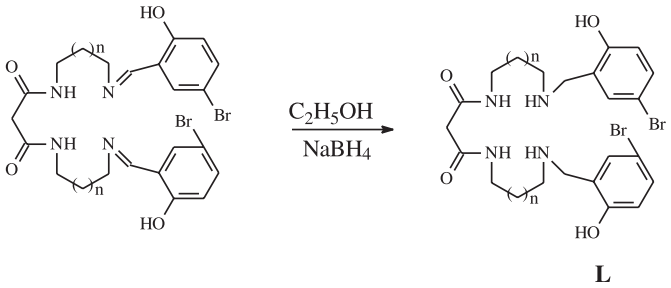
Received June 5, 2000. Published on the NRC Research Press Web site on May 3, 2001.

D. Cao, H.-K. Lin[1], Z.-F. Zhou, S.-R. Zhu, X.-C. Su, and Y.-T. Chen. Department of Chemistry, Nankai University, Tianjin 300071, P. R. China.

[1]Corresponding author (fax: 0086-022-23502458; e-mail: hklin@nankai.edu.cn).

 DOI: 10.1139/cjc-79-4-455 © 2001 NRC Canada

Fig. 1. Synthesis route of the ligands $\mathbf{L_1}$ (n = 0) and $\mathbf{L_2}$ (n = 1).



L

Experimental

Reagents

Dimethylmalonate, salicylaldehyde, ethylenediamine, and propylenediamine were of AR reagent grade and purified prior to use. *N*,*N*′-bis-(2-aminoethyl) malondiamide, *N*,*N*′-bis-(3-aminopropyl) malondiamide, and 5-Br-salicylaldehyde were synthesized according to the earlier reports (4, 5). $Mn(CH_3COO)_2{\cdot}4H_2O$ and $Mn(CH_3COO)_3{\cdot}2H_2O$ were used as received. Five-substituted *o*-phenanthroline (Rphen, R = CH_3, H, Cl, NO_2) were purchased from G. Friderik Smith Chemistry Corporation and used without further purification. In potentiometric experiments, all solutions were prepared from redistilled water. The Cu(II), Zn(II), Co(II), Mn(II), Mg(II), and Ca(II) nitrates were purchased from Tianjin Third Chemical Reagent Factory and recrystallized. All these metal ion solutions were standardized with EDTA.

Instruments

Elemental analyses were performed on a Perkin Elmer 240C elemental analyzer. IR spectra were obtained as KBr disks on a Nicolet 170 SX FT-IR spectrometer, and the ^{1}H NMR spectra were recorded with a Varian UNITY-plus 400 MHz spectrometer. The electronic absorption spectra of the complexes were measured in the range 190–500 nm using a Shimadzu UV-240 spectrometer.

Potentiometric measurements

The potentiometric technique was described in a previous paper (6), and the potentiometric measurements were carried out with a Beckman pH meter Model Φ71 equipped with a type 39841 combination electrode. Typical concentration of the experimental solutions for molar ratios M:**L** of 1:1 in binary systems and Cu(II):Rphen:**L** of 2:2:1 in ternary systems, was 5×10^{-4} mol dm^{-3}. The ionic strength was adjusted to 0.1 mol dm^{-3} with KNO_3. All the potentiometric measurements were carried out in a nitrogen atmosphere at 25.0 ± 0.1°C. The calculations of protonation and equilibrium constants were made using the SCMAR program (7) based on the improved TITFIT technique (8). For each system, at least three titrations were performed, and each titration contained ca. 50 experimental points.

Synthesis

Symmetric Schiff-base

5-Bromosalicylaldehyde (0.075 mol) and ethanol (50 cm^3) was placed in a 250 mL flask equipped with a magnetic stirrer. The solution of *N*,*N*′-bis-(2-aminoethyl)-malondiamide (0.026 mol) in water (40 mL) was added slowly at room temperature and a yellow precipitate was formed immediately. After the addition, the resulting solution was brought to reflux for 2 h and then allowed to cool. The precipitate was filtered off, washed with ethanol, and dried.

N,N′*-bis-(2-(*N″*-2-hydroxyl-5-bromobenzyl)aminoethyl) malondiamide (L_1)*

Solid $NaBH_4$ (0.76 g) was added in portions to solution at reflux of 0.005 mol (1.98 g) *N*,*N*′-bis-(2-(*N*″-5-bromosalicylaldehyde)aminoethyl) malondiamide in absolute methanol (30 mL). After heating an additional 2 h at reflux, the solution was cooled. The excess methanol was removed with a rotary evaporator and the pH was adjusted to about 8. The resulting solution was extracted with $CHCl_3$ three times. The removal of $CHCl_3$ gave a pale red powder as the crude product. It was then recrystallized as white powder from ethanol, 2.09 g (75%). IR (cm^{-1}): 3282.0 (N-H), 1637.9 (C=O), 814.3 (C-H benzene ring). ^{1}H NMR(DMSO) δ: 6.670–8.059 (6H), 2.506–3.740 (14H). Anal. calcd. for $C_{21}H_{26}N_4O_4Br_2$: C 45.16, N 10.03, H 4.67; found: C 45.17, N 9.83, H 4.60.

N,N′*-bis-(3-(*N″*-2-hydroxyl-5-bromobenzyl)aminopropyl) malondiamide (L_2)*

The method was similar to the synthesis of $\mathbf{L_1}$ and the yield was 73%. IR (cm^{-1}): 3288.0 (N-H), 1637.2 (C=O), 815.3 (C-H benzene ring). ^{1}H NMR (DMSO) δ: 6.648–8.004 (6H), 1.550–3.755 (18H). Anal. calcd. for $C_{23}H_{30}N_4O_4Br_2$: C 45.54, N 9.24, H 4.95; found: C 45.59, N 9.30, H 4.90.

MnL_1 complex

The ligand $\mathbf{L_1}$ (1.51 g, 2.7 mmol) was stirred with 2 equiv KOH (0.303 g, 5.4 mmol) for 30 min in methanol (40 cm^3) at room temperature. An aqueous solution of $Mn(CH_3COO)_2{\cdot}4H_2O$ (20 cm^3, 0.67 g, 2.7 mmol) was added slowly, and the solution gradually turned dark brown. The reaction mixture was allowed to reflux for 45 min, filtered, and then the product was washed with methanol and dried. The yield was 67%. The same product could be isolated in 58% yield by using $Mn(CH_3COO)_3{\cdot}2H_2O$ instead of the Mn(II) salt.

MnL_2 complex

A slightly different method was adopted for the synthesis of Mn$\mathbf{L_2}$. The methanol solution containing ligand $\mathbf{L_2}$ was stirred with 2 equiv of KOH for 30 min at 313 K, solid $Mn(CH_3COO)_2{\cdot}4H_2O$ (1 equiv) was added to the solution and the resulting solution turned dark brown. The reaction mixture was allowed to reflux for 45 min, then filtered at 313 K, washed with methanol and dried. The yield was 65%.

Results and discussion

Protonation constants of the ligands $\mathbf{L_1}$ and $\mathbf{L_2}$

The stepwise protonation of the ligands $\mathbf{L_1}$ and $\mathbf{L_2}$ have been studied by potentiometric titration in 1,4-dioxane–water (v/v = 15:100) at 25.0°C and I = 0.1 mol dm^{-3} in KNO_3. In a typical experiment, a solution containing the ligand and excess acid was titrated by the standard base. The equilibrium in the system can be written as in eq. [1], where β_{mlh} =

© 2001 NRC Canada

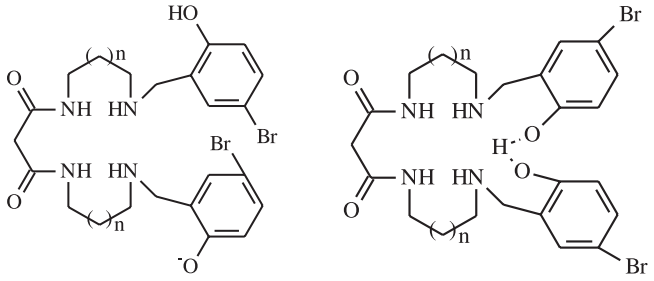
Table 1. Protonation constants for the ligands $\mathbf{L_1}$ and $\mathbf{L_2}$.

Ligand	log β_{011} (log K_1)	log β_{012} (log K_2)	log β_{013} (log K_3)	log β_{014} (log K_4)
$\mathbf{L_1}$	10.02 (10.02)	19.77 (9.75)	27.75 (7.98)	34.60 (6.85)
$\mathbf{L_2}$	10.33 (10.33)	20.39 (10.06)	28.83 (8.44)	36.06 (7.23)

Table 2. Stability constants of the binary complexes for Cu(II), Zn(II), Co(II), Mn(II), Mg(II), and Ca(II) with the ligand $\mathbf{L_1}$.

	Cu(II)	Zn(II)	Co(II)	Mn(II)	Mg(II)	Ca(II)
log β_{111}	22.09	—	15.48	15.22	15.00	13.90
log β_{110}	14.74	8.64	7.05	6.02	5.32	4.12
log β_{11-1}	5.47	–2.30	–2.96	—	—	—
log β_{11-2}	–5.42	–11.65	–13.33	–13.78	–14.95	–16.59

Fig. 2. The structures of model species 011.



$[M_m\mathbf{L}_lH_h]/[M]^m[\mathbf{L}]^l[H]^h$ in which charges are omitted for the sake of simplicity, and square brackets denote equilibrium concentrations. The *m*, *l*, and *h* are the stoichiometric numbers of the metal ions, the ligand (**L**), and hydrogen ions, respectively, and h has a negative value when H^+ is released during coordination. The value of *m* is zero for protonation constants of the ligands (**L**).

[1] $$m\mathrm{M} + l\mathbf{L} + h\mathrm{H} \rightleftharpoons \mathrm{M}_m\mathbf{L}_l\mathrm{H}_h$$

Within the investigated pH range (2.7–10.5), protonation reactions were found to occur in four steps, and the results are listed in Table 1. In fact, the ligand containing two amines, two phenols, and two amide groups might experience six-step protonation, but the basicity of both amide groups is so weak that their protonation constants can not be determined in the investigated pH range (2.7–10.5). For ligands $\mathbf{L_1}$ and $\mathbf{L_2}$, log K_1 and log K_2 can be ascribed to the protonation constants of both phenolic groups. It can be observed that log K_1 is larger than log K_2 for ligands $\mathbf{L_1}$ and $\mathbf{L_2}$. The species (011) might have two types of structures as show in Fig. 2, the structure *b* seems much more reasonable than *a* because of the bulky effect of the bromine group. Log K_3 and log K_4 are the protonation constants of both amine groups. The log K_3 values for ligands $\mathbf{L_1}$ and $\mathbf{L_2}$ are somewhat lower than the corresponding first step protonation constants of ethylene diamine (9) (log K_1 = 9.93) and 1,3-propanediamine (9) (log K_1 = 10.62). The lower log K_3 values obtained for ligands $\mathbf{L_1}$ and $\mathbf{L_2}$ indicated that the basicity of the amine group became weak due to some electron transfer to the "super conjugative" system of the 2-hydroxyl-5-bromobenzyl group when the proton of the amine group was substituted by the 2-hydroxyl-5-bromobenzyl. After the third step protonation was completed, the two amine groups were bridged by the same proton. Under this condition, both of the two amine groups have difficulty to become protonated due to the effect of electrostatic interaction, so for the ligands $\mathbf{L_1}$ and $\mathbf{L_2}$, log K_4 is smaller than log K_3.

The comparison of protonation constants of $\mathbf{L_1}$ and $\mathbf{L_2}$ shows that the later is higher than the former. Log K_3 and log K_4 of ligand $\mathbf{L_2}$ are higher than the corresponding constants of $\mathbf{L_1}$. This is consistent with the reported results of log K_1 and log K_2 in 1,3-propanediamine (9) (log K_1 = 10.61, log K_2 = 8.64), which are higher than those in ethylene diamine (9) (log K_1 = 9.93, log K_2 = 6.85). Since some electrons of the amine group may transfer to the super conjugative system of the 2-hydroxy-5-bromobenzyl group, and the amine group basicity of the ligand $\mathbf{L_2}$ is stronger than that of the ligand $\mathbf{L_1}$, we obtained a higher log K_1 and log K_2 for the ligand $\mathbf{L_2}$ than $\mathbf{L_1}$. On the whole, the comparison of the four-step protonation constants of ligand $\mathbf{L_2}$ with those of ligand $\mathbf{L_1}$ shows that the protonation capability of ligand $\mathbf{L_2}$ is stronger than that of ligand $\mathbf{L_1}$, which can also be deduced from the distribution curves of the protonation of ligands $\mathbf{L_1}$ and $\mathbf{L_2}$ (Fig. 3 and 4).

Stability constants of ligands $\mathbf{L_1}$ and $\mathbf{L_2}$ with Cu(II), Zn(II), Co(II), Mn(II), Ca(II), and Mg(II)

For ligands $\mathbf{L_1}$ and $\mathbf{L_2}$, the stability constants (log β_{mlh}) of binary systems are listed in Table 2 and Table 3, respectively. In Fig. 5 (the distribution curves of the Cu(II)-**L** binary complexes), only 80% maximal formation of complex Cu$\mathbf{L_1}$, while almost 100% formation for the complex Cu$\mathbf{L_2}$ occurred in a wide pH range, indicating that for the same metal ion (Cu(II)) the coordination capability of the ligand $\mathbf{L_1}$ is weaker than that of the ligand $\mathbf{L_2}$. Comparing the stability constants of $\mathbf{L_2}$ with Zn(II), Co(II), Mn(II), Ca(II), and Mg(II) with the corresponding ones of $\mathbf{L_1}$, the results are in line with our expectations as follows:

For the ligand $\mathbf{L_1}$ and $\mathbf{L_2}$, the model species (111) of Zn(II) was not detected at the lower pH due to the weak coordination capability of Zn(II) compared to Cu(II), and coordination did not take place, as shown in Table 2 and 3. In addition, the model species (11–1) of Mn(II) did not occur, because the two protons of the amides that coordinate with Mn(II) tend to dissociate simultaneously at a higher pH. From the determined stability constants of $\mathbf{L_1}$ (in Table 2) and $\mathbf{L_2}$ (in Table 3), the coordination capabilities of metal ions for the ligands are Mn(II) < Co(II) < Cu(II) > Zn(II),

© 2001 NRC Canada

Fig. 3. Distribution curves of the protonation of $\mathbf{L_1}$ (*a*) and $\mathbf{L_2}$ (*b*).

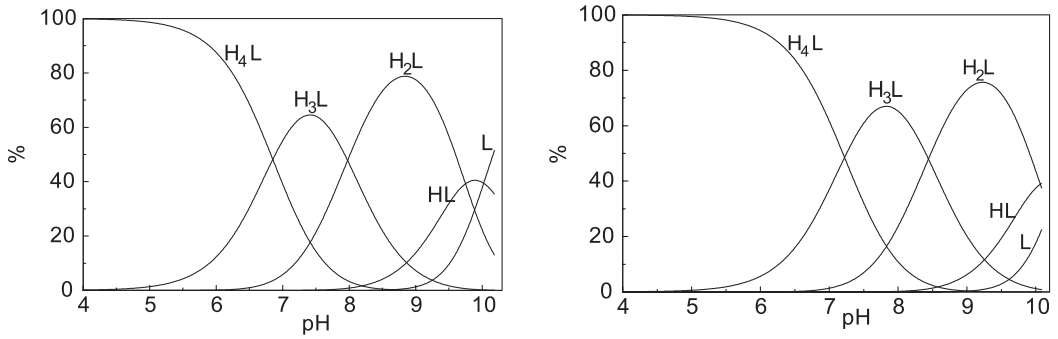
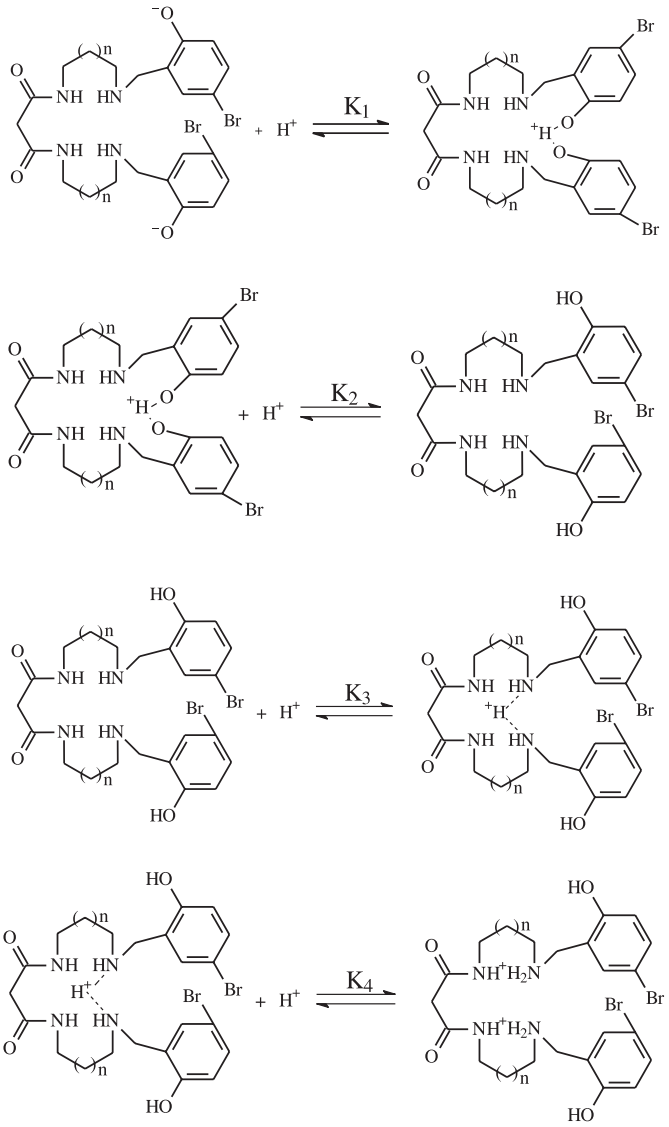


Fig. 4. Protonation style of $\mathbf{L_1}$ and $\mathbf{L_2}$.



which shows good agreement with the Irving–William sequence.

As expected, the ligands $\mathbf{L_1}$ and $\mathbf{L_2}$ have good deforming capability, so that for each ligand, not much difference appears between the corresponding log *K* for Mg(II)-**L** and Ca(II)-**L**, even though the radius of Mg(II) and Ca(II) differ greatly. In addition, the stability constants of Mg(II)-**L** or Ca(II)-**L** are not obviously smaller than for Co(II)-**L**, which may be due to the hard nature (from the hard-soft acid-base point of view) of coordination donors of ligands $\mathbf{L_1}$ and $\mathbf{L_2}$.

Stability constants of Cu-Rphen-L ternary (quasi-binary) complexes

It is well known (10) that Cu(II) can almost coordinate completely with Rphen in the pH range 2–7 due to the extremely strong coordination capability of Rphen. In this work, Cu(II)-Rphen binary complexes were prepared and employed in potentiometric measurements. The ligand $\mathbf{L_1}$ or $\mathbf{L_2}$ and Cu(II)-Rphen were mixed by a certain molar ratio and the system was defined as a quasi-binary system. In the above quasi-binary systems, the molar ratio of **L**:Cu(II)-Rphen may be 1:1 or 1:2. We failed to obtain rational results at molar ratio 1:1, but in contrast, we found that binuclear metal complexes formed at molar ratio 1:2 in quasi-binary systems. The stability constants obtained are summarized in Table 4. It seems that the appearance of **L** varied from a quasi-cycle to a torsional chain when coordinating with Cu(II)-Rphen, and binuclear complexes were formed as a result. The structure of binuclear complexes were determined only by the potentiometric method without separation. The structure of species 210 is suggested in Fig. 6*b*. Potentiometric titrations were performed in the pH range 2.7–6.7. Since the basicity of amide groups is too weak, only two amine groups and two phenolic donors coordinated with Cu(II) as shown in Fig. 6*b*. As shown in Table 4, the stability constant of the ligand $\mathbf{L_1}$ is lower than that of the ligand $\mathbf{L_2}$ for the same model species, which agrees with the weaker basicity of $\mathbf{L_1}$ vs. $\mathbf{L_2}$.

Comparing the stability constants for the Cu(II)-Rphen-**L** ternary (quasi-binary) systems in Table 4, it is found that the stability constants for Cu(II)-Rphen-**L** (R from CH_3 to NO_2) for $\mathbf{L_1}$ and $\mathbf{L_2}$ increase with corresponding increasing Hammett constant (–0.05, 0, 0.47, 0.63), and decreasing protonation constants of Rphen (5.028, 4.748, 4.125, 3.437) (11). The reasonable interpretation of the above phenomenon is that there exists a *d*–π feedback bond between Cu(II) and Rphen. Some *d* orbit electrons of Cu(II) feedback to Rphen and this decreases the density of the electron cloud around Cu(II). The lower the electron cloud density of Cu(II), the stronger the coordination of Cu(II) with **L**. From CH_3 to NO_2, the

© 2001 NRC Canada

Fig. 5. Distribution curves of the binary complexes (*a*) Cu$\mathbf{L_1}$ and (*b*) Cu$\mathbf{L_2}$.

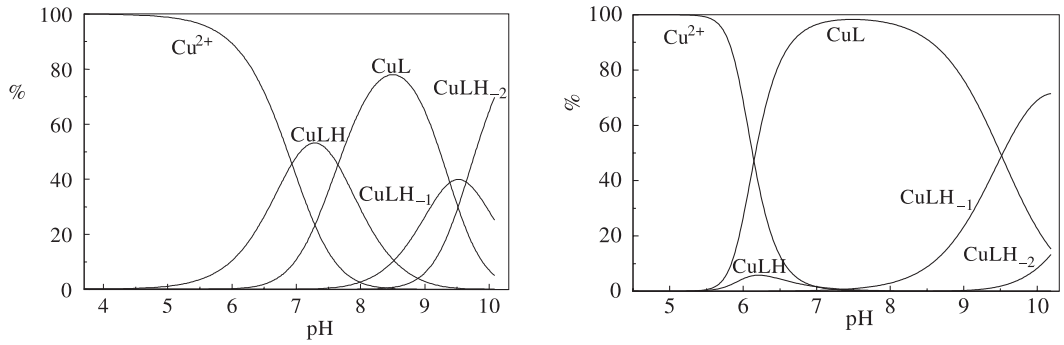


Table 3. Stability constants of the binary complexes for Cu(II), Zn(II), Co(II), Mn(II), Mg(II), and Ca(II) with the ligand $\mathbf{L_2}$.

	Cu(II)	Zn(II)	Co(II)	Mn(II)	Mg(II)	Ca(II)
log β_{111}	23.37	—	16.06	15.50	15.33	14.69
log β_{110}	15.14	9.26	7.20	6.41	5.55	4.26
log β_{11-1}	5.62	–1.23	–2.47	—	—	—
log β_{11-2}	–5.02	–11.54	–12.56	–13.10	–14.83	–16.47

Table 4. Stability constants of the ternary (quasi-binary) complexes for Cu(II)-Rphen with the ligand $\mathbf{L_1}$ and $\mathbf{L_2}$.

	CH_3	H	Cl	NO_2
$\mathbf{L_1}$				
log β_{212}	29.25	29.38	29.76	30.01
log β_{210}	16.01	16.10	16.37	16.54
$\mathbf{L_2}$				
log β_{212}	29.75	29.84	30.13	30.31
log β_{210}	16.57	16.62	16.90	17.10

density of the electron cloud of the ligand decreases gradually, *d*–π feedback increases, and the stability constants of the Cu(II)-Rphen-**L** ternary (quasi-binary) complexes (for the same model species) also increase gradually. In the quasi-binary systems studied, it was also found that linear relationships exists between log β_{212} or log β_{210} and the protonation contants of Rphen with the following equations:

for $\mathbf{L_1}$: $\log \beta_{212} = 31.72 - 0.49 \log \beta_{Rphen}$ $r = -0.994$
$\log \beta_{210} = 17.74 - 0.34 \log \beta_{Rphen}$ $r = -0.993$

and $\mathbf{L_2}$: $\log \beta_{212} = 31.58 - 0.36 \log \beta_{Rphen}$ $r = -0.992$
$\log \beta_{210} = 18.31 - 0.35 \log \beta_{Rphen}$ $r = -0.994$

In our work, linear relationship was also obtained between the Hammett constant (σ) and stability constants of complexes in quasi-binary system. The relevant equations are as follows:

for $\mathbf{L_1}$: $\log \beta_{212} = 29.33 + 1.02\sigma$ $r = 0.990$

and $\mathbf{L_2}$: $\log \beta_{212} = 29.81 + 0.76\sigma$ $r = 0.992$

The coordination nature of complexes

As shown in Table 5, for the complexes Mn$\mathbf{L_1}$ and Mn$\mathbf{L_2}$, analytical results agree well with theoretical calculations. In

Table 5. Analytical data for the complexes of Mn(III) with the ligands $\mathbf{L_1}$ and $\mathbf{L_2}$.

		Analysis (%)[a]		
Compound	Color	C	H	N
Mn$\mathbf{L_1}$	Brown	40.89 (41.11)	3.70 (3.92)	9.10 (9.14)
Mn$\mathbf{L_2}$	Brown	42.95 (43.06)	4.12 (4.37)	8.23 (8.74)

[a]Calculated values are given in parentheses.

the two complexes, the valence state of manganese ion is +3 (12). We also studied solid powder ESR spectra of complexes Mn$\mathbf{L_1}$ and Mn$\mathbf{L_2}$ at room temperature and did not observe any peaks, which also supports our conclusion.

Infrared Spectroscopy

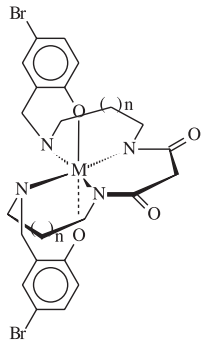
The spectra of the solid state complex Mn$\mathbf{L_1}$ and Mn$\mathbf{L_2}$ are assigned and given in Table 6. For the complex Mn$\mathbf{L_1}$, the phenol's coordination is suggested by the shift of ν (Ar-O) to 1271 cm^{-1} towards the peak of the ligand $\mathbf{L_1}$ at 1253 cm^{-1} (13). From comparison of the ν (CO) and δ (NH) of $\mathbf{L_1}$ with those of the complex Mn$\mathbf{L_1}$, the coordination of amide with Mn(III) could be determined. For the complex Mn$\mathbf{L_2}$, the coordination nature is suggested by the presence of absorption due to the metal-bound amide ν (CO) at 1654 cm^{-1}, δ (NH) at 1545 cm^{-1}, and stretching frequency ν (Ar-O) at 1272 cm^{-1} (14).

Electronic Spectroscopy

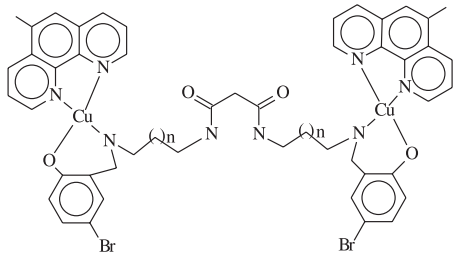
Electronic spectra in DMSO solution of $\mathbf{L_1}$, Mn$\mathbf{L_1}$, $\mathbf{L_2}$, and Mn$\mathbf{L_2}$ over the 190–500 nm region (298 K) are reported in Table 7. For the complex Mn$\mathbf{L_1}$, the σ(N) → Mn(III) LMCT transition occurs as a single broad band centering at 390 nm (15). Intense bands at 262 nm and 283 nm are assignable to absorptions of the benzene ring. Comparing these with the 287 nm band of $\mathbf{L_1}$, it was found that new absorptions of the benzene ring are due to phenolic group coordination with Mn(III). For the complex Mn$\mathbf{L_2}$ similar

© 2001 NRC Canada

Fig. 6. Proposed structures for the Cu**L** or Mn**L** binary complexes 110 (*a*) and Cu-Rphen-**L** ternary (quasi-binary) complex 210 (*b*), where L = $\mathbf{L_1}$, $\mathbf{L_2}$, and *n* = 0, 1, respectively.



(*a*)



(*b*)

Table 6. IR data (cm^{-1}) (KBr discs) for $\mathbf{L_1}$, $\mathbf{L_2}$, and their complexes of Mn(III).

Compound	Amide 1 (ν (CO))	Amide 2 (δ (NH))	ν (Ar-O)
$\mathbf{L_1}$	1638	1556	1253
Mn$\mathbf{L_1}$	1653	1545	1271
$\mathbf{L_2}$	1637	1558	1259
Mn$\mathbf{L_2}$	1654	1545	1272

Table 7. Electronic spectrum data in DMSO for $\mathbf{L_1}$, Mn$\mathbf{L_1}$, $\mathbf{L_2}$, and Mn$\mathbf{L_2}$.

Compound	λ_1 (nm)	λ_2 (nm)	λ_3 (nm)
$\mathbf{L_1}$	—	287	—
Mn$\mathbf{L_1}$	262	283	390
$\mathbf{L_2}$	—	287	—
Mn$\mathbf{L_2}$	259	286	391

peaks appear. Additionally, each of the complexes also exhibit a broad absorption near 500 nm, which may be due to the ligand field transitions.

Conclusion

In summary, two novel linear ligands $\mathbf{L_1}$ and $\mathbf{L_2}$ have been synthesized. The thermodynamic properties of these ligands and their metal complexes have been studied in aqueous solutions using potentiometric methods. The results show that the ligands are of great interest in coordination to metal ions. In addition, two mangantic complexes have been prepared and their structures have been extensively studied. The amides coordinated complexes Mn$\mathbf{L_1}$ and Mn$\mathbf{L_2}$ are indicated by the blue shift of ν (CO) in IR spectra, so it is reasonable to conclude that amides coordinate with Mn(III) without dissociating protons. The complexes Mn$\mathbf{L_1}$ and Mn$\mathbf{L_2}$ are both of octahedral geometry and the possible structures are given in Figs. 6*a*, *b.*

Acknowledgments

This project, 29971018, was supported by the National Natural Science Foundation of China, the Nature Science Foundation of Tianjin, and the National Key Laboratory of Coordination Chemistry, Nanjing University.

References

1. J.M. Dominguez-Vera, J.M. Moreno, N. Galvez, J. Suarez-Varela, E. Colacio, R. Kivekas, and M. Klinga. Inorg. Chim. Acta, **95**, 281 (1998).
2. V.L. Pecoraro, M.J. Baldwin, and A. Gelasco. Chem. Rev. **94**, 807 (1994).
3. K. Wieghardt. Angew. Chem. Int. Ed. Engl. **28**, 1153 (1989).
4. H.A.O. Hill and K.A. Raspin. J. Chem. Soc. (A), 3036 (1968**)**.
5. Friedrich Richter (*Editor*). Beilsteins Handbuch der Organischen Chemie. Vol. 2, 4th ed. Springer, Berlin. 1974–1958. **8**,54.
6. E. Chinea, S. Dominguez, A. Mederos, F. Brito, J.M. Arrieta, A. Sanchez, and G. Germain. Inorg. Chem. **34**, 1579 (1995).
7. H. Sun. Ph.D. Thesis, Nankai University. 1997. pp. 145–153.
8. A.D. Zuberbuhlen, and T.A. Kaden. Talanta, **29**, 201 (1982).
9. Y. Yao, T. Xie, and Y. Gao. Handbook of physical chemistry, Shanghai Science and Technique Press, Shanghai. 1985. p. 791, 797 (in Chinese).
10. H. Sigle and R.B. Martin. Chem. Rev. **82**, 385 (1982).
11. H. Xia, H. Lin, and Y. Chen. Wuji Huaxue Xuebao, **10**(4), 365 (1994).
12. G. Das, R. Shukla, S. Mandal, R. Singh, and P.K. Bharadwaj. Inorg. Chem. **36**, 323 (1997).
13. J. Wang, Sh. Gao, X. Liao, and F. Liu. Chem. Res. Chin. Univ. **14**(5), 646 (1993).
14. R.M. Silverstein, G.C. Bassler, and T.C. Morrill. Spectrometric identification of organic compounds. John Wiley, New York. 1974. p. 94 (Chinese, translation H. Yao, J. Ma, and J. Huang).
15. A. van den Bergen, K.S. Murray, M.J. Connor, and B.O. West. Aust. J. Chem. **22**, 39 (1969); L.J. Boucher and V.B. Day. Inorg. Chem. **16**, 1360 (1977); R. Shukla and P.K. Bharadwaj. Indian J. Chem. **32**A, 767 (1993).

© 2001 NRC Canada

Addendum

Bis(trimethylsilyl)methanesulfonyl and tris(trimethylsilyl)methanesulfonyl chlorides and their reactions by way of sulfenes: Addendum[1]

James F. King, Kim M. Baines, Matthew R. Netherton, and Vinod Dave

In footnote 4 of this paper we expressed reservations about the reliability of a report by Skrypnik and Lyashchuk in *Sulfur Letters* (ref. 10), on the preparation by reaction of Arduengo's carbene with sulfur dioxide of a sulfene "stable at low temperature." We now wish to note further that the editor of *Sulfur Letters* in an Editorial Note has concluded as follows with respect to the paper by Skrypnik and Lyashchuk: "In the absence of self-consistent convincing proof of the claims made in this paper we suggest that it should be stricken from the scientific record." (A. Senning, *Sulfur Letters*, **1996**, *20*, 105). We thank Professor Senning for drawing this Note to our attention.

Received March 13, 2001. Published on the NRC Research Press Web site on May 3, 2001.

J.F. King[2], K.M. Baines[2], M.R. Netherton, and V. Dave. Department of Chemistry, The University of Western Ontario, London, ON N6A 5B7, Canada.

[1]Original paper J.F. King, K.M. Baines, M.R. Netherton, and V. Dave. 2000. Canadian Journal of Chemistry, **78**: 1642–1646.
[2]Corresponding authors (scijfk@julian.uwo.ca and kbaines2@uwo.ca).

 DOI: 10.1139/cjc-79-4-461 © 2001 NRC Canada

Synthesis, characterization, and C—N bond cleavage of tungsten(VI)arylimido-calix[4]arene complexes

Martyn Brown and Chet Jablonski

Abstract: The tetradentate, partially flattened cone tungsten(VI) imido-calix[4]arene derivative $[W(NC_6H_5)(t\text{-BucalixH})]^+Cl^-$, **(4)**, is formed in good yield from reaction of *p-tert*-butyl-calix[4]arene (t-BucalixH_4), and $W(NC_6H_5)Cl_4$. A reaction mechanism involving a putative, bidentate calixarene intermediate $W(NC_6H_5)(t\text{-Bucalix}H_2)Cl_2$ (**3**), which partitions by reversible cleavage of the imido group to give the known tetradentate calixarene complex W(t-Bucalix)Cl_2 (**2**), and elimination of HCl to form the thermodynamic imido product **4** is proposed. A series of isostructural $[W(NAr)(t\text{-BucalixH})]^+Cl^-$ (Ar = C_6H_5 or *o,m,p*-$C_6H_4CH_3$) imido derivatives (**4**–**7**), which adopt a partially flattened cone conformation in solution has been prepared by reaction of dichloride **2** with H_2NAr (Ar = C_6H_5, *o,m,p*-$C_6H_4CH_3$). Reaction of W(t-Bucalix)Cl_2 with aliphatic amines affords a red product formulated as the nitrido complex, **9**, which results from facile cleavage of the imido C—N bond.

Key words: calix[4]arene complex, imido complex, nitrido complex, C—N bond cleavage, conformation, metallocalixarene.

Résumé : Le dérivé imidocalix[4]arène $[W(NC_6H_5)(t\text{-BucalixH}]^+Cl^-$ (**4**), un tétradentate du tungstène(VI) en cône partiellement aplati, se forme avec un bon rendement par réaction du *p-tert*-butyl-calix[4]arène, (t-BucalixH_4) et du $W(NC_6H_5)Cl_4$. On suggère que la réaction implique un mécanisme dans lequel un intermédiaire calixarène bidentate putatif, le $W(NC_6H_5)(t\text{-Bucalix}H_2)Cl_2$ (**3**), subit une partition par un clivage réversible du groupe imido pour conduire à la formation du complexe calixarène tétradentate connu W(t-Bucalix)Cl_2 (**2**) et à une élimination de HCl pour former le produit imido **4**. Faisant appel à la réaction du dichlorure **2** avec H_2NAr (Ar = C_6H_5 ou *o,m,p*-$C_6H_4CH_3$), on a préparé une série de dérivés imido isostructuraux $[W(NAr)(t\text{-BucalixH}]^+Cl^-$ (**4**–**7**) qui, en solution, adoptent une conformation en cone partiellement déformé. La réaction du W(t-Bucalix)Cl_2 avec des amines aliphatiques conduit à la formation d'un produit rouge dont la formule correspond à celle du complexe nitrido **9** qui résulte d'un clivage facile de la liaison C—N de l'imido.

Mots clés : complexe du calix[4]arène, complexe imido, complexe nitrido, clivage d'une liaison C—N, conformation, métallocalixarène.

Introduction

Interest in organotransition–imido complexes derives from their recognized ability to function as active homogeneous olefin metathesis catalysts, CVD thin-film metal nitride precursors, and as models for intermediates in catalytic oxidation–deoxygenation and hydro-denitrogenation (1–5). Imido ligands are excellent π-donors which can contribute 2–6 electrons depending on the geometry of the M—N—R bond, properties of the supporting ligands, oxidation state, and the relative energy levels of the nitrogen–metal frontier orbitals (3, 6–11). Our interest in the synthesis of nonracemic macrocyclic coordination complexes with conformationally stable cavities as host–guest models for biological systems led us to explore the possibility of employing asymmetric transition metal–imido functionalities as a route to the easy resolution of inherently chiral metallocalixarenes which are expected to have interesting supramolecular properties (12–16). In this report we describe the synthesis and spectroscopic characterization of a series of model tungsten(VI) tetradentate imido-calix[4]arene derivatives $[W(NAr)(t\text{-BucalixH})]^+Cl^-$ (Ar = C_6H_5, *o,m,p*-$C_6H_4CH_3$) (**4**–**7**) as well as an unusual, mild, reversible, imido C—N bond cleavage reaction which forms the nitrido complex $[W(N)(t\text{-BucalixH})]\cdot HCl$ (**9**).

Received December 17, 1999. Published on the NRC Research Press Web site at http://canjchem.nrc.ca on May 23, 2001.

Dedicated to Professor Brian R. James on the occasion of his 65th birthday.

M. Brown and C. Jablonski.[1] Department of Chemistry, Memorial University of Newfoundland, St. John's, NF A1B 3X7, Canada.

[1]Corresponding author (telephone: (709) 737-8089; fax: (709) 737-3702; e-mail: cjablons@mun.ca).

Experimental

Apparatus and procedures

Solvents were purified and dried by conventional methods and were distilled from an atmosphere of dry nitrogen. Reactions were carried out under a nitrogen atmosphere. Elemental analyses were performed by the MicroAnalytical Service Laboratory, Department of Chemistry, University

 DOI: 10.1139/cjc-79-5/6-463 © 2001 NRC Canada

of Alberta. Hexamethyldisiloxane, phenyl isocyanate and *p-tert*-butyl-calix[4]arene were purchased from Aldrich and used as received. Aniline, toluidines, and aliphatic amines were dried by refluxing over NaOH(s) and were distilled under nitrogen before use. Preparative radial, thick-layer chromatography separations were carried out unprotected from the ambient atmosphere on 2 or 4 mm silica gel (Merck TLC grade 7749) plates using a Chromatotron (Harrison Research). NMR spectra were measured on Varian INOVA 500 MHz (Palo Alto) or GE GN-300-NB instruments. NOe measurements were determined using steady-state difference (GE instrument) or selective excitation (Varian instrument) techniques. Chemical shifts are reported in ppm referenced to internal tetramethylsilane. IR spectra were measured on a Mattson Polaris instrument as Nujol mulls. $WOCl_4$, $W(NPh)Cl_4$, and W(*t*-Bucalix)Cl_2 were prepared using literature methods (7, 17, 18). Electrospray mass spectra (ESMS) were measured at DFO, St. John's, on a Micromass triple quadrupole mass spectrometer (OCP-v3.2–3-QUATT 4000) equipped with an electrospray ionization source. The temperature of the electrospray ionization source was maintained at 65°C. The capillary voltage was maintained at 3.50 kV. Cone voltage settings varied from 30 to 300 V. Samples were injected as methanol–chloroform solutions. X-ray data was collected at the University of Alberta on a Bruker P4/CCD system with graphite monochromated Mo-Kα radiation and a rotating anode generator.

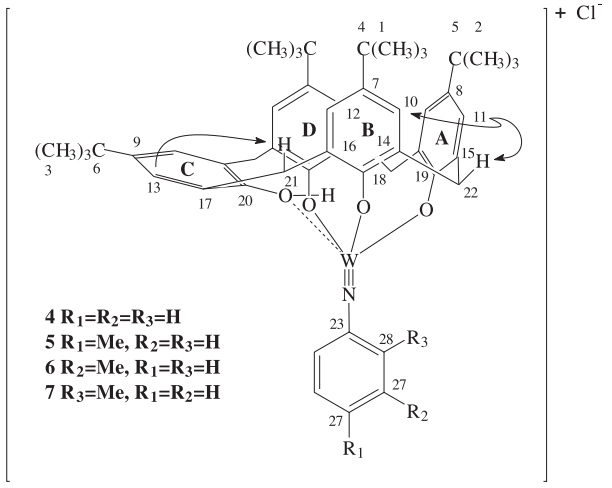
Reaction of W(NPh)Cl_4 with p-tert-*butyl-calix[4]arene*

Solid $W(NPh)Cl_4$ (0.64 g, 1.54 mmol) was added to a stirred suspension of *p-tert*-butyl-calix[4]arene (1.0 g, 1.54 mmol) in toluene (20 mL)and refluxed for 12 h. The resulting black violet solution deposited black crystals of W(*t*-Bucalix)Cl_2 (**2**) at room temperature which were filtered and collected. δ_H ($CDCl_3$): 7.35 (s, 4H, calix[4]arene Ar), 7.13 (s, 4H, calix[4]arene Ar), 4.57 (d, 4H, J = 13.3, -CH_2-), 3.55 (d, 4H, -CH_2-), 1.40 (s, 18H, C(CH_3)$_3$), 1.22 (s, 18H, C(CH_3)$_3$). δ_C ($CDCl_3$): 164.4 (Ar ipso-O), 151.0 (Ar ipso-CH_2), 149.2 (Ar ipso-CH_2), 139.5 (Ar ipso-*t*-Bu), 131.9 (Ar ipso-*t*-Bu), 126.8 (Ar *C*H), 124.0 (Ar *C*H), 34.7 (*C*H_2), 34.1 (*C*H_2), 32.2 (C(*C*H_3)), 32.1 (C(*C*H_3)). Anal. calcd. for $C_{44}H_{52}O_4WCl_2$: C 58.7, H 5.7; found: C 58.7, H 5.9.

The remaining solution was reduced in volume and cooled. A purple powder precipitated which was determined by NMR analysis to be W(*t*-Bucalix)Cl_2·2($C_6H_5CH_3$). δ_H ($CDCl_3$): 7.41–7.27 (m, 18H, $C_6H_5CH_3$ + *t*-Bucalix Ar), 4.71 (d, 4H, J = 14.0 Hz, CH_2), 3.69 (d, 4H, CH_2), 2.51 (s, 6H, $C_6H_5CH_3$), 1.54 (s, 18H, C(CH_3)$_3$), 1.35 (s, 18H, C(CH_3)$_3$). δ_C ($CDCl_3$): 163.2 (Ar ipso-O), 158.2 (Ar ipso-O), 151.1 (Ar ipso-CH_2), 149.3 (Ar ipso-CH_2), 139.5 (Ar ipso-*t*-Bu), 132.0 (Ar ipso-*t*-Bu), 129.4 ($C_6H_5CH_3$), 128.5 ($C_6H_5CH_3$), 126.9 (*C*H-*t*-Bucalix), 125.2 ($C_6H_5CH_3$), 124.1 (*C*H-*t*-Bucalix), 35.1 (C(*C*H_3)$_3$), 34.8 (*C*H_2), 34.2 (C(*C*H_3)$_3$), 32.3(CH_2), 22.2 ($C_6H_5CH_3$).

Removal of solvent from the filtrate left a dark solid which was purified by preparative TLC using 4 mm silica gel plates and hexane as the initial elutant followed by increasing amounts of $CHCl_3$. An initial orange fraction was collected followed by a violet band of the dichloride, W(*t*-Bucalix)Cl_2 (**2**). Removal of solvent from the orange fraction left an orange solid, 20 mg, 1.2%, which analyzed

Fig. 1. Important nOe correlations for the imido complexes **4**–**7**.



for the imido complex [W(NPh)(*t*-BucalixH)]$^+Cl^-$ (**4**). Anal. calcd. for $C_{50}H_{58}O_4NClW$: C 62.8, H 6.1, N 1.5; found: C 62.3, H 6.3, N 1.6.

*Preparation of the aniline adduct, (**4**) ([W(NPh)(*t*-BucalixH)]$^+Cl^-$)*

Repetition of the reaction with a reflux time of 24 h resulted in a deep red – brown solution which gave orange **4** as the major product (1.1 g, 65.4%) upon removal of solvent. Although imido complexes have been reported (1) to hydrolyze readily, complex **4** appears stable to hydrolysis and can be purified by preparative TLC on silica gel plates. ESMS (-ve ion, *m*/*z* calculated for $^{180}W/^{37}Cl$ + $^{182}W/^{35}Cl$ isotopomers): *m*/*z* = 952 (M-H)$^-$, 875 (952-C_6H_5)$^{-\cdot}$, 861 (952-NC_6H_5)$^{-\cdot}$, 647 (*t*-BucalixH_4-H)$^-$. IR (Nujol) ν_{max} cm^{-1}: 1 193 (WN), 730 (aromatic C-H). δ_H ($CDCl_3$, see Fig. 1 for numbering scheme): 7.17 (d, 2H, J = 2.3 Hz, H_{10}), 7.04 (d, 2H, J = 2.1 Hz, H_{12}), 6.9 (t, 2H, J = 6.1 Hz, H_{25} + H_{27}), 6.72 (s, 2H, H_{11}), 6.73 (s, 2H, H_{13}), 6.63 (t, 1H, J = 6.2 Hz, H_{26}), 6.44 (d, 2H, J = 7.5 Hz, H_{24} + H_{28}), 5.62 (d, 2H, J = 12.2 Hz, H_{22} *syn* to W), 4.73 (d, 2H, J= 14.4 Hz, H_{21} *syn* to W), 3.43 (d, 2H, H_{22} *anti* to W), 3.35 (d, 2H, H_{21} *anti* to W), 1.21 (s, 18H, C(CH_3)$_3$), 1.07 (s, 9H, C(CH_3)$_3$), 0.88 (s, 9H, C(CH_3)$_3$). δ_C ($CDCl_3$): 167.7 (C_{23}), 161.1 (C_{20}), 154.3 (C_{18}), 150.4 (C_{19}), 146.1 (C_{17}), 145.1 (C_{16}), 133.9 (C_{14}), 133.6 (C_{15},), 129.5 (C_9), 129.0 (C_7), 128.9 (C_8), 126.7 (C_{24}), 125.7 (C_{26}), 124.4 (C_{25}), 124.0 (C_{12}), 123.7 (C_{10}), 122.6 (C_{11}), 36.4 (C_{21}), 34.3 (C_{22}), 33.8 (*C*-*t*-Bu) 31.8 (C(*C*H_3)$_3$), 31.5 ((C(*C*H_3)$_3$), 31.2 (C(*C*H_3)$_3$).

Crystallization from toluene over a period of two weeks gave **4** as red–orange plates which lost solvent readily when removed from the mother liquor and failed to diffract. Repeated attempts to generate and mount X-ray diffraction quality crystals failed.

*Reaction of W(*t*-Bucalix)Cl_2 (2) with aniline and* o-, m-, p-*toluidines*

Amine (7.5 mmol) was added via syringe to a stirred solution of W(*t*-Bucalix)Cl_2 (**2**) (2.25 g, 2.50 mmol) in 20 mL of toluene and refluxed for 24 h. The resulting deep red solution was cooled to room temperature and the precipitated [$ArNH_3$]$^+$ Cl^- (2.1–2.3 mmol) was removed by filtration.

© 2001 NRC Canada

Partial evaporation of solvent deposited a yellow solid which analyzed for W(O)(*t*-Bucalix)·H_2O (**8**). Yield: aniline 25.5%, *p*-toluidine 26.8%, *o*-toluidine 34.3%, *m*-toluidine 27.8%. IR (Nujol) ν_{max} cm^{-1} : 983 (W=O). ^1H NMR (C_6D_6) δ: 7.1 (s, 8H, calix aromatic), 4.98 (d, 4H, CH_2), 3.21 (d, 4H, CH_2), 1.22 (s, 36H, *t*-Bu). Anal. calcd. for $C_{44}H_{54}O_6W$: C 61.3, H 6.3%; found: C 61.0, H 6.0%.

The remaining solution was evaporated and the products separated by preparative TLC with hexane as the initial elutant followed by a steadily increasing $CHCl_3$ gradient. The orange imido adducts **4**–**7** were collected as the first fraction. With aniline, the product (isolated yield 35.5%) was identical to **4** obtained from the reaction of W(NPh)Cl_4 with *p-tert*-butylcalix[4]arene.

p-*Toluidine adduct (**5**) ([W(NC$_6$H$_4$CH$_3$)(*t*-BucalixH)]$^+$Cl$^-$)*: Yield 30.1%. ESMS (–ve ion, $^{180}W/^{37}Cl$ + $^{182}W/^{35}Cl$ isotopomers): *m*/*z* = 966 (M-H)$^-$, 875 (966-$C_6H_4CH_3$)$^-$, 861 (M-$NC_6H_4CH_3$)$^-$, 647 (Bu^{t}calixH_4-H)$^-$. IR(Nujol) ν_{max} (cm^{-1}): 3 500–3 200 (OH), 1 200 (WN). ^1H NMR ($CDCl_3$) δ (ppm): 7.22 (d, 2H, *J* = 1.9 Hz, H_{10}), 7.05 (d, 2H, *J*= 1.9 Hz, H_{12}), 6.80 (d, 2H, *J* = 8.5 Hz, H_{25} + H_{27}), 6.75 (d, 2H, *J* = 8.5 Hz, H_{24} + H_{28}), 6.41 (s(br), 4H, H_{11} + H_{13}), 5.67 (d, 2H, *J* = 13.9 Hz, H_{22} *syn* to W), 4.85 (d, 2H, *J* = 13.1Hz, H_{21} *syn* to W), 3.45 (d, 2H, H_{22} *anti* to W), 3.42 (d, 2H, H_{21} *anti* to W), 2.35 (s, 3H, Me(toluidine)), 1.18 (s, 18H, C(CH_3)$_3$), 1.02 (s, 9H, C(CH_3)$_3$), 0.91 (s, 9H, C(CH_3)$_3$). ^{13}C NMR ($CDCl_3$) δ (ppm): 167.6 (C_{23}), 161.0 (C_{20}), 153.6 (C_{18}), 148.4 (C_{19}), 147.5 (C_{17}), 146.0 (C_{16}), 144.9 (C_{14}), 139.0 (C_{15}), 133.9 (C_{26}), 133.5 (C_9), 129.5 (C_7), 129.0 (C_8), 127.2 (C_{24},C_{28}), 126.7 (C_{25}, C_{27}), 125.7 (C_{13}), 124.4 (C_{10}), 124.2 (C_{11}), 123.9 (C_{12}), 36.5 (C_{21}), 34.3 (C_{22}), 33.9 (*C*(CH_3)$_3$), 32.0 (C(*C*H_3)$_3$), 31.9 (C(*C*H_3)$_3$), 31.5 (C(*C*H_3)$_3$), 21.4 (Me, toluidine). Anal. calcd. for $C_{51}H_{60}O_4NWCl$: C 63.2, H 6.2; found: C 62.9, H 6.4.

m-*Toluidine adduct (**6**) ([W(NC$_6$H$_4$CH$_3$)(*t*-BucalixH)]$^+$Cl$^-$)*: Yield 25.2%. ESMS (–ve ion, $^{180}W/^{37}Cl$ + $^{182}W/^{35}Cl$ isotopomers): *m*/*z* = 966 (M-H)$^-$, 875 (966-$C_6H_4CH_3$)$^-$, 861 (M-$NC_6H_4CH_3$)$^-$, 647 (*t*-BucalixH_4-H)$^-$. IR (Nujol) ν_{max} (cm^{-1}): 3 500–3 300 (OH), 1 206 (WN). ^1H NMR ($CDCl_3$) δ (ppm): 7.15 (s, 2H, H_{10}), 7.08 (s, 2H, H_{12}), 6.90 (t, 1H, H_{25}, *J* = 4.5 Hz), 6.79 (s, 4H, H_{11} + H_{13}), 6.41 (d, 1H, H_{24}, *J* = 4.5 Hz), 6.15 (m(br), 2H, H_{26} + H_{28}), 5.82 (d, 2H, *J* = 13.7 Hz, H_{22} *syn* to W), 4.89 (d, 2H, *J* = 13.1 Hz, H_{21} *syn* to W), 3.40 (d, 4H, H_{21} + H_{22} *anti* to W), 2.05 (s, 3H, Me toluidine), 1.30 (s, 18H, C(CH_3)$_3$), 1.08 (s, 9H, C(CH_3)$_3$), 0.97(s, 9H, C(CH_3)$_3$). ^{13}C NMR ($CDCl_3$) δ (ppm): 167.9 (C_{23}), 161.1(C_{20}), 153.6 (C_{18}), 150.3 (C_{19}), 147.5 (C_{17}), 146.1 (C_{16}), 144.9 (C_{14}), 135.9 (C_{15}), 133.9 (C_{27}), 133.6 (C_{25}), 130.6 (C_9), 129.5 (C_{26}), 128.9 (C_{24}), 127.5 (C_7), 126.3 (C_8), 125.7 (C_{13}), 124.9 (C_{10}), 124.7 (C_{11}), 123.5 (C_{12}), 36.3 (C_{21}), 34.5(C_{22}), 34.0 (*C*(CH_3)$_3$), 31.3 (C(*C*H_3)$_3$), 31.1 (C(*C*H_3)$_3$), 30.0 (C(*C*H_3)$_3$), 21.3 (Me, toluidine). Anal. calcd. for $C_{51}H_{60}O_4NWCl$: C 63.2, H 6.2; found C 63.1, H 6.0.

o-*Toluidine adduct (**7**) ([W(NC$_6$H$_4$CH$_3$)(*t*-BucalixH)]$^+$Cl$^-$)*: Yield 27.5%. ESMS (–ve ion, $^{180}W/^{37}Cl$ + $^{182}W/^{35}Cl$ isotopomers): *m*/*z* = 966 (M-H)$^-$, 875 (966-$C_6H_4CH_3$)$^-$, 861 (M-$NC_6H_4CH_3$)$^-$, 647 (*t*-BucalixH_4-H)$^-$. IR (Nujol) ν_{max} (cm^{-1}): 3 500–3 300 (OH), 1 206 (WN). ^1H NMR ($CDCl_3$) δ (ppm): 7.23 (s(br), 2H, H_{10}), 7.02 (s, 2H, H_{12}), 6.85 (t, 1H, H_{26}), 6.79 (s, 4H, H_{11} + H_{13}), 6.45 (d, 1H, H_{24}), 6.30 (m, 2H, H_{25} + H_{27}), 5.81 (d, 2H, *J* = 13.6 Hz, H_{22} *syn* to W), 4.82 (d, 2H, *J* = 13.3 Hz, H_{21} *syn* to W), 3.42 (m, 4H, H_{21} + H_{22} *anti* to W), 2.05 (s, 3H, Me toluidine), 1.15 (s, 18H, C(CH_3)$_3$), 1.05 (s, 9H, C(CH_3)$_3$), 0.95 (s, 9H, C(CH_3)$_3$). ^{13}C NMR ($CDCl_3$) δ: 167.9 (C_{23}), 161.0 (C_{20}), 153.6 (C_{18}), 150.3 (C_{19}), 147.8 (C_{17}), 146.1 (C_{16}), 145.0 (C_{14}), 136.0 (C_{15}), 134.0 (C_{28}), 133.6 (C_{24}), 129.9 (C_9), 129.5 (C_{25}), 129.0 (C_{26}), 127.9 (C_7), 126.3 (C_8), 125.7 (C_{10} + C_{11}), 125.3 (C_{12}), 36.5 (C_{21}), 34.5 (C_{22}), 33.8 (*C*(CH_3)$_3$), 31.9 (C(*C*H_3)$_3$), 31.4 (C(*C*H_3)$_3$), 29.9 (C(*C*H_3)$_3$), 21.6 (Me, toluidine). Anal. calcd. for $C_{51}H_{60}O_4NWCl$: C 63.2, H 6.2; found: C 63.1, H 6.4.

A second, red fraction was collected in all cases. Evaporation gave [W(N)(*t*-BucalixH)]·HCl (**9**) as a red solid. ESMS (–ve ion, $^{180}W/^{37}Cl$ + $^{182}W/^{35}Cl$ isotopomers): *m*/*z* = 875 (M-H)$^-$, 647 (*t*-BucalixH_4-H)$^-$. ^1H NMR ($CDCl_3$, 60°C) δ (ppm): 7.27 (m, aromatic), 7.18 (m, aromatic), 7.12 (s, aromatic), 7.08 (s, aromatic), 7.05 (d, aromatic), 6.99 (d, aromatic), 6.93 (m, aromatic), 6.85 (m, aromatic), 6.38 (d, CH_2), 5.03 (d, CH_2), 4.42 (d, CH_2), 4.27 (d, CH_2), 3.93 (d, CH_2), 3.51 (d, CH_2), 3.44 (d, CH_2), 3.29 (d, CH_2), 3.27 (d, CH_2), 1.39 (s, *t*-Bu), 1.21 (s, *t*-Bu), 1.20 (s, *t*-Bu), 1.11 (s, *t*-Bu). ^{13}C NMR ($CDCl_3$) δ (ppm): 162.4, 161.8, 158.4, 156.3, 149.1, 147.1, 146.7, 146.3, 142.7, 135.7, 135.1, 134.8, 131.2 (CH), 130.6 (CH), 128.2 (CH), 127.4 (CH), 126.8 (CH), 16.5 (CH), 125.4 (CH), 125.1 (CH), 124.1 (CH), 123.9 (CH), 36.1 (*C*Me$_3$), 35.3 (CH_2), 35.1 (CH_2), 34.7 (CMe_3), 34.26 (CH_2), 34.1 (CH_2), 33.4 (CMe_3), 32.2 (Me), 32.0 (Me), 31.7 (Me). Anal. calcd. for $C_{44}H_{54}O_4NWCl$: C 60.0, H 6.2, N 1.6; found: C 60.5, H 6.1, N 1.5.

*Reaction of diisopropylamine, diethylamine, benzylamine, and (S)-(–)-α-methylbenzylamine with W(*t*-Bucalix)Cl$_2$ (**2**)*

The procedure was identical to that used for the aromatic amines. Amine (3 mmol) was added via syringe to a stirred solution of the dichloride **2** (1 mmol) under N_2 in 15 mL of toluene. After 24 h reflux, the cooled solution deposited crystals of the oxo compound (**8**), which were removed by filtration (yields: diisopropyl amine 35.5%, diethylamine 32.4%, benzylamine 38.6%, methylbenzylamine 45.3%). The filtrate showed a single spot on TLC (silica gel, hexane:$CHCl_3$, 10:1). Removal of solvent gave a red solid which was identical by NMR with complex **9** obtained as a trace product from the reaction with anilines. No imido-calixarene derivatives were isolated.

*Reaction of imido adduct **4** ([W(NPh)(*t*-BucalixH)]$^+$Cl$^-$) with AgPF$_6$*

0.1 mmol of the imido adduct **4** was dissolved in $CDCl_3$ (1 mL) in an NMR tube. $AgPF_6$ (0.1mmol) was then added as a solid. After initial dissolution, precipitation of a white solid took place. The ^1H NMR spectrum of the solution was identical with that of the starting [W(NPh)(*t*-BucalixH)]Cl complex (**4**).

*Reaction of imido adducts **4**–**7** ([W(NAr)(*t*-BucalixH)]$^+$Cl$^-$) with ClSiMe$_3$ and CH$_3$COCl*

1.0 mmol of the imido adduct and 1.1 mmol of $ClSiMe_3$ or CH_3COCl were refluxed in 20 mL of toluene. The orange solution turned violet after 3 h. After 24 h, the solvent was

© 2001 NRC Canada

removed to leave a black solid which was identified as W(*t*-Bucalix)Cl_2 (**2**) by NMR.

*Attempted reaction of imido adducts **4** ([W(NPh)(*t*-BucalixH)]$^+Cl^-$) with HCl*

Imido complex **4** (1 mmol) was dissolved in 20 mL of toluene and stirred under N_2. HCl(g) (3 mmol) was added via syringe and the mixture refluxed for 12 h. No reaction occurred, even upon addition of a total of 10 equiv of HCl(g).

*Crystal structure determination of **8** (W(O)(t-Bucalix)·H_2O)*

A pale yellow plate crystal of **8** having approximate dimensions of 0.36 × 0.03 × 0.37 mm was selected and mounted on a glass fibre. All measurements were made on a Bruker P4/CCD system with graphite monochromated Mo-Kα radiation and a rotating anode generator. The data were collected at a temperature of –80 ± 1°C. The full hemisphere of data was collected with 30 s, 0.3 deg. frames to a maximum 2θ value of 51.55°.

Of the 19 634 reflections which were collected, 2 382 were unique, R_{int} = 0.048). The linear absorption coefficient, μ, for Mo-Kα radiation is 28.1 cm^{-1}. The Siemens area detector absorption routine (SADABS) was used to correct the data with max and min effective transmissions of 0.942192 and 0.706867, respectively. The data were corrected for Lorentz and polarization effects. A correction for secondary extinction was applied (coefficient = 8.90850e-008).

Collection, solution, and refinement all proceeded normally. Hydrogens were introduced in calculated or difference map positions with isotropic thermal parameters set 20% greater than those of their bonding partners at the time of their inclusion. They were not refined. All non-hydrogen atoms were refined anisotropically with the exception of a second, disordered water molecule located near the upper rim of the calixarene. The structure was solved by direct methods (19, 20) and expanded using Fourier techniques (21). The final cycle of full-matrix least-squares refinement (least-squares function minimized: $\Sigma w(|F_o| - |F_c|)^2$ where $w = 1/[\sigma^2(F_o)] = [\sigma^2_c(F_o) + p^2F_o^2/4]^{-1}$; $\sigma_c(F_o)$ = esd based on counting statistics; p = p-factor) on F was based on 1329 observed reflections ($I > 2.00\sigma(I)$) and 123 variable parameters and converged (largest parameter shift was 0.00 times its esd) with unweighted and weighted agreement factors of: $R = \Sigma||F_o| - |F_c||/\Sigma|F_o| = 0.045$ and $R_w = [\Sigma w(|F_o| - |F_c|)^2/\Sigma wF_o^2]^{1/2} = 0.061$.

The standard deviation of an observation of unit weight $([\Sigma w(|F_o| - |F_c|)^2/(N_o - N_V)]^{1/2}$ where N_o = number of observations and N_V = number of variables) was 2.63. The weighting scheme was based on counting statistics. Plots of $\Sigma w(|F_o| - |F_c|)^2$ vs. $|F_o|$, reflection order in data collection, sin θ/λ and various classes of indices showed no unusual trends. The max and min peaks on the final difference Fourier map corresponded to 1.21 and –0.77 $e^-/Å^3$, respectively.

Neutral atom scattering factors were taken from Cromer and Waber (22). Anomalous dispersion effects were included in Fcalc (23); the values for Df′ and Df″ were those of Creagh and McAuley (24). The values for the mass attenuation coefficients are those of Creagh and Hubbell (25). All calculations were performed using the teXsan (26) crystallographic software package of Molecular Structure Corporation. The crystallographic data are summarized in Table 1.

Results

Synthesis and characterization

Our investigations began by studying model reactions of tungsten tetrachloro-aryl imido derivatives with *p-tert*-butylcalix[4]arene with the expected, direct formation of the tetradentate-calix[4]arene imido tungsten product (**1**) (Scheme 1). Instead, refluxing an equimolar suspension of W(NPh)Cl_4 and *p-tert*-butyl-calix[4]arene for 12 h in toluene afforded a black–violet solution which deposited black crystals, identified as the known (18) dichlorocalix[4]arene complex W(*t*-Bucalix)Cl_2 (**2**) on cooling. Continued reflux for an additional 12 h resulted in a deep red – brown solution which yielded an orange solid on removal of solvent. Complex **2** was shown to be an intermediate in the formation of the orange thermodynamic product which was spectroscopically characterized as the imido calix[4]arene complex [W(NPh)(*t*-BucalixH)]$^+Cl^-$ (**4**) (cf. discussion below).

Complex **4** along with a series of isostructural imido complexes, **5**–**7**, were rationally synthesized (1) by reaction of aniline or *o*-, *m*-, or *p*-toluidine with the dichlorocalix[4]arene complex **2** in refluxing toluene. The insoluble, yellow oxo complex W(O)(*t*-Bucalix)·H_2O (**8**) which was spectroscopically and structurally characterized, precipitated directly from the reaction mixture as a major by-product in all cases. Complex **8**, which has been previously prepared from the reaction of $WOCl_4$ and *p-tert*-butylcalix[4]arene (18), presumably results from hydrolysis of **2**. Chromatographic work-up of the toluene soluble fraction afforded the orange imido complexes **4**–**7** in reasonable yield. A second red, slower moving band which afforded trace quantities of a red solid, formulated as the nitrido species W(N)(*t*-BucalixH)·HCl (**9**) was also isolated in each case.

Reaction of the dichlorocalixarene complex **2** with aliphatic amines gave a very different result. Refluxing **2** with diisopropylamine, diethylamine, or (*S*)-(–)-α-methylbenzylamine gave the oxo complex **8**, and the nitrido species **9** as major products. No imido products were detected.

The toluene soluble, orange thermodynamic product isolated from the reaction of W(NPh)Cl_4 and *p-tert*-butyl-calix[4]arene or from the reaction of W(*t*-Bucalix)Cl_2 (**2**) with aniline was characterized by analysis and spectroscopic data as the cationic calix[4]arene phenol–phenolate imido complex [W(NPh)(*t*-BucalixH)]$^+Cl^-$ (**4**) (cf. experimental). An alternate, neutral structure [W(NPh)(*t*-Bucalix)]·HCl (**4′**) in which the HCl is present as an inclusion compound could not be ruled out. Negative ion ESMS showed a mass envelope corresponding to $[M-H]^-$ at m/z = 952 (calculated for $^{180}W/^{37}Cl + ^{182}W/^{35}Cl$ isotopomers) as well as major fragments at 875 $(952\text{-}C_6H_5)^-$, 861 $(952\text{-}NC_6H_5)^-$ and 647 (*t*-BucalixH_4-H)$^-$. Formulation as **4** or **4′** is supported by its +ve ion ESMS which gave a peak at m/z = 919 assigned to [M + H]-Cl^+ which was not present in the –ve ion ESMS data. Similarly, the negative ion ESMS spectra of the toluidine analogs **5**–**7** all showed characteristic fragments at m/z = 966 $(M-H)^-$, 875 $(966\text{-}C_6H_4CH_3)^-$, 861 $(M\text{-}NC_6H_4CH_3)^-$ and 647 (*t*-BucalixH_4-H)$^-$. Facile aryl cleavage (5) in the ESMS of the imido series gives a base peak at m/z = 875 assigned to the nitrido species.

© 2001 NRC Canada

Table 1. Crystallographic data for complex **8**.

Empirical formula	$C_{44}H_{56}O_7W$
Formula weight	880.77
Crystal colour, habit	colourless, plate
Crystal dimensions	0.36 × 0.03 × 0.37 mm
Crystal system	tetragonal
Lattice type	Primitive
Lattice parameters	a = 12.897(1) Å
	c = 25.193(2) Å
	V = 4190.4(5) Å^3
Space group	*P*4/*nnc* (no. 126)
Z value	4
D_{calc}	1.396 g/cm^3
F_{000}	1 800.00
μ(Mo-Kα)	28.07 cm^{-1}
Diffractometer	Bruker P4/CCD/RA
Radiation	Mo-Kα (λ = 0.71073 Å) graphite monochromated
Temperature	–80.0°C
Scan rate	30 s, 0.3 deg. frames
θ_{max}	51.55°
No. of reflections measured	Total: 19 634
	Unique: 2 382 (R_{int} = 0.048)
Corrections	Lorentz polarization
	SADABS correction
	(trans. factors: 0.942192–0.706867)
	Secondary extinction
	(coefficient: 8.90850e-008)
Structure solution	Direct Methods (SHELX97)
Refinement	Full-matrix least-squares on F
Function Minimized	$\Sigma w(\|F_o\| - \|F_c\|)^2$
Least-squares weights	$1/\sigma^2(F_O) = 4F_o^2/\sigma^2(F_o^2)$
p-factor	0.0000
Anomalous dispersion	All non-hydrogen atoms
No. observations ($I > 2.00\sigma(I)$)	1 329
No. variables	123
Reflection/parameter ratio	10.80
Residuals: R, R_w	0.045, 0.061
Goodness-of-fit indicator	2.63
Max shift/error in final cycle	0.00
Max peak in final diff. map	1.21 (e$^-$ Å^{-3})
Min peak in final diff. map	–0.77 (e$^-$ Å^{-3})

Proton NMR spectra of **4**–**4′** in $CDCl_3$ showed two characteristic pairs of calix[4]arene -CH_2-AB doublets and three *t*-Bu singlets which integrated in a 2:1:1 ratio. Very similar spectra were reported for tetradentate niobium (27) and tantalum (28) calix(4)arene complexes. The calixarene portion of the NMR spectra of the toluidine imido complexes **5**–**7** were nearly identical (cf. Experimental) and we therefore propose that they are isostructural with **4**–**4′**.

Two imido structures, which are difficult to distinguish on the basis of spectroscopic information, are reasonable for isostructural series **4**–**7**. We were, however, unable to distinguish between formulation as cationic phenol–phenolates, [W(NAr)(*t*-BucalixH)]$^+$Cl$^-$, or neutral hydrochlorides, [W(NAr)(*t*-Bucalix)]·HCl. For consistency in mechanistic arguments, we have selected the former (cf. Scheme 1).

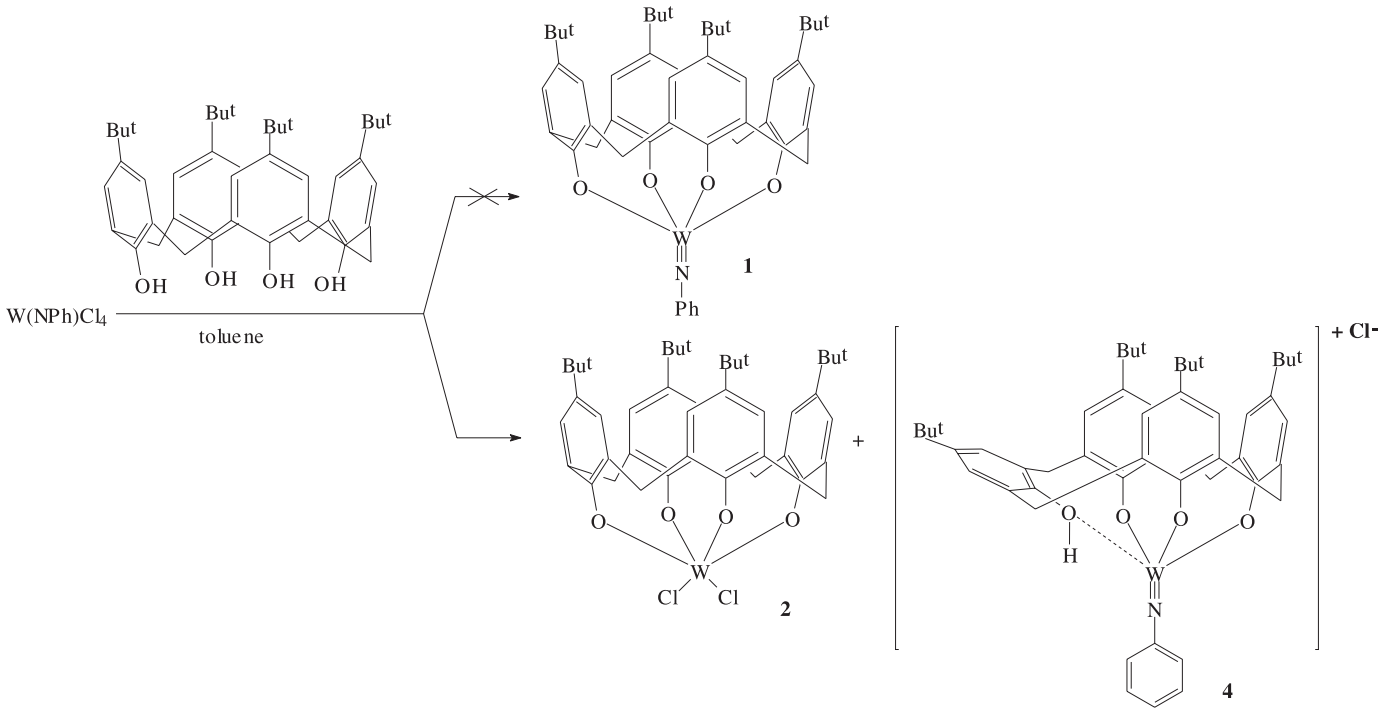
Attempts to confirm the cationic structure on the basis of reactivity failed. For example, a similar phenol–phenolate tetra coordinate calix[4]arene complex had been successfully derivatized by Floriani and co-workers (27), hence we treated **4** with excess acetyl chloride or trichloromethylsilane but isolated only W(*t*-Bucalix)Cl_2 (**2**). The chloride in **4**–**7** was easily precipitated by reaction with $AgPF_6$ to give a soluble fraction which showed a ^{1}H NMR spectrum unchanged from the starting material. Although this result is more consistent with an ionic rather than a covalent (eg. W-Cl) and hence supports a tetra-coordinated calix[4]arene, it does not conclusively distinguish between the two structures (**4**, **4′**) in question.

Conformational analysis of 4–7 ([W(NAr)(*t*-BucalixH)]$^+$Cl$^-$)

Variable temperature ^{1}H NMR experiments on the imido complex **4** in toluene-d_8 and benzene-d_6 showed no substantive changes in the range –10 to 80°C and were therefore

© 2001 NRC Canada

Scheme 1.



congruent with the presence of a single, stable conformation. A cone, flattened cone, or partial cone conformation of **4** could conceivably give the ^{1}H spectrum observed (29–33) but ^{1}H nOe experiments and ^{13}C methylene shift arguments are more in accord with a partially flattened cone conformation.

In an nOe experiment, partial selective saturation of the singlet assigned to the two equivalent *t*-Bu groups at 1.21 ppm, $H_1/H_{1'}$, resulted in a positive enhancement of the signals assigned to the *ortho* aromatic doublets at 7.17 and 7.04 ppm on rings **B** and **D** respectively (cf. Fig. 4). Therefore, the remaining two closely spaced singlets at ca 6.7 ppm must be $H_{11}/H_{11'}$ and $H_{13}/H_{13'}$ on rings **A** and **C** respectively. Subsequent nOe experiments identified the remaining *t*-Bu groups. The fact that the *ortho* protons of rings **B** and **D** are nonequivalent requires that each side of the rings be in a distinctly different chemical environment, a result not consistent with a cone conformation but which does support a partial cone or partially flattened cone conformation.

Selective partial saturation of the ortho resonance at 7.17 ppm resulted in a positive enhancement of the 3.35 ppm doublet (-CH_2- *exo* to W) as well as the 6.73 ppm signal (ring $\mathbf{A}_{ortho}$). A parallel experiment on the ortho resonance at 7.04 ppm resulted in a positive enhancement of the 3.43 ppm doublet (-CH_2- exo to W) but had no effect on the aryl region. Clearly, the aromatic protons on ring **C** (cf. Fig. 4) are not proximal to the aromatic protons on rings **B** and **D**, a result which supports a flattened cone conformation. Ring **C** cannot be orthogonal to the axis of the cone as in a partial cone conformation since, if this were the case, both *anti* and *syn* methylene protons $H_{21}/H_{21'}$ would be expected to experience a +ve nOe enhancement on irradiation of the aromatic protons in ring **C**.

The empirical Mendoza and co-workers (34) formalism for determining calixarene conformations suggests that the methylene carbons bridging *syn*-oriented calixarene rings have a ^{13}C shift of 31–34 ppm and a shift closer to 37 ppm when the rings are *anti*. Applied to complex **4**, the observed chemical shifts of C_{21} (36 ppm) and C_{22} (34 ppm) suggest that rings **C**/**D**/**B** are not *syn*. These predictions must be viewed with caution, especially in the case of the metallo-calixarenes in this study. Nevertheless, both the partial cone and partially flattened cone conformations are consistent with ^{13}C chemical shift data.

Characterization of 9 ([W(N)(*t*-BucalixH)]·HCl)

Attempts to obtain a X-ray quality single crystal of the red complex isolated as the major toluene soluble product from the reaction of **2** with 1° or 2° aliphatic amines failed. It is formulated as the phenol–phenolate nitrido complex **9** (cf. Scheme 2) on the basis of analytical, NMR, and ESMS data. The latter shows a $(M-H)^-$ molecular ion at m/z = 875 ($^{180}W/^{37}Cl$ + $^{182}W/^{35}Cl$ isotopomers). An alternate, parent imido structure, W(NH)(*t*-Bucalix)·HCl, seems less likely since we were unable to detect a ^{1}H NMR signal assignable to the imido hydrogen.

The ^{1}H NMR spectrum of **9** in $CDCl_3$ is complex and our assignments are based on the assumption that several distinct conformations are present. A total of 10 calixarene -CH_2- doublets corresponding to three conformations **a**, **b**, **c** (cf. Fig. 2) were observed. The presence of three calixarene conformers is supported by variable temperature ^{1}H NMR experiments which showed a small but measurable dependence of the integrated ratio of the sets of resonances assigned to the conformers and by a 2-D COSY experiment which was consistent with three distinct, mutually coupled spin systems. A cone conformation was assigned to the two AB doublets at 5.03 and 3.44 ppm. Two sets of four doublets at 6.38, 3.93, 3.51, 3.27 ppm and at 4.42, 4.27, 3.29, and

© 2001 NRC Canada

Scheme 2.

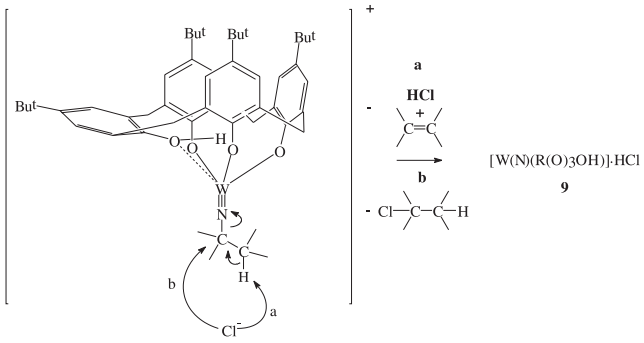
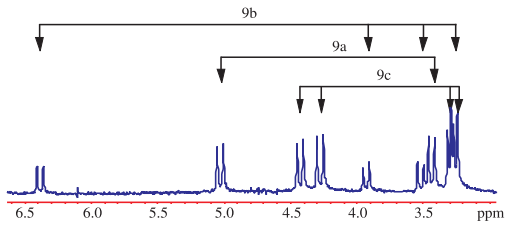


Fig. 2. Partial 300 MHz NMR spectrum (-CH_2- region) of **9** in $CDCl_3$ at 60°C showing three conformers.



3.27 ppm correspond to two partial cone or partially flattened cone conformations.

Solid state structure of 8 (W(O)(*t*-Bucalix)·H_2O)

The solid state structure of complex **8** was determined from a single crystal X-ray study. Tables 1, 2, and 3 list crystallographic data, positional parameters, and selected bond distances and angles for **8**. As Fig. 3 shows, the coordination sphere of the tungsten atom in the oxo-complex **8** establishes a distorted MO_6 octahedral coordination geometry. The O_2-W-O_1 angles of 99.7° allow the tungsten atom to ride slightly above the calixarene O_4 plane. The loosely coordinated clathrate water shows a long W—O(3) bond length of 2.37(1) Å compared to the 1.910(6) Å value for the four calixarene oxygen atoms. Atypically for tetradentate complexes of calixarenes in the cone conformation (2, 18), **8** retains C_{4v} symmetry. Accordingly, unlike the elliptically distorted parent W(O)(calix[4]arene) complex (18) which shows *para* carbon atom distances for opposing phenyl rings of 9.04 Å/7.88 Å, the calixarene cavity of **8** is spherical with a corresponding distance of 8.60 Å and identical O1-C1-C6-C7 dihedral angles of 4.4°.

Table 2. Positional parameters and *B*(eq) for complex **8**.

Atom	*x*	*y*	*z*	*B*(eq)
W(1)	0.2500	0.2500	0.53845(2)	1.596(6)
O(1)	0.3164(3)	0.3800(3)	0.5256(2)	1.50(9)
O(2)	0.2500	0.2500	0.6055(3)	2.3(1)
O(3)	0.2500	0.2500	0.4445(3)	1.9(1)
O(4)	0.222(4)	0.323(2)	0.278(1)	11(1)
C(1)	0.3417(4)	0.4314(4)	0.4800(3)	1.5(1)
C(2)	0.2715(3)	0.5020(4)	0.4579(2)	1.2(1)
C(3)	0.3006(5)	0.5578(4)	0.4134(3)	1.4(1)
C(4)	0.3996(5)	0.5481(4)	0.3908(3)	1.6(1)
C(5)	0.4663(5)	0.4756(5)	0.4136(2)	1.5(1)
C(6)	0.4394(4)	0.4158(4)	0.4574(2)	1.5(1)
C(7)	0.1627(4)	0.5146(4)	0.4804(3)	1.5(1)
C(8)	0.4297(5)	0.6183(5)	0.3443(3)	2.4(2)
C(9)	0.4221(6)	0.7324(6)	0.3621(3)	3.6(2)
C(10)	0.3530(6)	0.6021(6)	0.2978(3)	3.9(2)
C(11)	0.5386(6)	0.6003(6)	0.3249(3)	3.5(2)

Table 3. Selected bond distances and angles for complex **8**.

(A) Intramolecular bond distances involving the non-hydrogen atoms

Bond	Distance (Å)
W(1)—O(1)	1.910(6)
W(1)—O(2)	1.69(1)
W(1)—O(3)	2.37(1)

(B) Intramolecular bond angles involving the non-hydrogen atoms

Bond angles	Angle (deg)	Bond angles	Angle (deg)
O(1)-W(1)-O(1)	160.5(4)	O(1)-C(1)-C(2)	119.7(8)
O(1)-W(1)-O(1)	88.36(7)	O(1)-C(1)-C(6)	119.2(8)
C(2)-C(1)-C(6)	121.0(9)	O(1)-W(1)-O(2)	99.7(2)
C(1)-C(2)-C(3)	119.1(8)	O(1)-W(1)-O(3)	80.3(2)
C(1)-C(2)-C(7)	121.2(9)	C(3)-C(2)-C(7)	119.7(8)
C(2)-C(3)-C(4)	121.9(9)	O(1)-W(1)-O(2)	99.7(2)
C(3)-C(4)-C(5)	117.0(9)	O(1)-W(1)-O(3)	80.3(2)
C(3)-C(4)-C(8)	119.2(9)	O(1)-W(1)-O(1)	160.5(4)
C(5)-C(4)-C(8)	123.8(9)	C(4)-C(5)-C(6)	123(1)
C(1)-C(6)-C(5)	118.0(9)	C(1)-C(6)-C(7)	121.2(9)
C(5)-C(6)-C(7)	120.8(9)	O(2)-W(1)-O(3)	180.0(2)
C(2)-C(7)-C(6)	113.9(8)	W(1)-O(1)-C(1)	132.5(6)

Note: Distances are in Å. Angles are in deg. Estimated standard deviations in the least significant figure are given in parentheses.

Discussion

Mechanistic considerations

Figure 4 shows the % mol fraction vs. reaction time for the ^{1}H NMR observed species formed from the reaction of $W(NPh)Cl_4$ with *p-tert*-butylcalix(4)arene in toluene-d_8 at 80°C. The dichloride species W(*t*-Bucalix)Cl_2 (**2**), rapidly forms initially and, subsequent to an induction period, remains essentially constant as the thermodynamic imido product [W(NPh)(*t*-BucalixH)]$^+$Cl$^-$ (**4**) begins to accumulate. Clearly, the formation of **2** from the starting complex $W(NPh)Cl_4$ requires an imido W—N cleavage. There is precedent for imido cleavage in a related reaction of $Mo(NAr)_2(OR)_2$ with *t*-BucalixH_4 (35). We propose a similar mechanism which involves initial replacement of two equiv of chloride to form a putative, bidentate, calix[4]arene imido intermediate W(NPh)(*t*-BucalixH_2)Cl_2 (**3**) which subsequently partitions by reversible imido cleavage to give **2** and loss of a third equiv of chloride as HCl to give **4** as depicted in Scheme 3. The conversion of **3** → **4** is essentially irreversible since **2** is not present at the end of the reaction and attempts to react **4** with HCl failed.

© 2001 NRC Canada

Fig. 3. ORTEP representation of the solid-state structure of W(O)(*t*-Bucalix)·H_2O (**8**).

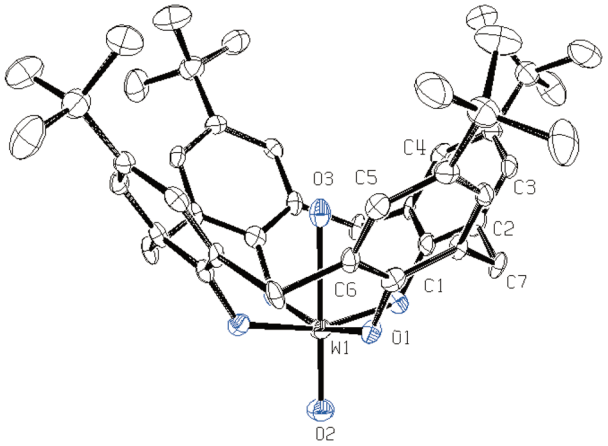
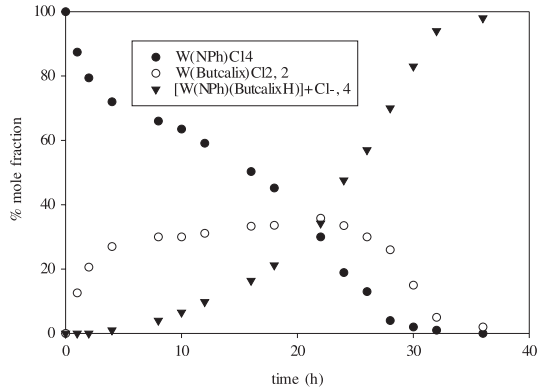
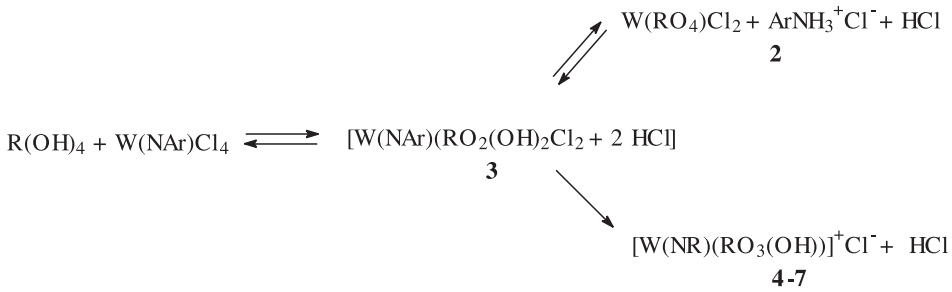


Fig. 4. Mol fraction $W(NPh)Cl_4$, **2** and **4** vs. time at 80°C in toluene-d_8.



Scheme 3.



Early transition metal – imido ligands are typically nucleophilic and are readily cleaved by HCl to produce the corresponding metal dichloride and the ammonium salt (3, 10, 36). It can be argued that the imido link in the tungsten complex, **3**, would be particularly susceptible to protonation since coordination of two π-donor oxygen atoms increase electron density on the imido nitrogen atom. Although we are unable to provide direct structural evidence establishing the geometry of the imido link in these complexes, imido reactivity would be enhanced by bending the imido bond (9, 10, 37) which forces the lone pair to reside on nitrogen, thereby making it more nucleophilic. Further, calculations by Nugent et al. (8) support enhanced imido nucleophilicity for early 5*d* metals since the LUMO is essentially localized on the nitrogen *p* orbital.

Figure 4 and the mechanism shown in Scheme 3 require a reversible W—N imido cleavage. Such reactions are well-known and indeed imido formation by reaction of metal chlorides with amines (1, 3, 38) represents a general synthetic route. Excess base is often required to remove the HCl produced. Consistent with this requirement, reaction of the calixarene dichloride complex W(*t*-Bucalix)Cl_2 (**2**) with 2 equiv of aniline, gave the partial cone adduct **4** in 35% yield, presumably via facile, sequential amine and amido deprotonation (3). The conformational properties of the putative bidentate calixarene intermediate W(NPh)(*t*-BucalixH_2)Cl_2 (**3**) are unknown. However, significant ligand preorganization may present the metal—imido bond in such a way that reversible cleavage is facilitated. Similar results were obtained for reactions with *o*-, *m*-, and *p*-toluidines.

In contrast, **4** survives extended reflux in toluene or reaction with HCl and therefore appears to be the thermodynamic product under the reaction conditions investigated. The fact that the imido complexes **4**–**7** carry a formal positive charge may account for the observed resistance toward protonation and the failure to form derivatives with $ClSiMe_3$ or MeCOCl (cf. experimental).

Formation of the proposed nitrido-derivative W(N)(*t*-BucalixH) (**9**) as a major toluene soluble product from the reaction of W(*Bu*^{t}calix)Cl_2 (**2**) with aliphatic 1° and 2° amines but not from aniline or toluidines requires explanation. Literature precedent for related C—N bond cleavage reactions, which form the basis for use of imido complexes as CVD sources of metal nitrides (39), derives from a thermal, Hoffman-like β-elimination (40, 41) observed for the conversion of the amido $Ta(NEt_2)_5$ to the imido–amido product (EtN) = $Ta(NEt_2)_3$ and ethylene. The proposed mechanism for the aliphatic analogs of **4**–**7** is illustrated in Scheme 3. Further examples involving an alternative S_N, N—C cleavage of $Os(O)_3$(N*t*-Bu) can be found in Nugent and Mayer's (42) anthology on metal—ligand multiple bonds. Alternatively, the C—N bond cleavage may be viewed as the reverse of nitrido alkylation (1) in which S_N2 nucleophilic attack (42) (cf. Scheme 3) of chloride at C_α results in formation of alkyl halide and **9**. The observation that benzylamine also provides **9** in good yield suggests that the S_N2 mechanism may in fact be more likely in the present case.

Clearly, either mechanism is impossible for the aniline-and toluidine-derived imido complexes **4**–**7** hence **9** is only observed in trace amounts.

© 2001 NRC Canada

Conclusion

A tetradentate tungsten(VI) imido calix[4]arene complex $[W(NPh)(t\text{-BucalixH})]^+Cl^-$ (**4**) has been isolated from the reaction of $W(NPh)Cl_4$ with *p-tert*-butyl-calix[4]arene (t-BucalixH_4) as the thermodynamic product in a series of reactions involving formation of a putative bidentate calix[4]arene tungsten-imido intermediate $W(NPh)(t\text{-Bu calix}H_2)Cl_2$ (**3**) which partitions by reversible cleavage of the W-imido link to form $W(t\text{-Bucalix})Cl_2$ and HCl, and elimination of a further equiv of HCl to form the isolated imido product **4**. Imido complex **4** and an isostructural series of cationic tetradentate tungsten-imido species of the type $[W(NAr)(t\text{-BucalixH})]^+Cl^-$ (**5**–**7**) with a partially flattened cone conformation have been rationally synthesized from the reaction of $W(t\text{-Bucalix})Cl_2$ (**2**) and NH_2Ar. The imido substituent determines the stability of the imido adduct and reaction of **2** with aliphatic 1° and 2° amines results in an unstable imido complex which cleaves the C—N bond to form the nitrido adduct **9**.

Acknowledgements

CRJ gratefully acknowledges financial support from the Natural Sciences and Engineering Research Council of Canada (NSERC) and Memorial University. We thank Dr. J. Banoub, DFO, St John's, for the ESMS data and Dr. S. Cheatham, Varian Associates, Palo Alto, for the 500 MHz NMR data. We are indebted to Dr. R. McDonald, University of Alberta for collecting the crystallographic data and to Mr. D. Miller, Memorial X-ray Unit, for refinement of the X-ray structure of complex **8**.

References

1. W.A. Nugent and B.L. Haymore. Coord. Chem. Rev. **31**, 123 (1980).
2. C. Wieser, C.B. Dieleman, and D. Matt. Coord. Chem. Rev. **165**, 93 (1997).
3. D.E. Wigley. Prog. Inorg. Chem. **42**, 239 (1994).
4. R.J. Schrock, C.D. Dewan, and C.J. Schaverien. J. Am. Chem. Soc. **108**, 2771 (1986).
5. T.S. Lewkebandara, P.H. Sheridan, M.J. Heeg, A.L. Rheingold, and C.H. Winter. Inorg. Chem. **33**, 5879 (1994).
6. T.I. Gountchev and T.D. Tilley. J. Am. Chem. Soc. **119**, 12831 (1997).
7. S.F. Pederson and R.R. Schrock. J. Am. Chem. Soc. **104**, 7483 (1982).
8. W.A. Nugent, R.J. McKinney, R.V. Kasowski, and F.A. Van-Catledge. Inorg. Chim. Acta, **65**, L91 (1982).
9. D.C. Bradley, S.R. Hodge, J.D. Runnacles, M. Hughes, J. Mason, and L.R. Raymond. J. Chem. Soc. Dalton Trans. 1663 (1992).
10. R.R. Schrock, R.T. DePue, J. Feldman, K.B. Yap, D.C. Yang, W.M. Davis, L. Park, M. Dilare, M. Schofield, J. Anhaus, E. Walborsky, E. Evitt, C. Kruger, and P. Betz. Organometallics, **9**, 2262 (1990).
11. T.R. Cundari. J. Am. Chem. Soc. **114**, 7879 (1992).
12. W. Verboom, P.J. Bodewes, G. Vanessen, P. Timmerman, G.J. Vanhummel, S. Harkema, and D.N. Reinhoudt. Tetrahedron, **51**, 499 (1995).
13. D.K. Fu, B. Xu, and T.M. Swager. J. Org. Chem. **61**, 802 (1996).
14. T. Mochizuki, S. Hayakawa, and K. Narasaka. Bull. Chem. Soc. Jpn. **69**, 2317 (1996).
15. G.D. Andreetti, V. Bohmer, J.G. Jordon, M. Tabatabai, F. Ugozzoli, W. Vogt, and A. Wolff. J. Org. Chem. **58**, 4023 (1993).
16. S. Caccamese, G. Principato, C. Geraci, and P. Neri. Tetrahedron: Asymmetry, **8**, 1169 (1997).
17. V.C. Gibson, T.P. Kee, and A. Shaw. Polyhedron, **7**, 579 (1988).
18. F. Corazza, C. Floriani, A. Chiesi-Villa, and C. Rizzoli. Inorg. Chem. **30**, 4465 (1991).
19. G.M. Sheldrick. SHELX-97. Program for the refinement of crystal structures. University of Göttingen, Germany. 1997.
20. A. Altomare, M. Cascarano, C. Giacovazzo, and A. Guagliardi. J. Appl. Crystallogr. **26**, 343 (1993).
21. P.T. Beurskins, G. Admiraal, G. Beurskins, W.P. Bosman, R. deGelder, R. Israel, and J.M.M. Smits. Technical Report of the Crystallography Laboratory, University of Nijmegen, The Netherlands. 1994.
22. D.T. Cromer and J.T. Waber. *In* International tables for x-ray crystallography. Vol. 4. Kynoch Press, Birmingham. 1974. Table 2.2A.
23. J.A. Ibers and W.C. Hamilton. Acta Crystallogr. **17**, 781 (1964).
24. D.C. Creagh and W.J. McAuley. *In* International tables for crystallography. Vol. C. Kluwer Academic Publishers, Boston. 1992. pp. 219–222.
25. D.C. Creagh and J.H. Hubbell. *In* International tables for crystallography. Vol. C. Kluwer Academic Publishers, Boston. 1992. pp. 200–206.
26. teXsan. teXsan for Windows: crystal structure analysis package. Molecular Structure Corp. 1997.
27. F. Corazza, C. Floriani, A. Chiesi-Villa, and C. Guastini. J. Chem. Soc. Chem. Commun. 1083 (1990).
28. B. Castellano, A. Zanotti-Gerosa, E. Solari, C. Floriani, A. Chiesi-Villa, and C. Rizzoli. Organometallics, **15,** 4894 (1996).
29. A. Lehtonen and R. Sillanpaa. Polyhedron, **17**, 3327 (1998).
30. U. Radius and J. Attner. Eur. J. Inorg. Chem. 299 (1998).
31. J. McInness, D. Swallow, A.J. Blake, and P. Mountford. Inorg. Chem. **37**, 5970 (1998).
32. C.D. Gutsche, B. Dhawan, J.A. Levine, H.K. No, and L.J. Bauer. Tetrahedron, **39**, 409 (1983).
33. J.L. Atwood, M.G. Gardiner, C. Jones, C.L. Raston, B.W. Skelton, and A.H. White. Chem. Comm. (Cambridge), 2487 (1996).
34. C. Jaime, J. de Mendoza, P. Prados, P.M. Nieto, and C. Sanchez. J. Org. Chem. **56**, 3372 (1991).
35. V.C. Gibson, C. Redshaw, W. Clegg, and M.R. Elsegood. J. Chem. Soc. Chem. Commun. 2371 (1995).
36. R.R. Schrock. J. Am. Chem. Soc. **110**, 2686 (1988).
37. D.C. Bradley, R.J. Errington, M.B. Hursthouse, and R.L. Short. J. Chem. Soc. Dalton Trans. 1043 (1990).
38. S.V. Shevchuk, E.A. Alexeeva, N.V. Rusakova, Y.V. Korovin, V.A. Bacherikov, and A.I. Gren. Mendeleev Commun. 112 (1998).
39. C.J. Carmalt, S.R. Whaley, P.S. Lall, A.H. Cowley, R.A. Jones, B.G. McBurnett, and J.G. Ekerdt. J. Chem. Soc. Dalton Trans. 553 (1998).
40. D.C. Bradley and I.M. Thomas. Can. J. Chem. **40**, 1355 (1962).
41. Y. Takahashi, N. Onoyama, and Y. Ishikawa. Chem. Lett. 525 (1978).
42. W. Nugent and J.M. Mayer. *In* Metal-ligand multiple bonds: the chemistry of transition metal complexes containing oxo, nitrido, imido, alkylidene, or alkylidyne ligands. Wiley-Interscience, New York. 1988.

© 2001 NRC Canada

On the reduction of rhodium trichloride in the presence of triisopropylphosphine

David C.D. Butler, Duncan W. Bruce, Philip Lightfoot, and David J. Cole-Hamilton

Abstract: The reduction of $RhCl_3 \cdot 3H_2O$ by sodium amalgam in the presence of P-*i*-Pr_3 has been reexamined. Reaction of $RhCl_3 \cdot 3H_2O$ with P-*i*-Pr_3 in THF gives *i*-Pr_3PO and $[RhHCl_2(P\text{-}i\text{-}Pr_3)_2]$ or $[RhDCl_2(P\text{-}i\text{-}Pr_3)_2]$ if D_2O is added. Further reaction of $[RhHCl_2(P\text{-}i\text{-}Pr_3)_2]$ with P-*i*-Pr_3 gives $[i\text{-}Pr_3PH][RhHCl_3(P\text{-}i\text{-}Pr_3)_2]$, which reversibly dissociates to $[RhHCl_2(P\text{-}i\text{-}Pr_3)_2]$ and $[i\text{-}Pr_3PH]Cl$ at high temperatures in solution. Sodium amalgam reduction of $[RhHCl_2(P\text{-}i\text{-}Pr_3)_2]$ in THF containing P-*i*-Pr_3 gives $[RhH(P\text{-}i\text{-}Pr_3)_3]$ if water is rigorously excluded, but $[RhH_2Cl(P\text{-}i\text{-}Pr_3)_2]$ if water is present.

Key words: rhodium, trisiopropylphosphine, hydride, reduction.

Résumé : On a réétudié la réduction du $RhCl_3 \cdot 3H_2O$ par l'amalgame de sodium en présence de P-*i*-Pr_3 . La réaction du $RhCl_3 \cdot 3H_2O$ avec le P-*i*-Pr_3 dans le THF conduit à la formation de $[RhHCl_2(P\text{-}i\text{-}Pr_3)_2]$ ou au $[RhDCl_2(P\text{-}i\text{-}Pr_3)_2]$ si on ajoute du D_2O. Une réaction subséquente de $[RhHCl_2(P\text{-}i\text{-}Pr_3)_2]$ avec un excès de P-*i*-Pr_3 conduit à la formation de $[i\text{-}Pr_3PH][RhHCl_3(P\text{-}i\text{-}Pr_3)_2]$ qui, en solution à haute température, se dissocie de façon réversible en $[RhHCl_2(P\text{-}i\text{-}Pr_3)_2]$ et $[i\text{-}Pr_3PH]Cl$. La réduction du $[RhHCl_2(P\text{-}i\text{-}Pr_3)_2]$ par l'amalgame de sodium dans du THF qui contient du P-*i*-Pr_3 conduit à la formation de $[RhHCl(P\text{-}i\text{-}Pr_3)_3]$ si le milieu est strictement anhydre; toutefois, si le solvant contient de l'eau, il y a formation de $[RhH_2Cl(P\text{-}i\text{-}Pr_3)_2]$.

Mots clés : rhodium, trisisopropylphosphine, hydrure, réduction.

[Traduit par la Rédaction]

Introduction

$[RhH(P\text{-}i\text{-}Pr_3)_3]$ has been shown to be an active catalyst for the water gas shift reaction (WGSR) (1, 2) and for the photochemical dehydrogenation of alcohols (3, 4). It also reacts oxidatively with water (5), and ketones (6). It has generally been prepared from the reaction of $RhCl_3 \cdot 3H_2O$ with P-*i*-Pr_3 under nitrogen, followed by evaporation to dryness and reduction with sodium amalgam in dry THF (7). The source of the hydride was believed to be the THF. During the course of studies of a variety of catalytic reactions using low-valent rhodium trialkylphosphine complexes (3, 4, 8), we have reexamined this reaction, as well as a number of similar reactions carried out under related conditions. We now report the results of these studies. An alternative synthesis of $[RhH(P\text{-}i\text{-}Pr_3)_3]$ by reaction of $[RhH_2Cl(P\text{-}i\text{-}Pr_3)_2]$ with KO-*t*-Bu has been reported (9).

Received September 7, 2000. Published on the NRC Research Press Web site at http://canjchem.nrc.ca on May 30, 2001.

Dedicated to Professor Brian James on the occasion of his 65th birthday.

D.C.D. Butler, P. Lightfoot, and D.J. Cole-Hamilton.[1] School of Chemistry, University of St. Andrews, St. Andrews, Fife, KY16 9ST, Scotland.
D.W. Bruce. School of Chemistry, University of Exeter, Stocker Road, Exeter, EX4 4QD, U.K.

[1]Corresponding author (telephone: (44) 1334-463805; fax: (44) 1334-463808; e-mail: djc@st-and.ac.uk).

Experimental

Microanalyses were done by the Universities of Liverpool's and St. Andrews' Microanalytical Services. NMR spectra were recorded on a Varian Gemini 2000 or a Brüker Associates AM 300 spectrometer operating in the Fourier transform mode with, for ^{31}P, broadband proton decoupling, and FT IR spectra were recorded as Nujol™ mulls between CsI plates on Nicolet Protégé 460 Magna or PerkinElmer PE 1710 spectrometers.

All manipulations were carried out using standard Schlenk line catheter tubing techniques under nitrogen purified by passing through a glass column containing Cr(II) absorbed onto silica. Petroleum ether (boiling range 40–60°C), diethylether, and THF were distilled over sodium diphenylketyl and degassed before use. Dichloromethane was dried by refluxing over CaH_2.

$RhCl_3 \cdot 3H_2O$ (Johnson Matthey, Royston, England), and other commercial chemicals were used as received. P-*i*-Pr_3 was either purchased from Strem, Royston, England or prepared by a standard method (10).

Dichlorohydridobis(triisopropylphosphine)rhodium(I)

$RhCl_3 \cdot 3H_2O$ (0.49 g, 1.86 mmol) was refluxed in THF (35 cm^3) with P-*i*-Pr_3 (0.8 cm^3, 4 mmol) for 3 h. On cooling, the orange solution was filtered, reduced in vacuo and cooled to –30°C for 72 h. The resulting orange crystals were recovered by filtration and washed with light petroleum (2 × 10 cm^3) to remove any free P-*i*-Pr_3. Recrystallization was from CH_2Cl_2–light petroleum. Yields of this reaction are very variable (20–50%). Anal. calcd. for $C_{18}H_{43}Cl_2P_2Rh$ (%): C 43.7, H 8.7, P 12.5, Cl 14.3; found: C 43.6, H 8.7,

 DOI: 10.1139/cjc-79-5/6-472 © 2001 NRC Canada

P 12.5, Cl 14.8. It was identified by comparison with a sample prepared by lit. method (11).

An increased yield could be obtained as follows: $RhCl_3 \cdot 3H_2O$ (1.04 g, 4.97 mmol) was dissolved in THF (50 cm^3). Water (10 cm^3), P-*i*-Pr_3 (2.5 cm^3, 12.5 mmol), and HCl (4 drops, concd) were added and the mixture was refluxed with stirring for 18 h under argon. The resulting red solution was dried in vacuo at 45°C to remove residual water, then washed with diethyl ether (2 x 15 cm^3) and water (2 × 5 cm^3) before drying thoroughly. Yield: 2.4 g, 99%. The spectroscopic data from samples prepared in this way were identical to those from samples prepared as above, but the microanalytical data suggests some contamination with HCl. Anal. calcd. for $C_{18}H_{43}Cl_2P_2Rh$ (%): C 43.7, H 8.7; found: C 41.5, H 8.5. Anal. cald. for $C_{18}H_{44}Cl_3P_2Rh$ (%): C 40.6, H 8.2.

Dichlorodeuteridobis(triisopropylphosphine)rhodium(I)

Prepared as above but using $RhCl_3 \cdot 3H_2O$ (0.49 g, 1.86 mmol), P-*i*-Pr_3 (1.2 cm^3, 6 mmol), and D_2O (5 cm^3) containing DCl (1 cm^3, 20% in D_2O) in THF (35 cm^3). The final product was not washed with H_2O. FT IR λ_{max} (cm^{-1}): 1380 (RhD). ^{2}D NMR (46.076 MHz, CH_2Cl_2) δ: –30.1 (RhD).

Triisopropylphosphonium trichlorohydridobis(triisopropylphosphine)rhodium(I) tetrahydro-uran

$[RhHCl_2(P\text{-}i\text{-}Pr_3)_2]$ (0.14 g, 0.28 mmol) prepared by the higher yield method described above, and therefore containing HCl, was refluxed for 3 h in THF (4 cm^3) containing P-*i*-Pr_3 (0.3 cm^3, 1.5 mmol). On cooling slowly, orange crystals separated. These were stored under the mother liquors to prevent decomposition and collected by filtration to obtain the NMR spectra. The instability of this complex and the requirement to store it under the mother liquors means that the yield has not been measured. FT IR λ_{max} (cm^{-1}): 1943 (RhH). ^{1}H NMR (300.13 MHz, CD_2Cl_2) δ: (298 K): –30.3 (br s, RhH), 8.1 (d, $J_{P,H}$ = 492 Hz, PH); (193 K) δ: –21.0 (br s, RhH), 8.1 (d, $J_{P,H}$ = 492 Hz, PH); (308 K): –30.3 (dt, $J_{Rh,H}$ = 12.8, $J_{P,H}$ = 31.3 Hz, RhH), 8.1 (d, $J_{P,H}$ = 492 Hz, PH). ^{31}P NMR (121.497 MHz, CD_2Cl_2) δ: (298 K): 43.5 (br d, $J_{Rh,P}$ = 96 Hz, RhP), 32.7 (s, HP); (183 K): 29.2 (d, $J_{Rh,P}$ = 97 Hz, RhP), 32.2 (s, HP); (308 K): 44.5 (br d, $J_{Rh,P}$ = 97 Hz, RhP), 32.8 (s, HP). Microanalytical data were variable, but an example is: anal. calcd. for $C_{31}H_{68}Cl_3OP_3Rh$ (%): C 50.0, H 9.1; found: C 47.4, H 9.5.

Reduction of $[RhHCl_2(P\text{-}i\text{-}Pr_3)_2]$ in dry THF

A suspension of $[RhHCl_2(P\text{-}i\text{-}Pr_3)_2]$ (0.5 g, 1.01 mmol), prepared by lit. method (11), in THF containing P-*i*-Pr_3 (1.5 cm^3, 7.5 mmol) was stirred with Na–Hg (140 g, 0.7%) for 18 h. The resulting solution was decanted from the amalgam, which was washed with THF (5 cm^3), and the washing combined with the original solution. The solvent was removed in vacuo and the resulting yellow-brown tar was extracted with light petroleum (3 × 5 cm^3) to give a yellow solution, which was filtered through Celite. The volume was reduced to 3 cm^3 and P-*i*-Pr_3 (15 drops) added, prior to cooling to –30°C for 24 h. The yellow crystals that formed were collected by filtration and washed with cold light petroleum. The crystals were unstable to air and slowly melted in the solid state even under argon when stored at 4°C. Solutions in light petroleum were more stable.

The spectroscopic properties of the product from this reaction were identical to those of a batch obtained by the reaction of $[RhH_2Cl(P\text{-}i\text{-}Pr_3)_2]$ with KO-*t*-Bu (9), but differed from the literature values. FT IR λ_{max} (cm^{-1}): 1960 (RhH) (lit. 7 value 1975). ^{1}H NMR (300.13 MHz, CD_2Cl_2) δ: (298 K): –11.6 (dd on a br hump, RhH) (lit. 7 value –10.5, complex multiplet); (213 K): –11.2 (second order pattern, resembles dddd, RhH). ^{31}P NMR (121.497 MHz, CD_2Cl_2) δ: (298 K): 53.6 (d, $J_{Rh,P}$ = 157 Hz) (lit. 5 value 58.8 (d, $J_{Rh,P}$ = 157 Hz)) (lit. 12 value 32.2 (d, $J_{Rh,P}$ = 157 Hz)). The properties of the compound including the exchange of Rh-H for D in C_6D_6 or in $C_6D_4CD_3$ (5), make us confident that the product is $[RhH(P\text{-}i\text{-}Pr_3)_3]$.

Chlorodihydridobis(triisopropylphosphine)rhodium(I)

A suspension of $[RhHCl_2(P\text{-}i\text{-}Pr_3)_2]$ (1.44 g, 2.90 mmol), prepared by lit. method (11), in THF containing P-*i*-Pr_3 (0.4 cm^3, 2 mmol) and water (0.2 cm^3, 11 mmol) was stirred with Na–Hg (60 g, 0.3%) under argon until the solution turned yellow (ca. 2 h). This solution was worked up as for $[RhH(P\text{-}i\text{-}Pr_3)_3]$ to give light yellow crystals contaminated with a darker material. This solid was collected by filtration and recrystallized from light petroleum at –30°C. The resulting pale yellow crystals were collected by filtration at –78°C. Yield: 0.7 g, 52%. The complex was identified crystallographically and by comparison of its spectroscopic properties with those in the literature (13). FT IR λ_{max} (cm^{-1}): 2140.

X-ray crystallography

X-ray data were collected at 220 K on a Rigaku AFC7S diffractometer using graphite-monochromated Mo Kα radiation (λ = 0.71069 Å). The structures were solved using direct methods (14) and expanded using Fourier techniques. The non-hydrogen atoms were refined anisotropically. For $[RhH_2Cl(P\text{-}i\text{-}Pr_3)_2]$, the hydrogen atoms on Rh were refined isotropically, the rest were included in fixed positions. For $[i\text{-}Pr_3PH][RhHCl_3(P\text{-}i\text{-}Pr_3)_2]$, hydrogen atoms were included but not refined. Neutral atom scattering factors were taken from the literature (15). Anomolous dispersion effects, Lorentz, and polarization corrections were applied. All calculations were performed using the teXsan (16) crystallographic software package. Crystal data, along with the structure solution and refinement parameters are listed in Table 1. CCDC reference numbers: $[RhH_2Cl(P\text{-}i\text{-}Pr_3)_2]$ 163 735, $[i\text{-}Pr_3PH][RhHCl_3(P\text{-}i\text{-}Pr_3)_2]$ 163 736.[2]

Results and discussion

Reaction of $RhCl_3 \cdot 3H_2O$ with excess P-*i*-Pr_3 in THF produces $[RhHCl_2(P\text{-}i\text{-}Pr_3)_2]$, which has also been prepared by refluxing $RhCl_3 \cdot 3H_2O$ with P-*i*-Pr_3 in wet propan-2-ol (11, 17), and shown crystallographically to be square pyramidal with an apical hydride (18). *i*-Pr_3PO is also a product,

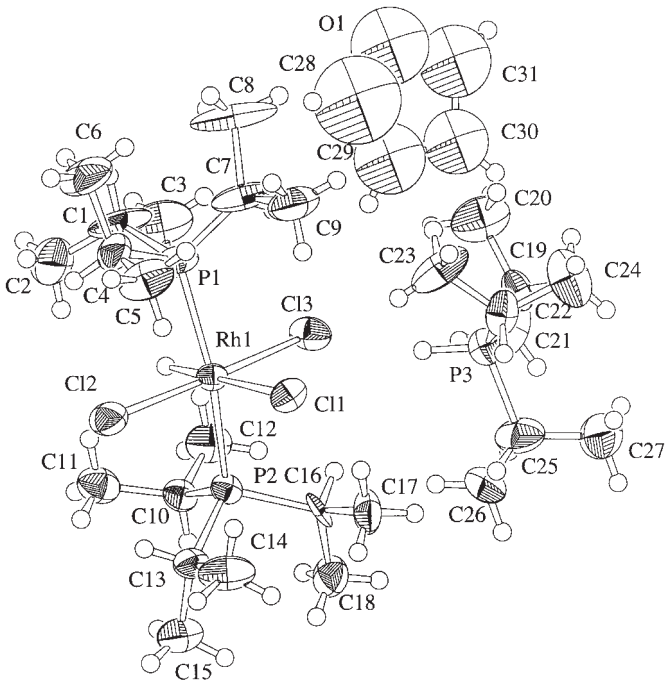
[2] This supplementary material has also been deposited with, and may be purchased from, the Depository of Unpublished Data, Document Delivery, CISTI, National Research Council Canada, Ottawa, ON K1A 0S2, Canada, DUD No. 3275. For information on obtaining material electronically go to http://www.nrc.ca/cisti/irm/unpub_e.shtml.

© 2001 NRC Canada

Table 1. Summary of data collection, structure solution, and refinement for [*i*-Pr_3PH][$RhHCl_3$(P-*i*-$Pr_3)_2$] and [$RhHCl_2$(P-*i*-$Pr_3)_2$].

Compound	[*i*-Pr_3PH][$RhHCl_3$(P-*i*-$Pr_3)_2$]·THF	[RhH_2Cl(P-*i*-$Pr_3)_2$]
Empirical formula	$C_{31}H_{69}Cl_3OP_3Rh$	$C_{18}H_{44}ClP_2Rh$
Formula weight	759.06	460.85
Crystal system	Triclinic	Monoclinic
Lattice parameters		
a (Å)	11.60(1)	13.095(2)
b (Å)	15.86(2)	12.614(4)
c (Å).	11.345(4)	14.621(4)
α (°)	95.55(5)	—
β (°)	93.33(5)	100.17(2)
γ (°)	94.66(9)	—
V (Å^3)	2066(2)	2377(1)
Space group	*P*1 (no. 2)	$P2_1/n$ (no. 14)
Z value	2	4
μ (Mo Kα) (cm^{-1})	7.42	9.61
Temperature (K)	220.0	220.0
No. of observations ($I > 3.00\sigma(I)$)	3303	3313
No. of variables	327	207
Reflection / parameter ratio	10.10	16.00
Residuals: *R*, *Rw*	0.099, 0.136	0.025, 0.023
Goodness of Fit indicator	6.79	1.92

Fig. 1. X-ray structure and numbering scheme for [*i*-Pr_3PH][$RhHCl_3$(P-*i*-$Pr_3)_2$]·THF.



suggesting that the reaction may proceed via reduction of the rhodium by P-*i*-Pr_3. The final product is then formed by oxidative addition of HCl. That the hydride comes from the water in $RhCl_3·3H_2O$ rather than from THF is confirmed by carrying out the reaction in THF in the presence of D_2O to give [$RhDCl_2$(P-*i*-$Pr_3)_2$] (FT IR: 1380 cm^{-1} (RhD) ($\nu_{Rh,H}$ / $\nu_{Rh,D}$ = 1.41), ^{2}D NMR δ: –30.1 (RhD)).[3] The need for water and excess P-*i*-Pr_3 in this reaction means that the yield of [$RhHCl_2$(P-*i*-$Pr_3)_2$] can be increased by carrying out the reaction in the presence of excess P-*i*-Pr_3, added water, and HCl, but it is difficult to remove the last traces of HCl.

Further reaction of [$RhHCl_2$(P-*i*-$Pr_3)_2$], produced from the reaction of $RhCl_3·3H_2O$ with P-*i*-Pr_3 in THF containing aqueous HCl, produced a yellow solution, from which yellow-orange crystals could be isolated. The NMR spectra of this compound were broad at room temperature (see below), but an X-ray structural determination (Fig. 1, Table 2) showed it to be [*i*-Pr_3PH][$RhHCl_3$(P-*i*-$Pr_3)_2$] with an octahedral rhodium centre and mutually *trans* phosphine ligands. At room temperature, the ^{1}H NMR spectrum shows a doublet at δ 8.1 ($J_{P,H}$ = 492 Hz) from the H of the phosphonium ion, and a broad hydride signal at δ –30.3, a position similar to that of [$RhHCl_2$(P-*i*-$Pr_3)_2$], whilst the ^{31}P NMR spectrum consists of a broad doublet at δ 43.5 ($J_{Rh,P}$ = 95.5 Hz). Variable-temperature ^{31}P and ^{1}H NMR studies (Figs. 2 and 3) show the phosphonium cation does not exchange with the bound P-*i*-Pr_3, resonating as a singlet (δ = 32–34 at all temperatures). The broadening of this signal in the spectrum measured at 308 K may indicate that exchange would occur at higher temperatures. Changes do occur, however, in the resonance due to the rhodium bound phosphines, which exhibit a doublet at δ –29.2 ($J_{Rh,P}$ = 97 Hz) at –183 K. On warming, this doublet broadens and shifts to lower field before sharpening to a doublet at δ 43 ($J_{Rh,P}$ = 95.6 Hz). The hydride resonance in the ^{1}H NMR spectrum at 193 K is a singlet at δ –21, but this also broadens on warming and moves to higher field sharpening to a doublet of triplets at δ –30.3 (dt, $J_{Rh,H}$ = 12.8, $J_{P,H}$ = 31.3 Hz). The high-temperature limiting spectrum of the rhodium containing

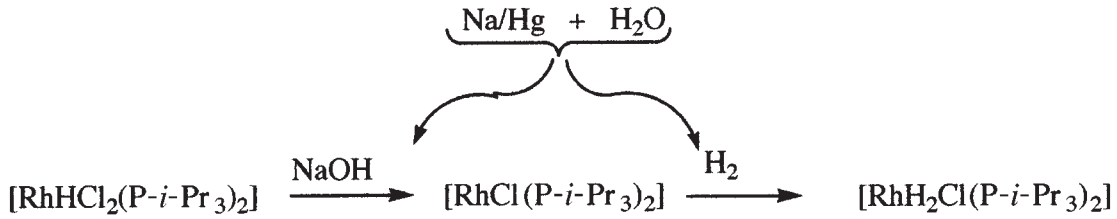
[3] It is also possible that D could be incorporated by exchange of [$RhHCl_2$(P-*i*-$Pr_3)_2$] with D_2O after its formation, but the increased yield in the presence of water suggests that water is the direct source of the hydride.

© 2001 NRC Canada

Table 2. Selected bond lengths (Å) and angles (°) for [*i*-Pr_3PH][$RhHCl_3$(P-*i*-Pr_3)$_2$]·THF, compared with related data for [$RhHCl_2$(P-*i*-Pr_3)$_2$] (18).

	[*i*-Pr_3PH][$RhHCl_3$(P-*i*-Pr_3)$_2$]·THF	[$RhHCl_2$(P-*i*-Pr_3)$_2$]
Bond lengths		
Rh(1)—Cl(1)	2.578(6)	—
Rh(1)—Cl(2)	2.362(7)	2.342(1)
Rh(1)—Cl(3)	2.360(7)	2.342(1)
Rh(1)—P(1)	2.365(6)	2.367(1)
Rh(1)—P(2)	2.366(6)	2.367(1)
P(1)—Cl(1)	3.88	—
Bond angles		
Cl(1)-Rh(1)-Cl(2)	92.3(2)	—
Cl(1)-Rh(1)-Cl(3)	91.1(3)	—
Cl(1)-Rh(1)-P(1)	96.2(2)	—
Cl(1)-Rh(1)-P(2)	99.0(2)	—
P(1)-Rh(1)-P(2)	164.8(2)	—
Cl(2)-Rh(1)-P(1)	90.0(2)	90.05(0)
Cl(2)-Rh(1)-P(2)	89.2(2)	89.95(2)
Cl(3)-Rh(1)-P(1)	89.4(2)	89.95(2)
Cl(3)-Rh(1)-P(2)	90.5(2)	90.05(2)

Scheme 1. Proposed reactions involved in the formation of [RhH_2Cl(P-*i*-Pr_3)$_2$] from Na–Hg reduction of [$RhHCl_2$(P-*i*-Pr_3)$_2$] in the presence of water.



species is the same as that for [$RhHCl_2$(P-*i*-Pr_3)$_2$] (18), so that [*i*-Pr_3PH][$RhHCl_3$(P-*i*-Pr_3)$_2$] is only stable at lower temperatures, losing Cl^- from the rhodium on warming.

Reduction of [$RhHCl_2$(P-*i*-Pr_3)$_2$] with Na–Hg in THF containing P-*i*-Pr_3 leads to the formation of [RhH(P-*i*-Pr_3)$_3$] as might be expected. However, the reaction shows poor reproducibility and variable yield, and is better carried out under argon. If the reaction is carried out under nitrogen, spectroscopic studies show the presence of a mixture of compounds, possibly [RhH(P-*i*-Pr_3)$_2$] or [RhH(P-*i*-Pr_3)$_2$]$_2$ (μ-N_2) (δ = 66 (d, $J_{P,Rh}$ = 162 Hz, P); δ = –15.0 (dt, $J_{Rh,H}$ = 17.0, $J_{P,H}$ = 20.8 Hz, RhH)) (7) and [RhH(N_2)(P-*i*-Pr_3)$_2$] (δ = 67 (d, $J_{P,Rh}$ = 158 Hz, P); δ = –13.6 (dt, $J_{Rh,H}$ = 18.4, $J_{P,H}$ = 18.2 Hz, RhH)) (7), but [RhH(P-*i*-Pr_3)$_3$] can be recovered from this solution by evaporation to dryness and recrystallization from light petroleum in the presence of excess P-*i*-Pr_3.

On some occasions, attempts to prepare [RhH(P-*i*-Pr_3)$_3$] from the reaction of $RhCl_3$·$3H_2O$ with P-*i*-Pr_3 followed by evaporation to dryness and reduction with sodium amalgam led to a different yellow complex, which crystallizes as yellow plates, for which the spectroscopic properties suggest [RhH_2Cl(P-*i*-Pr_3)$_2$]. This formulation has been confirmed crystallographically, although a different polymorph is obtained from that described previously (18). Detailed studies have shown that this product arises if water remains after evaporation of the solution formed in the first step of the reaction to "dryness". The probable mechanism of formation of the dihydrido complex is shown in Scheme 1 and involves NaOH formed from the reaction of water with Na–Hg, removing HCl from [$RhHCl_2$(P-*i*-Pr_3)$_2$] to give [RhCl(P-*i*-Pr_3)$_2$] (13), which reacts with hydrogen, also produced from water and Na–Hg, to give the final product. This mechanism is supported by the reports that [$RhHCl_2$(P-*i*-Pr_3)$_2$] reacts with H_2 in 50% NaOH–benzene mixtures under phase transfer conditions to give [RhH_2Cl(P-*i*-Pr_3)$_2$] (19), and that [RhCl(P-*i*-Pr_3)$_2$] gives the same product on reaction with H_2 in benzene (13). We find the yield from these reactions can be quite low and variable, but a reproducible synthesis of the dihydride, which occurs in 50% yield, involves reaction of [$RhHCl_2$(P-*i*-Pr_3)$_2$], prepared by the lit. method (11), over sodium amalgam in the presence of THF, P-*i*-Pr_3, and water for 2 h. Prolonged stirring leads to a green solution, from which we have not isolated any pure complexes.

X-ray crystal and molecular structure of [RhH_2Cl(P-*i*-Pr_3)$_2$]

A previous structure of [RhH_2Cl(P-*i*-Pr_3)$_2$] (18) showed it to be triclinic with space group *P*1 and containing two independent molecules in the asymmetric unit. One of these had a pseudo-twofold axis passing through the Rh and Cl atoms, whilst in the other, this axis was destroyed by different orientations in the P-*i*-Pr_3 groups. Samples of [RhH_2Cl(P-*i*-

© 2001 NRC Canada

Fig. 2. Variable temperature ^{31}P NMR spectra for [*i*-Pr_3PH][$RhHCl_3$(P-*i*-Pr_3)$_2$] (in CD_2Cl_2).

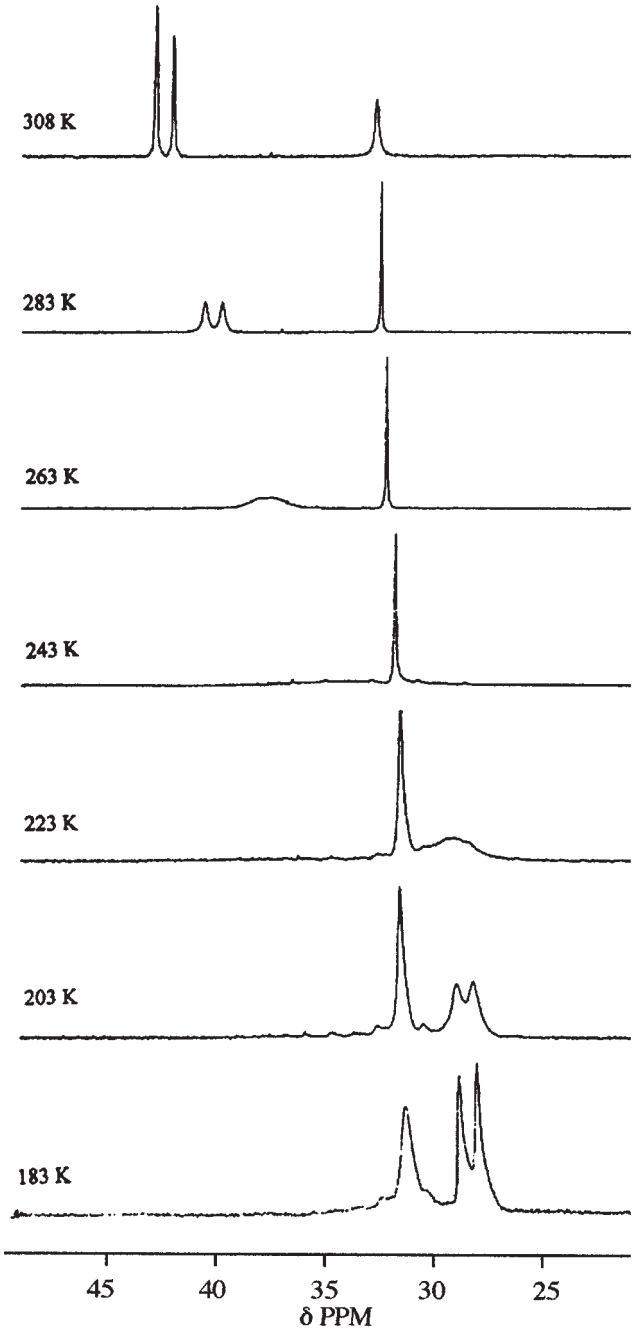
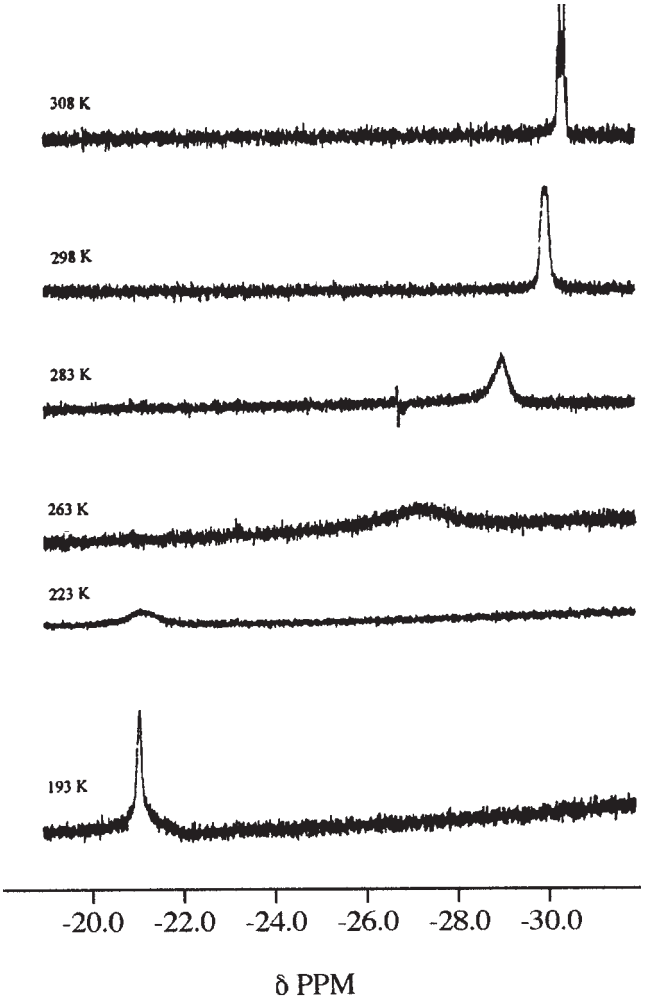


Fig. 3. Variable temperature ^1H NMR spectra for [*i*-Pr_3PH][$RhHCl_3$(P-*i*-Pr_3)$_2$] (in CD_2Cl_2).



$Pr_3)_2$] prepared from the reaction of $RhCl_3 \cdot H_2O$ with P-*i*-Pr_3 in THF crystallized in a different space group ($P2_1/n$) and contained only one type of molecule with no pseudo-twofold axis (Fig. 4 and Table 3). The H-Rh-H angle (71°) is slightly more obtuse and the Rh—H distances (1.45(4), 1.51(3) Å) are similar to but less unequal than those previously reported. The amount of "T"-square pyramidal geometry character in our structure is slightly greater, as indicated by the relatively acute Cl-Rh-H(43) angle of 132° and the rather more obtuse Cl-Rh-H(44) angle of 155°. This results in a noticeable distortion of H(43) away from the Cl-Rh-H(44) plane towards one of the P-*i*-Pr_3 ligands. The H—H distance is 1.74 Å, confirming the complex to be a dihydride. The P-Rh-P angle (176.6°) is very similar to those reported for the two independent molecules of the triclinic system (176.6, 175.6°), so it can be concluded that the slight "T"-distortion in our structure is responsible for the longer Rh—Cl, Rh—P, and Rh—H bond lengths (see Table 3).

Crystal and molecular structure of [*i*-Pr_3PH][$RhHCl_3$(P-*i*-Pr_3)$_2$]

The X-ray crystal structure and numbering scheme for [*i*-Pr_3PH][$RhHCl_3$(P-*i*-Pr_3)$_2$] are shown in Fig. 4, with selected bond lengths and angles in Table 2. The crystals are triclinic, space group *P*1 (no. 2). The complex is octahedral with meridional chlorides and Rh-Cl *trans* to hydride being longer by 0.21 Å than those for the mutually *trans* chlorides (which are similar to those observed for [$RhHCl_2$(P-*i*-Pr_3)$_2$]), as expected on account of the large *trans* influence of hydride and possibly weak H-bonding of this Cl atom to the phosphonium cation (see below). The similarity between the structural parameters for [*i*-Pr_3PH][$RhHCl_3$(P-*i*-Pr_3)$_2$], omitting the chloride *trans* to H, and those for [$RhHCl_2$(P-*i*-Pr_3)$_2$] (18) (Table 2) is striking and consistent with the ready loss of Cl^- observed by NMR spectroscopy (see above). The [*i*-Pr_3PH]$^+$ cation is orientated in such a way that the H atom is directed towards the Cl atom *trans* to H, but the P—Cl

© 2001 NRC Canada

Scheme 2. Summary of reactions of rhodium complexes of P-*i*-Pr_3 discussed in this paper.

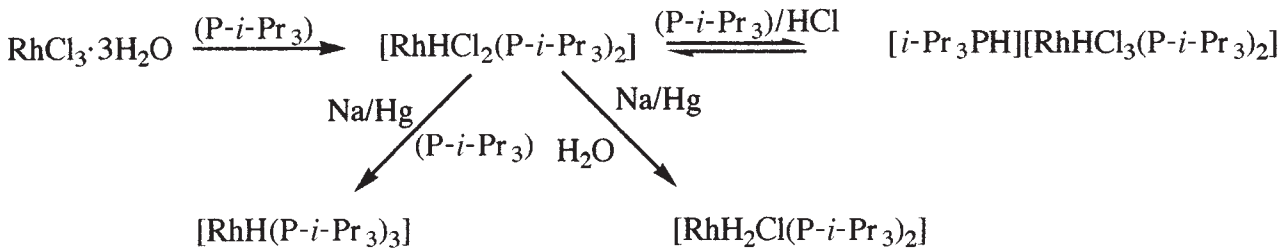
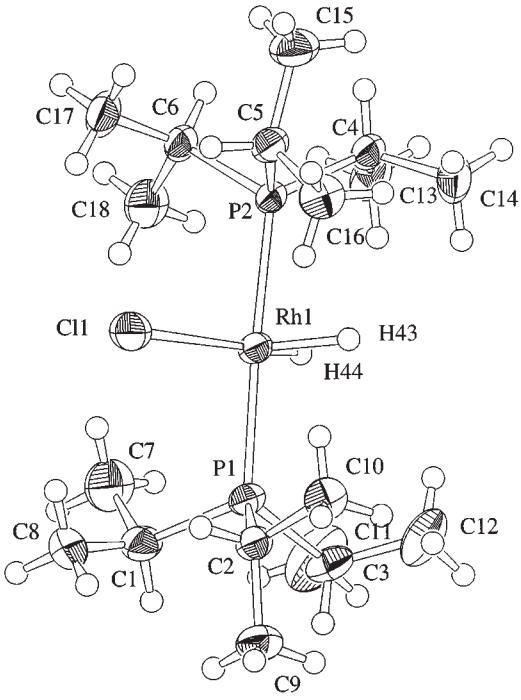


Fig. 4. X-ray structure and numbering scheme for $[RhH_2Cl(P\text{-}i\text{-}Pr_3)_2]$.



distance is 3.88 Å, suggesting that if hydrogen-bonding occurs in the solid state, it is very weak. The reactions discussed in this paper are outlined in Scheme 2.

Conclusions

We conclude that reaction of $RhCl_3 \cdot 3H_2O$ with P-*i*-Pr_3 in THF can lead to $[RhHCl_2(P\text{-}i\text{-}Pr_3)_2]$ or $[i\text{-}Pr_3PH][RhHCl_3(P\text{-}i\text{-}Pr_3)_2]$, depending upon the conditions, with the hydride being derived from the water in $RhCl_3 \cdot 3H_2O$. A better synthesis of $[RhHCl_2(P\text{-}i\text{-}Pr_3)_2]$ involves carrying out the reaction in propan-2-ol (11). Sodium amalgam reduction of in-situ prepared $[RhHCl_2(P\text{-}i\text{-}Pr_3)_2]$ in the presence of excess P-*i*-Pr_3 leads to $[RhH(P\text{-}i\text{-}Pr_3)_3]$ only if water has been rigorously removed. If water is present, $[RhH_2Cl(P\text{-}i\text{-}Pr_3)_2]$, which crystallizes in a different polymorph from that previously reported (18), is obtained.

Acknowledgements

We thank Johnson Matthey plc (D.C.D. Butler), the Engineering and Physical Sciences Research Council (EPSRC) and Shell Agrochemicals (D.W.B.) for studentships, and Johnson Matthey plc, for generous loans of rhodium salts.

Table 3. Selected bond lengths (Å) and angles (°) for $[RhH_2Cl(P\text{-}i\text{-}Pr_3)_2]$, compared with related data for the two molecules of another polymorph of $[RhH_2Cl(P\text{-}i\text{-}Pr_3)_2]$ (18).

		$[RhH_2Cl(P\text{-}i\text{-}Pr_3)_2]$	
	$[RhH_2Cl(P\text{-}i\text{-}Pr_3)_2]$	1	2
Bond lengths			
Rh(1)—Cl(1)	2.4275(9)	2.413(1)	2.422(1)
Rh(1)—P(1)	2.3123(8)	2.307(1)	2.308(1)
Rh(1)—P(2)	2.3097(8)	2.303(1)	2.302(1)
Rh(1)—H(43)	1.45(4)	1.38(3)	1.40(4)
Rh(1)—H(44)	1.51(3)	1.52(3)	1.50(4)
Bond angles			
Cl(1)-Rh(1)-H(43)	132(1)	152(1)	146(2)
P(1)-Rh(1)-H(43)	98(1)	87(1)	85(2)
P(2)-Rh(1)-H(43)	79(1)	89(1)	93(2)
H(43)-Rh(1)-H(44)	71(1)	65(2)	65(2)
Cl(1)-Rh(1)-H(44)	155(1)	143(1)	148(1)
P(1)-Rh(1)-H(44)	89(1)	92(1)	89(1)
P(2)-Rh(1)-H(44)	87(1)	86(1)	87(1)
P(1)-Rh(1)-P(2)	176.60(3)	176.6(1)	175.6(1)
Cl(1)-Rh(1)-P(1)	92.84(3)	92.09(3)	90.67(3)
Cl(1)-Rh(1)-P(2)	90.55(3)	91.20(2)	92.91(3)

References

1. T. Yoshida, T. Okano, and S. Otsuka. J. Am. Chem. Soc. **102**, 5967 (1980).
2. T. Yoshida, T. Okano, Y. Ueda, and S. Otsuka. J. Am. Chem. Soc. **103**, 3411 (1981).
3. D. Morton, D.J. Cole-Hamilton, I.D. Utuk, M. Panaque-Sosa, and M. Lopez-Poveda. J. Chem. Soc. Dalton Trans. 489 (1989).
4. E. Delgado-Lieta, M.A. Luke, R.F. Jones, and D.J. Cole-Hamilton. Polyhedron, **1**, 839 (1982).
5. T. Yoshida, T. Okano, K. Saito, and S. Otsuka. Inorg. Chim. Acta, **44**, L135 (1980).
6. T. Okano and T. Yoshida. Yuki Gosei Kagaku Kyokaishi, **41**, 359 (1983).
7. T. Yoshida, T. Okano, D.L. Thorn, T.H. Tulip, S. Otsuka, and J.A. Ibers. J. Organomet. Chem. **181**, 183 (1979).
8. M.C. Simpson and D.J. Cole-Hamilton. Coord. Chem. Rev. **155**, 163 (1996).
9. J. Wolf, O. Nornberg, and H. Werner. Chem. Ber. **126**, 1409 (1993).
10. A.H. Cowley and J.L. Mills. J. Am. Chem. Soc. **91**, 2915 (1969).
11. V.V. Grushin and H. Alper. Organometallics, **10**, 1620 (1991).
12. T. Yoshida, D.L. Thorn, T. Okano, S. Otsuka, and J.A. Ibers. J. Am. Chem. Soc. **102**, 6451 (1980).

© 2001 NRC Canada

13. H. Werner, J. Wolf, and A. Hohn. J. Organomet. Chem. **287**, 395 (1985).
14. (*a*) SIR 92, A. Altomare, G. Cascarano, G. Giacovazzo, and A. Guagliardi. J. Appl. Crystallogr. **27**, 1045 (1994); (*b*) A. Altomare, C. Giacovazzo, and A. Moltierni. Acta. Crystallogr. Sect. A: Fundam. Crystallogr. **50**, 585 (1994).
15. D.T. Cromer and J.T. Cromer. *In* International tables for X-ray crystallography. Vol. 4. Kynoch Press, Birmingham. 1974. Table 2.2A.
16. TeXsan. Crystal structure analysis package. Molecular Structure Corp., Houston, TX. 1985 and 1992.
17. G.M. Intille. Inorg. Chem. **11**, 695 (1972).
18. R.L. Harlow, D.L. Thorn, R.T. Baker, and N.L. Jones. Inorg. Chem. **31**, 993 (1992).
19. V.V. Grushin, A.B. Vymenits, and M.E. Vol'pin. J. Organomet. Chem. **382**, 185 (1990).

© 2001 NRC Canada

In-depth NMR and IR study of the proton transfer equilibrium between [{(MeC(CH_2PPh_2)$_3$}Ru(CO)H_2] and hexafluoroisopropanol

Vladimir I. Bakhmutov, Ekaterina V. Bakhmutova, Natalia V. Belkova, Claudio Bianchini, Lina M. Epstein, Dante Masi, Maurizio Peruzzini, Elena S. Shubina, Evgenii V. Vorontsov, and Fabrizio Zanobini

Abstract: The (carbonyl)dihydride complex [(triphos)Ru(CO)H_2] (**2**) has been synthesized by reaction of the ruthenate [(triphos)RuH_3]K (triphos = MeC(CH_2PPh_2)$_3$) with ethanol saturated with CO. A single crystal X-ray analysis and IR and NMR experiments have shown that **2** adopts in both the solid state and solution an octahedral coordination geometry with a *facial* triphos ligand, two *cis* terminal hydrides, and a terminal carbonyl. The reaction of hexafluoro-2-propanol (HFIP) with **2** has been studied in CH_2Cl_2 solution by IR and NMR spectroscopy. The proton donor interacts with a terminal hydride of **2** forming a rather strong hydrogen bond. The resulting H-bonded adduct [{(triphos)Ru(CO)(H)H}$\cdots${HOCH(CF_3)$_2$}] (**2a**) has fully been characterized by in situ NMR and IR techniques. Compound **2a** is in equilibrium with the nonclassical η^2-H_2 complex [(triphos)Ru(CO)H(H_2)]$^+$ (**2b**), which can independently be prepared by protonation of **2** with a strong protic acid at low temperature. Unequivocal characterization of the dihydrogen complex (**2b**) has been achieved by a multifaceted spectroscopic investigation (T_{1min}^{obs} = 0.005 s (200 MHz), $J_{H,D} \approx$ 30 Hz, DQCC = 78.3 kHz). A combined IR and NMR study of the proton transfer reaction involving **2** and HFIP in CH_2Cl_2 to give, first, the H-bonded adduct (**2a**) and, then, the dihydrogen complex (**2b**) has demonstrated that all these species are in equilibrium in the temperature range from 190 to 260 K. The thermodynamic parameters for the formation of **2a** have independently been determined by NMR and IR methods, while those for the formation of **2b** have been obtained by IR spectroscopy. An energetic profile for the reaction sequence **2** $\rightarrow$ **2a** $\rightarrow$ **2b** is proposed and discussed.

Key words: hydrides, hydrogen bonding, ruthenium, IR spectroscopy, NMR spectroscopy.

Résumé : On a synthétisé le complexe [(triphos)Ru(CO)H_2] (**2**) (triphos = MeC(CH_2PPh_2)$_3$), un (carbonyl)dihydrure, en faisant réagir le ruthénate [(triphos)RuH_3]K avec de l'éthanol saturé de CO. La diffraction des rayons X sur un cristal unique et des expériences d'IR et de RMN ont permis de montrer que le composé **2**, tant à l'état solide qu'en solution, adopte une géométrie de coordination octaédrique comportant un ligand triphos *facial*, deux hydrures terminaux *cis* et un carbonyle terminal. Faisant appel à la spectroscopie IR et RMN, on a étudié la réaction du composé **2** avec l'hexafluoropropan-2-ol (HFIP) en solution dans le CH_2Cl_2. Le donneur de proton interagit avec un hydrure terminal du composé **2** en formant une liaison hydrogène relativement forte. Faisant appel in situ d'IR et de RMN, on a fait un caractérisation complète de l'adduit à liaison hydrogène qui en résulte [{(triphos)Ru(CO)(H)H}$\cdots${HOCH(CF_3)$_2$}] (**2a**). Le composé **2a** est en équilibre avec le complexe non classique η^2-H_2, [(triphos)Ru(CO)(H_2)]$^+$ (**2b**) que l'on peut préparer de façon indépendante en procédant à la protonation du composé **2** à l'aide d'un acide protique fort, à basse température. On a effectué la caractérisation non ambiguë du complexe dihydrogéné, **2b**, en faisant appel à une étude spectroscopique à multiples facettes (T_{1min}^{obs} = 0,005 s (200 MHz), $J_{H,D} \approx$ 30 Hz, DQCC = 78,3 kHz). Faisant appel à une combinaison de techniques d'IR et de RMN, on a étudié la réaction de transfert de proton du composé **2** avec l'HFIP, dans le CH_2Cl_2, qui donne premièrement l'adduit à liaison hydrogène **2a** et ensuite le complexe dihydrogéné **2b**; ces études ont démontré que toutes ces espèces sont en équilibre sur toute la plage de températures allant de

Received August 30, 2000. Published on the NRC Research Press Web site at http://canjchem.nrc.ca on May 23, 2001.

Dedicated to Professor Brian James on the occasion of his 65th birthday in recognition of his outstanding work in organometallic chemistry and homogeneous catalysis.

V.I. Bakhmutov,[1,2] E.V. Bakhmutova,[1] N.V. Belkova, L.M. Epstein,[1,2] E.S. Shubina, and E.V. Vorontsov. A.N. Nesmeyanov Institute of Organoelement Compounds, Vavilov str. 28, V-334, Moscow, Russia, 117813.
C. Bianchini,[2] D. Masi, M. Peruzzini, F. Zanobini. Istituto per lo Studio della Stereochimica ed Energetica dei Composti di Coordinazione, ISSECC-CNR, Via Jacopo Nardi, 39, 50132, Firenze, Italy.

[1]Present Address: Centro de Investigación y de Estudios Avanzados del I.P.N., Apdo postal 14–740, 07000, México D.F., México.

[2]Corresponding authors (fax: 39-055-247-8366; e-mail: bianchini@fi.cnr.it; vladimir@mail.cinvestav.mx; epst@ineos.ac.ru; peruz@fi.cnr.it).

 DOI: 10.1139/cjc-79-5/6-479 © 2001 NRC Canada

190–260 K. Faisant appel à l'IR et à la RMN, on a déterminé de façon indépendante les paramètres thermodynamiques pour la formation du composé **2a** alors que ceux pour la formation de **2b** ont été obtenus par spectroscopie IR. On propose et on discute d'un profil énergétique pour la séquence des réactions **2** → **2a** → **2b**.

Mots clés : hydrures, liaison hydrogène, ruthénium, spectroscopie IR, spectroscopie RMN.

[Traduit par la Rédaction]

Introduction

The occurrence of intra- and intermolecular hydrogen bonds between transition-metal hydride complexes and Brønsted acids has recently been established for a variety of metals and proton donors (1). It is proposed that such M-H···H-X interactions in solution may lead to the formation of dihydrogen (η^2-H_2) complexes; however, well-documented examples of proton transfers involving the formation of η^2-H_2 metal complexes via M-H···H-X intermediates are still very scarce (2). This scarcity of data is essentially due to the low temperature at which the M-H···H-X ⇆ $M(H_2)^+$ + X^- equilibrium becomes spectroscopically visible (2*b*, *d*, *f*). Nonetheless, the energetic profile associated with the M-H + ROH ⇆ M-H···HOR ⇆ $M(H_2)^+$ + RO^- sequence relative to the reaction of the rhenium(I) complex [(triphos)Re$(CO)_2$H] (triphos = MeC$(CH_2PPh_2)_3$) (**1**) with perfluoro-*tert*-butanol has recently been estimated using a combined NMR–IR approach (2*e*). In particular, the H-bonded adduct [(triphos)Re$(CO)_2$H···HOR] (**1a**) was unambiguously intercepted by in situ IR and NMR experiments before degradation to the thermodynamically stable dihydrogen complex [(triphos)Re$(CO)_2(\eta^2$-$H_2)]^+$ (**1b**) (2*b*). The energy associated with each step of the conversion of **1a** to **1b** was determined, and a neat energy profile for the whole proton transfer process was obtained (2e). Prior to the rhenium study, thermodynamic parameters relative to the (M-H + HOR ⇆ M-H···HOR)→ M-(η^2-H_2) step had been reported exclusively for the reaction of the dihydride *trans*-[RuH_2(dppm)$_2$] (dppm = bis-diphenylphosphinomethane) with phenol in toluene (2*a*).

This paper is aimed at expanding our knowledge on proton-transfer reactions involving transition metal hydrides, as well as showing the reliability and wide applicability of the combined NMR–IR approach to study M-H + ROH ⇆ M-H···HOR ⇆ $M(H_2)^+$ + RO^- solution equilibria. To this purpose, the new dihydride complex [(triphos)Ru$(CO)H_2$] (**2**) has been synthesized, and the energetic profile associated with the formation of the hydrogen-bonded adduct [{(triphos)Ru(CO)(H)H}···{HOCH$(CF_3)_2$}] (**2a**) and of the dihydrogen complex [(triphos)Ru(CO)H$(H_2)]^+$ (**2b**) has been determined by means of low-temperature NMR and IR experiments.

Experimental

General procedures

Tetrahydrofuran (THF) was purified by distillation under nitrogen over $LiAlH_4$. All other reagents and chemicals were reagent grade and, unless otherwise stated, were used as received by commercial suppliers. All reactions and manipulations were routinely performed under a dry nitrogen atmosphere by using standard Schlenk-tube techniques. The solid complexes were collected on sintered glass-frits and washed with ethanol and light petroleum ether (bp 40–60°C) before being dried with a stream of nitrogen. The complex [(triphos)RuH(η^2-BH_4)] (**3**) was prepared as described in the literature (3).

NMR studies were carried out in standard 5-mm-NMR tubes in either CD_2Cl_2 or THF-d_8. The deuterated solvents were dried by using conventional procedures and were freshly distilled under inert atmosphere prior to use. ^{1}H and ^{2}H NMR spectra were recorded on Bruker AC200, WP-200 or AMX-400 spectrometers and were calibrated with respect to tetramethylsilane. ^{31}P NMR spectra were recorded on the Bruker AC200 instrument operating at 81.01 MHz. Chemical shifts were measured relative to external 85% H_3PO_4 with downfield values taken as positive. ^{13}C NMR spectra were recorded on Varian VXR 300 or Bruker AC200 spectrometers operating at 75.42 or 50.32 MHz, respectively. Peak positions are relative to tetramethylsilane and were calibrated against the residual solvent resonance. The conventional inversion-recovery method (180-τ-90) was used to determine the variable-temperature longitudinal-relaxation time (T_1). The relaxation times were calculated using the nonlinear three-parameter fitting routine of the spectrometers. In each experiment, the waiting period was five times larger than the expected relaxation time and 16–20 variable delays were employed. The duration of the pulses were controlled at every temperature. The errors in T_1 determinations were lower than 5% (this was checked with different samples). The proton donor-hydride reactions were carried out in cold (195–250 K) CD_2Cl_2 solutions in 5-mm-NMR tubes and all the NMR experiments were run starting at low temperature with precooled probe-heads.

Infrared spectra were recorded as Nujol™ mulls on a PerkinElmer 1600 series FT-IR spectrometer between KBr plates or in CH_2Cl_2 solutions on a Specord M82 spectrometer using 0.01–0.2 cm CaF_2 cells. The latter measurements were performed under a dry argon atmosphere. Low-temperature IR measurements were carried out in CH_2Cl_2 solutions using a Carl Zeiss Jena cryostat. The accuracy of the experimental temperature was ±0.5 K. The cells width was 0.04–0.12 cm.

Elemental analyses (C, H) were performed at ISSECC CNR using a Carlo Erba model 1106 elemental analyzer.

Preparation of [(triphos)Ru(CO)H_2] (2)

A vigorously stirred suspension of [(triphos)RuH(η^2-BH_4)] (**3**) (600 mg, 0.81 mmol) in THF (30 mL) was treated with solid KO-*t*-Bu (270 mg, 2.41 mmol) added in small portions. After 30 min stirring, the starting pale yellow complex dissolved to yield a colorless solution which was layered with absolute ethanol (20 mL) saturated with carbon monoxide (CO). After 15 min, the CO flow was stopped and a brisk stream of nitrogen was passed throughout the solution until ivory colored crystals of **2** separated. Yield: 415 mg (78%). Slow crystallization of the mother liquor in the air gave a second crop of **2** (80 mg, 15%). Ivory-colored truncated prisms of **2** suitable for an X-ray crystal analysis

© 2001 NRC Canada

were obtained by slow evaporation of the solvent from a diluted CH_2Cl_2–EtOH solution (2:1 v/v). IR (KBr, Nujol™) (cm^{-1}): 1920 (CO), 1884 (RuH), 1859; (CH_2Cl_2 solution) 1934 (CO), 1871 (RuH). $^{31}P\{H\}$ NMR (22°C, CD_2Cl_2, 81.01 MHz) δ: 34.71 (AM_2 spin system, t, $^2J_{P_A,P_M}$ = 32.9 Hz, P_A), 27.07 (d, $^2J_{P_M,P_A}$ = 32.9 Hz, P_M). ^1H NMR (22°C, CD_2Cl_2, 200.13 MHz) δ: 7.8–6.9 (m, 30H, aromatic protons), 2.4–2.1 (m, 6H, $CH_{2(triphos)}$), –1.48 (q, $^4J_{H,P}$ = 2.9 Hz, 3H, $CH_{3(triphos)}$), –7.32 (AA′XX′Y, $^2J_{H_A,H_{A'}}$ = 6.0 Hz, $^2J_{H_A,P_X}$ = 18.2 Hz, $^2J_{H_A,P_{X'}}$ = 66.1 Hz, $^2J_{H_A,P_Y}$ = 18.0 Hz, $^2J_{P_X,P_{X'}}$ = 38.0 Hz, 2H, RuH). $^{13}C\{H\}$ NMR (22°C, CD_2Cl_2, 50.32 MHz) δ: 209.98 (dt, $^2J_{C,P_{trans}}$ = 77.5 Hz, $^2J_{C,P_{cis}}$ = 7.8 Hz, CO), 142, 138 (m, aromatic ipso carbons), 134–128 (m, aromatic *meta*, *ortho*, and *para* carbons), 39.36 (q, $^3J_{C,P}$ = 9.4 Hz, CH_3), 39.11 (q, $^2J_{C,P}$ = 7.0 Hz, CCH_3), 35.71 (td, $J = J_{C,P_{equat}} + J_{C,P'_{equat}}$ = 12.5 Hz, $J_{C,P_{axial}}$ = 4.7 Hz, CH_2P_{equat}), 33.98 (dt, $J_{C,P_{axial}}$ = 20.3 Hz, $J_{C,P_{equat}}$ = 6.2 Hz, CH_2P_{axial}). Anal. calcd. for $C_{42}H_{41}OP_3Ru$: C 66.8, H 5.5; found C 66.4, H 5.6.

Preparation of [(triphos)Ru(CO)D_2] (2-d_2)

The perdeuterated isotopomer [(triphos)Ru(CO)D_2] (**2b**-d_2) was prepared as described above using [(triphos)RuD(η²-BD_4)] (**3**-d_4) in the place of **3** and C_2H_5OD instead of ethanol. IR (KBr) (cm^{-1}): 1349 (m) (RuD). ^1H NMR analysis confirmed an isotopic purity higher than 95%.

Preparation of [(triphos)Ru(CO)H(H_2)]$^+$ (2b)

A 5-mm screw-cap NMR tube was charged with **2** (40 mg, 5.3×10^{-2} mmol) and degassed dichloromethane-d_2 (0.8 mL). Into this solution, cooled to –78°C with a dry ice–acetone bath, was added via syringe an excess of $HBF_4 \cdot OMe_2$ (20 μL, 0.16 mmol). The tube was immediately inserted into the spectrometer precooled at –80°C and a $^{31}P\{H\}$ NMR spectrum, immediately recorded at this temperature, revealed the quantitative transformation of **2** into **2b**. $^{31}P\{H\}$ NMR (–80°C, CD_2Cl_2, 81.01 MHz) δ: 20.19 (AM_2 spin system, t, $^2J_{P_M,P_A}$ = 35.3 Hz, P_A), 22.90 (d, $^2J_{P_A,P_M}$ = 35.3 Hz, P_M). ^1H NMR (–80°C, CD_2Cl_2, 200.13 MHz) δ: 7.7–7.0 (m, 30H, aromatic protons), 2.7–2.1 (m, 6H, $CH_{2(triphos)}$), 1.58 (br, 3H, $CH_{3(triphos)}$), –5.39 (br, 3H, RuH).

Monitoring the reaction between 2 and HFIP

Interception of the hydrogen-adduct [{(triphos)Ru(CO)(H)H}···{HOCH(CF_3)$_2$}] (2a)

Under similar experimental conditions, two equiv of HFIP (11.2 μL, 0.11 mmol) were added via syringe to a solution of **2** prepared as described above. Low temperature NMR spectra showed the complete conversion of **2** into the hydrogen-adduct **2a**. $^{31}P\{H\}$ NMR (–80°C, CD_2Cl_2, 81.01 MHz) δ: 30.95 (AM_2 spin system, t, $^2J_{P_M,P_A}$ = 34.5 Hz, P_A), 24.47 (d, $^2J_{P_A,P_M}$ = 34.5 Hz, P_M). ^1H NMR (–80°C, CD_2Cl_2, 200.13 MHz) δ: 8.1–6.8 (m, 30H, aromatic protons), 2.4–2.0 (m, 6H, $CH_{2(triphos)}$), 1.43 (br, 3H, $CH_{3(triphos)}$), –7.79 (br, 2H, RuH).

Transformation of the hydrogen-adduct into [(triphos)Ru(CO)H(H_2)]$^+$ (2b)

Addition of a large excess of HFIP (12 equiv, 67 μL) to the above solution at –80°C immediately transformed the hydrogen-adduct **2a** into the molecular hydrogen complex **2b**. ^{31}P NMR spectroscopy showed that the transformation of **2a** in **2b** occurred in almost quantitative yield. Complex **2b** was also obtained by addition 10–12 equiv of HFIP to a dichloromethane-d_2 solution of **2** (NMR tube experiment carried out at –80°C).

Preparation of [(triphos)Ru(CO)$_2$H](BPh$_4$) (5)

A solution of **2** (250 mg, 0.33 mmol) in THF (15 mL) was saturated with CO and then 1 equiv of MeOTf (40 μL, 0.36 mmol) was added via syringe under stirring. After 15 min, CO was replaced by nitrogen, and $NaBPh_4$ (300 mg, 0.88 mmol) in ethanol (15 mL) was added. Slow concentration of the resulting colorless solution gave off-white crystals of **5** in ca. 95% yield. The IR and NMR characteristics of **5** are fully coincident with those reported in the literature for the same compound prepared by a different route (4).

X-ray diffraction study of [(triphos)Ru(CO)H$_2$] (2)

An ivory-colored crystal of **2** with the dimensions 0.22 × 0.12 × 0.17 mm was chosen for an X-ray analysis. A summary of crystal and intensity data for the compound is presented in Table 1. Experimental data were recorded at room temp on a PHILIPS PW1100-FEBO diffractometer using a graphite-monochromated Cu Kα radiation. A set of 25 carefully centered reflections in the range $10° \le \theta \le 15°$ was used for determining the lattice constants. As a general procedure, the intensity of three standard reflections was measured periodically every 2 h for orientation and intensity control. This procedure did not reveal any decay of intensities. The data were corrected for Lorentz and polarization effects. Atomic scattering factors were those tabulated by Cromer and Waber (5) with anomalous dispersion corrections taken from ref 6. An empirical absorption correction was applied via Ψ scan with transmission factors in the range 1.8794–1.0042. The computational work was performed with a Pentium-II™ personal computer using the programs SHELXL 93 (7) and ZORTEP (8). Final atomic coordinates with equivalent isotropic thermal parameters of all atoms and structure factors are available as supplementary material.

The structure was solved via the heavy atom technique using the program SIR 92 (9) and all the non-hydrogen atoms were found through a series of F_0 Fourier maps. Refinement was done by full-matrix least-squares calculations, initially with isotropic thermal parameters, and then, in the last least-squares cycle, with anisotropic thermal parameters for ruthenium, phosphorus, and carbon and oxygen atoms of the carbonyl ligand. All of the phenyl rings were treated as rigid bodies with D_{6h} symmetry and C—C distances fixed at 1.39 Å. Hydrogen atoms of the triphos ligand were introduced in calculated positions, but not refined. At an advanced stage of the refinement, two hydrogen atoms were located in the Fourier map and successfully refined as ruthenium coordinated hydrides.

Results and discussion

Synthesis and characterization of the dihydride complex [(triphos)Ru(CO)H$_2$] (2)

Treatment of the known (tetrahydroborate)hydride complex [(triphos)RuH(η²-BH_4)] (**3**) with a slight excess of KO-*t*-Bu in anhydrous THF at room temp gave a yellow-orange solution of the trihydride [(triphos)RuH_3]K (**4**) as the only Ru-containing product (Scheme 1) (10). Although **4** can be

© 2001 NRC Canada

Table 1. Crystal data and structure refinement for **2**.

Empirical formula	$C_{42}H_{41}OP_3Ru$
Formula weight	755.78
Temperature (K)	293(2)
Wavelength (Å)	1.54180
Crystal system	Orthorombic
Space group	*P*21/*b*
Unit cell dimensions	*a* = 16.886(6) Å
	α = 90.00(2)°
	b = 20.845(9) Å
	β = 90.00(2)°
	c = 10.2770(10) Å
	γ = 90.00(2)°
Volume (Å^3)	3617(2)
Z	4
Density (calcd.) (Mg m^{-3})	1.388
Absorption coefficient (mm^{-1})	5.003
F(000)	1560
Crystal size (mm)	0.22 × 0.12 × 0.17
Theta range for data collection (°)	4.24–50.02
Index ranges	$-2 \le h \le 16$; $0 \le k \le 20$; $-2 \le l \le 10$
Reflections collected	1832
Independent reflections	1831 (*R(int)* = 0.0374)
Refinement method	Full-matrix least-squares on F^2
Data/restraints/parameters	1831/1/158
GoF on F^2	1.074
Final *R* indices [$I > 2\sigma(I)$]	R_1 = 0.0796, wR_2 = 0.2039
R indices (all data)	R_1 = 0.0836, wR_2 = 0.2107
Absolute structure parameter	–0.03(3)
Largest diff. peak and hole (e Å^{-3})	1.286 and –1.400

isolated as potassium salt in the presence of a 18-crown-6 ether, its difficult storage, due to remarkable sensitivity to water and protic solvents, makes freshly prepared THF solutions excellent vehicles to study the chemistry of the ruthenate **4** and, in particular, to generate the 16e$^-$ fragment [(triphos)Ru(H)$_2$]. As a matter of fact, a THF solution of **4** reacts with protic solvents such as water or alcohols to give quantitatively the tetrahydrido complex [{(triphos)RuH}$_2$(μ-H)$_2$] and H_2 via spontaneous dimerization of the coordinatively unsaturated fragment [(triphos)RuH$_2$].[3] In the presence of σ-donor ligands, this 16e$^-$ system can be intercepted to form stable octahedral complexes of the formula [(triphos)Ru(L)H$_2$] (L = nitriles, phosphines, arsines, CO, etc.).[3] With carbon monoxide, the new carbonyl dihydride complex [(triphos)Ru(CO)H$_2$] (**2**) was readily obtained by simply adding ethanol saturated with CO to a THF solution of **4**. Once formed, **2** is stable in THF and can be isolated in the solid state. Compound **2** is air-stable in both the solid state and solution (THF, halocarbons, acetone) and has been characterized by multinuclear (^{1}H, ^{31}P, and ^{13}C) NMR and IR spectroscopy, and elemental and X-ray diffraction analyses (vide infra).

The AM$_2$ pattern featured in the ^{31}P NMR spectrum of **2** and the typical AA′XX′Y (X, X′, Y = ^{31}P) pattern of the high-field hydride resonance (δ = –7.32) are consistent with the presence of two *cis*-disposed hydride ligands in an octahedral coordination with three positions taken by a *facial* (*fac*) triphos and three other positions occupied by two hydrides and one carbon monoxide ligand (11). A narrow doublet of triplets is contained in the ^{13}C NMR spectrum at δ 209.98 for the CO carbon atom, which agrees with the proposed structural formulation for **2**.

Complex **2** is stereochemically rigid on the NMR time scale; neither the ^{31}P nor the ^{1}H NMR spectrum show significant changes over the temperature window of dichloromethane. In keeping with a classical dihydride nature, a variable-temperature analysis of the spin-lattice relaxation time (T_1) of the isochronous hydride ligands gave a quite long minimum value of 0.178 s at 200 K using a 200 MHz instrument (12). The solid state IR spectrum contains a ν(CO) band at 1920 cm^{-1} and two ν(RuH) bands at 1884 and 1859 cm^{-1}. The observation of a medium intensity absorption at ca. 1350 cm^{-1} in the spectrum of the deuterated isotopomer **2b-*d*$_2$** confirmed the correctness of our ν(RuH) assignment ($k_{H/D}$ = 1.39). The IR spectrum in CH_2Cl_2 solution shows ν(CO) at 1934 cm^{-1} and ν(RuH) at 1871 cm^{-1}. This latter band is a combination of both ν_s(RuH) and ν_{as}(RuH), which are well-resolved in the solid state (ν_s(RuH) 1884 cm^{-1} and ν_{as}(RuH) 1859 cm^{-1}).

Well-shaped crystals of **2** were grown from a dilute dichloromethane–ethanol solution. Figure 1 shows a ORTEP view of the complex molecule, while crystallographic data and selected bond distances and angles are presented in Tables 1 and 2, respectively. The results of a single crystal

[3] C. Bianchini and M. Peruzzini, unpublished results.

© 2001 NRC Canada

Scheme. 1.

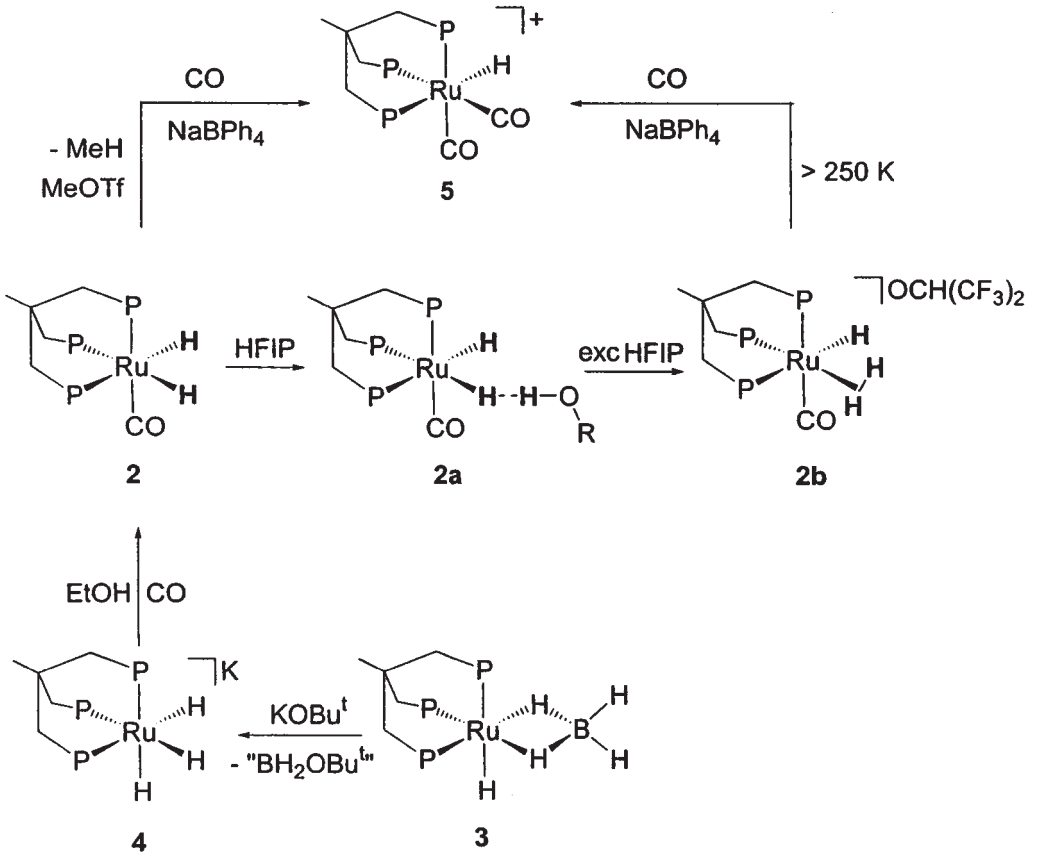
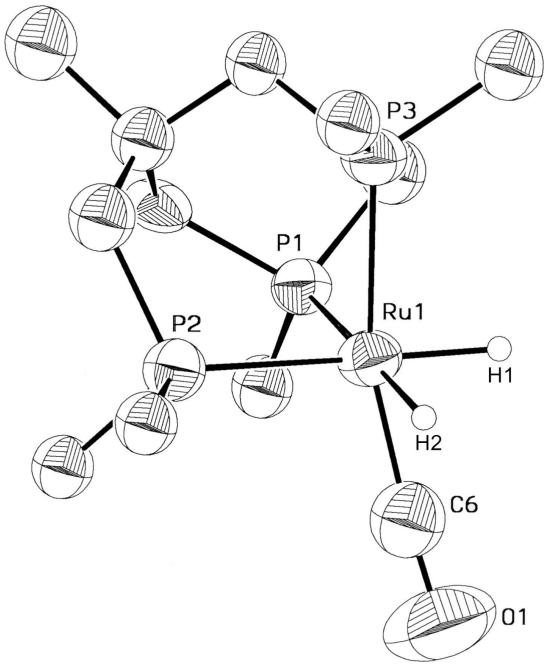


Fig. 1. ORTEP drawing of the molecular structure of **2**. Only the ipso carbons of the six triphos phenyl rings are shown.



X-ray diffraction analysis are consistent with the solution structure determined by NMR spectroscopy.

The ruthenium atom is octahedrally coordinated by a *fac* triphos ligand, by two *cis* hydrides, and by a terminal carbonyl. The observed distortions from a regular octahedron are typical of triphos complexes containing hydride ligands (13). The three Ru—P distances are very similar to each other (average Ru—P = 2.34 Å), and reflect comparable *trans* influence exerted by the hydride and the carbonyl ligands. The Ru—CO distance of 1.84(2) Å is typical for ruthenium(II) carbonyl complexes (14). The two hydride ligands were located in the difference Fourier maps and refined as isotropic atoms together with the rest of the non-hydrogen atoms of the structure, giving Ru—H(1) and Ru—H(2) separations of 1.46(18) and 1.50(11) Å, respectively.

Synthesis and spectroscopic characterization of the dihydrogen complex [(triphos)Ru(CO)(H)(H_2)]$^+$ (2b)

Treatment of **2** with strong protic acids (HBF_4, $HOSO_2CF_3$) at room temp gave a mixture of products that denied first-order analysis, thus indicating that the molecular hydrogen complex [(triphos)Ru(CO)(H)(H_2)]$^+$ (**2b**), which actually forms upon protonation of **2** (vide infra), is unstable at room temp. This behavior agrees with the results by Michos et al. (15) for the protonation of [{PhP($CH_2CH_2PPh_2$)$_2$}RuH_2L] (L = CO, P(OCH_2)$_3$CEt, PMe_2Ph), which did not afford isolable molecular hydrogen complexes, although the spectroscopic data were provided. However, when the protonation was repeated in the presence of carbon monoxide, the known octahedral hydrido dicarbonyl complex [(triphos)Ru($CO)_2$H]$^+$ was quantitatively produced and isolated as the tetraphenylborate salt [(triphos)Ru($CO)_2$H](BPh_4) (**5**). Complex **5** has previously been synthesized by oxidation of the ruthenium(0) complex

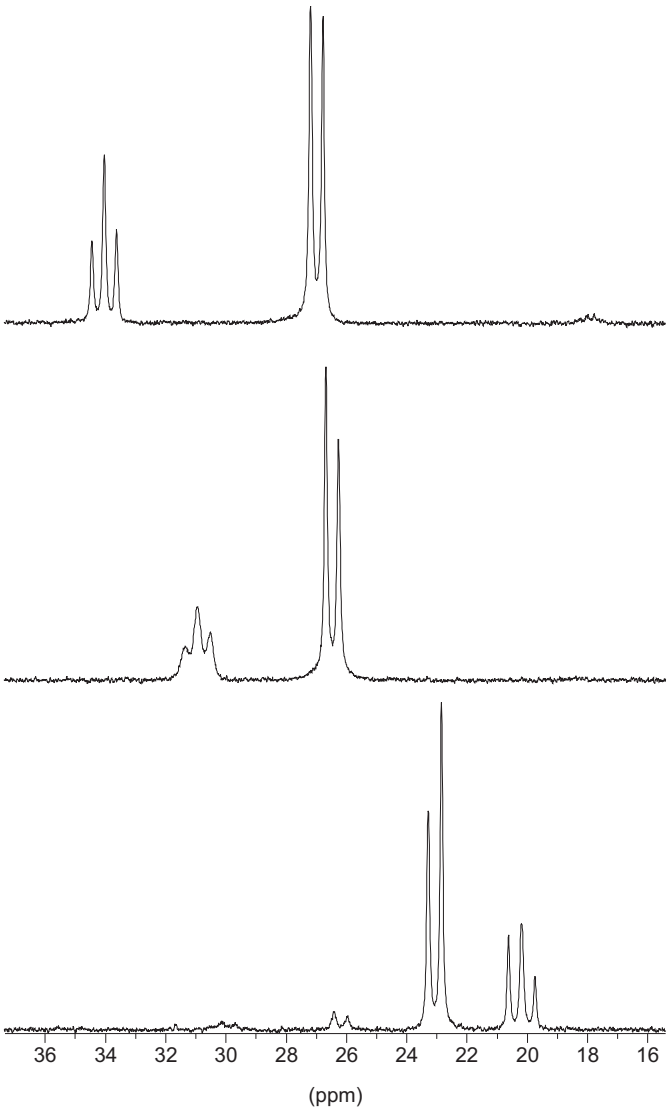
© 2001 NRC Canada

Table 2. Selected bond lengths and angles for **2**.

Bond lengths (Å)	
Ru(1)—C(6)	1.84(2)
Ru(1)—P(1)	2.334(5)
Ru(1)—P(2)	2.340(5)
Ru(1)—P(3)	2.344(5)
Ru(1)—H(1)	1.46(18)
Ru(1)—H(2)	1.50(11)
O(1)—C(6)	1.20(3)
P(1)—C(1)	1.873(19)
P(2)—C(2)	1.881(19)
P(3)—C(3)	1.856(18)
C(1)—C(4)	1.56(2)
C(2)—C(4)	1.50(3)
C(3)—C(4)	1.57(2)
C(4)—C(5)	1.58(3)
Bond angles (°)	
C(6)-Ru(1)-P(1)	107.4(7)
C(6)-Ru(1)-P(2)	101.9(7)
P(1)-Ru(1)-P(2)	89.54(17)
C(6)-Ru(1)-P(3)	162.1(8)
P(1)-Ru(1)-P(3)	87.17(18)
P(2)-Ru(1)-P(3)	88.19(17)
C(6)-Ru(1)-H(1)	81(8)
P(1)-Ru(1)-H(1)	110(7)
P(2)-Ru(1)-H(1)	158(7)
P(3)-Ru(1)-H(1)	84(8)
C(6)-Ru(1)-H(2)	65(4)
P(1)-Ru(1)-H(2)	172(4)
P(2)-Ru(1)-H(2)	96(4)
P(3)-Ru(1)-H(2)	99(4)
H(1)-Ru(1)-H(2)	66(8)
O(1)-C(6)-Ru(1)	176(2)

[(triphos)Ru(CO)$_2$] with HCl or MeCOCl (4). To intercept the molecular hydrogen complex **2b**, the protonation of **2** was then carried out in CH_2Cl_2 solution at low-temperature (200 K) using either a stoichiometric amount of strong acid or a large excess (10–12 equiv) of a medium-strength proton donor such as the activated alcohol hexafluoroisopropanol (HFIP). Indeed, the addition of 12 equiv of HFIP to a CD_2Cl_2 solution of **2** in a 5 mm NMR tube cooled to 195 K generated a new broad hydride resonance centered at ca. –5.4 ppm (3H) featured by a very short T_{1min} value of 0.005 s at 190 K (200 MHz), which is typical for a nonclassical dihydrogen structure (16, 17). The appearance of the η^2-H_2 resonance in the proton spectrum of **2b** was paralleled by that of a well-resolved AMM′ pattern with δ_{P_A} 20.19 and δ_{P_M} 22.90 ppm (J_{P_A,P_M} = 35.3 Hz) in the ^{31}P NMR spectrum. The P_A donor atom, *trans* to the CO ligand, undergoes a significant high-field shift ($\Delta\delta \approx 14.5$ ppm) in line with the formation of a cationic carbonyl complex. Figure 2 collects the NMR spectra illustrating the stepwise transformation of **2** into **2b** via the H-bonded adduct [{(triphos)Ru(CO)(H)H}$\cdots${HOCH(CF$_3$)$_2$}] (**2a**). Indeed, this latter compound is formed in very low concentration when a large excess of HFIP is employed (Fig. 2*c*), while it is the only product visible on the ^{31}P NMR timescale when **2** is reacted with two equiv of alcohol (vide infra).

Fig. 2. ^{31}P NMR spectra (81.01 MHz) illustrating the stepwise transformation of **2** (4.63×10^{-5} M solution in CD_2Cl_2) (top trace), into **2a** (middle trace) upon addition of HFIP (2 equiv) and, eventually, into **2b** (bottom trace) upon addition of further 10 equiv of HFIP. All the spectra were taken at 193 K.

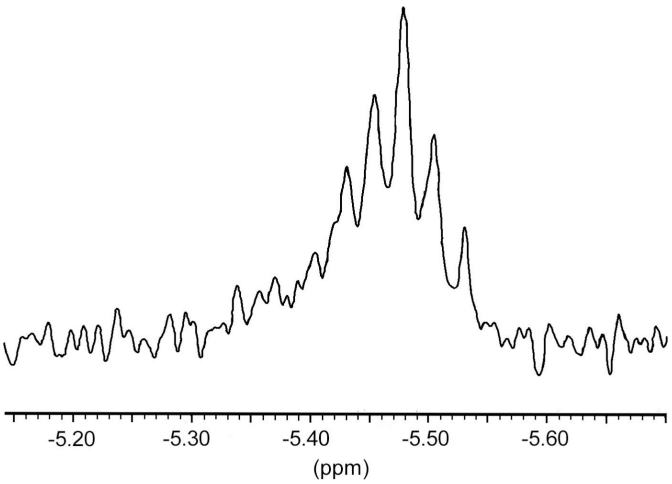


The dihydrogen complex **2b** is highly fluxional in CD_2Cl_2 solution as a consequence of a fast hydride-dihydrogen exchange occurring even at the lowest temperature investigated (180 K). Compound **2b** is quite stable in solution below 250 K but slowly eliminates H_2 above this temperature as shown by the appearance of the typical H_2 resonance at 4.56 ppm in the proton NMR spectrum. The decomposition of **2b** is not chemoselective; in fact, a single, well-defined product was obtained only in the presence of external ligands, like carbon monoxide, which are capable of trapping the 16e$^-$ fragment [(triphos)Ru(CO)H]$^+$.

The nonclassical nature of **2b** was confirmed by deuterium labeling experiments. A ^{1}H{^{31}P} NMR spectrum, recorded after addition of excess CF_3COOD to a solution of **2** in CD_2Cl_2 at 200 K, exhibits a poorly resolved resonance at –5.48 ppm, which, upon increasing the temperature to 250 K, transforms into a nonbinomial quintet with a line separation of ca. 10 Hz. Accordingly, this resonance can

© 2001 NRC Canada

Fig. 3. Hydride region of the $^1H\{^{31}P\}$ NMR spectrum of the **2-*d*$_2$** isotopomer (250 K, 400 MHz) prepared by low-temperature protonation of **2** with an excess of CF_3COOD in CD_2Cl_2.



safely be assigned to the bis-deuterated isotopomer $[(triphos)Ru(CO)HD_2]^+$ (**2b-*d*$_2$**) (Fig. 3). In the ^1H NMR spectrum, the typical 1:1:1 triplet of free HD is also observed at 4.51 ppm. In agreement with the formation of a deuterated isotopomer of **2b**, the deuteration results in a high-field isotopic shift of the "HD_2" signal of 120 ppb. Similar isotopic shifts are commonly observed for HD metal complexes (17) and may be due to the IPR effect. A $J_{H,D}$ constant of ca. 30 Hz can be calculated for **2b** assuming a very fast H–H_2 exchange (17). Introducing this value in the empirical correlation, $r_{(HH)} = (1.42 - 0.0167)J_{H,D}$ Å, recently proposed by Morris and co-workers (18) for dihydrogen complexes, a rather elongated H—H distance of 0.92 Å may be figured out for the nonclassical ligand in **2b**.

An independent estimation of the H—H separation can also be obtained from the relaxation data. The T_{1min} measured for both the hydride signals in **2** (T_{1min} (**2**$_{Ru,H2}$) = 0.178 s) and **2b** (T^{obs}_{1min} (**2b**$_{Ru,H3}$) = 0.005 s) allows one to calculate the T_{1min} for the dihydrogen ligand in **2b** by means of eq. [1], and hence the T_{1min} ($Ru(H_2)$) applying eq. [2].

$$[1]\qquad 1/T^{obs}_{1min}(\mathbf{2b}_{Ru,H3}) = (1/3)/T_{1min}\ (\mathbf{2}_{Ru,H2}) + (2/3)/T^{obs}_{1min}(\mathbf{2b}_{Ru(H2)})$$

$$[2]\qquad 1/T^{obs}_{1min}\ (\mathbf{2b}_{Ru(H2)}) = 1/T_{1min}\ (\mathbf{2}_{Ru,H2}) + 1/T_{1min}\ (\mathbf{2b}_{Ru(H2)})$$

As a result, a T_{1min} (**2b**$_{Ru(H2)}$) value of 0.0035 s, exclusively occasioned by hydride–hydride dipole–dipole interactions in the dihydrogen ligand, is obtained, which ultimately gives an H—H distance ranging from 0.74 to 0.94 Å depending on the spinning model adopted (fast or slow rotation) for the motion of the dihydrogen ligand (19*a*). As the separation of 0.94 Å calculated using the low-spinning model is very close to the distance determined from the $J_{H,D}$ coupling constant in **2b-*d*$_2$**, it is conceivable that **2b** contains, as usually, a rather "immobile" H_2 ligand (19*b*).

Since the relaxation properties of the deuterium nucleus are a powerful tool to investigate the dynamic behavior of dihydrogen ligands (16*b*, 21), ^2H-T_1 spin-lattice measurements were carried out on complexes **2b-*d*$_2$** and **2b-*d*$_3$** in CH_2Cl_2. The perdeuterated isotopomer **2b-*d*$_3$** has been prepared by low-temperature protonation of **2b-*d*$_2$** with CF_3COOD. The ^2H NMR spectrum of **2b-*d*$_3$** contains a broad resonance at ca. –5.4 ppm that can safely be assigned to the three freely exchanging deuterides. Like **2b**, the ^2H resonance of **2b-*d*$_3$** remains unchanged even at 180 K due to fast deuteride–deuterium exchange.

The ^2H-T_1 relaxation experiments on the parent classical deuteride **2b-*d*$_2$** give a T_{1min} (**2**$_{Ru,D2}$) value of 0.0149 s at 61.402 MHz. By applying eq. [3] and introducing therein $\eta = 0$ (21), a deuterium quadrupole coupling constant (DQCC) (22) as large as 78.3 kHz can be calculated for **2b-*d*$_2$**

$$[3]\qquad DQCC = 1.2201(1 + \eta^2/3)^{-1/2}\ (\nu/T_{1min})^{1/2}$$

where DQCC, ν, and T_{1min} are given in kHz, MHz, and s, respectively.

The DQCC value for **2-*d*$_2$** is very close to those recently determined for classical deuteride ligands in the related complexes $[(dppe)_2RuD(D_2)]BPh_4$ (dppe = $PPh_2CH_2CH_2PPh_2$) (DQCC = 79 kHz) (20*b*) and $[(PP_3)RuD_2]$ (PP_3 = $P(CH_2CH_2PPh_2)_3$) (DQCC = 73–76 kHz) (20*a*). The average ^2H resonance in **2b-*d*$_3$** exhibits a T_{1min} (**2b**$_{Ru,D3}$) time of 0.0174 s. Taking into account a fast D–D_2 exchange (see eq. [1]), it is then possible to calculate a T_{1min} value of 0.0190 s for the nonclassical D_2 ligand in **2b-*d*$_3$**. Nonclassical transition metal hydride complexes have been reported to display longer ^2H-T_{1min} times as compared to classical polyhydrides due to motions of the dihydrogen ligands (20). The elongation observed on going from **2b-*d*$_2$** to **2b-*d*$_3$**, however, is very weak, which may be due to a slow-rotating dihydrogen ligand. Thus, the evaluation of ^2H-T_{1min} (or DQCC) is important because it provides an additional support for the genuine nonclassical nature of **2b**.

The IR spectrum of the dihydrogen complex **2b**, obtained by treatment of **2** with HBF_4 at 200 K in dichloromethane solution, shows a ν(CO) band at 2023 cm^{-1}, which is shifted at higher energy as compared to the ν(CO) band of the initial complex. Such high-frequency shifts are commonly observed for transformations of hydride(carbonyl) complexes into cationic nonclassical molecular hydrogen-carbonyl derivatives (2*b*, *f*).

Synthesis and spectroscopic characterization of the H-bonded adduct [{(triphos)Ru(CO)(H)H}···{HOCH(CF$_3$)$_2$}] (2a)

Upon addition of **2** (0.07 M) to a CH_2Cl_2 solution of trifluoroethanol (TFE), HFIP, MeOH, or monofluoroethanol (MFE) at 298 K, significant changes were observed in the ν_{OH} region of the corresponding IR spectrum. To avoid self-association, proton-donor concentrations in the range 0.01–0.03 M were used, so as to work with an excess of **2**. Irrespective of the proton donor, the changes affecting the OH stretching region (Table 3) were indicative of a hydrogen bonding interaction between the alcohol and the hydride ligands in the ruthenium complex.[4] Indeed, the intensity of the

[4] A hydrogen-bonding interaction between the activated alcohol and the oxygen atom of the carbonyl ligand was ruled out in view of the high-frequency shift encompassed by ν_{CO} upon addition of HFIP (1*d*, 2*b*).

© 2001 NRC Canada

Table 3. Spectral characteristics of the H-bonded adducts [{(triphos)Ru(CO)(H)H}···{HOR}] and enthalpy values ($-\Delta H$) relative to their formation in CH_2Cl_2.

ROH	ν_{OH}^{bonded} (cm^{-1})	$\Delta\nu_{OH}$ (cm^{-1})	$-\Delta H$ (kcal mol^{-1})	E_j
CH_3OH	3415	212	4.1	1.41
MFE	3355	254	4.7	1.38
TFE	3254	346	5.8	1.40
HFIP	3160	420	6.6	1.37

band due to the free OH groups decreased, while a new broad and intense band was formed at lower frequency. As previously observed (1*d*, 2*f*), the frequency shifts ($\Delta\nu = \nu_{OH}^{free} - \nu_{OH}^{bonded}$) increase with the proton-donor ability of the alcohol in the order MeOH < MFE < TFE < HFIP.

The Iogansen correlation shown in eq. [4] may be used to estimate the hydrogen-bonding enthalpy values at 298 K from the experimental frequency shifts listed in Table 3 (1*d*, 2*b*).

$$[4] \qquad -\Delta H^\circ = 18\ \Delta\nu/(720 + \Delta\nu)$$

On decreasing the temperature, the band shift ($\Delta\nu_{CO}$) gradually moved to high-frequency reaching a maximum of +15 cm^{-1} at 190 K for a 10-fold excess of alcohol, while a band shift to low-frequency was displayed by the Ru—H stretching of **2**. Indeed, after addition of HFIP (2 to 3 equiv) and cooling down the solution, the ν_{RuH} band at 1871 cm^{-1} moved to low-frequency by 20 cm^{-1}, which is consistent with a hydrogen bonding interaction between the alcohol and a hydride ligand of **2** (1*d*, 2*f*). This behavior led us to assign the two bands at 1949 (ν_{CO}) and 1851 (ν_{RuH}) cm^{-1} to the H-bonded complex **2a**. In contrast, when both the parent hydride **2** and the H-bonded adduct **2a** were contemporaneously present in solution, a unique ν_{CO} and ν_{RuH} band was observed in a position intermediate between the two limits and depending on the molar fraction of **2a** (p(**2a**)). This latter can readily be calculated from eq. [5]

$$[5] \qquad p(\mathbf{2a}) = \frac{\nu_{CO}(\mathbf{2} + \mathbf{2a}) - \nu_{CO}(\mathbf{2})}{\nu_{CO}(\mathbf{2a}) - \nu_{CO}(\mathbf{2})}$$

Using the p(**2a**) data obtained in this way, the formation constants $K_{\mathbf{2-2a}} = [\mathbf{2a}]/[\mathbf{2}][\text{HFIP}]$ have been determined in the temperature range from 200 to 260 K, and hence the enthalpy and entropy values associated with the formation of **2a** have been calculated by the van't Hoff method. The corresponding temperature dependence of ln $K_{\mathbf{2-2a}}$ vs. $1/T$ shown in Fig. 4 gave a $-\Delta H^\circ_{\mathbf{2a}}$ value of 6.7 kcal mol^{-1} in fairly good agreement with the value calculated from eq. [4]. A $-\Delta S^\circ_{\mathbf{2a}}$ value of 19.6 eu was similarly determined from the plot.

Following the method reported by Iogansen (23), the basicity factor (E_j) of the hydride ligand in **2** was calculated as 1.39 ± 0.02 (1*d*, 2*b*). It is worth noticing that this parameter, which characterizes the absolute proton accepting ability of the hydride ligand, irrespective of both proton donor partner and solvent, is significantly greater than those reported for rhenium hydride **1** (E_j = 0.97) and other metal hydride complexes (2*b*) as well as organic bases such as Et_2O (E_j = 1.0) and DMSO (E_j = 1.27) (23). The relatively high E_j value of **2** might explain why this dihydride complex is easily protonated to give the dihydrogen complex **2b** even with relatively weak proton donors such as HFIP and PFTB.

Fig. 4. Temperature-dependence of the equilibrium constant ($K_{\mathbf{2-2a}}$) for the formation of **2a** from **2** and HFIP in CH_2Cl_2 (obtained from IR data).

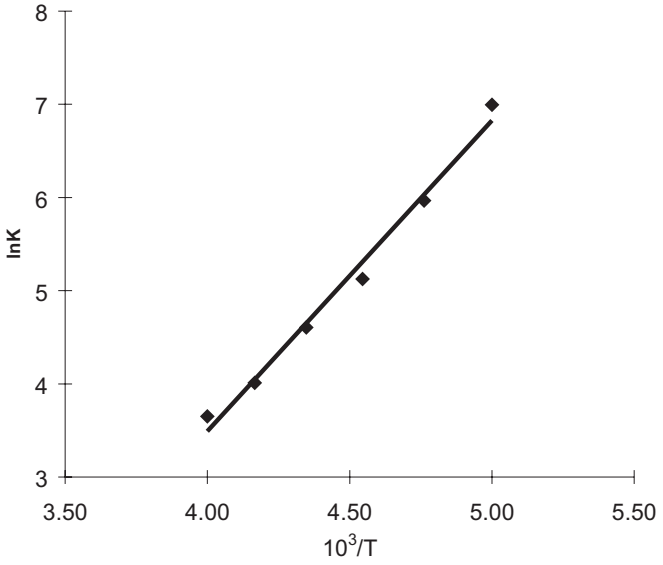
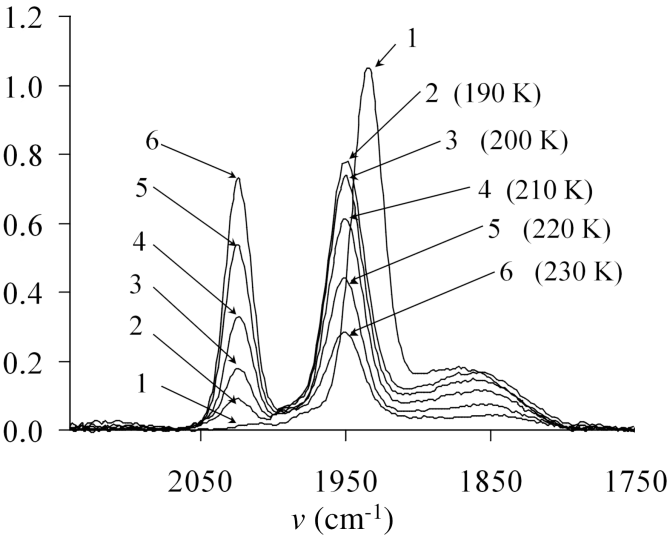


Fig. 5. Variable-temperature IR spectra (ν_{CO} range) of complex **2** (0.006 M) in CH_2Cl_2 at 190 K (curve 1) and in the presence of a 10-fold excess of HFIP in the temperature range between 230 and 190 K (curves 2–6).



Variable-temperature IR and NMR studies of the proton transfer reactions between 2 and HFIP

The reaction of **2** with HFIP (10–12 equiv) was followed by IR spectroscopy in CH_2Cl_2 starting from 200 K. Selected variable-temperature spectra in the ν_{CO} region are reported in Fig. 5. The spectrum at 200 K showed the presence of the dihydrogen complex **2b**, with ν_{CO} at 2023 cm^{-1}, and of the H-bonded adduct **2a** with ν_{CO} at 1949 cm^{-1}. When the temperature was increased to 260 K, the ν_{CO} band of **2b** decreased in intensity while that of **2a** increased.

© 2001 NRC Canada

Table 4. Temperature-dependence of the equilibrium constants between **2**, **2a**, and **2b** in the presence of HFIP determined from the variable-temperature ^{1}H NMR and IR spectra (range 200–240 K).

T (K)	$K_{\mathbf{2-2a}}$ (mol^{-1})[a]	$K_{\mathbf{2a-2b}}$[b]	$K_{\mathbf{2-2b}}$ (mol^{-1})[b]
200	4.6×10^3	2.9×10^3	2.7×10^0
210	1.8×10^3	3.4×10^3	8.6×10^{-1}
215	1.0×10^3		
220	8.3×10^2	4.9×10^1	2.9×10^{-1}
225	5.2×10^2		
230	3.7×10^2	1.6×10^1	1.6×10^{-1}
240	2.6×10^2		

[a]Determined from NMR data.
[b]Determined from IR data.

Concomitantly, an enhancement of the ν_{RuH} band due to **2a** at ca. 1855–1860 cm^{-1} was observed.

Since the equilibrium between **2a** and **2b** is reversible in the temperature range from 200 to 260 K, the IR spectra allowed us to determine the equilibrium constants $K_{\mathbf{2a-2b}}$ = [**2b**]/[**2a**] and the overall constant $K_{\mathbf{2-2b}}$ = [**2b**]/[**2**][HFIP] for the proton transfer from HFIP to a terminal hydride of **2** to give the dihydrogen complex **2b** via the intermediate H-bonded complex **2a**.

The equilibrium concentrations [**2b**] were obtained directly from the IR experiments. The equilibrium concentrations [**2**], [**2a**], [**2b**], and [HFIP] are related to each other and to the total concentration of hydride (c_2) and proton donor (c_{HFIP}) by the mass-balance eqs. [6*a*] and [6*b*].

$$[6a] \quad c_2 = [\mathbf{2}] + [\mathbf{2a}] + [\mathbf{2b}]$$

$$[6b] \quad c_{HFIP} = [HFIP] + [\mathbf{2a}] + [\mathbf{2b}]$$

Substituting for [**2**] and [HFIP] from eqs. [6*a*] and [6*b*] into equation for $K_{\mathbf{2-2a}}$ and rearranging, eq. [7] was obtained whose solution gave [**2a**].

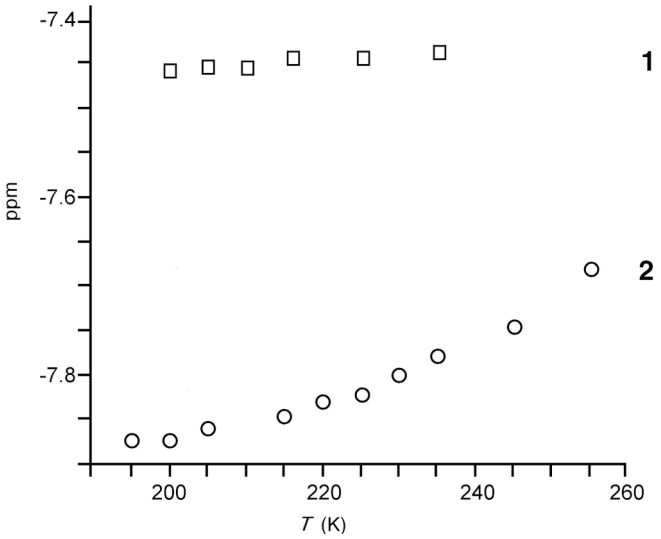
$$[7] \quad [\mathbf{2a}]^2 + [\mathbf{2a}]\left\{2[\mathbf{2b}] - c_2 - c_{HFIP} - \frac{1}{K_{\mathbf{2-2a}}}\right\} + \{c_2 c_{HFIP} + [\mathbf{2b}]^2 - [\mathbf{2b}](c_2 + c_{HFIP})\} = 0$$

Once the concentrations of each species participating in the proton transfer equilibrium were known, the calculation of the equilibrium constants $K_{\mathbf{2a-2b}}$ and $K_{\mathbf{2-2b}}$ in the temperature range from 200 to 230 K was straightforward (Table 4).

The temperature dependencies of the equilibrium constants with inverse temperature (1/T) are linear and provide the following thermodynamic parameters: $-\Delta H^\circ_{\mathbf{2a-2b}}$ = 8.7 kcal mol^{-1}, $-\Delta S^\circ_{\mathbf{2a-2b}}$ = 42 eu for the formation of **2b** from **2a** and $-\Delta H^\circ_{\mathbf{2-2b}}$ = 16.1 kcal mol^{-1}, $-\Delta S^\circ_{\mathbf{2-2b}}$ = 65 eu for the overall proton transfer. Since the formation of **2a** has been found to involve a $-\Delta H^\circ_{\mathbf{2-2a}}$ value of 6.7 kcal mol^{-1}, it is apparent that the formation of **2a** plays the major role in the proton transfer reaction.

The proton transfer reaction for the system (**2** + HFIP) has also been studied by NMR spectroscopy. The low-temperature addition (200 K) of a twofold excess of HFIP to a CH_2Cl_2 solution of **2** results in a high-field shift of the hydride resonance to –7.86 ppm. Figure 6 illustrates the temperature dependence of the hydride chemical shift observed

Fig. 6. Temperature-dependence of the chemical shift of the hydride resonance of **2** in CD_2Cl_2 (□), and in the presence of a twofold excess of HFIP (○).



for this solution. The hydride chemical shift of **2** is practically independent from the temperature in the absence of the proton donor (curve 1), while it reaches a plateau at –7.87 ppm below 200 K (curve 2). Therefore, the resonance at –7.87 ppm can be assigned to the H-bonded adduct **2a**. Obviously, the observed hydride resonance is averaged between two nonequivalent positions and, therefore, the chemical shift of the hydride involved in hydrogen bonding can be calculated as –8.29 ppm by eq. [8].

$$[8] \quad \delta(RuH)^{obs} = 0.5\ \delta(RuH^{free}) + 0.5\ \delta(RuH\cdots HOR)$$

From curve 2 in Fig. 6, the molar fractions of **2** (p_{free}) and **2a** (p_{bonded}) were obtained at different temperatures (eq. [9]) and the corresponding equilibrium constants for the formation of the H-bonded complex could be calculated (Table 4). Finally, the $-\Delta H°$ (7.1 kcal mol^{-1}) and $-\Delta S°$ (19.0 eu) values relative to the formation of **2a** were obtained from a standard ln K vs. 1/T plot.

$$[9] \quad \delta(RuH)^{obs} = p_{free}\ \delta(RuH^{free}) + p_{bonded}\ \delta(RuH^{bonded})$$

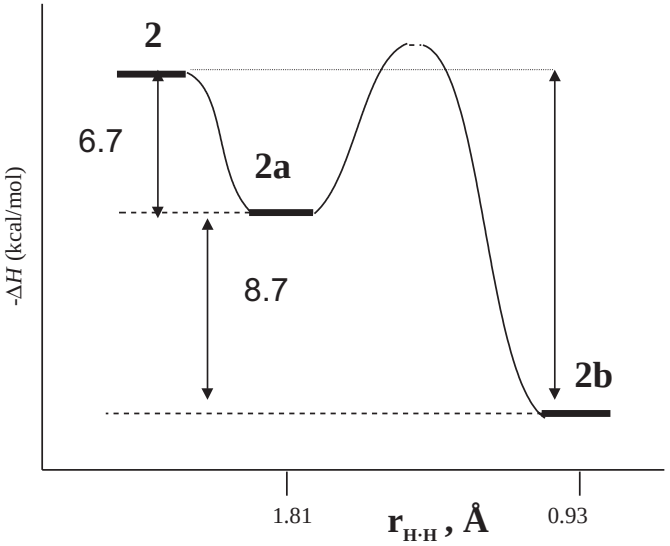
It is worth noticing that the thermodynamic parameters calculated using variable-temperature NMR and IR experiments are in good agreement with each other.

Positive enthalpy and entropy changes ($\Delta H°$ = 17 kcal mol^{-1}, $\Delta S°$ = 75.8 eu) obtained by NMR methods have been reported for the proton transfer from phenol to the hydride ligand in [RuH_2(dppm)$_2$] (2*a*), while the thermodynamic parameters for the proton transfer to [RuH_2(dmpe)$_2$] (dmpe = bis(dimethylphosphino)ethane) in ethanol (the H-bonded complex was not observed, however) exhibit a negative sign and are only slightly smaller than ours ($-\Delta H°$= 6.0 kcal mol^{-1}, $-\Delta S°$ = 19.9 eu) (24).

It is also worth noticing that the H-bonded complex (**2a**) is thermodynamically more stable than corresponding rhenium complex (**1a**) ($-\Delta H°$ = 4.8 kcal mol^{-1}) (2*b*), which

© 2001 NRC Canada

Scheme 2.



reflects the lower basicity of the hydride ligand in **1** (see the E_j factor).

The variable-temperature spin-lattice relaxation data for a CH_2Cl_2 solution of **2** in the presence of a twofold excess of HFIP showed that the relaxation time of the observed hydride resonance reaches a minimum at 200 K (T_{1min}^{obs} = 0.119 s at 200 MHz). As it is evident from Fig. 5, under these conditions the equilibrium is completely shifted towards the formation of **2a**. Using eq. [10], the observed T_{1min}^{obs} value was employed to calculate T_{1min}^{obs} (RuH···HFIP) (0.0894 s) for the H-bonded hydride ligand in **2a**. Finally, the combination of T_{1min}^{obs} (RuH···HFIP) and of T_1 (0.178 s) measured for **2** (see above) provided a T_{1min} (H···H) value of 0.183 s for **2a**, which is exclusively due to hydride–proton dipole–dipole interactions (12).

$$[10] \quad 1/T_{1min}^{obs} = 0.5/0.178 + 0.5/T_{1min}^{obs} \ (\mathrm{RuH\cdots H})$$

Using the procedure described by Halpern and co-workers (12), the T_{1min} (H···H) relaxation time has been employed to calculate a hydride—proton distance of 1.81 Å in **2a**, which is quite comparable to the value reported for the rhenium system (**1** + PFTB) (1.83 Å) (2*b*). This H—H distance lies in the expected range (1.7–2.0 Å) for transition metal hydride complexes with either intra- (1*a–c*) or intermolecular hydrogen bonds (1*d*, *e*).

We have already shown that **2** (0.008 M) is converted to **2b** in the presence of a 12-fold excess of HFIP in CD_2Cl_2. The dihydrogen complex is clearly observed in the ^{1}H NMR spectrum at 183 K (see above), which also contains an averaged hydride resonance for **2** and **2a**. Consistent with the IR data, it has been found that increasing the temperature leads to a completely reversible redistribution of integral intensities of both signals, thus indicating that all these species are in equilibrium.

An energetic profile for the overall hydrogen-transfer reaction is illustrated in Scheme 2. It is worth noticing that: (*i*) the hydride—proton distance represents the reaction coordinate (determined by NMR spectroscopy); (*ii*) the energy of **2a** is obtained by IR and NMR data; (*iii*) the depth of the second well corresponds to the enthalpy value obtained from the IR data; and (*iv*) the energy level of the transition state for the proton transfer **2a** → **2b** has a purely qualitative character.

Notwithstanding the qualitative character of the profile, the proposed energy levels are quite reasonable. Indeed, it is well known that the formation of H-bonded adducts is a diffusion-controlled process with no energy barrier (25). The observation of separated signals for the hydride ligands in **2a** and **2b**, with no broadening of the resonances at low-temperature, is consistent with a lifetime longer than 10 s for this reaction (26). Accordingly, an upper limit of 10^{-1} s^{-1} can be envisaged for the corresponding rate constant. The bottom limit of rate constant may roughly be estimated considering that our IR technique does not allow one to monitor band-intensity changes for processes faster than 1×10^{-2} s^{-1} (2*e*). Since no intensity change with time is observed, it may be assumed that the lifetime of the proton transfer is shorter than 1 to 2 min, which provides a lower limit of 1×10^{-2} s^{-1} for the rate constant. It may be thus concluded that the transformation of **2a** into **2b** has an activation barrier $-\Delta G^{\ddagger}$ (200 K) of ca. 12 to 13 kcal mol^{-1}, which is in nice agreement with the barrier previously calculated for the related rhenium system [(triphos)Re(CO)$_2$H] with PFTB (2*e*) as well as other literature data. In particular, theoretical studies of proton transfer to Re- and Ru-hydrides have recently shown that the proton-transfer barriers depend on both the metal complex basicity and the strength of the acid and may vary from 10 to 0.7 kcal mol^{-1} (27). On the other hand, rather low rates of proton transfer and dihydrogen complex generation (varying from 1×10^6 to 1×10^{-1} s^{-1} with corresponding activation barriers of ca. 6.5–12 kcal mol^{-1}) have been reported for the reactions of Fe- and Ru-hydrido complexes with strong acids (28).

Conclusions

The (carbonyl)dihydride complex [(triphos)Ru(CO)H$_2$] (**2**) has been found to react with hexafluoro-2-propanol to give the new dihydrogen complex [(triphos)Ru(CO)H(H$_2$)]$^+$ (**2b**) through the H-bonded adduct [{(triphos)Ru(CO)(H)H}···{HOCH(CF$_3$)$_2$}] (**2a**). All these compounds have been characterized by in situ NMR and IR techniques. Variable-temperature IR and NMR studies in CH_2Cl_2 solution have shown that **2**, **2a**, and **2b** are in equilibrium in the temperature range from 190 to 260 K. An energetic profile describing the formation of the dihydrogen complex via the H-bonded adduct has been proposed on the basis of thermodynamic parameters determined experimentally. The proposed energy profile suggests that, at least in thermodynamic terms, the formation of the H-bonded adduct contributes substantially to the overall proton transfer leading to the dihydrogen complex.

Acknowledgments

Thanks are due to NATO (contract "^{2}H-relaxation as a tool to study hydrogen transfer reactions", grant HTECH-CRG 972 135), CNR (Italy) – RAS (Russian Federation) agreement, and RFBR (project No 99–03–33270) for financial support. Support from COST Chemistry Action D17/WG003 is also acknowledged.

© 2001 NRC Canada

References

1. (*a*) A.J. Lough, S.Park, R. Ramashandrar, and R.H. Morris. J. Am. Chem. Soc. **116**, 8356 (1994); (*b*) J.C. Lee, E. Peris, A. Rheinhold, and R.H. Crabtree. J. Am. Chem. Soc. **116**, 11014 (1994); (*c*) E. Peris, J.C. Lee, J.R. Rambo, O. Eisenstein, and R.H. Crabtree. J. Am. Chem. Soc. **117**, 3485 (1995); (*d*) E.S. Shubina, N.V. Belkova, A.N. Krylov, E.V. Vorontsov, L.M. Epstein, D.G. Gusev, M. Niedermann, and H. Berke. J. Am. Chem. Soc. **118**, 1105 (1996); (*e*) N.V. Belkova, E.S. Shubina, A.V. Ionidis, L.M. Epstein, H. Jacobsen, A. Messmer, and H. Berke. Inorg. Chem. **36**, 1522 (1997).
2. (*a*) J.A. Ayllon, C. Gervaux, S. Sabo-Etienne, and B. Chaudret. Organometallics, **16**, 2000 (1997); (*b*) E.S. Shubina, N.V. Belkova, E.V. Bakhmutova, E.V. Vorontsov, V.I. Bakhmutov, A.V. Ionidis, C. Bianchini, L. Marvelli, M. Peruzzini, and L.M. Epstein. Inorg. Chim. Acta, **280**, 302 (1998); (*c*) Y. Guari, J.A. Aylonn, S. Sabo-Etienne, and B. Chaudret. Inorg. Chem. **37**, 640 (1998); (*d*) S. Grundemann, S. Ulrich, H.H. Limbach, N.S. Golubev, G.S. Denisov, L.M. Epstein, S. Sabo-Etienne, and B. Chaudret. Inorg. Chem. **38**, 2550 (1999); (*e*) N.V. Belkova, E.V. Bakhmutova, E.S. Shubina, C. Bianchini, M. Peruzzini V.I. Bakhmutov and L.M. Epstein. Eur. J. Inorg. Chem. 2163 (2000); (*f*) N.V. Belkova, E.S. Shubina, E.I. Gutsul, L.M. Epstein, I.L. Eremenko, and S.E. Nefedov. J. Organomet. Chem. (2000) in press.
3. L.F. Rhodes and L.M. Venanzi. Inorg. Chem. **26**, 2692 (1987).
4. S.I. Hommeltoft and M.C. Baird. Organometallics, **5**, 190 (1986).
5. D. Cromer and J. Waber. Acta Crystallogr. **18**, 104 (1965).
6. A.J.C. Wilson (*Editor*). International tables for X-ray crystallography. Vol. C. Kluwer Academic Press, Dordrecht. 1992. p. 219
7. G.M. Sheldrick. SHELXL. 93 Program for crystal structure refinement. University of Göttingen, Germany. 1993.
8. C.K. Johnson. Report ORNL-5138. Oak Ridge National Laboratory, Oak Ridge, TN. 1976; as modified by L. Zsolnai and H. Pritzkow. University of Heidelberg, Germany. 1994.
9. A. Altomare, G. Cascarano, G. Giacovazzo, and A. Gualandi. J. Appl. Crystallogr. **26**, 343 (1993).
10. C. Bianchini, A. Meli, S. Moneti, and F. Vizza. Organometallics, **17**, 2636 (1998).
11. (*a*) P. Barbaro, C. Bianchini, A. Meli, M. Peruzzini, and F. Vizza. Organometallics, **10**, 2227 (1991); (*b*) C. Bianchini, S. Moneti, M. Peruzzini, and F. Vizza. Inorg. Chem. **36**, 5818 (1997); (*c*) C. Bianchini, A. Meli, M. Peruzzini, F. Vizza, P. Frediani, and J.A. Ramirez. Organometallics, **9**, 226 (1990).
12. P.J. Desrosiers, L. Cai, Z. Lin, R. Richards, and J. Halpern. J. Am. Chem. Soc. **113**, 4173 (1991).
13. J. Ott, L.M. Venanzi, C.A. Ghilardi, S. Midollini, and A. Orlandini. J. Organomet. Chem. **291**, 89 (1985).
14. A.G. Orpen, L. Brammer, F.H. Allen, O. Kennard, D.G. Watson, and R. Taylor. J. Chem. Soc. Dalton Trans. S1 (1989).
15. D. Michos, X.-L. Luo, and R.H. Crabtree. Inorg. Chem. **31**, 4245 (1992).
16. (*a*) P.G. Jessop and R.H. Morris. Coord. Chem. Rev. **121**, 155 (1992); (*b*) V.I. Bakhmutov and E.V. Vorontsov. Rev. Inorg. Chem. **18**, 183 (1998).
17. W.J. Oldham, A.S. Hinkle, and D.M. Heinekey. J. Am. Chem. Soc. **119**, 11028 (1997).
18. P.A. Maltby, M. Schlaf, M. Steinbeck, A.J. Lough, R.H. Morris, W.T. Klooster, T.F. Koetzle, and R.C. Srivastava. J. Am. Chem. Soc. **118**, 5396 (1996).
19. (*a*) R.H. Morris and R.J. Witterbort. Magn. Reson. Chem. **35**, 243 (1997); (*b*) D.G. Gusev, R.L. Kuhlman, K.B. Renkema, O. Eisenstein, and K.G. Caulton. Inorg. Chem. **35**, 6775 (1996).
20. (*a*) V.I. Bakhmutov, C. Bianchini, F. Maseras, A. Lledos, M. Peruzzini, and E.V. Vorontsov. Chem. Eur. J. **5**, 3318 (1999); (*b*) G.A. Facey, T.P. Fong, D. Gusev, P.M. Macdonald, R.H. Morris, M. Schlaf, and W. Xu. Can. J. Chem. **77**, 1899 (1999); (*c*) V.I. Bakhmutov, C. Bianchini, M. Peruzzini, F. Vizza, and E.V. Vorontsov. Inorg. Chem. **39**, 1655 (2000).
21. D. Nietlispach, V.I. Bakhmutov, and H. Berke. J. Am. Chem. Soc. **115**, 9191 (1993).
22. (*a*) H. Guo, W.L. Jarret, and L.G. Butler. Inorg. Chem. **26**, 3001 (1987); (*b*) L.G. Butler and E.A. Keiter, J. Coord. Chem. **32**, 121 (1992); (*c*) A.J. Kim, F.R. Fronczek, L.G. Butler, S. Chen, and E.A. Keiter. J. Am. Chem. Soc. **113**, 9090 (1991).
23. A.V. Iogansen. Theor. Experim. Khim. **7**, 302 (1971).
24. L.D. Field, T.W. Hambley, and B.C.K. Yau. Inorg. Chem. **33**, 2009, (1994).
25. S. Scheiner. Hydrogen bonding: a theoretical perspective. Oxford University Press, Oxford, N.Y. 1997.
26. H. Gunter. NMR spectroscopy. John Wiley & Sons, Chichester, N.Y. 1980.
27. (*a*) G. Orlova and S. Scheiner. J. Phys. Chem. A, **102**, 4813 (1998); (*b*) G. Orlova, S. Scheiner, and T. Kar. J. Phys. Chem. A, **103**, 514 (1999).
28. (*a*) M.G. Basallote, J. Duran, M.J. Fernandez-Trujillo, M.A. Manez, and J.R. Torre. J. Chem. Soc. Dalton Trans. 7445 (1998); (*b*) M. G.Basallote, J. Duran, M.J. Fernandez-Trujillo, and M.A. Manez. J. Chem. Soc. Dalton Trans. 2205 (1998).

© 2001 NRC Canada

Iron complexes of the $N(CH_2CH_2S)_3^{3-}(NS_3)$ ligand with isocyanide co-ligands.

Lyndsey Cooper, Sian C. Davies, Jonathan R. Dilworth, David L. Hughes, Marcin Konkol, Raymond L. Richards, J. Roger Sanders, and Piotr Sobota

Abstract: The complexes $NEt_4[Fe(NS_3)(CNR)]$ (**1**), $[Fe\{Fe(NS_3)(CNR)\}_2\text{-}S,S']$ (**2**), $[Co\{Fe(NS_3)(CNMe)\}_2\text{-}S,S']$ (**3**), and $[Ni\{Fe(NS_3)(CNMe)\}_2\text{-}S,S']$ (**4**) (R = Me, *t*-Bu, or C_6H_{11}(Cy)) have been prepared and the X-ray crystal structures of $NEt_4[Fe(NS_3)(CNMe)]$ (**1a**) and $[Fe\{Fe(NS_3)(CNCy)\}_2\text{-}S,S']$ (**2c**) have been determined. Mössbauer and IR spectroscopic data and room temperature magnetic moments for these complexes are reported.

Key words: iron, cobalt, nickel, thiolate, isocyanide.

Résumé : On a préparé les complexes de $NEt_4[Fe(NS_3)(CNR)]$ (**1**), $[Fe\{Fe(NS_3)(CNR)\}_2\text{-}S,S']$ (**2**), $[Co\{Fe(NS_3)(CNMe)\}_2\text{-}S,S']$ (**3**) et $[Ni\{Fe(NS_3)(CNMe)\}_2\text{-}S,S']$ (**4**) (R = Me, *t*-Bu ou C_6H_{11} (Cy)) et on a déterminé les structures de $NEt_4[Fe(NS_3)(CNMe)]$ (**1a**) et de $[Fe\{Fe(NS_3)(CNCy)\}_2\text{-}S,S']$ (**2c**) par diffraction des rayons X. Pour chacun de ces complexes, on a déterminé les spectres de Mössbauer et IR ainsi que les moments magnétiques à la température ambiante.

Mots clés : fer, cobalt, nickel, thiolate, isocyanure.

[Traduit par la Rédaction]

Introduction

We have been exploring the chemistry of the tripodal NS_3 ligand $N(CH_2CH_2S)_3^{3-}(NS_3)$ in order to investigate the ability of metal sites carrying this ligand to mimic the behaviour of metal–sulfur sites in enzymes such as hydrogenases and nitrogenase. In the former study, some of us have shown that sulfur-bridged, binuclear complexes containing the $\{Fe(\mu\text{-}NS_3)Ni\}$ unit model structural aspects of iron–nickel hydrogenase (1). Recently a rich chemistry of the tripodal nitrogen-donor ligand $[N(CH_2CH_2NSiMe_3)_3]^{3-}(NN_3)$, and its analogues has been developed, including the preparation of the tris(μ-dinitrogen) complex $[Fe\{N_2Mo(NN_3)\}_3]$ as well as the monomer $[Mo(NN_3)(N_2)]$ (2). This prompted us to investigate the ability of metal sites carrying the (NS_3) ligand to bind species on the route from N_2 to NH_3 such as N_2H, N_2H_2, and N_2H_4 and their derivatives, and alternative substrates to N_2 such as CO, cyanides, isocyanides, and azide. We have already reported or communicated some of our results for Mo (3), V (4), and Fe (5). The $Fe(NS_3)$ site is able to bind CO with biologically relevant values of ν(C=O) (5). We, therefore, searched for interactions of this site with other small molecules which are able to function as alternative substrates for dinitrogen, and have developed chemistry of isocyanides as detailed below.

Received August 30, 2000. Published on the NRC Research Press Web site at http://canjchem.nrc.ca on May 23, 2001.

Dedicated to Professor Brian R. James on the occasion of his 65th birthday.

L.Cooper and J.R. Dilworth. Inorganic Chemical Laboratory, University of Oxford, South Parks Road, Oxford OX1 3QR, U.K.
S.C. Davies, D.L. Hughes, R.L. Richards[1], and J.R. Sanders. Department of Biological Chemistry, John Innes Centre, Colney Lane, Norwich NR4 7UH, U.K.
M. Konkol and P. Sobota. Faculty of Chemistry, University of Wroclaw, 14 F Joliot Curie, 50–383 Wroclaw, Poland.

[1]Corresponding author (present address: School of Chemistry, Physics and Environmental Science, University of Sussex, Brighton, Sussex BN1 9RQ, U.K.; telephone: 01 273 877 711; fax: 01 273 677 196; e-mail: r.richards@sussex.ac.uk).

Results and discussion

The blue, mononuclear, terminal RNC complexes $NEt_4[Fe(NS_3)(CNR)]$ (R = Me (**1a**); *t*-Bu (**1b**); or C_6H_{11} (Cy) (**1c**)) were obtained either by treatment of $[Fe(acac)_3]$ and NS_3H_3 with RNC in presence of $Et_4N(OAc)$, or by reduction of $NEt_4[FeCl(NS_3)]$ (5) with sodium amalgam in presence of RNC (rxn. [1]). Compounds **1a** and **1b** form blue crystals, but **1c** could not be crystallized, nor obtained analytically pure, although its spectroscopic data show it clearly to be the analogue of **1a** and **1b**. In the solid, compounds **1** are moderately stable to air, decomposing over 2 to 3 days, but they are more sensitive in solution.

[1] $NEt_4[FeCl(NS_3)] + Na + RNC \rightarrow NEt_4[Fe(NS_3)(CNR)] + NaCl$
(R = Me (**1a**), *t*-Bu (**1b**), or Cy **(1c)**)

The complexes have the RNC ligand bound to five-coordinated Fe in the linear mode as revealed by the X-ray crystal structure of **1a**. The structure (Fig. 1) is similar to that of the carbonyl analogue (5), and consists essentially of a trigonal bipyramid with the terminal MeNC ligand linearly bound in the position *trans* to the apical N atom of the NS_3 ligand, with the three S atoms lying in the equatorial plane.

 DOI: 10.1139/cjc-79-5/6-490 © 2001 NRC Canada

Fig. 1. The anion of $NEt_4[Fe(NS_3)(CNMe)]$ (**1a**) showing the disorder in the NS_3 ligand and the atom numbering scheme.

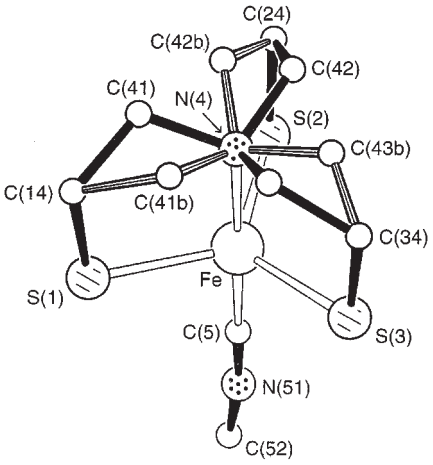


Table 1. Selected molecular dimensions in complex **1a**.

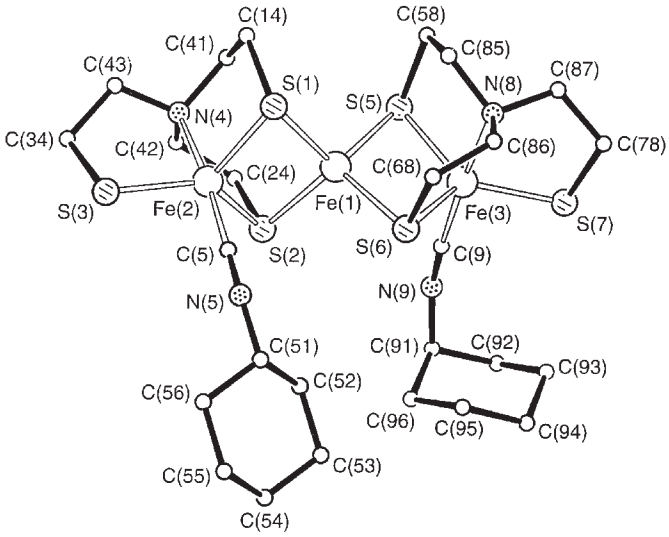
(*a*) About the iron atom			
Fe—S(1)	2.2953(5)	Fe—N(4)	2.049(2)
Fe—S(2)	2.2908(5)	Fe—C(5)	1.805(2)
Fe—S(3)	2.2926(6)		
S(2)-Fe-S(1)	119.09(2)	N(4)-Fe-S(2)	87.24(5)
S(3)-Fe-S(1)	118.73(2)	C(5)-Fe-S(2)	90.48(6)
N(4)-Fe-S(1)	87.87(5)	N(4)-Fe-S(3)	87.37(5)
C(5)-Fe-S(1)	92.35(6)	C(5)-Fe-S(3)	94.69(6)
S(2)-Fe-S(3)	121.61(2)	C(5)-Fe-N(4)	177.51(7)
(*b*) In the isocyanide ligand			
C(5)—N(51)	1.169(3)	N(51)-C(5)-Fe	178.2(2)
N(51)—C(52)	1.411(3)	C(5)-N(51)-C(52)	169.3(2)

Note: Bond lengths are in angstroms (Å), angles in degrees (°), Esds are in parentheses.

Principal structural parameters are presented in Table 1 and show that the Fe—N distance (2.049(2) Å) and average Fe—S distances (2.2929(14) Å) are close to those of the CO analogue, 2.035(7) and 2.274(5) Å respectively (5). The iron atoms are displaced similarly toward the apical C atom, 0.1003(2) and 0.0893(11) Å in **1a** and the CO analogue, respectively, from the 3S equatorial plane. The Fe—C distance 1.805(2) Å and Fe-C-N angle 178.2(2)° are in the expected ranges for linear RNC at an Fe(II) site.

As expected, compounds **1** have NC stretching frequencies in the terminal range (2061–1940 cm^{-1}). These values are lower than those of the corresponding free ligands, in keeping with the lowering of the CO stretching frequency on binding CO to this site, which is clearly electron releasing. The lowering of the NC frequency caused by binding to the d^6 $Fe(NS_3)^-$ site is similar to that produced by binding the analogous d^4 $Re(NS_3)$ site e.g., both **1b** and $[Re(NS_3)(CN\text{-}t\text{-}Bu)]$ (6) have ν(N≡C) at 1975 cm^{-1}, some 162 cm^{-1} lower than the value for the free ligand. The d^3 complex analogues $[V(NS_3)(CNR)]$ (R = *t*-Bu or Cy) do not show such a lowering of the CN stretching frequency (ν(N≡C) = 2173 cm^{-1} in both cases) (4). The electron-releasing properties of the

Fig. 2. View of the trinuclear complex $[Fe\{Fe(NS_3)(CNCy)\}_2]$ (**2c**) with the pseudo-twofold symmetry axis vertical in the plane of the paper. Only the major components of the disordered NS_3 ligands are shown.



V(NS_3) site is clearly less than that of the iron and rhenium systems, in keeping with the inability of the vanadium site to bind CO (4).

Compounds **1** are paramagnetic, with μ_{eff} values in the range 2.61–2.58 μ_B corresponding to an S = 1 state, as observed for the CO analogue (μ_{eff} = 2.79 μ_B) (5). Like the CO analogue, their Mössbauer spectra show a doublet, but the parameters (in the ranges: IS 0.36–0.32, QS 1.27–1.30 mm s^{-1}), are somewhat larger than those of the CO analogue (IS 0.22, QS 0.99 mm s^{-1}) (5).

In addition to the mononuclear complexes, the paramagnetic homo- and hetero-metallic linear cluster complexes $[Fe\{Fe(NS_3)(CNR)\}_2\text{-}S,S']$ (**2**), $[Co\{Fe(NS_3)(CNR)\}_2\text{-}S,S']$ (**3**), and $[Ni\{Fe(NS_3)(CNR)\}_2\text{-}S,S']$ (**4**) have been obtained by two routes. The first route, which involves treatment of $[Fe(acac)_3]$ with RNC and NS_3H_3, gives the very dark green "all iron" complexes (**2 a**–**c**). The second and more general route exploits the donor properties of the ligating S-atoms of complexes **1** and allows the controlled synthesis of the green-black hetero-atom linear clusters **3** and **4**, as shown in rxn. [2].

[2] $2NEt_4[Fe(NS_3)(CNR)] + MCl_2 \rightarrow [M\{Fe(NS_3)(CNR)\}_2\text{-}S,S'] + 2NEt_4Cl$

(M = Fe, R = Me (**2a**), *t*-Bu (**2b**), Cy **(2c)**;
M = Co, R = Me (**3)**; M = Ni, R = Me (**4**))

The linear structure of complexes **2a**–**c** is proven by the X-ray crystal structure of **2c**, shown in Fig. 2. The structure consists of two trigonal bipyramidal $Fe(NS_3)(CNCy)$ units, each of which bridges through two of its S atoms to a central Fe, which has distorted tetrahedral symmetry and lies on an approximate twofold symmetry axis. Principal structural parameters are presented in Table 2. Within the $Fe(NS_3)(CNCy)$ units, the Fe—S distances involving the four bridging S atoms average 2.265(4) Å, but those to the non-bridging S atoms are shorter, mean 2.221(4) Å. The

© 2001 NRC Canada

Table 2. Selected molecular dimensions in complex **2c**.

(*a*) About the iron atoms			
Fe(1)···Fe(2)	2.716(2)	Fe(1)···Fe(3)	2.705(2)
Fe(1)—S(1)	2.293(2)	Fe(1)—S(5)	2.301(2)
Fe(1)—S(2)	2.318(2)	Fe(1)—S(6)	2.315(2)
S(1)-Fe(1)-S(2)	105.00(8)	S(5)-Fe(1)-S(2)	110.76(8)
S(1)-Fe(1)-S(5)	114.10(8)	S(6)-Fe(1)-S(2)	112.99(8)
S(1)-Fe(1)-S(6)	109.40(8)	S(5)-Fe(1)-S(6)	104.80(8)
Fe(2)—S(1)	2.275(2)	Fe(3)—S(5)	2.258(2)
Fe(2)—S(2)	2.264(2)	Fe(3)—S(6)	2.262(2)
Fe(2)—S(3)	2.217(3)	Fe(3)—S(7)	2.224(2)
Fe(2)—N(4)	2.059(6)	Fe(3)—N(8)	2.044(6)
Fe(2)—C(5)	1.822(9)	Fe(3)—C(9)	1.835(9)
S(2)-Fe(2)-S(1)	107.40(8)	S(5)-Fe(3)-S(6)	108.02(8)
S(3)-Fe(2)-S(1)	121.59(10)	S(7)-Fe(3)-S(5)	127.71(9)
N(4)-Fe(2)-S(1)	88.3(2)	N(8)-Fe(3)-S(5)	88.5(2)
C(5)-Fe(2)-S(1)	98.5(3)	C(9)-Fe(3)-S(5)	94.6(2)
S(3)-Fe(2)-S(2)	130.61(10)	S(7)-Fe(3)-S(6)	123.98(9)
N(4)-Fe(2)-S(2)	87.8(2)	N(8)-Fe(3)-S(6)	88.5(2)
C(5)-Fe(2)-S(2)	89.2(3)	C(9)-Fe(3)-S(6)	93.5(3)
N(4)-Fe(2)-S(3)	87.8(2)	N(8)-Fe(3)-S(7)	87.7(2)
C(5)-Fe(2)-S(3)	89.5(3)	C(9)-Fe(3)-S(7)	87.9(3)
C(5)-Fe(2)-N(4)	173.1(3)	C(9)-Fe(3)-N(8)	175.6(3)
Fe(2)-S(1)-Fe(1)	72.95(7)	Fe(3)-S(5)-Fe(1)	72.78(7)
C(14)-S(1)-Fe(1)	106.1(3)	C(58)-S(5)-Fe(1)	107.5(3)
Fe(2)-S(2)-Fe(1)	72.70(7)	Fe(3)-S(6)-Fe(1)	72.43(7)
C(24)-S(2)-Fe(1)	106.9(3)	C(68)-S(6)-Fe(1)	105.8(3)
(*b*) In the isocyanide ligands			
C(5)—N(5)	1.148(9)	C(9)—N(9)	1.153(9)
N(5)—C(51)	1.448(11)	N(9)—C(91)	1.431(10)
N(5)-C(5)-Fe(2)	175.3(7)	N(9)-C(9)-Fe(3)	176.2(7)
C(5)-N(5)-C(51)	160.3(8)	C(9)-N(9)-C(91)	160.2(8)

Note: Bond lengths are in angstroms (Å), angles in degrees (°), Esds are in parentheses.

Fe—S distances about the central Fe have a mean value of 2.307(6) Å. The iron atoms Fe(2) and Fe(3) are displaced from the planes of their three equatorially-arranged sulfur atoms by 0.0805(11) and 0.0696(10) Å, respectively, similar to the values above for complex **1a** and its CO analogue. The apical N-Fe-C-N-C units are basically linear, with dimensions resembling those in **1a**. The isocyanide C-N-C angles in both ligands of **2c** however, essentially identical at 160.25(1)°, deviate more from linearity than in **1a** where the angle is 169.3(2)°. Even greater deviations have been noted in the Re^{III} complexes $[Re(NS_3)(CN\text{-}t\text{-}Bu)]$ and $[Re(NS_3)(CNCH_2COOMe)]$ where the C-N-C angles are 154.0(10) and 150.8(9)°, respectively (6). The limit of the pseudo-symmetry is reached at the cyclohexyl ring junction; both Cy rings have the chair conformation but the C(51)—N(5) bond is equatorial with respect to the ring in one isocyanide ligand, whereas, in the second, C(91)—N(9) is axially orientated.

All the Fe atoms can be regarded as formally in oxidation state two, but solid **2c** has μ_{eff} = 1.72 μ_B per molecule at 20°C showing considerable electronic coupling, and **2a**, **2b**, **3**, and **4** also show similar behaviour (see *Experimental*). The detailed magnetic and electrochemical properties of these and related complexes will form a separate study.

The Mössbauer spectrum of complex **2c** is in accord with its structure, showing resonances corresponding to two different iron(II) sites, one having twice the intensity of the other (*Experimental*). Since the Mössbauer spectra of **2a**, **2b**, **3**, and **4** all have similar IS and QS values to those of **2c**, all of these complexes are considered to have an analogous linear cluster structure. The CO analogue has the same linear structure also (5) and the members of this class of complex have structural similarities to the linear clusters $[NEt_4]_3[Fe_3S_4(SPh)_4]$ (7) and $[NEt_4]_3[VFe_2S_4Cl_4]$ (8).

The NC stretching frequencies of **2**, **3**, and **4** are increased relative to the corresponding monomeric precursors (*Experimental*). A similar increase was observed for the CO analogue on passing from the monomer to the linear cluster complexes (5). Clearly the ability of the $Fe(NS_3)$ site to release electron density to CO or RNC is reduced in the linear clusters as a consequence of the loss of anionic charge and by two of its sulfur ligands utilising lone pairs to bind a central metal atom.

Conclusions

The $Fe(NS_3)$ site is able to support a number of co-ligands including isocyanides, and its tendency to bridge through sulfur can be used to synthesise linear cluster complexes. The stretching frequencies of CO at mononuclear and linear cluster $Fe(NS_3)$ sites have values which are similar to those observed in stop-flow IR studies of *Klebsiella pneumoniae* nitrogenase (5). Corresponding data for RNC interactions with the enzyme are not yet available to ascertain how extensively the behaviour of the $Fe(NS_3)$ sites resembles that of the enzyme.

Experimental

General

All operations were carried out under a dry dinitrogen atmosphere, using standard Schlenk techniques. Solvents were distilled under dinitrogen from the appropriate drying agents prior to use. Starting materials were obtained from Aldrich Chemical Co. and used without further purification unless stated otherwise. Methyl isocyanide was made by the reaction of *N*-methylformamide with *p*-toluenesulfonyl chloride in quinoline at 75°C and purified by trap-to-trap distillation at 15 mm Hg (1 mm Hg = 133.222 Pa). NS_3H_3 was made by a modification of the literature method (4, 9–11) via tris(chloroethyl)amine hydrochloride (CAUTION-VESICANT) This work was carried out in an enclosed Schlenk apparatus whilst wearing heavy duty gloves and a face mask.

$[FeCl_2(MeCN)_2]$, $[FeCl_2(DMSO)_3]$ (DMSO = dimethylsulfoxide), and their cobalt and nickel analogues were made by heating the anhydrous metal chlorides in MeCN or DMSO until they dissolved and crystallizing by adding diethyl ether. IR spectra were recorded on PerkinElmer 883 or Shimadzu FT-IR 810M instruments in Nujol™ mulls. Mössbauer parameters were determined at 77 K by Dr D.J. Evans and Mrs E. Barclay of this laboratory, using an ES-technology MS105 spectrometer having a 925 MBq ^{57}Co source in a rhodium matrix at ambient temperature, referenced against a 25 μm iron foil at 295 K. Magnetic moment determinations at 293 K were in the solid state, using a

© 2001 NRC Canada

Johnson Matthey Gouy balance. Microanalyses were by Mr A. Saunders of the University of East Anglia (CHN) or by Southern Science, Falmer Laboratories, East Sussex (metals).

Syntheses

*Preparation of $Et_4N[Fe(NS_3)(CNMe)]\cdot MeCN$ (**1a**)*

$[Fe(acac)_3]$ (0.71 g, 2.0 mmol), $Et_4NOAc\cdot 4H_2O$ (0.65 g, 2.5 mmol), and MeNC (0.4 g, 10 mmol) were stirred in MeCN (10 mL) for a few minutes, then NS_3H_3 (0.6 g, 3 mmol) in MeCN (5 mL) was added, whereupon the solution turned blue. After 1 h it was filtered and MeCN (5 mL) and ether (20 mL) were added as a layer. After 3 days large blue crystals deposited, which were filtered off, washed with MeCN:ether and then ether, and dried in a vacuum; yield 0.35 g (38%). Mössbauer (mm s^{-1}): IS 0.36, QS 1.27. μ_{eff} = 2.61 μ_B (S = 1). IR (cm^{-1}): 2291, 2246 (C≡N), 2061 (N≡C). Anal. calcd. for $C_{18}H_{38}FeN_4S_3$: C 46.8, H 8.2, N 12.1; found: C 46.3, H 8.2, N 11.7.

*Preparation of $Et_4N[Fe(NS_3)(CN\text{-}t\text{-}Bu)]$ (**1b**)*

$Et_4N[FeCl(NS_3]$ (0.83 g, 2 mmol) was treated with sodium amalgam (70 g, 0.5% Na) in MeCN (20 mL). After 20 min the solution became yellow and was filtered through Celite™. *t*-BuNC (0.8 g, 10 mmol) was added immediately to the filtrate, which became blue. Ether (60 mL) was then added as a layer to give, after 2 h, dark blue microcrystals (0.14 g, 15%), which were filtered off, washed with ether, and dried in a vacuum. Mössbauer (mm s^{-1}): IS 0.32, QS 1.30. μ_{eff} = 2.58 μ_B (S = 1). IR (cm^{-1}): 1975 (N≡C). Anal. calcd. for $C_{19}H_{41}FeN_3S_3$: C 49.2, H 8.9, N 9.1; found: C 48.1, H 8.9, N 8.7.

*Preparation of $Et_4N[Fe(NS_3)(CNCy)]$ (**1c**)*

This was made similarly from reduced $Et_4N[FeCl(NS_3)]$ by treatment with CyNC, in 35% yield. A good analysis was not obtained (see text). Mössbauer (mm s^{-1}): IS 0.33, QS 1.29. IR (cm^{-1}): 2023, 1940 (N≡C). Anal. calcd. for $C_{21}H_{43}FeN_3S_3$: C 51.5, H 8.8, N 8.6; found: C 49.1, H 8.2, N 9.1.

*Preparation of $[Fe\{Fe(NS_3)(CNMe)\}_2$-S,S′] (**2a**)*

$[Fe(acac)_3]$ (0.71 g, 2 mmol) and MeNC (0.4 g, 10 mmol) were dissolved in MeCN (40 mL), and NS_3H_3 (0.6 g, 3 mmol) in MeCN (5 mL) was added. The solution turned dark red, but within 30 min it turned dark green and deposited black needles after 3 h which were filtered off, washed with ether, and dried in a vacuum (yield: 0.13 g, 0.2 mmol, 30% with respect to iron). Mössbauer (mm s^{-1}): IS 0.59, QS 2.06 (rel. intensity 1); IS 0.33, QS 1.38 (rel. intensity 2). μ_{eff} = 2.92 μ_B. IR (cm^{-1}): 2099 (N≡C). Anal. calcd. for $C_{16}H_{30}Fe_3N_4S_6$: C 30.1, H 4.6, N 8.8; found: C 30.1, H 4.6, N 8.9.

*Preparation of $[Fe\{Fe(NS_3)(CN\text{-}t\text{-}Bu)\}_2$-S,S′] (**2b**)*

$[Fe(acac)_3]$ (2.13 g, 6 mmol) and *t*-BuNC (3 g, 36 mmol) were dissolved in ether (40 mL) and NS_3H_3 (1.2 g, 6 mmol) was added. The mixture was stirred overnight and a brown precipitate was formed which turned dark green on standing overnight. It was filtered off, washed with ether, and dried in a vacuum; yield 1.0 g (70% with respect to Fe). Mössbauer (mm s^{-1}): IS 0.58, QS 2.04 (rel. intensity 1); IS 0.32, QS 1.39 (rel. intensity 2). μ_{eff} = 1.72 μ_B. IR (cm^{-1}): 2098, 2065 (N≡C). Anal. calcd. for $C_{22}H_{42}Fe_3N_4S_6$: C 36.6, H 5.8, N 7.8; found: C 36.7, H 5.6, N 7.7.

*Preparation of $[Fe\{Fe(NS_3)(CNCy)\}_2$-S,S′] (**2c**)*

This was made similarly using CyNC in ether, in 82% yield with respect to Fe. Mössbauer (mm s^{-1}): IS 0.67, QS 2.01 (rel. intensity 1); IS 0.30, QS 1.47 (rel. intensity 2). μ_{eff} = 1.72 μ_B. IR (cm^{-1}): 2084, 2060 (N≡C). Anal. calcd. for $C_{26}H_{46}Fe_3N_4S_6$: C 40.3, H 5.9, N 7.2; found: C 40.4, H 5.9, N 7.4.

*Preparation of $[Co\{Fe(NS_3)(CNMe)\}_2$-S,S′] (**3**)*

$[CoCl_2(DMSO)_3]$ (0.10 g, 0.3 mmol) in methanol (10 mL) was added to $Et_4N[Fe(NS_3)(CNMe)]$ (0.24, 0.6 mmol) in methanol (20 mL). A black precipitate formed. The next day this was filtered off, washed with methanol and ether, and dried in a vacuum (yield: 0.06 g, 34%). Mössbauer (mm s^{-1}): IS 0.29, QS 1.52. IR (cm^{-1}): 2105 (N≡C). Anal. calcd. for $C_{16}H_{30}CoFe_2N_4S_6$: C 30.0, H 4.7, N 8.7, Co 9.2, Fe 17.5; found: C 29.7, H 4.9, N 8.2, Co 9.9, Fe 17.3.

*Preparation of $[Ni\{Fe(NS_3)(CNMe)\}_2$-S,S′] (**4**)*

This was made similarly from $[NiCl_2(DMSO)_3]$ in 76% yield. Mössbauer (mm s^{-1}): IS 0.27, QS 1.61. μ_{eff} = 2.26 μ_B. IR (cm^{-1}): 2103 (N≡C). Anal. calcd. for $C_{16}H_{30}Fe_2N_4NiS_6$: C 30.0, H 4.7, N 8.7, Fe 17.5, Nil 9.2; found: C 30.0, H 4.9, N 8.2, Fe 15.6, Nil 9.1.

Crystal structure analyses

*$NEt_4[Fe(NS_3)(CNMe)]\cdot MeCN$ (**1a**)*

Crystal data: $C_8H_{20}N\cdot C_8H_{15}FeN_2S_3\cdot C_2H_3N$, MW = 462.5. Orthorhombic, space group $P2_12_12_1$ (No. 19), a = 16.664(2), b = 14.2340(12), c = 9.929(2) Å, V = 2355.1(6) $Å^3$, Z = 4, D_c = 1.31 g cm^{-3}, $F(000)$ = 992, T = 140 K, μ (Mo Kα) = 9.2 cm^{-1}, λ (Mo Kα) = 0.71069 Å.

Crystals are black, irregular octahedra; in thin section they are blue, decomposing in air to orange over two to three days. Most are twinned, and from preliminary photographic examination, some crystals show small variations in cell parameters and diffraction intensities. One, ca. 0.83 × 0.48 × 0.48 mm, sealed in a capillary tube, was mounted on an Enraf–Nonius CAD4 diffractometer (with monochromated radiation) for determination, at room temperature, of accurate cell parameters (from the settings of 25 reflections, θ = 10 to 11°, each centred in four orientations). The sample, shown to be twinned, was then cooled to 140 K, the cell parameters were re-determined, and diffraction intensities of the major twin were recorded. Of the 3825 unique reflections to θ_{max} = 30°, 3537 were "observed" with $I > 2\sigma_I$; the 00l reflections, common to both twins, were removed from the data set, leaving 3819 and 3532 reflections, respectively.

During processing, corrections were applied for Lorentz polarization effects, absorption (by semi empirical ψ-scan methods), and to eliminate negative net intensities (by Bayesian statistical methods). No deterioration correction was necessary. The structure was determined by the direct methods routines in the SHELXS program (12) and refined by full-matrix least-squares methods, on F^2's, in SHELXL (13). There is disorder in the N-bonded methylene groups in

© 2001 NRC Canada

the NS_3 ligand, with occupancy ratio of 0.736:0.264(2). All the non-hydrogen atoms were refined with anisotropic thermal parameters. Hydrogen atoms were included in idealised positions; later, the parameters of those in the cation, the major component of NS_3 ligand and the solvent molecule were refined freely, while the remainder were set to ride on those of the parent carbon atoms. At the conclusion of the refinement, $wR_2 = 0.051$ and $R_1 = 0.026$ (13) for all 3819 reflections weighted $w = [\sigma^2(F_o^2) + 0.180P]^{-1}$ with $P = (F_o^2 + 2F_c^2)/3$; for the observed data only, $R_1 = 0.022$. In the final difference map, the highest peaks (to ca. 0.2 e Å^{-3}) were close to a methylene group in the cation. Scattering factors for neutral atoms were taken from ref. 14. Computer programs used in this analysis have been noted above or in Table 4 of ref. 15, and were run on a DEC-Alpha Station 200 4/100 in the Department of Biological Chemistry, John Innes Centre.

[Fe{Fe(NS$_3$)(CNCy)}$_2$-S,S′]·nH$_2$O ***(2c)***

Crystal data: $C_{26}H_{46}Fe_3N_4S_6{\cdot}n(H_2O)$, with *n* ca. 0.2, MW = 778.2. Monoclinic, space group $P2_1/n$ (equiv. to No. 14), $a = 17.112(2)$, $b = 11.3486(8)$, $c = 17.313(2)$ Å, $\beta = 97.693(8)°$, $V = 3331.7(5)$ Å^3, $Z = 4$, $D_c = 1.551$ g cm^{-3}, $F(000) = 1624$, $T = 293$ K, μ (Mo Kα) = 16.9 cm^{-1}, λ (Mo Kα) = 0.71069 Å.

Crystals are black polyhedra. One, ca. 0.36 × 0.21 × 0.17 mm, was mounted on a glass fibre and coated with epoxy resin. Following a similar procedure to that described above, 4058 unique reflections to $\theta_{max} = 22°$ were measured at room temperature; 2523 were observed with $I > 2\sigma_I$. One reflection, whose intensity measurement was suspect, was not included in the refinement process.

During refinement, both NS_3 ligands were both found to have two alternative conformations; these were refined independently, each with its complement of hydrogen atoms included in idealised positions and with temperature factors riding on those of the parent carbon atoms. Hydrogen atoms were included similarly in the cyclohexyl groups. The non-hydrogen atoms, except for those in the minor components in the disordered ligands, were refined with anisotropic thermal parameters. A persistent difference peak was included as a partially occupied water molecule. At the conclusion of the refinement, $wR_2 = 0.132$ and $R_1 = 0.086$ (12) for the 4057 reflections weighted $w = [\sigma^2(F_o^2) + (0.0593P)^2]^{-1}$; for the observed data only, $R_1 = 0.051$. In the final difference map, the highest peaks (to ca. 0.8 e Å^{-3}) were all in the region of the iron-sulfur core of the molecule.

Acknowledgments

We thank the BBSRC and the EU (SOCRATES programme) for support and Dr A. Trzeciak for helpful discussions.

References

1. S.C. Davies, D.J. Evans, D.L. Hughes, S.Longhurst, and J.R. Sanders. Chem. Commun. 1935 (1999).
2. (*a*) M.B. O'Donoghue, N.C. Zanetti, W.M. Davis, and R.R. Schrock. J. Am. Chem. Soc. **119**, 2753 (1997); (*b*) M. B. O'Donoghue, W. M. Davis, R. R. Schrock, and W. M. Reiff. Inorg. Chem. **38**, 243 (1999).
3. S.C. Davies, D.L. Hughes, R.L. Richards, and J.R. Sanders. J. Chem. Soc. Dalton Trans. 719 (2000).
4. (*a*) S.C. Davies, D.L. Hughes, Z. Janas, L. Jerzykiewicz, R.L. Richards, J.R. Sanders, and P. Sobota. Chem. Commun. 1261 (1997); (*b*) S.C. Davies, D.L. Hughes, Z. Janas, L. Jerzykiewicz, R.L. Richards, J.R. Sanders, J.E. Silverston, and P. Sobota. Inorg. Chem. **39**, 3485 (2000).
5. S.C. Davies, D.L. Hughes, R.L. Richards, and J.R. Sanders. Chem. Commun. 2699 (1998).
6. M. Glaser, H. Spies, T. Lügger, and F.E. Hahn. J. Organomet. Chem. **503**, C 32 (1995) and refs. therein.
7. K.S. Hagen, A.D. Watson, and R.H. Holm. J. Am. Chem. Soc. **105**, 3905 (1983).
8. Y. Do, E.D. Simhon, and R.H. Holm. Inorg. Chem. **24**, 4635 (1985).
9 K. Ward. J. Am. Chem. Soc. **57**, 914 (1935).
10. J. Harley-Mason. J. Chem. Soc. 320 (1947).
11. P. Barbaro, C. Bianchini, G. Scapacci, D. Masi, and P. Zanello. Inorg. Chem. **33**, 3180 (1994).
12. G.M. Sheldrick. Acta Crystallogr. Sect. A: Fundam. Crystallogr. **A46**, 467 (1990).
13. G.M. Sheldrick. SHELXL. Program for crystal structure refinement. University of Göttingen, Germany. 1993.
14. International tables for X-ray crystallography. Vol. C. Kluwer Academic Publishers, Dordrecht, Netherlands. 1992. pp. 500, 219, and 193.
15. S.N. Anderson, R.L. Richards, and D.L. Hughes. J. Chem. Soc. Dalton Trans. 245 (1986).

© 2001 NRC Canada

Synthesis, characterization, and reactivity of manganese(II) and iron(II) trifluoroacetates. Crystal and molecular structure of two linkage isomers of polynuclear $[Mn(CF_3COO)_2(THF)_2]_n$

Fausto Calderazzo, Ulli Englert, Guido Pampaloni, Vincenzo Passarelli, Giovanna Serni, and Ruimin Wang

Abstract: The trifluoroacetates of manganese(II) and iron(II) have been prepared as THF or DMF adducts by reaction of metallic manganese or pentacarbonyliron(0) in THF or DMF, respectively, with CF_3COOH–$(CF_3CO)_2O$. Crystals of two linkage isomers of polynuclear $[Mn(CF_3COO)_2(THF)_2]_n$ have been obtained differing in the distribution of the bridging trifluoroacetato groups within the repeating units, namely $[(THF)_2Mn(\mu\text{-}CF_3COO)_3Mn(THF)_2(\mu\text{-}CF_3COO)]$ and $[(THF)_2Mn(\mu\text{-}CF_3COO)_2Mn(\mu\text{-}CF_3COO)_2(THF)_2]$. Photolysis of $Fe(CO)_5$ in CF_3COOH–$(CF_3CO)_2O$ mixtures or in neat $(CF_3CO)_2O$ gives the trifluoroacetato of iron(II) $Fe(CF_3COO)_2$, whose formation may occur through the intermediacy of $Fe_2(CO)_9$.

Key words: linkage isomers, manganese, iron, carboxylates, X-ray structure.

Résumé : Par réaction du manganèse métallique ou du pentacarbonylfer(0) avec du CF_3COOH–$(CF_3CO)_2O$, en solution dans le THF ou le DMF, il est possible de préparer les trifluoroacétates de manganèse(II) ou de fer(II) sous la forme d'adduits avec du THF ou du DMF. On a obtenu des cristaux pour deux isomères de liaison de l'entité polynucléaire $[Mn(CF_3COO)_2(THF)_2]_n$; ils ne diffèrent que par la distribution des groupes trifluoroacétato qui forment les ponts dans les motifs de la chaîne, soit le $[(THF)_2Mn(\mu\text{-}CF_3COO)_3Mn(THF)_2(\mu\text{-}CF_3COO)]$ et $[(THF)_2Mn(\mu\text{-}CF_3COO)_2Mn(THF)_2(\mu\text{-}CF_3COO)_2(THF)_2]$. La photolyse du $Fe(CO)_5$ dans des mélanges de CF_3COOH–$(CF_3CO)_2O$ ou dans du $(CF_3CO)_2O$ pur conduit à la formation du trifluoroacétatofer(II), $Fe(CF_3COO)_2$, dont la formation peut se produire par l'intermédiaire de $Fe_2(CO)_9$.

Mots clés : isomères de liaison, manganèse, fer, carboxylates, structure par diffraction des rayons X.

[Traduit par la Rédaction]

Introduction

Carboxylates of transition- and nontransition elements occupy a central position in coordination chemistry (1). More recently, the discovery of new applications has increased the interest in the chemistry of metal carboxylates. Trifluoroacetates are important in the production of ferroelectrics, and in the thin-film coating of complex oxides in the high-T_c superconductor field (2).

Moreover, trifluoroacetates offer a number of advantages with respect to unsubstituted carboxylates: they are generally more soluble in common organic solvents and in some cases they can be sublimed at relatively low temperature. Moreover, trifluoroacetic acid being a relatively strong acid, the conjugated base ($[CF_3COO]^-$) is weakly basic and may be easily displaced from the coordination sphere of a metal or at least can easily behave as a monodentate ligand, leaving a free coordination position.

In continuation of our recent work (3) on triflato- or trifluoracetato complexes of vanadium(II), it was believed that homoleptic[3] trifluoroacetato derivatives should be further explored, as these derivatives of transition metals are limited in

Received August 30, 2000. Published on the NRC Research Press Web site at http://canjchem.nrc.ca on May 23, 2001.

Dedicated to Professor Brian James on the occasion of his 65th birthday and in recognition of his outstanding scientific achievements.

F. Calderazzo, G. Pampaloni[1], V. Passarelli[2], and G. Serni. Università degli Studi di Pisa, Dipartimento di Chimica e Chimica Industriale, Via Risorgimento 35, I-56126 Pisa, Italy.
U. Englert and R. Wang. Institut für Anorganische Chemie der RWTH, Professor-Pirlet-Strasse 1, D-52074 Aachen, Germany.
V. Passarelli. Scuola Normale Superiore, Piazza dei Cavalieri 7, I–56126 Pisa, Italy.

[1]Corresponding author (telephone: + 50-918 221; fax: + 50-20 237; e-mail: pampa@dcci.unipi.it).
[2]Present address: Scuola Normale Superiore, Piazza dei Cavalieri 7, I-56126 Pisa, Italy.

[3]In the context of this paper, a homoleptic derivative is a compound which contains trifluoroacetato ligands only, their number corresponding to the formal oxidation state of the metal.

 DOI: 10.1139/cjc-79-5/6-495 © 2001 NRC Canada

number. A few compounds have been crystallographically characterized, namely $M_2(CF_3COO)_4$, M = Mo (4), W (5), $Ru_2(CF_3COO)_5$ (6), $Rh_2(CF_3COO)_4$ (7), $Pd_n(CF_3COO)_{2n}$, n = 3 (8), 4 (9), and $Ag(CF_3COO)$ (10). We therefore decided to study the manganese(II) and iron(II) carboxylato systems and in this paper we report the synthesis of the trifluoroacetates of manganese(II) and iron(II) and their complexes with Lewis bases. In the course of this work we have encountered an unusual type of linkage isomerism for the manganese(II) derivatives.

Experimental

All operations were carried out using standard Schlenk-tube techniques, under an atmosphere of prepurified nitrogen. The reaction vessels were oven dried prior to use. Solvents were dried by conventional methods.

Elemental analyses were performed with a Carlo Erba Mod. 1106 elemental analyzer. Infrared spectra were recorded with a PerkinElmer mod. FT 1725X instrument on solutions or Nujol or polychlorotrifluoroethylene mulls of the compounds prepared under rigorous exclusion of moisture and oxygen. The presence of solvent (THF, DMF, or trifluoroacetic acid) in the compounds reported in this paper was qualitatively established by IR spectroscopy and quantitatively confirmed by gravimetric determination of the liquid collected at liquid nitrogen temperature upon thermal decomposition at about 250°C/10^{-1} torr (1 torr = 133.322 Pa). Photolytic reactions were performed in a quartz apparatus equipped with a 150 W mercury lamp.

Pentacarbonyliron (Fluka) and finely divided manganese (Fluka) were commercially available and were used without further purification. Di-iron enneacarbonyl ($Fe_2(CO)_9$) was prepared according to literature (11).

Synthesis of $Mn(CF_3COO)_2 \cdot n$THF

A mixture of CF_3COOH (60 mL) and $(CF_3CO)_2O$ (10 mL) was treated with finely divided manganese (2.58 g, 46.96 mmol) at room temperature. Evolution of gas and formation of a colourless solid were observed. After 12 h stirring at room temperature, the mixture, still containing unreacted manganese, was refluxed for 6 h. The volatiles were evaporated to dryness in vacuo and the colourless residue (with broad absorptions above 3000 and at 1781(s) cm^{-1} due to trifluoroacetic acid) was dissolved in THF (100 mL). After filtration, the volatiles were removed in vacuo at room temperature and the residue was heated at 120°C/10^{-2} torr (1 torr = 133.322 Pa) for 5 h obtaining 12.4 g (76% yield) of $Mn(CF_3COO)_2 \cdot 0.9$ THF.[4] IR (Nujol – polychlorotrifluoroethylene mull) $\bar{\nu}$ (cm^{-1}): 2964 m-w, 2915 m-w, 1721 s, 1685 vs (ν_{as} (COO)), 1663 w, 1462 m-s (ν_s (COO)), 1375 w, 1211 vs (ν_{as} (CF_3)), 1151 s (ν_s (CF_3)), 1027 m (ν_{as} (COC)), 920 w, 875 m-s (ν_s (COC)), 851 m-s, 798 s, 726 s, 616 w, 524 w, 475 w. Magnetic data: $\chi_M^{corr} = 1.1 \times 10^{-2}$ cgsu, diam. corr. = -1.36×10^{-4} cgsu, μ_{eff} (293 K) = 5.08 BM. Anal. calcd. for $C_{7.6}H_{7.2}F_6MnO_{4.9}$: C 26.4, H 2.1, Mn 15.9; found: C 26.0, H 2.4, Mn 16.0. The compound was recrystallized from THF–heptane affording colourless crystals.

Table 1. Crystallographic data and details of structure refinement for $[(THF)_2Mn(\mu\text{-}CF_3COO)_3Mn(THF)_2(\mu\text{-}CF_3COO)]_n$.

Compound	$Mn(CF_3COO)_2(THF)_2$
FW	425.19
Crystal system	monoclinic
Space group (no)	$P2_1/c$ (no. 14)
a (Å)	9.659(3)
b (Å)	19.706(12)
c (Å)	18.064(12)
β (deg)	90.89(5)
V (Å^3)	3438(5)
Z	8
D_{calc} (g cm^{-3})	1.643
μ (cm^{-1})	8.207
Crystal dimensions (mm)	1.20 × 0.60 × 0.40
Diffractometer	Enraf–Nonius CAD4
T (K)	203
F(000)	1720
$\Theta_{min,\ max}$	2.0, 26.0
Scan type	ω
Absorption correction	empirical
(min, max)	(0.866, 0.999)
Reflections collected	7502
Reflections unique	6065
Observations in refinement	5253 [$I > 1.0\ \sigma(I)$]
Variables refined	451
R	0.078
R_w	0.086
Goodness of fit	1.709
Max residual electron density (e Å^{-3})	0.75

$R = \Sigma||F_o| - |F_c|| / \Sigma|F_o|$. $R_w = [\Sigma w(|F_o| - |F_c|)^2 / \Sigma w|F_o|^2]^{1/2}$.

Crystal structure solution and refinement $(Mn(CF_3COO)_2(THF)_2)$[5]

Crystals suitable for the X-ray structural determination were chosen within the mother liquor (heptane + THF) to avoid their collapse upon filtration and drying in vacuo. Crystal data, data collection parameters, and refinement results are in Table 1.

Structure solution based on direct methods (12) and refinement on structure factors (13) were straightforward. Highly anisotropic displacement parameters for the trifluoromethyl groups and the five-membered THF rings are considered to be responsible for the relatively high R factors.

[4] On several preparations, the amount of THF retained by the compound depends on the drying time in vacuo. The THF content of the solid was determined by collecting the volatiles (THF by IR spectroscopy) in a liquid nitrogen trap upon heating the sample at 250°C/10^{-2} torr (1 torr = 133.322 Pa). The compound darkens at ca. 220°C without melting.

[5] Copies of material on deposit may be purchased from the Depository of Unpublished Data, Document Delivery, CISTI, National Research Council Canada, Ottawa, ON K1A 0S2, Canada (http:\\www.nrc.ca/cisti/irm/unpub_e.shtml for information on ordering electronically). Some of this material has also been deposited with the Cambridge Crystallogrpahic Data Centre. Copies of the data can be obtained, free of charge, on application to the Director, CCDC, 12 Union Road, Cambridge CB2 1EZ, U.K. (Fax: 44-1223-336033 or e-mail: deposit@ccdc.cam.ac.uk).

© 2001 NRC Canada

While choosing the crystals for the X-ray diffractometric experiment, it was noted that some of them had a different shape. The low quality of these crystals prevented a conventional refinement of the structure, although it was possible to establish the atom connectivity.[6]

Synthesis of $Fe(CF_3COO)_2 \cdot n$DMF from $Fe(CO)_5$

A golden yellow solution of $Fe(CO)_5$ (2 mL, 15.2 mmol) in DMF (25 mL) was treated with a mixture of CF_3COOH (2.34 mL, 30.4 mmol) and $(CF_3CO)_2O$ (0.43 mL, 3.04 mmol). After 15 h reflux, no carbonyl derivatives were detected in the solution (IR spectrum in the carbonyl stretching region). The colourless solution was evaporated at 80°C/10^{-2} torr (1 torr = 133.322 Pa), thus obtaining a pale yellow liquid residue. After addition of toluene (25 mL) the mixture was evaporated (80°C/10^{-2} torr (1 torr = 133.322 Pa)) affording a colourless solid. In some instances, this operation should be repeated at least three times to obtain a microcrystalline solid. The residue was suspended in heptane (25 mL). After filtration and washing with heptane (2 × 5 mL), the solid was dried in vacuo at room temperature affording 4.0 g (67% yield) of $Fe(CF_3COO)_2 \cdot 1.5$DMF.[7] IR (Nujol – polychlorotrifluoroethylene mull) $\bar{\nu}$ (cm^{-1}): 2943 m-w, 1729 m, 1646 vs (ν_{as} (COO)), 1496 m-s, 1456 m-s (ν_s (COO)), 1435 m-s, 1376 s, 1208 vs (ν_{as} (CF_3)) 1144 s ($\nu_s(CF_3)$), 844 m-s, 795 m-s, 724 s, 670 m-w, 453 s, 409 m-w. Magnetic data: χ_M^{corr} = 1.1 × 10^{-2} cgsu, diam. corr. = –1.60 × 10^{-4} cgsu, μ_{eff} (293 K) = 5.08 BM. Anal. calcd. for $C_{8.5}H_{10.5}F_6FeN_{1.5}O_{5.5}$: C 26.1, H 2.7, N 5.4, Fe 14.3; found: C 25.7, H 2.4, N 5.1, Fe 14.5.

The compound was heated in vacuo at 120°C for 4 h which caused partial loss of DMF and gave $Fe(CF_3COO)_2 \cdot 0.9$DMF as established by elemental analysis. Attempts to remove DMF completely produced darkening and decomposition.

Synthesis of $Fe(CF_3COO)_2 \cdot n CF_3COOH$

By photolysis of $Fe(CO)_5$ in CF_3COOH–$(CF_3CO)_2O$

A golden yellow solution of $Fe(CO)_5$ (2 mL, 15.2 mmol) in CF_3COOH (100 mL) and $(CF_3CO)_2O$ (2 mL) was photolyzed at 20°C for 2 h. Evolution of gas and formation of a colourless solid were observed. The solid was filtered off and dried in vacuo at room temperature affording 4.54 g (58.5% yield) of $Fe(CF_3COO)_2.2CF_3COOH$. IR (Nujol – polychlorotrifluoroethylene mull) $\bar{\nu}$ (cm^{-1}): 3200 m-br, 1781 m, 1697 vs (ν_{as} (COO)), 1450 m-s (ν_s (COO)), 1204 vs (ν_{as} (CF_3)), 1140 s ($\nu_s(CF_3)$), 855 m-s, 820 w, 796 m-s, 728 s, 705 m-s, 522 m-w, 458 m-w, 420 m-w. Magnetic data: χ_M^{corr} = 1.04 × 10^{-2} cgsu, diam. corr. = –1.69 × 10^{-4} cgsu, μ_{eff} (293 K) = 4.94 BM. Anal. calcd. for $C_8H_2F_{12}FeO_8$: C 18.9, H 0.4, Fe 10.8; found: C 18.3, H 0.3, Fe 10.7. The solution was evaporated to dryness at 60°C/10^{-2} torr (1 torr = 133.322 Pa) and 1.1 g of $Fe(CF_3COO)_2 \cdot CF_3COOH$ was thus obtained. Anal. calcd. for $C_6HF_9FeO_6$: C 18.2, H 0.2 Fe 14.1; found: C 17.7, H 0.1, Fe 13.8.

By photolysis of $Fe(CO)_5$ in CF_3COOH

A golden yellow solution of $Fe(CO)_5$ (2 mL, 15.2 mmol) in CF_3COOH (100 mL), was photolyzed at 20°C. Evolution of gas (H_2 and CO by gas chromatography) took place. After 9 h, an IR spectrum of the solution showed unreacted $Fe(CO)_5$ as the only carbonyl species. The solution was evaporated to dryness in vacuo at room temperature affording 1.87 g (28% yield) of $Fe(CF_3COO)_2 \cdot 1.4CF_3COOH$. IR (Nujol – polychlorotrifluoroethylene mull) $\bar{\nu}$ (cm^{-1}): 3200 m-br, 1785 m, 1698 vs (ν_{as} (COO)), 1455 m-s (ν_s (COO)), 1204 vs ($\nu_{as}(CF_3)$), 1140 s ($\nu_s(CF_3)$), 855 m-s, 820 w, 796 m-s, 728 s, 705 m-s, 522 m-w, 458 m-w. Anal. calcd. for $C_{6.8}H_{1.4}F_{10.2}FeO_{6.8}$: C 18.5, H 0.3, Fe 12.6; found: C 18.3, H 0.4, Fe 12.6.

By photolysis of $Fe(CO)_5$ in $(CF_3CO)_2O$

A golden-yellow solution of $Fe(CO)_5$ (2 mL, 15.2 mmol) in $(CF_3CO)_2O$ (45 mL), was photolyzed at 20°C. Evolution of gas (CO by gas chromatography) and separation of a colourless solid took place during photolysis (7 h). The mixture was filtered and the solid was dried in vacuo at room temperature affording 2.3 g (48% yield) of $Fe(CF_3COO)_2 \cdot 0.3CF_3COOH$. IR (Nujol – polychlorotrifluoroethylene mull) $\bar{\nu}$ (cm^{-1}): 3200 w-br, 1751 w, 1694 vs (ν_{as} (COO)), 1455 m-s (ν_s (COO)), 1206 vs (ν_{as} (CF_3)) 1160 s (ν_s (CF_3)), 858 m-s, 797 m-s, 729 s, 614 m-w, 523 m-w, 461 m-w. Magnetic data: χ_M^{corr} = 1.17 × 10^{-2} cgsu, diam. corr. = –1.00 × 10^{-4} cgsu, μ_{eff} (293 K) = 5.26 BM. Anal. calcd. for $C_{4.6}H_{0.3}F_{6.9}FeO_{4.6}$: C 17.5, H 0.1, Fe 17.7; found: C 17.5, H 0.0, Fe 17.6. The mother liquor was evaporated at 80°C/10^{-2} torr (1 torr = 133.322 Pa) in a trap cooled at liquid nitrogen temperature and the distillate showed (GC–MS) the presence of hexafluoro–2,3-butanedione ($(CF_3CO)_2$).

By reaction of $Fe_2(CO)_9$ in CF_3COOH–$(CF_3CO)_2O$

An orange suspension of $Fe_2(CO)_9$ (0.651 g, 1.8 mmol) in a 85:15 mixture (v/v) of CF_3COOH–$(CF_3CO)_2O$ (30 mL) was stirred in the dark for 12 h at room temperature, thus obtaining a pale yellow solution (free from absorptions in the carbonyl stretching region) which was evaporated to dryness in vacuo at room temperature. The pale yellow $Fe(CF_3COO)_2 \cdot 0.8CF_3COOH$ (0.43 g, 64%) was obtained as a microcrystalline solid. IR (Nujol – polychlorotrifluoroethylene mull) $\bar{\nu}$ (cm^{-1}): 3210 w-br, 1783 w, 1694 vs-br (ν_{as} (COO)), 1457 m-s (ν_s (COO)), 1203 vs (ν_{as} (CF_3)), 1166 s (ν_s (CF_3)), 852 m-s, 797 m-s, 729 s, 702 w, 615 m-w, 522 w, 455 m-w. Anal. calcd. for $C_{5.6}H_{0.8}F_{8.4}FeO_{5.6}$: C 18.0, H 0.2, Fe 15.0; found: C 17.7, H 0.1, Fe 15.0.

Reaction of $Fe(CF_3COO)_2 \cdot 2CF_3COOH$ with THF

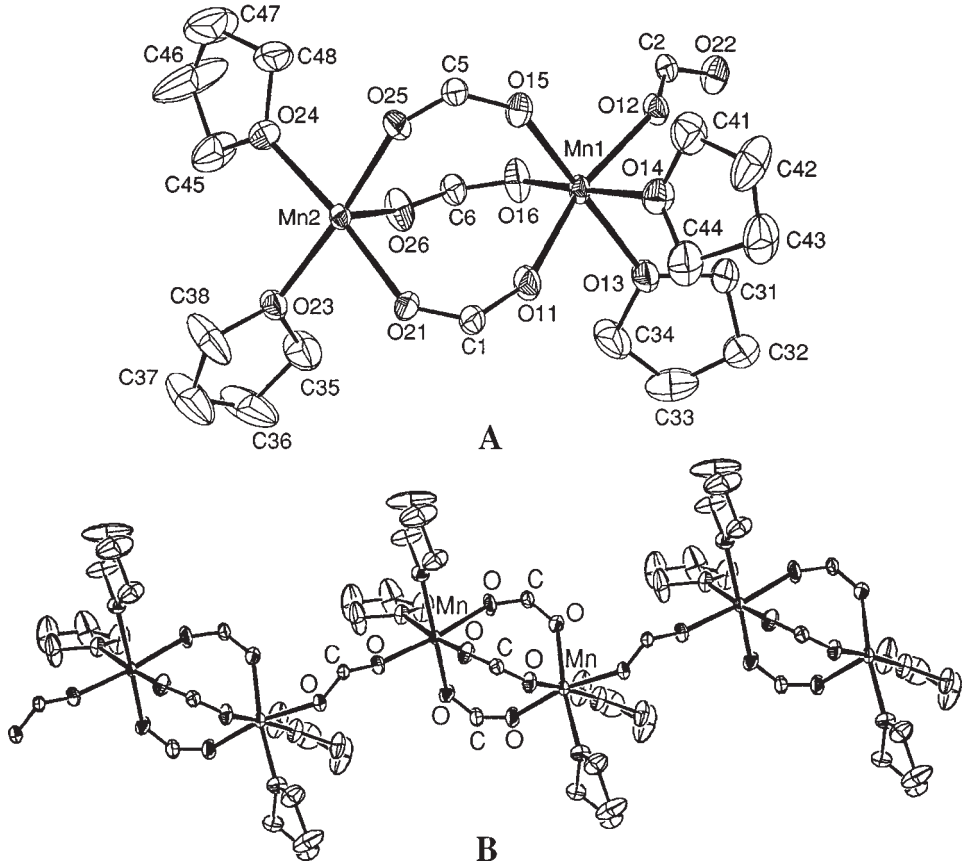
A solution of $Fe(CF_3COO)_2 \cdot 2CF_3COOH$ (1.273 g, 2.5 mmol) in THF (10 mL) was stirred at room temperature for 4 h. The solid which formed on addition of heptane (30 mL) was filtered off, washed with heptane (2 × 10 mL), and dried in vacuo at room temperature affording 0.80 g

[6] Crystal data: MW = 425.19; crystal system: monoclinic; space group: $P2_1/c$ (no. 14); a = 8.21(5) Å, b = 10.88(5) Å, c = 19.52(5) Å; V = 1743(1) Å^3; Z = 4; D_c = 1.62 g cm^{-3}; μ = 8.09 cm^{-1}; $F(000)$ = 860; T = 203 K. The structure was solved by direct methods. 1164 independent reflections with $I > 2\,\sigma(I)$ and 101 variables were used in the refinement which converged at values of R = 0.216 and Rw = 0.238.

[7] On several preparations, the amount of DMF retained by the compound was found to depend on the isolation procedure. The DMF content of the solid was determined by collecting the volatiles (DMF by IR spectroscopy) in a liquid nitrogen trap upon heating the sample at 250°C/10^{-2} torr (1 torr = 133.322 Pa).

© 2001 NRC Canada

Fig. 1. View of the dinuclear unit (A) and of the polynuclear chain (B) of $[(THF)_2Mn(\mu\text{-}CF_3COO)_3Mn(THF)_2(\mu\text{-}CF_3COO)]_n$.



(78% yield) of $Fe(CF_3COO)_2 \cdot 1.8THF$ as a microcrystalline solid. IR (Nujol – polychlorotrifluoroethylene mull) $\bar{\nu}$ (cm^{-1}): 2989 m-s, 2898 m-s, 1713 s, 1454 s, 1374 w, 1346 m-w, 1208 vs, 1143 vs, 1044 s (ν_{as} (COC)), 921 m-s, 885 m-s (ν_s (COC)), 841 m, 795 s, 679 w, 610 m-w, 524 m-w. Magnetic data: $\chi_M^{corr} = 1.13 \times 10^{-2}$ cgsu, diam. corr. = -1.8×10^{-4} cgsu, μ_{eff} (293 K) = 5.16 BM. Anal. calcd. for $C_{11.2}H_{14.4}F_6FeO_{4.8}$: C 32.7, H 3.5, Fe 13.6; found: C 32.0, H 3.8, Fe 13.6.

Results and discussion

Manganese

The reaction of finely divided manganese with CF_3COOH in the presence of $(CF_3CO)_2O$ (see rxn. [1]) gives a colourless solid containing CF_3COOH as suggested by the broad absorption above 3000 cm^{-1} and the strong absorption at 1781 cm^{-1}. The product is massively soluble in THF (concentrations as high as 12% w/w can be obtained at 20°C) and from the colourless solution the highly moisture sensitive THF adduct crystallizes out on addition of heptane. The treatment of the crude material with THF is also important to eliminate small amounts of unreacted metallic manganese. Depending on the drying procedure, compounds with THF–Mn molar ratios lower than 2 were isolated. The THF-containing species decompose at ca. 210°C (14) without melting (15; this paper reports that the reaction of manganese with CF_3COOH gives $Mn(CF_3COO)_2$ as a colourless solid melting at 63°C).

[1] $$Mn \xrightarrow[2)\ THF]{1)\ CF_3COOH/(CF_3CO)_2O} Mn(CF_3COO)_2 * n\text{THF}$$

The IR spectrum of the THF adduct of $Mn(CF_3COO)_2$ shows strong bands at 1670 (ν_{as} (COO)) and 1470 (ν_s (COO)) cm^{-1}, the difference between the two absorptions being typical of chelating bridging trifluoroacetato groups (16). The presence of THF in this species is indicated by the two absorptions of medium intensity at 1027 and 851 cm^{-1}.

Colourless crystals of $Mn(CF_3COO)_2(THF)_2$ were obtained by recrystallization from THF–heptane and used for the crystallographic study. The compound is polynuclear with bridging trifluoroacetato groups giving a sequence of one-three bridges between neighboring metal centres. Consequently, two different intermetallic distances are observed along the chain (Mn1···Mn2 = 4.371 Å ; Mn2···Mn1 = 6.128 Å) (Fig. 1A) and the asymmetric unit contains two manganese atoms. The two manganese atoms are bonded in a distorted octahedral coordination to the oxygen atoms of the triple bridge, to two oxygen atoms of two THF ligands, and to one oxygen atom of the single trifluoroacetato bridge (see Fig. 1B). The chain is therefore constituted by the $[(THF)_2Mn(\mu\text{-}CF_3COO)_3Mn(\mu\text{-}CF_3COO)(THF)_2]$ repeating unit. Table 2 reports a selection of bond distances and angles of this compound.

The trifluoroacetato groups of the triple bridge are arranged in a *syn-syn* bidentate mode; nevertheless, one of the bridges is substantially symmetric (Mn—O distances: 2.133(3) and 2.135(3) Å), while the remaining two groups

© 2001 NRC Canada

Table 2. Table of bond distances (Å) and angles (deg) for $[(THF)_2Mn(\mu\text{-}CF_3COO)_3Mn(THF)_2(\mu\text{-}CF_3COO)]_n$.

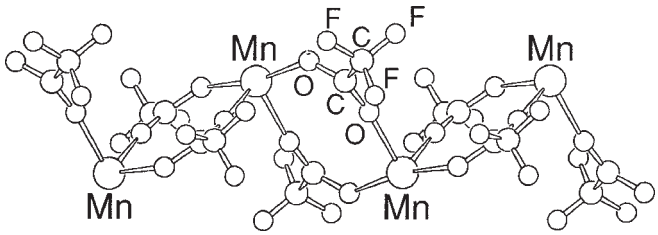
Bond distances (Å)			
Mn1—O11	2.133(3)	O11—C1	1.224(5)
Mn1—O12	2.148(3)	O12—C2	1.234(4)
Mn1—O13	2.239(3)	O15—C5	1.226(4)
Mn1—O14	2.207(3)	O16—C6	1.226(5)
Mn1—O15	2.130(3)	O21—C1	1.218(5)
Mn1—O16	2.126(3)	O22—C2	1.230(4)
Mn2—O21	2.135(3)	O25—C5	1.224(5)
Mn2—O22	2.124(3)	O26—C6	1.212(5)
Mn2—O23	2.213(3)		
Mn2—O24	2.231(3)		
Mn2—O25	2.116(3)		
Mn2—O26	2.151(3)		
Bond angles (deg)			
O11-Mn1-O12	166.2(1)	O23-Mn2-O25	174.6(1)
O11-Mn1-O13	83.2(1)	O23-Mn2-O26	86.2(1)
O11-Mn1-O14	85.5(1)	O24-Mn2-O25	87.5(1)
O11-Mn1-O15	94.7(1)	O24-Mn2-O26	83.7(1)
O11-Mn1-O16	100.2(1)	O25-Mn2-O26	93.2(1)
O12-Mn1-O13	86.8(1)	Mn1-O11-C1	151.5(3)
O12-Mn1-O14	84.9(1)	Mn1-O12-C2	142.3(3)
O12-Mn1-O15	94.7(1)	Mn1-O15-C5	139.4(3)
O12-Mn1-O16	88.5(1)	Mn1-O16-C6	137.9(3)
O13-Mn1-O14	89.1(1)	Mn2-O21-C1	137.2(3)
O13-Mn1-O15	176.3(1)	Mn2-O22-C2	165.3(3)
O13-Mn1-O16	85.8(1)	Mn2-O23-C35	122.4(3)
O14-Mn1-O15	87.7(1)	Mn2-O25-C5	149.8(3)
O14-Mn1-O16	171.9(1)	Mn2-O26-C6	149.1(3)
O15-Mn1-O16	97.5(1)	O11-C1-O21	131.5(4)
O21-Mn2-O22	88.6(1)	O11-C1-C11	114.9(4)
O21-Mn2-O23	85.1(1)	O21-C1-C11	113.5(4)
O21-Mn2-O24	171.8(1)	O12-C2-O22	127.3(4)
O21-Mn2-O25	100.3(1)	O12-C2-C21	117.0(3)
O21-Mn2-O26	93.3(1)	O22-C2-C21	115.7(4)
O22-Mn2-O23	88.4(1)	O15-C5-O25	130.8(4)
O22-Mn2-O24	93.7(1)	O15-C5-C51	114.2(4)
O22-Mn2-O25	91.9(1)	O25-C5-C51	115.0(4)
O22-Mn2-O26	174.1(1)	O16-C6-O26	130.8(4)
O23-Mn2-O24	87.1(1)	O16-C6-C61	114.8(3)
		O26-C6-C61	114.4(4)

Note: Numbers in parentheses are estimated standard deviations in the least significant digits.

form two asymmetric bridges (Mn—O distances: 2.151(3) and 2.126(3); 2.116(3) and 2.130(3) Å). The mean C—O bond distance (1.224 Å) is in agreement with a bidentate coordination of the ligand (17). The single trifluoroacetato bridge shows two significantly different Mn—O bond distances (Mn1—O12 = 2.148(3), Mn2—O22 = 2.124(3) Å); moreover, the O12-C2-O22 bond angle (127.3(4)°) is smaller than the average O-C-O bond angles of the triple bridge (131°).

The two THF groups occupy *cis*-positions around the manganese at Mn—O bond distances comprised between 2.213(3) and 2.239(3) Å, in agreement with the Mn—O bond distances observed in THF-adducts of manganese(II) (some selected examples are found in ref. 18).

Fig. 2. View of the atom connectivity in $[(THF)_2Mn(\mu\text{-}CF_3COO)_2Mn(\mu\text{-}CF_3COO)_2(THF)_2]$. The THF ligands have been omitted for clarity.



Crystals of a different shape were noticed and found to correspond to a *linkage isomer* of $Mn(CF_3COO)_2(THF)_2$ with the symmetric repeating unit $[(THF)_2Mn(\mu\text{-}CF_3COO)_2\text{-}Mn(\mu\text{-}CF_3COO)_2(THF)_2]$. The low quality of the crystals prevented a conventional refinement of the structure; nevertheless, the atom connectivity was established, as reported in Fig. 2. The Mn···Mn distance was found to be 4.87 Å, to be compared with the Mn···Mn distances of 4.371 and 6.128 Å observed in the asymmetric isomer.

It is interesting to note that the manganese centres show a similar coordination sphere (six oxygen atoms belonging to two *cis*-THF groups and four bridging trifluoroacetates), the difference between the two isomers consisting of the different distribution of the trifluoroacetates along the polynuclear chain. Thus, the two species represent an interesting case of linkage isomerism which is rather uncommon in the literature, previous examples being bis(hydrotris(1,2,4-triazolyl)borato)zinc (19), and $[Rh_2(CF_3COO)_4(TCNE)]_x$ (20).

Although many carboxylato derivatives of manganese(II) exist (21), trifluoroacetato complexes are not common. Examples of structurally characterized derivatives are: the mononuclear $Mn(CF_3COO)_2(pyridine)_4$ (15), $Mn(CF_3COO)_2(tmen)_2$ (tmen = *N,N,N′N′* -tetramethylethylenediamine (22)), $Mn(CF_3COO)_2(2,2'\text{-dipyridyl})_2$ (22), the trinuclear $Mn_3(CF_3COO)_6(C_6H_5CN)_6$(15), and the polynuclear chain of the 1,10-phenanthroline adduct $[Mn(CF_3COO)_2(1,10\text{-phenanthroline})]_n$ (23) whose structure is reminiscent of the more symmetric linkage isomer of $[Mn(CF_3COO)_2(THF)_2]_n$.

Iron

Iron(II) trifluoroacetate was obtained many years ago by reacting $Ba(CF_3COO)_2$ with $FeSO_4$ in water (24). According to an earlier report, $Fe(CO)_5$ slowly reacts with acetic acid in boiling DMF to give high yields of $Fe(CH_3COO)_2$ (25). The reaction with the stronger acid CF_3COOH is faster and after some hours at the boiling point of the mixture, no IR carbonyl absorptions were detected in solution and DMF-solvated $Fe(CF_3COO)_2$ was isolated (see rxn. [2]).

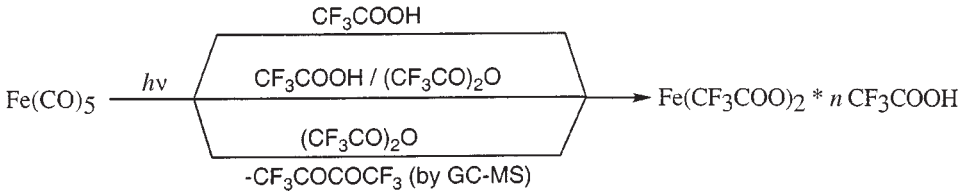
$$[2]\qquad Fe(CO)_5 \xrightarrow[DMF]{CF_3COOH/(CF_3CO)_2O} Fe(CF_3COO)_2{}^{*}\, n\ DMF$$

Some DMF was retained by the product, the amount depending on the drying conditions (see *Experimental*).

The IR spectrum of the solid has strong absorptions at 1729 and 1645 cm^{-1}; additional absorptions were observed at 1435 (ν_{sym} (COO)), 1208 (ν_{asym} (CF_3)), and 1144 (ν_{sym} (CF_3)) cm^{-1}. The magnetic moment of 5.08 BM at room

© 2001 NRC Canada

Scheme 1.



temperature is in agreement with the presence of high-spin d^6 iron(II) (26).

Having shown that $Fe(CO)_5$ is oxidized thermally to iron(II) by CF_3COOH in DMF, it was of interest to see which products are obtained in the reaction of $Fe(CO)_5$ with neat CF_3COOH. As a matter of fact, it is known that the photolysis of $Fe(CO)_5$ in acetic acid or in acetic anhydride gives quantitative yields of $Fe_2(CO)_9$ (11). Unexpectedly, we have found that $Fe(CO)_5$ is easily converted into $Fe(CF_3COO)_2$ by photolysis in neat CF_3COOH, in CF_3COOH–$(CF_3CO)_2O$ mixtures, or in neat $(CF_3CO)_2O$ (see Scheme 1). No traces of $Fe_2(CO)_9$ were observed, although that this species may be an intermediate cannot be excluded. As a matter of fact, an independent experiment has shown $Fe_2(CO)_9$ to react with CF_3COOH in the dark at room temperature to give $Fe(CF_3COO)_2 \cdot nCF_3COOH$ (see rxn. [3]).

[3] $$Fe_2(CO)_9 \xrightarrow{CF_3COOH/(CF_3CO)_2O} Fe(CF_3COO)_2 * n\,CF_3COOH$$

The presence of CF_3COOH in the iron-containing product obtained from $Fe(CO)_5$–$(CF_3CO)_2O$ is presumably due to some adventitious acid present in the reaction mixture. Moreover, the detected formation of $CF_3COCOCF_3$ suggests cleavage of the anhydride, i.e., an oxidative addition process through the C—O bond of $(CF_3CO)_2O$. Our data are in agreement with the observation that $Ni(CF_3COO)_2$ can be obtained from $(CF_3CO)_2O$ and $Ni(CO)_4$ (27).

Bis(trifluoroacetato)iron(II) was isolated as a CF_3COOH adduct with quantities of acid depending on the drying procedures. It is a colourless microcrystalline solid, soluble in water and DMF, slightly soluble in hydrocarbons and THF. It is paramagnetic (magnetic moments about 5 BM, see *Experimental*) in agreement with the value expected for a high-spin d^6 ion in an octahedral field (26). The IR spectrum in the solid-state shows strong absorptions at 1697 (ν_{as} (COO)) and 1450 (ν_s (COO)) cm^{-1} suggesting the presence of bridging trifluoroacetato groups (16). A strong multiple absorption at 1781 cm^{-1} and a broad one above 3000 cm^{-1} are diagnostic of the presence of CF_3COOH in our compound. As a matter of fact, these absorptions disappear upon treatment with THF (see rxn. [4]) and the THF-adduct $Fe(CF_3COO)_2 \cdot n$THF has been isolated in good yields.

[4] $$Fe(CF_3COO)_2 * 2CF_3COOH + n\,THF \longrightarrow Fe(CF_3COO)_2 * n\,THF + 2CF_3COOH$$

Conclusions

Metallic manganese or iron pentacarbonyl are useful precursors in the preparation of the corresponding trifluoroacetates, $M(CF_3COO)_2$. In the case of the polynuclear THF-adduct of $Mn(CF_3COO)_2$, the existence of linkage isomerism has been observed. For donor atoms of the same type (oxygen in this case) linkage isomerism is a rather uncommon phenomenon. As a matter of fact, the two isomers essentially differ in the distribution of the bridging ligands along the polynuclear chain. As far as iron is concerned, the results of the present work have established that, at variance with the $Fe(CO)_5$–CH_3COOH system under photolytic conditions, $Fe_2(CO)_9$ is not the product when the photolysis of $Fe(CO)_5$ is carried out in CF_3COOH. The higher autoionization constant of CF_3COOH with respect to CH_3COOH may be responsible for the present experimental findings.

Acknowledgments

The authors wish to thank the Ministero dell' Università e della Ricerca Scientifica e Tecnologica (MURST), Programma di Ricerca Scientifica di Notevole Interesse Nazionale, Cofinanziamento MURST 1998–1999, for financial support, and the Vigoni Programme for an exchange between the Università di Pisa and the RWTH Aachen.

References

1. C. Oldham. *In* Comprehensive coordination chemistry. Vol. 2. *Edited by* G. Wilkinson, R.D. Gillard, and J.A. McCleverty. Pergamon Press, Oxford. 1987. p. 435.
2. A. Gupta. Chemistry of high temperature superconductors II. *Edited by* D.L. Nelton. American Chemical Society, Washington, D.C. 1988. p. 265.
3. F. Calderazzo, G.E. De Benedetto, S. Detti, and G. Pampaloni. J. Chem. Soc. Dalton Trans. 3319 (1997).
4. F.A. Cotton, and J.G. Norman, Jr. J. Coord. Chem. **1**, 161 (1971).
5. D.J. Santure, K.W. McLaughlin, J.C. Huffman, and A.P. Sattelberger. Inorg. Chem. **22**, 1877 (1983).
6. F.A. Cotton, M. Matusz, and B. Zhong. Inorg. Chem. **27**, 4368 (1988).
7. F.A. Cotton, E.V. Dikarev, and X.J. Feng. Inorg. Chim. Acta, **237**, 19 (1995).
8. A.S. Batsanov, G.A. Timko, Yu.T. Struchkov, N.V. Gerbeleu, K.M. Indrichan, and G.A. Popovich. Koord. Khim. **15**, 688 (1989).
9. N.V. Gerbeleu, G.A. Timko, K.M. Indrichan, A.S. Batsanov, O.S. Manole, and Yu.T. Struchkov. Koord. Khim. **20**, 846 (1994).
10. R.G. Griffin, J.D. Ellett Jr., M. Mehring, J.G. Bullitt, and J.S. Waugh. J. Chem. Phys. **57**, 2147 (1972).
11. E.H. Braye, and W. Hübel. Inorg. Synth. **8**, 178 (1966).
12. G.M. Sheldrick. SHELXS86. Program for structure solution. University of Göttingen, Göttingen, Germany. 1986.
13. ENRAF-Nonius SDP Version 5.0. Delft, The Netherlands. 1989.

© 2001 NRC Canada

14. M.J. Baillie, D.H. Brown, K.C. Moss, and D.W.A. Sharp. J. Chem. Soc. A, 3110 1968.
15. K. Hübner, H.W. Roesky, M. Noltemeyer, and R. Bohra. Chem. Ber. **124**, 515 (1991).
16. G.B. Deacon, and R.J. Phillips. Coord. Chem. Rev. **33**, 227 (1980).
17. J.T. Gleghorn, and R.W.H. Small. Acta Crystallogr. Sect B: Struct. Sci. **B51**, 346 (1995).
18. (*a*) D. Sekutowski, R. Jungst, and G.D. Stucky. Inorg. Chem. **17**, 1848 (1978); (*b*) F. Bottomley, P.N. Keizer, and P.S. White. J. Am. Chem. Soc. **110**, 137 (1988); (*c*) P. Stolz and S. Pohl. Z. Naturforsch. B: Chem. Sci. **43**, 175 (1988); (*d*) H.W. Roesky, M. Scholz, and M. Noltemeyer. Chem. Ber. **123**, 2303 (1990).
19. C. Janiak and H. Hemling. J. Chem. Soc. Dalton Trans. 2947 (1994).
20. F.A. Cotton, Y. Kim, and J. Lu. Inorg. Chim. Acta, **221**, 1 (1994).
21. L. Que Jr. and A.E. True. Prog. Inorg. Chem. **38**, 97 (1990); R.L. Rardin, W.B. Tolman, and S.J. Lippard. New J. Chem. **15**, 417 (1991); G. Christou. Acc. Chem. Res. **22**, 328 (1989).
22. M. Andruh, K. Hübner, M. Noltemeyer, and H.W. Roesky, Z. Naturforsch. B: Chem. Sci. **48**, 591 (1993).
23. M. Andruh, H.W. Roesky, M. Noltemeyer, and H.-G. Schmidt. Polyhedron, **12**, 2901 (1993).
24. F. Swarts. Bull. Soc. Chim. Belg. **48**, 176 (1939).
25. F. Calderazzo, C. Floriani, R. Henzi, and F. L'Eplattenier. J. Chem. Soc. A, 1378 (1969).
26. N. Figgis and J. Lewis. Prog. Inorg. Chem. **6**, 37 (1964).
27. D.E. Tevault, R.L. Mowery, R.A. DeMarco, and A.D. Berry. Inorg. Chim. Acta, **60**, 59 (1982).

© 2001 NRC Canada

Synthesis, characterization, and properties of some cyclopentadienyl molybdenum nitrosyl benzyl complexes

Peter Legzdins, Kevin M. Smith, and Steven J. Rettig

Abstract: Reaction of $CpMo(NO)(CH_2Ph)Cl$ with Me_2Mg, Ph_2Mg, or PhCCLi reagents in THF affords the corresponding alkyl, aryl, or alkynyl $CpMo(NO)(CH_2Ph)R$ (R = hydrocarbyl) complexes as orange powders in good yields. Unlike related 16-electron $CpMo(NO)R_2$ complexes, these 18-electron species exhibit good thermal stability due to their η^2-benzyl-Mo interactions. Treatment of $CpMo(NO)(CH_2Ph)Cl$ with Na(DME)Cp provides dark green $Cp_2Mo(NO)(CH_2Ph)$, whose solid-state molecular structure has been established by a single-crystal X-ray crystallographic analysis. The two Cp rings display different binding modes to the Mo atom, while the benzyl ligand is coordinated to the metal centre in an η^1 fashion. The triflate complex, $CpMo(NO)(CH_2Ph)(OTf)$, is obtained by addition of AgOTf to the benzyl chloride precursor. The covalent Mo—OTf bond in this compound can be disrupted by the addition of Lewis bases (L) such as PPh_3 or pyridine, leading to the corresponding $[CpMo(NO)(CH_2Ph)(L)][OTf]$ salts. Attempts to generate neutral benzylidene complexes by deprotonation of $[CpMo(NO)(CH_2Ph)(PPh_3)][OTf]$ have not yet been successful.

Key words: nitrosyl, molybdenum, benzyl, hydrocarbyl, triflate.

Résumé : La réaction du $CpMo(NO)(CH_2Ph)Cl$ avec les réactifs Me_2Mg, Ph_2Mg et PhCCLi dans le THF conduit aux complexes alkyles, aryles ou alkynyles correspondants, $CpMo(NO)(CH_2Ph)R$ (R = hydrocarbyle), des poudres oranges obtenues avec des bons rendements. Contrairement à ce qui se produit avec les complexes à seize électrons du type $CpMo(NO)R_2$, ces espèces à dix-huit électrons présentent une bonne stabilité thermique en raison de leurs interactions η^2-benzyl-Mo. Le traitement du $CpMo(NO)(CH_2Ph)Cl$ par du Na(DME)Cp conduit au $Cp_2Mo(NO)(CH_2Ph)$ vert foncé dont on a déterminé la structure moléculaire à l'état solide par une analyse cristallographique réalisée par diffraction des rayons X par un cristal unique. Les deux noyaux Cp présentent des modes de liaison avec le Mo qui sont différents alors que le ligand benzyle est coordiné au centre métallique de façon η^1. On a obtenu le complexe au triflate, $CpMo(NO)(CH_2Ph)(OTf)$ en additionnant du AgOTf au précurseur avec du chlorure de benzyle. La liaison covalente Mo—OTf de ce composé peut être perturbée par l'addition de bases de Lewis (L), telles que la PPh_3 ou la pyridine, qui conduisent à la formation des sels $[CpMo(NO)(CH_2Ph)(L)][OTf]$ correspondants. Les essais effectués en vue de générer des complexes benzylidènes neutres par déprotonation de $[CpMo(NO)(CH_2Ph)(PPh_3)][OTf]$ se sont avérés infructueux jusqu'à maintenant.

Mots clés : nitrosyle, molybdène, benzyle, hydrocarbyle, triflate.

Introduction

We (1) recently reported the intermolecular C—H bond activation of alkane substrates by thermolysis of the 16-electron (16e) bis(hydrocarbyl) complexes, $Cp^*W(NO)(CH_2CMe_3)_2$ and $Cp^*W(NO)(CH_2CMe_3)(CH_2Ph)$. Labeling and kinetic studies established that these reactions proceed via initial elimination of CMe_4 to form the unsaturated alkylidene complexes, $Cp^*W(NO)(=CHCMe_3)$ and $Cp^*W(NO)(=CHPh)$, respectively. However, the generation of these reactive alkylidene species requires reaction temperatures in the range of 70–80°C, and little control can be exerted on the steps following the initial, rate-determining α-hydrogen abstraction step. This practical limitation could be avoided by either lowering the activation barrier of the neopentane elimination process or by finding an alternative route to the reactive alkylidene compounds.

Previous studies in these laboratories have demonstrated that the related $CpMo(NO)(=CHCMe_3)$ fragment is readily produced by the *room temperature* transformation of the 16e $CpMo(NO)(CH_2CMe_3)_2$ compound (2), or by the facile loss of pyridine (py) from the 18e adduct $CpMo(NO)(=CHCMe_3)(py)$ (3). Like the Cp*W analogues, $CpMo(NO)(=CHCMe_3)$ can also activate element—hydrogen bonds. Thus, isolable $CpMo(NO)(CH_2CMe_3)(ER)$ complexes are obtained when the ER group can act as a π-donor

Received August 24, 2000. Published on the NRC Research Press Web site at http://canjchem.nrc.ca on May 23, 2001.

This paper is dedicated to Professor Brian R. James on the occasion of his 65th birthday.

P. Legzdins,[1] K.M. Smith,[2] and S.J. Rettig.[3] Department of Chemistry, The University of British Columbia, 2036 Main Mall, Vancouver, BC V6T 1Z1, Canada.

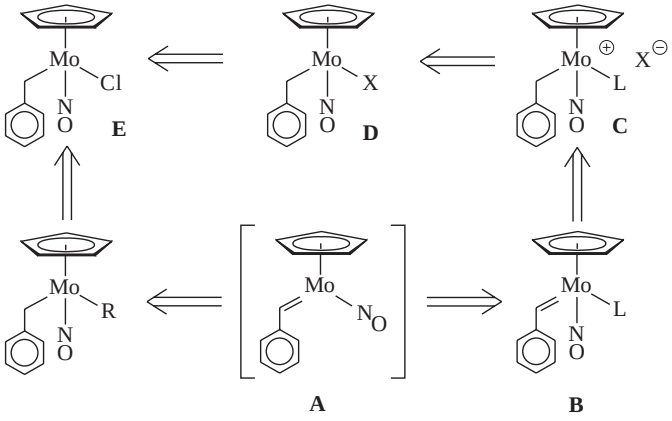
[1]Corresponding author (telephone: (604) 822-2987; fax: (604) 822-2847; e-mail: legzdins@chem.ubc.ca)
[2]Permanent address: Department of Chemistry, University of Prince Edward Island, 550 University Avenue, Charlottetown, PE C1A 4P3, Canada.
[3]Deceased.

 DOI: 10.1139/cjc-79-5/6-502 © 2001 NRC Canada

ligand (e.g., HER = HOPh, H_2NCMe_3, $HSCMe_3$), thereby resulting in 18e products (3). However, stable $CpMo(NO)(CH_2CMe_3)R$ compounds resulting from activation of hydrocarbon RH substrates have not yet been observed, and this may well be a manifestation of the marked thermal instability of 16e $CpMo(NO)(R)_2$ complexes. For instance, diaryl species can be observed in situ when $[CpMo(NO)Cl_2]_2$ is treated with $(aryl)_2Mg$ reagents at low temperature, but these 16e complexes decompose at ambient temperatures even in the presence of trapping agents (4). The differing reactivities of Mo and W cyclopentadienyl nitrosyl alkyl complexes have recently been analyzed using density functional theoretical techniques (5).

The current study was undertaken with a view to developing a non-thermolytic route to an electronically unsaturated alkylidene species, specifically the benzylidene fragment [CpMo(NO)(=CHPh)] (**A**). As shown in the retrosynthetic strategy outlined below in Scheme 1, the reactive 16e species **A** should be accessible by loss of a labile, neutral ligand L from the 18e CpMo(NO)(=CHPh)(L) complex (**B**). The neutral benzylidene compound could be formed by deprotonation of the cationic complex $[CpMo(NO)(CH_2Ph)(L)]^+$ (**C**). The cationic complex could, in principle, be synthesized by nucleophilic displacement of a weakly bound anionic ligand X from $CpMo(NO)(CH_2Ph)(X)$ (**D**), which in turn would be derived by salt metathesis from the known $CpMo(NO)(CH_2Ph)(Cl)$ compound (**E**) (6).

Scheme 1.

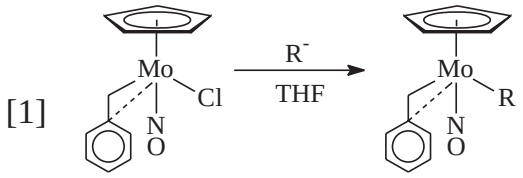


Benzyl chloro complex **E** also provides a metathetical route to the benzyl hydrocarbyl complexes expected to result from the C—H bond activation of RH substrates by the [CpMo(NO)(=CHPh)] target species. Indeed, the prototypal complex, $CpMo(NO)(CH_2Ph)(CH_2SiMe_3)$, has previously been synthesized using just this methodology (6). The independent synthesis of additional $CpMo(NO)(CH_2Ph)R$ compounds was thus undertaken to assess their thermal stability and to establish their diagnostic spectroscopic properties. It was anticipated that these alkyl complexes, as well as compounds **C** and **D**, might well be stabilized as 18e species by the η^2-benzyl-metal interactions characteristic of other $Cp'M(NO)(CH_2Ph)(X)$ complexes (Cp′ = Cp or Cp*, M = Mo or W) (6, 7), some of which are analogues of those depicted above in Scheme 1.

This paper describes the synthesis of several $CpMo(NO)(CH_2Ph)R$ compounds by salt metathesis and outlines their spectroscopic and physical properties. The solid-state molecular structure of one of these compounds, namely $Cp_2Mo(NO)(CH_2Ph)$, as determined by X-ray crystallography is described. The synthesis and characterization of $CpMo(NO)(CH_2Ph)(OTf)$, (OTf = triflate, OSO_2CF_3) and $[CpMo(NO)(CH_2Ph)(L)]^+[OTf]^-$, corresponding to target molecules **D** and **C** in Scheme 1, respectively, are also presented. Finally, the various attempts to generate alkylidene complexes from these precursors are summarized.

Results and discussion

Direct synthesis of $CpMo(NO)(CH_2Ph)R$ complexes



As shown in eq. [1] above, $CpMo(NO)(CH_2Ph)Cl$ is a useful precursor to a range of $CpMo(NO)(CH_2Ph)R$ complexes, where R is methyl **1**, phenyl **2**, phenylalkynyl **3**, or cyclopentadienyl **4**. The metathesis reactions proceed cleanly in THF as determined by monitoring the change in ν (NO) during the course of the reaction by solution IR spectroscopy. The conversions can be accomplished using a diverse range of hydrocarbylating reagents, including organolithium and organosodium species as well as the more typical organomagnesium reagents. Analytically pure, crystalline samples of the $CpMo(NO)(CH_2Ph)R$ complexes may be obtained by chromatography of the crude products on Alumina I using toluene as eluant, followed by recrystallization from toluene:hexanes solvent mixtures. The colour, yield, and elemental analysis data for the new compounds are listed in Table 1. Their IR and mass spectral data are collected in Table 2, and Table 3 contains their ^1H and ^{13}C NMR data.

The replacement of the electronegative Cl ligand with more covalently bound hydrocarbyl groups has the expected effect on the electron density at the metal centres. This is indicated by the ν(NO) bands in the Nujol mull IR spectra of the $CpMo(NO)(CH_2Ph)R$ compounds which are from 14 to 44 cm^{-1} lower in energy than the 1620 cm^{-1} value exhibited by $CpMo(NO)(CH_2Ph)Cl$ (6). The magnitude of this decrease in ν (NO) follows the trend C≡CPh < Cp ~ Ph ~ CH_2Ph < CH_2SiMe_3 ~ Me, which is consistent with the electron-donating abilities of these hydrocarbyl ligands. The IR spectrum of **3** also displays a ν(C≡C) band at 2091 cm^{-1} (8).

In their ^1H NMR (C_6D_6) spectra, the C_5H_5 signals of compounds **1**–**4** lie in the 4.80–5.20 ppm region and are diagnostic indicators of these complexes. Also useful is the signal at –0.88 ppm characteristic of a Me ligand in the ^1H NMR (C_6D_6) spectrum of **1**. The ^{13}C NMR spectra of complexes **1**–**3** are important chiefly for the ipso carbon signals of the CH_2Ph ligands which fall in the 110–113 ppm range indicative of η^2-benzyl-molybdenum interactions (6, 7). In contrast, complex **4** does not appear to possess a η^2-benzyl ligand according to its ^1H and ^{13}C NMR spectra. The benzyl methylene ^1H NMR signal appears as a singlet at room

© 2001 NRC Canada

Table 1. Numbering scheme, colour, yield, and elemental analysis data for the new complexes.

Complex	Cmpd no.	Colour (yield, %)[a]	Anal. found (calcd.) C	H	N
$CpMo(NO)(CH_2Ph)(CH_3)$	**1**	orange (63)	52.67 (52.54)	5.11 (5.09)	4.78 (4.71)
$CpMo(NO)(CH_2Ph)(Ph)$	**2**	orange (72)	60.03 (60.18)	4.75 (4.77)	3.89 (3.90)
$CpMo(NO)(CH_2Ph)(C{\equiv}CPh)$	**3**	orange (68)	62.73 (62.67)	4.45 (4.47)	3.66 (3.65)
$Cp_2Mo(NO)(CH_2Ph)$	**4**	dark green (65)	58.29 (58.80)	4.84 (4.93)	3.91 (4.03)
$CpMo(NO)(CH_2Ph)(OTf)$	**5**	orange (83)	36.35 (36.21)	2.81 (2.80)	3.16 (3.25)
$[CpMo(NO)(CH_2Ph)(PPh_3)][OTf]$	**6**	yellow (79)	53.31 (53.69)	3.95 (3.92)	1.89 (2.02)
$[CpMo(NO)(CH_2Ph)(py)][OTf]$	**7**	yellow (82)	42.51 (42.36)	3.29 (3.36)	5.22 (5.49)

[a]Yield calculated from crude isolated product.

Table 2. Infrared ν(NO) and mass spectral data for the new complexes.

Complex	Cmpd no.	IR (ν(NO) cm^{-1}) Nujol	CH_2Cl_2	FAB-MS (*m*/*z*) P+
$CpMo(NO)(CH_2Ph)(CH_3)$	**1**	1576	1591	299
$CpMo(NO)(CH_2Ph)(Ph)$	**2**	1592	1603	361
$CpMo(NO)(CH_2Ph)(C{\equiv}CPh)$	**3**	1604	1620	385
$Cp_2Mo(NO)(CH_2Ph)$	**4**	1592	1607	349
$CpMo(NO)(CH_2Ph)(OTf)$	**5**	1654	1657	284
$[CpMo(NO)(CH_2Ph)(PPh_3)][OTf]$	**6**	1655	1655	546

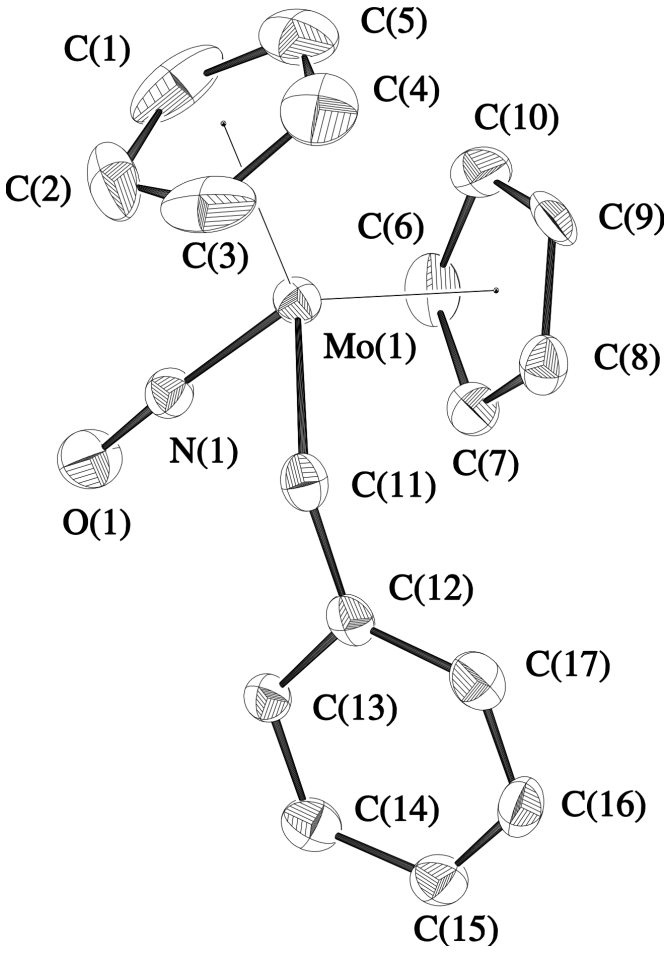
temperature, and the ipso carbon signal occurs at 152.3 ppm in the ^{13}C NMR spectrum of **4**. There is also only a single ^1H NMR peak for the two Cp ligands at room temperature. Consequently, a single-crystal X-ray crystallographic analysis of **4** was undertaken to establish definitively its solid-state molecular structure. The results of this analysis are discussed in the next section.

Solid-state molecular structure of $Cp_2Mo(NO)(CH_2Ph)$

The nature of the Cp—Mo bonds in $Cp_2Mo(NO)X$ complexes has been the subject of debate since their initial synthesis over 30 years ago (9, 10). If these compounds possessed two η^5-Cp groups and a linear nitrosyl ligand, they would have a formal valence electron count of 20 (11*e*). Early suggestions that this unfavourable situation might be avoided by the complexes adopting an asymmetric η^5-Cp/η^3-Cp binding mode (11*a*, *b*) were *not* supported by subsequent X-ray crystallographic studies. The solid-state molecular structures of $Cp_2Mo(NO)(\eta^1$-Cp) (11*c*), $Cp_2Mo(NO)(CH_3)$ (11*d*), and Cp*(Cp)Mo(NO)(CH_3) (11*f*) all exhibit linear Mo-N-O angles (>172°) and essentially planar but skewed Cp′ groups with all 10 multihapto ring C atoms lying within bonding distance of the Mo centres. This observation contrasts with the situation in $Cp_2W(CO)_2$ which possesses distinct η^5-Cp and η^3-Cp ligands (12). The η^3-Cp group contains a localized C—C double bond, with the two unique C atoms bent 20° away from the plane containing the three Cs bound to the W centre. Calhorda and co-workers (13) have recently investigated via DFT calculations the phenomenon of ring slippage in Cp_2MoL_2 species and related Cp and indenyl complexes of Mo(II).

The solid-state molecular structure of $Cp_2Mo(NO)(CH_2Ph)$ **4** (Fig. 1) exhibits features intermediate between those displayed by $Cp_2W(CO)_2$ and the previously reported $Cp_2Mo(NO)R$ structures. All 10 Cp carbons in **4** are within 2.336–2.700 Å (avg = 2.475 Å) of the Mo centre, and the

Fig. 1. The solid-state molecular structure of $Cp_2Mo(NO)(CH_2Ph)$ (**4**); 50% probability thermal ellipsoids are shown.



© 2001 NRC Canada

Table 3. ^{1}H and ^{13}C NMR data for the new complexes.

Compound (solvent)	^{1}H NMR (δ)[a]	^{13}C NMR (δ)
1	7.5–6.8 (m, 5H, Ph)	131.0–127.5 (Ph)
(C_6D_6)	4.99 (s, 5H, C_5H_5)	112.2 (*C* ipso)
	3.19 (d, 1H C*H*H)	99.3 (C_5H_5)
	2.21 (d, 1H, CH*H*)	37.8 (CH_2)
	–0.88 (s, 3H, CH_3)	1.34 (CH_3)
2	7.2–6.4 (m, 10H, Ph)	196.9 (*C* ipso Ph)
(C_6D_6)	5.04 (s, 5H, C_5H_5)	140.4–124.2 (Ph)
	3.12 (d, 1H C*H*H)	112.1 (*C* ipso Bz)
	2.83 (d, 1H, CH*H*)	100.1 (C_5H_5)
		40.1 (CH_2)
3	7.6–7.0 (m, 10H, Ph)	136.1–131.4 (Ph)
(C_6D_6)	5.13 (s, 5H, C_5H_5)	112.7 (*C* ipso Bz)
	3.19 (d, 1H C*H*H)	108.8 (*C*≡C)
	2.66 (d, 1H, CH*H*)	106.1 (C_5H_5)
		42.8 (CH_2)
4	7.6–7.0 (m, 5H, Ph)	152.3 (*C* ipso Bz)
(C_6D_6)	5.17 (s, 10H, C_5H_5)	128.0, 127.7, 123.8 (*C* Ph)
	3.45 (s, 2H CH_2)	109.0 (C_5H_5)
		25.1 (CH_2)
5	7.5–6.8 (m, 5H, Ph)	137.2–127.7 (Ph)
(C_6D_6)	5.04 (s, 5H, C_5H_5)	112.4 (*C* ipso)
	3.12 (d, 1H C*H*H)	102.7 (C_5H_5)
	2.83 (d, 1H, CH*H*)	50.5 (CH_2)
6	7.8–6.5 (m, 20H, Ph)	136.3–126.8 (Ph)
(CD_3NO_2)	5.78 (s, 5H, C_5H_5)	110.1 (*C* ipso)
	3.92 (d, 1H C*H*H)	103.1 (C_5H_5)
	3.63 (d, 1H, CH*H*)	44.7 (CH_2)
7	7.9–7.0 (m, 10H, Ph, NC_5H_5)	156.1–127.8 (Ph, NC_5H_5)
(CD_3NO_2)	6.18 (s, 5H, C_5H_5)	112.7 (*C* ipso)
	3.95 (d, 1H C*H*H)	104.9 (C_5H_5)
	3.78 (d, 1H, CH*H*)	50.2 (CH_2)

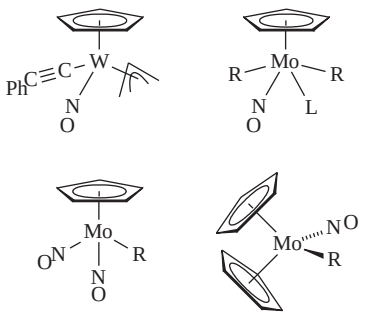
[a]The H—H coupling constants of the diastereotopic benzyl hydrogens, while not specifically measured, appear to be in the normal 4.5–7.0 Hz range expected for these complexes (6).

difference between the two Cp groups is not as marked as in the $Cp_2W(CO)_2$ structure. However, the C(1)-C(5) ring exhibits characteristics more typical of an η^3-Cp ligand than previously observed for any other structurally characterized $Cp_2Mo(NO)R$ species. The C(4) and C(5) atoms are 2.700(3) and 2.667(3) Å away from the Mo atom, respectively, and the C(4)—C(5) bond length of 1.317(5) Å is significantly shorter than the other C—C distances in the ring (1.392(5)–1.407(5) Å, avg = 1.401 Å). The C(1)-C(2)-C(3)-C(4) and C(3)-C(2)-C(1)-C(5) torsion angles of 7.0(4)° and 8.0(4)°, respectively, are also reminiscent of, if less pronounced than, those found in $Cp_2W(CO)_2$. The crystallographic and experimental data for **4** are presented in Table 4. Table 5 lists the positional and thermal parameters of its constituent atoms, while selected bond lengths and angles are collected in Tables 6 and 7, respectively.

Stabilizing effects of η^2-CH_2Ph ligands

The coordinative and electronic saturation imparted by their η^2-benzyl ligands is deemed to be responsible for the thermal stability of compounds **1**–**3**. Of the known $Cp'M(NO)R_2$ (Cp′ = Cp, Cp*; M = Mo, W) complexes, the CpMo-containing species are the most Lewis acidic, the most prone to M—C bond hydrolysis, and the most thermally sensitive (14). The general fragility of the 16e $CpMo(NO)R_2$ species is in marked contrast to the robust 18e complexes shown below.

These latter compounds achieve a saturated electronic configuration via additional σ-donor ligation (15), lower oxidation state (9), or multihapto ancillary ligand bonding (11, 14). All of the species shown above are thermally stable at ambient temperature, and several are remarkably tolerant of air and (or) water. The range of hydrocarbyl ligands available to these 18e complexes extends to groups which are difficult to synthesize (e.g., Me, Ph) or entirely unknown



© 2001 NRC Canada

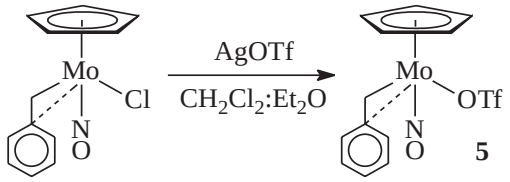
Table 4. Crystallographic and experimental data for $Cp_2Mo(NO)(CH_2Ph)$ (**4**).

Colour	Green-black
Formula	$C_{17}H_{17}MoNO$
Formula weight	347.27
Crystal system	Orthorhombic
Space group	*Pbca*
a (Å)	11.120(2)
b (Å)	15.2821(3)
c (Å)	16.8371(6)
V (Å^3)	2861.4(3)
Z	8
d_{calcd}(g cm^{-1})	1.612
F(000)	1408.00
μ (Mo Kα) (cm^{-1})	9.09
T (K)	180(1)
Crystal dimensions (mm^3)	0.50 × 0.40 × 0.10
Scan type	(ω and φ) 0.5°
2θ (max)(deg)	60.1
Total reflections	26 363
Unique reflections	3639
Reflections with $I \geq 3\sigma(I)$	2083
No. of variables	181
R_1 (on *F*, $I \geq 3\sigma(I)$)	0.030
R_2 (on F^2, all data)	0.021
Goodness of fit	1.53
Max Δ/σ (final cycle)	0.0003
Residual density (e Å^{-3})	–0.83 to 1.09

(e.g., Et, *i*-Bu, C≡CR, C_6F_5) for the 16e Cp′M(NO)(R)(R′) compounds.

Synthesis of [CpMo(NO)(CH$_2$Ph)(L)][OTf]

The stabilizing influence of the η^2-benzyl ligand is also of critical importance to the target molecule CpMo(NO)(CH$_2$Ph)(OTf) **5** which can be synthesized in high yields as illustrated below in eq. [2].

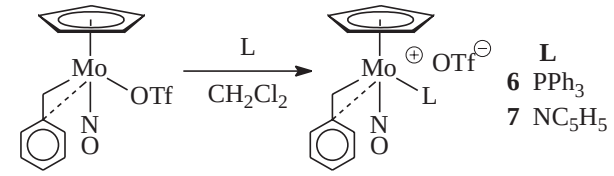
[2] 

5

Silver salts have been previously utilized to abstract halide ligands from Cp′M(NO)$_x$-containing complexes. For instance, if the abstraction from CpMo(NO)(CH$_2$Ph)Cl is performed using $AgBF_4$ in acetonitrile, NCMe-solvated organometallic cations can be isolated (16). Furthermore, treatment of Cp′M(NO)$_2$Cl with $AgBF_4$ in CH_2Cl_2 generates the reactive Cp′M(NO)$_2$(FBF$_3$) species (17) which have been used to synthesize lactones (17*b*) and pyrones (17*c*). Halide-abstraction reactions with AgO_2CR (R = 2-phenylbutyrate) (16e) or AgO_3SR (R = *p*-tolyl, camphor) (18) in CH_2Cl_2 afford neutral nitrosyl complexes with covalent M—O bonds.

As shown in eq. [2], the synthesis of **5** is best accomplished in a 1:1 solvent mixture of CH_2Cl_2 and Et_2O. The thermal stability of CpMo(NO)(CH$_2$Ph)(OTf), which is isolable as a orange powder that can even be handled briefly in air without deleterious effects, can be contrasted with that of CpMo(NO)(η^3-(*Z*)-crotyl)(OTs) (which was not isolated, but was generated at low temperature and used in situ) (18*a*) and that of Cp*W(NO)(CH$_2$SiMe$_3$)(OTf) (which decomposes upon being generated in non-coordinating arene or chlorinated solvents).[4] The existence of a covalent Mo—OSO_2CF_3 bond in **5** is inferred from its solubility in poor ion-supporting solvents such as toluene, C_6D_6 and Et_2O, and by its IR spectrum (Nujol) (19). The highly electron-withdrawing nature of the OTf group in **5** is evidenced by the ν(NO) (Nujol) value of 1654 cm^{-1} which is much higher in energy than that exhibited by the hydrocarbyl products **1**–**4** or the benzyl chloride starting material.

As shown above in eq. [3], reaction of isolated or in situ generated CpMo(NO)(CH$_2$Ph)(OTf) with PPh_3 or pyridine

[3] 

L	
6	PPh_3
7	NC_5H_5

results in the formation of complexes **6** and **7**, respectively. As expected, these [CpMo(NO)(CH$_2$Ph)(L)][OTf] salts display decreased solubility as compared to the neutral complexes **1**–**5**. Thus, **6** and **7** are only moderately soluble even in THF, and dissolve readily only in good ion-supporting solvents such as CH_2Cl_2 and CH_3NO_2. As solids, **6** and **7** appear to be relatively inert with respect to O_2 and water, since the yellow powders may be handled briefly in air without noticeable decomposition. The decrease in the highest frequency ν(SO) band of the triflate group from 1321 cm^{-1} in the IR spectrum of **5** to ~1260 cm^{-1} in **6** and **7** is consistent with the displacement of the OTf group from the Mo centre (19). The ^{1}H and ^{13}C NMR spectra of **6** and **7** help demonstrate that only one L ligand is present in each molecule and that the η^2-benzyl-molybdenum interaction is preserved in each complex.

Attempted deprotonation of [CpMo(NO)(CH$_2$Ph)(PPh$_3$)][OTf]

In an attempt to form a benzylidene compound such as CpMo(NO)(=CHPh)(PPh_3) or [CpMo(NO)(=CHPh)]$_2$, cationic complex **6** was treated with a variety of Brønsted bases (e.g., KO-*t*-Bu, LiN(SiMe$_3$)$_2$, 1,8-diazabicyclo[5.4.0]undec-7-ene (DBU), NEt_3, HN-*i*-Pr$_2$) in THF and CH_2Cl_2. In each case, monitoring of the reaction by solution IR spectroscopy revealed the complete consumption of starting material and the formation of a broad band at ~1600 cm^{-1}. However, ^{1}H NMR spectra of the crude reaction mixtures resulting from these reactions were devoid of signals characteristic of alkylidene Hs. None of the attempts to purify, chromatograph, crystallize, or precipitate the products from

[4] P. Legzdins and S.F. Sayers. Unpublished results.

© 2001 NRC Canada

Table 5. Positional and thermal parameters, with esds in parentheses, for $Cp_2Mo(NO)(CH_2Ph)$ (**4**).

Atom	*x*	*y*	*z*	*B*(eq)
Mo(1)	0.08242(2)	0.174875(14)	0.10364(2)	1.677(5)
O(1)	0.2723(2)	0.04584(12)	0.06261(13)	3.26(6)
N(1)	0.1903(2)	0.09618(13)	0.07689(14)	1.91(6)
C(1)	0.0288(3)	0.2235(3)	–0.0257(2)	4.54(11)
C(2)	–0.0204(4)	0.1401(2)	–0.0150(3)	4.80(12)
C(3)	–0.1140(4)	0.1501(2)	0.0392(3)	4.26(11)
C(4)	–0.1299(3)	0.2401(2)	0.0532(2)	3.94(10)
C(5)	–0.0468(4)	0.2833(2)	0.0135(2)	3.82(10)
C(6)	0.2373(3)	0.2644(2)	0.1512(2)	2.64(8)
C(7)	0.1964(3)	0.2139(2)	0.2146(2)	2.23(7)
C(8)	0.0807(3)	0.2434(2)	0.2347(2)	2.25(7)
C(9)	0.0539(3)	0.3156(2)	0.1863(2)	2.35(7)
C(10)	0.1470(3)	0.3265(2)	0.1333(2)	2.71(7)
C(11)	–0.0068(3)	0.0705(2)	0.1781(2)	2.00(7)
C(12)	0.0635(3)	0.03364(15)	0.2457(2)	1.79(7)
C(13)	0.1632(3)	–0.0209(2)	0.2334(2)	1.93(7)
C(14)	0.2284(3)	–0.0541(2)	0.2959(2)	2.31(8)
C(15)	0.1970(3)	–0.0354(2)	0.3735(2)	2.47(8)
C(16)	0.0975(3)	0.0163(2)	0.3869(2)	2.66(7)
C(17)	0.0320(3)	0.0494(2)	0.3248(2)	2.45(8)

Table 6. Selected bond lengths (Å) for $Cp_2Mo(NO)(CH_2Ph)$ (**4**).[a]

Bond lengths (Å)			
Mo(1)—CP(1)	2.23	Mo(1)—CP(2)	2.12
Mo(1)—N(1)	1.757(2)	C(2)—C(3)	1.392(5)
Mo(1)—C(1)	2.377(4)	C(3)—C(4)	1.407(5)
Mo(1)—C(2)	2.362(4)	C(4)—C(5)	1.317(5)
Mo(1)—C(3)	2.469(3)	C(6)—C(7)	1.394(4)
Mo(1)—C(4)	2.700(3)	C(6)—C(10)	1.414(4)
Mo(1)—C(5)	2.667(3)	C(7)—C(8)	1.404(4)
Mo(1)—C(6)	2.340(3)	C(8)—C(9)	1.404(4)
Mo(1)—C(7)	2.336(3)	C(9)—C(10)	1.377(4)
Mo(1)—C(8)	2.442(3)	C(11)—C(12)	1.492(4)
Mo(1)—C(9)	2.581(3)	O(1)—N(1)	1.217(3)
Mo(1)—C(10)	2.477(3)	C(1)—C(2)	1.398(5)
Mo(1)—C(11)	2.258(3)	C(1)—C(5)	1.407(5)

[a]CP(1) and CP(2) refer to the unweighted centroids of the C(1–5) and C(6–10) rings, respectively.

Table 7. Selected bond angles (°) for $Cp_2Mo(NO)(CH_2Ph)$ (**4**).[a]

Bond angles (°)			
N(1)-Mo(1)-C(11)	87.7(1)	N(1)-Mo(1)-CP(1)	116.8
N(1)-Mo(1)-CP(2)	115.3	C(11)-Mo(1)-CP(1)	103.5
C(11)-Mo(1)-CP(2)	106.6	CP(1)-Mo(1)-CP(2)	119.8
Mo(1)-N(1)-O(1)	174.1(2)	C(2)-C(1)-C(5)	107.3(3)
C(1)-C(2)-C(3)	106.1(3)	C(2)-C(3)-C(4)	108.1(3)
C(3)-C(4)-C(5)	108.5(4)	C(1)-C(5)-C(4)	109.3(3)
C(7)-C(6)-C(10)	107.7(3)	C(6)-C(7)-C(8)	107.8(3)
C(7)-C(8)-C(9)	107.9(3)	C(8)-C(9)-C(10)	108.1(3)
C(6)-C(10)-C(9)	108.3(3)	Mo(1)-C(11)-C(12)	117.4(2)
C(11)-C(12)-C(13)	121.8(3)	C(11)-C(12)-C(17)	122.0(3)

[a]CP(1) and CP(2) refer to the unweighted centroids of the C(1–5) and C(6–10) rings, respectively.

the attempted deprotonation reactions resulted in any tractable material.

Related attempts to form alkylidene complexes by deprotonation of neutral $Cp^*M(NO)(CH_2CMe_3)(PMe_3)Cl$ (M = Mo, W) (16*a*) or $Cp^*Mo(NO)(CH_2SiMe_3)_2$ (20) complexes with $LiNR_2$ reagents have been shown to result in metallated η^5,η^1-$C_5Me_4CH_2$ species due to attack on the Cp* methyl groups. From the reaction of LiN-*i*-Pr_2 with $Cp^*Mo(NO)(CH_2SiMe_3)_2$, the anionic "tucked-in" compound goes on to rearrange to $[Cp^*Mo(NO)(=CHSiMe_3)(CH_2SiMe_3)]_2[Li_2(THF)_3]$ (20).

Experimental

Methods

All reactions and subsequent manipulations were conducted under anaerobic conditions using an atmosphere of N_2. $CpMo(NO)(CH_2Ph)Cl$ (6) and the $R_2Mg{\cdot}x$(dioxane) (6) and Na(DME)Cp (21) reagents were prepared according to the published procedures. All other reagents were used as received from commercial suppliers. Filtrations were performed through Celite (1 × 2 cm) supported on a medium-porosity glass frit unless specified otherwise. For the low-temperature alkylation reactions, solvents were transferred via trap-to-trap distillation from the drying reagent directly onto the reactants contained in a flask cooled by a liquid nitrogen bath.

Synthesis of $CpMo(NO)(CH_2Ph)R$ (R = Me (1), Ph (2), C≡CPh (3), Cp (4))

All four complexes were prepared in a similar manner, and the synthesis of $CpMo(NO)(CH_2Ph)Me$ (**1**) is described as a representative example.

THF (~25 mL) was vacuum transferred onto $CpMo(NO)(CH_2Ph)Cl$ (0.186 g, 0.59 mmol) and $Me_2Mg{\cdot}x$(dioxane) (0.089 g, 0.59 mmol). The mixture was stirred while being allowed to warm slowly to room temperature. After ~1 h, the solvent was removed from the final red

© 2001 NRC Canada

solution in vacuo. The residue was extracted with a 2:1 solvent mixture of Et_2O:CH_2Cl_2, and the extracts were filtered. The solvent was again removed from the filtrate in vacuo, and the residue was triturated with Et_2O twice to obtain CpMo(NO)(CH_2Ph)Me (**1**) as an orange powder (0.110 g, 63% yield). Analytically pure samples of **1** were obtained by extraction of the crude powder with a 1:1 solvent mixture of THF:toluene, followed by chromatography using an Alumina I column with toluene as eluant. The resulting orange eluate was then reduced in volume in vacuo, hexanes were added, and the solution was chilled to –30°C overnight to induce the deposition of orange crystals.

CpMo(NO)(CH_2Ph)Ph (**2**), CpMo(NO)(CH_2Ph)(C≡CPh) (**3**), and Cp_2Mo(NO)(CH_2Ph) (**4**) were synthesized from CpMo(NO)(CH_2Ph)(Cl) in an analogous manner, using $Ph_2Mg{\cdot}x$(dioxane), LiC≡CPh, and Na(DME)Cp, respectively, instead of $Me_2Mg{\cdot}x$(dioxane) as the hydrocarbylating reagent.

Synthesis of CpMo(NO)(CH_2Ph)(OTf) (5)

First CH_2Cl_2 (20 mL) and then Et_2O (20 mL) were added via syringe to CpMo(NO)(CH_2Ph)Cl (0.433 g, 1.36 mmol) and AgOTf (0.350 g, 1.36 mmol). After ~10 min, a flocculent white precipitate had formed in the orange solution. The mixture was filtered, and the Celite plug was washed with Et_2O (3 × 5 mL). The combined filtrates were taken to dryness in vacuo, and the residue was triturated twice with Et_2O (10 mL) to obtain CpMo(NO)(CH_2Ph)(OTf) (**5**) as an orange powder (0.529 g, 83% yield).

Synthesis of [CpMo(NO)(CH_2Ph)(L)][OTf] (L = PPh_3 (6), NC_5H_5 (7))

Both triflate salts **6** and **7** may be obtained from either isolated or in situ generated **5**. The two-step synthesis of [CpMo(NO)(CH_2Ph)(PPh_3)][OTf] from CpMo(NO)(CH_2Ph)Cl is described as a representative example.

First CH_2Cl_2 (10 mL) and then Et_2O (10 mL) were added to CpMo(NO)(CH_2Ph)Cl (0.115 g, 0.36 mmol) and AgOTf (0.092 g, 0.36 mmol). After ~10 min, the mixture was filtered through Celite onto solid PPh_3 (0.096 g, 0.36 mmol). The solution was stirred briefly, and then hexanes (10 mL) were added. The total volume of the solution was reduced to ~25 mL, and it was chilled to –30°C overnight to obtain [CpMo(NO)(CH_2Ph)(PPh_3)][OTf] **6** as a yellow powder (0.198 g, 79% yield).

X-ray crystallographic analysis of Cp_2Mo(NO)(CH_2Ph) (4)

A green/black plate of **4** having approximate dimensions of 0.50 × 0.40 × 0.10 mm was mounted in a glass capillary. All measurements were made on a Rigaku/ADSC CCD area detector with graphite monochromated Mo Kα radiation. Data were collected in 0.50° oscillations with 60.0 s exposures. A sweep of data was done using ϕ oscillations from 0.0 to 190.0° at χ = –90° and a second sweep was performed using ω oscillations between –23.0 and 18.0° at χ = –90°. The crystal-to-detector distance was 39.20(3) mm. The detector swing angle was –10°. The data were corrected for Lorentz and polarization effects.

The structure was solved by heavy-atom Patterson methods (22) and expanded using Fourier techniques (23). The non-hydrogen atoms were refined anisotropically. Hydrogen atoms were fixed in calculated positions with C—H = 0.98 Å. Neutral atom scattering factors were taken from Cromer and Waber (24). Anomalous dispersion effects were included in *F*calc (25); the values for $\Delta f'$ and $\Delta f''$ were those of Creagh and McAuley (26). The values for the mass attenuation coefficients are those of Creagh and Hubbell (27). All calculations were performed using the teXsan (28) crystallographic software package of Molecular Structure Corp.

Acknowledgement

We are grateful to the Natural Sciences and Engineering Research Council of Canada (NSERC) for support of this research in the form of grants to P.L.

References

1. (*a*) E. Tran and P. Legzdins. J. Am. Chem. Soc. **119**, 5071 (1997); (*b*) C.S. Adams, P. Legzdins, and E. Tran. J. Am. Chem. Soc. **123**, 612 (2001).
2. P. Legzdins, S.J. Rettig, J.E. Veltheer, R.J. Batchelor, and F.W.B. Einstein. Organometallics, **12**, 3575 (1993).
3. P. Legzdins, J.E. Veltheer, M.A. Young, R.J. Batchelor, and F.W.B. Einstein. Organometallics, **14**, 407 (1995).
4. N.H. Dryden, P. Legzdins, S.J. Rettig, and J.E. Veltheer. Organometallics, **11**, 2583 (1992).
5. R. Poli and K.M. Smith. Organometallics, **19**, 2850 (2000).
6. N.H. Dryden, P. Legzdins, J. Trotter, and V.C. Yee. Organometallics, **10**, 2857 (1991).
7. P. Legzdins, R.H. Jones, E.C. Phillips, V.C. Yee, J. Trotter, and F.W.B. Einstein. Organometallics, **10**, 986 (1991).
8. J. Ipaktschi, F. Mirzaei, G.J. Demuth-Eberle, J. Beck, and M. Serafin. Organometalics, **16**, 3965 (1997).
9. J.K. Hoyano, P. Legzdins, and J.T. Malito. J. Chem. Soc. Dalton Trans. 1022 (1975).
10. (*a*) M.W. Hunt, W.G. Kita, B.E. Mann, and J.A. McCleverty. J. Chem. Soc. Dalton Trans. 467 (1978); (*b*) M.W. Hunt, W.G. Kita, and J.A. McCleverty. J. Chem. Soc. Dalton Trans. 474 (1978); (*c*) M.W. Hunt and J.A. McCleverty. J. Chem. Soc. Dalton Trans. 480 (1978).
11. (*a*) R.B. King. Inorg. Chem. **7**, 90 (1968); (*b*) F.A. Cotton and P. Legzdins. J. Am. Chem. Soc. **90**, 6232 (1968); (*c*) J.L. Calderon, F.A. Cotton, and P. Legzdins. J. Am. Chem. Soc. **91**, 2528 (1969); (*d*) F.A. Cotton and G.A. Rusholme. J. Am. Chem. Soc. **94**, 402 (1972); (*e*) J.W. Lauher and R. Hoffmann. J. Am. Chem. Soc. **98**, 1729 (1976); (*f*) E. de Jesús, A. Vázquez de Miguel, P. Royo, A.M.M. Lanfredi, and A. Tiripicchio. J. Chem. Soc. Dalton Trans. 2779 (1990).
12. G. Huttner, H.H. Brintzinger, L.G. Bell, P. Friedrich, V. Bejenke, and D. Neugebauer. J. Organomet. Chem. **145**, 329 (1978).
13. (*a*) M.J. Calhorda and L.F. Veiros. Coord. Chem. Rev. **185–186**, 37 (1999); (*b*) M.J. Calhorda, C.A. Gamelas, C.C. Romão, and L.F. Veiros. Eur. J. Inorg. Chem. 331 (2000).
14. P. Legzdins and J.E. Veltheer. Acc. Chem. Res. **26**, 41 (1993).
15. B. Alegre, E. de Jesús, A. Vázquez de Miguel, P. Royo, A.M.M. Lanfredi, and A. Tiripicchio. J. Chem. Soc. Dalton Trans. 819 (1988).
16. (*a*) J.D. Debad, P. Legzdins, S.J. Rettig, and J.E. Veltheer. Organometallics, **12**, 2714 (1993); (*b*) P. Legzdins and C.R. Nurse. Inorg. Chem. **21**, 3110 (1982); (*c*) T.T. Chin, P. Legzdins, J. Trotter, and V.C. Yee. Organometallics, **11**, 913 (1992); (*d*) P. Legzdins, S.J. Rettig, and S.F. Sayers. J. Am.

© 2001 NRC Canada

Chem. Soc. **116**, 12 105 (1994); (*e*) N.H. Dryden, P. Legzdins, S.F. Sayers, J. Trotter, and V.C. Yee. Can. J. Chem. **73**, 1035 (1995); (*f*) J.A. McCleverty and A.J. Murray. Transition Met. Chem. **4**, 273 (1979).
17. (*a*) P. Legzdins and D.T. Martin. Organometallics, **2**, 1785 (1983); (*b*) P. Legzdins, G.B. Richter-Addo, F.W.B. Einstein, and R.H. Jones. Organometallics, **9**, 431 (1990); (*c*) P. Legzdins, W.S. McNeil, E.G. Vessey, R.J. Batchelor, and F.W.B. Einstein. Organometallics, **11**, 2718 (1992).
18. (*a*) J.W. Faller, M.J. DiVerdi, and J.A. John. Tetrahedron Lett. **32**, 1271 (1991); (*b*) J.W. Faller, J.T. Nguyen, and M.R. Mazzieri. Organometallics, **12**, 1434 (1993); (*c*) J.W. Faller, K.J. Chase, and M.R. Mazzieri. Inorg. Chim. Acta, **229**, 39 (1995).
19. G.A. Lawrance. Chem. Rev. **86**, 17 (1986).
20. (*a*) P. Legzdins and S.F. Sayers. Organometallics, **15**, 3907 (1996); (*b*) P. Legzdins and S.F. Sayers. Chem. Eur. J. **3**, 1579 (1997).
21. J.C. Smart and C.J. Curtis. Inorg. Chem. **16**, 1788 (1977).
22. P.T. Beurskens, G. Admiraal, G. Beurskens, W.P. Bosman, S. Garcia-Granda, R.O. Gould, J.M.M. Smits, and C. Smykalla. PATTY: The DIRDIF program system. Technical Report of the Crystallography Laboratory, University of Nijmegen, The Netherlands. 1992.
23. P.T. Beurskens, G. Admiraal, G. Beurskens, W.P. Bosman, R. de Gelder, R. Israel, and J.M.M. Smits. DIRDIF94: The DIRDIF-94 program system. Technical Report of the Crystallography Laboratory, University of Nijmegen, The Netherlands. 1994.
24. D.T. Cromer and J.T. Waber. International tables for X-ray crystallography. Vol. IV. Kynoch Press, Birmingham, U.K. 1974. Table 2.2A.
25. J.A. Ibers and W.C. Hamilton. Acta Crystallogr. **17**, 781 (1964).
26. D.C. Creagh and W.J. McAuley. International tables for crystallography. Vol. C. *Edited by* A.J.C. Wilson. Kluwer Academic Publishers, Boston. 1992. Table 4.2.6.8, pp. 219–222.
27. D.C. Creagh and J.H. Hubbell. International tables for crystallography. Vol. C. *Edited by* A.J.C. Wilson. Kluwer Academic Publishers, Boston. 1992. Table 4.2.4.3, pp. 200–206.
28. teXsan: Crystal structure analysis package. Molecular Structure Corp. 1985 and 1992.

© 2001 NRC Canada

Synthesis of 5-fluoro-β-D-glucopyranosyluronic acid fluoride and its evaluation as a mechanistic probe of *Escherichia coli* β-glucuronidase

Alexander W. Wong, Shouming He, and Stephen G. Withers

Abstract: Synthesis of the potential mechanism-based inactivator of β-D-glucuronidases (5-fluoro-β-D-glucopyranosyluronic acid fluoride) was accomplished via a six-step process from D-glucuronic acid that involved radical bromination at C-5 and displacement of the bromide by fluoride. A key step in this process was the masking of the carboxylic acid as a phenacyl ester. This group is uniquely stable to conditions of photobromination and fluoride displacement, yet removable under very mild conditions. Incubation of the *Escherichia coli* β-glucuronidase with 5-fluoro-β-D-glucopyranosyluronic acid fluoride resulted in time-dependent inactivation of the enzyme through the accumulation of a covalent 5-fluoro-α-D-glucopyranosyluronic acid-enzyme. Peptic digestion of the 5-fluoro-α-D-glucopyranosyluronic acid-enzyme intermediate and subsequent analysis by liquid chromatography coupled to an electrospray ionization triple quadrupole mass spectrometer indicated the presence of a 5-fluoro-α-D-glucopyranosyluronic acid-modified peptide. This peptide was partially purified by HPLC and its sequence determined by tandem mass spectrometry in the daughter ion scan mode, permitting the identification of Glu504 as the catalytic nucleophile within the sequence IT**E**YGVD. This new reagent is therefore useful for the specific, mechanism-based inactivation of glycuronidases and has good potential in other studies of enzymes of this general class.

Key words: β-glucuronidase, catalytic nucleophile, 5-fluoro-β-D-glucopyranosyluronic acid fluoride, electrospray MS.

Résumé : Utilisant une voie en six étapes au départ de l'acide D-glucuronique qui implique une bromation radicalaire en C-5 et une substitution du brome par du fluor, on a réalisé la synthèse du fluorure de l'acide 5-fluoro-β-D-glucopyranosyluronique, un inhibiteur potentiel des β-D-glucuronidases en raison du mécanisme. Dans une étape clé de la synthèse, on masque l'acide carboxylique sous la forme d'ester phénacyle. Ce groupe, particulièrement stable dans les conditions de photobromation et de déplacement par le fluorure, peut facilement être enlevé dans des conditions très douces. L'incubation de la β-glucuronidase de l'*Escherichia coli* avec du fluorure de l'acide 5-fluoro-β-D-glucopyranosyluronique donne lieu à une inactivation de l'enzyme qui dépend du temps et qui résulte d'une accumulation d'un dérivé covalent l'acide 5-fluoro-α-D-glucopyranosyluronique-enzyme. L'hydrolyse peptique de cet intermédiaire et l'analyse subséquente du produit par chromatographie liquide couplée à un spectromètre de masse quadripolaire à triple ionisation par électronébulisation met en relief la présence d'un peptide modifié par l'acide 5-fluoro-α-D-glucopyranosyluronique. Ce peptide a été partiellement purifié par CLHP et on a déterminé sa séquence par spectrométrie de masse en tandem dans le mode de balayage de l'ion fille qui a permis d'identifier le Glu504 comme nucléophile catalytique dans la séquence IT**E**YGVD. Ce nouveau réactif est donc utile pour les inactivations spécifiques de glycuronidases liées à des mécanismes et il offre de bons potentiels dans d'autres études d'enzymes de cette classe générale.

Mots clés : β-glucurononidase, nucléophile catalytique, fluorure de l'acide 5-fluoro-β-D-glucopyranosyluronique, SM par électronébulisation.

[Traduit par la Rédaction]

Introduction

β-Glucuronidases are enzymes responsible for the cleavage of the β-glucuronide linkages that occur in a number of contexts, of which the most prevalent are probably the glycosaminoglycans. β-Glucuronides are also formed as conjugates with toxins to assist in their clearance from the body. Gene sequences for a number of β-glucuronidases have been determined and on this basis these enzymes have been assigned to glycoside hydrolase family 2 (1) (see also the following Web site http://afmb.cnrs-mrs.fr/~pedro/CAZY). This is a large family also containing β-galactosidases and β-mannosidases. Three-dimensional structures of several enzymes from this family have been determined, including that

Received September 12, 2000. Published on the NRC Research Press Web site at http://canjchem.nrc.ca on May 29, 2001.

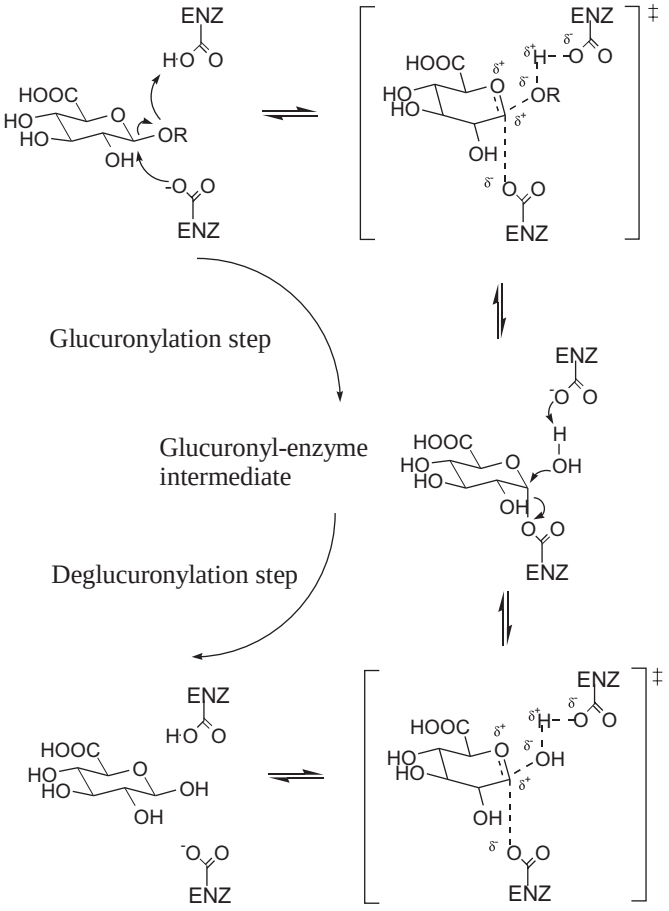
Dedicated to Professor Brian James on the occasion of his 65th birthday.

A.W. Wong, S. He, and S.G. Withers.[1] Protein Engineering Network Centres of Excellence of Canada and Department of Chemistry, University of British Columbia, Vancouver, BC V6T 1Z1, Canada.

[1]Corresponding author (telephone: (604) 822-3402; fax: (604) 822-2847; e-mail: withers@chem.ubc.ca).

 DOI: 10.1139/cjc-79-5/6-510 © 2001 NRC Canada

Fig 1. Proposed mechanism for a retaining β-glucuronidase.



of the human lysosomal β-glucuronidase (2), an enzyme whose deficiency results in Sly syndrome (3). Members of this family are all retaining enzymes, which catalyze glycosidic bond cleavage with net retention of anomeric configuration. Such enzymes employ a two step mechanism involving the formation and hydrolysis of a covalent glycosyl-enzyme intermediate via oxacarbenium ion-like transition states. Two carboxylic acids at the active site play direct roles in the mechanism, one acting as an acid and (or) base catalyst and the other functioning as the nucleophile that attacks at the substrate anomeric centre to form the intermediate (Fig. 1).

Inhibitors of these enzymes are useful in several ways, and of particular value are those that function by trapping the enzyme in its glycosyl-enzyme intermediate form. Such reagents can be used to identify the catalytic nucleophile at the active site, and to allow the determination of the three-dimensional structure of this key species along the reaction coordinate. They also have potential value as therapeutic agents, for example as inhibitors of the heparanase (a β-glucuronidase) associated with cancer metastasis (4). They are also of interest to us in our efforts to develop positron emission tomographic (PET) imaging agents for the in vivo localization and quantitation of glycosidase activity. Two such classes of inhibitor have been developed, the 2-deoxy-2-fluoroglycosides and the 5-fluoroglycosides. Both classes function by the same mechanism, the fluorine substituent serving to inductively destabilize the oxacarbenium ion-like transition states for both the formation and the hydrolysis of the glycosyl-enzyme intermediate, thereby slowing *both* steps. The presence of a good leaving group (typically fluoride) at the anomeric centre accelerates the first step, thereby ensuring that the intermediate is kinetically accessible, thus that it accumulates.

The synthetic strategy employed for the 5-fluorosugar inhibitors hinges upon a radical bromination reaction at C-5, followed by fluoride displacement of the bromide so installed. It is important that the anomeric substituent be correctly installed prior to bromination since these C-5 halo derivatives actually contain two reactive anomeric centres, thus are quite labile. In addition, once the C-5 fluorine substituent has been installed it is not possible to generate intermediates with free hemiacetals at C-1 since they would rapidly decompose via ring opening and elimination of HF. This synthetic approach has been applied to the generation of 5-fluoro glucosides, galactosides, mannosides, and even *N*-acetylhexosaminides, but has never been used to generate 5-fluoroglucuronyl derivatives. Indeed, glucuronides are particularly attractive candidates for such chemistry since generation of a radical at C-5 should be considerably facilitated by the adjacent acid and (or) ester functionality.

We report here the synthesis of 5-fluoro-β-D-glucopyranosyluronic acid fluoride (5FGlcAF), the kinetic analysis of its interaction with the *Escherichia coli* β-glucuronidase, and the identification of the active site nucleophile so labelled via proteolysis of the tagged enzyme and subsequent sequencing of the labelled peptide via liquid chromatography – tandem mass spectrometry (LC–MS–MS).

Experimental procedures

General procedures

All buffer chemicals and other reagents were obtained from Sigma and (or) Aldrich unless otherwise noted. *E. coli* β-glucuronidase (EBG) was purchased from Sigma in lyophilized form. Pepsin (from porcine gastric mucosa) was obtained from Boehringer Mannheim. Dichloromethane and carbon tetrachloride were distilled from calcium hydride under dry nitrogen. Methanol was distilled from magnesium hydride under dry nitrogen.

^{1}H NMR spectra chemical shifts are externally referenced to tetramethylsilane and for samples dissolved in D_2O, the spectra are externally referenced to 2,2-dimethyl-2-silapentane-5-sulfonate (δ = 0.015 ppm). ^{19}F NMR shifts are referenced to $CFCl_3$, although the samples were externally referenced to trifluoroacetic acid (δ = –76.53 ppm).

Syntheses

1,2,3,4-Tetra-O-*acetyl*-β-D-*glucuronic acid (2)*

D-Glucuronic acid (20 g, 103 mmol) was suspended in 200 mL acetonitrile. To it was added acetic anhydride (60 mL, 636 mmol, 6.2 equiv) and concentrated sulfuric acid (1 mL). The mixture was stirred at room temperature for 16 h. The solvent was then removed in vacuo and the remaining acetic acid was removed by coevaporation with toluene. To the concentrated syrup was added 100 mL of water and the mixture stirred at room temperature for 2 h. The

© 2001 NRC Canada

resulting white solids were filtered off, rinsed with water, and dried over P_2O_5 under vacuum. The yield of the product was 23 g (62%). ^{1}H NMR data (CD_3OD, 200 MHz) δ: 5.89 (d, 1 H, $J_{1,2}$ = 8.0 Hz, H-1), 5.39 (t, 1 H, $J_{3,2}$ = 9.0 Hz, $J_{3,4}$ = 9.4 Hz, H-3), 5.19 (t, 1 H, $J_{4,3}$ = 9.4 Hz, $J_{4,5}$ = 9.6 Hz, H-4), 5.06 (t, 1 H, $J_{2,1}$ = 8.0 Hz, $J_{2,3}$ = 9.0 Hz, H-2), 4.35 (d, 1 H, $J_{5,4}$ = 9.6 Hz, H-5), 1.97–2.09 (4 s, 12 H, -OAc).

Phenacyl 2,3,4-tri-O-*acetyl*-α-D-*glucopyranuronate (**3**)*

1,2,3,4-Tetra-*O*-acetyl-D-glucuronic acid **2** (7.59 g, 20.9 mmol) was dissolved in 70 mL HPLC-grade acetonitrile. To this solution was added hydrazine acetate (3.86 g, 41.8 mmol, 2 equiv). The resulting suspension was warmed until most of the solid had dissolved and the solution then stirred at room temperature for 15 min. The reaction was quenched with the addition of 100 mL 0.5 M HCl, the acetonitrile was evaporated in vacuo, and the aqueous layer extracted with ethyl acetate (8 × 50 mL). The organic layer was dried over magnesium sulfate, filtered, and evaporated. The crude gum was dissolved in 100 mL ethyl acetate and 2-bromoacetophenone (4.62 g, 23.2 mmol, 1.1 equiv) followed by addition of triethylamine (4 mL, 28.7 mmol, 1.4 equiv). After stirring at room temperature overnight, the mixture was washed with 1 M HCl and saturated sodium bicarbonate, dried with magnesium sulfate, filtered, and evaporated. The crude material was purified by flash chromatography using 1:1 ethyl acetate:petroleum ether to yield **3** as a white solid (4.3 g, 47% over 2 steps). ^{1}H NMR data (CD_3OD, 400 MHz) δ: 7.82–7.90 (m, 2 H, H-2′, H-6′), 7.56–7.62 (m, 1 H, H-4′), 7.42–7.51 (m, 2 H, H-3′, H-5′), 5.57–5.63 (m, 2 H, H-1, H-3), 5.41 (d, 1 H, *J* = 16.4 Hz, -CH-*H*-), 5.35 (d, 1 H, *J* = 16.4 Hz, -CH-*H*-), 5.29 (dd, 1 H, $J_{4,3}$ = 9.5 Hz, $J_{4,5}$ = 10.0 Hz, H-4), 4.94 (dd, 1 H, $J_{2,1}$ = 3.5 Hz, $J_{2,3}$ = 10.1 Hz, H-2), 4.80 (d, 1 H, $J_{5,4}$ = 10.0 Hz, H-5), 3.60 (s, -OH), 1.98–2.10 (3 s, 9 H, -OAc).

Phenacyl (2,3,4-tri-O-*acetyl*-β-D-*glucopyranosyl fluoride)uronate (**4**)*

Hemiacetal **3** (4.3 g, 9.8 mmol) was dissolved in 100 mL dry dichloromethane, cooled to –30°C under N_2, then DAST (2.5 mL, 18.9 mmol, 1.9 equiv) was added dropwise to the stirring solution. After the addition, the solution was allowed to warm gradually to room temperature. When the reaction was complete, as determined by TLC, the solution was cooled to 0°C and methanol (5 mL) was added dropwise and the solution stirred for 15 min. The mixture was then worked up according to the general procedure. The crude material was passed through a silica gel plug using 1:1 ethyl acetate:petroleum ether. The β-anomer was selectively crystallized using dichloromethane and petroleum ether to yield white needles of **4** (2.41 g, 56%). ^{1}H NMR data ($CDCl_3$, 200 MHz) δ: 7.82–7.92 (m, 2 H, H-2′, H-6′), 7.56–7.68 (m, 1 H, H-4′), 7.42–7.53 (m, 2 H, H-3′, H-5′), 5.54 (t, 1 H, $J_{4,3}$ = 8.5 Hz, $J_{4,5}$ = 9.2 Hz, H-4), 5.48 (dd, 1 H, $J_{H1\text{-}F}$ = 51.0 Hz, $J_{1,2}$ = 4.9 Hz, H-1), 5.42 (s, 2 H, -CH_2-), 5.26 (t, 1 H, $J_{3,2}$ = 7.1 Hz, $J_{3,4}$ = 8.5 Hz, H-3), 5.13 (ddd, 1 H, $J_{2,1}$ = 5.0 Hz, $J_{2,3}$ = 7.1 Hz, $J_{2,F}$ = 9.4 Hz, H-2), 4.49 (d, 1 H, $J_{5,4}$ = 9.2 Hz, H-5), 2.00–2.18 (3 s, 9 H, OAc). ^{19}F NMR data ($CDCl_3$, 188 MHz) δ: –57.87 (dd, 1 F, $J_{H1\text{-}F}$ = 51.1 Hz, $J_{H2\text{-}F}$ = 9.4 Hz, F-1).

Phenacyl (5-bromo-2,3,4-tetra-O-*acetyl*-β-D-*glucopyranosyl fluoride)uronate (**5**)*

Phenacyl (2,3,4-tri-*O*-acetyl-β-D-glucopyranosyl fluoride)uronate **4** was suspended in dry CCl_4 (50 mL), recrystallized *N*-bromosuccinimde (3.23 g, 4 equiv) added, and the mixture irradiated with two 200 W light bulbs. After 2 h, the resulting orange mixture was filtered through glass wool, washed with saturated sodium bicarbonate, dried with magnesium sulfate, filtered, and evaporated. The crude material was purified by flash chromatography using 1:5 ethyl acetate:petroleum ether to yield **5** as a gum (1.02 g, 43%). ^{1}H NMR data ($CDCl_3$, 200 MHz) δ: 7.82–7.92 (m, 2 H, H-2′, H-6′), 7.56–7.68 (m, 1 H, H-4′), 7.42–7.53 (m, 2 H, H-3′, H-5′), 5.70 (dd, 1 H, $J_{1,2}$ = 7.5 Hz, $J_{1,F}$ = 51.3 Hz, H-1), 5.38–5.54 (m, 4 H, H-3, H-4, -CH_2-), 5.26 (ddd, 1 H, $J_{2,1}$ = 7.5 Hz, $J_{2,3}$ = 2.3 Hz, $J_{2,F}$ = 13.5 Hz, H-2), 1.94–2.08 (3 s, 9 H, -OAc). ^{19}F NMR data ($CDCl_3$, 188 MHz) δ: –74.42 (dd, 1 F, $J_{H1,F}$ = 51.3 Hz, $J_{H2,F}$ = 13.5 Hz, F-1).

Phenacyl (5-fluoro-2,3,4-tri-O-*acetyl*-β-D-*glucopyranosyl fluoride)uronate (**6**) and phenacyl (5-fluoro-2,3,4-tri*-O-*acetyl*-α-L-*idopyranosyl fluoride)uronate (**7**)*

Phenacyl (2,3,4-tri-*O*-acetyl-5-bromo-β-D-glucopyranosyl fluoride)uronate **5** (0.176 g, 0.339 mmol) was dissolved in dry diethyl ether (3.5 mL) and cooled to 10°C. To this solution was added silver tetrafluoroborate (0.166 g, 0.850 mmol, 2.5 equiv). After stirring the mixture at room temperature in the dark for 1 h, the mixture was diluted with ethyl acetate (10 mL), and washed with water. The aqueous phase was extracted once more with ethyl acetate, then the organic phase was washed with brine, dried with magnesium sulfate, filtered, and evaporated. The crude material was purified by flash chromatography using 1:3 ethyl acetate:petroleum ether to yield **6** as a white solid (0.0192 g, 12%) and **7** as a gum (0.0512 g, 32%). ^{1}H NMR data of **6** ($CDCl_3$, 400 MHz) δ: 7.82–7.90 (m, 2 H, H-2′, H-6′), 7.58–7.64 (m, 1 H, H-4′), 7.44–7.51 (m, 2 H, H-3′, H-5′), 5.81 (dd, 1 H, $J_{4,3}$ = 9.4 Hz, $J_{4,F5}$ = 22.4 Hz, H-4), 5.72 (dd, 1 H, $J_{1,2}$ = 5.7 Hz, $J_{1,F1}$ = 51.7 Hz, H-1), 5.53 (d, 1 H, *J* = 16.1 Hz, -CH-*H*-), 5.43 (dd, 1 H, $J_{3,2}$ = 6.8 Hz, $J_{3,4}$ = 9.4 Hz, H-3), 5.39 (d, 1 H, *J* = 16.1 Hz, -CH-*H*-), 5.27 (ddd, 1H, $J_{2,1}$ = 5.7 Hz, $J_{2,3}$ = 6.8 Hz, $J_{2,F1}$ = 10.6 Hz, H-2), 2.00–2.21 (3 s, 9 H, -OAc). ^{19}F NMR data of **6** ($CDCl_3$, 188 MHz) δ: –51.11 (dd, 1 F, $J_{F5,H4}$ = 22.4 Hz, $J_{F5,F1}$= 9.4 Hz, F-5), –64.67 (dt, 1 F, $J_{F1,H1}$ = 51.7 Hz, $J_{F1,H2}$ = 10.6 Hz, $J_{F1,F5}$ = 9.4 Hz, F-1). ^{1}H NMR data of **7** ($CDCl_3$, 400 MHz) δ: 7.83–7.89 (m, 2 H, H-2′, H-6′), 7.57–7.62 (m, 1 H, H-4′), 7.44–7.51 (m, 2 H, H-3′, H-5′), 5.75 (d, 1 H, $J_{1,F1}$ = 50.1 Hz, H-1), 5.61–5.67 (m, 1 H, H-4), 5.58 (d, 1 H, *J* = 16.1 Hz, -CH-*H*-), 5.39 (d, 1 H, *J* = 16.1 Hz, -CH-*H*-), 5.31–5.36 (m, 1 H, H-3), 5.21–5.29 (m, 1 H, H-2), 2.05–2.20 (3 s, 9 H, -OAc). ^{19}F NMR data of **7** ($CDCl_3$, 188 MHz) δ: –30.40 (dd, 1 F, $J_{F5,H4}$ = 9.4 Hz, $J_{F5,F1}$= 15.6 Hz, F-5), -47.77 (ddd, 1 F, $J_{F1,H1}$ = 50.1 Hz, $J_{F1,H2}$ = 9.1 Hz, $J_{F1,F5}$ = 15.6 Hz, F-1).

(5-Fluoro-2,3,4-tri-O-*acetyl*-β-D-*glucopyranosyl fluoride)uronic acid (**8**)*

The phenacyl ester **6** (0.050 g, 0.109 mmol) was dissolved in 4:1 methanol:water (5 mL). To this solution was added a spatula tip of 10% Pd/C. The mixture was stirred under an atmosphere of hydrogen gas at room temperature for 1 h.

© 2001 NRC Canada

The suspension was then filtered through a plug of Celite 545 and the filtrate concentrated in vacuo. The crude material was purified by flash chromatography using initially 1:1 ethyl acetate:petroleum ether, followed by 4:1 ethyl acetate:methanol to yield **8** as a gum (0.033 g, 90%). ^{1}H NMR data (CD_3OD, 400 MHz) δ: 5.69 (dd, 1 H, $J_{1,2}$ = 6.6 Hz, $J_{1,F1}$ = 53.0 Hz, H-1), 5.69 (dd, 1 H, $J_{4,3}$ = 9.8 Hz, $J_{4,F5}$ = 22.0 Hz, H-4), 5.35 (t, 1 H, $J_{3,2}$ = 8.7 Hz, $J_{3,4}$ = 9.8 Hz, H-3), 5.23 (ddd, 1 H, $J_{2,1}$ = 6.6 Hz, $J_{2,3}$ = 8.7 Hz, $J_{2,F1}$ = 12.6 Hz, H-2), 1.96–2.12 (3 s, 9 H, -OAc).

*(5-Fluoro-β-D-glucopyranosyl fluoride)uronic acid (**9**)*

5-Fluoro-2,3,4-tri-*O*-acetyl-β-D-glucopyranosyl fluoride)uronic acid (0.033 g, 0.097 mmol) was dissolved in 5 mL dry methanol and cooled to 0°C. Anhydrous ammonia was bubbled through the solution until it was saturated. The solution was allowed to warm to room temperature and stirred for 30 min. The solution was then concentrated in vacuo. The crude material was purified by flash chromatography using 17:2:1 ethyl acetate:methanol:water to yield a gum (0.019 g, 90%). This was then dissolved in minimal ddH_2O and eluted through a column of Bio-Rad AG 1X-8 resin (H^+ form) using ddH_2O as the eluant. Fractions obtained were lyophilized to yield a white powder (0.016 g, 85%). ^{1}H NMR data (D_2O, 400 MHz) δ: 5.48 (dd, 1 H, $J_{1,2}$ = 7.3 Hz, $J_{1,F1}$ = 53.9 Hz, H-1), 3.95 (dd, 1 H, $J_{4,3}$ = 9.6 Hz, $J_{4,F5}$ = 22.8 Hz, H-4), 3.76 (t, 1 H, $J_{3,2}$ = 9.4 Hz, $J_{3,4}$ = 9.6 Hz, H-3), 3.67 (ddd, 1 H, $J_{2,1}$ = 7.3 Hz, $J_{2,3}$ = 9.4 Hz, $J_{2,F1}$ = 14.8 Hz, H-2). ^{19}F NMR data (D_2O, 188 MHz) δ: –30.40 (dd, 1 F, $J_{F5,H4}$ = 22.8 Hz, $J_{F5,F1}$= 15.6 Hz, F-5), -47.77 (ddd, 1 F, $J_{F1,H1}$ = 53.9 Hz, $J_{F1,H2}$ = 14.8 Hz, $J_{F1,F5}$ = 15.6 Hz, F-1). Anal. calcd. for $C_6H_8O_6F_2 \cdot 0.5H_2O$: C 32.30, H 4.07; found: C 32.33, H 4.09.

Enzyme kinetics

All studies on *E. coli* β-glucuronidase were performed in 30 mM potassium phosphate buffer, pH 6.8 (buffer A) at 37°C. A continuous spectrophotometric assay based on the hydrolysis of *p*-nitrophenyl-β-D-glucuronide (pNPGlcA) was used to monitor enzyme activity by measurement of the rate of *p*-nitrophenolate release upon hydrolysis (λ = 400 nm, ε = 7.28 × 10^3 M^{-1} cm^{-1}) using a UNICAM 8700 UV–vis spectrophotometer equipped with a circulating water bath. Michaelis–Menten parameters for the substrate, previously undetermined with this enzyme, were determined by measuring initial rates at a series of substrate concentrations and fitting these data to the Michaelis–Menten equation using the program GraFit (5). Values of K_m = 87 (±10) μM and k_{cat} = 226 (±20) s^{-1} were determined.

Inactivation studies

The inactivation of EBG by 5FGlcAF was monitored by incubation of the enzyme (~25 ng μL^{-1}) under the above conditions in the presence of various concentrations (30–500 μM) of 5FGlcAF at 37°C in a total volume of 100 μL. Residual enzyme activity was determined at the appropriate time intervals by addition of a 5 μL aliquot of the inactivation mixture to a solution of pNPGlcA (1 mM, 700 μL) in 30 mM potassium phosphate buffer and measurement of rates of *p*-nitrophenolate release over a period of 1 min. Pseudo-first-order inactivation rate constants at each inactivator concentration (k_{obs}) were determined by fitting each curve to a first-order equation using the program GraFit. Values of the inactivation parameters (k_i and K_i) for the kinetic model eq. [1] shown below, were determined by fitting values of k_{obs} and inactivator concentration [*I*] to eq. [2] shown below using the program GraFit:

$$[1] \qquad E + I \overset{K_i}{\rightleftharpoons} E \cdot I \xrightarrow{k_i} E\text{-}I$$

$$[2] \qquad k_{obs} = \frac{k_i [I]}{K_i [I]}$$

Turnover (reactivation) of the 5-fluoro-glucuronyl-enzyme intermediate

5-Fluoro-α-D-glucuronyl enzyme was generated by incubating EBG in the presence of 500 μM 5FGlcAF in buffer A at 37°C for 10 min. The trapped intermediate (100 μL, ~8 μg mL^{-1}) was freed of excess inactivator by dilution of the inactivated enzyme with buffer A to a final volume of 2000 μL followed by concentration to a volume of ~200 μL using 10 kDa nominal molecular weight cut-off centrifugal concentrators (Amicon Centricon-10). Fourfold repetition of this process ensured a 1000-fold (>99%) reduction in the free 2FGlcAF concentration. The inactivated enzyme, freed from 5FGlcAF, was then incubated at 37°C in buffer A. Reactivation was monitored by removing aliquots (5 μL) at several time intervals and assaying for activity as described above.

Labeling and proteolysis

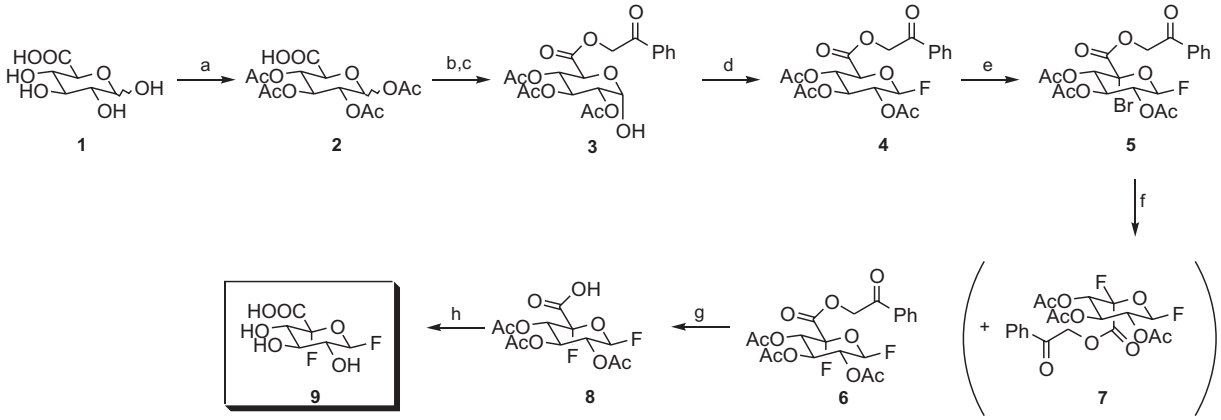
EBG (36 μL, 4.2 mg mL^{-1}) was incubated with 5FGlcAF (4 μL, 10 mM) or 2FGlcAF (4 μL, 50 mM) at 37°C for 15 min in buffer A; complete inactivation (>99%) was confirmed by enzyme assay as above. These mixtures were immediately subjected to peptic digestion: the samples were mixed with pepsin (40 μL, 1.2 mg mL^{-1} in 2.1 M sodium phosphate buffer, pH 1.6) followed by 2.1 M sodium phosphate, pH 1.6 buffer (40 μL). The mixture was incubated at 37°C for 30 min, frozen, and analyzed immediately by liquid chromatography – mass spectrometry (LC–MS) upon thawing.

Electrospray mass spectrometry

Mass spectra were recorded on a PE-Sciex API 300 triple quadrupole mass spectrometer (Sciex, Thornhill, Ontario, Canada) equipped with an Ionspray ion source. Peptides were separated by reverse phase HPLC on an Ultrafast Microprotein Analyzer (Michrom BioResources Inc., Pleasanton, California) directly interfaced with the mass spectrometer. In each of the MS experiments, the proteolytic digest was loaded onto a C18 column (Reliasil, 1 × 150 mm) equilibrated with solvent A (solvent A: 0.05% trifluoroacetic acid (TFA), 2% acetonitrile in water). Elution of the peptides was accomplished using a gradient (0–60%) of solvent B over 60 min followed by 100% solvent B over 2 min (solvent B: 0.045% TFA, 80% acetonitrile in water). Solvents were pumped at a constant flow rate of 50 μL min^{-1}. Spectra were obtained in the single quadrupole scan mode (LC–MS) or the tandem MS product ion scan mode (MS–MS).

© 2001 NRC Canada

Fig 2. Reaction scheme used in the synthesis of 5-fluoro-glucopyranosyluronic acid fluoride (**8**): (*a*) acetic anhydride, acetonitrile, H_2SO_4 (cat.); (*b*) hydrazine acetate, DMF; (*c*) phenacyl bromide, triethylamine, ethyl acetate; (*d*) DAST, CH_2Cl_2; (*e*) NBS, CCl_4; (*f*) $AgBF_4$, diethyl ether; (*g*) 10% Pd-C, H_2; (*h*) NH_3, MeOH; AG 1X-8 (H^+) resin.



In the single quadrupole mode (LC–MS), the quadrupole mass analyzer was scanned over a mass to charge ratio (*m*/*z*) range of 400–2200 Da with a step size of 0.5 Da and a dwell time of 1.0 ms per step. The ion source voltage (ISV) was set at 5.5 kV and the orifice energy (OR) was 45 V. In the tandem MS daughter ion scan mode, the spectrum was obtained by selectively introducing the parent ion (*m*/*z* = 974 or 990) from the first quadrupole (Q1) into the collision cell (Q2) and observing the product ions in the third quadrupole (Q3). Thus, Q1 was locked on *m*/*z* = 974 or 990; Q3 scan range was 50–1000; the step size was 0.5; dwell time was 2.0 ms; ion source voltage (ISV) was 5 kV; orifice energy (OR) was 45 V; Q0 = –10 V; IQ2 = –48 V.

Results and discussion

Synthesis of the 5-fluoro inactivators

The synthesis of 5-fluoroglycosyl fluorides is generally achieved via a route involving radical bromination of an acyl-protected sugar at C-5 (6), displacement of the bromide by fluoride (7), and then deprotection using methoxide in methanol. A major stumbling block in the synthesis of 5FGlcAF was the choice of protecting group for the acid functionality. Simple alkyl esters such as a methyl ester are unsuitable since the conditions required for their removal result in decomposition of the difluoride product. Benzyl esters, which could be removed hydrogenolytically, are also of no use, being incompatible with the photobromination conditions. Silicon-based protecting groups are also out of the question since fluoride would rapidly remove them at the displacement stage. The protecting group ultimately employed was the phenacyl ester, which is compatible with all the reaction conditions employed, and removable by hydrogenolysis (8).

As illustrated in Fig. 2, acetylation of D-glucuronic acid was carried out with acetic anhydride under acidic conditions to yield the 1,2,3,4-tetra-*O*-acetate. Selective anomeric deprotection was achieved by the use of hydrazine acetate, the product partially purified by extraction, and then directly converted to the phenacyl ester via reaction with 2-bromoacetophenone in the presence of triethylamine. Conversion of this protected hemiacetal (**3**) to the β-glycosyl fluoride (**4**) was achieved by reaction with DAST, yielding a mixture of the β- and α-anomers, of which the β-anomer was the predominant species. Bromination at C-5 to yield **5** was performed under radical conditions using *N*-bromosuccinimide and light. While this reaction proceeds slowly for the per-*O*-acetylated β-glucosyl fluoride (over 4 h), bromination of the phenacyl 2,3,4-tri-*O*-acetyl-β-D-glucopyranosyluronic acid fluoride is complete within two hours, presumably reflecting captodative stabilization of the radical generated at C-5 by the adjacent carbonyl group (electron-withdrawing) and the adjacent oxygen atom (electron-donating) (6).

Reaction of the 5-bromo sugar with silver tetrafluoroborate in diethyl ether afforded a mixture of the 5-fluoro D-gluco and L-ido uronic acid fluorides (**6** and **7**), but unfortunately only in low yields (12 and 32%, respectively). Use of silver fluoride in acetonitrile yielded only the ido-epimer. However, the bromide displacement step provided sufficient material for deprotection, characterization, and testing as an inactivator. Deprotection was achieved via a two-step process: the phenacyl protecting group was removed via hydrogenolysis in methanol:water to give **8** while the acetate groups were cleaved using ammonia in methanol to yield the desired final product **9**.

Inactivation kinetics

Incubation of EBG with 5FGlcAF resulted in inactivation of the enzyme in a time dependent manner according to pseudo-first-order kinetic behaviour, allowing measurement of pseudo-first-order rate constants for inactivation at each concentration of 5FGlcAF (Fig. 3A). A plot of these observed rate constants versus inactivator concentration revealed that full saturation of the enzyme was not achieved, even at the highest inactivator concentrations studied (Fig. 3B). Unfortunately, higher concentrations could not be investigated due to the rapidity of inactivation, which precluded accurate sampling. Nevertheless, approximate values for the inactivation rate constant of $k_i = 4.8 \pm 0.6$ min^{-1} and of the reversible dissociation constant $K_i = 455 \pm 95$ μM were determined, and an accurate value of the second-order rate constant $k_i/K_i = 10.4 \pm 1.9$ min^{-1} mM^{-1} was extracted from the initial slope of this plot (obtained by performing a linear regression on the first three points of the data).

© 2001 NRC Canada

Fig 3. Inactivation of human β-glucuronidase by 5FGlcAF. Lines shown in each case are those for the best fit to the data. (A) Plot of residual activity vs. time at the indicated inactivator concentrations: (○) 30 μM, (●) 60 μM, (□) 100 μM, (■) 200 μM, (△) 300 μM, (▲) 400 μM, (▽) 500 μM; (B) replot of the first-order rate constants from panel A. The dashed line represents the initial slope of the plot.

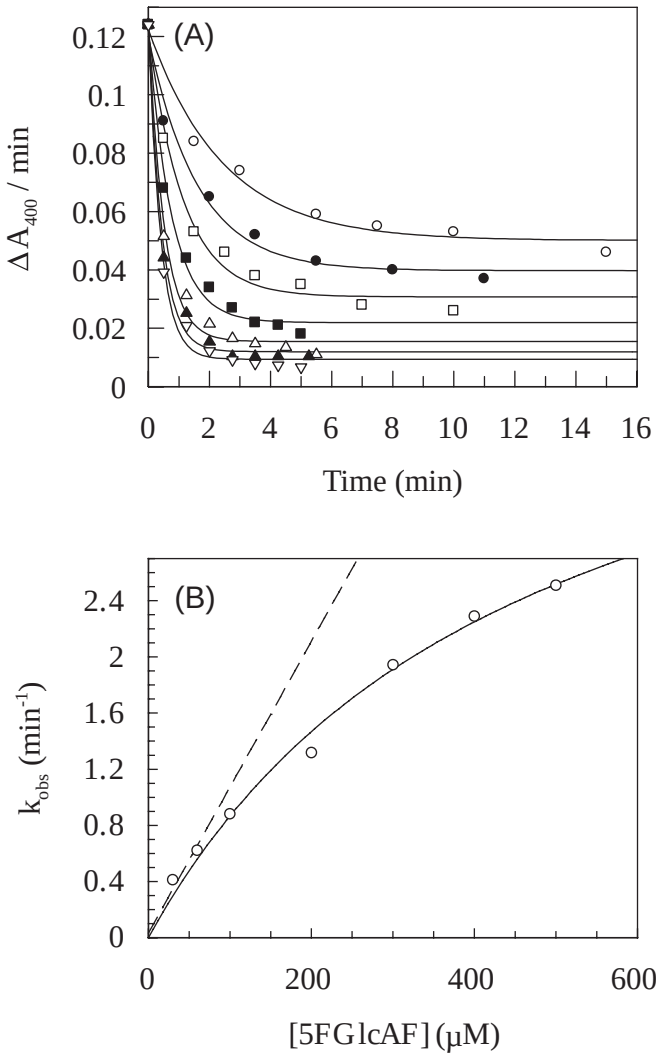
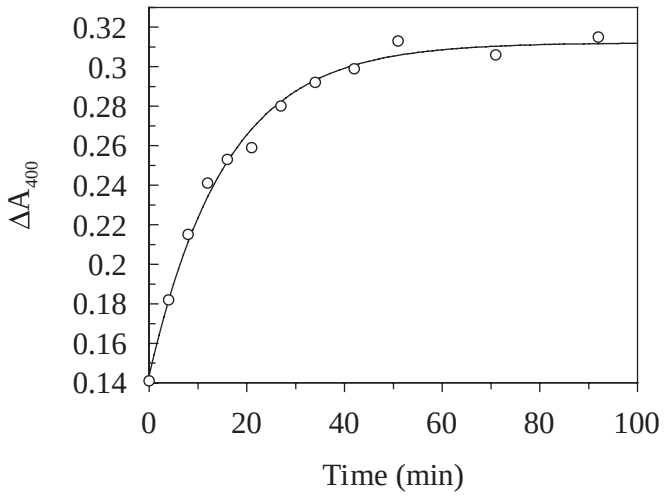


Fig 4. Reactivation of 5F-glucuronyl glucuronidase. Plot of enzyme activity vs. time.



Catalytic competence

Further evidence supporting the trapping of a relevant covalent 5F-glucuronyl-enzyme arises from demonstration of the catalytic competence of the trapped intermediate. Following removal of excess inactivator from the labelled enzyme, the sample was incubated at 37°C in the presence of buffer A and the recovery of activity associated with the regeneration of the free enzyme was monitored. Reactivation of the 5F-glucuronyl-enzyme in buffer followed a first order process with an apparent rate constant of k_{re} = 0.0642 ± 0.0045 min^{-1} ($t_{1/2}$ = 10.8 ± 0.8 min) (Fig. 4).

Identification of the labelled active site peptide by ESMS

The strategy for identification of the active site nucleophile involved first labelling a sample of EBG with 5FGlcAF, then carrying out comparative LC–MS analyses of samples of labelled and unlabelled enzyme that had been subjected to proteolytic digestion. Searching of these chromatograms for a pair of unique peptides differing in mass by exactly the mass of the 5-fluoroglucuronyl moiety (195 Da) should identify a candidate peptide, which could then be sequenced by tandem mass spectrometry.

Peptic hydrolysis of native EBG or 5F-glucuronyl-enzyme resulted in a mixture of peptides that were separated by reverse-phase HPLC using the ESMS as detector. When scanned in the normal LC–MS mode, the total ion chromatograms (TIC) showed a large number of peaks, each corresponding to one or more peptides in the digest mixture. The masses under each peak in the labelled sample were compared with the masses of the corresponding peptides in the native sample, searching for a peptide present only in the labelled sample that was 195 Da greater than a peptide present only in the unlabelled sample. However, no peptide was found matching this criterion.

The absence of such a match did not rule out the presence of a labelled peptide in the treated sample since it was possible that the presence of the sugar moiety could modify the cleavage pattern of pepsin, thereby masking the mass difference. Comparative mapping was therefore performed between EBG labelled with 5FGlcAF and EBG labelled with the previously synthesized 2FGlcAF (9). The latter reagent has previously been shown to label human glucuronidase and was shown here to also inactivate EBG. The difference in mass between 5FGlcAF and 2FGlcAF is 16, allowing for comparative searching of the chromatograms from proteolytic digests of the two labelled samples. These samples would likely have very similar proteolytic digestion profiles, thereby sidestepping the problem of different digestion patterns. Only one pair of peaks with this difference in mass was found, these being a peak with *m*/*z* 990 in the 5FGlcAF-treated sample, which was not observed in the 2FGlcAF-treated sample (Fig. 5) and a peak with *m*/*z* 974 in the 2FGlcAF-treated sample that was not observed in that of the 5FGlcAF-treated sample (Fig. 5). The labelled parent ions (*m*/*z* 974 and 990) thus appear as singly charged species. Subtracting 179 and 195 (the masses of the 2FGlcAF and

© 2001 NRC Canada

Fig 5. Electrospray mass spectrometry experiments on EBG proteolytic digests. (A) Total ion chromatogram (TIC) of EBG+2FGlcAF; (B) mass spectrum of peptides at 26 min in A; (C) TIC of EBG+5FGlcAF; (D) mass spectrum of peptides at 23 min in C. Vertical grey lines in (A) and (C) indicate the regions of the chromatograms for which mass spectra are shown in (B) and (D).

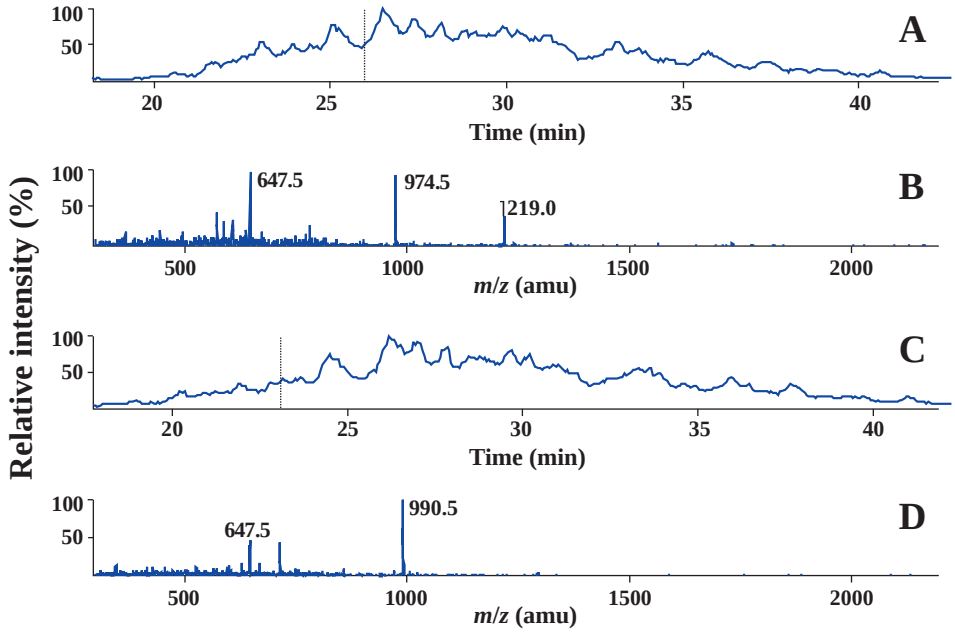


Table 1. Conserved active site residues of Family 2 glycosidases.

Group	Sequence	Species
Galactosidases	507 PRIIC**EY**AHAM	*E. coli* α-subunit
	520 PYISC**EY**MHSM	*Clostridium acetobutylicum*
	532 PLILC**EY**AHAM	*E. coli*
	539 PLILC**EY**AHAM	*Klebsiella pneumoniae*
	546 PLILC**EY**GHAM	*Kluyveromyces lactis*
	526 PFISV**EY**AHAM	*Lactobacillus delbrueckii*
	529 PFLNC**EY**MHDM	*Leuconostoc lactis*
	640 PYISC**EY**MHTM	*Streptococcus thermophilus*
	457 PYLVT**EY**NGHM	*Thermoanaerobacter thermosulfurogenes*
Glucuronidases	534 PIIQS**EY**GAET	*Canis familiaris*
	499 PIIIT**EY**GVDT	*E. coli*
	535 PIIQS**EY**GAET	*Homo sapiens*
	531 PIIQS**EY**GADA	*Mus musculus*
	531 PIIQS**EY**GADA	*Rattus norvegicus*
Mannosidases	549 ARFVS**EY**GYQS	*Bos taurus*
	549 ARFVS**EY**GYQS	*Capra hircus*
	549 ARFVS**EY**GYQS	*H. sapiens*
	554 PRCAS**EY**GVQS	*Caenorhabditis elegans*

Note: The enzymes are grouped according to substrate specificity.

5FGlcAF labels) from these observed masses gives the molecular weight of the native peptide as 795.

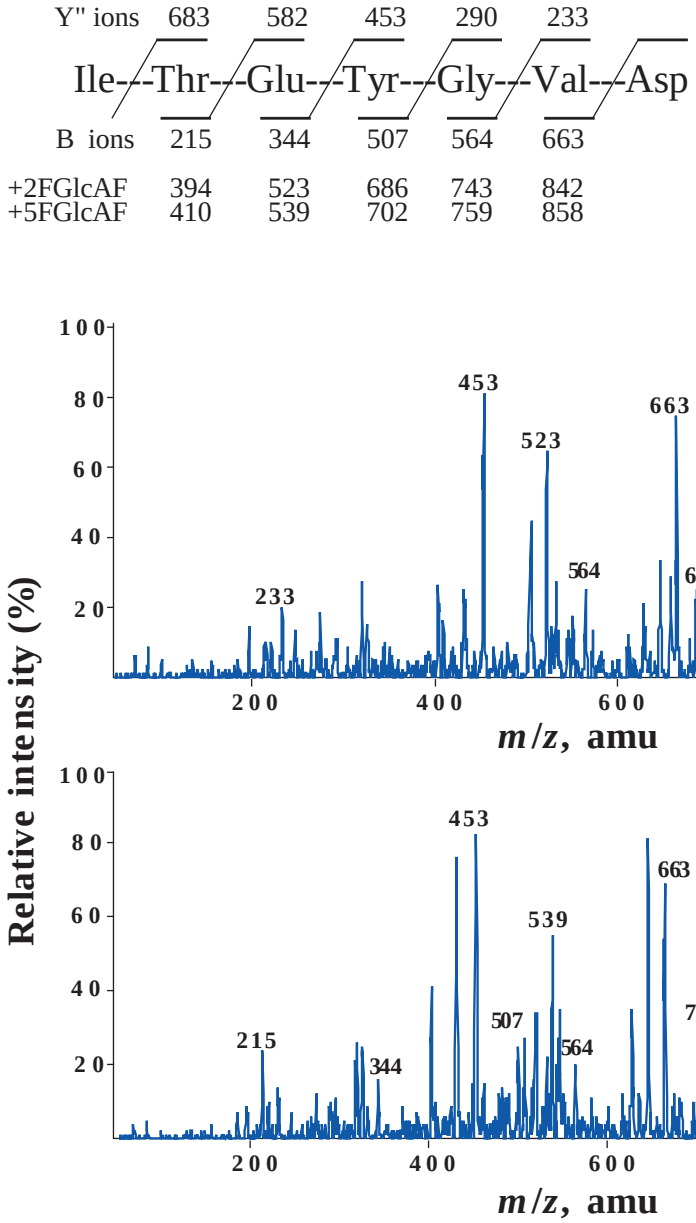
Candidate peptides with a mass of 795 ± 1 Da were then identified by inspection of the amino acid sequence of the enzyme and searching for all possible peptides with this mass. Three such peptides were identified, but one of these was eliminated because its sequence did not contain either an aspartate or a glutamate residue. Precedent with retaining glycosidases to date would predict that the nucleophile should be one of these two amino acids (10). The candidate peptides are $_{115}$EADVTPY$_{121}$ and $_{502}$ITEYGVD$_{507}$. The sequence of the peptide was then unambiguously determined by tandem mass spectrometry.

Peptide sequencing

Information on the sequence was obtained by additional fragmentation of the peptides of interest (*m/z* 974 and 990) in the daughter ion scan mode (Fig. 6). The parent ion of interest was selected in the first quadrupole and subjected to collision-induced fragmentation, and then the masses of the

© 2001 NRC Canada

Fig 6. Electrospray tandem MS daughter ion spectrum of labelled peptides. (A) Observed fragments for peptide labelled with 2FGlcAF; (B) observed fragments for peptide labelled with 5FGlcAF. The sizes of the observed B and Y″ series fragments are shown above.



daughter ions were detected in the third quadrupole. In each sample, peaks with a mass difference of 16 arising from B ions bearing either a 2FGlcAF or a 5FGlcAF label include ITE (*m*/*z* 523 and 539), ITEY (*m*/*z* 686 and 702), ITEYG (*m*/*z* 743 and 759), and ITEYGV (*m*/*z* 842 and 858). Because the B ions bearing the label include only a glutamic acid, we can infer that the label is linked to Glu504. This information, in conjunction with the mass of the labelled peptide and the primary sequence of the enzyme, permits identification of the peptide containing the active site nucleophile as $_{502}$ITEYGVD$_{507}$. Comparison of this sequence with those of the other Family 2 glycosidase sequences shows that the dipeptide EY is conserved throughout the known family members (Table 1). However, the amino acids around this dipeptide are conserved only within a particular glycosidase category, i.e., galactosidase vs. glucuronidase vs. mannosidase. From this we can assign Glu504 as the catalytic nucleophile.

Conclusion

Synthesis of a new mechanism-based inactivator for β-glucuronidases (5-fluoro-β-D-glucuronosyl fluoride) is described and the reagent shown to be an effective inactivator of the β-glucuronidase from *E. coli*. The reagent functions via the formation of a stable, catalytically competent 5-fluoroglucuronosyl-enzyme intermediate. Proteolysis of this labelled enzyme coupled with tandem mass spectrometric analysis revealed the labelled residue as Glu504 within the sequence ITEYGVD.

© 2001 NRC Canada

Acknowledgments

We thank the Natural Sciences and Engineering Research Council of Canada (NSERC) and the Protein Engineering Network of Centres of Excellence of Canada for financial support. Alexander W. Wong was funded by a Medical Research Council of Canada Studentship Award.

References

1. B. Henrissat and G. Davies. Curr. Opin. Struct. Biol. 637 (1997).
2. S. Jain, W.B. Drendel, Z.-W. Chen, F.S. Mathews, W.S. Sly, and J.H. Grubb. Nat. Struct. Biol. **3**, 375 (1996).
3. V. Gieselmann. Biochim. Biophys. Acta, 103 (1995).
4. M.D. Hulett, C. Freeman, B.J. Hamdorf, R.T. Baker, M.J. Harris, and C.R. Parish. Nature Med. **5**, 803 (1999).
5. R.J. Leatherbarrow. GraFit 3.09b. Erithacus Software Ltd., Staines, U.K. 1996.
6. L. Somsák and R.J. Ferrier. Adv. Carbohydr. Chem. Biochem. **49**, 37 (1991).
7. K. Igarashi, T. Honma, and J. Irisawa. Carbohydr. Res. **11**, 577 (1969).
8. G.C. Stelakatos, A. Paganou, and L. Zervas. J. Chem. Soc. C, 1191 (1966).
9. A.W. Wong, S. He, J.H. Grubb, W.S. Sly, and S.G. Withers. J. Biol. Chem. **273**, 34 057 (1998).
10. D.L. Zechel and S.G. Withers. Acc. Chem. Res. 11 (2000).

© 2001 NRC Canada

Homobinuclear Ru–Ru and heterobinuclear Ru–Rh complexes with alkynyl and vinylidene ligands as molecular units

Helmut Werner, Petra Bachmann, and Marta Martin

Abstract: The chelate complex [$RuCl_2\{\kappa^2(P,O)$-*i*-$Pr_2PCH_2CH_2OMe\}_2$] (**1**) reacted, in the presence of CF_3SO_3Ag, with 1 equiv of $C_6H_4(C{\equiv}CH)_2$-*p* (**4**) to afford the mononuclear vinylidene compound [$RuCl(C{=}CHC_6H_4$-*p*-$C{\equiv}CH)\{\kappa^2(P,O)$-*i*-$Pr_2PCH_2CH_2OMe\}_2](CF_3SO_3)$ (**3**). From **1** and 0.5 equiv of **4**, the binuclear bis(vinylidene) complex [$RuCl\{\kappa^2(P,O)$-*i*-$Pr_2PCH_2CH_2OMe\}_2(C{=}CHC_6H_4$-*p*-$CH{=}C)RuCl\{\kappa^2(P,O)$-*i*-$Pr_2PCH_2CH_2OMe\}_2](CF_3SO_3)_2$ (**6**) was obtained. The related compound [$RuCl\{\kappa^2(P,O)$-*i*-$Pr_2PCH_2CH_2OMe\}_2(C{=}CHC_6H_4$-*m*-$CH{=}C)RuCl\{\kappa^2(P,O)$-*i*-$Pr_2PCH_2CH_2OMe\}_2](CF_3SO_3)_2$ (**7**) was prepared from **1**, 0.5 equiv of $C_6H_4(C{\equiv}CH)_2$-*m* (**5**), and silver triflate. The reaction of **2** or **3** with $[RhCl(P$-*i*-$Pr_3)_2]_2$ (**8**) in the molar ratio of 2:1 yields, by addition of the 14-electron fragment [$RhCl(P$-*i*-$Pr_3)_2$] to the uncoordinated C—C triple bond, the heterobinuclear complexes [$RuCl\{\kappa^2(P,O)$-*i*-$Pr_2PCH_2CH_2OMe\}_2(C{=}CHC_6H_4$-*m*/*p*-$C{\equiv}CH)RhCl(P$-*i*-$Pr_3)_2](CF_3SO_3)$ (**9**, **10**) which slowly rearrange at room temperature to give the bis(vinylidene) isomers [$RuCl\{\kappa^2(P,O)$-*i*-$Pr_2PCH_2CH_2OMe\}_2(C{=}CHC_6H_4$-*m*/*p*-$CH{=}C)RhCl(P$-*i*-$Pr_3)_2](CF_3SO_3)$ (**11**, **12**).

Key words: ruthenium, rhodium, vinylidene complexes, alkyne complexes, phosphine complexes.

Résumé : En présence de CF_3SO_3Ag, le chélate complexe [$RuCl_2\{\kappa^2(P,O)$-*i*-$Pr_2PCH_2CH_2OMe\}_2$] (**1**) réagit avec un équivalent de $C_6H_4(C{\equiv}C)_2$-*p* (**4**) pour conduire à la formation du composé vinylidène mononucléaire [$RuCl(C{=}CHC_6H_4$-*p*-$C{\equiv}C)\{\kappa^2(P,O)$-*i*-$Pr_2PCH_2CH_2OMe\}_2](CF_3SO_3)_2$ (**3**). À partir de **1** et d'un demi-équivalent de **4**, on obtient le complexe bis(vinylidène) binucléaire [$RuCl\{\kappa^2(P,O)$-*i*-$Pr_2PCH_2CH_2OMe\}_2(C{=}CHC_6H_4$-*p*-$C{=}C)RuCl\{\kappa^2(P,O)$-*i*-$Pr_2PCH_2CH_2OMe\}_2](CF_3SO_3)_2$ (**6**). On a préparé le composé apparenté [$RuCl\{\kappa^2(P,O)$-*i*-$Pr_2PCH_2CH_2OMe\}_2(C{=}CHC_6H_4$-*m*-$C{=}C)RuCl\{\kappa^2(P,O)$-*i*-$Pr_2PCH_2CH_2OMe\}_2](CF_3SO_3)_2$ (**7**) en faisant réagir le composé **1** un demi-équivalent de $C_6H_4(C{\equiv}CH)_2$-*m* (**5**) en présence de triflate d'argent. Par le biais d'une addition du fragment à quatorze électrons [$RhCl(P$-*i*-$Pr_3)_2$] à la triple liaison qui n'est pas coordinée, les réactions des composés **2** ou **3** avec le $[RhCl(P$-*i*-$Pr_3)_2]_2$ (**8**), dans un rapport molaire de 2:1, conduisent aux complexes hétérobinucléaires [$RuCl\{\kappa^2(P,O)$-*i*-$Pr_2PCH_2CH_2OMe\}_2(C{=}CHC_6H_4$-*m*/*p*-$C{\equiv}C)RhCl(P$-*i*-$Pr_3)_2](CF_3SO_3)_2$ (**9**, **10**) qui se réarrangement lentement à la température ambiante pour conduire aux isomères bis(vinylidènes) [$RuCl\{\kappa^2(P,O)$-*i*-$Pr_2PCH_2CH_2OMe\}_2(C{=}CHC_6H_4$-*m*/*p*-$C{=}C)RhCl(P$-*i*-$Pr_3)_2](CF_3SO_3)_2$ (**11**, **12**).

Mots clés : ruthénium, rhodium, complexes de vinylidènes, complexes d'alcynes, complexes de phosphines.

[Traduit par la Rédaction]

Introduction

Recently, we (1) described an efficient method for the preparation of the chelate complex [$RuCl_2\{\kappa^2(P,O)$-*i*-$Pr_2PCH_2CH_2OMe\}_2$] (**1**) using $[(1.5\text{-}C_8H_{12})RuCl_2]_n$ as the starting material. Due to the *hemilabile* coordination mode of the two phosphinoether ligands (for the term hemilabile see ref. 2*a*; for reviews see ref. 2*b*), compound **1** is quite reactive and affords with CO or PhC≡CH by cleavage of one of the Ru—O bonds the corresponding carbonyl and vinylidene complexes, [$RuCl_2(CO)\{\kappa^1(P)$-*i*-$Pr_2PCH_2CH_2OMe\}\{\kappa^2(P,O)$-*i*-$Pr_2PCH_2CH_2OMe\}$] and [$RuCl_2(C{=}CHPh)\{\kappa^1(P)$-*i*-$Pr_2PCH_2CH_2OMe\}\{\kappa^2(P,O)$-*i*-$Pr_2PCH_2CH_2OMe\}$], respectively, (3). Moreover, treatment of **1** with terminal alkynes RC≡CH, in the presence of silver triflate, led to the formation of the cationic compounds [$RuCl(C{=}CHR)\{\kappa^2(P,O)$-*i*-$Pr_2PCH_2CH_2OMe\}_2](CF_3SO_3)$ which reacted with base by deprotonation of the vinylidene ligand to give the alkynyl derivatives [$RuCl(C{\equiv}CR)\{\kappa^2$-$(P,O)$-*i*-$Pr_2PCH_2CH_2OMe\}_2$] (1). Since we used in the course of these studies apart from alkynes RC≡CH with *R* = H, Ph, and C_6H_4Me-*p* also the diyne $C_6H_4(C{\equiv}CH)_2$-*m* as a substrate, we isolated a cationic complex with a ligand containing an uncoordinated C≡CH unit in the side chain.

Received September 12, 2000. Published on the NRC Research Press Web site at http://canjchem.nrc.ca on May 29, 2001.

This paper is dedicated to Professor Brian R. James on the occasion of his 65th birthday, in recognition of his manifold contributions to organometallic chemistry and homogeneous catalysis.

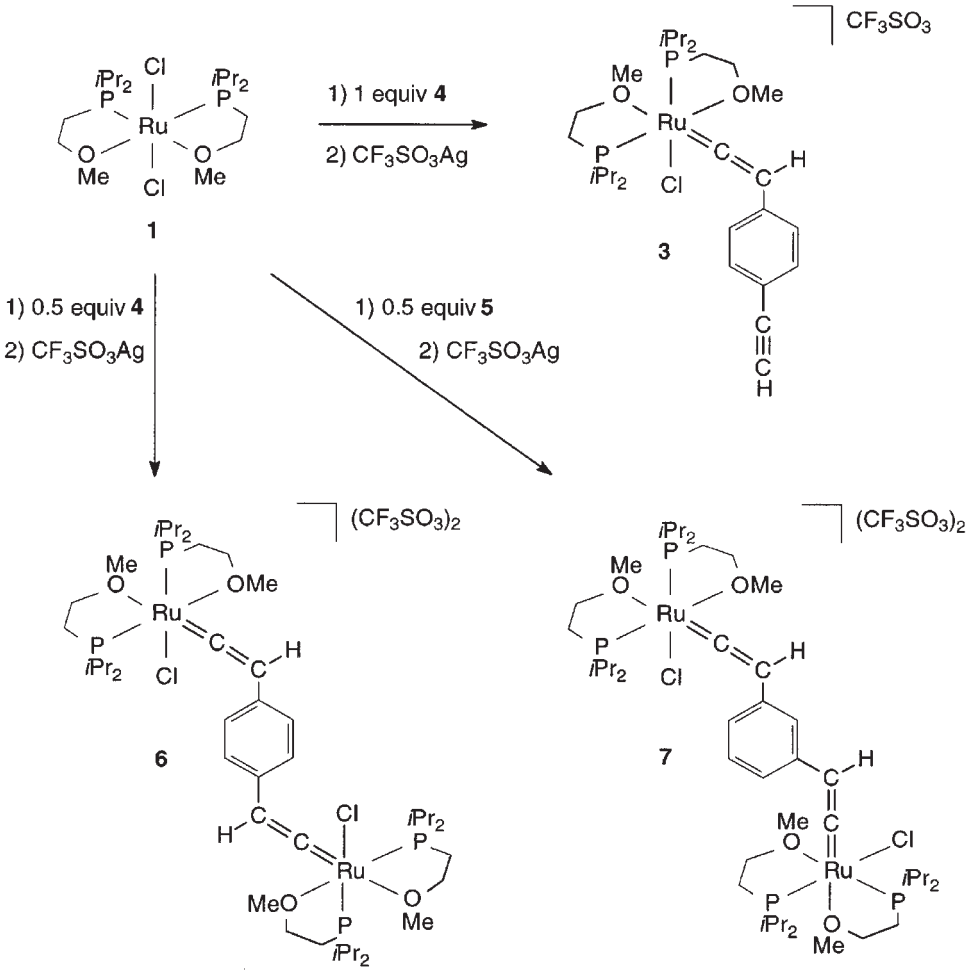
H. Werner,[1] P. Bachmann, and M. Martin.[2] Institut für Anorganische Chemie der Universität, Am Hubland, D-97074 Würzburg, Germany.

[1]Corresponding author (fax: +49-931-888-4605; e-mail: helmut.werner@mail.uni-wuerzburg.de

[2]Present adress: Departamento de Quimica Inorganica, Universidad de Zaragoza, CSIC, E-50009 Zaragoza, Spain.

 DOI: 10.1139/cjc-79-5/6-519 © 2001 NRC Canada

Scheme 1.



Based on this result, the question arose whether this ruthenium cation behaves like an ordinary terminal alkyne and reacts with coordinatively unsaturated precursors to give bimetallic products.

In answering this question, we report in the present paper the synthesis of some homo- and hetero-binuclear Ru–Ru and Ru–Rh complexes, the latter of which revealing different coordination spheres around the two metal centers.

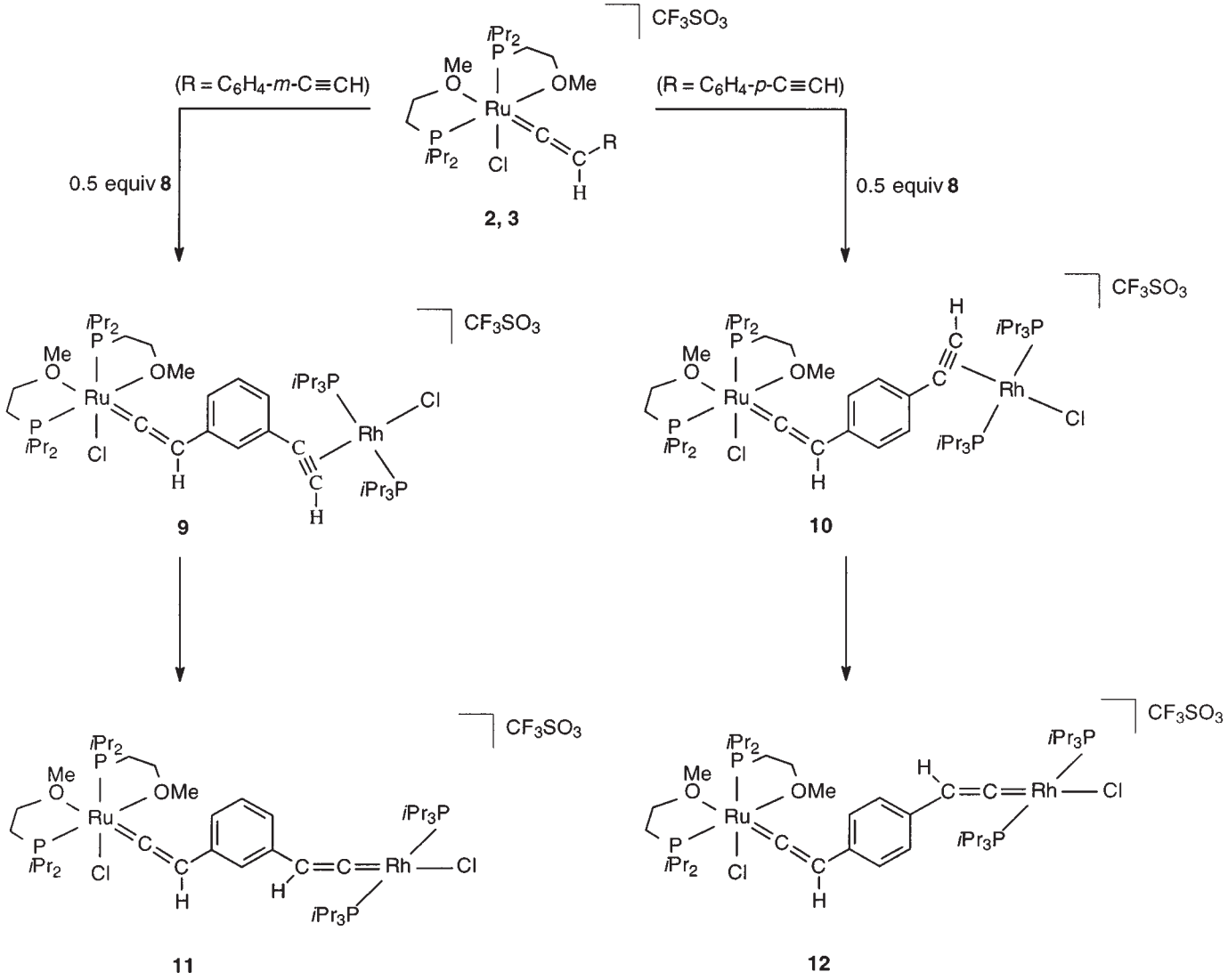
Results and discussion

The preparation of the mononuclear complex **3** (see Scheme 1) followed the route which we had already used for the analogous compound **2** (1). Stepwise treatment of the starting material **1** in acetone with the diyne **4** and silver triflate led, after separation of AgCl, to the formation of a yellow solution from which **3** was isolated in 72% yield. The proposed structure with the *cis*-disposed P-*i*-Pr_2 groups is supported by the ^{31}P NMR spectrum which displays the typical pattern of an AB spin system showing two doublets with a small P—P coupling constant of 24.1 Hz. Further characteristic features are the triplet resonance for the =C*H*R proton in the ^1H NMR spectrum at δ 5.09 and the low-field signals at δ 355.5 and 117.2 in the ^{13}C NMR spectrum which, in agreement with DEPT measurements, are assigned to the α- and β-C atoms of the vinylidene unit. The resonances for the ^{13}C NMR nuclei of the uncoordinated C≡C bond appear as singlets at δ 83.8 and 77.4, respectively.

The reaction of **1** with an equimolar amount of CF_3SO_3Ag but with 0.5 equiv instead of 1 equiv of the diyne **4** led, under the same conditions as used for the preparation of **3**, to the binuclear complex **6** (see Scheme 1). Similarly to **3**, compound **6** is also an orange, only slightly air-sensitive solid which is easily soluble in polar solvents such as acetone or dichloromethane. In contrast to **3**, the IR spectrum of **6** shows no stretching vibrations in the regions at about 3200 and 2100 cm^{-1}, indicating that no C≡CH unit is present. The ^{13}C NMR spectrum of **6** displays the signals for the vinylidene carbon atoms at almost the same positions as found for the mononuclear complex **3**.

© 2001 NRC Canada

Scheme 2.



The starting material **1** reacts not only with **4** but also with the *meta*-isomer **5** of the diyne $C_6H_4(C{\equiv}CH)_2$ in the molar ratio of 2:1 to give the binuclear compound **7**. Due to the related structure of **6** and **7**, it is not surprising that both the chemical properties and the spectroscopic data of the two isomers are in most respects quite similar. The slightly lower symmetry of **7** compared to **6** is indicated, inter alia, by the appearance of a broad multiplet instead of a singlet for the protons of the C_6H_4 fragment and equally by the observation of eight instead of two singlet resonances for the carbon atoms of the phenylene ring. We also note that apart from **6** and **7**, three isomeric binuclear rhodium complexes with the *ortho*-, *meta*-, and *para*-isomers of the bis(vinylidene) unit $C{=}CHC_6H_4CH{=}C$ have been prepared in our laboratory (4).

The uncoordinated alkyne functionality of both **2** and **3** can also be used for the preparation of the mixed-metal ruthenium–rhodium compounds **9**–**12** shown in Scheme 2. The mononuclear precursors react, analogously as terminal alkynes RC≡CH (5), with the dimer $[RhCl(P\text{-}i\text{-}Pr_3)_2]_2$ (**8**) under mild conditions to give the Ru–Rh complexes **9** and **10** as orange microcrystalline solids in ca. 60% yield. In the IR spectra of **9** and **10**, the ν (≡CH) and ν (C≡C) modes appear at significantly lower wave numbers than in the spectra of **2** and **3** which is in agreement with the coordination of the triple bond to the rhodium center. The proposed *trans*-disposition of the two triisopropylphosphine ligands at Rh is supported by the ^{1}H NMR spectra of **9** and **10**, each of which displays two doublets of virtual triplets for the protons of the diastereotopic methyl groups of the P-*i*-Pr_3 units.

Both **9** and **10** slowly rearrange, in toluene at room temperature, to the isomeric species **11** and **12** which are isolated as green, relatively air-stable solids in ca. 70% yield. The ^{13}C NMR spectra of **11** and **12** exhibit in the low-field region two signals for the metal-bound carbon atoms at about δ 355 and 292 which is consistent with the presence of two different carbene-like vinylidene units in the molecule. Another characteristic feature in the ^{31}P NMR spectra of **11** and **12** is the appearance of two doublets for the phosphorus atoms linked to ruthenium and of one doublet for the phosphorus atoms linked to rhodium, the latter showing a rather large Rh—P coupling of ca. 135 Hz. With regard to the course of the rearrangement of **9** and **10** to **11** and **12**, we

© 2001 NRC Canada

failed to find any evidence for the generation of an intermediate containing an alkynyl(hydrido)rhodium moiety RhH(C≡CR)Cl(P-*i*-Pr_3)$_2$ as a building block, and therefore a concerted mechanism is most likely (6). This result is in contrast to that for the isomerization reaction of *trans*-[RhCl(HC≡C*t*Bu)(P-*i*-Pr_3)$_2$] to *trans*-[RhCl(=C≡CH-*t*-Bu)(P-*i*-Pr_3)$_2$] for which a five-coordinate intermediate [RhH(C≡C-*t*-Bu)Cl(P-*i*-Pr_3)$_2$] could not only be detected but even isolated (7).

Experimental

All experiments were carried out under an atmosphere of argon by using standard Schlenk techniques. The starting materials [$RuCl_2${κ^2(*P,O*)-*i*-$Pr_2PCH_2CH_2OMe$}$_2$] (**1**) (1), C_6H_4(C≡CH)$_2$-*p* and -*m* (**4**, **5**) (8), [RuCl-(C=CHC_6H_4C≡CH-*m*){κ^2(*P,O*)-*i*-$Pr_2PCH_2CH_2OMe$}$_2$](CF_3SO_3) (**2**) (1), and [RhCl(P-*i*-Pr_3)$_2$]$_2$ (**8**) (9) were prepared as described previously. IR spectra were recorded on a PerkinElmer 1420 IR spectrometer and NMR spectra on Bruker AC 200 and WM 400 instruments. Melting points (dec. temp.) were determined by DTA.

Preparation of [RuCl(C=CHC_6H_4-*p*-C≡CH){κ^2(*P,O*)-*i*-$Pr_2PCH_2CH_2OMe$}$_2$](CF_3SO_3) (3)

A solution of **1** (262 mg, 0.50 mmol) and **4** (63 mg, 0.50 mmol) in 10 mL of acetone was cooled to 0°C and then treated with CF_3SO_3Ag (128 mg, 0.50 mmol). After the reaction mixture was stirred for 20 min in the dark, the precipitate (AgCl) was separated by filtration through Kieselgur and the filtrate concentrated to ca. 0.5 mL in vacuo. A yellow microcrystalline solid was formed which was washed twice with ether and dried. Yield: 275 mg (72%). IR (KBr) (cm^{-1}): ν(≡CH) 3200, ν(C≡C) 2080, ν(C=C) 1620, 1590. ^{1}H NMR (400 MHz, CD_2Cl_2) δ: 7.37, 7.30 (AB spin system, *J* (HH) = 7.8 Hz, C_6H_4), 5.09 (t, *J* (PH) = 3.2 Hz, =CH), 4.18, 4.13, 4.04, 3.80 (all m, C*H*$_2$OCH$_3$), 3.84, 3.65, (both s, OCH$_3$), 3.10 (s, ≡CH), 2.88, 2.50, 2.40, 2.34, 2.30, 2.00, 1.85 (all m, PC*H*CH$_3$ and PCH$_2$), 1.53–1.29 (br m, PCHC*H*$_3$). ^{13}C NMR (100.6 MHz, CD_2Cl_2) δ: 355.5 (dd, *J* (PC) = 18.1 and 15.1 Hz, Ru=C), 132.7, 130.5, 126.5, 119.9 (all s, C_6H_4), 121.4 (q, *J* (FC) = 320.9 Hz, CF_3), 117.2 (s, =*C*HR), 83.8 (s, C≡*C*H), 77.4 (s, *C*≡CH), 72.8, 71.7 (both s, *C*H$_2$OCH$_3$), 63.2, 63.1, 61.7, 61.6 (all s, OCH$_3$), 37.7 (d, *J* (PC) = 33.2 Hz, P*C*HCH$_3$), 29.5 (d, *J* (PC) = 26.0 Hz, P*C*HCH$_3$), 26.6 (d, *J* (PC) = 28.6 Hz, P*C*HCH$_3$), 25.8 (d, *J* (PC) = 20.0 Hz, P*C*HCH$_3$), 25.4 (d, *J* (PC) = 22.0 Hz, PCH$_2$), 23.2 (d, *J* (PC) = 24.0 Hz, PCH$_2$), 20.1, 19.8, 19.7, 19.65, 19.6, 19.5, 19.1, 19.0 (all s, PCH*C*H$_3$). ^{31}P NMR (162.0 MHz, CD_2Cl_2) δ: 67.9, 56.3 (both d, *J* (PP) = 24.1 Hz). ^{19}F NMR (376.5 MHz, CD_2Cl_2) δ: –78.6 (s). Anal. calcd. for $C_{29}H_{48}ClF_3O_5P_2RuS$: C 45.58, H 6.33, S 4.19; found: C 45.19, H 6.22, S 4.22.

Preparation of [RuCl{κ^2(*P,O*)-*i*-$Pr_2PCH_2CH_2OMe$}$_2$(C=CHC_6H_4-*p*-CH=C)RuCl{κ^2(*P,O*)-*i*-$Pr_2PCH_2CH_2OMe$}$_2$](CF_3SO_3)$_2$ (6)

The procedure was analogous to that described for **3**, using **1** (262 mg, 0.50 mmol), **4** (31 mg, 0.25 mmol), and CF_3SO_3Ag (128 mg, 0.50 mmol) in 20 mL of acetone as starting materials. An orange microcrystalline solid was obtained. Yield: 298 mg (85%). IR (kBr) (cm^{-1}): ν(C=C) 1600. ^{1}H NMR (400 MHz, CD_2Cl_2) δ: 7.21 (s, C_6H_4), 5.08, 5.06 (both t, *J* (PH) = 3.6 Hz, =CH), 4.19, 4.11, 4.04, 3.77 (all m, C*H*$_2$OCH$_3$), 3.84, 3.82, 3.64 (all s, OCH$_3$), 2.86, 2.48, 2.37, 2.32, 2.20, 2.01, 1.89 (all m, PC*H*CH$_3$ and PCH$_2$), 1.54–1.28 (br m, PCHC*H*$_3$). ^{13}C NMR (100.6 MHz, CD_2Cl_2) δ: 355.5 (dd, *J* (PC) = 18.1 and 15.1 Hz, Ru=C), 127.1, 126.3 (both s, C_6H_4), 121.4 (q, *J* (FC) = 320.9 Hz, CF_3), 117.8 (s, =CH), 72.7, 71.7 (both s, *C*H$_2$OCH$_3$), 63.2, 63.1, 61.8 (all s, OCH$_3$), 37.5 (d, *J* (PC) = 33.3 Hz, P*C*HCH$_3$), 28.6, 28.5 (both d, *J* (PC) = 26.0 Hz, P*C*HCH$_3$), 26.6 (d, *J* (PC) = 31.2 Hz, P*C*HCH$_3$), 25.8 (d, *J* (PC) = 20.0 Hz, P*C*HCH$_3$), 25.7 (d, *J* (PC) = 19.0 Hz, PCH$_2$), 23.3 (d, *J* (PC) = 23.6 Hz, PCH$_2$), 20.1, 19.8, 19.75, 19.7, 19.6, 19.2, 19.1, 19.0 (all s, PCH*C*H$_3$). ^{31}P NMR (162.0 MHz, CD_2Cl_2) δ: 68.1, 56.2 (both d, *J* (PP) = 24.3 Hz). ^{19}F NMR (376.5 MHz, CD_2Cl_2) δ: –78.6 (s). Anal. calcd. for $C_{48}H_{90}Cl_2F_6O_{10}P_4Ru_2S_2$: C 41.11, H 6.47, S 4.57; found: C 41.37, H 6.30, S 4.42.

Preparation of [RuCl{κ^2(*P,O*)-*i*-$Pr_2PCH_2CH_2OMe$}$_2$(C=CHC_6H_4-*m*-CH=C)RuCl{κ^2(*P,O*)-*i*-$Pr_2PCH_2CH_2OMe$}$_2$](CF_3SO_3)$_2$ (7)

The procedure was analogous to that described for **3**, using **1** (262 mg, 0.50 mmol), **5** (31 mg, 0.25 mmol), and CF_3SO_3Ag (128 mg, 0.50 mmol) in 20 mL of acetone as starting materials. An orange microcrystalline solid was obtained. Yield: 161 mg (46%). IR (KBr) (cm^{-1}): ν(C=C) 1610, 1580. ^{1}H NMR (400 MHz, CD_2Cl_2) δ: 7.22–6.95 (br m, C_6H_4), 5.06, 5.05 (both t, *J* (PH) = 3.7 Hz, =CH), 4.20, 4.12, 4.04, 3.80 (all m, C*H*$_2$OCH$_3$), 3.87, 3.82, 3.65 (all s, OCH$_3$), 2.88, 2.48, 2.42, 2.33, 2.22, 2.03, 1.91 (all m, PC*H*CH$_3$ and PCH$_2$), 1.55–1.28 (br m, PCHC*H*$_3$). ^{13}C NMR (100.6 MHz, CD_2Cl_2) δ: 357.4 (dd, *J* (PC) = 19.1 and 15.1 Hz, Ru=C), 129.5, 129.4, 129.3, 127.2, 125.7, 125.5, 123.0, 122.8 (all s, C_6H_4), 121.4 (q, *J* (FC) = 319.9 Hz, CF_3), 117.8, 117.7 (both s, =CH), 72.8, 72.7, 71.7 (all s, *C*H$_2$OCH$_3$), 63.2, 63.1, 61.7 (all s, OCH$_3$), 37.5 (d, *J* (PC) = 31.2 Hz, P*C*HCH$_3$), 29.6, 29.4 (both d, *J* (PC) = 26.3 Hz, P*C*HCH$_3$), 26.7, 26.5 (both d, *J* (PC) = 28.8 Hz, P*C*HCH$_3$), 25.7 (d, *J* (PC) = 20.2 Hz, P*C*HCH$_3$), 25.6 (d, *J* (PC) = 19.6 Hz, PCH$_2$), 23.3 (d, *J* (PC) = 23.0 Hz, PCH$_2$), 20.2, 20.1, 19.7, 19.65, 19.6, 19.1, 19.0, 18.9 (all s, PCH*C*H$_3$). ^{31}P NMR (162.0 MHz, CD_2Cl_2) δ: 68.0, 56.1 (both d, *J* (PP) = 24.3 Hz). ^{19}F NMR (376.5 MHz, CD_2Cl_2) δ: –78.6 (s). Anal. calcd. for $C_{48}H_{90}Cl_2F_6O_{10}P_4Ru_2S_2$: C 41.11, H 6.47, S 4.57; found: C 41.49, H 6.21, S 4.49.

Preparation of [RuCl{κ^2(*P,O*)-*i*-$Pr_2PCH_2CH_2OMe$}$_2$(C=CHC_6H_4-*m*-C≡CH)RhCl(P-*i*-Pr_3)$_2$](CF_3SO_3) (9)

A solution of **8** (101 mg, 0.11 mmol) in 15 mL of freshly distilled THF was cooled to –60°C and then treated with **2** (160 mg, 0.21 mmol). A characteristic change of color from violet to orange-yellow occurred. After the reaction mixture was warmed to room temperature and stirred for 10 min, the solvent was removed, the remaining orange solid washed three times with 5 mL portions of pentane (–20°C), and dried in vacuo. Yield: 159 mg (62%), mp 114°C (dec.). IR (CH_2Cl_2) (cm^{-1}): ν(≡CH) 3070, ν(C≡C) 1790, ν(C=C) 1570. ^{1}H NMR (200 MHz, CD_2Cl_2) δ: 7.59–6.75 (br m, C_6H_4), 5.10 (t, *J* (PH) = 3.1 Hz, =CH), 4.16, 4.14, 4.02, 3.83 (all m,

© 2001 NRC Canada

CH_2OCH_3), 3.81, 3.67 (both s, OCH_3), 3.71 (d, *J* (RhH) = 2.8 Hz, ≡CH), 2.87, 2.51, 2.37, 2.33, 2.32, 2.10, 1.87 (all m, RuPC*H*CH_3 and PCH_2), 2.74 (m, RhPC*H*CH_3), 1.51–1.39 (br m, RuPCHC*H*$_3$), 1.24 (dvt, *N* = 15.7, *J* (HH) = 7.5 Hz, RhPCHC*H*$_3$), 1.04 (dvt, *N* = 13.8, *J* (HH) = 6.7 Hz, RhPCHC*H*$_3$). ^{31}P NMR (81.0 MHz, CD_2Cl_2) δ: 66.6, 55.7 (both d, *J* (PP) = 24.0 Hz, RuP), 31.3 (d, *J* (RhP) = 117.7 Hz, RhP). ^{19}F NMR (376.5 MHz, CD_2Cl_2) δ: –78.4 (s). Anal. calcd. for $C_{47}H_{90}Cl_2F_3O_5P_4RhRuS$: C 46.16, H 7.42, S 2.62; found: C 46.09, H 7.35, S 2.26.

Preparation of [RuCl{κ^2(*P,O*)-*i*-Pr$_2$PCH$_2$CH$_2$OMe}$_2$(C=CHC$_6$H$_4$-*p*-C≡CH)RhCl(P-*i*-Pr$_3$)$_2$](CF$_3$SO$_3$) (10)

The procedure was analogous to that described for **9**, using **3** (153 mg, 0.20 mmol) and **8** (94 mg, 0.10 mmol) as starting materials. An orange microcrystalline solid was obtained. Yield: 147 mg (60%), mp 120°C (dec.). IR (CH_2Cl_2) (cm^{-1}): ν(≡CH) 3070, ν(C≡C) 1780, ν(C=C) 1570. ^{1}H NMR (200 MHz, CD_2Cl_2) δ: 7.65–6.78 (br m, C_6H_4), 5.08 (t, *J* (PH) = 3.0 Hz, =CH), 4.13, 4.11, 4.01, 3.81 (all m, C*H*$_2$OCH$_3$), 3.78, 3.68 (both s, OCH$_3$), 3.67 (d, *J* (RhH) = 2.7 Hz, ≡CH), 2.87, 2.50, 2.35, 2.34, 2.31, 2.10, 1.88 (all m, RuPC*H*CH$_3$ and PCH$_2$), 2.73 (m, RhPC*H*CH$_3$), 1.49–1.37 (br m, RuPCHC*H*$_3$), 1.23 (dvt, *N* = 15.8, *J* (HH) = 7.3 Hz, RhPCHC*H*$_3$), 1.02 (dvt, *N* = 13.7, *J* (HH) = 6.5 Hz, RhPCHC*H*$_3$). ^{31}P NMR (81.0 MHz, CD_2Cl_2) δ: 66.2, 55.6 (both d, *J* (PP) = 24.3 Hz, RuP), 31.5 (d, *J* (RhP) = 116.8 Hz, RhP). ^{19}F NMR (376.5 MHz, CD_2Cl_2) δ: –78.6 (s). Anal. calcd. for $C_{47}H_{90}Cl_2F_3O_5P_4RhRuS$: C 46.16, H 7.42, S 2.62; found: C 46.23, H 7.51, S 2.74.

Preparation of [RuCl{κ^2(*P,O*)-*i*-Pr$_2$PCH$_2$CH$_2$OMe}$_2$(C=CHC$_6$H$_4$-*m*-CH=C)RhCl(P-*i*-Pr$_3$)$_2$](CF$_3$SO$_3$) (11)

A solution of **9** (162 mg, 0.13 mmol) in 15 mL of toluene was stirred for 4 h at room temperature. A change of colour from orange to dark brown occurred. The solvent was removed in vacuo, the remaining residue was dissolved in 2 mL of toluene, and the solution was chromatographed on Al_2O_3 (neutral, activity grade V, height of column = 7 cm). With toluene, a green fraction was eluted which was evaporated to dryness in vacuo. The green solid was washed twice with 2 mL portions of pentane (0°C) and dried in vacuo. Yield: 113 mg (71%), mp 105°C (dec.). IR (CH_2Cl_2) (cm^{-1}): ν(C=C) 1610, 1570. ^{1}H NMR (200 MHz, CD_2Cl_2) δ: 7.55–6.74 (br m, C_6H_4), 4.80 (t, *J* (PH) = 3.1 Hz, Ru=C=CH), 4.17, 4.15, 4.02, 3.85 (all m, C*H*$_2$OCH$_3$), 3.80, 3.63 (both s, OCH$_3$), 2.88, 2.48, 2.39, 2.35, 2.31, 2.14, 1.92 (all m, RuPC*H*CH$_3$ and PCH$_2$), 2.74 (m, RhPC*H*CH$_3$), 1.53–1.42 (br m, RuPCHC*H*$_3$), 1.30 (dvt, *N* = 12.8, *J* (HH) = 6.3 Hz, RhPCHC*H*$_3$), the signal of Rh=C=CH could not be exactly located. ^{13}C NMR (100.6 MHz, CD_2Cl_2) δ: 355.3 (dd, *J* (PC) = 17.9 and 14.8 Hz, Ru=C), 292.7 (dt, *J* (RhC) = 59.6, *J* (PC) = 15.5 Hz, Rh=C), 133.8, 130.0 127.3, 122.2 (all s, C_6H_4), 119.6 (q, *J* (FC) = 319.1 Hz, CF_3), 117.9 (s, Ru=C=*C*), 112.2 (dt, *J* (RhC) = 15.3, *J* (PC) = 7.0 Hz, Rh=C=*C*), 62.3, 61.3 (both s, OCH$_3$), 36.9 (d, *J* (PC) = 31.8 Hz, RuP*C*HCH$_3$), 29.0 (d, *J* (PC) = 24.2 Hz, RuP*C*HCH$_3$), 26.0 (d, *J* (PC) = 28.0 Hz, RuP*C*HCH$_3$), 25.6 (d, *J* (PC) = 24.2 Hz, PCH$_2$), 25.5 (d, *J* (PC) = 20.5 Hz, PCH$_2$), 25.4 (d, *J* (PC) = 20.3 Hz, RuP*C*HCH$_3$), 24.0 (vt, *N* = 17.8 Hz, RhP*C*HCH$_3$), 20.4 (s, RhPCH*C*H$_3$), 20.2, 20.1, 19.8, 19.6, 19.5, 19.4, 19.3, 19.1 (all s, RuPCH*C*H$_3$). ^{31}P NMR (81.0 MHz, CD_2Cl_2) δ: 68.6, 57.7 (both d, *J* (PP) = 24.7 Hz, RuP), 43.2 (d, *J* (RhP) = 135.1 Hz, RhP); ^{19}F NMR (376.5 MHz, CD_2Cl_2) δ: –77.5 (s). Anal. calcd. for $C_{47}H_{90}Cl_2F_3O_5P_4RhRuS$: C 46.16, H 7.42, S 2.62; found: C 45.99, H 7.50, S 2.27.

Preparation of [RuCl{κ^2(*P,O*)-*i*-Pr$_2$PCH$_2$CH$_2$OMe}$_2$(C=CHC$_6$H$_4$-*p*-CH=C)RhCl(P-*i*-Pr$_3$)$_2$](CF$_3$SO$_3$) (12)

The procedure was analogous to that described for **11**, using **10** (115 mg, 0.09 mmol) in 10 mL of toluene as starting material. A green microcrystalline solid was obtained. Yield: 78 mg (71%), mp 108°C (dec.). IR (CH_2Cl_2) (cm^{-1}): ν(C=C) 1610, 1570. ^{1}H NMR (200 MHz, CD_2Cl_2) δ: 7.53–6.72 (br m, C_6H_4), 4.78 (t, *J* (PH) = 3.0 Hz, Ru=C=CH), 4.21, 4.17, 4.12, 3.97 (all m, C*H*$_2$OCH$_3$), 3.87, 3.67 (both s, OCH$_3$), 2.78, 2.45, 2.40, 2.36, 2.34, 2.16, 1.97 (all m, RuPC*H*CH$_3$ and PCH$_2$), 2.80 (m, RhPC*H*CH$_3$), 1.51–1.39 (br m, RuPCHC*H*$_3$), 1.32 (dvt, *N* = 12.6, *J* (HH) = 6.2 Hz, RhPCHC*H*$_3$), the signal of Rh=C=CH could not be exactly located. ^{13}C NMR (100.6 MHz, CD_2Cl_2) δ: 355.2 (dd, *J* (PC) = 18.2 and 15.1 Hz, Ru=C), 291.5 (dt, *J* (RhC) = 58.2, *J* (PC) = 15.9 Hz, Rh=C), 134.1, 129.7, 127.2, 122.3 (all s, C_6H_4), 120.2 (q, *J* (FC) = 321.1 Hz, CF_3), 118.3 (s, Ru=C=*C*), 112.4 (dt, *J* (RhC) = 15.4, *J* (PC) = 7.1 Hz, Rh=C=*C*), 62.5, 61.6 (both s, OCH$_3$), 37.1 (d, *J* (PC) = 31.6 Hz, RuP*C*HCH$_3$), 29.3 (d, *J* (PC) = 24.1 Hz, RuP*C*HCH$_3$), 26.1 (d, *J* (PC) = 28.2 Hz, RuP*C*HCH$_3$), 25.7 (d, *J* (PC) = 24.2 Hz, PCH$_2$), 25.3 (d, *J* (PC) = 20.5 Hz, PCH$_2$), 25.2 (d, *J* (PC) = 20.1 Hz, RuP*C*HCH$_3$), 23.7 (vt, *N* = 17.5 Hz, RhP*C*HCH$_3$), 20.3 (s, RhPCH*C*H$_3$), 20.1, 19.9, 19.7, 19.6, 19.5, 19.4, 19.2, 19.1 (all s, RuPCH*C*H$_3$). ^{31}P NMR (81.0 MHz, CD_2Cl_2) δ: 68.3, 57.6 (both d, *J* (PP) = 24.3 Hz, RuP), 43.7 (d, *J* (RhP) = 135.9 Hz, RhP). ^{19}F NMR (376.5 MHz, CD_2Cl_2) δ: –77.7 (s). Anal. calcd. for $C_{47}H_{90}Cl_2F_3O_5P_4RhRuS$: C 46.16, H 7.42, S 2.62; found: C 46.29, H 7.45, S 2.67.

Acknowledgements

We thank the Deutsche Forschungsgemeinschaft (SFB 347), the European Community (Network ERBCHRXCT 930147) for financial support, and the Spanish Ministry of Education for a scholarship (to M. M., EX94 25143294). We also gratefully acknowledge support by Dr. W. Buchner and Mrs. M.-L. Schäfer (NMR spectra), Mrs. R. Schedl and Mr. C. P. Kneis (DTA measurements and elemental analyses), and Degussa AG (chemicals).

References

1. M. Martin, O. Gevert, and H. Werner. J. Chem. Soc. Dalton Trans. 2275 (1996).
2. (*a*) T.B. Rauchfuss and D.M. Roundhill. J. Am. Chem. Soc. **96**, 3098 (1974); (*b*) A. Bader and E. Lindner. Coord. Chem. Rev. **108**, 27 (1991); E. Lindner, S. Pautz, and M. Haustein. Coord. Chem. Rev. 155, 145 (1996); P. Braunstein and F. Naud. Angew. Chem. Int. Ed. **40**, 680 (2001).

© 2001 NRC Canada

3. H. Werner, A. Stark, M. Schulz, and J. Wolf. Organometallics, **11**, 1126 (1992).
4. (*a*) H. Werner, T. Rappert, and J. Wolf. Isr. J. Chem. **30**, 377 (1990); (*b*) H. Werner, P. Bachmann, M. Laubender, and O. Gevert. Eur. J. Inorg. Chem. 1217 (1998).
5. (*a*) H. Werner, F.J. Garcia Alonso, H. Otto, and J. Wolf. Z. Naturforsch. B: Chem. Sci. **43b**, 722 (1988); (*b*) T. Rappert, O. Nürnberg, N. Mahr, J. Wolf, and H. Werner. Organometallics, **11**, 4156 (1992).
6. (*a*) J. Silvestre and R. Hoffmann. Helv. Chim. Acta, **68**, 1461 (1985); (*b*) Y. Wakatsuki, N. Koga, H. Werner, and K. Morokuma. J. Am. Chem. Soc. **119**, 360 (1997).
7. H. Werner and U. Brekau. Z. Naturforsch. B: Chem. Sci. **44b**, 1438 (1989).
8. (*a*) R. Diercks, J.C. Armstrong, R. Boese, and K.P.C. Vollhardt. Angew. Chem. Int. Ed. Engl. **25**, 268 (1986); (*b*) B.C. Berris, G.H. Hovakeemian, Y.-H. Lai, H. Mestdagh, and K.P.C. Vollhardt. J. Am. Chem. Soc. **107**, 5670 (1985).
9. H. Werner, J. Wolf, and A. Höhn. J. Organomet. Chem. **287**, 395 (1985).

© 2001 NRC Canada

Mechanistic study of ligand substitution processes in TpIr(III) complexes

David M. Tellers and Robert G. Bergman

Abstract: The synthesis of the cationic hydridotris(pyrazolyl)borate iridium(III) complex [Tp(PMe_3)IrMe($ClCH_2Cl$)][BAr_f] (**2-CH_2Cl_2**) is reported. Spectroscopic characterization of **2-CH_2Cl_2** in CH_2Cl_2 solution indicates that exchange of bound CH_2Cl_2 with free CH_2Cl_2 is slow on the NMR time scale. Under 50 atm (1 atm = 101.325 kPa) of N_2, the CH_2Cl_2 in **2-CH_2Cl_2** is displaced by N_2 to yield [Tp(PMe_3)IrMe(N_2)][BAr_f] (**2-N_2**). The stronger nucleophile CH_3CN reacts rapidly with **2-CH_2Cl_2** to produce [Tp(PMe_3)IrMe($NCCH_3$)][BAr_f] (**4**). A kinetic study was performed on CH_2Cl_2 substitution in **2-CH_2Cl_2** by CD_3CN. The data are most consistent with dissociative loss of CH_2Cl_2 to generate the unsaturated species ([Tp(PMe_3)IrMe][BAr_f]) which then reacts with CD_3CN to generate [Tp(PMe_3)IrMe($NCCD_3$)][BAr_f]. Further evidence for a dissociative mechanism was obtained by comparison of ligand substitution rates for the Tp complexes with the analogous Tp^{Me2} complexes (Tp^{Me2} = hydridotris(3,5-dimethylpyrazolyl)borate). The relevance of these substitution experiments to C—H activation by cationic iridium(III) complexes is discussed.

Key words: iridium, hydridotris(pyrazolyl)borate, methylene chloride and dinitrogen complexes, dissociative substitution.

Résumé : On a réalisé la synthèse du complexe cationique hydridotris(pyrazolyl)borate d'iridium(III) ([Tp(PMe_3)IrMe($ClCH_2Cl$)][BAr_f]) (**2-CH_2Cl_2**). Une caractérisation spectroscopique du **2-CH_2Cl_2** en solution dans le CH_2Cl_2 indique que l'échange des CH_2Cl_2 liés et libres est lente sur l'échelle de temps de la RMN. Sous 50 atm (1 atm = 101.325 kPa) de N_2, le CH_2Cl_2 du **2-CH_2Cl_2** est déplacé par le N_2 pour conduire à la formation de [Tp(PMe_3)IrMe(N_2])[BAr_f] (**2-N_2**). Le CH_3CN, un nucléophile plus puissant, réagit rapidement avec le **2-CH_2Cl_2** pour conduire à la formation de [Tp(PMe_3)IrMe($NCCH_3$)][BAr_f] (**4**). On a réalisé une étude cinétique sur la vitesse de remplacement du CH_2Cl_2 de **2-CH_2Cl_2** par du CD_3CN. Les données sont plutôt en accord avec une perte dissociative du CH_2Cl_2 générant l'espèce insaturée [Tp(PMe_3)IrMe][BAr_f] qui réagit alors du CH_3CN pour générer le [Tp(PMe_3)IrMe($NCCD_3$)][BAr_f]. On a obtenu d'autres données favorisant un mécanisme dissociatif en comparant les vitesses de substitution des complexes Tp avec celles des complexes analogues Tp^{Me2} (Tp^{Me2} = hydridotris(3,5-diméthylpyrazolyl)borate). On discute de la pertinence de ces expériences de substitution sur l'activation des liaisons C—H par les complexes cationiques de l'iridium(III).

Mots clés : iridium, hydridotris(pyrazolyl)borate, complexes avec le chlorure de méthylène et le diazote, substitution dissociative.

We recently reported the synthesis of [Tp^{Me2}(PMe_3)IrMe(L)][BAr_f] (L = CH_2Cl_2 (**1-CH_2Cl_2**); L = N_2 (**1-N_2**); BAr_f = $B[3,5\text{-}C_6H_3(CF_3)_2]_4$) salts of a cationic complex that is capable of activating the C—H bonds of arenes and aldehydes (1). We envision these reactions occurring by one of the pathways illustrated in Scheme 1. The first mechanism involves dissociative loss of L and subsequent reaction with the hydrocarbon while the second involves an associative displacement of L by the hydrocarbon. Notably, complex **1** activates C—H bonds at rates slower than those reported for the corresponding Cp* compounds (2). Interest in understanding these differences prompted us to undertake a detailed study of the mechanism of substitution of L in these TpIr(III) complexes. Additional impetus was provided by the fact that relatively few mechanistic studies have been carried out on TpM-ligand exchange reactions (3–6; for a general review on Tp chemistry see ref. 7). Herein we communicate the synthesis of two new cationic hydridotris(pyrazolyl)borate iridium complexes, [Tp(PMe_3)IrMe(L)][BAr_f] (L = CH_2Cl_2 (**2-CH_2Cl_2**); L = N_2 (**2-N_2**)), and provide evidence that these complexes undergo substitution in a dissociative manner.

Preliminary kinetic experiments with the Tp^{Me2} system **1-CH_2Cl_2** were too fast to monitor. As a result, we shifted our focus to the hydridotris(pyrazolyl)borate analogue in hopes that it might prove easier to study. The synthesis of [Tp(PMe_3)IrMe(L)][BAr_f] (**2**) is illustrated in Scheme 2 and is analogous to a method reported by Heinekey and coworkers (8) for the synthesis of Tp(PMe_3)IrH_2. Dissolution of Cp*(PMe_3)$IrMe_3OTf$ (9) in CH_3CN produces

Received August 31, 2000. Published on the NRC Research Press Web site at http://canjchem.nrc.ca on May 30, 2001.

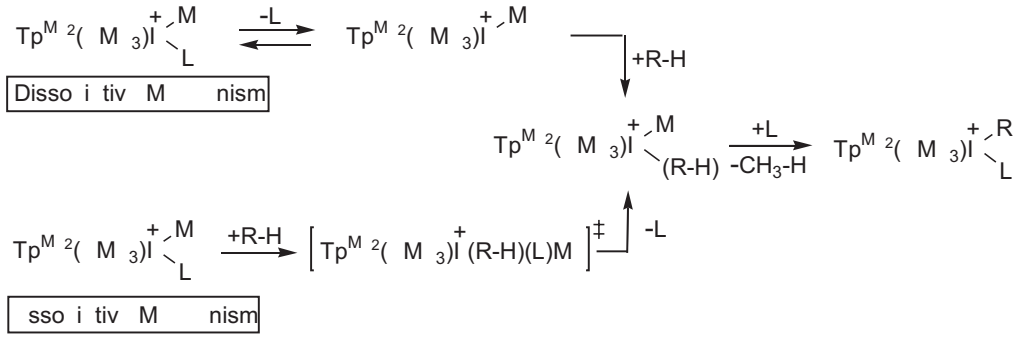
This paper is dedicated to Professor Brian James in recognition of his outstanding contributions to Organometallic Chemistry

D.M. Tellers and R.G. Bergman.[1] Department of Chemistry and Center for New Directions in Organic Synthesis (CNDOS), University of California, Berkeley CA and Division of Chemical Sciences, Lawrence Berkeley National Laboratory, Berkeley CA 94720, U.S.A.

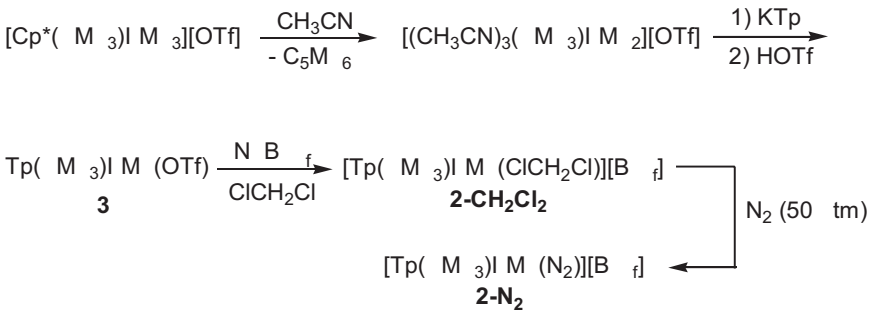
[1]Corresponding author (telephone: (510) 642-2156; fax: (510) 642-7714; e-mail: bergman@cchem.berkeley.edu).

 DOI: 10.1139/cjc-79-5/6-525 © 2001 NRC Canada

Scheme 1. Proposed mechanisms for displacement of L in the reaction of **1-L** with hydrocarbons.



Scheme 2. Synthesis of **2-CH_2Cl2** and **2-N_2**.



$[(CH_3CN)_3(PMe_3)IrMe_2][OTf]$ and hexamethylcyclopentadiene (C_5Me_6).[2] Subsequent addition of KTp to $[(CH_3CN)_3(PMe_3)IrMe_2][OTf]$ yields $Tp(PMe_3)IrMe_2$ (87%). Protonolysis of this product with HOTf yields $Tp(PMe_3)Ir(Me)OTf$ (**3**) (53%). Treatment of **3** with $NaBAr_f$ in CH_2Cl_2 under a dinitrogen atmosphere produces *only* **2-CH_2Cl_2** (40%). This was unexpected since under identical conditions the preparation of the Tp^{Me2} analogue yields only **1-N_2**. The identity of **2-CH_2Cl_2** was confirmed by ^{13}C NMR spectroscopy. In CH_2Cl_2 a triplet is observed at 61.3 ppm ($^1J_{C\text{-}H}$ = 183 Hz; free CH_2Cl_2 = 54.0 ppm, $^1J_{C\text{-}H}$ = 180 Hz). This resonance is assigned to the dichloromethane molecule bound to the cationic iridium center. The fact that it does not disappear at elevated temperatures (60°C) indicates that exchange with the solvent is slow on the NMR time scale. The slow rate of exchange appears to be unique to **2-CH_2Cl_2** since other cationic dichloromethane complexes, including **1-CH_2Cl_2**, require the use of low-temperature NMR spectroscopy to observe the bound dichloromethane resonance (for leading references see refs. 10 and 11).

Consistent with the observation that CH_2Cl_2 is bound to iridium relatively strongly, the synthesis of the dinitrogen complex **2-N_2** from **2-CH_2Cl_2** necessitates the use of high dinitrogen pressures. Placing a dichloromethane solution of **2-CH_2Cl_2** under 50 atm (1 atm = 101.325 kPa) of dinitrogen for 12 h yields **2-N_2** (60%, ν_{NN} (KBr) = 2237 cm^{-1}). Interestingly, **2-N_2** is thermodynamically more stable than **2-CH_2Cl_2**; **2-N_2** does not react to form **2-CH_2Cl_2** after 5 days in CH_2Cl_2 (1 atm N_2 (1 atm = 101.325 kPa)). The slow rate of formation of **2-N_2** compared to that of **1-N_2** is therefore the result of a relatively large kinetic barrier to dichloromethane loss. Stronger nucleophiles, however, displace CH_2Cl_2 from **2-CH_2Cl_2** at a more rapid rate. For example, treatment of **2-CH_2Cl_2** with 1 equiv of acetonitrile at 22°C yields $[Tp(PMe_3)IrMe(NCCH_3)][BAr_f]$ (**4**) ($t_{1/2}$ = 5 min, 74% yield).

As demonstrated above, it was more convenient to carry out exchange kinetics with **2-CH_2Cl_2** as it is significantly less reactive than the Tp^{Me2} complex **1-CH_2Cl_2**. We therefore elected to investigate the mechanism of formation of **4** from **2-CH_2Cl_2** and acetonitrile. A kinetic study was performed in CD_2Cl_2 at 0°C using ^1H NMR spectroscopy to monitor the reaction between **2-CH_2Cl_2** (0.004 M) and excess concentrations of CD_3CN (0.29–3.6 M).[3] A plot of k_{obs} vs. $[CH_3CN]$ is shown in Fig. 1. For an associative mechanism, we would expect a strictly linear relationship between k_{obs} and $[CH_3CN]$. As illustrated in Fig. 1, the reaction begins to deviate from linear behavior at high $[CH_3CN]$.[4] While this deviation may be the result of a solvent effect caused by the high $[CH_3CN]$, we believe the data are most consistent with the dissociative mechanism shown in Scheme 3, which leads to the rate law shown in eq. [1]. The

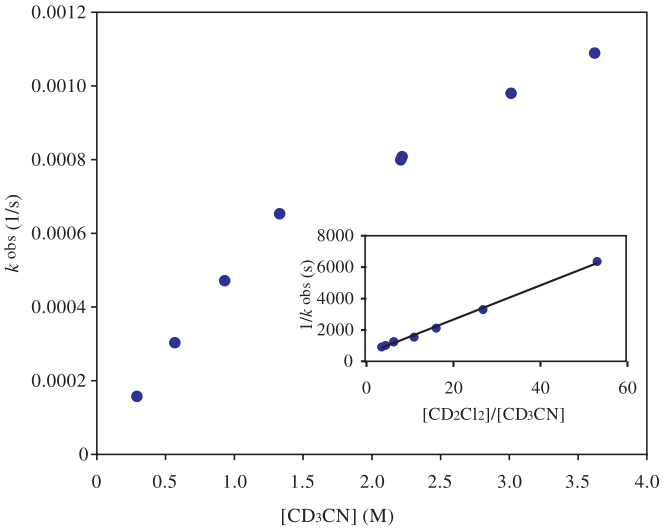
$$[1] \qquad \frac{d[\mathbf{4}]}{dt} = \frac{k_1 k_2[\mathbf{2\text{-}CH_2Cl_2}][CD_3CN]}{k_{-1}[CH_2Cl_2] + k_2[CD_3CN]}$$

first step (k_1) involves dichloromethane loss to generate the unsaturated 16-electron cation $[Tp(PMe_3)IrMe]$. This complex is subsequently trapped by added acetonitrile to

[2] Spectroscopic and analytical data can be found in the supplementary material.
[3] Deuterated material was used to avoid saturating the NMR receiver by the acetonitrile proton signals.
[4] Reactions at much higher concentrations were not run because the reaction rates became too fast to measure.

© 2001 NRC Canada

Fig. 1. Plot of k_{obs} vs. [CD_3CN] for the reaction of **2-CH_2Cl_2** with acetonitrile-d_3 to produce **4** at 0 ± 0.1°C. The inset is a plot of $1/k_{obs}$ vs. [CD_2Cl_2]/[CD_3CN]. This solid line is a linear least squares fit of the data (R^2 = 0.997).



generate **4**. As predicted by eq. [2], a linear plot is ob-

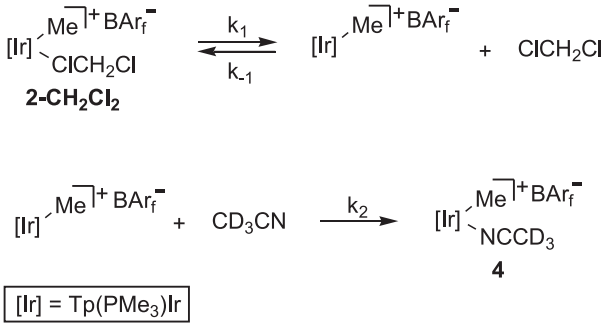
$$[2] \qquad \frac{1}{k_{obs}} = \left(\frac{k_{-1}}{k_2 k_1}\right)\frac{[CH_2Cl_2]}{[CD_3CN]} + \frac{1}{k_1}$$

tained when $1/k_{obs}$ is plotted against [CD_2Cl_2]/[CD_3CN] (Fig. 1). The rate constant for methylene chloride dissociation (k_1) from **2-CH_2Cl_2** at 0°C can be determined from the value of the *y*-intercept of this plot, which is equal to $1/k_1$. The value of k_1 is 2.1 ± 0.2 × 10^{-3} s^{-1} at 0°C.

Because of our inability to experimentally reach the limiting dissociation rate of **2-CH_2Cl_2**, the reaction of **1-CH_2Cl_2** with acetonitrile ([CD_3CN] = 0.27 M) to produce [Tp^{Me2}(PMe_3)IrMe($NCCD_3$)][BAr_f] (**6**) (1) was also examined. At 0°C, this reaction was too fast to monitor by NMR spectroscopy ($t_{1/2} \leq 5$ s). Under identical conditions, the Tp analogue (**2-CH_2Cl_2**) was found to have a $t_{1/2} \approx 75$ min. The difference in reaction rates between the Tp and Tp^{Me2} complexes for this reaction and for dichloromethane substitution by dinitrogen (vide supra) also supports the dissociative mechanism shown in Scheme 3. If substitution were to occur by an associative mechanism (i.e., via a seven-coordinate complex or transition state), the less sterically congested Tp compound should react at a faster rate.[5] Instead, the Tp^{Me2} ligand, which is more sterically encumbering and a stronger electron donor than the Tp ligand (12), serves to increase the rate of ligand loss at the metal center, as would be expected for a dissociative mechanism.

Our results are consistent with recent work done by Kirchner and co-workers (3) who demonstrated that the iso-

Scheme 3. Proposed dissociative mechanism for the formation of **4**.



electronic Ru(II) compound [$TpRu(NCCH_3)_3$]$^+$ undergoes dissociative exchange with free acetonitrile. Furthermore, displacement of $OPPh_3$ by pyridine on $TpReCl_2(OPPh_3)$ was shown to be dissociative by Seymore and Brown (5). It seems likely that the Tp ligand's ability to enforce an octahedral geometry about the metal center, coupled with its steric bulk, prevents the formation of a transient seven-coordinate species (i.e., an associative mechanism) (3). It should be noted, however, that Mayer and co-workers (4) recently demonstrated that triflate displacement from Tp(Ph)Re(NtBu)OTf by various dative ligands occurs via an associative mechanism. Consistent with this, and in constrast to our results, they observed that substitution in the Tp complex was *faster* than that observed for the more sterically encumbered Tp^{Me2} complex.[6]

In conclusion, we have synthesized two cationic iridium complexes and demonstrated that complex **2-CH_2Cl_2** undergoes ligand substitution by initial dissociation of CH_2Cl_2. Based upon this work, it is likely that the Tp-containing compounds **1** and **2** and the corresponding Cp* analogue react with the C—H bonds of hydrocarbons in a similar manner (Scheme 1, Dissociative pathway). Current work is focused on understanding the differences in the relative rates of C—H activation by these complexes.[7]

Acknowledgments

This work was supported by the Director, Office of Energy Research, Office of Basic Energy Sciences, Chemical Sciences Division, U. S. Department of Energy, under Contract no. DE-AC03-76SF00098. We thank Mr. J.S. Yeston and Professor J. M. Mayer for helpful discussions. The Center for New Directions in Organic Synthesis is supported by Bristol-Myers-Squibb as a founding member. Boehringer-Ingelheim Pharmaceuticals Inc. is acknowledged for a graduate fellowship to D.M.T.

References

1. D.M. Tellers and R.G. Bergman. J. Am. Chem. Soc. **122**, 954 (2000).

[5] Our experiments do not rule out a mechanism involving rate-determining dechelation of one pyrazole arm. It is unlikely, however, that dissociation of a Tp arm is more favorable than dissociation of what should be a relatively weakly bound methylene chloride molecule.

[6] In the TpRe system, the imido group can potentially serve to shuttle electron density away from the metal center as the nucleophile attacks prior to ligand substitution (similar to the mechanism of organic carbonyl substitution reactions). This type of mechanism would also generate an associative rate law.

[7] Supplementary material may be purchased from the Depository of Unpublished Data, Document Delivery, CISTI, National Research Council Canada, Ottawa, ON K1A 0S2, Canada (http://www.nrc.ca/cisti/irm/unpub_e.shtml for information on ordering electronically).

© 2001 NRC Canada

2. B.A. Arndtsen and R.G. Bergman. Science (Washington, D.C.), **270**, 1970 (1995).
3. E. Rüba, W. Simanko, K. Mereiter, R. Schmid, and K. Kirchner. Inorg. Chem. **39**, 382 (2000).
4. W.S. McNeil, D.D. Dumez, Y. Matano, S. Lovell, and J.M. Mayer. Organometallics, **18**, 3715 (1999).
5. S.B. Seymore and S.N. Brown. Inorg. Chem. **39**, 325 (2000).
6. W.J. Oldham and D.M. Heinekey. Organometallics, **16**, 467 (1997).
7. S. Trofimenko. Scorpionates: The coordination chemistry of polypyrazolylborate ligands. Imperial College, London. 1999.
8. W.J. Oldham, A.S. Hinkle, and D.M. Heinekey. J. Am. Chem. Soc. **119**, 11 028 (1997).
9. P.J. Alaimo and R.G. Bergman. Organometallics, **18**, 2707 (1999).
10. J. Vincent-Huhmann, B.L. Scott, and G.J. Kubas. J. Am. Chem. Soc. **120**, 6808 (1998).
11. T. Peng, C.H. Winter, and J.A. Gladysz. Inorg. Chem. **33**, 2534 (1994).
12. D.M. Tellers, S.J. Skoog, B.T. Gunnoe, W.D. Harman, and R.G. Bergman. Organometallics, **19**, 2428 (2000).

© 2001 NRC Canada

Evaluation of ruthenium-based complexes for the controlled radical polymerization of vinyl monomers

François Simal, Dominique Jan, Lionel Delaude, Albert Demonceau, Marie-Rose Spirlet, and Alfred F. Noels

Abstract: New complexes of the type $RuCl_2$(*p*-cymene)L where the ligand L is either a phosphine or a stable triazolinylidene carbene have been tested and compared to the Grubbs' benzylidene complex $RuCl_2(=CHPh)(PCy_3)_2$ as catalyst precursors for the controlled atom transfer radical polymerization (ATRP) of methyl methacrylate and of various *para*-substituted styrenes. Kinetic data and Hammett ρ constants are reported, as well as the X-ray structure of the *ortho*-metallated triazolinylidene-ruthenium(II) complex RuCl(*p*-cymene)[1,2-phenylene[3,4-diphenyl-1*H*-1,2,4-triazol-1-yl-5(4*H*)-ylidene]].

Key words: ruthenium, carbene, chelate complex, homogeneous catalysis, atom transfer radical polymerization.

Résumé : De nouveaux complexes du type $RuCl_2$(*p*-cymène)L où le ligand L désigne une phosphine ou un carbène triazolinylidène ont été testés et comparés au complexe benzylidène de Grubbs $RuCl_2(=CHPh)(PCy_3)_2$ comme précurseurs de catalyseurs pour la polymérisation radicalaire contrôlée par transfert d'atome (ATRP) du méthacrylate de méthyle et de divers styrènes *para*-substitués. Des données cinétiques et les constantes de Hammett ρ sont rapportées ainsi que la structure cristallographique du complexe ruthénium(II)-triazolinylidène *ortho*-métallé RuCl(*p*-cymène)[1,2-phénylène[3,4-diphényl-1*H*-1,2,4-triazol-1-yl-5(4*H*)-ylidène]].

Mots clés: ruthénium, carbène, complexe chélaté, catalyse homogène, polymérisation radicalaire par transfert d'atome.

Introduction

The advent of well-defined organometallic complexes which may be used as initiators for controlled radical polymerization has opened new vistas in macromolecular synthesis. A major advance in this field came from the development of the so-called atom transfer radical polymerization (ATRP), which takes advantage of the redox properties of transition-metals (1–3). ATRP is based on a dynamic equilibration between active propagating radicals and dormant species. This equilibrium is established through the reversible transition-metal-catalyzed homolytic cleavage of the covalent carbon—halogen bond in the dormant species (Scheme 1) (4).

Catalytic engineering at the metal center aims to shift this equilibrium toward the dormant species. Thus, the concentration of propagating radicals remains low thorough the whole polymerization process and a high degree of control ensues, allowing not only the synthesis of polymers of predictable molecular weights and low polydispersities, but also the preparation of novel, functionalized, block copolymers amenable to further transformations (5, 6).

Polymerization systems utilizing the ATRP concept have been developed with complexes of Cu, Ru, Ni, Pd, Rh, and Fe during the last five years (7–10). We recently reported on the exceptional efficiency and versatility of new catalysts based on $RuCl_2$(*p*-cymene)(PR_3) (**1**) for promoting the ATRP of vinyl monomers (*p*-cymene is 4-isopropyltoluene) (11). The choice of the phosphane ligand proved to be crucial. Only phosphanes which were both strongly basic and which possessed a well-defined steric bulk led to both high catalytic activity and high control of the polymerization process (high initiation efficiency f and narrow molecular weight distribution, M_w/M_n = 1.1). Along these guidelines, the most suitable phosphines in our hands were tricyclohexylphosphine (PCy_3) and triisopropylphosphine (P-*i*-Pr_3). The corresponding catalyst precursors **1** are conveniently and quantitatively prepared by reacting the ruthenium dimer $[RuCl_2$(*p*-cymene)$]_2$ with 2 equiv of the phosphine (12, 13). They exhibit a high tolerance to heteroatom functionality in

Received August 8, 2000. Published on the NRC Research Press Web site at http://canjchem.nrc.ca on May 30, 2001.

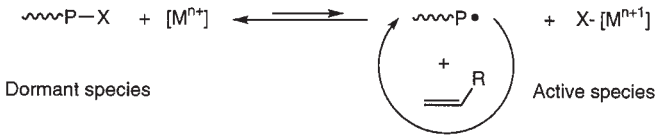
Dedicated to Professor Brian James on the occasion of his 65th birthday.

F. Simal, D. Jan, L. Delaude, A. Demonceau, and A.F. Noels.[1] Center for Education and Research on Macromolecules (CERM), Institut de Chimie (B6a), Université de Liège, Sart-Tilman, B-4000 Liège, Belgium. **M.-R. Spirlet.** Physique expérimentale, Institut de Physique (B5), Université de Liège, Sart-Tilman, B-4000 Liège, Belgium.

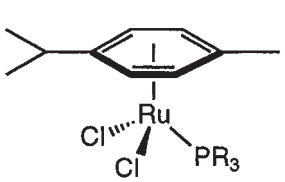
[1]Corresponding author (telephone: +32 (4) 366-3463; fax: +32 (4) 366-3497; e-mail: AF.Noels@ulg.ac.be).

 DOI: 10.1139/cjc-79-5/6-529 © 2001 NRC Canada

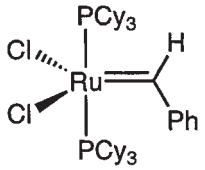
Scheme 1.



the monomer, as well as to ubiquitous impurities such as oxygen and water.



1



2

Surprisingly, the best catalysts for ATRP were also the most active ones for the ring-opening metathesis polymerization (ROMP) of cycloolefins, a reaction where metal–carbene moieties (in equilibrium with metallacyclobutanes) are known to play a key role (14). This prompted us to test preformed metal–carbene complexes such as $RuCl_2(=CHPh)(PCy_3)_2$ (**2**) — a ruthenium-benzylidene catalyst precursor commonly used for olefin metathesis (15) — under ATRP conditions (16). The results were most gratifying and we further expanded our investigations in this field by substituting *N*-heterocyclic stable carbenes for the phosphine ligands (17).

In this article, we present further studies on the scope and limitations of: (*i*) new arene–ruthenium(II)-phosphine complexes; and (*ii*) new arene–ruthenium(II)-triazolinylidene complexes as potential catalysts for the controlled radical polymerization of methyl methacrylate (MMA) and of substituted styrenes.

Results and discussion

Polymerization of MMA with $RuCl_2$(*p*-cymene)PR_3 catalyst precursors

In a previous communication from our group, the catalytic activity of numerous $RuCl_2$(*p*-cymene)PR_3 complexes based on trialkyl-, triaryl-, or mixed alkylarylphosphines was investigated under ATRP conditions. Methyl methacrylate was chosen as a model substrate and polymerizations were initiated by ethyl 2-bromo-2-methylpropanoate at 85°C (11). Ruthenium–arene complexes containing the tricyclohexylphosphine (**1a**) and, to a slightly lesser extent, triisopropylphosphine (**1b**) emerged from this study as the most efficient catalyst precursors.

To complement our initial screening, we have tested new complexes based on tricyclopentylphosphine (**1c**), *tert*-butyldicyclohexylphosphine (**1d**), and dicyclohexylphosphine (**1e**) using the same experimental conditions for MMA polymerization. The results are summarized in Table 1. For comparison sake, data previously obtained with **1a** (PR_3 = PCy_3) and **1b** (PR_3 = P-*i*-Pr_3) are also included.

Table 1. Polymerization of methyl methacrylate with various $RuCl_2$(*p*-cymene)PR_3 catalyst precursors.[a]

Catalyst	PR_3	Polymer yield (%)	M_n (kg mol^{-1})[b]	M_w/M_n	f [c]
1a	PCy_3	100	41.5	1.12	0.95
1b	P-*i*-Pr_3	80	40.5	1.10	0.8
1c	PCp_3	99	66	1.12	0.6
1d	PCy_2-*t*-Bu	99	63	1.14	0.65
1d[d]	PCy_2-*t*-Bu	84	45	1.11	0.75
1e	PCy_2H	32	150	1.8	0.1

[a] Reaction conditions: MMA 1 mL, initiator (ethyl 2-bromo-2-methylpropanoate) 0.0234 mmol, catalyst 0.0117 mmol, 16 h at 85°C.
[b] Determined by size-exclusion chromatography with PMMA calibration.
[c] Initiation efficiency $f = M_{n,\,theor.}/M_{n,\,exp.}$ with $M_{n,\,theor.} = ([monomer]_0/[initiator]_0) \times MW\ (monomer) \times conversion$.
[d] Reaction at 60°C.

Both PCp_3 and PCy_2-*t*-Bu fulfill the requirements previously defined for achieving a high catalytic activity, namely a strong basicity and a well-defined steric bulk (160° < θ < 170°, θ = cone angle of the phosphine). Accordingly, complexes **1c** and **1d** are more than satisfactory catalyst precursors for MMA polymerization. On the other hand, PCy_2H is a much less efficient ligand, probably because of its smaller cone angle (θ = 143°) (18) and weaker basicity (pK_a $H_2PCy_2^+$ = 4.55) (19) compared to PCy_3 (θ = 170°, pK_a $HPCy_3^+$ = 9.70).

A detailed examination of the polymerization kinetics reveals that complexes based on the PCy_3 or PCp_3 ligands deserve the title of best catalyst precursors, because they display slightly faster reaction rates and afford better molecular weight control than the ones ligated to P-*i*-Pr_3 or PCy_2-*t*-Bu. For instance, the apparent propagation constants k_p^{app} calculated for **1a** and **1d** are 1.05×10^{-4} s^{-1} and 7.9×10^{-5} s^{-1}, respectively. Data analysis also confirms the living nature of the polymerization process with the most efficient catalytic systems. The plots of ln ($[M]_0/[M]$) and of M_n vs. monomer conversion are linear (not shown), and polymerization resumes when a second feed of MMA is added to an (almost) completely polymerized reaction mixture. Last but not least, the polymer samples were all colorless after a single precipitation step, a feature that catalytic systems based on other types of transition-metal complexes often lack (10, 20).

Polymerization of styrene and of *p*-substituted styrenes with $RuCl_2$(*p*-cymene)PR_3 catalyst precursors

To broaden the scope of our study on ruthenium(II)-phosphine complexes, a comparison of various catalyst precursors for the polymerization of different *para*-substituted styrenes was carried out. Prior reports strongly suggest that the same stereoelectronic requirements for the phosphine ligand apply to the polymerization of styrene and of MMA (11,21). Therefore, we have tested only three $RuCl_2$(*p*-cymene)PR_3 complexes which contain sterically demanding basic phosphines, viz. **1a** (PR_3 = PCy_3), **1b** (PR_3 = P-*i*-Pr_3), and **1d** (PR_3 = PCy_2-*t*-Bu). The polymerization of unsubstituted styrene initiated by ethyl 2-bromopropanoate at 110°C served as a model reaction in a first set of experiments. A comparative run in the presence of the Grubbs' benzylidene catalyst **2** was included and the results are summarized in Table 2.

© 2001 NRC Canada

Table 2. Polymerization of styrene with various $RuCl_2$(*p*-cymene)PR_3 and $RuCl_2$(=CHPh)$(PCy_3)_2$ catalyst precursors.[a]

Catalyst	PR_3	Polymer yield (%)	M_n (kg mol^{-1})[b]	M_w/M_n	f [c]
1a	PCy_3	58	27	1.25	0.85
1b	P-*i*-Pr_3	45	18	1.11	0.95
1d	PCy_2-*t*-Bu	57	23.5	1.85	0.95
2	PCy_3	61	27	1.38	0.9

[a]Reaction conditions: styrene 1 mL, initiator (ethyl 2-bromopropanoate) 0.0234 mmol, catalyst 0.0117 mmol, 16 h at 110°C.
[b]Determined by size-exclusion chromatography with PS calibration.
[c]See footnote *c*, Table 1 for a definition of *f*.

Table 3. Polymerization of styrene and of *p*-substituted styrenes with $RuCl_2$(*p*-cymene)PCy_3 as catalyst precursor.[a]

Monomer	Polymer yield (%)	M_n (kg mol^{-1})[b]	M_w/M_n	k_p^{app} (1×10^5 s^{-1})
4-Chlorostyrene[c]	68	18	1.27	2.01
Styrene	58	27	1.25	1.52
4-Methylstyrene	45	16	1.38	0.97
4-Methoxystyrene[c]	51	1.4	2.5	1.11

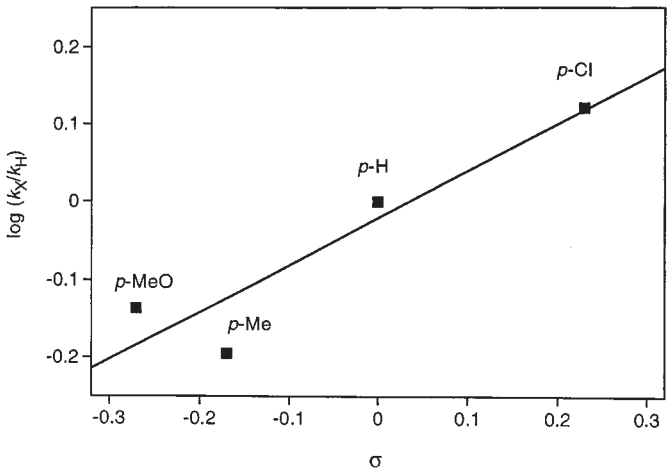
[a]Reaction conditions: 4-X-styrene 1 mL, initiator (ethyl 2-bromopropanoate) 0.0234 mmol, catalyst (**1a**) 0.0117 mmol, 16 h at 110°C.
[b]Determined by size-exclusion chromatography with PS calibration.
[c]Reaction time 24 h.

Although styrene is less prone to ATRP than MMA, catalysts **1a**, **b**, **d**, and **2** permit a moderate to satisfactory control of its polymerization. The narrowest molecular weight distribution was obtained with complex **1b**, while Grubbs' benzylidene complex **2** displayed the fastest reaction kinetics. Thus, the apparent propagation constants k_p^{app} (expressed in 10^5 s^{-1}) follow the order: 1.85 (**2**) > 1.52 (**1a**) > 1.25 (**1d**) > 1.16 (**1b**). In all cases, a linear relationship was observed between the number-average molecular weight (M_n) of the polystyrene samples and the monomer conversion.

To gain further insight into the reaction mechanism and kinetics, the polymerization of various *para*-substituted styrenes was carried out at 110°C with ethyl 2-bromopropanoate as initiator. The results obtained with styrene, 4-chloro-, 4-methyl-, and 4-methoxystyrene are listed in Table 3. They clearly show that the polymerization process is favored when an electron-withdrawing group is present on the aromatic ring. The relative reaction rates k_X/k_H follow the sequence: 1.32 (4-chlorostyrene) > 1 (styrene) > 0.73 (4-methoxystyrene) > 0.63 (4-methylstyrene). The decrease in rates is furthermore associated with an increase in the polydispersity ratio M_w/M_n.

No high molecular weight polymer was formed with 4-methoxystyrene, although the monomer conversion reached ca. 50%. This indicates that transfer reactions take over propagation, a likely consequence of competing ionic processes induced by the electron-donating substituent on styrene that could favor the heterolytic cleavage of the carbon—halogen bond in the active species. Yet, we opted for not excluding the data acquired with *p*-methoxystyrene from the Hammett plot presented in Fig. 1. With all four points, the correlation between log (k_X/k_H) and the substituent σ constant (22) leads to a ρ value of 0.60 and a correlation coefficient of 0.93. The ρ value becomes 0.78 when the 4-methoxy point is discarded, but the conclusion remains the same: one is dealing with a *nucleophilic* active radical species which favors the polymerization of electron-poor olefins.

Fig. 1. Hammett plot for the polymerization of *p*-substituted styrenes initiated by ethyl 2-bromopropanoate and mediated by $RuCl_2$(*p*-cymene)PCy_3 at 110°C.



Synthesis and evaluation of new RuCl(*p*-cymene)(triazolinylidene) catalyst precursors

In this section, we describe our attempts at further improving the ATRP of vinyl monomers by replacing the phosphine ligands in ruthenium complexes with *N*-heterocyclic carbenes (NHC). These new, stable, nucleophilic divalent carbon species are increasingly used in organometallic synthesis (23). They are very strong σ-donating ligands, while the extent of their π-back-bonding is negligible. Many representatives of this new class of compounds isolated so far also bear large substituents, such as benzyl or mesityl groups, on the ring nitrogen atoms. Because of these combined electron-donating properties and steric bulkiness, *N*-heterocyclic carbenes seemed to us to be promising alternatives to strongly basic, sterically crowded phosphines as ligands in our catalyst precursors.

Presently, derivatives of the imidazole and of the triazole ring systems constitute the most widely studied NHC. Our investigations concerning the diaza heterocyclic ligands have been reported elsewhere (17) and we shall focus here solely on the use of a commercially available triazolinylidene carbene, viz. 1,3,4-triphenyl-4,5-dihydro-1*H*-1,2,4-triazol-5-ylidene (**3**) (24). The stoichiometric reaction between this ligand and the ruthenium dimer $[RuCl_2(p\text{-cymene})]_2$ is depicted in Scheme 2. The addition of a base (EtN-*i*-Pr_2 in excess) is required to obtain selectively and quantitatively a single adduct. Indeed, the reaction proceeds via the opening of the μ-chloro bridges of the dimer and the coordination of the incoming carbene to the ruthenium atom. An *ortho*-metallation of the phenyl substituent in position 1 occurs and 1 equiv of HCl is released. It is trapped by the base, which therefore helps driving the reaction to its completion and prevents side-reactions between the protic acid and the highly reactive free carbene species.

© 2001 NRC Canada

Scheme 2.

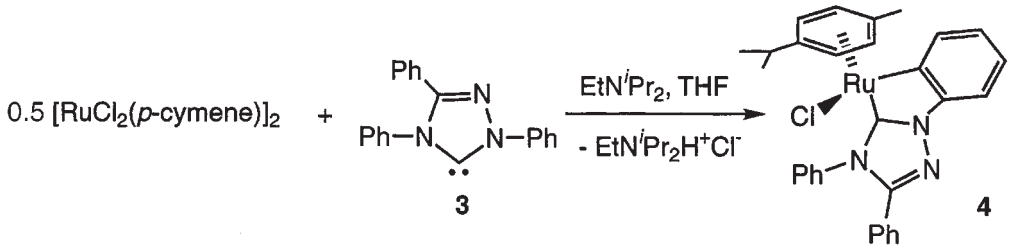
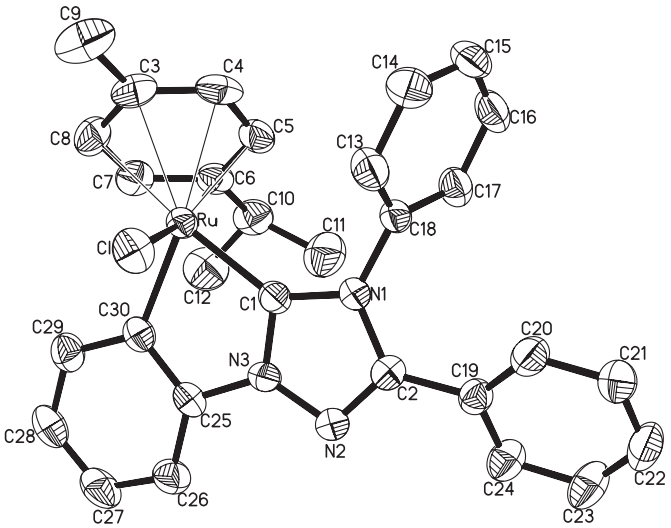


Table 4. Selected bond distances (Å) and bond angles (°) for complex **4**.

Bond distances (Å)					
Ru—Cl	2.4187(8)	Ru—C(4)	2.284(3)	Ru—C(7)	2.198(3)
Ru—C(1)	2.004(3)	Ru—C(5)	2.185(3)	Ru—C(8)	2.267(3)
Ru—C(3)	2.300(3)	Ru—C(6)	2.207(3)	Ru—C(30)	2.071(3)
Bond angles (°)					
Cl-Ru-C(1)	84.06(8)				
Cl-Ru-C(30)	87.63(8)				
C(1)-Ru-C(30)	76.77(11)				

Fig. 2. Molecular structure of complex **4** showing the numbering system; ORTEP diagram with 50% probability ellipsoids.



Complex **4** was isolated as a yellow, air- and water-stable powder and its structure in the solid state was determined by X-ray crystallography. A plot of its molecular structure and a listing of selected bond distances and bond angles are reported in Fig. 2 and Table 4, respectively.

The structure of **4** is close to that reported by Enders et al. (25) for similar complexes. The ruthenium atom lies in a *pseudo*-tetrahedral environment, and the C(1)-Ru-C(30) angle formed between the metal and the two carbon atoms from the chelating ligand equals 76.11(11)° (see Fig. 2 for atom numbering). The triazolinylidene ring is planar and the interatomic distances are in agreement with those observed in other ruthenium–nucleophilic carbene complexes (26, 27). The ruthenium-carbene carbon bond length is 2.004(3) Å, and the *ortho*-metallation takes place with the phenyl ring located at N(3) rather than N(1). At 2.071(3) Å the ruthenium-carbon σ bond to the phenyl ring (Ru—C(30)) is comparable to the values obtained for other *ortho*-metallated *N*-arylcarbenes (25). Furthermore, the *p*-cymene ligand is tilted, the distances ruthenium to C(8), C(3), and C(4) (2.267(3)–2.300(3) Å) are longer than the distances ruthenium to C(7), C(6), and C(5) (2.185(3)–2.207(3) Å). We attribute this distortion to a relatively important *trans* effect of the *ortho*-metallated carbene ligand.

^{1}H and ^{13}C NMR spectra corroborate the X-ray analysis and bring over additional structural information on complex **4** (see *Experimental section* for detailed assignments). The carbene-carbon resonates at 192.8 ppm, a typical value for this type of complex. Due to chirality, all aromatic hydrogen and carbon atoms from the *p*-cymene ligand are inequivalent. The aromatic protons appear as 2 AB systems and the aromatic carbons as 6 different singlets in ^{1}H and proton-decoupled ^{13}C NMR spectra, respectively. The two methyls from the isopropyl group give rise to two doublets (^{1}H NMR) or two singlets (^{13}C NMR). No changes in the NMR spectra were observed even at temperatures as high as 110°C, indicating that dissociation of the *p*-cymene ligand does not take place under these conditions.

Addition of 1 equiv of silver tetrafluoroborate to the neutral complex **4** led to the corresponding cationic species **5** ligated to an extra molecule of solvent (CH_3CN) (Scheme 3). As expected, the cationic complex displayed after purification the same NMR characteristics than its neutral precursor, i.e., inequivalent C and H atoms for the arene ligand.

Both **4** and **5** were tested as ATRP catalysts. Cationic complex **5** was practically inactive at promoting the polymerization of MMA and of styrene, whereas its neutral counterpart **4** proved to be an active catalyst precursor for the ATRP of vinyl monomers. Because a reversible oxidation of Ru(II) into Ru(III) is central to the ATRP mechanism (cf. Scheme 1), one could argue that the already charged species **5** is less prone to oxidation than its neutral counterpart **4**, thus explaining the large difference in reactivity between the two of them. Results obtained with MMA, styrene, and two *para*-substituted styrenes using complex **4**

© 2001 NRC Canada

Scheme 3.

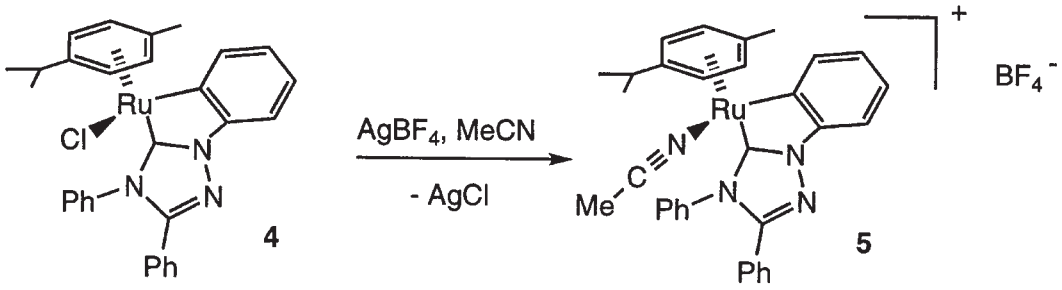


Table 5. Polymerization of methyl methacrylate and of styrenes mediated by complex **4**.

Monomer	Polymer yield (%)	M_n (kg mol^{-1})[a]	M_w/M_n	f [b]
MMA[c]	80	56.5	1.6	0.55
Styrene[d]	81	35	1.4	0.9
4-Chlorostyrene[d]	83	42	1.5	0.98
4-Methylstyrene[d]	80	38.5	1.5	0.8

[a]Determined by size-exclusion chromatography with PMMA or PS calibration.
[b]See footnote *c*, Table 1 for a definition of *f*.
[c]Reaction conditions: MMA 1 mL, initiator (ethyl 2-bromo-2-methylpropanoate) 0.0234 mmol, catalyst (**4**) 0.0117 mmol, 16 h at 85°C.
[d]Reaction conditions: 4-X-styrene 1 mL, initiator ((1-chloroethyl)benzene) 0.0234 mmol, catalyst (**4**) 0.0117 mmol, 16 h at 110°C.

as catalyst precursor are summarized in Table 5. Standard polymerization conditions were applied with ethyl 2-bromo-2-methylpropanoate and (1-chloroethyl)benzene as initiators for MMA and styrenes, respectively.

The molecular weight distributions are slightly narrower for polystyrenes than for PMMA. However, the *ortho*-metallated triazolinylidene complex **4** does not afford a better control of the polymerization than the phosphine-based catalysts **1a**–**d**. It also loses more rapidly its efficiency when the reaction temperature is lowered, since the polymer yield drops to 16% when MMA is reacted at 75°C instead of 85°C and no more PMMA is isolated when the reaction is carried out at 60°C. Thus, catalyst **4** is presently no match for complexes **1** and **2**, whose synthesis is also more straightforward. Further studies concerning the relationship between ATRP and ATRA (atom transfer radical addition, Kharasch reaction) as a function of the electronic tuning and other variations of the carbene ligand are in progress.

Experimental Section

General information

All the solvents and monomers were dried, distilled, and degassed prior to use. They were stored under nitrogen at –20°C in the absence of light. NMR spectra were recorded on a Brucker AM 400 spectrometer (400 and 100 MHz for ^{1}H and ^{13}C NMR, respectively). Chemical shifts are listed in ppm downfield from TMS with the solvent as the internal standard. Infrared spectra were recorded on a PerkinElmer 1720X series FT-IR spectrometer from KBr discs. Elemental analyses were performed at the Laboratory of Pharmaceutical Chemistry, University of Liège.

Materials

Complexes **1a**–**e** were prepared according to the literature (12, 13). $RuCl_2(=CHPh)(PCy_3)_2$ (**2**) was used as received from Strem. 1,3,4-Triphenyl-4,5-dihydro-1*H*-1,2,4-triazol-5-ylidene (**3**) was purchased from Acros.

*Chloro[(1,2,3,4,5,6-η)-1-methyl-4-(1-methylethyl) benzene][1,2-phenylene[3,4-diphenyl-1*H*-1,2,4-triazol-1-yl-5(4*H*)-ylidene]]ruthenium (**4**)*

A 0.44 g sample of 1,3,4-triphenyl-4,5-dihydro-1*H*-1,2,4-triazol-5-ylidene **3** (0.48 mmol) was weighted in a glove box and dissolved in 15 mL of THF. This solution was added via a cannula to a mixture of $[RuCl_2(p\text{-cymene})]_2$ (0.40 g, 0.65 mmol) and *N*,*N*-diisopropylethylamine (0.75 g, 5.74 mmol) in 40 mL of THF under inert atmosphere. The initial red suspension was stirred 4.5 h at room temperature. It progressively turned into an orange then a yellow solution. After 4.5 h the solvent was removed on a rotary evaporator and the yellow residue was purified by column chromatography on silica gel with CH_2Cl_2. The eluate was washed with H_2O (3 × 20 mL) to remove the ammonium salt, dried over sodium sulfate, and evaporated. The residue was rinsed with Et_2O (2 × 10 mL) and *n*-pentane (2 × 15 mL) to afford the title compound as a bright yellow powder. Yield: 0.59g (79%); mp 215°C (dec.). IR (cm^{-1}): 3052(m), 2959(m), 2915(m), 2865(m), 1593(m), 1533(m), 1497(s), 1143(s), 1336(s), 1013(m), 750(s), 702(s). ^{1}H NMR ($CDCl_3$, δ ppm): 8.13 (d, 1H, C*H* Ph, $^3J_{H\text{-}H}$ = 8.4 Hz), 7.60–7.31 (m, 11H, C*H* Ph), 7.05 (t, 2H, C*H* Ph, $^3J_{H\text{-}H}$ = 5.0 Hz), 5.43 (d, 1H, C*H* *p*-cym, C*H* Ph, $^3J_{H\text{-}H}$ = 6.4 Hz), 5.19 (d, 1H, C*H* *p*-cym, C*H* Ph, $^3J_{H\text{-}H}$ = 6.4 Hz), 4.63 (d, 1H, C*H* *p*-cym, C*H* Ph, $^3J_{H\text{-}H}$ = 6.4 Hz), 4.55 (d, 1H, C*H* *p*-cym, C*H* Ph, $^3J_{H\text{-}H}$ = 6.4 Hz), 2.12 (sept, 1H, C*H*CH$_3$, $^3J_{H\text{-}H}$ = 6.8 Hz), 1.92 (s, 3H, ArC*H*$_3$), 0.83 (d, 3H, CHC*H*$_3$, $^3J_{H\text{-}H}$ = 6.8 Hz), 0.66 (d, 3H, CHC*H*$_3$, $^3J_{H\text{-}H}$ = 6.8 Hz). ^{13}C NMR ($CDCl_3$, δ ppm): 192.81 (Ru=*C*), 160.78 (Ru-*C*$_{ar}$), 152.06 (N-*C*$_{ar}$), 144.76 (N-*C*$_{ar}$), 141.30 (=C-*C*$_{ar}$), 137.47, 131.03, 130.27, 128.88, 127.36, 125.51, 125.37, 122.59, 121.96, 112.93 (Ph), 105.07, 99.81 (*C*$_{ar}$CH$_3$, *C*$_{ar}$CH(CH$_3$)$_2$), 93.12, 90.57, 89.80, 82.60 (*C*H *p*-cym), 30.88 (*C*HMe$_2$), 23.34 (CH(*C*H$_3$)$_2$), 21.16 (CH(*C*H$_3$)$_2$), 18.89 (ArC*H*$_3$ *p*-cym). Anal. calcd. for $C_{30}H_{28}ClN_3Ru$ (%): C 63.53, H 4.95, N 7.41; found: C 63.13, H 5.40, N 7.48.

*(Acetonitrile)[(1,2,3,4,5,6-η)-1-methyl-4-(1-methylethyl)benzene][1,2-phenylene[3,4-diphenyl-1H-1,2,4-triazol-1-yl-5(4*H*)-ylidene]]ruthenium tetrafluoroborate (**5**)*

Complex **4** (151 mg, 0.266 mmol) and $AgBF_4$ (104 mg, 0.532 mmol) were dissolved in 40 mL of acetonitrile under nitrogen. The initial yellow suspension was stirred 18 h at room temperature. It progressively turned into a green then a

© 2001 NRC Canada

purple solution. After 18 h the mixture was filtered on a Celite pad and the solvent was removed on a rotary evaporator. The blue residue was purified by column chromatography on silica gel (eluent CH_2Cl_2:CH_3OH, 10:1). Evaporation of the eluent afforded **5** as a blue powder which was rinsed with Et_2O (3 × 20 mL) and dried. Yield: 0.13 g (76%); mp 140°C (dec.). IR (cm^{-1}): 3055(w), 2964(w), 2930(w), 1596(w), 1498(m), 1446(m), 1399(m), 1338(m), 1262(m), 1062(s), 700(m). ^{1}H NMR (CD_2Cl_2, δ ppm): 8.00 (d, 1H, C*H* Ph, $^3J_{H\text{-}H}$ = 6.4 Hz), 7.73–7.09 (m, 13H, C*H* Ph), 5.60 (d, 1H, C*H* *p*-cym, C*H* Ph, $^3J_{H\text{-}H}$ = 6.2 Hz), 5.37 (d, 1H, C*H* *p*-cym, C*H* Ph, $^3J_{H\text{-}H}$ = 6.2 Hz), 5.04 (d, 1H, C*H* *p*-cym, C*H* Ph, $^3J_{H\text{-}H}$ = 6.2 Hz), 4.94 (d, 1H, C*H* *p*-cym, C*H* Ph, $^3J_{H\text{-}H}$ = 6.2 Hz), 2.22 (s, 3H, CH_3CN), 2.12 (sept, 1H, C*H*CH_3, $^3J_{H\text{-}H}$ = 6.4 Hz), 1.93 (s, 3H, ArCH_3), 0.84 (d, 3H, CHCH_3, $^3J_{H\text{-}H}$ = 6.4 Hz), 0.73 (d, 3H, CHCH_3, $^3J_{H\text{-}H}$ = 6.4 Hz). ^{13}C NMR (CD_2Cl_2, δ ppm): 188.52 (Ru=*C*), 154.81 (Ru-C_{ar}), 153.70 (N-C_{ar}), 145.42 (N-C_{ar}), 141.61 (=C-C_{ar}), 136.95, 131.38, 131.06, 130.93, 130.67, 129.18, 128.80, 128.41, 126.60, 124.53 (Ph, CH_3*C*N), 113.85, 106.34 ($C_{ar}CH_3$, $C_{ar}CH(CH_3)_2$), 95.47, 93.53, 90.88, 87.84 (*C*H *p*-cym), 31.60 (*C*HMe_2), 23.19 (CH(*C*H_3)$_2$), 21.64 (CH(*C*H_3)$_2$), 19.18 (Ar*C*H_3 *p*-cym), 4.30 (*C*H_3CN).

X-ray crystallography

Crystals of **4** suitable for X-ray diffraction analysis were obtained by slow diffusion of *n*-pentane in a CH_2Cl_2 solution at –18°C. A summary of the crystal data and parameters for data collection is given in Table 6. Data were collected at 293 K on a four circle Brucker P4 diffractometer using monochromated Mo K_α radiation (0.71073 Å). The structure was solved by direct method and refinement was performed on F^2 using the SHELXL-96 solution package programs (28). All non-hydrogen atoms were refined anisotropically. Hydrogen atoms were located on difference Fourier map and refined isotropically. Complete tables of bond distances and angles, final atomic coordinates, and anisotropic displacement parameters have been deposited as supplementary material.[2]

Table 6. Crystallographic data for complex **4**.

Formula	$C_{30}H_{28}ClN_3Ru$
Formula weight	567.07
Crystal system	Monoclinic
Space group	$P2_1/c$
a (Å)	9.6322(13)
b (Å)	17.970(2)
c (Å)	15.128(2)
α (°)	90
β (°)	107.930(12)
γ (°)	90
V (Å^3)	2491.3(6)
Z	4
$\rho_{calc.}$ (g cm^{-3})	1.512
μ (mm^{-1})	0.761
F(000)	1160
Crystal size (mm)	0.30 × 0.4 × 0.35
Temperature (K)	293(2)
2θ limits (°)	1.8–25.0
Total reflections	5543
Unique reflections	4350
No. of variables	428
Goodness-of-fit	1.019
R_1 [$I > 2\sigma(I)$][a]	0.0285
wR_2 (all data)[b]	0.0692
Max, min resid. density (e Å^{-3})	1.362 and –0.495

[a] $R_1 = \Sigma||F_0| - |F_c||\Sigma|F_0|$.
[b] $wR_2 = [\Sigma[w(F_0^2 - F_c^2)^2]/\Sigma[w(F_0^2)_2]]^{0.5}$.

Typical polymerization procedure

A ruthenium complex (0.0117 mmol) was placed in a glass tube containing a magnet bar and capped by a three-way stopcock. Air was expelled by three vacuum–nitrogen cycles before methyl methacrylate (1 mL, 9.35 mmol) and the initiator solution (0.1 M in toluene, 0.234 mL) were added. All liquids were handled with dried syringes under nitrogen. The reaction mixture was heated for 16 h at 85°C under inert atmosphere. After cooling, it was diluted with THF and poured in *n*-heptane (600 mL) under vigorous stirring. The precipitated polymer was filtered with suction and dried overnight at 80°C under vacuum.

Styrene and the *p*-substituted styrenes were polymerized according to the same procedure and precipitated from methanol. In all experiments, 1 mL of monomer was used (see the Tables for further information on the initiator, the temperature, and the reaction time).

Polymer characterization

Molecular weight distributions were determined by SEC in THF at 40°C using a Hewlett–Packard 1090 liquid chromatograph equipped with a Hewlett–Packard 1037A refractive index detector. PMMA and PS standards (Polymer Laboratories) were used for calibration. Before SEC analysis, the polymers were purified by passing solutions through a short Al_2O_3-filled column. ^{1}H NMR spectra were recorded at room temperature in $CDCl_3$ with TMS as internal reference on a Brucker AM 400 apparatus.

Conclusions

A major advantage of utilizing transition-metal complexes as catalysts is the possibility to fine tune their electronic and steric properties through the design of their ligands. Our research on the potential of various ruthenium(II)-phosphine or ruthenium(II)-triazolinylidene complexes to promote atom transfer radical polymerization of vinyl monomers nicely illustrates this concept. Polymerizations of methyl methacrylate and of styrene were chosen as model reactions with ethyl 2-bromo-(2-methyl)propanoate or (1-chloroethyl)benzene serving as initiators. Very efficient catalyst precursors were

[2] Copies of material on deposit may be purchased from the Depository of Unpublished Data, Document Delivery, CISTI, National Research Council Canada, Ottawa, Ontario, Canada K1A OS2 ((http://www.nrc.ca/cisti/irm/unpub_e.shtml for information on ordering electronically). Copies of the data can be obtained, free of charge, on application to the Director, CCDC, 12 Union Road, Cambridge CB2 1EZ, U.K. (Fax: 44-1223-336033 or e-mail: deposit@ccdc.cam.ac.uk).

© 2001 NRC Canada

obtained when bulky and basic phosphines were ligated to the metal. Ligands that did not meet these requirements gave much poorer or inefficient catalyst systems for ATRP.

Acknowledgments

Financial support from the Fonds National de la Recherche Scientifique (F.N.R.S.), Belgium, for the purchase of major instrumentation is gratefully acknowledged. We also thank the EU TMR program (HPRN-CT-2000-10) for generous support.

References

1. M. Sawamoto and M. Kamigaito. CHEMTECH. June, 30 (1999).
2. K. Matyjaszewski. *In* Education in advanced chemistry, mechanistic aspects of molecular catalysis. Vol. 6. *Edited by* K. Matyjaszewski. and B. Marciniec. Wydawnictwo Poznanskie, Poznan-Wroclaw. 1999. pp. 95–105.
3. K. Matyjaszewski (*Editor*). Controlled/living radical polymerization: Progress in ATRP, NMP, and RAFT. Vol. 768. ACS Symposium Series. ACS, Washington, D.C. 2000.
4. K. Matyjaszewski. Chem. Eur. J. **5**, 3095 (1999).
5. C.J. Hawker. Acc. Chem. Res. **30**, 373 (1997).
6. M. Sawamoto and M. Kamigaito. *In* Materials science and technology. A comprehensive treatment. *Edited by* R.W. Cahn, P. Haasen, and E.J. Kramer. Synthesis of polymers. A.-D. Schlüter (*Volume Editor*). Wiley-VCH, Weinheim. 1999. pp. 163–194.
7. K. Matyjaszewski. Macromolecules **31**, 4710 (1998); Macromolecules **31**, 4718 (1998).
8. D.M. Haddleton, M.C. Crossman, B.H. Dana, D.J. Duncalf, A.M. Heming, D. Kukulj, and A.J. Shooter. Macromolecules **32**, 2110 (1999).
9. H. Uegaki, Y. Kotani, M. Kamigaito, and M. Sawamoto. Macromolecules **30**, 2249 (1997).
10. T. Ando, M. Kamigaito, and M. Sawamoto. Macromolecules **30**, 4507 (1997).
11. F. Simal, A. Demonceau, and A.F. Noels. Angew. Chem. Int. Ed. Engl. **38**, 538 (1999).
12. A. Demonceau, A.W. Stumpf, E. Saive, and A.F. Noels. Macromolecules **30**, 3127 (1997).
13. D. Jan, L. Delaude, F. Simal, A. Demonceau, and A.F. Noels. J. Organomet. Chem. **606**, 55 (2000).
14. K.J. Ivin and J.C. Mol. Olefin metathesis and metathesis polymerization. Academic Press Ltd., London. 1997.
15. A. Amir-Ebrahimi, D.A. Corry, J.G. Hamilton, J.M. Thompson, and J.J. Rooney. Macromolecules **33**, 717 (2000).
16. F. Simal, A. Demonceau, and A.F. Noels. Tetrahedron Lett. **40**, 5689 (1999).
17. F. Simal, A. Demonceau, A.F. Noels, F. Kohl, T. Weskamp, and W.A. Herrmann. Chem. Eur. J. **7** (2001) accepted for publication.
18. D. White and N.J. Coville. Adv. Organomet. Chem. **36**, 95 (1994).
19. W.A. Henderson, Jr. and C.A. Streuli. J. Am. Chem. Soc. **82**, 5791 (1960).
20. G. Moineau, P. Dubois, R. Jérôme, T. Senninger, and P. Teyssié. Macromolecules **31**, 545 (1998).
21. F. Simal, L. Delaude, D. Jan, A. Demonceau, and A.F. Noels. Polym. Prepr. (Am. Chem. Soc. Div. Polym. Chem.) **40**, 336 (1999).
22. J. March. Advanced organic chemistry. 3rd ed. Wiley-Interscience, New York. 1985. pp. 242–250.
23. T. Weskamp, V.P.W. Böhm, and W. A. Herrmann. J. Organomet. Chem. **600**, 12 (2000).
24. D. Enders, K. Breuer, G. Raabe, J. Runsink, J.H. Teles, J.P. Melder, K. Ebel, and S. Brode. Angew. Chem. Int. Ed. Engl. **34**, 1021 (1995).
25. H. Enders, H. Gielen, G. Raabe, J. Runsink, and J.H. Teles. Chem. Ber./Recl. **130**, 1253 (1997) and refs. cited therein.
26. J. Huang, E.D. Stevens, S.P. Nolan, and J.L. Petersen. J. Am. Chem. Soc. **121**, 2674 (1999).
27. T. Weskamp, W.C. Schattenmann, M. Spiegler, and W.A. Herrmann. Angew. Chem. Int. Ed. Engl. **37**, 2490 (1998).
28. G. Sheldrick. SHELXL-96. University of Göttingen, Göttingen, Germany. 1996.

© 2001 NRC Canada

Formation and reactivity of the zirconium ethylene complexes [η^5-C_5H_3-1,3-($SiMe_2CH_2PR_2$)$_2$]Zr(η^2-CH_2=CH_2)(X) (R = Me, Pr^i; X = Br, C_5H_5)

Michael D. Fryzuk, Paul B. Duval, and Steven J. Rettig

Abstract: The formation and reactivity of the zirconium ethylene complexes ^{R}[P_2Cp]Zr(η^2-CH_2=CH_2)(X) (**2a**: R = Pr^i, X = Br; **2b**: R = Me, X = Br; **4a**: R = Pr^i, X = C_5H_5; ^{R}[P_2Cp] = (η^5-C_5H_3-1,3-($SiMe_2CH_2PR_2$)$_2$)) are described. Ethylene complexes **2a** and **2b** are prepared from a reaction of ^{R}[P_2Cp]ZrCl_3 (**1a**: R = Pr^i; **1b**: R = Me) with 2 equiv of EtMgBr, presumably via β-H elimination from the diethyl intermediate ^{R}[P_2Cp]ZrCl(CH_2CH_3)$_2$. The structure of **2b** was determined by X-ray crystallography. Addition of carbon monoxide to 16-electron **2** displaces the ethylene ligand to generate the carbonyl complex ^{R}[P_2Cp]Zr(CO)$_2$Br (**5a**: R = Pr^i; **5b**: R = Me), which is stable only under an atmosphere of CO. The corresponding CO reaction with 18-electron **4a** to give the metallocene monocarbonyl analogue ^{Pr}[P_2Cp]Zr(η^5-C_5H_5)(CO) (**6a**) is considerably slower. **2a** exhibits fluxional exchange of one carbonyl ligand with bulk ^{13}CO in solution; the kinetic parameters for this exchange process are $\Delta H^{\ddagger}$ = 9.2(5) kcal mol^{-1} and $\Delta S^{\ddagger}$ = –17(2) cal mol^{-1} K^{-1}. The addition of diphenylacetylene to **2a** yields the alkyne complex ^{Pr}[P_2Cp]Zr(η^2-PhCCPh)Br (**7a**), which exists in solution as two isomers in equilibrium. A solid-state X-ray structure determination for the minor isomer ***syn*-7a** was performed.

Key words: zirconium, cyclopentadienyl phosphine, alkyne, metallocyclopropane.

Résumé : On décrit la formation et la réactivité de complexes de l'éthylène zirconium ^{R}[P_2Cp]Zr(η^2-CH_2=CH_2)(X) (**2a** : R = *i*Pr, X = Br; **2b** : R = Me, X = Br; **4a** : R = *i*Pr, X = C_5H_5; ^{R}[P_2Cp] = (η^5-C_5H_3-1,3-($SiMe_2CH_2PR_2$)$_2$)). On a préparé les complexes **2a** et **2b** par réaction du ^{R}[P_2Cp]ZrCl_3 (**1a** : R = *i*Pr; **1b** : R = Me) avec deux équivalents de EtMgBr, probablement par le biais d'une élimination β d'hydrogène à partir de l'intermédiaire diéthylé ^{R}[P_2Cp]ZrCl(CH_2CH_3)$_2$. On a déterminé la structure du complexe **2b** par diffraction des rayons X. L'addition de monoxyde de carbone au complexe **2** à seize électrons conduit à un déplacement du ligand éthylène et à la formation du complexe carbonylé ^{R}[P_2Cp]Zr(CO)$_2$Br (**5a**: R = *i*Pr; **5b**: R = Me) qui n'est stable que sous une atmosphère de CO. La réaction correspondante du CO avec le complexe **4a** à dix-huit électrons, qui conduit à la formation du métallocène monocarbonylé analogue, ^{R}[P_2Cp]Zr(η^5-C_5H_5)(CO) (**6a**) est beaucoup plus lente. Le complexe **2a** donne lieu à un échange fluxionnel d'un ligand carbonyle avec le ^{13}CO qui se trouve dans l'ensemble de la solution; les paramètres cinétiques pour ce processus d'échange sont $\Delta H^{\ddagger}$. = 9,2(5) kcal mol^{-1} et $\Delta S^{\ddagger}$ = –17,2 cal mol^{-1} K^{-1}. L'addition de diphénylacétylène au complexe **2a** conduit à la formation de ^{R}[P_2Cp]Zr(η^2-PhCCPh)Br (**7a**) qui, en solution, existe sous la forme de deux isomères à l'équilibre. Faisant appel à la diffraction des rayons X, on a effectué une détermination de la structure en phase solide de l'isomère mineur, le ***syn*-7a**.

Mots clés : zirconium, cyclopentadiényl phosphine, alcyne, métallocyclopropane.

[Traduit par la Rédaction]

Introduction

The coordination of ethylene to transition metal centers is one of the foundations of organometallic chemistry (1) and dates back to the synthesis of Zeise's salt (K[Pt(η^2-CH_2=CH_2)Cl_3]) in 1827. Currently, the chemistry of metal-alkene complexes encompasses numerous important catalytic industrial processes, such as alkene polymerization using Ziegler–Natta catalysts, olefin metathesis (2, 3) (which includes both ring-opening (4) and ring-closing (5) metathesis type processes), alkene hydrogenation (6), and the Wacker process (7). In addition, there is continued interest in the bonding aspects of the metal-alkene interaction (8), which has been the focus of theoretical studies (9).

Received September 5, 2000. Published on the NRC Research Press Web site at http://canjchem.nrc.ca on May 23, 2001.

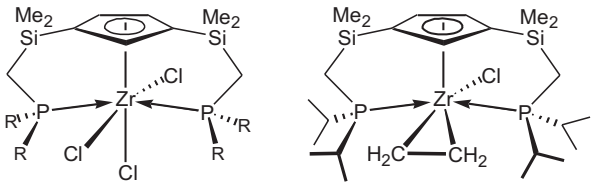
Dedicated to Professor B. R. James, in recognition of his distinguished contributions to homogeneous catalysis, on the occasion of his 65th birthday.

M.D. Fryzuk[1], P.B. Duval, and S.J. Rettig.[2] Department of Chemistry, University of British Columbia, 2036 Main Mall, Vancouver, BC V6T 1Z1, Canada.

[1]Corresponding author (e-mail: fryzuk@chem.ubc.ca).
[2]Deceased.

 DOI: 10.1139/cjc-79-5/6-536 © 2001 NRC Canada

We have been examining the reactivity of zirconium complexes stabilized by the hybrid donor ancillary ligand η^5-C_5H_3-($SiMe_2CH_2PR_2$)$_2$ (^{R}[P_2Cp], R = Pr^i, Me). Deployment of bulky isopropyl substituents on the side-arm phosphines has enabled the isolation of Zr(IV) alkylidene complexes, ^{Pr}[P_2Cp]Zr=CHR(Cl), (10, 11) from which reaction with ethylene yields the ethylene adduct ^{Pr}[P_2Cp]Zr(η^2-CH_2=CH_2)Cl (**2c**) (11). An interest in studying the reactivity of this product as a probe into the nature of the metal-alkene bonding in this formally Zr(II) species led to a more direct synthetic route from the starting chloride ^{Pr}[P_2Cp]$ZrCl_3$ (**1a**). One advantage of this alternate preparation is the ability to obtain the analogous but less bulky ^{Me}[P_2Cp]Zr ethylene derivative (^{Me}[P_2Cp]Zr(η^2-CH_2=CH_2)Br (**2b**)) directly from ^{Me}[P_2Cp]$ZrCl_3$ (**1b**).



1a R = Pr^i
1b R = Me

2c

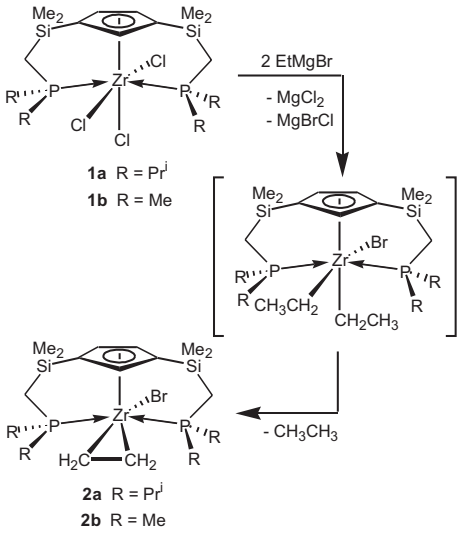
Although zirconium–alkene complexes are proposed as intermediates in several important synthetic transformations, (12, 13) the number of characterizable species has been restricted to a few metallocene-type systems, (14–17) the majority of which are isolated by the use of a trapping donor (typically a phosphine) to stabilize these complexes. The ethylene derivatives introduced in this report expand this sample to include 16-electron mono(cyclopentadienyl) complexes and a related 18-electron metallocene analogue; in addition, some substitution studies are included.

Preparation of ^{R}[P_2Cp]Zr(η^2-CH_2=CH_2)Br (R = Pr^i, Me)

A toluene solution of the starting Zr(IV) trichloride **1** reacts with 2 equiv of EtMgBr at –78°C to give a bright yellow solution, which upon warming to room temperature produces the ethylene complex ^{R}[P_2Cp]Zr(η^2-CH_2=CH_2)Br (**2a**: R = Pr^i; **2b**: R = Me) in excellent yield, either as dark purple (**2a**) or dark red (**2b**) crystals (Scheme 1). The yellow precursor is presumed to be the diethyl species ^{R}[P_2Cp]$ZrBr(CH_2CH_3)_2$, although no direct proof of its existence was obtained. The putative reaction sequence is completed by a β-H abstraction reaction with the elimination of ethane to generate the ethylene product. A quantitative halide exchange incorporates a bromide ligand in the final product, based on elemental analyses and an X-ray structural determination for **2b** (see below).

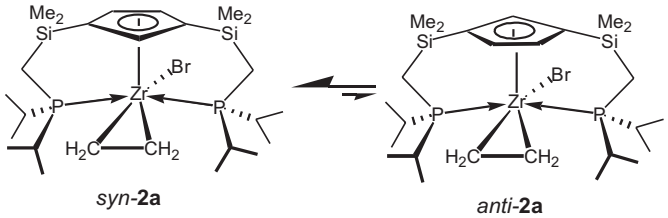
The ^{1}H and ^{31}P NMR spectra of purple **2a** are nearly identical to that of the crystallographically characterized chloro derivative ^{Pr}[P_2Cp]Zr(η^2-CH_2=CH_2)Cl (**2c**), a red product formed from the reaction of either alkylidene complex ^{Pr}[P_2Cp]Zr=CHR(Cl) (R = Ph, $SiMe_3$) with ethylene (18). As with **2c**, the NMR spectra for **2a** show the presence of two species in a 9:1 ratio assigned as *syn* (major) and *anti* (minor) isomers, designated according to the orientation of the ethylene ligand as being directed either *syn* or *anti* with respect to the unique carbon of the cyclopentadienyl (Cp) ring, as shown below (eq. [1]). Each isomer of **2a** displays a separate singlet in the ^{31}P NMR spectrum and corresponding resonances in the ^{1}H NMR spectrum.

Scheme 1.



1a R = Pr^i
1b R = Me

2a R = Pr^i
2b R = Me



syn-**2a** *anti*-**2a**

The ethylene protons give rise to a complex multiplet centred near 1.0 ppm in the ^{1}H NMR spectrum, originating from an AA′BB′XX′ spin system due to additional $^3J_{PH}$ coupling from the side-arm phosphines. The upfield location of these resonances in the ^{1}H NMR spectrum is indicative of an ethylene fragment coordinated to Zr. As with **2c**, definitive assignment of stereochemistry was unfortunately not possible (via ^{1}H NMR NOEDIFF experiments, for example) and so our designation of *syn* or *anti* is presumed.

In contrast to **2a**, only a single species is seen in solution for the ^{Me}[P_2Cp] derivative **2b**; we speculate that the reduced steric hindrance from the smaller methyl substituents at phosphorus reduces the tendency for phosphine dissociation which in turn discourages a *syn*/*anti* exchange process in this complex. The solid-state molecular structure of **2b** is shown in Fig. 1, along with the atom numbering scheme. A summary of the crystallographic data is given in Table 1; selected bond distances and bond angles are listed in Table 2. The structure reveals that the ethylene unit is coordinated parallel to the Cp ring and oriented *syn* to the unique Cp carbon atom C(2), precisely as found for the solid state structure for **2c** (18). Presumably, this orientation reduces steric interactions between the bound ethylene molecule and the Cp ring; moreover, it situates the ethylene π*-orbital to overlap favorably with the filled metal d_{xy} orbital (in this

© 2001 NRC Canada

Table 1. Crystallographic data.

Compound	**2b**[a]	***syn*-7a**[b]
Formula	$C_{25}H_{51}ClP_2Si_2Zr$	$C_{31}H_{53}ClOP_2Si_2Zr$
Fw	596.48	686.55
Crystal system	Triclinic	Monoclinic
Space group	*P*-1 (no. 2)	$P2_1/c$ (no. 14)
a (Å)	15.432(3)	8.666(1)
b (Å)	20.483(3)	24.244(1)
c (Å)	20.995(7)	17.543(1)
α (deg)	76.50(3)	90
β (deg)	83.12(7)	100.936(8)
γ (deg)	88.52(4)	90
V (Å^3)	6407(3)	3618.9(6)
Z	8	4
D_{calc} (g cm^{-3})	1.24	1.260
F(000)	2528	1448
μ (cm^{-1})	6.0	5.53
Crystal size (mm)	0.30 × 0.40 × 0.45	0.25 × 0.35 × 0.45
Transmission factors	0.903–1.00	0.96–1.00
Scan type	ω-2θ	ω-2θ
Scan range (deg in ω)		0.79 + 0.35 tan θ
Scan speed (deg min^{-1})		16 (up to 9 scans)
Data collected	±*h*, +*k*, ±*l*	
$2\theta_{max}$ (deg)	40	60
Crystal decay (%)		2.0
Total reflections	11 928	11 425
Unique reflections	11 917	10 783
R_{merge}	0.023	0.036
No. with $I \geq 3\sigma(I)$	7589	5598
No. of variables		344
R (F) ($I \geq 3\sigma(I)$)	0.055	0.034
R_w (F) ($I \geq 3\sigma(I)$)	0.060	0.031
R (F^2) (all data)	0.055	—
R_w (F^2) (all data)	0.060	—
Gof	3.71	1.49
Max Δ/σ (final cycle)	0.000	0.003
Residual density (e Å^{-3})	–0.550 to 0.640	–0.35 to 0.31

[a]Temperature 294 K, Nonius CAD-4 diffractometer, Mo K_α radiation (λ = 0.70930 Å), graphite monochromator, takeoff angle 6.0°, aperture 6.0 × 6.0 mm at a distance of 285 mm from the crystal, stationary background counts at each end of the scan (scan:background time ratio, 2:1), $\sigma^2(F^2) = [S^2(C + 4B)]/Lp^2$ (S = scan rate, C = scan count, B = normalized background count), function minimized $\Sigma w(|F_o| - |F_c|)^2$ where $w = 4F_o^2/\sigma^2(F_o^2)$, R (F) = $\Sigma||F_o| - |F_c||/\Sigma|F_o|$, R_w (F) = $(\Sigma w(|F_o| - |F_c|)^2/\Sigma w|F_o|^2)^{1/2}$, and Gof ($F$) = $[\Sigma w(|F_o| - |F_c|)^2/(m - n)]^{1/2}$.

[b]Temperature 294 K, Rigaku AFC6S diffractometer, Mo K_α radiation (λ = 0.71069 Å), graphite monochromator, takeoff angle 6.0°, aperture 6.0 × 6.0 mm at a distance of 285 mm from the crystal, stationary background counts at each end of the scan (scan:background time ratio, 2:1), $\sigma^2(F^2) = [S^2(C + 4B)]/Lp^2$ (S = scan rate, C = scan count, B = normalized background count), function minimized $\Sigma w(|F_o| - |F_c|)^2$ where $w = 4F_o^2/\sigma^2(F_o^2)$, R (F) = $\Sigma||F_o| - |F_c||/\Sigma|F_o|$, R_w (F) = $(\Sigma w(|F_o| - |F_c|)^2/\Sigma w|F_o|^2)^{1/2}$, and Gof ($F$) = $[\Sigma w(|F_o| - |F_c|)^2/(m - n)]^{1/2}$.

representation the *z*-axis passes through the Cp-centroid). Previous investigations into bonding interactions in electron-rich complexes with piano-stool geometries suggest that the metal d_{xy} orbital offers the best electron donation to a π-acceptor ligand (19, 20). The C(16)—C(17) bond distance of 1.431(6) Å in **2b** is comparable to the corresponding value of 1.433(17) Å for **2c**, which illustrates that the degree of

Fig. 1 Molecular structure of $^{Me}[P_2Cp]Zr(\eta^2\text{-}CH_2{=}CH_2)Br$ (**2b**); 33% probability thermal ellipsoids are shown. Hydrogen atoms are omitted for clarity.

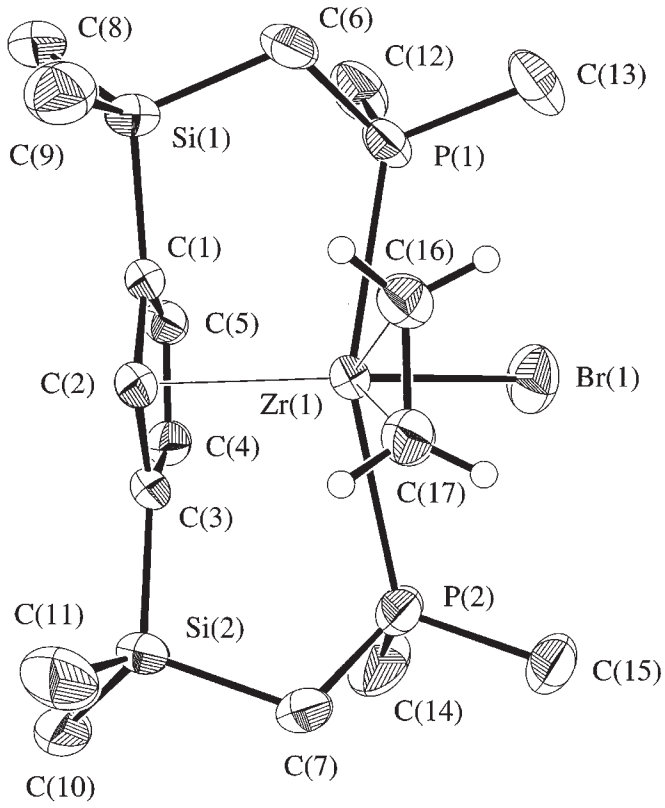


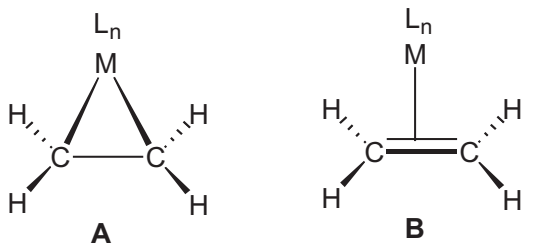
Table 2. Selected bond lengths (Å) and bond angles (°) for $^{Me}[P_2Cp]Zr(\eta^2\text{-}CH_2{=}CH_2)Br$ (**2b**).

Bond lengths (Å)		Bond angles (°)	
Zr(1)—Br(1)	2.6744(6)	Br(1)-Zr(1)-P(1)	78.28(3)
Zr(1)—P(1)	2.730(1)	Br(1)-Zr(1)-P(2)	76.94(3)
Zr(1)—P(2)	2.703(1)	Br(1)-Zr(1)-C(16)	109.7(1)
Zr(1)—C(16)	2.293(5)	Br(1)-Zr(1)-C(17)	109.7(1)
Zr(1)—C(17)	2.312(5)	P(1)-Zr(1)-P(2)	155.17(4)
Zr(1)—Cp′	2.23	P(1)-Zr(1)-C(16)	75.6(1)
C(16)—C(17)	1.431(6)	P(1)-Zr(1)-C(17)	111.0(1)
		C(16)-Zr(1)-C(17)	36.2(2)

backbonding is not significantly altered upon substituting either the halide (Br for Cl) or the groups attached to the phosphines (methyl for isopropyl). However, the phosphines are bound considerably closer to the metal in **2b**, with Zr—P bond distances averaging 2.72 Å in comparison to 2.86 Å for **2c**. The C—C bond distance of the ethylene ligand is similar in these complexes to that found for other monomeric Zr(II) ethylene complexes (14, 16, 21). The lengthening of this bond compared to 1.337 Å found in free ethylene (22) is indicative of significant back-bonding from the metal as represented in the Dewar–Chatt–Duncanson model (23, 24) and supports a Zr(IV) metallacyclopropane bonding depiction (**A**). Also consistent with this formalism are the short Zr—C bond lengths (average 2.30 Å) in **2b**, which are within the range of typical Zr—C single bonds

© 2001 NRC Canada

(12) and considerably shorter than the Zr—C distance of 2.68 (2) in a cationic Zr(IV) olefin complex in which *d*-π* back-bonding is unavailable (25).



By NMR spectroscopy, only one isomer is seen for **2b** in solution, thus it is assumed that it corresponds to the *syn* structure observed in the solid state. The similarities between the ^{1}H NMR spectrum of the major isomer of **2a** with that of the single species seen for **2b**, particularly in the distinctive Cp region, suggests that the major isomer of **2a** is the *syn* isomer as well.

The formation of the ethylene complexes **2a** and **2b** directly from the respective starting trichlorides offers a facile alternative to the multistep approach to **2c** (i.e., via an alkylidene complex) (18). This general synthetic route has been employed elsewhere to obtain a number of early metal alkene complexes (15). Unfortunately, this procedure could not be extended to other Zr alkene complexes with this system. For example, propylene complexes could not be isolated by using Grignard reagents such as Pr^{n}MgBr or Pr^{i}MgCl, nor was Bu^{n}Li effective in obtaining a coordinated butene species. All of these attempts resulted in complete consumption of the starting materials, but no isolable alkene complexes were forthcoming; this is reminiscent of the reactions of substituted alkenes with the related alkylidene complexes (18). The apparent instability of these complexes incorporating higher alkenes may be due to a combination of greater steric hindrance from the bulky ancillary ligand along with weaker bonding of these alkenes relative to ethylene.

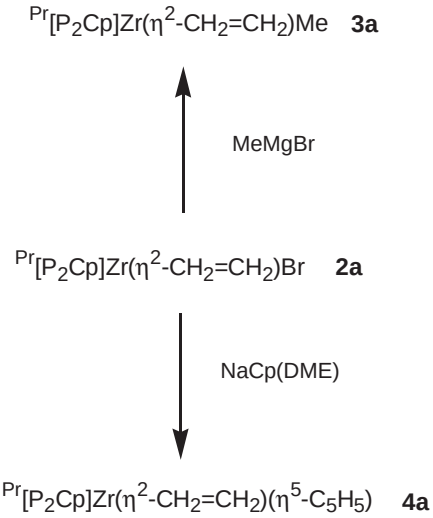
Preparation of ^{Pr}[P$_2$Cp]Zr(η^2-CH$_2$=CH$_2$)R′ (R′ = Me, C$_5$H$_5$)

In an attempt to expand the scope of ethylene complexes for which reactivity studies could be compared, we examined the preparation of alkyl-ethylene derivatives by standard metathesis reactions involving the bromide ligand (Scheme 2).

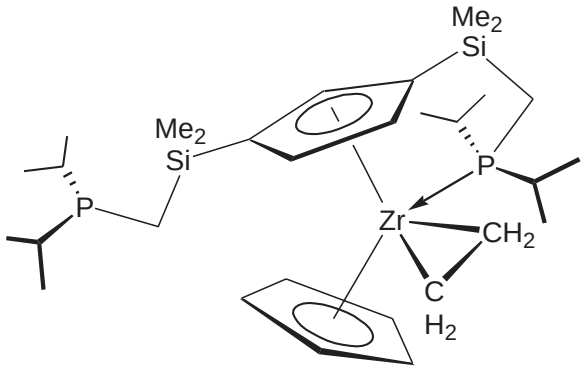
The characteristic spectroscopic feature of the methyl derivative **3a** is the triplet ($^3J_{PH}$ = 10 Hz) at –0.67 ppm in the ^{1}H NMR spectrum for the methyl group attached to Zr. The distinctive Cp region of this spectrum is nearly identical to that of the major *syn* isomer of **2**, suggesting that the solution structure of **3a** (only one species is seen) is exclusively the *syn* isomer. Unfortunately this complex was only characterized in solution as it could not be isolated as a solid, despite many attempts; decomposition with the elimination of ethylene to give unidentified products was observed.

The Cp derivative **4a** could be isolated as reddish-orange crystals. There are two equal intensity singlets in the ^{31}P NMR spectrum for **4a** at –5.3 ppm and 42.3 ppm; the peak

Scheme 2.



at –5.3 ppm for this ligand system is indicative of an uncoordinated phosphine, while the other resonance at 42.3 corresponds to a bound phosphine donor. The ^{1}H NMR spectrum shows a doublet ($^3J_{PH}$ = 2 Hz) at 5.20 ppm for the five protons of the C_5H_5 ring; the downfield chemical shift suggests that this ligand is coordinated in an η^5-mode. As the array of ligands in this complex is similar to that found in the structurally characterized metallocene derivative Cp$_2$Zr(η^2-CH$_2$=CH$_2$)(PMe$_3$), (14, 21) it is reasonable to consider an analogous structure for **4a** as shown below.



4a

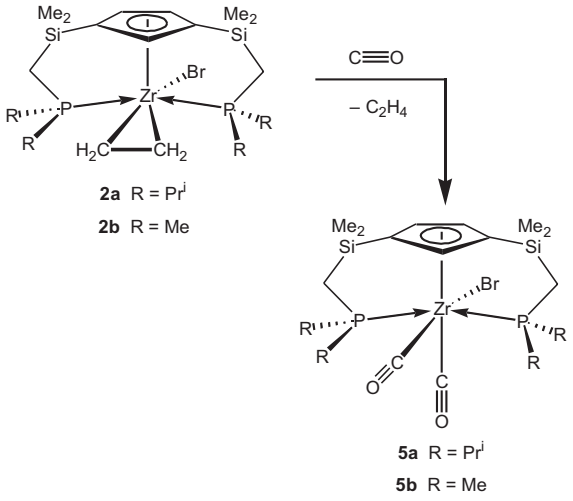
The asymmetric geometry renders all four ethylene protons inequivalent, thus generating a complicated second order splitting pattern in the ^{1}H NMR spectrum (with additional coupling to the coordinated phosphine). This asymmetry is also evident from the three separate resonances observed for the cyclopentadienyl portion of the P$_2$Cp ancillary ligand. The presence of only one coordinated phosphine in **4a** supports the view of the C_5H_5 ligand as η^5-bound; the steric and electronic saturation provided by this coordination mode yields an 18-electron species which would force one side-arm to remain dangling, as observed. The ethylene unit and the coordinated phosphine thus can be

© 2001 NRC Canada

considered to be occupying the metallocene wedge, with the other side-arm left out of the coordination sphere.

Ligand substitution reactions with CO

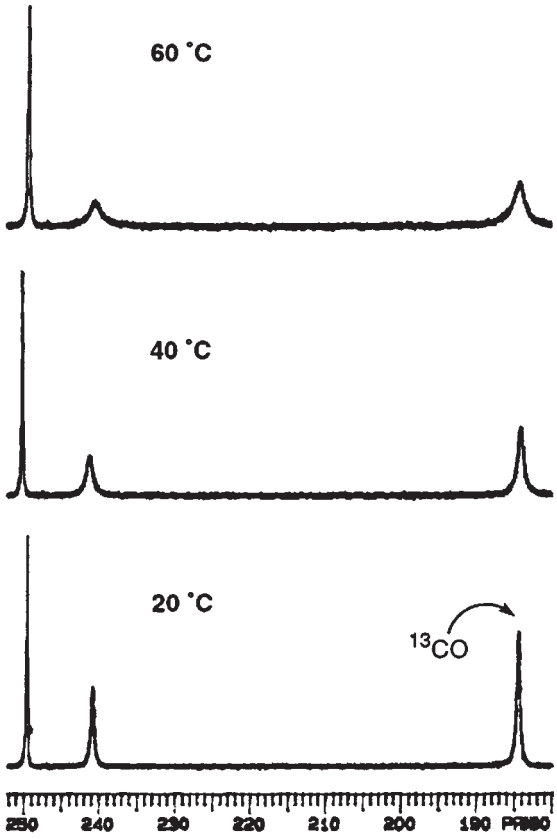
A purple toluene solution of the ethylene complex **2a** reacts instantly under an atmosphere of CO to generate a dark greenish-orange solution that shows a single resonance in the ^{31}P NMR spectrum at 29.1 ppm. In the ^{1}H NMR spectrum the only resonances observed are attributed to the ancillary ligand, and a sealed NMR tube reaction reveals a singlet at 5.25 ppm for the evolution of free ethylene. A similar result is obtained in the reaction with **2b**. Therefore, it is apparent in both instances that the coordinated ethylene unit has been replaced by CO in a ligand substitution reaction to give a carbonyl complex (eq. [2]).



For the reaction of **2a** with ^{13}CO the downfield region of the ^{13}C NMR spectrum displays two carbonyl peaks at 241 and 249 ppm for **5a** in addition to a third resonance at 184 ppm for excess free ^{13}CO, indicating that an 18-electron dicarbonyl species has been formed from the 16-electron precursor. In **5b** the carbonyl resonances are located at 240 and 245 ppm, respectively. These complexes have a ligand arrangement that is similar to known derivatives such as $CpZr(CO)_2(dmpe)Cl$ (26). The presence of a carbonyl ligand is supported by absorptions in the IR spectra at 1890 and 1898 cm^{-1} for **5a** and **5b**, respectively, which shift to 1865 and 1855 cm^{-1} for the ^{13}C labeled isotopomers. The low ν_{CO} values of the coordinated carbonyl ligands in comparison to free CO (ν_{CO} = 2143 cm^{-1}) are due to strong back-bonding from the electron-rich Zr(II) centre to the π^* orbital of the CO ligand and is consistent with the stretching frequency in analogous Zr(II) carbonyls (i.e., $CpZr(CO)_2(dmpe)Cl$, ν_{CO} = 1940 cm^{-1}) (26). Unfortunately, although both carbonyl complexes **5a** and **5b** are stable indefinitely in solution in the presence of excess CO, attempts to isolate these species in the absence of CO led to decomposition. This instability outside of a protective CO atmosphere has been noted with other Zr carbonyl derivatives (26–28), demonstrating the labile nature of these ligands with early metals.

A notable feature of the ambient temperature ^{13}C NMR spectrum of **5a** is that the peak for free CO at 184 ppm is broadened, as is the carbonyl peak at 241 ppm. This observation suggests that this CO ligand is undergoing an exchange process with free CO in solution; the remaining ligand is either not involved in this process or is at the slow exchange limit at this temperature, since the peak for this ligand at 249 ppm is quite sharp in comparison. This exchange process was monitored by variable temperature ^{13}C NMR spectroscopy and a selection of the spectra are shown in Fig. 2; these spectra demonstrate an increase in line broadening as the temperature is raised, in agreement with an increase in the exchange rate between free CO and the exchanging carbonyl ligand.

Fig. 2 Variable temperature ^{13}C NMR spectra of $^{Pr}[P_2Cp]Zr(CO)_2Br$ (**5a**).

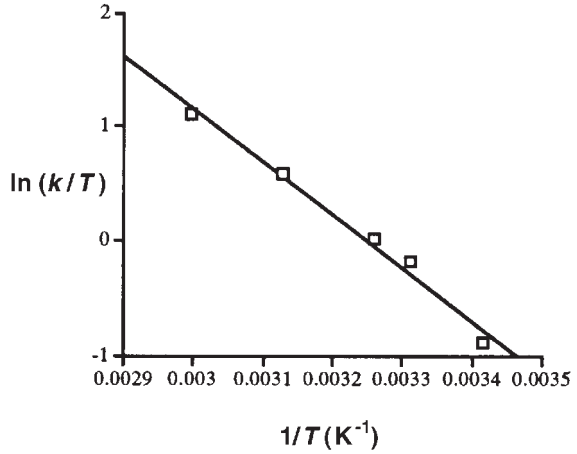


The NMR spectra were simulated (using DNMR-5)® to obtain rate constants at each temperature, which were used in the resulting Eyring plot shown in Fig. 3. The kinetic parameters $\Delta H^{\ddagger}$ = 9.2(5) kcal mol^{-1} and $\Delta S^{\ddagger}$ = –17(2) cal mol^{-1} K^{-1} were calculated from this plot. The negative entropy term is unexpected, as ligand exchange from this saturated 18-electron species is anticipated to proceed in a dissociative mechanism that should produce a positive entropy term for a less ordered transition state. A concerted mechanism involving dissociation of a pendant phosphine may therefore be a factor in this exchange. An associative process has also been suggested from a separate kinetic study into similar CO ligand exchange in other 18-electron Zr carbonyl species (27, 28).

Ligand exchange is common for early metal carbonyl complexes. In the related complex $Cp^*Hf(CO)_2(dmpe)Cl$ (28) both CO ligands are observed to rapidly and quantitatively exchange with excess ^{13}CO. One can speculate as to

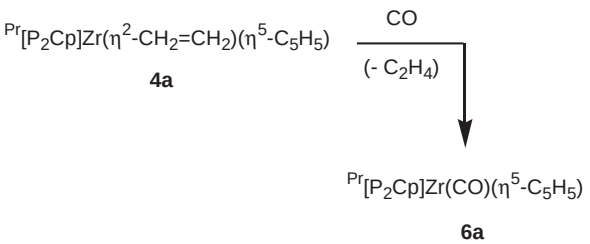
© 2001 NRC Canada

Fig. 3 Eyring plot for the CO ligand exchange process in $^{Pr}[P_2Cp]Zr(CO)_2Br$ (**5a**).

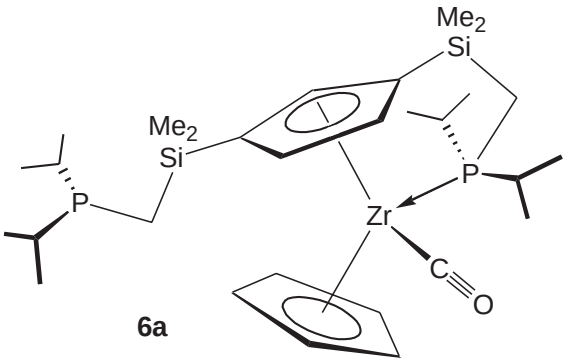


why only one carbonyl ligand in **5a** undergoes this exchange. If we assume that the quasioctahedral geometry shown in eq. [2] holds here, then for such mono(cyclopentadienyl) type complexes the ligand located *trans* to the Cp donor is typically weakly bound, (29) with labile coordination observed in some instances (30). Thus for **5a**, it is the carbonyl ligand located at this labile site that undergoes exchange while the other *trans* to the bromide remains unaffected. To rationalize this observation, one can invoke two complementary effects: first, the strong labilizing trans effect of the Cp donor contrasts with the weak trans effect of the electron withdrawing bromide, and second, and as noted for **2b**, backbonding from the zirconium in monocyclopentadienyl complexes is optimized by the d_{xy} orbital (and to a lesser extent the d_z2 orbital), which is well suited to stabilize the carbonyl *trans* to the bromide but of negligible use for the other carbonyl ligand *trans* to the Cp group.

The reactivity of the 18-electron ethylene complex **4a** with CO was examined to compare with the results observed for the 16-electron analogue **2a**. As opposed to **2a**, which coordinates CO almost instantly, the reaction of **4a** with CO is considerably slower, requiring more than two weeks for completion under the same reaction conditions (eq. [3]). This remarkable difference in reaction times can be traced to the electronic saturation in **4a**, adding further evidence that the C_5H_5 donor in this complex is η^5-coordinated. As a result, in lieu of a 20-electron intermediate in this reaction, either a ligand must dissociate or alternatively the Cp ring must undergo η^5-η^3 ring slippage, prior to the coordination of a CO molecule.



The eventual product from the above reaction is the carbonyl species $^{Pr}[P_2Cp]Zr(CO)(\eta^5\text{-}C_5H_5)$ (**6a**), which is accompanied by the evolution of free ethylene as observed with the analogous reaction that forms carbonyl **5**. The ^{31}P NMR spectrum of **6a** is similar to that of the precursor **4a**, with one singlet at 58.7 ppm and another at –4.8 ppm. In the ^1H NMR spectrum only resonances attributed to the ancillary ligand and the Cp ligand are evident. The presence of the carbonyl ligand is indicated in the ^{13}C NMR spectrum by a single downfield resonance at 308 ppm ($^2J_{PC}$ = 2 Hz) in the reaction of **4a** with ^{13}CO. As an analogue of the 18-electron metallocene carbonyl species $Cp_2Zr(CO)(PMe_3)$ (31), the proposed structure of **6a** is depicted as shown below.



6a

In contrast to **5a**, the line width of the carbonyl peak for **6a** is very narrow, with no evidence for exchange with the narrow peak at 184 ppm due to excess ^{13}CO. The difference in the respective lability of the carbonyl ligands in **5a** vs. **6a** may originate from the presence of one less CO ligand in **6a**, which is not in competition for backbonding and hence is less labile. The contrasting rapid CO exchange observed for the similar metallocene analogue $Cp_2Zr(CO)_2$ (27) is in accord with this view, where two carbonyl ligands are in competition for backbonding from the same filled donor orbital (32).

Preparation of $^{Pr}[P_2Cp]Zr(\eta^2\text{-PhCCPh})Br$

Given the facile ligand substitution reaction observed for the ethylene derivatives **2a** and **2b** with CO, and the observed tendency for early metal alkene complexes to undergo substitution reactions with alkynes, (33, 34) the reaction with diphenylacetylene was examined with this system. A toluene solution of ethylene **2a** reacts with 1 equiv of diphenylacetylene (PhCCPh) under ambient conditions to displace the ethylene ligand and generate the alkyne complex $^{Pr}[P_2Cp]Zr(\eta^2\text{-PhCCPh})Br$ (**7a**), which can be isolated as pale yellow crystals (Scheme 3). In contrast to the immediate displacement of ethylene by CO to give carbonyl **5a**, the corresponding ligand substitution reaction of **2a** with diphenylacetylene is slower, requiring 24 h for completion. This observation is consistent with steric factors inducing a slower rate for the bulky alkyne in comparison to the small linear CO molecule, and points to a probable requirement that a phosphine must dissociate to allow room for the incoming alkyne.

In solution alkyne **7a** exists as two isomers in a 3:2 ratio, based on the ^1H and ^{31}P NMR spectra. There are two singlets in the ^{31}P NMR spectrum, one each for the major (8.5 ppm) and minor isomer (11.6 ppm), respectively, and a

© 2001 NRC Canada

Scheme 3.

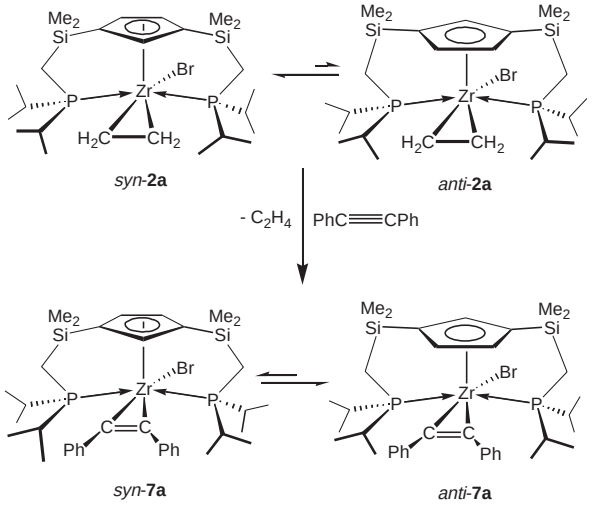


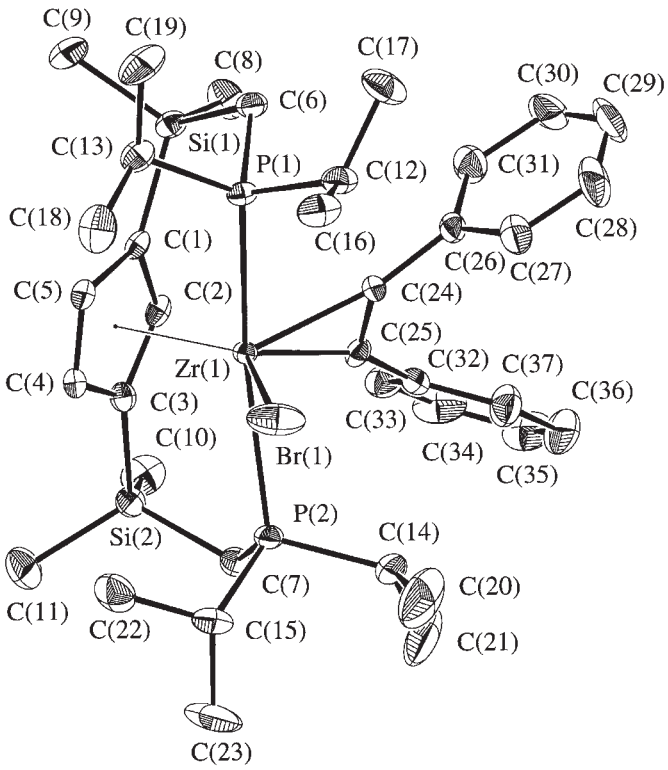
Table 3. Selected bond lengths (Å) and bond angles (°) for $^{Pr}[P_2Cp]Zr(\eta^2\text{-PhCCPh})Br$ (***syn*-7a**).

Bond lengths (Å)		Bond angles (°)	
Zr(1)—Br(1)	2.6771(5)	Br(1)-Zr(1)-P(1)	78.61(2)
Zr(1)—P(1)	2.8367(8)	Br(1)-Zr(1)-P(2)	76.35(2)
Zr(1)—P(2)	2.8129(8)	Br(1)-Zr(1)-C(24)	102.85(8)
Zr(1)—C(24)	2.197(3)	Br(1)-Zr(1)-C(25)	116.88(8)
Zr(1)—C(25)	2.182(2)	P(1)-Zr(1)-P(2)	154.87(4)
Zr(1)—Cp′	2.264	P(1)-Zr(1)-C(24)	77.57(7)
C(24)—C(25)	1.322(6)	Zr(1)-C(24)-C(26)	111.0(1)
C(24)—C(26)	1.471(4)	C(25)-C(24)-C(26)	126.8(2)

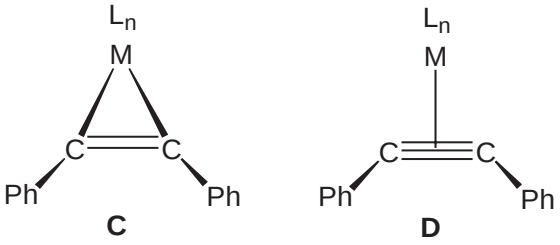
corresponding set of resonances in the ^{1}H NMR spectrum for each species. As found with other complexes having this ancillary ligand system (18) and observed for **2a**, the two species seen for **7a** are likely the *syn* and *anti* stereoisomers. A variable temperature NMR study indicates that these isomers interconvert, as evidenced by increased line broadening in both peaks in the ^{31}P NMR spectrum as the temperature is raised. Curiously, a change in the equilibrium ratio of these species was not detected from this experiment. A ^{1}H NOEDIFF NMR experiment was performed, from which it was determined that the *anti* isomer is the major species in solution. Irradiation of the resonance assigned to the two equivalent protons in the Cp ring of the major isomer showed an enhancement of the signals for the ortho protons of the phenyl ring; no effect was detected when the unique Cp proton resonance was irradiated.

The molecular structure of alkyne **7a** was determined by an X-ray crystal structure analysis and is shown in Fig. 4. Selected bond lengths and bond angles are listed in Table 3. The solid-state structure corresponds to the minor *syn* isomer, with the alkyne coordinated parallel to the Cp ring as found for the ethylene ligand in **2b**. However, in ***syn*-7a** the alkyne unit is tilted from this parallel orientation by approximately 9°. The short Zr(1)—C(24) and Zr(1)—C(25) bond lengths of 2.20 Å and 2.18 Å, respectively, are indicative of strong back-bonding from the metal. This is also reflected in the C(25)-C(24)-C(26) bond angle of 127° that illustrates the

Fig. 4 Molecular structure of $^{Pr}[P_2Cp]Zr(\eta^2\text{-PhCCPh})Br$ (***syn*-7a**); 33% probability thermal ellipsoids are shown. Hydrogen atoms are omitted for clarity.



degree to which the phenyl rings are pulled back from the metal as a result of this back-donation. This geometry of the coordinated alkyne resembles that of a metallacyclopropene **C**, rather than a simple π-bound alkyne as shown in **D** (6). The double bond character of the coordinated alkyne is indicated by the C(24)—C(25) bond distance of 1.322(6) Å. These structural parameters are similar to those of the structurally characterized Zr alkyne complex $Cp_2Zr(\eta^2\text{-PhCCPh})(PMe_3)$ (34).



A comparison of the bonding in ***syn*-7a** with that of the ethylene complex **2b** shows in each case that back-bonding from the metal induces lengthening of the coordinated C—C bond (compared to the free substrate). In addition, alkynes have a second π-orbital that can overlap with a metal *d* orbital of suitable symmetry to form a π-bond, such that this ligand can potentially be represented as a four-electron donor. However, in **7a** this interaction is in competition with one of the π-donor orbitals from the Cp ring, which diminishes the ability of the alkyne to donate electron density from this second π-orbital. But the observation that alkyne

© 2001 NRC Canada

7a is unreactive in the presence of CO is in direct contrast to the rapid reaction seen for ethylene **2a**, which otherwise has the same ligand coordination sphere. Assuming that steric considerations are minimal for a small nucleophile such as CO, this difference in reaction times suggests that the alkyne complex **7a** is a fully saturated 18-electron species, implying that there is at least some component present to the additional π-bond from the alkyne to the metal centre.

Experimental section

General considerations

Unless otherwise stated all manipulations were performed under an atmosphere of prepurified nitrogen in a Vacuum Atmospheres HE-553–2 glove box equipped with a MO-40–2H purification system or in standard Schlenk-type glassware on a dual vacuum–nitrogen line. Reactions involving gaseous reagents were conducted in Pyrex vessels (bombs) designed to withstand pressures up to 10 atm (1 atm = 101.325 kPa). ^{1}H NMR spectra (referenced to either C_6D_5H or $C_6D_5CD_2H$ for benzene and toluene, respectively) were performed on one of the following instruments depending on the complexity of the particular spectrum: Bruker WH-200, Varian XL-300, or a Bruker AM-500. ^{13}C NMR spectra (referenced to solvent peaks) were run at 50.323 MHz on the Bruker WH-200 or at 75.429 MHz on the XL-300 instrument, and ^{31}P NMR spectra (referenced to external $P(OMe)_3$ at 141.0 ppm) were run at 121.421 MHz and 202.33 MHz, on the XL-300 and Bruker AM-500 instruments, respectively. All chemical shifts are reported in ppm and all coupling constants are reported in Hz. Infrared spectra were recorded on a BOMEM MB-100 spectrometer. Solution samples were recorded on a 0.1 mm KBr cell and solid samples were recorded as pellets. Elemental analyses (Mr. P. Borda) and GC–MS were performed within this department.

Reagents

Ethylene and carbon monoxide were obtained as lecture bottles from Matheson and dried over P_2O_5 before use. Labeled ^{13}CO (Cambridge Isotopes) was used as received. Diphenylacetylene (Aldrich) was sublimed before use. MeMgBr (1.4 M solution in THF–toluene) and EtMgBr (3.0 M solution in ether) were purchased from Aldrich and used as received. NaCp(DME) (DME = dimethoxyethane) was prepared according to published literature procedure (35). Hexanes, tetrahydrofuran (THF), and toluene were predried over CaH_2 followed by distillation under argon from either sodium metal or sodium-benzophenone ketyl; pentane was distilled from sodium-benzophenone ketyl. The deuterated solvents C_6D_6 and $C_6D_5CD_3$ were dried over sodium, vacuum transferred to a bomb, and degassed by freeze–pump–haw technique before use. The procedures for the preparation of $^R[P_2Cp]ZrCl_3$ (**1a**: R = Pr^i (36); **1b**: R = Me[3]) have been described elsewhere.

*$^{Pr}[P_2Cp]Zr(\eta^2$-CH_2=$CH_2)Br$ (**2a**)*

A solution of 3.0 M EtMgBr (2.15 mL, 6.45 mmol) was diluted in 20 mL of toluene and added dropwise with stirring to a cooled (–78°C) solution of **1a** (2.06 g, 3.23 mmol) dissolved in 100 mL of toluene. The pale yellow colour of the solution turned to bright yellow upon addition. The mixture was stirred at –78°C for 1 h and allowed to slowly warm to room temperature, whereupon the colour of the solution gradually changed to a dark reddish purple. The volatiles were then removed under vacuum and the residue extracted with pentane and filtered. Dark purple crystals of **2a** were obtained from a cold (–40°C) concentrated pentane solution. Yield: 1.86 g (90%). ^{1}H NMR (20°C, C_6D_6) δ: 0.21 and 0.23 (s, 6H, $Si(CH_3)_2$), 0.82 and 0.85 (d, 2H, $^2J_{PH}$ = 8 Hz, $SiCH_2P$), 0.98 and 1.01 (m, 2H, $^3J_{PH}$ = 7 Hz, CH_2=CH_2), 1.08, 1.15, 1.26, and 1.31 (dd, 6H, $^2J_{HH}$ = 7 Hz, $^2J_{PH}$ = 7 Hz, $CH(CH_3)_2$), 2.23 and 2.35 (sept, 2H, $^3J_{HH}$ = 7 Hz, $CH(CH_3)_2$), 4.37 (t, 1H, $^4J_{HH}$ = 1 Hz, Cp-*H*), 6.31 (d, 2H, $^4J_{HH}$ = 2 Hz, Cp-*H*). ^{31}P NMR (20°C, C_6D_6) δ: 19.5 (s). Anal. calcd. for $C_{25}H_{51}BrP_2Si_2Zr$: C 46.85, H 8.02; found: C 46.89, H 8.06.

*$^{Me}[P_2Cp]Zr(\eta^2$-CH_2=$CH_2)Br$ (**2b**)*

A solution of 3.0 M EtMgBr (1.50 mL, 4.50 mmol) was diluted in 20 mL of toluene and added dropwise with stirring to a cooled (–78°C) solution of **1b** (1.19 g, 2.26 mmol) dissolved in 40 mL of toluene. The reaction mixture was allowed to warm to room temperature and stirred for 3 h, during which a dark reddish brown colour was generated. The solvent was removed and the residue extracted with hexanes and filtered. Reducing this solution to 5 mL permitted the isolation of dark red crystals at –40°C, which were washed with cold pentane and dried. Yield: 0.93 g (79%). ^{1}H NMR (20°C, C_6D_6) δ: 0.09 and 0.16 (s, 6H, $Si(CH_3)_2$), 0.84 and 1.15 (d, 2H, $^2J_{HH}$ = 12 Hz, $SiCH_2P$), 0.88 and 1.33 (d, 2H, $^3J_{PH}$ = 9 Hz, CH_2=CH_2), 1.24 and 1.27 (d, 6H, $^2J_{PH}$ = 7 Hz, $P(CH_3)_2$), 4.15 (t, 1H, $^4J_{HH}$ = 1 Hz, Cp-*H*), 6.02 (d, 2H, $^4J_{HH}$ = 1 Hz, Cp-*H*). ^{31}P NMR (20°C, C_6D_6) δ: 0.0 (s). Anal. calcd. for $C_{17}H_{35}BrP_2Si_2Zr$: C 38.62, H 6.67; found: C 38.54, H 6.74.

*$^{Pr}[P_2Cp]Zr(\eta^2$-CH_2=$CH_2)Me$ (**3a**)*

A solution of 1.4 M MeMgBr (0.75 mL, 1.05 mmol) was diluted in 10 mL of toluene and added dropwise with stirring to a cooled (–78°C) solution of **2a** (620 mg, 0.97 mmol) dissolved in 30 mL of toluene. The mixture was allowed to slowly warm to room temperature, during which the colour of the solution gradually changed from a deep purple to a dark reddish orange. The reaction mixture was stirred for another 24 h, the volatiles were then removed under vacuum and the residue extracted with hexanes and filtered. An impure pale pink solid was obtained by slow evaporation of the filtrate, which gradually decomposed with the evolution of free ethylene. ^{1}H NMR (20°C, C_6D_6) δ: –0.67 (t, 3H, $^3J_{PH}$ = 10 Hz, $ZrCH_3$), 0.24 and 0.26 (s, 6H, $Si(CH_3)_2$), 0.86 (m, 4H, $^2J_{PH}$ = 8 Hz, $SiCH_2P$), 1.05 (m, 2H, $^3J_{PH}$ = 8 Hz, $Zr(CH_2$=$CH_2)$), 1.10 (m, 24H, $CH(CH_3)_2$), 2.09 (sept, 4H, $^3J_{HH}$ = 7 Hz, $CH(CH_3)_2$), 4.61 (t, 1H, $^4J_{HH}$ = 2 Hz, Cp-*H*), 6.32 (d, 2H, $^4J_{HH}$ = 2 Hz, Cp-*H*). ^{31}P NMR (20°C, C_6D_6) δ: 20.1 (s).

*$^{Pr}[P_2Cp]Zr(\eta^2$-CH_2=$CH_2)(\eta^5$-$C_5H_5)$ (**4a**)*

A solution of NaCp(DME) (106 mg, 0.59 mmol) in 30 mL of toluene was added dropwise with stirring to a cooled (–78°C) solution of **2a** (410 mg, 0.59 mmol) dis-

[3] M.D. Fryzuk, P.B. Duval, V.J. Young, Jr., and G.P.A. Yap. Manuscript in preparation.

© 2001 NRC Canada

solved in 50 mL of toluene. The mixture was stirred at –78°C for 2 h, then allowed to slowly warm to room temperature and stirred for another 24 h The colour of the solution gradually changed from a deep purple to a orange-red. The volatiles were then removed under vacuum and the residue extracted with hexanes and filtered. Orange crystals were obtained from a cold (–40°C) concentrated hexamethyldisiloxane–hexanes mixture. The crystals were washed with cold hexamethyldisiloxane and dried. Yield: 310 mg (84%). ^{1}H NMR (20°C, C_6D_6) δ: 0.08, 0.13, 0.52 and 0.58 (s, 3H, Si(CH_3)$_2$), 0.42, 0.75, and 0.85 (ddt, 1H, $^3J_{HH}$ = 10 Hz (*cis* and *trans*), $^3J_{PH}$ = 6 Hz, CH*H*=CH$_2$), 0.74 and 0.81 (dd, 2H, $^2J_{HH}$ = 15 Hz, $^2J_{PH}$ = 4 Hz, SiCH_2P), 0.94, 1.00, 1.02, 1.03, 1.04, 1.05, 1.05, and 1.13 (dd, 3H, $^3J_{HH}$ = 7 Hz, $^3J_{PH}$ = 7 Hz, CH(CH_3)$_2$), 1.59 and 1.60 (sept, 1H, $^3J_{HH}$ = 7 Hz, C*H*(CH$_3$)$_2$), 1.74 (d of sept, 1H, $^3J_{HH}$ = 7 Hz, $^2J_{PH}$ = 3 Hz, C*H*(CH$_3$)$_2$), 1.98 (d of sept, 1H, $^3J_{HH}$ = 7 Hz, $^2J_{PH}$ = 7 Hz, C*H*(CH$_3$)$_2$), 5.21 (t, 1H, $^4J_{HH}$ = 2 Hz, Cp-*H*), 5.35, (s, 5H, $^3J_{PH}$ = 1 Hz, C$_5H_5$), 5.61 and 5.62 (dd, 1H, $^3J_{HH}$ = 6 Hz, $^4J_{HH}$ = 2 Hz, Cp-*H*). ^{31}P NMR (20°C, C_6D_6) δ: –5.3 (s), 42.3 (s). Anal. calcd. for $C_{30}H_{56}P_2Si_2Zr$: C 57.55, H 9.01; found: C 57.25, H 9.15.

^{Pr}[P_2Cp]Zr(CO)$_2$Br (**5a**)

A benzene-d_6 solution of **2a** was placed in a sealable NMR tube and affixed to a dual vacuum–nitrogen line. A small portion of solvent was removed under vacuum, and an atmosphere of carbon monoxide introduced at –78°C. The colour of the solution instantly changed from dark purple to dark green. ^{1}H NMR spectroscopy revealed the evolution of free ethylene and the formation of one clean product with resonances associated solely with the ancillary ligand, while the ^{31}P NMR spectrum showed a single new resonance. Repeating the reaction in a sealed tube with the addition of ^{13}CO yielded diagnostic peaks for the carbonyl ligands in the ^{13}C NMR spectrum. Conducting the reaction on a larger scale in toluene generated the same colour change in solution as noted before upon addition of CO, although removal of the volatiles induced a subtle degradation of the green colour to this solution. A hydrocarbon-soluble, thermally labile dark orange-green oil was obtained after workup in hexanes. IR (C_6D_6) ν_{CO} (cm^{-1}): 1890, 1865 (^{13}CO). ^{1}H NMR (20°C, C_6D_6) δ: 0.12 and 0.28 (s, 6H, Si(CH_3)$_2$), 0.51 and 0.82 (dd, 2H, $^2J_{HH}$ = 15 Hz, $^2J_{PH}$ = 9 Hz, SiCH_2P), 0.97, 1.22, 1.29 and 1.32 (dd, 6H, $^3J_{HH}$ = 7 Hz, $^3J_{PH}$ = 7 Hz, CH(CH_3)$_2$), 1.95 and 2.48 (sept, 2H, $^3J_{HH}$ = 7 Hz, C*H*(CH$_3$)$_2$), 5.16 (d, 2H, $^4J_{HH}$ = 1 Hz, Cp-*H*), 5.19 (t, 1H, $^4J_{HH}$ = 1 Hz, Cp-*H*). ^{13}C NMR (20°C, C_6D_6) δ: 241.1 (br s, Zr(*C*O)), 249.1 (s, Zr(*C*O)). ^{31}P NMR (20°C, C_6D_6) δ: 29.1 (s).

^{Me}[P_2Cp]Zr(CO)$_2$Br (**5b**)

The procedure followed was similar to that for **5a**, reacting ethylene **2b** in an atmosphere of CO. The colour of the solution gradually changed from dark red to a dull purplish red after the addition of CO. Once again, a scaled up version of this reaction permitted only the isolation of a thermally labile oil. IR (C_6D_6) ν_{CO} (cm^{-1}): 1898, 1855 (^{13}CO) ^{1}H NMR (20°C, C_6D_6) δ: 0.09 and 0.18 (s, 6H, Si(CH_3)$_2$), 0.57 and 1.03 (d, 2H, $^2J_{PH}$ = 7 Hz, SiCH_2P), 1.41 and 1.50 (t, 6H, $^2J_{PH}$ = 5 Hz, P(CH_3)$_2$), 4.82 (d, 2H, $^4J_{HH}$ = 1 Hz, Cp-*H*), 5.08 (t, 1H, $^4J_{HH}$ = 1 Hz, Cp-*H*). ^{13}C NMR (20°C, C_6D_6) δ: 240.5 and 245.1 (s, Zr(*C*O)). ^{31}P NMR (20°C, C_6D_6) δ: –12.0 (s).

^{Pr}[P_2Cp]Zr(η^5-C_5H_5)(CO) (**6a**)

A benzene-d_6 solution of **4a** was placed in a sealable NMR tube and affixed to a dual vacuum–nitrogen line. A small portion of solvent was removed under vacuum, and an atmosphere of carbon monoxide introduced at –78°C. The contents within the sample were continually mixed under ambient temperature by a constant inversion of the sample by mechanical method. The reaction was monitored by ^{1}H and ^{31}P NMR spectroscopy until the reaction was complete (approximately 2 weeks). There was no obvious colour change associated with this reaction. **6a** was observed to be the major product (90%) based on the NMR spectra. Repeating the procedure in a sealed tube with the addition of ^{13}CO yielded a strong diagnostic peak at 308 ppm for the carbonyl ligand in the ^{13}C NMR spectrum. Conducting the reaction on a larger scale in toluene generated a thermally sensitive hydrocarbon-soluble orange oil after workup that gradually decomposed at –40°C. ^{1}H NMR (20°C, C_6D_6) δ: 0.13, 0.24, 0.35, and 0.47 (s, 3H, Si(CH_3)$_2$), 0.42 and 0.63 (dd, 1H, $^2J_{HH}$ = 11 Hz, $^2J_{PH}$ = 9 Hz, SiCH_2P), 0.69 (d, 2H, $^2J_{PH}$ = 7 Hz, SiCH_2P), 0.75, 0.78, 0.90, and 0.91 (dd, 3H, $^3J_{HH}$ = 7 Hz, $^3J_{PH}$ = 7 Hz, CH(CH_3)$_2$), 1.05 (m, 12H, CH(CH_3)$_2$), 1.29 and 1.55 (sept, 1H, $^3J_{HH}$ = 7 Hz, C*H*(CH$_3$)$_2$), 1.59 (sept, 2H, $^3J_{HH}$ = 7 Hz, C*H*(CH$_3$)$_2$), 4.95 (s, 5H, $^3J_{PH}$ = 1 Hz, C$_5H_5$), 5.08, 5.55, and 5.62 (dd, 1H, $^4J_{HH}$ = 1 Hz, Cp-*H*). ^{13}C NMR (20°C, C_6D_6) δ: 308.0 (d, $^2J_{PC}$ = 3 Hz, Zr(*C*O)). ^{31}P NMR (20°C, C_6D_6) δ: –4.8 and 58.7 (s).

^{Pr}[P_2Cp]Zr(η^2-PhCCPh)Br (**7a**)

Diphenylacetylene (106 mg, 0.59 mmol) was dissolved in 30 mL of toluene and added dropwise with stirring to a cooled (–78°C) solution of **2a** (410 mg, 0.59 mmol) dissolved in 50 mL of toluene. The mixture was slowly warmed to room temperature and stirred for another 24 h. The colour of the solution gradually changed from a deep purple to a dark brown. The volatiles were then removed under vacuum and the residue extracted with hexanes and filtered. Pale yellow crystals were obtained from slow evaporation of a concentrated hexamethyldisiloxane–hexanes mixture. The crystals were washed with two aliquots of cold hexamethyldisiloxane and dried. Yield: 313 mg (67%). Anal. calcd. for $C_{37}H_{57}P_2Si_2Zr$: C 56.18, H 7.26; found: C 56.15, H 7.31.

Major isomer (60%): ^{1}H NMR (20°C, C_6D_6) δ: 0.27 and 0.46 (s, 6H, Si(CH_3)$_2$), 0.84 and 1.28 (dd, 2H, $^2J_{HH}$ = 15 Hz, $^2J_{PH}$ = 4 Hz, SiCH_2P), 0.80, 0.98, 1.04, and 1.13 (dd, 6H, $^3J_{HH}$ = 7 Hz, $^3J_{PH}$ = 7 Hz, CH(CH_3)$_2$), 1.74 and 2.53 (sept, 2H, $^3J_{HH}$ = 7 Hz, C*H*(CH$_3$)$_2$), 6.75 (d, 2H, $^4J_{HH}$ = 1 Hz, Cp-*H*), 6.86 (t, 1H, $^4J_{HH}$ = 1 Hz, Cp-*H*), 7.00 (t, 2H, *p*-C_6H_5), 7.24 (t, 4H, *m*-C_6H_5), 7.45 (d, 4H, *o*-C_6H_5). ^{31}P NMR (20°C, C_6D_6) δ: 9.3 (s).

Minor isomer (40%): ^{1}H NMR (20°C, C_6D_6) δ: 0.21 and 0.33 (s, 6H, Si(CH_3)$_2$), 0.67 and 1.14 (dd, 2H, $^2J_{HH}$ = 14 Hz, $^2J_{PH}$ = 5 Hz, SiCH_2P), 0.75, 1.19, 1.29, and 1.35 (dd, 6H, $^3J_{HH}$ = 7 Hz, $^3J_{PH}$ = 7 Hz, CH(CH_3)$_2$), 2.10 and 2.15 (sept, 2H, $^3J_{HH}$ = 7 Hz, C*H*(CH$_3$)$_2$), 6.46 (t, 1H, $^4J_{HH}$ = 1 Hz, Cp-*H*), 6.80 (d, 2H, $^4J_{HH}$ = 1 Hz, Cp-*H*), 6.94 (t, 2H, *p*-C_6H_5),

© 2001 NRC Canada

7.18 (t, 4H, *m*-C_6H_5), 7.35 (d, 4H, *o*-C_6H_5). ^{31}P NMR (20°C, C_6D_6) δ: 6.9 (s).

Concluding remarks

In this paper a series of zirconium complexes stabilized by the ancillary P_2Cp ligand are presented in which the formal oxidation state can be regarded as Zr(II). The ethylene complexes **2** and **4a** react with CO via loss of ethylene to generate carbonyl derivatives, and **2a** undergoes a similar reaction with diphenylacetylene to produce alkyne **7a**. The slow reaction of the saturated 18-electron complex **4a** with CO demonstrates that phosphine dissociation is required to provide a reactive site. The lack of reactivity of alkyne **7a** with CO presumably originates from the same electronic saturation of that species. In comparison, the immediate incorporation of CO by the 16-electron ethylene complexes **2a** or **2b** suggests an associative mechanism. The displacement of a coordinated ethylene molecule by CO is a rare occurrence in early metal complexes (33). It might have been anticipated that strong back-bonding should confer a degree of Zr(IV) metallacycle character in the metal—ethylene bonding as shown in **A**; however, it is apparent from the resulting ligand substitution reactions that considerable Zr(II) character is still present in these ethylene derivatives.

References

1. J.P. Collman, L.S. Hegedus, J.R. Norton, and R.G. Finke. Principles and applications of organotransition metal chemistry. University Science Books, Mill Valley, California. 1987. Chap. 3.
2. M. Schuster and S. Blechert. Angew. Chem. Int. Ed. Engl. **36**, 2036 (1997).
3. K.J. Ivin and J.C. Mol. Olefin metathesis and metathesis polymerization. Academic Press, London, U.K. 1997.
4. N.A. Petasis and D.-K. Fu. J. Am. Chem. Soc. **115**, 7208 (1993).
5. R.H. Grubbs, S.J. Miller, and G.C. Fu. Acc. Chem. Res. **28**, 446 (1997).
6. R.H. Crabtree. The organometallic chemistry of the transition metals. John Wiley & Sons, New York. 1994. Chap. 9.
7. G.W. Parshall. Science (Washington, D.C.), **208**, 1221 (1990).
8. M.R. Sievers, L.M. Jarvis, and P.B. Armentrout., J. Am. Chem. Soc. **120**, 1891 (1998).
9. M.L. Steigerwald and W.A. Goddard. J. Am. Chem. Soc. **107**, 5027 (1985).
10. M.D. Fryzuk, S.S.H. Mao, M.J. Zaworotko, and L.R. MacGillivray. J. Am. Chem. Soc. **115**, 5336 (1993).
11. M.D. Fryzuk, P.B. Duval, S.S.H. Mao, M.J. Zaworotko, and L.R. MacGillivray. J. Am. Chem. Soc. **121**, 2478 (1999).
12. G. Wilkinson, F.G.A. Stone, and E.W. Abel. Comprehensive organometallic chemistry II. Vol. 4. Pergamon Press, Oxford. 1995. Chap. 12.
13. E. Negishi and T. Takahashi. Acc. Chem. Res. **27**, 124 (1994).
14. H.G. Alt, C.E. Denner, U. Thewalt, and M.D. Raush. J. Organomet. Chem. **356**, C83 (1988).
15. T. Takahashi, M. Murakama, M. Kunishige, M. Saburi, Y. Uchida, K. Kozawa, T. Uchida, D.R. Swanson, and E. Negishi. Chem. Lett. 761 (1989).
16. H. Lee, T. Hascall, P.J. Descrosiers, and G. Parkin. J. Am. Chem. Soc. **120**, 5830 (1998).
17. R. Fischer, D. Walther, P. Gebhardt, and H. Görls. Organometallics, **19**, 2532 (2000).
18. M.D. Fryzuk, P.B. Duval, S.S.H. Mao, S.J. Rettig, M.J. Zaworotko, and L.R. MacGillivray. J. Am. Chem. Soc. **121**, 1707 (1999).
19. P. Kubácek, R. Hoffmann, and Z. Havias. Organometallics, **1**, 180 (1982).
20. R. Poli. Organometallics, **9**, 1892 (1990).
21. P. Binger, P. Muller, R. Benn, A. Rufinska, B. Gabor, and C. Kruger. Chem. Ber. **122**, 1035 (1989).
22. L.S. Bartell, E.A. Roth, C.D. Hollowell, K. Kuchitsu, and J.E. Young. J. Chem. Phys. **42**, 2683 (1965).
23. J. Chatt and L.A. Duncanson. J. Chem. Soc. 2939 (1953).
24. M.J.S. Dewar. Bull. Soc. Chim. Fr. **18**, C79 (1951).
25. Z. Wu, R.F. Jordan, and J.L. Petersen. J. Am. Chem. Soc. **117**, 5867 (1995).
26. Y. Wielstra, S. Gambarotta, and J.B. Roedelof. Organometallics, **7**, 2177 (1988).
27. G.T. Palmer, F. Basolo, L.B. Kool, and M.D. Rausch. J. Am. Chem. Soc. **108**, 4417 (1986).
28. B.K. Stein, S.R. Frerichs, and J.E. Ellis. Organometallics, **6**, 2017 (1987).
29. U. Zucchini, E. Albiizzati, and U. Gianni. J. Organomet. Chem. **26**, 357 (1971).
30. G. Erker, C. Sarter, M. Albrecht, S. Dehnicke, C. Krüger, E. Raabe, R. Schlund, R. Benn, A. Rufínska, and R. Mynott. J. Organomet. Chem. **382**, 89 (1990).
31. B. Demerseman, G. Bouquet, and M. Bigorne. J. Organomet. Chem. **132**, 223 (1977).
32. J.W. Lauher and R. Hoffmann. J. Am. Chem. Soc. **98**, 1729 (1976).
33. A.D. Poole, V.C. Gibson, and W. Clegg. J. Chem. Soc. Chem. Commun. 237 (1992).
34. T. Takahashi, D.R. Swanson, and E. Negishi. Chem. Lett. 623 (1987).
35. J.C. Smart and C.J. Curtis. Inorg. Chem. **16**, 1788 (1977).
36. M.D. Fryzuk, S.S.H. Mao, P.B. Duval, and S.J. Rettig. Polyhedron, **14**, 11 (1995).

© 2001 NRC Canada

Molecular characterization of petroporphyrins in crude oil by electrospray ionization Fourier transform ion cyclotron resonance mass spectrometry

Ryan P. Rodgers, Christopher L. Hendrickson, Mark R. Emmett, Alan G. Marshall, Mark Greaney, and Kuangnan Qian

Abstract: Petroporphyrin compositional analysis of a heavy crude oil has been realized by isolation and subsequent ESI–FT-ICR mass spectrometric analysis of the porphyrin-containing fractions. Vanadium octaethyl (V=O(II)OEP) and nickel octaethyl (Ni(II)OEP) porphyrin standards were analyzed to determine favorable electrospray ionization conditions and provide insight as to the molecular species present (e.g., adducts, multimers). Standard V=O(II)OEP and Ni(II)OEP solutions revealed the presence of both monomer and dimer species with a greater relative abundance of monomers. In contrast, mass spectral analysis of a porphyrin fraction from Cerro Negro crude oil was dominated by dimeric species. MS^3 analysis identified a dioctylphthalate (DOP) contaminant, likely introduced during fractionation of the crude oil. DOP-porphyrin complexes and porphyrin–porphyrin dimers were then identified. Infrared multiphoton dissociation (IRMPD) of dimeric species produced the corresponding monomers with minimal fragmentation. The monomeric petroporphyrins were analyzed to reveal the metal (Ni(II) or V=O(II)), porphyrin type (e.g., etio vs. DPEP), and distribution of alkylation.

Key words: petroporphyrin, porphyrin, petroleum, electrospray ionization, mass spectrometry, Fourier transform, ion cyclotron resonance, ICR, FT-ICR, FTMS.

Résumé : On a réalisé une analyse de la composition en pétroporphyrines d'une huile brute lourde en procédant à l'isolement et à une analyse subséquente des fractions contenant des porphyrines par spectrométrie de masse par la technique « ESI–FT-IRC.» Dans le but de déterminer les conditions les plus favorables pour obtenir une ionisation par électronébulisation ainsi que pour évaluer la nature des espèces moléculaires présentes (par exemple, adduits, multimères), on a procédé à l'analyse d'échantillons de référence d'octaéthylvanadium- (V=O(II)OEP) et d'octaéthylnickel-(Ni(II)OEP) porphyrines. Des solutions de référence d'échantillons de V=O(II)OEP et de Ni(II)OEP montrent la présence d'espèces monomères ainsi que dimères; l'abondance relative des espèces monomères est plus importante que celle des dimères. Par ailleurs, l'analyse par spectrométrie de masse d'une fraction de porphyrines d'une huile brute de Cerro Negro est dominée par les espèces dimères. Une analyse par la méthode MS^3 révèle la présence de phtalate de dioctyle (« DOP ») comme contaminant introduit vraisemblablement durant le fractionnement de l'huile brute. On a alors identifié des complexes de DOP-porphyrine et des dimères porphyrine–porphyrine. Une dissociation multiphotonique par infrarouge (« IRMPD ») des espèces dimères a conduit aux monomères correspondants avec un minimum de fragmentation. Les pétroporphyrines monomères ont été analysées et ont mis en évidence la nature du métal (Ni(II) ou V=O(II)), le type de porphyrine (par exemple, etio vs. DPEP) ainsi que la distribution de l'alkylation.

Mots clés : pétroporphyrine, porphyrine, pétrole, ionisation par électronébulisation, spectrométrie de masse, transformation de Fourier, résonance gyromagnétique des ions, ICR, FT-CR, FTMS.

Received May 15, 2000. Published on the NRC Research Press Web site at http://canjchem.nrc.ca on May 29, 2001.

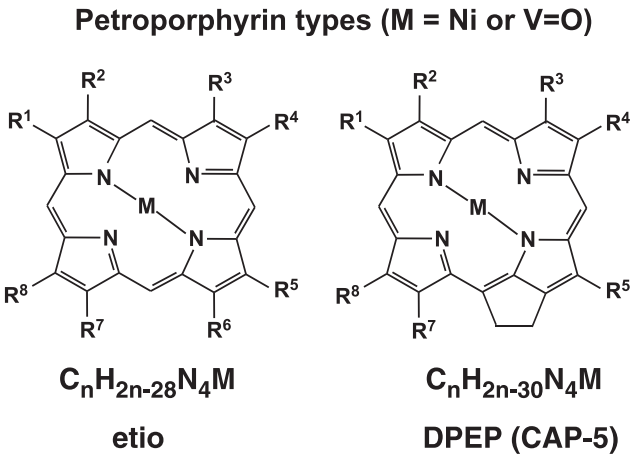
Dedicated to Professor Brian R. James on the occasion of his 65th birthday.

R.P. Rodgers, C.L. Hendrickson, M.R. Emmett, and A.G. Marshall.[1,2] Center for Interdisciplinary Magnetic Resonance, National High Magnetic Field Laboratory, Florida State University, 1800 East Paul Dirac Dr., Tallahassee, FL 32310, U.S.A.
M.A. Greaney and K. Qian.[2] ExxonMobil Research and Engineering, 1545 Route 22 East, Annandale, NJ 08801, U.S.A.

[1]Member of the Department of Chemistry, Florida State University, Tallahassee, Fla.
[2]Corresponding authors (AGM: telephone: (850) 644-0529; fax: (850) 644-1366; e-mail: marshall@magnet.fsu.edu; KQ: telephone: (908) 730-2013; fax: (908) 730-3314; e-mail: kqian@erenj.com).

 DOI: 10.1139/cjc-79-5/6-546 © 2001 NRC Canada

Fig. 1. Structures of two common types of petroporphyrins.



Introduction

The presence of petroporphyrins (also known as geoporphyrins) in crude oils is significant to the petroleum industry in both upstream (exploration and production) and downstream (refinery) sectors of the business. Petroporphyrins originate from the degradation of biological materials and are regarded as important biomarkers. The distribution of porphyrin types, such as the ratio of etioporphyrin (etio) (i.e., porphyrins that bear no exocyclic ring) to deoxophyllerythro-etioporphyrin (DPEP) (see Fig. 1) is widely used as a measure of the maturity of a crude oil (1, 2). For example, degradation of the heme, from hemoglobin or the cytochromes, by decarboxylation of the acids and reduction of the vinyl groups generates etioporphyrin-III. Similarly, degradation of chlorophyll can generate the five-membered ring of the DPEP family. DPEP is an example of the more general classification of cycloalkanoporphyrins (CAP), which may contain one or more five-, six-, or seven-membered rings (3).

Petroporphyrins are also an important class of metal-containing compounds in crude oil. Metals are known to poison catalysts in various catalytic refinery processes, such as catalytic cracking, hydrocracking, etc. (4–6). As world-wide petroleum supplies become richer in heteroatomic content, research on processing such heavy petroleum becomes increasingly important. Knowledge of the molecular composition of metal-containing species, including petroporphyrins in crude, is important to the development of an effective demetallation process for heavy petroleum processing.

Characterization of petroporphyrins, developed over the past several decades, traditionally involves separations of petroporphyrins by open column, thin-layer, or reverse-phase HPLC (7–10). Demetallation by methane sulfonic acid is often performed to facilitate spectroscopic analysis, including mass spectrometric analysis. Various petroporphyrin types, such as etio, DPEP, Di-DPEP, rhodo-etio and rhodo-DPEP, have been identified in petroleum products (1).

Mass spectrometry provides molecular weight and elemental composition of porphyrin homologs, from which porphyrin "type" (rings plus double bonds) may be determined. Additional structural information may be obtained by tandem mass spectrometry (3). Direct mass spectrometric characterization of petroporphyrins in crude oil without prior chromatographic separation remains difficult and a subject of continued research interest. Direct analysis would not only avoid potential modification of petroporphyrin structures during chromatography, but also make it possible to track directly molecular transformations of porphyrin structures in crude oil processing. The latter is critical to the understanding of fundamental chemistry occurring in the refinery process. Direct mass spectrometric analysis is difficult for at least two reasons. First, the low concentration and high-boiling nature of petroporphyrins render traditional vaporization and ionization methods ineffective. Second, the complexity of the hydrocarbon matrix in the high-boiling region demands ultra-high mass resolving power that cannot be met by traditional mass spectrometric methods. The development of electrospray ionization high-field Fourier transform ion cyclotron resonance mass spectrometry (ESI–FT-ICR–MS) technology offers an opportunity to characterize polar molecules, such as petroporphyrins in heavy petroleum, at an unprecedented level of detail.

In an effort to develop a strategy to speciate directly petroporphyrins in crude oil, we have evaluated the use of ESI–FT-ICR–MS for petroporphyrin characterization. Here, we report elemental compositional analyses of two petroporphyrin standards (nickel and vanadyl octaethyl porphyrins (Ni(II)OEP and V=O(II)OEP) and two petroporphyrin fractions isolated from Cerro Negro extra heavy crude oil. Cerro Negro was selected not only for its high VO/Ni content, but also because it has been previously characterized by other researchers (11). High-resolution ($m/\Delta m_{50\%} \approx 100\,000$) broadband (200 m/z 1200) mass analysis allows for resolution and identification of ~300 distinct elemental compositions in a complex mass spectrum. Furthermore, IRMPD of dimeric species present in the broadband mass spectrum allows for the detection and subsequent identification of the monomer petroporphyrins present in the crude despite strong signals from dioctylphthalate contamination. Both porphyrin:porphyrin and porphyrin:DOP dimers could be dissociated into their respective monomers in the ICR ion trap, leading to a much simplified mass spectrum.

Experimental

Sample preparation

Vanadyl octaethyl porphyrin (V=O(II)OEP) and nickel octaethyl porphyrin (Ni(II)OEP) were purchased from Aldrich Chemical Co. and used as received. Standard solutions of Ni(II)OEP and V=O(II)OEP were prepared by dissolution in either methanol (V=O(II)OEP) or acetonitrile (ACN) (Ni(II)OEP) to a concentration of 10 μM, with the addition of acetic acid (1% v/v). Preparation of the isolated petroporphyrin fractions went as follows. The basic procedure used for petroporphyrin isolation is a slightly modified version of that described by Grigsby and Green (11). The isolation scheme is illustrated in Fig. 2. Six grams of extra heavy crude oil from Cerro Negro, Venezuela was diluted with 10 mL of toluene and loaded onto a dry packed column of neutral aluminum oxide (Alfa, 60 mesh, 100 g). Three dark bands were eluted with 100 mL of toluene, then 100 mL of a 1:1 toluene–methylene chloride (CH_2Cl_2)

© 2001 NRC Canada

Fig. 2. Separation scheme employed to isolate the petroporphyrin fractions from Cerro Negro crude oil. The second and third bands (A2 and A3 fractions) exhibited Soret peaks at 408 nm in their UV–vis absorption spectra, indicating the presence of petroporphyrins. Therefore, both A2 and A3 were further processed to yield the A2-S(5–7) and A3-S7 fractions, whose UV–vis spectra are shown at the bottom of the diagram.

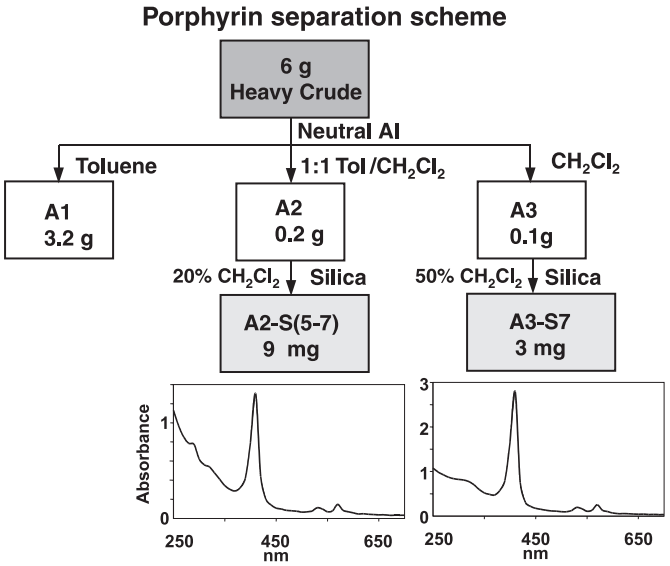
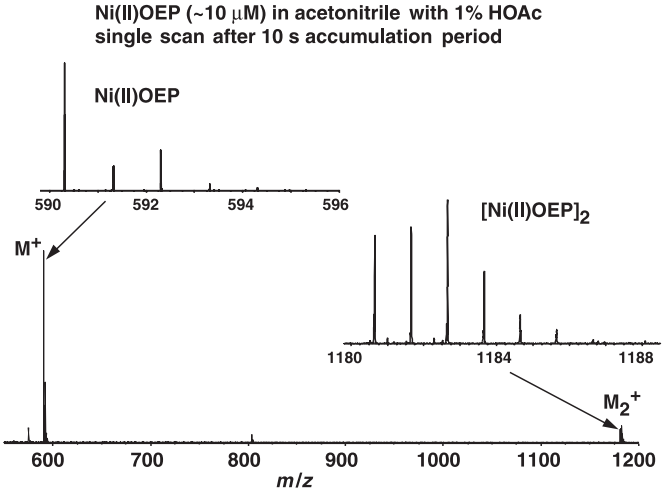


Fig. 3. Broadband single-scan ESI–FT-ICR mass spectrum of a 10 μM Ni(II) octaethyl porphyrin solution in acetonitrile with 1% acetic acid (v/v) at an average mass resolving power ($m/\Delta m_{50\%} \approx 100\,000$) and a signal-to-noise ratio (S/N) > 1000). The two dominant isotopic distributions at m/z = 590 (left zoom inset) and 1180 (right zoom inset) are the Ni(II)OEP monomer and dimer.



mixture and finally with 50 mL of pure CH_2Cl_2. The second and third bands (A2 and A3 fractions) exhibited Soret peaks at 408 nm in their UV–vis absorption spectra indicating the presence of petroporphyrins. A2 and A3 fractions were dried under a nitrogen stream and weighed 200 and 100 mg, respectively.

Further purification was achieved by passing A2 and A3 fractions through silica gel (J.T. Baker, 60–200 mesh, 40 g) that was slurried into the column after mixing with 200 mL of 10 vol% CH_2Cl_2 in hexane. The column was eluted sequentially with 10, 20, 30, 40, and 50% CH_2Cl_2. For A2, elution with 20% CH_2Cl_2 led to isolation of a red-pink band, with a UV–vis spectrum characteristic of a porphyrin, with absorbance maxima at 408, 537, and 573 nm. The fraction was labeled as A2-S(5–7) and weighed 9 mg after solvent evaporation. A3 was separated by a similar scheme. A red band was isolated by elution with 50% CH_2Cl_2 in hexane. The fraction was labeled as A3-S7 and weighed 3 mg after solvent evaporation. It exhibited absorbance maxima in the UV–vis region at 408, 533, and 572 nm, and a shoulder peak at 588 nm. Portions of the dried Cerro Negro fractions (both A2-S(5–7) and A3-S7) were first dissolved in a small amount of methylene chloride (~500 μL) and then added to 10 mL of methanol with 1% (v/v) acetic acid. If precipitation occurred, methylene chloride was added dropwise until the solution cleared. The samples were then microelectrosprayed into the FT-ICR mass spectrometer.

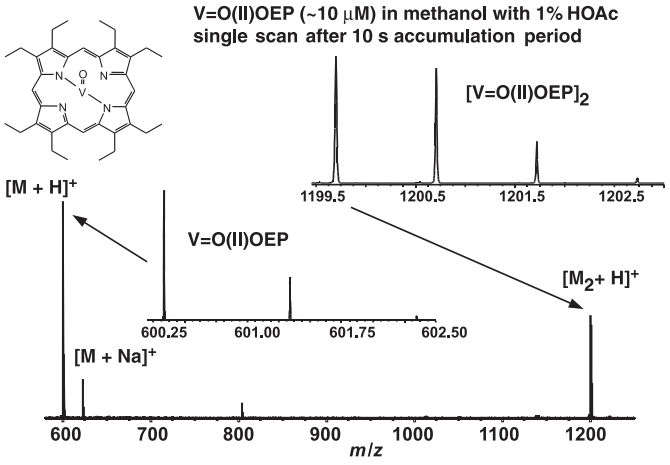
Instrumentation

All mass analyses were carried out on a homebuilt FT-ICR mass spectrometer (12) equipped with a 22 cm horizontal room temperature bore 9.4 Tesla magnet (Oxford Corp., Oxney Mead, England) and a modular ICR data station (13). Positive ions were generated from a microelectrospray source (14) at a flow rate of 300 nL min^{-1} and a source potential of ~2.2 kV before external accumulation (5–30 s) in a 67 cm long octopole (15). Ions were then transferred through a 200 cm long rf-only octopole into an open cylindrical ICR cell (10 cm i.d. × 30 cm long) prior to broadband frequency chirp excitation (50 kHz – 1.44 MHz at a sweep rate of 150 Hz s^{-1} and amplitude, $V_{p\text{-}p}$ = 210 V) and direct mode image current detection to yield 512 K word time-domain data. The data were processed by an in-house FT-ICR–MS analysis package (13). The time-domain data was Hanning-apodized, followed by a single zero-fill before FFT and magnitude calculation. Frequency-to-mass conversion was based on assumed three-dimensional axial quadrupolar trapping potential (16, 17), to generate the spectra shown in Figs. 3–6. For the Cerro Negro fractions, VOEP served as an internal calibrant. External calibration was used for the two porphyrin standards, VOEP and NiOEP. IRMPD studies were performed by irradiation for 2 s by a Synrad (Mukilteo, WA) 50 W cw CO_2 (λ = 10.6 μm) laser aligned on-axis with the ion cloud. The laser was operated at 20 W and focused to a ~1 cm beam diameter at the center of the Penning trap.

Mass spectral data were converted to the Kendrick mass scale to facilitate separation and identification of pseudohomologous series (i.e., a series of compounds differing in mass by 14.01565 Da (CH_2) from one member to the next). In the Kendrick mass scale (18), each mass value is multiplied by (14.00000/14.01565), so that the Kendrick mass of CH_2 becomes 14.00000. With this convention, members of a homologous series differing by multiples of CH_2 each have identical mass defect. All of the Kendrick mass values may then be scanned to find each series of ions differing by (say) 14.000 ± 0.001 Kendrick mass units. The type for each such series is then determined from the z-value

© 2001 NRC Canada

Fig. 4. Broadband single-scan ESI–FT-ICR mass spectrum of a 10 μM V=O(II) octaethyl porphyrin solution in methanol with 1% acetic acid (v/v) at an average mass resolving power ($m/\Delta m_{50\%} \approx 100\,000$) and a signal-to-noise ratio (S/N) > 1000). The two dominant isotopic distributions at m/z = 600 (left zoom inset) and 1200 (right zoom inset) are the V=O(II)OEP monomer and dimer.



(C_nH_{2n+z}) to locate porphyrins containing V=O, Ni, and Na (see below).

Results and discussion

Porphyrin standards analysis

Solutions of Ni(II)OEP and V=O(II)OEP (each ~10 μM) were separately electrosprayed (19, 20) into the FT-ICR mass spectrometer to yield in each case a relatively simple positive ion mass spectrum. Figure 3 shows the ESI–FT-ICR mass spectrum of the Ni(II)OEP stock solution at an average mass resolving power ($m/\Delta m_{50\%} \approx 100\,000$ (in which $m_{50\%}$ denotes the magnitude-mode peak full-width at half-maximum peak height)) and a signal-to-noise ratio (S/N) 1000. The two prominent isotopic distributions centered about m/z 590 and 1180 correspond to the singly charged Ni(II)OEP monomer molecular ion and its (proton-bound) dimer. The experimental nominal mass isotopic relative abundance distributions (not shown) for Ni(II)OEP monomer and dimer match the theoretical distributions quite well, and are quite diagnostic because of the distinctive isotopic distribution of Ni (68.3% ^{58}Ni, 26.1% ^{60}Ni).

Similarly, Fig. 4 shows the ESI–FT-ICR mass spectral analysis of the V=O(II)OEP stock solution at an average mass resolving power $m/\Delta m_{50\%} \approx 100\,000$ and a S/N 1000. Again, the two prominent isotopic distributions (m/z = 600 and 1200, shown in the zoom mass insets) represent both the VOEP monomer and dimer. Interestingly, whereas Ni(II)OEP monomer and dimer become positively charged by loss of an electron, V=O(II)OEP and its dimer gain positive charge by addition of H^+ (or Na^+). The tendency of the porphyrins to dimerize is important for the analysis of the crude oil extracts (see below).

Petroporphyrin fraction analysis

Both A2-S(5–7) and A3-S7 porphyrin-containing fractions isolated from Cerro Negro crude were micro-

Fig. 5. Broadband ESI–FT-ICR mass spectrum of A3-S7 fraction isolated as in Fig. 1, shown before (top) and after (bottom) infrared multiphoton dissociation. Top: Three dimer distributions in the range, 800 < m/z < 1100. The species at m/z 800 was identified by MS^3 experiments as dioctyl phthalate (DOP) dimer. The remaining two dimer distributions were then identified as petroporphyrin:dioctyl phthalate (900 < m/z < 1000) and petroporphyrin:petroporphyrin (1000 < m/z < 1100) dimers. Bottom: broadband mass spectrum of the same isolated petroporphyrin fraction after IRMPD. IRMPD dissociates the dimers to yield solely monomers. Each spectrum was the result of 20 co-added time-domain transients, and the sample was spiked with V=O(II)OEP as an internal mass calibrant.

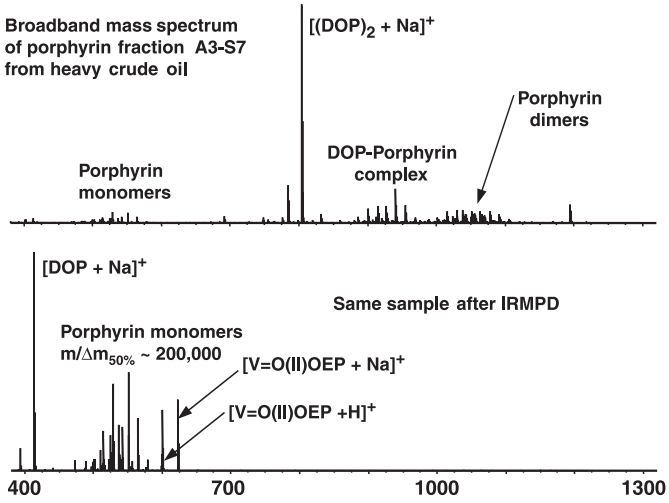
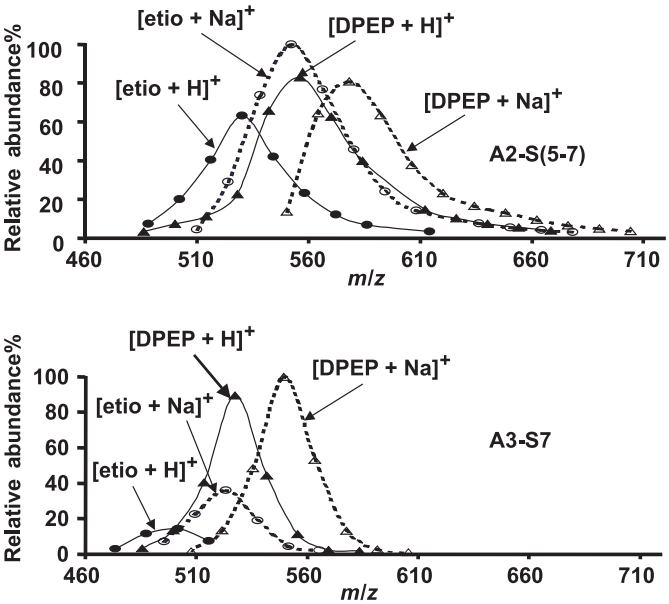


Fig. 6. Molecular weight distribution of vanadyl etio and DPEP monomer series in A2-S(5–7) (top) and A3-S7 (bottom) fractions isolated from heavy crude oil.



electrosprayed into the FT-ICR mass spectrometer to yield a complex mass spectrum containing ~400 peaks at mass resolving power of ~100 000. Because similar species were identified in both fractions, data from only one fraction (A3-S7)

© 2001 NRC Canada

Table 1. Measured and theoretical Kendrick masses for a series of $C_nH_{2n-30}N_4VONa$ (DPEP) porphyrins electrosprayed from heavy crude oil.

Measured Kendrick mass	Theoretical Kendrick mass	Mass difference (millimass units)	Mass error (ppm)	Relative abundance (%)
535.5774	535.5770	+0.4	+0.8	0.4
549.5769	549.5770	–0.1	–0.1	1.7
563.5766	563.5770	–0.4	–0.7	8.2
577.5774	577.5770	+0.4	+0.8	10.2
591.5766	591.5770	–0.4	–0.7	8.0
605.5777	605.5770	+0.7	+1.1	4.8
619.5771	619.5770	+0.1	+0.1	2.9
633.5768	633.5770	–0.2	–0.3	2.1
647.5776	647.5770	+0.6	+0.9	1.7
661.5778	661.5770	+0.8	+1.2	1.2
675.5774	675.5770	+0.4	+0.6	0.8
689.5775	689.5770	+0.5	+0.7	0.6
703.5771	703.5770	+0.1	+0.2	0.5
717.5769	717.5770	–0.1	–0.1	0.4
731.5773	731.5770	+0.3	+0.4	0.3
745.5774	745.5770	+0.4	+0.6	0.2

Note: Kendrick mass increases by exactly 14 mass units for every additional CH_2 group, making it easy to recognize such a series of alkylated molecules.

will be presented. Figure 5 (top) shows the broadband mass spectrum of the isolated porphyrin fraction spiked with the V=O(II)OEP standard solution to provide an internal calibrant. Petroporphyrins in the mass range 500 *m*/*z* 600 are barely observable. However, the V=O(II)OEP dimer is clearly evident at 1200 Da as are many other dimeric species from 800–1100 Da. Two separate groups of dimers are apparent in the mass range spanning 900–1000 Da and 1000–1100 Da. A third homodimer of large relative abundance at *m*/*z* 800 was SWIFT-isolated (21, 22) and fragmented by IRMPD for identification. Subsequent MS^3 experiments identified the dimer species as a dioctyl phthalate (DOP) contaminant, most likely introduced (e.g., from bottle cap lining) in the fractionation of the Cerro Negro crude oil. Identification of the DOP contaminant led to the assignment of the two heterodimer distributions as petroporphyrin:dioctyl phthalate (900–1000 Da) and petroporphyrin–petroporphyrin (1000–1100 Da) dimer series. The laser power and duration were varied in an attempt to dissociate the dimer complexes so as to reveal the true petroporphyrin monomer distributions present in the Cerro Negro crude oil. Figure 5 (bottom) shows the broadband mass spectrum of the same isolated porphyrin fraction (Fig. 5, top) after IRMPD to yield both the petroporphyrin, DOP, and VOEP monomers at a mass resolving power of ~200 000 and S/N 1000.

Petroporphyrin type and alkylation analysis

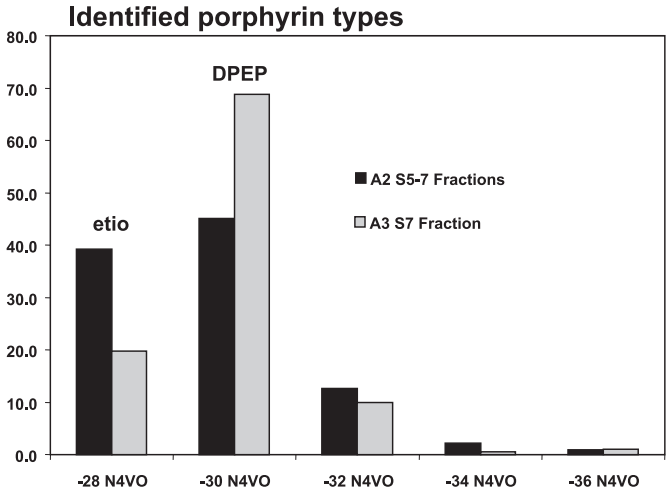
Table 1 shows how the members of a particular vanadyl petroporphyrin family are identified. First, the masses of all resolved peaks are converted to Kendrick mass scale. For a particular petroporphyrin ion type (in this case, $C_nH_{2n-30}N_4VONa$) the mass values calculated from the elemental composition constitute a series of masses separated by 14.000 Kendrick mass units, with identical Kendrick mass defect. Examination of the experimental masses then immediately results in identification of all of the members of the $C_nH_{2n-30}N_4VONa$ (DPEP) porphyrin family shown in the table.

Two types of petroporphyrin homolog series (VO(II)etio and VO(II)DPEP) identified in this way are shown in Fig. 6, for A2-S(5–7) and A3-S7 fractions isolated as shown in Fig. 1. The average molecular weight (MW) of petroporphyrins in A2-S(5–7) is higher than that in A3-S7. Molecular ions with mass up to 700 Da were observed. This observation is consistent with the higher polarity of the A3-S7 fraction compared to the A2-S(5–7) fraction. The MW profile reflects the distribution of alkylation of the porphyrins: for example, the most probable carbon number observed for the DPEP family in A3-S7 is 31. Given that the porphyrin skeleton itself (including the five-membered ring) contains 22 carbons, the most probable number of alkyl carbon substituents is nine. It is satisfying to note that both the M+H and the M+Na ion series yield very similar alklyation patterns, suggesting that the mass spectrometric ion relative abundances may well correlate to the relative abundances of the petroporphyrins in solution. Figure 6 also suggests that short chain porphyrins have a higher tendency to form Na adducts than do long chain porphyrins. Moreover, etio-type form Na adducts to a greater degree than the DPEP-type. Grigsby and Green (11) have characterized by low-voltage high-resolution mass spectrometry a vanadyl fraction isolated from the 700°C residual of Cerro Negro heavy crude oil. Their carbon number distribution for the etio type accords with our observation. Their carbon number distribution for the DPEP type, however, is about two carbon higher than our result. It is also interesting to note that the average number of carbon atoms in vanadyl petroporphyrins from another heavy crude (Boscan) oil (35–40) (23) is somewhat higher than the value (33) that we observe for Cerro Negro heavy crude oil.

Listings like that in Table 1 reveal additional homolog series for the petroporphyrins in Fig. 6. The results are conveniently summarized in Fig. 7, which shows the relative

© 2001 NRC Canada

Fig. 7. Relative abundances of various porphyrin types identified by ESI–FT-ICR mass analysis. The indicated type is denoted according to its elemental composition, in which the carbon and hydrogen values are abbreviated by their "*z*"-value in the formula, $C_nH_{2n+z}N_4VO$. Thus, ETIO and DPEP porphyrins have $z = -28$ and $z = -30$, respectively. The species with $z = -32$, –34, and –36 presumably contain 2, 3, and 4 additional rings.



abundances of different petroporphyrins according to type and isolated fraction. For example, the etio and DPEP porphyrins are comparably abundant in the A2 S(5–7) fraction, whereas the DPEP porphyrins are much more abundant in the A3-S7 fraction.

In conclusion, we are able to resolve and classify petroporphyrins from extracts of a heavy crude oil by ESI–FT-ICR–MS. First, we can identify the metal (Ni(II) or V=O(II)) in the porphyrin. Second, we can determine the porphyrin type (i.e., rings plus double bonds). Third, for each type, we can determine the distribution of alkylation of the porphyrin skeleton. Finally, tandem mass spectrometry, previously available only for pure porphyrins (3), should now be available for petroporphyrins from crude oil isolates, making it possible to determine the chain lengths of individual alkyl substituents. In summary, petroleum chemists now have access to a much higher level of compositional and structural detail in characterizing metallopetroporphyrins. This work provides a valuable reference base for direct speciation of petroporphyrins in crude oil.

Acknowledgments

The authors thank Daniel McIntosh for machining the custom parts required for the 9.4 T instrument construction and John P. Quinn for his help with instrumental modifications. This work was supported by NSF (CHE-94-13008 and CHE 99-09502), Florida State University, and the National High Magnetic Field Laboratory at Tallahassee, Florida. The authors also thank ExxonMobil for permission to publish this data.

References

1. E.W. Baker, T.F. Yen, J.P. Dickie, R.E. Rhodes, and L.F. Clark. J. Am. Chem. Soc. **89**, 3631 (1967).
2. Z. Frakman, T.M. Ignasiak, D.S. Montgomery, and O.P. Strausz. AOSTRA J. Res. **4**, 171 (1988).
3. J.M.E. Quirke. *In* The porphyrin handbook. Vol. 7. *Edited by* K.M. Kadish, K.M. Smith, and R. Guilard. Academic Press, 2000. pp. 371–422.
4. M. Ushio and T. Ino. Shokubai, **35**, 250 (1993).
5. P. O'Connor and A.C. Pouwels. Stud. Surf. Sci. Catal. **88**, 129 (1994).
6. J.W. Gosselink and W.H. Stork. J. Ind. Eng. Chem. Res. 3354 (1997).
7. J.V. Johnson, E.D. Britton, R.A. Yost, J.M.E. Quirke, and L.L. Cuesta. Anal. Chem. **58**, 1325 (1986).
8. A.L. Johnson and D.H. Freeman. Energy & Fuel, **4**, 695 (1990).
9. W.A.J. Dewaal, S. Heemstra, J.C. Kraak, and R.J. Jonker. Chromatographia, **30**, 38 (1990).
10. C.J. Boreham and C.J.R. Fookes. J. Chromatogr. **467**, 195 (1989).
11. R.D. Grigsby and J.B. Green. Energy & Fuels, **11**, 602 (1997).
12. M.W. Senko, C.L. Hendrickson, L. Pasa-Tolic, J.A. Marto, F.M. White, S. Guan, and A.G. Marshall. Rapid Commun. Mass Spectrom. **10**, 1824 (1996).
13. M.W. Senko, J.D. Canterbury, S. Guan, and A.G. Marshall. Rapid Commun. Mass Spectrom. **10**, 1839 (1996).
14. M.R. Emmett, F.M. White, C.L. Hendrickson, S.D.-H. Shi, and A.G. Marshall. J. Am. Soc. Mass Spectrom. **9**, 333 (1998).
15. M.W. Senko, C.L. Hendrickson, M.R. Emmett, S.D.-H. Shi, and A.G. Marshall. J. Am. Soc. Mass Spectrom. **8**, 970 (1997).
16. E.B. Ledford, Jr., D.L. Rempel, and M.L. Gross. Anal. Chem. **56**, 2744 (1984).
17. S.D.-H. Shi, J.J. Drader, M.A. Freitas, C.L. Hendrickson, and A.G. Marshall. Int. J. Mass Spectrom. **195**/**196**, 591 (2000).
18. E. Kendrick. Anal. Chem. **35**, 2146 (1963).
19. G.J. Van Berkel, S.A. McLuckey, and G.L. Glish. Anal. Chem. **63**, 1098 (1991).
20. G.J. Van Berkel, M.A. Quinones, and J.M.E. Quirke. Energy & Fuels, **7**, 411 (1993).
21. A.G. Marshall, T.-C.L. Wang, and T.L. Ricca. J. Am. Chem. Soc. **107**, 7893 (1985).
22. S. Guan and A.G. Marshall. Int. J. Mass Spectrom. Ion Processes, **157**/**158**, 5 (1996).
23. J.J.E. Quirke, L.L. Cuesta, R.A. Yost, J. Johnson, and E.D. Britton. Org. Geochem. **14**, 43 (1989).

© 2001 NRC Canada

Structural, electronic and spectroscopic features of the dihydride $Pd_4(dppm)_4(H)_2^{2+}$ cluster catalyst

Daniel Meilleur and Pierre D. Harvey

Abstract: ^{1}H NMR, vibrational, and UV–vis spectroscopic measurements for $Pd_2(dppm)_2Cl_2$ (dppm = $Ph_2PCH2PPh_2$), $[Pd_4(dppm)_4(X)_2](BF_4)_2$ (X = Cl, H), and $[Pd_4(dmpm)_4(H)_2](Br)_2$ (dmpm = $Me_2PCH_2PMe_2$) were performed to address the structure of the recently identified title cluster. Its dmpm analogue was prepared from the reaction between $Pd_2(dmpm)_2Br_2$ and $NaBH_4$ in methanol under inert atmosphere, and exhibits the expected nonet (rel. int. 1:8:28:56:70:56:28:8:1) at –5.21 ppm (in $(CD_3)_2CO$), contrasting with that of $Pd_4(dppm)_4(H)_2^{2+}$ (δ + 5.15 ppm, $(CD_3)_2CO$). This significant difference is explained by the presence of the PdH residues in the deshielding region of the dppm-phenyl groups. The vibrational spectra in the low-frequency region are consistent with a centrosymmetric structure, and a scattering at 144 cm^{-1} in the FT-Raman spectra is observed; a peak that is assigned to $\nu(Pd_2)$ on the basis of a comparison with the well established M_2-bonded $Pd_2(dppm)_2Cl_2$ data ((Pd_2) = 149 cm^{-1}). On the basis of the qualitative temperature behavior of the band maxima and width, the two lowest energy absorption bands in the UV–vis spectra are assigned to $d\sigma \rightarrow d\sigma^*$ type transition. EHMO computations predict four well-isolated frontier MO levels, defined as $d\sigma^*(Pd_2)/d\sigma^*(PdH)$ (LUMO + 1), $d\sigma^*(Pd_2)$ (LUMO), $d\sigma^*(Pd_2)/d\sigma^*(PdH)$ (HOMO), and $d\sigma$ (Pd_2) (HOMO –1), and simple selection rules ($u \leftrightarrow g$) indicate that only two low-energy electronic transitions are orbitally allowed, consistent with the UV–vis findings. Computer modelings show the presence of large cavities above and under the Pd_4 plane, described by inner-cavity nonbonded H···H distances of ~5–8 Å.

Key words: cluster, palladium, hydride, structure, spectroscopy.

Résumé : Afin de pouvoir étudier la structure du composé mentionné dans le titre, qui a récemment été identifié comme un agrégat, on a déterminé les spectres RMN du ^{1}H et les spectres vibrationnels et UV–vis du $Pd_2(dppm)_2Cl_2$ (dppm = $Ph_2CH_2PPh_2$), $[Pd_4(dppm)_4(X)_2](BF_4)_2$ (X = Cl, H) et du $[Pd_4(dmpm)_4(H)_2](Br)_2$ (dmpm = $Me_2PCH_2PMe_2$). L'analogue dmpm a été préparé par réaction d $Pd_2(dmpm)_2Br_2$ avec du $NaBH_4$ dans du méthanol, dans une atmosphère inerte; son spectre RMN comporte le nonet attendu (int. rel. 1:8:28:56:70:56:28:8:1) à –5,21 ppm (dans le $(CD_3)_2CO$); ce résultat est en contraste avec les résultats obtenus avec le $Pd_4(dppm)_4(H)_2^{2+}$ pour lequel la valeur de δ est de +5,15 ppm dans le $(CD_3)_2CO$. Cette différence significative est expliquée par la présence de résidus PdH dans la région de déblindage des groupes dppm-phényles. Les spectres vibrationnels dans la région des basses fréquences sont en accord avec une structure centrosymétrique et on observe un étalement de 144 cm^{-1} dans les spectres Raman à TF; on attribue un pic à la vibration $\nu(Pd_2)$ en se basant sur une comparaison avec des données bien établies de M_2-lié dans $Pd_2(dppm)_2Cl_2$ ($(Pd)_2$ = 149 cm^{-1}). Sur la base du comportement qualitatif des maxima et des largeurs de bandes en fonction de la température, on a attribué les deux bandes d'absorption de basse énergie du spectre UV–vis à une transition de type $d\sigma \rightarrow d\sigma^*$. Des calculs d'OM "EH" permettent de prédire quatre niveaux d'OM frontières bien isolées qui sont définies comme $d\sigma^*(Pd_2)/d\sigma^*(PdH)$ (BV + 1), $d\sigma^*(Pd_2)$ (HO), $d\sigma^*(Pd_2)/d\sigma^*(PdH)$ (HO) et $d\sigma(Pd_2)$ (HO –1) et des règles de sélection simple (u $\leftrightarrow$ g) indiquent qu'il n'y a que deux transitions électroniques de basse énergie qui sont permises, ce qui est en accord avec ce qui a été observé dans les spectres UV–vis. Des modélisations à l'ordinateur montrent la présence de larges cavités au-dessus et en-dessous du plan Pd_4 qui est décrit par des distances H···H non liées dans la cavité interne d'environ 5 à 8 Å.

Mots clés : agrégat, palladium, hydrure, structure, spectroscopie.

[Traduit par la Rédaction]

Received May 23, 2000. Published on the NRC Research Press Web site at http://canjchem.nrc.ca on May 29, 2001.

Dedicated to Professor Brian R. James on the occasion of his 65th birthday.

D. Meilleur and P.D. Harvey.[1] Département de Chimie, Université de Sherbrooke, 2500, boul de l'université, Sherbrooke (PQ) JlK 2R1.

[1]Corresponding author (telephone: (819) 821-8001 (ext. 2005), or (819) 821-7092; fax. (819) 821-8017; (e-mail: pharvey@courrier.usherb.ca).

Introduction

In 1983, Kirss and Eisenberg (1) reported the preparation of a new material arising from the reaction of $Pd_2(dppm)_2Cl_2$ with sodium borohydride which analysed as C 57.28%, H 4.68%, P 11.57%, Pd 19.84%, and correctly identified the presence of a hydride species. Although the analysis did not add to 100%, the authors proposed the general formula "PddppmH$_x$". In 1998, our group in collaboration with Mugnier's group (2) in Dijon, more appropriately reformulated the description of this purple compound as

 DOI: 10.1139/cjc-79-5/6-552 © 2001 NRC Canada

$Pd_4(dppm)_4(H)_2Cl_2$. This discovery was important because the cluster is a catalyst or precatalyst for various reactions. Interestingly, the title compound can be electrochemically generated from the reduction of $Pd_2(dppm)_2Cl_2$ in the presence of carbon dioxide in protic media (3). In aprotic media, this reaction leads to the known cluster $Pd_3(dppm)_3(CO)^{2+}$, and carbonate (4). The title cluster can be electrochemically reduced to its neutral form, which in turn catalyses the hydrogen evolution, via the generation of the $Pd_4(dppm)_4(H)_3^+$ species (5). This same trihydride species can also electrocatalytically decompose the formate ion into dihydrogen and carbon dioxide, under oxidation conditions. Kirss and Eisenberg (1) also briefly described experiments on *para*-H_2 during the catalytical hydrogenation of phenylacetylene using this same cluster. Our group[2] recently reported a more complete description of this catalytical activity, and some new interesting and important features. First, under mild conditions, styrene is the only product observed at a turnover rate of ~67 h^{-1}, but at 100 atm, ethylbenzene is obtained selectively and quantitatively. Upon increasing the temperature, a similar behavior is seen, but cluster decomposition interfers with the catalyst. More importanly, no hydrogenation of diphenylacetylene occurs at room temperature and 1 atm. This regioselectively (internal vs. external) is tentatively explained by steric hindrance, which is governed by host–guest interactions somewhat similar to that described for the cyclic $M_3(dppm)_3(CO)^{2+}$ species (M = Pd, Pt) (6, 7). However, upon increasing the pressure to ~8 atm, 1,2-diphenylethane is unexpectedly obtained quantitatively. These surprising new results suggest the presence of a dissociative equilibrium between these $Pd_4(dppm)_4(H)_2^{2+}$ and a hypothetical active intermediate formulated as $Pd_2(dppm)_2(H)(solvent)^+$. Unfortunately, the X-ray structure for the title cluster has never been reported, despite the numerous attempts to obtain single crystals of suitable quality (5).

We now wish to report some key spectroscopic features (electronic, vibrational, NMR) in comparison with related clusters, along with some qualitative EHMO calculations and computer modeling. We will address both the electronic and molecular structures of this important species, in more detail, to corroborate and explain new and important experimental results.

Experimental section

Materials

$Pd_2(dppm)_2X_2$ (X = Cl, Br) (8), $Pd_2(dmpm)_2Br_2$ (9), $[Pd_4(dppm)_4(H)_2](BF_4)_2$ (5), and $[Pd_4(dppm)_4(Cl)_2](BF_4)_2$ (10, 11) have been prepared according to literature procedures. The solvents methanol (BDH), ethanol (BDH), tetrahydrofuran, and 2-methyltetrahydrofuran (both from Aldrich Chemical Co.) were purified according to standard procedures (12).

$Pd_4(dmpm)_4(H)_2(Br)_2$

This compound was prepared using the same methodology employed for $Pd_4(dppm)_4(H)_2(Br)_2$ (2), except dmpm (Aldrich) was used instead of dppm. 100 mg (0.18 mmol) of $Pd_2(dmpm)_2Br_2$ was dissolved in 10 mL of methanol in a cold bath maintained in an ice bath (~4°C) and under inert atmosphere. The Br-derivative was selected because previous works on $Pd_4(dppm)_4(H)_2(X)_2$ (X = Cl, Br)(2) indicated better stability. To this solution, 68 mg (1.8 mmol) of $NaBH_4$ was dissolved in 5 mL of degassed ethanol, and added dropwise by canular to the $Pd_2(dmpm)_2Br_2$ solution. Over a period of 1 h, the bright yellow solution turned dark blue, and a deep purple product was obtained from evaporation to dryness. Yield: 85 mg (83%). UV–vis (MeOH): 500 (m), 570 nm (sh). ^{1}H NMR $(CD_3)_2CO$: 2.81 ppm (br, fwhm = 13.5 Hz, 8H, PCH_2P), 1.72 ppm (s, 48 H, CH_3), –5.21 ppm (nonet, rel. int. = 1:8:28:56:70:56:28:8:1, ^2J (H,P) = 13.5 Hz, 2H, Pd-H). ^{31}P NMR $(CD_3)_2CO$: –10.12 (s). FAB mass obs.: 658, 637, 621, 605, 582, 559, 488; calcd. for: $Pd_2(dmpm)_2Br_2(O)$ 660.8, $Pd_2(dmpm)_3(O)$ 637.2, $Pd_2(dmpm)_3$ 621.2, $Pd_3(dmpm)_2(O)$ 607.6, $Pd_2(dmpm)(Br)(O)$ 580.9, $Pd_2(dmpm)_2Br$ 564.9, $Pd_2(dmpm)_2$ 485.1. The compound proved air-sensitive, and unstable in solutions at room temperature and decomposed slowly with time. The presence of oxide fragments in the mass spectra is not surprising when the samples are handled in air.

Apparatus

The UV–vis spectra were acquired on a Hewlett–Packard 8452A diode array spectrophotometer. The emission spectra were obtained on a PTI LS-100 spectrophotometer. The phosphorescence lifetime measurements were performed on the same PTI instrument using the phosphorimeter assembly. The solid state Raman data were acquired using a Bruker IFS 66/CS FT-IR spectrometer coupled with an FRA 106 FT-Raman module and using a Nd:YAG laser (1064 nm excitation) and a Notch filter (cut off ~50 cm^{-1}). The mass spectra were measured on a Krator MS-50 TCTA spectrometer using an Iontech model FAB 11NF saddle field source operating at 70 kV with 2 mA current. The samples were in thiolglycerol matrices. The NMR data were obtained on a Bruker instrument 300 MHz (^{1}H NMR: 300.15 MHz, ^{31}P NMR: 121.497 MHz). The reference was the residual nondeuterated solvent. The chemical shifts are reported with respect to TMS (^{1}H NMR) and H_3PO_4 (^{31}P NMR).

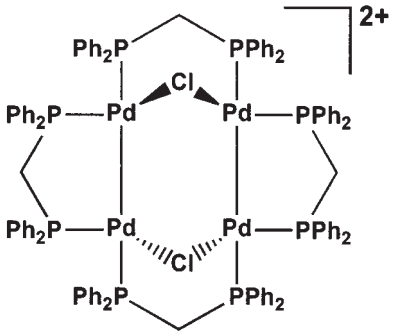
EHMO computations

All the molecular orbital calculations were of the extended Hückel type (13) using a modified version of the Wolfsberg–Helmholz formula (14). The atomic parameters used for C (12), H (12), P (14), and Pd (15, 16) were from the literature. Because of the size of the molecules handled, dppm was replaced by 2 PH_3 groups to simplify the resulting MO diagram. In this case the $P(C_6H_5)_2$ fragments do not contribute to the frontier orbitals and complicate needlessly the MO diagram. This methodology is standard (17). The bond distances and angles are close to those reported in the X-ray structures of the related $Pd_4(dppm)_4(Cl)_2^{2+}$ cluster (10, 11), and are as follows: d (Pd_2) = 2.64 Å, d (Pd···Pd) = 3.60 Å, d (Pd—P_{axial}) = 2.35 Å, and d (Pd—$P_{equa.}$) = 2.23 Å. The d (Pd—H) value was set at 1.80 Å, an average value known for Pd—H species (18).

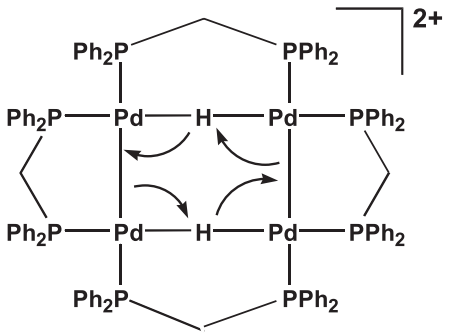
[2] D. Meilleur (MSc. Université de Sherbrooke), unpublished results.

© 2001 NRC Canada

Scheme 1.



Scheme 2.



Computer modelings

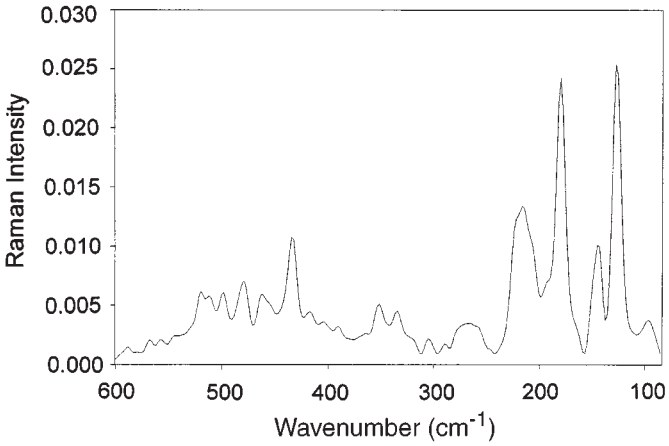
The computer modelings were performed using a commercially available program called PC-Model version 7.0. On occasion, some distances, notably the *d* (Pd_2) and *d* (PdH) values, were fixed to retain the planar structure of the cluster.

Results and discussion

Hydride ^{1}H NMR data

The $Pd_4(dppm)_4(H)_2^{2+}$ cluster exhibits a nonet signal at +5.15 ppm in $(CD_3)_2CO$ of relative intensity 1:8:28:56:70:56:28:8:1 in the ^{1}H NMR spectra (2), which suggests that the cluster has a four-fold symmetry. The T_1 data (0.5 s) (2) confirms the presence of hydrides (19), but the formulation of μ^4-bridging coordinates over and under the Pd_4 plane appears inconsistent as computer models indicate that the H···H separation would be close or within the H_2 bond length (≤0.74 Å) (20), assuming Pd—Pd distances of 2.60–2.70 Å generally encountered for Pd_2 single bonds (21). The highly deshielded hydride ^{1}H NMR signal is also curious, and suggests that the hydrides are located within the deshielding region of the anisotropy cones of the dppm-phenyl substituents. Kirss and Eisenberg (1) noted that the surprisingly deshielded signal was not unprecedented. Indeed Lloyd and Puddephatt (22) reported the hydride resonance for the $[Pt_3(\mu^3\text{-}H(dppm)_3]^+$ cluster at δ 4.16 ppm. To prove this point the dmpm analogue was prepared using the $NaBH_4$ procedure published by Kirss and Eisenberg (1), adapted for dmpm using the $Pd_2(dmpm)_2Br_2$ starting material. This compound exibits the same nonet signal, but appears in the normally expected region for hydride species (at –5.21 ppm in $(CD_3)_2CO$). As with the highly related cluster $Pd_4(dppm)_4(Cl)_2^{2+}$ (Scheme 1) reported by Braunstein et al. (10, 11), the hydrides must be placed more closely to the Pd_4 plane to be within the deshielding region of the phenyl groups. To explain the four-fold symmetry recurrently deduced from the ^{1}H NMR spectra, one should consider a rapid fluxionnality process of the bridged Pd-H-Pd fragments, as shown in Scheme 2. The nonet signal remains even at –70°C.

Fig. 1. Low-frequency FT-Raman (up) and FT-IR (down) spectra of solid $[Pd_4(dppm)_4(H)_2](BF_4)_2$ at room temperature. Experimental conditions: FT-Raman, resolution = 4 cm^{-1}, number of scans = 500.



The ν (Pd_2) data

The IR, Raman and resonance Raman spectra of the Pd_2-bonded dimers $M_2(dppm)_2X_2$ (M = Pd, Pt; X = Cl, Br, $SnCl_3$) and $Pd_2(dppm)_2(SnCl_3)Cl$ have been fully interpretted by Sourisseau and co-workers (23). Using resonance Raman, the authors have securely assigned ν (M_2) which appears between 140 and 150 cm^{-1} in all cases, except for $Pd_2(dppm)_2Br_2$ (ν (Pd_2) = 120 cm^{-1}) (23). $[Pd_4(dppm)_4(H)_2](BF_4)_2$ proved to be extremely laser sensitive in solutions, and resonance Raman spectra could not be acquired in this case. Using FT-Raman, lower laser power, and multi-scan conditions, Raman data for solid samples have been obtained and are shown in Fig. 1 and Table 1. For comparison purposes, both $Pd_2(dppm)_2Cl_2$ and $[Pd_4(dppm)_4(Cl)_2]$-$(BF_4)_2$ are investigated in this work. The comparison of the IR and Raman data, particularly in the low-frequency region associated with skeleton deformations, illustrates clearly the centrosymmetric geometry of the molecules. ν (Pd_2) is easily localized at 144 cm^{-1} as expected, except that the relative intensity is somewhat lower than anticipated. Such behavior is however, not uncommon, and not shocking for 4*d* row elements (24, 25). The structure indicated in Scheme 2 exhibits two independent Pd_2 vibrators (i.e., no coupling between the two should occur), and therefore the symmetric and assymmetric stretches should have about the same frequency. This frequency predicts that the Pd_2 bond length should be in the same order of magnitude as what is generally encountered in the literature for "Pddppm" fragments

© 2001 NRC Canada

Table 1. Low-frequency vibrational data.[a]

$Pd_4(dppm)_4(H)_2^{2+}$		$Pd_2(dppm)_2Cl_2$		$Pd_4(dppm)_4(Cl)_2^{2+b}$	
R	IR	R	IR	R	Assignation
	82 (w)		81 (w)	80 (vs,br)	
97 (m)					skeleton def.
	109 (w,br)	115 (sh)	118 (m)		
127 (s)		125 (sh)	128 (w,sh)	125 (ms)	
144 (m)		149 (s)		?	ν (Pd-Pd)
160 (w,sh)		164 (ms)		165 (ms)	ν (Pd-P)
180 (s)	182 (w)		184 (w)		
		198 (sh)		198 (m)	dppm modes
	205 (w)	209 (mw)			δ (PPh2) + Γ (Ph)
216 (m)	217 (w)	222 (m)	220 (m)	219 (m)	
			247 (ms)		ν $(Pd\text{-}Cl)_{ass}$
266 (w)	262 (w)	258 (sh)			dppm (Γ (Ph))
		269 (m)		271 (mw)	ν $(Pd\text{-}Cl)_{svm}$
	279 (w)	278 (sh)	281 (w)		dppm (Γ (Ph))

[a]The far-IR spectrum of $[Pd_4(dppm)_4(Cl)_2](BF_4)_2$ was not acquired. Code: s (strong), m (medium), w (weak), sh (shoulder), br (broad), ν (stretching), δ (deformation), Γ (torsion), ass (assymmetric), sym (symmetric).

[b]This cluster proved very laser sensitive and the power was reduced to 10 mW at the sample. This peaks are broad, and ν (Pd_2) expected at ~150 cm^{-1} was not observed, presumably hidden under the stronger and broad scattering at 165 cm^{-1} associated with the ν (Pd-P) modes.

Fig. 2. UV–vis spectra of $Pd_2(dppm)_2Cl_2$ in 2-MeTHF at 293 K (---) and 77 K (___).

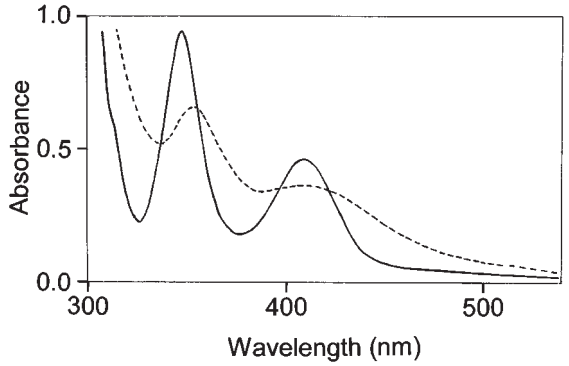
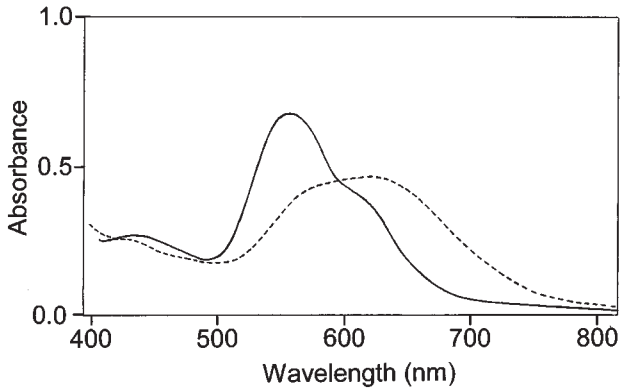


Fig. 3. Uv–vis spectra of $[Pd_4(dppm)_4(H)_2](BF_4)_2$ at 293 K (---) and 77 K (___) in 2-MeTHF.



(2.6 to 2.7 Å) (10, 11, 26, 27). The spectra are provided in the Supporting information.[2]

Numerous attempts to locate ν (Pd-H) in both the IR and Raman spectra were made, but were unsuccessful.

Absorption spectra

Electronic bands associated with $d\sigma \rightarrow d\sigma^*$ electronic transitions for M_2-bonded species generally exhibit low energies, high intensities ($\varepsilon > 10\,000\ M^{-1}\ cm^{-1}$), and are often narrow ($2000 < FWHM < 4000\ cm^{-1}$ at room temperature) (20). The most striking piece of evidence for such a band in the UV–vis spectra is the high sensitivity of the λ_{max} and FWHM, with the temperature. Upon cooling the samples, either in the solid state or in solutions, the $d\sigma \rightarrow d\sigma^*$ bands experience a significant blue shift and decrease in FWHM. This well-known phenomena is due to lower energy "hot bands" of vibronic origin, which disappear upon cooling (28). The presence or absence of such hot bands depends upon the vibrational frequency of the Franck–Condon active modes in the electronic transitions. For $d\sigma \rightarrow d\sigma^*$ transitions, this mode is ν (M_2), which is generally of low frequency, leading to significant hot bands contributions in the $d\sigma \rightarrow d\sigma^*$ spectral envelope. For MLCT or *d*—*d* transitions, higher frequency Franck–Condon active modes are generally present, such as intraligand and M–L stretches. Because of their greater energy gap, the higher vibrational levels are not heavily populated. As a consequence, there is no or little intensity arising from hot bands and upon cooling the samples, the band shape does not change greatly and the hot bands' intensity is weak or nil. For comparison purposes and reference point, the $Pd_2(dppm)_2Cl_2$ UV–vis spectra at 77 and 293K are investigated (Fig. 2). Sourrisseau and co-workers (23) used resonance Raman to demonstrate the $d\sigma \rightarrow d\sigma^*$ assignment of the lowest energy absorption band at ~420 nm. Indeed, there is a ~10 nm blue shift (408 vs. 418 nm) and a notable 2800 cm^{-1} decrease in FWHM (1200 vs. 4000 cm^{-1}, at 77 and 293 K, respectively). Such values are comparable to other Pd_2-bonded species (21). The UV–vis spectra for $[Pd_4(dppm)_4(H)_2](BF_4)_2$ under the same experimental conditions are presented in Fig. 3 in which a drastic change in band shape is depicted for the lowest

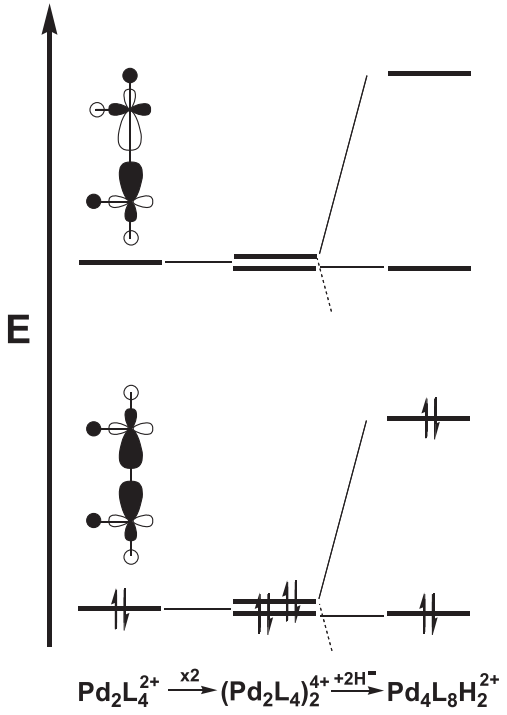
© 2001 NRC Canada

Table 2. Atomic contributions of the frontier MOs for the planar $Pd_4(PH_3)_8(H)_2^{2+}$ model cluster.[a]

EHMO energy	Pd%				P%	H%	
(eV)	d_{x2-y2}	p_x	p_y	s	p_x or p_y (n)	s	Assignation
–8.681	56				24	12	LUMO +1
–9.977	60	12			24		LUMO
–10.657	48		16	8	12	8	HOMO
–11.214	64		8		18		HOMO –1

[a]Contributions less than 1% per atom are not included.

Fig. 4. MO diagrams of the frontier orbitals for the model compounds $Pd_2L_4^{2+}$, $(Pd_2L_4)_4^{4+}$ (intermolecular distance = 3.60 Å), and $Pd_4L_8H_2^{2+}$ (L = PH_3).



energy absorption bands. The blue shifts of the two features are striking (615 vs. 629 nm, and 557 vs. 583 nm, at 77 and 293 K, respectively), and the decrease in FWHM is easily noted as well. Based on these observations $d\sigma \rightarrow d\sigma^*$ assignments can be made for these bands.

Frontier MOs

Scheme 2 best describes the $Pd_4(dppm)_4(H)_2^{2+}$. The static molecule exhibits two Pd_2 single bonds and two Pd-H-Pd bridges, and is very probably planar. Using d (PdH) = 1.80 Å (an average value found for other Pd—H species) (19) and d (Pd2) = 2.64 Å, the model compound $Pd_4(\mu\text{-}H)_2(PH_3)_8^{2+}$ is designed for EHMO computational purposes.

The analysis indicates the presence of four well-separated frontier MO levels depicted as LUMO +1, LUMO, HOMO, and HOMO –1. They originate from interactions between the HOMO and the LUMO of two double-T shaped $Pd_2L_4^{2+}$ fragments (L = PH_3), as shown in Fig. 4. These precursor MOs exhibit atomic contributions primarily localized within the metal centers (~75%), using the d_{x2-y2}, p_x, and p_y orbitals. Minor contributions from the nonbonding lone pairs of the phosphine ligands (either as p_x or p_y depending upon the molecular axis), are also calculated. The $Pd_2L_4^{2+}$ HOMO and LUMO show the expected bonding $d\sigma$ and antibonding $d\sigma^*$ M_2 interactions, respectively, in agreement with previous studies on similar systems (21, 29).

The side-by-side dimerization of the $Pd_2L_4^{2+}$ fragments provides the intermediate species $Pd_2L_4^{4+}$. These are placed at 3.60 Å from each other allowing the hydrides to occupy the vacant sites half way between the two dimers. At such a distance, practically no or very weak Pd···Pd interactions are anticipated (30). Indeed, the $(Pd_2L_4)_2^{4+}$ MO diagram consists of two degenerated HOMO and LUMO levels (Fig. 4).

The addition to the two hydride centers in this $(Pd_2L_4)_2^{4+}$ frame lead to six MO levels. The bonding PdHPd interactions (+++ and —-) generate two strongly stabilized MOs (not shown in Fig. 4). Similarly, the antibonding PdHPd interactions (+-+ and -+-) produce two destabilized MOs (HOMO and LUMO +1). The remaining two MOs are the HOMO –1 and LUMO and do not involve any atomic contribution from the hydrides (Table 2). Their interactions are essentially nonbonding, and therefore have no effect on either the atomic contributions of three MOs, nor their relative energies (Fig. 4). The overall result is that the lowest electronic transition energy should be smaller in the title compound than that of the dimeric $Pd_2L_4^{2+}$. This observation is readily corroborated by the UV–vis spectra of the $Pd_2(dppm)_2Cl_2$ and $Pd_4(dppm)_4(H)_2^{2+}$ complexes, where the lowest energy absorptions are located at 420 and 600 nm, respectively. In addition, for a $D2h$ local symmetry, the LUMO +1, LUMO, HOMO, HOMO –1 possess the u, g, u and g symmetry, respectively. Selection rules indicate that only two orbitally allowed $u \leftrightarrow g$ transitions are possible (HOMO –1 $\rightarrow$ LUMO +1, and HOMO $\rightarrow$ LUMO), and therefore only two bands should be observed. This is obviously the case (Fig. 3). The atomic contributions are listed in Table 2, and orbital drawings are presented in Fig. 5.

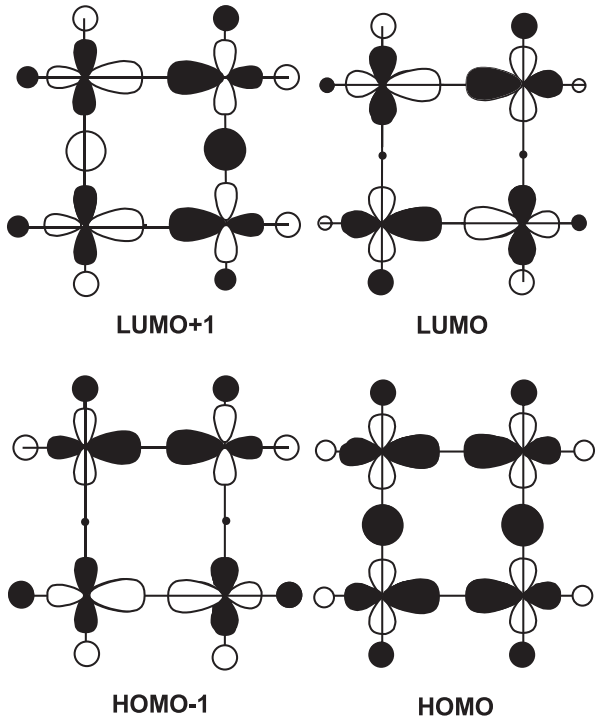
Upon the one- or two-electron reduction of the title cluster, this MO diagram predicts a weakening in the Pd_2 bond, as the bond order decreases formally by a half with no influence to the hydrides. There should be no cluster dissociation due to the dppm ligands and the presence of Pd2 bonding during reductive electrolysis to $Pd_4(dppm)_4(H)_2^0$. This is indeed the case as the reductive waves are found electrochemically reversible (2) and that this neutral species could be characterized from ^{31}P NMR (5). In addition, the related $Pd_4(dppm)_4(S)$ which also contains a Pd_4^{2+} core, has successfully been characterized crystallographically (31) and exhibits a rectangular geometry with longer Pd—Pd bonds (2.675(1) Å) in comparison to that reported for $Pd_4(dppm)_4(Cl)_2^{2+}$ (2.594(2) Å).

© 2001 NRC Canada

Table 3. Comparison of the modelized structures.

	$Pd_4(dppm)_4(Cl)_2^{2+}$		$Pd_4(dppm)_4(H)_2^{2+}(C_{2v})$
	X-ray (11,12)	Modelings	Modelings
d (Pd—Pd) (Å)	2.594	2.63	2.65
d (Pd···Pd) (Å)	3.742	3.20	3.30
d $(Pd—P)_{axial}$ (Å)	2.351 (av)	2.32	2.35
d $(Pd—P)_{equa.}$/(Å)	2.225 (av)	2.28	2.35
d (Pd—X) (Å)	2.422, 2.391	2.30	1.65
∠ Pd-X-Pd (°)	102.1	88	167

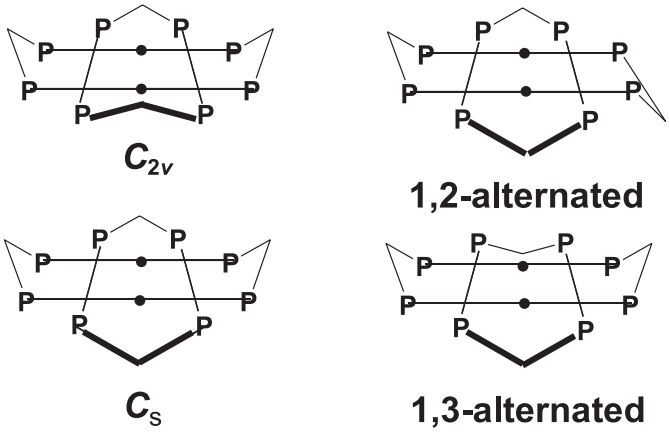
Fig. 5. MO drawings of the LUMO +1, LUMO, HOMO and HOMO –1 for $Pd_4L_8H_2^{2+}$ model compound (L = PH_3). The atomic contributions are listed in Table 2.



A two-electron oxidation of the title cluster should, on one hand, also decrease the Pd—Pd bond order by a half as well, but more importantly it should also remove electrons from an MO exhibiting some significant hydride character. One can also predict that a two-electron oxidation should not lead to cluster dissociations for the same bridging ligand and Pd_2-bonding, but H_2 loss is highly anticipated. The cyclic voltammograms do indeed exhibit an irreversible two-electron wave for $Pd_4(dppm)_4(H)_2^{2+}$ (2), and the FAB analysis of the bulk electrolysis product, provides clear evidence that the Pd_4 cluster is not dissociated, as expected (Supporting information)[2].

Under these frontier orbitals lie many other MO levels which are close in energy to each other (16 MOs within 1 eV). These are the expected $d\pi$, $d\pi^*$, $d\delta$, and $d\delta^*$ orbitals issued from M_{2-} bonding interactions. Below these levels are the two $d\sigma(Pd_2)/d\sigma(PdH)$ and $d\sigma^*(Pd_2)/d\sigma^*(PdH)$ MOs briefly mentionned above. None of these sublevels will be discussed in this work.

Scheme 3.



Molecular modelings

The title cluster may exist under four different conformations depending upon the relative orientation of the dppm-methylene groups (Scheme 3). These are called the C_{2v}, C_s, 1,2-alternated, and 1,3-alternated structures in this work. The $Pd_4(dppm)_4(Cl)_2^{2+}$ (10, 11) and $Pd_4(dppm)_4(S)$ (31) clusters are found in their 1,2- and 1,3-alternated structures, respectively, in the solid state. The ^1H NMR data do not exhibit the presence of a coupling constant ^2J (HCH) as the ^{31}P-irradiated CH_2 signal exhibits a singlet of 1.5 width (2). The results clearly indicate that these protons have the same chemical environment, and must be fluxional as well. This behavior is not uncommon for $Pt_4(dppm)_4$ clusters (32).

All four structures were modelized, and a comparison between the known compound ($Pd_4(dppm)_4(Cl)_2^{2+}$) and its computer modeling was made (Table 3). A positive charge of +1 was added to the Pd atoms, and a fixed distance of 3.60 Å between the non-Pd_2-bonded atoms, was set. After minimization, this fixed distance was removed, and the model was reminimized. The comparison between the X-ray and computed data is reasonable as the bond distances of the skeleton are all within ±0.06. The Pd-Cl-Pd fragment was somewhat poorly modeled (Table 3), as the program does not include the ionic character of the Pd—Cl coordination bond. As a result the computed Pd···Pd, and Pd—Cl distances, and Pd-Cl-Pd angles were smaller than expected. For the $Pd_4(dppm)_4(H)_2^{2+}$ structures, the computed data are very similar in all four conformations and only one typical example is provided in Table 2. The interrelated Pd—H and Pd···Pd distances are shorter than expected, but are not disturbing as the 1.65 Å distance for a bridged palladium

© 2001 NRC Canada

Fig. 6. CPK model of the 1,3-alternated structure. This geometry provides the smallest opening to the Pd_4H_2 center, on one face.

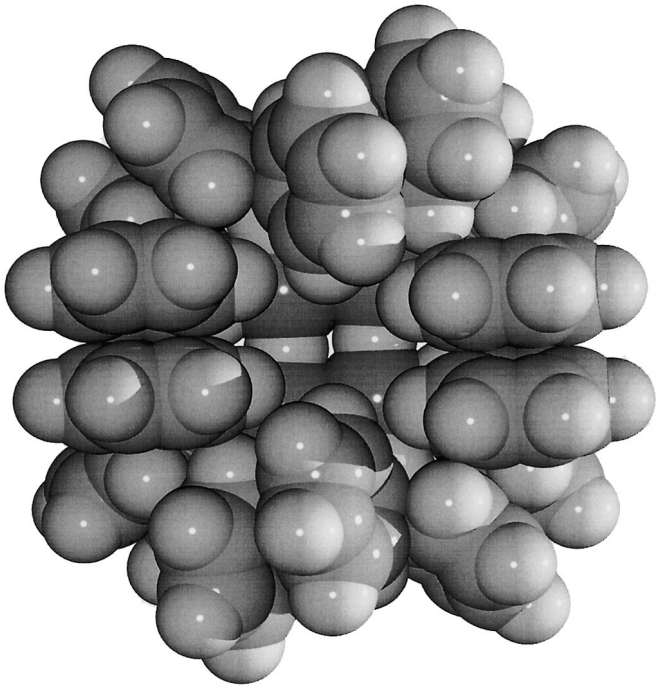
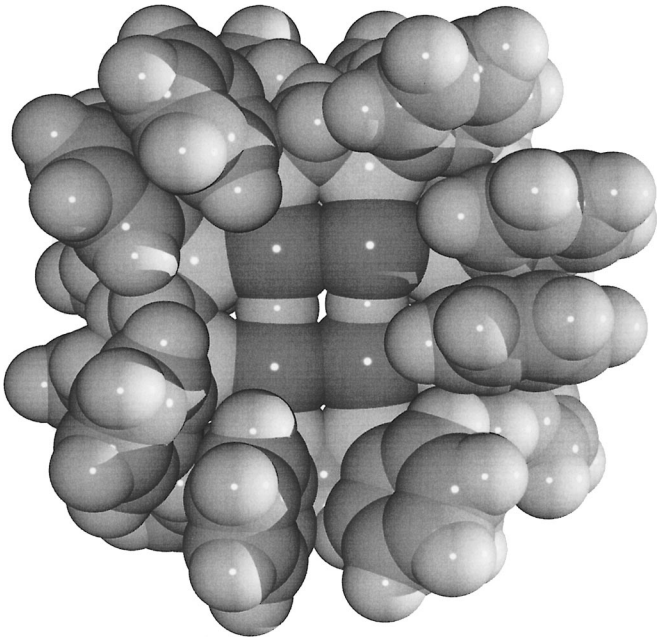


Fig. 7. CPK model of the C_s structure. This geometry provides the largest openings to the Pd_4H_2 center, for both faces.



hydride bond lies at the lower end of what is known in the literature (18).

All four models exhibit two quasiplanar unsaturated Pd_4H_2 faces located well inside picket-fence cavities described by the dppm-phenyl groups, similar to that described for the $Pd_3(dppm)_3(CO)^{2+}$ species (6, 7). Depending on the structure, the cavity openings vary expectedly, where the C_s geometry offers the greatest access to the Pd_4H_2 center, while the 1,3-alternated one, provides the least for one face. Inner-cavity nonbonded H···H distances in the order of 5.5–8.7 Å (typically 6.5–7.5 Å), are computed for the C_s structure. The 1,3-alternated structure exhibits two different cavities: a large and a small one. The inner-cavity nonbonded H···H distances are in the order of 7.6–8.0 Å for the large cavity, while separations of 4.6–5.1 Å are calculated for the smaller one. The two other structures exhibit large cavities somewhat similar in dimensions to that of the C_s model. Typical examples are shown in Figs. 6 and 7 for the two cases discussed. Taking into account the uncertainties of the calculated models, the computation results clearly show the presence of large openings allowing substrates of about 5–6 Å in size to penetrate the cavities, and leaving access for interactions with the Pd_4H_2 faces.

Concluding remarks

This work has compiled spectroscopic results which rationalize the $Pd_4(dppm)_4(H)_2^{2+}$ structure, and based upon that structure simple EHMO analysis has reassuringly confirmed, or supported, many of the experimental findings. The most important feature is undoubtedly the presence of unsaturated sites at the Pd centers, somewhat analoguous to the well known reactive Pd—Pd bonded $Pd_2(dppm)_2Cl_2$ dimer. The presence of cavities above and under the Pd_4 plane is also evident, and explains in part, the selectivity for catalytical hydrogenation of phenylacetylene vs. diphenylacetylene under mild conditions. Further attemps to obtain suitable crystals for X-ray structure determination, and a full investigation on the reactivity and catalytical activity are clearly in order.

Acknowledgments

This research is supported from the Natural Sciences and Engineering Research Council of Canada (NSERC) and the Fond Concerté pour l'Avancement de la Recherche (FCAR).

References

1. R.U. Kirss and R.Eisenberg. Inorg. Chem. **28**, 3372 (1983).
2. I. Gauthron, J. Gagnon, T. Zhang, D. Rivard, D. Lucas, Y. Mugnier, and P.D. Harvey. Inorg. Chem. **37**, 1112 (1998).
3. I. Gauthron. Ph.D. Thesis. Université de Bourgogne, Dijon France. 1997.
4. I. Gauthron, Y. Mugnier, K. Hierso, and P.D. Harvey. New. J. Chem. **22**, 237 (1998).
5. D. Meilleur, D. Rivard, P.D. Harvey, I. Gauthron, D. Lucas, and Y. Mugnier. Inorg. Chem. **39**, 2909 (2000).
6. T. Zhang, M. Drouin, and P.D. Harvey. J. Chem. Soc. Chem. Commun. 877 (1996).
7. R. Provencher, K.T. Aye, M. Drouin, J. Gagnon, N. Boudreault, and P.D. Harvey. Inorg. Chem. **33**, 3686 (1994), and refs. therein.
8. R.G. Holloway, B.R. Penfold, R. Cotton, and M.J. McCormick. J. Chem. Soc. Chem. Commun. 485 (1976).
9. (*a*) J.A. Davies, S. Dutremez, and M. Vilmer. J. Prakt. Chem. Chem. Ztg. **334**, 34 (1992); (*b*) M.L. Kullberg, C.P. Kubiak. Organometallics **3**, 632 (1984); (*c*) M.L. Kullberg, F.R. Lemke, D.R. Powell, C.P. Kubiak. Inorg. Chem. **24**, 3589 (1985).
10. P. Braunstein, M.A. Luke, A. Tiripicchio, and M.T. Camellini. Angew. Chem. **26**, 768 (1987).

© 2001 NRC Canada

11. P. Braustein, M.A. Luke, A. Tiripicchio, and M.T. Camellini. New. J. Chem. **12**, 429 (1988).
12. (*a*) D.D. Penin, W.L.F. Armarego, and D.R. Penin. Purifications of laboratory chemicals. Pergamon Press, Oxford. 1966; (*b*) A.J. Gordon and R.A. Ford. The chemist's companion, a handbook of practical data, techniques, and references. Wiley, New York. 1972. p. 436.
13. (*a*) R. Hoffmann and W.N. Lipscomb. J. Chem. Phys. **36**, 2179 (1962); (*b*) R. Hoffmann and W.N. Lipscomb. J. Chem. Phys. **36**, 2872 (1962); (*c*) R. Hoffmann. J. Chem. Phys. **39**, 1397 (1963).
14. J.H. Ammeter, H.B. Burgi, J.C. Thibeault, and R. Hoffmann. J. Am. Chem. Soc. **100**, 3686 (1978).
15. R.H. Summerville, and R. Hoffmann. J. Am. Chem. Soc. **98**, 7240 (1976).
16. K. Tatsumi, R. Hoffmann, A. Yamamoto, and J.K. Stille. Bull. Chem. Soc. Jpn. **54**, 1857 (1981).
17. C. Mealli. J. Am. Chem. Soc. **107**, 2245 (1985).
18. V.V. Grushin. Chem. Rev. **96**, 2011 (1996).
19. P.G. Jessop and R.H. Morris. Coord. Chem. Rev. **121**, 155 (1992).
20. K.P. Huber and G. Herzberg. Molecular spectra and molecular structure constants of diatomic molecules. Van Nostrand, New York. 1979.
21. P.D. Harvey and Z. Murtaza. Inorg. Chem. **32**, 4721 (1993), and refs. therein.
22. B.R. Lloyd and R.J. Puddephatt. J. Am. Chem. Soc. **107**, 7785 (1985).
23. O.L. Alves, M.-C. Vitorge, and C. Sourrisseau. Nouv. J. Chim. **7**, 231 (1983).
24. R.J.H. Clark, A.J. Hempleman, and C.D. Flint. J. Am. Chem. Soc. **108**, 518 (1986).
25. V.M. Miskowski, R.F. Dallinger, G.G. Christoph, D.E. Morris, G.H. Spies, and W.H. Woodruff. Inorg. Chem. **26**, 2127 (1987).
26. R.G. Holloway, B.R. Penfold, R. Cotton, and J. McCormick. J. Chem. Soc. Chem. Commun. 485 (1976).
27. M.M. Olmstead, L.S. Brenner, H. Hope, and A.L. Balch. Inorg. Chim. Acta, **32**, 193 (1979).
28. V.M. Miskowski, T.P. Smith, T.M. Loehr, and H.B. Gray. J. Am. Chem. Soc. **107**, 7925 (1985).
29. R. Provencher and P.D. Harvey. Inorg. Chem. **35**, 2113 (1996).
30. D. Perreault, M. Drouin, A. Michel, and P.D. Harvey. Inorg. Chem. **32**, 1903 (1993).
31. M. Maekawa, M. Munakata, T. Kuroda-Sowa, and T. Goto. Inorg. Chim. Acta, **239**, 159 (1995).
32. T. Zhang and P.D. Harvey. J. Cluster Sci. **9**, 165 (1998), and refs. therein.

© 2001 NRC Canada

Study of the hydroformylation of 2,5-dihydrofuran catalyzed by rhodium diphosphine complexes

Inmaculada del Río, Piet W.N.M. van Leeuwen, and Carmen Claver

Abstract: Rhodium diphosphine systems, including chiral ones, were used as catalyst precursors for the hydroformylation of 2,5-dihydrofuran. The effect of the reaction conditions and the bite angle on the activity and selectivity of the reaction were studied. The solution structures of the species present have been investigated spectroscopically through HP-NMR experiments during the hydroformylation reaction.

Key words: hydroformylation, dihydrofuran, rhodium complexes, diphosphines, HP-NMR.

Résumé : On a utilisé des systèmes diphosphines de rhodium, y compris des systèmes chiraux, comme précurseurs de catalyseurs pour l'hydroformylation du 2,5-dihydrofurane. On a étudié l'effet des conditions de la réaction et l'angle d'accès sur l'activité et la sélectivité de la réaction. On a étudié les structures des espèces présentes en solution à l'aide de la spectroscopie, impliquant des expériences de RMN du phosphore et de l'hydrogène au cours de la réaction d'hydroformylation.

Mots clés : hydroformylation, dihydrofurane, complexes du rhodium, diphosphines, RMN du phosphore et de l'hydrogène.

[Traduit par la Rédaction]

Introduction

Considerable effort has been made to synthesize derivatives of heterocyclic compounds such as tetrahydrofuran and tetrahydropyran (1–3). These derivatives are of interest for the preparation of intermediates for the synthesis of natural products or pharmaceuticals (4).

The great development of the rhodium-catalyzed hydroformylation is shown for the amount of modified systems using monofunctional and chelate phosphorus ligands. Furthermore, the hydroformylation reactions have been applied for different substrates to obtain intermediates in organic syntheses (5–7). The hydroformylation of heterocyclic olefins would provide a potential synthetic tool for preparing derivatives of tetrahydrofuran and tetrahydropyran.

Few systems have proved to be successful in the hydroformylation of internal cyclic alkenes. In most cases, selectivities are only moderate, probably because of the drastic reaction conditions required (8, 9).

In the case of the hydroformylation of dihydrofurans with rhodium/phosphine catalysts, high pressures and temperatures have been used and low selectivities towards tetrahydrofuran-2-carbaldehyde were obtained (10, 11).

In recent years, the use of bulky phosphites in rhodium–phosphorus catalytic systems has been found to be useful in the hydroformylation of cycloalkenes (12–15).

We reported on the hydroformylation of 2,3-dihydrofuran and 2,5-dihydrofuran under mild conditions using rhodium systems with PPh_3 and tris(*o*-*tert*-butylphenyl)phosphite ($P(OC_6H_4$-2-*t*-$Bu)_3$) as catalyst precursors (16, 17). By modifying the reaction conditions we succeeded in selectively introducing a formyl group in the 2- or 3-position of tetrahydrofuran, starting from 2,3- and 2,5-dihydrofuran (16). The influence of the phosphorus co-catalyst, pressure, and temperature on the reaction selectivity has also been studied and a reaction mechanism proposed (17).

Although only the tetrahydrofuran-3-aldehyde would be expected to form in the hydroformylation of 2,5-dihydrofuran, it has been shown (16) that the tetrahydrofuran-2-aldehyde can also form through an isomerization process (Scheme 1). This isomerization is taking place simultaneously with the hydroformylation reaction. When the 2,5-dihydrofuran reacts with the rhodium hydride complex, the 3-alkyl intermediate is formed, which can evolve to the 2,3-dihydrofuran via the β-hydride elimination reaction. This new substrate can evolve to give either of the metal alkyl intermediates, 2-alkyl or 3-alkyl. The 3-alkyl intermediate is thermodynamically favoured according to Ojima et al. (18) because the metal—carbon bond is formed at the carbon with the highest electron density regardless of the phosphorus ligand used. However, because the C-2—metal bond in the 2-alkyl intermediate is more polarized than the C-3—metal bond in the 3-alkyl intermediate, the acyl complex forms more quickly from the 2-alkyl than from the 3-alkyl rhodium intermediate (Scheme 1).

Received August 8, 2000. Published on the NRC Research Press Web site at http://canjchem.nrc.ca on May 23, 2001.

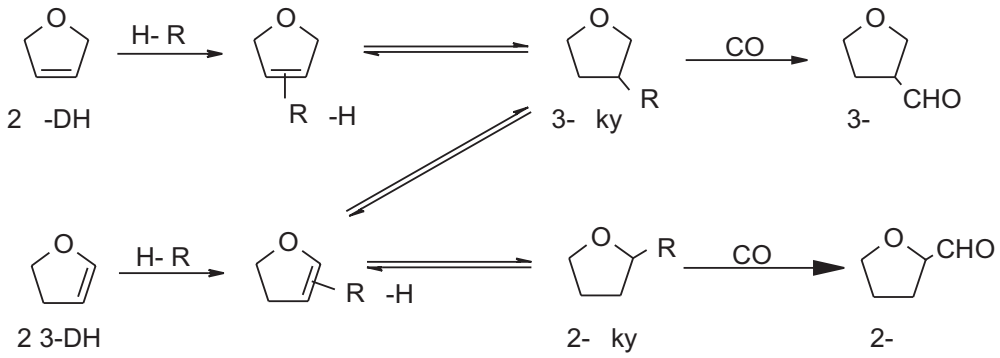
Dedicated to Professor Brian James on the occasion of his 65th birthday.

I. del Rio and C. Claver.[1] Departament de Química Física i Inorgànica, Universitat Rovira i Virgili, Pl. Imperial Tarraco I, 43005 Tarragona, Spain.
P.W.N.M. van Leeuwen. Institute of Molecular Chemistry, Nieuwe Achtergracht 166, NL-1018 WV Amsterdam, The Netherlands.

[1]Corresponding author (telephone: +34-977-559574; fax: +34-977-559563; e-mail: claver@quimica.urv.es).

 DOI: 10.1139/cjc-79-5/6-560 © 2001 NRC Canada

Scheme 1.



Therefore, according to the proposed model, there is a fast preequilibrium between the metal alkyl species, via the β-elimination process. The selectivity is dominated by the rate of formation of the acyl complex, provided that the hydrogen pressure is high enough for the hydrogenolysis of the metal–acyl complex not to be the rate-determining step (Scheme 1).

The asymmetric hydroformylation of heterocyclic olefins has been studied very little and enantiomeric excesses below 10% ee have been published (19, 20). Only a successful enantioselective hydroformylation of oxygen- and nitrogen-containing internal cyclic olefins was reported in which phosphine-phosphite ((*R*,*S*)-BINAPHOS and (*R*,*S*)-BIPHEMPHOS) were used as ligands (21). Enantiomeric excesses between 60–70% were obtained in the hydroformylation of 2,5-dihydrofuran, using these rhodium phosphine-phosphite systems.

If diphosphines are used as ligands in homogeneous catalysis, not only is there the possibility of chiral control but also the possibility of stabilizing a specific geometry that depends on the bite angle of the diphosphine. In recent years a correlation has been observed between the bite angle of the diphosphines and the catalytic activity or selectivity in rhodium-catalyzed hydroformylation (22–25), nickel hydrocyanation (26, 27), palladium-catalyzed allylic alkylation (28), cross coupling reactions of Grignard reagents with organic halides (29, 30), and palladium hydroxycarbonylation (31). In hydroformylation, ligands with wider bite angles tend to give little isomerization of the alkenes at relatively low ligand-to-metal ratios, while retaining a high activity.

Nowadays high-pressure NMR is often used to identify organometallic compounds under high pressure, although the reaction intermediates during rhodium-catalyzed hydroformylation have scarcely been characterized (32–37).

We report here a study of the hydroformylation of 2,5-dihydrofuran using rhodium diphosphine systems as the catalytic precursor. We studied the effect of the bite angle on the activity of the system and tested different chiral diphosphines. We performed in situ HP-NMR experiments during the catalysis to determining the nature of the catalytic species.

Experimental section

General techniques

Rhodium complexes were synthesized using standard Schlenk techniques under a nitrogen atmosphere. The diphosphines DPEphos and Xantphos were synthesized via published methods (23). Solvents were distilled and deoxygenated before use. All other reagents were commercial samples and were used as purchased. Gas chromatography analyses were performed on a Hewlett–Packard 5840A, a gas chromatograph with a flame ionization detector and an Ultra-2 (5% diphenylsilicone:95% dimethylsilicone) (25 m × 0.2 mm Ø) capillary column.

Catalysis

Hydroformylation experiments were carried out in a specially designed autoclave with magnetic stirring and electrical heating. The catalytic solution was contained in a glass vessel. The inside part of the cover was made from Teflon® to protect the solution from direct contact with the stainless steel. These experiments were not performed at constant pressure, but for the amount of substrate used the drop of pressure was never more than 3 bar.

Standard experiment

A solution of the substrate (5 mmol) (previously stirred with alumina for 24 h), the catalyst (0.05 mmol), and the diphosphine were placed in the evacuated autoclave. The gas mixture ($CO–H_2$) was introduced, the system was heated, and the stirring initiated when the thermal equilibrium was reached. Conversion and regioselectivities were determined by GC analysis of the crude samples.

Determination of the enantiomeric excess

The reaction mixture was treated to obtain the corresponding carboxylic acids as has been previously reported (21). The crude acid was dissolved in ether and treated with diazomethane in an Aldrich MNNG diazomethane generation apparatus (38) to afford the methyl ester. The enantiomeric excess was determined by ^{1}H NMR spectroscopy using $Eu(hfc)_3$ as the chiral shift reagent. The absolute configuration of the enantiomers was previously determined by comparing the optical rotation of the corresponding alcohol by reduction of the methyl ester (21).

The in situ HP-NMR experiments

In a typical experiment, the in situ HP-NMR experiments were carried out in a sapphire tube (ϕ = 10 mm). The rhodium complex $[Rh(\mu\text{-}OMe)(COD)]_2$ (0.04 mmol), dppb (0.08 mmol), and substrate (0.05 mmol) were dissolved in toluene-d_8 (2 mL) under nitrogen, and the sapphire tube was

© 2001 NRC Canada

closed. After pressurizing the mixture with H_2–CO, the tube was placed in the NMR spectrometer and the spectra were recorded.

Results and discussion

Catalysis experiments

The catalytic species were prepared in situ by mixing $[Rh(\mu\text{-OMe})(COD)]_2$ with the corresponding diphosphine. After a screening with different diphosphines, the diphosphine dppb (bis(diphenylphosphino)butane) was chosen to study the effect of the parameters and the reaction conditions on the hydroformylation of 2,5-dihydrofuran with Rh–diphosphine systems.

Preliminary experiments were undertaken to establish how the P-P:[Rh] molar ratio affected the hydroformylation of 2,5-dihydrofuran with dppb (Table 1).

It is important to note that when the rhodium precursor was used without the phosphorus ligand, conversion into aldehyde was high but the reaction was not regioselective (Table 1, entry 1). A P-P:[Rh] molar ratio of 1 was required to obtain high conversion and regioselectivity in the tetrahydrofuran-3-aldehyde (Table 1, entry 3). When the P-P:[Rh] ratio was increased the regioselectivity increased to 100% but the conversion decreased (Table1, entries 4, 5). This effect contrasts with previous results in the hydroformylation styrene where an excess of phosphine is required to allow the active species to be formed (39, 40).

The fact that the regioselectivity increased as the P-P:[Rh] molar ratio increased can be explained in terms of ligand dissociation phenomena (Scheme 1). Since an excess of ligand shifts the equilibrium toward coordinatively saturated species, the β-elimination processes are not favoured.

The effects of pressure and temperature were examined using dppb as the ligand (Table 2). At 30 bar, the conversion decreased when the temperature decreased. However, the regioselectivity in tetrahydrofuran-3-carbaldehyde increased (Table 2, entries 6–9). To obtain total regioselectivity in the 3-formyl derivative of the tetrahydrofuran, the temperature had to be 40°C but conversion was only 51% (Table 2, entry 9). There was a slightly increase in conversion when the total pressure of the system was increased (Table 2, entries 9, 10). Finally, conversion and of regioselectivity were 96 and 99%, respectively at 34 bar of CO–H_2 pressure, 50°C of temperature, and substrate:Rh = 100. The substrate:Rh ratio was increased to 200 but the conversion fell to 84% and the regioselectivity to 90:10.

The effect of pressure and temperature on the hydroformylation of this substrate can be explained in terms of the proposed mechanism for the hydroformylation of 2,5-dihydrofuran (Scheme 1). When the temperature was decreased, selectivity for the formation of the tetrahydrofuran-3-aldehyde was higher (Table 2, entries 6–9). Thus, in the range of temperatures explored it seems that only the β-elimination is significantly affected. Therefore by increasing the temperature, a fast preequilibrium is established between the metal alkyl species, via the β-elimination process, and the regioselectivity towards the tetrahydrofuran-3-aldehyde decreases. At constant temperature (Table 2, entries 9, 10) the total pressure increased from 30 to 60 bar, and the rate of formation of the rhodium acyl species increased because of the higher partial pressure of CO. In this situation, CO insertion is much faster than β-elimination. In our case, the temperature was relatively low (40°C) and the β-elimination was not predominant so the regioselectivity was not affected, and there was only a slight increase in conversion into aldehydes.

Once the conditions allowing high conversion and regioselectivity had been selected, the effect of the bite angle of different diphosphines was studied (Table 3).

Diphosphines with bite angles smaller than 90° such as dppe and dppp (Table 3, entries 12, 13) provided low conversions to aldehyde. Systems containing diphosphines with a wider bite angle such as dppb, 1,1′-bis(diphenylphosphino)ferrocene (dppf), and 9,9-dimethyl-4,6-bis(diphenylphosphino)xanthene (Xantphos) provided high conversions (Table 3, entries 14–16). After 6 h of reaction activity was seen to increase with the bite angle (Table 3).

Table 1. Influence of the P-P:Rh molar ratio on conversion and regioselectivity in the hydroformylation of 2,5-dihydrofuran with dppb.[a]

Run	P-P:Rh	*P* (bar)	Conv. (%)	3-Ald. (%)[b]
1	—	60	96	51
2	0.5	60	84	71
3	1	60	97	90
4	1.5	60	37	100
5	2.5	80	5	100

[a]Conditions: 0.05 mmol $[Rh(\mu\text{-OMe})(COD)]_2$, 5 mmol 2,5-dihydrofuran, 15 mL of dichloroethane, T = 80°C, t = 20 h.
[b]% Tetrahydrofuran-3-carbaldehyde.

Table 2. Effect of the pressure and temperature on the hydroformylation of 2,5-dihydrofuran with the [Rh]–dppb system.[a]

Run	*P* (bar)	*T* (°C)	Conv. (%)	3-Ald. (%)[b]
6	30	80	97	84
7	30	60	97	94
8	30	50	90	99
9	30	40	51	100
10	60	40	59	100
11	34	50	96	99

[a]Conditions: 0.05 mmol $[Rh(\mu\text{-OMe})(COD)]_2$, 5 mmol 2,5-dihydrofuran, in 15 mL of dichloroethane, t = 20 h, P-P:Rh = 1.
[b]% Tetrahydrofuran-3-carbaldehyde.

Table 3. Effect of the bite angle on the hydroformylation of 2,5-dihydrofuran with diphosphines.[a]

Run	Phosphine	Bite angle[b] (°)	Conv. (%) (6 h)	Conv. (%) (20 h)	3-Ald. (%)[c]
12	dppe	78	26	71	97
13	dppp	86	22	79	99
14	dppb	98	42	96	99
15	dppf	99	56	96	99
16	Xantphos	112	79	97	96

[a]Conditions: 0.05 mmol $[Rh(\mu\text{-OMe})(COD)]_2$, 5 mmol 2,5-dihydrofuran, in 15 mL of dichloroethane, P = 34 bar, T = 50°C, P-P:Rh = 1.
[b]Calculated by molecular modelling (46).
[c]% Tetrahydrofuran-3-carbaldehyde.

© 2001 NRC Canada

Scheme 2.

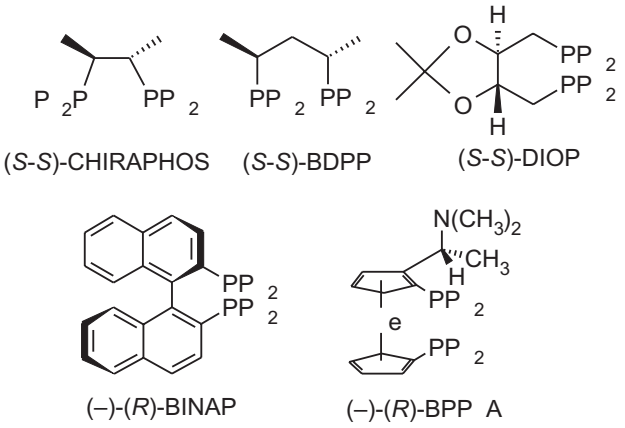


Table 4. Hydroformylation of 2,5-dihydrofuran with chiral diphosphines.[a]

Run	Phosphine	Conv. (%)	3-Ald. (%)[b]	ee (%)
17	CHIRAPHOS	98	98	3 *R*
18	BDPP	91	98	14 *S*
19	DIOP	96	94	3 *R*
20	BINAP	100	88	5 *R*
21	BPPFA	100	99	4 *S*

[a]Conditions: 0.05 mmol [Rh(μ-OMe)(COD)]$_2$, 5 mmol 2,5-dihydrofuran, in 15 mL of dichloroethane, P = 34 bar, T = 50°C, t = 20 h, P-P:Rh = 1.
[b]% Tetrahydrofuran-3-carbaldehyde.

Xantphos-type diphosphines have been shown to give excellent regioselectivities in the rhodium-catalyzed hydroformylation of 1-octene (23). In the hydroformylation of 2,5-dihydrofuran under the conditions chosen, it seems that the bite angle has no influence on the regioselectivity (Table 3) as for all ligands tested the selectivity is high. Within the Xantphos series of ligands one also observes an increase of the rate at wider bite angles, which is ascribed to the stabilization of the unsaturated species obtained after CO dissociation (25).

We tested several chiral diphosphines in the asymmetric hydroformylation of 2,5-dihydrofuran (Scheme 2).

Conversions into aldehydes were higher than 90% with regioselectivities as high as 99% in the tetrahydrofuran-3-aldehyde. However, only in the case of BDPP the enantiomeric excess was 14% (Table 4). It has been previously found that [Rh]–BDPP systems provide enantiomeric excesses that are higher than other rhodium diphosphine systems in the hydroformylation of styrene (39, 40).

Rhodium systems with DIOP and related ligands have previously been used in the hydroformylation of 2,5-dihydrofuran at higher pressures and temperatures. The enantiomeric excesses observed were in the same range (3 to 4%) (19, 20).

It has been reported that an excess of chiral ligand may increase the enantiomeric excess (33–37). However, when the same experiments were performed with P-P:Rh = 1.25 conversions into aldehydes were very low. It seems that an excess of ligand quenches the system forming species that are not active in the hydroformylation reaction.

Scheme. 3

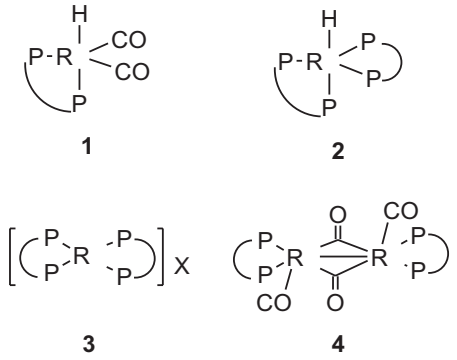


Table 5. ^{31}P and ^{1}H NMR data of the species formed in the reaction of [Rh(μ-OMe)(COD)]$_2$ with dppb under hydroformylation conditions.[a]

	^{31}P NMR		1H NMR		
Complex	δ	$^{1}J_{Rh-P}$ (Hz)	δ	$^{1}J_{H-Rh}$ (Hz)	$^{2}J_{P-H}$ (Hz)
1	26.7	116	–8.8	11	49
2	19.6	147	–9.3	—	—
3	16.7	131	—	—	—
4	13.7	155	—	—	—

[a]Conditions: 0.04 mmol [Rh(μ-OMe)(COD)]$_2$, in 2 mL of toluene-d_8, P = 30 bar CO–H_2, T = 25°C, dppb:Rh = 1.

High-pressure NMR study

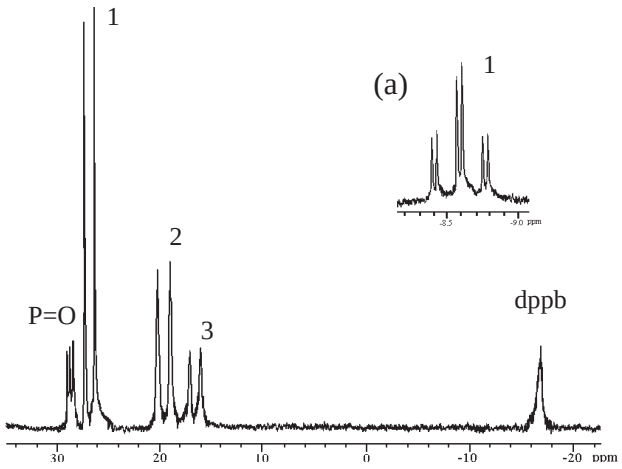
HP-NMR experiments were performed with dppb under hydroformylation conditions with and without 2,5-dihydrofuran to observe the species present during the hydroformylation reaction.

The HP-NMR spectroscopic study was performed at 30 bar H_2–CO, room temperature, and a dppb:Rh ratio of 1 in toluene-d_8, which has been found to provide the same catalytic behaviour as dichloroethane. The ^{31}P NMR spectrum of the solution has four doublets at δ 26.7 ($^{1}J_{Rh-P}$ = 116 Hz), 19.6 ($^{1}J_{Rh-P}$ = 147 Hz), 16.7 ($^{1}J_{Rh-P}$ = 131 Hz), and 13.7 ($^{1}J_{Rh-P}$ = 155 Hz) (Table 5). The ^{1}H NMR of this solution revealed a double triplet in the hydride region at –8.8 ppm ($^{1}J_{Rh-H}$ = 11 Hz, $^{2}J_{P-H}$ = 49 Hz), which is indicative of the coupling of a hydride with the rhodium and with two equivalent phosphorus nuclei. The ^{1}H NMR spectrum also shows a broad signal at –9.3 ppm (Table 5).

We assigned the doublet at 26.7 ppm and the double triplet in the hydride region to the mononuclear rhodium complex [HRh(dppb)(CO)$_2$] (**1**) (Scheme 3) in accordance with data for BDPP from the literature (32). We suggest that this species has trigonal–bipyramidal geometry with the dppb coordinated to the rhodium centre. In the present case, the intermediate phosphorus-hydride coupling constant ($^{2}J_{P-H}$ = 49 Hz) and the averaged coupling constant ($^{1}J_{Rh-P}$ = 115 Hz) suggest that there is an apical–equatorial coordination of the diphosphine with an exchange of the phosphorus atoms (32, 34, 41, 42), although small amounts of the equatorial–equatorial isomer cannot be discounted. The doublet at 19.6 ppm with $^{1}J_{Rh-P}$ = 147 Hz and the broad hydride observed in the ^{1}H NMR were attributed to the mononuclear rhodium complex **2**, which has four equivalent phosphorus

© 2001 NRC Canada

Fig. 1. ^{31}P NMR spectrum during hydroformylation of 2,5-dihydrofuran at room temperature. (*a*) Hydride region of the ^{1}H NMR.



atoms with an average coupling constant (43). The doublet at 16.7 ppm is attributed to a square-planar rhodium complex **3** with two dppb coordinating to the metal (Scheme 3) (44). Finally, the doublet at 13.7 ppm had previously been observed by James et al. (45) and assigned to the carbonyl diphosphine dimer $[Rh(CO)_2dppb]_2$ (**4**) which has a Rh—Rh bond and two CO groups bridging the metal atoms.

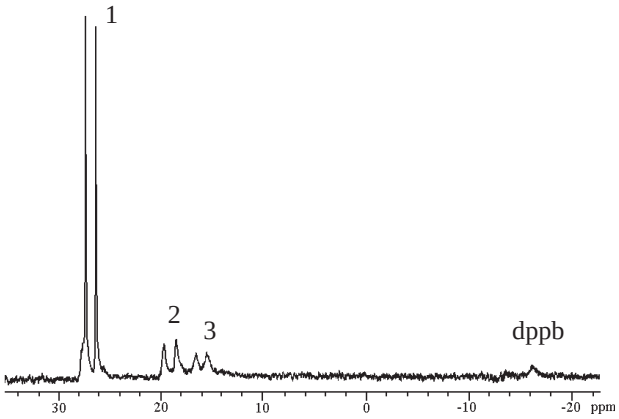
When the temperature was increased to 50 and 90°C, the ^{31}P NMR spectrum showed a major signal at 26.7 ppm, which was attributed to complex **1**. Two minor doublets were observed at 19.6 and 16.7 ppm and assigned to compounds **2** and **3**. The hydrides of complexes **1** and **2** were also observed in the ^{1}H NMR. No formation of the dinuclear rhodium complex **4** was observed in the ^{31}P NMR spectrum.

The HP-NMR tube was then depressurized at room temperature and the 2,5-dihydrofuran was added (0.05 mL) under nitrogen. The HP-NMR spectrum at 30 bar $CO–H_2$ and room temperature remained unchanged (Fig. 1). Three doublets at δ 26.7, 19.6, and 16.7 ppm were assigned to complexes **1**, **2**, and **3**, respectively. The resonance of the free dppb was observed at –17 ppm and three singlets were attributed to oxidized phosphine at δ 29 ppm. In the ^{1}H NMR spectra the double triplet was assigned to complex **1** (Fig. 1).

The temperature was increased to 80°C to reach hydroformylation conditions, and the formation of the aldehydes was observed in the ^{1}H NMR during the hydroformylation reaction. Simultaneously the species observed in the ^{31}P NMR were the ones that had previously been observed without the addition of substrate at these temperatures (Fig. 2). Complex **1** was the major compound observed and the other two doublets were assigned to complexes **2** and **3**. Since complexes **2** and **3** are not active under hydroformylation conditions, complex **1** can be considered as one of the species present in the catalytic cycle of the hydroformylation reaction.

It is well known that diphosphines containing at least one alkyl substituent are prone to oxidation. The three signals for oxidized diphosphine observed at room temperature (Fig. 1) indicate the possible presence of rhodium species with partially oxidized monocoordinated diphosphine. This oxidation

Fig. 2. ^{31}P NMR spectrum during hydroformylation of 2,5-dihydrofuran at 80°C.



can be due to the difficulty to avoid the presence of oxygen in these HP-NMR experiments.

At higher P-P:Rh ratios, conversion into aldehydes decreases drastically. In the case of dppb, this can be because in the presence of high P-P:[Rh] ratios inactive species **2** and **3** can be easily formed, as was observed in the HP-NMR experiments.

Conclusions

The effect of pressure and temperature was explained in terms of the described isomerization process via β-elimination during the hydroformylation of 2,5-dihydrofuran.

The rhodium–diphosphine systems provide high activity by using diphosphines with wider bite angles. The regioselectivity depends on the pressure and temperature conditions. High pressures and low temperatures favour the selective formation of the tetrahydrofuran-3-carbaldehyde.

HP-MR experiments performed with and without the substrate during the hydroformylation of 2,5-dihydrofuran show that the rhodium hydride $[HRh(dppb)(CO)_2]$ (**1**) is the predominant species during the hydroformylation.

The addition of an excess of ligand decreased conversion because inactive species **2** and **3** were formed with two coordinated diphosphines in the case of dppb.

Acknowledgements

This work was supported by Spanish Ministerio de Educación y Ciencia (DGES PB-97-0407-C05-01) and the Generalitat de Catalunya (CIRIT) with a research grant to I. del Río.

References

1. C. Botteghi. Gazz. Chim. Ital. **105**, 233 (1975).
2. L.F. Walker, S. Connolly, and M. Wills. Tetrahedron Lett. **39**, 5273 (1998).
3. A.R. Katritzky and C.W. Rees. (*Editors*). Comprehensive heterocyclic chemistry. Vol. 1. Pergamon Press Ltd., Oxford. 1984.
4. H. Siegel and W. Himmele. Angew. Chem. Int. Ed. Engl. **19**, 178 (1980).

© 2001 NRC Canada

5. C.D. Frohning and C.W. Kohlpaintner. *In* Applied Homogeneous Catalysis with Organometallic Compounds. *Edited by* B. Cornils and W.A. Herrmann. Springer–Verlag, New York. 1996. pp. 29.
6. P.W.N.M. van Leeuwen. *In* Catalysis. *Edited by* J.A. Moulijn, P.W.N.M. van Leeuwen, and R.A. van Santen. Elsevier, Amsterdam. 1993. Chap. 6.2.
7. P.W.N.M. van Leeuwen and C. Claver. (*Editors*). Recent advances in rhodium catalyzed hydroformylation. Kluwer-CMC, Dordrecht. 2000.
8. M.E. Garst and D. Lukton. J. Org. Chem. **46**, 4433 (1981).
9. A.L. Lapidus, I.G. Priudze, G.A. Korneyeva, M.M. Vartanyan, A.P. Rodin, Y.V. Slivinskii, A.V. Dolidze, and S.M. Loktev. Neftekhimiya, **33**, 102 (1993).
10. D. E. Vietti, III. C. U. S. Patent 4 376 208. 1983.
11. E.Y. Volf, T.Y. Soloveva, M.M. Vartanyan, L.Y. Brezhnev, and A.L. Lapidus. Izv. Akad. Nauk. SSSR, Ser. Khim. **11**, 2569 (1989).
12. P.W.N.M. van Leeuwen and C.F. Roobeek. J. Organomet. Chem. **258**, 343 (1983).
13. T. Jongsma, G. Challa, and P.W.N.M. van Leeuwen. J. Organomet. Chem. **421**, 121 (1991).
14. A. van Rooy, E.N. Orij, P.C.J. Kamer, and P.W.N.M. van Leeuwen. Organometallics, **14**, 34 (1995).
15. E. Fernández, A. Ruiz, C. Claver, and S. Castillón. Organometallics, **17**, 2857 (1998).
16. A. Polo, J. Real, C. Claver, S. Castillón, and J. C. Bayón, J. Chem. Soc. Chem. Commun. **8**, 600 (1990).
17. A. Polo, C. Claver, S. Castillón, A. Ruiz, J.C. Bayón, J. Real, C. Mealli, and D. Masi. Organometallics, **11**, 3525 (1992).
18. I. Ojima, K. Kato, M. Okabe, and T. Fuchikami. J. Am. Chem. Soc. **109**, 7714 (1987).
19. C. Botteghi, M. Branca, G. Micera, F. Piacenti, and G. Menchi. Chim. Ind. (Milan) **60**, 16 (1978).
20. S. Gladiali, G. Faedda, M. Marchetti, and C. Botteghi. J. Organomet. Chem. **244**, 289 (1983).
21. T. Horiuchi, T. Ohta, E. Shirakawa, K. Nozaki, and H. Takaya. J. Org. Chem. **62**, 4285 (1997).
22. C.P. Casey, G.T. Whiteker, M.G. Melville, L.M. Petrovich, J.A. Gavney, and D.R. Powell. J. Am. Chem. Soc. **114**, 5535; J. Am. Chem. Soc. **114**, 10 680 (1992).
23. M. Kranenburg, Y.E.M. van der Burgt, P.C.J. Kamer, P.W.N.M. van Leeuwen, K. Goubitz, and J. Fraanje. Organometallics, **14**, 3081 (1995).
24. K. Yamamoto, S. Momose, M. Funahashi, S. Ebata, H. Ohmura, H. Komatsu, and M. Miyazawa. Chem. Lett. 189 (1994).
25. L.A. van der Veen, P.H. Keeven, G.C. Schoemaker, J.N.H. Reek, P.C.J. Kamer, P.W.N.M. van Leeuwen, M. Lutz, and A.L. Spek. Organometallics, **19**, 872 (2000).
26. W. Goertz, P.C.J. Kamer, P.W.N.M. van Leeuwen, and D. Vogt. Chem. Commun. 1521 (1997).
27. M. Kranenburg, P.C.J. Kamer, P.W.N.M. van Leeuwen, D. Vogt, and W. Keim. J. Chem. Soc. Chem. Commun. 2177 (1995).
28. M. Kranenburg, P.C.J. Kamer, and P.W.N.M. van Leeuwen. Eur. J. Inorg. Chem. 25 (1998).
29. T. Hayashi, M. Konishi, and M. Kumada. Tetrahedron Lett. **21**, 1871 (1979).
30. T. Hayashi, M. Konishi, Y. Kobori, M. Kumada, T. Higuchi, and K. Hirotsu. J. Am. Chem. Soc. **106**, 158 (1984).
31. I. del Río, N. Ruiz, C. Claver, L.A. van der Veen, and P.W.N.M. van Leeuwen. J. Mol. Catal. A: Chem. **161**, 39 (2000).
32. A. Castellanos-Páez, S. Castillón, C. Claver, P.W.N.M. van Leeuwen, and W.G.J. de Lange. Organometallics, **17**, 2543 (1998).
33. C.J. Elsevier. J. Mol. Catal. **92**, 285 (1994).
34. I. Horvath. Organometallics, **5**, 2333 (1986).
35. J.M. Brown and A.G. Kent. J. Chem. Soc. Perkin Trans. 2, 1597 (1987).
36. L.A. van der Veen, M.D.K. Boele, F.R. Bregman, P.C.J. Kamer, P.W.N.M. van Leeuwen, K. Goubitz, J. Fraanje, H. Schenk, and C. Bo. J. Am. Chem. Soc. **120**, 11616 (1998).
37. C. Bianchini, H.M. Lee, A. Meli, and F. Vizza. Organometallics, **19**, 849 (2000).
38. F. Ngan and M. Toofan. J. Chromatogr. Sci. **29**, 8 (1991).
39. A.M. Masdeu-Bultó, A. Orejón, A. Castellanos, S. Castillón, and C. Claver. Tetrahedron: Asymmetry, **7**, 1829 (1996).
40. I. del Río, W. G. J. de Lange, P. W. N. M. van Leeuwen, and C. Claver. J. Chem. Soc. Dalton Trans. 1293 (2001).
41. G.J.H. Buisman, E.J. Vos, P.C.J. Kamer, and P.W.N.M. van Leeuwen. J. Chem. Soc. Dalton Trans. 409 (1995).
42. C.P. Casey, G.T. Whiteker, M.G. Melville, L.M. Petrovich, J.A. Gavney, Jr., and D.R. Powell. J. Am. Chem. Soc. **114**, 5535 (1992).
43. B.R. James and D. Mahajan. Can. J. Chem. **57**, 180 (1979).
44. A. Sanger. J. Chem. Soc. Dalton Trans. 120 (1977).
45. B.R. James, D. Mahajan, S.J. Rettig, and G.M. Williams. Organometallics, **2**, 1452 (1983).
46. P. Dierkes and P.W.N.M. van Leeuwen. J. Chem. Soc. Dalton Trans. 1519 (1999).

© 2001 NRC Canada

An easy-to-use heterogeneous catalyst for the Knoevenagel condensation

Bernd Siebenhaar, Bruno Casagrande, Martin Studer, and Hans-Ulrich Blaser

Abstract: Physical mixtures of alkali and earth alkali metal carbonates and commercially available zeolites were investigated as solid catalysts for the Knoevenagel condensation. Best results for the model reaction between benzaldehyde and ethyl cyanoacetate were obtained for a 1:4 mixture of Na_2CO_3 with 4 Å molecular sieves (MS). The effects of the following parameters were investigated: structure of substrate, type and basicity of metal carbonate and zeolite, and temperature. Between 50 and 90°C chemical yields up to >90% were obtained without continuous removal of water and with reasonable catalyst activities and reaction times. Na_2CO_3 – MS 4 Å proved to be active for the condensation of several aldehydes and ketones with a variety of active methylene components.

Key words: Knoevenagel condensation, solid basic catalysts, zeolite – sodium carbonate mixtures.

Résumé : On a évalué la possibilité d'utiliser des mélanges physiques de carbonates de métaux alcalins ou alcalinoterreux et de zéolites commercialement disponibles comme catalyseurs solides pour des condensations de Knoevenagel. Les meilleurs résultats pour la réaction modèle entre le benzaldéhyde et le cyanoacétate d'éthyle ont été obtenus avec un mélange 4:1 de Na_2CO_3 avec du MS 4 Å. On a étudié les effets des paramètres suivants: structure du substrat; type et basicité du carbonate métallique et du zéolite; température. Entre 50 et 90°C, on a obtenu des rendements chimiques allant jusqu'à plus de 90 % sans nécessité d'enlever l'eau de façon continue, avec des activités catalytiques et des temps de réaction raisonnables. Le mélange Na_2CO_3 – MS 4 Å s'avère actif pour la condensation de plusieurs aldéhydes et cétones avec une grande variété de composés comportant un méthylène actif.

Mots clés : condensation de Knoevenagel, catalyseurs basiques solides, mélanges de zéolite – carbonate de sodium.

[Traduit par la Rédaction]

Introduction

The Knoevenagel condensation is a valuable tool in synthetic chemistry (1, 2). Starting from aldehydes or ketones and activated methylene compounds the synthesis of a wide variety of tri- or tetra-substituted olefins is possible (usually *trans* products are favored). This type of reaction is classically carried out in presence of an organic bases such as pyridine and piperidine and water is removed continuously. While yields are generally good, relatively high temperatures are needed and work up can be cumbersome (Fig. 1).

To overcome some of these problems, solid basic catalysts were developed using zeolites (3, 4), clays (5, 6), alumina (7, 8), as well as amines immobilized on montmorillonite (9), silica (10, 11), and ion exchanged resins (12, 13). Although many of these catalysts indeed have helped to solve some of the problems mentioned above, they are not very practical for the synthetic organic chemist. Most of them are not available commercially, many are difficult to prepare, and even though there are cases where the reaction occurs at room temperature (14), some catalysts are not very active. In this contribution we describe the application of a physical mixture of molecular sieves (MS) and sodium carbonate as very effective solid catalysts for the Knoevenagel condensation of several types of starting materials. The catalysts are easy to prepare starting from commercially available materials, are highly active and selective, and lead to very pure condensation products at relatively low temperatures.

Received September 20, 2000. Published on the NRC Research Press Web site at http://canjchem.nrc.ca on May 31, 2001.

Dedicated to Professor Brian James on the occasion of his 65th birthday.

B. Siebenhaar,[1] B. Casagrande, M. Studer, and H.-U. Blaser. Solvias AG, P.O. Box, CH-4002 Basel, Switzerland.

[1]Corresponding author (telephone: +41 61 686 64 26; fax: +41 61 686 63 11; e-mail: bernd.siebenhaar@solvias.com).

Results and discussion

As already pointed out, zeolites have been used as solid catalysts before (3, 4). However, in order to get reasonable activities, quite elaborate modification of the commercially available materials is usually necessary. On the other hand, alkaline carbonates have also been used with good activity , but due to various side reactions, selectivities were reported to be rather low (1, 15). We thought that a combination of a metal carbonate with a readily available zeolite might eliminate these deficiencies and a catalyst screening was carried out with different carbonates and zeolites using the reaction of benzaldehyde with ethyl cyanoacetoactetate as model reaction. The results were very promising and selected results are presented in Table 1 and Fig. 2. The most important finding was that with several catalyst combinations, conversions up to 99% and selectivities of 98 to 99% of ethyl cyanocinnamate were reached at low temperature within reasonable reaction times. No further Michael addition

 DOI: 10.1139/cjc-79-5/6-566 © 2001 NRC Canada

Fig. 1. Knoevenagel condensation.

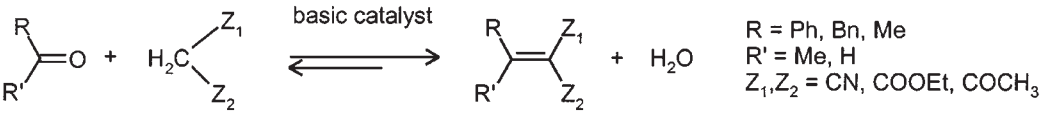


Table 1. Effect of zeolite type, counter ion, temperature on conversion, and reaction time for the condensation of benzaldehyde and ethyl cyanoacetate.

Zeolite	Metal	*T* (°C)	Conversion (%) (5 min)	Conversion (%) (max)	t_{max} (min)	Comments
MS 4 Å	K	22	60	83	30	1 g zeolite
MS 4 Å	K	50	80	85	20	1 g zeolite
MS 4 Å	K	70	93	95	15	1 g zeolite
MS 4 Å	K	90	93	96	10	1 g zeolite
MS 4 Å	Li	70	80	98	90	2 g zeolite
MS 4 Å	Na	70	61	96	90	2 g zeolite
MS 4 Å	K	70	94	97	30	2 g zeolite
MS 4 Å	Rb	70	95	97	15	2 g zeolite
MS 4 Å	Cs	70	72	97	15	2 g zeolite
MS 4 Å	Ca	90	14	96	150	2 g zeolite
MS 4 Å	Ba	90	22	96	150	2 g zeolite
MS 4 Å	Sr	90	55	98	150	2 g zeolite
H-MOR	K	50	—	76[a]	[a]	2 g mordenite, 0.45 g K_2CO_3
Na-X	K	50	—	78[a]	[a]	2 g zeolite X, 0.45 g K_2CO_3
Na-Y	K	50	—	80[a]	[a]	2 g zeolite Y, 0.45 g K_2CO_3
SiO_2	K	50	—	70[a]	[a]	2 g SiO_2, 0.45 g K_2CO_3

Note: Reaction conditions: 0.1 mol substrates, 0.55 g metal carbonate.
[a]Reaction time 15 min.

reactions to the product molecules were ever observed. As expected, the strongest correlation was found between catalyst activity (expressed as mmol/g catalyst * h) and the basicity of the two components (see Fig. 3), but the amount of zeolite also plays a role. Similar dependencies have been reported before (3). The overall preferred combination used for further investigations was the easily available MS 4 Å and K_2CO_3 at a weight ratio of ca. 1:4, respectively. This means that the molecular sieve can absorb about 50% of the water formed (pore volume of 0.45 mL g^{-1}) (16), which seems to be enough to allow high conversions under these conditions. Control experiments in absence of molecular sieves gave similar conversions but much lower yields due to side reactions, confirming the documented observations (1, 15) mentioned above.

To determine the scope and limitations of the new catalyst system we investigated the effect of variations in the substrate structure. On the one hand, this is important for the preparative applications of the catalysts, and on the other hand the dependence on the pK_a of the methylene component allows an indirect catalyst characterization (3, 5, 6). The best results for each combination of starting materials are listed in Table 2 and the following trends are noteworthy: (*i*) The scope of the Na_2CO_3 – MS 4 Å combination is quite broad, and a variety of different substrates can be condensed with moderate to very high conversions and low to very high yields. (*ii*) For the reaction with benzaldehyde, the catalyst activity (see Fig. 3), as well as the product yields, are related to the pK_a of the starting methylene compound with a limiting value of ca. 13; this is inferred to correspond to an approximate pK_a value for the solid catalyst. (*iii*) As for the classical version of the Knoevenagel condensation, products are predominantly *trans*, and aldehydes are much more reactive than ketones, which give generally low conversions but acceptable selectivities.

Conclusions

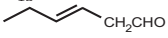
As a result of their ready availability and very good overall catalytic performance, a 1:4 physical mixture of Na_2CO_3 with MS 4 Å is a very useful catalyst for the preparative Knoevenagel condensation for a variety of aldehydes and ketones with different active methylene compounds. The most important parameters affecting the catalytic performance were the structure of starting materials and the catalyst basicity. From the correlation between the catalyst activity and the pK_a of different methylene components, it is concluded that the Na_2CO_3 – MS 4 Å catalyst has a pK_a of approximately 13. Optimal reaction temperatures are between 50 and 90°C, and chemical yields of up to >90% can be obtained without continuous removal of water and with reasonable catalyst activities and reaction times.

Experimental

All organic starting materials were obtained from Fluka (purum) and were used without further purification. The following reference compounds were used: benzylidenemalononitrile (Aldrich), ethyl cyanocinnamate (Aldrich), diethyl benzylidenemalonate (Fluka). The inorganic salts

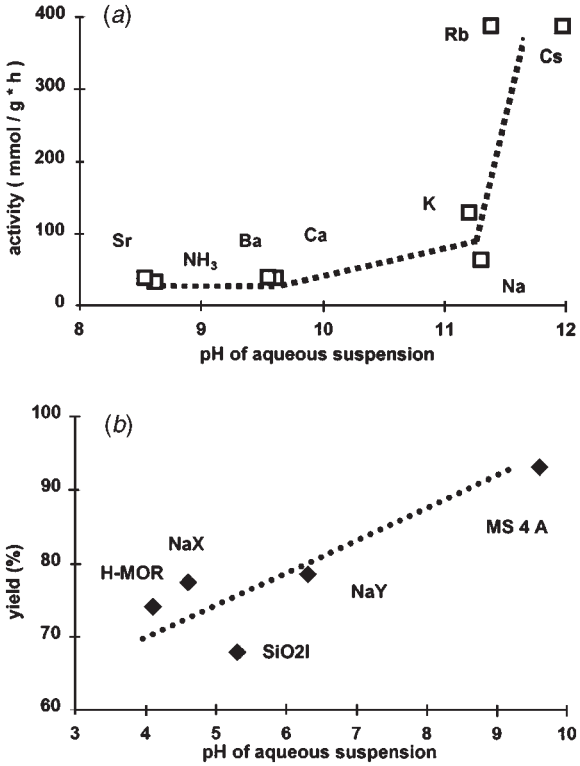
© 2001 NRC Canada

Table 2. Best results at the optimal temperature for the Knoevenagel condensation with different substrates using a mixture of Na_2CO_3 and MS 4 Å.

Z_1	Z_2	pK_a	R	R′	T (°C)	Time (h)	Conversion (%)	Yield (%)	Activity (mmol/g catalyst * h)
CN	CN	~8	Ph	H	70	0.25	98	97	872
CN	COOEt	9	Ph	H	90	0.25	94	93[a]	736
Ac	COOEt	10.7	Ph	H	90	0.5	63	62[a,b]	282
COOEt	COOEt	13.3	Ph	H	130	1.5	69	61[a,b]	102
Br	COOEt	>14	Ph	H	120	6	0	0	0
CN	COOEt	9	Vanillin		30	3	59	57[a,b]	43
CN	COOEt	9	2-OH-Ph	H	25	1.25	90	58[b]	161
CN	COOEt	9	C_7H_{15}	H	50	2	90	82[b]	99
CN	COOEt	9			50	0.25	63	35[b]	562
CN	COOEt	9	$BnCH_2$	Me	90	5	8	8	4
CN	COOEt	9	$PhCHCH_2$	Me	90	5	82	80	36
CN	COOEt	9	Ph	Me	120	4	5	5	3
CN	COOEt	[c]	Ph	H	150	2	98[c]	97[c]	—

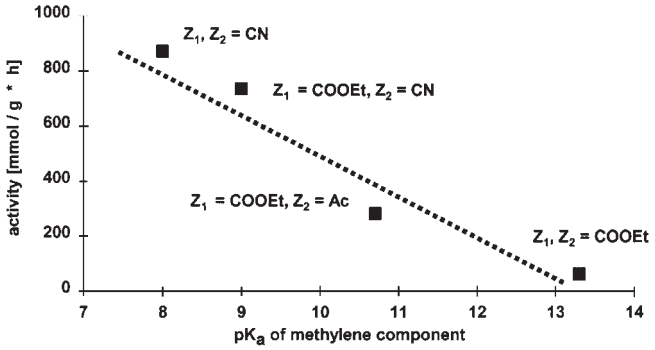
Note: Reaction conditions: 0.1 mol substrates, 0.45 g Na_2CO_3, 2 g MS 4 Å.
[a]>95% *trans* according to ^{1}H NMR, not determined for the other substrates.
[b]Isolated yield after purification (see *Experimental*), product with >95% purity.
[c]Reference experiment: β-alanine as homogeneous catalyst, with continuous removal of water with toluene (1).

Fig. 2. Condensation of benzaldehyde and ethyl cyanoacetate. (*a*) Correlation between pH of different metal carbonates and catalyst activity mmol/g catalyst * h); (*b*) correlation between product yield and pH value of aqueous suspensions of different zeolites. For the determination of the pH value see *Experimental*.



were p.A. grade and supplied by Fluka or Merck. The zeolites used were obtained from Strem (H-mordenite, zeolite X and Y) and from Merck (MS 4 Å).

Fig. 3. Condensation of benzaldehyde with different methylene compounds using a mixture of Na_2CO_3 and MS 4 Å at 70–90°C; correlation between pK_a and catalyst activity.



General procedure for Knoevenagel condensations

In a 50 mL three-necked flask with reflux condenser the carbonyl compound (0.1 mol) and the methylene compound (0.1 mol) were heated to reaction temperature. A mixture of carbonate (0.45 g) and MS 4 Å (2.0 g) was added and the reaction started immediately. After 0.25–4 h (depending on the nature of the carbonyl and methylene compound) the hot reaction mixture was filtered to remove the catalyst and yields were determined by GLC. In many cases the crude product was obtained with high yield and purity and did not need further purification. Otherwise the crude product was dissolved in hot ethanol and slowly cooled down to room temperature. Crystals of the product appeared and after filtration and drying under vacuum the product was obtained with high yield and purity.

Analytics

The course of reaction was monitored by GLC (OV 101, 40°C, 10°C min^{-1}; 220°C, 5°C min^{-1}). Conversion was calculated on the basis of peak area of the carbonyl compound,

© 2001 NRC Canada

the product peak, and byproduct areas. The selectivity was defined as %desired product/%all products. To verify the GLC results, an ^{1}H NMR analysis of the crude product mixture was carried out directly after filtration on a Bruker ARX 250 instrument in $CDCl_3$ at room temperature.

Procedure for the determination of the pH values of catalyst slurries

To the inorganic compound (0.5g) (zeolite or carbonate–zeolite mixture) was added de-ionized water (10 mL). The flask was shaken from time to time, and after 24 h the pH of the water phase was measured with a glass electrode.

Acknowledgment

We would like to thank Reto Fankhauser for careful experimental work.

References

1. Organikum. VEB Deutscher Verlag der Wissenschaften, Berlin. 1981. p. 571
2. G. Jones. Org. React. (N.Y.), **15**, 204 (1967).
3. A. Corma, V. Fornes, R.M. Martin-Aranda, H. Gracia, and J. Primo. Appl. Catal. **59**, 237 (1990).
4. P.E. Hathaway and M.E. Davis. J. Catal. **116**, 263 (1989); 278 (1989).
5. A. Corma and R.M. Martin-Aranda. J. Catal. **130**, 130 (1991).
6. A. Corma, V. Fornes, R.M. Martin-Aranda, and F. Rey. J. Catal. **134**, 58 (1992).
7. P.S. Kwon, Y.M. Kim, C.J. Kang, and T.W. Kwon. Synth. Commun. **27**, 4091 (1997).
8. J.A. Cabello, J.M. Campelo, A. Gracia, D. Luna, and J.M. Marinas. J. Org. Chem. **49**, 5195 (1984).
9. B.M. Choudary. Synth. Commun. **21**, 1163 (1991).
10. E. Angeletti, C. Canepa, G. Martinetti, and P. Venturello. J. Chem. Soc. Perkin Trans. 1, 105 (1989).
11. D.J. Macquarrie. Green Chem. **1**, 195 (1999).
12. T. Saito, H. Goto, K. Honda, and T. Fuji. Tetrahedron Lett. **33**, 7535 (1992).
13. J. Simpson, D.L. Rathbone, and D.C. Billington. Tetrahedron Lett. **40**, 7031 (1999).
14. M. Lakshimi Kantam, B.M. Choudary, Ch. Venkat Reddy, K. Koteswara Rao, and F. Figueras. Chem. Commun. 1033 (1998).
15. M.A. Aramendia, V. Brau, J.M. Marinas, and F.J. Romero. Chem. Lett. 574 (2000).
16. R.M. Barrer. Zeolites and clay minerals as sorbents and molecular sieves. Academic Press, New York. 1978. p. 23.

© 2001 NRC Canada

Synthesis and spectroscopic (^{1}H NMR, ESR) characterization of new aryloxy–Mn(II) complexes: steric control over *O*– vs. phenyl–π-coordination of ArO^- ligands (ArO^- = $C_6H_5O^-$, 4-methyl-$C_6H_4O^-$, 3,5-dimethyl-$C_6H_3O^-$, 2,6-di-*tert*-butyl-$C_6H_3O^-$, 2,6-dimethyl-$C_6H_3O^-$) to the "Mn(II)Cp" moiety, and their reactivity with carbon dioxide

M. Aresta, I. Tommasi, C. Dileo, A. Dibenedetto, M. Narracci, J. Ziolkowski, and A. Jezierski

Abstract: The coordination chemistry of phenoxide ligands, such as $C_6H_5O^-$, 4-(CH_3)-$C_6H_4O^-$, 3,5-$(CH_3)_2$-$C_6H_3O^-$, 2,6-(*tert*-butyl)$_2$-$C_6H_3O^-$, 2,6-$(CH_3)_2$-$C_6H_3O^-$, to Mn(II) has been investigated because of the possible implication of Mn(II)–phenoxide complexes as intermediates in the phenylphosphate carboxylase enzyme, a protein which catalyses the selective carboxylation of phenylphosphate to 4-OH-benzoic acid using CO_2. We report here the synthesis and characterization of $[CpMn(\mu\text{-}OAr)(THF)]_2$ (ArO = $C_6H_5O^-$, 4-(CH_3)-$C_6H_4O^-$, 3,5-$(CH_3)_2$-$C_6H_3O^-$, 2,6-$(CH_3)_2$-$C_6H_3O^-$) and $[CpMn(\eta^5\text{-}ArO)]$ (ArO = 2,6-(*tert*-butyl)$_2$-$C_6H_3O^-$ and 2,6-$(CH_3)_2$-$C_6H_3O^-$) complexes, the first examples of mixed-sandwich complexes with Cp and phenate as π-ligands. The latter bear the 2,6-substituted phenoxide π-coordinated to the $[Mn(Cp)]^+$ moiety. The different mode of bonding of the phenoxide ligands to Mn(II), substantiated by ^{1}H NMR and electron spin resonance (ESR) spectroscopy, is controlled by the steric hindrance of substituents at the 2- and 6-position. The reactivity of the π-bonded ligand towards CO_2 is also reported as a quite rare example of nucleophilic attack at the cumulene by the ring-carbon of the phenoxide, which is driven by electron density localization at the 4-position generated upon π-coordination to Mn(II).

Key words: Mn(II)-complexes, phenoxide ligands, ^{1}H NMR spectroscopy, ESR spectroscopy, reaction with carbon dioxide.

Résumé : On a étudié la chimie de coordination des ligands phénolates, tels que $C_6H_5O^-$, 4(CH_3)-$C_6H_4O^-$, 3,5-$(CH_3)_2$-$C_6H_3O^-$, 2,6-(*tert*-butyl)$_2$-$C_6H_3O^-$ et 2,6-$(CH_3)_2$-$C_6H_3O^-$, avec le Mn(II) en raison de l'implication possible des complexes Mn(II)-phénolates comme intermédiaires dans l'enzyme carboxylase du phosphate de phényle, une protéine qui catalyse la carboxylation sélective du phosphate de phényle en 4-HO-C_6H_4-C(O)OH à l'aide de CO_2. On a synthétisé et caractérisé les complexes $[CpMn(\mu\text{-}OAr)(THF)]_2$ (ArO = $C_6H_5O^-$, 4(CH_3)-$C_6H_4O^-$, 3,5-$(CH_3)_2$-$C_6H_3O^-$ et 2,6-$(CH_3)_2$-$C_6H_3O^-$) et $[CpMn(\eta^5\text{-}ArO)]$ (ArO = 2,6-(*tert*-butyl)$_2$-$C_6H_3O^-$ et 2,6-$(CH_3)_2$-$C_6H_3O^-$), le premier exemple d'un complexe sandwiche mixte comportant un Cp et un phénate comme ligands π. Dans le dernier, le phénolate 2,6-disubstitué est fixée par une coordination π à la partie $[Mn(Cp)]^+$. Les différents modes de fixation des ligands phénolates au Mn(II), tels que confirmés par RMN du ^{1}H et par spectroscopie RPE, sont contrôlés par l'encombrement stérique des substituants en positions 2 et 6. On a aussi déterminé la réactivité des ligands fixés d'une façon π vis à vis du CO_2; il s'agit d'un rare exemple d'attaque nucléophile au niveau du cumulène par l'atome de carbone du cycle du phénolate alors que celle-ci est amenée par la localisation de la densité électronique en position 4 sous l'influence d'une coordination π avec le Mn(II).

Mots clés : complexes du Mn(II), ligands phénolates, spectroscopie RMN du ^{1}H, spectroscopie RPE, réaction avec le bioxyde de carbone.

[Traduit par la Rédaction]

Received August 8, 2000. Published on the NRC Research Press Web site at http://canjchem.nrc.ca on May 31, 2001.

Dedicated to Professor Brian James on the occasion of his 65th birthday.

M. Aresta[1], I. Tommasi, C. Dileo, M. Narracci, and A. Dibenedetto. Department of Chemistry and CNR-MISO, University of Bari, Campus Universitario, 70126 Bari, Italy.
J. Ziolkowski and A. Jezierski. Institute of Chemistry, University of Wroclaw, F. Joliot-Curie 14, 50383, Wroclaw, Poland.

[1]Corresponding author (telephone: +39 080 544-2430; fax: +39 080 544-2429; e-mail: aresta@meteo.uniba.it).

 DOI: 10.1139/cjc-79-5/6-570 © 2001 NRC Canada

Introduction

Phenol and its derivatives have been shown to act as ligands to transition metal systems (1) through either the *O*-atom or the phenyl π-electron system. Bulky substituents in both 2- and 6-position of the phenyl ring, as well as an unsaturated coordination of the metal, may force π-phenyl bonding to the metal center (2). Such a situation has been structurally documented for diamagnetic Rh(I) complexes (3). Although both diamagnetic and paramagnetic phenoxide-complexes are extensively described in the literature, no examples of phenoxide π-coordination to a paramagnetic center have been reported to date.

Iron(III) complexes bearing phenol or substituted phenols, which are exclusively η^1–*O*-bonded, have been extensively studied as model compounds of catechol oxidase (4). The importance of Mn(II) systems in several biosystems (5) and in material science has prompted investigatations of complexes or clusters bearing the η^1–*O*-bonded phenoxide anion (6). Only a single case of π-bonded phenate to Mn(I) is reported in the literature (7). Despite this interest practically no reports are available in the literature that describe both modes of bonding of phenol and (or) its substituted forms to manganese(II).

Very recently we have extracted a phenol carboxylase enzyme from the anaerobic bacteria *Thauera aromatica* (8). The extracted enzyme was supported onto an organic matrix and shown to catalyse very selectively the conversion of phenylphosphate into 4-OH-benzoic acid in mesophilic conditions (9) with significant turnover frequency (TOF) and turnover number (TON). While information about the structure of the active site is still not available, it is known that the enzymatic activity is Mn(II) dependent (8) and that if the enzyme is incubated with phenol this activity is strongly retained. This finding prompted us to investigate the coordination of phenol and its derivatives to Mn(II) in order to gain information about the relevance of the mode of bonding to reactivity. Therefore, we decided to investigate the reaction of $Mn(Cp)_2$ with C_6H_5OH, 4-(CH_3)-C_6H_4OH, 3,5-$(CH_3)_2$-C_6H_3OH, 2,6-(*tert*-butyl)$_2$-C_6H_3OH, and 2,6-$(CH_3)_2$-C_6H_3OH.

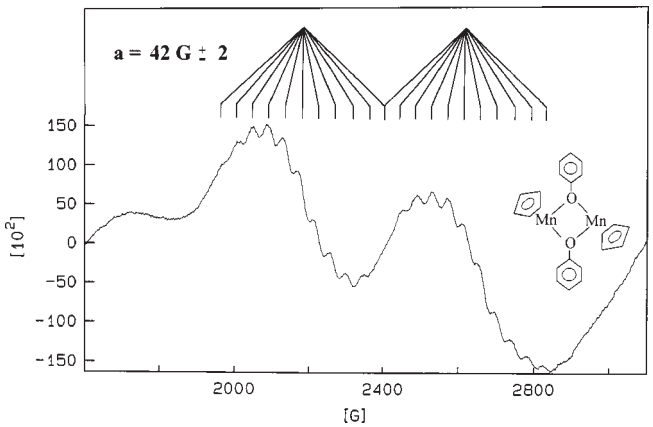
In this paper, we report the synthesis of complexes of the formula [CpMn(ArO)(THF)] (ArO = $C_6H_5O^-$, 4-(CH_3)-$C_6H_4O^-$, 3,5-$(CH_3)_2$-$C_6H_3O^-$, 2,6-(*tert*-butyl)$_2$-$C_6H_3O^-$, and 2,6-$(CH_3)_2$-$C_6H_3O^-$), which are quite rare examples of paramagnetic complexes bearing one Cp and one phenoxide ligand. The different mode of bonding of phenoxide anion to Mn(II) is substantiated by ^{1}H NMR, electron spin resonance (ESR), and IR spectroscopy, and by the reactivity of Mn–phenoxides with CO_2. A unique example of ring carboxylation of phenol derivatives to substituted 4-OH-benzoic acid under ambient conditions, which is fully mimetic of the above mentioned biological carboxylation of phenol, is also reported.

Results and discussion

Synthesis and characterization of the [Cp(THF)Mn(μ-*O*-C_6H_5)]$_2$ complex (1)

Cp_2Mn reacts with PhOH (in THF) in a 1:1 molar ratio at room temp to afford a white solid (**1**), which separates quantitatively from the reaction mixture (eq. [1]). This reaction is very clean and can be followed by GC that allowed the reaction stoichiometry to be determined for eq. [1].

Fig. 1. ESR sectrum of [Cp(THF)Mn(μ-*O*-C_6H_5)]$_2$ (in THF, *T*= 77 K, mod amplitude: 2.299 G, frequency: 9.4247866 GHz, power: 2.00e + 01 mW).



[1] $2Cp_2Mn + 2C_6H_5OH \xrightarrow[298K]{THF} [Cp(THF)Mn(\mu\text{-}O\text{-}C_6H_5)]_2 + 2C_5H_6$

GC analysis of the reaction solution after precipitation of the solid, shows that one mol of C_5H_6 per mol of Cp_2Mn is released after addition of phenol. Residual phenol is not found in solution.

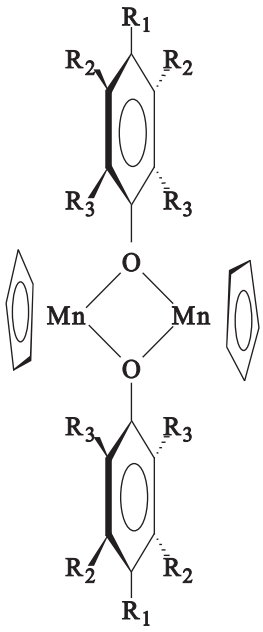
Complex **1** is very oxygen- and moisture-sensitive. The white solid is pyrophoric and could not be correctly characterized by conventional elemental analysis techniques. In spite of this, it was possible to ascertain its composition by acidolysis of the compound and quantitative determination, via GC, of the ligands released (see *Experimental*). Analysis of **1**, by this methodology, ascertained that Cp and PhO^- are coordinated to the metal in a 1:1 ratio and that one mol of solvent (THF) per mol of Cp and PhO^- is also present in the metal coordination sphere. Quantitative determination of Mn was achieved by atomic absorption after acidolysis of the compound in aqueous solution and was determined to be present in a 1:1 ratio with the other ligands (PhOH, Cp, THF). When **1** was suspended in pentane under continuous stirring for approximately two days, the analysis of the recovered compound, after acidolysis, still gave a 1:1:1:1 ratio for Cp, THF, phenol, and Mn, respectively, indicating that the THF ligand remains quite strongly bound to the metal when the solid is suspended in non-coordinating solvents.

Complex **1** has been also characterized by spectroscopic techniques (ESR, IR, ^{1}H NMR) and by magnetic measurements. The IR spectrum (Nujol™ suspension) shows bands at 1587 (s, (C=C)) and 1260 (m, (C-O)) cm^{-1}. The ESR spectrum of **1** (Fig. 1), measured at 77 K in frozen THF, shows several not well resolved absorptions in the range 0–5000 G.

The two transitions in the range 1800–2800 G show an hyperfine structure consisting of 11 lines with a hyperfine coupling constant of 42 ± 2 G, in which the intensities follow quite well the 1:2:3:4:5:6:5:4:3:2:1 ratio. The observed value (42 G) is approximately half the value (85–90 G) found for monomeric complexes (10). Preliminary theoreti-

© 2001 NRC Canada

Fig. 2. Proposed structure of dimeric Mn-complexes.



Compound **1** $R_1 = H, R_2 = H, R_3 = H$
Compound **2** $R_1 = CH_3, R_2 = H, R_3 = H$
Compound **3** $R_1 = H, R_2 = CH_3, R_3 = H$
Compound **5** $R_1 = H, R_2 = H, R_3 = CH_3$

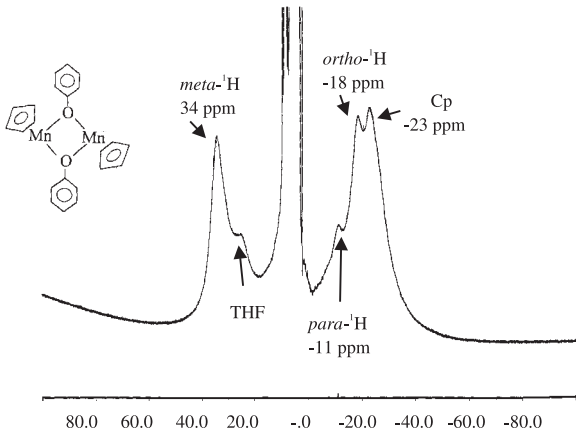
cal calculations[2] also support the presence of a dimeric system. The above reported spectral features indicate the presence of two ^{55}Mn centers ($I = 5/2$) with strong electron spin exchange interaction through the bridging *O*-bonded phenoxide ligands. Such features are common to other Mn(II)-complexes bearing *O*-bridging ligands (11). The proposed structure for compound **1** is shown in Fig. 2 and accounts for a 17 electron-system.

Complex **1** has a magnetic moment of $\mu_{eff} = 5.35\ \mu_B$ per Mn atom measured at room temp and $4.54\ \mu_B$ at 80 K. The product $(\chi_m \cdot \theta)$ is almost constant over the entire range of temperature. This value may indicate the presence of high spin antiferromagnetically coupled Mn(II) centers (12).

Unfortunately, it was not possible to obtain the ^{13}C NMR spectrum of **1**. The ^1H NMR spectrum of **1** (Fig. 3), however, shows a very complex pattern with broad signals (half-widths of ca. 4 kHz) at 34, 24, –11, –18, and –23 ppm. The ^1H NMR spectra reported throughout this paper are quite rare examples of proton NMR spectra of Mn(II) complexes, for which very often it is reported that it was not possible to obtain the ^1H NMR spectrum due to sensivity reasons.

The observed pattern in the ^1H NMR spectra strongly indicates the dominance of the spin density polarisation effect through the aromatic ring (5). As the integral and the chemical shifts were not helpful for the assignment of the resonances for the phenoxide, THF, and Cp protons, a systematic study of the ^1H NMR spectra of half-sandwich Mn(II) complexes with *ortho*-, *meta*-, and *para*-substituted phenols ($4\text{-}(CH_3)\text{-}C_6H_4OH$, $3,5\text{-}(CH_3)_2\text{-}C_6H_3OH$, $2,6\text{-}(tert\text{-butyl})_2\text{-}C_6H_3OH$), and $2,6\text{-}(CH_3)_2\text{-}C_6H_3OH$) was undertaken. This study was reputed useful for the following reasons. (*i*) As

Fig. 3. ^1H NMR spectrum of $[Cp(THF)Mn(\mu\text{-}O\text{-}C_6H_5)]_2$ in THF-d_8, $T = 298$ K.



documented in the literature, the ^1H NMR signals of CH_3-protons attached to aromatic systems in paramagnetic complexes are narrower with respect to the signals of protons directly attached to the carbon atoms of the phenyl ring and, thus, they can be more easily recognized in the spectrum. (*ii*) If strong spin density polarisation is taking place through the aromatic ring, the substitution of H with a CH_3 group is expected to significantly shift the proton resonance. This feature is often very helpful in proton assignment.

In fact, a comparative analysis of the variation of the CH_3-proton shifts with the position of the substituents in the ring made possible the assignment of almost all resonances for the complexes with the different ligands listed above; the results are reported in Table 1.

On the basis of the total spectral assignments for the complexes bearing coordinated phenoxide and its substituted forms, we can, for complex **1**, attribute the signal at 34 ppm to phenolate-*meta*-protons and the signals at –18 and –11 ppm to the phenolate *ortho*- and *para*-protons, respectively. The signal at –23 ppm is assigned to the coordinated Cp protons. This value is in agreement with the data reported in the literature for half-sandwich complexes with facial coordination of the Cp ligand (13). The band at 24 ppm is assigned to the coordinated THF molecule. When the spectrum was registered in THF-d_8 this signal was not observed, because of the exchange with the deuterated solvent. By adding small amounts of THF directly to the solution in the NMR tube, the resonance at 24 ppm did finally appear.

Reaction of Cp_2Mn with $4\text{-}CH_3\text{-}C_6H_4OH$

The reaction of Cp_2Mn with $4\text{-}(CH_3)\text{-}C_6H_4OH$ in a 1:1 molar ratio in THF affords compound **2**, which is soluble in THF and can be separated from a very concentrated solution.

$$[2] \quad 2Cp_2Mn + 2(4\text{-}CH_3\text{-}C_6H_4OH) \xrightarrow[298\ K]{THF} [Cp(THF)Mn(\mu\text{-}O\text{-}4\text{-}(CH_3)\text{-}C_6H_4)]_2 + 2C_5H_6$$

[2] V. Minin. Kurnakov Institute of General and Inorg. Chem. of the Russian Academy of Sciences, Moscow, Russia (personal communication).

© 2001 NRC Canada

Table 1. ^{1}H NMR data for Mn-complexes.

	H-*ortho*	H-*meta*	H-*para*	Cp
[Cp(THF)Mn(μ-C_6H_5)]$_2$ (**1**)	–18	34	–11	–23
[Cp(THF)Mn(μ-*O*-4-(CH_3)-C_6H_4)]$_2$ (**2**)	n.a.	26[a]	31 (CH_3)	–26
[Cp(THF)Mn(μ-*O*-3,5-(CH_3)$_2$-C_6H_3)]$_2$ (**3**)	–2	–5 (CH_3)	–18	–26
[CpMn(η^5–2,6-(*tert*-butyl)$_2$-C_6H_3O)] (**4**)	10 (*t*-Bu)	31	–22	3
[Cp(THF)Mn(μ-*O*-2,6-(CH_3)$_2$-C_6H_3)]$_2$ (**5**)	28 (CH_3)	35	–18	–29
[CpMn(η^5–2,6-(CH_3)$_2$-C_6H_3O)] (**6**)	–24 (CH_3)	25	–18	2

Note: n.a. = not assigned.
[a]Tentative assignment.

In this case, GC analysis of the reaction solution is not helpful for monitoring the amount of Cp released upon the reaction of Cp_2Mn with 4-(CH_3)-C_6H_4OH. In fact, because the product is soluble in the reaction solvent, the GC technique cannot distinguish the free Cp in solution from that generated upon decomposition of the complex in the injector. It was, however, possible to follow the reaction by monitoring the IR spectrum of the reaction solution. In fact, just minutes after the addition of 4-CH_3-(C_6H_4)OH, the band at 3600 cm^{-1} due to the free phenol ν(OH) completely disappears, allowing one to conclude that the added substituted phenol has completely reacted with Mn(II). Complex **2** was analyzed by GC and atomic absorption analysis after acidolysis of the solution (see *Experimental*) and shown to bear Mn in a 1:1 ratio to Cp, THF, and 4-(CH_3)-C_6H_4OH. The analytical data do not change if complex **2** is suspended in pentane (even for 2 days), indicating that THF is always strongly bound to the metal. The ESR spectrum of **2** measured at 77 K, as a frozen THF solution, is very similar to that of **1**, including the presence of the 11 line hyperfine structure for bands in the range 1800–2800 G with hyperfine coupling of 42 ± 2 G. These features suggest a dimeric structure for complex **2**, with μ-*O*-bonded phenoxide ligands. The ^{1}H NMR spectrum of **2** shows only two intense signals at 31 and –26 ppm, assigned to the CH_3-*para*-protons of the phenoxide ligand and the cyclopentadienyl protons, respectively. The shift towards lower fields of the CH_3-*para*-phenoxide protons is in agreement to what is observed for CH_3-*para*-protons of 4-(CH_3)-$C_6H_4O^-$ coordinated to Fe(III)–salen complexes (5), and the observed value of –26 ppm, is in the correct range for Cp protons. The signals of the *ortho*- and *meta*-protons of the phenoxide ligand are probably obscured by the two large signals reported above. The structure for compound **2** is shown in Fig. 2.

Reaction of Cp_2Mn with 3,5-(CH_3)$_2$-C_6H_3OH

The reaction of Cp_2Mn with 3,5-dimethylphenol (1:1 molar ratio) in THF closely matches the reaction reported for **2**. A white powder is isolated from a very concentrated solution, which was analyzed to be [Cp(THF)Mn(μ-*O*-3,5-(CH_3)$_2$-C_6H_3)]$_2$ (**3**).

[3] $$2Cp_2Mn + 2(3,5\text{-}(CH_3)_2\text{-}C_6H_3OH) \xrightarrow[298\ K]{THF} [Cp(THF)Mn(\mu\text{-}O\text{-}3,5(CH_3)_2\text{-}C_6H_3)]_2 + 2C_5H_6$$

THF is strongly bound as shown by the stability of **3** in pentane even for a long period of time (2 days).

The ESR spectrum of **3** in frozen THF solution at 77 K consists of bands in the range 1800–2800 G, with a hyperfine structure comprised of 11 lines, and hyperfine coupling of 42 ± 2 G. A dimeric structure is also assigned to complex **3** (Fig. 2).

The ^{1}H NMR spectrum of compound **3** in THF-d_8 shows that the CH_3-*meta*-protons (–5 ppm) and the Cp protons (–26 ppm) almost overlap the signals found at –2.5 and –18 ppm, which are assigned to the *para*- and *ortho*-phenoxide protons, respectively, in the dimeric μ-*O*-bonded phenoxide complex (compound **3**, Fig. 2). This is in agreement with a negative spin density delocalization on the CH_3-*meta*-protons of the μ-*O*-coordinated phenoxide anion and confirms the spectral analogies between Mn(II)– and Fe(III)–phenoxide complexes (5). In fact, the pattern of the isotropic shifts of CH_3-*meta*- or *para*-protons in compound **3** or **2,** respectively, is very similar to what observed for (salen)Fe(III) – methyl-substituted-phenoxide complexes, and demonstrates the presence of a strong spin polarization through the aromatic ring. On this basis, a positive spin density delocalization is expected and revealed for protons of CH_3-group *ortho*- or *para*- in the phenoxide ligand, as found also in relevant (salen)Fe(III) complexes.

Reaction of Cp_2Mn with 2,6-(*tert*-butyl)$_2$-C_6H_3OH

When Cp_2Mn is reacted in anhydrous THF with 2,6-(*tert*-butyl)$_2$-C_6H_3OH in a 1:1 molar ratio a white solid product (**4**) is isolated. (eq. [4])

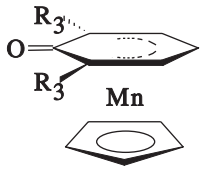
[4] $$Cp_2Mn + 2,6\text{-}(tert\text{-butyl})_2\text{-}C_6H_3OH \xrightarrow[298\ K]{THF} [CpMn(\eta^5\text{–}2,6\text{-}(tert\text{-butyl})_2\text{-}C_6H_3O)] + C_5H_6$$

Again, the reaction cannot be followed by GC analysis because of the solubility of the reaction product, but can be isolated and analyzed by GC after acidolysis. The ligands (Cp, THF, and 2,6-(*tert*-butyl)$_2$-C_6H_3OH) are determined to be in a 1:1:1 reciprocal ratio and each in 1:1 ratio to Mn. If **4** is suspended in pentane for 12 h, analysis of the solid shows that THF has been released almost quantitatively (less than 5% of product still contains coordinated THF, as demonstrated by GC analyses).

The ESR spectrum of **4** measured at 77 K, in a frozen THF solution, shows only one large signal at g = 2.003 G due to a low spin Mn(II) with a six line hyperfine structure. The coupling constant (A = 85 ± 3 G) and the six lines clearly indicate the presence of a monomeric species (10). When 2,6-(*tert*-butyl)$_2$-C_6H_3OH is added in a 1:1 ratio to a

© 2001 NRC Canada

Fig. 4. Proposed structure of monomeric [CpMn(η^5–2,6-(*tert*-butyl)$_2$-C_6H_3O)].



R_3 = *t*-Bu; Compound **4**
R_3 = CH_3; Compound **6**

solution of Cp_2Mn and the ESR spectrum of the reaction mixture is measured at low temperature (80 K) with time, several changes are observed. Immediately after the addition of 2,6-(*tert*-butyl)$_2$-C_6H_3OH, a complex pattern of signals appears, similar to that observed for compounds **1**–**3**. If the solution is allowed to warm to room temp, and after 30 min the spectrum is repeated at low temperature (80 K), one single signal is observed as specified above. These features indicate the initial formation of a high spin species (most probably, the *O*-bonded phenoxide complex is the kinetic product), which in a short time converts into a low spin species. The complex bearing the phenol moiety π-bonded to the metal is the thermodynamic product.

Since, Cp_2Mn and substituted cyclopentadienyl manganocenes show a spin cross-over effect at temperature close to room temp that depends on the matrix that contains the compound, a detailed analysis of the dependence of the high spin ⇄ low spin equilibrium for **4** is in progress.

Complex **4** is soluble enough in benzene at room temp for preparing a 1×10^{-2} M solution, which was not possible for dimeric compounds described above, to allow for molecular mass determination of **4** by cryoscopy (14). The molecular mass of **4** was found to be 355 g mol^{-1} (calculated 325 g mol^{-1}), thus, confirming the monomeric structure of the complex. The ^{1}H NMR of **4** in THF-d_8 shows a signal at 10 ppm for the *tert*-butyl-protons. As the *tert*-butyl-protons are one C—C bond further away from the aromatic ring with respect to the CH_3-protons, the slight shift to lower fields confirms that in this complex the same mechanism of spin density delocalization is operative as described for the other complexes in this paper. The signal due to Cp protons overlaps with that of the solvent and is found around 3 ppm. The ^{1}H NMR spectrum of **4** in C_6D_6 shows the same features of that measured in THF-d_8, demonstrating that both benzene and THF do not coordinate to the metal center and, thus, validates the cryoscopic measurement of the molecular mass made in C_6H_6. The monomeric structure of **4**, as shown by ESR and cryoscopic measurements, can be explained by considering a π-coordination of the aromatic ring to the metal center (Fig. 4).

A single *O*-bonded phenoxide to the CpMn moiety should, in fact, give a coordinatively unsaturated 13e$^-$ species. While in the literature, one example of a dimeric Mn–phenoxide complex (15) which formally accounts for 11e$^-$, is reported, all known momeric cyclopentadienyl complexes account for 17–19e$^-$.

Reaction of Cp_2Mn with 2,6-$(CH_3)_2$-C_6H_3OH

The reaction of Cp_2Mn with 2,6-$(CH_3)_2$-C_6H_3OH in a 1:1 molar ratio in THF affords a mixture of solid products. Analysis shows the ligands and Mn to all be in a 1:1 ratio. However, the suspension of the white solid in pentane for 12 h allows for isolation of a powder showing, after acidolysis, a Cp:THF:phenoxide ratio of 1:0.5:1, indicating that THF is released from the coordination sphere even in non-coordinating solvents. Such finding must be related to a possible change of the coordination mode of the ligand.

Spectroscopic data of the white solid clearly show the presence of two products (**5** and **6**) (see discussion below) formed according to eq. [5]:

$$[5]\quad 3Cp_2Mn + 3(2,6\text{-}(CH_3)_2\text{-}C_6H_3OH) \xrightarrow[298\ K]{THF} [Cp(THF)Mn(\mu\text{-}O\text{-}2,6\text{-}(CH_3)_2\text{-}C_6H_3)]_2 + [CpMn(\eta^5\text{-}2,6\text{-}(CH_3)_2\text{-}C_6H_3O)] + 3C_5H_6$$

Such data can be rationalized considering the features of complexes **1**–**4** described above. The ESR spectrum of the reaction product measured at 77 K in a frozen THF solution shows a quite complex pattern of signals, only in part similar to the ESR spectrum of compound **1**. The most important differences are related to: (*i*) the absence of the hyperfine structures in the bands in the range 1800–2800 G; and (*ii*) the presence of hyperfine splitting in the region of 500 G. In this region a six-line pattern is observed. Such a hyperfine structure suggests the presence of a monomeric species, as found for complex **4**. The analysis of the ^{1}H NMR spectrum (in THF-d_8) shows two broad and partially overlapping signals at 35 and 28 ppm. One very broad strong signal appears at –28 ppm with two less intense signals in the high field region at –18 and –24 ppm. The signals at 28 and –24 ppm are easily recognized as CH_3-protons on the basis of their half-width of ca. 1 kHz. The signal at 28 ppm is assigned to CH_3-protons of a dimeric compound (compound **5**, Fig. 1). The difference in the absolute value of the isotropic shift for the *tert*-butyl-protons of compound **4** compared with the CH_3-protons of compound **6** is due to the absence of the strong hyperconjugation effect operative in the case of the CH_3-protons. While the presence of the CH_3-proton signal at 28 ppm is in agreement with the above discussed pattern, the signal at –24 ppm deviates strongly if a μ-*O*-structure is considered. The latter signal is assigned to a species bearing the *O*-2,6-$(CH_3)_2$-C_6H_3 moiety π-coordinated to the Mn(II) center. The signals at 35 and –18 ppm are assigned to the *meta*- and *para*-protons, respectively, of compound **5**. The Cp ligand in this complex is found at –29 ppm. In **6** the Cp signal is shifted to lower field (2 ppm), and partially overlaps with the solvent signal.

Both the ESR and ^{1}H NMR spectra and the analytical data support the conclusion that two products (**5** and **6**) are formed as shown in eq. [5]. The experimental evidence that half of the coordinated THF is released after suspension of the solid in pentane, indicates that approximately half of the solid is a species in which THF is not strongly bound to the metal and can be removed by the action of a non-coordinating solvent. By simply taking into account electron-counting, compound **5** can reach a 17e$^-$ configuration by being a dimer with a molecule of THF in the coordination

© 2001 NRC Canada

sphere. The monomeric species (**6**), which on the basis of the analytical data is composed of Mn, Cp, and phenoxide in 1:1:1 ratio, does not need THF to reach the $17e^-$ configuration as it bears the π-coordinated phenoxide ligand. In compound **6**, the presence of two methyl groups in the 2- and 6-positions, forces the η^5-coordination of the substituted phenoxide, but the steric hindrance is not such to afford the π-coordination as the only form, as observed in the case of **4**. Attempts to isolate compounds **5** and **6** as pure solids have been done. By crystallization from benzene or toluene it is possible to obtain a compound richer in **6**, but not totally free of **5**. The interconversion (**5** ⇄ **6**) is not operating at room temp or lower.

Reaction of 4 and 6 with CO_2

When complex **4** (or **6**) is exposed to CO_2, 4-OH-3,5-di-*tert*-butyl-benzoic acid (or 4-OH-3,5-dimethyl-benzoic acid) is isolated (yield ca. 10%). When Mn-complexes bearing *O*-bonded phenols are used, ring-carboxylation is not observed. The behaviour of μ-*O*- and π-bonded phenols can be explained by taking into account that the π-coordination forces electron-dislocation in the 4-position to facilitate nucleophilic attack on CO_2. This produces the ring carboxylation, as also observed for similar Rh-complexes (4*a*), and benzene electro-carboxylation, via electron-transfer, to the ring coordinated Cr(0)-system upon electrochemical reduction of the metal center (16). Conversely, the μ-*O*-bonded phenols undergo CO_2 insertion into the Mn—O bond. Subsequent acidolysis produces the semi-carbonate (ROC(O)OH), which promptly decomposes into ROH and CO_2.

Experimental

General procedure

Unless otherwise stated, all reactions and manipulations were conducted under a nitrogen (N_2) atmosphere by using vacuum-line techniques. Samples for ESR studies were prepared using a Brown glove-box under N_2 atmosphere. All solvents were dried as described in the literature (17) and stored under nitrogen. FT-IR spectra were recorded using a Bruker 113V Fourier transform interferometer. Frequencies are accurate to ±1 cm^{-1}. Solid samples were studied as Nujol™ mulls (Nujol™ was previously dried on sodium wires and bubbled with argon). GC analyses were performed with a Dani 3800 gas chromatograph equipped with a FID detector and a packed SE30 column. Quantitative Mn determination was performed with an PerkinElmer 3110 atomic absorption spectrometer equipped with Mn lamp.

NMR spectra were recorded using a AM 500 Bruker spectrometer. ESR spectra were recorded at 9.4247866 GHz (power = 2.00×10^1 mW) on a Bruker ESP300E spectrometer, which has a 100 kHz magnetic field modulation and is equipped with a Bruker NMR gaussmeter (ER 035M) and a Hewlett–Packard microwave frequency counter (HP 5350B).

Acidolysis, GC, and atomic absorption analysis of compounds

All described compounds were pyrophoric and could not be analysed by conventional analytical techniques. The following methodology allowed for compositional analysis: (*i*) 20–30 mg of the compound, carefully weighted out of the contact with air, was put in a Schlenck tube cooled to 0°C with an ice water bath and, under vigorous stirring, was added dry toluene (2 mL) previously saturated with dry, gaseous HCl. A brown solid immediately separated. After deposition of the solid, the liquid fraction was analysed by GC using a temperature program, which allowed for the separation of cyclopentadiene (1.07 min), THF (1.72 min), toluene (7.8 min), and phenols (C_6H_5OH, 10.40 min; 4-CH_3-C_6H_4OH, 12.38 min; 3,5-$(CH_3)_2$-C_6H_3OH, 14.5 min; 2,6-(*tert*-butyl)$_2$-C_6H_3OH, 15.3 min; 2,6-$(CH_3)_2$-C_6H_3OH, 12.87 min). (*ii*) Alternatively, the solid sample was treated with a large (>100 molar ratio) excess of propionic acid. The solution was analysed by the same GC procedure (propionic acid retention time is 5.5 min in the reaction conditions and does not interfere with other species).

For the quantitative determination of Mn, the following procedure was applied: to 15–20 mg of carefully weighted compound was put in a Schlenck tube under N_2 and was added, under vigorous stirring, distilled water (2 mL) and concentrated H_2SO_4 (analytical grade) (1 mL). The light pink solution obtained was quantitatively transferred into a 50 mL analytical flask and diluted with distilled water. The solution was then analysed by atomic absorption spectroscopy.

Synthesis of [Cp(THF)Mn(μ-*O*-C_6H_5)]$_2$ (1)

To a solution of Cp_2Mn (400 mg, 2.1 mmol) in anhydrous THF (30 mL) under a N_2 atmosphere was added, with vigorous stirring, phenol (200 mg, 2.1 mmol) dissolved in THF (10 mL). A white solid immediately precipitated. After stirring for 1 h, the mixture was filtered and the white solid washed with THF (10 mL), pentane (20 mL), and finally dried in vacuo. The compound was isolated in 95% yield. The GC and atomic absorption analysis, carried out after acidolysis of **1** (as previously described), revealed the presence of Cp, THF, phenol, and Mn in a 1:1:1:1 ratio.

Compound **1** was suspended in anhydrous pentane (30 mL) under a N_2 atmosphere with vigorous stirring for 2 days. The solvent was eliminated and the complex washed and dried in vacuo. Analysis, after acidolysis, of the isolated product showed the same composition as reported above. FT-IR (Nujol/KBr) (cm^{-1}): (PhO-ligand) 1587 (vs) (C=C), 1260 (m) (C-O), 753 (s) (γC-H), 693 (s) (γC-H); (cyclopentadienyl ligand) 1025 (vs) (δC-H), 1006 (s) (δC-H), 760 (s) (γC-H). ^{1}H NMR (THF-d_8) δ: 34 (H-*meta*), –11 (H-*para*), –18 (H-*ortho*), –23 (Cp).

Synthesis of [Cp(THF)Mn(μ-*O*-4-(CH_3)-C_6H_4)]$_2$ (2) and [Cp(THF)Mn(μ-*O*-3,5-(CH_3)$_2$-C_6H_3)]$_2$ (3)

(*i*) A solution of 4-CH_3-C_6H_4OH (292 mg, 2.7 mmol) dissolved in anhydrous THF (15 mL) was added to Cp_2Mn (500 mg, 2.7 mmol) in THF (35 mL) (under N_2 atmosphere) with stirring. The resulting mixture was stirred for 4 h and then concentrated in vacuo to 5–7 mL. A light-brown solid separated from the solution and the organic phase was removed. The solid was washed anhydrous THF (2 × 5 mL), anhydrous pentane (10 mL), and dried in vacuo. The compound, isolated as a grey powder in 90% yield, was determined to be [Cp(THF)Mn(μ-*O*-4-(CH_3)-C_6H_4)]$_2$ by GC analysis after acidolysis (as previously described).

Compound **2** was suspended in anhydrous pentane following the same procedure as described for compound **1**. Analysis,

© 2001 NRC Canada

showed that no change had occurred. FT-IR (Nujol/KBr) (cm^{-1}): (4-CH_3-$C_6H_4O^-$ ligand) 1589 (s) (C=C), 1260 (vs) (C-O), 750 (s) (γC-H), 700 (s) (γC-H); (cyclopentadienyl ligand) 1025 (vs) (δC-H), 1006 (s) (δC-H), 770 (s) (γC-H). ^{1}H NMR (THF-d_8) δ: 26 (H-*meta*), 31 (CH_3-*para*), –26 (Cp).

(*ii*) A solution of 3,5-$(CH_3)_2$-C_6H_3OH (278 mg, 2.28 mmol) in anhydrous THF (10 mL) was added, under N_2 flow and vigorous stirring, at room temp to a flask containing Cp_2Mn (420 mg, 2.28 mmol) dissolved in THF (30 mL). The mixture was worked up as described above and [Cp(THF)Mn(μ-*O*-3,5-$(CH_3)_2$-C_6H_3)]$_2$ was isolated in 90% yield.

Compound **3** in anhydrous pentane did not change its composition after two days. FT-IR (Nujol/KBr) (cm^{-1}): (3,5-$(CH_3)_2$-$C_6H_3O^-$ ligand) 1585 (s) (C=C), 1155 (vs) (C-O), 750 (s) (γC-H), 690 (s) (γC-H); (cyclopentadienyl ligand) 1025 (vs) (δ C-H), 1006 (s) (δC-H). ^{1}H NMR (THF-d_8) δ: –5 (CH_3-*meta*), –2 (H-*ortho*), –18 (H-*para*), –26 (Cp).

Synthesis of [CpMn(η^5-2,6-(*tert*-butyl)$_2$-C_6H_3O)] (4)

A solution of Cp_2Mn (300 mg, 1.62 mmol) dissolved in anhydrous THF (20 mL) under a N_2 atmosphere was added to 2,6-(*tert*-butyl)$_2$-C_6H_3OH (334 mg, 1.62 mmol) dissolved in THF (10 mL). The mixture was stirred for 4 h and then worked up as for **2**. A white solid compound was isolated in 90% yield which analysis, after acidolysis, showed Cp, THF, 2,6-(*tert*-butyl)$_2$-C_6H_3OH, and Mn to be in a 1:1:1:1 ratio. Compound **6** was suspended in anhydrous pentane (30 mL) and stirred for 12 h. The solvent was eliminated and the product obtained was dried in vacuo. The analysis after acidolysis of the obtained complex showed Cp, THF, phenoxide, and Mn to be in a 1:0.05:1:1 ratio. FT-IR (Nujol/KBr) (cm^{-1}): (2,6-(*tert*-butyl)$_2$-$C_6H_3O^-$ ligand) 1575 (s) (C=O and C=C), 1181 (vs) (C-O), 840 (m) (γC-H), 610 (m) (γC-H); (cyclopentadienyl ligand) 1000 (s) (δC-H), 775 (s) (γC-H). ^{1}H NMR (THF-d_8) δ: 31 (H-*meta*), –22 (H-*para*), 10 (*t*-Bu-*ortho*), 3 (Cp).

Synthesis of [Cp(THF)Mn(μ-*O*-2,6-$(CH_3)_2$-C_6H_3)]$_2$ (5) and [CpMn(η^5-2,6-$(CH_3)_2$-C_6H_3O)] (6)

To a solution of Cp_2Mn (450 mg, 2.4 mmol) in THF (35 mL) was added 297 mg (2.4 mmol) of 2,6-$(CH_3)_2$-C_6H_3OH dissolved in 10 mL of the same solvent. The mixture was stirred for 4 h and then worked up as for **2**. A white powder was isolated in 90% yield. GC analysis, carried out after acidolysis, revealed the presence of Cp, THF, 2,6-$(CH_3)_2$-C_6H_3OH, and Mn in a 1:1:1:1 ratio. The white solid obtained was suspended in anhydrous pentane (30 mL) under N_2 atmosphere with vigorous stirring for 12 h. The solvent eliminated and the complex dried in vacuo. Analysis, after acidolysis, of the obtained product showed the Cp, THF, phenoxide, and Mn in a 1:0.5:1:1 ratio. FT-IR (Nujol/KBr) (cm^{-1}): (2,6-$(CH_3)_2$-$C_6H_3O^-$ ligand) 1585(s) (C=O and C=C), 1250 (vs) (C-O), 750(s) (γC-H), 690(s) (γ C-H); (cyclopentadienyl ligand) 1025(w) (δC-H), 995(s) (δC-H), 760(s) (γC-H).

Crystallization from benzene–pentane allowed separating almost pure samples of **5** and **6**. ^{1}H NMR (THF-d_8) δ: (compound **5**) 35 (H-*meta*), –18 (H-*para*), 28 (CH_3-*ortho*), –29 (Cp); (compound **6**) 25 (H-*meta*), –18 (H-*para*), –24 (CH_3-*ortho*), 2 (Cp).

Reaction of 4 and 6 with CO_2

Complex **4** (180 mg, 0.5 mmol) (180 mg (0.7 mmol) for **6**) was dissolved in THF and the solution exposed to 0.1 MPa of CO_2 at room temp. After 6 h stirring, the solution was dried in vacuo and the residual solid treated with BF_3–CH_3OH. Water was added to eliminate the excess of BF_3 and the mixture extracted with diethyl ether. The GC analysis of the resulting ether solution showed the formation of the methyl ester of 4-OH-3,5-(*tert*-butyl)-benzoic acid if starting from **4** (or of 4-OH-3,5-$(CH_3)_2$-benzoic acid if starting from complex **6**).

Conclusions

The results reported above demonstrate that bulky substituents at the 2,6-positions of the phenyl ring may force the η^5-coordination to Mn(II) of substituted phenoxides. Coupling ESR and ^{1}H NMR spectroscopy proved to be a useful tool for structure determination in solution. The η^5-coordination of the phenol prompts the phenyl-ring to a nucleophilic attack of CO_2, which produces the ring carboxylation.

Acknowledgements

This work was supported by MURST, project no. 9 803 026 360. A partial financial support to J. Ziolkowski and A. Jezierski from the TEMPUS Programme (JEP 8164) is also acknowledged. Professor Claudio Luchinat is gratefully thanked for helpful discussions. Mr. Giuseppe Cosmai is thanked for skillful technical assistance in hardware construction for the manipulation of compounds.

References

1. D.C. Bradley, R.C. Mehrotra, and D.P. Gaur. Metal alkoxides. Academic Press, London. 1980.
2. (*a*) S.D. Loren, B.K. Campion, R.H. Heyn, T.D. Tilley, B.E. Bursten, and K.W. Luth. J. Am. Chem. Soc. **111**, 4712 (1989); (*b*) B. Chaudret, X. He, and Y. Huang. J. Chem. Soc. Chem. Commun. 1844 (1989); (*c*) U. Koelle, M. Homg Wang, and G. Raabe. Organometallics, **10**, 2573 (1991); (*d*) W.S. Trahanovsky and R.A. Hall. J. Am. Chem. Soc. **99**, 4850 (1977).
3. (*a*) D.J. Cole-Hamilton, R.J. Young, and G. Wilkinson. J. Chem. Soc. Dalton Trans. 1995 (1976); (*b*) M. Aresta, E. Quaranta, A. Dibenedetto, M. Pascale, and I. Tommasi. J. Organomet. Chem. **605**, 143 (2000); (*c*) H. El-Amouri, M. Gruselle, and J. Veissermann. Organometallics **9**, 2871 (1990); (*d*) M.D. Fryzuk, M.L. Yang, T. Jones, and F.W.B. Einstein. Can. J. Chem. **664**, 174 (1986); (*e*) L. Dahlenburg and N. Hock. J. Organomet. Chem. **284**, 129 (1985); (*f*) B. Cetinkaya, P.B. Hitchcock, M.L. Lappert, S. Torroni, J.L. Atwood, W.E. Hunter, and M.J. Zaworotko. J. Organomet. Chem. **188**, C31, (1980); (*g*) C. White, S.J. Thompson, and P.M. Maitlis. J. Organomet. Chem. **127**, 415 (1977); (*h*) V.F. Kuznetsov, G.P.A. Yap, C. Bensimon, and H. Alper. Inorg. Chim. Acta, **280**, 172 (1998).
4. (*a*) R.H. Heistand II, R.B. Lauffer, E. Fikrig, and L. Que. J. Am. Chem. Soc. **104**, 2789 (1982); (*b*) G.N. La Mar, G.R. Eaton, R.H. Holm, and F.A. Walker. J. Am. Chem. Soc. **95**, 63 (1973).
5. V.K. Yachandra, K. Sauer, and M.P. Klein. Chem. Rev. **96**, 2927 (1996).

© 2001 NRC Canada

6. (*a*) L.E. Pence, A. Caneschi, and S.J. Lippard. Inorg. Chem. **35**, 3069 (1996); (*b*) B. Horvath, R. Möseler, and E.G. Horvath. Z. Anorg. Allg. Chem. **41**, 449 (1979); (*c*) H.W. Roesky, M. Scholz, and M. Noltemeyer. Chem Ber. **123**, 2303 (1990); (*d*) M. Wesolek, D. Meyer, J.A. Osborn, A. De Cian, J. Fischer, A. Derory, P. Legoll, and M. Drillon. Angew. Chem. Int. Ed. Engl. **33**, 1592 (1994); (*e*) R.A. Bartlett, J.J. Ellison, P.P. Power, and S.C. Shoner. Inorg. Chem. **30**, 2888 (1991); (*f*) D. Meyer, J.A. Osborn, and M. Wesolek. Polyhedron, **9**, 1311 (1990) and refs. therein.
7. K.K. Bhasin, W.G. Balkeen, and P.L. Pauson. J. Organomet. Chem. **204**, C25 (1981).
8. A. Lack, M. Aresta, G. Fuchs, and I. Tommasi. Eur. J. Biochem. **197**, 471 (1991).
9. M. Aresta, E. Quaranta, R. Liberio, C. Dileo, and I. Tommasi. Tetrahedron, **54**, 8841 (1998).
10. A. Hudson and M.J. Kennedy. Inorg. Nucl. Chem. Letters, **7**, 333 (1971).
11. P. Mathur and G.C. Dismukes. J. Am. Chem. Soc. **105**, 7093 (1983).
12. (*a*) D.R. Eaton and W.D. Phillips. Advan. Magn. Resonance, **1**, 103 (1965); (*b*) R.L. Martin. *In* New pathways in inorganic chemistry. *Edited by* E.A.V. Ebsworth, A.G. Maddock, and A.G. Sharpe. Cambridge University Press, London. 1968. p. 175.
13. N. Hebendanz, F.H. Kohler, G. Muller, and J. Riede. J. Am. Chem. Soc. **108**, 3281 (1986).
14. M. Aresta, C.F. Nobile, and A. Sacco. Inorg. Chem. Acta, **12**, 167 (1975).
15. R.A. Jones, S.U. Koschmieder, and C.M. Nunn. Inorg. Chem. **27**, 4526 (1988).
16. J.A. Corella II and N.J. Cooper. J. Am. Chem. Soc. **112**, 2832 (1990).
17. D.D. Perrin, W.L.F. Amarego, and D.R. Perrin. Purification of laboratory chemicals. Pergamon Press, Oxford, U.K. 1986.

© 2001 NRC Canada

$Rh_2Cl_2(CO)_4$ adsorbed and tethered on gold powder: IR spectroscopic characterization and olefin hydrogenation activity

Hanrong Gao and Robert J. Angelici

Abstract: Catalysts were prepared by adsorbing $Rh_2Cl_2(CO)_4$ directly on gold powder or on gold that contained the tethered ligands 2-(diphenylphosphino)ethane-1-thiol (DPET) or methyl 2-mercaptonicotinate (MMNT). Infrared (IR) studies (diffuse reflectance infrared Fourier transform (DRIFT)) of the catalyst Rh–Au prepared by adsorbing $Rh_2Cl_2(CO)_4$ directly on Au indicate that a $Rh^I(CO)_2$ species is present. IR studies of Rh–DPET-Au suggest that tethered *cis*-Rh(DPET)$(CO)_2$Cl is the major species at relatively high $Rh_2Cl_2(CO)_4$ loadings, but *trans*-Rh$(DPET)_2$(CO)Cl is observable at low $Rh_2Cl_2(CO)_4$ loadings. Spectral investigations of the catalyst Rh–MMNT-Au prepared by adsorbing $Rh_2Cl_2(CO)_4$ on MMNT-Au suggest that tethered [*cis*-Rh$(MMNT)_2(CO)_2]^+Cl^-$ and (or) Rh(MMNT)$(CO)_2$Cl are the major species at low $Rh_2Cl_2(CO)_4$ loadings, while a new unidentified species predominates at high $Rh_2Cl_2(CO)_4$ loadings. All three catalysts are active 1-hexene hydrogenation catalysts under the mild conditions of 40°C and 1 atm of H_2; they are much more active than Au powder or $Rh_2Cl_2(CO)_4$ in solution. Of the three catalysts, Rh–Au is the most active with a maximum turnover frequency (TOF) of 800 mol H_2 per mol Rh per min while its turnover (TO) is 29 600 mol H_2 per mol Rh during a 2-hour run. Under the conditions of 1-hexene hydrogenation, the catalysts lose their CO ligands. Thus, it appears that a form of Rh metal on Au is the catalytically active species.

Key words: catalysis, olefin hydrogenation, gold powder, tethered rhodium complexes, infrared studies, adsorption, rhodium complexes.

Résumé : On a préparé les catalyseurs mentionnés dans le titre en faisant absorber du $Rh_2Cl_2(CO)_4$ directement sur de l'or en poudre ou sur de l'or qui contient les ligands fixés 2-(diphénylphosphino)éthane-1-thiol (DPET) ou 2-mercaptonicotinate de méthyle (MMNT). Des études infrarouges («DRIFT») du catalyseur (Rh–Au) préparé par adsorption de $Rh_2Cl_2(CO)_4$ directement sur de l'or indiquent la présence d'une espèce $Rh^I(CO)_2$. Les études IR du Rh–DPET-Au suggèrent que, pour des chargements relativement élevés de $Rh_2Cl_2(CO)_4$, le *cis*-Rh(DPET)$(CO)_2$Cl est l'espèce fixée principale; on peut toutefois observer la formation de *trans*-Rh$(DPET)_2$(CO)Cl avec des chargements faibles de $Rh_2Cl_2(CO)_4$. Des études spectrales du catalyseur (Rh–MMNT-Au) préparé par adsorption de $Rh_2Cl_2(CO)_4$ sur du MMNT-Au suggèrent que, pour des chargements faibles de $Rh_2Cl_2(CO)_4$, le [*cis*-Rh$(MMNT)_2(CO)_2]^+Cl^-$ et (ou) le Rh(MMNT)$(CO)_2$Cl sont les espèces fixées principales; toutefois, pour des chargements élevés de $Rh_2Cl_2(CO)_4$, l'espèce principale est une nouvelle espèce qui n'a pas été identifiée. Les trois catalyseurs sont des catalyseurs actifs pour l'hydrogénation de l'hex-1-ène dans des conditions douces, soit 40°C et 1 atm. de H_2; en solution, ils sont beaucoup plus actifs que l'or en poudre ou le $Rh_2Cl_2(CO)_4$. Des trois catalyseurs, le Rh–Au est le plus actif avec une valeur maximale de "TOF" de 800 mol H_2/mol Rh·min alors que son "TO" est de 29,600 mol H_2/mol Rh pour une expérience de deux heures. Dans les conditions d'hydrogénation de l'hex-1-ène, les catalyseurs perdent leurs ligands CO. Il semble donc que l'espèce catalytiquement active soit une forme métallique de Rh sur de l'or.

Mots clés : catalyseur, hydrogénation d'oléfines, poudre d'or, complexes de rhodium fixés, études infrarouges, complexes de rhodium.

[Traduit par la Rédaction]

Introduction

Heterogenized transition-metal complex catalysts, which offer distinct advantages over their homogeneous counterparts, have been extensively studied in the past few decades (1). Much work in this area has been dedicated to tethering organometallic complexes to insoluble organic polymers or inorganic oxides (2). Little information, however, has been reported on transition-metal complexes tethered to metallic surfaces (3).

The adsorption of organic molecules on solid metal surfaces has been extensively studied in recent years (4). Gold

Received July 12, 2000. Published on the NRC Research Press Web site at http://canjchem.nrc.ca on May 30, 2001.

Dedicated with best wishes to Professor Brian James on the occasion of his 65th birthday.

H. Gao and R.J. Angelici.[1] Ames Laboratory and Department of Chemistry, Iowa State University, Ames, IA 50011, U.S.A.

[1]Corresponding author (telephone: (515) 294-2603; fax: (515) 294-0105; e-mail: angelici@iastate.edu).

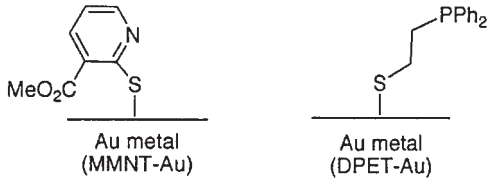
 DOI: 10.1139/cjc-79-5/6-578 © 2001 NRC Canada

metal has been investigated extensively because it does not form a surface oxide under atmospheric conditions at room temperature (5, 6). Among the organic compounds (7, 8) that adsorb on gold are thiols (RSH) and disulfides (RSSR), which produce RS groups on the surface (9). For example, terminal alkyl thiols, $X(CH_2)_nSH$ ($n \geq 1$ and X = COOH, $CONH_2$, CN, CH_2NH_2, etc.) adsorb on gold films as $X(CH_2)_nS$ groups (10).

Various transition-metal complexes have been tethered on polymer or inorganic oxide supports using a ligand that coordinates to the transition-metal complex through a donor ligand at one end and to the support through a surface-reactive group at the other end (11). Some of these tethered complexes have been used as catalysts (2). In our previous studies, we formed catalysts by tethering complexes on silica that also contained a supported metal, e.g., Pd (12). These tethered complex on a supported metal (TCSM) catalysts are unusually active for the hydrogenation of arene substrates. In the present report, we describe catalysts that are prepared by tethering a Rh complex directly to the surface of a metal (Au). The tethering ligand is attached to the Au through a thiol group and to the Rh complex by a phosphine or pyridine donor group. It was hoped that an unsaturated organic substrate would be activated by coordination to the Rh complex and hydrogen would be activated by Au to give a catalyst that was more active than either the complex or the Au metal separately. Although gold is generally considered to be a poor catalyst, small-particle gold has recently been reported (13) to be active for alkene hydrogenation. Although there are a few examples (14) of metal complexes tethered on gold, none have been used in catalytic hydrogenation reactions.

In this study, the tethering ligands, methyl 2-mercaptonicotinate (MMNT) or 2-(diphenylphosphino)ethane-1-thiol (DPET), were adsorbed on gold powder to give the ligand-modified gold powders MMNT-Au and DPET-Au (Scheme 1). These modified gold powders were reacted with $Rh_2Cl_2(CO)_4$ to give Au powders with tethered rhodium-carbonyl complexes. We also observed that $Rh_2Cl_2(CO)_4$ could be adsorbed directly onto Au powder without a tether. All three of these rhodium-complex – Au-metal materials were characterized by diffuse reflectance infrared Fourier transform (DRIFT) spectroscopy and evaluated for their catalytic activities in the hydrogenation of 1-hexene under the mild conditions of 40°C and 1 atm of H_2.

Scheme 1.



Experimental

Materials

$Rh_2Cl_2(CO)_4$ and $HAuCl_4{\cdot}xH_2O$ (Au, 49%) were purchased from Strem. The 2-(diphenylphosphino)ethane-1-thiol (DPET) (15) and methyl 2-mercaptonicotinate (MMNT) (16) tethers were prepared by the literature methods. Toluene was dried over CaH_2 before use, while THF, ethanol, and olefin substrates were used directly as commercial products without further purification.

The gold powder was prepared by reducing anhyd $AuCl_3$ (17) with $Li[(C_2H_5)_3BH]$ in THF using the following modified literature procedures (18). Hydrogen tetrachloroaurate ($HAuCl_4{\cdot}3H_2O$) (2.00 g) was heated under reflux with $SOCl_2$ (20 mL) in a 250 mL flask connected to a mineral oil bubbler in order to prevent moisture from contaminating the reaction mixture. Evolution of SO_2 and HCl was observed while the suspension was heated at reflux, and a red precipitate of anhyd gold(III) chloride was visible in the reaction flask. When the evolution of SO_2 and HCl ceased, the remaining $SOCl_2$ was removed by syringe and the red solid was dried in vacuum (1 mm Hg, 1 mm Hg = 133.322 Pa) at 65°C for 4 h. Then THF (100 mL) was added to the reaction flask, and 20 mL (1.0 M) of a THF solution of $Li[B(C_2H_5)_3H]$ was added dropwise with stirring at room temperature. After stirring for 12 h at room temperature, the mixture was filtered and the solid was washed successively with 80 mL aliquots of THF, methanol, THF, pentane, and water, and then dried under vacuum (0.02 mm Hg) at 80°C. The resulting Au powder was cleaned with freshly prepared "piranha" solution (20 mL) composed of a 50:50 mixture of concd H_2SO_4 and 30% aq H_2O_2 (caution: carefully add the H_2SO_4 to the H_2O_2) in a 250 mL beaker with slow stirring. Nitrogen was blown over the mixture to reduce gold loss due to foaming. The mixture was stirred for 10 min, filtered on a coarse frit, washed with water (10 × 50 mL) and ethanol (2 × 20 mL), and dried under a nitrogen stream. The Au powder was then baked in an oven at 120°C overnight. Routine BET surface area measurements were performed on a Micromeritics AccuSorb 2100 E instrument. With Kr as the adsorbate gas at 77 K, the surface area of the resulting Au powder was determined to be 0.96 ± 0.07 m^2 g^{-1}. An XPS analysis (on an AEI 200B spectrometer) of the Au powder showed it to be pure Au(0). Neither Au(I) nor other impurities such as lithium and boron were detected.

Infrared spectroscopy

All FT-IR and DRIFT spectra were recorded on a Nicolet 710 spectrophotometer equipped with a TGS detector in the main compartment and a MCT detector in the auxiliary experimental module (AEM). The AEM housed a Harrick diffuse reflectance accessory. All solution IR spectra were recorded using a NaCl cell (0.50 mm thickness) in the main compartment with the instrument set for 4 cm^{-1} resolution and 128 scans. All DRIFT spectra were recorded with samples in the Harrick microsampling cup using 600 scans and 4 cm^{-1} resolution. The background spectrum used for the DRIFT spectra was clean gold powder. Spectra were routinely baseline and purge corrected. The abscissa of the spectra were recorded and are reported in absorbance units even though the radiation collected is actually reflectance. Kubelka–Munk transformations of the spectra were not possible because of the low intensities of all bands; the bands were eliminated by the transformation. The pseudo-absorbance units used do appear to obey Beer's law, at least approximately.

© 2001 NRC Canada

Preparation of ligand-modified Au powders

MMNT-Au

The Au powder (300 mg) was mixed with a THF solution (1 mL) of methyl 2-mercaptonicotinate (MMNT) (3 mM) in a test tube and shaken for 2 min on a Genie Vortex mixer. After allowing the mixture to stand overnight at room temperature, the solution was separated by centrifugation and analyzed for the amount of MMNT by measuring the intensity of the ester ν(C=O) absorption at 1720 cm^{-1} and converting it to MMNT concentration using Beer's law. Subtracting this concentration from the original concentration of the MMNT solution gave the amount of MMNT (0.30 μmol) adsorbed on the 300 mg sample of Au powder. Increasing the original concentration of MMNT in the THF solution did not change the amount of MMNT adsorbed on the Au powder. The Au solid was washed with THF (1 mL) and dried in vacuum at room temperature to give the MMNT-modified Au powder (MMNT-Au). The DRIFT spectrum of MMNT-Au shows a carbonyl band at 1728 cm^{-1}. This 8 cm^{-1} increase from that of free MMNT (1720 cm^{-1}) is similar to that observed in the adsorption of $MeO_2C(CH_2)_nSH$ on a Au film (10*a*, 19).

DPET-Au

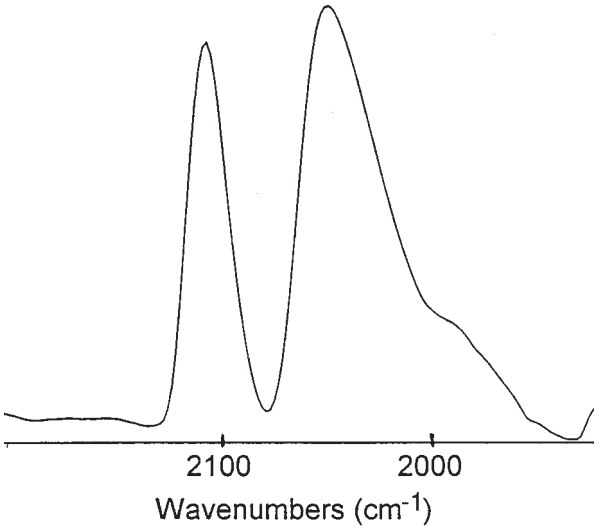
The Au powder (300 mg) was mixed with a 1,2-dichloroethane (DCE) solution (1 mL) of 2-(diphenylphosphino)ethane-1-thiol (DPET) (5 mM). After being shaken for 2 min on a Genie Vortex mixer, the mixture was allowed to stand at room temperature overnight. The solution was separated by centrifugation and analyzed for the amount of DPET by measuring the intensity of the C-H stretching absorption at 3073 cm^{-1} and converting it to DPET concentration using Beer's law. Subtracting this concentration from the original concentration of the DPET solution gave the amount (0.63 μmol) of DPET adsorbed on the 300 mg sample of Au powder. Increasing the original concentration of DPET in the DCE solution did not change the amount of DPET adsorbed on the Au powder. The Au solid was washed with DCE (1 mL) and dried in vacuum at room temperature to give the modified Au powder, DPET-Au.

Preparation of $Rh_2Cl_2(CO)_4$-modified Au powder catalysts

$Rh_2Cl_2(CO)_4$ adsorbed on Au powder (Rh–Au)

The Au powder (300 mg) was mixed with a toluene solution (1 mL) of $Rh_2Cl_2(CO)_4$ (0.6 mM), and the mixture was stirred at room temperature overnight under an N_2 atmosphere. The solution was separated by centrifugation and analyzed for the amount of $Rh_2Cl_2(CO)_4$ by measuring the intensity of the ν(CO) band at 2088 cm^{-1} and converting it to $Rh_2Cl_2(CO)_4$ concentration using Beer's law. Subtracting this concentration from the original concentration of the $Rh_2Cl_2(CO)_4$ solution gave the amount of $Rh_2Cl_2(CO)_4$ (0.72 μmol) adsorbed on the 300 mg sample of Au powder. The gold powder was washed with toluene (4 × 1 mL) and dried at room temperature under vacuum to give the catalyst Rh–Au. IR (DRIFT) (cm^{-1}): 2105 (s) (CO), 2045 (s) (CO) (Fig. 1).

Fig. 1. DRIFT spectrum of Rh–Au.



$Rh_2Cl_2(CO)_4$ tethered on MMNT-Au (Rh–MMNT-Au)

A mixture of MMNT-Au (300 mg) and a toluene solution (1 mL) of $Rh_2(CO)_4Cl_2$ of the desired concentration was stirred at room temperature overnight under an N_2 atmosphere. The mixture was centrifuged for 5 min to separate the toluene solution. The separated toluene solution was analyzed by the same IR method that was used in the preparation of the Rh–Au catalyst to determine the amount of $Rh_2Cl_2(CO)_4$ adsorbed on the 300 mg of MMNT-Au powder. The Au solid was washed (4 × 1 mL) with toluene and dried in vacuum at room temperature to give the tethered $Rh_2Cl_2(CO)_4$ catalyst Rh–MMNT-Au. The mol of tethered $Rh_2Cl_2(CO)_4$, and the DRIFT spectra of the Rh–MMNT-Au catalysts prepared by using different concentrations of $Rh_2Cl_2(CO)_4$ solutions are shown in Table 1 and Fig. 2.

$Rh_2Cl_2(CO)_4$ tethered on DPET-Au (Rh–DPET-Au)

Rh–DPET-Au was prepared by the same procedure as that used for the preparation of Rh–MMNT-Au using DPET-Au instead of MMNT-Au. The mol of tethered $Rh_2Cl_2(CO)_4$, and DRIFT spectra of the Rh–DPET-Au catalysts prepared by using different concentrations of $Rh_2Cl_2(CO)_4$ solutions are shown in Table 2 and Fig. 3.

Hydrogenation reactions

The hydrogenation reactions were carried out in a 50 mL three-necked jacketed glass-vessel closed with a self-sealing silicon rubber cap and connected to a vacuum–hydrogen line and a constant pressure (1 atm) gas buret. The temperature of the ethylene glycol circulating through the jacket was maintained at 40.0°C by a constant temperature bath. After the catalyst was added and the atmosphere in the vessel was replaced with hydrogen, solvent was added and the mixture was stirred for about 5 min. Then, the substrate was added and the hydrogen volume uptake was followed by the constant-pressure gas buret. The products were analyzed by gas chromatography on a Varian 3400 GC using a 25 m HP-1 capillary column with a FID detector. When the catalyst was used in several successive 1-hexene hydrogenations, the reaction mixture after the first cycle was filtered, and the solid

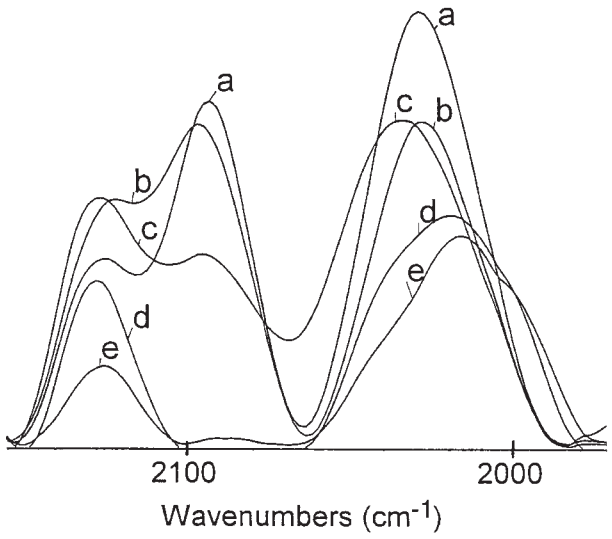
© 2001 NRC Canada

Table 1. Adsorption of $Rh_2Cl_2(CO)_4$ from a 1 mL toluene solution on 300 mg of MMNT-Au powder.

Entry	Concentration of $Rh_2Cl_2(CO)_4$ before adsorption (mM)	Rh:MMNT mol ratio[a]	Rh adsorbed (μmol)[b]	MMNT:Rh[c]
a	1.00	9	0.56	0.53
b	0.60	4	0.56	0.53
c	0.30	2	0.42	0.71
d	0.15	1	0.30	1.0
e	0.075	0.5	0.15	2.0

[a]Mol ratio of rhodium in the initial toluene solution to the MMNT ligand adsorbed on 300 mg of MMNT-Au.
[b]On 300 mg of MMNT-Au.
[c]Ratio on Rh–MMNT-Au.

Fig. 2. DRIFT spectra of the Rh–MMNT-Au samples containing various amounts of rhodium (μmol) per 300 mg catalyst: (*a*) 0.56; (*b*) 0.56; (*c*) 0.42; (*d*) 0.30; (*e*) 0.15.



catalyst was washed with ethanol, dried under vacuum, and used for the hydrogenation of the second batch of 1-hexene by following the same procedure as that used in the first cycle. After the second cycle, the catalyst was treated as after the first cycle; the isolated catalyst was then used for the third cycle.

Results and discussion

IR characterization of catalysts consisting of $Rh_2Cl_2(CO)_4$ adsorbed or tethered on Au powder

Rh–Au

After stirring a mixture of $Rh_2Cl_2(CO)_4$ and Au powder in toluene at room temperature overnight, IR analyses of both the solution and the Au solid showed that rhodium-carbonyl species were present on the Au powder surface. A DRIFT spectrum (Fig. 1) of the resulting Au powder (Rh–Au) shows two ν(CO) bands at 2105 (s) and 2045 (s) cm^{-1}. The DRIFT spectrum of Rh–Au remained the same after it was washed with toluene several times, which indicates that the rhodium-carbonyl species is strongly adsorbed on the Au surface. Although the ν(CO) bands of Rh–Au are similar to those of $Rh_2Cl_2(CO)_4$ (2115 (w), 2095 (s), and 2045 (s) cm^{-1} in Nujol™ mull (20)), they are also similar to those of $Rh^I(CO)_2$ (approximately 2095 (s) and 2032 (s) cm^{-1}) on SiO_2 or Al_2O_3 (21). Thus, the Rh carbonyl group on Rh–Au appears to be some type of $Rh^I(CO)_2$ species, perhaps associated with Cl^- ligands in some way. The broadness of the 2045 cm^{-1} absorption suggests that other species, perhaps monocarbonyl $Rh^I(CO)$ species, are also present. It is unlikely that any of these species is associated with CO adsorbed on Au as CO does not adsorb on pure Au powder under these conditions.

Rh–MMNT-Au

The tethered $Rh_2Cl_2(CO)_4$ catalyst Rh–MMNT-Au was obtained by stirring a mixture of $Rh_2Cl_2(CO)_4$ and MMNT-Au in toluene at room temperature overnight. Table 1 gives the number of mol of rhodium anchored on 300 mg of MMNT-Au when 1 mL toluene solutions of $Rh_2Cl_2(CO)_4$ in concentrations ranging from 0.075 to 1.0 mM were used. The MMNT:Rh ratio on the Au surface ranges from 0.53 to 2.0. In Table 1, it is evident that the number of mol of rhodium anchored on 300 mg of MMNT-Au increases as the initial concentration of $Rh_2Cl_2(CO)_4$ in the toluene solution increases. When the initial concentration of $Rh_2Cl_2(CO)_4$ in the toluene solution reaches 0.60 mM (Table 1, entry *b*), the amount of Rh anchored on 300 mg of MMNT-Au is 0.56 μmol and does not increase further when the initial concentration of $Rh_2Cl_2(CO)_4$ in the toluene solution is increased to 1.0 mM. To gain some insight into the structure of the rhodium species, DRIFT spectra (Fig. 2) were recorded on the five Rh–MMNT-Au samples. When the amount of Rh on the MMNT-Au is relatively low (Table 1, entries *d* and *e*), the DRIFT spectra (Fig. 2*d* and *e*) show one relatively sharp ν(CO) band at 2120 (s) cm^{-1} and one broad band in the region 2060–2000 cm^{-1}; these absorptions are somewhat similar to those of the Rh–Au catalyst (2105 (s) and 2045 (s) cm^{-1}). Although this suggests that the structure of the major rhodium-carbonyl species formed on these two Rh–MMNT-Au samples might be similar to that on Rh–Au, the two ν(CO) bands at 2120 (s) and 2060–2000 (vs, br) could also be assigned to the square planar $[(cis\text{-}Rh(MMNT)_2(CO)_2]^+Cl^-$; the related $cis\text{-}Rh(py)_2(CO)_2^+$ complex is known to have ν(CO) bands at 2095 (vs) and 2020 (vs) cm^{-1} in $CHCl_3$ solution (22*a*). In pyridine solution under a CO atmosphere, $cis\text{-}Rh(py)_2(CO)_2^+$ has bands at 2100 and 2038 cm^{-1} (22*b*). Still another possible assignment for the species with bands at

© 2001 NRC Canada

Table 2. Adsorption of $Rh_2Cl_2(CO)_4$ from a 1 mL toluene solution on 300 mg of DPET-Au powder.

Entry	Concentration of $Rh_2Cl_2(CO)_4$ before adsorption (mM)	Rh:DPET mol ratio[a]	Rh adsorbed (μmol)[b]	DPET:Rh[c]
a	3.00	9	0.52	1.2
b	1.00	3	0.48	1.3
c	0.30	1	0.45	1.4
d	0.15	0.5	0.28	2.3

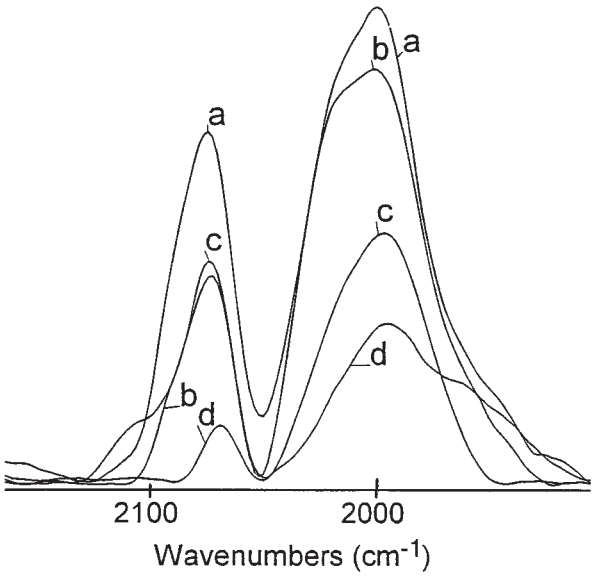
[a]Mol ratio of rhodium in the initial toluene solution to the DPET ligand adsorbed on 300 mg of DPET-Au.
[b]On 300 mg of DPET-Au.
[c]Ratio on Rh–DPET-Au.

2120 (s) and 2060–2000 (vs, br) cm^{-1} is $Rh(MMNT)(CO)_2Cl$; this assignment is based on the ν(CO) spectrum of $Rh(py)(CO)_2Cl$ which has bands at 2090 (s) and 2020 (s) cm^{-1} in $CHCl_3$ solution (23). In fact, there may be an equilibrium (eq. [1]) between $[Rh(MMNT)_2(CO)_2]^+Cl^-$ and $Rh(MMNT)(CO)_2Cl$ as the MMNT:Rh ratio on the surface decreases from 2.0 to 1.0. This equilibrium may account for the change in band shapes between spectra in Fig. 2*d* and *e*. The shoulder on the low-energy side of the 2060–2000 cm^{-1} absorption in Rh–MMNT-Au might be attributed to a $[Rh(MMNT)_3(CO)]^+Cl^-$ species based on a 1993 cm^{-1} band reported for $Rh(py)_3(CO)^+$, which was observed in pyridine (22*b*).

$$[1]\quad [Rh(MMNT)_2(CO)_2]^+Cl^- + 1/2Rh_2Cl_2(CO)_4 \rightleftarrows 2Rh(MMNT)(CO)_2Cl$$

When the initial mol ratio of Rh–MMNT increases to 2, the Rh–MMNT-Au sample (Table 1, entry *d*) has ν(CO) absorptions at 2120 (s), 2095 (m), and 2030 (s) cm^{-1}. As the initial mol ratio of Rh–MMNT increases further, the relative intensity of the ν(CO) band at 2120 cm^{-1} decreases, but the relative intensity of the ν(CO) band at 2095 cm^{-1} increases. The growth of the 2095 cm^{-1} band (Fig. 2*a*–*c*) is in samples in which the MMNT:Rh ratio is less than 1.0, which means that there is less than one MMNT ligand per Rh. A species with only one MMNT per two Rh atoms is $Rh_2Cl_2(CO)_3(MMNT)$; however, the model complex $Rh_2Cl_2(CO)_3(py)$ for this species is unknown. Another possible species for the 2095 cm^{-1} band (and probably a companion band at 2030 cm^{-1}) is one in which Rh is bonded to the sulfur atom tethered to the surface. At this point, it is not possible to make an assignment to these new bands. It was also observed that when the Rh–MMNT-Au sample (Table 1, entry *d*) was stirred in a toluene solution (1 mL) of $Rh_2Cl_2(CO)_4$ (0.60 mM), an additional 0.24 μmol of $Rh_2Cl_2(CO)_4$ was tethered on the Au powder, giving a sample with 0.56 μmol of Rh, which is the same as that of the Rh–MMNT-Au (0.56 μmol) sample used in Table 1, entry *b*. The DRIFT spectra of these two Rh–MMNT-Au samples are similar as well. Because of the broadness of the ν(CO) bands, these assignments are tentative, and it is not possible to exclude the presence of the $Rh^I(CO)_2$ species resulting from the adsorption of $Rh_2Cl_2(CO)_4$ directly on the Au.

Fig. 3. DRIFT spectra of the Rh–DPET-Au samples containing various amounts of rhodium (μmol) per 300 mg catalyst: (*a*) 0.52; (*b*) 0.48; (*c*) 0.45; (*d*) 0.28.

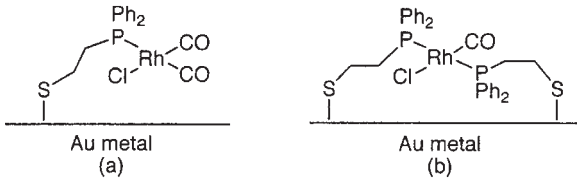


Rh–DPET-Au

The tethered $Rh_2Cl_2(CO)_4$ catalyst Rh–DPET-Au was prepared by reacting DPET-Au with toluene solutions (1 mL) of $Rh_2Cl_2(CO)_4$ ranging in concentration from 3.0 to 0.15 mM to give Au powders (Rh–DPET-Au) containing different amounts of tethered $Rh_2Cl_2(CO)_4$. The data in Table 2 show that the amount of rhodium anchored on 300 mg of DPET-Au increases with an increase in the amount of $Rh_2Cl_2(CO)_4$ in the initial toluene solution; the DPET:Rh ratio on the Au surface increases from 1.2 to 2.3 in the samples. Figure 3 shows that the DRIFT spectra of the four Rh–DPET-Au samples (Table 2) change as the DPET:Rh ratio increases. All of the samples exhibit one relatively sharp ν(CO) band at about 2070 cm^{-1} and one broad ν(CO) band in the region 2025–1975 cm^{-1}, and as expected, the intensities of the bands increase as the loading of $Rh_2Cl_2(CO)_4$ increases. The reaction of $Rh_2Cl_2(CO)_4$ with PPh_3 in solution is known (24) to give a complicated distribution of various mononuclear $[RhCl(CO)_{3-n}(PPh_3)_n]$ and dinuclear $[Rh_2(\mu\text{-}Cl)_2(CO)_{4-m}(PPh_3)_m]$ complexes depending on the ratio of reactants. The complex *cis*-$Rh(PPh_3)(CO)_2Cl$ is assigned to the two ν(CO) absorptions at 2090 (s) and 2005 (s) cm^{-1}, which are in a

© 2001 NRC Canada

Scheme 2.



similar position (2070 and 2025–1975 cm^{-1}) to those (Fig. 3*a*–*c*) of the samples in which the DPET:Rh ratio is near unity (1.2–1.4). In the spectrum (Fig. 3*d*), in which the DPET:Rh ratio is higher (2.3), there is evidence of another band at lower energy, which is similar in position to that reported for *trans*-$Rh(PPh_3)_2(CO)Cl$ (1959 cm^{-1}) (24). Thus, the spectra in Fig. 3 are consistent with *cis*-$Rh(DPET)(CO)_2Cl$ (Scheme 2*a*) as the predominant species at high $Rh_2Cl_2(CO)_4$ loadings where the DPET:Rh ratio is 1.2–1.4, whereas *trans*-$Rh(DPET)_2(CO)Cl$ (Scheme 2*b*) becomes a contributing species when the DPET:Rh ratio is higher (24). It should be noted that none of the four Rh–DPET-Au samples exhibit ν(CO) bands that are characteristic of $Rh^I(CO)_2$ resulting from the adsorption of $Rh_2Cl_2(CO)_4$ directly on Au.

Decarbonylation of $Rh_2Cl_2(CO)_4$ adsorbed and tethered on Au powder

The decarbonylation of the Rh–Au and Rh–DPET-Au catalysts was examined by heating under vacuum. Figure 4 shows changes in the ν(CO) bands for the Rh–Au catalyst as a function of treatment under vacuum (0.1 mm Hg) and at different temperatures (no absorptions in the 1700–1900 cm^{-1} range were observed in the DRIFT spectra of any of the heat-treated samples). After treatment at 50–60°C under vacuum for 1.5 h, the ν(CO) band at 2105 cm^{-1} disappeared but the band at 2045 cm^{-1} remained, although its intensity decreased (Fig. 4*b*); this suggests that the original $Rh^I(CO)_2$ species has been lost and small amounts of perhaps a monocarbonyl $Rh^I(CO)$ species remain. After further treatment at 70–80°C for 1.5 h, the ν(CO) band at 2045 cm^{-1} shifted to about 2025 cm^{-1} and broadened (Fig. 4*c*). After this sample was further treated at 100–110°C for 1.5 h, only a weak, broad band at 2005 cm^{-1} remained (Fig. 4*d*). However, when this final sample was stirred in toluene under a CO atmosphere at room temperature overnight, the DRIFT spectrum (Fig. 4*e*) of the resulting sample was similar to that of the original Rh–Au catalyst, although the ν(CO) bands are at slightly lower values, which suggests the formation of a $Rh^I(CO)_2$ species that is not identical to the original $Rh^I(CO)_2$ species.

After a sample of Rh–DPET-Au containing 0.45 μmol Rh per 300 mg of DPET-Au was heated at 60°C under vacuum (0.1 mm Hg) for 1.5 h, the DRIFT spectrum showed only three weak ν(CO) bands at 2105 (sh), 2076 (s), and 2007 (s, br) cm^{-1} (Fig. 5*b*). When the heat-treated sample was stirred in toluene under a CO atmosphere at room temperature overnight, the sample exhibited ν(CO) bands at 2105 (sh), 2076 (s), and 2007 (s, br) cm^{-1}. The absorptions at 2076 (s) and 2007 (vs, br) indicate that at least some of the original Rh–DPET-Au (2076 (s) and 2008 (s) cm^{-1}) has been regenerated. The ν(CO) band at 2105 (sh) corresponds to a $Rh^I(CO)_2$ species with ν(CO) bands at 2105 and 2045 cm^{-1} (the band at 2045 cm^{-1} would overlap with that of *cis*-$RhCl(CO)_2(DPET)$ (Scheme 2). Thus, it appears that during the heat treatment, some of the rhodium is deposited on the Au surface and is carbonylated to $Rh^I(CO)_2$ under CO.

Fig. 4. DRIFT spectra of Rh–Au as a function of treatment under vacuum (0.1 mm Hg) at different temperatures: (*a*) original; (*b*) 50–60°C for 1.5 h; (*c*) 70–80°C for 1.5 h; (*d*) 100–110°C for 1.5 h; (*e*) after stirring sample (*d*) in toluene under CO (1 atm) at room temperature overnight.

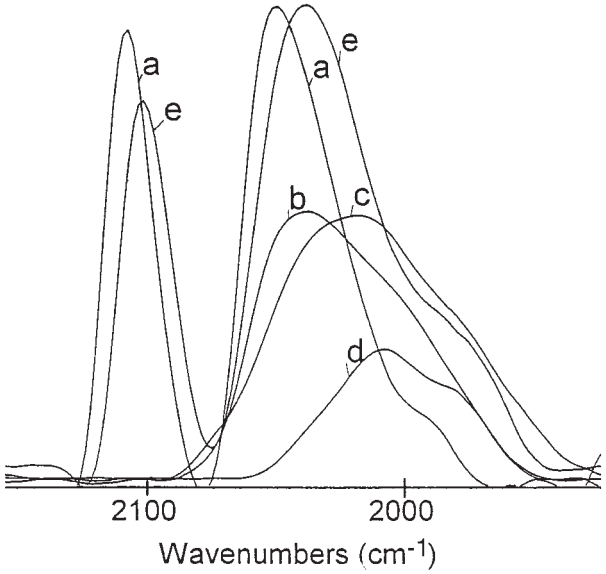
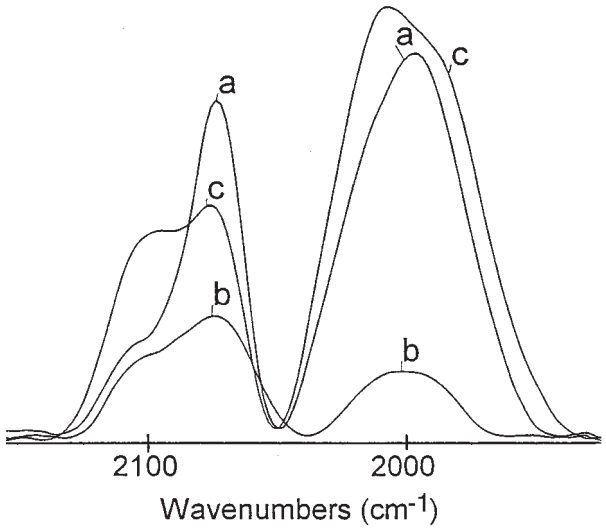


Fig. 5. DRIFT spectra of Rh–DPET-Au with heat and CO treatment: (*a*) original; (*b*) heating at 50–60°C under vacuum for 1.5 h; (*c*) stirring sample (*b*) in toluene at room temperature overnight under CO (1 atm).



Hydrogenation of 1-hexene with catalysts consisting of $Rh_2Cl_2(CO)_4$ adsorbed and tethered on Au powder

The Rh–Au, Rh–MMNT-Au, and Rh–DPET-Au materials were used to catalyze the hydrogenation of 1-hexene under the conditions of 40°C and 1 atm of H_2. Table 3 gives hydrogenation activities for the homogeneous $Rh_2Cl_2(CO)_4$ and

© 2001 NRC Canada

Table 3. Hydrogenation of 1-hexene catalyzed by $Rh_2Cl_2(CO)_4$ adsorbed and tethered on gold powder.[a]

Catalyst	Rh (μmol)	Reaction time (h)	Conversion (%)[b]	Max TOF[c]	TO[d]	Yields of products (%)[e]		
						Hexane	*trans*-2-Hexene	*cis*-2-Hexene
Au	—	7.5	9.2	—	—	0.7	5.9	2.6
Rh–Au[f]	0.12	2	100	800	29 600	100	0	0
Rh–DPET-Au[g]	0.08	6	89.7	116	14 500	49	24	16.7
Rh–MMNT-Au[h]	0.08	6	56.3	23.2	6 900	23.3	17.4	15.6
$Rh_2Cl_2(CO)_4$	10	5	0	0	0	0	0	0
$Rh_2Cl_2(CO)_4$ + PPh_3 (1:1)	10	6	0	0	0	0	0	0

[a]Reaction conditions: catalyst (50–55 mg), 1-hexene (0.5 mL), ethanol (5 mL), 40°C, 1 atm of H_2.
[b]Conversion of 1-hexene determined by GC at the indicated reaction time.
[c]Maximum TOF defined as mol of H_2 uptake per mol rhodium per min.
[d]Turnover (mol of H_2 uptake per mol Rh) at the indicated reaction time.
[e]Yields of products determined by GC.
[f]0.72 μmol Rh per 300 mg catalyst.
[g]0.48 μmol Rh per 300 mg catalyst.
[h]0.42 μmol Rh per 300 mg catalyst.

Table 4. Hydrogenation of 1-hexene using Rh–MMNT-Au catalysts with different amounts of rhodium.[a]

Rh on 300 mg of Rh–MMNT-Au (μmol)	Max TOF[b]	TO[c]
0.15	48.0	10 800(5)
0.30	23.2	6 900(6)
0.42	16.0	3 280(5)
0.56	7.0	1 740(5)

[a]Reaction conditions are the same as those in Table 3.
[b]TOF defined as mol of H_2 uptake per mol Rh per min.
[c]TO (mol of H_2 uptake per mol rhodium) at the indicated reaction time (h) shown in parentheses.

Table 5. Durability of the Rh–Au and Rh–DPET-Au catalysts in the hydrogenation of 1-hexene.[a]

Catalyst	Cycle	Max TOF[b]	TO[b]
Rh–Au	1st	800	29 600(2)
	2nd	528	29 500(2.5)
	3rd	350	28 500(3)
Rh–DPET-Au	1st	116	18 400(6)
	2nd	35	9 640(6)

[a]Reaction conditions are the same as those in Table 3.
[b]Footnotes are the same as those in Table 4.

$Rh_2Cl_2(CO)_4$-PPh_3 (1:1) catalysts, Au powder, Rh–Au, Rh–DPET-Au (0.48 μmol Rh per 300 mg of DPET-Au), and Rh–MMNT-Au (0.42 μmol Rh per 300 mg of MMNT-Au). From the data in Table 3, it can be seen that the homogeneous rhodium complex catalysts $Rh_2Cl_2(CO)_4$ and $Rh_2Cl_2(CO)_4$-PPh_3 are inactive for 1-hexene hydrogenation under these mild conditions. The Au powder exhibits a very low activity for the hydrogenation. However, Rh–Au, Rh–MMNT-Au, and Rh–DPET-Au are all active for the hydrogenation of 1-hexene under these reaction conditions. Their activities decrease in the following order: Rh–Au > Rh–DPET-Au > Rh–MMNT-Au. The maximum turnover frequency (TOF) and turnover (TO) values for the Rh–Au catalyst are 800 mol H_2 per mol Rh per min and 29600 mol H_2 per mol Rh in 2 h. To the best of our knowledge, this activity is greater than that of any homogeneous or immobilized rhodium complex catalyst for the hydrogenation of 1-hexene reported in the literature (11*f*, 25–27). For the Rh–DPET-Au and Rh–MMNT-Au catalysts, substantial amounts of isomerization to the 2-hexenes also occur.

Table 4 gives the results of hydrogenation of 1-hexene over Rh–MMNT-Au catalysts with different amounts of rhodium, prepared as described in Table 1. It can be seen that the activities (per mol of Rh) of the Rh–MMNT-Au catalysts decrease as the amount of rhodium on the catalyst increases. This decrease may be due to changes in the catalyst precursor complexes present on the surface at different Rh loadings. Table 5 shows the durability of the Rh–Au and Rh–DPET-Au catalysts during repeated use in the hydrogenation of 1-hexene. The activities of both catalysts in the second cycle are lower than in the first cycle. The DRIFT spectra of the used Rh–Au and Rh–DPET-Au catalysts, which were isolated from the reaction mixtures after Rh–Au was used for three cycles and Rh–DPET-Au was used for two cycles, show no ν(CO) absorptions. Even after these two used catalysts were stirred in toluene under CO (1 atm) overnight, no ν(CO) bands were observed in the DRIFT spectra of the samples. Thus, the nature of the Rh species on the Au has changed dramatically during the hydrogenation. It seems unlikely that all of the rhodium has leached from the surface since the catalysts still have appreciable activity after two or three runs even though they exhibit no ν(CO) absorptions.

Conclusions

Although the original goal of this investigation was to probe the hydrogenation activities of catalysts that consist of metal complexes tethered on a gold surface, we find that the most active catalyst is Rh–Au in which $Rh_2Cl_2(CO)_4$ is simply adsorbed on gold. This catalyst is far more active than Au metal or $Rh_2Cl_2(CO)_4$ separately. While the initial rhodium species on the Au appears to be some type of $Rh^I(CO)_2$ unit, it loses CO under 1-hexene hydrogenation conditions (40°C, 1 atm H_2). Thus, the active catalyst is a noncarbonyl Rh species, which also does not adsorb CO. Although the active form of the Rh is not known, it is possibly small Rh metal aggregates. The formation of this active Rh species is

© 2001 NRC Canada

apparently facilitated in some manner by the Au. This is supported by the observation that Rh–Au and Rh–DPET-Au undergo decarbonylation even at 55°C under vacuum (0.1 mm Hg), as described above. In contrast, Bhaduri and Khwaja (26*c*) reported that the catalyst prepared by the reaction of a phosphinated polystyrene with $Rh_2Cl_2(CO)_4$ does not undergo decarbonylation even when heated at 120°C under vacuum (1×10^{-3} mm Hg) for 24 h. It has also been reported that the intensities and positions of the ν(CO) bands for a material prepared by adsorbing $Rh_2Cl_2(CO)_4$ from toluene solution onto Al_2O_3 do not change when it is heated at 80°C under 1 atm of H_2 for 1 h (2l). This suggests that the Au powder facilitates the decarbonylation of the rhodium carbonyl complex adsorbed or tethered on it. Another possible role played by the Au powder support is the creation of an unusually active form of Rh for 1-hexene hydrogenation.

While less active, the tethered Rh complex catalysts, Rh–DPET-Au and Rh–MMNT-Au, also catalyze the hydrogenation of 1-hexene. Under the hydrogenation conditions, the Rh complexes that are present in the unused catalysts lose their CO ligands to generate a noncarbonyl form of Rh, perhaps the same as that formed from Rh–Au, which is the catalytically active species. The activities of the Rh–Au and Rh–DPET-Au catalysts decrease upon repeated use. This decrease may be due to migration of the Rh(0) into the Au to form an inactive alloy.

These studies demonstrate that it is possible to form active hydrogenation catalysts by adsorbing Rh complexes on Au metal. Although Au is too expensive to be used as a catalyst support for most studies, the results do suggest that the adsorption of metal complexes on less expensive metal supports may lead to unusually active hydrogenation catalysts.

Acknowledgement

This work was supported by the U.S. Department of Energy, Office of Science, Office of Basic Energy Sciences, Chemical Sciences Division, under contract W-7405-Eng-82 with Iowa State University.

References

1. (*a*) F.R. Hartley. Supported metal complexes. Reidel, Dordrecht, Netherlands. 1985; (*b*) T. Iwasawa. Tailored metal catalysts. Reidel, Tokyo. 1986; (*c*) P. Panster and S. Wieland. *In* Applied homogeneous catalysis with organometallic compounds. *Edited by* B. Cornils and W.A Herrmann. VCH, Weinheim. 1996. pp. 605–623; (*d*) W.T. Ford. Polymeric reagents and catalysts. ACS, Washington, D.C. 1986.
2. (*a*) B.J. Pugin. J. Mol. Catal. A: Chem. **107**, 273 (1996); (*b*) A. Kinting, H. Krause, and M.J. Capka. J. Mol. Catal. **33**, 215 (1985); (*c*) A. Carmona, A. Corma, M. Iglesias, A. José, and F.J. Sánchez. J. Organomet. Chem. **492**, 11 (1995); *(d)* J. Cermák, M. Kvícalová, V. Blechta, M. Capka, and Z. Bastl. J. Organomet. Chem. **509**, 77 (1996); (*e*) A. Corma, M. Iglesias, C. Del Pino, and F.J. Sánchez. J. Organomet. Chem. **431**, 233 (1992); (*f*) A. Carmona, A. Corma, M. Iglesias, and F. Sánchez. Inorg. Chim. Acta, **244**, 79 (1996); (*g*) P.C. L'Argentière, D. Liprandi, D.V. Marconetti, and N.S. Fígoli. J. Mol. Catal. A: Chem. **118**, 341 (1997); (*h*) F. Verpoort, A.R. Bossuyt, L. Verdorck, and B.J. Coussens. J. Mol. Catal. A: Chem. **115**, 207 (1997); (*i*) R. Giannandrea, P. Mastrorilli, G. Zaccaria, and C.F. Nobile. J. Mol. Catal. A: Chem. **109**, 113 (1996); (*j*) W. Kein, P. Mastrorilli, C.F. Nobile, N. Ravasio, B. Corain, and M. Zecca. J. Mol. Catal. **81**, 167 (1993); (*k*) S. Shimazu, K. Ro, T. Sento, N. Ichikuni, and T. Uematsu. J. Mol. Catal. A: Chem. **107**, 297 (1996); (*l*) P.M. Lausarot, G.A. Vaglio, and M. J. Valle. J. Organomet. Chem. **204**, 249 (1981); (*m*) K.G. Allum, R.D. Hancock, I.V. Howell, T.E. Lester, S. McKenzie, R.C. Pitkethly, and P.J. Robinson. J. Catal. **43**, 331 (1976).
3. (*a*) J.J. Hickman, D. Ofer, C. Zou, M.S. Wrighton, P.E. Laibinis, G.M. Whitesides. J. Am. Chem. Soc. **113**, 1128 (1991); (*b*) D. Kang and M.S. Wrighton. Langmuir, **7**, 2169 (1991); (*c*) E.W. Wollman, D. Kang, C.D. Fribsbie, I.V. Lorkovic, and M.S. Wrighton. J. Am. Chem. Soc. **116**, 4395 (1994); (*d*) J.P. Collman, M.S. Ennis, D.A. Offord, L.L. Chng, and J.H. Griffin. Inorg. Chem. **35**, 1751 (1996).
4. (*a*) J.D. Swalen, D.L. Allar, J.D. Andrade, E.A. Chandross, S. Garoff, J. Israelachvili, T.J. McCarthy, R. Murray, R.F. Passe, J.F. Robolt, K.J. Wynne, and H. Yu. Langmuir, **3**, 932 (1987); (*b*) T.R. Lee, P.E. Laibinis, J.P. Folkers, and G.M. Whitesides. Pure Appl. Chem. **63**, 821 (1991); (*c*) E.L. Muetterties. Angew. Chem. Int. Ed. Engl. **17**, 545 (1978); (*d*) A. Ulman. Introduction to ultrathin organic films from Langmuir Blodgett to self-assembly. Academic Press, New York. 1991; (*e*) P.E. Laibinis, G.M. Whitesides, D.L. Allara, Y.T. Tao, A.N. Parikh, and R.G. Nuzzo. J. Am. Chem. Soc. **113**, 7152 (1991).
5. (*a*) W. Andreoni and C.M. Varma. Phys. Rev. B: Condens. Matter, **23**, 437 (1981); (*b*) P.V. Kamath, S. Yashonath, A. Srinivason, P.K. Basu, and C.N.R. Rao. J. Indian Chem. Soc. **59**, 153 (1982).
6. (*a*) J.J. Pireaux, M. Chlaib, J.P. Delrue, P.A. Thiry, M. Liehr, and R. Caudano. Surf. Sci. **141**, 211 (1984); (*b*) N.D.S. Canning, D. Outka, and R.J. Madix. Surf. Sci. **141**, 240 (1984); (*c*) A.G. Sault, R.J. Madix, and C.T. Campbell. Surf. Sci. **169**, 347 (1986).
7. (*a*) M.J. Robertson and R.J. Angelici. Langmuir, **10**, 1488 (1994); (*b*) K.C. Shih and R.J. Angelici. Langmuir, **11**, 2539 (1995); (*c*) A.C. Ontko and R.J. Angelici. Langmuir, **14**, 1684 (1998); (*d*) A.C. Ontko and R.J. Angelici. Langmuir, **14**, 3071 (1998).
8. (*a*) D.N. Batchelder, S.D. Evans, T.L. Freeman, L. Häussling, H. Ringsdorf, and H. Wolf. J. Am. Chem. Soc. **116**, 1050 (1994); (*b*) N. Mohri, M. Inoue, and Y. Arai. Langmuir, **11**, 1612 (1995); (*c*) U.B. Steiner, P. Neuenschwander, W.R. Caseri, and U.W. Suter. Langmuir, **8**, 90 (1992); (*d*) R.I. Carey, J.P. Folkers, and G.M. Whitesides. Langmuir, **10**, 2228 (1994); (*e*) C.D. Bain, E.B. Troughton, Y.T. Tao, J. Evall, G.M. Whitesides, and R.G. Nuzzo. J. Am. Chem. Soc. **111**, 321 (1989); (*f*) L. Zhang, T. Lu, G.M. Gokel, and A.E. Kaifer. Langmuir, **9**, 786 (1993); (*g*) A.J. Black, T.T. Wooster, W.E. Geiger, and M.N. Paddon-Row. J. Am. Chem. Soc. **115**, 7924 (1993); (*h*) I. Willner, M. Lion-Dagan, S. Marx-Tibbon, and E. Katz. J. Am. Chem. Soc. **117**, 6581 (1995); (*i*) S.K. Tam-Chang, H.A. Biebuyck, G.M. Whitesides, N. Jeon, and R.G. Nuzzo. Langmuir, **11**, 4371 (1995).
9. (*a*) C.D. Bain and G.M. Whitesides. J. Am. Chem. Soc. **110**, 3665 (1988); (*b*) C.D. Bain, J. Evall, and G.M. Whitesides. J. Am. Chem. Soc. **111**, 7155 (1989); (*c*) T. Arndt, H. Schupp, and W. Schrepp. Thin Solid Films, **178**, 319 (1989); (*d*) M.A. Bryant and J.E. Pemberton. J. Am. Chem. Soc. **113**, 8284 (1991); (*e*) C.E.D. Chidsey and D. N. Loiacono. Langmuir, **6**, 682 (1990); (*f*) P.E. Laibinis and G.M. Whitesides. J. Am. Chem. Soc. **114**, 1990 (1992); (*g*) C.A. Alves and M.D. Porter. Langmuir, **9**, 3507 (1993); (*h*) C.A. Alves and M.D. Porter.

© 2001 NRC Canada

J. Am. Chem. Soc. **114**, 1222 (1992); (*i*) H. Sellers, A. Ulman, Y. Shnidman, and J.E. Eilers. J. Am. Chem. Soc. **115**, 9389 (1993); (*j*) A. Ulman. Chem. Rev. **96**, 1533 (1996).

10. (*a*) R.G. Nuzzo, L.H. Dabois, and D.L. Allara. J. Am. Chem. Soc. **112**, 558 (1990); (*b*) E.B. Trought, C.D. Bain, G.M. Whitesides, R.G. Nuzzo, D.L. Allara, and M.D. Porter. Langmuir, **4**, 365 (1988).
11. (*a*) J. Blumel. Inorg. Chem. **33**, 5050 (1994); (*b*) M.G.L. Petrucci and A.K. Kakkar. J. Chem. Soc. Chem. Commun. 1577 (1995); (*c*) T. Kitamura, T. Joh, and N. Hagihara. Chem. Lett. 203 (1975); (*d*) Y. Nakamura and H. Hirai. Chem. Lett. 823 (1975); (*e*) N.J. Holy. J. Org. Chem. **44**, 239 (1979); (*f*) U. Deschler, P. Kleinschmit, and P. Penster. Angew. Chem. Int. Ed. Engl. **25**, 236 (1989); (*g*) L. Bemi, H.C. Clark, J.A. Davies, C.A. Fyfe, and R.E. Waysylishen. J. Am. Chem. Soc. **104**, 438 (1982); (*h*) A.K. Smith, J.M. Basset, and P.M. Maitlis. J. Mol. Catal. **2**, 223 (1977); (*i*) F. Ciardelli, C. Carlini, P. Pertici, and G. Valentini. J. Macromol. Sci. A, Pure Appl. Chem. **A26**, 327 (1989); (*j*) U. Deschler, P. Kleinschmit, and P. Panster. Angew. Chem. Int. Ed. Engl. **25**, 236 (1986).
12. (*a*) H. Gao and R.J. Angelici. J. Am. Chem. Soc. **119**, 6937 (1997); (*b*) H. Gao and R.J. Angelici. Organometallics, **18**, 989 (1999); (*c*) H. Gao and R.J. Angelici. J. Mol. Catal. A: Chem. **145**, 83 (1999); (*d*) H. Gao and R.J. Angelici. New J. Chem. **23**, 633 (1999); (*e*) H. Gao and R.J. Angelici. J. Mol. Catal. A: Chem. **149**, 63 (1999); (*f*) M.A. Perera and R.J. Angelici. J. Mol. Catal. A: Chem. **149**, 99 (1999); (*g*) H. Yang, H. Gao and R.J. Angelici. Organometallics, **19**, 622 (2000).
13. (*a*) H.G. Ahn, Y. Sieun, K. Imamura, R. Nakamura, and H. Niiyama. Proc. 57th Ann. Meeting Chem. Eng. Soc. Jpn. 1992. p. 300; (*b*) M. Shibata, N. Kawata, T. Masumoto, and H. Kimura. J. Chem. Soc. Chem. Commun. 154 (1988); (*c*) M. Haruta. Catal. Surveys Japan, **1**, 61 (1997).
14. (*a*) R.L. Bretz and H.D. Abruna. J. Electroanal. Chem. **408**, 199 (1996); (*b*) I.C.N. Diógenes, F.C. Nart, and I.S. Moreira. Inorg. Chem. **38**, 1646 (1999); (*c*) K.V. Gobi and T. Ohsaka. J. Electroanal. Chem. **465**, 177 (1999); (*d*) M. Bartz, J. Küther, R. Seshadri, and W. Tremel. Angew. Chem. Int. Engl. Ed. **37**, 2466 (1998).
15. J. Chatt, J.R. Dilworth, J.A. Schmuts, and J.A. Zubieta. J. Chem. Soc. Dalton Trans. 1595 (1979).
16. L. Katz, W. Schroeder, and M. Cohen. J. Org. Chem. **19**, 711 (1954).
17. D. BelliDell'Amico. Inorg. Synth. **24**, 236 (1986).
18. H. Bönnemann, R. Brijoux, R. Fretzen, T. Joussen, R. Köppler, B. Korall, P. Neiteler, and J. Richter. J. Mol. Catal. **86**, 129 (1994).
19. (*a*) R.G. Nuzzo, F.A. Fusco, and D.L. Allara. J. Am. Chem. Soc. **109**, 2358 (1987); (*b*) D.L. Allara, and R.G. Nuzzo. Langmuir, **1**, 52 (1985).
20. R. Colton, R.H. Farthing, and J.E. Knapp. Aust. J. Chem. **23**, 1351 (1970).
21. (*a*) H.F.J. van't Blik, J.B.A.D. van Zon, T. Huizinga, J.C. Vis, D.C. Koningsberger, and R. Prins. J. Am. Chem. Soc. **107**, 3139 (1985); (*b*) S. Trautmann and M. Baerns. J. Catal. **150**, 335 (1994); (*c*) A.C. Yang and W.C. Garland. J. Phys. Chem. **61**, 1504 (1957); (*d*) P. Basu, D. Panayotov, and J.T. Yates. J. Am. Chem. Soc. **110**, 2074 (1988).
22. (*a*) B. Denise and G. Pannetier. J. Organomet. Chem. **63**, 423 (1973); (*b*) G. Fachinetti, T. Funaioli, and F. Zanazzi. J. Organomet. Chem. **460**, C34 (1993); (*c*) C. Cocevar, G. Mestroni, and A. Camus. J. Organomet. Chem. **35**, 389 (1972); (*d*) C. Longo, J. Alvarez, M. Fernandez, A.J. Pardey, S.A. Moya, P. Baricelli, and M. Mdleleni. Polyhedron, **19**, 487 (2000).
23. (*a*) D.N. Lawson and G. Wilkinson. J. Chem. Soc. 1900 (1965); (*b*) P. Fougeroux, B. Denise, R. Bonnaire, and G. Pannetier. J. Organomet. Chem. **60**, 375 (1973).
24. (*a*) J. Gallary, D.D. Montauzon, and R. Poilblanc. J. Organomet. Chem. **38**, 179 (1972); (*b*) P. Uguagliati, G. Deganello, and U. Belluco. Inorg. Chim. Acta, **9**, 203 (1974).
25. (*a*) C. O'Conner and G. Wilkinson. J. Chem. Soc. A. 2665 (1968); (*b*) S. Montelatici, A. VanderEnt, J.A. Osborn, and G. Wilkinson. J. Chem. Soc. A. 1054 (1968).
26. (*a*) F.H. Jardine. Prog. Inorg. Chem. **28**, 63 (1981); (*b*) Z. Nagy-Magos, B. Heil, and L. Markó. Transition Met. Chem. **1**, 215 (1976); (*c*) S. Bhaduri and H. Khwaja. J. Chem. Soc. Dalton Trans. 419 (1983); (*d*) P.W. Linder and W.P. Bryan. J. Am. Chem. Soc. **93**, 3062 (1971); (*e*) M. Capka, P. Svoboda, M. Cerny, and J. Hetfleje. Tetrahedron Lett. 4787 (1971). *(f)* K.G. Allum, R.D. Hancock, I.V. Howell, T.E. Lester, S. McKenzie, R.C. Pitkethy, and P.J. Robinson. J. Organomet. Chem. **107**, 393 (1976).
27. (*a*) M. Czaková and M. Capka. J. Mol. Catal. **11**, 313 (1981); (*b*) M. Capka, M. Czaková, W. Urbaniak, and U. Schuber. J. Mol. Catal. **74**, 335 (1992).

© 2001 NRC Canada

Palladium-catalyzed alternating copolymerization of carbon monoxide with olefins bearing carbamate and amide functionalities

Christophe Moineau, Giuseppe Mele, and Howard Alper

Abstract: The copolymerization of carbon monoxide with different olefins bearing carbamate and amide functionalities was effected using $[Pd(CH_3CN)_4](BF_4)_2$ as the catalyst and (*R*,*R*)-Me-DUPHOS (2:1 (v/v) $MeNO_2$–MeOH or CH_2Cl_2 as the solvent). The products constitute a new class of functionalized copolymers, and were found to be optically active with a mixture of 1,4-ketone and spiroketal repeating units in the backbone. The influence of different parameters on the copolymerization of methyl *N*-(3-butenyl)carbamate with carbon monoxide was examined.

Key words: copolymerization, carbon monoxide, olefins bearing carbamate and amide functionalities.

Résumé : On a réalisé la copolymérisation du monoxyde de carbone avec diverses oléfines portant des fonctions carbamate et amide en utilisant du $[Pd(CH_3CN)_4](BF_4)_2$ en présence de (*R*,*R*)-Me-DUPHOS comme catalyseur et du CH_2Cl_2 ou un mélange 2:1 (v/v) de $MeNO_2$–MeOH comme solvant. Les produits constituent une nouvelle classe de copolymères fonctionnalisés et on a observé qu'ils sont optiquement actifs avec un squelette comportant un mélange de motifs 1,4-dicétone et spirocétal. On a évalué l'influence de divers paramètres sur la copolymérisation du *N*-(but-3-ényl)carbamate de méthyle avec le monoxyde de carbone.

Mots clés : copolymérisation, monoxyde de carbone, oléfines portant des fonctions carbamate et amide.

Introduction

Since 1982, there has been great interest in the development of the metal-catalyzed alternating copolymerization reaction of alkenes with carbon monoxide (1). The reasons for this interest are the low monomer costs, the potential photodegradability of the copolymers (2), and the possibility to modify them (3). Another important area is the use of functional alkenes as monomers. This is an interesting strategy to obtain highly functionalized copolymers which can find a large number of applications.

The advantage of the palladium complex as a catalyst is the greater stability when compared with early transition-metal complexes which allow the polymerization of a limited number of polar monomers due to their sensitivity to electron-donating functional groups (4). However, few papers describe the alternating copolymerization of functional alkenes with carbon monoxide using a palladium catalyst. In these studies (5), olefins bearing alcohol and acid functionalities were used but it had been observed that the copolymerization stopped or became very slow when the functional group and the C=C bond were proximate to each other. This was due to a strong coordination between the functional group and the metal. This problem was recently addressed by using a bulky chelate phosphine such as Me-DUPHOS (Fig. 1), instead of a classic bidentate phosphine, which allowed the formation of chiral functionalized copolymers with isotactic sequences (6).

To our knowledge there have been no studies concerning the copolymerization of alkenes bearing amide and carbamate functionalities with carbon monoxide catalyzed by metal complexes. Herein we present some interesting results for the copolymerization, with novel features of the reaction such as an excess of ligands, or reactions without solvent.

Received July 7, 2000. Published on the NRC Research Press Web site at http://canjchem.nrc.ca on May 30, 2001.

Dedicated to Brian James, who has made outstanding contributions to inorganic chemistry and catalysis.

C. Moineau, G. Mele, and H. Alper.[1] Centre for Catalysis Research and Innovation, Department of Chemistry, University of Ottawa, 10 Marie Curie Street, Ottawa, ON K1N 6N5, Canada.

[1]Corresponding author (telephone: (613) 562-5189; fax: (613) 562-5871; e-mail: halper@science.uottawa.ca).

Results and discussion

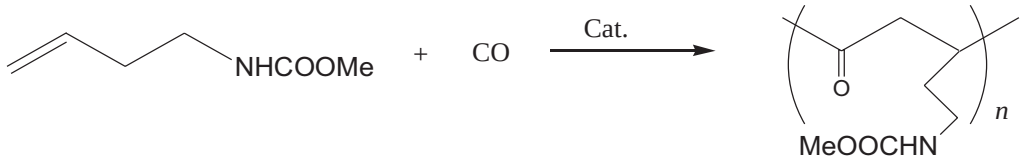
Copolymerization of methyl *N*-(3-butenyl)carbamate with carbon monoxide

The copolymerization with carbon monoxide of methyl *N*-(3-butenyl)carbamate was investigated under various conditions. The catalyst used for the reaction was the dicationic complex $[Pd(CH_3CN)_4](BF_4)_2$ with added bidentate phosphine ((*R*,*R*)-Me-DUPHOS). Other synthetic procedures and different kinds of palladium catalysts were not effective in giving the desired copolymer.

We first examined the reaction using a 2:1 (v/v) $MeNO_2$–MeOH solvent mixture (Table 1). In all cases the formed

 DOI: 10.1139/cjc-79-5/6-587 © 2001 NRC Canada

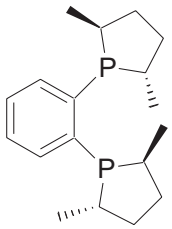
Table 1. Influence of reaction conditions on the copolymerization of methyl *N*-(3 butenyl)carbamate with carbon monoxide.[a]



Entry	Pd/L	% Cat.	T (°C)	P_{CO} (psi)	Yield (%)	M_w (M_w/M_n)[b]	$[\alpha]_D^{25}$ (c, solvent)
1	1/2	0.4	40	1000	—	—	—
2	1/1.5	0.4	25	1000	73	6800 (1.5)	+23 (c 1.0, CH_3OH)
3	1/1.5	0.1	25	1000	70	6500 (1.5)	+12 (c 1.1, CH_3OH)
4	1/1.5	0.4	40	1000	78	13 200 (1.4)	+5 (c 1.2, CH_3OH)
5	1/1.5	0.05	40	1000	70	10 200 (1.4)	+6 (c 1.1, CH_3OH)
6	1/1.5	0.4	80	1000	40	3900 (1.2)	+4 (c 1.3, CH_3OH)
7	1/1	0.1	25	1000	49	5100 (1.4)	+9 (c 1.3, CH_3OH)
8	1/1	0.05	40	1000	67	9200 (1.5)	+8 (c 0.9, CH_3OH)
9	1/1	0.4	40	1000	66	9700 (1.5)	+1 (c 1.1, CH_3OH)
10	1/1	0.05	40	800	62	5500 (1.5)	+3 (c 1, CH_3OH)

[a]Reaction conditions: olefin 10 mmol, catalyst Pd/L = $[Pd(CH_3CN)_4](BF_4)_2$/(*R*,*R*)-Me-DUPHOS, solvent CH_3NO_2–CH_3OH 2:1 (v/v) 3 mL, time 48 h.
[b]The molecular weight of the polymers were measured by GPC using Styragel HT columns (HPLC-grade THF as eluant) and based on calibration with polystyrene standards.

Fig. 1. 1,2-Bis((2*R*,5*R*)-2,5-dimethylphospholano)benzene((*R*,*R*)-Me-DUPHOS).



copolymer was found to be a mixture of 1,4-ketone and spiroketal repeating units in the polymer backbone. The structure of the polymer was characterized by IR and NMR spectroscopy and was supported by elemental analysis results.

The ^{13}C NMR spectrum (in $CDCl_3$) of the product showed resonances at 212.4 ppm due to the carbonyl group and at 114.2 ppm due to the ketal group. We also observed two resonances at 157.1 and 154.2 ppm due to carbamate groups branched on the 1,4-polyketone and on the polyketal backbone. The methylene and methine carbons in the polymer displayed resonances at 46.1, 40.1, and 29.1 ppm, and the signal for the methyl carbon occurred at 51.8 ppm. The ^1H NMR spectrum in $CDCl_3$ displayed a signal at 3.58 ppm due to the methyl group and broad resonances at 6.50–4.50 ppm due to the NH unit, and at 3.11 and 2.75–1.05 ppm for the $CH_2CHCH_2CH_2$ units.

These polymers showed some optical rotation (Table 1). The magnitude of the optical rotation may depend on the ratio of ketone to spiroketal units present in the backbone. These copolymers appeared as amorphous white solids soluble in $CHCl_3$, THF, CH_3OH, CH_2Cl_2, and CH_3COCH_3, and insoluble in diethyl ether, hexane, and toluene. The molecular weight and the yield of the copolymer are significantly increased if an excess of (*R*,*R*)-Me-DUPHOS is used ([Pd]/L = 1/1.5) relative to palladium. For example, at 40°C and under 1000 psi CO-pressure, the use of 0.4% of the catalytic system [Pd]/Me-DUPHOS = 1/1.5 (entry 4) gave a copolymer with a molecular weight of 13 200 g mol^{-1} in 78% yield, compared with a molecular weight of 9700 g mol^{-1} and a yield of 66% for 1/1 [Pd]/Me-DUPHOS. The same enhancement can be seen with entries 3, 7 and 5, 8. To our knowledge, this is the first obsrvation of the increase in molecular weight resulting from the addition of more phosphine. Note, however, that no copolymer forms when too much (*R*,*R*)-Me-DUPHOS is used (entry 1). We assume, in the latter case, that the result is a consequence of bis-ligand complex formation.

Increasing the amount of catalyst afforded a slight increase in molecular weight (entries 2–5 and 8, 9). The temperature has an important effect on the molecular weight as well as on the yield (entries 2, 4). At 40°C the molecular weight is approximately double that at 25°C (13 200 g mol^{-1} compared to 6800 g mol^{-1}). However, higher temperatures have a detrimental effect on the reaction: at 80°C (entry 6) the molecular weight was only 3900 g mol^{-1} with a polymer yield of 40%. The influence of the CO-pressure was also analyzed (entries 8, 10). At lower pressure (800 psi instead of 1000 psi), a lower molecular weight of copolymer was obtained (5500 g mol^{-1} instead of 9200 g mol^{-1}).

Table 2 shows the influence of dilution on the reaction. Reaction at higher dilution appreciably lowers the yield (to 5%), and the molecular weight decreases significantly (3800 g mol^{-1}). The copolymerization reaction was also run neat and in CH_2Cl_2 (Table 3). A polar olefin such as methyl *N*-(3 butenyl)carbamate is capable of solubilizing the palladium catalyst. At 40°C and 1000 psi of CO, the copolymer was obtained in 30% yield with a molecular weight of 60 500 g mol^{-1} (entry 1). Higher temperatures (80°C, entry 2) gave essentially the same yield and also had a significant effect in lowering the molecular weight. The limitation of this reaction may be the solubility of the polymer in the

© 2001 NRC Canada

Table 2. Effect of solvent dilution on the copolymerization of methyl *N*-(3 butenyl)carbamate with carbon monoxide.[a]

Entry	$V_{solvent}$ (mL)	Yield (%)	M_w (M_w/M_n)[b]	$[\alpha]_D^{25}$ (c, solvent)
1	3	70	6500 (1.5)	+12 (c 1.1, CH_3OH)
2	15	5	3800 (1.3)	+41 (c 0.4, CH_3OH)

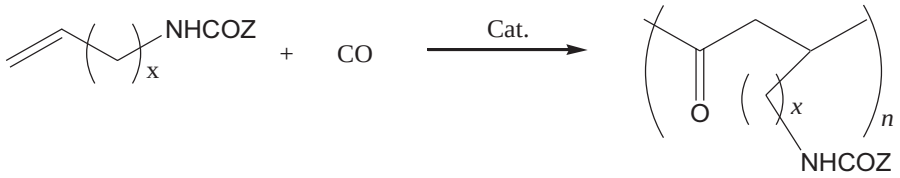
[a]Reaction conditions: olefin 10 mmol, $[Pd(CH_3CN)_4](BF_4)_2$ 1×10^{-2} mmol, (*R*,*R*)-Me-DUPHOS 1.5×10^{-2} mmol, solvent CH_3NO_2–CH_3OH 2:1 (v/v), CO pressure 1000 psi, temperature 40°C, time 48 h.
[b]The molecular weight of the polymers were measured by GPC using Styragel HT columns (HPLC-grade THF as eluant) and based on calibration with polystyrene standards.

Table 3. Copolymerization of methyl *N*-(3 butenyl)carbamate with carbon monoxide without solvent and with CH_2Cl_2.[a]

Entry	Solvent	*T* (°C)	Yield (%)	M_w (M_w/M_n)[b]	$[\alpha]_D^{25}$ (c, solvent)
1	—	40	30	60 500 (2.3)	+19 (c 0.9, CH_2Cl_2)
2	—	80	31	9700 (1.5)	+6 (c 1.0, CH_3OH)
3	CH_2Cl_2[c]	40	80	30 400 (1.8)	+19 (c 1.0, CH_2Cl_2)

[a]Reaction conditions: olefin 10 mmol, $[Pd(CH_3CN)_4](BF_4)_2$ 1×10^{-2} mmol, (*R*,*R*)-Me-DUPHOS 1.5×10^{-2} mmol, CO pressure 1000 psi, time 48 h.
[b]The molecular weight of the polymers were measured by GPC using Styragel HT columns (HPLC-grade THF as eluant) and based on calibration with polystyrene standards.
[c]CH_2Cl_2 1.3 mL.

Table 4. Copolymerization of carbon monoxide with different olefins bearing carbamate and amide functionalitiies.[a]



Entry	*x*	*Z*	Solvent	Yield (%)	M_w (M_w/M_n)[b]	T_m (°C)[c]	$[\alpha]_D^{25}$ (c, solvent)
1	1	OMe	A	—	—	—	—
2			B	75	6300 (1.3)	190–200	+83 (c 1.1, CH_2Cl_2)
3	1	OPh	A	44	4500 (1.2)	180–190	+44 (c 1.2, CH_2Cl_2)
4			B	55	<1000	160–170	+27 (c 1.1, DMSO)
5	2	Me	A	30	<1000	145–155	+24 (c 1.2, CH_3OH)
6			B	—	—	—	—
7	2	Ph	A	53	3300 (1.2)	150–165	–53 (c 0.1, DMSO)
8			B	62	6400 (1.2)	155–170	+40 (c 0.2, DMSO)
9	1	Ph	A	20	3400 (1.2)	140–150	+33 (c 1.1, DMSO)
10			B	55	3600 (1.2)	140–150	+29 (c 1.0, DMSO)

[a]Reaction conditions: olefin 10 mmol, $[Pd(CH_3CN)_4](BF_4)_2$ 4×10^{-2} mmol, (*R*,*R*)-Me-DUPHOS 6×10^{-2} mmol, solvent: A, CH_3NO_2–CH_3OH 2:1 (v/v) 3 mL; B, CH_2Cl_2 1.3 mL, CO pressure 1000 psi, temperature 40°C, time 48 h.
[b]The molecular weight of the polymers were measured by GPC using Styragel HT columns (HPLC-grade THF as eluant) and based on calibration with polystyrene standards.
[c]T_m = melting temperature.

monomer. One can also use CH_2Cl_2 as the solvent with the yield of the functionalized polyketone being 80% and a molecular weight of 30 400 g mol^{-1}. Note that unreacted monomer was recovered without isomerization of the double bond, in contrast with isomerization observed using 2:1 (v/v) $MeNO_2$–MeOH mixture as the solvent.

Copolymerization of other olefins bearing carbamate and amide functionalities

The methodology described for the copolymerization of methyl *N*-(3-butenyl)carbamate and carbon monoxide, was applied to different unsaturated carbamates and amides using CH_2Cl_2 or 2:1 (v/v) $MeNO_2$–MeOH as the solvent. The results are summarized in Table 4. All copolymers were found to be a mixture of 1,4-ketone and spiroketal repeating units in the polymer backbone.

One cannot predict, a priori, which solvent would give the best results for the copolymerization of unsaturated carbamates and amides with carbon monoxide. For example, when 2:1 (v/v) $MeNO_2$–MeOH is used, no polymer was obtained with methyl *N*-(2-propenyl)carbamate (entry 1) and only an oligomer with a molecular weight less than 1000 g mol^{-1} was formed (30% yield, entry 5) with methyl *N*-(3-butenyl)amide. Also, using phenyl *N*-(2-propenyl)amide

© 2001 NRC Canada

as the olefin (entry 9), a copolymer with molecular weight of 3400 g mol^{-1} was obtained with a yield of only 20%. On the other hand, when CH_2Cl_2 is used as the solvent, no polymer was formed with methyl *N*-(3-butenyl)amide (entry 6) and only an oligomer with a molecular weight less than 1000 g mol^{-1} was obtained with phenyl *N*-(3-propenyl)carbamate (55% yield, entry 4).

Concerning the other cases, copolymers were obtained in moderate molecular weight, and in good yield (44–75%). All copolymers melted without decomposition, and were optically active. Concerning the latter, two interesting results merit comment: the copolymer obtained with methyl *N*-(3-propenyl)carbamate and carbon monoxide (entry 2) showed a high optical rotation, especially when compared with the other results. Also, it was observed for the first time that the copolymerization of phenyl *N*-(3-butenyl)amide in two different solvents (entries 7 and 8) gave two chiral copolymers with specific rotations of opposite sign.

Experimental section

Materials

Most chemicals were purchased from Aldrich Chemical Co. and were used as received. $[Pd(CH_3CN)_4](BF_4)_2$ and 1,2-bis((2*R*,5*R*)-2,5-dimethylphospholano)benzene ((*R*,*R*)-Me-DUPHOS) were purchased from Strem Chemicals. Solvents were appropriately dried and distilled (under nitrogen if necessary) before use.

General methods

Methyl *N*-(2-propenyl)carbamate, phenyl *N*-(2-propenyl)carbamate, methyl *N*-(3-butenyl)carbamate, phenyl *N*-(2-propenyl)amide, methyl *N*-(3-butenyl)amide, and phenyl *N*-(3-butenyl)amide were prepared according to literature methods (7, 8).

All ^1H and ^{13}C NMR spectra were recorded on either a Gemini-200 or Bruker AMX 500 NMR spectrometer using $CDCl_3$, CD_3OD, or DMSO-d_6 as solvent and TMS as the internal standard. Infrared spectra were recorded on a Bomem-100 FT-IR spectrometer. Gel permeation chromatography (GPC) was run using a Waters 510 HPLC pump operating on a 1 mL min^{-1} flow rate with three consecutive Styragel HT columns effective from 5×10^2 to 4×10^6 and detected using a Waters 410 differential refractometer detector. HPLC-grade THF was used as the eluant. The molecular weight for the polymers are based on calibration with polystyrene standards. Optical rotation measurements of chiral polymers were performed on a PerkinElmer 241 polarimeter using a sodium lamp.

Methyl *N*-(2-propenyl)carbamate

Allyl amine (5.0 g) afforded methyl *N*-(2-propenyl)carbamate (5.6 g, 55%) as a colorless oil, $bp_{0.3}$ = 39°C. IR (neat) (cm^{-1}): 3340, 3084, 2952, 1712, 1537, 1258, 1021, 994, 921, 780. ^1H NMR ($CDCl_3$) (ppm): 5.79 (1H, ddt, *J* = 17.2, 10.2, 5.4 Hz), 5.13 (1H, d, *J* = 17.2 Hz), 5.07 (1H, d, *J* = 10.2 Hz), 4.90 (1H, br), 3.75 (2H, br), 3.63 (3H, s). ^{13}C NMR ($CDCl_3$) (ppm): 157.6, 135.2, 116.4, 52.7, 44.0. Anal. calcd.: C 52.16, H 7.88, N 12.17; found: C 52.01, H 7.91, N 12.10.

Phenyl *N*-(2-propenyl)carbamate

Allyl amine (5.0 g) afforded phenyl *N*-(2-propenyl)carbamate (10.9 g, 70%) as a colorless oil. R_f = 0.16 (hexane – ethyl acetate, 10:1). IR (neat) (cm^{-1}): 3332, 3073, 1731, 1646, 1594, 1537, 1487, 1205, 1024, 990, 931, 758, 689. ^1H NMR ($CDCl_3$) (ppm): 7.35 (2H, dl, *J* = 7.4 Hz), 7.27–7.08 (3H, m), 5.88 (1H, ddt, *J* = 16.2, 10.3, 6.5 Hz), 5.23 (1H, d, *J* = 16.2 Hz), 5.17 (1H, d, *J* = 10.3 Hz), 5.29–5.10 (1H, br), 3.86 (2H, br). ^{13}C NMR ($CDCl_3$) (ppm): 155.2, 134.6, 130.0, 129.9, 126.0, 122.2, 117.2, 44.3. Anal. calcd.: C 67.78, H 6.26, N 7.90; found: C 68.03, H 6.51, N 7.46.

Methyl *N*-(3-butenyl)carbamate

3-Butenylamine (7) (5.0 g) afforded methyl *N*-(3-butenyl)carbamate (6.0 g, 66%) as a colorless oil, $bp_{0.1}$ = 37°C. IR (neat) (cm^{-1}): 3347, 2953, 1710, 1535, 1263, 1144, 1034, 917, 779. ^1H NMR ($CDCl_3$) (ppm): 5.68 (1H, m), 5.01 (1H, d, *J* = 16.7 Hz), 5.00 (1H, d, *J* = 10.4 Hz), 3.58 (3H, s), 3.20 (2H, m), 2.18 (2H, m). ^{13}C NMR ($CDCl_3$) (ppm): 156.9, 135.1, 117.2, 52.0, 40.0, 34.1. Anal. calcd.: C 55.80, H 8.58, N 10.84; found: C 55.91, H 8.64, N 10.72.

Phenyl *N*-(2-propenyl)amide

Allyl amine (5.0 g) afforded phenyl *N*-(2-propenyl)amide (7.8 g, 55%) as a light yellow oil. R_f = 0.15 (hexane – ethyl acetate, 10:1). IR (neat) (cm^{-1}): 3317, 3084, 3067, 1633, 1556, 1488, 1308, 993, 804, 694. ^1H NMR ($CDCl_3$) (ppm): 7.76 (2H, d, *J* = 7.8 Hz), 7.47–7.33 (3H, m), 6.48 (1H, br), 5.88 (1H, ddt, *J* = 17.2, 10.2, 5.6 Hz), 5.22 (1H, d, *J* = 17.2 Hz), 5.14 (1H, d, *J* = 10.2 Hz), 4.04 (2H, br). ^{13}C NMR ($CDCl_3$) (ppm): 168.2, 135.0, 134.8, 132.0, 129.1, 127.7, 117.0, 43.0. Anal. calcd.: C 74.51, H 6.88, N 8.69; found: C 74.40, H 6.83, N 8.50.

Methyl *N*-(3-butenyl)amide

3-Butenylamine (7) (5.0 g) afforded methyl *N*-(3-butenyl)amide (4.8 g, 60%) as a colorless oil, $bp_{0.3}$ = 85°C. IR (neat) (cm^{-1}): 3333, 3084, 2952, 1698, 1538, 1258, 994, 921. ^1H NMR ($CDCl_3$) (ppm): 5.84–5.62 (2H, m), 5.06 (1H, d, *J* = 16.1 Hz), 5.05 (1H, d, *J* = 10.3 Hz), 3.28 (2H, dt, *J* = 5.9, 6.7 Hz), 2.22 (2H, dt, *J* = 6.7 Hz), 1.93 (3H, s). ^{13}C NMR ($CDCl_3$) (ppm): 172.7, 135.6, 117.8, 39.1, 34.3, 23.9. Anal. calcd.: C 63.68, H 9.79, N 12.38; found: C 63.60, H 9.80, N 12.35.

Phenyl *N*-(3-butenyl)amide

3-Butenylamine (7) (5.0 g) afforded phenyl *N*-(3-butenyl)amide (7.4 g, 60%) as a light yellow oil, R_f = 0.33 (hexane – ethyl acetate, 2:1). IR (neat) (cm^{-1}): 3318, 3077, 2979, 2933, 1642, 1543, 1311, 1150, 1076, 992, 917, 803, 695. ^1H NMR ($CDCl_3$) (ppm): 7.73 (2H, d, *J* = 7.9 Hz), 7.50–7.24 (3H, m), 6.34 (1H, br), 5.80 (1H, *J* = 17.1, 10.2, 6.9 Hz), 5.11 (1H, d, *J* = 17.1 Hz), 5.10 (1H, d, *J* = 10.2 Hz), 3.50 (2H, dt, *J* = 6.9, 6.7 Hz), 2.35 (2H, dt, *J* = 6.7, 6.7 Hz). ^{13}C NMR ($CDCl_3$) (ppm): 168.2, 135.9, 135.3, 132.0, 129.1, 127.4, 117.9, 39.5, 34.4. Anal. calcd.: C 75.40, H 7.48, N 7.99; found: C 75.79, H 7.46, N 7.89.

Copolymerization of methyl *N*-(3-butenyl)carbamate

To a solution containing 4.0×10^{-2} mmol of $[Pd(CH_3CN)_4](BF_4)_2$ and 6.0×10^{-2} mmol of (*R*,*R*)-Me-

© 2001 NRC Canada

DUPHOS in 3 mL of a 2:1 (v/v) mixture of CH_3NO_2 and MeOH was added 10 mmol of methyl *N*-(3-butenyl)carbamate. The resultant solution was place in a 45 mL autoclave and charged with 1000 psi of CO. After stirring for 48 h at 40°C, the excess carbon monoxide was released and the solution was diluted with CH_2Cl_2 and filtered. Diethyl ether was added to the filtrate to precipitate out the polymer (1.2 g). The polymer was washed with diethyl ether and dried under vacuum. The formed polymer was found to be a mixture of 1,4-ketone and spiroketal repeating units in the polymer backbone. $[\alpha]_D^{25}$ = +8 (c = 0.9, MeOH). $M_w = 1.3 \times 10^4$, M_w/M_n = 1.4. T_m = 145–155°C. IR (KBr) (cm^{-1}): 3342, 2982, 1706, 1534, 1448, 1374, 1259, 1139, 1034, 835, 781. ^{1}H NMR ($CDCl_3$) (ppm): 6.50–4.50 (1H, br), 3.58 (3H, s), 3.11 (2H, br), 2.75–1.05 (5H, m). ^{13}C NMR ($CDCl_3$) (ppm): 212.4, 157.1, 154.2, 114.2, 51.8, 46.1, 40.1, 29.1. Anal. calcd. for the poly(spiroketal–1,4-ketone): C 53.49, H 7.05, N 8.91; found: C 53.73, H 7.06, N 8.73.

Copolymerization of methyl *N*-(2-propenyl)carbamate

The copolymerization was carried out following the same procedure as the one employed for *N*-(3-butenyl)carbamate using 10 mmol of methyl *N*-(2-propenyl)carbamate in 1.3 mL of CH_2Cl_2. The formed polymer (1.1 g) was a mixture of 1,4-ketone and spiroketal repeating units in the polymer backbone. $[\alpha]_D^{25}$ = +83 (c = 1.1, CH_2Cl_2). $M_w = 6.3 \times 10^3$, M_w/M_n = 1.3. T_m = 190–200°C. IR (KBr) (cm^{-1}): 3349, 2954, 1709, 1536, 1449, 1262, 1195, 1147, 824. ^{1}H NMR ($CDCl_3$) (ppm): 7.0–5.0 (1H, br), 3.62 (3H, s), 3.40 (2H, br), 2.88–1.40 (3H, m). ^{13}C NMR ($CDCl_3$) (ppm): 215.0, 158.0, 115.1, 52.9, 47.5, 43.5, 40.8. Anal. calcd. for the poly(spiroketal–1,4-ketone): C 50.35, H 6.34, N 9.79; found: C 50.05, H 6.53, N 9.49.

Copolymerization of phenyl *N*-(2-propenyl)carbamate

The copolymerization was carried out following the same procedure as the one employed for *N*-(3-butenyl)carbamate using 10 mmol of phenyl *N*-(2-propenyl)carbamate in 3 mL of a 2:1 (v/v) mixture of CH_3NO_2 and MeOH. The formed polymer (0.9 g) was a mixture of 1,4-ketone and spiroketal repeating units in the polymer backbone. $[\alpha]_D^{25}$ = +44 (c = 1.2, CH_2Cl_2). $M_w = 4.5 \times 10^3$, M_w/M_n = 1.2. T_m = 180–190°C. IR (KBr) (cm^{-1}): 3352, 2942, 1736, 1491, 1376, 1206, 952, 826, 762, 689. ^{1}H NMR ($CDCl_3$) (ppm): 7.60–6.60 (5H, m), 5.96 (1H, br), 3.36 (2H, br), 3.00–1.40 (3H, m). ^{13}C NMR (DMSO-d_6) (ppm): 209.9, 154.4, 151.0, 129.2, 124.9, 121.7, 47.5, 43.7, 41.2. Anal. calcd. for the poly(spiroketal–1,4-ketone): C 64.38, H 5.40, N 6.83; found: C 64.59, H 5.47, N 6.62.

Copolymerization of methyl *N*-(3-butenyl)amide

The copolymerization was carried out following the same procedure as the one employed for *N*-(3-butenyl)carbamate using 10 mmol of methyl *N*-(3-butenyl)amide in 3 mL of 2:1 (v/v) CH_3NO_2–MeOH. The formed polymer (0.4 g) was a mixture of 1,4-ketone and spiroketal repeating units in the polymer backbone. $[\alpha]_D^{25}$ = +24 (c = 1.2, MeOH). $M_w < 10^3$. T_m = 145–155°C. IR (KBr) (cm^{-1}): 3289, 3093, 2936, 1708, 1655, 1560, 1440, 1374, 1297, 1212, 1149, 1096, 1040, 954, 823. ^{1}H NMR (CD_3OD) (ppm): 7.72 (1H, br), 2.79 (2H, br), 1.56 (3H, s), 2.30–0.94 (5H, m). ^{13}C NMR (CD_3OD) (ppm): 172.9, 135.1, 114.9, 42.7, 41.9, 39.2, 29.8, 22.5. Anal. calcd. for the poly(spiroketal–1,4-ketone): C 63.68, H 9.80, N 12.38; found: C 63.40, H 9.91, N 12.51.

Copolymerization of phenyl *N*-(3-butenyl)amide

The copolymerization was carried out following the same procedure as the one employed for *N*-(3-butenyl)carbamate using 10 mmol of phenyl *N*-(3-butenyl)amide in 1.3 mL of CH_2Cl_2. The formed polymer (1.3 g) consisted of a mixture of 1,4-ketone and spiroketal repeating units in the polymer backbone. $[\alpha]_D^{25}$ = +40 (c = 0.2, DMSO). $M_w = 6.4 \times 10^3$, M_w/M_n = 1.2. T_m = 155–170°C. IR (KBr) (cm^{-1}): 3318, 3066, 2930, 1638, 1542, 1309, 1148, 955, 822, 694. ^{1}H NMR (DMSO-d_6) (ppm): 8.42 (1H, br), 7.75 (2H, br), 7.60–7.00 (3H, br), 3.16 (2H, br), 2.47 (1H, br), 2.05 (2H, br), 1.73 (2H, br). ^{13}C NMR (DMSO-d_6) (ppm): 166.8, 134.7, 130.8, 128.1, 127.0, 38.1, 30.7, 41.0. Anal. calcd. for the poly(spiroketal–1,4-ketone): C 70.92, H 6.45, N 6.89; found: C 70.51, H 6.25, N 7.01.

Copolymerization of phenyl *N*-(2-propenyl)amide

The copolymerization was carried out following the same procedure as the one employed for *N*-(3-butenyl)carbamate using 10 mmol of phenyl *N*-(2-propenyl)amide in 1.3 mL of CH_2Cl_2. The formed polymer (1.0 g) was a mixture of 1,4-ketone and spiroketal repeating units in the polymer backbone. ^{1}H NMR (DMSO-d_6) (ppm): 8.58 (1H, br), 8.15–6.80 (5H, m), 3.17 (2H, br), 2.92–1.00 (3H, m). ^{13}C NMR (DMSO-d_6) (ppm): 209.9, 166.5, 134.3, 131.2, 128.3, 127.2, 46.1, 43.5, 41.7. IR (KBr) (cm^{-1}): 3353, 3066, 2939, 1647, 1541, 1308, 823, 712. Anal. calcd. for the poly(spiroketal–1,4-ketone): C 69.83, H 5.86, N 7.40; found: C 69.40, H 5.71, N 7.31.

Conclusion

The solubilization of the palladium catalyst in unsaturated carbamates and amides enables copolymerization with carbon monoxide to take place without any solvent. While the yield may be only 30%, the fact that the unreacted olefin can be recovered without isomerization of the C=C bond is of interest. For the first time, an excess of phosphine was found to be effective for obtaining polyketones in higher molecular weight. Finally the new copolymers formed may be of value for subsequent modification of the polymer (*e-g* polyurethane-polyketone).

Acknowledgment

We are grateful to Dow Chemical Co. for support of this research.

References

1. (*a*) A. Sen and T.-N. Lai. J. Am. Chem. Soc. **104**, 3520 (1982); (*b*) A. Sen. Adv. Polym. Sci. **73**/**74**, 125 (1986); (*c*) E. Drent, J.A.M. van Broekhoven, and M.J. Doyle. J. Organomet. Chem. **417**, 235 (1991); (*d*) A. Sen. Acc. Chem. Rev. **26**, 303 (1993); (*e*) Z. Ziang, G.M. Dahlen, and A. Sen. *In* New advances in polyolefins. *Edited by* T.C. Chung. Plenum, New York. 1993. p. 47; (*f*) E. Drent and P.H.M. Budzelaar. Chem.

© 2001 NRC Canada

Rev. **96**, 663 (1996); (*g*) E. Drent and W.W. Jager. Polym. Mater. Sci. Eng. **76**, 100 (1997).
2. (*a*) J. Guillet. Polymer Photophysics and Photochemistry. Cambridge University, Cambridge, U.K. 1985. p. 261; (*b*) F.Y. Xu and J.C.W. Chien. Macromolecules, **26**, 3485 (1993); (*c*) M.D.E. Forbes, S.R. Ruberu, D. Nachtigallova, K.D. Jordan, and J.C. Barborak. J. Am. Chem. Soc. **117**, 3946 (1995).
3. (*a*) A. Sen, Z. Jiang, and J.-T. Chen. Macromolecules, **22**, 2012 (xxxx); (*b*) Z. Jiang and A. Sen. Macromolecules, **25**, 880 (1992); (*c*) Z. Jiang, S. Sanganeria, and A. Sen. J. Polym. Sci. A: Polymer Chem. **32**, 841 (1994).
4. (*a*) D.J. Crowther, N.C. Baenziger, and R.F. Jordan. J. Am. Chem. Soc. **113**, 1455 (1991); (*b*) M.R. Kesti, G.W. Coates, and R.M. Waymouth. J. Am. Chem. Soc. **114**, 9679 (1992); (*c*) X. Yang, C.L. Stern, and T.J. Marks. J. Am. Chem. Soc. **116**, 10015 (1994).
5. (*a*) E. Drent. Eur. Pat. Appl. EP 272 727, 1988; Chem. Abstr. **109**, 191 089n (1988); (*b*) E. Drent. Eur. Pat. Appl. EP 463 689, 1992; Chem. Abstr. **116**, 129 879m (1992);(*c*) A. Sen and Z. Jiang. Macromolecules, **26**, 911 (1993).
6. (*a*) Z. Jiang and A. Sen. J. Am. Chem. Soc. **117**, 4455 (1995); (*b*) S. Kacker, Z. Jiang, and A. Sen. Macromolecules, **29**, 5852 (1996).
7. N.M. Yoon and H.C. Brown. J. Am. Chem. Soc. **90**, 2931 (1968).
8. N.O.V. Sonntag. Chem. Rev. **52**, 237 (1953).

© 2001 NRC Canada

Alternating copolymerization of ω-perfluoroalkyl-1-alkenes with carbon monoxide catalyzed by homogeneous and polymer-supported Pd-complexes

Kyoko Nozaki, Fumitoshi Shibahara, Stephan Elzner, and Tamejiro Hiyama

Abstract: Alternating copolymerization of fluorinated olefins $(C_nF_{2n+1})(CH_2)_mCH=CH_2$ (**1**) and carbon monoxide was carried out using cationic Pd(II)-(*R*,*S*)-BINAPHOS complexes (**2**) as catalysts. To obtain polymeric products sufficiently, existence of at least two methylenes in **1** were essential ($m \geq 2$). The products thus obtained formed polyspiroketal (**4**) rather than polyketone (**3**), the structures being determined by solid- and solution-state NMR and IR analyses. The water contact angle was 108° for a sample of **4f** when it was casted on a glass surface from C_6F_6 solution.

Key words: copolymer, fluoroalkene, carbon monoxide, palladium, contact angle.

Résumé : Utilisant des complexes cationiques Pd(II)-(*R*,*S*)-BINAPHOS (**2**) comme catalyseurs, on a effectué une copolymérisation alternative d'oléfines fluorées $(C_nF_{2n+1})(CH_2)_mCH=CH_2$ (**1**) et de monoxyde de carbone. Pour obtenir des quantités suffisantes de polymères, il est essentiel que **1** comporte au moins deux méthylènes ($m \geq 2$). Les produits ainsi obtenus forment des polyspirocétals (**4**) plutôt que des polycétones (**3**); les structures ont été déterminées par analyses IR et par RMN à l'état solide et en solution. L'angle de contact avec l'eau est de 108° pour un échantillon de **4f** déposé sur une surface de verre à partir d'une solution de C_6F_6.

Mots clés : copolymère, fluoroalcène, monoxyde de carbone, palladium, angle de contact.

[Traduit par la Rédaction]

Introduction

The Pd(II)-catalyzed alternating copolymerization of alkenes with carbon monoxide provides polyketones whose carbonyl groups are potentially convertible to other functional groups (1). Meanwhile, employment of alkenes bearing functional groups is also of interest to obtain highly functionalized polymers. For example, Sen and co-workers (2) successfully applied alkenols and alkenoic acids to the copolymerization. We put a trialkoxysilyl group to the alkene, that opens the possibility of silane coupling of the polyketones on silica gels (3). In the course of our study, we became interested in the introduction of perfluoroalkyl groups into the polyketone. While our research was going on, Sen and co-workers (4) reported elegant success in the alternating copolymerization of fluorinated allylbenzenes with carbon monoxide catalyzed by a Me-DuPHOS complex of Pd(II) (for another example of fluoroalkene–CO copolymerization see ref. 5). Potential utility of the copolymer was suggested as new materials to alter the surface properties when blended with polar polymers. Here, we report the alternating olefin–CO copolymerization catalyzed by Pd(II)-(*R*,*S*)-BINAPHOS employing ω-perfluoroalkyl-1-alkenes. Our attempt to produce the copolymer using a polymer-supported catalyst is also described. Supercritical CO_2 was examined as a solvent in addition to the conventional CH_2Cl_2 because CO_2 is known to possess high affinity with perfluoroalkyl groups.

Received September 26, 2000. Published on the NRC Research Press Press Web site at http://canjchem.nrc.ca on May 30, 2001.

This paper is dedicated to Professor Brian James on the occasion of his 65th birthday.

K. Nozaki[1], S. Elzner, and T. Hiyama. Department of Material Chemistry, Graduate School of Engineering, Kyoto University, Yoshida, Sakyo-ku, Kyoto 606-8501, Japan.
F. Shibahara. TOREST, Japan Science and Technology Corporation (JST).

[1]Corresponding author (telephone: (+81)-75-753-5545; fax (+81)-75-753-5555; e-mail nozaki@npc05.kuic.kyoto-u.ac.jp).

Results and discussions

Monomer synthesis

Other than commercially available 3,3,3-trifluoropropene, we synthesized fluoroalkenes which have either one or two methylene groups between the C=C double bond and the perfluoroalkyl groups. 3-Perfluoroalkyl-1-propenes (**1b**–**d**) were prepared from perfluoroalkyl halides and allyl(trimethyl)silane according to the literature (eq. [1]). Between the two catalysts proposed in the literature (6), $Ru_3(CO)_{12}$ was preferably used rather than $Fe_3(CO)_{12}$ because of its easy separation from the products by simple filtration. 4-Perfluoroalkyl-1-butenes **1e** and **1f** were prepared from (2-perfluoroalkyl)ethyl

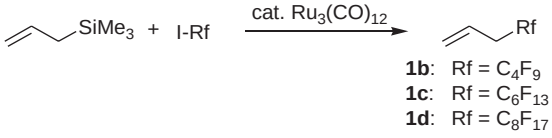
 DOI: 10.1139/cjc-79-5/6-593 © 2001 NRC Canada

Table 1. Copolymerization of fluorinated alkenes with carbon monoxide.[a]

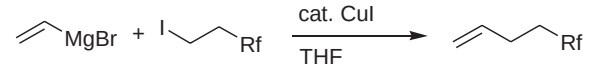
Run	Alkene	Catalyst (mol%)	Time (h)	Turnover ($^{-}$h)	Yield (%)
1	**1a**	—[b]	41	0	0
2	**1b**	0.19	24	0.7	3
3	**1c**	0.23	88	0.5	10
4	**1c**	1.00	100	0.1	10
5	**1d**	0.20	63	0.6	8
6	**1e**	0.40	71	2.2	63
7	**1f**	0.20	89	3.2	57

[a]In CH_2Cl_2, under CO pressure of 20 atm, at 50°C. Details of the reaction conditions are described in the *Experimental* part.
[b]A large excess of olefin was introduced.

iodide and vinylmagnesium bromide according to the literature (eq. [2]) (7).

[1] 

1b: Rf = C_4F_9
1c: Rf = C_6F_{13}
1d: Rf = C_8F_{17}

[2] 

1e: Rf = C_4F_9
1f: Rf = C_6F_{13}

Alternating copolymerization of fluoroalkenes with CO in CH_2Cl_2

Fluorinated alkenes were subjected to the alternating copolymerization with carbon monoxide. The employed catalyst was a cationic Pd(II) complex of a chiral phosphine-phosphite ([PdMe(MeCN){(*R*,*S*)-BINAPHOS}][B{3,5-$(CF_3)_2C_6H_3$}$_4$] (**2a**)) (8). In the presence of **2a**, a CH_2Cl_2 solution of fluoroalkenes (**1a**–**f**) were treated under CO pressure in an autoclave. The product polymers were allowed to precipitate from methanol. The results are summarized in Table 1. With 3,3,3-trifluoropropene (**1a**), no polymeric material was produced. Starting from 3-perfluoroalkyl-1-propenes (**1b**–**d**), insoluble products were obtained in low yields as shown in runs 2–5. With 4-perfluoroalkyl-1-butenes (**1e**–**f**), the products were given in higher yields. The polymers thus obtained were insoluble in most of organic solvents, except for hexafluorobenzene (C_6F_6). In THF, which was reported to dissolve poly(fluorine-substituted allylbenzene-*alt*-CO) (4), only oligomers with low molecular weights were soluble and most of the polymeric materials remained insoluble. Accordingly, the copolymers here obtained were characterized on the basis of solid-state and solution-state (in C_6F_6) NMR and IR spectra. The representative spectra of poly(**1f**-*alt*-CO) are shown in Figs. 1 and 2. Solid-phase ^{13}C NMR (Fig. 1(*a*)) shows a peak at 114 ppm suggesting the presence of spiroketal **4f** (9). No peak was detectable around 213 ppm where polyketone **3f** would exhibit a peak due to C=O, with the S/N ratio of 32. The solution NMR chart taken in C_6F_6 (Fig. 1(*b*)) is essentially superimposable on the solid-state NMR Fig. 1(*a*). By IR, an extremely weak absorption was observed at 1710 cm^{-1}, attributed to carbonyl. The peak at 840 cm^{-1} may be assigned as the C—O—C bond of spiroketal **4f**. Thus, the polymer exists mainly as spiroketal

Fig. 1. (*a*) Solid-phase ^{13}C NMR (CP-MAS) of poly(**1f**-*alt*-CO). The peak at 114 ppm suggests the presence of spiroketal **4f**. No peak is detectable around 213 ppm where polyketone **3f** would exhibit a peak due to C=O. (*b*) Solution-phase ^{13}C NMR (C_6F_6). The chart is essentially superimposable on (*a*).

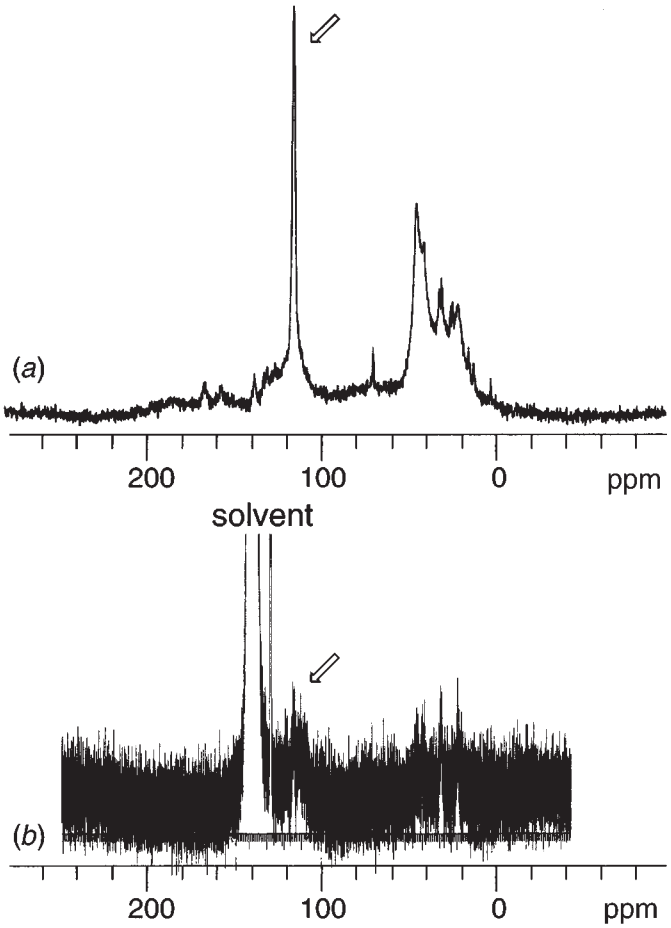
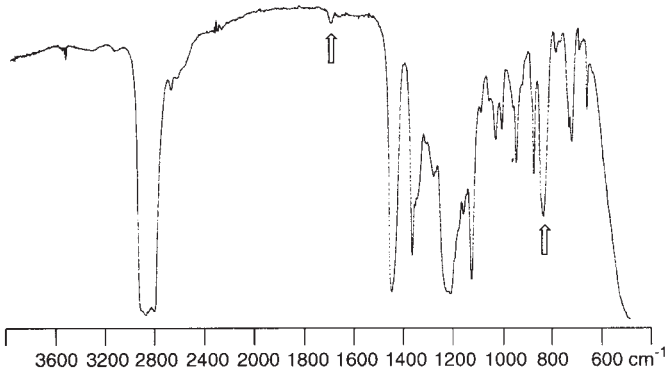
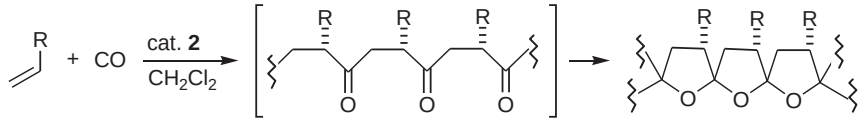


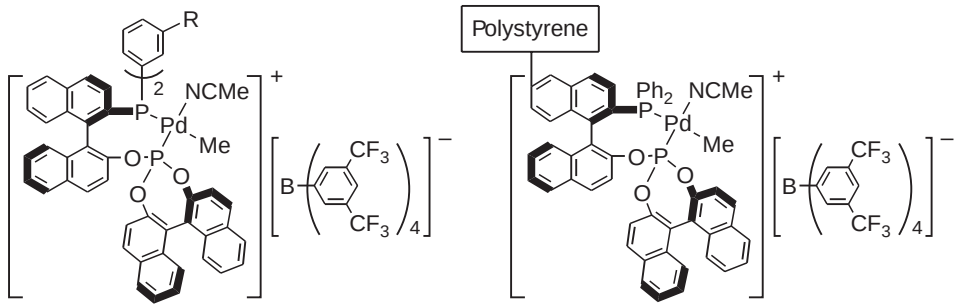
Fig. 2. Infrared spectrum (Nujol) of poly(**1f**-*alt*-CO). A small peak is observed at 1710 cm^{-1}, attributed to the C=O absorption due to polyketone **3f**. Absorption around 840 cm^{-1} may be assigned as the C—O—C of spiroketal **4f**.



© 2001 NRC Canada

[3] 

1a: R = CF_3
1b: R = $CH_2C_4F_9$
1c: R = $CH_2C_6F_{13}$
1d: R = $CH_2C_8F_{17}$
1e: R = $CH_2CH_2C_4F_9$
1f: R = $CH_2CH_2C_6F_{13}$

[4] 

2a: R = H
2b: R = $CH_2CH_2C_6F_{13}$

2c

4f, and at max, 3% of the polymer may form polyketone **3f** (the **4f**/**3f** ratio was estimated from the S/N ratio of the solid-state ^{13}C NMR). This is unchanged when the polymer is dissolved in C_6F_6. Also, characterization by IR was carried out for the copolymers obtained from **1b–e** to reveal that all of them exist as spiroketals **4b–e** but not polyketones **3b–e**.

Alternating copolymerization of fluoroalkenes with CO in supercritical CO_2

Fluorinated compounds are known to have strong affinity with supercritical (sc.) CO_2 (10) (for examples of fluoroalkene polymerization in sc. CO_2 see ref. 11). In sc. CO_2, no polymeric material was obtained in the attempted copolymerization of **1f** with CO when Pd-complex **2a**, which was insoluble in sc. CO_2, was employed as a catalyst. Meanwhile **2b**, a perfluoroalkyl-substituted analog of **2a**, (12*a*; for fluoroalkyl-substituted complexes in general see ref. 12*b*) was soluble in sc. CO_2 and the corresponding copolymer **4f** was produced in 3% yield. Polymer production with polymer-supported catalyst was also possible (for preparation of alternating olefin–CO copolymers under heterogeneous conditions, e.g., see ref. 13). A cationic Pd(II) complex of polystyrene-supported (*R*,*S*)-BINAPHOS (14), complex **2c**, was treated with olefin **1f** and CO in sc. CO_2 for 72 h at 50°C. After removal of the residual monomers by filtration, the product polymer **4f** was obtained in 0.08% yield when it was separated from the catalyst polymer **2c** by extracting the filter cake with C_6F_6.

Water contact angle

Taking advantage of the hydrophobic nature of the perfluoroalkyl side chain, the water contact angle was measured for a sample of **4f** by casting on glass surface. The observed contact angle of 108° is larger than the value 96° reported by Sen (4) for a related polymer (poly[(allyl)pentafluorobenzene-*alt*-CO]). The value 108° is even comparable to that of poly(tetraflueoroethylene) (PTFE).

Experimental

General

All manipulations involving the air- and moisture-sensitive compounds were carried out using standard Schlenk techniques under an argon purified by passing through a hot column packed with BASF catalyst R3-11. Solid-state ^1H–^{13}C CP-MAS NMR at 67.94 MHz was measured by a JEOL GSX270 spectrometer. Infrared spectra were recorded by a Jasco IR810 spectrometer after mixing the polymers with Nujol. Most of reagents were purchased from Wako Pure Chemical Industries Ltd., Daikin Fine Chemical, or Aldrich Chemical Co. Inc., and were used without further purification unless otherwise specified. Solvents were purified by distillation under argon after drying over standard drying agents. Carbon monoxide (99.9%) was obtained from Teisan Co.

Alternating copolymerization of 3-perfluoroalkyl-1-propenes 1a–d with CO in CH_2Cl_2

A solution of Pd(Me)(Cl){(*R*,*S*)-BINAPHOS} (23.8 mg, 26 μmol) in CH_2Cl_2 (1.5 mL) was added to a solution of Na[B(3,5-$(CF_3)_2C_6H_3$)] (24.9 mg, 28 μmol) in MeCN (0.5 mL). After the solution was stirred at 20°C for 1 h, the solvents were removed in vacuo to give [Pd(Me)(MeCN){(*R*,*S*)-BINAPHOS}]·[B{3,5-$(CF_3)_2C_6H_3$}$_4$] (**2**). The resulting NaCl was not removed from **2**. Palladium complex **2** was dissolved in 2 mL of CH_2Cl_2 and to this, fluoroalkenes **1** (13 mmol) were added. The solution was

© 2001 NRC Canada

degassed by three freeze–thaw cycles and transferred into an autoclave. In the case of highly volatile olefin (**1a**), the olefin was directly introduced into the autoclave. The solution was stirred with a stirring bar in the atmosphere of CO at 50°C. After removal of the volatile materials in vacuo, the residual trace amounts of waxy compounds were analyzed by IR without separation of the catalyst. For the samples of runs 2–5, IR absorptions were observed both at 1710 cm^{-1} (C=O of polyketone **3b**–**d**) and 840 cm^{-1} (C—O—C of spiroketal **4b**–**d**).

Alternating copolymerization of 4-perfluoroalkyl-1-butenes 1e and 1f with CO in CH_2Cl_2

The procedure used for **1b**–**d** was employed for the copolymerization process. When reactions were completed, the CO pressure was released, and the products were reprecipitated from MeOH–CH_2Cl_2. For characterization of **4f**, solid-state ^{13}C NMR, solution-phase ^{13}C NMR (C_6F_6), and IR spectrum were taken and the charts are shown in Figs. 1(*a*), 1(*b*), and 2. Due to the limited solubility of the polymer in C_6F_6, the S/N could not be improved further. **4f**: $[\alpha]_D^{23}$ –62.9 (*c* 0.5, C_6F_6). Polymer **4e** was less soluble in C_6F_6 and was characterized by IR. Absorptions were observed both at 1710 cm^{-1} (C=O of polyketone **3e**) and 840 cm^{-1} (C—O—C of spiroketal **4e**).

Attempted copolymerization of 1f with CO in sc. CO_2 catalyzed by 2a

In a 33-mL autoclave equipped with a window, complex **2a** (4.9 μmol) was prepared by the method mentioned above. The autoclave was charged with olefin **1f** (2.5 mmol) and CO (20 atm), and then cooled down to –78°C. After introduction of liquid CO_2, the system was heated up to 50°C whereupon the total pressure reached 125 atm. The catalyst did not get dissolved and stayed at the bottom of the autoclave. The monomers were soluble in sc. CO_2. After stirring for 20 h at 50 C, the autoclave was cooled down to –78°C and the pressure was slowly released. No polymeric products were obtained.

Copolymerization of 1f with CO in sc. CO_2 catalyzed by perfluoroalkyl-substituted complex 2b

The same reaction as mentioned above was repeated with complex **2b** (0.005 mmol). The catalyst was soluble in CO_2 in this case. After 3 days at 50°C, 3% of the monomer was converted into a black waxy solid whose IR showed peaks at 1710 cm^{-1} (C=O of polyketone **3f**) and 840 cm^{-1} (C—O—C of spiroketal **4f**).

Copolymerization of 1f with CO in sc. CO_2 catalyzed by polymer-supported complex 2c

Polymer-supported (*R*,*S*)-BINAPHOS (14) (0.55 g as a polymer, corresponding to 0.10 mmol of the ligand) was allowed to swell in 5.0 mL of benzene in a Schlenk tube. To this was added a benzene (3.0 mL) solution of Pd(Me)(Cl)(cod) (0.10 mmol). After standing for 4 h at 25°C, the solvents were removed in vacuo, and the polymers were freeze-dried, washed with CH_2Cl_2 and Et_2O. Polymer-supported neutral Pd complex thus prepared was placed in a Schlenk tube and was allowed to swell in 5.0 mL of CH_2Cl_2. To this was added a solution of Na[B(3,5-$(CF_3)_2C_6H_3$)] (0.10 mmol) in MeCN (4.0 mL). The mixture was stirred for ca. 10 min and then allowed to stand for 20 h at 25°C. The solvents were removed in vacuo to produce polymer-supported cationic Pd complex **2c**. Complex **2c** was placed at the bottom of a 33-mL autoclave, equipped with a window. The autoclave was charged with a solution of **1f** (11 mmol) in C_6F_6 (5 mL) and CO (20 atm at 25°C), and then cooled down to introduce CO_2 at –78°C. At 50°C, the total pressure was 110 atm. After stirring by a stirring bar for 81 h at 50°C, the pressure was slowly released at –78°C, and then the autoclave was charged with 0.5 mL of methanol and CO (20 atm at 25°C). After stirring for 1 h at 50°C, the pressure was released, and the resulting mixture was poured into 50 mL of methanol, filtered through a Celite pad, washed with methanol and CH_2Cl_2, and then extracted with C_6F_6. The extracts were evaporated and dried under vacuum to yield **4f** as a white waxy solid (3.5 mg, 0.08% yield).

Contact angle measurement

Polymer **4f** (19.0 mg) was dissolved in C_6F_6 (0.50 mL) and an aliquot (0.1 mL) was placed on the surface of a piece of slide glass (MATSUNAMI precleaned micro slide glass, thickness 0.8 ~ 1.0 mm). The solution was spread over the glass by the aid of a gas blow (HFC 134a, OKEN Bioden gas spray)) and air-dried at room temperature. Contact angle was measured by dropping 3.5 μL of water drops on the surface. Contact angles were measured on either side of eleven drops and averaged to be 108°.

Conclusion

The olefin–CO copolymerization resulted in low conversion with monomers in which a carbon-carbon double bond and a perfluoroalkyl chain is either directly attached or separated only by one methylene group. On the other hand, when they were separated by two methylenes, the corresponding alternating copolymers were obtained in satisfactory yields. Apparently, two methylenes were required to cancel the influence of the perfluoroalkyl group upon the electronic nature of the C=C double bond. The polymers thus produced contain substantial amount of polyspiroketal structure **4** as was characterized by solid-state and solution-phase ^{13}C NMR and IR. The high density of fluorine in **4f** endowed the polyspiroketal with a hydrophilic nature. The highest level of water contact angle of 108° was observed when **4f** was cast on a glass surface. By using super critical CO_2 as a solvent, a small amount of copolymer was obtained from fluoroalkene **1f** and CO employing either a CO_2-soluble Pd complex **2b** or a polymer-supported catalyst **2c**.

Acknowledgements

We thank Dr. Tatsuya Takeguchi (Kyoto University) and Dr. Mutsuo Matsumoto (Kyoto University) for their help in measuring solid-state NMR and contact angle, respectively. Financial support from the Ministry of Education, Science, Sports and Culture, Japan, for the Grant-in-Aids for COE Research on Elements Science, no. 12CE2005 is acknowledged. We are grateful to the Integrated Study-Abroad Program between Johannes Gutenberg Universität, Mainz and Kyoto University by Deutscher Akademischer

© 2001 NRC Canada

Austauschdienst (DAAD) for its support to S.E.'s stay in Kyoto.

References

1. (*a*) A. Sen. Chemtech. **48**, (1986), and refs. cited therein; (*b*) Z. Jiang, S. Sanganeria, and A. Sen. J. Polym. Sci. Part A: Polymer Chem. **32**, 841 (1994); (*c*) P. Wong, E. Drent, A. A. Smaardijk, and A. H. Kramer. Eur. Pat. Appl. EP 322 976; Chem. Abstr. **111**, 195 667p (1989); (*d*) A. A. Smaardijk and A. H. Kramer. Eur. Pat. Appl. EP 372602; Chem. Abstr. **113**, 173 476q (1990); (*d*) Y. Watanabe, M. Takeda, J. Ookago, and S. Seo. Jpn. Kokai Tokkyo Koho JP 01 149 828; Chem. Abstr. **112**, 57 079t (1990); (*e*) C. Ito and K. Takatani. Jpn. Kokai Tokkyo Koho JP 05 339 367; Chem. Abstr. **120**, 299 571e (1994); (*f*) M. J. Green, A. R. Lucy, S. Lu, and R. M. Paton. J. Chem. Soc. Chem. Commun. 2063 (1994); (*g*) K. Nozaki, N. Kosaka, S. Muguruma, and T. Hiyama. Macromolecules, **33**, 5340 (2000).
2. S. Kacker, Z. Jiang, and A. Sen. Macromolecules, **29**, 5852 (1996).
3. K. Nozaki, Y. Kawashima, K. Nakamoto, and T. Hiyama. Polymer J. (Tokyo), **31**, 1057 (1999).
4. S. Murtuza, S. B. Harkins, and A. Sen. Macromolecules, **32**, 8697 (1999).
5. S. Di Benedetto and G. Consiglio. Helv. Chim. Acta, **80**, 2204 (1997).
6. T. Fuchikami and I. Ojima. Tetrahedron Lett. **25**, 307 (1984).
7. F. Derguini-Boumechal and G. Linstrumelle. Tetrahedron Lett. **36**, 3225 (1976).
8. (*a*) K. Nozaki, N. Sato, and H. Takaya. J. Am. Chem. Soc. **117**, 9911 (1995); (*b*) K. Nozaki, N. Sato, Y. Tonomura, M. Yasutomi, H. Takaya, T. Hiyama, T. Matsubara, and N. Koga. J. Am. Chem. Soc. **119**, 12 779 (1997).
9. Z. Jiang and A. Sen. J. Am. Chem. Soc. **117**, 4455 (1995).
10. P.G. Jessop and W. Leitner (*Editors*). Chemical synthesis using supercritical fluids. Wiley–VCH, Weinheim. 1999.
11. (*a*) J. M. DeSimone, Z. Guan, and C.S. Elsbernd. Science (Washington, D.C.), **257**, 945 (1992); (*b*) J.K. Kendall, D.A. Canelas, J.F. Young and J.M. DeSimone. Chem. Rev. **99**, 543 (1999) and refs. cited therein.
12. (*a*) W. Leitner and G. Franciò. Chem. Commun. 1663 (1999); (*b*) J.A. Darr and M. Poliakoff. Chem Rev. **99**, 495 (1999).
13. Preparation of alternating olefin-CO copolymers under heterogeneous conditions, e.g., (*a*) A. Sommazzi, G. Lugli, F. Calderazzo, D.D. Belli, and F. Garbassi. Eur. Patent Appl. EP 559 288 (1993); Chem. Abstr. **120**, 192 571c (1994); (*b*) W.P. Mul, H. Oosterbeek, G.A. Beitel, G.J. Kramer, and E. Drent. Angew. Chem. Int. Ed. **39**, 1848 (2000).
14. (*a*) K. Nozaki, Y. Itoi, F. Shibahara, E. Shirakawa, T. Ohta, H. Takaya, and T. Hiyama. J. Am. Chem. Soc. **120**, 4051 (1998); (*b*) K. Nozaki, F. Shibahara, Y. Itoi, E. Shirakawa, T. Ohta, H. Takaya, and T. Hiyama. Bull. Chem. Soc. Jpn. **72**, 1911 (1999); (*c*) K. Nozaki, F. Shibahara, T. Hiyama. Chem. Lett. 694 (2000).

© 2001 NRC Canada

Studies on transition-metal nitrido and oxo complexes. Part 20. Oxoruthenates and oxo-osmates in oxidation catalysis; *cis*-$[Os(OH)_2O_4]^{2-}$ as a catalytic oxidant for primary amines and for alcohols

William P. Griffith and Maria Suriaatmaja

Abstract: *cis*-$[Os(OH)_2O_4]^{2-}$ with $[Fe(CN)_6]^{3-}$ and other co-oxidants has been studied as a catalytic reagent for the oxidative dehydrogenation of primary aromatic and aliphatic amines to nitriles, the oxidation of primary alcohols to carboxylic acids and of secondary alcohols to ketones. Electronic and Raman spectroscopy have been used to elucidate the nature of the oxoruthenates and oxo-osmates present in a number of reported organic oxidations catalyzed by ruthenium and osmium species.

Key words: oxidation catalysis, ruthenium, osmium, amine dehydrogenation, alcohol oxidation.

Résumé : On a évalué les possibilités d'utiliser le *cis*-$[Os(OH)_2O_4]^{2-}$, avec le $[Fe(CN)_6]^{2-}$ ou d'autres cooxydants, comme réactif catalytique pour la déshydrogénation oxydante d'amines aromatiques et aliphatiques primaires en nitriles, pour l'oxydation d'alcools primaires en acides carboxyliques et d'alcools secondaires en cétones. On a fait appel aux spectroscopies électronique et Raman pour élucider la nature des oxoruthénates et oxo-osmates présents dans un certain nombre de réactions d'oxydations connues, catalysées par des espèces contenant du ruthénium et de l'osmium.

Mots clés : oxydation, catalyse, ruthénium, osmium, déshydrogénation d'amine, oxydation d'alcool.

[Traduit par la Rédaction]

Introduction

Homogeneous oxidation reactions catalyzed by transition metal complexes are a subject of much current interest, and those catalyzed by ruthenium and osmium complexes have been much studied in recent years (for Part 19 see ref. 1) (2, 3). The reagent *trans*-$[Ru^{VI}(OH)_2O_3]^{2-}$ – $S_2O_8^{2-}$ is effective in aqueous base for a fairly unusual catalyzed reaction, the oxidative dehydrogenation of primary amines to nitriles at room temperatures (4), a reaction also studied by the dedicatee of this paper using ruthenium porphyrinato complexes (5). We have reported that *cis*-$[Os^{VIII}(OH)_2O_4]^{2-}$ – $[Fe(CN)_6]^{3-}$ in aqueous base at room temperatures will oxidize primary alcohols and primary alkyl halides to aldehydes (6). Here we show that *cis*-$[Os(OH)_2O_4]^{2-}$ – $[Fe(CN)_6]^{3-}$ is, in the presence of CH_3CN, comparable in efficacy with *trans*-$[Ru(OH)_2O_3]^{2-}$ – $S_2O_8^{2-}$ for oxidative amine dehydrogenation, and is much more effective for the oxidations of secondary alcohols than we had previously observed (6) in the absence of CH_3CN.

A second purpose of this paper is to use spectroscopic methods, principally electronic spectroscopy but also Raman solution studies, to establish the nature of the active catalytic intermediates, or their precursors, in systems described in a number of reports of organic oxidations catalyzed by ruthenium and osmim complexes with a variety of co-oxidants. Since in some cases the procedures are used for organic preparations a knowledge of the nature of the catalyst (or its active precursor) is of value.

Received August 30, 2000. Published on the NRC Research Press Web site at http://canjchem.nrc.ca on May 30, 2001.

This paper is dedicated to Brian James, a good friend for many years and a continuing source of inspiration for his catalytic and ruthenium work in particular, on the occasion of his 65th birthday.

W.P. Griffith[1] and M. Suriaatmaja. Department of Chemistry, Imperial College of Science, Technology and Medicine, London SW7 2AY, U.K.

[1]Corresponding author (telephone: +0207 594 475 9; fax: +0207 594 580 4; e-mail: w.griffith@ic.ac.uk).

Results and discussion

I. Oxidations catalyzed by *cis*-$[Os^{VIII}(OH)_2O_4]^{2-}$ with $[Fe(CN)_6]^{3-}$ and other co-oxidants

(i) Oxidative dehydrogenation of primary amines

In earlier work we attempted, with very limited success, to use *cis*-$[Os(OH)_2O_4]^{2-}$ with $S_2O_8^{2-}$, BrO_3^-, and $[Fe(CN)_6]^{3-}$ as co-oxidants for the oxidative dehydrogenation of amines to nitriles (6). Here we examine the utility of *cis*-$[Os(OH)_2O_4]^{2-}$ as a catalyst for the oxidative dehydrogenation of primary amines to nitriles with a variety of co-oxidants in the presence of CH_3CN. Acetonitrile is

 DOI: 10.1139/cjc-79-5/6-598 © 2001 NRC Canada

Table 1. Oxidative dehydrogenation of primary amines to nitriles by *cis*-$[Os^{VIII}(OH)_2O_4]^{2-}$ – $[Fe(CN)_6]^{3-}$.

Substrate	Product	Yield (%) [Turnover]	Time (h)
Benzylamine	Benzonitrile	94 [24]	2
4-Methoxybenzylamine	4-Methoxybenzonitrile	81 [21]	1.5
2-Chlorobenzylamine	2-Chlorobenzonitrile	75 [19]	1.5
4-Chlorobenzylamine	4-Chlorobenzonitrile	74 [19]	1.5
2-Bromobenzylamine·HCl	2-Bromobenzonitrile	82 [21]	1.5
3-Bromobenzylamine·HCl	3-Bromobenzonitrile	80 [20]	1.5
4-Bromobenzylamine·HCl	4-Bromobenzonitrile	80 [20]	1.5
Octylamine	Octanenitrile	84 [22]	1.5
With BrO_3^- co-oxidant the following were obtained:			
Benzylamine	Benzonitrile	51 [13]	2
Octylamine	Octanenitrile	63 [16]	2

Note: Conditions: 2 mmol of the amine in 25 cm^3 of the *cis*-$[Os^{VIII}(OH)_2O_4]^{2-}$ – $[Fe(CN)_6]^{3-}$ or the *cis*-$[Os^{VIII}(OH)_2O_4]^{2-}$ – BrO_3^- reagent, each with 5 cm^3 of CH_3CN at room temperature.

known to improve yields in a number of ruthenium-catalyzed reactions (7, 8).

We tried the three co-oxidants used previously with *cis*-$[Os(OH)_2O_4]^{2-}$, viz. $S_2O_8^{2-}$, BrO_3^-, and $[Fe(CN)_6]^{3-}$. Persulfate gave rather poor yields of nitriles (ca. 15%) as was the case with *trans*-$[Ru(OH)_2O_3]^{2-}$ with $S_2O_8^{2-}$ (4). Ferricyanide gave the best results while bromate was of intermediate efficiency (Table 1). The success of $[Fe(CN)_6]^{3-}$ is perhaps not surprising since with *cis*-$[Os^{VIII}(OH)_2O_4]^{2-}$ for oxidation of alcohols, aldehydes, and alkyl halides it was the most effective co-oxidant (6) (and the related *trans*-$[OS^{VI}O_2(OH)_4]^{2-}$ is widely used in the asymmetric *cis*-hydroxylation of alkenes (3, 9)). Results in terms of product yields, turnovers and times for amine dehydrogenations by *cis*-$[Os(OH)_2O_4]^{2-}$ – $[Fe(CN)_6]^{3-}$ are comparable with those found (4) for *trans*-$[Ru(OH)_2O_3]^{2-}$ – $S_2O_8^{2-}$.

In the absence of $[Fe(CN)_6]^{3-}$, addition of benzylamine to the orange *cis*-$[Os(OH)_2O_4]^{2-}$ in base gives an immediate purple colour of *trans*-$[OsO_2(OH)_4]^{2-}$, identified by its electronic spectrum. Reaction of *trans*-$[Ru(OH)_2O_3]^{2-}$ with benzylamine gave a transient green amine complex (4), but there is no evidence of such a species being formed with *cis*-$[Os(OH)_2O_4]^{2-}$ or *trans*-$[OsO_2(OH)_4]^{2-}$. In the presence of excess $[Fe(CN)_6]^{3-}$ with *cis*-$[Os(OH)_2O_4]^{2-}$ in base the colour darkens on addition of amine, but when the reaction is complete the original orange returns, so the reagent is self-indicating. Comparisons of the electronic spectra of $[Fe(CN)_6]^{3-}$ and of a mixture of $[Fe(CN)_6]^{3-}$ with *cis*-$[Os(OH)_2O_4]^{2-}$ in molar NaOH show, in addition to bands due to $[Fe(CN)_6]^{3-}$, maxima at 225, 325, and 380 nm due to *cis*-$[Os(OH)_2O_4]^{2-}$. Raman spectra of a similar mixture show the symmetric Os=O stretch (ν^s (OsO_4)) of *cis*-$[Os(OH)_2O_4]^{2-}$ known[2] to lie at 915 cm^{-1} in addition to bands from $[Fe(CN)_6]^{3-}$. Electronic spectra also show that excess $[Fe(CN)_6]^{3-}$ with *trans*-$[Os^{VI}O_2(OH)_4]^{2-}$ gives *cis*-$[Os^{VIII}(OH)_2O_4]^{2-}$, as shown by appearance of bands due to the latter at 325 and 380 nm, and again Raman spectra confirm this by the appearance of the same 915 cm^{-1} band. It thus seems clear that $[Fe(CN)_6]^{3-}$ oxidizes *trans*-$[OsO_2(OH)_4]^{2-}$ to *cis*-$[Os(OH)_2O_4]^{2-}$, and we conclude that this is the effective catalyst precursor in the system.

As indicated above the yields of nitriles are much improved by addition of CH_3CN. It has long been known that acetonitrile substantially improves yields, selectivities, and catalytic turnovers in ruthenium-catalyzed reactions (7), and we have recently observed a similar effect in the $RuCl_3.nH_2O$–$IO(OH)_5$ system for alkene and alkyne cleavage (8). The action of CH_3CN is not clear; Sharpless and co-workers (7) have suggested, in the case of ruthenium complexes, that CH_3CN, itself resistant to oxidation, may stabilize intermediate lower oxidation states of ruthenium involved in the catalytic cycle, and it is possible that there is a similar effect with osmium.

Attempts were made to use *N*-methylmorpholine-*N*-oxide (nmo) as a co-oxidant since this is very effective in nonaqueous solutions for alcohol oxidations with $[RuO_4]^-$ (10, 11). Although some oxidation of 4-methoxybenzylamine to the nitrile was observed, black OsO_2 was formed during the reaction, so such dehydrogenation as did occur was probably via a heterogeneously catalyzed route. With hypochlorite as co-oxidant primary aromatic amines gave only ca. 15% of nitriles. GC–MS studies on the oxidation products of benzylamine, 2-methoxy-, 2-methyl-, 4-methylbenzylamine, and octylamine showed in all cases a clean conversion to the nitrile. For benzylamine no formation of the imine ($PhCH_2N{=}CHPh$) was observed, though this was a significant side-product (4) in the oxidation of benzylamine by *trans*-$[Ru(OH)_2O_3]^{2-}$ – $S_2O_8^{2-}$.

(ii) Oxidation of primary and secondary alcohols

Our earlier use of *cis*-$[Os(OH)_2O_4]^{2-}$ as a catalyst for alcohol oxidations with $[Fe(CN)_6]^{3-}$, BrO_3^-, and $S_2O_8^{2-}$ as co-oxidants showed that $Fe(CN)_6]^{3-}$ was the most efficient co-oxidant, but no acetonitrile was added to the reaction mixture (6). In the presence of CH_3CN (Table 2) we again find that $[Fe(CN)_6]^{3-}$ is the most effective co-oxidant, and secondary alcohols (found to give relatively poor yields of ketones in our earlier work in the absence of acetonitrile (6))

[2] A.M. El-Hendawy, W.P. Griffith, M. Suriaatmaja. To be submitted.

© 2001 NRC Canada

Table 2. Oxidations of alcohols by *cis*-$[Os^{VIII}(OH)_2O_4]^{2-}$ – $[Fe(CN)_6]^{3-}$.

Substrate	Product	Yield (%) [Turnover]	Time (h)
Benzyl alcohol	Benzoic acid	81 [21]	2
1-Hexanol	1-Hexanoic acid	70 [18]	2
Cyclopentanol	Cyclopentanone	>99 [25]	2
Cylohexanol	Cyclohexanone	66 [17]	0.5
Cylohexanol	Cyclohexanone	69 [18]	1
Cylohexanol	Cyclohexanone	>99 [25]	2
Cycloheptanol	Cycloheptanone	>99 [25]	2
Cyclooctanol	Cyclooctanone	>99 [25]	2
2-Hexanol	2-Hexanone	>99 [25]	2
2-Octanol	2-Octanone	90 [23]	0.5
2-Octanol	2-Octanone	>99 [25]	2
4-Methylcyclohexanol	4-Methylcyclohexanone	>99[25]	2
Citronellol	Citronellal	90 [24]	2
Geraniol	Citral	91 [24]	2

Note: Conditions: 2 mmol of the alcohol in 25 cm^3 of the *cis*-$[Os^{VIII}(OH)_2O_4]^{2-}$ – $[Fe(CN)_6]^3$ reagent with 25 cm^3 of CH_3CN at room temperature.

gave good yields and turnovers if CH_3CN is used. Thus cyclopentanol, cyclohexanol, cycloheptanol, cyclooctanol, 2-methyl-cyclohexanol, 2-hexanol, and 2-octanol give the corresponding ketones in >99% yield with catalytic turnovers of ca. 25 over a two-hour period. With primary alcohols however, the yields and turnovers of carboxylic acids are only slightly improved by addition of acetonitrile. Unsaturated alcohols (citronellol, geraniol) do not suffer competing double bond cleavage and give the corresponding unsaturated aldehydes in good yield. The same colour changes as with amines are observed when alcohols are added to orange *cis*-$[Os(OH)_2O_4]^{2-}$ in base, without and with $[Fe(CN)_6]^{3-}$.

II. Identification of ruthenium and osmium catalyst precursors in published oxidation procedures

Over the past 20 years there have been numerous reports on oxidations catalyzed by ruthenium and, in a smaller number of cases, osmium complexes. Usually $RuCl_3 \cdot nH_2O$ or OsO_4 are the reagents initially used, but there is often doubt about the nature of the species involved in the catalysis. We have tried (Table 3) to establish the nature of such species by measuring the electronic and, in some cases, Raman spectra of the solutions used in typical literature reports. Often, particularly in kinetic studies, a range of concentrations was used by the original investigators. We have used conditions typical of these and they are listed (catalyst and its concentration, co-oxidant, substrate, solvent and solutes, pH). In the last two columns of Table 3 the active catalyst precursor is given as suggested by the literature and that which we favour from spectra which we have measured of the reaction solutions. Occasionally our catalyst concentrations differ from those in the cited publications to be able to obtain reasonable spectra.

In most cases the ruthenium precursors are likely to be the oxo species ruthenium tetroxide ($Ru^{VIII}O_4$), perruthenate ($[Ru^{VII}O_4]^-$), or ruthenate (*trans*-$[Ru^{VI}(OH)_2O_3]^{2-}$); these are easily distinguished by their electronic (13–15) or Raman[2] (15, 16) spectra. For the osmium-catalyzed reactions, likely intermediates are osmium tetroxide ($Os^{VIII}O_4$), perosmate (*cis*-$[Os^{VIII}(OH)_2O_4]^{2-}$), or osmate (*trans*-$[Os^{VI}O_2(OH)_4]^{2-}$). These can be distinguished by their electronic (17–19) or Raman[2] (6, 15) spectra, and here again we use electronic spectra to help in the identification of such species in published procedures. An earlier paper of ours (20) covered some literature for oxoruthenate but not oxo-osmate species up to 1994.

A. Oxidations with ruthenium catalysts

(i) Electronic spectra of oxoruthenates

In Fig. 1 we reproduce the electronic spectra of: (*a*) RuO_4, (*b*) $[RuO_4]^-$, and (*c*) of *trans*-$[Ru(OH)_2O_3]^{2-}$ in aqueous media; they are close to those reported earlier for all three species (12), for $[RuO_4]^-$ (13), and of *trans*-$[Ru(OH)_2O_3]^{2-}$ (13, 14).

(ii) Hypochlorite as co-oxidant

Recently Mills and Holland (21) studied the oxidation of 2-octanol to 2-octanone by RuO_4 using ClO^- as co-oxidant, and gave a speciation diagram for the oxoruthenates produced from RuO_4 at different pH. From pH 5–7 RuO_4 is the predominant species, $[RuO_4]^-$ from pH 7.5–10.5, and *trans*-$[Ru(OH)_2O_3]^{2-}$ at higher pH, essentially in agreement with the classic work of Connick and Hurley (12)). They noted for oxoruthenates in hypochlorite solutions that, although at pH 11–14 the orange *trans*-$[Ru(OH)_2O_3]^{2-}$ might be expected to be present, in fact the yellow-green $[RuO_4]^-$ is the predominant species. This was ascribed to a kinetic effect, the oxidation of *trans*-$[Ru^{VI}(OH)_2O_3]^{2-}$ to $[Ru^{VII}O_4]^-$ by ClO^- being much more rapid than the reduction of RuO_4 to *trans*-$[Ru^{VI}(OH)_2O_3]^{2-}$ by OH^-, unless the pH is very high (>5 M OH^-). However, they did not show spectroscopically that $[RuO_4]^-$ is present in such hypochlorite solutions. Here we demonstrate both with electronic and Raman spectroscopies that this is the case.

In Table 3 (entries 1–7 (22–26)) we list a number of ruthenium-catalyzed oxidations with hypochlorite, all used as preparative methods and thus of particular interest. The electronic spectra of both aqueous and organic layers were mea-

© 2001 NRC Canada

Table 3. Oxidation reactions catalyzed by ruthenium and osmium complexes.

No.	Precursor (mmol dm^{-3})	Co-oxidant (mol dm^{-3})	Substrate	Solvent[a]	Aqueous solute (mol dm^{-3})	pH measured	Claimed catalyst	Actual catalyst[b]	Ref.
1	$RuCl_3 \cdot nH_2O$ (0.4)	NaOCl (0.3)	1-Pentadecene	aq–CH_2Cl_2	NaOH (0.8)	14	RuO_4	$[RuO_4]^-$	(22)
2	$RuCl_3 \cdot nH_2O$ (3.4)	NaOCl (0.3)	Methylbenzenes	aq–DCE	—	13	RuO_4	$[RuO_4]^-$	(23)
3	$RuCl_3 \cdot nH_2O$ (1.0)	NaOCl (0.3)	Epoxybornane	aq–CH_3CN–CCl_4	—	13	RuO_4	$[RuO_4]^-$	(24)
4	RuCl3·nH_2O (0.4)	NaOCl (0.3)	1-Decanol	aq–CCl_4	—	13	$[RuO_4]^-$	$[RuO_4]^-$	(25)
5	$RuCl_3 \cdot nH_2O$ (2.5)[c]	NaOCl (0.3)	1-Decanol	aq–CCl_4	—	13	$[RuO_4]^-$	$[RuO_4]^-$	(25)
6	$RuCl_3 \cdot nH_2O$ (5.2)	NaOCl (0.3)	Cyclopentene	aq–CCl_4	NaOH (1)	14	$[RuO_4]^{2-}$	$[RuO_4]^-$	(26)
7	$RuCl_3 \cdot nH_2O$ (0.4)	$Ca(OCl)_2$ (0.3)	Alcohols	aq–CH_3CN	—	13	—	$[RuO_4]^-$	(27)
8	$RuCl_3 \cdot nH_2O$ (1.1)	$NaIO_4$ (0.2)	Epoxybornane	aq–CH_3CN–CCl_4	—	7	RuO_4	RuO_4	(24)
9	$RuCl_3 \cdot nH_2O$ (0.4)	$NaIO_4$ (0.3)	Alcohols	aq–CH_3CN	—	7	—	RuO_4	(27)
10	$RuCl_3 \cdot nH_2O$ (0.4)	$NaIO_4$ (0.04)	DMF	aq	NaOH (0.02)	12	Ru^I/Ru^{III}	RuO_4	(31)
11	$RuCl_3 \cdot nH_2O$ (0.05)	$NaIO_4$ (0.1)	Acetaldehyde	aq	NaOH (0.1)	13	Ru^I/Ru^{III}	$[RuO_2(HIO_6)_2]^{6-}$	(32)
12	$RuCl_3 \cdot nH_2O$ (0.4)	$KBrO_3$ (0.1)	Bordeaux	aq	H_2SO_4 (1) – K_2SO_4 (0.5)	3	—	RuO_4	(33)
13	$[Ru(OH)_2O_3]^{2-}$ (0.2)	$KBrO_3$ (0.014)	Cyclopentanol	aq	NaOH (0.4)	13	$[RuO_4]^{2-}$	$[Ru(OH)_2O_3]^{2-}$	(34)
14	$RuCl_3 \cdot nH_2O$ (0.24)	$K_3(Fe(CN)_6)$ (0.2)	Ethanediol	aq	NaOH (3)	14	Ru^{III}	Ru^{III}	(36)
15	$RuCl_3 \cdot nH_2O$ (0.3)	$K_3(Fe(CN)_6)$ (1)	Propan-2-ol	aq	NaOH (0.2)	13	Ru^{III}	Ru^{III}	(37)
16	$RuCl_3 \cdot nH_2O$ (0.3)	$K_3(Fe(CN)_6)$ (1)	Hexyleneglycol	aq	NaOH (0.1)	13	Ru^{III}	Ru^{III}	(38)
17	$RuCl_3 \cdot nH_2O$ (0.06)	$Ce(SO_4)_2$ (0.04)	Butyric acid	aq	H_2SO_4 (1)	1	Ru^{III}-complex	See text	(39)
18	$RuCl_3 \cdot nH_2O$ (1.78)	$Ce(SO_4)_2$ (0.01)	DMSO	aq	H_2SO_4 (0.8)	1	Ru^{III}-complex	See text	(40)
19	OsO_4 (0.8)	—	Sugars	aq	NaOH (0.1)	13	$[Os(OH)_2O_4]^{2-}$	$[Os(OH)_2O_4]^{2-}$	(43)
20	OsO_4 (6)	NaOCl (0.3)	Oleate	aq	NaOH(0.8)	13	—	$[Os(OH)_2O_4]^{2-}$	(44)
21	OsO_4 (0.45)	$NaIO_4$ (0.01)	Acetaldehyde	aq	NaOH (1)	14	??	$[Os(OH)_2O_4]^{2-}$	(27)
22	OsO_4 (0.35)	$NaIO_4$ (0.04)	DMF	aq	NaOH (2)	14	$[Os(OH)_2O_4]^{2-}$	$[Os(OH)_2O_4]^{2-}$	(46)
23	OsO_4 (0.45)	$NaIO_4$ (0.04)	Allylalcohol	aq	NaOH (1)	14	$[Os(OH)_2O_4]^{2-}$	$[Os(OH)_2O_4]^{2-}$	(47)
24	OsO_4 (4.7×10^{-4})	$K_3(Fe(CN)_6)$ (0.2)	2-Bromopropionate	aq	NaOH (1)	14	Os^{VIII}	$[Os(OH)_2O_4]^{2-}$	(48)
25	OsO_4 (0.7)	$K_3(Fe(CN)_6)$ (0.01) (0.2)	Tartrate	aq	NaOH (3.3)	14	Os^{VI}-complex	$[Os(OH)_2O_4]^{2-}$	(49)
26	$RuCl_3 \cdot nH_2O$ (0.45) + OsO_4 (0.45)	$NaIO_4$ (0.1)	Allyalcohol	aq	NaOH (0.5)	14	See text	See text	(47)
27	$RuCl_3 \cdot nH_2O$ (0.7) + OsO_4 (0.7)	$NaIO_4$ (0.1)	Acetaldehyde	aq	NaOH (0.1)	13	See text	See text	(50)

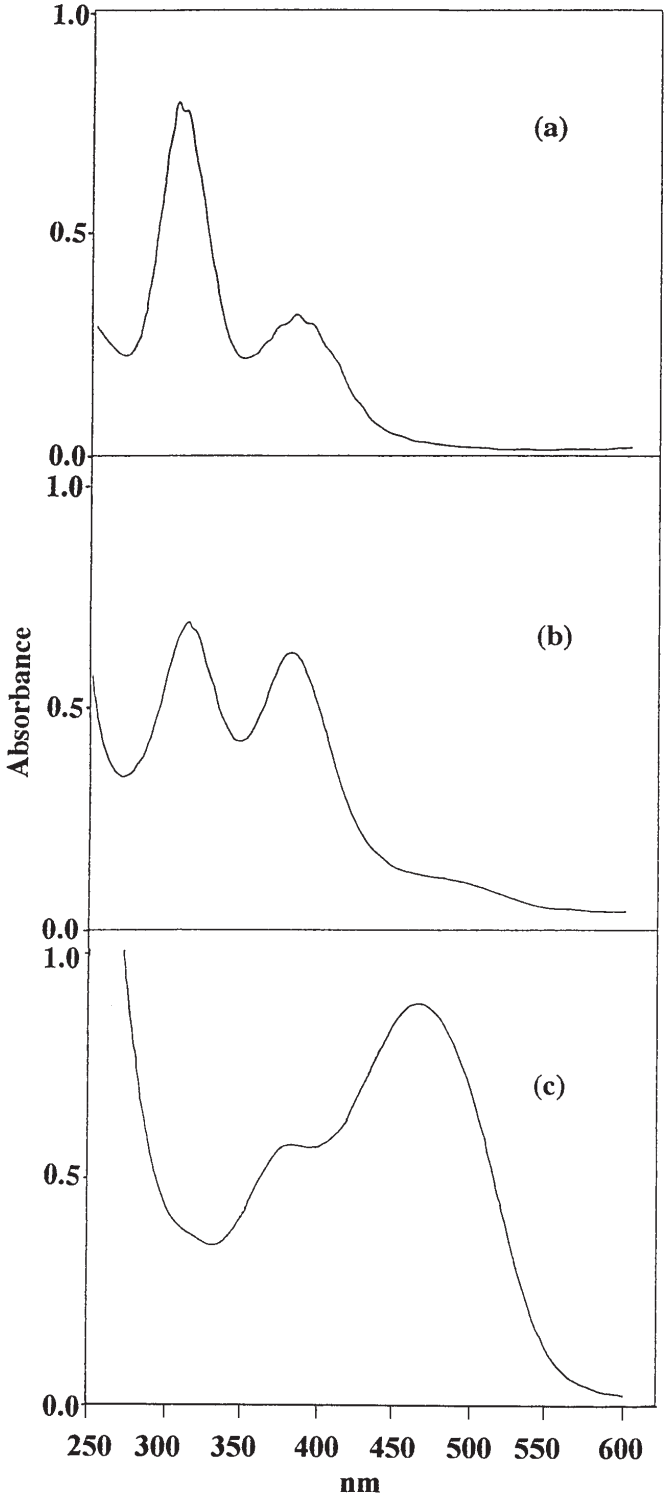
[a]Electronic spectra of aqueous layer measured at 60°C.

[b]Species present in aqueous layer according to electronic spectra.

[c]Electronic spectra of aqueous layer measured at room temperature.

© 2001 NRC Canada

Fig. 1. Electronic spectra in aqueous solutions of: (*a*) RuO_4 in water at pH 7 (ca. 2.6×10^{-4} M RuO_4); (*b*) $[Ru^{VII}O_4]^-$ in water at pH 10; 0.09 g dm^{-3} (3.5×10^{-4} M) $RuCl_3 \cdot 3H_2O$ in 0.2 M $NaBrO_3$ and molar Na_2CO_3; (*c*) *trans*-$[Ru^{VI}(OH)_2(O_3]^{2-}$ in water at pH 14; 0.15 g dm^{-3} (6×10^{-4} M) $RuCl_3 \cdot 3H_2O$ in 0.05 M $K_2S_2O_8$ and molar KOH.



sured. In the organic solvent RuO_4 is always present, clearly shown by its bands at 315 and 385 nm with attendant vibrational fine structure particularly for the 385 nm band. The aqueous layer could contain RuO_4, $[RuO_4]^-$ or *trans*-$[Ru(OH)_2O_3]^{2-}$, depending on the pH. Unfortunately for such layers the electronic spectrum of ClO^- obscures the 315 nm band and part of the 385 nm band of $[RuO_4]^-$. Nevertheless the latter is visible as a shoulder without the fine structure always observed on this band for RuO_4, as well as the weak shoulder near 480 nm present in the spectrum of $[RuO_4]^-$ but not RuO_4. Study of the Raman spectra of more concentrated solutions of $RuCl_3 \cdot nH_2O$ (0.01 M) in 0.3 M hypochlorite clearly show the ν^s (RuO_4) band of $[RuO_4]^-$ at 853 cm^{-1}, close to the literature values for this mode in the perruthenate ion (15, 16).

For entries 1 and 2, RuO_4 was suggested as the oxidant (22, 23), but certainly for the aqueous layers our electronic spectra showed $[RuO_4]^-$ to be present, although no phase-transfer reagent was used in our measurements. For entries 3 (24), 4, and 5 (25) the pH of the aqueous layers are 13 and our electronic spectra show that they contain $[RuO_4]^-$ rather than the RuO_4 which we had earlier suggested (20). For the solution at 60°C this is still the case for entry 5. For entry 6 (26) $[RuO_4]^-$ is clearly present rather than the claimed "$[RuO_4]^{2-}$".

In entry 7 $Ca(OCl)_2$ is used in a small quantity of concentrated water – CH_3CN (27). Little of the co-oxidant dissolves under the conditions described and the mixture separates into two layers. The upper, predominantly acetonitrile, layer contains RuO_4 and the lower, predominantly aqueous layer $[RuO_4]^-$.

Thus in all the solutions studied with hypochlorite as the co-oxidant we observe $[RuO_4]^-$ in the aqueous layer and RuO_4 in the organic layer ($[RuO_4]^-$, being a charged species, does not extract into the organic layer in the absence of a phase-transfer agent).

(iii) With periodate as co-oxidant

We have isolated salts of *trans*-$[Ru^{VI}O_2\{I(OH)O_5\}_2]^{6-}$ from reaction of $RuCl_3 \cdot nH_2O$ with periodates and persulfate (28, 29) and have shown that with excess periodate these function as catalysts for the oxidation of primary alcohols and alkyl halides to carboxylic acids, and for secondary alcohols and halides to ketones (29). The X-ray crystal structure of *trans*-$NaK_5[Ru^{VI}O_2\{I(OH)O_5\}_2] \cdot 8H_2O$ was determined (28), and the electronic spectrum of *trans*-$[RuO_2\{I(OH)O_5\}_2]^{6-}$ in aqueous base has bands at 221 and 389 nm (29). Rozovskii et al. (30) have proposed the formation of a ruthenium(VII) periodato complex from *trans*-$[Ru(OH)_2O_3]^{2-}$ and periodate in base (0.04–2 M KOH) and such a species, possibly *trans*-$[Ru^{VII}O_2\{I(OHO)O_5\}_2]^{5-}$, seems to be associated with a band near 380 nm.

For those oxidations effected in neutral solution (entries 8, 9 (24, 27)) it is clear that RuO_4 is produced, as expected. At 60°C, at which some of these oxidations (entry 8) were conducted (24), electronic spectra show that there is surprisingly still some RuO_4 remaining in both layers. Raman spectra also show, in addition to bands due to $(IO_4)^-$, the ν^s (RuO_4) and ν^{as} (RuO_4) bands at 883 and 915 cm^{-1}, in agreement with the literature data (15).

At high pH (entries 10 and 11 (31, 32)) problems arise from the very low solubilities of $NaIO_4$ or KIO_4 at such pH. We observe inflections in the electronic spectra of the

© 2001 NRC Canada

solutions near 380 nm which could well arise from *trans*-$[RuO_2\{I(OH)O_5\}_2]^{6-}$ which has a band near this wavelength and is an effective catalytic oxidant with periodate as co-oxidant (29). Unfortunately, Raman spectra could not be recorded owing to the low concentrations at this pH. We believe the effective oxidation precursor to be the periodato species abbreviated as $[RuO_2(HIO_6)_2]^{6-}$ in Table 3.

(iv) With bromate and iodate as co-oxidant

Aqueous bromate is an effective co-oxidant at pH 10 for $[RuO_4]^-$ and *trans*-$[Ru(OH)_2O_3]^{2-}$ at pH 14 (13). For entry 12 our electronic spectra show that RuO_4 is produced, as expected, since the pH ~ 7. The substrate was "Bordeaux" (disodium-2-hydroxy-4-(1-naphthylazo)-naphthalen-3,6-disulphonate) being oxidized to an unspecified product; the effective oxidant was not identified (33). Raman spectra also show the ν^s (RuO_4) and ν^{as} (RuO_4) bands of RuO_4 at 883 and 915 cm^{-1} in addition to those due to bromate. Entry 13 involves the initial use of *trans*-$[Ru(OH)_2O_3]^{2-}$ (incorrectly formulated in (34) as $[RuO_4]^{2-}$) with BrO_3^- in 0.01 M OH^-. Bands in the electronic spectra at 385 and 460 nm show that *trans*-$[Ru(OH)_2O_3]^{2-}$ is indeed the effective oxidant precursor.

There are references to the use of iodate (IO_3^-) as a co-oxidant with $RuCl_3{\cdot}nH_2O$ as the catalyst for kinetic data on certain oxidations (35). However, under the conditions reported, we found no evidence of electronic spectral change on addition of iodate to $RuCl_3{\cdot}nH_2O$.

(v) With ferricyanide as co-oxidant

We have shown the viability of using $[Fe(CN)_6]^{3-}$ on a preparative scale for the oxidation of primary alcohols to aldehydes and carboxylic acids and for secondary alcohols to ketones with *trans*-$[Ru(OH)_2O_3]^{2-}$ as the catalyst (20) and, above (section I), with *cis*-$[Os(OH)_2O_4]^{2-}$. Three recent reports concern oxidations with $RuCl_3{\cdot}nH_2O$ with $[Fe(CN)_6]^{3-}$ as co-oxidant (entries 14–16). As before (20), there is no evidence of formation of oxoruthenates in such mixtures in the absence of organic substrate. It is likely, as the authors suggest (36–38), that a ruthenium(III) species is responsible for the catalysis.

(vi) With cerium(IV) sulfate

With cerium(IV) sulfate as co-oxidant and $RuCl_3{\cdot}nH_2O$ (entries 17, 18 (39, 40)) a strong electronic absorption at 315 nm in the aqueous layer is observed, but extraction of the solutions with CCl_4 shows RuO_4 to be present in the organic layer. It may be that the band at 315 nm arises from a ruthenium(IV) chloro-aquo complex, the existence of which was suggested by Giddings and Mills (41) from their studies on cerium(IV) sulfate at pH 5 with $RuO_2{\cdot}nH_2O$.

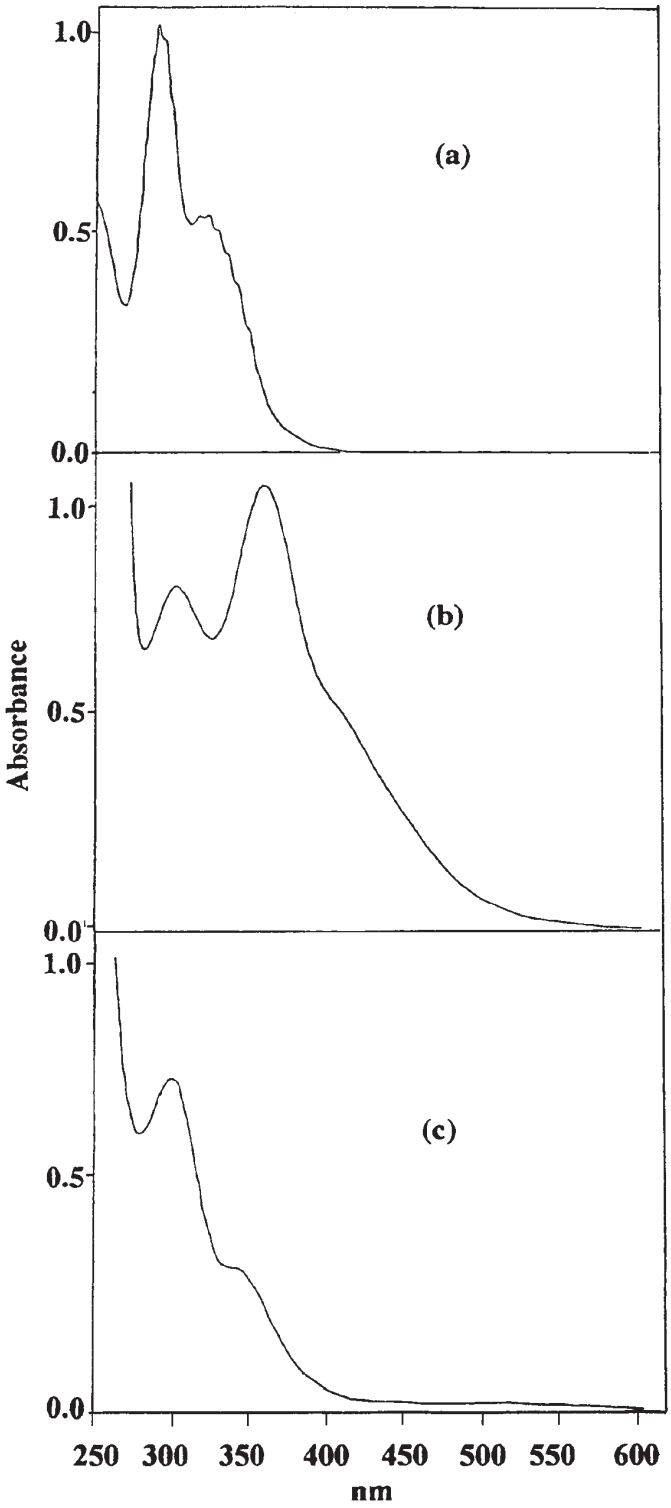
B. Oxidations reported catalyzed by osmium complexes

There is an early but comprehensive review of reactions catalyzed by OsO_4 in base by a variety of co-oxidants (42).

(i) Electronic spectra of oxo-osmates

In Fig. 2 we give the spectra of: (*a*) OsO_4, (*b*) *cis*-$[Os^{VIII}(OH)_2O_4]^{2-}$, and (*c*) *trans*-$[Os^{VI}O_2(OH)_4]^{2-}$; again these are close to those reported for these species (17–19). No molar extinction coefficients (ε) values have been given in the literature (17) for OsO_4 in aqueous solution, but for the 251 and 288 nm bands we measured the ε values to be 1905 and 1048 mol^{-1} cm^{-1}, respectively. For *trans*-$[Os^{VI}O_2(OH)_4]^{2-}$ we measured the spectrum of a known

Fig. 2. Electronic spectra in aqueous solutions of: (*a*) $Os^{VIII}O_4$ in water at pH 7 (0.13 g dm^{-3} (5.2×10^{-4} M) OsO_4); (*b*) *cis*-$[Os^{VIII}(OH)_2O_4]^{2-}$ (0.11 g dm^{-3} (4.5×10^{-4} M) OsO_4 in molar NaOH); (*c*) *trans*-$[Os^{VI}O_2(OH)_4]^{2-}$ (0.165 g dm^{-3} (4.5×10^{-4} M) *trans*-$K_2[OsO_2(OH)_4$ in 0.1 M NaOH).



© 2001 NRC Canada

amount of *trans*-$K_2[Os^{VI}O_2(OH)_4]^{2-}$ dissolved in 0.1 M NaOH. Essentially identical spectra were obtained by reduction of *cis*-$[Os^{VIII}(OH)_2O_4]^{2-}$ in molar KOH with 2-propanol.

(ii) Oxidations by OsO_4 with no co-oxidant

Entry 19 concerns stoichiometric oxidations by OsO_4 in base. *cis*-$[Os(OH)_2O_4]^{2-}$ was suggested as the catalyst precursor (43) and our spectra, showing bands at 325 and 375 nm, confirm this.

(iii) Oxidations with hypochlorite as co-oxidant

Foglia et al. (44) report oxidations with OsO_4 in alkaline hypochlorite (entry 20) and implied that OsO_4 is the active species. We observe a shoulder at 380 nm which probably arises from *cis*-$[Os(OH)_2O_4]^{2-}$ which has a band here (its 300 nm band would be obscured by absorption from hypochlorite).

(iv) With periodate as co-oxidant

The complex *trans*-$Na_6[Os^{VI}O_2\{I(OH)O_5\}_2]\cdot 18H_2O$ is made from *trans*-$K_2[OsO_2(OH)_4]$ and $NaIO_4$ in NaOH (45). Its electronic spectrum in aqueous base shows bands at 325 and 385 nm and it functions as a catalyst, with periodate as co-oxidant, for the oxidation of primary alcohols and alkyl halides to carboxylic acids and of secondary alcohols to ketones (29).

For entries 21–23 (27, 46, 47) in which oxidations are carried out at high pH our electronic spectra show a clearly pronounced shoulder at 380 nm which could arise either from *trans*-$[Os^{VI}O_2\{I(OH)O_5\}_2]^{6-}$ or *cis*-$[Os(OH)_2O_4]^{2-}$. We think it likely that, from the known ease of oxidation of osmium(VI) to (VIII), that the latter is the more likely effective catalyst precursor. Again, as was the case with the analogous ruthenium system, low solubilities prevent Raman spectra being obtained.

(v) With ferricyanide as co-oxidant

The use of $[Fe(CN)_6]^{3-}$ with *trans*-$[Os^{VI}O_2(OH)_4]^{2-}$ at pH 10 is common in organic synthesis for the *cis*-hydroxylation of alkenes (3, 9); in our earlier work (6) we showed that *cis*-$[Os^{VIII}(OH)_2O_4]^{2-}$ is not present in such mixtures at that pH. In entries 24 and 25 (48, 49) the oxidations were carried out at high pH, and our electronic spectra show a band at 325 nm in addition to bands due to $[Fe(CN)_6]^{3-}$. We ascribe this (as discussed above in section I) to *cis*-$[Os(OH)_2O_4]^{2-}$; the 380 nm band of the latter is obscured by the broad 425 nm band of $[Fe(CN)_6]^{3-}$. The Raman data alluded to above also suggest that that *cis*-$[Os(OH)_2O_4]^{2-}$ is present in these mixtures.

C. Oxidations reported catalyzed by osmium and ruthenium complexes

The last entries in Table 3 (26, 27 (47, 50)) concern oxidations with a mixture of OsO_4 and $RuCl_3\cdot nH_2O$ with periodate in base. The mixtures show electronic spectral bands at 325 and 385 nm; it is possible that a mixture of *trans*-$[RuO_2\{I(OH)O_5\}_2]^{6-}$ (which has a band at 389 nm (29)) and *cis*-$[Os(OH)_2O_4]^{2-}$ (bands at 325 and 385 nm (6)) is present in both cases. Unfortunately, low solubilities prevented the collection of Raman data.

Experimental

Materials

Chemicals were purchased from Aldrich (hydrated ruthenium trichloride and osmium tetroxide were obtained from Johnson, Matthey) and used without further purification.

The use of *cis*-$[Os^{VIII}(OH)_2O_4]^{2-}$ as a catalyst for oxidative amine dehydrogenation and alcohol oxidations.

Preparation of the cis-*$[Os(OH)_2O_4]^{2-}$ – $[Fe(CN)_6]^{3-}$ reagent*

OsO_4 (0.02 g, 0.08 mmol) was dissolved in 25 cm^3 of aqueous molar NaOH and excess $K_3[Fe(CN)_6]$ (9.9 g, 30 mmol) was added to give an orange solution.

Preparation of cis-*$[Os(OH)_2O_4]^{2-}$ – $S_2O_8^{2-}$ and* cis-*$[OsO_4(OH)_2]^{2-}$ – BrO_3^-*

OsO_4 (0.02 g, 0.08 mmol) was dissolved in 25 cm^3 of aqueous molar NaOH to give an orange solution of *cis*-$[OsO_4(OH)_2]^{2-}$. Excess $K_2S_2O_8$ (9.9 g, 30 mmol) or 1.5 g (10 mmol) of $NaBrO_3$ was then added.

Catalytic dehydrogenation of amines to nitriles

The reactions (Table 1) were performed at room temperature by dropwise addition of the amines (RCH_2NH_2, 2 mmol) over a period of 5 min to a vigorously stirred solution (25 cm^3) of the *cis*-$[Os(OH)_2O_4]^{2-}$ – $[Fe(CN)_6]^{3-}$ reagent and acetonitrile (25 cm^3). Subsequent work with benzylamine and 2-chlorobenzylamine shows that the same results were obtained with only 5 cm^3 of CH_3CN. The initial colour of the reaction mixture is orange; on addition of amine the solution darkens and some pale-yellow $K_4[Fe(CN)_6]$ is deposited. When the reaction is complete the original orange colour of the mixture reappears. The mixture was then extracted with chloroform (3 × 25 cm^3), these extracts dried over anhyd $MgSO_4$, and the chloroform removed. Products were characterized by ^1H NMR, IR spectra, and melting points of solids; liquids were characterized by GC–MS.

Catalytic oxidation of alcohols

Reactions (Table 2) were carried out at room temperature, and the oxidation of cyclohexanol is typical. To 25 cm^3 of the *cis*-$[Os(OH)_2O_4]^{2-}$ – $[Fe(CN)_6]^{3-}$ reagent made as described above was added 0.22 g (2 mmol) of cyclohexanol and 25 cm^3 of acetonitrile, and the mixture stirred for the stated time. The colour changes are similar to those observed for the amine dehydrogenations. The mixture was then extracted with chloroform (3 × 25 cm^3), the extracts combined and dried over anhyd $MgSO_4$, the chloroform evaporated off, and the product characterized by GC or, in the cases of carboxylic acids, by isolation.

The nature of oxoruthenates or oxo-osmates present in solutions

In all cases (Table 3) the cited literature procedure was followed but no substrate added. The solvent after mixture of the ruthenium or osmium precursor, co-oxidant and buffer (if appropriate) was diluted if necessary, using the same solvent or solvent mixture at the same pH as in the literature so that good quality electronic spectra could be obtained.

© 2001 NRC Canada

Spectroscopic data

In general the optimum ruthenium or osmium concentrations for measurements of electronic spectra were ca. 4×10^{-4} M (see also legends for Figs. 1 and 2. Note that for Fig. 1(*a*) the concentration of RuO_4 given is approximate since the solution was made by passing RuO_4 vapour into water). For the less sensitive Raman technique the ruthenium or osmium concentrations had to be substantially higher: for *cis*-$[Os(OH)_2O_4]^{2-}$ in $[Fe(CN)_6]^{3-}$ 0.02 M of the former and 0.6 M of the latter in molar NaOH was used, while for Raman spectral demonstration of the oxidation of *trans*-$[OsO_2(OH)_4]^{2-}$ to *cis*-$[OsO_4(OH)_2]^{2-}$ by $[Fe(CN)_6]^{3-}$ in base the same concentrations were used. For detection of $[RuO_4]^-$ in hypochlorite 0.01 M $RuCl_3 \cdot nH_2O$ was used in aqueous 0.3 M hypochlorite. For detection of RuO_4 in periodate and also in bromate, 0.25 M $RuCl_3 \cdot nH_2O$ was used in molar aq $NaIO_4$ and in 2 M aq $NaBrO_3$, respectively.

Instrumentation

Electronic spectra were measured in 1 cm quartz cuvettes on a PerkinElmer Lambda 2 instrument. Raman spectra were measured on a PerkinElmer 1760X Fourier Transform Raman instrument with 1064 nm Nd-YAG excitation with a power of 2 W, and on a Dilor LabRam Infinity instrument with 632 nm. He–Ne excitation and 532 nm frequency-doubled Nd-YAG excitations, as appropriate, each at 5 mW.

Mass spectra were measured on a PerkinElmer Autosystem instrument with a PerkinElmer stainless-steel column packed with 5% Carbowax 20M on Chromosorb (DCMS treated). GC–MS characterization was carried out on a Micromass Autospec with a Hewlett–Packard 5890 gas chromatograph and an SGE BPX5 column.

Conclusions

The *cis*-$[Os(OH)_2O_4]^{2-}$ – $[Fe(CN)_6]^{3-}$ reagent will, in the presence of acetonitrile, oxidatively dehydrogenate primary amines to nitriles and oxidise primary alcohols to carboxylic acids and secondary alcohols to ketones at room temperatures. Ferricyanide is the best co-oxidant while others (persulfate, bromate, hypochlorite) are less effective.

Studies by electronic and Raman spectroscopies of solutions in a wide variety of procedures in the literature using ruthenium or osmium catalysts with a number of co-oxidants (hypochlorite, periodate, bromate, iodate, ferricyanide, and cerium(IV)) were made to identify the nature of the catalyst or catalyst precursor.

Acknowledgements

We thank the University of London Intercollegiate Research Service (ULIRS) for the Raman facilities, Mr. John Barton for the GC–MS studies, and Johnson Matthey for loan of ruthenium trichoride and osmium tetroxide.

References

1. A.J. Bailey, W.P. Griffith, S.P. Marsden, A.J.P. White, and D.J. Williams. J. Chem. Soc. Dalton Trans. 3673 (1998).
2. T. Naota, H. Takaya, and S.I. Murahashi. Chem. Rev. **98**, 2599 (1998).
3. H.C. Kolb, M.S. van Nieuwenzhe, and K.B. Sharpless. Chem. Rev. **94**, 2483 (1994).
4. W.P. Griffith, B. Reddy, A.G.F. Shoair, M. Suriaatmaja, A.J.P. White, and D.J. Williams. J. Chem. Soc. Dalton Trans. 2819 (1998).
5. A.J. Bailey and B.R. James. J. Chem. Soc. Chem. Commun. 2343 (1996); J. Chem. Soc. Chem. Commun. 507 (1997).
6. A.J. Bailey, M.G. Bhowon, W.P. Griffith, A.G.F. Shoair, A.J.P. White, and D.J. Williams. J. Chem. Soc. Dalton Trans. 3245 (1997).
7. P.H.J. Carlsen, T. Katsuki, V.S. Martín, and K.B. Sharpless. J. Org. Chem. **46**, 3936 (1981).
8. W.P. Griffith, A.G. Shoair, and M. Suriaatmaja. Synth. Commun. **30**, 3091 (2000).
9. H.-L. Kwong, C. Sorato, Y. Ogino, H. Chen, and K.B. Sharpless. Tetrahedron Lett. **31**, 2999 (1990).
10. W.P. Griffith, S.V. Ley, J. Norman, W.P. Griffith, and S.P. Marsden. Synthesis 639 (1994); W.P. Griffith, S.V. Ley, G.P. Whitcombe, and A.D. White. J. Chem. Soc. Chem. Commun. 1625 (1987).
11. D.G. Lee, Z. Wang, and W.D. Chandler. J. Org. Chem. **57**, 3276 (1992).
12. R.E. Connick and C.R. Hurley. J. Am. Chem. Soc. **74**, 5012 (1952).
13. A.J. Bailey, W.P. Griffith, and P.A. Sherwood. Inorg. Chem. **32**, 268 (1993).
14. J.L. Woodhead and J.M. Fletcher. J. Chem. Soc. 5039 (1961).
15. W.P. Griffith. J. Chem. Soc. (A), 1663 (1968)
16. A.C. Dengel, R.A. Hudson, and W.P. Griffith. Transition Met. Chem. (Dordrecht, Neth.), **10**, 98 (1985).
17. R.H. Pettit, R. Brist, A. Mullerand, and E. Diemann. Mol. Phys. **27**, 1373 (1974).
18. J.S. Mayell. Ind. Eng. Chem. Prod. Res. Dev. **7**, 129 (1968).
19. K.A.K. Lott and M.C.R. Symons. J. Chem. Soc. 973 (1960).
20. A.J. Bailey, L.D. Cother, W.P. Griffith, and D.M. Hankin. Transition Met. Chem. (Dordrecht, Neth.), **20**, 590 (1995).
21. A. Mills and C. Holland. J. Chem. Res. Synop. 368 (1997).
22. T.A. Foglia, P.A. Barr, and A.J. Malloy. J. Am. Oil Chem. Soc. **54**, 858A (1977)
23. Y. Sasson, G.D. Zappi, and R. Neumann. J. Org. Chem. **51**, 2880 (1986).
24. A. Tenaglia, E. Terranova, and B. Waegell. Tetrahedron Lett. **31**, 1157 (1990); Tetrahedron Lett. **30**, 5275 (1989).
25. Y.N. Ogibin, A.I. Ilovaiskii, and G.I. Nikishin. Bull. Acad. Sci. USSR. 99 (1991).
26. H. Orita, T. Hayakawa, and K. Takehira. Bull. Chem. Soc. Jpn. **59**, 2637 (1986).
27. J.P. Genet, D. Pons, and S. Jugé. Synth. Commun. **19**, 1712 (1989).
28. A.M. El-Hendawy, W.P. Griffith, B. Piggott, and D.J. Williams. J. Chem. Soc. Dalton Trans. 1983 (1988).
29. A.C. Dengel, A.M. El-Hendawy, W.P. Griffith, S.I. Mostafa, and D.J. Williams. J. Chem. Soc. Dalton Trans. 3489 (1992).
30. G.I. Rozovskii, Z.A. Porshkute, A.Y. Prokopchik, and P.K. Norkus. Russ. J. Inorg. Chem. **18**, 1432 (1973).
31. D.L. Kamble and S.T. Nandibewoor. J. Phys. Org. Chem. **1**, 171 (1998).
32. L. Timmanagoudar, G.A. Hiremath, and S.T. Nandibewoor. J. Ind. Chem. Soc. **74**, 296 (1997).
33. J.T. Ayodele. Ghana J. Chem. **2**, 57 (1996).
34. D. Singh, S.B. Singh, V.P. Sahay, M. Prasad, and J. Prasad. Asian J. Chem. **11**, 666 (1999).
35. A. Brahmaiah and P. Manikyamba. Oxid. Commun. **22**, 228 (1999); Oxid. Commun. **19**, 94 (1996); Indian J. Chem. Sect. A: Inorg. Phys. Theor. Anal. Chem. **34A**, 900 (1995).

© 2001 NRC Canada

36. A.E. Mucientes, F.J. Poblete, F. Santiago, and M.A. Rodriguez. J. Chim. Phys. Phys.-Chim. Biol. **94**, 1642 (1997).
37. A.E. Mucientes, F.J. Poblete, M.A. Rodriguez, and F. Santiago. J. Phys. Org. Chem. **10**, 662 (1997).
38. A.E. Mucientes, F.J. Poblete, R.E. Gabaldon, M.A. Rodriguez, and F. Santiago. J. Chem. Res. Synop. 286 (1997).
39. R.K. Mohanty, M. Das, and A.K. Das. Indian J. Chem. Sect. A: Bio-inorg. Phys. Theor. Anal. **37A**, 663 (1998).
40. Y.R. Rao and M.K. Reddy. Oriental J. Chem. **14**, 13 (1998).
41. S. Giddings and A. Mills. J. Org. Chem. **53**, 1103 (1988).
42. M.C. Agrawal and S.K. Upadhya. J. Sci. Ind. Res. **42**, 508 (1983).
43. S. Singh, A. Gupta, and A.K. Singh. Transition Met. Chem. (Dordrecht, Neth.), **23**, 277 (1998).
44. T.A. Foglia, P.A. Barr, A.J. Malloy, and M.J. Costanzo. J. Am. Oil Chem. Soc. **54**, 870A (1977).
45. J. Evans, W. Levason, and M.D. Spicer. J. Chem. Soc. Dalton Trans. 2307 (1990).
46. G.H. Hugar and S.T. Nandibewoor. Transition Met. Chem. (Dordrecht, Neth.), **19**, 215 (1994).
47. G.A. Hiremath, P.L. Timanagoudar, R.B. Chougale, and S. T. Nandibewoor. J. Ind. Chem. Soc. **75**, 363 (1998).
48. B. Singh, B.B. Singh, and R.P. Singh. J. Inorg. Nucl. Chem. **43**, 1283 (1981).
49. N.P. Singh, V.N. Singh, H.S. Singh, and M.P. Singh. Aust. J. Chem. **23**, 921 (1970).
50. D.L. Kamble and S.T. Nandibewoor. Oxid. Commun. **21**, 396 (1998).

© 2001 NRC Canada

Synthesis and molecular structures of monooxo aryl complexes of osmium(VI)

Man-Kit Lau, Joyce L.C. Chim, Wing-Tak Wong, Ian D. Williams, and Wa-Hung Leung

Abstract: Reaction of [OsO_4] with C_7H_7MgBr (C_7H_7 = 2-methylphenyl) followed by column chromatography afforded the reported osmium tetraaryl [$Os(C_7H_7)_4$] along with the oxo-osmium(VI) ([$OsO(C_7H_7)_4$]) (**1**) (13%) and the dioxo-osmium(VI) ([$OsO_2(C_7H_7)_2$]) (**2**) (25%) complexes. Treatment of [OsO_4] with C_8H_9MgBr (C_8H_9 = 2,5-dimethylphenyl) gave a mixture of [$Os(C_8H_9)_4$] (**3**) (34%) and [$OsO(C_8H_9)_4$] (**4**) (4%) while that with C_8H_9OMgBr (C_8H_9O = 4-methoxy-2-methylphenyl) afforded [$OsO(C_8H_9O)_4$] (**5**) in 20% yield. Oxidation of **3** with 3-chloroperoxybenzoic acid afforded **4** in good yield. The solid-state structures of **1** and **4** have been established by X-ray crystallography. Crystals of **1** are tetragonal with a = 13.080(1) and c = 6.6506(5) Å, V = 1137.9(1) Å^3, Z = 2, and space group of $P4/n$; while those of **4** are tetragonal with a = 13.593(2) and c = 7.377(2) Å, V = 1363.0(5) Å^3, Z = 4, and space group of $P4/n$. The geometry around osmium in both complexes is square pyramidal with the oxo ligand occupying apical position. The Os—O and Os—C distances in **1** are 1.652(2) and 2.084(1) Å, respectively, while those in **4** are 1.688(7) and 2.088(4) Å, respectively. The cyclic voltammograms of the monooxo aryl osmium(VI) compounds show reversible Os(VI/V) couple at around –1.4 V vs. ferrocene/ferrocenium couple.

Key words: osmium(VI), oxo aryl complexes.

Résumé : La réaction du [OsO_4] avec du C_7H_7MgBr (C_7H_7 = 2-méthylphényle), suivie d'une chromatographie sur colonne permet d'isoler le tétraarylosmium attendu [$Os(C_7H_7)_4$] aux côtés de complexes oxo-osmium(VI) [$OsO(C_7H_7)_4$] (**1**) (13%) et dioxo-osmium(VI) [$OsO_2(C_7H_7)_2$] (**2**) (25%). Le réaction du [OsO_4] avec du C_8H_9MgBr (C_8H_9 = 2,5-diméthylphényle) conduit à un mélange de [$Os(C_8H_9)_4$] (**3**) (34%) et de [$OsO(C_8H_9)_4$] (**4**) (4%) alors que celle avec C_8H_9MgOBr (C_8H_9 = 4-méthoxy-2-méthylphényle) conduit au [$OsO(C_8H_9O)_4$] (**5**) avec un rendement de 20%. L'oxydation du produit **3** par de l'acide 3-chloroperbenzoïque conduit au produit **4** avec un bon rendement. Les structures des composés **1** et **4** ont été déterminées à l'état solide par diffraction des rayons X. Les cristaux de **1** sont tétragonaux, groupe d'espace $P4/n$, avec a = 13,080(1) et c = 6,6506(5) Å, V = 1137,9(1) Å^3 et Z = 2 alors que ceux du composé **4** sont tétragonaux, groupe d'espace $P4/n$, avec a = 13,593(2) et c = 7,3776(2) Å et Z = 4 V = 1363,0(5) Å^3. Dans chacun des complexes, la géométrie autour de l'osmium est de type pyramide carrée de laquelle le ligand oxo se trouve en position apicale. Les distances Os—O et Os—C dans le composé **1** sont respectivement de 1,652(2) et 2,084(1)Å alors que celles dans le composé **4** sont respectivement de 1,688(7) et 2,088(4) Å. Dans les voltampérogrammes cycliques des composés monooxo aryl osmium(VI), on observe le couple réversible Os(VI/V) aux environs de –1,4 V par rapport au couple ferrocène/ferrocénium.

Mots clés : osmium(VI), complexes oxo aryles.

[Traduit par la Rédaction]

Introduction

Organometallic oxides are of interest due to their relevance to the active intermediates in metal-catalyzed oxidation of organic compounds (1, 2). Some transition metal oxo alkyls, notably [$Re(CH_3)O_3$], are also used as stoichiometric and catalytic reagents for organic transformations (2). While oxo alkyls of oxophilic early transition metals are well-documented, there are relatively few examples of the later transition-metal congeners. Wilkinson and co-workers (3, 4) first reported the synthesis of high-valent osmium aryls and oxo aryls by arylation of [OsO_4] with Grignard reagents ArMgBr (Ar = aryl). It was found that the *ortho*-methyl substituent in Ar has a significant effect on the nature of the arylation products. Thus, reaction of [OsO_4] with di*ortho*-substituted mesMgBr (mes = 2,4,6-trimethylphenyl) afforded [$OsO_2(mes)_2$] (3) whereas interactions of [OsO_4] with mono*ortho*-substituted or unsubstituted ArMgBr (e.g., Ar = 2-methylphenyl or phenyl) gave homoleptic Os(IV) aryls [$Os(Ar)_4$] (4). However, to our knowledge, no oxo(tetraaryl)osmium(VI) complexes have been isolated al-

Received August 30, 2000. Published on the NRC Research Press Web site at http://canjchem.nrc.ca on July 2, 2001.

This paper is dedicated to Professor Brian R. James on the occasion of his 65th birthday.

M.-K. Lau, J.L.C. Chim, I.D. Williams, and W.-H. Leung.[1] Department of Chemistry, The Hong Kong University of Science and Technology, Clear Water Bay, Kowloon, Hong Kong, China.
W.-T. Wong. Department of Chemistry, The University of Hong Kong, Pokfulam Road, Hong Kong, China.

[1]Corresponding author (e-mail: chleung@ust.hk).

 DOI: 10.1139/cjc-79-5/6-607 © 2001 NRC Canada

though oxo(tetraalkyl)osmium(VI) complexes have been prepared by alkylation of [OsO_4] (5) or oxo-osmium glycolates (6). In view of the low yield for the synthesis of [$Os(C_7H_7)_4$], we suspect that there may be other unidentified product(s) for the arylation of [OsO_4]. To this end, we set out to reinvestigate the reaction between [OsO_4] and ArMgBr, and to separate the products by column chromatography. We here describe the isolation, molecular structures, and electrochemistry of the first monooxo aryl complexes of osmium(VI).

Experimental

All manipulations, unless otherwise stated, were carried out in air. Solvents were purified, dried, and distilled prior to use. [OsO_4] was obtained from Strem Ltd. ArMgBr in Et_2O were prepared from commercially available aryl bromides and Mg.

Spectrometers used were as follows: IR spectra (in KBr discs) PerkinElmer 16 PC FT IR; mass spectra on a Finnigan TSQ 7000; UV–vis spectra Milton-Roy Spectronic 3000 diode array; 300 MHz ^{1}H NMR spectra Bruker ALX 300 (chemical shifts in ppm relative to $SiMe_4$). Cyclic voltammetry was performed with a Princeton Applied Research (PAR) Model 273A potentiostat. The working and reference electrodes were glassy carbon and $Ag/AgNO_3$ (0.1 M in acetonitrile), respectively, and the scan rate was 100 mV s^{-1}. Formal potentials ($E_{1/2}$) were measured in CH_2Cl_2 solutions with 0.1 M [*n*-NBu_4][PF_6] as supporting electrolyte and reported with reference to the ferrocenium/ferrocene couple ($Cp_2Fe^{+/0}$). Elemental analyses were performed by Medac Ltd., Surrey, U.K.

[$OsO(C_7H_7)_4$] (1) and [$OsO_2(C_7H_7)_2$] (2) (C_7H_7 = 2-methylphenyl)

These complexes were synthesized using a modification of the Wilkinson's procedure. To a solution of [OsO_4] (1 g, 3.94 mmol) in THF (30 mL) at –78°C were added 7 equiv of 2-methylphenylmagnesium bromide (17.3 mL of a 1.6 M solution in Et_2O), and the mixture was stirred for 45 min. The resulting purple mixture was then warmed to room temperature, stirred for a further 2 h, and evaporated to dryness. The residue was extracted into CH_2Cl_2 in air and subjected to column chromatography (silica gel). Elution with hexane, CH_2Cl_2–hexane (1:4), and acetone afforded purple [$Os(C_7H_7)_4$] (10%), orange **1** (13%), and green **2** (25%), respectively. Recrystallization of **1** from CH_2Cl_2–hexane led to isolation of orange blocks, which were suitable for X-ray diffraction.

*Characterization data for **1***

FT IR (KBr, cm^{-1}): 986 (Os=O). FAB-MS *m*/*z*: 572 (M^+). ^{1}H NMR (300 MHz, $CDCl_3$) δ: 2.32 (s, 12H, CH_3), 5.96 (d, J = 7.6 Hz, 4H, H_o), 6.87 (t, J = 7.6 Hz, 4H, H_m), 6.96 (t, J = 7.6 Hz, 4H, H_p), 7.27 (d, J = 7.6 Hz, 4H, H_m'). $E_{1/2}$ (V): –1.41 [Os(VI/V)]. Anal. calcd. for $C_{28}H_{28}OOs$: C 59.0, H 4.9; found: C 58.3, H 4.9.

*Characterization data for **2***

FT IR (KBr, cm^{-1}): 912, 956 (OsO_2). FAB-MS *m*/*z*: 407 [M + 1]$^+$. UV–vis (CH_2Cl_2) λ_{max} (nm) (ε_{max} (M^{-1} cm^{-1})): 248 (23 000), 350 (8700). ^{1}H NMR (300 MHz, $CDCl_3$) δ: 2.57 (s, 6H, CH_3), 7.04–7.13 (m, 4H, H_m and H_p), 7.19 (d, J = 7.8 Hz, 2H, H_o), 7.40 (d, J = 7.8 Hz, 2H, H_m'). $E_{1/2}$ (V): –1.14 [Os(VI/V)]. Anal. calcd. for $C_{14}H_{14}O_2Os$: C 41.6, H 3.5; found: C 41.3, H 3.9.

[$Os(C_8H_9)_4$] (3) and [$OsO(C_8H_9)_4$] (4)

To a solution of [OsO_4] (0.5 g, 2.0 mmol) in Et_2O (20 mL) at –78°C were added 7 equiv of 2,5-dimethylphenylmagnesium bromide (11.5 mL of a 1.2 M solution in Et_2O, 14 mmol) dropwise under nitrogen. The resulting reddish-brown mixture was warmed to room temperature, stirred for 2 h, and evaporated to dryness. The dark yellow sticky residue was extracted into CH_2Cl_2, filtered through a Celite pad, and subjected to column chromatography (silica gel). Elution with hexane and hexane–Et_2O (7:3) afforded purple **3** (34%) and orange **4** (2%), respectively.

*Characterization data for **3***

FAB-MS *m*/*z*: 612 (M^+). ^{1}H NMR (300 MHz, $CDCl_3$) δ: 2.22 (s, 12H, CH_3), 2.27 (s, 12H, CH_3), 6.57 (d, J = 8.5 Hz, 4H, H_p), 6.68 (d, J = 8.5 Hz, 4H, H_m), 6.70 (s, 4H, H_o). $E_{1/2}$ (V): –1.48 [Os(IV/III)] and 0.24 [Os(V/IV)]. Anal. calcd. for $C_{32}H_{36}Os$: C 62.9, H 5.9; found: C 63.0, H 6.0.

*Characterization data for **4***

FT IR (KBr, cm^{-1}): 986 (Os=O). FAB-MS *m*/*z*: 572 (M^+). UV–vis (CH_2Cl_2) λ_{max} (nm) (ε_{max} (M^{-1} cm^{-1})): 248 (22 000), 350 (8250). ^{1}H NMR (300 MHz, $CDCl_3$) δ: 1.99 (s, 12H, CH_3), 2.25 (s, 12H, CH_3), 5.78 (s, 4H, H_o), 6.75 (d, J = 7.5 Hz, 4H, H_p), 7.13 (d, J = 7.5 Hz, 4H, H_m). $E_{1/2}$ (V): –1.35 [Os(VI/V)]. Anal. calcd. for $C_{32}H_{36}OOs$: C 59.0, H 4.9; found: C 58.3, H 4.9.

*Preparation of **4** from **3***

To a solution of **3** (0.5 g, 0.08 mmol) in CH_2Cl_2 (10 mL) was added 1.5 equiv of 3-chloroperoxybenzoic acid or *t*-BuOOH at room temperature. The reaction mixture was stirred for 2 h, evaporated to dryness, and subjected to column chromatography (silica gel). The product was eluted with hexane and recrystallized from CH_2Cl_2–hexane to give orange crystals (80% yield), which was identified as **4** by ^{1}H NMR spectroscopy and mass spectrometry. Recrystallization of **4** from CH_2Cl_2–hexane afforded orange blocks, which were suitable for X-ray diffraction study.

[$OsO(C_8H_9O)_4$] (5)

To a solution of [OsO_4] (0.5 g, 2.0 mmol) in Et_2O (20 mL) at –40°C was added 7 equiv of 4-methoxy-2-methylphenylmagnesium bromide (20.6 mL of a 0.67 M solution in Et_2O), and the mixture was slowly warmed to room temperature and stirred for 2 h. The solvent was pumped off and the residue was extracted into CH_2Cl_2 in air. Column chromatography (silica gel, eluant: CH_2Cl_2–Et_2O (1:5)) followed by recrystallization from CH_2Cl_2–hexane afforded a brown solid. Yield: 0.25 g, 20%. FAB-MS *m*/*z*: 693 [M + 1]$^+$. FT IR (KBr, cm^{-1}): 982 (OsO). UV–vis (CH_2Cl_2) λ_{max} (nm) (ε_{max} (M^{-1} cm^{-1})): 254 (26 700), 350 (11 700). ^{1}H NMR (300 MHz, $CDCl_3$) δ: 2.28 (s, 12H, CH_3), 3.76 (s, 12H, OCH_3), 5.77 (d, J = 8.8 Hz, 4H, H_o), 6.41 (d, J = 8.8 Hz,

© 2001 NRC Canada

Table 1. Crystallographic data for $[OsO(C_7H_7)_4]$ (**1**) and $[OsO(C_8H_9)_4]$ (**4**).

Compound	**1**	**4**
Formula	$C_{28}H_{28}OOs$	$C_{36}H_{36}OOs$
Formula weight	570.73	626.81
Crystal system	Tetragonal	Tetragonal
Space group	*P*4/*n*	*P*4/*n*
a (Å)	13.080(1)	13.593(2)
c (Å)	6.6505(5)	7.377(2)
V (Å^3)	1137.9(1)	1363.0(5)
Z	2	2
ρ_{calcd} (g cm^{-3})	1.666	1.527
μ (Mo Kα) (cm^{-1})	56.16	46.99
F(000)	560	624
Crystal size (mm)	0.22 × 0.12 × 0.12	0.7 × 0.6 × 0.2
Transmission factor	—	—
Total reflections	6851	1636
Unique reflections	—	1522 (R_{int} = 0.0221)
No. of observed reflections	6217 ($I > 1.5\sigma(I)$)	—
No. of variables	70	79
R (*F*)	0.022	—
R_w (*F*)	0.037	—
R (F^2) (all data)	—	0.0304
wR_2 (F^2) (all data)	—	0.0842
GoF	1.38	1.088
Max Δ / σ (final cycle)	0.04	—
Residual density (e Å^{-3})	–0.51–1.06	–0.549–1.153

4H, H_m), 6.88 (s, *J* = 8.8 Hz, 4H, H_m'). $E_{1/2}$ (V): –1.37 [Os(VI/V)] and 0.93 irreversible [Os(VII/VI)]. Anal. calcd. for $C_{32}H_{36}O_5Os$: C 57.0, H 5.3; found: C 56.0, H 5.3.

X-ray crystallography

Pertinent crystallographic data and other experimental details for complexes **1** and **4** are summarized in Table 1. Data for **1** and **4** were collected on a Bruker CCD diffractometer and a Siemens P4 diffractometer, respectively, at room temperature using graphite-monochromated Mo K_α radiation (λ = 0.71073 Å). Data were corrected for Lorentz and polarization effects. Absorption corrections are semiempirical based on ψ-scan data. Structures **1** and **4** were solved by direct methods and refined by full-matrix least-squares on *F* and F^2, respectively. Hydrogen atoms were included and fixed in their idealized positions (C-H 0.95 Å). Calculations were carried out using the teXsan (7) (for **1**) and SHELXL (8) (for **4**) crystallographic software packages. Complete listings of bond lengths and angles, final atomic coordinates of non-hydrogen atoms with thermal parameters, and anisotropic thermal parameters are included as supplementary material.[2]

Results and Discussion

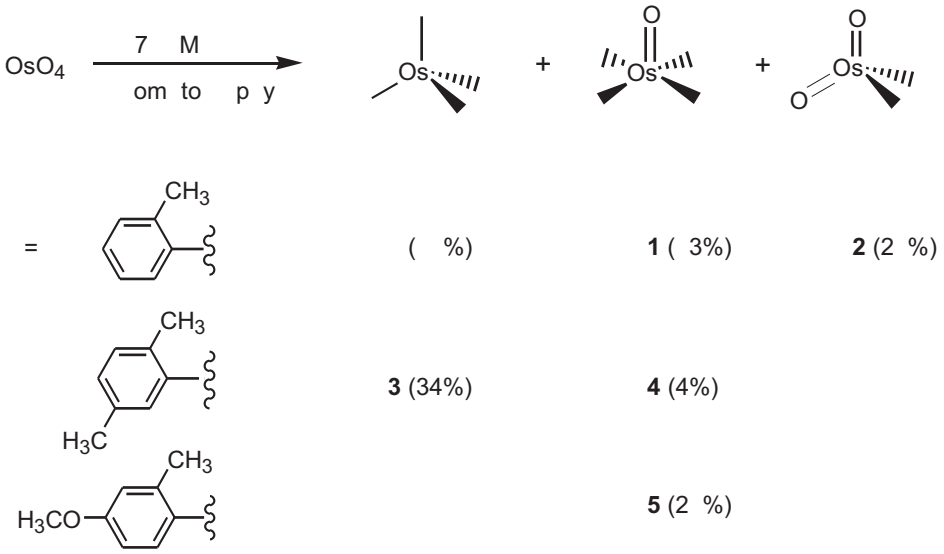
Synthesis

The preparations of osmium oxo aryl complexes are summarized in Scheme 1. Wilkinson and co-workers (4*a*) first reported the synthesis of $[Os(C_7H_7)_4]$ by the reaction of $[OsO_4]$ with C_7H_7MgBr. The osmium tetraaryl was obtained in 29% yield after extraction into light petroleum and subsequent recrystallization under nitrogen. However, we found that when the reaction mixture was exposed to air and then chromatographed (silica gel) in air, in addition to $[Os(C_7H_7)_4]$, the oxo-osmium species $[OsO(C_7H_7)_4]$ (**1**) and $[OsO_2(C_7H_7)_2]$ (**2**) species were isolated in 13 and 25% yield, respectively. The relative yields of $[Os(C_7H_7)_4]$, **1**, and **2** for the reaction were, however, found to be dependent on reaction conditions, workup procedure, and some unknown factors that have not been optimized yet. It appears that the oxo complexes **1** and **2** were derived directly from reaction of $[OsO_4]$ with C_7H_7MgBr, instead of via aerobic oxidation of $[Os(C_7H_7)_4]$, because $[Os(C_7H_7)_4]$, **1**, and **2** are all air stable in solution and under chromatographic conditions. Like $[Os(C_7H_7)_4]$ (3*a*), complex **1** exhibits a symmetric ^{1}H NMR spectrum featuring a single *ortho*-methyl resonance at δ 2.32 at room temperature, indicating that the 2-methylphenyl ligands are free to rotate around the Os—C bonds at the NMR timescale. The UV–vis spectrum of **1** in CH_2Cl_2 displays absorption bands at ca. 350 (ε_{max} = 8700 M^{-1} cm^{-1}) and 248 nm (sh, ε_{max} = 23 000 M^{-1} cm^{-1}). The former band is tentatively attributed to a charge transfer transition due to the Os=O moiety while the latter probably arises from an intraligand transition because a similar absorption was also found for $[Os(C_7H_7)_4]$. The IR Os—O

[2] Crystal data for **1** and **4** may be purchased from the Depository of Unpublished Data, Document Delivery, CISTI, National Research Council Canada, Ottawa, ON K1A 0S2, Canada DUD No. 3276. For information on obtaining material electronically go to http://www.nrc.ca/cisti/irm/unpub_e.shtml. This supplementary material has also been deposited with the Cambridge Crystallographic Centre (deposition nos. 148 810 and 148 809, respectively), and can be obtained on request from: The Director, Cambridge Crystallographic Centre, University Chemical Laboratory, 12 Union Road, Cambridge, CB2 1EZ, U.K.

© 2001 NRC Canada

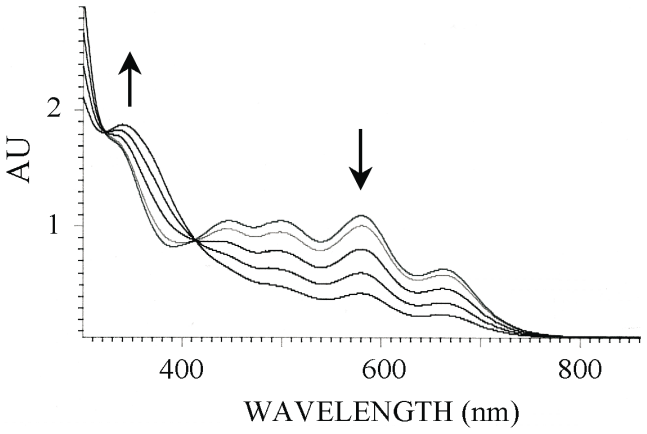
Scheme 1.



stretching frequency for **1** was observed at 990 cm^{-1}, which is comparable to that for $[OsO(CH_3)_4]$ (994 cm^{-1}) (6*a*) but is lower than that for $[OsO(CH_2SiMe_3)_4]$ (1054 cm^{-1}) (5*b*). Complex **2**, which presumably has a similar tetrahedral geometry as $[OsO_2(mes)_2]$ (4*a*), exhibits $\nu(OsO)_{as}$ at 1000 and 980 cm^{-1}. Neither **1** nor **2** reacted with oxygen abstractors such as tertiary phosphines and Si_2Cl_6. Attempts to reduce **2** by cobaltocene led to recovery of the starting material.

To further investigate the substituent effect of Ar on the arylation of $[OsO_4]$, disubstituted phenyl Grignard were used as the alkylation agents. Treatment of $[OsO_4]$ with 7 equiv of 2,5-dimethylphenylmagnesium bromide (C_8H_9MgBr) in Et_2O afforded purple $[Os(C_8H_9)_4]$ (**3**) (33%) and orange $[OsO(C_8H_9)_4]$ (**4**) (4%), which were separated by column chromatography. On the other hand, reaction of $[OsO_4]$ with 4-methoxy-2-methylphenylmagnesium bromide (C_8H_9OMgBr) in Et_2O gave the oxo-Os(VI) compound $[OsO(C_8H_9O)_4]$ (**5**) as the sole isolable product in 20% yield. Complexes **3**–**5** are soluble in common organic solvents including hexanes, ether, and methanol. They are air-stable in solution and could be chromatographed in air without decomposition. It appears that the presence of the 5-methyl substituent in the aryl group enhances the production of Os(IV) tetraaryl while the 4-methoxy substituent favors oxo-Os(VI) formation although the origin of such a substituent effect is not well understood. The ^1H NMR spectrum of **3** shows two singlets at δ 2.22 and 2.27 due to the *ortho*- and *meta*-methyl protons. Oxidation of **3** with $[Ag(CF_3SO_3)]$ afforded the osmium(V) species $[Os(C_8H_9)_4]^+$, which exhibits an isotropic EPR signal at $g = 2.04$ at –120°C. A similar *g* value was found for the structurally characterized osmium(V) complex $[Os(C_7H_7)_4][CF_3SO_3]$ (3*b*, 9). Treatment of **3** with single-oxygen donors such as 3-chloroperoxybenzoic acid and *t*-BuOOH gave **4** in good yield. Figure 1 shows a spectral trace for the reaction of **3** with *t*-BuOOH in CH_2Cl_2. Upon addition of ca. 1 equiv of *t*-BuOOH, the d-d bands for **3** centered at 447, 579, and 662 nm disappeared and concomitantly an absorption at 352 nm attributable to the charge transfer band for **4** appeared. The observation of isosbestic points at ca. 325 and 420 nm suggests that the oxo transfer

Fig. 1. Optical spectral trace for the reaction between $[Os(C_8H_9)_4]$ (**3**) and *t*-BuOOH in CH_2Cl_2.



from *t*-BuOOH to **3** is a clean, single-step process. The charge transfer band for methoxy-substituted **5** (385 nm) was found at a longer wavelength relative to those for **4** (352 nm) and **1** (350 nm). The ^1H NMR spectrum of **4** shows two singlets at δ 1.99 and 2.25 due to the *meta*- and *ortho*-methyl protons while the methyl and methoxy proton signals for **5** were observed at δ 2.28 and 3.76, respectively. The IR Os—O stretching frequencies for **4** and **5** (982 and 986 cm^{-1}, respectively) are comparable to that for **1**.

Crystal structures

Complexes **1** and **4** have been unambiguously characterized by X-ray crystallography. The corresponding molecular structures with selected bond lengths and angles are shown in Figs. 2 and 3. Complex **1** is isostructural with the previously reported Re(VI) analogue $[ReO(C_7H_7)_4]$, which also exhibits a fourfold molecular symmetry (10). The geometry around osmium in **1** and **4** is pseudo-square pyramidal with the oxo ligand occupying the apical position. The Os atoms are situated above the C4 plane with the O-Os-C angles of 110.4(4) and 110.82(12)° for **1** and **4**, respectively, (cf.

© 2001 NRC Canada

Fig. 2. Molecular structure of $[OsO(C_7H_7)_4]$ (**1**). Selected bond lengths and angles are: Os(1)—O(1) 1.652(2) and Os(1)—C(1) 2.084(1) Å; O(1)-Os(1)-C(1) 110.04(4), C(1)-Os(1)-C(1*) 82.59(3), and C(1)-Os(1)-C(1*) 137.91(8)°.

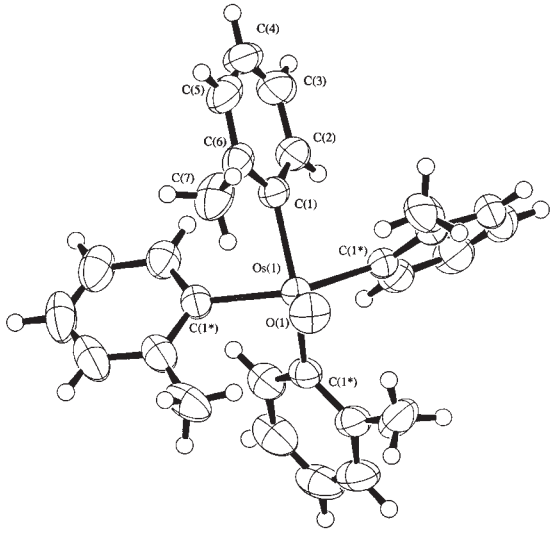
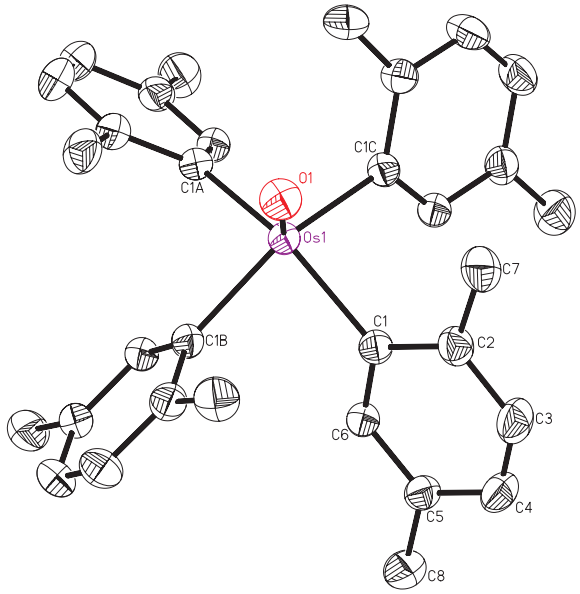
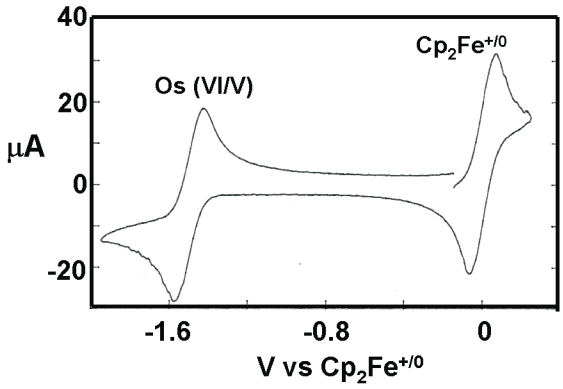


Fig. 3. Molecular structure of $[OsO(C_8H_9)_4]$ (**4**). Selected bond lengths and angles are: Os(1)—O(1) 1.688(7) and Os(1)—C(1) 2.088(4) Å; O(1)-Os(1)-C(1) 110.82(12), C(1)-Os(1)-C(1B) 82.74(8), and C(1)-Os(1)-C(1A) 138.4(2)°.



106.0(2)° for $[ReO(C_7H_7)_4]$ (10)). Like $[ReO(C_7H_7)_4]$, the *ortho*-methyl groups in **1** and **4** are found on the same side as the oxo function possibly due to steric reasons. The Os—O and average Os—C distance for **1** are 1.652(2) and 2.084(1) Å, respectively, while those for **4** are 1.688(7) and 2.088(4) Å, respectively. The Os—C distances are comparable to those in $[OsO(CH_2SiMe_3)_4]$ (average 2.078 Å) (5*b*) and $[ReO(C_7H_7)_4]$ (2.063 Å) (10) but is slightly shorter than that in $[Os(C_7H_7)_4]$ (average 1.997 Å) (4*a*). The Os—O distances are short and similar to that in $[OsO(CH_2SiMe_3)_4]$ (1.692(6) Å) (5*b*).

Fig. 4. Cyclic voltammogram of $[OsO(C_8H_9)_4]$ (**4**) in CH_2Cl_2 at a glassy carbon electrode. Scan rate = 100 mV s^{-1}.



Electrochemistry

The formal potentials for the osmium aryl complexes have been determined by cyclic voltammetry in CH_2Cl_2. The tetraaryl complex **3** exhibits reversible couples at 0.24 and –1.48 V vs. $Cp_2Fe^{+/0}$, which are assigned to the metal-centered Os(V/IV) and Os(IV/III) couples, respectively. The $E_{1/2}$ ([Os(V/IV)]) for **3** is less anodic than that for $[Os(C_7H_7)_4]$ (0.33 V) due to inductive effect of *meta*-methyl substitutents in the aryl groups. The cyclic voltammogram of **4** (Fig. 4) shows a reversible reduction couple at –1.35 V, which is assigned to the Os(VI/V) couple. Similarly, the Os(VI/V) couples for **1** and **5** were observed at –1.41 and –1.37 V, respectively. An irreversible oxidation wave at 0.93 V, which is tentatively assigned to the Os(VII/VI) oxidation, was also found for **5**. For comparison, the Os(VII/VI) couple for $[Os(O)(CH_2SiMe_3)_4]$ was observed at 1.19 V vs. Ag/AgCl (5*b*). The dioxo-osmium(VI) complex **2** exhibits the Os(VI/V) couple at –1.14 V, which is similar to that for $[OsO_2(mes)_2]$ (–1.28 V) (4*b*). In general, the $E_{1/2}$ ([Os(VI/V)]) for $[OsO(aryl)_4]$ are more negative than those for $[OsO_2(aryl)_2]$, indicating that the σ-aryls are very strong donor ligands.

Conclusions

In summary, we found that depending on the nature of aryl ligand, reaction of $[OsO_4]$ with arylmagnesium bromide produced a mixture of osmium(IV) tetraaryl, oxo(tetraaryl)osmium(VI), and dioxo(diaryl)osmium(VI) complexes, which could be separated by column chromatography. It appears that the presence of the 5-methyl substituent in the aryl ligand enhances the formation of Os(IV) tetraaryl while the 4-methoxy substituent favors the formation of $[OsO(aryl)_4]$. Oxidation of $[Os(C_8H_9)_4]$ with 3-choroperoxybenzoic acid gave $[OsO(C_8H_9)_4]$ in good yield. The oxo(tetraaryl)osmium(VI) complexes exhibit reversible Os(V/IV) couples at ca. –1.4 V while the Os(VI/V) couples for dioxodiarylosmium(VI) occur at ca. –1.1 V vs. $Cp_2Fe^{+/0}$.

Acknowledgement

The work described in this paper was supported by a grant from the Research Grants Council of the Hong Kong SAR, China (project no. HKUST 6189/00P).

© 2001 NRC Canada

References

1. F. Bottomley and L. Sutin. Adv. Organomet. Chem. **28**, 339 (1988), and references cited therein.
2. (*a*) W.A. Herrmann. J. Organomet. Chem. **500**, 149 (1995); (*b*) W.A. Herrmann. Acc. Chem. Res. **30**, 169 (1997).
3. (*a*) P. Stavropoulos, P.G. Edwards, T. Behling, G. Wilkinson, M. Motevalli, and M.B. Hursthouse. J. Chem. Soc. Dalton Trans. 169 (1987); (*b*) B.S. McGilligan, J. Arnold, G. Wilkinson, B. Hussain-Bates, and M.B. Hursthouse. J. Chem. Soc. Dalton Trans. 2465 (1990).
4. (*a*) P. Stavropoulos, P.D. Savage, R.P. Tooze, G. Wilkinson, B. Hussain, M. Motevalli, and M.B. Hursthouse. J. Chem. Soc. Dalton Trans. 557 (1987); (*b*) J. Arnold, G. Wilkinson, B. Hussain, and M.B. Hursthouse. J. Chem. Soc. Dalton Trans. 2149 (1989).
5. (*a*) A.S. Alves, D.S. Moore, R.A. Andersen, and G. Wilkinson. Polyhedron, **1**, 83 (1982); (*b*) R.W. Marshman, W.S. Bigham, S.R. Wilson, and P.A. Shapley. Organometallics, **9**, 1341 (1990).
6. (*a*) W.A. Herrmann, S.J. Eder, P. Kiprof, K. Rypdal, and P. Watzlowik. Angew. Chem. Int. Ed. Engl. **29**, 1445 (1990); (*b*) W.A. Herrmann, S.J. Eder, P. Kiprof, and P. Watzlowik. J. Organomet. Chem. **428**, 187 (1992).
7. TeXsan. Crystal structure package. Molecular Structure Corp., Houston, TX. 1985 and 1992.
8. G.M. Sheldrick. SHELXTL-97 software reference manual. Bruker AXS Inc., Madison, Wisconsin, U.S.A. 1997.
9. J. Arnold, G. Wilkinson, B. Hussain, and M.B. Hursthouse. J. Chem. Soc. Chem. Commun. 1349 (1988).
10. P.D. Savage, G. Wilkinson, M. Motevalli, and M.B. Hursthouse. J. Chem. Soc. Dalton Trans. 669 (1988).

© 2001 NRC Canada

One-electron reduction of the γ*-isomer of $[S_2W_{18}O_{62}]^{4-}$ leads to isolation of the α-isomer

Peter J.S. Richardt, Jonathon M. White, Peter A. Tregloan, Alan M. Bond, and Anthony G. Wedd

Abstract: Bu_4N^+ salts of $[S_2W_{18}O_{62}]^{5-}$ and $[S_2W_{18}O_{62}]^{6-}$ can be isolated by electro reduction of γ*-$(Bu_4N)_4[S_2W_{18}O_{62}]$ in MeCN. α-$(Bu_4N)_5[S_2W_{18}O_{62}]\cdot 4MeCN$ crystallizes in space group *C*2/*c* with *a* = 26.226(2) Å, *b* = 15.570(2) Å, *c* = 38.407(2) Å, β = 115.59(2)°, *V* = 14 145(2) Å^3, and *Z* = 8. The observations indicate that a γ* ↔ α isomerization is associated with the $[S_2W_{18}O_{62}]^{4-}$– $[S_2W_{18}O_{62}]^{5-}$ couple. However, the transformation could not be detected on the timescale of cyclic voltammetry up to a scan rate of 10 V s^{-1}. The available data suggest that either: (*i*) the γ* ↔ α equilibrium favors one of the isomers in solution for both redox states, or (*ii*) the isomerization is slow on the cyclic voltammetric timescale but the differences in $E_{1/2}$ values for the α-$[S_2W_{18}O_{62}]^{4-}$–$[S_2W_{18}O_{62}]^{5-}$ and γ*-$[S_2W_{18}O_{62}]^{4-}$–$[S_2W_{18}O_{62}]^{5-}$ couples cannot be resolved by cyclic voltammetry.

Key words: polyoxometalates, synthesis, electrochemistry, isomerization.

Résumé : On peut isoler les sels de Bu_4N^+ de $[S_2W_{18}O_{62}]^{5-}$ et de $[S_2W_{18}O_{62}]^{6-}$ par électroréduction du γ*-$(Bu_4N)_4[S_2W_{18}O_{62}]$ dans le MeCN. Le α-$(Bu_4N)_5[S_2W_{18}O_{62}]\cdot 4MeCN$ cristallise dans groupe d'espace *C*2/*c*, avec *a* = 26,226(2) Å, *b* = 15,570(2) Å et *c* = 38,407(2) Å, β = 115,59(2)°, *V* = 14 145(2) Å^3 et *Z* = 8. Les observations indiquent qu'une isomérisation γ* ↔ α est associée au couple $[S_2W_{18}O_{62}]^{4-}$–$[S_2W_{18}O_{62}]^{5-}$. Toutefois, il n'est pas possible de détecter cette transformation à l'échelle de temps de la voltampérométrie cyclique jusqu'à des vitesses de balayage de 10 V s^{-1}. Les données disponibles suggèrent (*i*) que, en solution, l'équilibre γ*↔ α favorise l'un des isomères pour les deux états redox ou (*ii*) que l'isomérisation est lente à l'échelle de temps de la voltampérométrie cyclique, mais que les différences dans les valeurs de $E_{1/2}$ pour les couples α-$[S_2W_{18}O_{62}]^{4-}$–$[S_2W_{18}O_{62}]^{5-}$ et γ*-$[S_2W_{18}O_{62}]^{4-}$–$[S_2W_{18}O_{62}]^{5-}$ ne peuvent pas être résolues par voltampérométrie cyclique.

Mots clés : polyoxométalates, synthèse, électrochimie, isomérisation.

Introduction

The $[S_2Mo_{18}O_{62}]^{4-}$ ion as its Bu_4N^+ salt exists as the α-isomer of nominal D_{3h} point symmetry (Fig. 1) (1). In contrast, the equivalent tungsten salt contains the γ*-isomer (Fig. 1, D_{3d}) (2), derived formally from the α-form by 60° rotation of one half of the ion relative to the other, followed by 60° rotation of both trinuclear "caps" (3). The two hexanuclear "belts" are eclipsed in the α-form but staggered in the γ*-form.

The rich electrochemistries of both α-$[S_2Mo_{18}O_{62}]^{4-}$ and γ*-$[S_2W_{18}O_{62}]^{4-}$ have been explored recently (2, 4, 5). These studies have provided an understanding of the complex but highly reversible electrochemical behavior characteristic of these anions and those of polyoxometalate systems in general (6). Multiple pathways for correlated reduction and protonation are present in both the molybdenum and tungsten systems, but only a single fast oxidation pathway is available. As the reduced forms of $[S_2W_{18}O_{62}]^{4-}$ are weaker bases than those of $[S_2Mo_{18}O_{62}]^{4-}$, the individual oxidation pathways are different (2).

A number of reduced forms of $[S_2Mo_{18}O_{62}]^{4-}$ have been isolated in substance[2] (4, 7, 8). The α-isomer is present in structurally characterized salts of the oxidized form and (2 e$^-$, H$^+$)- and (4 e$^-$, 3H$^+$)-reduced forms[2] (8).

The present work reports synthesis and characterization of Bu_4N^+ salts of 1 e$^-$- and 2 e$^-$-reduced forms of $[S_2W_{18}O_{62}]^{4-}$. Intriguingly, one-electron reduction of the γ*-isomer of $[S_2W_{18}O_{62}]^{4-}$ converts it to the α-isomer. A number of systems that exhibit reversible changes in molecular geometry upon simple electron-transfer are known (9, and refs. therein), but not with the multiple breaking and making of bonds characteristic of the present example.

Received September 12, 2000. Published on the NRC Research Press Web site at http://canjchem.nrc.ca on May 31, 2001.

Dedicated to Professor Brian R. James on the occasion of his 65th birthday.

P.J.S. Richardt, J.M. White, P.A. Tregloan, and A.G. Wedd.[1] School of Chemistry, University of Melbourne, Parkville, Victoria 3010, Australia.
A.M. Bond. School of Chemistry, Monash University, Clayton, Victoria 3800, Australia.

[1]Corresponding author (telephone: +61 3 8344 6813; fax: +61 3 9347 5180; e-mail: agw@unimelb.edu.au.

[2]S. Juraja, T. Vu, A.M. Bond, T.J. Cardwell, J.D. Cashion, G. Fallon, G. Lazarev, B. Moubaraki, K.S. Murray, and A.G. Wedd. Submitted for publication (2001).

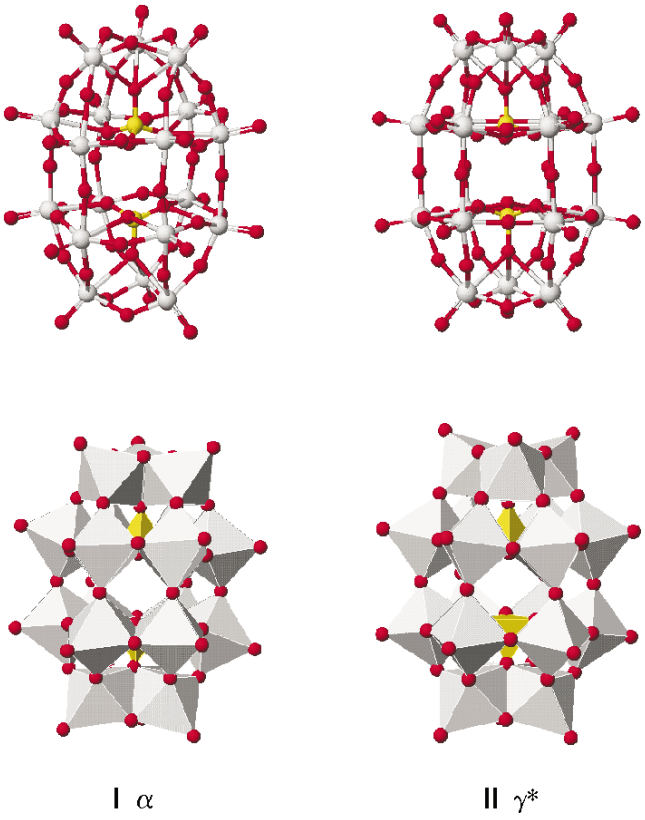
Experimental

Reagents

$Na_2WO_4\cdot 2H_2O$ and $Na_2MoO_4\cdot 2H_2O$ were reagent grade chemicals from APS Ajax Finechem, Melbourne, Australia.

 DOI: 10.1139/cjc-79-5/6-613 © 2001 NRC Canada

Fig. 1. Ball-and-stick and polyhedral representations of the α- and γ*-isomers of $[S_2W_{18}O_{62}]^{4-}$.



CH_3CN, Et_2O, and EtOH were analytical grade chemicals from APS Ajax Finechem. Bu_4NBr was purchased from Aldrich, Milwaukee, WI. The Bu_4N^+ salt of γ*-$[S_2W_{18}O_{62}]^{4-}$ was synthesized as described previously (2).

Synthesis

α-$(Bu_4N)_5[S_2W_{18}O_{62}]$·4MeCN

Controlled potential electrolysis was carried out at a carbon-tube- or mercury-pool-working electrode. A solution of γ*-$(Bu_4N)_4[S_2W_{18}O_{62}]$ (2.0 mM, 1×10^{-4} mol) in MeCN (50 cm^3, 0.1 M Bu_4NClO_4) was electrolyzed at –0.40 V vs. Fc^+/Fc. The reduction was monitored by coulometry, and the average oxidation state of the product confirmed by the position of zero current in a rotating-disk electrode-voltammogram (RDEV). Complete precipitation of the dark blue product occurred upon addition of EtOH with vigorous stirring. The solid was filtered off, washed with EtOH (× 2) and Et_2O, and dried under vacuum (0.46 g, 82%). Recrystallization from hot MeCN yielded dark blue microcrystals. Anal. calcd. for $C_{80}H_{180}N_5O_{62}S_2W_{18}$ (%): C 17.23, H 3.25, N 1.26, S 1.15, W 59.33; found: C 17.46, H 3.13, N 1.30, S 1.18, W 59.60. The MeCN molecules of crystallization detected by X-ray crystallography (see below) appear to be absent in the analytical samples, which were dried under vacuum. UV–vis (MeCN) λ_{max} (nm) (ε (M^{-1} cm^{-1})): 855 (4.2×10^3), 740 (3.7×10^3). FT-IR (KBr pellet) (cm^{-1}): 1175 (m) (WOS), 1075 (m) (WOS), 975 (vs) (W=O), 960 (sh) (W=O), 880 (sh) (WOW), 840 (s) (WOW), 740 (sh) (WOW).

$(Bu_4N)_6[S_2W_{18}O_{62}]$

This salt was prepared similarly via electrolysis at –0.80 V. Isolation was also similar except that anaerobic techniques were employed due to the oxygen sensitivity of the product. Recrystallization from MeCN yielded dark blue microcrystals (0.14 g, 26%). UV–vis (MeCN) λ_{max} (nm) (ε (M^{-1} cm^{-1})): 685 (1.5×10^4). FT-IR (KBr pellet) (cm^{-1}): 1165 (w) (WOS), 1155 (sh) (WOS), 1110 (vw) (WOS), 965 (vs) (W=O), 950 (sh) (W=O), 880 (sh) (WOW), 830 (s) (WOW), 735 (sh) (WOW). Anal calcd. for $C_{96}H_{216}N_6O_{62}S_2W_{18}$ (%): C 19.81, H 3.74, N 1.44, S 1.10, W 56.86; found: C 20.01, H 3.83, N 1.33, S 1.04, W 56.75.

Instrumental techniques

Elemental analysis was performed by the Analytische Laboratorien, Elbach, Germany. Electronic spectra were recorded on a Cary 1C UV–vis spectrophotometer. IR spectra of pressed KBr discs were recorded on a Bio-Rad FTS-165 Fourier-transform spectrometer. Data collection employed a generic 486 PC running Cary ver. 2.50 software on an OS/2 WARP ver. 3 operating platform. The spectrometric cells were quartz with a 1 cm path length. A rectangular OTTLE cell (path length 1 mm) with a 3 mL solution reservoir was utilized for spectro-electrochemistry (10). A Pt gauze (ca. 4 cm^2, ca. 75% transmission) working electrode was used to generate reduced species. A silver-wire quasireference electrode and Pt counter electrode were separated from the electroactive solution by salt bridges located in the upper reservoir of the cell. Electrolysis was performed with a PAR 273A potentiostat. Potentials were held at about 200 mV more negative than the half-wave potential of the appropriate redox process. All spectra were corrected for background electrolyte absorption.

Voltammograms were obtained using a Cypress Systems model CS1087E electroanalysis system. The standard three-electrode arrangement was employed with a Pt-wire auxiliary electrode, glassy-carbon working electrode and Ag/AgCl reference electrode for both rotating-disk voltammetry and cyclic voltammetry. The reference electrode was calibrated against the ferricenium/ferrocene (Fc^+/Fc) couple. All potentials are quoted relative to this standard. The glassy-carbon working electrodes (dia 2.8 mm) were polished with alumina (3 μm) on LECO Inc. polishing pads, then rinsed with distilled water and dried before each experiment. The cell was purged with N_2 for at least ten minutes before each experiment. Rotating-disk voltammetric measurements were undertaken with a Metrohm 2.8 mm diameter glassy-carbon working electrode that was rotated by a variable speed Metrohm 628–10 rotator.

X-ray crystallography

Crystal data

Large hexagonal shaped plates were grown by dissolving $(Bu_4N)_5[S_2W_{18}O_{62}]$ in MeCN (ca. 0.01 M) at 40°C, allowing the solution to cool to room temperature and then stand at 4°C. The large crystals could not be cut without causing significant damage and so large uncut crystals were selected for data collection. The crystals decomposed rapidly during room temperature data collection using Mo Kα radiation. Instrument problems in our laboratories at the time dictated that low-temperature data could be collected only with a Cu

© 2001 NRC Canada

Table 1. Crystallographic data for α-$(Bu_4N)_5[S_2W_{18}O_{62}]$·4MeCN.

Empirical formula	$C_{88}H_{152}N_9O_{64}SW_{18}$
Formula weight (g mol^{-1})	5701.6
Temperature (K)	130.0(1)
Wavelength (Å)	1.54180
Crystal system	Monoclinic
Space group	*C*2/*c*
Unit cell dimensions (Å)	*a* = 26.226(4)
	b = 15.570(2)
	c = 38.407(8)
β (deg)	115.59(2)
Volume ($Å^3$)	14 145(4)
Z, Calculated density (Mg m^{-3})	4, 2.677
Absorption coefficient (mm^{-1})	27.198
F (000)	10 412
Crystal size (mm)	1.0 × 0.5 × 0.09
θ range for data collection (deg)	2.55–60.00
Limiting indices	*h* (0–29), *k* (–17–0), *l* (–43–38)
Reflections collected, unique (*R* (int) = 0.1299)	10 553, 10 284
Completeness to θ = 60.00 (%)	98.1
Refinement method	Full-matrix least-squares on F^2
Data, restraints, parameters	10 284, 0, 656
GoF on F^2	1.135
Final *R* indices ($I > 2\sigma(I)$)[a]	R_1 = 0.0693, wR_2 = 0.1911
R indices (all data)[a]	R_1 = 0.0738, wR_2 = 0.1947
Absorption method	Analytical
Faces (distance to centroid) (mm)	0 0 1 (0.044)
	0 0 –1 (0.044)
	1 0 –1 (0.25)
	–1 0 1 (0.25)
	1 1 –1 (0.5)
	–1 –1 1 (0.5)
Max, min trans.	0.18, 0.006
Extinction coefficient	0.0000191(17)
Largest difference peak and hole (e A^{-3})	4.468, –3.553

[a] $R = \Sigma||Fo| - |Fc||/\Sigma Fo$; $Rw = [\Sigma w(Fo^2\text{-}Fc^2)^2/\Sigma w(Fo^2)^2]^{0.5}$.

radiation source with the attendant problems of absorption. However, the crystal faces were well-formed and easily measured and indexed. Crystals were mounted on a drop of paraffin oil and flash cooled to 130 K using an Oxford Cryostream low-temperature device. Although the reflection peaks showed high mosaicity, data collection was continued. Intensity data were collected using an Enraf–Nonius CAD-4 MachS single crystal X-ray diffractometer using the ω:2θ scan method, with Cu Kα (Ni filtered) λ = 1.5418. Accurate values of the unit cell parameters and crystal orientation were obtained by a least-squares procedure from the angular settings of 25 carefully centered reflections. The crystal showed a deterioration of ca. 5% during the data collection. A total of 10 553 reflections were collected $2 < \theta < 60$, with 10 284 unique (*R* (int) = 0.1299), and used in the subsequent solution and refinement. Crystallographic data are summarized in Table 1. Three different crystals selected from different crops exhibited the same crystallographic parameters.

The structure was solved by a combination of direct methods and difference synthesis (11, 12). It was refined using a full-matrix least-squares refinement procedure based on F^2 and with ansiotropic displacement parameters assigned to all nonhydrogens excluding the oxygen atoms in the cluster. The anion and one of the Bu_4N^+ cations lie on a crystallographic twofold axes while the remaining Bu_4N^+ cations are in general positions. The latter four cations in general positions, were relatively well-ordered while the terminal carbon atoms of the fifth Bu_4N^+ cation and the MeCN solvent showed large temperature factors suggesting disorder. Hydrogen atoms were constrained to idealized positions. The largest peaks in the difference map were in the vicinity of the tungsten cage and may reflect some disorder in the anion. The molecular structure of the anion is shown in Fig. 2, while selected interatomic distances and angles are included in Table 2.[3]

Results and discussion

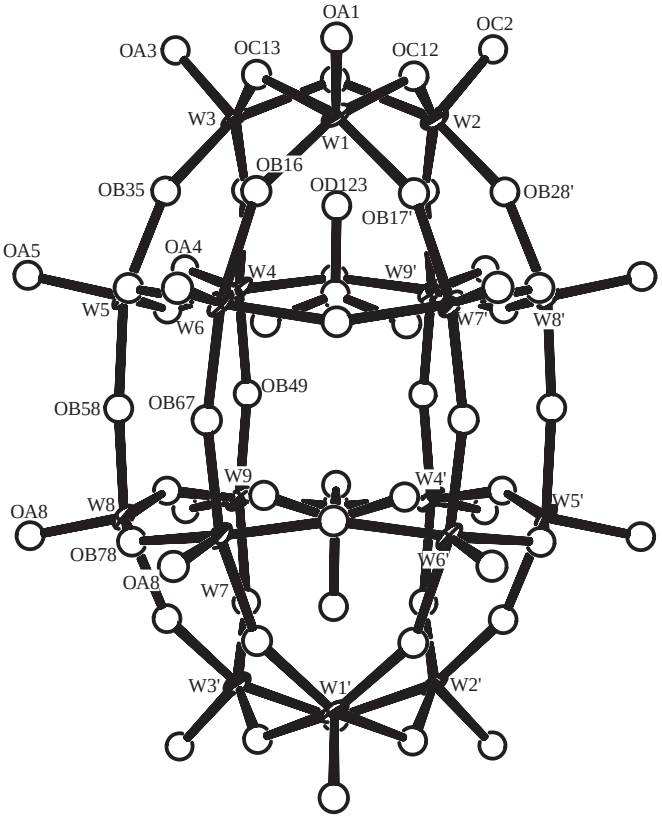
Electrosynthesis and characterization

The first four redox processes (**I**–**IV**) observed for

[3] Supporting information available: An X-ray crystallographic file for $(Bu_4N)_5[S_2W_{18}O_{62}]$·4MeCN in CIF format is available from the authors.

© 2001 NRC Canada

Fig. 2. Molecular structure and labelling scheme of the anion in $(Bu_4N)_5[S_2W_{18}O_{62}]\cdot 4MeCN$. Primed atoms are related to the unprimed atoms by the symmetry operator $1 - x, y, 1/2 - z$.



γ^*-$(Bu_4N)_4[S_2W_{18}O_{62}]$ in MeCN are reversible one-electron processes (2). Controlled potential electrolysis was carried out in MeCN at potentials slightly more negative than those of processes **I** and **II** until the current had decayed to zero (Fig. 3). Coulometry indicated that, respectively, 1.03 and 1.92 electron equiv were transferred. The positions of zero current in RDEV confirmed the presence of stable 1 e^-- and 2 e^--reduction products (Fig. 3). Intense absorption bands characteristic of reduced polyoxo anions appeared in the wavelength range 400–2000 nm (Fig. 4) (13). Quantitative oxidation of the 2 e^--reduction product cleanly regenerated the spectra of the 1 e^--product and of the oxidized anion. In addition, the 2 e^--reduction product was oxidized quantitatively to the 1 e^--level upon exposure to air. Solutions of the latter were stable in air.

This information defined conditions for the isolation in substance of Bu_4N^+ salts of the 1 e^-- and 2 e^--reduced anions $[S_2W_{18}O_{62}]^{5-}$ and $[S_2W_{18}O_{62}]^{6-}$ (see *Synthesis*). Solutions of these salts in MeCN reproduced the spectra of Fig. 4 quantitatively.

X-ray crystal structure of α-$(Bu_4N)_5[S_2W_{18}O_{62}]\cdot 4MeCN$

The 1 e^--reduced anion $[S_2W_{18}O_{62}]^{5-}$ adopts the α-isomeric structure (D_{3h}, Fig. 3), rather than the γ^*-structure (D_{3d}) seen in the oxidized form (2). Upon electrolytic reduction by one electron, γ^*-$[S_2W_{18}O_{62}]^{4-}$ undergoes isomerization to α-$[S_2W_{18}O_{62}]^{5-}$. Attempts to confirm the physical reversibility of this process by X-ray powder diffraction of α-$(Bu_4N)_5[S_2W_{18}O_{62}]\cdot 4MeCN$ and its 1 e^- oxidation product were frustrated by loss of crystallinity caused by solvent loss.

Fig. 3. Rotating-disk electrode voltammograms for: γ^*-$[S_2W_{18}O_{62}]^{4-}$ (——); its 1 e^--reduced (——); and 2 e^--reduced (·····) electrolysis products (2×10^{-3} M in MeCN, 0.1 M Bu_4NClO_4, ν 0.010 V s^{-1}, N_r 2000 min^{-1}).

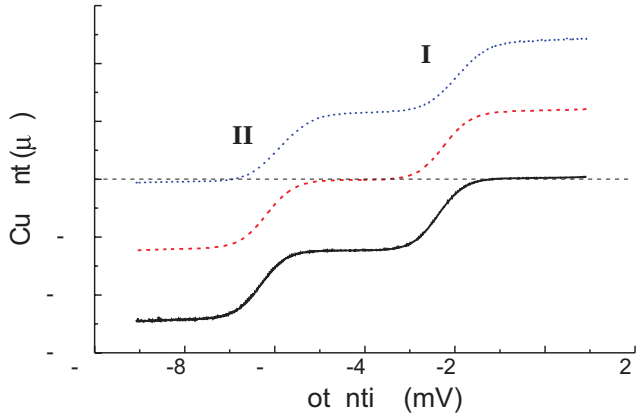
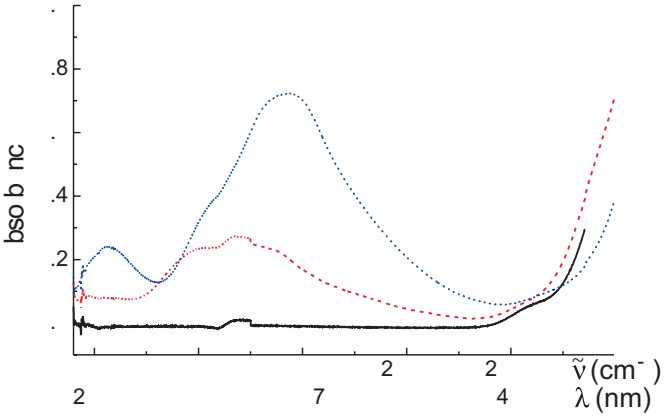


Fig. 4. Electronic spectra generated by electrolysis of γ^*-$(Bu_4N)_4[S_2W_{18}O_{62}]$ (5×10^{-4} M) in MeCN (0.1 M Bu_4NClO_4): before reduction (——); after reduction by 1 e^- equiv (——-); after reduction by 2 e^- equiv (·····). Note baseline artefact at 800–900 nm.



Comparison of structural parameters of α-$[S_2W_{18}O_{62}]^{5-}$ with γ^*-$[S_2W_{18}O_{62}]^{4-}$ and α -$[S_2Mo_{18}O_{62}]^{4-}$ may be made from Tables 2 and 3. The most significant differences between the tungsten isomers are the changes in the ranges observed in bond angles M(μ-O)M at the oxygen atoms O_{b2}, which link the caps with the belts (e.g., W3OB35W5: $\gamma^* = 161 \pm 1°$, $\alpha = 154 \pm 1°$), and at the oxygen atoms O_{b3}, which link the two belts (e.g., W5OB58W8: $\gamma^* = 179 \pm 1°$, $\alpha = 167 \pm 1°$). These differences occur in the regions of major topological change induced by the relative rotation of the belts and caps (2, 3). Table 3 details the O···O nonbonded separations in these anions. The smaller hexagons of bridging atoms (O_{b1}), which link the belts with the caps each feature alternating shorter and longer nonbonding separations. The difference is more pronounced in the α-isomers. On the other hand, the larger hexagon of bridging atoms (O_{b3}),

© 2001 NRC Canada

Table 2. Mean interatomic distances (Å), bond angles (°), and observed ranges[a] in Bu_4N^+ salts of α-$[S_2Mo_{18}O_{62}]^{4-}$, γ*-$[S_2W_{18}O_{62}]^{4-}$, and α-$[S_2W_{18}O_{62}]^{5-}$.

	α-$[S_2Mo_{18}O_{62}]^{4-}$, [b]	γ*-$[S_2W_{18}O_{62}]^{4-}$, [c]	α-$[S_2W_{18}O_{62}]^{5-}$, [d]
Bond lengths (Å)			
$M{=}O_{a1}$	1.66 ± 0.04	1.70 ± 0.01	1.71 ± 0.02
$M{=}O_{a2}$	1.66 ± 0.03	1.69 ± 0.03	1.69 ± 0.03
$M{-}O_{b1}$ (from cap)	1.91 ± 0.14	1.90 ± 0.04	1.88 ± 0.01
$M{-}O_{b1}$ (from belt)	1.94 ± 0.15	1.90 ± 0.03	1.93 ± 0.02
$M{-}O_{b2}$	1.90 ± 0.06	1.89 ± 0.03	1.90 ± 0.03
$M{-}O_{b3}$	1.92 ± 0.14	1.89 ± 0.02	1.89 ± 0.03
$M{-}O_{c1}$	1.91 ± 0.13	1.89 ± 0.05	1.92 ± 0.03
$M{-}O_{c2}$	1.91 ± 0.07	1.92 ± 0.03	1.91 ± 0.03
$M{-}O_{d1}$	2.47 ± 0.04	2.52 ± 0.05	2.51 ± 0.03
$S{-}O_{d1}$	1.46 ± 0.04	1.47 ± 0.01	1.45 ± 0.01
$M{-}O_{d2}$	2.49 ± 0.05	2.53 ± 0.03	2.47 ± 0.01
$S{-}O_{d2}$	1.50 ± 0.02	1.46 ± 0.01	1.51 ± 0.01
S···S	3.92	3.77	3.81
Bond angles (°)			
O_{d2}-M-O_{a1}	171 ± 2	172 ± 1	173 ± 1
O_{d1}-M-O_{a2}	170 ± 2	172 ± 2	173 ± 2
M-O_{b1}-M	153 ± 6	151 ± 2	152 ± 2
M-O_{b2}-M	153 ± 2	161 ± 1	154 ± 1
M-O_{b3}-M	164 ± 1	179 ± 1	167 ± 1
M-O_{c1}-M	128 ± 2	132 ± 2	127 ± 1
M-O_{c2}-M	129 ± 3	131 ± 1	131 ± 2
M-O_{d1}-M	89 ± 2	87 ± 1	87 ± 1
M-O_{d1}-S	128 ± 4	127 ± 2	128 ± 2
M-O_{d2}-M	87 ± 1	86 ± 1	88 ± 1
M-O_{d2}-S	127 ± 3	128 ± 2	127 ± 1

[a]The observed values are indicated as a ± range. The key to the labelling of specific oxygen atoms is in Fig. 2.
[b]Taken from ref. 1.
[c]Taken from ref. 3.
[d]Typical esd values (Å or °) for α-$(Bu_4N)_5[S_2W_{18}O_{62}]$·4MeCN are: W-O, 0.01; S-O, 0.01; S···S, 0.008; OWO, 0.6; WOW, 0.6; WOS, 0.6.

Table 3. Observed ranges of O···O distances (Å)[a] in α-$(Bu_4N)_4[S_2Mo_{18}O_{62}]$, γ*-$(Bu_4N)_4[S_2W_{18}O_{62}]$, and α-$(Bu_4N)_5[S_2W_{18}O_{62}]$.

Hexagon[b]	Corner (c)- or edge (e)-shared octahedra	α -$[S_2Mo_{18}O_{62}]^{4-}$, [c]	γ*-$[S_2W_{18}O_{62}]^{4-}$, [c]	α-$[S_2W_{18}O_{62}]^{5-}$
Larger	c	4.18 ± 0.04		4.13 ± 0.02
	c, e		3.63 ± 0.01	
	e	3.08 ± 0.03		3.16 ± 0.01
Smaller	c	2.58 ± 0.01	3.29 ± 0.04	2.57 ± 0.03
	e	3.17 ± 0.04	2.53 ± 0.03	3.20 ± 0.03

[a]The observed values are indicated as a ± range. Data taken from references footnoted in Table 2.
[b]The larger hexagon is formed by atoms O_{b3}, which bridge the two hexanuclear belts; the smaller hexagon is formed by atoms O_{b1}, which bridge the hexanuclear belts and the trinuclear caps (see Fig. 2).
[c]Esd values for O···O distances are typically 0.02 Å.

which link the two halves of the molecules, have similar separations in the γ*-isomer but alternating shorter and longer separations in the α-isomers.

It is surprising to find that upon reduction by a single electron, γ*-$[S_2W_{18}O_{62}]^{4-}$ undergoes relative rotation of both caps and belts, which would require the breaking of multiple W—O bonds. In particular, the two hexanuclear belts are eclipsed in the α form but staggered in the γ* form (Fig. 1).

Resonance and spectroscopic data on the 1 e^-- and 2 e^--reduced forms of α-$[P_2M_{18}O_{62}]^{6-}$ (M = Mo, W) indicate that the additional electrons are localized on the metal atoms of the belts (14–18). There is now direct structural evidence of this phenomenon in the series of α-anions $[S_2Mo_{18}O_{62}]^{4-}$ (oxidized), $[HS_2Mo_{18}O_{62}]^{5-}$ (reduced by 2 e^-, 1H^+), and $[H_3S_2Mo_{18}O_{62}]^{5-}$ (reduced by 4 e^-, 3H^+)[2] (8). As two and then four electrons are added, the average Mo···Mo distance across the belts decreases. As equivalent octahedra in each belt are linked by a bridging O_{b3} ligand, the conclusion is consistent with the known stability of the spin-paired $[Mo^VO]_2(\mu\text{-}O)$ fragment, stabilized by exchange correlations

© 2001 NRC Canada

Table 4. Cyclic voltammetry data for α-$(Bu_4N)_5[S_2W_{18}O_{62}]$ (1.0×10^{-3} M) in MeCN (0.1 M Bu_4NClO_4).[a]

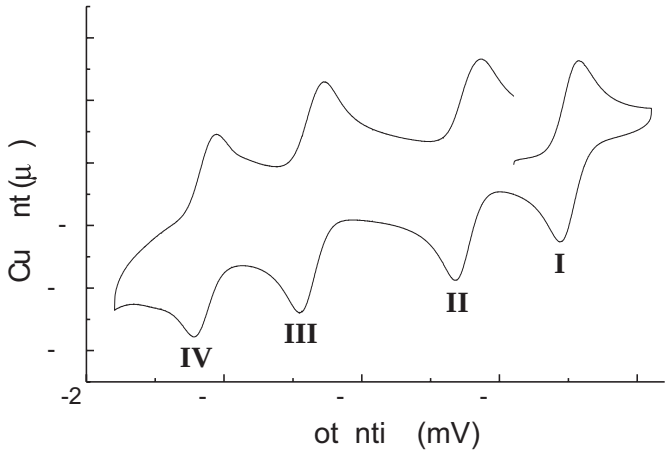
	ν ($V\ s^{-1}$)	$E_{1/2}$ (V)	E_{pc} (V)	ΔE_p (V)	i_{pc} ($\mu A\ mM^{-1}$)	$i_{pc}v^{-1/2}$ ($\mu A\ s^{1/2}\ V^{-1/2}$)	i_{pa}/i_{pc}
I	0.020	–0.245	–0.275	0.060	6.1	1.4	1.0
	0.050	–0.245	–0.280	0.070	9.4	1.3	1.0
	0.100	–0.245	–0.280	0.070	13.2	1.3	1.0
	0.200	–0.245	–0.280	0.070	18.0	1.3	1.0
	0.500	–0.245	–0.285	0.080	29.1	1.3	0.9
	1.000	–0.245	–0.290	0.090	40.4	1.3	1.0
II	0.020	–0.615	–0.650	0.070	5.9	1.3	1.0
	0.050	–0.615	–0.650	0.070	9.1	1.3	1.0
	0.100	–0.620	–0.660	0.080	12.9	1.3	1.0
	0.200	–0.625	–0.660	0.070	17.5	1.2	1.0
	0.500	–0.625	–0.660	0.070	28.1	1.3	1.1
	1.000	–0.625	–0.665	0.080	39.6	1.3	1.1
III	0.020	–1.175	–1.210	0.070	6.3	1.4	1.0
	0.050	–1.180	–1.220	0.080	9.6	1.4	1.0
	0.100	–1.185	–1.225	0.080	13.0	1.3	1.0
	0.200	–1.185	–1.225	0.080	18.1	1.3	1.0
	0.500	–1.190	–1.230	0.080	28.6	1.3	1.0
	1.000	–1.190	–1.235	0.090	40.5	1.3	1.0
IV	0.020	–1.560	–1.590	0.060	4.7	1.0	1.2
	0.050	–1.560	–1.600	0.080	7.0	1.0	1.2
	0.100	–1.565	–1.600	0.070	10.2	1.0	1.2
	0.200	–1.565	–1.600	0.070	13.7	1.0	1.2
	0.500	–1.570	–1.610	0.080	22.1	1.0	1.2
	1.000	–1.570	–1.615	0.090	31.8	1.0	1.2

[a]Potentials relative to the Fc^+/Fc couple.

mediated by the bridging O_{b3} atom (19). EPR investigations of 1 e^--reduced α-$[S_2Mo_{18}O_{62}]^{5-}$ indicate that the unpaired electron is delocalized over the entire molecular framework (7). However, cyclic voltammetry in MeCN revealed pairs of 1 e^--reductions (separation ~0.2 V) with a larger separation between pairs (~0.6 V) (4). This result suggests a significant contribution from exchange via M_2^V pairs.

The presence of additional electron density on the belts of $[S_2W_{18}O_{62}]^{5-}$ may lower the activation energy for rotation of the belts from the staggered (γ*) to the eclipsed (α) conformation (Fig. 1). Such rotation converts the similar O···O nonbonding separations in the large central hexagons of O_{b3} atoms in γ*-$[S_2W_{18}O_{62}]^{4-}$ to the alternating long and short distances characteristic of an α-isomer (Table 3). The effect of this conversion on the smaller, upper hexagon of the belt is to invert the pattern of long and short O···O separations. This would destabilize the caps in their original orientation and favor rotation to that characteristic of the α-isomer.

Fig. 5. Cyclic voltammogram of α-$(Bu_4N)_5[S_2W_{18}O_{62}]$ (1.0×10^{-3} M) in MeCN (0.1 M Bu_4NClO_4, ν 0.100 V s^{-1}).



Electrochemistry in MeCN

RDE voltammetry for the isolated reduced salts $(Bu_4N)_5[S_2W_{18}O_{62}]$ and $(Bu_4N)_6[S_2W_{18}O_{62}]$ in MeCN mimics that of the electrolyzed solutions (Fig. 3). The reversible half-wave potential ($E_{1/2}$) and diffusion coefficient (D_f) were the same, within experimental error, for each salt and the same as those observed for $(Bu_4N)_4[S_2W_{18}O_{62}]$ (2). Cyclic voltammetry operates on a faster timescale. Results for the two reduced salts revealed four one-electron processes that are essentially reversible (Fig. 5, Table 4). A comparison of data for processes **I**–**IV** of 1 e^--reduced α-$[S_2W_{18}O_{62}]^{5-}$ with those (2) of oxidized γ*-$[S_2W_{18}O_{62}]^{4-}$ indicate that all parameters are the same within experimental error. No evidence of interconversion of α- and γ*-isomers could be detected on the timescale of the cyclic voltammetry. Addition of acid in MeCN–H_2O (95:5 v/v) solutions also allowed no discrimination. Processes **III** and **IV** coalesced as the acid concentration increased to produce the new 2 e^--process *III*. This was accompanied at higher acid concentrations by new 2 e^--process *IV*. This is clearly evident in RDE

© 2001 NRC Canada

Fig. 6. RDE voltammogram of α-$(Bu_4N)_5[S_2W_{18}O_{62}]$ (1.0×10^{-3} M) in MeCN:H_2O (95:5 v/v, 0.1 M Bu_4NClO_4, N_r 2000 min^{-1}) with 100 mol equiv $HClO_4$.

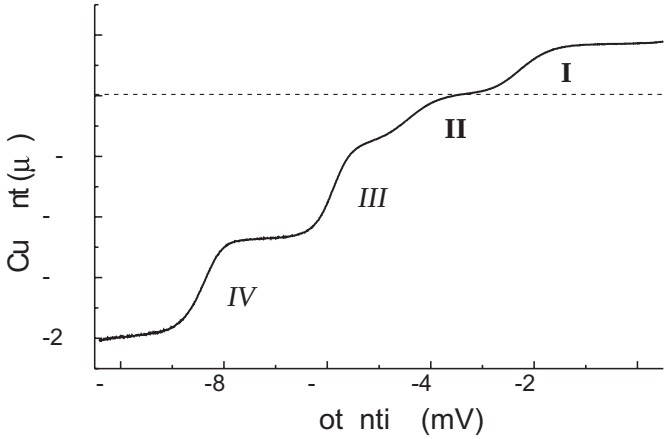
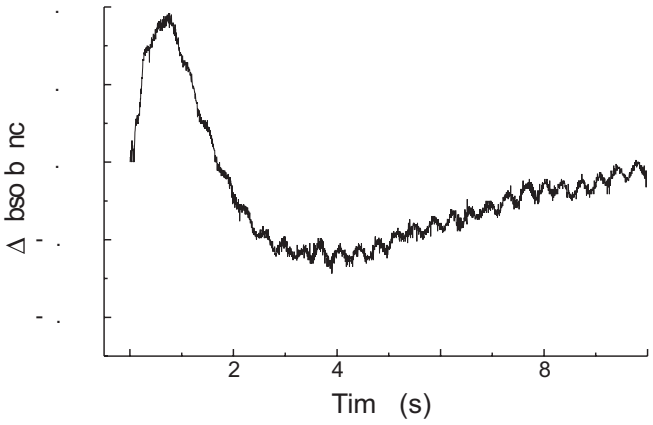


Fig. 7. Plot of absorbance difference vs. time for α-$(Bu_4N)_4[S_2Mo_{18}O_{62}]$ (3.2×10^{-5} M) and α-$(Bu_4N)_5[S_2W_{18}O_{62}]$ (9.8×10^{-5} M) in MeCN (λ = 410 nm).



voltammetry, where the ratios of limiting currents for processes **I**:**II**:*III*:*IV* = 1:0.96:1.96:1.93 (Fig. 6). Again the behavior mimics that of oxidized γ*-$[S_2W_{18}O_{62}]^{4-}$ under equivalent conditions (2).

Isomerization

Reduction of γ*-$[S_2W_{18}O_{62}]^{4-}$ by 1 e^--equiv by electrolysis leads to the isolation of α-$[S_2W_{18}O_{62}]^{5-}$ as the Bu_4N^+ salt. This transformation was not detected on the timescale of cyclic voltammetry, even at the fast scan rate of 10 V s^{-1}. The $E_{1/2}$ values derived by cyclic voltammetry were the same, within experimental error, for γ*-$[S_2W_{18}O_{62}]^{4-}$ and α-$[S_2W_{18}O_{62}]^{5-}$. This observation may be attributed to one of three possibilities: (*i*) the γ* ↔ α equilibrium favors one of the isomers in solution (presumably the α-form) for both redox states and the electrochemistry accesses that form; (*ii*) the isomerization is fast on the voltammetric timescale; or (*iii*) the isomerization is slow on that timescale but the difference in $E_{1/2}$-values for processes **I**–**IV** cannot be resolved by the techniques available up to the present work.

In the only comparable system available, RDE voltammetry (carbon-working electrode) examined $[As_2W_{18}O_{62}]^{6-}$ in aq solution at pH 1 (NaCl 0.9 M, HCl 0.1 M) (3). The voltammetries of the β- and γ*-isomers were indistinguishable within the resolution limit of 20 mV. Three processes were reported for each of the α- and γ*-isomers. The differences in $E_{1/2}$-values were 30 mV for each process, close to the resolution limit, with those for the γ*-isomer being more positive. However, the second process was reported as a 1 e^--process for the α-isomer and as a 2 e^--process for the γ*-isomer. In nonaqueous systems, Bu_4N^+ salts of the α-, β-, and γ-isomers of the Keggin system $[SiW_{12}O_{40}]^{4-}$ are available (20, 21). Cyclic voltammetry in MeCN demonstrated that the α- and β-isomers can be distinguished on the basis of $E_{1/2}$-values (three 1 e^--processes that are 80–110 mV more positive for the α-isomer), and that 1 e^--reduction of the γ-isomer converts it to the α-isomer on the voltammetric timescale (22).

Examination of the half potentials for the $[S_2W_{18}O_{62}]^{4-}$–$[S_2W_{18}O_{62}]^{5-}$ and α-$[S_2Mo_{18}O_{62}]^{4-}$–α-$[S_2Mo_{18}O_{62}]^{5-}$ couples (Table 5 and ref. 2) indicated that the following reaction would proceed to completion:

$$\alpha\text{-}[S_2W_{18}O_{62}]^{5-} + \alpha\text{-}[S_2Mo_{18}O_{62}]^{4-} \rightarrow [S_2W_{18}O_{62}]^{4-} + \alpha\text{-}[S_2Mo_{18}O_{62}]^{5-}$$

Mixing experiments confirmed this prediction as the electronic spectra of each of the four species is known (see *Synthesis* and ref. 2). Exploratory stopped-flow experiments were carried out in the wavelength range 820–340 nm at a range of relative concentrations of reactants. Typical results are presented in Fig. 7. Data fitting was not attempted due to the complex nature of the system. However, different transformations are occurring on time scales of about ~1 s, ~2 s, and >10 s. The simplest interpretation is that electron transfer is completed in the first process and that the slower processes are associated with subsequent relaxation of the product anions. Whether this includes isomerization of initial product α-$[S_2W_{18}O_{62}]^{4-}$ to final product γ*-$[S_2W_{18}O_{62}]^{4-}$ cannot be discerned.

The available data suggest that either: (*i*) the γ* ↔ α equilibrium favors one of the isomers in solution (presumably the α-form) for both redox states, or (*ii*) the γ* ↔ α isomerization associated with the $[S_2W_{18}O_{62}]^{4-}$–$[S_2W_{18}O_{62}]^{5-}$ couple is slow on the cyclic voltammetric timescale and that the differences in $E_{1/2}$ values for the α-$[S_2W_{18}O_{62}]^{4-}$– α-$[S_2W_{18}O_{62}]^{5-}$ and γ*-$[S_2W_{18}O_{62}]^{4-}$–γ*-$[S_2W_{18}O_{62}]^{5-}$ couples cannot be resolved by cyclic voltammetry.

Acknowledgements

A.G.W and A.M.B thank the Australian Research Council for support via Grants A29531579 and A294801726.

References

1. T. Hori, O. Tamada, and S. Himeno. J. Chem. Soc. Dalton Trans. 1491 (1989).
2. P.J.S. Richardt, R.W. Gable, A.M Bond, and A.G. Wedd. Inorg. Chem. **40**, 703 (2001).
3. R. Contant and R. Thouvenot. Inorg. Chim. Acta, **212**, 41 (1993).
4. D.M. Way, A.M. Bond, and A.G. Wedd. Inorg. Chem. **36**, 2826 (1997).

© 2001 NRC Canada

5. D.M. Way, J.B. Cooper, M. Sadek, T. Vu, P.J. Mahon, A.M. Bond, R.T.C. Brownlee, and A.G. Wedd. Inorg. Chem. **36**, 4227 (1997); erratum: Inorg. Chem. **37**, 604 (1998).
6. P.D. Prenzler, C. Boskovic, A.M. Bond, and A.G. Wedd. Anal. Chem. **71**, 3650 (1999).
7. J.B. Cooper, D.M. Way, A.M. Bond, and A.G. Wedd. Inorg. Chem. **32**, 2416 (1993).
8. R. Neier, C. Trojanowski, and R. Mattes. J. Chem. Soc. Dalton Trans. 2521 (1995).
9. S. Zahn and J.W. Canary. Science **288**, 1404 (2000).
10. C.M. Duff and G.A. Heath. Inorg. Chem. **30**, 2528 (1991).
11. G.M. Sheldrick. SHELXS-97, program for crystal structure solution. University of Gottingen, Germany. 1997.
12. G.M. Sheldrick. SHELXL-97, program for crystal structure refinement. University of Gottingen, Germany, 1997.
13. M.T. Pope. Heteropoly and isopoly oxometalates. Springer-Verlag, Berlin. 1983. pp. 109–112.
14. R.A. Prados and M.T. Pope. Inorg. Chem. **15**, 2547 (1976).
15. L.P. Kazanskii and M.A. Fedotov. J. Chem. Soc. Chem. Commun. 644 (1980).
16. J.N. Barrows and M.T. Pope. Inorg. Chim. Acta, **213**, 91 (1993).
17. M. Kozik, C.F. Hammer, and L.C.W. Baker. J. Am. Chem. Soc. **108**, 2748 (1986).
18. N. Casan-Pastor and L.C.W. Baker. J. Am. Chem. Soc. **114**, 10384 (1992).
19. E.I. Steifel. Prog. Inorg. Chem. **22**, 1 (1977).
20. A. Tézé and G. Hervé. Inorg. Synth. **27**, 85 (1990).
21. C. Rocchiccioli-Deltcheff, M. Fournier, R. Franck, and R. Thouvenot. Inorg. Chem. **22**, 207 (1983).
22. P.J.S. Richardt. B.Sc. (Hons.) Thesis. University of Melbourne, Melbourne, Australia. 1993.

© 2001 NRC Canada

Thioacetalization of aldehydes and ketones in the presence of hydroxo complexes of platinum(II): An example of Lewis acid catalytic activity

Lorenzo Battaglia, Francesco Pinna, and Giorgio Strukul

Abstract: The complex $[(dppb)Pt(\mu\text{-}OH)]_2(BF_4)_2$ displays high catalytic activity in the thioacetalization of a variety of aldehydes and ketones with mercaptoethanol under very mild conditions. The reaction rate is greatly enhanced by the addition to the reaction mixture of magnesium perchlorate as drying agent and molar turnovers as high as 9700 can be observed. The effect of different desiccating agents is also reported. The reactivity pattern observed, the similarity with other reactions and NMR spectroscopic investigations confirm the possible role of the complex as Lewis acid catalyst in promoting the reaction.

Key words: thioacetalization, catalysis, aldehydes, ketones, platinum complex.

Résumé : Le complexe $[(dppb)Pt(\mu\text{-}OH)]_2(BF_4)_2$ présente une activité catalytique élevée dans les réactions de thioacétalisation d'une grande variété d'aldéhydes et de cétones par réaction avec le mercaptoéthanol, sous des conditions expérimentales douces. La vitesse de la réaction est augmentée par l'addition au mélange réactionnel de perchlorate de magnésium comme agent desséchant; on peut alors observer des taux de renouvellement chimique qui peut aller jusqu'à 9,700. On rapporte aussi l'effet de divers agents desséchant. Le type de réactivité observé, la similarité avec d'autres réactions et les études par spectroscopie RMN confirment la possibilité que le complexe agit comme un catalyseur acide de Lewis pour promouvoir la réaction.

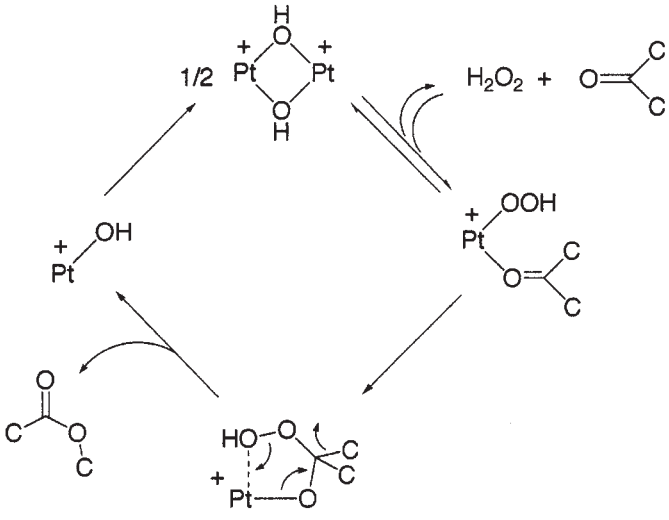
Mots clés : thioacétalisation, catalyseur, aldéhydes, cétones, complexe du platine.

[Traduit par la Rédaction]

Introduction

The acetalization reaction is a process that is widely used in organic synthesis to protect the carbonyl group of aldehydes and ketones (1) and for the synthesis of end products (acetals), including enantiomerically pure compounds (see for example ref. 2), that find practical application in the field of synthetic carbohydrate (3), steroids (4), pharmaceuticals and fragrances (5), and as polymers and copolymers (6). This reaction is normally acid catalyzed, although the use of transition-metal complexes as Lewis acid catalysts has been occasionally reported in the literature (7). In the past two decades we have extensively studied the properties of cationic Pd(II) and Pt(II) complexes in a variety of oxidation reactions using hydrogen peroxide as oxidant (for reviews on this subject see ref. 8). A typical feature displayed by the metal in the latter reactions is the ability to increase the reactivity of the substrate by coordination thereby making it more prone to attack by the peroxidic oxidant. An essential requirement to promote this kind of reactivity is the presence of a positive charge on the metal which, therefore, possesses a significant Lewis acidity. An example of this behavior is shown in Scheme 1 which illustrates the mechanism of the Baeyer–Villiger oxidation of ketones catalyzed by $[(P\text{-}P)Pt(\mu\text{-}OH)]_2^{2+}$ complexes [9] (P-P = a variety of different disphosphines, including chiral ones for asymmetric transformations (10)). The Lewis acidity of these complexes

Scheme 1.



Received September 14, 2000. Published on the NRC Research Press Web site at http://canjchem.nrc.ca on May 31, 2001.

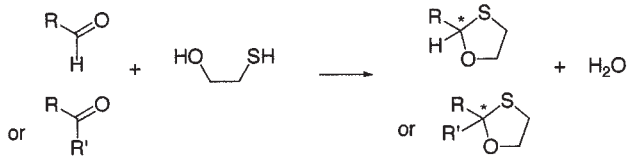
G. Strukul wishes to dedicate this work to Professor Brian R. James, mentor and friend of a lifetime.

Lorenzo Battaglia, Francesco Pinna, and Giorgio Strukul.[1] Department of Chemistry, University of Venice, Dorsoduro 2137, 30123 Venezia, Italy.

[1]Corresponding author (telephone: +39 041 257 8551; fax: +39 041 257 8517; e-mail: strukul@unive.it).

 DOI: 10.1139/cjc-79-5/6-621 © 2001 NRC Canada

Scheme 2.



has been recently exploited to catalyze the acetalization of a variety of aldehydes and ketones (11), where some unusual selectivities with respect to ordinary Brønsted acids were observed, especially in the case of α,β-unsaturated substrates (12).

In this paper we wish to report the first example of a transition-metal catalyzed thioacetalization reaction. This reaction is potentially very useful in organic synthesis as, for example, the use of 2-mercaptoethanol as the acetalizing agent leads to the formation of 1,3-oxathiolanes (Scheme 2) and opens an easy access to a class of chiral compounds that can be obtained starting from every aldehyde or unsymmetrically substituted ketones.

Results and discussion

The complex used as catalyst in the present study is $[(dppb)Pt(\mu\text{-}OH)]_2(BF_4)_2$. This cationic complex displays a significant Lewis acidity as was already observed in the catalysis of the above mentioned acetalization reactions (11, 12) and in the Baeyer–Villiger oxidation of ketones with hydrogen peroxide (9). The choice of this complex is due to the fact that it proved to be the most active among the homologous complexes of Pt in both the acetalization and the Baeyer–Villiger oxidation. Moreover, compared to homologous complexes of Pd, it is more thermally stable and can be used as catalyst up to 90°C without any problems. It can be easily obtained starting from the corresponding dichloro complex by addition of 2 equiv of $AgBF_4$ in acetone (13) according to eq. [1]. However, we found that the reported synthetic procedure (13) may lead to the adsorption of significant amounts of HBF_4 on the complex upon precipitation. To avoid possible ambiguities in the catalytic tests, the complex, dissolved in CH_2Cl_2, was extracted several times with water until neutrality was attained.

Initially, the search for the best reaction conditions in the thioacetalization reaction was carried out. To this purpose, 2-mercaptoethanol was tested in the reaction with benzaldehyde and a summary of the results obtained is reported in Table 1. Initial tests were carried out with benzaldehyde at 25°C using 0.05% equivalents of the dimeric catalyst with respect to the substrate corresponding to 0.1% Pt. At room temperature, no activity was observed even increasing the equivalents of Pt to 1% (run 2). Upon increasing the reaction temperature to 82°C, a quick reaction takes place leading to about 60% conversion in about 10 h and to the neat formation (>99% selectivity) of 2-phenyl-1,3-oxathiolane. During the same reaction time, a blank reaction without catalyst shows no conversion. Similar results were observed using other aldehyde and ketone substrates, with the exception of acetophenone where a much lower conversion was observed (Table 1). Since no attempt was made to remove water formed during the reaction (Scheme 2), in all cases the reaction stops at equilibrium concentration, preventing the achievement of higher conversions.

Table 1. Thioacetalization of different substrates with 2-mercaptoethanol catalyzed by $[(dppb)Pt(\mu\text{-}OH)]_2\ (BF_4)_2$.

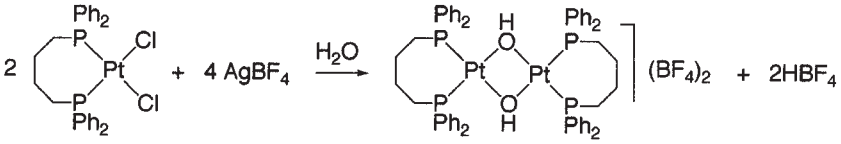
Run	Substrate	Temperature (°C)	Max conversion (%)	Time (min)
1	Benzaldehyde	25	0	1440
2		25[a]	0	1450
3		82	62	600
4	Propanal	82	57	500
5	Acetophenone	82	9	1800
6	*p*-Anisaldehyde	82	80	300
7	Cyclohexanone	82	58	350
8	2-Hexanone	82	21	1500

Note: Experimental conditions: Pt (5 μmol), substrate (5 mmol), 2-mercaptoethanol (5 mmol), 1,2-dichloroethane (2.2 mL).
[a]Pt (0.05 mmol).

For this reason the reaction was tested in the presence of a desiccating agent. This is not unusual for equilibrium reactions forming water, for example Gorla and Venanzi (7*e*) in their study on catalyzed acetalization reactions found the use of molecular sieves very useful to maximize conversions and reaction rates. In the present case, $Mg(ClO_4)_2 \cdot 2H_2O$ was added to the initial reaction mixture in 20% excess with respect to the theoretical amount of water formed at full conversion. At the reaction temperature used in the previous experiments (82°C) the thioacetalization reaction is extremely fast (>99% conversion in 1 min) both for the catalyzed and the non-catalyzed blank reaction. For this reason a new series of catalytic tests was carried out at 25°C. The results for a variety of aldehydes and ketones are shown in Tables 2 and 3 where a comparison with the non-catalyzed reaction is also reported.

As can be seen, in the case of aldehydes the reaction is always very fast and catalyst amounts as low as 0.01% with respect to the substrate were used. A comparison with the non-catalyzed reactions indicate that the catalytic effect is not very pronounced except in the case of *p*- and *m*-anisaldehyde, where the non-catalyzed reaction is considerably slower. The case of ketones is different. In all cases the catalytic effect is very strong (perhaps with the exception of cyclohexanone). In a few hours a variety of ketones can be converted almost quantitatively with the catalyst performing 8500–9700 turnovers, opening some interesting synthetic perspectives.

Other desiccating agents have been tested in the thioacetalization of 2-butanone taken as the test reaction, namely sodium sulfate, magnesium sulfate, and molecular

[1] 

© 2001 NRC Canada

Table 2. Thioacetalization of aldehydes with 2-mercaptoethanol in the presence of magnesium perchlorate.

Substrate	With catalyst		Without catalyst	
	Conversion (%)	Time (min)	Conversion (%)	Time (min)
Propanal	99	5	90	4
Benzaldehyde	90	210	85	415
3-Chlorobenzaldehyde	96	140	98	130
p-Anisaldehyde	85	200	78	1650
m-Anisaldehyde	84	55	87	1335
Octanal	94	4	92	25

Note: Comparison between the catalyzed (by $[(dppb)Pt(\mu\text{-}OH)]_2(BF_4)_2$) and the non-catalyzed reaction. Experimental conditions: Pt (2 μmol), substrate (20 mmol), 2-mercaptoethanol (20 mmol), $Mg(SO_4)_2\cdot 2H_2O$ (1.555 g), 1,2-dichloroethane (8.8 mL).

Table 3. Thioacetalization of ketones with 2-mercaptoethanol in the presence of magnesium perchlorate.

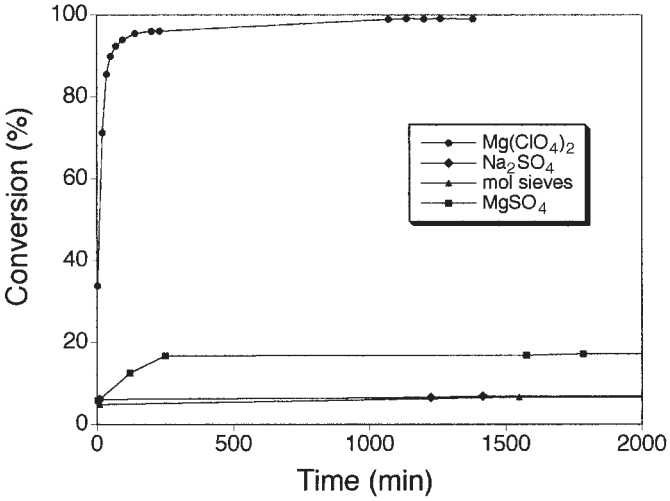
Substrate	With catalyst		Without catalyst	
	Conversion (%)	Time (min)	Conversion (%)	Time (min)
2-Butanone	96	200	3	1260
2-Hexanone	90	400	1	1700
Cyclohexanone	97	270	86	1080
Acetophenone	85	5400	0	5400
Phenylacetone	84	1065	2	1260

Note: Comparison between the catalyzed (by $[(dppb)Pt(\mu\text{-}OH)]_2(BF_4)_2$) and the non-catalyzed reaction. Experimental conditions: Pt (2 μmol), substrate (20 mmol), 2-mercaptoethanol (20 mmol), $Mg(SO_4)_2\cdot 2H_2O$ (1.555 g), 1,2-dichloroethane (8.78 mL).

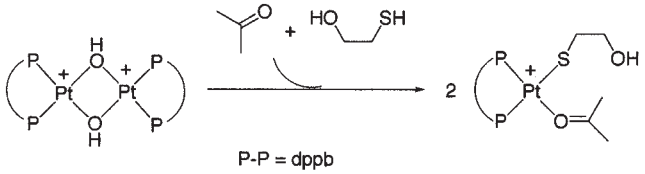
sieves. The results are summarized in Fig. 1 and show that $Mg(ClO_4)_2\cdot 2H_2O$ is by far the most effective desiccating agent. Since all desiccants tested are based on poorly coordinating anions, an interpretation of the data of Fig. 1 on this basis seems unlikely. Indeed, they differ significantly in the water absorption rate and, to a minor extent, in the water absorption capacity, in this respect magnesium perchlorate being the best option (14). This view may constitute a possible explanation for the behavior shown in Fig. 1, where the different rates correlate with the absorption rate, while the maximum conversions could be associated to different amounts of residual water at the equilibrium. The possible direct involvement of Mg^{2+} through the formation of soluble species similar to the complex $[(PPh_3)_2Pt(\mu\text{-}O)]_2LiBF_4$ as reported by Sharp and co-workers (13*a*) seems less likely in view of the very different behavior between magnesium perchlorate and magnesium sulfate observed in Fig. 1.

From Table 3, it appears that aliphatic ketones are more reactive and their reactivity can be correlated to the inductive effect of substituents as for example in the sequence: 2-butanone > phenylacetone > acetophenone. This seems to suggest that the role of the catalyst can be associated to Lewis acidity, where the electrophilicity of the carbonyl compound is increased by coordination making it more prone to nucleophilic attack by the alcohol (thiol). In this respect, Scheme 1 provides a rationale for the understanding of the mechanism with which the thioacetalization reaction occurs. The similarities between the formation of the

Fig. 1. Effect of four desiccating agents on the thioacetalization of 2-butanone with 2-mercaptoethanol in the presence of $[(dppb)Pt(\mu\text{-}OH)]_2(BF_4)_2$ as catalyst. $Mg(ClO_4)_2\cdot 2H_2O$ (circles), Na_2SO_4 (diamonds), molecular sieves (triangles), $MgSO_4$ (squares). Experimental conditions: Pt (2 μmol), 2-butanone (20 mmol), 2-mercaptoethanol (20 mmol), 1,2-dichloroethane (8.8 mL), $Mg(ClO_4)_2\cdot 2H_2O$ (1.555 g), Na_2SO_4 (0.341 g), molecular sieves (3.6 g), $MgSO_4$ (0.413 g).



Scheme 3.

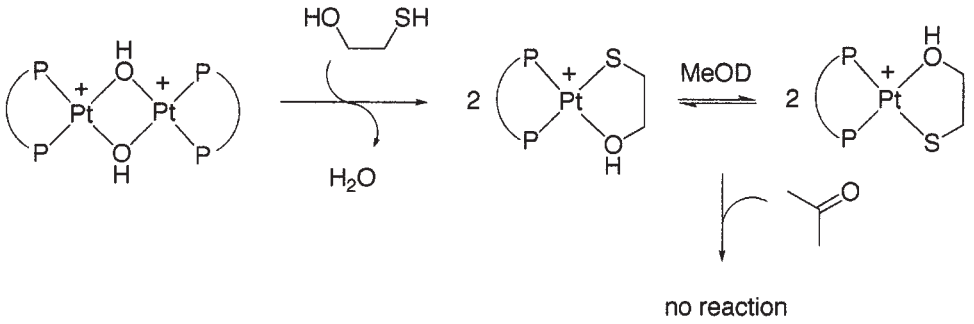


hydroperoxyplatinum ketone complex and the process depicted in Scheme 3 are evident.

We tried to find some experimental evidence for the formation of the intermediate indicated in Scheme 3. First of all, the reaction between $[(dppb)Pt(\mu\text{-}OH)]_2^{2+}$ and 2-mercaptoethanol was carried out (Scheme 4). A formulation of the new complex isolated as in Scheme 4 is supported by its spectroscopic features. It shows in the solid-state a strong, characteristic IR band at ~1090 cm^{-1} (BF_4), a broad band at 3360 cm^{-1}, and a weak band at 3521 cm^{-1}. The latter can be assigned respectively to the H-bonded and free O—H stretching vibrations of coordinated 2-mercaptoethanol. Consistently, in 1,2-dicholoroethane (DCE) solution only a weak band at 3533 cm^{-1} can be observed. No bands are observed in the region 2500–2600 cm^{-1} that can be assigned to the presence of SH ligands. Conductivity measurements (1×10^{-3} M in MeOH) are consistent with the presence of a 1:1 electrolyte (Λ_M 91 Ω^{-1} mol^{-1} cm^2) (15). In contrast to the inequivalence of the two phosphorus donors, the ^{31}P NMR spectrum in CD_3OD at 25°C shows only a sharp singlet at 15.82 ppm with a $^1J_{P\text{-}Pt}$ of 2904 Hz. When the temperature is lowered the signal broadens significantly and, at –70°C, the signal is so broad that it can hardly be distinguished from the base line. These observations may be consistent with the presence of a fast interchange equilibrium between the O and S donors as depicted in Scheme 4 promoted by a revers-

© 2001 NRC Canada

Scheme 4.



ible displacement of the OH moiety by MeOD. Unfortunately, the poor solubility of the new complex in solvents such as dichloromethane and acetone did not allow to confirm this hypothesis in other solvents.

Subsequently, the complex isolated from the previous reaction was dissolved in a large amount of 1,2-dichloroethane (the solvent used for the catalytic reactions) followed by addition of a 10-fold excess of *p*-anisaldehyde. The mixture was allowed to react both at 25°C and at 65°C for 2 h, however, no new product formation was observed by GC analysis. Isolation of the Pt species followed by spectroscopic analysis indicated that its features were identical to those of the starting complex. These observations are apparently in contrast with the observed catalytic effects displayed by $[(dppb)Pt(\mu\text{-}OH)]_2^{2+}$ and seem to indicate that the chelating effect of 2-mercaptoethanol as indicated in Scheme 4 is quite strong and is not reverted by the addition of a moderate excess of a mild ligand such as an aldehyde (or a ketone). However, it can be observed that under catalytic conditions, the carbonyl compound is added before 2-mercaptoethanol and in a much larger excess (1000–10 000 times with respect to the catalyst). In addition, the desiccating agent is present which allows the reaction to proceed at room temperature. These conditions are practically impossible to meet on a stoichiometric basis. In any case, the results reported in the above experiments show that the bridging hydroxy ligand can be promptly opened under catalytic conditions and support the plausibility of Scheme 3 as the activating process.

In conclusion, the platinum complex reported here appears to be a very interesting Lewis acid catalyst for the thioacetalization of a variety of aldehydes and ketones showing productivities that are attractive also for synthetic purposes. The easy modification of this class of complexes with chiral diphosphines seems to open also a viable access to the asymmetric transformation.

Experimental

Apparatus

Infrared spectra were taken on a Nicolet FT-IR Magna 750 and on a Digilab FTS 40 interferometer either in solid (KBr pellets) or in CH_2Cl_2 solution using CaF_2 windows. ^{31}P NMR spectra were recorded on a Bruker AC 200 spectrometer operating in FT mode, using as external reference 85% H_3PO_4. Conductivity measurements were performed on a Radiometer instrument using 1×10^{-3} M solutions in MeOH at 25°C. Gas chromatographic measurements were taken on a Hewlett–Packard 5790A gas chromatograph equipped with a 3390 automatic integrator. GC–MS measurements were performed on a Hewlett–Packard 5971 mass selective detector connected to a Hewlett–Packard 5890 II gas chromatograph. Identification of products was made with GC or GC–MS by comparison with authentic samples.

Materials

Solvents were dried and purified according to standard methods (14). Aldehyde and ketone substrates, 2-mercaptoethanol employed in the thioacetalization reactions and the desiccating agents ($Mg(ClO_4)_2 \cdot 2H_2O$, Na_2SO_4, molecular sieves 3A, $MgSO_4$) were commercial products (purum or puriss quality) used without purification.

The complex $[(dppb)Pt(\mu\text{-}OH)]_2(BF_4)_2$ was prepared according to literature procedures (13).

Thioacetals used as standards for gas chromatography in the individual catalytic reactions were synthesized from the starting aldehyde–ketone (20 mmol) and the stoichiometric amount of 2-mercaptoethanol in 25 mL DCE (1,2-dicholoroethane), to which 0.2 mmol PTSA (*p*-toluenesulfonic acid) were added under N_2 with stirring. The solution containing the acetal was used for qualitative identification in the GC analysis.

Reaction between $[(dppb)Pt(\mu\text{-}OH)]_2(BF_4)_2$ and 2-mercaptoethanol

The complex $[(dppb)Pt(\mu\text{-}OH)]_2(BF_4)_2$ (120 mg, 0.083 mmol) was dissolved in 20 mL of dry N_2 saturated 1,2-dichloroethane. 2-Mercaptoethanol (11.6 μL, 0.166 mmol) was added under N_2 and the solution was stirred for 2 h at room temperature. Addition of 20 mL of Et_2O lead to the precipitation of a white solid, which was filtered, washed with Et_2O, and dried in vacuo. (Yield: 92%). Anal. calcd. for $C_{30}H_{33}BF_4OP_2PtS$: C 45.87, H 4.23; found: C 46.01, H 4.11.

Catalytic reactions

These were carried out in a 25-mL round-bottomed flask equipped with a stopcock for vacuum–N_2 operations and a side-arm fitted with a screw-capped silicone septum to allow sampling. Constant temperature (±0.1°C) was maintained by water circulation through an external jacket connected with a thermostat. For reactions carried out at temperatures >25°C the reaction vessel was equipped with a reflux condenser and heating was ensured by a thermostatted external oil bath. Stirring was performed by a teflon-coated bar driven externally by a magnetic stirrer.

© 2001 NRC Canada

The following general procedure was followed: the required amount of catalyst was placed solid in the reactor which was evacuated and filled with N_2. Nitrogen-saturated solvent was added followed by aldehyde–ketone in the appropriate amount under N_2 flow. After thermostatting at the required temperature for a few min, 2-mercaptoethanol was injected through the septum and time was started.

All reactions were monitored with GC by direct injection of samples taken periodically from the reaction mixtures with a microsyringe. Separation of the products was performed on 25 m capillary columns using a flame ionization detector. Prior quenching of the catalyst using an excess of LiCl showed no differences in randomly selected analyses.

Acknowledgements

The financial support of MURST (Cofin 98) is gratefully acknowledged.

References

1. T.W. Greene. *In* Protective groups in organic synthesis, Wiley–Interscience, New York. 1981.
2. (*a*) W.S. Johnson, C.A. Harbert, and R.D. Stipanovic. J. Am. Chem. Soc. **90**, 5279 (1968); (*b*) W.S. Johnson, C.A. Harbert, B.E. Ratcliffe, and R.D. Stipanovic. J. Am. Chem. Soc. **98**, 6188 (1976); (*c*) P.A. Bartlett, W.S. Johnson, and J.D. Elliott. J. Am. Chem. Soc. **105**, 2088 (1983); (*d*) A. Mori and H. Yamamoto. J. Org. Chem. **50**, 5444 (1985); (*e*) K. Narasaka, M. Inoue, T. Yamada, J. Sugimori, and N. Iwasawa. Chem. Lett. 2409 (1987); (*f*) D. Seebach, R. Imwinkelried, and T. Weber. *In* Modern synthetic methods. Vol 4. *Edited by* R. Scheffold. Springer, Berlin. 1986.
3. D.M. Clode. Chem. Rev. **79**, 491 (1979).
4. J.R. Bull, J. Floor, and G.J. Kruger. J. Chem. Res. Synop. 224 (1979).
5. (*a*) K.A.M. Walker. U.S. Patent 4 150 153 (1979); (*b*) K. Bruns. J. Conrad, and A. Steigel Tetrahedron **35**, 2523 (1979).
6. A.J. Elliot. *In* Comprehensive heterocyclic polymers. Vol. 6. *Edited by* A.J. Elliot. Pergamon Press, Oxford. 1984.
7. (*a*) J. Ott, G.M. Ramos Tombo, B. Schmid, L.M. Venanzi, G. Wang, and T.R. Ward. Tetrahedron Lett. **30**, 6151 (1989); (*b*) W. Voelter and C. Djerassi. Chem. Ber. **101**, 1154 (1986); (*c*) R.V. Hoffman. Tetrahedron Lett. 2415 (1974); (*d*) J.F. Biellmann, M.J. Jung, and W.R. Pilgrim. Bull. Soc. Chim. Fr. **7**, 2720 (1971); (*d*) Z. Zhu and J.H. Espenson. Organometallics **16**, 3658 (1997); (*e*) F. Gorla and L.M. Venanzi. Helv. Chim. Acta, **73**, 690 (1990).
8. For reviews on this subject see: (*a*) G. Strukul. *In* Catalytic oxidations with hydrogen peroxide as oxidant. *Edited by* G. Strukul. Kluwer, Dordrecht. 1992. Chap. 6. p. 177; (*b*) G. Strukul *In* Advances in catalyst design. Vol. 2. *Edited by* M. Graziani and C.N.R. Rao. World Scientific, Singapore. 1993. p. 53; (*c*) G. Strukul. Angew Chem. Int. Ed. **37**, 1198 (1998).
9. R. Gavagnin, M. Cataldo, F. Pinna, and G. Strukul. Organometallics **17**, 661 (1998).
10. C. Paneghetti, R. Gavagnin, F. Pinna, and G. Strukul. Organometallics **18**, 5057 (1999).
11. M. Cataldo, E. Nieddu, R. Gavagnin, F. Pinna, and G. Strukul. J. Mol. Catal. A: Chem. **142**, 305 (1999).
12. E. Nieddu, M. Cataldo, F. Pinna, and G. Strukul. Tetrahedron Lett. **40**, 6987 (1999).
13. (*a*) J.J. Li, W. Li, and P.R. Sharp Inorg. Chem. **35**, 604 (1996); (*b*) A.L. Bandini, G. Banditelli, F. Demartin, M. Manassero, and G. Minghetti. Gazz. Chim. Ital. **123**, 417 (1993).
14. D.D. Perrin and W.L.F. Amarego. *In* Purification of laboratory chemicals. 3rd ed. Pergamon Press, Oxford. 1988.
15. W.J. Geary. Coord. Chem. Rev. **7**, 81 (1971).

© 2001 NRC Canada

Synthetic and solution calorimetric investigations of chelating phosphine ligands in Ru(allyl)$_2$(PP) complexes (PP = diphosphine)

Dale C. Smith, Jr., Jérémie Cadoret, Laleh Jafarpour, Edwin D. Stevens, and Steven P. Nolan

Abstract: Reaction enthalpies of (COD)Ru(allyl)$_2$ (COD = η^4-1,5-cyclooctadiene; allyl = 2-methylpropenyl) with a series of bidentate phosphines (dppm, dppf, dppe, dppb, dppp, depe, dmpe) have been measured by anaerobic solution calorimetry. The relative stability of the resulting complexes is strongly influenced by the electronic donor properties of the bidentate phosphine ligand. Reactions involving ligands that are better σ donors result in higher enthalpy values and, therefore, more thermodynamically stable complexes. Additionally, the synthesis and characterization of two new ruthenium allyl complexes Ru(allyl)$_2$(dppf) (**3**) and Ru(allyl)$_2$(depe) (**8**) and the X-ray crystal structure of **3** are reported.

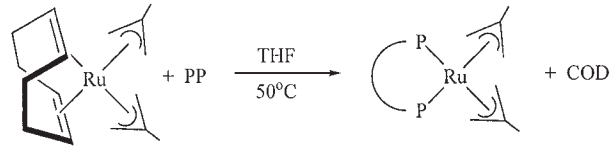
Key words: ruthenium, allyl, solution calorimetry, thermodynamics, X-ray structure.

Résumé : Les enthalpies de réaction entre (COD)Ru(allyl)$_2$ (COD = η^4-cycloocta-1,4-diène; allyl = 2-méthylpropényl) et une série de phosphines bidentates (dppm, dppf, dppe, dppb, dppp, depe, dmpe) ont été mesurées par calorimétrie de solution sous des conditions anaérobiques. La stabilité relative des complexes est fortement influencée par les propriétés électroniques du ligand. Les réactions impliquant des ligands ayant un fort caractère σ mènent à des valeurs enthalpiques élevées et des complexes thermodynamiquement plus stables. De plus, la synthèse et la caractérisation de deux nouveaux complexes allyles du ruthénium, Ru(allyl)$_2$(dppf) (**3**) et Ru(allyl)$_2$(depe) (**8**) ainsi qu'une étude par diffraction des rayons X de **3** sont décrites.

Mots clés : ruthénium, allyle, calorimétrie en solution, thermodynamique, diffraction des rayons X.

Introduction

Thermochemical measurements have been applied for some time to the quantitative assessment of metal–ligand interactions in organometallic systems (1). We have previously investigated the steric and electronic contributions present in tertiary phosphine-based organoruthenium systems by means of solution calorimetry (2). The present study extends our earlier thermochemical investigations to the reaction of (COD)Ru(allyl)$_2$ (**1**) with a series of diphosphine ligands [bis(diphenylphosphino)ethane (dppe), bis(diphenylphosphino)propane (dppp), bis(diphenylphosphino)butane (dppb), bis(diphenylphosphino)ferrocene (dppf), bis(dimethylphosphino)ethane (dmpe), and bis(diethylphosphino)ethane (depe)] as shown in the following general reaction:

[1] 

1

PP = dppm, dppf, dppe, dppp, dppb, dmpe, depe

Ruthenium complexes containing allylic ligands have found a wide range of useful applications in organic synthesis. Allylic ruthenium(IV) catalysts have been used for the ring opening polymerization of cyclic olefins (3) and in the allylation of carbon and nitrogen nucleophiles (4). Additionally, allylic ruthenium catalysts can be used in the C–C coupling of alkynes with allyl alcohol (5) and the *anti*-Markovnikov addition of carboxylic acids to terminal alkynes yielding (*Z*)-alk-1-en-1-yl esters (6, 7). The (PP)Ru(allyl)$_2$ complexes have shown to be effective catalyst precursors for the thermal cleavage of nonactivated sp^3 C—H bonds (8) and important catalysts in the formation of *o*-1-(1,3-dienyl) carbamates from the regioselective addition of CO_2 and secondary amines to isopropenylacetylene (9). Ruthenium allyl complexes bearing chiral phosphine lig-

Received August 8, 2000. Published on the NRC Research Press Web site at http://canjchem.nrc.ca on June 30, 2001.

This paper is dedicated to Professor Brian James on the occasion of his 65th birthday.

D.C. Smith, Jr., J. Cadoret, L. Jafarpour, E.D. Stevens, and S.P. Nolan.[1] Department of Chemistry, University of New Orleans, New Orleans, LA 70148, U.S.A.

[1]Corresponding author (telephone: (504) 280-6445; fax: (504) 280-6860; e-mail: snolan@uno.edu).

 DOI: 10.1139/cjc-79-5/6-626 © 2001 NRC Canada

ands have been extensively studied as catalysts precursors in the asymmetric hydrogenation of numerous unsaturated organic substrates (10, 11). In the present contribution we report thermochemical studies on the reaction of (COD)Ru(allyl)$_2$ (**1**) with a wide variety of chelating diphosphines: dppe, dppp, dppb, dppf, dmpe, and depe in tetrahydrofuran (THF) at 50°C. Additionally, we report the synthesis and characterization of two new complexes Ru(allyl)$_2$(dppf) (**3**) and Ru(allyl)$_2$(depe) (**8**), and present the crystal structure of **3**.

Experimental

General

All manipulations involving organoruthenium complexes were performed under an inert atmosphere of argon, using standard high vacuum or Schlenk techniques, or in a MBraun glove box containing less than 1 ppm oxygen and water. Only materials of high purity as indicated by NMR spectroscopy were used in the calorimetric experiments. Multinuclear NMR spectra were recorded using a Gemini 300 MHz or Varian 400 MHz spectrometer. Calorimetric measurements were performed using a Calvet calorimeter (Setaram C-80), which was periodically calibrated using the TRIS reaction (12) or the enthalpy of solution of KCl in water (13). The calorimeter has been previously described (14, 15). The experimental enthalpies for these two standard reactions compared closely with literature values. Control reactions with diphosphine ligands and Hg showed no reaction or enthalpy contribution.

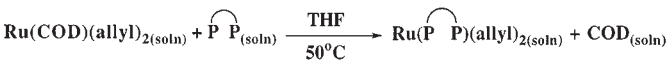
NMR titrations

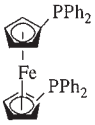
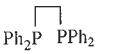
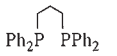
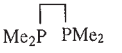
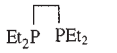
Prior to every set of calorimetric experiments involving a new ligand, a precisely measured amount (5.0 ± 0.1 mg) of (COD)Ru(allyl)$_2$ (**1**) was placed in an NMR tube along with THF-d_8 and >1.2 equiv of ligand and placed in a oil bath at 50°C. All ^{31}P NMR spectra were recorded within 1.5 h of mixing, which indicated the reactions were clean and quantitative. These conditions are necessary for accurate and meaningful calorimetric results and were satisfied for all reactions investigated.

Solution calorimetry

In a representative experimental trial, the mixing vessels of the Setaram C-80 calorimeter were cleaned, dried in an oven maintained at 150°C, and then taken into the glove box. A sample of (COD)Ru(allyl)$_2$ (**1**) (15.7 mg, 0.049 mmol) was loaded into the lower vessel, which was closed and sealed with 1.5 mL of mercury. A solution of dmpe (9.0 mg, 0.060 mmol) in THF (4 mL) was added, and the remainder of the cell was assembled, removed from the glove box, and inserted into the calorimeter. The reference vessel was loaded in an identical fashion with the exception that no ruthenium complex was added to the lower vessel. After the calorimeter had reached thermal equilibrium at 50.0 ± 0.2°C (ca. 2 h), it was inverted thereby allowing the reactants to mix. The reaction was considered complete after the calorimeter had once again reached thermal equilibrium (ca. 2 h). Control reactions with Hg and phosphine show no reaction. The enthalpy of ligand substitution (–30.0 ± 0.3 kcal mol^{-1}) listed in Table 1 represents the average of at least three individual calorimetric determinations with all species in solution. The enthalpy of solution of (COD)Ru(allyl)$_2$ (**1**) (+6.2 ± 0.2 kcal mol^{-1}) in THF was determined using identical methodology.

Table 1. Enthalpies of substitution (kcal mol^{-1}) in the reaction.



	P P	-ΔH$_{rxn}$[a]
dppm		12.0 (0.2)
dppf		13.9 (0.2)
dppe		16.6 (0.2)
dppp		16.6 (0.2)
dppb		17.6 (0.2)
dmpe		30.0 (0.3)
depe		30.5 (0.3)

[a]Enthalpies of reaction are reported with 95% confidence limits.

Synthesis of diallyldiphosphineruthenium(II) complexes

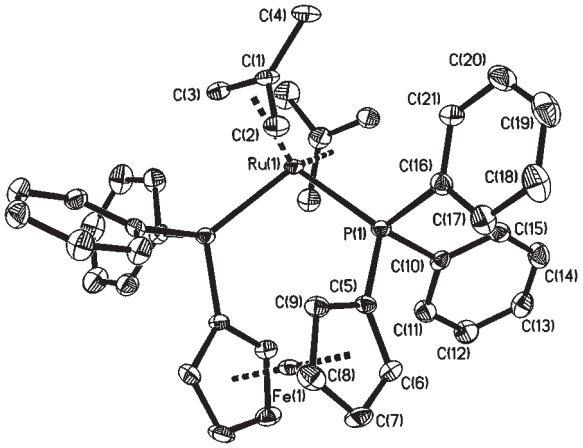
Unless otherwise noted, all new complexes were prepared according to the following typical procedure. The bis(phosphine) ligands dppm, dppe, dppp, dppb, dppf, dmpe, and depe were obtained from Strem and used as received. Synthesis of (COD)Ru(allyl)$_2$ (**1**) was conducted according to the method in the literature (16). Experimental synthetic procedures leading to the isolation of the previously unreported complexes are described below.

*Synthesis of (bis(diphenylphosphino)ferrocene)(allyl)$_2$ruthenium (**3**)*

In the glovebox, **1** (102 mg, 0.319 mmol), bis(diphenylphosphino)ferrocene (179 mg, 0.322 mmol), and THF (5 mL) were loaded to a 50 mL Schlenk tube. The tube was removed from the glovebox and interfaced to a Schlenk line. The Schlenk tube was placed in an oil bath at 50°C and vigorously stirred for 18 h. The solvent was removed in vacuum and the resulting residue was triturated with pentane. The orange residue was recrystallized from a CH_2Cl_2–pentane mixture, yielding orange blocks. Yield: 215 mg (88%). ^{1}H NMR (400 MHz, C_6D_6) δ: 0.86 (m, 2H, allylic CH_2), 1.41 (m, 2H, allylic CH_2), 1.49 (m, 2H, allylic CH_2), 2.25 (s, 6H, allylic Me), 2.32 (m, 2H, allylic CH_2), 4.01 (s, 2H, Cp), 4.22 (s, 2H, Cp), 4.26 (s, 2H, Cp), 4.88 (s, 2H, Cp), 6.90–7.50 (m, 20H, Ph). ^{31}P NMR (162 MHz, C_6D_6) δ: 49.84. Anal. calcd. for $C_{42}H_{42}P_2FeRu\cdot H_2O$: C 64.37, H 5.66; found: C 64.06, H 5.26.

© 2001 NRC Canada

Fig. 1. An ORTEP diagram of $Ru(allyl)_2(dppf)$ (**3**). Selected bond lengths: Ru—P, 2.3457(7) Å; Ru—C(1), 2.193(3) Å. Selected bond angles: P(1)-Ru-P(2), 104.18(3)°; C(1)-Ru-P(1), 106.1(2)°; C(1)-Ru-P(2), 116.9(1)°.



*Synthesis of (bis(diethylphosphino)ethane)(allyl)$_2$ruthenium (**8**)*

In a similar manner, **1** (153 mg, 0.479 mmol) and bis(diethylphosphino)ethane (103.5 mg, 0.5018 mmol) were reacted in THF (5 mL); after removing the solvent in vacuum and trituration with pentane, a yellow microcrystalline solid was isolated. Yield: 179 mg (90%). ^{1}H NMR (400 MHz, C_6D_6) δ: 0.81–1.42 (m, 8H, allylic; m, 20H, CH_2CH_3), 1.72 (m, 2H, PCH_2), 1.96 (m, 2H, PCH_2), 2.23 (s, 6H, allylic, Me). ^{31}P NMR (162 MHz, C_6D_6) δ: 64.38. Anal. calcd. for $C_{18}H_{38}P_2Ru$: C 51.78, H 9.17; found: C 51.41, H 8.93.

X-ray crystal structure determination and crystallographic data

A suitable crystal of **3** was mounted on the glass fiber of a goniometer head in a random orientation and placed in the cold stream of N_2 in an automated diffractometer using Mo Kα radiation. The structure of **3** was determined from data collected on a Bruker diffractometer with CCD detection equipped with Mo Kα radiation and a low-temperature apparatus (170 K). The cell dimensions were determined from at least 25 centered reflections, and standard reflections were monitored during data collection. The structure was solved by direct methods using the SHELXS program, and an azimuthal absorption correction was applied. The structure of **3** was refined in a full-matrix least-squares refinement on *F*, using anomalous terms for Ru and P, with all non-hydrogen atoms refined anisotropically. The hydrogen atoms were located from a Fourier difference map and used as the basis of H atom positions in the final structure. The structures have idealized and fixed H atoms, after attempts to refine them proved unsatisfactory. An ORTEP diagram of **3** and selected bond distances and angles are both given in Fig. 1. Positional and equivalent isotropic parameters for all non-hydrogen atoms and torsion angles are given as supplementary materials.[2]

Results and discussion

Organoruthenium synthesis

Two new complexes, $Ru(allyl)_2(dppf)$ (**3**) and $Ru(allyl)_2(depe)$ (**8**), were prepared by reacting $(COD)Ru(allyl)_2$ (**1**) (COD = η^4-1,5-cyclooctadiene; allyl = 2-methylpropenyl) with the appropriate bis(phosphine) ligand in THF at 50°C for 18 h. The colorless solution of **8** slowly turned yellow, whereas the reaction forming **3** remained orange throughout the ligand exchange process. When the solvent was removed, a yellow-orange oil was isolated (in both cases), which was triturated with pentane and filtered to give the resulting microcrystalline complexes in high yields. All complexes are moderately air-stable in the solid state and can be stored over several months under an argon atmosphere. The new complexes were characterized by ^{1}H and ^{31}P NMR and elemental analysis. The ^{31}P NMR spectra of the complexes display a single peak for both **3** and **8**, which is consistent with C_2 symmetrical molecule. The ^{1}H NMR spectra of the complexes are similar to that of other $(PP)Ru(allyl)_2$ complexes (8). Importantly, both complexes possess a five-resonance pattern characteristic of the allyl fragments.

X-ray crystal structure of 3

Crystallization by slow diffusion of a layered CH_2Cl_2–pentane solution leads to the formation of single crystals of **3**. The solid-state structure of **3** was found to crystallize in the monoclinic crystal system (space group *C*2/*c*), and an ORTEP diagram of **3** is presented in Fig. 1.

The central ruthenium atom is coordinated to two phosphorus atoms and two η^3-allyl ligands. The coordination geometry can be considered as a slightly distorted octahedral (outer two carbon atoms of both η^3-allyl ligands and the phosphorus atoms) or as a slightly distorted tetrahedral (coordination center of the η^3-allyl fragments and the phosphorus atoms). Specific details concerning structure determination are given in Table 2, and selected metrical parameters are given in Fig. 1. The Ru—P bond length of **3** is similar to that found in related ruthenium complexes (8, 10*b*, 17). The P-Ru-P angle in **3** (104.18°) is dictated by the six-membered chelate ring, and this angle is very different from the five-membered rings found in both $Ru(allyl)_2(dcpe)$ (85.03°) (8) and $Ru(allyl)_2(CHIRAPHOS)$ (85.0°) (10*b*). The P-Ru-P angle of **3** is very similar to that found for the monodentate complex $Ru(allyl)_2(PPh_3)_2$ (109.9°) (17). The Ru—C bond lengths of the allyl fragment are typical: the short bonds to the outer carbon (1.415(3) and 1.430(5) Å) and longer bonds to the central carbon (1.505(4) Å) of the η^3-allyl fragment.

Solution calorimetry

We have previously observed in organoruthenium phosphine systems (2) that steric, electronic, and structural parameters such as the Tolman's (18) cone angle (θ) and electronic parameter (χ) and metal–ligand bond lengths can be correlated with solution thermochemical data. These relationships can

[2] Supplementary material may be purchased from the Depository of Unpublished Data, Document Delivery, CISTI, National Research Council Canada, Ottawa, ON K1A 0S2, Canada. For information on obtaining material electronically go to http://www.nrc.ca/cisti/irm/unpub_e.shtml. Crystallographic information has been deposited with the Cambridge Crystallographic Data Centre. Copies of the data can be obtained, free of charge, on application to the Director, CCDC, 12 Union Road, Cambridge CB2 1EZ, U.K. (Fax: 44-1223-336033 or e-mail: deposit@ccdc.cam.ac.uk).

© 2001 NRC Canada

Table 2. Crystallographic data for Ru(dppf)(allyl)$_2$ (**3**).

Formula	$C_{42}H_{42}FeP_2Ru$
FW	765.62
Crystal system	Monoclinic
Space group	*C*2/*c*
a (Å)	13.123(2)
b (Å)	15.962(2)
c (Å)	16.328(2)
α (Å)	90
β (°)	97.328(3)
γ (°)	90
R_1 ($I > 2\sigma$)[a]	0.0509
R_w ($I > 2\sigma$)[b]	0.1206
R_1 (all data)	0.0839
R_w (all data)	0.1381
GoF	0.993

[a] $R = \sum(||F_o| - |F_c||)/\sum|F_o|$.
[b] $R_w = \sum w(|F_o| - |F_c|)^2/\sum w|F_o|^2$.

be used to indicate the relative contribution of steric and electronic effects in transition-metal systems. All (PP)Ru(allyl)$_2$ complexes have a central ruthenium atom coordinated by four groups: two methyl(allyl) ligands and the two coordinating phosphorus atoms of a bidentate ligand. In view of the rather unhindered geometry, any variation in the enthalpy of reaction could principally be attributable to the steric and electronic effects provided by the pnictide ligand. The general reaction illustrated in eq. [1] is notably fast (<2 h), clean, and quantitative for the chelating diphosphines, dppe, dppp, dppb, dppf, dmpe, and depe, at 50°C in THF, as determined by ^{1}H and ^{31}P NMR spectroscopy. The enthalpies of ligand substitution measured range from –12.0(2) kcal mol^{-1} for **2** to –30.5(3) kcal mol^{-1} for **8**.[3] The overall order of stability is as follows: dppm < dppf < dppe < dppp < dppb < dmpe < depe. As the Tolman electronic parameter scale predicts, the relative stability of the resulting complexes is strongly influenced by the electronic donor properties of the bidentate phosphine ligand in the absence of any steric factors. Reaction enthalpies involving better σ donor (or more basic) phosphine ligands result in more thermodynamically stable complexes, as shown in Table 1. This trend can be quantitatively illustrated by a plot of enthalpy of substitution versus pK_{a1} (H_2O) (19) of selected bidentate phosphine ligands (20) as illustrated in Fig. 2.[4]

The basicity of the free ligand is defined as the pK_{a1} value for the conjugated acid ($HPR_2P{\sim}PR_2^+$) and can be used to provide a measure of the ligand's ability to donate in a σ fashion to the metal (21) The good correlation between these two parameters (R = 0.974) clearly indicates the enthalpy of substitution to be related to the basicity of the bis(phosphine) ligand, and thus the electronic donating ability of the bis(phosphine).

The present enthalpy data allow for comparison to prior thermochemical studies on the Cp′Ru(PP)Cl (Cp′ either Cp* = η^5-C_5Me_5; or Cp = η^5-C_5H_5) systems (2*g*, *h*). The rel-

Fig. 2. Plot of pK_{a1} vs. –ΔH of substitution (kcal mol^{-1}) for selected bis(phosphine) ligands (pK_{a1} for H_2O (21); slope = 0.27, R = 0.97).

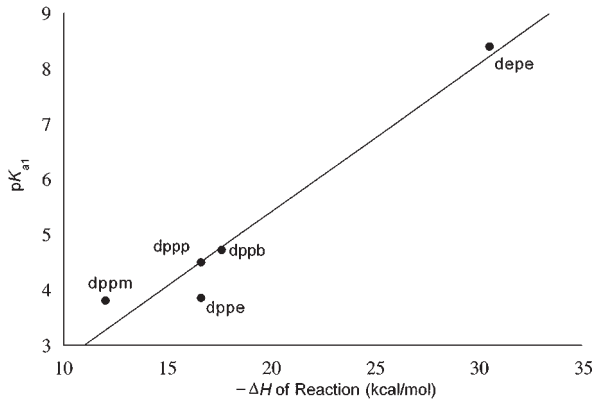
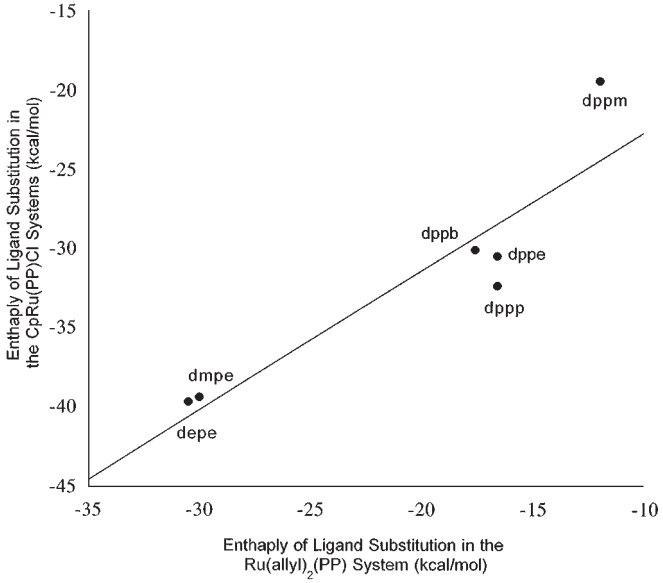


Fig. 3. Comparison between the enthalpies of ligand substitution (kcal mol^{-1}) in the CpRu(PP)Cl andRu(allyl)$_2$ (PP) systems (slope = 0.88, R = 0.91).



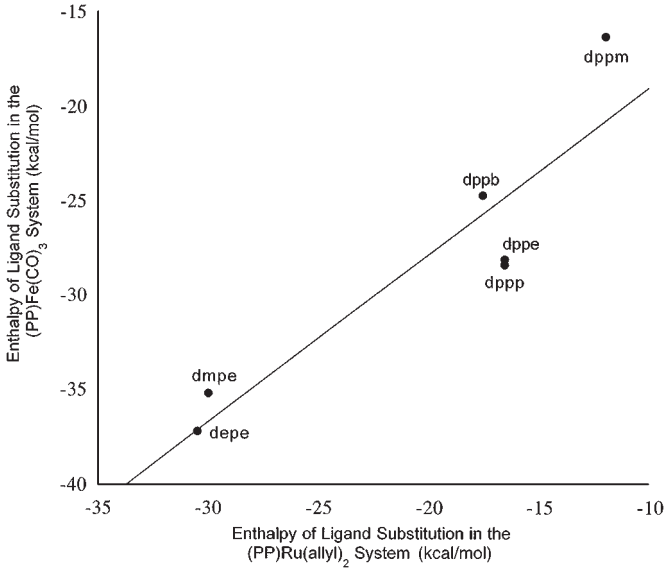
ative order of stability of the resulting complexes for both the Cp*Ru(PP)Cl and CpRu(PP)Cl systems follows a trend similar to that of the (PP)Ru(allyl)$_2$ system. A relationship between ΔH_{rxn} for PP ligand substitution in the CpRu(PP)Cl and (PP)Ru(allyl)$_2$ systems is presented in Fig. 3.[5]

A fair correlation (R = 0.91) is found for this quantitative comparison. A similar relationship is found to exist in the Cp*Ru(PP)Cl system (R = 0.89). The average difference between enthalpies of substitution in (PP)Ru(allyl)$_2$ and Cp*Ru(PP)Cl (2*g*) is found to be worth 8.6 kcal mol^{-1}, favoring the Cp* system. The same comparison with the CpRu(PP)Cl (2*h*) data yields an 11.4 kcal mol^{-1} difference, favoring the Cp system. These differences indicate that the metal center in the Ru(allyl)$_2$ moiety is more electron rich than either of

[3] Reported enthalpies of reaction include enthalpy values for the reaction with all species in solution. No correction is made for solvation enthalpy differences of free ligands which have previously been determined to cancel in neutral organometallic systems (14, 15).
[4] pK_a values for dppf and dmpe are not available.
[5] The enthalpy values for dppf in the CpRu(PP)Cl and (PP)Fe(CO)$_3$ are not available.

© 2001 NRC Canada

Fig. 4. Comparison between the enthalpies of ligand substitution (kcal mol^{-1}) in the $Fe(PP)(CO)_3$ and $Ru(allyl)_2(PP)$ systems (slope = 0.88, R = 0.91).



the Cp′RuCl moieties. The metal center in the $Ru(allyl)_2$ moiety is, therefore, not as good of an electron acceptor as the Cp′RuCl moieties, which leads to lower enthalpies of ligand substitution.

We have also previously observed that the ruthenium system and the $(PP)Fe(CO)_3$ system (22) presented similar trends in terms of thermodynamic stability. As expected, the relative order of stability of the resulting complexes of the $(PP)Ru(allyl)_2$ system is similar to that of the $(PP)Fe(CO)_3$ system. For reactions involving the same PP ligand with either $(bda)Fe(CO)_3$ (bda = benzylideneacetone) or $(COD)Ru(allyl)_2$, a fair correlation (R = 0.91) is found. This linear relationship between ΔH_{rxn} for PP ligand substitution in both the $(PP)Fe(CO)_3$ and $(PP)Ru(allyl)_2$ systems is presented in Fig. 4. The lack of steric hindrance in the iron system and the fairly linear correlation presented in Fig. 4 suggest that the main factors dictating the magnitude of the reaction enthalpies in the $(PP)Ru(allyl)_2$ system are the Lewis acidic character of the metal center and the electronic properties of the diphosphine ligand. The dppm entries in Figs. 3 and 4 appear to deviate the most from linearity. We attribute this deviation to the previously measured ring strain attributable to a metallacyclopropane-like structure. This strain energy, worth some 7–10 kcal mol^{-1} (2*g*, *h*, 22) if independently considered, would lead to enthalpy values significantly closer to those predicted from the linear relations.

Conclusions

The reaction enthalpies for the complex $(COD)Ru(allyl)_2$ with a series of bidentate phosphines have been measured by anaerobic solution calorimetry. The correlation between the $pK_{a1}(H_2O)$ (19) of the bis(phosphines) and the enthalpies of substitution demonstrates that the relative stability of the resulting complexes is influenced by the electronic donor abilities or basicity of the bidentate phosphine ligand. Thus, phosphine ligands that are better σ donors result in more thermodynamically stable $(PP)Ru(allyl)_2$ complexes. The present results are similar to those of prior studies on the Cp′Ru(PP)Cl systems (Cp′ = Cp, Cp^*) (2*g*, *h*) which established the thermodynamic stability of these complexes to be governed by electronic factors of the metal center and electronic properties characteristic of the incoming phosphine ligand.

Acknowledgments

We gratefully acknowledge the National Science Foundation, the Louisiana Board of Regents, and DuPont for partial financial support of this research.

References

1. (*a*) S.P. Nolan. *In* Encyclopedia of inorganic chemistry. *Edited by* R.B. King. John Wiley & Sons, New York. 1994; (*b*) C.D. Hoff. Prog. Inorg. Chem. **40**, 503 (1992); (*c*) J.A. Martinho Simões and J.L. Beauchamp. Chem. Rev. **90**, 629 (1990); (*d*) T.J. Marks (*Editor*). Bonding energetics. *In* Organotransition metal compounds. ACS Symp. Ser. 428. American Chemical Society, Washington, D.C. 1990; (*e*) T.J. Marks (*Editor*). Bonding energetics. *In* Organotransition metal compounds. Polyhedron Symp. Print, **7** (1988); (*f*) H.A. Skinner and J.A. Connor. *In* Molecular structure and energetics. Vol. 2. *Edited by* J.F. Liebman and A. Greenberg. VCH Publishers Inc., New York. 1987. Chap. 6.
2. (*a*) D.C. Smith, Jr., C.M. Haar, L. Luo, C. Li, M.E. Cucullu, C.H. Malher, S.P. Nolan, W.J. Marshall, N.L. Jones, and P.J. Fagan. Organometallics, **18**, 2357 (1999); (*b*) C. Li, S. Serron, and S.P. Nolan. Organometallics, **15**, 4020 (1996); (*c*) S.A. Serron, L. Luo, C. Li, M.E. Cucullu, and S.P. Nolan. Organometallics, **14**, 5290 (1995); (*d*) S.A. Serron and S.P. Nolan. Organometallics, **14**, 4611 (1995); (*e*) L. Luo, C. Li, M.E. Cucullu, and S.P. Nolan. Organometallics, **14**, 1333 (1995); (*f*) M.E. Cucullu, L. Luo, S.P. Nolan, P.J. Fagan, N.L. Jones, and J.C. Calabrese. Organometallics, **14**, 289 (1995); (*g*) L. Luo, N. Zhu, N.J. Zhu, E.D. Stevens, S.P. Nolan, and P.J. Fagan. Organometallics, **13**, 669 (1994); (*h*) C. Li, M.E. Cucullu, R.A. McIntyre, E.D. Stevens, and S.P. Nolan. Organometallics, **13**, 3621 (1994); (*i*) L. Luo and S.P. Nolan. Organometallics, **13**, 4781 (1994); (*j*) L. Luo, P.J. Fagan, and S.P. Nolan. Organometallics, **12**, 4305 (1993); (*k*) S.P. Nolan, K.L. Martin, E.D. Stevens, and P.J. Fagan. Organometallics, **11**, 3947 (1992).
3. S. Wache, W.A. Herrmann, G. Artus, O. Nuykne, and D. Wolf. J. Organomet. Chem. **491**, 181 (1995).
4. T. Kondo, H. Ono, N. Stake, T. Mitsudo, and Y. Watanabe. Organometallics, **14**, 1945 (1995).
5. S. Dérien and P.H. Dixneuf. J. Chem. Soc. Chem. Commun. 2551 (1994).
6. H. Doucet, B. Vaca-Martin, C. Bruneau, and P.H. Dixneuf. J. Org. Chem. **60**, 7247 (1995).
7. H. Doucet, J. Höfer, N. Derrien, C. Bruneau, and P.H. Dixneuf. J. Soc. Chim. Fr. **133**, 939 (1996).
8. C. Six, B. Gabor, H. Görls, R. Mynott, P. Phillips, and W. Leitner. Organometallics. **18**, 3316 (1999).
9. J. Höfer, H. Doucet, C. Bruneau, and P.H. Dixneuf. Tetrahedron Lett. **32**, 7409 (1991).
10. (*a*) M.J. Burk, T.G.P. Harper, and C.S. Kalberg. J. Am. Chem. Soc. **117**, 4423 (1995); (*b*) J.P. Genêt, C. Pinel, V. Ratovelomenanana-Vidal, S. Mallart, X. Pfister, M.C. Caño De Andrade, and J.A. Laffitte. Tetrahedron: Asymmetry, **5**, 665 (1994); (*c*) J.P. Genêt, C. Pinel, V. Ratovelomenanana-Vidal, C. Pinel, and J.A. Liffitte. Tetrahedron Lett. **35**, 4559 (1994);

© 2001 NRC Canada

(*d*) J.P. Genêt, C. Pinel, S. Mallart, S. Juge, N. Cailhol, and J.A. Laffitte. Tetrahedron Lett. **37**, 5343 (1992); (*e*) J.P. Genêt, C. Pinel, S. Mallart, S. Juge, S. Thorimbert, and J.A. Laffitte. Tetrahedron: Asymmetry, **2**, 555 (1991).
11. J.P. Genêt. Acros Organics Acta, **1**, 4 (1995).
12. G. Ojelund and I. Wadsö. Acta Chem. Scand. **22**, 1691 (1968).
13. M.V. Kilday. J. Res. Natl. Bur. Stand. (U.S.), **85**, 467 (1980).
14. S.P. Nolan, C.D. Hoff, and J.T. Landrum. J. Organomet. Chem. **282**, 357 (1985).
15. S.P. Nolan, R. Lopez de la Vega, and C.D. Hoff. Inorg. Chem. **25**, 4446 (1986).
16. J. Powell and B.L. Shaw. J. Chem. Soc. A. 159 (1969).
17. A.E. Smith. Inorg. Chem. **11**, 2306 (1972).
18. (*a*) C.A. Tolman. Chem. Rev. **77**, 313 (1977); (*b*) C.A. Tolman, D.W. Reutter, and W.C. Seidel. J. Organomet. Chem. **117**, C30 (1976); (*c*) L.E. Manzer and C.A. Tolman. J. Am. Chem. Soc. **97**, 1955 (1975).
19. S.J. Bersner-Price, R.E. Norman, and P.J. Sadler. J. Inorg. Biochem. **31**, 197 (1987).
20. R.J. Angelici. Acc. Chem. Res. **28**, 51 (1995).
21. M. Rahman, H.-L. Liu, K. Eriks, A. Prock, and W.P. Giering. Organometallics, **8**, 1 (1989).
22. C. Li, M.E. Cucullu, R.A. McIntyre, E.D. Stevens, and S.P. Nolan. Organometallics, **13**, 3221 (1994).

© 2001 NRC Canada

Addition of bridging-hydrosulfido ligands in diiridium complex to acrylonitrile. Synthesis of diiridium cyanoethylthiolato complexes and $RuIr_2$ sulfido-cyanoethylthiolato cluster

Fusao Takagi, Hidetake Seino, Yasushi Mizobe, and Masanobu Hidai

Abstract: Treatment of [Cp*Ir(μ-SH)$_3$IrCp*]Cl (Cp* = η^5-C_5Me_5) with acrylonitrile and NEt_3 in MeCN or $ClCH_2CH_2Cl$ gave [Cp*Ir(μ-$SCH_2CH_2CN)_3$IrCp*]$^+$, [Cp*Ir(μ-S)(μ-$SCH_2CH_2CN)_2$IrCp*] (**3**), or [Cp*Ir(μ-$SCH_2CH_2CN)_2$(μ-SCH_2CH_2Cl)IrCp*]$^+$, depending upon the conditions employed. From the reaction of **3** with [(Cp*Ru)$_4$(μ-Cl)$_4$], a sulfido-thiolato cluster [Cp*$_3$$RuIr_2$(μ$_3$-S)(μ-$SCH_2CH_2CN)_2$Cl] was obtained.

Key words: diiridium complex, thiolate, sulfide, ruthenium, cluster.

Résumé : Le traitement du [Cp*Ir(μ-SH)$_3$IrCp*]Cl (Cp* = η^5-C_5H_5) avec de l'acrylonitrile et du NEt_3, dans du MeCN ou du $ClCH_2CH_2Cl$, conduit à la formation de [Cp*Ir(μ-$SCH_2CH_2CN)_3$IrCp*]$^+$, [Cp*Ir(μ-S)(μ-$SCH_2CH_2CN)_2$IrCp*] (**3**) ou [Cp*Ir(μ-$SCH_2CH_2CN)_2$(μ-SCH_2CH_2Cl)IrCp*]$^+$ suivant les conditions utilisées. La réaction du composé **3** avec du [(Cp*Ru)$_4$(μ-Cl)$_4$] conduit à la formation d'un agrégat sulfido-thiolato [Cp*$_3$$RuIr_2$(μ$_3$-S)(μ-$SCH_2CH_2CN)_2$Cl].

Mots clés : complexe de diiridium, thiolate, sulfure, ruthénium, agrégat.

[Traduit par la Rédaction]

In contrast to extensive studies on the reactions of transition metal complexes with organic thiols and their derivatives, those with H_2S as well as the reactivities of the hydrosulfido complexes thus formed are still poorly developed (1). Previously we have shown that treatment of chloro-bridged dinuclear complexes [Cp*MCl(μ-Cl)$_2$MCp*Cl] (M = Ir, Rh (2), Ru (3); Cp* = η^5-C_5Me_5) with H_2S results in the formation of hydrosulfido-bridged complexes [Cp*MCl(μ-SH)$_2$MCp*Cl]. Under certain conditions, triply bridged complexes [Cp*MCl(μ-SH)$_3$MCp*Cl]Cl were also available for M = Ir (**1**) and Rh (2). Although various reactions of the former doubly bridged neutral complexes have already been demonstrated (3, 4), the reactivities of the latter cationic complexes are not yet explored. In this paper, we report the addition of the hydrosulfido ligands in **1** to acrylonitrile (AN) in the presence of base to give the cyanoethylthiolato-bridged diiridium complexes, one of which is transformed into a $RuIr_2$ cluster by reaction with a ruthenium complex.

When a mixture of **1** and 4 equiv of AN in MeCN was treated with 4 equiv of NEt_3 at –40°C, an immediate color change from yellow to red was observed. The mixture was warmed to 40°C and stirred continuously for 70 h, affording [Cp*Ir(μ-$SCH_2CH_2CN)_3$IrCp*][PF_6] (**2**)[3] as yellow needles in 36% yield after anion metathesis using [H_4N][PF_6] (Scheme 1). In the absence of NEt_3, addition of the SH ligands to AN did not take place under otherwise similar conditions. If **1** is treated with only 2 equiv of AN and 4 equiv of NEt_3 at –40°C, followed by stirring of the resulting red solution at room temperature for 24 h, the neutral complex [Cp*Ir(μ-S)(μ-$SCH_2CH_2CN)_2$IrCp*] (**3**)[3] is obtained as red prisms in 70% yield (Scheme 1). Complex **3** is the apparent result of insertion of 2 equiv of AN into two S—H bonds

Received August 30, 2000. Published on the NRC Research Press Web site at http://canjchem.nrc.ca on June 30, 2001.

Dedicated to Professor Brian James on the occasion of his 65th birthday.

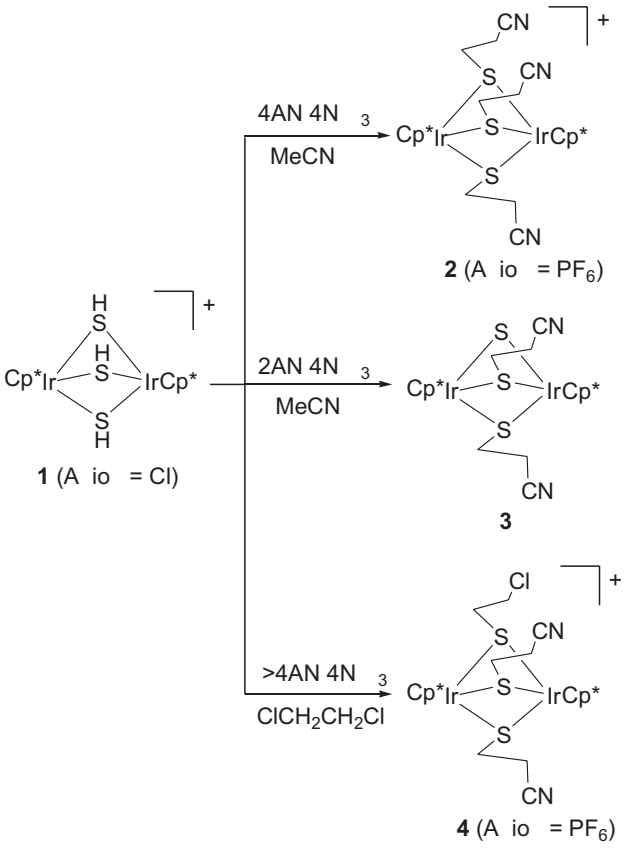
F. Takagi, H. Seino, and Y. Mizobe.[1] Komaba, Meguro-ku, Tokyo 153-8505, Japan.
M. Hidai.[2] Department of Materials Science and Technology, Faculty of Industrial Science and Technology, Science University of Tokyo, Noda, Chiba 278-8510, Japan.

[1]Corresponding author (telephone: +81-3-3402-6231; fax: +81-3-3402-6303; e-mail: ymizobe@iis.u-tokyo.ac.jp).
[2]Corresponding author (telephone: +81-471-24-1501 ext. 433; fax: +81-471-24-1699; e-mail: hidai@mail.rs.noda.sut.ac.jp).

[3]**2**: IR (KBr) (cm^{-1}): 2246 (C≡N). ^{1}H NMR (400 MHz, $CDCl_3$) δ: 1.85 (s, 30H, Cp*), 2.70, 2.95 (t, 6H each, CH_2). Anal. calcd. for $C_{29}H_{42}F_6N_3PS_3Ir_2$: C 32.91, H 4.00, N 3.97; found: C 32.76, H 4.04, N 4.00. **3**: IR (KBr) (cm^{-1}): 2241 (C≡N). ^{1}H NMR (400 MHz, C_6D_6) δ: 1.47 (s, 30H, Cp*), 2.20 (br t, 4H, CH_2), 2.4–3.0 (br, 4H, CH_2). Anal. calcd. for $C_{26}H_{38}N_2S_3Ir_2$: C 36.34, H 4.46, N 3.26; found: C 36.36, H 4.55, N 3.55. **4**: IR (KBr) (cm^{-1}): 2249 (C≡N). ^{1}H NMR (400 MHz, $CDCl_3$) δ: 1.84 (s, 30H, Cp*), 2.70 (m, 4H, CH_2), 2.96 (m, 6H, CH_2), 3.60 (m, 2H, CH_2). Anal. calcd. for $C_{28}H_{42}ClF_6N_2PS_3Ir_2$: C 31.50, H 3.96, N 2.62; found: C 31.18, H 4.05, N 2.96. **5**·0.5benzene·0.5hexane: IR (KBr) (cm^{-1}): 2245 (C≡N). ^{1}H NMR (400 MHz, C_6D_6) δ: 1.45, 1.52, 1.83 (s, 15H each, Cp*), 0.93, 1.97 (m, 2H each, CH_2), 1.72, 2.36, 2.78, 3.28 (m, 1H each, CH_2). Anal. calcd. for $C_{42}H_{63}ClN_2S_3Ir_2Ru$: C 41.58, H 5.23, N 2.31; found: C 41.76, H 5.28, N 2.30.

 DOI: 10.1139/cjc-79-5/6-632 © 2001 NRC Canada

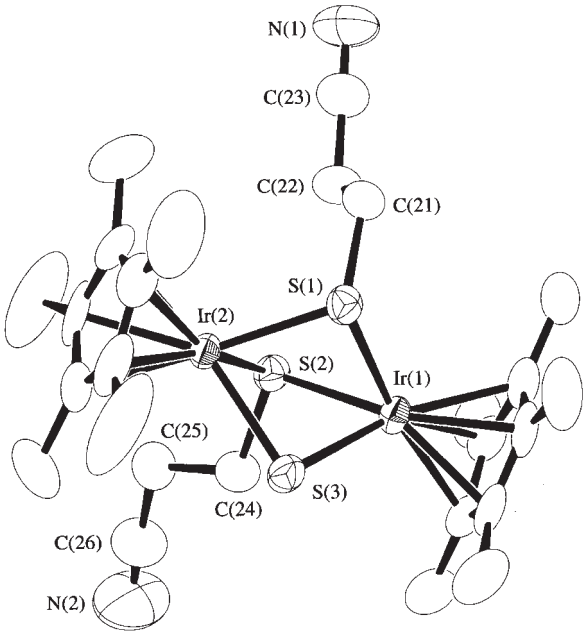
Scheme 1.



and deprotonation of the third thiolato group, and might represent one of the intermediate stages on the route from **1** to **2**.[4] Differences in the reaction conditions required for the isolation of **2** and **3** suggest that incorporation of the third AN is somehow much slower than that of the first or second AN.

Interestingly, when the reaction of **1** with 4 or more equiv of AN in the presence of 4 equiv of NEt_3 was performed in $ClCH_2CH_2Cl$ in place of MeCN, $[Cp^*Ir(\mu\text{-}SCH_2CH_2CN)_2(\mu\text{-}SCH_2CH_2Cl)IrCp^*][PF_6]$ (**4**)[3] was isolated as yellow crystals in 52% yield by treatment with $[H_4N][PF_6]$ (Scheme 1). Formally, two SH ligands in **1** underwent the addition to AN, while the remaining SH group was subjected to electrophilic substitution of the SH proton by the chloroethyl moiety. Addition to the third AN is so slow that the substitution may preferentially proceed at the third bridging sulfur atom. Indeed, it has been confirmed that **3** readily reacts with $ClCH_2CH_2Cl$ to give $[Cp^*Ir(\mu\text{-}SCH_2CH_2CN)_2(\mu\text{-}SCH_2CH_2Cl)IrCp^*]^+$ at room temperature.

Fig. 1. A molecular structure of **3**. Hydrogen atoms are omitted.



The structures of **3** and **4**·$ClCH_2CH_2Cl$ were determined in detail by X-ray crystallography.[5] The ORTEP drawing of **3** is shown in Fig. 1, whose Ir_2S_3 core structure is quite analogous to that in **4**. The Ir···Ir distances at 3.324(1) and 3.330(1) Å in **3** and **4**, respectively, which are elongated only slightly from 3.2954(7) Å of the hydrosulfido-bridged cation in **1**, indicate the absence of any bonding interactions between two Ir atoms. There exist no significant differences between the Ir—$S_{sulfido}$ and Ir—$S_{thiolate}$ bond lengths in **3**, which fall in the range 2.382(2)–2.395(2) Å and are comparable to the Ir—$S_{thiolate}$ bond distances in **4** (2.370(5)–2.399(5) Å).

With respect to the SH ligand, a considerable number of addition reactions toward unsaturated C—C bonds have been known for some time, which include, for example, the reactions of bridging SH ligands in dinuclear complexes such as $[\{Fe(CO)_3\}_2(\mu\text{-}SH)_2]$ (5), $[(Cp^*Rh)_2(\mu\text{-}CH_2)_2(\mu\text{-}SH)]^+$ (6), $[(Cp'Mo)_2(\mu\text{-}S)_2(\mu\text{-}SH)_2]$ (Cp′ = η^5-C_5H_4Me) (7), $[Rh(CO)(\mu\text{-}SH)(\mu\text{-}Ph_2PCH_2PPh_2)_2Mn(CO)_3]^+$ (8), and $[\{(\eta^5\text{-}C_5H_5)_2\}Ti(\mu\text{-}SH)_2Mo(CO)_4]$ (9) with alkynes and (or) alkenes. Nucleophilic substitution of the SH complexes with alkyl halides is also precedented for, e.g., $[(Cp'Mo)_2(\mu\text{:}\eta^2\text{-}$

[4] It has been confirmed that **3** dissolved in MeCN reacts with AN in the presence of $[Et_3NH]Cl$ to give **2**.

[5] **3**: MW = 859.22 g mol^{-1}; monoclinic; space group $P2_1/c$ (No. 14); a = 11.384(4), b = 16.097(3), and c = 16.368(2) Å; β = 104.93(2)°, V = 2898(1) $Å^3$ (room temp); Z = 4; μ (Mo Kα) = 94.33 cm^{-1}; R = 0.048 and R_w = 0.061 for 6650 reflections with $I > 3\sigma(I)$ and 299 variables. **4**·$ClCH_2CH_2Cl$: MW = 1166.65 g mol^{-1}; monoclinic; space group $P2_1/c$ (No. 14); a = 11.132(3), b = 19.431(4), and c = 19.259(3) Å; β = 98.96(2)°, V = 4115(1) $Å^3$ (room temp); Z = 4, μ (Mo Kα) = 69.15 cm^{-1}, R = 0.070 and R_w = 0.081 for 4741 reflections with $I > 3\sigma(I)$ and 425 variables. **5**·0.5benzene·0.5hexane: MW = 1213.12 g mol^{-1}; triclinic; space group $P\bar{1}$ (No. 2); a = 12.531(1), b = 14.223(1), and c = 15.012(1) Å; α = 75.305(7), β = 68.366(7), γ = 66.391(7)°, V = 2261.3(4) $Å^3$ (room temp); Z = 2; μ (Mo Kα) = 64.44 cm^{-1}; R = 0.026 and R_w = 0.029 for 6690 reflections with $I > 3\sigma(I)$ and 454 variables. The supplementary material has been deposited. Copies may be purchased from: The Depository of Unpublished Data, Document Delivery, CISTI, National Research Council Canada, Ottawa, ON K1A OS2, Canada. For information on obtaining material electronically go to http://www.nrc.ca/cisti/irm/unpub_e.shtml. Supplementary material referred to in this paper has also been deposited with the Cambridge Crystallographic Data Centre. Copies of the data can be obtained, free of charge, on application to the Director, CCDC, 12 Union Road, Cambridge CB2 1EZ, U.K. (Fax: 44-1223-336033 or e-mail: deposit@ccdc.cam.ac.uk).

© 2001 NRC Canada

Equation 1.

[1] **3** + 1 4[$(Cp^*Ru)_4(\mu_3\text{-}Cl)_4$] $\xrightarrow{THF}$ **5**

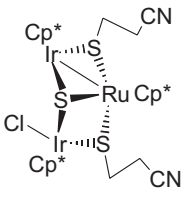
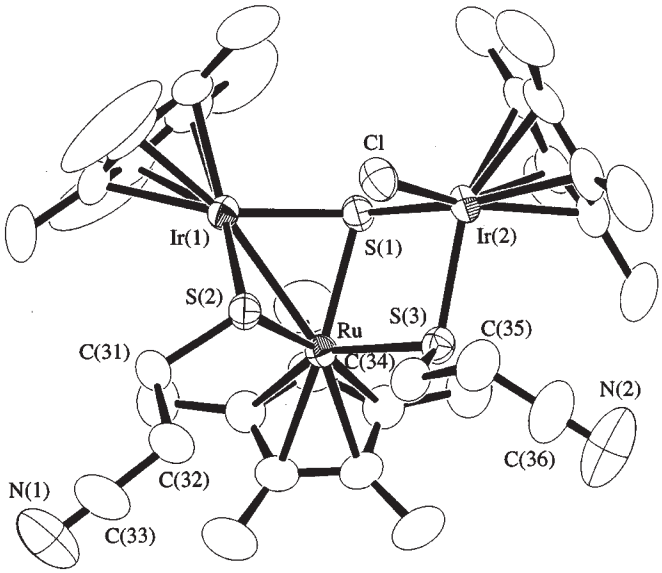


Fig. 2. A molecular structure of **5**. Hydrogen atoms are omitted.



S_2CH_2)(μ-SMe)(μ-SH)] (10) and [{$IrH(PPh_3)_2$}$_2$(μ-H)(μ-$SH)_2$]$^+$ (11).

Recent studies in this group have focused on the syntheses of mixed-metal sulfido clusters containing noble metals, which have revealed that the dinuclear complexes containing sulfido bridge(s) can serve as good precursors to such clusters (12). As expected, treatment of **3** with 0.25 molar equiv of [$(Cp^*Ru)_4(\mu_3\text{-}Cl)_4$] in THF at room temperature afforded a trinuclear bimetallic cluster [$Cp^*_3RuIr_2(\mu_3\text{-}S)(\mu\text{-}SCH_2CH_2CN)_2Cl$] (**5**)[3] in 70% yield (eq. [1]). Complex **5**, obtained as black needles, was also characterized by X-ray analysis.[5] As shown in Fig. 2, **5** has a sulfido-capped $RuIr_2$ core, which is further bridged by two cyanoethylthiolato ligands at each Ru—Ir edge. For the $RuIr_2$ triangle, there exists only one metal—metal single bond, thus satisfying the 18-e count for all metals. Thus, the Ru—Ir(1) distance at 2.8362(5) Å is consistent with the presence of a Ru—Ir single bond, while the separation of the Ru atom from Ir(2), having a terminal Cl ligand (3.6922(6) Å), as well as that between two Ir atoms (4.1529(3) Å), are apparently indicative of the absence of any bonding interaction.

Further studies are now in progress to clarify the reactivities of **1** towards more diversified unsaturated C—C bonds and also to synthesize a series of bimetallic clusters from **3**.

We are grateful to the Ministry of Education, Science, Sports, and Culture of Japan for financial support.

References

1. (*a*) B.R. James. Pure Appl. Chem. **69**, 2213 (1997); (*b*) S. Kuwata and M. Hidai. Coord. Chem. Rev. **213**, 211 (2001).
2. Z. Tang, Y. Nomura, Y. Ishii, Y. Mizobe, and M. Hidai. Inorg. Chim. Acta, **267**, 73 (1998).
3. K. Hashizume, Y. Mizobe, and M. Hidai. Organometallics, **15**, 3303 (1997).
4. (*a*) T. Kochi, Y. Nomura, Z. Tang, Y. Ishii, Y. Mizobe, and M. Hidai. J. Chem. Soc. Dalton Trans. 2575 (1999); (*b*) Z. Tang, Y. Nomura, S. Kuwata, Y. Ishii, Y. Mizobe, and M. Hidai. Inorg. Chem. **37**, 4909 (1998); (*c*) S. Kuwata, M. Andou, K. Hashizume, Y. Mizobe, and M. Hidai. Organometallics, **17**, 3429 (1998).
5. D. Seyferth, G.B. Womack, R.S. Henderson, M. Cowie, and B.W. Hames. Organometallics, **5**, 1568 (1986).
6. Y. Kaneko, N. Suzuki, A. Nishiyama, T. Suzuki, and K. Isobe. Organometallics, **17**, 4875 (1998).
7. M. Rakowski DuBois, M.C. VanDeveer, D.L. DuBois, R.C. Haltiwanger, and W.K. Miller. J. Am. Chem. Soc. **102**, 7456 (1980).
8. L.-S. Wang, R. McDonald, and M. Cowie. Inorg. Chem. **33**, 3735 (1994).
9. C.J. Ruffing and T.B. Rauchfuss. Organometallics, **4**, 524 (1985).
10. C.J. Casewit and M. Rakowski DuBois. J. Am. Chem. Soc. **108**, 5482 (1986).
11. A.M. Mueting, P.D. Boyle, R. Wagner, and L.H. Pignolet. Inorg. Chem. **27**, 271 (1988).
12. M. Hidai, S. Kuwata, and Y. Mizobe. Acc. Chem. Res. **33**, 46 (2000).

© 2001 NRC Canada

(*para*-Diphenylphosphino)benzenesulfonic acid and its ruthenium(II) complexes: an old water soluble phosphine ligand in a new perspective

Gábor Papp, József Kovács, Attila Cs. Bényei, Gábor Laurenczy, Levente Nádasdi, and Ferenc Joó

Abstract: Chloro- and hydrido-complexes of ruthenium(II) with potassium (4-diphenylphosphino)benzenesulfonate (pTPPMS) were prepared and their properties were compared with those of the related complexes of (3-diphenylphosphino)benzenesulfonates. An X-ray crystal structure determination revealed that the *para*-sulfonated ligand has a Tolman cone angle slightly smaller than that of PPh_3. It was established by pH-potentiometric measurements and by ^1H and ^{31}P NMR studies that the distribution of the hydride derivatives $[RuClH(pTPPMS)_3]$ and $[RuH_2(pTPPMS)_{3,4}]$ is strongly pH-dependent. Hydrogenation of *trans*-cinnamaldehyde in aqueous–organic mixtures is catalyzed by $[RuCl_2(pTPPMS)_4]$ and is also strongly influenced by the pH of the aqueous phase due to the pH-dependent formation of the above hydrides. In acidic solutions (pH < 2) an exclusive C=C reduction takes place, while in alkaline solutions (pH > 6) a selective C=O hydrogenation was observed.

Key words: ruthenium, water soluble, hydrogenation, hydrides, sulfonated phosphines, biphasic.

Résumé : On a préparé les complexes chloro- et hydrido de ruthénium(II) avec le (4-diphénylphosphino)benzènesulfonate de potassium (pTPPMS) et on a comparé leurs propriétés avec celles des complexes apparentés des (3-diphénylphosphino)benzènesulfonates. Une détermination de structure par diffraction des rayons X a permis de mettre en évidence que le ligand *para*-sulfoné présente un cône de Tolman qui est légèrement inférieur à celui du PPh_3. Des mesures potentiométriques de pH et des études de RMN du ^1H et du ^{31}P ont permit de déterminer que la distribution des dérivés hydrures $[RuClH(pTPPMS)_3]$ et $[RuH_2(pTPPMS)_{3,4}]$ dépend beaucoup du pH. L'hydrogénation du *trans*-cinnamaldéhyde, dans des mélanges eau/solvant organique, est catalysée par le $[RuCl_2(pTPPMS)_4]$ et qu'elle est fortement influencée par le pH de la phase aqueuse en raison de la formation des hydrures mentionnés plus haut qui est influencée par le pH. En solutions acides (pH < 2), on observe exclusivement la réduction de la liaison C=C alors qu'en solutions alcalines (pH > 6), on observe une hydrogénation sélective de C=O.

Mots clés : ruthénium, soluble dans l'eau, hydrogénation, hydrures, phosphines sulfonées, à deux phases.

[Traduit par la Rédaction]

Introduction

Aqueous organometallic chemistry and catalysis has attracted a great deal of interest recently mostly as a consequence of the relatively easy and cheap regeneration of the catalysts and isolation of products in aqueous–organic biphasic systems (1–3). Although by far not exclusive, water soluble tertiary phosphines are the most important ligands in this field; the best known example being 3,3′,3″-phosphinetriylbenzenesulfonic acid (Na^+ or K^+ salts) (TPPTS) or more precisely, mTPPTS (4, 5). The simplest way of preparation of sulfonated arylphosphines is the sulfonation of the parent triarylphosphine by fuming sulfuric acid. In fact, the first water soluble phosphine ligand (3-diphenylphosphino)benzenesulfonic acid (mTPPMS) (as a Na^+ or K^+ salt), introduced into coordination chemistry by Ahrland et al. (6), was prepared this way as early as 1958. As a result of the protonation of phosphorus in fuming sulfuric acid these compounds contain the $-SO_3$ moiety in the *meta* position to the P donor atom. Based on a large body of experimental findings in coordination chemistry (7) and in organometallic catalysis (1–3, 8, 9) it could be concluded that such a modification of triarylphosphines did not lead to spectacular changes in complexation properties of these ligands despite

Received September 5, 2000. Published on the NRC Research Press Web site at http://canjchem.nrc.ca on June 30, 2001.

Dedicated to Professor Brian R. James on the occasion of his 65th birthday.

G. Papp, J. Kovács, and F. Joó.[1,2] Research Group of Homogeneous Catalysis, Hungarian Academy of Sciences, University of Debrecen, 4010 Debrecen, P.O. Box 7, Hungary.
A.Cs. Bényei and L. Nádasdi. Institute of Physical Chemistry, University of Debrecen, 4010 Debrecen, P.O. Box 7, Hungary.
G. Laurenczy. Institute of Inorganic and Analytical Chemistry, University of Lausanne, 1015 Lausanne-Dorigny, Switzerland.

[1]Corresponding author (telephone: (36-52)-512900; fax: (36-52)-512915; e-mail: jooferenc@tigris.klte.hu).
[2]Present address: Institute of Physical Chemistry, University of Debrecen, 4010 Debrecen, P.O. Box 7, Hungary.

 DOI: 10.1139/cjc-79-5/6-635 © 2001 NRC Canada

the somewhat diminished electron density on phosphorus and the obvious increase in size. Nevertheless, a few distinct changes have been noticed. For example, although $[RuCl_2(PPh_3)_3]$, $[RuCl_2(PPh_3)_4]$, and $[\{RuCl_2(PPh_3)_2\}_2]$ are all known in solid form (10, 11), with the *meta*-monosulfonated triphenylphosphine only $[\{RuCl_2(mTPPMS)_2\}_2]$ could be isolated (12, 13). Furthermore, the water soluble analog of the easily isolable $[RhH(PPh_3)_4]$, i.e., $[RhH(mTPPMS)_4]$ could not be prepared at all (14). There are only a few X-ray crystal structures of complexes with sulfonated arylphosphines available (15–17) that would allow comparison of ligands having the sulfonate substituent in different positions; no systematic study was devoted to this question. Both (4-diphenylphosphino) benzenesulfonates (pTPPMS) (18) and 4,4′,4″-phosphinetriylbenzenesulfonates (pTPPTS) (19, 20) have already been described in the literature. The *para*-monosulfonated triphenylphosphine, pTPPMS was first prepared by Schindlbauer (18) in 1965, but since then only one study (21) concerned its use in catalysis. Ruthenium(II)–phosphine complexes play an important role in catalysis (22) and the dissociation equilibria and reactivity of $[RuCl_2(PPh_3)_3]$ was thoroughly studied in this context (23, 24). Therefore, it seemed of interest to us to prepare ruthenium(II) complexes of pTPPMS and compare them to the well known Ru(II) complexes of mTPPMS. Herein, we report the results of our structural and catalytic studies.

Experimental

All manipulations were done under an argon or nitrogen atmosphere. All solvents were purified by distillation and carefully deaerated before use. Doubly distilled water was used throughout.

Chlorodiphenylphosphine, triphenylphosphine, chlorosulfonic acid, and fluorobenzene were obtained from Aldrich. Fuming sulfuric acid (30% SO_3) was supplied by Merck. $RuCl_3$ (aq) was a loan from Johnson Matthey. D_2O (99.9%) was purchased from Cambridge Isotope Laboratories. H_2, N_2, and Ar were acquired from Carbagas-CH or from Messer (Hungary). *trans*-Cinnamaldehyde (Aldrich) was distilled at reduced pressure before use. All other reagents were obtained from Aldrich and used without further purification.

Infrared spectra were recorded on a PerkinElmer Paragon 1000 PC FT-IR spectrometer on KBr discs. ^1H and proton decoupled ^{31}P NMR measurements were run on Bruker AC 200, AM 360, DRX 400, and DRX 600 NMR spectrometers and are referenced to 3-(trimethylsilyl)-1-propanesulfonic acid sodium salt (TSPSA, Fluka) and 85% phosphoric acid, respectively. The spectra were fitted with WIN-NMR, GNMR 4.0, and NMRICMA/MATLAB programs using a PC. Conditions of the pH-potentiometric measurements are described in detail in refs. 25 and 26, and those of HPLC analysis of the sulfonated phosphines in ref. 13.

The sulfonated phosphines pTPPMS (K^+ salt, monohydrate) (21) and mTPPMS (Na^+ salt) (13), as well as the complexes $[RuCl_2(PPh_3)_3]$ (10), $[\{RuCl_2(mTPPMS)_2\}_2]$ (13), and $[\{Ru(H_2O)_6\}(tosylate)_2]$ (27) were prepared as described in the literature. The purity of pTPPMS was checked by ^{31}P NMR (D_2O, δ = –5.87 ppm, s) and by HPLC (13); both methods revealed a uniform compound with no phosphine oxide present. X-ray quality crystals of the pTPPMS–Cs^+ salt could be obtained by recrystallization of 0.1 mmol of the pTPPMS–K^+ salt from 12 mL of a 0.4 M CsCl solution.

$[RuCl_2(pTPPMS)_4]$ was prepared by an adaptation of the method of Borowski et al. (28) for the preparation of various mTPPMS complexes. To a solution of $[RuCl_2(PPh_3)_3]$ (288 mg, 0.3 mmol) in tetrahydrofuran (THF) (50 mL) was added pTPPMS (570 mg, 1.5 mmol). The resulting clear solution was stirred at room temperature for 24 h during which the THF-insoluble $[RuCl_2(pTPPMS)_4]$ (as a stable tetrahydrate) precipitated as a light brown powder. For several batches the yields were consistently higher than 90%. The ruthenium and phosphorus content was determined on a Spectroflame ICP-AES (λ_{Ru} = 267.876 nm, λ_P = 178.287 nm). Anal. calcd. for $C_{72}H_{64}Cl_2K_4O_{16}P_4S_4Ru$: Ru 5.72, P 7.02, [P]/[Ru] = 4; found: Ru 5.58, P 7.02, [P]/[Ru] = 4.10.

Catalytic hydrogenation of *trans*-cinnamaldehyde (50 μL, 0.4 mmol) was carried out in a thoroughly stirred two-phase liquid mixture comprised of an aqueous phosphate buffer (3.00 mL) of known pH, containing KCl (45 mg), and chlorobenzene (5.00 mL) at 80°C. The reaction was started by the addition of $[RuCl_2(pTPPMS)_4]$ (13.0 mg, 7.4 μmol) together with pTPPMS (12.0 mg, 30 μmol), and the organic layer was analyzed by gas chromatography after 240 min reaction time. GC conditions: Chrom 5; packed column, Carbowax 20M on Chromosorb, 240 cm; injector 220°C, column 200°C, detector (FID) 200°C; carrier Ar.

X-ray crystal structure determination of $Ph_2PC_6H_4$-4-$SO_3Cs\cdot H_2O$

A colourless prism of dimensions of 0.35 × 0.20 × 0.15 mm was mounted on a glass fiber with epoxy cement. Data collection was performed on an Enraf–Nonius MACH3/PC diffractometer in non-profiled ω/2θ scans with θ_{max} = 23.01°. A total of 7775 independent reflections were collected. The structure was solved with the use of direct methods (29) and refined by using SHELXL 97 (30). Hydrogen atoms were treated by a mixture of independent and constrained refinement. Scattering factors for all atoms and anomalous dispersion corrections for the non-hydrogen atoms were taken from ref. 31. Pertinent crystal data are shown in Table 1.

Results and discussion

Preparation and properties of pTPPMS

Potassium (4-diphenylphosphino)benzenesulfonate (pTPPMS) was prepared by the reaction of potassium 4-fluorobenzenesulfonate and $KPPh_2$ in THF as described by Novak and co-workers (21). In some cases we have observed formation of small amounts of the water insoluble 1,4-bis(diphenylphosphino)benzene. In fact, the latter compound was prepared in high yield by Schindlbauer (18) by heating at reflux (160–180°C) 1,4-$ClC_6H_4SO_3Na$ and $KPPh_2$ in β,β′-diethoxy-diethyl ether. Similar to mTPPMS, in aqueous solutions pTPPMS behaves as a surfactant, which may result in solubilization of unsulfonated phosphines (13). Infrared stretching frequencies of the $-SO_3$ group in pTPPMS are very close to those in mTPPMS (13): 1038 and 1042 cm^{-1} (A_1) and 1200 and 1196 cm^{-1} (E), respectively.

We could obtain X-ray quality crystals of the cesium salt of pTPPMS by recrystallization of the K-salt from a CsCl

© 2001 NRC Canada

Table 1. Crystallographic parameters for $Ph_2PC_6H_4$-4-$SO_3Cs\cdot H_2O$.

Formula	$C_{36}H_{32}Cs_2O_8P_2S_2$
MW	984.5
Crystal dimensions (mm)	0.35 × 0.2 × 0.15
Crystal system	Triclinic (colourless prism)
Space group	$P\bar{1}$
a (Å)	9.271(2)
b (Å)	10.561(2)
c (Å)	21.30(4)
α (°)	92.948(10)
β (°)	90.136(10)
γ (°)	108.314(10)
V (× 10^9) (pm^3)	1.997(4)
Z	2
D_x (Mg m^{-3})	1.65
μ (mm^{-1})	2.078
Data collection	
Radiation (λ (Å))	Mo Kα (0.71073)
T (K)	293(2)
T min/max	0.2031/0.7128
Measured reflections	7775
Independent reflections	7775
Index ranges	h = –3–11, k = –12–12, l = –20–20
(Δ/σ)max	0.076
Extinction correction	SHELXL
Data/restraints/parameters	7775/0/464
R(*F*)	0.0667
wR(F^2)	0.224
GoF (*S*)	1.063
Δρ min/max (e $Å^{-3}$)	1.796/–1.429 (around Cs atoms)

Fig. 1. ORTEP representation of $Ph_2PC_6H_4$-4-$SO_3Cs\cdot H_2O$. Probability displacement ellipsoids are drawn to 50%.

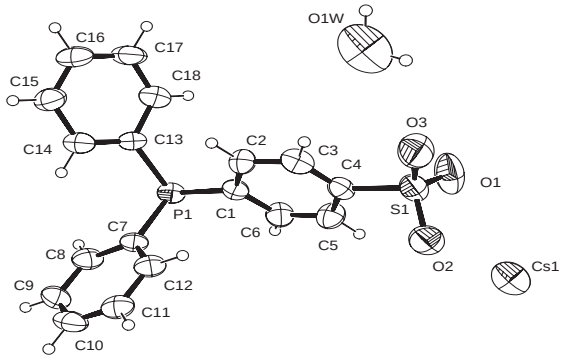


Table 2. Selected X-ray crystallographic parameters for $Ph_2PC_6H_4$-4-$SO_3Cs\cdot H_2O$.

Interatomic distances (pm)		Interatomic angles (°)	
C1—P1	182.9(8)	C1-P1-C7	101.4(3)
C7—P1	183.7(7)	C1-P1-C13	101.7(3)
C13—P1	184.5(7)	C7-P1-C13	101.5(3)
C1′—P1′	183.9(8)	C1′-P1′-C7′	101.4(4)
C7′—P1′	182.6(8)	C1′-P1′-C13′	103.1(4)
C13′—P1′	183.8(8)	C7′-P1′-C13′	102.2(0)

Note: Primed values refer to a second phosphine molecule in the unit cell.

solution. The structure of the pTPPMS–Cs^+ salt was determined by X-ray diffraction and this gives an opportunity to compare it to a recently published structure (32) of the benzyltriethylammonium salt of mTPPMS. An ORTEP representation is shown in Fig. 1. Each unit cell contains two phosphine molecules and one H_2O molecule. The two molecules consistently have slightly different geometric parameters, however, the difference is within the error of structure determination. Selected interatomic distances and angles are given in Table 2.[3]

As expected, the geometry around the phosphorus atom is trigonal pyramidal, and the average value (for both phosphine moieties in the asymmetric unit) of the three P—C bonds is 183.6 pm and that of the C-P-C angles is 101.9°. These values are insignificantly different from those determined for PPh_3 (182.8 pm and 103.0° (33) and 183.1 pm and 102.8° (34)), and from those obtained in the case of the mono- and tri-sulfonated triphenylphosphines $[N(CH_2C_6H_5)(C_2H_5)_3^+](Ph_2PC_6H_4$-3-$SO_3^-\cdot H_2O]$ (182.6 pm and 102.5° (32)) and $[P(C_6H_4$-4-$SO_3K)_3\cdot KCl\cdot 0.5H_2O]$ (184.3 pm and 103.5° (20)), respectively. The cone angle, as defined by Tolman (35), was determined from these structural data essentially as described by Darensbourg et al. (16, 17). To this end, a virtual H atom was placed at a distance of 228 pm from the phosphorus atom and the cone angle of the *smallest* cone which originates from the coordinates of this hydrogen and circumscribes the whole molecule (without the cation) was computed. For comparison, similar calculations were made using X-ray crystal structural data of other tertiary arylphosphines taken from the Cambridge Structural Database. In the case of *para*-subsituted arylphosphines it is also important to consider the space requirement of the hydrogen atoms in *ortho*-positions of the aryl rings; this was accounted for by using the Bohr radius of H (52.9 pm). Cone angles of several substituted triphenylphosphines and that of PPh_3 are collected in Table 3.

Our calculations resulted in a cone angle of 141.5° for PPh_3, which is in a reasonable agreement with the value of 145° reported by Tolman (35). More interestingly, the cone angles for pTPPMS and pTPPTS are slightly *smaller* (by 4° and 2°, respectively), while for mTPPMS and mTPPTS are considerably *larger* (approximately by 35°) than that of PPh_3. It can be concluded, therefore, that the space requirement of *para*-sulfonated triphenylphosphines is practically the same as that of PPh_3 itself, *meta*-sulfonated triphenylphosphines, however, are much more space-demanding. Furthermore, it is the position and not the number of the -SO_3 substituents

[3] Supplementary material may be purchased from the Depository of Unpublished Data, Document Delivery, CISTI, National Research Council Canada, Ottawa, ON K1A 0S2, Canada. For information on obtaining material electronically go to http://www.nrc.ca/cisti/irm/unpub_e.shtml. Crysallographic information has been deposited with the Cambridge Crystallographic Data Centre. Copies of the data can be obtained (deposition number 157 706), free of charge, on application to the Director, CCDC, 12 Union Road, Cambridge CB2 1EZ, U.K. (Fax: 44-1223-336033 or e-mail: deposit@ccdc.cam.ac.uk).

© 2001 NRC Canada

Table 3. Cone angles of tertiary arylphosphines calculated from crystallographic data.

Phosphine	Cone angle (°)	Ref. for crystallographic data
pTPPMS	137.7	This work
pTPPTS	139.2	20
PPh_3	141.5	34
mTPPMS	177.6	32
mTPPTS	170.0	16, 17

that defines the size of these ligands (at least in terms of their cone angles).

Preparation and reactions of $[RuCl_2(pTPPMS)_4]$ and its catalytic activity in hydrogenation of *trans*-cinnamaldehyde

When a THF solution of $[RuCl_2(PPh_3)_3]$ was reacted with 5 equiv of pTPPMS, metathesis of the phosphine ligands produced the title compound, which is only sparingly soluble in THF, in high yield.

The overall composition of the complex in solid form as $[RuCl_2(pTPPMS)_4]$ was confirmed by determination of its ruthenium–phosphorus content (1:4). This is an interesting difference in comparison with mTPPMS. Ruthenium(II) complexes of (3-diphenylphosphino)benzenesulfonic acid (Na salt) can be prepared either by heating at reflux ethanolic solutions of aq $RuCl_3$ with an excess of mTPPMS, or by phosphine metathesis in THF (13), similar to the procedure described above with pTPPMS. However, in both reactions the product is $[\{RuCl_2(mTPPMS)_2\}_2]$. While one can expect a larger extent of phosphine dissociation, and hence, an increased probability of dimerization at reflux temperature, the exclusive formation of the dimeric mTPPMS derivative in room temperature metathesis reactions is in contrast to the formation of $[RuCl_2(PPh_3)_3]$ in refluxing ethanol and to that of $[RuCl_2(PPh_3)_4]$ in cold methanol (10). On the other hand, the relative stability of the various monomeric and dimeric compounds correlates well with the space requirement of PPh_3, pTPPMS, and mTPPMS as represented by the respective Tolman cone angles. Such a lowering of the number of coordinated phosphine ligands was also observed in the case of $[Pd(mTPPMS)_3]$ (15) and in the failed attempts to prepare $[RhH(mTPPMS)_4]$ (14) (Na^+ or K^+ salts).

Characterization of the new water soluble phosphine complexes by NMR spectroscopy presented considerable difficulties. Unfortunately, in all measurements described below the signals were found to be very broad (50–150 Hz) and were basically uneffected by ^1H decoupling, changes in the temperature between 0–50°C, or by addition of small amounts of MeOD, which were found to be useful in other cases (14). Although the line width of the signals refer to intra- and (or) intermolecular dynamic processes or fast relaxation, insufficient solubility of the compounds in the ususal NMR solvents other than D_2O (alcohols, THF, acetone etc.) precluded measurements in a wide temperature range.

In D_2O solutions of $[RuCl_2(pTPPMS)_4]$ the ^{31}P NMR spectra showed two overlapping unresolved, symmetric resonances at 54.5 and 53.7 ppm in addition to resonances representing some phosphine oxide (36.0 ppm, br s) and some free phosphine (–5.8 ppm, br s). Upon addition of pTPPMS in excess (up to [P]/[Ru] = 15) the signal at 53.7 ppm became dominant at the expense of the signal at 54.5 ppm, which shows the existence of at least two ruthenium complexes in the solution. However, the signals were still unresolved, and therefore, unsuitable for structural characterization. To obtain more information we wanted to study the ^{19}F NMR spectra of related fluoro complexes. Addition of KF to solutions of $[RuCl_2(pTPPMS)_4]$ ($[F^-]/[Ru]$ = 2–10) produced complex spectra, therefore, chloride-free samples were prepared in the reaction of $[Ru(H_2O)_6]^{2+} + 2F^- + 8(pTPPMS)$. The only major ^{31}P NMR signal was observed at 53.2 ppm (broad but symmetric) accompanied by several small peaks at 54.0, 52.0, 45.1, and 39.2 ppm (in addition to free pTPPMS and some of its oxide). ^1H or ^{19}F decoupling did not reveal any structure of the resonances either, as it did not cause any noticable line sharpening (for technical reasons simultaneous decoupling was not possible). The ^{19}F NMR spectrum of the same solution was more informative. Remarkably, it showed no signs of free F^- indicating that the dominant peak in the ^{31}P NMR spectrum should belong to a *difluoro* species. Furthermore, a well resolved triplet of triplets centered at –108.70 ppm was observed with coupling constants $^2J_{P_{trans},F}$ = 8.5 Hz and $^2J_{P_{cis},F}$ = 5.2 Hz. ^{31}P decoupling resulted in partial collapse of the structure of the ^{19}F signal, although with our technical capabilities full collapse to a singlet could not be observed. These data are consistent with the presence of a *cis*-$[RuF_2(pTPPMS)_4]$ complex, and the small values of the coupling constants explain the insensitivity of the ^{31}P NMR signals for fluorine decoupling. Such a species should show two ^{31}P resonances of equal intensity, which we do not observe separately as they may overlap or be hidden underneath the broad envelope at 53.2 ppm. Although one may not extrapolate with certainty the conclusions regarding the fluoro-complex(es) to the case of the chloride-containing species, the similarity of the ^{31}P NMR spectra at high pTPPMS excess allows us to believe that at least some of the ruthenium is present as *cis*-$[RuCl_2(pTPPMS)_4]$. Stabilization of higher phosphine species by hydrogen bonding as in case of sulfonated phosphine complexes relative to the analogous PPh_3 compounds has already been observed and quantitatively established for the phosphine dissociation equilibria of $[Rh(CO)H(mTPPTS)_3]$ vs. $[Rh(CO)H(PPh_3)_3]$ (36).

We have described earlier that $[\{RuCl_2(mTPPMS)_2\}_2]$ is prone to hydrolysis in water (25, 26). This complex activates H_2 via heterolytic fission, and therefore, formation of both $[RuClH(mTPPMS)_3]$ and $[RuH_2(mTPPMS)_4]$ is accompanied by proton production. All these reactions were followed by pH-potentiometry and the resulting ruthenium complexes were identified by ^1H and ^{31}P NMR spectroscopy (25, 26). Similarly, in aqueous solutions at slightly elevated temperatures $[RuCl_2(pTPPMS)_4]$ readily reacts with molecular hydrogen. A combined potentiometric–NMR study of this reaction was undertaken. In short, $[RuCl_2(pTPPMS)_4]$ was dissolved under an inert gas atmosphere (Ar) in a solution of a supporting electrolyte (KCl) and excess pTPPMS at a preset *constant pH*. In case of any hydrolysis the pH was kept constant by delivering KOH solution of known concentration by an autoburette. The volume of the KOH solution consumed is proportional to the extent of hydrolysis at that particular pH. After attaining equilibrium the solution was

© 2001 NRC Canada

Fig. 2. Proton production upon dissolution (middle set of bars) and further hydrogenation (front set) of solutions of $[RuCl_2(pTPPMS)_4]$ as a function of pH. Total proton production is shown by the back set of bars (220 mg $[RuCl_2(pTPPMS)_4]$, 200 mg pTPPMS, 10 mL 0.2 M KCl, H_2O:D_2O = 9:1, 60°C, 1 bar of Ar or H_2).

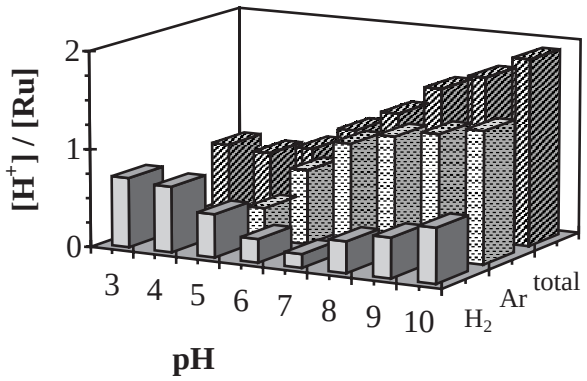
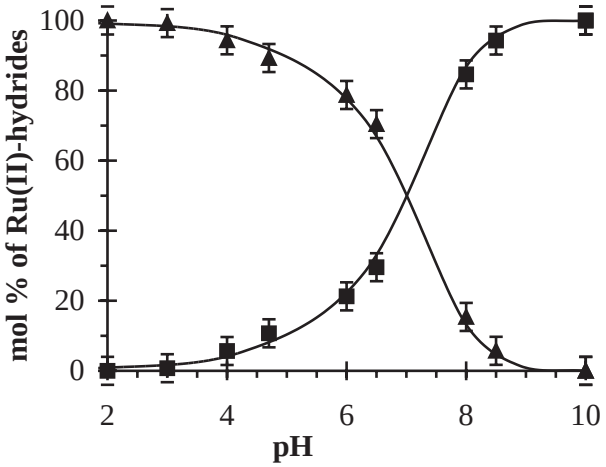


Fig. 3. Distribution of ruthenium into $[RuClH(pTPPMS)_3]$ (▲) and $[RuH_2(pTPPMS)_{3,4}]$ (■) in aqueous solution as a function of pH (220 mg $[RuCl_2(pTPPMS)_4]$, 200 mg pTPPMS, 10 mL 0.2 M KCl, H_2O:D_2O = 9:1, 60°C, 1 bar of Ar or H_2).



placed under hydrogen gas. Formation of any ruthenium hydrides with heterolytic splitting of H_2 was, again, indicated by further KOH consumption until the reaction attained a new equilibrium position at the particular (preset) pH. This way the whole pH-range, amenable to measurements with a glass electrode, was investigated for hydrolysis of and hydride formation from $[RuCl_2(pTPPMS)_4]$ under H_2. The results are shown in Figs. 2 and 3.

It is seen from Fig. 2 that below pH 5 there is no or negligible proton production upon dissolution of $[RuCl_2(pTPPMS)_4]$. However, hydrogenation of the same solutions results in the formation of 1 mol of H^+ for 1 mol of Ru. During this reaction the colour of the solution turns deep cherry red. The ^1H and ^{31}P NMR spectra of these solutions were recorded (90% H_2O – 10% D_2O, 50°C). ^1H NMR δ: –17.9 (q, $^2J_{P,H}$ = 24.9 Hz). ^{31}P NMR δ: 58.7 (br s). These data are consistent with the formation of $[RuHCl(pTPPMS)_3]$; similar $[RuHCl(P)_3]$ complexes have already been reported with PPh_3 (37), mTPPMS (25, 26), and mTPPTS ligands (38, 39).

In basic solutions significant proton production is observed upon dissolution of $[RuCl_2(pTPPMS)_4]$ with excess pTPPMS under argon indicating extensive hydrolysis. Bubbling hydrogen through these solutions resulted in further proton production (Fig. 2) giving $[H^+]_{total}/[Ru]$ = 2 at pH 10. Above pH 9 the hydrogenated solutions are bright yellow. ^{31}P NMR spectra of these yellow solutions recorded at 81.01 and 161.94 MHz (90% H_2O – 10% D_2O, 50°C) showed broad singlets at δ = 41.5, 52.0, and 54.6 ppm in a ratio of 2:2:1, respectively. However, at 242.94 MHz the signal at 41.5 ppm split into two resonances of equal intensity at 41.39 and 41.57 ppm. The only ^1H NMR signal was observed at –10.3 ppm (br td or pseudo q) with the coupling constants $^2J_{P_a,H}$ = 34.4 Hz and $^2J_{P_b,H}$ = 35.0 Hz. Selective ^{31}P decoupling at 41.5 ppm caused this signal to collapse into a triplet while irradiation at 52.0 ppm resulted in a doublet in the hydride region. According to the results of the pH-static hydrogenation (2 mol H^+ is produced for 1 mol Ru) the hydride species present should be *dihydride(s)*, so any monohydride which otherwise would fit the NMR data can be disregarded. Consequently, one pair of the ^{31}P NMR signals, one of those at 41.39 and 41.57 ppm together with the resonance at 52.0 (intensity ratio 1:2) is assigned to trisphosphine species, i.e., we suggest that part of the ruthenium(II) is present as the trigonal bipyramidal *cis*-$[RuH_2(pTPPMS)_3]$ and (or) the structurally close octahedral *trans*-$[RuH_2(H_2O)(pTPPMS)_3]$ (analogous to $[RuH_2(PPh_3)_3(THF)]$ (40)). Such complexes have been identified as the catalytically active species in transfer hydrogenation experiments (42, 44).

Based on literature reports (40–43), *exclusive* formation of trisphosphine complexes is unlikely in the presence of excess phosphine such as pTPPMS used in our experiments ($[P]_{total}/[Ru]$ = 8). In agreement with the above, the two other ^{31}P NMR signals at around 41.5 and 54.6 ppm (intensity ratio 1:1) may belong to *cis*-$[RuH_2(pTPPMS)_4]$. In two earlier studies the analogous *cis*-$[RuH_2(TPPTS)_4]$ was found to have ^{31}P chemical shifts at δ = 42.4 (br s) and 55.0 (br s) (38) and at δ = 41.9 and 53.9 ppm (39). The same authors observed the hydride signal of *cis*-$[RuH_2(TPPTS)_4]$ at δ = –10.6 ppm ("pseudo-quartet," $^2J_{P,H}$ = 33 Hz) (38) and at δ = –10.5 ppm ("four intense merging lines," $^2J_{P,H}$ = 35 Hz) (39). In our case the putative *cis*-$[RuH_2(pTPPMS)_4]$ species is also expected to show a pseudo-quartet in ^1H NMR around δ = –10.3 ppm which may coincide with the signal(s) of the above *trans*-$[RuH_2(H_2O)(pTPPMS)_3]$ or *cis*-$[RuH_2(pTPPMS)_3]$ complexes. Selective ^{31}P decoupling of either P_a or P_b of *cis*-$[RuH_2(pTPPMS)_4]$ should result in collapse of the pseudo-quartet to a triplet, however, this may be obscured by the changes in the ^1H NMR spectra of the trisphosphine hydride complexes. The presence of both kinds of dihydrides is further supported by the simulation of the hydride resonance. The experimental spectrum could not be fitted properly with either *trans*-$[RuH_2(H_2O)P_3]$ or *cis*-$[RuH_2P_3]$ alone, however, an acceptable fit was obtained by considering a mixture of the trisphosphine complexes with *cis*-$[RuH_2(pTPPMS)_4]$ around 1:1 ratio. These simulations gave coupling constants for the td part of the spectrum as $^2J_{P_a,H}$ = 33 Hz and $^2J_{P_b,H}$ = 39 Hz (compared to 34.4 and 35.0 Hz, respectively, from the ^{31}P NMR spectrum) and for the supposed pseudo-quartet as $^2J_{P,H}$ = 44 Hz, its center being shifted by 11 Hz from the center of the td signal. Based on these considerations we conclude

© 2001 NRC Canada

Fig. 4. Hydrogenation of *trans*-cinnamaldehyde.

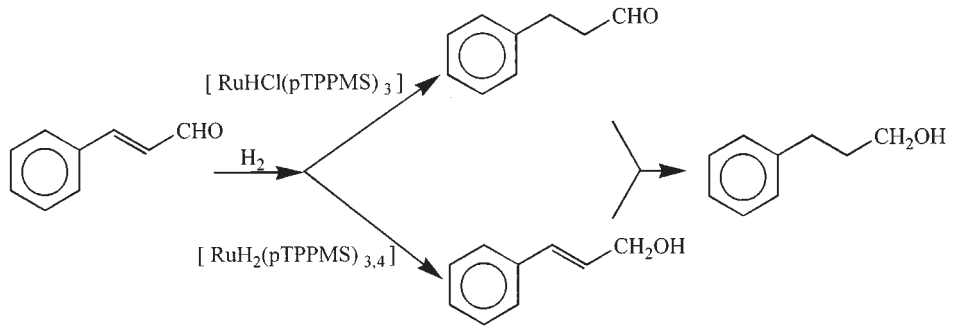
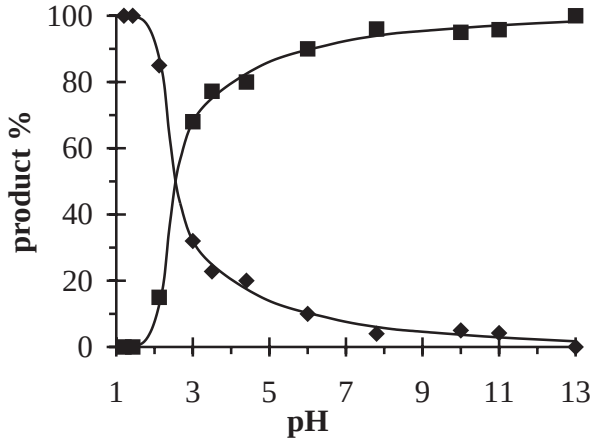


Fig. 5. Selectivity of the hydrogenation of *trans*-cinnamaldehyde to saturated aldehyde (◆) and unsaturated alcohol (■) catalyzed by $[RuCl_2(pTPPMS)_4]$ as a function of pH. For conditions see *Experimental*.



that in our solutions prepared from $[RuCl_2(pTPPMS)_4]$ with excess pTPPMS under hydrogen at high pH (>9) ruthenium is present in form of a mixture of tris- and tetrakisphosphine dihydrides, $[RuH_2X(pTPPMS)_3]$ (X = nothing or H_2O) and *cis*-$[RuH_2(pTPPMS)_4]$; for a general description of the ruthenium hydrides in such solutions in the following we use $[RuH_2(pTPPMS)_{3,4}]$.

In the intermediate pH range (5 < pH < 9) both mono- and dihydrides are present and their concentration distribution was calculated from the integrated intensities of the respective hydride ^1H NMR signals. Under these conditions a small amount of a third complex was also detected (90% H_2O – 10% D_2O, 50°C). ^1H NMR δ: –8.7 (td, $^2J_{P,H}$ = 37.7 Hz, $^2J_{P,H}$ = 7.9 Hz). ^{31}P NMR δ: 51.4 (br s). These data are very close to those of $[\{RuClH(mTPPMS)_2\}_2]$ identified earlier by Sánchez-Delgado et al. (45) (^1H NMR δ: –8.7 (td, $^2J_{P,H}$ = 38 Hz, $J_{H,H}$ = 9 Hz). ^{31}P NMR δ: 52.11 (AB q, $J_{A,B}$ = 38 Hz)) and suggest the presence of $[\{RuClH(pTPPMS)_2\}_2]$. No signs of other hydrides, such as e.g., the analogs of $[RuClH(PPh_3)_3]_2$ (46) and $[(PPh_3)_2(H)Ru(\mu\text{-}H)(\mu\text{-}Cl)RuH(PPh_3)_2]^-$ (47) were seen by NMR spectroscopy in solutions of any pH.

As expected, both the ^1H and ^{31}P NMR data of the Ru-pTPPMS complexes are very close to the corresponding parameters of $[RuHCl(mTPPMS)_3]$ and $[RuH_2(mTPPMS)_4]$, since in these hydrides the steric requirements of the phosphine ligands seem to play no important role. However, the higher stability of the corresponding pTPPMS complexes manifests itself in the onset of the formation of $[RuH_2(pTPPMS)_{3,4}]$ at somewhat lower pH, than for $[RuH_2(mTPPMS)_4]$. Under strictly comparable conditions there is only a negligible fraction of Ru(II) in the form of $[RuH_2(mTPPMS)_4]$ at pH 6 (25, 26), while $[RuH_2(pTPPMS)_{3,4}]$ represents about 20% of all ruthenium at this pH and $[RuH_2(pTPPMS)_{3,4}]$ can be detected in a small relative concentration already at pH ≈ 2 (Fig. 3). This has important consequences in catalysis.

Selective reduction of an aldehyde or ketone function in the presence of an olefinic C=C bond is a challenge in catalysis and ruthenium phosphine complexes are among the best catalysts of such processes (25, 38, 44, 48). Hydrogenation of *trans*-cinnamaldehyde (Fig. 4) is actively catalyzed by the hydrido-complexes formed from $[RuCl_2(pTPPMS)_4]$. Depending on the pH, overall turnover frequencies up to 13 h^{-1} were determined under the conditions specified in *Experimental* (complete conversion of cinnamaldehyde). However, the selectivity of the reaction was a striking function of the pH (Fig. 5). In acidic solutions, around and below pH 2 slow hydrogenation of *trans*-cinnamaldehyde yields the saturated aldehyde, 3-phenylpropanal (C=C reduction). An increase in the pH of the aqueous phase results in a sharp increase in the overall rate and more importantly in the selectivity of hydrogenation in favour of the unsaturated alcohol, 3-phenyl-2-propenol (C=O reduction), which represents about 80% of all products already at pH 4. Although this change in selectivity does not strictly parallel the concentration distribution of $[RuClH(pTPPMS)_3]$ and $[RuH_2(pTPPMS)_{3,4}]$ as a function of the pH, it can be easily rationalized by assuming a higher specific rate of C=O reduction catalyzed by $[RuH_2(pTPPMS)_{3,4}]$ than that of C=C reduction catalyzed by $[RuClH(pTPPMS)_3]$. In comparison to catalysis of hydrogenation of *trans*-cinnamaldehyde by $[RuHCl(mTPPMS)_3]$ and $[RuH_2(mTPPMS)_4]$, the basic characteristics are very similar except that the change in the selectivity happens in a lower pH range with complexes of pTPPMS (pH 2–4 compared to 4.5–6.5 with mTPPMS). This may be a useful feature of catalysis by $[RuCl_2(pTPPMS)_{3,4}]$ in cases where lower pH is beneficial, such as the hydrogenation of bicarbonates (49, 50) under CO_2 pressure. The mechanism of the reaction is thought to be similar to that of the hydrogenation of unsaturated aldehydes with $[\{RuCl_2(mTPPMS)_2\}_2]$ + mTPPMS (25, 26), however, elucidation of a detailed picture requires further measurements.

© 2001 NRC Canada

Conclusions

In this study we have shown that the (4-diphenylphosphino)benzenesulfonate anion pTPPMS has approximately the same Tolman cone angle (determined by X-ray diffraction as its Cs^+ salt) as PPh_3. Consequently, the steric requirements for its coordination are considerably smaller than those of the closest analog, the (3-diphenylphosphino)benzenesulfonate anion, mTPPMS. NMR data of the two phosphines and their Ru(II)-complexes showed the ligand electronic properties to be very similar. Due to its smaller size (cone angle) pTPPMS forms more stable tetrakisphosphino–Ru(II) complexes, such as $[RuCl_2P_4]$ and $[RuH_2P_4]$ than mTPPMS; this is manifested in the distribution of the hydride complexes and the resulting selectivity of hydrogenation of *trans*-cinnamaldehyde as a function of pH.

Acknowledgments

This work was supported by the Hungarian National Research Foundation (OTKA T29934 and D25136) and by the Office Fédéral de l'Education et de la Science, Suisse (OFES 98.0011). The generous loan of aq $RuCl_3$ by Johnson Matthey is gratefully acknowledged. This research is part of the collaboration within the COST Action D10–Working Group 0001.

References

1. B. Cornils and W.A. Herrmann (*Editors*). Aqueous phase organometallic catalysis: concepts and applications. Wiley-VCH, Weinheim. 1998.
2. F. Joó and Á. Kathó. J. Mol. Catal. A: Chem. **116**, 3 (1997).
3. I.T. Horváth and F. Joó (*Editors*). Aqueous organometallic chemistry and catalysis. NATO ASI Series 3/5. Kluwer Academic, Dordrecht. 1995.
4. E. Kuntz. CHEMTECH. **17**, 570 (1987).
5. W.A. Herrmann and C.W. Kohlpaintner. Inorg. Synth. **32**, 8 (1998).
6. S. Ahrland, J. Chatt, N.R. Davies, and A.A. Williams. J. Chem. Soc. 276 (1958).
7. J.C. Chang and J. Bjerrum. Acta Chem. Scand. **26**, 815 (1972).
8. P.A. Chaloner, M.A. Esteruelas, F. Joó, and L.A. Oro. Homogeneous hydrogenation. Kluwer Academic, Dordrecht. 1994. Chap. 5.
9. B. Driessen-Hölscher. Adv. Catal. **42**, 473 (1998).
10. T.A. Stephenson and G. Wilkinson. J. Inorg. Nucl. Chem. **28**, 945 (1966).
11. P.R. Hoffmann and K.G. Caulton. J. Am. Chem. Soc. **97**, 4221 (1975).
12. Z. Tóth, F. Joó, and M.T. Beck. Inorg. Chim. Acta, **42**, 153 (1980).
13. F. Joó, J. Kovács, Á. Kathó, A.C. Bényei, T. Decuir, and D.J. Darensbourg. Inorg. Synth. **32**, 1 (1998).
14. F. Joó, J. Kovács, A. Cs. Bényei, L. Nádasdi, and G. Laurenczy. Chem. Eur. J. **7**, 193 (2001).
15. A.L. Casalnuovo and J.C. Calabrese. J. Am. Chem. Soc. **112**, 4324 (1990).
16. D.J. Darensbourg and C.J. Bischoff. Inorg. Chem. **32**, 47 (1993).
17. D.J. Darensbourg, C.J. Bischoff, and J.H. Reibenspies. Inorg. Chem. **30**, 1144 (1991).
18. H. Schindlbauer. Monatsh. Chem. **96**, 2051 (1965).
19. O. Herd, K.P. Langhans, O. Stelzer, N. Weferling, and W.S. Sheldrick. Angew. Chem. Int. Ed. Engl. **32**, 3058 (1993).
20. O. Herd, A. Heβler, K.P. Langhans, O. Stelzer, W.S. Sheldrick, and N. Weferling, J. Organomet. Chem. **475**, 99 (1994).
21. T.I. Wallow, F.E. Goodson, and B.M. Novak. Organometallics, **15**, 3708 (1996).
22. B.R. James. Homogeneous hydrogenation. John Wiley & Sons, New York. 1973. Chap. IX.B.
23. B.R. James and L.D. Markham. Inorg. Chem. **13**, 97 (1974).
24. B.R. James, L.K. Thompson, and D.K. Wang. Inorg. Chim. Acta, **29**, L237 (1978).
25. F. Joó, J. Kovács, A. Cs. Bényei, and Á. Kathó. Angew. Chem. Int. Ed. **37**, 969 (1998).
26. F. Joó, J. Kovács, A. Cs. Bényei, and Á. Kathó. Catal. Today, **42**, 441 (1998).
27. P. Bernhard, M. Biner, and A. Ludi. Polyhedron, **9**, 1095 (1990).
28. A.F. Borowski, D.J. Cole-Hamilton, and G. Wilkinson. Nouv. J. Chim. **2**, 137 (1978).
29. A. Altomare, G. Cascarano, C. Giacovazzo, and A. Guagliardi. J. Appl. Crystallogr. **26**, 343 (1993).
30. G.M. Sheldrick. SHELXL 97. Program for crystal structure refinement. University of Göttingen, Germany. 1997.
31. A.J.C. Wilson (*Editor*). International tables for crystallography. Vol C. Kluwer Academics, Dordrecht. 1992.
32. P.J. Roman Jr., D.P. Paterniti, R.F. See, M.R. Churchill, and J.D. Atwood. Organometallics, **16**, 1484 (1997).
33. J.J. Daly. J. Chem. Soc. 3799 (1964).
34. B.J. Dunne, R.B. Morris, and A.G. Orpen. J. Chem. Soc. Dalton Trans. 653 (1991).
35. C.A. Tolman. Chem. Rev. **77**, 313 (1977).
36. I.T. Horváth, R.V. Kastrup, A.A. Oswald, and E.J. Mozeleski. Catal. Lett. **2**, 85 (1989).
37. R.U. Kirss, T.C. Eisenschmid, and R. Eisenberg. J. Am. Chem. Soc. **110**, 8564 (1988).
38. M. Hernandez and P. Kalck. J. Mol. Catal. A: Chem. **116**, 117 (1997).
39. E. Fache, C. Santini, F. Senocq, and J.M. Basset. J. Mol. Catal. A: Chem. **72**, 331 (1992).
40. D.E. Linn and J. Halpern. J. Am. Chem. Soc. **109**, 2969 (1987).
41. J.J. Levison and S.D. Robinson. J. Chem. Soc. A, 2947 (1970).
42. Y. Lin and Y. Zhou. J. Organomet. Chem. **381**, 135 (1990).
43. L.S. Van Der Sluys, G.J. Kubas, and K.G. Caulton. Organometallics, **10**, 1033 (1991).
44. A. Aranyos, G. Csjernyik, K.J. Szabó, and J.-E. Bäckvall. Chem. Commun. 351 (1999).
45. A. Sánchez-Delgado, M. Medina, F. López-Linares, and A. Fuentes. J. Mol. Catal. A: Chem. **116**, 167 (1997).
46. J.M. Towarnicky and E.P. Schram. Inorg. Chim. Acta, **41**, 55 (1980).
47. K.S. MacFarlane, A.M. Joshi, B.R. James, and S.J. Rettig. Chem. Commun. 1363 (1997).
48. J.M. Grosselin, C. Mercier, G. Allmang, and F. Grass. Organometallics, **10**, 2126 (1991).
49. F. Joó, G. Laurenczy, L. Nádasdi, and J. Elek. Chem. Commun. 971 (1999).
50. G. Laurenczy, F. Joó, and L. Nádasdi. Inorg. Chem. **39**, 5083 (2000).

© 2001 NRC Canada

Synthesis and structural features of complexes $[(P^{\frown}P)_2Rh][hfacac]$ containing hexafluoroacetylacetonate as a noncoordinating anion

Roland Fornika, Christian Six, Helmar Görls, Magnus Kessler, Carl Krüger, and Walter Leitner

Abstract: The synthesis and characterization of complexes $[(P^{\frown}P)_2Rh][hfacac]$ ($P^{\frown}P$ = chelating bidentate phosphine ligand $R_2P(CH_2)_nPR_2$ (**2a**–**g**), hfacac = hexafluoroacetylacetonate anion) (**4**) is reported. The molecular structures of **4a** (R = Ph, *n* = 1) and **4f** (R = Cy, *n* = 2) in the solid state were determined by single-crystal X-ray diffraction. The complexes crystallize in the monoclinic space groups *C*2/*c* (No. 15) and $P2_1/n$ (No. 14), respectively. No coordinative interaction between the rhodium center of the cation $[(P^{\frown}P)_2Rh]^+$ (**4a**$^+$, **4f**$^+$) and the hfacac anion is evident in either cases. In the crystal structure of **4a**, hydrogen bonds between the oxygen atoms of the hfacac anion and methylene protons of the CH_2 bridges of the phosphine ligand lead to highly symmetric chains of regularly alternating cations and anions. The coordination geometry around the rhodium center in **4a**$^+$ is ideally square-planar, whereas **4f**$^+$ is significantly distorted towards a tetrahedron with an angle between the two P_2Rh moieties of 18.6°. The cation **4b**$^+$ (R = Cy, *n* = 1) was investigated in form of the tetrafluoroborate salt for comparison. The compound $[\{Cy_2P(CH_2)PCy_2\}_2Rh][BF_4]$ crystallizes as a THF solvate (**4b′**) in the triclinic space group $P\bar{1}$ (No. 2) containing ideally square-planar $[(P^{\frown}P)_2Rh]^+$ cations.

Key words: rhodium, chelating ligands, coordination modes, 1,3-diketonates, phosphorus ligands.

Résumé : On a effectué la synthèse et la caractérisation de complexes $[(P^{\frown}P)_2Ph][hfacac]$ (**4**) ($P^{\frown}P$ = ligand phosphine chélatant bidentate $R_2P(CH_2)_nPR_2$, **2a**–**g**, hfacac = anion hexafluoroacétylacétonate). On a déterminé les structures moléculaires de **4a** (R = Ph, *n* = 1) et **4f** (R = Cy, *n* = 2) à l'état solide par diffraction des rayons X par des cristaux uniques. Les complexes cristallisent respectivement dans les groupes d'espace monocliniques *C*2/*c* (No. 15) et $P2_1/n$ (No. 14). Dans chacun de ces cas, on n'observe aucune interaction de coordination entre le centre rhodium du cation $[(P^{\frown}P)_2Rh]^+$ (**4a**$^+$, **4f**$^+$) et l'anion hfacac. Dans la structure cristalline du produit **4a**, des liaisons hydrogènes entre les atomes d'oxygène de l'anion hfacac et les protons méthyléniques des ponts CH_2 du ligand phosphine conduisent à des chaînes fortement symétriques comportant une alternance régulière de cations et d'anions. La géométrie de coordination autour du centre rhodium de **4a**$^+$ se présente comme un plan carré idéal alors que dans le cas du **4f**$^+$ on observe une déformation importante vers un tétraèdre avec un angle de 18,6° entre les deux portions de P_2Rh. Pour fins de comparaison, on a étudié le cation **4b**$^+$ (R = Cy, *n* = 1) sous la forme de sel de tétrafluoroborate. Les cristaux du composé $[\{Cy_2P(CH_2)PCy_2\}_2Rh][BF_4]$ qui est solvaté par le THF (**4b′**) sont tricliniques, groupe d'espace $P\bar{1}$ (No. 2) et ils comportent des cations $[(P^{\frown}P)_2Rh]^+$ qui sont dans un plan carré idéal.

Mots clés : rhodium, ligands chélatant, modes de coordination, 1,3-dicétonates, ligands phosphorés.

[Traduit par la Rédaction]

Introduction

1,3-Diketonates are frequently used as ligands in coordination chemistry (1). Metal complexes containing the acetylacetonate ligand (acac), and its trifluoro (tfacac) and hexafluoro (hfacac) analogues have found widespread applications. Such compounds are intensively studied in cancer chemotherapy (2), for metal extraction (3), as precursors for CVD applications (4), and as catalyst precursors (for example rhodium(I) 1,3-diketonates are frequently used as precur-

Received October 4, 2000. Published on the NRC Research Press Web site at http://canjchem.nrc.ca on June 30, 2001.

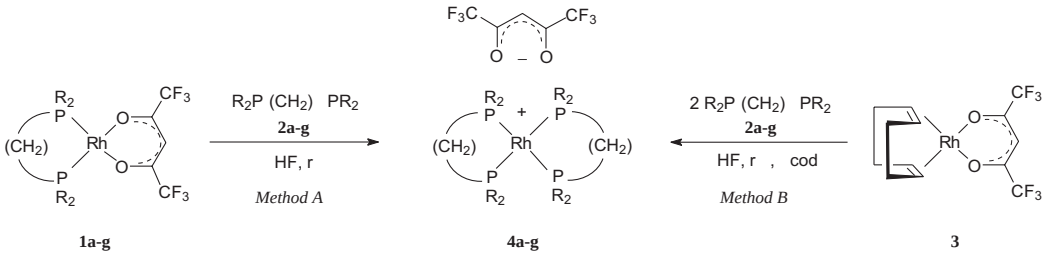
Dedicated to Professor Brian James on the occasion of his 65th birthday.

C. Six, M. Kessler, C. Krüger, and W. Leitner.[1] Max-Planck-Institut für Kohlenforschung, Kaiser-Wilhelm-Platz 1, D-45470 Mülheim/Ruhr, Germany.
H. Görls. Institut für Anorganische und Analytische Chemie, Friedrich-Schiller-Universität Jena, Lessingstr. 8, D-07743 Jena, Germany.
R. Fornika. Stockhausen GmbH, GB Acrylic Monomers, Paul-Baumann-Straβe 1, D-45764 Marl, Germany.

[1]Corresponding author (fax: +49 (0)208-306-2993; e-mail: leitner@mpi-muelheim.mpg.de).

 DOI: 10.1139/cjc-79-5/6-642 © 2001 NRC Canada

Scheme 1.



sors for olefin hydroformylation, see ref. 5*a*) to name just some of the most prominent fields of their uses.[2] We have utilized neutral complexes of type $[(P_2)Rh(hfacac)]$ (P_2 = phosphine ligand of general formula $R_2P\text{-}X\text{-}PR_2$) as model compounds to study the intrinsic influence of chelating phosphine ligands on catalytic active rhodium centers (6, 7*a*, and for a related discussion concerning complexes of the nickel triad see ref. 7*b*).

The classical coordination mode for 1,3-diketonates is the κ^2O,O′ bonding, which is favored by the generally strong M—O bond energy and the chelate effect of the planar six membered ring (1). Although less ubiquitous, the unidentate coordination modes κO (for an example see ref. 8) and κC (for a recent application of Ir(III)-acac complexes in benzene alkylation see ref. 5*b*, for other examples see ref. 9*a*, 9*b*) are also well-documented in the literature. A number of bridging coordination modes are known for acac-type anions, some of which have been described for the first time quite recently (5*b*, 10). However, there are very few cases of structurally characterized compounds with noncoordinating 1,3-diketonate anions in transition-metal chemistry (only one example could be localized in the Cambridge structure database, see ref. 11). For simple alkali and ammonium salts of acac-type anions, see ref. 12. Here, we report results on the synthesis and structure of complexes $[(P^{\frown}P)_2Rh][hfacac]$ ($P^{\frown}P$ = chelating bidentate phosphine ligand $R_2P(CH_2)_nPR_2$) (**4**), which consist of discrete anions and cations in solution and in the solid state. Structural features of the four coordinated d^8 cations $[(P^{\frown}P)_2Rh]^+$ ($\mathbf{4}^+$) related to the tendency of their formation are also discussed.

Results and discussion

Complexes $[(P^{\frown}P)_2Rh][hfacac]$ (**4a**–**g**) are readily synthesized in almost quantitative yield by treating either neutral complexes $[(P^{\frown}P)Rh(hfacac)]$ (**1a**–**g)** or [(cod)Rh(hfacac)] (cod = 1,5-cyclooctadiene) (**3**) with the $P^{\frown}P$-ligands **2a**–**g** in the appropriate stoichiometry (Scheme 1) (13, 14). The apparent simple cod substitution from **3** (15*a*, *b*; for a classical contribution to ligand exchange in complexes $[L_2Rh(acac)]$ see ref. 15*c*) has been shown to involve rather subtle ligand exchange equilibria (for recent examples see ref. 6*b*). The same is true for the addition of the second phosphine ligand to **1**; if **1g** is reacted with **2d**, only small amounts of the expected unsymmetrical [(**2d**)Rh(**2g**)][hfacac] are detected in solution by ^{31}P NMR, the main components being homoleptic complexes **4d** and **4g**. Similar observations have been made for acac-type rhodium complexes with monodentate phosphine ligands (14*d*) and upon addition of a second chelating phosphine to $[(P_2)Rh(L_2)]^+$ cations (L_2 = norbornadiene, cod) (16).

Table 1. Selected NMR data of complexes $[(R_2P(CH_2)_nPR_2)_2Rh]$-[hfacac)] (**4a**–**g**) and $[(Cy_2PCH_2PCy_2)_2Rh][BF_4]$ (**4b′**).

Complex	Ligand	R	*n*	δ (^{31}P)	$J_{Rh,P}$	δ (^{1}H)[a]	δ (^{19}F)
4a	**2a**	Ph	1	–20.9	116	5.36	–76.2
4b	**2b**	Cy	1	–17.6	110	n.d.[b]	–74.8
4b′	**2b**	Cy	1	–17.9	111	—	—
4c	**2c**	Ph	2	58.8	133	5.25	–75.2
4d	**2d**	Me	2	36.2	124	5.35	–77.0
4e	**2e**	*i*-Pr	2	74.3	129	5.27	–76.9
4f	**2f**	Cy	2	67.1	129	5.29	–77.0
4g	**2g**	Ph	3	8.9	132	5.39	–76.1

[a]Resonances of the hfacac anion only.
[b]n.d., not determined.

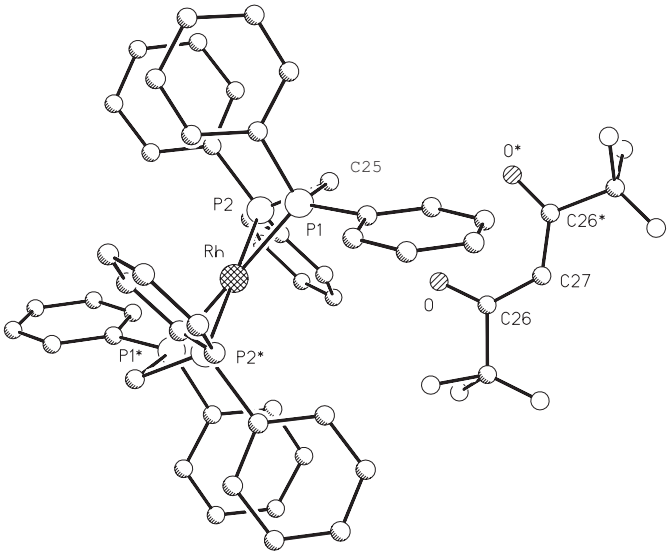
The influence of the ligand structure on the incorporation of a second chelating phosphine at the rhodium center to form $\mathbf{4}^+$ is reflected in the rate of reaction of **1** with a second equivalent of the corresponding phosphine ligand. The incorporation of the second ligand occurs almost immediately in the case of ligands **2a**–**d**, but requires approximately 3 h for the cyclohexyl analogue **2f**, as estimated from the colour change from dark red-brown to bright orange of the reaction solution. Notably, no reaction at all is observed with ligands $R_2P(CH_2)_4PR_2$ (R = Ph (**2h**), R = Cy (**2i**)) even upon prolonged heating, although the cation $[(\mathbf{2h})_2Rh]^+$ is a stable compound and has been obtained via cod substitution from $[\{(cod)Rh(\mu\text{-}Cl)\}_2]$ (17). It is interesting to note that the decreasing tendency of formation of $\mathbf{4}^+$ from **1** correlates with the increase of steric repulsion and thus the tetrahedral distortion within the $[(P^{\frown}P)_2Rh]^+$ cations (vide infra).

Selected NMR-spectroscopic data of complexes **4a**–**g** are listed in Table 1 together with the value for $[(\mathbf{2b})_2Rh][BF_4]$ (**4b′**). The tetrafluoroborate complex was isolated in the form of the crystalline THF solvate **4b′**·2THF as a by-product from the reaction of $[(cod)_2Rh][BF_4]$ with 1 equiv of **2b** at room temperature. The ^{31}P NMR spectroscopic data of the double substituted cation $\mathbf{4b}^+$ are independent from the counterion within experimental limits. The same holds for all other cations listed in Table 1 for which literature data are available. This observation strongly supports the formulation of compounds **4** as ionic complexes containing free cations $[(P^{\frown}P)_2Rh]^+$ ($\mathbf{4}^+$). It has been suggested, however, that coordination of hfacac to the unsaturated 16e$^-$ metal

[2]For a recent application of Ir(III)-acac complexes in benzene alkylation see ref. 5*b*.

© 2001 NRC Canada

Fig. 1. Molecular structure of [(**2a**)2Rh][hfacac] (**4a**) as determined by single-crystal X-ray diffraction analysis. Heavy atoms are represented as spheres, and hydrogen atoms have been omitted for clarity. Selected bond distances (Å) and angles (°): Rh—P(1), 2.283(1); Rh—P(2), 2.290(1); P(1)—C(25), 1.843(3); P(2)—C(25), 1.847(3); O—C(26), 1.234(4); C(26)—C(27), 1.391(4) Å; P(1)-Rh-P(2), 70.80(2); P(1)*-Rh-P(2), 109.20(2); P(1)-Rh-P(1)*, 180; P(2)-Rh-P(2)*, 180; Rh-P(1)-C(25), 94.44(8); Rh-P(2)-C(25), 94.07(8); P(1)-C(25)-P(2), 91.8(1); C(26)-C(27)-C(26*), 123.9(4)°.



centers could not be ruled out completely in solution and especially in the solid state on basis of NMR data (14*d*). Table 1 reveals indeed very small variations in the ^{1}H and ^{19}F NMR shifts of the hfacac anion, which might be indicative for some ion pairing in solutions of **4**.[3,4] The X-ray crystal structure analyses of complexes **4a** and **4f**, however, demonstrate unambiguously that there are no coordinative interactions between the hfacac anion and the rhodium centers of these compounds in the solid state.

Solid state structures

Yellow to orange crystals suitable for X-ray diffraction were obtained by slow cooling of warm solutions of **4a** and **4f** in acetone or THF to room temperature. The crystallographic data of both complexes are summarized in the *Experimental* section. No coordinative interaction between the hfacac moiety and the rhodium center is observed in the solid-state structure of **4a** (Fig. 1), although five coordinated derivatives of the cation $\mathbf{4a}^{+}$ are well known and can adopt either trigonal bipyramidal (18) or square pyramidal (19*d*) arrangements.

The cation $\mathbf{4a}^{+}$ has a centro-symmetric structure with the transition metal at the center of inversion. The coordination geometry at rhodium is ideally planar with a P-Rh-P bite angle of 70.8°. The four-membered chelate rings are puckered with an intersecting angle between the P-Rh-P and the P-C-P planes of 30.3°. The two pseudo-axial phenyl rings are oriented nearly parallel to each other. This contrasts the edge-to-face arrangement commonly encountered for phenyl rings in chelating phosphines. It appears from this structure and from published data (for structurally characterized examples with two molecules **2a** at rhodium see ref. 19) that the four-membered ring in the [(**2a**)Rh] moiety preferably adopts one of two different stable conformations in the solid state; one is characterized by a wider P-Rh-P angle (71.8–72.8°), less puckering (15–20°), and edge-to-face orientated phenyl rings. The other one, which includes the present example, is characterized by a bite angle of 70 to 71°, a puckering of 30°, and a parallel orientation of two of the phenyl groups.

The number of structurally characterized free 1,3-diketonate anions in transition-metal complexes is remarkably small (11), and no example involving the hfacac ligand could be retrieved in the Cambridge database. The free hfacac anion in **4a** has the symmetrical and entirely planar skeleton expected for a delocalized heteroatom-*p*-system and also observed in the simple salts [M][acac] (for simple alkali and ammonium salts of acac-type anions see ref. 12). Interestingly, a hydrogen bond between one of the fairly acidic (19*b*; for a discussion of dppm as hydrogen bond donor see ref. 19*e*) methylene protons of coordinated **2a** and one of the oxygen atoms of hfacac is indicated by a short distance of 3.394 Å between C(25) and O. This interaction leads to highly symmetrical indefinite chains of alternating cations and anions in the crystal structure without any coordinative interaction between the metal center and the hfacac anion (Fig. 2).

The molecular structure of **4f** is represented together with selected bond distances and angles in Fig. 3. As with **4a**, discrete cations and anions are present in the crystal lattice of complex **4f**. The structural data of the hfacac anion are very similar to those obtained for **4a**, but no short interatomic distances are observed between any of the hydrogen atoms of the cation and the anion. In contrast to planar $\mathbf{4a}^{+}$, the cation $\mathbf{4f}^{+}$ is significantly distorted towards a tetrahedral arrangement with a dihedral angle of $\theta = 18.6°$. Similar distortions have been observed for this cation with typical noncoordinating anions.[5]

In general, the amount of tetrahedral distortion in cations $[(P^{\frown}P)_2Rh]^{+}$ can be rationalized as a compromise between the preferred square planar arrangement of a d^8 transition-metal center and the steric repulsion of the four PR_2 groups[6] (17). This is nicely reflected within the series of cations containing two adjacent five-membered rings, where the amount of distortion increases steadily with R = Me (0°, $\mathbf{4d}^{+}$) (20), R = Ph (3.6–8.8°, $\mathbf{4c}^{+}$) (21), and R = Cy (18.6°, $\mathbf{4f}^{+}$). Ideal planar arrangements are only possible when 1,3-interactions between adjacent PR_2 groups of two different chelates are negligible. These interactions will be minimized with ligands featuring small R groups but also by small P-Rh-P bite

[3] Alternatively, the variations may partly arise from temperature and concentration effects, at least in the case of the fluorine resonances.
[4] The ligand exchange reactions observed in the P_2–Rh–hfacac system are likely to proceed via associative mechanisms (15), which may involve short lived intermediates or transition states of type $[(P_2)_2Rh(\kappa O\text{-hfacac})]$ or $[(P_2)(L_2)Rh(\kappa O\text{-hfacac})]$.
[5] B.R. James, private communication.
[6] For a detailed discussion of the structural features of $[(P^{\frown}P)_2Rh]^{+}$ and the impact of distortion for the ^{103}Rh NMR shifts see ref. 7*a*.

© 2001 NRC Canada

Fig. 2. Symmetrical chains of alternating cations and anions in the crystal structure of **4a** without any coordinative interaction between the metal center and the hfacac anion.

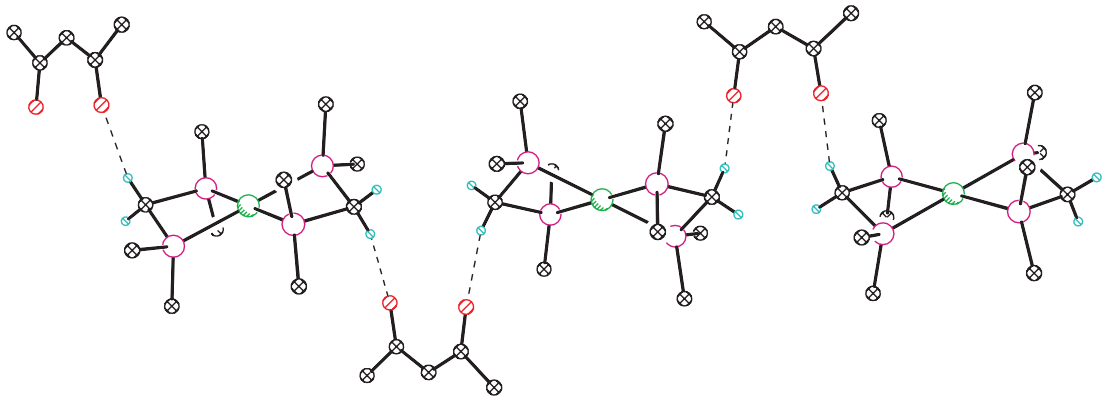
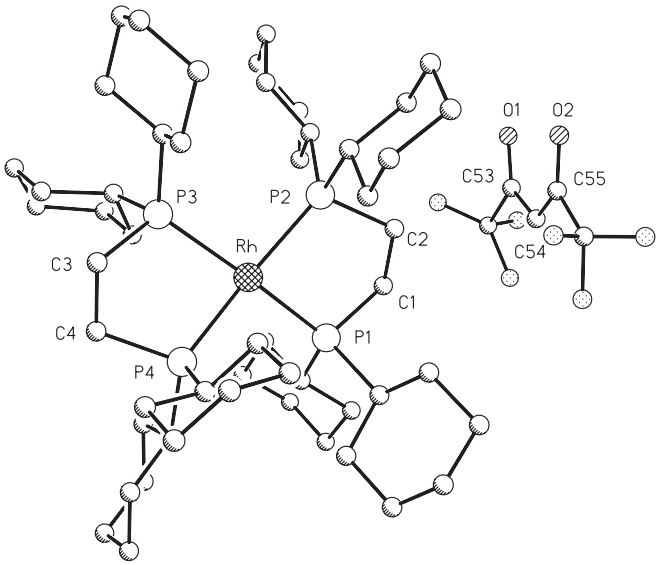


Fig. 3. Molecular structure of $[(\mathbf{2f})_2Rh][hfacac]$ (**4f**) as determined by single-crystal X-ray diffraction analysis of **4f**·0.5THF. Heavy atoms are represented as spheres and hydrogen atoms have been omitted for clarity. Selected bond distances (Å) and angles (°): Rh—P(1), 2.332(2); Rh—P(2), 2.332(2); Rh—P(3), 2.328(2); Rh—P(4), 2.343(2); P(1)—C(1), 1.844(6); P(2)—C(2), 1.854(7); P(3)—C(3), 1.842(6); P(4)—C(4), 1.846(6) Å; C(1)—C(2), 1.497(8); C(3)—C(4), 1.503(6); O(1)—C(53), 1.208(12); O(2)—C(55), 1.234(8); C(53)—C(54), 1.385(9); C(54)—C(55), 1.373(9) Å; P(1)-Rh-P(2), 84.03(6); P(3)-Rh-P(4), 82.71(6); P(1)-Rh-P(4), 98.61(6); P(2)-Rh-P(3), 97.34(6); P(1)-Rh-P(3), 168.43(7); P(2)-Rh-P(4), 166.65(6); Rh-P(1)-C(1), 109.2(2); Rh-P(2)-C(2), 108.9(2); Rh-P(3)-C(3), 109.2(2); Rh-P(4)-C(4), 108.8(2); C(53)-C(54)-C(55), 124.4(7)°.



angles within the chelate. In this context, it appeared interesting to investigate the solid state structure of the cation $[\{Cy_2P(CH_2)PCy_2\}_2Rh]^+$ (**4b**$^+$) containing bulky cyclohexyl groups embedded in two adjacent four-membered chelate rings.

As depicted in Fig. 4, the cation **4b**$^+$ has a C_2-symmetric molecular structure in the crystal lattice of compound **4b′**. The P-Rh-P angle and the P—Rh distance are with 72.4° and 2.32 Å, slightly larger than the corresponding values in **4a**$^+$. The four-membered chelates in **4b**$^+$ appear to be essentially planar, in contrast to the strongly puckered rings observed in **4a**$^+$. However, the large thermal ellipsoids of the bridging methylene carbon in **4b**$^+$ may indicate some statistical disorder at this position. Most significantly, the ideally square planar coordination geometry at rhodium indicates that the small P-Rh-P angle is sufficient to prevent severe steric interaction between the PCy_2 groups of the individual chelates.

Conclusion

Complexes $[(P^{\frown}P)_2Rh][hfacac]$ (**4**) can be readily synthesized according to the reaction sequences shown in Scheme 1. The crystallographic and spectroscopic data show that the compounds exist as discrete cations and anions in solution and in the solid state without any direct evidence for coordinative interaction between the rhodium center and the hfacac anion. The cations $[(P^{\frown}P)_2Rh]^+$ have ideally planar coordination geometries when both phosphines form four-membered chelate rings as in **4a**$^+$ and **4b**$^+$, regardless of the size of the R group at phosphorus. In contrast, the cation **4f**$^+$ containing a five-membered chelate ligand with cyclohexyl groups at phosphorus shows considerable tetrahedral distortion (θ = 18.6°). The hfacac anion has the symmetrical structure expected for the delocalized 1,3-diketonate anion and can form hydrogen bridges to acidic sites of the complex cations in the solid state.

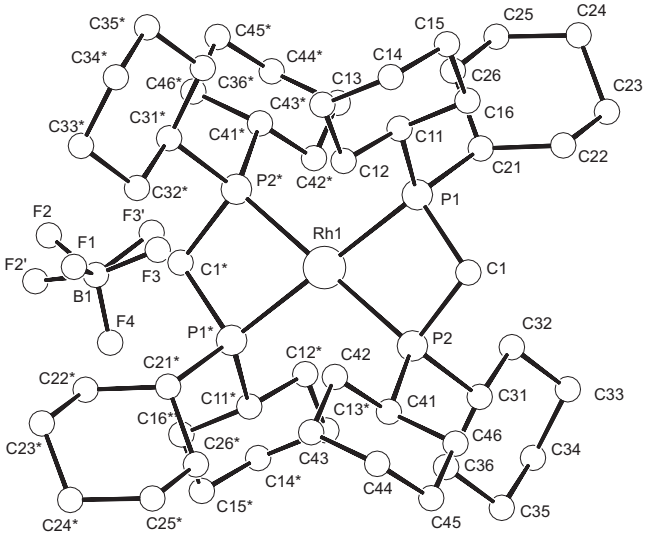
Experimental

General

The starting complexes [(cod)Rh(hfacac)] (**3**) (6) and $[Rh(cod)_2][BF_4]$ (22) were prepared as described in the literature. The bidentate phosphines **2a**–**g** were commercial products (Aldrich or Strem) and used as received. All reactions involving air- or moisture-sensitive materials were performed under argon using standard Schlenk techniques. Glassware was either oven-dried for at least 24 h or flame-dried under vacuum before use. Solvents were dried and deoxygenated by standard methods and freshly distilled prior to use.

© 2001 NRC Canada

Fig. 4. Molecular structure of $[(\mathbf{2b})_2Rh][BF_4]$ (**4b′**) as determined by single-crystal X-ray diffraction analysis of **4b′**·2 THF. Heavy atoms are represented as spheres. Hydrogen atoms and THF solvent molecule have been omitted for clarity. Selected bond distances (Å) and angles (°): Rh(1)—P(1), 2.324(1); Rh(1)—P(2), 2.315(1); P(1)—C(1), 1.852(3); P(2)—C(1), 1.847(3) Å; P(2)-Rh(1)-P(1), 72.4(1); P(1)*-Rh(1)-P(2), 107.6(1); P(2)-C(1)-P(1), 95.7(1); C(1)-P(1)-Rh(1), 95.3(1); C(1)-P(2)-Rh(1), 95.7(1)°.



Crystallographic data collection and processing

For all structures, data were collected on an Enraf–Nonius CAD4 diffractometer in the ω–2θ scan mode using graphite monochromated Mo Kα radiation. Unit cell parameters were determined from least-squares refinement of setting angles for 25 reflections. Data were corrected for Lorentz and polarization effects (23*a*). There was no correction for crystal decay. No absorption correction was applied. The structures were solved by direct methods (SHELXS (23*b*)) refined by full-matrix least-squares techniques against F_o^2 (SHELXL-97) (23*c*). The hydrogen atoms of the molecules were included at calculated positions with fixed thermal parameters. All non-hydrogen atoms were refined anisotropically (27*c*). XP (SIEMENS Analytical X-ray Instruments Inc.) was used for structure representations.[7]

NMR spectroscopy

Spectra were recorded on a Bruker AC 200 or AM 200 spectrometer operating at 200.13, 50.29, 188.15, or 81.00 MHz for ^1H, ^{13}C, ^{19}F, and ^{31}P NMR, respectively. Chemical shifts are given in ppm downfield from TMS (^1H and ^{13}C NMR), 85% H_3PO_4 (^{31}P NMR), and $CFCl_3$ (^{19}F NMR) as external standards. The solvent resonances were used as secondary standards if possible.

Further analytic methods

FAB-MS were obtained using a Finnigan MAT SSQ 710 spectrometer and DMBA as a matrix. Elemental analyses were performed on a LECO CHNS 932 analyzer at the laboratory of organic chemistry of the Friedrich-Schiller-Universität, Jena, Germany.

General procedures for the preparation of complexes $[(\mathbf{2a–g})_2Rh][hfacac]$ (4a–g)

Method A

[(**2a**–**g**)Rh(hfacac)] (**1a**–**g**) (ca. 200 mg) and 1 equiv amount of the corresponding phosphine **2a**–**g** were separately dissolved in THF (5 and 10 mL, respectively) at room temperature. The phosphine solution was added dropwise to the stirred solution of the rhodium complex using a cannula. The completeness of the reaction was indicated by a colour change from red-brown to yellow-orange. Within a few minutes an orange precipitate was formed. The supernatant was removed using a cannula and the solid dried 4 h under vacuum. The crude products were recrystallized from acetone or THF (ca. 5–15 mL) to give **4a**–**g** in >90% yield.

Method B

[(cod)Rh(hfacac)] (3) (150 mg, 0.36 mmol) and 2 equiv of the desired phosphine **2a**–**g** were separately dissolved in THF (15 mL) at room temperature. The phosphine solution was added dropwise to the stirred solution of the rhodium complex using a cannula. After addition was complete, stirring was continued until the colour of the reaction mixture had changed to yellow-orange. Work-up and isolation was identical as described for method A.

$[\{Ph_2P(CH_2)PPh_2\}_2Rh][hfacac]$ (4a)

Preparation according to method B; mp 273–281°C. (FAB+)-MS *m*/*z* (%): 871 (**4a**$^+$, 35), 487 ([**4a** – **2a**]$^+$, 10). (FAB–)-MS *m*/*z* (%): 207 ([hfacac]$^-$, 100). ^1H NMR (200.13 MHz, acetone-d_6) δ: 7.61–7.51 (m, 16H, *ortho*-C*H* of Ph), 7.47–7.26 (m, 24H, *meta*-, *para*-C*H* of Ph), 5.36 (s, 1H, C*H*C(O)CF_3), 4.83 (dt, $^2J_{P,H}$ = 4 Hz, $^3J_{Rh,H}$ = 2 Hz, 4H, CH_2PPh_2). $^{13}C\{^1H\}$ NMR (50.29 MHz, acetone-d_6) δ: 171.5 (q, $^2J_{F,C}$ = 28 Hz, *C*O), 134.0 (vt, $^1J_{P,C} + {}^3J_{P,C}$ = 26 Hz, ipso-*C*(Ph)), 133.5 (s br, *ortho*-*C*(Ph)), 131.5 (s br, *para*-*C*(Ph)), 129.4 (s, *meta*-*C*(Ph)), 119.3 (q, $^1J_{F,C}$ = 294 Hz, CF_3), 82.5 (s, *C*HC(O)CF_3), 46.3 (vt, $^1J_{P,C} + {}^3J_{P,C}$ = 24 Hz, CH_2PPh_2). $^{19}F\{^1H\}$ NMR (188.15 MHz, acetone-d_6) δ: –76.2. $^{31}P\{^1H\}$ NMR (81.00 MHz, THF-d_8) δ: –20.9 (d, $^1J_{Rh,P}$ = 116 Hz).

X-ray crystal structure determination of ***4a***

Suitable crystals were obtained as prisms by recrystallization from acetone at room temperature.

Crystal data: $C_{55}H_{45}F_6O_2P_4Rh$; MW = 1078.75 g mol^{-1}; monoclinic; space group *C*2/*c* (No. 15); *a* = 12.550(3), *b* = 23.269(5), and *c* = 17.598(2) Å; β = 102.55(1)°; *V* = 5016(2) Å^3; λ = 0.71069 Å; *Z* = 4; ρ_c = 1.43 g cm^{-3}; *F*(000) = 2200; crystal size: 0.40 × 0.35 × 0.32 mm; μ = 5.2 cm^{-1}.

Data collection and processing: *T* = 183(1) K; 5888 reflections measured ($1.75 \le \theta \le 27.40$, $-16 \le h \le 15$, $0 \le k \le 30$, $0 \le l \le 20$); 5705 independent reflections (R_{int} = 0.019); 4458

[7] Further details of the crystal structure investigations are available on requests from the director of the Cambridge Crystallographic Data Center, 12 Union Road, GB-Cambridge CB2 1 EZ, on quoting the depository number CCSD-101 851 (**4a**), CCSD-101 852 (**4f**·0.5THF), and CCSD-139 466 (**4b′**·2THF), the names of the authors, and the journal citation.

© 2001 NRC Canada

significant reflections with $I < 2\sigma(I)$; 444 parameters; final R indices: R_{1obsd} = 0.034, wR_{2obsd} = 0.085, R_{1all} = 0.056, wR_{2all} = 0.098; GoF = 1.028; largest difference peak and hole: 0.60, –0.48 e Å^{-3}.

[{$Cy_2P(CH_2)PCy_2$}$_2$Rh][hfacac] (4b)

Preparation according to method B. $^{19}F\{^1H\}$ NMR (188.15 MHz, acetone-d_6) δ: –74.8. $^{31}P\{^1H\}$ NMR (81.00 MHz, THF-d_8) δ: –17.6 (d, $^1J_{Rh,P}$ = 110 Hz). Anal. calcd. for $C_{55}H_{93}F_6O_2P_4Rh$ (MW = 1126.51 g mol^{-1}): C 58.61, H 8.32; found: C 58.82, H 8.39.

[{$Ph_2P(CH_2)_2PPh_2$}$_2$Rh][hfacac] (4c)

Preparation according to method B; mp 156–160°C. (FAB+)-MS *m*/*z* (%): 899 (**4c**$^+$, 40), 501 ([**4c** – **2c**]$^+$, 60). (FAB–)-MS *m*/*z* (%): 207 ([hfacac]$^-$, 100). ^1H NMR (200.13 MHz, THF-d_8) δ: 7.43–7.24 (m, 40H, *ortho*-, *meta*-, *para*-C*H* of Ph), 5.25 (s, 1H, C*H*C(O)CF_3), 2.21 (s, 8H, CH_2PPh_2). $^{19}F\{^1H\}$ NMR (188.15 MHz, acetone-d_6) δ: –75.2. $^{31}P\{^1H\}$ NMR (81.00 MHz, THF-d_8) δ: 58.8 (d, $^1J_{Rh,P}$ = 133 Hz). Anal. calcd. for $C_{57}H_{49}F_6O_2P_4Rh$ (MW = 1106.16 g mol^{-1}): C 61.86, H 4.41; found: C 61.96, H 4.45.

[{$Me_2P(CH_2)_2PMe_2$}$_2$Rh][hfacac] (4d)

Preparation according to method B; mp 72°C (dec). (FAB+)-MS *m*/*z* (%): 403 (**4d**$^+$, 100), 253 ([**4d** – **2d**]$^+$, 80). (FAB–)-MS *m*/*z*: 207 ([hfacac]$^-$). ^1H NMR (200.13 MHz, acetone-d_6) δ: 5.35 (s, 1H, C*H*C(O)CF_3), 1.71–1.61 (m, 8H, CH_2PMe_2), 1.48–1.33 (m, 24H, CH_3). $^{13}C\{^1H\}$ NMR (50.29 MHz, acetone-d_6) δ: 172.0 (q, $^2J_{F,C}$ = 29 Hz, *C*O), 119.5 (q, $^1J_{F,C}$ = 294 Hz, *C*F_3), 83.3 (s, *C*HC(O)CF_3), 29.8 (vt, $^1J_{P,C} + {}^3J_{P,C}$ = 54 Hz, CH_2PMe_2), 15.8 (vt, $^1J_{P,C} + {}^3J_{P,C}$ = 26 Hz, P(CH_3)$_2$. $^{19}F\{^1H\}$ NMR (188.15 MHz, acetone-d_6) δ: –77.0. $^{31}P\{^1H\}$ NMR (81.00 MHz, THF-d_8) δ: 36.2 (d, $^1J_{Rh,P}$ = 124 Hz). Anal. calcd. for $C_{17}H_{33}F_6O_2P_4Rh$ (MW = 610.04 g mol^{-1}): C 33.46, H 5.45; found: C 33.55, H 5.51.

[{*i*-$Pr_2P(CH_2)_2P$-*i*-Pr_2}$_2$Rh][hfacac] (4e)

Preparation according to method A; mp 121–123°C. (FAB+)-MS *m*/*z* (%): 627 (**4e**$^+$, 100), 365 ([**4e** – **2e**]$^+$, 20). (FAB–)-MS *m*/*z* (%): 207 ([hfacac]$^-$, 100). ^1H NMR (200.13 MHz, acetone-d_6) δ: 5.27 (s, 1H, C*H*C(O)CF_3), 2.42 (sept., $^3J_{C,H}$ = 7.8 Hz, 8H, $CH_2PCH(CH_3)_2$), 1.86 (m, 8H, $CH_2PCH(CH_3)_2$), 1.27 (m, 48H, $CH_2PCH(CH_3)_2$). $^{19}F\{^1H\}$ NMR (188.15 MHz, acetone-d_6) δ: –76.9. $^{31}P\{^1H\}$ NMR (81.00 MHz, THF-d_8) δ: 74.3 (d, $^1J_{Rh,P}$ = 129 Hz). Anal. calcd. for $C_{33}H_{65}F_6O_2P_4Rh$ (MW = 834.29 g mol^{-1}): C 47.49, H 7.85; found: C 47.63, H 7.98.

[{$Cy_2P(CH_2)_2PCy_2$}$_2$Rh][hfacac] (4f)

Preparation according to method A; mp 259–263°C. (FAB+)-MS *m*/*z* (%): 947 (**4f**$^+$, 100). (FAB–)-MS *m*/*z* (%): 207 ([hfacac]$^-$, 100). ^1H NMR (200.13 MHz, acetone-d_6) δ: 5.29 (s, 1H, C*H*C(O)CF_3), 2.25–1.15 (m, 96H, aliphatic H). $^{13}C\{^1H\}$ NMR (50.29 MHz, acetone-d_6) δ: 171.3 (q, $^2J_{F,C}$ = 29 Hz, *C*O), 119.6 (q, $^1J_{F,C}$ = 294 Hz, *C*F_3), 82.4 (s, *C*HC(O)CF_3), 40.2 (s br, C-1(Cy)), 29.9 (s, C-2(Cy)), 28.5 (s, C-3(Cy)), 26.9 (s, C-4(Cy)), 20.9 (dvt, $^2J_{Rh,C}$ = 12 Hz, $^1J_{P,C} + {}^3J_{P,C}$ = 46 Hz, *C*H_2PCy_2). $^{19}F\{^1H\}$ NMR (188.15 MHz, acetone-d_6) δ: –77.0. $^{31}P\{^1H\}$ NMR (81.00 MHz, THF-d_8) δ: 67.1 (d, $^1J_{Rh,P}$ = 129 Hz). Anal. calcd. for $C_{57}H_{89}F_6O_2P_4Rh{\cdot}0.5C_4H_8O$ (MW = 1154.54 g mol^{-1}): C 59.27, H 8.46; found: C 59.04, H 8.22.

X-ray crystal structure determination of ***4f***·*0.5THF*

Suitable crystals were obtained as prisms by recrystallization from THF at room temperature.

Crystal data: $C_{57}H_{89}F_6O_2P_4Rh{\cdot}0.5C_4H_8O$; MW = 1155.19 g mol^{-1}; monoclinic; space group $P2_1/n$ (No. 14); a = 13.413(3), b = 19.649(4), and c = 23.997(3) Å; β = 90.65(1)°; V = 6324(2) Å^3; λ = 0.71069 Å; Z = 4; ρ_c = 1.24 g cm^{-3}; F(000) = 2504; crystal size: 0.40 × 0.38 × 0.36 mm; μ = 4.2 cm^{-1}.

Data collection and processing: T = 293(1) K; 10 149 reflections measured ($1.34 \le \theta \le 23.98$, $-15 \le h \le 15$, $0 \le k \le 22$, $0 \le l \le 26$); 9889 independent reflections (R_{int} = 0.018); 8520 significant reflections with $I < 2\sigma(I)$, 730 parameters; final R indices: R_{1obsd} = 0.049, wR_{2obsd} = 0.147, R_{1all} = 0.080, wR_{2all} = 0.192; GoF = 1.002; largest difference peak and hole: 1.04, –0.43 e Å^{-3}.

[{$Ph_2P(CH_2)_3PPh_2$}$_2$Rh][hfacac] (4g)

Preparation according to method B; mp 84°C (dec). (FAB+)-MS *m*/*z* (%): 927 (**4g**$^+$, 10), 515 ([**4g** – **2g**]$^+$, 10). (FAB–)-MS *m*/*z* (%): 207 ([hfacac]$^-$, 100). ^1H NMR (200.13 MHz, acetone-d_6) δ: 7.90–7.05 (m, 40H, *ortho*-, *meta*-, *para*-C*H* of Ph), 5.39 (s, 1H, C*H*C(O)CF_3), 2.50–2.35 (m, 8H, $CH_2CH_2PPh_2$), 2.10–1.75 (m, 4H, $CH_2CH_2PPh_2$). $^{19}F\{^1H\}$ NMR (188.15 MHz, acetone-d_6) δ: –76.1. $^{31}P\{^1H\}$ NMR (81.00 MHz, THF-d_8) δ: 8.9 (d, $^1J_{Rh,P}$ = 132 Hz). Anal. calcd. for $C_{59}H_{53}F_6O_2P_4Rh$ (MW = 1134.20 g mol^{-1}): C 62.44, H 4.71; found: C 62.16, H 4.56.

[{$Cy_2P(CH_2)PCy_2$}$_2$Rh][BF_4] (4b′)

[(Cod)$_2$Rh][BF_4] (49.5 mg, 0.12 mmol) and **2b** (53.4 mg, 0.13 mmol) were placed together in a Schlenk tube as solids and dissolved in THF (5 mL). Deep orange crystals separated from the solution upon standing at room temperature within a few days. The supernatant was removed using a cannula and the precipitate was washed with small portions of THF to give **4b′**·2THF (22 mg, 17%) as orange crystals suitable for X-ray analysis; mp 259–263°C. ^1H NMR (200.13 MHz, CD_2Cl_2) δ: 3.02 (dt, 4H, $^2J_{P,H}$ = 3.9 Hz, CH_2PCy_2), 2.20–1.07 (m, 88H, aliphatic H). $^{13}C\{^1H\}$ NMR (50.29 MHz, CD_2Cl_2) δ: 36.9 (vt, $^1J_{P,C} + {}^3J_{P,C}$ = 10.6 Hz, C-1(Cy)), 30.1 (s, C-2(Cy)), 28.7 (s, C-2′(Cy)), 27.7 (vt, $^3J_{P,C} + {}^5J_{P,C}$ = 6.1 Hz, C-3(Cy)), 27.3 (vt, $^3J_{P,C} + {}^5J_{P,C}$ = 5.2 Hz, C-3′(Cy)), 26.4 (dt, $^2J_{Rh,C}$ = not resolved, $^1J_{P,C}$ = 15 Hz, CH_2PCy_2), 26.3 (s, C-4(Cy)). $^{19}F\{^1H\}$ NMR (188.15 MHz, CD_2Cl_2) δ: –153.4. $^{31}P\{^1H\}$ NMR (81.00 MHz, THF-d_8) δ: –17.9 (d, $^1J_{Rh,P}$ = 111 Hz).

X-ray crystal structure determination of ***4b′***·*2THF*

Suitable crystals were obtained directly from the reaction mixture.

Crystal Data: $C_{58}H_{108}BF_4O_2P_4Rh$; MW = 1151.04 g mol^{-1}; triclinic; space group $P\bar{1}$ (No. 2); a = 10.5726(11), b = 11.3976(11), and c = 13.786(3) Å; α = 78.80(2)°; β = 87.823(14)°; γ = 82.771(9)°; V = 1616.5(5) Å^3; λ = 0.71069

© 2001 NRC Canada

Å; $Z = 1$; $\rho_c = 1.182$ g cm^{-3}; $F(000) = 618$; crystal size: 0.70 × 0.60 × 0.67 mm; $\mu = 4.11$ cm^{-1}.

Data collection and processing: $T = 293(1)$ K; 7770 reflections measured ($2.59 \leq \theta \leq 27.48$, $0 \leq h \leq 13$, $-14 \leq k \leq 14$, $-17 \leq l \leq 17$); 7371 independent reflections ($R_{int} = 0.010$); final R indices: $R_{1obsd} = 0.046$, $wR_{2obsd} = 0.148$, $R_{1all} = 0.061$, $wR_{2all} = 0.156$; GoF = 1.035; largest difference peak and hole: 1.0, –0.5 e Å^{-3}.

Acknowledgements

This work was supported by the Max-Planck-Gesellschaft and the Fonds der Chemischen Industrie. W.L. wishes to thank Professor B.R. James (Vancouver), Professor M.A. Bennett (Canberra), and Professor T.B. Marder (Durham) for communicating results prior to publication. Generous loans of $RhCl_3 \cdot H_2O$ were provided by Degussa AG.

References

1. (*a*) R.C. Mehrotra, R. Bohra, and D.P. Gaur. Metal β-diketonates and allied derivatives. Academic Press, London. 1978; (*b*) S. Kawaguchi. Variety in coordination modes of ligands in metal complexes in inorganic chemistry concepts. Vol. 11. Springer-Verlag, Heidelberg. 1988. Chap. 5. p. 75.
2. M. Hartmann and B.K. Keppler. Comments Inorg. Chem. **16**, 339 (1995).
3. N.G. Smart, T. Carleson, T. Kast, A.A. Clifford, M.D. Burford, and C.M. Wai. Talanta, **44**, 137 (1997).
4. (*a*) T.T. Kodas and M.J. Hampden-Smith. Chemical vapor deposition of assorted metals in chem. met. CVD. *Edited by* T.T. Kodas and M.J. Hampden-Smith. VCH, Weinheim. 1994. p. 357; (*b*) C. Xu, M.J. Hampden-Smith, and T.T. Kodas. Adv. Mater. **6**, 746, 1994; (*c*) W. Lin, B.C. Wiegand, R.G. Nuzzo, and G.S. Girolami. J. Am. Chem. Soc. 5977 (1996); (*d*) W. Lin, R.G. Nuzzo, and G.S. Girolami. J. Am. Chem. Soc. **118**, 5988 (1996).
5. (*a*) C.D. Frohning and C.W. Kohlpaintner. *In* Applied homogeneous catalysis with organometallic compounds. *Edited by* B. Cornils and W.A. Herrmann. VCH, Weinheim. 1996. p. 47; (*b*) R.A. Periana et al. J. Am. Chem. Soc. **122**, 7414 (2000).
6. (*a*) R. Fornika, H. Görls, B. Seemann and W. Leitner. J. Chem. Soc. Chem. Commun. 1479 (1995); (*b*) K. Angermund, W. Baumann, E. Dinjus, R. Fornika, H. Görls, M. Kessler, C. Krüger, W. Leitner and F. Lutz. Chem. Eur. J. **3**, 755 (1997); (*c*) F. Hutschka, A. Dedieu, M. Eichberger, R. Fornika and W. Leitner. J. Am. Chem. Soc. **119**, 4432 (1997).
7. (*a*) W. Leitner, M. Bühl, R. Fornika, C. Six, W. Baumann, E. Dinjus, M. Kessler, C. Krüger and A. Rufinska. Organometallics, **18**, 1196 (1999); (*b*) D.E. Berning, B.C. Noll and D.L. DuBois. J. Am. Chem. Soc. **121**, 11432 (1999).
8. T. Kurauchi, M. Matsui, Y. Nakamura, S. Ooi, S. Kawaguchi and H. Kuroya. Bull. Chem. Soc. Jpn. **47**, 3049 (1974), and refs. therein.
9. (*a*) P. Maitlis. J. Chem. Soc. Dalton Trans. 387 (1979); (*b*) C. Xu, M.J. Hampden-Smith, T.T. Kodas, E.N. Duesler, A.L. Rheingold and G. Yap. Inorg. Chem. **34**, 4767 (1995), and references therein.
10. A. Bailey, T.S. Corbitt, M.J. Hampden-Smith, E.N. Duesler and T.T. Kodas. Polyhedron, **12**, 1785 (1993).
11. S. Kotake, T. Sei, K. Miki, Y. Kai, N. Yasuoka and N. Kasai. Bull. Chem. Soc. Jpn. **53**, 10 (1980).
12. (*a*) F.A. Schröder and H.P. Weber. Acta Crystallogr. Sect. B: Struct. Crystallogr. Cryst. Chem. **31**, 1745 (1975); (*b*) S. Shibata, S. Onuma, Y. Matsui and S. Motegi. Bull. Chem. Soc. Jpn. **48**, 2516 (1975); (*c*) J. Emsley, N.J. Freeman, R.J. Parker, H.M. Dawes and M.B. Hursthouse. J. Chem. Soc. Perkin Trans. 1, 471 (1986).
13. R. Fornika. PhD Thesis. Friedrich-Schiller-Universität, Jena, Germany. 1994.
14. (*a*) D.M. Barlex, J. Hacker and R.D.W. Kemmit. J. Organomet. Chem. **43**, 425 (1972); (*b*) W. Partenheimer and E.F. Hoy. J. Am. Chem. Soc. **95**, 2842 (1973); (*c*) P.J. Fennis, H.M. Budzelaar, H.G. Frijns and A.G. Orpen. J. Organomet. Chem. **393**, 287 (1990); (*d*) Z. Duan, M.J. Hampden-Smith and E.N. Duesler. Polyhedron, **13**, 609 (1994).
15. (*a*) J.H. Potgieter. J. Organomet. Chem. **36**, 389 (1989); (*b*) J.G. Leipoldt and E.C. Grobler. Transition Met. Chem. **11**, 110 (1986); (*c*) S.J. Lippard and S.M. Morehouse. J. Am. Chem. Soc. **91**, 2504 (1969).
16. (*a*) J.M. Ernsting, C.J. Elsevier, W.G. J. de Lange and K. Timmer. Magn. Reson. Chem. **29**, S118 (1991); (*b*) A.G. Avent, R.B. Bedford, P.A. Chaloner, S.Z. Dewa and P.B. Hitchcock. J. Chem. Soc. Dalton Trans. 4633 (1996).
17. P.M. Anderson and L.H. Pignolet. Inorg. Chem. 20, 4101 (1981).
18. H. Pignolet, D.H. Doughty, S.C. Nowicki and A.L. Casalnuovo. Inorg. Chem. **19**, 2172 (1980).
19. (*a*) M. Cowie and S.K. Dwight. Inorg. Chem. **18**, 1209 (1979); (*b*) D.E. Chebi, P.E. Fanwick and I.P. Rothwell. Organometallics, **9**, 2948 (1990); (*c*) F.A. Cotton, K.R. Dunbar, C.T. Eagle, L.R. Falvello, S.-J. Kang, A.C. Price and M.G. Verbruggen. Inorg. Chim. Acta, **184**, 35 (1991); (*d*) C.-P. Shao, G.-B. Cheng, J.-Y. Wang and H.-F. Guo. Jiegou Huaxue (J. Struct. Chem.), **12**, 343 (1993). (*e*) P.G. Jones and B. Ahrens. Chem. Commun. 2307 (1998).
20. T.B. Marder and T.D. Williams. J. Chem. Soc. Chem. Commun. 1478 (1987).
21. (*a*) R.R. Burch and J.C. Calabrese. J. Am. Chem. Soc. **108**, 5359 (1986); (*b*) M.C. Hall, B.T. Kilbourn and K.A. Taylor. J. Chem. Soc. A, 2539 (1970).
22 M. Green, T.A. Kuc and S.H. Taylor. J. Chem. Soc. A, 2334 (1971).
23. (*a*) MOLEN. An interactive structure solution procedure. Enraf–Nonius, Delft, the Netherlands. 1990; (*b*) G.M. Sheldrick. Acta Crystallogr. Sect. A: Fundam. Crystallogr. **46**, 467 (1990); (*c*) G.M. Sheldrick. SHELXL-97. University of Göttingen, Germany. 1993.

© 2001 NRC Canada

A relationship between the catalytic carbonylation of (*N*-arenesulfonyl)imides and iodonium ylides

Gábor Besenyei, András Neszmélyi, Sándor Holly, László I. Simándi, and László Párkányi

Abstract: Reactivities of various sulfonamide derivatives of general formula $ArSO_2N{=}XPh_n$ (X = I; n = 1; X = S, Se, n = 2; X = P, As, n = 3) in catalytic carbonylations have been explained by structural properties of the substrates. Based on crystallographic data reported in the literature, it has been concluded that the two-step catalytic oxidative carbonylation of sulfonylimides proceeds only when the N=X double bond is strongly polarized. The structural requirement observed within the sulfonamide derivatives has been found to be applicable for iodonium ylides. Catalytic carbonylation of the phenyliodonium methylide (**3a**) prepared from dimedone (5,5-dimethyl-1,3-cyclohexanedione) and (diacetoxyiodo)benzene, resulted in a new spirobenzofuranone derivative (**5a**) which was characterized by X-ray single crystal diffraction, $^1J_{C,C}$ coupling constants, ^{13}C-T_1 relaxation times, as well as by IR and Raman spectroscopic methods. Crystals of **5a** are monoclinic, space group $P2_1/c$, a = 7.187(1), b = 21.129(1), and c = 10.636(1) Å, β = 92.81(1)°, V = 1613.2(3) Å^3, and Z = 4. A ketene intermediate has been postulated in the catalytic carbonylation of the iodonium ylide. A survey of databases has revealed that the triacyl dihydrofuranone moiety in **5a** constitutes a new structural unit.

Key words: oxidative carbonylation, palladium catalyst, iodonium ylides, spirobenzofuranone.

Résumé : Les réactivités de divers dérivés du sulfonamide, de formule générale $ArSO_2N{=}XPh_n$ (X = I, n = 1; X = S, Se, n = 2; X = P, As, n = 3), dans des réactions de carbonylations catalytiques sont expliquées par des propriétés structurales des substrats. En se basant sur des données cristallographiques rapportées dans la littérature, on a conclu que la réaction de carbonylation oxydante, catalysée et en deux étapes, de sulfonylimides ne se produit que lorsque la double liaison N=X est fortement polarisée. On a trouvé que les conditions structurales observées dans les dérivés sulfonamides s'appliquent aussi aux ylures d'iodonium. La carbonylation catalytique du méthylure de phényliodonium (**3a**) préparé à partir de la dimédone (5,5-diméthylcyclohexane-1,3-dione) et de (diacétoxyiodo)benzène, conduit à la formation d'un nouveau dérivé spirobenzofuranone (**5a**) qui a été caractérisé par diffraction des rayons X sur un cristal unique, par les constantes de couplage $^1J_{C,C}$, les temps de relaxation ^{13}C-T_1 ainsi que par spectroscopies IR et Raman. Les cristaux de **5a** sont monoclinique, groupe d'espace $P2_1/c$ avec a = 7,187(1), b = 21,129(1) et c = 10,636(1) Å, β = 92,81°, V = 1613,2(3) Å^3 et Z = 4. On suggère l'existence d'un intermédiaire cétène lors de la carbonylation catalytique de l'ylure d'iodonium. Une revue des bases de données indique que la partie triacyldihydrofuranone du composé **5a** correspond à une nouvelle unité structurale.

Mots clés : carbonylation oxydante, catalyseur de palladium, ylures d'iodonium, spirobenzofuranone.

[Traduit par la Rédaction]

Introduction

The practical importance of organic isocyanates and their derivatives like urethanes and ureas has attracted continuous interest in catalytic carbonylation at nitrogen atoms (1, 2). Reductive carbonylation of aromatic nitro and nitroso compounds and oxidative carbonylation of aromatic amines are the most representative cases of these catalytic transformations.

During our search for phosgene-free methods for the preparation of arenesulfonyl isocyanates, we have discovered three new reactions leading to the formation of these target molecules (3–5). The catalytic transformation of *N*-chloroarenesulfonamidates (**1**) and (*N*-arenesulfonyl)imides (**2**) are shown by eqs. [1] and [2].

$$[1]\quad \underset{\mathbf{1}}{[ArSO_2NCl]M} + CO \xrightarrow[25^\circ C,\ 5\text{–}30\ bar]{\text{Pd–complex}} ARSO_2NCO + MCl$$

$$M = Na^+,\ K^+$$

Received October 13, 2000. Published on the NRC Research Press Web site http://canjchem.nrc.ca on June 30, 2001.

Dedicated to Brian James on the occasion of his 65th birthday.

G. Besenyei,[1] A. Neszmélyi, S. Holly, L.I. Simándi, and L. Párkányi. Chemical Research Center, Institute of Chemistry, Hungarian Academy of Sciences, 1525 Budapest P.O. Box 17, Hungary.

[1]Corresponding author (telephone: (36-1) 325-7900 exts. 197 or 339; fax: (36-1) 325-7554; e-mail: besenyei@cric.chemres.hu).

 DOI: 10.1139/cjc-79-5/6-649 © 2001 NRC Canada

Table 1. A compilation of d_{NX} bond lengths in (*N*-arenesulfonyl)imides ($ArSO_2N{=}XPh_n$).

Compound	d_{NX} (Å)	d_{NX} (obsd. or calcd.) (Å)		Ref.
		Single bond	Double bond	
$Ar^1SO_2N{=}IAr^2$	1.997(8)–2.039(3)	1.99	—	10–12
$CH_3C_6H_4SO_2N{=}SePh_2$	1.787(6)	1.824(6)–1.846(4)	1.64	13
$C_6H_5SO_2N{=}SePh_2$	1.82(1)	—	—	14
$CH_3C_6H_4SO_2N{=}SPh_2$	1.628(7)	1.76(2)	1.53	6*a*, 8, 9
$CH_3C_6H_4SO_2N{=}PPh_3$	1.579(4)	1.77(2)	1.60	6
$CH_3C_6H_4SO_2N{=}AsPh_3$	1.755(3)	1.87	—	7

[2] $$\underset{\mathbf{2}}{ArSO_2N{=}XPh_n} + CO \xrightarrow[25\text{–}50^\circ C,\ 30\ bar]{Pd\text{–}complex} ArSO_2NCO + Ph_nX$$

2a X = I, $n = 1$; **2b** X = Se, $n = 2$

Although the products are isocyanates, resembling those of the catalytic carbonylation of nitro arenes, rxns. [1] and [2] cannot be described as reductive carbonylations. As substrates **1** and **2** are prepared via oxidative reactions, these transformations of sulfonamide derivatives have been classified as two-step oxidative carbonylations and constitute a new class of catalytic reactions taking place at nitrogen atoms.

To check if other sulfonylimides have a tendency to undergo the reaction described by eq. [2], we prepared several known imidocompounds of general formula $4\text{-}CH_3C_6H_4SO_2N{=}XPh_n$ (**2c** X = S, $n = 2$; **2d** X = P, $n = 3$; **2e** X = As, $n = 3$) and subjected them to catalytic carbonylation. No CO consumption could be detected, however, under reaction conditions successfully applied earlier for the catalytic transformation of *N*-chloroarenesulfonamidates, [(*N*-arenesulfonyl)imino]phenyliodinanes, and imido selenium compounds.

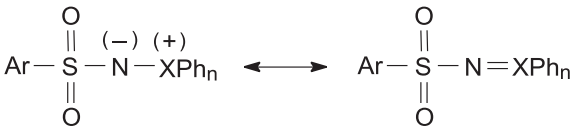
It seemed to us of interest to find an explanation for why compounds possessing seemingly close structural features behave differently under the same reaction conditions. To elucidate this problem, we examined various structural and chemical properties of the substrates. As the reaction takes place via the cleavage of nitrogen-heteroatom bonds, special attention was paid to data characterizing the bonding properties within the SO_2NX fragments.

Results and discussion

As a result of the long-standing interest toward the sulfonamide derivatives used here as model compounds, crystallographic data are available for the typical representatives of these substrates, providing us with the necessary structural information to discuss a structure–reactivity relationship. A compilation of selected crystallographic data is shown in Table 1.

The phosphorus—nitrogen bond length of **2d** (1.579(4) Å) is much shorter than a P—N single bond (1.77(2) Å), therefore a bond order of 2 is most probable in the (*N*-*p*-toluenesulfonyl)iminotriphenylphosphorane (6). A comparison of the experimentally determined arsine—nitrogen distance in **2e** (1.755(3) Å) with the As—N single bond length of ca. 1.87 Å makes feasible a similar conclusion (7). Based on a systematic study of sulfur—nitrogen bonds, the S(IV)—N bond order in **2c** can be estimated to be ca. 1.5 (d = 1.628(7) Å) (8, 9).

On the contrary, available structural data for the [(*N*-arenesulfonyl)imino]phenyliodinanes ($ArSO_2N{=}IPh$) and the theoretical calculations as well, have suggested little evidence for the iodine-nitrogen multiple bonding (10–12). Single crystal diffraction studies have revealed the strongly polarized nature of the I=N bonds, which brings about secondary interactions between the amide nitrogen, sulfonyl oxygen, and iodine atoms. In $4\text{-}CH_3C_6H_4SO_2N{=}IPh$ (**2a**, Ar = $4\text{-}CH_3C_6H_4$), the I—N bond length is 2.039(2) Å (12), which together with other iodine—nitrogen covalent bonds found in this series of imidocompounds (1.997(8)–2.027(3) Å) (10, 11), compares well with the value of 1.99 Å calculated for a single bond (12). Although the nitrogen—selenium bond length in **2b** (Ar = $4\text{-}CH_3C_6H_4$) falls somewhat out of the range observed for a selenium—nitrogen single bond (1.824(6)–1.846(4) Å), the experimentally determined value of 1.787(6) Å is still much greater than that predicted for a selenium nitrogen double bond (1.64 Å) (13). X-ray diffraction studies may indicate a further loss of Se—N multiple bonding in $C_6H_5SO_2N{=}SePh_2$ (1.82(1) Å) (14). These observations suggest that resonance structure **A** makes a major contribution to the distribution of valence electrons in **2a** and **2b,** while formula **B** is thought to be a good approximation for the structural description of **2c–e**. The N—Cl bond length in the sodium *N*-chloro-*p*-toluenesulfonamidate **1** (1.750(2) Å) was found to be equal to the mean N—Cl distance in NCl_3 and was described as a single bond (15).



A **B**

Apart from the crystallographic data, the other structural parameter considered was the position of the $\nu_{as}SO_2$ band in the IR spectra of the substrates (recorded in KBr pellets) because the wave number of this absorption can vary considerably depending on the nature of the bonds surrounding the sulfonyl group. The extent of these shifts, however, does not have a predictive power by itself with respect to the reactivity of a given imide. The $\nu_{as}SO_2$ for the inert phosphorane **2d** and for the highly reactive [(*N*-*p*-toluenesulfonyl)imino]-phenyliodinane were equally found to appear at 1266 cm^{-1}.

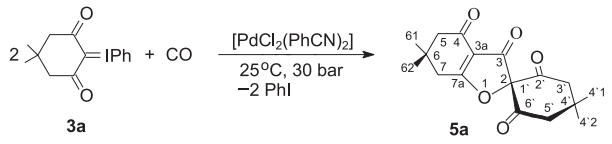
This overview of the available structural data clearly shows that the same structural formulas may hide completely

© 2001 NRC Canada

different structural properties within the SO_2NX system and a bond order of close to unity is a precondition of the carbonylation reaction. It seems plausible to assume that it is the strength of the SO_2N—X bond that is reflected by the reactivity of the substrates, and strongly polarized, consequently weaker, double bonds make the imide more reactive. The polarization of the N—X bond is not important just for weakening the bond but certainly facilitates the initial interaction with the catalyst.[2] Different reactivities of *N*-sulfonylimides in copper-catalyzed aziridination of olefins have also been observed by Evans et al. (16) by demonstrating that **2a** (Ar = *p*-tolyl) resulted in the highest yield, while the imido sulfur compound $PhMeS{=}NSO_2Ph$ gave no reaction in copper-catalyzed aziridination of olefins.

All these observations may be viewed as indirect evidence for the intermediacy of palladium–nitrene complexes that may emerge in the catalytic *N*-carbonylation of sulfonamide derivatives.

[(*N*-arenesulfonyl)imino]phenyliodinanes and phenyliodonium methylides of general formulas $ArSO_2N{=}IPh$ and $E^1E^2C{=}IPh$ (E represents electron-withdrawing groups like RC(O), RSO_2, R_FSO_2), respectively, have been mentioned as nitrogen and carbon analogues of iodosylbenzene (PhIO) and have been postulated as sources of arylsulfonylnitrene (16) and diacylcarbene species (17). Considerations regarding the structural properties of iodonium ylides (18) and available crystallographic data for them (19) have turned our attention toward the structural similarities of **2a** and iodonium ylides and have made the latter promising candidates as substrates for two-step oxidative carbonylations.

[3] 

Iodonium ylides were first described in the pioneering works of Neiland and co–workers (20), and their chemical and physical properties have been extensively studied (18, 21). However, to our knowledge, catalytic carbonylation of phenyliodonium methylides has not been described.

As expected, catalytic carbonylation of the iodonium ylide **3a** prepared from 5,5-dimethyl-1,3-cyclohexanedione and (diacetoxyiodo)benzene was accompanied by CO consumption, but the IR spectrum of the final reaction mixture did not reveal any absorption that could have been explained by the formation of ketene **4**. Based on X-ray crystallographic data as well as on NMR and IR-Raman studies, structure **5a** was ascribed to the product. The carbonyl group in position 3 clearly indicates that the isolated compound is a product of catalytic carbonylation.

A survey of various databases has shown (22) that compound **5a** has not been synthesized earlier although benzofuranones and their derivatives have been the subject of extensive research for decades. Moreover, a recent search of the CA on-line registry file has revealed that the central triacyl dihydrofuranone ring as well (shown as formula **6**) is a structural element that has not been observed in any cyclic or open-chain molecule ("A" represents a hydrogen atom, any organic moiety, or forms a ring with other units defined as "A"). Therefore, catalytic carbonylation of iodonium ylides can be viewed as a promising method to prepare formerly unknown heterocyclic compounds.

Based on two-dimensional routine ^1H and ^{13}C NMR methods (including HMQC) it was not feasible to conclusively establish the connectivity of the carbon atoms. Determination of the $^1J_{C,C}$ coupling constants and T_1 relaxation times for all carbon atoms and the assignment of the ν(C=C) band both in IR and Raman spectra together with Raman depolarization measurements have unequivocally proved, however, that the product is a hexahydrobenzofuranone derivative.

The results of spectroscopic studies carried out on bulk samples are in agreement with the results of crystallographic studies on a single crystal. NMR data are collected in Table 2. Crystallographic data, data collection parameters, and selected bond lengths and angles are summarized in Tables 3 and 4. A molecular diagram of **5a** is shown in Fig. 1.

Apart from the large difference between the angles C(3)-C(3a)-C(4) (130.8°) and C(7)-C(7a)-O(1) (118.3°), compound **5a** is quite regular from a structural point of view. The atoms in the hexahydrobenzofuranone ring are coplanar with the exception of the C(6) atom that bends above the plane by 0.6 Å and this feature turns this portion of the molecule into an envelope conformation. The cyclohexanedione moiety adopts a chair conformation with the two carbonyl groups pointing toward the side of the O(1) atom.

The relaxation times for methylene and methyl carbon atoms (see Fig. 2) result in average values of 0.58 s and 3.2 s, respectively. The averaging of carbon chemical shifts in the saturated rings reflect conformational transitions (envelope–envelope transitions probably). In addition, the methyl substituents have a nearly complete rotational freedom (methyl relaxation times are approximately nine times longer than expected for a rigid methyl carbon). From these observations and the individual T_1 values of the protonated carbons along the skeleton we may deduce that the microdynamics of the molecule in solution corresponds to that of a virtual rigid body.

We feel noteworthy that the NMR and IR-Raman spectroscopic data supported by crystallographic investigations reported here for **5a** may be of help in recognizing similar structural units.

We suppose that **5a** is formed via the intermediate ketene **4**, which is thought to be the primary product of the reaction. The postulated formation of **4** is in agreement with previous reports on the intermediacy of diketocarbene species generated from **3a**. Compound **5a** seems to be a product of the interaction of **4** with the unreacted starting substrate **3a**. The feasibility of a thermal reaction of diphenylketene with **3a** has been demonstrated (23) and was found to produce heterocycles formally composed of the ketene and the alicyclic fragment of the iodonium ylide. Compound **5a** is, however, structurally different from those described as major products of the interaction of **3a** with diphenylketene. It seems reasonable to postulate that the presence of a

[2] This point was raised by one of the reviewers.

© 2001 NRC Canada

Table 2. NMR spectroscopic data of compound **5a**.

Carbon No.	^{1}H NMR		^{13}C NMR[a]	
	δ (ppm)	$^2J_{H,H}$ (Hz)	δ (ppm)	$^1J_{C,C}$ (Hz)
2 or 1′	—	—	107.0	$J_{2,3}$ = 34, $J_{2,2'} \approx 34$, $J_{2,6'} \approx 34$
3	—	—	181.4	$J_{3,2}$ = 32, $J_{3,3a}$ = 61
3a	—	—	108.5	$J_{3a,3}$ = 61, $J_{3a,4} \approx 61$, $J_{3a,7a} \approx 61$
4	—	—	202.6	$J_{4,3a}$ = 64, $J_{4,5}$ = 44
5	2.91 (2H) (s)	—	39.5	$J_{5,4}$ = 44, $J_{5,6}$ = 33
6	—	—	33.4	$J_{6,5}$ = 33, $J_{6,61}$ = 36, $J_{6,62} \approx 36$, $J_{6,7} \approx 33$
61	1.18 (3H) (s)	—	27.9	$J_{61,6}$ = 36
62	1.18 (3H) (s)	—	27.9	$J_{62,6}$ = 36
7	2.38 (2H) (s)	—	51.5	$J_{7,6}$ = 33, $J_{7,7a}$ = 38
7a	—	—	189.7	$J_{7a,7}$ = 41, $J_{7a,3a}$ = 59
2′	—	—	191.1	$J_{2',2}$ = 35, $J_{2',3'}$ = 42
3′	2.56 (1H), 3.26 (1H)	13.6	50.0	$J_{3',2'}$ = 42, $J_{3',4'}$ = 32
4′	—	—	30.2	$J_{4',3'}$ = 32, $J_{4',5'}$ = 32, $J_{4',4'1}$ = 35
4′1	0.96 (3H) (s)	—	26.6	$J_{4',4'}$ = 36
4′2	1.30 (3H) (s)	—	29.8	$J_{4'2,4'}$ not determined
5′	2.56 (1H), 3.26 (1H)	13.6	50.0	$J_{5',4'}$ = 32, $J_{5',6'}$ = 42
6′	—	—	191.1	$J_{6',5'}$ = 42, $J_{6',2}$ = 35

[a]Spectra were recorded at 500–125 MHz (DRX-500, Bruker) at room temperature, 400 mg of **5a** in 2 mL of $CDCl_3$ with internal TMS as reference; $^1J_{C,C}$ coupling constants were measured using the one-dimensional INADEQUATE method.

Table 3. Crystallographic data and data collection parameters for compound **5a**.

Empirical formula	$C_{17}H_{20}O_5$
Formula weight	304.33
Crystal system	Monoclinic
Space group	$P2_1/c$
Unit cell dimensions	
a (Å)	7.187(1)
b (Å)	21.129(1)
c (Å)	10.636(1)
β (°)	92.81(1)
Volume (Å^3)	1613.2(3)
Z	4
Density (calcd.) (Mg m^{-3})	1.253
Absorption coefficient, μ (mm^{-1})	0.759
F(000)	648
Theta range for data collection (°)	$4.18 \le \theta \le 74.86$
Index ranges	$0 \le h \le 8$; $0 \le k \le 26$; $-13 \le l \le 13$
Reflections collected	3564
Completeness to 2θ	0.966
Decay (%)	4
Independent reflections	3197 [*R*(int) = 0.0093]
Reflections $I > 2\sigma(I)$	2637
Data, restraints, parameters	3197, 0, 205
Goodness-of-fit on F^2	1.067
Final *R* indices [$I > 2\sigma(I)$]	R_1 = 0.0338, wR_2 = 0.0958
R indices (all data)	R_1 = 0.0453, wR_2 = 0.1001
Max and mean shift–esd	0.099, 0.007
Extinction coefficient	0.0031(6)
Largest difference peak and hole (e Å^{-3})	0.176 and –0.121

Table 4. Selected bond lengths (Å) and angles (°) for **5a**.

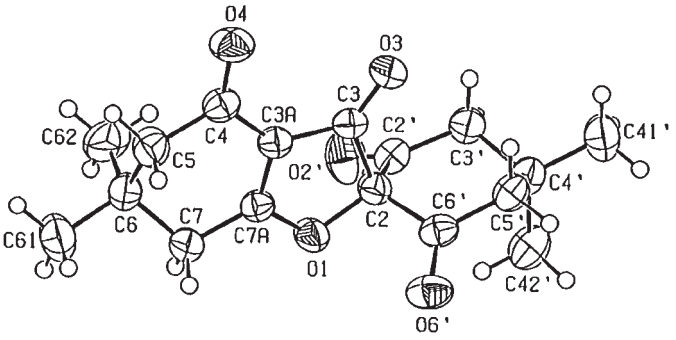
Bond length (Å)	
C(3)—O(3)	1.209(1)
C(4)—O(4)	1.215(2)
C(3a)—C(7a)	1.356(2)
C(3)—C(3a)	1.449(2)
C(3a)—C(4)	1.462(2)
C(2′)—O(2′)	1.203(2)
C(6′)—O(6′)	1.205(2)
C(2)—C(3)	1.574(2)
C(2)—O(1)	1.430(1)
Bond angle (°)	
C(5)-C(4)-C(3a)	114.0(1)
C(4)-C(3a)-C(3)	130.8(1)
C(3a)-C(3)-C(2)	103.1(1)
C(4)-C(3a)-C(7a)	120.9(1)
C(7)-C(7a)-O(1)	118.3(1)
O(1)-C(2)-C(2′)-O(2′)	–18.9(2)
O(1)-C(2)-C(6′)-O(6′)	9.7(2)

palladium catalyst induces a reaction path different from that followed in the thermal interaction.

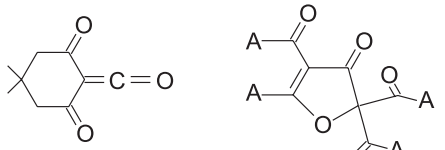
Further support for the intermediacy of **4** was obtained when carbonylation of **3a** was accomplished in the presence of 2-amino-4-methyl-6-methylthiotriazine. The solid material isolated upon carbonylation could be identified as amide **7**. It is believed that **7** is formed by trapping the primarily formed ketene **4** by the aminotriazine reactant to give an *N*-substituted-1,3-cyclohexanedione-2-carboxamide derivative, which is rearranged into its enol form.

© 2001 NRC Canada

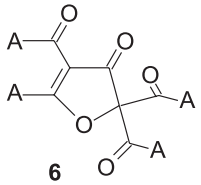
Fig. 1. Molecular structure of the spirobenzofuranone derivative **5a**. Atomic displacement parameters represent 50% probabilities.



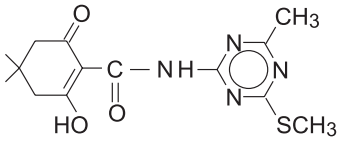
Our preliminary experiments with phenyliodonium methylide **3b,** synthesized from dibenzoylmethane and (diacetoxyiodo)benzene, have demonstrated that the catalytic reaction is accompanied by a pressure drop indicating the incorporation of carbon monoxide from the gas phase. The isolated product has proved to contain two major components, one of them having a molecular mass of 472.1311 amu (±5 ppm). The expected product (**5b**), formally composed of two dibenzoyl methanide moieties and one molecule of carbon monoxide, corresponds to the formula $C_{31}H_{20}O_5$ (theoretical molecular mass: 472.1311 amu).



4

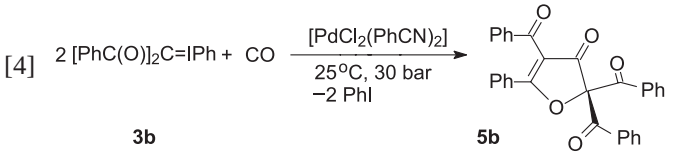


6



7

This strongly suggests that rxn. [3] takes place with **3b** as well but a combination of crystallographic and nonroutine spectroscopic methods should be applied to obtain unquestionable proof for the connectivity of the quaternary carbon atoms. Further studies on catalytic carbonylation of iodonium ylides are in progress in our laboratory.

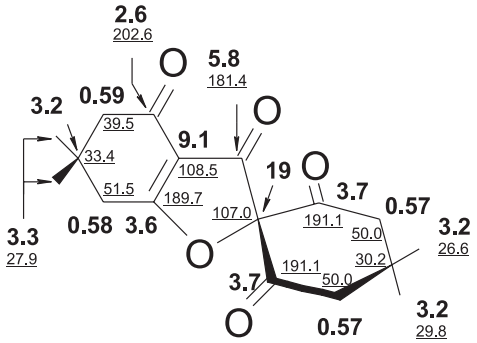


3b **5b**

Experimental

Iodonium ylides **3a** and **b** were prepared according to described procedures (24). Catalytic carbonylations were carried out in a pressure vessel (Parr Model 4712) with a total volume of 45 mL. NMR spectra were recorded on Bruker DRX-500 and Varian Unity Inova (400 MHz) spectrometers. IR spectroscopic investigations were carried out on a Magna 750 (Nicolet) fourier-transform spectrometer equipped with a DTGS detector at a resolution of 4 cm^{-1}. Raman shifts were measured in the range of 4000–100 cm^{-1} on a Nicolet System 950 FT Raman spectrometer using Nd:YAG laser. Mass spectroscopic analyses were performed on a VG ZAB-2SEQ instrument.

Fig. 2. NMR relaxation times (T_1, s) of the carbon atoms of **5a** measured at 125 MHz and room temperature in 0.2 M $CDCl_3$ solution. Underlined numbers represent the ^{13}C NMR chemical shifts in ppm.



X-ray diffraction studies

Intensity data were collected on an Enraf–Nonius CAD4 diffractometer (graphite monochromator, Cu Kα radiation, λ = 1.54180 Å) at 293(2) K using ω–2θ scans. An experimental (ψ-scan) absorption correction (25) was applied to the data (the min and max transmission factors were 0.896 and 0.998, respectively). The structure was solved by direct methods (26) (and subsequent difference syntheses). The structure was refined on F^2 (27). Hydrogen atomic positions were calculated from assumed geometries. Hydrogen atoms were included in structure factor calculations but they were not refined. The isotropic displacement parameters of the hydrogen atoms were approximated from the U_{eq} value of the atom they were bonded to. Data collection and refinement data are shown in Table 3.

Carbonylation of iodonium ylide 3a

1.84 g (5.4 mmol) of ylide **3a** and 0.1 g of $[PdCl_2(PhCN)_2]$ were charged in a pressure vessel equipped with a glass lining and 10 mL of dried (stored over activated 3 Å molecular sieve) CH_2Cl_2 was added. The reactor was flushed and pressurized to 32 bar with CO. The reaction mixture was stirred at 20°C until the pressure drop ceased. Evaporation of the solvent and precipitation with ethanol resulted in a grayish powder (414 mg), which was redissolved in dichloromethane, filtered through a Celite™ layer and precipitated again with EtOH. Yield: 355 mg (43%). Anal. calcd. for $C_{17}H_{20}O_5$: C 67.09, H 6.62; found: C 67.11, H 6.52.

Physical data of compound 5a

EI-MS (70 eV) *m/z* (%) (MF = $C_{17}H_{20}O_5$, molecular ion = 304.1448): 304 (M^+, 38), 289 (55), 276 (11), 261 (15), 207 (15), 193 (64), 83 (100). IR (cm^{-1}) (17 mg of **5a** in 1 mL of

© 2001 NRC Canada

CH_2Cl_2, KBr cell, d = 0.016 cm): 1757 (vw) and 1732 (vs) (ν_sCO and ν_{as}CO of 2′ and 6′ carbonyls), 1717 (s) and 1676 (m) (νCO of carbonyl groups at positions 3 and 4), 1592 (νC=C). Raman-IR (measured on the same solution, cm^{-1}): 1755 (s) (ρ = 0.19) and 1733 (m) (ρ = 0.72) (ν_sCO and ν_{as}CO of 2′ and 6′ carbonyls), 1719 (m) (ρ = 0.47) and 1677 (s) (ρ = 0.60) (νCO of carbonyl groups at 3 and 4), 1594 (s) (ρ = 0.22) (νC=C); (ρ denotes the depolarization ratio). NMR data are shown in Table 2.

Carbonylation of iodonium ylide 3a in the presence of 2-amino-4-methyl-6-methylthiotriazine

2.02 g (5.9 mmol) of iodonium ylide **3a** and 0.95 g (6.0 mmol) of 2-amino-4-methyl-6-methylthiotriazine were carbonylated overnight in 10 mL of CH_2Cl_2 in the presence of 96 mg of $[PdCl_2(PhCN)_2]$. The solvent was distilled off under vacuum and the oily residue was treated with diethyl ether. The white precipitate proved to be an analytically pure compound (0.74 g, 39%). Based on MS, NMR, and IR data the product was formulated as *N*-(4-methyl-6-methylthio-triazin-2-yl)-5,5-dimethyl-1,3-cyclohexanedione-2-carboxamide (**7**) observed in its enol form in solution, as shown by NMR spectra. Anal. calcd. for $C_{14}H_{18}N_4O_3S$: C 52.16, H 5.63, N 17.38, S 9.96; found: C 52.45, H 5.87, N 17.46, S 9.85.

Physical data of compound 7

EI-MS (70 eV) m/*z* (%): 322 (M^+, 86), 307 (4), 294 (4), 266 (22), 251 (18), 183 (25), 156 (100), 110 (27). IR (KBr, cm^{-1}): 3500–2800 (O*H*, N*H*, C*H*), 1661, 1624, 1579, 1526, 1479, 1423, 1387, 1276. ^{1}H NMR ($CDCl_3$) δ: 1.12 (6H, s), 2.44 (2H, s), 2.57 (6H, s, methyl and S-methyl protons on the triazine ring), 2.59 (2H, s), 12.33 (1H, N*H*), 16.77 (1H, O*H*). ^{13}C NMR ($CDCl_3$) δ: 197.3, 194.5, 183.5, 176.4, 170.0, 161.7, 103.2, 51.2, 45.2, 30.9, 28.0 (2C), 25.7, 13.4 (S*C*H_3).

Conclusions

A survey of available structural data on (*N*-arenesulfonyl)imides and the outcome of carbonylation experiments with them and with iodonium ylides have shown that: (*i*) the feasibility of two-step catalytic oxidative carbonylation is not restricted to sulfonamide derivatives; and (*ii*) the occurrence of transformation of this kind is associated with structural properties of the substrates rather than with the presence of special functional groups. We may conclude as well that other ylides like $(ArSO_2)_2C{=}IPh$ or $(R_FSO_2)_2C{=}IPh$ (where R_F represents a perfluoroalkyl group), may also prove suitable starting materials for catalytic carbonylation. The catalytic transformation of iodonium ylides described here is expected to open a new route for the preparation of heterocyclic compounds.

Acknowledgements

The authors are indebted to Dr. Pál Kolonits, Department of Organic Chemistry, Technical University, Budapest for taking the nonroutine NMR spectra and for his invaluable help in their interpretation. This work was supported by the Hungarian Research Fund (OTKA Grants T 25 870 and T 25 967).

References

1. F. Paul. Coord. Chem. Rev. **203**, 269 (2000).
2. F. Ragaini and S. Cenini. J. Mol. Catal. A: Chem. **109**, 1 (1996).
3. G. Besenyei, S. Németh, and L.I. Simándi. Angew. Chem. Int. Ed. Engl. **29**, 1147 (1990).
4. G. Besenyei and L.I. Simándi. Tetrahedron Lett. **34**, 2839 (1993).
5. G. Besenyei, S. Németh, and L.I. Simándi. Tetrahedron Lett. **35**, 9609 (1994).
6. (*a*) A.F. Cameron, N.J. Hair, and D.G. Morris. Acta Crystallogr. Sect. B: Struct. Crystallogr. Cryst. Chem. **B30**, 221 (1974); (*b*) F.H. Allen, O. Kennard, D.G. Watson, L. Brammer, A.G. Orpen, and R. Taylor. J. Chem. Soc. Perkin Trans. 2, S1 (1987).
7. H.-J. Mai, F. Weller, K. Dehnicke, C. Maichle-Mössmer, and J. Strähle. Z. Anorg. Allg. Chem. **620**, 851 (1994).
8. A. Kálmán, B. Duffin, and Á. Kucsman. Acta Crystallogr. Sect. B: Struct. Crystallogr. Cryst. Chem. **B27**, 586 (1971).
9. A. Kálmán, G. Argay, E. Fischer, and G. Rembarz. Acta Crystallogr. **B35**, 860 (1979).
10. M. Boucher, D. Macikenas, T. Ren, and J.D. Protasiewicz. J. Am. Chem. Soc. **119**, 9366 (1997).
11. R.L. Cicero, D. Zhao, and J.D. Protasiewicz. Inorg. Chem. **35**, 275 (1997).
12. A.K. Mishra, M.M. Olmstead, J.J. Ellison, and P.P. Power. Inorg. Chem. **34**, 3210 (1995).
13. H.W. Roesky, K-L. Weber, U. Seseke, W. Pinkert, M. Noltemeyer, W. Clegg, and G.M. Sheldrick. J. Chem. Soc. Dalton Trans. 565 (1985) and refs. therein.
14. H.G. Furmanova, R.G. Gerr, V.P. Krasnov, and V.I. Naddaka. Zh. Strukt. Khim. **25**, 166 (1984).
15. M.M. Olmstead and P.P. Power. Inorg. Chem. **25**, 4057 (1986).
16. D.E. Evans, M.M. Faul, and M.T. Biledeau. J. Am. Chem. Soc. **116**, 2742 (1994).
17. Y. Hayasi, T. Okada, and M. Kawanisi. Bull. Chem. Soc. Jpn. **43**, 2506 (1970).
18. G.F. Koser. *In* The chemistry of functional groups. Supplement D. *Edited by* S. Patai and Z. Rappoport. Wiley, New York. 1983. pp. 721–811.
19. (*a*) R.-Y. Yang, L.-X. Dai, and C.-G. Chen. J. Chem. Soc. Chem. Commun. 1487 (1992); (*b*) S.-Z. Zhu and Q.-Y. Chen. J. Chem. Soc. Chem. Commun. 1459 (1992); (*c*) U. Drück and W. Littke. Acta Crystallogr. Sect. B: Struct. Crystallogr. Cryst. Chem. **B34**, 3092 (1978).
20. E. Gudriniece, O. Neiland and G. Vanag. Zh. Obshch. Khim. **27**, 2737 (1957).
21. A. Varvoglis. Tetrahedron, **53**, 1179 (1997).
22. (*a*) CA on-line registry file; (*b*) CSD, Ver. 5.19. April, 2000.
23. G.F. Koser and S.-M. Yu. J. Org. Chem. **40**, 1166 (1975).
24. (*a*) O. Neiland. Zh. Org. Khim. **1**, 1858 (1965); (*b*) O.J. Neiland and B.J. Karele. Zh. Org. Khim. **7**, 1611 (1971).
25. A.C. North, D.C. Philips, and F. Mathews. Acta Crystallogr. Sect. A: Fundam. Crystallogr. **A24**, 350 (1968).
26. G.M. Sheldrick. SHELXS-97. Program for crystal structure solution. University of Göttingen, Germany. 1997.
27. G.M. Sheldrick. SHELXL-97. Program for crystal structure refinement. University of Göttingen, Germany. 1997.

© 2001 NRC Canada

Mono- and bis-(acetylacetonato) complexes of arene–ruthenium(II) and arene–osmium(II): variation of the binding mode of η^1-acetylacetonate with the nature of the arene

Martin A. Bennett, Thomas R.B. Mitchell, Mark R. Stevens, and Anthony C. Willis

Abstract: The mono(acetylacetonato) complexes [MCl(*O*,*O*′-acac)(η^6-arene)] (M = Ru, Os, arene = C_6H_6, 1,3,5-$C_6H_3Me_3$, C_6Me_6; M = Os, arene = 1,2-$C_6H_4Me_2$, 1,2,3-$C_6H_3Me_3$), which are formed from [MCl_2(η^6-arene)]$_2$ and thallium or sodium acetylacetonate, react with thallium acetylacetonate to give bis(acetylacetonato) complexes [M(*O*,*O*′-acac)(η^1-acac)(η^6-arene)]. The η^1-acac ligand is bound through the γ-carbon atom for M = Ru, Os, arene = C_6H_6; M = Os, arene = 1,2-$C_6H_4Me_2$, 1,2,3-$C_6H_3Me_3$ and through a keto-oxygen atom for M = Ru, Os, arene = 1,3,5-$C_6H_3Me_3$, C_6Me_6, the difference being attributed to a combination of steric and electronic effects. Cationic ruthenium(II) derivatives [Ru(L)(*O*,*O*′-acac)(η^6-arene)]$^+$ (arene = C_6H_6, 1,3,5-$C_6H_3Me_3$, C_6Me_6; L = DMSO, MeCN, py, PPh_3) and [Ru(CO)(*O*,*O*′-acac)(η^6-arene)]$^+$ (arene = 1,3,5-$C_6H_3Me_3$,C_6Me_6), and neutral osmium(II) η^1-acetato derivatives [Os(η^1-OAc)(*O*,*O*′-acac)(η^6-arene)] (arene = C_6H_6, 1,2-$C_6H_4Me_2$, 1,2,3-$C_6H_3Me_3$, 1,3,5-$C_6H_3Me_3$, C_6Me_6) are also described. The molecular structures of the following complexes have been determined by X-ray crystallography: [Os(*O*,*O*′-acac)(η^1-*C*-acac)(η^6-1,2-$C_6H_4Me_2$)], triclinic, space group $P\bar{1}$ (No. 2), a = 9.922(2), b = 9.974(2), and c = 11.001(2) Å, α = 68.33(1), β = 64.18(1), and γ = 62.38(1)°, V = 849.0(3) Å^3, Z = 2; [Os(*O*,*O*′-acac)(η^1-*O*-acac)(η^6-1,3,5-$C_6H_3Me_3$)], monoclinic, space group $C2/c$ (No. 15), a = 16.032(4), b = 11.989(3), and c = 21.562(7) Å, β = 108.91(2)°, V = 3921(2) Å, Z = 8; [Os(η^1-OAc)(*O*,*O*′-acac)(η^6-C_6H_6)], triclinic, space group $P\bar{1}$ (No. 2), a = 8.368(4), b = 8.402(4), and c = 11.008(4) Å, α = 71.68(3), β = 69.35(3), and γ = 69.77(3)°, V = 663.0(6) Å^3, Z = 2.

Key words: arene–ruthenium, arene–osmium, acetylacetone, crystal structures.

Résumé : Les complexes mono(acétylacétonato) [MCl(*O*,*O*′-acac)(η^6-arène)] (M = Ru, Os, arène = C_6H_6, 1,3,5-$C_6H_3Me_3$, C_6Me_6; M = Os, arène = 1,2-$C_6H_4Me_2$, 1,2,3-$C_6H_3Me_3$), qui se forment par réaction de [MCl_2(η^6-arène)]$_2$ avec l'acétylacétonate de thallium ou de sodium, réagissent avec l'acétylacétonate de thallium pour donner des complexes bis(acétylacétonato) [M(*O*,*O*′-acac)(η^1-acac)(η^6-arène)]. Le ligand η^1 est lié par le carbone γ dans les cas où M = Ru, Os, arène = C_6H_6; M = Os, arène = 1,2-$C_6H_4Me_2$, 1,2,3-$C_6H_3Me_3$ et par l'atome d'oxygène de la cétone lorsque M = Ru, Os, arène = 1,3,5-$C_6H_3Me_3$, C_6Me_6; on attribue les différences à une combinaison d'effets stériques et électroniques. On décrit aussi les dérivés cationiques du ruthénium [Ru(L)(*O*,*O*′-acac)(η^6-arène)]$^+$ (arène = C_6H_6, 1,3,5-$C_6H_3Me_3$, C_6Me_6; L = DMSO; MeCN; py, PPh_3) et [Ru(CO)(*O*,*O*′-acac)(η^6-arène)]$^+$ (arène = 1,3,5-$C_6H_3Me_3$, C_6Me_6) et les dérivés neutres η^1-acétato de l'osmium(II) [Os(η^1-OAc)(*O*,*O*′-acac)(η^6-arène)] (arène = C_6H_6, 1,2-$C_6H_4Me_2$, 1,2,3-$C_6H_3Me_3$, 1,3,5-$C_6H_3Me_3$, C_6Me_6). Les structures moléculaires des complexes suivants ont été déterminées par diffraction des rayons X: [Os(*O*,*O*′-acac)(η^1-*C*-acac)(η^6-1,2-$C_6H_4Me_2$)], triclinique, groupe d'espace $P\bar{1}$ (No. 2), avec a = 9,922(2), b = 9,974(2) et c = 11,001(2) Å, α = 68,33(1), β = 64,18(1) et γ = 62,38(1)°, V = 849,0(3) Å^3 et Z = 2; [Os(*O*,*O*′-acac)(η^1-*O*-acac)(η^6-1,3,5-$C_6H_3Me_3$)], monoclinique, groupe d'espace $C2/c$ (No. 15), avec a = 16,032(4), b = 11,989(3) et c = 21,562(7) Å, β = 108,91(2), V = 3921(2) Å^3 et Z = 8; [Os(η^1-OAc)(*O*,*O*′-acac)(η^6-C_6H_6)], triclinique, groupe d'espace $P\bar{1}$ (No. 2), avec a = 8,368(4), b = 8,402(4) et c = 11,008(4) Å, α = 71,68(3), β = 69,35(3) et γ = 69,77(3)°, V = 663,0(6) Å^3 et Z = 2.

Mots clés : arène–ruthénium, arène–osmium, acétylacétone, structures cristallines.

[Traduit par la Rédaction]

Received November 17, 2000. Published on the NRC Research Press Web site at http://canjchem.nrc.ca on June 30, 2001.

This paper is dedicated to Brian James on the occasion of his 65th birthday, and in recognition of his many contributions to organometallic chemistry, coordination chemistry, and homogeneous catalysis.

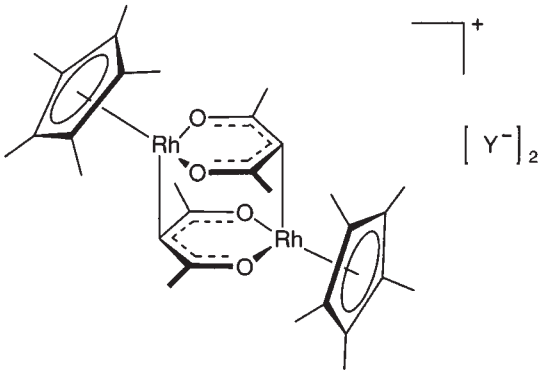
M.A. Bennett,[1] T.R.B. Mitchell, M.R. Stevens, and A.C. Willis. Research School of Chemistry, Australian National University, Canberra, ACT 0200, Australia.

[1]Corresponding author (telephone: (61) 6249-3639; fax: (61) 6249-3216; email: bennett@rsc.anu.edu.au).

 DOI: 10.1139/cjc-79-5/6-655 © 2001 NRC Canada

Introduction

Although the acac anion $(CH_3COCHCOCH_3)^-$ (see *List of abbreviations*),[2] and the mono-anions of other β-dicarbonyl compounds, usually behave as bidentate chelate *O*,*O*′-donors to transition metal ions, the more electronegative elements towards the end of the 4*d*- and 5*d*-series, especially Hg(II), Au(I), Au(III), Pt(II), Pd(II), Pt(IV), and Ir(III), display a pronounced tendency to bind to the γ-carbon atom of acetylacetonate ion (Fig. 1) (1–3). There are fewer examples of this behaviour in the coordination chemistry of rhodium, ruthenium, and osmium, which form stable chelate complexes such as [M(*O*,*O*′-acac)$_3$]. Starting from the η^5-pentamethylcyclopentadienyl complexes $[MCl_2(\eta^5\text{-}C_5Me_5)]_2$ (M = Rh, Ir), Maitlis et al. (4) have prepared [MCl(*O*,*O*′-acac)(η^5-C_5Me_5)], [Ir(*O*,*O*′-acac)(η^1-*C*-acac)(η^5-C_5Me_5)], and $[Rh_2(\mu\text{-}O,O',C\text{-acac})_2(\eta^5\text{-}C_5Me_5)_2]Y_2$ (Y = BF_4, PF_6) (**1**); in **1** each acac anion is bound as an *O*,*O*′-bidentate ligand to one rhodium atom and as a γ-*C*-donor to the other. Some



1, Y = BF_4, PF_6

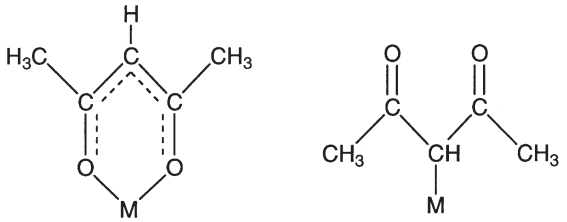
analogous compounds are known in the isoelectronic η^6-*p*-cymene–ruthenium(II) and –osmium(II) systems. The complexes [MCl(*O*,*O*′-acac)(η^6-cym)] have been obtained by reaction of $[MCl_2(\eta^6\text{-cym})]_2$ with acetylacetone and base (5, 6), and [Os(*O*,*O*′-acac)(η^1-*C*-acac) (η^6-cym)] is formed by treatment of the *tert*-butylimido compound [Os(N-*t*-Bu) (η^6-cym)] with acetylacetone (6). We report here the preparation and structural characterization of a wider range of (η^6-arene)ruthenium(II) and (η^6-arene)osmium(II) acetylacetonato complexes, and show that the mode of binding of a second acetylacetonate anion to the [M(*O*,*O*′-acac)(η^6-arene)] moiety depends on the nature of the arene.

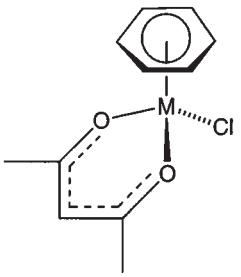
Results and discussion

Mono(acetylacetonato) complexes

Chloro(acetylacetonato) complexes of arene–ruthenium(II) or arene–osmium(II) of general formula [MCl(acac)(η^6-arene)] (M = Ru, Os; arene = C_6H_6, 1,3,5-$C_6H_3Me_3$, C_6Me_6; M = Os, arene = 1,2-$C_6H_4Me_2$, 1,2,3-$C_6H_3Me_3$) have been prepared in yields of 60–80% by reaction of 1 mol of the dichloride dimers $[MCl_2(\eta^6\text{-arene})]_2$ with 2 mol of thallium acetylacetonate or sodium acetylacetonate in dichloromethane or dichloromethane–methanol at room temperature. The ruthenium compounds can also be obtained, in generally lower yield, by heating $[RuCl_2(\eta^6\text{-arene})]_2$ with acetylacetone in DMF in the presence of anhyd Na_2CO_3 for 2–10 min at 100°C; longer periods or higher temperatures cause the formation of $[Ru(acac)_3]$. The complexes are orange or yellow, air-stable, microcrystalline solids that are very soluble in chloroform, dichloromethane, or methanol and are poorly soluble in benzene or ether. Molecular weight determinations in dichloromethane confirm that the ruthenium compounds are monomeric. Selected spectroscopic data are collected in Tables 1 and 2. In addition to the expected resonances in the region of δ 5 arising from the protons of the complexed arene, the ^{1}H NMR spectra show a 1H singlet at δ 4.9–5.1 and a 6H singlet at δ ca. 1.9 due to the γ-proton and the methyl protons of the acac group, respectively. The IR spectra show a pair of strong bands at ca. 1570 and 1510 cm^{-1}, which are assignable to coupled ν(C=O) + ν(C=C) modes of the bidentate *O*,*O*′-acetylacetonate (1–3, 7). Thus, the data are in agreement with the half-sandwich formulation **2**, similar to that proposed for the *p*-cymene–ruthenium and –osmium analogues (5, 6).

Fig. 1. Common binding modes of acetylacetonate to metal ions.





M = Ru, Os; arene = C_6H_6, 1,3,5-$C_6H_3Me_3$, C_6Me_6
M = Os; arene = 1,2-$C_6H_4Me_2$, 1,2,3-$C_6H_3Me_3$

2

In a similar manner, we have also made the corresponding hexafluoroacetylacetonato complexes [RuCl(η^6-arene)(*O*,*O*′-hfacac)] (arene = C_6H_6, 1,3,5-$C_6H_3Me_3$,C_6Me_6), whose

[2] Supplementary material may be purchased from the Depository of Unpublished Data, Document Delivery, CISTI, National Research Council Canada, Ottawa, ON K1A 0S2, Canada. For information on obtaining material electronically go to http://www.nrc.ca/cisti/irm/unpub_e.shtml. Crystallographic information has been deposited with the Cambridge Crystallographic Data Centre. Copies of the data can be obtained, free of charge, on application to the Director, CCDC, 12 Union Road, Cambridge CB2 1EZ, U.K. (Fax: 44-1223-336033 or e-mail: deposit@ccdc.cam.ac.uk).

© 2001 NRC Canada

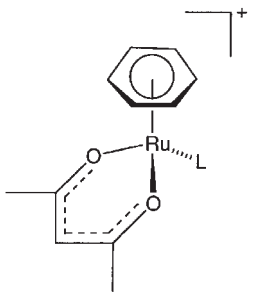
Table 1. ^{1}H NMR data and characteristic IR bands for Ru(acac)(η^6-arene) and Ru(hfacac)(η^6-arene) complexes.

	^{1}H NMR (δ)					
Complex	Solvent	acac-*Me*	acac-γ-*H*	Arene ring-*H*	Arene ring-*Me*	IR[a]
[RuCl(*O*,*O*′-acac)(η^6-C_6H_6)]	$CDCl_3$	1.97 (s, 6H)	5.16 (s, 1H)	5.61 (s, 6H)		1572, 1525
[RuCl(*O*,*O*′-acac)(η^6-1,3,5-$C_6H_3Me_3$)]	$CDCl_3$	1.98 (s, 6H)	5.15 (s, 1H)	4.84 (s, 3H)	2.12 (s, 9H)	1583, 1516
[RuCl(*O*,*O*′-acac)(η^6-C_6Me_6)]	$CDCl_3$	1.92 (s, 6H)	4.94 (s, 1H)		1.97 (s, 18H)	1584, 1513
[Ru(*O*,*O*′-acac)(dmso)(η^6-C_6H_6)]BF_4	CD_2Cl_2	2.04 (s, 6H)	5.28 (s, 1H)	5.77 (s, 6H)		1555, 1519
[Ru(*O*,*O*′-acac)(dmso)(η^6-1,3,5-$C_6H_3Me_3$)]BF_4	$CDCl_3$	2.10 (s, 6H)	5.27 (s, 1H)	4.98 (s, 3H)	2.06 (s, 9H)	1565, 1523
[Ru(*O*,*O*′-acac)(dmso)(η^6-C_6Me_6)]BF_4	$CDCl_3$	2.04 (s, 6H)	5.27 (s, 1H)		2.01 (s, 18H)	1562, 1520
[Ru(*O*,*O*′-acac)(NCMe)(η^6-C_6H_6)]BF_4	CD_2Cl_2	2.00 (s, 6H)	5.21 (s, 1H)	5.20 (s, 6H)		1569, 1514
[Ru(*O*,*O*′-acac)(NCMe)(η^6-C_6Me_6)]BF_4	$CDCl_3$	2.01 (s, 6H)	5.13 (s, 1H)		2.05 (s, 18H)	1569, 1518
[Ru(*O*,*O*′-acac)(py)(η^6-C_6H_6)]BF_4	$CDCl_3$	1.92 (s, 6H)	4.96 (s, 1H)	5.75 (s, 6H)		nm
[Ru(*O*,*O*′-acac)(py)(η^6-1,3,5-$C_6H_3Me_3$)]BF_4	$CDCl_3$	1.93 (s, 6H)	4.96 (s, 1H)	5.01 (s, 3H)	1.95 (s, 9H)	nm
[Ru(*O*,*O*′-acac)(py)(η^6-C_6Me_6)]BF_4	$CDCl_3$	1.96 (s, 6H)	4.90 (s, 1H)		1.96 (s, 18H)	nm
[Ru(*O*,*O*′-acac)(CO)(η^6-1,3,5-$C_6H_3Me_3$)]BF_4	$CDCl_3$	2.03 (s, 6H)	5.42 (s, 1H)	5.63 (s, 3H)	2.23 (s, 9H)	1580, 1519
[Ru(*O*,*O*′-acac)(CO)(η^6-C_6Me_6)]BF_4	$CDCl_3$	2.04 (s, 6H)	5.41 (s, 1H)		2.16 (s, 18H)	1566, 1522
[Ru(*O*,*O*′-acac)(PPh_3)(η^6-C_6H_6)]BF_4	$CDCl_3$	1.66 (s, 6H)	4.71 (s, 1H)	5.59 (s, 6H)		nm
[Ru(*O*,*O*′-acac)(PPh_3)(η^6-1,3,5-$C_6H_3Me_3$)]BF_4	$CDCl_3$	1.67 (s, 6H)	4.71 (s, 1H)	4.91 (s, 6H)	1.84 (s, 9H)	nm
[Ru(*O*,*O*′-acac)(PPh_3)(η^6-C_6Me_6)]BF_4	$CDCl_3$	1.73 (s, 6H)	4.60 (s, 1H)		1.73 (s, 18H)	nm
[RuCl(*O*,*O*′-hfacac)(PPh_3)(η^6-C_6H_6)]	$CDCl_3$		5.85 (s, 1H)	5.77 (s, 6H)		1628, 1605 (m), 1558
[RuCl(*O*,*O*′-hfacac)(η^6-1,3,5-$C_6H_3Me_3$)]	$CDCl_3$		5.85 (s, 1H)	4.84 (s, 3H)	2.12 (s, 9H)	1629, 1584 (m), 1554
[RuCl(*O*,*O*′-hfacac)(η^6-C_6Me_6)]	$CDCl_3$		5.79 (s, 1H)		2.06 (s, 18H)	1624, 1574 (m), 1547

[a]ν(C=O), ν(C=C) of acac (KBr, cm^{-1}); bands are very strong except where indicated; nm = not measured.

IR spectra show strong ν(C=O), ν(C=C) bands in the region of 1630–1550 cm^{-1} typical of bidentate *O*,*O*′-coordination of hfacac (7–9). The far-IR spectra of the [RuCl(acac)(η^6-arene)] and [RuCl(hfacac)(η^6-arene)] complexes contain a medium-intensity band at ca. 280 cm^{-1} that may be assigned to ν(RuCl).

Treatment of the [RuCl(*O*,*O*′-acac)(η^6-arene)] complexes with $AgBF_4$ or $AgPF_6$ in an acetone solution containing neutral ligands (L = dimethylsulfoxide (DMSO), acetonitrile, pyridine (py), triphenylphosphine) generates cationic complexes [Ru(L)(*O*,*O*′-acac)(η^6-arene)]$^+$, which can be isolated in good yield as their BF_4 or PF_6 salts. The IR spectra all show the characteristic pair of bands at ca. 1570 and 1510 cm^{-1} due to bidentate, O-bonded acac. The spectroscopic data (Table 1) are consistent with the half-sandwich structure **3**. In the solid state, the IR spectra of the DMSO complexes



L = DMSO, MeCN, py, PPh_3;
arene = C_6H_6, 1,3,5-$C_6H_3Me_3$, C_6Me_6
L = CO; arene = 1,3,5-$C_6H_3Me_3$, C_6Me_6

3

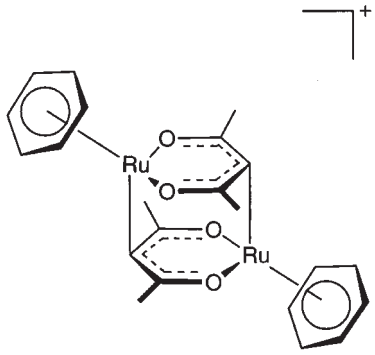
© 2001 NRC Canada

Table 2. ^{1}H NMR data and characteristic IR bands for Os(η^6-arene)(acac) complexes.

Complex	^{1}H NMR (δ)[a] Solvent	acac-*Me*	acac-γ-*H*	Arene ring-*H*	Arene ring-*Me*	IR[b]
[OsCl(*O*,*O*′-acac)(η^6-C_6H_6)]	C_6D_6	1.90 (s, 6H)	5.28 (s, 1H)	5.42 (s, 6H)		1570, 1527
[OsCl(*O*,*O*′-acac)(η^6-1,2-$C_6H_4Me_2$)]	C_6D_6	1.87 (s, 6H)	5.25 (s, 1H)	5.39 (m, 2H), 5.46 (m, 2H)	1.89 (s, 6H)	1579, 1520
	$CDCl_3$	1.99 (s, 6H)	5.35 (s, 1H)	5.84 (m, 2H), 5.93 (m, 2H)	2.14 (s, 6H)	
[OsCl(*O*,*O*′-acac)(η^6-1,2,3-$C_6H_3Me_3$)]	C_6D_6	1.87 (s, 6H)	5.23 (s, 1H)	5.29 (d, 2H), 5.53 (t, *J* = 5, 1H)	1.76 (s, 3H), 1.95 (s, 6H)	1578, 1516
	CD_2Cl_2	1.94 (s, 6H)	5.30 (s, 1H)	5.68 (d, 2H), 5.87 (t, *J* = 5, 1H)	1.95 (s, 3H), 2.10 (s, 6H)	
[OsCl(*O*,*O*′-acac)(η^6-1,3,5-$C_6H_3Me_3$)]	C_6D_6	1.88 (s, 6H)	5.26 (s, 1H)	5.00 (s, 3H)	2.02 (s, 9H)	1580, 1520
	$CDCl_3$	1.98 (s, 6H)	5.35 (s, 1H)	5.46 (s, 3H)	2.17 (s, 9H)	
[OsCl(*O*,*O*′-acac)(η^6-C_6Me_6)]	C_6D_6	1.83 (s, 6H)	5.14 (s, 1H)		1.91 (s, 18H)	1580, 1518
	$CDCl_3$	1.95 (s, 6H)	5.22 (s, 1H)		2.03 (s, 18H)	
[Os(OAc)(*O*,*O*′-acac)(η^6-C_6H_6)][c]	C_6D_6	1.87 (s, 6H)	5.23 (s, 1H)	5.72 (s, 6H)		1625,[d] 1580, 1525
[Os(OAc)(*O*,*O*′-acac)(η^6-1,2-$C_6H_4Me_2$)][e]	C_6D_6	1.85 (s, 6H)	5.19 (s, 1H)	5.79 (m, 2H), 6.06 (m, 2H)	1.83 (s, 6H)	1631,[d] 1581, 1519
[Os(OAc)(*O*,*O*′-acac)(η^6-1,2,3-$C_6H_3Me_3$)][e]	C_6D_6	1.89 (s, 6H)	5.14 (s, 1H)	5.78 (d, 2H), 6.50 (t, *J* = 5, 1H)	1.65 (s, 3H), 1.83 (s, 6H)	1634,[d] 1579, 1522
[Os(OAc)(*O*,*O*′-acac)(η^6-1,3,5-$C_6H_3Me_3$)][e]	C_6D_6	1.83 (s, 6H)	5.11 (s, 1H)	5.29 (s, 3H)	2.08 (s, 9H)	1626,[d] 1576, 1530
[Os(OAc)(*O*,*O*′-acac)(η^6-C_6Me_6)][f]	C_6D_6	1.84 (s, 6H)	5.06 (s, 1H)		2.01 (s, 18H)	1635,[d] 1575, 1524

[a]Coupling constants (*J*) in Hz.
[b]ν(C=O), ν(C=C) of acac (KBr, cm^{-1}); bands are very strong.
[c]δ 2.37 (s, 3H, C*H*$_3$CO$_2$).
[d]ν(C=O) of acetate.
[e]δ 2.38 (s, 3H, C*H*$_3$CO$_2$).
[f]δ 2.35 (s, 3H, C*H*$_3$CO$_2$).

contain a band at ca. 1120 cm^{-1}, which is assigned to ν(S=O) of S-bonded DMSO (10*a*). The region 950–1100 cm^{-1} where ν(S=O) of O-bonded DMSO is expected to appear is masked by an intense ν(BF) absorption of the BF_4 anion, but the spectrum of [Ru(DMSO)(*O*,*O*′-acac)(η^6-C_6H_6)]PF_6 showed no band attributable to ν(S=O) of O-bonded DMSO. However, the IR spectrum of [Ru(DMSO)(*O*,*O*′-acac)(η^6-C_6H_6)]PF_6 in CD_2Cl_2 contains a strong band at 1055 cm^{-1} due to free DMSO, in addition to the band at 1112 cm^{-1} due to S-coordinated DMSO, showing that this ligand is readily lost from the coordination sphere. The ^{1}H NMR spectra of the DMSO complexes in CD_2Cl_2 show a 6H singlet at δ 2.6 due to *Me*$_2$SO, the chemical shift being similar to that of free DMSO (δ 2.53), and addition of DMSO to the solution shifts the resonance towards that of free DMSO; hence, there is rapid exchange on the NMR timescale between free and coordinated DMSO. This conclusion was confirmed by adding DMSO-d_6 (6 mol) to [Ru(*O*,*O*′-acac) (DMSO)(η^6-C_6H_6)] in CH_2Cl_2; the ^{1}H NMR spectrum of the recovered complex showed the presence of only about one-sixth of the original DMSO methyl protons. Since the observations imply the existence of the coordinatively unsaturated or solvent-stabilized species [Ru(*O*,*O*′-acac)(η^6-arene)]$^+$, we treated the [RuCl(*O*,*O*′-acac)(η^6-arene)] complexes with $AgBF_4$ or $AgPF_6$ in acetone. Silver chloride is precipitated, and yellow solutions are formed that presumably contain [Ru(acetone)(*O*,*O*′-acac)(η^6-arene)]$^+$. Addition of ether precipitates yellow powders that are insoluble in chloroform, dichloromethane, or methanol and do not redissolve in acetone. They do dissolve in acetonitrile or DMSO-d_6 to generate solutions of the appropriate cations [Ru(L)(*O*,*O*′-acac)(η^6-arene)]$^+$ (L = MeCN, DMSO-d_6), as shown by ^{1}H NMR spectroscopy. Elemental analyses of the yellow solids were not completely satisfactory, but the presence of a strong ν(C=O) band at 1620 cm^{-1} in the IR spectra suggests that the complexes are the (η^6-arene)ruthenium(II) analogues (**4**) of the binuclear Rh(η^5-C_5Me_5) complex **1**, containing bridging *O*,*O*′,*C*-acac groups.

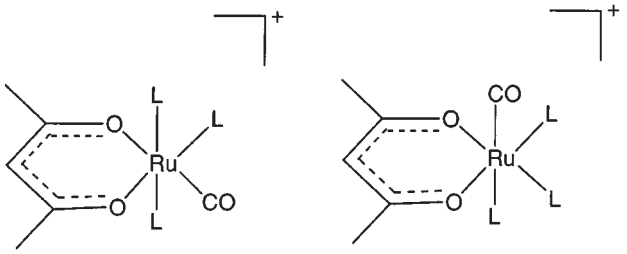


4

Cationic carbonyl complexes [Ru(CO)(*O*,*O*′-acac)(η^6-arene)]$^+$ (arene = 1,3,5-$C_6H_3Me_3$, C_6Me_6) can be isolated as their BF_4

© 2001 NRC Canada

salts by bubbling CO through the yellow solutions containing [Ru(acetone)(*O*,*O*′-acac)(η^6-arene)]$^+$. The mesitylene complex is unstable in chloroform over a period of hours and decomposes slowly in air. The IR spectra show an intense ν(CO) band at ca. 2030–2050 cm^{-1}. Attempts to prepare ethylene analogues were unsuccessful. Under the same conditions, CO displaces benzene from solutions of [Ru(L)(*O*,*O*′-acac)(η^6-C_6H_6)]BF_4 (L = Me_2CO, MeCN) to give an intractable brown oil. Addition of ether to an acetonitrile solution gave a low yield of a pale yellow crystalline salt formulated as [Ru(*O*,*O*′-acac)(CO)$(MeCN)_3$]BF_4 on the basis of spectroscopic data. In addition to the usual resonances of coordinated acac there are two singlets in a 2:1 ratio in the ^{1}H NMR spectrum at δ ca. 2.5 corresponding to the methyl protons of coordinated acetonitrile. The IR spectrum contains a pair of weak bands in the region of 2300 cm^{-1} arising from ν(CN) of coordinated acetonitrile, a strong ν(CO) band at 1982 cm^{-1}, and the usual pair of *O*,*O*′-acac bands at ca. 1570 and 1510 cm^{-1}. These data are consistent with either of the octahedral structures **5a** or **5b** in which the acetonitrile ligands adopt a *mer* or *fac* arrangement about ruthenium, respectively.



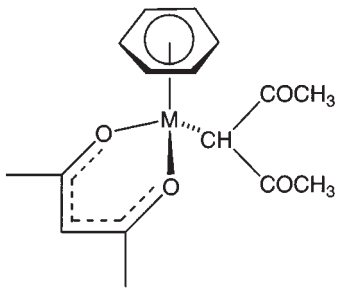
5a **5b**

Chloride ion can also be abstracted from the osmium complexes [OsCl(*O*,*O*′-acac)(η^6-arene)], which react with silver acetate to give the acetato complexes [Os(η^1-OAc)(*O*,*O*′-acac)(η^6-arene)]. Their IR spectra (Table 2) show, in addition to the usual *O*,*O*′-acac bands at ca. 1580 and 1520 cm^{-1}, a strong ν(C=O) absorption at ca. 1630 cm^{-1} characteristic of either monodentate or asymmetric bidentate acetate (10b); the ^{1}H NMR spectra show the expected 3H singlet at δ ca. 1.9. The structure of the η^6-benzene complex has been confirmed by X-ray crystallography (see below).

Bis(acetylacetonato) complexes

The [RuCl(*O*,*O*′-acac)(η^6-arene)] complexes react with an equimolar quantity of Tl(acac) in methanol at –20°C to give orange-red (benzene) or yellow (mesitylene, hexamethylbenzene) microcrystalline solids of formula [Ru$(acac)_2$(η^6-arene)]. Attempts to prepare analogous bis(hfacac) complexes were unsuccessful. The benzene complex decomposes both as a solid and in solution, and satisfactory elemental analyses could not be obtained. The mesitylene and hexamethylbenzene complexes are stable for short periods in the solid state at room temperature, but they also decompose in solution at room temperature over periods ranging from minutes in chloroform to several days in methanol. The corresponding thermally more stable osmium compounds [Os$(acac)_2$(η^6-arene)] (arene = C_6H_6, 1,2-$C_6H_4Me_2$, 1,2,3-$C_6H_3Me_3$, 1,3,5-$C_6H_3Me_3$, C_6Me_6) are obtained similarly from [OsCl(*O*,*O*′-acac)(η^6-arene)], and the benzene compound can also be isolated from the reaction of [$OsCl_2$(η^6-C_6H_6)]$_2$ with Tl(acac) in a 1:4 mol ratio in methanol. At a late stage of the study, during attempts to grow single crystals of [Os$(acac)_2$(η^6-C_6H_6)], we realized that the η^1-acetato complexes [Os(η^1-O_2CMe)(*O*,*O*′-acac)(η^6-arene)] are formed as byproducts in these reactions; these complexes have been prepared independently and have been fully characterized (see above). We have not established whether the byproducts arose from adventitious thallium acetate impurity in the sample of Tl(acac), or more likely, from a catalyzed process similar to the known base-promoted decomposition of acetylacetonate ion to acetate ion (11). In most cases the less soluble acetato complexes could be separated from the bis(acetylacetonato) complexes by fractional crystallization.

The key spectroscopic data for the [M$(acac)_2$(η^6-arene)] complexes are collected in Table 3. For the ruthenium compound [Ru$(acac)_2$(η^6-C_6H_6)], and for the osmium compounds [Os$(acac)_2$(η^6-arene)] (arene = C_6H_6, 1,2-$C_6H_4Me_2$, 1,2,3-$C_6H_3Me_3$), these data indicate a structure (**6**) in which one acac group is still bidentate (*O*,*O*′) while the other is bound as a monodentate ligand through the γ-carbon atom.



M = Ru, Os; arene = C_6H_6
M = Os; arene = 1,2-$C_6H_4Me_2$, 1,2,3-$C_6H_3Me_3$

6

Thus, the solid state and solution IR spectra show two pairs of strong bands in the ν(C=O), ν(C=C) region, one due to *O*,*O*′-acac at ca. 1580 and 1520 cm^{-1}, the other at 1650–1680 and 1620 cm^{-1} assignable to $CH(COMe)_2$ (7). Correspondingly, the ^{1}H NMR spectra contain a singlet acac methyl resonance at δ 1.9–2.3 (6H) and a γ-CH resonance at δ 4.3–4.7 assignable to C-bonded acac, in addition to a methyl resonance at δ ca. 1.8 (6H) and a γ-CH resonance at ca. δ 5.2 due to *O*,*O*′-acac. In contrast, although the ^{1}H NMR spectra of [M$(acac)_2$(η^6-arene)] (M = Ru, Os; arene = 1,3,5-$C_6H_3Me_3$, C_6Me_6) contain resonances typical of *O*,*O*′-acac, the η^1- acac group in each case gives rise to two methyl singlets at δ ca. 2.5 and 3.0, and a γ-CH singlet at δ ca. 5.0, consistent with binding through a keto-oxygen atom (structure **7**). The IR spectra show two pairs of strong bands in the ν(C=O), ν(C=C) region, one due to *O*,*O*′-acac at ca. 1580 and 1520 cm^{-1}, the other at ca. 1620 and 1500 cm^{-1}. The bands in the second pair clearly differ from those due to η^1-C-bonded acac and are similar to those reported for the structurally characterized compound [Rh(η^1-*O*-acac)(CO){P(*i*Pr)$_3$}$_2$] (1613 (w), 1515 (m) cm^{-1})) (12). However, the bands reported for *trans*-[Pt(η^1-*O*-acac)$_2$(PEt_3)$_2$] and

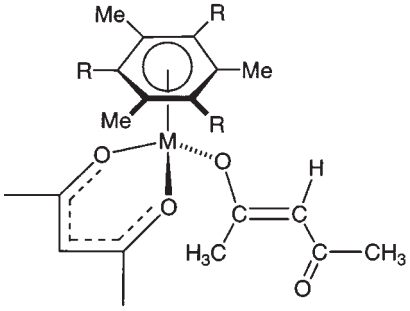
© 2001 NRC Canada

Table 3. ^{1}H NMR data and characteristic IR bands for M(acac)$_2$(η^6-arene) complexes (M = Ru, Os).

Complex	^{1}H NMR (δ) Solvent	acac-*Me*	acac-γ-*H*	Arene ring-*H*	Arene ring-*Me*	IR[a]
[Ru(*O,O′*-acac)(η^1-*C*-acac)(η^6-C_6H_6)]	C_6D_6	1.77 (s, 6H) (*O,O′*); 2.06 (s, 6 H) (η^1-*C*)	5.04 (s, 1H) (*O,O′*); 3.35 (s, 1 H) (η^1-*C*)	4.71 (s, 6H)		1574, 1520 (*O,O′*); 1672, 1623 (m) (η^1-*C*)
	CD_2Cl_2	1.83 (s, 6H) (*O,O′*); 1.98 (s, 6H) (η^1-*C*)	5.60 (s, 1H) (*O,O′*); 3.12 (s, 1 H) (η^1-*C*)	5.26 (s, 6H)		
[Ru(*O,O′*-acac)(η^1-*O*-acac)(η^6-1,3,5-$C_6H_3Me_3$)]	CD_2Cl_2	1.89 (s, 6H) (*O,O′*); 1.91 (s, 3H), 2.17 (s, 3H) (η^1-*O*)	5.43 (s, 1H) (*O,O′*); 4.97 (s, 1H) (η^1-O)	4.77 (s, 3H)	2.08 (s, 9H)	1579, 1525 (*O,O′*); 1616 (m), 1500 (η^1-*O*)
[Ru(*O,O′*-acac)(η^1-*O*-acac)(η^6-C_6Me_6)]	CD_2Cl_2	1.89 (s, 6H) (*O,O′*); 1.84 (s, 3H), 2.14 (s, 3H) (η^1-*O*)	5.14 (s, 1H) (*O,O′*); 4.94 (s, 1H) (η^1-*O*)		1.96 (s, 18H)	1582, 1519 (*O,O′*); 1613 (m), 1489 (η^1-*C*)
[Os(*O,O′*-acac)(η^1-*C*-acac)(η^6-C_6H_6)]	C_6D_6	1.88 (s, 6H) (*O,O′*)	5.27 (s, 1H) (*O,O′*); 4.64 (s, 1H) (η^1-*C*)	5.22 (s, 6H)		1570, 1520 (*O,O′*); 1678, 1631 (m) (η^1-*C*)
		2.28 (s, 6H) (η^1-*C*)				1583, 1523 (*O,O′*); 1678 1650 (sh), 1633 (η^1-*C*)[b]
[Os(*O,O′*-acac)(η^1-*C*-acac)(η^6-1,2-$C_6H_4Me_2$)]	C_6D_6	1.84 (s, 6H) (*O,O′*); 2.29 (s, 6H) (η^1-*C*)	5.22 (s, 1H) (*O,O′*); 4.69 (s, 1H) (η^1-*C*)	5.23 (m, 2H), 5.38 (m, 2H)	1.57 (s, 6H)	1573, 1520 (*O,O′*); 1646, 1630 (η^1-*C*)
	CD_2Cl_2	1.90 (s, 6H) (*O,O′*); 1.94 (s, 6H) (η^1-*C*)	5.42 (s, 1H) (*O,O′*); 4.30 (s, 1H) (η^1-*C*)	5.33 (s, 2H), 5.47 (s, 2H)	1.88 (s, 6H)	1581, 1523 (*O,O′*); 1675, 1650 (sh), 1632 (η^1-C)[b]
[Os(*O,O′*-acac)(η^1-*C*-acac)(η^6-1,2,3-$C_6H_3Me_3$)]	C_6D_6	1.82 (s, 6H) (*O,O′*)	5.17 (s, 1H) (*O,O′*); 4.73 (s, 1H) (η^1-*C*)	4.87 (d, 2H), 6.08 (t, 1H)	1.48 (s, 3H), 1.58 (s, 6H)	1575, 1527 (*O,O′*); 1646, 1626 (m) (η^1-*C*)
		2.34 (s, 6H) (η^1-*C*)				1581, 1522 (*O,O′*); 1673. 1631 (η^1-*C*)[b]
[Os(*O,O′*-acac)(η^1-*O*-acac)(η^6-1,3,5-$C_6H_3Me_3$)]	C_6D_6	1.77 (s, 6H) (*O,O′*); 2.47 (s, 3H), 3.05 (s, 3H) (η^1-*O*)	5.85 (s, 1H) (*O,O′*); 5.05 (s, 1H) (η^1-*C*)	4.95 (s, 3H)	1.95 (s, 9H)	1576, 1531 (*O,O′*); 1618 (m), 1502 (η^1-*C*)
	CD_2Cl_2	1.89 (s, 6H) (*O,O′*); 1.93 (s, 3H), 2.23 (s, 3H) (η^1-*O*)	5.46 (s, 1H) (*O,O′*); 5.23 (s, 1H) (η^1-*O*)	5.41 (s, 3H)	2.16 (s, 9H)	1582, 1524 (*O,O′*); 1617 (w), 1503 (η^1-*O*)[b]
[Os(*O,O′*-acac)(η^1-*O*-acac)(η^6-C_6Me_6)]	C_6D_6	1.76 (s, 6H) (*O,O′*)	5.52 (s, 1H) (*O,O′*); 5.00 (s, 1H) (η^1-*O*)		1.84 (s, 18H)	1580, 1526 (*O,O′*); 1624 (m), 1499 (η^1-*O*)
		2.46 (s, 3H), 2.99 (s, 3H) (η^1-*O*)				1579, 1523 (*O,O′*); 1620 (w), 1502 (η^1-*O*)[b]

[a] ν(C=O), ν(C=C) of acac (KBr, cm^{-1}); bands are strong or very strong except where indicated.
[b] In CH_2Cl_2.

© 2001 NRC Canada



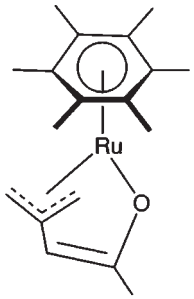
M = Ru, Os; R = H, Me

7

trans-[Pt(η^1-*O*-acac)$_2$($C_5H_{10}NH)_2$] appear at somewhat different frequencies, namely 1650 (s) and 1605 (m) cm^{-1} (13) and 1621 (vs) and 1583 (w) cm^{-1} (14), respectively, so that conclusions based on IR data must be treated with caution. Nevertheless, the proposed structures have been confirmed by single crystal X-ray diffraction studies (see below).

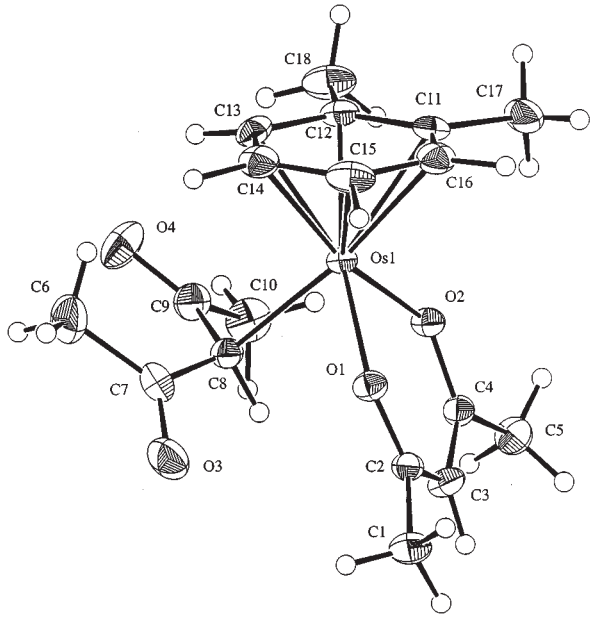
Although the ^{1}H NMR spectrum of [Ru(acac)$_2$(η^6-C_6Me_6)] in coordinating solvents such as acetone and acetonitrile is similar to that in $CDCl_3$ or CD_2Cl_2, the behaviour in methanol is different and suggestive of selective protonation of the acac ligands. At 28°C in methanol-d_4 there is one broad resonance at δ ca. 1.97 arising from the methyl protons of both acac ligands; the methine protons exchange rapidly with residual protons in the solvent and appear as a singlet at δ 4.77 (2H). It should be noted that the methine proton of [RuCl(acac)(η^6-C_6Me_6)] undergoes a similar but slower process at room temperature, complete exchange requiring ca. 100 h. At 7°C the ^{1}H NMR spectrum of [Ru(acac)$_2$(η^6-C_6Me_6)] in methanol-d_4 contains two broad methyl singlets of approximately equal intensity at δ 1.93 and ca. 2.01, the latter being partly obscured by the C_6Me_6 singlet. At this temperature, protonation of the monodentate ligand and subsequent rapid exchange between coordinated and uncoordinated acetylacetone averages the methyl environments of the enolate ligand, whereas at 28°C this process is rapid for both acac ligands. Only at –3°C in methanol-d_4 do the expected three acac methyl singlets appear.

The acac methyl protons of [Ru(acac)$_2$(η^6-C_6Me_6)] exchange completely with CH_3OD over a period of 3 days at room temperature, and the IR spectrum of the resulting deuterated complex shows characteristic shifts of the ν(C=O), ν(C=C) bands to ca. 1560 and 1480 cm^{-1} (15). A plausible intermediate in this process is **8**, which contains



8

Fig. 2. Molecular structure of [Os(*O*,*O*′-acac)(η^1-*C*-acac)(η^6-1,2-$C_6H_4Me_2$)] with selected atom labeling. Thermal ellipsoids in the ORTEP plot show 30% probability levels.



η^3-acetylacetonate dianion derived by deprotonation of the intermediate [Ru(*O*,*O*′-acac) (solvent)(η^6-C_6Me_6)]$^+$. Examples of this mode of coordination are known for palladium(II) (16) and platinum(II) (17).

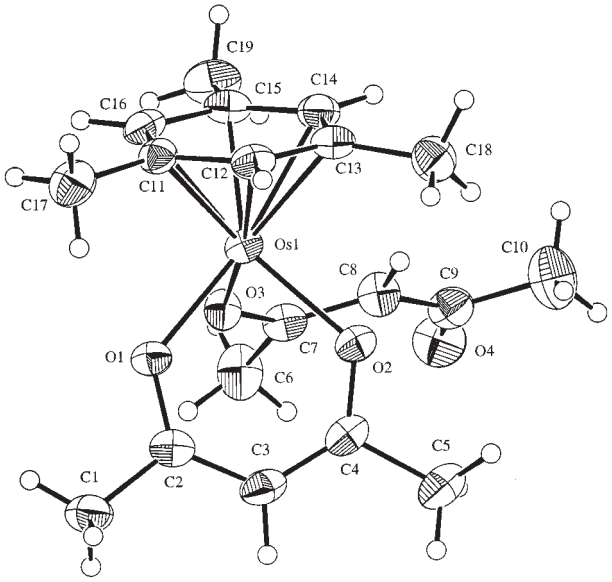
Structures determined by X-ray crystallography

The molecular structures of [Os(*O*,*O*′-acac)(η^1-*C*-acac)(η^6-1,2-$C_6H_4Me_2$)], [Os(*O*,*O*′-acac)(η^1-*O*-acac)(η^6-1,3,5-$C_6H_3Me_3$)], and [Os(η^1-OAc)(*O*,*O*′-acac)(η^6-C_6H_6)] are shown in Figs. 2–4, respectively, with atom labeling. They confirm the conclusions drawn above on the basis of spectroscopic data. Selected bond lengths and angles of these three compounds are listed in Tables 4–6, respectively.

All three compounds contain an almost planar η^6-arene ring attached to an osmium atom that is coordinated trigonally by a bidentate *O*,*O*′-bonded acac and a monodentate ligand. In the first compound, the η^1-acac group is bound through carbon atom C(8), the Os(1)–C(8) vector approximately eclipsing one of the Os–C(arene) vectors (Os(1)–C(13)). The orientation of the η^6-arene ring places its two methyl groups well away from the $COCH_3$ substituents of the η^1-acac group. The C=O groups of η^1-acac adopt a mutually *anti*-orientation, and their bond lengths are as expected (1.221(5), 1.235(5) Å). The Os(1)—C(8) bond length (2.233(4) Å) is slightly but significantly greater than the limited number of reported Os(II)—CH_3 and Os(II)—C sp^3 distances, which fall in the range of 2.17–2.21 Å (18–21). In the second compound, the η^1-acac group is bound through one of the keto-oxygen atoms, i.e., it acts as a η^1-enolate; the Os—O vectors of the trigonal array almost eclipse the methyl-bearing carbon atoms of the η^6-arene ring. The Os—O(η^1-acac) distance (2.099(5) Å) is just significantly greater than the Os—O (*O*,*O*′-acac) distances (2.078(5), 2.072(5) Å). The geometry and metrical parameters of the enolate fragment are similar to those observed in the acetylacetonato derivatives *trans*-[Rh(η^1-*O*-acac)(CO)L_2] (L = P(*i*Pr)$_3$, PCy_3) (12, 22),

© 2001 NRC Canada

Fig. 3. Molecular structure of [Os(*O,O′*-acac)(η^1-*O*-acac)(η^6-1,3,5-$C_6H_3Me_3$)] with selected atom labeling. Thermal ellipsoids in the ORTEP plot show 30% probability levels.



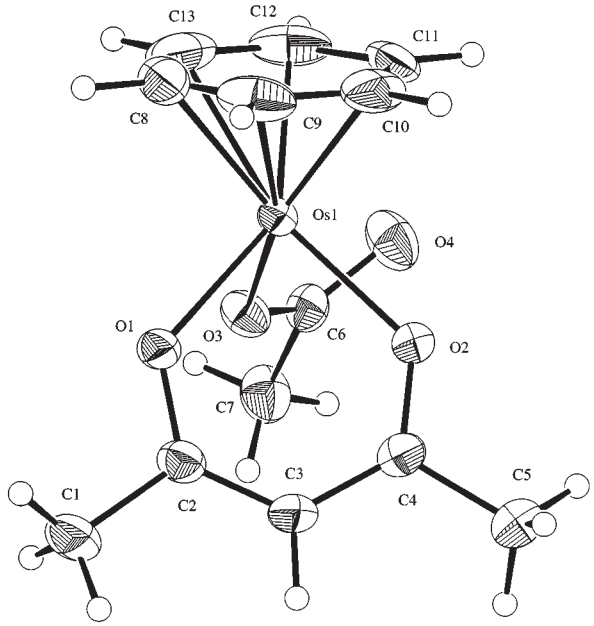
[$Cr(CO)_5${$PPh(\eta^1$-*O*-acac$)_2$}] (23), and [$Mn(\eta^5$-$C_5H_5)(CO)_2${$PPh_2(\eta^1$-*O*-acac)}] (24), and in the trifluoroacetylacetonato complex [Pd(*O,O′*-tfac)(η^1-*O*-tfac){P(*o*-tolyl)$_3$}] (25); the enolate group is almost planar, the Os-O and $COCH_3$ groups are mutually *trans* about the C—C bond, and the C=C and C=O groups are mutually *cis*. As expected, the C—O bond length of the bound enolate (1.301(9) Å) is greater than that of the uncoordinated C=O group (1.23(1) Å). The structure of [Os(η^1-OAc)(*O,O′*-acac)(η^6-C_6H_6)] confirms that the acetato group is monodentate, the Os—O bond length (2.077(3) Å) being similar to those to the *O,O′*-acac unit (2.074(3), 2.064(3) Å). In contrast to the two structures discussed above, the Os—O vectors of the trigonal array do not eclipse the arene carbon atoms.

Experimental

General procedures

All experiments were performed under an inert atmosphere with use of Schlenk techniques, and all solvents were dried and degassed by standard methods before use. ^{1}H NMR spectra were measured on Varian HA-100 or Jeol MH-100 spectrometers at 100 MHz or on Varian Gemini 300-BB or VXR-300 spectrometers at 300 MHz. Chemical shifts (δ) are in ppm referenced to residual proton signals of the solvent; coupling constants (*J*) are in Hz. IR spectra in the range 4000–400 cm^{-1} were recorded as KBr discs or Nujol™ mulls, or as CH_2Cl_2 solutions in 0.1 mm pathlength cells, on PerkinElmer PE 457 or 683 spectrometers. IR spectra in the range 450–150 cm^{-1} were measured as polythene discs on a PerkinElmer FT-1800 instrument. Electron impact (EI) mass spectra at 70 eV were measured on AEI–MS 902 or VG Micromass 7070 F spectrometers. ^{1}H NMR and selected IR data are collected in Tables 1–3; elemental analyses, which were carried out in-house, are listed in Tables 7 and 8.

Fig. 4. Molecular structure of [Os(*O,O′*-acac)(η^1-O_2CMe)(η^6-C_6H_6)] with selected atom labeling. Thermal ellipsoids in the ORTEP plot show 30% probability levels.



Starting materials

Hydrated ruthenium chloride and osmium tetraoxide were obtained from Johnson Matthey, U.K. The acetylacetonates of sodium and thallium were prepared by literature procedures (34, 35). Most of the [$MCl_2(\eta^6$-arene)]$_2$ complexes were made by reaction of the appropriate cyclohexa-1,3-diene or cyclohexa-1,4-diene with hydrated $RuCl_3$ or Na_2OsCl_6 in refluxing ethanol (27–29). The previously unknown compound [$OsCl_2$ (η^6-1,2,3-$C_6H_3Me_3$)]$_2$ was made in this way as orange microcrystals in 67% yield from Na_2OsCl_6 and a mixture of dihydro-isomers obtained by Li–NH_3 reduction of the arene. Anal. calcd. for $C_9H_{12}Cl_2Os$: C 28.35, H 3.2; found: C 27.8, H 2.8. The hexamethylbenzene complexes [$MCl_2(\eta^6$-$C_6Me_6)]_2$ were prepared by fusion of the corresponding *p*-cymene complexes with an excess of hexamethylbenzene (19, 30, 31). Since cyclohexa-1,3-diene undergoes extensive polymerization on heating with osmium chlorides, we prepared [$OsI_2(\eta^6$-$C_6H_6)]_2$ (32), converted it into the bis(acetate) by treatment with AgOAc for 2 days, and treated the bis(acetate) with conc. HCl to give [$OsCl_2(\eta^2$-$C_6H_6)]_2$ (33).

Preparations

*[RuCl(*O,O′*-acac)(η^6-arene)]*

(*i*) A mixture of [$RuCl_2(\eta^6$-$C_6H_6)]_2$ (200 mg, 0.40 mmol) and Tl(acac) (244 mg, 0.80 mmol) suspended in dichloromethane (15 mL) was stirred for 2 h and then filtered through Celite™ to remove the precipitated TlCl. The orange crystalline product [RuCl(*O,O′*-acac)(η^6-C_6H_6)], which formed on cooling the filtrate, was separated by filtration, washed with ether, and dried in vacuo. The yield was 165 mg (66%). Similarly prepared from [$RuCl_2(\eta^6$-1,3,5-$C_6H_3Me_3)]_2$ or [$RuCl_2(\eta^6$-$C_6Me_6)]_2$ and Tl(acac) with periods of stirring of 2 h and 10 min, respectively, were

© 2001 NRC Canada

Table 4. Selected bond distances and angles in [Os(*O,O′*-acac)(η^1-*C*-acac)(η^6-1,2-$C_6H_4Me_2$)].

Bond distances (Å)			
Os(1)—O(1)	2.076(2)	Os(1)—O(2)	2.078(2)
Os(1)—C(8)	2.233(4)	Os(1)—C(11)	2.207(4)
Os(1)—C(12)	2.195(3)	Os(1)—C(13)	2.156(3)
Os(1)—C(14)	2.189(4)	Os(1)—C(15)	2.177(4)
Os(1)—C(16)	2.218(4)	O(1)—C(2)	1.289(4)
O(2)—C(4)	1.277(4)	O(3)—C(7)	1.221(5)
O(4)—C(9)	1.235(5)	C(1)—C(2)	1.503(5)
C(2)—C(3)	1.388(5)	C(3)—C(4)	1.389(5)
C(4)—C(5)	1.506(5)	C(6)—C(7)	1.511(6)
C(7)—C(8)	1.481(6)	C(8)—C(9)	1.483(5)
C(9)—C(10)	1.495(6)	C—C(arom)	1.405(6)–1.431(6)
C(arom)—CH_3	1.508(6), 1.509(6)		
Bond angles (°)			
O(1)-Os(1)-O(2)	86.82(9)	O(1)-Os(1)-C(8)	83.6(1)
O(2)-Os(1)-C(8)	83.0(1)	O(1)-C(2)-C(1)	114.8(3)
O(1)-C(2)-C(3)	125.7(3)	C(2)-C(3)-C(4)	125.7(3)
O(2)-C(4)-C(3)	125.4(3)	O(2)-C(4)-C(5)	115.1(3)
Os(1)-O(1)-C(2)	126.8(2)	Os(1)-O(2)-C(4)	127.5(2)
Os(1)-C(8)-C(7)	108.7(3)	Os(1)-C(8)-C(9)	107.7(3)
C(7)-C(8)-C(9)	120.2(3)	C(6)-C(7)-C(8)	120.7(4)
O(3)-C(7)-C(8)	120.8(4)	O(4)-C(9)-C(8)	124.4(4)
O(4)-C(9)-C(10)	119.2(4)	C(8)-C(9)-C(10)	116.4(3)

Table 5. Selected bond distances and angles in [Os(*O,O′*-acac)(η^1-*O*-acac)(η^6-1,3,5-$C_6H_3Me_3$)].

Bond distances (Å)			
Os(1)—O(1)	2.078(5)	Os(1)—O(2)	2.072(5)
Os(1)—O(3)	2.099(5)	Os(1)—C(11)	2.175(8)
Os(1)—C(12)	2.172(8)	Os(1)—C(13)	2.173(8)
Os(1)—C(14)	2.172(8)	Os(1)—C(15)	2.159(8)
Os(1)—C(16)	2.178(8)	O(1)—C(2)	1.278(9)
O(2)—C(4)	1.282(9)	O(3)—C(7)	1.301(9)
O(4)—C(9)	1.23(1)	C(1)—C(2)	1.50(1)
C(2)—C(3)	1.40(1)	C(3)—C(4)	1.37(1)
C(4)—C(5)	1.51(1)	C(6)—C(7)	1.50(1)
C(7)—C(8)	1.36(1)	C(8)—C(9)	1.43(1)
C(9)—C(10)	1.51(1)	C—C(arom)	1.39(1)–1.45(1)
C(arom)—CH_3	1.49(1)–1.51(1)		
Bond angles (°)			
O(1)-Os(1)-O(2)	87.2(2)	O(1)-Os(1)-O(3)	78.4(2)
O(2)-Os(1)-O(3)	83.5(2)	O(1)-C(2)-C(1)	114.7(8)
O(1)-C(2)-C(3)	126.0(8)	C(2)-C(3)-C(4)	125.1(8)
O(2)-C(4)-C(3)	126.7(8)	O(2)-C(4)-C(5)	113.2(8)
C(1)-C(2)-C(3)	119.3(8)	C(3)-C(4)-C(5)	120.1(8)
Os(1)-O(1)-C(2)	126.2(6)	Os(1)-O(2)-C(4)	125.4(6)
Os(1)-O(3)-C(7)	128.8(5)	O(3)-C(7)-C(8)	125.9(7)
C(6)-C(7)-C(8)	122.5(8)	C(7)-C(8)-C(9)	128.4(8)
O(4)-C(9)-C(8)	127.4(9)	O(4)-C(9)-C(10)	116.6(8)
C(8)-C(9)-C(10)	116.0(8)		

Table 6. Selected bond distances and angles in [Os(η^1-OAc)(*O,O′*-acac)(η^6-C_6H_6)].

Bond distances (Å)			
Os(1)—O(1)	2.074(3)	Os(1)—O(2)	2.064(3)
Os(1)—O(3)	2.077(3)	Os(1)—C(8)	2.135(7)
Os(1)—C(9)	2.131(7)	Os(1)—C(10)	2.126(6)
Os(1)—C(11)	2.148(6)	Os(1)—C(12)	2.128(6)
Os(1)—C(13)	2.152(7)	O(1)—C(2)	1.282(6)
O(2)—C(4)	1.272(6)	O(3)—C(6)	1.283(6)
O(4)—C(6)	1.219(6)	C(1)—C(2)	1.501(7)
C(2)—C(3)	1.368(8)	C(3)—C(4)	1.390(8)
C(4)—C(5)	1.489(8)	C(6)—C(7)	1.503(8)
C(7)—C(8)	1.481(6)	C(8)—C(9)	1.483(5)
C—C(arom)	1.32(1)–1.46(1)		
Bond angles (°)			
O(1)-Os(1)-O(2)	87.4(1)	O(1)-Os(1)-O(3)	77.9(1)
O(2)-Os(1)-O(3)	82.4(1)	Os(1)-O(1)-C(2)	126.9(3)
Os(1)-O(2)-C(4)	127.2(3)	Os(1)-O(3)-C(6)	126.1(3)
O(1)-C(2)-C(1)	114.7(5)	O(1)-C(2)-C(3)	125.0(5)
C(1)-C(2)-C(3)	120.2(5)	C(2)-C(3)-C(4)	127.1(5)
O(2)-C(4)-C(3)	125.3(5)	O(2)-C(4)-C(5)	114.8(5)
C(3)-C(4)-C(5)	119.8(5)	O(3)-C(6)-O(4)	126.1(5)
O(3)-C(6)-C(7)	113.2(5)		

[RuCl(*O,O′*-acac)(η^6-1,3,5-$C_6H_3Me_3$)] (81%) and [RuCl(*O,O′*-acac)(η^6-C_6Me_6)] (82%).

(*ii*) A suspension of [$RuCl_2$(η^6-C_6H_6)]$_2$ (200 mg, 0.40 mmol) and Na(acac) (99 mg, 0.81 mmol) in dichloromethane–methanol (1:1) (15 mL) was stirred for 2 h at room temperature. The solution was evaporated to dryness under reduced pressure. The residue was extracted with dichloromethane and the solution was filtered. Addition of ether to the filtrate and cooling gave orange crystals of the product, which were separated by filtration, washed with ether, and dried in vacuo. The yield was 150 mg (60%). The complexes [RuCl(*O,O′*-acac)(η^6-arene)] (arene = 1,3,5-$C_6H_3Me_3$, C_6Me_6) were prepared similarly, with periods of stirring of 2 h and 15 min, respectively, in yields of 60 and 85%, respectively.

(*iii*) A mixture of [$RuCl_2$(η^6-C_6H_6)]$_2$ (200 mg, 0.40 mmol) and an excess of anhyd Na_2CO_3 (1 g) was suspended in DMF (5 mL) and stirred for 10 min at 100°C. The solution was filtered and methanol was added to the filtrate. The orange crystals that separated on cooling were washed with ether and dried in vacuo. The yield was 65 mg (26%).

Similarly prepared were [RuCl(*O,O′*-acac)(η^6-1,3,5-$C_6H_3Me_3$)] (63%) and [RuCl(*O,O′*-acac)(η^6-C_6Me_6)] (29%), the mixture being heated for only 2 min in the latter case.

*[RuCl(*O,O′*-hfacac)(η^6-arene)]*

(*i*) A solution of Tl(hfacac) (197 mg, 0.48 mmol) in dichloromethane (20 mL) was cooled to 0°C and treated with [$RuCl_2$(η^6-C_6H_6)]$_2$ (200 mg, 0.40 mmol). The suspension was stirred for 1 min and filtered at 0°C. Addition of ether to the filtrate gave [RuCl(*O,O′*-hfacac)(η^6-C_6H_6)] as an orange crystalline solid, which was separated by filtration, washed with ether, and dried in vacuo. The yield was 135 mg (67%). The complex [RuCl(*O,O′*-hfacac)(η^6-1,3,5-$C_6H_3Me_3$)] was

© 2001 NRC Canada

Table 7. Elemental analyses for Ru(acac)(η^6-arene) complexes.

	%C		%H		%Other	
Complex	Calcd.	Found	Calcd.	Found	Calcd.	Found
[RuCl(*O,O′*-acac)(η^6-C_6H_6)][a]	42.0	42.15	4.5	4.4	11.3 (Cl)	12.0 (Cl)
[RuCl(*O,O′*-acac)(η^6-1,3,5-$C_6H_3Me_3$)][b]	47.2	47.6	5.7	5.6	9.9 (Cl)	9.8 (Cl)
[RuCl(*O,O′*-acac)(η^6-C_6Me_6)][c]	51.3	51.25	6.3	6.3	8.9 (Cl)	8.7 (Cl)
[RuCl(*O,O′*-hfacac)(η^6-C_6H_6)]	31.3	31.6	1.7	1.7	8.4 (Cl)	8.7 (Cl)
[RuCl(*O,O′*-hfacac)(η^6-1,3,5-$C_6H_3Me_3$)]	36.3	35.5	2.8	3.1	7.6 (Cl)	8.1 (Cl)
[RuCl(*O,O′*-hfacac)(η^6-C_6Me_6)]	40.4	40.2	3.8	4.1	7.0 (Cl)	7.25 (Cl)
[Ru(*O,O′*-acac)(dmso)(η^6-C_6H_6)]BF_4	35.2	34.9	4.3	4.3	7.0 (S)	7.2 (S)
[Ru(*O,O′*-acac)(dmso)(η^6-1,3,5-$C_6H_3Me_3$)]BF_4	39.6	39.1	5.2	5.35	6.6 (S)	6.3 (S)
[Ru(*O,O′*-acac)(dmso)(η^6-C_6Me_6)]BF_4	43.3	43.4	5.9	5.9	6.1 (S)	5.7 (S)
[Ru(*O,O′*-acac)(MeCN)(η^6-C_6H_6)]BF_4	38.4	38.2	4.0	4.2	3.45 (N)	3.0 (N)
[Ru(*O,O′*-acac)(MeCN)(η^6-C_6Me_6)]BF_4	46.5	46.8	5.8	5.9	2.9 (N)	2.8 (N)
[Ru(*O,O′*-acac)(py)(η^6-C_6H_6)]BF_4	43.3	43.3	4.1	4.2	3.15 (N)	3.0 (N)
[Ru(*O,O′*-acac)(py)(η^6-1,3,5-$C_6H_3Me_3$)]BF_4	46.9	46.7	5.0	5.1	2.9 (N)	2.9 (N)
[Ru(*O,O′*-acac)(py)(η^6-C_6Me_6)]BF_4	50.0	49.8	5.7	5.9	2.65 (N)	2.5 (N)
[Ru(*O,O′*-acac)(CO)(η^6-1,3,5-$C_6H_3Me_3$)]BF_4	41.4	41.4	4.4	4.2		
[Ru(*O,O′*-acac)(CO)(η^6-C_6Me_6)]BF_4	45.3	45.2	5.3	5.3		
[Ru(*O,O′*-acac)(PPh_3)(η^6-C_6H_6)]BF_4	55.5	56.0	4.5	4.9		
[Ru(*O,O′*-acac)(PPh_3)(η^6-1,3,5-$C_6H_3Me_3$)]BF_4	57.4	57.3	5.1	5.2		
[Ru(*O,O′*-acac)(PPh_3)(η^6-C_6Me_6)]BF_4	59.1	59.1	5.7	5.7		
[Ru(*O,O′*-acac)(η^6-C_6H_6)]$_n$(BF_4)$_n$	36.4	36.2	4.8	3.2		
[Ru(*O,O′*-acac)(η^6-1,3,5-$C_6H_3Me_3$)]$_n$(BF_4)$_n$	42.5	41.3	5.0	4.8		
[Ru(*O,O′*-acac)(η^1-*O*-acac)(η^6-1,3,5-$C_6H_3Me_3$)]	54.4	53.1	6.3	6.2		
[Ru(*O,O′*-acac)(η^1-*O*-acac)(η^6-C_6Me_6)][d]	57.25	56.5	7.0	7.2		

[a]MW calcd.: 315; found: 300 (osmometry in CH_2Cl_2).
[b]MW calcd.: 356; found: 364 (osmometry in CH_2Cl_2).
[c]%Ru calcd.: 25.4; found: 25.4. MW calcd.: 398; found: 392 (osmometry in CH_2Cl_2).
[d]%Ru calcd.: 21.9; found: 21.8. MW calcd.: 461; found: 407.

prepared similarly from [RuCl(η^6-1,3,5-$C_6H_3Me_3$)]$_2$ and Tl(hfacac).

(*ii*) A solution of [$RuCl_2$(η^6-C_6Me_6)]$_2$ (150 mg, 0.22 mmol) in dichloromethane (15 mL) was stirred for 1 min with Tl(hfacac) (185mg, 0.45 mmol) at room temperature and then filtered. The filtrate was evaporated to ca. half the volume and ether was added to give [RuCl(*O,O′*-hfacac)(η^6-C_6Me_6)] as a red crystalline solid. The yield was 143 mg (63%).

*[Ru(*O,O′*-acac)(η^6-arene)(L)]BF_4 (L = DMSO, MeCN, py, PPh_3)*

Equimolar quantities of [RuCl(*O,O′*-acac)(η^6-arene)] and $AgBF_4$ were stirred in acetone at room temperature for 5 min. The solution was filtered through Celite™, the filtrate was treated with an equimolar quantity of ligand L, and the solution stirred for 1 h. Evaporation to ca. half the volume and addition of ether gave the products as yellow microcrystalline solids, which could be recrystallized from dichloromethane–ether. Yields were 40–80%. L = DMSO: arene = C_6H_6: IR (KBr, cm^{-1}): 1124 (s) (S=O). ^{1}H NMR ($CDCl_3$) δ: 2.66 (s, *Me*$_2$SO). Arene = 1,3,5-$C_6H_3Me_3$: IR (KBr, cm^{-1}): 1123 (s) (S=O). ^{1}H NMR ($CDCl_3$) δ: 2.64 (s, *Me*$_2$SO). Arene = C_6Me_6: IR (KBr, cm^{-1}): 1124 (s) (S=O). ^{1}H NMR ($CDCl_3$) δ: 2.57 (s, *Me*$_2$SO). L = MeCN: arene = C_6H_6: IR (KBr, cm^{-1}): 2295 (w) (CN). ^{1}H NMR (CD_2Cl_2) δ: 2.32 (s, *Me*CN). Arene = C_6Me_6: IR (KBr, cm^{-1}): 2290 (w) (CN). ^{1}H NMR ($CDCl_3$) δ: 2.42 (s, *Me*CN). L = py: arene = C_6H_6: ^{1}H NMR ($CDCl_3$) δ: 7.44 (m, 2H), 7.84 (m, 1H), 8.47 (m, 2H) (py). Arene = 1,3,5-$C_6H_3Me_3$: ^{1}H NMR ($CDCl_3$) δ: 7.49 (m, 2H), 7.87 (m, 1H), 8.50 (m, 2H) (py). Arene = C_6Me_6: ^{1}H NMR ($CDCl_3$) δ: 7.52 (m, 2H), 7.88 (m, 1H), 8.14 (m, 2H) (py).

*[Ru(*O,O′*-acac)(η^6-arene)(CO]BF_4*

A solution of $AgBF_4$ (55 mg, 0.28 mmol) in acetone (15 mL) was saturated with CO and treated with [RuCl(*O,O′*-acac)(η^6-1,3,5-$C_6H_3Me_3$)] (100 mg, 0.28 mmol). The solution was stirred for 5 min while CO was bubbled into it, then filtered, and evaporated under reduced pressure to ca. 5 mL volume. Addition of ether caused the product, [RuCl(*O,O′*-acac)(η^6-1,3,5-$C_6H_3Me_3$)(CO)]BF_4, to form as a yellow microcrystalline solid, which was separated by filtration, washed with ether, and dried in vacuo. The yield was 50 mg (41%). IR (KBr, cm^{-1}): 2045 (vs) (CO). A similar procedure was used to prepare [RuCl(*O,O′*-acac)(η^6-C_6Me_6)(CO)]BF_4 from [RuCl(*O,O′*-acac)(η^6-C_6Me_6)]. Evaporation to dryness of the filtered acetone solution gave an oil, which was dissolved in the minimum volume of dichloromethane. Addition of ether gave the product as a pale yellow solid in 45% yield. IR (KBr, cm^{-1}): 2026 (vs) (CO).

[Ru(acac)(arene)]$_n$(BF_4)$_n$

To a solution of $AgBF_4$ (64 mg, 0.33 mmol) in acetone (15 mL) was added [RuCl(*O,O′*-acac)(η^6-C_6H_6)] (100 mg, 0.32 mmol). The mixture was stirred for 15 min and filtered. Evaporation of the filtrate to ca. 5 mL volume and addition of ether gave [Ru(acac)(η^6-C_6H_6)]$_n$(BF_4)$_n$ as a pale yellow

© 2001 NRC Canada

Table 8. Elemental analyses for Os(acac)(η^6-arene) complexes.

	%C		%H	
Complex	Calcd.	Found	Calcd.	Found
[OsCl(*O,O′*-acac)(η^6-C_6H_6)]	32.8	32.0	3.2	3.2
[OsCl(*O,O′*-acac)(η^6-1,2-$C_6H_4Me_2$)][a]	36.2	36.0	4.0	3.9
[OsCl(*O,O′*-acac)(η^6-1,2,3-$C_6H_3Me_3$)]	37.8	37.5	4.3	3.95
[OsCl(*O,O′*-acac)(η^6-1,3,5-$C_6H_3Me_3$)]	37.8	38.1	4.3	4.5
[OsCl(*O,O′*-acac)(η^6-C_6Me_6)]	41.9	42.5	5.2	5.6
[Os(η^1-O_2CMe)(*O,O′*-acac)(η^6-C_6H_6)]	36.6	37.2	3.8	4.4
[Os(η^1-O_2CMe)(*O,O′*-acac)(η^6-1,2-$C_6H_4Me_2$)]	39.6	40.3	4.4	4.7
[Os(η^1-O_2CMe)(*O,O′*-acac)(η^6-1,2,3-$C_6H_3Me_3$)]	41.0	40.4	4.7	5.1
[Os(η^1-O_2CMe)(*O,O′*-acac)(η^6-1,3,5-$C_6H_3Me_3$)]	41.0	40.6	4.7	5.0
[Os(η^1-O_2CMe)(*O,O′*-acac)(η^6-C_6Me_6)]	44.7	44.6	5.5	5.4
[Os(*O,O′*-acac)(η^1-*C*-acac)(η^6-C_6H_6)]	41.2	40.8	4.3	4.1
[Os(*O,O′*-acac)(η^1-*C*-acac)(η^6-1,2-$C_6H_4Me_2$)]	43.7	43.3	4.9	4.7
[Os(*O,O′*-acac)(η^1-*C*-acac)(η^6-1,2,3-$C_6H_3Me_3$)]	44.9	43.9	5.15	4.9
[Os(*O,O′*-acac)(η^1-*O*-acac)(η^6-1,3,5-$C_6H_3Me_3$)]	44.9	43.1	5.15	5.7
[Os(*O,O′*-acac)(η^1-O-acac)(η^6-C_6Me_6)]	48.0	46.7	5.9	5.7

[a]%Cl calcd.: 8.2; found: 8.2.

powder, which was separated by filtration and washed with ether. The yield was 30 mg (26%). IR (KBr, cm^{-1}): 1620 (vs) (C=O)–(C=C). The mesitylene analogue was prepared similarly in 31% yield. IR (KBr, cm^{-1}): 1620 (vs) (C=O), (C=C).

*[Ru(*O,O′*-acac)(CO)(MeCN)$_3$]BF$_4$*

Carbon monoxide was bubbled into a solution of [Ru(*O,O′*-acac)(η^6-C_6H_6) (MeCN)] BF_4 (100 mg, 0.24 mmol) in acetone (15 mL) for 5 min. The solution was filtered and the filtrate evaporated under reduced pressure to give a brown oil. This was dissolved in acetonitrile and to the filtered solution was added ether dropwise to precipitate [Ru(*O,O′*-acac)(CO)$(MeCN)_3$]BF_4 (20mg, 18%) as a pale yellow solid. IR(KBr, cm^{-1}): 2300 (vw) (CN), 1980 (vs) (CO), 1570 (vs) (C=O), (C=C) of acac. ^{1}H NMR ($CDCl_3$) δ: 2.00 (s, 6H, acac-CH_3), 2.51 (s, 3H), 2.54 (s, 6H, MeCN), 5.31 (s, 1H, acac-γ-C*H*). Anal. calcd. for $C_{12}H_{16}BF_4N_3O_3Ru$: C 32.9, H 3.8, N 9.6; found: C 32.9, H 3.7, N 9.6.

*[OsCl(*O,O′*-acac)(η^6-arene)]*

(*i*) A mixture of [$OsCl_2$(η^6-1,3,5-$C_6H_3Me_3$)]$_2$ (200 mg, 0.26 mmol) and Tl(acac) (160 mg, 0.53 mmol) was stirred in dichloromethane (10 mL) for 2 h at room temperature. The yellow solution was separated from the precipitated TlCl by decantation and filtered through Celite™. The solution was concentrated in vacuo and ether was added. Cooling in dry ice – acetone gave [OsCl(*O,O′*-acac)(η^6-1,3,5-$C_6H_3Me_3$)] as a yellow-brown solid (176 mg, 75%). Evaporation of the supernatant liquid gave more yellow-brown solid, which was shown by ^{1}H NMR spectroscopy to be an approximately 1:1 mixture of [OsCl(*O,O′*-acac)(η^6-1,3,5-$C_6H_3Me_3$)] and the acetato complex [Os(η^1-O_2CMe)(*O,O′*-acac)(η^6-1,3,5-$C_6H_3Me_3$)].

The complexes [OsCl(*O,O′*-acac)(η^6-arene)] (arene = 1,2-$C_6H_4Me_2$, 1,2,3-$C_6H_3Me_3$, and C_6Me_6) were prepared similarly from the corresponding [$OsCl_2$(η^6-arene)]$_2$ complexes in yields of 83, 74, and 73%, respectively.

(*ii*) The benzene complex can be made from [$OsCl_2$(η^6-C_6H_6)]$_2$ and Na(acac) as described for the ruthenium analogue (1(*ii*)) or as follows.

Addition of a few drops of acetyl chloride to a solution of [Os(*O,O′*-acac)(η^1-*C*-arene) (η^6-C_6H_6)](125 mg, 0.27 mmol) (see below) in methanol (4 mL) caused a precipitate to form immediately. The solvent was removed in vacuo and the residue was extracted with dichloromethane. The extract was filtered through Celite™, concentrated under reduced pressure, and cooled to give [OsCl(*O,O′*-acac)(η^6-C_6H_6)] (73 mg, 67%) in two crops.

*[Os(*η^1-O$_2$CMe*)(*O,O′*-acac)(*η^6-arene*)]*

A suspension of [OsCl(*O,O′*-acac)(η^6-C_6H_6)] (48 mg, 0.12 mmol) and silver acetate (21 mg, 0.13 mmol) in benzene (10 mL) was stirred overnight. The yellow solution was separated by decantation from the precipitated AgCl, filtered through Celite™, and evaporated to dryness. The resulting yellow solid [Os(η^1-O_2CMe)(*O,O′*-acac)(η^6-C_6H_6)] (47 mg, 92%) was spectroscopically and analytically pure.

The corresponding complexes containing 1,2-$C_6H_4Me_2$, 1,2,3-$C_6H_3Me_3$, 1,3,5-$C_6H_3Me_3$, and C_6Me_6 were prepared similarly in yields of 71, 95, 59, and 95%, respectively.

*[Ru(acac)$_2$(*η^6-arene*)]*

A mixture of [RuCl(*O,O′*-acac)(η^6-C_6H_6)] (200 mg, 0.64 mmol) and Tl(acac) (190 mg, 0.63 mmol) was stirred in methanol (10 mL) at –20°C for 2 h. The solution was evaporated to dryness, the residue was extracted with ether, and the extract was filtered, the temperature being kept below 0°C at all times. The filtrate was concentrated under reduced pressure to give [Ru(*O,O′*-acac)(η^1-*C*-acac)(η^6-C_6H_6)] as a microcrystalline red solid, which darkened when warmed to room temperature. The yield was 120 mg (51%).

The complexes [Ru(*O,O′*-acac)(η^1-*O*-acac)(η^6-arene)] (arene = 1,3,5-$C_6H_3Me_3$, C_6Me_6) were prepared similarly from [RuCl(*O,O′*-acac)(η^6-arene)] in yields of 40 and 60%, respectively.

© 2001 NRC Canada

Table 9. Crystallographic data collection parameters for (η^6-arene)osmium complexes.

Complex	[Os(*O*,*O*′-acac)(η^1-*C*-acac)(η^6-1,2-$C_6H_4Me_2$)]	[Os(*O*,*O*′-acac)(η^1-*O*-acac)(η^6-1,3,5-$C_6H_3Me_3$)]	[Os(η^1-OAc)(*O*,*O*′-acac)(η^6-C_6H_6)]
Formula	$C_{18}H_{24}O_4Os$	$C_{19}H_{26}O_4Os$	$C_{13}H_{16}O_4Os$
FW	494.59	508.61	426.47
Crystal system	Triclinic	Monoclinic	Triclinic
Space group	$P\bar{1}$ (No. 2)	*C*2/*c* (No. 15)	$P\bar{1}$ (No. 2)
a (Å)	9.922(2)	16.032(4)	8.368(4)
b (Å)	9.974(2)	11.989(3)	8.402(4)
c (Å)	11.001(2)	21.562(7)	11.008(4)
α (°)	68.33(1)		71.68(3)
β (°)	64.18(1)	108.91(2)	69.35(3)
γ (°)	62.38 (1)		69.77(3)
V (Å^3)	849.0(3)	3921(2)	663.0(6)
Z	2	8	2
$\rho_{calcd.}$ (g cm^{-3})	1.935	1.723	2.133
Crystal size (mm)	0.38 × 0.37 × 0.08	0.25 × 0.20 × 0.17	0.40 × 0.23 × 0.04
Temperature (K)	296 ± 1	296 ± 1	296 ± 1
F (000)	480.00	1984.00	404.00
Colour, habit	Yellow, plate	Yellow, multifaceted	Orange, wedge
μ (cm^{-1})	75.22 (Mo Kα)	65.18 (Mo Kα)	96.01 (Mo Kα)
Diffractometer	Philips PW 1100/20	Philips PW 1100/20	Philips PW 1100/20
Data collection method	ω–2θ	ω–2θ	ω–2θ
ω-Scan width (°)	1.20 + 0.35 tan θ	1.0 + 0.35 tan θ	1.20 + 0.34 tan θ
2θ limits (°)	60.0	55.0	55.2
Total unique reflections	4949	4721	3064
Total observed reflections[a]	4508	2717	2738
Max/min transmission factor[b]	0.104–0.578	0.318–0.436	0.127–0.582
No. of parameters	281	217	164
Largest difference peak and hole (e Å^{-3})	1.73, –1.17	0.56, –1.63	0.85, –0.72
R[c]	0.023	0.032	0.023
R_w[c]	0.026	0.034	0.027
GoF[d]	1.54	1.53	1.50

[a] $I > 3\sigma(I)$.
[b] Analytical absorption correction.
[c] $R = \Sigma||F_o| - |F_c||/\Sigma|F_o|$; $R_w = [\Sigma\{w(|F_o| - |F_c|)\}/\Sigma(w|F_o|)^2]^{1/2}$.
[d] $\{\Sigma w(|F_o| - |F_c|)^2/(N_o - N_v)\}^{1/2}$, where N_o = number of observations, N_v = number of variables.

[Os(acac)$_2$(η^6-arene)]

(*i*) A mixture of [OsCl$_2$(η^6-C_6H_6)]$_2$ (100 mg, 0.15 mmol) and Tl(acac) (179 mg, 0.59 mmol) in methanol (10 mL) was stirred for 2 h. The solvent was removed under reduced pressure and the residue was extracted with dichloromethane. The extracts were filtered through Celite™ and again evaporated to dryness. The residue was extracted with ether (ca. 20 mL) and the ether solution passed down a short column of Celite™. Concentration and cooling gave two crops (34 mg in total) of a yellow solid containing [Os(*O*,*O*′-acac)(η^1-*C*-acac)(η^6-C_6H_6)] contaminated by the acetato complex [Os(η^1-O_2CMe)(*O*,*O*′-acac)(η^6-C_6H_6)] (ca. 10–15%) as shown by ^{1}H NMR spectroscopy. An X-ray quality crystal of the latter was obtained by evaporation of the ether solution. A crystalline, spectroscopically and analytically pure sample of [Os(*O*,*O*′-acac)(η^1-*C*-acac)(η^6-C_6H_6)] was obtained by diffusion of pentane into a dichloromethane solution.

(*ii*) A mixture of [OsCl(*O*,*O*′-acac)(η^6-1,2-$C_6H_4Me_2$)] (130 mg, 0.30 mmol) and Tl(acac) (95 mg, 0.31 mmol) in methanol (10 mL) was stirred for 2 h giving a yellow solution and a colourless precipitate. The methanol was removed in vacuo and the residue was extracted with ether and filtered through Celite™. Concentration of the filtrate and cooling gave a yellow solid containing mainly [Os(*O*,*O*′-acac)(η^1-*C*-acac)(η^6-1,2-$C_6H_4Me_2$)], as shown by ^{1}H NMR spectroscopy. The yield was 82 mg (55%). Evaporation of the supernatant liquid gave a further 34 mg of less pure product. Yellow-brown X-ray quality crystals of [Os(*O*,*O*′-acac)(η^1-*C*-acac)(η^6-1,2-$C_6H_4Me_2$)] were obtained by diffusion of hexane into a benzene solution of the first solid; these crystals also gave satisfactory microanalytical data. EI-MS (70 eV) *m*/*z* : 496.1 (M$^+$, based on ^{192}Os), 397 ([M – acac]$^+$).

(*iii*) Similarly prepared from OsCl(*O*,*O*′-acac)(η^6-1,2,3-$C_6H_3Me_3$)] (123 mg, 0.28 mmol) and Tl(acac) (85 mg, 0.28 mmol) in methanol, after extraction with dichloromethane (10 mL), was crude [Os(*O*,*O*′-acac)(η^1-*C*-acac)(η^6-1,2,3-$C_6H_3Me_3$)] (127 mg, 89%). Purification was carried out by extraction with ether as described above.

(*iv*) Reaction of [OsCl(*O*,*O*′-acac)(η^6-1,3,5-$C_6H_3Me_3$)] (150 mg, 0.34 mmol) with Tl(acac) (103 mg, 0.34 mmol) in

© 2001 NRC Canada

Table 10. Positional parameters and isotropic thermal parameters for non-hydrogen atoms of [Os(*O*,*O′*-acac)(η¹-*C*-acac)(η⁶-1,2-$C_6H_4Me_2$)].

Atom	*x*	*y*	z	B_{eq}[a]
Os(1)	0.18151(1)	0.29901(1)	0.29616(1)	2.147(2)
O(1)	0.0834(2)	0.5387(2)	0.2434(2)	2.66(4)
O(2)	0.2262(2)	0.3002(2)	0.0929(2)	2.58(3)
O(3)	0.3610(3)	0.5716(3)	0.2550(3)	4.90(7)
O(4)	0.6139(3)	0.0977(3)	0.2733(3)	5.25(6)
C(1)	0.0263(4)	0.7945(3)	0.1137(4)	3.79(7)
C(2)	0.0971(3)	0.6232(3)	0.1205(3)	2.53(4)
C(3)	0.1658(4)	0.5690(3)	–0.0004(3)	3.10(5)
C(4)	0.2185(3)	0.4161(3)	–0.0087(3)	2.60(5)
C(5)	0.2720(4)	0.3779(4)	–0.1467(3)	3.46(6)
C(6)	0.4659(5)	0.3523(5)	0.4125(5)	5.3(1)
C(7)	0.4089(4)	0.4306(4)	0.2879(4)	3.66(6)
C(8)	0.4134(3)	0.3380(3)	0.2066(3)	2.93(5)
C(9)	0.5454(4)	0.1867(4)	0.1873(4)	3.59(6)
C(10)	0.5934(4)	0.1407(4)	0.0553(4)	4.40(7)
C(11)	0.0695(4)	0.1278(3)	0.3566(3)	3.20(6)
C(12)	0.2231(4)	0.0511(3)	0.3749(3)	2.99(5)
C(13)	0.2572(4)	0.1076(4)	0.4562(3)	3.21(6)
C(14)	0.1433(5)	0.2344(4)	0.5184(3)	3.59(6)
C(15)	–0.0062(4)	0.3093(4)	0.4961(3)	3.81(6)
C(16)	–0.0450(4)	0.2542(4)	0.4196(4)	3.50(6)
C(17)	0.0315(6)	0.0780(5)	0.2650(4)	4.8(1)
C(18)	0.3515(5)	–0.0832(4)	0.3089(4)	4.65(8)

[a] $B_{eq} = 8\pi^2/3\{U_{11}(aa^*)^2 + U_{22}(bb^*)^2 + U_{33}(cc^*)^2 + 2U_{12}aa^*bb^*\cos\gamma + 2U_{13}aa^*cc^*\cos\beta + 2U_{23}bb^*cc^*\cos\alpha\}$.

Table 11. Positional parameters and isotropic thermal parameters for non-hydrogen atoms of [Os(*O*,*O′*-acac)(η¹-*O*-acac)(η⁶-1,3,5-$C_6H_3Me_3$)].

Atom	*x*	*y*	*z*	B_{eq}[a]
Os(1)	0.19613(2)	–0.00494(3)	0.07174(1)	3.272(6)
O(1)	0.1366(4)	0.1412(4)	0.0270(3)	3.7(1)
O(2)	0.3051(3)	0.0912(4)	0.1204(3)	3.9(1)
O(3)	0.1456(3)	0.0597(4)	0.1427(3)	3.8(1)
O(4)	0.2731(5)	0.0444(5)	0.3525(3)	6.3(2)
C(1)	0.1030(6)	0.3303(7)	0.0065(4)	5.1(2)
C(2)	0.1626(6)	0.2405(7)	0.0447(4)	4.2(2)
C(3)	0.2398(6)	0.2700(7)	0.0949(5)	4.7(2)
C(4)	0.3048(6)	0.1972(7)	0.1282(4)	4.1(2)
C(5)	0.3877(6)	0.2402(8)	0.1782(5)	5.8(3)
C(6)	0.1229(6)	0.1159(9)	0.2389(5)	6.1(3)
C(7)	0.1809(6)	0.0591(6)	0.2062(4)	3.9(2)
C(8)	0.2600(6)	0.0126(7)	0.2407(4)	4.5(2)
C(9)	0.3027(6)	0.0113(8)	0.3100(4)	4.9(2)
C(10)	0.3951(7)	–0.037(1)	0.3333(5)	7.3(3)
C(11)	0.1396(5)	–0.0884(6)	–0.0222(4)	3.7(2)
C(12)	0.2331(6)	–0.0928(6)	0.0035(4)	4.0(2)
C(13)	0.2842(6)	–0.1326(6)	0.0573(4)	4.2(2)
C(14)	0.2417(6)	–0.1736(6)	0.1006(4)	4.4(2)
C(15)	0.1507(6)	–0.1695(6)	0.0859(4)	4.2(2)
C(16)	0.0976(6)	–0.1284(6)	0.0219(5)	4.2(2)
C(17)	0.0858(6)	–0.0386(8)	–0.0861(4)	5.5(2)
C(18)	0.3836(6)	–0.1249(8)	0.0787(5)	5.7(3)
C(19)	0.1055(7)	–0.2042(8)	0.1340(5)	6.0(3)

[a] B_{eq} defined as in Table 10.

methanol (10 mL) and work-up as described for the *o*-xylene preparation gave 150 mg (88%) of crude [Os(*O*,*O′*-acac)(η¹-*O*-acac)(η⁶-1,3,5-$C_6H_3Me_3$)] contaminated with the acetato complex. Yellow X-ray quality crystals of the former were obtained by diffusion of hexane into a benzene solution.

(*v*) Reaction of [OsCl(*O*,*O′*-acac)(η⁶-C_6Me_6)] (94 mg, 0.19 mmol) with Tl(acac) (60 mg, 0.20 mmol) in methanol (10 mL) and work-up as described above gave [Os(*O*,*O′*-acac)(η¹-*O*-acac)(η⁶-C_6Me_6)] (38 mg, 36%), which was ca. 90% pure, although ^{1}H NMR spectroscopy and elemental analyses indicated the presence of some of the acetato complex.

Molecular structure determinations

Crystals of [Os(*O*,*O′*-acac)(η¹-*C*-acac)(η⁶-1,2-$C_6H_4Me_2$)] and [Os(*O*,*O′*-acac)(η¹-*O*-acac)(η⁶-1,3,5-$C_6H_3Me_3$)] suitable for X-ray diffraction studies were obtained by vapour diffusion of hexane into benzene solutions. Crystals of [Os(*O*,*O′*-acac)(η¹-OAc)(η⁶-C_6H_6)] were obtained fortuitously from an ether solution of the crude η¹-*C*-acac complex. The crystal data and parameters for data collection are summarized in Table 9. The structures were solved by heavy atom Patterson methods (36) and expanded by use of Fourier techniques (37). Non-hydrogen atoms were refined anisotropically. Most of the hydrogen atoms were located in the difference electron density maps and the positions used to generate all the hydrogen atoms, assuming idealized geometry. For the *o*-xylene complex, the positional parameters for the hydrogen atoms were refined, the isotropic *B*-values being held fixed and tight restraints being imposed on distances and angles for the methyl groups only. For the mesitylene and benzene complexes, the hydrogen atoms were periodically recalculated but

Table 12. Positional parameters and isotropic thermal parameters for non-hydrogen atoms of [Os(*O*,*O′*-acac)(η¹-O_2CMe)(η⁶-C_6H_6)].

Atom	*x*	*y*	*z*	B_{eq}[a]
Os(1)	0.18666(2)	0.08777(2)	0.23193(2)	2.743(4)
O(1)	–0.0167(4)	0.2837(4)	0.3121(4)	3.53(7)
O(2)	0.2701(5)	0.2798(4)	0.0746(3)	3.61(7)
O(3)	0.3100(5)	0.1704(5)	0.3257(4)	3.77(8)
O(4)	0.5922(5)	0.0402(6)	0.2379(5)	5.2(1)
C(1)	–0.1831(9)	0.5568(8)	0.3596(7)	5.7(2)
C(2)	–0.0321(7)	0.4477(6)	0.2725(6)	3.8(1)
C(3)	0.0726(9)	0.5251(7)	0.1585(6)	4.8(1)
C(4)	0.2120(8)	0.4433(6)	0.0651(5)	3.9(1)
C(5)	0.2991(9)	0.5496(8)	–0.0612(6)	5.3(1)
C(6)	0.4775(7)	0.1353(7)	0.3078(5)	3.5(1)
C(7)	0.5256(8)	0.2229(9)	0.3847(6)	4.9(2)
C(8)	0.022(1)	–0.086(1)	0.326(1)	7.3(2)
C(9)	0.024(1)	–0.0307(9)	0.197(1)	6.4(2)
C(10)	0.183(2)	–0.0470(9)	0.0991(7)	7.4(2)
C(11)	0.346(1)	–0.127(1)	0.139(1)	7.7(2)
C(12)	0.327(1)	–0.1789(8)	0.275(1)	6.6(2)
C(13)	0.171(2)	–0.1610(9)	0.3631(8)	7.6(3)

[a] B_{eq} defined as in Table 10.

© 2001 NRC Canada

not refined. The function minimized was $\Sigma w(|F_o| - |F_c|)^2$ with the weights w given by $w = |\sigma^2(F_o)|^{-1}$. The software packages used were Xtal (38) for data reduction and teXsan (39) for structure solution, refinement, and graphics. Neutral atom scattering factors were taken from ref. 40. Anomalous dispersion effects were included in F_{calc} (41); values of $\Delta f'$ and $\Delta f''$ and of mass attenuation coefficients were taken from standard compilations (42, 43). Selected bond distances and angles are given in Tables 4–6, atomic coordinates are listed in Tables 10–12.

Crystal data, complete tables of bond distances and angles, atomic coordinates, anisotropic thermal parameters for the non-hydrogen atoms, non-bonded contacts, and selected least-squares planes have been deposited.[2]

Conclusion

In this work, we have shown that the [M(*O*,*O*′-acac)(η^6-arene)] (M = Ru, Os) fragments are capable of binding a range of ligands containing nitrogen, phosphorus, oxygen, and sulfur donor atoms. The mode of binding of a second acac group depends on the nature of the arene. The fact that the preferred binding mode changes from η^1-*C* to η^1-*O* in going from 1,2,3- to 1,3,5-$C_6H_3Me_3$ suggests that there is a delicate balance, possibly mediated by a steric effect. The more symmetrical arrangement of ring methyl groups could give rise to an unavoidable steric repulsion between them and the $COCH_3$ groups of a η^1-*C*-acac group, thus favouring coordination of the sterically less demanding η^1-*O*- enolate form. However, on this basis alone, it is difficult to see why η^1-*C*-bonding should be favoured for the isoelectronic complexes of rhodium(III) and iridium(III) [M(*O*,*O*′-acac)(η^1-*C*-acac)(η^5-C_5Me_5)] (4), since the estimated average cone angles of Rh^{III}-C_5Me_5 and Ru^{II}-$C_6H_3Me_3$ are likely to be very similar (ca. 188°) (26). Another possibility is that, since the charge separation in an arene–metal bond in the sense (arene)(δ^+)–metal(δ^-) is probably greater than that in its isoelectronic C_5Me_5–metal counterpart, the negative charge on the metal may be better accommodated by the more electronegative oxygen atom of an O-bound enolate.

References

1. S. Kawaguchi. Coord. Chem. Rev. **70**, 51 (1986).
2. S. Kawaguchi. Variety in coordination modes of ligands in metal complexes. Springer-Verlag, Berlin. 1988. Chap. 5.
3. A.R. Siedle. *In* Comprehensive coordination chemistry. Vol. 2. *Edited by* G. Wilkinson, R.D. Gillard, and J.A. McCleverty. Pergamon, Oxford. 1987. p. 365.
4. W. Rigby, H-B. Lee, P.M. Bailey, J.A. McCleverty, and P.M. Maitlis. J. Chem. Soc. Dalton Trans. 387 (1979).
5. D. Carmona, J. Ferrer, L.A. Oro, M.C. Apreda, C. Foces-Foces, F.H. Cano, J. Elguero, and M.L. Jimeno. J. Chem. Soc. Dalton Trans. 1463 (1990).
6. R.J. Michelman, G.E. Ball, R.G. Bergman, and R.A. Andersen. Organometallics, **13**, 869 (1994).
7. K. Nakamoto. Infrared and Raman spectra of inorganic and coordination compounds. 5th ed. Part B. Wiley Interscience, New York. 1997. pp. 91–100.
8. M.L. Morris, R.W. Moshier, and R.E. Sievers. Inorg. Chem. **2**, 411 (1963).
9. M. Kilner, F.A. Hartman, and A. Wojcicki. Inorg. Chem. **6**, 406 (1967).
10. (*a*) K. Nakamoto. Infrared and Raman spectra of inorganic and coordination compounds. 5th ed. Part B. Wiley Interscience, New York. 1997. pp. 102–104; (*b*) pp. 59–62.
11. J. March. Advanced organic chemistry. 4th ed. Wiley Interscience, New York. 1992. p. 631.
12. S.I. Yoshida, Y. Ohgomori, Y. Watanabe, K. Honda, M. Goto, and M. Kurabashi. J. Chem. Soc. Dalton Trans. 895 (1988).
13. T. Ito, T. Kiriyama, and A. Yamamoto. Chem. Lett. 835 (1976).
14. S. Okeya, F. Egawa, Y. Nakamura, and S. Kawaguchi. Inorg. Chim. Acta, **30**, L 319 (1978).
15. B. Bock, K. Flatau, H. Junge, M. Kuhr, and H. Musso. Angew. Chem. Int. Ed. Engl. **10**, 225 (1971).
16. N. Yanase, Y. Nakamura, and S. Kawaguchi. Inorg. Chem. **19**, 1575 (1980).
17. S. Okeya, Y. Nakamura, S. Kawaguchi, and T. Hinimoto. Bull. Chem. Soc. Jpn. **55**, 477 (1982).
18. E. Lindner, R.M. Jansen, W. Hiller, and R. Fawzi. Chem. Ber. **122**, 1403 (1989).
19. W.A. Kiel, R.G. Ball, and W.A.G. Graham. J. Organomet. Chem. **383**, 481 (1990).
20. M.A. Esteruelas, F.J. Lahoz, J.A. Lopez, L.A. Oro, C. Schlünken, C. Valero, and H. Werner. Organometallics, **11**, 2034 (1992).
21. G. Bellachioma, G. Cardaci, A. Macchioni, and P. Zanazzi. Inorg. Chem. **32**, 547 (1993).
22. G.B. Ansell, S. Leta, A.A. Oswald, and E.J. Mozeleski. Acta Crystallogr. Sect. C: Cryst. Struct. Commun. **42**, 1516 (1986).
23. J. von Seyerl, D. Neugebauer, G. Huttner, C. Krüger, and Y-H. Tsay. Chem. Ber. **112**, 3637 (1979).
24. G. Huttner, J. von Seyerl, and D. Neugebauer. Cryst. Struct. Commun. **9**, 1093 (1980).
25. S. Ooi, T. Matsushita, K. Nishimoto, S. Okeya, Y. Nakamura, and S. Kawaguchi. Bull. Chem. Soc. Jpn. **56**, 3297 (1983).
26. P.M. Maitlis. Chem. Soc. Rev. **10**, 1 (1981).
27. M.A. Bennett and A.K. Smith. J. Chem. Soc. Dalton Trans. 233 (1974).
28. M.A. Bennett and A.M.M. Weerasuria. J. Organomet. Chem. **394**, 481 (1990).
29. M.A. Bennett, M. Bown, L.Y. Goh, D.C.R. Hockless, and T.R.B. Mitchell. Organometallics, **14**, 1000 (1995).
30. M.A. Bennett, T.N. Huang, T.W. Matheson, and A.K. Smith. Inorg. Synth. **21**, 74 (1982).
31. M. Bown, X.L.R. Fontaine, N.N. Greenwood, and J.D. Kennedy. J. Organomet. Chem. **325**, 233 (1987).
32. G. Winkhaus, H. Singer, and M. Kricke. Z. Naturforsch. B, **21**, 1109 (1966).
33. A.M.M. Weerasuria. Ph.D. thesis, Australian National University, Australia. 1988.
34. R. West and R. Riley. J. Inorg. Nucl. Chem. **5**, 295 (1958).
35. E. Kurowski. Ber. Dtsch. Chem. Ges. A, **43**, 1078 (1910).
36. P.T. Beurskens, G. Admiraal, G. Beurskens, W.P. Bosman, S. Garcia-Granda, R.O. Gould, J.M.M. Smits, and C. Smykalla. PATTY: The DIRDIF program system. Technical report of the crystallography laboratory. University of Nijmegen, The Netherlands. 1992.
37. P.T. Beurskens, G. Admiraal, G. Beurskens, W.P. Bosman, R. de Gelder, R. Israel, and J.M.M. Smits. DIRDIF-94: The DIRDIF-94 program system. Technical report of the crystallography laboratory. University of Nijmegen, The Netherlands. 1994.
38. S.R. Hall, G.S.D. King, and J.M. Stewart (*Editors*). Xtal 3.4. University of Western Australia, Perth, Australia. 1995.

© 2001 NRC Canada

39. teXsan: crystal structure analysis package. Molecular Structure Corp. 3200 Research Forest Drive, The Woodlands, Texas 77381, U.S.A. 1985 and 1992.
40. D.T. Cromer and J.T. Waber. International tables for X-ray crystallography. Vol 4. Kynoch Press, Birmingham. 1974. Table 2.2A.
41. J.A. Ibers and W.C. Hamilton. Acta Crystallogr. **17**, 781 (1964).
42. D.C. Creagh and W.J. McAuley. International tables for crystallography. Vol C. *Edited by* A.J.C. Wilson. Kluwer Academic Publishers, Boston. 1992. Table 4.2.6.8, pp. 219–222.
43. D.C. Creagh and J.H. Hubbell. International tables for crystallography. Vol C. *Edited by* A.J.C. Wilson. Kluwer Academic Publishers, Boston. 1992. Table 4.2.4.3, pp. 200–206.

List of Abbreviations

acac = acetylacetonate, 2,4-pentanedionato, $CH_3COCHCOCH_3$; tfacac = trifluoroacetylacetonato, 1,1,1-trifluoro-2,4-pentanedionato, $CF_3COCHCOCH_3$; hfacac = hexafluoroacetylacetonato, 1,1,1,5,5,5-hexafluoro-2,4-pentanedionato, $CF_3COCHCOCF_3$; cym = *p*-cymene, 1,4-$MeC_6H_4CHMe_2$; DMSO = dimethylsulfoxide; py = pyridine.

© 2001 NRC Canada

BINAPS — An axially chiral *P,S*-heterodonor ligand for asymmetric catalysis based on binaphthalene backbone

Serafino Gladiali, Serenella Medici, Giovanna Pirri, Sonia Pulacchini, and Davide Fabbri

Abstract: The chelating *P,S*-heterodonor ligand 2-diphenylphosphanyl-1,1′-binaphthalene-2′-thiol (**11**) (BINAPS), which features a chiral axis as the unique stereogenic element, has been prepared in both racemic and enantiopure form through a multistep reaction sequence using 2,2′-dihydroxy-1,1′-binaphthalene (BINOL) as the starting material. The reaction sequence is completely stereoconservative and (*S*)-**11** is obtained with no loss of enantiopurity from pure (*S*)-BINOL. (*R*)-**11** can be alternatively obtained by resolution of racemic **11** using the chiral (*S*)-benzylaminato Pd(II)-complex **19** as the resolving agent. The *S*-methyl or the *S*-*i*-propyl derivatives **14** have been used as chiral ligands in the Rh(I)-catalyzed asymmetric hydroformylation of styrene and in the hydrogen transfer reduction of acetophenone with modest success (up to 20% ee). In the presence of suitable Pd-complexes the same ligands provide higher ees in the hydrosilylation of styrene (50% ee) and in the allylic alkylation of 1,3-diphenylprop-2-enyl acetate (60% ee).

Key words: heterodonor ligands, binaphthalene derivatives, enantioselective catalysis, transition metal catalysts, allylic alkylation.

Résumé : Utilisant le 2,2′-dihydroxy-1,1′-binaphtalène (BINOL) comme produit de départ d'une synthèse en plusieurs étapes, on a préparé les formes racémiques et énantiopures du ligand chélatant *P,S*-hétérodonneur 2-diphénylphosphanyl-1,1′-binaphtalène-2′-thiol, **11** (BINAPS), qui ne comporte qu'un axe chiral comme seul élément stéréogène. La séquence de réaction est complètement stéréoconservatrice et l'isomère (*S*)-**11** a été obtenu sans perte d'énantiopureté à partir du (*S*)-BINOL pur. On peut aussi obtenir l'isomère (*R*)-**11** en procédant au dédoublement du produit **11** racémique en utilisant le complexe chiral **19** (*S*)-benzylaminato Pd(II) comme agent de résolution. On a utilisé avec des succès mitigés (ee allant jusqu'à 20%) les dérivés *S*-méthyle ou *S*-*i*-propyle, **14**, comme ligands chiraux dans l'hydroformylation asymétrique du styrène catalysée par le Rh(I) et dans la réduction par transfert de proton de l'acétophénone. En présence de complexes de Pd appropriés, les mêmes ligands conduisent des ee beaucoup plus élevés lors de l'hydrosilylation du styrène (ee de 50%) et de l'alkylation allylique de l'acétate de 1,3-diphénylprop-2-ényle (ee de 60%).

Mots clés : ligands hétérodonneurs, dérivés du binaphtalène, catalyse énantiosélective, catalyseurs dérivés de métaux de transition, alkylation allylique.

[Traduit par la Rédaction]

Introduction

The preparation of BINAP **1** reported in 1980 has marked a landmark in asymmetric catalysis and has illustrated the peculiar stereorecognitive properties inherent with the axially chiral 1,1′-binaphthalene framework (1). Since then, a great deal of work has been devoted to the preparation of binaphthalene-templated ligands of related design. These efforts have resulted in the generation of a library of bidentate binaphthyl ligands featuring equal (or diverse) substituents with the same (or different) donors on the 2,2′-positions of the binaphthalene backbone (for a review on C_2-symmetric binaphthyl derivatives see ref. 2).

In the course of the last five years, binaphthyl P,X-heterodonor ligands **2** where the P-donor is flanked by a different heteroatom which aids at the chelate coordination of the ligand to the metal, have increased in their number and variety. After the first term of this family (**2**, X = OMe, MOP) was reported by Uozumi and Hayashi (3) almost one decade ago, a range of derivatives where one of the

Received November 7, 2000. Published on the NRC Research Press Web site at http://canjchem.nrc.ca on June 30, 2001.

Dedicated to Professor Brian James on the occasion of his 65th birthday, and in recognition of his pioneering contributions to the field of asymmetric catalysis.

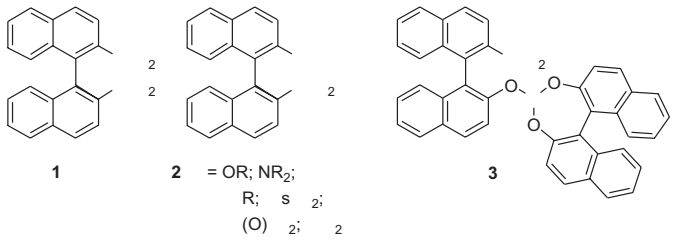
S. Gladiali,[1] S. Medici, G. Pirri, and S. Pulacchini. Dipartimento di Chimica, Università di Sassari, Via Vienna 2, 07100 Sassari, Italia.
D. Fabbri. Istituto C. N. R. per L'Applicazione delle Tecniche Chimiche Avanzate ai Problemi Agrobiologici, Via Vienna 2, 07100-Sassari, Italia.

[1]Corresponding author (telephone: +39-079-229546; fax: +39-079-229559; e-mail: gladiali@ssmain.uniss.it).

 DOI: 10.1139/cjc-79-5/6-670 © 2001 NRC Canada

diphenylphosphanyl substituent of BINAP is retained while the other is substituted by a group containing a donor different from phosphorus, have been synthesized and used in enantioselective catalysis more or less successfully (for a review on axially chiral bidentate ligands see ref. 4).

Scheme 1.



Several structural modifications of BINAP have been pursued in these investigations and the family of these C_1-symmetry axially chiral inducers now comprises a range of structures where the chelate coordination of the P-donor is supported by a group which contains either oxygen (5), or nitrogen, both sp^2- (6) and sp^3- (7), or sulfur (8), or arsenic (9) as the donor.

There are also some derivatives with two not equivalent phosphorus donors. The oxidation state of the two P-centres may be different, as in the case of the extraordinarily efficient phosphane-phosphite ligand BINAPHOS **3** (10), or identical, as in the case of the heterotopic diphosphines BINAPP′ (**2**, X = PAr_2), quite recently reported by us (11), which feature two not equivalent diarylphosphanyl groups.

We were among the first groups involved in this chemistry and, as the result of our initial efforts, a few years ago we (8) reported in a short communication the synthesis of BINAPS (**2**, X = SR), a heterobidentate version of BINAP, where one alkylthio group takes up the position of one of the two diphenylphosphanyl substituents.

At the time of our preliminary report (1994), there was no significant precedent for the use of chiral *P,S*-heterobidentate ligands in transition-metal-catalyzed asymmetric processes. Thus, BINAPS was the first representative of this class of chiral auxiliaries which had been synthesized for this purpose and exploited with some success in asymmetric catalysis. Since then, however, the use of chiral *P,S*-heterodonor ligands, has attracted increasing interest and several examples of their use in asymmetric catalysis have appeared in the recent literature.

P,S-Chelating derivatives with quite varied chiral skeletal backbones, where the P centre is part of a phosphanyl or a phosphito group, have been exploited more or less successfully by several authors in the asymmetric allylic alkylation–amination with Pd catalysts (12) and in the asymmetric hydrogenation with Rh (13) and Ir (14) complexes. The scope of these ligands in asymmetric catalysis spans also over other enantioselective processes such as the hydrosilylation of ketones (15) and the hydroformylation of styrene (14). The efficiency of chiral *P,S*-ligands to promote the Co-catalyzed Pauson–Khand reaction with quite high stereoselectivity has been very recently demonstrated (16).

In this paper we like to report the details of the chemistry underlying the preparation and resolution of BINAPS **11** and its derivatives **14**, as well as some aspects of its coordination chemistry and some further application of this type of ligands in Rh- and Pd-catalyzed asymmetric reactions

Results and discussion

The preparation of unsymmetrically 2,2′-disubstituted binaphthyl derivatives can be dealt with either by heterocoupling of the appropriate pair of 2-substituted naphthalenes, or by asymmetrization of a suitable C_2-symmetric 2,2′-homodisubstituted binaphthalene. The second route is more practical and, with just one notable exception (6*a*), it has been consistently exploited for the synthesis of C_1-symmetric P,X-binaphthyl derivatives **2** using 1,1′-binaphthalene 2,2′-diol (BINOL) as the starting material.

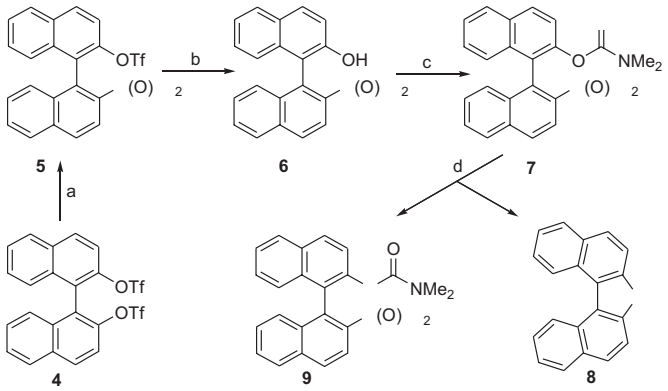
Accordingly, the synthesis of *S*-alkyl (2′-diphenylphosphanyl-1,1′-binapht)-2-yl sulfides **14** has been accomplished in eight steps starting from BINOL. Dissymmetrization of the substrate is achieved in the second step of the synthetic scheme where the phosphorated substituent is introduced in the form of a diphenylphosphinyl group by Pd-catalyzed displacement of one triflate of **4** following a reported procedure (17). This reaction is remarkable in that only one single triflate undergoes susbtitution. Due to this selectivity it has been exploited by several authors in the preparation of various C_1-symmetry binaphthalene-templated P-donor ligands (5–11).

The key intermediate **9** is obtained by Newmann–Kwart thermo-rearrangement of the thiocarbamate **7** at 260–270°C. In this reaction, the pentahelicenic thiophene **8** is simultaneously formed as a byproduct to a variable extent.

It has been previously pointed out that the selectivity of this reaction is strongly dependent on the quality of the starting material, highly crystalline samples providing better returns in the rearranged carbamate (18). The same result was observed in the rearrangement of **7**. Short reaction times and fast heating of the reactor are crucial factors for obtaining satisfactory yields of **9** in this stage.

It is worth to stress that, in spite of the harsh conditions required and of the capricious nature of this reaction, if properly performed the Newmann–Kwart rearrangement proceeds with retention of the original stereochemistry (19). Actually, we have checked that no loss of enantiomeric pu-

Scheme 2.



(a) 2 (O)H, Et_3N, d(cO)$_2$/1,4-bis-dip enylp osp inobutane, DM O, 100°C, 14 ; 78% yield.
(b) NaOH, H_2O/THF, 25°C, 12 ; 98% yield.
(c) Me_2C( )Cl, Et_3N, DM , THF, 25°C, 48 ; 78% yield.
(d) Neat, 260-270°C, 10'; 75% yield.

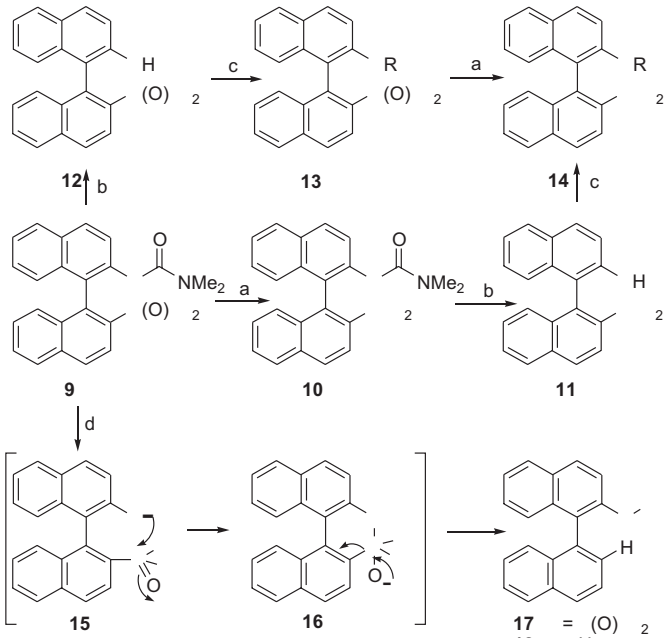
© 2001 NRC Canada

rity occurred in this transformation when enantiopure samples of **7** were used as the starting material (vide infra).

Conversion of **9** into the phosphanyl sulfides **14** has been accomplished through two different but basically equivalent three-step routes. The first involves hydrolysis of the carbamate **9**, alkylation at sulfur, and deoxygenation of the phosphinyl group (Scheme 3, upper part). In the second route deoxygenation precedes hydrolysis (Scheme 3, middle part).

The attempt to prepare the phosphanyl thiol **11** straight from **9** by performing hydrolysis and deoxygenation in a single step by treatment with an excess of $LiAlH_4$ in boiling THF met with a modest success. The product isolated at the end of this reaction consisted of a mixture of hardly separable compounds. One of this did not contain anymore phosphorus and was identified as 1,1′-binaphthyl-2-thiol (**18**). Its formation could proceed through an intramolecular nucleophilic attack of an intermediate thiolate anion to the phosphinyl centre (as in **15**), leading to the cyclic species **16** (Scheme 3, lower part). Ring-opening of **16** should result in the transfer of the phosphinyl group to the sulfur to give the thiol phosphonite **17** which is readily cleaved to the relevant thiol by $LiAlH_4$.

Scheme 3.



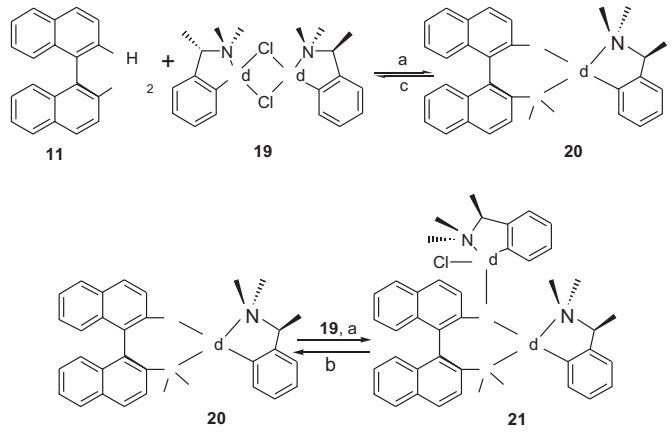
(a) H iCl$_3$, Et$_3$N, xylene, 120°C, 6 ; 85% yield.
(b) Li lH$_4$, THF, 0°C, 5 ; 98% yield.
(c) RB o RI, MeOH, 25°C, 6-12 ; 90-98% yield.
(d) Li lH$_4$, THF, 66°C, 8 ; 65% yield (= H).

The (*S*)-(–)-enantiopure phosphane thiol **11** has been prepared as illustrated above from enantiopure (*S*)-BINOL. Its enantiomeric purity has been checked by NMR on the relevant cyclopalladated complex **20** obtained by reaction with (–)-di-μ-chloro-bis[(*S*)-*N*,*N*-dimethyl(α-methylbenzyl)aminate-2-*C*,*N*]dipalladium(II) ((*S*)-**19)** (20). The presence of only one ^{31}P NMR resonance and of a single set of peaks of the two shown by the same complex prepared from racemic **11** in the ^{1}H NMR demonstrated that the ligand (*S*)-**11** was enantiopure. This proved that the Newmann–Kwart rearrangement has proceeded with complete retention of stereochemistry.

The (+)-(*R*)-enantiomer could be obtained as well by resolution of the racemic compound with the same (*S*)-α-methylbenzylaminato Pd-complex **19** (21). Treatment of racemic **11** with 1 molar equiv of **19** in the presence of triethylamine gave the mononuclear derivatives **20** which could not be separated by chromatography or fractional crystallization (Scheme 4). Upon addition of 1 further equiv of **19**, **20** was converted into the dinuclear-thiolato-bridged species **21** (22) which could be separated by chromatography allowing to isolate the less polar diastereoisomer (R_{ax}, *S*,*S*-configurations) in pure form.

Stirring a dichloromethane solution of this product with an aqueous solution of 1,2-diaminoethane converted the dipalladium complex **21** back into the mononuclear species **20** (R_{ax},*S*-configurations). The enantiopure ligand (*R*)-**11** ($[\alpha]_D^{25}$ + 31.4 (*c* = 1, $CHCl_3$)) could be liberated from this complex by reaction with diphenylphosphinoethane–LiCl in methanol in the presence of methanesulfonic acid. This last step constitutes an improvement of the previously reported procedure which required the sulfur to be previously alkylated for the ligand to be displaced from the complex (22).

Scheme 4.



(a) Et$_3$N, CHCl$_3$, 25°C, 1 ; quantit.
(b) Et ylenediamine, H$_2$O/CH$_2$Cl$_2$, 25°C, 15'; 85% yield.
(c) LiCl, MeOH, Me O$_3$H, t en D E, 25°C, 2 ; quantit.

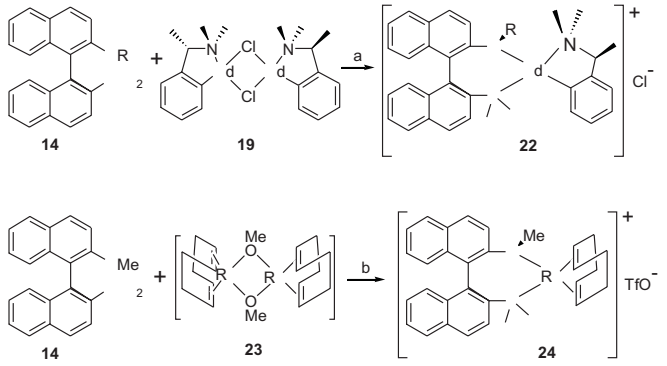
(*R*)-Configured enantiopure sulfides **14** (**14a**, R = Me or **14b**, R = *i*-Pr) have been obtained by *S*-alkylation of (*R*)-**11** obtained from the resolution. They have been as well prepared from (*R*)-BINOL **4** according to the synthetic procedure outlined in Schemes 2 and 3.

The enantomeric purity of (*R*)-**14a** was determined by ^{31}P NMR of the cationic Pd(II) complexes **22** obtained by reaction with **19** in the NMR tube (one single peak detectable at 48.9 ppm) and confirmed by HPLC on chiral phase. Chelate coordination of the ligand is confirmed, inter alia, by the upfield shift of the S-CH$_3$ peak which appears as a singlet at 2.15 δ (2.32 δ in the free ligand). Given that the sulfur becomes sterogenic upon coordination to the metal, the formation of more than one stereoisomer should be possible. These NMR data are in keeping with the presence of one single species in solution. Thus it seems reasonable to

© 2001 NRC Canada

assume that the binding of (*R*)-**14a** to the Pd-centre has proceeded stereoselectively.

Scheme 5.



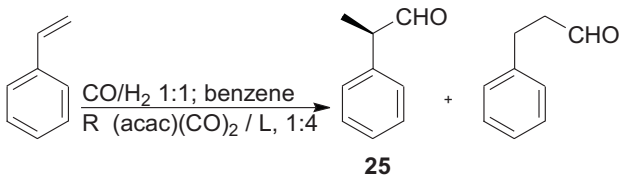
Reaction of the μ-methoxo-bridged dinuclear Rh(I) complex **23** with (*R*)-**14a** in the presence of trimethylsilyl triflate (8) produced the cationic Rh(I)-complex **24**. In this compound, the phosphorus resonance showed the expected downfield shift (36 ppm) appearing as a doublet at 23.03 ppm ($^1J_{P\text{-}Rh}$ = 145.8 Hz). The chelate coordination of the ligand was demonstrated in the ^{1}H NMR by the downfield shift of the *S*-methyl resonance (from 2.32 to 2.59 δ) and by the presence in the ^{13}C NMR of a coupling (J = 10.2 Hz) between the *S*-methyl group and the Rh. Notably, the ^{1}H NMR showed the *S*-methyl peak as a sharp singlet. From these data it seem reasonable to assume that: (*i*) the binding of the Rh to the sulfur centre has occurred with complete stereoselectivity affording only one diastereoisomer; (*ii*) at room temperature inversion of configuration of the *S*-stereocentre, if occurring, is slow on the NMR time scale; (*iii*) at room temperature the complex **24** is locked in a single conformation, where most probably the methyl takes up an equatorial position in the puckered seven-membered ring. All these facts have significant bearings in view of the use of this complex in asymmetric catalysis.

Both the preformed derivative **24** or slightly different Rh(I)-catalysts prepared in situ from enantiopure **14** (R = Me or *i*-Pr) and suitable Rh-complexes have been inspected for their catalytic activity in the asymmetric hydroformylation of styrene and in the H-transfer reduction of acetophenone.

In the hydroformylation at 40°C (Scheme 6) the in situ catalyst obtained from [Rh(acac)(CO)$_2$] and the *i*-Pr sulfide (*R*)-**14b** produced the branched aldehyde (*S*)-**25** with a very high positional selectivity (96% at 100% conversion after 14 h), but with low stereoselectivity (ee 14%). Both the ee and the regioselectivty decreased (10 and 94%, respectively) when the reaction was run in the presence of the same ligand **14b** at higher temperature (60°C for 4 h). A more consistent decrease (only 90% of branched isomer) was observed even at 40°C when the methyl derivative **14a** was used in the place of **14b**. In this case the aldehyde was practically racemic (2% ee).

We are confident that these low ees reflect the real enantioselection of the reaction and are not the consequence of a racemization suffered by the branched aldehyde after its formation, because the extent of the racemization of **25** is negligible under the conditions we have performed the hydroformylation experiments (for a review on asymmetric hydroformylation see ref. 23).

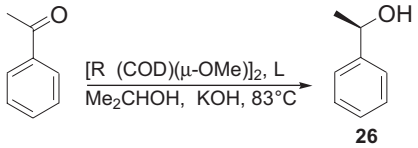
Scheme 6.



Comparable ees (20%) but lower conversions (15–25%) were observed in 1 h when the complex prepared in situ from [Rh(COD)(μ-OMe)]$_2$ and (*R*)-**14** was used as the catalyst in the hydrogen transfer reduction of acetophenone in boiling 2-propanol (Scheme 7). Longer reaction times (12–14 h) led to higher conversions, but the ee decreased (3–5%) due to the concurrent racemization suffered by the chiral carbinol **26** in the presence of base (for a comprehensive overview on H-transfer reduction see ref. 24). The *i*-Pr derivative **14b** was again more efficient of the methyl substituted counterpart **14a**, but the differences were not really impressive (20% vs. 14% ee).

In this same reaction, the Ir(I)-catalyst prepared in situ from [Ir(COD)Cl]$_2$ and (*R*)-**14b** displayed a catalytic activity lower than the Rh(I)-catalyst (6% conversion in 1 h) and provided an even lower ee of (*R*)-**26** (11%).

Scheme 7.



Ligand (*R*)-**14**	*t* ( )	conv.(%)	ee (%)
R = Me	1 (12)	12 (55)	14 (3)
R = *i*-	1 (14)	21 (75)	20 (5)
R = *i*- [a]	1	6	11

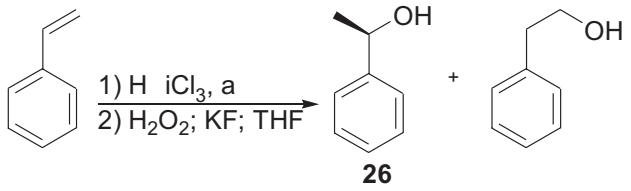
(a) Catalyst p epa ed f om [I (COD)Cl]$_2$.

The phosphanyl sulfide ligands **14** performed better in some Pd-catalyzed asymmetric processes. In the hydrosilylation of styrene, after 40 h at 25°C the (*R*)-*i*-Pr derivative **14b** gave the (*S*)-configured branched derivative in more than 70% conversion and 90% regioselectivity (50% ee) (Scheme 8). The corresponding methyl derivative **14a** was by far less efficient and led to a lower conversion (40% with 82% branched) and a negligible ee (4%).

The use of the methyl derivative **14a** as chiral ligand in the Pd-catalyzed allylic alkylation of 1,3-diphenyl allyl acetate with dimethylmalonate has been explored a few years ago by Kang et al. (25) who scored a remarkably high ee (91%). We have limited our screening to check whether this

© 2001 NRC Canada

Scheme 8.

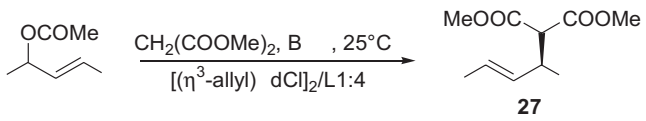


Ligand (*R*)-**14**	*t* ( )	conv. (% **26**)	ee (config.)
R = Me	39	41 (82)	4 (*S*)
R = *i*-	41	72 (91)	51 (*R*)

(a) [(η^3-allyl) dCl]$_2$/L1:4; ty ene/ d 1000:1; 25°C

range could be maintained or not by changing the alkyl substituent on the sulfur. The reaction was run at room temperature in dichloromethane solution using [Pd(η^3-C_3H_5)Cl]$_2$ as the catalytic precursor in the presence of (*R*)-**14b** as the chiral ligand at a Pd:ligand ratio of 1:2. In these conditions, the (*R*)-configured alkylated product **27** was formed in almost quantitative yield within minutes and showed 60% ee (Scheme 9).

Scheme 9.



Experimental

General procedures

Nuclear magnetic resonance spectra were recorded in $CDCl_3$ on a Varian VXR-300 spectrometer at 300 MHz for ^{1}H, 75 MHz for ^{13}C, and 121.4 for ^{31}P. Chemical shifts are reported in ppm downfield from internal Me_4Si or external H_3PO_4. Gas chromatographic analysis were performed on a 25 m × 0.25 mm capillary column coated with diethyl-*tert*-butylsilyl-β-cyclodextrin using a Hewlett Packard 5890A gas chromatograph equipped with a HP 3396 integrator. Mesitylene (20% w/w to the substrate) was employed as an internal standard. Optical rotations were measured on a PerkinElmer Model 241 polarimeter. Elemental analyses were performed on samples purified by crystallization with a PerkinElmer Analyzer 240B by Mr. A. Canu (Dipartimento di Chimica, Università di Sassari). MS Spectra were recorded with a HP 5988A spectrometer. Melting points were obtained with a Leitz Laborlux S melting point apparatus and are not corrected. Solvents were dried and distilled under nitrogen before use. Commercial reagents (Aldrich) were used as received. Racemic and enantiopure 2-(diphenylphosphinyl)-1,1′-binaphth-2′-ol (**6**) was prepared from BINOL as described in the literature (3).

(*S*)-(+)-2-(Diphenylphosphinyl)-1,1′-binaphth-2′-ol-*N*,*N*-dimethylthiocarbamate ((*S*)-7)

To a solution of (*S*)-(–)-2-(diphenylphosphinyl)-1,1′-binaphth-2′-ol **6** (13.2 g, 28.1 mmol) in DMF (170 mL), cooled at 0°C, NaH (1.6 g, 39.4 mmol) was added and the mixture was stirred at 80°C for 1 h. Then *N*,*N*-dimethylthiocarbamoyl chloride (5.0 g, 39.4 mmol) was added and stirring was continued at 90°C for 3 h. The mixture was cooled to room temperature and poured into water (1 L). The solid thus formed was washed with water, taken up with CH_2Cl_2, and dried (Na_2SO_4). The solvent was removed and the crude product was purified by flash chromatography (ethyl acetate:light petroleum, 6:1) to give 11.3 g (72%) of (*S*)-**7** as a white solid, mp 128 to 129°C (CH_2Cl_2–hexane). $[\alpha]_D^{25}$ = 149 (*c* = 1, $CHCl_3$).EI-MS (*m*/*z*): 557.2 (M^+), 453.0 (100%), 283.9 (48%), 200.9 (27%), 87.9 (53%). ^{1}H NMR δ: 2.98 (s, CH_3, 3H), 3.05 (s, CH_3, 3H), 6.80–8.00 (series of m, Ar, 22H). ^{31}P NMR δ: 27.25. Anal. calcd. for $C_{35}H_{28}NO_2PS$: C 75.39, H 5.06, N 2.51; found: C 75.22, H 5.12, N 2.60.

(*S*)-(–)-2-(Diphenylphosphinyl)-1,1′-binaphthyl-2′-thiol-*N*,*N*-dimethylcarbamate ((*S*)-9)

In a Kugelrohr apparatus (*S*)-(+)-2-(diphenylphosphinyl)-1,1′-binaphth-2′-ol-*N*,*N*-dimethylthiocarbamate **7** (1 g, 1.79 mmol) was heated to 250°C for 9 min. After cooling to room temperature, the brown solid was taken up with CH_2Cl_2, and purified by flash chromatography (light petroleum:acetone, 4:1) to give, after a forerun of the binaphthyl thiophene **8** (0.6 g (60%)) of (*S*)-**9** as a white solid, mp 118 to 129°C (CH_2Cl_2–hexane). $[\alpha]_D^{25}$ = –5.7 (*c* = 1, $CHCl_3$). EI-MS (*m*/*z*): 557.2 (100%, M^+), 284 (58%), 201 (36%). ^{1}H NMR δ: 2.73 (bs, CH_3, 6H), 6.80–8.10 (series of m, Ar, 22H). ^{31}P NMR δ: 28.99. Anal. calcd. for $C_{35}H_{28}NO_2PS$: C 75.39, H 5.06, N 2.51; found: C 75.44, H 5.15, N 2.68.

(*S*)-(–)-2-(Diphenylphosphanyl)-1,1′-binaphthyl-2′-thiol-*N*,*N*-dimethylcarbamate ((*S*)-10)

To a solution of (*S*)-(–)-2-(diphenylphosphinyl)-1,1′-binaphthyl-2′-thiol-*N*,*N*-dimethylcarbamate **9** (1.7 g, 3.04 mmol) and Et_3N (3.6 g, 35.8 mmol) in xylene (50 mL), cooled at 0°C, $HSiCl_3$ (1.21 g, 8.9 mmol) was added. After stirring at 120°C for 6 h, the mixture was cooled to room temperature and ether (50 mL) and a saturated solution of aq $NaHCO_3$ (100 mL) were added. The organic layer was separated and the aqueous phase was extracted with ether. The combined organic phase was dried (Na_2SO_4) and the solvent evaporated. The crude product was purified by flash chromatography ($CHCl_3$), to give 1.32 g (80%) of (*S*)-**10**, mp 178–180°C (CH_2Cl_2–hexane). $[\alpha]_D^{25}$ = –15 (*c* = 0.1, THF). ^{1}H NMR δ: 2.65 (bs, CH_3, 6H), 6.87–8.00 (series of m, Ar, 22H). ^{31}P NMR δ: –14.87. Anal. calcd. for $C_{35}H_{28}NOPS$: C 77.61, H 5.21, N 2.59; found: C 77.84, H 5.38,, 2.61.

(*S*)-(–)-2-(Diphenylphosphanyl)-1,1′-binaphthyl-2′-thiol ((*S*)-11)

To a suspension of $LiAlH_4$ (510 mg, 13.78 mmol) in THF (40 mL), cooled to 0°C, a solution of (*S*)-(–)-2-(diphenylphosphanyl)-1,1′-binaphthyl-2′-thiol-*N*,*N*-dimethylcarbamate **10** (867 mg, 1.6 mmol) in THF (30 mL) was added. After stirring for 5 h at room temperature, the

© 2001 NRC Canada

suspension was cooled to 0°C and water (0.5 mL), then NaOH (0.5 mL, 4 M) and again water (3 × 0.5 mL) were added. The insoluble aluminium salts were separated by centrifugation, and the solvent evaporated to give 730 mg (97%) of (*S*)-**11**, mp 198–200°C (benzene–hexane). $[\alpha]_D^{25}$ = –33.4 (*c* = 0.1, THF). ^{1}H NMR δ: 3.17 (s, SH, 1H), 6.67–7.94 (series of m, Ar, 22H). ^{31}P NMR δ: –13.43. Anal. calcd. for $C_{32}H_{23}PS$: C 81.68, H 4.93; found: C 81.49, H 4.84.

S-Alkyl derivatives of (*S*)-(–)-2-(diphenylphosphanyl)-1,1′-binaphthyl-2′-thiol ((*S*)-14)

To a stirred solution of (*S*)-(–)-2-(diphenylphosphanyl)-1,1′-binaphthyl-2′-thiol **11** (282 mg, 0.6 mmol) in DMF (15 mL) containing *t*-BuOK (84 mg, 0.75 mmol) methyl iodide (or *i*-propyl bromide) (0.62 mmol) was added. The solution turned from red to yellow. Stirring was continued at room temperature for 1 h (16 h in the case of *i*-propyl halide). The solution was diluted with water, neutralized with 3 N HCl, and extracted with CH_2Cl_2. The organic phase was washed with water, dried (Na_2SO_4), and the solvent evaporated. The crude product was purified by flash chromatography using ether–acetone (6:1) as the eluent.

*(S)-(–)-**14a***

90% yield, mp 95 to 96°C (CH_2Cl_2–hexane). $[\alpha]_D^{25}$ = –52.6 (*c* = 0.5, $CHCl_3$). EI-MS (*m*/*z*): 484.2 (M^+), 469.2 (9%), 437.1 (100%), 281.0 (32%), 218.1 (19%). ^{1}H NMR δ: 2.32 (s, CH_3, 3H), 6.70–8.00 (series of m, Ar, 22H). ^{31}P NMR δ: –13.56. Anal. calcd. for $C_{33}H_{25}PS$: C 81.79, H 5.20; found: C 81.58, H 5.35.

*(S)-(–)-**14b***

60% yield, mp 90–93°C (CH_2Cl_2–hexane). $[\alpha]_D^{25}$ = –81.2 (*c* = 0.5, $CHCl_3$). EI-MS (*m*/*z*): 512.6 (M^+), 437.1 (100%), 281.0 (22%), 218.1 (45%). ^{1}H NMR δ: 1.18 (d, *J* = 6.6 Hz, 3H), 1.22 (d, *J* = 6.6 Hz, 3H), 3.67 (sept, 1H), 6.60–8.00 (series of m, Ar, 22H). ^{31}P NMR δ: –13.82. Anal. calcd. for $C_{35}H_{29}PS$: C 82.00, H 5.70; found: C 82.29, H 5.95.

(*S*)-(–) 2-(Diphenylphosphinyl)-1,1′-binaphthyl-2′-thiol ((*S*)-12)

To a stirred solution of (*S*)-(–)-2-(diphenylphosphinyl)-1,1′-binaphthyl-2′-thiol-*N*,*N*-dimethylcarbamate **9** (3.9 g, 7.0 mmol) in THF (50 mL), $LiAlH_4$ (270 mg, 7.17 mmol) was slowly added at 0°C. The reaction mixture was stirred for 12 h at room temperature. Water (50 mL) was added and the precipitate was dissolved with 10% HCl. The aqueous phase was extracted with ether (3 × 50 mL), the combined organic phase was dried (Na_2SO_4), and the solvent evaporated to give 3.06 g (90%) of (*S*)-**12**, mp 100–102°C (benzene). $[\alpha]_D^{25}$ = –42.3 (*c* = 1, $CHCl_3$). EI-MS (*m*/*z*): 486.6 (M^+), 284.0 (100%), 201.0 (15%). ^{1}H NMR δ: 3.48 (s, SH, 1H), 6.80–8.10 (series of m, Ar, 22H). ^{31}P NMR δ: –28.73. Anal. calcd. for $C_{32}H_{23}POS$: C 78.99, H 4.76; found: C 79.18, H 4.84.

S-Alkyl derivatives of (*S*)-(–) 2-(diphenylphosphinyl)-1,1′-binaphthyl-2′-thiol ((*S*)-13)

To a solution of 2-(diphenylphosphinyl)-1,1′-binaphthyl-2′-thiol **12** (1.5 g, 3.0 mmol) in methanol (15 mL) and Et_3N (8 mL) methyl iodide (or *i*-propyl bromide) (3.1 mmol) was added. The reaction mixture was stirred for 5 h (16 h in the case of *i*-propyl halide). The solvent was removed and the residue was dissolved with CH_2Cl_2. The organic phase was washed with water, dried (Na_2SO_4), and the solvent evaporated to give **13**.

*(S)-(–)-**13a***

94% yield, mp 154 to 155°C (ether–hexane). $[\alpha]_D^{25}$ = –126.2 (*c* = 0.5, $CHCl_3$). ^{1}H NMR δ: 2.27 (s, 3H), 6.88–8.00 (series of m, Ar, 22H). ^{31}P NMR δ: 28.89. EI-MS (*m*/*z*): 500.2 (M^+), 453.1 (100%), 282.0 (12%), 226.1 (9%). Anal. calcd. for $C_{33}H_{25}POS$: C 79.18, H 5.03; found: C 79.35, H 5.25.

*(S)-(–)-**13b***

90% yield, mp 88 to 89°C (ether–hexane). $[\alpha]_D^{25}$ = –117.8 (*c* = 0.5, $CHCl_3$). ^{1}H NMR δ: 1.09 (d, *J* = 6.6 Hz, 3H), 1.16 (d, *J* = 6.6 Hz, 3H), 3.43 (sept, *J* = 6.6 Hz, 1H), 6.85–8.00 (series of m, Ar, 22H). ^{31}P NMR δ: 29.27. EI-MS (*m*/*z*): 528.2 (M^+), 453.1 (100%), 282.0 (18%). Anal. calcd. for $C_{33}H_{25}POS$: C 79.52, H 5.53; found: C 79.68, H 5.40.

Deoxygenation of (*S*)-13b — preparation of 2-(diphenylphosphanyl)-)-2′-isopropylthio-1,1′-binaphthalene ((*S*)-14b)

To a solution of (*S*)-(2-(diphenylphosphinyl)-2′-isopropylthio-1,1′-binaphthalene **13b** (660 mg, 1.25 mmol) in xylene (10 mL) containing Et_3N (10.5 mL) stirred at 0°C, $HSiCl_3$ (0.85 mL, 6.2 mmol) was added and the mixture was stirred at 120°C for 8 h. After cooling to room temperature, 10% HCl (10 mL) was added and the organic phase was separated. The aqueous layer was extracted with ether (3 × 20 mL), the combined organic phase was dried (Na_2SO_4), and the solvent was evaporated. The residue was purified by flash chromatography, using ethyl acetate:light petroleum (1:1) as the eluent. Compound (*S*)-(–)-**14b** was isolated in 95% yield.

Resolution of (*R*,*S*)-2-(diphenylphosphanyl)-1,1′-binaphthyl-2′-thiol (11)

*[(*S*)-N,N-Dimethyl(α-methylbenzyl)aminate-2-*C,N*][(*R,S*)-2-(diphenylphosphino)-1,1′-binaphthyl-2′-thiolate]palladium(II) (**20**)*

To a solution of (*R*,*S*)-2-(diphenylphosphanyl)-1,1′-binaphthyl-2′-thiol (**11**) (730 mg, 1.46 mmol) in $CHCl_3$ (10 mL) and Et_3N (1 mL), a solution of (–)-di-μ-chloro-bis[(*S*)-*N*,*N*-dimethyl(α-methylbenzyl)aminate-2-*C*,*N*]dipalladium(II) **19** (450 mg, 0.7 mmol) in $CHCl_3$ (7 mL) was added. The mixture turned to a brillant red and was stirred at room temperature 10 min. Then 2% HCl was added to neutralize and the organic phase was separated and washed with water. After drying (Na_2SO_4), the solvent was evaporated to give the (R_a,*S*)- and (S_a,*S*)-complexes **20.** Purification by flash chromatography (*n*-hexane–$CHCl_3$, 1:1) provided **20** as a 1:1 mixture of diastereoisomers in quantitative yield.

(R_a,S)-20: ^{1}H NMR δ: 1.73 (d, *J* = 6.3 Hz, C-CH_3, 3H), 2.84 (d, *J* = 3.6 Hz, N-CH_3, 3H), 2.96 (s, N-CH_3, 3H), 3.51 (m, CH, 1H), 6.13–6.21 (series of m, Ar, 2H), 6.34 (d, *J* = 8.1 H,

© 2001 NRC Canada

Ar, 1H), 6.62–7.47 (series of m, Ar, 18H), 7.71–7.85 (series of m, Ar, 5H). ^{31}P NMR δ: 42.87.

(S_a,S*)-**20***: ^{1}H NMR δ: 1.43 (d, *J* = 6.6 Hz, C-CH_3, 3H), 2.73 (s, N-CH_3, 3H), 3.04 (d, *J* = 2.7 Hz, N-CH_3, 3H), 4.49 (m, CH, 1H), 6.08–7.86 (series of m, Ar, 26H). ^{31}P NMR δ: 44.41.

Chlorobis-[(*S*)-*N*,*N*-dimethyl(α-methylbenzyl)aminate-2-*C*,*N*][μ-(*R*,*S*)-2-(diphenylphosphanyl)-1,1′-binaphthyl-2′-thiolate-*P*,*S*,*S*]dipalladium(II) (21)

To a solution of 2-(diphenylphosphanyl)-1,1′-binaphthyl-2′-thiol (**11**) (1.06 g, 2.3 mmol) in CH_2Cl_2 (10 mL), (–)-di-μ-chloro-bis[(*S*)-*N*,*N*-dimethyl(α-methylbenzyl)aminate-2-*C*,*N*]dipalladium(II) (1.3 g, 2.3 mmol) and Et_3N (8 mL) were added. The mixture was stirred at room temperature for 10 min. Then 2% HCl was added to neutralize and the organic phase was separated and washed with water. The organic layers were dried (Na_2SO_4) and the solvent evaporated. The two diastereomeric complexes **21** were isolated in quantitative yield and were separated by flash chromatography (*n*-hexane–tetrahydrofuran, 4:1).

Less polar isomer (R_a,S,S*)-21*

^{1}H NMR δ: 0.85 (d, *J* = 6.6 Hz, C-CH_3, 3H), 1.93 (d, *J* = 6.6 Hz, C-CH_3, 3H), 1.94 (m, CH, 1H), 2.16 (s, N-CH_3, 3H), 2.28 (s, N-CH_3, 3H), 2.96 (s, N-CH_3, 3H), 3.14 (d, *J* = 3.6 Hz, N-CH_3, 3H), 3.50 (dq, *J* = 6.3 Hz, 12 Hz, CH, 1H), 6.01–7.99 (series of m, Ar, 29H), 9.01 (m, Ar, 1H). ^{13}C NMR δ: aliphatic carbon only 18.21 (s), 33.75 (s), 51.39 (s), 56.17 (d), 56.90 (s), 58.89 (d), 86.42 (d), 86.50 (d). ^{31}P NMR δ: 40.82.

More polar isomer (S_a,S,S*)-**21***

^{1}H NMR δ: 0.57 (d, *J* = 6.6 Hz, C-CH_3, 3H), 1.39 (d, *J* = 6.6, C-CH_3, 3H), 2.64 (d, *J* = 3.6 Hz, N-CH_3, 9H), 3.37 (d, *J* = 3.6 Hz, N-CH_3, 3H), 3.51 (m, CH, 1H), 4.85 (m, CH, 1H), 6.01–7.99 (series of m, Ar, 29H), 9.01 (m, Ar, 1H). ^{31}P NMR δ: 41.78.

A solution of (*R*$_a$,*S*,*S*)-**21** (670 mg, 0.66 mmol) in CH_2Cl_2 (5 mL) was vigorously stirred for 15 min at room temperature with a solution of ethylenediamine (110 mg, 1.8 mmol) in water (2.5 mL). The organic phase was separated, washed with water, and dried (Na_2SO_4). The solvent was evaporated and the residue was purified by flash chromatography, using CH_2Cl_2 as the eluent, to give 420 mg (88%) of (*R*$_a$,*S*)-**20**. A solution of this product (0.93 g, 1.3 mmol) in methanol (20 mL) containing LiCl (0.51 g, 12 mmol) and two drops of methansulfonic acid was stirred 10 min at room temperature. Then, bis(diphenylphosphino)ethane (0.51 g, 1.3 mmol) was added and stirring was continued for 2 h, while a precipitate was formed. The solid was filtered and dried to give 610 mg (99%) of (*R*)-(+)-**11**. $[\alpha]_D^{25}$ = +31.4 (*c* = 1, $CHCl_3$).

(+)-(1,5-Cyclooctadiene)[(*R*)-2-(diphenylphosphanyl)-2′-methylthio-1,1′-binaphthalene]rhodium(I) trifluoromethanesulfonate ((*R*)-24)

To a solution of [Rh(μ-OMe)(COD)]$_2$ (400 mg, 0.82 mmol) in CH_2Cl_2 (5 mL), $CF_3SO_3SiMe_3$ (184 mg, 0.82 mmol) was added. The mixture was stirred for 10 min at room temperature, then a solution of (*R*)-(+)-2-(diphenylphosphanyl)-2′-methylthio-1,1′-binaphthalene (422 mg, 0.82 mmol) in CH_2Cl_2 (10 mL) was added. Stirring was continued for 30 min, then the solvent was concentrated and the solid precipitated was filtered and recrystallized from CH_2Cl_2–Et_2O to give 640 mg (91%) of (*R*)-**24**, mp 208 to 209°C. $[\alpha]_D^{25}$ = +118.9 (*c* = 0.5, $CHCl_3$). ^{1}H NMR δ: 1.90 (bs, COD, 2H), 2.35 (bs, COD, 4H), 2.51 (series of m, COD, 2H), 2.54 (s, CH_3, 3H), 4.50 (bs, COD, 2H), 6.10 (d, *J* = 9.9 Hz, Ar, 1H), 6.65 (bs, COD, 2H), 6.85 (m, Ar, 3H), 7.24 (series of m, Ar, 5H), 7.55 (m, Ar, 6H), 7.69 (m, Ar, 2H), 7.95–8.10 (series of m, Ar, 5H). ^{13}C NMR δ (aliphatic carbons only): 16.20 (d, $^2J_{C\text{-}Rh}$ = 10.2 Hz), 29.4 (s), 32.8 (s). ^{31}P NMR δ: 23.03 (d, $^1J_{P\text{-}Rh}$ = 145.8 Hz). Anal. calcd. for $C_{42}H_{37}F_3O_3PS_2Rh$: C 59.76, H 4.41; found: C 58.97, H 4.54.

(+)-[(*S*)-*N*,*N*-Dimethyl(α-methylbenzyl)aminate-2-*C*,*N*][(R)-2-(diphenylphosphanyl)-)-2′-methylthio-1,1′-binaphthalene]palladium(II) ((*R*$_a$,*S*)-22)

To a solution of (–)-di-μ-chloro-bis[(*S*)-*N*,*N*-dimethyl(α-methylbenzyl)aminate-2-*C*,*N*]dipalladium(II) (226 mg, 0.4 mmol) in $CHCl_3$ (5 mL), a solution of (*R*)-(+)-2-(diphenylphosphanyl)-2′-methylthio-1,1′-binaphthalene (*R*)-**14a** (360 mg, 0.8 mmol) in $CHCl_3$ (15 mL) was added. The mixture was stirred for 30 min, then the solvent was evaporated and the residue was washed with ether. The solid obtained was filtered and crystalized from CH_2Cl_2–EtO_2 to give 520 mg (89%) of (*R*$_a$,*S*)-**22**, mp 155–158°C. $[\alpha]_D^{25}$ = +171.4 (*c* = 0.5, $CHCl_3$). ^{1}H NMR δ: 1.61 (d, *J* = 5.4 Hz, CH_3, 3H), 2.15 (s, S-CH_3, 3H), 2.68 (bs, N-CH_3, 3H), 2.95 (bs, N-CH_3, 3H), 3.96 (m, CH, 1H), 5.95 (m, Ar, 1H), 6.15 (m, Ar, 1H), 6.70–7.98 (series of m, Ar, 24H). ^{13}C NMR δ (aliphatic carbons only): 15.69, 17.28, 44.60, 49.55, 73.87. ^{31}P NMR δ: 48.91. Anal. calcd. for $C_{43}H_{39}NPSPdCl$: C 66.67, H 5.07, N 1.81; found: C 66.84, H 5.06, N 1.77.

Hydroformylation of styrene

In a typical experiment, 0.005 mmol of Rh(acac)(CO)$_2$ and 0.02 mmol of **14** (R = *i*-Pr or Me) were dissolved in benzene (6 mL) in a Schlenk tube under argon and styrene (2 mL) was added. The solution was transferred into a 100 mL autoclave and pressurized by CO–H_2 = 1:1 mixture at 60–120 bar. The reaction mixture was agitated by a magnetic stirrer in a thermostatted oil bath at the required temperature. At the end of the reaction, the mixture was cooled to room temperature, vented, and immediately analyzed. Conversions, chemo-, regio-, and enantioselectivities were determined by GC analysis: initial temperature: 60°C, heating rate: 2°C/min; final temperature: 150°C: mesitylene (20% w/w to the substrate) as an internal standard. Retention times (min): branched aldehyde: 21 ((*S*)-isomer), 21.5 ((*R*)-isomer); linear aldehyde (min): 26.7.

H-transfer reduction of acetophenone

A solution of [Rh(COD)(μ-OMe)]$_2$ (3.3 mg, 0.007 mmol) and the ligand **14b** (7 mg, 0.014 mmol) in *i*-Pr-OH (11 mL) containing KOH (0.1 mL, 0.5M in *i*-Pr-OH) was heated to reflux under nitrogen for 1 h. A solution of acetophenone (0.41 mL, 3.5 mmol) in *i*-Pr-OH (11 mL) was then added to the resulting yellow solution and heating was continued while the reaction mixture was monitored by GC. Yield, conversion, and ee were determined by GC analysis at

© 2001 NRC Canada

105°C. Retention times (min): 13.8 ((*R*)-phenylethanol), 14.8 ((*S*)-phenylethanol).

Hydrosilylation of styrene

To a solution of $[Pd(\eta^3\text{-}C_3H_5)Cl]_2$ (4.4 mg, 0.012 mmol) and the ligand (R)-**14b** (R = *i*-Pr) (20.5 mg, 0.04 mmol) in benzene (2.5 mL), then styrene (3.9 g, 37 mmol) was added. A solution of $HSiCl_3$ (6.1 g, 45 mmol) in benzene (5 mL) was added dropwise and the reaction was followed via gc after work-up: 0.5 mL of the reaction mixture were treated with MeOH (0.2 mL) and Et_3N (0.4 mL), then diethyl ether (25 mL) was added. The solvent was evaporated, then MeOH and THF (4 mL each) were added, followed by KF (58mg, 1mmol) and $KHCO_3$ (100 mg, 1 mmol), and then H_2O_2 30% (1 mL). The mixture was stirred overnight, then treated with $Na_2S_2O_5$, extracted with diethyl ether, the organic phase dried over Na_2SO_4, and the solvent evaporated. GC Analysis at 105°C showed a 50% ee for (*S*)-phenyl methyl carbinol **26** with 72% conversion and 91% branched selectivity. Retention times (min): 13.8 ((*R*)-phenylethanol), 14.8 ((*S*)-phenylethanol), 14.1 (2-phenylethanol).

Asymmetric allylic alkylation of 1,3-diphenylallyl acetate with dimethyl malonate

A solution of $[Pd(\eta^3\text{-}C_3H_5)Cl]_2$ (4.4 mg, 0.012 mmol) and the ligand (R)-**14b** (R = *i*-Pr) (20.5 mg, 0.04 mmol) in CH_2Cl_2 (1 mL) was stirred at room temperature under nitrogen. After 30 min, a solution of 1,3-diphenylprop-2-enyl acetate (100 mg, 0.4 mmol) in CH_2Cl_2 (0.5 mL) was added. A solution of dimethyl malonate (160 mg, 1.2 mmol), *N*,*O*-bis(trimethylsilyl)acetamide (BSA) (244 mg, 1.2 mmol), and potassium acetate (1.2 mg, 0.012 mmol) in CH_2Cl_2 (3.5 mL) was then added and stirring was continued at room temperature until complete conversion was attained. The reaction mixture was diluted with ether (25 mL) and washed with saturated NH_4Cl. The organic phase was dried (Na_2SO_4), concentrated under reduced pressure, and the residue purified by flash chromatography (light petroleum:ether, 3:1) to give dimethyl [(*R*)-1,3-diphenylprop-2-enyl]malonate **27** (60% ee). The enantiomeric purity was determined from the integrals of the methoxy groups of (1,3-diphenylprop-2-enyl)malonate, as split by the chiral shift reagent europium tris[3-(heptafluoropropylhydroxymethylene)-(+)camphorate].

Conclusions

The results obtained in the course of this study show that, unlike the corresponding oxygenated counterpart MOP (3), neutral *P,S*- heterobidenate ligands such as BINAPS derivatives **14** display a sharp propensity to act as chelating ligands towards transition-metal centres in low oxidation state. Unlike the case of the corresponding binaphthyl dithioethers (26), no evidence either of the formation of different stereoisomers or of a fluxional behaviour has been noticed in the NMR for the Pd(II)- and Rh(I)-complexes (**22** and **24**) prepared in this work. Thus, it seems that the presence of a strongly coordinating arm such as the phosphanyl phosphorus aids both at the chelation and at the stabilization of the configurational integrity of the new stereocentre originated upon binding of the *S*-donor.

This reaction apparently affords one single diastereoisomer which, in the case of Rh-complex **24**, is most probably the one with the *S*-methyl group in the equatorial position of a boat-like chelate ring, as we have recently determined for a related complex.[2] Assuming that the same occurs also in catalysis, a matching or a mismatching combination of the chiral elements can be envisaged.

The stereochemistry of the binding is basically determined by the chiral array of the binaphthalene backbone and, to a lower extent, by the steric demand of the alkyl group onto the sulfur atom. When these two effects are cooperative, we have almost no chance to steer the stereochemistry of the binding and can only hope that the final result is coincident with the matching case. If the two effects are contrasting, then the introduction of substituents of different steric demand may be exploited as a tool for controlling to some extent the configuration of the new stereocentre. Further work along this direction is in progress and will be published in due time.

Acknowledgements

Work carried out in the frame of the COST Chemistry Action D12 — Organic Transformations: Selective Processes and Asymmetric Catalysis, project 0009/98. The financial support of the University of Sassari and of MURST (Rome) is gratefully acknowledged by S.G.

References

1. A. Miyashita, A. Yasuda, H. Takaya, K. Toriumi, T. Ito, T. Souchi, and R. Noyori. J. Am. Chem. Soc. **102**, 7932 (1980).
2. C. Rosini, L. Franzini, A. Raffaelli, and P. Salvadori. Synthesis, 503 (1992).
3. Y. Uozumi and T. Hayashi. J. Am. Chem. Soc. **113**, 9887 (1991).
4. M. McCarthy and P.J. Guiry. Tetrahedron, **57**, 3809 (2001).
5. (*a*) S. Gladiali, S. Pulacchini, D. Fabbri, M. Manassero, and M. Sansoni. Tetrahedron: Asymmetry, **9**, 391 (1998); (*b*) S. Gladiali, E. Alberico, S. Pulacchini, and L. Kollàr. J. Mol. Catal. A, **143**, 155 (1999); (*c*) S. Gladiali, S. Medici, T. Kégl, and L. Kollàr. Monatsh. Chem. **131**, 1351 (2000).
6. (*a*) Y. Imai, W. Zhang, T. Kida, Y. Nakatsuji, and I. Ikeda. Tetrahedron Lett. **39**, 4343 (1998); (*b*) M. Ogasawara, K. Yoshida, H. Kamei, K. Kato, Y. Uozumi, and T. Hayashi. Tetrahedron: Asymmetry, **9**, 1779 (1998).
7. (*a*) S. Vyskocil, M. Smrcina, V. Hanus, M. Polasek, and P. Kocovsky. J. Org. Chem. **63**, 7738 (1998); (*b*)) S. Vyskocil, M. Smrcina, and P. Kocovsky. Tetrahedron Lett. **39**, 9289 (1998); (*c*) K. Ding, Y. Wang, H. Yun, J. Liu, Y. Wu, M. Terada, Y. Okubo, and K. Mikami. Chem. Eur. J. **5**, 1734 (1999); (*d*) A. Aranyos, D.W. Old, A. Kiyomori, J.P. Wolfe, J.P. Sadighi, and S.L. Buchwald. J. Am. Chem. Soc. **121**, 4369 (1999); (*e*) K. Sumi, T. Ikariya, and R. Noyori. Can. J. Chem. **78**, 697 (2000).
8. S. Gladiali, A. Dore, and D. Fabbri, Tetrahedron: Asymmetry, **5**, 1143 (1994).
9. S.Y. Cho and M. Shibasaki. Tetrahedron Lett. **39**, 1773 (1998).
10. (*a*) N. Sakai, S. Mano, K. Nozaki, and H. Takaya. J. Am. Chem. Soc. **115**, 7033 (1993); (*b*) K. Nozaki, N. Sakai, T.

[2] S. Gladiali, F. Grepioni, S. Medici, A. Zucca, Z. Berente, L. Kollàr. To be published.

© 2001 NRC Canada

Nanno, T. Higashjima, S. Mano, T. Horiuchi, and H. Takaya. J. Am. Chem. Soc. **119**, 4413 (1997).
11. S. Gladiali, A. Dore, D. Fabbri, S. Medici, G. Pirri, and S. Pulacchini. Eur. J. Org. Chem. **3**, 2861 (2000).
12. (*a*) A. Albinati, J. Eckert, P. Pregosin, H. Ruegger, R. Salzmann, and C. Stossel. Organometallics, **16**, 579 (1997) and refs. therein; (*b*) K. Hiroi and Y. Suzuki. Tetrahedron Lett. **39**, 6499 (1998); (*c*) D.A. Evans, K.R. Campos, J.S. Tedrow, F.E. Michael, and M.R. Gagné. J. Org. Chem. **64**, 2994 (1999); (*d*) D.A. Evans, K.R. Campos, J.S. Tedrow, F.E. Michael, and M.R. Gagné. J. Am. Chem. Soc. **122**, 7905 (2000).
13. E. Hauptmann, P.J. Fagan, and W. Marshall. Organometallics, **18**, 2061 (1999).
14. O. Pàmies, M. Diéguez, G. Net, A. Ruiz, and C. Claver. Organometallics, **19**, 1488 (2000).
15. M. Hiraoka, A. Nishikawa, T. Morimoto, and K. Achiwa. Chem. Pharm. Bull. **46**, 704 (1998).
16. X. Verdaguer, A. Moyano, M.A. Pericàs, A. Riera, M.A. Maestro, and J. Mahìa. J. Am. Chem. Soc. **122**, 10 242 (2000).
17. L. Kurz, G. Lee, D. Morgans, Jr., M.J. Waldike, and T. Ward. Tetrahedron Lett. **31**, 1665 (1990).
18. (*a*) U.K. Bandarage, J. Simpson, R.A.J. Smith, and R.T. Weavers. Tetrahedron, **50**, 3463 (1994); (*b*) S. Cossu, O. De Lucchi, D. Fabbri, G. Valle, G.F. Painter, and R.A.J. Smith. Tetrahedron, **53**, 6073 (1997).
19. (*a*) D. Fabbri, G. Delogu, and O. De Lucchi. J. Org. Chem. **58**, 1748 (1993); (*b*) A. Dore, D. Fabbri, S. Gladiali, and G. Valle. Tetrahedron: Asymmetry, **6**, 779 (1995).
20. K. Tani, L.D. Brown, J. Ahmed, J.A. Ibers, M. Yokota, A. Nakamura, and S. Otsuka. J. Am. Chem. Soc. **99**, 7876 (1977).
21. N.K. Roberts and S.B. Wild. J. Am. Chem. Soc. **101**, 6254 (1979).
22. P.H. Leung, A.C. Willis, and S.B. Wild. Inorg. Chem. **31**, 1406 (1992).
23. S. Gladiali, J.C. Bayón, and C. Claver. Tetrahedron: Asymmetry, **6**, 1453 (1995).
24. S. Gladiali and G. Mestroni. Transferhydrogenations. *In* Transition-metals for organic synthesis. Vol. 2. pp 97–119. *Edited by* M. Beller and C. Bolm. Wiley–VCH, Weinheim, Germany. 1998.
25. J. Kang, S. Hoon Yu, J.I. Kim, and H.G. Cho. Bull. Korean Chem. Soc. **16**, 439 (1995).
26. S. Gladiali, D. Fabbri, L. Kollàr, C. Claver, N. Ruiz, A. Alvarez-Larena, and J.F. Piniella. Eur. J. Inorg. Chem. **1**, 113 (1998).

© 2001 NRC Canada

Sulfate as a ligand in ruthenium(II) and (III) ammines

Hildo Antonio dos Santos Silva, Bruce R. McGarvey, Regina Helena de Almeida Santos, Mauro Bertotti, Vânia Mori, and Douglas Wagner Franco

Abstract: The *trans*-$[RuSO_4(NH_3)_4(L)]Cl$ complexes, (L = nicotinamide (nia), L-histidine (L-hist), 4-picoline (4-pic), 4-chloropyridine (4-Clpy), isonicotinamide (isn), pyrazine (pyz), 4-aminopyridine (4-NH_2py), 4-cyanopyridine (4-CNpy), pyridine (py), imidazole (Him), and water (H_2O)), were characterized by elemental analysis cyclic voltammetry, UV–vis, IR, and electron paramagnetic resonance spectroscopies. From the four ν (SO_4^{2-}) observed only ν_3 and ν_4 split in two bands each for the sulfate unidentate coordination. The values of Δ/ξ parameters, extracted from *g* values, allow us to write the following order of increasing π-donation ability: pyz < (py, 4-CNpy, 4-Clpy. 4-pic, isn, nia) < Him < L-hist < 4-NH_2py. The intense absorption in the 317–347 nm ($\varepsilon \sim 2.3–5.6 \times 10^3$ M^{-1} cm^{-1}) region was tentatively assigned to sulfate-to-metal charge transfer (LMCT) and the absorption in the range of 230–270 nm ($\varepsilon \sim 2 – 6 \times 10^3$ M^{-1} cm^{-1}) assigned to an internal (IL) π-π^* transition in the heterocyclic ligands. The rate for the sulfate aquation in *trans*-$[RuSO_4(NH_3)_4L]^0$ complexes was evaluated through chronopotentiometric measurements and are in the 2.6 s^{-1} (chloropyridine) to 20 s^{-1} (pyrazine) range. The SO_4^{2-} is aquated in *trans*-$[Ru^{III}SO_4(NH_3)_4(4\text{-pic})]Cl$ at the specific rate constant of $(1.4 \pm 0.4) \times 10^{-5}$ s^{-1}, which is very much slower than in *trans*-$[Ru^{II}SO_4(NH_3)_4(4\text{-pic})]$ (5.4 s^{-1}). The X-ray crystal structure data show that the Ru—Cl (2.3444(9) Å) and Ru—NH_3 (2.100(2) Å) mean distances in *trans*-$[RuCl(NH_3)_4(4\text{-pic})]Cl_2 \cdot H_2O$ are similar to the ones observed in other tetraammineruthenium(III) complexes.

Key words: ruthenium, sulfate, ammines.

Résumé : Les complexes *trans*-$[RuSO_4(NH_3)_4(L)]Cl$ (L = nicotinamide (nia), L-histidine (L-hist), 4-picoline (4-pic), 4-chloropyridine (4-Clpy), isonicotinamide (isn), pyrazine (pyz), 4-aminopyridine (4-NH_2py), 4-cyanopyridine (4-CNpy), pyridine (py), imidazole (Him) et eau (H_2O)) ont été caractérisés par analyse élémentaire, voltampérométrie cyclique, spectroscopies UV–vis, infrarouge et de résonance paramagnétique électronique. Sur la base des quatre ν (SO_4^{2-}) observées, il n'y a que ν_3 et ν_4 qui se dédoublent pour la coordination unidentate du sulfate. Les valeurs des paramètres Δ/ξ extraites des valeurs de *g* permettent de proposer l'ordre suivant pour la facilité croissante à donner des électrons π: pyz < (py, 4-CNpy, 4-Clpy, 4-pic, isn, nia) < Him < L-hist < 4-NH_2py. L'absorption intense dans la région de 317 à 347 nm (ε d'environ 2,3 à 5,6 × 10^3 M^{-1} cm^{-1}) a été attribuée provisoirement au transfert de charge sulfate à métal (« LMCT ») et l'absorption aux environs de 230–270 nm (ε d'environ 2 à 6 × 10^3 M^{-1} cm^{-1}) est attribuée à une transition π-π* interne (« IL ») dans les ligands hétérocycliques. On a évalué la vitesse d'aquation dans les complexes *trans*-$[RuSO_4(NH_3)_4L]^0$ à l'aide de mesures chronopotentiométriques et sa valeur varie de 2.6 s^{-1} (chloropyridine) à 20 s^{-1} (pyrazine). La constante de vitesse d'aquation du SO_4^{2-} dans le *trans*-$[Ru^{III}SO_4(NH_3)_4(4\text{-pic})]Cl$ est de $(1,4 \pm 0,4) \times 10^{-5}$ s^{-1}, valeur qui est beaucoup inférieure à celle observée dans le *trans*-$[Ru^{II}SO_4(NH_3)_4(4\text{-pic})]$, 5,4 s^{-1}. Les données structurales obtenues par diffraction des rayons X établissent que les distances moyennes Ru—Cl [2,3444(9) Å] et Ru—NH_2 [2,100(2) Å] dans le *trans*-$[RuCl(NH_3)_4(4\text{-pic})]Cl_2 \cdot H_2O$ sont semblables à celles observées dans d'autres complexes tétraammineruthénium(III).

Mots clés : ruthénium, sulfate, ammines.

[Traduit par la Rédaction]

Received October 3, 200. Published on the NRC Research Press Web site at http://canjchem.nrc.ca on July 20, 2001.

Dedicated to Professor Brian James on the occasion of his 65th birthday.

H.A.S. Silva, R.H. de Almeida Santos, V. Mori and D.W. Franco.[1] Instituto de Química de São Carlos-USP, Universidade de São Paulo, Av. Trabalhador Sãocarlense, 400, Caixa Postal 780, 13560-970, São Carlos-SP – Brasil.
B.R. McGarvey. Department of Chemistry and Biochemistry, University of Windsor, Windsor, Ontario, N9B 3P4 Canada.
M. Bertotti. Instituto de Química-USP, Universidade de São Paulo, São Paulo, Caixa Postal 26077, 05508-900, Brasil.

[1]Corresponding author (telephone: (55) 21-16-273-997; fax: (55) 21-16-273-9976; e-mail: douglas@iqsc.sc.usp.br).

 DOI: 10.1139/cjc-79-5/6-679 © 2001 NRC Canada

Introduction

The oxidation of SO_2 to SO_4^{2-}, catalyzed by transition-metal complexes is an important reaction for the environmental control of sulfur dioxide (1, 2). Therefore, the knowledge of the behavior of sulfate as a ligand holds a considerable relevance. The metal center in ruthenium(II)ammines strongly bonds (3) to SO_2, HSO_3^-, and SO_3^{2-}, but has a very low affinity for SO_4^{2-}. Conversely, the Ru(III) center exhibits high affinity for SO_4^{2-}. In addition, sulfate complexes are useful intermediate (3) complexes in the preparation of *trans*-$[Ru^{II}{}_4L_1L_2(NH_3)]^n$ species ($L_1 = L_2$, $L_1 \neq L_2$).

The NH_3 ligands in tetraammineruthenium are innocent ligands and inert regarding substitution reactions (3), therefore making *trans*-$[Ru^{II}L_1L_2(NH_3)_4]^{n+}$ a good model to study the chemical properties of L_1 and L_2 as a function of the metal center oxidation state.

This paper describes the aspects of the electrochemical and spectroscopic properties of 11 ruthenium-sulfate complexes (where L_1 = nicotinamide (nia), pyrazine (pyz), L-histidine (L-hist), imidazole (Him), pyridine (py), 4-cyanopyridine (4-CNpy), 4-chloropyridine (4-Clpy), 4-picoline (4-pic), 4-aminopyridine (4-NH_2py), isonicotinamide (isn), and water (H_2O).

Since the electron paramagnetic resonance spectrum (EPR) of strong field d^5 complexes is very sensitive to the energy gap of t_{2g} orbitals, which are π-bonding in character, it was used to analyze the strength of the ligand–metal π-interaction. The aquation of the sulfate ion in *trans*-$[Ru^{II}SO_4(NH_3)_4(L_1)]^0$ and *trans*-$[Ru^{III}SO_4(NH_3)_4(4\text{-pic})]^+$ species is also reported, as well as the crystal structure analysis of *trans*-$[RuCl(NH_3)_4(4\text{-pic})]Cl_2\cdot H_2O$.

Experimental section

Reagents

All chemicals were reagent grade (Aldrich or Merck). The L = nicotinamide (nia), L-histidine (L-hist), 4-picoline (4-pic), 4-chloropyridine (4-Clpy), isonicotinamide (isn), pyrazine (pyz), 4-aminopyridine (4-NH_2py), 4-cyanopyridine (4-CNpy), pyridine (py), imidazole (Him), and water (H_2O) were used as supplied. The $RuCl_3\cdot nH_2O$ was obtained from Johnson Matthey and also used as supplied. The acetone and ethyl alcohol (Merck), used to precipitate the sulfate complexes were purified just before use according to the literature (4). Doubly distilled water was used throughout the experiment.

All preparation and measurements were carried out under argon using standard techniques (5) for the manipulation of air sensitive compounds.

Synthesis of complexes

The $[RuCl(NH_3)_5]Cl_3$ (6), *trans*-$[Ru(HSO_3)_2(NH_3)_4]$ (7), and *trans*-$[RuCl(NH_3)_4SO_2]Cl$ (8) were prepared as described in the literature.

The *trans*-$[RuSO_4(NH_3)_4L]Cl$ complexes were prepared (9, 10) as follows: 0.100 g of the *trans*-$[RuCl(SO_2)(NH_3)_4]Cl$ was dissolved in a min volume of aq 1.0×10^{-1} mol L^{-1} $NaHCO_3$ (about 3.5 mL), previously argon-degassed. A 10-fold excess of the corresponding L-ligand (except for L-hist) was added and after about 20 min, 1.0 mL of 6 mol L^{-1} HCl and 2.5 mL of 30% H_2O_2 were added to the system, resulting in a faint yellow solution. For L-hist, only twofold ligand excess was used to prevent oil formation. The sulfate complex was precipitated by the addition of acetone (70 mL) and the mixture was kept in the refrigerator for one night (12 h). The solid product was collected by filtration, washed with ethanol or acetone, and kept in vacuum in the dark The overall yield ranged from 83% (L-hist) to 90% (4-pic). All the elemental analyses were consistent with the *trans*-$[RuSO_4(NH_3)_4(L)]Cl$ formulation. According to the hexacoordinate nature of Ru(III), the SO_4^{2-} behaves as a unidentate ligand in these complexes. Elemental analyses for sulfate complexes: Anal. calcd. for L = nia: C 17.0, N 19.9, H 4.3, Ru 23.9; found: C 16.4, N 18.6, H 4.4, Ru, 24.7. Anal. calcd. for L = L-hist: C 14.6, N 19.9, H 5.0, Ru 20.6; found: C 13.8, N 19.0, H 4.9, Ru 20.6. Anal. calcd. for L = 4-pic: C 18.3, N 17.9, H 4.9, Ru 25.7; found: C 18.0, N 17.1, H 4.9, Ru 25.8. Anal. calcd. for L = 4-Clpy: C 13.5, N 16.9, H 4.0, Ru 24.4; found: C 14.0, N 14.7, H 3.1, Ru 22.1. Anal. calcd. for L = isn: C 17.0, N 19.9, H 4.3, Ru 23.9; found: C 16.5, N 19.4, H 4.5, Ru 23.2. Anal. calcd. for L = pyz: C 12.6, N 22.1, H 4.2, Ru 26.5; found: C 12.1, N 22.0, H 4.3, Ru 26.3. Anal. calcd. for L = 4-NH_2py: C 15.2, N 21.3, H 4.6, Ru 25.8; found: C 14.7, N 20.4, H 4.8, Ru 25.4. Anal. calcd. for L = 4-CNpy: C 17.8, N 20.8, H 4.0, Ru 25.2; found: C 17.1, N 20.2, H 4.2, Ru 24.8. Anal. calcd. for L = py: C 15.8, N 18.4, H 4.5, Ru 26.6; found: C 16.0, N 18.2, H 4.5, Ru 26.4. Anal. calcd. for L = Him: C 9.8, N 22.8, H 4.4, Ru 27.4; found: C 9.6, N 22.1, H 4.2, Ru 26.9.

Apparatus and methods

The elemental analyses were carried out at the Instituto de Química at Universidade de São Paulo. The atomic absorption analysis of ruthenium was performed using a Hitachi polarized Zeeman atomic absorption spectrophotometer (model Z-8100) and following Rowston and Ottaway's method (11), modified by Clarke (12).

A Bruker spectrometer model ESP 300E operating in the X-band and coupled to a standard cavity was used to obtain the EPR spectra. All experiments were carried out at liquid nitrogen temperature (77 K) and the samples were both solid powders and frozen solutions in 70% ethylene glycol – 30% water mixture.

The IR spectra were recorded in KBr pellets using a Bomem FT IR spectrometer (model MB-102) in the range of 3000–400 cm^{-1}.

The UV–vis spectra were recorded using a Hitachi U-3501 spectrophotometer. The spectra of the complexes were carried out in aqueous solutions μ = 0.1 mol L^{-1} (CF_3COOH–$NaCF_3COO$) and (pH $\cong$ 3.0) and in a 1.0 cm quartz cell.

Voltammetric measurements were carried out with a Princepton applied research polarographic voltammeter system (model 264) coupled with a IBM compatible microcomputer. The formal reduction potentials ($E_{1/2}$) were measured by cyclic voltammetry using a three electrode cell: (*i*) saturated calomel (SCE) (reference electrode); (*ii*) glassy carbon (working electrode); and (*iii*) platinum (auxiliary electrode). The measurements were carried out in CF_3COOH–$NaCF_3COO$ (pH 2.0, μ = 0.1) and at 4.0 ± 0.2°C. The double potential step chronoamperometry technique was used in

© 2001 NRC Canada

Table 1. Crystal data and details of the structure determination for *trans*-$[RuCl(NH_3)_4(4\text{-pic})]Cl_2 \cdot H_2O$.

Empirical formula	$C_6H_{19}ClN_5Ru$, H_2O, 2(Cl)
Formula weight	386.70
Crystal system	Monoclinic
Space group	$P2_1/m$
a (Å)	9.7488(8)
b (Å)	7.4805(9)
c (Å)	10.693(1)
β (°)	91.96(1)
V (Å^3)	779.4(1)
Z	2
D(calc) (g cm^{-3})	1.648
F(000)	390
μ(Mo Kα) (cm^{-1})	15.11
Crystal size (mm)	0.15 × 0.20 × 0.30
Temperature (K)	243
Radiation Mo Kα (Å)	0.71073
θ Min-max (°)	2.8, 30.0
Data set	–13:13, –10:0, –15:0
Tot., Uniq. Data, R(int)	2527, 2412, 0.029
Observed data [$I > 2.0\sigma(I)$]	2036
Nref, Npar	2412, 94
R, wR, S	0.0287, 0.0742, 1.04
$w = 1/(\sigma^2(Fo^2) + (0.0366P)^2 + 0.0750P)$ where $P = (Fo^2 + 2Fc^2)/3$	
Max and avg shift/error	0.00, 0.00
Min and max resd. dens. (e Å^{-3})	–0.46, 0.39

the determination of the aquation rate constant values (13). The calculation was based on work curves described in the literature (14). Current values corresponding to the reduction and oxidation processes of the material generated in the surface of the working electrode were measured at specific times after the potential steps. Chronoamperometric measurements were performed in millimolar solutions of ruthenium complexes in CF_3COOH (pH = 2.0) by using a CV-27 potentiostat (Bioanalytical Systems). In these studies, a glassy carbon electrode (r = 1.5 mm) was used as working electrode and a silver–silver chloride (saturated KCl) and a platinum wire were used as reference and auxiliary electrodes, respectively. The oxygen from solutions was removed by bubbling argon for at least 10 min.

The kinetic measurements of sulfate aquation in *trans*-$[RuSO_4(NH_3)_4(4\text{-pic})]^{2+}$ ions were followed spectrophotometrically at 326 nm (where the sulfate species absorb) and 348 nm (where the chloro species absorbs). The temperature of cells were held constant at 40 ± 0.2°C. The measurements were carried out in HCl 1.0 × 10^{-2} M and μ = 2.0 (NaCl). The plots of log $A_\infty - A_t$ vs. t were linear for at least three half-lives. The $k_SO_4^{2-}$ values calculated from log $A_\infty - A_t$ vs. t plots using the absorbance data measured at 348 and 326 nm are in very good agreement.

The X-ray crystal data were obtained on a CAD4 Enraf–Nonius diffractometer, at the Laboratório de Cristalografia do Departamento de Química e Física Molecular do Instituto de Química de São Carlos.

Table 2. Positional and thermal parameters for *trans*-$[RuCl(NH_3)_4(4\text{-pic})]Cl_2 \cdot H_2O$.

Atom	x	y	z	U(eq) (Å^2)
Ru	0.17835(3)	0.2500	0.82493(2)	0.0266(1)
Cl1	0.0992(1)	0.2500	1.02948(8)	0.0435(3)
N	0.2449(3)	0.2500	0.6428(2)	0.0291(8)
N1	0.3212(2)	0.4531(3)	0.8724(2)	0.0369(6)
N2	0.0353(2)	0.0492(3)	0.7778(2)	0.0368(6)
C1	0.3792(3)	0.2500	0.6178(3)	0.040(1)
C2	0.4268(4)	0.2500	0.4989(3)	0.045(1)
C3	0.3362(4)	0.2500	0.3965(3)	0.038(1)
C4	0.1973(4)	0.2500	0.4228(3)	0.037(1)
C5	0.1560(3)	0.2500	0.5436(3)	0.0347(9)
C6	0.3844(5)	0.2500	0.2650(3)	0.060(2)
Cl2	0.2263(1)	0.7500	0.64199(8)	0.0470(3)
Cl3	0.6290(1)	0.2500	0.88750(9)	0.0470(3)
O1W	–0.1877(3)	0.2500	0.6503(3)	0.067(1)
H1O	–0.2379	0.3461	0.6706	0.0870[a]

Note: U(eq) = 0.3333 of the trace of the orthogonalized U tensor.
[a]Isotropic 1.3 times U(eq) of O1W.

Crystal structure of *trans*-$[RuCl(NH_3)_4(4\text{-pic})]Cl_2 \cdot H_2O$

Crystals for X-ray diffraction were obtained from acidic solution (0.5 mol L^{-1} HCl) kept at room temperature for a week. A summary of crystal data and refinement conditions are in Table 1. The intensity data were measured at 243 K with graphite monochromatized Mo Kα radiation using the ω-2θ mode, and three standards measured every 7200 s with no significant decay. Unit cell parameters in Table 1 were obtained by least-squares refinement of 25 reflections (θ min = 12.42° and max = 18.39°). The absorption correction was performed by the PSISCAN method (15) (μMo Kα = 15.11 cm^{-1}).

All the calculations were made using WinGX (16). The heavy atom positions were obtained by the Patterson function and the structure was completed using Fourier difference. The refinement was by full-matrix least-squares (17). The hydrogen atoms of the water molecule were found in DF map and not refined, (d (H-O) = 0.900 Å) and the others were located in their ideal positions and not refined, using d (N-H) = 0.940 Å, and d (C-H) = 0.970 Å; with isotropic thermal vibration equal to 1.3 times the isotropic equivalent thermal parameter of the attached atom. All non-hydrogen atoms were refined anisotropically, and the atomic scattering factors were taken from *International Tables for X-ray Crystallography* (18). The final atomic coordinates and the equivalent isotropic temperature factors are shown in Table 2. Anisotropic thermal parameters, a complete list of distance and angles, a complete table of hydrogen bonds, and final structure factors are available as supplementary data.[2]

The Ru, Cl atoms, and the 4-pic group lie on the crystallographic mirror plane, with the CH_3 hydrogen atoms disordered with occupancy factors of 0.5. The oxygen atom of the water molecule lies also in the mirror plane. Figure 1 shows

[2] Copies of material on deposit may be purchased from the Depository of Unpublished Data, Document Delivery, CISTI, National Research Council Canada, Ottawa, Canada K1A 0S2. Copies of the data can be obtained, free of charge, on application to the Director, CCDC, 12 Union Road, Cambridge CB2 1EZ, U.K. (Fax: 44-1223-336033 or e-mail: deposit@ccdc.cam.ac.uk).

© 2001 NRC Canada

Fig. 1. ORTEP representation for the *trans*-$[RuCl(NH_3)_4(4\text{-pic})]Cl_2 \cdot H_2O$, with the label scheme.

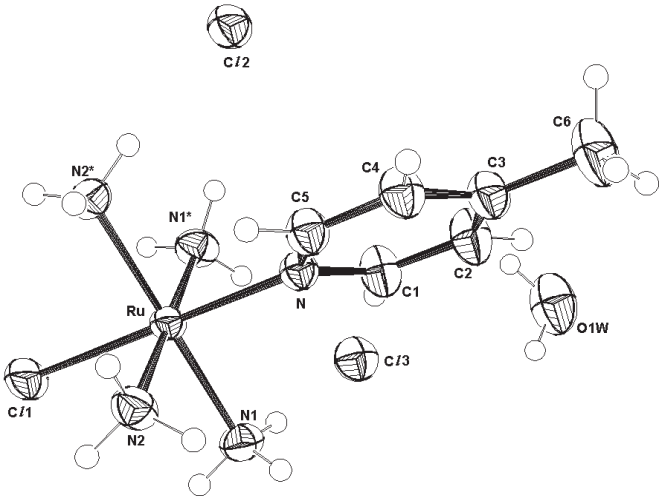


Table 3. Selected interatomic distances (Å) and angles (°) for *trans*-$[RuCl(NH_3)_4(4\text{-pic})]Cl_2 \cdot H_2O$.

Interatomic distances (Å)	
Ru—Cl1	2.3444(9)
Ru—N	2.074(2)
O1W—H1O	0.900
Ru—N1	2.111(2)
Ru—N2	2.099(2)
Interatomic angles (°)	
Cl1-Ru-N1	90.66(5)
N-Ru-N1	90.03(8)
N1-Ru-N2	179.64(8)
N1-Ru-N1[a]	92.06(8)
Cl1-Ru-N	179.01(8)
Cl1-Ru- N2	89.25(6)
N-Ru-N2	90.05(8)
N1[a]-Ru-N2	88.29(8)
N2-Ru-N2[a]	91.37(8)
H1O-O1W-H1O[b]	106.0

[a] x, 0.5 – y, z.
[b] x, 0.5 – y, z.

the compound with the label scheme. Some selected distances and angles are presented in Table 3.

Results and discussion

The EPR portion of the study was undertaken to see if one could get a semiquantitative measure of the π donor ability of a ligand from the EPR g tensor of a Ru(III) ion, to which the ligand was bonded. It is well known that the g tensor of a strong field d^5 is strongly dependent upon the relative energies of the three π bonding t_2 orbitals in which the unpaired electron resides. Ligand field distortions combined with the spin-orbit interaction produce three Kramer's doublet states, which are mixtures of the three t_2 orbitals with different m_s values for the spin. EPR of powders at low temperatures and frozen solutions is capable of measuring the three principal g values associated with the Zeeman splitting of the ground-state doublet by the magnetic field. In powder spectra, the labeling of the principle axes is arbitrary, but it has been shown (19, 20) that much confusion about these systems can be eliminated by defining the z direction to be perpendicular to the orbital whose energy is furthest away from the energy of the two other orbitals. This will become clearer by considering the two energy parameters defined below:

Table 4. EPR g values for *trans*-$[RuSO_4(NH_3)_4L]^+$.

	Frozen solution		Powder	
L	$g_{\|}$	$g_{\perp}$	$g_{\|}$	$g_{\perp}$
Him	1.21	2.60	1.40	2.46
isn	≤0.8	2.59	≤0.8	2.58
nia	≤0.8	2.56	≤0.8	2.58
4-pic	≤0.8	2.61	≤0.8	2.63
4-Clpy	≤0.8	2.57	≤0.8	2.59
4-CNpy	≤0.8[b]	2.80–2.30[b]	≤0.8	2.56
4-NH_2py	?[a]	2.58[a]	1.39	2.56
L-hist	1.24	2.60	?[c]	2.58
py	≤0.8	2.59	≤0.8[d]	2.30[d]
pyz	1.56	2.03	?[d]	2.40[d]

[a] Low solubility, hence weak signal-to-noise.
[b] Multiple signals.
[c] Bad baseline in high field region.
[d] Very broad lines (~2000 gauss) and poor baseline.

$$[1] \qquad \Delta = E\,(d_{xy}) - 0.5[E\,(d_{xz}) + E\,(d_{yz})]$$

$$[2] \qquad V = E\,(d_{xz}) - E\,(d_{yz})$$

V cannot be greater than $2\Delta/3$ in magnitude because that is when we would have to change our designated z axis because $E\,(d_{xy})$ becomes too close to one of the other energy states. This z axis depends only on relative energy spacing and has nothing to do with geometry. This will become clearer below when we find that this z axis in *trans*-$[RuSO_4(NH_3)_4L]^+$ is perpendicular to the L-Ru-SO_4 axis.

The theoretical treatment (19, 20) shows that the three g values depend on three parameters: (Δ/ξ), (V/ξ), and the orbital reduction parameter k. ξ is the one electron spin-orbit parameter, which is approximately 1000 cm^{-1} in Ru(III). The appropriate method of extracting these parameters from the g values is given in two recent reviews (19, 20). There are always two possible solutions, but it is nearly always possible to choose the more likely values by either an unreasonable size for k or Δ/ξ in one of the solutions.

The unpaired electrons in *trans*-$[RuSO_4(NH_3)_4L]^+$ are in *anti*-bonding π-type MOs (molecular orbitals) which are raised in energy proportional to the ability of the ligands that π bond to the given d orbital. As can be seen from Table 4, all complexes studied have $g_x = g_y = g_{\perp}$ and $g_z = g_{\|}$ with $g_{\|} < g_{\perp}$. This means that $V = 0$ and Δ is positive and therefore two of the three t_2 orbitals are degenerate with the third being higher in energy. As will be shown below, this means that the only significant π bonding occurs with the L ligand.

We take the x axis to be the SO_4RuL axis, the y axis perpendicular to both the SO_4RuL axis and the plane of L, and the z axis perpendicular to the SO_4RuL axis and in the plane

© 2001 NRC Canada

Fig. 2. Cartesian axes orientation.

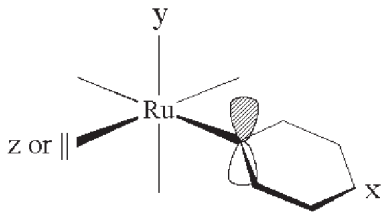
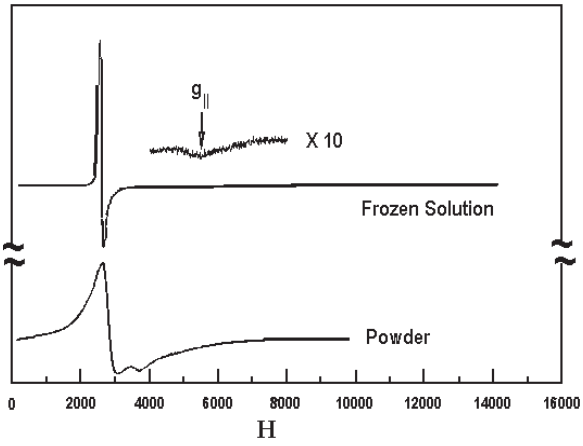


Fig. 3. EPR spectra for *trans*-[$Ru^{III}SO_4(NH_3)_4$(Him)]Cl powder and in a frozen 70% ethylene glycol – 30% H_2O solution. Both spectra were taken at 77 K.



of L. L has only one pair of π electrons to donate, so it interacts only with d_{xy} (see Fig. 2).

Unidentate SO_4^{2-} has two pairs of π electrons, so it interacts with d_{xy} and d_{xz} Using the AOM (atomic orbital method) the energies for the three MOs can be written as:

[3] $$E^*(xy) = \varepsilon_\pi(L) + 2\varepsilon_\pi(NH_3) + \varepsilon_\pi(SO_4)$$

[4] $$E^*(yz) = 2\varepsilon_\pi(NH_3) + \varepsilon_\pi(SO_4)$$

[5] $$E^*(xz) = 4\varepsilon_\pi(NH_3)$$

There are only two ways to produce two degenerate states lower in energy than the third state. One is to make $\varepsilon_\pi(L) = 0$ but this would require us to assume that $\varepsilon_\pi(NH_3) > \varepsilon_\pi(SO_4)$, This is absurd since NH_3 is the only ligand with no π electrons to donate. The second way is assume $\varepsilon_\pi(SO_4) \approx \varepsilon_\pi(NH_3) \approx 0$ and is, therefore, the only reasonable choice. Thus our results show very strongly that the NH_3 and SO_4^{2-} ligands are not π donors with Ru(III) and $\Delta = \varepsilon_\pi(L)$. Also the $g_{||}$ axis is not the SO_4RuL axis as some researchers have assumed. This problem of the location of the $g_{||}$ axis has been discussed more thoroughly in an article (21) on the EPR and NMR of $[Ru^{III}(NH_3)_5(H_2O)]^{3+}$.

We tried to run both the powder and frozen solution spectrum of all the compounds studied. Solution spectra in general give sharper spectra and are to be preferred but in some cases low solubility prevented our obtaining a satisfactory spectrum. We then used an automatic simulation program (B.R. McGarvey, personal communication) to find the best fit between calculated and experimental spectra by adjusting the two *g* values and line widths. Both the powder and frozen solution spectra for L = Him are shown in Fig. 3.

Table 5. Parameters[a] derived from *g* values of *trans*-$[RuSO_4(NH_3)_4(L)]^+$.

L	*k*	Δ/ξ
Him	0.90	2.06
isn	0.88–0.95	1.51–0.98
nia	0.85–1.05	1.53–0.98
4-pic	0.89–0.96	1.52–0.99
4-Clpy	0.86–0.93	1.51–0.97
4-CNpy	0.85–0.97	1.50–0.97
4-NH_2	0.89	2.31
L-hist	0.90	2.05
py	0.88–0.95	1.51–0.98
pyz	0.91	0.18

[a]See *Apparatus and methods* section.

These spectra demonstrate some of the problems encountered in this research. The broadness of the powder line makes the determination of $g_{||}$ difficult. The extra bump in the lower portion of the derivative cannot be simulated under any assumptions except as an extra peak. It remains under repeated syntheses but goes away in the solution spectrum. In most of the systems studied, the solid and solution spectra are in reasonable agreement but in this case the solid gives a $g_\perp = 2.46$, which is not what the solution spectrum gives. This is the only compound for which there are *g* values (22) reported in the literature. It was run in the same solution and agrees very well with the values we report. In general we used the solution values wherever possible. The only cases (3) where the $g_\perp$ values differ markedly between the solution and powder samples all had very large line widths (>1000 gauss) in the powder.

In some cases we list a value for $g_{||}$ of < 0.8. In these cases no $g_{||}$ dip could be observed. We have found by simulation that the intensity of such a peak is very difficult to detect for *g* values less than 0.8. In such cases, we have used both a value of 0.9 and 0.0 to estimate a range of values for the parameters.

In Table 5 are given the values of Δ/ξ and *k* that were extracted from these *g* values. We tried to include H_2O as a ligand but the spectra in solution and solid were useless for our purposes. Using the Δ/ξ parameters we find the following order of increasing π donating ability: pyz < (py, 4-CNpy, 4-Clpy. 4-pic, isn, nia) < Him < L-hist < 4-NH_2py. This series is in agreement with the previous one deduced on basis of ν_{NO} data for *trans*-$[Ru(NH_3)_4(L)NO](BF_4)_3$ complexes (23). It is unfortunate that six of these lie in the region $1 > \Delta/\xi > 1.5$ where it was impossible to determine $g_{||}$. One way to get around this would be to obtain Os(III) analogs since its value of ξ (~3000 cm^{-1}) would allow us to determine the $g_{||}$ values. We do have an estimate for the Δ/ξ parameter to be in the region of 1–1.5 from the EPR studies (21) of $[Ru^{III}(NH_3)_5(H_2O)]^{3+}$.

During our attempts to grow *trans*-$[RuSO_4(NH_3)_4$(4-pic)]Cl crystals in HCl medium, we observed the sulfate substitution by the chloride ion yielding as a product *trans*-$[RuCl(NH_3)_4$(4-pic)]$Cl_2 \cdot H_2O$.

© 2001 NRC Canada

Table 6. Vibrational frequencies[a] from SO_4^{2-} group of *trans*-$[RuSO_4(NH_3)_4L]Cl$ complexes (cm^{-1}).

Ligand	ν_1	ν_2	ν_3	ν_4
SO_4^{2-} (ligand free) (27)			1104(vs)	613 (s)
py	932 (s)	473 (w)	1179–1141(s)	612 (m)
	915 (s)		1025–1020 (s)	593 (m)
4-pic	940 (s)	498 (m)	1168–1042 (s)	615 (m)
			1049–1038 (s)	580 (m)
pyz	914 (w)	477 (m)	1167–1122 (m)	668 (w)
			1096–1065 (m)	658 (w)
nia	935 (s)	479 (w)	1180–1162 (s)	613 (w)
			1048–1020 (s)	578 (w)
isn	942 (m)	478 (w)	1184–1146 (s)	639 (w)
			1049 (s)–1035 (m)	613 (w)
				581 (w)
4-Clpy	939 (s)	507(m)	1171 (s)–1120 (m)	616 (m)
			1050–1039 (s)	580 (m)
4-CNpy	933 (s)	465 (w)	1189–1163 (s)	614 (w)
			1065–1034 (s)	579–563 (w)
Him	921 (m)	458 (w)	1150–1129 (s)	587 (w)
	908 (m)		1080–1030 (s)	612 (m)
L-hist	929 (m)	462 (w)	1177–1111 (s)	618 (m)
			1039 (s)	596 (m)
4-NH_2py	935 (m)	467 (w)	1162–1138 (s)	588 (w)
			1043–1028 (s)	614 (w)

[a]KBr pellets; vs very strong, s strong, m medium, w weak.

The analysis of the crystalline structure of *trans*-$[RuCl(NH_3)_4(4\text{-pic})]Cl_2$ by X-ray diffraction shows that the distances Ru—Cl and Ru—NH_3 (media) are 2.3444(9)and 2.100(2) Å, respectively. These values are similar to the ones found for other ruthenium complexes: Ru—Cl 2.34(1) Å; Ru—NH_3 2.10(1) Å for $[RuCl(NH_3)_5]Cl_2$ (24), Ru—Cl 2.36 Å, Ru—NH_3 2.11(4) Å for *cis*-$[RuCl_2(NH_3)_4]Cl$ (25); and Ru—Cl 2.336(1) Å, Ru—NH_3 2.105(4) Å for *trans*-$[RuCl_2(NH_3)_4]Cl$ (25). The crystal packing shows two short hydrogen bonds between the Cl3 atom and the water molecule using the H1O atom from the water molecule, with *d* (O-Cl) = 3.152(3) Å; and Cl3···H1*n*1-N1 (amine group) with *d* (N-Cl) equal to 3.282(2) Å. The other chlorine atoms hydrogen bond with hydrogen atoms of the amine groups (*d* (N-Cl) 3.362(2), 3.417(2), 3.341(2), 3.421(2) Å), and the oxygen atom of the water is hydrogen bonded to the hydrogen attached to the N2 amine atom with *d* (N-O) = 2.939(3) Å. This hydrogen bond scheme is probably responsible for the high symmetry of the crystal, and shows the importance of the crystallization of water. The Ru coordination geometry in the complex is best described as a slightly distorted octahedron, as shown by the values in Table 3.

The free sulfate ion belongs to the group of high symmetry T_d. Of the four vibrational frequencies only ν_3 and ν_4 are active in the IR. The interaction of SO_4^{2-} with metal ion acts as a perturbation, which decreases the sulfate symmetry. For the *trans*-$[Ru(SO_4)(NH_3)_4(L)]^+$ complex both ν_1 and ν_2 appear with medium and strong intensity, and moreover, ν_3 and ν_4 split into two bands each (see Table 6). These IR data, consistent with the sulfate group in C_{3v} symmetry (26, 27), shows that the sulfate is coordinate to the metal ion as a unidentate ligand.

The most relevant information in the UV–vis spectra of the sulfate complexes are summarized in Table 7. All the assignments are tentative and based on data described in the literature (28). The most significant bands observed were in the 314–347 nm range ($\varepsilon \sim 2.3–5.6 \times 10^3$ M^{-1} cm^{-1}), attributed to the ligand to metal charge transfer (LMTC), and $SO_4^{2-} \rightarrow$ (Ru(III)), in the 230–270 nm range ($\varepsilon \sim 2 – 6 \times 10^3$ M^{-1} cm^{-1}), attributed to the IL π-π^* of the heterocyclic ligand. A value of ~3.0×10^3 cm^{-1} can be calculated for the shift on the LMCT band energy when L changes from pyz to Him (see Table 7).

The $E_{1/2}$ values for the Ru(III)–Ru(II) couple in *trans*-$[RuSO_4(NH_3)_4(L)]^{1+/0}$, *trans*-$[Ru(H_2O)(NH_3)_4(L)]^{3+/2}$, and the specific rate constant data for the sulfate aquation in *trans*-$[RuSO_4(NH_3)_4(L)]$ are shown in Table 8.

Figure 4 shows a typical cyclic voltammogram for the *trans*-$[RuSO_4(NH_3)_4(L)]^{1+/0}$ species. The voltammograms for all sulfate complexes exhibit a general behavior, which can be explained by the following scheme:

[6] $$trans\text{-}[Ru^{III}SO_4(NH_3)_4(L)]^+ + e^- \underset{}{\overset{\text{fast}}{\rightleftharpoons}} trans\text{-}[Ru^{II}SO_4(NH_3)_4(L)]^0$$

[7] $$trans\text{-}[Ru^{II}SO_4(NH_3)_4(L)]^0 + H_2O \xrightarrow{\text{fast}} trans\text{-}[Ru^{II}(NH_3)_4(L)H_2O]^{2+} + SO_4^{2-}$$

[8] $$trans\text{-}[Ru^{II}(NH_3)_4(L)H_2O]^{2+} \underset{}{\overset{\text{fast}}{\rightleftharpoons}} trans\text{-}[Ru^{III}(NH_3)_4(L)H_2O]^{3+} + e^-$$

© 2001 NRC Canada

Table 7. UV–vis spectra[a] data for *trans*-$[RuSO_4(NH_3)_4(L)]^+$ species.

L	λ_{max} (nm)	ε (mol^{-1} L cm^{-1} × 10^3)	L	λ_{max} (nm)	ε (mol^{-1} L cm^{-1} × 10^3)
py	252	4.9	nia	256	6.0
	330	3.1		332	3.0
4-CNpy	230	3.2	4-pic	255	5.0
	274	3.8		281	2.1
	334	3.5		326	3.2
4-Clpy	258	4.6	pyz	244	3.0
	285	4.4		270	3.8
	326	3.3		347	2.3
4-NH_2py	251	1.4	L-hist	226	2.7
	324	4.0		318	3.0
	480	3.45		448	0.3
isn	264	5.3	Him	228	1.8
	345	5.6		314	3.0
				420	0.3
H_2O	265	9.8			
	320	2.9			
	480	3.7			

[a] Spectra obtained for aqueous solution at 25° C, pH ~ 3, ionic strength μ = 0.10 (CF_3COOH– $NaCF_3COO$), $C_{Ru(III)}$ from 1 to 5 × 10^{-4} M.

Table 8. Specific rate constants ($k_SO_4^{2-}$) and ($E_{1/2}$) data for the Ru(III)–Ru(II) couple in *trans*-$[RuSO_4(NH_3)_4(L)]^{+/0}$ complex ions.

Ligand	$k_SO_4^{2-}$ (s^{-1})[a]	$(E_{1/2})_1$ (V)[b]	$(E_{1/2})_2$ (V)[b]	(ΔE) (V)[b]
4-NH_2py	17	–0.306	–0.120	0.186
Him	16	–0.280	–0.143	0.137
L-hist	11	–0.418	–0.302	0.116
4-pic	5.4	–0.088	0.049	0.153
py	4.3	–0.048	0.094	0.142
4-Clpy	2.6	–0.016	0.126	0.142
nia	5.2	0.014	0.156	0.142
isn	16	0.047	0.186	0.139
4-CNpy	4.9	0.012	0.264	0.137
pyz	20	0.246	0.391	0.145

[a] $k_SO_4^{2-}$ (at (25 ± 0.2)°C), for the reaction *trans*-$[RuSO_4(NH_3)_4(L)]^+ + H_2O \rightarrow$ *trans*-$[Ru(NH_3)_4(L)H_2O]^+ + SO_4^{2-}$.
[b] $(E_{1/2})_1$ = Ru(III)–Ru(II) in *trans*-$[RuSO_4(NH_3)_4(L)]^{3+/2}$; $(E_{1/2})_2$ = Ru(III)–Ru(II) in *trans*-$[Ru(NH_3)_4H_2O(L)]^{3+/2}$; t = 4 ± 0.2°C, μ = 0.10 (CF_3COOH– $NaCF_3COO$), pH ~ 2.0.

which suggest an ECE mechanism (14).

At scan rates up to 0.2 V s^{-1} the electrochemical process involving the *trans*-$[Ru^{III}SO_4(NH_3)_4(L)]^{+/0}$ complex ($(E_{1/2})_1$) depicted irreversible behavior due to the fast aquation of the sulfate group from the electrogenerated Ru(II) center. The other redox couple ($(E_{1/2})_2$), which corresponds to the Ru(III)–Ru(II) couple in the aquo species, shows a reversible behavior even at room temperature and scan rate as low as 0.010 V s^{-1}. This assignment was confirmed by addition of the respective aquo compounds to the solution containing the sulfate complex.

At short-time window conditions (scan rate ≥ 0.5 V s^{-1}) and low temperatures (4.0 ± 0.2°C), a good definition for the Ru(III)–Ru(II) couple in the sulfate complexes was obtained, therefore, allowing the $(E_{1/2})_2$ calculation.

The aquation rate constants for the sulfate ion in all these Ru(II) complexes has been estimated through chronoamperometric measurements as being in the range of 2.6 (4-Clpy) to 20 (pyz).

As expected due to the sulfate σ donor ability, the Ru(III)–(II) couple in the *trans*-$[Ru^{III}SO_4(NH_3)_4(L)]^+$ ions is electroactive at more negative potentials than the corresponding aqua species. Since σ bonding is more relevant for Ru(III) than for Ru(II), this shift would reflect the stabilization of Ru(III) relative to Ru(II) due to the $SO_4^{2-} \rightarrow$ Ru(III) interaction.

As observed in Table 8, the $(\Delta E_{1/2})_{1,2}$ for the Ru(III)–Ru(II) redox couple in the sulfate and in the corresponding aqua species, for all the compounds studied, differ by about 0.14 ± 0.02 V. This difference is likely to be more credited to the SO_4^{2-} σ basicity abilities, than to the L ligand σ characteristics.

As mentioned earlier, *trans*-$[RuSO_4(NH_3)_4(4\text{-pic})]^+$ is quantitatively converted into *trans*-$[RuCl(NH_3)_4(4pic)]^+$ in the presence of excess of chloride ion. The sulfate complex has an LMCT band (λ_{max} = 326 nm, ε = 3.2 × 10^3) that is red-shifted by 22 nm when the sulfate is replaced by the chloride ion (see Fig. 5). This red-shift suggests that SO_4^{2-} is a poorer π-donor ligand than Cl^-, which is not surprising in

© 2001 NRC Canada

Fig. 4. Consecutive cyclic voltammograms for an aqueous solution of 1.7×10^{-3} M *trans*-$[RuSO_4(NH_3)_4(nic)]^+$, $\mu = 0.10$ (CF_3COOH–$NaCF_3COO$, pH ≅ 2.0, scan rate 0.20 V s^{-1}, E_i 0.50 V and E_f 0.5 V, $t = 4.0 \pm 0.1$°C; 1a, 1c couple corresponds to *trans*-$[Ru(NH_3)_4(H_2O)L]^{3+/2+}$, 2a, 2c couple corresponds to *trans*-$[RuSO_4(NH_3)_4(L)]^{+/0}$.

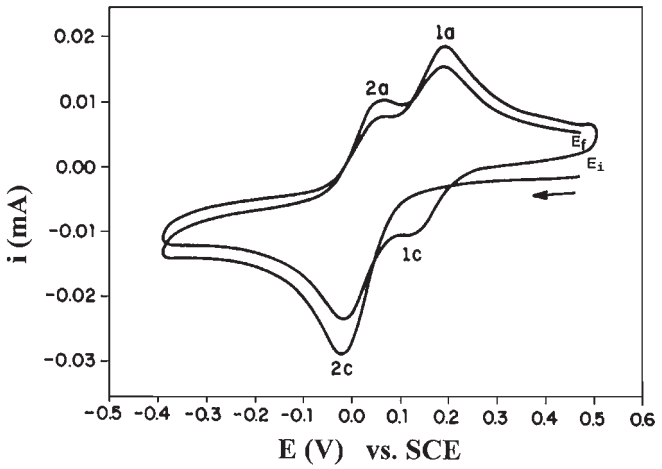
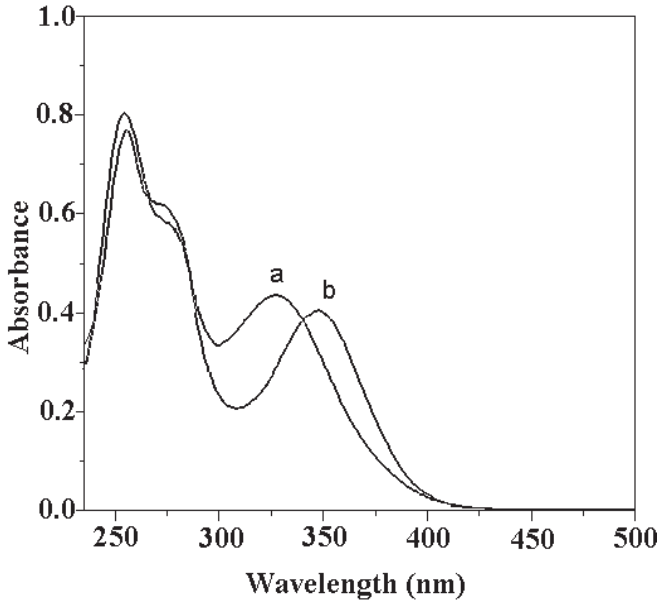


Fig. 5. Electronic spectra for conversion of aqueous 1.5×10^{-3} M *trans*-$[RuSO_4(NH_3)_4(4\text{-pic})]^+$ into *trans*-$[RuCl(NH_3)_4(4pic)]^{2+}$, $t = 40 \pm 0.2$°C, HCl 1.0×10^{-2} M, and $\mu = 2.0$ (NaCl). (*a*) Initial; (*b*) final.



[9] $$trans\text{-}[RuSO_4(NH_3)_4(L)]^+ + H_2O \xrightarrow[\text{slow}]{k\text{-}SO_4^{2-}} trans\text{-}[Ru(NH_3)_4(L)H_2O]^{3+} + SO_4^{2-}$$

[10] $$trans\text{-}[Ru(NH_3)_4(L)H_2O]^{3+} + Cl^- \underset{\text{fast}}{\rightleftharpoons} trans\text{-}[RuCl(NH_3)_4(L)]^{2+} + H_2O$$

view of the EPR results, which show that the SO_4^{2-} is ineffective as a π donor.

The aquation of the SO_4^{2-} in the *trans*-$[RuSO_4(NH_3)_4(4\text{-pic})]^+$ was studied using Cl^- as the auxiliary ligand, assuming eqs. [9] and [10] give the mechanism for the replacement reaction.

The value of $k_SO_4^{2-}$ calculated from measurements at chloride concentrations of 0.5, 1.0, and 2.0 M (40.0 ± 0.10°C) is $(1.4 \pm 0.4) \times 10^{-5}$ s^{-1}. Despite the difference in temperature, the $k_SO_4^{2-}$ data for the two 4-picoline complexes show that sulfate is aquated in Ru(III) complex ions at least 105 times slower than in *trans*-$[RuSO_4(NH_3)_4(4\text{-pic})]^0$ species.

It is also interesting to point out that, SO_4^{2-} dissociation from *trans*-$[RuSO_4(NH_3)_4(4\text{-pic})]^0$, (5.4 s^{-1}) is about the same as the Cl^- (29) aquation from $[RuCl(NH_3)_5]^+$ (6.3 s^{-1}), probably reflecting the difference in the anionic charge.

Efforts to grow a sulfate complex crystal and to perform a quantum mechanical calculation to explain the sulfate and sulfur dioxide complexes' spectra are in progress and will be reported upon in the future.

Conclusion

The EPR spectrum analysis of a strong d^5 field metal complex allows the extraction of valuable information about the nature of the π interactions with aromatic ligands. The values of Δ/ξ parameters, extracted from *g* values, allow the following order of π increasing donation ability to be written: pyz < (py, 4-CNpy, 4-Clpy, 4-pic, isn, nia) < Him < L-hist < 4-NH_2py.

The vibrational modes (ν_1, ν_2, ν_3, ν_4) of SO_4^{2-} in which ν_3 and ν_4 each split into two, were observed in the IR spectra of the sulfate complexes, confirming the unidentate coordination of SO_4^{2-}.

A variation of one order of magnitude in the aquation rates of sulfate in *trans*-$[RuSO_4(NH_3)_4(L)]^+$ was observed suggesting the following order of L *trans-effect*: pyz > 4-NHz py ~ Him ~ isn ~ L-hist > 4-pic ~ nia ~ 4-CNpy ~ py > 4.

As inferred from the sulfate aquation in *trans*-$[RuSO_4(NH_3)_4(4\text{-pic})]^+$ and *trans*-$[RuSO_4(NH_3)_4(4\text{-pic})]^0$, the increase of one unit charge in the metal center oxidation state leads to a decrease on the SO_4^{2-} rate of at least 300 times.

Comparing the ($E_{1/2}$) values for the Ru(III)–Ru(II) couple in the aqua and in the sulfate species, it was possible to observe a $(\Delta E_{1/2})_{1,2}$ value of 0.14 ± 0.02 V ($\Delta G° \sim -3.2$ kcal mol^{-1} (1 kcal = 4184 J)), which should be credited to the SO_4^{2-} presence in the coordination sphere.

Acknowledgements

The authors are indebted to C.W.W. Bezerra for recording the UV–vis spectra of the sulfate complexes. The authors are also very grateful to the Brazilian research foundations

© 2001 NRC Canada

CAPES, CNPq, and FAPESP for their financial support. The loan of a $RuCl_3$ sample from Johnson & Matthey is very much appreciated.

References

1. J.P. Dunn, H.G. Stenger Jr., and I.E. Watchs. Catal. Today, **51**, 301 (1999).
2. C.D. Cook and G.S. Jahaul. J. Am. Chem. Soc. **89**, 3066 (1967).
3. (*a*) H. Taube. Surv. Prog. Chem. **6**, 1 (1973); (*b*) H. Taube. Comments Inorg. Chem. **1**, 17 (1981); (*c*) P.C. Ford. Coord. Chem. Rev. **5**, 75 (1970). (*d*) C.G. Kuehn and S.S. Isied. Prog. Inorg. Chem. **27**, 1048 (1980).
4. W.L.F. Armarego and D.D. Perrin. *In* Purification of laboratory chemicals. 4th ed. Butterworth Heinemann, New York. 1996. pp. 66–67, 209–210.
5. D.F. Shriver and M.A. Drezdzon. *In* The manipulation of air-sensitive Compounds. John Wiley & Sons, New York. 1986. pp. 99–117.
6. A.D. Allen, F. Bottomley, R.D. Harris, V.P. Reinslau, and C.V. Senaff. Inorg. Synth. **12**, 2 (1972).
7. K. Gleu, W.*Z.* Breuel, and K. Rehm. Z. Anor. Allg. Chem. **235**, 211 (1938).
8. L.H. Vogt, Jr., L. Katz, and S.E. Wiberley. Inorg. Chem. **4**, 1157 (1965).
9. G.M. Brown, J.E. Sutton, and H. Taube. J. Am. Chem. Soc. **100**, 2767 (1978**)**.
10. S.S. Isied and H. Taube. J. Am. Chem. Soc. **95**, 8198 (1973).
11. W.B. Rowston and J.M. Ottaway. Anal. Lett. **8**, 3411 (1970).
12. M.J. Clark. J. Am. Chem. Soc. **100**, 5068 (1978).
13. W.M. Schwarz and I. Shain. J. Phys. Chem. **69**, 30 (1965).
14. A.J. Bard and L.R. Faulkner. *In* Electrochemical methods: fundamentals and applications. Wiley, New York. 1980. pp. 176–183.
15. A.C.T. North, D.C. Phillips, and F.S. Mathews. Acta Crystallogr. Sect. A: Cryst. Phys. Diffr. Theor. Gen. Crystallogr. **A24**, 351 (1968).
16. L.J. Farrugia. J. Appl. Crystallogr. **32**, 837 (1999).
17. G.M. Sheldrick. Programs for crystal structure analysis. Release 97–2. Institüt für Anorganische Chemie der Universität, Tammanstrasse 4, D-3400 Göttingen, Germany. 1998.
18. A.J.C. Wilson (*Editor*). International tables for crystallography. Vol. C. Kluwer Academic Publishers, Dordrecht, The Netherlands. 1995.
19. B.R. McGarvey. Quim. Nova, **21**, 206 (1998).
20. B.R. McGarvey. Coord. Chem. Rev. **170**, 75 (1998).
21. B.R. McGarvey, N.C. Batista, C.W.B. Bezerra, M.S. Schultz, and D.W. Franco. Inorg. Chem. **37**, 2865 (1998).
22. J. Clarke, V.M. Bailey, P.E. Doan, C. Hiller, K.J. LaChance-Galang, H. Daghlian, S. Mandal, C. Basto, and D. Lang. Inorg. Chem. **35**, 4896 (1996).
23. S.S.S. Borges, C.U. Davanzo, E.E. Castelano, J.-Z. Schpector, S.C. Silva, and D.W. Franco. Inorg. Chem. **37**, 2670 (1998).
24. C.K. Prout and H.M. Powell. J. Am. Chem. Soc. 137 (1962).
25. C.M.C. Picchi. Dissertação, Universidade de São Paulo. 2000.
26. K. Nakamoto, J. Fujita, S. Tanaka, and M. Kobayashi. J. Am. Chem Soc. **79**, 4904 (1957).
27. J. Reed, S.L. Soled, and R. Eisenberg. Inorg. Chem. **13**, 3001 (1974).
28. J.E. Sutton, H. Krentzien, and H. Taube. Inorg. Chem. **21**, 2842 (1982).
29. G.N. Coleman, J.W. Gesler, F.A. Shirley, and J.R. Kuempel. Inorg. Chem. **12**, 1036(1973).

© 2001 NRC Canada

Amide directed hydrocarboxylation of *N*-allylacetamide catalyzed by the aqueous Pd – tppts – Brønsted acid system (tppts = $P(C_6H_4$-*m*-$SO_3Na)_3$)[1]

Göran Verspui, Gábor Besenyei, and Roger A. Sheldon

Abstract: The Pd – tppts – HOTs (tppts = $P(C_6H_4$-*m*-$SO_3Na)_3$, HOTs = *p*-toluenesulfonic acid) catalyzed hydrocarboxylation of *N*-allylacetamide in an aqueous medium afforded 4-acetamidobutyric acid and 3-acetamido-2-methylpropanoic acid under mild conditions, with a high regioselectivity towards the linear isomer. During the hydrocarboxylation an acid catalyzed hydrolysis of the amide moieties of both the substrate and the products took place, as well as the formation of acetamide and propanal, presumably via a Pd-catalyzed allylic substitution reaction of *N*-allylacetamide. The hydrolysis reaction was suppressed by lowering the amount of Brønsted acid cocatalyst (HOTs) or by employing a weaker Brønsted acid such as propanoic acid. The allylic substitution reaction was minimized by increasing the CO pressure but unfortunately this caused a decrease in the regioselectivity. A sudden inhibition took place after ca. 70% conversion, presumably caused by one of the side products. By increasing the tppts concentration to 13.1 mmol L^{-1} (20 equiv per Pd) the inhibition was circumvented and a quantitative conversion of *N*-allylacetamide was achieved.

Key words: aqueous media, olefins, palladium, hydrocarboxylation, *N*-allylacetamide.

Résumé : Le complexe Pd – tppts – HOTs (tppts = $P(C_6H_4$-*m*-$SO_3Na)_3$, HOTs = acide *p*-toluènesulfonique) catalyse l'hydrocarboxylation du *N*-allylacétamide, en solution aqueuse et dans des conditions douces, pour conduire à la formation des acides 4-acétamidobutyrique et 3-acétyl-2-méthylpropanoïque, avec une régiosélectivité élevée en faveur de l'isomère linéaire. Au cours de la réaction d'hydrocarboxylation, il se produit une hydrolyse acidocatalysée des portions amides tant du substrat que du produit ainsi que la formation d'acétamide et de propanal, probablement par le biais d'une réaction de substitution allylique du *N*-allylacétamide, catalysée par le Pd. La réaction d'hydrolyse peut être supprimée en abaissant la quantité de l'acide de Brønsted utilisé comme cocatalyseur (HOTs) ou en utilisant un acide de Brønsted plus faible, tel que l'acide propanoïque. On peut minimiser la réaction de substitution allylique en augmentant la pression de CO; toutefois, ceci provoque une diminution de la régiosélectivité. Après environ 70% de conversion, il se produit une inhibition soudaine de la réaction qui est probablement causée par l'un des produits secondaires. En augmentant la concentration de tppts jusqu'à une valeur de 13,1 mmol L^{-1} (20 équivalents par Pd), on peut prévenir l'inhibition et obtenir une conversion quantitative du *N*-allylacétamide.

Mots clés : milieu aqueux, oléfines, palladium, hydrocarboxylation, *N*-allylacétamide.

[Traduit par la Rédaction]

Introduction

Organometallic catalysis in aqueous media currently attracts much attention due to the advantages of using the safe, environmentally friendly and economically attractive process solvent: water (1). Recently, we and others have developed a novel aqueous biphasic system for the hydrocarboxylation of olefins (2). In the presence of a Brønsted acid cocatalyst consisting of weakly coordinating anions, the Pd–tppts catalyst efficiently converts partly water-soluble olefins, such as ethene, propene, or isobutene, into their corresponding hydrocarboxylation products: propionic acid, *n*- and isobutyric acid and 3-methylbutyric acid, respectively. Unfortunately, when higher olefins were applied, e.g., 1-octene, due to phase transfer limitations, the reaction rate decreased dramatically, accompanied by the decomposition of the catalyst.

We have also shown that a hetero-atom substituted olefin, *N*-allylacetamide, was smoothly converted into 4-acetamidobutanal and 3-acetamido-2-methylpropanal by a Rh–tppts catalyzed hydroformylation reaction in water (3). In comparison with the conventional Rh–PPh_3 catalyst in an

Received October 10, 2000. Published on the NRC Research Press Web site at http://canjchem.nrc.ca on June 30, 2001.

Dedicated to Professor Brian R. James on the occasion of his 65th birthday.

G. Verspui and R.A. Sheldon.[2] Delft University of Technology, Laboratory of Organic Chemistry and Catalysis, Julianalaan 136, 2628 BL DELFT, The Netherlands.
G. Besenyei. Hungarian Academy of Sciences, Chemical Research Institute Centre, Institute of Chemistry, P.O. box 17, H-1525 Budapest, Hungary.

[1]Catalytic conversions in water, part 20.
[2]Corresponding author (telephone: +31 15 278 2675; fax: +31 15 278 1415; e-mail: r.a.sheldon@tnw.tudelft.nl).

 DOI: 10.1139/cjc-79-5/6-688 © 2001 NRC Canada

Scheme 1. The hydrocarboxylation of *N*-allylacetamide.

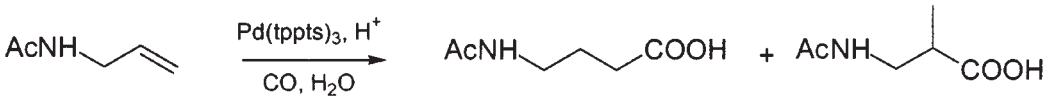


Table 1. The Pd–tppts catalyzed hydrocarboxylation of *N*-allylacetamide.

Experiment[a]	Temperature (°C)	Pressure (bar)	Time (h)	Yield (%)		1:b Ratio	Allylic substitution (%)[b]	Hydrolysis (%)[c]
				n	iso			
1/1	80	10	2	21.2	0.7	29.1	7.7	0
			8	27.8	1.7	16.0	8.0	1.7
1/2	60	10	8	30.3	2.1	14.6	9.6	0
			24	41.5	3.3	12.5	12.8	1.3
1/3	40	10	8	4.0	0.3	11.5	2.9	0
			24	14.9	1.1	13.6	7.4	0
1/4[d]	60	10	8	37.3	2.8	13.4	14.0	0
			24	41.6	3.7	11.4	14.4	11.6
1/5[d]	60	30	8	38.8	5.8	6.7	9.2	3.5
			24	44.1	8.3	5.3	12.1	10.5
1/6[d]	60	50	8	38.4	8.5	4.5	8.9	2.9
			24	43.6	11.5	3.8	9.5	9.0

[a]Reaction conditions: 50 μmol $PdCl_2$, 0.50 mmol tppts, 0.50 mmol *p*-toluenesulfonic acid, 10.0 mmol *N*-allylacetamide, 2.0 mmol *n*-BuOH (internal standard), 76.5 g total amount of reaction mixture.
[b]Both propanal and acetamide, were formed in equal amounts.
[c]Calculated from the amount of HOAc formed.
[d]2.50 mmol *p*-toluenesulfonic acid.

organic solvent, e.g., toluene or THF, the reaction in water proceeded considerably faster and in a higher selectivity towards the aldehydes. The rapid hydroformylation of *N*-allylacetamide in water suggested that the Pd–tppts catalyzed hydrocarboxylation reaction of this water-soluble olefin, affording 4-acetamidobutyric acid and 3-acetamido-2-methylpropanoic acid (Scheme 1), might proceed smoothly in a neat aqueous medium as well. The de-acetylated derivative of the linear product, γ-aminobutyric acid (GABA), is a well-known neurotransmitter with interesting pharmacological properties.

The hydrocarboxylation and alkoxycarbonylation of amide-functionalized olefins have been sporadically reported. Becker et al. (4) described the $PdCl_2(PPh_3)_2$ catalyzed methoxycarbonylation of *N*-vinylphtalimide in 2-butanone. After a 21 h reaction time at 70°C and 100 bar CO pressure, in the presence of 1% catalyst, 48% of the olefin was converted into the methylester of 2-phthalimidopropanoic acid. Ojima and Zhang (5) reported the methoxycarbonylation of *N*-allylbenzamide in the presence of $PdCl_2(PPh_3)_2$ in benzene at 80°C and a CO pressure of 100 bar. The products methyl-4-benzamidobutanoate and methyl-3-methyl-3-benzamidopropanoate were obtained in 18% and 71% yield, respectively. Magnus and Slater (6) studied the $Co_2(CO)_8$ catalyzed carbonylation of *N*-allylacetamide in ethylacetate, in the presence of 1 equiv of water. Under forcing conditions (140–160°C), a mixture of 2-acetamidobutyric acid and 2-acetamido-2-methylpropanoic acid was obtained in a 3.8:1 ratio. The formation of the linear hydrocarboxylation product 4-acetamidobutyric acid was not observed. When a combination of Co and Rh carbonyl precursors was used, the selectivity increased towards 2-acetamidobutyric acid.

In this paper we report on the hydrocarboxylation of *N*-allylacetamide in water catalyzed by the Pd – tppts – Brønsted acid system. The high water-solubility of *N*-allylacetamide enabled us to study this reaction in a single phase aqueous medium, i.e., in the absence of phase transfer limitations.

Results and discussion

In the hydrocarboxylation experiments we started with a freshly prepared catalyst solution by codissolving $PdCl_2$ and 10 equiv of tppts in water. We previously observed by NMR that under these conditions a cationic $[PdCl(tppts)_3]^+$ intermediate is formed, which is rapidly reduced to $[Pd(tppts)_3]$ in the presence of CO (7). We assume that this reduction is complete before the autoclave has reached the reaction temperature (within 8 min). We have also established by multinuclear NMR experiments, that $[Pd(tppts)_3]$ is protonated by the acid cocatalyst to afford the cationic $[PdH(tppts)_3]^+$, which reacts with ethene and CO to give a relatively stable Pd–acyl intermediate (8). The rate determining hydrolysis of the Pd—acyl bond affords propanoic acid and the Pd–hydride which returns to the catalytic cycle. Since we did not observe any induction period in our hydrocarboxylation reactions, we assume that the generation of the active catalyst is complete when the reaction temperature was reached.

When the hydrocarboxylation of *N*-allylacetamide was carried out under similar reaction conditions to those which we previously applied for ethene and propene (110°C, 50 bar) (2*a*), severe catalyst decomposition took place. In contrast, at a reaction temperature below 80°C the catalyst remained

© 2001 NRC Canada

Table 2. The Pd – tppts – Brønsted acid catalyzed hydrocarboxylation of *N*-allylacetamide.

Experiment[a]	Brønsted acid (mmol)	Time (h)	Yield (%)		1:b Ratio	Allylic substitutuion (%)	Hydrolysis (%)
			n	iso			
2/1	HOTs (0.5)	8	30.3	2.1	14.6	9.6	0
		24	41.5	3.3	12.5	12.8	1.3
2/2	HOTs (2.5)	8	37.3	2.8	13.4	14.0	0
		24	41.6	3.7	11.4	14.4	11.6
2/3	HOTs (5.0)	8	37.0	2.8	13.3	11.1	7.9
		24	35.3	3.8	9.2	11.4	21.2
2/4	HCl (2.5)	8	27.9	2.3	12.4	8.1	3.1
		24	38.6	4.8	8.0	11.1	10.8
2/5	$HOOCCH_2CH_3$ (2.5)	8	26.4	2.0	13.0	11.6	0
		24	36.9	3.2	11.4	14.7	1.6

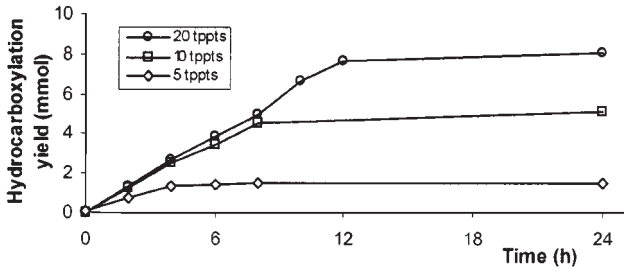
[a]Reaction conditions: see Table 1; 60°C, 10 bar CO.

Table 3. The Pd – tppts – Brønsted acid catalyzed hydrocarboxylation of *N*-allylacetamide.

Experiment[a]	Tppts–Pd	Time (h)	Yield (%)		1:b Ratio	Allylic substitution (%)	Hydrolysis (%)
			n	iso			
3/1[b]	5	8	12.5	1.2	10.8	4.3	2.8
		24	12.3	1.7	7.2	5.1	5.3
	Extra tppts	60	55.9	4.8	11.6	22.9	15.4
3/2	10	8	37.3	2.8	13.4	14.0	0
		24	41.6	3.7	11.4	14.4	11.6
3/3	20	8	44.0	2.7	16.1	14.1	3.4
		12	61.7	3.6	17.2	21.0	5.4
		24	61.4	4.0	15.9	21.3	10.6

[a]Reaction conditions: see Table 1; 2.50 mmol *p*-toluenesulfonic acid, 60°C, 10 bar CO.
[b]10 equiv of tppts added at t = 24 h.

Fig. 1. The effect of the tppts concentration on the progress of the reaction (reaction conditions: see Table 3).



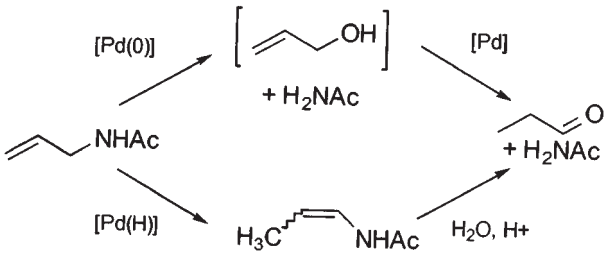
intact and converted *N*-allylacetamide into 4-acetamidobutyric acid and 3-acetamido-2-methylpropanoic acid (Table 1). During the reaction some acetic acid was formed via an acid-catalyzed hydrolysis of the amide moieties in *N*-allylacetamide and both carboxylic acid products. Decreasing the amount of HOTs to 0.50 mmol led to a slower hydrolysis (1.3% after 24 h reaction time (Table 2, Experiment 2/1)) with only a small compromise in the initial hydrocarboxylation rate. The hydrolysis reaction was also suppressed by using a much weaker Brønsted acid cocatalyst (we chose propionic acid for analysis reasons).

In addition to hydrocarboxylation and hydrolysis products we also observed the formation of acetamide, propanal, and traces of allylalcohol. The formation of these side products continues at room temperature, in the absence of CO, which necessitated immediate analysis of the samples (within 5 min) as soon as they were withdrawn from the reaction mixture. The formation of acetamide and propanal could be suppressed to some extent by increasing the CO pressure, but unfortunately, this also resulted in a considerably lower regioselectivity (1:b = 4 at 50 bar CO, Experiment 1/6). We suggest that a Pd-catalyzed allylic substitution reaction of *N*-allylacetamide takes place, affording acetamide and allylalcohol, of which the latter is isomerized to propanal (Scheme 2). In basic media, such an allylic hydrolysis reaction occurs readily at room temperature (9). The reaction apparently also proceeds under our mildly acidic conditions. Alternatively, *N*-allylacetamide might undergo an isomerization reaction to 1-acetamidopropene, followed by a fast acid-catalyzed hydrolysis, which would also afford acetamide and propanal. However, the absence of 1-acetamidopropene in the reaction mixtures and the high stability of the related enamide, *N*-methyl-*N*-vinylacetamide, under representative reaction conditions are not consistent with the latter explanation and, thus, would favour the allylic substitution mechanism.

The much higher regioselectivity towards the linear carboxylic acid in the hydrocarboxylation of *N*-allylacetamide, compared to propene (1:b = 1.3–1.6, irrespective of the conditions applied) suggests that the amide moiety has a directing effect. During the insertion of the C=C bond into the Pd—hydride bond, at which stage the regioselectivity is determined, the amide might coordinate to the palladium. We envisage two possible mechanisms that explain the higher selectivity to the linear isomer compared to the hydrocarboxylation of the nonfunctionalized olefin

© 2001 NRC Canada

Scheme 2. Possible mechanisms for the formation of propanal and acetamide.



propene (Scheme 3): (*i*) coordination takes place via the nitrogen which favours the formation of the anti-Markovnikov addition product (1) while there is not a large difference in reactivity of both Pd–alkyl intermediates (**1** and **2**) towards CO; (*ii*) coordination takes place via the oxygen; Markovnikov addition of Pd-H to *N*-allylacetamide affords the six-membered chelate (**4**), which is more stable but less reactive towards CO compared to the anti-Markovnikov addition product (**3**).

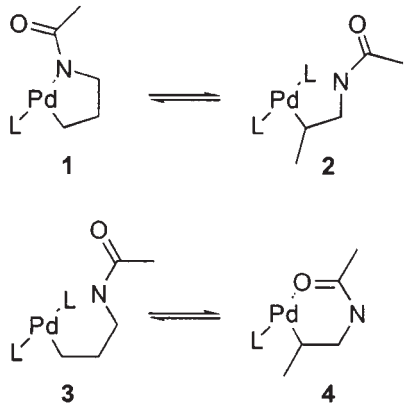
The experiments in Tables 1 and 2 reveal that the 1:b ratio decreases at higher pressures, indicating that the amide moiety competes with CO for coordination to the palladium. The rate of hydrocarboxylation is, however, independent of the pressure, which suggests that the first mechanism is operative, since a higher reactivity at higher pressures would be expected if inhibition is due to the formation of a putative stable intermediate such as **4**.

In all experiments reported in Tables 1 and 2, conducted at 60°C, the reaction rates remained constant up to ca. 70% conversion, after which inhibition was observed. Although the catalyst decomposes at temperatures >80°C, at 60°C we did not observe a black precipitate, indicating that this sudden decrease in reaction rate is not due to decomposition of the catalyst. Neither the Brønsted acid concentration, the type of Brønsted acid, the pressure, nor temperature had a significant effect on the inhibition. Addition of extra *N*-allylacetamide at t = 24 h also gave no further reaction, which rules out a possible need for a threshold substrate concentration. Only by increasing the concentration of the ligand to 13.1 mmol L^{-1} (20 equiv per Pd) were we able to achieve full conversion. In the absence of tppts the catalyst decomposed, while when 5 equiv of phosphine were added, the reaction was already inhibited after 24% conversion. Addition of more tppts as a solid to the latter reaction mixture (Experiment 3/1) led to an almost quantitative conversion.

As previously shown by a number of groups, tppts reacts with unsaturated compounds, such as acrylic acid esters, unsaturated alcohols and aldehydes, in the presence of an acid, to afford phosphonium salts (10). However, under our reaction conditions (60°C, [tppts] = 6.5 mmol L^{-1}, [*N*-allylacetamide] = 0.13 mol L^{-1}, [HOTs] = 6.5 mmol L^{-1}) the tppts ligand remained unchanged; no formation of phosphonium salts from tppts, *N*-allylacetamide, and HOTs or phosphine oxide was observed by ^{31}P NMR spectrometry. We assume that the observed inhibition of the hydrocarboxylation is caused by the coordination of byproducts that can only be displaced by an excess of tppts.

By adding 4-acetamidobutyric acid and 3-acetamido-2-methylpropanoic acid to the reaction mixture at the beginning of the experiment, we again observed an inhibition after ca. 70% conversion, just as in the case of the previously described experiments. We conclude that not the hydrocarboxylation products, but one (or more) of the side products formed in the competing hydrolysis and allylic substitution reaction, are responsible for the lower reaction rate. Further studies should reveal the identity of the actual inhibitor.

Scheme 3. Possible intermediates in the hydrocarboxylation of *N*-allylacetamide.



Finally, we observed that during the hydrocarboxylation reaction the 1:b ratio decreases with time. Since the rate of hydrolysis of both carboxylic acid products is similar, the decrease in regioselectivity must be due to changes in the coordination sphere of the palladium. We suggest that a coordinating compound can alter the coordination sphere in such a manner that the amide substituent of allylacetamide can no longer fulfil its directing effect during the insertion of the C=C bond into the Pd—hydride bond (Scheme 2). This phenomenon is also the subject of further investigations.

Experimental details

All manipulations were done under an nitrogen atmosphere. Tppts (11), *N*-allylacetamide (12), *N*-acetyl-4-aminobutyric acid, and *N*-acetyl-3-amino-2-methylpropanoic acid (13) were prepared according to previously described procedures. All other chemicals are commercially available. HPLC analyses were done using a Phenomenex organic acid collumn using a solution of 0.01 M trifluoroacetic acid in water as eluent.

Hydrocarboxylation reactions

Tppts and $PdCl_2$ were codissolved in water and the resulting bright yellow solution was transferred into a 300 mL Hasteloy C Parr autoclave that contains an aqueous solution of the Brønsted acid, the substrate, and *n*-BuOH (standard). The autoclave was closed, the nitrogen atmosphere was replaced by CO, and the autoclave was heated. When the contents reached reaction temperature (t = 0) samples were taken at regular time intervals (t = 0. 2, 4, 6, 8, and 24 h). The samples were analyzed by HPLC immediately (within 5 min). The products were identified by LC–MS and by comparing the ^{1}H and ^{13}C NMR spectra and the retention times with those of the authentic samples.

© 2001 NRC Canada

Conclusions

In comparison with the Rh–tppts catalyzed hydroformylation, the Pd–tppts catalyzed hydrocarboxylation of *N*-allylacetamide in water proceeds considerably less facile. Nevertheless, in comparison with related Pd chemistry in organic media, the results obtained are encouraging. The hydrocarboxylation of *N*-allylacetamide proceeds with a high regioselectivity towards 4-acetamidobutyric acid under mild reaction conditions, but the reaction is complicated by the hydrolysis of amide moieties in the substrate and the products, a competing allylic substitution reaction and a sudden inhibition, caused by side products. Amide hydrolysis was suppressed by optimization of the concentration of the Brønsted acid cocatalyst and the formation of acetamide and propanal was minimized by increasing the CO pressure. Unfortunately a higher CO pressure led to a lower regioselectivity. The inhibition could be circumvented by increasing the concentration of the ligand.

Acknowledgements

Financial support by the Netherlands foundation for Chemical Research (NWO-CW) is gratefully acknowledged. G.B. thanks the Royal Dutch Academy of Sciences for their financial support for his stay at the Delft Laboratories.

References

1. (*a*) B. Cornils and W.A. Herrmann (*Editors*). Aqueous-phase organometallic catalysis. Wiley–VCH, Weinheim, Germany. 1998; (*b*) G. Verspui, G.J. ten Brink, and R.A. Sheldon. Chemtracts: Org. Chem., **12**, 777 (1999)
2. (*a*) G. Verspui, J. Feiken, G. Papadogianakis, and R.A Sheldon. J. Mol. Catal. A: Chem. **146**, 299 (1999); (*b*) G. Papadogianakis, G. Verspui, L. Maat, and R.A. Sheldon. Catal. Lett. **47**, 43 (1997); (*c*) B. Xie, Y. Kou, and Y.Ying. Fenzi Cuihua, **11**, 81 (1997); (*d*) S. Tilloy, E. Monflier, F. Bertoux, Y. Castanet, and A. Mortreux. New J. Chem. **21**, 529 (1997); (*e*) F. Bertoux, S. Tilloy, E. Monflier, Y. Castanet, and A. Mortreux. J. Mol Catal. A: Chem. **138**, 53 (1999).
3. G. Verspui, G. Elbertse, F.A. Sheldon, M.A.P.J. Hacking, and R.A. Sheldon. Chem. Commun. 1363 (2000).
4. Y. Becker, A. Eisenstadt, and J.K. Stille. J. Org. Chem. **45**, 2145 (1980).
5. I. Ojima and Z. Zhang. J. Org. Chem. **53**, 4422 (1988).
6. P. Magnus and M. Slater. Tetrahedron Lett. **28**, 2829 (1987).
7. G. Papadogianakis, J.A. Peters, L. Maat, and R.A. Sheldon. Chem. Commun. 1105 (1995).
8. G. Verspui, I.I. Moiseev, and R.A. Sheldon. J. Organomet. Chem. **586**, 196 (1999).
9. (*a*) J.P. Genêt, E. Blart, M. Savignac, J.M. Paris, and J.M. Bernard. Tetrahedron Lett. **34**, 4189 (1993); (*b*) S. Lemaire-Audoire, M. Savignac, E. Blart, G. Pourcelot, J.P. Genêt, and J.M. Bernard. Tetrahedron Lett. **35**, 8783 (1994); (*c*) J.P. Genêt, E. Blart, M. Savignac, S. Lemeune, S. Lemaire-Audoire, J.M. Paris, and J.M. Bernard. Tetrahedron, **50**, 497 (1994); (*d*) S. Lemaire-Audoire, M. Savignac, G. Pourcelot, J.P. Genêt, and J.M. Bernard. J. Mol. Catal. A: Chem. **116**, 247 (1997).
10. (*a*) C. Larpent and H. Patin. Tetrahedron Lett. **29**, 4577 (1988); (*b*) C. Larpent and H. Patin. Tetrahedron, **44**, 6107 (1988); (*c*) C. Larpent, G. Meignan, J. Priol, and H. Patin. C.R. Acad. Sci. Ser. II: 493 (1990); (*d*) D.J. Darensbourg, F. Joó, A. Kathó, J.N. White Stafford, A. Bényei, and J.H. Reibenspies. Inorg. Chem. **33**, 175 (1994); (*e*) M. Hernandez and P. Kalck. J. Mol. Catal. A: Chem. **116**, 131 (1997).
11. W.A. Herrmann and C.W. Kohlpaintner. Inorg. Synth. **32**, 8 (1998).
12. G. Schlegel and H.J. Schaefer. Chem. Ber. **117**, 1400 (1984).
13. A. Mori. J. Biochemistry, **46**, 60 (1959).

© 2001 NRC Canada

Binap and MeO-Biphep complexes of Ru(II). Dicationic ligands as 6e donors. Unexpected cyclometallation in connection with P—C bond breaking

Carolien J. den Reijer, Pascal Dotta, Paul S. Pregosin, and Alberto Albinati

Abstract: A series of cationic and dicationic Ru-arene complexes with Binap (**1a**) and MeO-Biphep (**1b**) have been prepared. ^{13}C NMR studies are shown to be useful in connection with recognising the 6e-bonding mode of **1a** and **1b** in the dications [Ru(**1a** or **1b)**(η^6-arene)]$(SbF_6)_2$ (**8**, **9**). Reaction of **8**, **9** with: (*a*) $(Bu_4N)(Ph_3SiF_2)$ leads to a cyclometallated product which arises via P—C bond breaking and P—F bond making; (*b*) methanol provides a straightforward synthesis of the corresponding hydrides. ^{13}C NMR *p*-cymene chemical shifts are reported.

Key words: P—C bond cleavage, 6e donors, cyclometallation, hydrides, ^{13}C NMR.

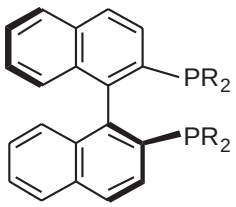
Résumé : On a préparé une série de complexes cationiques et dicationiques Ru-arène avec du Binap (**1a**) et MeO-Biphep (**1b**). Des études de RMN du ^{13}C se sont avérées utiles pour reconnaître le mode de liaison à 6-e de **1a** et **1b** dans les dications [Ru(**1a** ou **1b**)(η^6-arène)]$(SbF_6)_2$ (**8**, **9**). Les réactions des composés **8** et **9** avec : (*a*) du $(Bu_4N)(Ph_3SiF_2)$ conduisent à la formation des produits cyclométallés qui découlent de la scission d'une liaison P—C et de la formation d'une liaison P—F; (*b*) du méthanol conduisent à une synthèse directe des hydrures correspondants. On rapporte les déplacements chimiques du *p*-cymène en RMN du ^{13}C.

Mots clés : scission du liaison P—C, donneurs à 6-e, cyclométallation, hydrures, RMN du ^{13}C.

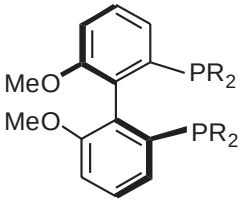
[Traduit par la Rédaction]

Introduction

The atropisomeric chelating bidentate phosphines Binap (**1a**) and MeO-Biphep (**1b**) have enjoyed substantial success in enantioselective homogenous catalysis (1, 2).



1a, R = Ph



1b, R = Ph, **1c** R = *i*-Pr

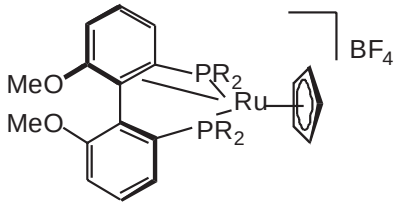
Received July 19, 2000. Published on the NRC Research Press Web site at http://canjchem.nrc.ca on July 9, 2001.

Dedicated to Professor Brian James on the occasion of his 65th birthday.

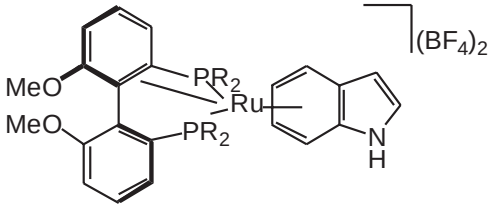
C.J. den Reijer, P. Dotta, and P.S. Pregosin.[1] Laboratory of Inorganic Chemistry, ETH-Zentrum, CH-8092 Zürich, Switzerland.
A. Albinati. Institute of Pharmaceutical Chemistry, University of Milan, Milan I-20131, Italy.

[1]Corresponding author (telephone: ++41-1-6322915; fax: ++41-1-6321090; e-mail: pregosin@inorg.chem.ethz.ch).

Interestingly, it is now known that both of these ligands can function as six (3, 4), e.g., in **3** and **4**, and even eight (5) electron donors for Ru(II).



3, R = 3,5-di-*t*-BuC_6H_3

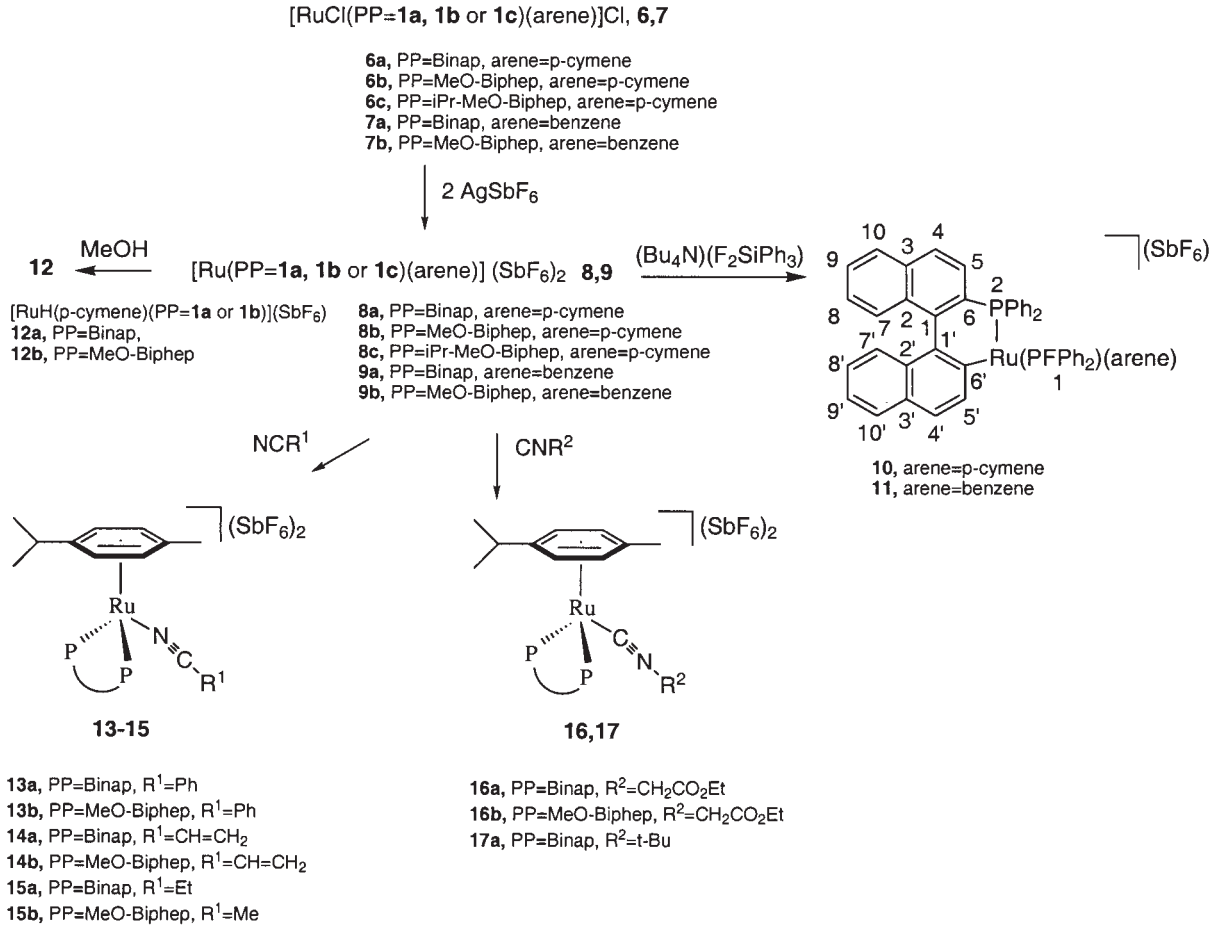


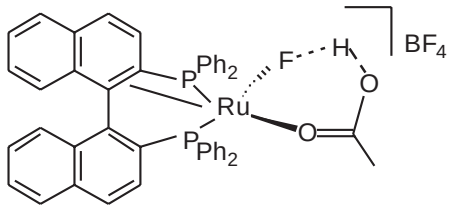
4, R = 3,5-di-*t*-BuC_6H_3

The 6e bonding mode, in which a biaryl double bond proximate to one P-donor coordinates to Ru(II), has been found both at ambient temperature as well as in low-temperature NMR studies (6) of reactive intermediates, e.g.,

 DOI: 10.1139/cjc-79-5/6-693 © 2001 NRC Canada

Scheme 1. Preparative pathway.





5

5. We report here preparative and spectroscopic studies on new dicationic η^6-arene Ru-complexes which extend our understanding of this 6e-bonding mode.

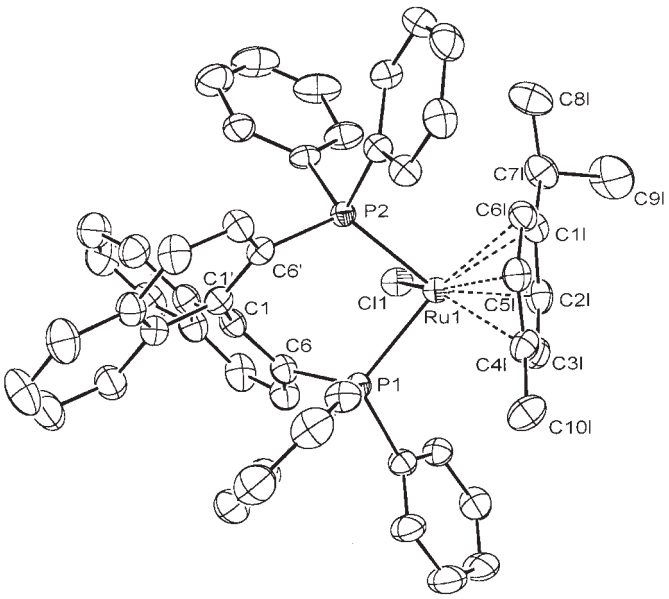
Results and discussion

The new Ru-complexes were prepared as described in Scheme 1. This chemistry starts from the cationic chloro-Ru-derivatives [RuCl(**1a** or **1b**)(η^6-arene)]Cl (**6** or **7**, respectively), which can be prepared from [$RuCl_2(\eta^6$-arene)]$_2$ (7) and the appropriate bidentate phosphine (see experimental part).

X-ray structure of 6a·1.5CH_2Cl_2

The solid-state structure of the Binap *p*-cymene analogue (**6a**) has been determined via X-ray diffraction and a view of the cation is shown in Fig. 1. The immediate coordination sphere consists of the two P-donors, the chloride, and the six carbon atoms of the η^6 p-cymene arene ligand. The six Ru-C(arene) separations fall in the range 2.258(5)–2.315(5) Å

Fig. 1. An ORTEP view of the structure of the cation of **6a**, (ellipsoids at 50% probability). The η^6-complexation is indicated by dotted lines.



and are all fairly routine (8–11). The two Ru—P distances (Ru—P(1), 2.345(1) Å and Ru—P(2), 2.380(1) Å) are somewhat long but not unusual (12). Both the Ru—Cl bond

© 2001 NRC Canada

Table 1. Selected bond lengths (Å) and bond angles (deg) for the cation in **6a**.

Bond lengths (Å)			
Ru(1)—C(1L)	2.315(5)	Ru(1)—C(4L)	2.294(5)
Ru(1)—C(2L)	2.258(5)	Ru(1)—C(5L)	2.262(5)
Ru(1)—C(3L)	2.281(5)	Ru(1)—C(6L)	2.280(5)
Ru(1)—P(1)	2.345(1)	P(1)—C(111)[a]	1.848(5)
Ru(1)—P(2)	2.380(1)	P(1)—C(121)[a]	1.831(5)
Ru(1)—Cl(1)	2.394(1)	P(2)—C(211)[b]	1.838(4)
P(1)—C(6)	1.836(5)	P(2)—C(221)[b]	1.840(5)
P(2)—C(6′)	1.851(5)		
Bond angles (deg)			
C(1L)-Ru(1)-P(1)	159.02(13)	C(4L)-Ru(1)-P(1)	93.34(13)
C(2L)-Ru(1)-P(1)	122.62(14)	C(5L)-Ru(1)-P(1)	116.94(13)
C(3L)-Ru(1)-P(1)	96.70(13)	C(6L)-Ru(1)-P(1)	153.26(13)
C(1L)-Ru(1)-P(2)	110.94(13)	C(4L)-Ru(1)-P(2)	129.16(13)
C(2L)-Ru(1)-P(2)	146.02(14)	C(5L)-Ru(1)-P(2)	99.79(13)
C(3L)-Ru(1)-P(2)	164.29(13)	C(6L)-Ru(1)-P(2)	92.28(13)
C(1L)-Ru(1)-Cl(1)	89.91(13)	C(4L)-Ru(1)-Cl(1)	139.91(13)
C(2L)-Ru(1)-Cl(1	82.12(14)	C(5L)-Ru(1)-Cl(1)	155.42(13)
C(3L)-Ru(1)-Cl(1)	103.96(13)	C(6L)-Ru(1)-Cl(1)	121.68(13)
P(1)-Ru(1)-P(2)	89.51(4)		
P(1)-Ru(1)-Cl(1)	84.95(4)		
P(2)-Ru(1)-Cl(1)	90.91(4)		

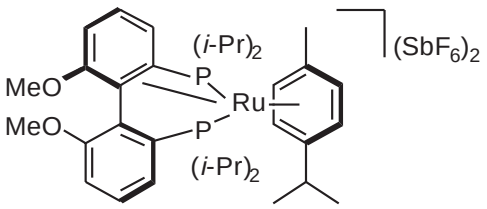
[a]C(111) and C(121) are the ipso-carbons of the phenylsubstituents of P1.
[b]C(211) and C(221) are the ipso-carbons of the phenylsubstituents of P2.

length (2.394(1) Å) and the P(1)-Ru-P(2) angle (89.51(4)°) are normal.

A list of selected bond lengths and bond angles is given in Table 1. The structure of the cation $[RuCl(Binap)(benzene)]^+$ has been reported previously (13). Taken together, the X-ray data show a classical "piano stool" structure with relatively little distortion.

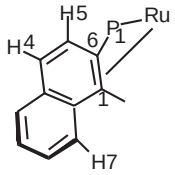
Recognition of 8 and 9

Treatment of **6**, **7** with 2 equiv of $AgSbF_6$ for prolonged periods affords the compounds **8** and **9**, as *p*-cymene and benzene derivatives, respectively, in which the chelating ligands act as 6e-donors.



8c (using ligand **1c**)

The Binap derivatives **8a** and **9a** as well the MeO-Biphep complex (**8c**) containing *i*-Pr groups on the MeO-Biphep phosphorus donors, could be isolated and afforded satisfactory analytical data. MeO-Biphep analogues **8b** and **9b**, exist in solution together with an aquo-complex. This latter assignment is based on the observation that addition of water to a solution of **9b** and the presumed aquo-species, results in a marked increase in the concentration of this second species, at the expense of **9b**. Proof of the coordination mode for **8** and **9** stems from the low frequency ^{13}C NMR coordination chemical shifts for C1 and C6 of the complexed biaryl double bond (see Table 2 and Fig. 2). The chemical shifts of C1 and C6 were determined via their three bond long-range couplings to H4, H5, and H7.



(Fragment of **9a** showing the protons used for the correlation)

The chemical shifts of the corresponding C1′ and C6′-carbons (in the second biaryl ring) fall at ca. 135–140 ppm so that the $\Delta\delta$ values for the two coordinated carbons (C1 and C6) are ca. 30–40 ppm for C1 and ca. 60–70 ppm for C6. It is tempting to use the observed relatively low-frequency ^{31}P NMR resonance of P1 (see Table 2) as an indication of this bonding mode. This chemical shift empiricism (3, 4, 6), also noted early on by James and co-workers (14), but not explored, is not always a reliable indicator since cyclometallated Ru-complexes can show similar ^{31}P NMR chemical shifts (15, 16).

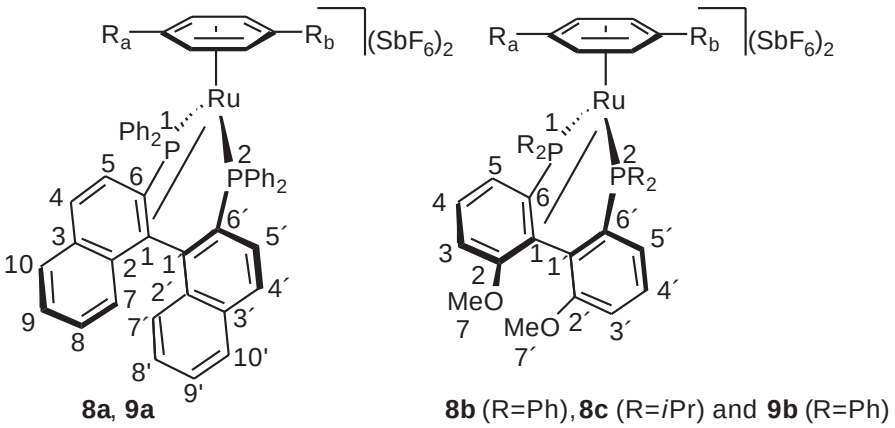
It is interesting that the observed ^{31}P frequencies for complexed **1a** vs. **1b**, do not depend markedly on the structure of the bidentate phosphine, however the ^{13}C chemical shifts values for C1 and C6 in these dications do vary as a function of the chelate (see Table 2).

P—C bond cleavage

We (6) previously reported that P—C bond splitting together with carbon protonation resulted from reaction of $Ru(OAc)_2$(**1a** or **1b**) with wet HBF_4 under relatively mild conditions (see eq. [1]). The product contains a complexed

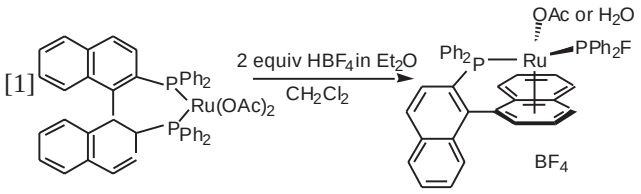
© 2001 NRC Canada

Table 2. Selected NMR chemical shifts for the carbon and phosphorus donors in **8**, **9**.



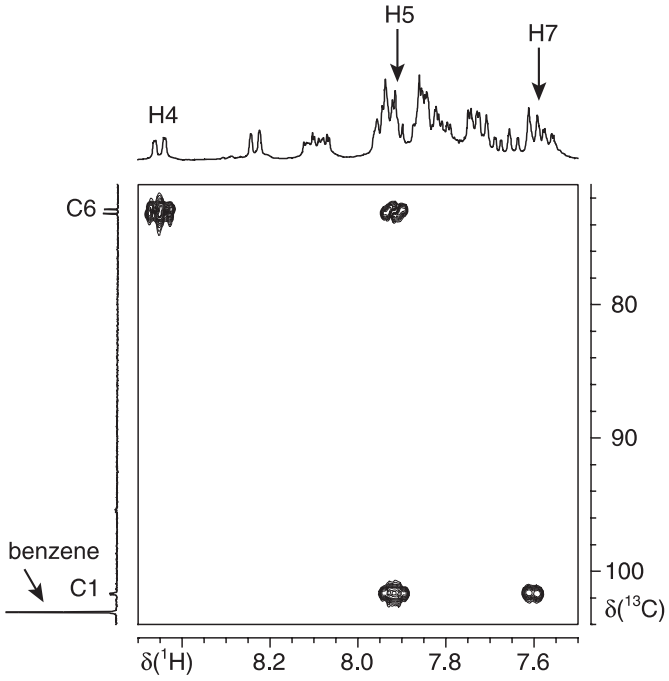
8, p-cymene = R_a=CH_3, R_b=$CH(CH_3)_2$
9, benzene = R_a=H, R_b=H

Complex	^{13}C1	^{13}C6	^{31}P1	^{31}P2
8a	98.0	67.5	3.3	68.7
8b	93.0	80.1	7.7	67.1
8c	102.5	79.1	27.3	82.6
9a	101.7	73.0	19.0	64.0
9b	90.9	86.0	15.4	64.7



diphenyl-fluoro-phosphine ligand with the BF_4^- anion functioning as the source of the fluoride. Complex **5** is an intermediate in this reaction. We know of only one related reaction (17) in which a P—C bond is so easily cleaved to form a fluorophosphine. It seemed of interest to attempt the preparation of a Ru-F species via an independent route, as the fluoride is transferred initially to the metal and only later to the P-atom. To this end we allowed $(Bu_4N)(Ph_3SiF_2)$ (18), a soluble fluoride source, to react with the Binap dications **8a** and **9a**. As shown in Scheme 1 the products are the cyclometallated fluorophosphine derivatives **10** and **11**. Obviously the complexed P-donor is sufficiently electrophilic to accept the fluoride anion with resulting cleavage of the P—C bond. In **10** and **11** the Ru(II) coordinates the (formally) negative charged carbon, whereas in the chemistry of eq. [1], where wet HBF_4 was used, one observes protonation. Compounds **10** and **11** were identified by ^{1}H, ^{13}C, ^{19}F and ^{31}P NMR spectroscopy. The $PFPh_2$ ligand is readily identified via its large $^1J(^{31}P, ^{19}F)$ value (936 Hz (**10**), 951 Hz (**11**)) and its high frequency ^{31}P NMR chemical shift (181.7 ppm (**10**), 180.4 ppm (**11**)) (19). The cyclometallated carbons are observed at 147.0 and 145.6 ppm for **10** and **11**, respectively. Figure 3 shows the ^{19}F and ^{31}P NMR spectra of the cation of compound **11**.

Fig. 2. ^{13}C-^{1}H long-range correlation for **9a** showing cross-peaks for the two olefinic carbons with the three Binap backbone protons.



Hydride synthesis from 8

The dications **8a**, **b** react smoothly on stirring in MeOH as solvent at room temperature to afford the hydride complexes [RuH(*p*-cymene)(**1a** or **1b**)]SbF_6 (**12a**, **b**). No base is necessary and the yields are good. This straightforward ap-

© 2001 NRC Canada

Fig. 3. ^{19}F and ^{31}P NMR spectra of the cation of **11**. Top: $PFPh_2$ region showing the ^{19}F NMR resonance for the F atom of the new $PFPh_2$-ligand with a large $^1J(^{31}P\text{-}^{19}F)$ coupling constant and the smaller $^3J(^{31}P\text{-}^{19}F)$ coupling constant. Bottom: the nonequivalent ^{31}P NMR resonances. The high frequency signal shows the large $^1J(^{31}P\text{-}^{19}F)$ coupling as well as the $^2J(^{31}P\text{-}^{31}P)$ interaction.

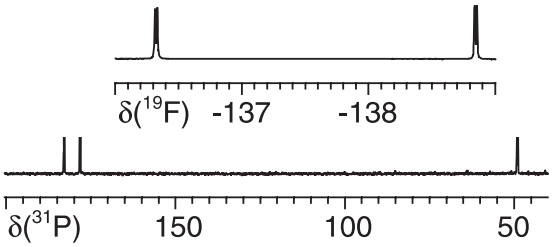
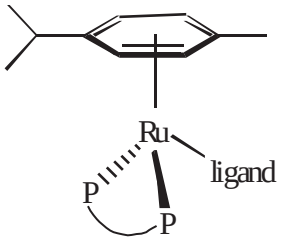


Table 3. Averaged CH-arene ^{13}C NMR chemical shifts in Ru(*p*-cymene) complexes.[a]



Ligand	Binap	MeO-Biphep
Cl (**6**)	98.5	98.3
η-2 olefin (**8**)	101.9	96.8
H (**12**)	96.0	95.8
PhCN (**13**)	99.9	99.7
CH_2=CHCN (**14**)	99.8	99.7
CH_3CH_2CN (**15a**)	99.5	—
CH_3CN (**15b**)	—	99.1
$(CO_2Et)CH_2NC$ (**16**)	104.1	103.8
t-BuNC (**17**)	104.2	—

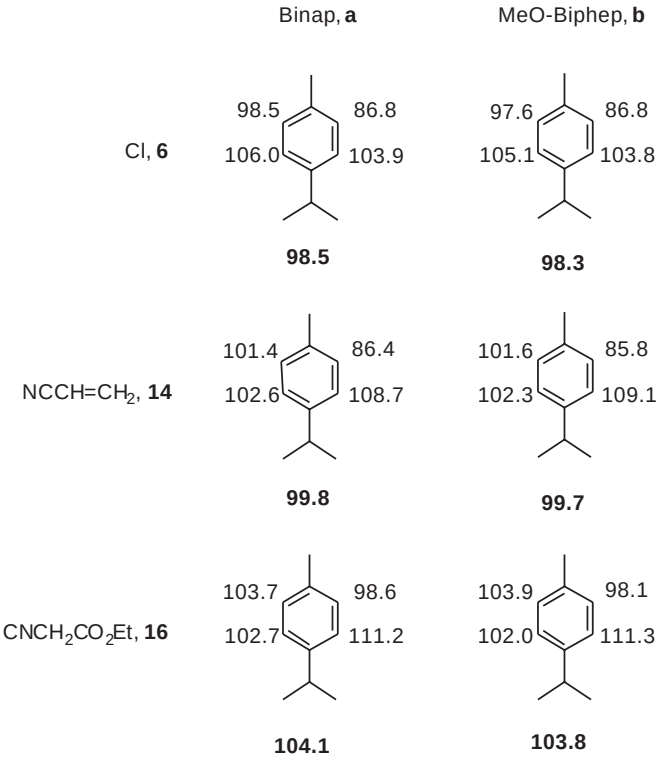
[a]As mono- or di-SbF_6 cations.

proach to hydride synthesis provides a useful alternative to synthetic routes involving molecular hydrogen or boron or aluminium hydrides. The ^1H NMR spectra for **12a**, **b** show the hydride resonances as a doublet of doublets at δ = –9.79 and δ = –10.10 for **12a** and **12b**, respectively. The *p*-cymene ^{13}C NMR resonances are shifted to lower frequency and fall in the region δ = 91.5–116.8, with the four CH-carbons of the *p*-cymene appearing in the narrow range 91.5–98.3 ppm. Interestingly, the MeO-Biphep complex (**8b**) reacts to afford product ca. 10 times faster than the Binap analogue (**8a**). We have made similar qualitative observations with respect to relative kinetics in other reactions, as well, i.e., MeO-Biphep is generally faster than Binap in our Ru-chemistry. There are relatively few well-characterised Ru-H complexes of **1a** and **1b** (20, 21).

^{13}C NMR data for the *p*-cymene ligand

The carbon-13 chemical shifts for the complexed arenes in e.g., **6**–**12** are readily determined in that they fall in a convenient region (ca. 70–110 ppm). Having noticed that this NMR parameter varies somewhat for the η^2-olefin of **8**, **9** we

Scheme 2. ^{13}CH-chemical shifts (ppm) for selected arene complexes. The averages of the chemical shifts, i.e., the sum divided by four, are written in bold (ppm).



considered it interesting to compare the ^{13}C NMR η^6 *p*-cymene characteristics in several Binap and MeO-Biphep compounds. To this end we prepared the dicationic nitrile and isonitrile complexes (**13**–**15** and **16**, **17**, respectively), and show examples in Scheme 2 (and the remaining data in the experimental part). It is interesting that the four CH=*p*-cymene ^{13}C NMR signals are well separated suggesting asymmetric bonding for this arene. It is equally interesting that these ^{13}C NMR chemical shifts in **6** and **14** do not vary very much, either as a function of charge on the complex or as a function of the chelate ligand. Moreover, the averages of the four δ CH= values (98.5 for **6a**, 98.3 for **6b**, 99.8 for **14a**, and 99.7 ppm for **14b**) are quite close. Thus, it appears that the total charge on the molecule, i.e., monocationic for the chloride complexes and dicationic for the acrylonitrile complexes, is of secondary importance in this connection. The nature of the donor is the more important factor as shown by the averages for **16a** (104.1) and **16b** (103.8), i.e., ca. 4–5 ppm larger than the previous averages. This suggests that the isocyanoacetate ligand is a better π-acceptor ligand than either the cloride or the acrylonitrile. In Table 3 we show averages for the four cymene CH= signals for a larger data set. The olefin and isonitrile π-acceptor ligands result in higher frequency positions whereas the hydride, due to its stronger σ-donor character, affords a lower frequency result. For the Binap series, we have carried out a similar analysis using all six carbons of the *p*-cymene. Inclusion of the two fully substituted carbon chemical shifts moves the averaged results to higher frequency by ca. 5–6 ppm, but does not change any of the conclusions.

© 2001 NRC Canada

Table 4. Experimental data for the X-ray diffraction study of compound **6a** ($1.5CH_2Cl_2$).

Formula	$C_{55.5}H_{49}Cl_5P_2Ru$
Mol wt	1056.26
Crystal size (mm)	0.32 × 0.26 × 0.20
Data coll. *T* (K)	200 (2)
Diffractometer	SMART CCD
Cryst syst	monoclinic
Space group (no.)	$P2_1/c$ (14)
a (Å)	12.5980 (2)
b (Å)	21.8156 (1)
c (Å)	19.4865 (3)
β (deg)	107.869 (2)
V (Å^3)	5097.2 (1)
Z	4
$\rho_{(calcd)}$ (g cm^{-3})	1.371
μ (cm^{-1})	6.15
Radiation	Mo Kα (graphite monochrom. λ = 0.71073 Å)
θ Range (deg)	1.94 < θ < 27.47
Scan type	ω
No. of measured frames	2142
*t*ime per frame (s)	20
Scan width per frame (deg)	0.3
No. independent data	11 569
No. obs. reflct. (n_o) [$\|F_o\|^2 > 2.0\sigma(\|F\|^2)$]	8741
Transmission coeff.	0.83–0.93
No. of param. refined (n_v)	564
R_{av}	0.057
R (obs. reflct.)	0.058
R^2_w (obs. reflct.)	0.124
GOF	0.738

Note: $R_{av} = \Sigma|F_o^2 - F_o^2{}_{,av}|/\Sigma_i|F_o^2|$; $R = \Sigma(|F_o - (1/k)F_c|)/\Sigma|F_o|$; $R^2_w = [\Sigma w(F_o^2 - (1/k)F_c^2)^2/\Sigma w|F_o^2|^2]$ where $w = 1/[\sigma^2(F_o^2) + (0.1717P)^2 + 30.9364P]$ and $P = (F_o^2 + 2F_c^2)/3.0$; GOF = $[\Sigma_w(F_o^2 - (1/k)F_c^2)^2/(n_o - n_v)]^{1/2}$.

Conclusions

The biaryl phosphine ligands **1a** and **1b** readily complex an adjacent biaryl double bond. This co-ordination introduces some strain in the molecule so that reaction with a fluoride source readily leads to P—C bond cleavage and the formation of a cyclometallated complex. The complexes **8a** and **8b** react easily with MeOH to give the respective hydride complexes **12a** and **12b** in good yield. Interestingly, the *p*-cymene ^{13}C NMR chemical shifts do not depend on the formal positive charge on the cation, but rather the nature of the donor ligands.[2]

Experimental section

Crystallography

Air stable, orange crystals of compound **6a** were obtained via slow diffusion of diethyl ether into a solution of **6a** in dichloromethane.

For the data collection, a prismatic single crystal was mounted on a Bruker SMART CCD diffractometer. The space group was determined from the systematic absences, while the cell constants were refined, at the end of the data collection with the data reduction software SAINT (22). The collected intensities were corrected for Lorentz and polarization factors (22) and empirically for absorption using the SADABS program (23). Selected crystallographic and other relevant data collection and refinement parameters are listed in Table 4.

The standard deviations on intensities were calculated in term of statistics alone, while those on F^2_o were calculated as shown in Table 4. The structure was solved by direct and Fourier methods and refined by full-matrix least-squares (24), minimizing the function $(\Sigma w(F_o^2 - (1/k)F_c^2)^2)$ and using anisotropic displacement parameters for all atoms. Toward the end of the refinement a disordered solvent (CH_2Cl_2) molecule was located in a difference Fourier map and successfully refined, allowing two orientations for the Cl atoms (with occupancy factors of 0.75 and 0.25, respectively). After refinement, a second CH_2Cl_2 molecule was located in the difference Fourier map but refined satisfactorily (with isotropic temperature factors) only with partial occupancy of the site (0.5). No extinction correction was deemed necessary. Upon convergence (max parameter shift $\Delta p/\sigma < 0.3$) the final difference Fourier map showed no significant peaks.

The contribution of the hydrogen atoms, in their calculated position (C—H = 0.95 Å, B(H) = 1.5 × $B(C_{bonded})$ Å^2), was included in the refinement using a riding model; the hydrogen atoms bonded to the disordered solvent molecules were not included.

All calculations were carried out by using the PC version of the SHELX-97 programs (22). The scattering factors used, corrected for the real and imaginary parts of the anomalous dispersion, were taken from the literature (25).

General

All manipulations were carried out under argon atmosphere. Methanol was distilled from magnesium. Diethyl ether was distilled from sodium-benzophenone ketyl. Dichloromethane and pentane were distilled from CaH_2. Hexane and toluene were distilled from sodium. $[Ru(benzene)Cl_2]_2$ (**7a**) (7), [Ru(Binap)(benzene)Cl]Cl (13) as well as tetrabutylammonium difluorotriphenylsilicate ($(Bu_4N)(F_2SiPh_3)$) (18) were prepared according to the literature. $[Ru(p\text{-cymene})Cl_2]_2$ is commercially available at Aldrich, and was purified before use. Rac-2,2′-bis(diphenylphosphino)-1,1′-binaphthyl (Binap) was purchased from Strem Chemicals. *S*-(6,6′-Dimethoxybiphenyl-2,2′-diyl)bis(diphenylphosphine) (*S*-MeO-Biphep) and *R*-*i*-Pr-MeO-Biphep were provided by

[2] Supplementary material may be purchased from the Depository of Unpublished Data, Document Delivery,CISTI, National Research Council Canada, Ottawa, ON K1A 0S2, Canada (http://www.nrc.ca/cisti/irm/unpub_e.shtml for information on ordering electronically). Copies of the data can be obtained, free of charge, on application to the Director, CCDC, 12 Union Road, Cambridge CB2 1EZ, U.K. (Fax: 44-1223-336033 or e-mail: deposit@ccdc.cam.ac.uk).

© 2001 NRC Canada

F. Hoffmann-La Roche AG. All the other chemicals were commercial products used as received. NMR Spectra were measured on a Bruker AVANCE 400 MHz spectrometer. Chemical shifts are given in ppm, coupling constants in Hz.

Synthesis of [RuCl(Binap)(*p*-cymene)]Cl (6a)

$[Ru(p\text{-cymene})Cl_2]_2$ (60.9 mg, 0.10 mmol) and Binap (130.0 mg, 0.21 mmol) were dissolved in 3 mL methanol and then stirred for 15 h at room temperature. The solution was then heated for 8 h at 40°C. The reaction mixture was filtered through Celite and then the solvent was evaporated in vacuo. The resulting orange powder was washed with 2 × 3 mL Et_2O and 1 × 2 mL pentane and then dried in vacuo. Color: orange. Yield: 62.2 mg (67%). FAB-MS calcd. M^+: 892.6; found: M^+-*p*-cymene: 758.5; M^+-Cl: 857.6. ^{1}H NMR (298 K, CD_2Cl_2): 1.03 (d, $^3J_{HH}$ = 6.8, CH(CH_3)$_2$), 1.37 (d, $^3J_{HH}$ = 6.8, CH(CH_3)$_2$), 1.99 (s, CH_3), 3.08 (m, CH(CH$_3$)$_2$), 4.41 (d, $^3J_{HH}$ = 3.7, cyH), 4.42 (d, $^3J_{HH}$ = 6.8, cyH), 6.00 (d, $^3J_{HH}$ = 6.8, cyH), 6.50 (d, $^3J_{HH}$ = 3.7, cyH). ^{13}C NMR (298 K, CD_2Cl_2): 19.4 (*C*H$_3$), 21.8 (CH(*C*H$_3$)$_2$), 23.2 (CH(*C*H$_3$)$_2$), 30.6 (*C*H(CH$_3$)$_2$), 86.8 (cy), 97.1 (cy), 103.9 (cy), 106.0 (cy), 110.8 (cy), 113.6 (cy). ^{31}P NMR (298 K, CD_2Cl_2): 41.5 (d, $^2J_{PP}$ = 63), 26.7 (d, $^2J_{PP}$ = 63). Anal. calcd. for $C_{54}H_{46}P_2Cl_2Ru\cdot 0.5CH_2Cl_2$ (928.1): C 67.39, H 4.88; found: C 66.67, H 5.67.

Synthesis of [RuCl(*S*-MeO-Biphep)(*p*-cymene)]Cl (6b)

$[Ru(p\text{-cymene})Cl_2]_2$ (151.7 mg, 0.25. mmol) and *S*-MeO-Biphep (292.3 mg, 0.50. mmol) were dissolved in 3 mL methanol and then stirred for 3 h at room temperature. Then the orange solution was filtered through Celite. The solvent was evaporated in vacuo to afford the orange product. Color: orange. Yield: 410.1 mg (93%). Anal. calcd. for $C_{48}H_{42}O_2P_2Cl_2Ru\cdot 3MeOH$ (884.78): C 62.42, H 5.49; found: C 62.44, H 5.51. FAB-MS calcd. M^+: 849.4; found: M^+-Cl-*p*-cymene: 679.7. ^{1}H NMR (298 K, CD_2Cl_2): 1.04 (d, $^3J_{HH}$ = 6.9, CH(CH_3)$_2$), 1.39 (d, $^3J_{HH}$ = 6.9, CH(CH_3)$_2$), 1.99 (s, CH_3), 3.09 (m, CH(CH$_3$)$_2$), 3.38 (s, OCH_3), 3.45 (s, OCH_3), 4.38 (d, $^3J_{HH}$ = 7.0, cyH), 4.52 (br d, $^3J_{HH}$ = 6.2, cyH), 5.97 (d, $^3J_{HH}$ = 7.0, cyH), 6.52 (d, $^3J_{HH}$ = 6.2, cyH). ^{13}C NMR (298 K, CD_2Cl_2): 19.2 (*C*H$_3$), 21.6 (CH(*C*H$_3$)$_2$), 23.0 (CH(*C*H$_3$)$_2$), 30.4 (*C*H(CH$_3$)$_2$), 55.3 (O*C*H$_3$), 55.5 (O*C*H$_3$), 86.0 (cy), 97.5 (cy), 103.9 (cy), 105.2 (cy). ^{31}P NMR (298 K, CD_2Cl_2): 41.5 (d, $^2J_{PP}$ = 63), 28.3 (d, $^2J_{PP}$ = 63).

Synthesis of [RuCl(*R*-*i*-Pr-MeO-Biphep)(*p*-cymene)]Cl (6c)

$[Ru(p\text{-cymene})Cl_2]_2$ (65.3 mg, 0.11 mmol) and R-*i*-Pr-MeO-Biphep (95.5 mg, 0.22 mmol) were dissolved in 2 mL methanol and then stirred for 3 h at room temperature. Then the orange solution was filtered through Celite and the solvent was evaporated in vacuo to afford an orange powder. The product was then washed with 3 × 1 mL Et_2O and dried in vacuo. Color: orange. Yield: 130.2 mg (79%). HR-MALDI-MS calcd. M^+: 717.3; found: M^+-*i*-Pr: 701.2; M^+-*p*-cymene: 583.1; M^+-*p*-cymene-Cl: 545.2. ^{1}H NMR (298 K, CD_2Cl_2) : 0.78–1.85 (overlapping *i*-Pr protons and *p*-cymene Me-protons), 2.71 (m, CH(CH$_3$)$_2$), 3.75 (s, OCH$_3$), 3.78 (s, OCH$_3$), 5.60 (br d, cyH), 6.06 (d, $^3J_{HH}$ = 5.8, cyH), 6.68 (br d, cyH), 7.00, 7.16, 7.40, 7.62, 7.72 (overlapping cyH and MeO-biphep backbone protons). ^{31}P1H NMR (298 K, CD_2Cl_2): 41.6 (d, $^2J_{PP}$ = 46), 34.4 (d, $^2J_{PP}$ = 46). Anal. calcd. for $C_{36}H_{54}O_2P_2Cl_2Ru\cdot 2MeOH$ (752.74): C 55.88, H 7.59; found: C 55.88, H 7.56.

Synthesis of [RuCl(*S*-MeO-Biphep)(benzene)]Cl (7b)

$[Ru(benzene)Cl_2]_2$ (122.0 mg, 0.24 mmol) and *S*-MeO-Biphep (286.8 mg, 0.49 mmol) were dissolved in 6 mL of a 2:1 mixture of methanol and toluene. Stirring at room temperature for 3 h was followed by the filtration through Celite. The solvents were evaporated in vacuo and then the yellow powder was washed with 3 × 1 mL Et_2O and dried in vacuo. Color: yellow. Yield: 367.8 mg (90%). FAB-MS calcd. M^+: 832.8; found M^+-benzene: 718.9; M^+ -benzene -Cl: 684.0. ^{1}H NMR (298 K, CD_2Cl_2): 3.46 (s, OCH_3), 3.57 (s, OCH_3), 5.76 (s, C_6H_6), 6.50, 6.82, 6.76, 6.96, 7.17, 7.24 (all 6 MeO-Biphep backbone). ^{13}C NMR (298 K, CD_2Cl_2): 55.5 (O*C*H$_3$), 55.6 (O*C*H$_3$), 97.4 (*C*$_6$H$_6$), 113.0, 113.2, 125.1, 126.0, 126.6, 127.2, 127.5, 129.1, 129.6, 130.9, 158.0, 159.0 (all 12 MeO-Biphep backbone). ^{31}P NMR (298 K, CD_2Cl_2): 39.1 (d, $^2J_{PP}$ = 64), 32.3 (d, $^2J_{PP}$ = 64). Anal. calcd. for $C_{44}H_{38}O_2P_2Cl_2Ru$ (832.75): C 63.47, H 4.60; found: C 63.04, H 5.22.

Synthesis of 8a–9b

The reactions are quantitative, however due to the small scales, losses occurred in the work-up.

Synthesis of [Ru(Binap)(*p*-cymene)][SbF_6]$_2$ (8a)

[RuCl(Binap)(*p*-cymene)]Cl (**6a**) (185.0 mg, 0.20 mmol) and $AgSbF_6$ (137.0 mg, 0.40 mmol) were dissolved in 6 mL dichloromethane. The resulting suspension was stirred for 24 h at 40°C. Then the precipitate of AgCl was filtered and the solvent was removed in vacuo to afford the product. Color: red. Yield: 216.2 mg (87%). ^{1}H NMR (253 K, CD_2Cl_2): 0.00 (d, CH(CH_3)$_2$), 0.02 (m, CH(CH$_3$)$_2$), 0.71 (d, CH(CH_3)$_2$), 1.78 (s, CH_3), 4.55 (d, cyH), 5.59 (d, cyH), 5.79 (d, cyH), 6.27 (d, cyH), 5.56 (H7′), 7.22 (H10′), 7.34 (H5′), 7.44 (H9′), 7.54 (H7′), 7.57 (H4′), 7.59 (H8′), 7.60 (H8), 7.77 (H9), 8.31 (H10), 8.56 (H5), 8.66 (H4). ^{13}C NMR (253 K, CD_2Cl_2): 17.4 (*C*H$_3$), 18.3 (CH(*C*H$_3$)$_2$), 24.1 (CH(*C*H$_3$)$_2$), 29.2 (*C*H(CH$_3$)$_2$), 67.5 (C6), 92.0 (cy), 98.0 (C1), 104.0 (cy), 104.0 (cy), 107.6 (cy), 114.0 (cy), 124.7 (C5′), 125.1 (C7′), 125.4 (C5), 126.0 (cy), 128.6 (C7), 128.8 (C8′), 129.7 (C9′), 129.8 (C10′), 130.2 (C3), 131.6 (C10), 131.7 (C6′), 133.0 (C8), 133.2 (C2′), 133.8 (C4′), 134.0 (C9), 135.5 (C3′), 138.3 (C4), 142.0 (C2), 145.3 (C1′). ^{31}P NMR (253 K, CD_2Cl_2): 68.7 (d, $^2J_{PP}$ = 44), 3.3 (d, $^2J_{PP}$ = 44). Anal. calcd. for $C_{54}H_{46}F_{12}P_2RuSb_2\cdot H_2O$ (1242.6): C 48.13, H 3.59; found: C 48.10, H 3.85. FAB-MS calcd. M^{2+}: 857.9; found: M^{2+} + SbF_6: 1092.6; M^{2+} + SbF_6-*p*-cymene: 958.6; M^{2+}: 857.9; M^{2+}-*p*-cymene 721.2.

Synthesis of [Ru(*S*-MeO-Biphep)(*p*-cymene)][SbF_6]$_2$ (8b)

[RuCl(*S*-MeO-Biphep)(p-cymene)]Cl (**6b**) (58.6 mg, 0.07 mmol) and $AgSbF_6$ (41.6 mg, 0.12 mmol) were dissolved in 1 mL dichloromethane and the resulting suspension was refluxed overnight. Then the precipitate of AgCl was filtered through Celite and the solvent was removed in vacuo to afford the product. Color: red. Yield: 68.2 mg (76%). FAB-MS calcd. M^{2+}: 818.0; found: M^{2+}: 818.9; M^{2+}-*p*-cymene: 683.0. ^{1}H NMR (243 K, CD_2Cl_2): 0.47 (d, CH(CH_3)$_2$), 1.01 (d, CH(CH_3)$_2$), 1.77 (m, CH(CH$_3$)$_2$), 2.16 (s, CH_3), 3.58 (s, OCH_3), 3.92 (s, OCH_3), 4.29, (d, cyH),

© 2001 NRC Canada

5.17 (d, cyH), 5.57 (d, cyH), 5.95 (d, cyH), 6.56 (H3′), 6.57 (H5′), 7.03 (H4′), 7.36 (H3), 7.88 (H5), 8.23 (H4). ^{13}C NMR (243 K, CD_2Cl_2): 17.9 (CH(CH_3)$_2$), 18.6 (CH_3), 25.1 (CH(CH_3)$_2$), 29.5 (CH(CH_3)$_2$), 56.5 (H7′), 57.7 (H7), 80.1 (C6), 92.5 (cy), 93.0 (C1), 100.7 (cy), 103.6 (cy), 103.8 (cy), 107.7 (C3), 108.0 (cy), 115.0 (C3′), 121.4 (C5), 121.8 (C5′), 123.4 (cy), 132.6 (C4′), 134.7 (C6′), 141.0 (C4), 157.0 (C2′), 172.3 (C2). ^{31}P NMR (243 K, CD_2Cl_2): 67.1 (d, $^2J_{PP}$ = 45), 7.7 (d, $^2J_{PP}$ = 45). Anal. calcd. for $C_{48}H_{46}F_{12}P_2RuSb_2$ (1289.4): C 44.71, H 3.60; found: C 44.97, H 3.90.

Synthesis of [Ru(*R*-*i*-Pr-MeO-Biphep)(*p*-cymene)][SbF_6]$_2$ (8c)

[RuCl(*R*-*i*-Pr-MeO-Biphep)(*p*-cymene)]Cl (**6c**) (39.6 mg, 0.05 mmol) and $AgSbF_6$ (34.1 mg, 0.10 mmol) were dissolved in 1 mL dichloromethane and the resulting suspension was refluxed overnight. Then the precipitate of AgCl was removed by filtration through Celite. The evaporation of the solvent in vacuo afforded the product. Color: red. Yield: 42.5 mg (74%). FAB-MS calcd. M^{2+}: 681.9; found: M^{2+} + SbF_6: 917.7; M^{2+}: 682.1; M^{2+}-*p*-cymene: 548.0. ^{1}H NMR (298 K, CD_2Cl_2) : 1.08 (d, CH(CH_3)$_2$), 1.21 (d, CH(CH_3)$_2$), 1.79 (m, CH(CH_3)$_2$), 2.40 (s, CH_3), 3.54 (s, H7′), 3.78 (s, H7), 5.06 (d, cyH), 5.75 (d, cyH), 5.95 (d, cyH), 6.71 (d, cyH), 6.95 (H3′), 7.08 (H5′), 7.24 (H3), 7.61 (H4′), 7.61 (H5), 8.01 (H4). ^{13}C NMR (298 K, CD_2Cl_2): 19.7 (CH_3), 19.9 (CH(CH_3)$_2$), 24.6 (CH(CH_3)$_2$), 29.1 (CH(CH_3)$_2$), 56.0 (C7′)), 57.0 (C7), 79.1 (C6), 90.5 (cy), 93.0 (C1), 95.7 (cy), 98.6 (cy), 100.8 (cy), 102.4 (cy), 102.5 (C1), 107.7 (C3), 115.4 (C3′), 122.7 (C5′), 124.5(C5), 126.3 (cy), 132.3 (C1′), 133.3 (C4′), 134.2 (C6′), 138.6 (C4), 168.7 (C2),157.8 (C2′). ^{31}P NMR (298 K, CD_2Cl_2): 82.6 (d, $^2J_{PP}$ = 39), 27.3 (d, $^2J_{PP}$ = 39). Anal. calcd. for $C_{36}H_{54}O_2F_{12}P_2RuSb_2$ (1153.4): C 37.49, H 4.72; found: C 37.51, H 5.32.

Synthesis of [Ru(Binap)(benzene)][SbF_6]$_2$ (9a)

[RuCl(Binap)(benzene)]Cl (**7a**) (226.9 mg, 0.26 mmol) and $AgSbF_6$ (178.4 mg, 0.52 mmol) were dissolved in 2 mL dichloromethane and the resulting suspension was refluxed overnight. Then the precipitate of AgCl was filtered using Celite and then the solvent was removed in vacuo to afford the product. Color: red. Yield: 285.6 mg (86%). FAB-MS calcd. M^{2+}: 801.9; found M^{2+} + SbF_6: 1036.3; M^{2+} + SbF_6-benzene: 958.2; M^{2+}: 801.4; M^{2+}-benzene: 730.4. ^{1}H NMR (298 K, CD_2Cl_2): 5.72 (s, C_6H_6), 5.94 (H7′), 7.40 (H5′), 7.42 (H8′), 7.61 (H7), 7.66 (H9′), 7.71 (H8), 7.85 (H9), 7.92 (H4′), 7.92 (H5), 7.95 (H10′), 8.23 (H10), 8.45 (H4). ^{13}CNMR (298 K, CD_2Cl_2): 73.0 (C6), 101.7 (C1), 103.1 (C_6H_6), 125.2 (C7′), 126.1 (C5′), 126.8 (C5), 129.3 (C10′), 130.0 (C8′), 131.2 (C10), 133.4 (C3), 133.4 (C4′), 133.6 (C8), 133.8 (C2′), 136.1 (C3′), 138.3 (C4), 144.9 (C2), 146.8 (C1′). ^{31}P NMR (298 K, CD_2Cl_2): 64.0 (d, $^2J_{PP}$ = 46), 19.0 (d, $^2J_{PP}$ = 46). Anal. calcd. for $C_{50}H_{38}F_{12}P_2RuSb_2$ (1273.4): C 47.16, H 3.01; found: C 47.06, H 3.12.

Synthesis of [Ru(*S*-MeO-Biphep)(benzene)][SbF_6]$_2$ (9b)

[RuCl(*S*-MeO-Biphep) (benzene)]Cl (**7b**) (219.8 mg, 0.26 mmol) and $AgSbF_6$ (179.2 mg, 0.52 mmol) were dissolved in 1 mL dichloromethane and the resulting suspension was refluxed overnight. The precipitate of AgCl was filtered using Celite and the the solvent was removed in vacuo to afford the product. Color: red. Yield: 296.2 mg (92%). FAB-MS calcd. M^{2+}: 761.8; found: M^{2+} + SbF_6-benzene: 919.3; M^{2+}: 761.4; M^{2+}-benzene: 688.5. ^{1}H NMR (298 K, CD_2Cl_2): 3.78 (s, H7′), 4.16 (s, H7), 5.68 (s, C_6H_6), 6.75 (H5′), 6.99 (H3′), 7.26 (H3), 7.27 (H4′), 7.38 (H5), 8.15 (H4). ^{13}CNMR (298 K, CD_2Cl_2): 56.7 (C7′), 58.3 (C7), 100.8 (C_6H_6), 86.0 (C6), 90.9 (C1), 107.6 (2), 115.4 (C3′), 120.9 (C5), 123.0 (C5′), 134.0 (C4), 134.1 (C1′), 134.2 (C4′), 135.6 (C6′), 157.6 (C2′), 176.6 (C2). ^{31}P NMR (298 K, CD_2Cl_2): 64.7 (d, $^2J_{PP}$ = 49), 15.4 (d, $^2J_{PP}$ = 49). Anal. calcd. for $C_{44}H_{38}F_{12}P_2RuSb_2$ (1233.3): C 42.85, H 3.11; found: C 42.79, H 3.61.

Reaction of [Ru(Binap)(*p*-cymene)][SbF_6]$_2$ (8a) with (Bu_4N)(F_2SiPh_3) (10)

[Ru(Binap)(*p*-cymene)][SbF_6]$_2$ (**8a**) (18.8 mg, 0.014 mmol) was dissolved in 1 mL CD_2Cl_2 in an NMR tube. The resulting red solution was cooled to –78°C before (Bu_4N)(F_2SiPh_3) (7.9 mg, 0.014 mmol), under a continous Ar flow, was added. The color of the solution changed from red to yellow. A ^{31}P NMR spectrum of the cooled solution, measured immediately, showed complete conversion of the starting Ru-compound to a single new Ru-complex, **10**. The solution was allowed to come to room temperature and the complex **10** was characterised by NMR spectroscopic methods. Then the solvent was evaporated in vacuo and washed 3 × 3 mL Et_2O. The yellow powder was dried in vacuo. FAB-MS calcd. M^+: 877.0; found: M^+: 877.3; M^+ -*p*-cymene: 743.3. ^{1}H NMR (298 K, CD_2Cl_2): 0.13 (d, $^3J_{HH}$ = 6.9, CH(CH_3)$_2$), 1.03 (d, $^3J_{HH}$ = 6.9, CH(CH_3)$_2$), 1.67 (s, CH_3), 2.56 (m, CH(CH_3)$_2$), 5.56 (br d, $^3J_{HH}$ = 6.5, cyH), 5.71 (d, $^3J_{H7',H8'}$ = 8.8, H7′), 5.84 (br d, $^3J_{HH}$ = 6.7, cyH), 6.09 (br d, $^3J_{HH}$ = 6.5, cyH), 6.12 (br d, $^3J_{HH}$ = 6.9, cyH), 6.67 (ddd, $^3J_{H7',H8'}$ = 8.8, $^3J_{H8',H9'}$ = 7.8, $^3J_{H8',H10'}$ = 1.2, H8′), 6.33 (d, $^3J_{H7,H8}$ = 8.6, H7), 6.79 (H8), 7.19 (H9), 7.30 (H5′), 7.32 (H4′), 7.33 (H9′), 7.48 (H4), 7.70 (H10), 7.76 (br d, $^3J_{H8',H9'}$ = 8.3, H10′), 8.39 (d, $^3J_{H4,H5}$ = 8.4, H5). ^{13}C NMR (298 K, CD_2Cl_2): 17.4 (CH_3), 20.1 (CH(CH_3)$_2$), 23.8 (CH(CH_3)$_2$), 31.0 (CH(CH_3)$_2$), 99.4 (cy), 102.0 (cy), 102.3 (cy), 103.8 (cy), 114.1 (cy), 125.0 (C5′), 124.2 (C9), 124.9 (C8), 125.9 (C7), 129.3 (C8′), 127.3 (C7′), 127.2 (C10), 126.2 (C10′), 128.0 (C9′), 127.6 (C4′), 131.9 (C3), 132.3 (cy), 133.3 (C2′), 134.3 (C2), 134.8 (C3′), 140.3 (C1), 144.1 (C5), 147.0 (C6), 147.7 (C6′), 140.3 (C1′). ^{31}P NMR (298 K, CD_2Cl_2): 181.7 (dd, $^1J_{PF}$ = 936, $^2J_{PP}$ = 50), 50.9 (dd, $^2J_{PP}$ = 50, $^3J_{PF}$ = 13). ^{19}F NMR (298 K, CD_2Cl_2): –139.1 (dd, $^1J_{PF}$ = 936, $^3J_{PF}$ = 13).

Reaction of [Ru(Binap)(benzene)][SbF_6]$_2$ (9a) with (Bu_4N)(F_2SiPh_3) (11)

[Ru(Binap)(benzene)][SbF_6]$_2$ (**9a**) (33.5 mg, 0.03 mmol) was dissolved in 1 mL CD_2Cl_2 in an NMR tube. The resulting red solution was cooled to –78°C before (Bu_4N)(F_2SiPh_3) (13.9 mg, 0.03 mmol), under a continous Ar flow, was added. The color of the solution changed immediately from red to yellow. A ^{31}P NMR spectrum of the cooled solution, measured immediately, showed complete conversion of the starting Ru-compound to a single new Ru-complex (**11**). The solution was allowed to come to room temperature and the complex **11** was characterised by NMR spectroscopic methods. ^{1}H NMR (298 K, CD_2Cl_2): 5.68 (br d, $^3J_{H7',H8'}$ = 8.8, $^3J_{H7',H9'}$ = 1.1, H7′), 6.56 (ddd, $^3J_{H7,H8}$ =

© 2001 NRC Canada

8.8, $^3J_{H8,H9}$ = 7.7, $^4J_{H8,H10}$ = 1.5, H8), 6.60 (ddd, $^3J_{H7',H8'}$ = 8.8, $^3J_{H8',H9'}$ = 7.6, $^3J_{H8',H19'}$ = 1.3, H8′), 7.08 (H9), 7.33 (ddd, $^3J_{H9',H10'}$ = 8.4, $^3J_{H8',H9'}$ = 7.5, $^3J_{H7',H9'}$ = 1.1, H9′), 7.54 (H4), 7.64 (br d, $^3J_{H9,H10}$ = 8.3, $^4J_{H8,H10}$ = 1.5, H10), 7.71 (H5′), 7.83 (br d, $^3J_{H9',H10'}$ = 8.4, $^4J_{H8,H10}$ = 1.5, H10′), 7.91 (dd, $^3J_{H4',H5'}$ = 8.6, $^4J_{P2,H4'}$ = 2.4, H4′), 8.53 (d, $^3J_{H4,H5}$ = 8.6, H5). ^{13}C NMR (298 K, CD_2Cl_2): 102.1 (C_6H_6), 124.3 (C5′), 124.3 (C9), 124.7 (C8), 125.7 (C7), 126.6 (C8′), 127.2 (C7′), 127.3 (C10), 128.1 (C10′), 128.6 (C9′), 128.9 (C4′), 131.9 (C3), 133.2 (C2′), 134.2 (C2), 134.7 (C3′), 140.3 (C1), 144.2 (C5), 145.6 (C6), 146.8 (C6′). ^{31}P NMR (298 K, CD_2Cl_2): 180.4 (dd, $^1J_{PF}$ = 950, $^2J_{PP}$ = 48), 49.0 (dd, $^2J_{PP}$ = 48, $^3J_{PF}$ = 7). ^{19}F NMR (298 K, CD_2Cl_2): –137.2 (dd, $^1J_{PF}$ = 950, $^3J_{PF}$ = 7).

In an attempt to separate the metal complex **11** from (Bu_4N)(SbF_6) and $FSiPh_3$, a second reaction was carried on a 2.5-fold larger scale following the same procedure described previously but using dichloromethane at room temperature. After 5 min the solvent was evaporated in vacuo. The resulting yellow powder was washed with 3 × 1 mL Et_2O. Slow diffusion of Et_2O into a dichloromethane solution resulted in two crystalline materials (i.e., yellow and white crystals). X-ray diffraction measurements on the yellow crystals failed to give a structure. An attempt was made to separate the two species on basis of the color of the crystals. However, this solid did not afford satisfactory microanalytic data. The isolated yellow product is stable under Ar and affords the same ^{31}P, ^{19}F, and ^{1}H NMR characteristics described above. However, in solution it decomposes over a short period of time. FAB-MS calcd. M^+: 820.9; found M^+: 820.2; M^+ -benzene: 742.8; M^+ -PPh_2F: 614.0.

Synthesis of [RuH(Binap)(*p*-cymene)]SbF_6 (12a)

[Ru(Binap)(*p*-cymene)][(SbF_6)$_2$] (**8a**) (74.4 mg, 0.06 mmol) was dissolved in 2 mL methanol. The resulting orange solution was then stirred at room temperature. After 15 min the yellow product began to precipitate. The suspension was stirred for another 2 h after which the orange solution was removed using a syringe. The remaining powder was washed 2 × 1 mL methanol. The resulting yellow product was dried in vacuo. Color: yellow. Yield: 48.4 mg (71%). FAB-MS calcd. M^+: 858.5; found M^+: 858.4; M^+ -*p*-cymene: 722.8. ^{1}H NMR (298 K, CD_2Cl_2): –9.79 (q, $^2J_{PH}$ = 29.2, $^2J_{PH}$ = 40.6, RuH), 0.93 (d, $^3J_{HH}$ = 6.6, CH(CH_3)$_2$), 1.23 (d, $^3J_{HH}$ = 6.6, CH(CH_3)$_2$), 2.10 (s, CH_3), 2.41 (m, CH(CH_3)$_2$), 3.84 (d, $^3J_{HH}$ = 5.8, cyH), 4.08 (d, $^3J_{HH}$ = 5.8, cyH), 5.71 (d, $^3J_{HH}$ = 5.8, cyH), 5.97 (d, $^3J_{HH}$ = 5.8, cyH). ^{13}C NMR (298 K, CD_2Cl_2): 20.5 (*C*H_3), 23.4 (CH(*C*H_3)$_2$), 23.8 (CH(*C*H_3)$_2$), 32.3 (*C*H(CH_3)$_2$), 91.7 (cy), 96.5 (cy), 97.3 (cy), 98.3 (cy), 113.0 (cy), 116.8 (cy). ^{31}P NMR (298 K, CD_2Cl_2): 52.8 (d, $^2J_{PP}$ = 47), 52.0 (d, $^2J_{PP}$ = 47). Anal. calcd. for $C_{54}H_{47}F_{12}P_2RuSb_2\cdot H_2O$ (1132.8): C 58.28, H 4.40; found: C 57.92, H 4.80.

Synthesis of [RuH(*S*-MeO-Biphep)(*p*-cymene)]SbF_6 (12b)

[Ru(*S*-MeO-Biphep)(*p*-cymene)]Cl (**6b**) (156.3 mg, 0.18 mmol) and $AgSbF_6$ (120.4 mg, 0.35 mmol) were dissolved in 1 mL dichloromethane. The resulting suspension was refluxed overnight. The precipitate of AgCl was filtered using Celite and the solvent was evaporated in vacuo; 5 mL methanol was added to the remaining powder. The color changed from red to yellow. A ^{31}P NMR spectrum of the sample recorded within 5 min, showed complete conversion. The solution was concentrated to 1 mL methanol during which time the yellow product precipitated. After 1 h the orange solution was removed by use of a syringe and then the remaining powder was washed with 2 × 3 mL methanol. The yellow product was dried in vacuo. Color: yellow. Yield: 158.2 mg (83%). FAB-MS calcd. M^+: 818.0; found: M^+ + SbF_6: 1053.3; M^+ + SbF_6-*p*-cymene: 902.2; M^+: 817.4; M^+-*p*-cymene-H: 683.0. ^{1}H NMR (298 K, CD_2Cl_2): –10.10 (q, $^2J_{PH}$ = 31.6, $^2J_{PH}$ = 39.7, RuH), 0.92 (d, $^3J_{HH}$ = 7.0, CH(CH_3)$_2$), 1.26 (d, $^3J_{HH}$ = 7.0, CH(CH_3)$_2$), 2.12 (s, CH_3), 2.44 (m, 1CH(CH_3)$_2$), 3.19 (s, OCH_3), 3.26 (s, OCH_3), 3.74 (d, $^3J_{HH}$ = 6.6, cyH), 4.05 (d, $^3J_{HH}$ = 6.6, cyH), 5.74 (d, $^3J_{HH}$ = 6.6, cyH), 6.00 (d, $^3J_{HH}$ = 6.6, cyH), 6.27, 6.30, 7.03. 7.07, 7.12, 7.40 (all 6 MeO-Biphep backbone). ^{13}C NMR (298 K, CD_2Cl_2): 20.4 (*C*H_3), 23.2 (CH(*C*H_3)$_2$), 23.5 (CH(*C*H_3)$_2$), 32.2 (*C*H(CH_3)$_2$), 54.6 (O*C*H_3), 54.7 (O*C*H_3), 91.5 (cy), 96.3 (cy), 97.5 (cy), 97.8 (cy), 110.6 (MeO-Biphep backbone), 111.2 (MeO-Biphep backbone), 112.4 (cy), 115.7 (cy), 119.2, 121.0, 125.7, 127.0, 134.2, 137.2, 157.0, 157.3 (all 8 MeO-Biphep backbone). ^{31}P NMR (298 K, CD_2Cl_2): 51.0 (d, $^2J_{PP}$ = 46), 50.4 (d, $^2J_{PP}$ = 46). Anal. calcd. for $C_{48}H_{46}O_2F_6P_2RuSb_2\cdot$MeOH (1053.7): C 54.26, H 4.52; found: C 54.21, H 4.66.

Synthesis of [Ru(NCC_6H_5)(Binap)(*p*-cymene)][SbF_6]$_2$ (13a)

Benzonitrile (3.3 μL, 0.03 mmol) was added to a solution of [Ru(Binap)(*p*-cymene)][SbF_6]$_2$ (**8a**) (39.1 mg, 0.03 mmol) in 1 mL dichloromethane. After an immediate color change from orange to yellow, the solvent was evaporated. The remaining yellow powder was washed with 4 × 3 mL Et_2O and dried in vacuo. Color: yellow. Yield: 34.8 mg (81%). FAB-MS calcd. M^{2+}: 961.2; found: M^{2+} + SbF_6: 1196.0; M^{2+}-benzonitrile: 858.1. ^{1}H NMR (298 K, CD_2Cl_2): 1.10 (d, $^3J_{HH}$ = 6.0, CH(CH_3)$_2$), 1.48 (d, $^3J_{HH}$ = 6.0, CH(CH_3)$_2$), 1.86 (s, CH_3), 3.01 (m, CH(CH_3)$_2$), 4.69 (d, $^3J_{HH}$ = 7.0, cyH), 5.18 (d, $^3J_{HH}$ = 6.1, cyH), 5.94 (d, $^3J_{HH}$ = 7.0, cyH), 7.09 (d, $^3J_{HH}$ = 6.1, cyH). ^{13}C NMR (298 K, CD_2Cl_2): 19.2 (*C*H_3), 21.6 (CH(*C*H_3)$_2$), 23.7 (CH(*C*H_3)$_2$), 32.3 (*C*H(CH_3)$_2$), 86.4 (cy), 101.3 (cy), 102.6 (cy), 109.2 (cy), 118.3 (cy), 118.7 (cy). ^{31}P NMR (298 K, CD_2Cl_2): 44.5 (d, $^2J_{PP}$ = 51), 29.9 (d, $^2J_{PP}$ = 51). Anal. calcd. for $C_{61}H_{51}F_{12}NP_2RuSb_2\cdot H_2O$ (1432.6): C 50.50, H 3.68, N 0.97; found: C 50.48, H 3.78, N 1.09.

Synthesis of [Ru(NCC_6H_5)(*S*-MeO-Biphep)(*p*-cymene][SbF_6]$_2$ (13b)

[RuCl(*S*-MeO-Biphep)(*p*-cymene)]Cl (**6b**) (67.8 mg, 0.08 mmol) and $AgSbF_6$ (52.2 mg, 0.15 mmol) were dissolved in 1 mL dichloromethane and the resulting suspension was refluxed overnight. The precipitate of AgCl was filtrated using Celite. Acrylonitrile (20 μL, 0.19 mmol) was added to the remaining red solution. The color change from red to yellow and then the solvent was evporated in vacuo. The remaining yellow powder was washed with 5 × 1 mL Et_2O and then dried in vacuo. Color: yellow. Yield: 109.2 mg (98%). FAB-MS calcd. M^{2+}: 921.0; found: M^{2+} + SbF_6: 1158.1; M^{2+}-benzonitrile: 818.2. ^{1}H NMR (298 K, CD_2Cl_2): 1.12 (d, $^3J_{HH}$ = 7.0, CH(CH_3)$_2$), 1.51 (d, $^3J_{HH}$ = 6.8, CH(CH_3)$_2$), 1.89 (s, CH_3), 3.02 (m, CH(CH_3)$_2$), 3.46 (s, OCH_3), 3.60 (s, OCH_3), 4.08 (br d, $^3J_{HH}$ = 6.4, cyH), 5.12 (d, $^3J_{HH}$ = 7.3, cyH), 6.01 (d, $^3J_{HH}$ = 6.4, cyH), 6.57, 6.60, 6.59, 6.84, 6.96 (all 5 MeO-

© 2001 NRC Canada

Biphep backbone), 7.07 (cyH), 7.08 (MeO-Biphep backbone). ^{13}C NMR (298 K, CD_2Cl_2): 19.1 (CH_3), 21.3 ($C(CH_3)_3$), 23.5 ($C(CH_3)_3$), 32.1($C(CH_3)_3$), 55.5 (OCH_3), 56.0 (OCH_3), 85.6 (cy), 101.3 (cy), 102.3 (cy), 109.4 (cy), 114.3 (MeO-Biphep backbone), 114.3 (MeO-Biphep backbone), 117.9 (cy), 118.4 (cy), 123.7, 125.1, 125.8, 126.1, 128.9, 129.8, 130.0, 130.2, 158.2, 159.8 (all 10 MeO-Biphep backbone). ^{31}P NMR (298 K, CD_2Cl_2): 43.7 (d, $^2J_{PP}$ = 51), 28.8 (d, $^2J_{PP}$ = 51). Anal. calcd. for $C_{55}H_{51}F_{12}NO_2P_2RuSb_2$ (1392.5): C 47.44, H 3.69, N 1.01; found: C 47.56, H 3.81, N 1.15.

Synthesis of [Ru(NCCH=CH$_2$)(Binap)(*p*-cymene)][SbF$_6$]$_2$ (14a)

Acrylonitrile (1.6 μL, 0.02 mmol) was added to a solution of [Ru(Binap)(*p*-cymene)][SbF_6]$_2$ (**8a**) (28.3 mg, 0.02 mmol) in 1.5 mL dichloromethane solution. After the immediate color change from orange to yellow, the solvent was evaporated in vacuo. The yellow remaining powder was washed with 2 × 3 mL Et_2O and then dried in vacuo. Color: yellow. Yield: 15.2 mg (55%). FAB-MS calcd. M^{2+}: 911.1; found: M^{2+} + SbF_6: 1148.1; M^{2+}-acrylonitrile: 858.1. ^{1}H NMR (298 K, CD_2Cl_2): 1.08 (d, $^3J_{HH}$ = 6.8, CH(CH_3)$_2$), 1.47 (d, $^3J_{HH}$ = 6.8, CH(CH_3)$_2$), 1.84 (s, CH_3), 3.01 (m, CH(CH$_3$)$_2$), 3.75 (q, $^3J_{HH}$ = 15, $^2J_{HH}$ = 3, CH_2CHCN), 4.68 (d, $^3J_{HH}$ = 5.9, cyH), 5.04 (d, $^3J_{HH}$ = 6.8, cyH), 5.60 (d, $^2J_{HH}$ = 3, CH_2CHCN), 5.66 (d, $^3J_{HH}$ = 15, $^2J_{HH}$ = 3, CH$_2$CHCN), 5.92 (d, $^3J_{HH}$ = 5.9, cyH), 6.95 (d, $^3J_{HH}$ = 6.8, cyH). ^{31}P NMR (298 K, CD_2Cl_2): 44.3 (d, $^2J_{PP}$ = 50), 29.5 (d, $^2J_{PP}$ = 50). ^{13}C NMR (75.48 MHz, CD_2Cl_2): 19.2 (CH_3), 22.1 (CH(CH_3)$_2$), 23.0 (CH(CH_3)$_2$), 31.9 (CH(CH$_3$)$_2$), 86.6 (cy), 101.4 (cy), 102.4 (cy), 106.2 (CH$_2$CHCN), 108.7 (cy), 117.6 (cy), 117.6 (cy), 129.6 (CH$_2$CHCN), 143.6 (CH$_2$CHCN). Anal. calcd. for $C_{57}H_{49}F_{12}NP_2RuSb_2$ (1382.6): C 49.52, H 3.57, N 1.01; found: C 49.38, H 3.71, N 1.04.

Synthesis of [Ru(NCCH=CH$_2$)(*S*-MeO-Biphep)(*p*-cymene)][SbF$_6$]$_2$ (14b)

[RuCl(*S*-MeO-Biphep)(*p*-cymene)]Cl (**6b**) (46.7 mg, 0.05 mmol) and $AgSbF_6$ (35.4 mg, 0.10 mmol) were dissolved in 1 mL dichloromethane. The resulting suspension was refluxed overnight. The precipitate of AgCl was filtrated using Celite. Acrylonitrile (3 μL, 0.08 mmol) was added to the remaining red solution. After the color changed from red to yellow, the solvent was evporated in vacuo. The remaining powder was washed with 5 × 1 mL Et_2O and was dried in vacuo. Color: yellow. Yield: 65.4 mg (97%). FAB-MS calcd. M^{2+}: 871.0; found: M^{2+} + SbF_6: 1106.2; M^{2+}-acrylonitrile: 818.0. ^{1}H NMR (298 K, CD_2Cl_2): 1.10 (d, $^3J_{HH}$ = 6.9, CH(CH_3)$_2$), 1.49 (d, $^3J_{HH}$ = 6.9, CH(CH_3)$_2$), 1.86 (s, CH_3), 3.00 (m, CH(CH$_3$)$_2$), 3.46 (s, OCH_3), 3.58 (s, OCH_3), 4.77 (d, $^3J_{HH}$ = 6.4, cyH), 4.95 (d, $^3J_{HH}$ = 7.2, cyH), 5.01 (d, $^3J_{HH}$ = 12.0, CH_2CHCN), 5.50 (dd, $^3J_{HH}$ = 17.8, $^3J_{HH}$ = 12.0, CH$_2$CHCN), 5.98 (d, $^3J_{HH}$ = 12, CH_2CHCN), 6.00 (d, $^3J_{HH}$ = 6.4, cyH), 6.54, 6.78, 6.82 (all 3 MeO-Biphep backbone), 6.94 (d, $^3J_{HH}$ = 7.2, cyH), 7.07, 7.10, 7.19 (all 3 MeO-Biphep backbone). ^{13}C NMR (298 K, CD_2Cl_2): 19.3 (CH_3), 22.1 (CH(CH_3)$_2$), 23.2 (CH(CH_3)$_2$), 32.1 (CH(CH$_3$)$_2$), 55.3 (OCH3), 56.0 (OCH3), 85.8 (cy), 101.6 (cy), 102.3 (cy), 106.1 (CH$_2$CHCN), 109.1 (cy), 114.1, 114.5 (both MeO-Biphep backbone), 117.8 (cy), 118.0 (cy), 123.8, 125.5, 125.9, 125.9, 126.0, 129.1 (all 6 MeO-Biphep backbone), 130.1 (CH$_2$CHCN), 130.3, 130.4 (both MeO-Biphep backbone), 143.9 (CH$_2$CHCN), 158.3, 160.0 (both MeO-Biphep backbone). ^{31}P NMR (298 K, CD_2Cl_2): 43.8 (d, $^2J_{PP}$ = 50), 28.6 (d, $^2J_{PP}$ = 50). Anal. calcd. for $C_{51}H_{49}F_{12}NO_2P_2RuSb2\cdot H_2O$ (1342.5): C 44.99, H 3.75, N 1.03; found: C 44.94, H 3.99, N 0.94.

Synthesis of [Ru(NCCH$_2$CH$_3$)(Binap)(*p*-cymene)][SbF$_6$]$_2$ (15a)

Propionitrile (1.7 μL, 0.02 mmol) was added to a solution of [Ru(Binap)(*p*-cymene)][SbF_6]$_2$ (**8a**) (31.5 mg, 0.02 mmol) in 1 mL dichloromethane. After the immediate color change from orange to yellow, the solvent was evaporated in vacuo. The remaining yellow product was dried in vacuo. Color: yellow. Yield: 27.7 mg (99%). FAB-MS calcd. M^{2+}: 913.1; found: M^{2+} + SbF_6: 1147.5; M^{2+}-propionitrile: 857.7. ^{1}H NMR (298 K, CD_2Cl_2): 0.38 (t, CH_3CH$_2$CN) 1.10 (d, $^3J_{HH}$ = 6.8, CH(CH_3)$_2$), 1.49 (d, $^3J_{HH}$ = 6.8, CH(CH_3)$_2$), 1.84 (s, CH_3), 1.86 (m, CH$_3$CH_2CN), 2.52 (m, CH$_3$CH_2CN), 3.00 (m, CH(CH$_3$)$_2$), 4.66 (d, $^3J_{HH}$ = 6.4, cyH), 5.06 (d, $^3J_{HH}$ = 6.8, cyH), 5.86 (d, $^3J_{HH}$ = 6.4, cyH), 6.87 (d, $^3J_{HH}$ = 6.8, cyH). ^{13}C NMR (298 K, CD_2Cl_2): 8.4 (CH$_3$CH$_2$CN), 14.1 (CH$_3$CH$_2$CN), 19.1 (CH_3), 22.2 (CH(CH_3)$_2$), 23.1 (CH(CH_3)$_2$), 31.9 (CH(CH$_3$)$_2$), 86.2 (cy), 100.8 (cy), 102.3 (cy), 108.5 (cy), 118.0 (cy), 118.0 (cy), 135.5 (CH$_3$CH$_2$CN). ^{31}P NMR (298 K, CD_2Cl_2): 44.2 (d, $^2J_{PP}$ = 51), 29.4 (d, $^2J_{PP}$ = 51). Anal. calcd. for $C_{57}H_{51}F_{12}NP_2RuSb_2$ (1384.6): C 49.45, H 3.71, N 1.01; found: C 49.46, H 3.91, N 1.07.

Synthesis of [Ru(NCCH$_3$)(*S*-MeO-Biphep)(*p*-cymene)][SbF$_6$]$_2$ (15b)

[RuCl(*S*-MeO-Biphep) (*p*-cymene)]Cl (**6b**) (32.1 mg, 0.035 mmol) and $AgSbF_6$ (24.9 mg, 0.072 mmol) were dissolved in 1 mL dichloromethane. The resulting suspension was refluxed overnight. The precipitate of AgCl was filtrated using Celite. Acetonitrile (6 μL, 0.11 mmol) was added to the remaining red solution. After the color change from red to yellow, the solvent was evporated in vacuo. The remaining powder was washed with 3 × 1 mL Et_2O and was dried at in vacuo. Color: yellow. Yield: 42.6 mg (92%). FAB-MS calcd. M^{2+}: 859.0; found: M^{2+} + SbF_6: 1096.1; M^{2+}-acetonitrile: 818.2. ^{1}H NMR (298 K, CD_2Cl_2): 1.09 (d, $^3J_{HH}$ = 6.8, CH(CH_3)$_2$), 1.48 (d, $^3J_{HH}$ = 6.8, CH(CH_3)$_2$), 1.72 (s, CH_3CN), 1.87 (s, CH_3), 3.03 (m, CH(CH$_3$)$_2$), 3.46 (s, OCH_3), 3.60 (s, OCH_3), 4.78 (br d, $^3J_{HH}$ = 6.2, cyH), 4.88 (br d, $^3J_{HH}$ = 7.0, cyH), 5.97 (cyH), 6.55, 6.83, 6.85 (all 3 MeO-Biphep backbone), 6.86 (d, $^3J_{HH}$ = 6.2, cyH), 7.08, 7.18, 7.31 (all 3 MeO-Biphep backbone). ^{13}C NMR (298 K, CD_2Cl_2): 4.7 (CH$_3$CN), 19.2 (CH_3), 22.4 (CH(CH_3)$_2$), 22.6 (CH(CH_3)$_2$), 31.7 (CH(CH$_3$)$_2$), 55.6 (OCH3), 56.0 (OCH3), 85.6 (cy), 101.3 (cy), 101.4 (cy), 108.3 (cy), 114.0 (MeO-Biphep backbone), 114.4 (MeO-Biphep backbone), 117.2 (cy), 117.8 (cy), 123.9, 125.8, 125.9, 126.0, 129.5, 129.5, 129.9, 130.4 (all 8 MeO-Biphep backbone), 132.1(CH$_3$CN), 158.1 (MeO-Biphep backbone), 159.9 (MeO-Biphep backbone). ^{31}P NMR (298 K, CD_2Cl_2): 43.7 (d, $^2J_{PP}$ = 51), 28.9 (d, $^2J_{PP}$ = 51). Anal. calcd. for $C_{57}H_{51}F_{12}NO_2P_2RuSb_2$ (1330.4): C 45.14, H 3.71, N 1.05; found: C 45.13, H 3.88, N 0.94.

© 2001 NRC Canada

Synthesis of [Ru(CNCH$_2$CO$_2$Et)(Binap)(*p*-cymene)][SbF$_6$]$_2$ (16a)

Ethyl isocyanoacetate (4.5 μL, 0.04 mmol) was added to a solution of [Ru(Binap)(*p*-cymene)][SbF$_6$]$_2$ (**8a**) (50.3 mg, 0.04 mmol) in 1 mL dichloromethane. An immediate color change from orange to yellow occurred. ^{31}P NMR recorded within 5 min after adding the isocyanoacetate, showed complete conversion of the starting material to the product. The solvent was evaporated in vacuo and then the remaining powder was washed with 2 × 3 mL Et$_2$O. The yellow product was dried in vacuo. Color: yellow. FAB-MS calcd. M^{2+}: 971.1; found: M^{2+} + SbF$_6$: 1207.9; M^{2+}-*p*-cymene: 836.9. ^{1}H NMR (298 K, CD_2Cl_2): 0.94 (d, $^3J_{HH}$ = 6.8, CH(C*H*$_3$)$_2$), 1.37 (d, $^3J_{HH}$ = 6.8, CH(C*H*$_3$)$_2$), 1.42 (t, CNCH$_2$CO$_2$CH$_2$C*H*$_3$), 1.95 (s, C*H*$_3$), 3.23 (d, $^2J_{HH}$ = 19, CNC*H*$_2$CO$_2$CH$_2$CH$_3$), 3.37 (m, C*H*(CH$_3$)$_2$), 4.24 (d, $^2J_{HH}$ = 19, CNC*H*$_2$CO$_2$CH$_2$CH$_3$), 4.41 (m, CNCH$_2$CO$_2$C*H*$_2$CH$_3$), 4.75 (d, $^3J_{HH}$ = 6.0, cyH), 4.77 (d, $^3J_{HH}$ = 6.6, cyH), 6.80 (d, $^3J_{HH}$ = 6.6, cyH), 7.15 (d, $^3J_{HH}$ = 6.0, cyH). ^{13}C NMR (298 K, CD_2Cl_2): 14.1 (CNCH$_2$CO$_2$CH$_2$*C*H$_3$), 19.6 (*C*H$_3$), 20.5 (CH(*C*H$_3$)$_2$), 24.4 (CH(*C*H$_3$)$_2$), 31.2 (*C*H(CH$_3$)$_2$), 47.3 (CN*C*H$_2$CO$_2$CH$_2$CH$_3$), 64.3 (CNCH$_2$*C*O$_2$CH$_2$CH$_3$), 98.6 (cy), 102.7 (cy), 103.7 (cy), 111.2 (cy), 123.2 (cy), 125.7 (cy), 142.8 (*C*NCH$_2$CO$_2$CH$_2$CH$_3$), 163.7 (CNCH$_2$*C*O$_2$CH$_2$CH$_3$). ^{31}P NMR (298 K, CD_2Cl_2): 46.0 (d, $^2J_{PP}$ = 40), 29.8 (d, $^2J_{PP}$ = 40). Anal. calcd. for $C_{59}H_{53}F_{12}NO_2P_2RuSb_2$ (1442.6): C 49.12, H 3.70, N 0.97; found: C 48.39, H 4.14, N 1.27.

Synthesis of [Ru(CNCH$_2$CO$_2$Et)(*S*-MeO-Biphep)(*p*-cymene)][SbF$_6$]$_2$ (16b)

[RuCl(*S*-MeO-Biphep)(*p*-cymene)]Cl (**6b**) (35.0 mg, 0.04 mmol) and AgSbF$_6$ (25.3 mg, 0.08 mmol) were dissolved in 1 mL dichloromethane. The resulting suspension was refluxed overnight. The precipitate of AgCl was filtrated using Celite. Ethyl isocyanoacetate (7 μL, 0.06 mmol) was added to the remaining red solution. An immediate color change from red to yellow occurred after which the solvent was evaporated. The remaining powder was washed with 3 × 1 mL Et$_2$O and 3 × 1 mL pentane. The yellow product was dried in vacuo. Color: yellow. Yield: 54.1 mg (95%). FAB-MS calcd. M^{2+}: 931.0; found: M^{2+} + SbF$_6$: 1165.9. ^{1}H NMR (298 K, CD_2Cl_2): 0.97 (d, $^3J_{HH}$ = 6.8, CH(C*H*$_3$)$_2$), 1.40 (t, CNCH$_2$CO$_2$CH$_2$C*H*$_3$), 1.41 (d, $^3J_{HH}$ = 6.8, CH(C*H*$_3$)$_2$), 2.00 (s, C*H*$_3$), 3.46 (s, OC*H*$_3$), 3.55 (s, OC*H*$_3$), 3.56 (d, $^2J_{HH}$ = 18.9, CNC*H*$_2$CO$_2$CH$_2$CH$_3$), 3.32 (m, C*H*(CH$_3$)$_2$), 4.12 (d, $^2J_{HH}$ = 18.9, CNC*H*$_2$CO$_2$CH$_2$CH$_3$), 4.45 (m, CNCH$_2$CO$_2$C*H*$_2$CH$_3$), 4.68 (d, $^3J_{HH}$ = 7.0, cyH), 4.87 (d, $^3J_{HH}$ = 6.8, cyH), 6.55, 6.84, 6.84 (all 3 MeO-Biphep backbone), 6.86 (d, $^3J_{HH}$ = 6.8, cyH), 7.08 (d, $^3J_{HH}$ = 7.0, cyH), 7.08, 7.17, 7.30 (all 3 MeO-Biphep backbone). ^{13}C NMR (298 K, CD_2Cl_2): 14.1 (CNCH$_2$CO$_2$CH$_2$*C*H$_3$), 19.6 (*C*H$_3$), 20.6 (CH(*C*H$_3$)$_2$), 24.1 (CH(*C*H$_3$)$_2$), 31.2 (*C*H(CH$_3$)$_2$), 47.1 (CN*C*H$_2$CO$_2$CH$_2$CH$_3$), 55.6 (O*C*H$_3$), 55.8 (O*C*H$_3$), 63.9 (CNCH$_2$CO$_2$*C*H$_2$CH$_3$), 98.1 (cy), 102.0 (cy), 103.9 (cy), 111.3 (cy), 114.3, 114.5 (both MeO-Biphep backbone), 122.8 (cy), 122.9, 125.2 (both MeO-Biphep backbone), 125.4 (cy), 125.8, 126.4, 129.3, 129.4, 130.4, 131.7 (all 6 MeO-Biphep backbone), 144.2 (*C*NCH$_2$CO$_2$CH$_2$CH$_3$), 158.2, 159.8 (both MeO-Biphep backbone), 163.7 (CNCH$_2$*C*O$_2$CH$_2$CH$_3$). ^{31}P NMR (298 K, CD_2Cl_2): 44.8 (d, $^2J_{PP}$ = 40), 28.5 (d, $^2J_{PP}$ = 40). Anal. calcd. for $C_{53}H_{53}F_{12}NO_2P_2RuSb_2$ (1402.50): C 45.39, H 3.81, N 1.00; found: C 45.11, H 4.05, N 1.10.

Synthesis of [Ru(CNC(CH$_3$)$_3$)(Binap)(*p*-cymene)(][SbF$_6$]$_2$ (17a)

tert-Butyl isocyanide (4.2 μL, 0.04 mmol) was added to a solution of [Ru(Binap)(*p*-cymene)][SbF$_6$]$_2$ (**8a**) (50.0 mg, 0.04 mmol) in 1 mL dichloromethane. A color change from orange to yellow occurred immediately. A ^{31}P NMR recorded within 5 min after adding the *tert*-butyl isocyanide, showed complete conversion of the starting material to the product. The solvent was evaporated in vacuo and then the remaining powder was washed with 3 × 3 mL Et$_2$O and 1 × 2 mL pentane. As ^{1}H NMR indicated still free *tert*-butyl isocyanide, the powder was washed another time with 2 × 3 mL Et$_2$O. The yellow product was dried in vacuo. Color: yellow. FAB-MS calcd. M $^{2+}$: 941.1; found: M^{2+} + SbF$_6$: 1176.2; M^{2+}-*p*-cymene: 807.1. ^{1}H NMR (298 K, CD_2Cl_2): 1.03 (d, $^3J_{HH}$ = 6.8, CH(C*H*$_3$)$_2$), 1.06 (s, C(C*H*$_3$)$_3$), 1.48 (d, $^3J_{HH}$ = 6.8, CH(C*H*$_3$)$_2$), 1.89 (s, C*H*$_3$), 2.94 (m, C*H*(CH$_3$)$_2$), 4.68 (d, $^3J_{HH}$ = 5.8, cyH), 4.84 (d, $^3J_{HH}$ = 6.7, cyH), 6.76 (d, *C*N(C(CH$_3$)$_3$, 7.16 ($^3J_{HH}$ = 6.7, cyH). ^{13}C NMR (298 K, CD_2Cl_2): 19.6 (*C*H$_3$), 21.8 (CH(*C*H$_3$)$_2$), 23.3 (CH(*C*H$_3$)$_2$), 29.1 (C(*C*H$_3$)$_3$), 32.0 (*C*H(CH$_3$)$_2$), 62.5 (*C*(CH$_3$)$_3$), 97.5 (cy), 102.6 (cy), 103.2 (cy), 113.3 (cy), 120.8 (cy), 126.2 (cy). ^{31}P NMR (298 K, CD_2Cl_2): 46.3 (d, $^2J_{PP}$ = 42), 30.0 (d, $^2J_{PP}$ = 42). Anal. calcd. for $C_{59}H_{55}F_{12}NP_2RuSb_2$ (1412.6): C 50.17, H 3.92, N 0.99; found: C 49.93, H 4.01, N 1.12.

Acknowledgements

P.S.P. thanks the Swiss National Science Foundation, and the ETH Zürich for financial support. A.A. thanks MURST and the Vigoni program for support and Dr. F. Eisentraeger for helping with the data collection. We also thank Johnson Matthey for the loan of RuCl$_3$ and F. Hoffmann La Roche, Basel, for the MeO-Biphep ligands.

References

1. R. Noyori. Chimia, **42**, 215 (1988); M. Kitamura, T. Ohkuma, S. Inoue, N. Sayo, H. Kumobayashi, S. Akutagawa, T. Ohta, and R. Noyori. J. Am. Chem. Soc. **110**, 629 (1988); R. Noyori and H. Takaya. Acc. Chem. Res. **23**, 345 (1990); H. Takaya, T. Ohta, K. Mashina, and R. Noyori. Pure Appl. Chem. **62**, 1135 (1990); H. Takaya and R. Noyori Comprehensive organic synthesis. *Edited by* B.M. Trost and I. Flemming. Pergamon Press, Oxford. 1991; R. Noyori. Asymmetric catalysis in organic synthesis. John Wiley and Sons, Inc., London. 1994; R. Noyori and S. Hashiguchi. Acc. Chem. Res. **30**, 97 (1997); K. Mikami, T. Korenaga, M. Terada, T. Ohkuma, T. Pham, and R. Noyori. Angew. Chem. **111**, 517 (1999).
2. R. Schmid, M. Cereghetti, B. Heiser, P. Schönholzer, and H.J. Hansen. Helv. Chim. Acta, **71**, 897 (1988); R. Schmid, J. Foricher, M. Cereghetti, and P. Schönholzer. Helv. Chim. Acta, **74**, 370 (1991); R. Schmid, E.A. Broger, M. Cereghetti, Y. Crameri, J. Foricher, M. LaLonde, R.K. Mueller, M. Scalone, G. Schoettel, and U. Zutter. Pure Appl. Chem. **68**, 131 (1996); Y. Crameri, J. Foricher, U. Hengartner, C. Jenny, F. Kienzle, H. Ramuz, M. Scalone, M. Schlageter, R. Schmid, and S. Wang. Chimia, **51**, 303 (1997); K. Mauthner, C. Slugovc, K. Mereiter, R. Schmid, and K. Kirchner. Organometallics, **16**,

© 2001 NRC Canada

1956 (1997); M.J. Fehr, G. Consiglio, M. Scalone, and R. Schmid. J. Org. Chem. **16**, 5768 (1999).
3. N. Feiken, P.S. Pregosin, G. Trabesinger, and M. Scalone. Organometallics, **16**, 537 (1997).
4. N. Feiken, P.S. Pregosin, and G. Trabesinger. Organometallics, **16**, 5756 (1997).
5. N. Feiken, P.S. Pregosin, G. Trabesinger, A. Albinati, and G.L. Evoli. Organometallics, **16**, 3735 (1997).
6. C.J. den Reijer, M. Wörle, and P.S. Pregosin. Organometallics, **19**, 309 (2000).
7 M.A. Bennet and A.K. Smith. J. Chem. Soc. Dalton Trans. 233 (1974).
8. J.W. Faller and J. Parr. Organometallics, **19**, 1829 (2000); J.W. Faller, B.P. Patel, M.A. Albrizzio, and M. Curtis. Organometallics, **18**, 3096 (1999).
9. G. Trabesinger, A. Albinati, N. Feiken, R.W. Kunz, P.S. Pregosin, and M. Tschoerner. J. Am. Chem. Soc. **119**, 6315 (1997).
10. P. Steenwinkel, S.L. James, R.A. Gossage, D.M. Grove, H. Koojman, W.J.J.S. Smeets, A.L. Spek, and G. van Koten. Organometallics, **17**, 4680 (1998).
11. N.C. Zanetti, F. Spindler, J. Spencer, A. Togni, and G. Rihs. Organometallics, **15**, 860 (1996).
12. N.D. Jones, K.S. Macfarlane, M.B. Smith, R.P. Schutte, S.J. Rettig, and B.R. James. Inorg. Chem. **38**, 3956 (1999); D.D. Pathak, H. Adams, N.A. Bailey, P.J. King, and C. White. J. Organomet. Chem. **479**, 237 (1994).
13. K. Mashima, K. Kusano, T. Ohta, R. Noyori, and H. Takaya. J. Chem. Soc. Chem. Commun. 1208 (1989); K. Mashima, K.H. Kusano, N. Sato, Y. Matsumura, K. Nozaki, H. Kumobayashi, N. Sayo, Y. Hori, T. Jshizaki, S. Akutagawa, H. Takaya, J. Org. Chem. **59**, 3064 (1994).
14. A.M. Joshi, I.S. Thorborn, S.J. Rettig, and B.R. James. Inorg. Chim. Acta, **198**–**200**, 283 (1992).
15. K. Umezawa-Vizzini and T.R. Lee. Organometallics, **16**, 5613 (1997).
16. M. Fryzuk, C.D. Montgomery, and S.J. Rettig. Organometallics, **10**, 467 (1991).
17. R.H. Morris, J.F. Sawer, C.T. Schweitzer, and A. Sella. Organometallics, **8**, 2099 (1989).
18. A.S. Pilcher, H.L. Ammon, and P.J. DeShong. J. Am. Chem. Soc. **117**, 5166 (1995).
19. J.G. Verkade and J.A. Mosbo. Stereospecificity in ^{1}J coupling to metals. *Edited by* J.G. Verkade and J.A. Mosbo. VCH, Deerfield Beach, Fla. **8**, 425 (1987).
20. J.A. Wiles, C.E. Lee, R. McDonald, and S. Bergens. Organometallics, **15**, 3782 (1996); J.A. Wiles and S.H. Bergens. Organometallics, **17**, 2228 (1998); J.A. Wiles and S.H. Bergens. Organometallics, **18**, 3709 (1999); J.A. Wiles, S.H. Bergens, K.P.M. Vanhessche, D.A. Dobbs, V. Rautenstrauche. Angew. Chem. Int. Edit. **40**, 914 (2001).
21. A. Currao, N. Feiken, A. Macchioni, R. Nesper, P.S. Pregosin, and G. Trabesinger. Helv. Chim. Acta, **79**, 1587 (1996).
22. SAINT: area detector integration. Bruker Analytical X-ray systems, Madison, WI, (1996).
23 G.M. Sheldrick. SADABS. Universität Göttingen, Germany. 1996.
24 G.M. Sheldrick. SHELX-97. Structure solution and refinement package. Universität Göttingen, Germany. (1997).
25. A.J.C. Wilson (*Editor*). International tables for X-ray crystallography. Vol. C. Kluwer Academic Publisher, Dordrecht, The Netherlands. 1992.

List of Symbols

cy aromatic carbon of *p*-cymene
cyH aromatic proton of *p*-cymene

© 2001 NRC Canada

A temperature-controlled reversible ionic liquid – water two phase – single phase protocol for hydrogenation catalysis

Paul J. Dyson, David J. Ellis, and Thomas Welton

Abstract: An ionic liquid – water system that undergoes a reversible two phase – single phase transformation dependent upon temperature has been used as a novel medium for the transition-metal-catalyzed hydrogenation of a water soluble substrate. At room temperature, the ionic liquid 1-octyl-3-methylimidizolium tetrafluoroborate, containing $[Rh(\eta^4\text{-}C_7H_8)(PPh_3)_2][BF_4]$ catalyst, forms a separate layer to water containing 2-butyne-1,4-diol. In a stirred autoclave the mixture was pressurized with hydrogen to 60 atm (1 atm = 101.325 kPa) and heated to 80°C giving a homogeneous single phase solution. On cooling to room temperature, two phases reform, with the ionic liquid phase containing the catalyst and the aqueous phase containing a mixture of 2-butene-1,4-diol and butane-1,4-diol products that can be simply removed without catalyst contamination.

Key words: ionic liquids, biphasic catalysis, hydrogenation, rhodium.

Résumé : Un système liquide ionique – eau soumis à une transformation réversible de deux à une phase suivant la température est utilisé comme nouveau milieu pour l'hydrogénation, catalysée par des métaux de transition, de substrats solubles dans l'eau. À la température ambiante, le liquide ionique tétrafluoroborate de 1-méthyl-3-méthylimidizolinium contenant le catalyseur $[Rh(\eta^4\text{-}C_7H_8)(PPh_3)_2][BF_4]$ forme une couche séparée de l'eau qui contient du but-2-yne-1,4-diol. Dans un autoclave sous agitation, le mélange est soumis à une pression d'hydrogène de 60 atm (1 atm = 101.325 kPa) et chauffé à 80°C pour donner une solution homogène comportant une seule phase. Par refroidissement à la température ambiante, les deux phases se reforment avec la phase du liquide ionique qui contient le catalyseur et la phase aqueuse qui contient un mélange de but-2-ène-1,4-diol et de but-2-yne-1,4-diol qui peut être enlevé sans contamination par le catalyseur.

Mots clés : liquides ioniques, catalyse biphasique, hydrogénation, rhodium.

[Traduit par la Rédaction]

Introduction

Room temperature ionic liquids are emerging as excellent alternatives to organic solvents in homogeneous and biphasic processes and several excellent reviews are available (1). For example, liquids composed of various imidazolium cations with aluminium chloride based anions have replaced organic solvents in Friedel–Crafts reactions (2) and in polyethylene cracking (3) (both being catalyzed by aluminium chloride). More inert ionic liquids, also composed of imidazolium cations, but with counter anions such as tetrafluoroborate or hexafluorophosphate, have been used as catalyst supports in biphasic processes for a wide range of reactions as outlined in the reviews cited in ref. 1. Specific examples include hydrogenation (4) and hydroformylation, (5) Heck, (6) Trost–Tsuji (7), and Sukuzi (8) coupling reactions, the Diels–Alder reaction (9), alkylation (10), and polymerization (11) reactions.

While comparisons between ionic liquid – biphasic systems and others such as water and fluorous biphasic systems have been widely discussed from an environmental perspective, detailed assessment of the influence of the solvent regime on the catalyst has not been widely made (1). One of the most impressive aspects of some ionic liquids is that the liquid is essentially non-nucleophilic and as a consequence extends the lifetime of supported catalysts giving higher turnover numbers, clearly demonstrated for the hydroformylation of methyl-3-pentenoate using rhodium-based catalysts supported in the ionic liquid 1-butyl-3-methylimidazolium hexafluorophosphate (5*b*). When the reaction is carried out in organic solvents such as dichloromethane and toluene deactivation of the catalysts takes place rapidly, whereas in the reactions conducted in the ionic liquid, the catalyst remains active for considerably longer periods with turnover numbers typically 600% greater. This feature is especially important since concerns have been expressed that homogeneous catalysts tend to have short lifetimes and therefore there is little point in trying to recover them.

Received September 9, 2000. Published on the NRC Research Press Web site at http://canjchem.nrc.ca on July 6, 2001.

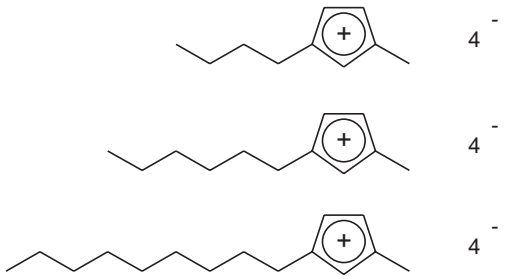
This paper is dedicated to Professor Brian James whose energy and enthusiasm for chemistry has inspired us.

P.J. Dyson[1] and D.J. Ellis. Department of Chemistry, The University of York, Heslington, York YO10 5DD, U.K.
T. Welton. Department of Chemistry, Imperial College of Science, Technology and Medicine, South Kensington, London SW7 2AY, U.K.

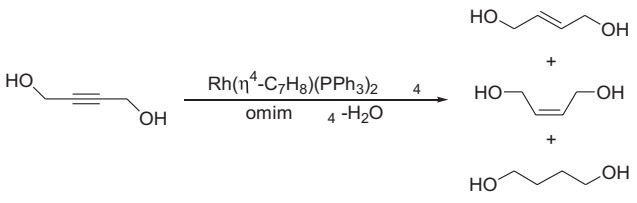
[1]Corresponding author (telephone: +(0)1904-434076; fax: +(0)1904-432516; e-mail: pjd14@york.ac.uk).

 DOI: 10.1139/cjc-79-5/6-705 © 2001 NRC Canada

Chart 1.



Scheme 1.



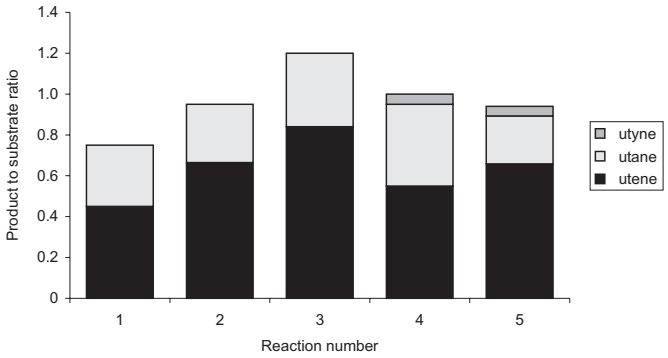
In this paper we describe an ionic liquid – water biphasic system employing a cationic rhodium catalyst that has been applied to the hydrogenation of a water soluble substrate. At higher temperatures, the ionic liquid and water form a single phase allowing truly homogeneous catalysis to be carried out, whereas at lower temperatures the ionic liquid and water form two phases allowing easy separation of the product in the aqueous phase from the catalyst supported in the ionic liquid. As far as we are aware this represents the first example of an ionic liquid to be employed in such a process although a related process has been used in fluorous phase – organic systems (12).

Results and discussion

The ionic liquids 1-butyl-3-methylimidizolium tetrafluoroborate ([bmim][BF_4]), 1-hexyl-3-methylimidizolium tetrafluoroborate ([hmim][BF_4]), and 1-octyl-3-methylimidizolium tetrafluoroborate ([omim][BF_4]) (see Chart 1) reported previously (13) have been shown to exhibit pH dependent reversible partitioning with water (14). These liquids also exhibit temperature-dependent reversible-phase separation with water. The temperature at which the [omim][BF_4] ionic liquid and water form a homogeneous system (established by measuring w/w) is 80°C which is ideally suited to chemical reactions. At room temperature (20°C) the [omim][BF_4] ionic liquid contains 12% water (w/w). This provides a potential method of conducting homogeneously catalyzed reactions at 80°C with the combined advantages of biphasic separation at 20°C (or below).

The solubility of numerous catalysts in the ionic liquid – water systems has been examined. To effectively dissolve a catalyst into an ionic liquid the catalyst must be a salt (recently a new cobaltacenium-based diphosphine ligand was specifically made with this in mind) (5*c*). To induce water solubility hydrophilic groups must be present and a wide range of water soluble phosphine ligand have been developed over the years (15). One of the most widely used hydrophilic groups is sulphate, and for example, P(C_6H_4-*m*-$SO_3Na)_3$ has been extensively employed in biphasic aqueous – organic catalysis (for recent examples see ref. 16) with very little contamination of the catalyst observed in the organic phase after reaction. We have found that complexes containing P(C_6H_4-*m*-$SO_3Na)_3$ ligands are also reasonably soluble in ionic liquids but they are clearly unsuitable for the ionic liquid – aqueous regime described herein due to preferential solubility in water. Since the triphenylphosphine complex [Rh(η^4-C_7H_8)($PPh_3)_2$][BF_4] is a hydrophobic salt, with high solubility in [omim][BF_4] and other ionic liquids (4*a*), it is ideally suited to the [omim][BF_4]–water system. Furthermore, cationic rhodium(I) compounds of formula [Rh(diene)$P_2]^+$ (where P_2 represents two monophosphines or a single diphosphine) have been used extensively as hydrogenation catalysts (17) and show excellent activity and have even been used in ionic liquid – organic biphasic hydrogenations (18). The P(C_6H_4-*m*-$SO_3Na)_3$ derivative has been used in aqueous – organic biphasic catalysis (19).

Fig. 1. Graphic representation of the relative components obtained from a consecutive series of hydrogenations of 2-butyne-1,4-diol (10 g of substrate was introduced into each batch).



Based on the above criteria [Rh(η^4-C_7H_8)($PPh_3)_2$][BF_4] was used to catalyze the hydrogenation of maleic acid and 2-butyne-1,4-diol in [omim][BF_4]–water at 80°C. The succinic acid product obtained quantitatively from the hydrogenation of maleic acid was not significantly more water soluble than ionic liquid soluble and presented separation problems that offer no advantage over other methodologies (20). In contrast, the hydrogenation of 2-butyne-1,4-diol afforded preferentially water soluble 2-butene-1,4-diol and butane-1,4-diol products (see Scheme 1) that were easily separated from the ionic liquid – catalyst phase after cooling the reaction mixture to room temperature. The results obtained from a series of consecutive batch hydrogenation reactions of 2-butyne-1,4-diol are presented graphically in Fig. 1.

Over the series of five reactions the catalyst decomposes slightly, as evidenced by the formation of a black precipitate and slight decoloration of the ionic liquid phase. The presence of a black precipitate often indicates the active catalyst species is colloidal, however, tests using mercury as a selective poison proved this not to be the case. Figure 1 shows that over the five batch reactions the conversion not only remains high, but also the recovery of the products remains high.

The initial relatively low recovery level of the product, stems from the fact that 2-butyne-1,4-diol and the hydrogenation products (as well as water) show some degree of solubility in the [omim][BF_4] ionic liquid. Once the ionic liquid

© 2001 NRC Canada

solution becomes saturated with these compounds higher recovery is observed.

Experimental

The ionic liquids 1-butyl-3-methylimidizolium tetrafluoroborate, 1-hexyl-3-methylimidizolium tetrafluoroborate, and 1-octyl-3-methylimidizolium tetrafluoroborate (13) and the catalyst $[Rh(\eta^4\text{-}C_7H_8)(PPh_3)_2][BF]_4$ (21) were prepared according to the literature methods. 2-Butyne-1,4-diol was purchased from Aldrich and used without further purification; water was distilled before use.

Hydrogenations were carried in a Parr stainless steel autoclave (300 mL) fitted with a PTFE liner. The catalyst was dissolved in ionic liquid and added directly to the autoclave. The autoclave was then sealed and purged with nitrogen. The reaction substrate was then dissolved in water and added through the liquid inlet port via a syringe. The autoclave was then purged thoroughly with hydrogen gas (99.9995% purity) and the pressure was then set at room temperature to 60 atm (1 atm = 101.325 kPa). The autoclave was then heated to 10°C and stirred for 2 h. Once the desired time period had elapsed, heating and stirring was stopped. The autoclave was allowed to cool and the pressure released. Substrate and catalyst layers were separated in a separating funnel.

The products were identified by ^{1}H NMR spectroscopy on a JEOL JNM-EX270 FT-NMR instrument and quantified gas chromatographic analysis using a Varian gas chromatograph with a capillary carbowax column (30 m) using injection, oven and detector temperatures 10–30°C above the boiling points of the substrate–product being studied. Such conditions typically gave good separations within 10 min although *cis* and *trans* isomers of the 2-butene-1,4-diol could not be resolved.

Concluding remarks

We have demonstrated the use of a temperature-controlled reversible ionic liquid – water partitioning system for the catalytic hydrogenation of 2-butyne-1,4-diol. However, the process still requires some optimization as it operates under fairly harsh conditions (cf. the hydrogenation of cyclohexene with a related rhodium(I) catalyst in a similar ionic liquid occurs at 10 atm (1 atm = 101.325 kPa) H_2 compared to 60 atm (1 atm = 101.325 kPa) H_2 used here) and some catalyst decomposition takes place. Furthermore, since the amount of water in the ionic liquid at lower temperatures remains relatively high (and visa versa) some contamination of the aqueous product phase with the catalyst or catalyst decomposition products is observed. However, it is likely that this problem could be largely overcome by selection of an alternative ionic liquid. In fact, by simply using the PF_6^- anion in place of BF_4^- in the ionic liquid the solubility with water drops considerably. Despite these problems the ease of catalyst–substrate separation combined with the isolation of product largely uncontaminated by the catalyst does indicate that this type of method could become highly desirable for certain processes. For example, the synthesis of pharmaceuticals, many of which are water soluble, using this approach, could help to overcome product contamination by toxic metal residues.

Acknowledgements

We would like to thank the Royal Society for a University Research Fellowship (PJD) and the University of York for a studentship (DJE).

References

1. (*a*) R.T. Carlin and J.S. Wilkes. *In* Advances in nonaqueous chemistry. *Edited by* G. Mamantov and A. Popov. VCH, New York. 1994; (*b*) Y. Chauvin and H. Olivier-Bourbigou. CHEMTECH, **25**, 26 (1995); (*c*) K.R. Seddon. Kinet. Catal. **37**, 693 1996; (*d*) K.R. Seddon. J. Chem. Technol. Biotechnol. **68**, 351 (1997); (*e*) H. Olivier-Bourbigou. *In* Aqueous-phase organometallic catalysis: concepts and applications. *Edited by* B. Cornils and W.A. Herrmann. Wiley–VCH, Weinheim. 1998; (*f*) T. Welton. Chem. Rev. **99**, 2071 (1999); (*g*) H. Olivier. J. Mol. Catal. A: Chem. **146**, 285 (1999).
2. (*a*) J.K.D. Surette, L. Green, and R.D. Singer. Chem. Commun. 2753 (1996); (*b*) C.J. Adams, M.J. Earle, G. Roberts, and K.R. Seddon. Chem. Commun. 2097 (1998); (*c*) P.J. Dyson, M.C. Grossel, N. Srinivasan, T. Vine, T. Welton, D.J. Williams, A.J. White, and T. Zigras. J. Chem. Soc. Dalton Trans. 3465 (1997).
3. C.J. Adams, M.J. Earle, and K.R. Seddon. Green Chem. 21 (2000).
4. (*a*) P.A.Z. Suarez, J.E.L. Dullius, S. Einloft, R.F. DeSouza, and J. Dupont. Polyhedron, **15**, 1217 (1996); (*b*) P.A.Z. Suarez, J.E.L. Dullius, S. Einloft, R.F. DeSouza, and J. Dupont. Inorg. Chim. Acta, **255**, 207 (1997); (*c*) A.L. Monteiro, F.K. Zinn, R.F. DeSouza, and J. Dupont. Tetrahedron: Asymmetry, **8**, 177 (1997); (*d*) P.J. Dyson, D.J. Ellis, D.G. Parker, and T. Welton. Chem. Commun. 25 (1999).
5. (*a*) Y. Chauvin, L. Mussmann, and H. Olivier. Angew. Chem. Int. Ed. Engl. **34**, 2698 (1995); (*b*) W. Keim, D. Vogt, H. Waffenschmidt, and P. Wasserscheid. J. Catal. **186**, 481 (1999); (*c*) C. C. Brasse, U. Englert, A. Salzer, H. Waffenschmidt, and P. Wasserscheid. Organometallics, **19**, 3818 (2000).
6. (*a*) A.J. Carmichael, M.J. Earle, J.D. Holbrey, P.B. McCormac, and K.R. Seddon. Org. Lett. **1**, 997 (1999); (*b*) V.P.W. Böhm and W.A. Herrmann. Chem. Eur. J. **6**, 1017 (2000); (*c*) L. Xu, W. Chen, and J. Xiao. Organometallics, **19**, 1123 (2000).
7. C. De Bellefon, E. Pollet, and P. Grenouillet. J. Mol. Catal. A: Chem. **145**, 121 (1999).
8. C.J. Mathews, P.J. Smith, and T. Welton. Chem. Commun. 1249 (2000).
9. T. Fischer, A. Sethi, T. Welton, and J. Woolf. Tetrahedron Lett. **40**, 793 (1999).
10. M.J. Earle, P.B. McCormac, and K.R. Seddon. Chem. Commun. 2245 (1998).
11. A.J. Carmichael, D.M. Haddleton, S.A.F. Bon, and K.R. Seddon. Chem. Commun. 1237 (2000).
12. (*a*) B. Cornils. Agnew. Chem. Int. Ed. Engl. **36**, 2057 (1997); (*b*) A. Stanislaus and B.H. Cooper. Catal. Rev. Sci. Eng. **36**, 75 (1993).
13. J.D. Holbrey and K.R. Seddon. J. Chem. Soc. Dalton Trans. 2133 (1999).
14. A.E. Visser, R.P. Swatloski, and R.D. Rogers. Green Chem. 1 (2000).
15. (*a*) P. Kalck and F. Monteil. Adv. Organomet. Chem. **34**, 219 (1992); (*b*) O. Stelzer. *In* Aqueous-phase organometallic catalysis: concepts and applications. *Edited by* B. Cornils and W.A.

© 2001 NRC Canada

Herrmann. Wiley–VCH, Weinheim. 1998; (*c*) M. Schreuder Goedheijt and P. van Leeuwen. *In* Aqueous-phase organometallic catalysis: concepts and applications. *Edited by* B. Cornils and W.A. Herrmann. Wiley–VCH, Weinheim. 1998.

16. (*a*) N. Tanchoux and C. De Bellefon. Eur. J. Inorg. Chem. 1495 (2000); (*b*) S. Jayasree, A. Seayad, and R.V. Chaudhari. Chem. Commun. 1239 (2000); (*c*) B.M. Bhanage, M. Shirai, and M. Arai. J. Mol. Catal. A: Chem. **145**, 69 (1999); (*d*) P.J. Dyson, D.J. Ellis, D.G. Parker, and T. Welton. J. Mol. Catal. A: Chem. **150**, 71 (1999).
17. (*a*) R.H. Crabtree. Acc. Chem. Res. **12**, 331 (1979); (*b*) Z.X. Zhou, G. Facey, B.R. James, and H. Alper. Organometallics, **15**, 2496 (1996); (*c*) M.A. Esteruelas, I. González, J. Herrero, and L.A. Oro. J. Organomet. Chem. **551**, 49 (1998).
18. Y. Chauvin, L. Muβmann, H. Olivier. Angew. Chem. Int. Edit. **34**, 2698 (1995).
19. M.H. Bortoletto, L. Lavenot, C. Larpent, A. Roucoux, and H. Patin. Appl. Catal. A, **156**, 347 (1997).
20. A. Benyei, J.N.W. Stafford, A. Katho, D.J. Darensbourg, and F. Joo. J. Mol. Catal. **84**, 157 (1993).
21. E.W. Abel, M.A. Bennett, and G. Wilkinson. J. Chem. Soc. 3178 (1978).

© 2001 NRC Canada

Transmetalation reactions with nitrogen-containing "pincer"-class ligands on platinum(II) centers

Martin Albrecht, Stuart L. James, Nora Veldman, Anthony L. Spek, and Gerard van Koten

Abstract: The transmetalation reaction of the aryllithium compound $[Li(NCN)]_2$ (NCN is the monoanionic "pincer" ligand $[C_6H_3(CH_2NMe_2)_2\text{-}2,6]^-$) with the cyclometalated arylplatinum complex [PtCl(NCN)] afforded the bisaryl platinum(II) complex $[Pt(NCN)_2]$ (**3**) containing one η^3-*N,C,N*-terdentate and the other η^1-*C*-monodentate-bonded pincer ligand. Spectroscopic analyses on **3** suggest that η^3 to η^1 interconversion of the ligand binding mode (or vice versa) is inhibited. Two independent X-ray structure determinations on crystals of **3** revealed the existence of a rare polymorph containing one and three crystallographically independent molecules, respectively, in the unit cell. A similar transmetalation reaction with lithium and platinum complexes containing heteroleptic $NCN^{RR'}$ ligands ($NCN^{RR'}$ is $[C_6H_3(CH_2NRR')\text{-}2,6]^-$ with R = R′ = Me or R = Me, R′ = Et) pointed to the formation of a heterodinuclear cationic bisaryl platinum lithium species as an intermediate of a preequilibrium to the final transmetalation products, involving, rapid transcyclometalation (TCM) reactions. These TCM reactions comprise the exchange of the monoanionic $NCN^{RR'}$ ligands between the platinum(II) and lithium centers. A consequence of the latter properties is that the strong Pt—N bonds in [PtX(NCN)] complexes are considerably weakened by the presence of Li^+ cations.

Key words: transmetalation, transcyclometalation (TCM), platinum, bisaryl complex, polymorphism.

Résumé : La réaction de transmétallation du composé aryllithium $[Li(NCN)]_2$ (NCN = ligand « en pince » monoanionique $[C_6H_3(CH_2NMe_2)_2\text{-}2,6]^-$) avec le complexe d'arylplatine cyclométallé [PtCl(NCN)] conduit à la formation du complexe bisaryle de platine(II) $[Pt(NCN)_2]$ (**3**) qui contient un ligand η^3-*N,C,N*-terdentate et l'autre ligand en forme de pince lié de façon η^1-*C*-monodentate. Les analyses spectroscopiques de **3** suggèrent qu'il y a une inhibition à l'interconversion η^3 à η^1 (ou vice versa) du mode de fixation du ligand. Deux déterminations indépendantes de la structure des cristaux de **3** par diffraction des rayons X révèlent l'existence d'une polymorphie rare dans laquelle chacune des formes comprend respectivement une et trois molécules cristallographiquement indépendantes par maille. Une réaction de transmétallation semblable avec des complexes de lithium et de platine contenant les ligands hétéroleptiques $NCN^{RR'}$ ($NCN^{RR'}$ = $[C_6H_3(CH_2NRR')\text{-}2,6]^-$ avec R = R′ = Me ou R = Me, R′ = Et) suggère qu'il y a formation d'une espèce bisaryle de platine et de lithium hétérodinucléaire cationique comme intermédiaire d'un prééquilibre vers les produits finaux de transmétallation et qu'il implique des réactions rapides de transcyclométallation (TCM). Ces réactions de TCM incluent l'échange des ligands monoanioniques $NCN^{RR'}$ entre les centres de platine(II) et de lithium. En conséquence de ces propriétés, les fortes liaisons Pt—N présentes dans les complexes de [PtX(NCN)] sont de beaucoup affaiblies par la présence des cations Li^+.

Mots clés : transmétallation, transcyclométallation (TCM), platine, complexe bisaryle, polymorphie.

[Traduit par la Rédaction]

Introduction

The reversible formation of an intermediate metal-to-carbon bond is a crucial step in many catalytic cycles (1). In particular, making and breaking of C_{aryl}—M σ-bonds is of great significance, e.g., in C_{aryl}—C_R cross coupling reactions (Heck: R = alkene; Sonogashira: R = alkyne; Suzuki:

Received October 18, 2000. Published on the NRC Research Press Web site at http://canjchem.nrc.ca on July 9, 2001.

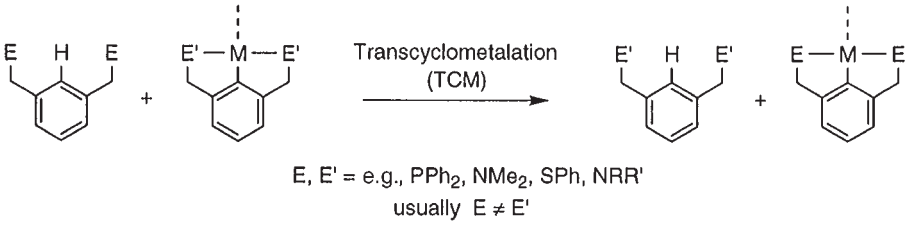
Dedicated to Brian James on the occasion of his 65th birthday in admiration for his great contribution to homogeneous catalysis and our friendship.

M. Albrecht, S.L. James, and G. van Koten.[1] Debye Institute, Department of Metal-Mediated Synthesis, Utrecht University, Padualaan 8, 3584 CH Utrecht, The Netherlands.
N. Veldman[2] **and A.L. Spek.**[3] Bijvoet Center for Biomolecular Research, Department of Crystal and Structure Chemistry, Utrecht University, Padualaan 8, 3584 CH Utrecht, The Netherlands.

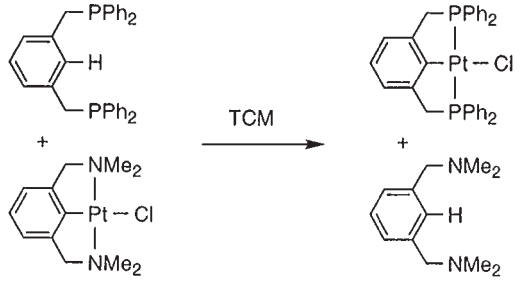
[1]Corresponding author (telephone: +31-30-253-3120; Fax: +31-30-252-3615; e-mail: g.vankoten@chem.uu.nl).
[2]Deceased.
[3]Corresponding author pertaining to crystallographic details (e-mail: a.l.spek@chem.uu.nl).

 DOI: 10.1139/cjc-79-5/6-709 © 2001 NRC Canada

Scheme 1. General representation of TCM reactions with terdentate coordinating ligands; interconversion of one metallacycle into another.



Scheme 2. TCM reaction of [PtCl(NCN)] with PCHP to give [PtCl(PCP)] and NCHN (12*d*).



R = aryl) and in C_{aryl}—E bond activation processes (E = carbon or heteroatom) (for examples of cross coupling see ref. 2*a*; for examples of bond activation see ref. 2*b*). Intramolecular stabilization of this C—M bond by heteroatom coordination, i.e., formation of metallacycles, has been demonstrated to be an efficient methodology for stabilizing the metal-to-carbon bond. As a consequence, the rate of (catalytic) processes is often considerably reduced, which provides insight into mechanistic details and thus important information for efficient catalyst design (3, 4). Other applications of transition metal complexes containing C_{aryl} σ–bonding chelates include the engineering and processing of materials properties, e.g., for gas storage (5) and sensoring purposes (6).

Up to now, cyclometalated complexes containing C—M σ-bonds have been accessible predominantly via two different methods: (*i*) transmetalation of (main group) organometallics (C-Mg, C-Li, C-Sn) with a suitable metal precursors (7); or (*ii*) direct cyclometalation via C—E bond activation (E = e.g., C, Si, halide) (8). Recently, transcyclometalation (TCM) reactions have been introduced as a new methodology for the generation of cyclometalated transition-metal complexes. In close relation to (organic) transesterification reactions (9), TCM reactions consist of the substitution of one (monoanionic) cyclometalated ligand by another one (Scheme 1). In some cases, this has the advantage of being a cleaner reaction than direct cyclometalation. Previous examples, though at that time not recognized as TCM reactions, include a variety of ligand systems, which were predominantly activated with palladium complexes (10). More recently, the TCM reaction of a terdentate coordinated NCN-type pincer-ligand (11) by another bis(*ortho*)-chelating PCP pincer-ligand has been described to occur on a ruthenium(II) (i.e., M in Scheme 1 is $RuCl(PPh_3)$) and a platinum(II) (Scheme 2) metal center, respectively, (12). As a primary conclusion of these studies (12*a*), the higher bond strength of the M—P bond compared to the analogous M—N bond is anticipated to be the driving force. Indeed, the selective and quantitative replacement of the amines by phosphorus donors has been demonstrated to initiate the TCM process. In this report we present evidence that also cyclometalated aryllithium and platinum compounds can undergo TCM reactions. This leads even for η^3-coordinated NCN ligands to the formation of mixtures of cyclometalated compounds.

Results and discussion

Initial attempts to transcyclometalate aryl ligands of the type $NC(H)N^{RR'}$ ($NCN^{RR'}$ denotes the monoanionic bis(*ortho*)-substituted aryl ligand $[C_6H_3(CH_2NRR')_2\text{-}2,6]^-$) with either the neutral cyclometalated complex $[PtCl(NCN^{Me_2})]$ (**2**), or its cationic analogue $[Pt(NCN^{Me_2})(H_2O)](BF_4)$ (13) gave no detectable reaction. Obviously, the Pt—N bond in [PtCl(NCN)] cannot be displaced by an amino group of the $NCHN^{RR'}$ ligand, and consequently, a TCM process is prevented since in these reactions ligand substitution has been identified as an initial step. Hence, half an equivalent of the dimeric aryllithium species $[Li(NCN^{Me_2})]_2$ (**1-Li**) (14) was reacted with the arylplatinum(II) complex **2** in polar solvents and at elevated temperatures (THF, reflux temperature). This afforded the bisaryl platinum(II) complex $[Pt(\eta^3\text{–}NCN^{Me_2})(\eta^1\text{–}C\text{–}NCN^{Me_2})]$ (**3**) in 60% yield (Scheme 3). This complex contains two differently bonded pincer ligands, one monodentate η^1-*C* and the other terdentate η^3-*N*,*C*,*N* coordinating. This compound may be envisaged as an intermediate in the full substitution of one NCN ligand by another in the TCM reaction, cf. the isolation of $[Pt(\eta^3\text{–}P,C,P\text{–PCP})(\eta^1\text{–}C\text{–NCN})]$ in the TCM reaction of **1** with PCHP (Scheme 2). This is further underlined by the reactivity of **3** towards aq HCl, which results in rapid Pt—C bond cleavage of the η^1-coordinated ligand and formation of the starting materials **2** and **1** as the diprotonated chloride salt (Scheme 3). Remarkably, these conditions affect neither the Pt—N nor the Pt—C bonds of the η^3-*N*,*C*,*N* chelating ligand, and are a good indication for the excellent stability of the [Pt(NCN)] unit. This is also in concert with the fact that **2** does react with the bis-phosphinoarene PCHP but not with the bis-aminoarene NCHN.

Unambiguous confirmation of the connectivity pattern in **3** was accomplished by detailed X-ray structure analyses of single crystals, which were grown by slow evaporation of a saturated Et_2O solution.

Solid-state structure of 3

The molecular structure of **3**, measured at room temperature, is shown in Fig. 1 and reveals a platinum(II) center that is ligated by a terdentate, η^3-*N*,*C*,*N*-bound, and a mono-

© 2001 NRC Canada

Scheme 3. Synthesis of the homoleptic bisaryl platinum(II) complex **3** and its reactivity towards MeI.

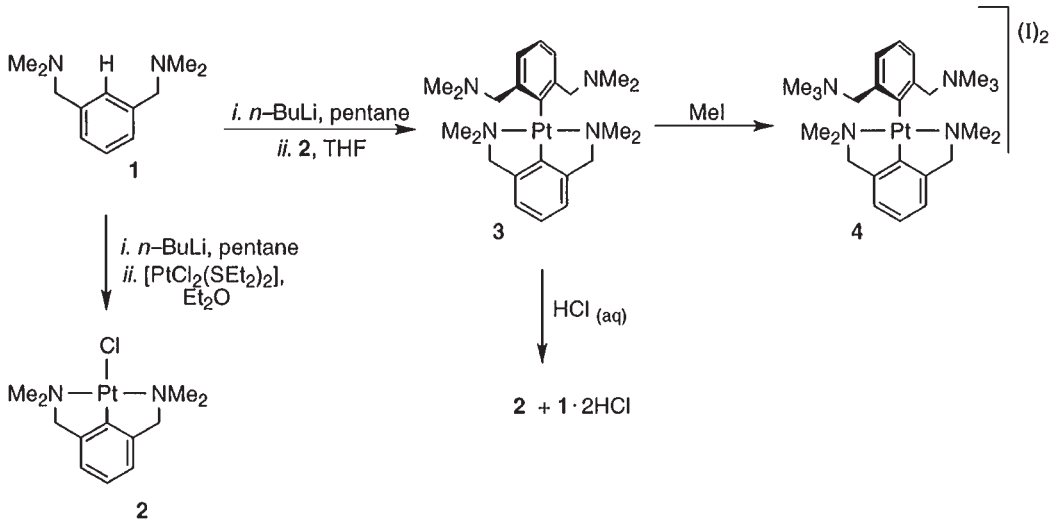
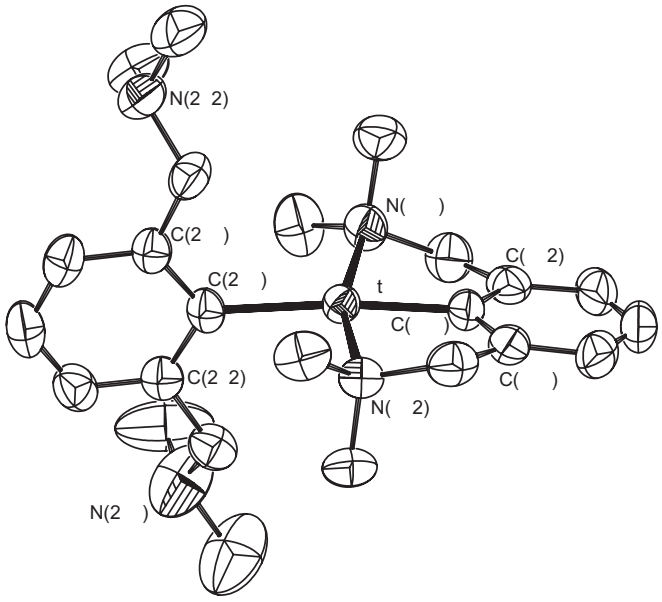


Fig. 1. Perspective view of the molecular structure of **3** (50% probability level, crystal **I**).



dentate, η^1-*C*-bound, NCN pincer ligand, resulting in a *trans* positioning of the two aryl groups across the metal square plane. The puckered five-membered chelate ring conformations, bond lengths, and bond angles of the [Pt(η^3-NCN^{Me_2})] moiety are normal for square planar platinum(II) complexes containing this ligand (Table 1) (13, 15). As a consequence of the different denticity of the ligands, the metal-to-carbon σ-bond of platinum to the monodentate bonded NCN ligand is considerably longer (Pt—C(201) 2.126(5) Å) than the one to the terdentate coordinating NCN ligand (Pt—C(101) 1.963(6) Å). Moreover, the aromatic ring of the η^1-*C*-bonded ligand system is considerably distorted (the internal angle at C_{ipso} is 114.3(5)° for the η^1-*C*-NCN, and 121.4(5)° for the η3-*N*,*C*,*N*-bonded ligand), which is presumably a consequence of the steric crowding around the platinum nucleus. The noncoordinating tertiary amines are directed away from the metal center.

Two different structural motifs have been identified, for the orientation of the CH_2NMe_2 groups with respect to the arylplatinum unit. The first comprises short interatomic C-H···N contacts between the aryl protons H(201) and H(203) and the nitrogen atoms of the η^1-coordinated NCN ligand (C_{aryl}-H···N 2.627 and 2.679 Å, respectively; see Fig. 2 and Table 2). The second motif has the benzylic protons H(205) and H(212) of the η^1-coordinating pincer ligand positioned near the virtual *z* axis of the platinum center (Pt···H 2.803 and 2.704 Å, respectively). The filled d_z2 orbitals in such d^8 metal centers, particularly in bisaryl platinum(II) complexes, have been established to be important frontier orbitals. As a consequence, the observed C-H···Pt arrangement provides additional stabilization to this particular CH_2NMe_2 conformer (12*a*, 16).

Surprisingly, a second crystal structure determination, which was performed at 150 K, revealed a polymorph (17). While the overall connectivity was the same as established for the first X-ray analysis, distinctly different intramolecular orientations for the CH_2NMe_2 substituents were identified for the crystal structures. Representative sections of the two polymorphous crystal structures (**I** and **II**) are shown in Fig. 3. Form **I** (data collected at room temperature, Fig. 3*a*) contains one molecule per asymmetric unit, in which the two free amine arms are both positioned on the same side of the aryl ring to which they are connected, i.e., they have a *cisoid* arrangement. The asymmetric unit in the polymorph **II** (150 K), however, contains three independent molecules, two of which have the *cisoid* conformation as observed in **I**, while the third (molecule 3, Fig. 3*b*) has the free amine groups positioned on opposite sides of the aryl ring (*transoid*). It is noteworthy that no phase transition was observed on cooling of crystal **I** to 150 K.

Structural aspects of 3 in solution

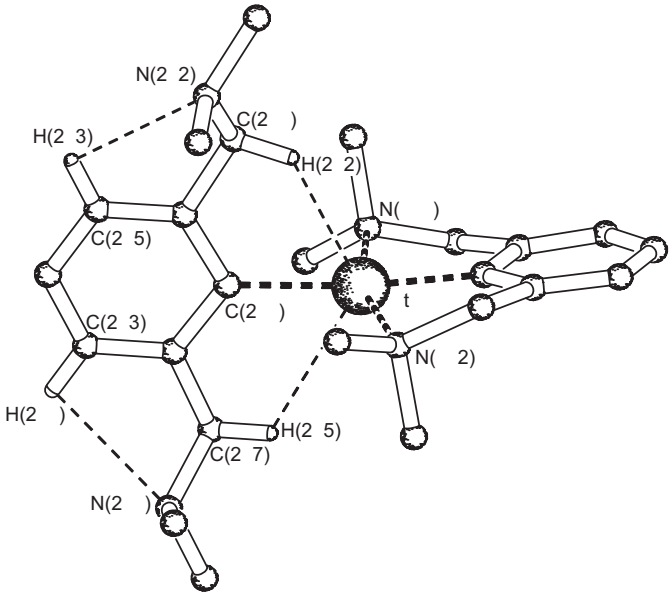
As a result of the ligand arrangement at the platinum center (viz. two metal-bound aryl units and two noncoordinating *tert*-amine moieties), complex **3** displays good solubility in apolar solvents (e.g., in Et_2O and pentane) which is unusual for related platinum-halide species such as **2** (13). In the ^{1}H NMR spectrum (C_6D_6 solution), two distinct signals for the

© 2001 NRC Canada

Table 1. Interatomic bond lengths (Å) and angles (deg) of **3**.

		Crystal **II**		
	Crystal **I**	Molecule 1	Molecule 2	Molecule 3
Bond lengths				
Pt—C(101)	1.963(6)	1.92(2)	1.95(2)	2.00(2)
Pt—C(201)	2.126(5)	2.131(19)	2.15(2)	2.12(2)
Pt—N(101)	2.104(5)	2.096(14)	2.117(14)	2.075(18)
Pt—N(102)	2.107(5)	2.102(16)	2.104(16)	2.090(17)
C(101)—C(102)	1.385(8)	1.42(3)	1.40(3)	1.34(3)
C(101)—C(106)	1.388(9)	1.41(3)	1.38(3)	1.39(3)
C(201)—C(202)	1.419(8)	1.41(3)	1.41(3)	1.40(2)
C(201)—C(206)	1.424(8)	1.39(3)	1.41(3)	1.40(3)
Bond angles				
C(101)-Pt-C(201)	174.1(2)	177.7(8)	177.6(7)	176.8(8)
C(101)-Pt-N(101)	80.9(2)	79.4(7)	80.9(7)	78.4(7)
C(101)-Pt-N(102)	80.1(2)	80.8(7)	80.2(7)	81.1(8)
C(201)-Pt-N(101)	97.8(2)	102.4(7)	101.4(7)	101.0(7)
C(201)-Pt-N(102)	101.3(2)	97.3(6)	97.5(7)	99.4(7)
N(101)-Pt-N(102)	160.9(2)	160.3(6)	161.1(6)	159.5(7)
C(102)-C(101)-C(106)	121.4(5)	123.5(19)	119.3(19)	125(2)
C(202)-C(201)-C(206)	114.3(5)	116.5(18)	116.4(18)	113.8(17)

Fig. 2. Short intramolecular contacts of the noncoordinating *ortho*-substituents from the η^1-coordinating pincer ligand.



NMe_2 groups are observed, which are located at 2.41 and 2.58 ppm, respectively. The resonance at 2.41 ppm is typical for noncoordinating amine methyl groups, but is shifted to higher frequency when compared to free ligand (δ_H (NMe_2) = 2.21 ppm in **1**). In contrast, the signal at 2.58 ppm displays a coupling pattern ($^3J_{HPt}$ = 42 Hz) which is diagnostic for nitrogen coordination to the metal center, even though these nuclei seem to be considerably shielded when compared to related groups, in **2** and analogues where the chloride in **2** is replaced by another halide or a *para*-tolyl ligand, cf. δ_H (NMe_2) = 2.95–3.18 (13*a*). Similar features are also observed for the resonances at 4.38 and 3.57 ppm, which, on the basis of either the absence or presence of ^{195}Pt coupling ($^3J_{HPt}$ = 47.0 Hz),

Table 2. Short intramolecular distances (Å) and angles (deg) in **3**.

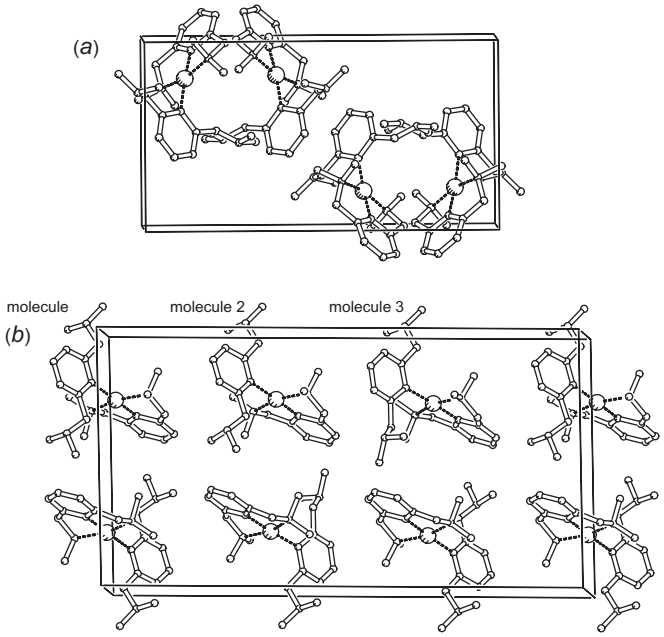
Donor–acceptor system	Distances (Å)		Angles (deg)
D-H···A	H···A	D···A	D-H···A
C(207)-H(205)···Pt	2.803	3.391(6)	119.8
C(210)-H(212)···Pt	2.704	3.324(6)	122.2
C(203)-H(201)···N(201)	2.627	2.914(9)	98.5
C(205)-H(203)···N(202)	2.679	2.960(9)	98.3

were assigned to the $ArCH_2N$ protons of the η^1-*C* and the η^3-*N,C,N*-coordinating pincer systems, respectively, (12*a*, 13). The low field shift of the noncoordinating CH_2N protons is remarkable and points to additional deshielding of these nuclei. Such effects may originate from weak intramolecular interactions (e.g., hydrogen bonding) with the nucleophilic platinum(II) center (Fig. 2) (12*a*, 18). The properties of the platinum(II) center as hydrogen bond acceptor have recently been applied for the fabrication of organometallic proton sponges (12*a*, 19). Further confirmation of the structure of **3** was obtained from ^{13}C NMR spectroscopy. In particular, the two signals at 172.6 and 182.2 ppm are characteristic for Pt(NCN) type complexes containing an aryl anion in mutual *trans*-position to the metal-bound pincer-carbon N*C*N (13). As expected, two sets of benzylic carbons (at 68.4 and 80.8 ppm) and nitrogen-bound methyl carbons (at 45.9 and 54.7 ppm) were observed, which belong to the monodentate coordinating and to the chelating ligand, respectively. The symmetric structure in solution, indicated by ^{1}H and ^{13}C NMR spectra, is consistent with a purely *transoid* arrangement of the free arms, or fast exchange between *transoid* and *cisoid* forms on the NMR time scale.

Variable temperature NMR experiments were carried out to probe in particular whether dynamic processes could be feasible involving a fluxional switch between η^3- and η^1-bonding of each of the pincer ligands. At low temperature (–80°C, CD_2Cl_2) the signals due to the free amine arms broaden. Although this may be due to the onset of freezing

© 2001 NRC Canada

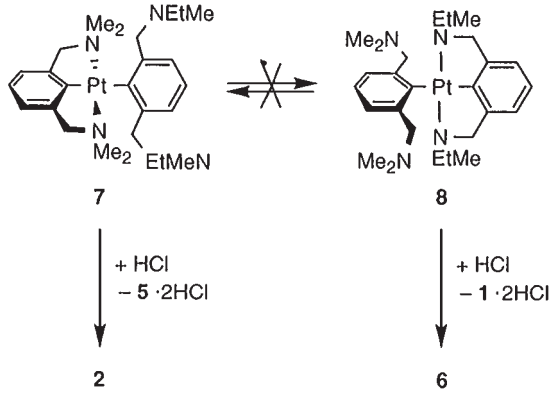
Fig. 3. Polymorphism in crystalline **3**: (*a*) crystal structure of crystal **I**, which is characterized by one single independent molecule of **3**. Note that the noncoordinating nitrogens are in *cisoid* configuration with respect to the bisecting aryl plane of the η^1-bound ligand; (*b*) the second polymorph, crystal **II**, contains three independent molecules of **3** in the unit cell. Molecule 1 and 2 display a similar *cisoid* confirmation as identified for crystal **I**, whereas molecule 3 contains the non-coordinating amines in a *transoid* position.



out of a *cisoid–transoid* equilibrium, temperatures low enough to resolve the interconverting species could not be attained. Fluxional processes involving coordination of the free amine groups with associated decoordination of the bonded amine groups could also occur at higher temperatures. However, neither ^{1}H NMR spectra in toluene-d_8 solution at 110°C nor spin saturation transfer experiments revealed any evidence for a dynamic behavior of **3** on the NMR time scale. These results show that even *intra*molecular substitution of coordinated amines by free amine sites is not occurring (vide infra).

The presence of noncoordinating tertiary amines in **3** was further established by derivatization with MeI, which gave the bis-ammonium salt [Pt(η^3-NCN^{Me_2})(η^1-NCN^{Me_3})](I)$_2$ (**4**) (Scheme 3). Interestingly, no arenium species was formed, as might be expected on basis of previous results related to the reaction of NCN platinum(II) aryl complexes with MeI (20). Two different explanations may rationalize these observations: Either the bulk of the noncoordinating CH_2NMe_2 groups of the η^1-monodentate bound pincer ligand efficiently reduce the accessibility of the platinum center or alternatively, oxidative addition of MeI may take place to form an intermediate platinum(IV) species (4*a*, 21), followed by irreversible trapping of the platinum-bound methyl group by the noncoordinated amine groups, and formation of a cationic ammonium structure as **4**. The accumulation of positive charges and (or) steric crowding in close proximity to the metal center apparently prevents the reaction of **4** with another equivalent of MeI. The methyl groups of the terdentate pincer ligand in **4** are chemically inequivalent (viz. two singlet resonances with ^{195}Pt couplings in the ^{1}H NMR spectrum at δ_H = 2.69 and 2.74, respectively). Also, the benzylic protons of the η^3-bonded ligand in **4** became diastereotopic as shown by the AB-type pattern with δ_A at 3.83 ppm and δ_B at 5.03 ppm, respectively. These observations suggest a reduced symmetry in **4**, which may be due to a frozen wagging of the methylene CH_2 groups of the five-membered metallacycles. In solution, puckering effects are usually fast and cannot be slowed down significantly by cooling (22). However, the steric constraints of the bulky ammonium groups on the η^1-bonded ligand may reduce the fluxionality of the metallacycles considerably. This is corroborated by the anticipated relative position of the aryl planes of the η^1-bonded and η^3-bonded pincer ligands, which are most likely significantly tilted from an ideal perpendicular orientation, cf. the solid-state structure of related bis-ammonium complexes (12*a*).

Scheme 4. Selective acid-mediated cleavage of the unsupported Pt—C bond.



Bisaryl platinum(II) complexes containing heteroleptic pincer ligands

It must be noted that during the formation of **3**, a TCM type reaction could be operative, which is undetectable as it is degenerative in the products. To distinguish a transmetalation reaction, i.e., Li–Pt exchange on NCN, from an eventually competitive TCM type process, a chemical modification in one ligand framework was introduced. Ideally, such a modification should allow to distinguish between the different amine donors but not cause significantly different coordination properties. Therefore, the prochiral pincer ligand precursor NCHN^{EtMe} (**5**) containing one methyl and one ethyl group bound to each nitrogen donor, was used as a marker.[4] Lithiation and subsequent transmetalation of this ligand readily afforded the corresponding platinum complex [PtCl(NCN^{EtMe})] (**6**) (23).

[4] It has been shown previously that replacement of all methyl groups by ethyl substituents severely disturbes nitrogen coordination and reduces the accessibility of the metal center rigorously. As a consequence, the platinum center in complexes such as [PtX(NCN^{Et_2})] is not available anymore for, e.g., SO_2 (23) or I_2 (4*b*) coordination. Moreover, X-ray structure analyses revealed that the puckering of the metallacycle in, e.g., [PtI(NCN^{Et_2})] is considerably smaller than in the corresponding NCN^{Me_2} complexes (23).

© 2001 NRC Canada

Scheme 5. Heteroleptic bisaryl platinum(II) complex formation by using modified pincer ligands containing ethyl-labeled amino groups.

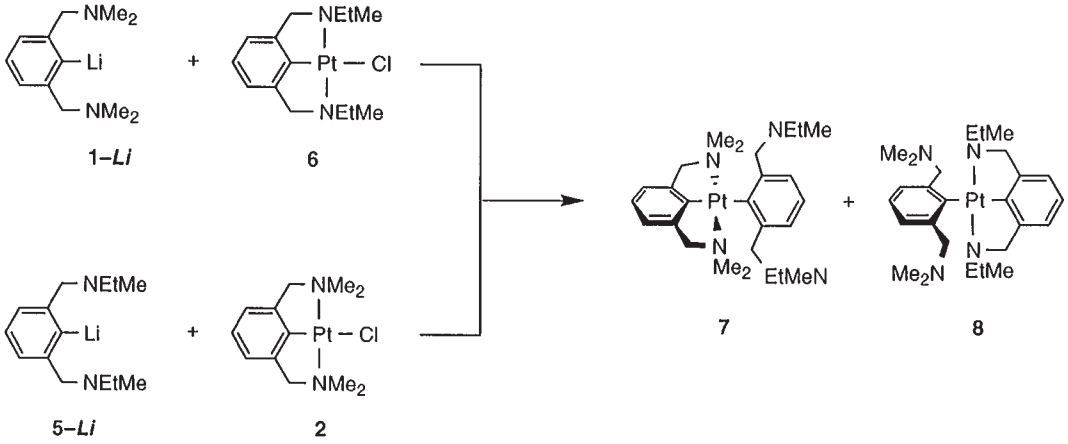
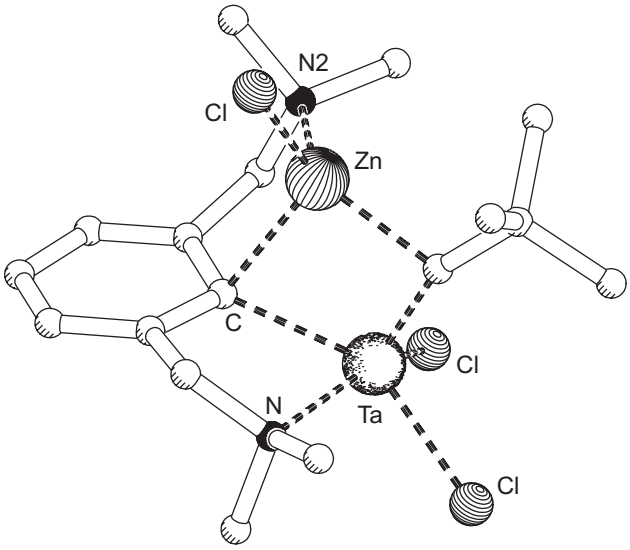


Fig. 4. Snapshot of the transmetalation reaction between tantalum and zinc on a pincer ligand. Note the structural analogy of this complex with intermediate **A** as proposed for the transcyclometalation between platinum and lithium (see Scheme 6).



Reaction of **6** with **1-Li** is anticipated to give selectively the bisaryl complex **8** containing the NEtMe groups coordinated to the platinum center, provided the reaction is a straightforward transmetalation reaction involving substitution of the Li^+ cation in **1-Li** by $[Pt(NCN^{EtMe})]^+$ (Scheme 5). Analogously, the product of a transmetalation of **5-Li** with **2** would afford complex **7** as the exclusive product. On the contrary, an eventually operative TCM reaction would be indicated in these cross-experiments by the concomitant presence of both complexes **7** and **8**, since this process involves (repetitive) formation and cleavage of metallacycles with reformation of the corresponding $[Li(NCN^{RR'})]$ compounds.

Analysis of the product mixtures obtained from the cross-experiments (performed under experimental conditions that were analogous to those applied for the formation of **3**) pointed to the presence of both **7** and **8**. The NMR spectra of the product mixtures of both reactions were complicated (24). However, they were remarkably consistent, irrespective of whether the ethyl-labeled nitrogen donors were in the lithium species or in the cyclometalated starting material. The high field region of the ^1H NMR spectra is diagnostic: the signals at δ_H = 2.69 and 2.10 are indicative for platinum-bound and noncoordinated NMe_2 groups, respectively. Furthermore, two sets of resonances were observed for the nitrogen-bound ethyl substitutents. The set at lower field (δ_H = 2.64 (q) and 1.16 (t)) is located at frequencies similar to those observed for nonmetalated **5**, whereas the set at higher field (δ_H = 2.33 (m) and 0.99 (t)) showed the expected pattern for nitrogen coordination to platinum (24), with characteristic coupling constants of the methylene NCH_2 protons to the platinum center ($^3J_{HPt}$ = 78 Hz). A product ratio between **7** and **8** of 3:5 was estimated based on the signals due to the NCH_2CH_3 methyl groups. Interestingly, this ratio is nearly constant and independent of the chosen starting materials, i.e., the cycloplatinated starting materials **2** or **6**. This implies an equilibrium situation which precedes the ultimate formation of the transmetalation products.

Product analyses using variable temperature ^1H NMR lead to similar results as obtained for **3**. In the measured temperature range (–80 to +100°C, toluene-d_8 solution), no significant line-broadening was observed. More importantly, the product ratio between **7** and **8** remained constant, implying a high kinetic barrier for the transition of **7** to **8** and vice versa (Scheme 4). These results exclude a potential equilibrium situation *after* the transmetalation sequence.

When the complexes **3**, or **7** and **8** were treated with an excess of aq HCl, rapid fission of the unsupported Pt—C bond was observed, thus giving the cyclometalated platinum chloride complexes **2** and **6**, respectively, along with the protonated pincer ligands **1**·2HCl and **5**·2HCl (Scheme 4). Since the non-chelating Pt—C bond is cleaved selectively (the Pt—C bond in complex **2** was stable towards HCl at 60°C for several hours), quantification of the product ratio between **2** and **6** provides an a posteriori method for the determination of the ratio between **7** and **8**.

Mechanistic consequences for TCM reactions with $[Li(NCN^{RR'})]$ complexes

Related transmetalation studies have emphasized the relevance of bimetallic intermediates comprising an aryl carbanion bridging to two (different) metal centers through 3*c*—2*e* or 3*c*—4*e* bonding (Fig. 4) (25). A similar

© 2001 NRC Canada

Scheme 6. Rapid and reversible TCM process in a preequilibrium of the transmetalation reaction. Note that structure **A** is the common intermediate of both the TCM and the transmetalation process.

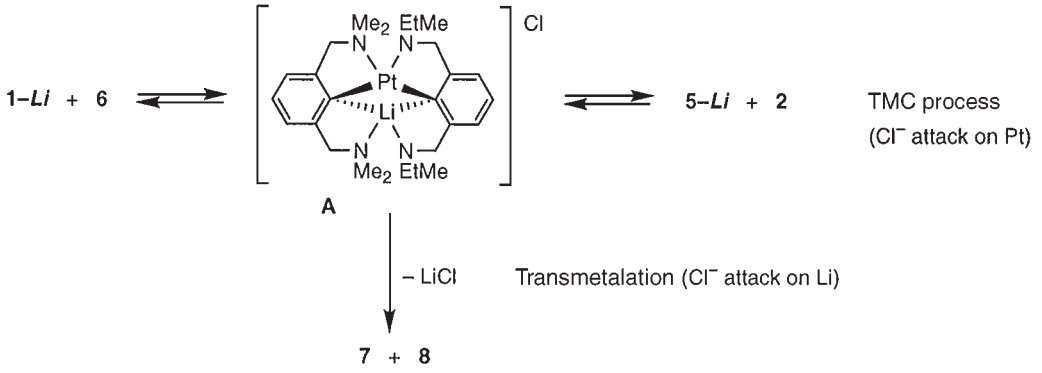


Table 3. Crystallographic data for both polymorphs of complex **3**.

	Crystal **I**	Crystal **II**
Empirical formula	$C_{24}H_{38}N_4Pt$	$C_{24}H_{38}N_4Pt$
Formula weight	577.67	577.67
T (K)	298	150
Crystal system	Monoclinic	Monoclinic
Space group	$P2_1/c$ (no. 14)	$P2_1/c$ (no. 14)
Crystal size (mm)	0.50 × 0.50 × 0.50	0.38 × 0.38 × 0.15
Crystal color	Colorless	Colorless
Unit cell dimensions		
a (Å)	10.3234(7)	16.954(2)
b (Å)	19.1763(12)	27.422(2)
c (Å)	12.3632(8)	18.023(2)
β (deg)	93.271(5)	121.271(10)
V (Å^3)	2443.5(3)	7161.8(15)
Z	4	12
D_{calc} (g cm^{-3})	1.5703(2)	1.6073(3)
μ (mm^{-1}) (Mo Kα)	5.76	5.89
Abs. correction	PLATON (DELABS)	PLATON (DELABS)
Transmission range	0.386–1.000	0.585–1.000
(sin θ/λ) Max (Å^{-1})	0.65	0.65
Reflections collected, unique	8598, 5592	14374, 13561
R_{int}	0.0301	0.0581
Parameters, restraints	271, 0	538, 0
R_1,[a] wR_2,[b] *S*	0.0372, 0.0811, 1.027	0.0680, 0.1363, 1.017
w^{-1} [c]	$\sigma^2(F_o^2) + (0.0250P)^2 + 5.13P$	$\sigma^2(F_o^2) + (0.0170P)^2 + 100.31P$
Resid. density (e Å^{-3})	–0.79 < 1.18	–1.99 < 2.13

[a] $R_1 = \Sigma||F_o| - |F_c||/\Sigma|F_o|$, for all $I > 4\sigma(I)$.
[b] $wR_2 = [\Sigma[w(F_o^2 - F_c^2)^2]/\Sigma[w(F_o^2)^2]]^{1/2}$.
[c] $P = (\max(F_o^2, 0) + 2F_c^2)/3$.

intermediate (A) is likely to be involved in the transmetalation of **1-Li** or **5-Li** by the cyclometalated platinum(II) complexes **6** and **2**, respectively, (Scheme 6). Due to the low stability of such complexes, it is expected that intermediate **A** equilibriates rapidly with the starting materials. Notably, it is not possible to deduce the precursors, i.e., **2** and **5-Li** or **6** and **1-Li**, from complex **A** and formation of either of these two sets of starting materials occurs on nucleophilic attack of Cl^- on the platinum center. This interconversion of **2** and **5-Li** to **6** and **1-Li** and vice versa corresponds to a transcyclometalation (TCM) reaction between the platinum and lithium centers. Alternative attack of the Cl^- nucleophile on the lithium center in intermediate **A** induces the formation of LiCl and the respective bisaryl platinum(II) product, which is probably an irreversible reaction sequence. Apparently, the equilibrium situation of the TCM reaction with complex **A** as an intermediate must be reached rapidly. This is an interesting further reaction trajectory for a TCM process and contrasts to earlier established reactions where one starting material was metal-free. The relatively low selectivity of this TCM reaction (Scheme 6) in terms of product distribution (nearly equal yields of **7** and **8**) is most likely a direct consequence of the only small differences in the bond strength of the platinum center to either N^{Me_2} or N^{EtMe} type amines. Similar arguments account for the Li—N^{Me_2} and Li—N^{EtMe} bond strengths. According to

© 2001 NRC Canada

spectroscopic analyses (NMR signal integration), there is a slight preference for initial Li—N^{EtMe} bond cleavage rather than Li—N^{Me_2} fission, since the major product of the transmetalation is complex **8** having metallacycles containing N^{EtMe} type amines. The low product selectivity contrasts with previously reported TCM processes, which involved amine and phosphines donors on the pincer ligands (Scheme 2). In those systems, exclusive formation of [PtCl(PCP)] and NCHN resulted from a more pronounced donor-metal bond strength difference, since the Pt—P bond is significantly more stable than the corresponding M—N bond.

Experimental

Reactions involving organolithium derivatives were carried out using standard Schlenk techniques under an inert atmosphere of dry, oxygen-free nitrogen. Hexane, Et_2O, and THF were distilled from Na–benzophenone, CH_2Cl_2 from CaH_2 prior to use. All ^1H and ^{13}C NMR spectra were recorded on a Bruker AC300 or a Varian Inova 300 spectrometer, operating at 300 and 75 MHz, respectively. Spectra were obtained at 25°C, unless stated otherwise, and are referenced to external TMS (δ = 0.00 ppm, *J* in Hz). Elemental analyses were obtained from Kolbe, Mikroanalytisches Laboratorium (Mülheim, Germany).

The ligand precursors $NC(H)N^{Me_2}$ (**1**), $NC(H)N^{EtMe}$ (**5**), and the platinum complexes [PtCl(NCN^{Me_2})] (**2**) and [PtCl(NCN^{EtMe})] (**6**), were prepared according to described procedures (13, 15, 23).

[Pt(η³-NCN^{Me2})(η¹-NCN^{Me2})] (3)

To a pentane solution of **1** (0.25 g, 1.3 mmol in 4 mL) was added *n*-BuLi (1.5 M hexane solution, 0.87 mL, 1.3 mmol) at –80°C. The reaction mixture was allowed to warm to room temperature over 14 h. All volatiles were then removed in vacuo and the residue was redissolved in THF. To this solution was added the platinum complex **2** (0.50 g, 1.2 mmol) and the mixture was heated to reflux temperature for 4 h. After cooling to room temperature, the solvents were removed and the residue was extracted with Et_2O (3 × 20 mL). The combined ether layers were concentrated to 5 mL and pentane was overlayered, which caused slow crystallization of the product. Yield: 0.41 g (60%). ^1H NMR (C_6D_6) δ: 7.70 (d, 2H, $^3J_{HH}$ = 7.0, Ar*H*), 7.40 (t, 1H, $^3J_{HH}$ = 7.0, Ar*H*), 7.17 (t, 1H, $^3J_{HH}$ = 8.0, Ar*H*), 6.93 (d, 2H, $^3J_{HH}$ = 8.0, Ar*H*), 4.38 (s, 4H, CH_2N), 3.57 (s, $^3J_{HPt}$ = 47, 4H, CH_2NPt), 2.58 (s, $^3J_{HPt}$ = 42, 12H, $PtNCH_3$), 2.41 (s, 12H, NCH_3). ^{13}C NMR (C_6D_6) δ: 182.2 (C_{ipso}, $^1J_{HPt}$ not resolved), 172.6 (C_{ipso}, $^1J_{HPt}$ not resolved), 147.4, 145.1, 127.4, 122.7, 122.3, 119.0 (all Ar*C*), 80.8 (CH_2NPt), 68.4 (CH_2N), 54.7 ($PtNCH_3$), 45.9 (NCH_3). Anal. calcd. for $C_{24}H_{38}N_4Pt$ (587.66): C 49.90, H 6.63, N 9.70; found: C 50.07, H 6.90, N 9.59.

[Pt(η³-NCN^{Me3})(η¹-NCN^{Me3})]$(I)_2$ (4)

To a stirred solution of **3** (0.50 g, 0.87 mmol) in CH_2Cl_2 (5 mL) was added a solution of MeI (0.28 g, 2.0 mmol) in CH_2Cl_2 (2 mL) and the mixture stirred for 3 h. The volatiles were removed to leave **4** as an off-white solid (0.72 g, 97%). Analytically pure **4** was obtained by recrystallization from H_2O–acetone. ^1H NMR (D_2O, 200 MHz) δ: 7.41 (d, 4H, $^3J_{HH}$ = 7.3, Ar*H*), 7.27 (t, 2H, $^3J_{HH}$ = 7.3, Ar*H*), 5.04 (d, 2H, $^3J_{HH}$ = 13.2 Hz, $^3J_{HPt}$ not observed, C*H*$HNMe_2$), 4.84 (d, 2H, $^3J_{HH}$ = 11.6, C*H*$HNMe_3$), 4.52 (d, 2H, $^3J_{HH}$ = 11.6, C*H*$HNMe_3$), 3.83 (d, 2H, $^3J_{HH}$ = 13.4, $^3J_{HPt}$ not observed, CH*H*NMe_2), 3.24 (s, 18H, NMe_3), 2.75 (s, 6H, $^3J_{HPt}$ = ca. 40, NCH_3Me), 2.73 (s, 6H, $^3J_{HPt}$ = 36.2, $NMeCH_3$). ^{13}C NMR (D_2O) δ: 175.8 (C_{ipso}), 149.2, 132.8, 130.5, 123.6, 123.5 (all Ar*C*), 78.9 (CH_2NPt), 74.9 (CH_2N), 56.1 ($PtNCH_3Me$), 52.9 (NMe_3), 51.7 ($PtNMeCH_3$). Anal. calcd. for $C_{26}H_{44}I_2N_4Pt \cdot H_2O$ (879.57): C 35.50, H 5.27, N 6.37; found: C 35.50, H 5.42, N 6.21.

[Pt(η³-NCN^{Me2})(η¹-NCN^{EtMe})] (7) and [Pt(η³-NCN^{EtMe})(η¹-NCN^{Me2})] (8)

These complexes have been prepared following a similar protocol as for **3**. The products were obtained as mixtures, which precipitated as off-white powders from pentane–Et_2O systems. All attempts to separate the products were unsuccessful.

Method A

From **1** (0.17 g, 0.89 mmol) in pentane (4 mL), *n*-BuLi (1.5 M in hexane, 0.60 mL, 0.9 mmol), and **6** (0.37 g, 0.82 mmol). Yield: 0.22 g (44%).

Method B

From **5** (0.26 g, 1.2 mmol) in pentane (6 mL), *n*-BuLi (1.5 M in hexane, 0.8 mL, 1.2 mmol), and **2** (0.46 g, 1.1 mmol). Yield: 0.35 mg (53%).

^1H NMR (C_6D_6) δ: 7.83 (d, $^3J_{HH}$ = 7.4, Ar*H*), 7.55 (s, Ar*H*), 7.43 (t, $^3J_{HH}$ = 7.4, Ar*H*), 7.31–7.19 (m, Ar*H*), 7.04 (t, $^3J_{HH}$ = 7.5, Ar*H*), 6.93 (d, $^3J_{HH}$ = 7.4, Ar*H*), 6.64 (d, $^3J_{HH}$ = 7.5, Ar*H*), 4.47 (s, CH_2N (**8**)), 3.57 (s, $^3J_{HPt}$ = 43.7, CH_2NPt (**7**)), 3.40 (s, CH_2N (**7**)), 3.29 (s, $^3J_{HPt}$ = 30.3, CH_2NPt (**8**)), 2.69 (s, $^3J_{HPt}$ = 38.0, $PtNCH_3$ (**8**)), 2.64 (q, $^3J_{HH}$ = 7.1, NCH_2CH_3 (**7**)), 2.58 (s, $^3J_{HPt}$ = 43.6, $PtNCH_3$ (**7**)), 2.41 (s, NCH_3 (**8**)), 2.33 (q, $^3J_{HH}$ = 7.1, $^3J_{HPt}$ = 78.0, $PtNCH_2CH_3$ (**8**)), 2.10 (s, NCH_3 (**7**)), 1.16 (t, $^3J_{HH}$ = 7.1, 2.25H, NCH_2CH_3 (**7**)), 0.99 (t, 3.75H, $^3J_{HH}$ = 7.1, $PtNCH_2CH_3$ (**8**)). ^{13}C NMR (C_6D_6) δ: 181.6 (C_{ipso}), 172.7 (C_{ipso}), 147.5, 145.1, 143.8, 140.2, 130.0, 127.4, 126.9, 122.9, 122.6, 122.5, 119.2, 119.0 (all Ar*C*), 80.9 ($^2J_{CPt}$ = 28.0, CH_2NPt (**8**)), 77.7 ($^2J_{CPt}$ = 65.0, CH_2NPt (**7**)), 66.8 (CH_2N (**7**)), 62.6 (CH_2N (**8**)), 54.8 ($^2J_{CPt}$ not resolved, $PtNCH_3$ (**8**)), 54.0 ($^2J_{CPt}$ = 15.3, $PtNCH_3$ (**7**)), 52.0 (NCH_2CH_3 (**7**)), 51.6 ($PtNCH_2CH_3$ (**8**)), 42.0 (NCH_3 (**7**)), 41.6 (NCH_3 (**8**)), 13.5 (NCH_2CH_3 (**7**)), 12.8 ($PtNCH_2CH_3$ (**8**)).

Reaction with HCl

A solution of the bisarylplatinum complex **3**, or **7** and **8** in CH_2Cl_2 was saturated with freshly prepared anhyd HCl. Stirring was maintained for 1 h and all volatiles removed in vacuo. Identification of the products (^1H NMR) was performed by comparison with authentic samples of **2** and **6**, respectively.

Structure determination and refinement of 3

Intensities were measured on an Enraf–Nonius CAD4-T diffractometer with rotating anode (Mo Kα, λ = 0.71073 Å). Crystal data and details on data collection and refinement

© 2001 NRC Canada

are collected in Table 3.[5] The structures were solved with Patterson methods (DIRDIF-92 (26)) and refined against F^2 of all reflections (SHELXL-93 (27)). Non-hydrogen atoms were refined freely with anisotropic displacement parameters, hydrogen atoms were introduced at calculated positions and refined riding on their carrier atoms. Weights were optimized in the final refinement cycles. Neutral atomic scattering factors and anomalous dispersion corrections were taken from the *International Tables of Crystallography*. All calculations, graphical illustrations, and checking for higher symmetry were performed with the PLATON package (28).

Conclusions

The use of labeled NCN pincer ligands suggested that the transmetalation of [Li(NCN)] with cyclometalated [PtCl(NCN)] precursors is preceded by a comparatively fast and reversible TCM process between lithiated and platinated metallacycles. Such a TCM reaction does not involve C—H bond activation and therefore follows a distinctly different reaction coordinate than previously analyzed TCM processes. Importantly, in this case the product distribution is most likely determined by steric preferences rather than metal-to-heteroatom bond strength arguments as established previously. A cationic heterodinuclear bisaryl platinum lithium species has been suggested as a key intermediate. Attack of chloride on the platinum center of this intermediate induces a TCM reaction, whereas attack on lithium completes the transmetalation trajectory with formation of the corresponding bisaryl platinum(II) complex and LiCl. Investigations towards the stabilization and characterization of the proposed intermediate of this novel TCM process are currently in progress.

Acknowledgements

This work was supported in part (N.V., A.L.S.) by the Dutch Council for Chemical Sciences (CW-NWO).

References

1. S. Murai, F. Kakiuchi, S. Sekine, Y. Tanaka, A. Kamatani, M. Sonoda, and N. Chatani. Nature (London), **366**, 529 (1993).
2. (*a*) N. Miyaura and A. Suzuki. Chem. Rev. **95**, 2457 (1995); (*b*) G. Oláh, S. Kuhn, and A. Pavláth. Nature (London), **178**, 693 (1956); (*c*) B. Chauder, G. Laine, and V. Snieckus. Pure Appl. Chem. **71**, 1521 (1999); (*d*) A.E. Shilov and G.B. Shul'pin. Chem. Rev. **97**, 2897 (1997); (*e*) W.D. Jones and F.J. Feher., Acc. Chem. Res. **22**, 91 (1989).
3. M.E. van der Boom, C.L. Higgitt, and D. Milstein. Organometallics, **18**, 2413 (1999), and refs. therein.
4. (*a*) M. Albrecht, R.A. Gossage, A.L. Spek, and G. van Koten. J. Am. Chem. Soc. **121**, 11 898 (1999); (*b*) R.A. Gossage, A.D. Ryabov, A.L. Spek, D.J. Stufkens, J.A.M. van Beek, R. van Eldik, and G. van Koten. J. Am. Chem. Soc. **121**, 2488 (1999); (*c*) J.A.M. van Beek, G. van Koten, W.J.J. Smeets, and A.L. Spek. J. Am. Chem. Soc. **108**, 5010 (1986).
5. (*a*) M. Gupta, C. Hagen, W.C. Kaska, R.E. Cramer, and C.M. Jensen. J. Am. Chem. Soc. **119**, 840 (1997); (*b*) C.M. Jensen. Chem. Commun. 2443 (1999); (*c*) F. Liu, E.B. Pak, B. Singh, C.M. Jensen, and A.S. Goldman. J. Am. Chem. Soc. **121**, 4086 (1999).
6. (*a*) M. Albrecht, M. Lutz, A.L. Spek, and G. van Koten. Nature (London), **406**, 970 (2000); (*b*) M. Albrecht and G. van Koten. Adv. Mater. **11**, 171 (1999); (*c*) M. Albrecht, R.A. Gossage, A.L. Spek, and G. van Koten. Chem. Commun. 1003 (1998).
7. J.P. Collman, L.S. Hegedus, J.A. Norton, and R.G. Finke. Principles and applications of organotransition metal chemistry. University Science Books, Mill Valley, California. 1987. p. 279.
8. (*a*) J. Dehand and M. Pfeffer. Coord. Chem. Rev. **18**, 327 (1976); (*b*) I. Omae. Coord. Chem. Rev. **53**, 261 (1984); (*c*) G.R. Newkome, W.E. Puckett, V.K. Gupta, and G.E. Kiefer. Chem. Rev. **86**, 451 (1986); (*d*) A.D. Ryabov. Chem. Rev. **90**, 403 (1990); (*e*) C.G. Anklin, P.S. Pregosin, F.J. Wombacher, and H.J. Rüegg. Organometallics, **9**, 1953 (1990); (*f*) P. Steenwinkel, R.A. Gossage, and G. van Koten. Chem. Eur. J. **4**, 759 (1998).
9. J. McMurry. Advanced organic chemistry. 4th ed. Pergamon Press, Oxford, U.K. 1994. p. 749.
10. (*a*) J. Dupont, N. Beydoun, and M. Pfeffer. J. Chem. Soc. Dalton Trans. 1715 (1989); (*b*) F. Maassarani, M. Pfeffer, A.L. Spek, A.M.M. Schreurs, and G.van Koten. J. Am. Chem. Soc. **108**, 4222 (1986); (*c*) J.-P. Djukic, A. Maisse, and M. Pfeffer. J. Organomet. Chem. **567**, 65 (1998); (*d*) P.S. Pregosin, F. Wombacher, A. Albinati, and F. Lianza. J. Organomet. Chem. **418**, 249 (1991); (*e*) A.D. Ryabov and R. van Eldik. Angew. Chem. **106**, 922 (1994); Angew. Chem. Int. Ed. Engl. **33**, 917 (1994); (*f*) A.D. Ryabov. *In* Perspectives in coordination chemistry. *Edited by* A.F. Williams, C. Floriani, and A.E. Merbach. Verlag Helvetica Chimica Acta, Basel, Switzerland. 1992. p. 271.
11. G. van Koten. Pure Appl. Chem. **61**, 1681 (1989).
12. (*a*) M. Albrecht, P. Dani, M. Lutz, A.L. Spek, and G. van Koten. J. Am. Chem. Soc. **122**, 11 822 (2000); (*b*) P. Dani, M. Albrecht, G.P.M. van Klink, and G. van Koten. Organometallics, **19**, 4468 (2000).
13. (*a*) J. Terheijden, G. van Koten, F. Muller, D.M. Grove, K. Vrieze, E. Nielsen, and C.H. Stam, J. Organomet. Chem. **315**, 401 (1986); (*b*) D.M. Grove, G. van Koten, J.N. Louwen, J.G. Noltes, A.L. Spek, and H.J.C. Ubbels. J. Am. Chem. Soc. **104**, 6609 (1982).
14. (*a*) E. Wehman, J.T.B.H. Jastrzebski, J.-M. Ernsting. D.M. Grove, and G. van Koten. J. Organomet. Chem. **353**, 145 (1988); (*b*) J.T.B.H. Jastrzebski, G. van Koten, M. Konijn, and C.H. Stam. J. Am. Chem. Soc. **104**, 5490 (1982).
15. (*a*) M. Albrecht, M. Lutz, A.M.M. Schreurs, E.T.G. Lutz, A.L. Spek, and G. van Koten. J. Chem. Soc. Dalton Trans. 3797 (2000); (*b*) M.H.P. Rietveld, D.M. Grove, and G. van Koten. New J. Chem. **21**, 751 (1997).
16. (*a*) I.C.M. Wehman-Ooyevaar, D.M. Grove, H. Kooijman, P. van der Sluis, A.L. Spek, and G. van Koten. J. Am. Chem. Soc. **114**, 9916 (1992); (*b*) I.C.M. Wehman-Ooyevaar, D.M. Grove, P. van der Sluis, A.L. Spek, and G. van Koten. J.

[5] Copies of material on deposit may be purchased from The Depository of Unpublished Data, CISTI, National Research Council Canada, Ottawa, ON K1A 0S2, Canada (http://www.nrc.ca/cisti/irm/unpub_e.shtml for information on ordering electronically). Crystallographic data (excluding structure factors) for the structures reported in this paper have also been deposited with the Cambridge Crystallographic Data Centre as deposition no. CCDC-149 827 (crystal **I**) and CCDC-149 828 (crystal **II**). Copies of the data can be obtained, free of charge, on application to the Director, CCDC, 12 Union Road, Cambridge, CB2 1EZ, U.K. (Fax: +44-1223-336 033, e-mail: deposit@ccdc.cam.ac.uk).

© 2001 NRC Canada

Chem. Soc. Chem. Commun. 1367 (1990); (*c*) A. Albinati, F. Lianza, P.S. Pregosin, and B. Müller. Inorg. Chem. **33**, 2522 (1994).
17. (*a*) J.D. Dunitz and J. Bernstein. Acc. Chem. Res. **28**, 193 (1995); (*b*) S. Isz, I. Weissbuch, K. Kjaer, W.G. Bouwman, J. Als-Nielsen, S. Palacin, A. Ruaudel-Teixier, L. Leiserowitz, and M. Lahav. Chem. Eur. J. **3**, 930 (1997); (*c*) D. Braga and F. Grepioni. Chem. Soc. Rev. **29**, 229 (2000).
18. J.C. Muijsers, J.W. Niemantsverdriet, I.C.M. Wehman-Ooyevaar, D.M. Grove, and G. van Koten. Inorg. Chem. **31**, 2655 (1992).
19. (*a*) P.S. Pregosin, H. Rüegger, F. Wombacher, G. van Koten, D.M. Grove, and I.C.M. Wehman-Ooyevaar. Magn. Reson. Chem. **30**, 548 (1992); (*b*) R.W. Alder. Chem. Rev. **89**, 1215 (1989).
20. (*a*) J. Terheijden, G. van Koten, I.C. Vinke, and A.L. Spek. J. Am. Chem. Soc. **107**, 2891 (1985); (*b*) G. van Koten, K. Timmer, J.G. Noltes, and A.L. Spek. J. Chem. Soc. Chem. Commun. 250 (1978).
21. J.V. Ortiz, Z. Havlas, and R. Hoffmann. Helv. Chim. Acta, **67**, 1 (1984).
22. M. Albrecht, R.A. Gossage, U. Frey, A.W. Ehlers, E.J. Baerends, A.E. Merbach, and G. van Koten. Inorg. Chem. **40**, 850 (2001).
23. M. Albrecht, R.A. Gossage, M. Lutz, A.L. Spek, and G. van Koten. Chem. Eur. J. **6**, 1431 (2000).
24. (*a*) M. Oki. Pure Appl. Chem. **61**, 699 (1989); (*b*) M. Oki and M. Ohira. Chem. Lett. 1267 (1982); (*c*) J.A.M. van Beek, G. van Koten, G.P.C.M. Dekker, E. Wissing, M.C. Zoutberg, and C.H. Stam. J. Organomet. Chem. **394**, 659 (1990).
25. (*a*) H.C.L. Abbenhuis, N. Feiken, H.F. Haarman, D.M. Grove, E. Horn, H. Kooijman, A.L. Spek, and G.van Koten. Angew. Chem. **103**, 1046 (1991); Angew. Chem. Int. Ed. Engl. **30**, 996 (1991); (*b*) H.C.L. Abbenhuis, N. Feiken, H.F. Haarman, D.M. Grove, E. Horn, H. Kooijman, A.L. Spek, and G.van Koten. Organometallics, **12**, 2227 (1993); (*c*) A.J. Canty and G. van Koten. Acc. Chem. Res. **28**, 406 (1995).
26. P.T. Beurskens, G. Admiraal, G. Beurskens, W.P. Bosman, S. Garcia-Granda, R.O. Gould, J.M.M. Smits, and C. Smykalla. The DIRDIF program system. Technical report of the crystallography laboratory. University of Nijmegen, The Netherlands. 1992.
27. G.M. Sheldrick. SHELXL-93. Program for crystal structure refinement. B test version. University of Göttingen, Germany. 1993.
28. A.L. Spek. Acta Crystallogr. Sect. A: Fundam. Crystallogr. **A46**, C-34 (1990).

© 2001 NRC Canada

Hydrogenation of carbon dioxide catalyzed by ruthenium trimethylphosphine complexes — Effect of gas pressure and additives on rate in the liquid phase

Colin A. Thomas, R. Jason Bonilla, Yong Huang, and Philip G. Jessop

Abstract: Kinetic and mechanistic studies of CO_2 hydrogenation were performed in liquid triethylamine and at subcritical CO_2 pressures to avoid complications from phase behaviour that are observed under supercritical conditions. Kinetic measurements of the hydrogenation of CO_2 to formic acid, catalyzed by $RuCl(O_2CMe)(PMe_3)_4$, support a CO_2 insertion mechanism. The reaction is first-order in both H_2 and CO_2 under most conditions. The rate is strongly dependent on the choice of additive, with methanol giving the greatest rates. Because only trace amounts of methanol are needed, the effect of the additive is believed to involve direct interactions with the catalyst rather than changes in the physical properties of the reaction medium. The optimized rates exceed 3500 h^{-1}. Addition of an inert gas affects the rate of the reaction, probably via the phenomenon of gas expansion of the liquid phase.

Key words: carbon dioxide, homogeneous catalysis, hydrogenation, formic acid, expanded liquids.

Résumé : On a réalisé des mesures de cinétique et de mécanisme d'hydrogénation du CO_2 en opérant dans la triéthylamine liquide et à des pressions sous critiques de CO_2 pour éviter les complications résultant du comportement de la phase observées dans des conditions supercritiques. Les mesures cinétiques d'hydrogénation du CO_2 dans l'acide formique, catalysée par le $RuCl(O_2CMe)(PMe_3)_4$, supportent le mécanisme impliquant une insertion de CO_2. Dans la plupart des conditions, la réaction est du premier ordre en H_2 ainsi que CO_2. La vitesse dépend grandement du choix d'additif; le méthanol est celui qui donne les vitesses les plus élevées. En raison du fait que des traces de méthanol sont suffisantes, on croit que l'effet de l'additif implique des interactions directes avec le catalyseur plutôt que des changements dans les propriétés physiques du milieu réactionnel. Les vitesses optimisées dépassent 3500 h^{-1}. L'addition d'un gaz inerte affecte la vitesse de la réaction, probablement en raison du phénomène de l'expansion du gaz dans la phase liquide.

Mots clés : bioxyde de carbone, catalyse homogène, hydrogénation, acide formique, expansion des liquides.

[Traduit par la Rédaction]

Introduction

Carbon dioxide is a renewable and inexpensive C_1 carbon source, but the lack of very efficient methods for its reduction has restricted its utility to only a few industrial processes (1–3). In the past few years, there have been a number of studies of homogeneously catalyzed CO_2 hydrogenation to formic acid (eq. [1]) with ever-increasing rates of reaction (4–14). Principal among the breakthroughs have been the development of improved catalysts (primarily Rh and Ru phosphine complexes) and identification of optimal solvents (such as DMSO and supercritical carbon dioxide). Previous studies by one of us (9–11, 15) showed that ruthenium trimethylphosphine complexes, particularly $RuH_2(PMe_3)_4$, were highly active for the hydrogenation of supercritical CO_2. Under such conditions the rate was very high, but was unfortunately a strong function of phase behaviour. All attempts at determining the chemical rate dependence on the concentration of reagents or the partial pressures of the gases were frustrated by the occurrence of phase changes, which altered the rate and therefore obscured the kinetic information. To circumvent this problem, we have reopened the investigation and decided to concentrate on determining the factors that control the rate of the reaction *in liquid triethylamine*. The goals of this study are to determine the mechanism of the reaction, to find the reasons for the rapid rate, to explore the role of additives such as methanol, and to optimize the liquid phase reaction. This note describes our early findings.

Received August 30, 2000. Published on the NRC Research Press Web site at http://canjchem.nrc.ca on July 5, 2001.

Dedicated with best wishes to Professor Brian James on the occasion of his 65th birthday.

C.A. Thomas, R.J. Bonilla, Y. Huang, and P.G. Jessop.[1] Department of Chemistry, University of California, Davis, CA 95616-5295, U.S.A.

[1]Corresponding author (telephone: (530) 754-9426; fax: (530) 759-9773; e-mail: jessop@chem.ucdavis.edu).

[1] $CO_2 + H_2 + NEt_3 \xrightarrow[Y = C\ H\ O_2CM]{Ru(\ )(Y)(\ M\ 3)_4} HCO_2H\ _2NEt_3$

 DOI: 10.1139/cjc-79-5/6-719 © 2001 NRC Canada

Fig. 1. The dependence of the rate of CO_2 hydrogenation on the pressure of CO_2. Conditions: 50°C, 0.5 h reaction time, 31 mL vessel, 40 bar H_2, 2.5 mmol MeOH, 3.6 mmol NEt_3, 3.0 μmol $RuCl(O_2CMe)(PMe_3)_4$.

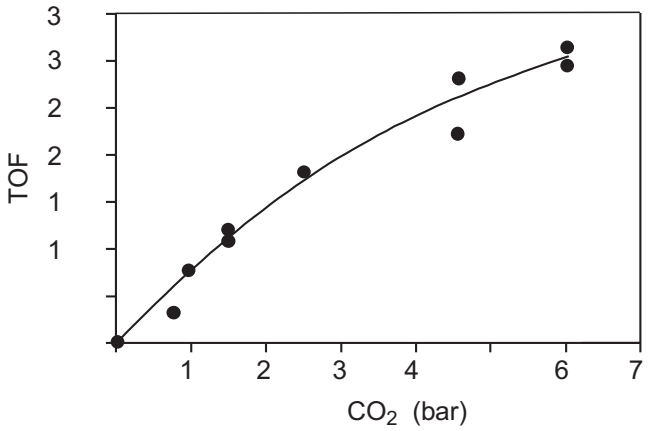
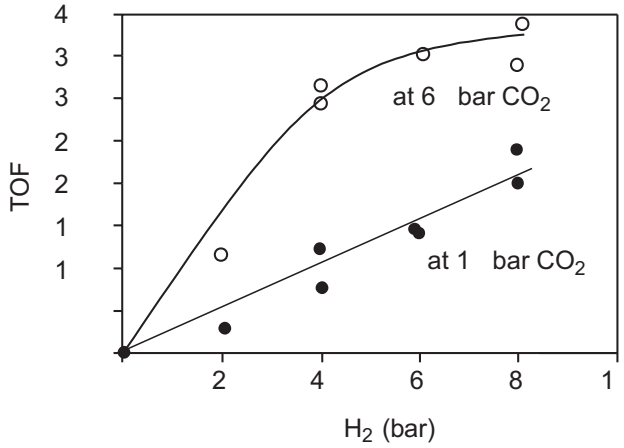


Fig. 2. The dependence of the rate of CO_2 hydrogenation on the pressure of H_2 at 10 and 60 bar CO_2. Conditions: 50°C, 0.5 h reaction time, 31 mL vessel, 2.5 mmol MeOH, 3.6 mmol NEt_3, 3.0 μmol $RuCl(O_2CMe)(PMe_3)_4$.



Results and discussion

The reaction system consists of CO_2 and H_2 gases, liquid triethylamine, an additive, and a catalyst precursor. Although the earlier studies focused on the $RuH_2(PMe_3)_4$ catalyst precursor, we now prefer the related complex $RuCl(O_2CMe)(PMe_3)_4$ because it is equally active (11), more stable, and far easier to prepare. The triethylamine serves as a base, which stabilizes the formic acid product as a 2:1 adduct (eq. [1]). Although additives, usually water in the earlier studies, are known to accelerate the reaction in the supercritical phase, the reason for this is not clear. In the present study, methanol was chosen as the additive, although a number of other additives were tested (vide infra). The rate is reported as the turnover frequency (TOF), meaning the number of turnovers per hour, where turnover number (TON) is mol of formic acid per mol of catalyst. The yield is reported as the formic acid to triethylamine molar ratio (acid to amine ratio, AAR), where the highest possible AAR is 2.0 (based upon eq. [1]) and the highest practically attainable AAR is 1.8.

Pressure dependence of rate

We have now found that the rate of the reaction is a function of the CO_2 and the H_2 pressures. At lower pressures of CO_2, the rate is first-order with respect to CO_2, while the order declines somewhat at higher pressure (Fig. 1). The rate dependence on H_2 pressure was measured at two pressures of CO_2 (Fig. 2). At 10 bar of CO_2, the rate is first-order with respect to H_2, while at 60 bar of CO_2 the rate shows saturation kinetics with respect to H_2 (i.e., it is first-order at low H_2 pressure and lower order at higher pressure).

Of the several mechanisms that have been observed in homogeneously catalyzed CO_2 hydrogenation (12, 14), only one (Scheme 1, L = PMe_3) is consistent with a first-order H_2 dependence, a decreasing order dependence on CO_2, and the previously observed (11) CO_2 insertion into the Ru—H bond in $Ru(H)_2(PMe_3)_4$. The first step is the presumed conversion of the acetate group (and possibly also the chloride group) of the catalyst precursor to a hydride ligand; this is considered likely because there are no reasonable mechanisms for CO_2 hydrogenation which do not involve a hydride ligand (12, 14). The mechanism continues with CO_2 insertion into the Ru—H bond, a step which may be preceded by phosphine dissociation. The insertion of CO_2 into the Ru—H bond of $Ru(H)_2(PMe_3)_4$, giving $RuH(O_2CH)(PMe_3)_4$, has been directly observed in an in situ NMR experiment (11). A similar reaction has been observed with $RuH_2(PPh_3)_3$ (16). The hydrogenolysis of the ruthenium formate, giving formic acid, presumably proceeds via a molecular hydrogen complex $RuCl(O_2CH)(H_2)(PMe_3)_3$, a classical dihydride $RuCl(O_2CH)(H)_2(PMe_3)_3$, or by concerted hydrogenolysis with unbound H_2. Of these options, the molecular hydrogen complex should be thermodynamically preferred over the dihydride (11) based upon ligand additivity calculations (17).

If one assumes that the CO_2 insertion and the phosphine dissociation reactions of Scheme 1 are fully reversible and rapid and that the reaction of H_2 with the formate complex is the slow step in the catalytic cycle, then one can predict the following rate law (L = PMe_3, $[Ru_{tot}]$ = initial concentration of the catalyst precursor (for derivation see *Appendix*)):

$$[2] \quad \frac{d\,HCO_2H}{dt} = \frac{k_4K_2\,H_2\;CO_2\;Ru_{tot}}{\left(\frac{L}{K_1} + 1 + K_2\,CO_2 + K_2K_3\,CO_2\;L\right)}$$

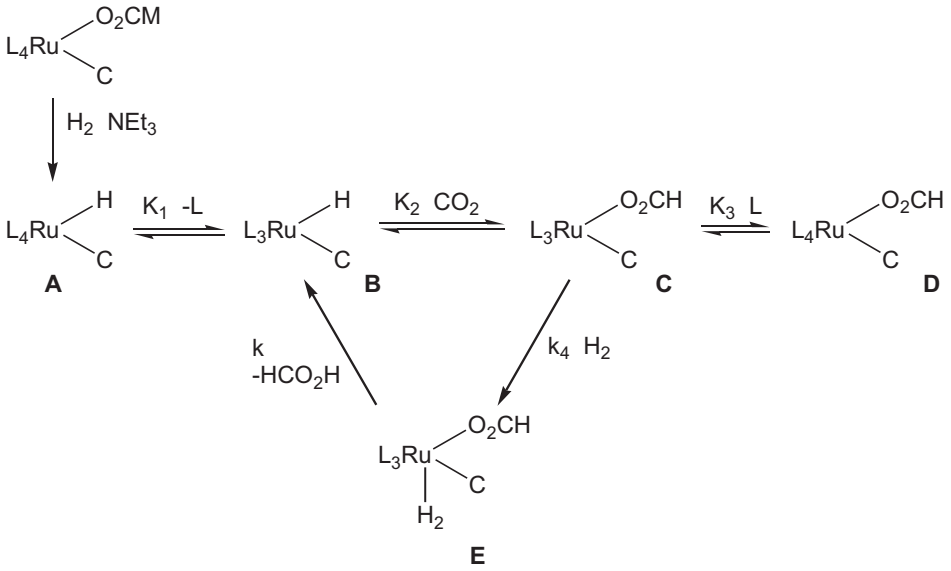
which simplifies, at very low [L], to:

$$[3] \quad \frac{d\,HCO_2H}{dt} = \frac{k_4K_2\,H_2\;CO_2\;Ru_{tot}}{1 + K_2\,CO_2}$$

This rate law predicts that the rate will be first-order with respect to $[H_2]$ and will show saturation kinetics with respect to $[CO_2]$, as observed (here we are assuming that the concentrations of the gases in the liquid phase are proportional to their pressures in the gas phase). This rate law does not, however, explain the decline in the order with respect to H_2 at high H_2 and CO_2 pressures. A satisfactory explanation for that observation has not yet been found. The rate law also does not explain why, in the earlier studies, a small excess of

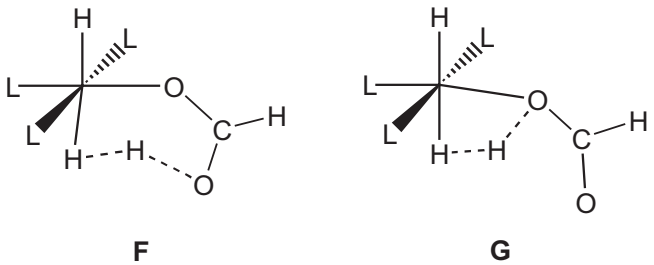
© 2001 NRC Canada

Scheme 1.



PMe_3 failed to slow down the reaction (11). Our further studies will explore these questions.

Musashi and Sakaki (18) have completed ab initio calculations for the reaction catalyzed by $RuH_2(PH_3)_4$. While this is not exactly the same as the catalyst used in the present study, it can be considered to be roughly analogous to species A in Scheme 1. They found that for the CO_2 insertion step, the path with phosphine dissociation was more energetically demanding (30.5 kcal mol^{-1} relative to $RuH_2(PH_3)_4$) than the path without phosphine dissociation (26.7 kcal mol^{-1}). However, for the hydrogenolysis step, the path with phosphine dissociation (i.e., via $RuH(O_2CH)(\eta^2\text{-}H_2)(PH_3)_3$) was less energetically demanding than the path without phosphine dissociation (reductive elimination of HCO_2H). Most importantly, they found that the hydrogenolysis takes place via a six-membered ring transition state (structure F below), not the four-membered ring that was anticipated (structure G). With or without phosphine dissociation, they predicted that the rate-determining step would be the CO_2 insertion, which would result in the reaction being first order in CO_2 and zero-order in H_2. The contradiction with the experimentally observed results could be the slight difference in the catalyst or the fact that the liquid phase conditions have a low H_2 concentration, which could cause the hydrogenolysis to become rate limiting.



Kinetic studies of CO_2 hydrogenation by other homogeneous catalysts have been reported. The first such study used $PdCl_2$ as the catalyst under rather extreme conditions (240°C) in aqueous KOH solution (19). The rate was zero-order with respect to CO_2 pressure and exhibited saturation kinetics with respect to H_2. The mechanism was proposed to be hydrogenation of HCO_3^- anion, with rate-limiting binding of that ion to the active catalyst. Taquikhan et al. (20) observed that the reaction catalyzed by $K[Ru(EDTA\text{-}H)Cl]\cdot 2H_2O$ in water was first-order in both H_2 and CO_2 (EDTA-H refers to deprotonated EDTA). They proposed a mechanism involving abnormal CO_2 insertion into a Ru—H bond, giving a metallocarboxylic acid; such a step has no confirmed literature precedent (12). Tsai and Nicholas (5) found that the reaction catalyzed by $[Rh(NBD)(PMe_2Ph)_3]BF_4$ was also first-order in both H_2 and CO_2. Their proposed mechanism involved H_2 oxidative addition to $[Rh(solvent)(PMe_2Ph)_3]^+$, CO_2 insertion, and reductive elimination of HCO_2H. Such a reductive elimination pathway, although feasible for Rh, is likely to be energetically unfavourable for Ru (18). Leitner's group (6–8, 13, 21–25) has extensively studied Rh catalysts for this reaction in a variety of solvents. Their kinetic study using Rh(hfacac)(dppp) (where hfacac = hexafluoroacetylacetonate and dppp = 1,3-bis(diphenylphosphino)propane) in DMSO–NEt_3 showed that the reaction is nearly first-order in CO_2 and has saturation kinetics with respect to H_2 pressure (25). With assistance from ab initio calculations, they proposed a mechanism of initial hydrogenolysis of the catalyst precursor to give the active catalyst RhH(dppp), followed by CO_2 insertion (giving $Rh(O_2CH)$(dppp)), H_2 coordination (giving $Rh(O_2CH)(H_2)$(dppp)), and then hydrogenolysis. The rate-limiting step was proposed to be the product-eliminating hydrogenolysis. The Leitner mechanism is the closest of those described in the literature to the mechanism proposed in Scheme 1; it is therefore noteworthy that H_2 saturation kinetics were observed in both Leitner's system and our own.

Gas expansion of the liquid phase

At high pressures of CO_2 (above ca. 40 bar), the phenomenon of gas expansion of liquids takes place. In this phenomenon, a gas (either CO_2 or another gas commonly used

© 2001 NRC Canada

Table 1. Effect of added inert gas on the rate of hydrogenation of CO_2 in the liquid phase.[a]

Added gas (bar)	AAR	TON	TOF (h^{-1})
None	0.32	390	770
Ethane (40)	0.072	79	160
Fluoroform (40)	0.40	455	910
Fluoroform (50)	0.40	450	900

[a]Conditions: 50°C, 0.5 h reaction time, 31 mL vessel, 40 bar H_2, 10 bar CO_2, 2.5 mmol MeOH, 3.6 mmol NEt_3, 3.0 μmol $RuCl(O_2CMe)(PMe_3)_4$.

as a SCF) dissolves in a liquid to such an extent that the liquid phase increases substantially in volume (26). The increase in volume, which can be over 10-fold, is accompanied by many changes in the physical properties of the liquid phase, including its dielectric constant (27), viscosity (28), diffusion rates (29), and its ability to dissolve hydrogen (30). Therefore, the higher pressures of CO_2 in the present study could result not only in the expected increase in [CO_2] in the liquid phase, but also in many other changes, any of which could affect the rate of the reaction in the liquid phase. We speculated in an earlier paper that this may play a role in the reaction (11), but evidence of this was not obtained.

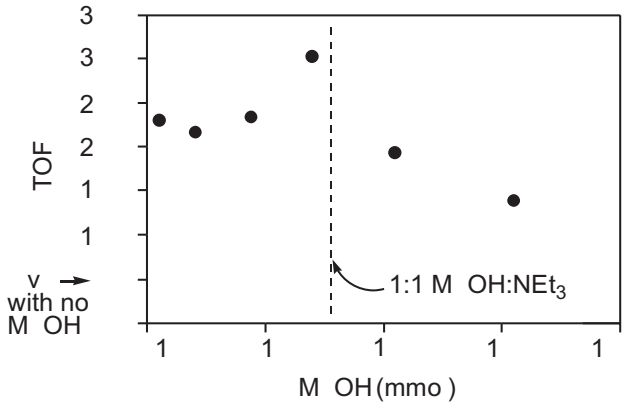
We have now evaluated the effect of this phenomenon by using inert gases (i.e., other than CO_2) to expand the liquid phase. Adding an inert gas in addition to the CO_2 and H_2 indeed changes the rate of the reaction. With H_2 and CO_2 pressures roughly constant, adding 40 bar of ethane (T_c = 32°C, P_c = 49 bar) causes the rate to drop greatly, but adding 40 or 50 bar of fluoroform (CHF_3, T_c = 26°C, P_c = 48 bar) causes the rate to rise slightly (demonstrated with multiple experiments, typical results shown in Table 1). Because ethane and fluoroform are very similar in their critical parameters but differ primarily in their dipole moments, one could speculate that the contrasting rates with these two gases are a result of their differing polarity; ethane renders the liquid phase less polar, while fluoroform does not. A similar decrease in rate is observed if liquid hexane is added instead of ethane, further evidence that a low polarity reaction medium is detrimental to the rate.

The role of the additive

The role of the methanol additive has not been satisfactorily explained, and [MeOH] is not shown in the above mechanism or rate law. To further explore this question, we determined the dependence of the rate of reaction on the concentration of methanol (Fig. 3). The rate in the absence of any added methanol was 500 h^{-1}. Poor reproducibility is encountered at very low [MeOH], but it can be clearly seen that rate is improved by the addition of methanol. With the addition of any amount of methanol from 0.124 to 1 mmol (41–333 equiv of methanol per Ru atom) the rate was approximately 2300 h^{-1}, a significant increase over that without methanol. The observation that only a trace of alcohol or water is required to increase the rate of CO_2 hydrogenation has been observed previously for other catalysts such as $Pd(dpppe)_2$ (4) and $[Rh(NBD)(PMe_2Ph)_3]BF_4$ (5).

Possible roles for the methanol additive are: (*i*) to raise the dielectric constant of the liquid phase; (*ii*) to bind to and therefore stabilize the 16 e complexes in the mechanism (18); (*iii*) to bind to the $RuHCl(PMe_3)_3$ intermediate and facilitate CO_2 insertion through secondary interactions (5); (*iv*) to provide a proton source during the preheating time to facilitate the conversion of the catalyst precursor to the active catalyst; or (*v*) to help solubilize the complex in the triethylamine. The fact that only trace amounts of methanol were needed to enhance the rate suggests that it is not a true solvent effect. The amount of methanol (3 mol% in NEt_3) was too small to have any significant effect on the dielectric constant or other physical properties of the liquid phase, or on the ability of the triethylamine to dissolve the catalyst. At these very small amounts, the only likely role of the additive is to interact with the catalyst in some manner.

Fig. 3. The dependence of the rate of CO_2 hydrogenation on the amount of MeOH additive. Conditions: 50°C, 0.5 h reaction time, 31 mL vessel, 60 bar CO_2, 40 bar H_2, 3.6 mmol NEt_3, 3.0 μmol $RuCl(O_2CMe)(PMe_3)_4$.

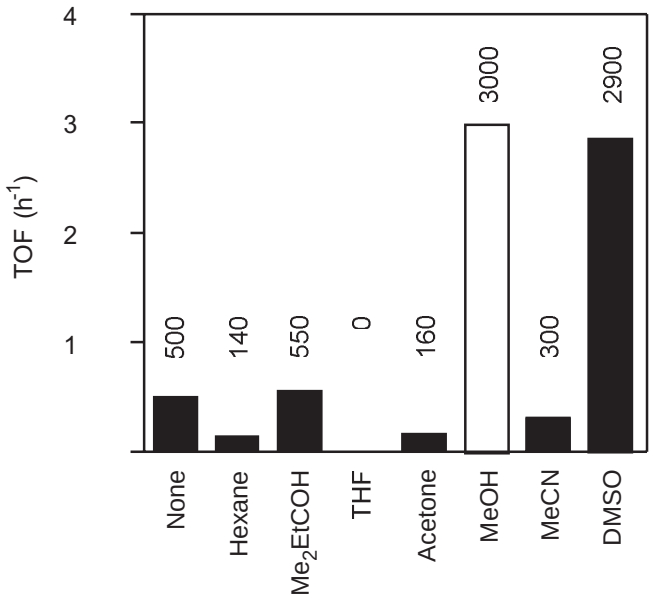


Increasing the amount of methanol to approximately a 1:1 mol ratio with the triethylamine causes a further increase in the rate to 3100 h^{-1}. An even greater amount of methanol causes a decline in the rate, which suggests that bulk methanol is a poor solvent, relative to triethylamine containing trace methanol, in which to perform these hydrogenations. This parallels the earlier observation (11) that bulk methanol as a solvent is inferior to supercritical CO_2 with methanol and triethylamine dissolved therein.

The result of a comparison of different additives (Fig. 4) shows that the identity and not so much the amount of the additive affects the reaction rate most significantly. The most effective additive, methanol, is protic, polar, sterically unencumbered, and mildly coordinating. The use of a sterically bulky alcohol, *t*-amyl alcohol instead of methanol, causes the rate to drop significantly. This supports the notion that binding of the alcohol to the metal centre is necessary, although the low dielectric constant of *t*-amyl alcohol (5.78 (31)) may also have contributed to the low rate. Aprotic polar additives had mixed results. DMSO nearly duplicated the high rate seen with methanol, while MeCN and acetone were ineffective. Carefully dried DMSO gave the same result as undried DMSO. Aprotic solvents that are less polar and coordinating (e.g., THF and hexane) caused the rate to decrease relative to the rate without an additive. We have been unable to discern a trend in these results; although, the two most effective additives both have high dielectric constants. Similarly polar solvents such as MeCN are ineffective. The rate does not correlate with the coordinating ability of the additive; MeCN and DMSO are known to be able to

© 2001 NRC Canada

Fig. 4. The rate of CO_2 hydrogenation in the presence of various additives, presented in order of increasing dielectric constant. Conditions: 50°C, 0.5 h reaction time, 31 mL vessel, 60 bar CO_2, 40 bar H_2, 3.6 mmol NEt_3, 2.6 mmol additive, 3.0 μmol $RuCl(O_2CMe)(PMe_3)_4$.



coordinate to vacant sites on Ru complexes, but only one of these additives accelerates the reaction. The rate also does not correlate with the miscibility of the additive with triethylamine; methanol is miscible and DMSO is not. Further investigation of the role of the additive is underway.

Experimental

Safety warning

Operators of high-pressure equipment such as that required for these experiments should take proper precautions, including but not limited to the use of blast shields and pressure relief mechanisms, to minimize the risk of personal injury.

General

All liquid reagents and solvents were degassed before use. The gases H_2 (99.99% purity, Praxair) and C_2H_6 (99.995% purity, Nellcor Puritan Bennett) were used as received, but CHF_3 (99.995% purity, AGA), and CO_2 gas (99.9999% purity, SFC/SFE grade product of Air Products) were passed through an oxygen trap before use. Liquid additives, deuterated solvents, and triethylamine were degassed by freeze–vacuum–thaw cycles and then stored under nitrogen. $RuCl(O_2CMe)(PMe_3)_4$ was prepared as described in the literature (32). Acetone was dried with $MgSO_4$ and then freshly activated molecular sieves — in addition to being degassed. Similarly treated DMSO gave the same result as DMSO that had not been dried.

The high-pressure equipment, similar to that published previously (11), consists of stainless steel 31 mL reaction vessels, a Jasco PU-980 HPLC pump fitted with a liquid CO_2 reservoir cooled by an Isotemp 1016S coolant circulator, and a constant-temperature water bath, underneath which is a magnetic stir plate known to be able to couple to a stir bar inside the reaction vessels. The vessels are equipped with burst disks (345 bar) and a pressure transducer.

CO_2 hydrogenation method

Standard reaction conditions are described below. Parameters were varied accordingly from those conditions. Reaction time was measured from the introduction of CO_2 to the time that the vessel was placed in the cooling bath; this leads to a minor ambiguity in the actual reaction stopping time (<2 min).

Triethylamine (3.6 mmol), methanol (2.5 mmol), a stir bar, and the catalyst precursor $RuCl(O_2CMe)(PMe_3)_4$ (3 μmol) were introduced into a pressure vessel in a nitrogen filled glove box and the vessel was sealed. Upon removal from the glove box, the vessel was flushed with 15 bar H_2 three times after which 95% of the final pressure of H_2 was added to the vessel. The vessel was placed into a 50°C water bath and stirring was begun. The vessel was allowed to equilibrate to this temperature for 1 h. Further H_2 was added until the required pressure of 40 bar was attained, and CO_2 was added as rapidly as possible to a total pressure of 100 bar (CO_2 pressure was assumed to be the difference between the total pressure and the H_2 pressure). After 30 min reaction time, the vessel was half submerged in an ice water bath. Once the pressure ceased to decline (typically after 10 min), the vessel was placed in a dry ice–acetone bath. After the pressure in the vessel dropped below the original pressure of H_2, the pressure was slowly vented. The vessel was then allowed to return to room temperature venting the CO_2 as it sublimed. 250 μL (2.35 mmol) of toluene was added to the vessel contents as an internal reference. A sample of the vessel contents was dissolved in CD_3OD and analysed by ^1H NMR spectroscopy (300 MHz). The following parameters were determined from the integration: the formic acid to triethylamine molar ratio (acid to amine ratio, AAR), the yield of formic acid, the turnover number, and the turnover frequency.

Experiments with other gases in addition to CO_2 and H_2 had the gases added in the following order: H_2, CO_2, and then the extra gas.

Acknowledgements

We gratefully acknowledge valuable advice from Dr. John Linehan of the Pacific Northwest National Laboratory and support from the Division of Chemical Sciences, Office of Basic Energy Sciences, Office of Science, U. S. Department of Energy (grant no. 069 628). This support does not constitute an endorsement by DOE of the views expressed in this article.

Conclusions

This liquid phase study shows that meaningful kinetic data can be obtained without the interference of phase changes when subcritical CO_2 pressures are used. The results are consistent with the CO_2 insertion mechanism. One can optimize the reaction by adjusting the gas partial pressures to obtain rates of reaction over 3500 h^{-1}, even without

© 2001 NRC Canada

resorting to supercritical pressures. If these results can be extrapolated to the hydrogenation of supercritical CO_2, then one can conclude that the rapid rate that was observed in earlier studies in the supercritical phase was a direct result of *both* the high CO_2 and the high H_2 concentrations.

References

1. W. Keim. *In* Carbon dioxide as a source of carbon. NATO ASI Series C. 206. *Edited by* M. Aresta and G. Forti. D. Reidel Publishing Co., Dordrecht. 1986. p. 23.
2. R.P.A. Sneeden. *In* Comprehensive organometallic chemistry. Vol. 8. *Edited by* S.G. Wilkinson. Pergamon Press, Oxford. 1982. p. 225.
3. M.M. Halmann. Chemical fixation of carbon dioxide: methods for recycling CO_2 into useful products. CRC Press, Boca Raton, Florida. 1993. p. 172.
4. Y. Inoue, H. Izumida, Y. Sasaki, and H. Hashimoto. Chem. Lett. 863 (1976).
5. J.-C. Tsai and K.M. Nicholas. J. Am. Chem. Soc. **114**, 5117 (1992).
6. E. Graf and W. Leitner. J. Chem. Soc. Chem. Commun. 623 (1992).
7. T. Burgemeister, F. Kastner, and W. Leitner. Angew. Chem. Int. Ed. Engl. **32**, 739 (1993).
8. F. Gassner and W. Leitner. J. Chem. Soc. Chem. Commun. 1465 (1993).
9. P. G. Jessop, T. Ikariya, and R. Noyori. Nature (London), **368**, 231 (1994).
10. T. Ikariya, P. G. Jessop, and R. Noyori. Japan Tokkai 5-274721, ERATO, Patent Appl. 4 Nov. 1993, published 11 July 1995, Patent no. 7-173 098.
11. P. G. Jessop, Y. Hsiao, T. Ikariya, and R. Noyori. J. Am. Chem. Soc. **118**, 344 (1996).
12. P. G. Jessop, T. Ikariya, and R. Noyori. Chem. Rev. **95**, 259 (1995).
13. W. Leitner, E. Dinjus, and F. Gaβner. J. Organomet. Chem. **475**, 257 (1994).
14. W. Leitner. Angew. Chem. Int. Ed. Engl. **34**, 2207 (1995).
15. T. Ikariya, Y. Hsiao, P. G. Jessop, R. Noyori. Eur. Patent Appl. 94 308 144.8, filed 4 November 1994, published 10 May 1995, No. 0 652 202 A1.
16. S. Komiya and A. Yamamoto. Bull. Chem. Soc. Jpn. **49**, 784 (1976).
17. R. H. Morris. Inorg. Chem. **31**, 1471 (1992).
18. Y. Musashi and S. Sakaki. J. Am. Chem. Soc. **122**, 3867 (2000).
19. K. Kudo, N. Sugita, and Y. Takezaki. Nihon Kagaku Kaishi, 302 (1977).
20. M. M. Taquikhan, S. B. Halligudi, and S. Shukla. J. Mol. Catal. **57**, 47 (1989).
21. R. Fornika, H. Göris, B. Seemann, and W. Leitner. J. Chem. Soc. Chem. Commun. 1479 (1995).
22. F. Hutschka, A. Dedieu, and W. Leitner. Angew. Chem. Int. Ed. Engl. **34**, 1742 (1995).
23. F. Gassner, E. Dinjus, H. Görls, and W. Leitner. Organometallics, **15**, 2078 (1996).
24. K. Angermund, W. Baumann, E. Dinjus, R. Fornika, H. Gorls, M. Kessler, C. Kruger, W. Leitner, and F. Lutz. Chem. Eur. J. **3**, 755 (1997).
25. F. Hutschka, A. Dedieu, M. Eichberger, R. Fornika, and W. Leitner. J. Am. Chem. Soc. **119**, 4432 (1997).
26. A. Kordikowski, A.P. Schenk, R.M. Van Nielen, and C.J. Peters. J. Supercrit. Fluids, **8**, 205 (1995).
27. V. Roskar, R.A. Dombro, G.A. Prentice, C.R. Westgate, and M.A. McHugh. Fluid Phase Equilib. **77**, 241 (1992).
28. S.D. Yeo and E. Kiran. Macromolecules, **32**, 7325 (1999).
29. C. Dariva, L.A.F. Coelho, and J.V. Oliveira. Fluid Phase Equilib. **160**, 1045 (1999).
30. N.P. Freitag and D.B. Robinson. Fluid Phase Equilib. **31**, 183 (1986).
31. C. Reichardt. Solvents and solvent effects in organic chemistry. VCH, Weinheim. 1988.
32. V.V. Mainz and R.A. Andersen. Organometallics, **3**, 675 (1984).

Appendix

The rate law was derived from the mechanism in Scheme 1 by making the following assumptions: (*i*) that k_5 is faster than k_4; (*ii*) that all the catalyst precursor was converted to the hydrido or formato complexes shown in the scheme; and (*iii*) that K_1, K_2, and K_3 are able to maintain equilibrium.

$$[4] \qquad \text{rat} = \frac{d\,HCO_2H}{dt} = k\,E = k_4\,H_2\,C$$

Define $[Ru_{tot}] = [A] + [B] + [C] + [D]$
From the equilibrium equations.

$$[5] \qquad B = \frac{C}{K_2\,CO_2} \qquad D = K_3\,C\,L \qquad A = \frac{B\,L}{K_1} = \frac{C\,L}{K_1K_2\,CO_2}$$

$$Ru_{tot} = \frac{C\,L}{K_1K_2\,CO_2} + \frac{C}{K_2\,CO_2} + C + K_3\,C\,L$$

Solve for [C] and plug into eq. [4]:

$$[6] \qquad \frac{d\,HCO_2H}{dt} = \frac{k_4\,H_2\,Ru_{tot}}{\left(\frac{L}{K_1K_2\,CO_2} + \frac{1}{K_2\,CO_2} + 1 + K_3\,L\right)}$$

Simplify by multiplying top and bottom by $K_2[CO_2]$:

$$[7] \qquad \frac{d\,HCO_2H}{dt} = \frac{k_4K_2\,H_2\,CO_2\,Ru_{tot}}{\left(\frac{L}{K_1} + 1 + K_2\,CO_2 + K_2K_3\,L\,CO_2\right)}$$

© 2001 NRC Canada

Asymmetric hydroformylation of styrene catalyzed by platinum complexes of chiral diphosphites with atropisomeric terminal moieties

J. Bakos, S. Cserépi-Szűcs, Á. Gömöry, C. Hegedüs, L. Markó, and Á. Szöllősy

Abstract: To study the nature of steric and electronic effects of diphosphites, a novel diphosphite was synthesized and tested with regard of its catalytic performance in the hydroformylation of styrene catalyzed by platinum complexes. The novel ligand **3** was prepared by the reaction of enantiomerically pure pentane-2,4-diol with (*S*)-2-chloro-5,5′,6,6′,7,7′,8,8′-octahydro-dinaphtho[2,1-*d*:1′,2′-*f*][1,3,2]dioxaphosphepine based on H_8-BINOL (H_8-BINOL = 5,5′,6,6′,7,7′,8,8′-octahydro-1,1′-bi-2-naphthol). For a comparative study, the BINOL (1,1′-bi-2-naphthol) based analogue **4** of **3** has also been synthesized. The highest chemoselectivity to aldehyde (71%) and regioselectivity to branched aldehyde (85%) with an enantiomer excess (ee) of 86% was obtained with the platinum(II)–$SnCl_2$ catalytic system associated with (2*S*,4*S*)-bis(*S*)-**3**.

Key words: asymmetric hydroformylation, chirality, homogeneous catalysis, P ligands, platinum.

Résumé : Dans le but d'étudier la nature des effets stériques et électroniques des diphosphites, on a synthétisé un nouveau diphosphite et on a évalué sa performance catalytique dans l'hydroformylation du styrène catalysée par des complexes de platine. On a préparé le nouveau ligand **3** par réaction du pentane-2,4-diol énantiomériquement pur avec de la (*S*)-2-chloro-5,5′,6,6′,7,7′,8,8′-octahydrodinaphto[2,1-*d*:1′,2′-*f*][1,3,2]dioxaphosphépine préparé à partir de H_8-BINOL (H_8-BINOL = 5,5′,6,6′,7,7′,8,8′-octahydro-1,1′-binapht-2-ol). Pour fins d'études comparatives, on a aussi synthétisé l'analogue **4** du composé **3**, préparé à partir du BINOL (1,1′-binapht-2-ol). Les niveaux les plus élevés de chimiosélectivité pour conduire à l'aldéhyde (71%) et de régiosélectivité pour conduire à l'aldéhyde ramifié (85%) avec un ee de 86% ont été obtenus avec un système platine(II)-$SnCl_2$ associé au (2*S*,4*S*)-bis(*S*)-**3**.

Mots clés : hydroformylation asymétrique, chiralité, catalyse homogène, ligands phosphorés, platine.

[Traduit par la Rédaction]

Introduction

Homogeneously catalyzed asymmetric hydroformylation represents a rapidly growing field because of its industrial potential and academic challenge. Applying this synthetic method aldehydes of great value can be obtained, which are attractive building blocks in organic synthesis (1). High activity and stability of the catalyst, high enantiomeric excess (ee), and an almost exclusive chemoselectivity to aldehydes and regioselectivity to branched aldehydes are required for an efficient catalytic system. These challenges prompted us to continue our research in the field of asymmetric hydroformylation by matching the structure of the ligand (for recent reviews, see ref. 2).

Although the investigation of the phosphine-modified rhodium (3) and platinum (4) systems is still overwhelming, the importance of applying phosphite (5) and phosphine-phosphite (6) modified systems is increasing. For example, rhodum complexes of the chiral phosphinephosphite ligand, (*R*)-2-(diphenylphosphino)-1,1′-binaphthalene-2′-yl-(*S*)-1,1′-binaphthalene-2,2′-diyl phosphite ((*R*,*S*)-BINAPHOS) catalyze asymmetric hydroformylation of styrene with an outstanding level of regio- and enantio-control (94% ee, iso:normal = 88:12). The catalyst system was also effective for a variety of other alkenes.

Surprisingly, however, there have been only a few reports on the application of bisphosphite-Pt(II)–$SnCl_2$ complexes in asymmetric hydroformylation (7). We have already reported that in the asymmetric hydroformylation of styrene by Pt-complexes containing chiral diphosphites with terminal atropisomeric substituents, the handiness of the product is dictated by the configuration of the stereogenic carbons of

Received September 5, 2000. Published on the NRC Research Press Web site at http://canjchem.nrc.ca on June 30, 2001.

Dedicated to Professor Brian James on the occasion of his 65th birthday.

J. Bakos[1] and C. Hegedüs. Department of Organic Chemistry, University of Veszprém, H-8201 Veszprém, P.O. Box 158, Hungary.
S. Cserépi-Szűcs and L. Markó. Research Group for Petrochemistry, Hungarian Academy of Science, H-8201 Veszprém, P.O. Box 158, Hungary.
Á. Gömöry. Chemical Research Center, H-1027 Budapest, P.O. Box 5967, Hungary.
Á. Szöllősy. Department of General and Analytical Chemistry, Technical University of Budapest, H-1521 Budapest, Hungary.

[1]Corresponding author (telephone: (36) 88 422022 (4355); fax: (36) 88 427492; e-mail: bakos@almos.vein.hu).

 DOI: 10.1139/cjc-79-5/6-725 © 2001 NRC Canada

the chiral backbone (7). Thus, for example, by using (2*S*,4*S*)-bis[((*S*)-dinaphtho[2,1-*d*:1′,2′-*f*][1,3,2]dioxaphosphepin-2-yl)oxy]pentane **4** (matched structure) as the ligand remarkably high catalytic activity and enantioselectivity (91% ee in CH_2Cl_2 at 17°C) were achieved, however, the hydrogenation activity of this heterobimetallic Pt–Sn catalytic system was still rather high (7*a*). In contrast to this, the use of the diastereomeric pair of **4**, (2*R*,4*R*)-bis(*S*) (mismatched constellation), leads to the opposite prevailing configuration of the product with a considerably lower asymmetric induction.

We have established that phosphites with enhanced π-acceptor ability give higher hydrogenation activity. The best chemoselectivity for hydroformylation was achieved when bisphosphites, based on the pentanediol backbone associated with dioxaphosphorinane terminal units, were used in the hydroformylation of styrene catalyzed by platinum complexes (7*b*). Based on these findings, we set up our hypothesis that retaining the appropriate structure of **4** and decreasing the π-acceptor ability of the terminal groups could improve chemoselectivity and regioselectivity and simultaneously retain high enantioselectivity. With this consideration in mind, we synthesized a new diphosphite **3** and the previously described diphosphite **4** (7*a*).

This paper describes the preparation and the catalytic properties of the chiral bisphosphites **3** and **4** in asymmetric hydroformylation of styrene. Both diphosphites **3** and **4** bear two methyl groups on the backbone and two atropisomeric 1,1′-bitetralin or 1,1′-binaphthyl frameworks on the phosphorus atoms.

Experimental

General

All reaction were carried out in oven-dried glasswork using Schlenk techniques under an atmosphere of argon. Benzene and toluene were distilled from sodium–benzophenone. Triethylamine and dichloromethane were distilled from CaH_2 and stored under an atmosphere of argon. Infrared (IR) spectra were recorded on a Specord IR-75A spectrometer. ^{31}P (202.45 MHz), ^{13}C (125.77 MHz), and ^{1}H (500.13 MHz) NMR spectra were obtained on a Bruker DRX-500 or on Varian Unity 300 spectrometer (121 MHz for ^{31}P, 75.4 MHz for ^{13}C, and 300.15 MHz for ^{1}H). Optical rotations were measured on Schmidt Haensch 21245. Gas chromatographic analyses were run on a Hewlett–Packard 5830A gas chromatograph (SPB-1 30 m column, film thickness 0.1 μm, carrier gas 2 mL min^{-1}). Mass spectrometric measurements were performed using a PE SCIEX API 2000 triple quadrupole instrument. Electrospray ionization (ES) was used and positive ions were detected. Samples were dissolved in acetonitrile. LiI was added to the solution to obtain abundant adduct ion with the molecule, because protonoted molecular ions were observed only in very low abundance.

Mass spectrum of (*S*)-**2** was obtained using a VG ZAB2-SEQ instrument with electron impact ionization (EI). Electron energy was 70 eV. The sample was introduced via a direct inlet system.

Materials and methods

Enantiomerically pure pentane-2,4-diol was synthesized by asymmetric hydrogenation of 2,4-pentanedione over Raney nickel catalyst modified with the corresponding enantiomer of tartaric acid and NaBr (TA-NaBr-MRNi) (8). 2,2′-Dihydroxy-1,1′-binaphthyl (BINOL) was obtained from Merck–Schuchardt. 2,2′-Dihydroxy-5,5′,6,6′,7,7′,8,8′-octahydro-1,1′-binaphthyl (H_8-BINOL) was prepared according to the literature procedure (9).

Catalytic experiments

In a typical experiment, $Pt(PhCN)_2Cl_2$ (0.0125 mmol), ligand (0.014 mmol), $SnCl_2$ (0.0125 mmol), CH_2Cl_2 (2 mL), and then styrene (25 mmol) (for a substrate:catalyst mol ratio of 5000:1, 62.5 mmol of styrene was used) and decane (5 mmol) (as an internal standard) were placed into a Schlenk-tube under argon. A stainless-steel autoclave (20 mL) was filled with this solution and then purged with syn gas ($CO:H_2$ (1:1)) and pressurized to the appropriate initial pressure with this gas mixture. At the end of the reaction the autoclave was cooled and depressurized. The reaction mixture was directly vacuum distilled to remove the catalyst. The reaction mixture and the distilled products were analyzed by gas chromatography. The enantiomeric excess of the aldehyde was determined by GC analysis of the distilled product (Hewlett–Packard HP 4890 gas chromatograph, split–splitless injector, β-DEX 225, 30 m, internal diameter 0.25 mm, film thickness 0.25 μm, carrier gas: 100 kPa nitrogen, FID detector; the retention times of the enantiomers are 30.5 min (*R*), 32.1 min (*S*)). The configuration of the prevailing enantiomer in the product was determined by the sign of optical rotation of the corresponding aldehyde. Conversions and composition of the reaction mixture (**5**:**6**:**7**, branched:linear:hydrogenated) were determined by GC (SPB-1) using decane as an internal standard.

Preparation of (*S*)-2-chloro-5,5′,6,6′,7,7′,8,8′-octahydro-1,1′-dinaphtho[2,1-*d*:1′,2′-*f*][1,3,2]dioxaphosphepine ((*S*)-2)

(*S*)-H_8-BINOL **1** (4.2 g, 14 28 mmol) was dried azeotropically with toluene (3 × 20 mL), and then the solvent was evaporated. The residue was dissolved in dry THF (50 mL) and added slowly (30 min) to a solution of PCl_3 (1.6 mL, 18.6 mmol) and Et_3N (4.4 mL, 31.4 mmol) in THF (20 mL) at 0°C. The reaction mixture was stirred overnight at room temperature. The formed amine salts were removed by filtration. Evaporation to dryness gave the pale yellow phosphorochloridite, which was washed with ether (2 × 30 mL) to give the product as a white solid (4.92 g, 95.9%). This product was used without any further purification. mp 109–111°C, $[\alpha]_D^{20}$ = +391.52° (*c* = 1.18, CH_2Cl_2). EI-MS *m*/*z*: 358 (M^+). ^{1}H NMR ($CDCl_3$, 300.15 MHz) δ: 1.48–1.64 (m, 2H, CH_2), 1.70–1.85 (m, 6H, CH_2), 2.26 (dt, *J* = 16.6, 6.4 Hz, 2H, CH_2), 2.58–2.70 (m, 2H, CH_2), 2.76–2.88 (m, 4H, CH_2), 6.91 and 7.01 (d, *J* = 8.3 Hz, 2H, H_3, $H_{3'}$), 7.09 (d, *J* = 8.3 Hz, 2H, H_4, $H_{4'}$). ^{13}C NMR ($CDCl_3$, 75.42 MHz) δ: 23.00 (s, CH_2), 23.06 (s, CH_2), 23.15 (s, CH_2), 23.24 (s, CH_2), 28.5 (s, CH_2), 29.8 (s, CH_2), 29.9 (s, CH_2), 119.42 (d, $J_{P,C}$ = 15.1 Hz), 119.42 (d, $J_{P,C}$ = 18.1 Hz), 128.3 (d, $J_{P,C}$ = 3.0 Hz), 129.8 (d, $J_{P,C}$ = 5.0 Hz), 129.9 (s), 130.5 (s), 135.7 (d, $J_{P,C}$ = 2.0 Hz), 136.7 (d, $J_{P,C}$ = 2.0 Hz) 139.5 (d, $J_{P,C}$ = 2.0 Hz), 145.9 (d, $J_{P,C}$ = 5.0 Hz) 147.4 (d,

© 2001 NRC Canada

$J_{P,C}$ = 3.0 Hz). $^{31}P\{^1H\}$ NMR ($CDCl_3$, 121.42 MHz) δ: 171.5 (s).

Preparation of (2*S*,4*S*)-2,4-bis[(*S*)-5,5′,6,6′,7,7′,8,8′-octahydro-dinaphtho[2,1-*d*:1′,2′-*f*][1,3,2]dioxaphosphepin-2-yloxy]-pentane ((2*S*,4*S*)-bis(*S*)-3)

To a solution of **2** (2.00 g, 5.57 mmol) and Et_3N (2.25 mL, 16.0 mmol) in toluene (20 mL) was added slowly a solution of optically pure (*S*,*S*)-pentane-2,4-diol (281.0 mg, 2.7 mmol, azeotropically dried with toluene, 3 × 3 mL) in toluene (25 mL) at 0°C. The reaction mixture was stirred for 30 min at 0°C and then at room temperature overnight. The formed hydrochloride salt was removed by filtration. Evaporation to dryness gave a pale yellow foam, which was washed with ether (2 × 30 mL) to give the product as a white solid (1.92 g, 95.0%). mp 158–160°C, $[\alpha]_D^{20}$ = +269.23° (*c* = 1.04, CH_2Cl_2). EI-MS *m*/*z*: 755 ($[M + Li]^+$). ^1H NMR ($CDCl_3$, 500.13 MHz) δ: 1.38 (d, *J* = 6.3 Hz, 6H, CH_3), 1.56–1.65 (m, 4H, CH_2), 1.76 (m, 2H, CH_2), 1.79–1.86 (m, 12H, CH_2), 2.29–2.36 (m, 4H, CH_2), 2.66–2.74 (m, 4H, CH_2), 2.77–2.89 (m, 8H, CH_2), 4.65 (m, 2H, CH) 6.88 (d, *J* = 8.2 Hz, 2H, CH), 7.05 (d, *J* = 8.2 Hz, 2H, CH) 7.06 (d, *J* = 8.2 Hz, 2H, CH), 7.09 (d, *J* = 8.2 Hz, 2H, CH). ^{13}C NMR ($CDCl_3$, 125.75 MHz) δ: 22.91 (s), 22.95 (s), 23.10 (s), 23.16 (s), 23.76 (s), 28.21 (s), 29.61 (s), 29.65 (s), 46.60 (m, CH_2), 69.00 (t, $J_{P,C}$ = 12.1 Hz, CH), 119.20 (s), 119.60 (s), 125.70 (s), 128.50 (s), 128.60 (s), 129.3 (s), 129.40 (s), 129.70 (s), 129.90 (s), 131.20 (s), 134.10 (s), 134.90 (s), 137.50 (s), 137.90 (s), 138.60 (s), 146.40 (s) 146.90 (s). $^{31}P\{^1H\}$ NMR ($CDCl_3$, 202.45 MHz) δ: 146.2 (s).

(*S*)-2-chloro-dinaphhtho[2,1-*d*:1′,2′-*f*][1,3,2]dioxaphosphepine

This compound was prepared according to the literature procedure (10). mp 113–115°C, $[\alpha]_D^{20}$ = +709.25° (*c* = 1.135, CH_2Cl_2).

(2*S*,4*S*)-2,4-bis[(*S*)-dinaphtho[2,1-d:1′,2′-*f*][1,3,2]dioxaphosphepin-2-yloxy]-pentane ((2*S*,4*S*)-bis(*S*)-4)

To a solution of (*S*)-2-chloro-dinaphhtho[2,1-*d*:1′,2′-*f*][1,3,2]-dioxaphosphepine (5.3 g, 15.11 mmol) and Et_3N (6.3 mL, 16.0 mmol) in toluene (10 mL) was added slowly a solution of optically pure (*S*,*S*)-pentane-2,4-diol (0.755 g, 7.25 mmol, azeotropically dried with toluene, 3 × 8 mL) in toluene (30 mL) at 0°C. The reaction mixture was stirred for 30 min at 0°C and then at room temperature overnight. The formed hydrochloride salt was removed by filtration. Evaporation to dryness gave a pale yellow residue, which was washed with ether (2 × 20 mL) to give the product as a white solid (5.2 g, 97.9%). mp 100–102°C, $[\alpha]_D^{20}$ = +509.43° (*c* = 1.06, CH_2Cl_2). EI-MS *m*/*z*: 739 ($[M + Li]^+$). ^1H NMR ($CDCl_3$, 500.13 MHz) δ: 1.43 (d, *J* = 6.3 Hz, 6H, CH_3), 1.78 (m, 2H, CH_2), 4.80 (m, 2H, CH), 7.19–7.34 (m, 4H, CH), 7.41–7.50 (m, 10H, CH), 7.60 (d, *J* = 8.8 Hz, 2H, CH), 7.94–8.01 (m, 8H, CH). ^{13}C NMR ($CDCl_3$, 125.75 MHz) δ: 23.85 (s, CH_3), 46.50 (m, CH_2), 69.71 (t, $J_{P,C}$ = 10.9 Hz, CH), 122.30 (s), 122.40 (s), 123.40 (s), 124.80 (s), 125.20 (s), 125.3 (s), 125.70 (s), 126.50 (s), 126.60 (s), 127.50 (d, $J_{P,C}$ = 3.6 Hz), 128.70 (s), 128.80 (s), 129.40 (s), 130.10 (s), 130.70 (s), 131.60 (s), 132.00 (s), 133.10 (s), 133.30 (s), 148.00 (s) 148.30 ppm (s). $^{31}P\{^1H\}$ NMR ($CDCl_3$, 202.45 MHz) δ: 153.5 (s).

Results and discussion

H_8-BINOL **1** can be readily derived from BINOL using the protocol of Cram et al. (9). The reaction of racemic H_8-BINOL with PCl_3 in the presence of triethylamine in THF gave phosphorochloridite, (*S*,*R*)-2-chloro-5,5′,6,6′,7,7′,8,8′-octahydro-dinaphtho[2,1-*d*:1′,2′-*f*][1,3,2]dioxaphosphepine ((*S*,*R*)-**2**). The $^{31}P\{^1H\}$ NMR spectrum of the compound showed one absorption at 171.5 ppm, which is in the region expected for a chlorodioxaphosphepine. It is noteworthy that there is a substantial upfield ^{31}P chemical shift relative to the BINOL-based chlorophosphepine (179.0 vs. 171.5 ppm, Δδ = 7.5 ppm) (10). A similar upfield shift was observed when the chemical shift of phosphorochloridite based on 2,2′-bisphenol was compared to the value of that based on 2,2′-bisphenol bearing bulky *tert*-butyl substituents at the *ortho* and *para* positions (180.2 vs. 172.1 ppm) (5*b*).

Two equivalents of the racemic chloro-compound (*S*,*R*)-**2** were reacted with optically pure (2*S*,4*S*)-pentane-2,4-diol in the presence of triethylamine to give a diastereomeric mixture of **3** (Scheme 1). In the $^{31}P\{^1H\}$ NMR spectrum of the product at ambient temperature, six lines are observed with relative intensities and splittings consistent with the expected three diastereomers. An obvious explanation is that a pair of doublets arises from the diastereomer, (2*S*,4*S*)-(*S*,*R*) = (2*S*,4*S*)-(*R*,*S*). The absolute configuration of the diastereomers is given in a shorthand notation as (2*S*,4*S*)-(*R*,*S*), (2*S*,4*S*)-bis(*R*), and (2*S*,4*S*)-bis(*S*). Where (2*S*,4*S*) refer to the absolute configurations of carbon atoms C(2) and C(4) in the pentane-2,4-diol backbone, and (*R*) or (*S*) refer to the configuration of the axial chirality. The 2D homonuclear ^{31}P COSY NMR spectrum of the product confirms the existence of coupling ($^6J_{P,P}$ = 8.8 Hz) between the P atoms (δ 140.9 and 145.7 ppm) six bonds apart (11). Two singlets (δ 146.2 for (2*S*,4*S*)-bis(*S*)-**3** and 141.1 for (2*S*,4*S*)-bis(*R*)-**3**) are attributed to the presence of the other two diastereomers. This was supported by the NMR spectrum of the optically pure diastereomer, (2*S*,4*S*)-bis(*S*)-**3** obtained from (*S*)-**2** and (2*S*,4*S*)-pentane-2,4-diol. In this case the other diastereomers were not detected by $^{31}P\{^1H\}$ NMR, implying that diastereomer **3** was obtained in optically pure form.

The "like" (*S*,*S*,*S*) diastereomers of **3** and **4** give ^{31}P resonances at 146.2 and 153.6 ppm, respectively. The "unlike" (*S*,*S*,*R*) diastereomers of **3** and **4** give signals at 141.1 and 147.1 ppm, respectively. In both cases there are substantial upfield shifts relative to the BINOL based bisphosphite (146.2 to 153.6 ppm, Δδ = 7.4 ppm and 141.6 to 147.1 ppm, Δδ = 6.0 ppm), which might be primarily due to the change of the electronic character of the phosphorus, rather than to an increase of strain of the partially hydrogenated dioxaphosphepine ring.

Phosphites **3** and **4** form phosphite–platinum complexes. For example, treatment of **4** with $PtCl_2(PhCN)_2$ in CD_2Cl_2 resulted in displacement of PhCN by the ligand. The $^{31}P\{^1H\}$ NMR spectrum of $PtCl_2$[(2*S*,4*S*)-bis(*S*)-**4**] consists of a singlet supplemented with *J* ^{195}Pt–^{31}P satellites (δ = 87.5, $J_{Pt,P}$ = 5672 Hz). The phosphorus resonance is 66.1 ppm upfield from that of the free ligand (153.6 ppm). From the magnitude of the coordination shift and the coupling constant ($J_{Pt,P}$) a *cis* P-Pt-P disposition in a square pla-

© 2001 NRC Canada

Scheme 1.

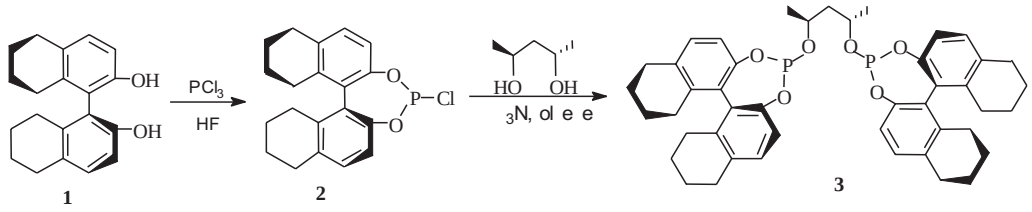


Table 1. Hydroformylation of styrene with ligands **3** and **4**.

Run	Ligand	Time (h)	*T* (°C)	Conv. (%)[a]	RCHO (%)[b]	**5**:**6**[a]	ee of **5** (%)[c]
1	**3**	1	80	93	65	57:43	54 (*R*)
2	**3**	1.5	60	95	68	70:30	67 (*R*)
3	**3**	2	40	77	69	80:20	79 (*R*)
4	**3**	20	23	62	71	85:15	86 (*R*)
5[d]	**3**	4	23	27	63	84:16	94 (*R*)
6[d]	**3**	20	23	83	62	84:16	88 (*R*)
7	**4**	2	60	100	53	59:41	71 (*R*)
8[e]	**4**	4	60	100	53	58:42	75 (*R*)
9[e]	**4**	70	17	90	46	60:40	91 (*R*)
10[d]	**4**	1	100	100	41	59:41	62 (*R*)
11[d]	**4**	2	60	100	45	60:40	73 (*R*)
12[d]	**4**	67	17	76	45	58:42	88 (*R*)

Note: Reaction conditions: solvent CH_2Cl_2; substrate:Pt ratio = 2000.

[a]Conversions and composition of the reaction mixture of branched:linear:hydrogenated (**5:6:7**) were determined by GC (SPB-1) using decane as an internal standard.

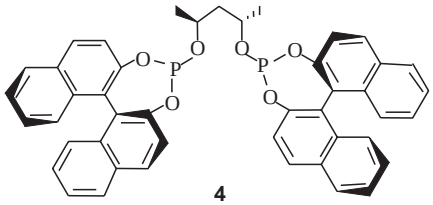
[b]Aldehydes/(aldehydes + ethylbenzene).

[c]Determined by GC analysis of the distilled product (β-DEX 225, 30 m, id 0.25 mm). Stereochemisty determined by the sign of optical rotation of the corresponding aldehyde.

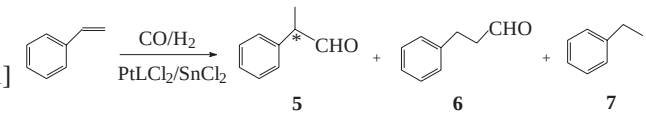
[d]Solvent, toluene.

[e]Substrate:Pt ratio = 5000.

nar arrangement can be confidently assigned (7). Both diphosphites form eight-membered chelate rings upon coordination of the Pt metal center, and afford only the *cis* complexes without any oligomeric species. Oligomeric platinum complexes of diphospholes, dibenzophospholes, and bisnaphthophospholes have been reported with *trans* P-Pt-P arrangement (4*d* and *e*).



Catalysts were prepared in situ from $PtCl_2(PhCN)_2$ and 1.12 equiv. of ligand in dichloromethane using a 6.25 mM solution of platinum–diphosphite catalyst. It is noteworthy that, in contrast to rhodium systems modified with phosphines or phosphinephosphites, there is no need for an excess of phosphite ligand in the platinum system. Anhydrous $SnCl_2$ was used as a co-catalyst. Addition of $SnCl_2$ is essential for catalytic activity (12). Catalytic reactions were carried out under classical conditions to give a mixture of the branched 2-phenylpropanal **5**, the normal 3-phenylpropanal aldehyde regioisomers **6**, and the hydrogenated ethylbenzene product **7**. Some representative results are given in Table 1.

[1] 

Several studies (2) have shown that regio- and enantioselectivity of platinum-catalyzed asymmetric hydroformylation can be very sensitive to the nature of the solvent. Dichloromethane and toluene, having medium polarity, give the highest reaction rate and the best enantioselectivity and therefore were chosen as the routine solvents. It is interesting to note that the chemoselectivity and the activity of the catalysts are significantly lower in toluene than in dichloromethane. For example, although the highest ee of 94% was obtained at a conversion of 27% in toluene (Table 1, run 5) the enantioselectivity is not constant in time, i.e., after 20 h (run 6) at a conversion of 83% the ee is 88%.

The data show that the in situ platinum catalyst is most effective for hydroformylation of styrene when the reaction is performed at room temperature. As usual, on lowering the temperature enantioselectivity improves at the expense of reaction rate (Table 1, runs 1–4 compared to runs 10–12). At higher temperature the activity of the catalyst increases from 83 to 1200 mol mol^{-1} h^{-1} (runs 4–1, TOF in mol aldehydes

© 2001 NRC Canada

(mol Pt)$^{-1}$ h^{-1} determined at the reaction time indicated in Table 1). In dichloromethane the highest enantioselectivity is obtained (91%, *R*) when ligand **4** is used, but in case of ligand **3** the enantioselectivity is only slightly lower (86%). At the same time, chemoselectivity to hydroformylation (71%) and regioselectivity to branched aldehyde (85%) of the catalyst improved substantially (run 4). Thus, an important feature of this diphosphite system in combination with platinum is the relatively high regioselectivity of the reaction. The branched isomer forms with these ligands in a significantly higher amount than with the usual mono- and ditertiary phosphines (4*e*).

Regioselectivity of the reaction depends largely on the reaction temperature in case of **3**; with decreasing temperature regioselectivity to branched aldehyde increases markedly. This can be explained by the enhanced rate of isomerization of the initially formed Pt-*i*-alkyl complex to the thermodynamically more stable *n*-alkyl complex, which leads to a higher percentage of *n*-aldehyde. It is interesting to note that the regioselectivity is less dependent on temperature in the case of ligand **4.**

We have shown recently that with the platinum phosphite systems the *relative* configuration of the stereogenic elements in the backbone and in the terminal units play crucial roles in the degree of enantioselectivities and the sense of enantioface discrimination. In the case of styrene, the latter is mainly determined by the configuration of the backbone of the ligand. Accordingly, both ligands used in this study gave (*R*)-2-phenylpropanal as the prevailing enantiomer. It is not surprising because **3** and **4** can be considered "like" sytems (2*S*,4*S*)-bis(*S*) and the relative spatial arrangement around the stereogenic elements of the backbone is the same.

When **3,** a partially hydrogenated analogue of **4**, was used as the bisphosphite ligand for the catalyst precursor, the branched:linear ratio of hydroformylation products was found to increase from ~1.5 to 5.7 (i.e., 85:15).

Enhancing the electron-donating ability of the ligand resulted in an increase of chemoselectivity to hydroformylation from 53% with **4** (run 7) to 68% with **3** (run 2) at 60°C. The regioselectivity to branched aldehyde were 59 and 70%, respectively. The increase of the branched:linear ratio with increasing phosphite basicity (ligand **3** vs. ligand **4**) probably results from the different behaviour of branched and linear platinum alkyls toward β-hydrogen elimination. The linear alkyls, the anti-Markovnikov products of the insertion of styrene into the Pt–H bond, are mainly converted to linear aldehyde, while the branched alkyls partially regenerate styrene through enhanced β-hydrogen elimination. Selective β-hydrogen elimination from the branched alkyl metal intermediate was already observed by Lazzaroni et al. (13) for rhodium systems. In our case increasing electrophilicity of the platinum center may result in higher reactivity of the branched alkyl platinum species toward β-hydrogen elimination (14).

Recently, RajanBabu and Ayers (15) studied the electronic effect of the ligands on the enantioselectivity of hydroformylation of vinylarenes using rhodium diphosphinites and found that the introduction of electron-withdrawing aryl groups on the phosphorus increased the enantioselectivity of the catalyst. The mechanistic aspects of the electronic effects on rhodium diphosphine catalyzed hydroformylation were investigated by Casey et al. (16) and van Leeuwen et al. (17).

Similarly, Ir(I)- and Ru(II)-complexes of H_8-BINAP served as more effective catalyst precursors for asymmetric hydrogenation of some substrates, than did the analogous complexes of BINAP (18). Furthermore, the Pd(II) complex of (*R*,*S*)-H_8-BINAPHOS is a more active catalyst compared to that of (*R*,*S*)-BINAPHOS for alternating copolymerization of propene with carbon monoxide. A completely isotactic copolymer was obtained in high optical purity with (*R*,*S*)-H_8-BINAPHOS (19). It is noteworthy that in [Rh{(*S*)-H_8-BINAP}(COD)]ClO_4 the dihedral angle between the two phenyl rings of the bitetralin moiety (18*a*) is markedly larger (80.3°) than that between the two naphthalene rings in [Rh{(*R*)-BINAP}(NBD)]ClO_4 (74.4°) (20). Recently, we have reported the X-ray structure of the complex [$PtCl_2$(2,2′-bis[(4*R*,6*R*)-4,6-dimethyl-1,3,2-dioxaphosphorinan-2-yloxy]-1,1′-binaphtyl)] and that of the free ligand (7*c*). It is interesting to note that the dihedral angle defined by the planes of the naphthyl rings is 77.6° in the complex and 103.0° in the free ligand, while in the free ligand of the octahydro analogue it is 98.2° (7*d*). The dihedral angles in these structures suggest that ligands having H_8-BINOL based backbone possess a quite different axial flexibility, however, in our case the seven-membered dioxaphosphepine ring restricts this flexibility. Unfortunately, suitable crystals of the free ligand **3** or its platinum complex for X-ray analysis could not be obtained.

Conclusion

As an the extension of our study on asymmetric hydroformylation, we reported herein a comparative study of the catalytic performance of bisphoshites **3** and **4**. Chiral bisphosphites with C_2 symmetry afforded highly active platinum catalysts for asymmetric hydroformylation of styrene. High enantioselectivities (86–91%) have been obtained with the platinum(II)–$SnCl_2$ catalytic system containing ligands **3** and **4.** Retaining the favorable structure of ligand **4** but increasing the electron density in the terminal group significantly improved the catalytic performance, i.e., higher regioselectivity to branched aldehyde (85%) and lower hydrogenation activity were achieved with almost unchanged enantioselectivity. Although the chemoselectivity of the process could be improved, the level is still modest. The observed changes of activity, chemoselectivity, and regioselectivity may have their origin in electronic effects, but steric factors like the bite angle of the ligands cannot be excluded.

Acknowledgments

Financial support from Hungarian National Science Foundation (OTKA T 032 004) is gratefully acknowledged. We are grateful to Mr. Béla Édes for skillful assistance in the synthetic and catalytic experiments.

© 2001 NRC Canada

References

1. C. Botteghi, S. Paganelli, A. Schionato, and M. Marchetti. Chirality, **3**, 355 (1991).
2. (*a*) S. Gladiali, J. Bayón, and C. Claver. Tetrahedron: Asymmetry, **7**, 1453 (1995); (*b*) F. Agbossou, J.F. Carpentier, and A. Mortreux. Chem. Rev. **95**, 2485 (1995); (*c*). G. Consiglio. *In* Catalytic asymmetric syntheses. *Edited by* I. Ojima. VCH Publishers, Weinheim. 1993. p. 273; (*c*) M. Beller, B. Cornils, C.D. Frohning, and C.D.J. Kohlpainter. J. Mol. Catal. **104**, 17 (1995).
3. A.M. Masdeu-Bultó, A. Orejon, A. Castellanos, S. Castillón, and C. Claver. Tetrahedron: Asymmetry, **7**, 1834 (1996).
4. (*a*) J.K. Stille, H. Su, P. Brechot, G. Parrinello, and L.S. Hegedus. Organometallics, **10**, 1183 (1991); (*b*) G. Consiglio, S.C.A. Nefkens, and A. Borer. Organometallics, **10**, 2046 (1991); (*c*) A. Scrivanti, S. Zeggio, V. Beghetto, and U. Matteoli. J. Mol. Catal. **101**, 217 (1995); (*d*) G. Consiglio and S.C.A. Nefkens. Tetrahedron: Asymmetry, **1**, 417 (1990); (*e*) S. Gladiali, D. Fabbri, and L. Kollár. J. Organomet. Chem. **491**, 91 (1995); (*f*) S. Gladiali, E. Alberico, E.S. Pulacchini, and L. Kollár. J. Mol. Catal. A: Chem., **143,** 155 (1999).
5. (*a*) J.E. Babin and G.T.W.O. Whiteker. U. S. Pat. 911 518. 1992. (to Union Carbide Corp.); (*b*) G.J.H. Buisman, P.C.J. Kamer, and P.W.N.M. van Leeuwen. Tetrahedron: Asymmetry, **4**, 1625 (1993); (*c*) G.J.H. Buisman, M.E. Martin, E.J. Vos, A. Klootwijk, P.C.J. Kamer, and P.W.N.M. van Leeuwen. Tetrahedron: Asymmetry, **7**, 719 (1995).
6. (*a*) N. Sakai, K. Nozaki, K. Mashima, and H. Takaya. Tetrahedron: Asymmetry, **3**, 583 (1992); (*b*) N. Sakai, S. Mano, K. Nozaki, and H. Takaya. J. Am. Chem. Soc. **115**, 7033 (1993); (*c*) T. Horiuchi, T. Ohta, K. Nozaki, and H. Takaya. Chem. Commun. 155 (1996).
7. (*a*) S. Cserépi-Szűcs and J. Bakos. Chem. Commun. 635 (1997); (*b*) S. Cserépi-Szűcs, I. Tóth, L. Párkányi, and J. Bakos. Tetrahedron: Asymmetry, **9**, 3135 (1998); (*c*) S. Cserépi-Szűcs, G. Huttner, L. Zsolnai., and J. Bakos. J. Organomet. Chem. **586**, 70 (1999); (*d*) S. Cserépi-Szűcs, G. Huttner, L. Zsolnai, Á. Szöllősy, C. Hegedüs, and J. Bakos. Inorg. Chim. Acta, **296**, 222 (1999); (*e*) R. Kadyrov, D. Heller, and R. Selke. Tetrahedron: Asymmetry, **9**, 329 (1998).
8. (*a*) K. Ito, T. Harada, A. Tai, and Y. Izumi. Chem. Lett. 1049 (979); (*b*) K. Ito, T. Harada, and A. Tai. Bull. Chem. Soc. Jpn. **53**, 3367 (1980).
9. D.J. Cram, R.C. Helgeson, S.C. Peacock, L.J. Kaplan, L.A. Domeier, P. Moreau, K. Koga, J.M. Mayer, Y. Chao, M.G. Siegel, D.H. Hoffman, and G.D.Y. Sogah. J. Org. Chem. **43**, 1930 (1978).
10. J. Scherer, G. Huttner, M. Büchner, and J. Bakos. J. Organomet. Chem. **520**, 45 (1996).
11. G. Szalontai, J. Bakos, I. Tóth, and B. Heil. Magn. Reson. Chem. **25**, 761 (1987).
12. (*a*) A. Scrivanti, A. Berton, L. Toniolo, and C. Botteghi. J Organomet. Chem. **314**, 369 (1986); (*b*) A. Scrivanti, C. Botteghi, L. Toniolo, L. Berton. J Organomet. Chem. **314**, 369 (1986); (*c*) I. Tóth, T. Kégl, C. J. Elsevier, and L. Kollár. Inorg. Chem. **33**, 5708 (1994); (*d*) R.W. Rocho, W.B. De Almeida. Organometallics, **17**, 1961 (1998).
13. R. Lazzaroni, R. Settambolo, and G. Uccello-Baretta. Organometallics, **14**, 4644 (1995) and refs. therein.
14. J.D. Unruh and J.R.J. Christensen. J. Mol. Catal. **14**, 19 (1982).
15. T.V. RajanBabu and T.A. Ayers. Tetrahedron Lett. **35**, 4295 (1994).
16. C.P. Casey, E.L. Paulsen, E.W. Beuttenmueller, B.R. Proft, B.A. Matter, and D.R. Powel. J. Am. Chem.Soc. **121**, 63 (1999).
17. L.A. van der Veen, M.D. Boele, F.R. Bergman, P.C.J. Kamer, P.W.N.M. van Leeuwen, K. Goubitz; J. Fraanje, H. Schenk, and C. Bo. J. Am. Chem. Soc. **120**, 11 616 (1998).
18. (*a*) X. Zhang, K. Mashima, K. Koyano, N. Sayo, H. Kumabayashi, S. Akutagawa, and H. Takaya. J. Chem. Soc. Perkin. Trans. 1, 2309 (1994); (*b*) T. Taketomi, Y. Yoshizumi, H. Kumobayashi, S. Akutagawa, and H. Takaya. J. Am. Chem. Soc. **115**, 3318 (1993).
19. K. Nozaki, M. Yasutomi, K. Nakamoto, and T. Hiyama. Polyhedron, **17**, 1159 (1998).
20. R. Schmid, M. Cereghetti, B. Heiser, P. Schönholzer, and H.-J. Hansen. Helv. Chim. Acta, **71**, 897 (1988).

© 2001 NRC Canada

Chiral metallocenes: the synthesis and X-ray crystal structures of $TiCl_2(\eta^5{:}\eta^5\text{-}C_5Me_4SiMe_2C_5H_3R^*)$ (R^* = menthyl or neomenthyl) and related compounds

Paul Beagley, Philip Davies, Harry Adams, and Colin White

Abstract: The syntheses of the chiral ansa-metallocene complexes $TiCl_2(\eta^5{:}\eta^5\text{-}C_5Me_4SiMe_2C_5H_3R^*)$ (R^* = menthyl (**4a**) or neomenthyl (**4b**)) are reported; initially **4a** was obtained as a 3:1 mixture of (*R*:*S*) diastereoisomers, which differ only in which face of the asymmetrically substituted cyclopentadienyl ring is bonded to the titanium (chiral descriptor shown). The major diastereomer $\mathbf{4a}_{\boldsymbol{R}}$ was crystallized out optically pure from the initial reaction mixture, whereas the $\mathbf{4a}_{\boldsymbol{S}}$ diastereoisomer was isolated after isomerizing a racemic mixture of **4a** to a 1:3 mixture of (*R*:*S*) diastereoisomers using UV irradiation. The corresponding neomenthyl complex **4b** was obtained as a 1.3:1 mixture of diastereoisomers that could not be separated. The optically pure $\mathbf{4a}_{\boldsymbol{R}}$ was converted stereoselectively into the corresponding (*R*)-$TiMe_2(\eta^5{:}\eta^5\text{-}C_5Me_4SiMe_2C_5H_3R^*)$ (R^* = menthyl). Syntheses of the related indenyl ligand system $C_5Me_4SiMe_2C_9H_7$ (**3**) is reported but complexation to titanium proved to be problematic although $ZrCl_2(\eta^5{:}\eta^5\text{-}C_5Me_4SiMe_2C_9H_6)$ (**6**) was isolated. The crystal structures of both $\mathbf{4a}_{\boldsymbol{R}}$ and $\mathbf{4a}_{\boldsymbol{S}}$ are reported and compared. Crystals of $\mathbf{4a}_{\boldsymbol{R}}$ are orthorhombic, a = 27.857(11), b = 9.985(5), and c = 9.596(4) Å, Z = 4, space group $P2_12_121$ (D_2^4, No. 19), and those of $\mathbf{4a}_{\boldsymbol{S}}$ are monoclinic, a = 8.5810(10), b = 38.679(4), and c = 8.5842(10) Å, β = 113.001(2)°, Z = 4, space group $P2_1$ (C_2^2, No. 4). The structures were solved by the Patterson method and $\mathbf{4a}_{\boldsymbol{R}}$ was refined by blocked-cascade least-squares procedures to R = 0.0628 (R_ω = 0.0503) for 902 reflections with $|F|/\sigma(|F|) \geq 3.0$, whereas $\mathbf{4a}_{\boldsymbol{S}}$ was refined by full-matrix least-squares procedures to R = 0.0646 (wR_2 = 0.1829) for 5734 reflections with $|F|/\sigma(|F|) \geq 4.0$. Both diastereomers of **4a** catalyze hydrosilylation of ketones, but as expected from a comparison of the two crystal structures, the $\mathbf{4a}_{\boldsymbol{R}}$ isomer is the more stereoselective catalyst, i.e., hydrosilylation of acetophenone followed by hydrolysis gives 82% enantiomeric excess (ee) of (*S*)-PhCH(Me)OH with $\mathbf{4a}_{\boldsymbol{R}}$ whereas only 16% ee of (*R*)-PhCH(Me)OH with $\mathbf{4a}_{\boldsymbol{S}}$.

Key words: titanium, metallocene, chiral, structure, catalyst.

Résumé : On a réalisé la synthèse des complexes ansa-métallocènes chiraux $TiCl_2(\eta^5{:}\eta^5\text{-}C_5Me_4SiMe_2C_5H_3R^*)$ (R^* = menthyle **(4a)**; R^* = néomenthyle (**4b**)). Originalement **4a** a été obtenu sous la forme d'un mélange 3:1 des diastéréomères (*R*) et (*S*) qui ne diffèrent que par quelle face du noyau cyclopentadiényle substitué de façon asymétrique est liée au titane (on explicite le descripteur chiral). Le diastéréomère principal, $\mathbf{4a}_{\boldsymbol{R}}$ a été retiré optiquement pur par cristallisation du mélange réactionnel initial; le diastéréomère $\mathbf{4a}_{\boldsymbol{S}}$ n'a été isolé qu'après avoir isomérisé un mélange racémique de **4a** en un mélange 1:3 des diastéréomères (*R*) et (*S*) par irradiation UV. Le complexe néomenthylique correspondant **4b** a été obtenu sous la forme d'un mélange 1:4:1 de diastéréomères qui n'a pas pu être séparé. Le produit $\mathbf{4a}_{\boldsymbol{R}}$ a été optiquement pur a été transformé stéréosélectivement en (*R*)-$TiMe_2(\eta^5{:}\eta^5\text{-}C_5Me_4SiMe_2C_5H_3R^*)$ (R^* = menthyle) correspondant. On rapporte aussi la synthèse du système de ligand indényle apparenté $C_5Me_4SiMe_2C_9H_7$ (**3**), mais sa complexation avec le titane s'est avérée être problématique même si on a pu isoler le $ZrCl_2(\eta^5{:}\eta^5\text{-}C_5Me_4SiMe_2C_9H_6)$ (**6**). On a déterminé les structures cristallines des composés $\mathbf{4a}_{\boldsymbol{R}}$ et $\mathbf{4a}_{\boldsymbol{S}}$ et on en a fait une comparaison. Les cristaux de $\mathbf{4a}_{\boldsymbol{R}}$ sont orthorhombiques, groupe d'espace $P2_12_12_1$ (D_2^4, No. 19), avec a = 27,857(11), b = 9,985(5) et c = 9,596(4) Å et Z = 4 alors que ceux de $\mathbf{4a}_{\boldsymbol{S}}$ sont monocliniques, groupe d'espace $P2_1$ (C_2^2, No. 4), avec a = 8,5810(10), b = 38,679(4) et c = 8,5842(10) Å, β = 113,001(2)° et Z = 4. Les structures ont été résolues par la méthode de Patterson et celle de $\mathbf{4a}_{\boldsymbol{R}}$ a été affinée par des méthodes de moindres carrés à cascade bloquée jusqu'à des valeurs de R = 0,0628 (R_ω = 0,0503) pour 902 réflexions avec $|F|/\sigma|F| \geq 3,0$ alors que celle de $\mathbf{4a}_{\boldsymbol{S}}$ a été affinée par la méthode des moindres carrés (matrice complète) jusqu'à des valeurs de R = 0,0646 (wR_2 = 0,1829) pour 5734 réflexions avec $|F|/\sigma|F| \geq 4,0$. Les deux diastéréomères de **4a** catalyzent l'hydrosilylation des cétones mais, comme on peut s'y attendre sur la base d'une comparaison des deux structures cristallines, l'isomères $\mathbf{4a}_{\boldsymbol{R}}$ est plus stéréosélectif; par exemple l'hydrosilylation de l'acétophénone, suivie d'une hydrolyse, conduit à un mélange avec 82% d'ee du (*S*)-PhCH(Me)OH avec $\mathbf{4a}_{\boldsymbol{R}}$ alors que l'on n'obtient que 16% d'ee de (*R*)-PhCH(Me)OH avec $\mathbf{4a}_{\boldsymbol{S}}$.

Received September 12, 2000. Published on the NRC Research Press Web site at http://canjchem.nrc.ca on June 30, 2001.

Dedicated to Professor Brian James on the occasion of his 65th birthday.

P. Beagley, P. Davies, H. Adams, and C. White.[1] Department of Chemistry, The University Sheffield S3 7HF, England.

[1]Corresponding author (telephone: +44 (0)114-222-9310; fax: +44 (0)114-273-8673; e-mail: Colin.white@sheffield.ac.uk).

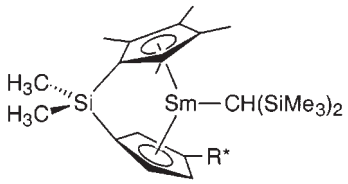
 DOI: 10.1139/cjc-79-5/6-731 © 2001 NRC Canada

Mots clés : titane, métallocène, chiral, structure, catalyseur.

[Traduit par la Rédaction]

Introduction

Chiral metallocenes have attracted considerable attention in the last decade (1) fueled by their spectacular successes in catalyzing stereoselectively a wide range of organic transformations (2), including the stereospecific polymerization of α-olefins (3). We were particularly impressed by the report of Marks and co-workers (4) that lanthanide complexes, containing a chiral ansa-bis(cyclopentadienyl)[2] ligand (**1**), cata-



1 (R* = menthyl or neomenthyl)

lyzed the hydrogenation of nonfunctionalized alkenes in up to 96% enantiomeric excess (ee). To put this in context, the best result that we know of for the hydrogenation of a nonfunctionalized alkene using a rhodium(I)–chiral bis(phosphine) catalyst is 48% ee (5), and results of 0–20% ee are typical even with well-known phosphines such as Diop (6) and Binap (7). Organolanthanide complexes are, however, notoriously moisture-sensitive, and synthesizing and handling them requires special techniques. We, therefore, wondered if the chiral ansa-bis(cyclopentadienyl) ligand developed by Marks and co-workers (4), and related ligands, could be complexed to less moisture-sensitive transition metals and still give impressive results in enantioselective synthesis. We report herein our studies involving the syntheses of the corresponding titanium complexes. Our choice of titanium was influenced by the fact that two other research groups had reported impressive results for the hydrogenation of nonfunctionalized alkenes using titanocene systems, but with C_2-symmetric chiral ligands (8). We should also point out that, after the start of this work, hydrogenation of nonfunctionalized alkenes with ee's of up to 98% were reported using an iridium – chiral phosphanodihydrooxazole system (9) and also using a cationic zirconocene catalyst (10).

Results and discussion

Ligand syntheses

The ansa-cyclopentadiene ligands consisting of a 2,3,4,5-tetramethylcyclopentadienyl ring linked via a dimethylsilyl bridge to a menthyl- (**2a)** or neomenthyl- (**2b**) cyclopentadienyl moiety were synthesized by a modification of the procedure reported by Marks and co-workers (4) (Scheme 1). In our experience, the key to successful synthesis of these ligands is to use freshly prepared 1-(chlorodimethylsilyl)-2,3,4,5-tetramethylcyclopentadiene; if this is not possible then this reagent should be distilled immediately before use. The corresponding indenyl analogue (**3**) was synthesized using similar procedures (Scheme 1).

Metal complexes

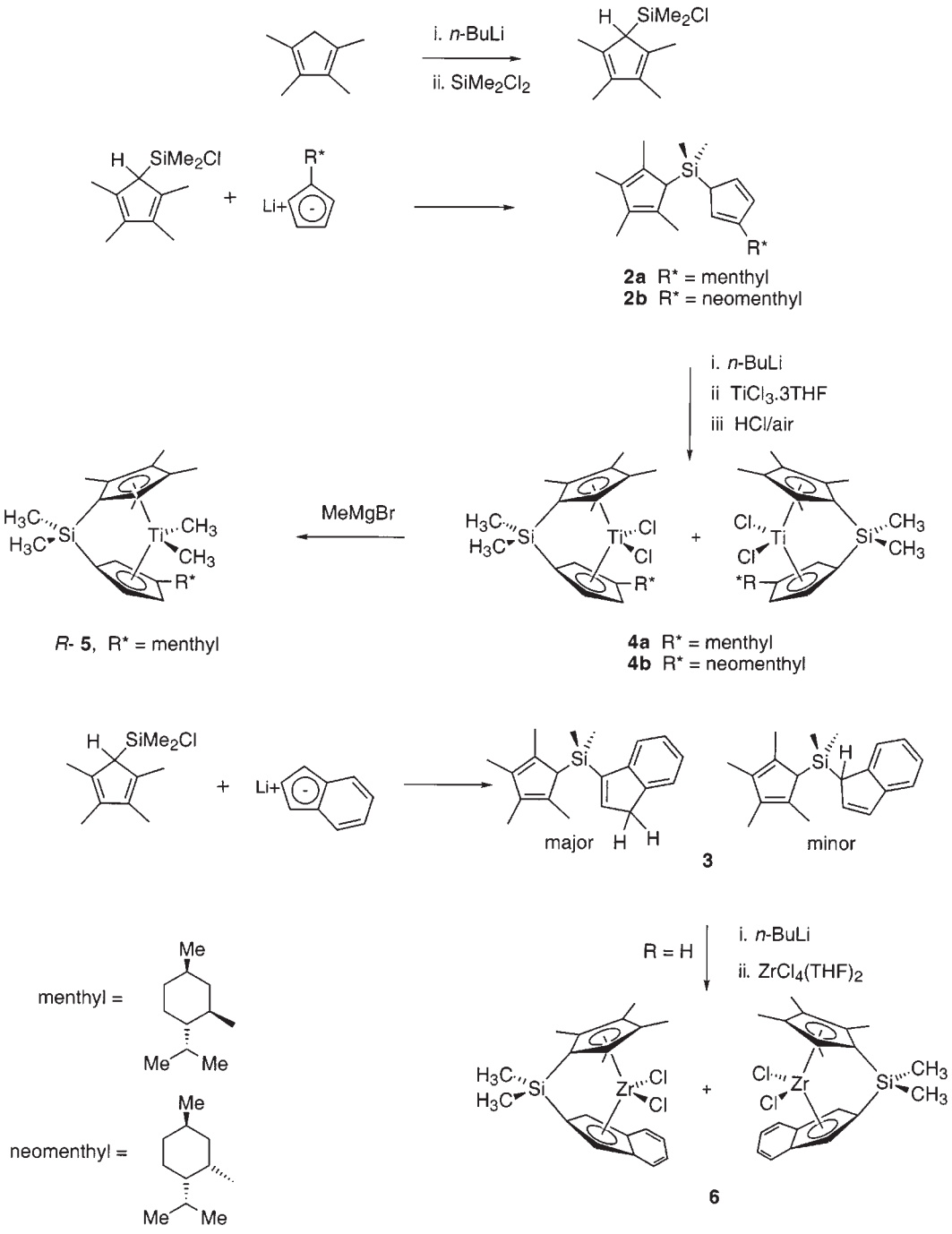
Complexation of ligands **2a** and **2b** to titanium was carried out as shown in Scheme 1. The dilithium salt of the appropriate ligand precursor was formed via double deprotonation with two equiv of *n*-butyllithium in THF and was then reacted in situ with one equiv of $TiCl_3 \cdot 3THF$ in refluxing THF for 12 h. The resulting Ti(III) complex was then oxidized to the desired Ti(IV) complex by stirring with concentrated hydrochloric acid, open to the air, and worked up, followed by removal of solvent to give the crude products **4a** and **4b** as red solids. The ligands **2a** and **2b** are chiral by virtue of the menthyl or neomenthyl substituent, but in addition, the two faces of the asymmetrically substituted cyclopentadiene ring are different and, therefore, complexation to titanium introduces an element of planar chirality into the system. Hence, the titanium complexes **4a** and **4b** are obtained as a mixture of diastereoisomers. This is readily apparent from the ^{1}H NMR spectra; the asymmetry of the complex renders all four methyl groups on the tetramethyl-substituted cyclopentadienyl ring chemically inequivalent and the four methyl signals corresponding to each diastereoisomer are readily assigned from their relative intensity. Thus, the diastereoisomeric ratio can be easily measured via integration of a major and its corresponding minor peak. In this way the diastereoisomeric ratios were found to be 3.0:1 for **4a** and 1.3:1 for **4b**, i.e., 75 and 57% diastereoselectivities, respectively. In contrast, Marks and co-workers (4) found that both these ligands complexed to lanthanides with much higher diastereoselection (>80%) under similar reaction conditions. In both cases ligand complexation takes place to the metal in the +3 oxidation state, and we had expected that complexation to the smaller titanium atom would have led to an increase in the diastereoselection compared to that observed for the lanthanides. We can only presume that as a result of solvent coordination the lanthanides are more sterically congested and hence more stereo-differentiating.

In the case of the menthyl derivative **4a**, which was formed in a diastereomeric ratio of 3:1, cooling a hexane solution to –60°C resulted in the selective crystallization of the major isomer, presumed to be the kinetically favoured isomer. By X-ray crystallography (see below) we were able to show that this was the $\mathbf{4a}_{\boldsymbol{R}}$ diastereomer where the *R* chiral descriptor refers to the planar chirality of the asymmetric cyclopentadienyl ring. There are several reports of photo-induced racemate–meso interconversions of group IV ansa-metallocene dichlorides, which it is generally agreed, proceed via photolytic homolytic cleavage of a Ti-(η^5-cyclopentadienyl) bond, rotation of the cyclopentadienyl radical about the linking-Cp bond, and recombination of the Ti(III) centre with the opposite face of the cyclopentadienyl

[2] Prefix ansa Latin for bent handle, attached at both ends.

© 2001 NRC Canada

Scheme 1.



ligand (11). We were, therefore, interested to see the effect of photolysis upon these chiral titanium complexes. Photolyzing the mother liquor left from the recrystallization of the $\mathbf{4a}_{R}$ diastereomer, which now consisted of an approximately equal mixture of diastereomers, with UV radiation at –30°C slowly led to a change in this isomeric ratio with preferential formation of the most thermodynamically stable product, i.e., the $\mathbf{4a}_{S}$ diastereomer, which was initially the minor isomer. Thus, after irradiating for 1 week, the solution contained a 1:3 ratio of $\mathbf{4a}_{R}$:$\mathbf{4a}_{S}$, and upon cooling to –60°C the $\mathbf{4a}_{S}$ diastereomer selectively crystallized out. Hence, both diastereomers could be obtained and the crystal structures of both were determined.

In contrast, the separation of the two diastereoisomers of the neomenthyl complex **4b** by recrystallization was not possible because of the high solubility of both diastereoisomers in hydrocarbon solvents. For example, no crystals were formed even after cooling a hot, saturated hexane solution of **4b** to –30°C for a number of days. Attempts to significantly increase the diastereomeric ratio by UV irradiation were also unsuccessful. Thus, the initial diastereomeric ratio of 1.3:1 changed to only 1:1.4 after UV irradiation for 1 week at

© 2001 NRC Canada

–30°C. Further irradiation had no effect upon this ratio. Crystallization from pentane was attempted, but no single diastereoisomer was isolated by this method.

The use of silanized silica as a stationary phase in liquid chromatography has proved successful for the purification of ansa-bis(η^5-cyclopentadienyl)dichlorotitanium complexes (12). Therefore, silica gel was modified via treatment with chlorotrimethylsilane (see *Experimental*), and the resulting silanized silica gel was used as a stationary phase for the attempted separation of the two diastereoisomers of **4b**. Unfortunately, no separation of the two diastereoisomers occurred, although there were no visible signs of decomposition either. Attempts to separate the diastereoisomers by converting the dichloride complex into a less soluble derivative by reaction with either 1,2-benzenedimethanol or (*R*)-(–)-acetylmandelic acid failed to yield stable characterizable products.

From the diastereoselectivity observed in the initial formation of the titanium complexes it is clear that the difference in free energy between the two menthyl diastereomers is greater than the difference in free energy between the two neomenthyl diastereomers. The initial diastereomeric ratio is determined by kinetic control but under UV irradiation the diastereomers are in equilibrium and the ratio is determined by their relative thermodynamic stabilities. Hence, it is possible to estimate the difference in free energy between the two diastereoisomers of the menthyl substituted complex (**4a**$_R$ and **4a**$_S$) at –30°C as 2.2 kJ mol^{-1} and that of the neomenthyl diastereomers as 0.7 kJ mol^{-1}.

The NMR spectra of the titanium complexes **4a** and **4b** are worthy of comment; the three cyclopentadienyl protons are grouped together in a similar manner in both diastereoisomers of both catalysts with one proton exhibiting a greater degree of deshielding than the other two protons adjacent to the silicon bridge. This proton sits directly over one of the chloride ligands, and the magnetic anisotropy of the halogen atom has been ascribed as the origin of the low-field shift of such protons (13).

The optically pure dichloro-complex **4a**$_R$ was reacted with methylmagnesium bromide to give the corresponding (*R*)-$TiMe_2(\eta^5{:}\eta^5\text{-}C_5Me_4SiMe_2C_5H_3R^*)$ (R^* = menthyl) (**5**$_R$). We were surprised and disappointed to find that this compound was rather unstable, like the corresponding $Ti(C_5H_5)_2Me_2$ (14), as compared to the more robust $Ti\{(C_5H_4)_2SiMe_2\}Me_2$ (15). Similarly, although synthesis of the related indenyl ligand system $C_5HMe_4SiMe_2C_9H_7$ (**3**) proved to be relatively straightforward, complexation of this ligand was not. The reaction of $TiCl_3{\cdot}3THF$ with the dilithium salt of **3** using similar reaction conditions as those successfully used for the syntheses of the titanium complexes **4a** and **4b** repeatedly failed to yield $TiCl_2(\eta^5{:}\eta^5\text{-}C_5Me_4SiMe_2C_9H_7)$. Titanium indenyl complexes are notoriously difficult to synthesize or are unstable and, therefore, these are often prepared and reduced in situ to the corresponding more stable tetrahydroindenyl titanium complexes using hydrogen in the presence of a PtO_2 catalyst (12*a*, 16); unfortunately, even this strategy failed to yield a stable complex. More successful was the synthesis of the corresponding zirconium indenyl complex $ZrCl_2(\eta^5{:}\eta^5\text{-}C_5Me_4SiMe_2C_9H_6)$ (**6**), although this too proved to be unstable in solution.

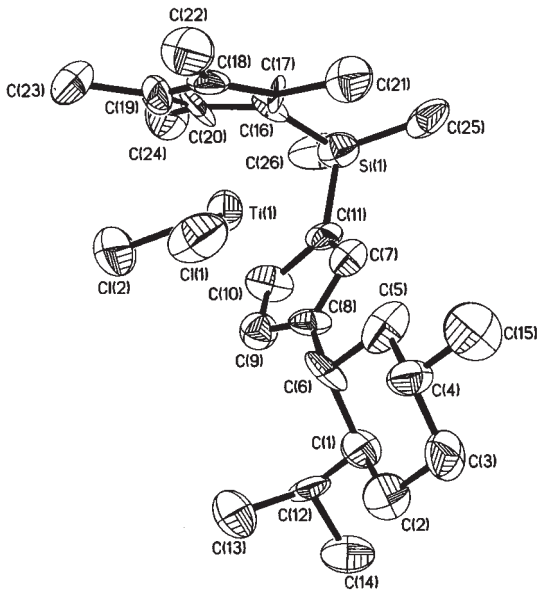


Fig. 1. Molecular structure of $TiCl_2\{\eta^5{:}\eta^5\text{-}C_5Me_4SiMe_2C_5H_3(menthyl)\}$, (*R*)-diastereoisomer **4a**$_R$. Hydrogen atoms are omitted for clarity.

Comparison of the X-ray crystal structures of the diastereoisomers 4a$_R$ and 4a$_S$

Crystallographic data are presented in Table 1 and atomic cooordinates are listed in Table 2.[3] The crystal stucture of the menthyl complex with *R* planar chirality (**4a**$_R$) is shown in Fig. 1; the corresponding diastereoisomer with *S* planar chirality crystallized as two independent molecules per unit cell and these are shown as **4a**$_S$ and **4a**$_{S'}$ in Figs. 2*a* and *b*, respectively. As expected, the bond distances in all the diastereoisomers are essentially similar taking into account that the face of the menthyl-Cp is reversed on going from **4a**$_R$ to **4a**$_S$ and **4a**$_{S'}$ (Table 3). In all the structures each cyclopentadienyl ring is asymmetrically pentahapto bonded to the titanium (Ti—C in the range 2.35–2.59 Å), with the greater asymmetry for the menthylated ring in which the menthylated carbon C(8) is always more distant from the titanium than any other ring carbon. All these Ti—C distances are within the range reported for similar titanium complexes (17). In each complex both five-membered rings are planar with the four methyl groups of the tetramethylcyclopentadienyl ring bent away from the titanium by up to 0.24 Å from the mean plane of the cyclopentadienyl ring. A consequence of the short bridging unit and the bulky menthyl substituent is that the angle between the planes of the two Cp rings (i.e., the bite angle) is relatively large at 58.0 and 59.2° for **4a**$_R$ and **4a**$_S$, respectively, (Table 4) compared to

[3] Supplementary material may be purchased from the Depository of Unpublished Data, Document Delivery, CISTI, National Research Council Canada, Ottawa, ON K1A 0S2, Canada. For information on obtaining material electronically go to http://www.nrc.ca/cisti/irm/unpub_e.shtml. Crystallographic information has been deposited with the Cambridge Crystallographic Data Centre. Copies of the data can be obtained, free of charge, on application to the Director, CCDC, 12 Union Road, Cambridge CB2 1EZ, U.K. (fax: 44-1223-336033 or e-mail: deposit@ccdc.cam.ac.uk).

© 2001 NRC Canada

Table 1. Crystallographic data for diffraction studies of **4a$_R$** and **4a$_S$**.

	4a$_R$	**4a$_S$**
Crystal parameters		
Empirical formula	$C_{26}H_{40}Cl_2SiTi$	$C_{26}H_{40}Cl_2SiTi$
Formula weight	499.49	499.49
Color	Red	Red
Solvent	*n*-Pentane	*n*-Pentane
Crystal size (mm)	0.80 × 0.20 × 0.05	0.07 × 0.04 × 0.03
Habit	Elongated thin plates	Red plates
Crystal system	Orthorhombic	Monoclinic
Space group	$P2_12_12_1$ (D_4^2, No. 19)	$P2_1$ (C_2^2, No. 4)
a (Å)	27.857(11)	8.5810(10)
b (Å)	9.985(5)	38.679(4)
c (Å)	9.596(4)	8.5842(10)
β (°)		113.001(2)
V (Å^3)	2669.1(18)	2622.6(5)
Z	4	4
D_{calcd} (Mg m^{-3})	1.243	1.265
μ (cm^{-1})	5.73	5.87
F(000)	1064	1064
Intensity data		
Diffractometer	Stoe Stadi-2 2-circle	Nicolet R3 4-circle
λ (Mo Kα radiation) (Å)	0.71073	0.71073
Monochromator	Graphite, incident beam	Graphite, incident beam
Reflections measured	$+h, +k, \pm l$	$+h, +k, \pm l$
2θ range (°)	6.5–50	2.11–23.32
Temperature (K)	293	150(2)
Scan type	ω	ω
Standard reflections	2 every 50 reflections	3 every 100 reflections
No. of reflections collected	2701	11784
No. of reflections used	902	5734
Acceptance criterion	$\|F\|/\sigma(\|F\|) > 3.0$	$\|F\|/\sigma(\|F\|) > 4.0$
Absorption coefficient (mm^{-1})	0.573	0.587
Transmissionn coefficient (min)	0.882	0.9601
Transmissn coefficient (max)	0.972	0.9826
Absorption correction	Gaussian integration	Semi-empirical
Structure solution		
Method	Patterson–Fourier	Patterson–Fourier
Programs	SHELXTL (25)	SHELXTL (25)
Scattering factors	Ref. 26	Ref. 26
Refinement method	Blocked-cascade least-squares	Full-matrix least-squares on F^2
R	0.0628	0.0646
wR_2		0.1829
R_ω	0.0503 (266 parameters)	
Weighting scheme	$\omega^{-1} = [\sigma^2(F) + 0.00021(F)^2]$	$\omega^{-1} = [\sigma^2(F_0^2) + (0.1148P)^2 + 0.3205P]$
Absolute structure parameter		0.00(5)
Largest diff. peak and hole (e Å^{-3})	+0.30 and −0.37	+0.494 and −0.536
H refinement	Riding mode	Riding mode

other ansa-dichlorotitanocenes; for example, $[TiCl_2\{(\eta^5{:}\eta^5\text{-}C_5H_4)_2SiMe_2\}]$ has a bite angle of 56.2° (17a).

The Cl(1)-Ti-C(11) and Cl(1)-Ti-C(16) bond angles are 131(4) and 131.1(3)°, respectively, for **4a$_R$**, whereas the coresponding angles for **4a$_S$** are 124.1(2) and 123.11(19)°, showing the different relative orientations of the ligands about the titanium. However, the differences between the two diastereoisomers are best viewed by comparison of the space-filling models (Fig. 3). With the bulky C_5Me_5 ligand occupying the top face of the complex it can be seen that the bottom face of **4a$_R$** is more sterically crowded because the *i*-Pr group of the menthyl substituent points across this face, whereas in **4a$_S$** the menthyl group is orientated such that the *i*-Pr group points away from this face. This steric crowding presumably accounts for the smaller Cl-Ti-Cl bond angle of 95.3(2)° found in **4a$_R$** compared to that of 97.75(8)° found in **4a$_S$**. If the structures of the diastereoisomers are similar in solution this would imply that the diastereoisomer **4a$_R$**

© 2001 NRC Canada

Table 2. Atomic coordinates (1 x 10^4) and equivalent isotropic displacement parameters (U_{eq}) (1 x 10^3) for the two diastereoisomers of [$TiCl_2(\eta^5:\eta^5$-$C_5Me_4SiMe_2C_5H_3$(menthyl)].

Atom	*x*	*y*	*z*	U_{eq} (Å^2)
4a$_R$				
Ti(1)	3419(1)	3009(3)	4031(3)	53(1)*
Cl(1)	3908(2)	1180(4)	4427(5)	92(2)*
Cl(2)	2932(2)	1940(6)	2376(4)	113(2)*
Si(1)	3200(1)	6117(5)	4854(4)	55(2)*
C(1)	5008	3654(15)	1535(11)	54(6)*
C(2)	5498	3008(17)	1617(15)	66(7)*
C(3)	5746	3136(18)	3004(15)	64(7)*
C(4)	5455	2532(14)	4157(14)	53(7)*
C(5)	4955	3225(16)	4182(15)	70(7)*
C(6)	4689	3053(15)	2756(13)	48(5)*
C(7)	4054	4672(14)	3928(16)	42(6)*
C(8)	4207	3773(16)	2851(14)	44(6)*
C(9)	3814	3754(14)	1921(13)	52(4)
C(10)	3467	4674(14)	2303(13)	57(6)*
C(11)	3604	5277(14)	3590(13)	46(6)*
C(12)	4767	3519(12)	135(12)	53(6)*
C(13)	4680(5)	2087(14)	–352(12)	68(6)*
C(14)	5060(4)	4259(14)	–976(13)	67(7)*
C(15)	5701(4)	2694(15)	5549(12)	82(8)*
C(16)	3016(4)	4455(13)	5595(12)	39(5)*
C(17)	3327(4)	3600(15)	6376(14)	39(6)*
C(18)	3153(6)	2341(15)	6397(14)	48(6)*
C(19)	2739(5)	2308(14)	5508(15)	58(7)*
C(20)	2649(4)	3617(15)	5083(13)	62(6)*
C(21)	3740(5)	4040(13)	7288(14)	68(7)*
C(22)	3335(6)	1159(13)	7299(13)	84(7)*
C(23)	2415(5)	1045(15)	5306(16)	106(9)*
C(24)	2224(4)	4044(17)	4236(15)	88(8)*
C(25)	3512(4)	7278(13)	6011(15)	77(7)*
C(26)	2723(5)	7099(16)	4014(14)	89(7)*
4a$_S$				
Ti(1)	2610(1)	3540(1)	1003(1)	32(1)
Ti(1A)	1003(1)	398(1)	2610(1)	31(1)
Si(1)	–864(2)	3538(1)	–2404(2)	41(1)
Si(1A)	–2409(2)	401(1)	–866(2)	40(1)
Cl(1)	3090(3)	3568(1)	3851(2)	48(1)
Cl(1A)	3853(2)	370(1)	3082(2)	48(1)
Cl(2)	5432(2)	3511(1)	1308(2)	51(1)
Cl(2A)	1311(2)	426(1)	5433(2)	51(1)
C(1)	1476(13)	2413(3)	3246(13)	71(3)
C(2)	1848(14)	2306(5)	5067(16)	114(6)
C(3)	3785(16)	2274(5)	6124(16)	112(5)
C(4)	4743(15)	2594(3)	6109(12)	75(3)
C(5)	4280(10)	2720(3)	4279(11)	54(2)
C(6)	2408(11)	2769(2)	3333(11)	50(2)
C(7)	517(10)	3117(2)	656(9)	39(2)
C(8)	1992(9)	2924(2)	1585(9)	39(2)
C(9)	2964(10)	2912(2)	620(10)	42(2)
C(10)	2068(10)	3082(2)	–950(9)	41(2)
C(11)	482(9)	3196(2)	–998(9)	39(2)
C(12)	–399(12)	2399(3)	2089(14)	76(3)
C(13)	–1511(14)	2602(4)	2782(17)	101(5)
C(14)	–1011(17)	2023(5)	1700(20)	124(6)
C(15)	6647(13)	2538(3)	7040(13)	75(3)
C(16)	562(8)	3884(2)	–1089(8)	35(2)
C(17)	603(8)	3993(2)	540(8)	33(2)
C(18)	2167(9)	4167(2)	1437(9)	35(2)
C(19)	3139(9)	4156(2)	418(8)	35(2)
C(20)	2176(9)	3979(2)	–1085(8)	36(2)
C(21)	–766(9)	3967(2)	1194(9)	40(2)
C(22)	2652(10)	4362(2)	3067(9)	47(2)
C(23)	4776(9)	4333(3)	852(10)	52(2)
C(24)	2762(10)	3929(3)	–2523(8)	55(3)
C(25)	–967(12)	3492(3)	–4605(11)	68(3)
C(26)	–3064(9)	3541(3)	–2472(11)	55(2)
C(1A)	3246(14)	1527(3)	1498(12)	74(3)
C(2A)	5067(15)	1631(5)	1859(14)	111(6)
C(3A)	6121(16)	1665(5)	3752(15)	114(6)
C(4A)	6078(13)	1335(3)	4747(14)	76(3)
C(5A)	4279(10)	1215(2)	4297(9)	50(2)
C(6A)	3292(12)	1168(3)	2392(10)	55(2)
C(7A)	651(9)	822(2)	503(9)	37(2)
C(8A)	1600(10)	1014(2)	2000(9)	41(2)
C(9A)	610(10)	1023(2)	2980(10)	43(2)
C(10A)	–947(10)	854(2)	2066(9)	43(2)
C(11A)	–990(9)	741(2)	469(9)	40(2)
C(12A)	2086(15)	1538(3)	–379(11)	74(3)
C(13A)	2710(17)	1338(4)	–1521(13)	108(5)
C(14A)	1690(20)	1917(5)	–1034(16)	125(6)
C(15A)	7045(14)	1394(3)	6664(13)	80(3)
C(16A)	–1075(9)	52(2)	564(8)	37(2)
C(17A)	–1092(9)	–40(2)	2184(9)	40(2)
C(18A)	409(10)	–216(2)	3102(8)	36(2)
C(19A)	1424(9)	–230(2)	2159(9)	35(2)
C(20A)	534(9)	–61(2)	600(8)	33(2)
C(21A)	–2517(10)	13(3)	2773(10)	53(2)
C(22A)	824(11)	–391(3)	4798(10)	54(2)
C(23A)	3032(10)	–426(2)	2666(11)	50(2)
C(24A)	1214(10)	–30(2)	–774(9)	42(2)
C(25A)	–4631(10)	436(3)	–971(12)	67(3)
C(26A)	–2454(11)	396(3)	–3057(9)	56(2)

[a] U_{eq} is defined as one third of the trace of the orthogonalized U_{ij} tensor.

should be a more stereoselective catalyst. Preliminary results from hydrosilylation experiments (Table 5) are in keeping with this statement (18).

Experimental

All reactions of moisture sensitive reagents were performed under nitrogen. THF was heated under reflux over sodium benzophenone ketyl and distilled under nitrogen. Hexane, toluene, and diethyl ether were heated under reflux over sodium and freshly distilled under nitrogen prior to use.

Menthyltosylate [(1*R*, 2*S*, 5*R*)-(–)-2-isopropyl-5-methylcyclohexyl tosylate] and neomenthyltosylate [(1*S*, 2*S*, 5*R*)-(+)-2-isopropyl-5-methylcyclohexyl tosylate] were prepared by modifications of the literature procedures (19, 20) as we have previously described (21). (+)-Neomenthyl tosylate is thermally unstable, therefore, it is best stored at –10°C.

© 2001 NRC Canada

Table 3. Selected bond lengths (Å) with estimated standard deviations for the two diastereoisomers of [$TiCl_2(\eta^5{:}\eta^5$-$C_5Me_4SiMe_2C_5H_3$(menthyl)].

	$4a_R$	$4a_S$	$4a_{S'}$
Ti(1)—Cl(1)	2.310(5)	2.3171(18)	2.3201(19)
Ti(1)—Cl(2)	2.346(5)	2.3349(19)	2.3352(17)
Ti(1)—C(7)	2.428(14)	2.359(8)	2.347(8)
Ti(1)—C(8)	2.585(14)	2.530(9)	2.535(9)
Ti(1)—C(9)	2.421(13)	2.484(8)	2.477(9)
Ti(1)—C(10)	2.352(13)	2.358(7)	2.370(8)
Ti(1)—C(11)	2.360(14)	2.366(7)	2.367(7)
Ti(1)—C(16)	2.366(12)	2.370(7)	2.367(7)
Ti(1)—C(17)	2.340(14)	2.381(7)	2.391(8)
Ti(1)—C(18)	2.479(14)	2.508(8)	2.500(8)
Ti(1)—C(19)	2.468(14)	2.516(8)	2.509(8)
Ti(1)—C(20)	2.448(13)	2.392(7)	2.398(7)
Si(1)—C(11)	1.855(14)	1.856(8)	1.852(9)
Si(1)—C(16)	1.877(14)	1.866(9)	1.882(8)
C(7)—C(8)	1.434(21)	1.416(11)	1.433(11)
C(7)—C(11)	1.431(19)	1.441(10)	1.432(11)
C(8)—C(9)	1.413(19)	1.387(11)	1.410(11)
C(9)—C(10)	1.383(19)	1.424(11)	1.418(11)
C(10)—C(11)	1.426(18)	1.417(11)	1.425(10)
C(16)—C(17)	1.430(18)	1.448(10)	1.441(10)
C(16)—C(20)	1.409(18)	1.432(10)	1.437(11)
C(17)—C(18)	1.347(22)	1.428(11)	1.397(11)
C(18)—C(19)	1.435(21)	1.426(10)	1.402(10)
C(19)—C(20)	1.393(20)	1.409(11)	1.416(11)

Trichlorotris(tetrahydrofuran)titanium was synthesized by the procedure reported by Manzer (22).

Preparation of silanized silica gel

Dichloromethane (1500 cm^3) was added to silica gel (150 g) and the resulting slurry rapidly stirred by an overhead stirrer. Chlorotrimethylsilane (150 cm^3) was added and the slurry stirred for a further 1 h. The slurry was washed with saturated sodium hydrogencarbonate solution (100 cm^3) and then with water until the washings were neutral. The resulting silanized silica gel was washed with acetone and dried in an oven at 100°C overnight.

Menthylcyclopentadiene

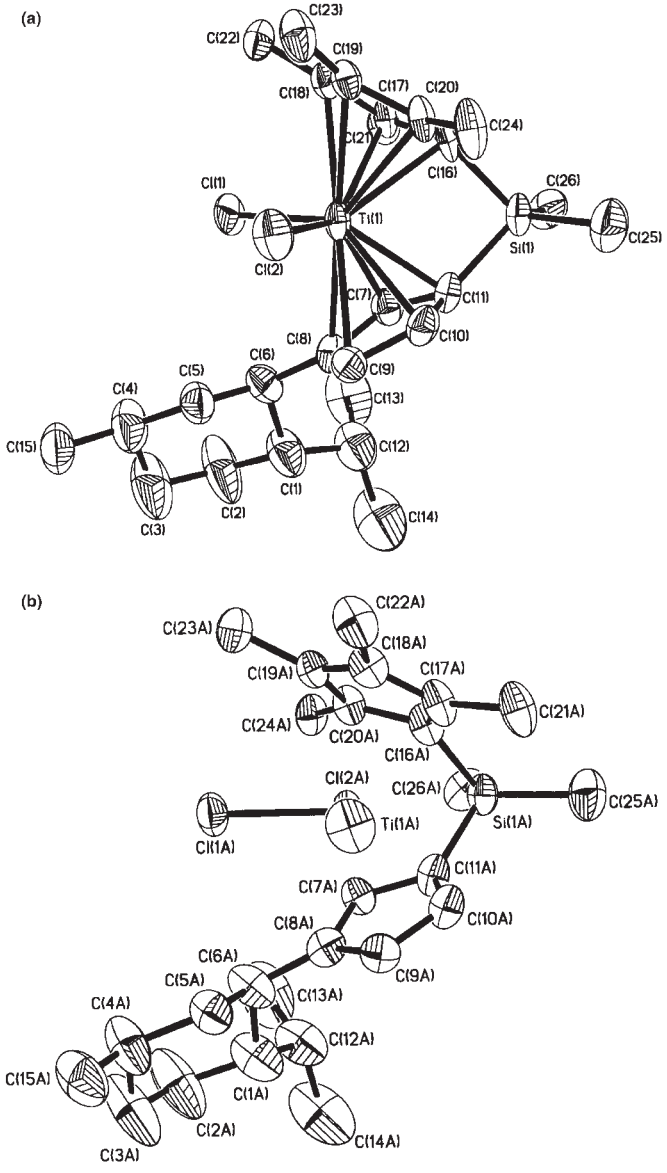
This was prepared by the following modification of the literature procedure (23). NaH (9.6 g, 0.4 mol, i.e., 19.2 g 50% dispersion) was washed with hexane, and freshly distilled THF (150 cm^3) was added. Freshly cracked cyclopentadiene (26 g, 0.4 mol) in THF (50 cm^3) was added slowly over a 2 h period and the mixture stirred until the bubbling stopped and the NaH was consumed (approximately 30 min). The resulting pale red solution of sodium cyclopentadienide was added to a solution of (1*S*, 2*S*, 5*R*)-5-methyl-2-(2-propyl)-cyclohexyl tosylate (63.4 g, 0.2 mol) in THF (200 cm^3) at 0°C via cannula. This mixture was heated under reflux for 6 h producing a sodium tosylate precipitate. Then the mixture was cooled, filtered, and the solvent removed in vacuo. The brown viscous residue was redissolved in diethyl ether and washed with water (5 × 100 cm^3). After drying the organic layer over Na_2SO_4, the solvent was

Table 4. Bond angles (°) with estimated standard deviations for the two diastereoisomers of [$TiCl_2(\eta^5{:}\eta^5$-$C_5Me_4SiMe_2C_5H_3$(menthyl)].

	$4a_R$	$4a_S$	$4a_{S'}$
Cl(1)-Ti(1)-C1(2)	95.3(2)	97.75(8)	97.86(8)
Cl(1)-Ti(1)-C(8)	78.7(4)	78.52(18)	78.26(19)
Cl(2)-Ti(1)-C(8)	109.2(3)	102.76(19)	102.77(17)
Cl(1)-Ti(1)-C(11)	131.3(4)	124.1(2)	123.7(2)
Cl(2)-Ti(1)-C(11)	116.2(4)	121.8(2)	122.3(2)
Cl(1)-Ti(1)-C(16)	131.1(3)	123.11(19)	122.64(19)
Cl(2)-Ti(1)-C(16)	115.6(3)	122.77(18)	122.89(18)
C(11)-Ti(1)-C(16)	68.4(4)	68.4(3)	68.5(3)
C(11)-Si(1)-C(16)	90.8(6)	91.3(3)	91.1(3)
C(6)-C(8)-C(7)	126.8(12)	125.2(7)	125.2(7)
C(6)-C(8)-C(9)	129.7(12)	127.6(7)	128.3(7)

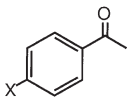
Symmetry transformations used to generate equivalent atoms:

Fig. 2. Molecular structure of the two independent molecules of $TiCl_2\{\eta^5{:}\eta^5$-$C_5Me_4SiMe_2C_5H_3$(menthyl)}, (*S*)-diastereoisomer $\mathbf{4a_S}$. Hydrogen atoms are omitted for clarity.



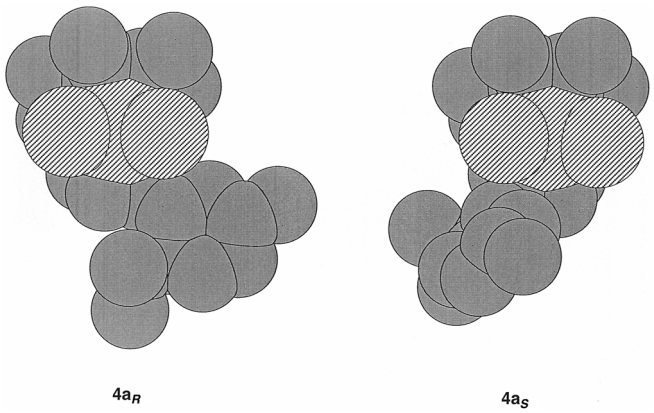
© 2001 NRC Canada

Table 5. Catalytic hydrosilylations of ketones in toluene.

Substrate		Catalyst $\mathbf{4a}_R$		Catalyst $\mathbf{4a}_S$	
	Temperature (°C)	Conversion (%)	ee (%)[a]	Conversion (%)	ee (%)[a]
X = H	25	100[b]	82 (*S*)	100[b]	16 (*R*)
X = F	65	100[c]	66 (*S*)	38[c]	12 (*R*)
X = OMe	65	100[c]	65 (*S*)	100[c]	23 (*R*)

[a]Absolute configurations of the product alcohols are shown in parentheses.
[b]After 24 h.
[c]After 1 h.

Fig. 3. The structures of the two diastereoisomers $\mathbf{4a}_R$ and $\mathbf{4a}_S$ compared.



removed in vacuo to yield a brown oil which was distilled[4] to yield the product as a colourless liquid ($bp_{0.1}$ 70°C, 23.84 g, 58%). ^{1}H NMR (250 MHz, $CDCl_3$) δ: 0.71 (d, $^3J_{H,H}$ = 6 Hz, 3H, CH_3), 0.84 (d, $^3J_{H,H}$ = 6 Hz, 3H, CH_3), 0.88 (d, $^3J_{H,H}$ = 6 Hz, 3H, CH_3), 0.95–1.84 (m, 9H, CH_2's and CH's), 2.31–2.48 (m, 1H, CH), 2.83–2.98 (m, 2H, allylic), 5.97–6.54 (m, 3H, vinylic). 95% pure by GC.

Preparation of neomenthylcyclopentadiene

An analagous procedure to that employed for the preparation of menthylcyclopentadiene but using menthyltosylate yielded the title product as a colourless liquid ($bp_{0.01}$ 70°C, 42%, 95% pure by GC). ^{1}H NMR (250 MHz, $CDCl_3$) δ: 0.79–0.90 (m, 9H, CH_3), 0.90–1.86 (m, 9H, CH_2's and CH's), 2.90–3.12 (m, 3H, CH and allylic), 6.08–6.58 (m, 3H, vinylic).

Preparation of 1,2,3,4-tetramethylcyclopentadiene

The synthesis was based on the method reported by Marks and co-workers (4). 2,3,4,5-Tetramethylcyclopent-2-enone (24) (18.8 g, 0.13 mol) in diethyl ether (50 cm^3) was added over 1 h to a suspension of lithium aluminium hydride (2.5 g, 0.07 mol) in diethyl ether (200 cm^3) and the mixture was stirred for 2 h. Aqueous hydrochloric acid (1.0 M, 300 cm^3) was added slowly and the mixture stirred for 16 h in air. The organic layer was separated and the aqueous layer washed with diethyl ether (3 × 100 cm^3). Both organic layers were combined, washed with a saturated sodium carbonate solution (2 × 50 cm^3), and dried over Na_2SO_4. Removal of the solvent in vacuo gave a yellow liquid that was distilled to produce the title product as colourless liquid (30–35°C, 0.5 mm Hg, 6.59 g, 37%). (EI) GC–MS *m*/*z* (%): 122 (M^+, 60). ^{1}H NMR (250 MHz, $CDCl_3$) δ: 1.80 (br s, 6H, $2CH_3$), 1.95 (br s, 6H, $2CH_3$), 2.75 (br s, 2H, $C_5Me_4H_2$).

Preparation of 1-(chlorodimethylsilyl)-2,3,4,5-tetramethylcyclopentadiene

The literature procedure (4) was modified as follows. 1,2,3,4-Tetramethylcyclopentadiene (6 g, 0.05 mol) was dissolved in dry petroleum ether (bp 40–60°C) and a solution of *n*-butyllithium (2.5 M, 20 cm^3, 0.05 mol) was added at 0°C over 1 h. The mixture was stirred for 15 h at room temp to produce a milky white suspension which was thinned by the addition of THF (45 cm^3). A solution of dichlorodimethylsilane (9.7 g, 0.075 mol) in THF (30 cm^3) was added at 0°C over 1 h and the mixture stirred for 15 h. The yellow solution was filtered under nitrogen through Celite previously dried at 100°C under vacuum to remove the lithium chloride precipitate. The solvent was removed in vacuo to give the crude product as a yellow-brown oil which was distilled to give the title product as a yellow-green liquid; $bp_{0.1}$ 60–65°C (lit. $bp_{0.1}$ 56–60°C), 7.05 g (67%). EI-MS *m*/*z* (%): 214 (M^+, 60), 121 ([M – $SiMe_2Cl$]$^+$), 97, 106 ([M – $SiMe_2Cl$ –Me]$^+$), 100). IR (neat) cm^{-1}: 2961s, 2916s, 2861s, 1445m, 1380m, 1258s, 1058br, 844s, 811br, 656m. ^{1}H NMR (250 MHz, $CDCl_3$) δ: 0.30 (s, 6H, 2Si-CH_3), 1.9 (s, 6H, $2CH_3$), 2.06 (s, 6H, $2CH_3$) 3.06 (br s, 1H, Cp-H).

Preparation of 1-(2,3,4,5)-tetramethylcyclopentadiene)-1′-(3′(-1*R*, 2*S*, 5*R*)-5-methyl-2-(2-propyl)-cyclohexylcyclopentadiene)dimethylsilane (2a)

The synthesis was based on the procedure reported by Marks and co-workers (4). A solution of lithium menthylcyclopentadienide was prepared by adding a solution of *n*-butyllithium (2.5 M, 5.6 cm^3, 0.014 mol) to a solution of (1*R*, 2*S*, 5*R*)-5-methyl-2-(2-propyl)-cyclohexylcyclopentadiene (2.81 g, 0.014 mol) in THF (50 cm^3) at 0°C and stirring the mixture for 30 min at room temp. The solution was then transferred via cannula at room temp to a solution of freshly distilled 1-(chlorodimethylsilyl)-2,3,4,5-tetramethylcyclopentadiene (3.8 g, 0.018 mol) in THF (25 cm^3). The

[4]The vacuum distillation must be performed at high vacuum since the product decomposes at higher temperatures and this is probably the main reason for the low yields. A two stage distillation and washing the condenser after the CpH–$(CpH)_2$ is distilled at 30°C is also recommended to ensure no CpH contaminates the product.

© 2001 NRC Canada

mixture was heated under reflux for 12 h, cooled to room temp, and filtered to remove the lithium chloride formed. Solvent was removed in vacuo to yield a brown residue which was redissolved in diethyl ether, washed with water (3×10 cm^3), dried over Na_2SO_4,and the solvent removed in vacuo to yield a yellow-brown oil. Excess 1-(chlorodimethylsilyl)-2,3,4,5-tetramethylcyclopentadiene was removed by distillation (heating to 80°C, 0.01 mm Hg) to yield the isomers of the desired menthyl product **2a** as a brown residue. Yield 3.55 g (67%). EI-MS *m*/*z* (%): 382 (M^+, 10), 261 ([M – TMCp]$^+$, 31), 204 ([M – TMCpSiMe$_2$]$^+$, 100). ^{1}H NMR (250 MHz, $CDCl_3$) δ:–0.35–0.10 (m, 6H, Si-CH_3), 0.62 (d, $^3J_{H,H}$ = 6 Hz, 3H, CH_3), 0.75 (d, $^3J_{H,H}$ = 6 Hz, 3H, CH_3), 0.80 (d, $^3J_{H,H}$ = 6 Hz, 3H, CH_3), 0.85–1.60 (m, 9H, CH_2's), 1.60–1.75 (m, 6H, Cp-CH_3), 1.78 (s, 3H, Cp-CH_3), 1.90 (s, 3H, Cp-CH_3), 2.29 (m, 1H, menthyl CH), 2.61–3.21 (m, 2H, allylic), 5.8–6.60 (m, 3H, Cp-H). ^{13}C NMR (63 MHz, $CDCl_3$) δ: 151.9, 150.4, 145.5, 136.1, 133.5 (Cp tertiary), 143.0, 142.0, 133.9, 138.5, 131.1, 131.0, 130.4, 127.3, 126.8, 126.6 (Cp quaternary), 47.4, 46.6, 41.9, 33.0, 27.9, 27.7, 22.6, 21.6, 15.3, 14.7, 14.2, 11.3, 11.1 (CH_3's and CH's), 43.7, 35.4, 24.5, (CH_2's), 1.0, –4.0 (Si-CH_3).

Preparation of 1-(2,3,4,5-tetramethylcyclopentadienyl)-1′-(3′-(1*S*, 2*S*, 5*R*)-5-methyl-2-(2-propylcyclohexyl-cyclopentadienyl)dimethylsilane (2b)

An analogous procedure to that employed for the preparation of 1-(2,3,4,5-tetramethylcyclopentadienyl)-1′-[3′-menthylcyclopentadienyl]dimethylsilane but employing neomenthylcyclopentadiene yielded the desired neomenthyl product **2b** as a yellow oil (70%) found to be 91% pure by GC. (EI) GC–MS *m*/*z* (%): 382 (M^+, 12), 261 ([M – TMCp]$^+$, 78), 179 ([M – nmCp]$^+$, 100). ^{1}H NMR (250 MHz, $CDCl_3$) δ:–0.05–0.33 (m, 6H, Si-CH_3), 0.90–1.11 (m, 9H, neomenthyl CH_3), 1.07–1.85 (m, 9H, CH_2's and CH's), 1.85–2.20 (m, 12H, Cp-CH_3's), 3.00–3.40 (m, 3H, allylic, neomenthyl CH), 6.15 (br s, 1H, olefinic), 6.36–6.48 (m, 1H, olefinic), 6.61–6.72 (m, 1H, olefinic). ^{13}C NMR (63 MHz, $CDCl_3$) δ: 156.5, 147.7, 147.3, 142.6, 136.1, 135.2, 133.2, 132.4, 129.0, 119.7 (Cp's), 48.0, 47.9, 37.8, 37.7 (CH's), 42.4, 35.8, 26.1 (neomenthyl CH_2's), 30.2, 26.5, 22.8, 21.4, 21.3, 14.7, 11.3 (CH_3's), 1.1, –2.6 ($SiMe_2$).

Synthesis of (*R*/*S*)-dichloro[1-(η^5-3′-(1*R*, 2*S*, 5*R*)-5-methyl-2-(2-propyl)cyclohexyl-cyclopentadienyl)-1′-(η^5-2,3,4,5-tetramethylcyclopentadienyl)dimethylsilane]titanium (4a$_{R/S}$)

1-(2,3,4,5-Tetramethylcyclopentadiene)-1′-[3′-menthylcyclopentadiene]dimethylsilane (3.02 g, 7.9 mmol) was dissolved in THF (45 cm^3). A solution of *n*-butyllithium (2.5 M, 6.3 cm^3, 15.8 mmol) in hexanes was added at 0°C and the mixture stirred at room temp for 30 min. The solution was cooled to –78°C and $TiCl_3$·3THF (2.9 g, 7.9 mmol) was added rapidly against a stream of nitrogen and the mixture was allowed to warm to room temp before heating under reflux for 6 h. After cooling to room temp, chloroform (45 cm^3) and concentrated aqueous hydrochloric acid (1 M, 30 cm^3) were added and the mixture stirred at room temp in air for 30 min. The organic layer was separated, dried, and the solvent removed in vacuo to yield a red viscous oil which was shown by ^{1}H NMR to be a 3:1 mixture of *R*:*S*.

Isolation of (*R*)-dichloro[1-(η^5-3′-(1*R*, 2*S*, 5*R*)-5-methyl-2-(2-propyl)cyclohexyl-cyclopentadienyl)-1′-(η^5-2,3,4,5-tetramethylcyclopentadienyl)dimethylsilane]titanium (4a$_R$)

The above oil was dissolved in the minimium of boiling hexane and crystallized at –30°C, to yield the title product as red crystals. Yield 0.75g (19%), mp 162–164°C. [α]^{20} (*c* 0.032, DCM): –62.5° (589 nm), –103.1° (578 nm), and –256.3° (549 nm). EI-MS *m*/*z* (%): 498 (M^+, 10%), 463 ([M – Cl]$^+$, 100). ^{1}H NMR (250 MHz, $CDCl_3$) δ: 0.66 (m, 3H, CH_3), 0.76 (m, 3H, CH_3), 0.79 (m, 3H, CH_3), 0.82 (m, 3H, CH_3), 0.83 (m, 3H, CH_3), 0.88–1.76 (m, 9H, CH's, CH_2's), 1.84 (s, 3H, Cp-CH_3), 1.87 (s, 3H, Cp-CH_3), 2.00 (s, 3H, Cp-CH_3), 2.10 (s, 3H, Cp-CH_3), 2.69–2.81 (m, 1H, CH), 5.37 (t, $^4J_{H,H}$ = 3 Hz, 1H, Cp-H), 5.67 (t, $^3J_{H,H}$ = $^4J_{H,H}$ = 3 Hz, 1H, Cp-H), 6.50 (t, $^3J_{H,H}$ $^4J_{H,H}$ = 3 Hz, 1H, Cp-H). ^{13}C NMR (63 MHz, $CDCl_3$) δ: 155.2, 145.7, 139.1, 137.4, 128.7, 103.4, 96.8 (Cp quarterary), 126.7, 122.6, 114.3 (C1, C3, C4), 48.6 (C12), 41.7, 41.2 (C6, C7), 35.2, 32.3 (C10, C8), 27.0 (C13), 24.8 (C11) 22.8, 21.8, 16.7, 16.3, 16.2, 13.8, 12.8 (TMCp CH_3's and menthyl CH_3's), 0.36, –1.5 ($SiMe_2$). Anal calcd. for $C_{26}H_{40}Cl_2SiTi$: C 62.5, H 8.1, Cl 14.2; found: C 62.4, H 8.1, Cl 14.1.

Isolation of (*S*)-dichloro[1-(η^5-3′-(1*R*, 2*S*, 5*R*)-5-methyl-2-(2-propyl)cyclohexyl-cyclopentadienyl)-1′-(η^5-2,3,4,5-tetramethylcyclopentadienyl)dimethylsilane]titanium (4a$_S$)

A 1:1 diastereomeric mixture (2 g) of (*R*)- and (*S*)-dichloro{1-[η^5-3′-(menthylcyclopentadienyl)-1′-[η^5-2,3,4,5-tetramethylcyclopentadienyl)dimethylsilane]}titanium was dissolved in toluene (200 cm^3), cooled to –30°C, and irradiated with UV light using a Hanovair medium pressure 125 W lamp. After 7 d the solvent was removed in vacuo and the mixture filtered through a silanized silica column, eluting with 4% diethyl ether in pet ether (40–60 °C), resulting in a viscous red oil (1.1 g) which was shown by ^{1}H NMR spectroscopy to contain a *S*:*R* ratio of 3:1. The red oil was dissolved in boiling pentane and cooled to –30°C; the title compound crystallized as red-brown microcrystals which were collected by suction filtration (520 mg, 26%). FAB-MS m/z (%): 498 (M^+, 24), 463 ([M – Cl]$^+$, 100). ^{1}H NMR (250 MHz, $CDCl_3$) δ: 0.70 (s, 3H, CH_3), 0.72 (m, 3H, CH_3), 0.81 (m, 3H, CH_3), 0.83 (m, 3H, CH_3), 0.86 (m, 3H, CH_3), 0.85–1.60 (m, 8H, CH's, CH_2's), 1.69 (s, 3H, Cp-CH_3), 1.83 (s, 3H, Cp-CH_3), 2.05 (s, 3H, Cp-CH_3), 2.13 (s, 3H, Cp-CH_3), 2.25–2.88 (m, 1H, CH), 2.65–2.78 (m, 1H, CH), 5.05 (t, $^4J_{H,H}$ = $^4J_{H,H}$ = 3 Hz, 1H, Cp-H), 5.47 (t, $^3J_{H,H}$ = $^4J_{H,H}$ = 3 Hz, 1H, Cp-H), 6.81 (t, $^3J_{H,H}$ = $^4J_{H,H}$ = 3 Hz, 1H, Cp-H). ^{13}C NMR (63 MHz, $CDCl_3$) δ: 148.3, 145.3, 141.6, 132.7, 127.8, 101.8, 96.5 (Cp quaternary), 134.9, 117.7, 115.0 (C1, C3, C4), 50.1 (C12), 41.8, 40.3 (C6, C7), 35.6 (C10), 32.7 (C8), 27.3 (C13), 24.9 (C11), 22.8, 21.7, 16.3, 15.7 (TMCp CH_3's and menthyl CH_3's), 0.0, 1.0 ($SiMe_2$). Anal. calcd. for $C_{26}H_{40}Cl_2SiTi$: C 62.5, H 8.1, Cl 14.2; found: C 62.8, H 8.3, Cl 14.3.

Preparation of (*R*/*S*)-dichloro[1-(η^5-2,3,4,5-tetramethyl-cyclopentadienyl)-1′-(η^5-3′-(1*S*, 2*S*, 5*R*)-5-methyl-2-(2-propyl)-cyclohexylcyclopentadienyl)dimethylsilane]titanium (4b$_{R/S}$)

1-(2,3,4,5-Tetramethylcyclopentadienyl)-1′-[3′-neomenthyl-cyclopentadienyl]dimethylsilane (3.07 g, 8 mmol) was dissolved in THF (45 cm^3). A solution of *n*-butyllithium (2.5 M,

© 2001 NRC Canada

6.4 cm^3, 16 mmol) in hexanes was added at 0°C via syringe and the mixture stirred at room temp for 30 min. The solution was cooled to –78 °C and $TiCl_3$·3THF (3.1 g, 8 mmol) was added rapidly against a stream of nitrogen; the mixture was maintained at –78°C for 5 h then allowed to warm to room temp and heated under reflux for a further 6 h. After cooling to room temp, chloroform (45 cm^3), together with concentrated aqueous hydrochloric acid (30 cm^3), was added and the mixture stirred at room temp in air for 30 min. The organic layer was separated, dried over Na_2SO_4, and the solvent removed in vacuo to yield a red, viscous oil. This was chromatographed on a silanized silica column eluting with hexane to remove organic residues and then a 4% diethyl ether – hexane mixture to elute a red band. Removal of solvent in vacuo yielded the title product (2.74 g, 68%), which was found to consist of a 1.3:1 mixture of (*R*) and (*S*) diastereoisomers, mp 122–130°C. $[\alpha]^{20}$ (*c* 0.026, CH_2Cl_2): +7.6° (589 nm), +30.8° (546 nm), and –61.5° (378 nm). FAB-MS *m*/*z* (%): 499 ($[M + 1]^+$, 20), 463 ($[M – Cl]^+$ 100). ^1H NMR (250 MHz, $CDCl_3$) δ: 0.05 (s, 6H, Si-CH_3), 0.79–0.96 (m, 9H, neomenthyl CH_3's), 0.96–1.72 (m, 9H, neomenthyl CH's, CH_2's), 1.77 (s, CH_3 (minor)), 1.79 (s, CH_3 (major)), 1.87 (s, CH_3 (major)), 1.93 (s, CH_3 (minor)), 2.09 (s, CH_3 (minor)), 2.12 (s, CH_3 (major)), 2.13 (s, CH_3 (major)), 2.18 (s, CH_3 (minor)), 3.50–3.60 (m, CH (minor)), 3.63–3.71 (m, CH (major)), 5.20–5.29 (m, 1H, Cp-H), 5.53–5.61 (m, 1H, Cp-H), 6.85–7.01 (m, 1H, Cp-H). ^{13}C NMR (63 MHz, $CDCl_3$) δ: 150.1, 146.4, 144.9, 144.0, 142.0, 141.6, 134.0, 132.0, 129.8, 128.9, 102.5, 102.1, 97.5, 97.1 (Cp quaternary), 137.0, 132.1, 119.1, 118.0, 116.5, 115.7 (Cp tertiary), 51.1, 49.6, 37.9, 37.2, 29.4, 29.1, 28.7, 28.0, 22.8, 22.6, 22.3, 21.9, 20.8, 16.3, 16.2, 16.0, 13.8, 13.7, 13.6, 13.3, 13.2, 1.0 (CH's, CH_3's), 40.2, 38.8, 35.8, 35.7, 26.0, 25.0 (neomenthyl CH_2's), 0.4, –0.3, –0.7, –1.0 (Si-CH_3's). Anal. calcd. for $C_{26}H_{40}Cl_2SiTi$: C 62.5, H 8.1; found: C 61.2, H 8.2.

Synthesis of (*R*)-dimethyl[1-(η^5-3′-(–)-menthylcyclopentadienyl)-1′-(η^5-2,3,4,5-tetramethylcyclopentadienyl)dimethylsilane]titanium (5)

Methylmagnesium bromide (0.76 cm^3, 2.4 mmol, 3M in diethyl ether) was added to a red solution of $\mathbf{4a}_{R}$ in diethyl ether (15 cm^3) and the mixture stirred overnight in the dark. The diethyl ether was removed in vacuo from the resulting yellow solution and the product extracted by washing the residue with hexane (5 × 1 cm^3). The solvent was removed in vacuo. No further purification was attempted since previous attempts to crystallize the product or purify on a silanized silica column had failed. The product was stored under $Ar_{(g)}$ in a lightshielded flask at –30°C. FAB-MS *m*/*z*: 459 ($[M + 1]^+$), 429 ($[M + 1 – 2CH_3]^+$). ^1H NMR (250 MHz, C_6D_6) δ: –0.29 (s, 3H, Ti-CH_3), –0.19 (s, 3H, Ti-CH_3), 0.02 (s, 3H, Si-CH_3), 0.28, (s, 3H, Si-CH_3), 0.75 (d, *J* = 7 Hz, 3H, Me), 0.81 (d, *J* = 7 Hz, 3H, Me), 0.92 (d, *J* = 7 Hz, 3H, Me), 0.7–1.65 (m, 8H, menthyl-CH's, CH_2's), 1.49 (s, 3H, TMCp CH_3), 1.59 (s, 3H, TMCp CH_3), 1.75 (s, 3H, TMCp CH_3), 2.11 (s, 3H, TMCp CH_3), 2.40 (m, 1H, menthyl CH), 2.70 (m, 1H, menthyl CH), 4.94 (t, $^4J_{H,H}$ = 2 Hz, $^4J_{H,H}$ = 2 Hz, 1H), 5.47 (t, $^3J_{H,H}$ = 2 Hz, $^4J_{H,H}$ = 2 Hz,1H), 6.93 (t, $^3J_{H,H}$ = 2 Hz, $^4J_{H,H}$ = 2 Hz, 1H). ^{13}C NMR (63 MHz, C_6D_6) δ: 143.3, 132.3, 129.9, 128.5, 122.7, 99.7, 94.3 (quarternary Cp), 122.3, 119.8, 111.3 (C1, C3, C4), 50.7, 47.5 (Ti-CH_3), 41.6, 35.6, 25.2 (neomenthyl CH_2's), 47.9, 41.2, 33.0, 27.5, 23.0, 22.0, 16.3, 15.6, 15.4, 12.2, 12.1 (CH's, CH_3's), 1.35, –1.9 (Si-CH_3).

Synthesis of 1-indenyl-1′-(2,3,4,5-tetramethylcyclopentadienyl)dimethylsilane (3)

Freshly distilled indene (48°C, 0.5 mm Hg, 4.3 cm^3, 37 mmol) was dissolved in THF (100 cm^3), cooled to 0°C, and then *n*-butyllithiium (2.5 M, 14.8 cm^3, 37 mmol) in hexanes was added over 30 min. The resulting orange-red solution was stirred at room temp for 2 h. 1-(Chlorodimethylsilyl)-2,3,4,5-tetramethyl-cyclopentadiene (10.0 g, 46 mmol) was dissolved in THF (75 cm^3) and the indenide solution transferred to this solution via cannula. The reaction mixture was heated to reflux for 18 h. The suspension was cooled to room temp and transferred via cannula through Celite, under nitrogen, to remove lithium chloride. The solvent was removed in vacuo from the filtrate yielding a red-brown oil which was redissolved in diethyl ether and washed with water (3 × 20 cm^3). The organic layer was dried over Na_2SO_4, filtered, and the solvent removed in vacuo to give an oil, which was heated to 80°C under 0.01 mm Hg to remove excess starting material and to leave the title product as an orange oil (7.29 g, 67.0%; 98% pure by GC). Attempts to separate isomers by recrystallization from pentane at –30°C were unsuccessful. Similarly, chromatography on alumina, eluting with pentane, failed to separate the isomers but did yield a yellow oil. (EI) GC–MS *m*/*z* (%): major, 294 (M^+, 33), 179 ($[M – indenyl]^+$, 44), 173 ($[M – TMCp]^+$, 100); minor, 294 (M^+, 52), 179 ($[M – indenyl]^+$, 49), 173 ($[M – TMCp]^+$, 100). ^1H NMR (250 MHz, $CDCl_3$) δ: –0.61, –0.21, –0.05 (s, 12H, 2SiCH_3 (major), 2SiCH_3 (minor)), 1.59 (s, 6H, 2Cp″CH_3 (major)), 1.71 (s, 6H, 2Cp″CH_3 (major)), 1.82 (s, 6H, 2Cp″CH_3 (minor)), 1.89 (s, 6H, 2Cp″CH_3 (minor)), 2.86 (br s, 2H, Cp″ipso-CH (major)), 3.05 (br s, 1H, Cp″ ipso-CH (minor)), 3.26 (d, *J* = 3 Hz, 2H, indenyl CH_2 (minor)), 3.45 (d, *J* = 3 Hz, 1H, indenyl SiCH (major)), 6.39 (dd, *J* = 11, 3 Hz, 2H, indenyl olefinic CH (major)), 6.49 (t, *J* = 3 Hz, 1H, indenyl olefinic CH (minor)), 6.69–6.75 (m, 2H, indenyl olefinic CH (major)), 6.95–7.15 (m, 6H, 2 × indenyl CH (major) and 2 × indenyl CH (minor)), 7.12–7.39 (m, 6H, 2 × indenyl CH (major) and 2 × indenyl CH (minor)). ^{13}C NMR (32.44 MHz, $CDCl_3$) δ: –5.9, -5.1, –3.7 ($SiCH_3$), 11.1, 11.3 (Cp″CH_3 (major)), 14.7, 14.8 (Cp″CH_3 (minor)), 40.8 (indenyl CH_2 (minor)), 44.4 (indenyl ipso-C (major)), 54.2 (Cp″ ipso-C (minor)), 54.6, (Cp″ ipso-C (major)), 120.8 (indenyl CH (major)), 122.2 (indenyl CH (minor)), 122.9 (indenyl CH (major)), 124.4 (indenyl CH (minor)), 123.7 (indenyl CH (major)), 126.0 (indenyl CH (minor)), 124.8 (indenyl CH (major)), 128.8 (indenyl CH (minor)), 129.1 (indenyl olefinic CH (major)), 135.7 (olefinic indenyl CH (major)), 144.3 (indenyl ipso-C (minor)), 144.4 (olefinic indenyl CH (minor)), 133.1, 135.1, 136.4, 136.5 (Cp″), 144.5, 144.9, 148.0 (indenyl).

Synthesis of dichloro[(η^5-1-indenyl)-1′-(η^5-2,3,4,5-tetramethylcyclopentadienyl)dimethyl silane]zirconium (6)

1-Indenyl-1′-(2,3,4,5-tetramethylcyclopentadienyl)dimethylsilane (1.01 g, 3.45 mmol) was dissolved in THF (10.0 cm^3) and the solution cooled to –78°C. *n*-Butyllithium (2.3 M,

© 2001 NRC Canada

3.00 cm^3, 6.89 mmol) in hexanes was slowly added and the reaction mixture stirred at –78°C for 10 min, then at room temp for a further 1 h, giving a dark red solution. Tetrachloro-bis(tetrahydrofuran)zirconium (1.30 g, 3.45 mmol), was dissolved in THF (25 cm^3), cooled to 0°C, and transferred via cannula onto the dianion solution at 0°C. The reaction mixture was stirred at room temp for 20 h giving a yellow suspension in an orange solution. The reaction was heated to 40°C for 72 h causing the mixture to become increasingly yellow. The mixture was filtered and washed with toluene yielding a bright yellow solid (1.41 g, 90.0% crude). Solutions were prepared immediately prior to running NMR spectra since the solid was unstable in solution. FAB-MS m/z (%): 455 (M^+, 5), 419 ($[M - Cl]^+$, 14), 247 (24), 173 (80). ^1H NMR (400 MHz, $CDCl_3$) δ: 0.95, 1.15 (s, 6H, $2SiCH_3$), 1.89, 1.93, 1.45, 1.47 (s, 12H, $4Cp''CH_3$), 5.98, 7.24 (d, J = 3 Hz, 2H, indenyl), 7.06, 7.33, 7.50, 7.70 (m, 4H, indenyl).

Catalytic studies

Hydrosilylations were carried out by adding *n*-BuLi in toluene (1 cm^3, 0.08 M) to the titanium complex (20 mg, 0.04 mmol) at room temp. After stirring the mixture rapidly for 5 min., phenylsilane (108 μL, 0.88 mmol) was added followed 5 min later by the ketone (0.8 mmol). The mixture was then placed in a thermostatic bath and the reaction monitored by GC. The product alcohols were obtained by adding acetone and 0.1 M HCl to the mixture; after bubbling had ceased, excess HCl was neutralized with a saturated solution of $NaHCO_3$ and the product extracted into diethyl ether and run through a short plug of anhydrous $MgSO_4$. Enantiomeric excess was determined using chiral GC using a β-Dex support.

Acknowledgments

We thank the EPSRC for postgraduate studentships (to P.D. and P.B) and I.C.I. Specialties for financial support. Advice and constant encouragement from David J. Milner (I.C.I.) is gratefully acknowledged.

References

1. (*a*) R.L. Halterman. Chem. Rev. **92**, 965 (1992); (*b*) Metallocenes: synthesis, reactivity, applications. Vol. 1 and 2. *Edited by* A. Togni and R.L. Halterman. Wiley-VCH, New York. 1998; (*c*) N. Long. Metallocenes: an introduction to sandwich complexes. Blackwell Science Inc., Malden. 1998.
2 (*a*) X. Verdaguer, U.E.W. Lange, M.T. Reding, and S.L. Buchwald. J. Am. Chem. Soc. **118**, 6784 (1996); (*b*) C.A. Willoughby and S.L. Buchwald. J. Am. Chem. Soc. **116**, 8952 (1994); (*c*) R.L. Halterman, T.M. Ramsey, and Z.L. Chen. J. Org. Chem. **59**, 2642 (1994); (*d*) Z.L. Chen and R.L. Halterman. J. Am. Chem. Soc. **114**, 2276 (1992); (*e*) R.L. Halterman, K.P.C. Vollhardt, M.E. Welker, D. Blaser, and R. Boese. J. Am. Chem. Soc. **109**, 8105 (1987); (*f*) P. Pino, P. Cioni, and J.J. Wei. J. Am. Chem. Soc. **109**, 6189 (1987).
3. *(a)* L. Resconi, L. Cavallo, A. Fait, and F. Piemontesi. Chem. Rev. **100**, 1253 (2000); (*b*) M.A. Giardello, M.S. Eisen, C.L. Stern, and T.J. Marks. J. Am. Chem. Soc. **117**, 12114 (1995); (*c*) H.H. Brintzinger, D. Fischer, R. Mülhaupt, B. Rieger, and R.M. Waymouth. Angew. Chem. Int. Ed. Engl. **34**, 1143 (1995); (*d*) R. Mülhaupt and B. Rieger. Chimia, **49**, 486 (1995); (*e*) F. Langhauser, J. Kerth, M. Kersting, P. Kölle, D. Lilge, and P. Müller. Angew. Makromol. Chem. **223**, 155 (1994); (*f*) K.B. Sinclair and R.B.Wilson. Chem. Ind. (London) 857 (1994).
4 (*a*) V.P. Conticello, L. Brard, M.A. Giardello, Y. Tsuji, M. Sabat, C.L. Stern, and T.J. Marks. J. Am. Chem. Soc. **114**, 2761 (1992); (*b*) T.J. Marks, M.A. Giardello, V.P. Conticello, L. Brard, and M. Gagne. J. Am. Chem. Soc. **116**, 10241 (1994).
5 T. Hayashi, M. Tanaka, and I. Ogata. Tetrahedron Lett. 295 (1977).
6. (*a*) W. Dumont, J.C. Poulin, T.P. Dang, and H.B. Kagan. J. Am. Chem. Soc. **95**, 8295 (1973); (*b*) O. Samuel, R. Couffignal, M. Lauer, S.Y. Zhang, and H.B. Kagan. Nouv. J. Chim. **5**, 15 (1981).
7. Q. Jiang, D. Xiao, Z. Zhang, P. Cao, and X. Zhang. Angew. Chem. Int. Ed. **38**, 516 (1999).
8. (*a*) R.L. Halterman, K.P.C. Vollhardt, and M.E. Welker. J. Am. Chem. Soc. **109**, 8105 (1987); (*b*) R.D. Broene and S.L. Buchwald. J. Am. Chem. Soc. **115**, 12569 (1993).
9. A. Lightfoot, P. Schnider, and A. Pfaltz. Angew. Chem. Int. Ed. **37**, 2897 (1998).
10. M.V. Troutman, D.H. Appella, and S.L. Buchwald. J. Am. Chem. Soc. **121**, 4916 (1999).
11. *(a)* R.W. Harrigan, G.S. Hammond, and H.B. Gray. J. Organomet. Chem. **81**, 79 (1974); (*b*) Z.T. Tsai and C.H. Brubaker Jr. J. Organomet. Chem. **166**, 199 (1979); (*c*) P.B. Brindley, A.G. Davies, and J.A.-A. Hawari. J. Organomet. Chem. **250**, 247 (1983); (*d*) K. Schmidt, A. Reinmuth, U. Rief, J. Diebold, and H.H. Brintzinger. Organometallics, **16**, 1724 (1997); (*e*) S. Miyake, L.M. Henling, and J.E. Bercaw, Organometallics, **17**, 5528 (1998).
12. (*a*) T.K. Hollis, A.L. Rheingold, N.P. Robinson, J. Whelan, and B. Bosnich. Organometallics, **11**, 2812 (1992); (*b*) J.A. Smith and H.H. Brintzinger. J. Organomet. Chem. **218**, 159 (1981).
13. H.H. Brintzinger, S. Gutmann, and M.H. Prosenc. J. Organomet. Chem. **397**, 21 (1990).
14. G.J. Wilson, D.A. Erskine, and J.D. McCowan. J. Organomet. Chem. **114**, 119 (1976).
15. R. Gomez, T. Cuenca, P. Royo, and E. Hovestreydt. Organometallics, **10**, 2516 (1991).
16. (*a*) R.L. Halterman, D. Combs, and M.A. Khan. Organometallics, **17**, 3900 (1998); (*b*) H.H. Brintzinger, A. Schafer, E. Karl, L. Zsolnai, and G. Huttner. J. Organomet. Chem. **328**, 87 (1987).
17. (*a*) J.L. Petersen, W.R. Tikkanen, and C.S. Bajgur. Inorg. Chem. **24**, 233 (1985); (*b*) H.H. Brintzinger, G. Huttner, and J. von Seyerl. J. Organomet. Chem. **288**, 69 (1985); (*c*) N.P. Rath, J.Y. Corey, and R.M. Shalton. J. Organomet. Chem. **503**, 205 (1995).
18. C. White, P. Beagley, P. Davies, J.A. Blacker, and B.J. Mellor. PCT Int. Appl. WO 9 911 648 to Zeneca Ltd. 1999 (March 11).
19. H.J. Phillips. Chem. Soc. **127**, 2566 (1925).
20. S. Winstein, B.K. Morse, E. Grunwald, H.W. Jones, J. Corse, D. Trifan, and H. Marshall. J. Am. Chem. Soc. **74**, 1127 (1952) and refs. therein.
21. J.A. Ramsden, D.A. Milner, H. Adams, N.A. Bailey, A.J. Smith, and C. White. Organometallics, **14**, 2575 (1995).
22. L.E. Manzer. Inorg. Synth. **21**, 137 (1982).
23. H.B. Kagan, E. Cesarotti, R. Goddard, and C. Kruger. J. Organomet. Chem. **162**, 297 (1978).
24. F.X. Kohl and P. Jutzi. J. Organomet. Chem. **243**, 119 (1983).
25. G.M. Sheldrick. SHELXL TL, an integrated system for solving, refining and displaying crystal structures and diffraction data. University of Gottingen, Germany. 1978; revision 5.1, 1985.
26. International tables for X-ray crystallography. Vol IV. Kynoch Press, Birmingham, U.K. (present distributor Kluwer Academic Publishers, Boston, U.S.A.) 1974.

© 2001 NRC Canada

New pathways of site selective aromatic alkylation of palladium complexes: fragmentation to arenes vs. ring closure to hexahydromethano-fluorenes or -phenanthrenes

Marta Catellani, Federica Cugini, and Domenico Tiefenthaler

Abstract: Dimeric arylbicycloheptylpalladium halide complexes of type **1** undergo selective alkylation at the aromatic site by reaction with allyl, styryl, and benzyl bromides (RBr) via hexahydromethanopalladafluorenes (**2**). Ring closure of the resulting palladium complex (**7**) on sp^2 and sp^3 C–H bonds of a suitable R group then occurs with formation of hexahydromethanophenanthrene or hexahydromethanofluorene derivatives. Alternatively, substituted arenes derived from bicycloheptene deinsertion are formed. In some cases the latter can be obtained in substantial amounts when methyl isonicotinate is used as ligand.

Key words: alkylations, C–H activation, palladium, palladacycles.

Résumé : Les complexes dimères halogénure d'arylbicycloheptylpalladium de type **1** subissent des réactions d'alkylation sélective du site aromatique par réaction avec les bromures d'allyle, de styryle et de benzyle, RBr, via les hexahydrométhanopalladafluorènes, **2**. La réaction de fermeture de cycle du complexe de palladium **7** qui en résulte, par réaction avec les liaisons C–H sp^2 et sp^3 d'un groupe R approprié, se produisent alors avec formation de dérivés hexahydrométhanophénanthrène ou hexahydrométanoflurorène. Des arènes substitués dérivant d'une désinsertion du bicycloheptène peuvent aussi se former. Dans quelques cas, ces derniers peuvent être obtenus en assez grandes quantités en présence d'isonicotinate de méthyle comme ligand.

Mots clés : alkylations, activation C–H, palladium, palladacycles.

[Traduit par la Rédaction]

Introduction

Organic syntheses involving selective activation and functionalization of aromatic and aliphatic C–H bonds by means of transition metal complexes are important goals of chemistry (1– 4). To this end metallacycles have been proved to be particularly useful providing an easy route to direct C–H activation (5), in addition to many useful synthetic applications (6–9). Selective aromatic dialkylation of hexahydromethanopalladafluorenes (**2**) with aliphatic iodides and bromides with consequent expulsion of the cycloaliphatic moiety (bicycloheptene) has been obtained in our laboratory (10). Catalytic processes based on this method have been reported (11–14). The starting palladacycle **2**, resulting from aromatic C–H activation (15), can be readily formed in situ from the phenylbicycloheptylpalladium chloride precursor **1** (16–19) (Scheme 1, L = solvent or added ligand).

To get further insight into this chemistry we varied the type of organic halide used, passing to allyl, vinyl, and benzyl halides. We, thus, could discover new types of alkylation followed by ring closure involving attack of palladium–carbon bonds on sp^2 and sp^3 C–H bonds. The present paper offers an outlook on the observed behaviour.

Results and discussion

Experiments were performed with dimeric arylbicycloheptylpalladium chloride complexes and different organic bromides, which react much better than the corresponding chlorides, in the presence of potassium carbonate in dimethylacetamide (DMA). We shall consider the results in the following sequence: allyl bromide, styryl bromide, and benzyl bromide. Aromatic arylation with aryl iodides has been the subject of previous papers (20–22).

Allyl bromide was caused to react with the phenylbicycloheptylpalladium chloride dimer **1**, or with its aryl analogues, dissolved in DMA at room temperature in the presence of potassium carbonate, using a fivefold excess of allyl bromide, which was found beneficial to obtain complete conversion of the starting palladium complex. While the migration of two allyl groups occurred as expected (Scheme 1, R = $CH_2CH{=}CH_2$), the resulting palladium-bonded intermediate

Received September 26, 2000. Published on the NRC Research Press Web site at http://canjchem.nrc.ca on June 30, 2001.

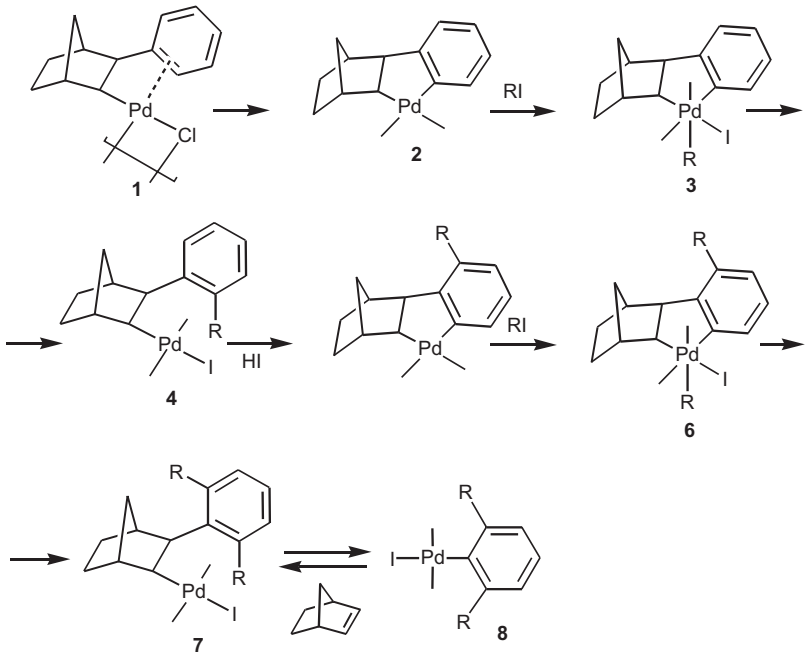
Dedicated to Professor Brian James in recognition of his outstanding contributions to organometallic chemistry.

M. Catellani,[1] F. Cugini, and D. Tiefenthaler. Dipartimento di Chimica Organica e Industriale dell'Università, Parco Area delle Scienze, 17/A, 43100 Parma, Italy.

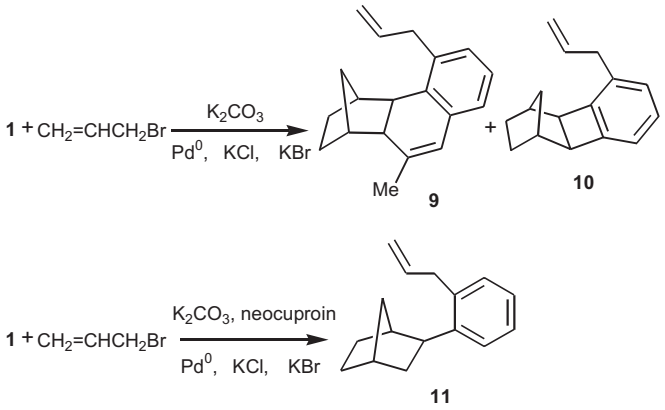
[1]Corresponding author (telephone: +39 0521 905 415; fax: +39 0521 905 472; e-mail: marta.catellani@unipr.it).

 DOI: 10.1139/cjc-79-5/6-742 © 2001 NRC Canada

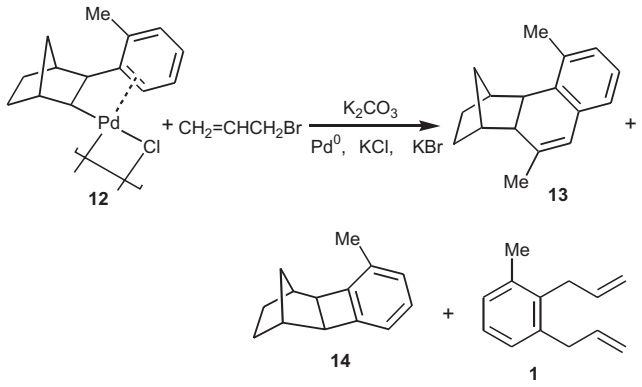
Scheme 1.



Scheme 2.



Scheme 3.



7 (R = $CH_2CH{=}CH_2$) underwent ring closure to hexahydromethanophenanthrene **9** in 62% yield (Scheme 2). It is worth noting that the entire process not only is stereoselective, leading to an *exo* C–C bond with the bicycloheptyl group, but also is regioselective, with the methyl group being placed near the bicycloheptyl site as ascertained by NMR spectra.

An allyl derivative of hexahydromethanobiphenylene **10**, resulting from reductive elimination of complex **5** (R = $CH_2CH{=}CH_2$), was formed in 26% yield as a by-product.

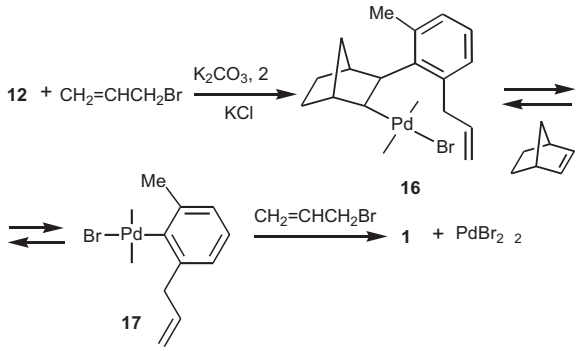
Under these conditions the previously observed deinsertion reaction of bicycloheptene from complex **7** to **8** (Scheme 1) did not take place because of the faster ring closure, probably involving previous coordination of the allyl double bond (23, 24). It is worth noting that the ring closure on the allylic double bond did not occur at the stage of the first allylation product **4** (R = $CH_2CH{=}CH_2$), when the formation of the benzocyclobutene derivative **10** was preferred, but only after the introduction of the second allyl group, when the only alternative would have been bicycloheptene deinsertion.

We also carried out the same reaction in the presence of nitrogen ligands. Pyridine and methyl isonicotinate (10:1 and 5:1 molar ratio to palladium, respectively) gave results similar to those of the previously reported reaction, however, a lower conversion (82%) was observed with the latter ligand. The addition of phenanthroline (1:1 molar ratio to palladium) blocked the reaction at the initial stage and phenylnorbornane was recovered almost quantitatively after treatment with sodium borohydride. Neocuproin (2,9-dimethyl-1,10-phenanthroline; 1:1 molar ratio to palladium), which is more dissociable than phenanthroline, allowed the reaction to proceed to the first allylation of the aromatic ring (complex **4**, R = $CH_2CH{=}CH_2$) to afford the organic product *exo*-2-[2′-(prop-2-enyl)phenyl]bicyclo[2.2.1]heptane (**11**) (92%) after addition of sodium borohydride as the reducing agent.

2-Methylphenylbicycloheptylpalladium chloride dimer **12** was then used as the starting complex in place of **1** under the standard conditions previously reported. The reaction (Scheme 3) gave products **13** (61%) and **14** (11%) (25), corresponding to analogous compounds **9** and **10**, respectively,

© 2001 NRC Canada

Scheme 4.



of Scheme 2. This time, however, a third product (**15**, 7%), was present.

Apparently compound **15** is formed via bicycloheptene deinsertion from complex **16** followed by coupling of the resulting species **17** with another molecule of allyl bromide (Scheme 4).

The fact that the presence of a methyl and an allyl group in the *ortho* positions leads to deinsertion only to a very small extent is probably due to stabilization of the complex by coordination of the allyl double bond (23, 24). The yield of **15** depends on the ability of the ligands to prevent coordination of the allyl group, as shown in Table 1.

While phenanthroline completely blocked the reaction, as with complex **1**, neocuproin gave only 51% conversion with yields for **13**, **14**, and **15** of 35, 9, and 5%, respectively. Monodentate ligands gave better results; pyridine (10:1 molar ratio to palladium) increased the yields to 41, 23, and 16%, respectively, while methyl isonicotinate (5:1 molar ratio to palladium) gave the best yield of product **15** (34%), resulting from deinsertion and coupling with an allyl group, along with **13** and **14** in 28 and 9% yield, respectively. The combined effect of the *ortho* methyl group and of the ligand thus allows deinsertion to be obtained to a substantial extent.

To get more information on the steric effect caused by the *ortho* methyl group, complexes **18**, **21**, and **24** were caused to react with allyl bromide under the same conditions adopted for **12**. As shown in Scheme 5 only **24** gave the deinsertion product.

Complex **18** gave compounds **19** and **20** (25) in 78 and 11% yield, respectively, and complex **21** gave **22**, **23**, and **20** (25) in 52, 35, and 11% yield, respectively.

It is worth noting that, contrary to what occurred in the case of compound **9** (Scheme 2), compound **19** was formed by ring closure on the allyl group in the absence of a second allyl substituent on the *ortho* position. This is probably due to the steric hindrance exerted by the *meta* methyl group to allylation in the second *ortho* position. While addition of methyl isonicotinate as the ligand to complexes **18** and **21** did not lead to significant amounts of products resulting from bicycloheptene deinsertion, complex **24** in the presence of methyl isonicotinate as the ligand (5:1 molar ratio to palladium) gave compounds **25**, **26**, and **27** (25) in 35, 31, and 15% yield, respectively. The yield of compound **26** (31%) compares well with the yield for compound **15** (34%) (derived from complex **12)** under the same conditions. In the absence of additional ligands compounds **25**, **26**, and **27** were obtained in 68, 9, and 13% yield, respectively.

Table 1. Ligand effect on the reaction of 2-methylphenylbicycloheptylpalladium chloride dimer (**12**) with allyl bromide.

Ligand	Yield of compound (%)		
	13	**14**	**15**
—	61	11	7
Phenanthroline[a]	n.a.	n.a.	n.a.
Neocuproin	35	9	5
Pyridine	41	23	16
Methyl isonicotinate	28	9	34

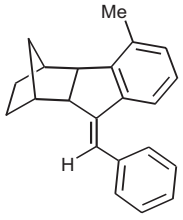
[a]n.a., not applicable.

These results offer further evidence that methyl isonicotinate competes with the allyl group for coordination to palladium, thus causing bicycloheptene deinsertion to occur to a substantial extent.

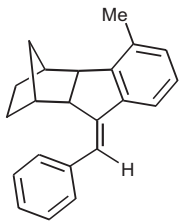
Styryl bromide

Under the conditions adopted for the previous reactions *E*-styryl bromide reacted with complex **1** to give the hexahydromethanofluorene derivatives **30a** (*Z*, 64%) and **30b** (*E*, 21%). The reaction is likely to proceed, as shown in Scheme 6, through oxidative addition of styryl bromide to give the palladium(IV) species **28** (for general overview of palladium(IV) intermediates, see ref. 26), followed by styryl migration on the metallacycle aryl site (**29**). At this point ring closure to the *syn* and *anti* phenylmethylenehexahydromethanofluorene derivatives **30a** and **30b** occurred according to (Scheme 6).

The situation did not change using complex **12**, instead of **1**, and methyl isonicotinate as the ligand. The corresponding *Z*- and *E*-5-methyl-9-phenylmethylenehexahydromethanofluorenes **31a** and **31b** were obtained in 74 and 24% yield, respectively. Apparently double bond coordination predominates over the steric and ligand effects.



31a



31b

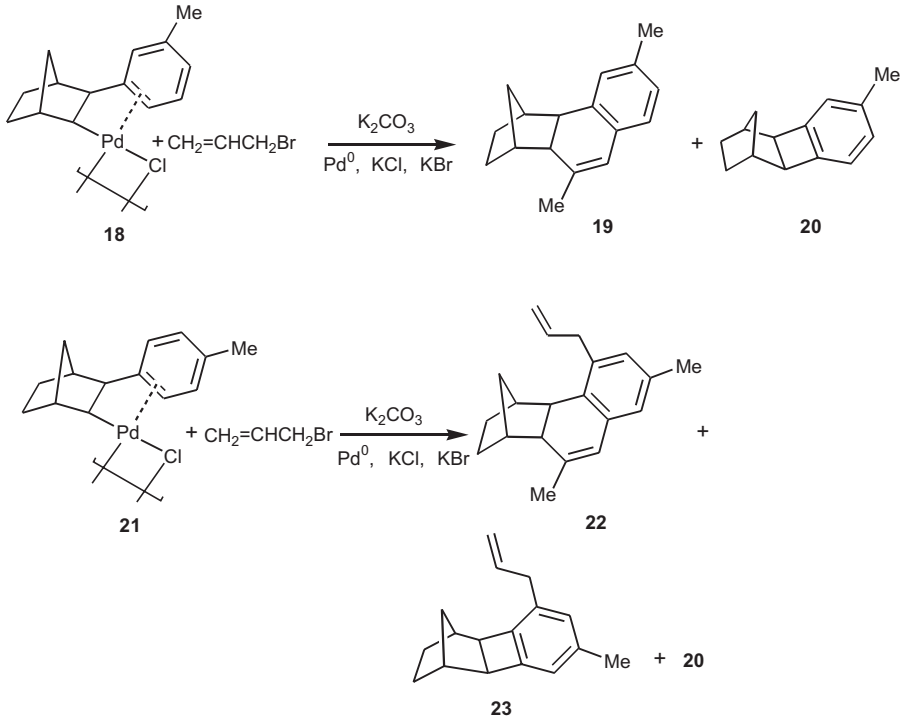
Benzyl bromide

Benzyl bromide had been previously shown to react with complex **1** to give the aromatic dibenzylated product resulting from bicycloheptene deinsertion in the same way shown in the general Scheme 1 (10).

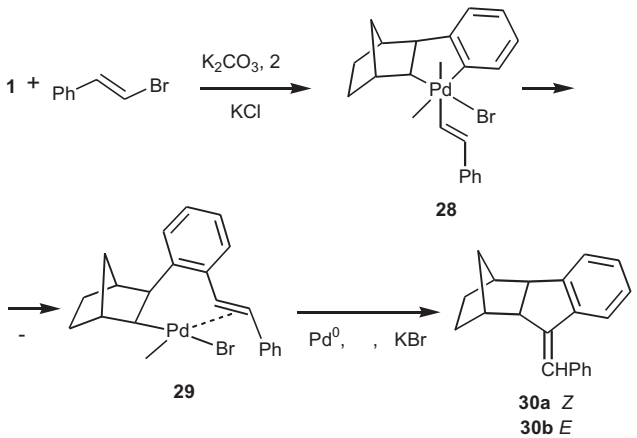
Starting from the *ortho* methyl-substituted complex **12**, however, an unexpected behaviour was observed. The complex underwent activation of the methyl group with ring closure to a hexahydromethanofluorene derivative; compounds **34a** and **34b** were obtained both in 77% yield using benzyl bromide and 4-methylbenzyl bromide, respectively (Scheme 7).

© 2001 NRC Canada

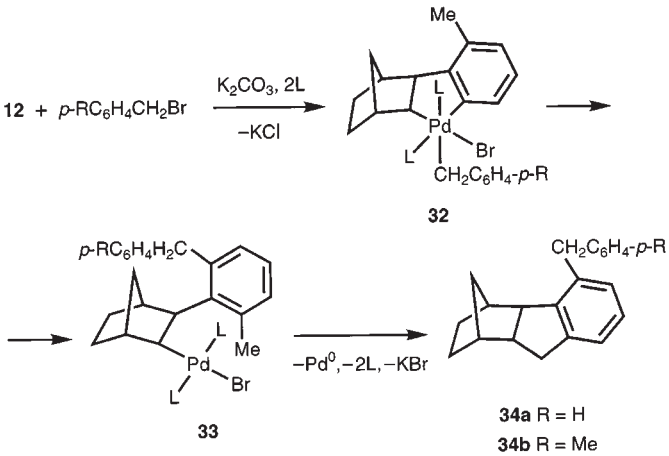
Scheme 5.



Scheme 6.

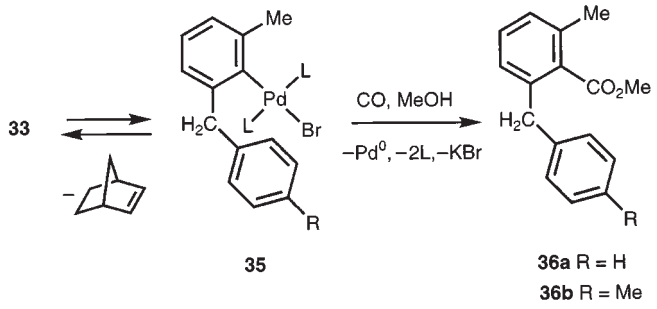


Scheme 7.



© 2001 NRC Canada

Scheme 8.

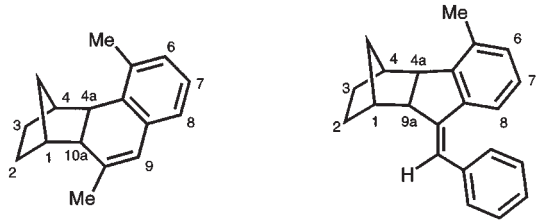


The reaction proceeds through the palladium(IV) complex **32** and the bicycloheptyl palladium species **33**. Complexes of this type (**32** and **33**) had been isolated with phenanthroline as the ligand (26–28). Ring closure between two sp^3 carbons, thus, appears to be preferred not only to bicycloheptene deinsertion and but also to ring closure on the benzylic CH_2. Catalytic reactions of this type have been derived from this observation (29). An agostic interaction of CH_3 with palladium might be at the origin of this behaviour (30). Bicycloheptene deinsertion has also occurred in small amount as evident by the isolation of the corresponding products **36a** and **36b** (14 and 10% yield, respectively) obtained after carbonylation in methanol (Scheme 8).

The situation changes completely in the presence of methyl isonicotinate as the ligand (fivefold excess with respect to palladium). This time complexes **33** (R = H, CH_3) undergo deinsertion almost quantitatively. The resulting arylpalladium complexes **35** (R = H, CH_3) were treated in situ with CO and methanol at room temperature and atmospheric pressure. Compounds **36a** and **36b** were obtained in 97 and 95% yield, respectively. The reaction of benzyl halides with complex **12**, thus offers the possibility to obtain deinsertion products (diphenylmethane derivatives) in the presence of methyl isonicotinate as the ligand or cyclization products (hexahydromethanofluorene derivatives) in its absence.

Ring size, regiochemistry, and stereochemistry of compounds 9, 13, 19, 22, 25, 30a, 30b, 31a, and 31b

The regiochemistry of the products was established from the NOESY spectra. For the hexahydromethanophenanthrene derivatives (**9**, **13**, **19**, **22**, **25**) the strong dipolar interaction of the methyl protons on C10 with both H10a and H1 clearly indicates that the methyl group is placed in the proximity of the bicycloheptyl unit. Accordingly, the vinyl proton on C9 shows an NOE effect with the facing aromatic proton on the adjacent C8. Although the NMR data were in agreement with the proposed phenanthrene structure, they could not, however, unambiguously proved it, as they were also compatible with fluorene systems such as in compounds **30a** and **31a**. The fluorene system was ruled out by carrying out a long range C–H correlation HMBC experiment. As expected for the phenanthrene structure, the vinyl proton of compound **13** shows correlations to CH_3C=, C10a, C8, C4b ($^3J_{^{13}C,^1H}$), and 8a ($^2J_{^{13}C,^1H}$) and the methyl protons on C10 correlate to C9, C10a ($^3J_{^{13}C,^1H}$), and C10 ($^2J_{^{13}C,^1H}$). For compounds **30a** and **31a** the strong NOE interactions between the vinyl proton and both H9a and H1 complement the correlation signal of the aromatic *ortho* protons of the styryl unit with H8, thus indicating that the phenyl ring of the styryl group is situated in the proximity of the aromatic side. The fluorene structure of **30a** and **31a** is, thus, confirmed since the formation of a six-membered ring would have placed the phenyl ring of the styryl unit adjacent to the bicycloheptyl moiety. Moreover, vicinal couplings ($^3J_{^1H,^1H}$) on the order of 7 to 8 Hz have been usually observed for the two *endo* protons (H4a and H9a) on the bicycloheptyl unit involved in a five-membered ring, while larger coupling constants, on the order of 10 Hz, have been encountered in six-membered rings for the corresponding H4a and H10a *endo* protons (31). The cross peaks present in the NOESY spectra of compounds **30b** and **31b** are in agreement with the assigned *E*-stereochemistry; moreover yield of these compounds increases with increased reaction times as a result of the *Z* to *E* isomerization process.



Experimental

General

Reagents were obtained from commercial sources and were used without further purification. Starting complexes were prepared using the procedure reported for the unsubstituted parent compound (16). Their structural characterization will be the subject of a forthcoming paper.[2] DMA was distilled under reduced pressure and stored under an atmosphere of dinitrogen over 4 Å molecular sieves. Reactions were carried out under dinitrogen using conventional Schlenk techniques. Column chromatography was performed on silica gel (Merck silica 70–230 mesh) using hexane or a mixture of hexane – ethyl acetate as the eluent. TLC analyses were carried out on precoated plates (Merck silica gel 60). GLC analyses were run with a Carlo Erba HRGC 5300 instrument equipped with a 30 m long capillary column (SE-30 as the stationary phase). Mass spectra (EI) were acquired with Finnigan MAT SSQ 710 spectrometer operating at 70 eV and are reported as *m/z* (relative intensity). Infrared spectra were run on a Nicolet 5PC FT-IR instrument and are reported in wave numbers (cm^{-1}). Melting points were determined by the capillary method on an electrothermal apparatus and are uncorrected. Elemental analyses were performed by using a Carlo Erba EA1108 elemental analyzer. Unless indicated otherwise, ^1H and ^{13}C NMR spectra were recorded in $CDCl_3$ at 20°C using the solvent as internal standard on a Bruker AC 300 operating at 300.1 and 75.4 MHz, respectively. The HMBC experiments were run on a Bruker AMX 400 using the program INVBTP supplied by Bruker. ^{13}C

[2] M. Catellani, C. Mealli, E. Motti, P. Paoli, and P. Pregosin, manuscript in preparation.

© 2001 NRC Canada

spectra were collected using TD = 16 or 64K; in the latter case two decimal figures were given. One or more asterisks (*) indicate interchangeable assignments.

General procedure for the reaction of arylnorbornylpalladium chloride dimer with allyl, styryl, and benzyl bromides

The palladium complex and potassium carbonate were introduced under dinitrogen into a 25 mL Schlenk-type flask. The appropriate ligand, if any, and the desired organic halide, separately dissolved in DMA, were then added and the resulting solution stirred at room temperature for 4–24 h. After addition of methanol (0.5–1 mL), dinitrogen was replaced by CO at atmospheric pressure and stirring was continued for 6 h until palladium black was formed. Alternatively, the reaction mixture was quenched by treatment with $NaBH_4$ in slight excess. The mixture was diluted with CH_2Cl_2 and extracted three times with a 5% solution of H_2SO_4. The combined organic layer was washed with water and dried over anhyd Na_2SO_4. The solvent was evaporated and the products were isolated by column chromatography using hexane or a mixture of hexane–EtOAc as the eluent. Yields, based on monomeric arylnorbornylpalladium chloride, were determined by GC. Conversions were obtained from the corresponding arylnorbornane formed by decomposition with $NaBH_4$ and were determined by GC. Compounds **14**, **20**, and **27** were previously reported (25).

*Reaction of **1** with allyl bromide*

Following the general procedure dimeric complex **1** (76 mg, 0.12 mmol), allyl bromide (145 mg, 1.20 mmol), and K_2CO_3 (100 mg, 0.72 mmol) in DMA (12 mL) were converted to yield **9** (37 mg, 62%) and **10** (13 mg, 26%). An isomer of **9** (ca. 3%) was also detected by GC–MS but not further characterized. Conversion of **1** was complete in 4 h. Similar results were obtained using pyridine or methyl isonicotinate as the ligand (10:1 and 5:1 molar ratio to palladium, respectively) in 4 and 8 h. Reaction with phenanthroline (43 mg, 0.24 mmol) for 24 h gave *exo*-2-phenylbicyclo[2.2.1]heptane (39 mg, 95%) (32) as the only product after treatment with $NaBH_4$, while using neocuproin (50 mg, 0.24 mmol) for 24 h gave 2-[2′-(prop-2-enyl)phenyl]bicyclo[2.2.1]heptane (**11**, 47 mg, 92%).

exo-*1,2,3,4,4a,10a-Hexahydro-10-methyl-5-(prop-2-enyl)-1,4-methanophenanthrene (**9**)*: EI-MS *m/z* (%): 250 (M^+, 87), 183 (67), 182 (67), 181 (78), 167 (100), 165 (62), 152 (40), 67 (66), 41 (85). IR (cm^{-1}): 1666.7, 1637.7, 992.5, 911.5. ^{1}H NMR δ: 7.02 (t, *J* = 7.4 Hz, 1H, H7), 6.95 (dd, *J* = 7.6, 1.7 Hz, 1H, H6), 6.72 (dd, *J* = 7.2, 1.7 Hz, 1H, H8), 5.98 (quint. partly overlapping with C*H*=CH_2, *J* = 1.4 Hz, 1H, H9), 5.95 (m, 1H, C*H*=CH_2), 5.07 (dt, *J* = 10.5, 1.5 Hz, 1H, =C*H*(H)), 5.06 (dt, *J* = 18.0, 1.7 Hz, 1H, =C*H*(H)), 3.42, 3.30 (part AB of an ABX system further coupled with the two terminal vinylic protons, *J* = 15.7, 6.5, 1.5 Hz, 2H, CH_2CH=), 3.07 (br d, *J* = 10.1 Hz, 1H, H4a), 2.54 (d, *J* = 10.1 Hz, 1H, H10a), 2.41 (m, 1H, H1), 2.20 (m, 1H, H4), 1.82 (t, *J* = 1.2 Hz, 3H, CH_3), 1.81–1.65 (m, 1H, $H2_{exo}$), 1.65–1.52 (m, 3H, $H3_{exo}$, $H3_{endo}$, $H11_{syn}$), 1.52–1.39 (m, 1H, $H2_{endo}$), 1.11 (d quint., *J* = 9.8, 1.5 Hz, 1H, $H11_{anti}$). ^{13}C NMR δ : 137.4 (C5), 137.3 (*C*H=CH_2), 135.9 (C10), 133.8 (C4b) 133.4 (C8a), 128.3 (C6), 126.1 (C7), 124.4 (C8), 123.7 (C9), 115.7 (=CH_2), 49.9 (C10a), 48.5 (C4), 43.5 (C4a), 41.4 (C1), 36.6 (*C*H_2CH=), 34.0 (C11), 30.6 (C3), 29.6 (C2), 22.0 (CH_3). Anal. calcd. for $C_{19}H_{22}$: C 91.14, H 8.86; found: C 90.93, H 9.07.

exo-*1,2,3,4,4a,8b-Hexahydro-5-(prop-2-enyl)-1,4-methanobiphenylene (**10**)*: EI-MS *m/z* (%): 210 (M^+, 11), 169 (100), 141 (45), 128 (27), 41 (32). IR (cm^{-1}): 1638.7, 992.5, 911.5. ^{1}H NMR δ: 7.14 (t, *J* = 7.5 Hz, 1H, H7), 6.98 (d, *J* = 7.5 Hz, 1H, H8), 6.84 (br d, *J* = 7.5 Hz, 1H, H6), 5.97 (ddt, *J* = 16.8, 10.2, 6.6 Hz, 1H, =CH), 5.06, 5.05 (two partly overlapping d further split, 2H, =CH_2), 3.28 (dt, *J* = 6.6, 1.5 Hz, 2H, CH_2CH=), 3.18–3.12 (m, 2H, H4a, H8b), 2.28 (m, 1H, H1*), 2.25 (m, 1H, H4*), 1.62–1.54 (m, 2H, $H2_{exo}$, $H3_{exo}$), 1.22–1.14 (m, 2H, $H2_{endo}$, $H3_{endo}$), 0.95 (d quint., *J* = 10.1, 1.4 Hz, 1H, $H9_{anti}$), 0.85 (d quint., *J* = 10.1, 1.9 Hz, 1H, $H9_{syn}$). ^{13}C NMR δ: 144.9 (q), 141.1 (q), 137.0 (*C*H=CH_2), 134.2 (q), 127.7 (C7), 127.1 (C6), 119.6 (C8), 115.5 (=CH_2), 49.9 (C4a*), 49.8 (C8b*), 36.5 (C1**), 36.2 (C4**, *C*H_2CH=), 31.9 (C9), 27.8 (C2, C3). Anal. calcd. for $C_{16}H_{18}$: C 91.37, H 8.63; found: C 91.18, H 8.82.

exo-*2-[2′-(Prop-2-enyl)phenyl]bicyclo[2.2.1]heptane (**11**)*: EI-MS *m/z (%)*: 212 (M^+, 22), 169 (35), 144 (77), 129 (100), 115 (45), 91 (85), 67 (60), 41 (45). IR (cm^{-1}): 1637.7, 993.5, 912.5. ^{1}H NMR δ: 7.27 (br d, 1H, H6′), 7.22–7.09 (m, 3H, H5′, H4′, H3′), 5.98 (ddt, *J* = 16.9, 10.1, 6.4 Hz, 1H, C*H*=CH_2), 5.07 (dq, *J* = 10.1, 1.7 Hz, 1H, =C*H*(H)), 5.03 (dq, *J* = 16.9, 1.7 Hz, 1H, =C*H*(H)), 3.43 (m, 2H, CH_2CH=), 2.88 (dd, *J* = 8.7, 5.6 Hz, 1H, H2), 2.35 (m, 2H, H1, H4), 1.80 (ddd, *J* = 11.6, 9.0, 2.2 Hz, 1H, $H3_{endo}$), 1.68–1.53 (m, 4H, $H3_{exo}$, $H5_{exo}$, $H6_{exo}$, $H7_{syn}$), 1.38–1.20 (m, 3H, $H5_{endo}$, $H6_{endo}$, $H7_{anti}$ centred at 1.24). ^{13}C NMR δ: 145.3 (q), 137.7 (q), 137.4 (CH=), 129.5, 126.1, 125.4 (C5′, C4′, C3′), 125.2 (C6′), 115.7 (CH_2=), 43.1 (C2), 42.1 (C1*), 39.3 (C3), 37.3 (*C*H_2CH=), 36.9 (C4*), 36.4 (C7), 30.6 (C5**), 29.0 (C6**). Anal. calcd. for $C_{16}H_{20}$: C 90.51, H 9.49; found: C 90.29, H 9.71.

*Reaction of **12** with allyl bromide*

Following the general procedure dimeric complex **12** (79 mg, 0.12 mmol), allyl bromide (145 mg, 1.20 mmol), and K_2CO_3 (100 mg, 0.72 mmol) in DMA (12 mL) were converted to yield **13** (33 mg, 61%), **14** (5 mg, 11%) (25), and **15** (3 mg, 7%). Conversion of **12** was complete in 4 h. In the presence of phenanthroline as the ligand (43 mg, 0.24 mmol) for 24 h only *exo*-2-(2′-methyl)phenylbicyclo[2.2.1]heptane (43 mg, 96%) (33) was obtained after treatment with $NaBH_4$. Reaction with neocuproin (50 mg, 0.24 mmol) for 24 h gave 2-(2′-methyl)phenylbicyclo[2.2.1]heptane (22 mg, 49%) (33) together with **13** (19 mg, 35%), **14** (4 mg, 9%), and **15** (2 mg, 5%), while using pyridine (190 mg, 2.4 mmol) for 4 h gave **13** (22 mg, 41%), **14** (10 mg, 23%), and **15** (7 mg, 16%). Methyl isonicotinate (166 mg, 1.2 mmol) for 8 h led to **13** (15 mg, 28%), **14** (4 mg, 9%), and **15** (14 mg, 34%).

exo-*1,2,3,4,4a,10a-Hexahydro-5,10-dimethyl-1,4-methanophenanthrene (**13**)*: EI-MS *m/z* (%): 224 (M^+, 65), 183 (22), 157 (64), 156 (100), 141 (44), 67 (25), 41 (23). IR (cm^{-1}): 1665.8. ^{1}H NMR δ: 6.98 (dd, *J* = 7.5, 7.0 Hz, 1H, H7), 6.93

© 2001 NRC Canada

(dd, *J* = 7.5, 1.9 Hz, 1H, H6), 6.70 (dd, *J* = 7.0, 1.9 Hz, 1H, H8), 5.98 (quint., *J* = 1.3 Hz, 1H, H9), 2.99 (br d, *J* = 10.1 Hz, 1H, H4a), 2.55 (br d, *J* = 10.1 Hz, 1H, H10a), 2.42 (m, 1H, H1), 2.26 (s, 3H, CH_3Ar), 2.21 (m, 1H, H4), 1.82 (t, *J* = 1.2 Hz, 3H, CH_3C=), 1.74 (m, 1H, $H2_{exo}$), 1.63–1.53 (m, 3H, $H3_{exo}$, $H3_{endo}$, $H11_{syn}$), 1.51–1.41 (m, 1H, $H2_{endo}$), 1.12 (d quint., *J* = 9.7, 1.4 Hz, 1H, $H11_{anti}$). ^{13}C NMR δ: 135.85 (C10), 135.67 (C5), 134.13 (C4b), 133.13 (C8a), 129.08 (C6), 125.88 (C7), 123.99 (C8), 123.65 (C9), 49.88 (C10a), 47.37 (C4), 44.18 (C4a), 41.28 (C1), 34.12 (C11), 30.52 (C3), 29.61 (C2), 22.06 (CH_3C=), 19.33 (CH_3Ar). Anal. calcd. for $C_{17}H_{20}$: C 91.01, H 8.99; found: C 91.28, H 8.72.

2,3-Diprop-2-enyl-1-methylbenzene (***15***): EI-MS *m*/*z* (%): 172 (M^+, 35), 157 (55), 144 (39), 143 (74), 142 (37), 129 (100), 128 (87), 115 (67), 91 (55), 77 (37), 51 (32), 41 (25). IR (cm^{-1}): 1637.8, 993.4, 912.7. ^{1}H NMR δ: 7.09 (t partly overlapping with the subsequent m, 1H, H5), 7.07–6.98 (m, 2H, H4, H6), 5.92 (m, 2H, 2CH=), 5.01 (m, 3H, =C*H*(H), $=CH_2$), 4.84 (dq, *J* = 17.1, 1.9 Hz, 1H, =C*H*(H)), 3.41, 3.38 (2 overlapping dt, 4H, $2CH_2CH$=), 2.30 (s, 3H, CH_3). Anal. calcd. for $C_{13}H_{16}$: C 90.64, H 9.36; found: C 90.54, H 9.46.

Reaction of ***18*** *with allyl bromide*

Following the general procedure dimeric complex **18** (79 mg, 0.12 mmol), allyl bromide (145 mg, 1.20 mmol), and K_2CO_3 (100 mg, 0.72 mmol) in DMA (12 mL) were converted to yield **19** (42 mg, 78%) and **20** (5 mg, 11%) (25).

exo-*1,2,3,4,4a,10a-Hexahydro-6,10-dimethyl-1,4-methanophenanthrene* (***19***): mp (hexane): 79 to 80°C. EI-MS *m*/*z* (%): 224 (M^+, 55), 209 (21), 183 (26), 165 (23), 157 (54), 156 (100), 155 (44), 128 (25), 115 (35), 67 (30), 41 (32). IR (cm^{-1}): 1656.1. ^{1}H NMR δ: 6.91 (br s, 1H, H5), 6.84 (d further split, 1H, H7), 6.72 (d, *J* = 7.6 Hz, 1H, H8), 5.95 (sext., *J* = 1.2 Hz, 1H, H9), 3.06 (d, *J* = 10.3 Hz, 1H, H4a), 2.42 (d, *J* = 10.3 Hz, 1H, H10a), 2.39 (m, 1H, H1), 2.35 (m, 1H, H4), 2.27 (s, 3H, CH_3Ar), 1.83 (t, *J* = 1.1 Hz, 3H, CH_3C=), 1.68–1.57 (m, 2H, $H2_{exo}$, $H3_{exo}$), 1.55–1.38 (m, 3H, $H2_{endo}$, $H3_{endo}$, $H11_{syn}$ centered at 1.50), 1.09 (d quint., *J* = 9.7, 1.5 Hz, 1H, $H11_{anti}$). ^{13}C NMR δ: 135.96 (C10*), 135.94 (C6*), 135.32 (C4b), 130.65 (C8a), 129.31 (C5), 126.59 (C7), 125.56 (C8), 122.35 (C9), 49.25 (C4), 48.97 (C10a), 46.39 (C4a), 42.51 (C1), 33.98 (C11), 30.34 (C2**), 29.88 (C3**), 22.58 (CH_3C=), 21.23 (CH_3Ar). Anal. calcd. for $C_{17}H_{20}$: C 91.01, H 8.99; found: C 90.93, H 9.07.

Reaction of ***21*** *with allyl bromide*

Following the general procedure dimeric complex **21** (79 mg, 0.12 mmol), allyl bromide (145 mg, 1.20 mmol), and K_2CO_3 (100 mg, 0.72 mmol) in DMA (12 mL) were converted to yield **22** (33 mg, 52%), **23** (19 mg, 35%), and **20** (5 mg, 11%) (25).

exo-*1,2,3,4,4a,10a-Hexahydro-7,10-dimethyl-5-(prop-2-enyl)-1,4-methanophenanthrene* (***22***): EI-MS *m*/*z* (%): 264 (M^+, 80), 197 (67), 196 (51), 195 (76), 181 (100), 179 (48), 165 (85), 141 (26), 67 (85), 41 (78). IR (cm^{-1}): 1666.7, 1637.7, 992.5, 909.5. ^{1}H NMR δ: 6.78 (d, *J* = 1.6 Hz, 1H, H6), 6.55 (d, *J* = 1.6 Hz, 1H, H8), 5.94 (m, 2H, H9, C*H*=CH_2), 5.07 (m, 2H, $=CH_2$), 3.45–3.22 (m, 2H, CH_2CH=), 3.03 (d, *J* = 10.1 Hz, 1H, H4a), 2.53 (d, *J* = 10.1 Hz, 1H, H10a), 2.40 (m, 1H, H1), 2.23 (s, 3H, CH_3Ar), 2.18 (m, 1H, H4), 1.81 (t, *J* = 1.9 Hz, 3H, CH_3C=), 1.72 (m, 1H, $H2_{exo}$), 1.61–1.51 (m, 3H, $H3_{exo}$, $H3_{endo}$, $H11_{syn}$), 1.45 (m, 1H, $H2_{endo}$), 1.10 (d quint., *J* = 9.7, 1.5 Hz, 1H, $H11_{anti}$). ^{13}C NMR δ: 137.4 (*C*H=CH_2), 137.3 (C5), 135.9 (C10), 135.4 (C7) 133.3 (C8a), 130.8 (C4b), 129.0 (C6), 125.2 (C8), 123.8 (C9), 115.7 (=*C*H_2), 49.9 (C10a), 48.4 (C4), 43.2 (C4a), 41.4 (C1), 36.6 (CH_2CH=), 34.0 (C11), 30.5 (C3), 29.6 (C2), 22.1 (CH_3C=), 20.8 (CH_3). Anal. calcd. for $C_{20}H_{24}$: C 90.85, H 9.15; found: C 90.61, H 9.39.

exo-*1,2,3,4,4a,8b-Hexahydro-7-methyl-5-(prop-2-enyl)-1,4-methanobiphenylene* (***23***): EI-MS *m*/*z* (%): 224 (M^+, 12), 183 (100), 165 (26), 155 (35), 153 (26), 141 (24), 115 (22), 41 (30). IR (cm^{-1}): 1638.7, 992.5, 910.5. ^{1}H NMR δ: 6.81 (br s, 1H, H6), 6.68 (br s, 1H, H8), 5.96 (ddt, *J* = 16.9, 10.1, 6.7 Hz, 1H, =CH), 5.11–5.00 (two partly overlapping d further split, 2H, $=CH_2$), 3.25 (br d, *J* = 6.7 Hz, 2H, CH_2CH=), 3.10, 3.09 (m, 2H, H4a, H8b), 2.30 (s, 3H, CH_3Ar), 2.26 (m, 1H, H1*), 2.23 (m, 1H, H4*), 1.62–1.53 (m, 2H, $H2_{exo}$, $H3_{exo}$), 1.16 (m, 2H, $H2_{endo}$, $H3_{endo}$), 0.95 (d quint., *J* = 10.1, 1.2 Hz, 1H, $H9_{anti}$), 0.87 (d quint., *J* = 10.1, 1.8 Hz, 1H, $H9_{syn}$). ^{13}C NMR δ: 146.4 (q), 141.6 (q), 137.3 (q), 137.1 (*C*H=CH_2), 133.9 (q), 127.9 (C6), 120.3 (C8), 115.4 (=*C*H_2), 49.5 (C4a*), 49.3 (C8b*), 36.5 (C1**), 36.2 (C4**, CH_2CH=), 31.9 (C9), 27.8 (C2***), 27.7 (C3***), 22.0 (CH_3Ar). Anal. calcd. for $C_{17}H_{20}$: C 91.01, H 8.99; found: C 91.09, H 8.91.

Reaction of ***24*** *with allyl bromide*

Following the general procedure dimeric complex **24** (82 mg, 0.12 mmol), allyl bromide (145 mg, 1.20 mmol), and K_2CO_3 (100 mg, 0.72 mmol) in DMA (12 mL) were converted to yield **25** (39 mg, 68%), **26** (4 mg, 9%), and **27** (6 mg, 13%) (25). The same reaction carried out in the presence of methyl isonicotinate (164 mg, 1.2 mmol) gave **25** (20 mg, 35%), **26** (14 mg, 31%), and **27** (7 mg, 15%).

exo-*1,2,3,4,4a,10a-Hexahydro-5,7,10-trimethyl-1,4-methanophenanthrene* (***25***): EI-MS *m*/*z* (%): 238 (M^+, 90), 197 (27), 171 (80), 170 (100), 156 (27), 155 (54), 67 (36), 41 (35). IR (cm^{-1}): 1665.7. ^{1}H NMR δ: 6.76 (br s, 1H, H6), 6.53 (br s, 1H, H8), 5.93 (quint., *J* = 1.4 Hz, 1H, H9), 2.95 (br d, *J* = 10.1 Hz, 1H, H4a), 2.52 (br d, *J* = 10.1 Hz, 1H, H10a), 2.40 (m, 1H, H1), 2.22 (s, 6H, $2CH_3Ar$), 2.18 (m, 1H, H4), 1.81 (t, *J* = 1.2 Hz, 3H, CH_3C=), 1.72 (m, 1H, $H2_{exo}$), 1.62–1.52 (m, 3H, $H3_{exo}$, $H3_{endo}$, $H11_{syn}$), 1.52–1.39 (m, 1H, $H2_{endo}$), 1.10 (d quint., *J* = 9.7, 1.5 Hz, 1H, $H11_{anti}$). ^{13}C NMR δ: 135.9 (C10), 135.6 (C5), 135.2 (C7), 133.1 (C4b*), 131.2 (C8a*), 129.9 (C6), 124.7 (C8), 123.7 (C9), 49.9 (C10a), 47.4 (C4), 43.9 (C4a), 41.3 (C1), 34.1 (C11), 30.5 (C3), 29.6 (C2), 22.1 (CH_3C=), 20.7 (CH_3Ar), 19.2 (CH_3Ar). Anal. calcd. for $C_{18}H_{22}$: C 90.70, H 9.30; found: C 90.52, H 9.48.

1,3-Dimethyl-5,6-diprop-2-enylbenzene (***26***): EI-MS *m*/*z* (%): 186 (M^+, 32), 171 (31), 157 (32), 148 (43), 128 (42), 115 (32), 44 (100). IR (cm^{-1}): 1637.8, 993.4, 912.3. ^{1}H NMR δ: 6.87 (br s, 1H, H2), 6.85 (br s, 1H, H4), 5.93 (m, 2H, 2CH=), 5.01 (m, 3H, =C*H*(H), $=CH_2$), 4.85 (dq, *J* = 17.1, 1.9 Hz, 1H, =C*H*(H)), 3.36 (m, 4H, $2CH_2CH$=), 2.27 (br s, 3H, CH_3(C1)), 2.26 (br s, 3H, CH_3(C3)). ^{13}C NMR δ: 137.6

© 2001 NRC Canada

(=CH), 136.9 (=CH), 136.0 (q), 135.5 (q), 132.7 (q), 129.2 (q), 128.1 (C2, C4), 115.4 (=CH_2), 114.8 (=CH_2), 37.4 (CH_2CH=), 32.7 (CH_2CH=), 19.8 (CH_3Ar), 19.2 (CH_3Ar). Anal. calcd. for $C_{14}H_{18}$: C 90.26, H 9.74; found: C 90.02, H 9.98.

*Reaction of **1** with styryl bromide*

Following the general procedure dimeric complex **1** (76 mg, 0.12 mmol), *E*-styryl bromide (110 mg, 0.60 mmol), and K_2CO_3 (100 mg, 0.72 mmol) in DMA (12 mL) in 8 h were converted to yield **30a** (42 mg, 64%) and **30b** (14 mg, 21%).

*2,3,4,4a,9,9a-Hexahydro-9-*Z*-phenylmethylene-1,4-methano-9*H*-fluorene (**30a**)*: EI-MS *m/z* (%): 272 (M^+, 100), 205 (85), 157 (32), 115 (16), 91 (24), 67 (27), 41 (15). IR (cm^{-1}): 1635.8. ^{1}H NMR δ: 7.39–7.35 (m, 4H, H2′, H3′, H5′, H6′), 7.28 (m, 1H, H4′), 7.23 (m, 1H, H5), 7.15 (m, 2H, H6, H8), 6.89 (m, 1H, H7), 6.62 (d, *J* = 2.0 Hz, 1H, =CH), 3.07 (br d, *J* = 7.2 Hz, 1H, H4a), 2.92 (dm, *J* = 7.3 Hz, 1H, H9a), 2.33 (m, 1H, H1), 2.30 (m, 1H, H4), 1.65 (m, 2H, $H2_{exo}$, $H3_{exo}$), 1.52–1.33 (m, 2H, $H2_{endo}$, $H3_{endo}$), 1.17 (d quint., *J* = 10.1, 1.9 Hz, 1H, $H10_{syn}$), 1.01 (d quint., *J* = 10.1, 1.5 Hz, 1H, $H10_{anti}$). ^{13}C NMR δ: 150.72 (q), 147.28 (q), 141.19 (q), 138.65 (q), 128.57 (C2′,C6′*), 128.39 (C6), 128.38 (C3′,C5′*), 126.62 (C4′), 125.90 (C7), 125.10 (C5), 123.50 (C8), 122.87 (=CH), 53.38 (C9a), 51.60 (C4a), 45.42 (C1), 42.69 (C4), 32.22 (C10), 29.42 (C2**), 28.57 (C3**). Anal. calcd. for $C_{21}H_{20}$: C 92.60, H 7.40; found: C 92.71, H 7.29.

*2,3,4,4a,9,9a-Hexahydro-9-*E*-phenylmethylene-1,4-methano-9*H*-fluorene (**30b**)*: mp (hexane) 72–74°C. EI-MS *m/z* (%): 272 (M^+, 100), 205 (79), 157 (21), 115 (16), 91 (25), 67 (31), 41 (15). IR (cm^{-1}): 1632.4. ^{1}H NMR δ: 7.57 (m, 3H, H2′, H6′, H8), 7.38 (m, 2H, H3′, H5′), 7.26–7.19 (m, 4H, H5, H6, H7, H4′), 6.92 (d, *J* = 2.3 Hz, 1H, =CH), 3.35 (dm, *J* = 6.9 Hz, 1H, H9a), 3.23 (br d, *J* = 6.9 Hz, 1H, H4a), 2.39 (m, 1H, H1), 2.34 (m, 1H, H4), 1.71–1.54 (m, 2H, $H2_{exo}$, $H3_{exo}$), 1.52–1.46 (m, 2H, $H2_{endo}$, $H3_{endo}$), 0.96, 0.91 (AB system further split, *J* = 10.1 Hz, 2H, $H10_{syn}$, $H10_{anti}$). ^{13}C NMR δ: 148.2, 147.0, 144.2, 137.6, 128.7, 128.5, 128.4, 126.8, 126.2, 124.9, 119.4, 119.2, 53.3, 50.8, 42.9, 40.3, 32.6, 28.9, 28.7. Anal. calcd. for $C_{21}H_{20}$: C 92.60, H 7.40; found: C 92.42, H 7.58.

*Reaction of **12** with styryl bromide*

Following the general procedure dimeric complex **12** (79 mg, 0.12 mmol), *E*-styryl bromide (110 mg, 0.60 mmol), and K_2CO_3 (100 mg, 0.72 mmol) in DMA (12 mL) in 8 h were converted to yield **31a** (51 mg, 74%) and **31b** (16 mg, 24%).

*2,3,4,4a,9,9a-Hexahydro-5-methyl-9-*Z*-phenylmethylene-1,4-methano-9*H*-fluorene (**31a**)*: EI-MS *m/z* (%): 286 (M^+, 98), 219 (100), 215 (47), 204 (74), 203 (76), 202 (70), 91 (29), 67 (19). IR (cm^{-1}): 1637.6. ^{1}H NMR (CD_2Cl_2) δ: 7.39–7.30 (m, 4H, H2′, H3′, H5′, H6′), 7.27 (m, 1H, H4′), 6.95 (two overlapping d, 2H, H6, H8), 6.79 (t, *J* = 7.6 Hz, 1H, H7), 6.60 (d, *J* = 2.0 Hz, 1H, =CH), 3.04 (br d, *J* = 7.2 Hz, 1H, H4a), 2.94 (dm, *J* = 7.2 Hz, 1H, H9a), 2.39 (m, 1H, H4), 2.35 (m, 1H, H1), 2.32 (s, 3H, CH_3), 1.68–1.61 (m, 2H, $H2_{exo}$, $H3_{exo}$), 1.48–1.44 (m, 1H, $H3_{endo}$), 1.43–1.39 (m, 1H, $H2_{endo}$), 1.19 (d quint., *J* = 10.0, 1.8 Hz, 1H, $H10_{syn}$), 1.02 (d quint., *J* = 10.0, 1.5 Hz, 1H, $H10_{anti}$). ^{13}C NMR (CD_2Cl_2) δ: 149.32 (q), 148.13 (q), 141.44 (q), 139.16 (q), 134.98 (q), 129.87 (C6), 128.93 (C2′*,C6′*), 128.70 (C3′*,C5′*), 126.91 (C4′), 126.47 (C7), 122.89 (=CH), 121.35 (C8), 53.90 (C9a), 51.14 (C4a), 45.74 (C1), 40.75 (C4), 32.47 (C10), 30.07 (C3**), 28.55 (C2**), 18.89 (CH_3). Anal. calcd. for $C_{22}H_{22}$: C 92.26, H 7.74; found: C 92.16, H 7.84.

*2,3,4,4a,9,9a-Hexahydro-5-methyl-9-*E*-phenylmethylene-1,4-methano-9*H*-fluorene (**31b**)*: mp (hexane) 74–76°C. EI-MS *m/z* (%): 286 (M^+, 93), 219 (100), 215 (49), 204 (72), 203 (77), 202 (71), 91 (29), 67 (21). IR (cm^{-1}): 1630.2. ^{1}H NMR δ: 7.55 (m, 2H, H2′, H6′), 7.40 (d further split and partly overlapping with H3′, H5′, 1H, H8), 7.37 (m, 2H, H3′, H5′), 7.20 (tt, *J* = 7.3, 1.2 Hz, 1H, H4′), 7.14 (t, *J* = 7.5 Hz, 1H, H7), 7.03 (dm, *J* = 7.3 Hz, 1H, H6), 6.89 (d, *J* = 2.4 Hz, 1H, =CH), 3.37 (dm, *J* = 6.9 Hz, 1H, H9a), 3.20 (br d, *J* = 6.9 Hz, 1H, H4a), 2.45 (m, 2H, H1, H4), 2.37 (s, 3H, CH_3), 1.68–1.57 (m, 2H, $H2_{exo}$, $H3_{exo}$), 1.50–1.44 (m, 2H, $H2_{endo}$, $H3_{endo}$), 1.04 (d quint., *J* = 10.1, 1.8 Hz, 1H, $H10_{syn}$), 0.91 (d quint., *J* = 10.1, 1.5 Hz, 1H, $H10_{anti}$). ^{13}C NMR δ: 147.44 (q), 146.42 (q), 144.18 (q), 137.66 (q), 134.51 (q), 129.55 (C6), 128.69 (C2′,C6′), 128.40 (C3′,C5′), 127.09 (C7), 126.13 (C4′), 119.00 (=CH), 116.97 (C8), 52.59 (C4a), 50.92 (C9a), 40.66 (C1*), 40.12 (C4*), 32.78 (C10), 29.06 (C2**), 28.72 (C3**), 18.66 (CH_3). Anal. calcd. for $C_{22}H_{22}$: C 92.26, H 7.74; found: C 91.99, H 8.01.

*Reaction of **12** with benzyl bromide*

Following the general procedure dimeric complex **12** (79 mg, 0.12 mmol), benzyl bromide (82 mg, 0.48 mmol), and K_2CO_3 (100 mg, 0.72 mmol) in DMA (12 mL) were converted to yield in 4 h **34a** (51 mg, 77%) and **36a** (8 mg, 14%). In the presence of methyl isonicotinate (165 mg, 1.2 mmol) only compound **36a** (56 mg, 97%) was obtained.

*1,2,3,4,4a,9a-Hexahydro-5-phenylmethylene-1,4-methano-fluorene (**34a**)*: EI-MS *m/z* (%): 274 (M^+, 25), 206 (27), 128 (20), 115 (18), 91 (100), 67 (49). ^{1}H NMR δ: 7.28 (m, 2H, H3′, H5′), 7.20 (m, 1H, H4′), 7.16 (m, 2H, H2′, H6′), 7.06 (t, *J* = 7.4 Hz, 1H, H7), 6.99 (d further split, *J* = 7.4 Hz, 1H, H8), 6.86 (m, 1H, H6), 4.10, 3.99 (m, 2H, $ArCH_2Ph$), 3.20 (dd, *J* = 17.2, 10.3 Hz, 1H, H9), 3.03 (br d, *J* = 7.9 Hz, 1H, H4a), 2.62 (ddd, *J* = 17.2, 4.3, 0.6 Hz, 1H, H9), 2.38 (m, 1H, H4), 2.35 (m, 1H, H9a), 2.10 (m, 1H, H1), 1.61–1.46 (m, 2H, $H2_{exo}$, $H3_{exo}$), 1.36–1.16 (m, 3H, $H2_{endo}$, $H3_{endo}$, $H10_{syn}$, centered at 1.20), 1.01 (d quint., *J* = 9.9, 1.5 Hz, 1H, $H10_{anti}$). ^{13}C NMR δ: 145.1 (q), 144.6 (q), 140.9 (q), 136.9 (q), 129.1 (C2′, C6′), 128.3 (C3′, C5′), 127.4 (C6), 126.7 (C7), 125.9 (C4′), 122.1 (C8), 54.4 (C4a), 45.0 (C9a), 43.5 (C1), 41.7 (C4), 39.6 (C9), 38.7 ($ArCH_2Ph$), 32.5 (C10), 29.2 (C2*), 28.5 (C3*). Anal. calcd. for $C_{21}H_{22}$: C 91.92, H 8.08; found: C 92.04, H 7.96.

*Methyl 6-methyl-2-phenylmethylenebenzoate (**36a**)*: EI-MS *m/z* (%): 240 (M^+, 5), 209 (30), 208 (100), 193 (15), 165 (36), 91 (12), 89 (19). IR (cm^{-1}): 1729.4. ^{1}H NMR δ: 7.28 (m, 2H, H3′, H5′), 7.20 (m, 2H, H4′, H4), 7.15 (m, 2H, H2′, H6′), 7.08 (d further split, 1H, H5), 7.00 (d further split, 1H, H3), 4.00 (s, 2H, $ArCH_2Ph$), 3.78 (s, 3H,

© 2001 NRC Canada

CO_2CH_3), 2.32 (s, 3H, CH_3Ar). ^{13}C NMR δ: 170.3 (CO), 140.2 (q), 138.0 (q), 135.1 (q), 133.8 (q), 129.4 (C4), 129.0 (C2′,C6′), 128.3 (C3′,C5′), 128.1 (C5), 127.6 (C3), 126.1 (C4′), 51.8 (CO_2CH_3), 39.4 ($ArCH_2Ph$), 19.7 (CH_3Ar). Anal. calcd. for $C_{16}H_{16}O_2$: C 79.97, H 6.71; found: C 79.74, H 6.90.

*Reaction of **12** with 4-methylbenzyl bromide*

Following the general procedure dimeric complex **12** (79 mg, 0.12 mmol), 4-methylbenzyl bromide (89 mg, 0.48 mmol), and K_2CO_3 (100 mg, 0.72 mmol) in DMA (12 mL) were converted to yield **34b** (53 mg, 77%) and **36b** (6 mg, 10%). In the presence of methyl isonicotinate (165 mg, 1.2 mmol) only compound **36b** (58 mg, 95%) was obtained.

*1,2,3,4,4a,9a-Hexahydro-5-(4′-methylphenylmethylene)-1,4-methanofluorene (**34b**)*: EI-MS *m*/*z* (%): 288 (M^+, 38), 220 (27), 196 (14), 129 (24), 128 (45), 105 (100), 67 (52), 41 (22). ^1H NMR δ: 7.11 -7.03 (m, 4H, H2′, H3′, H5′, H6′), 7.05 (t, *J* = 7.5 Hz, 1H, H7), 6.98 (d further split, *J* = 7.5 Hz, 1H, H8), 6.84 (d further split, 1H, H6), 4.10–3.91 (m, 2H, $ArCH_2Ar$), 3.20 (dd, *J* = 17.4, 10.2 Hz, 1H, H9), 3.04 (br d, *J* = 7.8 Hz, 1H, H4a), 2.61 (ddd, *J* = 17.4, 4.5, 0.9 Hz, 1H, H9), 2.39 (m, 1H, H4), 2.34 (m, 1H, H9a), 2.32 (s, 3H, CH_3Ar), 2.10 (m, 1H, H1), 1.61–1.46 (m, 2H, $H2_{exo}$, $H3_{exo}$), 1.36–1.16 (m, 3H, $H2_{endo}$, $H3_{endo}$, $H10_{syn}$, centered at 1.20), 1.00 (d quint., *J* = 10.2, 1.5 Hz, 1H, $H10_{anti}$). ^{13}C NMR δ: 145.1 (q), 144.5 (q), 137.7 (q), 137.2 (q), 135.3 (q), 129.0 (C2′, C6′*), 128.9 (C3′, C5′*), 127.3 (C6), 126.7 (C7), 122.0 (C8), 54.4 (C4a), 45.0 (C9a), 43.5 (C1), 41.7 (C4), 39.6 (C9), 38.2 ($CH_2(Ar)_2$), 32.5 (C10), 29.2 (C2**), 28.5 (C3**), 21.0 (CH_3Ar). Anal. calcd. for $C_{22}H_{24}$: C 91.61, H 8.39; found: C 91.37, H 8.63.

*Methyl 6-methyl-2-(4′-methylphenylmethylene)benzoate (**36b**)*: EI-MS *m*/*z* (%): 254 (M^+, 5), 223 (15), 222 (100), 165 (49), 91 (16). IR (cm^{-1}): 1727.2. ^1H NMR δ: 7.20 (t, *J* = 7.6 Hz, 1H, H4), 7.10–7.00 (m, 5H, H2′, H3′, H5′, H6′, H5), 6.98 (dm, *J* = 7.6 Hz, 1H, H3), 3.95 (s, 2H, $CH_2(Ar)_2$), 3.79 (s, 3H, CO_2CH_3), 2.31 (s, 3H, CH_3Ar), 2.30 (s, 3H, CH_3Ar). ^{13}C NMR δ: 170.3 (CO), 138.4 (q), 137.2 (q), 135.6 (q), 135.1 (q), 133.8 (q), 129.4 (C4), 129.0 (C2′*,C6′*), 128.9 (C3′*,C5′*), 128.1 (C5), 127.5 (C3), 51.8 (CO_2CH_3), 39.0 ($CH_2(Ar)_2$), 21.0 (CH_3Ar), 19.7 (CH_3Ar). Anal. calcd. for $C_{17}H_{18}O_2$: C 80.28, H 7.13; found: C 80.39, H 7.14.

Conclusions

In conclusion, we have shown that alkylation of palladacycles with allyl, styryl, and benzyl halides undergoes new pathways when the position *ortho* to the aryl-bicycloheptyl bond is or becomes occupied. Cyclization occurs either directly as in the case of the styryl group or after a second group (allyl, benzyl) has occupied the other *ortho* position. In all cases cyclization is regio and stereoselective. Ligands can interfere in the cyclization process leading to C–C cleavage between the aryl and bicycloheptyl groups with liberation of bicycloheptene.

Acknowledgments

Financial support was provided by Ministero dell'Università e della Ricerca Scientifica e Tecnologica (MURST, Roma) and Consiglio Nazionale delle Ricerche (CNR, Roma). We thank Prof. B.E. Mann (University of Sheffield) for carrying out and discussing some key NMR experiments. Mass and NMR facilities were provided by the Centro Interfacoltà di Misure of the University of Parma.

References

1. K. Tamao. *In* Comprehensive organic synthesis. Vol. 3. *Edited by* B.M. Trost and I. Fleming. Pergamon, Oxford. 1991. pp. 435–480.
2. W.W. Leong and R.C. Larock. *In* Comprehensive organometallic chemistry II. Vol. 12. *Edited by* E.W. Abel, F.G.A. Stone, and G. Wilkinson. Pergamon, Oxford. 1995. pp. 131–160.
3. G. Dyker. Angew Chem. Int. Ed. Engl. **38**, 1698 (1999).
4. T.-Y. Luh, M.-K. Leung, and K.-T. Wong. Chem. Rev. **100**, 3187 (2000).
5. A.D. Ryabov. Chem. Rev. **90**, 403 (1990).
6. B. Cornils and W.A. Herrmann. Applied homogeneous catalysis with organometallic compounds. Wiley, Weinheim. 1996.
7 J. Tsuji. Transition metal reagents and catalysts – innovations in organic synthesis. Wiley, Chichester, U.K. 1995.
8. E. Negishi. Pure Appl. Chem. **64**, 323 (1992).
9. H. Alper. Transition metal organometallics in organic synthesis. Academic Press, New York. 1976.
10. M. Catellani and M.C. Fagnola. Angew. Chem. Int. Ed. Engl. **33**, 2421 (1994).
11. M. Catellani, F. Frignani, and A. Rangoni. Angew. Chem. Int. Ed. Engl. **36**, 119 (1997).
12. M. Catellani and F. Cugini. Tetrahedron, **55**, 6595 (1999).
13. M. Catellani, E. Motti, and M. Minari. Chem. Commun. 157 (2000).
14. M. Lautens and S. Piguel. Angew. Chem. Int. Ed. Engl. **39**, 1045 (2000).
15. M. Catellani and G.P. Chiusoli. J. Organomet. Chem. **346**, C27 (1988).
16. H. Horino, M. Arai, and M. Inoue. Tetrahedron Lett. 647 (1974).
17. C.-S. Li, C.-H. Cheng, F.-L. Liao, and S.-L. Wang. J. Chem. Soc. Chem. Commun. 710 (1991).
18. B.A. Markies, P. Wijkens, H. Kooijman, A.L. Spek, J. Boersma, and G. van Koten. J. Chem. Soc. Chem. Commun. 1420 (1992).
19. M. Portnoy, Y. Ben-David, I. Rousso, and D. Milstein. Organometallics, **13**, 3465 (1994).
20. M. Catellani and E. Motti. New J. Chem. **22**, 759 (1998).
21. M. Catellani, E. Motti, L. Paterlini, G. Bocelli, and L. Righi, J. Organomet. Chem. **580**, 191 (1999).
22. K. Albrecht, O. Reiser, M. Weber, B. Knieriem, and A. de Meijere. Tetrahedron, **50**, 393 (1994).
23. R.P. Hughes and J. Powell. J. Organomet. Chem. **30**, C45 (1971).
24. M. Zocchi, G. Tieghi, and A. Albinati. J. Organomet. Chem. **33**, C47 (1971).
25. M. Catellani and L. Ferioli. Synthesis, 769 (1996).
26. A.J. Canty. *In* Comprehensive organometallic chemistry II. Vol. 9. *Edited by* E.W. Abel, F.G.A. Stone, and G. Wilkinson. Pergamon, Oxford. 1995. pp. 225–290.

© 2001 NRC Canada

27. M. Catellani and B.E. Mann. J. Organomet. Chem. **390**, 251 (1990).
28. G. Bocelli, M. Catellani and S.Ghelli. J. Organomet. Chem. **458**, C12 (1993).
29. M. Catellani, E. Motti, and S. Ghelli. Chem. Commun. 2003 (2000).
30. W. Baratta, E. Herdtweck, and P. Rigo. Angew. Chem. Int. Ed. Engl. **38**, 1629 (1999).
31. A.P. Marchand. Stereochemical applications of NMR studies in rigid bicyclic systems, VCI, Deerfield Beach, Florida. 1983. pp. 112–160.
32. L. Schmerling. U.S. Patent 2 480 267 (1949); Chem. Abstr. 44, 1136 (1950).
33. V.P. Yur'ev, G. Gailiunas, G.A. Tolstikov, V.I. Khvostenko, and E.G. Galkin. Zh. Obshch. Kim. **45**, 2741 (1975); Chem. Abstr. 84, 10 5062 (1976).

© 2001 NRC Canada

Structural studies of $PdCl_2L_2$ complexes with fluorinated phosphines, phosphites, and phosphinites as precursors of benzyl bromide carbonylation catalysts, and and X-ray crystal structure of *cis*-$PdCl_2[PPh_2(OEt)]_2$

Anna M. Trzeciak, Hubert Bartosz-Bechowski, Zbigniew Ciunik, Katarzyna Niesyty, and Józef J. Ziółkowski

Abstract: $PdCl_2L_2$-type complexes with phosphines (L = $PPh_x(C_6F_5)_{3-x}$ (x = 0–3)), phosphites (L = $P(OMe)_3$, $P(OPh)_3$, $P(OEt)_3$), and phosphinites (L = $PPh_2(OC_6F_5)$, PPh_2(O-3,5-$F_2C_6H_3$), $PPh_2(OEt)$, PPh_2(O-*n*-Bu), PPh_2(O-*t*-Bu)) were synthesized and characterized by UV–vis and ^{31}P NMR methods. $PdCl_2L_2$ complexes with less sterically demanding phosphines ($\Theta < 140°$) exist as *cis* isomers, which is confirmed by the X-ray structure of *cis*-$PdCl_2[PPh_2(OEt)]_2$. These complexes react with CO in the presence of NEt_3 forming $Pd(CO)_xL_y$ ($x + y = 4$) type carbonyls characterized by IR spectra. All $PdCl_2L_2$ complexes studied are active as precursors of benzyl bromide carbonylation catalysts at 40°C and 1 atm CO; however, the activity of the *cis* isomers is higher than that of the *trans* isomers. The highest yields of the carbonylation product, phenylacetic acid methyl ester, were obtained using *cis*-$PdCl_2[P(OMe)_3]_2$ (92%), *cis*-$PdCl_2[P(OPh)_3]_2$ (89%), and *cis*-$PdCl_2[PPh_2$(O-*n*-Bu)$]_2$ (78%) as catalyst precursors.

Key words: palladium complexes, fluorinated phosphines, benzyl bromide carbonylation.

Résumé : On a synthétisé des complexes de type $PdCl_2L_2$ comprenant des phosphines L = $PPh_x(C_6F_5)_{3-x}$ (x = 0–3), des phosphites L = $P(OMe)_3$, $P(OPh)_3$ et $P(OEt)_3$ et des phosphinites L = $PPh_2(OC_6F_5)$, PPh_2(O-3,5-$F_2C_6H_5$), $PPh_2(OEt)$, $PPh_2(OBu)$ et PPh_2(O-*t*-Bu) et on les a caractérisés par spectroscopie UV–vis et par RMN du ^{31}P. Les complexes $PdCl_2L_2$ comportant des phosphines stériquement moins encombrées ($\theta < 140°$) existent sous la forme d'isomères *cis*; cette situation a été confirmée par diffraction des rayons du *cis*-$PdCl_2[PPh_2(OEt)]_2$. Ces complexes réagissent avec le CO en présence de NEt_3 pour former des complexes carbonylés de type $Pd(CO)_xL_y$ ($x + y = 4$) qui ont été caractérisés par spectroscopie IR. À 40°C et 1 atm de CO, tous les complexes de type $PdCl_2L_2$ sont actifs comme précurseurs de catalyseurs pour la carbonylation du bromure de benzyle; toutefois, l'activité des isomères *cis* est supérieure à celle des isomères *trans*. Les rendements les plus élevés en produit de carbonylation, le phénylacétate de méthyle, ont été obtenus avec les *cis*-$PdCl_2[P(OMe)_3]_2$ (92%), *cis*-$PdCl_2[P(OPh)_3]_2$ (89%) et *cis*-$PdCl_2[P(OBu)_3]_2$ (78%) comme précurseurs de catalyseur.

Mots clés : complexes de palladium, phosphines fluorées, carbonylation du bromure de benzyle.

[Traduit par la Rédaction]

Introduction

The electronic and steric properties of fluorine-containing phosphorus ligands are quite different from those of their nonfluorinated analogues. The σ-electron-withdrawing character of fluorine reduces the basicity of the ligand, as has been demonstrated for *trans*-$MCl(CO)(PR_3)_2$ (M = Rh, Ir) by an increase of the ν(CO) frequency in the following series of PR_3 ligands: $PPh_3 < PPh_2(C_6F_5) < P(C_6F_5)_3$ (1). However, when only two fluorines are present in the phenyl ring of the phosphine coordinated in complexes of the same type ($PPh_x(2,6\text{-}F_2C_6H_3)_{3-x}$, x = 0–2), the ν(CO) remains constant and close to the value observed for $MCl(CO)(PPh_3)_2$ (1). On the basis of ligand displacement studies of $PtCl_2(PR_3)_2$ complexes, phosphorus ligands have been ordered according to their ligand exchange ability, which increases in the following order: $P(C_6F_5)_3 < PPh(C_6F_5)_2 < P(2,6\text{-}F_2C_6H_3)_3 < PPh_2(C_6F_5) < PPh_3$ (2). Rhodium and platinum complexes with fluorinated phosphines, diphosphines, phosphonites, and phosphinites have been studied (3–5). Examples of *ortho*-C–F bond activation in rhodium and iridium complexes with fluorinated diphosphines have been reported (6, 7).

Received September 14, 2000. Published on the NRC Research Press Web site at http://canjchem.nrc.ca on June 30, 2001.

Dedicated to Professor Brian James on the occasion of his 65th birthday.

A.M. Trzeciak, H. Bartosz-Bechowski, Z. Ciunik, K. Niesyty, and J.J. Ziółkowski.[1] Faculty of Chemistry, University of Wroclaw, 14 F. Joliot-Curie St., 50–383 Wroclaw, Poland.

[1]Corresponding author (telephone: +48 71 3402-270; fax: +48 71 3282-348; e-mail: jjz@wchuwr.chem.uni.wroc.pl).

 DOI: 10.1139/cjc-79-5/6-752 © 2001 NRC Canada

Table 1. UV-vis (in $CHCl_3$) and ^{31}P NMR (in $CDCl_3$) data of $PdCI_2L_2$ complexes.

No.	L	Isomer	UV–vis (λ, nm)	^{31}P NMR $PdCl_2L_2$ (δ, ppm)	$\Delta = \delta_{compl} - \delta_L$	^{31}P NMR OPR_3 (δ, ppm)	θ (°)[a]
1	PPh_2(O-*t*-Bu)	*trans*	348	79.0	37.5	34.0	155[b]
2	PPh_3	*trans* (15)	345	23.4	29.4	28.1	145 (8)
3	PCy_3	*trans* (17)	344	24.8	13.9	50.0	170
4	$PPh_2(C_6F_5)$	*trans*	342	12.8	37.7	20.9	158 (8)
5	$PPh_2(OC_6F_5)$	*trans*	342	79.0	–3.1	27.8	145
6	PPh_2(O-3,5-$F_2C_6H_3$)	*cis*	342	79.2	–35.4	32.9	139
7	$P(OCH_2CF_3)_3$	*cis*	334	94.8	–45.1	–3.4	115
8	$PPh(C_6F_5)_2$	*trans*	333	–5.93	40.5	7.9	167 (1), 171 (8)
9	PPh_2(OEt)	*cis*	330	109.5	–22.5	31.0	133 (8)
10	PPh_2(O-*n*-Bu)	*cis*	326	109.3	–2.8	31.7	133
11	$P(OPh)_3$	*cis* (18)	320	83.7	–42.3	–17.0	128 (8)
12	$P(C_6F_5)_3$	*trans* (16)	317	–26.8	47.6	–8.0	184 (8), 172 (1)
13	$P(OMe)_3$	*cis*	306	94.8	–30.5	2.0 (13)	107 (8)
14	$P(OEt)_3$[c]	*cis*	305	93.1	–46.3	–1.0 (13)	109 (8)

[a]Cone angle. References are given in parentheses.
[b]Calculated from the equation $\theta = 2/3\ \Sigma\theta_i/2$ (8).
[c]Not isolated.

The presence of fluorines in the phosphine phenyl ring, especially in *ortho*-positions, dramatically changes the steric properties of the ligand causing an increase of the cone angle (Θ), e.g., from 145° for PPh_3 to 184° for $P(C_6F_5)_3$ (8).

Long chain alkyl fluorinated phosphines, such as $P(CH_2CH_2(CF_2)_5CF_3)_3$, are successfully applied for catalytic processes in highly fluorinated solvents (9, 10).

Looking for good modifying ligands for palladium carbonylation catalysts, we selected fluorinated phosphorus ligands such as phosphines of the form $PPh_x(C_6F_5)_{3-x}$ (x = 0–2) and phosphinites of the form $PPh_2(OC_6F_5)$ and PPh_2(O-3,5-$F_2C_6H_3$) for systematic studies of the electronic and steric effects of ligands on the structural and catalytic properties of $PdCl_2L_2$-type palladium complexes.

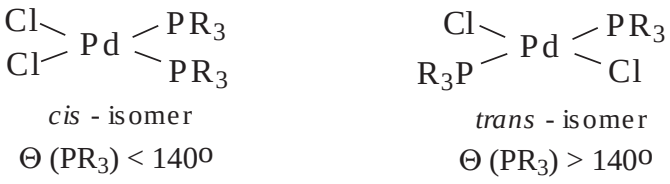
It was particularly interesting to test complexes with ligands that are bulky and simultaneously have a strong acceptor character (low basicity). Recently, we found a new Pd(0)–triphenylphosphite complex formation reaction when $PdCl_2[P(OPh)_3]_2$ was treated with NEt_3 (11). Although triphenylphosphite is a stronger π-acceptor, it has relatively small cone angle (Θ = 128°), and the question arises how the same reaction with NEt_3 would proceed in the case of more bulky fluorinated phosphines. To supplement the series of complexes under study and to be able to draw more general conclusions, we prepared palladium complexes with nonfluorinated phosphites ($P(OPh)_3$, $P(OMe)_3$, $P(OEt)_3$) and phosphinites (PPh_2(OEt), PPh_2(O-*n*-Bu), PPh_2(O-*t*-Bu)) for comparison.

Results and discussion

$PdCl_2L_2$-type complexes

The palladium complexes that we used for spectroscopic and catalytic studies were prepared by substitution of cyclooctadiene (cod) in $PdCl_2$(cod) with a suitable phosphorus ligand. All complexes were isolated and characterized by spectroscopic and analytical methods (Table 1, and see *Experimental*).

Scheme 1.



Square planar complexes of the $PdCl_2L_2$ type can exist as two isomers, *cis* and *trans* (14). Some of the compounds listed in Table 1, namely $PdCl_2L_2$ (L = PPh_3, $P(C_6F_5)_3$, $P(OPh)_3$, PCy_3) had been characterized earlier by X-ray crystallography (14–18), and the presence of *trans*-isomers was confirmed for complexes with bulky ligands, e.g., *trans*-$PdCl_2(PPh_3)_2$ (15), *trans*-$PdCl_2[P(C_6F_5)_3]_2$ (14), and *trans*-$PdCl_2(PCy_3)_2$ (17). The phosphites and phosphinites, on the other hand, preferentially formed *cis*-isomers (14), as was recently confirmed by the structure of *cis*-$PdCl_2[P(OPh)_3]_2$ (8) and the structure of *cis*-$PdCl_2[PPh_2(OEt)]_2$ in this paper. On the basis of the literature data (14–18), we assigned *cis* or *trans* geometry for all complexes under study (Table 1) according to the general rule shown in Scheme 1. The only doubtful structure is that of $PdCl_2[PPh_2(OC_6F_5)]_2$, which decomposes during recrystallization thereby making it impossible to determine the structure via X-ray crystallography. The cone angle of the $PPh_2(OC_6F_5)$ ligand, calculated from the molecular structure of the platinum complex (3), is 145°, and by analogy with *trans*-$PdCl_2(PPh_3)_2$ (Θ for PPh_3 = 145°), we proposed a *trans* geometry for $PdCl_2[PPh_2(OC_6F_5)]_2$.

It is important to note that the presence of only one ^{31}P NMR signal in the spectrum of each of the palladium complexes suggested the presence of only one isomer in solution.

UV–vis spectra

Spectroscopic data for the $PdCl_2L_2$ complexes are presented in Table 1. All of the complexes display one elec-

© 2001 NRC Canada

Fig. 1. Correlation between the UV–vis band position (λ, nm) of $PdCl_2L_2$ complexes in $CHCl_3$ and the ^{31}P NMR chemical shift (δ, ppm) of respective phosphine oxides OPR_3; **1** PPh_2(O-*t*-Bu), **2** PPh_3, **3** PCy_3, **4** $PPh_2(C_6F_5)$, **5** $PPh_2(OC_6F_5)$, **6** PPh_2(O-3,5-$F_2C_6H_3$), **7** $P(OCH_2CF_3)_3$, **8** $PPh(C_6F_5)_2$, **9** PPh_2(OEt), **10** PPh_2(O-*n*-Bu), **11** $P(OPh)_3$, **12** $P(C_6F_5)_3$, **13** $P(OMe)_3$, **14** $P(OEt)_3$. *cis*-$PdCl_2L_2$ (●), *trans*-$PdCl_2L_2$ (○).

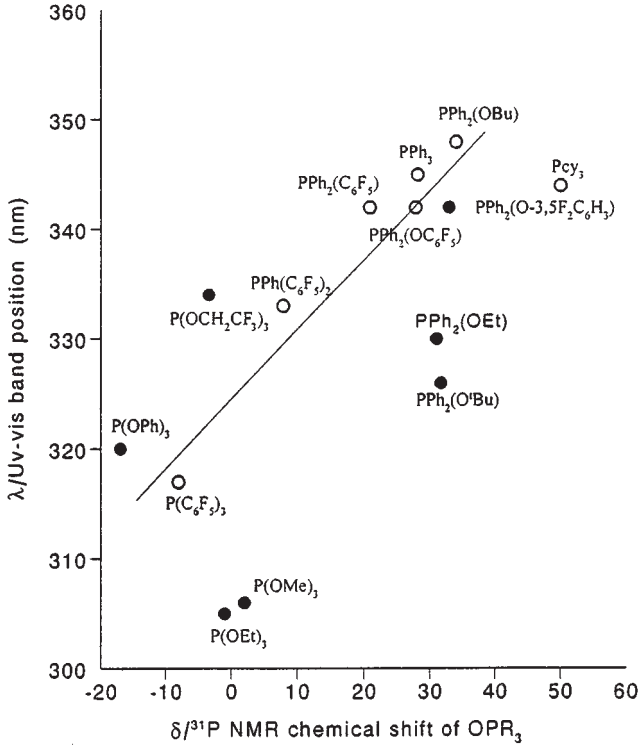
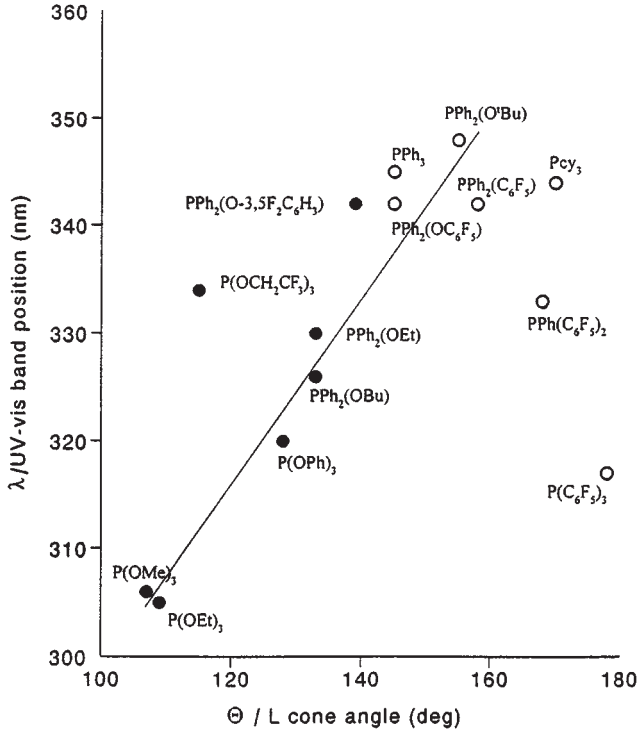


Fig. 2. Correlation between the UV–vis band position (λ, nm) of $PdCl_2L_2$ complexes in $CHCl_3$ and the cone angles (θ) of respective phosphines (L) **1** PPh_2(O-*t*-Bu), **2** PPh_3, **3** PCy_3, **4** $PPh_2(C_6F_5)$, **5** $PPh_2(OC_6F_5)$, **6** PPh_2(O-3,5-$F_2C_6H_3$), **7** $P(OCH_2CF_3)_3$, **8** $PPh(C_6F_5)_2$, **9** PPh_2(OEt), **10** PPh_2(O-*n*-Bu), **11** $P(OPh)_3$, **12** $P(C_6F_5)_3$, **13** $P(OMe)_3$, **14** $P(OEt)_3$. *cis*-$PdCl_2L_2$ (●), *trans*-$PdCl_2L_2$ (○).



tronic transition (λ) in the 300–350 nm region of the UV–vis spectrum, as similarly reported for other palladium(II) complexes with phosphorus ligands (12). In the group of complexes studied, the band is shifted from 348 nm for $PdCl_2[PPh_2$(O-*t*-Bu)$]_3$ to 305 nm for $PdCl_2[PPh_2(OEt)]_2$, showing a dependence on the type of phosphorus ligand coordinated to palladium. The influence of the phosphorus ligand on the spectroscopic properties of metal complexes can be discussed in terms of two types of effects; electronic and steric, which could not be separated and considered as totally independent effects. In the group of palladium complexes under study, we can however, discuss the domination of electronic or steric influence of the ligand on the spectroscopic properties of the compound.

To characterize the influence of the electronic properties of the phosphorus ligand coordinated to palladium on the UV–vis spectrum of the complex, we plotted the relationship between the band position (λ) and the ^{31}P NMR chemical shift of phosphine oxides (δ_{OPR_3}) (13) (Fig. 1).

The selection of this parameter was based on Derenesceyi's demonstration (13) that the carbonyl stretching frequency (ν(CO)) of $Ni(CO)_3PR_3$, being the measure of the electronic properties of PR_3, is linearly correlated with the ^{31}P NMR chemical shift of OPR_3 (δ). The linear correlation is fairly good only for *trans*-$PdCl_2L_2$ with fluorinated phosphines (L = $PPh_x(C_6F_5)_{3-x}$ (x = 0–3)) (Fig. 1).

Another correlation, between the UV–vis band position (λ) and the phosphine cone angle (Θ), was plotted because of the estimation of the influence of the steric effect of the ligand on the spectroscopic properties of palladium complexes (Fig. 2). This correlation is also not satisfactory as it still shows some deviations from linearity. However, it allows one to conclude that the band position in the spectra of $PdCl_2L_2$ complexes are dependent on both the electronic and steric properties of ligand L.

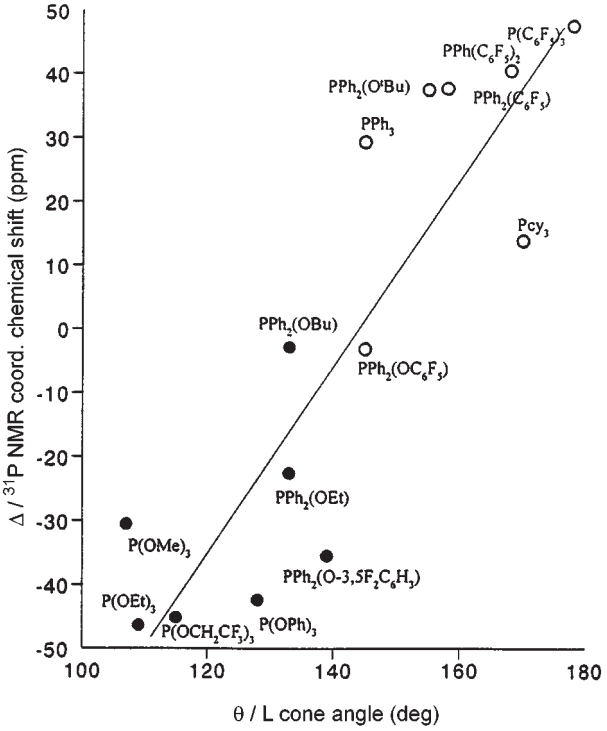
^{31}P NMR spectra

The chemical shift of the ^{31}P NMR signal, being strongly dependent on the kind of phosphorus ligand, is not very informative (Table 1). However, the coordination chemical shift (Δ), defined as the difference in the ^{31}P NMR chemical shift between coordinated and free phosphine ($\Delta = \delta_{coord.} - \delta_L$), can be used to compare structurally similar complexes with different phosphorus ligands (8). The coordination chemical shift can also be used for the estimation of bond strength, as was demonstrated for $PtCl_2L_2$ complexes with fluorinated phosphines (2).

We found that the coordination chemical shift (Δ) of complexes under study increases with increase of phosphine cone angle (Θ) (Fig. 3), as was similarly reported for $RhCl(CO)(PR_3)_2$ complexes (8). The lowest (negative) values of Δ were found for complexes with less bulky phosphorus ligands (Θ < 140°), existing as *cis*-isomers. The coordination of these ligands to palladium causes an upfield shift of

© 2001 NRC Canada

Fig. 3. Correlation between the ^{31}P NMR coordination chemical shift ($\Delta = \delta_{coord.} - \delta_L$) of $PdCl_2L_2$ complexes in $CHCl_3$ and the cone angles (θ) of the phosphorus ligand (L). **1** PPh_2(O-*t*-Bu), **2** PPh_3, **3** PCy_3, **4** $PPh_2(C_6F_5)$, **5** $PPh_2(OC_6F_5)$, **6** PPh_2(O-3,5-$F_2C_6H_3$), **7** $P(OCH_2CF_3)_3$, **8** $PPh(C_6F_5)_2$, **9** PPh_2(OEt), **10** PPh_2(O-*n*-Bu), **11** $P(OPh)_3$, **12** $P(C_6F_5)_3$, **13** $P(OMe)_3$, **14** $P(OEt)_3$. *cis*-$PdCl_2L_2$ (●), *trans*-$PdCl_2L_2$ (○).



the ^{31}P NMR signal as compared with the free ligand and as a consequence leads to a negative coordination shift. The highest (positive) values of Δ were noted for *trans*-complexes with bulky ligands ($\Theta > 140°$). Changes in coordination chemical shift (Δ) were explained by changes in SPS angles (angles between substituents on trivalent phosphorus upon coordination of phosphine to metal) (8).

Attempts to correlate both the ^{31}P NMR parameters; the coordination chemical shift (Δ) and the chemical shift of phosphine oxides (δ), failed.

Reactions of $PdCl_2L_2$ complexes with CO and NEt_3

A $PdCl_2L_2$ complex used as a carbonylation reaction catalyst precursor should first undergo reduction to a palladium(0) complex. We recently found that $PdCl_2[P(OPh)_3]_2$ is reduced to a Pd(0) species by NEt_3, even in aprotic solvents such as CH_2Cl_2 or C_6H_6 (11) (eq. [1]).

$$[1]\quad PdCl_2[P(OPh)_3]_2 + nNEt_3 \rightarrow Pd[(P(OPh)_3]_4 + Pd[P(OPh)_3]_x[(NEt_3)]_{4-x}$$

$x = 1–3$

The $PdCl_2(PPh_3)_2$ complex under similar conditions exhibits different reactivity, forming a carbomethoxy complex (eq. [2]) (19):

$$[2]\quad PdCl_2(PPh_3)_2 + CO + NEt_3 + MeOH \rightarrow PdCl(C(O)OMe)(PPh_3)_2 + HNEt_3Cl$$

Table 2. ν(CO) frequencies observed for $Pd(CO)_xL_y$ ($x + y = 4$) complexes in KBr.

L	ν(CO) (cm^{-1})
PPh_2(OEt)	1816 (m), 1876 (vs), 1896 (s), 1916 (vs)
PPh_2(OBu)	1809 (m), 1846 (s), 1876 (vs), 1896 (vs), 1942 (m)
$P(OCH_2CF_3)_3$	1876 (vs), 1920 (m)
$P(OPh)_3$	1810 (m), 1849 (m), 1876 (s), 1893 (s), 1926 (m)
$P(OMe)_3$	1822 (m), 1883 (vs), 1903 (vs), 1916 (vs)

When a tertiary amine was replaced by a secondary one, a mixture of Pd(0) carbonyls, $Pd(CO)_x(PPh_3)_y$ ($x + y = 4$), was identified in the reaction product (eq. [3]) (19):

$$[3]\quad PdCl_2(PPh_3)_2 + CO + HNR^1R^2 + MeOH \rightarrow Pd(CO)(PPh_3)_3 + Pd_3(CO)_3(PPh_3)_4 + H_2NR^1R^2Cl$$

The $PdCl_2L_2$ complexes react with CO in the presence of NEt_3, giving products depending on the phosphorus ligand used.

Palladium complexes with fluorinated phosphines ($PPh_x(C_6F_5)_{3-x}$ ($x = 0–2$)) treated with CO (1 atm) in methanol containing an excess of NEt_3 ([NEt_3]:[Pd] = 5) did not give any new products, even after 24 h. In contrast, complexes with less bulky phosphines react with CO forming the respective palladium carbonyls in about 20 min (eq. [4]). The carbonyls were identified by IR spectra and showed ν(CO) bands of terminally bonded CO-ligands at ca. 1900 cm^{-1} (Table 2).

$$[4]\quad PdCl_2L_2 + CO + NEt_3 + MeOH \rightarrow Pd(CO)_x(L)_y + HNEt_3Cl$$

$L = PPh_2$(OEt), PPh_2(O-*n*-Bu), $P(OPh)_3$, $P(OCH_2CF_3)_3$, $P(OMe)_3$

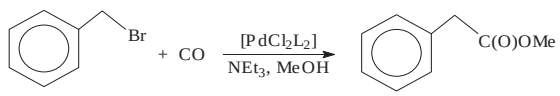
$x + y = 4$

It is worth mentioning that carbomethoxy complexes were not identified during rxn. [3] nor in its final product.

It is reasonable to propose that NEt_3 acts as a reducing agent with respect to all complexes mentioned in rxn. [4], and the presence of methanol is not necessary, as palladium carbonyls were also obtained in reactions of $PdCl_2[P(OPh)_3]_2$ or $PdCl_2[PPh_2(O\text{-}n\text{-}Bu)]_2$ with CO and NEt_3 in CH_2Cl_2 as a solvent.

Catalytic activity of $PdCl_2L_2$ complexes in benzyl bromide carbonylation

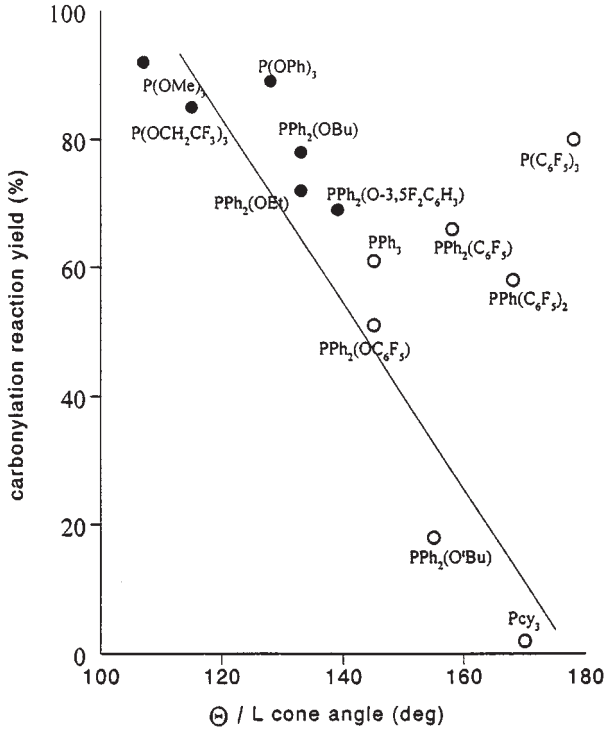
A test of the catalytic activity of $PdCl_2L_2$ complexes in the carbonylation of benzyl bromide to phenylacetic acid methyl ester was performed under standard conditions of 40°C and 1 atm of CO in MeOH (eq. [5]).

[5] 

The results are summarized in Fig. 4 in the form of a correlation between the yield of phenylacetic acid methyl ester and the cone angle of the phosphorus ligand (Θ). It can be

© 2001 NRC Canada

Fig. 4. Dependence of the benzyl bromide carbonylation reaction yield on the cone angle (θ) of phosphorus ligand (L) coordinated in $PDCl_2L_2$ complex. **1** PPh_2(O-*t*-Bu), **2** PPh_3, **3** PCy_3, **4** $PPh_2(C_6F_5)$, **5** $PPh_2(OC_6F_5)$, **6** PPh_2(O-3,5-$F_2C_6H_3$), **7** $P(OCH_2CF_3)_3$, **8** $PPh(C_6F_5)_2$, **9** PPh_2(OEt), **10** PPh_2(O-*n*-Bu), **11** $P(OPh)_3$, **12** $P(C_6F_5)_3$, **13** $P(OMe)_3$, **14** $P(OEt)_3$. *cis*-$PdCl_2L_2$ (●), *trans*-$PdCl_2L_2$ (○).



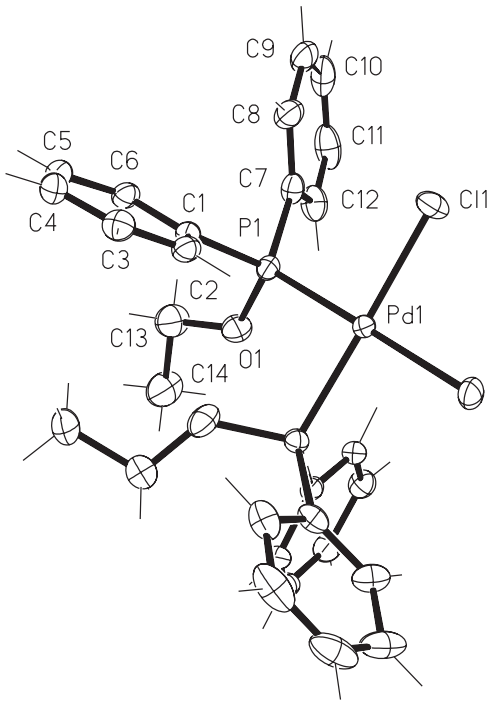
concluded that palladium complexes with less crowded phosphorus ligands ($P(OMe)_3$, $P(OPh)_3$, PPh_2(O-*n*-Bu)) exhibit higher catalytic activity, producing ca. 90% of the phenylacetic acid methyl ester. This is in agreement with the observation that these complexes undergo easier reduction to palladium(0) species when treated with CO and NEt_3 (eq. [4]). Therefore, the higher catalytic activity can be explained by the higher concentration of the active form of the catalyst, a Pd(0) complex, which activates benzyl bromide by an oxidative addition reaction. It is interesting to note that palladium complexes with fluorinated phosphines ($PPh_x(C_6F_5)_{3-x}$, x = 1 or 2) exhibit higher catalytic activity than expected on the basis of the correlation presented in Fig. 4. In these cases, the electronic effect of phosphine seems to be dominating over the steric effect.

The formation of black palladium metal at the end of some carbonylation reactions was observed, i.e., in reactions with *cis*-$PdCl_2[P(OCH_2CF_3)_3]_2$ and *cis*-$PdCl_2[P(OPh)_3]_2$. However, the good yields of carbonylation products in these reactions show that the benzyl bromide carbonylation reaction is faster than palladium reduction. It was found earlier (20) that palladium black is not catalytically active.

X-ray crystal structure of *cis*-$PdCl_2[PPh_2(OEt)]_2$

The molecular structure of the *cis*-$PdCl_2[PPh_2(OEt)]_2$ complex is shown in Fig. 5, and selected bond distances and angles are given in Table 3. The complex is of square-planar

Fig. 5. Molecular structure of *cis*-$PdCl_2[PPh_2(OEt)]_2$ (**9**).



geometry with P-Pd-Cl angles of 178.54(3) and 89.40(3)°, respectively.

The Pd—P distance (2.2474(8) Å) in *cis*-$PdCl_2[PPh_2(OEt)]_2$ is significantly shorter than corresponding Pd—P distances in *trans*-$PdCl_2L_2$ complexes with L = PPh_3 (15), $P(C_6F_5)_3$ (16), PCy_3 (17). In the series of these complexes, a gradual shortening of Pd—P distances is observed as ligand's (L) basicity decreases from 2.3628(9) Å in *trans*-$PdCl_2(PCy_3)_2$ (17) to 2.3051(12) Å in *trans*-$PdCl_2[P(C_6F_5)_3]_2$ (16). The basicity of PPh_2(OEt) is expected to be intermediate between that of PPh_3 and $P(C_6F_5)_3$, and therefore, the order of decreasing basicity is as follows: $PCy_3 > PPh_3 > PPh_2(OEt) > P(C_6F_5)_3$. Thus, the Pd—P bond in *cis*-$PdCl_2[PPh_2(OEt)]_2$ should be longer compared to that in *trans*-$PdCl_2[P(C_6F_5)_3]_2$, which was not observed. On the other hand, the Pd—P bond in complex *cis*-$PdCl_2[PPh_2(OEt)]_2$ is only slightly longer than that in *cis*-$PdCl_2(P(OPh)_3)_2$ (2.2299(11) and 2.2314(12) Å, respectively) (18), because of the higher basicity of the PPh_2(OEt) ligand compared with that of $P(OPh)_3$. The observed shortening of the Pd—P distance in the *cis*-$PdCl_2[PPh_2(OEt)]_2$ and other *cis*-$PdCl_2L_2$ complexes with respect to *trans*-$PdCl_2L_2$ complexes is consistent with the stronger *trans* influence of a phosphorus ligand than that of a chloride ligand. The Pd—Cl bond length in *cis*-$PdCl_2[PPh_2(OEt)]_2$ (2.3430(8) Å) is similar to those found in *cis*-$PdCl_2(P(OPh)_3)_2$ (2.3273(11) and 2.3354(11) Å) (18) and *cis*-$PdCl_2[PPh_2(OMe)]_2$ (2.349(8) and 2.358(6) Å) (21). In the *trans*-$PdCl_2L_2$ complexes mentioned above the respective distances are ca. 0.04 Å longer. The conformation of PPh_2(OEt) ligand is slightly different from that of PPh_2(OEt), which is illustrated by smaller Pd-P-O angles, 118.6(7) and 115.5(6)° in *cis*-$PdCl_2[PPh_2(OMe)]_2$ (21) and 108.19(10)° in *cis*-$PdCl_2[PPh_2(OEt)]_2$.

© 2001 NRC Canada

Table 3. Selected bond lengths (Å) and angles (°) for $PdCI_2[PPh_2(OEt)]_2$.

Bond lengths (Å)	
Pd(1)—P(1)	2.2474(8)
Pd(1)—P(1)′	2.2474(8)
Pd(1)—Cl(1)′	2.3430(8)
Pd(1)—Cl(1)	2.3430(8)
P(1)—O(1)	1.620(3)
P(1)—C(7)	1.804(4)
P(1)—C(1)	1.809(3)
O(1)—C(13)	1.409(5)
C(13)—C(14)	1.505(6)
Bond angles (°)	
P(1)-Pd(1)-P(1)′	89.97(4)
P(1)-Pd(1)-Cl(1)′	178.54(3)
P(1)′-Pd(1)-Cl(1)′	89.40(3)
P(1)-Pd(1)-Cl(1)	89.40(3)
P(1)′-Pd(1)-Cl(1)	178.54(3)
Cl(1)′-Pd(1)-Cl(1)	91.26(4)
O(1)-P(1)-C(7)	103.11(15)
O(1)-P(1)-C(1)	109.04(14)
C(7)-P(1)-C(1)	105.07(15)
O(1)-P(1)-Pd(1)	108.19(10)
C(7)-P(1)-Pd(1)	118.19(11)
C(1)-P(1)-Pd(1)	112.60(11)

Note: Symmetry transformations used to generate equivalent atoms (′): $-x + 1, y, -z + 1/2$.

Experimental

General

All syntheses were conducted under dry dinitrogen using the Schlenk technique. Ethyl ether and THF were dried prior the use by distilling over sodium. Methanol was distilled over Mg, triethylamine was dried over KOH and distilled. C_6H_6 and CH_2Cl_2 have been purified according to the standard methods (22). Compounds $C_6H_5CH_2Br$, $PClPh_2$, and PCl_2Ph were purchased from Aldrich and used without purification. $P(C_6F_5)_3$ was purchased from Strem Chemicals. $PdCl_2(cod)$ was obtained according to the literature method (23).

NMR spectra were recorded with Bruker 300 spectrometer and chemical shifts are given vs. TMS (^1H) and vs. 85% H_3PO_4 (^{31}P). Abbreviations used in multiplicities are: singlet (s), doublet (d), triplet (t), quartet (q), and virtual quartet (vq). IR spectra were measured with FT-IR Nicolet Impact 400 instrument. UV–vis spectra were measured with an HP 4852 Diode Array spectrophotometer. GC–MS analyses were carried out with HP 5890 II linked to an HP 5971 A mass detector.

Ligand syntheses

*Syntheses of fluorophenyl phosphines (**2**)*

Diphenyl pentafluorophenyl phosphine ($PPh_2(C_6F_5)$): Bromopentafluorobenzene (2.46 g, 10 mM) was added to a suspension of activated magnesium (0.3 g, 1.2 equiv) in freshly distilled THF (100 mL). The reaction mixture was stirred and heated under reflux until almost all magnesium reacted (~40 min). The reaction mixture was cooled to –30°C and distilled chlorodiphenyl phosphine (1.8 mL, 2.21 g, 10 mM) was added. The cooling bath was removed and the whole mixture was stirred overnight.

The THF was removed on rotary evaporator and the remaining oil was dissolved in methanol (30 mL) and evaporated (3 times). The oil was extracted with dry ethyl ether (3 times), the extracts were collected, and evaporated. The residue was extracted with hot petroleum ether (PE) (bp 40–60°C), the extracts were treated with charcoal, and evaporated. The crude phosphine (1.9 g, 54%) was recrystalized from PE–methanol to give 1.2 g (37.5%) of white crystals. mp 57–60°C (lit. mp (2) 65–68°C). GC–MS: single peak. MS *m*/*z*: 352. ^1H NMR ($CDCl_3$) δ: 7.35–7.45 (m). ^{31}P NMR ($CDCl_3$) δ: –24.9.

Phenyl di(pentafluorophenyl)phosphine ($PPh(C_6F_5)_2$): The compound was obtained in analogous manner as given above starting from bromopentafluorobenzene (20 mM) and dichlorophenylphosphine (1.38 mL, 1.82 g, 10 mM). The attempted crystallization failed so the phosphine was purified chromatographically on basic alumina with ethyl acetate – hexane (1:1 v/v) as the eluent. The obtained red oil was frozen at –10°C. A small sample of the waxy substance was dissolved in dry methanol and allowed to evaporate slowly. A few reddish crystals obtained were then used to initialize crystallization of the remaining wax. The reddish crystals were recrystallized from methanol (2 times) giving the 2.1 g of the white phosphine (38%). mp 68°C, (lit. (2) mp 68–70°C) GS–MS-MS *m*/*z*: 442. ^{31}P NMR ($CDCl_3$) δ: –46.4.

Syntheses of phosphinous esters and their palladium complexes ($PdCl_2L_2$)

Our attempts to synthesize pentafluorophenyl esters of (di)phenyl phosphinous acid by the literature method (applied for the synthesis of 2,6-difluorophenyldiphenyl phosphinite) (3) using pentafluorophenol, triethyl amine, and chlorodiphenyl phosphine failed. Based on NMR analysis (data not shown) we suppose that because of its acidic properties pentafluorophenol forms an adduct with the amine rather then reacting with chlorophosphine. Increasing the ratio of phenol and amine to chlorophosphine led to inhomogeneous mixture, which was very difficult to separate and purify. An additional problem of very fast hydrolysis of esters by atmospheric humidity was also observed. We, therefore, decided to use a less convenient indirect way based on the application of sodium methanolate for generation of appropriate phenolate, which in turn reacts with stoichiometric amounts of chlorodiphenyl phosphine in ethyl ether.

Preparation of sodium salts of phenols $Na(OC_6F_5)$ and $Na(O\text{-}3,5\text{-}F_2C_6H_3)$: Metallic sodium was reacted with dry methanol. When all the metal was dissolved, a stochiometric amount of appropriate phenol was added, mixed, and then the methanol was removed on rotary evaporator. To the white product was added dry ethyl ether, mixed, evaporated (3 times), and dried in vacuo.

*Preparation of pentafluorophenyl diphenylphosphinite and $PdCl_2[PPh_2(OC_6F_5)]_2$ (**5**)*: Dry sodium pentafluorophenolate (0.486 g, 2.3 mM) was dissolved in a Schlenk flask in dry ethyl ether and cooled. A solution of of chlorodiphenyl-

© 2001 NRC Canada

phosphine (0.42 mL, 0.52 g, 2.3 mM) in ethyl ether (10 mL) of was added at once. The formation of sodium chloride occurred immediately. The mixture was stirred overnight. The NaCl was filtered off and solid $PdCl_2$(cod) (0.5 equiv) was added to the filtrate. The mixture was stirred 30 min and the yellow product was filtrated off and dried. ^{1}H NMR ($CDCl_3$) δ: 7.22 (t), 7.36 (t), 7.55 (q, Ph). Anal. calcd. for $C_{36}H_{20}Cl_2F_{10}O_2P_2Pd$: C 47.3, H 2.2; found: C 47.5, H 2.6.

Preparation of (3,5-difluorophenyl) diphenylphosphinite and $PdCl_2[PPh_2(O\text{-}3,5\text{-}F_2C_6H_3)]_2$ ***(6)***: Dry sodium 3,5-difluorophenolate (0.746 g, 5.2 mM) was allowed to react at 0°C with chlorodiphenyl phosphine (0.66 mL, 0.86 g, 3.9 mM) for 2 days. The insoluble salts were filtered off and the solution was used immediately to prepare the palladium complex (**6**) by the method given for (**5**). Yield: 78%. ^{1}H NMR ($CDCl_3$) δ: 6.1 (dd, $J_{H,F}$ = 8 Hz, $J_{H,H}$ = 2.0 Hz), 6.5 (dt, 3,5-$F_2C_6H_3$), 7.38 (t), 7.51 (vt), 7.75 (vq, Ph). Anal. calcd. for $C_{36}H_{26}Cl_2F_4O_2P_2Pd$: C 53.7, H 3.3; found: C 52.7, H 3.3.

Preparation of tert-*butyl diphenylphosphinite and* $PdCl_2[PPh_2(O\text{-t-}Bu)]_2$ ***(1)***: PPh_2(O-*t*-Bu) was prepared by reacting potassium *tert*-butanolate (0.634 g, 5.2 mM) with chlorodiphenyl phosphine (0.70 mL, 0.86 g, 3.9 mM) for 2 days. To the filtrated ether solution was added $PdCl_2$(cod) (0.5 equiv), and the complex (**1**) was isolated after 10 h of stirring of the mixture as a dark yellow powder (yield 85%). ^{1}H NMR ($CDCl_3$) δ: 0.2 (CH_3), 7.22 (t), 7.34 (d), 7.54 (q, Ph). Anal. calcd. for $C_{32}H_{48}Cl_2O_2P_2Pd$: C 54.6, H 6.9; found: C 54.7, H 6.3.

Preparation of ethyl diphenylphosphinite and $PdCl_2[PPh_2(OEt)]_2$ ***(9)***: PPh_2(OEt) was synthesized analogously to the butyl analog using sodium ethanolate (0.316 g, 4.6 mM) and chlorodiphenyl phosphine (0.83 mL, 1.03 g) in ether (30 mL) for 3 days. The addition of $PdCl_2$(cod) (0.5 equiv) and stirring of the mixture for 30 min allowed the formation of complex (**9**) with 90% yield. The crystals for X-ray studies were obtained by recrystallization of the yellow powder from CH_2Cl_2–EtOH. ^{1}H NMR ($CDCl_3$) δ: 0.96 (t, $J_{H,H}$ = 7 Hz, CH_3), 3.67 (q, CH_2), 7.38 (m), 7.48 (m), 7.76 (m, Ph). Anal. calcd. for $C_{28}H_{30}Cl_2O_2P_2Pd$: C 52.7, H 4.7; found: C 52.1, H 4.4.

Other syntheses

The other $PdCl_2L_2$ complexes have been obtained in reaction of $PdCl_2$(cod) with 2 mol equiv of phosphorus ligands in C_6H_6, CH_2Cl_2, or $(C_2H_5)_2O$. Depending on the solubility they have been isolated as precipitates or after solvent evaporation. In all cases the products have been washed by ethyl ether and dried in vacuo. The preparation and spectroscopic data of $PdCl_2[PPh_2(O\text{-}n\text{-}Bu)]_2$ (**10**) and $PdCl_2[P(OPh)_3]_2$ (**11**) are reported in ref. 11.

$PdCl_2[PPh_2(C_6F_5)]_2$ ***(4)***: ^{1}H NMR ($CDCl_3$) δ: 7.42 (t), 7.51 (t), 7.86 (q, Ph). Anal. calcd. for $C_{36}H_{20}Cl_2F_{10}P_2Pd$: C 49.0, H 2.3; found: C 49.9, H 3.0.

$PdCl_2[PPh(C_6F_5)_2]_2$ ***(8)***: ^{1}H NMR ($CDCl_3$) δ: 7.40 (t), 7.48 (t), 7.83 (q, Ph). Anal. calcd. for $C_{36}H_{10}Cl_2F_{20}P_2Pd$: C 40.7, H 1.0; found: C 40.7, H 1.0.

$PdCl_2[PCy_3]_2$ ***(3)***: ^{1}H NMR ($CDCl_3$) δ: 1.24 (s), 1.68 (m), 1.95 (d), 2.49 (m, CH_2). Anal. calcd. for $C_{36}H_{66}Cl_2P_2Pd$: C 58.6, H 9.0; found: C 58.0, H 8.5.

$PdCl_2[P(OCH_2CF_3)_3]_2$ ***(7)***: Anal. calcd. for $C_{12}H_{12}Cl_2F_{18}O_6P_2Pd$: C 17.3, H 1.5; found: C 17.1, H 1.2.

$PdCl_2[P(OMe)_3]_2$ ***(13)***: Compound **13** was obtained in reaction of $PdCl_2$(cod) with a fourfold excess of $P(OPh)_3$ in MeOH (yield 50%). ^{1}H NMR ($CDCl_3$) δ: 1.2 (s, CH_3). Anal. calcd. for $C_6H_{18}Cl_2O_6P_2Pd$: C 16.3 H 4.1; found: C 16.9, H 4.3.

Reactions of $PdCl_2L_2$ complexes with CO and NEt_3

In the typical experiment, MeOH (1 mL) and NEt_3 (ca. 0.01 mL) were added consecutively under dinitrogen to the palladium complex (0.05 g). The Schlenk tube was filled twice with CO and the solution was stirred under CO atmosphere for 30 min. The resulting precipitate of palladium carbonyl complex was filtrated off, dried, and analyzed by IR. The products decompose in the presence of air in ca. 30 min.

Carbonylation reaction of benzyl bromide

To the thermostated glass reactor (40°C), was added under a N_2 atmosphere MeOH (1.5 mL), NEt_3 (1.5 mL), and benzyl bromide (0.5 mL), the mixture was stirred for 1 min and then the catalyst (2.45×10^{-5} mol) in small teflon vessel was added. The reactor was connected with the CO-container (1 atm), flushed twice with CO, and left for 2 h with magnetic stirring. After that time, the reaction mixture was treated with HCl up to pH ca. 7. The reaction products were extracted with ethyl ether (1 mL) and analyzed by GC–MS.

X-ray crystallography

X-ray crystal data, together with refinement details, are given in Table 4. All measurements of crystal were performed on a Kuma KM4CCD κ-axis diffractometer with graphite-monochromated Mo Kα radiation. The crystal was positioned at 65 mm from the KM4CCD camera, and 612 frames were measured at 0.75° intervals with a counting time of 20 s. The data were corrected for Lorentz and polarization effects. No absorption correction was applied. Data reduction and analysis were carried out with the Kuma Diffraction (Wroclaw) programs. The structure was solved by direct methods (program SHELXS 97 (24)) and refined by the full-matrix least-squares method on all F^2 data using the SHELXL 97 (25) programs. Nonhydrogen atoms were refined with anisotropic thermal parameters; hydrogen atoms were included from geometry of molecules and Δρ maps but were not refined.

Conclusions

The attempts to correlate the spectroscopic (UV–vis, ^{31}P NMR) data of $PdCl_2L_2$ complexes with the steric and electronic parameters of phosphorus ligands (L) show a dominating influence of the steric over the electronic effect. Correlations between ^{31}P NMR coordination chemical shifts (Δ) and the cone angles (Θ) of L on the other are not perfect, but strong enough to show the tendency and directions

© 2001 NRC Canada

Table 4. Crystal data and structure refinement.

Empirical formula	$C_{28}H_{30}O_2Cl_2P_2Pd$
FW	318.88
T (K)	100(1)
λ (Å)	0.71073
Crystal system	Orthorhombic
Space group	*Pbcn*
a (Å)	10.5041(6)
b (Å)	16.4709(10)
c (Å)	15.1275(11)
V (Å^3)	2617.2(3)
Z	4
D_c (Mg m^{-3})	1.619
μ (mm^{-1})	1.061
F(000)	1296
Crystal size (mm)	0.15 × 0.10 × 0.10
Diffractometer	Kuma KM4CCD
θ range for data collection (°)	3.42–28.74
h, k, and l ranges	–14–8, –21–21, –19–19
Reflections collected	17459
Independent reflections (R_{int})	3217 (0.0384)
Data/parameters	3217/160
Weighting scheme: a, b, c^a	0.0296, 9.32, 3
GoF (F^2)	1.141
Final R_1/wR_2 indices ($I > 2\sigma_I$)	0.0484/0.0975
Largest diff. peak and hole (e Å^{-3})	1.480/–1.022

[a] $w = 1/[\sigma^2(F_o^2) + (aP)^2 + bP]$ where $P = [\mathrm{Max}(F_o^2, 0) + F_c^2]/c$.

of changes. The most important conclusion of the reported studies is the finding that the catalytic activity of $PdCl_2L_2$ complexes in the carbonylation of benzyl bromide also depends mainly on the steric properties of L and thus on the *cis–trans* geometry of the starting complex. Complexes with less sterically hindered ligands (phosphites, phosphinites) having *cis* structure are more active than those with bulky ligands (Θ > 140°, e.g., PCy_3, PPh_2(O-*t*-Bu)). An exception should, however, be noted for complexes with bulky fluorinated phosphines ($PPh_x(C_6F_5)_{3-x}$, x = 0–2), which are *trans*-isomers that exhibit unexpectedly high catalytic activity.

Acknowledgments

This work was supported by KBN (State Committee for Research) project 3T09A 061 15. The authors would like thank Ms. Iwona Lankiewicz for technical assistance.

References

1. C. Corcoran, J. Fawcett, S. Friedrichs, J.H. Holloway, E.G. Hope, D.R. Russell, G.C. Saunders, and A.M. Stuart. J. Chem. Soc. Dalton Trans. 161 (2000).
2. R.D.W. Kemmitt, D.I. Nichols, and R.D. Peacock. J. Chem. Soc. A, 2149 (1968).
3. M.J. Atherton, J. Fawcett, A.P. Hill, J.H. Holloway, E.G. Hope, D.R. Russell, G.C. Saunders, and R.M.J. Stead. J. Chem. Soc. Dalton Trans. 1137 (1997).
4. M.J. Atherton, J. Fawcett, J.H. Holloway, E.G. Hope, D.R. Russell, and G.C. Saunders. J. Chem. Soc. Dalton Trans. 2217 (1997).
5. M.J. Atherton, K.S. Coleman, J. Fawcett, J.H. Holloway, E.G. Hope, A. Karacar, L.A. Peck, and G.C. Saunders. J. Chem. Soc. Dalton Trans. 4029 (1995).
6. M.J. Atherton, J. Fawcett, J.H. Holloway, E.G. Hope, A. Karacar, D.R. Russell, and G.C. Saunders. J. Chem. Soc. Dalton Trans. 3215 (1996).
7. M.J. Atherton, J. Fawcett, J.H. Holloway, E.G. Hope, S.M. Martin, D.R. Russell, and G.C. Saunders. J. Organomet. Chem. **555**, 67 (1998).
8. C.A. Tolman. Chem. Rev. **77**, 314 (1977).
9. U.S.A. Patent. 5 463 082 (1995).
10. J.J.J. Juliette, I.T. Horvath, and J.A. Gladysz. Angew. Chem. Int. Ed. Engl. **36**, 1610 (1997).
11. A.M. Trzeciak and J.J. Ziółkowski. Monatsh. Chem. **131**, 1281 (2000).
12. A.W. Verstuyft, D.A. Redfield, L.W. Cary, and J.H. Nelson. Inorg. Chem. **15**, 1128 (1976).
13. T.T. Derenesceyi. Inorg. Chem. **20**, 665 (1981).
14. A.T. Hutton and C.P. Morley. *In* Comprehensive coordination chemistry. The synthesis, reactions, properties and application of coordination compounds. Vol 5. *Edited by* G. Wilkinson. Pergamon Press, New York. 1987.
15. G. Ferguson, R. McCrindle, A.J. McAlees, and M. Parvez. Acta Crystallogr. Sect. B: Struct. Sci. **B38**, 2679 (1982).
16. B. Bertsch-Frank, and W. Frank. Acta Crystallogr. Sect. C: Cryst. Struct. Commun. **C52**, 328 (1996).
17. S.J. Sabounchei, A. Naghipour, and J.F. Bichley. Acta Cryst. **C56**, e280 (2000).
18. V.V. Grushin, C. Bensimon, and H. Alper. Inorg. Chem. **33**, 4804 (1994).
19. M. Hidai, M. Kokura, and Y. Uchida. J. Organomet. Chem. **52**, 431 (1973).
20. A.M. Trzeciak and J.J. Ziółkowski. J. Mol. Catal. A: Chem. **154**, 93 (2000).
21. D.R. Powell and R.A. Jacobson. Cryst. Struct. Comm. **9**, 1023 (1980).
22. D.D. Perrin, W.L.F. Armarego, and D.R. Perrin. Purifcation of laboratory chemicals. Pergamon, Oxford, England. 1986.
23. F.A. Cotton. Inorg. Synth. **XIII**, 52 (1972).
24. G.M. Sheldrick. SHELXS 97. Program for solution of crystal structures. University of Göttingen, Germany. 1997.
25. G.M. Sheldrick. SHELXL 97. Program for crystal structure refinement. University of Göttingen, Germany. 1997.

© 2001 NRC Canada

The fluxionality and crystal structures of $[Fe_3(CO)_{10}L_2]$ (L_2 = dppm, $(Ph_2P)_2NH$, $\{(EtO)_2P\}_2O$) and $[Fe_3(CO)_9(dppm)\{P(OMe)_3\}]$

Harry Adams, Sylvana C.M. Agustinho, Krystyna Chomka, Brian E. Mann, Stephen Smith, Clare Squires, and Sharon E. Spey

Abstract: The crystal structures of $[Fe_3(CO)_{10}L_2]$ (L_2 = dppm, $(Ph_2P)_2NH$, $\{(EtO)_2P\}_2O$) and $[Fe_3(CO)_9(dppm)\{P(OMe)_3\}]$ (dppm = $(Ph_2P)_2CH_2$) have been determined. $[Fe_3(CO)_{10}L_2]$ (L_2 = dppm, $(Ph_2P)_2NH$, $\{(EtO)_2P\}_2O$) adopt a stereochemistry in the crystal with the bidentate ligand across an unbridged Fe–Fe edge, resulting in one phosphorus ligand being unusually in the axial position. In contrast, $[Fe_3(CO)_9(dppm)\{P(OMe)_3\}]$ adopts a stereochemistry in the crystal with the bidentate ligand across the bridged Fe–Fe edge. The structures of the $[Fe_3(CO)_{10}L_2]$ (L_2 = dppm, $(Ph_2P)_2NH$, $\{(EtO)_2P\}_2O$) support the Mann concerted bridge – opening bridge – closing mechanism of carbonyl fluxionality rather than the Johnson libration mechanism. The fluxionality of the compounds in the ^{13}C NMR spectra is explained by a combination of the concerted bridge – opening bridge – closing, merry-go-round, and trigonal twist mechanisms, and $\Delta G^{\ddagger}$ values were determined.

Key words: iron carbonyls, crystal structures, ^{13}C NMR spectroscopy, fluxionality, mechanisms.

Résumé : On a déterminé les structures cristallines des complexes $[Fe_3(CO)_{10}L_2]$ (L_2 = dppm, $(Ph_2P)_2NH$, $\{(EtO)_2P\}_2O$) et $[Fe_3(CO)_9(dppm)[P(OMe)_3]$. Dans le cristal, le $[Fe(CO)_{10}L_2$ (L_2 = dppm, $(Ph_2P)_2NH$, $[(EtO)_2P]_2O$) adopte une stéréochimie comportant un ligand bidentate à travers une arête non pontée Fe–Fe; il en résulte qu'un ligand phosphoré se trouve de façon inhabituelle en position axiale. Par ailleurs, à l'état cristallin, le $[Fe_3(CO)_9(dppm)\{P(OMe)_3\}]$ adopte une stéréochimie avec un ligand bidentate à travers une arête Fe–Fe pontée. Les structures des complexes $[Fe_3(CO)_{10}L_2]$ (L_2 = dppm, $(Ph_2P)_2NH$, $\{(EtO)_2P\}_2O$) sont en accord le mécanisme d'ouverture et fermeture concertées de pont de Mann pour la fluxion du carbonyle plutôt que le mécanisme de libration de Johnson. La fluxion des composés dans les spectres RMN du ^{13}C est expliquée par les mécanismes d'ouverture et de fermeture concertées de pont et de carrousel et par des mécanismes trigonaux déformés et on a déterminé les valeurs de $\Delta G^{\ddagger}$.

Mots clés : fer-carbonyle, structures cristallines, spectroscopie RMN du ^{13}C, fluxion, mécanismes.

[Traduit par la Rédaction]

Introduction

$[Fe_3(CO)_{12}]$ is highly fluxional, and even at –150°C a singlet is observed in the ^{13}C NMR spectrum (1). Cotton and Hunter (1) proposed that the fluxionality is a result of the merry-go-round mechanism, see Scheme 1. In 1976, Johnson (2) proposed a mechanism going via a $[Fe_3(CO)_{10}(\mu_3\text{-}CO)_2]$ intermediate and (or) transition state **1** as a result of rotation of the $Fe(CO)_4$ moieties. To slow down the fluxionality of $[Fe_3(CO)_{12}]$ on the NMR timescale, it is necessary to introduce ligands that do not readily move between iron atoms, and hence, block dynamic pathways.

There have been a number of papers reporting dynamic NMR investigation of $[Fe_3(CO)_{12}]$ derivatives. In 1981, Johnson and co-workers (3) examined the ^{13}C NMR spectrum of $[Fe_3(CO)_{11}\{P(OR)_3\}]$ and concluded that at –90°C it shows CO signals in an intensity ratio of 6:4:1. They explained the fluxionality on the basis of an icosahedron $\rightleftharpoons$ cube octahedron $\rightleftharpoons$ icosahedron rearrangement. Subsequently Farrar and Lunniss (4) synthesized a number of di- and trisubstituted $[Fe_3(CO)_{12}]$ derivatives. Unfortunately, their interpretation of the fluxionality was flawed as it required the activation energy of the merry-go-round mechanism to vary wildly between similar derivatives.

In 1989, the fluxionality of $[Fe_3(CO)_{12-n}\{P(OMe)_3\}_n]$ was reexamined (5). It was found that at –101°C, the intensity of the carbonyl signals of $[Fe_3(CO)_{11}\{P(OMe)_3\}]$ are 5:5:1, not 6:4:1 as previously reported (3). As a result, a new mechanism for the fluxionality of $[Fe_3(CO)_{12}]$ and its derivatives was proposed (5). The mechanism involves the rotation of the Fe_3 triangle around the S_{10} axis of the carbonyl icosahedron defined by carbonyls C(6)O and C(10)O, see

Received August 31, 2000. Published on the NRC Research Press Web site at http://canjchem.nrc.ca on June 30, 2001.

Dedicated to Professor B.R. James on the occasion of his 65th birthday.

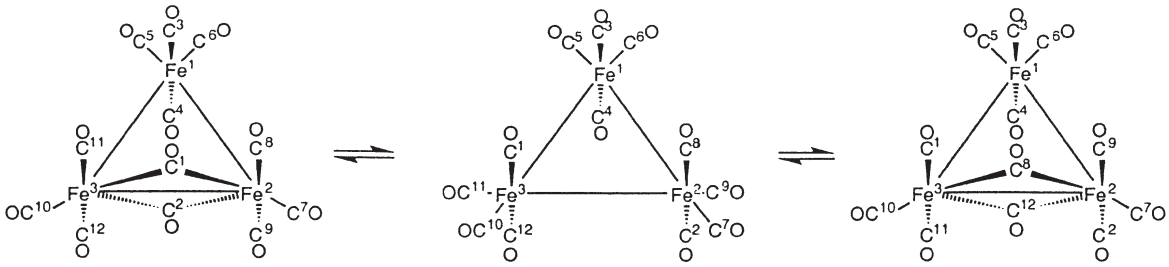
H. Adams, S.C.M. Agustinho,[1] K. Chomka, B.E. Mann,[2] S. Smith, C. Squires, and S.E. Spey. The Department of Chemistry, The University of Sheffield, Sheffield, S3 7HF, U.K.

[1]Permanent address: Institito de Quimica de São Carlos, Universidade de São Paulo, Cx Postal 780, CEP 13.560-970, São Carlos, São Paulo, Brazil.

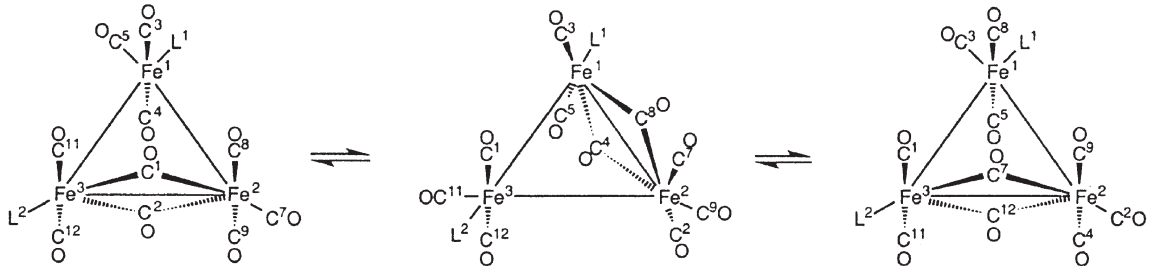
[2]Corresponding author (telephone: +44 (0) 114 222-9332; fax +44 (0) 114 273-8673; e-mail: B.Mann@sheffield.ac.uk).

 DOI: 10.1139/cjc-79-5/6-760 © 2001 NRC Canada

Scheme 1.



Scheme 2.



Scheme 2.[3] As the carbonyl bridge opens on one Fe–Fe edge, another closes on a second Fe–Fe edge, and hence, this mechanism is described as the concerted bridge – opening bridge – closing mechanism. The halfway stage of this carbonyl exchange has been observed in the crystal structure of $[Fe_3(CO)_{10}\{1,2\text{-}(Me_2As)_2C_6H_4\}]$ (6). This mechanism, when applied to $[Fe_3(CO)_{11}\{P(OMe)_3\}]$, causes the exchange of carbonyls C(1)O, C(2)O, C(7)O, C(11)O, and C(12)O as one set of five carbonyls, and C(3)O, C(4)O, C(5)O, C(8)O, and C(9)O as the second set of five carbonyls, leaving C(6)O as the unique carbonyl.

Subsequently Johnson and Bott (7) revised the Johnson mechanism, and showed how rotations of the $Fe(CO)_4$ groups about the axis going through the iron and the opposite edge of the Fe_3 triangle, called librations, could lead to the same exchange.

An investigation involving $[Fe_3(CO)_{10}(CN\text{-}t\text{-}Bu)\{P(OMe)_3\}]$ confirmed that the rotation of the two groups of five carbonyls is concerted (8).

To differentiate between the two mechanisms, an analysis of X-ray crystal structures was performed (9). A Bürgi–Dunitz analysis (10) was applied to then known crystal structures and a web movie was produced.[4]

The Johnson libration mechanism and the Mann concerted bridge – opening bridge – closing mechanism differ in the pathway followed by the iron triangle during fluxional pathway. However, the difference is best seen in terms of the location of the carbonyls with respect to the iron triangle. In the Johnson libration mechanism all the equatorial carbonyls (C(5)O, C(6)O, C(7)O, C(10)O) move out of the plane defined by the iron triangle. In the Mann concerted bridge – opening bridge – closing mechanism, C(5)O and C(7)O move out of the plane defined by the iron triangle, while C(6)O and C(10)O remain in the plane. The crystal structure of $[Fe_3(CO)_{10}\{1,2\text{-}(Me_2As)_2C_6H_4\}]$ (6) represents the half way stage for the exchange. The structure lies almost exactly on the ideal pathway predicted by the Mann concerted bridge – opening bridge – closing mechanism with the line joining C(6)O and C(10)O lying only 2.6° from the plane of the iron triangle. Although Johnson (11) published a rebuttal of the Mann concerted bridge – opening bridge – closing mechanism, he failed to address this key point. Johnson also claimed priority, but his mechanism is different going via **1**, which does not lie on the pathway mapped out by the Bürgi–Dunitz analysis (9).

The majority of crystal structures of $[Fe_3(CO)_{12}]$ and its derivatives have structures that are close to that found in $[Fe_3(CO)_{12}]$ and shed little light on the differences between the two mechanisms. In view of the distortion produced by $1,2\text{-}(Me_2As)_2C_6H_4$, a number of compounds containing bidentate ligands have been synthesized. $[Fe_3(CO)_{10}(dppe)]$ showed only minor distortions from the $[Fe_3(CO)_{12}]$ structure with the ligand bridging the $Fe(\mu\text{-}CO)_2Fe$ edge of the iron triangle (12, 13). To increase the distortions, ligands with a smaller bite angle were examined, and it is this that is reported in this paper.

Experimental

$[Fe_3(CO)_{12}]$ was synthesized according to the literature (14). $Me_3NO{\cdot}2H_2O$, $Ph_2PCH_2PPh_2$ ($Ph_2PCH_2PPh_2$ = dppm), $(EtO)_2POP(OEt)_2$, and $P(OMe)_3$ were purchased from Aldrich. $Ph_2PNHPPh_2$ was purchased from Strem Chemicals, Inc. $Me_3NO{\cdot}2H_2O$ was dehydrated by Dean–Stark distillation using toluene.

Synthesis of $[Fe_3(CO)_{10}L_2]$ (L_2 = dppm, $Ph_2PNHPPh_2$, $(EtO)_2POP(OEt)_2$)

$[Fe_3(CO)_{12}]$ (0.5 g, 0.992 mmol) was placed in a nitrogen purged three-neck round-bottom flask and dissolved in

[3] There is an identical axis through C(5)O and C(7)O.
[4] To observe movie go to http://www.shef.ac.uk/misc/personal/ch1bem/Fe3-carbonyl12A.html.

© 2001 NRC Canada

CH_2Cl_2 (150 cm^3). The flask was cooled to –78°C in a solid CO_2–acetone bath. The phosphorus ligand (0.992 mmol) was slowly added to the flask with stirring, followed by Me_3NO (0.15 g, 2.0 mmol). The flask was left in the solid CO_2–acetone bath and allowed to warm to room temperature. The reaction was then monitored by TLC; all the $[Fe_3(CO)_{12}]$ had been consumed in 4 h at room temperature. The solvent was removed and the product purified by chromatography on a 30 cm silica gel column, eluting with hexane–CH_2Cl_2 (3:1). The dark green compounds were recrystallized from acetonitrile.

$[Fe_3(CO)_{10}(dppm)]$

Yield: 47%. MS *m/z*: 832. IR (CH_2Cl_2) (cm^{-1}): 2114, 2048, 2008. ^{13}C NMR (–105°C) δ: 229.9, 225.5, 218.6, 205.9, 131.5 (t, $N_{P,C}$ = 48 Hz), 130.5 (*ortho*), 129.8 (*para*), 127.7 (*meta*), 47.8, ($J_{P,C}$ = 19 Hz, CH_2). ^{31}P NMR (CD_2Cl_2) δ: 47.

$[Fe_3(CO)_{10}(Ph_2PNHPPh_2)]$

Yield: 25%. IR (CH_2Cl_2) (cm^{-1}): 2062, 1998, 1815. ^{13}C NMR (CD_2Cl_2) δ: 220.4, 136.7 (t, $N_{P,C}$ = 55 Hz, ipso), 131.1 (*para*), 130.8 ($N_{P,C}$ = 12 Hz, *ortho*), 128.9 ($N_{P,C}$ = 10 Hz, *meta*). ^{31}P NMR (CD_2Cl_2) δ: 99. Anal. calcd. for $C_{34}H_{21}NO_{10}P_2Fe_3$: C 46.46, H 2.70, N 1.68; found: C 45.78, H 3.25, N 1.69.

$[Fe_3(CO)_{10}\{(EtO)_2POP(OEt)_2\}]$

Yield: 21%. IR (CH_2Cl_2) (cm^{-1}): 2069, 2009, 1955, 1909, 1750, 1711. ^{13}C NMR (CD_2Cl_2) (RT) δ: 218 (br), 63.2 (t, $N_{P,C}$ = 7.2 Hz, OCH_2), 15.8 (t, $N_{P,C}$ = 7.0 Hz, CH_3). ^{31}P NMR (CD_2Cl_2) δ: 155. Anal. calcd. for $C_{18}H_{20}O_{15}P_2Fe_3$: C 30.63, H 2.86; found: C 29.43, H 3.31.

Synthesis of $[Fe_3(CO)_9(dppm)\{P(OMe)_3\}]$

The same method as for $[Fe_3(CO)_{10}(dppm)]$ was followed with the exception that $[Fe_3(CO)_{10}(dppm)]$ was used in place of $[Fe_3(CO)_{12}]$ and 1 mol equiv of Me_3NO was used. Yield: 18%. MS *m/z*: 928. IR (CH_2Cl_2) (cm^{-1}): 2037, 1998, 1940, 1890, 1772, 1717. ^{13}C NMR (CD_2Cl_2) (RT) δ: 227.9, 223.4, 135.0 (t, $N_{P,C}$ = 45 Hz, ipso), 132.1 (t, $N_{P,C}$ = 10 Hz, *ortho*), 130.5 (*para*), 128.8 (t, $N_{P,C}$ = 9 Hz, *meta*), 52.9 ($J_{P,C}$ = 7 Hz, OMe), 43.9, ($J_{P,C}$ = 22 Hz, CH_2). ^{31}P NMR (CD_2Cl_2) δ: 166.4, 48.6. Anal. calcd. for $C_{37}H_{31}O_{12}P_3Fe_3$: C 47.93, H 3.26; found: C 47.70, H 3.37.

Crystallographic data for $[Fe_3(CO)_{10}(dppm)]\cdot 1.5NCCH_3$

Crystal data for $C_{76}H_{53}Fe_6N_3O_{20}P_4$: MW = 1787.19, crystallizes from acetonitrile as black blocks, crystal dimensions 0.10 × 0.02 × 0.02 mm^3. Triclinic, space group $P\bar{1}$, *a* = 11.3686(13), *b* = 17.2410(19), and *c* = 20.148(2) Å, α = 82.753(2), β = 83.366(2), and γ = 72.853(2)°, *U* = 3730.6(7) $Å^3$, *Z* = 2, D_c = 1.591 Mg m^{-3}, Mo Kα radiation (λ = 0.71073 Å), μ (Mo Kα) = 1.297 mm^{-1}, *F*(000) = 1812.

Data collected were measured on a Bruker Smart CCD area detector with Oxford Cryosystems low temperature system. Cell parameters were refined from the setting angles of 64 reflections (θ range 1.02 < 23.35°).

Reflections were measured from a hemisphere of data collected of frames each covering 0.3 degrees in omega. Of the 16769 reflections measured, all of which were corrected for Lorentz and polarization effects and for absorption by semi empirical methods based on symmetry-equivalent and repeated reflections (minimum and maximum transmission coefficients 0.8812 and 0.9745), 6546 independent reflections exceeded the significance level $|F|/\sigma(|F|) > 4.0$. The structure was solved by direct methods and refined by full-matrix least-squares methods on F^2. Hydrogen atoms were placed geometrically and refined with a riding model (including torsional freedom for methyl groups) and with U_{iso} constrained to be $1.2U_{eq}$ (1.5 for methyl groups) of the carrier atom. Refinement converged at a final *R* = 0.0598 (wR_2 = 0.2215, for all 10688 data, 984 parameters, mean and maximum δ/σ: 0.000, 0.001) with allowance for the thermal anisotropy of all non-hydrogen atoms. Minimum and maximum final electron density –0.834 and 1.540 e $Å^{-3}$.

A weighting scheme $w = 1/[\sigma^2(F_o^2) + (0.1390P)^2 + 0.00P]$ where $P = (F_o^2 + 2F_c^2)/3$ was used in the latter stages of refinement. Complex scattering factors were taken from the program package SHELXTL (15) as implemented on the Viglen Pentium computer.

Crystallographic data for $[Fe_3(CO)_{10}(Ph_2PNHPPh_2)]\cdot 0.5CH_2Cl_2$

Crystal data for $C_{34.5}H_{22}ClNO_{10}P_2Fe_3$: MW = 875.47, crystallizes from deuterated dichloromethane as dark green blocks, crystal dimensions 0.38 × 0.25 × 0.12 mm^3. Monoclinic, space group *C*2/*c*, *a* = 22.223(15), *b* = 20.984(17), and *c* = 16.229(15) Å, β = 106.46(6)°, *U* = 7258(10) $Å^3$, *Z* = 8, D_c = 1.602 Mg m^{-3}, Mo Kα radiation (λ = 0.71073 Å), μ (Mo Kα) = 1.402 mm^{-1}, *F*(000) = 3528.

Three-dimensional, room temperature X-ray crystal data were collected in the range 2.72 < 2θ < 50.20° on a Siemens P4 diffractometer by the omega scan method. Of the 7266 reflections measured, all of which were corrected for Lorentz and polarization effects, and for absorption by semi-empirical methods based on symmetry-equivalent and repeated reflections (minimum and maximum transmission coefficients 0.6178 and 0.8498), 3620 independent reflections exceeded the significance level $|F|/\sigma(|F|) > 4.0$. The structure was solved by direct methods and refined by full-matrix least-squares methods on F^2. Hydrogen atoms were placed geometrically and refined with a riding model and with U_{iso} constrained to be $1.2U_{eq}$ of the carrier atom. Refinement converged at a final *R* = 0.0908 (wR_2 = 0.2657 for all 6338 data, 465 parameters, mean and maximum δ/σ: 0.000, 0.000) with allowance for the thermal anisotropy of all non-hydrogen atoms. Minimum and maximum final electron density –0.709 and 1.402e $Å^{-3}$ (the latter 1.28 Å from Fe(1)). A weighting scheme $w = 1/[\sigma^2(F_o^2) + (0.1456P)^2 + 0.00P]$ where $P = (F_o^2 + 2F_o^2)/3$ was used in the latter stages of refinement. Complex scattering factors were taken from the program package SHELXTL (15) as implemented on the Viglen Pentium computer.

Crystallographic data for $[Fe_3(CO)_{10}\{(EtO)_2POP(OEt)_2\}]$

Crystal data for $C_{18}H_{20}Fe_3O_{15}P_2$: MW = 705.83, crystallizes from pet ether as black blocks, crystal dimensions 0.20 × 0.10 × 0.06 mm. Monoclinic, space group $P2_1/n$ (a non-standard setting of $P2_1/c$ C_h, No. 14), *a* = 9.175(5), *b* = 18.294(11), and *c* = 16.584(10) Å, β = 104.489(13)°, *U* =

© 2001 NRC Canada

2695(3) Å^3, Z = 4, D_c = 1.740 Mg m^{-3}, Mo Kα radiation (λ = 0.71073 Å), μ (Mo Kα) = 1.781 mm^{-1}, F(000) = 1424.

Data collected were measured on a Bruker Smart CCD area detector with Oxford Cryosystems low temperature system. Cell parameters were refined from the setting angles of 23 reflections (θ range 1.69 < 28.47°).

Reflections were measured from a hemisphere of data collected of frames each covering 0.3 degrees in omega. Of the 17546 reflections measured, all of which were corrected for Lorentz and polarization effects and for absorption by semi empirical methods based on symmetry-equivalent and repeated reflections (minimum and maximum transmission coefficients 0.7172 and 0.9007) 2572 independent reflections exceeded the significance level $|F|/\sigma(|F|) > 4.0$. The structure was solved by direct methods and refined by full-matrix least-squares methods on F^2. Hydrogen atoms were placed geometrically and refined with a riding model (including torsional freedom for methyl groups) and with U_{iso} constrained to be $1.2U_{eq}$ (1.5 for methyl groups) of the carrier atom. Refinement converged at a final R = 0.0766 (wR_2 = 0.2053 for all 6439 data, 343 parameters, mean and maximum δ/σ: 0.000, 0.000) with allowance for the thermal anisotropy of all non-hydrogen atoms. Minimum and maximum final electron density –0.762 and 0.890e Å^{-3}.

A weighting scheme $w = 1/[\sigma^2(F_o^2) + (0.0824P)^2 + 0.00P]$ where $P = (F_o^2 + F_c^2)/3$ was used in the latter stages of refinement. Complex scattering factors were taken from the program package SHELXTL (15) as implemented on the Viglen Pentium computer.

Crystallographic data for $[Fe_3(CO)_9(dppm)\{P(OMe)_3\}]\cdot 0.618NCCH_3\cdot 0.382CH_3CH_2OH$

Crystal data for $C_{39}H_{35.14}N_{0.62}O_{12.38}P_3Fe_3$ ($C_{37}H_{31}Fe_3O_{12}P_3$ and two disordered solvents – acetonitrile and ethanol): MW = 971.04, crystallizes from acetonitrile – pet. ether as black plates, crystal dimensions 0.26 × 0.15 × 0.02 mm^3. Monoclinic, space group $P2_1/n$ (a non-standard setting of $P2_1/c$ C_{2h}^5, No. 14), a = 11.1541(16), b = 10.3350(14), and c = 35.384(5) Å, β = 91.678(3)°, U = 4077.3(10) Å^3, Z = 4, D_c = 1.582 Mg m^{-3}, Mo Kα radiation (λ = 0.71073 Å), μ (Mo Kα) = 1.235 mm^{-1}, F(000) = 1982.

Data collected were measured on a Bruker Smart CCD area detector with Oxford Cryosystems low temperature system. Cell parameters were refined from the setting angles of 98 reflections (θ range 1.15 to 28.33°).

Reflections were measured from a hemisphere of data collected of frames each covering 0.3 degrees in omega. Of the 23908 reflections measured, all of which were corrected for Lorentz and polarization effects and for absorption by semi empirical methods based on symmetry-equivalent and repeated reflections (minimum and maximum transmission coefficients 0.7396 and 0.9757) 4145 independent reflections exceeded the significance level $|F|/\sigma(|F|) > 4.0$. The structure was solved by direct methods and refined by full-matrix least-squares methods on F^2. Hydrogen atoms were placed geometrically and refined with a riding model (including torsional freedom for methyl groups) and with U_{iso} constrained to be $1.2U_{eq}$ (1.5 for methyl groups) of the carrier atom. Refinement converged at a final R = 0.0648 (wR_2 = 0.1180 for all 9780 data, 522 parameters, mean and maximum δ/σ: 0.000, 0.000) with allowance for the thermal anisotropy of all non-hydrogen atoms with the exception of the solvent molecules. Minimum and maximum final electron density –0.613 and 1.004 e Å^{-3}. Two solvents of crystallization were found to be disordered and refined as 61.8% acetonitrile and 38.2% ethanol. A weighting scheme $w = 1/[\sigma^2(F_o^2) + (0.0225P)^2 + 0.00P]$ where $P = (F_o^2 + 2F_c^2)/3$ was used in the latter stages of refinement. Complex scattering factors were taken from the program package SHELXTL (15) as implemented on the Viglen Pentium computer.

NMR Investigations

NMR spectra were recorded on a Bruker AMX400 NMR spectrometer in CD_2Cl_2. Temperatures were calibrated using a Comark electronic thermometer, placing a thermocouple in an NMR tube containing ethanol and placing this tube in the probe. EXSY spectra were determined qualitatively using the Bruker pulse sequence "NOESYTP" which had been modified to include ^{1}H composite pulse decoupling.

$\Delta G^{\ddagger}$ values were obtained from line widths. In most cases the simple equation, $k = \pi\Delta\nu$ was used below coalescence, where Δν is the line broadening due to exchange. This was estimated from the spectrum. In the case of rotation about the C(7)O–P(1) axis in $[Fe_3(CO)_{10}\{(EtO)_2POP(OEt)_2]$, only a broad signal was obtained for C(1)O, C(3)O, C(4)O, and C(12)O at –106°C. It was assumed that in the absence of rotation about the C(7)O–P(1) axis they would give two signals of equal intensity separated by 15 ppm. The equation given below was used to determine the rate.

$$[1] \qquad k = \frac{\pi(\nu_A - \nu_B)^2}{2\Delta\nu}$$

Results and discussion

Crystallographic sudies

The crystal structures of $[Fe_3(CO)_{10}L_2]$ (L_2 = dppm, $(Ph_2P)_2NH$, $\{(EtO)_2P\}_2O$)

The crystal structures of $[Fe_3(CO)_{10}L_2]$ (L_2 = dppm, $(Ph_2P)_2NH$, $\{(EtO)_2P\}_2O$) are all similar and are shown in Figs. 1–4. Crystal intensity data, and collection and structural refinement information are summarized in Table 1. Positional parameters and isotropic thermal parameters are given for the four compounds in Tables 2–5. Key distances and angles are given in Table 6.

The phosphorus ligand substitutes an equatorial carbonyl on Fe(1) and an axial carbonyl on Fe(3). This contrasts with the structure of $[Fe_3(CO)_{10}(dppe)]$ where the ligand bridges the Fe(μ-CO)$_2$Fe edge of the iron triangle. For monodentate phosphorus ligands there is a strong preference for them to go into an equatorial position (12), and this is the first example where a phosphorus group goes into an axial position. As a result the structure distorts towards a geometry where this phosphorus is equatorial. This can be seen in a view down the C(6)O–C(10)O axis, see Fig. 5, where P(2) is markedly out of the plane of the Fe_3 triangle. The group of five ligands at the front of the projection, C(1)O, C(2)O, C(7)O, C(11)O, and P(1), have rotated clockwise from the position found in $[Fe_3(CO)_{12}]$. As a result of this rotation, carbonyls C(1)O and C(2)O have become semi-bridging.

© 2001 NRC Canada

Fig. 1. The molecular structure of $[Fe_3(CO)_{10}(dppm)]$ as an ORTEP diagram showing the numbering system. There are two independent molecules in the unit cell.

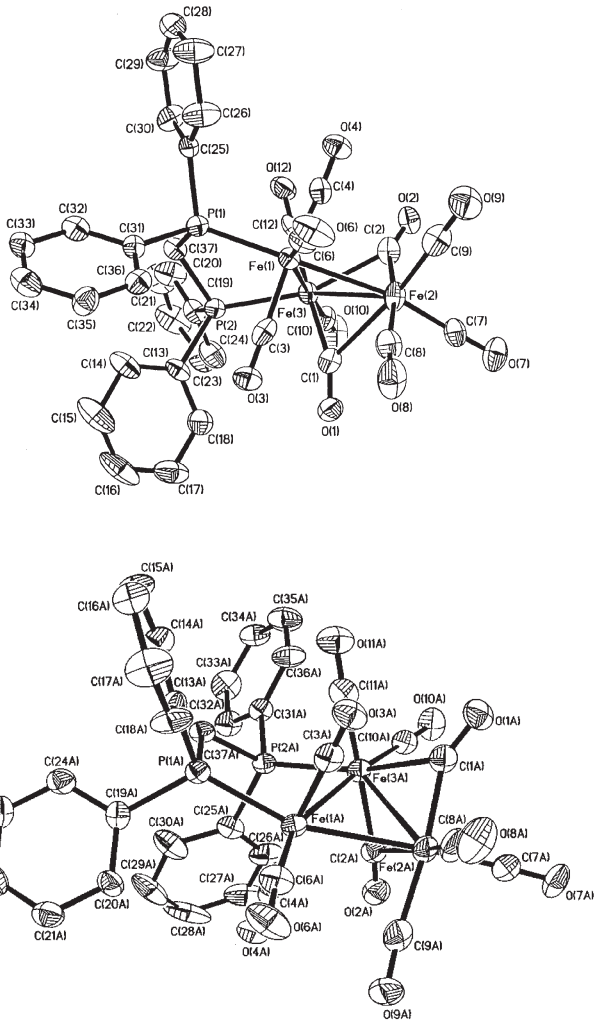


Fig. 2. The molecular structure of $[Fe_3(CO)_{10}(Ph_2PNHPPh_2)]$ as an ORTEP diagram showing the numbering system.

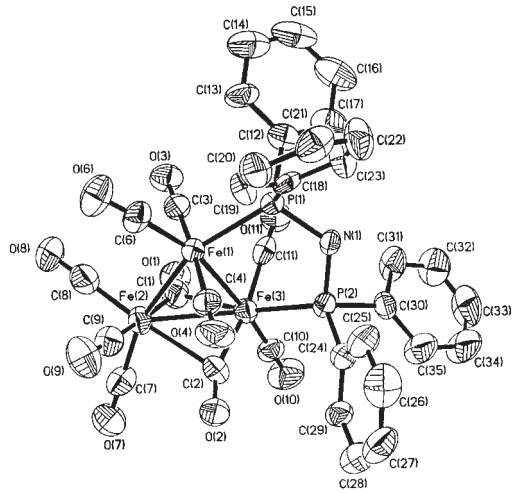


Fig. 3. The molecular structure of $[Fe_3(CO)_{10}\{(EtO)_2POPO(OEt)_2\}]$ as an ORTEP diagram showing the numbering system.

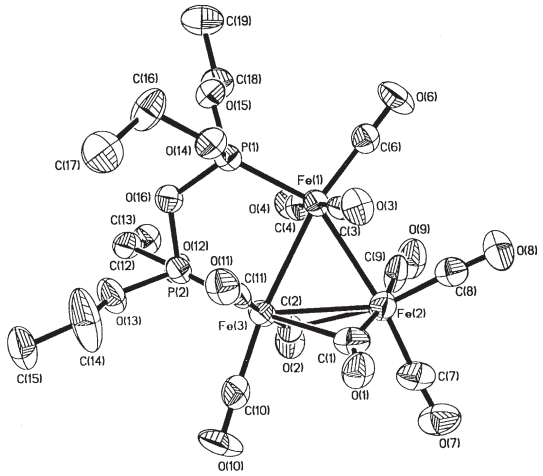
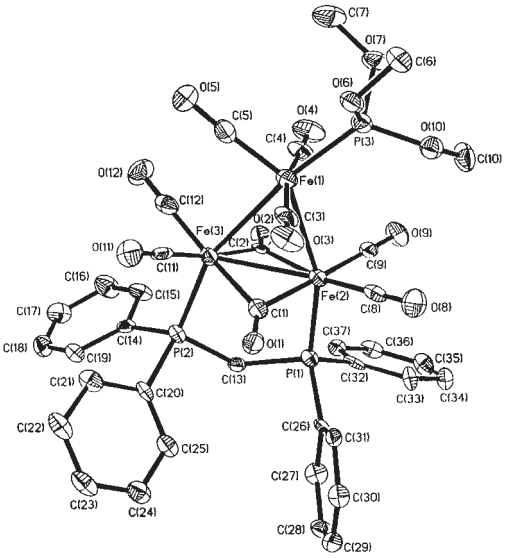


Fig. 4. The molecular structure of $[Fe_3(CO)_9(dppm)\{P(OMe)_3\}]$ as an ORTEP diagram showing the numbering system.



There has been a smaller clockwise rotation for C(3)O, P(1), C(4)O, C(9)O, and C(8)O.

In view of the strong tendency of phosphorus ligands to go into equatorial positions, it might be expected that the chelating ligands would prefer to coordinate in the positions occupied by C(5)O and C(6)O, or C(7)O and C(10)O. The only example of a similar bidentate ligand coordinating to a single iron in $[Fe_3(CO)_{12}]$ derivatives is $[Fe_3(CO)_{10}\{1,2\text{-}(Me_2As)_2C_6H_4\}]$ (6). It is possible that such a derivative is formed for $[Fe_3(CO)_{10}L_2]$ (L_2 = dppm, $(Ph_2P)_2NH$, $\{(EtO)_2P\}_2O$), but the compounds decompose. This leaves coordination in the positions of C(7)O and C(10)O. This geometry is adopted by $[Fe_3(CO)_{10}\{(Ph_2PC_5H_4\text{-}\eta^5)_2Fe\}]$ (16), $[Fe_3(CO)_{10}(dppe)]$ (13), and $[Fe_3(CO)_{10}\{1,2\text{-}(Me_2As)_2\text{-}$perfluorocyclobut-1-ene$\}]$ (17). For these compounds, the P···P–As···As distances are 4.797, 3.867, and 4.079–4.083 Å, respectively. This is a long distance for the ligands dppm, $(Ph_2P)_2NH$, and $\{(EtO)_2P\}_2O$ to bridge. The distance can be

© 2001 NRC Canada

Table 1. Crystal data and structure refinement for $[Fe_3(CO)_{10}L_2]$ (L_2 =dppm, $Ph_2PNHPPh_2$, $(EtO)_2POP(OEt)_2$), and $[Fe_3(CO)_9(dppm)\{P(OMe)_3\}]$.

	$[Fe_3(CO)_{10}(dppm)]$	$[Fe_3(CO)_{10}(Ph_2PNHPPh_2)]$	$[Fe_3(CO)_{10}\{(EtO)_2POP(OEt)_2\}]$	$[Fe_3(CO)_9(dppm)\{P(OMe)_3\}]$
Empirical formula	$C_{76}H_{53}Fe_6N_3O_{20}P_4$	$C_{34.50}H_{22}ClFe_3N\ O_{10}P_2$	$C_{18}H_{20}FeO_{15}P_2$	$C_{39}H_{35.14}Fe_3N_{0.62}O_{12.38}P_3$
FW	1787.19	875.47	705.83	971.04
Temperature (K)	150(2)	293(2)	150(2)	150(2)
Wavelength (Å)	0.71073	0.71073	0.71073	0.71073
Crystal system	Triclinic	Monoclinic	Monoclinic	Monoclinic
Space group	$P\bar{1}$	$C2/c$	$P2_1/n$	$P2_1/n$
a (Å)	11.3686(13)	22.223(15)	9.175(5)	11.1541(16)
b (Å)	17.2410(19)	20.984(17)	18.294(11)	10.3350(14)
c (Å)	20.148(2)	16.229(15)	16.584(10)	35.384(5)
α (°)	82.753(2)	90	90	90
β (°)	83.366(2)	106.46(6)	104.489(13)	91.678(3)
γ (°)	72.853(2)	90	90	90
Volume (Å^3)	3730.6(7)	7258(10)	2695(3)	4077.3(10)
Z	2	8	4	4
Density (Mg m^{-3}) (calcd.)	1.591	1.602	1.740	1.582
Absorption coefficient (mm^{-1})	1.297	1.402	1.781	1.235
F(000)	1812	3528	1424	1982
Crystal size (mm^3)	0.10 × 0.02 × 0.02	0.38 × 0.25 × 0.12	0.20 × 0.10 × 0.06	0.26 × 0.15 × 0.02
θ range for data collection (°)	1.02–23.35	1.36–25.10	1.69–28.47	1.15–28.33
Index ranges	$-12 \le h \le 11$, $-19 \le k \le 11$, $-22 \le l \le 21$	$-1 \le h \le 26$, $-1 \le k \le 24$, $-19 \le l \le 18$	$-9 \le h \le 12$, $-15 \le k \le 24$, $-22 \le l \le 21$	$-14 \le h \le 14$, $-12 \le k \le 13$, $-27 \le l \le 46$
Reflections collected	16769	7266	17546	23908
Independent reflections	10688 (R(int) = 0.0865)	6338 (R(int) = 0.1085)	6439 (R(int) = 0.1297)	9780 (R(int) = 0.1526)
Completeness to θ = 23.35° (%)	98.6	97.9	94.4	96.3
Absorption correction	Semi-empirical	Semi-empirical	Semi-empirical	Semi-empirical
Max. and min. transmission	0.9745 and 0.8812	0.8498 and 0.6178	0.9007 and 0.7172	0.9757 and 0.7396
Refinement method	Full-matrix least-squares on F^2	Full-matrix least-squares on F^2	Full-matrix least-squares on F^2	Full-matrix least-squares on F^2
Data/restraints/parameters	10688/0/984	6338/0/465	6439/0/343	9780/5/522
GoF on F^2	1.036	1.033	0.901	0.812
Final R indices [$I > 2\sigma(I)$]	R_1 = 0.0598, wR_2 = 0.1697	R_1 = 0.0908, wR_2 = 0.2199	R_1 = 0.0766, wR_2 = 0.1727	R_1 = 0.0648, wR_2 = 0.0961
R indices (all data)	R_1 = 0.0924, wR_2 = 0.2215	R_1 = 0.1587, wR_2 = 0.2657	R_1 = 0.1855, wR_2 = 0.2053	R_1 = 0.1740, wR_2 = 0.1180
Largest diff. peak and hole (e Å^{-3})	1.540 and –0.834	1.402 and –0.709	0.892 and –0.762	1.004 and –0.613

reduced by bridging between the positions occupied by C(5)O and C(12)O. In the case of $[Fe_3(CO)_{12}]$ at 100 K (18), the C(7)O···C(10)O carbon—carbon distance is 3.948 Å, while the C(5)O···C(12)O carbon—carbon distance is 3.480 Å. The distance is reduced further by decreasing the torsion angle from 46.9° for C(5)-Fe(1)-Fe(3)-C(12) found in $[Fe_3(CO)_{12}]$ at 100 K (18), to between 29.5 and 32.5° for P(1)-Fe(1)-Fe(3)-P(2). The P···P distances are L_2 = dppm (3.067(2), 3.053(2) Å), $Ph_2PNHPPh_2$ (2.978(4) Å), and $(EtO)_2POP(OEt)_2$ (2.836(3) Å).

The crystal structure of $[Fe_3(CO)_9(dppm)\{P(OMe)_3\}]$

The crystal structure of $[Fe_3(CO)_9(dppm)\{P(OMe)_3\}]$ is shown in Fig. 4, and key distances and angles are given in Table 1. In contrast with $[Fe_3(CO)_{10}L_2]$ (L_2 = dppm, $(Ph_2P)_2NH$, $\{(EtO)_2P\}_2O$) it is the Fe(μ-CO)$_2$Fe edge that is bridged by the dppm ligand. It would be wrong to attribute this change of geometry to the $P(OMe)_3$ ligand as it will be shown later by ^{13}C NMR spectroscopy that both geometries are present in solution. Hence, the geometry observed in the crystal structure is more a function of crystal packing than of intramolecular factors.

Comparison of the concerted bridge – opening bridge – closing and the libration mechanisms

The molecules $[Fe_3(CO)_{10}L_2]$ (L_2 = dppm, $(Ph_2P)_2NH$, $\{(EtO)_2P\}_2O$) provide excellent examples to compare the concerted bridge – opening bridge – closing and the libration mechanisms. The L_2 ligand bridges between the C(5)O and C(12)O coordination sites. The P···P distance is rather short and this will cause a torque to try to rotate the iron triangle within the icosahedron of ligands. If the

© 2001 NRC Canada

Table 2. Atomic coordinates (1 x 10^4) and equivalent isotropic displacement parameters (1 x 10^3, Å^2) for [$Fe_3(CO)_{10}$(dppm)].

Atom	*x*	*y*	*z*	U_{eq}
Fe(1)	6012(1)	7380(1)	870(1)	24(1)
Fe(2)	4261(1)	6742(1)	608(1)	32(1)
Fe(3)	6280(1)	6520(1)	–190(1)	25(1)
P(1)	7907(1)	7523(1)	769(1)	25(1)
P(2)	7643(1)	7199(1)	–654(1)	23(1)
O(1)	4188(4)	7792(3)	–774(2)	37(1)
O(2)	5706(4)	5021(3)	617(2)	39(1)
O(3)	4981(4)	8927(3)	47(2)	36(1)
O(4)	6880(4)	5812(3)	1694(2)	39(1)
O(6)	4850(5)	8203(3)	2053(2)	50(1)
O(7)	2315(4)	6233(3)	119(2)	50(1)
O(8)	2612(4)	8407(3)	724(3)	56(1)
O(9)	3774(5)	6164(3)	2022(2)	59(1)
O(10)	6284(4)	5619(3)	–1327(2)	50(1)
O(12)	8447(4)	5240(3)	298(2)	45(1)
C(1)	4830(5)	7308(4)	–431(3)	31(1)
C(2)	5424(5)	5721(4)	491(3)	33(1)
C(3)	5397(5)	8304(4)	341(3)	29(1)
C(4)	6533(5)	6391(4)	1354(3)	29(1)
C(6)	5332(6)	7874(4)	1591(3)	32(1)
C(7)	3098(6)	6428(4)	293(3)	35(2)
C(8)	3325(6)	7775(4)	671(3)	39(2)
C(9)	3954(6)	6406(4)	1480(3)	43(2)
C(10)	6273(5)	5973(4)	–891(3)	30(1)
C(12)	7608(6)	5748(4)	128(3)	33(2)
C(13)	7177(5)	8262(3)	–1033(3)	28(1)
C(14)	7747(6)	8831(4)	–884(3)	40(2)
C(15)	7386(8)	9620(4)	–1186(3)	57(2)
C(16)	6517(8)	9837(4)	–1643(4)	62(3)
C(17)	5969(7)	9282(5)	–1804(3)	55(2)
C(18)	6299(6)	8488(4)	–1492(3)	41(2)
C(19)	8663(6)	6679(4)	–1340(3)	31(1)
C(20)	9832(6)	6226(4)	–1296(3)	48(2)
C(21)	10537(7)	5812(4)	–1835(4)	57(2)
C(22)	10061(8)	5844(4)	–2415(4)	62(2)
C(23)	8804(7)	6250(5)	–2470(3)	55(2)
C(24)	8118(7)	6660(4)	–1941(3)	49(2)
C(25)	8934(5)	6930(3)	1415(3)	27(1)
C(26)	8545(6)	7102(4)	2073(3)	44(2)
C(27)	9295(7)	6700(5)	2594(3)	52(2)
C(28)	10410(6)	6149(4)	2441(3)	41(2)
C(29)	10773(6)	5973(4)	1803(3)	44(2)
C(30)	10028(5)	6362(4)	1294(3)	39(2)
C(31)	8108(5)	8531(3)	787(3)	25(1)
C(32)	9312(6)	8615(4)	676(3)	33(1)
C(33)	9514(6)	9378(4)	669(3)	32(1)
C(34)	8505(7)	10052(4)	762(3)	43(2)
C(35)	7328(6)	9976(4)	883(3)	36(2)
C(36)	7149(6)	9221(4)	896(3)	32(1)
C(37)	8717(5)	7183(3)	–40(3)	27(1)
Fe(1A)	4029(1)	7584(1)	4086(1)	23(1)
Fe(2A)	5732(1)	8268(1)	4355(1)	30(1)
Fe(3A)	3686(1)	8480(1)	5134(1)	25(1)
P(1A)	2162(1)	7388(1)	4195(1)	24(1)
P(2A)	2391(1)	7757(1)	5617(1)	23(1)
O(1A)	4249(4)	9982(3)	4337(2)	41(1)
O(2A)	5776(4)	7260(3)	5750(2)	37(1)
O(3A)	3140(4)	9130(3)	3234(2)	38(1)
O(4A)	5104(4)	6054(2)	4916(2)	36(1)
O(6A)	5314(5)	6745(3)	2926(2)	51(1)
O(7A)	7614(4)	8869(3)	4840(2)	44(1)
O(8A)	6210(4)	8859(3)	2945(2)	57(1)
O(9A)	7475(4)	6613(3)	4280(3)	58(1)
O(10A)	3550(4)	9468(3)	6230(2)	43(1)
O(11A)	1516(4)	9667(3)	4554(2)	43(1)
C(1A)	4533(5)	9281(4)	4464(3)	34(2)
C(2A)	5115(5)	7722(4)	5399(3)	29(1)
C(3A)	3475(5)	8553(4)	3580(3)	29(1)
C(4A)	4676(5)	6668(4)	4631(3)	29(1)
C(6A)	4760(6)	7078(4)	3374(3)	34(2)
C(7A)	6872(6)	8644(4)	4671(3)	33(2)
C(8A)	6025(6)	8606(4)	3483(3)	40(2)
C(9A)	6751(6)	7235(4)	4318(3)	41(2)
C(10A)	3619(5)	9075(4)	5807(3)	29(1)
C(11A)	2367(6)	9189(4)	4760(3)	33(2)
C(13A)	1116(5)	7967(3)	3562(3)	27(1)
C(14A)	–44(5)	8439(4)	3708(3)	34(2)
C(15A)	–820(6)	8836(4)	3202(3)	40(2)
C(16A)	–393(6)	8767(4)	2546(3)	39(2)
C(17A)	796(6)	8299(5)	2380(3)	50(2)
C(18A)	1553(6)	7904(4)	2889(3)	39(2)
C(19A)	1982(5)	6372(4)	4168(3)	27(1)
C(20A)	2979(6)	5697(3)	4012(3)	31(1)
C(21A)	2790(6)	4947(4)	4001(3)	37(2)
C(22A)	1628(6)	4843(4)	4146(3)	38(2)
C(23A)	616(6)	5498(4)	4291(3)	33(1)
C(24A)	801(5)	6257(4)	4298(3)	32(1)
C(25A)	2975(5)	6725(3)	6022(3)	28(1)
C(26A)	3757(5)	6629(4)	6532(3)	39(2)
C(27A)	4144(7)	5905(5)	6916(3)	54(2)
C(28A)	3774(8)	5250(5)	6781(4)	63(3)
C(29A)	3009(8)	5324(4)	6276(4)	55(2)
C(30A)	2586(7)	6077(4)	5893(3)	43(2)
C(31A)	1255(5)	8230(3)	6294(3)	26(1)
C(32A)	922(6)	7740(4)	6844(3)	37(2)
C(33A)	46(6)	8097(4)	7354(3)	44(2)
C(34A)	–481(6)	8936(4)	7307(3)	36(2)
C(35A)	–175(6)	9404(4)	6757(3)	45(2)
C(36A)	694(6)	9048(4)	6256(3)	39(2)
C(37A)	1334(5)	7691(3)	5014(3)	26(1)
N(1S)	8887(6)	2080(4)	898(3)	57(2)
C(1S)	7242(7)	3225(5)	1538(4)	66(2)
C(2S)	8176(7)	2579(5)	1176(4)	55(2)
N(2S)	5164(8)	2204(7)	2540(4)	105(3)
C(3S)	6125(10)	1657(7)	2446(4)	77(3)
C(4S)	7358(9)	1013(7)	2305(5)	102(4)
N(3S)	1106(6)	2858(4)	4202(3)	54(2)
C(5S)	1781(7)	2370(5)	3903(4)	51(2)
C(6S)	2659(7)	1755(5)	3509(4)	59(2)

Note: U_{eq} is defined as one third of the trace of the orthogonalized U_{ij} tensor.

© 2001 NRC Canada

Table 3. Atomic coordinates (1×10^4) and equivalent isotropic displacement parameters (1×10^3, Å^2) for $[Fe_3(CO)_{10}(Ph_2PNHPPh_2)]$.

Atom	*x*	*y*	*z*	U_{eq}
Fe(1)	2838(1)	1398(1)	2995(1)	36(1)
Fe(2)	2087(1)	1757(1)	1458(1)	46(1)
Fe(3)	1769(1)	781(1)	2232(1)	38(1)
P(1)	3105(1)	715(1)	4081(2)	33(1)
P(2)	1731(1)	459(1)	3528(2)	36(1)
N(1)	2456(4)	322(3)	4175(5)	39(2)
O(1)	2076(4)	566(4)	504(5)	64(2)
O(2)	1058(4)	1932(3)	2398(5)	57(2)
O(3)	3445(4)	662(3)	1911(5)	59(2)
O(4)	2237(4)	2214(3)	4031(5)	65(2)
O(6)	3889(4)	2286(4)	3274(6)	74(2)
O(7)	962(5)	2247(4)	203(6)	78(3)
O(8)	3027(5)	1973(5)	528(7)	101(4)
O(9)	2278(5)	3012(4)	2328(6)	83(3)
O(10)	596(4)	198(4)	1225(6)	80(3)
O(11)	2477(4)	–377(4)	2083(5)	65(2)
C(1)	2035(6)	944(5)	1032(7)	54(3)
C(2)	1402(5)	1573(4)	2268(6)	45(2)
C(3)	3182(5)	945(5)	2311(6)	45(2)
C(4)	2444(5)	1887(5)	3604(6)	43(2)
C(6)	3478(6)	1927(5)	3190(7)	47(3)
C(7)	1399(6)	2040(6)	678(7)	53(3)
C(8)	2673(6)	1905(5)	930(9)	67(3)
C(9)	2208(6)	2508(6)	2040(7)	59(3)
C(10)	1053(5)	432(5)	1623(7)	46(2)
C(11)	2228(5)	73(5)	2162(6)	46(2)
C(12)	3663(5)	77(4)	4035(6)	45(2)
C(13)	4248(5)	262(6)	3949(7)	56(3)
C(14)	4702(7)	–182(8)	3956(9)	79(4)
C(15)	4591(8)	–799(8)	4049(8)	83(5)
C(16)	4019(8)	–1008(6)	4143(10)	91(5)
C(17)	3546(7)	–546(5)	4126(8)	71(4)
C(18)	3469(4)	1027(4)	5167(5)	36(2)
C(19)	3663(5)	1650(4)	5301(6)	43(2)
C(20)	3950(6)	1868(5)	6134(7)	53(3)
C(21)	4041(5)	1463(6)	6822(7)	58(3)
C(22)	3845(6)	838(5)	6687(6)	63(3)
C(23)	3569(6)	632(5)	5876(6)	54(3)
C(24)	1347(5)	948(4)	4157(6)	38(2)
C(25)	1643(6)	1093(5)	5014(7)	57(3)
C(26)	1326(8)	1440(5)	5501(8)	73(4)
C(27)	717(7)	1638(6)	5125(9)	68(3)
C(28)	425(6)	1515(5)	4263(8)	59(3)
C(29)	744(5)	1176(4)	3788(7)	44(2)
C(30)	1350(5)	–320(4)	3526(6)	44(2)
C(31)	1635(7)	–862(4)	3323(8)	68(4)
C(32)	1325(8)	–1440(6)	3276(9)	79(4)
C(33)	772(8)	–1493(6)	3415(10)	87(5)
C(34)	497(7)	–982(6)	3656(12)	99(5)
C(35)	769(6)	–379(5)	3669(10)	79(4)
C(1S)	5000	1186(14)	2500	138(11)
Cl(1S)	5336(3)	1607(3)	3398(5)	172(3)

Note: U_{eq} is defined as one third of the trace of the orthogonalized U_{ij} tensor.

Table 4. Atomic coordinates (1×10^4) and equivalent isotropic displacement parameters (1×10^3, Å^2) for $[Fe_3(CO)_{10}\{(EtO)_2POP(OEt)_2\}]$.

Atom	*x*	*y*	*z*	U_{eq}
Fe(1)	2009(1)	1220(1)	2570(1)	35(1)
Fe(2)	–545(1)	684(1)	1606(1)	43(1)
Fe(3)	–488(1)	1134(1)	3110(1)	36(1)
P(1)	3261(2)	1592(1)	3780(1)	34(1)
P(2)	381(2)	2057(1)	3912(1)	35(1)
O(1)	–1141(7)	–489(3)	2673(4)	49(2)
O(2)	–2097(7)	2205(3)	1875(4)	51(2)
O(3)	2573(7)	–322(3)	3035(4)	46(2)
O(4)	1305(6)	2730(3)	1980(4)	46(2)
O(6)	4383(7)	1160(4)	1694(4)	62(2)
O(7)	–3545(8)	377(4)	565(4)	70(2)
O(8)	1057(8)	–422(4)	885(4)	60(2)
O(9)	–177(9)	1820(4)	412(4)	69(2)
O(10)	–3381(7)	900(4)	3493(5)	67(2)
O(11)	992(7)	85(3)	4409(4)	47(2)
O(12)	–12(6)	2832(3)	3502(3)	37(1)
O(13)	–61(8)	2168(4)	4758(4)	60(2)
O(14)	3909(6)	967(3)	4424(3)	40(1)
O(15)	4680(6)	2107(3)	3912(3)	41(1)
O(16)	2208(6)	2074(3)	4243(3)	39(1)
C(1)	–833(9)	69(6)	2434(6)	47(2)
C(2)	–1421(10)	1728(5)	2239(5)	43(2)
C(3)	2294(9)	265(5)	2849(5)	37(2)
C(4)	1510(9)	2137(5)	2216(5)	37(2)
C(6)	3461(10)	1188(5)	2026(5)	40(2)
C(7)	–2375(12)	512(5)	985(7)	52(3)
C(8)	452(10)	13(5)	1173(5)	43(2)
C(9)	–253(12)	1421(5)	934(6)	53(3)
C(10)	–2254(12)	999(4)	3355(6)	47(2)
C(11)	484(9)	496(5)	3906(5)	33(2)
C(12)	431(10)	3509(4)	3976(6)	45(2)
C(13)	188(11)	4110(5)	3363(6)	51(2)
C(14)	–252(19)	1669(7)	5315(7)	106(5)
C(15)	–848(13)	1942(6)	5981(6)	66(3)
C(16)	4793(11)	1109(6)	5278(5)	56(3)
C(17)	4054(13)	849(8)	5908(7)	88(4)
C(18)	4704(10)	2773(5)	3457(6)	49(2)
C(19)	6270(11)	3066(6)	3706(7)	63(3)

Note: U_{eq} is defined as one third of the trace of the orthogonalized U_{ij} tensor.

libration mechanism is the lowest energy pathway, then the ligands P(1), C(6)O, C(7)O, and C(10)O will all be out of the plane of the iron triangle. If the concerted bridge – opening bridge – closing mechanism is the lowest energy pathway, then P(1) and C(7)O are permitted to move out of the plane of the iron triangle, but C(6)O and C(10)O should remain in it. Examination of the data in Table 7 shows that C(6)O and C(10)O do remain in the plane of the iron triangle, while P(1) and C(7)O move substantially out of the plane. This is strong evidence for the concerted bridge – opening bridge – closing mechanism over the libration mechanism.

Although it has been shown that the two groups, each composed of five ligands, rotate about the S_{10} axis of the

© 2001 NRC Canada

Table 5. Atomic coordinates (1×10^4) and equivalent isotropic displacement parameters (1×10^3, Å^2) for $[Fe_3(CO)_9(dppm)\{P(OMe)_3\}]$.

Atom	*x*	*y*	*z*	U_{eq}
Fe(1)	4709(1)	2027(1)	839(1)	22(1)
Fe(2)	5083(1)	301(1)	1413(1)	18(1)
Fe(3)	3058(1)	284(1)	1079(1)	19(1)
P(1)	4724(1)	–1213(1)	1841(1)	18(1)
P(2)	2181(1)	–1216(1)	1436(1)	19(1)
P(3)	6159(1)	3340(1)	720(1)	22(1)
O(1)	3164(3)	1685(3)	1807(1)	26(1)
O(2)	4646(3)	–1855(3)	866(1)	25(1)
O(3)	3937(4)	4006(4)	1377(1)	37(1)
O(4)	5902(4)	61(4)	377(1)	41(1)
O(5)	3052(4)	2953(4)	244(1)	45(1)
O(6)	5702(3)	4803(3)	714(1)	25(1)
O(7)	6850(3)	3176(3)	335(1)	28(1)
O(8)	6301(4)	2311(4)	1866(1)	35(1)
O(9)	7301(3)	–932(4)	1169(1)	35(1)
O(10)	7289(3)	3478(3)	1002(1)	28(1)
O(11)	1257(3)	2373(4)	1091(1)	35(1)
O(12)	2332(4)	–573(4)	313(1)	42(1)
C(1)	3570(5)	1078(5)	1558(2)	22(1)
C(2)	4369(4)	–896(5)	1026(2)	17(1)
C(3)	4224(5)	3185(5)	1175(2)	26(2)
C(4)	5436(5)	771(5)	567(2)	27(2)
C(5)	3701(5)	2568(5)	479(2)	29(2)
C(6)	6502(5)	5861(5)	643(2)	30(2)
C(7)	6229(6)	3185(6)	–26(2)	39(2)
C(8)	5817(5)	1534(5)	1690(2)	22(1)
C(9)	6460(5)	–420(5)	1263(2)	22(1)
C(10)	8171(5)	2482(5)	1033(2)	38(2)
C(11)	1955(5)	1561(5)	1081(2)	21(1)
C(12)	2615(5)	–235(5)	609(2)	29(2)
C(13)	3374(4)	–2143(5)	1695(2)	17(1)
C(14)	1368(5)	–2552(5)	1204(2)	18(1)
C(15)	1962(5)	–3272(5)	935(2)	28(2)
C(16)	1404(6)	–4316(5)	755(2)	36(2)
C(17)	234(5)	–4635(5)	833(2)	32(2)
C(18)	–363(5)	–3920(5)	1094(2)	31(2)
C(19)	184(5)	–2877(5)	1272(2)	21(1)
C(20)	1150(4)	–672(5)	1789(2)	19(1)
C(21)	106(5)	–21(5)	1665(2)	27(1)
C(22)	–741(5)	338(5)	1924(2)	33(2)
C(23)	–563(5)	79(5)	2307(2)	32(2)
C(24)	468(5)	–535(5)	2432(2)	28(2)
C(25)	1307(5)	–904(5)	2173(2)	25(1)
C(26)	4471(4)	–837(5)	2333(2)	16(1)
C(27)	4270(5)	–1857(5)	2585(2)	24(1)
C(28)	3996(5)	–1640(5)	2956(2)	27(1)
C(29)	3893(5)	–369(5)	3087(2)	27(1)
C(30)	4093(4)	635(5)	2847(2)	22(1)
C(31)	4382(4)	420(5)	2473(2)	19(1)
C(32)	5887(5)	–2451(5)	1888(2)	18(1)
C(33)	6886(4)	–2163(5)	2114(2)	23(1)
C(34)	7857(5)	–3010(5)	2146(2)	28(1)
C(35)	7808(5)	–4176(5)	1951(2)	27(2)
C(36)	6827(5)	–4471(5)	1724(2)	23(1)
C(37)	5872(5)	–3618(5)	1689(2)	23(1)
C(1SA)	9427(10)	9372(9)	450(3)	45(3)
C(2SA)	9025(18)	8284(14)	239(5)	109(4)
N(1SA)	9711(8)	10221(9)	621(3)	62(3)
C(1SB)	9672(14)	8022(14)	70(5)	30(4)
C(2SB)	9080(30)	8600(30)	378(8)	104(5)
O(1SB)	9940(20)	7740(20)	–268(5)	199(11)

Note: U_{eq} is defined as one third of the trace of the orthogonalized U_{ij} tensor.

icosahedron concertedly (7), the crystal structures of $[Fe_3(CO)_{10}L_2]$ (L_2 = dppm, $(Ph_2P)_2NH$, $\{(EtO)_2P\}_2O$) show that it is possible to distort the icosahedron by slightly rotating one set of five ligands with respect to the other. This can be seen qualitatively in Fig. 5, where the L_2 ligand closes the angle between the two sets of ligands, C(1)O, C(11)O, P2, C(2)O, and C(7)O with C(3)O, P(1), C(4)O, C(9)O, and C(8)O. This can be seen most easily by comparing the projected angle between P(1)-Fe(1)-Fe(3)-P(2) with the angles between P(1)-Fe(1)-Fe(2)-C(11) and C(4)-Fe(1)-Fe(2)-P(2). The distortion is localized to that side of the icosahedron and is barely apparent around C(7). This can be verified by comparing the projected angles between C(8)-Fe(2)-C(7) and C(7)-Fe(2)-C(9) in Fig. 5.

NMR spectra and fluxionality

For $[Fe_3(CO)_{10}L_2]$ (L_2 = dppm, $(Ph_2P)_2NH$, $\{(EtO)_2P\}_2O$) the ^{13}C carbonyl NMR spectrum in CD_2Cl_2 consists of a singlet at approximately δ 223. On cooling to ca. –40°C two new signals appear at approximately δ 206 and 230 giving intensity ratios of 2:6:2, respectively. These two signals are not observed at room temperature as they are exchanging at an intermediate rate of exchange, and hence, give a signal too broad to observe. Because at room temperature the signal at δ 223 is broadened, presumably by exchange with these two signals, it is possible that all three signals are exchanging by a single dynamic process. Pairwise exchange between the signals at approximately δ 206 and 230 was demonstrated using exchange spectroscopy (EXSY), see Fig. 6. It will be shown later that these signals are due to C(2)O–C(8)O and C(7)O–C(9)O, and the free energies of activation were derived for this pairwise exchange for all three compounds, see Table 8.

A similar exchange is observed between C(2)O–C(8)O and C(9)O in $\{Fe_3(CO)_9(dppm)\{P(OMe)_3\}]$, and the activation energy for this is also given in Table 8.

On further cooling of $[Fe_3(CO)_{10}(dppm)]$, the ^{13}C NMR signal at ca. δ 223 broadened and split into two signals at δ 225.4 and 218.6, in a 2:4 ratio (Fig. 7). In the case of $[Fe_3(CO)_{10}\{(EtO)_2POP(OEt)_2\}]$, the ^{13}C NMR signal at δ 223 split into two very broad signals at δ 223 and 206, in a 4:2 intensity ratio (Fig. 8). In the case of $[Fe_3(CO)_{10}(Ph_2PNHPPh_2)]$, the low temperature limit was not achieved and the central signal of intensity 6 produced a broad hump, as seen in Fig. 9.

The variable temperature behaviour of the ^{13}C NMR spectra of $[Fe_3(CO)_{10}L_2]$ (L_2 = dppm, $(Ph_2P)_2NH$, $\{(EtO)_2P\}_2O$) proved difficult to explain until the low temperature ^{13}C NMR spectrum of $[Fe_3(CO)_9(dppm)\{P(OMe)_3\}]$ was recorded. The presence of the $P(OMe)_3$ ligand acted as a block, and the low temperature ^{13}C NMR spectrum consisted

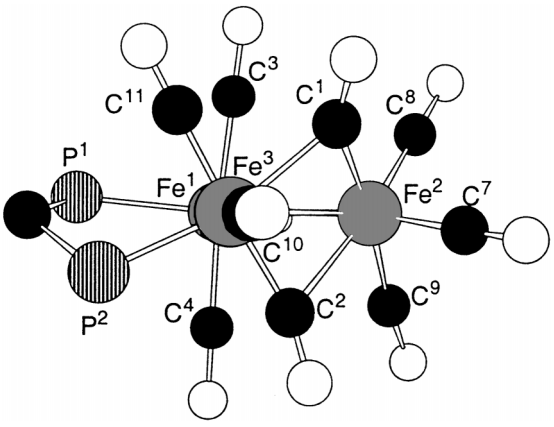
© 2001 NRC Canada

Table 6. Selected bond distances and angles in $[Fe_3(CO)_{10}L_2]$ (L_2 = dppm, $(Ph_2P)_2NH$, $\{(EtO)_2P\}_2O$) and $[Fe_3(CO)_9(dppm)\{P(OMe)_3\}]$.

	$[Fe_3(CO)_{10}$ (dppm)]^a	$[Fe_3(CO)_{10}$ $\{(Ph_2P)_2NH\}]$	$[Fe_3(CO)_{10}$ $\{(EtO)_2P\}_2O]$	$[Fe_3(CO)_9(dppm)$ $\{P(OMe)_3\}]$	$[Fe_3(CO)_{12}]$ at 100 K
Bond distances (Å)					
Fe(1)—Fe(2)	2.6804(12)	2.687(3)	2.671(2)	2.7262(11)	2.677
	2.6707(12)				
Fe(1)—Fe(3)	2.6966(11)	2.679(3)	2.665(2)	2.7313(11)	2.683
	2.6889(11)				
Fe(2)—Fe(3)	2.6099(11)	2.602(2)	2.614(2)	2.5176(11)	2.551
	2.6046(11)				
Fe(1)—P(1)	2.2279(17)	2.218(3)	2.158(3)		
	2.2224(17)				
Fe(3)—P(2)	2.2608(17)	2.234(3)	2.175(3)	2.2411(16)	
	2.2599(17)				
Fe(2)—C(1)	1.893(6)	1.833(12)	1.843(9)	1.952(6)	2.103
	2.301(6)				
Fe(2)—C(2)	2.314(6)	2.309(11)	2.229(10)	1.994(5)	1.986
	1.887(6)				
Fe(3)—C(1)	2.162(7)	2.215(11)	2.412(9)	1.953(6)	1.969
	1.870(6)				
Fe(3)—C(2)	1.846(6)	1.860(10)	1.839(10)	1.918(5)	2.109
	2.175(6)				
P(1)—C or NH or O	1.859(5)	1.705(8)	1.634(6)	1.847(5)	
	1.849(5)				
P(2)—C or NH or O	1.838(5)	1.681(8)	1.629(6)	1.859(5)	
	1.829(6)				
P(1)···P(2)	3.067(2)	2.978(4)	2.836(3)	3.1392(19)	
Fe(2)—P(1)	3.053(2)			2.2220(16)	
Bond angles (°)					
P(1)-C-P(2)	112.1(3)	123.2(4)	120.8(3)	115.8(3)	112.2(3)
P(1)-Fe(1)-Fe(2)-P(2)	30.0	30.6	29.5	32.5	1.0

[a]Two independent molecules in each unit cell. Note that the two molecules are mirror images of each other to the first approximation. This results in reversal of bond lengths involving C(1)O and C(2)O.

Fig. 5. A projection of the crystal structure of $[Fe_3(CO)_{10}(dppm)]$ looking along the S_{10} axis from C(6)O to C(10)O.



of five signals with an intensity ratio of 2:2:2:2:1, see Fig. 10.

Previous work has shown that only two dynamic processes need to be considered at ca. –100°C (5). In $[Fe_3(CO)_{12}]$ and its derivatives, the concerted bridge – opening bridge – closing mechanism is very fast unless blocked by a ligand, and $\Delta G^{\ddagger}$ is less than 16 kJ mol^{-1}. In general, the merry-go-round mechanism is just stopped at –100°C with $\Delta G^{\ddagger}$ around 40 kJ mol^{-1}. However, with the dppm, $Ph_2PNHPPh_2$, and $(EtO)_2POP(OEt)_2$ ligands used in this paper, the ligands are trying to open the Fe(μ-CO)$_2$Fe bridge as shown by the asymmetric nature of the bridge, and the barrier for the merry-go-round mechanism could be lowered.

There are two types of the concerted bridge – opening bridge – closing mechanism possible in these complexes. The rotation may occur about the C(6)O–C(10)O axis, see Scheme 3, or about the C(7)O–P(1) axis, see Scheme 4.

Rotation about the C(6)O–C(10)O axis in Scheme 3 has the effect of exchanging the role of the two phosphorus atoms and making the carbonyl ligands pairwise exchange. There is no apparent reason for this dynamic process to be of much higher energy than in $[Fe_3(CO)_{12}]$ and is expected to be fast on the NMR timescale at –100°C. Substitution of C(7)O by $P(OMe)_3$ in $[Fe_3(CO)_9(dppm)\{P(OMe)_3\}]$ will result in the blockage of this pathway, as there is a substantial barrier to the phosphorus ligands going into the axial position.

The ease of rotation about the C(7)O–P(1) axis will depend on the accessibility of the isomer with the chelating phosphorus ligand along the Fe(μ-CO)$_2$Fe edge. This should

© 2001 NRC Canada

Table 7. Deviations (in Å) of chosen atoms from the Fe_3 plane for $[Fe_3(CO)_{10}L_2]$ (L_2 = dppm, $(Ph_2P)_2NH$, $\{(EtO)_2P\}_2O$), and $[Fe_3(CO)_9(dppm)\{P(OMe)_3\}]$.

	$[Fe_3(CO)_{10}$ (dppm)]^a	$[Fe_3(CO)_{10}$ $\{(Ph_2P)_2NH\}]$	$[Fe_3(CO)_{10}$ $\{(EtO)_2P\}_2O]$	$[Fe_3(CO)_9(dppm)$ $\{P(OMe)_3\}]$	$[Fe_3(CO)_{12}]$ at 100 K
C(5)				0.072	–0.195
C(6)	–0.025	0.051	0.023		0.103
C(7)	–0.240	–0.584	–0.323		0.139
C(10)	–0.024	0.025	0.054		–0.117
P(1)	0.200	0.165	0.182	0.092	
P(2)	–0.968	–0.953	–1.009	0.137	
P(3)				0.067	

^{a}Two independent molecules in the unit cell.

Table 8. Free energies of activation ($\Delta G^{\ddagger}$) for fluxional processes in $[Fe_3(CO)_{10}L_2]$ (L_2 = $Ph_2PCH_2PPh_2$, $Ph_2PNHPPh_2$, $(EtO)_2POP(OEt)_2$), and $[Fe_3(CO)_{10}(Ph_2PCH_2PPh_2)\{P(OMe)_3\}]$.

	C(7)O—P(1) rotation (kJ mol^{-1})	Merry-go-round (kJ mol^{-1})	C(2)O, C(8)O and C(7)O, C(9)O exchange (kJ mol^{-1})
$[Fe_3(CO)_{10}\{dppm\}]$	<24	33.7 ± 1.0	46.4 ± 1.0
$[Fe_3(CO)_{10}\{Ph_2PNHPPh_2\}]$			52.2 ± 1.0
$[Fe_3(CO)_{10}\{(EtO)_2POP(OEt)_2\}]$	33 ± 1.0	ca. 28	49.5 ± 1.0
$[Fe_3(CO)_{10}\{dppm\}\{P(OMe)_3\}]$		37.3 ± 1.0	42.8 ± 1.0

Fig. 6. A partial 100.62 MHz ^{13}C NMR 2D EXSY NMR spectrum of $[Fe_3(CO)_{10}(dppm)]$ in CD_2Cl_2 at –36.2°C

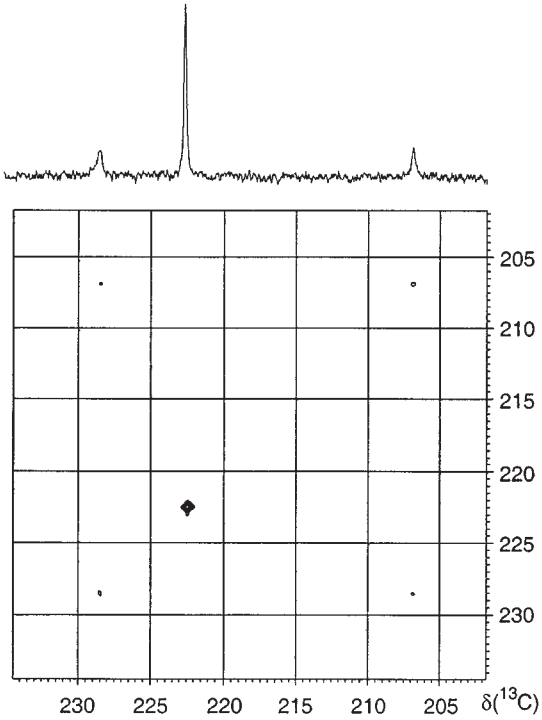
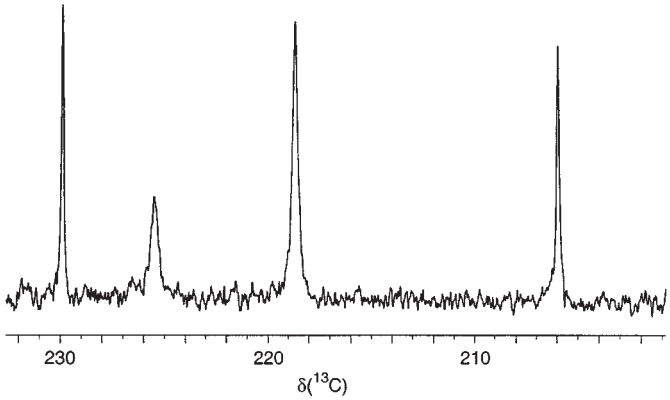


Fig. 7. A partial 100.62 MHz ^{13}C NMR spectrum of $[Fe_3(CO)_{10}(dppm)]$ in CD_2Cl_2 at –105°C.



be accessible for $[Fe_3(CO)_{10}(dppm)]$ as this bonding arrangement is found in the crystal structure of $[Fe_3(CO)_9(dppm)\{P(OMe)_3\}]$. However, as the P···P distance shortens on going to $[Fe_3(CO)_{10}(Ph_2PNHPPh_2)]$ and $[Fe_3(CO)_{10}\{(EtO)_2POP(OEt)_2\}]$, the barrier to this pathway should increase. As C(7)O lies on the axis of rotation, substitution by $P(OMe)_3$ should not block the pathway based on this rotation, but it will block the pathway based on rotation about the C(9)O–P(2) given in Scheme 4.

The effect of the merry-go-round mechanism is given in Scheme 5. At ca. –40°C, the ^{13}C carbonyl spectrum of $[Fe_3(CO)_{10}L_2]$ (L_2 = dppm, $(Ph_2P)_2NH$, $\{(EtO)_2P\}_2O$) consists of a 2:6:2 set of signals. No single mechanism produces six exchanging carbonyls, nor does a combination of two mechanisms. To achieve this pattern all three mechanisms shown in Schemes 3–5 have to be combined. This produces the exchanging sets of carbonyls: C(2)O and C(8)O; C(1)O, C(3)O, C(4)O, C(6)O, C(10)O, and C(12)O; C(7)O and C(9)O.

On cooling to around –105°C, the carbonyl ^{13}C NMR signals split to give a 2:2:4:2 pattern for $[Fe_3(CO)_{10}(dppm)]$ and a 2:4:2:2 pattern for $[Fe_3(CO)_{10}\{(EtO)_2POP(OEt)_2\}]$. The behaviour is markedly different for the two compounds with the new signal of intensity 2 being at δ 225.6 for $[Fe_3(CO)_{10}(dppm)]$ and δ 206 for $[Fe_3(CO)_{10}\{(EtO)_2POP(OEt)_2]$. The behaviour is substantially different and suggests for one the mechanism in Scheme 4 is freezing out, while for the other it is the mechanism in Scheme 5 that is freezing out. Combining the mechanisms in Schemes 3 and 4 produces

© 2001 NRC Canada

Fig. 8. A partial 100.62 MHz ^{13}C NMR spectrum of $[Fe_3(CO)_{10}\{(EtO)_2POP(OEt)_2\}]$ in CD_2Cl_2 at –106°C.

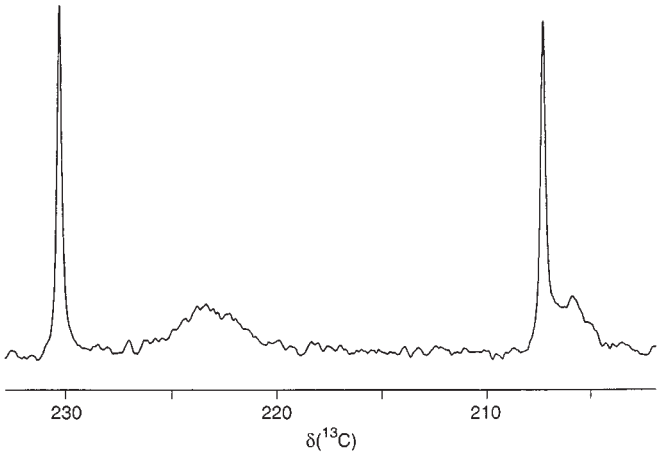
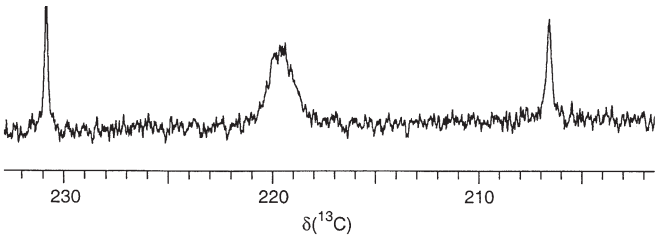


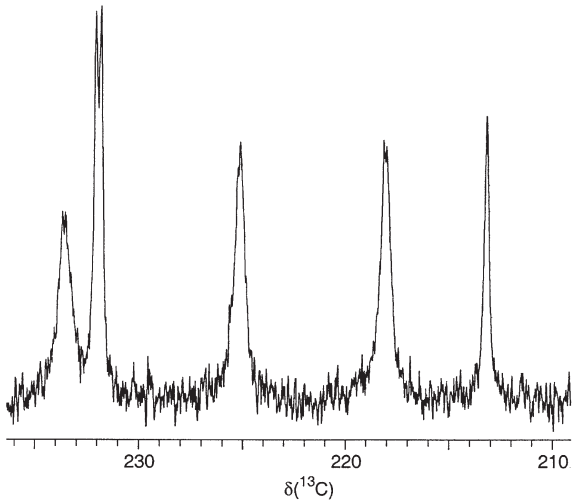
Fig. 9. A partial 100.62 MHz ^{13}C NMR spectrum of $[Fe_3(CO)_{10}(Ph_2PNHPPh_2)]$ in CD_2Cl_2 at –105°C.



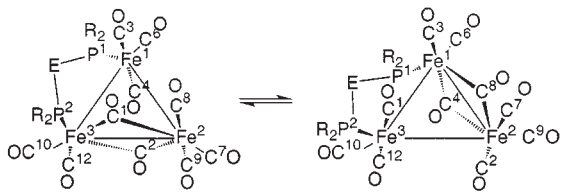
four sets of exchanging carbonyls: C(2)O and C(8)O; C(3)O and C(12)O; C(1)O, C(4)O, C(6)O, and C(10)O; C(7)O and C(9)O. Combining the mechanisms in Schemes 3 and 5 produces the exchanging sets of carbonyls: C(2)O and C(8)O; C(1)O, C(3)O, C(4)O, and C(12)O; C(6)O and C(10)O; C(7)O and C(9)O. This analysis works very well for $[Fe_3(CO)_{10}\{(EtO)_2POP(OEt)_2]$ with the mechanism in Scheme 4 freezing out. Figure 11 shows the estimated chemical shifts for the carbonyls at the various positions of $[Fe_3(CO)_{12}]$. This can be used to estimate the ^{13}C chemical shifts for the carbonyls of $[Fe_3(CO)_{10}\{(EtO)_2POP(OEt)_2]$ assuming that the fluxional mechanisms are according to Schemes 3 and 5. The calculated shifts (δ) based on Fig. 11 are as follows: 233.5 for C(2)O, C(8)O; 227.8 for C(1)O, C(3)O, C(4)O, C(12)O; 207 for C(6)O, C(10)O; and 209 for C(7)O, C(9)O, which are in tolerable agreement with the observed shifts (Table 9). A perfect agreement would not be expected as the effects of substitution and distortion from an ideal geometry would produce deviations from the predicted values.

When this approach is applied to $[Fe_3(CO)_{10}(dppm)]$ with the mechanism in Scheme 5 frozen out, there is a problem. The predicted chemical shifts (δ), based on the crystal structure, for the four sets of exchanging carbonyls are: 233.5 for C(2)O, C(8)O; 218.5 for C(3)O, C(12)O; 222 for C(1)O, C(4)O, C(6)O, C(10)O; and 209 for C(7)O, C(9)O. The agreement is very poor for C(3)O and C(12)O. However, as the crystal structure of $[Fe_3(CO)_9(dppm)\{P(OMe)_3\}]$ shows that the geometry with the chelate ligand across the Fe(μ-$CO)_2$Fe edge is accessible the chemical shifts would be very different. It follows from the position of the ligands in

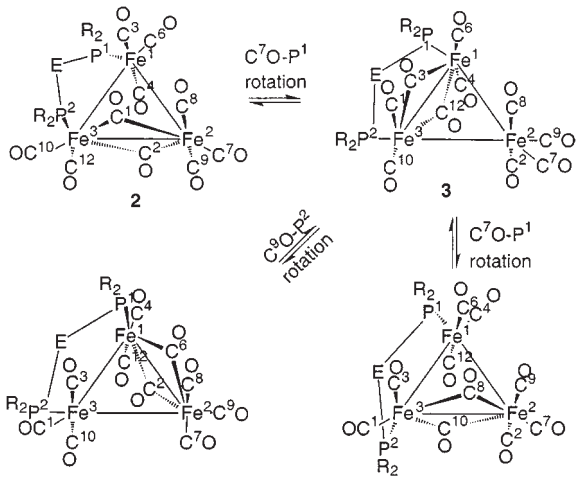
Fig. 10. A partial 100.62 MHz ^{13}C NMR spectrum of $[Fe_3(CO)_9(dppm)\{P(OMe)_3\}]$ in CD_2Cl_2 at –97°C.



Scheme 3.



Scheme 4.



Scheme 3, that if this geometry was exclusively present, the chemical shifts would be δ: 222 C(2)O, C(8)O; 252 C(3)O, C(12)O; 215 C(1)O, C(4)O, C(6)O, C(10)O; and 203 C(7)O, C(9)O. Hence, to account for the observed shifts, it is necessary to conclude that isomers **2** and **3** are present in solution in a ratio of approximately 3:1.

The low temperature ^{13}C NMR spectrum of $[Fe_3(CO)_9(dppm)\{P(OMe)_3\}]$ is shown in Fig. 10. By analogy with $[Fe_3(CO)_{10}(dppm)]$, only the mechanism in Scheme 4 should be operating as the presence of the $P(OMe)_3$ blocks the mechanism shown in Scheme 3. This leads to the following exchange: C(1)O ⇌ C(10)O, C(4)O ⇌ C(6)O, C(3)O ⇌ C(12)O, C(2)O ⇌ C(8)O, C(6)O ⇌ C(10)O,

© 2001 NRC Canada

Scheme 5.

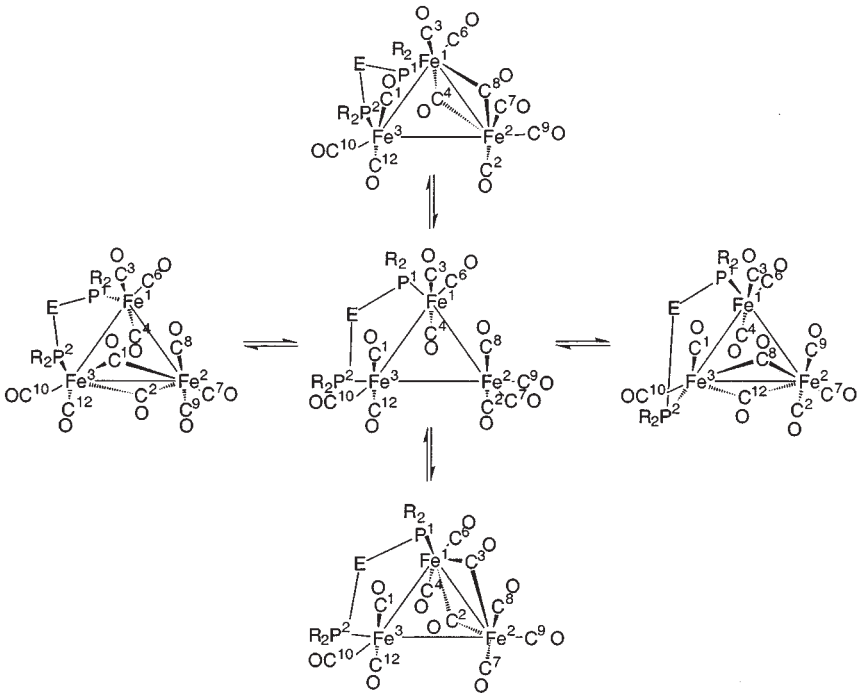
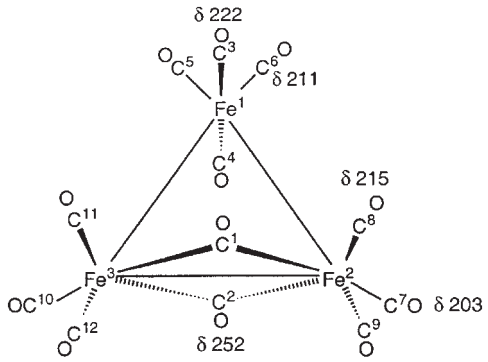


Fig. 11. Estimated ^{13}C NMR chemical shifts for carbonyls on $[Fe_3(CO)_{12}]$ based on the reported chemical shifts for $[Fe_3(CO)_{12-n}\{P(OMe)_3\}_n]$, n = 2, 3.



and C(9)O is left unaffected. If the structure in solution is **2**, then the predicted chemical shifts are δ: 227.5 C(1)O, C(10)O; 216.5 C(4)O, C(6)O; 218.5 C(3)O, C(12)O; 233.5 C(2)O, C(8)O; and 215 C(9)O. If the structure in solution is **3**, then the predicted chemical shifts are δ: 215 C(1)O, C(10)O; 215 C(4)O, C(6)O; 252 C(3)O, C(12)O; 222 C(2)O, C(8)O; 211 C(7)O and C(9)O. Comparison of these shifts with the spectrum and the observation of $J_{P,C}$ on the signal at δ 232 makes the probable assignments δ: 225 C(1)O, C(10)O; 218 C(4)O, C(6)O; 233 C(3)O, C(12)O; 232 C(2)O, C(8)O; 213 C(9)O. The ^{13}C chemical shifts suggest that **2** is the major isomer in solution despite the crystal structure being **3**.

The concerted bridge – opening bridge – closing mechanism

Usually the concerted bridge – opening bridge – closing mechanism is extremely facile and cannot be stopped. The only previous example of it being stopped is $[Fe_3(CO)_{11}(CNCF_3)]$ and related complexes, where the $CNCF_3$ is tightly held into a μ_2-bridging position (19). In the cases of the $[Fe_3(CO)_{10}L_2]$ (L_2 = dppm, $Ph_2PNHPPh_2$, $(EtO)_2POP(OEt)_2$) complexes, rotation about the S_{10} axis through C(6)O and C(10)O is fast on the NMR time scale even at –105°C. However, the barrier to rotation about the S_{10} axis through C(7)O and P(1) is increased because of the strain produced by the chelating ligand in **3**. The formation of a carbonyl bridge on the same edge as the chelate is bonding increases the ideal separation of the two phosphorus atoms. The barrier increases from <24 kJ mol^{-1} in $[Fe_3(CO)_{10}(dppm)]$ to 33 ± 2.0 kJ mol^{-1} in $[Fe_3(CO)_{10}\{(EtO)_2POP(OEt)_2\}]$ correlating with the P···P distance decreasing from 3.053(2)–3.067(2) to 2.836(3) Å.

The merry-go-round mechanism

The strain produced by the chelate ring has a tendency to open the Fe(μ-CO)$_2$Fe bridge. As the strain increases from $[Fe_3(CO)_{10}(dppm)]$ to $[Fe_3(CO)_{10}\{(EtO)_2POP(OEt)_2\}]$, the Fe(μ-CO)$_2$Fe bridge opens more easily and $\Delta G^{\ddagger}$ drops from 33.7 ± 1.0 to ca. 26 kJ mol^{-1}. The clearest demonstration of the merry-go-round mechanism occurs with $[Fe_3(CO)_{10}(dppm)\{P(OMe)_3\}]$, where an EXSY NMR spectrum clearly shows C(1)O, C(4)O exchanging with C(3)O, C(12)O and C(6)O, C(12)O as would be expected when the merry-go-round mechanism is applied to isomer **3**, see Fig. 12. No direct exchange is detected between the signals due to C(3)O, C(12)O and C(6)O, C(12)O. The exchange mechanism in Scheme 5 does not produce this exchange, and the merry-go-round mechanism has to operate around the edge Fe(1)–Fe(3), see Scheme 6.

For both the concerted bridge – opening bridge – closing and merry-go-round mechanism, $\Delta G^{\ddagger}$ for $[Fe_3(CO)_{10}(Ph_2PNHPPh_2)]$ is expected to be between the

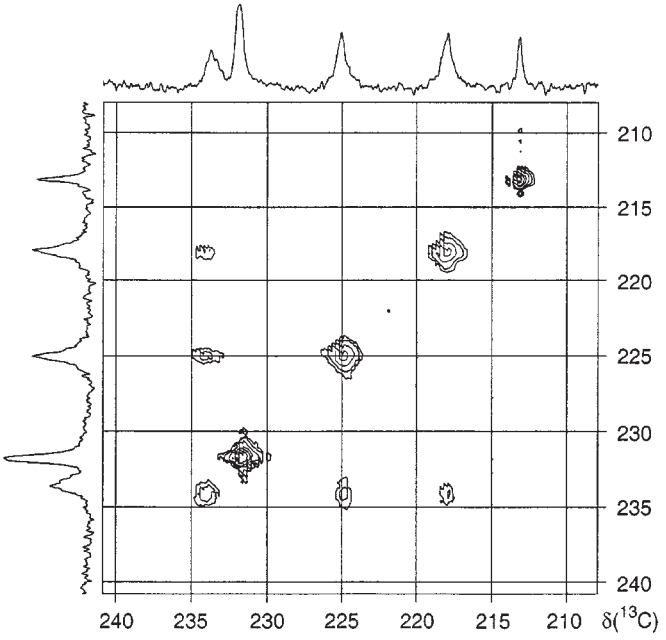
© 2001 NRC Canada

Table 9. ^{13}C NMR chemical shifts of the carbonyls of $[Fe_3(CO)_{10}L_2]$ (L_2 = dppm, $Ph_2PNHPPh_2$, $(EtO)_2POP(OEt)_2$) and $[Fe_3(CO)_{10}(Ph_2PCH_2PPh_2)\{P(OMe)_3\}]$ at ca. –100°C in CD_2Cl_2.

	C(1)O, C(4)O	C(2)O, C(8)O	C(3)O, C(12)O	C(6)O, C(10)O	C(7)O, C(9)O
$[Fe_3(CO)_{10}(Ph_2PCH_2PPh_2)]$	218.6[a]	229.9	225.5	218.6a	205.9
$[Fe_3(CO)_{10}(Ph_2PNHPPh_2)]$	219.1	230.5	219.1	219.1	206.2
$[Fe_3(CO)_{10}\{(EtO)_2POP(OEt)_2\}]$	224[a]	229.8	224[a]	206	206.6
$[Fe_3(CO)_{10}(Ph_2PCH_2PPh_2)\{P(OMe)_3\}]$	233.7	231.9 (24)	225.1	218.1	213.2

[a]Averaged.

Fig. 12. A partial 100.62 MHz ^{13}C EXSY NMR spectrum of $[Fe_3(CO)_{10}(dppm)\{P(OMe)_3\}]$ in CD_2Cl_2 at –96°C with a mixing delay of 0.002 s.

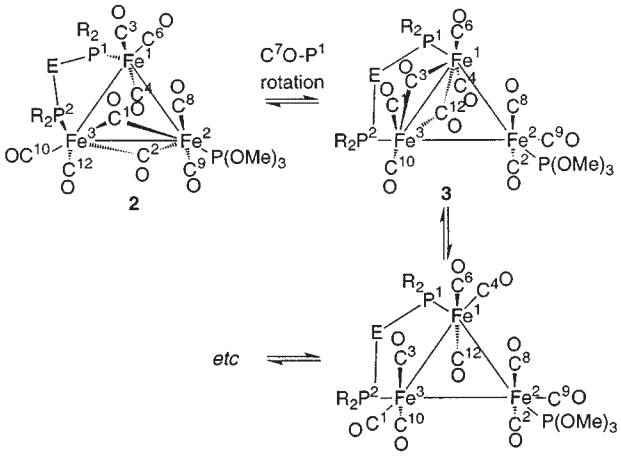


values determined for $[Fe_3(CO)_{10}(dppm)]$ and $[Fe_3(CO)_{10}\{(EtO)_2POP(OEt)_2\}]$. Hence, both values are expected to be less than 30 kJ mol^{-1}. As a result, neither mechanism is frozen out at –105°C and the resulting signal is broad. No value could be determined for $\Delta G^{\ddagger}$ as it is unknown if one or both mechanisms are freezing out.

Trigonal twist mechanism

All four complexes reported here show exchange between C(2)O, C(8)O and C(7)O, C(9)O, or just C(9)O in the case of $[Fe_3(CO)_{10}(dppm)\{P(OMe)_3\}]$. At the onset of the exchange, the exchange is localized to C(2)O, C(8)O and C(7)O, C(9)O for $[Fe_3(CO)_{10}L_2]$ (L_2 = dppm, $Ph_2PNHPPh_2$, $(EtO)_2POP(OEt)_2$), although this is not known for $[Fe_3(CO)_{10}(dppm)\{P(OMe)_3\}]$. The most likely mechanism to fit this exchange is the trigonal twist mechanism. It appears to have been facilitated in these compounds as in $[Fe_3(CO)_{11}\{P(OMe)_3\}]$ it is believed to occur with $\Delta G^{\ddagger}$ = 62 kJ mol^{-1} and in $[Fe_3(CO)_{10}\{P(OMe)_3\}2]$ with $\Delta G^{\ddagger}$ = 60 kJ mol^{-1}. It would, therefore, appear that substitution of the carbonyls facilitates the dynamic process.

Scheme 6.



Conclusions

The distortions observed in the crystal structures induced in the structure of $[Fe_3(CO)_{12}]$ by substitution with the small bite-angle ligands ($Ph_2PCH2PPh_2$, $Ph_2PNHPPh_2$, $(EtO)_2POP(OEt)_2$) follow from the predictions of the Mann concerted bridge – opening bridge – closing mechanism rather than the Johnson libration mechanism.

The dynamic processes observed in the ^{13}C NMR spectra can be fully explained using either the Mann concerted bridge – opening bridge – closing mechanism or the Johnson libration mechanism, the merry-go-round mechanism, and the trigonal twist mechanism.

The changes in $\Delta G^{\ddagger}$ from those previously observed with monodentate ligands are predictable as a consequence of using small bite-angle ligands.

References

1. F.A. Cotton and D.L. Hunter. Inorg. Chim. Acta, **11**, L9 (1974).
2. B.F.G. Johnson. J. Chem. Soc. Chem. Commun. 703 (1976).
3. R.E. Benfield, P.D. Gavens, B.F.G. Johnson, M.J. Mays, S. Aime, L. Milone, and D. Osella. J. Chem. Soc. Dalton Trans. 1535 (1981).
4. D.H. Farrar and J.A. Lunniss. J. Chem. Soc. Dalton Trans. 1249 (1987).
5. H.A. Adams, N.A. Bailey, G.W. Bentley, and B.E. Mann. J. Chem. Soc. Dalton Trans. 1831 (1989).
6. A. Bino, F.A. Cotton, P. Lahuerta, P. Puebla, and R. Usón. Inorg. Chem. **19**, 2357 (1980).

© 2001 NRC Canada

7. B.F.G. Johnson and A. Bott. J. Chem. Soc. Dalton Trans. 2437 (1990).
8. H. Adams, A.G. Carr, B.E. Mann, and R. Melling. Polyhedron, **14**, 2771 (1995).
9. B.E. Mann. J. Chem. Soc. Dalton Trans. 1457 (1997).
10. (*a*) H.B. Bürgi and J.D. Dunitz. Acc. Chem. Res. **16**, 153 (1983); (*b*) T.A.D. Heyde. Structure correlation. Vol 1 and 2. *Edited by* H.B. Bürgi and J.D. Dunitz. VCH, Weinheim. 1994. Chap. 8.
11. B.F.G. Johnson. J. Chem. Soc. Dalton Trans. 1472 (1997).
12. E. Stein and F.Y. Fujiwara. J. Organomet. Chem. **525**, 31 (1996).
13. H. Adam, S.C.M. Agusthino, B.E. Mann, and S. Smith. J. Organomet. Chem. **607**, 175 (2000).
14. W. McFarlane and G. Wilkinson. Inorg. Synth. **8**, 181 (1966).
15. G.M. Sheldrick. SHELXL. An integrated system for solving and refining crystal structures from diffraction data (Revision 5.1), Bruker AXS Ltd.
16. T.-J. Kim, S.-C. Kwon, Y.-H. Kim, N.H. Heo, M.M. Teeter, and A. Yamano. J. Organomet. Chem. **426**, 71 (1991).
17. P.J. Roberts, B.R. Penfold, and J.R. Trotter. Inorg. Chem. **9**, 2137 (1970).
18. D. Braga, F. Grepioni, L.J. Farrugia, and B.F.G. Johnson. J. Chem. Soc. Dalton Trans. 2911 (1994).
19. D. Lentz and R. Marschall. Organometallics, **10**, 1487 (1991).

© 2001 NRC Canada

Functionalization vs. degradation of 1,4-polybutadiene by ruthenium complex catalyzed reaction with vinylsilanes

Bogdan Marciniec, Ewa Małecka, Jacek Guliński, Monika Grundwald-Wyspiańska, and Mariusz Lewandowski

Abstract: Polybutadiene (**I**) containing 91% of 1,4-(*cis–trans*) units and 9% of 1,2-units in the presence of vinyltriethoxysilane (**II**) and ruthenium catalysts $RuCl_2(PPh_3)_3$ (**III**), $RuHCl(CO)(PPh_3)_3$ (**IV**), and $[RuCl_2(CO)_3]_2$ (**V**) at 100–130°C undergoes functionalization and (or) partial degradation as an effect of competitive silylative coupling of =C-H and cross-metathesis of **I** with **II**. Significant degradation of **I** occurs at lower temperatures (100–110°C) (particularly when the process is carried out in air), but exclusive functionalization of **I** is observed at higher temperature (120–130°C) regardless of the atmosphere (air or argon) used.

Key words: functionalization, degradation, polybutadiene, ruthenium complexes.

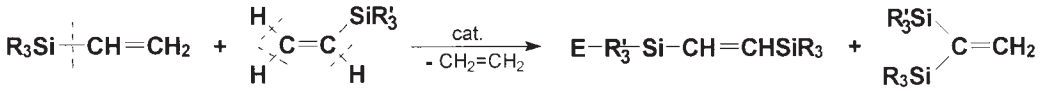
Résumé : Le polybutadiène (**I**) contenant 91% d'unités 1,4-(*cis–trans*) et 9% d'unités 1,2 mis en présence de vinyltriéthoxysilane (**II**) et des catalyseurs de ruthénium $RuCl_2(PPh_3)_3$ (**III**), $RuHCl(CO)(PPh_3)_3$ (**IV**) ou $[RuCl_2(CO)_3]_2$ (**V**), à 100–130°C, subit une fonctionnalisation et (ou) une dégradation partielle qui résultent d'un couplage silylisant de =C-H qui est en compétition avec une réaction de métathèse croisée de **I** avec **II**. À des températures plus faibles (100–110°C) (particulièrement lorsqu'on effectue la réaction en présence d'air), on observe une dégradation importante du composé **I**; toutefois, à des températures plus élevées (120–130°C), on n'observe que la fonctionnalisation du composé **I** quelle que soit la nature de l'atmosphère (air ou argon).

Mots clés : fonctionnalisation, dégradation, polybutadiène, complexes du ruthénium.

Introduction

Cross-metathesis of unsaturated polymers with olefins has been widely studied to follow their degradation and to determine their cross linked structure (1). The degradation of 1,4-polybutadiene by hex-2-ene (2), hex-3-ene (3, 4), as well as ethylene (5), occurs mostly in the presence of tungsten and molybdenum carbenes. Recently Grubbs ruthenium-carbenes have been used as degradation agents (6). Silicon-containing olefins, mainly allylsilanes, have been applied by Marmo and Wagener (7, 8) in metathetical (ADMET) degradation of 1,4-polybutadiene in the presence of a Schrock molybdenum catalyst to yield perfectly difunctional (f = 2.0) telechelic polybutadiene oligomers. Vinyl-substituted silanes are not active in ADMET depolymerization (M and W catalysts) (9, 10), however, they can be used for the reduction of the molar mass of polymers (11). Our recent study has shown that polybutadiene (**I**) containing 91% of 1,4-(*cis–trans*) units and 9% of 1,2-units in the presence of vinyltriethoxysilane and ruthenium carbenes undergoes partial degradation and functionalization (12).

On the other hand, olefins react readily via silylative coupling with vinylsilanes (*trans*-silylation) in the presence of ruthenium complexes containing or initially forming Ru—H and (or) Ru—Si bonds (13–16). Evidence has been found confirming nonmetathetical conversion of the olefins with vinylsilanes in the presence of such catalysts (14–16). Instead of the cleavage of the C=C bonds in olefin metathesis the process occurs via silylation of olefins by vinylsilanes (i.e., cleavage of vinyl C—H in the olefins and Si—C_{vinyl} bonds) according to eq. [1] (15):

[1] 

Received September 5, 2000. Published on the NRC Research Press Web site at http://canjchem.nrc.ca on June 30, 2001.

Dedicated to Professor Brian R. James in recognition of his great contribution to homogeneous catalysis.

B. Marciniec,[1] E. Małecka, J. Guliński, M. Grundwald-Wyspiańska, and M. Lewandowski. Faculty of Chemistry, Adam Mickiewicz University, Grunwaldzka 6, 60–780 Poznan, Poland.

[1]Corresponding author (telephone: (48-61) 8291 366 or (48-61) 8291 509; fax: (48-61) 8291 508; e-mail marcinb@main.amu.edu.pl).

 DOI: 10.1139/cjc-79-5/6-775 © 2001 NRC Canada

Table 1. The effect of the catalyst and temperature, under argon, on the average molecular weight (kDa) of the functionalized (M_n(**F**)) and degraded (M_n(**D**)) 1,4-polybutadiene with vinyltriethoxysilane.

Catalyst	100°C		110°C		120°C[a]	130°C[a]
	M_n(**F**)	M_n(**D**)[b]	M_n(**F**)	M_n(**D**)[b]	M_n(**F**)	M_n(**F**)
$RuCl_2(PPh_3)_3$ (**III**)	460.0	288.2 (9)	480.4	312.6 (19)	498.5	510.4
$Ru(H)Cl(CO)(PPh_3)_3$ (**IV**)	445.2	190.0 (2)	470.0	246.2 (4)	492.4	504.4
$[RuCl_2(CO)_3]_2$ (**V**)	434.8	164.2 (1.2)	443.2	230.7 (3)	451.6	467.2

Note: Reaction conditions: ratio of [C=C bond]:[catalyst]:[$ViSi(OEt)_3$] = $1:10^{-2}$:2; glass ampoules, 48 h. Initial polymer: 1,4-polybutadiene containing 9% of vinyl group; M_n = 400.0 kDa.
[a]Only polymers with higher mass than initial 1,4-polybutadiene were detected.
[b]Values in parentheses represent **F**:**D** ratio.

Table 2. The effect of the catalyst and temperature, under dry air, on the average molecular weight (kDa) of the functionalized (M_n(**F**)) and degraded (M_n(**D**)) 1,4-polybutadiene with vinyltriethoxysilane.

Catalyst	100°C		110°C		120°C		130°C
	M_n(**F**)	M_n(**D**)[a]	M_n(**F**)	M_n(**D**)[a]	M_n(**F**)	M_n(**D**)[a]	M_n(**F**)[b]
$RuCl_2(PPh_3)_3$ (**III**)	462.4	62.5 (0.11)	481.6	116.4 (0.82); (1.80)[c]	500.8	285.0 (9.0)	515.3 (1.13)[c]
$Ru(H)Cl(CO)(PPh_3)_3$(**IV**)	457.6	84.6 (0.33)	472.4	176.2 (1.50)	492.4[c]	—	505.7
$[RuCl_2(CO)_3]_2$ (**III**)	434.8	95.0 (0.54)	443.2	184.6 (1.91)	452.8[c]	—	467.2

Note: Reaction conditions: ratio of [C=C bond]:[catalyst]:[$ViSi(OEt)_3$] = $1:10^{-2}$:2; glass ampoules, 48 h. Initial polymer: 1,4-polybutadiene containing 9% of vinyl group; M_n = 400.0 kDa.
[a]Values in parentheses represent **F**:**D** ratio.
[b]Only polymers with higher mass than initial 1,4-polybutadiene were detected.
[c]M_w/M_n.

The vinyl group in 1,2-polybutadiene in the presence of various ruthenium complexes at elevated temperature undergoes facile silylation, which leads a new type of modification of unsaturated polymers (17).

In view of the catalytic activity of ruthenium–carbenes in degradation of 1,4-polybutadiene by vinylsilanes and effective catalysis by Ru–H and Ru–Si complexes for functionalization of 1,2-units of polybutadiene, a study was undertaken to show the suitability of vinyltriethoxysilane (**II**), not for depolymerization of 1,4-polybutadiene (**I**), but for its modification to synthesize silyl-substituted polymers.

Experimental

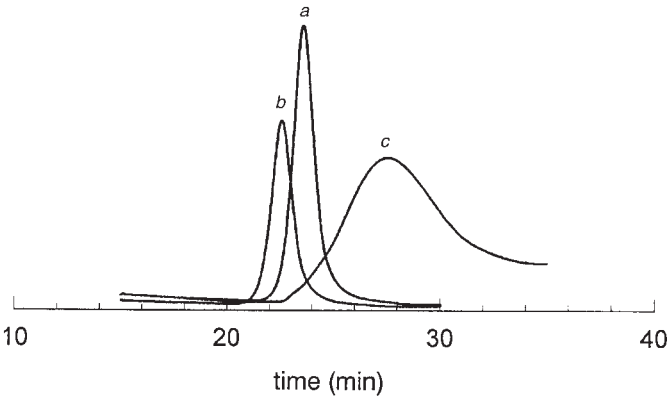
Materials

Polybutadiene (M_n = 400 000) (**I**) containing 91% of 1,4-(*cis–trans*) units and 9% of 1,2-units, was purchased from Polysciences, Inc. and used without additional purification. Vinyltriethoxysilane (**II**), purchased from Fluka, was distilled prior to use. $RuCl_2(PPh_3)_3$ (**III**) (18) and $RuHCl(CO)(PPh_3)_3$ (**IV**) (19) were prepared by standard procedures. $[RuCl_2(CO)_3]_2$ (**V**) was purchased from Strem Chemicals, Inc.

Functionalization and (or) degradation reactions

Reactions were carried out under dry air or under argon in a glass reactor equipped with a condenser and a heater or in sealed glass ampules. In a typical reaction, 1,4-polybutadiene (1.00 g, 0.001 mol), chlorobenzene (24 g), vinyltriethoxysilane (0.32 cm^3), and a catalyst (7.4×10^{-6} mol) were placed in the reaction system and heated for 24 h at the required temperature (100–130°C). Reaction mixtures were analyzed by gel permeation chromatography (GPC) and NMR techniques. GPC results are presented in Tables 1 and 2 and Fig. 1. Spectroscopic analyses (NMR) were performed both for the reaction mixtures and the isolated products. For example, for the reaction mixture of **I** with **II** in the presence of $RuCl_2(PPh_3)_3$ (dry air, 100°C) the following signals (ppm) were observed: 0.96 (t), 1.19 (t), 1.21 (t), 2.10 (s), 3.34 (t), 3.80 (t), 3.92 (t), 5.48 (s), 6.00 (m) (signals originating from solvent were omitted for clarity). Polymeric products were precipitated from the solution with methanol, filtered, washed with methanol, and dried under vacuum. IR and NMR spectra of the isolated polymer were also obtained.

Fig. 1. GPC spectra of initial 1,4-polybutadiene (**I**) and after undergoing functionalization and degradation with vinyltriethoxysilane in the presence of catalyst $RuCl_2(PPh_3)$: (*a*) initial polymer; (*b*) under argon, 130°C; (*c*) under dry air, 100°C.

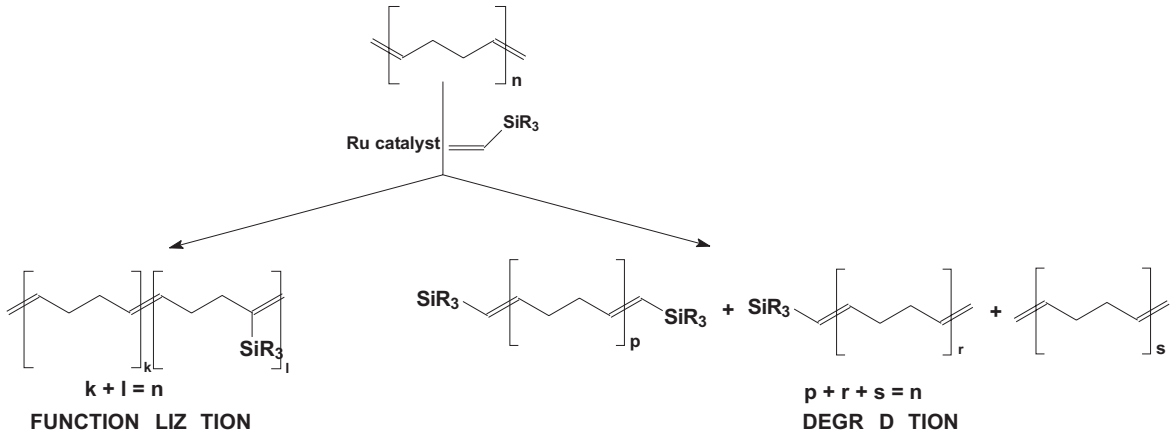


Equipment and analytical measurements

^1H and ^{13}C NMR spectra were recorded on a Varian XL300 spectrometer. GPC data were collected using a Gilson HPLC system with 2 × 250 × 10 mm, Jordi-Gel DVB

© 2001 NRC Canada

Scheme 1.



Column: 500 and 100 Å, using polystyrene standards (mobile phase, THF; flow rate, 1.2 mL min^{-1}; ambient temperature). The ratio (**F**:**D**) of GPC peak area coming from functionalized polybutadiene (higher M_n) to the area of GPC peak originating from degraded polybutadiene (lower M_n) were calculated for reaction products. IR spectra (film or KBr pellet) were recorded using a FT-Bruker JFS-113V instrument.

Results and discussion

Polybutadiene (**I**) was used as the substrate in its reaction with vinyltriethoxysilane (**II**) to synthesize polymers or oligomers containing alkoxy-substituted silyl groups, i.e., polymeric coupling agents (20). $RuCl_2(PPh_3)_3$ (**III**), $RuHCl(CO)(PPh_3)_3$ (**IV**), and $[RuCl_2(CO)_3]_2$ (**V**) were used as catalysts. All three Ru-complexes catalyze the cross-disproportionation (silylative coupling) of olefins with vinylsilanes according to eq. [1]. Oligomers obtained as a result of this reaction are the products of metathetical degradation (**D**) (cleavage of the C=C bond in the chain, followed by silylation of the newly formed $CH{=}CH_2$ unit). On the other hand, polymers of the molecular weight higher than the initial polybutadiene (**I**) are products of functionalization (silylation) (**F**) of starting **I**.

All experiments of **I** and any catalyst performed at different conditions (argon or oxygen) in the absence of vinyltriethoxysilane showed no changes (evidenced by IR, NMR, and GPC analysis) in the starting polybutadiene. No oxidation of polybutadiene, resulting in the formation of OH groups, is observed.

Scheme 1 illustrates both reactions (functionalization and degradation) occurring under the above specified conditions, but omits for clarity the reactions of the 1,2-units (present in 9% in **I**). To follow the effect of vinylsilane on the process, GPC was used to measure the functionalization and degradation of **I**. The GPC chromatograms of the initial 1,4-polybutadiene (*a*) and the same compound after heating with vinyltriethoxysilane in the presence of $RuCl_2(PPh_3)_3$ in argon (130°C) (*b*) and in air (100°C) (*c*), are presented in Fig. 1.

If the reaction occurs under oxygen-free conditions predominantly at higher temperature (i.e., 130°C) exclusive functionalization over degradation is observed (Table 1). On the basis of the results of GPC analysis (Fig. 1*b*) it is possible to distinguish the modified 1,4-polybutadiene from the degraded oligomers, and simultaneously to determine the degree of functionalization of **I** by vinyltriethoxysilane (**II**). The latter effect is observed to increase with increasing temperature to the optimum of 130°C.

$RuCl_2(PPh_3)_3$ is well-known as an effective unicomponent catalyst for the ring-opening metathesis polymerization (ROMP) of norbornene. The rate of the reaction increases as much as 100-fold when O_2 is bubbled through the reactor (21).

Our experiments carried out with catalysts **III**–**V** (see Table 2 and Fig. 1*c*) indicate that significant degradation of **I** via metathetical cleavage of C=C bonds, when compared to the functionalization of =C—H bonds, is taking place, but only at lower temperatures (100–110°C). At higher temperatures (120–130°C), even if the process occurs in the air, the functionalization of **I** is exclusively observed.

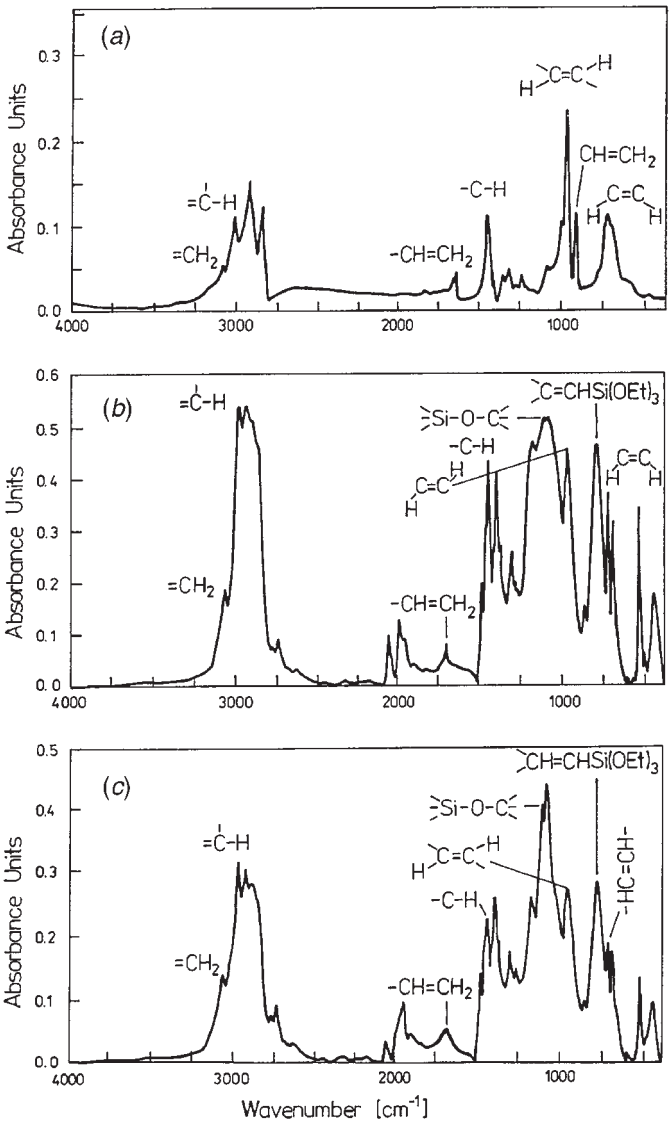
^1H and ^{13}C NMR spectrometry experiments as well as FT-IR studies of **I** heated with vinyltriethoxysilane were performed to find the possible evidence for functionalization, i.e., silylation or activation, of the =C—H bond of HC=CH units and (or) vinyl groups.

The ^1H NMR spectra of all the reaction products mixtures show not only resonances close to 6.00, 3.80, and 1.19 ppm (characteristic of the starting vinylsilane (22)), but also new signals (at about 3.40 and 1.00 ppm) attributed to ethoxy substituted silyl groups located in silylated unsaturated oligomers (polymers). Such signals, of different intensities, can be detected in the spectra of all systems, and they are convincing evidence for both functionalization and degradation of 1,4-polybutadiene (**I**) accompanied by the incorporation of triethoxysilyl groups into oligomer chain. The spectra of the isolated polymeric products are similar, however, in the air-free conditions with $RuCl_2(PPh_3)_3$ as the catalyst (i.e., when functionalization is most prevalent) the intensities of OCH_2CH_3 signals (3.34 and 0.96 ppm) are more than 10-fold higher than those observed for the dry-air reaction products (i.e., when degradation predominates) in relation to the CH_2 signals of polybutadiene network.

The IR spectrum (Fig. 2*a*) of 1,4-polybutadiene (**I**), shows a strong absorption at 964 cm^{-1} characterizing deformation vibrations of *trans* =C—H bonds (23). The spectrum recorded after the reaction of **I** with vinyltriethoxysilane (**II**) in argon ($RuCl_2(PPh_3)_3$ as the catalyst) (Fig. 2*b*) reveals the

© 2001 NRC Canada

Fig. 2. FT-IR spectra of: (*a*) initial 1,4-polybutadiene (**I**) and functionalized and (or) degraded with vinyltriethoxysilane; (*b*) $RuCl_2(PPh_3)_3$, argon, 120°C, 48 h; (*c*) $RuCl_2(PPh_3)_3$, dry air, 100°C, 48 h.



presence of new bands at 1078 and 1102 cm^{-1} attributable to the Si—O-C vibration in $CH=CHSi(OEt)_3$ and (or) in $CH=C[Si(OEt)_3]_2$, which proves the occurrence of the silylation of C—H bonds with vinyltriethoxysilane. Moreover, the spectra show the appearance of a new band at 789 cm^{-1} presumably characterizing deformation vibrations of $CH=CHSi(OEt)_3$ and (or) $CH=C[Si(OEt)_3]_2$. Simultaneously, a decrease in the intensity of the bands at 723 cm^{-1}, which are due to *cis*-CH=CH deformation, and the lack of changes in the absorption band assigned to *trans*-HC=CH vibration are observed. Figure 2*c* reflects the same effect, since it corresponds to the mixture of the functionalized and degraded oligomers when **I** is heated with vinylsilane in the presence of $RuCl_2(PPh_3)_3$ in air (100°C).

Thus, FT-IR analysis may be valuable proof for activation of C—H in the chain (to get $CH=C[Si(OEt)_3]_2$ fragments) and simultaneously in the terminal vinyl groups of the degradated oligomers and pendant groups of 1,2-polybutadiene units (to yield $CH=CHSi(OEt)_3$ fragments). The former effect can be accounted for by activation of *cis*-HC=CH units in the silylation of (**I**) by vinylsilanes, while the latter by a well-known process of silylation of most vinylic olefins with vinylsilanes (13).

All the results on the silylative coupling (the functionalization) vs. cross-metathesis (the degradation) of vinyltriethoxysilane with 1,4-polybutadiene are strongly supported in detail by previous examination of the reaction of the vinylsilanes with alkenes catalyzed by Ru–H and Ru–Si containing complexes (16, 24) or ruthenium carbenes (24–26).

Acknowledgment

Financial support by the State Committee for Scientific Research project No. K012/T09/2000 is gratefully acknowledged.

References

1. K.J. Ivin and J.C. Mol. Olefin metathesis and metathesis polymerization. Academic Press, San Diego. 1997. Chap. 16.
2. W. Ast and K. Hummel. Naturwiss. **545**, 57 (1970).
3. H.Abendroth and E.Canji. Makromol. Chem. **176**, 775 (1975).
4. E. Canji and H. Perner. Rec. Trav. Chim. Pays-Bas, **96**, M70, (1978).
5. K.B. Wagener, R.D. Puts, and D.W. Smith. Makromol. Chem. Rapid Commun. **12**, 419 (1991).
6. M.D. Watson and K.B. Wagener. Am. Chem. Soc. Polymer Prep. **37**, 1 (1996).
7. J.C. Marmo and K.B. Wagener. Macromolecules, **26**, 2137 (1993).
8. J.C. Marmo and K.B. Wagener. Macromolecules, **28**, 2602 (1995).
9. D.W. Smith and K.B. Wagener. Macromolecules, **26**, 1633 (1993).
10. E.S. Finkelshtein and B. Marciniec. *In* Progress in organosilicon chemistry. *Edited by* B. Marciniec and J. Chojnowski. Gordon and Breach, Basel. 1995. p. 445.
11. R. Streck. J. Mol. Catal. A: Chem. **15**, 3 (1982).
12. B. Marciniec, M. Lewandowski, J. Gulinski, A.F. Noels, A. Demonceau, E. Malecka, and D. Jan. Polymer, **41**, 827 (2000).
13. B. Marciniec. New J. Chem. **21**, 815 (1997).
14. Y. Wakatsuki, H. Yamazaki, M. Nakano, and Y. Yamamoto. J. Chem. Soc. Chem. Commun. 703 (1991).
15. B. Marciniec and C. Pietraszuk. J. Chem. Soc. Chem. Commun. 2003 (1995).
16. B. Marciniec and C. Pietraszuk. Organometallics, **16**, 4320 (1997).
17. B. Marciniec, M. Lewandowski, C. Pietraszuk, and Z. Foltynowicz. Polymer, **38**, 5169 (1997).
18. P.S. Hallman, T.A. Stephenson, and G. Wilkinson. Inorg. Synth. Vol. XII. 1973. p. 237.
19. N. Ahmad, J.J. Levison, S.D. Robinson, and M.F. Uttey. Inorg. Synth. Vol. XII. 1973. p. 45.
20. M.P. McGrath, E.D. Sall, and S.J. Tremont. Chem. Rev. **95**, 381 (1995).
21. K.J. Ivin, B.S. Reddy, and J.J. Rooney. J. Chem. Soc Chem. Commun. 1062 (1981).

© 2001 NRC Canada

22. A.L. Smith (*Editor*). Analysis of silicones. John Wiley & Sons, New York. 1974.
23. L.J. Bellamy. The infrared spectra of complex molecules. John Wiley & Sons, New York. 1958.
24. B. Marciniec, Z. Foltynowicz, C. Pietraszuk, J. Gulinski, and H. Maciejewski. J. Mol. Catal. A: Chem. **90**, 213 (1994).
25. C. Pietraszuk, B. Marciniec, and H. Fischer. Organometallics, **29**, 913 (2000).
26. C. Pietraszuk, H. Fisher, M. Kujawa, and B. Marciniec. Tetrahedron Lett. **42**, 1175 (2001).

© 2001 NRC Canada

Synthesis and coordination studies of new aminoalcohol functionalized tertiary phosphines

Sean E. Durran, Martin B. Smith, Alexandra M.Z. Slawin, Thomas Gelbrich, Michael B. Hursthouse, and Mark E. Light

Abstract: The synthesis of two new aminoalcohol functionalized tertiary phosphines *o*-$Ph_2PCH_2N(H)C_6H_4(OH)$ (**I**) and *o*-$Ph_2PCH_2N(H)C_6H_4(CH_2OH)$ (**II**) are reported. Oxidation with aqueous H_2O_2 gave the corresponding phosphine oxides *o*-$Ph_2P(O)CH_2N(H)C_6H_4(OH)$ (**III**) and *o*-$Ph_2P(O)CH_2N(H)C_6H_4(CH_2OH)$ (**IV**) (^{31}P NMR evidence only). The ligating ability of **I**, **II** and, in several cases, the known ligand 2,3-$Ph_2PCH_2N(H)C_5H_3N(OH)$ (**V**), was investigated with a range of late transition-metal precursors. Accordingly, reaction of 2 equiv of **I** (or **II**) with [MCl_2(cod)] (M = Pd or Pt, cod = cycloocta-1,5-diene) gave the corresponding dichloro metal(II) complexes [MCl_2(**I**)$_2$] (M = Pd **1**; M = Pt **2**) and [MCl_2(**II**)$_2$] (M = Pd **3**; M = Pt **4**) in which **I** (and **II**) *P*-coordinate. Solution NMR studies reveal that **2** and **4** are exclusively *cis* whereas **1** and **3** are present as a mixture of *cis* and (or) *trans* isomers [4.7:1 (for **1**); 2.2:1 (for **3**)]. Reaction of 2 equiv of **II** with [$Pt(CH_3)_2$(cod)] gave the neutral complex [$Pt(CH_3)_2$(**II**)$_2$] (**5**) whose X-ray structure confirmed a *cis* disposition of "hybrid" ligands. In contrast, reaction of **I** with [$Pt(CH_3)_2$(cod)] gave initially [$Pt(CH_3)_2$(**I**)$_2$] (**6**) which, upon standing, afforded several products possibly reflecting an increased acidity of the phenolic groups of ligated **I**. Chloro bridge cleavage reactions of [{Ru(μ-Cl)Cl(*p*-cymene)}$_2$] or [{Rh(μ-Cl)Cl{$C_5(CH_3)_5$}}$_2$] with **I** (or **II**) proceeds smoothly and gave the mononuclear complexes [$RuCl_2$(*p*-cymene)**I**] (**7**), [$RuCl_2$(*p*-cymene)**II**] (**8**), [$RhCl_2${$C_5(CH_3)_5$}**I**] (**9**), and [$RhCl_2${$C_5(CH_3)_5$}**II**] (**10**) in good yield. X-ray crystallography confirms both ruthenium complexes bear *P*-coordinated **I** (or **II**) ligands. Molecules of **7** are linked into linear chains via O-H···Cl_{coord} intermolecular hydrogen bonding, a feature absent in the closely related compound **8**. Reaction of [AuCl(tht)] (tht = tetrahydrothiophene) with 1 equiv of **I** (or **II**) gave the corresponding gold(I) complexes [AuCl(**I**)] (**11**) and [AuCl(**II**)] (**12**). Bridge cleavage of the cyclometallated palladium(II) dimers [{Pd(μ-Cl)(C~N)}$_2$] [C~N = *C*,*N*-$C_6H_4CH_2N(CH_3)_2$, *C*,*N*-$C_{10}H_6N(CH_3)_2$, *C*,*N*-$C_6H_4N{=}NC_6H_5$] with **V** (or **I**) gave the neutral complexes [PdCl(C~N)**V**] (**13**–**15**) (or [PdCl($C_9H_{12}N$)**I**] (**16**)), respectively. Chloride abstraction from **13** (or **15**) with Ag[BF_4] gave the cationic complexes [Pd(C~N)**V**][BF_4] (**17**) (or **18**) in which **V** *P*,$N_{pyridyl}$-chelates to the palladium(II) metal centre. The X-ray structures of **13** and **18** have been determined and confirm the expected coordination environments. An array of intra- and intermolecular H-bonding contacts are also observed. All compounds have been characterized by a combination of spectroscopic and analytical studies.

Key words: phosphines, crystal structures, alcohols, precious metals.

Résumé : On a réalisé la synthèse de deux nouvelles phosphines tertiaires fonctionnalisées par un aminoalcool, *o*-$Ph_2PCH_2N(H)C_6H_4(OH)$ (**I**) et *o*-$Ph_2PCH_2N(H)C_6H_4(CH_2OH)$ (**II**). Leur oxydation par du peroxyde d'hydrogène aqueux conduit aux oxydes de phosphines correspondantes, *o*-$Ph_2P(O)CH_2N(H)C_6H_4(OH)$ (**III**) et *o*-$Ph_2P(O)CH_2N(H)C_6H_4(CH_2OH)$ (**IV**) (uniquement démontré par RMN du ^{31}P). On a étudié l'habilité des composés **1** et **2** et, dans plusieurs cas, du ligand bien connu 2,3-$Ph_2PCH_2N(H)C_5H_3N(OH)$ (**V**), d'agir comme coordinats pour une variété des précurseurs contenant des métaux de transition lourds. En conséquence, la réaction de deux équiv de **I** (ou **II**) avec du [MCl_2(cod)] (M = Pd ou Pt, cod = cycloocta-1,5-diène) conduit à la formation de complexes dichlorométalliques [MCl_2(**I**)$_2$] (M = Pd **1**; M = Pt **2**) et [MCl_2(**II**)$_2$] (M = Pd **3**; M = Pt **4**) dans lesquels les phosphines **I** (et **II**) sont coordinées au phosphore. Des études de RMN en solution révèlent que les composés **2** et **4** existent exclusivement sous la forme *cis* alors que les composés **1** et **3** existent sous la forme de mélanges d'isomères *cis*/*trans* [4,7:1 pour **1** et 2,2:1 pour **3**]. La réaction de deux équiv de **II** avec le [$Pt(CH_3)_2$(cod)] conduit à la formation du complexe neutre [$Pt(CH_3)_2$(**II**)], **5**, dont la structure telle que déterminée par diffraction des rayons X confirme la présence d'une disposition *cis* des ligands hybrides. Par opposition, la réaction de **I** avec le [$Pt(CH_3)_2$(cod)] conduit initialement à la formation de [$Pt(CH_3)_2$(**I**)$_2$], **6**, qui laissé à lui-même conduit à la formation

Received October 10, 2000. Published on the NRC Research Press Web site at http://canjchem.nrc.ca on July 9, 2001.

This article is dedicated to Brian James on the special occasion of his 65th birthday.

S.E. Durran and M.B. Smith.[1] Department of Chemistry, Loughborough University, Loughborough, Leics, LE11 3TU U.K.
A.M.Z. Slawin. School of Chemistry, University of St. Andrews, St Andrews, Fife, KY16 9ST U.K.
T. Gelbrich, M.B. Hursthouse and M.E. Light. EPSRC X-Ray Crystallography Service, Department of Chemistry, University of Southampton, Highfield, Southampton, SO17 1BJ U.K.

[1]Corresponding author (telephone: +44 (0)1509 222553; fax: +44 (0)1509 213925; e-mail: m.b.smith@lboro.ac.uk).

 DOI: 10.1139/cjc-79-5/6-780 © 2001 NRC Canada

de plusieurs produits et ceci est vraisemblablement un reflet d'une augmentation de l'acidité des groupes phénoliques de la phosphine (**I**) qui est liée. Les réactions de clivage du pont chloro du [{Ru(μ-Cl)Cl(*p*-cymène)}$_2$] ou du [{Rh(μ-Cl)Cl{C$_5$(CH$_3$)$_5$}}$_2$] avec **I** (ou **II**) se produisent facilement et conduisent à la formation de complexes mononucléaires [RuCl$_2$(*p*-cymène)**I**], **7**, [RuCl$_2$(*p*-cymène)**II**], **8**, [RhCl$_2$l{C$_5$(CH$_3$)$_5$}**I**], **9**, et [RhCl$_2$l{C$_5$(CH$_3$)$_5$}**II**], **10** avec de bons rendements. La diffraction des rayons X permet de confirmer que les deux complexes du ruthénium comportent des ligands **I** (ou **II**) qui sont coordinés au phosphore. Les molécules de **7** forment des chaînes linéaires par le biais d'une liaison hydrogène intermoléculaire, O–H···Cl$_{coord}$, une caractéristique qui est absente dans le composé **8** qui lui est fortement apparenté. La réaction de [AuCl(tht)] (tht = tétrahydrothiophène) avec un équivalent de **I** (ou **II**) conduit à la formation des complexes d'or correspondants [AuCl(**I**)], **11**, et [AuCl(**II**)], **12**. Le clivage du pont des dimères cyclométallés du palladium [{Pd(μ-Cl)(C~N)}$_2$] [C~N = *C*,*N*-C$_6$H$_4$CH$_2$N(CH$_3$)$_2$, *C*,*N*-C$_{10}$H$_6$N(CH$_3$)$_2$ et *C*,*N*-C$_6$H$_4$N=NC$_6$H$_5$] à l'aide des phosphines **V**
(ou **I**) conduit respectivement à la formation des complexes neutres [PdCl(C~N)**V**], **13–15**, ou [PdCl(C$_9$H$_{12}$N)**I**], **16**. L'enlèvement du chlorure à partir des composés **13** (ou **15**) à l'aide de Ag[BF$_4$] conduit à la formation des complexes cationiques [Pd(C~N)**V**][BF$_4$], **17** (ou **18**) dans lesquels le *P*,*N*-$_{pyridyl}$ de la phosphine **V** se chélate au centre métallique du palladium(II). Les structures des composés **13** et **18** ont été déterminées par diffraction des rayons X et elles confirment les environnements attendus par la coordination. On a aussi observé un arrangement de contacts par liaisons hydrogènes intra- et intermoléculaires. Tous les composés ont été caractérisés par une combinaison d'études analytiques et spectroscopiques.

Mots clés : phosphines, structures cristallines, alcools, métaux précieux.

[Traduit par la Rédaction]

Introduction

Tertiary phosphines continue to engage a quintessential role in the development of many avenues of coordination and organometallic chemistry and in catalysis. The ability to modify a ligand structure, in a precise and controlled fashion, explains the recent significant advances made in catalytic selectivity and activity, facile catalyst separation and enhanced enantiomeric excesses in asymmetric transformations.

Recent impressive progressions in the synthesis and chemistry of new functionalized tertiary phosphines have been made, one notable class are the so-called "hemilabile" ligands (1). Alcohol functionalized tertiary phosphines (2–10) which, in addition to a mismatch of "soft" and "hard" donor centres, have several attractive attributes: (*i*) reactive site(s) for further functionalization. The ligand Ph$_2$PCH$_2$OH is an excellent precursor for tertiary phosphines containing macrocycle (11), β-cyclodextrin (12), chitosan (13), or even dendrimer (14) backbones. Recently, we (15) prepared a hydroxy-functionalized pyridylphosphine while Faraone and co-workers (16) described the synthesis and catalytic applications of new mixed phosphine-phosphonite ligands, in both cases using Ph$_2$PCH$_2$OH as a convenient starting material; (*ii*) the hard oxygen donor can further be utilized in forming heterobimetallic complexes, e.g., Ph$_2$PCH$_2$OH can function as a uninegative *P*,*O*-bridging ligand (17); (*iii*) the presence of several hydroxy groups can render transition-metal complexes water soluble. The groups of Pringle (18,19), Katti (20), and more recently Fukuoka (21) made extensive use of this unique property in various coordination, catalytic, and biomedical studies.

As part of an ongoing programme, we reported (15) the synthesis and characterization of a new alcohol functionalized, potentially terdendate, pyridylphosphine and demonstrated its suitability for further functional group inclusion. Herein we describe the synthesis of two new "hybrid" ligands and demonstrate their coordination capabilities with selected precious metal precursors. To the best of our knowledge, there are very few reports (22–24) of hydroxy-functionalized tertiary phosphines in which the connectivity between disparate P and O donors bears an additional nitrogen donor atom, itself potentially capable of metal complexation. One interesting aspect we wished to probe further is what hydrogen bonding motifs would be expected upon coordination and accordingly, subtle variations in the ligand structures described here enable such a comparison to be tested. Previously we noted that Ph$_2$PCH$_2$N(H)C$_5$H$_3$N(X) (X = H, OH) can adopt a range of H-bonding motifs (e.g., **A**–**D**) (15) and in this work, two new network arrangements (**E** and **F**) are presented.

Experimental

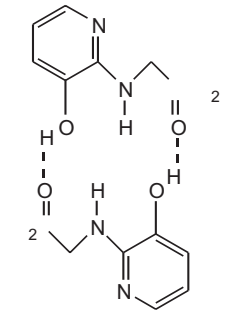
Chemicals

All reactions were performed under nitrogen unless otherwise stated. The starting materials [MCl$_2$(cod)] (M = Pd, Pt) (25, 26), [Pt(CH$_3$)$_2$(cod)] (27), [{Ru(μ-Cl)Cl(*p*-cymene)}$_2$] (28), [{Rh(μ-Cl)Cl{C$_5$(CH$_3$)$_5$}}$_2$] (29), [AuCl(tht)] (30), and [{Pd(C~N)(μ-Cl)}$_2$] (C~N = C$_9$H$_{12}$N, C$_{12}$H$_{12}$N, C$_{12}$H$_9$N$_2$) (31) were prepared according to previous reported procedures. The ligands Ph$_2$PCH$_2$OH (32) and Ph$_2$PCH$_2$N(H)C$_5$H$_3$N(OH) (15) were synthesized according to known literature methods. The compounds *o*-H$_2$NC$_6$H$_4$(OH) and *o*-H$_2$NC$_6$H$_4$(CH$_2$OH) were purchased from Aldrich Chemical Co. and used directly without further purification.

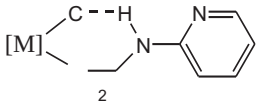
Physical techniques and methods

Infrared spectra were recorded as KBr pellets in the range 4000–220 cm^{-1} on a PerkinElmer System 2000 Fourier transform spectrometer. ^{1}H NMR spectra (250 MHz) were recorded on a Bruker AC250 FT spectrometer with chemical shifts (δ) in ppm to high frequency of SiMe$_4$ and coupling constants (*J*) in Hz. ^{31}P NMR spectra (36.2 MHz) were recorded on a JEOL FX90Q spectrometer with chemical shifts (δ) in ppm to high frequency of 85% H$_3$PO$_4$ and coupling constants (*J*) in Hz. All spectra were measured in CDCl$_3$ unless otherwise stated. Elemental analyses (PerkinElmer 2400

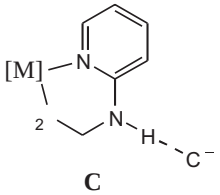
© 2001 NRC Canada



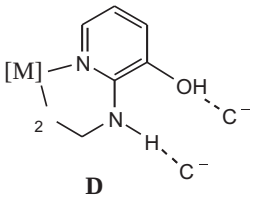
A



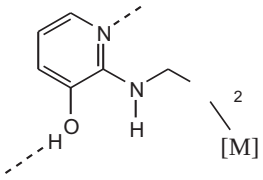
B



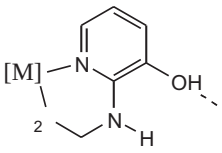
C



D



E



F

CHN Elemental Analyzer) were performed by the Loughborough University Analytical Service within the Department of Chemistry.

Precious metal salts were provided on loan by Johnson Matthey PLC.

Ligand syntheses

*o-$Ph_2PCH_2N(H)C_6H_4(CH_2OH)$ (**II**)*

To a solution of *o*-$H_2NC_6H_4(CH_2OH)$ (0.286 g, 2.32 mmol) in CH_3OH (5 mL) was added a solution of Ph_2PCH_2OH (0.501 g, 2.23 mmol) in CH_3OH (3 mL). After stirring the solution for 30 min, toluene (13 mL) was added and the solution heated at ca. 65°C for 18 h. The solution was evaporated to dryness under reduced pressure and triturated with several portions of petroleum ether (bp 40–60°C). The solid was collected by suction filtration and dried in vacuo. (yield 0.36 g, 48%). A similar method was used for the synthesis of *o*-$Ph_2PCH_2N(H)C_6H_4(OH)$ (**I**) (53%) from *o*-$H_2NC_6H_4(OH)$.

*NMR reaction of aq H_2O_2 with (**II**)*

To a $CDCl_3$ (0.5 mL) solution of *o*-$Ph_2PCH_2N(H)C_6H_4(CH_2OH)$ (0.020 g, 0.067 mmol) was added H_2O_2 (30% w/w, 0.1 mL) and a ^{31}P NMR spectrum recorded. Only *o*-$Ph_2P(O)CH_2N(H)C_6H_4(CH_2OH)$ **IV** was formed as inferred by a new ^{31}P NMR resonance of characteristic downfield shift (δ (P) 30.9 ppm). In a similar manner we observed the formation of *o*-$Ph_2P(O)CH_2N(H)C_6H_4(OH)$ (**III**).

Complexes

*[$PtCl_2${*o*-$Ph_2PCH_2N(H)C_6H_4(CH_2OH)$}$_2$] (**4**)*

To a CH_2Cl_2 (10 mL) solution of [$PtCl_2$(cod)] (0.050 g, 0.134 mmol) was added *o*-$Ph_2PCH_2N(H)C_6H_4(CH_2OH)$ (0.089 g, 0.277 mmol). The solution turned immediately deep yellow and progressively faded to pale yellow. After ca. 15 min, solid **4** deposits from solution and was collected by suction filtration and dried in vacuo (yield 0.094 g, 74%).

Using a similar procedure the following complexes were prepared: [$PdCl_2${*o*-$Ph_2PCH_2N(H)C_6H_4(OH)$}$_2$] (**1**) (93%), [$PtCl_2${*o*-$Ph_2PCH_2N(H)C_6H_4(OH)$}$_2$] (**2**) (72%), and [$PdCl_2${*o*-$Ph_2PCH_2N(H)C_6H_4(CH_2OH)$}$_2$] (**3**) (68%).

*[$Pt(CH_3)_2${*o*-$Ph_2PCH_2N(H)C_6H_4(CH_2OH)$}$_2$] (**5**)*

To the solids [$Pt(CH_3)_2$(cod)] (0.025 g, 0.075 mmol) and **II** (0.048 g, 0.149 mmol) was added toluene (ca. 1 mL) and the solution left to stand. After ca. 12 d crystalline **5** was isolated from solution (yield 0.038 g, 58%).

*[$RuCl_2$(*p*-cymene){*o*-$Ph_2PCH_2N(H)C_6H_4(OH)$}] (**7**)*

To the solids [{Ru(μ-Cl)Cl(*p*-cymene)}$_2$] (0.100 g, 0.163 mmol) and *o*-$Ph_2PCH_2N(H)C_6H_4(OH)$ (0.100 g, 0.326 mmol) was added CH_2Cl_2 (20 mL) and the deep red solution stirred for 15 min. The solvent was reduced in volume to ca. 1 to 2 mL under reduced pressure and diethyl ether (5 mL) added. The solid was isolated by suction filtration and additional crops isolated from the filtrate (yield 0.181 g, 91%). Using a similar procedure the following compounds were prepared: [$RuCl_2$(*p*-cymene){*o*-$Ph_2PCH_2N(H)C_6H_4(CH_2OH)$}] (**8**) (78%), [$RhCl_2${$C_5(CH_3)_5$}{*o*-$Ph_2PCH_2N(H)C_6H_4(OH)$}] (**9**) (90%), and [$RhCl_2${$C_5(CH_3)_5$}{*o*-$Ph_2PCH_2N(H)C_6H_4(CH_2OH)$}] (**10**) (63%).

*[AuCl{*o*-$Ph_2PCH_2N(H)C_6H_4(OH)$}] (**11**)*

To a CH_2Cl_2 (ca. 5 mL) solution of [AuCl(tht)] (0.030 g, 0.094 mmol)) was added *o*-$Ph_2PCH_2N(H)C_6H_4(OH)$ (0.029 g, 0.094 mmol) and stirred for ca. 15 min. The volume was concentrated in vacuo to ~1 mL and petroleum ether (bp 60–80°C, 20 mL) added. The solid was collected by suction filtration and dried in vacuo (yield 0.035 g, 70%). In a similar manner [AuCl{*o*-$Ph_2PCH_2N(H)C_6H_4(CH_2OH)$}] (**12**) was prepared (74%).

*[PdCl($C_{12}H_{12}N$){$Ph_2PCH_2N(H)C_5H_3N(OH)$}] (**14**)*

To a CH_2Cl_2 (15 mL) solution of [{Pd($C_{12}H_{12}N$)(μ-Cl)}$_2$] (0.099 g, 0.159 mmol) was added $Ph_2PCH_2N(H)C_5H_3N(OH)$

© 2001 NRC Canada

(0.100 g, 0.324 mmol) as a solid. After stirring for ca. 1 h, **14** was filtered under reduced pressure and dried in vacuo (yield 0.160 g, 81%). Using a similar procedure the following complexes were prepared: [$PdCl(C_9H_{12}N)\{Ph_2PCH_2N(H)C_5H_3N(OH)\}$] (**13**) (94%), [$PdCl(C_{12}H_9N_2)\{Ph_2PCH_2N(H)C_5H_3N(OH)\}$] (**15**) (91%), and [$PdCl(C_9H_{12}N)\{o\text{-}Ph_2PCH_2N(H)C_6H_4(OH)\}$] (**16**) (86%).

*[$Pd(C_{12}H_9N_2)\{Ph_2PCH_2N(H)C_5H_3N(OH)$-*P,N*$\}][BF_4$] (**18**)*

To a CH_2Cl_2 (30 mL) suspension of $Ag[BF_4]$ (0.040 g, 0.206 mmol) was added [$PdCl(C_{12}H_9N_2)\{Ph_2PCH_2N(H)C_5H_3N(OH)\}$] (0.100 g, 0.158 mmol) and stirred, in the dark, for ca. 2 h. The AgCl was removed by filtration through a small Celite plug and reduced in vacuo to ca. 1 to 2 mL. Addition of diethyl ether (25 mL) gave **18** which was collected by suction filtration and dried in vacuo (yield 0.086 g, 80%). In a similar manner [$Pd(C_9H_{12}N)\{Ph_2PCH_2N(H)C_5H_3N(OH)$*P,N*$\}][BF_4$] (**17**) (93%) was prepared.

X-ray Crystallography

Crystals of **5** were grown by allowing a toluene solution of [$Pt(CH_3)_2$(cod)] and 2 equiv of **II** to stand for ca. 12 days. For **7** and **8** suitable crystals for X-ray crystallography were grown by slow diffusion of either Et_2O (for **7**) or petroleum ether (bp 60–80°C) (for **8**) into $CDCl_3$ solutions over several days. Suitable crystals of **13** were grown by slow diffusion of Et_2O into a $CDCl_3$–CH_3OH solution over 7 days whereas for **18**, X-ray quality crystals were obtained by allowing $CDCl_3$ solutions to stand for several days.

The crystal structures of compounds **7**, **8**, and **13** were obtained using a Rigaku AFC7S serial diffractometer with graphite-monochromated Mo Kα radiation (λ = 0.71069 Å) and ω scans. Details of the crystal data collection and refinement are given in Table 1. Intensities were collected by ω scans over a single quadrant of reciprocal space. All data were corrected for Lorentz polarization and long-term intensity fluctuations. Absorption effects were corrected on the basis of multiple equivalent reflections or by empirical methods (33). Structures were solved by direct methods and refined by full-matrix least-squares against *F* (teXsan) (34) for data with $I > 2\sigma(I)$. The weighting scheme used was as previously reported (35). Refinements converged to residuals given in Table 1. All calculations were made with programs of the teXsan systems.

Data were collected (for **5** and **18**) using a Nonius κ CCD area detector diffractometer mounted at the window of a rotating molybdenum anode. Ω scans were employed such that 95% of the unique data were recorded at least once. Data collection and processing were carried out using the programs COLLECT (36), DENZO (37), and maXus (38) and an empirical absorption correction was applied using SORTAV (39, 40). The structures were solved via direct methods (41) and refined by full-matrix least-squares (41) on F^2. Non-hydrogen atoms were refined anisotropically and hydrogen atoms were treated using a riding model.

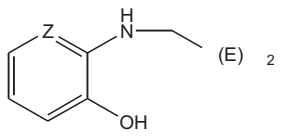
Copies of material on deposit may be purchased from The Depository of Unpublished Data, Document Delivery, CISTI, National Research Council Canada, Ottawa, ON K1A 0S2, Canada (http://www.nrc.ca/cisti/irm/unpub_e.shtml for information on ordering electronically). Crystallographic data (excluding structure factors) have also been deposited with the Cambridge Crystallographic Data Centre as supplementary publication no. CCDC 148 356 (**5**), 149 218 (**7**), 149 219 (**8**), 149 220 (**13**), and 148 357 (**18**) and can be obtained, free of charge, on request from The Director, CCDC, 12 Union Road, Cambridge, CB2 1EZ, U.K. (Fax: 44-1223-336033 or e-mail: deposit@ccdc.cam.ac.uk).

Results and discussion

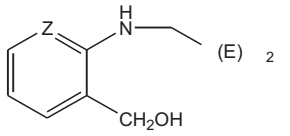
Ligand syntheses

Reaction of Ph_2PCH_2OH (32) with commercially available aminoalcohols *o*-$H_2NC_6H_4(OH)$ and *o*-$H_2NC_6H_4(CH_2OH)$ in toluene–methanol at ca. 65°C for 18 h, gave after workup, the new hybrid ligands *o*-$Ph_2PCH_2N(H)C_6H_4(OH)$ (**I**) and *o*-$Ph_2PCH_2N(H)C_6H_4(CH_2OH)$ (**II**), respectively, in reasonable yields. A similar procedure was used recently for the preparation of the pyridyl analogue $Ph_2PCH_2N(H)C_5H_3N(OH)$ (**V**) (15). The ^{31}P NMR spectra of **I** and **II** both displayed single ^{31}P NMR resonances at ca. δ (P) –18 ppm, some 8 ppm upfield of that observed for Ph_2PCH_2OH (δ (P) –9.9 ppm). One feature noted upon monitoring the stability of these ligands, when $CDCl_3$ solutions are allowed to stand, is the formation of a second new phosphorus species. Thus for **I**, after ca. 3 h, a new species at δ (P) –25.6 ppm was observed and confidently assigned as the diphosphine *o*-$(Ph_2PCH_2)_2NC_6H_4(OH)$. Independently *o*-$(Ph_2PCH_2)_2NC_6H_4(OH)$ can be prepared by reaction of *o*-$H_2NC_6H_4(OH)$ with 2 equiv of Ph_2PCH_2OH under similar conditions.[2] Other supporting data for **I** and **II** are given in Tables 2 and 3.

Oxidation of **I** (or **II**) with aq H_2O_2 proceeds smoothly affording (as confirmed by ^{31}P NMR spectroscopy, Table 3) the corresponding tertiary phosphine oxides *o*-$Ph_2P(O)CH_2N(H)C_6H_4(OH)$ (**III**) and *o*-$Ph_2P(O)CH_2N(H)C_6H_4(CH_2OH)$ (**IV**).



Z = CH, E = lone pair **I**
Z = CH, E = O **III**
Z = N, E = lone pair **V**



Z = CH, E = lone pair **II**
Z = CH, E = O **IV**

Palladium(II) and platinum(II) chemistry

Reaction of 2 equiv of either **I** (or **II**) with [MCl_2(cod)] (cod = cycloocta-1,5-diene) gave the corresponding metal(II) complexes [$PdCl_2$(**I**)$_2$] (**1**), [$PtCl_2$(**I**)$_2$] (**2**), [$PdCl_2$(**II**)$_2$] (**3**), and [$PdCl_2$(**II**)$_2$] (**4**). Previously, we (15) showed that reaction of 2 equiv of **V** with [$PtCl_2$(cod)] gave the bis *P*,$N_{pyridyl}$-chelate complex [$Pt\{Ph_2PCH_2N(H)C_5H_3N(OH)$-*P,N*$\}_2]Cl_2$. The platinum(II) complexes **2** and **4** in solution have a *cis* configuration as inferred by large ^1J (Pt-P) coupling constants (3678 Hz for **2**, 3660 Hz for **4**) whereas **1** and **3** are present as a mixture of both *cis* and (or) *trans* isomers (4.7:1 (for **1**); 2.2:1 (for **3**)). For comparison the spectral data of

[2] S.E. Durran and M.B. Smith. Unpublished work.

© 2001 NRC Canada

Table 1. Details of the X-ray data collections and refinements for compounds **5**, **7**, **8**, **13**, and **18**.

Compound	**5**	**7**	**8**	**13**	18
Empirical Formula	$C_{42}H_{46}N_2O_2P_2Pt{\cdot}C_7H_8$	$C_{29}H_{32}NOPCl_2Ru$	$C_{30}H_{34}NOPClRu{\cdot}0.5CHCl_3$	$C_{27}H_{29}N_3OPClPd{\cdot}0.5CHCl_3$	$C_{30}H_{26}N_4OPPdBF_4{\cdot}H_2O$
MW	959.97	613.53	687.24	644.06	700.74
Crystal system	Triclinic	Monoclinic	Monoclinic	Monoclinic	Monoclinic
Unit cell dimensions					
a (Å)	11.2761(3)	9.877(3)	11.041(3)	11.078(7)	10.4438(3)
b (Å)	11.8122(3)	16.430(3)	15.885(4)	26.974(4)	9.5206(3)
c (Å)	16.7161(5)	17.078(3)	35.394(7)	11.354(9)	14.6711(5)
α (°)	103.9790(12)				
β (°)	96.4490(11)	93.64(3)	96.07(3)	115.76(4)	99.7840(10)
γ (°)	91.8270(10)				
Volume ($Å^3$)	2142.87(10)	2766(1)	6173(3)	3055(3)	1437.55(8)
Temperature (K)	150(2)	293(2)	293(2)	293(2)	150(2)
Space group	*P*-1	$P2_1/n$	$P2_1/n$	$P2_1/c$	$P2_1$
Z	2	4	8	4	2
μ (mm^{-1})	3.390	0.829	0.887	0.902	0.764
Reflections collected	19 755	5358	11 902	5798	4758
Independent reflections	8366	5051	11 279	5503	3944
	(*R* (int) = 0.0645)	(*R* (int) = 0.044)	(*R* (int) = 0.075)	(*R* (int) = 0.022)	[*R*(int) = 0.027]
Final *R* indices	*R*1 = 0.045,	*R*1 = 0.030,	*R*1 = 0.041,	*R*1 = 0.062,	*R*1 = 0.031,
($I > 2\sigma(I)$)[a]	*wR*2 = 0.085	*wR*1 = 0.027	*wR*1 = 0.043	*wR*1 = 0.075	*wR*2 = 0.077

[a] $R = \sum ||F_o| - |F_c|| / \sum |F_o|$. $wR\,2 = (\sum [w(F_o^2 - F_c^2)^2] / \sum [w(F_o^2)^2])^{1/2}$.

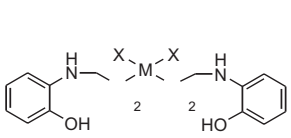
© 2001 NRC Canada

Table 2. Microanalytical data[a] for compounds **I**, **II**, **1**–**5**, and **7**–**18**.

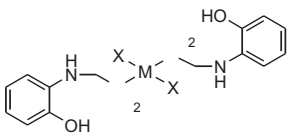
Compound	Analysis (%)		
	C	H	N
I	74.03 (74.24)	5.80 (5.92)	4.60 (4.56)
II	74.06 (74.74)	5.98 (6.29)	4.23 (4.36)
1	57.51 (57.62)	4.62 (4.59)	3.09 (3.54)
2	51.85 (51.82)	4.51 (4.13)	3.06 (3.18)
3	57.44 (58.59)	4.91 (4.92)	3.36 (3.42)
4	52.20 (52.86)	4.45 (4.45)	2.85 (3.08)
5[b]	61.35 (61.30)	5.57 (5.68)	2.94 (2.92)
7	56.10 (56.77)	5.12 (5.26)	2.05 (2.28)
8	56.67 (57.42)	5.31 (5.46)	2.18 (2.23)
9	55.92 (56.51)	5.25 (5.40)	2.12 (2.27)
10[c]	55.72 (55.75)	5.82 (5.45)	2.02 (2.15)
11	41.71 (42.28)	3.12 (3.36)	2.39 (2.60)
12	42.90 (43.38)	3.46 (3.64)	2.36 (2.53)
13	55.45 (55.48)	4.90 (5.01)	7.10 (7.19)
14	57.62 (58.07)	4.60 (4.72)	6.67 (6.77)
15	56.63 (57.06)	4.08 (4.16)	8.79 (8.87)
16	57.84 (57.64)	5.34 (5.19)	4.81 (4.80)
17	50.85 (51.01)	4.54 (4.61)	6.24 (6.61)
18	53.06 (52.77)	3.96 (3.85)	8.14 (8.21)

[a]Calculated values in parentheses.
[b]Contains 1 mol toluene as solvate.
[c]Contains 0.25 mol CH_2Cl_2 as solvate.

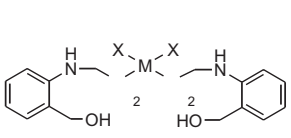
1–**4** are similar to $[MCl_2\{Ph_2PCH_2OH\}_2]$ (δ (P) 7.3 ppm, ^1J (Pt-P) 3687 Hz, M = Pt (42); δ (P) 27.8 and 13.7 ppm, M = Pd (recorded in CH_2Cl_2–C_6D_6)). Further support comes from the IR spectra (KBr disc) of **2** and **4** which display two ν_{PtCl} bands (Table 3). Apparently in the solid-state only the *cis* isomer is observed for the palladium(II) complexes **1** and **3**.



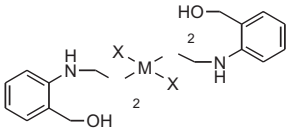
X = Cl, M = Pd **1a**
X = Cl, M = Pt **2**
X = CH_3, M = Pt **6**



X = Cl, M = Pd **1b**



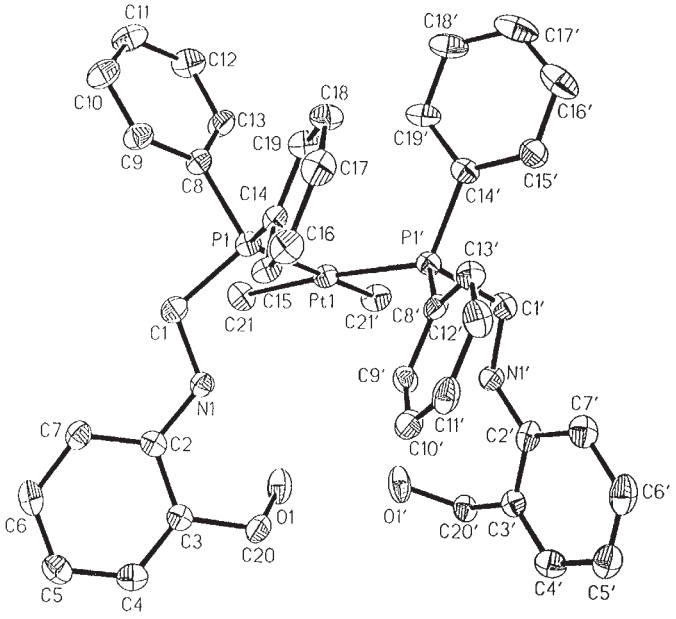
X = Cl, M = Pd **3a**
X = Cl, M = Pt **4**
X = CH_3, M = Pt **5**



X = Cl, M = Pd **3b**

Reaction of 2 equiv of **II** with $[Pt(CH_3)_2(cod)]$ in toluene gave a white solid which analyzed, by microanalysis, as $[Pt(CH_3)_2(\mathbf{II})_2]$·toluene (**5**·toluene). The ^{31}P NMR spectrum showed a single ^{31}P NMR resonance at δ (P) 17.2 ppm, with a considerably reduced ^1J (Pt-P) of 1830 Hz and in keeping with **II** *trans* to a methyl group (43). The Pt-CH_3 signals appear in the ^{1}H NMR spectrum as phosphorus coupled multiplets with ^{195}Pt satellites (J (Pt-H) = 68.4 Hz). In contrast, reaction of 2 equiv of **I** with $[Pt(CH_3)_2(cod)]$ in $CDCl_3$ gave initially **6** which, upon standing at ambient temperature for 20 h, gave a new major species tentatively assigned as *trans*-$[Pt(CH_3)Cl(\mathbf{I})_2]$ (δ (P) 21.4 ppm, ^1J (Pt-P) 3106 Hz). After ca. 5 days the intensity of this species diminishes and a new, as yet unidentified compound at δ (P) 22.9 ppm (^1J(Pt-P) 4469 Hz) is the major species present. Clearly, either the acidity of the phenolic group of *P*-coordinated **I** or residual traces of HCl (in $CDCl_3$) may account for methane elimination observed here. No attempts to identify methane formation were pursued. Further reactivity studies are underway and will be reported in due course.

Fig. 1. Crystal structure of **5** (solvent omitted for clarity). Thermal ellipsoids set at 50% probability level.



The X-ray structure of **5** (Fig. 1, Table 4) shows the expected near square-planar geometry (C(21)-Pt(1)-C(21′) 83.2(2)°, C(21)-Pt(1)-P(1) 86.84(15)°, C(21′)-Pt(1)-P(1′) 92.26(18)°, P(1)-Pt(1)-P(1′) 98.05(5)°) and comprises two aminoalcohol functionalized tertiary phosphines and two methyl ligands arranged in a *cis* configuration. The Pt—P and Pt—C bond distances are comparable with those recently reported (43) for $[Pt(CH_3)_2(PR_3)_2]$ complexes. Hydrogen bonds involving both hydroxy groups of each molecule result in a tetrameric $(OH)_4$ eight-membered ring that contain two intramolecular O(1)-H···O(1̇) (O(1)···O(1̇) 2.69 Å, H···O(1̇) 2.00 Å; O(1)-H···O(1′) 150°) and two intermolecular O(1′)-H···O(1̈) (where i = –x, –y, –z + 1; O(1′)···O(1̈) 2.76 Å, H···O(1̈) 1.95 Å; O(1′)-H···O(1̈) 169°] interactions (Fig. 2). The two hydrogen bonded molecules in each dimer are related by inversion symmetry. Additional short intramolecular N(1)···O(1) and N(1̇)···O(1̇) contacts, both in the range of 2.87 Å, show less favourable N-H···O angles (113 and 128°), so we conclude they are probably the result of steric restrictions rather than hydrogen bonds.

© 2001 NRC Canada

Table 3. Selected spectroscopic data for compounds **I**–**IV** and **1**–**18**.

Compound	δ (P)	*J* (Pt-P)	*J* (Rh-P)	δ (H) (arom.)	δ (H) (CH_2)[a]	IR ($\nu_{NH/OH}$)	IR ($\nu_{C=N}$)	*m*/*z*
I	–18.8[b]			7.52–6.61[c]	3.83 (3.7)	3480, 3414, 3349		307 (*M*)
II	–18.5			7.51–6.65[c]	4.49, 3.86 (4.2)	3479, 3386		321 (*M*)
III	32.2							
IV	30.9							
1	26.3			7.82–6.47[d,e]	4.45 (5.8)	3380[f]		756 (*M-Cl*)
	14.2[g]							
2	6.4	3678		7.57–6.53	4.11	3387[h]		845 (*M-Cl*)
3	26.5			7.82–6.58[d,e]	4.52, 4.28	3364, 3298[f]		785 (*M-Cl*)
	14.0[g]							
4	5.8	3660		7.57–6.49[e,i]	4.32 (5.1)[j]	3369, 3293[h]		908 (*M*)
5	17.2	1830		7.54–6.41[k]	4.46, 3.59	3384, 3309		867 (*M*)
6	17.4	1817						
7	23.9[l]			7.87–6.03[m]	4.32 (6.5)	3418, 3245		614 (*M*)
8	22.2			7.86–6.24[e,n]	4.30 (5.1), 4.10 (5.3)	3394		628 (*M*)
9	28.8		141	7.94–6.47[o,p]	4.50	3392, 3300		616 (*M*)
10	26.4		145	7.97–6.45[q]	4.51, 4.41	3396		630 (*M*)
11	24.7[l]			7.78–6.74	4.26	3424, 3372[r]		539 (*M*)
12	30.2			7.73–6.58[p]	4.57, 4.38	3356[r]		
13	34.5[l]			7.87–6.30[e,s]	4.61 (3.7)	3272	1613	547 (*M-Cl*)
14	38.6[l]			8.02–6.26[e,t]	4.71 (4.8)	3326	1611	584 (*M-Cl*)
15	33.7			8.06–6.04[p]	4.35	3293, 3268	1611	595 (*M-Cl*)
16	34.2			7.93–6.39[u]	4.11	3383, 3275		583 (*M*)
17	33.2[l]			7.70–6.42[e,v]	4.31	3406, 3339	1624	548 (*M-BF_4*)
18	31.5			8.10–6.02[w]	4.25 (4.6)	3409, 3361	1627	595 (*M-BF_4*)

[a] *J* (P-H) in parentheses.
[b] After ca. 3 h, a second species at δ (P) –25.6 ppm was observed.
[c] Other resonance at δ (H): 3.99 (NH) (for **I**), 4.90 (NH) (for **II**).
[d] Other resonances at δ (H): 9.46, 9.36 (OH); 4.87 (NH) (for **1**); 5.36, 5.06 (NH–OH) (for **3**).
[e] Recorded in $(CD_3)_2SO$.
[f] PdCl at 307 and 285 cm^{-1} (for **1**); PdCl at 316 and 290 cm^{-1} (for **3**).
[g] Mixture of *cis* and (or) *trans* isomers, recorded in $CDCl_3$–$(CH_3)_2SO$.
[h] PtCl at 311 and 284 cm^{-1} (for **2**); PtCl at 318 and 293 cm^{-1} (for **4**).
[i] Other resonances at δ (H): 5.35, 5.11 (NH–OH).
[j] Overlapping signals.
[k] Other resonances at δ (H): 5.14 (NH); 1.75 (OH); 0.58 (Pt-CH_3), *J* (Pt-H) 68.4 Hz, *J* (P-H) 14.1 Hz.
[l] Recorded in $CDCl_3$–CH_3OH.
[m] Other resonances at δ (H): 9.03 (OH); 4.45 (NH): 5.49, 5.33, 2.32, 1.82, 0.77 [$CH_3C_6H_4\{CH(CH_3)_2\}$].
[n] Other resonances at δ (H): 5.09, 4.85 (NH–OH); 5.51, 5.35, 2.33, 1.83, 0.79 [$CH_3C_6H_4\{CH(CH_3)_2\}$].
[o] Other resonance at δ (H): 1.39 (*J* (P-H) 3.5 Hz, $C_5(CH_3)_5$).
[p] δ (H) OH–NH not observed.
[q] Other resonances at δ (H): 5.25 (NH); 1.40 (*J* (P-H) 3.5 Hz, $C_5(CH_3)_5$).
[r] AuCl at 322 cm^{-1} (for **11**); 321 cm^{-1} (for **12**).
[s] Other resonances at δ (H): 9.78 (OH); 6.17 (NH); 4.08 (*J* (P-H) 1.4 Hz, CH_2), 2.75 (*J* (P-H) 2.1 Hz, $N(CH_3)_2$).
[t] Other resonances at δ (H): 9.67 (OH); 6.24 (NH); 3.43 ($N(CH_3)_2$).
[u] Other resonances at δ (H): 5.75 (OH); 4.76 (NH); 4.05 (*J* (P-H) 2.1 Hz, CH_2), 2.86 (2.3 Hz, $N(CH_3)_2$).
[v] Other resonances at δ (H): 10.77 (OH); 7.30 (*J* (P-H) 13.7 Hz, NH); 4.11 (CH_2); 2.54 ($N(CH_3)_2$).
[w] Other resonance at δ (H): 6.47 (*J* (P-H) 16.3 Hz, NH). OH not observed.

Ruthenium(II), rhodium(III), and gold(I) chemistry

Reaction of **I** (or **II**) with [{Ru(μ-Cl)Cl(*p*-cymene)}$_2$] in CH_2Cl_2 at ambient temperature gave the mononuclear ruthenium complexes [$RuCl_2$(*p*-cymene)**I**] (**7**) and [$RuCl_2$(*p*-cymene)**II**] (**8**). The ^{31}P NMR spectra show, in both cases, a single phosphorus resonance at δ (P) 23.9 (for **7**) and 22.2 (for **8**) ppm [cf. 16.3 ppm for [$RuCl_2$(*p*-cymene)(Ph_2PCH_2OH)] (**G**)]. Upon inspection of the coordination chemical shifts (Δ_{coord}) (Δ_{coord} = 42.7 (for **7**), 40.7 (for **8**), 25.3 (for **G**)) we observe a larger Δ_{coord} for complexes bearing **I** and **II**. Other spectroscopic and microanalytical data (Tables 2 and 3) confirm the constitution of **7** and **8**. The X-ray structures of both ruthenium compounds have been determined (Figs. 3 and 4, Table 5). Both molecules display similar overall structures — pseudo-octahedral geometries at ruthenium comprising an η^6-*p*-cymene, two chlorides and one phosphorus bound ligand completing the metal coordination sphere. The Ru—Cl and Ru—P distances in **7** and **8** are similar (44), broadly as expected, and furthermore in the case of **8** comparable to those values for [$RuCl_2$(*p*-

© 2001 NRC Canada

Fig. 2. Hydrogen bond interactions in **5**.

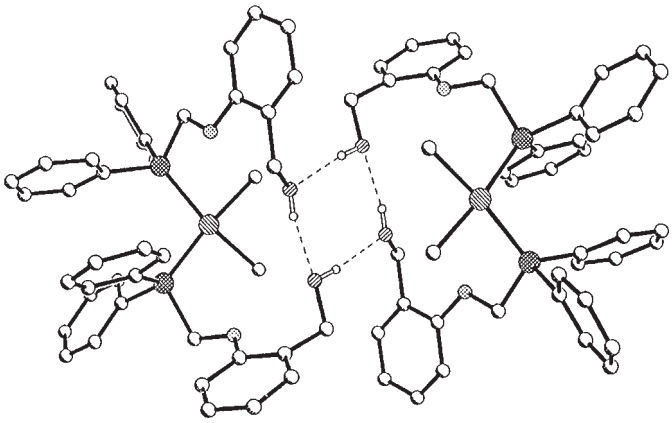
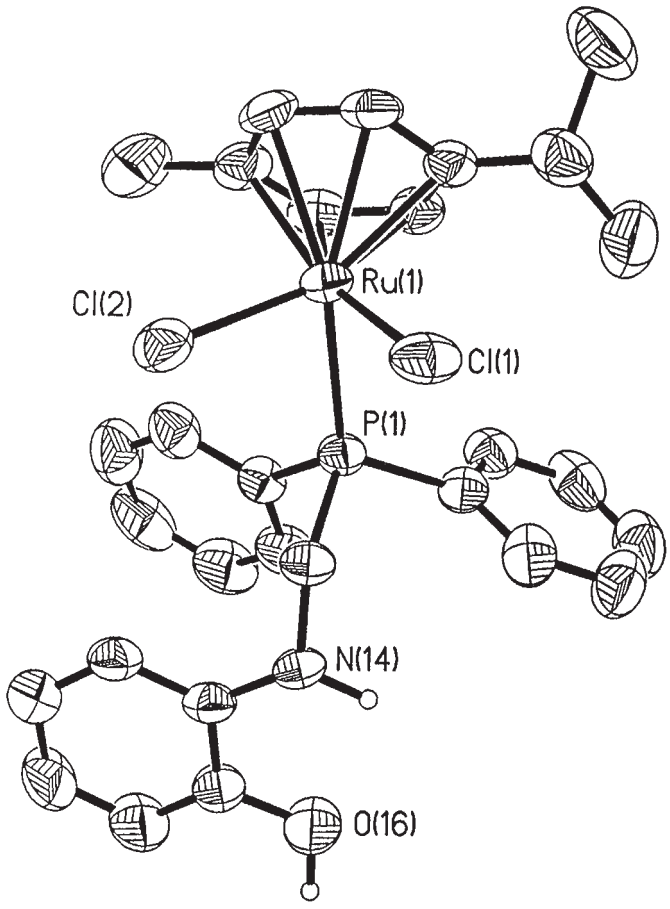


Fig. 3. Crystal structure of **7**. Thermal ellipsoids set at 50% probability level.

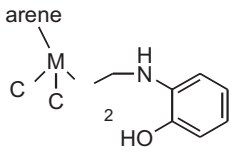


cymene){*o*-$Ph_2PCH_2CH_2C_6H_4(CH_2OH)$}] (5). In **7**, molecules are linked into one-dimensional chains through O-H···Cl_{coord} intermolecular hydrogen bonds (O(16)···Cl(1) 3.10 Å, H(16o)···Cl(1) 2.11 Å; O(16)-H(16o)···Cl(1) 162°). Short intramolecular N···O contacts (N(14)···O(16) 2.62 Å, H(14n)···O(16) 2.23 Å; N(14)-H(14n)···O(16) 100° for **7**; O(16)···N(14) 2.88 Å, H(16o)···N(14) 2.17 Å; O(16)-H(16o)···N(14) 128° and O(46)···N(44) 2.87 Å, H(46o)···N(44) 2.25 Å; O(46)-H(46o)···N(44) 143° for **8**) are also present which again are probably a consequence of steric limitations. The related complex [RuCl(*p*-cymene){$Ph_2PCH_2N(H)C_5H_3N(OH)$-*P*,*N*}]Cl exists in the solid-state (15) as a dimer pair through simultaneous N-H···Cl_{anion} and O-H···Cl_{anion} hydrogen bonding (**D**).

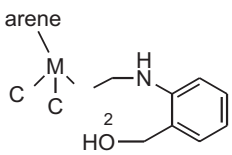
Table 4. Selected bond distances (Å) and angles (°) for compound **5**.

Bond distances (Å)	**5**
Pt(1)—C(21)	2.095(5)
Pt(1)—C(21′)	2.116(5)
Pt(1)—P(1)	2.2849(13)
Pt(1)—P(1′)	2.2817(14)
Bond angles (°)	
C(21)-Pt(1)-C(21′)	83.2(2)
C(21)-Pt(1)-P(1)	86.84(15)
C(21′)-Pt(1)-P(1′)	92.26(18)
P(1)-Pt(1)-P(1′)	98.05(5)
C(21′)-Pt(1)-P(1)	168.67(17)
C(21′)-Pt(1)-P(1′)	174.05(15)

We also studied the reaction of **I** (and **II**) with the rhodium(III) precursor [{Rh(μ-Cl)Cl{$C_5(CH_3)_5$}}$_2$]. Chloro bridge cleavage of [{Rh(μ-Cl)Cl{$C_5(CH_3)_5$}}$_2$] with **I** (and **II**) in dichloromethane gave the rhodium(III) complexes [$RhCl_2${$C_5(CH_3)_5$}**I**] (**9**) and [$RhCl_2${$C_5(CH_3)_5$}**I**] (**10**). The ^{31}P and ^{1}H NMR data are consistent with the proposed structures (Table 3). Hence δ (P) and ^{1}J (Rh-P) for **9** (28.8 ppm, 141 Hz) and **10** (26.4 ppm, 145 Hz) are similar as expected. In the ^{1}H NMR spectra clear, well-resolved doublets at ca. 1.40 ppm (*J* (P-H) 3.5 Hz) confirm the presence of η^5-ligated $C_5(CH_3)_5$ ligands. The gold(I) complexes **11** and **12** were prepared from [AuCl(tht)] and 1 equiv of either **I** (or **II**).



M = Ru **7**
M = Rh **9**



M = Ru **8**
M = Rh **10**

Cyclometallated palladium(II) chemistry

Treatment of the cyclometallated palladium(II) dimers [{Pd(C~N)(μ-Cl)}$_2$] [C~N = $C_9H_{12}N$, $C_{12}H_{12}N$, $C_{12}H_9N_2$] with 2 equiv of **V** gave the mononuclear complexes [PdCl(C~N)**V**] ($C_9H_{12}N$ (**13**), $C_{12}H_{12}N$ (**14**), $C_{12}H_9N_2$ (**15**)) in high yields (>80%) (Scheme 1). The ^{31}P NMR spectra (Table 3) of **13**–**15** show single ^{31}P NMR resonance at δ (P) 34.5 (**13**), 38.6 (**14**), and 33.7 ppm (**15**) indicating similar structures. We also prepared the related complex [PdCl(C~N)**I**] **16** (C~N = $C_9H_{12}N$) whose ^{31}P NMR reveals a singlet at δ (P) 34.2 ppm indicating that pyridyl or phenyl group inclusion has a marginal influence on δ (P). The trans N-Pd-P geometry was inferred from the magnitude of the *J* (P-H) couplings observed in the ^{1}H NMR spectra (Table 3) which correspond well with related compounds and by X-ray crystallography. The X-ray structure of **13** (Fig. 5,

© 2001 NRC Canada

Table 5. Selected bond distances (Å) and angles (°) for compounds **7** and **8**.

Bond distances (Å)	**7**	8[a]	
Ru(1)—l(1)	2.424(2)	2.442(4)	(2.412(3))
Ru(1)—Cl(2)	2.418(2)	2.400(3)	(2.425(4))
Ru(1)—P(1)	2.351(1)	2.354(3)	(2.344(3))
Ru(1)—C_{arene}	2.172(5)–2.247(5)	2.18(1)–2.24(1)	(2.16(1)–2.23(1))
Bond angles (°)			
Cl(1)-Ru(1)-Cl(2)	88.12(6)	87.3(1)	(88.4(1))
Cl(1)-Ru(1)-P(1)	83.53(5)	86.6(1)	(84.2(1))
Cl(2)-Ru(1)-P(1)	86.11(5)	85.0(1)	(86.0(1))
Cl(1)-Ru(1)-C_{arene}	90.0(2)–157.4(2)	88.5(3)–156.9(4)	(88.3(3)–157.6(4))
Cl(2)-Ru(1)-C_{arene}	90.4(2)–156.0(2)	91.9(4)–158.1(4)	(89.2(4)–156.7(4))
P(1)-Ru(1)-C_{arene}	94.5(1)–159.0(2)	93.5(3)–159.9(4)	(94.9(4)–161.1(4))
C_{arene}-Ru(1)-C_{arene}	35.7(2)–80.5(2)	35.6(5)–78.9(5)	(35.5(4)–81.0(5))

[a]Values in brackets are the equivalent parameter in the second molecule.

Fig. 4. Crystal structure of **8** (solvent omitted for clarity). Thermal ellipsoids set at 50% probability level.

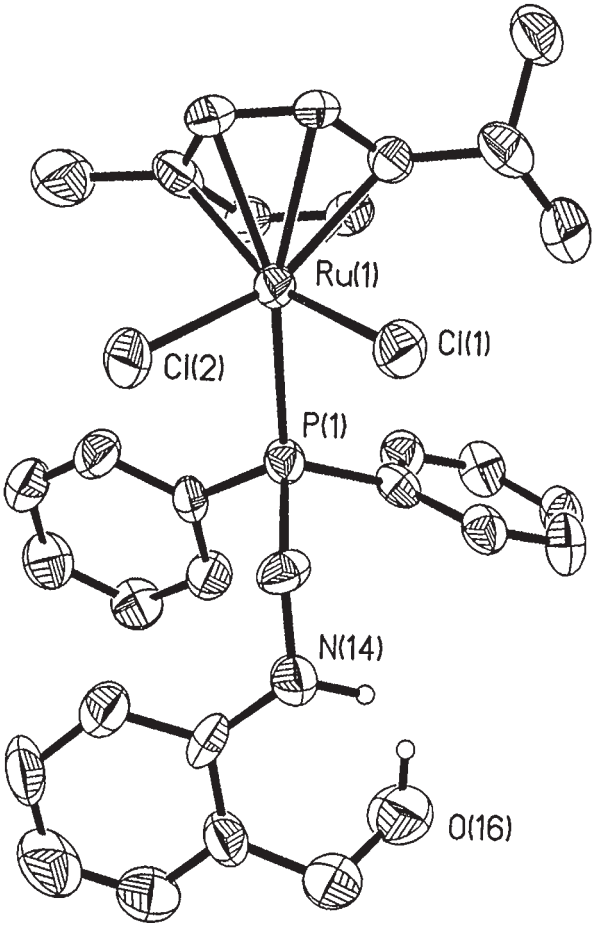


Fig. 5. Crystal structure of **13** (solvent omitted for clarity). Thermal ellipsoids set at 50% probability level.

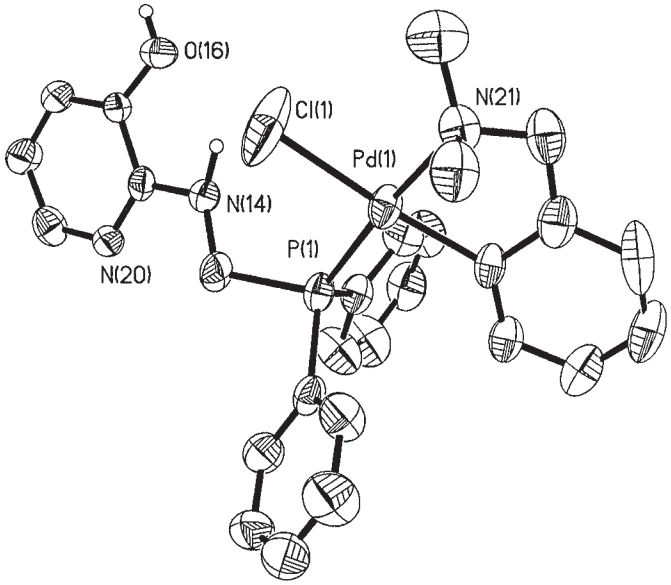
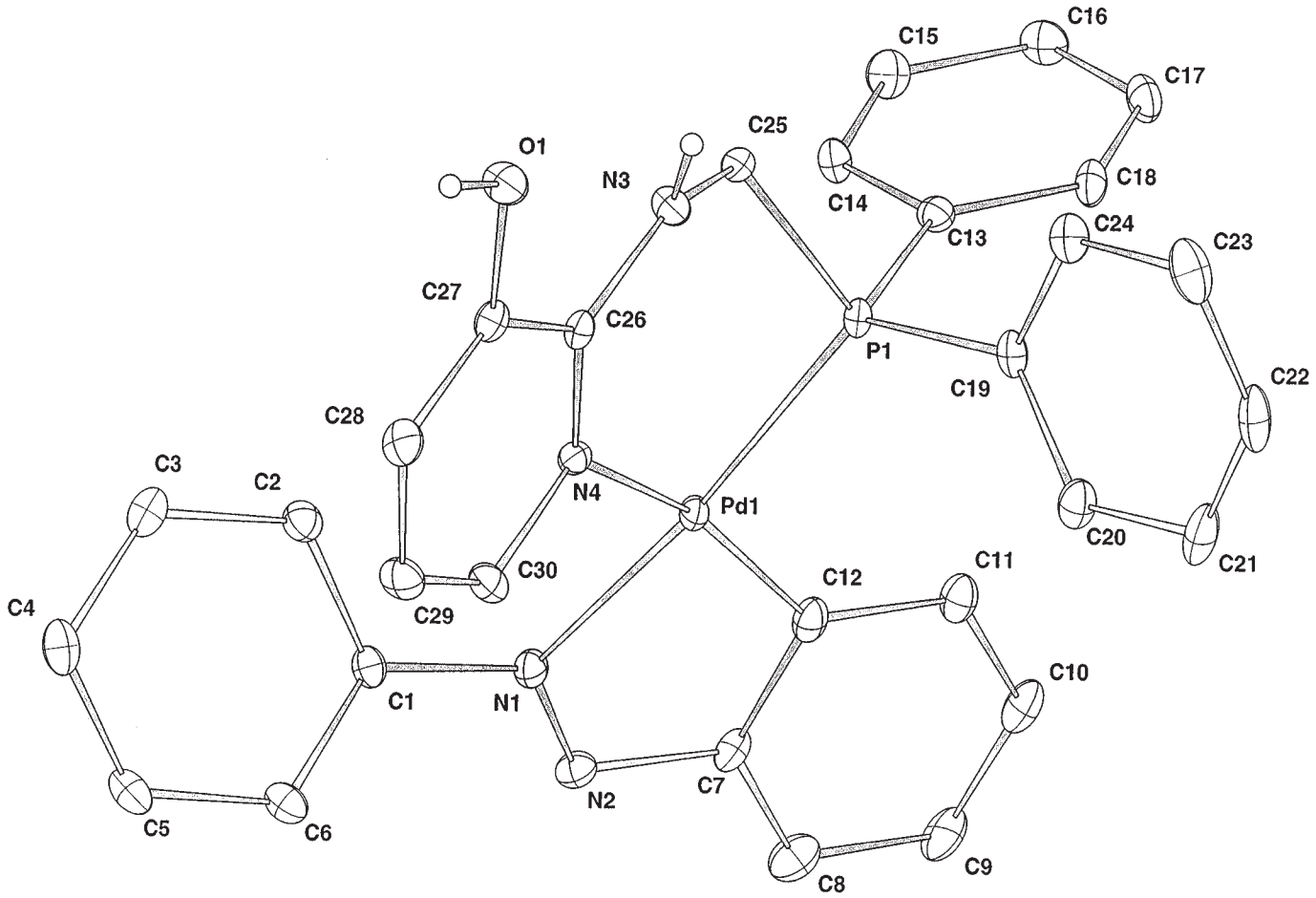


Table 6) shows a near square-planar geometry around the palladium(II) centre (N(21)-Pd(1)-C(25) 83.0(3)°, Cl(1)-Pd(1)-N(21) 90.2(2)°, P(1)-Pd(1)-C(25) 92.9(3)°, and Cl(1)-Pd(1)-P(1) 93.7(1)°) and comprises a chelating cyclometallated $C_9H_{12}N$, a chloride, and a *P*-bound **V** ligand. The P donor is *trans* to the dimethylamino group of the cyclometallated ligand. The Pd—C, Pd—N, Pd—P, and Pd—Cl distances are all broadly as anticipated (45). Molecules are arranged into linear chains through O-H···$N_{pyridyl}$ intermolecular H-bonding (O(16)···N(20A) 2.64 Å, H(16o)···N(20A) 1.82 Å; O(16)-H(16o)···N(20A) 179°). There is also an intramolecular N···O contact (N(14)···O(16) 2.64 Å, H(14n)···O(16) 2.09 Å; N(14)-H(14n)···O(16) 114°) but like **5**, **7**, and **8** is probably not a legitimate H-bond.

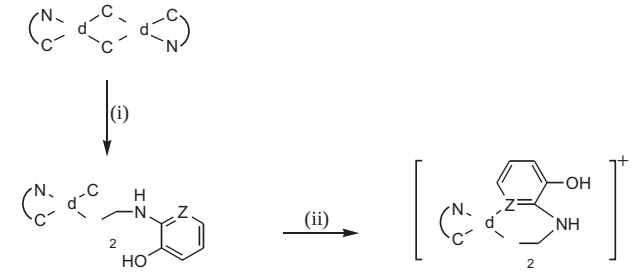
Unlike complexes of **I** (or **II**) for which no further coordination studies were probed, reaction of **13** or **15** with $Ag[BF_4]$ in dichloromethane gave the *P,N*-chelate complexes $[Pd(C\sim N)\{Ph_2PCH_2N(H)C_5H_3N(OH)\}][BF_4]$ (C~N = $C_9H_{12}N$ (**17**); $C_{12}H_9N_2$ (**18**)). Slight upfield shifts were

© 2001 NRC Canada

Fig. 6. Crystal structure of **18** (solvent and tetrafluoroborate anion omitted for clarity). Thermal ellipsoids set at 50% probability level.



Scheme 1. (*i*) 2 equiv **V** (or **I**), CH_2Cl_2; (*ii*) $Ag[BF_4]$, CH_2Cl_2.



C~N = $C_9H_{12}N$, Z = N **13**
C~N = $C_{12}H_{12}N$, Z = N **14**
C~N = $C_{12}H_9N_2$, Z = N **15**
C~N = $C_9H_{12}N$, Z = CH **16**

C~N = $C_9H_{12}N$, Z = N **17**
C~N = $C_{12}H_9N_2$, Z = N **18**

observed in the ^{31}P NMR spectra while the IR spectra showed small (typically ca. 10–15 cm^{-1}) downfield shifts in $\nu_{C=N(pyridyl)}$ (Table 3). The X-ray structure of **18** (Fig. 6, Table 7) confirms *P*,*N*-co-ordination of **V** with the pyridyl nitrogen *trans* to the orthometallated carbon. The Pd—N bond lengths (Pd(1)-N(1) 2.098(3) Å (N *trans* to P) and Pd(1)-N(4) 2.176(3) Å (N *trans* to C)) differ and reflect the higher *trans*-influence of the aryl ligand compared to the tertiary phosphine. The tetrafluoroborate and water molecules are alternately linked via hydrogen bonds to form single chains running along the 2_1 screw axis (Fig. 7 shows these hydrogen bonded chains viewed along the *a* axis, only the core of the palladium complex is drawn). This involves both protons on the water (H1W and H2W) and two of the tetrafluoroborate fluorines (F2 and F3). The hydrogen bonds formed are: O2-H1W···F2^{ii} where *ii* = $-x + 1$, $y + 0.5$, $-z$ (O2···F2^{ii} 2.72 Å, H1W···F2^{ii} 2.14 Å; O2-H1W···F2^{ii} 168°) and O2-H2W···F3 (O2···F3 2.82 Å, H2W···F3 2.09 Å; O2-H2W···F3 165°). The palladium complex is connected, in a branch like manner, to these chains by a single hydrogen

Table 6. Selected bond distances (Å) and angles (°) for compound **13**.

Bond distances (Å)	**13**
Pd(1)—Cl(1)	2.386(3)
Pd(1)—P(1)	2.250(2)
Pd(1)—N(21)	2.139(7)
Pd(1)—C(25)	2.015(8)
Bond angles (°)	
N(21)-Pd(1)-C(25)	83.0(3)
Cl(1)-Pd(1)-N(21)	90.2(2)
P(1)-Pd(1)-C(25)	92.9(3)
Cl(1)-Pd(1)-P(1)	93.7(1)
Cl(1)-Pd(1)-C(25)	173.2(3)
P(1)-Pd(1)-N(21)	174.7(2)

© 2001 NRC Canada

Fig. 7. Hydrogen bonded chains in **18** (viewed along the *a* axis).

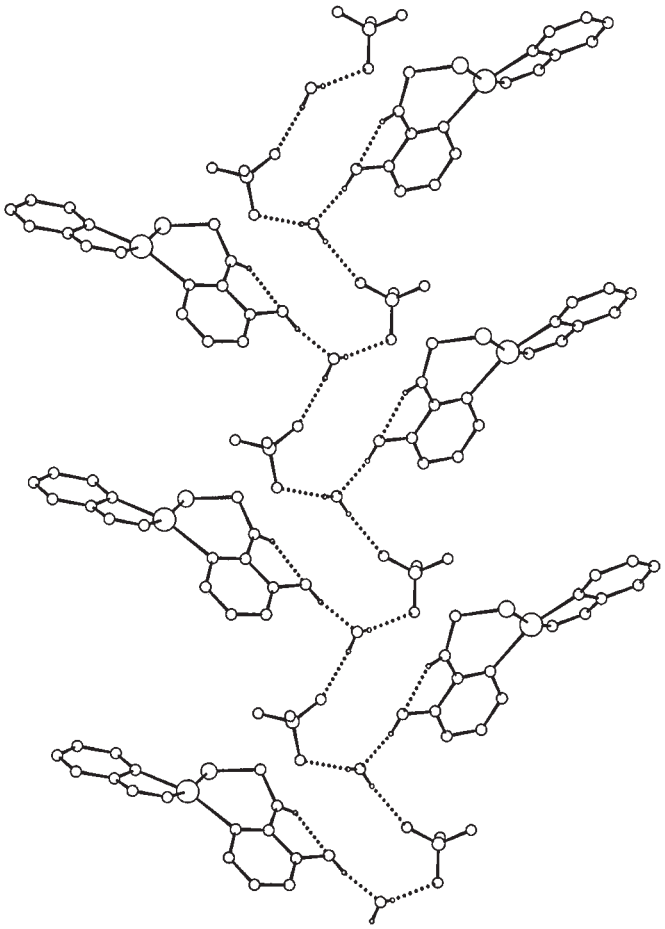


Table 7. Selected bond distances (Å) and angles (°) for compound **18**.

Bond distances (Å)	**18**
Pd(1)—C(12)	1.998(4)
Pd(1)—N(1)	2.098(3)
Pd(1)—N(4)	2.176(3)
Pd(1)—P(1)	2.2302(11)
Bond angles (°)	
C(12)-Pd(1)-N(1)	77.81(15)
N(4)-Pd(1)-P(1)	90.39(9)
N(1)-Pd(1)-N(4)	97.24(14)
C(12)-Pd(1)-P(1)	97.53(13)
C(12)-Pd(1)-N(4)	164.27(14)
N(1)-Pd(1)-P(1)	166.66(13)

bond from the hydroxy group to the oxygen of every water molecule (O1-H1···O2^{i} (where $i = -x + 1, y + 0.5, -z + 1$), O1··· O2^{i} 2.70 Å, H1···O2^{i} 1.88 Å; O1-H1···O2^{i} 164.5°). No interaction between chains is possible due to the shielding effect of the bulky palladium complex. In addition to the three unique intermolecular hydrogen bonds there is an intramolecular N(3)-H(3)···O(1) close contact (N(3)···O(1) 2.59 Å, H(3)···O(1) 2.22 Å) however, this has an acute angle of 105.4° and is most likely imposed by the stereochemistry and not a genuine hydrogen bond.

Acknowledgements

We should like to thank the EPSRC for funding and the EPSRC Mass Spectrometry Service at Swansea. Johnson Matthey are gratefully acknowledged for loans of precious metals.

References

1. A. Bader and E. Linder. Coord. Chem. Rev. **108**, 27 (1991).
2. J. Heinicke, M. He, A. Dal, H.-F. Klein, O. Hetche, W. Keim, U. Flörke, and H.-J. Haupt. Eur. J. Inorg. Chem. 431 (2000).
3. F. Connac, Y. Lucchese, M. Gressier, M. Dartiguenave, and A.L. Beauchamp. Inorg. Chim. Acta, **304**, 52 (2000).
4. L. Dahlenburg and V. Kurth. J. Organomet. Chem. **585**, 315 (1999).
5. B. Therrien, T.R. Ward, M. Pilkington, C. Hoffmann, F. Gilardoni, and J. Weber. Organometallics, **17**, 330 (1998).
6. J.-C. Shi, D.-X. Wu, T.-B. Weng, M.-C. Hong, Q.-T. Liu, B.-S. Kang, S.-J. Lu, and H.-Q. Wang. J. Chem. Soc. Dalton Trans. 2911 (1996).
7. J. Scherer, G. Huttner, O. Walter, B.C. Janssen, and L. Zsolnai. Chem. Ber. **129**, 1603 (1996).
8. J. Scherer, G. Huttner, and M. Büchner. Chem. Ber. **129**, 697 (1996).
9. S.B. Sembiring, S.B. Colbran, D.C. Craig, and M.L. Scudder. J. Chem. Soc. Dalton Trans. 3731 (1995).
10. A.W.G. Platt and P.G. Pringle. J. Chem. Soc. Dalton Trans. 1193 (1989).
11. H. Hope, M. Viggiano, B. Moezzi, and P.P. Power. Inorg. Chem. **23**, 2550 (1984).
12. M.T. Reetz and S.R. Waldvogel. Angew. Chem. Int. Ed. Engl. **36**, 865 (1997).
13. W. Henderson, G.M. Olsen, and L.S. Bonnington. J. Chem. Soc. Chem. Commun. 1863 (1994).
14. M.T. Reetz, G. Lohmer, and R. Schwickardi. Angew. Chem. Int. Ed. Engl. **36**, 1526 (1997).
15. S.E. Durran, A.M.Z. Slawin, M.B. Smith, and J. Steed. J. Chem. Soc. Dalton Trans. 2771 (2000).
16. C.G. Arena, D. Drommi, and F. Faraone. Tetrahedron: Asymmetry, **11**, 2765 (2000).
17. S.M. Baxter, G.S. Ferguson, and P.T. Wolczanski. J. Am. Chem. Soc. **110**, 4231 (1988).
18. P.A.T. Hoye, P.G. Pringle, M.B. Smith, and K. Worboys. J. Chem. Soc. Dalton Trans. 269 (1993).
19. J.W. Ellis, K.N. Harrison, P.A.T. Hoye, A.G. Orpen, P.G. Pringle, and M.B. Smith. Inorg. Chem. **31**, 3026 (1992).
20. K.V. Katti, H. Gali, C.J. Smith, and D.E. Berning. Acc. Chem. Res. **32**, 9 (1999); and refs. therein.
21. A. Fukuoka, W. Kosugi, F. Morishita, M. Hirano, L. McCaffrey, W. Henderson, and S. Komiya. Chem. Commun. 489 (1999).
22. G. Scherhag and M.D. Spicer. J. Chem. Soc. Dalton Trans. 1237 (2000).
23. I.D. Kostas and C.G. Screttas. J. Organomet. Chem. **585**, 1 (1999).
24. J. Andrieu, B.R. Steele, C.G. Screttas, C.J. Cardin, and J. Fornies. Organometallics, **17**, 839 (1998).
25. J.X. McDermott, J.F. White, and G.M. Whitesides. J. Am. Chem. Soc. **98**, 6521 (1976).
26. D. Drew and J.R. Doyle. Inorg. Synth. **13**, 47 (1972).

© 2001 NRC Canada

27. E. Costa, P.G. Pringle, and M. Ravetz. Inorg. Synth. **31**, 284 (1997).
28. M.A. Bennett and A.K. Smith. J. Chem. Soc. Dalton Trans. 233 (1974).
29. C. White, A. Yates, and P.M. Maitlis. Inorg. Synth. **29**, 228 (1992).
30. R. Uson, A. Laguna, and M. Laguna. Inorg. Synth. **26**, 85 (1989).
31. A.C. Cope and E.C. Friedrich. J. Am. Chem. Soc. **90**, 909 (1968); A.C. Cope and R.W. Siekman. J. Am. Chem. Soc. **87**, 3272 (1965); G.E. Hartwell, R.V. Lawrence, and M.J. Smas. Chem. Commun. 912 (1970).
32. H. Hellmann, J. Bader, H. Birkner, and O. Schumacher. Liebigs Ann. Chem. **659**, 49 (1962).
33. N.G. Walker and D. Stuart. Acta Crystallogr. Sect. A: Fundam. Crystallogr. **A39**, 158 (1983).
34. teXsan. Crystal analysis package. Molecular Structure Corporation, The Woodlands, Texas. 1985 and 1992.
35. A.M.Z. Slawin, M.B. Smith, and J.D. Woollins. J. Chem. Soc. Dalton Trans. 3659 (1996).
36. "Collect" data collection software. Nonius B. V. 1998.
37. Z. Otwinowski and W. Minor. Processing of X-ray diffraction data collected in oscillation mode. *In* Methods in enzymology Vol. 276; C. W. Carter, Jr. and R. M. Sweet (*Editors*). Macromolecular crystallography. Part A. Academic Press, 1997. p. 307–326.
38. S. Mackay, C.J. Gilmore, C. Edwards, M. Tremayne, N. Stuart, and K. Shankland. maXus: a computer program for the solution and refinement of crystal structures from diffraction data. University of Glasgow, Scotland, U.K., Nonius B.V., Delft, The Netherlands, and MacScience Co. Ltd., Yokohama, Japan, 1998.
39. R.H. Blessing. Acta Crystallogr. Sect. A: Fundam. Crystallogr. **A51**, 33 (1995).
40. R.H. Blessing. J. Appl. Crystallogr. **30**, 421 (1997).
41. G.M. Sheldrick. SHELX97: Programs for crystal structure analysis. Institüt für Anorganische Chemie der Universität, Tammanstrasse 4, D-3400 Göttingen, Gemany. 1998.
42. D.L. Davies, J. Neild, L.J.S. Prouse, and D.R. Russell. Polyhedron, **12**, 2121 (1993).
43. D.G. Smith Jr., C.M. Haar, E.D. Stevens, S.P. Nolan, W.J. Marshall, and K.G. Moloy. Organometallics, **19**, 1427 (2000).
44. K.Y. Ghebreyessus and J.H. Nelson. Organometallics, **19**, 3387 (2000).
45. J.-F. Ma and Y. Yamamoto. Inorg. Chim. Acta, **299**, 164 (2000).

© 2001 NRC Canada

Highly efficient and stable catalyst for peroxynitrite decomposition

Yurii V. Geletii, Alan J. Bailey, Jennifer J. Cowan, Ira A. Weinstock, and Craig L. Hill

Abstract: The new cobalt substituted-polyoxometalate $K_7[CoAlW_{11}O_{39}]\cdot 15H_2O$ and the simple $CoCl_2\cdot 6H_2O$ salt are efficient catalysts for peroxynitrite decomposition. These compounds also catalyze the oxidation of ascorbic acid and the nitration of phenol by peroxynitrite.

Key words: peroxynitrite, polyoxometalates, antioxidant.

Résumé : Le nouveau polyoxométalate substitué du cobalt, $K_7[CoAlW_{11}O_{39}]\cdot 15H_2O$ ainsi que le simple sel $CoCl_2\cdot 6H_2O$ sont des catalyseurs efficaces pour la décomposition du peroxynitrite. Ces composés catalysent aussi l'oxydation de l'acide ascorbique et la nitration du phénol par le peroxynitrite.

Mots clés : peroxynitrite, polyoxométalates, antioxydant.

[Traduit par la Rédaction]

Introduction

The recent interest in peroxynitrite[1], a compound known for many years (1), was inspired by Beckman et al. (2), who suggested it was formed in vivo from NO and $O_2^{\bullet -}$. Under physiological conditions, $ONOO^-$ is partially protonated to HOONO (pK_a = 6.8), which rapidly ($k \sim 1\ s^{-1}$, pH = 7.0, 25°C) decomposes to highly reactive radical species in a unimolecular reaction (1–4). Peroxynitrite also reacts with many compounds in bimolecular reactions, and it is a powerful oxidant with substantial toxicity (1–4). There is accumulating evidence for peroxynitrite formation in vivo, which naturally has led to a search for compounds that can intercept this powerful oxidant and destroy it safely. The discovery of a fast peroxynitrite reaction with myeloperoxidase ($6.2 \times 10^6\ M^{-1}\ s^{-1}$ at pH = 7.2) (5) inspired studies of peroxynitrite reactions with synthetic, water-soluble Fe- and Mn-porphyrin complexes (6–11). Reactions of peroxynitrite with combinations of these metalloporphyrins and antioxidants were found to be even more rapid. Recently, several nonheme catalysts for peroxynitrite decomposition were reported (9, 12, 13); however, they appeared to be unstable and less active.

Here we report that a simple cobalt salt, $CoCl_2\cdot 6H_2O$, and the Co-substituted polyoxometalate, $K_7[Co^{II}AlW_{11}O_{39}]\cdot 15H_2O$, catalytically decompose peroxynitrite at neutral pH (6.5–7.4) with high turnover numbers. Their activity is comparable to MnTMPyP, where TMPyP is the dianion of tetrakis(*N*-methyl-4′-pyridyl) porphyrin. All species also catalyze ascorbic acid oxidation and phenolic nitration by peroxynitrite.

Results and discussion

Peroxynitrite decay in the absence and in the presence of representative catalysts is exponential and follows the rate law in eq. [1].

$$[1] \qquad -d[ONOO^-]/dt = k_{obs}[ONOO^-] = k_o[ONOO^-] + k_{cat}[ONOO^-][cat]$$

When k_{obs} values are plotted as a function of catalyst concentrations ([cat]) straight lines are obtained. The *y*-intercepts provide k_o and the slopes of each line provide k_{cat}. The data are summarized in Table 1. The following compounds were evaluated and found to be minimally active ($k_{cat} < 1 \times 10^3\ M^{-1}\ s^{-1}$): $CuCl_2\cdot 2H_2O$, $FeCl_2\cdot 4H_2O$, $K_9[AlW_{11}O_{39}]\cdot 13H_2O$, $Na_5[AlW_{12}O_{40}]\cdot 13H_2O$, $K_7[V^{IV}AlW_{11}O_{40}]\cdot 8H_2O$, and $K_5[Co^{III}W_{12}O_{40}]\cdot 13H_2O$ (the reproducible value for the uncatalyzed rate constant, $k_o = 0.35 \pm 0.03\ s^{-1}$ at pH 7.4).

The stabilities of the three most active catalysts, $CoCl_2$, $K_7[Co^{II}AlW_{11}O_{39}]$, and MnTMPyP, were evaluated by comparing their activities, indicated by experimental k_{obs} values, before and after reaction with large excesses of peroxynitrite (for concentrations see Table 2). The resistance of each catalyst to irreversible decomposition was estimated by $n = [NaOONO]_d/\Delta[cat]$, where $[NaOONO]_d$ is the total amount of peroxynitrite decomposed and $\Delta[cat]$ is the amount of the catalytic activity lost in the catalytic reaction. The latter term

Received September 29, 2000. Published on the NRC Research Press at http://canjchem.nrc.ca Web site on June 30, 2001.

Dedicated to Professor Brian R. James on the occasion of his 65th birthday.

Yu.V. Geletii, A.J. Bailey, J.J. Cowan, I.A. Weinstock, and C.L. Hill.[2] Department of Chemistry, Emory University, 1515 Pierce Drive, Atlanta, GA. 30322, U.S.A.

[1]The term peroxynitrite is used to refer to peroxynitrite anion ($O{=}NOO^-$) and peroxynitrous acid (ONOOH) unless otherwise indicated. The IUPAC-recommended names are oxoperoxonitrate (–1) and hydrogen oxoperoxonitrate, respectively.

[2]Corresponding author (telephone: (404) 727-6611; fax: (404) 727-6076; e-mail: chill@emory.edu).

 DOI: 10.1139/cjc-79-5/6-792 © 2001 NRC Canada

Table 1. The rate constants (k_{cat}) of representative compounds used to catalyze peroxynitrite decomposition at 25°C.

Catalyst	k_{cat} (1×10^{-4}) (M^{-1} s^{-1})
MnTMPyP	2.1 ± 0.2
$CoCl_2$	3.0 ± 0.3
$K_7[CoAlW_{11}O_{39}]$	1.9 ± 0.15

Note: For all experiments the pH = 7.0 ± 0.05, 75 mM phosphate buffer, $[ONOO^-]_o$ = 300–400 μM, $[cat]_o$ = 0–40 μM (0–14 μM for MnTMPyP).

was calculated as $\Delta[cat] = [cat]_o(k^\circ_{obs} - k'_{obs})/(k^\circ_{obs} - k_o)$, where $[cat]_o$ is the initial concentration of the catalyst, k_{obs} is the decomposition rate in the presence of the catalyst that has been pretreated with a large excess of peroxynitrite, and k°_{obs} and k_o are the decomposition rates in the presence and the absence of the catalyst, respectively.[3] The results, presented in Table 2, show that both $K_7[Co^{II}AlW_{11}O_{39}]$ and MnTMPyP are substantially more stable than Co^{2+} (as $CoCl_2$).

The self-decomposition of peroxynitrite at neutral pH is known to form nitrate and nitrite, and the formation of nitrite is accompanied by dioxygen evolution in a 2:1 ratio (14). The addition of $K_7[Co^{II}AlW_{11}O_{39}]$ increases the yield of nitrite (from 11 to 23% based on peroxynitrite, if 20 μM of $K_7[Co^{II}AlW_{11}O_{39}]$ is added at pH 7.4).

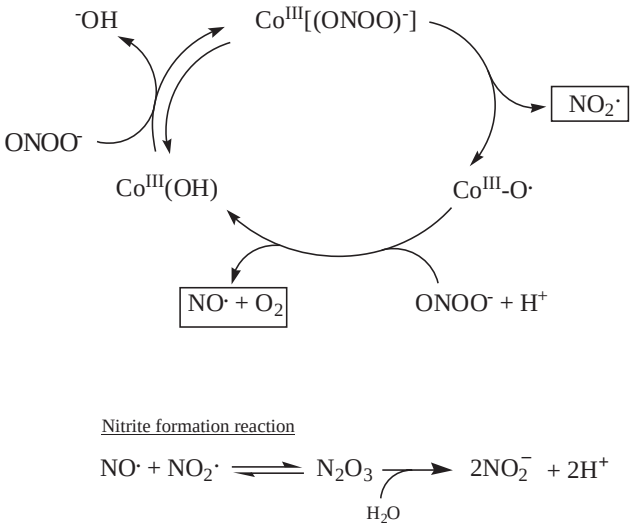
Since $CoCl_2$ is more active than $K_7[Co^{II}AlW_{11}O_{39}]$, the activity of the latter could be attributed to Co^{2+} ions formed via dissociation of $K_7[Co^{II}AlW_{11}O_{39}]$ (eq. [2]). However, the activity of a mixture of $CoCl_2$ and $K_7[Co^{II}AlW_{11}O_{39}]$ was the same as the sum of the activities of each of the individual components, suggesting that $K_7[Co^{II}AlW_{11}O_{39}]$ itself is also an active catalyst.

$$[2] \qquad [Co^{II/III}AlW_{11}O_{39}]^{7-/6-} \rightleftharpoons Co^{2+/3+} + [AlW_{11}O_{39}]^{9-}$$

Treatment of the starting $K_7[Co^{II}AlW_{11}O_{39}]$ with peroxynitrite results in its immediate oxidation to $K_6[Co^{III}AlW_{11}O_{39}]$ (λ_{max} shifts from 560 to 680 nm). The mechanism in Scheme 1 (proposed mechanism of peroxynitrite decomposition catalyzed by $K_7[Co^{II}AlW_{11}O_{39}]$, where Co^{II} represents $[Co^{II}AlW_{11}O_{39}]^{7-}$) is consistent with all the above data and is based on that proposed for catalysis of peroxynitrite decomposition by Fe-porphyrins (7, 11) and sulfito-bound Co(III) (*cis*-$[Co(NH_3)_4(SO_3)_2]^-$) (12).[4] The rate-limiting step is likely to be a homolysis of the O—O bond in a Co^{III} peroxonitrito intermediate to form Co^{III}-$O^\bullet$ and $NO_2^\bullet$. Previously, a Co(III) peroxynitrito complex has been isolated and characterized (15). The reaction is thought to occur by an outer-sphere mechanism. However, since the lability of Co(III) increases when its geometry is perturbed from rigorous O_h symmetry (16), as is the case in $K_7[Co^{II}AlW_{11}O_{39}]$, an inner-sphere mechanism cannot definitely be ruled out. Further investigations are ongoing.

The addition of ascorbic acid significantly increases the rate of peroxynitrite consumption in reactions catalyzed by $K_7[Co^{II}AlW_{11}O_{39}]$, i.e., the observed second-order rate constant (k_{cat}, eq. [1]), increases from 1.9×10^4 to 12.7×10^4 M^{-1} s^{-1} in the presence of 7.4 mM ascorbic acid at pH 7.4. However, the rate of $K_6[Co^{III}AlW_{11}O_{39}]$ reduction by ascorbic acid is too slow to account for the observed increase in the total rate of peroxynitrite decomposition. Therefore, ascorbic acid is likely to reduce the $Co^{III}[(OONO)^-]$ intermediate complex, thus accelerating the total rate.

Scheme 1.



The nitration of phenols by peroxynitrite has long been known (17), and Beckman et al. (18) were the first, to our knowledge, to report a catalytic version of this process. To assess phenol nitration activity by the Co systems, the yield and the rate of 3-nitro-4-hydroxyphenylacetic acid (3-NO_2-4-HPA) from the nitration of 4-hydroxyphenylacetic acid (4-HPA) were quantified. The yield of 3-NO_2-4-HPA, and the rate of its formation, both increase with increasing $K_7[Co^{II}AlW_{11}O_{39}]$ concentration. Based on the initial peroxynitrite concentration, the 3-NO_2-4-HPA yield was 7% in the absence of a catalyst and 40% in the presence of 82 μM of $K_7[CoAlW_{11}O_{39}]$ (pH 7.4, [4-HPA] = 6.0 mM, $[NaOONO]_o$ = 1.1 mM). However, unlike in the catalyzed oxidation of ascorbic acid by peroxynitrite, the observed second-order rate constant (k_{cat}, eq. [1]) does not increase with 4-HPA concentration. The mechanism of nitration may involve a fast reduction of Co^{III}-$O^\bullet$ by the phenolic species; subsequent coupling of the resulting phenoxy radical and $NO_2^\bullet$ gives nitrophenol. Mn- and Fe-porphyrins active in peroxynitrite decomposition have also been found to catalyze the nitration of phenols (6, 8–11, 19) likely through the coupling of phenoxy and $NO_2^\bullet$ radicals (19).

Experimental

MnTMPyP (ICN Biomedicals Inc.) was standardized in aqueous solution using $\varepsilon_{462} = 1 \times 10^5$ M^{-1} cm^{-1} (20). Peroxynitrite was synthesized from H_2O_2 and nitrite in a simple flow reactor (21, 22) and its concentration was deter-

[3] $k'_{obs} = k_o + k_{cat}[cat]$, see eq. [1].
[4] The reaction decelerates at $[OH^-]$ = 0.4 M, $[NaOONO]_o$:[cat] ~ 10–15, as a result of catalyst decomposition.

© 2001 NRC Canada

Table 2. The observed reaction rate constants before (k°_{obs}) and after (k'_{obs}) reaction of the catalyst with a large excess of peroxynitrite, and n values.

Catalyst	k°_{obs} (s^{-1}) [a]	k'_{obs} (s^{-1}) [a]	$(k^{\circ}_{obs} - k'_{obs})/(k^{\circ}_{obs} - k_o)$ [b]	n [c]
$CoCl_2$	1.85 ± 0.07	1.33 ± 0.07	0.3	~3×10^3
$K_7[CoAlW_{11}O_{39}]$	1.33 ± 0.05	1.30 ± 0.05	<0.03	>3×10^4
MnTMPyP	1.10 ± 0.04	1.09 ± 0.04	<0.03	>3×10^4

Note: All experiments carried out at 25°C. Pretreatment conditions: $[NaOONO]_o$ = 24 mM, $[cat]_o$ = 25 μM, pH 6.8, 0.15 M phosphate buffer.

[a] $[NaOONO]_o$ = 0.4 mM, $[cat]_o$ = 15 μM, pH 7.4, 0.11 M phosphate buffer.

[b] $k_o = 0.35 \pm 0.03\ s^{-1}$.

[c] $n = [NaOONO]_d/\Delta[cat]$; see text for details.

mined by UV–vis spectroscopy, $\varepsilon_{302} = 1.7 \times 10^3\ M^{-1}\ cm^{-1}$ (23).

The new transition-metal-substituted POM (α-$K_7[CoAlW_{11}O_{39}]\cdot 15H_2O$) was prepared by metallation of the lacunary complex α-$K_9[AlW_{11}O_{39}]\cdot 15H_2O$ (24) by $Co(NO_3)_2\cdot 6H_2O$. A 10 g portion of $K_9[AlW_{11}O_{39}]$ (3.05 mmol) was stirred in water (100 mL), and a solution of $Co(NO_3)_2\cdot 6H_2O$ (0.88 g, 3.05 mmol, in 10 mL water) was added dropwise to the slurry via a pipette. The reaction mixture was stirred in a hot water bath (70–80°C) until the solution became clear. The resulting solution was dark pink (pH 6.2), and after cooling to room temperature, a red powder deposited. The product was recrystallized from a minimum of warm (60°C) water.[5]

Kinetic experiments were studied using a SF-61 stop flow instrument (Hi-Tech Scientific, U.K.). A buffer solution with the reactants and peroxynitrite diluted in aqueous NaOH were mixed and the absorbance at 302 nm was measured. The first-order reaction rate constants were determined using standard software (KISS 5.1 for Macintosh computer). The yields of nitrite and 3-NO_2-4-HPA were determined after a small amount of highly concentrated (~0.6 M) peroxynitrite solution was mixed with a buffer solution containing all other ingredients. Yields of nitrite were determined as previously described (25) and 3-NO_2-4-HPA was quantified from its absorbance at 430 nm after adjusting the pH to 10–11 (18).

Acknowledgements

We thank Dr. Eric A. Boring for the preparation of $K_5[CoW_{12}O_{40}]\cdot 13H_2O$, and Professor W. H. Koppenol and Dr. R. Kissner for helpful discussions. This work was funded by the National Science Foundation (to CLH) and in part by INTAS (grant 99–209, to YVG).

References

1. J.O. Edwards and R.C. Plumb. Prog. Inorg. Chem. **41**, 599 (1994).
2. J.S. Beckman, T.W. Beckman, J. Chen, P.A. Marshal, and B.A. Freeman. Proc. Natl. Acad. Sci. U.S.A. **87**, 1620 (1990).
3. W.A. Pryor and G.L. Squadrito. Am. J. Physiol. **268**, L699 (1995).
4. J.S. Beckman and W.H. Koppenol. Am. J. Physiol. **271**, C1424 (1996).
5. R. Floris, S.R. Piersma, G. Yang, P. Jones, and R. Wever. Eur. J. Biochem. **215**, 767 (1993).
6. J.T. Groves and S.S. Marla. J. Am. Chem. Soc. **117**, 9578 (1995).
7. M.K. Stern, M.P. Jensen, and K. Kramer. J. Am. Chem. Soc. **118**, 8735 (1996).
8. G.G.A. Balavoine, Y.V. Geletii, and D. Bejan. Nitric Oxide. **1**, 507 (1997).
9. G. Ferrer-Seuta, I. Batinic-Haberle, I. Spasojevic, I. Fridovich, and R. Radi. Chem. Res. Toxicol. **12**, 442 (1999).
10. J. Lee, J.A. Hunt, and J.T. Groves. J. Am. Chem. Soc. **120**, 6053 (1998).
11. J. Lee, J.A. Hunt, and J.T. Groves. J. Am. Chem. Soc. **120**, 7493 (1998).
12. A.M. Al-Ajlouni, P.C. Paul, and E.S. Gould. Inorg. Chem. **37**, 1434 (1998).
13. X. Zhang and D.H. Busch. J. Am. Chem. Soc. **122**, 1229 (2000).
14. S. Pfeiffer, A.C.F. Gorren, K. Schmidt, E.R. Werner, B. Hansert, D.S. Bohle, and B. Mayer. J. Biol. Chem. **272**, 3465 (1997).
15. P.K. Wick, R. Kissner, and W.H. Koppenol. Helv. Chim. Acta, **83**, 748 (2000).
16. R.W. Hay, R. Bembi, F. McLaren, and W.T. Moodie. Inorg. Chim. Acta, **85**, 23 (1984).
17. M.S. Ramezanian, S. Padmaja, and W.H. Koppenol. Chem. Res. Toxicol. **9**, 232 (1996).
18. J.S. Beckman, H. Ischiropoulos, L. Zhu, M. Van der Woerd, C. Smith, J. Chen, J. Harrison, J.C. Martin, and M. Tsai. Arch. Biochem. Biophys. **298**, 438 (1992).
19. J.P. Crow. Arch. Biochem. Biophys. **371**, 41 (1999).
20. J. Bernadou, G. Pratviel, F. Bennis, M. Girardet, and B. Meunier. Biochem. **28**, 7268 (1989).
21. N. Hogg, V. Darley-Usmar, M.T. Wilson, and S. Moncada. FEBS Lett. **326**, 199 (1993).
22. W.H. Koppenol, R. Kissner, and J.S. Beckman. Methods Enzymol. **269**, 296 (1996).
23. D.S. Bohle, B. Hansert, S.C. Paulson, and B.D. Smith. J. Am. Chem. Soc. **116**, 7423 (1994).
24. I.A. Weinstock, J.J. Cowan, E.M.G. Barbuzzi, H. Zeng, and C.L. Hill. J. Am. Chem. Soc. **121**, 4608 (1999).
25. R.C. Plumb, J.O. Edwards, and M.A. Herman. Analyst, **117**, 1639 (1992).

[5] Yield: 7.31 g (74%). IR (KBr pellet) (cm^{-1}): 952 (m), 935 (s), 891 (s), 798 (m), 697 (m), 533 (w), 486 (w). Anal. calcd. for $K_7[CoAlW_{11}O_{39}]\cdot 15H_2O$: H 0.92, Al 0.82, Co 1.80, K 8.35, W 61.73; found: H 0.91, Al 0.88, Co 1.73, K 8.16, W 62.26.

© 2001 NRC Canada

Hetero trinuclear oxo-bridged complexes of ruthenium porphyrin and iron phthalocyanine

Fabio Zobi and Dennis V. Stynes

Abstract: New diamagnetic hetero bi- and trinuclear oxo-bridged metal complexes of formula (L)(Pc)Fe-O-Ru(TPP′)(O) and (L)(Pc)Fe-O-Ru(TPP′)-O-Fe(Pc)(L) have been prepared from Ru(TPP′)$(O)_2$ and Fe(Pc)$(L)_2$ (TPP′ = tetrakis(4-methoxyphenyl)porphyrinate, Pc = phthalocyanate ion, L = monodentate ligand). The trinuclear complex binds a variety of ligands (4,4′-bipy, 4-MePy, $P(OEt)_3$, pip, NH_3, 1-MeIm, $P(Me)_2Ph$) *trans* to the oxo-bridge. ^{1}H NMR spectra are characterized by large ring current shifts (rcs) due to the TPP′ and Pc ions. The complexes show an unusually weak Pc Q band in their visible spectra at 700 nm and two CT bands in the near-IR region from 1000 to 1500 nm, which are sensitive to the *trans* ligand. The trinuclear complex can be reversibly oxidized to the +1 and +2 ions, formally Fe(IV)-O-Ru(IV)-O-Fe(III) and Fe(IV)-O-Ru(IV)-O-Fe(IV) at 0.4 and 0.76 V. The +1 ion is chemically obtained by reaction of the neutral species with $(Cp)_2Fe^+$ for L = 4-MePy and this reaction is reversed upon addition of L′ = $P(Me)_2Ph$. Reductive cleavage by hydroquinone, phosphines and phosphites are the slowest of all RuTPP[$O(FeN_4)$]$_2$ systems studied to date ($t_{1/2}$ = 8 h at 40°C).

Key words: ruthenium, iron, porphyrin, phthalocyanine, oxo.

Résumé : En faisant réagir du Ru(TPP′)$(O)_2$ et du Fe(Pc)$(L)_2$ (TPP′ = tétrakis(4-méthoxyphényl)porphyrinate, Pc = ion phtalocyanate, L = ligand monodentate), on a préparé de nouveaux complexes métalliques diamagnétiques, hétéro-bi et -trinucléaires, à ponts oxo, de formules (L)(Pc)Fe-O-Ru(TPP′)(O) et (L)(Pc)Fe-O-Ru(TPP′)-O-Fe(Pc)(L). Le complexe trinucléaire se fixe à une variété de ligands (4,4′-bipy, 4-MePy, $P(OEt)_3$, pip, NH_3, 1-MeIm, $P(Me)_2Ph$), de façon *trans* par rapport au pont oxo. Les spectres de RMN du ^{1}H sont caractérisés par d'importants déplacements de courant de cycle causés par les ions TPP′ et Pc. Dans leurs spectres dans le visible, ces complexes comportent une bande Q anormalement faible pour le Pc, à 700 nm, et deux bandes CT dans la région du proche infrarouge, entre 1000 et 1500 nm, qui sont sensibles au ligand *trans*. À des valeurs de 0,4 et 0,76 V suivant le cas, le complexe trinucléaire peut être oxydé de façon réversible vers les ions +1 et +2 qui sont formellement le Fe(IV)-O-Ru(IV)-O-Fe(III) et le Fe(IV)-O-Ru(IV)-O-Fe(IV). On peut obtenir l'ion +1 de façon chimique par réaction de l'espèce neutre avec $(Cp)_2Fe^+$, pour L = 4-MePy, et cette réaction est renversée par l'addition de L′ = $P(Me)_2Ph$. De tous les clivages réducteurs par l'hydroquinone, les phosphines et les phosphites observés à date avec des systèmes RuTPP[$O(FeN_4)$]$_2$, ce sont les plus lents ($t_{1/2}$ = 8 h, à 40°C).

Mots clés : ruthénium, fer, porphyrine, phtalocyanine, oxo.

[Traduit par la Rédaction]

Introduction

The study of oxo-bridged multinuclear metal complexes has continued to attract interest both for their biological relevance (1) and as the most common example of single atom bridged systems (2). Oxo-bridged metal complexes have been prepared by hydrolytic processes (3), by one-electron redox reactions in which a high valent metal-oxo compound is reacted with a lower valent metal complex (4), and by autoxidation (5). We and others have employed a $Ru^{VI}(O)_2$ porphyrin as a route to μ-oxo trinuclear species (6, 7) In this study we extend this reaction to a new class of oxo-bridged heterotrinuclear complexes containing the iron phthalocyanine (FePc) moiety.

Received August 31, 2000. Published on the NRC Research Press Web at http://canjchem.nrc.ca site on June 30, 2001.

Dedicated to Professor Brian James on the occasion of his 65th birthday.

F. Zobi and D.V. Stynes.[1] Department of Chemistry York University, Toronto, ON M3J 1P3, Canada.

[1]Corresponding author (telephone: (416) 736-2100, ext. 22308; e-mail: stynes@yorku.ca).

Experimental

Materials

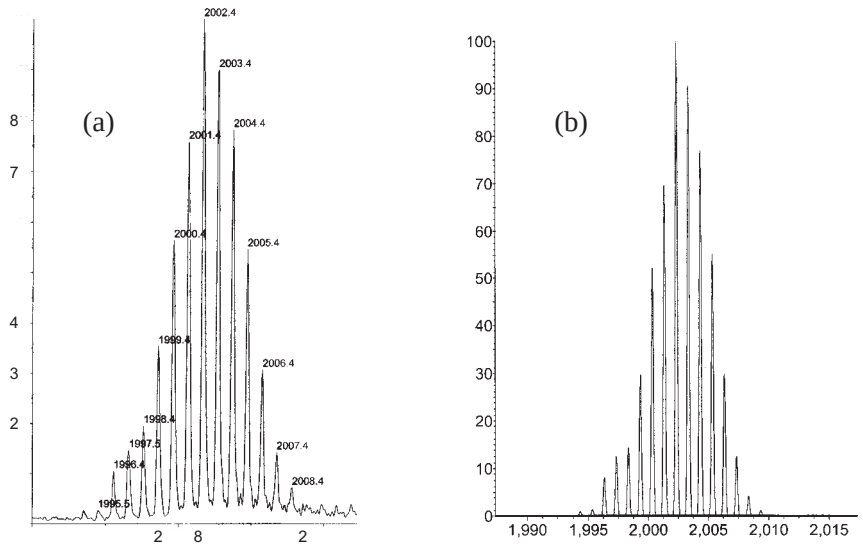
Common ligands were obtained from standard sources and were used as received. Solvents were distilled and kept over molecular sieves (3 Å). $CDCl_3$ was dried over activated molecular sieves (3 Å) and freed of acid by filtering through vacuum dried $Al(OH)_3$. Tetrakis(4-methoxyphenyl) porphyrin (H_2TPP′), Ru(TPP′)(CO)(C_2H_5OH), and Ru(TPP′)$(O)_2$ were prepared by literature methods (8–10).

Physical measurements

Visible spectra were recorded on a HP-8451 Diode array UV–vis spectrometer in 1 cm glass cuvettes thermostated at 25°C. ^{1}H NMR spectra were obtained on a Bruker ARX 400 MHz spectrometer at 300 K using $CDCl_3$ as the solvent

 DOI: 10.1139/cjc-79-5/6-795 © 2001 NRC Canada

Fig. 1. Experimental (*a*) and simulated (*b*) MS spectra of **2**. Shown is the isotopic distribution of the peak at *m*/*z* 2002, assigned to the $[(Pc)FeO]_2Ru(TPP')$ skeleton.



with TMS as an internal standard. Near-IR spectra were recorded on a Cary 2400 UV–vis – near-IR spectrometer at 25°C. Electrochemical data were collected with a computer-controlled Electroanalytical Cypress System model CS-1090. Cyclic voltammetry experiments were performed under a nitrogen atmosphere in a CH_2Cl_2 solution containing 0.1 M $(TBA)PF_6$ and ~5 × 10^{-3} M complex at −42°C. A platinum disk sealed in glass was used as a working electrode. Graphite was used as a counter electrode and AgCl/Ag was used as the reference electrode. Ferrocene was used as an internal reference (Fc+/Fc = 0.46 V in CH_2Cl_2 vs. SCE). Mass spectra were collected with a Perseptive Biosystems MALDI spectrometer, model Voyager-DE STR operating in the positive-ion mode.

Fe(Pc)(L)$_2$ (L = 4-MePy, 1-MeIm)

Fe(Pc) (Pc = phthalocyanate ion) (Aldrich) (1 g, 1.76 mmol) was dissolved in a $CHCl_3$ solution (25 mL) containing 4-MePy (5 mL, 51.4 mmol). After stirring the solution for 10 h at room temperature a purple crystalline precipitate was collected by filtration through paper. The product was then washed with hexane and dried in vacuo. Yield: 579 mg, 44%. $Fe(Pc)(1\text{-MeIm})_2$ was prepared by a similar procedure. Yield: 697 mg, 54%.

[(1-MeIm)Fe(Pc)O]Ru(TPP′)(O) (1)

Freshly made $Ru(TPP')(O)_2$ (5 mg, 5.8 × 10^{-3} mmol) and $Fe(Pc)(1\text{-MeIm})_2$ (10 mg, 1.36 × 10^{-2} mmol) were dissolved in a N_2 purged $CDCl_3$ solution (5 mL) and the reaction followed by NMR. When all $Ru(TPP')(O)_2$ had reacted (indicated by the disappearance of the H_β peak at 9.11 ppm) the reaction was quenched by slowly adding hexane (10 mL). The ppt was filtered through paper and dried in vacuo. Yield: 6.9 mg, 80%. The complex was very reactive and it formed an insoluble precipitate both in solution (within minutes) and in the solid state even when stored in vacuo at –20°C.

[(4-MePy)Fe(Pc)O]$_2$Ru(TPP′) (2)

Freshly made $Ru(TPP')(O)_2$ (100 mg, 0.116 mmol) and $Fe(Pc)(4\text{-MePy})_2$ (200 mg, 0.265 mmol) were mixed as solids and dissolved in a CH_2Cl_2–$CHCl_3$ solution (3:1, 18 mL). After 40 min hexane (50 mL) was slowly added depositing 223 mg of a black crude precipitate. The product was found to be contaminated by unreacted $Fe(Pc)(4\text{-MePy})_2$ and $[Ru(TPP')(OH)]_2O$, which were subsequently removed by recrystallizing the complex from a hexane–$CHCl_3$ solution. Yield: 199 mg, 79%. MALDI-MS ($CHCl_3$) *m*/*z*: 2188 ($[M]^+$). Other relevant peaks are at 2002 ($[(PcFeO)_2Ru(TPP')]^+$) (Fig. 1), 1418 ($[(Pc)FeORu(TPP')]^+$), 850 ($[Ru(TPP')(O)]^+$), 662 ($[Fe(Pc)(4\text{-MePy})]^+$), 569 ($[Fe(Pc)]^+$). Anal. calcd for $C_{124}H_{82}N_{22}O_6Fe_2Ru$: C 68.04, H 3.78, N 14.08; found: C 68.39, H 3.76, N 13.91. This complex is sensitive to trace acid normally present in $CDCl_3$, therefore, its ^1H NMR spectrum must be taken in acid free solvents. Various ligated derivatives of **2** were generated in situ in a NMR tube by addition of excess ligand L (L = 4,4′-bipy, pip, NH_3, 1-MeIm, $P(CH_3)_2Ph$) to the 4-MePy-ligated derivative in a chloroform solution. Solid samples were obtained in quantitative yields by precipitation with hexane (typically 1–3 mg).

Kinetic measurements

Neat phosphines, phosphites, or a dichloromethane solution of hydroquinone were injected via syringe into a thermostated (40°C) $CHCl_3$ solution of the complex (1 × 10^{-5} M) and the subsequent reaction followed by visible spectroscopy. Pseudo-first-order rate constants were obtained by monitoring the growth of the Soret band of the $Ru(TPP')L_2$ complex. Spectra were typically scanned between 380 and 820 nm under anaerobic conditions.

© 2001 NRC Canada

Fig. 2. Reaction sequence in the formation of [(4-MePy)Fe(Pc)O]2Ru(TPP′) (**2**). The intermediate binuclear species is indicated by **1**.

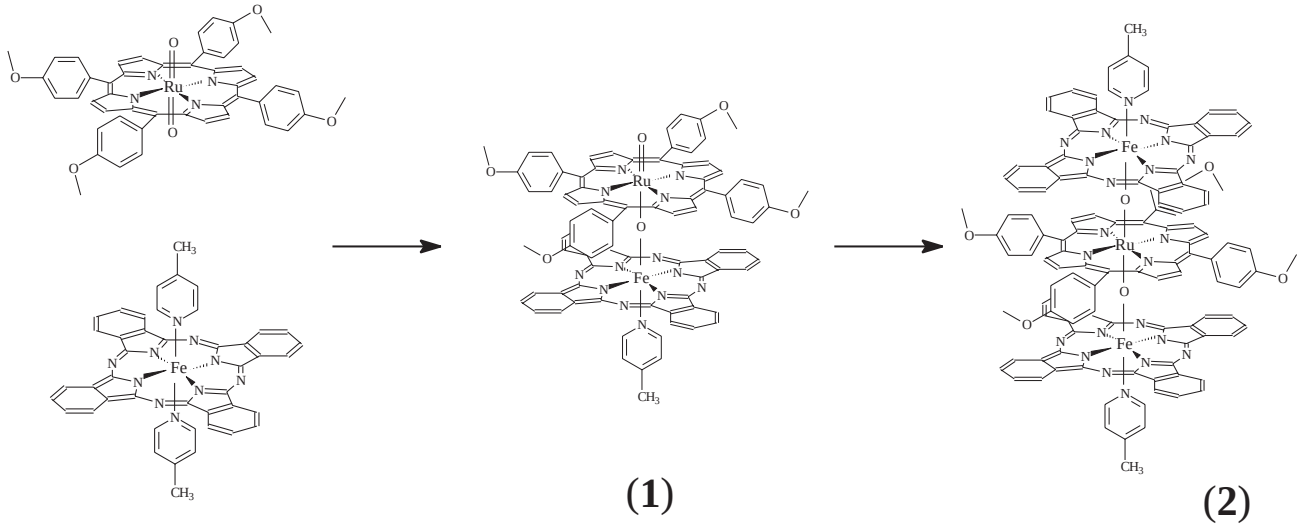
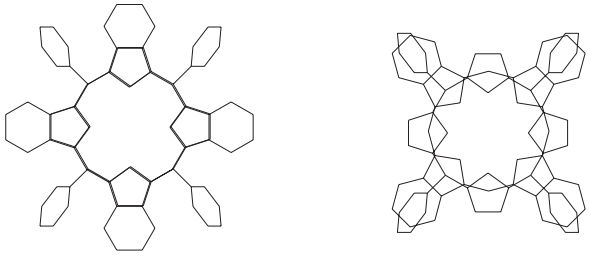


Fig. 3. Eclipsed (*a*) and staggered (*b*) conformations of stacked TPP and Pc rings. A staggered conformation leads to prohibited contacts between Pc benzopyrrole rings and TPP phenyls.



(a) (b)

Results and discussion

Synthesis

Formation of **2**, the trinuclear complex, proceeds through the initial formation of a reactive binuclear species **1** (Fig. 2). Both steps involve an inner-sphere oxidation of the Fe^{II} metal center by the dioxo Ru-porphyrin. Attempts to isolate the 4-MePy derivative of **1** proved unsuccessful as **1**-(4-MePy) is extremely reactive.

The 1-MeIm derivative was isolated but survives only long enough to obtain an NMR and observe its reactions with reductants. Oxidation of the Fe^{II} metal center by $Ru(TPP')(O)_2$ requires a vacant coordination site on Fe(Pc). Ligand dissociation in $Fe(Pc)(1\text{-MeIm})_2$ is about 50 times slower than $Fe(Pc)(4\text{-MePy})_2$ (11) and this allows for a better control over the reaction. Slow dissociation of 1-MeIm in the binuclear complex may also retard polymerization of **1**. While **1**-(4-MePy) is generated in situ by reacting $Ru(TPP')(O)_2$ with $Fe(Pc)(4\text{-MePy})_2$ in a 1:1 ratio, an excess of $Fe(Pc)(1\text{-MeIm})_2$ was used in the slower formation of **1**-(1-MeIm) to avoid formation of the $[Ru(TPP')(OH)]_2O$ dimer.

The binuclear complex is formally Fe^{IV}-O-Ru^{IV} and is the first example of a Ru porphyrin complex containing both a terminal and a bridging oxo ligand. The presence of the reactive terminal oxygen is inferred from the observation that the binuclear species reacts with a second Fe(Pc) unit to form the trinuclear compound and undergoes rapid reactions on mixing with hydroquinone, DMSO, or dimethylphenylphosphine. The oxidation products quinone, $DMSO_2$, and dimethylphenylphosphine oxide, respectively, were identified in the NMR spectrum.

^{1}H NMR spectra

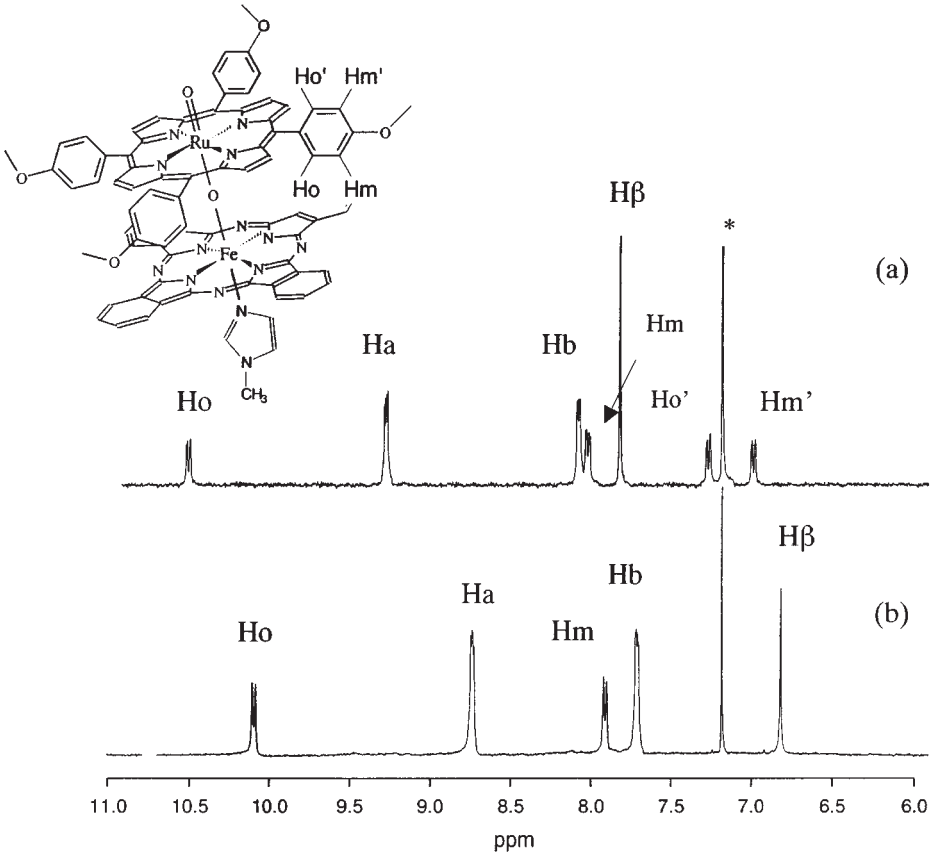
Both **1** and **2** are diamagnetic as expected for linear species with axial d_π^4 and d_π^8 configurations (6). ^{1}H NMR provides definitive characterization of the different ligated bi- and trinuclear μ-oxo species. All spectra are characterized by large ring current shifts (rcs) due to the TPP′ and Pc ions. Observed shifts are consistent with rcs calculations carried out on the basis of Abraham 12-loop model (12). An eclipsed conformation of the macrocycles is most consistent with the NMR data as this places the porphyrin H_β protons directly over the benzopyrrole rings. A staggered conformation would lead to prohibited contacts with the TPP′ phenyls (Fig. 3). An eclipsed structure is rare for X-bridged dimers and trimers (X = C, N, O). The only other known examples are $[(THF)(TPP)Fe\text{-}N\text{-}Fe(Pc)(H_2O)](I_5)$ (13), $[(Pc)Al]_2O$ (14), and $[Fe(OEP)]_2O$ (15). Complex **2** is the first example of a fully eclipsed macrocyclic trinuclear.[2]

^{1}H NMR spectra of the bi- and trinuclear complexes are shown in Figs. 4*a* and *b*, respectively. The binuclear species is identified on the basis of differentiated TPP′ phenyls protons. Phenyl protons directed toward the Fe(Pc) face project into the deshielding region of the Pc ring and experience a downfield shift, while those directed to the open face (denoted $H_{o'}$ and $H_{m'}$ in Fig. 4*a*) experience a small upfield shift. In the centrosymmetric trinuclear species a single set of ortho and meta phenyl resonances is observed (H_o and H_m in Fig. 4*b*). The porphyrin H_β protons are shifted upfield (rela-

[2] The $[Mo_3O_4(TPP)_3]^+$ ion shows partial eclipse of two Mo(TPP) moieties (16).

© 2001 NRC Canada

Fig. 4. Aromatic region of ^{1}H NMR spectra of (*a*) binuclear **1**-(1-MeIm); and (*b*) trinuclear **2**-(4-MePy)$_2$ species in $CDCl_3$ (* indicates solvent peak).



tive to Ru(TPP′)(O)$_2$) in both **1** and **2**. Axial ligand resonances are also shifted upfield as a result of the cumulative effect of Pc and TPP′ rcs. Hydrogen atoms at the *ortho* position in 4-MePy, for example, suffer a 8.5 ppm upfield shift in **1** and over 9 ppm upfield shift in **2** when compared to the free ligand. Spectral data are collected in Table 1.

Electronic spectra

The visible spectrum of **2** is given in Fig. 5. It shows a typical porphyrin Soret band at 410 nm in contrast to a red-shifted Soret band at about 435 nm in DMG and DPG trinuclears (6). A weak bathochromic shifted phthalocyanine Q band at about 700 nm is present in the visible spectrum of **2**. An unusually weak Pc Q band is also reported for the μ-nitrido (TPP)Mn-N-Fe(Pc) (17) and the μ-oxo (TPP)Cr-O-Fe(Pc) (18) complexes. This feature may be characteristic of X-bridged metal atoms containing face-to-face Pc and porphyrin rings. Additionally, two low energy charge transfer bands (CT1 and CT2) appear in the near-IR region at 1050 and 1330 nm (see Fig. 6 and Table 2).

The CT bands show significant shifts as a function of the axial ligand suggesting that MO's with substantial iron character are involved. The two bands are tentatively assigned to an oxo-to-metal (CT1) and to an intervalence metal-to-metal charge transfer (CT2). A similar assignment was made in DMG based systems (6). The lower oxidation potential of **2** translates in a smaller HOMO–LUMO gap and less energy is required for this transition. Consequently CT2 in **2** shifts 500 nm and is well-resolved in the IR. The same is true for CT1 (see Tables 3 and 4). Both CT bands undergo a bathochromic shift with increasing π-acceptor strength and (or) increasing basicity of the axial ligand. A typical change is shown in Fig. 6.

Ligation

The Fe(Pc) based heterotrinuclear complexes are substantially more stable in solution than borylated dioxime and paramagnetic heme or Fe(Schiff base)-derived Fe-O-Ru-O-Fe systems (6, 7). Ligand displacement at the Fe^{III} center can be followed at room temperature by both NMR and near-IR spectroscopy. 4-MePy in **2** is easily displaced by stonger σ-donors such as NH_3 and 1-MeIm, by π-acid ligands including P(Me)$_2$Ph, and by ligands capable of promoting chain elongation like 4,4′-bipy (eq. [1]). These substitution reactions are over on mixing at ambient temperature but are in the slow exchange limit in the ^{1}H NMR.

[1] $$[(4\text{-MePy})Fe(Pc)O]_2Ru(TPP') + 2L' \rightarrow [(L')Fe(Pc)O]_2Ru(TPP') + 2(4\text{-MePy})$$

The relative binding strength of the different ligands was obtained from spectrochemical titrations in the near-IR and follows the order:

$$4,4'\text{-bipy} < 4\text{-MePy} \sim P(OEt)_3 < pip < NH_3 < 1\text{-MeIm} < P(CH_3)_2Ph$$

© 2001 NRC Canada

Table 1. ^{1}H NMR data (δ, ppm) in $CDCl_3$.

Complex	H_β	H_o	H_m	OCH_3	H_a	H_b	Ligand
2-(4-MePy)$_2$	6.89	10.18	8.00	4.59	8.82	7.80	^{L}H$_o$ –0.90, ^{L}H$_m$ 3.59, ^{L}CH$_3$ 0.30
2-(1-MeIm)$_2$	6.88	10.15	7.97	4.58	8.80	7.77	H$_2$ –1.05, H$_4$ –0.61, H$_5$ 3.31, CH$_3$ 0.88
2-[P(Me$_2$Ph)]$_2$	6.81	10.00	7.92	4.54	8.67	7.70	Hα 2.60, Hβ 5.30, Hγ 6.00, CH$_3$ –4.12
2-(NH$_3$)$_2$	6.78	10.00	7.92	4.53	8.76	7.78	NH$_3$ –9.00
2-[P(OEt)$_3$]$_2$	6.84	10.10	7.93	4.55	8.76	7.69	CH$_3$ –1.29, CH$_2$ –0.36
2-(4-MePy) [P(OEt)$_3$]	6.86	10.15, 10.10	7.93, 7.91	4.57	8.85, 8.46	7.81, 7.68	^{L}H$_o$ –0.90, ^{L}H$_m$ 3.59, ^{L}CH$_3$ 0.30, ^{P}CH$_3$ –1.29, ^{P}CH$_2$ –0.36
2-(4,4′-bipy)$_2$	6.92	10.18	8.00	4.60	8.84	7.82	Hα –0.64, Hβ 3.90, Hγ 5.51, Hδ 7.72
1-(4-MePy)	7.89	10.59, 7.35	8.09, 7.07	4.30	9.37	8.16	^{L}H$_o$ –0.15, ^{L}H$_m$ 4.09, ^{L}CH$_3$ 0.61
1-(1-MeIm)	7.88	10.57, 7.37	8.09, 7.07	4.30	9.35	8.15	H$_2$ –0.38, H$_4$ 0.89, H$_5$ 3.82, CH$_3$ 1.37
Ru(TPP′)(O)$_2$	9.11	8.26	7.36	4.14			
Fe(Pc)(4-MePy)$_2$					9.30	7.95	H$_o$ 1.98, H$_m$ 4.81, CH$_3$ 1.07
Fe(Pc)[P(Me$_2$Ph)]$_2$					9.07	7.87	Hα 4.36, Hβ 6.24, Hγ 6.66, CH$_3$ –2.11
Fe(Pc)[P(OEt)$_3$]$_2$					9.26	7.91	CH$_3$ –0.20, CH$_2$ 1.27
3-(1-MeIm)[a]	9.20	8.77	7.46	4.15	1.56 (DMG CH$_3$)		H$_2$ 4.87, H$_4$ 4.49, H$_5$ 5.71, CH$_3$ 2.83

[a] **3** = [Fe((DMG)BF$_2$)$_2$O]$_2$Ru(TPP′), ref. 6.

Fig. 5. Visible spectrum of **2** in $CHCl_3$. Insert shows the growth of the Pc Q band during the reductive cleavage of the oxo-bridge.

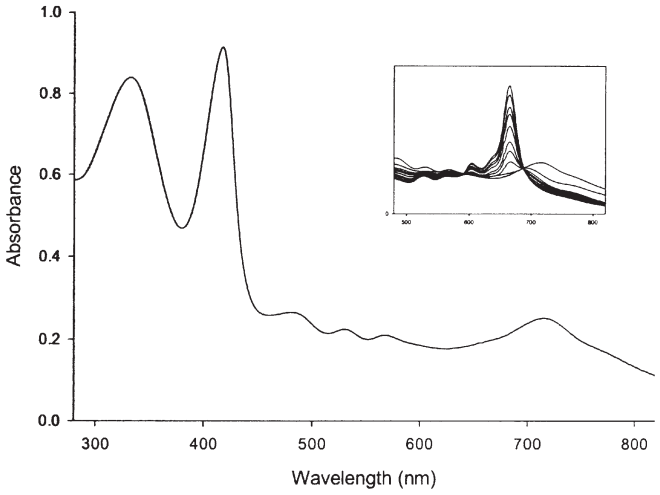
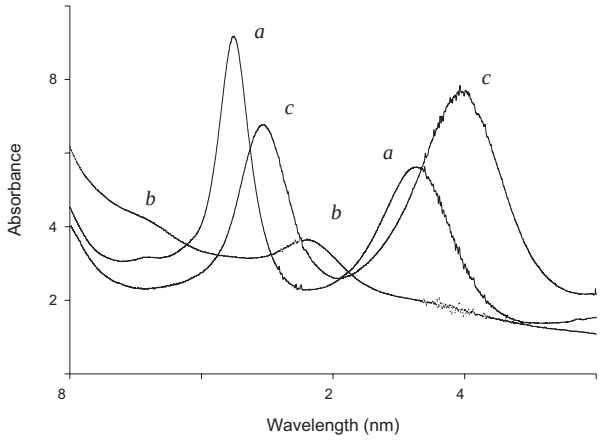


Fig. 6. Spectral changes in the near-IR region during the oxidation and subsequent reduction of **2**. (*a*) **2**-(4-MePy)$_2$; (*b*) [**2**-(4-MePy)$_2$]$^+$, obtained upon addition of 1 equiv. of [(η^5-Cp)$_2$Fe](PF$_6$); and (*c*) **2**-[(PMe$_2$Ph)]$_2$ obtained by addition of neat P(Me)$_2$Ph to the +1 ion.



Shifts in the near-IR as a function of axial ligand are similar to those previously described for Fe(DMG) systems (6).

Electrochemistry and redox reactions

Cyclic voltammetry experiments were carried out for **2** in CH_2Cl_2 containing 0.1 M (TBA)PF$_6$. Four reversible one-electron oxidation waves are observed for the 4-MePy adduct at –42°C and these occur at $E_{1/2}$ = 0.4, 0.76, 1.04, and 1.32 V (Fig. 7). The two lower oxidation waves are assigned to successive Fe$^{III/IV}$ oxidations in agreement with what previously reported for (PcFe)$_2$O (19). The third and fourth waves (1.04 and 1.32 V) are tentatively ascribed to successive oxidations of the Pc rings (20). Complex **2** shows a lower oxidation potential than the borylated dioxime-derived heterotrinuclear of Vernik (6) (Table 3).

The complex may be chemically oxidized to the +1 cation by using [(η^5-Cp)$_2$Fe](PF$_6$) ($E_{1/2}$ = 0.46 V in CH_2Cl_2). This chemical oxidation is reversible upon changing the axial ligand to P(CH$_3$)$_2$Ph. Figure 6 shows the change in the near-IR spectrum caused by the oxidation and subsequent reduction of the 4-MePy derivative. No reduction wave for **2** was detected up to –2.0 V. In related systems reduction normally results in irreversible oxo-bridge cleavage as electrons are added to antibonding orbitals (21).

Kinetics of reductive cleavage of oxo-bridge

The trinuclear complex undergoes slow reductive cleavage of the oxo-bridge with hydroquinones (H_2Q), phosphines, or phosphites. The kinetics of the reactions were studied at 40°C under anaerobic conditions and all changes were monitored by visible spectroscopy. Products were identified on the basis of distinctive visible–IR and ^{1}H NMR spectra and

© 2001 NRC Canada

Table 2. Visible and near-IR data for trinuclear $[(L)FeN_4O]_2Ru(TPP')$ oxo-bridged complexes (λ_{max}, nm).

N_4	Ligand	Soret	α	β	Q	CT1	CT2
Pc	4-$MePy_2$[a]	410	530	576	702	1050	1332
Pc	1-MeIm	410	528	566	702	1071	1325
Pc	$P(Me_2Ph)$	410	536	572	700	1096	1404
Pc	NH_3	412	526	572	702	1056	1312
Pc	CN^-	410	538	570	698	1130	1380
Pc	4,4′-bipy	412	532	572	702	1040	1340
Pc	pip	412	530	574	700	1088	1341
Pc	CH_3CN	410	530	568	702	1007	1300
$((DMG)BF_2)_2$[b]	1-MeIm	435	541	576		703	857
$((DMG)BPh_2)_2$[b]	1-MeIm	435	538	572		732	890
$((DPG)BF_2)_2$[b]	1-MeIm	433	542	577		714	836

[a]Extinction coefficient for **2**-(4-$MePy)_2$ log (ε): 4.70, 4.18, 4.15, 4.33, 4.17, 4.03 for Soret, α, β, Q, CT1, and CT2, respectively. Other derivatives of **2** give comparable values.
[b]Ref. 6.

Table 3. Electrochemical data for trinuclear $[(L)FeN_4O]_2Ru(TPP')$ oxo-bridged complexes.

N_4	Ligand	$E_{1/2}$ (V)[a]	CT1	CT2
Pc	4-MePy	0.40, 0.76, 1.04, 1.32	1050	1332
$((DMG)BF_2)_2$[b]	CH_3CN	0.80, 1.20	691	812
$((DMG)BPh_2)_2$[b]	CH_3CN	0.60, 1.06	709	839
	NH_3	0.51, 1.04	716	850
$((DPG)BF_2)_2$[b]	CH_3CN	1.00	686	799

[a]Half-wave potentials for reversible oxidation.
[b]Ref. 6.

Table 4. Kinetic data for the reductive μ-oxo cleavage of trinuclear $[(L)FeN_4O]_2Ru(TPP')$ complexes.

N_4	Reductant	K_{obs} (1×10^{-4}) (s^{-1})
Pc[a]	$P(Me_2Ph)$	0.074
Pc[a]	$P(OEt)_3$	0.078
Pc[a]	H_2Q[b]	0.069
$((DMG)BF_2)_2$	H_2Q[c]	453
$((DPG)BF_2)_2$	H_2Q[c]	1340

[a]$[2\text{-}(4\text{-}MePy)_2] = 1.0 \times 10^{-5}$ M. Reaction carried out in $CHCl_3$ at 40°C.
[b]In the presence of 4-MePy (1.0×10^{-3} M).
[c]Reaction carried out in CH_2Cl_2 at 25°C in the presence of 1 M CH_3CN. Ref. 6.

Fig. 7. Cyclovoltammogramm of **2** in CH_2Cl_2 at −42°C (Ag/Ag^+ used as the reference electrode).

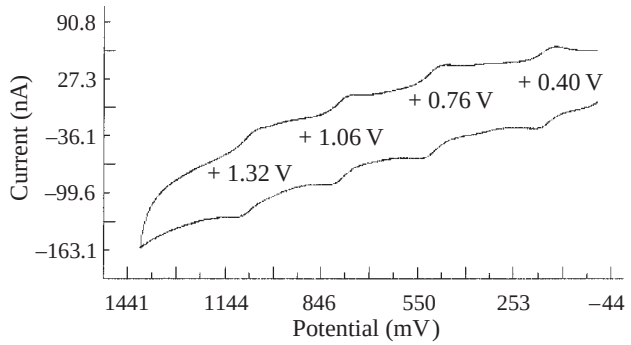
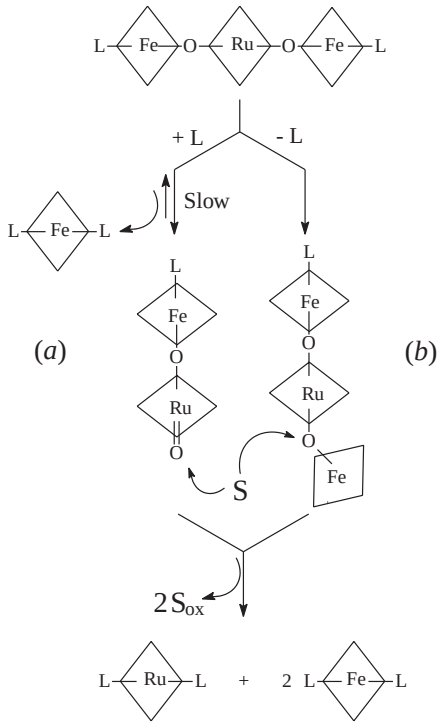


Fig. 8. Possible pathways of oxo-bridge reductive cleavage in trinuclear complexes. (*a*) Dissociative path; occurs in $[(L)Fe(N_4)O]_2Ru(TPP')$ complexes where N_4 is the Pc ring. The rate-determining step is the dissociation of a Fe(Pc) unit. (*b*) Bent μ-oxo path; occurs in $[(L)Fe(N_4)O]_2Ru(TPP')$ complexes where N_4 is the DMG or the DPG ring. The rate-determining step involves oxo-transfer from the trinuclear to S; S = reducing substrate (H_2Q, $P(Me_2Ph)$, or $P(OEt)_3$).



the overall stoichiometry shown in eqs. [2] and [3] was confirmed by NMR.

[2] **2**-(4-$MePy)_2$ + $8PX_3 \rightarrow 2Fe(Pc)(PX_3)_2$ +

$Ru(TPP')(PX_3)_2 + 2(O{=}PX_3)$

© 2001 NRC Canada

[3] **2**-$(L)_2$ + 4L + $2H_2Q \rightarrow 2Fe(Pc)(L)_2$ + $Ru(TPP')(L)_2$ + 2Q (where L = 4-MePy)

The rate constant for the reduction of **2** (7×10^{-6} s^{-1}) was found to be independent of the concentration or nature of the reductant used and it is at least four orders of magnitude slower than that of μ-oxo borylated dioxime systems (6) (see Table 4). The reaction proceeds cleanly (isosbestic point at 688 nm) with no binuclear or other intermediates detected. Mechanism A in Fig. 8 is proposed in which the rate determining step is the dissociation of a Fe(Pc) unit to generate a binuclear species, which is subsequently reduced to the monomeric $Ru^{II}(TPP')$ and $Fe^{II}(Pc)$ complexes. In contrast, mechanism B was proposed in DMG systems where reduction was found to show an inverse first-order dependence on the axial ligand concentration implying a loss of one ligand prior to the rate determining μ-oxo cleavage (6, 22). A folding back of the pentacoordinate FeN_4 fragment in a bent geometry permits direct attack at the oxo site in these systems. Mechanism B may be much more difficult in FePc-based trinuclears as the Pc ring lacks the flexibility of the DMG macrocycles. Thus, only a [L] independent dissociative path is observed in the FePc systems.

Acknowledgments

Financial support from NSERC (Canada) is gratefully acknowledged. The authors are also thankful to Christos Alexiou for his assistance in CV data collection, and Gianni Manno of the Department of Mathematics at the King's College, London, U.K. for his suggestions regarding rcs calculations.

References

1. (*a*) R.D. Holm. Chem. Rev. **87**, 1401 (1987); (*b*) D.M. Kurtz. Chem. Rev. **90**, 585 (1990); (*c*) R.D. Holm, P. Kennepohl, and E.I. Solomon. Chem. Rev. **96**, 2239 (1996); (*d*) B.J. Waller and J.D. Lipson. Chem. Rev. **96**, 2625 (1996); (*e*) P. Norlund, B.-M. Sjöberg, and H. Eklund. Nature (London), **345**, 593 (1990); (*g*) R.M. Buchanan, S. Chen, and J.F. Richardson. Inorg. Chem. **33**, 3208 (1994); (*h*) K. Neimann, R. Neumann, and A. Ribion. Inorg. Chem. **38**, 3575 (1999).
2. C. Ercolani and B. Floris. *In* Phthalocyanines. Properties and applications. Vol. 2. *Edited by* C.C. Leznoff and A.B.P. Lever. VCH Publishers, New York. 1993. pp. 1–42.
3. (*a*) R.D. Cannon and R.P. White. Prog. Inorg. Chem. **36**, 195 (1988); (*b*) M.H. Chisholm, K. Folting, and E.M. Kober. Inorg. Chem. **24**, 241 (1985).
4. (*a*) E.N. Baski, R.L. Elliott, K.S. Murray, P.J. Nichols, and B.O. West. Aust. J. Chem. **43**, 707 (1990); (*b*) B.O. West. Polyhedron, **8**, 219 (1989); (*c*) D.J. Liston, B.J. Kennedy, K.S. Murray, and B.O. West. Inorg. Chem. **24**, 1561 (1985); (*d*) R.J. Saxton, L.W. Olson, and L.J.J. Wilson. J. Chem. Soc. Chem. Commun. 984 (1982).
5. (*a*) A. Yamamoto, L.K. Phillips, and M. Calvin. Inorg. Chem. **7**, 847 (1968); (*b*) A.B.P. Lever, J.P. Wilshire, and K.S. Quan. Inorg. Chem. **20**, 761 (1981); (*c*) C. Ercolani, M. Gardini, F. Monacelli, G. Pennesi, and G. Rossi. Inorg. Chem. **22**, 2584 (1983); (*d*) C. Ercolani, G. Rossi, and F. Monacelli. Inorg. Chem. Acta, **44**, L215 (1980).
6. I. Vernik and D.V. Stynes. Inorg. Chem. **37**, 10 (1998).
7. (*a*) K.J. Berry, B. Moubaraki, K.S. Murray, P.J. Nichols, L.D. Schultz, and B.O. West. Inorg. Chem. **34**, 4123 (1995); (*b*) L.D. Schultz, G.D. Fallon, B. Moubaraki, K.S. Murray, and B.O. West. J. Chem. Soc. Chem. Commun. 971 (1992).
8. A.D. Alder, F.R. Longo, J.D. Finarelli, J. Goldmacher, J. Assour, and L. Koskakoff. J. Org. Chem. **32**, 476 (1967).
9. J.P. Collman, C.E. Barnes, P.J. Brothers, T.J. Collins, T. Ozawa, J.C. Gallucci, and J.A. Ibers. J. Am. Chem. Soc. **106**, 5151 (1984).
10. W. Leung and C.M. Che. J. Am. Chem. Soc. **111**, 8812 (1989).
11. D.V. Stynes and B.R. James. J. Am. Chem. Soc. **96**, 2733 (1974).
12. (*a*) R.J. Abraham, S.C.M. Fell, and K.M. Smith. Org. Magn. Reson. **9**, 367 (1977); (*b*) R.J. Abraham, G.R. Bedford, D. McNeillie, and B. Wright. Org. Magn. Reson. **14**, 418 (1980); (*c*) R.J. Abraham, G.R. Bedford, B. Wright. Org. Magn. Reson. **18**, 45 (1982); (*d*) R.J. Abraham, C.J. Medforth, K.M. Smith, D.A. Goff, and D.J. Simpson. J. Am. Chem. Soc. **109**, 4786 (1987).
13. C. Ercolani, J. Jubb, G. Pennesi, U. Russo, and G. Trigante. Inorg. Chem. **34**, 2535 (1995).
14. K.J. Wynne. Inorg. Chem. **24**, 1339 (1985).
15. M.T. Pinillos, A. Elduque, E. Martin, N. Navarro, J.F. Lahoz, J.A. Lopez, and L. Oro. Inorg. Chem. **34**, 111 (1995).
16. B.J. Hamstra, B. Cheng, and M.K. Ellison. Inorg. Chem. **38**, 3554 (1999).
17. M.P. Donzello, C. Ercolani, K.M. Kadish, Z. Ou, and U. Russo. Inorg. Chem. **37**, 3682 (1998).
18. D.J. Liston, B.J. Kennedy, K.S. Murray, and B.O. West. Inorg. Chem. **24**, 1567 (1985).
19. L.A. Bottomley, C. Ercolani, J.-N. Gorce, G. Pennesi, and G. Rossi. Inorg. Chem. **25**, 2338 (1986).
20. (*a*) M. Hannak, A. Lange, M. Rein, R. Behnisch, G. Renz, and A. Leverenz. Synth. Metal, **29**, F1 (1989); (*b*) R. Behnisch and M. Hannak. Synth. Metal, **36**, 387 (1990); (*c*) W. Kalz, H. Homborg, H. Kuppers, B.J. Kennedy, and K.S. Murray. Naturforsch. **B39b**, 1478 (1984); (*d*) Y. Orihashi, H. Ohno, E. Tsuchida, H. Matsuda, H. Nakanishi, and M. Kato. Chem. Lett. 601 (1987); (*e*) Y. Orihashi, N. Nishikawa, H. Ohno, E. Tsuchida, H. Matsuda, H. Nakanishi, and M. Kato. Bull. Chem. Soc. Jpn. **60**, 3731 (1987).
21. (*a*) M. Muller, B. Eckhard, T. Weyhermuller, and K. Wieghardt. Chem. Commun. 705 (1997); (*b*) J.D. Cohen, S. Payne, K.S. Hagen, and J. Sanders-Loehr. J. Am. Chem. Soc. **119**, 2960 (1997); (*c*) U. Bossek, H. Hummel, T. Weyhermuller, E. Bill, and K. Wieghardt. Angew. Chem. Int. Ed. Engl. **34**, 2642 (1995); (*d*) D.V. Stynes, H. Noglik, and D.W. Thompson. Inorg. Chem. **30**, 4567 (1991); (*e*) J.E. Early and T. Fealey. Inorg. Chem. **25**, 2015 (1986).
22. (*a*) I. Vernik and D.V. Stynes. Inorg. Chem. **35**, 2006 (1996); (*b*) J.M. Caroll and J.R. Norton. J. Am. Chem. Soc. **114**, 8744 (1992).

© 2001 NRC Canada

Derivatization of polyoxotungstates in aqueous solution. Exploration of the kinetic stability of cobalt(II)- and cobalt(III) derivatives of lacunary anions with pyridine and pyridine-type ligands

Joseph L. Samonte and Michael T. Pope

Abstract: Four complexes of cobalt(II) with lacunary polyoxotungstate ligands, α-$[PW_{11}O_{39}Co(H_2O)]^{5-}$, α-$[SiW_{11}O_{39}Co(H_2O)]^{6-}$, α_1-, and α_2-$[P_2W_{17}O_{61}Co(H_2O)]^{8-}$ have been examined as potential precursors to substitutionally inert derivatized polytungstates that are stable in aqueous solution at near neutral pH. Replacement of the terminal water ligand by pyridine is readily achieved and the rates of exchange between bound and free pyridine were determined from NMR line widths at temperatures between 24 and 48°C. Oxidation to the aquacobalt(III) and pyridinecobalt(III) polytungstates occurs at potentials between +0.64 V (for α_1-$P_2W_{17}O_{61}Co(py)]^{8-}$) and +1.00 V (for α_2-$[P_2W_{17}O_{61}Co(H_2O)]^{8-}$). The cobalt(III) complexes (with the exception of α-$[PW_{11}O_{39}Co(H_2O)]^{4-}$ which undergoes slow reduction by the solvent) were prepared by controlled potential electrolysis and by oxidation with potassium perdisulfate. The rates of pyridine substitution on the aquacobalt(III) complexes were determined and follow the sequence α_1-$[P_2W_{17}O_{61}Co(H_2O)]^{7-}$ (~0.5 M^{-1} s^{-1}) » α_2-$[P_2W_{17}O_{61}Co(H_2O)]^{7-}$ ~ α-$[SiW_{11}O_{39}Co(H_2O)]^{5-}$. Cesium salts of α_1-$[P_2W_{17}O_{61}Co^{III}(L)]^{7-}$ (L = pyrazine, 4,4′-bipyridine, isonicotinic acid, and the ethyl ester of isonicotinoylglycylglycine) and the "dumbbell" 2:1 complex with bridging 4,4′-bipyridine were isolated and characterized by cyclic voltammetry and ^{1}H NMR spectroscopy.

Key words: lacunary polyoxotungstates, cobalt, ligand substitution, kinetics, redox.

Résumé : On a étudié la possibilité d'utiliser quatre complexes de cobalt(II) avec des ligands polyoxotungtate lacunaires, α-$[PW_{11}O_{39}Co(H_2O)]^{5-}$, α-$[SiW_{11}O_{39}Co(H_2O)]^{6-}$, α_1 et α_2-$[P_2W_{17}O_{61}Co(H_2O)]^{8-}$, comme précurseurs potentiels à des dérivés de polytungstates, inertes vis-à-vis de la substitution, qui sont stables en solution aqueuse à de pH proches de la neutralité. On peut facilement effectuer le remplacement de la molécule d'eau agissant comme ligand terminal par une pyridine et les vitesses d'échange entre la pyridine liée et libre ont été déterminées par les largeurs des raies RMN à des températures entre 24 et 48°C. L'oxydation des polytungstates d'aquacobalt(III) et de pyridinecobalt(III) se produit à des potentiels allant de +0,64 V (pour le α_1-$[P_2W_{17}O_{61}Co(py)]^{8-}$) à 1,00 V (pour le α_2-$[P_2W_{17}O_{61}Co(H_2O)]^{8-}$). Les complexes de Co(III) (à l'exception du α-$[PW_{11}O_{39}Co(H_2O)]^{4-}$ qui subit une réduction lente par le solvant) ont été préparés par une électrolyse à potentiel contrôlé et par oxydation à l'aide de perdisulfate de potassium. On a déterminé les vitesses de substitution de la pyridine sur les complexes aquacobalt(III) qui sont dans la séquence suivante: α_1-$[P_2W_{17}O_{61}Co(H_2O)]^{7-}$ (environ 0,5 M^{-1} s^{-1}) » α_2-$[P_2W_{17}O_{61}Co(H_2O)]^{7-}$ ~ α-$[SiW_{11}O_{39}Co(H_2O)]^{5-}$. On a aussi isolé les sels de césium de α_1-$[P_2W_{17}O_{61}CO^{III}(L)]^{7-}$ (L = pyrazine, 4,4′-bipyridine, acide isonicotinique, isonicotinoylglycylglycinate d'éthyle) et le complexe 2:1 en forme d' « haltère » et on les a caractérisés par voltampérométrie cyclique et par spectroscopie RMN du ^{1}H.

Mots clés : polyoxotungstates lacunaires, cobalt, substitution du ligand, cinétique, redox.

[Traduit par la Rédaction]

Introduction

The current interest and research activity in the chemistry of polyoxometalates (1) is driven to a large extent by applications of these complexes in catalysis (2), and in recent years by their biological activity (3). Long known (and used) as electron-dense electron microscope stains ("phosphotungstic acid") polyoxometalates have recently been used for structural crystallographic investigation of very large biomolecules (4). We have been exploring ways of functionalizing the surfaces of large polytungstate anions for several reasons. In the biological context these species could be targeted towards specific sites on the surfaces of proteins for imaging and crystallographic purposes. Appropriately derivatized

Received August 8, 2000. Published on the NRC Research Press Web site at http://canjchem.nrc.ca on June 30, 2001.

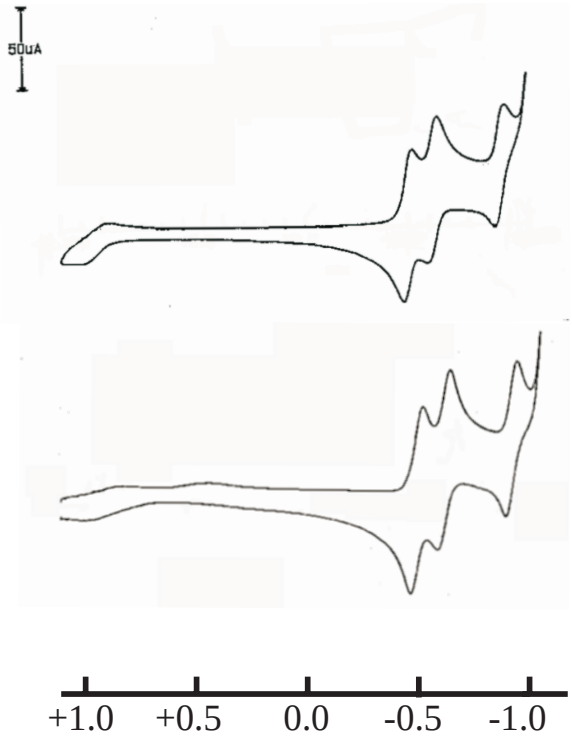
Dedicated to Professor Brian James on the occasion of his 65th birthday.

J.L. Samonte and M.T. Pope.[1] Department of Chemistry, Box 571227, Georgetown University, Washington, DC 20057, U.S.A.

[1]Corresponding author (telephone: (202) 687-6253; fax: (202) 687-6209; email: popem@georgetown.edu).

 DOI: 10.1139/cjc-79-5/6-802 © 2001 NRC Canada

Fig. 1. Cyclic voltammograms of (upper) α_1-$[P_2W_{17}O_{61}Co^{II}(H_2O)]^{8-}$ and (lower) α_1-$[P_2W_{17}O_{61}Co^{II}(py)]^{8-}$ at pH 4.7. Glassy carbon electrode (100 mV s^{-1}).



polyanions known to have antitumoral and antiviral activity in vitro might also be rendered membrane-permeable, thereby opening up pharmaceutical applications. The present investigation explores the possibility of using "substitution-inert" cobalt(III) to attach appropriate ligands to polytungstate anions in aqueous media at near neutral pH.

The first examples of polyoxoanions that contained transition-metal cations *in place of* a W^{VI} or Mo^{VI} atom were recognized by Baker et al. (5) and by numerous subsequent investigators (6) in the 1960s. In 1970, Baker and Figgis (7) pointed out that a *substituted* polyanion should be regarded as a coordination complex of the transition-metal cation with pentadentate polyoxometalate and (in most cases) monodentate aqua ligand. Since the terminal water molecule was susceptible to replacement by other ligands, the complexes were predicted to have an important role in catalysis (7). This prediction has been borne out by work from several groups within the past 10–15 years (2). There have been many qualitative observations of ligand substitution processes, including isolation of adducts, (1*a*, 8) but, to our knowledge, only two publications address the thermodynamic or kinetic parameters associated with these processes. Weakley (8) has reported conditional formation constants, *K*, for $[XW_{11}O_{39}Co^{II}(OH_2)]^{n-}$ + L ⇔ $[XW_{11}O_{39}Co^{II}(L)]^{n-}$ (X = B, P, As; L = pyridine, 3-cyano-, 2-methyl-, 4-methyl-pyridines, NCS^-, thiourea). In aqueous solution (no pH or ionic medium specified) *K*s range from 1.0 to 255 M^{-1} at 20°C. For the Co^{III} anion $[BW_{11}O_{39}Co(OH_2)]^{6-}$ the *K*s are somewhat larger (e.g., 16.0 M^{-1} for L = 2-methylpyridine vs. 1.0 M^{-1} for the corresponding Co^{II} derivative). More recently Finke and coworkers (9) have measured the nonaqueous equilibria, α_2-$[P_2W_{17}O_{61}Mn^{III}(solvent)]^{7-}$ + L ⇔ α_2-$[P_2W_{17}O_{61}Mn^{III}(L)]^{7-}$. In dichloromethane solution, *K*s range from 4100 ± 1700 M^{-1} (L = pyridine) to 6 ± 3 M^{-1} (L = triphenylphosphine). Kinetic data appear to be limited to Weakley's observation (8) that the second-order rate constant for substitution of water by pyridine on the Co^{III} complex $[BW_{11}O_{39}Co(OH_2)]^{6-}$ is ~0.1 M^{-1} s^{-1} at 20°C.

Results and discussion

The four lacunary tungstate anions, α-$[PW_{11}O_{39}]^{7-}$, α–$[SiW_{11}O_{39}]^{8-}$, α_1-$[P_2W_{17}O_{61}]^{10-}$, and α_2-$[P_2W_{17}O_{61}]^{10-}$ were converted to the red aquacobalt(II) derivatives, $[PW_{11}O_{39}Co(H_2O)]^{5-}$, etc., as described in the *Experimental section*. Cyclic voltammograms of these complexes revealed, in addition to reversible two-electron tungsten reduction waves at negative potentials, a quasireversible feature at positive potentials corresponding to the oxidation of cobalt(II) to cobalt(III) (see Fig. 1 (upper) for example).

The yellow cobalt(III) complexes, $[PW_{11}O_{39}Co(H_2O)]^{4-}$ etc., were obtained by controlled potential electrolysis or by oxidation with potassium perdisulfate. Solution features of the Co(II) and Co(III) derivatives are summarized in Table 1.

Addition of pyridine to solutions of the Co(II) complexes caused an intensification of the red color and the introduction of an additional redox feature at positive potentials corresponding to the Co(II/III) couple of the pyridine complex (see Fig. 1 (lower)).

^{1}H NMR spectra of solutions containing mixtures of the polyoxometalates and pyridine show signals from both free and coordinated pyridine, as has been observed by So and co-workers (10) for analogous polytungstate systems. Chemical shifts for the coordinated pyridine are given in Table 2.

The chemical shifts for the free pyridine in these solutions were constant within ±0.04 ppm. Consequently, it was possible to estimate the rate of exchange between free and coordinated pyridine from measurement of the line width of the α-proton signal of free pyridine using the equation appropriate for the slow exchange limit, i.e. $\frac{1}{T_2} = \frac{1}{t_2} + \frac{1}{\tau}$

where T_2' and T_2 are the transverse relaxation times for the proton in the presence and absence of the Co(II)-polyoxometalate respectively, and τ is the coordination lifetime of the free pyridine. Figure 2 illustrates the free pyridine signals in a solution containing a 1:1 molar mixture of α_2-$[P_2W_{17}O_{61}Co(H_2O)]^{8-}$ and pyridine at different temperatures.

Calculated rates for the four polyoxometalates are summarized in Table 3 and activation parameters in Table 4.

These data illustrate a clear distinction between isostructural anions of different charge and between the two isomers of $[P_2W_{17}O_{61}Co(H_2O)]^{8-}$. However, it is not possible with the present limited data set to establish whether the compensation effects (11) exhibited by the activation parameters are real or artifactual.[2]

Electrolytic oxidation of the pyridine-containing solutions yielded green solutions from which the pyridine complexes

[2] The slope of a plot of $\Delta H^{\ddagger}$ vs. $\Delta S^{\ddagger}$ (*Deposited material*) is not significantly different from the mean temperature of the experiments.

© 2001 NRC Canada

Table 1. Solution characterization of aquacobalt derivatives of some lacunary polyoxotungstates.

Anion	E_{pc}/V vs. Ag/AgCl $Co^{III/II}$	$W^{VI/V}$ [a]	λ_{max} (nm Co(II))	λ_{max} (nm Co(III))
α-$[PW_{11}O_{39}Co(H_2O)]^{4-/5-}$	[b]	–0.72, –0.90	548	[c]
α-$[SiW_{11}O_{39}Co(H_2O)]^{5-/6-}$	+0.94	–0.78, –0.90	548	708 (75)[d]
α_1-$[P_2W_{17}O_{61}Co(H_2O)]^{7-/8-}$	+0.98	–0.54, –0.68, –0.99	540	695 (77)
α_2-$[P_2W_{17}O_{61}Co(H_2O)]^{7-/8-}$	+1.00	–0.48, –0.62, –0.86	540	710 (76)

[a]Two-electron reductions.
[b]Cathodic peak for Co reduction not clearly resolved.
[c]Not observed due to partial reduction by solvent.
[d]Molar absorptivity (M^{-1} cm^{-1}).

Table 2. ^1H chemical shifts of coordinated pyridine of Co(II) derivatives at 24°C.

Anion	H_α	H_β	H_γ
α-$[PW_{11}O_{39}Co(py)]^{5-}$	117.7 (330)[a]	26.2 (280)	–5.5 (210)
α-$[SiW_{11}O_{39}Co(py)]^{6-}$	113.0 (280)	25.1 (50)	–5.4 (50)
α_2-$[P_2W_{17}O_{61}Co(py)]^{8-}$	112.8 (280)	21.8 (110)	–8.8 (170)
Pyridine	8.49	7.44	7.86

[a]Line width (±20 Hz) measured in solution with 3:1 ratio of pyridine to polyoxometalate.

Table 3. Pyridine exchange rates estimated from the line width of the α-proton signal of free pyridine.

Anion	Temperature (°C)	$\Delta\nu_{0.5}$ (Hz)	τ (ms)	k_{obs} (s^{-1})
α-$[PW_{11}O_{39}Co(H_2O)]^{5-}$	24	59.2	6.2	160
	30	74.9	4.4	210
	34	99.7	3.5	290
	41	132.5	2.6	390
	48	156.6	2.2	460
α-$[SiW_{11}O_{39}Co(H_2O)]^{6-}$	24	11.0	108.9	9
	30	11.7	95.2	10
	34	12.7	75.3	13
	41	13.9	64.8	15
	48	16.3	51.1	20
α_1-$[P_2W_{17}O_{61}Co(H_2O)]^{8-}$	24	18.7	30.0	33
	30	22.9	21.8	46
	34	28.1	16.2	62
	41	36.0	11.8	85
	48	55.1	7.1	140
α_2-$[P_2W_{17}O_{61}Co(H_2O)]^{8-}$	24	16.5	37.8	26
	30	20.9	25.2	40
	34	23.1	21.8	46
	41	25.4	19.4	52
	48	32.2	14.4	70

$[PW_{11}O_{39}Co(py)]^{4-}$, etc., were isolated as cesium salts. Spectroscopic features of the pyridine complexes are summarized in Table 5.

It was observed that the same Co(III) – pyridine complexes could be prepared by treatment of the Co(III) – aqua complexes by pyridine and warming the solution to 60°C for a few minutes. This observation led to an examination of the rate of pyridine substitution on the Co(III) – aqua complexes.

Fig. 2. ^1H NMR spectra of uncomplexed pyridine in a solution containing a 1:1 mixture of pyridine and α_2-$[P_2W_{17}O_{61}Co(H_2O)]^{8-}$ recorded at different temperatures. As indicated in the text, the signals for coordinated pyridine appeared at –8.8, +21.8, and +112.8 ppm at 24°C.

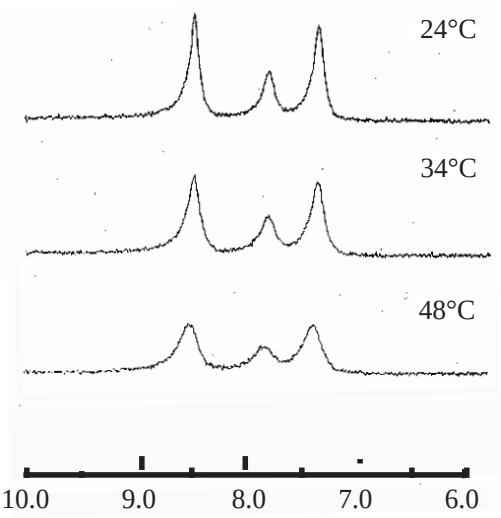


Table 4. Activation parameters for pyridine exchange with Co(II) heteropolytungstates.

Anion	$\Delta H^‡$ (kcal mol^{-1})	$\Delta S^‡$ (cal deg^{-1} mol^{-1})
α-$[PW_{11}O_{39}Co(H_2O)]^{5-}$	8.2(0.7)	–21(4)
α-$[SiW_{11}O_{39}Co(H_2O)]^{6-}$	5.5(0.4)	–36(2)
α_1-$[P_2W_{17}O_{61}Co(H_2O)]^{8-}$	10.8(0.5)	–15(3)
α_2-$[P_2W_{17}O_{61}Co(H_2O)]^{8-}$	6.5(0.8)	–30(4)

Preliminary spectrophotometric measurements established that: (*i*) $[PW_{11}O_{39}Co^{III}(H_2O)]^{4-}$ underwent slow reduction by the solvent to the Co(II) derivative in aqueous solution, but that the other three complexes were redox-stable for at least 4 h; and (*ii*) the Co(III) – pyridine derivatives (with the exception of $[PW_{11}O_{39}Co(py)]^{4-}$ as just noted) did not undergo aquation in aqueous solution over a period of 4 days. Kinetic measurements were therefore made on solutions of the three stable aqua-complexes under pseudo-first-order conditions (60-fold excess of pyridine) by following absorbance changes at 626–654 nm. The plots were linear over at least

© 2001 NRC Canada

Table 5. Solution characterization of pyridinecobalt(III) derivatives of some lacunary polyoxotungstates.

Anion	E_{pc} (Co)	λ_{max} (nm (ϵ /M^{-1} cm^{-1}))	δ (^{1}H) (ppm)
α-$[PW_{11}O_{39}Co(py)]^{4-}$	+0.95	638 (63)	7.91, 8.07, 7.58
α-$[SiW_{11}O_{39}Co(py)]^{5-}$	+0.62	626 (73)	8.12, 8.08, 7.61
α_1-$[P_2W_{17}O_{61}Co(py)]^{7-}$	+0.46	654 (66)	8.17, 7.85, 7.44
α_2-$[P_2W_{17}O_{61}Co(py)]^{7-}$	+0.64	634 (30)	8.03, 8.06, 7.59
Pyridine			8.50, 7.85, 7.44

Table 6. Pseudo-first-order rate data for the substitution of water by pyridine in tungstocobaltates(III) at 30°C at pH 4.7 in 1.0 M sodium perchlorate.

Anion	Half-life (s)	1×10^4 k_{obs} (s^{-1})
α-$[SiW_{11}O_{39}Co(H_2O)]^{5-}$	$1.6(2) \times 10^3$	4.4(2)
α_1-$[P_2W_{17}O_{61}Co(H_2O)]^{7-}$	27(4)	250(40)
α_2-$[P_2W_{17}O_{61}Co(H_2O)]^{7-}$	$1.8(2) \times 10^3$	3.7(2)

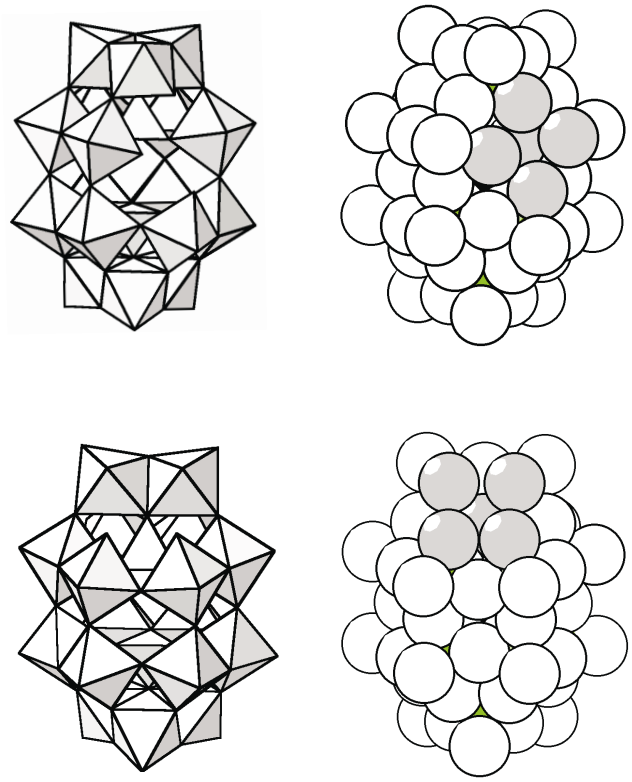
two half-lives (see *Deposited material*), and the derived rate constants are shown in Table 6.

With the exception of Weakley's result for $[BW_{11}O_{39}Co(H_2O)]^{7-}$ (8) noted above, these kinetic data are the first to have been reported regarding ligand substitution at a transition-metal center in a polyoxometalate. The rates are high for octahedral Co(III) substitution. Expressed as a second-order rate constant, k for α_1-$[P_2W_{17}O_{61}Co(H_2O)]^{7-}$ + py $\rightarrow$ α_1-$[P_2W_{17}O_{61}Co(py)]^{7-}$ + H_2O is ~0.5 M^{-1} s^{-1}. Although not reaching the astonishingly high rates for substitution on aquacobalamin (e.g., 2.3×10^3 M^{-1} s^{-1} for SCN^-) (12), the rates are two to six orders of magnitude greater than those involving classical Werner complexes (e.g., SCN^- on $[Co(NH_3)_5H_2O]^{3+}$, 1.3×10^{-6} M^{-1} s^{-1}) (13), and underscore the analogy that has been drawn between macrocyclic and lacunary polyoxometalate ligands (14). That substitution on the α_1-isomer of $[P_2W_{17}O_{61}Co(H_2O)]^{7-}$ is two orders of magnitude faster than on the α_2-isomer and the Keggin-derived anion is tentatively attributed to the more congested environment of the cobalt center (Fig. 3) that would favor a presumed pentacoordinate intermediate.

Based on the stability of the Co(III) – pyridine derivatives in aqueous solution, examples of complexes with other pyridine-type ligands were prepared using α_1-$[P_2W_{17}O_{61}Co^{II}(H_2O)]^{8-}$ as the starting material. It was possible to isolate products with pyrazine, 4,4′-bipyridine, isonicotinic acid, and isonicotinoylglycylglycylethyl ester. In each case, the complexes were isolated as cesium salts and characterized by cyclic voltammetry, electronic and NMR spectroscopy (see Table 7 and Fig. 4).

Although pyrazine and 4,4′-bipyridine are potentially capable of acting as bridging ligands, only in the case of the latter ligand were both 1:1 and 2:1 (dumbbell) complexes prepared. Earlier work (15) has shown that dumbbell complexes of Keggin derivatives can be detected, and it is possible that our inability to observe such complexes with α_1-$[P_2W_{17}O_{61}]^{10-}$ is a result of steric interactions between the bulky ligands.

Fig. 3. Polyhedral and space-filling representations of the structures of (upper) α_1- and (lower) α_2-$[P_2W_{17}O_{61}]^{10-}$. Oxygen atoms forming five-sixths of the coordination environment of the cobalt ions in $[P_2W_{17}O_{61}Co(H_2O)]^{n-}$ are indicated as gray spheres.



Experimental

Synthesis of Complexes

Salts of the lacunary anions, $K_7[\alpha$-$PW_{11}O_{39}]\cdot 13H_2O$, $K_8[\alpha$-$SiW_{11}O_{39}]\cdot 13H_2O$, $K_9[\alpha_1$-$LiP_2W_{17}O_{61}]\cdot 20H_2O$, and $K_{10}[\alpha_2$-$P_2W_{17}O_{61}]\cdot 20H_2O$ were prepared according to literature methods, and characterized by cyclic voltammetry, ^{31}P NMR, and IR spectroscopy (16).

The Co(II) derivatives were prepared following a modification of the method of Weakley and Malik (17). Five g (ca. 1 to 2 mmol) of the appropriate lacunary salt was dissolved in 500 mL 1.0 M lithium acetate buffer (pH 4.7). In a separate container, 0.25 g (10 mmol) cobalt(II) acetate tetrahydrate was dissolved in 10 mL of the same buffer solution. As the cobalt acetate solution was stirred into the heteropolyanion solution the mixture

© 2001 NRC Canada

Table 7. Properties of complexes of α_1-$[P_2W_{17}O_{61}Co(L)]^{7-}$ with pyridine-type ligands.

Ligand (L)	E_{pc} $Co^{III/II}$ (V)	λ_{max} (nm)	δ (^{1}H)[a] (ppm)	δ (^{1}H) free ligand (ppm)[a]
Pyrazine	0.610	654 (68)[b]	8.41, 8.68	8.64
4,4′-Bipyridine (1:1)	0.578	648 (88)	8.00, 8.14, 8.34, 8.84	7.80, 8.64
4,4′-Bipyridine (2:1)	0.430	650 (120)	8.19, 8.45	
Isonicotinic acid	0.479	652 (76)	7.89, 8.24	7.83, 8.78
ingge[c]	0.439	656 (80)	7.98, 8.39[d]	8.26, 8.83[d]

[a]All signals (except for free pyrazine) are doublets. $^3J_{H\text{-}H}$ ~ 5 Hz.
[b]Molar absorptivity (M^{-1} cm^{-1}).
[c]Ethyl ester of isonicotinoylglycylglycine.
[d]Spectra also show signals from methylene groups of glycine residues and the ethyl group.

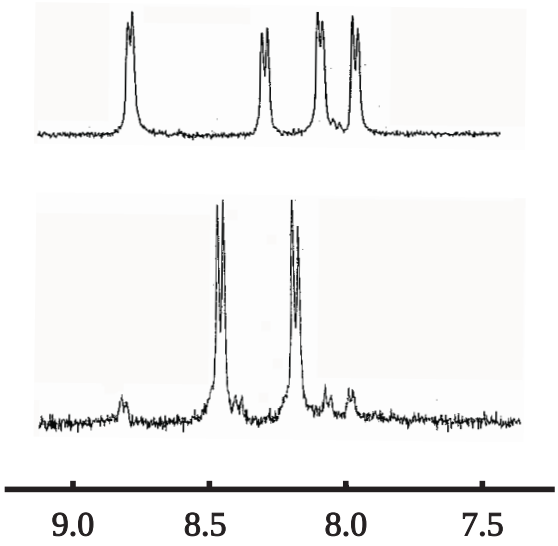
turned intensely red. The product was precipitated by adding saturated KCl solution, and was filtered off, and recrystallized from hot water. Yields: 92–94%. For characterization, see Table 1. TGA revealed the level of hydration corresponding to $K_5[PW_{11}O_{39}Co(H_2O)]\cdot 10H_2O$, $K_6[SiW_{11}O_{39}Co(H_2O)]\cdot 16H_2O$, α_1-$K_8[P_2W_{17}O_{61}Co(H_2O)]\cdot 19H_2O$, and α_2-$K_8[P_2W_{17}O_{61}Co(H_2O)]\cdot 18H_2O$.

The yellow Co(III) complexes were prepared either by oxidation with potassium perdisulfate (e.g., 100 mg polyoxometalate in 10 mL water with 160 mg $K_2S_2O_8$ heated to 90°C for 10 m) or by controlled potential electrolysis (see below). The oxidized anions were isolated as cesium salts by the addition of CsCl. For characterization, see Table 1. ^{31}P NMR α_1-$[P_2W_{17}O_{61}Co(H_2O)]^{7-}$ (ppm): –4.2, –13.2; α_2-$[P_2W_{17}O_{61}Co(H_2O)]^{7-}$ (ppm): –7.8, –13.1.

The Co(III) – pyridine complexes were prepared as follows: 300 mg $K_5[[PW_{11}O_{39}Co(H_2O)](aq)$ (ca. 0.1 mmol) dissolved in 50 mL 1.0 M lithium acetate buffer was treated with 80 μL (1.0 mmol) pyridine. The resulting solution was electrolyzed at a potential of 1.20 V and the product isolated in 60% yield by addition of CsCl. The other derivatives were prepared analogously: α-$[SiW_{11}O_{39}Co(py)]^{5-}$ (300 mg, 80 μL pyridine, guanidinium salt, 50% yield); α_1-$[P_2W_{17}O_{61}Co(py)]^{7-}$ (500 mg, 25 μL pyridine, cesium salt, 90% yield); α_2-$[P_2W_{17}O_{61}Co(py)]^{7-}$ (500 mg, 25μL pyridine, cesium salt, 90% yield). For characterization, see Table 5.

The cesium salts of the pyrazine, 4,4′-bipyridine, isonicotinic acid, and isonicotinoylglycylglycyl ethyl ester (ingge) derivatives of α_1-$[P_2W_{17}O\}61Co^{III}]^{7-}$ were prepared and isolated using the above-described method for the pyridine derivative, and the following quantities of $K_8[P_2W_{17}O_{61}Co(H_2O)]\cdot 19H_2O$ and ligand respectively: 500 mg (~100 mmol) and 25 mg (320 mmol) pyrazine; yield: 62%; 250 mg (~50 mmol) and 8 mg (50 mmol) 4,4′-bipyridine; yield: 60%; 500 mg and 37 mg (300 mmol) isonicotinic acid; yield: 72%; 500 mg and 83 mg (~300 mmol) ingge; yield: 77%. The 2:1 complex with 4,4′-bipyridine was prepared by mixing 1.00 g $K_8[P_2W_{17}O_{61}Co(H_2O)]$ (~200 mmol) with 4 mg (25 mmol) bipyridine in 50 mL lithium acetate buffer (pH 4.7). After electrolysis and precipitation with CsCl, the solid was slurried with 10 mL water and treated with solid $LiClO_4$. The resulting $KClO_4$ was removed by centrifugation and the centrifugate applied to a column of Sephadex G50. Upon elution with water two bands were separated; a faster-moving red band (unreacted polyoxometalate ligand, reduced to the Co(II) state) and a green fraction that was collected and characterized by absorption spectroscopy (λ_{max} 650 nm) and cyclic voltammetry (E_{pc} +0.43 V). The product was isolated as the cesium salt, which yielded the 4-line ^{1}H NMR spectrum shown in Fig. 4.

Fig. 4. ^{1}H NMR spectra of solutions of cesium salts of (upper) 1:1 and (lower) 2:1 complexes of α_1-$[P_2W_{17}O_{61}Co^{III}]^{7-}$ with 4,4′-bipyridine. Signals indicating the presence of about 10% of the 1:1 complex are also seen in the lower spectrum.



Instrumental

NMR spectra were recorded on a Bruker AM-300 instrument at a field of 7.05 T (300.10 MHZ for ^{1}H; 121.496 MHZ for ^{31}P). Chemical shifts are reported with respect to internal sodium 3-(trimethylsilyl)-1-propane sulfonate (^{1}H NMR) and external 85% phosphoric acid (^{31}P NMR). Variable temperature measurements were calibrated using external ethylene glycol as a temperature standard. Line widths were determined using a standard Lorentzian line-fitting program. Infrared and UV–vis spectra were recorded on MIDAC FT IR (KBr pellets) and Hewlett–Packard 8541A diode array instruments, respectively. Cyclic voltammetry was recorded using a BAS-100A electroanalyzer with a glassy carbon working electrode, platinum wire counter electrode, and Ag–AgCl reference electrode. All potentials are reported with respect to Ag–AgCl (+0.22 V vs. NHE). Scan rate: 100 mV s^{-1}. Controlled potential electrolyses were carried out using a Brinkmann/Wenking TS1

© 2001 NRC Canada

potentiostat and a Koslow Scientific Model 841 coulometer. The working electrode was graphite cloth (National Electrical Carbon Corporation) and the counter and reference electrodes were as for the voltammetry. The degree of hydration of the polyoxometalate salts was determined using a TA 2050 thermogravimetric analyzer.

Rate measurements

Pyridine exchange rates on the Co(II) complexes were made in 0.1 M sodium acetate buffer (pH 5.6). Five μL (60 μmol) of pyridine, previously deoxygenated by a 5-m stream of N_2 was injected into 10 mL of deoxygenated buffer to make a 6.0 mM solution of pyridine. Twelve μmol of the polyoxometalate salts (37–58 mg) were weighed into 2-mL volumetric flasks and dissolved in the pyridine-buffer solution. The resulting solutions contained 1:1 molar ratios of polyoxometalate and pyridine. One solution was also made up to contain no polyoxometalate. NMR spectra were recorded in triplicate at temperatures of 24, 30, 34, 41, and 48°C, using an external sample of ethylene glycol to calibrate the probe temperature. Sample tubes were equilibrated for 5 m at each temperature before data collection. Values of T_2 and T_2' as defined above were determined from the line widths using a Lorenztian line-fitting program.

The rates of pyridine substitution on the Co(III) derivatives were determined as follows:

Millimolar solutions of the potassium salts of the Co(II) derivatives of $[SiW_{11}O_{39}]^{8-}$ and both isomers of $[P_2W_{17}O_{61}]^{10-}$ in 0.1 M sodium acetate buffer, pH 4.7 (total ionic strength 1.0 M with sodium perchlorate) were electrolytically oxidized at 1.20 V as described above. One mL of the oxidized solution (containing 1.0 μmol polyoxometalate) was pipetted into a 1.0-cm quartz cell thermostated at 30°C. After 5 min, 5 μL pyridine (60 μmol) was introduced into the cell and the absorbance at 626 nm (Si anion), 654 nm (α_1-isomer), or 634 nm (α_2-isomer) was recorded as a function of time. Each kinetic run was carried out in triplicate. First-order plots (ln $[(A - A_\infty)/(A_0 - A_\infty)]$ vs. time, where A_0 is the initial absorbance (aqua complex) and A_∞ is the final absorbance (pyridine complex) were linear over at least two half-lives (*Deposited material*). Preliminary experiments to determine the stability of the Co(III) derivatives towards reduction by the solvent showed no change in the absorption spectra over a period of 4 days at 30°C. Under the same conditions solutions of $[PW_{11}O_{39}Co^{III}(H_2O)]^{4-}$ showed significant reduction to the Co(II) analogue within 1 h. The instability of this complex towards reduction by solvent has been noted before (16*a*).

Conclusions

Redox and ligand substitution processes involving cobalt derivatives of four lacunary polyoxotungstate anions have been investigated. As anticipated, the rates of exchange between free and coordinated pyridine on the cobalt(II) complexes, determined by NMR line-broadening, are moderately rapid (*k*s 10–260 s^{-1} at 30°C). The rates of substitution of pyridine on aquacobalt(III) derivatives of the polytungstates are also surprisingly fast and approach those of macrocyclic species such as the cobalamins. Substitution on the α_1-isomer (C_1 symmetry) of $[P_2W_{17}O_{61}Co(H_2O)]^{7-}$ is two orders of magnitude faster than on the α_2-isomer (C_s symmetry). Such lability may limit the value of cobalt(III) as a linker for the derivatization of polyoxometalates. Nevertheless binuclear dumbbell polytungstates linked by 4,4′-bipyridine, and anions incorporating the dipeptide glycylglycine moiety can be formed and characterized in aqueous solution, offering hope for further biochemical derivatization of polytungstates by this route.

Acknowledgment

Partial support by the NSF through grant CHE9215228 is gratefully acknowledged.

Deposited material

Figures S1–S4 showing first-order rate plots for substitution of pyridine on Co(III) complexes and activation parameters of pyridine exchange on Co(II) complexes may be purchased from the Depository of Unpublished Data, Document Delivery, CISTI, National Research Council Canada, Ottawa, ON K1A 0S2, Canada (http:/www.nrc.ca/cisti/irm/unpub_e.shtml for information on ordering electronically).

References

1. (*a*) M.T. Pope. Heteropoly and isopoly oxometalates. Springer–Verlag, New York. 1983; (*b*) M.T. Pope and A. Müller (*Editors*). Polyoxometalates: from platonic solids to anti-retroviral activity. Kluwer Academic Publishers, Dordrecht. 1994; (*c*) C.L Hill (*Editor*). Chem. Rev. **98**, 1 (1998).
2. (*a*) C.L. Hill and C.M. Prosser-McCartha. Coord. Chem. Rev. **143**, 407 (1995); (*b*) C.L. Hill (*Editor*). J. Mol. Catal. A: Chem. **114**, 1 (1996); (*c*) R. Neumann. Prog. Inorg. Chem. **47**, 317 (1998).
3. J.T. Rhule, C.L. Hill, D.A. Judd, and R.F. Schinazi. Chem. Rev. **98**, 327 (1998).
4. (*a*) N. Ban, B. Freeborn, P. Nissen, P. Penczek, R.A. Grassucci, R. Sweet, J. Frank, P. Moore, and A. Steitz. Cell (Cambridge, Mass.), **93**, 1105 (1998); (*b*) D. Janell, A. Tocili, I. Kolln, F. Schlunzen, M. Glühmann, H.A.S. Hansen, J. Harms, A. Rashan, I. Agmon, H. Bartels, M. Kessler, S. Weinstein, F. Franceschi, and A. Yonath. *In* Polyoxometalates: From topology via self assembly to applications. *Edited by* M.T. Pope and A. Müller. Kluwer Academic Publishers, Dordrecht. 2001.
5. L.C.W. Baker, V.S. Baker, K. Eriks, M.T. Pope, M. Shibata, O.W. Rollins, J.H. Fang, and L.L. Koh. J. Am. Chem. Soc. **88**, 2329 (1966).
6. (*a*) T.J.R. Weakley and S.A. Malik. J. Inorg. Nucl. Chem. **29**, 2935 (1967); (*b*) S.A. Malik and T.J.R. Weakley. Chem. Commun. 1094 (1967); (*c*) S.A. Malik and T.J.R. Weakley. J. Chem. Soc. A, 2647 (1968); (*d*) C. Tourné. C. R. Acad. Sci. Ser. C, **266**, 702 (1968); (*e*) C. Tourné and G. Tourné. Bull. Soc. Chim. Fr. 1124 (1969); (*f*) R. Ripan and M. Puscasiu. Z. Anorg. Allg. Chem. **358**, 83 (1968).
7. L.C.W. Baker and J.S. Figgis. J. Am. Chem. Soc. **92**, 3794 (1970).
8. T.J.R. Weakley. J. Chem. Soc. Dalton Trans. 341 (1973).
9. D.K. Lyon, W.K. Miller, T. Novet, P.J. Domaille, E. Evitt, D.C. Johnson, and R.G. Finke. J. Am. Chem. Soc. **113**, 7209 (1991).
10. (*a*) J.Y. Kim, S.M. Park, and H. So. Bull. Korean Chem. Soc. **18**,369 (1997); (*b*) J. Hyun and H. So. Bull. Korean Chem.

© 2001 NRC Canada

Soc. **18**, 961 (1997); (*c*) S.M. Park and H. So. Bull. Korean Chem. Soc. **18**, 1002 (1997); (*d*) J. Hyun, S.M. Park, and H. So. Bull. Korean Chem. Soc. **18**, 1090 (1997).
11. J. Halpern. Bull. Chem. Soc. Jpn. **61**, 13 (1988).
12. D. Thusius. J. Am. Chem. Soc. **93**, 2629 (1971).
13. H.R. Hunt and H. Taube. J. Am. Chem. Soc. **80**, 2642 (1958).
14. (*a*) D.E. Katsoulis and M.T. Pope. J. Am. Chem. Soc. **105**, 2737 (1984); (*b*) S.P. Harmalker and M.T. Pope. J. Inorg. Biochem. **28**, 85 (1986); (*c*) C.L. Hill and R.B. Brown Jr. J. Am. Chem. Soc. **108**, 536 (1986); (*c*) C. Rong and M.T. Pope. J. Am. Chem. Soc. **114**, 2932 (1992).
15. (*a*) L.C.W. Baker and J.S. Figgis. J. Am. Chem. Soc. **92**, 3794 (1970); (*b*) T.J.R. Weakley. J. Chem. Soc. Dalton Trans. 341 (1973); (*c*) A.M. Landis. Ph.D. Thesis, Georgetown University,Washington, DC. 1977; Diss. Abs. Int. B: **38**, 4225 (1978); (*d*) M. Ko, I. Rhyu, and H. So. Bull. Korean Chem. Soc. **14**, 500 (1993).
16. (*a*) C.M. Tourné and G.F. Tourné. Bull. Soc. Chim. Fr. 1124 (1969); (*b*) A. Tézé and G. Hervé. Inorg. Synth. **27**, 95 (1990); (*c*) R. Contant. Inorg. Synth. **27**, 107 (1990).
17. T.J.R. Weakley and S.A. Malik. J. Inorg. Nucl. Chem. **29**, 2935 (1967)**.**

© 2001 NRC Canada

A DFT study of Zr–S rotational barriers of $(\eta^5\text{-}C_5H_5)_2Zr(Cl)(SR)$; the origin of an inverse steric effect

P.K. Das, Susan Stanislav Alguindigue, and Michael T. Ashby

Abstract: We have previously reported the experimental rotational barriers about the M–S bonds of $16e^-$ bent metallocene monothiolates $(\eta^5\text{-}C_5H_5)_2Zr(Cl)(SR)$ (R = CH_3, CH_2CH_3, $CH(CH_3)_2$, $C(CH_3)_3$] (**1a**–**d**): 32, 33, 35, and 26 kJ mol^{-1}, respectively. The ground-state orientation about the Zr–S bonds of **1** that maximizes S($p\pi$) → M($d\pi$) bonding (Cl-Zr-S-R ≈ 90°) also maximizes Cp ↔ R (Cp = $\eta^5\text{-}C_5H_5$) steric interaction, whereas the rotational transition-state orientation (Cl-Zr-S-R ≈ 0°) is one that minimizes S($p\pi$) → M($d\pi$) bonding and maximizes Cl ↔ R steric interaction. Deviation from a ground-state orientation that is ideal for S($p\pi$) → M($d\pi$) bonding might be expected as the size of the R-group and Cp ↔ R steric interaction increases. The present study employs hybrid density function computational methods to reproduce the experimental rotational barriers. The computational rotational barriers decrease in the order **1a** (R = CH_3) > **1b** (R = CH_2CH_3) > **1c** (R = $CH(CH_3)_2$) at low temperature. However, opposing enthalpic factors reverse this trend at higher temperatures. The aberrant trend (unexpectedly low rotational barrier) that is observed for the **1d** (R = $C(CH_3)_3$) derivative is due to dominant ground-state steric (enthalpic) effects. We conclude the thiolate ligand of **1d** is misdirected in the ground-state with respect to the other thiolate derivatives.

Key words: misdirected ligands, metallocene, thiolate, structure, bonding, dynamics.

Résumé : On a rapporté antérieurement que les barrières expérimentales à la rotation autour des liaisons M–S des monothiolates de métallocènes repliés, à 16 électrons, $(\eta^5\text{-}C_5H_5)_2Zr(Cl)(SR)$ (R = CH_3, CH_2CH_3, $CH(CH_3)_2$, $C(CH_3)_3$) (**1a–d**) sont respectivement de 32, 33, 35 et 26 kJ mol^{-1}. L'orientation à l'état fondamental des liaisons Zr–S de **1** qui maximise la liaison S($p\pi$) → M($d\pi$) (Cl-Zr-S-R ≈ 90°) maximise aussi l'interaction stérique Cp ↔ R (Cp = $\eta^5\text{-}C_5H_5$) alors que l'orientation rotationnelle de l'état de transition (Cl-Zr-S-R ≈ 0°) en est un qui minimise la liaison S($p\pi$) → M($d\pi$) et qui maximise l'interaction stérique Cp ↔ R. Lorsque la taille du groupe R et que l'interaction sétrique Cp ↔ R augmentent, on peut s'attendre à une déviation par rapport à l'orientation de l'état fondamental qui est idéale pour une liaison S($p\pi$) → M($d\pi$). Dans le présent travail, on a fait appel à des méthodes de calcul de la fonction de densité hybride pour reproduire les barrières rotationnelles expérimentales. Les barrières rotationnelles calculées à basse température diminuent dans l'ordre **1a** (R = CH_3) < **1b** (R = CH_2CH_3) < **1c** (R = $CH(CH_3)_2$). Toutefois, des facteurs enthalpiques inverses provoquent une inversion de cette tendance à températures plus élevées. La tendance aberrante (barrière rotationnelle particulièrement basse) observée pour le dérivé **1d** (R = $C(CH_3)_3$) résulte d'effets stériques (enthalpiques) prédominants dans l'état fondamental. On en conclut que, dans l'état fondamental, le ligand thiolate du composé **1d** n'est pas bien orienté par rapport aux autres dérivés thiolates.

Mots clés : ligands mal orientés, métallocène, thiolate, structure, liaison, dynamique.

[Traduit par la Rédaction]

Introduction

Thiolate ligands are capable of stabilizing coordinatively unsaturated main-group and transition metal moieties via π-donation of the chalcogenide lone pair (1, 2). Since thiolates may be viewed as single-sided π-donors, rotational orientations about the M–S bonds of thiolate ligands are significant when the π-acceptor orbitals of the metal are not symmetric with respect to the M–S bonds (3). Asymmetrical M($d\pi$)–S($p\pi$) bonding is evident in the preferred rotational orientations of bent metallocene complexes of the type $(\eta^5\text{-}C_5H_5)_2MX_2$. The electronic structures of such bent metallocene complexes have been modeled using Extended Hückel (4), Fenske–Hall (5), and ab initio (6) methods and they have been experimentally investigated by single-crystal electron paramagnetic resonance spectroscopy (7, 8) and gas-phase photoelectron spectroscopy (9). The results of these studies indicate that the M *d*-orbital, that is π to X and spatially

Received September 5, 2000. Published on the NRC Research Press Web site at http://canjchem.nrc.ca on July 19, 2001.

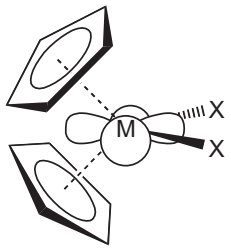
This paper is dedicated to Professor Brian James on the occasion of his 65th birthday.

P.K. Das. Phillips Petroleum Company, 327 PL, Bartlesville, OK 74004, U.S.A.
S.S. Alguindigue and M.T. Ashby.[1] Department of Chemistry and Biochemistry, The University of Oklahoma, 620 Parrington Oval, Rm. 208, Norman, Oklahoma 73019, U.S.A.

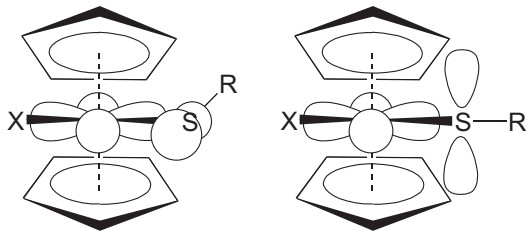
[1]Corresponding author (fax: (405) 325-6111; e-mail: mtashby@ou.edu).

 DOI: 10.1139/cjc-79-5/6-809 © 2001 NRC Canada

localized in the plane containing the MX_2 moiety, is the lowest unoccupied molecular orbitals (LUMO) of the d^1 derivatives, the singly occupied molecular orbital (SOMO) of the d^0 derivatives, and the highest occupied molecular orbitals (HOMO) of the d^2 derivatives.



Accordingly, the rotational orientations of the thiolate ligands of bent metallocenes $(\eta^5\text{-}C_5H_5)_2M(X)(SR)$ observed in the solid-state reflect the electron configuration of M (1). Thus, when the metal has a d^0 electron count an "*endo*" conformation (X-M-S-R angle of ca. 90°) is observed, when the metal has a d^2 electron count an "*exo*" conformation (X-M-S-R angle of ca. 180°) is observed, and when the metal has a d^1 electron count both "*endo*" and "*exo*" conformations are observed (for crystal structures of d^0 and d^2 derivatives see the citations in ref. 11). For the d^1 cases, the conformations are presumably dictated by subtle intramolecular steric and electronic effects (vide infra) and possibly intermolecular crystal packing effects (10).



endo *exo*

We have previously reported that the thiolate ligands of the d^0 bent metallocene thiolate complexes $(\eta^5\text{-}C_5H_5)_2Zr(Cl)(SR)$ (R = CH_3, CH_2CH_3, $CH(CH_3)_2$, $C(CH_3)_3$) (**1a**–**d**) exhibit rotational orientations in solution that favor M($d\pi$)–S($p\pi$) bonding, and we described the first experimental energy barriers associated with rotation about M–S bonds (11). Surprisingly, the rotational barriers do not appear to depend entirely upon the strength of the M($d\pi$)–S($p\pi$) bonding interaction, but rather they also apparently depend *inversely* on the steric size of the thiolate ligand (cf. R = CH_3, CH_2CH_3, $CH(CH_3)_2$ vs. R = $C(CH_3)_3$). Thus, rotational barriers about the Zr–S bond actually decrease if the R-group becomes significantly large. As explained previously (11), this trend might be attributed to either enthalpic or entropic effects. Unfortunately, it was not possible in our earlier study to measure the rates of rotation about the Zr–S bonds of **1** as a function of temperature. Consequently, we did not discern the significance of entropy. Furthermore, the issue of whether the apparent inverse steric dependency of the rotational barriers is due to a ground-state (GS) or transition-state (TS) phenomenon was not resolved. The computational results that are reported herein resolve the ambiguities that remained following our previous experimental study of the rotational barriers about Zr–S bonds of $(\eta^5\text{-}C_5H_5)_2Zr(Cl)(SR)$ complexes.

Methods and basis sets

The ab initio electronic structure computations were performed primarily using density functional theory (DFT) as implemented in GAUSSIAN 94 and 98 (12, 13). For **1a**–**d**, the B3LYP method (14) (Table 1, method A) based on Becke's 3-parameter hybrid exchange functionals (15) and Lee–Yang–Parr correlation functionals (16, 17) was used. Energetics, geometries, and analytical second derivatives were calculated at the B3LYP level with the following basis sets (18–24): LANL2DZ-ECP for Zr, Cl, and S; 3–21G for C and H atoms of the cyclopentadienyl (Cp) ligands; LANL2DZ for the remaining atoms. Optimized ground-state (GS) and transition-state (TS) geometries were obtained using nonredundant internal coordinates and starting Hessians calculated at the restricted Hartree-Fock (RHF) level. Analytical second derivatives were calculated to verify stationary points on the potential energy surface using the criteria of zero and one imaginary frequency for GS's and TS's, respectively. The analytical second derivatives were also used to calculate the real frequencies (using a scale factor of 1.0) that were subsequently used in the harmonic approximation of various thermodynamic properties: free energies ($\Delta G^{\ddagger}$), enthalpies ($\Delta H^{\ddagger}$), entropies ($\Delta S^{\ddagger}$), and zero-point energies (ZPE).

The role of the basis sets was tested for **1a** and **1d** by repeating the aforementioned calculations with a 6–31G basis set in place of the 3–21G basis set (Table 1, method B). The effect of the DFT functional was investigated by replacing the B3LYP method of A with the BLYP functional (i.e., Becke 88 exchange (25) and Lee–Yang–Parr correlation (16, 17)) with the same basis sets in method A (Table 1, method C). In both methods B and C, the geometries were fully optimized. To check the sensitivity of the computed energies with respect to correlation methodology, single-point calculations using second-order Moller–Plesset (26–31) perturbation theory (MP2) were performed on **1a** and **1d** using the optimized geometries that were obtained from method A (Table 1, method D).

Results

The GS minima and TS optimized structures for **1a**–**d** that were obtained using method A are shown in Figs. 1–4, respectively. Some relevant metric data for the computed structures are compiled in Table 2. Some of these metric data for **1a**–**d** are compared with the corresponding data that were determined by single-crystal X-ray crystallography for the analogous series of dithiolate complexes $(\eta^5\text{-}C_5H_5)_2Zr(SR)_2$ (R = CH_3, CH_2CH_3, $CH(CH_3)_2$, $C(CH_3)_3$) (**2a**–**d**) in Table 3. Tables 4 summarizes the computed rotational barriers at 0 K for **1a**–**d** using various methods. The previously reported experimental rotational energies and the temperature-corrected computed energies are compared in Table 5. For **1a** and **1d**, intrinsic rotational profiles were computed by constraining the Cl-Zr-S-C torsion angles at various values and optimizing the remainder of the molecules. The energy profile thus

© 2001 NRC Canada

Table 1. Details of the computational methods used.

Method	Geometry[a]	Exchange and correlation functional	Cp	Basis set	
				Zr, Cl, S	R-group
A (DFT)	A	B3LYP	3–21G	LANL2DZ/ECP	LANL2DZ
B (DFT)	B	B3LYP	6–31G	LANL2DZ/ECP	LANL2DZ
C (DFT)	C	BLYP	3–21G	LANL2DZ/ECP	LANL2DZ
D (MP2)[b]	A	—	3–21G	LANL2DZ/ECP	LANL2DZ

[a]Optimized at the indicated level.
[b]A single-point calculation.

Fig. 1. Ground-state (left) and transition-state (right) structures for $(\eta^5\text{-}C_5H_5)_2Zr(Cl)(SMe)$ (**1a**) optimized by method A.

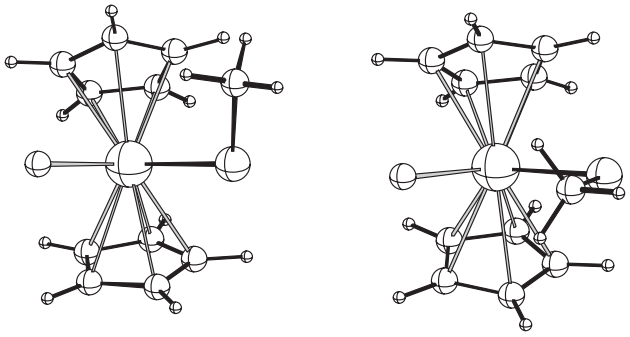
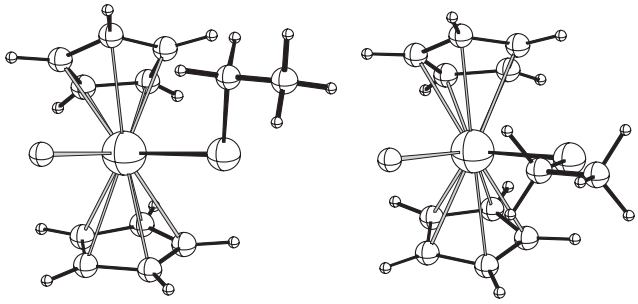


Fig. 2. Ground-state (left) and transition-state (right) structures for $(\eta^5\text{-}C_5H_5)_2Zr(Cl)(SEt)$ (**1b**) optimized by method A.



obtained for **1a** is given in Fig. 5. Details concerning the SCF energies, ZPE's, vibrational frequencies and intensities, and thermodynamic quantities are available as supplementary material.[2]

Discussion

Rotational barriers are determined by the difference between the energies of the GS and rotational TS structures. It is conceivable that the aberrant barrier that is observed experimentally is attributable to destabilization of the GS or stabilization of the TS of **1d**. For example, the lower rotational barriers that are associated with borates as compared to thioborates R_2BZR (Z = O, S) is attributed to stabilization of the TS of the former (32). In addition to stationary-state

Fig. 3. Ground-state (left) and transition-state (right) structures for $(\eta^5\text{-}C_5H_5)_2Zr(Cl)(S\text{-}i\text{-}Pr)$ (**1c**) optimized by method A.

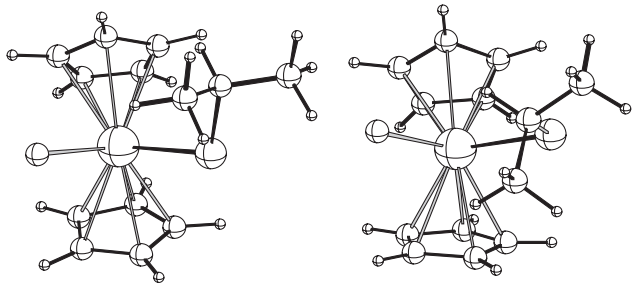
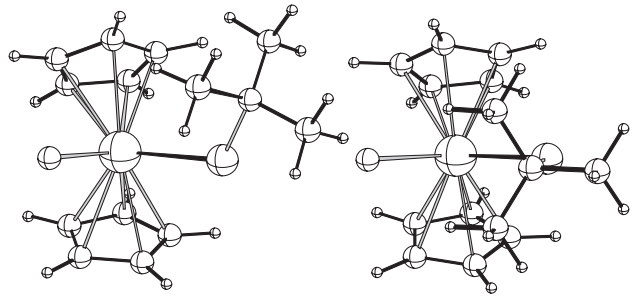


Fig. 4. Ground-state (left) and transition-state (right) structures for $(\eta^5\text{-}C_5H_5)_2Zr(Cl)(S\text{-}t\text{-}Bu)$ (**1d**) optimized by method A.



effects, entropic factors may be important in determining the difference in rotational barriers that are observed for **1** as a function of the R-group. We will first discuss GS vs. TS effects and the possible role of ligand misdirection. We will then describe the possible influence of entropy on the rotational barriers. Thus, by outlining the ambiguities that are associated with employing the available experimental data to discern the origin of the inverse steric effect associated with rotation about the Zr–S bonds of **1**, we will set the stage for resolution of these issues using the DFT method.

We have previously measured the rotational barriers about the Zr–S bonds of **1a**–**d** experimentally using variable-temperature nuclear magnetic resonance (11). These experiments were undertaken because of our interest in ligand misdirection (11, 33–37) and our expectation that larger R-groups would disfavor rotational orientations about the Zr–S bonds

[2]Supplementary material may be purchased from the Depository of Unpublished Data, Document Delivery, CISTI, National Research Council Canada, Ottawa, ON K1A OS2, Canada. For information on obtaining material electronically go to http://www.nrc.ca/cisti/irm/unpub_e.shtml.

© 2001 NRC Canada

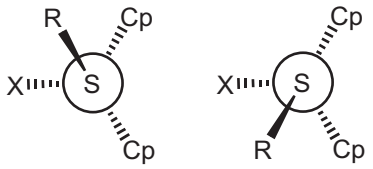
Table 2. Selected computed interatomic distances, angles, torsion angles, and dihedral angles for the ground-state and transition-state structures of $(\eta^5\text{-}C_5H_5)_2Zr(Cl)(SR)$ (R = Me, Et, *i*-Pr, *t*-Bu)

	Ground-state				Transition-state			
	Me	Et	*i*-Pr	*t*-Bu	Me	Et	*i*-Pr	*t*-Bu
Distances (Å)								
Zr—S	2.5401	2.5355	2.5330	2.5413	2.5972	2.5873	2.5778	2.4940
Zr—Cl	2.5020	2.5040	2.5080	2.5080	2.4840	2.4850	2.4880	2.4940
Zr—Cp	2.2533	2.2549	2.2555	2.2602	2.2660	2.2679	2.2702	2.2396
Zr—Cp′	2.2613	2.2624	2.2627	2.2679	2.2657	2.2670	2.2689	2.2677
Angles (°)								
Zr-S-C	109.08	109.44	112.32	120.66	104.89	109.44	108.11	116.00
Cl-Zr-S	99.40	99.33	100.58	101.07	99.57	99.34	99.42	103.13
Cp-Zr-Cp′	130.22	130.11	129.94	128.72	128.80	128.68	128.28	127.79
Cp-Zr-S	100.15	100.39	100.40	99.57	104.83	105.15	105.79	105.32
Cp′-Zr-S	109.87	110.00	110.11	112.57	106.44	106.60	106.51	106.17
Cp-Zr-Cl	108.18	108.06	107.49	106.85	107.46	107.37	107.43	106.95
Cp′-Zr-Cl	104.99	104.93	104.75	104.87	106.04	105.98	105.81	105.05
Torsion angles (°)								
Cl-Zr-S-C	–62.70	–62.44	–65.14	–60.04	1.99	2.25	3.13	3.47
Cp-Zr-S-C	–173.24	–172.89	–175.33	–169.46	–109.08	–108.73	–108.12	–108.51
Cp′-Zr-S-C	47.10	47.30	44.99	51.34	111.98	112.13	112.83	113.67
Dihedral angles (°)								
Cp-Zr-Cp′ – Cl-Zr-S	85.40	85.47	85.63	84.86	88.94	89.01	89.19	89.06
C_5–C_5'	51.65	51.73	52.01	53.11	53.48	53.51	53.99	54.28

Note: Cp and Cp′ are the centroids of the two cyclopentadienyl rings. C_5 and C_5' are the least-squares planes that contain the cyclopentadienyl rings.

of **1** that favor Zr($d\pi$)–S($p\pi$) bonding. Steric factors (steric conflict between a Cp ligand and the R-group in the GS) and electronic factors (orientation about the Zr–S bond that favors Zr($d\pi$)–S($p\pi$) bonding) are at odds for **1**. Recognizing that the S–C bond will be staggered with respect to the Cp_2ZrX moiety in the conformation of **1** that minimizes Cp ↔ R and X ↔ R steric contact, and the "X" substituent on Zr is far less sterically demanding than the Cp rings, there are two symmetry-related steric-minimized conformations of **1**:

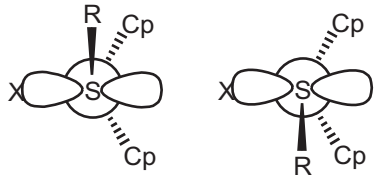
STERIC MINIMA



X Zr S R ~ 55° X Zr S R ~ 55°

Steric factors alone presumably do not dictate the ground-state conformations about the Zr–S bonds. Electronic minima will arise when Zr–S π-bonding is optimized:

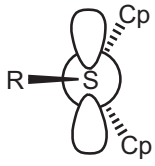
ELECTRONIC MINIMA



X-Zr-S-R ≈ 90° X-Zr-S-R ≈ –90°

Again, assuming that Cp ↔ R contact is more significant than X ↔ R contact, the saddle-point steric maximum would be for X-Zr-S-C = 0° (i.e., the X-Zr-S-C = 180° conformation is assumed to be unpopulated). Similarly, the electronic saddle-point would also be for X-Zr-S-C = 0°, when the π-type thiolate lone pair is orthogonal to the Zr-based $d\pi$ acceptor orbital (the LUMO). Thus, the rotational transition-state reflects both a steric and electronic maximum:

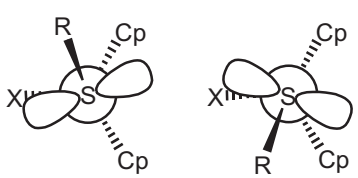
TRANSITION-STATE STRUCTURE



X-Zr-S-R = 0°

However, the ground-state structure represents a compromise between favorable S($p\pi$) → M($d\pi$) electronic interactions and unfavorable Cp ↔ R steric interactions:

GROUND-STATE STRUCTURES



X Zr S R ~ 60° X-Zr-S-R ~ –60°

© 2001 NRC Canada

Table 3. Comparison of selected metric data for the computed ground-state structures of $(\eta^5\text{-}C_5H_5)_2Zr(Cl)(SR)$ and experimental structures of $(\eta^5\text{-}C_5H_5)_2Zr(SR)_2$ (R = Me, Et, *i*-Pr, *t*-Bu).

	$(\eta^5\text{-}C_5H_5)_2Zr(Cl)(SR)$				$(\eta^5\text{-}C_5H_5)_2Zr(SR)_2$			
	Me	Et	*i*-Pr	*t*-Bu	Me	Et	*i*-Pr	*t*-Bu
Distances (Å)								
Zr—S	2.540	2.536	2.533	2.541	2.504	2.486	2.502	2.529
Zr—S′					2.507	2.511	2.502	2.529
Zr—Cp	2.253	2.255	2.256	2.260	2.203	2.211	2.211	2.220
Zr—Cp′	2.261	2.262	2.263	2.268	2.207	2.211	2.211	2.220
Angles (°)								
Zr-S-C	109.1	109.4	112.3	120.7	108.7	108.7	113.4	123.7
Zr-S′-C′					107.8	109.3	113.4	123.7
Cl-Zr-S	99.4	99.3	100.6	101.1				
S-Zr-S′					97.1	99.0	100.2	106.1
Cp-Zr-Cp′	130.2	130.1	129.9	128.7	129.8	130.4	129.4	127.7
Torsion angles (°)								
Cl-Zr-S-C	62.7	62.4	65.1	60.0				
S′-Zr-S-C					61.1	55.0	66.1	60.2
S-Zr-S′-C′					55.8	61.6	66.1	60.2
Dihedral angles (°)								
Cp-Zr-Cp′ – Cl-Zr-S	85.40	85.47	85.63	84.86				
Cp-Zr-Cp′ – S-Zr-S					82.4	82.7	84.2	81.5

Table 4. Computed rotational barriers (kcal mol^{-1}) about the Zr–S bonds of $(\eta^5\text{-}C_5H_5)_2Zr(Cl)(SR)$ at 0 K using various computational methods.

R	Method	Barrier (kcal mol^{-1})
Me	A	7.91
	B	7.20
	C	8.26
	D	7.72
Et	A	7.62
i-Pr	A	7.35
t-Bu	A	4.96
	B	4.50
	C	5.29
	D	4.92

Note: No ZPE corrections have been applied.

We previously hypothesized that the trend in slightly increasing (rather than decreasing) $\Delta G^{\ddagger}$ for R = CH_3, CH_2CH_3, $CH(CH_3)_2$ is due to either (*i*) an inductive effect, (*ii*) a dominant enthalpic effect that opposes the proposed entropic effect, or (*iii*) a transition-state steric effect (11). We will not repeat the detailed argument we have previously made for possible entropic effects and the literature precedence for such effects; however, we simply point out for the GS conformations of **1a**–**d** three, two, one, and three rotomers are likely, respectively. Accordingly, the decreasing number of populated GS rotomers relative to TS rotomers for **1a**–**c** should give rise to opposing enthalpic and entropic factors, which could account for the trend of slightly increasing barriers of rotation for **1a**–**c**. To assess the significance of entropic factors, it is necessary to measure the rates of rotation as a function of temperature. Unfortunately, because of the very small energies involved and the relatively small differences between the chemical shifts of the conformers, low temperatures were required that limited the temperature range over which variable temperature NMR data could be collected. Furthermore, **1a**–**d** disproportionate in solution to give approximately statistical 2:1:1 mixtures of **1a**–**d**, **2a**–**d**, and $(\eta^5\text{-}C_5H_5)_2Zr(Cl)_2$, respectively. The small temperature range and overlapping spectra conspire to make it difficult to separate enthalpic and entropic contributions to the free-energy of rotation. It is also conceivable that the measured values of $\Delta G^{\ddagger}$ for **1a**–**c** are within experimental error. These errors are difficult to estimate for the experimental method employed (coalescence temperature). The DFT calculations we will describe shortly suggest the entropy issue is in fact moot since the trends in rotational barriers that are observed experimentally for **1** are apparently due to enthalpic factors.

We reason that the origin of the rotational barrier trends might be discerned from trends in the metric data for **1a**–**d**. However, it proved impossible to crystallize these compounds because they scramble their ligands in solution (vide supra). We did manage to crystallize the corresponding series of dithiolate complexes **2a**–**d** and determine their molecular structures by single-crystal X-ray crystallography. However, our comparison of these structures was inconclusive as a result of the experimental errors that are associated with those data, crystal packing effects, and the relatively small effect the R-groups have on the metric data. Since the errors that are associated with the computed metric data are presumably systematic and the calculations were performed in the gas-phase, the DFT stationary-state structures offer considerable insight into the nature of the Zr–S rotational barriers of **1a**–**d**. The GS and TS structures of **1a**–**d** are illustrated in Figs. 1–4. Selected computed interatomic distances and angles for the GS and TS structures of **1a**–**d** are summarized in Table 2. The trends of some of these data are illustrated graphically in Fig. 6.

Importantly, most of the trends that are observed in Fig. 6 for the TS of the *t*-Bu derivative **1d** are regular with respect

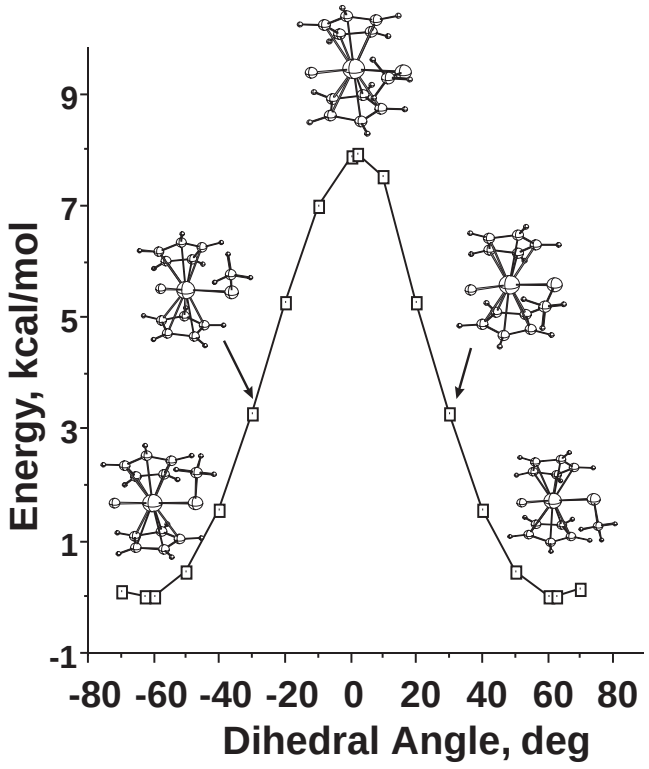
© 2001 NRC Canada

Table 5. Computed rotational barriers (kcal mol^{-1}) about the Zr–S bonds of (η^5-$C_5H_5)_2$Zr(Cl)(SR) above 0 K using method A.

R	Temp. (K)	$\Delta H^{\ddagger}$ (kcal mol^{-1})	$\Delta S^{\ddagger}$ (cal deg^{-1} mol^{-1})	$\Delta G^{\ddagger}$ (kcal mol^{-1})	$\Delta G^{\ddagger}_{expt}$ (kcal mol^{-1})[a]
Me	298	7.19	–0.38	7.30	
	148	7.40	0.58	7.31	7.7
Et	298	6.91	–0.99	7.21	
	169	7.11	–0.15	7.13	7.9
i-Pr	298	6.56	–2.39	7.27	
	164	6.74	–1.56	7.00	8.4
	178	6.73	–1.66	7.02	8.4
t-Bu	298	4.16	–2.29	4.84	
	133	4.42	–1.06	4.46	6.2

[a]The experimental data are from ref. 11.

Fig. 5. Zr–S conformational coordinate diagram for (η^5-$C_5H_5)_2$Zr(Cl)(SMe) (**1a**) (obtained using method A).



to the other derivatives (e.g., the Zr–S bond length, Zr-S-C bond angle, Cp-Zr-Cp′ angle, Cl-Zr-S-C torsional angle and the C5–C5′ angle). Only the Cl-Zr-S and Cp-Zr-Cp′ – S-Zr-S′ angles exhibit irregular trends. The more obtuse Cl-Zr-S bond angle for the TS of **1d** is expected because of the relative bulk of the R-group and the fact the TS is a steric maximum (vide supra), and it is in the direction of destabilizing Zr–S bonding. The trend that is observed for the Cp-Zr-Cp′ – S-Zr-S′ angles in the TS's of **1a**–**d** is the same trend that is observed in the GS's. In contrast to the trends that are observed for the TS's, many of the metric data for the GS of **1d** exhibit irregular trends (e.g., the Zr–S bond distance, Cl-Zr-S-C torsional angle and Cp-Zr-Cp′ – S-Zr-S′). These data indicate a destabilization of the GS of **1d** with respect to **1a**–**c**.

The influence of adding methyl groups on the total energy of the GS and TS of **1a**–**d** is illustrated in Fig. 7 as ΔE[(R = $CH_{3-(n+1)}Me_{(n+1)}$), (R = $CH_{3-n}Me_n$)] = E[**1**(R = $CH_{3-(n+1)}Me_{(n+1)}$)] – E[**1**(R = $CH_{3-n}Me_n$)]. Two features of Fig. 7 are notable: (*i*) the relative effects on the GS vs. the TS structures for a given comparison of ΔE(GS) vs. ΔE(TS), and (*ii*) the magnitudes of the stabilizations (ΔE) upon adding a methyl group. Figure 7 clearly illustrates that there is relatively little influence of adding methyl groups on the relative total energies of the GS and TS structures of **1a**–**c** (ΔE_{GT} vs. ΔE_{TS} for **1a**–**c**). However, a marked difference in the relative total energies of the GS and TS structures of the *i*-Pr and *t*-Bu derivatives (ΔE_{GS}[*t*-Bu, *i*-Pr] vs. ΔE_{TS}[*t*-Bu, *i*-Pr]) is observed, which we interpret as a larger steric destabilization of the GS of **1d** relative to its TS. The magnitudes of the effect on the total energies upon adding a methyl group are also telling. Dias and co-workers (38) have measured the standard enthalpies of formation for the series $Cp_2Mo(SR)_2$ (R = *n*-Pr, *i*-Pr, *n*-Bu, and *t*-Bu) and other thiolate complexes using reaction-solution calorimetery. Their investigation revealed that increasing the bulkiness of the alkyl group decreases the bond enthalpy (BE) and mean bond dissociation energy (BDE), whereas increasing the length of the alkyl chain increases the M–S BE and BDE. This trend was especially true for R = *t*-Bu. Thus in the absence of steric effects, adding methyl groups is expected to reduce the relative total energies by inductively strengthening the Zr–S bonds. Although such a trend is apparently reflected in the first two columns of Fig. 7, we note the small difference between the first two columns is negligibly small. Indeed, the apparent decreasing energies of the first two columns is reversed for ZPE-corrected room-temperature enthalpies. However, the magnitude of the relative total energies of the third column is substantially less than that of the first two, which we interpret as a counter destabilizing steric effect that partially negates the stabilizing inductive effect of adding a methyl group for **1c** → **1d**. This steric destabilization of **1d** is reflected in the magnitude of ΔE_{GS}[*t*-Bu, *i*-Pr] and ΔE_{TS}[*t*-Bu, *i*-Pr], albeit more so in the difference in GS energies.

Summary

We have previously measured rotational barriers about the M($d\pi$)–S($p\pi$) bonds of **1**. The trends in $\Delta G^{\ddagger}$ indicate that the strength of the M($d\pi$)–S($p\pi$) bonds and the steric interactions of the substituents of (η^5-$C_5H_5)_2$Zr(Cl)(SR) (**1**) both

© 2001 NRC Canada

Fig. 6. Graphical representations of selected computed metric data for the ground-state and transition-state structures of $(\eta^5\text{-}C_5H_5)_2Zr(Cl)(SR)$ for R = Me, Et, *i*-Pr, *t*-Bu. See Table 2 for definitions of the abbreviations. Note for the trends in the data for the R = *t*-Bu derivative are regular for the transition-state but irregular for the ground-state.

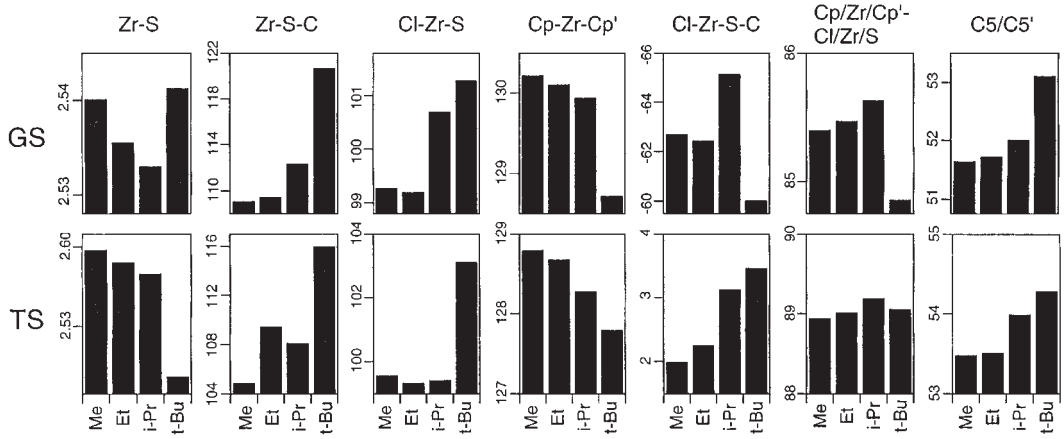
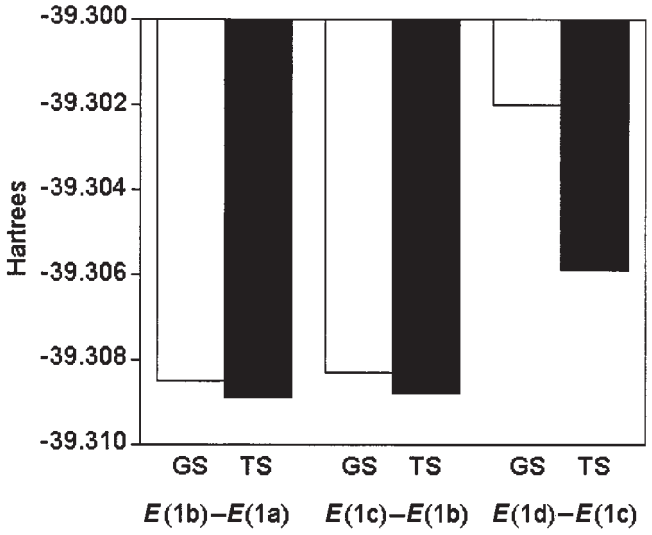


Fig. 7. Effect of adding a methyl group on the total energies of the GS and TS structures of **1a**–**d** (as calculated using method A and without a ZPE correction). Note the larger destabilizing effect on the GS of **1d** compared with its TS and the relative magnitudes of *E*(**1d**) – *E*(**1c**) vs. *E*(**1b**) – *E*(**1a**) and *E*(**1c**) – *E*(**1b**).



play important roles in determining the magnitude of the rotational barriers. For R = CH_3, CH_2CH_3, and $CH(CH_3)_2$, the experimental Zr–S rotational barriers are 32, 33, and 35 kJ mol^{-1}, respectively. However, the 26 kJ mol^{-1} barrier that was measured for R = $C(CH_3)_3$ is considerably less than the other derivatives. Previous studies of bond dissociation enthalpies of metal-thiolates suggest that *tert*-butyl thiolates have unusually weak bonds. This is presumably echoed in rotation about the Zr–S bond of **1**, where partial bond breakage takes place. The DFT calculations reported herein address the ambiguities that existed following the experimental study regarding the origin (enthalpy vs. entropy, electronic vs. steric, and GS vs. TS) of the irregular rotational barrier that was observed for **1d**. The trend of increasing rotational barriers for **1a**–**c** is attributed to inductive effects and overall stronger Zr–S bonds in the GS in the order $CH_3 < CH_2CH_3 < CH(CH_3)_2$. However, unfavorable Cp ↔ R steric contacts cannot be avoided for R = $C(CH_3)_3$. Consequently, the GS of **1d** is destabilized with respect to the other alkyl derivatives of **1**. The lower rotational barrier that was observed for **1d** is attributed to GS thiolate ligand π misdirection and overall weaker Zr(*d*π)–S(*p*π) overlap.

Acknowledgments

The financial support of the National Science Foundation (CHE-9612869) and the Petroleum Research (PRF# 29900-AC3) is gratefully acknowledged. SSA is a Department of Education G.A.A.N.N. Fellow. PKD is grateful to Prof. M. Hall of Texas AM University for valuable discussions.

References

1. M.T. Ashby. Comments Inorg. Chem. **10**, 297 (1990).
2. K.G. Caulton. New J. Chem. **18**, 25 (1994).
3. M.T. Ashby and J.H. Enemark. J. Am. Chem. Soc. **108**, 730 (1986).
4. J.W. Lauher and R. Hoffmann. J. Am. Chem. Soc. **98**, 1729 (1976).
5. J.L. Petersen and L.F. Dahl. J. Am. Chem. Soc. **96**, 2248 (1974).
6. C.Q. Simpson and M.B. Hall. New J. Chem. **15**, 763 (1991).
7. J.L. Petersen and L.F. Dahl. J. Am. Chem. Soc. **97**, 6416 (1975).
8. J.L. Petersen and L.F. Dahl. J. Am. Chem. Soc. **97**, 6422 (1975).
9. J.L. Petersen, D.L. Lichtenberger, R.F. Fenske, and L.F. Dahl. J. Am. Chem. Soc. **97**, 6433 (1975).
10. M.Y. Darensbourg, R. Silva, J. Reibenspies, and C.K. Prout. Organometallics, **8**, 1315 (1989).
11. M.T. Ashby, S.S. Alguindigue, and M.A. Khan. Inorg. Chim. Acta, 270, 227(1998).
12. M.J. Frisch, G.W. Trucks, H.B. Schlegel, G.E. Scuseria, M.A. Robb, J.R. Cheeseman, V.G. Zakrzewski, J.A. Montgonery, R.E. Stratmann, J.C. Burant, S. Dapprich, J.M. Millam, A.D. Daniels, K.N. Kudin, M.C. Strain, O. Farkas, J. Tomasi, V. Barone, M. Cossi, R. Cammi, B. Mennucci, C. Pomelli, C. Adamo, S. Clifford, J. Ochterski, G.A. Petersson, P.Y. Ayala, Q. Cui, K. Morokuma, D.K. Malick, A.D. Rabuck, K. Raghavachari, J.B. Foresman, J. Cioslowski, J.V. Ortiz, B.B. Stefanov, G. Liu, A. Liashenko, P. Piskorz, I. Komaromi, R.

© 2001 NRC Canada

Gomperts, R.L. Martin, D.J. Fox, T. Keith, M.A. Al-Laham, C.Y. Peng, A. Nanayakkara, C. Gonzalez, M. Challacombe, P.M.W. Gill, B. Johnson, W. Chen, M.W. Wong, J.L. Andres, C. Gonzalez, M.R. Head-Gordon, E. S., and J.A. Pople. Gaussian 98(R). Gaussian, Inc., Pittsburgh, PA, U.S.A. 1998.
13. M.J. Frisch, G.W. Trucks, H.B. Schlegel, P.M. Gill, B.G. Johnson, M.A. Robb, J.R. Cheeseman, T. Keith, G.A. Petersson, J.A. Montgonery, K. Raghavachari, M.A. Al-Laham, V.G. Zakrzewski, J.V. Ortiz, J.B. Foresman, J. Cioslowski, B.B. Stefanov, A. Nanayakkara, M. Challacombe, C.Y. Peng, P.Y. Ayala, W. Chen, M.W. Wong, J.L. Andres, E.S. Replogle, R. Gomperts, R.L. Martin, D.J. Fox, J.S. Binkley, D.J. Defrees, J. Baker, J.P. Stewart, M. Head-Gordon, C. Gonzalez, and J.A. Pople. Gaussian 94, Revision C.3. Gaussian, Inc., Pittsburgh, PA, U.S.A. 1995.
14. P.J. Stephens, F.J. Devlin, C.F. Chabalowski, and M.J. Frisch. J. Phys. Chem. **98**, 11623 (1994).
15. A.D. Becke. J. Chem. Phys. **98**, 5648 (1993).
16. C.T. Lee, W.T. Yang, and R.G. Parr. Phys. Rev. B: Condens. Matter, **37**, 785 (1988).
17. B. Miehlich, A. Savin, H. Stoll, and H. Preuss. Chem. Phys. Lett. **157**, 200 (1989).
18. W.J. Pietro, M.M. Francl, W.J. Hehre, D.J. Defrees, J.A. Pople, and J.S. Binkley. J. Am. Chem. Soc. **104**, 5039 (1982).
19. J.S. Binkley, J.A. Pople, and W.J. Hehre. J. Am. Chem. Soc. **102**, 939 (1980).
20. M.S. Gordon, J.S. Binkley, J.A. Pople, W.J. Pietro, and W.J. Hehre. J. Am. Chem. Soc. **104**, 2797 (1982).
21. J.T.H. Dunning and P.J. Hay. *In* Modern theoretical chemistry. Vol. 1. *Edited by* H.F. Schaefer. Plenum, New York. 1976. p. 1.
22. P.J. Hay and W.R. Wadt. J. Chem. Phys. **82**, 299 (1985).
23. P.J. Hay and W.R. Wadt. J. Chem. Phys. **82**, 270 (1985).
24. W.R. Wadt and P.J. Hay. J. Chem. Phys. **82**, 284 (1985).
25. A.D. Becke. Phys. Rev. A: At. Mol. Opt. Phys. **38**, 3098 (1988).
26. C. Moeller and M.S. Plesset. Phys. Rev. A: At. Mol. Opt. Phys. **46**, 618 (1934).
27. M. Headgordon, J.A. Pople, and M.J. Frisch. Chem. Phys. Lett. **153**, 503 (1988).
28. M. Headgordon and T. Headgordon. Chem. Phys. Lett. **220**, 122 (1994).
29. M.J. Frisch, M. Headgordon, and J.A. Pople. Chem. Phys. Lett. **166**, 275 (1990).
30. M.J. Frisch, M. Headgordon, and J.A. Pople. Chem. Phys. Lett. **166**, 281 (1990).
31. S. Saebo and J. Almlof. Chem. Phys. Lett. **154**, 83 (1989).
32. M.T. Ashby and N.A. Sheshtawy. Organometallics, **13**, 236 (1994).
33. M.T. Ashby, G.N. Govindan, and A.K. Grafton. Inorg. Chem. **32**, 3803 (1993).
34. M.T. Ashby. J. Am. Chem. Soc. **117**, 2000 (1995).
35. M.T. Ashby, G.N. Govindan, and A.K. Grafton. J. Am. Chem. Soc. **116**, 4801 (1994).
36. M.T. Ashby, S.S. Alguindigue, and M.A. Khan. Organometallics, **19**, 547 (2000).
37. S.S. Alguindigue, M.A. Khan, and M.T. Ashby. Organometallics, **18**, 5112 (1999).
38. M.J. Calhorda, M. Carrondo, A.R. Dias, C.F. Frazao, M.B. Hursthouse, J.A.M. Simoes, and C. Teixeira. Inorg. Chem. **27**, 2513 (1988).

© 2001 NRC Canada

Adsorption of etioporphyrin and Ni-etioporphyrin on a fractal silica

Josephine Mary Hill and Flora T.T. Ng

Abstract: Metal compounds are contaminants in heavy oil and must be removed using hydrodemetallization catalysts. To optimize the structure of hydrodemetallization catalysts it is useful to know the effective size of the metal compounds. To this end, fractal geometry has been used to determine the relationship between monolayer coverage and adsorbate size for silica by adsorbing a series of alcohols at 298 K. It was found that the silica had a fractal dimension of 2.923. Etioporphyrin and Ni-etioporphyrin were then adsorbed on the silica and their effective areas determined based on this fractal dimension. Cross-sectional areas of 4.58 and 14.8 nm^2 were determined for etioporphyrin and Ni-etioporphyrin, respectively. The areas are larger than those determined by X-ray methods and likely reflect the fact that the porphyrins are solvated with solvent (cyclohexane) molecules.

Key words: silica, adsorption, fractal dimension, etioporphyrin, Ni-etioporphyrin

Résumé : Les composés métalliques sont des contaminants des huiles lourdes qui doivent être éliminées par des catalyseurs d'hydrodémétallisation. Pour optimiser la structure des catalyseurs d'hydrodémétallisation, il est utile de connaître la taille effective des composés métalliques. À cette fin, on a fait appel à la géométrie fractale pour déterminer la relation entre la couverture de la monocouche et la taille de l'adsorbat d'une série d'alcools adsorbés à 298 K. On a trouvé que la dimension fractale de la silice est de 2,923. On y a ensuite adsorbé de l'étioporphyrine et de la Ni-éthioporphyrine et les superficies effectives ont été déterminées en se basant sur cette dimension fractale. On a déterminé que les superficies de section droite sont de 4,58 et 14,8 nm^2 respectivement pour l'étioporphyrine et la Ni-éthioporphyrine. Ces superficies sont supérieures à celles déterminées par diffraction des rayons X et elles reflètent probablement le fait que les porphyrines sont solvatées par des molécules de solvant (cyclohexane).

Mots clés : silice, adsorption, dimension fractale, étioporphyrine, Ni-étioporphyrine.

[Traduit par la Rédaction]

Introduction

There remains a high demand for fossil-based hydrocarbons for both energy and petrochemicals (1). At the same time, the world's reserves of crude oil are declining, and as a result, lower quality heavier crudes with more contaminants must be processed. Hydrodesulphurization (HDS) and hydrodemetallization (HDM) are two of the primary processes for upgrading heavy oil (2).

Both sulphur and metal contaminants are a problem in the process stream because they poison the cracking catalysts by depositing on the active sites and blocking pores. In addition, the metals can cause erosion of the furnace linings and turbine blades. Thus, the sulphur and metals are removed using HDS and HDM catalysts, respectively. Heavy oil contains Ni, V, and Fe in porphyrin type structure (Fig. 1), which generally precipitate with the asphaltenes. Ni is present in relatively high concentration and is a more severe poison for fluid catalytic cracking catalysts than V and Fe as a result of its high dehydrogenation activity, which results in coke formation. Therefore, it is particularly important to remove Ni.

Optimization of the HDM catalysts involves a balance between smaller pores for high surface area and larger pores to reduce diffusional resistance and pore-mouth plugging. Knowledge of the effective cross-sectional area of the metal compound, therefore, will help elucidate the optimum catalyst configuration. Various techniques can be used to determine the size of a metal compound. The size or cross-sectional area measured, however, will be technique dependent. That is, the diameter of a compound in dry powder form will be different than the effective area of the same compound fully solvated in solution or adsorbed on a surface. It is the latter effective area that is of interest for optimizing HDM catalysts.

To determine the effective area occupied by an adsorbed molecule, the surface area of the adsorbent must be known. Traditionally the surface area of a catalyst is determined by nitrogen BET adsorption, but this technique has the disadvantage that for a porous material, such as a catalyst support, the accessible area is dependent on the size of the adsorbate (i.e., larger molecules are excluded from smaller pores).

Received September 15, 2000. Published on the NRC Research Press Web site at http://canjchem.nrc.ca on July 19, 2001.

Dedicated to Professor Brian James on the occasion of his 65th birthday.

J.M. Hill[1] and F.T.T. Ng.[2] Department of Chemical Engineering, University of Waterloo, Waterloo, ON N2L 3G1, Canada.

[1]Present address: University of Calgary, Calgary, AB T2N 1N4, Canada.
[2]Corresponding author (telephone: (519) 888-4567, ext 3979; fax: (519) 746-4979; e-mail: fttng@cape.uwaterloo.ca).

 DOI: 10.1139/cjc-79-5/6-817 © 2001 NRC Canada

Fig. 1. Porphyrin structures: (*a*) etioporphyrin; (*b*) Ni-etioporphyrin; (*c*) Ni-chlorin.

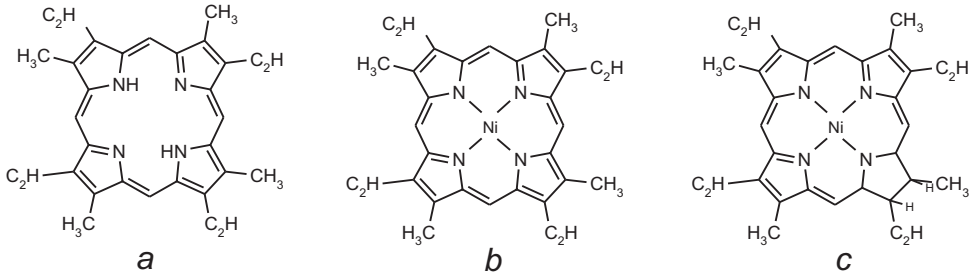


Table 1. Cross-sectional areas (σ) of adsorbates.

Adsorbate	σ (nm^2)
Nitrogen	0.162
Methanol	0.180
Ethanol	0.230
2-Methyl-2-propanol	0.317
2-Methyl-2-butanol	0.350
3-Ethyl-3-pentanol	0.414

Fractal analysis of materials offers a solution to this dilemma (3). For a material that is fractal in nature, the accessible surface area scales with the adsorbate size over a certain range. Given the fractal dimension of a surface and the monolayer coverage of an adsorbate on that surface, the effective cross-sectional area of the adsorbate can be calculated.

In the present study, this approach has been used to determine the effective size of etioporphyrin and Ni-etioporphyrin (Fig. 1) adsorbed on silica. First, the fractal dimension of the silica is determined by adsorbing a series of alcohols of different diameters onto the silica. Then the porphyrins are adsorbed and their cross-sectional areas determined.

Experimental

The two silica samples (Sigma) used for the adsorption studies had average pore diameters of 6 nm (S-2509 Lot 3 1H0 876, particle size range 63–200 μm) and 2.5 nm (S-4133 Lot 1 9F3 506, particle size range 70–140 μm). The alcohols and solvents used for the adsorption, methanol (Fisher Scientific A.C.S. grade), ethanol (absolute), 2-methyl-2-propanol (Aldrich HPLC grade), 2-methyl-2-butanol (Aldrich 99%), 3-ethyl-3-pentanol (Aldrich 98%), toluene (BDH Omnisolve), and cyclohexane (BDH Omnisolve), were dried and stored over 3 Å molecular sieves (BDH). Solutions of the alcohols in toluene were prepared gravimetrically.

Adsorption studies were carried out in test tubes with 1 to 2 g of silica dried at 450 K for 12 h under vacuum. The test tubes were sealed with a septum and purged with nitrogen (Linde Ultra High Purity). Solutions of alcohol in toluene, of known concentration, were then transferred using a cannula into the test tube. The solution and solid were stirred at 298 K for 2 to 3 h to allow equilibrium to be reached, and then a centrifuge was used to separate the solid and liquid phases. A sample of the liquid phase was taken using a gas-tight syringe (Hamilton). This liquid sample was analyzed in a gas chomatograph (PerkinElmer Sigma 3 B) with an FID detector and a 60 m × 0.32 mm diameter column (J&W Scientific DB1). The column temperature was ramped from 423 to 523 K at 15 K min^{-1}, and maintained at 523 K for 5 min. For the analysis of ethanol the temperature program was varied slightly, i.e., the temperature was held at 373 K for 4 min, ramped to 473 K at 15 K min^{-1}, and held at 473 for 2 min.

The adsorption experiments with the porphyrins (Midcentury Chemical Company) were done in a similar manner to those with the alcohols using both cyclohexane and toluene as solvents, but the analysis was done with an UV–vis Spectrophotometer (Varian Cary 219). Porphyrins are intensely coloured and their main absorption bands have very high molar extinction coefficients in the order of 2×10^5 (4). The Soret band around 400 nm is the most intense absorption band in the spectra of porphyrins. Etioporphyrin also has four characteristic bands in the visible region between approximately 500–630 nm (4). In contrast, Ni-etioporphyrin has only two bands in the visible region, around 515 and 555 nm, depending on the solvent (4). The bands in the visible region will be used to determine the solution concentrations of the porphyrins. Calibration curves were prepared for the porphyrins using the UV–vis spectrophotometer, and for the alcohols using the GC.

The nitrogen BET surface area of the silica was determined using a volumetric glass vacuum system with an MKS Baratron capacitance monometer and digital display (MKS 270B). The sample was pretreated for 16 h at 298 K under vacuum and then nitrogen was adsorbed at 77 K.

Determination of fractal dimension

The amount of a probe molecule adsorbed onto a surface can be given by the following relationship (5):

$$[1] \qquad n \propto \sigma^{-D/2}$$

or

$$[2] \qquad n = K\sigma^{-D/2}$$

where n is the monolayer value (mmol g^{-1}), K is a constant, σ is the cross-sectional area of the adsorbate (nm^2), and D is the fractal dimension, where $2 \leq D \leq 3$ for a surface. The fractal dimension (D) of a surface can be determined by adsorption of a series of adsorbates with different cross-sectional areas. Table 1 lists the cross-sectional areas of the probe molecules used for this work (6). The cross-sectional areas of the alcohols were determined by liquid density measurements. It should be noted that some of the areas reported in the literature for alcohols are incorrect because they were

© 2001 NRC Canada

Fig. 2. Effect of drying temperature on the adsorption of ethanol on silica at 298 K: 383 K (Δ); 423 K (○); and 450 K (□).

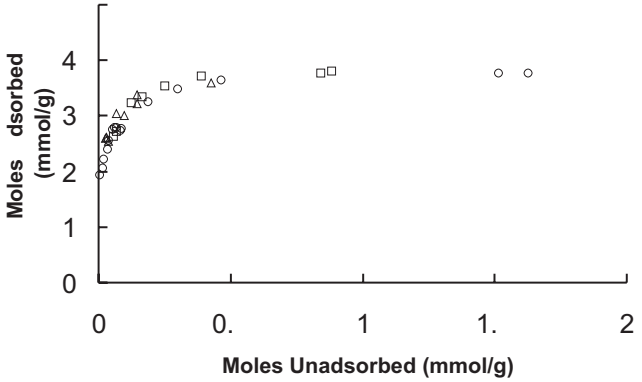
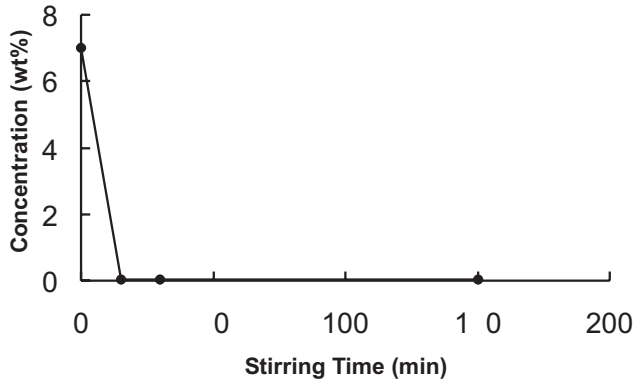


Fig. 3. Change in concentration with time for ethanol adsorbed on silica at 298 K.



determined by adsorption experiments on porous materials using the nitrogen BET surface area. In one study (7), alcohols were adsorbed on a silica that was later determined to have a fractal dimension of 2.94 (3). Monolayer coverages have been assumed for the adsorption of alcohols except for methanol, which was found to have more than a monolayer coverage (7).

The Langmuir Equation in the following form is used to determine the monolayer capacity:

$$[3] \qquad n' = \frac{bnC}{1+bC}$$

where C is the concentration of the adsorbate in the liquid phase at equilibrium, n' is the amount adsorbed, b is a constant, and n is the monolayer coverage. Nonlinear regression was performed using a Levenberg–Marquart algorithm (Sigmaplot 4.10, Jandel Corp.) to relate the amount adsorbed (n'), to the concentration in the liquid (C), and to calculate the monolayer coverage (n). Data from approximately 16 adsorption experiments with different initial concentrations of the alcohols or porphyrins were used to fit the Langmuir equation for each adsorbate.

Results and discussion

Experiments were carried out to establish the effects of drying temperature and mixing time on the uptake of alcohol from solution. The condition of the adsorbent surface was found to be very important in adsorption studies. That is, in the case of silica, the surface must be completely free of physisorbed water. To determine how best to pretreat the silica the adsorption of ethanol was studied on the smaller pore silica at three different temperatures. The results of drying the silica at 383, 423, and 450 K are shown in Fig. 2. The equilibrium absorptions are essentially the same for all three drying temperatures. Removal of surface hydroxyls groups begins at approximately 525 K (8). Thus, a drying temperature of 450 K is sufficient to remove physically adsorbed water but not so high as to remove surface hydroxyl groups. Figure 2 is a representative plot of the adsorption of all of the alcohols (except methanol as will be described below) and suggests that the alcohols adsorb in monolayer coverage on the silica.

Table 2. Monolayer coverages for nitrogen and alcohols on silica.

	Monolayer coverage (mmol g^{-1})[a]	
Adsorbent	Nonlinear regression	Linear regression
Nitrogen	4.84	4.84
Methanol	5.67(0.172)	5.87(0.143)
Ethanol	3.11(0.0585)	2.97(0.0543)
2-Methyl-2-propanol	1.79(0.0268)	1.80(0.0249)
2-Methyl-2-butanol	1.58(0.0663)	1.42(0.0644)
3-Ethyl-3-pentanol	1.14(0.0164)	1.16(0.0153)

[a]Standard error is given in parentheses.

It was also important to establish the length of time for equilibrium to be obtained between the solid and solution. Figure 3 shows the adsorption of ethanol from solution onto silica as a function of time. After 15 min of stirring the solution concentration decreased to 0.025 wt%. On stirring for an additional 135 min the amount adsorbed changed by less than 0.02% indicating the adsorption of ethanol on silica occurred quite rapidly. Solutions of alcohols with different initial concentrations and different weight of silica were stirred for 120 min before analyzing each solution concentration using the GC. This length of time allowed the solution and solid to come to equilibrium and also allowed the solution temperature to return to 298 K after the exothermic process of adsorption. Note that the smaller pore silica was used for these preliminary experiments. Unless otherwise noted all other references to silica refer to silica with an average pore size of 6 nm.

The monolayer coverages of nitrogen and the series of alcohols onto the silica are given in Table 2. All of the residuals from the nonlinear fit were randomly distributed, indicating that there is no bias in the experimental technique. It is apparent from Table 2 that methanol had adsorbed beyond a monolayer on the silica. Not only is the monolayer value higher for methanol than for the smaller molecule nitrogen, but the standard error is more than a factor of two larger for methanol than for any of the other adsorbates. Other studies have shown that methanol forms more than a monolayer when adsorbed on silica (7). Therefore, the data for methanol will not be used in the determination of the fractal dimension.

In Table 2 the results for the linear regression of eq. [3] are also given to illustrate that linear and nonlinear regres-

© 2001 NRC Canada

Fig. 4. Monolayer coverage vs. adsorbate size for a series of adsorbates on silica.

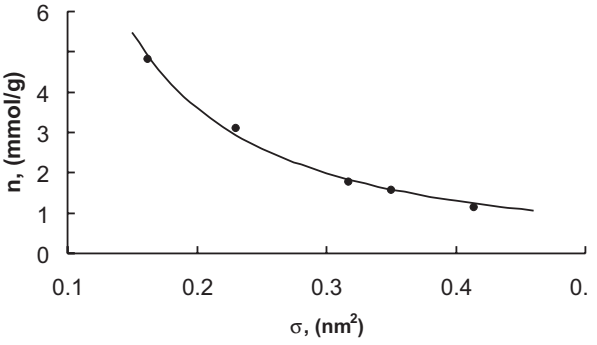


Table 3. Monolayer coverages for porphryins on silica.

Adsorbent	Monolayer coverage (mmol g^{-1})[a]
Etioporphyrin in cyclohexane	3.71×10^{-2} (0.00336)
Etioporphyrin in toluene	3.99×10^{-4} (2.88×10^{-5})
Ni-etioporphyrin in cyclohexane	6.7×10^{-3} (6.57×10^{-4})
Ni-etioporphyrin in toluene	Not measurable

[a]Standard error is given in parentheses.

sion give different results. Statistically it is not as accurate to plot a function of a variable against itself because it alters the error structure inherent in the measurement (9).

The nonlinear fit of eq. [2] is shown in Fig. 4 and is equal to:

$$[4] \qquad n = 0.3425\sigma^{-2.923/2}$$

for n in mmol g^{-1} and σ in nm^2. Thus, the resulting fractal dimension for this surface is 2.923 and the preexponential factor is 0.3425 with 95% confidence intervals of ±0.363 and ±0.1014, respectively. The calculated fractal dimension is close to the upper limit of 3.00, which implies that the surface is irregular and that the accessible surface area decreases rapidly as the adsorbate size increases. At the other end of the range, a fractal dimension of 2.00 indicates that the surface is relatively flat and the accessible surface area is independent of adsorbate size. The value obtained herein is in agreement with that obtained by other groups on similar silica gels using the adsorption of alcohols or alkanes (3, 10–12). Rearrangement of eq. [4] into linear form and conversion of units (i.e., σ in $Å^2$) yields a prefactor of 2.46, which is also consistent with that obtained for silicas with an average pore size of 6 nm (11, 12).

Similar to the alcohols, the porphyrins were adsorbed onto the silica, and the monolayer coverages determined (see Table 3). Equilibrium was achieved between the porphyrin solution and the silica within 2 to 3 h, as has been seen previously (13). The adsorption experiments with the porphyrins were difficult because of their limited solubility and smaller adsorption on the silica. As a result, the standard errors for the porphyrins are larger relative to the monolayer coverages than for the alcohols. The residuals from the nonlinear regression, however, show no trends or systematic errors.

Table 4. Calculated cross-sectional areas of the porphyrins.

Adsorbent	σ (nm^2)
Etioporphyrin in cyclohexane	4.58
Etioporphyrin in toluene	101
Ni-etioporphyrin in cyclohexane	14.8

The monolayer coverages are significantly higher for the porphyrins dissolved in cyclohexane than in toluene, consistent with other studies (13, 14). In fact, there was no measurable adsorption of the Ni-etioporphyrin from toluene onto silica. These results suggest that toluene competes for surface sites with the porphyrins. It has been reported that benzene competes with porphyrins for adsorption sites on silica–alumina catalysts (13). Aromatic molecules interact with surfaces through their conjugated rings. Mitchell and Scott (15) determined that nickel porphyrins lie flat on alumina and silica–alumina supports when adsorbed at 298 K, and that the delocalized π-system of the porphyrin ring is an electron donor and the Brønsted and (or) Lewis acid function of the catalyst is the electron acceptor.

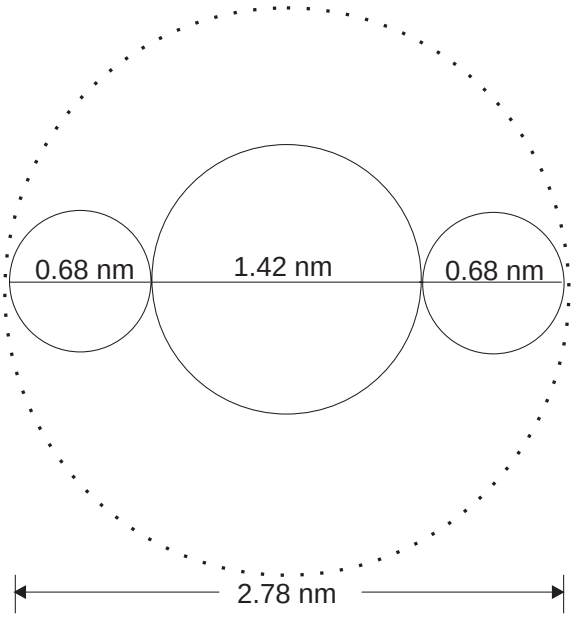
Interestingly, the silica in contact with a solution of etioporphyrin in cyclohexane changed colour after several days of aging. Initially the solution and the silica were a red colour, but the silica became green after approximately three days of aging. The silica was washed with toluene and the wash solution was analyzed in the UV–vis spectrophotometer. A new peak around 660 nm appeared in the spectra. This peak is characteristic of protonated porphyrins (15, 16). In the first step of hydrodemetallization, the metalloporphyrin is reversibly hydrogenated to a metal chlorin (2, 17, 18). The metal chlorin (see Fig. 1*c*) subsequently undergoes hydrogenolysis, which results in metal deposition.

Using eq. [4] the cross-sectional areas of the porphyrins have been calculated and are reported in Table 4. The cross-sectional area for Ni-etioporphyrin is calculated to be larger than that for the metal-free porphyrin. A larger cross-sectional area indicates that the addition of a metal centre to the porphyrin increases the interaction between the porphyrin and the solvent. This is supported by the observation that the Ni-etioporphyrin is an order of magnitude more soluble in cyclohexane than the metal-free etioporphyrin. In contrast, the solubilities of the two porphyrins are similar in toluene. The calculated value of 101 nm^2 for etioporphyrin in toluene is obviously too large and is likely a result of the toluene competing for adsorption sites on the silica. Because the etioporphyrin did not exclusively form a monolayer on the surface, the calculated cross-sectional area is too large.

The cross-sectional area for etioporphyrin in cyclohexane was calculated to be 4.58 nm^2 (Table 4). Based on X-ray data the diameter of Ni-etioporphyrin has been estimated to be 1.42 nm (19). Assuming that the porphyrin is circular, this diameter corresponds to a cross-sectional area of 1.58 nm^2 (i.e., $A = \pi r^2$). A value of 1.86 nm^2 has been suggested for the cross-sectional area of vanadyl etioporphyrin (14). These values are for unsolvated molecules. Galiasso and Morales (13) have studied the diffusion of vanadyl porphyrins in catalysts with varying silica–alumina ratios. Their studies showed that the vanadyl porphyrins interacted with the solvent (either cyclohexane, benzene, or thiophene) and

© 2001 NRC Canada

Fig. 5. Schematic drawing of porphyrin molecule with adjacent cyclohexane molecules, showing the effective cross-sectional area of the solvated molecule demarcated by the dashed line. Note that for simplicity only two cyclohexane molecules are shown.



that this interaction increased the hydraulic radius of the molecule while decreasing the diffusivity.

It is likely, therefore, that the cross-sectional areas measured in this study is that of the porphyrins solvated with cyclohexane. The cross-sectional area of Ni-etioporphyrin solvated with cyclohexane can be estimated based on the diameters of these molecules measured by X-ray and liquid density techniques. That is, the cross-sectional area of cyclohexane is 0.363 nm^2 (6) and corresponds to a diameter of 0.68 nm. If the Ni-etioporphyrin is solvated with cyclohexane molecules around the edge as shown in Fig. 5, the effective diameter of the solvated porphyrin is equal to the diameter of the porphyrin (1.42 nm) plus twice the diameter of cyclohexane (2 × 0.68 nm) or 2.78 nm. This diameter corresponds to a cross-sectional area of 6.07 nm^2 and is similar to an estimate of 3.0 nm, corresponding to a cross-sectional area of 7.1 nm^2, for the diameter of a solvated molecule of vanadyl etioporphyrin in cyclohexane (13).

Comparison of the calculated cross-sectional areas of 4.78 and 14.8 nm^2 for etioporphyrin and Ni-etioporphyrin (Table 4) to the estimated values for the cross-sectional areas of solvated metalloporphyrins seem to be reasonable although the cross-sectional area for the Ni-etioporphyrin is quite a bit larger than expected. We have no further data or explanation for this result. It should be noted that we have determined the fractal dimension of the silica using molecules between 0.162 and 0.414 nm^2 and then extrapolated the results to the much larger porphyrins molecules. It is possible that the fractal dimension of the silica is different outside of the range for which it was calculated. Galiasso and Morales (13) also performed HDM reactions and found that the solvated porphyrins were unable to diffuse to the active sites situated in the narrower pores. As a result, the number of accessible active sites was only a small fraction of the total number of active sites. Therefore, the effective area of the porphyrin (i.e., the area of a solvated molecule) is the relevant area for catalyst design.

Traditionally the nitrogen BET surface area is used to characterize catalysts, but using this technique, rather than the fractal dimension of the surface, gives considerably larger cross-sectional areas for the adsorbed molecules. For example, the surface area of the silica calculated using the monolayer coverage of nitrogen (Table 2) and a cross-sectional area for nitrogen of 0.162 nm^2, is 472 $m^2\ g^{-1}$. When this surface area is used to calculate the cross-sectional areas of the porphyrins, based on the uptakes in Table 3, the cross-sectional areas are 21.5 and 119 nm^2 for etiopophyrin and Ni-etioporphyrin, respectively, and much larger than the values calculated from the fractal dimension. This comparison demonstrates the utility of the fractal approach for highly porous supports. The nitrogen BET area does not describe the porous nature of the support or the pore size distribution. Conversely, fractal analysis allows the relationship between adsorbate size and accessible surface area to be determined.

Nonetheless, a few comments should be made about using fractal geometry for characterizing materials. First, it appears that the success of the approach depends on a number of factors, including the material itself as well as the method of determining the fractal dimension. We successfully applied the adsorption of a series of alcohols to determine the fractal dimension of silica with an average pore size of 6 nm. However, when we applied this same technique to silica with an average pore size of 2.5 nm we obtained a fractal dimension of 3.112 ± 0.293, which is slightly above the theoretical limit. Possibly the fractal dimension of the silica changed over the range of adsorbates used. The technique also failed for a γ-alumina support (10 nm average pore size). Unlike the silicas, the monolayer plots for the alumina were very scattered and it was evident immediately that the adsorption of alcohols was not the appropriate technique to use with alumina.

The values used for the cross-sectional areas of the adsorbates are also very important because the fractal dimension is quite sensitive to these values. For instance, if the cross-sectional areas in Table 1 are increased or decreased by 0.01 nm^2, the fractal dimension changes between 2.794 and 3.051, approximately ±10%. In addition, the use of nonlinear regression also makes a difference to the results.

As shown above, the nitrogen BET surface area gives exceedingly large values for the cross-sectional areas of the porphyrins because nitrogen is able to adsorb in pores that are too narrow for the porphyrin. This example illustrates the advantage of determining the fractal dimension of a surface. Although the fractal approach has limitations, and there has been controversy over the fractal nature of silica gels (8), we feel it is a useful technique for characterizing catalyst supports and determining the area occupied by an adsorbed molecule on a surface.

Conclusions

The fractal dimension of silica with an average pore diameter of 6 nm has been determined using nonlinear regression to be 2.923 with a preexponential factor of 0.3425 for the

© 2001 NRC Canada

monolayer coverage in mmol g^{-1} and cross-sectional areas in nm^2. It was found that methanol adsorbed beyond monolayer coverage on silica and so it was not used in the determination of the fractal dimension.

Etioporphyrin and Ni-etioporphyrin dissolved in cyclohexane were adsorbed onto silica and their cross-sectional areas were determined to be 4.58 and 14.8 nm^2, respectively, using fractal analysis. If the porphyrins were dissolved in toluene, monolayer coverage by the porphyrins was not achieved because the solvent competed for surface sites.

Acknowledgment

We wish to thank the Natural Sciences and Engineering Research Council (NSERC) of Canada for funding this work and for a graduate scholarship for JMH. Financial support from Canada Center for Mineral and Energy Technology (CANMET) is also gratefully acknowledged.

References

1. J.R. Katzer, M.P. Ramage, and A.V. Sapre. Chem. Eng. Prog. **July**, 41 (2000).
2. R.J. Quann, R.A. Ware, C.-W. Hung, and J. Wei. *In* Advances in chemical engineering. Vol 14. *Edited by* J. Wei. Academic Press, Toronto. 1988. pp. 96–251.
3. D. Avnir and P. Pfeifer. New J. Chem. **7**, 71 (1983).
4. J.E. Falk. Porphyrins and metalloporphyrins. *Edited by* K.M. Smith. Elsevier, New York. 1975.
5. D. Avnir, D. Farin, and P. Pfeifer. Nature, **308**, 261 (1984).
6. A.L. McClellan and H.F. Harnsberger. J. Colloid Interf. Sci. **23**, 577 (1967).
7. R.L. Hoffmann, D.G. McConnell, G.R. List, and C.D. Evans. Science, **157**, 550 (1967).
8. J. M. Drake, P. Levitz, and J. Klafter. Isr. J. Chem. **31**, 135 (1991).
9. G.E. Box, W.G. Hunter, and J.S. Hunter. Statistics for experimenters: an introduction to design, data analysis, and model building. John Wiley & Sons, Toronto. 1978.
10. P.A. Sermon, Y. Wong, and M.S.W. Vong. J. Colloid Interf. Sci. **168**, 327 (1994).
11. D. Farin, A. Volpert, and D. Avnir. J. Am. Chem. Soc. **107**, 3368 (1985).
12. D. Farin and D. Avnir. J. Chromatogr. **406**, 317 (1987).
13. R. Galiasso and A. Morales. Appl. Cat. **7**, 57 (1983).
14. P.C.H. Mitchell. Cat. Today, **7**, 439 (1990).
15. P.C.H. Mitchell and C.E. Scott. Polyhedron, **5**, 237 (1986).
16. P.C.H. Mitchell, C.E. Scott, J. Bonnelle, and J.G. Grimblot. J. Chem. Soc. Faraday Trans. 1, **81**, 1047 (1985).
17. R. Agarwal and J. Wei. Ind. Eng. Chem. Process Des. Dev. **23**, 505 (1984).
18. R.A. Ware and J. Wei. J. Catal. **93**, 100 (1985).
19. C. Hung and J. Wei. Ind. Eng. Chem. Process. Des. Dev. **19**, 250 (1980).

© 2001 NRC Canada

Selective dehydrogenation of alcohols and diols catalyzed by a dihydrido iridium PCP pincer complex

David Morales-Morales, Rocío Redón, Zhaohui Wang, Do W. Lee, Cathleen Yung, Kevin Magnuson, and Craig M. Jensen

Abstract: The PCP pincer complex, $IrH_2\{C_6H_3\text{-}2,6\text{-}(\mathbf{CH_2}P\text{-}t\text{-}Bu_2)_2\}$ (**1**) catalyzes the transfer dehydrogenation of primary and secondary alcohols. Dehydrogenation occurs across the C—O bond rather than the C—C bonds and the corresponding aldehydes or ketones are obtained as the sole products arising from the dehydrogenation reactions. Methanol is an exception to this pattern of reactivity and undergoes only stoichiometric dehydrogenation with **1** to give the carbonyl complex, $Ir(CO)\{C_6H_3\text{-}2,6\text{-}(\mathbf{CH_2}P\text{-}t\text{-}Bu_2)_2\}$ (**2**). The products are obtained in nearly quantitative yields when the reactions are carried out in toluene solutions. Under the same conditions, 2,5-hexanediol is converted to the annulated product, 3-methyl-2-cyclopenten-1-one which has been isolated in 91% yield in a preparative scale reaction.

Key words: alcohol, dehydrogenation, ketones, iridium pincer complex, annulation.

Résumé : Le complexe PCP en forme de pince, $IrH_2\{C_6H_3\text{-}2,6\text{-}(\mathbf{CH_2}P\text{-}t\text{-}Bu_2)_2\}$ (**1**) catalyse la réaction de déshydrogénation par transfert des alcools primaires et secondaires. La déshydrogénation se fait à travers la liaison C—O plutôt qu'à travers les liaisons C—C et on n'obtient que les aldéhydes et les cétones comme seuls produits de ces réactions de déshydrogénation. Le méthanol est une exception à ce mode de réactivité et il ne subit qu'une déshydrogénation stoechiométrique avec **1** pour conduire à la formation d'un complexe de carbonyle, $Ir(CO)\{C_6H_3\text{-}2,6\text{-}(\mathbf{CH_2}P\text{-}t\text{-}Bu_2)_2\}$ (**2**). Lorsqu'on effectue les réactions en solution dans le toluène, les produits sont obtenus en rendements pratiquement quantitatifs. Dans les mêmes conditions, l'hexane-2,5-diol est transformé en produit cyclique, la 3-méthylcyclopent-2-én-1-one qui a été isolée avec un rendement de 91% au cours d'une réaction à l'échelle préparative.

Mots clés : alcool; déshydrogénation, cétones, complexe de l'iridium en forme de pince, annellation.

[Traduit par la Rédaction]

Introduction

Ketones and aldehydes are most commonly prepared through the oxidation of alcohols (1). The large scale commercial production of acetone and 2-butanone is accomplished through aerobic dehydrogenation of alcohols using heterogenous catalysts such as copper chromite and silver (2). The high (>250°C) temperatures that are required for these processes, however, limits their application to production of only the simplest ketones. A remarkable homogeneous catalyst for the aerobic oxidation of alcohols has been discovered by James and co-workers (3) that operates at ambient temperature but proceeds at unpractical (1.5 turnovers/day) rates. Stoichiometric methods have been developed for the selective oxidation of alcohols to a variety of sensitive ketones and aldehydes. However, there are increasing environmental concerns about the highly toxic reagents employed in methods such as Moffatt (DMSO, DCC, and phosphoric acid), and Swern (oxalyl chloride) oxidations (1). Alternatively, the conversion of alcohols to ketones and aldehydes can be accomplished under mild conditions through transfer dehydrogenation. Oppenaurer oxidation, in which hydrogen is transferred from an alcohol to a ketone acceptor in the presence of a base (most commonly aluminum *tert*-butoxide in nearly stoichiometric amounts), has been widely employed in organic synthesis (1, 4). Several transition-metal complexes have been shown to catalyze the transfer of hydrogen from alcohols to olefins (5), acetylenes (6), or aldehydes and ketones (7, 8) acceptors. Other complexes have been found to catalyze "acceptor-less" dehydrogenation of alcohols (9, 10). Catalytic hydrogen transfer systems have been utilized in organic synthesis for the reduction of oxo-steriods to hydroxy-steriods (8) and its mircroreverse (10). More recently, enantioselective versions of this reaction have been developed for asymmetric synthesis (8*d–f*).

The iridium PCP pincer complex $IrH_2\{C_6H_3\text{-}2,6\text{-}(CH_2P\text{-}t\text{-}Bu_2)_2\}$ (**1**) has been found to be an efficient and robust catalyst for the transfer dehydrogenation of alkanes (11, 12),

Received September 20, 2000. Published on the NRC Research Press Web site at http://canjchem.nrc.ca on July 19, 2001.

This paper is dedicated to Professor Brian James on the occasion of his 65th birthday, in recognition of his inspirational pioneering spirit.

D. Morales-Morales, R. Redón, Z. Wang, D.W. Lee, C. Yung, K. Magnuson, and G.M. Jensen.[1] Department of Chemistry, University of Hawaii, Honolulu, Hawaii 96822, U.S.A.

[1]Corresponding author (telephone: (808) 956-6721; fax: (808) 956-5908; e-mail: jensen@gold.chem.hawaii.edu).

 DOI: 10.1139/cjc-79-5/6-823 © 2001 NRC Canada

Table 1. Crystallographic data for Ir(CO){C_6H_3-2,6-(CH_2P-*t*-Bu_2)$_2$} (**2**).

Formula	$C_{25}H_{43}OIrP_2$
Formula weight	613.73
T (K)	293(2)
Crystal system	Monoclinic
Space group	$P2_1/n$
Crystal dimensions (mm)	0.4 × 0.4 × 0.3
a (Å)	15.443(4)
b (Å)	11.619(3)
c (Å)	30.608(8)
α (deg)	90
β (deg)	93.22
γ (deg)	90
V (Å^3)	5483(3)
Z	8
μ (cm^{-1})	49.99
Transmission coeff. min, max	0.389, 1.000
λ (Å) (Mo Kα radiation)	0.71073
2θ range (deg)	3–45
Independent reflections	7143
Unique data with $I >> 2((I)$	5290
Parameter refined	526
Goodness-of-fit[a]	0.986
ρ calcd. (g cm^{-3})	1.487
Scan type	ω
R^b (%)	3.78
$R_w{}^c$ (%)	8.87

[a]GOF = $[w\sigma(|F_o| - |F_c|)^2/(N_o - N_v)]^{1/2}$.
[b]$R = \sigma|(F_o| - |F_c|/\sigma|F_o|$.
[c]$R_w = [w\sigma(|F_o| - |F_c|)^2/\sigma wF_o{}^2]^{1/2}$.

ethers (13), alkyl arenes (13), and amines (14). Thus it was of interest to examine the reactivity of **1** towards alcohols. We have found that **1** catalyzes the selective transfer dehydrogenation of primary and secondary alcohols to aldehydes and ketones in very high yields. We have also found that **1** catalyzes the unusual dehydrogenation and (or) annulation of 2,5-hexanediol to 3-methyl-cyclopenten-1-one. The results of these studies are reported herein.

Experimental

All manipulations were carried out using standard Schlenk and glovebox techniques under purified argon. Solvents were degassed and dried using standard procedures. The alcohols were purchased from Aldrich Chemicals Co. and used without further purification. The complex IrH_2{C_6H_3-2,6-(CH_2P-*t*-Bu_2)$_2$} (**1**) was synthesized by the literature methods (12). The ^{1}H NMR spectra were recorded on a Varian Unity Inova 400 spectrometer. Chemical shifts are reported in ppm down field of TMS using the solvent as internal standard ($CDCl_3$, 7.26 or cyclohexane-d_{12}, 1.38). ^{13}C and ^{31}P NMR spectra were recorded with complete proton decoupling and are reported in ppm down field of TMS with solvent as internal standard ($CDCl_3$, 77.0 or cyclohexane-d_{12}, 26.43) and external 85% H_3PO_4, respectively. Infrared spectra were recorded in a PerkinElmer Paragon FT IR spectrometer as Nujol mulls in NaCl plates. Gas chromatographic analyses were performed with a Hewlett–Packard 5890 instrument with a HP 5980A flame ionization detector and HP-1 capillary column (25.0 m). Gas chromatographic–mass spectral analyses were carried out using a HP 5890 Series II instrument with an 5971A mass selective detector and HP-1 capillary column (25.0 m).

Catalytic reactions

Solutions of the substrates (0.26 mmol), tbe (0.20 mL, 1.53 mmol), and 4 mL of toluene were charged with **1** (22 mg, 0.037 mmol) in sealed Schlenk tubes in a Vacuum Atmospheres glovebox under argon. The tubes were then fully immersed in a constant temperature bath at 200°C for the prescribed reaction times. After this time the tubes are allowed to cool down to room temperature. The products were identified by GC–MS analysis upon comparison to purchased samples of the authentic compounds. Product yields were calculated from the ratio of the integrated intensities of signals produced by the products and those of the toluene solvent after weighting the data by a predetermined relative molar response factor.

The attempted acceptor-less dehydrogenation reactions were carried out with mesitylene solutions of the substrates (0.26 mmol) and **1** (22 mg, 0.037 mmol) that were refluxed while passing a stream of argon above the condensor. Gas chromatographic analysis of the reaction mixtures following 72 h of rigorous reflux showed no traces of dehydrogenated products.

Preparative scale synthesis of 3-methyl-2-cyclopenten-1-one

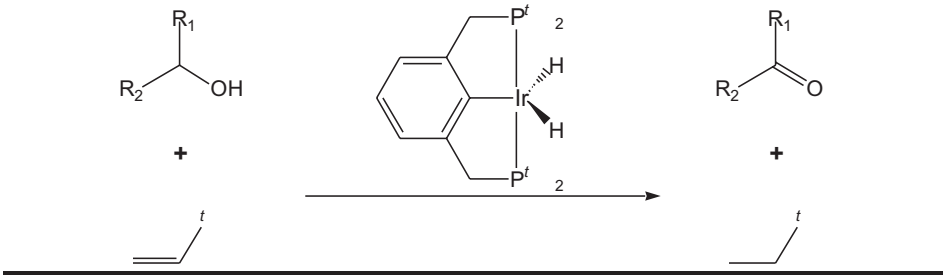
A solution of the 2,5-hexanediol (1.0 mL, 81 mmol), tbe (2.2 mL, 17 mmol), and 4 mL of toluene was charged with **1** (100 mg, 0.17 mmol) in a sealed Schlenk tube in a Vacuum Atmospheres glovebox under argon. The tube was then fully immersed in a constant temperature bath at 200°C for 78 h. After this time, the reaction mixture was cooled to room temperature and concentrated to ~1.4 mL. The product was then separated by column chromatography (Davisil (100–200 mesh silica gel) by eluting first with pentane and then with acetone. The product fraction was collected and concentrated under vacuum. The isolated product (yield: 0.73 mL, 91%) was identified as 3-methyl-2-cyclopenten-1-one by MS and NMR (^{1}H and ^{13}C) analysis upon comparison to an authentic sample. MS (*m*/*z*): $[M]^+$ 96, $[M\text{-}CH_3]^+$ 81. ^{1}H NMR (400.00 MHz, $CDCl_3$) δ: 5.91 (m, 1H, *H*C-2), 2.55 (m, 2H, H_2C-5), 2.38 (m, 2H, H_2C-4), 2.10 (s, 3H, CH_3). ^{13}C NMR (100.60 MHz, $CDCl_3$) δ: 210.15 (s, *C*=O), 178.82 (s, *C*-3), 130.62 (s, *C*-2), 35.66 (s, *C*-5), 32.97 (s, *C*-4), 19.30 (s, *C*H_3).

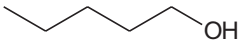
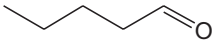
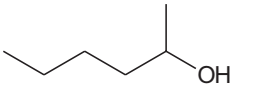
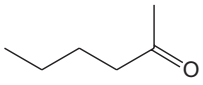
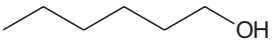
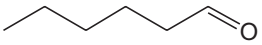
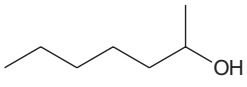
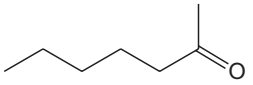
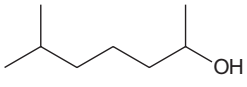
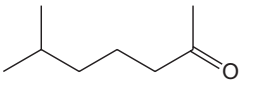
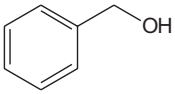
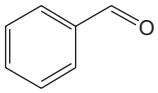
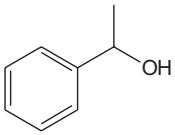
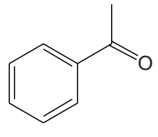
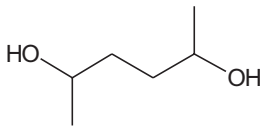
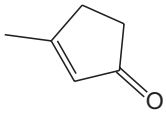
Synthesis of Ir(CO){C_6H_3-2,6-(CH_2P-*t*-Bu_2)$_2$} (2)

A pentane (5 mL) solution of **1** (20 mg, 0.034 mmol) was treated with *tert*-butylethylene (66 μL, 0.51 mmol) under 1 atm (1 atm = 101.325 kPa) of argon at 25°C. After 1 h of reaction, the resulting red-purple solution was treated with degassed methanol (0.1 mL, 5.6 mmol). Removal of the solvent in vacuo yields **2** as a deep yellow-orange solid. Yield: 19 mg, 90%. ^{1}H NMR (400.00 MHz, cyclohexane-d_{12}) δ: 6.93 (d, J_{HH} = 7.3 Hz, 2H, *m*-H), 6.67 (t, J_{HH} = 7.3 Hz, 1H, *p*-H), 3.42 (vt, J_{HH} = 3.0 Hz, 4H, CH_2), 1.28 (vt, J_{PH} =

© 2001 NRC Canada

Table 2. Dehydrogenation of alcohols using $IrH_2\{C_6H_3\text{-}2,6\text{-}(CH_2P\text{-}t\text{-}Bu_2)_2\}$ (**1**).[a]



Substrate	Product	Yield (%)[b]
		>99
		>99
		>99
		66[c]
		>99
		>99
		>99
		>99
		>99

[a]Reaction conditions: alcohol (0.26 mmol), tbe (1.53 mmol), 4 mL of benzene, and **1** (22 mg, 0.037 mmol) at 200°C for 18 h.
[b]Yields based on GC analysis.
[c]Traces of aldehyde were detected in the starting material; as a result, the performance of the catalyst was considerably reduced.

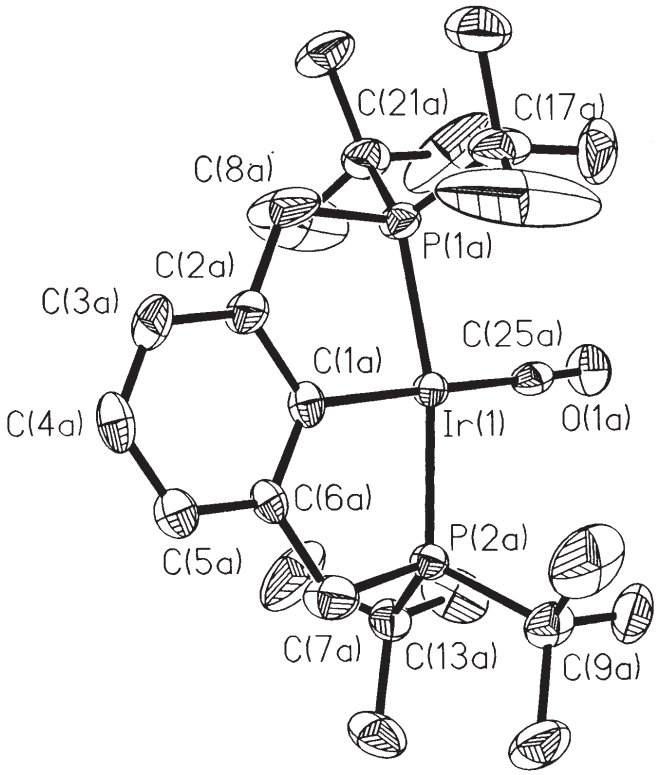
7.3 Hz, 36H, $C(CH_3)_3$). ^{13}C NMR (100.60 MHz, cyclohexane-d_{12}) δ: 197.6 (s, Ir-*C*-O), 168.8 (s, *C-1*), 155.3 (vt, J_{PC} = 12.0 Hz, *o-C*), 125.9 (s, *p-C*), 120.3 (vt, J_{PC} = 9.1 Hz, *m-C*), 39.6 (vt, J_{PC} = 13.9 Hz, CH_2P), 36.5 (vt, J_{PC} = 10.7 Hz, $C(CH_3)_3$), 30.1 (s, $C(CH_3)_3$). ^{31}P NMR (161.90 MHz, cyclohexane-d_{12}) δ: 82.8 (s). IR (KBr) (cm^{-1}): ν_{IrCO} = 1913 (s). Anal. calcd. for $C_{25}H_{43}OP_2Ir$ (613.77) (%): C 48.92, H 7.06; found: C 48.96, H 7.01.

Molecular structure determination of (2)

Yellow-orange crystals of **2** that were suitable for X-ray diffraction were obtained from slow evaporation of a pentane solution of the complex. Centering and data collection were performed with a Nicolet P3 diffractometer, graphite monochromator (λ = 0.71073 Å, Mo Kα) at room temperature using a crystal that was mounted on a glass fiber with epoxy. The unit cell was determined from the angular

© 2001 NRC Canada

Fig. 1. Thermal ellipsoid (50% probablity) drawing of Ir(CO){C_6H_3-2,6-(CH_2P-*t*-Bu_2)$_2$} (**2**). Hydrogen atoms have been omitted for clarity.



coordinates of 25 reflections with 2θ values between 15 and 30°. The diffractometer autoindexing routine found a monoclinic unit cell, which was confirmed by axial photographs.

Three check reflections, monitored every 100 reflections, showed no significant decay. The data were processed using SHELXTL program package (15), and an absorption correction was applied based upon ψ-scans of five reflections. Since the unit cell is triclinic, the space group *P*2(1)/*n* was assumed. The iridium was located by Patterson methods and the remainder of the structure was easily developed via a few cycles of least-squares refinement and difference Fourier maps. The unit cell was found to contain two symmetry-independent molecules of **2**. Hydrogen atoms were input at calculated positions, and allowed to ride on the atoms to which they are attached. Two group of thermal parameters were refined for hydrogen atoms, one each for methylene and methyl protons. The final cycle of refinement was carried out on all non-zero data using SHELXL-97 (6) and anisotropic thermal parameters for all non-hydrogen atoms. Crystal data and relevant information are summarized in Table 1.

Results

The catalytic activity of **1** was initially screened using solutions consisting of the saturated alcohol, and the hydrogen acceptor, *tert*-butylethylene (tbe). The orange solutions were sealed in tubes under argon and fully immersed in an oil bath at 200°C for 18 h. The solutions became red upon heating and gradually change color to yellow-orange during the reaction period. Gas chromatographic analysis of the reaction mixtures showed the substrates were converted to the corresponding dehydrogenated compounds with greater than 99% selectivity. However, only ≈1% yields were obtained in preliminary experiments with the neat reaction mixture even upon longer reaction times and increased catalyst loadings. This finding was not unanticipated as dehydrogenation reactions catalyzed by **1** have generally been found to be inhibited at low concentrations of the unsaturated products (11–14, 16). Apparently deactivation of the active catalyst through a coordinative interaction with the carbonyl groups prevents the occurrence of the slower process of catalytic dehydrogenation of aliphatic groups. In support of this hypothesis, 2-hexanone was found to be unreactive with **1** under the conditions employed for the dehydrogenation of the alcohols.

To obtain high yields, it was necessary to dilute the reaction mixtures. A similar strategy has been used to achieve high yields in the catalytic dehydrogenation of secondary amines to imines by **1** (14). Table 2 summarizes the results of the dehydrogenation experiments in which toluene solutions of the alcohols, **1**, and tbe were heated for 3 days at 200°C. The products were characterized by GC–MS analysis of the reaction mixtures. Excellent selectivities and yields were uniformly obtained without regio-restriction on the alcohol functionality. No traces of dehydrogenationated products were detected in acceptor-less experiments in which mesitylene solutions of alcohols and **1** were refluxed while passing a stream of argon above the condensor.

The dehydrogenation of 2,5-hexanediol produced an unexpected result. A single product arises upon heating dilute toluene solutions of the diol, **1**, and tbe for 3 days at 200°C. MS and NMR analysis showed the product to be the cyclic ketone, 3-methyl-2-cyclopenten-1-one. This product can be understood to arise upon dehydrogenation across both of the C—O bonds to produce the hexadione followed by an internal aldol reaction and subsequent dehydrogenation as in the final step of a Robinson annulation reaction (17). We are unaware of any previous reports of the catalytic dehydrogenation of diols resulting in the formation of cyclic unsaturated ketones. To probe the possible synthetic utility of this type of reaction, the dehydrogenation of 2,5-hexanediol was carried out on a preparative scale. Starting with 1.00 mL (81 mmol) of the diol, we were able to isolate 0.73 mL (74 mmol, 91% yield) of 3-methyl-2-cyclopenten-1-one upon work-up using silica gel column chromatography.

The pincer complex does not catalyze the dehydrogenation of methanol to formaldehyde but instead undergoes a stoichiometric reaction with methanol to yield the carbonyl compound Ir(CO){C_6H_3-2,6-(CH_2P-*t*-Bu_2)$_2$} (**2**). The presence of the carbonyl ligand of **2** is clearly indicated by the observation of a signal at 198.23 ppm in its ^{13}C NMR spectrum and strong absorption at 1911.8 cm^{-1} in the IR spectrum of the complex. Although carbonyl complexes commonly result upon the reaction of late transition-metal complexes with alcohols (for example see ref. 18; 19) it is surprising to find this partitioning in the reactivity of **1**. A similar dichotomy was previously observed for [Ru_2Cl_3(PMePh_2)$_6$]Cl which reacts with KOH in isopropanol

© 2001 NRC Canada

Table 3. Selected bond distances (Å) and angles (°) for Ir(CO){C_6H_3-2,6-(CH_2P-*t*-Bu_2)$_2$} (**2**).

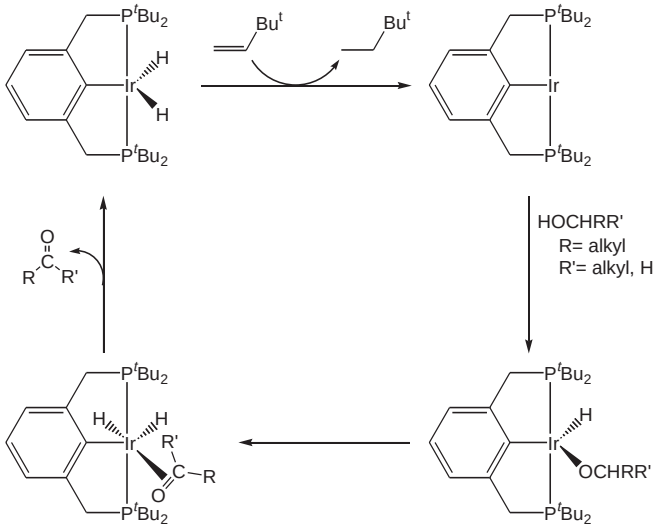
Molecule **1**		Molecule **2**	
Bond lengths			
Ir(1)—C(1A)	2.102(8)	Ir(2)—C(1B)	2.090(9)
Ir(1)—C(25A)	1.873(10)	Ir(2)—C(25B)	1.852(12)
Ir(1)—P(1A)	2.298(2)	Ir(2)—P(1B)	2.304(2)
Ir(1)—P(2A)	2.291(2)	Ir(2)—P(2B)	2.298(2)
C(25A)—O(1A)	1.167(10)	C(25B)—O(1B)	1.127(12)
Bond angles			
C(1A)-Ir(1)-P(2A)	81.800(2)	C(1B)-Ir(2)-P(2B)	82.300(3)
C(1A)-Ir(1)-P(1A)	82.900(2)	C(1B)-Ir(2)-P(1B)	82.400(3)
P(2A)-Ir(1)-P(1A)	164.510(8)	P(2B)-Ir(2)-P(1B)	163.080(9)
C(25A)-Ir(1)-C(1A)	178.100(3)	C(25B)-Ir(2)-C(1B)	179.400(4)
C(25A)-Ir(1)-P(2A)	97.700(3)	C(25B)-Ir(2)-P(2B)	98.300(3)
C(25A)-Ir(1)-P(1A)	97.700(3)	C(25B)-Ir(2)-P(1B)	97.100(3)
O(1A)-C(25A)-Ir(1)	176.800(8)	O(1B)-C(25B)-Ir(2)	175.600(12)

solution to give [*cis*-$Ru_2Cl_3(PMePh_2)_4$] but yields $RuH_2(CO)(PMePh_2)_3$ when the reaction is carried out in ethanol (19).

The molecular structure of **2** was determined through a single crystal X-ray diffraction study.[2] The structure consists of two molecules of **2** in the asymmetric unit. A thermal ellipsoid drawing of one of the molecules with atomic number scheme of the obtained structure is presented in Fig. 1. Selected bond angles and distances are listed in Table 3.

A distorted square-planar coordination geometry can be recognized about the iridium consisting of the tridentate PCP pincer and carbonyl ligands. While the vector between the metalated carbon in the aromatic ring and the carbonyl ligand O(1A)-C(25A)-Ir(1) is a nearly ideal 176.800(8)°, the vector between the two phosphorus atoms (P(2A)-Ir(1)-P(1A), 164.510(8)°), is much more distorted due to the geometric constraints imposed upon establishing the chelating interaction of the PCP ligand. The Ir-P and Ir-metalated C distances are comparable to those observed in similar PCP pincer complexes (12, 20, 21).

Scheme 1.



Discussion

A plausible mechanism for the catalytic reaction is depicted in Scheme 1.

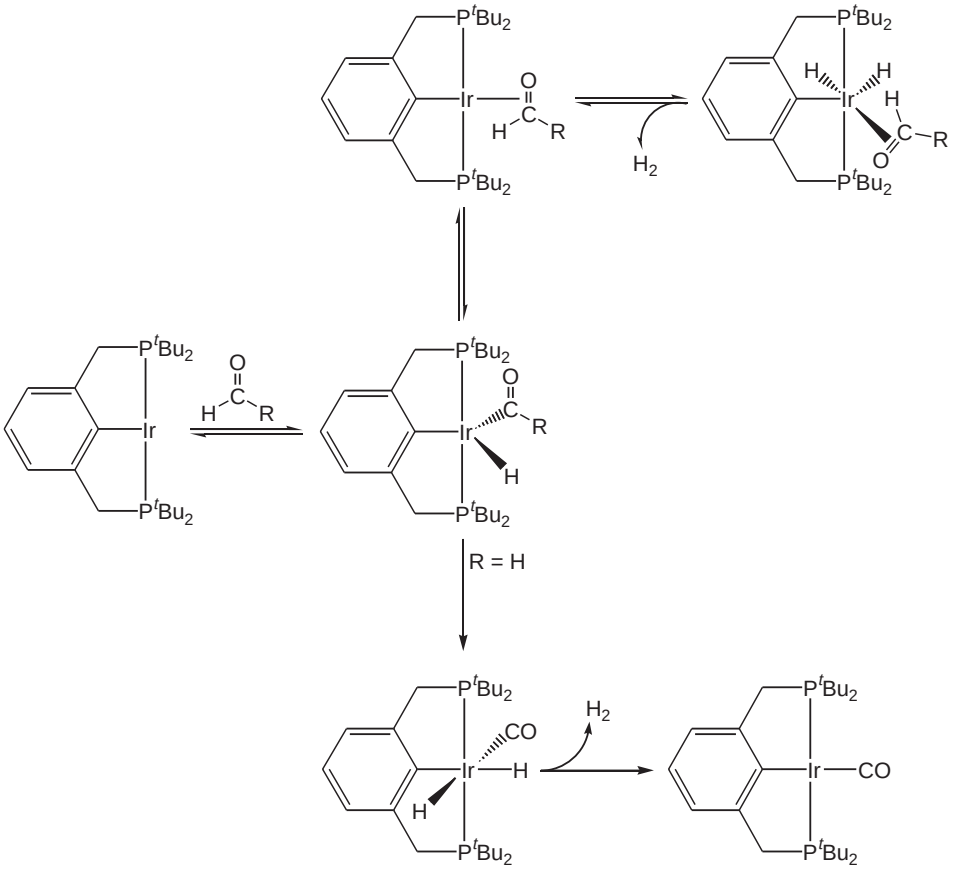
Alcohols apparently undergo O-H oxidative addition with the 14-electron complex arising upon dehydrogention of **1** by tbe to give intermediate alkoxy hydride complexes. In support of this hypothesis, the dehydrogenation of **1** in the presence of water produces the analogous hydroxy hydride complex IrH(OH)({C_6H_3-2,6-(CH_2P-*t*-Bu_2)$_2$}, that has been characterized spectroscopically and through a single crystal X-ray structure determination (22). The pincer alkoxide complexes would be expected to undergo the C-H β-elimination reaction that have generally been observed for metal alkoxide complexes (23) to produce η^2-aldehyde or ketone complexes. Dissociation of the dehydrogenated product then regenerates **1** and completes the catalytic sequence.

The alternate reaction pathway observed in the case of methanol can be rationalized in terms of the differing reactives of formyl and acyl complexes. As illustrated in Scheme 2, such intermediates could quite plausibly result from C-H oxidative addition of aldehydes in either: (*i*) an intermolecular process involving the 14-electron intermediate in the catalytic sequence; (*ii*) or an intramolecular process involving a 16-electron η^2-aldehyde species arising upon reductive elimination of H_2 from the 18-electron, η^2-aldehyde, dihydride intermediate in the catalytic sequence. Hydride elimination from a formyl ligand to generate a hydrido carbonyl complex is well known to be much more facile than the corresponding alkyl deinsertion from an acyl

[2] Copies of material on deposit (tables of crystal data, thermal parameters, bond distances, bond angles, and atomic coordinates for Ir(CO){C_6H_3-2,6-(CH_2P-*t*-Bu_2)$_2$}) may be purchased from the Depository of Unpublished Data, Document Delivery, CISTI, National Research Council Canada, Ottawa, ON K1A 0S2, Canada (http://www.nrc.ca/cisti/irm/unpub_e.shtml for information on ordering electronically). Some of this material has also been deposited with the Cambridge Crystallographic Data Centre. Copies of the data can be obtained, free of charge, on application to the Director, CCDC, 12 Union Road, Cambridge CB2 1EZ, U.K. (Fax: 44-1223-336033 or e-mail: deposit@ccdc.cam.ac.uk).

© 2001 NRC Canada

Scheme 2.



intermediate (24). Thus while all aldehydes are likely to undergo C-H oxidative addition in this catalytic system, subsequent deinsertion to form a carbonyl is competitive with the mircoreverse, reductive elimination of aldehyde only in the case of the formyl intermediate.

Conclusions

In summary, the PCP pincer complex **1** catalyzes the highly selective dehydrogenation of a variety of primary and secondary alcohols to aldehydes and ketones, respectively. The problem of product inhibition of the catalyst is eliminated by carrying out the dehydrogenation reactions in dilute solutions and dehydrogenated products have been uniformly obtained in nearly quantititative yields. The unusual dehydrogenation and (or) annulation of 2,5-hexanediol to 3-methyl-2-cyclopenten-1-one has been carried out on the preparative scale suggesting that the catalytic conversion of diols to cyclic enones could be utilized in organic synthesis.

Acknowledgements

The support of this research by the U.S. Department of Energy Hydrogen Program is gratefully acknowledged. DWL and ZW are the 1996 and 1999 J.J. Zuckermann fellows.

References

1. M.B. Smith and J. March. Advanced organic chemistry. Reactions, mechanisms, and structure. 5th ed. John Wiley and Sons, New York. 2001. Chap. 19. pp. 1514–1517.
2. (*a*) S. Sifniades. *In* Ullmann's encyclopedia of industrial chemistry. 5th ed. Vol. A 1. *Edited by* W. Gerhartz, Y.S. Yamamoto, F.T. Campbell, R. Pfefferkorn, and J.F. Rounsaville. VCH Verlagsgesellschaft, Weinheim, Germany. 1985. pp. 84–85; (*b*) W. Neier. *In* Ullmann's encyclopedia of industrial chemistry. 5th ed. Vol. A 4. *Edited by* W. Gerhartz, Y.S. Yamamoto, F.T. Campbell, R. Pfefferkorn, and J.F. Rounsaville. VCH Verlagsgesellschaft, Weinheim, Germany. 1985. p. 477.
3. S.Y.S. Cheng, N. Rajpakse, S. J. Rettig, and B.R. James. J. Chem. Soc. Chem. Commun. 2669 (1994).
4. (*a*) C. Djerassi. Org. React. (N.Y.), **6**, 207, (1951); (*b*) K.G. Akamanchi and B.A. Chaudhari. Tetrahedron Lett. **38**, 6925 (1997).
5. *(a)* J. Trocha-Grimshaw and H.B. Henbest. Chem. Commun. 544, (1967); (*b*) Y. Sasson and J. Blum. Tetrahedron Lett. 2167 (1971); *(c)* Y. Sasson and G.L. Rempel. Can. J. Chem. **52**, 3825 (1974); (*d*) H. Imai, T. Nishiguchi, and K. Fukizumi. J. Org. Chem. **39**, 1622 (1974); (*e*) Y. Sasson and J. Blum. J. Org. Chem. **40**, 1887 (1975); (*f*) A.S. Goldman and J. Halpern. J. Organomet. Chem. **382**, 237 (1990).
6. (*a*) J. Trocha-Grimshaw and H.B. Henbest. J. Chem. Soc. Chem. Commun. 757 (1968); (*b*) R. Zanella, F. Canziani, R. Ros, and M. Graziani. J. Organomet. Chem. **67**, 449 (1975).

© 2001 NRC Canada

7. *(a)* H.B. Henbest and T.R.B. Mitchell. J. Chem. Soc. C, 785 (1970); (*b*) V.Z. Sharf, K. Freidlin, V.N. Krutii, and G.T. Prokopenko. Kinet. Catal. **14**, 518 (1973); (*c*) M. Gullotti, R. Ugo, and S. Colonna. J. Chem. Soc. Chem. Commun. 2652 (1971); (*d*) R.A.W. Johnston, A.W. Wilby, and J.D. Entwistle. Chem. Rev. **85**, 129 (1985); (*e*) R. Noyori and H. Takaya. Acc. Chem. Res. **23**, 345 (1990); (*f*) J.E. Bäckvall, R.L. Choudhury, and U. Karlsson. J. Chem. Soc. Chem. Commun. 473 (1991).
8. (*a*) Y.M.Y. Haddad, H.B. Henbest, J. Husbands, and T.R.B. Mitchell. Proc. Chem. Soc. London, 361 (1964); (*b*) P.A. Browne and D.N. Kirk. J. Chem. Soc. C, 1653 (1969); (*c*) J.C. Orr, M. Mersereau, and A. Sanford. J. Chem. Soc. Chem. Commun. 162 (1970); (*d*) G. Zassinovich, G. Mestroni, and S. Gladiali. Chem. Rev. **92**, 1051 (1992); (*e*) R. Noyori and S. Hashiguchi. Acc. Chem. Res. **30**, 97 (1997); (*f*) D.A. Alonso, D. Guijarro, P. Pinho, O. Temme, and P.G. Andersson. J. Org. Chem. **63**, 2749 (1998), and refs. therein.
9. (*a*) H.B. Charman. J. Chem. Soc. B, 584 (1970); (*b*) A. Dobson and S.D. Robinson. Inorg. Chem. **16**, 137, 1977; (*c*) S. Shinoda, T. Kojima, and Y. Saito. J. Mol. Catal. **18**, 99 (1983).
10. Y. Lin, D. Ma., and X. Lu. Tetrahedron Lett. **28**, 3115 (1987).
11. (*a*) M. Gupta, C. Hagen, W.C. Kaska, R. Flesher, and C.M. Jensen. J. Chem. Soc. Chem. Commun. 2083 (1996); (*b*) W. Xu, G.P. Rosini, M. Gupta, C.M. Jensen, W.C. Kaska, K. Krough-Jespersen, and A.S. Goldman. J. Chem. Soc. Chem. Commun. 2273 (1997); (*c*) F. Liu, E.B. Pak, B. Singh, C.M. Jensen, and A.S. Goldman. J. Am. Chem. Soc. **121**, 4086 (1999).
12. M. Gupta, C. Hagen, W.C. Kaska, R. Cramer, and C.M. Jensen. J. Am. Chem. Soc. **119**, 840 (1997).
13. M. Gupta, W.C. Kaska, and C.M. Jensen. J. Chem. Soc. Chem. Commun. 461 (1997).
14. D. Morales-Morales, W. Chen, and C.M. Jensen. Paper INOR 0572 presented at the 218th American Chemical Society National Meeting, New Orleans, Louisiana. 1999.
15. G.M. Sheldrick. SHELXL-97. Program for crystal structure refinement. University of Göttingen, Germany. 1997.
16. C.M. Jensen. J. Chem. Soc. Chem. Commun. 2443 (1999).
17. E.M. Jung. Tetrahedron, **32**, 3 (1976).
18. (*a*) J. Chatt, B.L. Shaw, and A.E. Field. J. Chem. Soc. 3466 (1964); *(b)* J.A. Osborn, F.H. Jardine, J.F. Young, and G. Wilkinson. J. Chem. Soc. A, 1711 (1966); *(c)* M.S. Lupin and B.L. Shaw. J. Chem. Soc. A, 741 (1968).
19. R.H. Crabtree and A.J. Pearman. J. Organomet. Chem. **157**, 335 (1978).
20. S. Nemeh, C.M. Jensen, E. Binamira-Soriaga, and W.C. Kaska. Organometallics, **2**, 1442 (1983).
21. D.W. Lee, W.C. Kaska, and C.M. Jensen. Organometallics, **17**, 1 (1998).
22. D. Morales-Morales, D.W. Lee, Z. Wang, and C.M. Jensen. Organometallics, **21**, 1144 (2001).
23. *(a)* M.A. Bennett, G.B. Robertson, P.O. Whimp, and T. Yoshida. J. Am. Chem. Soc. **95**, 3028 (1973); (*b*) D.P. Arnold, M.A. Bennett, M.S. Bilton, and G.B. Robertson. J. Chem. Soc. Chem. Commun. 111 (1982); (*c*) H.E. Bryndza, S.A. Kretchmar, and T.H. Tulip. J. Chem. Soc. Chem. Commun. 977 (1985); (*d*) H.E. Bryndza, J.C. Calabrese, M. Marsi, D.C. Roe, W. Tam, and J.E. Bercaw. J. Am. Chem. Soc. **108**, 4805 (1986); (*e*) O. Blum and D. Milstein. J. Am. Chem. Soc. **117**, 4582 (1995).
24. R.H. Crabtree. The organometallic chemistry of the transition metals. 3rd ed. John Wiley and Sons, New York. 2001. Chap. 12. p. 342.

© 2001 NRC Canada

Synthesis, characterization, and protonation of octaethylporphyrin osmium nitrosyl complexes containing axial thiolate ligands — X-ray structures of an alkyl thionitrite (RSNO) and its (OEP)Os(NO)(SR) addition product

Jonghyuk Lee, Geun-Bae Yi, Douglas R. Powell, Masood A. Khan, and George B. Richter-Addo

Abstract: The (OEP)Os(NO)(SR) compounds (R = Me, Et, *i*-Pr, *t*-Bu) have been prepared in 33–48% isolated yields by the formal *trans*-addition of the precursor alkyl thionitrites (RSNO) across the metal center in (OEP)Os(CO). The nitrosyl thiolate compounds have been characterized by IR, ^{1}H NMR, and UV–vis spectroscopy, and by FAB mass spectrometry. Their IR spectra display bands in the 1751–1755 cm^{-1} (KBr) range, which is indicative of terminal *N*-bound NO ligands in this class of compounds. The thiolate–thiol (OEP)Os(NO)(SCH_2CH_2SH) complex has been prepared in 70% isolated yield from the reaction of (OEP)Os(NO)(O-*i*-C_5H_{11}) with ethane-1,2-dithiol. Nitrosation of the free -SH group in (OEP)Os(NO)(SCH_2CH_2SH) with *t*-BuONO, followed by reaction with (TTP)Ru(CO) gave [(OEP)Os(NO)](μ-SCH_2CH_2S-*S*,*S*′)[Ru(NO)(TTP)] in 70% yield by ^{1}H NMR spectroscopy. The (OEP)Os(NO)($SCR'_2CH_2NHC(O)Me$) compounds have also been prepared either by an alkoxide–thiolate exchange reaction (for R′ = H) or by RSNO addition to (OEP)Os(CO) (for R′ = Me). The solid-state molecular structures of the precursor RSNO thionitrite (for R′ = Me) and the metalloderivative have been determined by single-crystal X-ray crystallography. Protonation of these (OEP)Os(NO)($SCR'_2CH_2NHC(O)Me$) complexes gave the amide-bound [(OEP)Os(NO)($O=C(Me)NHCH_2CR'_2SH$)]BF_4 derivatives. The latter cationic compounds were also obtained by the sequential reaction of (OEP)Os(CO) with nitrosonium tetrafluoroborate, followed by addition of the amide–thiol reagent.

Key words: thionitrite, nitrosothiol, porphyrin, X-ray structure, nitric oxide, osmium.

Résumé : En procédant à une addition formelle *trans* des alkyl thionitrites (RSNO) précurseurs dans le centre métallique du (OEP)Os(CO), il a été possible de préparer les composés (OEP)Os(NO)(SR) (R = Me, Et, *i*-Pr et *t*-Bu), avec des rendements en produits isolés de 33 à 48%. Les composés thiolate de nitrosyle ont été caractérisés par IR, RMN du ^{1}H, spectroscopie UV–vis et spectrométrie de masse « FAB ». Les spectres IR présentent des bandes dans la plage allant de 1751 à 1755 cm^{-1} (KBr) qui, dans cette classe de composés, indiquent la présence de ligands NO terminaux liés par l'azote. Le complexe thiolate–thiol (OEP)Os(NO)(SCH_2CH_2S) a été préparé avec un rendement de 70% en produit isolé en faisant réagir du (OEP)Os(O-*i*-C_5H_{11}) avec de l'éthane-1,2-dithiol. La nitrosation du groupe -SH libre du (OEP)Os(NO)(SCH_2CH_2SH) avec du *t*-BuONO, suivie d'une réaction avec du (TTP)Ru(CO) conduit à la formation de [(OEP)Os(NO)](μ-SCH_2CH_2S-*S*,*S*′)[Ru(NO)(TTP)] avec un rendement de 70% sur la base de la spectroscopie RMN du ^{1}H. Faisant appel à une réaction d'échange alcoolate–thiolate (pour R′ = H) ou à une réaction d'addition de RSNO sur le composé (OEP)Os(CO) pour R′ = Me), il a aussi été possible de préparer les composés [OEP)Os(NO)($SCR'_2CH_2NHC(O)Me$)]. Les structures moléculaires à l'état solide du précurseur thionitrite RSNO (pour R′ = Me) et du dérivé métallique ont été déterminées par diffraction des rayons X sur un cristal unique. La protonation de ces complexes [(OEP)Os(NO)($SCR'_2CH_2NHC(O)Me$)] conduit à la formation des dérivés [(OEP)Os(NO)($O=C(Me)NHCH_2CR'_2SH$)]BF_4 liés par l'amide. On a aussi obtenu ces composés cationiques par la réaction en séquence du (OEP)Os(CO) avec le tétrafluoroborate de nitrosium, suivie par l'addition du réactif amide–thiol.

Mots clés : thionitrite, nitrosothiol, porphyrine, structure par diffraction des rayons X, oxyde nitrique, osmium.

[Traduit par la Rédaction]

Received August 30, 2000. Published on the NRC Research Press Web site at http://canjchem.nrc.ca on June 30, 2001.

Dedicated to Professor Brian R. James on the occasion of his 65th birthday.

J. Lee, G.-B. Yi, M.A. Khan, G.B. Richter-Addo.[1] Department of Chemistry and Biochemistry, University of Oklahoma, 620 Parrington Oval, Norman, OK 73019, U.S.A.
D.R. Powell. X-ray Structural Laboratory, Department of Chemistry, University of Wisconsin, 1101 University Avenue, Madison, WI 53706, U.S.A.

[1]Corresponding author (telephone: (405) 325-6401; fax: (405) 325-6111; e-mail: grichteraddo@ou.edu).

 DOI: 10.1139/cjc-79-5/6-830 © 2001 NRC Canada

The chemistry of the *S*-nitroso functional group in alkyl thionitrites (RSNO, nitrosothiols) is invariably linked to the biology of nitric oxide, although the exact physiological relationship between RSNO and NO remains to be discerned. For example, thiol groups on proteins can be nitrosated (1–4), and it has been shown that the βCys93 residue of hemoglobin can be nitrosated under some conditions (5–8). The X-ray structure of *S*-nitrosated hemoglobin has also been reported (9).

Nitrosation of thiols to give RSNO has a rather long history, and reviews on the chemistry of RSNOs have been published (10–16). A major breakthrough in the chemistry of RSNO compounds came when Butler and co-workers (17) reported that some trace metals (e.g., copper in buffered solutions) catalyze the decomposition of the *S*-nitroso functional group. We have also shown that metalloporphyrins of the group 8 metals react with RSNO to give formal *trans*-addition products, via initial *S*-coordination of the RSNO molecule (11, 18–22). We are interested in the chemical and spectroscopic properties of the resulting six-coordinate (por)M(NO)(SR) compounds, since these are potential structural models for the NO adducts of cytochrome P450, chloroperoxidase, and NO synthase (23). Prior to the current study, only three osmium (por)M(NO)(SR) derivatives had been reported in the literature, namely (TTP)Os(NO)(S-*i*-C_5H_{11}), (OEP)Os(NO)(S-*i*-C_5H_{11}), and the unstable (OEP)Os(NO)(SPh) (TTP = tetratolylporphyrinato dianion, OEP = octaethylporphyrinato dianion) (19, 21).

In this paper, we report the synthesis and characterization of an extended series of (OEP)Os(NO)(SR) compounds. We also report the single-crystal X-ray structures of an RSNO and (OEP)Os(NO)(SR) pair of compounds. It is surprising that only three crystal structures of organic RSNO compounds had been reported prior to this work, despite the recognized importance of RSNO chemistry. This manuscript contains, to the best of our knowledge, the first RSNO–metal-complex pair to be characterized by spectroscopy or crystallography.

Experimental section

All reactions were performed under an atmosphere of prepurified nitrogen using standard Schlenk glassware and (or) in an Innovative Technology Labmaster 100 dry box. Solutions for spectral studies were also prepared under a nitrogen atmosphere. Solvents were distilled from appropriate drying agents under nitrogen just prior to use: CH_2Cl_2 (CaH_2), hexane (CaH_2), toluene (Na).

Chemicals

(OEP)Os(CO) (24) and (TTP)Ru(CO) (25) were prepared by literature methods. HBF_4 (54 wt% solution in Et_2O), $NOBF_4$, MeOH (99.8%, anhyd), isoamyl nitrite (*i*-$C_5H_{11}ONO$, 97%), *t*-BuONO (96%), ethane-1,2-dithiol ($HSCH_2CH_2SH$, 90+%), methanethiol (CH_3SH, 99.5+%), ethanethiol (C_2H_5SH, 97%), 2-propanethiol ($(CH_3)_2CHSH$, 97+%), 2-methyl-2-propanethiol ($(CH_3)_3CSH$, 99%), and *N*-acetylcysteamine (95%) were purchased from Aldrich Chemical Co. and used as received. The thionitrite $MeC(O)NHCH_2C(Me)_2SNO$ was prepared by a literature procedure (26). Chloroform-*d* (99.8%) was obtained from Cambridge Isotope Laboratories. Elemental analyses were performed by Atlantic Microlab, Norcross, Georgia. The thionitrites (RSNO) were generated in situ from the reaction of *t*-BuONO and their thiol precursors either at low temperature (R = Me) or at room temperature (R = Et, *i*-Pr, *i*-Bu).

Instrumentation

Infrared spectra were recorded on a Bio-Rad FT-155 FT IR spectrometer. Proton NMR spectra were obtained on Varian 400 MHz or 300 MHz spectrometers and the signals referenced to the residual signal of the solvent employed. All coupling constants are in Hz. FAB mass spectra were obtained on a VG-ZAB-E mass spectrometer. UV–vis spectra were recorded on a Hewlett–Packard model 8453 diode array instrument. Wavelengths are reported with ε values or as %-intensities for the samples whose yields were too small for accurate concentration measurements.

Preparation of (OEP)Os(NO)(SR) compounds (R = Me, Et, *i*-Pr, *t*-Bu)

These compounds were synthesized via a formal *trans*-addition of the RSNO across the metal center. The following reaction is representative:

To a stirred CH_2Cl_2 solution (20 mL) of (OEP)Os(CO) (0.080 g, 0.107 mmol) was added a previously prepared green mixture of 2-methy-2-propanethiol and *t*-BuONO (1:1.1 ratio by volume, 1:1 mol ratio, 0.16 mL in 4 mL of CH_2Cl_2, 10 min mixing time). The mixture was stirred for 30 min, during which it turned from pink red to slightly dark red. The solvent was removed in vacuo, the residue was dissolved in a CH_2Cl_2–hexane (1:3, 5 mL) mixture, and filtered through a neutral alumina column (2 × 20 cm) in air. The bright red band was collected, and the filtrate was dried in vacuo for 5 h to give (OEP)Os(NO)(S-*t*-Bu)·$0.9CH_2Cl_2$ (0.041 g, 0.045 mmol, 42% isolated yield). Low-resolution FAB-MS *m*/*z*: 813 $[(OEP)Os(SC(CH_3)_3)]^+$ (13%), 754 $[(OEP)Os(NO)]^+$ (100%), 724 $[(OEP)Os]^+$ (28%). UV–vis (λ, CH_2Cl_2) (nm): 357 (100), 446 (49), 551 (20), 585 (16). IR (CH_2Cl_2, cm^{-1}): υ_{NO} = 1758. IR (KBr, cm^{-1}): υ_{NO} = 1754 s; also 2964 m, 2932 m, 2871 m, 1468 m, 1452 m, 1382 w, 1375 w, 1316 w, 1272 m, 1154 m, 1112 w, 1056 m, 1021 m, 994 m, 963 m, 842 m, 745 m, 737 m, 718 w. ^1H NMR ($CDCl_3$) δ: 10.29 (s, 4H, *meso*-H of OEP), 5.28 (s, CH_2Cl_2), 4.14 (m, 16H, CH_2CH_3 of OEP), 1.96 (t, *J* = 8, 24H, CH_2CH_3 of OEP), –2.19 (s, 9H, $SC(CH_3)_3$). Anal. calcd. for $C_{40}H_{53}N_5O_1S_1Os_1$·$0.9CH_2Cl_2$: C 53.48, H 6.01, N 7.62, Cl 6.95, S 3.49; found: C 53.42, H 5.95, N 7.43, Cl 6.75, S 3.29.

The other (OEP)Os(NO)(SR) compounds were generated similarly. The MeSNO reagent was prepared at low temperature (–78°C) by reacting condensed methanethiol with *t*-BuONO in CH_2Cl_2.

(OEP)Os(NO)(SMe)

Isolated yield: 48%. Low-resolution FAB-MS *m*/*z*: 771 $[(OEP)Os(SCH_3)]^+$ (11%), 754 $[(OEP)Os(NO)]^+$ (100%), 724 $[(OEP)Os]^+$ (20%). UV–vis (λ (ε, mM^{-1} cm^{-1}), 1.64 × 10^{-5} M in CH_2Cl_2) (nm): 354 (53), 439 (28), 551 (12), 585 (9). IR (CH_2Cl_2, cm^{-1}): υ_{NO} = 1759. IR (KBr, cm^{-1}): υ_{NO} = 1755 s; also 2962 m, 2927 m, 2869 m, 1905 w, 1467 m, 1447 m, 1424 w, 1374 m, 1316 w, 1303 w, 1270 m, 1229 w,

© 2001 NRC Canada

1153 m, 1111 w, 1056 m, 1021 m, 994 m, 963 m, 873 w, 841 m, 802 w, 747 m, 737 m, 717 w. ^{1}H NMR ($CDCl_3$) δ: 10.33 (s, 4H, *meso*-H of OEP), 4.17 (m, 16H, C*H*$_2$CH$_3$ of OEP), 2.01 (t, *J* = 8, 24H, CH$_2$C*H*$_3$ of OEP), –3.11 (s, 3H, SC*H*$_3$).

(OEP)Os(NO)(SEt)

Isolated yield: 37%. Low-resolution FAB-MS *m*/*z*: 815 [(OEP)Os(NO)(SCH$_2$CH$_3$)]$^+$ (6%), 754 [(OEP)Os(NO)]$^+$ (100%), 724 [(OEP)Os]$^+$ (22%). UV–vis (λ, CH_2Cl_2) (nm): 354 (100), 441 (55), 551 (22), 585 (17). IR (CH_2Cl_2, cm^{-1}): υ_{NO} = 1758. IR (KBr, cm^{-1}): υ_{NO} = 1753 s; also 2964 m, 2929 m, 2868 m, 1640 w, 1584 w, 1466 m, 1450 m, 1373 w, 1314 w, 1272 m, 1230 w, 1153 m, 1112 w, 1057 m, 1021 m, 994 m, 964 m, 842 m, 802 w, 737 m, 718 w. ^{1}H NMR ($CDCl_3$) δ: 10.30 (s, 4H, *meso*-H of OEP), 4.15 (m, 16H, C*H*$_2$CH$_3$ of OEP), 2.00 (t, *J* = 8, 24H, CH$_2$C*H*$_3$ of OEP), –1.85 (t, *J* = 8, 3H, SCH$_2$C*H*$_3$), –3.12 (q, *J* = 8, 2H, SC*H*$_2$CH$_3$).

(OEP)Os(NO)(S-i-*Pr)*

Isolated yield: 33%. Low-resolution FAB-MS *m*/*z*: 799 [(OEP)Os(SCH(CH$_3$)$_2$)]$^+$ (12%), 754 [(OEP)Os(NO)]$^+$ (100%), 724 [(OEP)Os]$^+$ (29%). UV–vis (λ, CH_2Cl_2) (nm): 354 (100), 441 (53), 551 (21), 585 (16). IR (CH_2Cl_2, cm^{-1}): υ_{NO} = 1754. IR (KBr, cm^{-1}): υ_{NO} = 1751 s; also 2963 m, 2928 m, 2869 m, 1471 m, 1464 m, 1457 m, 1442 w, 1374 w, 1314 w, 1271 m, 1230 w, 1154 m, 1110 w, 1056 m, 1020 m, 993 m, 963 m, 841 m, 746 m, 737 m, 718 w. ^{1}H NMR ($CDCl_3$) δ: 10.30 (s, 4H, *meso*-H of OEP), 4.15 (q, *J* = 8, 16H, C*H*$_2$CH$_3$ of OEP), 1.98 (t, *J* = 8, 24H, CH$_2$C*H*$_3$ of OEP), –1.95 (d, *J* = 7, 6H, SCH(C*H*$_3$)$_2$), –4.03 (m, 1H, SC*H*(CH$_3$)$_2$).

Preparation of (OEP)Os(NO)(SCH$_2$CH$_2$SH)

A mixture of (OEP)Os(NO)(O-*i*-C$_5$H$_{11}$) (0.100 g, 0.119 mmol) (21) and excess HSCH$_2$CH$_2$SH (0.1 mL, 1.073 mmol) in toluene (20 mL) was refluxed under N_2 gas with vigorous stirring for 48 h. Color change of the solution was apparent. The solvent was removed in vacuo, and a ^{1}H NMR spectrum of the residue in $CDCl_3$ showed the presence of the desired thiolate–thiol product and some unreacted thiol. The residue was dissolved in CH_2Cl_2–hexane (2:1, 10 mL), and the solution was transferred to the top of a silica gel column (2 × 20 cm). Elution with a CH_2Cl_2–hexane (2:1) mixture in air yielded a pale red band and a bright red band. The pale red band was discarded and the bright red band was collected by eluting with CH_2Cl_2. The filtrate was dried in vacuo, the residue was dissolved in CH_2Cl_2–hexane (10 mL, 3:1), and slow evaporation of the solvent mixture in air gave (OEP)Os(NO)(SCH$_2$CH$_2$SH)·0.85CH_2Cl_2 (0.076 g, 0.083 mmol, 70% isolated yield). Low-resolution FAB-MS *m*/*z*: 817 [(OEP)Os(SCH$_2$CH$_2$SH)]$^+$ (5%), 754 [(OEP)Os(NO)]$^+$ (100%), 724 [(OEP)Os]$^+$ (24%). UV–vis (λ (ε, mM^{-1} cm^{-1}), 1.31 × 10^{-5} M in CH_2Cl_2) (nm): 354 (75), 443 (39), 551 (15), 585 (11). IR (CH_2Cl_2, cm^{-1}): υ_{NO} = 1764. IR (KBr, cm^{-1}): υ_{NO} = 1756 s; also 2964 m, 2932 m, 2870 m, 1690 w, 1467 m, 1451 m, 1373 m, 1316 w, 1272 m, 1230 w, 1154 m, 1111 w, 1057 m, 1021 m, 994 m, 964 m, 842 m, 746 m, 737 m, 716 w. ^{1}H NMR ($CDCl_3$) δ: 10.35 (s, 4H, *meso*-H of OEP), 5.28 (s, C*H*$_2$Cl$_2$), 4.18 (m, 16H, C*H*$_2$CH$_3$ of OEP), 2.02 (t, *J* = 8, 24H, CH$_2$C*H*$_3$ of OEP), –0.30 (t, *J* = 8, 1H, SCH$_2$CH$_2$S*H*), –1.17 (m, 2H, SCH$_2$C*H*$_2$SH), –2.76 (m, 2H, SC*H*$_2$CH$_2$SH). Anal. calcd. for $C_{38}H_{49}N_5O_1S_2Os_1$·0.85$CH_2Cl_2$: C 50.81, H 5.56, N 7.63, Cl 6.56, S 6.98; found: C 50.67, H 5.46, N 7.46, Cl 6.88, S 7.32.

Preparation of [(OEP)Os(NO)](μ-SCH$_2$CH$_2$S-*S*,*S*′)[Ru(NO)(TTP)]

To a CH_2Cl_2 (20 mL) solution of (OEP)Os(NO)(SCH$_2$CH$_2$SH)·0.85CH_2Cl_2 (0.020 g, 0.022 mmol) was added *t*-BuONO (5 μL, 0.04 mmol), and the reaction mixture was stirred for 10 min. To this solution was added (TTP)Ru(CO) (0.018 g, 0.022 mmol), and the solution was stirred for a further 10 min, during which time its color turned from dark red to brown-purple. The solvent was removed in vacuo, and a ^{1}H NMR spectrum of the residue in $CDCl_3$ showed the formation of a mixture of the desired mixed bimetallic [(OEP)Os(NO)](μ-SCH$_2$CH$_2$S-*S*,*S*′)[Ru(NO)(TTP)] and [(OEP)Os(NO)]$_2$(μ-SCH$_2$CH$_2$S-*S*,*S*′) (a singlet at –6.27 ppm) in a 70:1 ratio (by ^{1}H NMR spectroscopy), together with several unidentified products in 29% yield total. Attempts to obtain spectroscopically pure [(OEP)Os(NO)](μ-SCH$_2$CH$_2$S-*S*,*S*′)[Ru(NO)(TTP)] were unsuccessful, since it is unstable in solution and there is little difference in solubility between this air-sensitive product and its by-products. ^{1}H NMR ($CDCl_3$) δ: 9.81 (s, 4H, *meso*-H of OEP), 8.51 (s, 8H, *pyrrole*–H of TTP), 7.87 (br d, *J* = 7, 4H of TTP), 7.46 (m, 12H of TTP), 3.85 (m, 16H, C*H*$_2$CH$_3$ of OEP), 2.73 (s, 12H, C*H*$_3$ of TTP), 1.71 (t, *J* = 8, 24H, CH$_2$C*H*$_3$ of OEP), –5.92 (app m (see text), 2H, SC*H*$_2$CH$_2$S), –6.01 (app m (see text), 2H, SCH$_2$C*H*$_2$S).

Preparation of (OEP)Os(NO)(SCH$_2$CH$_2$NHC(O)Me)

A mixture of (OEP)Os(NO)(O-*i*-C$_5$H$_{11}$) (0.050 g, 0.059 mmol) (21) and excess HSCH$_2$CH$_2$NHC(O)Me (20 μL, 0.178 mmol) in xylene (20 mL) was refluxed under N_2 gas with vigorous stirring for 48 h. The solvent was removed in vacuo, and an ^{1}H NMR spectrum of the residue in $CDCl_3$ showed the presence of the desired thiolate product and unreacted thiol. The residue was dissolved in a CH_2Cl_2–hexane mixture (1:10, 55 mL), and this solution was kept at –20°C overnight. Precipitation of the solid was enhanced by mixing of the CH_2Cl_2–hexane solution, and the supernatant solution was discarded. The remaining solid product was dried in vacuo, the residue was dissolved in a CH_2Cl_2–hexane (1:1, 5 mL) mixture, and the solution was transferred to the top of a neutral alumina column (1.5 × 15 cm). Elution with hexane in air removed unreacted thiol, and then elution with CH_2Cl_2 yielded a bright red band. This bright red band was collected and taken to dryness in vacuo. The residue was dissolved in a CH_2Cl_2–hexane (2:1, 15 mL) mixture, and slow evaporation of the solvent mixture in air gave (OEP)Os(NO)(SCH$_2$CH$_2$NHC(O)Me) (0.034 g, 0.039 mmol, 66% isolated yield). Low-resolution FAB-MS *m*/*z*: 842 [(OEP)Os(SCH$_2$CH$_2$NHC(O)Me)]$^+$ (3%), 754 [(OEP)Os(NO)]$^+$ (100%), 724 [(OEP)Os]$^+$ (29%). UV–vis (λ (ε, mM^{-1} cm^{-1}), 1.61 × 10^{-5} M in CH_2Cl_2) (nm): 354 (60), 441 (32), 551 (13), 585 (10). IR (CH_2Cl_2, cm^{-1}): υ_{NO} = 1765; υ_{CO} = 1665. IR (KBr, cm^{-1}): υ_{NO} = 1756 s; υ_{CO} = 1642 m br; also 2964 m, 2930 m, 2870 m, 1465 m, 1444 m, 1372 m,

© 2001 NRC Canada

1273 m, 1230 w, 1154 m, 1111 w, 1056 m, 1020 m, 994 m, 963 m, 843 m, 745 m, 736 m, 717 w. ^{1}H NMR ($CDCl_3$) δ: 10.34 (s, 4H, *meso*-H of OEP), 4.16 (m, 16H, C*H*$_2$CH$_3$ of OEP), 2.47 (br, 1H, SCH$_2$CH$_2$N*H*C(O)CH$_3$), 2.00 (t, *J* = 8, 24H, CH$_2$C*H*$_3$ of OEP), 1.10 (s, 3H, SCH$_2$CH$_2$NHC(O)C*H*$_3$), 0.22 (m, 2H, SCH$_2$C*H*$_2$NHC(O)CH$_3$), –2.98 (m, 2H, SC*H*$_2$CH$_2$NHC(O)CH$_3$).

Preparation of (OEP)Os(NO)(SC(Me)$_2$CH$_2$NHC(O)Me)

To a stirred CH_2Cl_2 solution (20 mL) of (OEP)Os(CO) (0.080 g, 0.107 mmol) was added MeC(O)NHCH$_2$C(Me)$_2$SNO (0.019 g, 0.108 mmol). The mixture was stirred for l h, during which it turned from pink red to slightly dark red. The solvent was removed in vacuo, the residue was dissolved in CH_2Cl_2 (10 mL), and the solution was transferred to the top of an alumina column (2 × 20 cm). Elution with CH_2Cl_2 in air yielded a pale brown band and a bright red band. The pale brown band was discarded, and the bright red band was collected and taken to dryness in vacuo. The resulting red product was identified as (OEP)Os(NO)(SC(Me)$_2$CH$_2$NHC(O)Me) (0.021 g, 0.023 mmol, 21% isolated yield). Low-resolution FAB-MS *m*/*z*: 870 [(OEP)Os(SC(Me)$_2$CH$_2$NHC(O)Me)]$^+$ (22%), 754 [(OEP)Os(NO)]$^+$ (100%), 724 [(OEP)Os]$^+$ (22%). UV–vis (λ, CH_2Cl_2) (nm): 357 (100), 443 (48), 552 (20), 585 (17). IR (CH_2Cl_2, cm^{-1}): υ_{NO} = 1773; υ_{CO} = 1681. IR (KBr, cm^{-1}): υ_{NO} = 1764 s; υ_{CO} = 1656 s br; also 2964 m, 2932 m, 2872 w, 1561 m, 1510 m, 1465 m, 1450 m, 1370 m, 1275 m, 1231 w, 1154 m, 1112 w, 1057 m, 1022 m, 995 m, 963 m, 845 m, 749 vs, 717 w. ^{1}H NMR ($CDCl_3$) δ: 10.35 (s, 4H, *meso*-H of OEP), 4.16 (m, 16H, C*H*$_2$CH$_3$ of OEP), 1.98 (t, *J* = 8, 24H, CH$_2$C*H*$_3$ of OEP), 1.52 (br, 1H, SC(CH$_3$)$_2$CH$_2$N*H*C(O)CH$_3$), 1.23 (s, 3H, SC(CH$_3$)$_2$CH$_2$NHC(O)C*H*$_3$), –0.88 (d, *J* = 4, 2H, SC(CH$_3$)$_2$C*H*$_2$NHC(O)CH$_3$), –2.08 (s, 6H, SC(C*H*$_3$)$_2$CH$_2$NHC(O)CH$_3$).

Preparation of disulfide {MeC(O)NHCH$_2$C(Me)$_2$S-}$_2$ (*R′SSR′*)

A MeOH solution of green thionitrite MeC(O)NHCH$_2$C(Me)$_2$SNO (0.010 g, 0.057 mmol) was refluxed with vigorous stirring for 3 h under a nitrogen atmosphere, during which the color of the solution turned colorless. The solvent was dried in air, and a ^{1}H NMR spectrum of the residue in $CDCl_3$ showed the quantitative formation of the disulfide. ^{1}H NMR ($CDCl_3$) δ: 5.80 (br, 2H), 3.30 (d, *J* = 6, 4H), 2.00 (s, 6H), 1.26 (s, 12H). Low-resolution FAB-MS *m*/*z*: 293 [*R′SSR′*+ H]$^+$ (76%), 146 [*R′S*]$^+$ (15%), 114 [*R′*]$^+$ (100%).

This previously unreported disulfide was also prepared from the decomposition of thionitrite MeC(O)NHCH$_2$C(Me)$_2$SNO in a CH_2Cl_2–MeOH solution (1:10) by light. Suitable crystals for X-ray crystallography were grown from a CH_2Cl_2–MeOH (1:10) mixture of the thionitrite precursor that had been left at –10°C under nitrogen for 2 weeks. The X-ray data has been deposited in the *Supplementary material*.

Preparation of [(OEP)Os(NO)(O=C(Me)NHCH$_2$CH$_2$SH)]BF$_4$

To a stirred CH_2Cl_2 solution (15 mL) of (OEP)Os(CO) (0.020 g, 0.027 mmol) was added $NOBF_4$ (0.003 g, 0.026 mmol). The color of the solution changed from pink red to slightly dark red over a 30 min period, and an IR spectrum (CH_2Cl_2) showed the replacement of the 1883 cm^{-1} assigned to the υ_{CO} of (OEP)Os(CO) with a new band at 1833 cm^{-1} assigned to the υ_{NO} of [(OEP)Os(NO)]BF_4. Liquid HSCH$_2$CH$_2$NHC(O)Me (6 μL, 0.053 mmol) was then added to the reaction solution, and the mixture was stirred for 5 h. The solvent was removed in vacuo, and a ^{1}H NMR spectrum of the residue in $CDCl_3$ showed the presence of the desired product and unreacted thiol. The residue was dissolved in CH_2Cl_2–hexane (1:10, 55 mL), and this solution was kept at –20°C for 2 days. Precipitation of the product was enhanced by mixing of the CH_2Cl_2–hexane solution, and the supernatant solution was discarded. The precipitate was washed with hexane (5 × 50 mL), and then dissolved in CH_2Cl_2–hexane (2:1, 6 mL). Slow evaporation of the solution in a dry box gave [(OEP)Os(NO)(O=C(Me)NHCH$_2$CH$_2$SH)] BF_4·CH_2Cl_2 (0.010 g, 0.010 mmol, 38% isolated yield). Low-resolution FAB-MS *m*/*z*: 873 [(OEP)Os(NO)(O=C(Me)NHCH$_2$CH$_2$SH)]$^+$ (11%), 754 [(OEP)Os(NO)]$^+$ (100%), 724 [(OEP)Os]$^+$ (15%). UV–vis (λ, CH_2Cl_2) (nm): 346 (sh, 91), 361 (94), 421 (100), 539 (26), 575 (42). IR (CH_2Cl_2, cm^{-1}): υ_{NO} = 1826; υ_{CO} = 1603. IR (KBr, cm^{-1}): υ_{NO} = 1814 s; υ_{CO} = 1605 m; also 2964 m, 2932 m, 2873 m, 1574 m, 1466 m, 1450 m, 1441 m, 1378 w, 1357 w, 1315 w, 1274 m, 1230 w,1207 w, 1155 m, 1085 s, 1056 s, 1022 s, 996 s, 964 m, 849 m, 745 m, 736 m, 714 w. ^{1}H NMR ($CDCl_3$) δ: 10.54 (s, 4H, *meso*-H of OEP), 5.74 (br, 1H, HSCH$_2$CH$_2$N*H*C(O)CH$_3$), 5.28 (s, C*H*$_2$Cl$_2$), 4.23 (q, *J* = 8, 16H, C*H*$_2$CH$_3$ of OEP), 2.02 (t, *J* = 8, 24H, CH$_2$C*H*$_3$ of OEP), –0.01 (t, *J* = 9, 1H, *H*SCH$_2$CH$_2$NHC(O)CH$_3$), –0.41 and –0.53 (m's, 4H of HSC*H*$_2$C*H*$_2$NHC(O)CH$_3$), –3.04 (s, 3H, HSCH$_2$CH$_2$NHC(O)C*H*$_3$). Anal. calcd. for $C_{40}H_{53}N_6O_2S_1Os_1B_1F_4$·$CH_2Cl_2$: C 47.17, H 5.31, N 8.05; found: C 47.24, H 5.39, N 8.00.

The analogous [(OEP)Os(NO)(O=C(Me)NHCH$_2$C(Me)$_2$SH)]BF_4 compound was prepared similarly, in 46% isolated yield, by the sequential reaction of (OEP)Os(CO) with $NOBF_4$ followed by addition of the solid HSC(Me)$_2$CH$_2$NHC(O)Me reagent. Data for [(OEP)Os(NO)(O=C(Me)NHCH$_2$C(Me)$_2$SH)]BF_4: Low-resolution FAB-MS *m*/*z*: 901 [(OEP)Os(NO)(O=C(Me)NHCH$_2$C(Me)$_2$SH)]$^+$ (9%), 754 [(OEP)Os(NO)]$^+$ (100%), 724 [(OEP)Os]$^+$ (27%). UV–vis (λ, CH_2Cl_2) (nm): 348 (sh, 90), 362 (93), 420 (100), 538 (26), 574 (39). IR (CH_2Cl_2, cm^{-1}): υ_{NO} = 1826; υ_{CO} = 1599. IR (KBr, cm^{-1}): υ_{NO} = 1816 vs; υ_{CO} = 1594 s br; also 2968 s, 2933 s, 2871 m, 1470 m, 1464 m, 1452 m, 1379 w, 1352 w, 1274 m, 1156 m, 1112 w, 1085 m, 1056 s, 1023 s, 996 m, 965 m, 849 m, 745 m, 736 w, 716 w. ^{1}H NMR ($CDCl_3$) δ: 10.53 (s, 4H, *meso*-H of OEP), 5.73 (br, 1H, HSC(Me)$_2$CH$_2$N*H*C(O)CH$_3$), 4.22 (q, *J* = 8, 16H, C*H*$_2$CH$_3$ of OEP), 2.02 (t, *J* = 8, 24H, CH$_2$C*H*$_3$ of OEP), –0.14 (s, 1H, *H*SC(Me)$_2$CH$_2$NHC(O)CH$_3$), –0.56 (s, 6H, HSC(*Me*)$_2$CH$_2$NHC(O)CH$_3$), –0.71 (d, *J* = 6, 2H, HSC(Me)$_2$C*H*$_2$NHC(O)CH$_3$), –2.98 (s, 3H, HSC(Me)$_2$CH$_2$NHC(O)C*H*$_3$).

Protonation of (OEP)Os(NO)(SCH$_2$CH$_2$NHC(O)Me)

To a CH_2Cl_2 (10 mL) solution of (OEP)Os(NO)(SCH$_2$CH$_2$NHC(O)Me) (0.010 g, 0.011 mmol) was added HBF_4·Et_2O (0.9 μL, 0.012 mmol). The mixture was stirred overnight. The solvent was removed in vacuo, and an ^{1}H NMR spectrum of the residue in $CDCl_3$ showed the formation of a mixture of [(OEP)Os(NO)(O=C(Me)NHCH$_2$CH$_2$SH)]BF_4

© 2001 NRC Canada

and the known (OEP)Os(NO)F (27) in a 78:15 ratio based on integrations of the *meso*-Hs of their OEP ligands.

Protonation of (OEP)Os(NO)(SC(Me)$_2$CH$_2$NHC(O)Me)

To a CH_2Cl_2 (10 mL) solution of (OEP)Os(NO)-(SC(Me)$_2$CH$_2$NHC(O)Me) (0.010 g, 0.011 mmol) was added $HBF_4 \cdot Et_2O$ (0.9 μL, 0.012 mmol). The reaction was monitored by IR spectroscopy, and the reaction stopped when the IR spectrum in CH_2Cl_2 was almost identical to that of authentic [(OEP)Os(NO)(O=C(Me)NHCH$_2$C(Me)$_2$SH)]BF_4 (ca. 30 min). The solvent was removed in vacuo, and an ^{1}H NMR spectrum of the residue in $CDCl_3$ showed the formation of [(OEP)Os(NO)(O=C(Me)NHCH$_2$C(Me)$_2$SH)]BF_4 in 29% yield (by ^{1}H NMR spectroscopy). The reaction mixture was stirred for a further 2 h, the solvent was removed in vacuo, and a ^{1}H NMR spectrum of the residue in $CDCl_3$ showed the presence of [(OEP)Os(NO)(O=C(Me)-NHCH$_2$C(Me)$_2$SH)]BF_4, and the known (OEP)Os(NO)F in a 56:4 ratio, together with other as yet unidentified products. Further reaction overnight yielded, by ^{1}H NMR spectroscopy, [(OEP)Os(NO)(O=C(Me)NHCH$_2$C(Me)$_2$SH)]BF_4 and (OEP)Os(NO)F in a 67:7 ratio.

Structural determinations by X-ray crystallography

Crystal data were collected using monochromated Mo Kα radiation (λ = 0.71073 Å). Displacement ellipsoids in Figs. 1 and 2 are drawn at the 50% probability level. Details of the crystal data and refinement are given in Table 1 and in the Supporting Information.

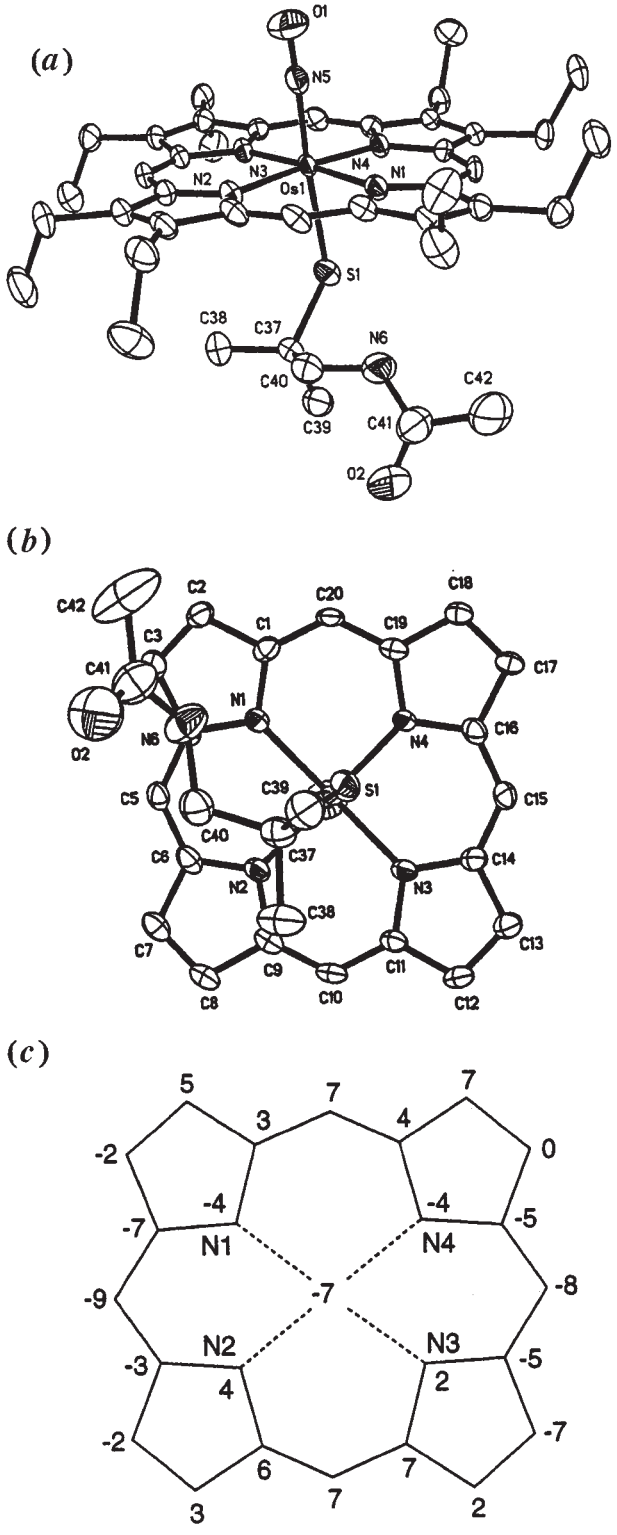
(i) (OEP)Os(NO)(SC(Me)$_2$CH$_2$NHC(O)Me)

A suitable crystal was grown from a CH_2Cl_2–hexane solution (5:1) left in air overnight. The data were corrected for Lorentz and polarization effects; and an empirical absorption correction based on ψ scans was applied. The structure was solved by the heavy atom method using the SHELXTL (Bruker) system, and refined by full-matrix least-squares on F^2 using all reflections (SHELXL-93). One of the methyl groups on the porphyrin ring (C24) is disordered at two sites, and both positions (C24a, C24b) were refined with 50% occupancy. Other atoms (C42, O1, and O2) are also slightly disordered as indicated by the large thermal motions of these atoms. The structure was solved and refined in both the noncentric space group $P1$ (no. 1) and the centric space group $P\bar{1}$ (no. 2). Better refinement was obtained in the $P\bar{1}$ space group. Hydrogen atoms were included in the refinement with idealized positions.

(ii) ONSC(Me)$_2$CH$_2$NHC(O)Me

The intensity data were measured as a series of ø oscillation frames each of 0.3° for 30 s per frame. Coverage of unique data was 99.6% complete to 25.00° in θ. Cell parameters were determined from a nonlinear least-squares fit of 3581 peaks in the range $2.63 < \theta < 26.76°$. The first 50 frames were repeated at the end of data collection and yielded 120 peaks showing a variation of 0.17% during the data collection. A total of 4483 data were measured in the range $2.98 < \theta < 27.10°$. A total of 100 parameters were refined against 1832 data to give $wR(F^2) = 0.1257$ and $S = 1.088$ for weights of $w = 1/[\sigma^2(F^2) + (0.0760P)^2 + 0.2300P]$, where $P = [F_o^2 + 2F_c^2]/3$. The final $R(F)$ was 0.0441 for the 1635 observed, $[F > 4\sigma(F)]$, data.

Fig. 1. (*a*) Molecular structure of (OEP)Os(NO)(SC(Me)$_2$CH$_2$NHC(O)Me). Hydrogen atoms have been omitted for clarity. (*b*) View along the general S(1)-Os(1) direction, showing the orientation of the axial thiolate with respect to the porphyrin skeleton. (*c*) Perpendicular atom displacements from the 24-atom porphyrin plane (in 0.01 Å units).

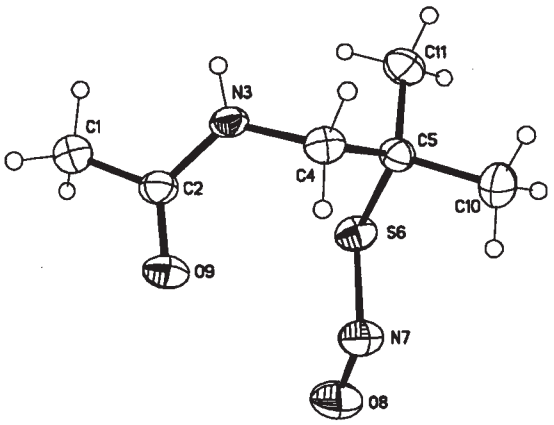


© 2001 NRC Canada

Table 1. Crystal data and structure refinement.

	$MeC(O)NHCH_2C(Me)_2SNO$	$(OEP)Os(NO)(S(Me)_2CH_2NHC(O)Me)$
Formula (fw)	$C_6H_{12}N_2O_2S$ (176.24)	$C_{42}H_{56}N_6O_2OsS$ (899.19)
T (K)	133(2)	173(2)
Diffractometer	Bruker SMART Platform CCD	Bruker P4
Crystal system	Monoclinic	Triclinic
Space group	$P2(1)/c$	$P\bar{1}$
Unit cell dimensions	a = 9.8139(7) Å, α = 90°	a = 10.445(2) Å, α = 84.657(9)°
	b = 9.8247(7) Å, β = 104.603(1)°	b = 11.116(2) Å, β = 78.327(13)°
	c = 9.7649(7) Å, γ = 90°	c = 17.173(2) Å, γ = 79.856(11)°
V (Å^3), Z	911.10(11), 4	1918.8(6), 2
D(calcd) (g cm^{-3})	1.285	1.556
Absorption coefficient (mm^{-1})	0.313	3.422
Max and min transmission	0.9231 and 0.8542	0.3415 and 0.2808
F(000)	376	916
Crystal size (mm)	0.52 × 0.52 × 0.26	0.32 × 0.22 × 0.14
θ range for data collection (deg)	2.98–27.10	1.86–25.00
Reflections collected	4483	7153
Independent reflections	1832 (R_{int} = 0.0306)	6753 (R_{int} = 0.0340)
Data / restraints / parameters	1832 / 0 / 100	6750 / 0 / 490
Goodness-of-fit on F^2	1.088	1.055
Observed no. of reflections [$I > 2\sigma(I)$]	1635	5959
R (F obsd data)	0.0441	0.0368
wR (F^2 all data)	0.1257	0.0927
Largest diff. peak and hole (e Å^{-3})	0.486 and –0.210	1.825 and –1.926

Fig. 2. Molecular structure of $ONSC(Me)_2CH_2NHC(O)Me$.

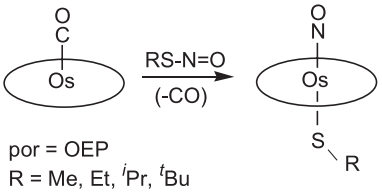


Results and discussion

Synthesis of nitrosyl thiolate complexes

The reaction of the alkyl thionitrites (RSNO: R = Me, Et, *i*-Pr, *t*-Bu) with the (OEP)Os(CO) compound generates, after appropriate work-up, the formal *trans*-addition products (OEP)Os(NO)(SR) in 33–48% isolated yields (eq. [1]).

[1]



The (OEP)Os(NO)(SR) nitrosyl thiolate products are red, moderately air-stable in solution, and can be stored in air in the solid state for at least 1 month with no noticeable decomposition. They are freely soluble in CH_2Cl_2 but only slightly soluble in hexane. These (OEP)Os(NO)(SR) nitrosyl thiolates are of the $\{OsNO\}^6$ formulation according to the Enemark–Feltham notation (28–30), and are expected to have linear Os-NO linkages. Their spectroscopic properties are consistent with their formulation as such. For example, their IR spectra reveal strong bands in the 1754–1759 cm^{-1} (CH_2Cl_2) or 1751–1755 cm^{-1} (KBr) ranges, which are indicative of terminal *N*-bound NO ligands for this class of compounds (23). This range is similar to that seen for related (OEP)Os(NO)(OR) alkoxide compounds (21, 31), but is higher than that seen for the organometallic (OEP)Os(NO)R compounds (1703–1748 cm^{-1}; R = alkyl, aryl) (27). In our previous work with the latter organometallic compounds, we showed that their υ_{NO}s decrease in the order (OEP)Os(NO)Me (1720 cm^{-1}) > (OEP)Os(NO)Et (1710 cm^{-1}) > (OEP)Os(NO)(*i*-Pr) (1703 cm^{-1}) ≈ (OEP)Os(NO)(*t*-Bu) (1703 cm^{-1}), consistent with increased electron donation of the R groups. Interestingly, however, the IR spectra of the alkyl *thiolate* (OEP)Os(NO)(SR) compounds in CH_2Cl_2 show that the υ_{NO}s fall in a very narrow range: (OEP)Os(NO)(SMe) (1759 cm^{-1}) ≈ (OEP)Os(NO)(SEt) (1758 cm^{-1}) ≈ (OEP)Os(NO)(S-*t*-Bu) (1758 cm^{-1}) > (OEP)Os(NO)(S-*i*-Pr) (1754 cm^{-1}). Clearly, the presence of the sulfur atom in these (OEP)Os(NO)(SR) compounds masks the direct interaction of the alkyl groups with the metal center, making a less dramatic variation in Os → NO back donation of electron density.

The ^{1}H NMR spectra of the (OEP)Os(NO)(SR) compounds in $CDCl_3$ reveal that the chemical shifts of the δ_{meso} protons of the OEP macrocycle decrease slightly from the (OEP)Os(NO)(SMe) (10.33 ppm) to the (OEP)Os(NO)(S-*t*-Bu) (10.29 ppm), consistent with a slight *cis*-influence of the

© 2001 NRC Canada

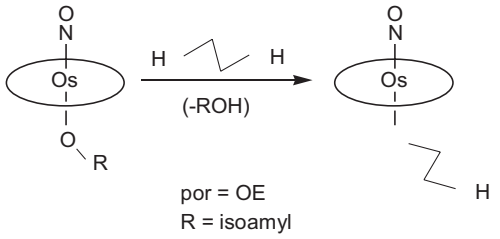
axial thiolate ligands. For comparison, the chemical shifts of the δ_{meso} protons in the related (OEP)Os(NO)(OR) *alkoxide* compounds are at 10.44 ppm (R = Me) or 10.32 ppm (R = Et, *i*-Pr, hexyl, cyclohexyl) (31). Buchler et al. (32) have previously examined similar *cis*-effects of axial ligands in (OEP)Os-containing compounds. The ^{1}H NMR spectra of these (OEP)Os(NO)(SR) compounds in $CDCl_3$ show that all the peaks due to the coordinated thiolate ligands are shifted upfield relative to those of the free thiols, consistent with the influence of the porphyrin ring current. Thus, the α-CH protons appear upfield at ca. –3.12 ppm (for the -SC*H*$_3$ and -SC*H*$_2$CH$_3$ compounds) and at –4.03 ppm for the SC*H*(CH$_3$)$_3$ derivative. Apparently, the presence of the two methyl substituents in the isopropyl group places the α-CH proton in closer proximity to the porphyrin ring current. The β-CH resonances for the thiolate ligands also appear upfield at –1.85 ppm (for SCH$_2$C*H*$_3$), –1.95 ppm (for SCH(C*H*$_3$)$_2$), and –2.19 ppm (for SC(C*H*$_3$)$_3$).

In general, the FAB-MS of the (OEP)Os(NO)(SR) compounds show ion fragments assigned to loss of the NO ligands or loss of the thiols. In the case of (OEP)Os(NO)(SEt), however, the mass spectrum also shows the parent ion at *m*/*z* 815.

Monometallic thiolate–thiol complex

The (OEP)Os(NO)(SCH$_2$CH$_2$SH) thiolate–thiol complex is prepared by an alkoxide–thiolate exchange reaction. Thus, the (OEP)Os(NO)(O-*i*-C$_5$H$_{11}$) alkoxide complex reacts with excess ethane-1,2-dithiol in toluene under refluxing conditions for 48 h to generate the monometallic thiolate–thiol derivative in 70% isolated yield as shown in eq. [2].

2



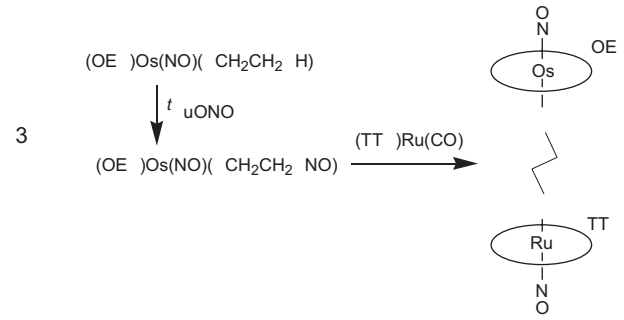
We note that high temperatures (e.g., refluxing toluene) and long reaction times (ca. 48 h by ^{1}H NMR spectroscopy) are required for this reaction to proceed with high yield. We found that this alkoxide–thiolate exchange method is more efficient in preparing this (OEP)Os(NO)(SCH$_2$CH$_2$SH) complex in high yields compared with the formal *trans*-addition reaction of eq. [1]. Unlike the ruthenium analog reported previously (22), this red (OEP)Os(NO)(SCH$_2$CH$_2$SH) compound is moderately air-stable in solution, showing no signs of decomposition for at least 8 h. It can also be stored in air in the solid state for at least 1 week without noticeable decomposition. This thiolate–thiol complex is freely soluble in CH_2Cl_2 but only slightly soluble in hexane.

The IR spectrum of this red product (as a KBr pellet) shows a band at 1756 cm^{-1} assigned to υ_{NO}. Its ^{1}H NMR spectrum shows, in addition to the characteristic OEP signals, peaks at –2.76 ppm (SC*H*$_2$CH$_2$SH), –1.17 ppm (SCH$_2$C*H*$_2$SH), and –0.30 ppm (SCH$_2$CH$_2$S*H*) assigned to the coordinated thiolate–thiol ligand. Although the FAB-MS does not show the parent ion, it shows ion fragments at *m*/*z* 817 (loss of the NO ligand) or at *m*/*z* 754 (loss of the thiolate–thiol ligand).

Bimetallic μ-dithiolate complex

Only a handful of bimetallic μ-dithiolate complexes are known (22, 33–40). We previously showed that the free -SH group in (por)Ru(NO)(SCH$_2$CH$_2$SH) can be nitrosated with *t*-BuONO (22). We have employed a similar methodology to prepare the intermediate (OEP)Os(NO)(SCH$_2$CH$_2$SNO) compound, which can then be reacted with (TTP)Ru(CO) to give the heterobimetallic [(OEP)Os(NO)](μ-SCH$_2$CH$_2$S-*S*,*S*′)[Ru(NO)(TTP)] derivative (eq. [3]) in 70% yield by ^{1}H NMR spectroscopy.

3



We have not yet been able to obtain a spectrocscopically pure sample of this air-sensitive compound. Thus, the ^{1}H NMR spectrum of the product mixture (of eq. [3]) shows, in addition to the signals for two porphyrin macrocycles (TTP and OEP), an AA′BB′ coupling pattern (41) consisting of two sets of peaks centered at ca. –5.92 ppm and –6.01 ppm (Fig. 3) assigned to the μ-SCH$_2$CH$_2$S- protons; spectral simulation gave $J_{AB'} = J_{A'B} = 13.4$ Hz, $J_{AA'} = J_{BB'} = -12.6$ Hz, $J_{AB} = 6$ Hz, $J_{A'B'} = 3.6$ Hz, and $\Delta\upsilon_{AB} = 43$ Hz. Due to the presence of two distinctly different metalloporphyrin moieties in this bimetallic derivative, it is not surprising that the AA′BB′ coupling pattern observed is almost identical to that of the related unsymmetrical [(TPP)Ru(NO)](μ-SCH$_2$CH$_2$S-*S*,*S*′)[Ru(NO)(OEP)] compound published previously (22).

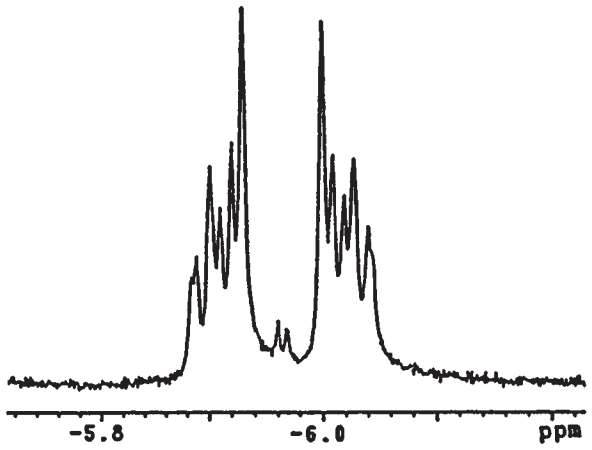
There are several notes of interest regarding the synthesis of [(OEP)Os(NO)](μ-SCH$_2$CH$_2$S-*S*,*S*′)[Ru(NO)(TTP)]. Reaction of the (OEP)Os(NO)(SCH$_2$CH$_2$SH) complex with (TTP)Ru(NO)(OR) did not produce the bimetallic derivative via the expected alkoxide–thiolate exchange reaction. In addition, we have found that the reaction of (OEP)Os(NO)(SCH$_2$CH$_2$SNO) with (TTP)Ru(CO) is more efficient in the formation of the desired bimetallic derivative than the reaction of (TTP)Ru(NO)(SCH$_2$CH$_2$SNO) with (OEP)Os(CO). Indeed, the latter reaction revealed the formation of the known [(TTP)Ru(NO)]$_2$(μ-SCH$_2$CH$_2$S-*S*,*S*′) (δ_{SCH_2} –5.73 ppm) compound (22) as a major product through an as yet unknown mechanism. In any event, the successful reaction of (OEP)Os(NO)(SCH$_2$CH$_2$SNO) with (TTP)Ru(CO) is consistent with our earlier observations that RSNO additions to (por)Ru(CO) were faster and cleaner than the analogous additions to (por)Os(CO) (19).

Amide-containing thiolate complexes

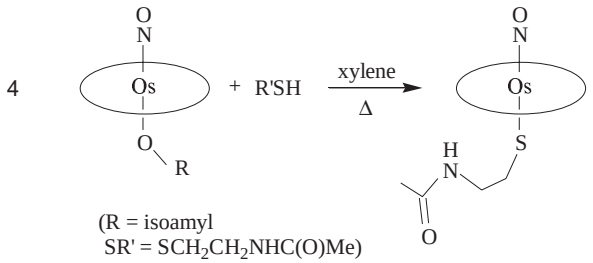
Organic thionitrites containing other heteroatoms are biologically relevant (10, 12). Examples of these include *S*-nitroso-*N*-acetyl-penicillamine, *S*-nitrosoglutathione, and *S*-nitrosocysteine. Part of our ongoing research effort is geared towards determining the preferred binding or reaction modes

© 2001 NRC Canada

Fig. 3. Upfield region of the 400 MHz ^{1}H NMR spectrum of [(OEP)Os(NO)](μ-SCH$_2$CH$_2$S-*S*,*S*′)[Ru(NO)(TTP)] in $CDCl_3$.



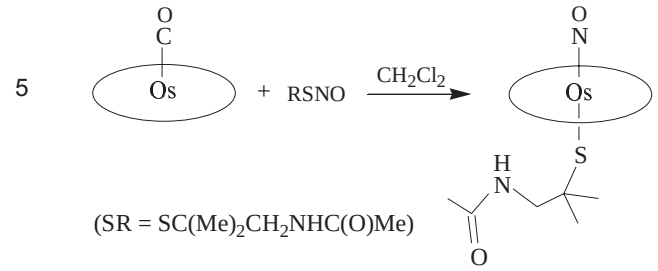
of such alkyl thionitrites with group 8 metalloporphyrins and heme. Reaction of the amide-containing *N*-acetylcysteamine thiol (containing a primary carbon atom next to sulfur) with (OEP)Os(NO)(O-*i*-C_5H_{11}) in refluxing xylene results in an alkoxide–thiolate exchange reaction to produce the desired (OEP)Os(NO)(SCH$_2$CH$_2$NHC(O)Me) product in 66% isolated yield (eq. [4]).



Relatively high temperatures are required for this reaction to proceed to completion. For example, the use of refluxing toluene (the solvent used in the related synthesis of (OEP)Os(NO)(SCH$_2$CH$_2$SH), vide supra) does not result in the reaction to form the product. Furthermore, the ^{1}H NMR spectrum of the crude product mixture in $CDCl_3$ (after reaction in refluxing xylene) only showed the presence of the desired thiolate complex and unreacted organic thiol, implying a quantitative conversion to the product in the high-temperature reaction.

This red (OEP)Os(NO)(SCH$_2$CH$_2$NHC(O)Me) product is moderately air-stable in solution and is stable in the solid state. It is readily soluble in CH_2Cl_2 and slightly soluble in hexane. Its IR spectrum shows bands at 1756 and 1642 cm^{-1} (KBr) assigned to υ_{NO} and υ_{CO}, respectively. The ^{1}H NMR spectrum of the compound in $CDCl_3$ shows that the chemical shift of the porphyrin *meso*-protons occur at 10.34 ppm, close to that observed for the other (OEP)Os(NO)(SR) complexes described earlier. All the peaks in the ^{1}H NMR spectrum due to the coordinated thiolate ligand are shifted upfield relative to those of the free thiol. For example, the peaks for the OsSC*H*$_2$- protons occur at –2.98 ppm, which is 5.63 ppm upshifted from that of the free thiol ligand (at 2.65 ppm). The FAB-MS of this compound shows ion fragments at *m*/*z* 842 (loss of the NO ligand) or at *m*/*z* 754 (loss of the thiol). We were not able to obtain suitable crystals of the compound for a crystallographic study.

We were successful in synthesizing the analogous (OEP)Os(NO)(SC(Me)$_2$CH$_2$NHC(O)Me) derivative (containing a tertiary carbon next to sulfur) by employing the formal *trans*-addition reaction described earlier in eq. [1]. Thus, reaction of 1 equiv of solid 1-(acetylamino)-2-methylpropane-2-thionitrite to the (OEP)Os(CO) compound results in the generation of the red (OEP)Os(NO)(SC(Me)$_2$CH$_2$NHC(O)Me) in 21% (nonoptimized) isolated yield (eq. [5]).



This red product can be stored in air in the solid state for at least 1 week without noticeable decomposition. Its IR spectrum as a KBr pellet shows bands at 1764 and 1656 cm^{-1} (KBr) assigned to υ_{NO} and υ_{CO}, respectively. The υ_{NO} band is slightly higher than those of the other (OEP)Os(NO)(SR) compounds described in this paper (1751–1756 cm^{-1}), however, it is within the range observed for linear NO ligands in (por)Os(NO)-containing complexes (23). The υ_{CO} of the amide group of the thiolate ligand is close to that of the precursor thionitrite (1655 cm^{-1}). The υ_{NO} and υ_{CO} bands of (OEP)Os(NO)(SC(Me)$_2$CH$_2$NHC(O)Me) are slightly shifted, by 8 cm^{-1} and 14 cm^{-1}, respectively, to higher wavenumbers relative to those of the (OEP)Os(NO)(SCH$_2$-CH$_2$NHC(O)Me) product of eq. [4]. The FAB-MS of this compound shows ion fragments at *m*/*z* 870 (loss of the NO ligand) or at *m*/*z* 754 (loss of the thiol). The ^{1}H NMR spectrum of (OEP)Os(NO)(SC(Me)$_2$CH$_2$NHC(O)Me) is also similar to that of the product of eq. [4], with the notable exception of the presence of the peak at –2.08 ppm due to the -SC(C*H*$_3$)$_2$CH$_2$- protons.

Prior to this study, only one X-ray structural determination of a (por)Os(NO)(SR) complex had been reported in the literature, namely that of (TTP)Os(NO)(S-*i*-C_5H_{11}) (19). We were able to obtain single crystals of the (OEP)Os(NO)(SC(Me)$_2$CH$_2$NHC(O)Me) product suitable for X-ray crystallography. The molecular structure is shown in Fig. 1*a*, and the thiolate orientation and porphyrin atom displacements are shown in Figs. 1*b* and 1*c*, respectively.

Selected bond lengths and angles are listed in Table 2. The Os—N(O) and N—O bond lengths are 1.781(5) and 1.126(6) Å, respectively, and the Os-N-O bond is essentially linear with a bond angle of 176.8(5)°. The Os—N(por) bond lengths range from 2.060(4)–2.068(4) Å, which is within the 2.03–2.068 Å range observed for other structurally characterized Os^{II} porphyrins. The Os atom is displaced by 0.07 Å from the porphyrin plane towards the axial NO ligand, and porphyrin moiety exhibits a *ruffled* distortion (Fig. 1*c*). The axial Os—S distance is 2.415(2) Å, which is longer than the Os—S distances found in the only other structurally characterized osmium alkanethiolate complexes: 2.298(3)–2.323(3) Å

© 2001 NRC Canada

Table 2. Selected bond lengths and angles for (OEP)Os(NO)($SC(Me)_2CH_2NHC(O)Me$).

Bond lengths (Å)			
N(5)—O(1)	1.126(6)	Os(1)—S(1)	2.415(2)
Os(1)—N(5)	1.781(5)	S(1)—C(37)	1.855(5)
Os(1)—N(1)	2.062(4)	C(37)—C(40)	1.525(8)
Os(1)—N(2)	2.060(4)	C(40)—N(6)	1.455(8)
Os(1)—N(3)	2.068(4)	N(6)—C(41)	1.349(9)
Os(1)—N(4)	2.060(4)	C(41)—O(2)	1.196(9)
Bond angles (°)			
O(1)-N(5)-Os(1)	176.8(5)	N(5)-Os(1)-N(3)	90.5(2)
C(37)-S(1)-Os(1)	121.8(2)	N(2)-Os(1)-N(3)	90.0(2)
C(41)-N(6)-C(40)	124.3(6)	N(5)-Os(1)-N(4)	95.2(2)
C(38)-C(37)-C(39)	109.2(5)	N(2)-Os(1)-N(4)	175.7(2)
C(38)-C(37)-C(40)	107.9(5)	N(3)-Os(1)-N(4)	90.0(2)
C(39)-C(37)-C(40)	110.0(5)	N(1)-Os(1)-N(2)	89.7(2)
C(38)-C(37)-S(1)	111.4(4)	N(1)-Os(1)-N(3)	176.4(2)
C(39)-C(37)-S(1)	104.4(4)	N(1)-Os(1)-N(4)	90.0(2)
C(40)-C(37)-S(1)	113.8(4)	N(1)-Os(1)-N(5)	93.1(2)
N(6)-C(40)-C(37)	114.0(5)	N(1)-Os(1)-S(1)	87.91(12)
O(2)-C(41)-N(6)	122.0(7)	N(2)-Os(1)-S(1)	96.43(12)
O(2)-C(41)-C(42)	121.6(7)	N(3)-Os(1)-S(1)	88.58(12)
N(6)-C(41)-C(42)	116.5(7)	N(4)-Os(1)-S(1)	79.26(12)
N(5)-Os(1)-N(2)	89.1(2)	N(5)-Os(1)-S(1)	174.36(14)

for $Os(SCH_2Ph)_2[(BA)_2en]$ (where $(BA)_2en$ is the bis(benzoylacetone) ethylenediimine dianion) (42), and 2.209(3) Å for (TTP)Os(NO)(S-*i*-C_5H_{11}) (19). The Os-S-C bond angle in (OEP)Os(NO)($SC(Me)_2CH_2NHC(O)Me$) is 121.8(2)°, which is larger than those observed in $Os(SCH_2Ph)_2[(BA)_2en]$ (107.8(4)–102.5(4)°) (42) and (TTP)Os(NO)(S-*i*-C_5H_{11}) (111.8(5)°) (19). The thiolate S—C37 bond essentially eclipses a porphyrin nitrogen, with the C37-S-Os-N2 torsion angle of 10.5(2)° (Fig. 1*b*). The thiolate Os-S-C37 angle is 121.8(2)°, and the corresponding S-C37-C40 angle is 113.8(4)°. The amide NH and C=O groups are in their usually favored *trans* arrangement (43), and the N6-C40-C37-S1 torsion angle is 52.8(6)°. The overall structure is similar to that seen for the ruthenium analogue reported earlier (20).

The molecular structure of the precursor $ONSC(Me)_2CH_2NHC(O)Me$ thionitrite is shown in Fig. 2, and selected bond lengths and angles are collected in Table 3.

Surprisingly, only three other RSNO solid-state structures have been reported in the literature, namely those of *S*-nitroso-*N*-acetylpenicillamine, Ph_3CSNO, and *S*-nitrosocaptopril (44–47). Their selected structural parameters are shown in Table 4, as are those for $ONSC(Me)_2CH_2NHC(O)Me$. The thionitrite functionality of $ONSC(Me)_2CH_2NHC(O)Me$ (Fig. 2) exists in an *anti* orientation, similar to that seen in *S*-nitroso-*N*-acetylpenicillamine and Ph_3CSNO. The N(7)-S(6)-C(5)-C(4) torsion angle is 66.65(12)°, whereas that of S(6)-C(5)-C(4)-N(3) is 54.10(17)°. Examination of the metrical parameters of $ONSC(Me)_2CH_2NHC(O)Me$ and those of its Os derivative (Fig. 1) reveal an expanded bond angle around the sulfur atom in the Os compound (121.8(2)°) relative to that in the free thionitrite (99.44(8)°). Furthermore, the amide C=O bond length of 1.232(2) Å in the free thionitrite is slightly longer than that in the Os derivative (1.196(9) Å), however, this may be a result of the moderate *inter*molecular C=O···HN hydrogen-bonding (48) observed in the crystal structure of the thionitrite (see *Supplementary material*).

Table 3. Selected bond lengths and angles for $ONSC(Me)_2CH_2NHC(O)Me$.

Bond lengths (Å)			
N(7)—O(8)	1.206(2)	C(2)—O(9)	1.232(2)
S(6)—N(7)	1.754(2)	C(2)—N(3)	1.343(2)
S(6)—C(5)	1.829(2)	N(3)···O(9)[a]	2.902(2)
Bond angles (°)			
O(8)-N(7)-S(6)	114.90(16)	C(4)-N(3)-C(2)	122.25(14)
N(7)-S(6)-C(5)	99.44(8)	N(3)-C(2)-C(1)	115.83(15)
S(6)-C(5)-C(4)	110.80(10)	N(3)-C(2)-O(9)	122.37(16)
C(5)-C(4)-N(3)	114.25(13)	C(1)-C(2)-O(9)	121.80(16)

[a]This represents an interaction between adjacent molecules, and is the distance between the amide nitrogen and the carbonyl group of a different molecule.

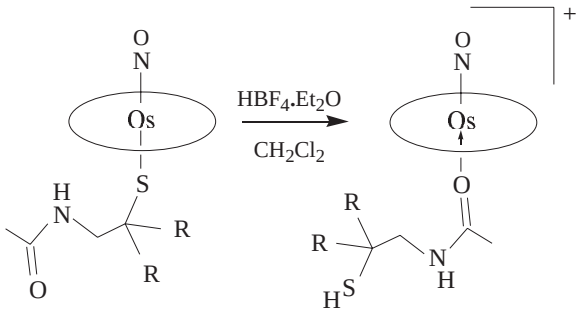
Protonation reactions

We have recently demonstrated that osmium nitrosyl porphyrins containing alkoxide ligands can be readily protonated to give the corresponding cationic derivatives containing labile alcohol ligands (e.g., eq. [6]) (31).

[6] $$(OEP)Os(NO)(OEt) \xrightarrow{H^+} [(OEP)Os(NO)(HOEt)]^+$$

We were thus interested in extending this protonation chemistry to the related thiolate ligated complexes. In general, protonation of the amide-containing (OEP)Os(NO)($SC(R)_2CH_2NHC(O)Me$) complexes (R = H, CH_3) with tetrafluoroboric acid in CH_2Cl_2 results in the formation of the amide-bound derivative shown in eq. [7].

7



(R = H, Me)

For the case where R = H, the amide-bound $[(OEP)Os(NO)(O=C(Me)NHCH_2CH_2SH)]BF_4$ derivative was obtained in 78% yield (by ^1H NMR spectroscopy). Monitoring this reaction (R = H) by IR and ^1H NMR spectroscopy reveals the simultaneous formation of the (OEP)Os(NO)F compound, the latter presumably from fluoride abstraction from the tetrafluoroborate anion in $[(OEP)Os(NO)]BF_4$. We also obtained the elementally pure amide-bound cationic [(OEP)Os(NO)(O=C(Me)NH-

© 2001 NRC Canada

Table 4. Metric parameters (in Å and deg) for structurally characterized alkyl thionitrites.

Compound	N-O	S-N	C-S	S-N-O	C-S-N	ϕ^a	Ref.
$ONSC(Me)_2CH_2NHC(O)Me$	1.206(2)	1.754(2)	1.829(2)	114.9(2)	99.44(8)	178.51	*This work*
S-Nitroso-*N*-acetyl-penicillamine[b]	1.199(2)	1.763(2)	1.833(1)	113.99(11)	100.80(7)	176.3	44, 45
S-Nitroso-*N*-acetyl-penicillamine[c]	1.206(3)	1.762(3)	1.842	114.9(2)	96.56(8)	179.7	46
Ph_3CSNO	1.177(6)	1.792(5)	1.867(3)	114.0(4)	102.1(2)	175.7	46
S-Nitrosocaptopril	1.206	1.766	1.800	117.7	103.7	0.68	47

[a]Defined as the O-N-S-C torsion angle.
[b]Crystallized from methanol–water.
[c]Crystallized from acetonitrile.

$CH_2CH_2SH)]BF_4$ product in 38% isolated yield from the sequential reaction of (OEP)Os(CO) with $NOBF_4$ (to produce $[(OEP)Os(NO)]BF_4$), followed by addition of the amide–thiol reagent. This cationic product of eq. [7] (R = H) is air-stable in the solid state. Its IR spectrum shows bands at 1814 and 1605 cm^{-1} (KBr) assigned to υ_{NO} and υ_{CO}, respectively. The υ_{NO} is 58 cm^{-1} higher than that of the neutral thiolate-bound precursor, consistent with less Os → NO back donation in this cationic complex. Furthermore, the shift in υ_{CO} of the coordinated amide–thiol ligand from 1642 cm^{-1} in the neutral precursor to 1605 cm^{-1} in the cationic derivative indicates a reduction in the C=O bond order in the cationic product complex, consistent with *O*-binding of the amide functional group. We have observed a similar IR spectral change in the related protonation reaction of $(OEP)Ru(NO)(SC(Me)_2CH_2NHC(O)Me)$, for which we were able to obtain X-ray crystal structures of both the thiolate-bound starting complex and the amide-bound product (20). The ^1H NMR spectrum of the cationic product of eq. [7] (R = H) shows that the SCH_2- and the amide N*H* peaks are shifted *downfield* from those of the coordinated thiolate in the precursor neutral complex (consistent with a placement of these groups further from the metal center). More striking is the upfield shift of the amide $C(CH_3) = O$ protons, indicative of an amide-bound form of the thiol ligand in the cationic product complex. The FAB-MS of this compound shows ion fragments at *m*/*z* 873 (loss of BF_4) or *m*/*z* 754 (loss of BF_4 and amide–thiol).

When R = CH_3 in eq. [7], the $[(OEP)Os(NO)(O=C(Me)NHCH_2C(Me)_2SH)]BF_4$ product is obtained in 67% yield (by ^1H NMR spectroscopy). The known fluoride (OEP)Os(NO)F compound (27) is the major by-product in this reaction. Not unexpectedly, we were also able to obtain this cationic product (in 46% isolated yield) from the reaction of in situ generated $[(OEP)Os(NO)]BF_4$ with the organic thiol. Similar by-products to those formed in the protonation reaction (eq. [7]) are also observed. This red compound is moderately air-stable in solution, showing signs of decomposition to the known (OEP)Os(NO)F complex in solution over a 1 week period. However, it is air-stable in the solid state. The υ_{NO} of the cationic product (as a KBr pellet) is 52 cm^{-1} higher than that of the neutral precursor. As was the case where R = H, the shift in υ_{CO} of the coordinated ligand from 1656 cm^{-1} in the neutral osmium thiolate precursor to 1594 cm^{-1} in the cationic derivative indicates a lowering of the C=O bond order in this amide-bound form of the thiol ligand in the cationic product complex. The ^1H NMR spectrum of this red compound (in $CDCl_3$) reveals that the $C(CH_3)$=O peak (at –2.98 ppm) is shifted by 4.21 ppm upfield from that of the thiolate precursor, a feature consistent with amide-binding to the metal center. We have not as yet been able to obtain suitable crystals of these cationic complexes for X-ray studies. We have also not been able to isolate or detect the putative thiol-bound $[(OEP)Os(NO)(HSR)]^+$ intermediates. Further studies to obtain stable thiol-bound derivatives are in progress.

Conclusion

In summary, we have prepared a new series of stable nitrosyl thiolate (OEP)Os(NO)(SR) complexes from (*i*) the formal *trans*-addition of thionitrites (RSNO) to the metal center in (OEP)Os(CO); or (*ii*) alkoxide–thiolate exchange reactions using (OEP)Os(NO)(OR) and the appropriate thiol. We have characterized these osmium nitrosyl thiolates by conventional spectroscopic techniques. Two such (OEP)Os(NO)(SR) complexes containing amide groups in the SR moieties have also been prepared. We have characterized, for the first time, a related pair of RSNO and (OEP)Os(NO)(SR) compounds by single-crystal X-ray crystallography. Protonation of the amide-containing thiolate complexes results in a net rearrangement of the protonated amide–thiol ligands to give the amide-bound cationic derivatives.

Acknowledgment

We thank the National Institutes of Health (GM53586) and the National Science Foundation (CHE-0076640) for support of this work. We also thank Dr. Li Chen for assistance during the preparation of this manuscript.

Supplementary material

Drawings and tables of crystallographic data for $(OEP)Os(NO)(SC(Me)_2CH_2NHC(O)Me)$, $ONSC(Me)_2CH_2NHC(O)Me$, and the disulfide $\{MeC(O)NHCH_2C(Me)_2S-\}_2$ may be purchased from the Depository of Unpublished Data, Document Delivery, CISTI, National Research Council Canada, Ottawa, ON K1A 0S2, Canada (http://www.nrc.ca/cisti/irm/unpub_e.shtml for information on ordering electronically). This material has also been deposited with the Cambridge Crystallographic Data Centre. Copies of the data can be obtained, free of charge, on application to the Director, CCDC, 12 Union Road, Cambridge CB2 1EZ, U.K. (Fax: 44-1223-336033 or e-mail: deposit@ccdc.cam.ac.uk).

© 2001 NRC Canada

References

1. J.S. Stamler, D.I. Simon, J.A. Osborne, M.E. Mullins, O. Jaraki, T. Michel, D.J. Singel, and J. Loscalzo. Proc. Natl. Acad. Sci. U.S.A. **89**, 444 (1992).
2. U.A. Mirza, B.T. Chait, and H.M. Lander. J. Biol. Chem. **270**, 17 185 (1995).
3. J.-W. Park. Biochem. Biophys. Res. Commun. **152**, 916 (1988).
4. J. S. Stamler. Cell (Cambridge, Mass.), **78**, 931 (1994).
5. M.P. Doyle, R.A. Pickering, and J. da Conceição. J. Biol. Chem. **259**, 80 (1984).
6. A.J. Gow and J.S. Stamler. Nature (London), **391**, 169 (1998).
7. T.J. McMahon and J.S. Stamler. Methods Enzymol. **301**, 99 (1999), and refs. therein.
8. R.P. Patel, N. Hogg, N.Y. Spencer, B. Kalyanaraman, S. Matalon, and V.M. Darley-Usmar. J. Biol. Chem. **274**, 15 487 (1999).
9. N.-L. Chan, P.H. Rogers, and A. Arnone. Biochemistry, **37**, 16 459 (1998).
10. A.R. Butler and P. Rhodes. Anal. Biochem. **249**, 1 (1997).
11. G.B. Richter-Addo. Acc. Chem. Res. **32**, 529 (1999).
12. D.L.H. Williams. Acc. Chem. Res. **32**, 869 (1999).
13. D.L.H. Williams. Nitrosation. Cambridge University Press, Cambridge, U.K. 1988.
14. A.R. Butler, F.W. Flitney, and D.L.H. Williams. TIPS, **16**, 18 (1995).
15. S. Oae and K. Shinhama. Org. Prep. Proced. Int. **15**, 165 (1983).
16. G.R. Upchurch Jr., G.N. Welch, and J. Loscalzo. Adv. Pharmacol. (San Diego), **34**, 343 (1995).
17. J. McAninly, D.L.H. Williams, S.C. Askew, A.R. Butler, and C. Russell. J. Chem. Soc. Chem. Commun. 1758 (1993).
18. G.-B. Yi, M.A. Khan, and G.B. Richter-Addo. Chem. Commun. 2045 (1996).
19. G.-B. Yi, L. Chen, M.A. Khan, and G.B. Richter-Addo. Inorg. Chem. **36**, 3876 (1997).
20. G.-B. Yi, M.A. Khan, D.R. Powell, and G.B. Richter-Addo. Inorg. Chem. **37**, 208 (1998).
21. L. Chen, M.A. Khan, and G.B. Richter-Addo. Inorg. Chem. **37**, 533 (1998).
22. J. Lee, G.-B. Yi, M.A. Khan, and G.B. Richter-Addo. Inorg. Chem. **38**, 4578 (1999).
23. L. Cheng and G.B. Richter-Addo. The porphyrin handbook. *Edited by* R. Guilard, K. Smith, and K.M. Kadish. New York. 2000. Chap. 33.
24. C.-M. Che, C.-K. Poon, W.-C. Chung, and H.B. Gray. Inorg. Chem. **24**, 1277 (1985).
25. D.P. Rillema, J.K. Nagle, L.F. Barringer Jr., and T.J. Meyer. J. Am. Chem. Soc. **103**, 56 (1981).
26. B. Roy, A. du Moulinet d'Hardemare, M. Fontecave. J. Org. Chem. **59**, 7019 (1994).
27. L. Cheng, L. Chen, H.-S. Chung, M.A. Khan, G.B. Richter-Addo, and V.G. Young Jr. Organometallics, **17**, 3853 (1998), and refs. therein.
28. J.H. Enemark and R.D. Feltham. Coord. Chem. Rev. **13**, 339 (1974).
29. R.D. Feltham and J.H. Enemark. Top. Stereochem. **12**, 155 (1981).
30. B.L. Westcott and J.H. Enemark. Transition metal nitrosyls. *Edited by* A.B.P. Lever and E.I. Solomon. New York. 1999.
31. L. Cheng, D.R. Powell, M.A. Khan, and G.B. Richter-Addo. Inorg. Chem. **40**, 125 (2001).
32. J.W. Buchler, W. Kokisch, and P.D. Smith. Struct. Bonding (Berlin), **34**, 79 (1978).
33. R. Narayanaswamy, M.A. Young, E. Parkhurst, M. Ouellette, M.E. Kerr, D.M. Ho, R.C. Elder, A.E. Bruce, and M.R.M. Bruce. Inorg. Chem. **32**, 2506 (1993).
34. W. Danzer, W.P. Fehlhammer, A.T. Liu, G. Thiel, and W. Beck. Chem. Ber. **115**, 1682 (1982).
35. D.W. Stephan. Organometallics, **10**, 2037 (1991).
36. T.D.P. Stack, M.J. Carney, and R.H. Holm. J. Am. Chem. Soc. **111**, 1670 (1989).
37. A. Aaliti, A.M. Masdeu, A. Ruiz, and C. Claver. J. Organomet. Chem. **489**, 101 (1995).
38. T.T. Nadasdi and D.W. Stephan. Organometallics, **11**, 116 (1992).
39. R.R. Holmes, S. Shafieezad, J.M. Holmes, and R.O. Day. Inorg. Chem. **27**, 1232 (1988).
40. H.M. Hoffmann and M. Dräger. Z. Naturforsch. B: Anorg. Chem. Org. Chem. **41B**, 1455 (1986).
41. F.A. Bovey, L. Jelinski, and P.A. Mirau. Nuclear magnetic resonance spectroscopy. Academic Press, San Diego. 1988. pp. 183–192.
42. W.E. Lynch, R.L. Lintvedt, and X.Q. Shui. Inorg. Chem. **30**, 1014 (1991).
43. H. Sigel and R.B. Martin. Chem. Rev. **82**, 385 (1982).
44. L. Field, R.V. Dilts, R. Ravichandran, P.G. Lenhert, and G.E. Carnahan. J. Chem. Soc. Chem. Commun. 249 (1978).
45. G.E. Carnahan, P.G. Lenhert, and R. Ravichandran. Acta Crystallogr. Sect. B: Struct. Crystallogr. Cryst. Chem. **B34**, 2645 (1978).
46. N. Arulsamy, D.S. Bohle, J.A. Butt, G.J. Irvine, P.A. Jordan, and E. Sagan. J. Am. Chem. Soc. **121**, 7115 (1999).
47. M.D. Bartberger, K.N. Houk, S.C. Powell, J.D. Mannion, K.Y. Lo, J.S. Stamler, and E.J. Toone. J. Am. Chem. Soc. **122**, 5889 (2000).
48. G.A. Jeffrey. An introduction to hydrogen bonding. *Edited by* D.G. Truhlar. Oxford University Press, New York. 1997. Table 2.1.

© 2001 NRC Canada

Pressure effects and solvent dynamics in the electrochemical kinetics of the tris(hexafluoroacetylacetonato)ruthenium(III)/(II) couple in nonaqueous solvents

Jinkui Zhou and Thomas W. Swaddle

Abstract: Rate constants and reactant diffusion coefficients for the $Ru(hfac)_3^{0/-}$ electrode reaction have been measured at 25°C as functions of pressure (0–200 MPa) in acetone, acetonitrile, methanol, and propylene carbonate. In sharp contrast to the negative volumes of activation $\Delta V_{ex}^{\ddagger}$ found for the corresponding bimolecular self-exchange reaction in organic solvents, the volumes of activation $\Delta V_{el}^{\ddagger}$ for the electrode reaction are markedly positive, ranging from 8 to 12 $cm^3\ mol^{-1}$. The volumes of activation $\Delta V_{diff}^{\ddagger}$ for reactant diffusion (which can be equated to the volume of activation $\Delta V_{visc}^{\ddagger}$ for viscous flow) range from 12 to 19 $cm^3\ mol^{-1}$. For the Debye solvents acetonitrile and acetone at least, $\Delta V_{el}^{\ddagger}$ is given within the experimental uncertainty by $\Delta V_{diff}^{\ddagger} + (\Delta V_{ex}^{\ddagger}/2)$. In this relation, the numerical value of $\Delta V_{diff}^{\ddagger}$ represents indirectly the dominant contribution of solvent dynamics (solvent friction) to $\Delta V_{el}^{\ddagger}$, and $\Delta V_{ex}^{\ddagger}/2$ represents the pressure dependence of the free-energy barrier height for the electrode reaction. It is proposed that solvent friction is important in nonaqueous electrode processes but not in the corresponding bimolecular self-exchange reactions because the free-energy activation barrier is twice as high in the latter.

Key words: electrode reaction kinetics, solvent dynamics, electron transfer mechanisms, pressure effects, volume of activation.

Résumé : On a mesuré les constantes de vitesse et les coefficients de diffusion des réactifs pour la réaction à l'électron du $Ru(hfac)_3^{0/-}$, à 25°C, en fonction de la pression (0–200 MPa), dans l'acétone, l'acétonitrile, le méthanol et le carbonate de propylène. En opposition avec les volumes négatifs observés pour les volumes d'activation, $\Delta V_{ex}^{\ddagger}$, de la réaction d'autoéchange bimoléculaire correspondante dans les solvants organiques, les volumes d'activation, $\Delta V_{el}^{\ddagger}$, pour la réaction à l'électrode sont très positifs, allant de 8 à 12 $cm^3\ mol^{-1}$. Les volumes d'activation, $\Delta V_{diff}^{\ddagger}$, pour la diffusion des réactifs (que l'on peut considérer comme égale au volume d'activation, $\Delta V_{visc}^{\ddagger}$, pour l'écoulement visqueux) vont de 12 à 19 $cm^3\ mol^{-1}$. Au moins pour les solvants de Debye, comme l'acétonitrile et l'acétone, $\Delta V_{el}^{\ddagger} = \Delta V_{diff}^{\ddagger} + (\Delta V_{ex}^{\ddagger}/2)$ aux erreurs expérimentales près. Dans cette équation, la valeur numérique de $\Delta V_{diff}^{\ddagger}$ représente indirectement la contribution dominante de la dynamique du solvant (friction du solvant) à $\Delta V_{el}^{\ddagger}$ alors que $\Delta V_{ex}^{\ddagger}/2$ représente la relation entre la pression et la hauteur de la barrière à l'énergie libre pour la réaction à l'électrode. On suggère que la friction du solvant est importante dans les processus non aqueux à l'électrode, mais qu'elle ne l'est pas dans les réactions correspondantes d'autoéchange bimoléculaire en raison du fait que, dans ce dernier cas, la barrière d'activation de l'énergie libre est deux fois plus élevée.

Mots clés : cinétique de la réaction à l'électrode, dynamique du solvant, mécanismes de transfert d'électron, effets de la pression, volume d'activation.

[Traduit par la Rédaction]

Introduction

It has recently been demonstrated (1–4) that, for transition-metal complex couples $ML_x^{z+/(z-1)}$ or $ML_x^{z-/(z+1)-}$ *in aqueous solutions*, a close proportionality exists between the volume of activation $\Delta V_{el}^{\ddagger}$ for the electrode reaction ($= -RT(\partial \ln k_{el}/\partial P)_T$, where k_{el} is the standard electrode reaction rate constant at zero driving force) and the corresponding parameter $\Delta V_{ex}^{\ddagger}$ for the bimolecular self-exchange reaction:

$$[1] \qquad \Delta V_{el}^{\ddagger} = (0.50 \pm 0.02)\Delta V_{ex}^{\ddagger}$$

This empirical observation, which is consistent with the corresponding relationship proposed by Marcus (5) for the free energies of activation

Received July 31, 2000. Published on the NRC Research Press Web site at http://canjchem.nrc.ca on June 30, 2001.

This article is dedicated to Professor Brian James — cherished friend, distinguished scholar, and inorganic kineticist par excellence.

J. Zhou and T.W. Swaddle.[1] Department of Chemistry, University of Calgary, Calgary, AB T2N 1N4, Canada.

[1]Corresponding author (telephone: (403) 220-5358; fax: (403) 284-1372; e-mail: swaddle@ucalgary.ca).

 DOI: 10.1139/cjc-79-5/6-841 © 2001 NRC Canada

[2] $\Delta G_{el}^{\ddagger} = \Delta G_{ex}^{\ddagger}/2$

holds with remarkable accuracy for all 15 couples tested to date, regardless of charge type,[2] and we therefore refer to it for convenience as the "50% rule". In the absence of complicating factors such as spin-state preequilibria (6) or catalysis by the counterions (7), $\Delta V_{ex}^{\ddagger}$ can be accounted for quantitatively (8) in terms of transition-state theory (TST) by an extension of Marcus' theory of adiabatic outer-sphere electron transfer reactions (9). The success of these calculations of $\Delta V_{ex}^{\ddagger}$ implies that, for couples in *aqueous* solution at least, $\Delta V_{el}^{\ddagger}$ can be also be accounted for theoretically.

The present paper addresses the question how $\Delta V_{el}^{\ddagger}$ relates to $\Delta V_{ex}^{\ddagger}$ in solvents *other than* water. As a first step in this direction, we recently examined the effects of pressure on the electrode kinetics of the $Co(bpy)_3^{3+/2+}$ couple in nonaqueous solvents as well as water (10)[3]. That choice was prompted by the discovery by Murray and co-workers (11, 12) that the electrode reaction rate constant k_{el} for $Co(bpy)_3^{3+/2+}$ in various organic solvents was proportional to the mean physical diffusion coefficient D of the complex ions and consequently (in accordance with the Stokes–Einstein relation — see below) inversely proportional to the viscosity η of the solvent over some 11 orders of magnitude. A marked viscosity dependence of the rate constant for any reaction that is plainly not diffusion-controlled is generally taken as evidence for control of the reaction rate by solvent dynamics (solvent "friction") (13–18). The relevant parameter is actually the longitudinal relaxation time τ_L of the solvent (19–27), but, for Debye solvents at least (i.e., ones in which dielectric relaxation can be modeled in terms of single spherical molecules rotating in a continuous viscous medium), η is usually proportional to τ_L.

These observations invite complementary variable-pressure kinetic studies, which have the advantage that the relevant nonaqueous solvent properties — notably η, but also the static dielectric constant ε_s and the optical dielectric constant ε_{op} ($\approx n^2$, where n is the refractive index) — can be "tuned" by varying the pressure for any one solvent individually without changing its chemical identity (10, 18). In particular, the assumption of a proportionality between η and τ_L is safer in pressure-tuning of a single solvent than in comparisons between solvents (18). Furthermore, because η is effectively *exponentially dependent* on pressure P over the first few hundred MPa for typical nonaqueous solvents but *almost independent* of P for water at near- or subambient temperatures (10), solvent dynamics in nonaqueous media can be expected to make a strongly positive contribution to $\Delta V_{el}^{\ddagger}$ in nonaqueous solvents but *none at all* in water at near-ambient temperatures. Thus, in organic solvents (but not in water), solvent dynamics, if rate-controlling, will make a large, positive contribution to $\Delta V_{el}^{\ddagger}$ that may overwhelm the moderately negative activation barrier height contribution expected from TST (10). Indeed, if solvent friction leads to a complete breakdown of TST, $\Delta V_{el}^{\ddagger}$ may be governed exclusively by the pressure dependence of τ_L (in effect, of η).

As anticipated, the observed $\Delta V_{el}^{\ddagger}$ values for $Co(bpy)_3^{3+/2+}$ in acetone, acetonitrile, and propylene carbonate turned out to be strongly positive (9–12 $cm^3\ mol^{-1}$, contrast –9 $cm^3\ mol^{-1}$ for water). The negative value of $\Delta V_{el}^{\ddagger}$ for *aqueous* $Co(bpy)_3^{3+/2+}$ is very similar to those found for $Co(en)_3^{3+/2+}$ and $Co(phen)_3^{3+/2+}$ (2) and can be accounted for theoretically (8), but it is not clear whether it implies that solvent friction is absent or simply that the near-independence of η on P for water fails to reveal it; in either case, $\Delta V_{el}^{\ddagger}$ in water can be equated with $\Delta V_{el(TST)}^{\ddagger}$. In any event, the difference in sign between $\Delta V_{el}^{\ddagger}$ in water and in nonaqueous media for the $Co(bpy)_3^{3+/2+}$ electrode reaction is a strong indication of solvent dynamical control of the reaction rate.

There remains, however, the possibility that association of $Co(bpy)_3^{2+}$ and particularly $Co(bpy)_3^{3+}$ with the supporting anions, which is expected to be of minor importance in water but dominant in typical organic solvents, could be responsible for the sharp contrast between the negative $\Delta V_{el}^{\ddagger}$ in water and the strongly positive $\Delta V_{el}^{\ddagger}$ in nonaqueous media. Indeed, the only known cases of positive $\Delta V_{el}^{\ddagger}$ or $\Delta V_{ex}^{\ddagger}$ for outer-sphere electron transfer reactions in water involve strong catalysis of anion–anion electron transfer by the counterions (cations) (3, 7). There is, however, no evidence for a comparable involvement of anions in cation-cation reactions, and furthermore Pyati and Murray (11) argue persuasively against ion pairing as a major contributor to the observed correlations of k_{el} for $Co(bpy)_3^{3+/2+}$ with D and η^{-1}. Nevertheless, the possibility of ion association introduces uncertainties into any analysis of $\Delta V_{el}^{\ddagger}$ data. A further limitation with respect to testing the 50% rule with $Co(bpy)_3^{3+/2+}$ is the absence of directly determined $\Delta V_{ex}^{\ddagger}$ values for this couple in any solvent (8).

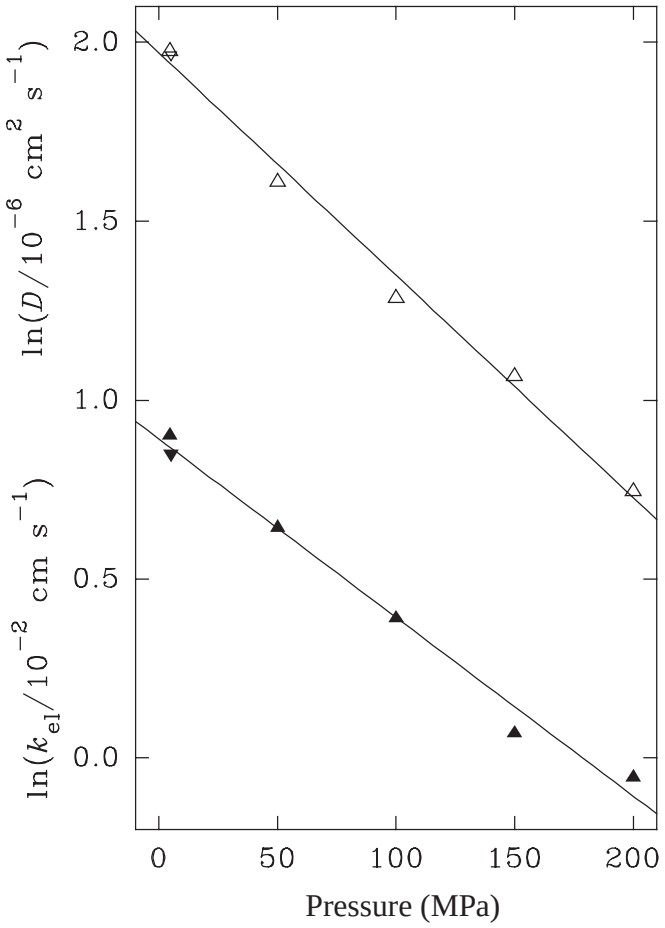
We have therefore turned our attention to the effects of pressure on the kinetics of electron transfer of the $Ru^{III}(hfac)_3/Ru^{II}(hfac)_3^-$ couple (28–31)[3] in polar organic solvents at an electrode, since $\Delta V_{ex}^{\ddagger}$ values are available for this couple in four organic solvents (29) and because ion pairing of the supporting electrolyte will not occur with the uncharged complex $Ru^{III}(hfac)_3$ and is expected to be minimal for $Ru^{II}(hfac)_3^-$ (indeed, Weaver and co-workers (32) found that ion pairing had only minor effects on the kinetics of the $Fe(\eta^5\text{-}C_5H_5)_2^{+/0}$ self-exchange in polar nonaqueous solvents). Furthermore, any effects of double-layer structure on electrode kinetics should be minimal for a neutral/low-charge couple (13). Similarly, Bjerrum–Brønsted–Christiansen theory predicts an absence of ionic strength effects on kinetics of reactions involving a zero-charged reactant, and coulombic work contributions to $\Delta V_{ex}^{\ddagger}$ and $\Delta V_{el}^{\ddagger}$ will also be effectively zero (8). Thus, since the contribution of internal reorganization is also expected to be very small (0 to +1 $cm^3\ mol^{-1}$), the theoretical $\Delta V_{ex(TST)}^{\ddagger}$ is given by the solvent reorganizational term $\Delta V_{SR}^{\ddagger}$ within the experimental uncertainty (29, 30). Values of $\Delta V_{ex}^{\ddagger}$ for the $Ru(hfac)_3^{0/-}$ self-

[2] The largest discrepancy in $\Delta V_{el}^{\ddagger}$ as predicted by eq. [1] was 1.7 $cm^3\ mol^{-1}$ for the diaminosarcophaginecobalt(III/II) couple $Co(diamsar)^{3+/2+}$ (6), which was also the only couple for which the measured electrochemical transfer coefficient α (= 0.27) deviated substantially from the ideal value of 0.5. In no other case did the discrepancy in $\Delta V_{el}^{\ddagger}$ exceed 1.0 $cm^3\ mol^{-1}$.

[3] 2,2′-Bipyridine (bpy), 1,2-diaminoethane (en), 1,10-phenanthroline (phen), 1,1,1,5,5,5-hexafluoroacetylacetonate ($hfac^-$), propylene carbonate (PC).

© 2001 NRC Canada

Fig. 1. Pressure dependences of the mean diffusion coefficient D ((△) ascending pressure, (▽) descending pressure) and electrode reaction rate constant k_{el} ((▲) ascending pressure, (▼) descending pressure) at 25.0°C for $Ru(hfac)_3^{0/-}$ ([Ru] = 2.25 mmol L^{-1}) in acetone containing 0.2 mol L^{-1} $[Bu_4N]PF_6$.



exchange reaction in methanol, acetonitrile, and acetone conform well to predictions based on TST (for chloroform, predictions are unrealistic because ε_s is too low) (30). Finally, there are no indications of solvent dynamical effects in this self-exchange reaction (28–31) or any other homogeneous self-exchange reaction for which $\Delta V_{ex}^{\ddagger}$ data are available (33), so that the experimental $\Delta V_{ex}^{\ddagger}$ can be identified with $\Delta V_{ex(TST)}^{\ddagger}$.

We show below that the experimental $\Delta V_{el}^{\ddagger}$ values for $Ru(hfac)_3^{0/-}$ turn out to be strongly positive, in contrast to the $\Delta V_{ex}^{\ddagger}$ values which are all negative (29). Unfortunately, the scope of our study was limited by the poor solubility of $Ru^{III}(hfac)_3$ in many solvents (notably water) and unsatisfactory electrochemical behavior in others (such as *N*,*N*-dimethylformamide). Of the four tractable solvent systems, methanol and propylene carbonate (PC) are non-Debye liquids and consequently pose difficulties in theoretical interpretation (13). Nevertheless, the positive $\Delta V_{el}^{\ddagger}$ observed for all these solvents are consistent with a substantial measure of rate control by solvent dynamics.

Experimental section

Materials

Acetonitrile (BDH, ACS Assured) was distilled three times. Acetone (EM Science, Omnisolv spectroscopic grade) was dried and distilled over $CaSO_4$ twice. Methanol (BDH, ACS Assured) was purified by refluxing over Mg for several hours, and then distilled. These solvents were stored over 4A molecular sieves. Propylene carbonate (Aldrich, Gold Label, sealed under N_2), tris(hexafluoroacetylacetonato)-ruthenium(III) (Strem), and tetrabutylammonium perchlorate and hexafluorophosphate (Fluka, puriss. electrochemical grade) were used as received.

Electrochemical measurements

Cyclic voltammetry (CV) and alternating current voltammetry (ACV) were carried out at 25.0 ± 0.1°C over ~50 MPa intervals, 0–200 MPa, as described previously (1–4, 10) with solutions containing 2.0–3.5 mmol L^{-1} $Ru(hfac)_3$ and 0.2 mol L^{-1} supporting electrolyte.[4] Solution samples were made up under dry N_2, placed in the three-electrode cell within the thermostated pressure vessel, and then purged with solvent-saturated N_2 for at least 40 min before the cell was closed. The working and counter electrodes were of Pt or Au wire (⌀ 0.5 mm). Results with Pt and Au electrodes were similar, but Pt gave better consistency and was used preferentially in the pressure experiments. The reference electrode was a silver rod in contact with a solution of 0.01 mol L^{-1} $AgClO_4$ and 0.2 mol L^{-1} Bu_4NClO_4 in CH_3CN. As the electrode reaction rates were rather low and decreased with rising pressure, the imposed AC frequency f was varied only between 25 and 45 Hz. Since the expression

$$[3] \qquad E_{max} = E_{1/2} + (RT/F) \ln [\alpha/(1 - \alpha)]$$

where E_{max} is the ACV peak potential and $E_{1/2}$ is the half-wave potential from the CVs, showed the transfer coefficient α to be 0.5 in all cases, the simplified relation

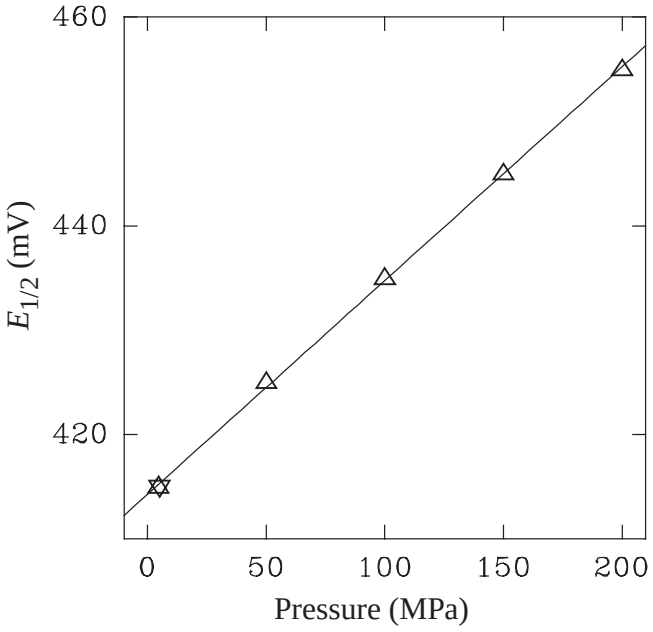
$$[4] \qquad \cot \phi = 1 + (D\omega/2)^{1/2}/k_{el}$$

where ϕ is the phase angle (corrected for the uncompensated resistance R_u) and $\omega = 2\pi f$, was used to calculate k_{el} (2, 10). R_u was measured directly at a relatively high frequency (8 kHz) and a potential at least 300 mV removed from $E_{1/2}$ (see *Supplementary information*). As expected for organic solvents, R_u was fairly high and increased markedly with rising pressure, especially for PC,[3] but the R_u values measured directly at each pressure were specifically used in calculating k_{el} as described previously (10). Thus, the k_{el} values and pressure dependence parameters reported here are not artifacts arising from R_u (cf. the concerns expressed by Weaver (19)). The useful range of f, though narrow, was sufficient to establish the linearity of the cot ϕ vs. $\sqrt{f}$ plots and to extract an average value of k_{el} (10). Only those cycles of variable-pressure measurements for which the initial and final low-pressure data agreed within the experimental uncertainty were accepted.

[4] Concentrations specified in this article are temperature- and pressure-independent, expressed as if at 22°C and 0.1 MPa.

© 2001 NRC Canada

Fig. 2. Pressure dependence of the half-wave potential $E_{1/2}$ ((△) ascending pressure, (▽) descending pressure) at 25.0°C for $Ru(hfac)_3^{0/-}$ ([Ru] = 2.25 mmol L^{-1}) in acetone containing 0.2 mol L^{-1} $[Bu_4N]PF_6$.



Results

Figures 1 and 2 show a sample set of pressure dependences of ln D, ln k_{el}, and $E_{1/2}$ for acetone as solvent; full details for all four solvents used are given in the *Supporting information*. The reaction volume ΔV_{cell} for $Ru(hfac)_3^{0/-}$ relative to Ag/Ag^+ ($= -F(\partial E_{1/2}/\partial P)_T$, where F is the faraday), the volume of activation $\Delta V_{diff}^{\ddagger}$ ($= -RT(\partial \ln D/\partial P)_T$) for diffusion of the reactants, and $\Delta V_{el}^{\ddagger}$ all appeared to be pressure-independent for a particular solvent over the experimental range (0–200 MPa) within the experimental uncertainty. Nevertheless, a small secondary dependence on pressure may be concealed (8), so that the values in Table 1 should be regarded as averages valid at 100 MPa, the midpoint of the pressure range. The derived electrochemical parameters are given in Table 1. To obtain optimal ACV measurements, it was necessary to adjust the electrode reaction rates by changing the identity or concentration of the supporting electrolyte between solvents, so that the k_{el} or ΔV_{cell} values given in Table 1 should not be directly compared. Fortunately, the pressure-dependence parameters are expected from past experience (34) to be rather insensitive to the nature or concentration of the supporting electrolyte in polar solvents such as those used in the present study. The lack of freedom of choice of supporting electrolyte precluded testing for ion pairing with the reactants, but in the $Ru(hfac)_3^{0/-}$ couple ion pairing is possible only for the reduced partner, and should be minimal in view of the large size and low charge of this anion (cf. Weaver and co-workers (32)). The values of k_{el} for $Ru(hfac)_3^{0/-}$ at the Pt electrode at atmospheric pressure are rather low, and may be compared with k_{el} = 0.015 cm s^{-1} reported by Weaver et al. (31) for the same couple at an annealed gold electrode in CH_3CN containing 0.1 mol L^{-1} tetraethylammonium perchlorate.

Discussion

A salient feature of the results in Table 1 is the sharp contrast between the moderately negative experimental values of the activation volumes for the $Ru(hfac)_3^{0/-}$ self-exchange reaction ($\Delta V_{ex}^{\ddagger}$ ~ –6 cm^3 mol^{-1}) and the strongly positive values for the electrode reaction ($\Delta V_{el}^{\ddagger}$ ~ +8 to +12 cm^3 mol^{-1}) in the same organic solvents. A rough correlation (but not equality) between $\Delta V_{el}^{\ddagger}$ and the activation volume $\Delta V_{diff}^{\ddagger}$ for the diffusion of the reactants is also clearly evident. We argue below that these facts indicate that the 50% rule (eq. [1]) does in fact hold for the solvents used here, but that its effect is swamped by a strongly positive contribution to $\Delta V_{el}^{\ddagger}$ from solvent dynamics, just as for the $Co(bpy)_3^{3+/2+}$ systems (10, 11, 12) but independently of any ion association effects that may have been present in the latter.

Solvent properties can affect the rate constant k for an electron transfer reaction directly in two principal ways. The first is through a contribution to the activation *barrier height*, represented by free energy of activation $\Delta G^{\ddagger}$ which comprises internal and solvent reorganizational components ($\Delta G_{IR}^{\ddagger}$ and $\Delta G_{SR}^{\ddagger}$, respectively):

$$[5] \qquad k = K_{prec}\kappa\nu_n\exp(-\Delta G^{\ddagger}/RT)$$

Here, κ is the electronic transmission coefficient (κ = 1 for adiabatic electron transfer) and ν_n the nuclear frequency factor, whereas K_{prec} is the equilibrium constant for assembly of a precursor state and effectively includes any coulombic work and medium (Debye–Hückel) terms (9). The second (solvent dynamical) way is through the influence of the *motions* of the solvent molecules on the electron transfer process, which can affect the *barrier crossing frequency* and hence influence k through ν_n. In an early paper, Kramers (35) treated the contribution of solvent dynamics to barrier climbing in the manner of a one-dimensional coupling of the Brownian motion to the reaction coordinate, an approach that has been further developed by others, notably Grote and Hynes (36). An alternative approach, originated by Agmon and Hopfield (37, 38) and developed first by Marcus and Sumi (39, 40) and Nadler and Marcus (41), and later by Basilevsky et al. (42, 43), treats the activation process in terms of a two-dimensional free energy surface with diffusive solvent motions represented along one coordinate and a low-frequency intramolecular vibration of the reactants along the other (21).

Following the Kramers–Grote–Hynes approach for the limiting case of adiabatic electron transfer in Debye liquids with a negligibly small $\Delta G_{IR}^{\ddagger}$ (10–17, 19–27), we have

$$[6] \qquad \nu_n = \tau_L^{-1}(\Delta G_{SR}^{\ddagger}/4\pi RT)^{1/2}$$

(Cases in which $\Delta G_{IR}^{\ddagger}$ is not negligible can be treated with the Sumi–Marcus theory (39, 40), considered below.) If the solvent behaves as a Debye liquid of Debye relaxation time τ_D, and V_M is the effective hard-sphere molar volume of the solvent molecules, τ_L can be obtained (at least approximately) (10–15, 23, 24, 27, 44) from

$$[7] \qquad \tau_L^{-1} = (\varepsilon_s/\varepsilon_{op})\tau_D^{-1} = (\varepsilon_s/\varepsilon_{op})RT/3V_M\eta$$

Here, η is properly the microscopic viscosity, but may be identified with the bulk viscosity of the solvent for our purposes. For a given reaction in different solvents, or (as in this work) in the same solvent over a range of pressure, the

© 2001 NRC Canada

Table 1. Electrochemical characteristics of $Ru(hfac)_3^{0/-}$ at a Pt wire electrode.[a]

Solvent	CH_3CN[b,c]	$(CH_3)_2CO$[d]	CH_3OH[e]	PC[f]
$E_{1/2}$ (mV)[g]	431 ± 2	414 ± 2	364 ± 2	369 ± 2
ΔV_{cell}^{g}	–24.8 ± 0.8	–19.8 ± 0.2	–18.3 ± 0.8	–13.0 ± 0.5
k_{el}^0 (10^{-2} cm s^{-1})	4.0 ± 0.1	2.44 ± 0.07	4.1 ± 0.1	2.26 ± 0.03
D^0 (10^{-6} cm^2 s^{-1})	8.1 ± 0.2	7.2 ± 0.2	7.3 ± 0.2	2.70 ± 0.03
$\Delta V_{el}^{\ddagger}$ (cm^3 mol^{-1})	8.4 ± 0.5	12.4 ± 0.7	9.9 ± 0.4	11.2 ± 0.3
$\Delta V_{diff}^{\ddagger}$ (cm^3 mol^{-1})	12.1 ± 0.7	15.4 ± 0.7	14.7 ± 0.7	18.5 ± 0.2
$\Delta V_{ex}^{\ddagger}$ (cm^3 mol^{-1})[h]	–5.5 ± 0.1	–6.1 ± 0.3	–5.8 ± 0.3	—
Q (cm^3 mol^{-1})[i]	–0.3	–0.3	–0.4	—
$\Delta V_{el}^{\ddagger}$ (calc)[i,j]	9.0 ± 0.7	12.1 ± 0.7	11.4 ± 0.7	—

[a][Ru] = 2.0–3.5 mmol L^{-1}, reference electrode Ag/(0.01 mol L^{-1} $AgClO_4$ – 0.20 mol L^{-1} Bu_4NClO_4-CH_3CN), 25.0°C.
[b]Supporting electrolyte 0.20 mol L^{-1} $[Bu_4N]ClO_4$.
[c]Weighted mean from two independent series of measurements.
[d]$[Bu_4N]PF_6$ (0.20 mol L^{-1}).
[e]$[Bu_4N]ClO_4$ (0.50 mol L^{-1}).
[f]$[Bu_4N]PF_6$ (0.50 mol L^{-1}).
[g]Relative to Ag/(0.0l mol L^{-1} $AgClO_4$ – 0.2 mol L^{-1} Bu_4NClO_4-CH_3CN).
[h]Reference 29.
[i]Calculated for the mid-range pressure of 100 MPa.
[j]Calculated from eq. [13].

dominant variable is η, and so in the simplest treatment we have

$$[8] \qquad \ln k \propto \ln k_{TST} - \ln \eta$$

From this follows an expression for the volume of activation $\Delta V^{\ddagger}$ for any reaction subject to Kramers–Grote–Hynes solvent dynamics:

$$[9] \qquad \Delta V^{\ddagger} = -RT(\partial \ln k/\partial P)_T = \Delta V_{TST}^{\ddagger} + RT(\partial \ln \eta/\partial P)_T = \Delta V_{TST}^{\ddagger} + \Delta V_{visc}^{\ddagger}$$

Literature values exist for the volume of activation $\Delta V_{visc}^{\ddagger}$ for viscous flow of acetonitrile (45), acetone (46), and methanol (46, 47) but are not entirely appropriate for the pressure range, temperature, and supporting electrolyte concentrations of our experiments. However, the Stokes–Einstein relation

$$[10] \qquad D = k_B T/C\pi a\eta$$

where a is the pressure-independent hydrodynamic radius, D is the mean diffusion coefficient of the reactant, and C is a constant (usually taken to be 6), allows us to substitute the volume of activation $\Delta V_{diff}^{\ddagger}$ for reactant diffusion (= $-RT(\partial \ln D/\partial P)_T$) for $\Delta V_{visc}^{\ddagger}$. Values of $\Delta V_{diff}^{\ddagger}$ are easily and accurately calculable from the variable-pressure CVs routinely obtained as a prerequisite for the ACV measurements (10), and have the advantage that they refer specifically to interactions between $Ru(hfac)_3^{0/-}$ and the solvent and (or) electrolyte of interest. Thus, we have

$$[11] \qquad \Delta V^{\ddagger} = \Delta V_{diff}^{\ddagger} + \Delta V_{TST}^{\ddagger}$$

or, more precisely from eqs. [6]–[10],

$$[12] \qquad \Delta V^{\ddagger} = \Delta V_{diff}^{\ddagger} + \Delta V_{TST}^{\ddagger} + Q$$

where $Q = -RT[(\partial \ln \varepsilon_s/\partial P)_T - 2(\partial \ln n/\partial P)_T + \Delta V_{SR}^{\ddagger}/2\Delta G_{SR}^{\ddagger}]$.

The solvent reorganizational terms $\Delta V_{SR}^{\ddagger}$ and $\Delta G_{SR}^{\ddagger}$ can be calculated as described elsewhere (8). If eqs. [1] and [2] apply, Q will be the same for self-exchange and electrode reactions, but in any case Q typically turns out to be small (Table 1). For the case where $\Delta G_{IR}^{\ddagger}$ is not negligible relative to $\Delta G_{SR}^{\ddagger}$ (we estimate $\Delta G_{IR}^{\ddagger}$ ~ 8.0 kJ mol^{-1} for the $Ru(hfac)_3^{0/-}$ self-exchange, cf. $\Delta G_{SR}^{\ddagger}$ ~ 8.5, 9.2, and 9.3 kJ mol^{-1} in acetone, acetonitrile and methanol respectively at 25°C and 0.1 MPa (31)), Q may be replaced by an analogous parameter Q' obtained by differentiation of eqs. [8.6] and [8.7] of ref. 39 with respect to pressure. It turns out that Q and Q' are the same within the experimental uncertainty — in other words, eq. [12] holds regardless of whether the internal reorganization barrier is negligible.

The strongly positive $\Delta V_{diff}^{\ddagger}$ and negative $\Delta V_{ex}^{\ddagger}$ values of Table 1 show that solvent dynamical effects on the *self-exchange* reaction kinetics are either minor or absent — the latter case is very likely because $\Delta V_{ex}^{\ddagger}$ for the $Ru(hfac)_3^{0/-}$ couple in CH_3CN, $(CH_3)_2CO$, and CH_3OH is accounted for fully by TST (29, 30). By the same token, however, the positive $\Delta V_{el}^{\ddagger}$ values imply that the electrode reaction is strongly influenced by solvent dynamics. Furthermore, for the Debye solvents acetonitrile and acetone at least, eq. [13] holds within the experimental uncertainty:

$$[13] \qquad \Delta V_{el}^{\ddagger} = \Delta V_{diff}^{\ddagger} + 0.5\Delta V_{ex}^{\ddagger} + Q$$

Comparison with eq. [12] indicates that, for the electrode reactions, $\Delta V_{TST}^{\ddagger}$ is given by $0.5\Delta V_{ex}^{\ddagger}$, i.e., that the 50% rule (eq. [1]) does in fact hold for nonaqueous solvents but the barrier-height contribution to $\Delta V_{el}^{\ddagger}$ is swamped by the pressure dependence of solvent friction.

Equation [13] is not expected to apply with methanol as solvent because of substantial hydrogen-bonding, in which case several solvent frequencies may contribute to the effective longitudinal relaxation time τ_L^{eff} leading to a non-Debye response (22, 48). Furthermore, although the Stokes–Einstein relation (eq. [10]) is valid for methanol, increasing the pressure in the range 0–400 MPa causes a shift from near the "sticking" boundary condition (C = 6.0) toward the "slipping" limit (C = 4.0) as pressure breaks up the methanol dimers

© 2001 NRC Canada

(49). This complication is absent in the cases of acetone and acetonitrile (50, 51). Not surprisingly, then, the agreement between the experimental $\Delta V_{el}^{\ddagger}$ and the prediction of eq. [13] for methanol is less close than for acetone and acetonitrile, yet it is better than might be expected, perhaps because of partial cancellation of the complicating factors. Unfortunately, $\Delta V_{ex}^{\ddagger}$ is not available for propylene carbonate, which in any event is a non-Debye solvent (13, 48).

The foregoing Kramers–Grote–Hynes-type treatment assumes that electron transfer in $Ru(hfac)_3^{0/-}$ at the electrode is adiabatic, i.e., that electronic coupling is sufficiently strong that solvent dynamics emerge as the rate-controlling factor. Certainly, the self-exchange reaction is as fast as other couples with low internal reorganization barriers (e.g., $Fe(phen)_3^{3+/2+}$ (33)), and the fact that $\Delta V_{ex}^{\ddagger}$ is accurately accounted for by the adiabatic TST model militates against significant nonadiabaticity which is expected to lead to anomalously negative $\Delta V_{ex}^{\ddagger}$ values (33). The $Ru(hfac)_3^{0/-}$ electrode reaction, however, is relatively slow (e.g., five times slower than the $Co(bpy)_3^{3+/2+}$ electrode reaction in CH_3CN, despite the greater $\Delta G_{IR}^{\ddagger}$ expected for the Co couple), and Weaver et al. (31) have proposed that it may be significantly nonadiabatic, i.e., that the electronic transmission coefficient κ may be substantially smaller than 1. This is unexpected, inasmuch as electrode reactions are ordinarily more fully adiabatic than the corresponding bimolecular self-exchange reactions, and in the case of $Ru(hfac)_3^{0/-}$ the latter appears to be adiabatic in nonaqueous solvents (29, 30). According to the Nadler–Marcus treatment (41) and experimental observations by McGuire and McLendon (52), the dependence of ν_n on τ_L can be more generally expressed as $\nu_n \propto \tau_L^{-\theta}$, where θ ranges from 1 when electron transfer is fully adiabatic and solvent coupling determines ν_n (cf. eq. [7]), to 0 for highly nonadiabatic cases where electronic coupling is completely dominant (21, 23, 24, 41, 52). For Debye solvents, eq. [13] can therefore be rewritten thus:

$$[14] \quad \Delta V_{el}^{\ddagger} = \theta[RT(\partial \ln \eta/\partial P)_T + Q] + \Delta V_{TST}^{\ddagger} = \theta(\Delta V_{diff}^{\ddagger} + Q) + (\Delta V_{ex}^{\ddagger}/2)$$

Here, $\Delta V_{TST}^{\ddagger}$ refers to the nonadiabatic case ($\kappa << 1$). The data of Table 1, however, suggest that $\theta \sim 0.87$–1.0, consistent with a high degree of adiabaticity of the $Ru(hfac)_3^{0/-}$ electrode reaction. Even if the contribution of $\Delta V_{TST}^{\ddagger}$ is simply ignored, $\theta \sim 0.6$–0.8, again suggesting only a small departure from adiabaticity.

If, however, we accept the conclusion of Weaver et al. (31) that the $Ru(hfac)_3^{0/-}$ electrode reaction is significantly nonadiabatic, we can estimate the contribution $\Delta V_{NA}^{\ddagger}$ of nonadiabaticity to $\Delta V_{el}^{\ddagger}$, as the electronic transmission coefficient κ_{el}, which depends on the electrode-reactant separation σ, will then approach 1 more closely as the pressure is increased (i.e., $\Delta V_{NA}^{\ddagger}$ will be *negative*) (53). This presupposes a Sutin model in which electron transfer occurs over a compressible reaction zone of thickness $\delta\sigma$ (nominally ~100 pm) rather than on hard contact (for which $\Delta V_{NA}^{\ddagger}$ would be 0), so that σ is pressure sensitive (54).

$$[15] \quad \kappa_{el} = \kappa_{el}^0 \exp[-\alpha(\sigma - \sigma^0)]$$

$$[16] \quad \Delta V_{NA}^{\ddagger} = -RT(\partial \ln \kappa_{el}/\partial P)_T = -\alpha\beta\sigma RT/3$$

In eqs. [15] and [16], κ_{el}^0 is the value of κ_{el} at the pressure-independent closest approach distance σ^0, β is the isothermal compressibility of the solvent, and the distance scaling factor α may be assumed to be about 16 nm^{-1} (54). For acetonitrile, acetone, and methanol, β is on the order of 6×10^{-10} Pa^{-1} at 25°C and the midrange pressure of 100 MPa (53). Taking the effective radius of $Ru(hfac)_3$ to be ~500 pm (so that $\sigma \sim 500$–600 pm), we find that $\Delta V_{NA}^{\ddagger}$ should not be more negative than about –5 $cm^3\ mol^{-1}$.

Thus, any contribution to $\Delta V_{el}^{\ddagger}$ from nonadiabaticity will be moderate in magnitude and *negative*, whereas our task is to explain why substantially *positive* values of $\Delta V_{el}^{\ddagger}$ are observed in nonaqueous media. In other words, any contribution of nonadiabaticity to $\Delta V_{el}^{\ddagger}$ would be far outweighed by that of solvent dynamics. The conflict between the conclusions of Weaver et al. (31) and the present findings may reflect difficulties inherent in making comparisons of electrochemical kinetics in chemically different solvents, a problem that the pressure-tuning approach circumvents.

Conclusions

An unequivocal result that emerges from the data of Table 1 is that the volumes of activation for the $Ru(hfac)_3^{0/-}$ electrode reaction in organic solvents are *all positive*, whereas for the corresponding parameters for self-exchange reactions are *all negative*. This is traceable to dependence of the electrode reaction rates on the organic solvent viscosities (which increase exponentially with pressure) because no such dichotomy in the direction of pressure effects on electrode and self-exchange reaction rates occurs in water (the viscosity of which is effectively independent of pressure at near-ambient temperatures). The viscosity-related pressure effect on nonaqueous electrode kinetics is attributable to the incursion of solvent friction; no such solvent dynamical influences are discernible in the homogeneous self-exchange reaction.

The numerical values of $\Delta V_{el}^{\ddagger}$ can be adequately accounted for by either the Kramers–Grote–Hynes or the Agmon–Hopfield–Sumi–Marcus approaches, at least for Debye solvents such as acetone and acetonitrile and surprisingly well for the non-Debye solvent methanol. The 50% rule (eq. [1]) appears still to be valid for nonaqueous solvents if the overwhelming solvent dynamical contributions to $\Delta V_{el}^{\ddagger}$ are taken into account.

It remains to be explained why solvent dynamics are manifest in electrode reactions but not self-exchange electron transfer, in nonaqueous systems (10). Equation [2] implies that $\Delta G^{\ddagger}$ for an electrode reaction is just one-half that for the corresponding self-exchange in homogeneous solution. In the case of $Ru(hfac)_3^{0/-}$ in the organic solvents considered here, the electrode reaction will therefore be over 1000-fold faster (on a common pseudo-first-order basis) than the already quite rapid self-exchange reaction on the basis of eq. [2] alone. Consequently, although the activation barrier height is kinetically dominant in bimolecular electron exchange, solvent dynamical control of barrier crossing can emerge in the electrode reaction.

The pressure dependence of rate constants in *aqueous* electron transfer reactions is not diagnostic of solvent friction at near-ambient temperatures because η for water is essentially independent of pressures on the order of 0–

© 2001 NRC Canada

200 MPa (10). It is possible, however, that electrode reactions in water may not be subject to solvent dynamical influences in the manner described above because of the extensive solvent–solvent hydrogen bonding and occurrence of ultrafast relaxation modes that are unique to water (55–57). Indeed, we have noted (10) that there appears to be an unidentified mechanistic difference between the electrode reactions of $Co(bpy)_3^{3+/2+}$ in organic solvents (where solvent friction is evidently dominant) and in water. Unfortunately, experimental comparison of organic and aqueous solutions is not possible for the $Ru(hfac)_3^{0/-}$ electrode reaction because of the insolubility of $Ru^{III}(hfac)_3$ in water.

Acknowledgements

We thank Dr. Noham Weinberg for discussions, and the Natural Sciences and Engineering Research Council of Canada (NSERC) for financial support.

Material on Deposit

Copies of material on deposit may be purchased from the Depository of Unpublished Data, Document Delivery, CISTI, National Research Council Canada, Ottawa, ON K1A 0S2, Canada (http://www.nrc.ca/cisti/irm/unpub_e.shtml for information on ordering electronically).

References

1. Y. Fu and T.W. Swaddle. Chem. Commun. 1171 (1996).
2. Y. Fu and T.W. Swaddle. J. Am. Chem. Soc. **119**, 7137 (1997).
3. Y. Fu and T.W. Swaddle. Inorg. Chem. **38,** 876 (1999).
4. P.D. Metelski, Y. Fu, K. Khan, and T.W. Swaddle. Inorg. Chem. **38**, 3103 (1999).
5. R.A. Marcus. Electrochim. Acta **13**, 995 (1968), and refs. therein.
6. R.D. Shalders and T.W. Swaddle. Inorg. Chem. **34**, 4815 (1995).
7. P.D. Metelski and T.W. Swaddle. Inorg. Chem. **38**, 301 (1999).
8. T.W. Swaddle. Can. J. Chem. **74**, 631 (1996), and refs. cited therein.
9. R.A. Marcus and N. Sutin. Biochim. Biophys. Acta, **811**, 265 (1985).
10. Y. Fu, A.S. Cole, and T.W. Swaddle. J. Am. Chem. Soc. **121**, 10410 (1999).
11. R. Pyati and R.W. Murray. J. Am. Chem. Soc. **118**, 1743 (1996).
12. M.E. Williams, J.C. Crooker, R. Pyati, L.J. Lyons, and R.W. Murray. J. Am. Chem. Soc. **119**, 10 249 (1997).
13. Z. Galus. Adv. Electrochem. Sci. Eng. **4**, 217 (1995).
14. X. Zhang, J. Leddy, and A.J. Bard. J. Am. Chem. Soc. **107**, 3719 (1985).
15. X. Zhang, H. Yang, and A.J. Bard. J. Am. Chem. Soc. **109**, 1916 (1987).
16. D.E. Khoshtariya, T.D. Dolidze, D. Krulic, N. Fatouros, and D Devilliers. J. Phys. Chem. B, **102**, 7800 (1998).
17. K. Winkler, N. McKnight, and W.R. Fawcett. J. Phys. Chem. B, **104**, 3575 (2000).
18. T. Asano. Pure Appl. Chem. **71**, 1691 (1999).
19. M.J. Weaver. Chem. Rev. **92**, 463 (1992).
20. M.J. Weaver. J. Mol. Liq. **60**, 57 (1994).
21. H. Heitele. Angew. Chem. Intl. Ed. Engl. **32**, 359 (1993).
22. J.T. Hynes. J. Phys. Chem. **90**, 3701 (1986).
23. W.R. Fawcett and M. Opallo. Angew. Chem. Int. Ed. Engl. **33**, 2131 (1994).
24. W.R. Fawcett and C.A. Foss, Jr. J. Electroanal. Chem. **270**, 103 (1989).
25. T. Gennett, D.F. Milner, and M.J. Weaver. J. Phys. Chem. **89**, 2787 (1985).
26. G.E. McManis, M.N. Golovin, and M.J. Weaver. J. Phys. Chem. **90**, 6563 (1986).
27. G. Grampp, W. Harrer, and W. Jaenicke. J. Chem. Soc. Faraday Trans. **1 83**, 161 (1987).
28. M.-S. Chan and A.C. Wahl. J. Phys. Chem. **86**, 126 (1982).
29. H. Doine and T.W. Swaddle. Inorg. Chem. **27**, 665 (1988).
30. H. Takagi and T.W. Swaddle. Chem. Phys. Lett. **248**, 207 (1996).
31. M.J. Weaver, D.K. Phelps, R.M. Neilson, M.N. Golovin and G.E. McManis. J. Phys. Chem. **94**, 2949 (1990).
32. R.M. Nielson, G.E. McManis, L.K. Safford, and M.J. Weaver. J. Phys. Chem. **93**, 2152 (1989).
33. H. Doine and T.W. Swaddle. Can. J. Chem. **66**, 2763 (1988).
34. T.W. Swaddle and P.A. Tregloan. Coord. Chem. Rev. **187**, 255 (1999).
35. H.A. Kramers. Physica (Amsterdam), **7**, 284 (1940).
36. R.F. Grote and J.T. Hynes. J. Chem. Phys. **73**, 2715 (1980).
37. N. Agmon and J.J. Hopfield. J. Chem. Phys. **78**, 6947 (1983).
38. N. Agmon and J.J. Hopfield. J. Chem. Phys. **79**, 2042 (1983).
39. H. Sumi and R.A. Marcus. J. Chem. Phys. **84**, 4894 (1986).
40. R.A. Marcus and H. Sumi. J. Electroanal. Chem. **204**, 59 (1986).
41. W. Nadler and R.A. Marcus. J. Chem. Phys. **86**, 3906 (1987).
42. M.V. Basilevsky, V.M. Ryaboy, and N.N. Weinberg. J. Phys. Chem. **94**, 8734 (1990).
43. M.V. Basilevsky, V.M. Ryaboy, and N.N. Weinberg. J. Phys. Chem. **95**, 5533 (1991).
44. D. Kivelson and H. Friedman. J. Phys. Chem. **93**, 7026 (1989).
45. O. Salman. Ph.D. Thesis, University of Illinois, 1982.
46. P.W. Bridgman. The physics of high pressure. G. Bell, London. 1931. p. 341.
47. H. Kubota, S. Tsuda, M. Murata, T. Yamamoto, Y. Tanaka, and T. Makita. Rev. Phys. Chem. Jpn. **49**, 59 (1979).
48. G. McManis and M.J. Weaver. J. Chem. Phys. **90**, 912 (1989).
49. J. Jonas and J.A. Akai. J. Chem. Phys. **66**, 4946 (1977).
50. T.E. Bull and J. Jonas. J. Chem. Phys. **52**, 2779 (1970).
51. T.E. Bull and J. Jonas. J. Chem. Phys. **53**, 3315 (1970).
52. M. McGuire and G. McLendon. J. Phys. Chem. **90**, 2549 (1986).
53. T.W. Swaddle. Inorg. Chem. **29**, 5017 (1990).
54. J.T. Hupp and M.J. Weaver. J. Electroanal. Chem. **152**, 1 (1983).
55. R. Jimenez, G.R. Fleming, P.V. Kumar, and M. Maroncelli. Nature (London), **369**, 471 (1994).
56. N. Agmon. J. Phys. Chem. **100**, 1072 (1996).
57. A. Nitzan. Nature (London), **402**, 472 (1999).

© 2001 NRC Canada

Kinetic modeling of homogeneous methanol synthesis catalyzed by base-promoted nickel complexes

Devinder Mahajan, Viwat Krisdhasima, and Robert D. Sproull

Abstract: Nickel complexes promoted by alkoxide bases can affect facile conversion of synthesis gas into methanol under thermodynamically favorable temperatures. At 100°C, syngas conversion of 99% with turnover frequency of 66 h^{-1} is reported. The reaction is truly catalytic in Ni as well as in base. A kinetic study of the $Ni(CO)_4$–KOMe catalyst system in 1,2-bis(2-methoxy ethoxy)ethane (triglyme)–MeOH solvent mixture is presented. The kinetic expression includes terms of zero-order in H_2 and first-order in CO with syngas of H_2–CO stoichiometry of ~2:1 and less than first-order in Ni (0.03–0.10 M), ~third-order in base (2.0–4.75 M), and an exponential dependence on methanol concentration (13.0–23.7 M at 2.0 M base; 15.8–22.6 M at 3.0 M base). The activation energy of 42.2 kJ mol^{-1} was estimated from the Arrhenius plot of the data between 374 and 393 K. Gas phase IR spectrum at the end of each run showed an intense signature peak at 2060 cm^{-1} for $Ni(CO)_4$. Process uncertainties to commercialization of this versatile homogenous catalyst system for CO hydrogenation to methanol are discussed.

Key words: homogeneous catalysis, syngas conversion, methanol synthesis, alkoxides, carbonyls of nickel.

Résumé : Des complexes de nickel activés par des bases de type alcoolate peuvent effectuer facilement la conversion du gaz de synthèse en méthanol, dans des conditions de température thermodynamiquement favorables. À 100°C, on observe une conversion à 99% du gaz de synthèse avec une fréquence de renouvellement de 66 h^{-1}. La réaction est vraiment catalytique tant en Ni qu'en base. On présente les résultats d'une étude cinétique du système $Ni(CO)_4$–KOMe dans un mélange de solvant 1,2-bis(2-méthoxyéthoxy)éthane (triglyme)–MeOH. L'expression cinétique comprend des termes d'ordre zéro en H_2 et du premier ordre en CO dans le gaz de synthèse de stoechiométrie H_2–CO d'environ 2:1, d'ordre inférieur à l'unité en Ni (0,03 à 0,10 M), du troisième ordre en base (2,0 à 4,75 M) et une dépendance exponentielle sur la concentration de méthanol (13,0 à 23,7 M à 2,0 M en base; 15,8 à 22,6 M à 3,0 M en base). On a évalué une énergie d'activation de 42,2 kJ mol^{-1} à l'aide d'une courbe d'Arrhenius des données entre 374 et 393 K. Les spectres infrarouges en phase gazeuse des produits à la fin de chaque réaction montrent tous une bande signature intense à 2060 cm^{-1} pour le $Ni(CO)_4$. On discute des incertitudes qui entourent les possibilités de commercialisation de ce système versatile de catalyseur homogène pour l'hydrogénation du CO en méthanol.

Mots clés : catalyse homogène, conversion du gaz de synthèse, synthèse du méthanol, alcoolates, carbonyls de nickel.

[Traduit par la Rédaction]

Introduction

A vast amount of natural gas is stranded in remote locations and economical transport of this clean fuel is highly desirable. Methanol and Fischer–Tropsch (F–T) hydrocarbons are considered shippable liquids that can be produced at remote locations from natural gas-derived synthesis gas (eqs. [1]–[3]) and as such, there is a renewed interest in catalytic synthesis gas conversions (also known as C_1 chemistry).

[1] $CH_4 + O_2\ (H_2O) \rightarrow CO + nH_2\ (n = 2, 3)$

[2] $CO + 2H_2 \rightarrow CH_3OH$

[3] $xCO + yH_2 \rightarrow (\text{-}CH_2\text{-})_n + pCO_2 + qH_2O$

Methanol has particularly attractive attributes as a fuel, an additive in conventional fuels, and a versatile building block in the synthesis of chemicals (1, 2). Methanol is presently manufactured from synthesis gas using supported Cu–ZnO heterogeneous catalyst at 250–300°C and between 5–10 MPa operating pressure (3). Reaction [2] is highly exothermic (ΔH_{298} = –128.6 kJ mol^{-1}) that poses thermodynamic limitations and together with poor process heat control allows <20% per pass gas conversion during the reaction (4). A homogeneous catalyst that affords high reaction rates at low temperatures would offer superior reaction heat management, higher yields per pass, and may afford attractive economics. Efforts have been made to synthesize

Received August 8, 2000. Published on the NRC Research Press Web site at http://canjchem.nrc.ca on June 30, 2001.

Dedicated to Professor Brian R. James on the occasion of his 65th birthday.

D. Mahajan,[1] V. Krisdhasima, and R.D. Sproull. Building 815, Advanced Fuels Group, Energy Sciences and Technology Department, Brookhaven National Laboratory, Upton, NY 11973–5000, U.S.A.

[1]Corresponding author (telephone: (631) 344-4985; fax: (631) 344-7905; e-mail: dmahajan@bnl.gov).

 DOI: 10.1139/cjc-79-5/6-848 © 2001 NRC Canada

oxygenates from synthesis gas using homogeneous systems. The use of transition-metal carbonyls especially those of Ru (5) and Rh (6) for synthesis of methanol, ethanol, other higher alcohols, and ethylene glycol is well documented for synthesis gas conversion but with these systems the overall reaction parameters are not economically attractive.

We previously reported (7) our approach to methanol synthesis from synthesis gas that utilized base-activated nickel tetracarbonyl as a catalyst for operation in homogeneous mode. In a follow-up paper (8), we reported on the kinetics of methanol synthesis catalyzed by the $Ni(CO)_4$–KOMe system in 1,4-dioxane–MeOH solvent mixture. Our further work on this catalyst suggested that 1,4-dioxane–MeOH was not particularly a good solvent mixture for this reaction because the solution homogeneity could not be maintained under a wide range of Ni and base concentrations. In this paper, we report on our work with other solvents for the reaction including a kinetic study in the MeOH–1,2-bis(2-methoxy ethoxy)ethane (triglyme) solvent mixture.

Experimental

Materials

Potassium methoxide (>95% pure) and nickel tetracarbonyl (>99.9% pure) were purchased from Alfa and used as received. Methanol, triglyme, and other solvents were obtained from Aldrich. For the kinetic study, methanol was distilled in 400mL batches with magnesium turnings and iodine under dry argon and triglyme was stored over molecular sieves prior to use. Pure CO, H_2, and syngas (H_2 and CO) mixtures were purchased in aluminum cylinders (to avoid any iron pentacarbonyl impurity) from Scott Specialty Gases.

Apparatus

A stainless steel MagneDrive II Packless Zipperclave 0.5 L reactor manufactured by Autoclave Engineers, Inc. (AE) was modified for this study. The reactor was equipped with a Dispersamax six-blade impeller mounted on a shaft driven by an AE variable speed motor. Ports were provided for loading nickel tetracarbonyl, reactant gases, and sampling vapor and liquid phases. The temperature of the reactor was maintained with a Parr 4831 temperature controller, which controlled an external heating mantle and an internal air-cooling system. The pressure was monitored with a Setra 204 pressure transducer (accuracy to ±1 psig). The transducer and temperature outputs were recorded using an Omega dual pen continuous chart recorder. The unit ratings were as follows: stirrer = 0–2000 rpm, T = 25–350°C, P = 0.1–14 MPa.

Run procedure and analysis

All runs containing nickel tetracarbonyl were performed under a well-ventilated fume hood (Caution: $Ni(CO)_4$ is volatile and extremely toxic!).[2] In a typical kinetic run, a specified amount of $KOCH_3$ was weighed inside a Labconco glove box under N_2 and was brought out in a closed vial. The methanol–triglyme solvent mixture (100mL) was degassed with N_2 and the weighed $KOCH_3$ in the vial was mixed with the degassed solvent mixture to obtain a light yellow homogeneous solution. The solution was poured into the pressure vessel and the vessel was quickly sealed and purged several times with N_2. A known amount of nickel tetracarbonyl was then injected into the base solution through the catalyst injection port and the vessel was immediately pressurized with syngas to about 750 psig. After 10 min, a gas sample was taken to establish the initial gas composition in the vessel. The automatic temperature controller and the stirrer were set at 120°C and 1600 rpm respectively. The stirring speed of 1600 rpm ensured that the reaction was operating out of the mass transfer regime. The vessel contents were then stirred for 15 min at room temperature to monitor initial gas absorption by the solvent and the base. At this time, methanol synthesis was initiated by heating the solution. The temperature and pressure were recorded as a function of time until the reaction became very slow. The reaction was quenched by replacing the heater with an ice water bath. Once the vessel cooled to room temperature, the final pressure and temperature were recorded. Gas and liquid samples were taken for analysis and the final liquid volume was measured. For this study, methanol synthesis was carried out under conditions with respect to nickel, base, and methanol concentrations that allowed collection of several data points during the runs. The data points were collected by analyzing the vapor-phase composition every 2 to 3 min during the run.

Gas samples were analyzed for H_2 and CO using Gow-Mac 550 gas chromatographs in the TCD mode: a molecular sieve column (8′ × 1/8″) with He carrier gas for CO and a molecular sieve column (6′ × 1/8″) with N_2 carrier gas for H_2 with data reproducibility within ±2%. Liquid phase samples (2μl) were analyzed on chromosorb-102 (8′ × 1/8″) column fitted in a PerkinElmer Model 8500 GC in the TCD mode with the data reproducibility within ±5%. All gas chromatographs were connected to HP Model 3390A integrators for peak quantification. A qualitative detection of $Ni(CO)_4$ in the vapor phase was achieved as follows. A 1-cm gas cell with KBr windows was evacuated and filled with the gas sample from the pressure vessel. The IR spectrum of the sample was recorded between 4000 and 400 cm^{-1} on a PerkinElmer Model 1330 IR spectrophotometer. The broad peaks at 2170, 2120 cm^{-1} (free CO), 2060 cm^{-1} ($Ni(CO)_4$), and 1760 cm^{-1} (CH_3O_2CH) were monitored.

For the kinetic study, the Redlich–Kwong equation of state was used to calculate the number of moles of H_2 and CO in the gas phase from the experimental data of syngas consumption vs. time. These data were further processed to yield rate constant values.

Results and discussion

Catalyst performance

It has been shown in an earlier study (8) that the $Ni(CO)_4$–KOMe system is a versatile catalyst to affect methanol synthesis from syngas. Table 1 lists representative runs

[2] Pure Ni is commercially manufactured via the Mond process (9) that involves the intermediacy of $Ni(CO)_4$. $Ni(CO)_4$ is volatile (bp = 43.2°C at 25°C; vapor pressure @ 20°C = 315 mmHg (1 mmHg = 133.322 Pa)) and extremely toxic. The OSHA limit for $Ni(CO)_4$ is set at 1 ppb in air for an 8-h daily exposure.

© 2001 NRC Canada

Table 1. Methanol synthesis catalyzed by the $Ni(CO)_4$–alkoxide base systems.[a]

Run	Solvent[b] (mL)	[Ni] (mmol)	Alkoxide (KOR)R (mmol)	Gas conversion (%)[c]	TOF (h^{-1})[d]
1	THF	5	2-Methyl-2-butyl (40)	93	24
2	THF	10	2-Methyl-2-butyl (100)	99	66
3	THF	1	2-Methyl-2-butyl (40)	92	6
4	THF	5	2-Methyl-2-propyl (40)	81	36
5	THF	5	Methyl (40)	97	41
6	1,4-Dioxane[e]	5	2-Methyl-2-butyl (40)	96	27
7	50% 1,4-Dioxane 50% MeOH	5	Methyl (400)	94	14
8	MeOH	5	Methyl (600)	92	1.4
9	Triglyme[e]	5	Methyl (200)	95	2.2

[a]All runs were carried out in 100mL solvent at 100°C under 2.1 MPa syngas (66% H_2:33%CO) per charge in a pressure vessel stirred at 1600 rpm. Typically, the reactor was charged twice in a given run.
[b]THF: tetrahydrofuran; triglyme: 1,2-bis(2-methoxyethoxy)ethane.
[c]Based on the final pressure at the end of the first charge.
[d]Turnover frequency is defined as g-mol MeOH g-mol catalyst (Ni + base)$^{-1}$ h^{-1}.

that demonstrate the performance of the alkoxide base-activated Ni catalyst for CO hydrogenation. A typical run proceeded as follows. For example in Run 1, on adding tetracarbonyl nickel to a light yellow solution of potassium 2-methyl-2-butoxide in tetrahydrofuran (THF) under argon, a deep red solution resulted. The red solution yielded an active catalyst when heated at 100°C under 2.1 MPa syngas (66% H_2:34% CO). During heating, syngas consumption commenced and within minutes the reactor pressure dropped below 0.2 MPa corresponding to an average gas consumption rate of 1 mmol s^{-1}. Gas chromatographic analysis of the final liquid and gas phases yielded >98% selectivity to methanol with the rest comprising of methyl formate and dimethyl ether as by-products. The total gas consumption during the run was 93%. Such analysis resulted in the data presented in Table 1 for all the runs. Gas phase IR spectrum taken at room temperature at the end of each run showed a sharp and intense signature peak at 2060 cm^{-1} for $Ni(CO)_4$. These data suggest the presence of free $Ni(CO)_4$ during these runs. The IR spectrum of the final solutions from these runs was somewhat complex that are being analyzed. It is known (10, 11) that basic solutions of $Ni(CO)_4$ yield multinuclear Ni species that are in facile equilibrium with $Ni(CO)_4$:

$$[4] \qquad Ni(CO)_4 \underset{CO}{\overset{Base}{\Leftrightarrow}} [Ni_x(CO)_y]^{n-}$$

Metal alkoxides as precursors for electronic and ceramic materials have been extensively studied (12). Alkali metal alkoxides are known to form hydrogen bonded homoconjugate anion. Specific hydrogen bonding is thought to contribute greatly to the solvation of alkoxides in protic solvents (13):

$$[5] \qquad RO^-M_{(s)} + HOR \Leftrightarrow [RO\cdots H\cdots OR] + M^+_{(s)}$$

Methoxides are strongly associated due to reduced steric effect and increased localization of charge compared to higher alkoxides. In the present catalyst system containing KOMe–MeOH, methanol is necessary to dissolve KOMe but the presence of methanol is likely to have a pronounced effect on the reaction rate. The data of Runs 6, 7, and 8 (Table 1) confirm the negative effect of methanol on rate with the slowest rate measured in neat methanol as solvent even at 6.0 M KOMe concentration. Thus in the present system, a suitable balance between methanol and base concentrations is needed to attain high reaction rates while maintaining solution homogeneity during the methanol synthesis reaction.

The screening runs in Table 1 also show that as a general trend, the reaction rate was dependent on Ni (0.01–0.10 M) and base (0.4–6.0 M) concentrations. Furthermore, the rate was affected by the nature of the alkyl group associated with potassium alkoxide. For example, in THF, at fixed Ni and alkoxide concentrations, the rate dependence followed the order: KOMe > KO-2-methyl-2-propyl > KO-2-methyl-2-butyl (Runs 5, 4, 1). KOMe was the preferred alkoxide because irrespective of the starting alkoxide, once MeOH is formed, methoxide is invariably produced via rxn. [6] and exists in equilibrium with the added alkoxide (13):

$$[6] \qquad KOR + MeOH \Leftrightarrow KOMe + ROH$$

It is thus clear that the use of KOMe as the alkoxide base yields the highest rates and avoids the complication of equilibrium [6].

The catalyst was evaluated in several different solvents (Runs 5–9). The reaction rate was solvent dependent and followed the order: 1,4-dioxane ~ THF > triglyme > MeOH. As stated earlier, methanol is necessary as a solvent to solubilize the base via rxns. [5] and [6] but the presence of a cosolvent appears to decrease methoxide association (rxn. [5]) and yield higher rates. Initially, THF was the solvent of choice based on the rate data in Table 1 but its similar boiling point (65°C) limited its use in the downstream separation from product methanol (bp: 65°C). 1, 4-dioxane (bp: 102°C) was then selected and a kinetic study in this solvent was reported (8). But the utility of the MeOH–1, 4-dioxane solvent mixture was limited due to its base solubility constraints. Triglyme boils at a higher temperature (216°C) and the MeOH–triglyme solvent mixture appeared to satisfy several reaction and process criteria. This led us to undertake a kinetic study on the $Ni(CO)_4$–KOMe catalyst system in MeOH–triglyme solvent mixture.

Kinetic study

Methanol synthesis requires syngas with H_2:CO ratio of 2:1 (eq. [2]). Therefore, all runs in this study were con-

© 2001 NRC Canada

Fig. 1. Typical log plots of CO consumption as a function of time during a typical kinetic run for the $Ni(CO)_4$–KOMe catalyst system. Solvent: 10% triglyme:90% MeOH = 100 mL. [Ni] = 0.05 M, [KOMe] = 3.0 M, T = 110°C. Stirring speed = 1600 rpm. Syngas: 66% H_2:34% CO = 5.0 MPa at 25°C.

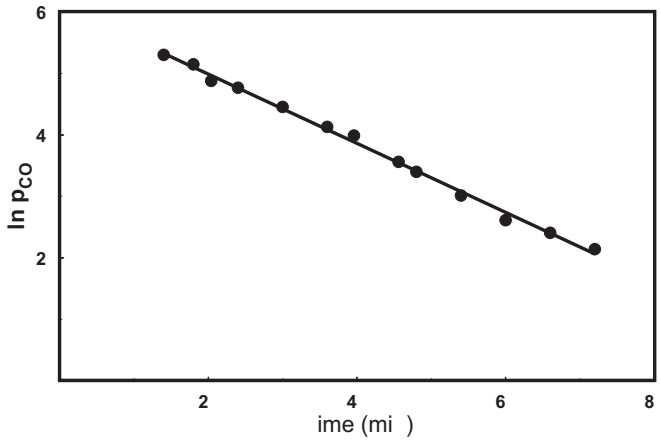
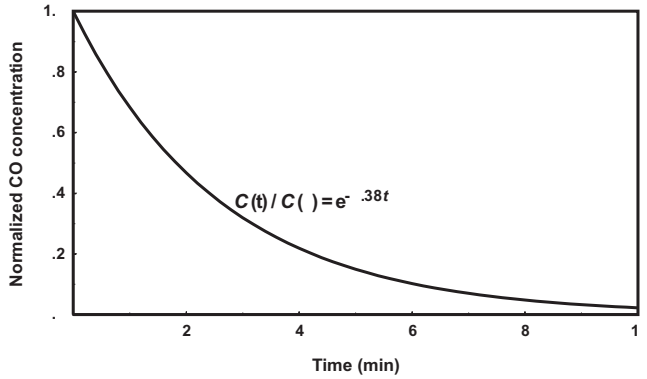


Fig. 2. Normalized CO concentration as a function of time during a typical kinetic run with the $Ni(CO)_4$–KOMe catalyst system. Solvent: 50% triglyme:50% MeOH = 100 mL. [Ni] = 0.05 M, [KOMe] = 3.0 M, T = 110°C. Stirring speed = 1600 rpm.

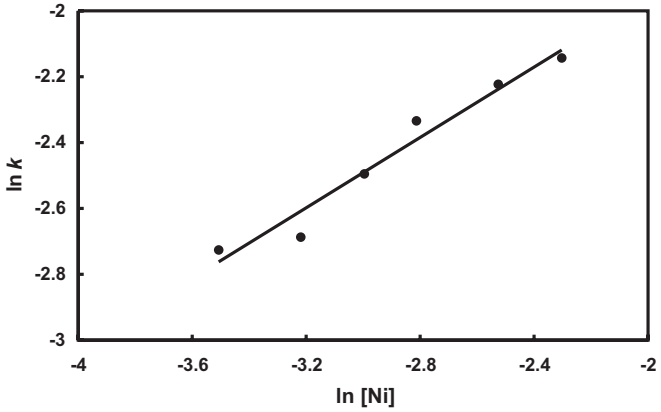


ducted with a constant syngas composition of 66% H_2:34% CO. The data in Table 1 show that under certain conditions, syngas consumption can be fast. For the kinetic runs, the catalyst composition was adjusted to allow enough reaction time for collection of several data points during each run. As shown below, four kinetic parameters were varied to collect the kinetic data on the $Ni(CO)_4$–KOMe system in MeOH–triglyme solvent mixture.

Rate of CO disappearance

The rate constants were calculated from the CO consumption data as follows. First, the Redlich–Kwong equation was used to calculate the individual H_2 and CO values from the experimentally measured values of the total syngas consumption. The time dependent CO values were corrected for solvent vapor pressure and liquid phase CO concentration factors. The variations of CO mol fraction as a function of time data were then used to determine the rate of disappearance of CO. Figure 1 shows one such plot for a run that was charged with 5.0 MPa syngas pressure at room temperature

Fig. 3. Effect of nickel concentration on the observed rate constant. Solvent: triglyme–MeOH = 100 mL. [KOMe] = 4.0 M, [MeOH] = 21.7 M, T = 110°C.



under the following reaction conditions: [Ni] = 0.05 M, [KOMe] = 3.0 M, T = 110°C; solvent: 100 mL triglyme–MeOH (10%:90%). The log of CO partial pressure vs. time plot yielded a straight line suggesting a first-order disappearance of CO:

$$[7] \qquad -dC_{co}/dt = kC_{co}$$

where C_{co} is the liquid-phase CO concentration and k is a first-order rate constant. Such analysis was carried out for all the runs. The data points could be used to construct a normalized CO concentration curves as a function of time during a kinetic run. Such a curve depicting CO consumption vs. time data is shown in Fig. 2 for a run that was carried out at: [Ni] = 0.05 M, [KOMe] = 3.0 M, T = 110°C; solvent: 100 mL triglyme–MeOH (50%:50%).

Effect of Ni concentration

The Ni concentration was varied between 0.03 and 0.10 M at fixed values of 4.0 M KOMe, 21.7 M MeOH, and a constant temperature of 110°C. In this Ni concentration range, the expression simplifies to:

$$[8] \qquad k = k_{Ni}C_{Ni}^{\alpha}$$

where α is the exponent of Ni concentration C_{Ni} and k_{Ni} is a constant. A plot of the experimental data in Fig. 3 shows that log k varied linearly with log C_{Ni}. The slope of this line yielded α of 0.534.

Effect of base concentration

The concentration of KOMe was varied between 2.0 and 4.75 M at fixed values of 0.05 M $Ni(CO)_4$ at a constant temperature of 110°C. Note that in this set, the methanol concentration was adjusted at 23.7, 24.0, 22.6, 21.7, 21.1 M, respectively, at KOMe concentrations of 2.0, 2.5, 3.0, 4.0, 4.75 M. Since the solution volume changes on dissolution of KOMe in the solvent mixture, this correction was necessary to keep the total solution volume constant. In this base concentration range, the rate constant can be modeled as a power function:

$$[9] \qquad k = k_bC_b^{\beta}$$

© 2001 NRC Canada

Fig. 4. Effect of base concentration on the observed rate constant. Solvent: triglyme–MeOH = 100 mL. [Ni] = 0.05 M, [MeOH] = 21.7 M, T = 110°C.

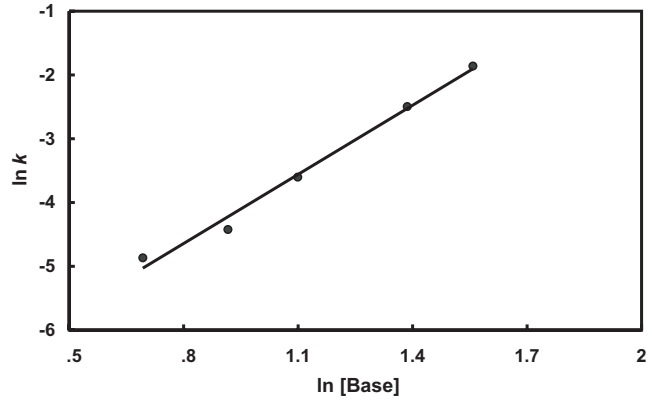
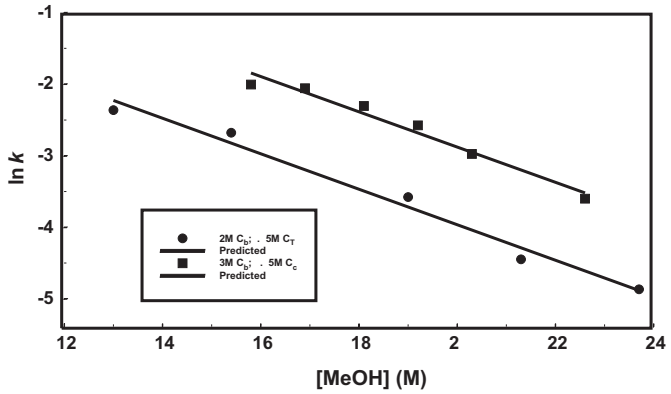


Fig. 5. Effect of methanol concentration on the observed rate constant. Solvent: triglyme–MeOH = 100 mL. [Ni] = 0.05 M, [KOMe] = 2.0, 3.0 M, T = 110°C.



where β is the exponent of base concentration C_b and k_b is a constant. A log–log plot of the experimental data in Fig. 4 shows that log k varied linearly with log C_b. The slope of this line yielded β of 2.89.

Effect of methanol concentration

We discussed earlier that a complex dependence of methanol and methoxide concentrations was noted during the methanol synthesis reaction. We, therefore, collected two sets of data, at 2.0 M and 3.0 M KOMe, in which MeOH concentration was varied. The plots in Fig. 5 show that there is a linear relation between log k and the liquid-phase methanol concentration (C_m). The slopes of the lines for both the both 2.0 M and 3.0 M data sets were the same (–0.248). From these data, the relationship between methanol concentration and the rate constant can be expressed as:

$$[10] \quad k = k_m \exp(-k_i C_m)$$

where k_m and k_i are methanol concentration dependent constants.

Effect of temperature

Rate constants were measured at 374, 383, and 393 K at constant 0.05 M Ni, 4.0 M base, 21.7 M MeOH in triglyme. An Arrhenius plot of the data yielded a straight line as shown in Fig. 6. This plot was used to calculate the frequency factor (A) and the energy of activation (E_{act}) of the reaction.

Fig. 6. An Arrhenius plot of the observed rate constant data at 101, 110, and 120°C. Solvent: triglyme–MeOH = 100 mL. [Ni] = 0.05 M, [KOMe] = 4.0 M, [MeOH] = 21.7 M.

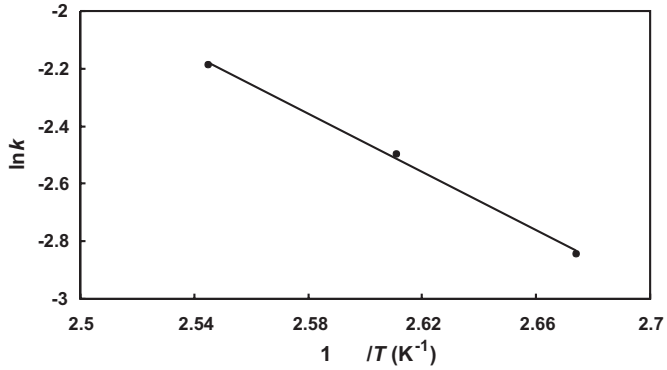


Table 2. Parameters in the kinetic model for methanol synthesis.

Parameter	Experimental	Calculated[a]
k_o	—	1.267×10^6
k_i	0.248	0.256
α	0.534	0.548
β	–2.89	–2.81
E_{act}	42.23	42.22

[a]For these values, regression constant (R^2) was 0.98.

$$[11] \quad k = A\exp(E_{act}/RT)$$

E_{act} was calculated by linear regression to be 42.2 kJ mol^{-1}. This value appears low compared to what is expected for a typical chemical reaction (83–126 kJ mol^{-1}). This value is also smaller compared to our previous data (97.6 kJ mol^{-1}) for the Ni–$^{-}$OMe catalyst system in 1,4-dioxane–MeOH solvent mixture (8). Interestingly, the measured E_{act} value is in the range of that measured for carbonylation of methanol to methyl formate (67.7 kJ mol^{-1} between 323 and 343 K) catalyzed by sodium methoxide (13). We are further analyzing the data to explain this discrepancy in the E_{act} values.

Kinetic model

The experimental data in Figs. 3–6 were used to estimate the respective parameters, α, β, k_i, and E_{act}. Next, all of the parameters were determined simultaneously by utilizing all the data points at one time. The proposed model is based on a combination of eqs. [8]–[11] that yields the following expression:

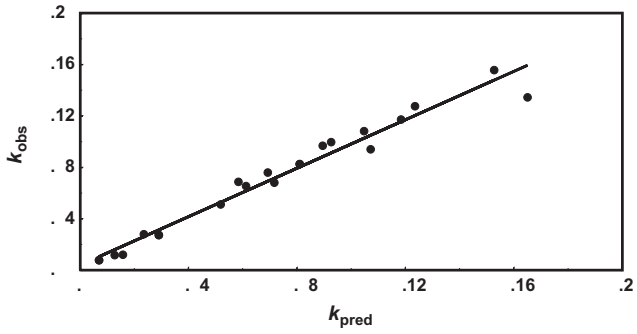
$$[12] \quad k = k_o \exp(-E_{act}/RT) C_{Ni}^{\alpha} C_b^{\beta} \exp(-k_i C_m)$$

A better estimate of the parameters in this model can be calculated by using multiple linear regression of eq. [11] (14). The parameter values from experimental data and the calculated values are given in Table 2. The final expression is then modified to:

$$[13] \quad k = (1.27 \times 10^6)\exp(-10\,084/RT) C_{Ni}^{0.548} C_b^{2.81} \exp(-0.256 C_m)$$

© 2001 NRC Canada

Fig. 7. A comparison of the observed and the predicted rate constants.



In Fig. 7, the observed rate constants (k_{obs}) are compared to the line based on the predicted rate constants (k_{pred}) from eq. [13]. The data are in excellent agreement.

The kinetic expression in eq. [13] includes terms for temperature, nickel, alkoxide base, and methanol concentrations. A less than first-order dependence on nickel may indicate the presence of more than one Ni species that are in equilibrium in solution. An approximate third-order dependence of rate on alkoxide base and a negative exponential methanol term likely result from ion-pairing due to hydrogen bonding in methanol, a protic solvent. Thus, the RO^-–ROH interaction results in slow reaction kinetics that is consistent with the presented data. Further work with different alkoxide bases in combination with various alkali metals in methanol will likely establish the effect of these parameters on thermodynamics and kinetics of the system.

Future direction

The potential use of methanol as a clean fuel including its use as a peak-shaving fuel in the integrated gasification combined cycle (IGCC) power plants is justifying further research in developing a simple and cost-effective methanol synthesis process. A catalyst that yields high reaction rates, high CO conversion, and high methanol selectivity would be applicable to such systems. In this paper, we have presented data to demonstrate that it is possible to develop such a catalyst system that operates in the homogeneous mode. The base activated $Ni(CO)_4$ system, in its present formulation, is not yet commercially attractive for two reasons. These are: (*i*) the presence of toxic $Ni(CO)_4$; and (*ii*) the sensitivity of the catalyst to CO_2 and H_2O. The latter is due to interaction of these molecules with the alkoxide base that yield alkyl carbonate and hydrolysis products respectively:

[14] $^-OMe + CO_2 \rightarrow {}^-OCO_2Me$

[15] $^-OMe + H_2O \rightarrow {}^-OH + MeOH$

Reaction [14] lies far to the right and the equilibrium constant (K_{eq}) for the NaOMe–CO_2 reaction is known to be ~2 × 10^{-8} (15). Both these reactions compete with presumably the initial methanol synthesis step that requires the availability of alkoxide base. This reaction has been studied for other metal carbonyls both with methoxide and hydroxide bases that result in methoxycarbonyl and hydroxycarbonyl adduct formation respectively via rxn. [16]:

[16] $M_x(CO)_y + RO^- \rightarrow M_x(CO)_{y-1}(CO_2R)^-$

(R = H or Me)

Rate constants have been reported for the reaction of $Ru_3(CO)_{12}$, $Ru(CO)_5$, $Fe_3(CO)_{12}$, and $Fe(CO)_5$ with ^-OMe and ^-OH ions at 25°C (16). The Ru carbonyls do yield methanol even in the absence of methoxide though at higher temperatures and pressures (5). A preliminary mechanistic study has appeared in literature for methanol synthesis catalyzed by the $Ni(CO)_4$–NaOMe catalyst system but the rate determining step (RDS) was not identified (17). The rate expression in eq. [13] is empirical and, as such, only limited information can be derived from the presented kinetic data. We are presently establishing a detailed mechanism of the KOMe–Ni catalyst system that will allow us to correlate the observed kinetic dependence and identify the rate-controlling step in methanol synthesis. A detailed study of our catalyst system will be the subject of a forthcoming publication[3] in which we also seek to establish the role of multinuclear Ni species (10, 11) in methanol synthesis.

Acknowledgments

The authors wish to thank the Electric Power Research Institute and the U.S. Department of Energy under Contract no. DE-AC02–98CH10886 for partial support of this work.

References

1. W. Keim (*Editor*). Catalysis in C_1 chemistry. D. Reidel Publishing Company, Dordrecht, The Netherlands. 1983; W. Keim. J. Organomet. Chem. **372**, 15 (1989).
2. I. Wender. Catal. Rev. Sci. Eng. **26**, 3 (1985).
3. S. Lee. Methanol synthesis technology. CRC Press, Inc., Boca Raton, Florida. 1990.
4. S Strelzoff. Chem. Eng. Prog. Symp. Ser. **66**, 98 (1970).
5. J.S. Bradley. J. Am. Chem. Soc. **101**, 7419 (1979).
6. R.L. Pruett and W.E. Walker. U.S. Patent 3 957 857 to Union Carbide, 1976.
7. D. Mahajan, R.S. Sapienza, W.A.R. Slegier, and T.E. O'Hare. U.S. Patent 4 935 395, 1990.
8. J.E. Wegrzyn, D. Mahajan, and M. Gurevich. Catal. Today, **50**, 97 (1999).
9. L. Mond. U.S. Patent 455230, 1891.
10. G. Longoni, P. Chini, and A. Cavalieri. Inorg. Chem. **15**, 3025 (1976), and refs. therein.
11. J.K. Beattie, T.W. Hambley, A.F. Masters, and J.T. Meyer. Inorg. Chim. Acta, **213**, 49 (1993).
12. D.C. Bradley. Chem. Rev. **89**, 1317 (1989).
13. S.P. Tonner, D.L. Trimm, M.S. Wainwright, and N.W. Cant. J. Mol. Catal. **18**, 215 (1983), and refs. therein.
14. J. Neter, W. Wasserman, and M. Kutner. Applied linear regression models. Richard D. Irwin, Inc., U.S.A. 1983.
15. C. Faurholt. Z. Phys. Chem. Stoechiom. Verwandtschaftsl. **126**, 72 (1927).
16. D.C. Gross and P.C. Ford. Inorg. Chem. **21**, 1704 (1982).
17. M. Marchionna, L. Basini, A. Arogno, M. Lami, and F. Ancilotti. J. Mol. Catal. **75**, 147 (1992).

[3] D. Mahajan. Manuscript in preparation.

© 2001 NRC Canada

Equilibrium thermodynamic studies for the formation of 1:1 complexes of CO and ethene with a rhodium(II) porphyrin metallo-radical

Leah Basickes, Andrew G. Bunn, and Bradford B. Wayland

Abstract: Tetra(2,4,6 triisopropropyl phenyl)porphyrinatorhodium(II) ((TTiPP)Rh^{II}·**1**) is a persistent metal-centered radical with the odd electron in the rhodium(II) dz^2 orbital. (TTiPP)Rh^{II}· forms 1:1 complexes with CO and CH_2CH_2 where the porphyrin ligand steric properties inhibit further reactions of the one-electron activated substrates. ^{1}H NMR paramagnetic shifts at a series of temperatures are used in evaluating the thermodynamics for CO complex formation with **1** to form [(TTiPP)Rh^{II}(CO)]·**2** ($\Delta H°$ = –5.5 ± 0.5 kcal mol^{-1}; $\Delta S°$ = –9 ± 1 cal K^{-1} mol^{-1}). Related ^{1}H NMR studies show that the bonding of **1** with ethene is less favorable than CO.

Key words: rhodium porphyrin, carbon monoxide, ethene, thermodynamics, complex formation, metal-centered radical.

Résumé : Le tétra(2,4,6-triisopropylphényl)porphyrinatorhodium(II) ((TTiPP)Rh^{II}·**1**) est un radical persistant centré sur un métal comportant un électron célibataire dans l'orbitale dz^2 du rhodium(II). Le (TTiPP)Rh^{II}· forme des complexes 1:1, avec le CO et le CH_2CH_2, dans lesquels les propriétés stériques du ligand porphyrine empêchent d'autres réactions avec des substrats à un électron activés. On a utilisé les déplacements paramagnétiques en RMN du ^{1}H à une série de températures pour évaluer les facteurs thermodynamiques de la réaction entre CO et **1** pour conduire à la formation du complexe [(TTiPP)Rh^{II}(CO)]·**2** ($\Delta H°$ = –5,5 ± 0,5 kcal mol^{-1}; $\Delta S°$ = –9 ± 1 cal K^{-1} mol^{-1}). D'autres études de RMN du ^{1}H montrent que la liaison entre **1** et l'éthène est moins favorable que celle avec le CO.

Mots clés : porphyrine-rhodium, monoxyde de carbone, éthène, thermodynamique, formation de complexe, radical centré sur un métal.

[Traduit par la Rédaction]

Introduction

Carbon monoxide and ethene are most often activated by binding with Lewis acid metal centers that promote two-electron reactions of nucleophiles at a substrate carbon site. The binding of carbon monoxide and ethene with rhodium(II) porphyrin metal-centered radicals results in complexes that manifest an alternate pattern of reactivity associated with one-electron activated substrates (1–6). Reactions of CO and ethene with rhodium(II) porphyrins that yield substrate bridged (Rh-C(O)-Rh (3, 4), Rh-CH_2CH_2-Rh (7, 8)) and coupled species (Rh-C(O)-C(O)-Rh (1–3), Rh-CH_2CH_2-CH_2CH_2-Rh (5, 6)) illustrate one-electron activated carbon centers in CO and ethene ligands. Direct investigation of complexes with one-electron activated substrates is usually precluded because they are highly reactive transient intermediates. However, steric constraints can be built into the porphyrin ligand which inhibit access to the reactive substrate site and provide persistent complexes containing one-electron activated CO and ethene (2, 5).

Tetra(2,4,6 triisopropyl phenyl)porphyrinatorhodium(II) ((TTiPP)Rh^{II}·) is an example of a metal-centered radical where the structural features sterically preclude Rh^{II}—Rh^{II} bonding and inhibit CO and ethene substrate reactions. This article reports on measurements of equilibrium thermodynamic values for complex formation of (TTiPP)Rh^{II}· with carbon monoxide and ethene.

Received September 15, 2000. Published on the NRC Research Press Web site at http://canjchem.nrc.ca on June 30, 2001.

This paper is dedicated to Professor Brian James on the occasion of his 65th birthday.

L. Basickes, A.G. Bunn, and B.B. Wayland.[1] Department of Chemistry, University of Pennsylvania, Philadelphia, PA 19104–6323, U.S.A.

[1]Corresponding author (telephone: (215) 898-8633; fax: (215) 573-6743; e-mail: wayland@mail.sas.upenn.edu).

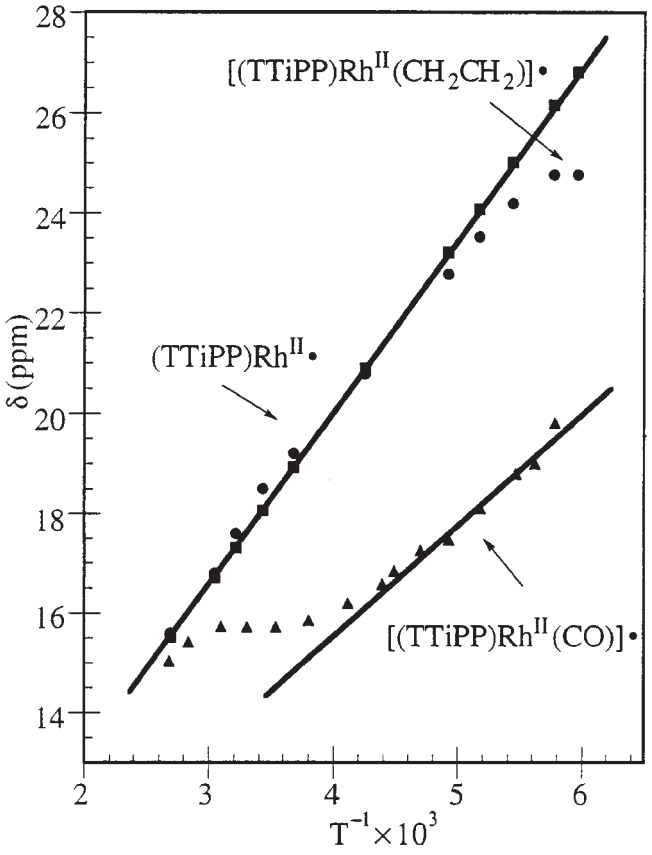
Results and discussion

(TTiPP)Rh^{II}·**1** is a stable persistent metal-centered radical with a $(d_{xy})^2(d_{xz,yz})^4(d_{z2})^1$ electron configuration as shown by the EPR spectral parameters in toluene glass (90 K) (g_{xx} = g_{yy} = 2.82, g_{zz} = 1.85) (9). ^{1}H NMR chemical shifts for (TTiPP)Rh^{II}· in toluene-d_8 solutions manifest an inverse dependence on temperature (T = 190–330 K) that is characteristic of Curie–Weiss paramagnetism (Fig. 1). There is no evidence from ^{1}H NMR, electronic spectra, or EPR for dimerization of (TTiPP)Rh^{II}· through Rh^{II}—Rh^{II} bonding in toluene solution (190–330 K) or frozen glass (160–90 K). The steric constraints for the TTiPP porphyrin ligand preclude dimerization through Rh^{II}—Rh^{II} bonding which occurs with less sterically demanding porphyrin ligands such as tetraphenyl porphyrin ([(TPP)Rh]$_2$) (10).

The EPR spectrum in toluene glass (90 K) for (TTiPP)Rh^{II}· in contact with ^{13}CO demonstrates the formation of a mono CO complex ([(TTiPP)Rh^{II}(CO)]·) through splitting of each

 DOI: 10.1139/cjc-79-5/6-854 © 2001 NRC Canada

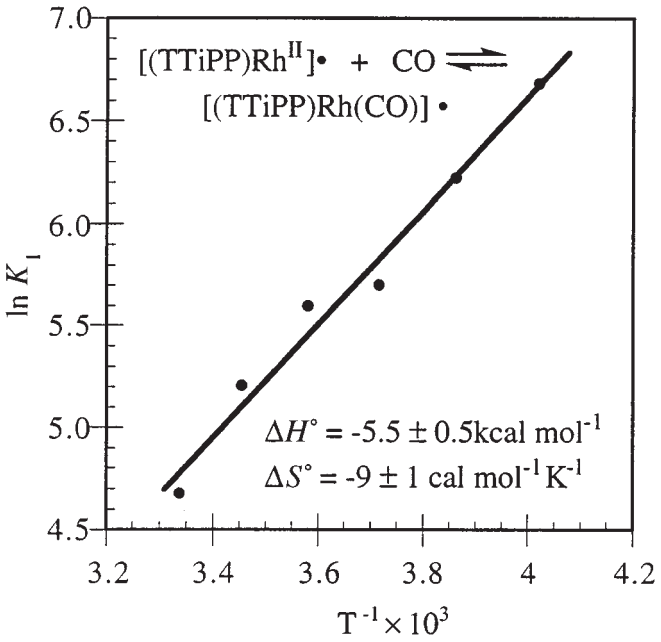
Fig. 1. Temperature dependence for the pyrrole ^{1}H NMR paramagnetic shift (δ (ppm)) for toluene-d_8 solutions of (TTiPP)Rh^{II}· (■), (TTiPP)Rh^{II}· (●) in contact with CH_2CH_2 (0.25 atm (1 atm = 101.325 kPa)), and (TTiPP)Rh^{II}· (▲) in contact with CO (0.855 atm (1 atm = 101.325 kPa)).



of the three *g* value transitions into a doublet by ^{13}C (9). The observed pyrrole ^{1}H NMR paramagnetic shifts for toluene-d_8 solutions of (TTiPP)Rh^{II}·**1** (1.0×10^{-3} M) in contact with carbon monoxide (P_{CO} = 0.855 atm (1 atm = 101.325 kPa)) are plotted vs. the inverse of temperature (T = 180–300 K) in Fig. 1. Sections of linearity are observed in both the higher and lower temperature regimes. The observed pyrrole chemical shifts in the higher temperature linear region coincide with the values for (TTiPP)Rh^{II}· ($\delta_1 = -1.86 + 3334\ T^{-1}$) and the lower temperature linear portion is assigned to the limiting shift values for a mono carbonyl complex ([(TTiPP)Rh^{II}(CO)]·**2** ($\delta_2 = -2.72 + 2376T^{-1}$)). The ratio of the slope of the pyrrole hydrogen paramagnetic shifts vs. T^{-1} plots for [(TTiPP)Rh^{II}(CO)]· to that for (TTiPP)Rh^{II}· equals 0.71 and this value is proportional to the ratio of the electron-pyrrole hydrogen coupling constants A_H (**2**)/A_H (**1**) and related pyrrole hydrogen spin densities (11). This ratio of the porphyrin pyrrole electron-hydrogen coupling constants (0.71) is similar to the ratio of 0.65 for the total rhodium spin density of [(TTiPP)Rh^{II}(CO)]· (0.62) to that of the (TTiPP)Rh^{II}· (0.95) which were estimated from EPR studies (9). In the temperature regime between 270 and 330 K, substantial amounts of both (TTiPP)Rh^{II}· and [(TTiPP)Rh^{II}(CO)]· are present in equilibrium with CO (eq. [1]). The

[1] $$[(TTiPP)Rh^{II}]\cdot + CO \rightleftharpoons [(TTiPP)Rh^{II}(CO)]\cdot$$

Fig. 2. van't Hoff plot for reaction of (TTiPP)Rh^{II}· with CO in toluene-d_8.



observed pyrrole shifts in this temperature range correspond to the mol fraction averaged positions for the (TTiPP)Rh^{II}· and [(TTiPP)Rh^{II}(CO)]· species in limiting fast exchange.

The pyrrole chemical shifts determined for (TTiPP)Rh^{II}·**1** ($\delta_1 = -1.86 + 3334\ T^{-1}$) and [(TTiPP)Rh^{II}(CO)]·**2** ($\delta_2 = -2.72 + 2376\ T^{-1}$) were used in determining the fraction of monocarbonyl complex from the observed mol fraction averaged chemical shifts (δ_{obs} = N(**1**)δ(**1**) + N(**2**)δ(**2**)), N(**2**) = [**2**]/[**1**] + [**2**]). The equilibrium constant expression for rxn. [1] (K_1 = [[(TTiPP)Rh^{II}(CO)]·]/[(TTiPP)Rh^{II}·][CO]) is evaluated using the ratio of mol fractions N(**2**):N(**1**) and the molar concentration of CO at each temperature (T). The plot of ln K_1 vs. T^{-1} (Fig. 2) gives an enthalpy change ($\Delta H_1°$) of –5.5 ± 0.5 kcal mol^{-1} and entropy change ($\Delta S_1°$) of –9 ± 1 cal K^{-1} mol^{-1} for the reaction of (TTiPP)Rh^{II}· with CO to form [(TTiPP)Rh^{II}(CO)]· (eq. [1]). The enthalpy change for complex formation of **1** with CO ($\Delta H_1° = -5.5 \pm 0.5$ kcal mol^{-1}) is very small even when compared to the reaction of CO with a related Rh^{II}—Rh^{II} bonded dimer [(OEP)Rh]$_2$ to form the mono CO adduct [(OEP)Rh]$_2$CO ($\Delta H° = -12$ kcal mol^{-1}) (3).

Reaction of (TTiPP)Rh^{II}· with ethene produces a 1:1 complex [(TTiPP)Rh^{II}(CH_2CH_2)]·**3** that is kinetically *meta*-stable relative to an ethene coupling product (Rh-$(CH_2)_4$-Rh).

[2] $$[(TTiPP)Rh^{II}]\cdot + CH_2CH_2 \rightleftharpoons [(TTiPP)Rh^{II}(CH_2CH_2)]\cdot$$

The g_{zz} transition in the EPR spectrum for the $^{13}C_2H_4$ derivative of **3** (90 K) occurs as a triplet of doublets arising from coupling of two equivalent ^{13}C nuclei on each ^{103}Rh transition which demonstrates that **3** is a 1:1 complex, [(TTiPP)Rh^{II}(CH_2CH_2)]· (5).

^{1}H NMR chemical shifts for the pyrrole hydrogens of (TTiPP)Rh^{II}· in contact with ethene (0.25 atm (1 atm = 101.325 kPa)) in toluene-d_8 over a wide range of tempera-

© 2001 NRC Canada

tures is shown in Fig. 1. At temperatures above 220 K the observed pyrrole ^{1}H NMR shifts are indistinguishable from the values for (TTiPP)$Rh^{II}\cdot$ and only below 200 K is there a clear indication of ethene complex formation with **1** to form **3**. Only a small temperature range is available for the study of **3** forming in toluene solutions and the regime with the limiting shift values and thus complete conversion to **3** was not attained. Qualitatively, the thermodynamics of ethene coordination with **1** are substantially less favorable than CO complexation.

Experimental

The synthesis of (TTiPP) has been described previously (2). All manipulations were performed under argon or by vacuum techniques. Reagents were purchased from Aldrich or Strem. Research grade carbon monoxide and ethene (Matheson) and ^{13}C-labeled carbon monoxide and ethene (Aldrich) were used without further purification. Benzene and toluene solvents used in the EPR and NMR studies were degassed, refluxed over sodium benzophenone, and then degassed again by freeze–pump–thaw cycles.

NMR Studies

Proton NMR spectra were recorded using a Bruker AF500 instrument equipped with a variable temperature FTS Refrigerator unit. NMR samples used toluene-d_8 as the solvent in a sealed NMR tube and low temperatures were obtained by utilizing the boil-off from liquid nitrogen. Temperature calibration was obtained by using methanol or ethylene glycol as an external standard.

Reaction of (TTiPP)$Rh^{II}\cdot$ with CO–CH_2CH_2

In a typical experiment, (TTiPP)$Rh^{II}\cdot$ was generated by photolysis of a benzene solution of (TTiPP)Rh-CH_3 (1×10^{-3} M) in a vacuum adapted NMR tube. Samples of (TTiPP)$Rh^{II}\cdot$ in vacuum adapted NMR tubes were then pressurized with CO (0.86 atm (1 atm = 101.325 kPa)) or ethene (0.25 atm (1 atm = 101.325 kPa)) and sealed. The solubility of CO and ethene in toluene was determined as a funtion of temperature. When measuring the concentration of disolved gas in solution at a temperature T_2, P is the pressure in atm (1 atm = 101.325 kPa) at the laboratory temperature T_1 in K when the gas was added into the tube. ([CO] (12) = $[a + b(T_2)][P][T_1/T_2]$ (a and b are solvent dependent in toluene, $a = 4.405 \times 10^{-3}$ and $b = 1.085 \times 10^{-5}$)); ([CO] (303 K) in toluene = 6.5×10^{-3} M), [ethene] (13) = $-0.4906 + (0.1850T_2)P$. ([ethene] (303 K) in toluene = 3.0×10^{-2} M).

Acknowledgements

This research was supported by grants from the Department of Energy, Division of Chemical Sciences, Office of Basic Energy Sciences, Grant DE-FG02–86ER 13615, and the National Science Foundation.

References

1. X.X. Zhang, G.F. Parks, and B.B. Wayland. J. Am. Chem. Soc. **119**, 7938 (1997).
2. B.B. Wayland, A.E. Sherry, G. Poszmik, and A.G. Bunn. J. Am. Chem. Soc. **114**, 1673 (1992).
3. V.L. Coffin, W. Brennen, and B.B. Wayland. J. Am. Chem. Soc. **110**, 6063 (1988).
4. B.B. Wayland, B.B. Woods, and V.L. Coffin. Organometallics, **5**, 5010 (1986).
5. A.G. Bunn and B.B. Wayland. J. Am. Chem. Soc. **114**, 6917 (1992).
6. B.B. Wayland and G. Poszmik. Organometallics, **11**, 3534 (1992).
7. H. Ogoshi, J. Setsume, and Z. Yoshida. J. Am. Chem. Soc. **99**, 3869 (1977).
8. (*a*) S.R. Paonessa, N.C. Thomas, and J. Halpern. J. Am. Chem. Soc. **107**, 4333 (1985); (*b*) B.B. Wayland, Y. Feng, and S. Ba. Organometallics, **8**, 1438 (1989).
9. B.B. Wayland, A.E. Sherry, and A.G. Bunn. J. Am. Chem. Soc. **115**, 7675 (1993).
10. B.B. Wayland, and S.L. Van Voorhees. Inorg. Chem. **25**, 4039, (1986).
11. I. Bertini and C. Luchinat. Nuclear magnetic resonance of paramagnetic substances in solution. *In* Physical methods in chemistry. 2nd ed. *Edited by* R.S. Drago. Saunders College Publishing, New York. 1992. p. 500.
12. (*a*) J.C. Gjaldbeak. Acta Chem. Scand. 623 (1952); (*b*) J.C. Gjaldbeak. Acta Chem. Scand. 1398 (1954); (*c*) L.R. Field, E. Wilhelm, and R. Battino. J. Chem. Thermodyn. **6**, 237 (1974).
13. S. Narasimhan and G. D. Nageshwar. Chem. Petro-Chem. J. **12**, 33 (1981).

© 2001 NRC Canada

Synthesis, characterization and chemistry of bis-(pentafluorophenyl)boryl ferrocene

Bryon E. Carpenter, Warren E. Piers, Masood Parvez, Glenn P.A. Yap, and Steven J. Rettig

Abstract: Bis-(pentafluorophenyl)boryl ferrocene, **1**, was prepared via borylation of ferrocene with $HB(C_6F_5)_2$ or via a transmetallation reaction involving FcHgCl and $ClB(C_6F_5)_2$ in 87–91% yield. The compound is characterized by a deep maroon colour. A significant intramolecular iron–boron interaction is manifested in the solution spectroscopic (Fe → B charge transfer band at ~230 nm, $\varepsilon = 1.33 \times 10^4$) and solid-state crystallographic data (Fe-B = 2.924 Å) This interaction has an impact on the Lewis acidity of the boron center which, unlike the related compound $B(C_6F_5)_3$, does not strongly bind Lewis bases such as acetone, THF, or acetonitrile. However, an adduct between the stronger base PMe_3 and **1** forms readily and this complex (**2**) was fully characterized. The electron withdrawing $-B(C_6F_5)_2$ group causes **1** to be oxidized at +450 mV relative to ferrocene. Oxidation of **1** with $[NO][BF_4]$, $AgOSO_2CF_3$, or AgC_6F_5 leads to the zwitterionic ferrocenium borates **3-F**, **3-OTf**, and **3-C_6F_5**, respectively. Each of these compounds was characterized spectroscopically and via X-ray crystallography. The properties of these compounds relative to **1** suggest that oxidation of the iron center significantly enhances the Lewis acidity of the boron center. Due to the σ-donating ability of the borate substituents, zwitterions **3** are weaker oxidizing agents than unsubstituted ferrocenium salts.

Key words: organoboranes, ferrocene derivatives, Lewis acids.

Résumé : On a préparé le bis-(pentafluorophénylboryl)ferrocène, **1**, par le biais d'une borylation du ferrocène à l'aide de $HB(C_6F_5)_2$ ou par une réaction de transmétallation impliquant le FcHgCl et le $ClB(C_6F_5)_2$; les rendements varient de 87 à 91%. Le composé est caractérisé par une couleur marron foncé. Il se manifeste une interaction intermoléculaire fer–bore significative tant en spectroscopie en solution (un transfert de bande Fe → B à environ 230 nm, $\varepsilon = 1{,}33 \times 10^4$) que dans les données cristallographiques à l'état solide (Fe-B = 2,924 Å). Cette interaction a une influence sur l'acidité de Lewis du bore qui, contrairement au composé $B(C_6F_5)_3$ apparenté, ne se lie pas fortement aux bases de Lewis telles que l'acétone, le THF ou l'acétonitrile. Toutefois, il se forme facilement un adduit entre le composé **1** et PMe_3, une base plus forte, et on a fait une caractérisation complète de ce complexe, **2**. La présence du groupe électroaffinitaire $B(C_6F_5)_3$ fait que le composé **1** peut s'oxyder à +450 mV par rapport au ferrocène. L'oxydation du composé **1** par $[NO][BF_4]$, $AgOSO_2CF_3$ ou AgC_6F_5 conduit suivant le cas à la formation des borates de ferrocénium zwitterioniques **3-F**, **3-Otf** et **3-C_6F_5**. Chacun de ces composés a été caractérisé par spectroscopie et par diffraction des rayons X. Les propriétés de ces composés, comparées à celles du composé **1**, suggèrent que l'oxydation du fer augmente de beaucoup l'acidité de Lewis du bore. En raison de la possibilité des substituants borates de donner des électrons σ, les zwitterions **3** sont des agents d'oxydation plus faibles que les sels de ferrocénium non substitués.

Mots clés : organoboranes, dérivés ferrocènes, acides de Lewis.

[Traduit par la Rédaction]

Introduction

Substituted ferrocenyl derivatives play an important role in many different areas of chemistry (1). While much activity has focussed on ferrocenes substituted with Lewis base donors as ligands for various transition metal catalysts, ferrocene derivatives with Lewis acid centers bonded to the cyclopentadienyl (Cp) ring have seen fewer applications. Nonetheless, borylated ferrocenes have been studied in some detail, initially due to the fact that they are isoelectronic to stable ferrocenyl carbocations (2), and are synthons for other substituted ferrocenes. Early examples involve mainly dihaloboryl derivatives, prepared by direct borylation of the metallocene with BX_3 (3). In these reactions, the ferrocene Cp rings can be borylated up to four times. These haloboryl derivatives can be further derivatized and used as precursors

Received August 8, 2000. Published on the NRC Research Press Web site at http://canjchem.nrc.ca on July 5, 2001.

Dedicated with warmth and deep respect to Professor Brian James on the occasion of his 65th birthday.

B.E. Carpenter, W.E. Piers,[1] and M. Parvez. Department of Chemistry, University of Calgary, 2500 University Drive N.W., Calgary, AB T2N 1N4, Canada.
G.P.A. Yap. Department of Chemistry, University of Ottawa, 10 Marie Curie, Ottawa, ON K1N 6N5, Canada.
S.J. Rettig.[2] Department of Chemistry, University of British Columbia, 2036 Main Mall, Vancouver, BC V6T 1Y6, Canada.

[1]Corresponding author (telephone: (403) 220-5746; fax: (403) 289-9488; e-mail: wpiers@ucalgary.ca).
[2]Deceased.

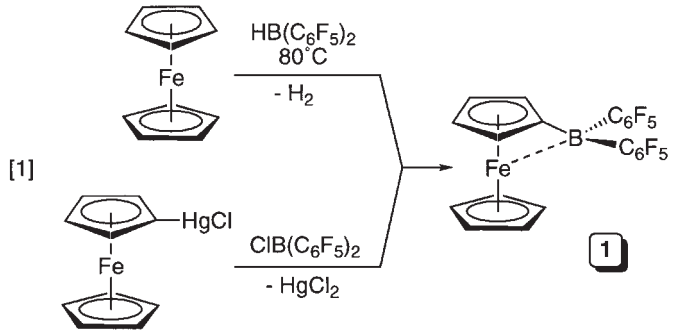
 DOI: 10.1139/cjc-79-5/6-857 © 2001 NRC Canada

to coordination polymer type materials (4). More recently, a class of *ansa*-ferrocenophanes utilizing a boron atom in the linking bridge have been prepared (5) and subjected to ring-opening polymerization reactions (5*c*).

Our interest in perfluoroaryl substituted boranes (6) led us to develop routes to bis-(pentafluorophenyl)boryl substituted boranes and to explore their properties as Lewis acids. In this paper, we detail the synthesis, properties, and reaction chemistry of the monoborylated ferrocene complex bis-(pentafluorophenyl)boryl ferrocene (**1**).

Results and discussion

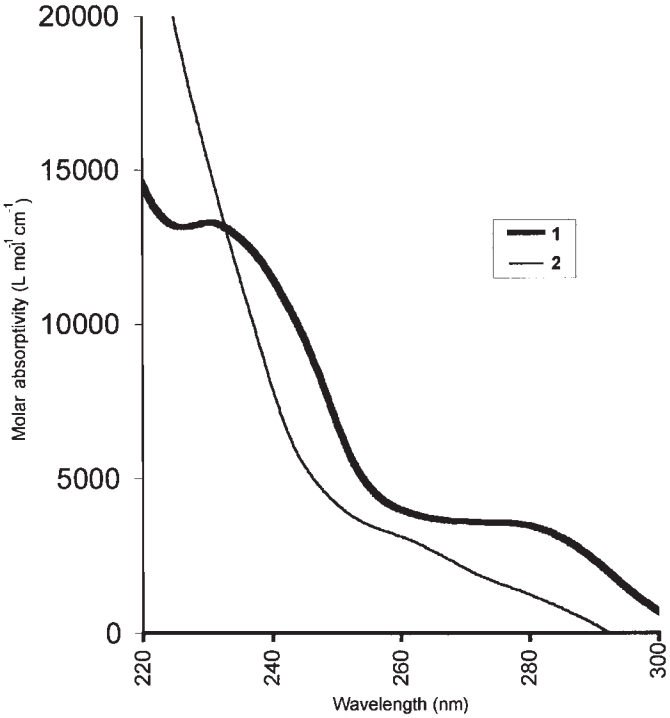
Previously, boryl-substituted ferrocenes have been prepared via direct borylation or transmetallation reactions (3). Accordingly, bis-(pentafluorophenyl)borylferrocene (**1**) can be synthesized either via borylation with bis-(pentafluorophenyl)borane, $HB(C_6F_5)_2$, (7) or through reaction of the well-known (chloromercuric)ferrocene, FcHgCl, (8) with bis-(pentafluorophenyl)chloroborane, $ClB(C_6F_5)_2$ (9) (eq. [1]). The former route requires heating for several hours and involves loss of H_2 during the course of the reaction, while the latter reaction occurs at room temperature and produces $HgCl_2$ as the by-product. Both routes are efficient, giving **1** in 87–91% isolated yield.



Boryl ferrocene **1** is a deeply maroon coloured solid which is highly soluble in common aliphatic and aromatic solvents. The UV–vis spectrum of **1** (Fig. 1) exhibits an intense absorption at ~230 nm ($\varepsilon = 1.33 \times 10^4$) likely assignable to an $Fe_{dz2/dx2-y2} \rightarrow B_p$ charge transfer process. Wagner and co-workers (3*j*) have detailed this Fe → B interaction in related dibromoboryl ferrocenes both experimentally and computationally and conclude that the occupied d_{z2} and d_{x2-y2} orbitals on the iron center have appropriate symmetry to interact with the empty *p*-orbital on the boron center, effectively forming a loose intramolecular Lewis acid–Lewis base adduct. A similar phenomenon accounts for the observed stability of ferrocenyl carbocations (2).

The NMR data for **1** also supports the notion that an Fe → B interaction is present in the compound. In perfluoroaryl substituted boranes, the chemical shift of the ^{11}B nucleus in the ^{11}B NMR spectrum is reflective of the coordination number and charge associated with the boron center (10). Neutral, three-coordinate boranes generally resonate in the 65–80 ppm range, neutral, four coordinate centers typically fall into the 5–25 ppm range, while anionic borates appear upfield at –10 to –35 ppm. Similarly, the chemical shift difference between the *meta* and *para* fluorines of the C_6F_5 rings is influenced by the amount of electron density at the boron center (11): as the boron proceeds from neutral, three-coordinate through four-coordinate adducts with Lewis bases, to anionic borates, the *para* fluorines become more shielded as the charge on boron increases, and shift upfield closer to the resonance for the *meta* fluorines. ^{11}B chemical shifts and $\Delta_{m,p}$ values for all the new compounds reported here as well as some comparable compounds are collected in Table 1. Inspection of this data shows that, for **1**, the ^{11}B chemical shift (53 ppm) and the $\Delta_{m,p}$ value (9.2 ppm) is intermediate to the numbers observed for purely neutral, three-coordinate examples and neutral, four-coordinate Lewis base adducts. These observations are consistent with the presence of a weak Fe → B interaction in **1**, which is maintained in nondonating solvents.

Fig. 1. UV–vis spectra of compounds **1** and **2** in 1,2-dichloroethane (concentration ~2×10^{-4} M).



This interaction is also manifested in the solid-state structure of **1**, determined by X-ray crystallography. Compound **1** crystallizes in the $P2_12_12_1$ space group with two crystallographically independent molecules in the asymmetric unit. Figure 2 shows the molecular structure of one of these molecules, along with selected metrical parameters; further details on this structure (and the others reported herein) can be found in the *Supplementary information*.[3] Immediately evident from the view shown is that the $B(C_6F_5)_2$ moiety is

[3] Copies of material on deposit may be purchased from the Depository of Unpublished Data, Document Delivery, CISTI, National Research Council Canada, Ottawa, ON K1A 0S2, Canada (http://www.nrc.ca/cisti/irm/unpub_e.shtml for information on ordering electronically). Some of this material has also been deposited with the Cambridge Crystallographic Data Centre. Copies of the data can be obtained, free of charge, on application to the Director, CCDC, 12 Union Road, Cambridge CB2 1EZ, U.K. (Fax: 44-1223-336033 or e-mail: deposit@ccdc.cam.ac.uk).

© 2001 NRC Canada

Fig. 2. ORTEP diagram of molecule one of **1**. Selected bond distances (Å): Fe(1)—C(13) 2.043(3), Fe(1)—C(14) 2.027(3), Fe(1)—C(17) 2.036(3), Fe(1)—C(15) 2.060(2), Fe(1)—C(16) 2.062(2), C(13)—C(14) 1.444(3), C(13)—C(17) 1.448(3), C(14)—C(15) 1.414(3), C(16)—C(17) 1.407(4), C(15)—C(16) 1.418(3), B(1)—C(13) 1.501(4), B(1)—C(6) 1.604(4), B(1)—C(12) 1.584(4). Selected nonbonded distance (Å): Fe(1)···B(1), 2.924. Selected bond angles (°): C(6)-B(1)-C(12) 118.4(2), C(6)-B(1)-C(13) 118.0(2), C(12)-B(1)-C(13) 122.5(2).

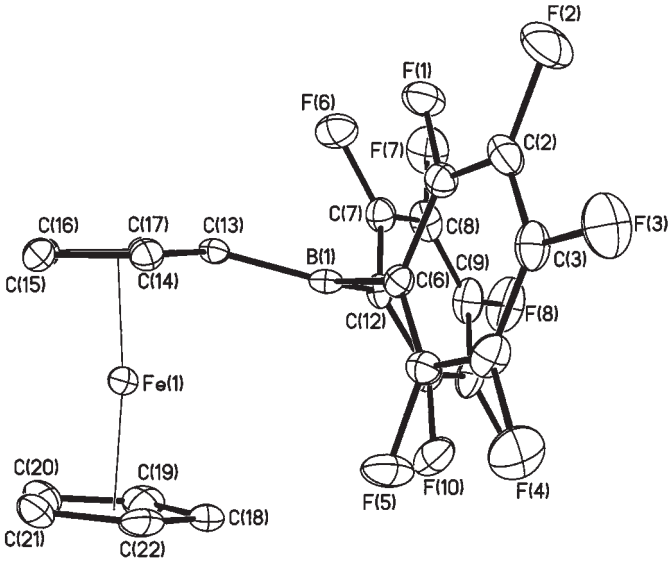


Table 1. ^{11}B and ^{19}F $\Delta_{m,p}$ values for various pentafluorophenyl-substituted boranes.

Compound	^{19}F $\Delta_{m,p}$	δ ^{11}B	Reference
$HB(C_6F_5)_2$	18.3	60.1	7
$B(C_6F_5)_3$	16.3	80	[a]
$C_6H_5B(C_6F_5)_2$	12.6	72.6	[b]
$FcBBr_2$	—	46.7	3*d*
1	9.2	53.0	
2	5.6	–13.5	
3-OTf	6.2	–4.8	
3-C_6F_5	6.8	–23.7	
4	3.7	–13.2	
$LiB(C_6F_5)_4$	3.7	–17.3	[b]

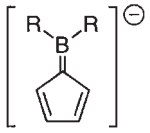
[a]A.G. Massey and A.J. Park. J. Organomet. Chem. **5**, 218 (1966).
[b]P.A. Deck, C.L. Beswick, and T.J. Marks. J. Am. Chem. Soc. **120**, 1771 (1998).

Table 2. Oxidation potentials for ferrocenyl boranes and borates vs. ferrocene$^{+1/0}$.

Compound	Solvent	$E_{1/2}$ (mV)
1	TFT[a]	+450
2	TFT	–100
3-C_6F_5	TFT	–472
$FcC(O)CH_3$	CH_2Cl_2	+270[b]

[a]α,α,α-Trifluorotoluene.
[b]Taken from ref. 22.

tilted towards the iron center such that the dip angle of the B(1)-C(13) vector out of the plane defined by the five Cp carbons is ~16°. This compares to the values of 17.7° and 18.9° found for the same parameter in crystallographically independent molecules of the related compound $Fc(BBr_2)$ (3*j*). As a consequence of this interaction in **1**, the B(1) center is slightly pyramidalized (the sum of the angles about B(1) is 358.2°) and the Fe(1)—B(1) distance is 2.924 Å. The metrical parameters for the borylated Cp ring suggest a partial contribution from a boratafulvene-like structure (12) akin to **I** is operative for this ligand. Furthermore, the B(1)—C(13) distance of 1.501(4) Å is intermediate between values found for a B(sp^2)-C(sp^2) double bond (e.g., 1.44 Å in $LiCH_2$=$B(mes)_2$ (13)) and that of a B(sp^2)-C(sp^2) single bond (e.g., 1.58 Å in BPh_3 (14)). Thus it appears that, in addition to accepting electron density directly from the iron center, the $B(C_6F_5)_2$ group withdraws π-electron density from the Cp ring as well.



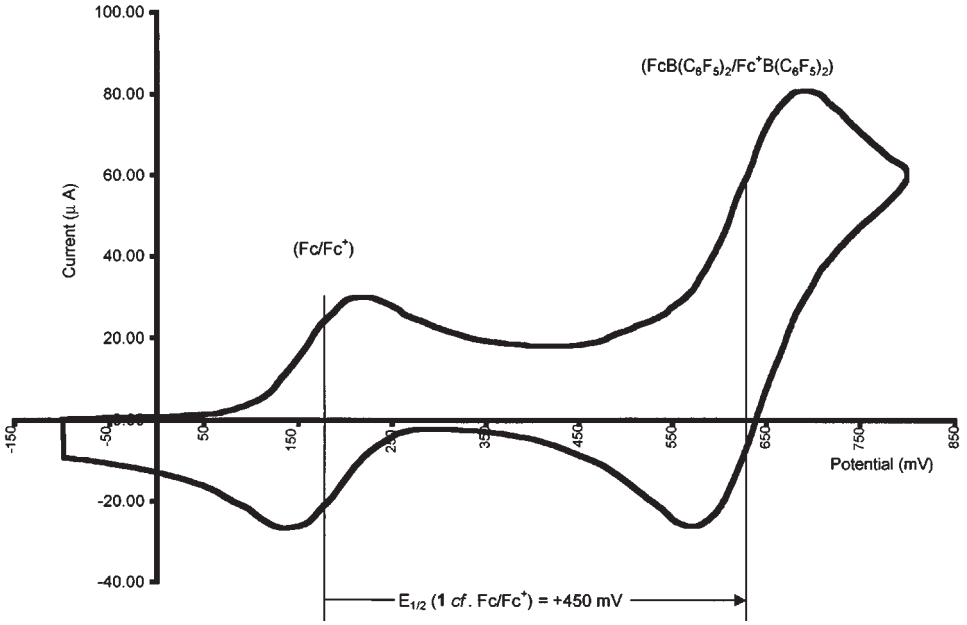
I

The electron-withdrawing capacity of the -$B(C_6F_5)_2$ group is manifested in the electrochemical behaviour of **1**. Cyclic voltammetric measurements were performed against a silver wire quasireference electrode in ≈100 mM solutions of substrate in α,α,α-trifluorotoluene (TFT) with $[NBu_4][B(C_6F_5)_4]$ as the supporting electrolyte (15). Use of the standard $[NBu_4][BF_4]$ electrolyte led to irreversible oxidations, a result of chemical reactions subsequent to oxidation (vide infra). An internal standard of ferrocene was employed; all $E_{1/2}$ values reported (Table 2) are relative to the Fc/Fc^+ couple under these conditions. As can be seen in Fig. 3, **1** exhibits a reversible oxidation wave at +450 mV relative to ferrocene, indicating that it is more difficult to oxidize owing to the electron-withdrawing -$B(C_6F_5)_2$ substituent.

The flow of electron density into the empty boron *p*-orbital dampens the Lewis acidity of **1** in comparison to other perfluoroaryl substituted boranes. For example, while carbonyl functions, (16) ethers and water, (17) isonitriles and nitriles (18) form strong adducts with $B(C_6F_5)_3$, when **1** is treated with oxygen nucleophiles such as acetophenone, acetylferrocene, *N*,*N*-di-iso-propylbenzamide or THF, the equilibrium for adduct formation lies far towards the reactants at room temperature. Treatment of **1** with 1 equiv of water leads to rapid formation of FcH and $HOB(C_6F_5)_2$ (9), indicating that coordination occurs to some extent. Toluene-d_8 solutions of **1** containing a few equiv of acetonitrile, when cooled, change in colour from the deep maroon of **1** to light yellow, indicative of disruption of the Fe → B interaction upon adduct formation. However, the acetonitrile ligand remains labile even at 193 K, as judged by the single resonance for free vs. bound acetonitrile in the sample's ^1H NMR spectrum at this temperature. Use of the Childs' method for assessing Lewis acid strength (19) shows that **1** has a Lewis acid strength of 0.37 ± 0.03 relative to BBr_3 at 1.00. Comparative values for other Lewis acids, for example,

© 2001 NRC Canada

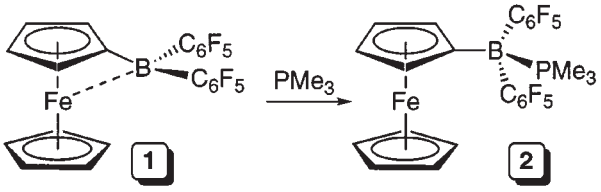
Fig. 3. Representative CV of **1** (1 mM) in α,α,α-trifluorotoluene with $[Bu_4N][B(C_6F_5)_4]$ (100 mM) as supporting electrolyte. Scan rate = 100 mV s^{-1}.



$AlCl_3$ (0.88 ± 0.03), $B(C_6F_5)_3$ (0.77) (20), and $SnCl_4$ (0.56 ± 0.03), show that **1** is a relatively weak Lewis acid by virtue of this Fe → B interaction.

Only strong Lewis bases, such as PMe_3, form adducts irreversibly with **1** (eq. [2]). When maroon solutions of **1** are exposed to PMe_3, an instantaneous colour change to a yellow hue signals formation of adduct **2**. This material was isolated and fully characterized. Notably, the UV–vis spectrum of **2** (Fig. 1) no longer contains a prominent charge transfer band, supporting the assignment of this band for **1** given above. The chemical shift of the ^{11}B nucleus in the NMR spectrum of **2** (–13.5 ppm) is somewhat upfield of the region expected for such four-coordinate adducts but is split into a doublet due to coupling to the ^{31}P nucleus ($J_{B\text{-}P}$ = 46 ± 10 Hz). The $\Delta_{m,p}$ value of 5.6 ppm (Table 1) is consistent with strong coordination of the phosphine to the boron center, although the relatively small value of $J_{B\text{-}P}$ suggests that the phosphine may be labile. The PMe_3 ligated boryl group is now a net electron donator to the Cp ring as judged by the $E_{1/2}$ value of –100 mV (relative to Fc/Fc^+, Table 2) in the cyclic voltammagram of **2**. Since the *p*-orbital on boron is plugged with the phosphine lone pair of electrons, the σ-donating ability of the boryl group now dominates the electronic effect of this group on the Fe(II)–Fe(III) redox couple of the iron center.

[2]

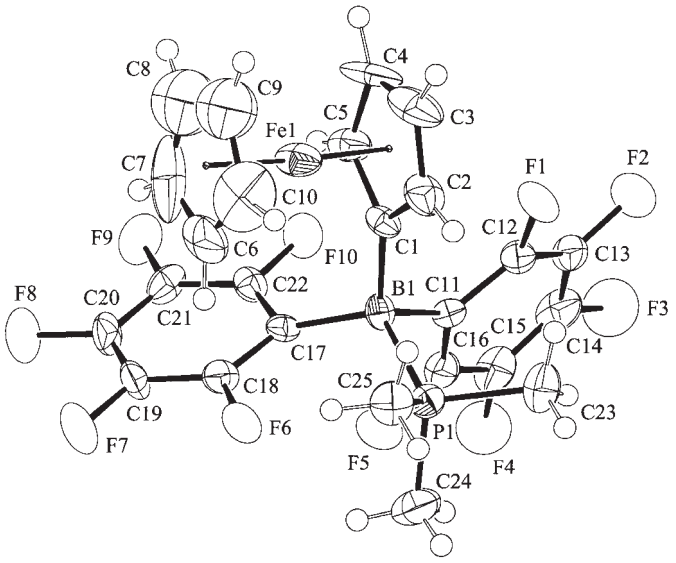


The solid-state structure of **2** was determined by X-ray crystallography, and an ORTEP diagram along with selected metrical data is given in Fig. 4. The B(1)—P(1) distance of 1.992(9) Å is comparable to the 2.046(8) Å and 2.015(3) Å values found for the PH_3 and *t*-$BuPH_2$ adducts, respectively, of $B(C_6F_5)_3$ (21). The now four-coordinate boron atom is tilted out of the Cp plane away from the iron center by 6.4°. As expected, the boratafulvene character of **1** is lost and the B(1)—C(1) distance of 1.61(1) Å is characteristic of a B(sp^3)—C(sp^2) bond.

Given the nature of the Fe → B interaction in **1** and related compounds and its dampening effect on the Lewis acidity of the boron center, it seemed logical to presume that oxidation of the iron center should weaken the Fe → B interaction and concommitantly impart stronger Lewis acidity on the borane. Experiments involving chemical oxidation of **1** appear to bear this out. For example, treatment of **1** with $[NO][BF_4]$, a common oxidizing agent for ferrocene derivatives (22), led to oxidation to a ferrocenium complex as indicated by a change in the solution's colour from maroon to dark green, with visible evolution of NO gas. ^{19}F NMR spectroscopy on the crude product showed that the BF_4 anion was no longer present and that one major $B(C_6F_5)_2$ containing product was present as ≈80% of the mixture. Due to the paramagnetism of this compound, ^1H and ^{11}B NMR spectroscopy provided little useful information; however, the C_6F_5 rings are far enough removed to be relatively unaffected by the paramagnetic iron center. While isolable quantities of pure product were not obtained, analysis of crystals isolated from this product mixture by X-ray crystallography, revealed the fluoroborate zwitterion **3-F** to be this major product (Fig. 5). Evidently, the boron center in the putative ferrocenium intermediate **3** (Scheme 1) is Lewis acidic enough to abstract a fluoride ion from the BF_4 counteranion. Fluoride abstraction by other perfluoroaryl boranes, specifi-

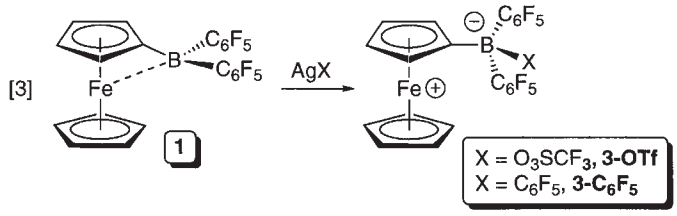
© 2001 NRC Canada

Fig. 4. ORTEP diagram of **2**. Selected bond distances (Å): Fe(1)—C(1) 2.098(7), Fe(1)—C(2) 2.044(8), Fe(1)—C(3) 2.012(9), Fe(1)—C(4) 2.037(8), Fe(1)—C(5) 2.022(8), C(1)—C(2) 1.447(9), C(1)—C(5) 1.424(10), C(2)—C(3) 1.400(12), C(4)—C(5) 1.425(10), C(3)—C(4) 1.401(12), B(1)—C(1) 1.609(11), B(1)—C(11) 1.665(10), B(1)—C(17) 1.637(10), B(1)—P(1) 1.992(9). Selected bond angles (°): P(1)-B(1)-C(1) 109.3(5), P(1)-B(1)-C(11) 102.1(5), P(1)-B(1)-C(17) 116.0(6), C(1)-B(1)-C(11) 110.6(6), C(1)-B(1)-C(17) 109.0(6), C(11)-B(1)-C(17) 109.8(6).



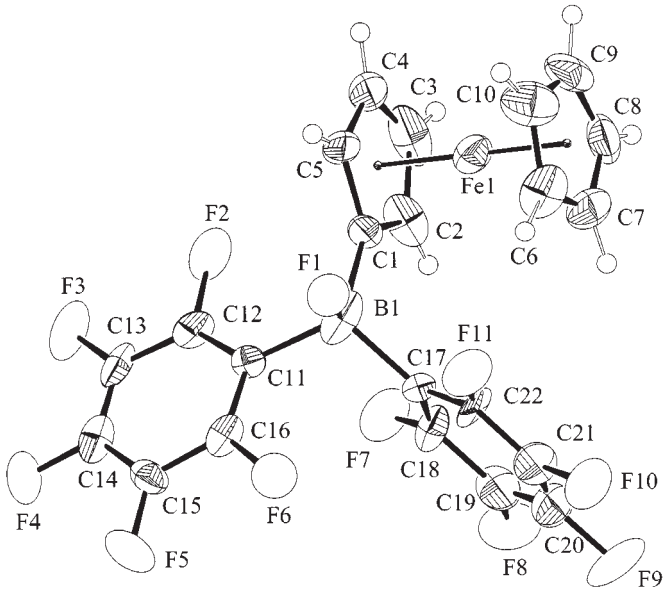
cally $B(C_6F_5)_3$ (23) and the chelating diboryl species 1,2-$C_6F_4[B(C_6F_5)_2]_2$ (24) has also been documented. Significantly, boryl ferrocene **1** does not react with $[NBu_4][BF_4]$, even upon heating. Recall, however, that electrochemical oxidation of **1** in the presence of this electrolyte was irreversible. Taken together, these observations suggest that oxidation of the iron center significantly increases the Lewis acidity of the boron center attached to the Cp ring.

Zwitterion **3-F** crystallizes as two independent molecules with essentially identical metrical parameters, differing only in the orientation of the fluoroborate moiety with respect to the Cp ligand plane. One of the molecules is shown in Fig. 5, along with selected metrical parameters; a picture of the other is given in the deposited material. The borate boron is tetrahedral in geometry and the B(1)—F(1) distance of 1.452(12) Å is typical of these bonding partners.

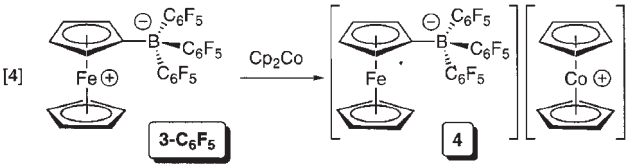


Two other zwitterionic ferrocenium compounds were prepared in high yield and purity by oxidation of **1** with AgOTf and AgC_6F_5 (25) as shown in eq. [3]. Formation of **3-OTf** was essentially immediate upon dissolution of the reactants

Fig. 5. ORTEP diagram of one molecule of **3-F**. Selected bond distances (Å): C(1)—B(1) 1.626(15), B(1)—F(1) 1.452(12), B(1)—C(11) 1.697(15), B(1)—C(17) 1.651(14). Selected bond angles (°): F(1)-B(1)-C(1) 108.1(11), F(1)-B(1)-C(11) 105.8(9), F(1)-B(1)-C(17) 109.2(8), C(1)-B(1)-C(11) 112.3(8), C(1)-B(1)-C(17) 111.5(10), C(11)-B(1)-C(17) 109.9(10).



in dichloromethane, whereas the reaction leading to **3-C_6F_5** required several hours in toluene solvent. Complex **3-OTf** exhibits a resonance at –89.6 ppm in the ^{19}F NMR spectrum, attributable to the triflate CF_3 group, in addition to those of the C_6F_5 fluorines. The solid-state structure of this compound was determined by X-ray crystallography and an ORTEP diagram and selected metrical data is given in Fig. 6. Again, the quaternized boron center is now directed away (6.0°) from the iron center. The metrical parameters associated with the OTf moiety are similar to other η^1-coordinated trifluoromethanesulfonates (26).



Zwitterion **3-C_6F_5** was also structurally characterized (Fig. 7). Consistent with boron quaternization, the boron atom is 3.59 Å away from the iron center (5.8° tilt). In addition, ^1H, ^{11}B, and ^{19}F NMR spectroscopy were fully consistent with the structure found in the solid state. Furthermore, one-electron reduction using cobaltocene gave a diamagnetic ion pair, $[FcB(C_6F_5)_3][Cp_2Co]$ (**4**, eq. [4]), which was also characterized spectroscopically and via elemental analysis. We were interested in **3-C_6F_5** as a potential activator for metallocene and related olefin polymerization catalyst precursors, since it is known that ferrocenium salts are capable of oxidizing neutral dialkyl metallocenes to the active cationic alkyl catalysts (27). Unfortunately, **3-C_6F_5** is not a strong enough oxidizing agent to remove an electron from Cp_2ZrMe_2. In fact, electrochemical measurements on this

© 2001 NRC Canada

Scheme 1.

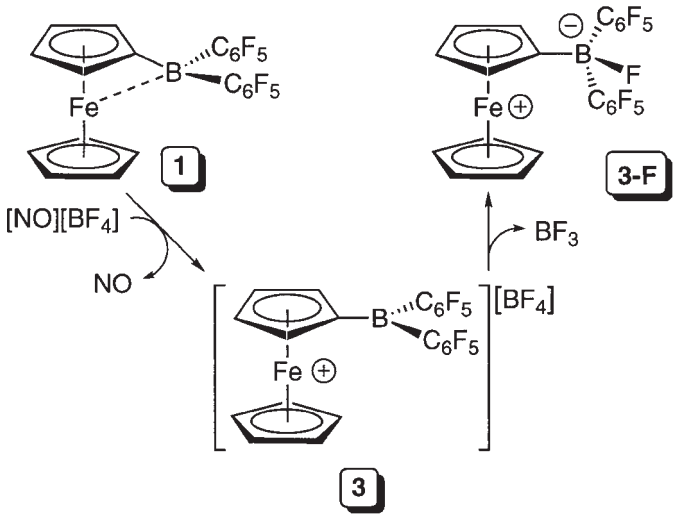
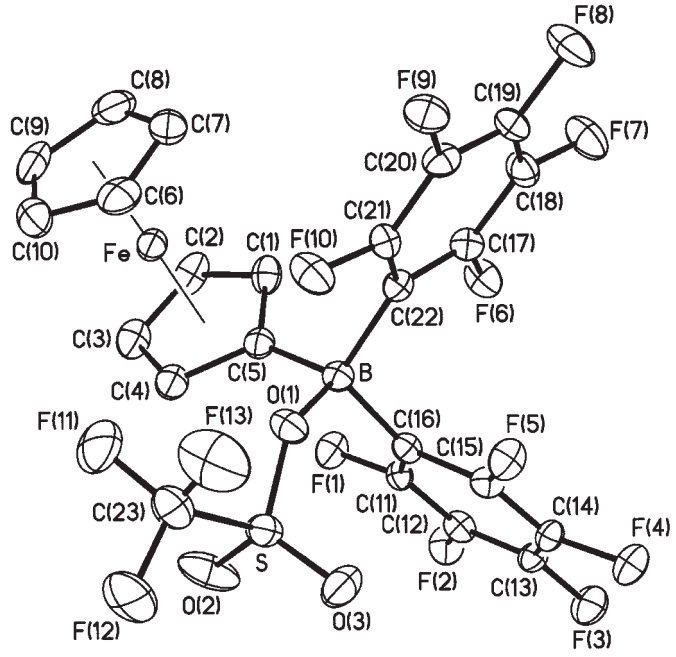
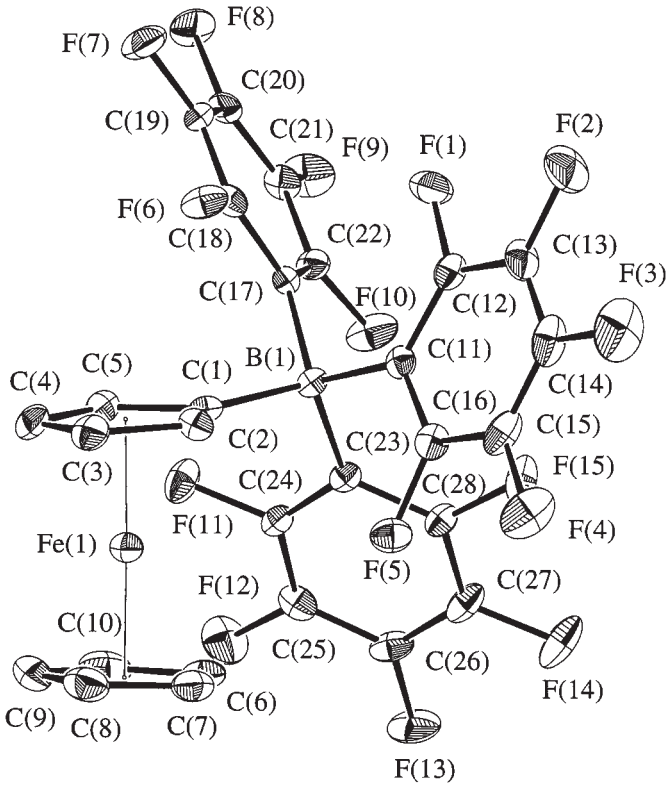


Fig. 6. ORTEP diagram of **3-OTf**. Selected bond distances (Å): B—C(5) 1.601(5), B—C(16) 1.624(5), B—C(22) 1.658(4), B—O(1) 1.575(4), S—O(1) 1.486(2), S—O(2) 1.416(7), S—O(3) 1.392(8), S—C(23) 1.824(6). Selected bond angles (°): O(1)-B-C(5) 107.7(3), O(1)-B-C(16) 109.0(3), O(1)-B-C(22) 104.8(2), C(5)-B-C(16) 112.7(3), C(5)-B-(C(22) 111.7(3), C(16)-B-C(22) 110.5(3).



zwitterion show that its oxidation potential is at –472 mV relative to Fc/Fc^+, indicating that the -$B(C_6F_5)_3$ borate moiety is a very good σ-donor to the Cp ring, stabilizing the Fe(III) center substantially relative to unsubstituted ferrocene. Structurally, there is nothing unusual about this compound; the borate boron is tetrahedral and the B—C bond lengths are normal. Compound **3-C_6F_5** is related to the zwitterion $Fc^+B(Fc)_3$, reported several years ago (28).

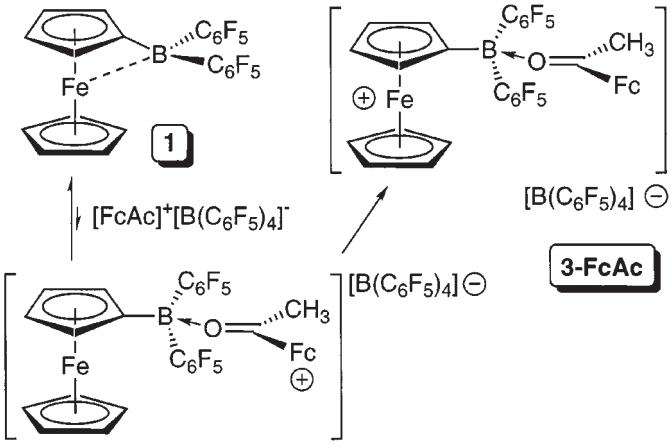
Fig. 7. ORTEP diagram of **3-C_6F_5**. Selected bond distances (Å): Fe(1)—C(1) 2.152(2), Fe(1)—C(2) 2.100(2), Fe(1)—C(3) 2.065(2), Fe(1)—C(4) 2.069(2), Fe(1)—C(5) 2.098(2), C(1)—C(2) 1.433(3), C(1)—C(5) 1.434(3), C(2)—C(3) 1.428(3), C(4)—C(5) 1.414(3), C(3)—C(4) 1.409(3), B(1)—C(1) 1.666(3), B(1)—C(11) 1.648(3), B(1)—C(17) 1.657(3), B(1)—C(23) 1.666(3). Selected bond angles (°): C(1)-B(1)-C(11) 106.0(2), C(1)-B(1)-C(17) 105.7(2), C(1)-B(1)-C(23) 112.0(2), C(11)-B(1)-C(17) 113.2(2), C(11)-B(1)-C(23) 110.9(2), C(17)-B(1)-C(23) 108.9(2).



The observations above infer that the boron center of the putative species **3** is more Lewis acidic than that of neutral borane **1**. Unfortunately, attempts to prepare **3** with a weakly coordinating anion, namely $[B(C_6F_5)_4]^-$ met with failure, although some of the experiments aimed at preparing **3** with this counteranion support the notion that **3** is a stronger Lewis acid than **1**. For example, **1** may be oxidized using the acetylferrocenium reagent $[FcAc]^+[B(C_6F_5)_4]^-$. Acetylferrocenium reagents have been used to oxidize other ferrocene derivatives, since its oxidation potential of +270 mV is higher than most substituted ferrocene derivatives (23). Interestingly, it should not be a strong enough oxidizing agent to oxidize **1**, whose potential is at +450 mV relative to ferrocene, and yet when **1** and $[FcAc]^+[B(C_6F_5)_4]^-$ are mixed together, a rapid redox reaction is observed. Presumably the carbonyl group of the acetyl substituent is able to weakly coordinate the boron center in **1**, converting the electron-withdrawing -$B(C_6F_5)_2$ substituent into an electron-donating (relative to H) -$B(L)(C_6F_5)_2$ group (Scheme 2). Thus, when the acetylferrocenium species coordinates to the boron center in **1**, oxidation is rapid, producing the complex **3-FcAc**. ^1H NMR spectroscopy suggests that the neutral

© 2001 NRC Canada

Scheme 2.



acetylferrocene product of the electron transfer reaction remains coordinated to the boron center. All attempts to remove the acetylferrocene failed; clearly, FcAc is bound much more tightly to the Lewis acid center in **3** compared to that in **1**.

In conclusion, we have prepared bis-(pentafluorophenyl)ferrocenylborane and examined its chemical and electrochemical behaviour. The Lewis acidity of the boron center is attenuated due to a significant Fe → B interaction in the Fe(II) species, but oxidation of the iron center to Fe(III) disrupts this interaction, resulting in a more strongly Lewis acidic boron center.

Experimental section

General

All reactions were carried out under an argon atmosphere either on a double manifold high vacuum line or in an Innovative Technology System One dry box. Standard inert atmosphere, Schlenk, vacuum line, and glove box techniques were used throughout, under purified argon. Nuclear magnetic resonance (NMR) spectra were obtained in d_2-methylene chloride (CD_2Cl_2), d_6-benzene, or d_8-toluene on either Bruker AMX400 (^{1}H NMR, 400.132 MHz, ^{13}C NMR, 100.623 MHz), Bruker AMX300 (^{1}H NMR, 300.138 MHz, ^{11}B NMR, 96.293 MHz, ^{19}F NMR, 282.371 MHz), Varian XL200 (^{13}C NMR, 50.310 MHz, ^{11}B NMR, 64.184 MHz, ^{31}P NMR, 80.988 MHz) or Bruker ACE-200 (^{1}H NMR, 200.134 MHz) spectrometers. ^{1}H and ^{13}C NMR spectra were referenced to tetramethylsilane ($SiMe_4$) via solvent resonances. ^{11}B NMR spectra were externally referenced to borane trifluoride diethyl etherate (δ 0.0 ppm) and ^{19}F NMR spectra were externally referenced to $CFCl_3$ (δ 0.00 ppm) using an external standard of hexafluorobenzene (δ –163.0 ppm) (29). ^{31}P NMR spectra were reference to the external standard H_3PO_4 in deuterium oxide (δ 0.00 ppm). UV–vis spectra were obtained in dry $ClCH_2CH_2Cl$ using a Cary 5E UV–vis and IR spectrometer. The samples were prepared in volumetric flasks (~2.0×10^{-4} M) and transferred to a 1 mm pathlength air-tight cell fused to a Kontes Teflon tap. A background spectrum of the solvent was collected and automatically subtracted from the spectrum collected of the substrate. The molar absorptivity was calculated using Beer's Law. Elemental analyses were performed by Mrs. Dorothy Fox (University of Calgary) on a Control Equipment Corporation 440 elemental analyzer.

Toluene, tetrahydrofuran (THF), and hexanes were purified using the Grubbs purification system (30) and stored in solvent pots over a drying agent. α,α,α-Trifluorotoluene (TFT) was predried over phosphorus pentoxide (P_2O_5) and stored over CaH_2 in a glass bomb. Deuterated solvents were purchased from Cambridge Isotopes Laboratories and dried analogously.

All chemicals were purchased from Aldrich–Sigma unless otherwise stated except tris-(pentafluorophenyl)borane and ferrocene, which were purchased from Boulder Scientific Company. The $B(C_6F_5)_3$ dried as previously described, while ferrocene was purified by sublimation under dynamic vacuum at 55°C. Literature procedures were used to prepare the following reagents: $[n\text{-}Bu_4N]^+[B(C_6F_5)_4]$ (15), ($ClB(C_6F_5)_2$) (9), ($HB(C_6F_5)_2$) (7), ($LiB(C_6F_5)_4\cdot Et_2O$) (31), (AgC_6F_5) (25), (FcHgCl) (8), and $[FcAc]^+[BF_4]^-$ (8).

Preparation of 1

Method A

Ferrocene (1.90 g, 10.2 mmol) and $HB(C_6F_5)_2$ (3.45 g, 9.98 mmol) were dissolved in toluene (60 mL), warmed slowly to 80°C, and stirred for 22.5 h under argon opened to a mercury bubbler. The reaction mixture was cooled and the toluene was removed under vacuum to afford a dark maroon solid. Boryl ferrocene product was extracted from unreacted $HB(C_6F_5)_2$ with hexanes. The hexanes were removed under vacuum to afford a crimson red crystalline solid. Residual ferrocene was removed from the product by sublimation (55°C under full vacuum). Yield of **1**: 4.39 g (8.28 mmol, 91%). X-ray quality crystals were grown from a saturated solution of **1** in dry hexamethyldisiloxane cooled to –35°C. UV (TFT) λ_{max} (nm) (ε): 231 (1.33×10^4). ^{1}H NMR (C_6D_6): 4.51 (t, 2H, J = 1.8 Hz, H_β), 4.03 (s, 5H, C_5H_5), 3.95 (bs, 2H, H_a). ^{13}C NMR (C_6D_6): 145.9 (d, $^1J_{CF}$ = 242 Hz), 141.9 (d, $^1J_{CF}$ = 242 Hz), 137.7 (d, $^1J_{CF}$ = 251 Hz), 115.0 (bs, WHM = 87 Hz, $C_{ipso}(C_6F_5)$), 79.5 (s, WHM = 7.4 Hz, C_β), 77.7 (s, WHM = 8 Hz, C_α), 70.5 (s, WHM = 7.4 Hz, C_5H_5). ^{11}B NMR (C_6D_6): 53.7 (bs, WHM = 650 Hz). ^{19}F NMR (C_6D_6): –129.3 (dd, 4F, F_o), –152.5 (t, 2F, F_p), –161.7 (dt, 4F, F_m). Anal. calcd. for $C_{22}H_9BF_{10}Fe$: C 49.86, H 1.71; found: C 49.69, H 1.90.

Method B

1-(Chloromercuric)ferrocene (2.403 g, 5.32 mmol) and $ClB(C_6F_5)_2$ (1.987 g, 5.23 mmol) were placed into a 100 mL bomb and hexanes (80 mL) added under vacuum transfer conditions. The mixture was warmed to room temperature and stirred for 22 h. The orange chalky suspension changed to a dark maroon solution with a green–grey precipitate. The suspension was cannula-transferred under argon flow into a 100 mL RBF and filtered to extract **1** from the mercuric chloride by-product. The $HgCl_2$ was washed with hexanes until the washings were colourless. The solvent was removed in vacuo to afford the maroon solid **1**. Yield: 2.461 g (4.64 mmol, 87%). The crude product was subjected to sublimation to remove any residual $ClB(C_6F_5)_2$.

© 2001 NRC Canada

Preparation of 2

Compound **1** (394 mg, 0.743 mmol) was dissolved in toluene and the solution degassed by a freeze–pump–thaw routine. At –196°C, an excess of PMe_3 (>15 cmHg in a 115 cm^3 bulb) was condensed into the flask. The reaction was warmed to –78°C during which time the maroon solution changed colour to light yellow. The solvent was removed in vacuo to afford a yellow powder. Yield: 443 mg (0.731 mmol, 98%). A single crystal was grown from a saturated toluene solution. ^{1}H NMR (d_8-toluene): 4.15 (t, 2H, J = 1.80 Hz, H_β), 3.99 (s, 5H, Fe(C_5H_5)), 3.62 (bs, 2H, H_a), 0.47 (d, 9H, $^2J_{PH}$ = 10.7 Hz, P(CH_3)$_3$). ^{13}C NMR (d_8-toluene): 148.1 (*d*, $^1J_{CF}$ = 234 Hz), 139.7 (*d*, $^1J_{CF}$ = 263 Hz, C_p), 137.7 (*d*, $^1J_{CF}$ = 246 Hz), 120.3 (bs, C_{ipso}(C_6F_5)), 80.2 (bs, C_{ipso}(C_5H_4)), 73.7 (*s*, C_α), 69.9 (*s*, C_β), 68.8 (*s*, Fe(C_5H_5)), 9.5 (*d*, $^1J_{CP}$ = 37 Hz, P(CH_3)$_3$). ^{11}B NMR (d_8-toluene): –13.5 (br d, $^1J_{BP}$ = 46 ± 10 Hz). ^{19}F NMR (d_8-toluene): –127.6 (d, 4F, F_o), –157.6 (t,2F, F_p), –163.2 (dt, 4F, F_m). ^{31}P NMR (d_8-toluene): –12.1 (br m, $^1J_{PB}$ = 46 ± 10 Hz).

Preparation of 3-F

Borane **1** (306 mg, 0.577 mmol) and nitrosonium tetrafluoroborate ($NOBF_4$) (65 mg, 0.557 mmol) were dissolved in CH_2Cl_2 (20 mL). The reaction vessel was placed into a 60°C oil bath and stirred for 30 min. The solution was cooled, degassed, and taken into the dry box where it was transferred to a flask fitted with a frit assembly. The solution was concentrated and the slurry sonicated; filtration afforded a dark blue solid. Yield: 250 mg (0.405 mmol, 72%). Crystals were grown by layering hexane on a concentrated solution in CH_2Cl_2 at 25°C. ^{1}H NMR: 33.1 (bs, WHM = 1360 Hz, 2H), 28.0 (bs, WHM = 700 Hz, 5H, Fe(C_5H_5)), 30.1 (bs, WHM = 2150 Hz, 2H). ^{19}F NMR: –157.1 (bs, 4F, F_o), –162.4 (t, 2F, F_p), –166.8 (bs, 4F, F_m); the B-F fluorine was not located.

Preparation of 3-Otf

Silver trifluoromethanesulfonate (245 mg, 0.953 mmol) and **1** (505 mg, 0.953 mmol) were placed into a flask fitted with a frit assembly. CH_2Cl_2 (25 mL) was condensed into the vessel under vacuum transfer conditions. The reaction was warmed to room temperature and stirred for 2 h during which time the solution changed from maroon to navy blue. The reaction mixture was filtered with a grey residue remaining on the frit and the solvent was removed under vacuum to afford 585 mg (0.858 mmol, 90%) of a paramagnetic dark blue solid of high purity by ^{19}F NMR. Crystals were grown at 25°C from a minimum amount of CH_2Cl_2 layered with hexane. UV (TFT) λ_{max} (nm) (ε): 256 (1.42×10^4). ^{1}H NMR: 42.0 (bs, WHM = 2780 Hz), 33.1 (bs, WHM = 2500 Hz), 30.1 (bs, WHM = 1050 Hz). ^{13}C NMR: 142.9 (d, $^1J_{CF}$ = 245 Hz), 137.7 (d, $^1J_{CF}$ = 257 Hz), 133.0 (d, $^1J_{CF}$ = 241 Hz), 92.1 (bs, C_{ipso}). ^{11}B NMR: –4.75 (bs, WHM = 394 Hz). ^{19}F NMR: –89.6 (s, 3F, CF_3), –155.8 (bs, 4F, F_o), –159.6 (s, 2F, F_p), –165.8 (s, 4F, F_m). Anal. calcd. for $C_{23}H_9BF_{13}FeO_3S$: C 40.68, H 1.34; found: C 40.51, H 1.13.

Preparation of 3-C_6F_5

Pentafluorophenyl silver(I) (AgC_6F_5) (614 mg, 2.23 mmol) and **1** (1.183 g, 2.23 mmol) were placed into a 100 mL bomb to which was added 50 mL of toluene. The vessel was sealed and warmed to 100°C in an oil bath for 23.5 h. The flask was cooled to room temperature and the green solution was cannula-transferred to a two-neck round-bottom flask with a frit assembly under an argon flow. The toluene was removed under vacuum and CH_2Cl_2 was condensed in at –78°C. The green solution was extracted from the silver powder by filtration and washed until the extracts were colourless. The solvent was removed in vacuo to afford a dark green solid. Yield: 1.397 g (2.00 mmol, 90%). Crystals of **3-C_6F_5** were grown at 25°C when dissolved into a minimum amount of dry CH_2Cl_2 layered with hexane. UV (TFT) λ_{max} (nm) (ε): 258 (1.33×10^4). ^{1}H NMR (d_8-toluene): 43.8 (bs, WHM = 1150 Hz), 30.2 (bs, WHM = 1400 Hz), 24.2 (bs, WHM = 780 Hz). ^{13}C NMR: 142.7 (d, 4C, $^1J_{CF}$ = 225 Hz), 139.3 (d, 2C, $^1J_{CF}$ = 246 Hz, C_p), 133.6 (d, 4C, $^1J_{CF}$ = 246 Hz). ^{11}B NMR: –23.7 (bs, 55 Hz). ^{19}F NMR: –139.6 (bs, 6F, F_o), –161.0 (s, 3F, F_p), –167.8 (d, 6F, F_m). Anal. calcd. for $C_{28}H_9BF_{15}Fe$: C 48.24, H 1.30; found: C 48.25, H 1.30.

Preparation of [FcB(C_6F_5)$_3$][Cp_2Co] (4)

3-C_6F_5 (420 mg, 0.619 mmol) and cobaltocene (117 mg, 0.619 mmol) were dissolved in dry CH_2Cl_2 (12 mL). The solution was stirred at room temperature for 2 h. The solution was run through a frit and the solvent removed to afford a brown crystalline solid. Yield: 490 mg (0.564 mmol, 91%). ^{1}H NMR: 5.60 (s, 10H, Co(C_5H_5)), 4.00 (t, 2H, J = 1.68 Hz, H_β), 3.94 (bs, 2H, H_α), 3.67 (s, 5H, Fe(C_5H_5)). ^{13}C NMR: 149.3 (d, $^1J_{CF}$ = 246 Hz), 138.4 (d, $^1J_{CF}$ = 245 Hz, C_p), 137.0 (d, $^1J_{CF}$ = 258 Hz), 85.2 (s, Co(C_5H_5)), 75.9 (s, C_α), 68.3 (s, Fe(C_5H_5)), 67.0 (s, C_β). ^{11}B NMR: –13.2 (bs, WHM = 39 Hz). ^{19}F NMR: –128.3 (d, 6F, F_o), –164.5 (dt, 3F, F_p), –168.0 (t, 6F, F_m). Anal. calcd. for $C_{38}H_{19}BCoF_{15}Fe$: C 51.51, H 2.16; found: C 51.30, H 2.34.

Preparation $[FcAc]^+[B(C_6F_5)_4]^-$

Acetylferrocenium tetrafluoroborate (298 mg, 0.946 mmol) and lithium tetrakis(pentafluorophenyl)borate etherate (843 mg, 0.947 mmol) were dissolved in CH_2Cl_2 and stirred for 12 h. The mixture was filtered and the solid washed with CH_2Cl_2 three times. The solvent was removed from the filtrate to afford a fluffy blue solid. Yield: 794 mg (0.875 mmol, 92%). ^{1}H NMR: 35.8 (bs, WHM = 750 Hz), 30.4 (bs, WHM = 1800 Hz), 0.90 (s, 3H, COOCH_3), –12.1 (bs, WHM = 120 Hz). ^{13}C NMR: 147.5 (d, $^1J_{CF}$ = 242 Hz), 138.2 (d, $^1J_{CF}$ = 232 Hz), 135.9 (d, $^1J_{CF}$ = 232 Hz), 126.3 (bs, C_{ipso}(C_6F_5)). ^{11}B NMR: –16.9 (s, WHM = 28 Hz). ^{19}F NMR: –135.6 (s, 8F, F_o), –164.4 (s, 4F, F_p), –169.4 (s, 8H, F_m). Anal. calcd. for $C_{36}H_{12}BF_{20}FeO$: C 47.66, H 1.33; found: C 46.88, H 1.53.

Preparation of 3-FcAc

Borane **1** (262 mg, 0.494 mmol) and $[FcAc]^+[B(C_6F_5)_4]^-$ (440 mg, 0.485 mmol) were loaded into flask fitted with a frit assembly. CH_2Cl_2 (15 mL) was condensed onto the solids under vacuum transfer conditions. The solution was warmed to room temperature and stirred for 80 min. The solvent was removed in vacuo to afford a violet solid which was triturated with dry hexanes and filtered to collect the

© 2001 NRC Canada

solid, which was washed with hexanes three times. Yield: 683 mg (0.475 mmol, 98%). IR (cm^{-1}): 3123, 1644 (C=O), 1516, 1464, 1277, 1089, 979. ^{1}H NMR: 45.2 (bs, 2H, WHM = 1630 Hz, $H_{\alpha/\beta}$); 31.9 (bs, 5H, WHM = 900 Hz, BCpFe(C_5H_5)), 22.3 (bs, 2H, WHM = 1900 Hz, $H_{\alpha/\beta}$), 7.21 (s, 2H), 6.85 (s, 5H, AcCpFe(C_5H_5)), 2.15 (s, 3H, CH_3). ^{11}B NMR: –17.0 (s, WHM = 17.4 Hz, $B(C_6F_5)_4$). ^{19}F NMR: –149.8 (s, 1F), –151.2 (s, 2F), –153.4 (s, 1F), –158.9 (s, 1F), 164.8 (s, 1F), –133.2 (s, F_o, 8F), –162.4 (s, F_p, 4F), –167.2 (s, F_m, 8F).

Relative Lewis acidity

In the dry box a known amount of Lewis acid was placed into an NMR tube, dissolved in a measured volume of CD_2Cl_2 and capped with a rubber septum. The sample was cooled to –78°C to which dry crotonaldehyde was added via microsyringe to the NMR tube. The tube was quickly shaken to ensure mixing. The ^{1}H NMR spectrum was collected at –20°C.

Cyclic voltammetry

Cyclic volammetric measurements were made on α,α,α-trifluorotolune (TFT) solutions under argon at 25°C, using a three-electrode cell attached to a Hitek Instruments of England Potentiostat (Type DT2101) and a Waveform Generator PPRI system. The electrolyte employed was $[n\text{-}Bu_4N]^+[B(C_6F_5)_4]^-$ with electrolyte:substrate concentrations of approximately 100:1. The air tight electrochemical cell consisted of a thick-walled glass bulb, Kontes Teflon tap, a set of platinum wire electrodes (working and secondary), and a silver wire quasireference electrode. Each experiment involved collecting the data for the substrate alone, which was then referenced to the Fc/Fc^+ couple in this medium. Samples were prepared in the dry box as follows: a known amount of electrolyte $[nBu_4N]^+[B(C_6F_5)_4]^-$ was dissolved into a minimum amount of dry TFT and added quantitatively to a volumetric flask. This solution was diluted to a known volume with additional TFT. The solution was mixed thoroughly and transferred to the electrochemical cell which contained the substrate and a small stir bar under argon. The Teflon tap was closed and a small amount of ferrocene was placed in a side arm. Outside the dry box, the electrochemical cell was attached to the potentiostat and the data were collected with a scan rate of 0.1 V s^{-1} without stirring. After the data for the substrate were collected the Teflon tap was opened to allow the ferrocene in the side arm to be added and dissolved. The stirring was halted and the CV data for the internal reference were collected along with the substrate. The half-wave potential of the substrate was referenced to that of the Fc/Fc^+ redox couple.

X-Ray crystallography

Suitable crystals were mounted on glass fibers using paraffin oil and cooled to the data collection temperature; details of crystal data, data collection, and structure refinement have been provided in Table 3.

*Structural determination of **1** and **3-Otf***

Data were collected on a Bruker AX SMART 1k CCD diffractometer using 0.3° ω-scans at 0, 90, and 180° in ϕ. Unit-cell parameters were determined from 60 data frames collected at different sections of the Ewald sphere. Semiempirical absorption corrections based on equivalent reflections were applied (32) to **1**. Attempts to correct the data set of **3-OTf** for absorption yielded T_{min}/T_{max} of unity and no correction was applied. Systematic absences in the diffraction data and unit-cell parameters were uniquely consistent with the reported space groups. The structures were solved by direct methods, completed with difference Fourier syntheses, and refined with full-matrix least-squares procedures based on F^2. Refinement of the Flack parameter for **1** yielded 0.39(1) indicating that the true hand of the data set could not be determined. All non-hydrogen atoms were refined with anisotropic displacement parameters. The triflate ion in **3-OTf** was located disordered in two positions with refined site occupancy of roughly 50/50. All hydrogen atoms were treated as idealized contributions. All scattering factors and anomalous dispersion factors are contained in the SHEXTL 5.1 program library (Sheldrick, 1997, WI.).

*Structural determination of **2** and **3-F***

Measurements were made on a Rigaku AFC6S diffractometer with graphite monochromated Mo Kα radiation for **2** and on an Enraf–Nonius CAD-4 diffractometer with graphite monochromated Cu Kα radiation for **3-F**. Cell constants and an orientation matrix for data collection were obtained from 25 reflections. The data were collected at a temperature of 170(2) K (**2**) and 295(2) K (**3-F**) using the ω-2θ scan technique. The intensities of three standard reflections were measured after every 200 reflections and decreased by 1.1% (**2**) and 0.69% (**3-F**). The data were corrected for decay, absorption (33), and for Lorentz and polarization effects. The structure of **2** was solved by direct methods (34) and expanded using Fourier techniques (35). The non-hydrogen atoms were refined anisotropically. The Cp and phenyl rings were constrained as regular pentagons and hexagons, respectively. H-atoms were included at geometrically idealized positions. The structure of **3-F** was solved by direct methods and expanded using Fourier techniques. There were two independent molecules in an asymmetric unit. The non-hydrogen atoms were refined anisotropically. H-atoms were included at geometrically idealized positions. For both structures, the weighting scheme was based on counting statistics and the final difference Fourier map was essentially featureless. Neutral atom scattering factors were taken from Cromer and Waber (36). Anomalous dispersion effects were included in *F*calc (37); the values for $\Delta f'$ and $\Delta f''$ were those of Creagh and McAuley (38). The values for the mass attenuation coefficients are those of Creagh and Hubbel (39). All calculations were performed using the teXsan (40) crystallographic software package of Molecular Structure Corporation.

*Structural determination of **3-C_6F_5***

Measurements were made on a Rigaku/ADSC CCD area detector with graphite monochromated Mo Kα radiation. The data were collected at a temperature of –93(1)°C to a max 2θ value of 61.1° in 0.50° oscillations with 14.0 s exposures. A sweep of data was done using ϕ oscillations from 0.0 to 190.0° at χ = –90° and a second sweep was performed

© 2001 NRC Canada

Table 3. Summary of data collection and structure refinement details for **1**, **2**, **3-F**, **3-OTf**, and **3-C_6F_5**.

	1	**2**	**3-F**	**3-OTf**	**3-C_6F_5**
Formula	$C_{22}H_9BF_{10}Fe$	$C_{25}H_{18}BF_{10}PFe$	$C_{22}H_9BF_{11}Fe$	$C_{23}H_9BF_{13}FeO_3S$	$C_{28}H_9BF_{15}Fe$
Fw	529.95	606.02	548.95	679.02	697.01
Temperature (K)	203(2)	170(2)	295(1)	203(2)	180(1)
λ (Å)	0.71073	0.71069	1.54178	0.71073	0.71069
Dimensions (mm^3)	0.4 × 0.2 × 0.1	0.42 × 0.38 × 0.4	0.5 × 0.4 × 0.22	0.1 × 0.1 × 0.2	0.45 × 0.40 × 0.40
Crystal system	Orthorhombic	Monoclinic	Triclinic	Monoclinic	Monoclinic
Space group	$P2_12_12_1$	$P2_1/n$	P	$P2_1/c$	$P2_1/n$
a (Å)	9.758(1)	10.899(3)	12.226(2)	10.909(3)	15.9529(13)
b (Å)	11.994	12.953(2)	13.1790(10)	12.896(4)	10.0171(7)
c (Å)	33.255(4)	17.012(3)	14.123(4)	17.017(5)	16.5882(3)
α (°)			109.40(2)		
β (°)		92.95(2)	108.87(2)	95.177(6)	111.1394(5)
γ (°)			93.150(10)		
V ($Å^3$)	3892.2(7)	2398.5(8)	1997.1(9)	2384(1)	2472.4(2)
Z	8	4	4	4	4
d_{calc} (mg m^{-3})	1.809	1.678	1.826	1.892	1.872
F(000)	2096	1216	1084	1340	1372
μ (mm^{-1})	0.878	0.786	0.7113	0.850	0.743
Max/min transmission	0.9281/0.5980	0.7334/7541	0.8082–1.000		0.8629–1.000
Scan type		ω-2θ	ω-2θ		
Scan range (°)	1.22–28.65	2.27–27.57	0.80+0.35θ 119.9	1.87–22.50	4.0–66.1
2θ (max) (°)		55.1			66.1
Reflections	29 867	5798	5953	5510	21 247
Unique reflections	9296	5531	5645	3039	6493
No. of variables	614	283	632	443	406
Restraints	0	0	0	38	0
R			0.063		0.035
R_w			0.033		0.032
$R1^a$	0.0373	0.0584		0.0327	
$wR2^a$	0.0616	0.1455		0.0621	
gof	1.008	1.010	2.73	1.082	1.26
Max Δ/σ (final cycle)			0.00		0.0003
Residual density (e $Å^{-3}$)	–0.588–0.585	–0.656–0.744	–0.46–0.58	–0.292–0.295	–0.61–0.59

[a]Final indices $I > 2\theta(I)$.

using ω oscillations between –23.0 and 18.0° at χ = –90°. The crystal-to-detector distance was 38.851(6) mm and the detector swing angle was –10.0°. The data were corrected for decay, absorption (33), and for Lorentz and polarization effects. The structure was solved by direct methods (34) and expanded using Fourier techniques.(35) The non-hydrogen atoms were refined anisotropically and hydrogen atoms were fixed in calculated positions with C-H = 0.98 Å. The final cycle of full-matrix least-squares refinement was based on all 6493 unique reflections and 406 variable parameters. Neutral atom scattering factors were taken from Cromer and Waber (36). Anomalous dispersion effects were included in *F*calc (37); the values for $\Delta f'$ and $\Delta f''$ were those of Creagh and McAuley (38). The values for the mass attenuation coefficients are those of Creagh and Hubbel (39). All calculations were performed using the teXsan (40) crystallographic software package of Molecular Structure Corporation.

Acknowledgments

Funding for this work from Nova Chemicals of Calgary, Alberta and the Natural Sciences and Engineering Research Council of Canada (NSERC) are gratefully acknowledged. BEC and WEP thank Professor Scott Hinman (Calgary) for use of his electrochemical equipment and helpful discussions. Also, we thank Professor Bill Gieger (Vermont) for details on the synthesis and use of $[Bu_4N][B(C_6F_5)_4]$ prior to publication.

References

1. A. Togni and T. Hayashi (*Editors*). Ferrocenes. VCH, Weinheim. 1995.
2. (*a*) W.E. Watts. J. Organomet. Chem. Libr. **7**, 399 (1979); (*b*) M.I. Rybinskaya, A.Z. Kreindlin, Y.T. Struchkov, and A.I. Yanovsky. J. Organomet. Chem. **359**, 233. (1989).
3. (*a*) J.C. Kotz and E.W. Post. Inorg. Chem. **9**, 1661 (1970); (*b*) E.W. Post, R.G. Cooks, and J.C. Kotz. Inorg. Chem. **9**, 1670 (1970); (*c*) T. Renk, W. Ruf, and W. Siebert. J. Organomet. Chem. **120**, 1 (1976); (*d*) W. Ruf, T. Renk, and W. Siebert. Z. Naturforsch. B: Anorg. Chem. Org. Chem. **31b**, 1028 (1976); (*e*) B. Wrackmeyer, U. Dörfler, and M. Heberhold. Z. Naturforsch. B: Chem. Sci. **48b**, 121 (1993); (*f*) B. Wrackmeyer, U. Dörfler, J. Rinck, and M. Heberhold. Z.

© 2001 NRC Canada

Naturforsch. B: Chem. Sci. **49b**, 1403 (1994); (*g*) B. Wrackmeyer, U. Dörfler, W. Milius, and M. Heberhold. Polyhedron, **14**, 1425 (1995); (*h*) M. Heberhold, U. Dörfler, and B. Wrackmeyer. Polyhedron, **14**, 2683 (1995); (*i*) A. Appel, H. Nöth, and M. Schmidt. Chem. Ber. **128**, 621 (1995); (*j*) A. Appel, F. Jäkle, T. Priermeier, R. Schmid, and M. Wagner. Organometallics, **15**, 1188 (1996).

4. (*a*) F. Jäkle, M. Mattner, T. Priermeier, and M. Wagner. J. Organomet. Chem. **502**, 123 (1995); (*b*) F. Jäkle, T. Priermeier, and M. Wagner. Chem. Ber. **128**, 1163 (1995); (*c*) M. Fontani, F. Peters, W. Scherer, W. Wachter, M. Wagner, and P. Zanello. Eur. J. Inorg. Chem. 1453 (1998).
5. (*a*) F. Jäkle, T. Priermeier, and M. Wagner. J. Chem. Soc. Chem. Commun. 1765 (1995); (*b*) E. Herdtweck, F. Jäkle, and M. Wagner. Organometallics, **16**, 4737 (1997); (*c*) H. Braunschweig, R. Dirk, M. Müller, P. Nguyen, R. Resendes, D.P. Gates, and I. Manners. Angew. Chem. Int. Ed. Engl. **36**, 2338 (1997); (*d*) M.J.G. Lesley, U. Mock, N.C. Norman, A.G. Orpen, C.R. Rice, and J. Starbuck. J. Organomet. Chem. **582**, 116 (1999); (*e*) A. Berenbaum, H. Braunschweig, R. Dirk, U. Englert, J.C. Green, F. Jäkle, A.J. Lough, and I. Manners. J. Am. Chem. Soc. **122**, 5765, (2000).
6. W.E. Piers and T. Chivers. Chem. Soc. Rev. 345 (1997).
7. D.J. Parks, W.E. Piers, and G.P.A. Yap. Organometallics, **17**, 5492 (1998).
8. R.W. Fish and M. Rosenblum. J. Org. Chem. **30**, 1253 (1965).
9. R.D. Chambers and T. Chivers. J. Chem. Soc. 3933 (1965).
10. R.G. Kidd. *In* NMR of newly accessible nuclei. Vol. 2. *Edited by* P. Laszlo. Academic Press, New York. 1983.
11. (*a*) A.D. Horton, J. de With, A.J. van der Linden, and H. van de Weg. Organometallics, **15**, 2672 (1996); (*b*) A.D. Horton and J. de With. Organometallics, **16**, 5425 (1997).
12. G.E. Herberich and A. Fischer. Organometallics, **15**, 58 (1996).
13. M.M. Olmstead, P.P. Power, K.J. Weese, and R.J. Doedens. J. Am. Chem. Soc. **109**, 2459 (1987).
14. F. Zettler, H.D. Hausen, and H.J. Hess. J. Organomet. Chem. **72**, 157 (1974).
15. R.J. LeSuer and W.E. Gieger. Angew. Chem. Int. Ed. **39**, 248 (2000).
16. D.J. Parks, W.E. Piers, M. Parvez, R. Atencio, and M.J. Zaworotko. Organometallics, **17**, 1369 (1998).
17. (*a*) A.R. Siedle and W.M. Lamanna. U.S. Patent no. 5 296 433, March 22, 1994; (*b*) L. Doerrer and M.L.H. Green. J. Chem. Soc. Dalton Trans. 4325 (1999); (*c*) A.A. Danopoulos, J.R. Galsworthy, M.L.H. Green, S. Cafferkey, L.H. Doerrer, and M.B. Hursthouse. Chem. Commun. 2529 (1998).
18. H. Jacobsen, H. Berke, S. Döring, G. Kehr, G. Erker, R. Fröhlich, and O. Meyer. Organometallics, **18**, 1724 (1999).
19. R.F. Childs, D.L. Mulholland, and A. Nixon. Can. J. Chem. **60**, 801 (1982).
20. L. Luo and T.J. Marks. Top. Catal. **7**, 97 (1999).
21. (*a*) D.C. Bradley, M.B. Husthouse, M. Motevalli, and Z. Dao-Hong. J. Chem. Soc. Chem. Commun. 7 (1991); (*b*) D.C. Bradley, I.S. Harding, A.D. Keefe, M. Motevalli, and D.H. Zheng. J. Chem. Soc. Dalton Trans. 3931 (1996).
22. N.G. Connelley and W.E. Geiger. Chem. Rev. **96**, 877 (1996).
23. C.J. Harlan, T. Hascall, E. Fujita, and J.R. Norton. J. Am. Chem. Soc. **121**, 7274 (1999).
24. V.C. Williams, G.J. Irvine, W.E. Piers, Z. Li, S. Collins, W. Clegg, M.R.J. Elsegood, and T.B. Marder. Organometallics, **19**, 1619 (2000).
25. K.K. Sun and W.T. Miller. J. Am. Chem. Soc. **92**, 6985 (1970).
26. G.A. Lawrance. Chem. Rev. **86**, 17 (1986).
27. R.F. Jordan, R.E. LaPointe, C.S. Bajgur, S.F. Echols, and R. Willett. J. Am. Chem. Soc. **109**, 4111 (1987).
28. D.O. Cowan, P. Shu, F.L. Hedberg, M. Rossi and T.J. Kistenmacher. J. Am. Chem. Soc. **101**, 1304 (1979).
29. R.K. Harris and B.E. Mann. NMR and the periodic table. Academic Press, New York. 1978. p. 99.
30. A.B. Pangborn, M.A. Giardello, R.H. Grubbs, R.K. Rosen, and F.J. Timmers. Organometallics, **15**, 1518, (1996).
31. J.B. Lambert, S. Zhang, and S.M. Ciro. Organometallics, **13**, 2430 (1994).
32. R.H. Blessing. Acta Crystallogr. Sect. A: Fundam. Crystallogr. **A51**, 33 (1995).
33. A.T.C. North, D.C. Phillips, and F.S. Mathews. Acta Crystallogr. **A24**, 351 (1964).
34. A. Altomare, M. Cascarano, C. Giacovazzo, and A. Guagliardi. J. Appl. Crystallogr. **26**, 343 (1993).
35. P.T. Beurskens, G. Admiraal, G. Beurskens, W.P. Bosman, R. de Gelder, R. Israel, and J.M.M. Smits. The DIRDIF-94 program system. Technical Report of the Crystallography Laboratory, University of Nijmegen, The Netherlands. 1994.
36. D.T. Cromer and J.T. Waber. International tables for X-ray crystallography. Vol. IV. The Kynoch Press, Birmingham, U.K. 1974. Table 2.2 A.
37. J.A. Ibers and W.C. Hamilton. Acta Crystallogr. **17**, 781 (1964).
38. D.C. Creagh and W.J. McAuley. International tables for crystallography. Vol C. *Edited by* A.J.C. Wilson. Kluwer Academic Publishers, Boston. 1992. pp. 219–222.
39. D.C. Creagh and J.H. Hubbell. International tables for crystallography. Vol C. *Edited by* A.J.C. Wilson. Kluwer Academic Publishers, Boston. 1992. pp. 200–206.
40. teXsan. Crystal structure analysis package. Molecular Structure Corporation. 1985 and 1992.

© 2001 NRC Canada

Tetraacetatodirhodium(II) complexes with tris(methoxyphenyl)phosphines, their reactivity, structure, and antitumor activity

Florian P. Pruchnik, Radosław Starosta, Zbigniew Ciunik, Adam Opolski, Joanna Wietrzyk, Elżbieta Wojdat, and Danuta Duś

Abstract: Reactions of $[Rh_2(\mu\text{-}OAc)_4(H_2O)_2]$ ($[\mathbf{1}\cdot(H_2O)_2]$) with tris(3-methoxyphenyl)phosphine at 1:1 and 1:2 molar ratios yield, first, the appropriate adducts: $[\mathbf{1}\cdot(H_2O)\{P(C_6H_4\text{-}3\text{-}OMe)_3\}]$ and $[\mathbf{1}\cdot\{P(C_6H_4\text{-}3\text{-}OMe)_3\}_2]$, and then $[Rh_2(\mu\text{-}OAc)_3\{\mu\text{-}(C_6H_3\text{-}3\text{-}OMe)P(C_6H_4\text{-}3\text{-}OMe)_2\}(HOAc)_2]$ ($[\mathbf{2}\cdot(HOAc)_2]$), and $[Rh_2(\mu\text{-}OAc)_2\{\mu\text{-}(C_6H_3\text{-}3\text{-}OMe)P(C_6H_4\text{-}3\text{-}OMe)_2\}_2(HOAc)_2]$ ($[\mathbf{3}\cdot(HOAc)_2]$) complexes, respectively. They have been characterized by spectroscopic methods. The molecular structure of $[\mathbf{3}\cdot(HOAc)(H_2O)]$ has been determined crystallographically. The complexes $[\mathbf{3}\cdot(HOAc)_2]$, $[Rh_2(\mu\text{-}OAc)_3\{\mu\text{-}(C_6H_3\text{-}4\text{-}OMe)P(C_6H_4\text{-}4\text{-}OMe)_2\}(HOAc)_2]$ ($[\mathbf{4}\cdot(HOAc)_2]$), and $[Rh_2(\mu\text{-}OAc)_2\{\mu\text{-}(C_6H_3\text{-}4\text{-}OMe)P(C_6H_4\text{-}4\text{-}OMe)_2\}_2(HOAc)_2]$ ($[\mathbf{5}\cdot(HOAc)_2]$) reversibly react with CO giving mono- and biadducts. Antitumor activity of binuclear rhodium(II) compounds $[\mathbf{3}\cdot(HOAc)_2]$, $[Rh_2(\mu\text{-}OAc)_3\{\mu\text{-}(C_6H_3\text{-}2\text{-}O)P(C_6H_3\text{-}2\text{-}OMe)_2\}(HOAc)]$ ($[\mathbf{6}\cdot($HOAc)]), and $[Rh_2(\mu\text{-}OAc)_3\{\mu\text{-}(C_6H_3\text{-}6\text{-}OMe\text{-}2\text{-}O)P[(C_6H_3\text{-}2,6\text{-}(OMe)_2]_2\}(HOAc)]$ ($[\mathbf{7}\cdot(HOAc)]$) have been investigated in vitro. The most active agent for investigated tumor lines is complex $[\mathbf{6}\cdot(HOAc)]$. It shows higher activity than cisplatin (*cis*-$[PtCl_2(NH_3)_2]$). Antitumor activity decreases in the series: $[\mathbf{6}\cdot(HOAc)] > [\mathbf{7}\cdot(HOAc)] > [\mathbf{3}\cdot(HOAc)_2]$. Activity of all investigated rhodium(II) complexes is higher than that of $[\mathbf{1}\cdot(H_2O)_2]$.

Key words: dirhodium(II) complexes, functionalized phosphines, aryl phosphines, ferrocenylmethylphosphines, adducts with CO, antitumor activity, orthometallation reactions.

Résumé : Les réactions du $[Rh_2(OAc)_4(H_2O)_2]$ ($[\mathbf{1}\cdot(H_2O)_2]$) avec la (3-méthoxyphényl)phosphine, à des rapports molaires de 1:1 et 1:2, conduisent à la formation d'adduits appropriés soit premièrement à $[\mathbf{1}\cdot(H_2O)\{P(C_6H_4\text{-}3\text{-}OMe)_3\}]$ et $[\mathbf{1}\cdot\{P(C_6H_4\text{-}3\text{-}OMe)_3\}_2]$ et ensuite à $[Rh_2(OAc)_3\{(C_6H_3\text{-}3\text{-}OMe)P(C_6H_4\text{-}3\text{-}OMe)_2\}(HOAc)_2]$ ($[\mathbf{2}\cdot(HOAc)_2]$) et $[Rh_2(OAc)_2\{(C_6H_3\text{-}3\text{-}OMe)P(C_6H_4\text{-}3\text{-}OMe)_2\}_2(HOAc)_2]$ ($[\mathbf{3}\cdot(HOAc)_2]$). Ces complexes ont été caractérisés par des méthodes spectroscopiques. La structure moléculaire du complexe $[\mathbf{3}\cdot(HOAc)(H_2O)]$ a été déterminée par cristallographie. Les complexes $[\mathbf{3}\cdot(HOAc)_2]$, $[Rh_2(OAc)_3\{(C_6H_3\text{-}4\text{-}OMe)P(C_6H_4\text{-}4\text{-}OMe)_2\}(HOAc)_2]$ ($[\mathbf{4}\cdot(HOAc)_2]$) et $[Rh_2(OAc)_2\{(C_6H_3\text{-}4\text{-}OMe)P(C_6H_4\text{-}4\text{-}OMe)_2\}_2(HOAc)_2]$ ($[\mathbf{5}\cdot(HOAc)_2]$) réagissent de façon réversible avec le CO pour donner des mono- et des bisadduits. On a évalué l'activité antitumorale in vitro des composés binucléaires de rhodium $[\mathbf{3}\cdot(HOAc)_2]$, $[Rh_2(OAc)_3\{(C_6H_3\text{-}2\text{-}O)P(C_6H_3\text{-}2\text{-}OMe)_2\}(HOAc)]$ ($[\mathbf{6}\cdot(HOAc)]$) et $[Rh_2(OAc)_3\{\mu\text{-}(C_6H_3\text{-}6\text{-}OMe\text{-}2\text{-}O)P[(C_6H_3\text{-}2,6\text{-}(OMe)_2]_2\}(HOAc)]$ ($[\mathbf{7}\cdot(HOAc)]$). Le complexe $[\mathbf{6}\cdot(HOAc)]$ est l'agent le plus actif pour les familles de tumeur étudiées. Il présente une activité supérieure à celle du cisplatine, *cis*-$[PtCl_2(NH_3)_2]$. L'activité antitumorale diminue dans la série $[\mathbf{6}\cdot(HOAc)] > [\mathbf{7}\cdot(HOAc)] > [\mathbf{3}\cdot(HOAc)_2]$. L'activité de chacun des complexes de rhodium(II) est supérieure à celle du $[\mathbf{1}\cdot(H_2O)_2]$.

Mots clés : complexes dirhodium(II), phosphines fonctionnalisées, arylphosphines, ferrocénylméthylphosphines, adduits avec le CO, activité antitumorale, réactions d'organométallation.

Introduction

The product of reaction of rhodium tetraacetate with triphenylphosphine, first reported by Cotton and co-workers (1) was one of the first examples of bimetallic *ortho*-metallated compounds. Since that time, attention has been paid to different *ortho*-metallated dirhodium(II) compounds with triaryl and alkyl–aryl phosphines because of the growing interest in the problem of activation of the C—H bond (2–14). However, reactions of tetraacetatodirhodium(II) with

Received September 12, 2000. Published on the NRC Research Press Web site at http://canjchem.nrc.ca on July 3, 2001.

This article is dedicated to Professor Brian R. James on his 65th birthday.

F.P. Pruchnik,[1] R. Starosta, and Z. Ciunik. Faculty of Chemistry, University of Wrocław, 14 F. Joliot-Curie Street, 50-383 Wrocław, Poland.
A. Opolski, J. Wietrzyk, E. Wojdat, and D. Duś. Institute of Immunology and Experimental Therapy, Polish Academy of Sciences, Wrocław, Poland.

[1]Corresponding author (telephone/fax: (+ 48 71) 32 04 232; e-mail: pruchnik@wchuwr.chem.uni.wroc.pl).

 DOI: 10.1139/cjc-79-5/6-868 © 2001 NRC Canada

Table 1. ^{31}P and ^{13}C NMR dirhodium(II) complexes (in $CDCl_3$, room temperature, broadened signal (*), signal from a metallated phenyl ring (^{m})).

Compound	^{31}P NMR: d (ppm), *J* (Hz)	^{13}C NMR: d (ppm), *J* (Hz)
MMP	–2.95 (s)	
[**1**·(H_2O)(MMP)]	–30.2 (dd), ^1J (P-Rh) = 97.7, ^2J (P-Rh) = 31.7	
[**1**·$(MMP)_2$]	–11.0 (s*)	
[**2**·$(HOAc)_2$]	25.0 (dd), ^1J (P-Rh) = 151.4, ^2J (P-Rh) = 4.9	
[**3**·$(HOAc)_2$]	22.6 (d*), ^1J (P-Rh) = 166.8	181.5 (s) (COO bridges); 179.5 (s) (COOH HOAc); $C6^m$: 158.4 (dd) ^1J (Rh-$C2^m$) = 33.3, ^2J (P-$C6^m$) = 12.7; 110–156 (aromatic carbon atoms); 55.33 (s), 54.7 (s), 55.3 (s), and 55.2 (s) (OMe groups); 22.8 (s) (CH_3 bridges); 22.4 (s), 22.3 (s) (CH_3–HOAc)
[**1**·(dhfmp)]	–43.2 (dd), ^1J (P-Rh) = 99.7, ^2J (P-Rh) = 22.4	
[**1**·(hfmp)]	–41.9 (dd), ^1J (P-Rh) = 101.5, ^2J (P-Rh) = 28.2	
[**7**·(hfmp)]	P_A: (dd) 10.66, ^1J (P_A-Rh_A) = 169.1, ^3J (P_A-P_B) = 6.4; P_B: (ddd) –41.34, ^1J (P_B-Rh_B) = 97.3, ^2J (P_B – Rh_A) = 27.3	
[**3**·(HOAc)(hfmp)]	P_A: (dd) 27.64, ^1J (P_A-Rh_A) = 183.1, ^2J (P_A-P_C) = 15.2; P_B: (d) 20.85, ^1J (P_B-Rh_B) = 155.1; P_C: (m) –37	
[**3**·$(hfmp)_2$]	P_A: (d) 24.24, ^1J (P_A-Rh) = 170.4; P_B: (t) –20.52, ^1J (P_B-Rh) = ^2J(P_B-Rh) = 49.6	

functionalized phosphines were not intensively studied. Water-soluble *ortho*-metallated complexes with tris(3-sodium sulfonatophenyl)phosphine (TPPTS), $[Rh_2(\mu\text{-}OAc)_3\{\mu\text{-}(C_6H_3\text{-}3\text{-}SO_3Na)P(C_6H_4\text{-}3\text{-}SO_3Na)_2\}]$, and $[Rh_2(\mu\text{-}OAc)_2\{\mu\text{-}(C_6H_3\text{-}3\text{-}SO_3Na)P(C_6H_4\text{-}3\text{-}SO_3Na)_2\}_2]$ have been investigated (15). It has been found that in reaction of tris(2,4,6-trimethoxyphenyl)phosphine (TMPP) (16–18), tris(2-methoxyphenyl)phosphine (OMP) (19, 20), and tris(2,6-dimethoxyphenyl)phosphine (DOMP) (20) with [**1**·$(H_2O)_2$], the O—CH_3 bond is split off and complexes with Rh-$P(C_6H_3(R)OMe)_2C_6H_2(R)(R')O$-Rh (where R, R′ = H or OMe) bridges are formed. In this paper we report on synthesis of $[Rh_2(\mu\text{-}OAc)_3\{\mu\text{-}(C_6H_3\text{-}3\text{-}OMe)P(C_6H_4\text{-}3\text{-}OMe)_2\}(HOAc)_2]$ ([**2**·$(HOAc)_2$]) and $[Rh_2(\mu\text{-}OAc)_2\{\mu\text{-}(C_6H_3\text{-}3\text{-}OMe)P(C_6H_4\text{-}3\text{-}OMe)_2\}_2(HOAc)_2]$ ([**3**·$(HOAc)_2$]) as well as properties and reactivity of binuclear rhodium(II) complexes containing other *ortho-C*- and *ortho-O*-metallated tris(methoxyphenyl)phosphines.

It has been known for many years, that rhodium(II) carboxylato complexes $[Rh_2(\mu\text{-}O_2CR)_4]$ and their derivatives (21–25), complexes $[Rh_2(\mu\text{-}O_2CR)_2(\mu\text{-}N\text{-}N)_2(H_2O)_2]^{2+}$ (N-N = bpy, phen) (25–31) are promising antitumor agents. However, antitumor properties of rhodium(II) complexes with phosphine bridges were not examined. Here we describe antitumor activity in vitro of some binuclear rhodium(II) compounds with methoxyphenylphosphines, namely complexes [**3**·$(HOAc)_2$], $[Rh_2(\mu\text{-}OAc)_3\{\mu\text{-}(C_6H_4\text{-}2\text{-}O)P(C_6H_4\text{-}2\text{-}OMe)_2\}(HOAc)]$ ([**6**·(HOAc)]) and $[Rh_2(\mu\text{-}OAc)_3\{\mu\text{-}(C_6H_3\text{-}6\text{-}OMe\text{-}2\text{-}O)P[(C_6H_3\text{-}2,6\text{-}(OMe)_2]_2\}(HOAc)]$ ([**7**·(HOAc)]), dhfmp as well as, for comparison, activity of *cis*-diaminadichloroplatinum(II).

Results and discussion

Syntheses of Rh(II) complexes with methoxyphenylphosphines

In reactions of [**1**·$(L)_2$] (L = Lewis base) and other dirhodium(II) carboxylates with phosphines, PR_3 ligands are first coordinated along the Rh-Rh axis forming reactive adducts [**1**·(PR_3)L] or [**1**·$(PR_3)_2$].

Formation of mono- and biadducts of [**1**·$(H_2O)_2$] with MMP ([**1**·(H$_2$O)(MMP)] and [**1**·$(MMP)_2$]) was followed with ^{31}P NMR spectroscopy. For the monoadduct in $CDCl_3$, a doublet of doublets at –30.2 ppm (^1J (P-Rh) = 97.7 Hz, ^2J (P-Rh) = 31.7 Hz) and for the biadduct, a broad singlet at –11.0 ppm have been observed (see Table 1). This indicates that axial phosphine ligands in the biadduct are labile. Coordination chemical shifts ($\Delta\delta$ (^{31}P) = δ (P_{adduct}) – δ (P_{ligand})) are –27.25 and –8.05 ppm for monoadduct and biadduct, respectively. $\Delta\delta$ (^{31}P) values are similar to those found in analogous dirhodium(II) compounds with other phosphines: ca. –30 and –10 ppm for monoadducts and biadducts, respectively, (2–4, 6–10, 12, 15, 18, 20, 32). Analogous adducts [**1**·(PR_3)] and [**1**·$(PR_3)_2$] were obtained with TPPTS (15) and PMP (21).

In the next step, phosphine ligands migrate to equatorial coordination sites and then the C—H bond of the PR_3 ligand can be activated giving the binuclear product of *ortho*-metallation.

In the reaction of [**1**·$(H_2O)_2$] with MMP complexes, $[Rh_2(\mu\text{-}OAc)_3\{\mu\text{-}(C_6H_3\text{-}3\text{-}OMe)P(C_6H_4\text{-}3\text{-}OMe)_2\}(HOAc)_2]$ ([**2**·$(HOAc)_2$]) and mainly [**3**·$(HOAc)_2$] were obtained.

In the contrast to the selective reactions of tris(4-methoxyphenyl)phosphine (PMP) with rhodium(II) acetate, which give $[Rh_2(\mu\text{-}OAc)_3\{\mu\text{-}(C_6H_3\text{-}4\text{-}OMe)P(C_6H_4\text{-}4\text{-}OMe)_2\}(HOAc)_2]$ ([**4**·$(HOAc)_2$]) and $[Rh_2(\mu\text{-}OAc)_2\{\mu\text{-}(C_6H_3\text{-}4\text{-}OMe)P(C_6H_4\text{-}4\text{-}OMe)_2\}_2(HOAc)_2]$ ([**5**·$(HOAc)_2$]) complexes at [**1**·$(H_2O)_2$]:PMP ratios equal to 1:1 and 1:2, respectively, (32), in the reactions of MMP with [**1**·$(H_2O)_2$] we obtained mainly [**3**·$(HOAc)_2$]. A mixture of compounds [**3**·$(HOAc)_2$], [**2**·$(HOAc)_2$], and [**1**·$(H_2O)_2$] was obtained even in the presence of excess of rhodium(II) acetate, at ratios of [**1**·$(H_2O)_2$]:MMP > 1. Thus complex [**2**·$(HOAc)_2$] is very reactive and can be easily transformed into compound [**3**·$(HOAc)_2$].

In the case of reactions of [**1**·$(H_2O)_2$] with methoxyphenylphosphines containing methoxy groups in *ortho* posi-

© 2001 NRC Canada

Table 2. ^{1}H NMR dirhodium(II) complexes (in $CDCl_3$, room temperature, broadened signal (*), signal from a metallated phenyl ring ($^{(m)}$)).

Compound	^{1}H NMR: d (ppm), *J* (Hz)
MMP	3.71 (s, 9H) (OMe groups); 6.8–7.3 (aromatic protons)
[**1**·(H_2O)(MMP)]	3.67 (s, 9H) (OMe groups); 1.73 (s*, 9H) (OAc bridges); 6.9–7.4 (aromatic protons)
[**1**·$(MMP)_2$]	3.66 (s, 18H^{OMe}) (OMe groups); 1.59 (s, 12H) (OAc bridges); 6.9–7.4 (aromatic protons)
[**2**·$(HOAc)_2$]	1.30 (s, 6H) (OAc bridges, *cis*); 2.32 (s, 3H) (OAc bridge, *trans*); 2.20 (s, 6H) (axial molecules of HOAc); 3.68 (s, 6H) (OMe groups); 3.65 (s, 3H) (OMe group$^{(m)}$); 6.5–8.5 (aromatic protons)
[**3**·$(HOAc)_2$]	1.20 (s, 6H) (OAc bridges); 2.14 (s, 6H) (axial molecules of HOAc); 3.43 (s, 6H) (OMe groups); 3.51 (s, 6H) (OMe groups); 3.76 (s, 6H) (OMe groups$^{(m)}$); 6.2–7.4 (aromatic protons)
[**1**·(dhfmp)]	1.84 (s) (OAc bridges); 2.0–4.4 (ligand's protons)
[**1**·(hfmp)]	1.87 (s) (OAc bridges); 2.0–4.5 (ligand's protons)
[**7**·(hfmp)]	1.25 (s, 3H) (OAc bridge); 1.27 (s, 3H) (OAc bridge); 1.72 (s, 3H) (OAc bridge); 2.08 (s, 3H) (molecule of HOAc); 3.14 (s, 3H) (OMe group); 3.30 (s, 3H) (OMe group); 3.33 (s, 3H) (OMe group); 3.40 (s, 3H) (OMe group); 4.09 (s, 10H^A) (cyclopentadienyl ring); 4.65 (s, 3H) (OMe group); 2.5–4.5 (other protons of hfmp) 6.11 (dd) ^3J (H-H) = 7.92, ^4J (H-P) = 4.20; 6.13 (dd) ^3J (H-H) = 7.92, ^4J (H-P) = 4.68; 6.34 (dd) ^3J (H-H) = 8.14, ^4J (H-P) = 3.49; 6.41 (dd) ^3J (H-H) = 8.15, ^4J (H-P) = 1.65; 6.50 (dd) ^3J (H-H) = 7.68, ^4J (H-P) = 4.89; 6.88 (dd) ^3J (H-H) = 8.16, ^4J (H-P) = 4.89; 6.95 (t) ^3J (H-H) ≈ ^4J (H-P) = 8.16; 7.02 (t) ^3J (H-H) ≈ ^4J (H-P) = 8.14; 7.35 (t) ^3J (H-H) ≈ ^4J (H-P) = 8.14
[**3**·(HOAc)(hfmp)]	1.14 (s, 3H) (OAc bridge); 1.12 (s, 3H) (OAc bridge); 2.07 (s, 6H) (molecule of HOAc); 4.13 (s, 10H^A) (cyclopentadienyl ring); 2.6–5.5 (OMe groups and protons of hfmp); 5.8–7.5 (aromatic protons)
[**3**·$(hfmp)_2$]	1.00 (s, 6H) (OAc bridges); 2.07 (s, 6H) (molecule of HOAc); 4.15 (s, 10H^A) (cyclopentadienyl ring); 2.6–5.5 (OMe groups and protons of hfmp); 5.8–7.5 (aromatic protons)

tions, the O—Me bond of the methoxy group is activated and a Rh-PC_6H_2RR'–2-O-Rh bridge is formed. Thus, tris(2-methoxyphenyl)phosphine (OMP) and tris(2,6-dimethoxyphenyl)phosphine (DOMP), at molar ratio [P]:[Rh_2] of 2:1, give complexes [**6**·(HOAc)] (19, 20) and [**7**·(HOAc)] (20) with only one bridging phosphine ligand. In these reactions, a methyl cation of one of the methoxy groups is split off and a $\{(CH_3)PAr_3\}^+$ cation is formed.

Complexes [**2**·$(HOAc)_2$] and [**3**·$(HOAc)_2$] have been characterized by a combination of ^{1}H, ^{13}C, and ^{31}P NMR spectroscopies (Table 2). The Chemical shift of OAc groups in *cis* positions is much lower (1.30 ppm, 6H) than that for the OAc bridge (2.32 ppm, 3H) in the *trans* position relative to the phosphine bridging ligand coordinated via P and C (*ortho*) atoms. Both coordination chemical shift and Rh-P coupling constants (^1J (P-Rh) = 151.4 Hz, ^2J (P-Rh) = 4.9 Hz) for complex [**2**·$(HOAc)_2$] (Table 2) are typical of *ortho*-metallated complexes [$Rh_2(\mu\text{-}OAc)_3\{\mu\text{-}(C_6H_3R)P(C_6H_4R)_2\}$]. In the case of complex [**4**·$(HOAc)_2$], ^1J (P-Rh) = 147.4 Hz and ^2J (P-Rh) = 6.1 Hz (22). The ^{1}H, ^{13}C, and ^{31}P NMR data indicate that complex [**3**·$(HOAc)_2$] has a head-to-tail structure. The ^1J (P-Rh) = 166.8 Hz for compound [**3**·$(HOAc)_2$] and is similar to that found for complex [**5**·$(HOAc)_2$] (168.9 Hz).

Molecular structure of [3·(H_2O)(HOAc)]

The molecular structure of [**3**·(H_2O)(HOAc)] shown in Fig. 1 confirms the structure of [**3**·$(HOAc)_2$] established with spectroscopic methods. Details of X-ray data collected are summarized in Table 3. Table 4 contains selected bond lengths and angles. The structure consists of a binuclear rhodium core bridged by two acetate groups and two MMP ligands in which *ortho*-metallation has occurred at one of the phenyl rings. The bridging phenyl rings are coordinated via C-6 atoms: C(46) and C(16). Phosphine ligands are in *cis* position to each other with H-T (head-to-tail) structure. One of the axial sites is occupied by a molecule of water and the second one by a molecule of acetic acid.

The molecular structure shows distorted octahedral coordination around the central atoms. The complex has an almost eclipsed conformation, torsion angles O(1)-Rh(1)-Rh(2)-O(2) and O(3)-Rh(1)-Rh(2)-O(4) are 19.4° and 17.6°, respectively. The torsion angles of the bridging *ortho*-metallated ligand are slightly smaller: P(1)-Rh(1)-Rh(2)-C(16) = 14.2° and P(2)-Rh(2)-Rh(1)-C(46) = 13.8°. The Rh(1)—Rh(2) distance is 2.4913(18) Å, indicating a rather strong single bond between two metal atoms. Rh(1)—P(1) and Rh(2)—P(2) bond lengths are 2.193 Å and Rh(1)—C(46) and Rh(2)—C(16) distances are 1.993(14) and 1.995(14) Å, respectively. Lengths of Rh—O^{equatorial} bonds change in the range 2.12–2.17 Å. The bond lengths between the phosphorus atom and carbon atom of the metallated ring are shorter than those between the phosphorus and carbon atoms of the nonmetallated rings. Methoxy substituents in the phosphine ligands lie approximately in the planes of the phenyl rings.

Lengths of rhodium – axial ligand bonds (Rh(1)—O(1w) = 2.313(9) Å, Rh(1)—O(5) = 2.363(12) Å) indicate rather weak bonding of these ligands. HOAc molecule is coordinating via oxygen atom of carbonyl group; the -OH group is involved in the formation of a strong hydrogen bond with the oxygen atom of the bridging acetato ligand (O(6)-H(6)···O(2), d_{O-O} = 2.565(18) Å).

A rather strong intermolecular hydrogen bond is formed between the axial molecule of water and the oxygen atom of the acetate bridge of another molecule of the compound (O(1w)-H(2w)···O(3) (1 –*x*, 2 – *y*, –*z*), d_{O-O} = 2.695(13) Å).

Reactions of *ortho*-metallated complexes

Complex [**3**·$(HOAc)_2$], as other dirhodium(II) carboxylates and their derivatives, reacts with ligands showing σ-donor and π-acceptor properties as well as with ligands

© 2001 NRC Canada

Fig. 1. Molecular structure of [**3**·(H_2O)(HOAc)] (an OTREP (49) drawing with 30% thermal ellipsoids).

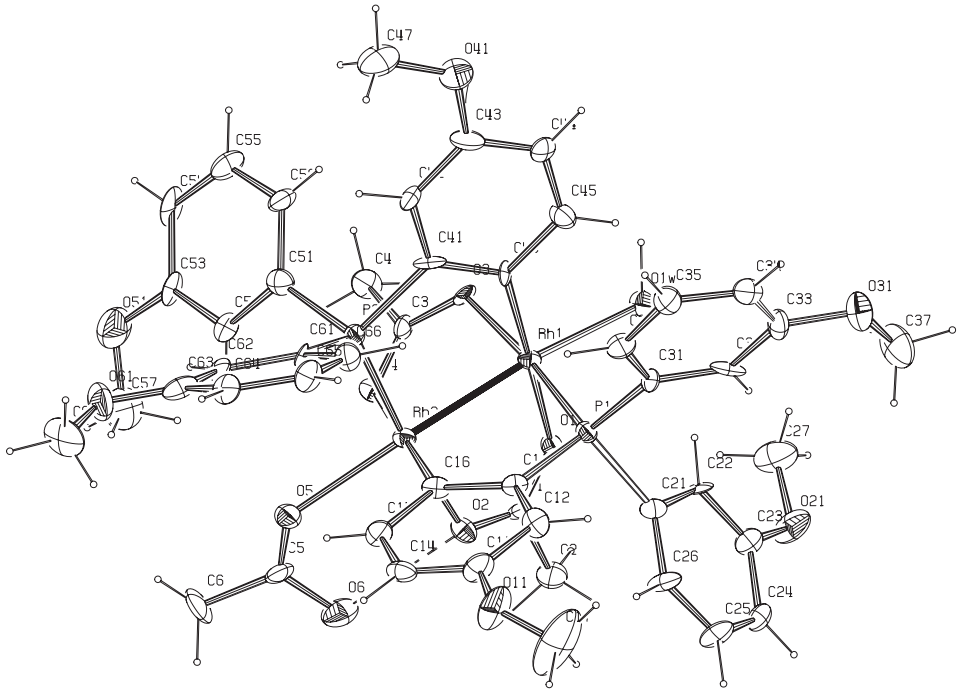


Table 3. Crystal data and details of the structure determination for [**3**·(H_2O)(HOAc)].

Empirical formula	$C_{48}H_{52}O_{13}P_2Rh_2$
Formula weight	1104.66
T (K)	170(2)
λ (Å)	0.71073
Crystal system	Triclinic
Space group	$P\bar{1}$
a (Å)	11.026(2)
b (Å)	15.290(3)
c (Å)	15.653(3)
α (°)	71.34(3)
β (°)	69.53(3)
γ (°)	75.69(3)
V (Å^3)	2314.9(10)
Z	2
D_c (mg m^{-3})	1.585
μ (mm^{-1})	0.8
F(000)	1128
Crystal size (mm)	0.1 × 0.05 × 0.02
Diffractometer	Kuma KM4CCD
θ range for data collection (°)	2.6–22.5
Index ranges	*h*:→ –11:11; *k*:→ –16:15; *l*:→ –16:16
Reflections collected	10 938
Independent reflections	5941
Data (parameters)	591
Weighting scheme: *a*, *b*, *c*[a]	0.00, 29.39, 3.00
Goodness-of-fit (F^2)	1.19
Final R_1 and wR_2 indices ($I > 2\sigma I$)	0.0973, 0.1907
Largest diff. peak and hole (e Å^{-3})	–0.72, 0.80

[a] $w = 1/[\sigma^2(F_o^2) + (a \times P)^2 + b \times P]$ where $P = [\max(F_o^2, 0) + 2 \times F_c^2]/c$.

possessing only σ-donor properties. Adducts [**3**·(L)] and [**3**·$(L)_2$] are the products of these reactions.

Reactions of complex [**3**·$(HOAc)_2$] with {(η^5-C_5H_5)Fe(η^5-C_5H_4)CH_2}$_2$$PCH_2OH$ (hfmp) (Table 2) give stable complexes. Pure adducts [**3**·(hfmp)(HOAc)] and [**3**·$(hfmp)_2$] can be obtained in chloroform at a [**3**·$(HOAc)_2$]:hfmp ratio equal to 1:1 and 1:2, respectively. However, $\Delta\delta$ (^{31}P) = δ (P_{adduct}) – δ (P_{ligand}) for axial hfmp ligands in this case are lower than those for adducts with arylphosphines: –19.1 and –2.6 ppm for [**3**·(hfmp)(HOAc)] and [**3**·$(hfmp)_2$], respectively, (Table 2). Coordination of the ferrocenylmethylphosphine ligand causes large changes in chemical shifts of the bridging MMP ligand; binding hfmp as axial ligand moves the signals of MMP to lower fields and raises the coupling constants between MMP and rhodium atom. In [**3**·(hfmp)(HOAc)], there are two signals of *ortho*-metallated MMP ligand: a doublet of doublets at 27.6 ppm (^1J (P-Rh) = 183.1 Hz, ^2J (P-P) = 15.2 Hz) and a doublet at 20.85 ppm (^1J (P-Rh) = 155.1 Hz); in biadduct [**3**·$(hfmp)_2$] there is only one doublet of MMP at 24.2 ppm (^1J (P-Rh) = 170.4 Hz).

For monoadducts [**1**·(hfmp)(H_2O)], [**1**(dhfmp)$(H_2O)_2$] (dhfmp = (η^5-C_5H_5)Fe(η^5-C_5H_4)$CH_2P(CH_2OH)_2$), and [**7**·(hfmp)], almost the same $\Delta\delta$ (^{31}P) were observed as for [**3**·(HOAc)(hfmp)].

Complex [**3**·$(HOAc)_2$] in methanol, acetone, and chloroform under a CO atmosphere very easily forms biadduct [**3**·$(CO)_2$] that is considerably more stable than adducts [**6**·(CO)], [**6**·$(CO)_2$], and [**7**·(CO)] (20). Complex [**3**·$(CO)_2$] is stable in these solvents in an air, nitrogen, or argon atmosphere at room temperature for several hours. The first band observed in the electronic spectrum of complex [**3**·$(HOAc)_2$] in acetone at 559 nm is shifted to 399 nm in biadduct [**3**·$(CO)_2$]. The spectrum of the starting compound can be observed after prolonged bubbling of nitrogen through solution, which proves reversibility of the binding of CO. The

© 2001 NRC Canada

Table 4. Selected bond lengths and angles in [**3**·(H_2O)(HOAc)].

Bond lengths	(Å)	Angles	(°)
Rh((1)—Rh(2)	2.4913(18)	Rh(2)-Rh(1)-P(1)	88.38(11)
Rh(1)—P(1)	2.193(4)	Rh(2)-Rh(1)-O(1)	83.9(3)
Rh(1)—O(1)	2.188(10)	Rh(2)-Rh(1)-O(1W)	162.3(3)
Rh(1)—O(1W)	2.313(9)	Rh(2)-Rh(1)-O(3)	86.8(3)
Rh(1)—O(3)	2.122(10)	Rh(2)-Rh(1)-C(46)	96.7(4)
Rh(1)—C(46)	1.993(14)	P(1)-Rh(1)-O(1)	94.8(3)
Rh(2)—P(2)	2.193(5)	P(1)-Rh(1)-O(1W)	99.8(3)
Rh(2)—O(2)	2.127(10)	P(1)-Rh(1)-O(3)	175.2(3)
Rh(2)—O(4)	2.177(10)	P(1)-Rh(1)-C(46)	90.5(4)
Rh(2)—O(5)	2.363(12)	O(1W)-Rh(1)-O(3)	84.9(4)
Rh(2)—C(16)	1.995(14)	Rh(1)-Rh(2)-P(2)	88.34(13)
P(1)—C(11)	1.805(13)	Rh(1)-Rh(2)-O(2)	86.0(3)
P(1)—C(21)	1.848(15)	Rh(1)-Rh(2)-O(4)	83.5(3)
P(1)—C(31)	1.813(17)	Rh(1)-Rh(2)-O(5)	163.7(3)
P(2)—C(41)	1.813(17)	Rh(1)-Rh(2)-C(16)	96.5(4)
P(2)—C(51)	1.833(16)	P(2)Rh(2)-O(2)	174.3(3)
P(2)—C(61)	1.824(16)	P(2)-Rh(2)-O(4)	93.1(3)
O(1)—C(1)	1.243(18)	P(2)-Rh(2)-O(5)	101.2(3)
O(2)—C(1)	1.236(19)	P(2)-Rh(2)-C(16)	90.2(4)
O(3)—C(3)	1.268(19)		
O(4)—C(3)	1.244(17)		

Hydrogen bonds: A-H (Å), H···B (Å), A-B (Å), A-H···B (°)
O(1W)-H(2W)···O(3) [1 −*x*, 2 − *y*, −*z*]: 1.0792, 1.7625, 2.695(13), 141.88

O(6)-H(6)···O(2): 0.8203, 1.7809, 2.565(18), 159.30

presence of [**3**·$(CO)_2$] was also demonstrated by the ^{1}H and ^{13}C NMR spectra of complex [**3**·$(HOAc)_2$] in $CDCl_3$ in an atmosphere of ^{13}CO (Tables 5 and 6). The AA′XX′ type spectrum of the ^{13}CO ligand has been observed at 243 K (d = 174.4 ppm, ^1J (C-Rh) = 46.5 Hz, ^2J (C-Rh) = 4.0 Hz, $^3J_{C-C}$ = 31.7 Hz, and ^1J (Rh-Rh) = 3.5 Hz) (Table 6, Fig. 2).

Relatively high stability of the Rh—CO bond in [**3**·$(CO)_2$] was confirmed by IR spectra. Stretching frequency ν (CO) for this adduct is low (2036 cm^{-1}) and similar to ν (CO) observed for [**5**·$(CO)_2$] (2032 cm^{-1}). This band is shifted to 1991 cm^{-1} for complex [**3**·$(^{13}CO)_2$], which agrees very well with the calculated value. For other adducts, the ν (CO) frequencies are higher, e.g., [**1**·$(CO)_2$] (2105 cm^{-1}), [**7**·(CO)] (2084 cm^{-1}), [**6**$(CO)_n$] (2085 and 2105 cm^{-1}).

Adducts [**4**·(CO)(HOAc)] and [**4**·$(CO)_2$] are less stable than [**3**·$(CO)_2$]. They are relatively stable in chloroform solutions and less stable in more polar solvents, methanol and acetone. At room temperature, in chloroform, the mixture of labile monoadduct [**4**·(CO)(HOAc)] and biadduct [**4**·$(CO)_2$] is formed. This was confirmed by ^{31}P and ^{13}C NMR spectra of these complexes in chloroform under CO atmosphere (Table 6). In the ^{31}P NMR spectrum only one doublet was observed at 11.7 ppm (^1J (P-Rh) = 140.2 Hz). This signal is shifted for 3 ppm to higher fields in comparison with complex [**4**·$(HOAc)_2$]. In the ^{13}C NMR spectrum at room temperature, ligand ^{13}CO gave a broad singlet at 165 ppm. However, the ^{31}P and ^{13}C spectra at 243 K indicate that monoadduct [**4**·(CO)(HOAc)] and biadduct [**4**·$(CO)_2$] are rigid. In the ^{31}P NMR spectrum, two doublets of the ratio of intensities 4.5:5.5 are observed. In the ^{13}C NMR spectrum of [**4**·$(^{13}CO)_2$] and [**4**·(^{13}CO)] at 243 K one can observe two broad singlets at 171.6 and 168.8 ppm which can be assigned to [**4**·$(CO)_2$] and a broad doublet at 156.1 ppm (^1J (C-Rh) = 45.8 Hz). Two signals of ^{13}CO in the biadduct are observed due to unequivalent axial positions in complex **4**. The doublet at 156.1 ppm should be assigned to [**4**·(CO)]. Similar chemical shift and ^1J (C-Rh) were found for monoadduct [**7**·(^{13}CO)] (δ (^{13}C) = 153 ppm, ^1J (P-Rh) = 42.0 Hz) (20). The approximate [**4**·(CO)(HOAc)]:[**4**·$(CO)_2$] ratio calculated from ^{13}C NMR is 3:7 and is similar to that determined from the ^{31}P NMR spectrum.

Antitumor activities of investigated complexes

We have investigated antitumor activity in vitro of some complexes against a few cell lines (KB (oral carcinoma), Hu1703 (bladder cancer), SW707 (colon adenocarcinoma), and T47D (breast cancer). Activities of investigated compounds [**3**·$(HOAc)_2$], [**6**·(HOAc)], [**7**(HOAc)], and dhfmp were compared to the activity of *cis*-diaminadichloroplatinum(II) (Table 7).

The most active agent against all investigated tumor lines is complex [**6**·(HOAc)]. It shows higher activity than cisplatin. Antitumor activity decreases in the series: [**6**·(HOAc)] > [**7**·(HOAc)] > [**3**·$(HOAc)_2$] > dhfmp. Activity of all investigated rhodium(II) complexes is higher than that of [**1**·$(H_2O)_2$].

To explain possible mechanisms of antitumor activity of these complexes we have investigated interactions in situ of complexes [**3**·$(HOAc)_2$] and [**6**·(HOAc)] with adenine, adenosine, AMP, ATP, guanine, guanosine, cytosine, cytidine, glutathione (GSH), oxidized glutathione (GSSG), and cysteine using UV–vis spectroscopy. Complex [**6**·(HOAc)] reacts immediately with adenine, adenosine, AMP, and ATP giving adducts most probably coordinated with the Rh atom via the N7 atom. This follows from the blue shift of the first band in the visible region from 618 nm for compound **5** to 564 nm for the adduct with adenine and 566 nm for the one with adenosine. The lowest shift, to 596 nm, was observed in the case of the adduct with ATP (Fig. 3). This observation is supported by literature data indicating that adenine and adenosine, when coordinated as axial ligands to dirhodium(II) complexes, usually interact via the N7 atom (33–35). Spectra of a solution containing [**6**·(HOAc)] and 10-fold excess of guanine, guanosine, cytidine, or cytosine are very similar to the spectrum of the pure complex. Thus, these nucleotide bases do not interact with complex [**6**·(HOAc)] or are coordinated through the O atom and therefore can be easily substituted by other oxygen-containing ligands present in cells (H_2O, $RCOO^-$, etc.). Interaction of adenine with complex [**3**·$(HOAc)_2$] is much weaker than with compound [**6**·(HOAc)]. The first band observed at 547 nm was shifted only to 545 nm after addition of 10 mol of adenine.

Complex [**6**·(HOAc)] easily reacts with compounds containing sulfhydryl groups, GSH, and cysteine. Even at a molar ratio [**6**·(HOAc)]:HSR of 1:1, the complex immediately is reduced to the diamagnetic mixed valence Rh(I)–Rh(II) complexes, most likely containing a Rh_4^{6+} core, showing a very intensive band at 552 nm (Fig. 4). It was found that complexes $[Rh_2(\mu\text{-}OAc)_2(\mu\text{-}N\text{-}N)_2(H_2O)_2]^{2+}$ can also be readily reduced with sulfhydryl compounds (GSH, cysteine,

© 2001 NRC Canada

Table 5. ^{1}H NMR spectra of [**3**·(HOAc)$_2$] and [**4**·(HOAc)$_2$] complexes with CO (broadened signal (*), signal from a metallated phenyl ring (^{m})).

Compound	^{1}H NMR: d (ppm), *J* (Hz)
[**4**·(HOAc)$_2$] + CO (MeOH-d_4, room temperature)	1.27 (s, 6H) (*cis* OAc bridges); 2.17 (s, 3H) (*trans* OAc bridge), 1.98 (s, 6H) (molecules of HOAc); 3.80 (s, 6H) (OMe groups), 3.84 (s, 3H) (OMe group$^{(m)}$); H2.6: 7.34 (dd, 4H), ^{3}J (H2.6-P) = 10.3, ^{3}J (H2.6- H3.5) = 8.9; H3.5: 6.93 (dd, 4H), ^{4}J (H3.5- P) = 1.8; H3^{m}: hidden under H2.6; H5^{m}: 6.46 (dt, 1H), ^{3}J (H5^{m}-H6^{m,}) = 8.5, ^{4}J(H5^{m}-P) ≈ ^{4}J(H5^{m}-H3^{m}) = 2.0; H6^{m}: 6.70 (dd, 1H), ^{3}J(H6^{m}-P) = 10.3
[**4**·(HOAc)$_2$] + ^{13}CO ($CDCl_3$, room temperature)	1.33 (s, 6H) (OAc bridges, *cis*); 2.25 (s, 3H) (OAc bridge, *trans*); 2.09 (s, 6H) (molecules of HOAc); 3.77 (s, 6H) (OMe groups); 3.86 (s, 3H) (OMe group$^{(m)}$); H2.6: 7.29 (dd, 4H), ^{3}J (H$^{2.6}$-P) = 10.8, ^{3}J (H2.6- H3.5) = 8.8; H3.5: 6.84 (dd, 4H), ^{4}J(H3.5- P) = 2.0; H3^{m}: 7.47 (s*, 1H); H5^{m}: 6.46 (dt, 1H), ^{3}J (H5^{m}-H6^{m,}) = 8.4, ^{4}J (H5^{m}-P) ≈ ^{4}J (H5^{m}-H3^{m}) = 2.0; H6^{m}: 6.70 (dd, 1H), ^{3}J (H6^{m}-P) = 10.3
[**4**·(HOAc)$_2$] + ^{13}CO ($CDCl_3$, 243 K)	1.32 (s*, 6H) (OAc bridges, *cis*); 2.27 (s*, 3H) (OAc bridge, *trans*); 2.11 (s*, 6H) (molecules of HOAc); 3.73 (s*, 6H) (OMe groups); 3.83 (s*, 3H) (OMe group$^{(m)}$); 7.4–6.3 (aromatic protons)
[**3**·(HOAc)$_2$] + CO (MeOH-d_4, room temperature)	1.17 (s, 6H) (OAc bridges); 1.98 (s, 6H) (molecules of HOAc); 3.52 (s, 6H) (OMe groups); 3.55 (s, 6H) (OMe groups); 3.78 (s, 6H) (OMe groups); 7.4–6.2 (aromatic protons)
[**3**·(HOAc)$_2$] + CO ($CDCl_3$, room temperature)	1.22 (s, 6H) (OAc bridges); 2.05 (s, 6H) (molecules of HOAc); 3.48 (s, 6H) (OMe groups); 3.51 (s, 6H) (OMe groups); 3.77 (s, 6H) (OMe groups); 7.3–6.2 (aromatic protons)
[**3**·(HOAc)$_2$] + ^{13}CO ($CDCl_3$, 243 K)	1.19 (s, 6H) (OAc bridges); 2.09 (s, 6H) (molecules of HOAc); 3.84 (s, 6H) (OMe groups); 3.51 (s, 6H) (OMe groups); 3.55 (s*, 6H) (OMe groups); 7.5–6.2 (aromatic protons)

Table 6. ^{31}P and ^{13}C NMR spectra of [**3**·(HOAc)$_2$] and [**4**·(HOAc)$_2$] complexes with CO (broadened signal (*), signal from a metallated phenyl ring (^{m})).

Compound	^{31}P NMR	^{13}C NMR
[**4**(HOAc)$_2$] + CO (MeOH-d_4, room temperature)	15.2 (d), ^{1}J (P-Rh) = 143	
[**4**·(HOAc)$_2$] + ^{13}CO ($CDCl_3$, room temperature)	11.7 (d), ^{1}J (P-Rh) = 140.2	
[**4**·(HOAc)$_2$] + ^{13}CO ($CDCl_3$, 243 K)	13.4 (d), ^{1}J (P-Rh) = 149.2 (55%); 11.7 (d), ^{1}J (P-Rh) = 124.3 (45%)	^{13}CO: 171.6 (s*), 168.8 (s*), 156.1 (d*) 45.8
[**3**·(HOAc)$_2$] + CO (MeOH-d_4, room temperature)	15.1 (d), ^{1}J (P-Rh) = 152.6	
[**3**·(HOAc)$_2$] + CO ($CDCl_3$, room temp.)	13.2 (d), ^{1}J (P-Rh) = 151.5	
[**3**·(HOAc)$_2$] + ^{13}CO ($CDCl_3$, 243 K)	14.2 (d), ^{1}J (P-Rh) = 149.0	^{13}CO: (AA′ part of AA′XX′): 174.38 ppm, ^{3}J (^{13}C–^{13}C) = 31.7, ^{1}J (Rh-Rh) = 3.5, ^{1}J (^{13}C-Rh) = 46.5, ^{2}J (^{13}C-Rh) = 4.0

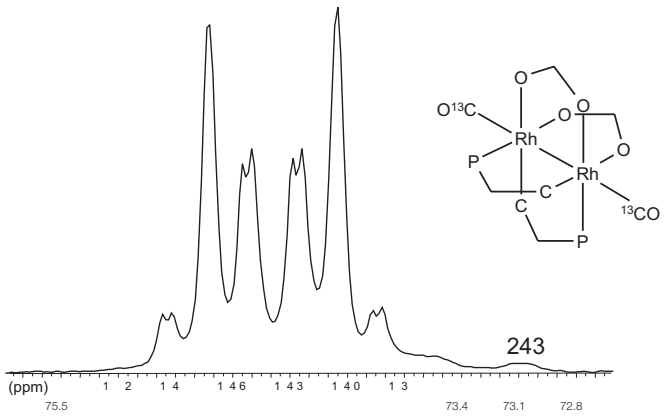
and coenzyme A) giving polynuclear rhodium compounds (36) intensively absorbing in the same region, at ca. 590 nm. Similar spectra were also observed for tetranuclear and polynuclear complexes with isocyanides $[Rh_4(\mu\text{-}CNRNC)_8]^{6+}$ (37–40), $[Rh_4(OAc)_4(N\text{-}N)_4](OAc)_2$ (41), and $\{[Rh_2(OAc)_2(N\text{-}N)_2]^{+}\}_nX_n^{-}$ (42), where N-N = bpy, phen and $X^{-} = BF_4^{-}$, PF_6^{-}. Interaction of complex [**6**·(HOAc)] with GSSG is very weak and the electronic spectrum of [**6**·(HOAc)] after addition of GSSG almost does not change. That proves that complex [**6**·(HOAc)] is easily reduced with GSH.

Absorbance of the reaction product of complex [**3**·(HOAc)$_2$] with GSH is considerably greater than the starting compound, however in the 750–400 nm region, only a shoulder at ca. 550 nm is present (Fig. 5). This suggests that reduction of compound [**3**·(HOAc)$_2$] with GSH proceeds less effectively than reduction of complex [**6**·(HOAc)].

Antitumor activity of complex [**6**·(HOAc)], reacting effectively with adenine and its derivatives and with sulfhydryl compounds, is much higher than the activity of complex [**3**·(HOAc)$_2$] that reacts with the same compounds much less intensely.

© 2001 NRC Canada

Fig. 2. Fragment of the ^{13}C NMR spectrum of [**3**·($^{13}CO)_2$] spectrum in $CDCl_3$ (temperature 243 K) (^{13}CO groups signal (AA′XX′ type)).



Experimental

Procedures and materials

Tris(4-methoxyphenyl)phosphine (PMP), tris(3-methoxyphenyl)phosphine (MMP), tris(2-methoxyphenyl)phosphine (OMP), and tris(2,6-dimethoxyphenyl)phosphine (DOMP) were purchased from Strem or Avocado and used without further purification. Adenine, adenosine, adenosine 5′-monophosphate (AMP), adenosine 5′-triphosphate (ATP), guanine, guanosine, cytosine, cytidine, glutathione (GSH), oxidized glutathione (GSSG), and cysteine were purchased from Reanal (Hungary) and also used as purchased. All solvents were deoxidized prior to use. Infrared spectrum (KBr pellet) was measured on a Bruker IFS 113v and UV–vis spectra on a Beckman DU 7500 spectrometer. ^1H NMR and ^{31}P NMR spectra were measured in $CDCl_3$ on a Bruker AMX 300 spectrometer with traces of $CHCl_3$ as an internal reference for ^1H (δ = 7.23 ppm) and 85% H_3PO_4 in H_2O as an external standard for ^{31}P. Mass spectra were measured on Finnigan Mat TSQ 700 ESI.

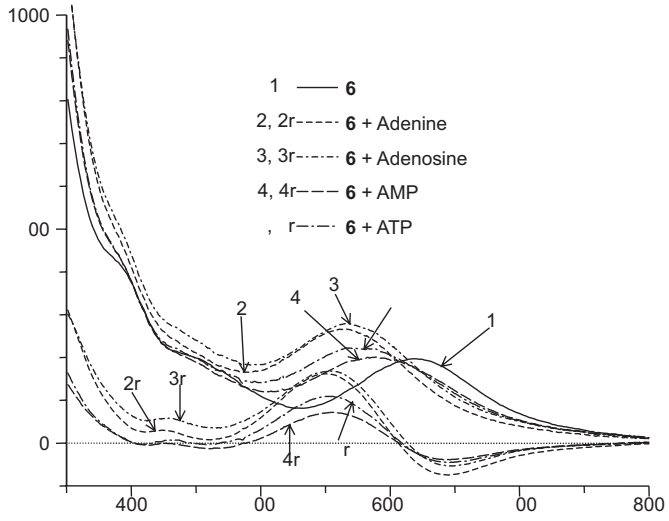
Syntheses

All operations were performed in dinitrogen or argon atmosphere using standard Schlenk technique. Complexes $[Rh_2(\mu\text{-}OAc)_4(H_2O)_2]$ ([**1**·$(H_2O)_2$]) (43), $[Rh_2(\mu\text{-}OAc)_3\{\mu\text{-}(C_6H_3\text{-}4\text{-}OMe)P(C_6H_4O\text{-}4\text{-}OMe)_2\}(HOAc)_2]$ ([**4**·$(HOAc)_2$]) (21), $[Rh_2(\mu\text{-}OAc)_2\{\mu\text{-}(C_6H_3\text{-}4\text{-}OMe)P(C_6H_4\text{-}4\text{-}OMe)_2\}_2(HOAc)_2]$ ([**5**·$(HOAc)_2$]) (21), $[Rh_2(\mu\text{-}OAc)_3\{\mu\text{-}(C_6H_4\text{-}2\text{-}O)P(C_6H_4\text{-}2\text{-}OMe)_2\}(HOAc)]$ ([**6**·(HOAc)]) (19), and $[Rh_2(\mu\text{-}OAc)_3\{\mu\text{-}(C_6H_3\text{-}6\text{-}OMe\text{-}2\text{-}O)P[(C_6H_3\text{-}2,6\text{-}(OMe)_2]_2\}(HOAc)]$ ([**7**·(HOAc)]) (20) were synthesized according to literature methods.

[Rh_2(μ-OAc)$_2${μ-(C_6H_3-3-OMe)P(C_6H_4-3-OMe)$_2$}$_2$(HOAc)$_2$] ([3·(HOAc)$_2$])

A suspension of [**1**·$(H_2O)_2$] (0.144 g, 0.3 mmol) and MMP (0.226 g, 0.6 mmol) in a mixture of 5 cm^3 of ethanol and 5 cm^3 of acetic acid was refluxed with stirring for 3 h. The initial orange color of the reaction mixture was replaced by brown-gray and then by deep violet solution. The solution was evaporated to dryness and the product was crystallized from mixture of chloroform (5 cm^3) and acetic acid (3 cm^3). Yield: 0.316 g, 69%. Mass spectrum (M = $Rh_2(\mu\text{-}OAc)_2\{\mu\text{-}(C_6H_3\text{-}3\text{-}OMe)P(C_6H_4\text{-}3\text{-}OMe)_2\}_2$) (signals of intensity higher than 16%): 367 (100%) ($MMP^+ + CH_3$), 926 (18%), 967 (30%) ($M^+ - OAc$), 1335 (20%) ($M^+ - OAc + MMP + CH_3$), 1993 (20%) ($M_2^+ - OAc$). Anal. calcd. for $C_{50}H_{54}O_{14}P_2Rh_2$: C 52.37, H 4.75; found: C 52.42, H 4.71.

Fig. 3. UV–vis spectra of the mixtures of [**6**·(HOAc)] with adenine, adenosine, AMP, and ATP (in molar ratios 1:10) in the mixture of H_2O and AcMe (1:1 by volume). *X* axis: λ (nm), *Y* axis: $e = Ac_0^{-1}\ L^{-1}$.



[(η^5-C_5H_5)Fe(η^5-C_5H_4)$CH_2P(CH_2OH)_2$ (dhfmp) and {(η^5-C_5H_5)Fe(η^5-C_5H_4)CH_2}$_2$$PCH_2OH$ (hfmp)

Both phosphines were synthesized according to literature methods (44, 45) describing the synthesis of dhfmp as a single product.

19.27 g of an 80% solution of $P(CH_2OH)_4Cl$ in H_2O was diluted with MeOH (20 cm^3), deoxidized, and placed under an Ar atmosphere; KOH (4.26 g, 0.076 mol) was added to the solution. The resulting mixture was stirred for 2 h at room temperature. Then $[C_5H_5FeC_5H_4CH_2N(CH_3)_3]I$ (10.0 g, 0.026 mol) suspension in methanol (20 cm^3) was slowly added and the reaction mixture was refluxed with stirring for 20 h. After that time two-thirds of the solvent was evaporated and H_2O (15 cm^3), diethyl ether (45 cm^3), and triethylamine (15 cm^3) were added. After 1 h of stirring, the water layer was removed and reextracted with diethyl ether (15 cm^3). The combined extracts were washed a few times with small portions (5 cm^3) of water (to dispel the characteristic smell of amine). After removing ether under reduced pressure, the products were recrystallized from the mixture of CH_2Cl_2 (5 cm^3), MeOH (5 cm^3), and light petroleum ether (35 cm^3). In all experiments, we have always obtained two products, which were isolated using the difference of their solubility in the mixture of water and methanol. In methanol–water (50:50 by mass) practically only dhfmp is dissolved. The purity of products was controlled using TLC (5 × 20 cm plates with reversed phase silicagel (C_{18}) from Alltech). Eluent: 90% solution of methanol in water. Intense yellow color of products facilitated the

© 2001 NRC Canada

Table 7. ID_{50} [μg mL^{-1}] ([mol dm^{-3}]).

	KB (oral carcinoma)	Hu1703 (bladder cancer)	SW707 (colon adenocarcinoma)	T47D (breast cancer)
[**6**·(HOAc)]	9.12 ± 2.00 (1.17×10^{-6})	0.309 ± 0.0013 (3.96×10^{-7})	0.427 ± 0.0012 (5.47×10^{-7})	0.302 ± 0.0012 (3.87×10^{-7})
[**7**·(HOAc)]	55.00 ± 1.90 (6.32×10^{-5})	5.100 ± 0.013 (5.86×10^{-6})	38.000 ± 0.001 (4.36×10^{-5})	3.550 ± 0.001 (4.08×10^{-6})
[**3**·$(HOAc)_2$]	66.00 ± 1.80 (5.76×10^{-5})	46.000 ± 0.001 (4.01×10^{-5})	49.000 ± 0.001 (4.27×10^{-5})	38.000 ± 0.001 (3.31×10^{-5})
dhfmp	74.0 ± 0.00 (2.53×10^{-4})	39.000 ± 0.001 (1.34×10^{-4})	40.000 ± 0.001 (1.37×10^{-4})	45.000 ± 0.001 (1.54×10^{-4})
$Pt(NH_3)_2Cl_2$ (*cis*-platin)	—	0.23 (7.66×10^{-7})	3.0 (1.00×10^{-5})	—

Fig. 4. UV–vis spectra of the mixtures of [**6**·(HOAc)] with GSH, GSSG, and cysteine (in molar ratios given in the figure) in the mixture of H_2O and AcMe (1:1 by volume). *X* axis: λ (nm), *Y* axis: $e = Ac_0^{-1}\ L^{-1}$.

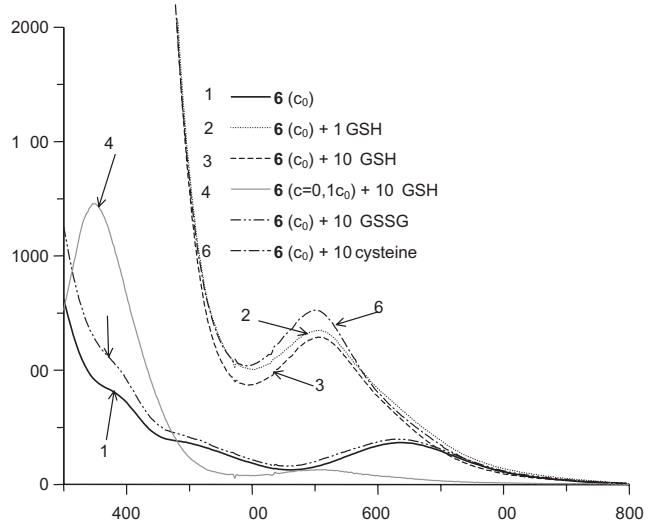
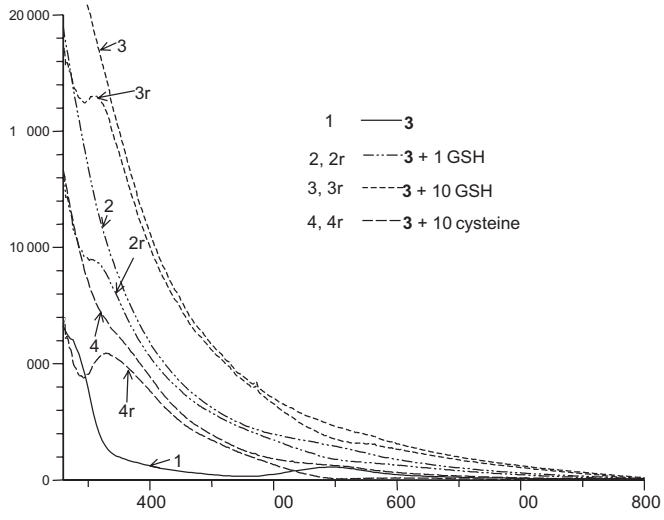


Fig. 5. UV–vis spectra of the mixtures of [**3**·$(HOAc)_2$] with GSH and cysteine (in molar ratios given in the figure) in the mixture of H_2O and AcMe (1:1.5 by volume). *X* axis: λ (nm), *Y* axis: $e = Ac_0^{-1}\ L^{-1}$.



observations. Yield: 47% for dhfmp and 21% for hfmp. Mass spectrum of dhfmp (M = $(C_5H_5)Fe(C_5H_4)CH_2P(CH_2OH)_2$) (signals of intensity higher than 16%): 199 (100%) $\{FcCH_2^+\}$, 292 (20%) $\{M^+\}$, 322 (42%) $\{M^+ + CH_2OH\}$, 460 (18%) $\{(FcCH_2)_2P(CH_2OH)^+\}$, 490 (20%) $\{(FcCH_2)_2PH(CH_2OH)_2\}$. Mass spectrum of hfmp (M = $\{(C_5H_5)Fe(C_5H_4)CH_2\}_2PCH_2OH$) (signals of intensity higher than 16%): 199 (72%) $\{FcCH_2^+\}$, 461 (100%) $\{M^+ + H\}$, 491 (68%) $\{M^+ + CH_2OH\}$. Anal. calcd. for $C_{13}H_{17}FeO_2P$ (dhfmp): C 53.46, H 5.87, P 10.60; found: C 53.4, H 5.6, P 9.8. Anal. calcd. for $C_{23}H_{25}Fe_2OP$ (hfmp): C 60.04, H 5.48, P 6.73; found: C 59.8, H 5.3, P 6.4.

X-ray structure determination

All measurements were made at 170(2) K on a Kuma KM4CCD κ-axis diffractometer with graphite monochromated Mo Kα radiation (λ = 0.71073 Å, 3.30 = θ = 27.00). The crystallographic data together with data collection and structure refinement details are given in Table 2. All the data were corrected for Lorentz and polarization effects but absorption and extinction were not applied. The crystal was positioned at 65 mm from the KM4CCD camera. Frames (612) were measured at 0.75° intervals with a counting time of 20 s. The data were corrected for Lorentz and polarization effects. Data reduction and analysis were carried out with the Kuma Diffraction programs (46, 47). The structure was solved by direct methods and refined by the full-matrix least-squares method on F^2 (48). The refinement was performed using the SHELXL program (49). Non-hydrogen atoms were refined with anisotropic thermal parameters; hydrogen atoms were included from the geometry of molecules and Δρ maps but were not refined.

Crystals of [**3**·(HOAc)(H_2O)] suitable for X-ray analysis were obtained from recrystallization of [**3**·$(HOAc)_2$] from the mixture of $CHCl_3$ and 96% EtOH in H_2O.

Cytotoxic activity in vitro

Compounds

Test solutions of the compounds tested (1 mg mL^{-1}) were prepared ex tempore by dissolving the substance in 100 μL of solvent completed with 900 μL of tissue culture medium. Afterwards, the tested compounds were diluted in culture medium (described below) to reach the final concentrations of 100, 10, 1, 0.1, and 0.01 μg mL^{-1}. The solvents (in dilu-

© 2001 NRC Canada

tion corresponding to its highest concentration applied to the tested compounds), did not exert any inhibitory effect on cell proliferation.

Cells

The below listed, established in vitro, human cancer cell lines were applied: SW707 (colon adenocarcinoma), Hu1703 (bladder cancer), T47D (breast cancer), KB (oral carcinoma). All lines were obtained from the American Type Culture Collection (Rockville, Maryland, U.S.A.) and are maintained in the Cell Culture Collection of the Institute of Immunology and Experimental Therapy, Wroclaw, Poland.

The cells were plated in 96-well plates (Sarstedt, U.S.A.) at a density of 1×10^4 cells per well, 24 h before addition of the tested agents. The cells were cultured in the opti-MEM medium supplemented with 2mM glutamine (Gibco, Warsaw, Poland), streptomycin (50 μg mL^{-1}), penicillin (50 U mL^{-1}) (both antibiotics from Polfa, Tarchomin, Poland), and 5% fetal calf serum (Gibco, Grand Island, New York). The cell cultures were maintained at 37°C in a humid atmosphere saturated with 5% CO_2.

Antiproliferative assay in vitro

SRB. The details of this technique were described by Skehan et al. (50). The cytotoxicity assay was performed after 72-h exposure of the cultured cells to varying concentrations (from 0.01 to 100 μg mL^{-1}) of the tested agents. The cells attached to the plastic were fixed by gently layering cold 50% TCA (trichloroacetic acid, Aldrich-Chemie, Germany) on the top of the culture medium in each well. The plates were incubated at 4°C for 1 h and then washed five times with tap water. The background optical density was measured in the wells filled with culture medium, without the cells. The cellular material fixed with TCA was stained with 0.4% sulforhodamine B (SRB, Sigma, Germany) dissolved in 1% acetic acid (POCh, Gliwice, Poland) for 30 min. Unbound dye was removed by rinsing (4×) with 1% acetic acid. The protein-bound dye was extracted with 10 mM unbuffered Tris base (tris (hydroksymethyl) aminomethane, POCh, Gliwice, Poland) for determination of optical density (at 540 nm) in a computer-interfaced, 96-well microtiter plate reader Multiskan RC photometer (Labsystems). Each compound in given concentration was tested in triplicates in each experiment, which was repeated 3–5 times.

The results of cytotoxic activity in vitro were expressed as ID_{50} — the dose of compound that inhibits proliferation rate of the tumor cells by 50% as compared to control untreated cells.

Supplementary material

Supplementary material may be purchased from the Depository of Unpublished Data, Document Delivery, CISTI, National Research Council Canada, Ottawa, ON K1A 0S2, Canada (for information on ordering electronically http://www.nrc.ca/cisti/irm/unpub_e.shtml). Crystallographic data (excluding structure factors) for the structure reported in this paper have been deposited with the Cambridge Crystallographic Data Centre. Copies of the data can be obtained, free of charge, on application to the Director, CCDC, 12 Union Road, Cambridge CB2, 1EZ, U.K. (Fax: (+44)1223-336-033 or e-mail: deposit@ccdc.cam.ac.uk).

References

1. A.R. Chakravarty, F.A. Cotton, D.A. Tocher, and J.H. Tocher. Organometallics, **4**, 8 (1985).
2. F.A. Cotton, F. Barcelo, P. Lahuerta, R. Llusar, J. Paya, and M.A. Ubeda. Inorg. Chem. **27**, 1010 (1988).
3. P. Lahuerta, J. Paya, E. Peris. M.A. Pellinghelli, and A. Tiripicchio. J. Organomet. Chem. **373**, C5 (1989).
4. M.V. Borrachero, F. Estevan, S. Garcia-Granda, P. Lahuerta, J. Latorre, E. Peris, and M. Sanau. J. Chem. Soc. Chem. Comm. 1864 (1993).
5. P. Lahuerta, J. Paya, X. Solans, and M.A. Ubeda. Inorg. Chem. **31**, 385 (1992).
6. P. Lahuerta, J. Paya, E. Peris, A. Aguirre, S. Garcia-Granda, and F. Gomez-Beltran. Inorg. Chim. Acta, **192**, 43 (1992).
7. P. Lahuerta, J. Paya, M.A. Pellinghelli, and A. Tiripicchio. Inorg. Chem. **31**, 1224 (1992).
8. A. Garcia-Bernabe, P. Lahuerta, M.A. Ubeda, S. Garcia-Granda, and P. Pertierra. Inorg. Chim. Acta, **229**, 203 (1995).
9. F. Estevan, S. Garcia-Granda, P. Lahuerta, J. Latorre, E. Peris, and M. Sanau. Inorg. Chim. Acta, **229**, 365 (1995).
10. P. Lahuerta, J. Paya, S. Garcia-Granda, F. Gomez-Beltran, and A. Anillo. J. Organomet. Chem. **443**, C14 (1993).
11. S. Garcia-Granda, P. Lahuerta, J. Latorre, M. Martinez, E. Peris, M. Sanau, and M.A. Ubeda. J. Chem. Soc. Dalton Trans. 539 (1994).
12. G. Gonzalez, M. Martinez, F. Estevan, A. Garcia-Bernabe, P. Lahuerta, E. Peris, M.A. Ubeda, M.R. Diaz, S. Garcia-Granda, and B. Tejerina. New J. Chem. **20**, 83 (1996).
13. G. Gonzalez, P. Lahuerta, M. Martinez, E. Peris, and M. Sanau. J. Chem. Soc. Dalton Trans. 545 (1994).
14. F. Estevan, G. Gonzalez, P. Lahuerta, M. Martinez, E. Peris, and R. van Eldik. J. Chem. Soc. Dalton Trans. 1045 (1996).
15. F.P. Pruchnik, R. Starosta, P. Smolenski, E. Shestakova, and P. Lahuerta. Organometallics, **17**, 1395 (1998).
16. S.J. Chen and K.R. Dunbar. Inorg. Chem. **29**, 588 (1990).
17. S.J. Chen and K.R. Dunbar. Inorg. Chem. **30**, 2018 (1991).
18. K.R. Dunbar, J.H. Matonic, and V.P. Saharan. Inorg. Chem. **33**, 25 (1994).
19. Z. Galdecki, E. Galdecka, A. Kowalski, F.P. Pruchnik, K. Wajda-Hermanowicz, and R. Starosta. Pol. J. Chem. **73**, 859 (1999).
20. F.P. Pruchnik, R. Starosta, M.W. Kowalska, E. Galdecka, Z. Galdecki, and A. Kowalski. J. Organomet. Chem. **597**, 20 (2000).
21. R.G. Hughes, J.L. Bear, and A.P. Kimball. Proc. Am. Assoc. Cancer Res. **13**, 120 (1972).
22. F.A. Cotton and R.A. Walton. Multiple bonds between metal atoms. Clarendon Press, Oxford. 1993.
23. E.B. Boyar and S.D. Robinson. Coord. Chem. Rev. **50**, 109 (1983).
24. N. Farrel and M.P. Hacker. Inorg. Chim. Acta, **166**, 35 (1989).
25. F.P. Pruchnik and D. Dus. J. Inorg. Biochemistry, **61**, 55 (1996).
26. F.P. Pruchnik, M. Bien, and T. Lachowicz. Met. Based Drugs, **3**, 185 (1996).
27. M. Bien, T.M. Lachowicz, A. Rybka, F.P. Pruchnik, and L. Trynda. Met. Based Drugs, **4**, 81 (1997).
28. M. Bien, F.P. Pruchnik, A. Seniuk, T.M. Lachowicz, and P. Jakimowicz. J. Inorg. Biochem. **73**, 49 (1999).
29. L. Trynda and F.P. Pruchnik. J. Inorg. Biochem. **58**, 69 (1995).

© 2001 NRC Canada

30. L. Trynda-Lemiesz and F.P. Pruchnik. J. Inorg. Biochem. **66**, 187 (1997).
31. F.P. Pruchnik, G. Kluczewska, A. Wilczok, U. Mazurek, and T. Wilczok. J. Inorg. Biochem. **65**, 25 (1997).
32. F.P. Pruchnik, R. Starosta, T. Lis, and P. Lahuerta. J. Organomet. Chem. **568**, 177 (1998).
33. N. Farrell. J. Inorg. Biochem. **14**, 261 (1981).
34. N. Alberding, N. Farrell, and E.D. Crozier. J. Am. Chem. Soc. **107**, 384 (1985).
35. J.R. Rubin, T.P. Haromy, and M. Sundaralingam. Acta Crystallogr. Sect. C: Cryst. Struct. Commun. **47**, 1712 (1991).
36. P. Jakimowicz, L. Ostropolska, and F.P. Pruchnik. Met. Based Drugs, **7**, 201 (2000).
37. V.M. Miskowski, I.S. Sigal, K.R. Mann, H.B. Gray, S.J. Milder, G.S. Hammond, and P.R. Ryason. J. Am. Chem. Soc. **101**, 4383 (1979).
38. V.M. Miskowski, G.L. Nobinger, D.S. Kliger, G.S. Hammond, N.S. Lewis, K.R. Mann, and H.B. Gray. J. Am. Chem. Soc. **100**, 485 (1978).
39. I.S. Sigal and H.B. Gray. J. Am. Chem. Soc. **103**, 2220 (1981).
40. N.S. Lewis, K.R. Mann, J.G. Gordon II, and H.B. Gray. J. Am. Chem. Soc. **98**, 7461 (1976).
41. E. Galdecka, Z Galdecki, F.P. Pruchnik, and P. Jakimowicz. Transition Met. Chem. (Dordrecht, Neth.), **25**, 315 (2000).
42. F.P. Pruchnik, P. Jakimowicz, Z. Ciunik, K. Stanislawek, L. Oro, C. Tejel, and M.A. Ciriano. Inorg. Chem. Comm. **4**, 19 (2001).
43. G.L. Rempel, P. Legzdins, H. Smith, and G. Wilkinson. Inorg. Synth. **13**, 90 (1972).
44. N.J. Goodwin, W. Henderson, and J.K. Sarfo. J. Chem. Soc. Chem. Comm. 1551 (1996).
45. N.J. Goodwin, W. Henderson, and B.K. Nicholson. J. Chem. Soc. Chem. Comm. 31 (1997).
46. KM4RED data reduction program. Kuma Diffraction Ltd., Wroclaw, Poland. 1997.
47. KM4CCD data collection program. Kuma Diffraction Ltd., Wroclaw, Poland. 1997.
48. G.M. Sheldrick. SHELXS 97. Program for the solution of crystal structures. University of Göttingen, Germany. 1997.
49. G.M. Sheldrick. SHELXL 97. Program for the refinement of crystal structures. University of Göttingen, Germany. 1997.
50. P. Skehan, R. Storeng, D. Scudiero, et al. J. Nat. Cancer Inst. **82**, 1107 (1990).

© 2001 NRC Canada

Octaarylethynyl and octaarylbutadiynyl phthalocyanines

Clifford C. Leznoff and Bohdan Suchozak

Abstract: 4,5-Diphenylethynylphthalonitrile, 4,5-di(*p*-*tert*-butylphenylethynyl)phthalonitrile, 4,5-di(*p*-neopentoxyphenylethynyl)phthalonitrile, and 4,5-di(*p*-neopentoxyphenyl-1,3-butadiynyl)phthalonitrile were prepared via 4,5-diiodophthalonitrile and the appropriate alkyne in palladium-catalyzed coupling reactions. Condensation of the above alkynylphthalonitriles with lithium 1-octanolate in 1-octanol afforded the desired polyalkynylphthalocyanines, but only 2,3,9,10,16,17,22,23-octa (*p*-neopentoxyphenylethynyl)phthalocyanine and 2,3,9,10,16,17, 22,23-octa (*p*-neopentoxyphenylbutadnyl)phthalocyanine were soluble enough to be suitably characterized.

Key words: phthalocyanines, phenylacetylenes, 1-phenyl-1,3-butadiynes.

Résumé : On a préparé le 4,5-diphényléthynylphtalonitrile, le 4,5-di(*p*-*tert*-butylphényléthynyl)phtalonitrile, le 4,5-di-(*p*-néopentoxyphényléthynyl)phtalonitrile, le 4,5-di-(*p*-néopentoxyphénylbuta-1,3-diynyl)phtalonitrile en procédant au couplage catalysé par le palladium du 4,5-diiodophtalonitrile avec l'alcyne approprié. La condensation des alcynylphtalonitriles mentionnés plus haut avec de l'octan-1-olate de lithium dans l'octan-1-ol permet d'obtenir les polyalcynylphtalocyanines recherchées; toutefois seules la 2,3,9,10,16,17,22,23-octa(*p*-néopentoxyphényléthynyl)phtalocyanine et la 2,3,9,10,16,17,22,23-octa-(*p*-néopentoxyphénylbutadiynyl)phtalocyanine sont suffisamment solubles pour être caractérisées de façon adéquate.

Mots clés : phtalocyanines, phénylacétylènes, 1-phénylbuta-1,3-diynes.

[Traduit par la Rédaction]

Introduction

2,3,9,10,16,17,23,24-Octa-substituted phthalocyanines are well-known (1), and have been studied for applications in a wide variety of areas, including dyes (2), chemical sensors (3), nonlinear optics (4), and photodynamic therapy of cancer (5, 6). Recently, poly(phenylalkynyl) benzenes (7) and alkynylporphyrins (8) have been described as possible compounds for use in nonlinear optics and arrays (8, 9). With this in mind, a series of 2,3,9,10,16,17,23,24-octaalkynylphthalocyanines were prepared (10) and their ^{1}H NMR spectra studied with respect to their variation in chemical shifts with concentration and temperature. Alkynyl-substituted phthalocyanines (Pcs) have been found to be particularly interesting in that each alkynyl group causes a red shift of 4–6 nm in the Q-band region of the spectrum, and can hence be applied in "fine-tuning" a Pcs absorption spectrum.

Not investigated in our original series of octaalkynylphthalocyanines were those substituted with phenylethynyl groups, which would be expected to give a greater red shift due to more extensive π-electron delocalization. Reports of enhanced nonlinear effects in molecules with extreme bond-length alternations (11), including conjugated diynyl systems (12) have also prompted our interest in butadiynyl substituted phthalocyanines. In this paper, the synthesis of some 2,3,9,10,16,17,23,24-octa(phenylethynyl)phthalocyanines will be described. The synthesis of a 4,5-di(butadiynyl)-substituted phthalonitrile is also outlined and its condensation reaction with lithium 1-octanolate will be discussed.

Received August 18, 2000. Published on the NRC Research Press Web site at http://canjchem.nrc.ca on July 3, 2001.

Dedicated to Professor Brian James on the occasion of his 65th birthday.

C.C. Leznoff[1] and B. Suchozak. Department of Chemistry, York University Toronto, ON M3J 1P3, Canada.
[1]Corresponding author (telephone: (416) 736-2100 ext. 33838; fax: (416) 736-5936; e-mail: leznoff@yorku.ca).

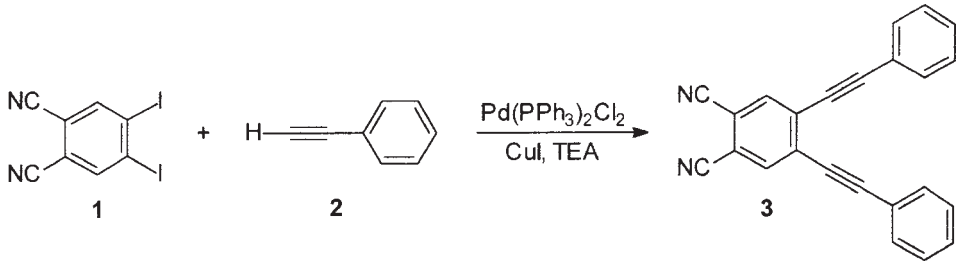
Results and discussion

Using catalytic quantities of $Pd(PPh_3)_2Cl_2$ and CuI in triethylamine (TEA), 4,5-diiodo-phthalonitrile (**1**) was coupled with 2 molar equiv of phenylacetylene (**2**), to afford 4,5-di(phenylethynyl)phthalonitrile (**3**) in 70% yield (Scheme 1). Subsequent condensation of **3** with lithium 1-octanolate in 1-octanol gave, after work-up, a dark green solid which was extremely insoluble in most organic solvents (see Scheme 3 below). Purification of this product, which is believed to be 2,3,9,10,16,17,23,24-octa(phenylethynyl)phthalocyanine (**4**), was made extremely difficult due to its insolubility, and consequently failed to afford satisfactory proton NMR or FAB mass spectra. A recently acquired MALDI-TOF mass spectrometer has allowed us to record the parent ion cluster at (1314) of **4**. However, a UV–vis spectrum of a probe from the reaction mixture at 20 h seems to suggest the formation of an MPc. This is indicated by a strong absorption maximum at 720 nm, which would correspond to the expected Q-Band absorption of the dilithium Pc.

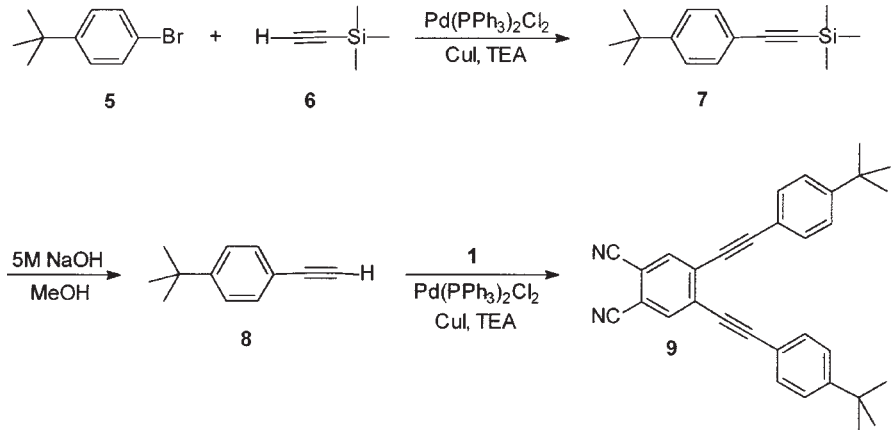
The high degree of insolubility displayed by the product of this reaction, assuming that it is indeed **4**, was believed to

 DOI: 10.1139/cjc-79-5/6-878 © 2001 NRC Canada

Scheme 1.



Scheme 2.



be due to aggregation. In an attempt to minimize these intramolecular aggregative effects, the phenylacetylene moiety was functionalized with the bulky *tert*-butyl group. Thus, 1-bromo-4-*tert*-butylbenzene (**5**) was coupled with trimethylsilylacetylene (**6**) using $Pd(PPh_3)_2Cl_2$ and CuI in TEA in a pressure bottle at 95°C, to give 1-trimethylsilyl-2-(*p*-*tert*-butylphenyl)acetylene (**7**) in 75% yield. This compound was then deprotected by treatment with aqueous 5 M NaOH in methanol to give *p*-*tert*-butylphenylacetylene (**8**) in 98% yield. This was subsequently coupled with 4,5-diiodophthalonitrile (**1**), again using $Pd(PPh_3)_2Cl_2$ and CuI, to afford 4,5-di(*p*-*tert*-butylphenylethynyl)phthalonitrile (**9**) in 88% yield (Scheme 2).

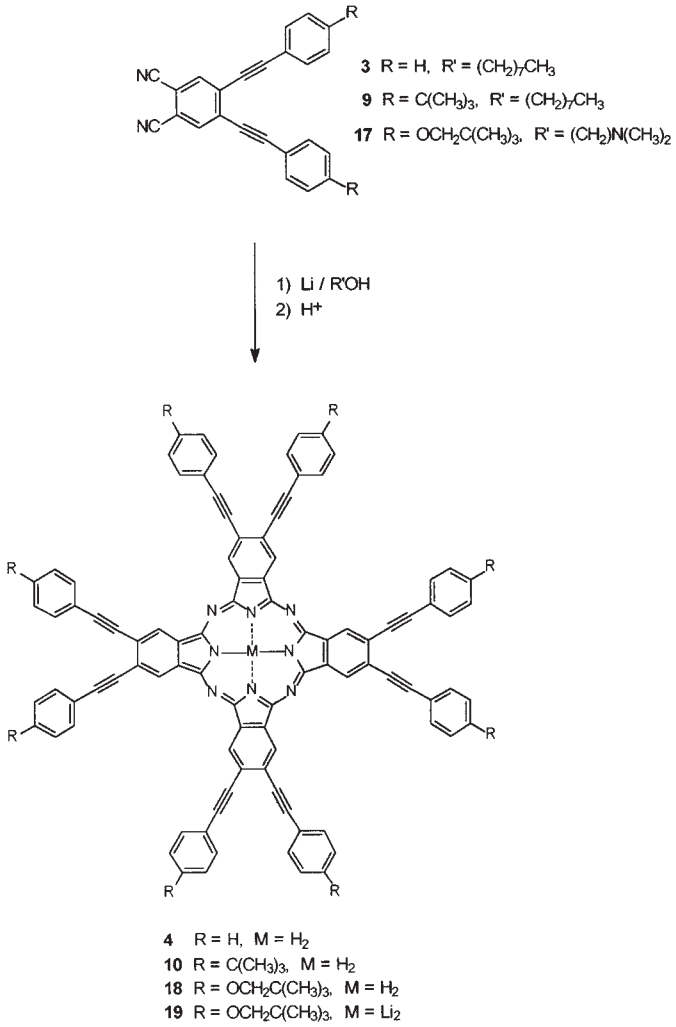
Condensation of **9** to the corresponding Pc (**10**) was performed using lithium 1-octanolate in 1-octanol at 100°C (see Scheme 3 below). A UV–vis probe of this reaction after 22 h revealed an absorption at 722 nm, believed to be the Q-band absorption of the intermediate dilithium Pc. An acid work-up of the reaction was performed to obtain the metal free Pc **10**, but the dark-green product isolated from this reaction was found to be just as insoluble in organic solvents as Pc **4**. Similar difficulties were also encountered in trying to obtain satisfactory NMR and mass spectra, although a MALDI-TOF mass spectrum of **10** exhibited a parent ion cluster at 1762 amu. If phthalocyanine **10** had indeed formed in this reaction, as suggested by the UV–vis spectrum, then it seemed evident that the *tert*-butyl groups did little to enhance the solubility of these Pcs in their metal-free state.

Previous work in our laboratory has shown that neopentoxy groups are highly effective at increasing the solubility of Pcs (13). It was therefore hoped that by replacing the *tert*-butyl groups with neopentoxy groups, a more soluble octaphenylethynyl Pc could be synthesized and full characterization might be facilitated. The synthesis was initiated with the tosylation of neopentyl alcohol (**11**) in pyridine to give neopentyl tosylate (**12**), which was obtained in 85% yield. Tosylate **12** then reacted with *p*-iodophenol (**13**) to give *p*-iodoneopentoxybenzene (**14**) in 82% yield. This was subsequently coupled with trimethylsilylacetylene (**6**) using $Pd(PPh_3)_2Cl_2$ to give 1-trimethylsilyl-2-(*p*-neopentoxyphenyl)acetylene (**15**) in 88% yield. The trimethylsilyl group was then cleaved from **15** using 5 M aq NaOH in methanol to give, in 97% yield, *p*-neopentoxyphenylacetylene (**16**). Terminal alkyne **16** was then coupled with 4,5-diiodophthalonitrile (**1**), again using $Pd(PPh_3)_2Cl_2$ as a catalyst, to give 4,5-di(*p*-neopentoxyphenylethynyl)phthalonitrile (**17**) in 70% yield (Scheme 4). Subsequent condensation of **17** in Li–DMAE at 100°C (Scheme 3) yielded 2,3,9,10,16,17,23,24-octa(*p*-neopentoxyphenylethynyl)phthalocyanine (**18**) as a dark green solid, after work-up. Although not exceedingly soluble, Pc **18** was found to dissolve appreciably well in benzene, toluene, $CHCl_3$, CH_2Cl_2, and THF. Purification of this compound was accomplished by column chromatography using flash silica gel and CH_2Cl_2 as eluent, followed by gel permeation chromatography using SX-2 Biobeads® and THF as eluent. This was followed by reprecipitation from benzene–ethanol and then further chromatography, again using flash silica gel and CH_2Cl_2. After exhaustive purification, **18** was obtained in an overall yield of 8%.

The UV–vis absorption spectrum of phthalocyanine **18** in THF is shown in Fig. 1. A broad absorption band was observed in the 600–800 nm region with an absorption max at 678 nm and a shoulder at 720 nm. Neither dilution of the so-

© 2001 NRC Canada

Scheme 3.



lution, nor heating to 60°C caused any observable changes in its spectral patterns. Although the known metal-free octa(*alkyl*)ethynyl phthalocyanines show a pair of sharp Q-band absorptions in the same region (10), this is not the case for **18**. The corresponding dilithium Pc (**19**) was formed by treating **18** with lithium metal in THF at 50°C. The UV–vis spectrum of this compound in THF, shown in Fig. 2, displays the same sharp Q-band absorption at 720 nm as observed in the spectral probes for the condensation reactions of **3** and **9**. This result lends evidence supporting the formation of Pcs **4** and **10** in the aforementioned reactions.

A comparison of the electronic spectrum of **19** with unsubstituted dilithium phthalocyanine, which displays a Q-band absorption at 688 nm (14), suggests that the eight peripheral *p*-neopentoxyphenylethynyl groups impart a red-shift of approximately 32 nm. Further comparison with the electronic spectrum of a representative octa*alkyl*ethynyl Pc, dilithium-2,3,9,10,16,17,23,24-octapentynylphthalocyanine, which displays a Q-band absorption at 700 nm (15), suggests that the eight peripheral phenyl groups on **19** have the effect of increasing the red-shift in dilithio-octaalkynylphthalocyanines by an additional 20 nm.

Phthalocyanines **18** and **19** were also characterized by ^{1}H NMR spectroscopy in toluene-d_8 at 300 K, at a concentration of 1.0×10^{-3} M. The spectrum of **18** exhibited three broad signals in the aromatic region, one corresponding to the protons on phthalocyanine itself, and the other two corresponding to the protons on the peripheral neopentoxyphenyl rings. The outer neopentoxy groups were observed as a pair of broad singlets, one at 3.48 ppm, corresponding to the OCH_2 hydrogens and the other at 1.16 ppm, corresponding to the hydrogens on the terminal $C(CH_3)_3$ groups. The two protons on the inner nitrogens however were not observed, and a series of high-temperature ^{1}H NMR experiments were subsequently conducted to determine whether aggregation may have any effect in obscuring this signal. The same sample was rerun at incrementally higher temperatures, ranging from 300 to 363 K, but the signal still remained absent. Only after extreme vertical expansion of the spectra was a very broad singlet detected at –4.8 ppm. Additionally, the previously broad aromatic singlets at 300 K began to sharpen, and eventually appeared as a pair of doublets (Fig. 3). FAB-MS analysis of **18** exhibited the parent ion (M + 1, m/z = 2004), but the elemental analysis exhibited somewhat low carbon values, typical of some Pc compounds. The MALDI-TOF mass spectrum also exhibited a parent ion at 2002 amu. The FAB-MS spectrum for **19** did not show a molecular ion peak, but exhibited rather, two ion clusters that are consistent with the loss of one and two lithium atoms; (M – Li) centred around m/z = 2010 and (M – 2 Li) centred around m/z = 2004.

The synthesis of a 4,5-di(butadiynyl)-substituted phthalonitrile was achieved via a palladium-catalyzed cross-coupling between a monosubstituted butadiyne and 4,5-diiodophthalonitrile (**1**). This was accomplished first, by treatment of **16** with an ethyl Grignard and iodine to give 1-iodo-2-(*p*-neopentoxyphenyl)acetylene (**20**) in 26% yield, along with an undesired by-product, 1,4-di(*p*-neopentoxyphenyl)-1,3-butadiyne (**21**). This was followed by a palladium-catalyzed coupling with trimethylsilylacetylene (**6**) to give 1-(trimethylsilyl)-4-(*p*-neopentoxyphenyl)-1,3-butadiyne (**22**) in 29% yield. Subsequent desilylation using 5 M aq NaOH in MeOH at room temperature afforded 1-(*p*-neopentoxyphenyl)-1,3-butadiyne (**23**) in 95% yield. This was followed immediately by a palladium-catalyzed cross-coupling with **1** to give 4,5-di[4-(*p*-neopentoxyphenyl)-1,3-butadiynyl]phthalonitrile (**24**) in 75% yield (Scheme 5). Slow heating of this compound on a melting point apparatus showed no melting point below 300°C, but the addition of a crystal on a hot Kofler block exhibited a sharp decomposition point at 223°C.

Condensation of **24** to 2,3,9,10,16,17,23,24-octa[4-(*p*-neopentoxyphenyl)-1,3-butadiynyl]phthalocyanine (**25**) was attempted using lithium 1-octanolate in 1-octanol at 80°C (Scheme 6). After 18 h, a UV–vis probe of the dark-green reaction mixture in THF revealed a sharp absorption at 738 nm, which was believed to correspond to the Q-band absorption of the dilithium derivative of **25**. A standard workup procedure was attempted whereby the reaction mixture was treated with dilute aqueous acid, followed by several dissolution–reprecipitation cycles from EtOH–H_2O. Unexpectedly, upon contact with aqueous acid or water, the previously dark-green reaction mixture turned brown and

© 2001 NRC Canada

Scheme 4.

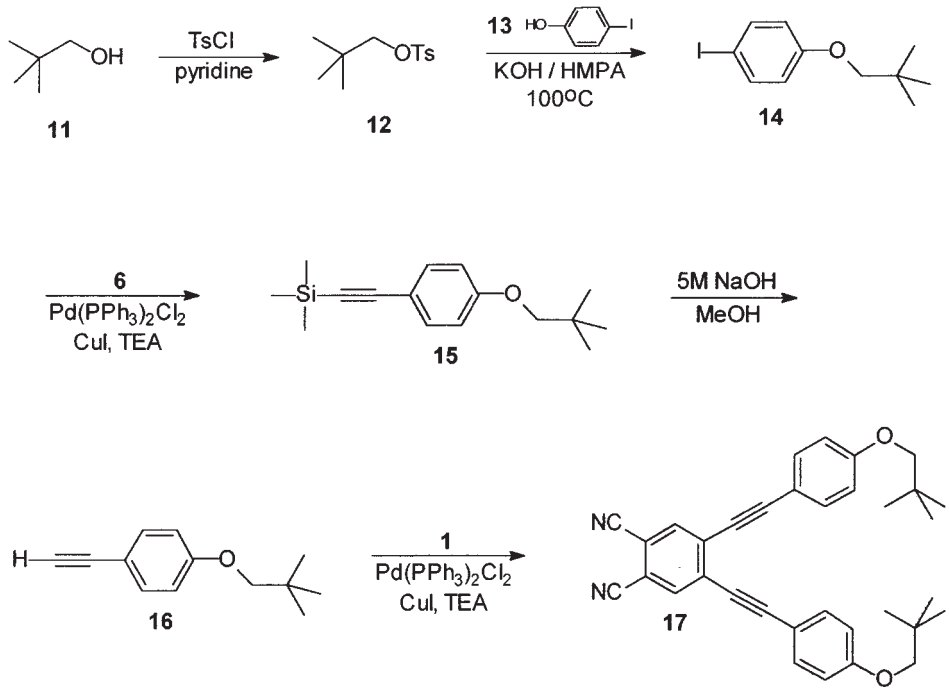


Fig. 1. The UV–vis absorption spectrum of Pc **18**.

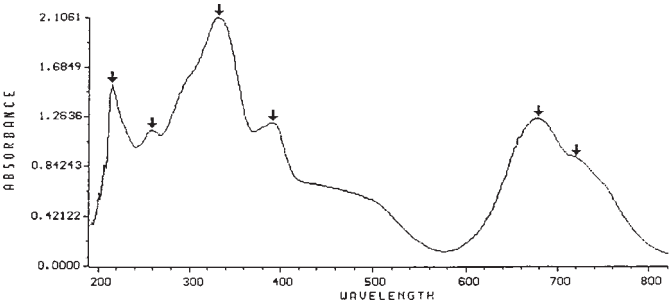
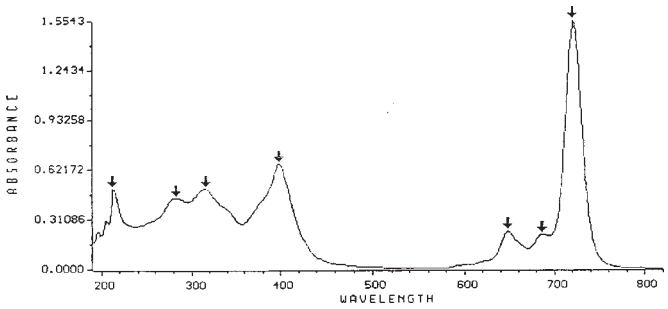


Fig. 2. The UV–vis absorption spectrum of Pc **19**.



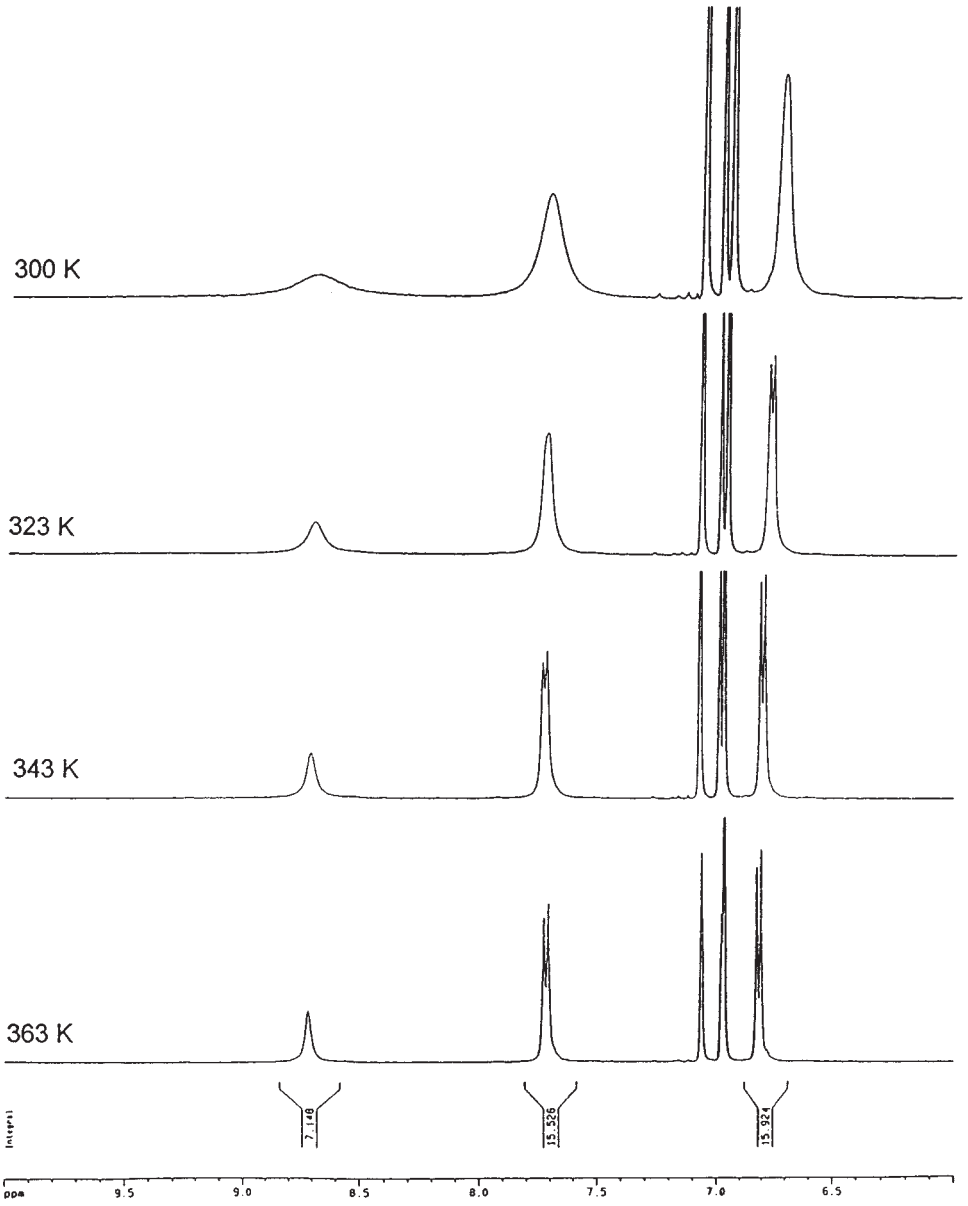
formed a highly insoluble precipitate. A UV–vis spectrum of this material showed almost no absorption in the Q-band region, a result which suggested to us that the Pc had decomposed or polymerized. Attempts were, therefore, made at isolating the intermediate dilithium Pc (**26**) under anhydrous conditions by precipitating the reaction mixture into hexane, followed by gel permeation chromatography of the crude product using dry THF and SX-2 Biobeads®. A dark-green solid was isolated from the column after evaporation of the solvent. An electronic spectrum of this material in THF is shown in Fig. 4. Proton NMR analysis of this material in pyridine-d_5 at 300 K showed a spectrum which was consistent with the structure of **26**. Two singlets were observed at 1.08 and 3.61 ppm, which would correspond to resonances arising from the protons of the eight neopentoxy groups. The aromatic signals arising from the outer neopentoxyphenyl groups corresponded to two doublets centered around 6.92 and 7.67 ppm, and the eight benzo protons on the Pc macrocycle corresponded to a singlet observed at 9.98 ppm. Although, this compound proved to be too unstable to give either a satisfactory elemental analysis or FAB mass spectrum, MALDI-TOF mass spectrometry of **26** did provide a parent ion minus one lithium ion at 2200 amu.

Experimental

Unless otherwise noted, all reaction processes were performed using magnetic stirring methods under an inert atmosphere of Matheson high-purity argon. All organic solvents were dried by appropriate methods and distilled before use. Ultrasound activation was carried out using a Branson 1200 sonicator. Thin layer chromatography (TLC) was performed using Merck silica gel 60 F_{254} polyester-backed plates and column chromatography was performed using Caledon flash grade silica gel 60 of particle size 40–63 μm. Gel permeation chromatography was performed with Bio-Rad SX-2 Biobeads®, using THF as the eluting solvent. Infrared (IR) spectra were recorded on a Unicam Mattson 3000 FT IR spectrometer using samples prepared as KBr discs, unless otherwise noted. Ultraviolet-visible (UV–vis) spectra were recorded on a Hewlett–Packard HP8451A diode array spectrophotometer using THF as the solvent. Melting points (mp) were determined using a Kofler hot stage melting point apparatus and are reported uncorrected. Nuclear magnetic resonance (NMR) spectra for proton and carbon were recorded on a Bruker ARX 400 high field Fourier transform

© 2001 NRC Canada

Fig. 3. The temperature dependent ^{1}H NMR spectra of Pc **18**.



instrument at room temperature unless otherwise stated. Chemical shifts are reported in ppm relative to a tetramethylsilane (TMS) internal standard. Splitting patterns of proton resonances are described as singlets (s), doublets (d), triplets (t), quartets (q), doublet of doublets (dd), multiplets (m), or as broad signals (br). Coupling constants for signals other than singlets and multiplets are reported in Hz. Resonances are reported as the proton decoupled chemical shifts for ^{13}C NMR spectra. Electron-impact mass spectral analyses (EI-MS) were performed by Dr. B. Khouw (York University, Toronto, Ontario, Canada) and Ms. Lisa Nelson (York University, Toronto, Ontario, Canada). MALDI-TOF mass spectra were performed neat using a Voyager Str instrument. Fast atom bombardment (FAB) and high resolution mass spectrometric analyses (HR-MS) were performed by Dr. R. L. Cerny (Nebraska Center for Mass Spectrometry, University of Nebraska-Lincoln, Lincoln, Nebraska, U.S.A.). Microanalyses were performed by Guelph Chemical Laboratories Ltd., Guelph, Ontario, Canada.

4,5-Diiodophthalonitrile (1)

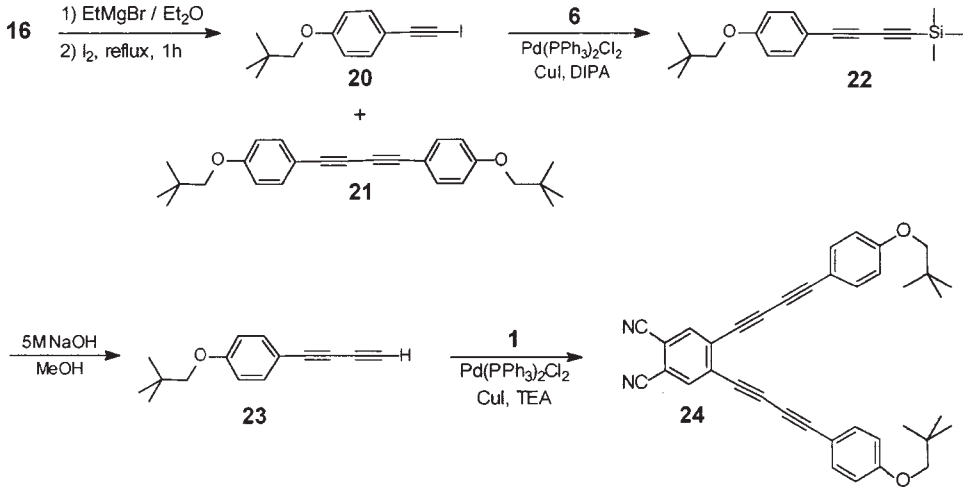
This compound was prepared in three steps according to a published procedure (10) (overall yield 50% from phthalimide); mp 216–217°C (lit. value (10), 216 to 217°C).

4,5-Di(phenylethynyl)phthalonitrile (3) general procedure

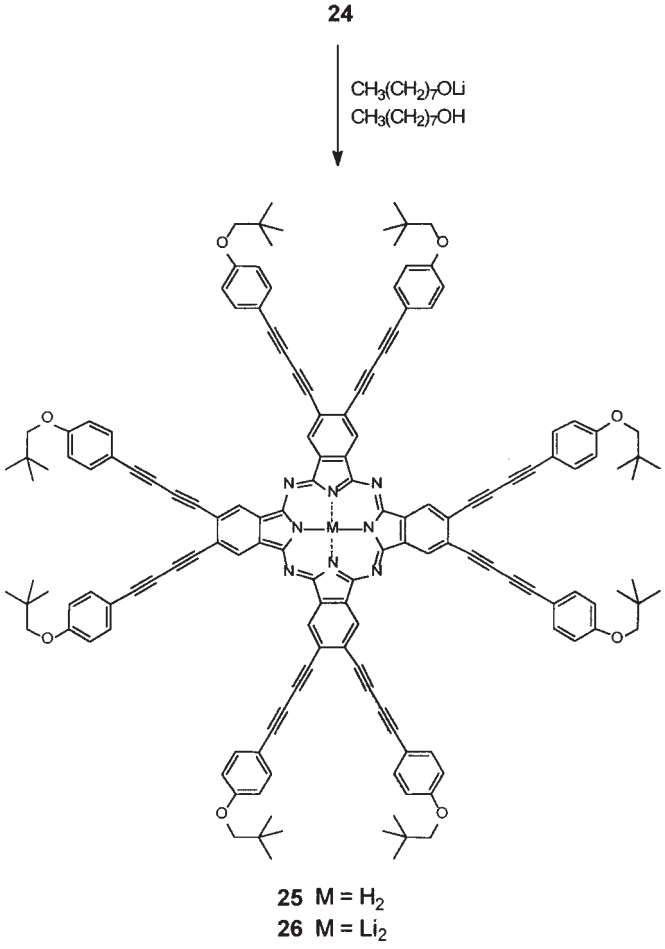
To a solution of 200 mg (0.53 mmol) of 4,5-diiodophthalonitrile (**1**) dissolved in 30 mL of triethylamine (TEA) was added 36 mg (0.051 mmol) of $Pd(PPh_3)_2Cl_2$, 10 mg (0.051 mmol) of CuI, and then 0.13 mL (0.11 g, 1.2 mmol) of phenylacetylene (**2**). The reaction was heated to 60°C for 2 h under argon and then allowed to cool to room temperature overnight. The reaction was analyzed by

© 2001 NRC Canada

Scheme 5.



Scheme 6.



TLC using benzene as eluent, and judged complete by the disappearance of the starting material. The solvent was removed by rotary evaporation at 40°C, the residue was suspended in ethyl acetate, suction filtered through celite, and then the solvent was removed from the filtrate in vacuo at 40°C. This brown residue was chromatographed with flash grade silica gel using 98:2 hexane:ethyl acetate to afford **3** as a yellow solid (121 mg, 70% yield), mp 190–192°C. EI-MS *m*/*z* (%): 328 (M^+, 100). UV–vis (THF) λ_{max} (nm): 222, 276, 301, 345. IR (KBr) (cm^{-1}): 2217 (C≡N). ^1H NMR ($CDCl_3$) δ: 7.93 (s, 2H), 7.59 (d, *J* = 7.1 Hz, 4H), 7.43 (m, 6H). ^{13}C NMR ($CDCl_3$) δ: 136.34, 132.22, 131.09, 130.21, 128.92, 121.72, 114.90, 114.27, 100.70, 85.74. Anal. calcd. for $C_{24}H_{12}N_2$: C 87.79, H 3.68, N 8.53; found: C 87.72, H 3.66, N 8.42.

2,3,9,10,16,17,23,24-Octa(phenylethynyl)phthalocyanine (4)

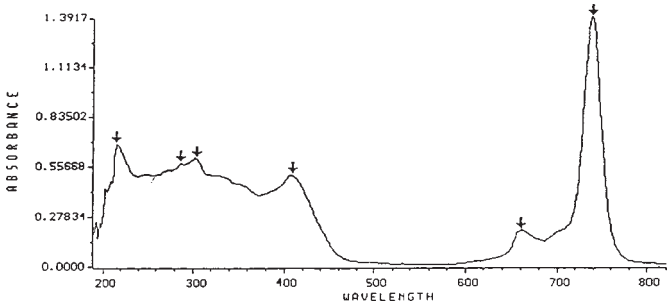
Lithium metal (20 mg, 2.9 mmol) was added to 2 mL of 1-octanol at 60°C and allowed to dissolve over 20 h under argon. After all of the lithium had dissolved, the mixture was cooled to room temperature and then 50 mg (0.15 mmol) of **3** was added. The reaction was heated to 80°C and allowed to stir at this temperature for 6 h. The reaction was monitored by TLC using benzene as the eluent. After all of the starting material had disappeared, the reaction was stopped by the addition of 20% ethanol–water and several drops of 1 M HCl. The reaction mixture was centrifuged, the precipitate was collected, and then washed several times with methanol until the filtrate was colourless. The remaining dark green solid was dried in vacuo to give 10 mg of **4** in a crude yield of 20%. Due to its extreme insolubility in most solvents, this material could not be further purified. MALDI-MS *m*/*z*: 1321.5 (M^+ + Li), 1315.5 (M^+). UV–vis (pyridine) λ_{max} (nm): 726, 650, 396, 306.

1-(*p*-*tert*-Butylphenyl)-2-trimethylsilylacetylene (7)

Into a 100 mL pressure bottle was placed 0.87 mL (1.1 g, 5.0 mmol) of 1-bromo-4-*tert*-butylbenzene (**5**), 0.23 g (0.32 mmol) of $Pd(PPh_3)_2Cl_2$, 19 mg (0.10 mmol) of CuI, and 50 mL of TEA. This yellow suspension was degassed with argon for approximately 5 min, and then 1.5 mL (1.0 g, 10 mmol) of (trimethylsilyl)acetylene (**6**) was added. The bottle was sealed and heated in an oil bath at 95°C overnight. The reaction mixture was allowed to cool to room temperature and was then filtered through celite. The solids were washed with ethyl ether until the washings were colourless and the filtrate was evaporated to dryness under reduced pressure. The residue was chromatographed with

© 2001 NRC Canada

Fig. 4. The UV–vis absorption spectrum of Pc **26**.



flash grade silica gel using hexane as the eluent to give **7** as a pale yellow oil (898 mg, 78% yield). EI-MS *m*/*z* (%): 230 (M^+, 58), 215 (100). ^{1}H NMR ($CDCl_3$) δ: 7.40 (d, *J* = 8.6 Hz, 2H), 7.31 (d, *J* = 8.5 Hz, 2H), 1.31 (s, 9H), 0.25 (s, 9H). The ^{1}H-NMR spectrum matched that of the previously reported compound (16).

p-*tert*-Butylphenylacetylene (8)

To a stirred solution of 200 mg (0.87 mmol) of 1-(*p*-*tert*-butylphenyl)-2-trimethylsilylacetylene (**7**) dissolved in 10 mL of MeOH was added 0.5 mL (2.5 mmol) of 5 M NaOH. After 15 min, the reaction mixture was acidified with 1 M HCl, extracted twice with hexane, and the extracts were dried over $MgSO_4$. Filtration, followed by evaporation of the filtrate in vacuo gave **8** as a pale yellow liquid (134 mg, 98%). IR (neat) (cm^{-1}): 2109 (C≡C). ^{1}HNMR ($CDCl_3$) δ: 7.44 (d, *J* = 8.6 Hz, 2H), 7.35 (d, *J* = 8.1 Hz, 2H), 3.03 (s, 1H), 1.32 (s, 9H). The ^{1}H NMR spectrum matched that of the previously reported compound (16).

4,5-Di(*p*-*tert*-butylphenylethynyl)phthalonitrile (9)

The same procedure was used as for the synthesis of **3**, using 1.0 g (2.6 mmol) of **1**, 1.0 g (6.3 mmol) of **8**, 222 mg (0.32 mmol) of $Pd(PPh_3)_2Cl_2$, 30 mg (0.16 mmol) of CuI, and 30 mL of TEA to give 1.0 g of **9** in 88% yield, mp 168 to 169°C. EI-MS *m*/*z* (%): 440 (M^+, 60), 426 (100). UV–vis (THF) λ_{max} (nm): 214, 279, 309, 354. IR (KBr) (cm^{-1}): 2213 (C≡N). ^{1}H NMR ($CDCl_3$) δ: 7.91 (s, 2H), 7.53 (d, *J* = 8.4 Hz, 4H), 7.43 (d, *J* = 8.6 Hz, 4H), 1.36 (s, 18H). ^{13}C NMR ($CDCl_3$) δ: 153.81, 136.36, 132.09, 131.23, 125.96, 118.79, 115.04, 113.99, 101.09, 85.45, 35.27, 31.34. Anal. calcd. for $C_{32}H_{28}N_2$: C 87.24, H 6.41, N 6.36; found: C 87.25, H 6.42, N 6.12.

2,3,9,10,16,17,23,24-Octa(*p*-*tert*-butylphenylethynyl)phthalocyanine (10)

Lithium metal (16 mg, 2.3 mmol) was added to 3 mL of 1-octanol at 80°C and allowed to dissolve over 20 h under argon. After all of the lithium had dissolved, the mixture was cooled to room temperature and then 200 mg (0.45 mmol) of **9** was added. The reaction was heated to 110°C and allowed to stir at this temperature for 15 h. The reaction was monitored by TLC using benzene as the eluent. After all of the starting material had disappeared, the reaction was stopped by the addition of 20% ethanol–water and several drops of 1 M HCl. The reaction mixture was centrifuged, the precipitate was collected, and then washed several times with methanol until the filtrate was colourless. The remaining dark-green solid was dried in vacuo to give 30 mg of **10** in a crude yield of 15%. Due to its extreme insolubility in most solvents, this material could not be further purified. MALDI-MS *m*/*z*: 1770.8 (M^+ + Li), 1764.8 (M^+). UV–vis (pyridine) λ_{max} (nm): 726, 656, 398, 316.

Neopentyl tosylate (12)

To a stirred, ice water cooled solution of 50 g (0.57 mol) of neopentyl alcohol (**11**) in 350 mL of pyridine was slowly added a solution of 162 g (0.85 mol) of *p*-toluenesulfonyl chloride in 200 mL pyridine. The resulting cloudy brown mixture was allowed to stir overnight at room temperature, after which time the pyridine was removed by rotary evaporation at 45°C. To the remaining residue was added 300 mL of ice-cold water, and the mixture was stirred for 1 h. The mixture was extracted three times with 200 mL portions of ethyl ether, and the combined organic layers were washed with successive 200 mL portions of 1 M HCl, sat. $NaHCO_3$, H_2O, and then brine. The extract was dried over $MgSO_4$, filtered, and the solvent was removed in vacuo to leave **12** as an amber oil. This crude product was crystallized from MeOH–H_2O to afford a white crystalline solid (116 g, 85% yield), mp 48 to 49°C (lit. value (17), 47 to 48°C). ^{1}H NMR ($CDCl_3$) δ: 7.76 (d, *J* = 8.4 Hz, 2H), 7.32 (d, *J* = 8.1 Hz, 2H), 3.63 (s, 2H), 2.42 (s, 3H), 0.87 (s, 9H). ^{13}C NMR ($CDCl_3$) δ: 144.75, 133.20, 129.91, 127.97, 79.59, 31.71, 26.10, 21.69.

p-Iodoneopentoxybenzene (14)

A mixture of 10 g (45 mmol) of 4-iodophenol (**13**), 12.1 g (50 mmol) of neopentyl tosylate (**12**), and 2.8 g (50 mmol) of potassium hydroxide in 30 mL of hexamethylphosphoramide (HMPA) (Caution: Carcinogen) was vigorously stirred at 100°C for 3 days. This mixture was then poured into 300 mL of H_2O and extracted three times with 100 mL portions of ethyl ether. The combined ether extracts were successively washed with 100 mL portions of H_2O, 1 M HCl, H_2O, and then brine, followed by drying over $MgSO_4$, filtration and removal of the solvent by rotary evaporation. The remaining amber oil was chromatographed using silica gel and hexane as eluent to afford **14** as a clear, colourless liquid (10.8 g, 82% yield). EI-MS *m*/*z* (%): 290 (M^+, 60), 220 (100). UV–vis (THF) λ_{max} (nm): 234, 282. ^{1}H NMR ($CDCl_3$) δ: 7.54 (d, *J* = 8.8 Hz, 2H), 6.68 (d, *J* = 8.8 Hz, 2H), 3.55 (s, 2H), 1.03 (s, 9H). ^{13}C NMR ($CDCl_3$) δ: 159.65, 138.27, 117.17, 82.50, 78.16, 32.05, 26.78. Anal. calcd. for $C_{11}H_{15}IO$: C 45.54, H 5.21; found: C 45.47, H 5.36.

1-Trimethylsilyl-2-(*p*-neopentoxyphenyl)acetylene (15)

The same procedure was used as for the synthesis of **3**, using 8.0 g (28 mmol) of **14**, 4.7 mL (3.3 g, 33 mmol) of trimethylsilylacetylene (**6**), 968 mg (1.4 mmol) of $Pd(PPh_3)_2Cl_2$, 263 mg (1.4 mmol) of CuI, and 300 mL of TEA, except that the entire reaction was carried out at room temperature. The crude product was chromatographed using silica gel and hexane as eluent to afford **15** as a white solid (6.3 g, 88% yield), mp 78 to 79°C. EI-MS *m*/*z* (%): 260 (M^+, 40), 245 (20), 190 (50), 175 (100). UV–vis (THF) λ_{max} (nm): 214, 261. IR (KBr) (cm^{-1}): 2157 (C≡C). ^{1}H NMR ($CDCl_3$) δ: 7.39 (d, *J* = 8.4 Hz, 2H), 6.81 (d, *J* = 8.6 Hz, 2H), 3.59 (s, 2H), 1.04 (s, 9H), 0.25 (s, 9H). ^{13}C NMR

© 2001 NRC Canada

($CDCl_3$) δ: 160.02, 133.62, 115.17, 114.60, 105.63, 92.39, 78.08, 32.08, 26.80, 0.32. Anal. calcd. for $C_{16}H_{24}OSi$: C 73.79, H 9.29; found: C 73.40, H 9.23.

p-Neopentoxyphenylacetylene (16)

The same procedure was used as for the synthesis of **8**, using 10 g (38 mmol) of **15**, 23 mL (115 mmol) of 5 M NaOH, and 600 mL of MeOH to afford **16**. The crude product was chromatographed using silica gel and hexane as eluent giving the title compound as a clear, colourless oil (6.5 g, 95% yield). EI-MS *m*/*z* (%): 188 (M^+, 10), 118 (100). UV–vis (THF) λ_{max} (nm): 213, 252, 293, 318, 343. IR (neat) (cm^{-1}): 2107 (C≡C). ^1H NMR ($CDCl_3$) δ: 7.42 (d, *J* = 8.7 Hz, 2H), 6.84 (d, *J* = 8.6 Hz, 2H), 3.60 (s, 2H), 2.99 (s, 1H), 1.04 (s, 9H). ^{13}C NMR ($CDCl_3$) δ: 160.21, 133.73, 114.71, 114.03, 84.05, 78.11, 75.81, 32.08, 26.78. Anal. calcd. for $C_{13}H_{16}O$: C 82.94, H 8.57; found: C 82.20, H 8.39.

4,5-Di(*p*-neopentoxyphenylethynyl)phthalonitrile (17)

The same procedure was used as for the synthesis of **3**, using 760 mg (2.0 mmol) of **1**, 791 mg (4.2 mmol) of **16**, 147 mg (0.32 mmol) of $Pd(PPh_3)_2Cl_2$, 40 mg (0.16 mmol) of CuI, and 25 mL of TEA to give 700 mg of **17** in 70% yield, mp 168–170°C. EI-MS *m*/*z* (%): 501 (M^+, 18), 500 (55), 360 (100). UV–vis (THF) λ_{max} (nm): 214, 252, 284, 325, 366. IR (KBr) (cm^{-1}): 2209 (C≡N). ^1H NMR ($CDCl_3$) δ: 7.87 (s, 2H), 7.51 (d, *J* = 8.6 Hz, 4H), 6.92 (d, *J* = 8.7 Hz, 4H), 3.64 (s, 4H), 1.06 (s, 18H). ^{13}C NMR (acetone-d_6) δ: 162.37, 137.24, 134.80, 131.70, 116.33, 116.03, 114.91, 114.66, 101.51, 86.12, 79.12, 32.69, 27.02. Anal. calcd. for $C_{34}H_{32}N_2O_2$: C 81.57, H 6.44, N 5.60; found: C 81.00, H 6.45, N 5.44.

2,3,9,10,16,17,23,24-Octa(*p*-neopentoxyphenylethynyl)phthalocyanine (18)

To 2.5 mL of dimethylaminoethanol (DMAE) was added 30 mg (4.3 mmol) of lithium metal. After the metal had completely dissolved, 200 mg (0.4 mmol) of **17** was added to the well-stirred alkoxide solution, and the reaction mixture was heated to 100°C for 15 h. After this time, the reaction mixture was cooled to room temperature and diluted with 10 mL of 20% MeOH–H_2O. After being allowed to stand for 90 min, the reaction mixture was centrifuged and the crude Pc was collected, dissolved in THF and precipitated from hexane. This crude pigment was chromatographed using silica gel and CH_2Cl_2 as eluent, followed by gel permeation chromatography using SX-2 Biobeads® and THF as eluent. This material was further purified by reprecipitation from benzene–ethanol and then by chromatography using silica gel and CH_2Cl_2 as eluent to give **18** as a dark green solid (64 mg, 8% yield). FAB-MS: 2004. MALDI-MS *m*/*z*: 2003.9 (M^+). UV–vis (THF) λ_{max} (nm) (log ϵ): 716 (6.08), 678 (6.19), 390 (6.18), 330 (6.41), 258 (6.14), 216 (6.23). ^1H NMR (toluene-d_8, 1.0×10^{-3} M, 363 K) δ: 8.71 (br, 8H), 7.71 (d, *J* = 7.8 Hz), 6.81 (d, *J* = 8.1 Hz), 3.58 (s, 16H), 1.14 (s, 72H), –4.81 (br, 2H). Anal. calcd. for $C_{136}H_{130}N_8O_8$: C 81.49, H 6.54, N 5.59; found: C 80.06, H 5.80, N 5.27.

[2,3,9,10,16,17,23,24-Octa(*p*-neopentoxyphenylethynyl)phthalocyaninyl]dilithium (19)

To a suspension of 10 mg (0.72 mmol) of lithium metal in 2 mL of dry THF was added 2 mg (1.0×10^{-3} mmol) of Pc **18**. The mixture was stirred at 50°C for 5 days, after which time the excess lithium was removed by filtration and the solvent was removed in vacuo at 40°C to give **19** (2 mg, 100% yield). FAB-MS: 2010 (M – Li), 2004 (M – 2Li). UV–vis (THF) λ_{max} (nm) (log ϵ): 720 (6.89), 686 (6.04), 648 (6.07), 398 (6.52), 316 (6.40), 282 (6.35), 212 (6.40). ^1H NMR (pyridine-d_5, 4.0×10^{-4} M, 333 K) δ: 8.86 (br, 8H), 7.75 (br, 16H), 6.79 (d, *J* = 7.4 Hz), 3.53 (s, 16H), 1.12 (s, 72H).

1-Iodo-2-(*p*-neopentoxyphenyl)acetylene (20)

To 11.5 mL (35 mmol) of ethylmagnesium bromide (3.0 M solution in ether) was slowly added a solution of 5.0 g (27 mmol) of *p*-neopentoxyphenylacetylene (**16**) in 15 mL of anhydrous ether. The reaction mixture was then heated to reflux as 6.7 g (23 mmol) of powdered iodine was slowly added through the top of the condenser. The solution was refluxed for another hour, allowed to cool to room temperature and then poured into 150 mL of H_2O. The mixture was acidified with glacial acetic acid, the ether layer was separated, and the aqueous layer was extracted twice with 50 mL portions of ether. The combined organic extracts were washed with sat. $Na_2S_2O_3$, sat. $NaHCO_3$, H_2O, and brine, then dried over $MgSO_4$, filtered and evaporated under reduced pressure. The title compound (**20**) was obtained as a white solid after recrystallization from MeOH–H_2O (2.2 g, 26% yield), mp 54 to 55°C. EI-MS *m*/*z* (%): 314 (M^+, 35), 244 (100), 118 (65). UV–vis (THF) λ_{max} (nm): 214, 262. IR (KBr) (cm^{-1}): 2166 (C≡C). ^1H NMR ($CDCl_3$) δ: 7.36 (d, *J* = 8.7 Hz, 2H), 6.83 (d, *J* = 8.7 Hz, 2H), 3.59 (s, 2H), 1.03 (s, 9H). ^{13}C NMR ($CDCl_3$) δ: 160.26, 133.94, 115.45, 114.62, 94.38, 78.13, 32.08, 26.79, 3.56. Anal. calcd. for $C_{13}H_{15}IO$: C 49.70, H 4.81; found: C 50.06, H 4.78.

The by-product, 1,4-di-(*p*-neopentoxyphenyl)-1,3-butadiyne (**21**), was obtained in 59% yield (2.9 g) as a white solid, mp 189–191°C. UV–vis (THF) λ_{max} (nm): 214, 269, 282, 300, 320, 343. IR (KBr) (cm^{-1}): 2388, 2139, 1601, 1503, 1291, 1247, 1166, 1016, 831. ^1H NMR ($CDCl_3$) δ: 7.44 (d, *J* = 8.7 Hz, 2H), 6.85 (d, *J* = 8.7 Hz, 2H), 3.60 (s, 2H), 1.04 (s, 9H). ^{13}C NMR ($CDCl_3$) δ: 160.50, 134.19, 114.89, 113.85, 81.59, 78.16, 73.10, 32.09, 26.78. EI-MS *m*/*z* (%): 374 (M^+, 50), 234 (100). Anal. calcd. for $C_{26}H_{30}O_2$: C 83.38, H 8.07; found: C 82.90, H 8.40.

1-(Trimethylsilyl)-4-(*p*-neopentoxyphenyl)-1,3-butadiyne (22)

To a solution containing 200 mg (0.64 mmol) of **20** dissolved in 5 mL of THF were added 22 mg (0.032 mmol) of $Pd(PPh_3)_3Cl_2$, 3.0 mg (0.016 mmol) of CuI, 0.16 mL (116 mg, 1.15 mmol) of diisopropylamine (DIPA), and then 0.36 mL (250 mg, 2.55 mmol) of trimethylsilylacetylene (**6**). The reaction mixture was allowed to stir overnight at room temperature, after which time the solvent was evaporated in vacuo, the residue was suspended in hexane and then filtered through a bed of celite. The filtrate was concentrated under reduced pressure, chromatographed using silica gel and hexane as eluent, and then recrystallized from EtOH–H_2O to

© 2001 NRC Canada

give **22** as a white, crystalline solid (53 mg, 29% yield). EI-MS *m*/*z* (%): 284 (M^+, 65), 214 (65), 199 (100). UV–vis (THF) λ_{max} (nm): 214, 240, 275, 291, 309. IR (KBr) (cm^{-1}): 2203, 2103, 1603, 1509, 1299, 1249, 1172, 1108, 1048, 1014, 847, 760, 694. ^1H NMR ($CDCl_3$) δ: 7.41 (d, *J* = 8.7 Hz, 2H), 6.83 (d, *J* = 8.7 Hz, 2H), 3.59 (s, 2H), 1.03 (s, 9H), 0.23 (s, 9H). ^{13}C NMR ($CDCl_3$) δ: 160.72, 134.49, 114.89, 113.06, 90.03, 88.41, 78.13, 77.48, 73.13, 32.08, 26.77, –0.10. Anal. calcd. for $C_{18}H_{24}OSi$: C 76.00, H 8.50; found: C 76.07, H 8.20.

1-(*p*-Neopentoxyphenyl)-1,3-butadiyne (23)

To a stirred solution of 1.0 g (3.5 mmol) of (**22**) dissolved in 50 mL of MeOH was added 2.1 mL (11 mmol) of 5 M NaOH. After 15 min, the reaction mixture was acidified with 1 M HCl, extracted twice with hexane, and the extracts were dried over $MgSO_4$. Filtration, followed by evaporation of the filtrate in vacuo gave a grey solid, which after chromatography through a plug of silica gel using hexane, afforded 709 mg of **23** as a white solid, which rapidly darkened on exposure to light and air (95% yield). (This material was used immediately in the synthesis of **24**). EI-MS *m*/*z* (%): 212 (M^+, 20), 142 (100). UV–vis (THF) λ_{max} (nm): 214, 281, 298. IR (KBr) (cm^{-1}): 2204, 1896, 1602, 1562, 1509, 1473, 1400, 1364, 1295, 1255, 1170, 1109, 1048, 1017, 921, 834, 624. ^1H NMR ($CDCl_3$) δ: 7.45 (d, *J* = 8.6 Hz, 2H), 6.85 (d, *J* = 8.7 Hz, 2H), 3.61 (s, 2H), 2.46 (s, 1H), 1.04 (s, 9H). ^{13}C NMR ($CDCl_3$) δ: 160.86, 134.59, 114.93, 112.74, 78.18, 75.99, 72.50, 70.87, 68.69, 32.09, 26.76.

4,5-Di[4-(*p*-neopentoxyphenyl)-1,3-butadiynyl]phthalonitrile (24)

The same procedure was used as for the synthesis of **3**, using 631 mg (1.66 mmol) of **1**, 740 mg (3.49 mmol) of **23**, 122 mg (0.174 mmol) of $Pd(PPh_3)_2Cl_2$, 33.2 mg (0.174 mmol) of CuI, and 40 mL of TEA, except that the entire reaction was carried out at room temperature. After 18 h, the solvent was removed in vacuo and then the residue was dissolved in CH_2Cl_2, washed with H_2O and brine, dried over $MgSO_4$ and filtered. The solvent was removed from the filtrate under reduced pressure and the brown residue was triturated twice with ethyl ether to leave **24** as a golden-yellow solid (683 mg, 75% yield), mp 233°C (decomp.). HR-MS (*m*/*z*) calcd. for $C_{38}H_{32}N_2O_2$: 548.2464; found: 548.2464. UV–vis (THF) λ_{max} (nm): 218, 262, 280, 294, 308, 386. IR (KBr) (cm^{-1}): 2203 (C≡N). ^1H NMR ($CDCl_3$) δ: 7.86 (s, 2H), 7.52 (d, *J* = 8.7 Hz, 4H), 6.89 (d, *J* = 8.7 Hz, 4H), 3.63 (s, 4H), 1.05 (s, 18H). ^{13}C-NMR (acetone-d_6) δ: 162.76, 138.72, 135.69, 131.19, 116.38, 116.24, 115.64, 113.14, 88.62, 85.03, 79.13, 77.41, 72.81, 32.67, 26.96. Anal. calcd. for $C_{38}H_{32}N_2O_2$: C 83.18, H 5.88, N 5.11; found: C 81.14, H 5.64, N 4.76.

Dilithium-2,3,9,10,16,17,23,24-octa[4-(*p*-neopentoxyphenyl)-1,3-butadiynyl]phthalocyanine (26)

To a vigorously stirred suspension containing 25 mg (0.046 mmol) of **24** in 0.4 mL of 1-octanol, was added 4 mg (0.58 mmol) of lithium metal (rolled to a foil in an argon purged plastic bag). The reaction mixture was heated to 80°C overnight, after which time the colour turned from bright yellow to dark green. The reaction mixture was diluted with 10 mL of hexane and then centrifuged. The supernatant liquid was discarded, the crude pigment was dissolved in anhydrous THF, reprecipitated into 5 mL of hexane and centrifuged again. This cycle was repeated four times until the octanol was removed and the supernatant liquid was colourless. The remaining crude Pc was dissolved in 2-mL of anhyd THF and loaded onto a gel permeation column consisting of SX-2 Biobeads® and anhyd THF as the eluting solvent. A single green band was collected in five, 2 mL fractions, each of which were analyzed by UV–vis spectroscopy. The fractions containing the least intense absorptions in the 200–500 nm region of the spectrum were combined and the solvent removed in vacuo to give what is believed to be **26** as a dark green solid (7 mg, 28% yield). MALDI-MS *m*/*z*: 2202 (M^+ – Li). UV–vis (THF) λ_{max} (nm): 214, 304, 408, 660, 738. ^1H NMR (pyridine-d_5, 4.53×10^{-4} M, 300 K) δ: 9.98 (br, 8H), 7.67 (d, *J* = 8.4 Hz, 16H), 6.92 (d, *J* = 8.4 Hz, 16H), 3.60 (s, 16H), 1.08 (s, 72H).

Conclusion

We have demonstrated that it is possible to prepare octaarylethynyl and octaarylbutadiynyl phthalocyanines, but that solubility and stability problems may make their use in nonlinear optics and other applications difficult. Solubilizing groups on the aryl groups *ortho* to the alkyne groups may provide the dual goal of solubilization and stabilization.

Note added in Proof

One different octaarylethynylphthalocyanine has recently been reported (see R. Faust and F. Mitzel. J. Chem. Soc. Perkin Trans. 1, 3746 (2000)).

Acknowledgement

We are grateful to the Natural Sciences and Engineering Research Council of Canada (NSERC) for financial support of this research.

References

1. (*a*). C.C. Leznoff. *In* Phthalocyanines: properties and applications. Vol. 1 *Edited by* C.C. Leznoff and A.B.P. Lever. VCH Publishers, New York. 1989. pp. 1–54; (*b*) G. De La Torre, C.G. Claessens, and T. Torres. Eur. J. Org. Chem. 2821 (2000); (*c*) N.B. McKeown, I. Chambrier, and M.J. Cook. J. Chem. Soc. Perkin Trans. 1, 1169 (1990); (*d*) C.C. Leznoff. Can. J. Chem. **78**, 167 (2000); (*e*). M. Hanack and M. Lang. Adv. Mater. (Weinheim Ger.), **6**, 819 (1994).
2. F.H. Moser and A.L. Thomas. The phthalocyanines. Vols. 1 and 2. CRC Press, Boca Raton, Florida. 1983.
3. A.W. Snow and W.R. Barger. *In* Phthalocyanines: properties and applications. Vol. 1. *Edited by* C.C. Leznoff and A.B.P. Lever. VCH Publishers, New York. 1989. pp. 341–392.
4. H.S. Nalwa and J.S. Shirk. *In* Phthalocyanines: properties and applications. Vol. 4. *Edited by* C.C. Leznoff and A.B.P. Lever. VCH Publishers, New York. 1996. pp. 79–181.
5. J.J. Dougherty. Photochem. Photobiol. **58**, 895 (1993).
6. R. Boyle and D. Dolphin. Photochem. Photobiol. **65**, 469 (1996).

© 2001 NRC Canada

7. K. Kondo, S. Yasuda, T. Sakaguchi, and M. Miya. J. Chem. Soc. Chem. Commun. 55 (1995).
8. O. Mongin, C. Papamicaël, N. Hoyler, and A. Gossauer. J. Org. Chem. **63**, 5568 (1998).
9. J.S. Lindsey. New J. Chem. **15**, 153 (1991).
10. D.S. Terekhov, K.J.M. Nolan, C.R. McArthur, and C.C. Leznoff. J. Org. Chem. **61**, 3034 (1996).
11. S.R. Marder, J.W. Perry, G. Bourhill. C.B. Gorman, B.G. Tiemann, and K. Mansour. Science (Washington, D.C.), **261**, 186 (1993).
12. C. Bosshard, R. Spreiter, P. Günter, R.R. Tykwinski, M. Schreiber, and F. Diederich. Adv. Mater. (Weinheim Ger.), **8**, 231 (1996).
13. C.C. Leznoff, S.M. Marcuccio, S. Greenberg, A.B.P. Lever, and K.B. Tomer. Can. J. Chem. **63**, 623 (1985).
14. A.B.P. Lever. Adv. Inorg. Radiochem. **7**, 28 (1965).
15. B. Suchozak. M.Sc. Thesis, York University, 2000.
16. J.A. John and J.M. Tour. Tetrahedron, **53**, 15 515 (1997).
17. D.D. Roberts and R.C. Snyder, Jr. J. Org. Chem. **45**, 4052 (1980).
18. S. Winstein, B.K. Morse, E. Grunwald, K.C. Schreiber, and J. Corse. J. Am. Chem. Soc. **74**, 1113, (1952).

© 2001 NRC Canada

Fluorous biphasic catalysis. 2. Synthesis of fluoroponytailed amine ligands along with fluoroponytailed carboxylate synthons, $[M(C_8F_{17}(CH_2)_2CO_2)_2]$ (M = Mn^{2+} or Co^{2+}): Demonstration of a perfluoroheptane soluble precatalyst for alkane and alkene functionalization in the presence of *tert*-butyl hydroperoxide and oxygen gas

Jean-Marc Vincent, Alain Rabion, Vittal K. Yachandra, and Richard H. Fish

Abstract: Fluorous biphasic catalysis (FBC) is a relatively new concept for homogeneous catalysis where the fluorocarbon soluble catalyst resides in a separate phase from the substrate and products. Therefore, separation of the catalyst and the products occurs by a facile decantation process. In this contribution, we present the synthesis of new R_f-fluoroponytailed synthons, 2-iodo-1-perfluorooctyl-3-propanol (**1**), 3-perfluorooctyl-1-propanol (**2**), and 3-perfluorooctyl-1-iodopropane (**3**), a variety of new R_f-fluoroponytailed ligands (**4**–**8**), with starting amines, 1,4,7-triazacyclononane, bis-picolylamine, and bis-picolylaminoethylenediamine, as well as new R_fMn^{2+} and R_fCo^{2+} fluoroponytailed carboxylate synthons, $[Mn(O_2C(CH_2)_2C_8F_{17})_2]$ (**9**), and $[Co(O_2C(CH_2)_2C_8F_{17})_2]$ (**10**), where R_f is C_8F_{17}. The only totally perfluoralkane soluble ligand we found was 1,4,7-tris-*N*-(4,4,5,5,6,6,7,7,8,8,9,9,10,10,11,11,11-heptadecafluoroundecyl)-1,4,7-triazacyclononane (R_fTACN, **4**), and it was utilized, along with synthons **9** and **10**, to generate in situ R_fMn^{2+}–R_fTACN and R_fCo^{2+}–R_fTACN complexes as precatalysts for functionalization of alkanes and alkenes. We will demonstrate that indeed this novel FBC approach for the separation of the precatalyst from the substrates and (or) products is viable for oxidation of alkanes and alkenes in the presence of the necessary oxidants, *tert*-butyl hydroperoxide (TBHP), and O_2 gas. We will also show that these oxidation reactions occur via an autoxidation mechanism under our FBC conditions, while using electron spin resonance (ESR) techniques to ascertain the redox chemistry occurring with the starting mononuclear R_fMn^{2+}–R_fTACN complex.

Key words: fluorous solvents, biphasic catalysis, alkane/alkene oxidation.

Résumé : La catalyse biphasique en milieu fluoré est un concept récent de catalyse homogène nécessitant l'emploi de catalyseurs solubles dans les perfluorocarbures. Le catalyseur se trouvant dans une phase différente du substrat et des produits de réaction, il peut être recyclé par une simple décantation. Nous présentons la synthèse de nouveaux synthons (**1**–**3**), et ligands (**4**–**8**), à chaîne perfluorée, ainsi que de nouveaux complexes métalliques à ligands carboxylates fluorés, $[Mn(O_2C(CH_2)_2C_8F_{17})_2]$ (**9**) et $[Co(O_2C(CH_2)_2C_8F_{17})_2]$ (**10**). Le ligand 1,4,7-tris-*N*-(4,4,5,5,6,6,7,7,8,8,9,9,10,10,11,11,11-heptadecafluoroundecyl)-1,4,7-triazacyclononane (R_fTACN, **4**) est le seul ligand à être soluble dans les perfluorocarbures. A partir des composé **9** et **10** et du ligand **4**, les complexes R_fMn^{2+}–TACN et Co^{2+}–TACN générés in situ servent de précatalyseurs pour les oxydations d'alcanes et alcènes. Les réactions sont réalisées en milieu biphasique en présence des oxydants TBHP et O_2 et les produits sont facilement séparés du catalyseur par simple décantation. Dans les

Received September 1, 2000. Published on the NRC Research Press Web site at http://canjchem.nrc.ca on July 5, 2001.

The senior author, RHF, wishes to dedicate this fluorous biphasic catalysis contribution to Brian James, a long-time friend and colleague, whose homogeneous catalysis studies/textbook have been an inspiration to several generations of chemists interested in this fascinating discipline.

J.-M. Vincent,[1] A. Rabion,[2] V.K. Yachandra, and R.H. Fish.[3] Lawrence Berkeley National Laboratory, University of California, Berkeley, CA 94720, U.S.A.

[1]Present address: Laboratoire de Chimie Organique et Organométallique, UMR CNRS 5802, Université Bordeaux 1, 351 Cours de la Libération, 33405 Talence CEDEX, France.
[2]Present address: Groupement de recherche de Lacq, BP 34, 64170 Artix, France.
[3]Corresponding author (fax: (510) 486-7303; e-mail: rhfish@lbl.gov).

 DOI: 10.1139/cjc-79-5/6-888 © 2001 NRC Canada

conditions utilisées les réactions se déroulent suivant un mécanisme radicalaire d'autoxydation.

Mots clés : solvants fluorés, catalyse biphasique, oxydation alcane/alcène.

[Traduit par la Rédaction]

Introduction

Recently, Horváth and Rábai (1) published an important paper on a new homogeneous catalysis concept, *fluorous biphasic catalysis* (FBC), that entailed the use of a fluorocarbon as one phase containing a modified fluoroponytailed catalyst, while the substrate and the product were soluble in a second hydrocarbon phase; this FBC concept was also reported in a Ph.D thesis that was not readily accessible by the catalysis community (2). More importantly, the Horváth and Rábai paper has been a virtual catalyst for chemists interested in new biphasic concepts, while this novel FBC approach has led to many contributions in a very short time frame (3). The process of developing a new paradigm for the separation of the homogeneous catalyst from the substrate and the product must start with the solvent system. Therefore, it is well-known that perfluorohydrocarbons have unusual properties that entail being extremely hydrophobic and lacking hydrogen bonding capabilities, which renders them to be relatively insoluble in their hydrocarbon analogs, and they are also able to dissolve various gases such as oxygen, hydrogen, and carbon dioxide, as examples (4). Thus, it is surprising that it took so long for this FBC approach to be discovered, since the above mentioned parameters would allow a number of critical catalytic reactions to be demonstrated using perfluorohydrocarbons as one phase in a biphasic solvent mode (1–3).

We have been interested in homogeneous oxidation catalysis for many years with the focus on functionalizing alkanes and alkenes at ambient temperatures (5). Our fascination with the FBC process provided an opportunity to also demonstrate this novel concept for the functionalization of alkanes and alkenes, and in a preliminary account (6), we did indeed verify this new biphasic approach for alkane and alkene functionalization, and in fact, a similar approach was also published by Pozzi et al. (7) very soon after. Therefore, in this full account, we present the synthesis of R_f-fluoroponytailed synthons (**1**–**3**), a variety of new R_f-fluoroponytailed ligands (**4**–**8**), with starting amines, 1,4,7-triazacyclononane (TACN), bis-picolylamine (BPA), and bis-picolylaminoethylenediamine (BisPICEN), as well as new R_fMn^{2+} and R_fCo^{2+} fluoroponytailed carboxylate synthons, $[Mn(O_2C(CH_2)_2C_8F_{17})_2]$ (**9**), and $[Co(O_2C(CH_2)_2C_8F_{17})_2]$ (**10**), where R_f is C_8F_{17}, and clearly demonstrate the critical need to pay close attention to the structures of the ponytailed ligands as it pertains to their solubility in perfluorocarbons.

To reiterate, we will further demonstrate the utilization of the FBC paradigm with the functionalization of alkanes and (or) alkenes, using in situ generated R_fMn^{2+}–R_fTACN and R_fCo^{2+}–R_fTACN as precatalysts that are totally soluble in the fluorous phase, and in the presence of the necessary oxidants, *tert*-butyl hydroperoxide (TBHP) and O_2 gas (6). In comparison to the new FBC concept presented in this paper, it is important to note that the oxidation of alkanes with TBHP in acetonitrile, and epoxidation of alkenes with hydrogen peroxide (H_2O_2) in acetone, were previously achieved in one homogeneous phase by the in situ preparation of Mn^{2+} catalysts, using 2,2′-bipyridine and tris-*N*-methyl-TACN ligands, respectively, and further state that separation of the Mn^{2+} catalyst from the product will be relatively difficult or impossible (8).

Results and discussion

Synthesis of fluoroponytailed ligands 4–8

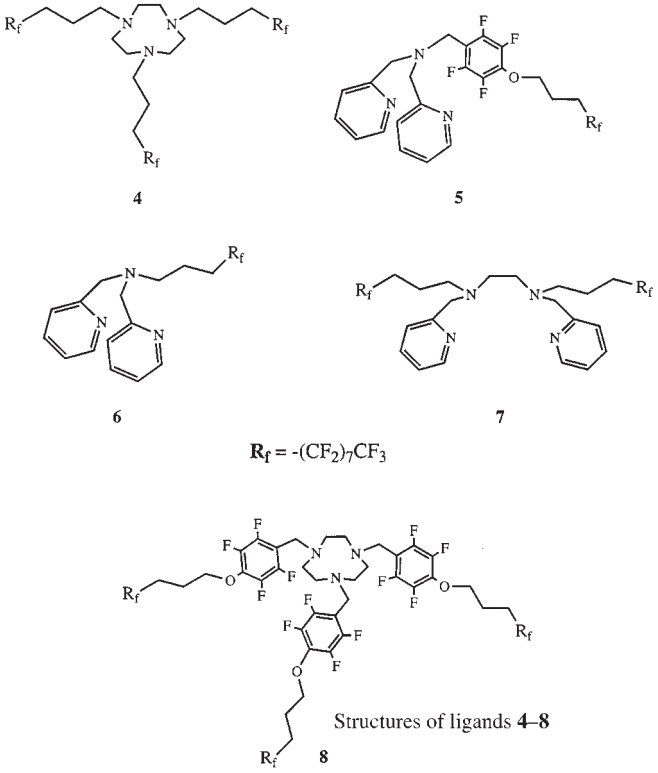
One of the key components of the FBC approach includes the synthesis of fluoroponytailed ligands that are totally soluble in fluorocarbon solvents at ambient temperature. Therefore, we set out initially to create a fluoroponytail synthon that we could append to our target ligands, which were aliphatic and aromatic substituted aliphatic amines. We chose aliphatic amines as ligands for several reasons that included their ease in appending fluoropontytails via alkylation reactions, and their metal complexes have been widely used in previous homogeneous oxidation chemistry of hydrocarbons (8). In our initial experiments to find a suitable fluoroponytailed synthon, we evaluated a compound that had a two-carbon spacer ($C_8F_{17}CH_2CH_2I$) but quickly found that in the presence of the aliphatic amine ligand that loss of HI prevailed rather than alkylation. Therefore, it is important to recognize that the three-methylene-carbon spacer in compound **3** was necessary, not only to insulate the amine from the powerful e-withdrawing effect of the perfluoroalkyl group, but also to avoid the above mentioned facile elimination reaction of HI that predominately occurs when a two-carbon spacer was used during the formation of ligands **4**–**8**.

The first step to the three-carbon spacer synthon, perfluoroalkyl iodide (**3**) proceeded by a free radical addition of a perfluoroalkyl iodide ($C_8F_{17}I$) to allyl alcohol that was initiated with AIBN to provide the perfluoroalkylated iodohydrin **1** (this procedure was slightly different than the one described by Kotora et al., who synthesized 3-perfluorohexyl-1-propanol ($C_6F_{13}(CH_2)_3OH$) using copper powder as a free radical initiator in neat solution followed by tin hydride reduction. See ref. 9). Compound **1** was then reduced to the perfluoroalkyl alcohol **2**, by using tributyltin hydride in dry benzotrifluoride. Iodination of **2** to form **3** was achieved using 85% phosphoric acid in the presence of phosphorous pentoxide and potassium iodide in 85% yield (Scheme 1).

The first alkylation approach we utilized to introduce the fluoroponytail, **2**, was the aromatic nucleophilic substitution with the *N*-pentafluorophenyl derivatives of the TACN and BPA ligands, leading to ligands **5** and **8** (Scheme 1). We introduced **2**, via a nucleophilic substitution of the *p*-fluoro substituent of the *N*-pentafluorophenyl group by using phase transfer catalysis in a mixture of 50% NaOH–trifluorotoluene, and in the presence of the phase transfer agent, Aliquat 336. The other alkylation approach, which directly alkylates

© 2001 NRC Canada

amine ligands (TACN), (BPA), and (BisPICEN) to provide **4**, **6**, and **7** with **3**, was conducted using K_2CO_3 in DMSO.



We were totally amazed to find that **4**, tris-*N*-(4,4,5,5,6,6,7,7,8,8,9,9,10,10,11,11,11-heptadecafluoroundecyl)-1,4,7-triazacyclononane (R_fTACN), *was the only fluoroponytailed ligand found to be soluble in perfluorocarbons, such as perfluoroheptane (PFH) or perfluoromethylcyclohexane (PFMC), at room temperature.* Fluoroponytailed ligands **5**–**8**, with a fluorine content for **5**–**8** of <60% were only soluble in hot perfluorocarbons (~50°C), while **4** had a fluorine content of 64.2%. These results vividly demonstrate that polar groups such as a pentafluorophenyl group or a nonfluorinated pyridine have to be avoided to obtain good solublity in perfluorocarbons; these are extremely nonpolar solvents. It also shows that the solubilzation of ligands, and moreover, the subsequent metal complexes, could represent an important limiting step in the FBC approach for oxidation chemistry. Moreover, it is of interest to also note that **4** represented at that time, to our knowledge, the first example of an R_f–amine ligand (6) to be found to be soluble in a perfluorocarbon solvent, subsequently also verified by Pozzi et al. (7) with their tetra-azamacrocycle systems.

Synthesis of Mn^{2+} and Co^{2+} fluoroponytailed carboxylate complexes 9 and 10

To insure fluorcarbon solvent solubility of the metal complexes of ligand **4**, the only amine ligand we found to have total fluorocarbon solubility at ambient temperature, we thought that appending fluoroponytailed groups to the metal complexes we were going to utilize as synthons would help in this important aspect, since metal complexes with multiple charges and counter anions, such as ClO_4^-, NO_3^-, PF_6^-, would be very difficult to solubilze in perfluorocarbons. Therefore, the new R_fMn^{2+} and R_fCo^{2+} complexes $[Mn(C_8F_{17}(CH_2)_2CO_2)_2]$ (**9**) and $[Co(C_8F_{17}(CH_2)_2CO_2)_2]$ (**10**) were synthesized by reaction of $Mn(ClO_4)_2\cdot 6H_2O$ or $Co(ClO_4)_2\cdot 6H_2O$ in acetone with 2 equiv of the triethylammonium salt of the 3-R_f-alkylpropionic acid $C_8F_{17}(CH_2)_2CO_2H$; elemental analysis of **9** and **10** provided a metal:carboxylate ligand ratio of 1:2, while **9** was found to be slightly soluble in perfluorocarbons, exhibited an intense and broad ESR signal at $g = 2$ (9 K), and displayed the broad six-line hyperfine structure ($J = 90$ G). This could be attributed either to an oligomeric Mn^{2+} structure, consistent with a $Mn(OAc)_2$ trimeric structure, or a mononuclear Mn^{2+} complex of low solubility in perfluorocarbons at 9K (10). In addition, it appears that the carboxylate group is chelating, rather than being in a monodentate coordination mode, in agreement with the small difference ($\Delta\nu = 132$ cm^{-1}) observed in the IR spectrum of **9** between the asymmetric and symmetric C—O stretch ($\nu = 1578$ and 1446 cm^{-1}), respectively. Complex **10** had a similar IR spectrum as **9** and we suggest that the Co^{2+} analog has a similar structure as the Mn^{2+} complex.

Interestingly, when 1 equiv of **4** was added to a solution of **9** in perfluoroheptane, the complete solubilization of **9** occurred concomitantly with the appearance of a new UV absorption band at 320 nm tentatively suggesting that a new $[R_fMn(R_fTACN)]^{2+}$ complex (**11**) was formed in situ. A similar result was also achieved when ligand **4** and complex **10** were added together to provide $[R_fCo(R_fTACN)]^{2+}$ (complex **12**).

Functionalization of alkanes and alkenes utilizing in situ generated $[R_fMn(R_fTACN)]^{2+}$ and $[R_fCo(R_fTACN)]^{2+}$ (complexes 11 and 12) as precatalysts

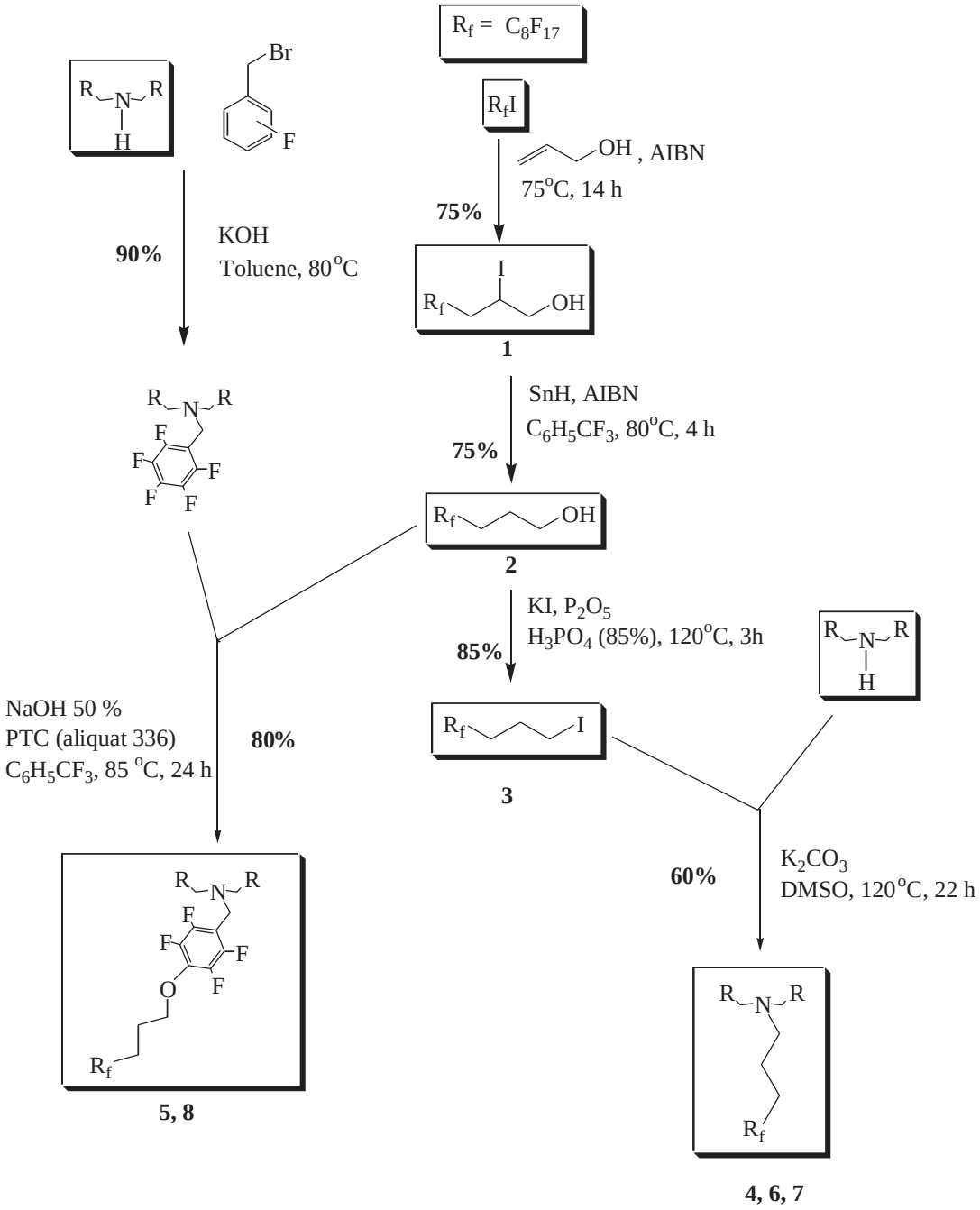
The FBC oxidation results for several substrates are presented in Table 1. All the experiments were carried out under biphasic conditions, generating complexes **11** or **12**, in situ in perfluoroheptane (Scheme 2), while the upper phase was the substrate itself. Importantly, the oxidation products were detected only in the colorless upper phase after decantation (GC), while the colored perfluoroheptane lower phase contains only traces (<5%) of product. Clearly, a facile and rapid separation of the products from the catalyst was achieved using this FBC approach.

Table 1 demonstrates that the olefin with allylic hydrogens, cyclohexene, provides the highest % yield of oxidation products (650%/TBHP in 3 h) with TBHP–O_2, while alkane oxidation was much lower as noted with cyclohexane to cyclohexanol–cyclohexanone (CyOH–CyONE, 12%/TBHP in 24 h) and toluene to benzyl alcohol–benzaldehyde ($PhCH_2OH$–PhCHO, 65%/TBHP in 24 h). In the presence of **11**, TBHP, and O_2 (1 atm (1 atm = 101.325 kPa)), and under vigorous stirring, cyclohexene was converted to a product ratio of 2-cyclohexen-1-one (CyenONE, ~65%), 2-cyclohexen-1-ol (CyenOH, ~35%), and a small amount of cyclohexene oxide (<2%), while with complex **12** similar oxidation results were obtained.

It is also important to note that styrene, with no allylic hydrogens, was not converted to styrene epoxide under these biphasic conditions. *In the absence of O_2 or TBHP, only negligible amounts of CyenOH and CyenONE were detected,*

© 2001 NRC Canada

Scheme 1. Preparation of fluoroponytailed synthon **3** and alkylation to provide ligands **4**–**8**.



indicative of an autoxidation reaction, i.e., both were necessary for oxidation to proceed. At the end of the reaction, the upper phase was removed and new aliquots of cyclohexene and TBHP were added to provide a 400% yield after 5 h, showing that the catalyst, after decantation, was only present in the lower fluorocarbon phase.

Autoxidation mechanism and fate of the Mn^{2+} precatalyst

The presented results are in agreement with an autoxidation mechanism involving alkoxy (RO·) or alkylperoxy (ROO·) radicals (11), where the reaction was initiated by *t*-BuO· or *t*-BuO_2· radicals produced from redox reactions (Haber–Weiss process with Mn^{2+}/Mn^{3+}). In the case of the substrate cyclohexene, the allylic radical that formed was then trapped by O_2 ($k > 1 \times 10^9$ M^{-1} s^{-1}) to provide cyclohexenylperoxy radicals, which were able (ROO-H = 90 kcal mol^{-1}) to homolytically remove a hydrogen from benzylic or allylic C—H bonds (85 kcal mol^{-1}), and hence, propagate the radical reactions. The secondary cyclohexenyl hydroperoxide that was formed then decomposes catalytically in the presence of the $R_fMn(R_fTACN)$ catalyst to give the alcohol and the ketone products (12). Scheme 3 defines the initiation, propagation, termination, and product-forming steps for the sequence of reactions (eqs. [1]–[8]).

Moreover, the lower yields observed in the case of cyclohexane are consistent with the stronger C—H bond strength

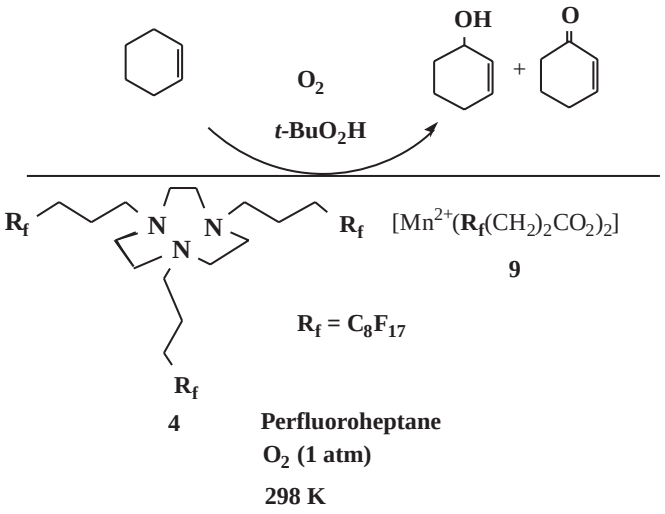
© 2001 NRC Canada

Table 1. Alkene and alkane functionalization under fluorous biphasic catalysis conditions.[a]

Precatalyst	Substrate	Oxidant	Products (μmol)	Yield (%)[b]	*t* (h)
11	Cyclohexene	TBHP–O_2	CyenOH (160) CyenONE (300)	650	3
11	Cyclohexene	TBHP	CyenOH (<2) CyenONE (<2)		7
11	Cyclohexene	O_2	CyenOH (<1) CyenONE (<1)		24
9	Cyclohexene	TBHP–O_2	CyenOH (130) CyenONE (160)	360	12
11	Styrene	TBHP–O_2	no epoxide		24
11	Toluene	TBHP–O_2	PhCHO (15) PhCH2OH (30)	65	24
11	Cyclohexane	TBHP–O_2	CyOH (5) CyONE (3.5)	12	24
12	Cyclohexene	TBHP–O_2	CyenOH (185) CyenONE (360)	750	20
12	Cyclohexane	TBHP–O_2	CyOH (7) CyONE (5.5)	17	24

[a]Conditions: [$M(R_f(CH_2)_2CO_2)_2$] (3.5 μmol), Mn or Co, and the R_fTACN ligand (3.5 μmol) were dissolved in hot perfluoroheptane (3 mL) and then the substrate (2 mL) was added. The reaction starts after the addition of TBHP (90%, 72 μmol) under an O_2 atmosphere at ambient termperature.
[b]Total yield was based on TBHP added.

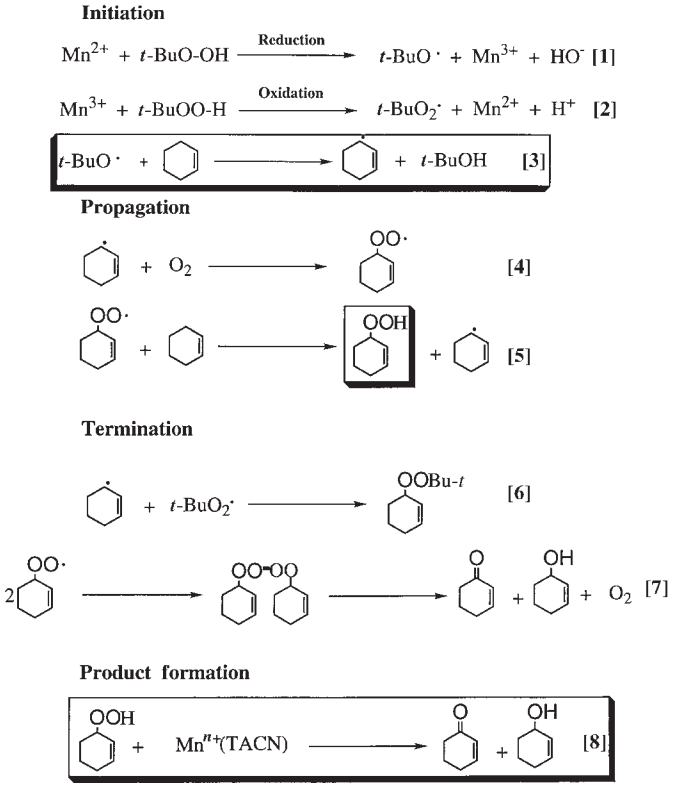
Scheme 2. Fluorous biphasic oxidation catalysis with cyclohexene as the substrate and complex **11** formed in situ from **4** and **9**.



(95 kcal mol^{-1}) (11), which implicates the cyclohexylperoxy radical, and thus causes a lowering of the rate of the propagation step. The chain termination step presumably comes mainly from the coupling of two cyclohexenylperoxy radicals to give alcohol, ketone, and O_2 (Russell-type mechanism (Scheme 3, eq. [7])) (11).

We found that the [R_fMn(R_fTACN)] complex, formed during the oxidation of **11**, was plausibly a $R_fMn^{3+}Mn^{4+}$ dimer. Therefore, when TBHP was added to the reaction mixture, the solution turns brown, and exhibits intense UV–vis absorptions (ε per atom is ~9000 and 1130 M^{-1} cm^{-1} at 300 and 500 nm, respectively, after 1 h) characteristic of dinuclear $Mn^{3+}Mn^{3+}$, $Mn^{3+}Mn^{4+}$, or $Mn^{4+}Mn^{4+}$ complexes (13). The occurrence of such a putative $R_fMn^{3+}Mn^{4+}$ dimer from starting complex **11** (Fig. 1, top spectrum), under oxidation conditions, was unambiguously confirmed by ESR studies at 9 K. Thus, a strong, distinctive 16-line signal of an antiferromagnetically coupled $R_fMn^{3+}Mn^{4+}$ dimer complex at $g = 2$ was observed in the perfluoroheptane phase, after 1 h of reaction in the presence of TBHP–O_2 and cyclohexene (Fig. 1, middle spectrum). Indeed, it has recently been shown that the decomposition of TBHP in the presence of a dinuclear

Scheme 3. Initiation, propagation, termination, and product forming steps with cyclohexene as substrate.

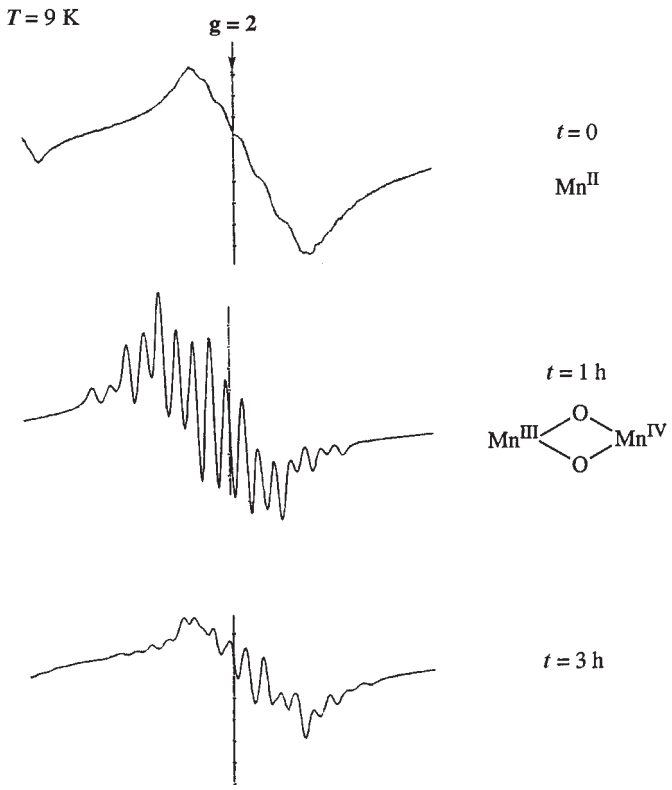


Mn_2^{3+}(2-OHsalpn)$_2$ complex resulted in the formation of *t*-BuO· radicals and a dinuclear $Mn^{3+}(\mu\text{-}O)_2Mn^{4+}$ complex (14).

Furthermore, rxn. [1] (Scheme 3) was favored over rxn. [2] with complex **11** for two important reasons: (*i*) it has been previously shown that in nonpolar solvents, eq. [2] was found to be very slow (15); and (*ii*) the $R_fMn^{3+}Mn^{4+}$ dimeric species formed upon the addtition of TBHP to complex **11** was not very efficient in the oxidation of TBHP. Interestingly, after 3 h (Fig. 1, lower spectrum), the 16-line ESR signal had almost disappeared, suggesting that this $R_fMn^{3+}Mn^{4+}$ dinuclear mixed valent species might be involved in the catalytic decomposition of the cyclohexenyl hydroperoxide intermediate to provide the alcohol and ketone products.

© 2001 NRC Canada

Fig. 1. ESR experiments at 20 K and 9 K (see *Experimental* for details). Top spectrum: $[R_fMn(R_fTACN)]^{2+}$ complex (**11**) at 20 K in benzotrifluoride; middle: after addition of TBHP–O_2 and cyclohexene (9 K); lower: after 3 h of reaction (9 K).



Conclusions

Finally, as we have clearly shown in this contribution, as well as being pointed out recently by Pozzi et al. (16), despite the apparent simplicity of the FBC concept, the concrete demonstration of this strategy is still a difficult challenge, since the solubilization of the fluoroponytailed metal complexes used in perfluorocarbons is one limiting step along with catalyst stability and the favorable recycling of the catalyst system. Thus, we were able to successfully solubilize complexes **11** and **12** in perfluoroheptane, using both the new R_fTACN ligand **4**, and the new R_fMn^{2+} and R_fCo^{2+} complexes **9** and **10**, with fluoroponytailed carboxylate ligands. Moreover, we have been able to perform alkane and alkene oxidations under FBC conditions in the presence of TBHP and O_2 as oxidants, and hence, separate the products from the catalyst by a simple decantation process. The oxidation process occurs via an autoxidation mechanism, with formation of alkenyl or alkyl hydroperoxides as the key intermediates, which then are catalytically decomposed by the R_fMn– or R_fCo–R_fTACN catalyst, probably at the solvent interface, to provide the alcohol and ketone products. Future studies will attempt to further the scope of the FBC approach to oxidation chemistry.

Experimental

Materials and instrumentation

The fluorocarbon solvents and some starting perfluoro derivatives were purchased from Pierce Chemical Co., while the alkenes and alkanes were from Aldrich Chemical Co. The oxidant, *tert*-butyl hydroperoxide (70% TBHP) was a commercial product from Aldrich Chemical Co., and all were used without further purification. The ^{1}H NMR spectra were obtained on a 500 MHz Brucker NMR spectrometer, while GC and GC–MS analysis were performed on Hewlett–Packard (HP) instruments. The UV–vis spectra were recorded on an HP diode array instrument with accompanying software. The ESR experiments were performed at the Calvin Laboratory at LBNL and the following describes the equipment used. EPR spectra were collected on a Varian E-109 spectrometer with an E-102 microwave bridge. The EPR spectra were collected using a home built signal averager and stored for further analysis on a VAX 4000-300. Samples were maintained at cryogenic temperatures using an Air Products Heli-tran liquid helium cryostat. For detecting the Mn^{2+} complex the conditions were as follows: 3300 ± 1000 G scan range, 10 mW microwave power, 20 K temperature, 32 G modulation amplitude, 100 kHz modulation frequency, 2 min/scan, 0.25 s time constant. Spectrometer conditions were as follows for detecting the 16 line spectrum from the coupled binuclear Mn^{3+}/Mn^{4+} complex: 2800 ± 500 G scan range, 30 mW microwave power, 9 K temperature, 32 G modulation amplitude, 100 kHz modulation frequency, 0.25 s time constant, 9.26 GHz microwave frequency. The amplitudes were calculated from the low-field and high-field peak-to-trough amplitudes for each designated peak.

2-Iodo-1-perfluorooctyl-3-propanol (1)

The R_fI ($R_f = C_8F_{17}$, 7 g, 12.8 mmol), allyl alcohol (1 mL, 14.7 mmol), and AIBN (84 mg, 0.51 mmol) were heated at 70–75°C under an inert atmosphere for 14 h. Every 2 h, a new portion of AIBN was added to the reaction mixture. The pale yellow solid obtained was recrystallized in refluxing hexane (40 mL). Compound **1** was obtained in 75% yield, mp 93–94°C. EI-MS: [M+] 604. ^{1}H NMR (400 MHz, $CDCl_3$, 25°C) δ: 4.45 (m, 1H, -C*H*I-), 3.79 (m, 2H, -C*H*$_2$-OH), 2.9 (2m, 2H, R_f-C*H*$_2$), 2.04 (t, -O*H*). Elemental anal. calcd. for $C_{11}H_6F_{17}IO$: C 21.87, H 1.00; found: C 22.06, H 0.97.

3-Perfluorooctyl-1-propanol (2)

Compound **1**, $R_fCH_2CHICH_2OH$ (8 g, 13.2 mmol), and AIBN (52 mg, 0.31 mmol) were partially dissolved in dry trifluorotoluene (40 mL). The tributyltin hydride (4.2 mL, 15.8 mmol) was then added dropwise and the reaction mixture was heated at 80°C under an inert atmosphere for 4 h (reaction followed by GC). After removing the solvent under vacuum, the resulting residue was dissolved in a perfluoroheptane–toluene mixture. After decantation, the lower phase was separated from the upper one, which mainly contains $(Bu)_3SnI$. By removing the perfluoroheptane, compound **2** was isolated as a white powder in 75% yield. Compound **2** can be recrystallized from hexane. EI-MS: [M+] 477. ^{1}H NMR (400 MHz, $CDCl_3$, 25°C) δ: 3.75 (m, 2H, -CH_2-OH), 2.20 (m, 2H, Rf-CH_2-), 1.88 (m, 2H, -CH_2-

© 2001 NRC Canada

CH_2-CH_2-), 1.57 (s, -OH). Elemental anal. calcd. for $C_{11}H_7F_{17}O$: C 27.63, H 1.46; found: C 27.72, H 1.63.

3-Perfluorooctyl-1-iodopropane (3)

The phosphorous pentaoxide (3.4 g) was added to phosphoric acid (85%, 7.1 mL) in a 50 mL round-bottom flask and then the mixture was cooled to 0°C. The KI (1.39 g, 8.2 mmol) was first added, followed immediately by $R_fCH_2CH_2CH_2OH$ (1.5 g, 3.1 mmol). The mixture was heated at 120°C for 3.5 h. At ambient temperature, 10 mL of water was added, and the resulting brown solution was extracted four times with 25 mL of diethyl ether. The organic layer was washed twice with 25 mL thiosulfate (0.1 M), then dried over Na_2SO_4. After removing the solvent, the iodo derivative was obtained as an oil, which solidified at 4°C. Compound **3** was used without further purification (yield 85%); however, **3** can be recrystallized from methanol. EI-MS: [M+] 588. ^{1}H NMR (400 MHz, $CDCl_3$, 25°C) δ: 3.26 (t, 2H, I-C*H*$_2$-), 2.16 (2m, 4H, -C*H*$_2$-C*H*$_2$-R_f). Elemental anal. calcd. for $C_{11}F_{17}H_6I$: C 22.47, H 1.02; found: C. 22.80, H 1.26.

Tris-*N*-(4,4,5,5,6,6,7,7,8,8,9,9,10,10,11,11,11-heptadecafluoroundecyl)-1,4,7-triazacyclononane (4)

The TACN (88.4 mg, 0.73 mmol), K_2CO_3 (423 mg, 3.1 mmol), and $R_fCH_2CH_2CH_2I$ (1.41 g, 2.41 mmol) were dissolved in DMSO (10 mL, distilled over CaH_2) and heated at 90°C for 24 h. Then perfluoroheptane (20 mL) was added to the reaction mixture and the brown fluorous lower phase was separated and then filtered. After removing the solvent, compound **4** was obtained as a brown oil. After crystallization from hot hexane, compound **4** was isolated as a yellowish powder in 50% yield. FAB-MS: [M + H$^+$] 1510. ^{1}H NMR (400 MHz, $CDCl_3$, 25°C) δ: 2.71 (s, 12H, -N-C*H*$_2$-C*H*$_2$-N), 2.55 (t, 6H, -N-C*H*$_2$-C*H*$_2$-), 2.17 (m, 6H, -CH_2-C*H*$_2$-CH_2), 1.58 (m, 6H, -CH_2-C*H*$_2$-Rf). Elemental anal. calcd. for $C_{39}H_{30}F_{51}N_3$: C 31.03, F 64.20, H 1.98, N 2.78; found: C 30.74, F 64.31, H 2.02, N 2.70.

Synthesis of the *N*-(pentafluorotoluene)-bis-picolylamine and ligand 5

This procedure for the preparation of **5** was similar to that used to prepare ligand **8**. At the end of the reaction, the toluene was removed under vacuum, and a brownish solid was obtained. This solid was triturated with pentane affording a beige powder. Ligand **5** was obtained in 85% yield and provided a satisfactory ^{1}H NMR spectrum. ^{1}H NMR (400 MHz, $CDCl_3$, 25°C) δ: 8.52 (d, 2H, aromatic H), 7.65 (t, 2H, aromatic H), 7.51 (d, 2H, aromatic H), 7.15 (m, 2H, aromatic H), 3.90 (s, 2H, -CH_2-C_6F_5), 3.85 (s, 4H, -C*H*$_2$-C_5H_4N).

Synthesis of ligand 6

BPA (59 mg, 0.296 mmol), K_2CO_3 (57 mg,), $R_fCH_2CH_2CH_2I$ (191 mg, 0.325 mmol) in DMSO (0.5 mL, distilled over CaH_2) were heated at 90°C for 16 h. The reaction mixture was filtered and the solvent removed in vacuo. Ligand **6** was purified by alumina column chromatography (CH_2Cl_2–MeOH) and was recovered as a beige oil, which solidifies at 4°C providing a yield of 60%. Ligand **6** was found to be soluble in hot, but not in cold perfluoroheptane. ^{1}H NMR (400 MHz, $CDCl_3$, 25°C) δ: 8.54 (d, 2H, pyr), 7.66 (t, 2H, pyr), 7.46 (d, 2H, pyr), 7.16 (m, 2H, pyr), 3.83 (s, 4H, -N-CH_2-pyr), 2.63 (t, 2H, -N-C*H*$_2$-CH_2-), 2.03 (m, 2H, -CH_2-C*H*$_2$-CH_2), 1.76 (m, 2H, -CH_2-C*H*$_2$-Rf). FAB-MS : [M + H$^+$] 660.

Synthesis of ligand 7

The BisPicen (50 mg, 0.206 mmol), K_2CO_3 (80 mg, 0.580 mmol), and $R_fCH_2CH_2CH_2I$ (266 mg, 0.450 mmol) were dissolved in DMSO (2.5 mL, distilled over CaH_2) and then heated at 90°C for 24 h. The solvent, benzotrifluoride, was added at room temperature to dissolve a brown oil, and then the solvent was removed under vaccum. To the sticky residue was added dichloromethane and then the solution was filtered, and the solvent removed under vaccum. The ligand (**7**) was purified first by alumina column chromatography (CH_2Cl_2–MeOH) and then by recrystallization from hexane to obtain a yellowish powder in 40% yield. ^{1}H NMR (400 MHz, $CDCl_3$, 25°C) δ: 8.54 (d, 2H, pyr), 7.66 (t, 2H, pyr), 7.46 (d, 2H, pyr), 7.16 (m, 2H, pyr), 3.83 (s, 4H, -N-CH_2-pyr), 2.63 (t, 2H, -N-C*H*$_2$-CH_2-), 2.03 (m, 2H, -CH_2-C*H*$_2$-CH_2), 1.76 (m, 2H, -CH_2-C*H*$_2$-R_f). FAB-MS: [M + H$^+$] 1163. Anal. calcd. for C_{36} H_{28} N_4 F_{34}: C 37.2, H 2.40, N 4.82; found: C 36.51, H 2.33, N 4.38.

Synthesis of tris-*N*-pentafluorophenyl-1,4,7-triazacyclononane and ligand 8

To a stirring solution of TACN (3.7 mmol) in anhydrous toluene (10 mL) in a glovebox was added powdered KOH (11 mmol) slowly, and then the resulting suspension was treated with $C_6F_5CH_2Br$ (11 mmol) dropwise. The reaction mixture was heated to 80°C and stirred at this temperature for 8 h. After being cooled to room temperature, it was then treated with an additional portion of powdered KOH and then $C_6F_5CH_2Br$. The mixture was stirred and heated to 80°C for another 8 h. After filtration, the toluene is removed under vacuum leading to a yellow solid, which gave a satisfactory NMR spectrum. Tris-*N*-pentafluorophenyl-1,4,7-triazacyclononane can be further purified by recrystallization from MeOH; mp 75°C. EI-MS: [M+] 669. ^{1}H NMR (400 MHz, $CDCl_3$, 25%C) δ: 2.70 (s, 12H, -CH_2-TACN), 3.71 (s, 6H, -CH_2-Ph). ^{13}C NMR (MHz, $CDCl_3$, 25°C) δ: 48.31, 54.69, 135.99, 138.50, 144.63, 146.62. ^{19}F NMR (MHz, $CDCl_3$–$CFCl_3$, 25°C) δ: –142.82 (2F), –156.11 (1F), –162.91 (2F). Elemental anal. calcd. for $C_{28}H_{18}F_{15}N_3$: C 48.4, F 42.5, H 2.7, N 6.3; found: C 48.3, F 42.4, H 2.8, N 6.2.

The PTC catalyst, Aliquat 336 (49 μmol), trifluorotoluene (5 mL), tris-*N*-pentafluorophenyl-1,4,7-triazacyclononane (1.49 mmol), $R_fCH_2CH_2CH_2OH$ (4.92 mmol), and NaOH 50% (5 mL) were stirred at 85°C for 22 h. After removing the solvent in vacuo, the solid was taken off with a mixture of trifluorotoluene, dichloromethane, and water. After stirring, the cloudy organic phase was isolated and the solvent stripped in vacuo. After washing the resulting orange solid with dichloromethane, compound **8** was obtained, after filtration, as a white powder (80%). Compound **8** can be further purified by alumina gel chromatography (CH_2Cl_2–MeOH, 0–2%). m p 98°C. FAB-MS: [M+H$^+$] 2044. ^{1}H NMR (400 MHz, $CDCl_3$, 25°C) δ: 4.27 (t, 6H, -O-CH_2-), 3.68 (s, 6H, N-CH_2-C_6F_4), 2.71 (s, 12H, CH_2-TACN), 3.37 (m, 6H, O-CH_2-C*H*$_2$), 2.10 (m, 6H, -CH_2-C*H*$_2$-Rf). ^{13}C NMR (MHz,

© 2001 NRC Canada

$CDCl_3$, 25°C) δ: 48.31, 54.69, 135.99, 138.50, 144.63, 146.62. ^{19}F NMR (MHz, $CDCl_3$–$CFCl_3$, 25°C) δ: –81.29 (3F), –114.92 (2F), –122.23 (2F), –122.43 (4F), –123.23 (2F), –124.00 (2F), –126.63 (2F), –144.16 (2F), –158.19 (2F). Anal. calcd. for $C_{60}H_{36}N_3F_{63}O_3$: C 35.3, H 1.8, N 2.1, F 58.6; found: C 35.6, H 1.9, N 2.1, F 59.6.

$[Mn(C_8F_{17}(CH_2)_2CO_2)_2(H_2O)_2]$ (9)

The $CF_3(CF_2)_7CH_2CH_2CO_2H$ (1.35 g, 2.80 mmol) was dissolved in acetone (15 mL) and to this solution was added triethylamine (380 mL, 2.80 mmol). This resulting solution was added dropwise to $Mn(ClO_4)_2 \cdot 6H_2O$ (500 mg, 1.37 mmol) dissolved in acetone (30 mL). The sticky precipitate which formed was vigorously stirred for 2 h. After filtration, **9** was obtained as a white powder in 75% yield. Elemental anal. calcd. for $C_{22}F_{34}H_{12}O_6Mn$: C 24.61, F 60.19, H 1.12, Mn 5.12; found: C 25.37, F 59.77, H 0.94, Mn 5.50.

$[Co(C_8F_{17}(CH_2)_2CO_2)_2(H_2O)_2]$ (10)

The same procedure, as conducted with complex **9**, was used for the synthesis of **10**, except with $Co(ClO_4)_2 \cdot 6H_2O$. A pink precipitate formed immediately, and after filtration, a pink powder was obtained in 100% yield. Elemental anal. calcd. for $C_{22}H_{12}F_{34}CoO_6$: C 24.53, H 1.11, F 59.98, Co 5.46; found: C 25.05, H 1.27, F 60.15, Co 5.35.

ESR–FBC experiment

The ESR spectrum for in situ generated **11** was conducted at 20 K in benzotrifluoride (top spectrum, Fig. 1). Using standard oxidation conditions for cyclohexene as outlined in Table 1, aliquots of the perfluoroheptane layer were removed and immediately frozen at 100 K in an ESR tube (middle and lower spectra, Fig. 1). ESR spectra were recorded at 9 K using microwave power at 10 mW, modulation amplitude 32 G, a time constant of 0.5 s, at a frequency of 9.18 GHz, and gain of 3.2×10^{-3}.

Acknowledgment

The studies at LBNL were generously supported by a gift grant (R.H.F.) and a postdoctoral fellowship to J.-M. V. from Elf Aquitaine Inc., and the Department of Energy under Contract no. DE-AC03–76SF00098. We thank Dr. István T. Horváth and Dr. Jozsef Rábai for many helpful discussions concerning our FBC program.

References

1. I. T. Horváth and J. Rábai. Science (Washington, D.C.), **266**, 72 (1994), and refs. therein.
2. M. Vogt. Ph.D Thesis. Technical University of Aachen, 1991.
3. (*a*) I.T. Horváth. Acc. Chem. Res. **31**, 641 (1998) and refs. therein; (*b*) I.T. Horváth. *In* Applied homogeneous catalysis with organometallic compounds. *Edited by* B. Cornils, W.A. Hermann). VCH, 1996. p. 601; (*c*) E. de Wolf, G. van Koten, and B.-J. Deelman. Chem. Soc. Rev. **28**, 37 (1999); (*d*) R.H. Fish. Chem. Eur. J. **5**, 1677 (1999), and refs. therein.
4. M. Hudlicky and A.E. Pavlath. Chemistry of organic compounds II. Ellis Horwood, Chichester, U.K. 1992.
5. K. Neimann, R. Neumann, A. Rabion, R.M. Buchanan, and R.H. Fish. Inorg. Chem. **38**, 3575 (1999), and refs. therein.
6. J.-M. Vincent, A. Rabion, V.K. Yachandra, and R.H. Fish. Angew. Chem. Int. Ed. Engl. **36**, 2346 (1997).
7. G. Pozzi, M. Cavazzini, S. Quici, and S. Fontana. Tetrahedron Lett. **38**, 7605 (1997).
8. (*a*) S. Ménage, M.-N. Collomb-Dunand-Sauthier, C. Lambeaux, and M. Fontecave. J. Chem. Soc. Chem. Commun. 1885 (1994); (*b*). D. De Vos and T. Bein. J. Chem. Soc. Chem. Commun. 917 (1996).
9. M. Kotora, M. Hajek, B. Ameduri, and B. Boutevin. J. Fluorine Chem. **68**, 85 (1994).
10. P. Mathur and G. Dismukes. J. Am. Chem. Soc. **105**, 7093 (1983).
11. R.A. Sheldon and J. K. Kochi. Metal-catalyzed oxidations of organic compounds. Academic Press, New York. 1981.
12. R.H. Fish, M.S. Konings, K.J. Oberhausen, R.H. Fong, W.M. Yu, G. Christou, J.B. Vincent, D.K. Coggin, and R.M. Buchanan. Inorg. Chem. **30**, 3002 (1991).
13. Y.-M. Frappart, A. Boussac, R. Albach, E. Anxolabéhère-Malhart, M. Delroisse, J.-B. Verlhac, G. Blondin, J.-J. Girerd, J. Guilhem, M. Cesario, A.W. Rutherford, and D. Lexa. J. Am. Chem. Soc. **118**, 2669 (1996).
14. M.T. Caudle, P. Riggs-Gelasco, A.K. Gelasco, J.E. Penner-Hahn, and V.L. Pecoraro. Inorg. Chem. **35**, 3577 (1996).
15. R.A. Sheldon and J.K. Kochi. Adv. Catal. **25**, 272 (1976).
16. G. Pozzi, S. Banfi, A. Manfredi, F. Montanari, and S. Quici. Tetrahedron, **52**, 36, 11 879 (1996).

© 2001 NRC Canada

Dithiophosphinates of gold (I); oxidative addition of Cl_2 to a neutral, dinuclear gold(I) dithiophosphinate complex, and X-ray crystal structures of $[AuS_2P(C_2H_5)_2]_2$, $[AuS_2PPh_2]_2$, $Au_2(CH_2)_2PMe_2(S_2PPh_2)$, and $Au_2Cl_2[(CH_2)_2PMe_2][S_2PPh_2]$

Werner E. van Zyl, José M. López-de-Luzuriaga, John P. Fackler, Jr., and Richard J. Staples

Abstract: The formation and characterization of dinuclear gold(I) dialkyl- and diaryl-dithiophosphinate complexes of the type $[AuS_2PR_2]_2$ are described. The complexes are readily prepared from the reaction between a chloro–gold(I) starting material and the corresponding dithiophosphinate salt. The structures of the complexes show both the absence (R = Et, **1**) and presence (R = Ph, **2a**) of intermolecular Au···Au interactions as confirmed by X-ray crystallographic study in the solid state. Reaction between $[AuS_2PPh_2]_2$ and $[Au(CH_2)_2PMe_2]_2$ in CH_2Cl_2 solution leads to a ligand transfer reaction to form the hetero-bridged complex $[Au_2\{(CH_2)_2PMe_2\}\{S_2PPh_2\}]$ (**3a**) in high yield. Additionally, the latter complex reacts with Cl_2 to form the oxidative addition product $[Au_2Cl_2\{(CH_2)_2PMe_2\}\{S_2PPh_2\}]$ (**4**), the first gold(II) complex with a S-P-S bridging moiety. The X-ray crystal structure of both **3a** and **4** exhibit rare boat conformations in the solid state, and **4** has a formal Au(II)—Au(II) single bond of 2.5611(5) Å. Reaction between $[AuS_2PPh_2]_2$ and dppm (dppm = $Ph_2PCH_2PPh_2$) leads to a sparsely soluble three-coordinate dinuclear gold(I) complex with the molecular formula $[Au_2\{dppm\}\{S_2PR_2\}_2]_n$ (n = 1 or ∞) (**5**).

Key words: dithiophosphinates, ylide, dithiols, gold–gold bond.

Résumé : On décrit la préparation et la caractérisation de complexes dinucléaires de dialkyl- et diaryldithiophosphinates d'or(I), du type $[AuS_2PR_2]_2$. Les complexes se forment facilement par réaction d'un produit de départ contenant du chloro-or(I) avec le sel de dithiophosphinate correspondant. Les structures des complexes montrent dans un cas l'absence (R = Et, **1**) et dans l'autre la présence (R = Ph, **2a**) d'interactions Au···Au intermoléculaires qui ont été confirmées par une étude cristallographique par diffraction des rayons X à l'état solide. La réaction entre le $[AuS_2PPh_2]_2$ et le $[Au(CH_2)_2PMe_2]_2$, en solution dans le CH_2Cl_2, donne lieu à une réaction de transfert de ligand qui conduit à la formation, avec un rendement élevé, du complexe hétéroponté $[Au_2\{(CH_2)_2PMe_2\}\{S_2PPh_2\}]$, **3a**. De plus, ce dernier complexe réagit avec le Cl_2 pour former le produit d'addition oxydante $[Au_2Cl_2\{(CH_2)_2PMe_2\}\{S_2PPh_2\}]$, **4**, le premier complexe d'or(II) comportant un pont S-P-S. Les structures de diffraction des rayons X des produits **3a** et **4** montrent toutes les deux la présence de conformations bateaux, rares à l'état solide; de plus, le produit **4** comporte aussi une liaison simple Au(II)—Au(II) de 2,5611(5)Å. La réaction du $[AuS_2PPh_2]_2$ avec le dppm (dppm = $Ph_2PCH_2PPh_2$) conduit à la formation d'un complexe d'or(I) dinucléaire, tricoordiné et à peine soluble de formule moléculaire $[Au_2\{dppm\}\{S_2PR_2\}_2]_n$ (n = 1 ou ∞), **5**.

Mots clés : dithiophosphinates, ylure, dithiols, liaison or–or.

[Traduit par la Rédaction]

Received August 16, 2000. Published on the NRC Research Press Web at http://canjchem.nrc.ca site on July 19, 2001.

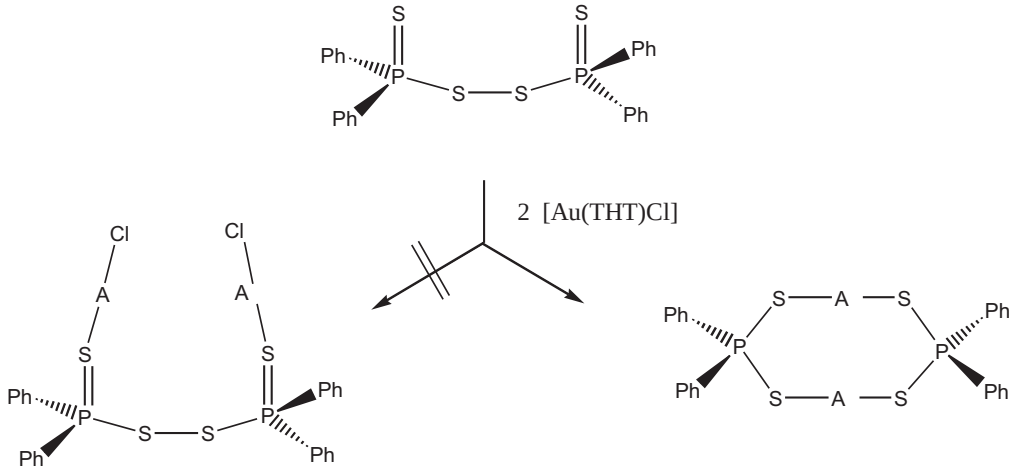
Best wishes to Professor Brian James on this occasion of his 65th birthday anniversary.

W.E. van Zyl, and J.P. Fackler, Jr.[1] Department of Chemistry and Laboratory for Molecular Structure and Bonding, Texas A&M University, P.O. Box 30012, College Station, TX 77842-3012, U.S.A.
J.M. López-de-Luzuriaga. Departamento de Química, Universidad de La Rioja, Obispo Bustamante 3, E-26001 Logroño, Spain.
R.J. Staples. Department of Chemistry and Chemical Biology, Harvard University, Cambridge, MA 02138, U.S.A.

[1]Corresponding author (telephone: (979) 845-2835; fax: (979) 845-2373; e-mail: Fackler@mail.chem.tamu.edu).

 DOI: 10.1139/cjc-79-5/6-896 © 2001 NRC Canada

Scheme 1.



Introduction

The chemistry of gold–sulfur compounds finds significant application ranging from surface science (1) to medicine (2). The use of gold(I) dithiophosphates as sensitizers in photographic films is well established (3). Recently the luminescent properties of gold(I) dithiocarbamates and related materials has been suggested for possible use as photosensors (4). The organophosphor-1,1-dithiolato class of compounds (which includes the dithiophosphinates) have found widespread use as anti-oxidant additives in the oil and petroleum industry (5), insecticide derivatives (6), and metal ore extraction reagents (7). Although the dithiophosphinic acids, $R_2P(S)SH$, have been known for more than a century (8), gold(I) complexes of these ligands have not been studied extensively. In 1968, Kuchen et al. (9) reported the first examples of gold(I) dithiophosphinate complexes. The complexes were obtained by reduction of gold(III) and required the separation of several by-products. Dinuclearity was suggested for the majority of these compounds based on osmometric molecular weight determinations in chloroform. Further research remained dormant until 1995 when Siasios and Tiekink (10) reported the structure of $[AuS_2PPh_2]_2$ as the first diaryldithiophosphinate complex of gold. The complex was obtained as a decomposition product, a non-reproducible synthesis, and the structure was determined in the wrong space group, *I*4.

The first systematic study of gold(I) dithiophosphinate complexes was reported by Schmidbaur and co-workers (11). The main focus of their study was to use dithiophosphinic acid anions $[R_2PS_2]^-$ as potential bidentate ligands to form efficient clustering centers for gold(I) cations, as exemplified by complexes such as $[Ph_2P\{SAu(PR_3)\}_2]^+$ and $Me_2P(S)SAuPR_3$.

As part of our ongoing studies of sulfur compounds of the Group 11 elements, the chemistry of the complexes of dithio-phosphorus ligands, $[AuS_2PR_2]_2$, sulfur analogs of the bis(ylide) complexes (for reviews of this chemistry see, ref. 12), is reported in this study. These materials show both the absence (R = Et) and the presence (R = Ph) of weak intermolecular Au···Au interactions in the solid state. The compound $[AuS_2PEt_2]_2$ was readily prepared from the sodium salt of the ligand, $Na[S_2PEt_2]$, and shows a solution ^1H NMR with $^3J_{P,H}$ larger than $^2J_{P,H}$. The analog $[AuS_2PPh_2]_2$ was obtained by a direct synthesis and its structure redetermined. A ligand transfer reaction with an ylide has led to a new, mixed ligand ylide–dithiophosphinate product, which like the previously studied bis(ylide), methylene-thiophosphinate and mixed ligand dithiocarbamate–bis(ylide) products (12), form stable Au(II) derivatives upon oxidation with halogens.

Results and discussion

Preparative methods

The reaction between [Au(tht)Cl] (tht= tetrahydrothiophene) and $Na[S_2PEt_2]\cdot 2H_2O$ in THF (molar ratio 1:1) leads to the cyclic dinuclear complex $[AuS_2PEt_2]_2$ (**1**). Following extraction of the product into CH_2Cl_2 solution and filtration through anhydrous $MgSO_4$ to remove water and NH_4Cl, complex **1** was isolated in >70% yield.

Different synthetic methodologies were investigated for the complex $[AuS_2PPh_2]_2$ (**2a**). Although **2a** and its analog $[AuS_2P(C_6H_4\text{-}p\text{-}Me)_2]_2$ (**2b**) were isolated in a manner similar to **1**, the yield for **2a** was only ~50% because of the product's sparse solubility in organic solvents, which hampered an efficient separation from by-products. Significantly improved yields (>75%) were obtained by extraction with water (in which **2a** remained stable) to remove NH_4Cl (from the ammonium salt of the ligand and the [Au(tht)Cl] and to obtain the product as a yellow paste, which was dried by consecutively washing with methanol and ether. A third method to prepare **2a** was discovered by accident in a reaction shown in Scheme 1. In hot benzene the disulfide $Ph_2P(S)S\text{-}SP(S)Ph_2$ was reduced by cleavage of the S–S bond, in the presence of [(tht)Au(I)Cl], to form the dinuclear complex **2a** in ~30% isolable yield. Organic by-products were not identified. Unlike the low thermal stability of the acid $Ph_2P(S)SH$, which decomposes through rapid elimination of hydrogen sulfide (11), the gold complex **2a** appears to have remarkable thermal stability. It was recovered nearly quantitatively from a boiling benzene solution exposed to air for 3 days.

© 2001 NRC Canada

Fig. 1. Drawings of two reasonable structures for the complex $[Au_2\{dppm\}\{S_2PPh_2\}_2]_n$ where $n = 1$ (top) or $n = \infty$ (bottom) following the reaction between **2a** and dppm.

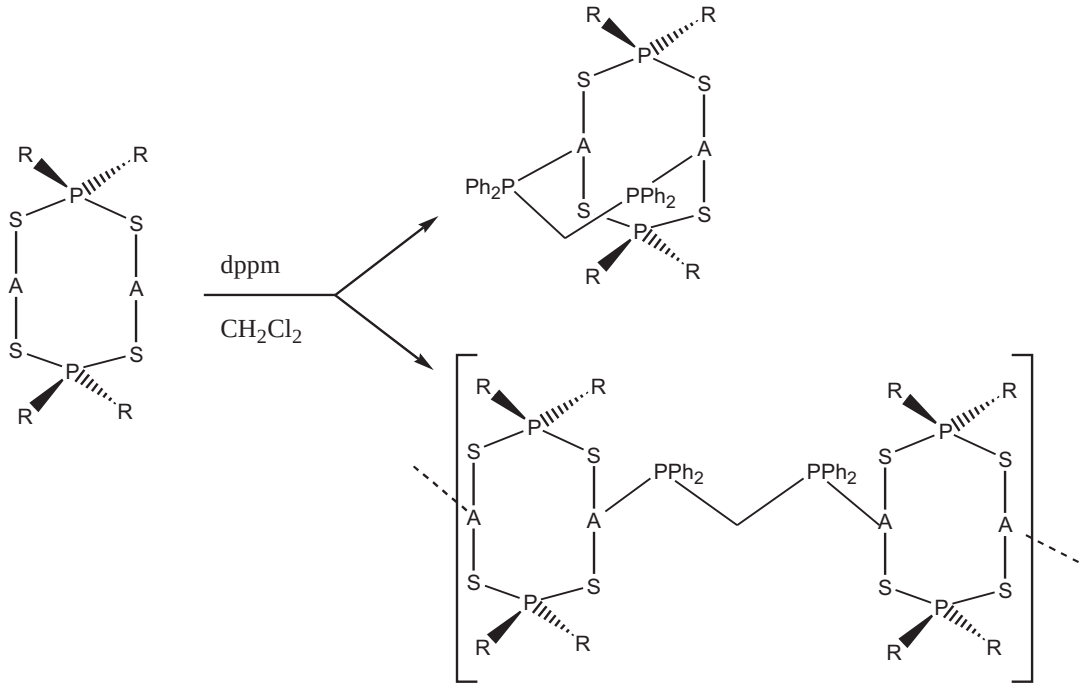
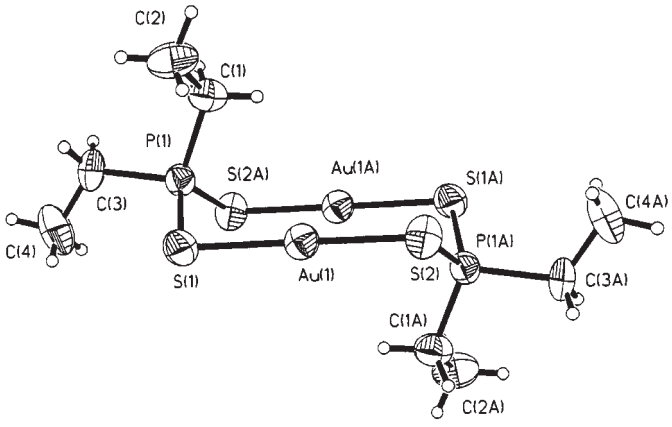


Fig. 2. View of the molecular structure (50% thermal ellipsoids) of complex **1** showing the atomic labeling scheme. Selected bond lengths (Å) and angles (°): Au(1)···Au(1A) 3.1822(13), Au(1)—S(1) 2.309(4), Au(1)—S(2) 2.310(4), S(1)—P(1) 2.035(5), P(1)—C(1) 1.780(14) Å; S(1)-Au(1)-S(2) 173.87(13), S(2)-Au(1)-Au(1A) 93.19(10), P(1)-S(1)-Au(1) 100.4(2), S(2A)-P(1)-S(1) 115.0(2)°.



Complexes **3a** and **3b** were formed in good yield (~80%) from the reaction between $[AuS_2PPh_2]$ (**2a**) and $[AuS_2PEt_2]$ (**1**), respectively, with $[Au(CH_2)_2PMe_2]_2$ (molar ratio 1:1) in a CH_2Cl_2 solution. The reaction was complete after 20 min. Complexes **3a** and **3b** are the first reported dinuclear gold(I) complexes with heterobridged phosphor-1,1-dithiolato moieties and bis(ylide) bridging ligands and show some unique structural features (vide infra). Laguna and co-workers (13) previously reported heterobridged complexes with dithiocarbamate $S_2CN(CH_2Ph)_2^-$, and xanthate S_2COR^-, along with bis(ylide) ligands bridging the two gold(I) centers.

Formation of the oxidative addition product $[Au_2Cl_2\{(CH_2)_2PMe_2\}\{S_2PPh_2\}]$ (**4**) was accomplished with Cl_2 in a CH_2Cl_2 solution. Upon Cl_2 addition the solution immediately turns from colorless to orange. Interestingly, following work-up and isolation of **4**, this solid product slowly releases chlorine gas at 140–160°C. The material gradually changes color from orange to colorless without additional decomposition. The compound melts at ~205°C, which is in the same range as the expected reductive elimination product **3a**. The elimination of chlorine gas was determined in a separate experiment wherein a saturated starch – NaI solution on filter paper was placed above ~100 mg of **4** that was heated. The chlorine released caused the filter paper to turn purple as expected for iodine formation. This apparently reversible reductive elimination appears related to the reversible CH_3Br addition–elimination observed with $[Au(CH_2)_2PPh_2]_2$ (12), but has not been observed previously with halogens.

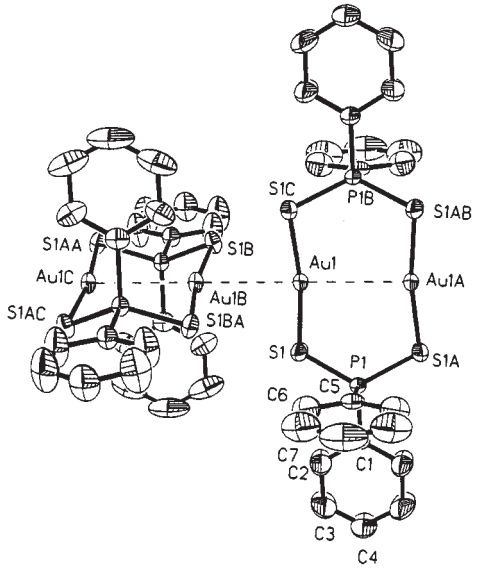
The gold(I) complex $[Au_2\{dppm\}\{S_2PPh_2\}_2]_n$ ($n = 1$ or ∞) (**5**) is formed from the reaction between **2a** and dppm (dppm = $Ph_2PCH_2PPh_2$) in CH_2Cl_2 in good yield. The complex is sparingly soluble in organic solvents, a result which hinders detailed spectroscopic investigation. However, based on limited ^1H NMR data and elemental analysis, two three-coordinate gold(I) structures are consistent with the available data. They are sketched in Fig. 1. Of these compounds, precedence exists for the molecular adduct with cationic complexes of dinuclear gold(I) dithiocarbamates, $[Au_2(\mu\text{-}S_2CNEt_2)\{\mu\text{-}PPh_2)_2C{=}CH_2\}_2]^+$, prepared and structurally established by X-ray crystallography (14). The limited solubility of **5** precluded $^{31}P\{^1H\}$ NMR studies.

Solution ^1H and ^{31}P NMR studies

All the complexes reported were studied in solution by ^1H and $^{31}P\{^1H\}$ NMR spectroscopy, except **5**. In several cases

© 2001 NRC Canada

Fig. 3. View of the molecular structure (50% thermal ellipsoids) of two adjacent units of the chain of complex **2a** showing the atom labeling scheme (determination 1). Atoms are shown as thermal ellipsoid plots at the 50% probability level. Selected bond lengths (Å) and angles (°): Au(1)—Au(1B) 2.9610(3), Au(1)—Au(1A) 3.0859(3), Au(1)—S(1) 2.3112(10), S(1)—P(1) 2.0265(11), P(1)—C(5) 1.817(6) Å; S(1C)-Au(1)-S(1) 171.29(4), P(1)-S(1)-Au(1) 100.84(5), C(1)-P(1)-C(5) 105.1(2), S(1)-P(1)-S(1A) 116.00(8)°.



interesting and somewhat unexpected NMR results were obtained. Due to the symmetry of **1**, the solution NMR spectrum is simple and consistent with the X-ray structure. Both CH_2 and CH_3 protons couple to the ^{31}P nuclei (I = 1/2) giving a doublet of quartets and a doublet of triplets, respectively. The $^3J_{P,H}$ coupling constant (21.78 Hz) is *larger* than the $^2J_{P,H}$ coupling constant (10.98 Hz). This phenomenon is not uncommon in ethyl derivatives of four-coordinate P(V) compounds, which often show a similar behavior (15) with the extent of the three bond coupling depending primarily on the P-C-C-H dihedral angle (16). The same observation was made for the heterobridged complex **3b**. The ethyl groups show coupling constants of $^3J_{P,H}$ = 21.3 Hz and $^2J_{P,H}$ = 7.8 Hz for the CH_3 and CH_2 groups, respectively.

The homoleptic complexes **1**, **2a**, and **2b** each show only a singlet in the $^{31}P\{^1H\}$ NMR resonating at δ 82.5, 67.4, and 66.6 ppm respectively. The heterobridged complexes **3a** and **3b** show a doublet, a $^4J_{P,P}$ coupling (8–11 Hz at 300 MHz) for each ^{31}P nuclei. This coupling was not observed for the oxidative addition product **4** wherein each ^{31}P appears as a single resonance. In complex **4** the chemical shift is down field with respect to the unoxidized precursor complex **3a**.

Structural studies

The dinuclear gold(I) structures reported in the present study are all neutral eight-membered ring metallocycles in an elongated chair or boat conformation with short transannular Au···Au interactions. Complex **1** does not contain intermolecular Au···Au interactions, which is as observed for the previously reported methyl derivative (10). The molecule crystallizes in the monoclinic space group $P2_1/n$ with an inversion center between the two gold atoms. The structure is shown in Fig. 2.

The structure of **2a** was previously reported (10), but several details raised suspicion causing us to further investigate the material. A significant concern was the absence of an inversion center (space group $I\bar{4}$) for this molecularly symmetrical molecule. Other troublesome indicators were the unequally sized thermal ellipsoids reported for gold atoms (Z = 79) and large variations in the presumably equal Au—S bond lengths which range from 2.23(2) to 2.38(2) Å. Following a rational synthesis (vide supra), high quality single crystals of **2a** were obtained, which allowed for successful structure refinement in the tetragonal space group $I4/m$. Unlike the methyl and ethyl derivatives which shows no intermolecular Au···Au interactions, the phenyl derivative shows short intermolecular Au···Au contacts of 2.9610(3) Å. This structure was determined at room temperature also for spectroscopic purposes. The results are statistically insignificant for the general structure but the intramolecular Au—Au distance is about 1% longer, and the intramolecular Au—Au distance about 1% shorter at room temperature than at –77°C. The structure of **2a** is shown in Fig. 3.

The complex **3a** crystallizes in the space group $P2_1/c$ with no intermolecular Au···Au interactions. An unusual feature of this structure is that the complex crystallizes in a boat conformation. Few examples of this form apparently exist for dimetallocycle Au(I) compounds (see Lin and co-workers (17)) when compared with the common chair conformation. The carbon atoms C(1) and C(2) were refined with some difficulty since the structure is close to that of a C-centered lattice, suggesting that the symmetry of the molecule is higher than the symmetry of the generated lattice. There also could be some ligand disorder, which would influence C(1) and C(2). The structure of **3a**, for which data was collected three times, is shown in Fig. 4.

Interestingly, the oxidative addition product of chlorine to **3a**, namely **4**, also crystallizes in a boat conformation. The single bond formed between the two Au(II) centers in **4** is clearly demonstrated by the crystallographic study. The intramolecular Au—Au distance decreases from 3.0966(7) Å (standard aurophilic bond) in **3a** to 2.5611(5) Å (single bond) in **4**. The structure is shown in Fig. 5. There is a significant twist of the two 5-membered rings in the molecule about the very short Au(II)–Au(II) bond which presumably arises from the constraints of the two different bridging ligands.

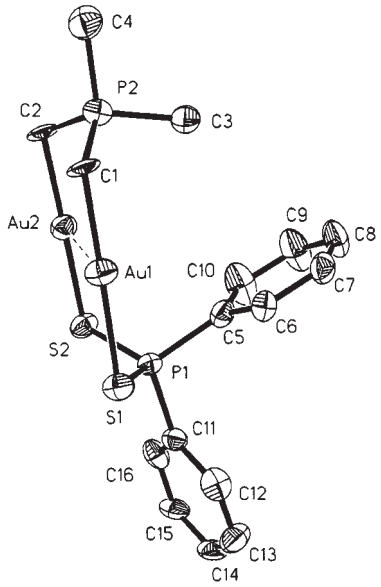
Experimental

General

All reactions and manipulations were carried out under an inert atmosphere with a positive nitrogen gas flow (pre-dried by two columns of Drierite) using standard Schlenk techniques. Solvents were distilled and kept under dinitrogen. The following chemicals were purchased from Aldrich: tetrahydrothiophene, aluminum trichloride, sodium sulfide nonahydrate, thiophosphoryl chloride, bis(diphenylphosphino)methane, ethylbromide. Elemental sulfur was obtained from J.T. Baker. The following compounds were prepared using literature procedures: $Et_2P(S)P(S)Et_2$ (18), $Na[S_2PEt_2]\cdot 2H_2O$ (19), $[NH_4][S_2PPh_2]$ (20),

© 2001 NRC Canada

Fig. 4. Thermal ellipsoid view (50%) of the boat form for the molecular structure of complex **3a** showing the atom labeling scheme. Atoms are represented by thermal ellipsoids at the 50% probability level. Selected bond lengths (Å) and angles (°): Au(1)—Au(2) 3.0966(7), Au(1)—S(1) 2.339(3), Au(2)—S(2) 2.317(3), Au(1)—C(1) 2.052(12), Au(2)—C(2) 2.080(12), C(1)—P(2) 1.756(14), P(1)—S(1) 2.031(4) Å; C(1)-Au(1)-S(1) 178.4(4), C(2)-Au(2)-Au(1) 87.9(4), C(5)-P(1)-S(2) 110.2(4),

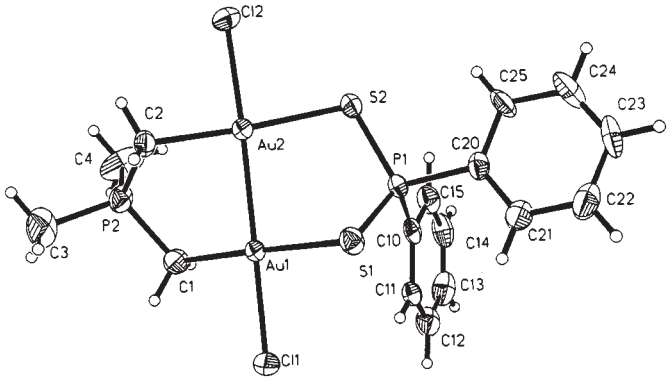


$Ph_2P(S)$-S-S-$P(S)Ph_2$ (21), $H[AuCl_4]\cdot 3H_2O$ (22), [Au(tht)Cl] (23), $[Au_2\{dppm\}_2]Cl_2$ (24), $[Au_2\{dppm\}Cl_2]$ (25), $[Au\{(CH_2)_2PMe_2\}]_2$ (26), and $PhI\cdot Cl_2$ (27). All chemicals were used as received.

Instrumentation

Melting points were measured on a Unimelt (A.H. Thomas Co, Philadelphia, PA) capillary melting point apparatus and are uncorrected. Elemental analyses were performed at Desert Analytics Inc., Tucson AZ. ^{1}H NMR spectra were obtained on a Varian XL-200 spectrometer operating at 200 MHz, or a Varian UnityPlus-300 spectrometer operating at 299.9 MHz. ^{1}H NMR data are expressed in parts per million (ppm) downfield referenced internally to the residual proton impurity in the deuterated solvent, and are reported as: chemical shift position (^{1}H NMR (δ)), multiplicity (s = singlet, d = doublet, t = triplet, q = quartet, m = multiplet, br = broad), coupling constant (*J* (Hz)), relative integral, and assignment. All $^{31}P\{^1H\}$ NMR spectra were obtained on either a Varian XL 200 MHz broadband spectrometer operating at 81 MHz, or a Varian UnityPlus-300 spectrometer operating at 121.4 MHz with chemical shifts reported relative to a 85% H_3PO_4 in D_2O external standard solution. Positive fast atom bombardment (+FAB–DIP) (DIP = direct insertion probe) mass spectra were acquired on a VG Analytical (Manchester, U.K.) 70S high resolution, double focusing mass spectrometer. Samples for analyses were prepared by dissolving the solid compound in appropriate solvent with a nitrobenzylalcohol (NBA) matrix added.

Fig. 5. Molecular structure of the Au(II)–Au(II) complex **4** showing the atom labeling scheme. Atoms are represented as thermal ellipsoids at the 50% probability level. There is a significant twist to the two chelate rings about the nearly linear Cl-Au-Au-Cl axis with the C(2)-Au(2)-S(2) axis offset by about 20° from the C(1)-Au(1)-S(1) axis. Selected bond lengths (Å) and angles (°): Au(1)—Au(2) 2.5611(5), Au(1)—C(1) 2.075(8), Au(2)—C(2) 2.063(8), Au(1)—Cl(1) 2.392(2), Au(1)—S(1) 2.401(2), Au(2)—S(2) 2.376(2) Å; C(1)-Au(1)-S(1) 177.8(3), Cl(1)-Au(1)-S(1) 91.05(7), S(1)-P(1)-S(2) 113.00(13)°.



X-ray crystallography

Crystals that were used in diffraction intensity measurements at room temperature were mounted on the tip of a quartz fiber with fast-adhesive glue. Single crystal diffraction analysis was carried out on complex **1** at Texas A&M using an automated Nicolet R3 four-circle diffractometer utilizing the Wyckoff scanning technique with graphite monochromated Mo Kα (λ = 0.71073 Å) radiation. Refined cell parameters were determined from setting angles of 25 reflections with 20° < 2θ < 30°. The unit cell was determined using search, center, index, and least-squares refinement routine. The Laue class and lattice dimensions were verified by axial oscillation photography. The intensity data were corrected for absorption, Lorentz, and polarization effects. An empirical absorption correction was performed based on ψ scans of five strong reflections spanning a range of 2θ values. All data processing were performed on a Data General Eclipse S140 minicomputer using the SHELXTL crystallographic package (version 5.1) and Siemens SHELXTL PLUS (Micro Vax II) (28). The systematic absences were consistent with the space group assigned. The structure was solved using direct-methods to determine the gold atom positions, while all other atoms were located with difference Fourier maps. Structure refinement was carried out using SHELX 93. The position of the hydrogen atoms were calculated by assuming idealized geometries, C—H = 0.93 Å.

X-ray data for complexes **2a**, **3a**, and **4** were collected at Harvard University on a Siemens (Bruker) SMART CCD (charge coupled device) based diffractometer equipped with a LT-2 low temperature apparatus operating at 213 K. Data for **2a** was collected three times including once at room temperature. A suitable crystal was chosen in each case and mounted on a glass fiber using grease. Data were measured

© 2001 NRC Canada

Table 1. Crystal data and structure refinement for compounds **1**, **2a**, **3a**, and **4**.

	1	**2a**	**3a**	**4**
Empirical formula	$C_8H_{20}Au_2P_2S_4$	$C_{24}H_{20}Au_2P_2S_4$	$C_{16}H_{20}Au_2P_2S_4$	$C_{16}H_{20}Au_2Cl_2P_2S_4$
FW	700.35	892.51	732.31	803.21
Crystal system	Monoclinic	Tetragonal	Monoclinic	Triclinic
Space group	$P2_1/n$	$I4/m$	$P2_1/c$	$P\bar{1}$
a (Å)	6.5660(10)	15.8963(4)	7.5146(6)	9.1519(9)
b (Å)	15.606(3)	15.8963(4)	9.0287(7)	9.669(1)
c (Å)	8.338(2)	12.0938(4)	28.734(2)	18.419(1)
α (°)	90	90	90	106.193(2)
β (°)	94.69(3)	90	97.346(2)	95.353(2)
γ (°)	90	90	90	102.084(2)
U (Å^3)	851.5(3)	3056.0(2)	1933.5(3)	1100(2)
D_c (g cm^{-1})	2.731	1.940	2.516	2.424
Z	2	4	4	2
F(000)	640	1664	1344	740
μ(Mo Kα) (mm^{-1})	17.863	9.979	15.532	13.893
T (K)	293(2)	213(2)	213(2)	213(2)
Theta range (°)	2.61–22.48	1.81–27.62	2.37–22.50	2.26–23.27
Reflections collected	1201	7028	5844	5638
Unique reflections	1093	1709	2508	3145
GoF on F^2	1.073	1.076	1.013	1.098
Final $R[I > 2\sigma(I)]/R_1$, wR_2	0.0389, 0.0973	0.0243, 0.0633	0.0421, 0.0967	0.0384, 0.1086
R (all data)/R_1, wR_2	0.0475, 0.1006	0.0305, 0.0683	0.0527, 0.1006	0.0411, 0.1130
ρ(max. min.) (e Å^{-3})	1.651 and –1.267	0.761 and –0.696	1.999 and –2.194	1.932 and –2.409

using omega scans of 0.3° per frame for 30 s, such that a hemisphere was collected. A total of 1271 frames were collected. The first 50 frames were collected again at the end of the data collection to monitor for decay. Cell parameters were retrieved using SMART software (29) and refined using SAINT on all observed reflections. Data reduction were performed using SAINT software (30) which corrects for Lp and decay. Absorption corrections were applied (semi-empirical from psi-scans) using SADABS (31) supplied by G. Sheldrick. The structures were solved by direct methods using the SHELXS 97 (32) program and refined by least-squares method on F^2, SHELXL 97 (33). The structures were solved in space groups consistent with analysis of systematic absences. All non-hydrogen atoms were refined anisotropically. The crystals used for diffraction showed no decomposition during data collection. Crystallographic data and structure refinement results are listed in Table 1. Bond lengths and angles are reported in the appropriate figure captions.

Preparation of compounds

*$[AuS_2PEt_2]_2$ (**1**) (9)*

A 50-mL Schlenk tube was charged with a solution of $Na[S_2PEt_2]\cdot 2H_2O$ (0.16 g, 0.72 mmol) and [Au(tht)Cl] (0.22 g, 0.70 mmol) in THF (35 mL) and stirred for 1 h at room temperature. The solvent was subsequently evaporated under reduced pressure, the crude mixture was extracted with CH_2Cl_2 (30 mL), active charcoal was added, and the mixture filtered through anhydrous $MgSO_4$ to remove water and NaCl. The volume of the filtrate was reduced in vacuo to 5 mL, and the clear solution transferred to a 10 mL test-tube, which was transferred to a larger vial that contained hexane. The larger vial was corked and after three days in the closed system the CH_2Cl_2 solvent diffused into the hexane yielding crystals and trace amounts of dark brown decomposition product (Au_2S?). Crystals of **1** suitable for X-ray crystallographic studies were obtained as colorless plates, yield 0.36 g (73%), mp 153°C. +FAB-MS (NBA/CH_2Cl_2) m/z: 701 ($[M + 1]^+$). ^{1}H NMR (200 MHz, $CDCl_3$, 19°C) δ: 1.36 (dt, $J_{P,H}$ = 21.78 Hz, 12H, $4CH_3$), 2.33 (dq, $J_{P,H}$ = 10.98 Hz, 8H, $4CH_2$). ^{31}P NMR (CH_2Cl_2 with 85% H_3PO_4 insert in 85% D_2O, 200 MHz, 20°C) δ: 82.59 (s). Anal. calcd. for $C_8H_{20}P_2S_4Au_2$: C 13.72, H 2.88; found: C 13.62, H 2.81.

*$[AuS_2PPh_2]_2$ (**2a**) (9)*

Method A: A 50-mL Schlenk tube was charged with a solution of $[NH_4][S_2PPh_2]$ (0.11 g, 0.415 mmol) in THF (40 mL) at room temperature. Upon dissolution, [Au(tht)Cl] (0.131 g, 0.408 mmol) was added in one portion. The solution immediately afforded a white precipitate (NH_4Cl). The mixture was stirred for 1 hour at room temperature. The solvent was removed in vacuo, and CH_2Cl_2 (40 mL) was added to extract the product. The mixture was filtered through anhydrous $MgSO_4$ (3 mm). The solvent was evaporated under reduced pressure, washed with dry ether, and vacuum dried for 1 hour.

Method B: Similar to Method A, but after THF was removed in vacuo, water (40 mL) was added to dissolve the NH_4Cl. The product (a wet yellow paste, stable in water) was filtered and washed consecutively with methanol and ether. The yellow product was dried in the air.

Method C: To a 100-mL beaker was added a solution of $Ph_2P(S)S\text{-}SP(S)Ph_2$ (0.2 g, 0.40 mmol) and [Au(tht)Cl] (0.26 g, 0.80 mmol) in benzene (40 mL) at room tempera-

© 2001 NRC Canada

ture. The mixture was heated to boiling for 20 min, which yielded a clear solution. Upon cooling, a yellow microcrystalline powder was obtained, which was filtered on a frit and washed with ether. Yields: Method A: 55% (some loss occurs due to the limited solubility of the product in CH_2Cl_2.); Method B: 78% (this was our best method); Method C: 28% (as crystallized product), mp 295°C (dec.). +FAB-MS (insolubility of product prevented satisfactory spectrum to be obtained). The complex is partially soluble in chlorinated solvents and THF, and insoluble in ether and hexane. ^{1}H NMR (300 MHz, $CDCl_3$, 20°C) δ: 8.06–7.92 (m, 8H, Ph), 7.58–7.38 (m, 12H, Ph). ^{31}P NMR (200 MHz, $CDCl_3$, 19°C) δ: 67.43 (s). Anal. calcd. for $C_{24}H_{20}P_2S_4Au_2$: C 32.32, H 2.24, S 14.33; found: C 32.92, H 2.13, S 13.86.

*$[AuS_2P(C_6H_4$-p-$Me)_2]_2$ (**2b**)*

Starting from $[NH_4][S_2P(C_6H_4$-*p*-$Me)_2]$ the toluene derivative was obtained in the same manner as described in Method A for **2a**, yield 77%, mp 275°C. ^{1}H NMR (200 MHz, $CDCl_3$, 20°C) δ: 7.90–7.78 (m, 8H, Ph), 7.22–7.12 (m, 8H, Ph), 2.37 (br s, 12H, 4Me). ^{31}P NMR (200 MHz, $CDCl_3$, 20°C) δ: 66.62 (s). Anal. calcd. for $C_{28}H_{28}P_2S_4Au_2$: C 35.45, H 2.97; found: C 35.62, H 3.08.

*$Au_2[(CH_2)_2PMe_2](S_2PPh_2)$ (**3a**)*

A 50-mL Schlenk tube was charged with a solution of **2a** (75.8 mg, 0.085 mmol) and $[Au(CH_2)_2PMe_2]_2$ (48 mg, 0.085 mmol) in CH_2Cl_2 (10 mL) at room temperature. An orange–yellow colored suspension was initially obtained since both starting materials are sparingly soluble in CH_2Cl_2. After the reaction mixture had been stirred for 10 min, a clear orange solution was obtained, and stirring was continued for an additional 20 min, followed by filtration through anhydrous $MgSO_4$. The filtrate solution was concentrated by evaporation of the solvent under reduced pressure, and ether was added to precipitate the product, which was filtered on a frit and air dried. Colorless blocky crystals suitable for X-ray studies were obtained from a concentrated CH_2Cl_2 solution layered with either ether or hexane, yield 52.3 mg (84%), mp 208°C (dec.). +FAB-MS (NBA/$CHCl_3$) *m*/*z*: 733 ($[M + 1]^+$). ^{1}H NMR (300 MHz, $CDCl_3$, 20°C) δ: 8.22–8.08 (m, 4H, Ph), 7.48–7.35 (m, 6H, Ph), 1.24 (d, $J_{P,H}$ = 13.2 Hz, 4H, $2CH_2$), 1.10 (d, $J_{P,H}$ = 12.6 Hz, 6H, $2CH_3$). ^{31}P NMR (300 MHz, $CDCl_3$, 20°C) δ: 68.52 (d, $J_{P,P}$ = 11.9 Hz, PPh_2), 34.78 (d, $J_{P,P}$ = 11.9 Hz, PMe_2). Anal. calcd. for $C_{16}H_{20}P_2S_2Au_2$: C 26.24, H 2.75; found: C 26.32, H 2.81.

*$[Au_2\{(CH_2)_2PMe_2\}\{S_2PEt_2\}]$ (**3b**)*

Prepared in the same fashion as **3a**, but **1** was used as a starting material instead of **2a**, yield 78%. ^{1}H NMR (300 MHz, $CDCl_3$, 20°C) δ: 2.30 (dq, $J_{P,H}$ = 7.8 Hz, 4H, $2CH_2CH_3$), 1.60 (d, $J_{P,H}$ = 12.3 Hz, 6H, 2P-CH_3), 1.38 (dt, $J_{P,H}$ = 21.3 Hz, 6H, $2CH_2CH_3$), 1.23 (d, $J_{P,H}$ = 12.3 Hz, 4H, 2P-CH_2-Au). ^{31}P NMR (300 MHz, $CDCl_3$, 20°C) δ: 81.93 (d, $J_{P,P}$ = 7.9 Hz, PEt_2), 34.20 (d, $J_{P,P}$ = 7.9 Hz, PMe_2).

*$Au_2Cl_2[(CH_2)_2PMe_2][S_2PPh_2]$ (**4**)*

A 50-mL Schlenk tube was charged with a solution of **3a** (60 mg, 0.082 mmol) in CH_2Cl_2 (8 mL) at room temperature. The solution was cooled to 0°C and PhI·Cl_2 (26 mg, 0.095 mmol) was added in one portion. The solution immediately turned deep orange. The reaction mixture was stirred for 30 min with a gradual increase of temperature until room temperature was reached. The solvent was partially removed under reduced pressure, and subsequently ether was added when the solution became sufficiently concentrated to induce precipitation of the product. The product was filtered, dried under vacuum for 2 h, and stored in a refrigerator, yield 78%, mp at ~ 205°C. +FAB-MS (NBA/$CHCl_3$) *m*/*z*: is similar to **3a**, ($[M - Cl_2]^+$). ^{1}H NMR ($CDCl_3$, 300 MHz, 20°C) δ: 8.05–7.90 (m, 4H, Ph), 7.60–7.40 (m, 6H, Ph), 2.05 (d, $J_{P,H}$ = 7.79 Hz, 4H, $2CH_2$), 1.81 (d, $J_{P,H}$ = 8.19 Hz, 6H, $2CH_3$). ^{31}P NMR (300 MHz, $CDCl_3$, 20°C) δ: 70.06 (s, no $^4J_{P,P}$ coupling detected, PPh_2), 42.02 (s, no $^4J_{P,P}$ coupling detected, PMe_2). Anal. calcd. for $C_{16}H_{20}Cl_2P_2S_2Au_2$: C 23.92, H 2.51; found: C 22.84, H 2.49 (some loss of Cl_2 is expected). Orange needles suitable for X-ray crystallographic studies were obtained from a concentrated CH_2Cl_2 solution layered with hexane.

*$[Au_2\{dppm\}\{S_2PPh_2\}_2]_n$ (**5**)*

A 50-mL Schlenk tube was charged with a solution of **2a** (0.1 g, 0.11 mmol) in CH_2Cl_2 (10 mL) at room temperature. To the yellow suspension was added dppm (0.043 g, 0.11 mmol) in one portion. The initial suspension became a clear solution after a few minutes, followed by formation of a white precipitate that emerged after 30–40 min. The solvent was subsequently removed under reduced pressure until a concentrated solution was obtained. Ether was added in excess to precipitate and consolidate the solid. The product was filtered on a frit and washed with ether. The product is a white solid and is sparingly soluble in polar and non-polar solvents, yield 72%, mp 227°C. ^{1}H NMR (300 MHz, $CDCl_3$, 20°C) δ: 8.28–8.12 (m, 8H, Ph), 7.80–7.62 (m, 12H, Ph), 7.50–7.35 (m, 8H, Ph), 7.26–7.10 (m, 12H, Ph), 4.26 (br s, 2H, PCH_2P). Anal. calcd. for $C_{49}H_{42}P_4S_4Au_2$: C 46.09, H 3.32, S 10.04; found: C 45.07, H 3.42, S 8.83.

Acknowledgments

The authors acknowledge the support of the Robert A. Welch Foundation for this work. J.M.L-de-L. also thanks the University of La Rioja for financial support and the opportunity to pursue these studies in 1998 at Texas A&M.

References

1. (*a*) R.P. Andres, J.D. Bielefeld, J.I. Henderson, D.B. Janes, V.R. Kolagunta, C.P. Kubiak, W.J. Mahoney, and R.G. Osifschin. Science, **273**, 1690 (1996); (*b*) M. Antler. Gold Bull. **16**, 2 (1983); (*c*) L.H. Dubois and R.G. Nuzzo. Ann. Rev. Phys. Chem. **43**, 437 (1992).
2. (*a*) R.V. Parish and S.M. Cottrill Gold Bull. **20**, 3 (1987); (*b*) D.R Haynes and M.W. Whitehouse. New developments in antiarthritic therapy. *Edited by* K.D. Rainsford and G.P. Velo. Kluwer Academic Publishers, Dordrecht. 1989. Chap. 8, pp. 207.
3. R. Lok, W.W. Weimar, and M.W. Marshall. Patent U.S 59 121 12A. U.S.A. 1999.
4. (*a*) W.E. van Zyl, J.M. López-de-Luzuriaga, and J.P. Fackler, Jr. J. Mol. Struct. **516**, 99 (2000); (*b*) M.A. Mansour, W.B. Connick, R.J. Lachicotte, H.J. Gysling, and R. Eisenberg. J. Am. Chem. Soc. **120**, 1329 (1998).

© 2001 NRC Canada

5. D. Klaman (*Editor*). Lubricants and related products. Verlag Chemie, Weinheim, Germany. 1984.
6. P. Patnaik. A comprehensive guide to the hazardous properties of chemical substances. 1st ed. Van Nostrand Reinhold, New York. 1992. Chap. 40.
7. (*a*) L. Bromberg, I. Lewin, and A. Warshawsky. Hydrometallurgy, **33**, 59 (1993); (*b*) S. Yu, J. Yu, and Z. Yu. Hydrometallurgy, **32**, 181 (1993).
8. A.W. van Hofmann and F. Mahla. Chem. Ber. **25**, 2436 (1892).
9. W. Kuchen, K. Strolenberg, and J. Metten. Chem. Ber. **101**, 3454 (1968).
10. G. Siasios and E.R.T. Tiekink. Z. Kristallogr. **210**, 698 (1995).
11. M. Preisenberger, A. Bauer, A. Schier, and H. Schmidbaur. J. Chem. Soc. Dalton Trans. 4753 (1997).
12. (*a*) J.P. Fackler, Jr. Polyhedron, **16**, 1 (1997); (*b*) A. Grohmann and H. Schmidbaur. *In* Comprehensive organometallic chemistry II. Vol. 3. *Edited by* E.W. Abel, F.G.A. Stone, and G. Wilkinson. Pergamon, Oxford. 1995. Chap. 1.
13. M. Bardaji, P.G. Jones, A. Laguna, and M. Laguna. Organometallics, **14**, 1310 (1995).
14. E.J. Fernández, J.M. López-de-Luzuriaga, M. Monge, E. Olmos, M.C. Gimeno, A. Laguna, and P.G. Jones. Inorg. Chem. **37**, 5532 (1998).
15. W.W. Simons and M. Zanger. The Sadtler guide to NMR spectra. Sadtler Research Laboratories Inc., Philadelphia. 1972.
16. E.A.V. Ebsworth, D.W.H. Rankin, and S. Cradock. Structural methods in inorganic chemistry. 2nd ed. Blackwell Scientific Publishers, London. 1991.
17. D.-F. Feng, S.S. Tang, C.W. Liu, I.J.B. Lin, Y.-S. Wen, and L.-K. Liu. Organometallics, **16**, 901 (1997).
18. (*a*) H. Niebergall and B. Langenfeld. Chem. Ber. **95**, 64 (1962); (*b*) W. Kuchen, H. Buchwald, K. Strolenberg, and J. Metten. Liebigs. Ann. Chem. **652**, 28 (1962).
19. W. Kuchen and H. Mayatepek. Chem. Ber. **96**, 1733 (1963).
20. (*a*) W.A. Higgins, P.W. Vogel, and W.G. Craig. J. Am. Chem. Soc. **77**, 1864 (1955); (*b*) R.G. Cavell, W. Byers, and E.D. Day. Inorg. Chem. **10**, 2710 (1971).
21. G. Peters. J. Org. Chem. **27**, 2198 (1962).
22. A. Haas, J. Helmbrecht, and U. Niemann. Handbuch der präparativen anorganischen Chemie. 3rd ed. *Edited by* G. Brauer. K. Enke, Stuttgart. 1975. p. 1014.
23. (*a*) R. Usón and A. Laguna. Organometallic synthesis. Vol. 3. *Edited by* R.B. King and J.J. Eisch. Elsevier Scientific Publishers, Amsterdam. 1986. p. 322; (*b*) R. Usón, A. Laguna, and M. Laguna. Inorg. Synth. **26**, 85 (1986).
24. H. Schmidbaur, A. Wohlleben, U. Schubert, A. Frank, and G. Huttner. Chem. Ber. **110**, 2751 (1977).
25. H. Schmidbaur, A. Wohlleben, O. Orama, and G. Huttner. Chem. Ber. **110**, 1748 (1977).
26. H. Schmidbaur. Acc. Chem. Res. **8**, 62 (1975).
27. (*a*) H.J. Lukas and E.R. Kennedy. Org. Synth. Coll. Vol. III. 1955. p. 482; (*b*) J.D. Protasiewicz. J. Chem. Soc. Chem. Commun. 1115 (1995).
28. G.M. Sheldrick. SHELXTL-Plus user's manual. Nicolet, XRD Corp. Madison, WI. 1988.
29. SMART V 4.050 Software for the CCD Detector System. Bruker Analytical X-ray Systems. Madison, WI. 1995.
30. SAINT V 4.050 Software for the CCD Detector System. Bruker Analytical X-ray Systems. Madison, WI. 1995.
31. SADABS Program for Absorption Corrections using Siemens CCD. Based on the Method of Robert Blessing. R.H Blessing. Acta Crystallogr. Sect. A: Fundam. Crystallogr. **A51**, 33 (1995).
32. G.M Sheldrick. SHELXS 97. Program for the solution of crystal structure. University of Göttingen, Germany. 1997.
33. G.M. Sheldrick. SHELXL 97. Program for the refinement of crystal structure. University of Göttingen, Germany. 1997.

© 2001 NRC Canada

Making a 16-electron bromo (or iodo) complex of ruthenium(II) and a C—F bond in one pot

Peter Barthazy, Diego Broggini, and Antonio Mezzetti

Abstract: The 16e$^-$ bromo or iodo complexes $[RuX(dppp)_2]^+$ (dppp = 1,3-bis(diphenylphosphino)propane, X = Br (**1c**), I (**1d**)) and $[RuX(dppe)_2]^+$ (dppe = 1,2-bis(diphenylphosphino)ethane, X = Br (**2c**), I (**2d**)) have been prepared exploiting the reaction of the fluoro complexes $[RuF(dppp)_2]^+$ (**1a**) and $[Tl(\mu\text{-}F)_2Ru(dppe)_2]^+$ (**3**) with activated alkyl bromides or iodides. The X-ray structures of **1c**, **1d, 2c**, and **2d** suggest that the distortion of the Y-shaped trigonal-bipyramidal structure of $[MX(P^\frown P)_2]^+$ is possibly related to the formation of intramolecular hydrogen bonds between the halide ligand and the *ortho*-hydrogen atoms of the neighbouring phenyl rings. The five-coordinate species **1c**, **1d**, **2c**, and **2d** react with H_2 to form the dihydrogen complexes $[RuX(\eta^2\text{-}H_2)(P^\frown P)_2]^+$. The reaction of the dppp derivatives **1c** and **1d** with H_2 (P = 1 atm, 1 atm = 101.322 kPa) is an equilibrium. Quantitative formation of $[RuBr(\eta^2\text{-}H_2)(dppp)_2]$ (**4c**) is obtained under H_2 pressure (100 bar, 1 bar = 100 kPa), whereas the iodo analogue is not stable under analogous conditions. The less crowded dppe derivatives **2c** and **2d** react quantitatively with H_2 under ambient pressure. The iodo and bromo derivatives $[RuX(\eta^2\text{-}H_2)(P^\frown P)_2]^+$ contain elongated dihydrogen ligands, as indicated by their transverse relaxation times T_1 (min). The present data suggest that Cl, Br, and I have similar donor properties in these dihydrogen complexes, and that the different chemical behaviour in the Cl, Br, I series is mainly a result of steric effects.

Key words: 16e$^-$ complexes, ruthenium, fluoro complexes, bromo complexes, iodo complexes, dihydrogen complexes.

Résumé : On a préparé les complexes bromés ou iodés à 16e$^-$ $[RuX(dppp)_2]^+$ (dppp = 1,3-bis(diphénylphosphino)propane, X = Br (**1c**), I (**1d**)) et $[RuX(dppe)_2]^+$ (dppe = 1,2-bis(diphénylphosphino)éthane, X = Br (**2c**), I (**2d**)) en mettant à profit la réaction des complexes fluorés $[RuF(dppp)_2]^+$ (**1a**) et $[Tl(\mu\text{-}F)_2(dppe)_2]^+$ (**3**) avec des bromures ou des iodures d'alkyles activés. Les structures des composés **1c**, **1d**, **2c** et **2d**, déterminées par diffraction des rayons X, suggèrent que la déformation de la structure trigonale-bipyramidale "en forme de Y" du cation $[MX(P^\frown P)_2]^+$ pourrait être reliée à la formation de liaisons hydrogènes intramoléculaires entre le ligand halogénure et les atomes d'hydrogène en *ortho* des noyaux phényles voisins. Les espèces pentacoordinées **1c**, **1d**, **2c** et **2d** réagissent avec H_2 pour former les complexes de dihydrogène $[RuX(\eta^2\text{-}H_2)(P^\frown P)_2]^+$. La réaction des dérivés dppp **1c** et **1d** avec H_2 (P = 1 atm, 1 atm = 101.322 kPa) est un équilibre. On arrive à une formation quantitative du $[RuBr(\eta_2\text{-}H_2)(dppp)_2]$ (**4c**) en opérant sous une pression de 100 bars (1 bar = 100 kPa) de H_2; le dérivé iodé analogue n'est toutefois pas stable dans des conditions analogues. Les dérivés dppe **2c** et **2d**, moins encombrés d'un point de vue stérique, réagissent quantitativement avec H_2, à la pression ambiante. Les dérivés iodés et bromés $[RuX(\eta^2\text{-}H_2)(P^\frown P)_2]^+$ comportent des ligands dihydrogènes "allongés" d'après leurs temps de relaxation transversale, T_1 (min). Les données présentées suggèrent que, dans ces complexes de dihydrogène, les atomes de Cl, Br et I possèdent des propriétés semblables comme donneurs et que le comportement chimique différent des atomes dans la série Cl, Br et I résulte principalement d'effets stériques.

Mots clés : complexes à 16e$^-$, ruthénium, complexes fluorés, complexes bromés, complexes iodés, complexes de dihydrogène.

[Traduit par la Rédaction]

Introduction

Ancillary ligands, such as halides, allow the fine-tuning of the electronic and steric properties of transition-metal complexes. This is particularly important in the case of coordinatively unsaturated complexes with a d^6 electron count such as the ruthenium(II) complexes $[RuX_2P_3]$ (X = halide, P = phosphine donor)[3], $[RuH(X)(CO)P_2]$[4], $[RuX_2NP_2]$ (N = nitrogen donor) (3), [RuX(P)(PCP)] (PCP = pincer ligand with a P_2C donor set) (4), $[RuX(CO)(R)P_2]$ (R = alkyl) (5), $[RuI(H)(\eta^2\text{-}H_2)(PCy_3)_2]$ (6), $[RuClP_2N_2]^+$ (7), or $[RuXP_4]^+$ (8) (P = phosphine donor). We have been studying

Received September 19, 2000. Published on the NRC Research Press Web site at http://canjchem.nrc.ca on July 9, 2001.

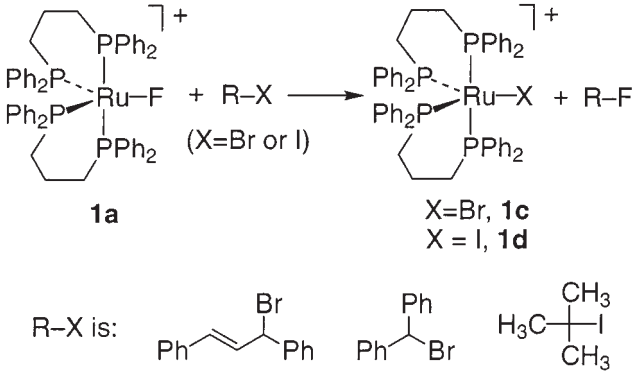
Dedicated to Professor B.R. James on the occasion of his 65th birthday.

P. Barthazy, D. Broggini,[1] and A. Mezzetti.[2] Laboratory of inorganic chemistry, Universitätstrasse 6, ETH Zentrum, CH-8092 Zürich, Switzerland.

[1]X-ray studies.
[2]Corresponding author (telephone: 0041 1 632 61 21; fax: 0041 1 632 13 10; e-mail: mezzetti@inorg.chem.ethz.ch).
[3]For selected examples of $[RuCl_2L_3]$ (L = phosphine donor), see ref. 1.
[4]For recent examples of $[RuH(X)(CO)P_2]$ and related complexes, see ref. 2.

 DOI: 10.1139/cjc-79-5/6-904 © 2001 NRC Canada

Scheme 1.



the 16e⁻ complexes of the type $[MXP_4]^+$ (M = Ru or Os) (8*b*, *c*, g) that exhibit a rich reactivity pattern, including the formation of (η^2-H_2)- (for review articles see ref. 9; for selected examples of H_2-activation by $[RuClP_4]^+$ complexes see ref. 10) and (η^2-O_2)-complexes (11). The halide ligand plays (at least) a twofold role in the stabilization of these five-coordinate complexes. As a bulky ligand, it favours the five-coordinate complexes relative to the corresponding six-coordinate ones as a result of the release of steric crowding in the former. As a π-donor, it stabilizes the 16e⁻ configuration even in the absence of strong σ-donor ligands, such as hydride (12). The resulting formally coordinatively unsaturated complexes adopt a typical distorted (Y-shaped) trigonal-bipyramidal structure to optimize the π-donation from the halide to the 16e⁻ metal center (12).

Recently, the nature of the halide ligand has been shown to play an essential role in a number of catalytic reactions. In particular, the use of fluoride as ligand in transition-metal catalysts, which has been reviewed recently (13). The addition of soluble fluoride sources to catalytic systems based on late transition metals (Pd, Ir) has been found to enhance the enantioselectivity in olefin hydrogenation (14) and hydroamination (15). Five-coordinate 16e⁻ complexes stabilized by π-donor ligands have recently been applied in a number of catalytic reactions that include the transfer hydrogenation of ketones (3*a*, 4*b*), olefin metathesis[5], oligomerization (5*a*, 17), hydrosilylation (3*a*, 18), cyclopropanation (8*g*, 19), and epoxidation (8*g*, 20). Although several types of 16e⁻ complexes are known, the effect of changing the halide ligand has been investigated systematically only for $[RuH(X)(CO)P_2]$ (X = F, Cl, Br, I), showing how their reactivity depends dramatically on the nature of X (21). In the other series, reports of bromo and iodo derivatives are sparse. Thus, besides $[RuCl_2(PPh_3)_3]$, only $[RuBr_2(PPh_3)_3]$ (22) is known in the $[RuX_2P_3]$ series. The five-coordinate vinylidene and vinyl complexes $[RuBr_2(C{=}CH\text{-}t\text{-}Bu)(PPh_3)_2]$ (23) and $[RuBr(CO)(\sigma\text{-}E\text{-}C(H){=}C(H)CH_2PPh_3)(PPh_3)_2]$ (24) have been reported, and the five-coordinate iodo complex $[RuI(PPh_3)(C_6H_3(CH_2NMe_2)_2\text{-}2,6)]$ has been characterized crystallographically (25). Some bromo and iodo five-coordinate complexes of the type $[RuXL_4]^+$ are also known (7*b*, 8*a*, *b*).

We have undertaken a systematic investigation of 16e⁻ complexes that are stabilized by different halides, including fluoride. Thus, we recently reported the fluoro complex $[RuF(dppp)_2]PF_6$ (**1a**), which is prepared by reaction of $[RuCl(dppp)_2]PF_6$ (dppp = 1,3-bis(diphenylphosphino)propane) (**1b**) with TlF (26). Complex **1a** reacts with activated haloalkanes R-X (X = Cl, Br, I) to give the fluoroalkane R-F and the corresponding halo complex $[RuX(dppp)_2]^+$ (X = Cl (**1b**), Br (**1c**), I (**1d**)) (Scheme 1). Reactivity trends for the haloalkanes have been discussed previously (26*b*). The halide-exchange reaction has a potential for both the organic and the inorganic chemist. Indeed, this reaction not only forms a C–F bond (a useful organic synthesis), but also cleanly introduces the desired halide in the five-coordinate complex $[RuX(P^{\frown}P)_2]^+$. This method allows avoidance of the halide metathesis with large excesses of inorganic salts (8*b*), a procedure that can result in mixed-halide complexes (27, 28). In this paper, we show the use of fluoro complexes in the synthesis of the five-coordinate complexes $[RuX(P^{\frown}P)_2]^+$ (X = Br or I, P⌒P = dppp or 1,2-bis(diphenylphosphino)ethane (dppe)) and investigate the reaction of the resulting bromo and iodo complexes with dihydrogen.

Experimental

All operations were carried out under argon using standard Schlenk techniques. All reagents and solvents were Fluka puriss. grade or had comparable purity. $[RuF(dppp)_2]PF_6$ (**1a**) (26), $[RuCl(dppe)_2]PF_6$ (8*d*), and 1,3-diphenylallyl bromide (29) were prepared according to literature methods. ^1H and ^{31}P NMR spectra were recorded on Bruker Avance 250 or 500 MHz spectrometers. Chemical shifts (δ) are in ppm relative to internal $SiMe_4$ (^1H) and to external 85% H_3PO_4 (^{31}P). Relaxation times were measured with a standard inversion–recovery experiment between 303 and 213 K (every 10 K). Equilibrium constants were measured as previously described (10*d*). IR spectra were recorded on a PerkinElmer Paragon 1000 FT-IR spectrophotometer. FAB⁺-MS were measured by the analytical service of Laboratorium für Organische Chemie of the ETH Zürich on a ZAB VSEQ instrument.

$[RuBr(dppp)_2]PF_6$ (1c)

Complex **1a** (22 mg, 20 μmol) and 1,3-diphenylallyl bromide (4.8 mg, 20 μmol) were dissolved in $CDCl_3$ (0.5 mL). Addition of 2-PrOH (1 mL) and evaporation of the $CDCl_3$ yielded a dark-brown crystalline product, which was filtered off and dried under vacuum. Yield: 21 mg (90%). Crystals for X-ray and elemental analyses were obtained by slow evaporation of CH_2Cl_2–2-PrOH solutions of the complex. FAB⁺-MS *m*/*z* (%): 1007 ($[M + H]^+$, 100), 926 ($[M - Br]^+$, 6), 511 ($[Ru(dppp)]^+$, 5). ^1H NMR (250 MHz, $CDCl_3$) δ: 7.80–7.90 (m, 4H, PhH), 7.10–7.60 (m, 24H, PhH), 6.80– 7.00 (m, 12H, PhH), 2.90–3.00 (m, 2H, CH_2), 2.60–2.70 (m, 2H, CH_2), 2.10–2.50 (m, 4H, CH_2), 1.60–1.70 (m, 2H, CH_2), 0.80–0.90 (m, 2H, CH_2). ^{31}P NMR (101 MHz, $CDCl_3$) δ: 43.5 (t, $J_{P,P}$ = 32 Hz), –4.4 (t, $J_{P,P}$ = 32 Hz), –143 (septet, $J_{P,F}$ = 710 Hz, PF_6). Anal. calcd. for $C_{54}H_{52}BrF_6P_5Ru{\cdot}0.25CH_2Cl_2$: C 55.59, H 4.51; found: C 55.63, H 4.63.

[5] Recent review on olefin metathesis, including the ruthenium-based Grubbs' catalysts, see ref. 16.

© 2001 NRC Canada

Table 1. Crystallographic data for **1c**, **1d**, **2c**, and **2d**.

	1c	**1d**	**2c**	**2d**
Formula	$C_{55}H_{54}BrCl_2F_6P_5Ru$	$C_{55}H_{54}Cl_2F_6IP_5Ru$	$C_{52}H_{48}BrF_6P_5Ru$	$C_{106}H_{100}Cl_4\ I_{10}P_8Ru_2Tl_2$
FW	1235.71	1282.70	1122.73	3643.30
Space group	$P2_1$	$P2_1$	$P2_1/c$	$P\bar{1}$
a (Å)	11.568(7)	11.628(4)	12.5409(2)	16.4029(4)
b (Å)	14.863(6)	14.836(4)	15.5269(2)	18.4970(5)
c (Å)	15.449(11)	15.766(5)	26.5846(1)	19.4795(5)
α (°)	90	90	90	97.965(1)
β (°)	94.54(5)	95.234(8)	95.728(1)	97.46
γ (°)	90	90	90	93.195(1)
V (Å^3)	2648(3)	2709(2)	5150.7(1)	5787.2(3)
Z	2	2	4	2
T (°C)	20	20	20	–40
λ (Å)	0.71073	0.71073	0.71073	0.71073
$\rho_{calcd.}$ (g cm^{-3})	1.550	1.573	1.448	2.091
μ (mm^{-1})	1.361	1.163	1.291	5.946
R ($I > 2\sigma(I)$)	0.0385	0.0625	0.0570	0.0545
wR_2 ($I > 2\sigma(I)$)	0.0979	0.1086	0.1159	0.0911
R_1 (all data)[a]	0.0419	0.1259	0.0840	0.1388
wR_2 (all data)[b]	0.0993	0.1363	0.1302	0.1182

[a] $R_1 = \Sigma||F_o|| - ||F_c|| / \Sigma|F_o|$.
[b] $wR_2 = [\Sigma w(F_o^2 - F_c^2)^2 / \Sigma w(F_o^2)^2]^{1/2}$.

[RuI(dppp)$_2$]PF$_6$ (1d)

Complex **1a** (22 mg, 20 μmol) and *t*-BuI (24 μL, 20 μmol) were dissolved in $CDCl_3$ (0.5 mL). After 6 h 2-PrOH (10 mL) was added, and the $CDCl_3$ was evaporated. The resulting dark-green crystalline product was filtered off and dried under vacuum. Yield: 19 mg (81%). Crystals for X-ray and elemental analyses were obtained by slow evaporation of CH_2Cl_2–2-PrOH solutions of the complex. FAB$^+$-MS *m*/*z* (%): 1052 ([M]$^+$, 100), 926 ([M – HI]$^+$, 9). ^{1}H NMR (250 MHz, $CDCl_3$) δ: 8.00–8.05 (m, 4H, PhH), 6.96–7.61 (m, 28H, PhH), 6.85–6.94 (m, 4H, PhH), 6.72–6.82 (m, 4H, PhH), 2.82–3.00 (m, 2H, CH_2), 2.48–2.67 (m, 2H, CH_2), 2.05–2.42 (m, 4H, CH_2), 1.15–1.52 (m, 4H, CH_2). ^{31}P NMR (101 MHz, $CDCl_3$) δ: 31.9 (t, $J_{P,P}$ = 31 Hz), 5.7 (t, $J_{P,P}$ = 31 Hz), –143 (septet, $J_{P,F}$ = 710 Hz, PF_6). Anal. calcd. for $C_{54}H_{52}F_6IP_5Ru\cdot 0.75CH_2Cl_2$: C 52.13, H 4.27; found: C 52.04, H 4.52.

Observation of [RuBr(η^2-H$_2$)(dppp)$_2$]PF$_6$ (4c)

Complex **1c** (20 mg, 17 μmol) was dissolved in $CDCl_3$ (0.5 mL) and treated with H_2 gas (100 bar, 1 bar = 100 kPa). After 1 h of reaction time at room temperature, the pressure was released, and the sample was removed from the autoclave. Its ^{31}P NMR spectrum shows a conversion of 40% to the dihydrogen complex **4c** as well as 60% of unchanged starting material. This sample was used to measure the longitudinal relaxation times (T_1 (min)). ^{1}H NMR (250 MHz, $CDCl_3$) δ: –10.3 (br s, 2H, Ru-(η^2-H$_2$)). ^{31}P NMR (101 MHz, $CDCl_3$) δ: 5.1 (s), –143 (septet, $J_{P,F}$ = 710 Hz, PF_6).

Observation of [RuI(η^2-H$_2$)(dppp)$_2$]PF$_6$ (4d)

Complex **1d** (20 mg, 17 μmol) was dissolved in $CDCl_3$ (0.5 mL) and treated with H_2 gas at 1 atm (1 atm = 101.322 kPa). After 3 h of reaction time, the ^{31}P NMR spectrum of the sample showed the signals of **1d** (93%) and **4d** (7%). ^{1}H NMR (250 MHz, $CDCl_3$) δ: –10.8 (br s, 2H, Ru-(η^2-H$_2$)). ^{31}P NMR (101 MHz, $CDCl_3$) δ: 5.1 (s, 4P, **4d**), –143 (septet, $J_{P,F}$ = 710 Hz, PF_6). After measuring the NMR spectra, the solution was pressurized to 100 bar H_2 for 16 h in an autoclave, the pressure was released, and the ^{1}H and ^{31}P NMR spectra were recorded again.

[RuBr(dppe)$_2$]PF$_6$ (2c)

Complex **3** (24 mg, 20 μmol) and 1,3-diphenylallyl bromide (4.8 mg, 20 μmol) were dissolved in $CDCl_3$ (0.5 mL). After 24 h of reaction time, addition of 2-PrOH (1 mL) and evaporation of the $CDCl_3$ precipitated a dark-brown crystalline product. Yield: 20 mg (86%). Crystals for X-ray and elemental analyses were obtained by slow evaporation of CH_2Cl_2–2-PrOH solutions of the complex. FAB$^+$-MS *m*/*z* (%): 979 ([M(^{81}Br)]$^+$, 100), 977 ([M(^{79}Br)]$^+$, 89), 897 ([M – HBr]$^+$, 16), 497 ([Ru(dppe)]$^+$, 3). ^{1}H NMR (250 MHz, $CDCl_3$) δ: 7.76–7.82 (m, 4H, PhH), 7.53–7.62 (m, 2H, PhH), 7.13–7.39 (m, 18H, PhH), 6.95–7.03 (m, 12H, PhH), 6.74–6.81 (m, 4H, PhH), 2.38–2.65 (m, 6H, CH_2), 1.40–1.62 (m, 2H, CH_2). ^{31}P NMR (101 MHz, $CDCl_3$) δ: 81.1 (t, $J_{P,P}$ = 12 Hz), 58.4 (t, $J_{P,P}$ = 12 Hz), –143 (septet, $J_{P,F}$ = 710 Hz, PF_6). Anal. calcd. for $C_{52}H_{48}BrF_6P_5Ru\cdot CH_2Cl_2$: C 52.71, H 4.17; found: C 52.94, H 4.46.

[RuI(dppe)$_2$]TlI$_4$ (2d)

Complex **3** (128 mg, 0.1 mmol) and *t*-BuI (0.6 mL, 0.5 mmol) were dissolved in CH_2Cl_2 (10 mL). Addition of 2-PrOH (10 mL) and evaporation of the $CDCl_3$ precipitated a dark green-brown crystalline product. Yield: 156 mg (90%). FAB$^+$-MS *m*/*z (%)*: 1153 ([M + I]$^+$, 100), 897 ([M – HI]$^+$, 50). ^{1}H NMR (250 MHz, $CDCl_3$) δ: 7.85–7.93 (m, 4H, PhH), 7.59–7.66 (m, 2H, PhH), 6.88–7.50 (m, 30H, PhH), 6.70–6.89 (m, 4H, PhH), 2.31–2.75 (m, 6H, CH_2), 1.75–1.96 (m, 2H, CH_2). ^{31}P NMR (101 MHz, $CDCl_3$) δ: 75.4 (t, $J_{P,P}$ = 12 Hz), 65.3 (t, $J_{P,P}$ = 12 Hz), –143 (septet, $J_{P,F}$ = 710 Hz,

© 2001 NRC Canada

Fig. 1. ORTEP drawing of $[RuBr(dppp)_2]^+$ (**1c**), ellipsoids at 30% probability level.

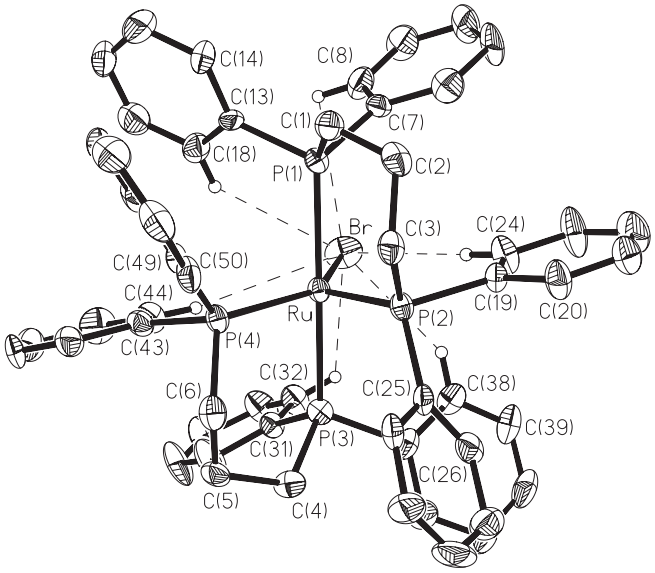
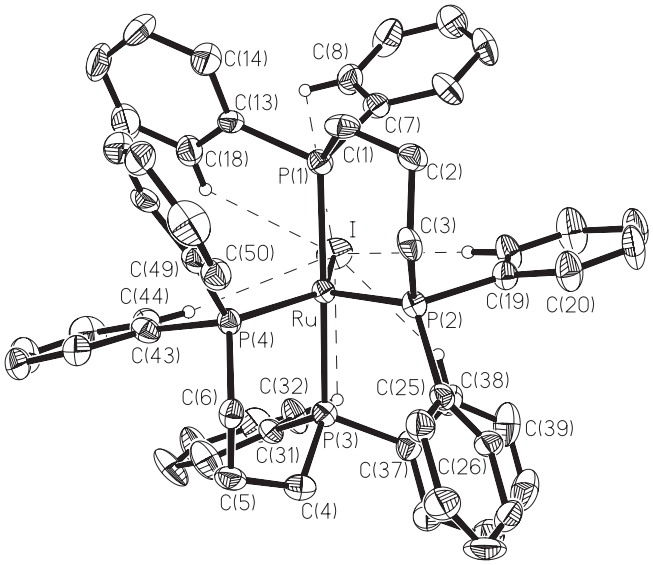


Fig. 2. ORTEP drawing of $[RuI(dppp)_2]^+$ (**1d**), ellipsoids at 30% probability level.



PF_6). Anal. calcd. for $C_{52}H_{48}I_5P_4RuTl \cdot 0.75CH_2Cl_2$: C 35.19, H 2.77; found: C 35.43, H 2.95.

Observation of $[RuBr(\eta^2\text{-}H_2)(dppe)_2]PF_6$ (5c)

Complex **2c** (24 mg, 21 μmol) was dissolved in $CDCl_3$ (0.5 mL) and treated with gaseous H_2 (1 bar, 4 h). ^{1}H NMR (250 MHz, $CDCl_3$) δ: 7.24–7.37 (m, 24H, PhH), 6.98–7.08 (m, 16H, PhH), 2.78–3.01 (m, 4H, CH_2), 2.21–2.46 (m, 4H, CH_2), –11.4 (br s, 2H, Ru-η^2-H_2). ^{31}P NMR (101 MHz, $CDCl_3$) δ: 50.9 (s), –143 (septet, $J_{P,F}$ = 710 Hz, PF_6).

Observation of $[RuI(\eta^2\text{-}H_2)(dppe)_2]TlI_4$ (5d)

Complex **2d** (24 mg, 20 μmol) was dissolved in $CDCl_3$ (0.5 mL) and treated with H_2 gas (1 bar, 10 min). ^{1}H NMR (250 MHz, $CDCl_3$) δ: 7.41–7.53 (m, 4H, PhH), 7.29–7.36 (m, 12H, PhH), 7.10–7.15 (m, 24H, PhH), 3.07–3.22 (m, 4H, CH_2), 2.40–2.57 (m, 4H, CH_2), –10.6 (br s, 2H, Ru-η^2-H_2). ^{31}P NMR (101 MHz, $CDCl_3$) δ: 47.3 (s), –143 (septet, $J_{P,F}$ = 710 Hz, PF_6).

X-ray structure determinations

Crystals of the complexes were grown by slow evaporation of CH_2Cl_2–*i*-PrOH solutions. Crystallographic data for **1c**, **1d**, **2c**, and **2d** are summarized in Table 1.[6]

1c

Dark-brown platelet. Data were collected on a four-circle Syntex $P2_1$ diffractometer. Unit cell dimensions determination and data reduction were performed by standard procedures. No absorption correction was applied. The structures were solved with SHELXS 96 using direct methods, and refined by full-matrix least-squares on F^2 with anisotropic displacement parameters for all non-H atoms. In addition to the complex cation and $[PF_6]^-$, the unit cell contains one CH_2Cl_2 molecule. Of the 2609 unique reflections with index ranges $0 \le h \le 11$, $0 \le k \le 14$, $14 \le l \le 14$, 2362 with $F > 2.0\sigma(F)$ were used in the refinement (631 parameters). Disordered atoms were refined isotropically. Hydrogen atoms were introduced at calculated positions, and refined with the riding model and individual isotropic thermal parameters for each group. Max and min difference peaks +0.636 and –0.795 e Å^{-3}; largest and mean Δ/σ = –0.003 and 0.000.

1d

Dark-green prism. Data were collected on a Siemens CCD SMART area detector system equipped with a normal focus Mo-target X-ray tube. Unit cell dimensions determination and data reduction were performed by standard procedures. An empirical absorption correction (SADABS) was applied. The structures were solved with SHELXS 96 using direct methods, and refined by full-matrix least-squares on F^2 with anisotropic displacement parameters for all non-H atoms. In addition to the complex cation and $[PF_6]^-$, the unit cell contains one CH_2Cl_2 molecule. Of the 9630 unique reflections with index ranges $-14 \le h \le 4$, $-17 \le k \le 18$, $-18 \le l \le 19$, 5908 with $F > 2.0\sigma(F)$ were used in the refinement (631 parameters). Max and min difference peaks +0.52 and –0.73 e Å^{-3}; largest and mean Δ/σ = 0.574 and 0.038.

2c

Dark-brown prism. Data collection, structure solution, and refinement were as described for **1d**. In addition to the complex cation and $[PF_6]^-$, the unit cell contains one severely disordered CH_2Cl_2 molecule, whose atomic positions were not refined. Of the 7390 unique reflections with index ranges

[6] Copies of material on deposit (tables of atomic coordinates, anisotropic displacement coefficients, extended lists of interatomic distances and angles, and calculated H atom positions) may be purchased from: The Depository of Unpublished Data, Document Delivery, CISTI, National Research Council Canada, Ottawa, Canada K1A 0S2. For information on obtaining material electronically go to http://www.nrc.ca/cisti/irm/unpub_e.shtml. This material has also been deposited with the Cambridge Crystallographic Data Centre. Copies of the data can be obtained, free of charge, on application to the Director, CCDC, 12 Union Road, Cambridge CB2 1EZ, U.K. (fax: 44-1223-336033 or e-mail: deposit@ccdc.cam.ac.uk).

© 2001 NRC Canada

Table 2. Comparison of coordination bond distances (Å) and angles (°) for $[RuF(dppp)_2]PF_6$ (**1a**), $[RuCl(dppp)_2]PF_6$ (**1b**), $[RuBr(dppp)_2]PF_6$ (**1c**), and $[RuI(dppp)_2]PF_6$ (**1d**).

	1a[a]	**1b**[b]	**1c**	**1d**[c]
Bond distance (Å)				
Ru—X	2.030(7) (2.033(9))	2.371(5)	2.491(2)	2.705(1)
Ru—P(1)	2.423(1)	2.402(4)	2.408(3)	2.421(3)
Ru—P(2)	2.261(1)	2.263(3)	2.249(3)	2.264(3)
Ru—P(3)	2.408(1)	2.431(4)	2.434(4)	2.443(3)
Ru—P(4)	2.254(1)	2.267(4)	2.259(3)	2.284(2)
X···H(8)	**2.11** (**2.27**)	3.00	3.08	3.30
X···H(18)	2.81 (**2.18**)	**2.83**	**2.83**	**2.99**
X···H(24)	**2.53** (3.14)	**2.62**	**2.75**	**2.96**
X···H(32)	**2.41** (**2.54**)	**2.65**	**2.75**	**3.10**
X···H(38)	**2.31** (2.97)	**2.55**	**2.67**	**2.81**
X···H(44)	2.88 (**2.24**)	3.02	3.07	3.23
Bond angle (°)				
P(1)-Ru-X	88.8(2) (85.8(2))	83.6(1)	84.22(9)	84.95(7)
P(2)-Ru-X	125.3(2) (145.5(2))	126.2(1)	128.09(10)	129.29(7)
P(3)-Ru-X	82.9(2) (85.5(2))	87.8(1)	88.34(9)	88.15(7)
P(4)-Ru-X	139.6(2) (119.7(2))	139.8(1)	137.78(9)	136.71(7)
P(1)-Ru-P(2)	89.41(4)	89.4(1)	89.47(11)	89.30(9)
P(1)-Ru-P(3)	171.26(4)	171.2(1)	172.31(12)	172.92(10)
P(1)-Ru-P(4)	96.51(4)	96.5(1)	95.83(11)	95.32(9)
P(2)-Ru-P(3)	97.40(4)	97.5(1)	96.69(11)	96.34(9)
P(2)-Ru-P(4)	94.85(4)	93.9(1)	94.10(11)	93.97(9)
P(3)-Ru-P(4)	88.39(4)	88.6(1)	88.36(12)	88.59(9)
ϕ	7.3 (–12.9)	6.8	4.9	3.8
X···H-C(18)	—	137	141	141
X···H-C(24)	—	169	172	174
X···H-C(32)	—	120	117	104
X···H-C(38)	—	144	147	148

[a]From ref. 26*b*.
[b]From ref. 30, atoms have been renumbered for consistency.
[c]The X···H distances are calculated assuming a C—H distance of 1.00 Å. Values in boldface are used to calculate average values in Table 3. Values in parentheses refer to the F position with lower occupancy.

Table 3. Properties of halides and selected metric data for **1a**–**d**.

	F	Cl	Br	I
$d_{Ru—X}$ (Å)	2.03	2.37	2.49	2.70
$\Delta d_{Ru—X}$ (Å)	0.00	0.34	0.46	0.67
r_{cov} (Å)	0.64	0.99	1.14	1.33
Δr_{cov} (Å)	0.00	0.35	0.50	0.69
r_{vdW} (Å)	1.50	1.80	1.95	2.15
cone angle (°)[a]	95	99	103	106
$r_{vdW}(C) + r_{vdW}(H)$ (Å)	2.70	3.00	3.15	3.35
$d(X\cdots H)_{av}$ (Å)	2.33 [2.31]	2.66[b]	2.75	2.96
$\Delta(d(X\cdots H)_{av})$ (Å)[c]	0.38	0.34	0.40	0.39

Note: Halogen data from J. E. Huheey, E. A. Keiter and R. L. Keiter. Inorganic chemistry: Principles of structure and reactivity. Harper Collins, New York, N.Y. 1993. p. 991.
[a]Calculated from the values of the van der Waals radius r_{vdW} and the experimental Ru—X distance.
[b]Calculated from atomic coordinates in ref. 30.
[c]$\Delta(d(X\cdots H)_{av})$ is the difference between the sum of the van der Waals radii of C and H ($r_{vdW}(C) + r_{vdW}(H)$) and the average of the four shortest C···H contacts ($d(X\cdots H)_{av}$).

$-13 \le h \le 7$, $-17 \le k \le 17$, $-29 \le l \le 29$, 5711 with $F > 2.0\sigma(F)$ were used in the refinement (586 parameters). Max and min difference peaks +0.64 and –0.80 e Å^{-3}; largest and mean Δ/σ = –0.005 and 0.000.

2d

Dark-green brown prism. Data collection and structure solution and refinement were as described for **1d**. The unit cell contains two crystallographically independent complex cations, two independent $[TlI_4]^-$ anions, one CH_2Cl_2 molecule in general positions, and a second CH_2Cl_2 molecule (0.5 occupancy) whose C atom lies close to a binary axis. Of the 28 299 unique reflections with index ranges $-22 \le h \le 19$, $-24 \le k \le 23$, $-26 \le l \le 23$, 14 820 with $F > 2.0\sigma(F)$ were used in the refinement (1175 parameters). Max and min difference peaks +1.46 and –1.47 e Å^{-3}; largest and mean Δ/σ = –0.298 and 0.003.

Results and discussion

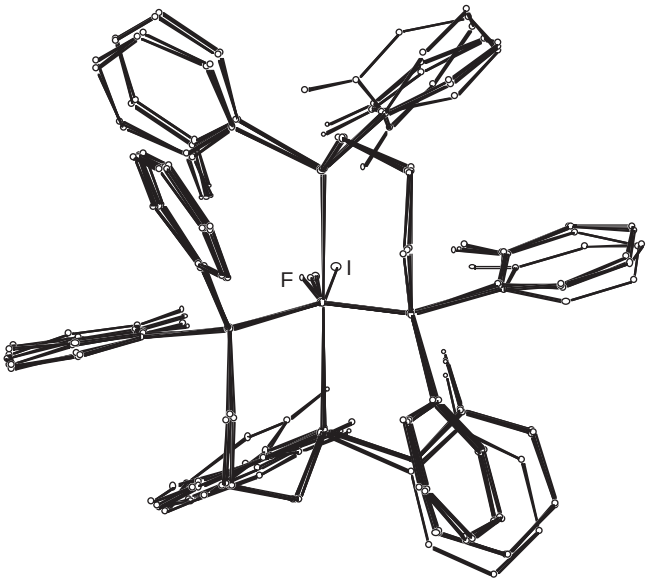
$[RuX(dppp)_2]^+$

The reaction of the fluoro complex $[RuF(dppp)_2]PF_6$ (**1a**) (26*a*) with 1,3-diphenylallyl bromide gives $[RuBr(dppp)_2]PF_6$ (**1c**) as shown in Scheme 1.[7]

[7]Complex **1c** has been previously prepared from $[RuBr_2(PPh_3)_3]$ (8*a*).

© 2001 NRC Canada

Fig. 3. Superposed structure drawings of **1a**–**d**.



The reaction is instantaneous at room temperature and gives the already known bromo complex in essentially quantitative yield. Alternatively to 1,3-diphenylallyl bromide, Ph_2CHBr or $(CH_3)_3CBr$ can be used as source of bromide. The iodo analogue $[RuI(dppp)_2]PF_6$ (**1d**) was prepared by reaction of **1a** with *tert*-butyl iodide (Scheme 1). The substitution reaction occurs within 5 h at room temperature and is favoured with respect to the elimination reaction, as only 9% of isobutene is formed with *t*-BuI. In contrast, *t*-BuBr reacted with **1a** only at 50°C giving isobutene as the major product, but with a quantitative yield of **1c** (26*a*). The identity of the fluoro alkyls and their yield have been ascertained as previously described (26). In the present paper, we focus the attention on the characterization of inorganic counterpart, i.e., the $[RuX(P^{\frown}P)_2]^+$ complexes (X = Br or I).

To study the effect of the diphosphine ligand parallel to that of the halide, we attempted the synthesis of the dppe analogue of **1a**, i.e., $[RuF(dppe)_2]PF_6$ by the same method followed for **1a** (halide exchange with TlF). Instead of the expected five-coordinate fluoro complex, the reaction of $[RuCl(dppe)_2]PF_6$ (**2b**) (8*d*) with TlF gave a doubly F-bridged thallium adduct $[Tl(\mu\text{-}F)_2Ru(dppe)_2]PF_6$ (**3**).[8] However, complex **3** reacts with alkyl bromides or iodides in the same way as **1a**. Thus, $[RuBr(dppe)_2]PF_6$ (**2c**) was obtained by treating **3** with 1,3-diphenylallyl bromide. Also, the reaction of **3** with *tert*-butyl iodide yielded $[RuI(dppe)_2]TlI_4$. However, in this case the Tl(I) ion activates the C–I bond, and $[TlI_4]^-$ is formed. Therefore, the reaction only goes to completion when an excess of *t*-BuI is added (approximately 5 equiv). Under these conditions, we isolated crystals of $[RuI(dppe)_2]TlI_4$ (**2d**), which contained tetraiodothallate(III) as counterion.

As a general comment, it should be noted that the above procedure requires neither the use of bromide- or iodide-containing precursors, nor the halide metathesis carried out with large excesses of halide salts (8*b*, *c*). Moreover, as the fluoride ion is effectively scavenged by the formation of R-F (or, in part, of HF), this method is safe with respect to the formation of mixed-halo complexes, whereas halide metathesis starting from chloro complexes occasionally fails because of the higher affinity of ruthenium(II) for chloride than for bromide or iodide (27, 28). Furthermore, the synthesis via the fluoro complexes **1a** and **2a** can also be applied in the cases where a suitable starting material is not available (e.g., a metal salt), which is the case of the iodo derivatives.

The characterization of **1c**, **1d**, **2c**, and **2d** is based on elemental analyses, FAB^+-MS, and ^{31}P and ^1H NMR spectroscopy. Additionally, their structures were determined crystallographically. As already observed for the fluoro and chloro analogues **1a** and **1b**, the ^{31}P NMR spectra of **1c** and **1d** are static at room temperature, which indicates that the exchange process between the axial and equatorial phosphines is slow on the NMR time-scale at 20°C. The AA′XX′ spin systems are indicative of C_2 symmetry. Also **2c** and **2d** give static AA′XX′ spectra at room temperature. The complexes have dark-brown (**1c**, **2c**), dark-green (**1d**), or intermediate colours (**2d**), and are stable in dichloromethane or chloroform solution for several days under inert gas.

X-ray structures of $[RuX(dppp)_2]^+$ (X = F, Cl, Br, I)

To get some insight into the effect of the halide on the structural features of the whole series $[RuX(dppp)_2]^+$ (X = F (**1a**), Cl (**1b**), Br (**1c**), I (**1d**)), we determined the X-ray structures of the new five-coordinate complexes **1c** and **1d** (Figs. 1 and 2, respectively), which will be discussed jointly and compared with those of the already known **1a** (26) and **1b** (30) (Table 2). The crystals of **1b**, **1c**, and **1d** are isomorphous, whereas **1a** crystallizes in the $P2_1/n$ space group with $Z = 4$ (Table 1).

The most striking aspect is the similarity of the five-coordinate structure throughout the series. The largest difference is obviously the Ru—X distance, which is expected to be indicative of the presence of a π-component of the Ru–X bond. Indeed, all Ru—X distances are in the lower range observed for the corresponding halide. The Ru—Br distance in **1c** (2.491(2) Å) is slightly shorter than the average observed for ruthenium bromo complexes (2.52(4) Å) (31). This value compares with the Ru—Br distances of other $16e^-$ bromo complexes reported, i.e., $[RuBr_2(PPh_3)_2]$ (2.515(1) and 2.526(1) Å) (22), $[RuBr_2(C{=}CH\text{-}t\text{-}Bu)(PPh_3)_2]$ (2.469(2) and 2.460(2) Å) (23), and $[RuBr(CO)(\sigma\text{-}E\text{-}C(H){=}C(H)CH_2PPh_3)(PPh_3)_2]$ (2.541(2) Å) (24). Taken together, however, these data do not show an unambiguous correlation between the Ru—Br bond length and the electron count of the metal.

In the iodo derivative **1d**, the Ru—I distance of 2.705(1) Å is close to the one of 2.710(1) Å observed in the $16e^-$ complex $[RuH(I)(\eta^2\text{-}H_2)(PCy_3)_2]$ (6). These compare with the Ru—I distances in six-coordinate Ru(II)-complexes from the CSD database, whose average and lower quartile are 2.74(3) and 2.716 Å, respectively, (31). The much longer Ru—I distance (2.8025(4) Å) found in the five-coordinate $[RuI(PPh_3)(C_6H_3(CH_2NMe_2)_2\text{-}2,6)]$ (25) is possibly a result of the high *trans* influence of the aryl ligand that occupies the position *trans* to I.

[8] Details of the preparation and characterization of **3** will be published elsewhere.

© 2001 NRC Canada

Table 4. Comparison between the selected bond distances (Å) and angles (°) for $[RuCl(dppe)_2]PF_6$ (**2b**), $[RuBr(dppe)_2]PF_6$ (**2c**), and $[RuI(dppe)_2]PF_6$ (**2d**).

	2b[a]	**2c**	**2d**
Bond distance (Å)			
Ru—X	2.395(1)	2.5363(8)	2.6856(8)
Ru—P(1)	2.243(2)	2.2485(17)	2.261(2)
Ru—P(2)	2.371(2)	2.3711(17)	2.394(2)
Ru—P(3)	2.238(2)	2.2469(16)	2.254(2)
Ru—P(4)	2.372(2)	2.3773(16)	2.369(2)
X···H(4)	2.77	2.86	3.07
X···H(16)	2.71	2.87	3.04
X···H(26)	2.83	2.93	3.21
X···H(30)	2.71	2.81	3.05
X···H(42)	2.80	2.94	3.39
X···H(48)	2.91	2.96	3.34
Bond angle (°)			
P(1)-Ru-X	135.8(1)	135.73(5)	133.30(6)
P(2)-Ru-X	92.1(1)	91.84(4)	94.49(6)
P(3)-Ru-X	129.1(1)	129.75(5)	132.69(6)
P(4)-Ru-X	90.9(1)	91.30(4)	88.15(5)
P(1)-Ru-P(2)	80.1(1)	80.40(6)	79.55(8)
P(1)-Ru-P(3)	95.0(1)	94.51(6)	93.91(8)
P(1)-Ru-P(4)	98.0(1)	97.55(6)	98.34(8)
P(2)-Ru-P(3)	98.2(1)	97.84(6)	97.57(8)
P(2)-Ru-P(4)	177.0(1)	176.84(6)	177.33(8)
P(3)-u-P(4)	79.6(1)	79.88(6)	80.89(8)
ϕ	3.4	3.0	0.4
X···H-C(4)	169	168	170
X···H-C(16)	128	120	119
X···H-C(30)	167	170	165

[a]From ref. 8*d*. Atoms have been renumbered for consistency with **2c** and **d**.

It has been proposed that the π-donation decreases in the series F > Cl > Br > I (32). However, comparison of the data of **1** suggests that the increase of the Ru—X bond length (Δd_{Ru-X}) along the series F, Cl, Br, and I parallels the increase of the covalent radius of the halogens (Δr_{cov}) (Table 3). Thus, the effect if any, is too small to be observed by X-ray crystallography.

Whatever the contribution of the π-donation from the halide ligand may be, all complexes show the typical geometrical features of the Y-shaped coordination that have been observed in a number of five-coordinate complexes of *d* metal ions (12). Thus, the equatorial P-Ru-P angle is reduced to a value close to 90°. This distortion rehybridizes the empty d_{xy} orbital towards the halide ligand and maximizes its overlap with one doubly occupied p_π orbital of the halide (12). In **1c** and **1d**, the two equatorial phosphorus atoms, the halide, and the ruthenium are coplanar within ±0.02 Å.

Interestingly, the average Ru—P distances remain constant throughout the series (2.34 Å for **1a**–**c** and 2.35 Å for **1d**), which is a strong indication that **1a**–**d** are very similar, both electronically and sterically. The bite angles of the chelate (88 and 89°) in the four dppp complexes **1a**–**d** match the usual value found for this ligand (26, 30). In **1a**–**d** the angles formed by an equatorial and axial phosphorus in different ligands is opened up to 95–98°, which is probably due to the sterically demanding Ph_2P groups.

The superimposition of molecular diagrams of the four complexes $[RuX(dppp)_2]^+$ (X = F, Cl, Br, or I) reveals a further structural trend (Fig. 3). The RuP_4 units fit nearly perfectly, as well as the phenyl groups on the equatorial P atoms (P_{eq}). In contrast, the position of the halide ligand changes monotonously on going from F to I. Inspection of the P_{eq}-Ru-H angles indicates that the Y-shape of the equatorial plane becomes more symmetric on going from F to I. In fact, an intriguing feature of many Y-shaped $16e^-$ complexes is the asymmetry of the Y-frame in the equatorial plane, which results in two largely different P_{eq}-M-P_{eq} angles (12*b*). In the case of the iridium-complexes $[IrX(QPh_3)_2(biph)]$ (Q = P or As; biph = biphenyl-2,2′-diyl), a hybrid quantum mechanical – molecular mechanics method predicts a C_2-symmetric structure instead, and it has been suggested that the distortion of the Y-frame is a result of steric effects (33). This distortion of the C_2-symmetric structure has been described in the case of $[IrX(QPh_3)_2(biph)]$ by means of φ, the angle between the M–X vector, and the ideal binary axis bisecting the L_{eq}-M-L_{eq} angle (L_{eq} is C in this case) (33). We have calculated the φ values for the complexes of the series $[RuX(dppp)_2]^+$ (**1a**–**d**) (Table 2). The data show clearly that fluoride gives the largest deviation from the C_2 symmetry, and that φ decreases on going to the heavier halides. The reason for this fact is not evident, and we tentatively suggest an explanation below.

First, it should be considered that although the cone angle remains nearly constant in the series F, Cl, Br, and I, the actual size of the halide does increase along these series as indicated by the van der Waals radii (Table 3). Figure 3 shows that the pocket formed by the four axial and two equatorial phenyl groups can also accommodate the largest halide(iodide) without major distortions. Thus, it is not evident why the smallest halide (fluoride) gives the larger distortion from the electronically favoured structure, and why the deviation from the ideal Y-shaped geometry decreases on going from **1a** to **1d**. The only explanation we can think of is based on the analysis of the nonbonded distances between the halide ligand and the *ortho*-hydrogen atoms of the neighbouring phenyl groups (Table 2). All four complexes exhibit short X···H-C contacts to the *ortho*-H atoms of the neighbouring phenyl rings. In the case of the fluoro analogue **1a**, the average of the four shortest F···H-C contacts between the disordered F atom and the *ortho*-H atoms of the phenyl rings are 0.38 Å shorter than the sum of the van der Waals radii of fluorine and hydrogen (ca. 2.7 Å) (26*b*), but the disorder of the fluoro ligand precludes a closer analysis. The chloro analogue **1b** shows four X—C distances that are shorter than 3.0 Å, the sum of the van der Waals radii of Cl and H. The Cl···H-C angles are in a range compatible with hydrogen bonding (137–169°) (Table 2). Two H atoms H(8) and H(44) lie further away. This pattern remains qualitatively similar in the bromo and iodo derivatives **1c** and **1d**, which exhibit X···H-C contacts ca. 0.4 Å shorter than the sum of the van der Waals radii (Table 3).

The above data suggest that the breakdown of the C_2 symmetry in the complexes of the lighter halides is due to an "attractive interaction" between the halide ligand and the C–H bonds of the neighbouring phenyl rings. A repulsive in-

© 2001 NRC Canada

Fig. 4. ORTEP drawing of $[RuBr(dppe)_2]^+$ (**2c**), ellipsoids at 30% probability level.

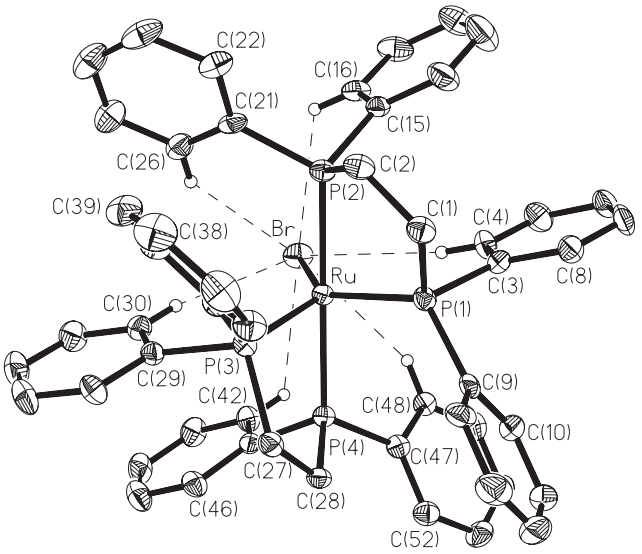
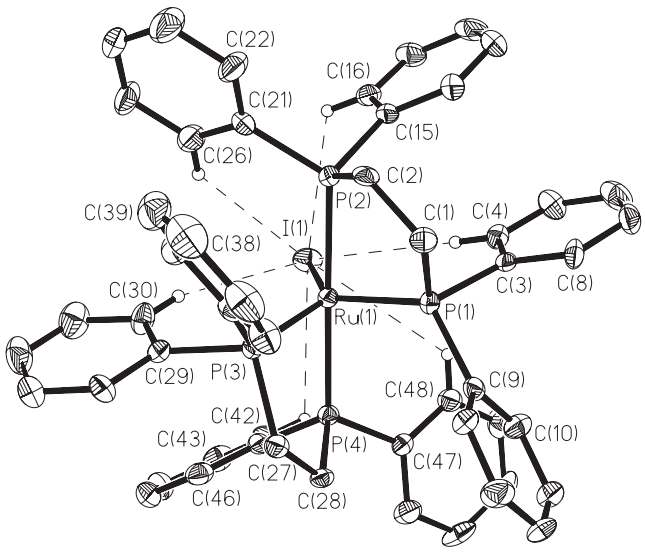


Fig. 5. ORTEP drawing of $[RuI(dppe)_2]^+$ (**2d**), ellipsoids at 30% probability level.



teraction would not explain why the smallest halide (fluoride) gives the largest distortion ϕ. Furtermore, the smallest P_{eq}-Ru-X angle is the one involved in the shortest X···H-C contacts, i.e., P(2)-Ru-X. Such interactions are apparently the hydrogen bonds X···H-C, whose structural features have been discussed above. Thus, the smaller and more electronegative halides move away from the pseudo-C_2 axis to optimize the contact to one of the equatorial phenyl rings.

The problem of the existence and relevance of C-H···B hydrogen bonds in crystals (B is a hydrogen bond acceptor) has been recently reviewed (34). Short C-H···Cl contacts involving chloride ions, found in a number of neutron-diffraction crystal structures, have been interpreted as hydrogen bonds (35). Moreover, the $16e^-$ complex $[RhCl_2(Ph)(PPh_3)_2]$ exhibits two short contacts (2.72(1) Å) to *ortho*-H atoms from the phenyl groups of PPh_3 that have been interpreted as hydrogen bonds on the basis of DFT calculations (36). A word of caution is required in the case of **1a**–**d**, as the X···H-C distances are based on "calculated" hydrogen positions (C—H = 1.00 Å) from X-ray data, and thus accurate H atom positions are not available. However, we consider these data as fairly significant because the van der Waals radii used are those calculated for Ru—X bonds in organic compounds (i.e., $CHCl_3$), which are considerably less polar than metal–halide bonds (37). Indeed, the ionicity of the metal–chloride bond increases the effective van der Waals radius of chloride to a value larger than 1.75 Å calculated for C—Cl bonds (37). Similar, albeit smaller, effects are expected for Br and I.

As a final comment, it should be noted that weaker Cl···H-C interactions are expected for an alyphatic than for an aromatic C–H bond. Indeed, $[RuCl(dcpe)_2]^+$ (dcpe = 1,2-bis(dicyclohexylphosphino)ethane) (8*b*), which contains cyclohexyl instead of phenyl groups, also features short Cl···H-C contacts to α-carbon atoms of three axial and one equatorial cyclohexyl groups (2.47, 2.69, 2.77, and 2.92 Å). However, as expected, the mean value of these contacts (2.71 Å) is slightly larger than in **1b** (2.66 Å).

X-ray structures of $[RuX(dppe)_2]^+$ (X = Cl, Br, I)

In the dppe series $[RuX(dppe)_2]^+$ (X = Cl (**2b**), Br (**2c**), I (**2d**)), the crystals of **2b** and **2c** are isomorphous, whereas those of **2d** are not, owing to the presence of the $[TlI_4]^-$ anion. The crystal of **2d** contains two crystallographically independent complex cations and two independent $[TlI_4]^-$ anions. All nonbonded Ru···Tl distances are longer than 9 Å, and the closest contacts between $[RuI(dppe)_2]^+$ and $[TlI_4]^-$ occur between the iodine atoms and the phenyl rings of dppe.

In the dppe series, the trend of the Ru—X bond lengths is less regular than in the $[RuX(dppp)_2]^+$ complexes. In particular, the Ru—Br distance in **2c** is somewhat longer than expected (Table 4). In **2c**, the two equatorial phosphorus atoms, the bromine, and the ruthenium lie in a perfect plane. In contrast, in **2d**, the iodo ligand is displaced by 0.11 Å from the Ru-P(1)-P(3) plane towards P(4). In both complexes, a further distortion derives from the bite angle of the dppe ligand (ca. 80°).

Interestingly, the equatorial plane of **2b**–**d** has a much more symmetric Y-shape than the dppp series **1a**–**d** (Figs. 4 and 5), as shown by the values of the ϕ angle (Table 4). We suggest that the C_2 symmetry is imposed by the 1,2-ethanediyl bridge of dppe, which is less flexible than the 1,3-propanediyl framework of dppp. Indeed, the "edge on" axial-phenyl groups C(13)–C(18) and C(38)–CC(43) of the dppp derivatives are pinned back as compared with the dppe complexes owing to the smaller chelate ring. Taking the bromo derivatives as example, one sees that H(26) and H(48) are 5.71 Å apart in $[RuBr(dppe)_2]^+$ (**2c**), whereas the equivalent H atoms of $[RuBr(dppp)_2]^+$ (**1c**), H(18) and H(38), are only 5.35 Å apart. Thus, in the dppp complex **1c**, the "edge on" axial-phenyl groups come closer to the halide than in **2c**, and the corresponding hydrogen bonds are shorter (2.83 and 2.67 Å vs. 2.93 and 2.96 Å). Under such conditions, the bromo ligand in **1c** forms short hydrogen bonds (<2.8 Å) to one equatorial phenyl (H(24)) and two axial ones (H(32) and H(38)). As all these Br··· contacts lie in

© 2001 NRC Canada

Table 5. ^{1}H NMR data for $[MXH_2(dppp)_2]^+$.

	X	*K*	δ (η^2-H_2) (ppm)	T_1 (min) (ms)	*T* (K)	Ref.
4b	Cl	72	–10.6	20[a]	223	10*d*
4c	Br	45	–10.3	23	253	this work
4d	I	16	–10.8	not measured	—	—
5b	Cl	*c*	–12.3	31[b]	250	8*d*
5c	Br	*c*	–11.4	32	253	this work
5d	I	*c*	–10.6	34	253	this work

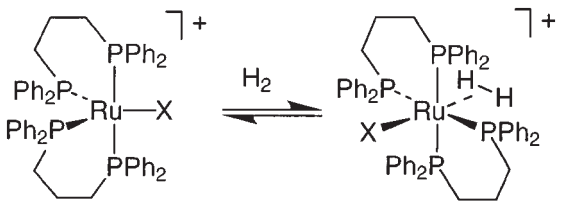
Note: CD_2Cl_2 solution, 500 MHz; *K* and δ values at room temperature; *T* values refer to T_1 measurements.

[a]Converted to 500 MHz from the original value of 8.2 ms at 200 MHz.

[b]Converted to 500 MHz from the original value of 25 ms at 400 MHz.

[c]Quantitative formation.

Scheme 2.



X = Br (**1c**)
X = I (**1d**)

X = Br (**4c**)
X = I (**4d**)

the same quadrant, their shortening goes at the expense of the H(44)···Br contact to the other equatorial phenyl, which is stretched to 3.07 Å. In contrast, the axial phenyl rings are essentially out of reach in the dppe complex **2c**, and the shortest contacts of the bromo ligand involve both equatorial phenyl rings. The Br···H—C contacts with the *ortho*-H atoms H(4) and H(30) are 2.86 and 2.81 Å, respectively. Thus, the X···H—C interactions in the dppe complexes **2** are distributed symmetrically and the Y-shape is least distorted.

In conclusion, we suggest that the higher flexibility of dppp as compared to dppe favours the formation of short hydrogen bonds to the axial phenyl groups and allows the formation of three short contacts within one quadrant. The latter feature enhances the asymmetry of the Y-shape in the dppp complexes.

$[RuX(\eta^2\text{-}H_2)(P^{\frown}P)_2]^+$

The 16e$^-$ complexes $[RuX(P^{\frown}P)_2]^+$ (X = H or Cl) are known to react with H_2 to give the corresponding dihydrogen complexes $[RuX(\eta^2\text{-}H_2)(P^{\frown}P)_2]^+$ (**4**) (9, 10). The properties of the complexes of type **4** strongly depend on nature of the ancillary ligand X. Thus, hydrido-complexes of d^6 metals such as $[MH(\eta^2\text{-}H_2)(P^{\frown}P)_2]^+$ generally feature a rapidly spinning (η^2-H_2) ligand with low acidity (9, 38), whereas their chloro analogues $[MCl(\eta^2\text{-}H_2)(P^{\frown}P)_2]^+$ contain elongated dihydrogen ligands (8*d*, 10). Moreover, both calculation and experiment show that the introduction of a halide as ancillary ligand enhances the acidity of the dihydrogen ligand, which makes the complexes of the type $[RuCl(\eta^2\text{-}H_2)(P^{\frown}P)_2]^+$ interesting for the heterolytic activation of dihydrogen (8*d*, 10*d*, 38–40). Thus, we investigated the reactivity of the bromo and iodo derivatives **1c**, **1d**, **2c**, and **2d** toward dihydrogen (Scheme 2). The resulting dihydrogen complexes $[RuX(\eta^2\text{-}H_2)(P^{\frown}P)_2]^+$ where characterized by ^{1}H and ^{31}P NMR and the minimum relaxation times of the (η^2-H_2) ligand (Table 5). Based on the singlet observed in the ^{31}P NMR spectrum, all dihydrogen complexes are formed as the *trans*-isomer.

The bromo derivative **1c** reacts with H_2 to give the dihydrogen complex $[RuBr(\eta^2\text{-}H_2)(dppp)_2]^+$ (**4c**). The formation of **4c** is an equilibrium reaction as already observed for $[RuCl(dppp)_2]^+$ (**1b**) (10*d*). When a 4×10^{-3} mol L^{-1} solution of **1c** is treated with 1 atm H_2 (1 atm = 101.322 kPa) for 24 h of reaction time, the resulting solution contains 90% of **1c** and 10% of the dihydrogen complex **4c**. The resulting equilibrium constant (*K*) of **1c** is 45, which compares with the value of 72 found for the chloro analogue **1b** (10*d*). The equilibrium is driven to completion when **1c** is treated with H_2 under high pressure (100 bar) in an autoclave for 24 h of reaction time.

The iodo analogue **1d** gives $[RuI(\eta^2\text{-}H_2)(dppp)_2]^+$ (**4d**) by reaction with H_2 at 1 atm. In a 1×10^{-3} mol L^{-1} solution of **1d**, 7% of starting **1d** is converted into **4d** after 3 h of reaction time. Complex **4d** is stable only for limited periods of time (ca. 12 h), and slowly reacts to give the already known $[RuH(\eta^2\text{-}H_2)(dppp)_2]$ and additional unidentified products. We estimate a constant *K* of 16 (under 1 atm H_2) for the equilibrium between **1d**, **4d**, and H_2 based on ^{1}H NMR measurements. Under these conditions the decomposition is slow, and **1d** and **4d** are the only complexes observed by ^{31}P NMR spectroscopy. We attempted to prepare the iodo derivative $[RuI(\eta^2\text{-}H_2)(dppp)_2]^+$ by reacting **1d** with H_2 in an autoclave under 100 bar H_2. However, the dihydrogen complex is formed in minor amounts (ca. 6%) together with the already known $[RuH(\eta^2\text{-}H_2)(dppp)_2]^+$ (ca. 13%) and other unidentified products after 16 h of reaction time. The hydride(dihydrogen) complex $[RuH(\eta^2\text{-}H_2)(dppp)_2]^+$ is apparently formed by elimination of HI from **4d**, followed by readdition of H_2, a reaction that has been observed for the reaction of the fluoro derivative $[RuF(dppp)_2]^+$ with H_2 (26*b*).

In contrast to the dppp complexes, the dppe derivatives **2c** and **2d** react quantitatively with H_2 at atmospheric pressure to give $[RuX(\eta^2\text{-}H_2)(dppe)_2]^+$ (X = Br (**5c**), I (**5d**)). The complexes $[RuX(\eta^2\text{-}H_2)(P^{\frown}P)_2]^+$ (X = halide) such as **4** and **5** are typical elongated dihydrogen complexes. Such complexes have attracted the attention both of synthetic chemists (6, 10) and of theoreticians (38, 40[9], 41) due to the enhanced

[9]For a review of theoretical studies of dihydrogen complexes, see ref. 9.

© 2001 NRC Canada

acidity and the puzzling nature of their dihydrogen ligand. The data in Table 5 show that the properties of the (η^2-H_2) ligand mainly depend on the nature of the diphosphine ligand, whereas the choice of the halide primarily affects the reactivity of $[RuX(P^{\frown}P)_2]^+$ with H_2. As for the effect of the halide ligand on the elongation of the dihydrogen ligand, it should be noted that the T_1 (min) data are nearly constant within each series **4b**, **4c**, and **5b**–**d**. Thus, the T_1 (min) values of **5b**–**d** can be considered identical within experimental error, and the *d*(H—H) bond length remains substantially unchanged troughout the halide series. Hence, the H—H distances in the bromo and iodo derivatives **4c**, **4d**, **5c**, and **5d** are close to those of the corresponding chloro derivatives **4b** and **5b** (1.02 and 1.16 Å, respectively), which were estimated from the value of the $J_{D,H}$ coupling constant (10*d*, 8*d*).

The insensitivity of the T_1 (min) values on the nature of X both in the dppp and in the dppe complexes indicates that the donor properties of the chloro, bromo, and iodo ligands are very similar. As there is ongoing debate on the electronic effects of halide ligands (37, 38, 40, 41), this result is in no way obvious. However, if one accepts that the slight differences observed are significant, then the T_1 (min) data suggest a slight increase of the electron density at the metal on going from Cl to I. This is not necessarily an effect of the π-donor capability of X alone, as the σ-donation (which is larger for iodide) also contributes. It is possible that the decrease of π-donor ability on going down the halide group (32) is counterbalanced by the increased σ-donation in the same sequence (39). In any case, it should be noted that an increase of the T_1 (min) values on going from chloride to bromide for the osmium analogues $[OsX(\eta_2\text{-}H_2)(dppe)_2]^+$ (X = Cl, Br) has been reported by Morris and co-workers (10*e*), although no effect on the *d* (H—H) distance was observed. Unfortunately, we do not have reliable *d* (H—H) values, as the $J_{D,H}$ coupling constants of **4b**, **4c**, and **5b**–**d** are not yet available.

The most remarkable effect of changing the halide is observed in the *K* values of the formation of the dppp derivatives **4** (Table 5). In contrast, the less crowded dppe derivatives **5b**–**d** also give stable dihydrogen complexes with iodide. Taken together, the above observations suggest that changing the halide ligand (Cl, Br, or I) affects the steric crowding of the complex rather than the electron density of the metal. Indeed, although the cone angle remains roughly constant from Cl to I, the van der Waals radius of X increases along the series (Table 3). The position of the equilibrium in Scheme 2 depends on the relative stability of the six-coordinate complex **4** relative to the five-coordinate complex **1**. Ceteris paribus, an increase of the coordination number from 5 to 6 increases the crowding of the complex. The X-ray structure of the osmium analogue $[OsCl(\eta^2\text{-}H_2)(dppp)]^+$ shows that the chloride ligand is fully embedded into a pocket formed by four phenyl groups (10*d*). In this kind of arrangement, the crowding around the metal depends on the van der Waals radius of X rather than on the cone angle, which explains why the stability of the dihydrogen complexes decreases along the series Cl > Br > I owing to increasing crowding in the six-coordinate complex. This is also an indication that besides π-donation, steric factors play an important role in the stabilization of the 16e$^-$ complexes of the heavier halogens as they destabilize the corresponding six-coordinate complexes (7*b*, 8*b*).

Finally, it is noteworthy that the hydrogenolysis of the Ru–X bond is the main reaction at both ends of the F, Cl, Br, and I series. Indeed, both $[RuF(dppp)_2]^+$ and $[RuI(dppp)_2]^+$ form (either quantitatively or in part) $[RuH(\eta^2\text{-}H_2)(dppp)_2]^+$ upon reaction with H_2. In the case of **1a**, we speculated that $[RuH(\eta^2\text{-}H_2)(dppp)_2]^+$ is formed by dissociation of the thermodynamically stable HF from the putative $[RuF(\eta^2\text{-}H_2)(dppp)_2]$ followed by addition of H_2. In the case of $[RuI(\eta^2\text{-}H_2)(dppp)_2]^+$, the same reaction may be triggered by the acidity of the dihydrogen ligand, as iodide is a much weaker base than fluoride. Indeed, a recent theoretical study has shown that the pseudo-aqueous pK_a value of $[MX(\eta^2\text{-}H_2)(H_2PCH_2CH_2PH_2)_2]$ (M = Ru, Os) increases on going from X = F to Br (38). Future work will be directed to assessing the acidity of the $[RuX(\eta^2\text{-}H_2)(P^{\frown}P)_2]^+$ complexes.

Conclusions

The reaction of the fluoro complex $[RuF(dppp)_2]^+$ affords easy access to five-coordinate bromo and, in particular, iodo complexes of ruthenium(II). In turn, the latter complexes are interesting for the investigation of steric and electronic effects of the heavier halogens as ancillary ligands in 16e$^-$ complexes. Preliminary results on H_2 activation suggest that Cl, Br, and I are very similar electronically, which is not obvious in view of their different electronegativities. Thus, one can take advantage of their different size to tune the steric properties of five-coordinate complexes (and of their six-coordinate addition products), while keeping the electron density at the metal constant.

Acknowledgement

We thank Dr. Heinz Rüegger (Laboratory of inorganic chemistry, ETH-Zürich) for the ^{1}H NMR spectroscopic measurements (T_1 (min)).

References

1. (*a*) S.J. La Placa and J.A. Ibers. Inorg. Chem. **4**, 778 (1965); (*b*) G. Jia, I.M. Lee, D.W. Meek, and J.C. Gallucci. Inorg. Chim. Acta, **177**, 81 (1990); (*c*) A. Albinati, Q. Jiang, H. Ruegger, and L.M. Venanzi. Inorg. Chem. **32**, 4940 (1993); (*d*) P. Barbaro, C. Bianchini, and A. Togni. Organometallics, **16**, 3004 (1997).
2. D. Huang, W.E. Streib, J.C. Bollinger, K.C. Caulton, R.F. Winter, and T. Scheiring. J. Am. Chem. Soc. **121**, 8087 (1999).
3. (*a*) Y. Nishibayashi, I. Takei, S. Uemura, and M. Hidai. Organometallics, **17**, 3420 (1998); (*b*) D.C. Mudalige, S.J. Rettig, B.R. James, and W.R. Cullen. Chem. Commun. 830 (1993); (*c*) C.R.S. Hampton, I.R. Butler, W.R. Cullen, B.R. James, J.-P. Charland, and J. Simpson. Inorg. Chem. **31**, 5509 (1992).
4. (*a*) P. Dani, G.P.M. van Klink, and G. van Koten. Eur. J. Inorg. Chem. 1465 (2000); (*b*) P. Dani, T. Karlen, R.A. Gossage, S. Gladiali, and G. van Koten. Angew. Chem. Int. Ed. Engl. **112**, 759 (2000); (*c*) G. Jia, H.M. Lee, and I.D. Williams. J. Organomet. Chem. **534**, 173 (1997).
5. (*a*) M.A. Esteruelas, F. Liu, E. Onate, E. Sola, and B. Zeier. Organometallics, **16**, 2919 (1997); (*b*) C.E.F. Rickard, W.R.

© 2001 NRC Canada

Roper, G.E. Taylor, J.M. Waters, and L.J. Wright. J. Organomet. Chem. **389**, 375 (1990).
6. B. Chaudret, G. Chung, O. Eisenstein, S.A. Jackson, F.J. Lahoz, and J.A. Lopez. J. Am. Chem. Soc. **113**, 2314 (1991).
7. (*a*) J.Y. Shen, C. Slugovc, P. Wiede, K. Mereiter, R. Schmid, and K. Kirchner. Inorg. Chim. Acta, **268**, 69 (1998); (*b*) L. Costella, A. Del Zotto, A. Mezzetti, E. Zangrando, and P. Rigo. J. Chem. Soc. Dalton Trans. 3001 (1993); (*c*) R.M. Stoop and A. Mezzetti. Green Chem. **1**, 39 (1999); (*d*) R.M. Stoop, S. Bachmann, M. Valentini, and A. Mezzetti. Organometallics, **19**, 4117 (2000).
8. (*a*) M. Bressan and P. Rigo. Inorg. Chem. **14**, 2286 (1975); (*b*) A. Mezzetti, A. Del Zotto, P. Rigo, and N. Bresciani Pahor. J. Chem. Soc. Dalton Trans. 1045 (1989); (*c*) A. Mezzetti, A. Del Zotto, and P. Rigo. J. Chem. Soc. Dalton. Trans. 2515 (1990); (*d*) B. Chin, A.J. Lough, R.H. Morris, C.T. Schweitzer, and C. D'Agostino. Inorg. Chem. **33**, 6278 (1994); (*e*) C. Bianchini, F. Laschi, M. Peruzzini, and P. Zanello. Gazz. Chim. Ital. **124**, 271 (1994); (*f*) I. de los Rios, M. Jiménez-Tenorio, M.C. Puerta, I. Salcedo, and P. Valerga. J. Chem. Soc. Dalton Trans. 4619 (1997); (*g*) R.M. Stoop, C. Bauer, P. Setz, M. Wörle, T.Y.H. Wong, and A. Mezzetti. Organometallics, **18**, 5691 (1999).
9. (*a*) P.G. Jessop and R.H. Morris. Coord. Chem. Rev. **121**, 155 (1992); (*b*) D.M. Heinekey and W.J. Oldham. Chem. Rev. **93**, 913 (1993); (*c*) R.H. Morris. Can. J. Chem. **74**, 1907 (1996); (*d*) M.A. Esteruelas and L.A. Oro. Chem. Rev. **98**, 577 (1998).
10. (*a*) E.P. Cappellani, P.A. Maltby, R.H. Morris, C.T. Schweitzer, and M.R. Steele. Inorg. Chem. **28**, 4437 (1989); (*b*) A. Mezzetti, A. Del Zotto, P. Rigo, and E. Farnetti. J. Chem. Soc. Dalton Trans. 1525 (1991); (*c*) A.K. Burrell, J.C. Bryan, and G.J. Kubas. J. Am. Chem. Soc. **116**, 1575 (1994); (*d*) E. Rocchini, A. Mezzetti, H. Rüegger, U. Burckhardt, V. Gramlich, A. Del Zotto, P. Martinuzzi, and P. Rigo. Inorg. Chem. **36**, 711 (1997); (*e*) P.A. Maltby, M. Schlaf, M. Steinbeck, A.J. Lough, R.H. Morris, W.T. Klooster, T.F. Koetzle, and R.C. Srivastava. J. Am. Chem. Soc. **118**, 5396 (1996).
11. (*a*) M. Jiménez-Tenorio, M.C. Puerta, and P. Valerga. Inorg. Chem. **33**, 3515 (1994); (*b*) A. Mezzetti, E. Zangrando, A. Del Zotto, and P. Rigo. J. Chem. Soc. Chem. Commun. 1597 (1994); (*c*) P. Barthazy, M. Wörle, and A. Mezzetti. J. Am. Chem. Soc. **121**, 480 (1999).
12. (*a*) K.G. Caulton. New J. Chem. **18**, 25 (1994); (*b*) J.-F. Riehl, Y. Jean, O. Eisenstein, and M. Pélissier. Organometallics, **11**, 729 (1992); (*c*) T.J. Johnson, K. Folting, W.E. Streib, J.D. Martin, J.C. Huffman, S.A. Jackson, O. Eisenstein, and K.G. Caulton. Inorg. Chem. **34**, 488 (1995).
13. B.L. Pagenkopf and E.M. Carreira. Chem. Eur. J. **5**, 3437 (1999).
14. Y.N.C. Chan and J.A. Obsorn. J. Am. Chem. Soc. **112**, 9400 (1990).
15. (*a*) R. Dorta, P. Egli, F. Zürcher, and A. Togni. J. Am. Chem. Soc. **119**, 10 857 (1997); (*b*) U. Burckhardt, M. Baumann, and A. Togni. Tetrahedron: Asymmetry, **8**, 155 (1997).
16. A. Fürstner. Angew. Chem. Int. Ed. Engl. **112**, 3012 (2000).
17. Y. Wakatsuki, H. Yamazaki, N. Kumegawa, T. Satoh, and J.Y. Satoh. J. Am. Chem. Soc. **113**, 9604 (1991).
18. (*a*) Y. Maruyama, K. Yamamura, T. Sagawa, H. Katayama, and F. Ozawa. Organometallics, **19**, 1308 (2000); (*b*) S.M. Maddock. C.E.F. Rickard, W.R. Roper, and L.J. Wright. Organometallics, **15**, 1793 (1996).
19. (*a*) H. Nishiyama. Enantiomer, **4**, 569 (1999); (*b*) C. Bianchini and H.M. Lee. Organometallics, **19**, 1833 (2000); (*c*) H.M. Lee, C. Bianchini, G. Jia, and P. Barbaro. Organometallics, **18**, 1961 (1999).
20. (*a*) M. Bressan and A. Morvillo. Inorg. Chem. **28**, 950 (1989); (*b*) A. Morvillo and M. Bressan. J. Mol. Catal. A: Chem. **125**, 119 (1997); (*c*) F. Maran, A. Morvillo, N. d'Alessandro, and M. Bressan. Inorg. Chim Acta, **288**, 122 (1999).
21. (*a*) J.T. Poulton, K. Folting, W.E. Streib, and K.G. Caulton. Inorg. Chem. **31**, 3190 (1992); (*b*) J.T. Poulton, M.P. Sigalas, O. Eisenstein, and K.G. Caulton. Inorg. Chem. **32**, 5490 (1993).
22. K.S. MacFarlane, A.M. Joshi, S.J. Rettig, and B.R. James. Inorg. Chem. **35**, 7304 (1996).
23. Y. Wakatsuki, N. Koga, H. Yamazaki, and K. Morokuma. J. Am. Chem. Soc. **116**, 8105 (1994).
24. N.W. Alcock, J. Cartwright, A.F. Hill, M. Marcellin, and H.M. Rawles. J. Chem. Soc. Chem. Commun. 369 (1995).
25. J.P. Sutter, S.L. James, P. Steenwinkel, T. Karlen, D.M. Grove, N. Veldman, W.J.J. Smeets, A.L. Spek, and G. van Koten. Organometallics, **15**, 941 (1996).
26. (*a*) P. Barthazy, L. Hintermann, R.M. Stoop, M. Wörle, A. Mezzetti, and A. Togni. Helv. Chim. Acta, **82**, 2448 (1999); (*b*) P. Barthazy, R.M. Stoop, M. Wörle, A. Togni, and A. Mezzetti. Organometallics, **19**, 2844 (2000).
27. P.R. Hoffman and K.G. Caulton. J. Am. Chem. Soc. **97**, 4221 (1975).
28. T.A. Stephenson and G. Wilkinson. J. Inorg. Nucl. Chem. **28**, 945 (1966).
29. R. Lespieau and R.L. Wakeman. Bull. Soc. Chim. Fr. **51**, 384 (1932).
30. A.A. Batista, L.A. Centeno Cordeiro, and G. Oliva. Inorg. Chim. Acta, **203**, 185 (1993).
31. A.G. Orpen, L. Brammer, F.H. Allen, O. Kennard, D.G. Watson, and R. Taylor. J. Chem. Soc. Dalton Trans. S1 (1989).
32. (*a*) N.M. Doherty and N.W. Hoffman. Chem. Rev. **91**, 553 (1991); (*b*) M. Tilset, J.-R. Hamon, and P. Hamon. Chem. Commun. 765 (1998).
33. G. Ujaque, F. Maseras, O. Eisenstein, L. Liabel-Sands, A.L. Rheingold, W. Yao, and R.H. Crabtree. New. J. Chem. 1493 (1998).
34. (*a*) G.A. Jeffrey. *In* An introduction to hydrogen bonding. Oxford University Press, Oxford, U.K. 1997. p. 85; (*b*) L. Brammer, J.C. Mareque Rivas, and D. Zhao. Inorg. Chem. **37**, 5512 (1998), and ref. therein.
35. (*a*) R. Taylor and O. Kennard. J. Am. Chem. Soc. **104**, 5063 (1982); (*b*) L. Brammer, J.M. Charnock, P.L. Goggin, R.J. Goodfellow, A.G. Orpen, and T.F. Koetzle. J. Chem. Soc. Dalton Trans. 1789 (1991).
36. R. Cini and A. Cavaglioni. Inorg. Chem. **38**, 3751 (1999).
37. G. Ujaque, F. Maseras, and O. Eisenstein. Theor. Chem. Acc. **96**, 146 (1997).
38. Z. Xu, I. Bytheway, G. Jia, and Z. Lin. Organometallics, **18**, 1761 (1999), and ref. 16 therein.
39. G. Jia, H.M. Lee, I.D. Williams, C.P. Lau, and Y. Chen. Organometallics, **16**, 3941 (1997).
40. F. Maseras and A. Lledos. Chem. Rev. **100**, 601 (2000).
41. R. Gelabert, M. Moreno, J.M. Lluch, and A. Lledos. J. Am. Chem. Soc. **120**, 8168 (1998).
41. (*a*) S. Dapprich and G. Frenking. Organometallics, **15**, 4547 (1996); (*b*) E. Clot and O. Eisenstein. J. Phys. Chem. A, **102**, 3592 (1998).

© 2001 NRC Canada

Hydrogen transfer from formic acid to alkynes catalyzed by a diruthenium complex

Yuan Gao, Michael C. Jennings, and Richard J. Puddephatt

Abstract: The diruthenium(0) complex $[Ru_2(\mu\text{-}CO)(CO)_4(\mu\text{-}dppm)_2]$ (**1**) (dppm = $Ph_2PCH_2PPh_2$), is a catalyst for the transfer hydrogenation, using formic acid as hydrogen donor, of the alkynes PhC≡CPh, PhC≡CMe, EtC≡CEt, and PrC≡CPr but not of the terminal alkynes HC≡CH, PhC≡CH, BuC≡CH, or the alkynes containing one or two electron-withdrawing substituents PhC≡CCO_2Me and MeO_2CC≡CCO_2Me. In the successful reactions, the formic acid is first decomposed to carbon dioxide and hydrogen, which then hydrogenates the alkynes in a slower reaction. In the unsuccessful reactions, the decomposition of formic acid is strongly retarded by the alkyne. In the case with the alkyne PhC≡CH, it is shown that the alkyne reacts with protonated **1** to give first $[Ru_2(\mu\text{-}CPh{=}CH_2)(CO)_4(\mu\text{-}dppm)_2][HCO_2]$, which then isomerizes to give the catalytically inactive, stable complex $[Ru_2(\mu\text{-}CH{=}CHPh)(CO)_4(\mu\text{-}dppm)_2][HCO_2]$. This complex has been structurally characterized and both of the μ-styrenyl complexes are shown to be fluxional in solution.

Key words: ruthenium, hydrogenation, catalysis, binuclear.

Résumé : Le complexe de diruthénium(0) $[Ru_2(\mu\text{-}CO)(CO)_4(\mu\text{-}dppm)_2]$ (**1**) (dppm = $Ph_2PCH_2PPh_2$) est un catalyseur pour l'hydrogénation par transfert dans laquelle l'acide formique est utilisé comme source d'hydrogène; cette réaction est efficace pour les alcynes tels que PhC≡CPh, PhC≡CMe, EtC≡CEt et PrC≡CPr, mais elle ne fonctionne pas avec les alcynes terminaux, tels que HC≡CH, PhC≡CH, BuC≡CH, ou avec les alcynes comportant un ou deux substituants électroaffinitaires, tels que PhC≡CCO_2Me et MeO_2CC≡CCO_2Me. Dans les réactions qui donnent les résultats espérés, l'acide formique est initialement décomposé en bioxyde de carbone et en hydrogène qui provoque l'hydrogénation des alcynes dans une réaction plus lente. Dans les réactions qui ne donnent pas les résultats espérés, la décomposition de l'acide formique est fortement ralentie par l'alcyne. Dans le cas de l'alcyne PhC≡CH, on a démontré que l'alcyne réagit avec le complexe **1** protoné pour donner dans une première étape le $[Ru_2(\mu\text{-}CPh{=}CH_2)(CO)_4(\mu\text{-}dppm)_2][HCO_2]$ qui s'isomérise alors pour donner le complexe stable et inactif $[Ru_2(\mu\text{-}CH{=}CHPh)(CO)_4(\mu\text{-}dppm)_2][HCO_2]$. On a caractérisé la structure de ce complexe et on a démontré que, en solution, les deux complexes μ-styrényles sont en état de fluxion.

Mots clés : ruthénium, hydrogénation, catalyseur, binucléaire.

[Traduit par la Rédaction]

Introduction

There has been increasing interest in using formic acid in catalytic transfer hydrogenation of multiple bonds, as an alternative to the traditional hydrogenation using hydrogen gas (1–3). Several active catalysts for this transfer hydrogenation have been identified, and all such catalysts are also active in the decomposition of formic acid to CO_2 and H_2 (1–4). All the catalysts studied so far have been mononuclear, and only a few of these have been studied in terms of reaction mechanisms (3, 4). Since the binuclear complex $[Ru_2(\mu\text{-}CO)(CO)_4(\mu\text{-}dppm)_2]$ (dppm = $Ph_2PCH_2PPh_2$) has been shown to have high activity toward the decomposition of formic acid (5), and also to react easily with terminal alkynes (6), it was considered likely that it might also be active for the catalytic transfer hydrogenation of alkynes using formic acid. This article reports that the desired catalysis is successful and also describes studies of the reaction mechanism.

Received August 8, 2000. Published on the NRC Research Press Web site at http://canjchem.nrc.ca on July 5, 2001.

Dedicated to Professor B.R. James, in recognition of his distinguished contributions to homogeneous catalysis, on the occasion of his 65th birthday.

Y. Gao, M.C. Jennings, and R.J. Puddephatt.[1] Department of Chemistry, University of Western Ontario, London, ON N6A 5B7, Canada.
[1]Corresponding author (telephone: (519) 679-2111; fax: (519) 850-2371; e-mail: pudd@uwo.ca).

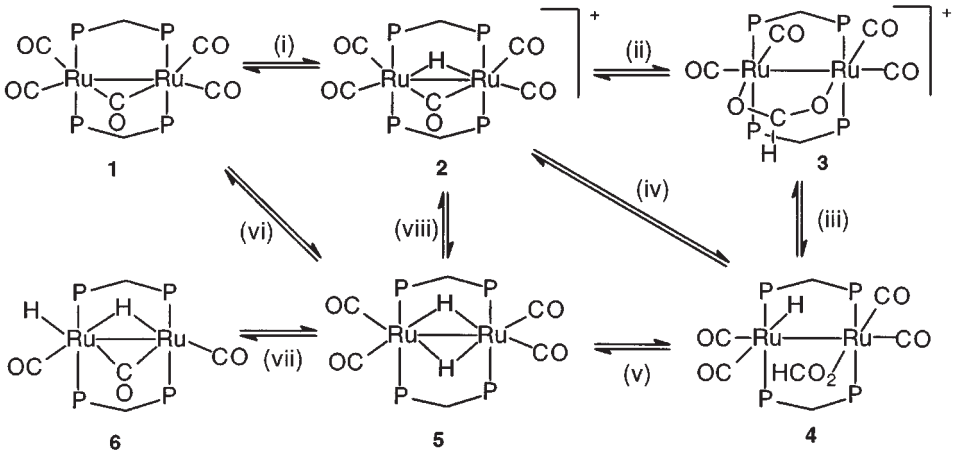
Results

Hydrogen transfer from formic acid to internal alkynes

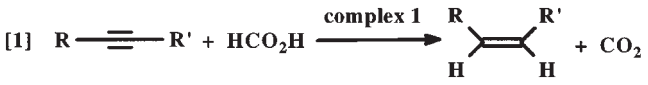
In the presence of $[Ru_2(\mu\text{-}CO)(CO)_4(\mu\text{-}dppm)_2]$ (**1**) the reaction of HCOOH with internal alkynes, containing either phenyl or alkyl substituents (diphenylacetylene, 1-phenyl-1-propyne, 3-hexyne, or 4-octyne), in acetone at room temperature gave the pure *cis*-alkene as shown in eq. [1]. No trace of *trans*-alkene, and no further hydrogenation of alkene to alkane, was detected when the reactions were monitored by ^{1}H NMR. Using a 20:10:1 ratio of formic acid to diphenylacetylene to complex **1**, the reaction to give *cis*-stilbene was complete in 1 day. Incomplete conversion of about 40% was observed when using equimolar amounts of formic acid and diphenylacetylene under similar conditions. The conversion rate of alkyne to alkene was found to follow

 DOI: 10.1139/cjc-79-5/6-915 © 2001 NRC Canada

Scheme 1. Reagents: (*i*) H^+; (*ii*) HCO_2H, H_2; (*iii*) H_2, H^+; (*iv*) HCO_2^-, CO; (*v*) CO_2; (*vi*) CO, H_2; (*vii*) CO; (*viii*) H^+, CO, H_2.



the sequence: diphenylacetylene > > 1-phenyl-1-propyne > 3-hexyne ≈ 4-octyne. For example, using a 10:10:1 molar ratio of HCO_2H:PhCCMe:complex **1**, the conversion was



about 15% after 1 day.

These catalytic hydrogenation reactions were all slower than the catalytic decomposition of formic acid by complex **1** (5). This reaction could be monitored independently by ^1H NMR and it was complete in about 20 min under the above conditions, to give CO_2 and H_2. It is therefore clear that the catalytic transfer hydrogenations occur in two steps. First, the formic acid is decomposed to give hydrogen and then, in a much slower reaction, catalytic hydrogenation of the alkyne occurs. Excess formic acid is required because excess hydrogen is needed for the slow second step. A similar reaction sequence has been proposed for catalytic transfer hydrogenation using formic acid and the mononuclear catalyst $[RuCl_2(PPh_3)_3]$, either alone or in combination with the heterogeneous hydrogenation catalyst Pd/C (7). Complex **1** was shown to be a catalyst for hydrogenation of diphenylacetylene using hydrogen gas at 1 atm (1 atm = 101.325 kPa) pressure, consistent with the above mechanism, and the hydrogenation is not affected by the presence or absence of free carbon dioxide.

The reactions were monitored at low temperature (–5 to –10°C) by NMR using $H^{13}COOH$. The catalytic decomposition of formic acid occurred by way of the intermediates shown in Scheme 1, and occurred at a similar rate as in the absence of alkyne (5). No new intermediates were observed and complex **1** was regenerated once the catalytic decomposition of formic acid was complete (5). No alkene was detected until the formic acid was completely decomposed to CO_2 and H_2. During the subsequent slow hydrogenation step, the only complex present in detectable quantity was complex **1**. This result is not unexpected since these internal alkynes without electronegative substituents (eq. [1]) do not react with complex **1**, but it does show that all reaction intermediates are short-lived (6).

Hydrogen transfer from formic acid to terminal alkynes and to internal alkynes with electron-withdrawing substituents

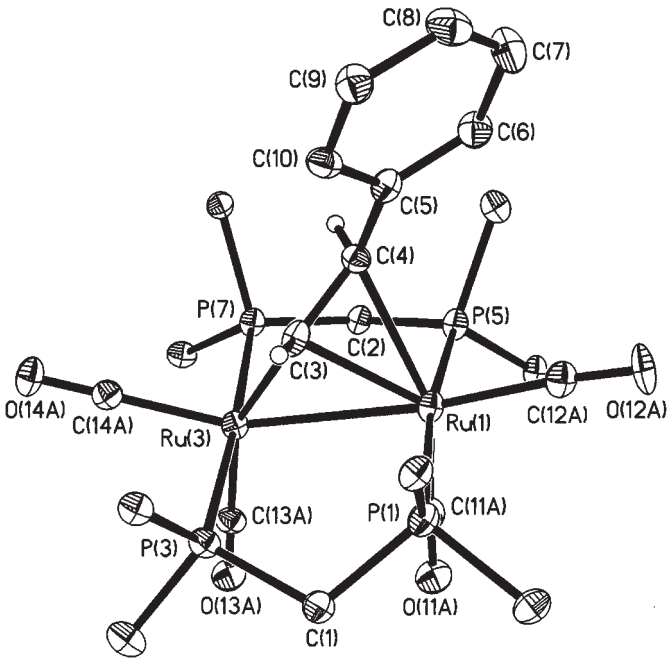
The terminal alkynes (PhCCH, HCCH, 1-hexyne) or internal alkynes with electron-withdrawing substituents ($PhCCCO_2Me$, MeO_2CCCCO_2Me) strongly inhibited the decomposition of formic acid to carbon dioxide and hydrogen. Thus, using $H^{13}CO_2H$ to allow detection of $^{13}CO_2$ by ^{13}C NMR, no CO_2 was detected at room temperature and only a trace was detected on warming the sample to 50°C. In terms of the ruthenium complexes present, in each case complexes **2** and **3** were formed first, in the same way as in the absence of the alkyne. This is consistent with the faster reaction of **1** with formic acid than with the alkynes (5, 6). However, the other intermediates of Scheme 1, including the important intermediate **4**, were not observed. Instead, products arising from reactions of **2** or **3** with the alkynes were observed. In the cases with the alkynes $PhC{\equiv}CCO_2Me$ or $MeO_2CC{\equiv}CCO_2Me$, the reactions gave complex mixtures that could not be identified but the terminal alkynes reacted more selectively, as described below.

The reaction of $PhC{\equiv}CH$ with complex **2** was relatively slow and thus was chosen for detailed study. At room temperature, the reaction occurred through several steps, as monitored by ^1H and ^{31}P NMR, to finally give a single product after 1 day at room temperature. This compound was characterized crystallographically as $[Ru_2(\mu\text{-}\eta^1{:}\eta^2\text{-}CHCHPh)(CO)_4(\mu\text{-}dppm)_2][HCOO]$ (**7**) and it is logical to suggest that it is formed from **2** by *cis*-insertion of phenylacetylene into the ruthenium hydride bond, with loss of a carbonyl ligand.

The molecular structure of the cation **7** is shown in Fig. 1 and selected interatomic distances and angles are listed in Table 1. The unit cell contains two independent cations **7** as well as formate anions and solvent molecules. Table 1 shows equivalent bond parameters for the two cations **7** in each row, and there are no major differences. The discussion will focus on the cation containing atoms Ru(1) and Ru(3) shown in Fig. 1. Each cation **7** contains a $Ru_2(\mu\text{-dppm})_2$ group in which the $Ru_2P_4C_2$ atoms adopt a slightly twisted, extended boat conformation. In addition each ruthenium is bound to two terminal carbonyl ligands and to the bridging styrenyl group. The α-carbon (C(3)) of the styrenyl group is σ-

© 2001 NRC Canada

Fig. 1. A view of the structure of the cation $[Ru_2(CO)_4(\mu\text{-}\eta^1,\eta^2\text{-}CH{=}CHPh)(\mu\text{-}dppm)_2]^+$. Only the ipso carbon atoms of the phenyl substituents of the dppm ligands are shown for clarity.



bonded to Ru(3) (Ru(3)C(3) = 2.09(1) Å) and the C=C unit is π-bonded to Ru(1) (Ru(1)C(3) = 2.27(1) Å, Ru(1)C(4) = 2.39(1) Å). Both C(3) and C(4) are chiral centers and the unit cell contains equal numbers of the *R,S* and *S,R* enantiomers: Fig. 1 shows the *S,R* enantiomer and the molecule containing Ru(2)Ru(4) is *R,S*. The distance C(3)—C(4) = 1.38(1) Å is slightly longer than a free double bond (1.34 Å) but significantly shorter than a single bond (1.53 Å), indicating relatively weak back-bonding to the C=C π*-orbital. The phenyl substituent of the styrenyl group is positioned between a sheath of phenyl substituents of the dppm ligands. The angles Ru(3)-C(3)-C(4) = 129.4(7) and C(3)-C(4)-C(5) = 123(1)° are each somewhat greater than the ideal angles of 120° for a double bond and, of course, significantly greater than the tetrahedral angle. Again this suggests that the carbon—carbon bond of the μ-styrenyl group is close to a double bond. The distortion of the angle Ru(3)-C(3)-C(4) is probably to maximize the Ru(1)-C(3-)C(4) π-bonding interaction. The distance Ru(1)—Ru(3) = 2.855(1) Å is consistent with a metal—metal single bond. Each ruthenium then has an 18-electron configuration if Ru(1) carries the positive charge. The structural features are consistent with those of other μ-alkenyl complexes (8).

The ^{31}P NMR spectrum of **7** contained only a very broad singlet at δ = 33 at room temperature and so **7** is clearly fluxional. The ^{1}H NMR spectrum at room temperature contained two vinyl resonances, each as a doublet of quintets, at δ = 8.4 and δ = 5.5, assigned to the hydrogen atoms on the α- and β-carbons [C(3) and C(4) in Fig. 1], respectively, (9). The magnitude of the doublet coupling constants ^3J (H-H) = 14 Hz confirm that these protons are *trans* within the vinyl group, and so confirms the stereochemistry shown crystallographically. Both vinyl hydrogen resonances show effectively equal coupling to the four phosphorus atoms, with J $(P\text{-}H)_{obs}$ = 7 and 3 Hz for the α- and β-protons, respectively. The phenyl protons of the bridging styrenyl ligand were observed δ = 6.9 (*para*), δ = 6.5 (*meta*), and at δ = 5.7 (*ortho*). These unusual chemical shifts for aryl protons are probably due to shielding by the surrounding four phenyl groups of the dppm ligands. Two broad, unresolved resonances were observed for the $CH^aH^bP_2$ protons at δ = 4.2 and 3.7 ppm.

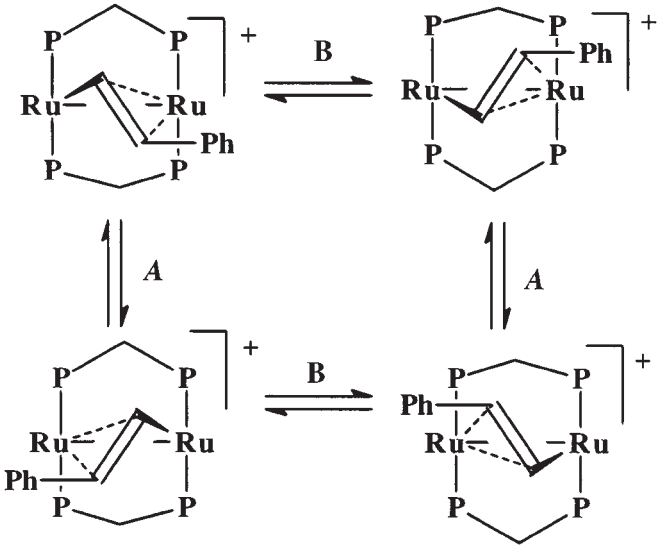
Table 1. Selected bond lengths (Å) and bond angles (°) for complex **7**.

Bond lengths (Å)			
Ru(1)—C(11A)	1.87(1)	Ru(4)—C(23B)	1.89(1)
Ru(1)—C(12A)	1.90(1)	Ru(4)—C(24B)	1.90(1)
Ru(1)—C(3)	2.27(1)	Ru(4)—C(13)	2.25(1)
Ru(1)—P(1)	2.378(3)	Ru(4)—P(8)	2.349(3)
Ru(1)—P(5)	2.387(3)	Ru(4)—P(4)	2.382(3)
Ru(1)—C(4)	2.39(1)	Ru(4)—C(14)	2.41(1)
Ru(1)—Ru(3)	2.855(1)	Ru(2)—Ru(4)	2.867(1)
Ru(3)—C(14A)	1.88(1)	Ru(2)—C(22B)	1.87(1)
Ru(3)—C(13A)	1.92(1)	Ru(2)—C(21B)	1.96(1)
Ru(3)—C(3)	2.09(1)	Ru(2)—C(13)	2.09(1)
Ru(3)—P(3)	2.347(3)	Ru(2)—P(6)	2.368(3)
Ru(3)—P(7)	2.363(2)	Ru(2)—P(2)	2.372(3)
C(3)—C(4)	1.38(1)	C(13)—C(14)	1.40(1)
C(4)—C(5)	1.49(1)	C(14)—C(15)	1.48(1)
Bond angles (°)			
C(4)-C(3)-Ru(3)	129.4(7)	C(14)-C(13)-Ru(2)	131.1(9)
C(4)-C(3)-Ru(1)	77.8(6)	C(14)-C(13)-Ru(4)	79.1(6)
Ru(3)-C(3)-Ru(1)	81.6(3)	Ru(2)-C(13)-Ru(4)	82.8(4)
C(3)-C(4)-C(5)	123(1)	C(13)-C(14)-C(15)	122(1)

At –50°C, complex **7** exhibits an ABCD pattern of peaks in the ^{31}P NMR spectrum, consistent with the structure established in the solid state by X-ray crystallography. The fluxional process that leads to the equivalence of phosphorus atoms must include not only the process A (Scheme 2), which can be considered to arise from an intermediate in which the plane of the vinyl group is perpendicular to the metal—metal bond (10–12), but also process B (Scheme 2), which requires an intermediate in which the plane of the vinyl group is parallel with the metal—metal bond. Process A is thought to occur through a $\mu\text{-}\eta^1$-vinyl intermediate (10–12), but it is likely that process B occurs by way of an intermediate with a terminal σ-vinyl group. Certainly the conventional ruthenium—alkene π-bond will be lost in the transition state in which the vinyl group and Ru—Ru bond are coplanar. At low temperature, four resonances were observed for the CH_2P_2 protons (one coupled pair at δ = 4.7 and 4.3 and the other at δ = 4.4 and 3.2), indicating that all are inequivalent. The chemical shifts of the vinyl protons did not change significantly but the appearance did. In particu-

© 2001 NRC Canada

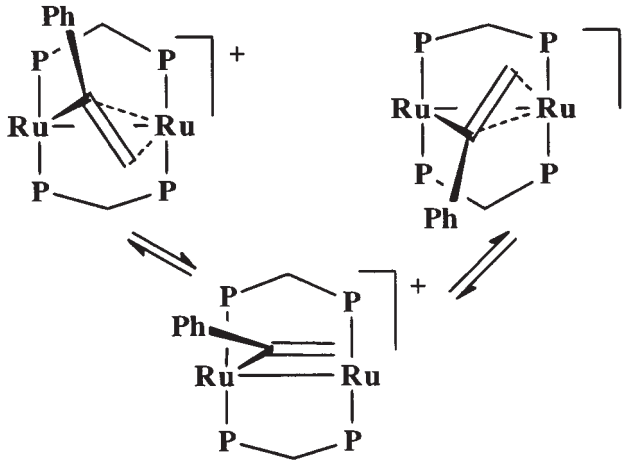
Scheme 2.



lar, the β-H resonance now appeared as a doublet of doublets with ^3J (H-H) = 14 Hz and J (P-H) = 10 Hz, thus showing coupling to only one phosphorus atom. The α-H resonance gave a complex unresolved multiplet, indicating nonequivalent couplings to several phosphorus atoms. These data are all easily rationalized in terms of the static structure determined crystallographically.

When the reaction of **1** with formic acid and phenylacetylene was monitored by NMR, a reaction intermediate was detected and characterized as $[Ru_2(\mu\text{-}\eta^1\text{:}\eta^2\text{-}CPhCH_2)(CO)_4(\mu\text{-dppm})_2][HCOO]$ (**8**). Complex **8** displays an AA′BB′ pattern of peaks in the ^{31}P NMR spectrum with δ (P) = 25.0 and 26.8 ppm. The vinyl protons appeared as broad singlets in the ^1H NMR spectrum at δ 4.8 and 5.5; the absence of resolved coupling between them indicates that these are geminal protons and this was confirmed by a $^1H^{13}C$ HSQC experiment which showed that both vinyl protons are attached to the same carbon atom at δ (C) = 111.5. The phenyl protons of the styrenyl group appeared at δ = 6.3 (ortho), 6.6 (*meta*), and 6.8 (*para*). The ^{31}P NMR spectrum broadened but did not split further at –90°C. Since the static structure is expected to give an ABCD pattern of peaks in the ^{31}P NMR spectrum, it is clear that the fluxionality differs from that of complex **7**. In particular, the two processes analogous to A and B of Scheme 2 must have different rates, one being fast and the other slow on the NMR time scale; it is likely that B is rapid but that A is slow. The distinction can be made on the basis of the CH_2P_2 resonances in the ^1H NMR spectrum. In each process, the styrenyl group stays on the same side of the $Ru_2(\mu\text{-dppm})_2$ unit, so each CH_2 group will have nonequivalent protons CH^aH^b. However, process A does not lead to equivalent dppm ligands, whereas process B does. Hence, if it is process A that is fast, four resonances (each 1H) are expected whereas, if process B is fast, two resonances (each 2H) are expected for the CH_2P_2 protons. The spectrum contains two resonances for the CH_2P_2 protons at δ = 3.2 (2H) and 3.4 (2H), indicating that it is process B that is fast. It is likely that steric hindrance in complex **8** prevents process A, which requires the phenyl substituent of the styrenyl group to swing by the phenyl substituents of the

Scheme 3.



dppm ligands. A much smaller motion of the α-phenyl substituent is required in process B. Following this line of reasoning, it is likely that process B is also fast for complex **7** (Scheme 2) and that process A is rate-determining. The proposed fluxionality of **8** is shown in Scheme 3.

The complex **8** was formed rapidly and isomerized to **7** slowly over a period of several hours at room temperature. Clearly then, **8** is the kinetic product arising from reaction of PhCCH with **2**, and it isomerizes slowly to the thermodynamic product **7**. The isomerization is suggested to occur by a β-elimination–reinsertion sequence (Scheme 4). The stereochemistry of the intermediate is uncertain, as is the mechanism of insertion and β-elimination, which could occur at one or across both metal centers.

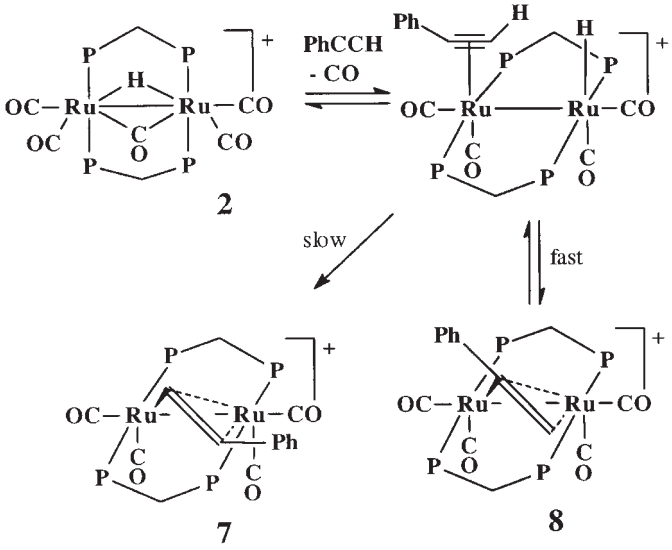
It is noteworthy that complex **7** is stable in solution in the presence of excess PhCCH, hydrogen gas, acids (HBF_4, HCO_2H), or bases (Et_3N, potassium *t*-butoxide). The strong inhibition of the catalytic decomposition of formic acid by phenylacetylene, and absence of catalytic transfer hydrogenation of phenylacetylene, can therefore be attributed to formation of the stable complex **7**, which is not an active catalyst. It has not been possible to characterize the products obtained when using the alkynes HCCH, BuCCH, MeO_2CCCCO_2Me, or $PhCCCO_2Me$, since intractable mixtures were obtained, but it is likely that they also give stable alkenyl or alkyne complexes that are not active catalysts.

Discussion

In catalytic transfer hydrogenation using formic acid, the donor must transfer two hydrogen atoms to the metal center (with loss of CO_2) to give metal hydride bonds, and the substrate must coordinate to the metal and accept the hydrogen atoms, typically by insertion followed by reductive elimination. However, within this framework there are many possible reaction sequences (1–3). One important classification is based on whether the hydrides react rapidly with substrate as they are formed, as is implied by the term transfer hydrogenation, or are first eliminated as free dihydrogen. The second case is then equivalent to hydrogenation with hydrogen gas, but with the hydrogen generated in situ from the formic acid (13). There is evidence for both cases in catalytic transfer hydrogenation using formic acid and mononuclear catalysts

© 2001 NRC Canada

Scheme 4.

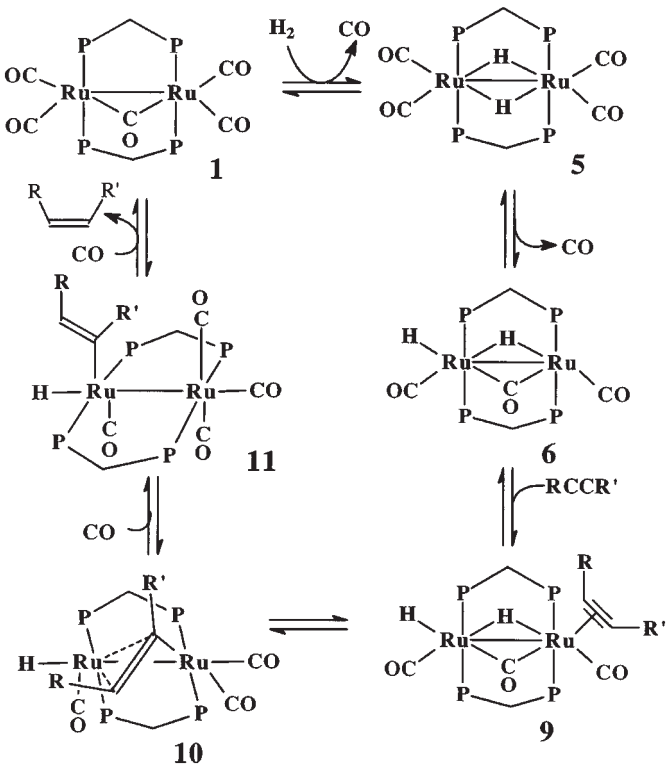


(1–3, 7). In the present case, the successful hydrogenations all occur by the mechanism in which formic acid is catalytically decomposed to carbon dioxide and hydrogen, followed by the slower catalytic hydrogenation of the alkyne.

In the successful catalytic reactions, no intermediates were detected in which the alkyne or its hydrogenation products were coordinated to ruthenium. This was the case when using any of HCOOH, HCOOH:Et_3N (5:2), or H_2 as the hydrogen source. It is likely that weak binding of the alkyne to the diruthenium complex is a prerequisite to successful catalysis, since those alkynes known to bind strongly (6) were not hydrogenated. On the other hand, alkenes are not hydrogenated by this catalyst system and they do not coordinate either. It seems there is a balance such that both substrates that bind strongly (terminal alkynes, alkynes with electon-withdrawing substituents) and those that cannot coordinate at all (alkenes) are not hydrogenated, and that substrates that are hydrogenated can probably bind transiently to the diruthenium center (internal alkynes without electron-withdrawing groups).

The mechanism of hydrogenation is necessarily speculative. The only difference in observed intermediates, compared to those observed in the catalytic decomposition of formic acid in the absence of alkynes, was that the hydride derivatives **5** and **6** were not observed. It is easy to understand how the coordinatively unsaturated hydride **6** might react with alkynes, and one possible mechanism based on this observation is shown in Scheme 5. Since none of the possible intermediates **9**–**11** of Scheme 5 is directly observed, the structures are very tentative. However, the overall mechanism involving oxidative addition of hydrogen with CO loss to give **5** and **6**, followed by rapid alkyne coordination (complex **9**), *cis*-insertion to give a vinyl derivative (complexes **10**, **11**), and reductive elimination of alkene with CO addition to regenerate the resting state complex **1**, is consistent with the observations. There are numerous instances of related mechanistic proposals with mononuclear ruthenium complexes, but the extension to binuclear catalysts is new (13, 14).

Scheme 5.



Experimental

All manipulations were operated under a dry nitrogen atmosphere using either standard Schlenk techniques or a glove box. Acetone was dried over 3 Å molecular sieves, toluene was dried by distillation from sodium benzophenone, and CH_2Cl_2 was distilled before use from CaH_2. The HCOOH (96%) and $H^{13}COOH$ (95%, 99 C^{13} atom%) contained 4 to 5% water and were used as purchased. [Ru_2(μ-CO)$(CO)_4$(μ-dppm)$_2$] (**1**) was synthesized according to literature procedure (15). ^1H, ^{13}C, and ^{31}P NMR spectra were recorded using Varian Inova 400 or Gemini 300 spectrometers.

Hydrogen transfer studies from HCOOH to alkynes

To a saturated solution of [Ru_2(μ-CO)$(CO)_4$(μ-dppm)$_2$] (**1**) (1.1×10^{-3} mmol) in acetone-d_6 (0.5 mL, 2.2 mM) in an NMR tube was added PhCCPh (1.98 mg, 1.1×10^{-2} mmol) and the tube was sealed with a septum. HCOOH (1.00 μL, 2.2×10^{-2} mmol) was then injected through the septum by syringe. The decay of formic acid and formation of *cis*-stilbene were monitored as a function of time by comparing the integrals of the formyl and vinyl hydrogen resonances with the integral of the CH_2P_2 resonance of **1** in the ^1H NMR spectrum. The decomposition of HCO_2H to H_2 and CO_2 was complete in 20 min, while the hydrogenation of PhCCPh to *cis*-stilbene was complete in 24 h at 20°C.

Reactions with diphenylacetylene, 1-phenyl-1-propyne, 3-hexyne, and 4-octyne were carried out in a similar way. For comparison of rates, the ratio of alkyne:formic acid:**1** was maintained at 10:10:1. Alkene products were characterized by their ^1H NMR spectra in acetone-d_6 as follows: *cis*-stilbene (16): δ (^1H) = 6.6 (s, =CH); *cis*-1-phenylpropene

© 2001 NRC Canada

(17): δ (^{1}H) = 7.3 (m, 5H, Ph), 6.42 (dq, *J* (H-H) = 13 Hz, *J* (H-H) = 2 Hz, PhCH=), 5.77 (dq, *J* (H-H) = 13 Hz, *J* (H-H) = 7 Hz, MeCH=), 1.85 (dd, *J* (H-H) = 7 Hz, *J* (H-H) = 2 Hz, Me); *cis*-3-hexene (18): δ (^{1}H) = 5.3 (m, =CH0, 2.03 (m, CH_2), 0.9 (t, *J* (H-H) = 6 Hz, Me); *cis*-4-octene (19): δ (^{1}H) = 5.3 (m, =CH), 2.03 (m, CH2)], 1.38 (m, CH_2), 0.9 (t, *J* (H-H) = 6 Hz, Me).

In the similar reaction using PhCCH (3 μL, 0.027 mmol), the complete decomposition of HCOOH (6.5 μL, 0.130 mmol) took 2 weeks to reach completion and no hydrogenation product (styrene) was detected. The only ruthenium complex present at the final stage was complex **7**. The alkynes HCCH, BuCCH, $PhCCCO_2Me$, and MeO_2CCCCO_2Me also retarded the decomposition of formic acid by complex **1** and failed to give the alkenes expected to be formed by catalytic hydrogenation.

Synthesis of $[Ru_2(CO)_4(\mu\text{-}\eta^1,\eta^2\text{-}CH{=}CHPh)(\mu\text{-}dppm)_2][HCOO]$ 7

To a saturated solution of $[Ru_2(\mu\text{-}CO)(CO)_4(\mu\text{-}dppm)_2]$ in acetone-d_6 (0.5 mL, 2.2 mM) in a septum-sealed NMR tube was added PhCCH (3 μL, 0.027 mmol) and HCOOH (6.5 μL, 0.130 mmol) by syringe. The solution was set aside for 18 h at room temperature to give complex **7** as the only product as determined by NMR. The same product was formed by heating to 45°C for 3 h, and using CD_2Cl_2 as solvent. Crystals were obtained from CD_2Cl_2 by slow diffusion of pentane. The crystals were formed with solvent occluded (see structure determination), which was partially lost on drying, thus making it difficult to obtain good analytical data. ^{1}H NMR (acetone-d_6, 20°C) δ: 8.4 (s, 1H, *H*COO], 8.2 (m, 1H, PhCH-C*H*), 5.4 (d quin, 1H, ^3J (H-H) = 14 Hz, *J* (P-H) = 3 Hz, PhC*H*-CH), 5.7 (d, 2H, ^3J (H-H) = 8 Hz, *Ph*CHCH), 6.5 (t, 2H, *J* (H-H) = 8 Hz, *Ph*CHCH), 6.8 (t, 1H, *J* (H-H) = 8 Hz, *Ph*CHCH), 5.05 (br s, 2H, P-C*H*-P), 3.65 (br s, P-C*H*-P). ^{31}P NMR δ: 33 (br s, dppm). ^{1}H NMR (acetone-d_6, –50°C) δ: 8.6 (s, 1H, *H*COO), 8.4 (m, 1H, PhC*H*-CH), 5.4 (dd, 1H, ^3J (H-H) = 14 Hz, ^3J (P-H) = 10 Hz, PhCH-C*H*), 5.6 (d, 2H, *J* (H-H) = 7 Hz, *Ph*CHCH), 6.44 (t, 2H, *J* (H-H) = 7 Hz, *Ph*CHCH), 6.8 (t, 1H, *J* (H-H) = 7 Hz, *Ph*CHCH), 4.7, 4.4, 4.3, 3.2 (m, each 1H, P-C*H*-P). ^{31}P NMR δ: 49.3 (ddd, *J* (P^a-P^b) = 56 Hz, *J* (P^a-P^c) = 237 Hz, *J* (P^a-P^d) = 30 Hz, P^a), 35.1 (ddd, *J* (P^a-P^b) = 56 Hz, *J* (P^b-P^c) = 38 Hz, *J* (P^b-P^d) = 267 Hz, P^b), 32.6 (ddd, *J* (P^a-P^c) = 237 Hz, *J* (P^b-P^c) = 30 Hz, *J* (P^c-P^d) = 73 Hz, P^c), 30.9 (ddd, *J* (P^a-P^d) = 30 Hz, *J* (P^b-P^d) = 267 Hz, *J* (P^c-P^d) = 73 Hz, P^d).

Structure determination

Crystals of $[(CO)_2Ru(\mu\text{-}dppm)_2(\mu\text{-}CHCHPh)Ru(CO)_2]\text{-}[HCOO]\cdot 1.5CH_2Cl_2\cdot 0.5C_5H_{12}\cdot 0.5H_2O$ were grown from CH_2Cl_2–pentane. A yellow block was mounted on a glass fibre at dry ice temperature. Data were collected at 200 K using a Nonius Kappa-CCD diffractometer using COLLECT software (20). The unit cell parameters were calculated and refined from the full data set. Crystal cell refinement and data reduction was carried out using the Nonius DENZO package. The data were scaled using SCALEPACK (21) and no other absorption corrections were applied. The SHELXTL 5.101 (22) program package was used to solve the structure by direct methods and refinement was by successive difference Fouriers. All non-hydrogen atoms were refined with anisotropic thermal parameters. One formate anion was poorly behaved and the C—O bond distances were fixed. The hydrogen atoms were calculated geometrically and were riding on their respective carbon atoms. There were several disordered solvent molecules in the lattice, and these were modeled isotropically and with partial occupancies. The crystal data and refinement parameters are listed in Table 2. The crystal was of poor quality, with disordered anion and solvent molecules, but the structure of the cations was well-defined.

Table 2. Crystal data and structure refinement for **7**$[HCO_2]\cdot 1.5CH_2Cl_2\cdot 0.5C_5H_{12}\cdot 0.5\ H_2O$.

Empirical formula	$C_{67}H_{60.75}Cl_3O_{6.50}P_4Ru_2$
Formula weight	1403.78
Temperature (K)	200(2)
Wavelength (Å)	0.71073
Crystal system	Triclinic
Space group	*P*-1
Cell dimensions	
a (Å)	14.8925(9)
b (Å)	21.6229(15)
c (Å)	23.2355(14)
α (°)	109.723(3)
β (°)	101.557(3)
γ (°)	100.677(3)
Volume (Å^3)	6636.0(7)
Z	4
Density (calculated) (mg m^{-3})	1.405
Absorption coefficient (mm^{-1})	0.722
F(000)	2858
Crystal size (mm^3)	0.46 × 0.14 × 0.11
θ range for data collection (°)	2.58–30.15
Refl., ind. refl.	72 876, 34 486 (*R*(int) = 0.0980)
Absorption correction	Scalepack
Max and min transmission	0.9248 and 0.7324
Data / restraints / parameters	34 486 / 22 / 1493
Goodness-of-fit on F^2	1.014
Final *R* indices [$I > 2\sigma(I)$]	*R*1 = 0.1131, *wR*2 = 0.2807
Largest diff. peak and hole (e Å^{-3})	1.591 and –0.769

Acknowledgments

We thank the Natural Sciences and Engineering Research Council of Canada (NSERC) for financial support.

References

1. R.A.W. Johnstone and A.H. Wilby. Chem. Rev. **85**, 129 (1985).
2. G. Zassinovich, G. Mestroni, and S. Gladiali. Chem. Rev. **92**, 1051 (1992).
3. (*a*) W. Leitner, J.M. Brown, and H. Brunner. J. Am. Chem. Soc. **115**, 152 (1993); (*b*) R. Noyori and S. Hashiguchi. Acc. Chem. Res. **30**, 97 (1997); (*c*) K. Matsumura, S. Hashiguchi, T. Ikariya, and R. Noyori. J. Am. Chem. Soc. **119**, 8738

© 2001 NRC Canada

(1996); (*d*) J. Yu and J.B. Spencer. Chem. Commun. 1935 (1998); Chem. Eur. J. **5**, 2237 (1999).
4. Y. Sasson and J. Blum. J. Org. Chem. **40**, 1887 (1975).
5. Y. Gao, J. Kuncheria, G.P.A Yap, and R.J. Puddephatt. Chem. Commun. 2365 (1998).
6. (*a*) J. Kuncheria, H.A. Mirza, J.J. Vittal, and R.J. Puddephatt. Inorg. Chem. Comm. **2**, 197 (1999); (*b*) J. Kuncheria, H.A. Mirza, J.J. Vittal, and R.J. Puddephatt. J. Organomet. Chem. **593**, 77 (2000); (*c*) H.A. Mirza, J.J. Vittal, and R.J. Puddephatt. J. Coord. Chem. **37**, 131 (1996); (*d*) H.A. Mirza, J.J. Vittal, and R.J. Puddephatt. Organometallics, **13**, 3063 (1994).
7. (*a*) Y. Watanabe, T. Ohta, and Y. Tsuji. Bull. Chem. Soc. Jpn. **55**, 2441 (1982); (*b*) B.T. Khai and A. Arcelli. J. Organomet. Chem. **309**, C63 (1986).
8. A.G. Orpen. J. Chem. Soc. Dalton Trans. 1427 (1983).
9. K.J. Edwards, J.S. Field, R.J. Haines, B.D. Homann, M.W. Stewart, J. Sundermeyer, and S.F. Woollam. J. Chem. Soc. Dalton Trans. 4171 (1996).
10. A.F. Dyke, S.A.R. Knox, M.J. Morris, and P.J. Naish. J. Chem. Soc. Dalton Trans. 1417 (1983).
11. M.D. Fryzuk, T. Jones, and F.W.B. Einstein. Organometallics, **3**, 185 (1984).
12. J.R. Shapley, S.I. Richter, M. Tachikawa, and J.B. Keister. J. Organomet. Chem. **94**, C43 (1975).
13. B.R. James. Homogeneous hydrogenation. Wiley, New York. 1973; (*b*) B.R. James. Catal. Today, **37**, 209 (1997).
14. R.B. Bedford and C.S.J. Cazin. J. Organomet. Chem. **598**, 20 (2000).
15. H.A. Mirza, J.J. Vittal, and R.J. Puddephatt. Inorg. Chem. **32**, 1327 (1993).
16. (*a*) L. Breau, N.K. Sharma, I.R. Butler, and T. Durst. Can. J. Chem. **69**, 185 (1991); (*b*) G. Bosser and J. Paris. J. Chem. Soc. Perkin Trans. 2, 2057 (1992).
17. L. Luan, J.S. Song, and R.M. Bullock. J. Org. Chem. **60**, 7170 (1995).
18. O.R. Brown and P.H. Middleton. J. Chem. Soc. Perkin Trans. 2, 955 (1984).
19. D.J. Hastings and A.C. Weedon. Can. J. Chem. **69**, 1171 (1991).
20. COLLECT. Nonius, Delft. 1998.
21. SCALEPACK. Nonius, Delft. 1998.
22. G.M. Sheldrick. SHELXTL Version 5.101. Madison, Wisconsin. 2000.

© 2001 NRC Canada

Oxidation of copper(II) hydroxyporphyrin (oxophlorin); oxidative ring opening and formation of an ester-linked, dinuclear copper complex

Shane Phillips, Bruce C. Noll, Marilyn M. Olmstead, and Alan L. Balch

Abstract: Addition of copper(II) acetate to octaethyl(*meso*-hydroxy)porphyrin (H_2OEPOH) in THF under a dinitrogen atmosphere produces Cu^{II}(OEPOH), which has been isolated as red crystals and shown to have a *meso*-hydroxyporphyrin structure by UV–vis and EPR spectroscopy. Cu^{II}(OEPOH) undergoes oxidation by dioxygen to form a novel dinuclear copper complex {Cu^{II}(OEPOC(O)OEB)Cu^{II}}. This dinuclear complex is composed of a copper(II) *meso*-substituted porphyrin portion (with a planar CuN_4 unit), which is attached through an ester linkage to a helical copper(II) tetrapyrrole that has been ring-opened through oxidative cleavage of a second molecule of Cu^{II}(OEPOH). The oxidative ring-opening reaction resembles that of natural heme catabolism but is arrested at a stage where the oxidized *meso*-carbon is still appended to the helical open tetrapyrrole. A mechanism is suggested for this process.

Key words: copper porphyrin, crystal structure, porphyrin oxidation, linear tetrapyrrole, hydroxy-porphyrin, oxophlorin.

Résumé : L'addition d'acétate de cuivre(II) à de l'octaéthyl(*méso*-hydroxy)porphyrine, H_2OEPOH, dans du tétrahydrofurane, sous atmosphère de diazote, conduit à la formation de Cu^{II}(OEPOH) que l'on a isolé sous la forme de cristaux rouges; sur la base des spectroscopies UV–vis et RPE, ces cristaux possèdent une structure *méso*-hydroxyporphyrine. Sous l'influence du dioxygène, le Cu^{II}(OEPOH) subit une oxydation conduisant à la formation d'un nouveau complexe dinucléaire du cuivre, le {Cu^{II}(OEPOC(O)OEB)Cu^{II}}. Ce complexe dinucléaire est formé d'une partie cuivre(II)/porphyrine substituée en *méso* (avec une unité CuN_4 planaire) qui est attachée par le biais d'une liaison ester à un cuivre(II)/tétrapyrrole hélicoïdal avec un cycle qui a été ouvert par un clivage oxydant d'une deuxième molécule de Cu^{II}(OEPOH). Cette réaction d'ouverture oxydante du cycle ressemble à celle du catabolisme naturel de l'hème, mais il s'arrête à un stade dans lequel le carbone *méso* oxydé est toujours attaché au tétrapyrrole hélicoïdal ouvert. On suggère un mécanisme pour ce processus.

Mots clés : cuivre porphyrine, structure cristalline, oxydation d'une porphyrine, tétrapyrrole linéaire, hydroxyporphyrine, oxophlorine.

[Traduit par la Rédaction]

Introduction

Classical studies of the interaction of porphyrins with dioxygen focused on the issue of reversible dioxygen binding and subsequently on the ability of metalloporphyrins and heme enzymes such as cytochrome P-450 to activate dioxygen toward the attack on various substrates (1). Dioxygen, especially in the presence of a reducing agent, can also cause the destruction of the metalloporphyrin itself (2, 3). This process generally occurs through attack on a *meso*-carbon atom of the porphyrin to produce the *meso*-substituted porphyrin shown as **1a** and **1b** in Scheme 1.

Received September 12, 2000. Published on the NRC Research Press Web site at http://canjchem.nrc.ca on July 9, 2001.

This paper is dedicated to Professor Brian James on the occasion of his 65th birthday.

S. Phillips, B.C. Noll, M.M. Olmstead, and A.L. Balch.[1] Department of Chemistry, University of California, Davis, CA, 95616, U.S.A.

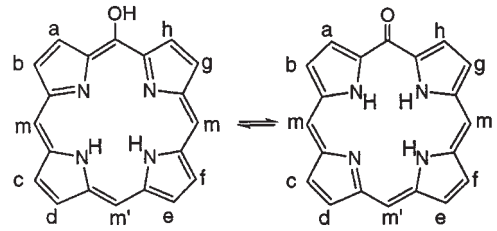
[1]Corresponding author (telephone (530) 752-0941; fax: (530) 752-8995; e-mail: albalch@ucdavis.edu).

This tetrapyrrole macrocycle can exist in two tautomeric forms, the *meso*-hydroxyporphyrin (**1a**) and the oxophlorin (**1b**) as seen in Scheme 1 (4). This relatively modest change to the porphyrin ligand core results in a tetrapyrrole that is more readily oxidized than the corresponding porphyrin and which has a rich coordination chemistry that involves not only the N_4 core but also can involve the exocyclic oxygen atom. Scheme 2 shows the principal structural forms that have been characterized to date for transition metal complexes of the octaethyl-substituted form of **1**. Four basic coordination modes have been identified (4). These modes include: **2** with porphyrin-like coordination mode and a *meso*-hydroxyl group, **3** with bridging coordination through the *meso*-oxygen atom, **4** with oxophlorin coordination and a *meso*-keto group, and **5** with ligand-based free radical coordination. Examples of each type of structure have been isolated and characterized through single crystal X-ray diffraction and by UV–vis, infrared (IR), and ^{1}H NMR spectroscopy. To simplify interpretation of the spectroscopic data this work has utilized the symmetric ligand, H_2OEPOH, **1a** with a–h = C_2H_5.

Metal complexes of **1a** are sensitive to oxidation, which can take several paths. In pyridine solution, air oxidizes the

 DOI: 10.1139/cjc-79-5/6-922 © 2001 NRC Canada

Scheme 1.



1a 1b

porphyrin-like complexes, Ni^{II}(OEPOH) and Zn^{II}(OEPOH), to produce stable free radical complexes $(py)_2Ni^{II}(OEPO^{\bullet})$ and $(py)Zn^{II}(OEPO^{\bullet})$, which have been isolated (5, 6). However, treatment of {$(py)Co^{II}$(OEPOH··py)} with either dioxygen or diiodine produces {$(py)_2Co^{III}$(OEPO)} in which the metal ion, not the ligand, has been oxidized (7). The behavior of iron complexes of H_2OEPOH is more complex and is summarized in Scheme 3. Note that in this Scheme the oxidation state of the iron in {$(py)_2$Fe(OEPO)} is not specified since the electrons can be apportioned between the ligand and iron in several different resonance structures (4). Not only are several reactions that result in ligand oxidation observed in Scheme 3, but the reactions shown at the lower right side of the Scheme involve ring-opening of the porphyrin to form the biliverdin complex {$(py)_2Fe^{III}$(OEB)}, and the verdoheme complex $[(py)_2Fe^{II}(OEOP)]^+$ (2, 8, 9). These ring-opening reactions are relevant to the operation of the enzyme heme oxygenase, which binds heme as substrate and uses it to activate dioxygen, which then attacks the heme at a *meso* carbon atom to yield the bile pigment biliverdin, carbon monoxide, and free iron ion (10).

Results

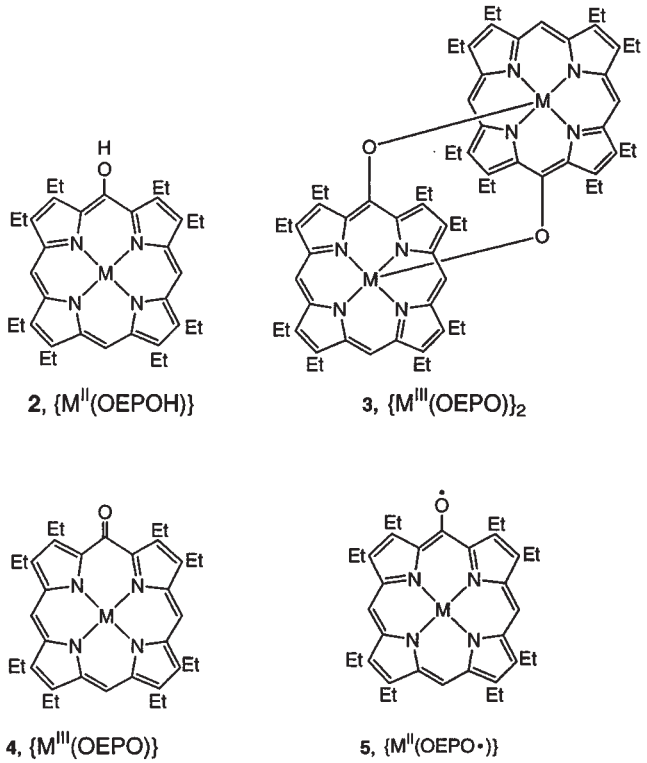
Formation and characterization of Cu^{II}(OEPOH) and its trifluoroacetic ester derivative, Cu^{II}(OEPTFA)

The synthetic work described here is summarized in Scheme 4.

Addition of a blue THF solution of copper(II) acetate to a blue THF solution of **1** (*a*–*h* = Et) under a dinitrogen atmosphere produces a red solution that contains Cu^{II}(OEPOH), which has been isolated as red crystals. After removing the solvent under vacuum, the red solids were dissolved in dichloromethane. This solution was washed with water, and the red organic layer was collected and dried to give a 89% yield of Cu^{II}(OEPOH). The trifluoroacetoxy analog, Cu^{II}(OEPTFA), was synthesized in 83% yield in a similar manner from H_2OEPTFA.

The electronic spectrum of Cu^{II}(OEPOH) in dichloromethane solution (Fig. 1*a*) consists of an intense Soret band at 404 nm and Q-bands at 528 and 560 nm. This spectrum is typical of the spectra of divalent metal complexes of type **2** in Scheme 2, such as Ni^{II}(OEPOH) and Zn^{II}(OEPOH) (5, 6). Cu^{II}(OEPTFA) in dichloromethane solution gives a very similar spectrum, with a Soret band at 400 nm and Q-bands at 526 and 564 nm. This similarity of the spectra of Cu^{II}(OEPOH) and Cu^{II}(OEPTFA) indicates that both have ligands that coordinate in the form **2** rather than **4**. The IR spectrum of Cu^{II}(OEPOH) as a mineral oil mull shows a broad peak at 3508 cm^{-1} corresponding to the hydroxyl functionality and no strong peaks above 1600 cm^{-1} where a carbonyl peak would be expected. Cu^{II}(OEPTFA), however, shows no hydroxyl peak above 3000 cm^{-1}, but does give a strong, sharp absorption at 1792 cm^{-1}, which is due to the C=O portion of the ester. The electron impact mass spectrum (EI-MS) of Cu^{II}(OEPOH) shows a molecular ion peak at 611 amu and *no peaks at higher masses*.

Scheme 2.



2, {M^{II}(OEPOH)} **3**, {M^{III}(OEPO)}$_2$

4, {M^{III}(OEPO)} **5**, {M^{II}(OEPO•)}

The electron spin resonance (ESR) spectra of these complexes are similar to those of other copper(II) d^9 porphyrin compounds (11). Cu^{II}(OEPTFA) produces an asymmetric quartet due to hyperfine coupling to the spin 3/2 copper atom centered at g = 2.10 with A_{Cu} = 96 G. The two high field signals are further split by superhyperfine coupling to the four nitrogen atoms with A_N = 16 G. The room temperature ESR spectrum of Cu^{II}(OEPOH) in dichloromethane solution is similar. The typical four band pattern is less well resolved for Cu^{II}(OEPTFA), but the signals are centered at g = 2.10 with a smaller copper hyperfine coupling constant of A_{Cu} = 86 G and a nitrogen superhyperfine coupling constant of A_N = 16 G.

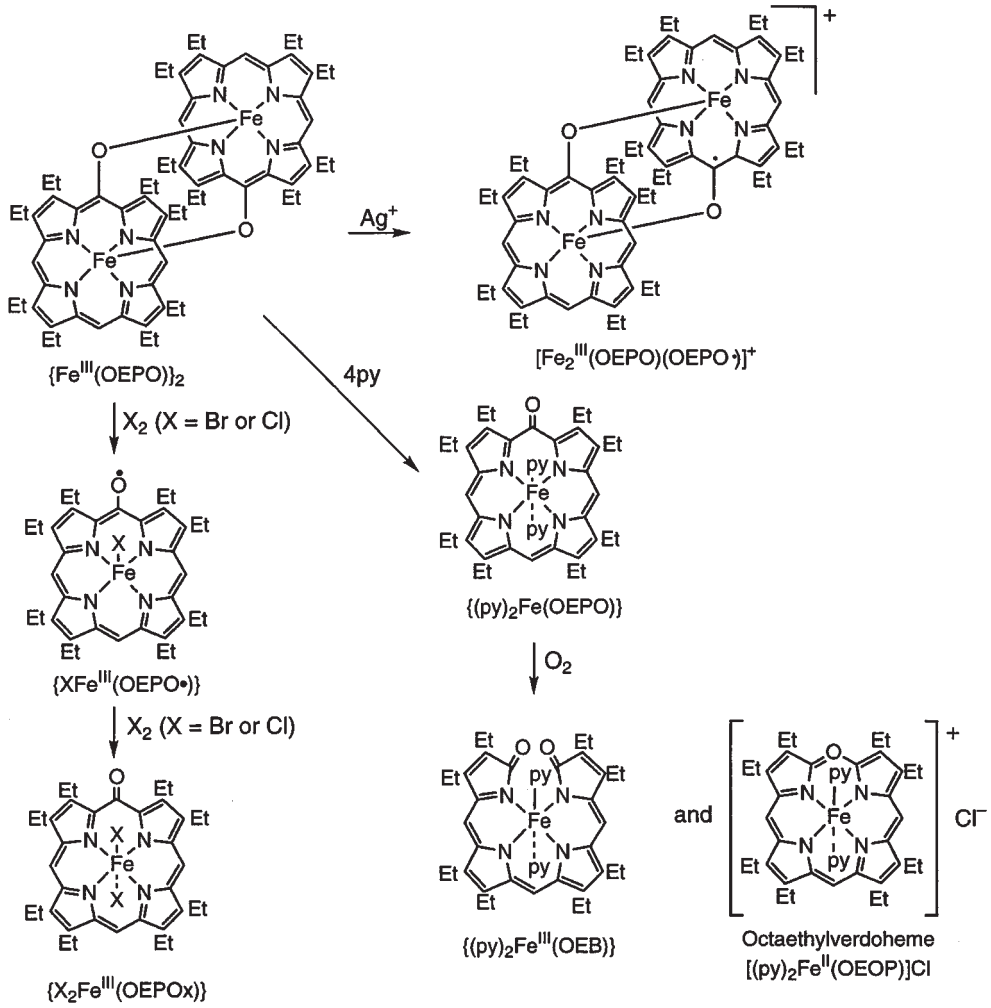
Cu^{II}(OEPTFA) can be hydrolyzed under basic conditions to form Cu^{II}(OEPOH). Washing a dichloromethane solution of Cu^{II}(OEPTFA) with a 1.0 M aqueous solution of KOH results in a color change from red to green. Subsequent washing with water generates the red complex, Cu^{II}(OEPOH), and this material gives electronic and IR spectra that match those observed previously.

Formation and structure of {Cu^{II}(OEPOC(O)OEB)Cu^{II}}

Cu^{II}(OEPOH) undergoes oxidation to form a novel dinuclear copper complex, {Cu^{II}(OEPOC(O)OEB)Cu^{II}}.

© 2001 NRC Canada

Scheme 3.



Slow diffusion of methanol into a chloroform–pyridine (9:1 v/v) solution of Cu^{II}(OEPOH) in air over a period of several weeks yielded large, single blocks. Fast atom bombardment mass spectrometry (FAB-MS) (1238 amu mass peak) and X-ray crystallography indicated that these red–purple crystals contain the unique binuclear complex, {Cu^{II}(OEPOC(O)OEB)Cu^{II}}. Representative crystals from the batch used in the crystallographic investigation also had an electronic spectrum that is similar to that of Cu^{II}(OEPOH). The electronic spectrum of {Cu^{II}(OEPOC(O)OEB)Cu^{II}}, which is shown in Fig. 1*b*, is dominated by the copper(II) porphyrin part of the dinuclear complex, which has a very large molar extinction coefficient. However, important spectral differences are seen in the broad shoulder at 460 nm and the broad feature seen at 748 nm. For comparison, the spectrum of Cu(OEFB), where OEFB is the dianion of octaethylformylbiliverdin (see Scheme 4), shows absorptions at 432, 752, and 844 nm, which have much lower absorptivities than those of Cu^{II}(OEPOH) (12). Thus, the feature at 748 nm in the spectrum of {Cu^{II}(OEPOC(O)OEB)Cu^{II}} is consistent with the presence of the ring-open tetrapyrrole portion of the molecule.

The structure of {Cu^{II}(OEPOC(O)OEB)Cu^{II}} has been determined by single crystal X-ray diffraction. A perspective view of the complex is given in Fig. 2. Atomic coordinates are given in Table 1. Selected bond distances and angles are given in Tables 2 and 3. The compound crystallizes with a molecule of {Cu^{II}(OEPOC(O)OEB)Cu^{II}} and a molecule of chloroform in the asymmetric unit. The dinuclear complex is composed of a copper(II) porphyrin portion, which is attached through an ester linkage to a second copper(II) tetrapyrrole that has been obtained through oxidative cleavage of a second molecule of Cu^{II}(OEPOH).

The porphyrin portion of the dinuclear complex contains a planar copper(II) ion bound to four pyrrole nitrogen atoms with an average Cu—N bond distance of 2.006 Å. This distance is comparable to the average Cu—N bond distance of 1.998 Å found in Cu^{II}(OEP) (13). Figure 3 shows a formal diagram that illustrates the out-of-plane displacements of the core atoms (in 0.01 Å units) of the porphyrin portion of the molecule from the mean plane defined by the copper atom, the four nitrogen atoms, and the 20 carbon atoms of the porphyrin's core. The core is nearly planar, but it does exhibit some unusual saddle-shaped distortions on its periphery in the vicinity of the *meso*-bound oxygen atom. The copper ion and the four pyrrole nitrogen atoms are distinctly planar.

The cleaved porphyrin portion of {Cu^{II}(OEPOC(O)OEB)Cu^{II}} also contains a copper(II) ion bound to the four pyrrole ni-

© 2001 NRC Canada

Scheme 4.

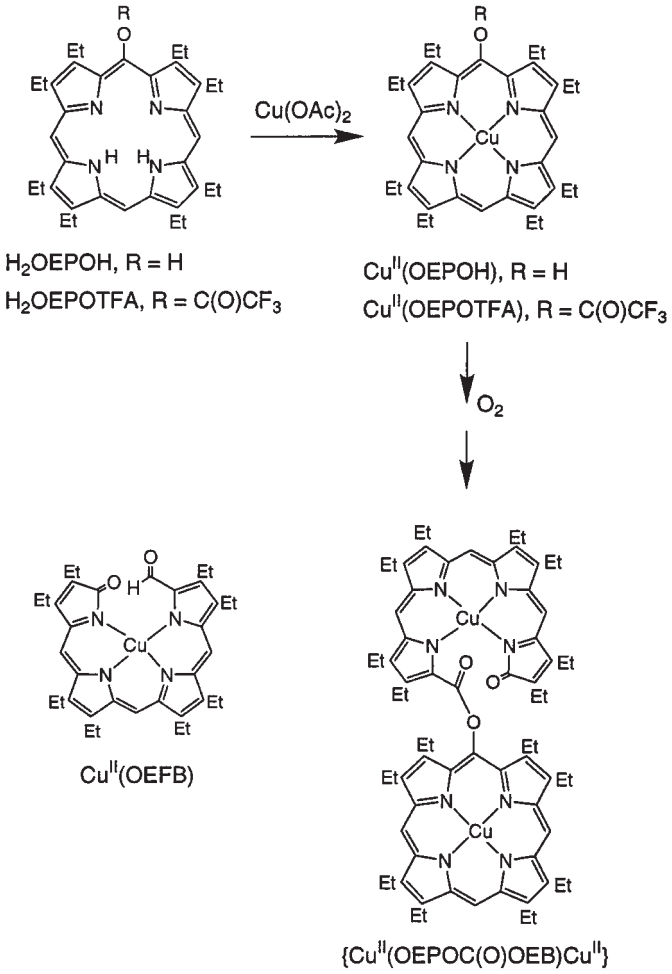
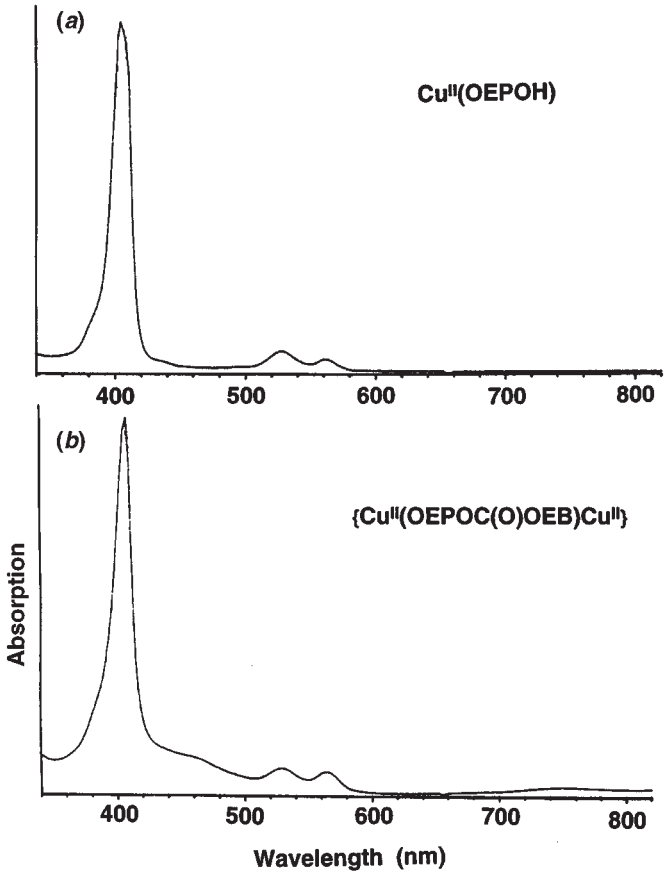


Fig. 1. Electronic absorption spectra of: (*a*) Cu^{II}(OEPOH) in dichloromethane solution; and (*b*) {Cu^{II}(OEPOC(O)OEB)Cu^{II}} in dichloromethane solution.



trogen atoms in an irregular geometry. The overall geometry of this portion is similar to that of Cu^{II}(OEFB), whose structure is diagrammatically shown in Scheme 4 (14). The Cu(2)—N bond distances (average Cu(2)—N distance, 1.953 Å) in {Cu^{II}(OEPOC(O)OEB)Cu^{II}} are slightly shorter than those found in the porphyrin part of the dinuclear complex, where the average Cu(1)—N distance is 2.006 Å, but they are similar to the Cu—N bond distances in the linear tetrapyrrole complex Cu^{II}(OEFB) where the average Cu—N distance in 1.953 Å (14). The Cu(2) atom is constrained to a geometry between planar and tetrahedral. Three of the *cis* N-Cu(2)-N angles (90.76(13), 91.14(13), and 90.28(13)°) are close to 90°, while the forth (N(5)-Cu(2)-N(8), 97.02(13)°) at the open end of the tetrapyrrole is wider. The pseudo-*trans* angles, N(5)-Cu(2)-N(7), 158.74(14)° and N(6)-Cu(2)-N(8), 154.44(14)°, are much narrower than the 180° required for planar coordination but wider than the 109.5° expected for tetrahedral coordination. As seen in Figs. 2 and 4, which shows a side-on view of each portion of the dinuclear complex, the macrocycle forms a helical arrangement around Cu(2). This arrangement allows the open ends of the ligand to avoid each other. The separation between O(3) and C(37) is 3.85 Å which is larger than the corresponding non-bonded O···O separations of 3.17 and 3.22 Å found in biliverdin complexes (15). The C(2)—O(1) and C(37)—O(1) bond lengths (1.419(5) and 1.370(5) Å, respectively) in the ester group are, as expected, longer than the C(37)—O(2) and C(56)—O(3) bond lengths (1.210(5) and 1.214(5) Å, respectively). The carbonyl oxygen of the ester link interacts weakly, if at all, with Cu(2). The Cu(2)—O(2) distance is 2.921(4) Å. This interaction may simply result from constraints of the bridge between the two parts of this dinuclear complex. The other carbonyl oxygen of the open chain tetrapyrrole is further away from Cu(2) with a Cu(2)···O(3) separation of 3.396(4) Å. The non-bonded Cu–Cu separation in {Cu^{II}(OEPOC(O)OEB)Cu^{II}} is 7.748(2) Å.

The formation of the dinuclear complex {Cu^{II}(OEPOC(O)OEB)Cu^{II}} is a complex process in which Cu^{II}(OEPOH) undergoes an oxidative ring opening that is somewhat similar to the behavior of iron porphyrins shown in Scheme 3, and some speculation in regard to the mechanism of this reaction is in order. Scheme 5 shows a proposed mechanism for the formation of the dinuclear complex, {Cu^{II}(OEPOC(O)OEB)Cu^{II}}. In the initial step dioxygen oxidizes a portion of Cu^{II}(OEPOH) to Cu^{II}(OEPO$^{\bullet}$). This step has precedent in the reactivity of both Ni^{II}(OEPOH) and Zn^{II}(OEPOH) with dioxygen in pyridine solution (5, 6). Moreover, solutions of Cu^{II}(OEPOH) in pyridine gradually develop a green color and new absorption bands at 440 (Soret) and 802 nm when exposed to dioxygen. An identical spectrum, which is characteristic of the formation of complexes of type **5**, is obtained rapidly by oxidizing

© 2001 NRC Canada

Fig. 2. A perspective view of {Cu^{II}(OEPOC(O)OEB)Cu^{II}}.

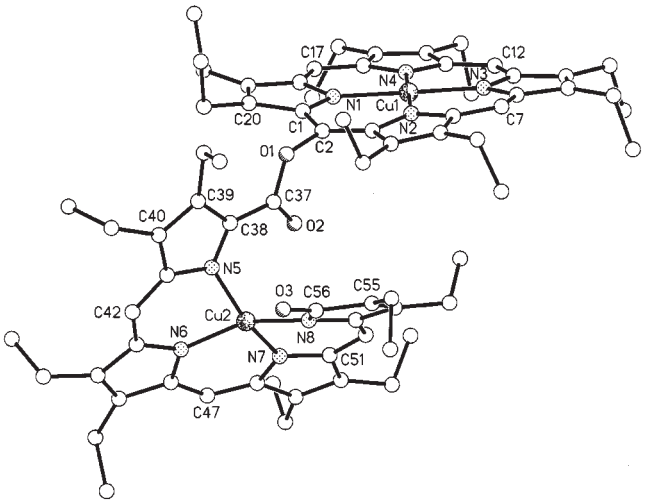


Table 1. Atomic coordinates (1×10^4) and equivalent isotropic displacement parameters (U_{eq}) ($Å^2$) for {Cu^{II}(OEPOC(O)OEB)Cu^{II}}·$CHCl_3$.

Atom	*x*	*y*	*z*	U_{eq} (1×10^3)[a]
Cu(1)	1682(1)	4829(1)	393(1)	34(1)
N(1)	2824(3)	3755(3)	410(2)	33(1)
N(2)	1114(3)	4136(2)	1306(2)	28(1)
N(3)	543(3)	5897(3)	368(2)	38(1)
N(4)	2268(3)	5530(3)	–510(2)	44(1)
O(1)	2819(2)	2031(2)	2161(2)	25(1)
C(1)	2999(3)	2933(3)	930(3)	34(1)
C(2)	2431(3)	2798(3)	1594(2)	26(1)
C(3)	1531(3)	3313(3)	1769(2)	27(1)
C(4)	880(3)	3075(3)	2389(2)	26(1)
C(5)	63(3)	3734(3)	2277(2)	27(1)
C(6)	227(3)	4408(3)	1626(2)	27(1)
C(7)	–410(3)	5235(3)	1394(3)	32(1)
C(8)	–272(3)	5943(3)	833(3)	34(1)
C(9)	–938(4)	6829(3)	635(3)	39(1)
C(10)	–521(4)	7314(4)	48(3)	49(1)
C(11)	397(4)	6730(3)	–126(3)	44(1)
C(12)	1052(5)	6965(4)	–687(3)	56(2)
C(13)	1913(4)	6425(4)	–871(3)	49(1)
C(14)	2595(5)	6679(5)	–1469(3)	64(2)
C(15)	3354(5)	5930(5)	–1472(3)	56(2)
C(16)	3128(4)	5220(4)	–878(3)	47(2)
C(17)	3715(4)	4341(4)	–714(3)	50(1)
C(18)	3572(4)	3645(4)	–127(3)	45(1)
C(19)	4213(3)	2743(4)	24(3)	46(1)
C(20)	3869(3)	2283(4)	677(3)	39(1)
C(21)	999(3)	2241(3)	3022(3)	30(1)
C(22)	715(3)	1391(3)	2719(3)	41(1)
C(23)	–831(3)	3810(3)	2762(3)	30(1)
C(24)	–855(3)	4395(3)	3468(3)	35(1)
C(25)	–1868(4)	7141(3)	1050(3)	45(1)
C(26)	–1813(4)	7661(4)	1781(3)	59(2)
C(27)	–925(5)	8286(4)	–368(3)	65(2)
C(28)	–555(6)	9052(4)	–46(4)	91(2)
C(29)	2435(6)	7639(5)	–1964(3)	90(3)

Table 1 (*continued*).

Atom	*x*	*y*	*z*	U_{eq} (1×10^3)[a]
C(30)	2849(10)	8336(7)	–1544(6)	212(8)
C(31)	4244(4)	5855(5)	–1961(3)	72(2)
C(32)	5100(6)	5889(8)	–1444(4)	168(6)
C(33)	5071(4)	2394(4)	–485(3)	58(2)
C(34)	4826(4)	1976(4)	–1210(3)	59(2)
C(35)	4260(3)	1282(4)	981(3)	48(1)
C(36)	3693(4)	628(4)	694(3)	57(2)
Cu(2)	4850(1)	2662(1)	4032(1)	22(1)
N(5)	4685(2)	1519(2)	3598(2)	24(1)
N(6)	6189(2)	2093(2)	4182(2)	22(1)
N(7)	5071(2)	3921(2)	4039(2)	21(1)
N(8)	3549(2)	3106(2)	4398(2)	23(1)
O(2)	3591(2)	3014(2)	2665(2)	32(1)
O(3)	3102(2)	1748(2)	4955(2)	28(1)
C(37)	3448(3)	2232(3)	2664(2)	25(1)
C(38)	3977(3)	1394(3)	3155(2)	25(1)
C(39)	3971(3)	412(3)	3172(2)	27(1)
C(40)	4727(3)	–55(3)	3639(2)	27(1)
C(41)	5169(3)	627(3)	3889(2)	26(1)
C(42)	6057(3)	471(3)	4234(2)	24(1)
C(43)	6572(3)	1136(3)	4315(2)	25(1)
C(44)	7552(3)	977(3)	4503(3)	28(1)
C(45)	7757(3)	1847(3)	4475(2)	26(1)
C(46)	6893(3)	2529(3)	4279(2)	24(1)
C(47)	6772(3)	3527(3)	4161(2)	22(1)
C(48)	5933(3)	4170(3)	4039(2)	23(1)
C(49)	5786(3)	5193(3)	3932(2)	23(1)
C(50)	4839(3)	5550(3)	3897(2)	25(1)
C(51)	4408(3)	4735(3)	3977(2)	23(1)
C(52)	3438(3)	4774(3)	4020(2)	25(1)
C(53)	3046(3)	4012(3)	4241(2)	23(1)
C(54)	2034(3)	4088(3)	4429(2)	25(1)
C(55)	1945(3)	3237(3)	4740(2)	23(1)
C(56)	2913(3)	2581(3)	4718(2)	23(1)
C(57)	3315(3)	–52(3)	2777(3)	30(1)
C(58)	2639(3)	–404(3)	3374(3)	40(1)
C(59)	5107(3)	–1108(3)	3777(3)	31(1)
C(60)	5902(3)	–1457(3)	3186(3)	42(1)
C(61)	8233(3)	30(3)	4616(3)	37(1)
C(62)	8740(4)	–246(4)	3830(3)	53(2)
C(63)	8671(3)	2076(3)	4677(3)	31(1)
C(64)	8678(3)	2272(4)	5557(3)	43(1)
C(65)	6551(3)	5719(3)	3831(2)	26(1)
C(66)	6878(3)	5845(3)	2949(2)	31(1)
C(67)	4308(3)	6553(3)	3797(3)	30(1)
C(68)	3942(4)	6873(3)	2953(3)	46(1)
C(69)	1302(3)	4991(3)	4289(3)	29(1)
C(70)	1177(3)	5336(3)	3401(3)	36(1)
C(71)	1139(3)	2894(3)	5145(2)	28(1)
C(72)	1232(3)	2799(3)	6057(2)	33(1)

[a] U_{eq} is defined as one third of the trace of the orthogonalized U_{ij} tensor.

Cu^{II}(OEPOH) with diiodine in pyridine, and the Cu^{II}(OEPO$^{\bullet}$) that forms is readily reduced to Cu^{II}(OEPOH) by addition of aqueous sodium dithionite. In the second step of Scheme 5, Cu^{II}(OEPO$^{\bullet}$) adds Cu^{II}(OEPOH) through the

© 2001 NRC Canada

Table 2. Selected bond distances (Å) for $\{Cu^{II}(OEPOC(O)OEB)Cu^{II}\}\cdot CHCl_3$.

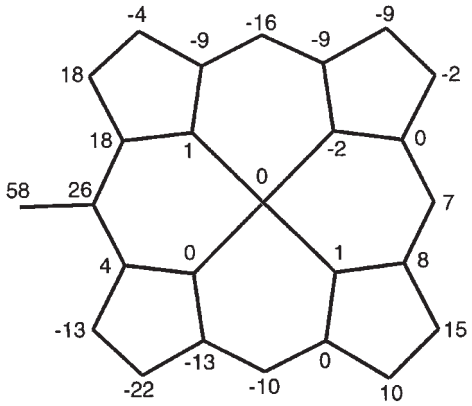
Cu(1)—N(3)	2.001(4)	Cu(2)—N(7)	1.945(3)
Cu(1)—N(2)	2.003(3)	Cu(2)—N(8)	1.954(3)
Cu(1)—N(1)	2.008(4)	Cu(2)—N(6)	1.956(3)
Cu(1)—N(4)	2.011(4)	Cu(2)—N(5)	1.958(3)
N(1)—C(18)	1.374(6)	N(5)—C(38)	1.353(5)
N(1)—C(1)	1.390(6)	N(5)—C(41)	1.383(5)
N(2)—C(6)	1.366(5)	N(6)—C(46)	1.355(5)
N(2)—C(3)	1.389(5)	N(6)—C(43)	1.382(5)
N(3)—C(11)	1.379(6)	N(7)—C(51)	1.348(5)
N(3)—C(8)	1.386(6)	N(7)—C(48)	1.391(5)
N(4)—C(16)	1.374(7)	N(8)—C(53)	1.364(5)
N(4)—C(13)	1.378(7)	N(8)—C(56)	1.396(5)
O(1)—C(37)	1.370(5)	O(2)—C(37)	1.210(5)
O(1)—C(2)	1.419(5)	O(3)—C(56)	1.214(5)
C(1)—C(2)	1.383(6)	C(37)—C(38)	1.478(6)
C(1)—C(20)	1.474(6)	C(38)—C(39)	1.436(6)
C(2)—C(3)	1.391(6)	C(39)—C(40)	1.381(6)
C(3)—C(4)	1.448(6)	C(40)—C(41)	1.414(6)
C(4)—C(5)	1.355(6)	C(41)—C(42)	1.401(6)
C(5)—C(6)	1.443(6)	C(42)—C(43)	1.382(6)
C(6)—C(7)	1.376(6)	C(43)—C(44)	1.439(6)
C(7)—C(8)	1.369(6)	C(44)—C(45)	1.371(6)
C(8)—C(9)	1.447(6)	C(45)—C(46)	1.442(6)
C(9)—C(10)	1.358(7)	C(46)—C(47)	1.424(6)
C(10)—C(11)	1.450(8)	C(47)—C(48)	1.370(6)
C(11)—C(12)	1.387(8)	C(48)—C(49)	1.456(6)
C(12)—C(13)	1.363(8)	C(49)—C(50)	1.362(6)
C(13)—C(14)	1.464(8)	C(50)—C(51)	1.466(6)
C(14)—C(15)	1.367(9)	C(51)—C(52)	1.404(6)
C(15)—C(16)	1.448(7)	C(52)—C(53)	1.381(6)
C(16)—C(17)	1.379(8)	C(53)—C(54)	1.480(6)
C(17)—C(18)	1.386(7)	C(54)—C(55)	1.333(6)
C(18)—C(19)	1.436(7)	C(55)—C(56)	1.516(6)
C(19)—C(20)	1.364(7)		

Table 3. Selected bond angles (°) for $\{Cu^{II}(OEPOC(O)OEB)Cu^{II}\}\cdot CHCl_3$.

N(3)-Cu(1)-N(2)	90.52(15)	N(7)-Cu(2)-N(8)	90.76(13)
N(3)-Cu(1)-N(1)	179.61(14)	N(7)-Cu(2)-N(6)	91.14(13)
N(2)-Cu(1)-N(1)	89.67(14)	N(8)-Cu(2)-N(6)	154.44(14)
N(3)-Cu(1)-N(4)	89.7(2)	N(7)-Cu(2)-N(5)	158.74(14)
N(2)-Cu(1)-N(4)	179.01(15)	N(8)-Cu(2)-N(5)	97.02(13)
N(1)-Cu(1)-N(4)	90.1(2)	N(6)-Cu(2)-N(5)	90.28(13)
C(18)-N(1)-C(1)	105.0(4)	C(38)-N(5)-C(41)	106.2(3)
C(18)-N(1)-Cu(1)	127.3(3)	C(38)-N(5)-Cu(2)	129.5(3)
C(1)-N(1)-Cu(1)	127.6(3)	C(41)-N(5)-Cu(2)	122.3(3)
C(6)-N(2)-C(3)	105.3(3)	C(46)-N(6)-C(43)	106.4(3)
C(6)-N(2)-Cu(1)	126.3(3)	C(46)-N(6)-Cu(2)	128.3(3)
C(3)-N(2)-Cu(1)	128.4(3)	C(43)-N(6)-Cu(2)	124.9(3)
C(11)-N(3)-C(8)	105.9(4)	C(51)-N(7)-C(48)	106.4(3)
C(11)-N(3)-Cu(1)	127.2(4)	C(51)-N(7)-Cu(2)	125.9(3)
C(8)-N(3)-Cu(1)	126.9(3)	C(48)-N(7)-Cu(2)	127.5(3)
C(16)-N(4)-C(13)	105.7(4)	C(53)-N(8)-C(56)	106.6(3)
C(16)-N(4)-Cu(1)	126.6(4)	C(53)-N(8)-Cu(2)	123.5(3)
C(13)-N(4)-Cu(1)	127.7(4)	C(56)-N(8)-Cu(2)	128.9(3)
C(37)-O(1)-C(2)	113.4(3)	O(2)-C(37)-O(1)	122.6(4)
C(20)-C(35)-C(36)	111.6(4)	O(2)-C(37)-C(38)	123.8(4)
		O(1)-C(37)-C(38)	113.4(3)

meso carbon to produce the crucial O–C bond that links the dinuclear complex. Subsequent addition of dioxygen to the resulting radical results in the eventual rupture of one of the *meso* C–C bonds. Finally, the process is terminated through reaction of the ring-open radical with superoxide via a RO_4H species (not shown) that is analogous to the termination of autoxidation though the interaction of two peroxy radicals as established by Russell (19). This mechanism predicts that the oxygen atom of the lactam ring is derived from molecular oxygen, while the other two oxygen atoms in the dinuclear product originate in the initial sample of Cu^{II}(OEPOH). Further studies of this oxidation process are clearly warranted. However, it is also clear from the present work that oxidative ring opening of metalloporphyrins can be stopped at a stage before the *meso*-carbon atom is removed (as carbon monoxide) from the tetrapyrrole. Of course the formation a dinuclear species analogous to $\{Cu^{II}(OEPOC(O)OEB)Cu^{II}\}$ is prohibited in enzymatic degradation of heme by the protein, which isolates the heme and prohibits interaction of one heme with another.

Fig. 3. A formal diagram that illustrates the out-of-plane displacements of the core atoms (in 0.01 Å units) of the porphyrin half of the dinuclear complex $\{Cu^{II}(OEPOC(O)OEB)Cu^{II}\}$ from the mean plane defined by the Cu(I), the four nitrogen atoms, and the 20 carbon atoms of the porphyrin's core.



Experimental

Preparation of compounds

Samples of H_2OEPOH and Cu^{II}(OEPTFA) were obtained by previously published methods (16–18).

Cu^{II}(OEPOH)

A sample of H_2OEPOH (47.5 mg, 0.086 mmol) dissolved in THF (50 mL) was mixed under nitrogen with a 50 mL THF solution containing copper(II) acetate monohydrate (18.0 mg, 0.090 mmol). The aqua blue solution immediately turned red and a precipitate begins to form. The solution was allowed to react for several hours before removing the solvent under vacuum. The solids were redissolved in dichloro-

© 2001 NRC Canada

Scheme 5.

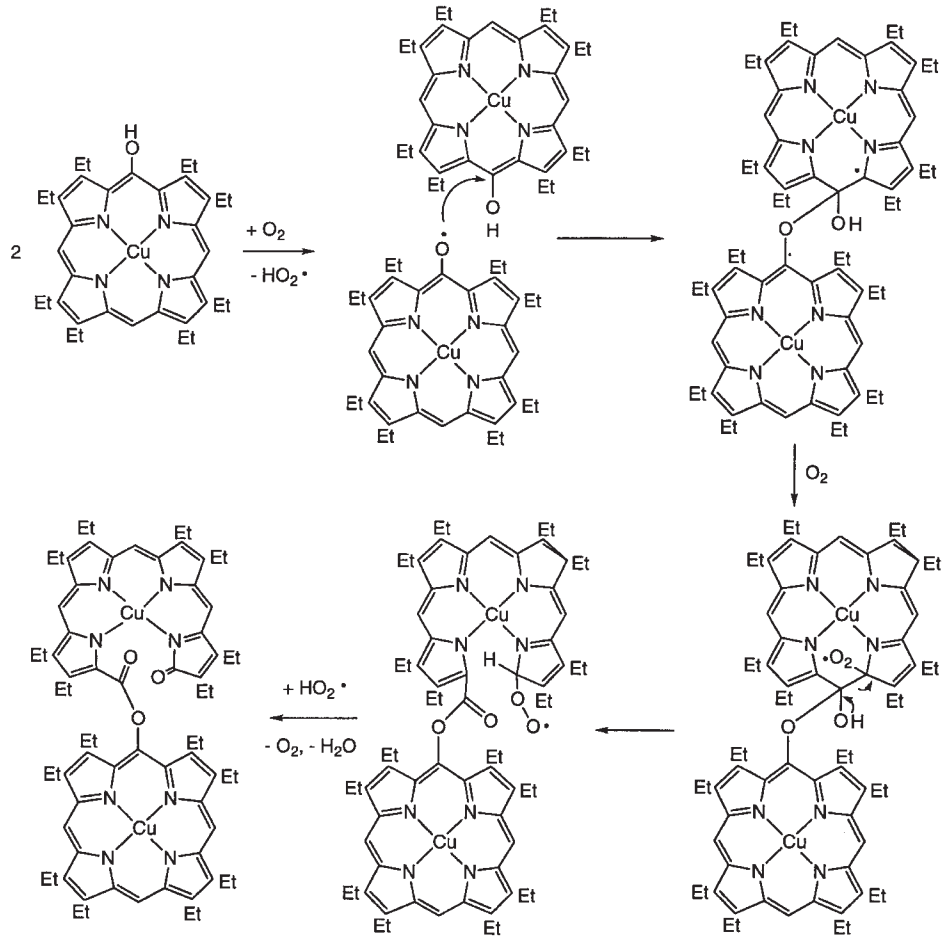
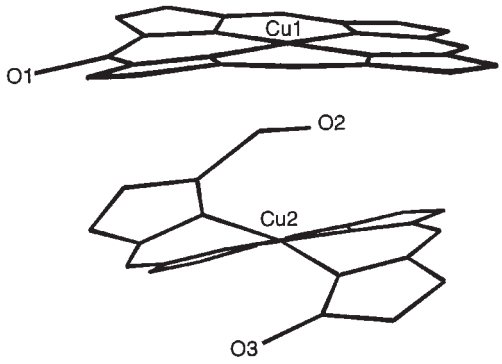


Fig. 4. Edge-on views of the two parts of {Cu^{II}(OEPOC(O)OEB)Cu^{II}}: the porphyrin-like environment surrounding Cu(1) (top); the linear tetrapyrrole unit surrounding Cu(2) (bottom).



methane and precipitated with methanol. The red crystalline product was collected by filtration, washed with methanol, and vacuum dried to give an 89% yield of Cu^{II}(OEPOH). UV–vis (in CH_2Cl_2) λ_{max} (nm) (ε (M^{-1} cm^{-1})): 404 (420 000), 528 (24 000), 560 (16 000). IR (mineral oil) (cm^{-1}): 3508 (s), 1592 (s), 1540 (w), 1501 (w), 1466 (m), 1389 (w), 1370 (w), 1275 (s), 1261 (m), 1226 (w), 1186 (m), 1155 (w), 1123 (w), 1099 (w), 1056 (m), 1018 (s), 957 (m), 830 (w), 794 (w), 692 (w).

Cu^{II}(OEPTFA)

The trifluoroacetoxy derivative was prepared in the same manner as Cu^{II}(OEPOH) to give an 83% yield of Cu^{II}(OEPTFA). UV–vis (in CH_2Cl_2) λ_{max} (nm) (ε (M^{-1} cm^{-1})): 400 (160 000), 526 (7 000), 564 (9 000). IR (mineral oil) (cm^{-1}): 1792 (s), 1591 (m), 1526 (w), 1477 (w), 1343 (m), 1275 (m), 1216 (s), 1176 (s), 1153 (m), 1130 (s), 1062 (m), 1019 (m), 957 (m), 845 (m), 753 (w).

X-ray data collection for {Cu^{II}(OEPOC(O)OEB)Cu^{II}}·$CHCl_3$

A homogeneous collection of red–purple blocks of {Cu^{II}(OEPOC(O)OEB)Cu^{II}}·$CHCl_3$ were obtained by slow diffusion of air-saturated methanol into an air-saturated chloroform–pyridine solution of Cu^{II}(OEPOH). The datum crystal was coated with a light hydrocarbon oil and mounted in the 121 K dinitrogen stream of a Siemens P4 rotating anode diffractometer that was equipped with a low-temperature device. Two check reflections showed less than a 2% decay during the data collection. The data were corrected for Lorentz and polarization effects. Crystal data and data collection parameters: $C_{73}H_{87}Cl_3N_8O_3Cu_2$, MW = 1357.94, triclinic, $P\bar{1}$, α = 14.6140(10), β = 14.642(2), γ = 16.690(2) Å, a = 84.18(2), b = 87.57(2), c = 76.55(2)°, V = 3454.8(7) $Å^3$, Z = 2, ρ_c = 1.305 g cm^{-3}, m = 2.233 mm^{-1} (121(2) K; Cu Kα (λ) = 1.54178). A complete set of unique data, 9017 re-

© 2001 NRC Canada

flections, was collected using $2\theta - \omega$ scans in the range $0 < h < 15$, $-15 < k < 15$, $-17 < l < 17$ on a needle cut to dimensions of 0.08 × 0.20 × 0.22 mm.

Solution and refinement

The structure was solved by direct methods using the SHELXS 86 suite of programs. Refinement (on F^2) was performed with the SHELX 93 software. Scattering factors for neutral atoms and corrections for anomalous dispersion were taken from a standard source (20). An absorption correction was applied to the data (21). Hydrogen atoms were placed at calculated positions and allowed to ride on the position of the parent carbon atom. Hydrogen atom thermal parameters were set to 1.2 times the equivalent isotropic thermal parameters of the adjacent carbon atom.

A badly disordered molecule of chloroform was located during refinement. The molecule appears to occupy more than three sites in a void space in the unit cell. No satisfactory model could be found to accommodate all of the observed electron density. The void space was analyzed with the SQUEEZE routine of PLATON (22). A volume of 237 Å^3 containing about 60 electrons was located. With 58 electrons, a single chloroform molecule is a good fit to the electron density. A new data file eliminating contributions from this electron density was created and used in subsequent cycles of refinement. The atoms of this chloroform molecule are thereby removed from the list of atom positional parameters. The density that was removed is incorporated in an output file that has been included in the refinement details of the cif.

Full-matrix least-squares refinement based on F^2 with 782 parameters and 9017 data yielded $R_1 = 0.077$, $wR_2 = 0.140$ for all data and a conventional $R_1 = 0.054$ computed for 6548 observed data ($I > 2\sigma(I)$). $R = \Sigma||F_o| - |F_c||/\Sigma|F_o|$ and $R_w = \Sigma||F_o| - |F_c||\sqrt{w}/\Sigma|F_o|\sqrt{w}$.

Tables of crystal data, bond lengths and angles, anisotropic displacement parameters, and hydrogen coordinates may be purchased from the Depository of Unpublished Data, Document Delivery, CISTI, National Research Council Canada, Ottawa, ON K1A 0S2, Canada. For information on obtaining material electronically go to http://www.nrc.ca/cisti/irm/unpub_e.shtml. Crystallographic information has also been deposited with the Cambridge Crystallographic Data Centre. Copies of the data can be obtained, free of charge, on application to the Director, CCDC, 12 Union Road, Cambridge CB2 1EZ, U.K. (fax: 44-1223-336033 or e-mail: deposit@ccdc.cam.ac.uk).

Instrumentation

Absorption spectra were recorded on a Hewlet–Packard 8452A diode array spectrophotometer. Infrared spectra were acquired on an IBM IR/32 spectrometer. EPR spectra were recorded in the X band on a Bruker spectrometer. EI (70 eV) mass spectrometry was performed on a VG Analytical ZAB-2F-HS mass spectrometer.

Acknowledgments

We thank the National Institutes of Health (GM-26226) for financial support and Prof. R. Koerner for assistance.

References

1. B.R. James. *In* The porphyrins. Vol. 5. *Edited by* D. Dolphin. Academic Press, New York. 1978. p. 205.
2. T.N. St Claire and A.L. Balch. Inorg. Chem. **38**, 684 (1999).
3. A.L. Balch, R. Koerner, L. Latos-Grayski, J.E. Lewis, T.N. St Claire, and E.P. Zovinka. Inorg. Chem. **36**, 3892 (1997).
4. A.L. Balch. Coord. Chem. Rev. **200**–**202**, 349 (2000).
5. A.L. Balch, B.C. Noll, S.L. Phillips, S.M. Reid, and E.P. Zovinka. Inorg. Chem. **32**, 4730 (1993).
6. A.L. Balch, B.C. Noll, and E.P. Zovinka. J. Am. Chem. Soc. **114**, 3380 (1992).
7. A.L. Balch, M. Mazzanti, and M.M. Olmstead. Inorg. Chem. **32**, 4737 (1993).
8. A.L. Balch, L.L. Latos-Grayski, B.C. Noll, M.M. Olmstead, and N. Safari. J. Am. Chem. Soc. **115**, 9056 (1993).
9. A.L. Balch, L. Latos-Grayski, B.C. Noll, M.M. Olmstead, L. Szterenberg, and N. Safari. J. Am. Chem. Soc. **115**, 1422 (1993).
10. P.R. Ortiz DeMontellano. Acc. Chem. Res. **31**, 543 (1998).
11. M. Iwaizumi, Y. Ohba, H. Iida, and M. Hirayama. Inorg. Chim. Acta, **82**, 47 (1984).
12. R. Koerner, M.M. Olmstead, A. Ozarowski, S.L. Phillips, P.M. VanCalcar, K. Winkler, and A.L. Balch. J. Am. Chem. Soc. **120**, 1274 (1998).
13. R. Pak and W.R. Scheidt. Acta Crystallogr. Sect. C: Cryst. Struct. Commun. **47**, 431 (1991).
14. R. Koerner, L. Latos-Grayski, and A.L. Balch. J. Am. Chem. Soc. **120**, 9246 (1998).
15. A.L. Balch, M. Mazzanti, B.C. Noll, and M.M. Olmstead. J. Am. Chem. Soc. **116**, 9114 (1994).
16. A.H. Jackson, G.W. Kenner, and K.M. Smith. J. Chem. Soc. C, 302 (1968).
17. R. Bonnett and M.J. Dimsdale. J. Chem. Soc. Perkin Trans 1, 2540 (1972).
18. G.H. Barnett, M.F. Hudson, S.W. McCombie, and K.M. Smith. J. Chem. Soc. Perkin Trans. 1, 691 (1973).
19 G.A. Russell. J. Am. Chem. Soc. **79**, 3871 (1957).
20. A.J.C. Wilson (*Editor*). International tables for crystallography. Kluwer Academic Publishers, Dordrecht. 1992.
21. S. Parkin, B. Moezzi, and H. Hope. J. Appl. Crystallogr. **28**, 53 (1995).
22. P. Vandersluis and A.L. Spek. Acta Crystallogr. Sect. A: Fundam. Crystallogr. **46**, 194 (1990).

© 2001 NRC Canada

Synthesis and characterization of the pentadentate macrobicyclic ligand, 14-thia-1,4,8,11-tetraazabicyclo[9.5.3]nonadecane (L1) and its nickel(II) complexes. X-ray crystal structure of $[Ni(L1)(ClO_4)](ClO_4)\cdot 2[Ni(L1)(OH_2)](ClO_4)_2\cdot 6H_2O$

Kevin R. Coulter, Alexander McAuley, and Steven Rettig

Abstract: The pentadentate macrobicycle,14-thia-1,4,8,11-tetraazabicyclo[9.5.3]nonadecane (L1), has been synthesized by high dilution cyclization of 1-thia-4,8-diazacyclododecane ([10]aneN$_2$S) (**2**) with *N*,*N*′-bis(α-chloro acetamido) propane (**3**) and subsequent reduction of the di-oxo intermediate. The structure of the $[Ni(L1)(ClO_4)](ClO_4)\cdot 2[Ni(L1)(OH_2)](ClO_4)_2\cdot 6H_2O$ complex (monoclinic, $P2_1/c$, a = 13.9261(4) Å, b = 30.279(2) Å, c = 17.1248(3) Å, β = 94.5065(3)°) at R = 0.039 (R_w = 0.034) for 911 parameters using 18 266 reflections with $I > 3\sigma I$ has been determined. The ligand adopts a *trans*-III configuration. The Ni(II) ion is pseudooctahedral with Ni—S = 2.3896(10) Å in $[Ni(L1)(ClO_4)]^+$ and 2.4193(10) Å, 2.4225(10) Å, in the two $[Ni(L1)(H_2O)]^{2+}$ cations. Both nickel(II) and nickel(III) complexes are six-coordinate in solution. Oxidation of the $[Ni(L1)(OH_2)]^{2+}$ complex with $K_2S_2O_8$ in aqueous solution yielded an ESR active Ni(III) species and the frozen solution spectrum displayed axial symmetry with $g_\perp$ = 2.159 and $g_\parallel$ = 2.024. In CH_3CN, the $[Ni(L1)(solv)]^{2+}$ complex showed two reversible redox waves corresponding to the $Ni^{2+/+}$ couple at $E_{1/2}$ = –1.807 V vs. $Fc^{+/0}$ and $Ni^{3+/2+}$ couple at $E_{1/2}$ = 0.715 V vs. $Fc^{+/0}$.

Key words: synthesis, structure, polydentate macrobicycle, nickel(II).

Résumé : On a synthétisé le macrobicycle pentadentate, 14-thia-1,4,8,11-tétrabicyclo[9.5.3]nonadécane (L1), en procédant à la cyclisation à haute dilution du 1-thia-4,8-diazacyclododécane (([10]aneN$_2$S) (**2**) avec le *N*,*N*′-bis(α-chloroacétamido)propane (**3**) et à une réduction subséquente de l'intermédiaire dioxo. On a déterminé la structure du complexe $[Ni(L1)(ClO_4)](ClO_4)\cdot 2[Ni(L1)(OH_2)](ClO_4)_2\cdot 6H_2O$ (monoclinique, $P2_1/c$, a = 13,9261(4) Å, b = 30,279(2) Å et c = 17,1248(3) Å, β = 94,5065(3)°) avec R = 0,039 (R_w = 0,034) pour 911 paramètres utilisant 18 266 réflexions avec $I > 3\sigma(I)$. Le ligand adopte une configuration *trans*-III. L'ion Ni(II) est pseudo-octaédrique avec Ni—S = 2,3896(10) Å dans le cation $[Ni(L1)(H_2O)]^{+2}$ et 2,4193(10) et 2,4225(10) Å dans les deux cations $[Ni(L1)(H_2O)]^{+2}$. En solution les complexes à nickel(II) et à nickel(III) sont tous les deux hexacoordiné. L'oxydation du complexe $[Ni(L1)(OH_2)]^{2+}$ par du $K_2S_2O_8$ en solution aqueuse fournit une espèce Ni(III) active en RPE et le spectre de la solution congelée présente une symétrie axiale avec $g_\perp$ = 2,159 et $g_\parallel$ = 2,024. Dans le CH_3CN, le complexe $[Ni(L1)(solv)]^{2+}$ présente deux vagues redox réversibles qui correspondent au couple $Ni^{2+/+}$ à $E_{1/2}$ = –1,807 V vs. $Fc^{+/0}$ et au couple $Ni^{3+/2+}$ à $E_{1/2}$ = 0,715 V vs. $Fc^{+/0}$.

Mots clés : synthèse, structure, macrobicycle polydentate, nickel(II).

[Traduit par la Rédaction]

Introduction

The coordination chemistry of the 14-membered tetraaza ligand cyclam (cyclam = 1,4,8,11-tetraazacyclotetradecane) has been studied extensively (1–7) owing to the propensity of various conformational isomers (8) to bind a wide range of first row transition-metal ions, forming complexes of considerable thermodynamic and kinetic stability. A detailed analysis has been presented recently of all nickel 14-membered macrocycles in the Cambridge data base (9), where

Received September 15, 2000. Published on the NRC Research Press Web site at http://canjchem.nrc.ca site on July 19, 2001.

This paper is dedicated to Brian James, colleague and friend.

A. McAuley.[1] Department of Chemistry, University of Victoria, Victoria, BC V8W 3V6, Canada.
K.R. Coulter. Cominco Chemical Company, Trail, BC V1R 3W0, Canada.
S. Rettig.[2] Department of Chemistry, University of British Columbia, Vancouver, BC V6T 1W5, Canada.

[1]Corresponding author (telephone: (250) 721-7164; fax: (250) 721-7147; e-mail: amcauley@uvic.ca).
[2]Deceased.

 DOI: 10.1139/cjc-79-5/6-930 © 2001 NRC Canada

it is seen that the majority of *trans*-I species are square-planar or square-pyramidal, and the *trans*-III conformation is associated with octahedral symmetry. Also, *N*-alkylation appears to confer additional thermodynamic stability to the *trans*-I configuration (10).

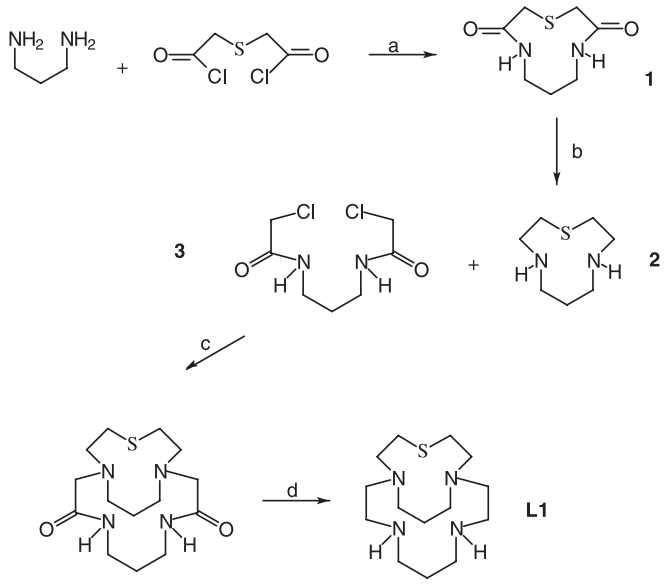
Previous studies in this laboratory (11–14)[3] have reported the syntheses of macrobicyclic pentacoordinate ligands 14-X-1,4,8,11-tetraazabicyclo[10.5.2]nonadecane (L2) in which a nine-membered cyclononane ring ([9]aneN_2X where X = NH, O, S) is fused to an ethylene segment of the 14-membered tetraaza cyclam ring. Each of the (L2) cations adopts the *trans*-I conformation in the solid state.

The coordination properties of sulfur donors continue to be of great interest (15–18), particularly those involving thioethers, which tend to be rare and of the weak apical type. Recently (15), the *s*- and *p*-donor properties have been examined in the possible use of macrocyclic thioethers in ^{99}Tc complexes with possible use as pharmaceuticals. Use has also been made (17) of the resistance of thioethers to aerial oxidation and hydrolysis to examine structure–function relationships in complex formation reactions with square-planar metal centers. Several studies have been presented (19–23) in which mixed *N*- and *S*-donor ligands, either open-chain or macrocyclic, form complexes with metal ions. This paper reports the synthesis of the (L1) macrobicycle, a structural isomer of (L2), which unlike the former, can also adopt a *trans*-III geometry. As a result of ligand conformation in these systems, if the sulfur binds, it must do so at the axial site. Also, since the electronic nature of the N_4S donor set is identical in both (L1) and (L2), any differences in the resulting coordination properties might be attributed principally to structural effects.

Experimental section

NMR spectra, both ^{1}H and ^{13}C, were recorded on Bruker AMX360 or Bruker AC300 high-field spectrometers with either D_2O (MeOH as external standard) or $CDCl_3$ (TMS) as the solvent. Mass spectra of the free ligands were recorded on a Finnegan 330 GC–MS instrument by methane chemical ionization and electron impact techniques. Mass spectra of acidified ligand perchlorate salts and metal complexes were recorded on a Kratos Concept spectrometer either by FAB or electrospray ionization techniques. Infrared spectra were recorded on either a Bruker IFS25 (FT IR) spectrometer or a PerkinElmer 1330 spectrometer. A Cary 5 UV–vis–NIR spectrophotometer was used to record spectra. Elemental analyses were performed by Canadian Microanalytical Services Ltd., Delta, BC, Canada. Electrochemistry was performed using a Princeton Applied Research model 273 potentiostat–galvanostat, interfaced with an IBM PC microcomputer. The data were recorded using the corrWare program (Scribner Associates Inc). The electrochemical cell employed the standard three electrode configuration: platinum working and counter electrodes with Ag–$AgNO_3$ or silver wire as the reference electrode and 0.1 M $(Bu)_4NClO_4$ as background electrolyte. The ferrocene–ferrocenium couple ($Fc^{0/+}$) was used as both an external and internal standard.

Scheme 1. (*a*) 2 mol equiv diaminopropane (C_6H_6), rapid stirring, high dilution, RT; (*b*) BH_3·THF; (*c*) 1:1 $CHCl_3$:CH_3CN–CH_3CN, Na_2CO_3, high dilution; (*d*) BH_3·THF.



Molecular mechanics calculations were carried out on a Power Macintosh 7100/80 computer using the CAChe Scientific Worksystem software package, version 3.7. This software uses Allinger's MM2 (24) force field modelling program.

Reagent grade starting materials were used without further purification. Liquid amines were purified by vacuum distillation. Chloroform was twice distilled over CaH_2 to remove the ethanol present as stabilizer. Benzene was dried with sodium metal and freshly distilled before use. Increased yields in cyclisation reactions were observed with rapid stirring, and an apparatus was constructed for this purpose (25) where solutions were stirred mechanically at 1900 rpm.

Syntheses

The [10]aneN_2S precursor ligand was synthesized via the high dilution cyclisation of thiodigylcolic acid chloride with diaminopropane. The synthetic route to ligand L1 from [10]aneN_2S is outlined in Scheme 1.

Thiodiglycolic acid chloride

This material was prepared by reaction of $SOCl_2$ with the corresponding acid (26). To a sample of 15 g (0.1 mol) of thioglycollic acid, was added 150 mL (2.1 mol) of thionyl chloride. The solution was stirred for 20 h at room temperature under a strictly monitored N_2 atmosphere. Unreacted $SOCl_2$ was removed by vacuum distillation leaving a dark oil from which the pure acid chloride was obtained by microdistillation in vacuo. Yield: 14.5 g (0.078 mol), 78%. ^{1}H NMR ($CDCl_3$): 3.86 (CH_2-S). ^{13}C NMR ($CDCl_3$): 44.3 (CH_2-S), 169.5 (*C*=O).

1-Thia-4,8-diazacyclodecane-3,9-dione (1)

Samples of diaminopropane (8.88 g, 0.12 mol) and thiodiglycolic acid chloride (11.22 g, 0.060 mol), each in 50 mL of benzene, were added simultaneously from the sy-

[3] T. Rodopoulos. Unpublished observations.

© 2001 NRC Canada

ringe pump apparatus over a period of 10 h to 2.5 L chloroform stirred under N_2 at room temperature. The resulting white precipitate of diaminopropane dihydrochloride was filtered off and the product recovered by evaporation of the colourless filtrate in vacuo. The major product was the 1:1 condensate (**1**), but some 2:2 adduct ([20]-aneN_4S_2 tetraamide) was also observed. Pure samples of (**1**) were obtained by washing the product with 50 mL of MeOH per gram of solid. Yield: 7.1 g (0.038 mol), 63%; mp > 200°C. CI-MS *m*/*e*: 189 (M+1), 217 (M+29), 229 (M+41). IR (cm^{-1}): C=O stretch, 1640 (s, brd). ^{1}H NMR (D_2O): 1.65 (m, C-C*H*$_2$-C), 3.12 (m, C*H*$_2$-S, C*H*$_2$-N). ^{13}C NMR (D_2O): 24.9 (C-*C*H$_2$-C), 36.4, 39.9 (*C*H$_2$-S, *C*H$_2$-N), 171.8 (*C*=O). Anal. calcd. for $C_7H_{12}N_2O_2S$: C 44.66, H 6.43, N 14.88; found: C 44.66, H 6.42, N 14.66.

1-Thia-4,8-diazacyclodecane (2)

To 2.0 g (11.0 mmol) (**1**) was added 45 mL of 1 M BH_3·THF (0.045 mol) under N_2. The slurry was stirred at room temperature for 20 min and then refluxed for 4 h. After cooling in an ice bath, the excess borane was destroyed by slow dropwise addition of distilled water (2 to 3 mL) and the resulting solution was taken to dryness on a rotary evaporator. The white solid produced was dissolved in 40 mL of 6 M HCl and refluxed for 2 h. After cooling, the solution was taken to dryness on a rotary evaporator and dried further in vacuo. The resulting pale orange solid was dissolved in 25 mL of 2.5 M NaOH and extracted into chloroform (6 × 50 mL). The organic layers were combined, dried over sodium sulfate, and taken to dryness yielding a pale yellow or colourless oil. Yield: 1.55g (9.7 mmol), 88%. CI-MS *m*/*e*: 161 (M+1), 189 (M+29), 201 (M+41). ^{1}H NMR ($CDCl_3$): 1.6 (quintet, C-C*H*$_2$-C), 2.6–2.8 (m, 12H). ^{13}C NMR ($CDCl_3$): 27.9 (C-*C*H$_2$-C), 35.3 (*C*H$_2$-S), 48.1, 49.7 (*C*H$_2$-N).

***N*,*N*′-Bis(α-chloro acetamido)propane (3)**

The procedure was essentially that of Bradshaw et al. (27). Reaction of chloroacetyl chloride (0.37 mol) with diaminopropane (14.8 g, 0.20 mol) in aqueous base and resulting work-up yielded 21.3 g (0.094 mol), 47% of **3**. CI-MS *m*/*e*: 227 (M+1), 255 (M+29). ^{1}H NMR ($CDCl_3$): 1.72 (quintet, C-C*H*$_2$-C), 3.18 (quartet, C*H*$_2$-N), 4.05 (singlet, C*H*$_2$Cl). ^{13}C NMR ($CDCl_3$): 29.4 (C-*C*H$_2$-C), 36.4 (*C*H$_2$-N), 42.6 (*C*H$_2$Cl), 166.8 (*C*=O).

14-Thia-1,4,8,11-tetraazabicyclo[9.5.3]nonadecane-3,9-dione (4)

Samples of ([10]aneN_2S) (**2**) 1.48 g (9.25 mmol) in 200 mL 50:50 $CHCl_3$–CH_3CN and (**3**) 2.1 g (9.25 mmol), in 200 mL CH_3CN, were added drop-wise simultaneously in four batches of 50 mL from the syringe pump apparatus over a period of 8–10 h per 50 mL batch (40 h total) to 2.5 L of refluxing distilled CH_3CN containing 2.5 g (2.5 equiv) of sodium carbonate under N_2. After cooling to room temperature and filtering, evaporation to dryness in vacuo, gave a white powdery solid. Yield: 2.1 g, (6.69 mmol), 71.5%; mp > 200°C. CI-MS *m*/*e*: 315 (M+1), 343 (M+29), 355 (M+41). IR (cm^{-1}): C=O stretch, 1645 (s, brd.). ^{1}H NMR ($CDCl_3$): 1.4–1.9 (m, C-C*H*$_2$-C), 2.4–2.6, 2.8–3.4, 3.6–3.8 (m, 20H, C*H*$_2$-S, C*H*$_2$-N). ^{13}C NMR ($CDCl_3$): 26.8 (C-*C*H$_2$-C), 27.9 (C-*C*H$_2$-C), 36.3, 39.5, 54.5, 55.2, 60.0 (*C*H$_2$-N, *C*H$_2$-S), 170.7 (C=O). Anal. calcd. for $C_{14}H_{26}N_4O_2S$: C 53.48, H 8.33, N 17.82; found: C 53.12, H 8.12, N 16.87. We have no explanation for the low figure for nitrogen analysis.

14-Thia-1,4,8,11-tetraazabicyclo[9.5.3]nonadecane (L1)

To 1.0 g (3.18 mmol) of the diamide (**4**) was added, under nitrogen, 20 mL of 1 M BH_3·THF (20 mmol, 6 equiv). The slurry was stirred for 20 min then refluxed for 4.5 h and processed as described earlier. After reflux in acid, cooling and drying in vacuo, the resulting material was dissolved in strongly basic NaOH and extracted with chloroform (6 × 40 mL). The combined organic layers were dried over anhyd Na_2SO_4 and taken to dryness in vacuo yielding a colourless oil. Yield: 0.72 g (2.52 mmol), 79%. The material was purified by dissolving 0.72 g (2.52 mmol) of crude L1 in 2 mL 1:1 v/v methanol and water, followed by dropwise addition of 70% $HClO_4$ (*CAUTION*) until the mixture was distinctly acidic. A colourless crystalline precipitate of composition $[H_4L1](ClO_4)_4$ formed overnight. The precipitate was filtered, washed successively with methanol, ether and dried in vacuo. Yield: 0.83 g (1.21 mmol). FAB-HR-MS calcd. for $[C_{14}H_{31}N_4S]^+$: 286.2269: found: 286.2255. ^{1}H NMR (D_2O): 1.6–1.8 (m, 4H, C-C*H*$_2$-C), 2.2–3.4 (m, 24H). ^{13}C NMR (D_2O): 18.9 (C-*C*H$_2$-C), 24.4 (C-*C*H$_2$-C), 28.5 (*C*H$_2$-S), 44.1, 49.9, 50.2, 52.7, 53.0 (5 × *C*H$_2$-N). The free ligand, L1, was obtained by dissolving the perchloric acid salt (0.83 g) in 15 mL of 5 M NaOH and extracting with chloroform (4 × 50 mL). The combined extracts were dried over anhyd Na_2SO_4 and taken to dryness in vacuo, leaving a viscous colourless oil. Yield: 0.191 g (0.67 mmol), 55%. CI-MS *m*/*e*: 287 (M+1), 315 (M+29), 327 (M+41). ^{1}H NMR ($CDCl_3$): 1.6–1.8 (m, 4H, C-C*H*$_2$-C), 2.4–2.9 (m, 24H). ^{13}C NMR ($CDCl_3$): 29.0 (C-*C*H$_2$-C), 29.3 (C-*C*H$_2$-C), 36.4 (*C*H$_2$-S), 46.7, 51.9, 55.2, 56.0, 57.9 (5 × *C*H$_2$-N).

CAUTION! Perchlorate salts are explosive and care should be taken when using these compounds. Only small quantities should be prepared. Experiments should be carried out only in designated fume hoods.

$[Ni(L1)(ClO_4)](ClO_4)\cdot 2[Ni(L1)(OH_2)](ClO_4)_2\cdot 6H_2O$

To 150 mg (0.52 mmol) of L1 and 192 mg (0.52 mmol) K_2CO_3 in 20 mL dry acetonitrile was added, with stirring, a solution of 72 mg (0.52 mmol) $[Ni(OH_2)_6](ClO_4)_2$ in 10 mL dry acetonitrile. The mixture was refluxed for 4 h to ensure complete coordination, filtered, and taken to dryness in vacuo. The pale pink residue was dissolved with heating in 8 mL of 5% $HClO_4$. Upon cooling, pale pink needle crystals formed which were removed by filtration and dried. Yield: 122 mg (0.069 mmol), 40%. The presence of the perchlorate cation was confirmed by FAB-HR-MS: calcd. for $[Ni(L1)(ClO_4)]^+$: 443.1029; found: 443.0966.

Crystallography

$[Ni(L1)(ClO_4)](ClO_4)\cdot 2[Ni(L1)(OH_2)](ClO_4)_2\cdot 6H_2O$

Pale pink crystals of dimension 0.35 × 0.25 × 0.20 mm, grown from dilute perchloric acid were used. X-ray measurements were made on a Rigaku/ADSC CCD area detector with graphite monochromated Mo Kα radiation (λ = 0.71069 Å). Data were collected in 0.30° oscillations with 12.5 s exposures. A sweep of data was done using φ oscilla-

© 2001 NRC Canada

Table 1. Crystallographic data.[a]

$[Ni(L1)(ClO_4)](ClO_4)\cdot 2[Ni(L1)(OH_2)](ClO_4)_2\cdot 6H_2O$			
Formula	$C_{42}H_{106}N_{12}Ni_3S_3Cl_6O_{32}$		
Crystal system	Monoclinic	Fw	1776.36
Space group	$P2_1/c$ (no. 14)		
a (Å)	13.9261(4)		
b (Å)	30.279(2)		
c (Å)	17.1248(3)		
α (°)	90		
β (°)	94.5065(3)		
γ (°)	90		
V (Å^3)	7198.7(4)	Z	4
ρ_{calc} (g cm^{-3})	1.639	Radiation	Mo
μ (cm^{-1})	11.78	Crystal size (mm)	0.15 × 0.2 × 0.3
Scan type	ω-2	Scan range (2θ, °)	4.0–60.1
φ Oscillation range (°)	0.0–190.2	ω Oscillation range (°)	–23–17.8
Crystal decay (%)	negligible		
Total reflections	68 135	Unique reflections	18 649
Observations	18 266		
No. of variables	911		
Max Δ/σ (final cycle)	0	Res. density (e Å^{-3})	–1.41–1.89
R_{merge} (R_w)	0.032 (0.034)	R (on $I > 3\sigma(I)$)	0.039

[a]Temperature 193(2) K, Mo Kα (λ = 71069 Å) radiation, graphite monochromator, Rigaku/ADSC CCD area detector, $R = \Sigma||Fo| - ||Fc||/\Sigma|Fo|$, $Rw = [(\Sigma w(|Fo| - |Fc|)^2/\Sigma wFo^2)]^{1/2}$.

tions from 0.0 to 190.2° at χ = –90° and a second sweep was performed using ω oscillations between –23.0 and 17.8° at χ = 90°. Corrections were made for Lorentz and polarization effects. The structure was solved by direct methods (28*a*) and expanded using Fourier techniques (28*b*). The asymmetric unit contained two $[Ni(L1)(H_2O)]^{2+}$, and one $[Ni(L1)(ClO_4)]^+$ cations, with five perchlorate anions and six water molecules in the lattice. Three perchlorate moieties were modelled as disordered. Two of these (containing Cl(1) and Cl(6) were mirror disordered with respect to a common O_3 plane and the third (containing Cl(3) was disordered by a rotation about one of the Cl—O bonds. Population parameters were adjusted to yield approximately equal thermal parameters for the corresponding components. All but two of the water hydrogen atoms (those associated with O(28)) were placed in difference map positions but were not refined. The location of the uncoordinated water hydrogen atoms is tentative and some of these hydrogen atoms may be disordered and (or) incorrectly placed. Some low occupancy non-hydrogen atoms were refined isotropically (Cl(1a), Cl(6a), O(4a), O(12a), O(13a), O(14a), and O(23a)) while the rest were refined anisotropically. N-H and C-H hydrogen atoms were fixed in calculated positions with N—H = 0.91 Å, C—H = 0.98 Å. Details of the crystallographic data are presented in Table 1. Neutral atom scattering factors were taken from Cromer and Weber (28*c*). Anomalous dispersion effects were included in *F*calc (28*d*) and the values for $\Delta f'$ and $\Delta f''$ were those of Creagh and McAuley (28*e*). The values for the mass attenuation coefficients are those of Creagh and Hubbell (28*f*). All calculations were performed using the teXsan (28*g*) crystallographic software package of Molecular Structure Corporation. Complete lists of atomic coordinates, angles and distances are presented in supplementary Table S1 (see *Supplementary material*).

Results and discussion

Synthetic aspects

The precursor (**1**) was synthesized by the high dilution cyclisation of thiodiglycolic acid chloride with diaminopropane (Scheme 1) as an alternative to the Richman–Atkins tosylate method (29, 30). The product yield depended considerably on the stirring conditions. High stirring speeds were employed to reduce any side products in the cyclisation of (**2**) with *N*,*N*′-bis(α-chloro acetamido)propane (**3**). Also, the analogous reaction (14) using 1-oxa-4,8-diazacyclododecane (**(**[10]aneN_2O) proceeded in 100% yield. This adaptation of the reactivity reported by Bradshaw et al. (27) appears to be both general and efficient, presumably due to preorientation of the C—Cl bonds in (**3**) owing to the presence of the adjacent amides. However, the reaction yield is dependent on the solubility of the reagents, which appears to be enhanced by the presence of small amounts of moisture. The borane reduction of (**4**) produced L1 in good yield. However, during extraction, if the aqueous layer was not >4 M NaOH, the chloroform extract consisted exclusively of colourless crystals of the mono-protonated ligand. An attempted crystallographic resolution[4] identified an extremely large unit cell containing the adduct $\{[HL1](ClO_4)\cdot CHCl_3\}_4$, confirming that the ligand acts as a proton sponge. The N_4S ligand structurally closest to those under consideration is the bicyclic species 12,17-dimethyl-5-thia-1,9,12,17-tetraazabicyclo[7.5.5]nonadecane, in which the N_4 donor set is part of a 12-membered cyclen ring (23). It is of interest

[4] S. Rettig. Unpublished results.

© 2001 NRC Canada

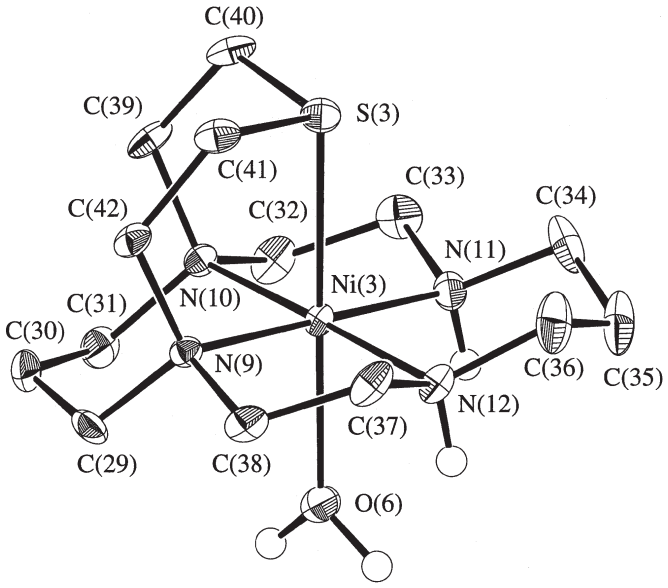
that this bicyclic ligand also acts as a very strong proton acceptor, with pK_a values for the *mono*- and *bis*-protonated species being 11.91 and 8.78, respectively.

The ligand L1 did not readily coordinate nickel(II) perchlorate in aqueous solution, presumably owing to the unique proton affinity observed for this isomer. Reaction of nickel(II) perchlorate with L1 in acetonitrile, followed by evaporation to dryness gave a white residue which, upon dissolution in hot 5% $HClO_4$, yielded reproducibly, upon cooling, pale pink needle crystals of $[Ni(L1)(ClO_4)](ClO_4)\cdot 2[Ni(L1)(OH_2)](ClO_4)_2\cdot 6H_2O$. Interestingly, if the pink-colored aqueous or acetonitrile solutions derived from the reaction residue were left to stand at room temperature for an extended period of time (days to weeks), the solution turned brown and yielded a brown solid residue. Recrystallization of the brown residue from 5% $HClO_4$ produced golden brown needle crystals similar in size and shape to the pale pink crystals. (Anal. calcd. for $[Ni(C_{14}H_{32}N_4S)](Cl_2O_9)$: C 29.93, H 5.74, N 9.97, S 5.71; found: C 29.74, H 5.23, N 9.75, S 5.79) of this golden brown form conforms to the formulation $[Ni(L1)](ClO_4)_2\cdot H_2O$. It may be in this case, that the S donor is detached and adopts the exo-configuration to give a square-planar nickel(II) center, since the HR-MS (FAB, calcd. = 443.1029; observed = 443.0970 *m*/*e*) is consistent with the $[Ni(L1)]^+$ cation and the colour of the material.

Molecular structures

In the nickel(II) cations, the four nitrogen donors of the cyclam ring are coordinated in a planar equatorial fashion and the thioether sulfur is coordinated axially. The cyclam ring adopts a *trans*-III conformation (8), in contrast to the isomeric $[Ni(L2)(ClO_4)]^+$ ions which are constrained to be *trans*-I. Extensive H-bonding was seen in the lattice of $[Ni(L1)(ClO_4)](ClO_4)\cdot 2[Ni(L1)(OH_2)](ClO_4)_2\cdot 6H_2O$, (supplementary Fig. 1, see *Supplementary material*). For clarity, only the structure of $[Ni(L1)(OH_2)]^{2+}$ is shown in Fig. 1. The ORTEP of the complex incorporating the perchlorate ion is shown in supplementary Fig. 2 (see *Supplementary material*). Principal values for bond distances and angles are presented in supplementary Table S2 (see *Supplementary material*). The geometry of the cations $[Ni(L1)(X)]^{n+}$ (X = ClO_4 or H_2O) is pseudooctahedral. In $[Ni(L1)(ClO_4)]^+$, the four nitrogen atoms show only minor deviations (0.053–0.071 Å) from coplanarity. In contrast to the 0.111 Å displacement observed (10) in $[Ni(L2)(ClO_4)]^+$, (*trans*-I) cation, the nickel in $[Ni(L1)(ClO_4)]^+$ is displaced from the N_4 plane by only 0.0045 Å towards the sulfur. The Ni—NH bond lengths (2.059 Å and 2.067 Å) are similar to those in $[Ni(L2)(ClO_4)]^+$. For the *trans*-III configuration, the hole size in free cyclam has been calculated (31) as 2.05 Å. However, the observed Ni—N(*tert*) distances (2.105 Å and 2.113 Å) are close to the calculated ideal high-spin Ni(II)—N bond (2.10 Å) (32, 33). In the present system, the implication is that the cyclam ring in L1 has expanded to accommodate the nickel(II) ion consistent with the coplanarity of the metal center and the N_4 framework. The Ni-S vector is tilted 5.7° from the perpendicular to the N_4 plane towards the tertiary nitrogens which is similar to the 6.5° tilt in the $[Ni(L2)(ClO_4)]^+$ cation. In the perchlorate complexes, the Ni—S bond lengths are virtually identical at 2.39 Å. In contrast, each of the two $[Ni(L1)(H_2O)]^{2+}$ cations has a slightly longer Ni—S bond distance at 2.42 Å which implies that a small *trans* effect exists for aquo vs. perchlorato coordination in the remaining sixth axial site. Also, in both $[Ni(L1)(H_2O)]^{2+}$ cations, the Ni—OH_2 bond vectors (2.18 Å and 2.19 Å) are tilted towards the two secondary nitrogens of the unbridged propylenediamine chelate. However, in $[Ni(L1)(ClO_4)]^+$, the Ni—$OClO_3$ bond vector is 2.24 Å and tilted 5.7° from the perpendicular to the N_4 plane, but now towards the N2-N3 ethylenediamine chelate.

Fig. 1. ORTEP diagram of $[Ni(L1)(OH_2)]^{2+}$ with 25% ellipsoids.



The relatively minor differences in the coordination geometries of the nickel(II) ions complexed with L1 and L2 suggests that the ligands are relatively flexible with the constraints of the metal ion dictating the observed geometry. However, there may exist some differences in ligand strain, if only due to the *trans*-III vs. *trans*-I conformations. Molecular mechanics calculations were undertaken to determine such variations. To optimize ligand geometries in their *trans*-I or III configurations, the fractional atomic coordinates of only the ligand atoms from the structures of the complexes were used. An iterative calculation was then conducted to find the minimum energy conformation of the free ligands. The difference in total energies of the coordinated versus free ligand forms is then an assessment of the ligand strain induced by coordination of the metal ion. The results of these calculations are provided in Table 3.

While the ligand isomers L1 and L2 are of comparable total energy (only 4 kJ mol^{-1} difference) in their *trans*-III and *trans*-I states, respectively, both ligands develop considerable strain (>95 kJ mol^{-1}) upon coordination. However, the Ni(II) ions with ligand L1 (*trans*-III) developed about 33 kJ mol^{-1} less strain energy than the L2 isomer which cannot adopt that configuration. In each case, bond stretch and van der Waals factors contributed most to the total strain. Although overall bond angle and torsional strain energies are less in magnitude, they differ significantly between L1 and L2. Owing to a lack of knowledge of the ligand structure in reduced metal complexes, no corresponding analysis was undertaken.

© 2001 NRC Canada

Table 2. Selected interatomic distances (Å) and bond angles (deg) for $[Ni(L1)(OH_2)]^{2+}$ (**2**) in the $[Ni(L1)(ClO_4)](ClO_4)\cdot 2[Ni(L1)(OH_2)](ClO_4)_2\cdot 6H_2O$ structure.

Bond distances			
Atom-atom	Distance (Å)	Atom-atom	Distance (Å)
Ni(3)—S(3)	2.4225(10)	Ni(3)—N(9)	2.103(3)
Ni(3)—N(10)	2.109(3)	Ni(3)—N(11)	2.057(3)
Ni(3)—N(12)	2.080(3)	Ni(3)—O(6)	2.189(3)
S(3)—C(40)	1.813(4)	S(3)—C(41)	1.810(4)
Bond angles			
Atom-atom-atom	Angle (deg)	Atom-atom-atom	Angle (deg)
S(3)-Ni(3)-O(6)	179.33(7)	S(3)-Ni(3)-N(9)	86.38(8)
S(3)-Ni(3)-N(10)	86.78(8)	S(3)-Ni(3)-N(11)	94.36(9)
S(3)-Ni(3)-N(12)	95.02(9)	N(9)-Ni(3)-N(10)	93.94(11)
N(9)-Ni(3)-N(11)	179.26(12)	N(9)-Ni(3)-N(12)	86.37(11)
N(10)-Ni(3)-N(11)	86.06(11)	N(9)-Ni(3)-N(12)	86.37(11)
N(10)-Ni(3)-N(12)	178.19(12)	N(11)-Ni(3)-N(12)	93.61(12)
Ni(3)-S(3)-C(40)	97.40(12)	Ni(3)-S(3)-C(41)	97.20(12)
C(40)-S(3)-C(41)	103.7(2)		

Table 3. Ligand strain energies induced by metal ion coordination.

Complex[a]	Total energy of coordinated ligand (kJ mol^{-1})	Total energy of minimized free ligand (kJ mol^{-1})	Ligand strain (ΔE) (kJ mol^{-1})
$[Ni(L2)(ClO_4)]$+	297	164	132
$[Ni(L1)(ClO_4)]$+	269	169	100
$[Ni(L1)(H_2O)]^{2+}$ (**1**)	268	169	99
$[Ni(L1)(H_2O)]^{2+}$ (**2**)	269	169	100

[a]Fractional atomic coordinates for $[Ni(L2)(ClO_4)]^+$ taken from ref. 10.

Table 4. UV–vis data.

Complex	λ_{max} (nm) (ε/M^{-1} cm^{-1})
$[Ni(L1)(OH_2)](ClO_4)_2$[a]	205 (1800), 260 (sh) 333 (23), 498 (11), 685 (7), 808 (sh), 848 (9), 989 (18)
$[Ni(L1)(OH_2)](ClO_4)_2$[b]	511 (10), 740 (sh), 842 (9), 930 (10)
$[Ni(L1)](ClO_4)_2]\cdot OH_2$[c]	390 (sh), 481 (8), 847 (sh), 940 (8)
$[Ni(L2)(OH_2)](ClO_4)_2$[d]	261 (1900), 330 (sh), 504 (14), 845 (sh), 1020 (18)

[a]Aqueous solution.
[b]Acetonitrile.
[c]Yellow, square-planar form, see text.
[d]Reference 11.

Solution studies

The UV–vis data are listed in Table 4 where data in aqueous and acetonitrile media are presented. Dissolution of the mixed aquo – perchlorato complex was considered to yield a solvento ion owing to the weak ligating properties of the perchlorate. In water, the spectrum of the pink pseudo-octahedral $[Ni(L1)(solv)]^{2+}$ ion is consistent with a water molecule as the sixth axial donor (14). This complex also exhibits exceptional kinetic stability, even in strongly acidic solutions. The $^3A_{2g} \rightarrow {}^3T_{1g}$ transition (498 nm) may be compared to the $[Ni(L2)(OH_2)]^{2+}$ isomer (504 nm) (11) which has a similar pattern of bands and intensities. The solution spectra of $[Ni(L1)(OH_2)]^{2+}$ and $[Ni(L2)(OH_2)]^{2+}$ ions differ slightly, possibly due to *trans*-III vs. *trans*-I configurations. The most significant difference in the spectra was observed in the bands at 989 nm for $[Ni(L1)(OH_2)]^{2+}$ and 1020 nm for $[Ni(L2)(OH_2)]^{2+}$. This may be a reflection of the differences in strain energy described earlier, deriving from the displacement of the nickel(II) from the N_4 plane in $[Ni(L2)(ClO_4)]^{2+}$. The yellow form of the complex is consistent with a square-planar ion.

EPR spectroscopy

Oxidation of the $[Ni(L1)(OH_2)]^{2+}$ cation with $K_2S_2O_8$ in aqueous solution yielded the EPR-active $[Ni(L1)(OH_2)]^{3+}$ ion with $g_\perp = 2.159$ and $g_\parallel = 2.024$ characteristic (34, 35) of a low-spin d^7 ion in a distorted octahedral environment of axial symmetry. There is the possibility of formation of some sulfato complex owing to the oxidant used, but it is unlikely that this would cause a significant change in the spectrum. The values are similar to the $g_\perp = 2.169$ and $g_\parallel = 2.025$ reported (10) for the $[Ni(L2)(solv)]^{3+}$ isomer suggesting that the coordination properties of the Ni(III) complexes

© 2001 NRC Canada

do not differ significantly. However, there is a difference between these values, and those for $[Ni([9]aneN_4O)(solv)]^{3+}$ [3] ($g_\perp$ = 2.200 and $g_\parallel$ = 2.028) and $[Ni(cyclam)(OH_2)_2]^{3+}$ (35) ($g_\perp$ = 2.219 and $g_\parallel$ = 2.033), respectively. Thus, the nature of the axial donor provides a much more dominant effect than the ligand structure probably owing to the presence of the electron in the d_{z2} orbital.

Electrochemistry

Studies of the $[Ni(L1)(solv)]^{2+}$ complex exhibited two waves in CH_3CN (0.1 M $(Bu)_4NClO_4$). The first at $E_{1/2}$ = –1.807 V vs. $Fc^{+/0}$, corresponding to the $[Ni(L1)(solv)]^{2+/+}$ couple was quasireversible ($E_{pc} - E_{pa}$ = 135 mV) and independent of scan rate. This value contrasts with the $[Ni(L2)(solv)]^{2+/+}$ potential of –1.685 V, suggesting that any structural rearrangement upon reduction favours the *trans*-I starting structure in which the nickel is displaced towards the sulfur. The second wave observed at $E_{1/2}$ = 0.715 V vs. $Fc^{+/0}$ for $[Ni(L1)(solv)]^{3+/2+}$ was chemically and electrochemically more reversible ($E_{pc} - E_{pa}$ = 87 mV). The half-wave potential of this couple is virtually identical to that of $[Ni(L2)(solv)]^{3+/2+}$ ($E_{1/2}$ = 0.719 V vs. $Fc^{+/0}$).[5] This result is somewhat surprising, given that the two isomers exhibited slight differences in their UV–vis and ESR spectra. It thus appears that the presence of the *trans*-III vs. *trans*-I configuration in the equatorial cyclam ring has no significant effect upon the stability of the $Ni^{3+/2+}$ redox couple. In contrast, Pierce et al. (36) have reported the isolation and characterization of *trans*-I-$[Ni(cyclam)]^{2+}$ and compared its electrochemical behavior to that of *trans*-III isomer (both complexes are low-spin square-planar perchlorate salts). In that study, it was found that, despite the similarity of the UV–vis spectra, the two configurational isomers showed markedly different electrochemical behaviour. The *trans*-I-$[Ni(cyclam)]^{2+}$ complex exhibited a broad, irreversible oxidation wave at 1.0–1.1 V (vs. 3.5 M NaCl calomel reference electrode) and then subsequently isomerized to the *trans*-III form which exhibits a reversible wave at 0.772 V. At higher sweep rates (>0.5 V s^{-1}), a reversible wave was observed for *trans*-I-$[Ni(cyclam)]^{2+}$ which permitted the formal potential to be estimated at $E_{1/2}$ = 0.92 V, 150 mV higher potential than the *trans*-III isomer. Clearly, further work is required on the present complexes to examine more closely any relationship between ring conformation and redox potentials.

Conclusion

The synthesis of L1 proceeded in high yield. Upon coordination of nickel(II), the ligand adopts the *trans*-III configuration of nitrogen donors which contrasts the *trans*-I configuration observed for the isomeric macrobicyclic ligand (L2). A stable protonated form $HL1^+$ has also been identified. In $[Ni(L1)(OH_2)]^{2+}$, the Ni(II) ion is coplanar with the N_4 donor set in contrast to the corresponding L2 ion where there is a marked displacement towards the S donor. These variations are reflected in slight differences in solution spectra and electrochemical potentials. Molecular mechanics calculations based on the solid-state structures also show an energy difference between the isomers.

Acknowledgements

We would like to thank the Natural Sciences and Engineering Research Council of Canada (NSERC) and the University of Victoria for their continued support of this research.

Supplementary material

Table S1 provides fractional coordinates, interatomic distances, and bond angles, for the $[Ni(L1)(ClO_4)](ClO_4)\cdot 2[Ni(L1)(OH_2)](ClO_4)_2\cdot 6H_2O$ complex. Detailed bond distances and angles for both $[Ni(L1)(OH_2)]^{2+}$ and $[Ni(L1)(ClO_4)]^{2+}$ cations are presented in Table S2. Figure S1 exhibits the extensive hydrogen bonding in $[Ni(L1)(ClO_4)](ClO_4)\cdot 2[Ni(L1)(OH_2)](ClO_4)_2\cdot 6H_2O$, and Fig. S2 shows an ORTEP of the $[Ni(L1)(ClO_4)]^{2+}$ cation. Copies of material on deposit may be purchased from the Depository of Unpublished Data, Document Delivery, CISTI, National Research Council Canada, Ottawa, ON K1A 0S2, Canada (http://www.nrc.ca/cisti/irm/unpub_e.shtml for information on ordering electronically). Tables of interatomic distances, bond distances, and bond angles have been deposited with the Cambridge Crystallographic Data Centre. Copies of the data can be obtained, free of charge, on application to the Director, CCDC, 12 Union Road, Cambridge CB2 1EZ, U.K. (Fax: 44-1223-336033 or e-mail: deposit@ccdc.cam.ac.uk).

References

1. D.K. Cabbiness and D.W. Margerum. J. Am. Chem. Soc. **91**, 6540 (1969).
2. L. Fabrizzi. Comments Inorg. Chem. **4**, 33 (1985).
3. G.A. Melson (*Editor*). Coordination chemistry of macrocyclic compounds. Plenum Press, New York. 1979.
4. L. Lindoy. Chemistry of macrocyclic ligand complexes. Cambridge University Press, Cambridge, U.K. 1989.
5. R.D. Hancock and A.E. Martell. Chem. Rev. **89**, 1875 (1989); R.D. Hancock. J. Chem. Ed. **69**, 615 (1992).
6. D.H. Busch. Acc. Chem. Res. **11**, 392 (1978); D.H. Busch. Adv. Chem. Ser. **100**, 44 (1971).
7. A. McAuley and S. Subramanian. Coord. Chem. Rev. **300**, 75 (2000).
8. B. Bosnich, C.K. Poon, and M.L. Tobe. Inorg. Chem. **4**, 1102 (1965).
9. M.A. Donnelly and M. Zimmer. Inorg. Chem**. 38**, 1650 (1999).
10. T.W. Hambley. J. Chem. Soc. Chem. Comm. 1228 (1984).
11. D.G. Fortier and A. McAuley. Inorg. Chem. **28**, 655 (1989).
12. D.G. Fortier and A. McAuley. J. Am. Chem. Soc. **112,** 2640 (1990).
13. K.A. Beveridge, A. McAuley, and C. Xu. Inorg. Chem. **30**, 2074 (1991).
14. A. McAuley, D.F. Fortier, D.H. Macartney, T.W. Whitcombe, and C. Xu. J. Chem. Soc. Dalton Trans. 2071 (1994).
15. R. Schibli, R. Alberto, U. Abram, S. Abram, A. Egli, P.A. Schubiger, and T.A. Kaden. Inorg. Chem. **37**, 3509 (1998).

[5] Note: to provide accurate comparisons, the $[Ni([9]aneN_4S)(solv)]^{2+/+}$ and $[Ni([9]aneN_4S)(solv)]^{3+/2+}$ couples were determined under the same conditions (cell, electrodes, and solution) as the respective $[Ni(L1)(solv)]^{2+/+}$ and $[Ni(L1)(solv)]^{3+/2+}$ couples.

© 2001 NRC Canada

16. E.I. Solomon, M.J. Baldwin, and M.D. Lowery. Chem. Rev. **92**, 521 (1992).
17. T. Shi and L.I. Elding. Inorg. Chem. **35**, 5941 (1996).
18. P. Comba. Coord. Chem. Rev. **200**–**202**, 217 (2000).
19. C. Beguin, P. Chautemps, A. El Marzouki, J.-L. Pierre, S.M. Refaif, G. Serratrice, E. Saint-Aman, and P. Rey. J. Chem. Soc. Dalton Trans. 1939 (1995).
20. U. Sivagnanam and M. Palaniandavar. J. Chem. Soc. Dalton Trans. 2277 (1994).
21. D.E. Nikles, M.J. Powers, and F.L. Urbach. Inorg. Chem. **22**, 3210 (1983).
22. H.J. Prochaska, W.F. Schwindinger, M. Schwartz, M.J. Burk, E. Bernaducci, R.A. Lalancette, J.A. Potenza, and H.J. Schugar. J. Am. Chem. Soc. **103**, 3446 (1981).
23. A. Bianchi, E. Garcia Espana, M. Micheloni, N. Nardi, and F. Vizza. Inorg. Chem. **25**, 4379 (1986).
24. N.L. Allinger. J. Am. Chem. Soc. **99**, 8127 (1977).
25. K. Coulter. Ph.D. dissertation, University of Victoria, 1997.
26. H.H. Bosshard, R. Mory, M. Schmid, and H. Zollinger. Helv. Chim. Acta, **42**, 1653 (1959).
27. J.S. Bradshaw, K.E. Krakowiak, and R.M. Izatt. J. Heterocycl. Chem. **26**, 1431 (1989).
28. (*a*) A. Altomare, M. Cascarano, C. Giacovazzo, and A. Guagliardi. J. Appl. Crystallogr. **26,** 343 (1993); (*b*) P.T. Beurskens, G. Admiral, G. Beurskens, W.P. Bosman, R. de Gelder, R. Israel, and J.M.M. Smits. The DIRDIF-94 program system. Technical Report of the Crystallography Laboratory, University of Nijmegen, The Netherlands. 1994; (*c*) D.T. Cromer and J.T. Weber. International tables for X-ray crystallography. Vol. IV. The Kynoch Press, Birmingham, U.K. 1974. Table 2.2 A.; (*d*) J.A. Ibers and W.C. Hamilton. Acta Crystallogr. **17**, 781 (1964); (*e*) D.C. Creagh and W.J. McAuley. International tables for crystallography. Vol C. *Edited by* A.J.C. Wilson. Kluwer Academic Publishers, Boston. 1992. pp. 219–222; (*f*) D.C. Creagh and J.H. Hubbell. International tables for crystallography. Vol C. *Edited by* A.J.C. Wilson. Kluwer Academic Publishers, Boston. 1992. pp. 200–206; (*g*) teXsan: Crystal structure analysis package. Molecular Structure Corporation. 1985, 1992.
29. J.E. Richman and T.J. Atkins. J. Am. Chem. Soc. **96**, 2268 (1974).
30. S. Chandrasekhar and A. McAuley. J. Chem. Soc. Dalton Trans. 2967 (1992).
31. J.C.A. Boeyens, S.M. Dobson, and R.D. Hancock. Inorg. Chem. **24**, 3073 (1985).
32. V.J. Thöm, C.F. Fox, J.C.A. Boeyens, and R.D. Hancock. J. Am. Chem. Soc. **106**, 5947 (1984).
33. K.R. Adam, M. Antolovich, L.G. Brigden, and L.F. Lindoy. J. Am. Chem. Soc. **113**, 3346 (1991).
34. R.I. Haines and A. McAuley. Coord. Chem. Rev. **39**, 77 (1981).
35. E.S. Gore and D.H. Busch. Inorg. Chem. **12**, 1 (1973).
36. D.T. Pierce, T.L. Hatfield, E.J. Billo, and Y. Ping. Inorg. Chem. **36**, 2950 (1997).

© 2001 NRC Canada

N,*N*-dimethylhydroxamidovanadium(V). Interactions with sulfhydryl-containing ligands: V(V) equilibria and the structure of a V(IV) dithiothreitolato complex

Sudeep Bhattacharyya, Anette Martinsson, Raymond J. Batchelor, F.W.B. Einstein, and Alan S. Tracey

Abstract: The major aqueous equilibrium complexation reactions of vanadate in the presence of *N*,*N*-dimethylhydroxylamine (DMHA) and with dithiothreitol (DTT), β-mercaptoethanol, glycine, or cysteine in solution have been studied using ^{51}V NMR spectroscopy. Previously unreported DMHA complexes of 2:1 and 2:3 V:DMHA stoichiometry were observed and characterized. Concentration studies showed that, for the three sulphur-containing ligands, the major product of sulphur coordination has a 1:2:1 stoichiometry of vanadate to dimethylhydroxylamine to heteroligand. These products do not carry a charge in neutral to moderately basic solution. A second product type of 1:1:1, V to DMHA to heteroligand, stoichiometry is also formed. These products carry a single negative charge. A reductive reaction between vanadate and excess DTT to form a V(IV) complex was also observed and a solid product was isolated. This product could also be obtained by direct reaction of vanadyl sulphate with DTT. It was characterized by X-ray diffraction studies. Crystal structure of $[\{VO(SCH_2CHOHCHOCH_2S)\}_2]$ $[AsPh_4]_2$: monoclinic, space group $P2_1/n$, $Z = 2$, $a = 10.1607(18)$ Å, $b = 17.8255(42)$ Å, $c = 15.1520(33)$ Å, $\beta = 104.\ 000(15)°$, $V = 2662.8$ Å^3, $R_F = 0.038$ for 2327 data ($I_o \geq 2.5\sigma(I_o)$) and 325 variables.

Key words: vanadate, vanadyl, dithiothreitol, mercaptoethanol, cysteine, glycine, equilibrium constants, crystal structure, X-ray, vanadium NMR.

Résumé : Faisant appel à la RMN du ^{51}V, on a étudié les principales réactions de complexation en équilibre aqueux du vanadate, en présence de *N*,*N*-diméthylhydroxylamine (DHMA), avec le dithiothréitiol (DTT), le β-mercaptoéthanol, la glycine et la cystéine. On a observé et caractérisé des complexes du DMHA de stoechiométries V:DMHA 2:1 et 2:3. Des études de concentrations montrent que, pour les trois ligands contenant du soufre, le produit principal de la coordination du soufre comporte une stoechiométrie 1:2:1 du vanadate par rapport à la diméthylhydroxylamine et à l'hétéroligand. En solution neutre ou faiblement basique, les produits ne portent pas de charge. Il se forme aussi un deuxième type de produit de stoechiométrie 1:1:1 du V au DMHA à l'hétéroligand. Ces produits portent une charge négative simple. On a observé une réaction réductrice entre le vanadate et l'excès de DTT; elle conduit à la formation du'un complexe V(IV) et on a isolé un produit solide. On peut aussi obtenir ce produit par réaction directe du sulfate de vanadyle avec le DTT. On l'a caractérisé par des études de diffraction des rayons X. Les cristaux de $[\{VO(SCH_2CHOHCHOCH_2S)\}_2][AsPh_4]_2$ sont monocliniques, groupe d'espace $P2_1/n$, $Z = 2$, $a = 10{,}1607(18)$ Å, $b = 17{,}8255(42)$ Å et $c = 15{,}1520(33)$ Å, $\beta = 104\ 000(15)°$, $V = 2662{,}8$ Å^3, $R_F = 0{,}038$ pour 2327 données ($I_0 \geq 2{,}5\sigma(I_o)$) et 325 variables.

Mots clés : vanadate, vanadyle, dithiothréiotol, mercaptoéthanol, cystéine, glycine, constantes d'équilibre, structure cristalline, rayons X, RMN du vanadium.

[Traduit par la Rédaction]

Received September 9, 2000. Published on the NRC Research Press Web site at http://canjchem.nrc.ca on July 11, 2001.

Dedicated to Professor Brian James on the occasion of his 65th birthday.

S. Bhattacharyya, A. Martinsson, and A.S. Tracey.[1] Department of Chemistry, Simon Fraser University, Burnaby, BC V5A 1S6, Canada.
R.J. Batchelor and F.W.B. Einstein. X-ray Crystal Laboratory, Department of Chemistry, Simon Fraser University, Burnaby BC V5A 1S6, Canada.

[1]Corresponding author (telephone: (604) 291-4464; fax: (604) 291-3765; email: tracey@sfu.ca).

 DOI: 10.1139/cjc-79-5/6-938 © 2001 NRC Canada

Introduction

It is frequently asserted that vanadium(V) oxides (vanadate) are rapidly reduced by thiolates but this is true only for specific conditions. Indeed, although stable V(IV) thiolates are frequently reported, it is not uncommon to have mixed vanadium (IV/V) states and even vanadium(V) thiolates can be quite stable in solution (1, 2). As a part of our ongoing studies on the reactivities of V(V) and thiolates, we have previously carried out a detailed study of the aqueous equilibria established between vanadate and dithiothreitol (DTT) and have proposed structures for the major product formed in that system (2). A crystal structure of the complex of β-mercaptoethanol with vanadate has also been reported and this structure correlated with aspects of the associated aqueous chemistry (1).

Our interest in these thiolate complexes has evolved from our studies of the insulin-mimetic effect of vanadium compounds and of protein tyrosine phosphatases (PTPases) that may be relevant to that effect. The PTPases are group of signal transduction enzymes that regulate a number of key cellular responses that are initiated by certain tyrosine phosphorylated proteins (3, 4). The event of dephosphorylation of the phosphotyrosine group of the substrate proteins by the PTPase regulates the cellular response. The dephosphorylation takes place via a concerted and cooperative mechanism effected by the catalytic active site residues of the enzyme. The chemistry of the process is complex, and involves the critical active site residues, aspartate and cysteine via a thiophosphate intermediate. Vanadate, a transition-metal analog of phosphate, is an excellent inhibitor of this hydrolytic process. Recently, it has been shown that *N*,*N*-dimethylhydroxylamine (DMHA) derivatives of vanadate (here referred to collectively as DMHAV) have a similar effect. Specifically, bis(*N*,*N*-dimethylhydroxamido)hydroxooxovanadate ($(dmha)_2V(O)OH$) is a very good inhibitor of PTPase activity (5). Furthermore, this compound is functional as an insulin-mimetic in some cell cultures where vanadate is inactive (6).

An understanding of the chemistry involved in the inhibition of PTPase function by the small molecules of DMHAV is important since it provides a basis for the design of other metallorganic inhibitors. To an extent, the identity of the actual inhibiting species is still speculative. The details of the specific interactions of DMHAV with the surrounding active site residues are not yet known although the interactions very likely involve direct reaction at the sulphur of the active site cysteine (7). The influence of externally added thiolate redox buffers like dithiothreitol (DTT) and β-mercaptoethanol is also not fully understood. Both of these buffers are known to form complexes with oxovanadium species (1, 8) and these, and various other sulphur-containing ligands are highly reactive with DMHAV (9). An understanding of the chemistry promoted by sulfur-containing reagents is critically important for the development of our understanding of the chemistry of the inhibition itself. Some time ago we reported a preliminary study of the reactions of DMHA complexes of vanadate with DTT (9). We are now able to provide a much more detailed description of the aqueous chemistry and also are able to draw some comparisons with the closely related ligand β-mercaptoethanol and with the amino acids glycine and cysteine. We also report an X-ray crystal structure of a V(IV) complex with DTT which is compared to and contrasted with the structure we propose for its V(V) analog.

Experimental section

Materials

All chemicals used in this work were of reagent or better quality. Divanadium(V) pentoxide, *N*,*N*-dimethylhydroxylamine hydrochloride, dithiothreitol, tetraphenylarsonium chloride, glycine, cysteine and β-mercaptoethanol were obtained from Sigma–Aldrich and used without further purification. Potassium chloride (99.5% analytical reagent) was from BDH Inc.

Solutions

Preparative methods for stock solutions of sodium vanadate, DMHA, KCl, and DTT are described elsewhere (9). The ionic strength of all solutions were maintained at 1.0 M with KCl. In each case, the solutions at different pH were prepared following a two-step addition. Initially, appropriate amounts, for the desired final concentrations, of the stock KCl, DMHA, and DTT solutions were combined. The pH of the solution was then adjusted, using appropriate amounts of HCl or KOH, to a value so that after, the addition of the stock vanadate solution, the pH would be close to, but below the desired value. In the second step the vanadate was added, the pH adjusted upward with KOH, and finally the final desired volume was made up with water previously brought to the particular pH. This procedure avoided the formation of decavanadate which tends to form in solutions below the neutral pH.

Synthesis of $As_2C_{56}H_{54}O_6S_4V_2$

At room temperature, an aqueous solution (2 mL) of DTT (0.15 g, 1 mmol), adjusted to pH 8.5, was added dropwise, with stirring, to a 2.5 mL aqueous solution of $VOSO_4.xH_2O$ (0.2 g, 1 mmol). The resultant solution gradually turned green. It was stirred for an additional 5 min and the desired compound was then precipitated by adding a warm saturated solution of tetraphenylarsonium chloride (0.42 g, 1 mmol), in 5 mL of water. The product, obtained in green microcrystalline form, was recrystallized from warm acetonitrile. Yield: (0.4 g) 67%. FT-IR (KBr) (cm^{-1}): 961, V=O stretching. Anal. calcd. for $As_2C_{56}H_{54}O_6S_4V_2$: C 55.9, H 4.5; found: C 55.78, H 4.52.

^{51}V NMR Spectroscopy

^{51}V NMR spectra were obtained either from a Bruker AMX400 NMR spectrometer operating at 105.2 MHz at ambient temperature or from a Bruker AMX600 operating at 157.7 MHz. Vanadium chemical shifts are reported relative to the chemical shift of the external reference $VOCl_3$ at 0 ppm. The following NMR parameters were used: pulse width 60°; spectral width 62.5 kHz; acquisition time 0.065 s. The data was process using the spectrometer manufacturers software WINNMR. A line-broadening factor of 40 Hz was applied to all spectra and after Fourier transformation, the

© 2001 NRC Canada

Table 1. Crystallographic data for the structure determination of $[\{VO(SCH_2CHOHCHOCH_2S)\}_2]$ $[AsPh_4]_2$.

Formula	$As_2V_2S_4O_6C_{56}H_{54}$	Crystal system	Monoclinic
Fw	1202.99	Space group	$P2_1/n$
a (Å)[a]	10.1607(18)	ρ_c (g cm^{-3})	1. 500
b (Å)	17.8255(42)	λ (Mo Kα_1) (Å)	0.70930
c (Å)	15.1520(33)	μ (Mo Kα) (cm^{-1})	17.7
b (°)	104. 000(15)	Min-max 2θ (°)	4–48
V (Å^3)	2662.8	Transmission[b]	0.634–0.818
Z	2	R_F[c]	0.038
Temperature (K)	295	R_{wF}[d]	0.040
Observed reflns[e]	2327	Parameters	325

[a]Cell dimensions were determined from 57 reflections ($40° < 2\theta < 46°$).
[b]The data were corrected for the effects of absorption by the Gaussian integration method.
[c]$R_F = \Sigma(|F_o| - |F_c|)/\Sigma|F_o|$ for observed data.
[d]$R_{wF} = [\Sigma(w(|F_o| - |F_c|)^2)/\Sigma(wF_o^2)]^{1/2}$ for observed data.
[e]$I_o \geq 2.5\sigma(I_o)$.

Table 2. Fractional atomic coordinates and equivalent isotropic or isotropic displacement parameters (Å^2) for the non-hydrogen atom sites $[\{VO(SCH_2CHOHCHOCH_2S)\}_2]$ $[AsPh_4]_2$.

Atom	x	y	z	U_{eq}[a]
As	0.28671(6)	0.07988(3)	0.11069(4)	0.0342(3)
V	0.56794(10)	0.53509(6)	–0.07304(6)	0.0374(6)
S(1)	0.80324(16)	0.52528(11)	–0.05604(12)	0.0557(11)
S(4)	0.41296(18)	0.33340(10)	0.06651(12)	0.0563(11)
O(1)	0.4998(4)	0.50966(23)	–0.1743(3)	0.051(3)
O(2)	0.8427(5)	0.4026(3)	0.0919(3)	0.057(3)
O(3)	0.5722(4)	0.44609(20)	0.0048(3)	0.0404(22)
C(1)	0.8221(7)	0.4248(4)	–0.0675(4)	0.060(5)
C(2)	0.7774(6)	0.3777(4)	0.0027(4)	0.052(4)
C(3)	0.6258(6)	0.3739(3)	–0.0068(4)	0.047(4)
C(4)	0.5853(7)	0.3192(3)	0.0583(4)	0.057(4)
C(11)	0.1451(6)	0.1396(3)	0.1361(4)	0.040(4)
C(21)	0.2471(5)	–0.0244(3)	0.1173(4)	0.034(3)
C(31)	0.4517(6)	0.1022(3)	0.1969(4)	0.036(3)
C(41)	0.2981(6)	0.1034(3)	–0.0099(4)	0.036(3)
C(12)	0.0591(7)	0.1122(4)	0.1845(4)	0.060(5)
C(13)	–0.0352(8)	0.1573(6)	0.2057(5)	0.090(7)
C(14)	–0.0445(9)	0.2312(6)	0.1792(6)	0.094(7)
C(15)	0.0417(8)	0.2590(4)	0.1313(6)	0.081(6)
C(16)	0.1366(7)	0.2141(4)	0.1088(5)	0.056(4)
C(22)	0.2434(6)	–0.0552(3)	0.2008(4)	0.047(4)
C(23)	0.2121(6)	–0.1295(4)	0.2053(5)	0.055(4)
C(24)	0.1855(7)	–0.1732(4)	0.1289(5)	0.059(5)
C(25)	0.1891(7)	–0.1431(4)	0.0468(5)	0.054(4)
C(26)	0.2199(6)	–0.0690(3)	0.0404(4)	0.043(4)
C(32)	0.5484(7)	0.0498(4)	0.2233(5)	0.071(5)
C(33)	0.6661(7)	0.0656(4)	0.2870(5)	0.079(5)
C(34)	0.6855(7)	0.1333(5)	0.3271(5)	0.066(5)
C(35)	0.5891(8)	0.1859(4)	0.3002(5)	0.079(5)
C(36)	0.4709(7)	0.1720(4)	0.2363(5)	0.063(5)
C(42)	0.1849(6)	0.0966(3)	–0.0796(4)	0.047(4)
C(43)	0.1908(7)	0.1088(4)	–0.1676(4)	0.055(5)
C(44)	0.3124(8)	0.1279(4)	–0.1850(4)	0.057(5)
C(45)	0.4250(7)	0.1369(4)	–0.1161(5)	0.056(4)
C(46)	0.4201(7)	0.1238(3)	–0.0273(4)	0.046(4)

[a]U_{eq} is the mean of the principal axes of the displacement ellipsoid.

spectra were baseline corrected before integration. Where necessary, signal deconvolution was also carried out using the WINNMR program.

Data analysis

The procedures for analysis of the NMR data are outlined in the text. All errors in parameters are reported at the 95% (3σ) confidence level.

X-ray crystallography

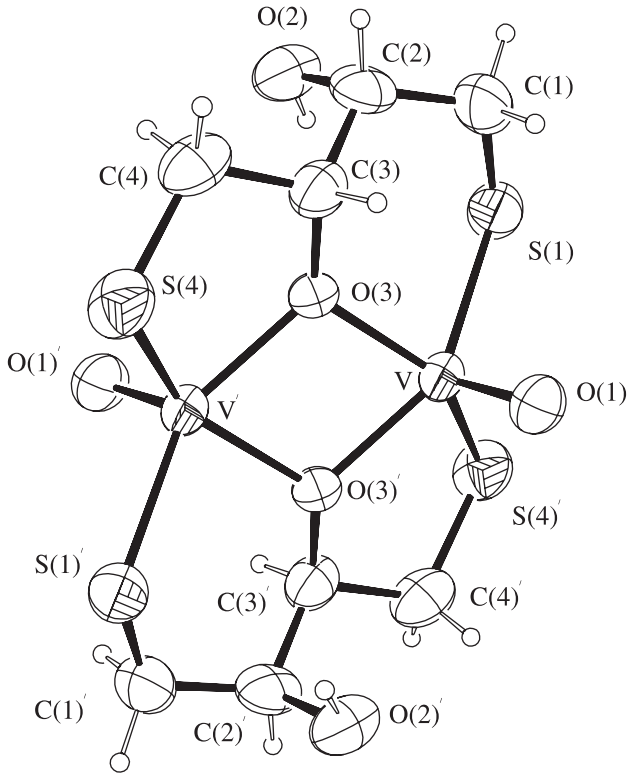
A cleaved segment of a light green, plate-shaped crystal was mounted on a glass fiber using epoxy glue as an adhesive. Data were recorded with an Enraf Nonius CAD4F diffractometer using graphite-monochromatized Mo K_α radiation. Data reduction included corrections for Lorentz and polarization effects.

All non-hydrogen atoms' coordinates and anisotropic displacement parameters as well as the hydroxyl hydrogen atoms' coordinates and isotropic displacement parameter were refined. All other hydrogen atoms were placed in calculated positions and their coordinates were linked with those of their respective carbon atoms during refinement. Isotropic displacement parameters for these latter hydrogen atoms were initially assigned proportionately to the equivalent isotropic displacement parameters of their respective carbon atoms. Subsequently, these hydrogen atom displacement parameters were refined, but were constrained such that those within each phenyl group or those within the vanadium complex had the same shifts.

The data collection was performed using the program DIFRAC (10). The programs used for absorption corrections, data reduction, structure solution, and graphical output were from the NRCVAX Crystal Structure System (11). Full-matrix least-squares refinement was carried out using CRYSTALS (12). Complex scattering factors for neutral atoms (13) were used in the calculation of structure factors. Crystal data and experimental details are given in Table 1. The atomic coordinates, equivalent isotropic thermal parameters, and site occupancies for the non-hydrogen atoms are listed in Table 2.

© 2001 NRC Canada

Fig. 1. Molecular structure of the complex anion formed from dithiothreitol and vanadyl sulphate. 50% probability ellipsoids are shown for all non-hydrogen atoms. Hydrogen atoms are indicated by spheres of arbitrary radius.



Results and discussion

The complexation of the vanadium(V) oxoanion, vanadate, by dithiothreitol (DTT) has been studied for the pH range 7.1–9.7 and reduction of V(V) to V(IV) reported to occur in about a 90 min timescale (2). In the solutions utilized for this study at pH levels above neutral pH, partial reduction of vanadium(V) to V(IV) was observable after about 1–1.5 h. Consequently, the formation of the various V(V) solution products was readily studied by ^{51}V NMR spectroscopy without needing to take into account the redox reactions. However, at pH values below neutrality, and particularly at the higher concentrations of DTT, the reduction rate increases substantially. For example, at pH 6.2, in the reaction of 40 mmol DTT with 3 mmol vanadate, discoloration of the solution as V(IV) is formed becomes clearly evident in about 20 min. In the presence of sufficient *N*,*N*-dimethylhydroxylamine (DMHA) to effectively remove any free vanadate from solution, the reduction of V(V) to V(IV) is greatly slowed.

Efforts to isolate a crystalline V(V)–DTT–DMHA complex was not successful. However, as a result of V(V) reduction to V(IV) in the reaction medium, a V(IV) complex was obtained in crystalline form. The product contained DTT but no DMHA. A successful procedure for preparation of this V(IV)–DTT product from vanadyl sulphate was developed and is reported in the *Experimental section* and summarized below.

Crystal structure

The formation of the V(IV) dithiothreitol complex ($As_2C_{56}H_{54}O_6S_4V_2$) was carried out in water by adding a stoichiometric amount of dithiothreitol to vanadyl sulphate. The product was precipitated from solution as the tetraphenylarsonium salt. The microcrystalline compound appeared to be chemically stable. It was found to have medium solubility in common organic solvents such as chloroform and acetone and, in solution, did not show signs of decomposition even after several days at ambient temperature. An acetonitrile solution of the compound was allowed to slowly evaporate to give green crystals suitable for X-ray crystallographic analysis.

The molecular structure of the $[\{VO(SCH_2CHOHCHOCH_2S)\}_2]^{2-}$ anion is shown in Fig. 1. The anion has crystallographic inversion symmetry and the associated tetraphenylarsonium cation is in a general position. There are no inter-ionic contacts significantly shorter than the appropriate sums of accepted van der Waals radii and there is no water in the cell. Each vanadium atom is coordinated to one thiolate and one bridging alkoxy group from two oppositely directed dithiothreitol molecules. One hydroxyl group of each DTT is not coordinated and there are no close intermolecular contacts of the oxygen of this hydroxyl group to any other group. Consequently, the hydroxyl group does not undergo hydrogen bonding interactions.

The bond distances and bond angles obtained for the anion are listed in Table 3. Each vanadium(IV) is in an irregular five-coordinate environment which is close to a square-pyramidal structure with the V=O (O(1)) in an axial position. The six-membered chelate ring (V-S(1)-C(1)-C(2)-C(3)-O(3)) has a chair conformation with the hydroxyl group (O(2)) in an axial position. The five-membered chelate ring (V′-S(4)-C(4)-C(3)-O(3)) has an envelope conformation with C(4) constituting the flap. The arrangement around O(3) is close to planar (cf. the sum of the three bond angles at O(3) is 356.8°).

Solution studies

In aqueous solution, both dithiothreitol (2) and *N*,*N*-dimethylhydroxylamine (14–16) react spontaneously with vanadate. If DTT is designated as T, then complexes of V_2T stoichiometry are formed with DTT. The chemistry with DMHA is quite complex but under moderate total vanadate concentrations, the predominent product stoichiometries with DMHA (L) are VL and VL_2. Additional mixed products of varying stoichiometry are formed when the two ligands are together in solution. In anticipation of the results summarized below, Fig. 2 identifies the various signals and Table 4 gives their ^{51}V chemical shifts.

These studies of vanadate complexation reactions with *N*,*N*-dimethylhydroxylamine and associated heteroligands have utilized overall vanadium concentrations considerably higher than we have previously used in studies of this type. One consequence of this was the observation of NMR signals that corresponded to multinuclear vanadium–DMHA complexes. The concentrations of these compounds were sufficiently high that it was necessary to identify them so that proper characterization of the mixed ligand complexes of predominant interest could be carried out. Initial studies indicated that the compounds were binuclear complexes of

© 2001 NRC Canada

Table 3. Selected intramolecular distances (Å) and angles (°) for $\{VO(SCH_2CHOHCHOCH_2S)\}_2]^{2-}$.

Distances (Å)			
V—S(1)	2.3484(20)	S(4)—C(4)	1.803(7)
V—S(4)′	2.3524(21)	O(2)—C(2)	1.424(7)
V—O(1)	1.589(4)	O(3)—V′	1.980(4)
V—O(3)	1.971(4)	O(3)—C(3)	1.424(7)
V—O(3)′	1.980(4)	C(1)—C(2)	1.510(10)
S(1)—C(1)	1.814(7)	C(2)—C(3)	1.514(9)
S(4)—V′	2.3524(21)	C(3)—C(4)	1.513(10)
Angles (°)			
S(1)-V-S(4)′	89.89(7)	V-O(3)-V′	105.16(18)
S(1)-V-O(1)	106.19(17)	V-O(3)-C(3)	127.4(4)
S(1)-V-O(3)	90.00(13)	V′-O(3)-C(3)	124.2(4)
S(1)-V-O(3)′	142.84(12)	S(1)-C(1)-C(2)	115.2(5)
S(4)′-V-O(1)	109.70(16)	O(2)-C(2)-C(1)	110.1(5)
S(4)′-V-O(3)	141.93(12)	O(2)-C(2)-C(3)	109.5(6)
S(4)′-V-O(3)′	82.63(12)	C(1)-C(2)-C(3)	115.5(5)
O(1)-V-O(3)	106.84(19)	O(3)-C(3)-C(2)	111.0(5)
O(1)-V-O(3)′	110.61(19)	O(3)-C(3)-C(4)	109.2(5)
O(3)-V-O(3)′	74.84(16)	C(2)-C(3)-C(4)	113.4(5)
V-S(1)-C(1)	101.03(23)	S(4)-C(4)-C(3)	112.1(4)
V′-S(4)-C(4)	94.09(21)		

Note: ′ represents the symmetry operation $1 - x, 1 - y, -z$.

V_2L and V_2L_3 stoichiometries. The stoichiometry of these complexes was most easily established through the use of the known mononuclear complex, VL (15), as a reference compound. Equations [1] –[3] then describe the formation of these products. The

$$[1] \quad V + L \overset{K_{110}}{\rightleftharpoons} VL \qquad [V][L]K_{110} = [VL]$$

$$[2] \quad 2VL \overset{K_{110,210}}{\rightleftharpoons} V_2L + L \qquad [VL]^2 K_{110,210} = [V_2L][L]$$

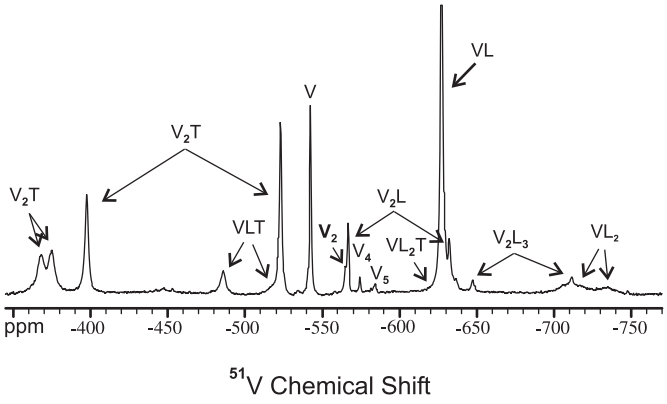
$$[3] \quad 2VL + L \overset{K_{110,230}}{\rightleftharpoons} V_2L_3 \qquad [VL]^2[L]K_{110,230} = [V_2L_3]$$

formation constant determined for VL ($K_{110} = (1.4 \pm 0.1) \times 10^3$ M^{-1}) agrees well with that previously reported (15).

The characterization of V_2L was complicated by the fact that one NMR signal (–632 ppm) from this compound occurred very close to that from VL while the second (–567 ppm) was partially superimposed on that of divanadate. As near as could be judged, both of these signals had the same intensity and exhibited the same concentration dependencies. They were therefore assigned to the individual vanadiums of the same product. On that basis, the formation constant was $K_{110,210} = (0.12 \pm 0.01)$.

Similarly to those of V_2L, two NMR signals (–648 ppm, –712 ppm) had a concentration dependence corresponding to a V_2L_3 stoichiometry. The second of these signals was superimposed on one of the VL_2 signals but appropriate concentrations of reactants could be obtained that allowed it to be established that these signals were of equal intensity. Consequently, they were assigned to the individual signals of V_2L_3. Fig. 3 shows the equilibrium data plotted according to

Fig. 2. ^{51}V NMR spectrum of vanadate in the presence of dithiothreitol (T) and *N*,*N*-dimethylhydroxylamine (L). The signals of various products discussed in the text are identified. Conditions of the experiment: vanadate (10 mM), dithiothreitol (10 mM), *N*,*N*-dimethylhydroxylamine (5 mM), KCl (1.0 M), pH 8.54.



eq. [3]. The value determined for the formation constant was $K_{110,230} = (4.2 \pm 0.2) \times 10^3$ M^{-2}.

From the relative values of $K_{110,210}$ and $K_{110,230}$ (note different units) it is evident that V_2L and V_3L_2 are found in equal proportions in solution when the free DMHA concentration is about 5 mM. Because of the L stoichiometry, the relative proportion of V_2L_3 increases with higher concentration of L free in solution and decreases with a lower concentration. This is evident in Fig. 2 where, as reflected in the NMR spectrum, the V_2L concentration is significantly higher than that of V_3L_2.

Of critical importance is the observation that VL (–627 ppm) and a mixed ligand product VL_2T (–626 ppm), have overlapping NMR signals. Products that have VLT stoichiometry have been assigned to NMR signals at –485 and –517 ppm. Both of these signals occur with low relative intensities, with the –515 ppm signal being much the smaller of the two. The identity of the –517 ppm product was inferred from that of the –485 ppm signal because the relative intensities of the two signals, as well as could be judged, maintained a constant proportionality throughout the various concentration studies. Because of the ligand and proton stoichiometries, the –485 ppm signal is observable at pH 6.73 only under low DMHA and quite high DTT concentrations. This condition also ensures formation of low amounts of VL_2T so that there is selective suppression of this –626 ppm product. The situation is quite different at pH 8.54 where the –485 ppm signal can be observed even when the concentration of DTT is low (Fig. 2).

Under neutral conditions, preliminary experiments identified the concentrations of vanadate, DMHA, and DTT, that provided a useful distribution of free vanadate and its products. Using appropriate concentrations of reactants, as established above, a pH variation study was carried out. At low pH (below 6.00), vanadate is a reasonably effective oxidant of DTT while at high pH (above 9.5) the vanadate complexes are highly dissociated. A pH range for the study of product formation from pH 6.7 to 8.7 was therefore adopted. Detailed solution studies were then carried out at both pH 6.73 and pH 8.54. In each case the concentrations of V,

© 2001 NRC Canada

Table 4. Equilibrium equations, product formation constants, and ^{51}V chemical shifts.[a]

Equilibrium equation	Formation constant	pH	ppm
$2VL \rightleftharpoons V_2L + L$	0.12 ± 0.01	8.54	–567, –632
$2VL + L \rightleftharpoons V_2L_3$	(4.2 ± 0.2) × 10^3 M^{-2}	8.54	–648, –712
$VL + T \rightleftharpoons VLT$[b]	13.4 ± 0.6 M^{-1}	6.73	–485
	12.6 ± 0.4 M^{-1}	8.54	–485
$VL + M \rightleftharpoons VLM$[b]	5.0 ± 0.2 M^{-1}	8.54	–487
$VL + Cys \rightleftharpoons VLCys$[b]	6.7 ± 1.2 M^{-1}	8.50	–496
$VL_2 + T \rightleftharpoons VL_2T$[b]	35.2 ± 0.9 M^{-1}	6.73	–626
	28.0 ± 1.0 M^{-1}	8.54	–626
$VL_2 + M \rightleftharpoons VL_2T$[b]	6.5 ± 0.6 M^{-1}	8.54	–628
$VL_2 + Gly \rightleftharpoons VL_2Gly$[c]	5.5 ± 0.4 M^{-1}	8.55	–700, –724, –734
$VL_2 + Cys \rightleftharpoons VL_2Cys$[c]	10.5 ± 3.5 M^{-1}	8.50	–729, –734, –741
$VL_2 + Cys \rightleftharpoons VL_2Cys$[b]	8.2 ± 0.5 M^{-1}	8.50	–632, –636

[a]Abbreviations: *N*,*N*-dimethylhydroxylamine (L), dithiothreitol (T), β-mercaptoethanol (M), cysteine (Cys), glycine (Gly). All formation constants are for aqueous 1.0 M ionic strength solutions maintained with KCl.
[b]Data is for sulphur-coordinated products.
[c]Data is for *N*,*O*-coordinated products.

Fig. 3. Graphical representation of the formation of V_2L_3 from VL and free *N*,*N*-dimethylhydroxylamine (L) according to the formalism of eq. [3]. Data for pH 8.54.

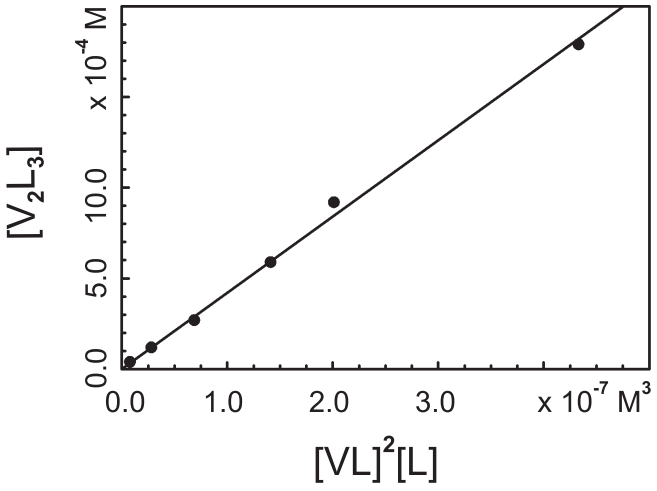
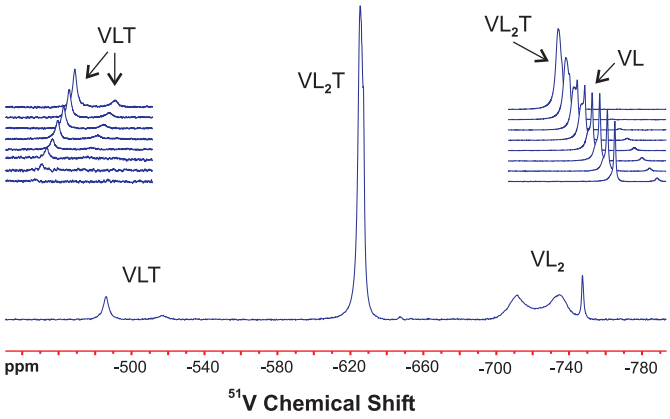


Fig. 4. ^{51}V NMR spectrum of vanadate in the presence of 60 mM dithiothreitol. The insets show the influences of varying amounts of dithiothreitol (T) with fixed total concentrations of vanadate and *N*,*N*-dimethylhydroxylamine (L). Conditions of the experiments: vanadate (5 mM), *N*,*N*-dimethylhydroxylamine (40 mM), dithiothreitol (60 mM) (main trace), pH 8.54, KCl (1.0 M); total dithiothreitol concentrations: 2, 5, 8, 10, 20, 30, 60, 120 mM bottom to top traces of the insets.



DMHA, and DTT were selectively varied in independent experiments. Figure 4 shows the results of one such concentration study.

There, however, is an analytical problem that arises because some product formation constants are large. Under certain reaction conditions, free DMHA ([L]) and free DTT ([T]) concentrations can be very low and thus difficult to accurately specify from the conservation equations. This arises because the errors in the determination of product concentrations are comparable to the free DMHA or free DTT concentrations. However, these problems were circumvented by a judicious choice of reactant concentrations. Studies were initially carried out under the assumption that the mixed ligand product at –626 ppm was of stoichiometry VLT, as previously assigned (5). It was possible to show that that assignment of stoichiometry was incorrect by studying first the formation of the minor product giving a signal at –485 ppm. The product giving rise to this latter signal could unequivocally be shown to have a VLT stoichiometry and also it could be shown that the stoichiometry of this product was different from the product giving rise to the partially obscured signal at –626 ppm.

The formation of two V_2T complexes (eq. [4]) has previously been reported (2) and, as is evident from Fig. 2, it was necessary to take them into account in this study.

$$[4] \qquad 2V + T \overset{K_{201}}{\rightleftharpoons} V_2T \qquad [V]^2[T]K_{201} = [V_2T]$$

The stoichiometry corresponding to the –485 ppm (and by inference the –517 ppm) signal was established by varying the total concentrations of V, L, and T in separate experiments. Figure 4 provides a graphical display of the influence of varying the concentration of DTT while total vanadate and total DMHA were maintained constant. The constant ratio of signal intensities of the –485 and –517 ppm signals is

© 2001 NRC Canada

Fig. 5. Correlation indicating the formation of VLT from VL_2 and dithiothreitol (T) with the release of 1 equiv of *N*,*N*-dimethylhydroxylamine (L) as described by eq. [8]. Data for pH 8.54.

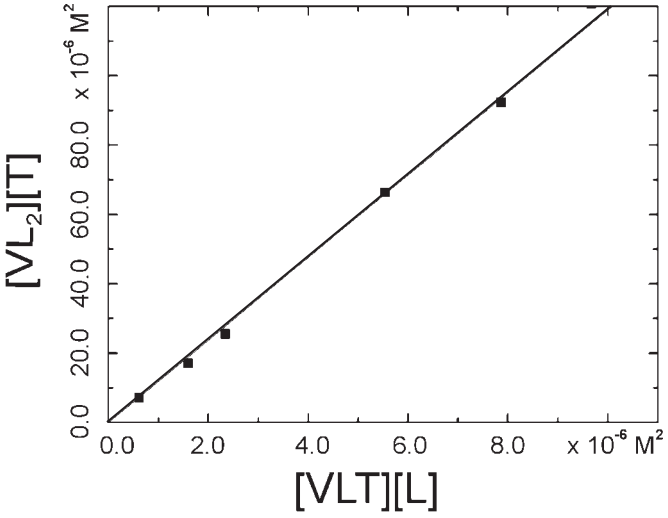
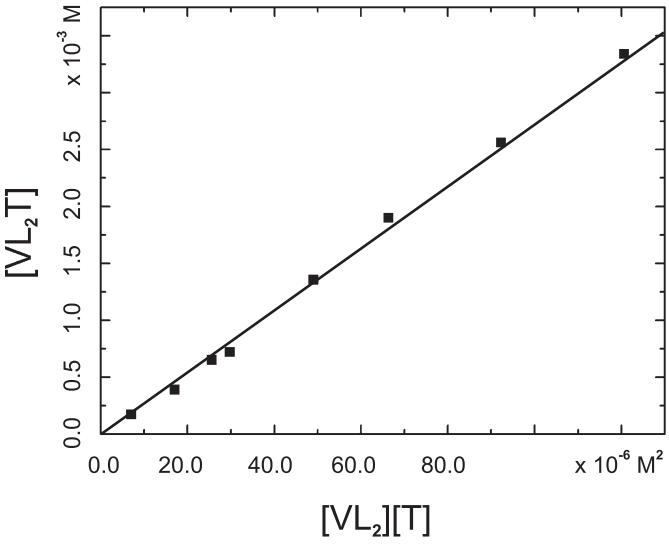


Fig. 6. Linear relationship between the product described as VL_2T and the VL_2 concentration multiplied by the dithiothreitol (T) concentration as required by eq. [9]. Data for pH 8.54.



evident in the inset of Fig. 4. In a similar experiment where DMHA was varied with constant total DTT, the two signals also maintained a constant proportionality with each. This indicates that these products have the same V to DMHA to DTT stoichiometry and therefore probably correspond to isomers, possibly arising from rotational isomerization of the hydroxamido group (15). From the concentration study, it was also evident that the signal corresponding to the product designated VL_2T at –626 ppm gained in magnitude relative to the VL and VLT signals as the L (DMHA) concentration was increased. These concentration studies are consistent with the equilibria expressed in eqs. [5] and [6] for the –485, –517 (eq. [5]), and –626 (eq. [6]) ppm products, respectively.

$$[5] \qquad V + L + T \overset{K_{111}}{\rightleftharpoons} VLT \qquad [V][L][T]K_{111} = [VLT]$$

$$[6] \qquad V + 2L + T \overset{K_{121}}{\rightleftharpoons} VL_2T \qquad [V][L]^2[T]K_{121} = [VL_2T]$$

Since, with a 600 MHz NMR spectrometer, it was possible to obtain a good enough resolution of the overlapped –626 and (or) –627 ppm signals to use lineshape fitting to resolve them into the two component parts it was possible to unambiguously establish the identity of the –485 (–517) and the –626 ppm products. The –627 ppm product is known to correspond to VL (15) and that identity has been confirmed in this study. Addition of 1 equiv of DTT to VL provides VLT (–485 ppm) as described by eq. [7]. Figure 5 shows the results of a concentration study carried out at pH 8.54 with the relevant quantities plotted according to eq. [7]. From this graph,

$$[7] \qquad VL + T \overset{K_{110,111}}{\rightleftharpoons} VLT \qquad [VL][T]K_{110,111} = [VLT]$$

$K_{110,111} = 12.8 \pm 0.9\ M^{-1}$. The corresponding value obtained for pH 6.73 was $13.0 \pm 1.1\ M^{-1}$. VL is singly negatively charged and, throughout the pH range of this study, does not form VL^{2-}. As a consequence of this, the finding that the formation constants are pH independent shows that VLT carries a single negative charge and, like VL^-, does not lose an additional proton.

It is possible to obtain the stoichiometry of the VLT product by an alternative method. Its formation can be written as occurring from VL_2, as described by eq. [8] so that VL_2 is the

$$[8] \qquad VL_2 + T \overset{K_{120,111}}{\rightleftharpoons} VLT + L$$

reference compound rather than VL. The observation of good straight lines when plotting the data according to eq. [8] was in accord with the assignment of VLT stoichiometry to the product providing the –485 ppm signal (and also, for the reasons described above, to the –517 ppm product).

The VL_2 complexes also provide a suitable reference for characterizing the product providing the –626 ppm signal, here assigned to VL_2T. Its formation can be written as in eq. [9], where cVL_2 represents the overall concentration of VL_2 complexes, and the

$$[9] \qquad VL_2 + T \overset{K_{120,121}}{\rightleftharpoons} VL_2T \qquad cVL_2[T]K_{120,121} = [VL_2T]$$

experimental results appropriately plotted. Figure 6 shows the good linear correlation obtained at pH 8.54, $K_{120,121} = (28.5 \pm 1.0)\ M^{-1}$. A similar correlation was obtained for the pH 6.73 study, $K_{120,121} = (35.6 \pm 0.9)\ M^{-1}$. The VL_2 complexes, which do not carry a charge in the slightly acidic to slight basic pH range, have a pK_a in the order of 9.0 (see below). The decrease in formation of VL_2T from VL_2 on going from pH 6.73 to pH 8.54 is fully accounted for by the averaged pK_a of VL_2 and therefore VL_2T does not have a pK_a within the range of pH of this study and is non-ionic.

The reactions of β-mercaptoethanol (M) with dimethylhydroxamidovanadates are quite similar to those of

© 2001 NRC Canada

Fig. 7. ^{51}V NMR spectra of vanadate in the presence of varying amounts of β-mercaptoethanol (M) with fixed total concentrations of vanadate and *N*,*N*-dimethylhydroxylamine (L). The chemical shift scale refers to the lower trace only, the remaining spectra are offset from that trace. Conditions of the experiments: vanadate (5 mM), *N*,*N*-dimethylhydroxylamine (40 mM), β-mercaptoethanol (as indicated), pH 8.54, KCl (1.0 M).

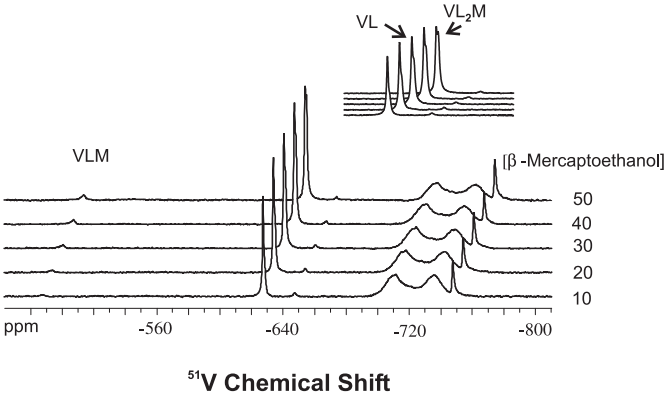
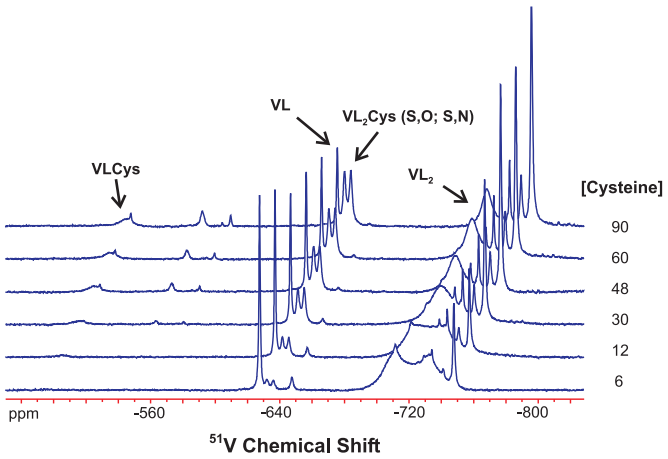


Fig. 8. The influence of varying amounts of cysteine on the ^{51}V NMR spectra of vanadate in the presence of a fixed total concentration of *N*,*N*-dimethylhydroxylamine (L). The chemical shift scale refers to the lower trace only, the remaining spectra are offset from that trace. Conditions of the experiments: vanadate (5.0 mM), *N*,*N*-dimethylhydroxylamine (40 mM), cysteine (as indicated), KCl (1.0 M), pH 8.50.



DTT. Figure 7 displays NMR spectra from a pH 8.54 β-mercaptoethanol concentration study. The VLM product gives a signal at –487 ppm, a 2 ppm shift to higher field of the corresponding VLT derivative at –485 ppm. This behaviour is mirrored in the VL_2M product where there is a small change of chemical shift to –628 ppm from –626 of the DTT complex. The formation of VLM can be described by an equation that is equivalent to eq. [7] and the data plotted appropriately. An excellent linear relationship was obtained. The formation constant for formation of VLM from VL and β-mercaptoethanol was 5.0 ± 0.2 M^{-1}. This value is close to one-half of that observed for formation of VLT and this is consistent with the fact that, structurally, DTT is equivalent to a dimer of β-mercaptoethanol and statistically, this will double the forward rate of complexation. There seems to be little stabilizing influence of the additional potentially ligating groups of the DTT ligand. In contrast to this, formation of VL_2M is less favoured by about a factor of four ($K_{120,121}$ = 6.5 ± 0.6 M^{-1}) compared to the formation of VL_2T ($K_{120,121}$ = 28.0 ± 1.0 M^{-1}).

The reaction of DMHA–vanadate with cysteine is considerably more complex than with DTT or β-mercaptoethanol. Figure 8 shows a cysteine concentration study carried out at pH 8.54. A previous study (9) has shown that bidentate complexation occurs through both *N*,*S* and *O*,*S* linkages and also through the *O*,*N*. However, there are problems arising because of a reaction involving the two VL_2 compounds with NMR signals at –710 and –732 ppm. With increase in cysteine content these signals collapsed into a single signal (–720 ppm, Fig. 8) corresponding to a complex of unknown identity. This behaviour was not observed with either dithiothreitol or β-mercaptoethanol. The reaction offered some complications in characterizing the cysteine system so an initial study of the simpler amino acid, glycine (G) was carried out. The coalescence of the –710 and –732 ppm signals was also observed with glycine, and, as for cysteine, new signals appeared in the –740 ppm region of the spectrum. Signals of the latter type have also been observed when simple peptides have been included in the medium (17) but the coalescence behaviour was not observed. The collapse of the –710 and –732 ppm signals into a single signal suggested the formation of a new product. However, a number of concentration studies, where the concentrations of V, L, or glycine were varied, showed that the single product signal corresponded to a VL_2 stoichiometry. If the formation of VL_2 is written from VL as described in eq. [10], and that of the glycine (N,O) complex as in eq. [11],

$$[10]\quad VL + L \overset{K_{110,120}}{\rightleftharpoons} VL_2 \qquad [VL][L]K_{110,120} = [VL_2]$$

$$[11]\quad VL_2 + G \overset{K_{120,121}}{\rightleftharpoons} VL_2G \qquad [VL_2][G]K_{120,121} = [VL_2G]$$

then summation and rearrangement of the two equations gives eq. [12] where cVL_2 refers to

$$[12]\quad cVL / [VL][L] = K_{110,120} + K_{110,120}K_{120,121}[G]$$

the total concentration of VL_2 + VL_2G products. Figure 9 shows the results plotted according to eq. [12]. A good linear correlation is in accord with this description of the equilibria. The intercept of the graph gives a value of 140 ± 3 M^{-1} for $K_{110,120}$ while the value for the slope (770 ± 50 M^{-2}) divided by the value for the intercept gives $K_{120,121}$ = 5.5 ± 0.4 M^{-1} for pH 8.54. This study is fully consistent with a VL_2 stoichiometry for the –720 ppm signal and suggests that the amino acid is catalyzing an exchange process between the VL_2 isomers. This might, for instance, be caused by the formation of a transient outer sphere complex that promotes rotational isomerization of the DMHA ligands. This isomerization already occurs in the timescale of a few milliseconds at room temperature (15).

© 2001 NRC Canada

Fig. 9. Relationship between the quantities, as described in eq. [12], for the formation of VL_2 and VL_2G from VL, L (*N*,*N*-dimethylhydroxylamine) and glycine (G). cVL_2 represents the sum of concentrations of VL_2 and VL_2G products.

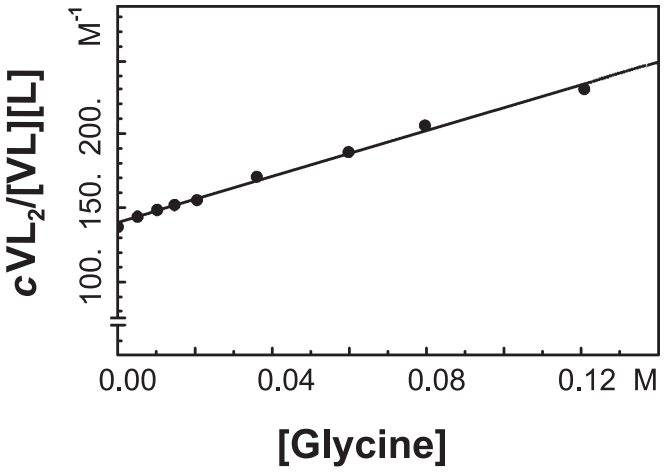
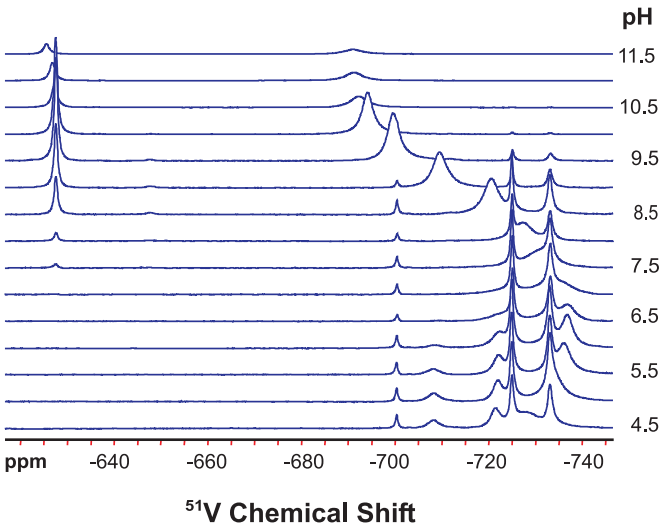
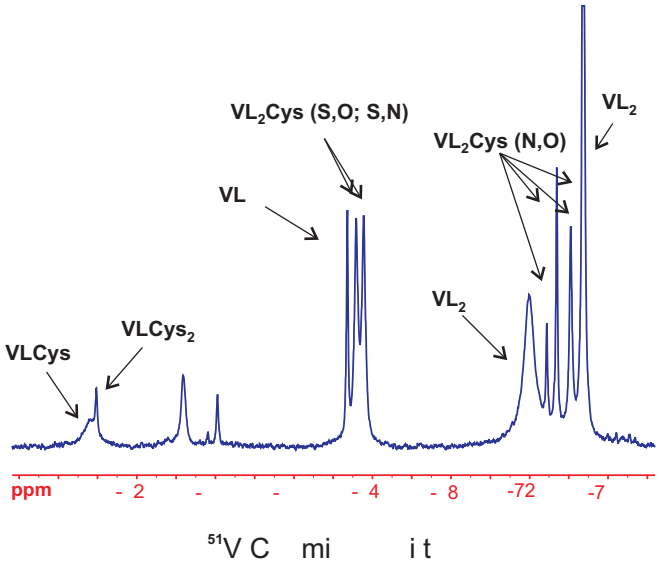


Fig. 10. Influence of pH on the NMR spectra of vanadate in the presence of *N*,*N*-dimethylhydroxylamine (DMHA) and glycine. Conditions of the experiments: vanadate (5 mM), DMHA (40 mM), glycine (120 mM) KCl (1.0 M), variable pH as indicated.



A pH variation study (pH 4.5–11.5) in the presence of 120 mM glycine revealed a systematic change in position of the –720 ppm signal (Fig. 10). Removal of glycine from the solution at pH 10 had no influence on peak position. Furthermore, a more detailed glycine concentration study at pH 10 revealed no reaction between glycine and any DMHA complex in solution. This is expected if the mixed ligand (glycine–DMHA) vanadate complexes do not have a pK_a in the high pH range. An additional pH study in the absence of glycine revealed that an increase in pH leads to generation of a single DMHA product signal above pH 9. Given then, that the –720 ppm signal is a time-averaged signal, the pH titration curve represents an averaged pK_a for the VL_2 products. Because of this, the pK_a from the titration curve (pK_a = 9.0) is not particularly meaningful. The VL_2 complexes can also be protonated at low pH to form cationic species (15) and this accounts for the downfield shifts observed in the spectral in the low pH region of Fig. 10. An interesting point to be made from Fig. 10 is that, near the high pH limit of the study, the signal of VL^- starts to change position. This indicates that VL has a second pK_a under strongly basic conditions.

Fig. 11. ^{51}V NMR spectrum of vanadate (5 mM) in the the presence of *N*,*N*-dimethylhydroxylamine (L, 40 mM) and cysteine (Cys, 120mM) obtained at pH 8.50 with 1.0 M KCl.

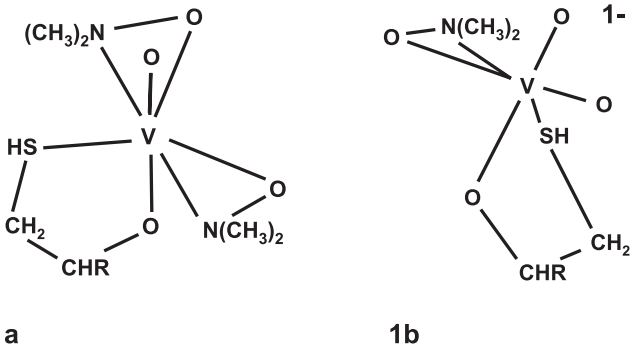


With the identification of the –720 ppm product signal as VL_2, characterization of the cysteine–DMHA complexes was reasonably straightforward. Cysteine (Cys) forms product complexes both with vanadate and with DMHA–vanadate. Vanadate, in the presence of only cysteine gives product complexes with ^{51}V NMR signals at –243, –309, –393, and –405 ppm. Under the conditions utilized in this study, oxidative instability precluded detailed characterization of these products. However, a cysteine concentration study suggested that the –243 and –309 ppm products contained at least two cysteine moieties per vanadium while the products giving signals at –393 and –405 contained less cysteine, most likely only one cysteine per vanadium.

In the presence of DMHA, both VLCys and VL_2Cys products were observed. Figure 11 shows a spectrum from a cysteine concentration study. The broad signal at –496 ppm derives from VLCys whiles those at –631 and –635 ppm arise from VL_2Cys products of *S*,*O* and *S*,*N* coordination. As for glycine, the broad VL_2 signals at –710 and –732 ppm collapsed into one signal (–720 ppm) with addition of cysteine. The sharp signal found at –747 ppm also arises from a VL_2 complex but the concentration studies revealed that an additional product signal is superimposed on the –747 ppm signal. The broad and sharp signals from VL_2 have been assigned to 6 ($(dmha)_2V(O)OH$) and 7 ($(dmha)_2V(O)(OH)H_2O$) coordinated products, respectively, (15, 18). Cysteine *N*,*O*-coordinated products give NMR signals at –729, –734, and –741 and, as mentioned, an additional product signal is found at –747 ppm. This latter

© 2001 NRC Canada

Scheme 1.



1a 1b

product was not observed at pH 7.3 (9) and apparently corresponds to a product of reaction with $(dmha)_2V(O)(OH)H_2O$. At pH 8.5, this coordination, relative to that of $(dmha)_2V(O)OH$, is much more highly favoured than it is at pH 7.3. The signals at –544, –556, and –561 apparently correspond to VLCys products. These latter signals are not observed in the absence of DMHA, so it seems likely that DMHA is complexed in an end-on fashion in these complexes. If so, the chemical shifts of these compounds suggest they are not coordinated through sulphur. The remaining NMR signal occurs at –500 ppm and is assigned to $VLCys_2$. Since the influence on chemical shift of this compound is small relative to the chemical shift of sulphur-coordinated VLCys (–496 ppm), it is likely that the second cysteine of $VLCys_2$ is not coordinated through a sulphur.

The formation constant for VLCys from VL and cysteine was 6.7 ± 1.2 M^{-1} while that of VL_2Cys was 8.2 ± 0.5 M^{-1} overall for the *S*,*O* and *S*,*N*-coordinated products from VL_2 and cysteine. As can be judged from Fig. 11, there is little selectivity of reaction of *N*,*S*- vs. *O*,*S*-coordination in these complexes. The magnitude of these formation constants is similar to those with the ligands DTT and β-mercaptoethanol. The overall constant for formation of the *N*,*O*-coordinated cysteine products was 11 ± 2 M^{-1}.

Discussion

^{51}V chemical shifts

The influence of ligating atoms on vanadium(V) chemical shifts has been of interest for a number of years (19–21) and various relationships have been drawn. Sulphur is known to have a large influence on chemical shifts compared to oxygen whereas the influence of nitrogen seems quite small. For instance, the complex formed between vanadate and β-mercaptoethanol (–362 ppm) is 160 ppm to low field of the structurally similar ethylene glycol complex (–522 ppm). The chemical shifts of VLT (–485 ppm) and VLM (–487 ppm) are 140 ppm to low field of the parent complex VL (–626 ppm) while those of VL_2T and VL_2M are about 95 ppm to low field of the precursor VL_2 complexes. Similarly, sulphur in cysteine complexes with VL_2 causes a shift of about +105 ppm compared to the *N*,*O* complexes of cysteine and serine (9). It seems evident then, that inclusion of a single sulphur in the coordination shell of vanadate complexes will cause a shift of about +100 to +150 ppm in the signal position compared to oxygen and changes in signal position of this magnitude should be looked for when studying thiolate complexes.

N,*N*-dimethylhydroxylamine has a large influence on vanadium chemical shifts that is comparable to the influence of hydrogen peroxide. Ligation of *N*,*N*-dimethylhydroxylamine causes a high field shift in resonance positions of about 100 ppm per ligand. This large change was used as a basis for assigning the individual vanadium signals of V_2L and V_2L_3. It is somewhat surprising that no product signals corresponding to the dimers V_2L_2 and V_2L_4, were observed in this study. It may be that the asymmetry in the V_2L and V_2L_3 complexes adds an additional element of stability to the formation of these dimer-like complexes. At higher overall vanadate concentrations, V_2L_2 and V_2L_4 dimers will probably be observable; certainly V_2L_4 ($\{(dmha)_2V(O)\}_2O$) is the crystalline form of the complex (15).

Coordination

The dimeric coordination of V_2L_4, $\{(dmha)_2VO\}_2O$, as observed in the crystal structure, and also assigned to the structure in aqueous solution (15) together with the observation of large differences in chemical shifts between the individual vanadiums (Fig. 2, Table 4), as expected from selective sulphur coordination, provides a firm foundation for assigning the coordination structures of V_2L and V_2L_3. The coordination is assigned here to be similar to that of V_2L_4 except that the compounds are not symmetrical, being $\{dmhaV(O)_2\}O\{V(O)_2OH\}^{2-}$ and $\{(dmha)_2VO\}O\{dmhaV(O)_2\}^{1-}$. No information about the acidity constants of these compounds was obtained in this study.

It seems likely that coordination of a thiolate sulphur does not induce a significant change in coordination geometry compared to oxygen. Certainly this is the case for the β-mercaptoethanol complex. The structure of this vanadate complex is not much different from the glycolate complexes with adenosine (22), with a glycoside (23), or with the proposed ethylene glycol complex (24). All are dimeric structures with the cyclic $[VO]_2$ core that is characteristic of many vanadium complexes.

X-ray structures of a number of VL_2 complexes with oxygen- and (or) nitrogen-coordinated bidentate heteroligands have been reported (14, 16) and their structures are very similar. It seems likely that the DTT and β-mercaptoethanol derivatives are, structurally, not very different from those complexes, all of which are pentagonal bipyramidal.

It is interesting to speculate on the position of the thiolate sulphur in the complex. Does it occupy an equatorial or apical position? A recent crystal structure of a tridentate $O(CH_2CH_2S)_2^{2-}$ complex of vanadium(V) shows both sulphurs in equatorial positions (25). In the β-mercaptoethanol–V(V) complex, the sulphur is also in an equatorial position but, in this case, the formation of the $[VO]_2$ core of the complex forces the equatorial location for the sulphur. It is suggested here that the sulphur will be found in the equatorial position in these complexes as indicated in Scheme 1a. Since VL_2T, like the parent VL_2 does not carry a charge under close to neutral conditions, then the ligand must retain one proton, either on the S or the O of the

© 2001 NRC Canada

ligating group. It seems likely that it is retained on the sulphur since the *S*-substituted cysteine (-SC(O)OBz) forms a product complex (–627 ppm) with VL_2 (9). In a related case where a bidentate ethylene glycol complex is formed under forcing conditions, a proton is retained on one of the oxygens of the ligand. The resultant bond to vanadium is, however, very long (2.321(4) Å) (26) compared to a more typical distance of about 1.9 Å for a V—O bond.

The assignment of a coordination geometry to VLT is complicated by the fact that there are no crystal structures of closely related compounds. However, if the bonding to the hydroxamido ligand is formally considered to be unidentate then the vanadiums in the crystalline dimer $\{(dmha)_2V(O)\}_2O$, can be considered to have a tetrahedral coordination (15). Since vanadate, itself, also has tetrahedral coordination, it seems unlikely that VL will have other than tetrahedral coordination. Bidentate complexation of the thiolate can reasonably be expected to expand the coordination sphere (Scheme 1b). On this basis, and if the DMHA ligand is formally considered unidentate, both VL_2T and VLT may be considered to be trigonal bipyramidal. Since there is no indication from these studies that more than one sulfhydryl or more than one hyroxyl group are involved in the complexation of DTT with VL or with VL_2, the β-mercaptoethanol complexes are unlikely to show significant structural differences from the corresponding DTT complexes.

These proposed coordination modes of Scheme 1 are very different from the coordination found in the V(IV) complex with DTT (V_2T_2, Fig. 1) and indeed from the structure previously proposed for the V(V) complex of DTT (2) where the stoichiometry is V_2T. The structure that was suggested for V_2T is quite similar to that observed here for the V(IV) complex. However, there is a significant difference in that the V(V) complex has only one DTT ligand that binds each vanadium differently while the V(IV) complex has two ligands and identical vanadiums. The proposed structures of Scheme 1 are similar to those observed for some amino acid and dipeptide complexes (16, 17) except that the latter complexes do not have sulphur ligation.

Although these β-mercaptoethanol and dithiothreitol complexes are of interest in their own right, they serve as useful models for the study of other thiolate complexes. In particular, they have aided in unraveling the complex equilibrium pattern of the cysteine ligand and have also provided critical information for the study of DMHAV complexation in the active site of protein tyrosine phosphatases (7). The structures of the VLCys and VL_2Cys complexes are probably not much different from those proposed above for the DTT and β-mercaptoethanol complexes except that, in the one case, a nitrogen takes the place of the oxygen. The fact that the *S,O* and *S,N* VL_2Cys complexes are formed in almost equal amounts suggests there is little to choose between nitrogen and oxygen in terms of binding affinity to vanadium in these types of complexes. Since only a single broad signal is observed for the VLCys products, it is not possible to know whether this observation also applies to this type of complex. Although, in VL_2Cys, *N,O*-coordination is as well favoured as is *S,O*- (*S,N*-) coordination at pH 8.5, this will be a pH-dependent phenomenon that is determined by the pK_a values of the various reactants and products.

Acknowledgements

Thanks are extended to Merck Frosst Canada, Inc. and to the Natural Sciences and Engineering Research Council of Canada (NSERC) for their financial support of this work.

References

1. S. Bhattacharyya, R.J. Batchelor, F.W.B. Einstein, and A.S. Tracey. Can. J. Chem. **77**, 2088 (1999).
2. P.C. Paul and A.S. Tracey J. Biol. Inorg. Chem. **2**, 644 (1997).
3. D. Barford. Curr. Opin. Struct. Biol. **5**, 728 (1995).
4. J.B. Vincent and M.W. Crowder. Phosphatases in cell metabolism and signal transduction: Structure, function and mechanism of action. R.G. Landes Company, Austin, Texas. 1995.
5. F. Nxumalo, N.R. Glover, and A.S. Tracey. J. Biol. Inorg. Chem. **3**, 534 (1998).
6. C. Cuncic, S. Desmarais, N. Detich, A.S. Tracey, M.J. Gresser, and C. Ramachandran. Biochem. Pharmacol. **58**, 1859 (1999).
7. S. Bhattacharyya and A.S. Tracey. J. Inorg. Biochem. **85**, 9 (2001).
8. G. Soman, Y.C. Chang, and D.J. Graves. Biochemistry, **22**, 4994 (1983).
9. F. Nxumalo and A.S. Tracey. J. Biol. Inorg. Chem. **3**, 527 (1998).
10. E.J. Gabe, P.S. White, and G.D. Enright. DIFRAC. A Fortran 77 control routine for 4-circle diffractometers. National Research Council Canada, Ottawa. 1995.
11. E.J. Gabe, Y. LePage, J.-P. Charland, F. L. Lee, and P.S. White. J. Appl. Crystallogr. **22**, 384 (1989).
12. D.J. Watkin, J.R. Carruthers, and P.W. Betteridge. CRYSTALS. Chemical Crystallography Laboratory, University of Oxford, Oxford, U.K. 1984.
13. J.A. Ibers and W.C. Hamilton (*Editors*). International tables for X-ray crystallography. Vol. IV. Kynoch Press, Birmingham. 1975.
14. S.J. Angus-Dunne, P.C. Paul, and A.S. Tracey. 31st International conference on coordination chemistry abstracts, 1P13. 1996.
15. P.C. Paul, S.J. Angus-Dunne, R.J. Batchelor, F.W.B. Einstein, and A.S. Tracey. Can. J. Chem. **75**, 429 (1997).
16. A.D. Keramidas, W. Miller, O.P. Anderson, and D.C. Crans. J. Am. Chem. Soc. **119**, 8901 (1997).
17. P.C. Paul, S.J. Angus-Dunne, R.J. Batchelor, F.W.B. Einstein, and A.S. Tracey. Can. J. Chem. **75**, 183 (1997).
18. S.J. Angus-Dunne, P.C. Paul, and A.S. Tracey. Can. J. Chem. **75**, 1002 (1997).
19. D. Rehder, C. Weidemann, A. Duch, and W. Priebsch. Inorg. Chem. **27**, 584 (1988).
20. D. Rehder. Z. Naturforsch. B: Anorg. Chem. Org. Chem. **32b**, 771 (1977).
21. O.W. Howarth. Prog. Nucl. Magn. Reson. Spectrosc. **22**, 453 (1990).
22. S.J. Angus-Dunne, R.J. Batchelor, A.S. Tracey, and F.W.B. Einstein J. Am. Chem. Soc. **117**, 5292 (1995).
23. B. Zhang, S. Zhang, and K. Wang. J. Chem. Soc. Dalton Trans. 3257 (1996).
24. W.J. Ray, Jr., D.C. Crans, J. Zheng, J.W. Burgner, II, H. Deng, and M. Mahroof-Tahir. J. Am. Chem. Soc. **117**, 6015 (1995).
25. S.C. Davies, D.L. Hughes, Z. Janas, L.B. Jerzykiewicz, R.L. Richards, J.R. Sanders, J.E. Silverston, and P. Sobota. Inorg. Chem. **39**, 3485 (2000).
26. S. Mondal, S.P. Rath, S. Dutta, and A. Chakravorty. J. Chem. Soc. Dalton Trans. 99 (1996).

© 2001 NRC Canada

Nature of the active silane alcoholysis catalyst in the $Ru_wCl_x(CO)_y(PMe_3)_z$ (*w*, *x*, *y*, *z* = 1 or 2) system; $Ru_2(\mu\text{-}Cl)_2Cl_2(CO)_4(PMe_3)_2$ as a new catalyst for silane alcoholysis in a polar solvent[1]

Mee-Kyung Chung, George Ferguson, Valerie Robertson, and Marcel Schlaf

Abstract: The dimeric complex $Ru_2(\mu\text{-}Cl)_2Cl_2(CO)_4(PMe_3)_2$ (**1**) forms an active silane alcoholysis complex in the polar solvent *N*,*N*-dimethylamino-acetamide (DMA). The dynamic behaviour of **1** in DMF-d_7 solution has been investigated by variable temperature (VT) ^1H NMR. The solid state structures of **1** and *cis,cis,trans*-$RuCl_2(CO)_2(PMe_3)_2$ (**3**) have been determined by single crystal X-ray diffractometry. Using ethylene glycol – triethylsilane as a model system, the catalytic activity of **1** in DMA is compared to that of a series of known silane alcoholysis catalysts, including $RhCl(PPh_3)_3$, PdX_2 (X = Cl^-, OAc^-), and *cis,cis,trans*-$[IrH_2S_2L_2]SbF_6$ (L = PPh_3, S = THF). Complex **3** is not an active silane alcoholysis catalyst in this solvent, but is active in nonpolar solvents. Its structure and spectroscopic signature is, however, different from that of a previously reported catalyst of the same composition.

Key words: silane alcoholysis, polar solvent, ruthenium catalyst.

Résumé : Dans un solvant polaire comme le *N*,*N*-diméthylacétamide (DMA), l'alcoolyse du complexe dimère $Ru_2(\mu\text{-}Cl)_2Cl_2(CO)_4(PMe_3)_2$ (**1**) donne lieu à la formation d'un complexe de silane actif. Faisant appel à la RMN du ^1H à température variable, on a étudié le comportement dynamique de **1** en solution dans le DMF-d_7. On a déterminé les structures de **1** et du *cis,cis,trans*-$RuCl_2(CO)_2(PMe_3)_2$ (**3**) à l'état solide par diffraction des rayons X par un cristal unique. Utilisant le système éthylèneglycol/triéthylsilane comme modèle, on a comparé l'activité catalytique de **1** dans le DMA avec celles d'une série de silanes connus comme catalyseurs de l'alcoolyse, y compris $RhCl(PPh_3)_3$, PdX_2 (X = Cl^-, OAc^-) et *cis,cis,trans*-$[IrH_2S_2L_2]SbF_6$ (L = PPh_3, S = THF). Dans ce solvant, ce composé **3** n'est pas un silane actif comme catalyseur de l'alcoolyse; il est toutefois actif dans les solvants non polaires. Sa structure et ses caractéristiques spectroscopiques sont toutefois différentes de celles rapportées antérieurement pour un catalyseur de même composition.

Mots clés : alcoolyse de silanes, solvant polaire, catalyseur de ruthénium.

[Traduit par la Rédaction]

Introduction

The silane alcoholysis reaction (eq. [1]) constitutes an exceptionally mild and efficient method of protecting hydroxyl functions by trialkyl or aryl-silyl groups.

[1] $$R'OH + HSiR_3 \xrightarrow{[cat.]} R'OSiR_3 + H_2(g)$$

Recieved August 20, 2000. Published on the NRC Research Press Web site at http://canjchem.nrc.ca on July, 11, 2001.

Dedicated to Professor Brian R. James on the occasion of his 65th birthday.

M.-K. Chung, G. Ferguson, V. Robertson, and M. Schlaf.[2] Department of Chemistry & Biochemistry, University of Guelph, Guelph, ON N1G 2W1, Canada.

[1]Contribution from the Guelph–Waterloo Centre for Graduate Work in Chemistry (GWC)[2].

[2]Corresponding author (telephone: (519) 824-4120 ext. 3002; fax: (519) 766-1499; e-mail: mschlaf@uoguelph.ca).

The high enthalpic driving force of the oxygen–silicon bond formation, together with the entropically favourable generation of 1 equivalent of hydrogen gas, generally results in clean and quantitative conversions. The reaction is catalyzed by a large variety of transition metal complexes (1–7). Specific examples of highly active catalysts are *cis,cis,trans*-$[IrH_2S_2L_2]SbF_6$ (L = PPh_3, S = THF) (8), *all-cis*-$RuCl_2(CO)_2(PMe_3)_2$ (9), $Co_2(CO)_8$ (10), $RhCl(PPh_3)_3$ (11–13), $IrX(CO)L_2$ (L = PR_3) (14), and $[IrCl(C_8H_{14})_2]_2$ (14). Most simply, palladium metal, generated in situ by reduction of PdX_2 (X = OAc^-, Cl^-) (15) also catalyzes the reaction. Another commercially available and metal-free catalyst system is $B(C_6F_5)_3$, recently described by Blackwell et al. (16).

Common to all these catalyst systems is that, to date, they have only been tested in nonpolar, non-coordinating organic solvents such as benzene, toluene, pentane, or methylene chloride. We are interested in applying the silane alcoholysis reaction to highly polar polyol and sugar substrates with multiple hydroxyl functions, which are insoluble in these solvents, but soluble in chemically largely inert amides such as *N*,*N*-dimethylformamide (DMF), *N*-methyl-pyrrolidin-2-one (NMP), and *N*,*N*-dimethylacetamide (DMA). In order to establish which of a selection of the known catalyst systems

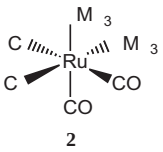
 DOI: 10.1139/cjc-79-5/6-949 © 2001 NRC Canada

would tolerate the anticipated *coordinative inhibition* by the donor atoms (O, N) in these solvents, we conducted an activity evaluation of a series of catalysts in DMA using ethylene glycol and triethylsilane as a model system. In the course of this study we found that the most active homogeneous catalyst system in DMA is derived from the general composition $Ru_wCl_x(CO)_y(PMe_3)_z$ (w, x, y, z = 1 or 2), but that the structures of the active catalyst precursors are in fact $Ru_2(\mu\text{-}Cl)_2Cl_2(CO)_4(PMe_3)_2$ (**1**) or *cis,cis,trans*-$RuCl_2(CO)_2(PMe_3)_2$ (**3**) rather than *all-cis*-$RuCl_2(CO)_2(PMe_3)_2$ (**2**) as previously reported (17). The dynamic solution behaviour of dimer **1** in amide solvents, as well as the solid state structures of the complex **1** and **3** as determined by single crystal X-ray structure analysis, are reported.

Results

The conditions and reagents for the synthesis of the catalyst system $Ru_wCl_x(CO)_y(PMe_2)_z$ as published are shown in eq. [2] (17).

[2] RuC$_3$ + 2 M$_3$ + CO( ) —u→ M = 2-m t o y- t no

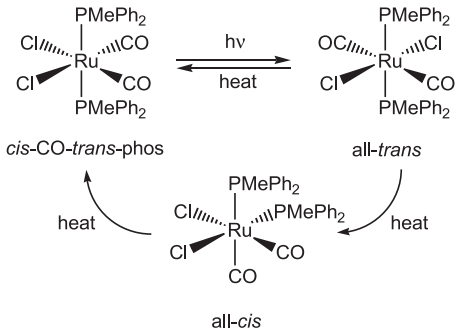


2

Following this procedure we obtained materials that gave inconsistent results with respect to catalytic activity and whose NMR and IR spectra in no case matched the previously reported data. Singer et al. (17) assigned the *all-cis* configuration **2** to their reaction product based on ^{1}H NMR and IR data.[3] They reported a single doublet at 1.78 ppm with $J_{H,P}$ = 12 Hz in $CDCl_3$ and two ν(CO) stretching frequencies at 2085 and 2022 cm^{-1} in Nujol. While the IR data and symmetry considerations support a *cis* position of the two CO ligands, the assignment does not match with the position of the phosphine ligands. In an *all-cis* arrangement one of the phosphines must be *trans* to the σ-donor – π-acceptor CO, while the other must be *trans* to the σ-donor – π-donor Cl^-. Two different chemical environments and chemical shifts should, therefore, result for the phosphorus and by extension carbon and proton nuclei on the two phosphine ligands, unless their shifts are fortuitously equivalent. This, however, appears to be unlikely, as the structurally very closely related complex *all-cis*-$RuCl_2(CO)_2(PMePh_2)_2$ shows two separate doublets for the methyl substituents on the phosphine ligands (18). Also the *all-cis* configuration of this complex is thermally unstable against isomerization to *cis,cis,trans*-$RuCl_2(CO)_2(PMePh_2)_2$ and only accessible through a photochemical reaction via the even more unstable *all-trans* form (Fig. 1).

The expected ^{1}H NMR of the *all-trans* form, i.e., a doublet of doublet or pseudo triplet for the methyl signals due to coupling to the two phosphorus nuclei, equally would not match the literature spectral data. These considerations together with wide variations of catalyst activity in the silane alcoholysis reactions using the material isolated by us, prompted us to reinvestigate the $Ru_wCl_x(CO)_y(PMe_3)_z$ system in more detail.

Fig. 1. Photochemically and thermally induced stereochemical rearrangements observed for $RuCl_2(CO)_2(PMePh_2)_2$.



Synthesis and isolation

The reaction of eq. [2] gives an amorphous solid from which two different products of different crystal habit are obtained by fractional crystallization, first from CH_2Cl_2–Et_2O and subsequently from EtOH–H_2O. The latter solvent system is also the one used by Singer et al. (17). Single crystal X-ray diffraction analysis revealed the structure of the first product to be the dimeric complex $Ru_2(\mu\text{-}Cl)_2Cl_2(CO)_4(PMe_3)_2$ (**1**) and that of the second component to be the mononuclear complex *cis,cis,trans*-$RuCl_2(CO)_2(PMe)_2$ (**3**). The yields for both products (**1** and **3**) are between 30 and 40%, with a total yield of about 70% with respect to ruthenium. By ^{1}H and ^{31}P NMR, both compounds are present in about the same ratio in the crude product, i.e., the product identity and distribution is not an artifact of the fractional crystallization.

Structure determinations

ORTEP diagrams (19) of the structures of the dimer $Ru_2(\mu\text{-}Cl)_2Cl_2(CO)_4(PMe_3)_2$ (**1**) and that of the mononuclear complex *cis,cis,trans*-$RuCl_2(CO)_2(PMe)_2$ (**3**) are shown in Figs. 2 and 3, respectively.

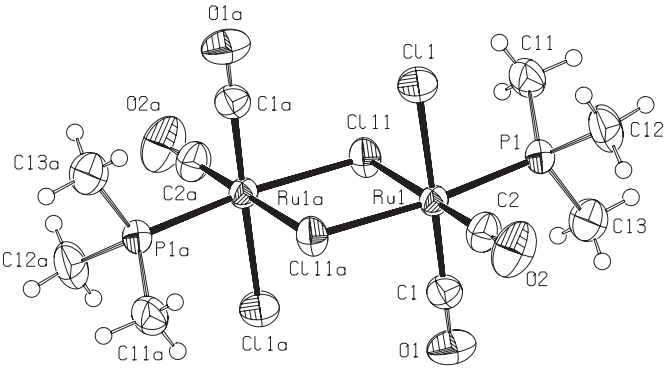
Selected bond angles and distances of complexes **1** and **3** are summarized in Tables 1 and 2, respectively. The dimer **1** has a center of inversion in the plane defined by the two ruthenium centers and the bridging chloride ligands. The two Ru—Cl bond distances in this plane are, however, not equivalent, but slightly shorter (2.457 Å) for the bond *trans* to the strong π-acceptor CO and slightly longer (2.496 Å) for the bond *trans* to the phosphine, resulting in a distorted diamond shape with Cl-Ru-Cl and Ru-Cl-Ru bond angles in this plane of 83.95 and 96.04°, respectively. The Ru—Cl bond distance of the terminal chloride ligand is very close to that of an average value of 2.409 Å as reported by Orpen et al. (20) The other bond angles around ruthenium closely approach that of an idealized octahedral environment with bond lengths in the expected ranges.

All ruthenium ligand bond lengths in the mononuclear complex **3** are pairwise equivalent within the 3σ level and

[3] The original formulation in the paper by Singer et al. is: "The dérivé III (i.e., $RuCl_2(CO)_2(PMe_3)_2$) isolé possède tous ses ligands en position *cis*."

© 2001 NRC Canada

Fig. 2. Molecular structure of the dimer complex $Ru_2(\mu\text{-}Cl)_2Cl_2(CO)_4(PMe_3)_2$ (**1**) as determined by single crystal X-ray diffraction (ORTEP plot at 30% probability level).



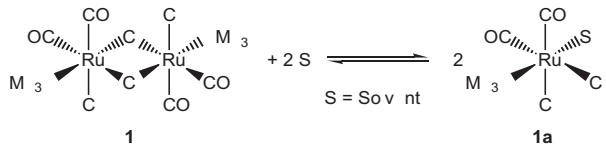
fall within the expected ranges and bond angles approach that of an idealized octahedral environment around the ruthenium center. In the solid state the two PMe_3 ligands are staggered about the P-Ru-P axis by 63.93° breaking the otherwise high symmetry of the ligand arrangement.

Spectroscopy

The spectroscopic data of **1**, **1a**, and **3** are summarized in Table 3.

Dissolving an authentic sample of X-ray grade crystals of **1** in either $CDCl_3$ or DMF-d_7 results in an ^{1}H NMR spectrum that displays two doublets for the PMe_3 ligands at the chemical shifts listed in Table 3 in relative intensities of 0.42:1, with the lower shift component as the more abundant one. Based on the high symmetry of the solid state structure of **1**, whose center of inversion would render the two phosphines chemically and magnetically equivalent, this spectral appearance immediately suggests a breakup of the dimer in solution, most likely through solvent coordination in the manner indicated in eq. [3], which retains the mutual *trans* arrangement of the π-donor chloride and π-acceptor carbonyl.

[3]

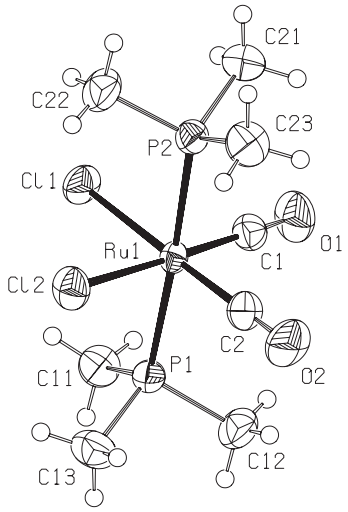


1 **1a**

The variable temperature (VT) ^{1}H NMR spectrum of the methyl signals of a sample of **1** in DMF-d_7 is shown in Fig. 4 and reveals the existence of a dynamic process in solution, which supports the above hypothesis.

The two doublets coalesce at ~100°C and reemerge as a time averaged doublet above ~120°C. In order to simplify a more quantitative analysis of this process through simulations, the VT experiment was repeated with phosphorus decoupling, which collapses the doublets into two simple coalescing singlets. Using the MEX program by Bain and Duns (21) a set of spectra were simulated that matched the these decoupled spectra over the temperature range from 65 to 124°C. From an Eyring plot of the rate constants calculated by the program vs. $1/T$ (in Kelvin) the approximate activation parameters of the process were determined to $\Delta H^{\ddagger}$ =

Fig. 3. Molecular structure of complex *cis,cis,trans*-$RuCl_2(CO)_2(PMe_3)_2$ (**3**) as determined by single crystal X-ray diffraction (ORTEP plot at 30% probability level).



18.0 ± 0.4 kcal mol^{-1} and $\Delta S^{\ddagger}$ = –2.7 ± 0.9 cal mol^{-1} K^{-1} for the reaction of the minor to the major component ($k_{reverse}$: **1a** → **1**) and through $K_{eq} = k_f/k_r$ to $\Delta H^{\ddagger}$ = 18.4 ± 0.9 kcal mol^{-1} and $\Delta S^{\ddagger}$ = –3.0 ± 0.9 cal mol^{-1} K^{-1} for the reaction of the major to the minor component ($k_{forward}$: **1** → **1a**). Within the experimentally achievable error ranges the activation parameters are the same for the forward and the reverse reaction, which reflects an equilibrium constant K_{eq} close to unity. K_{eq} ranges from 0.45 to 0.49 in the temperature range used and was determined from the integral ratios of the ^{31}P decoupled signals at low temperatures and extrapolated for the higher temperatures, where beginning coalescence makes a reliable integration impossible.

Further support for the reaction of eq. [3] comes from the ^{13}C and ^{1}H NMR spectra of the same sample at ambient temperature. In addition to the 1:1:1 triplet for the carbonyl carbon of free DMF-d_7 at 162.7 ppm, a second small 1:1:1 triplet ($J_{C,D}$ = 30 Hz) is observed at 169.2 ppm, which we assign to the coordinated DMF-d_7 in complex **1a**. This ^{13}C signal is matched by a very small singlet at 8.45 ppm in ^{1}H NMR, which disappears with the beginning coalescence of the methyl signals and which we assign to the aldehyde proton of coordinated DMF-d_6. The signal reversibly reappears upon cooling to ambient temperature.

An unambiguous assignment of the larger and smaller sets of peaks to **1** and **1a**, respectively follows from the ^{13}C NMR signals of the carbonyl ligands. In the dimer **1** the two carbonyl ligands are chemically and magnetically inequivalent and should give rise to two doublets due to coupling to the phosphorus nucleus. In complex **1a** both carbonyl ligands are chemically and magnetically equivalent and should, thus, result only in a single doublet. Two larger doublets of approximately equal intensity are observed at 198.12 and 192.93 ppm, the latter of which overlaps with a smaller doublet at 193.08 ppm. The larger peaks must, therefore, belong to complex **1**, bearing the two nonequivalent carbonyl ligands. By extension, the larger peaks in the ^{1}H and ^{31}P NMR spectra are assigned to the dimer **1**, which is

© 2001 NRC Canada

Table 1. Selected bond lengths (Å) and angles (°) in complex **1**.

Bond lengths (Å)		**Bond angles** (°)			
Ru(1)—C(1)	1.885(3)	C(2)-Ru(1)-C(1)	91.19(11)	C(2)-Ru(1)-Cl(11a)	94.92(8)
Ru(1)—C(2)	1.855(2)	C(2)-Ru(1)-P(1)	89.85(8)	C(1)-Ru(1)-Cl(11a)	90.70(7)
Ru(1)—P(1)	2.3018(6)	C(1)-Ru(1)-P(1)	93.21(7)	P(1)-Ru(1)-Cl(11a)	173.77(2)
Ru(1)—Cl(1)	2.4018(7)	C(2)-Ru(1)-Cl(1)	89.16(9)	Cl(1)-Ru(1)-Cl(11a)	88.30(2)
Ru(1)—Cl(11)	2.4573(6)	C(1)-Ru(1)-Cl(1)	178.97(8)	Cl(11)-Ru(1)-Cl(11a)	83.955(19)
Ru(1)—Cl(11a)	2.4967(6)	P(1)-Ru(1)-Cl(1)	87.77(2)	Ru(1)-Cl(11)-Ru(1a)	96.043(19)
Cl(11)—Ru(1a)	2.4967(6)	C(2)-Ru(1)-Cl(11)	178.45(8)		
Cl(11a)—Ru(1a)	2.4573(6)	C(1)-Ru(1)-Cl(11)	89.89(7)		
O(1)—C(1)	1.126(3)	P(1)-Ru(1)-Cl(11)	91.20(2)		
O(2)—C(2)	1.128(3)	Cl(1)-Ru(1)-Cl(11)	89.74(2)		

Table 2. Selected bond lengths (Å) and angles (°) in complex **3**.

Bond lengths (Å)		**Bond angles** (°)			
Ru(1)—Cl(1)	2.4403(9)	Cl(1)-Ru(1)-Cl(2)	91.31(4)	Cl(2)-Ru(1)-P(2)	87.55(4)
Ru(1)—Cl(2)	2.4323(6)	Cl(1)-Ru(1)-P(1)	92.23(2)	Cl(2)-Ru(1)-C(1)	178.29(11)
Ru(1)—P(1)	2.3888(11)	Cl(1)-Ru(1)-P(2)	85.64(4)	Cl(2)-Ru(1)-C(2)	88.86(10)
Ru(1)—P(2)	2.3905(9)	Cl(1)-Ru(1)-C(1)	86.97(10)	P(1)-Ru(1)-P(2)	177.17(4)
Ru(1)—C(1)	1.851(2)	Cl(1)-Ru(1)-C(2)	178.77(9)	P(1)-Ru(1)-C(1)	89.45(10)
Ru(1)—C(2)	1.861(3)	Cl(2)-Ru(1)-P(1)	90.63(4)	P(1)-Ru(1)-C(2)	88.99(9)

therefore the major component in solution at ambient temperature.

The IR spectrum of the same sample of **1** dissolved in $CDCl_3$ displays only two well defined bands at 2068 and 2010 cm^{-1}, i.e., does not show the presence of two components in solution as observed by NMR. This can be rationalized by the fact that in both complexes (**1** and **1a**) both carbonyl ligands are *trans* to the same π-donor chloride and the ν(CO) stretching frequencies are, therefore, presumably very close to or even identical with each other in both complexes.

The NMR spectra of complex **3** show no dynamic phenomena and display the expected coupling patterns for the *cis*,*cis*,*trans*-arrangement. The pseudo triplet observed for the methyl signals of **3**, also establishes that it cannot have been the compound originally isolated by Singer et al. (17), whose identity remains unknown.

Evaluation of the catalysts in DMA

The catalytic activity of the new complexes **1** and **3** was evaluated using the ethylene glycol – triethylsilane system as the model reaction (eq. [4]) and compared to a series of catalyst systems consisting of *cis*,*cis*,*trans*-$[IrH_2S_2L_2]SbF_6$ (L = PPh_3, S = THF) (8), $RhCl(PPh_3)_3$ (11–13), $Co_2(CO)_8$ (10), and PdX_2, (X = Cl^-, OAc^-) (15).

[4] $$HOCH_2CH_2OH + n\ Et_3SiH \xrightarrow[-n\ H_2(\ )]{[c\ t.]} \begin{matrix} HOCH_2CH_2OSiEt_3 \\ + \\ Et_3SiOCH_2CH_2OSiEt_3 \end{matrix}$$

In all reactions ethylene glycol (2.5 mmol) in DMA (6 mL) were reacted with one or two equivalents of triethylsilane at a catalyst concentration of 3 mol% with respect to metal content. Complexes **3** and $Co_2(CO)_8$ are inactive in DMA, however, **3** is an active catalyst in THF, the solvent used by Oehmichen and Singer (9). All other tested catalysts are active in the DMA solvent and quantitative results as determined by direct quantitative GC analysis of the reaction mixtures are summarized in Table 4. The data gives a direct comparison of the relative activity of the catalyst systems in the amide solvent, total yields of silylated products, as well as their selectivity towards mono- and disilylation of the diol substrate in the presence of one or two equiv of silane, respectively. The reaction times given in Table 4 refer to the end point of the reaction as indicated by the end of hydrogen gas evolution and by the complete consumption of triethylsilane as indicated by the GC trace of the reaction mixture.

Of all the catalyst systems tested, by far the most active is the dimer **1**, which even surpasses the activity of the heterogeneous palladium systems. The true catalyst of unknown structure and composition formed from **1** and triethylsilane in DMA, therefore, does not suffer from coordinative inhibition by the solvent. This contrasts with the behaviour of complex **3**, which does suffer inhibition by the solvent to the point of being inactive in the amide solvent, and the iridium system $[IrH_2(PPh_3)(THF)_2]SbF_6$, which shows as many as 130 000 turnovers per hour in methylene chloride solvent at 25°C (8), but requires heating to 45°C to achieve acceptable reaction rates in DMA. Consistent with the latter result, Crabtree et al. (22) had previously shown that the same iridium complex suffers strong inhibition by even trace amounts of coordinating solvents when used as an olefin hydrogenation catalyst. The active catalyst resulting from $RhCl(PPh_3)_3$ also must suffer coordinative inhibition, as it has been reported to give complete conversion to silane alcoholysis products within minutes in benzene solution at 20°C and catalyst concentrations as low as 0.05 mol% (13).

The yields of monosilylated product achieved by the catalysts in DMA solvent are moderate to good, but in no case

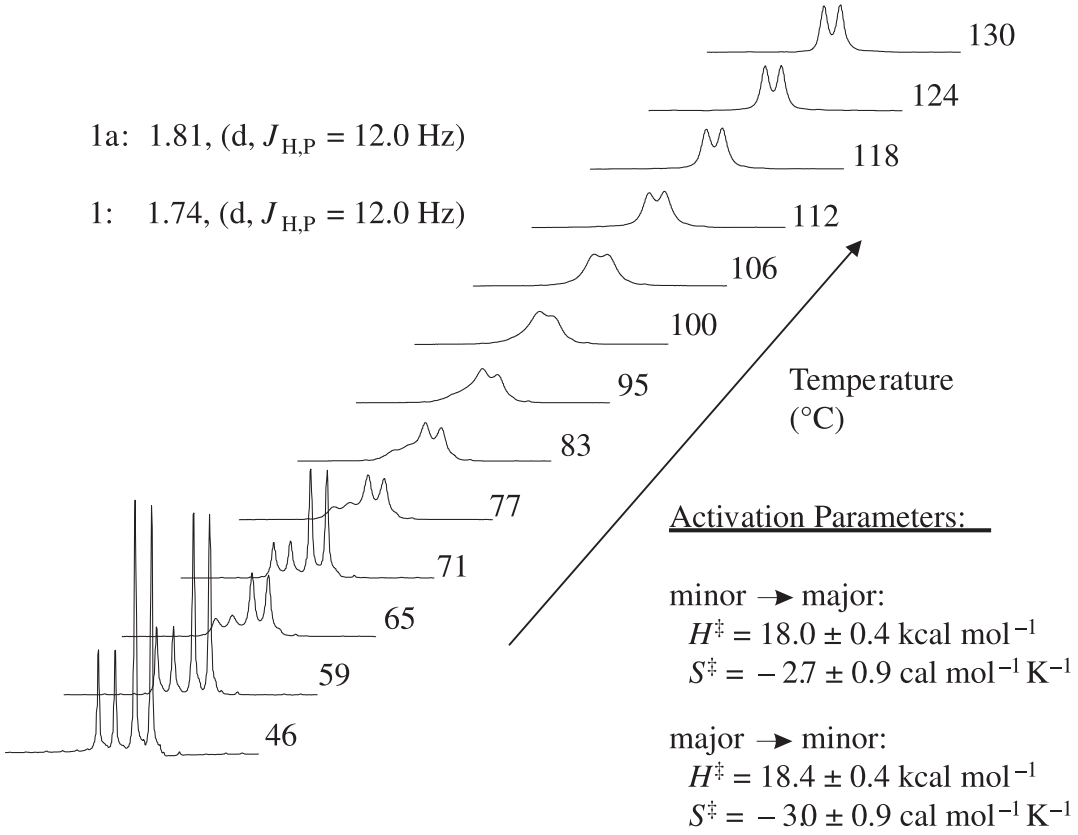
© 2001 NRC Canada

Table 3. Summary of spectroscopic data for $Ru_2(\mu\text{-}Cl)_2Cl_2(CO)_4(PMe_3)_2$ (**1**), $RuCl_2(CO)_2(PMe_3)(O{=}C(CD_3)N(CD_3)_2$ (**1a**), and *cis,cis,trans*-$RuCl_2(CO)_2(PMe)_2$ (**3**).

	1	**1a**	**3**
^{1}H NMR			
$CDCl_3$	1.67 (d, $J_{H,P}$ = 11.6 Hz)	1.70 (d, $J_{H,P}$ = 11.6 Hz)	1.68 (t, $J_{H,P}$ = 4.0 Hz)
DMF-d_7	1.74 (d, $J_{H,P}$ = 12.0 Hz)	1.81 (d, $J_{H,P}$ = 12.0 Hz)	
^{31}P{^{1}H} NMR ($CDCl_3$)	22.83 (s)	20.74 (s)	–6.70 (s)
^{13}C{^{1}H} NMR			
$CDCl_3$	too insoluble in $CDCl_3$	too insoluble in $CDCl_3$	193.27 (t, $J_{C,P}$ = 11.4 Hz, CO)
DMF-d_7	15.73 (dd, $J_{C,P}$ = 36.9, < 2 Hz, CH_3), 198.12 (d, $J_{C,P}$ = 14.8 Hz, CO), 192.93 (d, $J_{C,P}$ = 12.6 Hz, CO)	17.70 (dd, $J_{C,P}$ = 39.1, < 2 Hz, CH_3), 169.2 (t, $J_{C,D}$ = 30.0 Hz, coordinated DMF-d_7), 193.08 (d, $J_{C,P}$ = 16.2 Hz, CO)	14.86 (t, $J_{C,P}$ = 16.6 Hz, CH_3)
IR ν(CO) ($CDCl_3$)	2068, 2010	2068, 2010	2049, 1985

Note: All NMR data is reported in ppm, IR data in cm^{-1}.

Fig. 4. VT ^{1}H NMR spectrum of **1** and **1a** in DMF-d_7.



reach the near quantitative conversions to silylated products typically observed in this reaction with equimolar amounts of silane and alcohol in nonpolar solvents. Even with rigorous drying of the hygroscopic DMA solvent by distillation from barium oxide[4] under argon and subsequent storage over activated 4 Å molecular sieves, some of the silane is consumed by the reaction with adventitious water forming the silanol and siloxane side products Et_3SiOH and $Et_3SiOSiEt_3$. A control experiment in the absence of ethylene glycol also yielded Et_3SiOH and $Et_3SiOSiEt_3$ confirming the presence of water in the solvent. By GC–MS no disilane $Et_3SiSiEt_3$ could be detected in either the control or any of the actual alcoholysis reactions. Both observed side products were identified and authenticated by GC, ^{1}H NMR, and GC–MS, but not quantified. However, qualitatively the amounts of the side products formed appeared to be insufficient to explain the low yields. Even though we found no direct evidence of the solvent itself reacting with the silane,

[4] This drying agent has been suggested by Andrews (23) to be very effective for amide solvents.

© 2001 NRC Canada

Table 4. Comparison of relative catalyst activity and reaction yields (A = $Et_3SiOCH_2CH_2OH$, B = $Et_3SiOCH_2CH_2OSiEt_3$) for the silylation of ethyleneglycol with triethylsilane in DMA.

Catalyst	Et_3SiH–glycol (equiv.)	Rxn. temp. (°C)	Rxn. time (h)[a]	Yield A (%)[b]	Yield B (%)[b]	Total yield (%)[b]
$[IrH_2(PPh_3)(THF)_2]SbF_6$	1	ambient	>300	44	11	55
		45	4.2	42	11	53
	2	ambient	>300	46	40	86
		45	45	29	69	98
$Ru_2(\mu\text{-}Cl)_2Cl_2(CO)_4(PMe_3)_2$	1	ambient	<0.1	54	9	63
		0	1.1	50	8	58
	2	ambient	<0.1	58	32	90
		0	2.3	55	41	96
$RhCl(PPh_3)_3$	1	ambient	50	50	9	59
		45	12.5	44	7	51
	2	ambient	71	61	29	90
		45	14.8	39	61	100
$PdCl_2$	1	ambient	0.9	41	11	52
		0	1.7	46	19	65
	2	ambient	1.2	44	44	88
		0	4.5	22	78	100
$Pd(OAc)_2$	1	ambient	0.2	56	11	67
		0	4.75	46	6	52
	2	ambient	0.8	61	28	89
		0	4.0	61	28	S 89

Note: Reaction conditions in all cases: 2.5 mmol ethylene glycol in 6 mL of DMA, 3 mol% metal.
[a]End point of reaction indicated by the end of hydrogen gas evolution and complete consumption of Et_3SiH as confirmed by GC.
[b]By quantitative GC with respect to ethylene glycol.

i.e., there are no unaccounted peaks in the GC traces of the silylation reactions, we cannot exclude the possibility that the DMA solvent signal observed in the GC contains such reaction products that do not chromatographically separate as a result of hydrogen bond interactions within the solvent.[5] Another possible explanation is that larger amounts of silanol are actually formed in the reactions, but are not detected because of a reaction with the GC injector liner and (or) the column itself.

The selectivity to monosilylation:disilylation with one equivalent of silane ranges from 1:2.4 to 1:7.7. Interestingly, the most active catalyst **1** gives some of the best selectivity at a ratio of 1:6.2 at yields comparable to those of the other catalyst systems. As expected with two equiv of triethylsilane the selectivities increasingly favour disilylation. Good yields of disilylated products are, however, only achieved by $PdCl_2$ and the iridium system.

The temperature range investigated was limited to 0–45°C, as we were only interested in reaction conditions that could ultimately be applied to more complex and very temperature sensitive polyols and sugars. Within this range no clear trend of temperature dependency of yields and selectivities can be extracted from the data. Instead the conditions for the optimization of these two goals are unique to the catalyst used.

Equation [5] shows a possible pathway of an HCl catalyzed silane alcoholysis, which is conceivable for the chloride containing catalysts.

$$[5]\quad \begin{aligned} &L_nM\text{-}Cl + H\text{-}SiR_3 \longrightarrow L_nM\text{-}SiR_3 + HCl \\ &HCl + H\text{-}SiR_3 \longrightarrow Cl\text{-}SiR_3 + H_2(g) \\ &Cl\text{-}SiR_3 + R'OH \longrightarrow R'O\text{-}SiR_3 + HCl \\ &R' = H,\ CH_2CH_2OH \end{aligned}$$

Such a pathway may, in particular, be possible in the DMA solvent, which should be capable of stabilizing highly polar intermediates. The HCl would be generated from the chloride content of the catalysts through the reaction with triethylsilane. In order to exclude this possibility, we carried out a control reaction with concentrated aq HCl added in an amount equimolar to the metal catalysts used, i.e., 3 mol% $H_3O^+Cl^-$ with respect to ethylene glycol. The control reaction asserted that HCl catalyzed processes are irrelevant, as only very small amounts of silane hydrolysis and glycol silylation products were detected even at greatly extended reaction times compared to the metal catalyzed reactions in Table 4.

Discussion

While the selectivities and yields achieved so far are only moderate, the use of DMA as a solvent extends the utility of

[5]GC columns of various polarity did not result in further resolution of the solvent DMA peak. A GC–MS investigation of the solvent peak itself is not practical as it is entirely dominated by the solvent fragmentation pattern.

© 2001 NRC Canada

Table 5. Selected single crystal X-ray crystallography parameters for **1** and **3**.

	1	**3**
Empirical formula	$C_{10}H_{18}Cl_4O_4P_2Ru_2$	$C_8H_{18}Cl_2O_2P_2Ru$
FW	608.12	380.14
Crystal size (mm)	0.40 × 0.40 × 0.20	0.41 × 0.11 × 0.08
Crystal system	Monoclinic	Monoclinic
Space group	$P2_1/c$	$P2_1/c$
a (Å)	7.8533(6)	6.6145(6)
b (Å)	11.0683(9)	8.5160(6)
c (Å)	12.4603(8)	13.6041(18)
β (°)	100.577(7)	102.010(13)
Volume (Å^3)	1064.68(14)	749.53(13)
Unit cell data range 2Θ (°)	19.11–21.02	19.10–24.50
T (K)	294(1)	294(1)
Z	2	2
$\rho_{calcd.}$ (g cm^{-3})	1.897	1.684
X-ray source (graphite monochromator)	Mo Kα; λ = 0.71073 Å	Mo Kα; λ = 0.71073 Å
μ (cm^{-1})	2.079	1.597
Refinement	F^2	F^2
Reflections measured	2442	3404
Independent reflections	2442	3268
Observed reflections	2205	3085
Observation criterion	>2σ (*I*)	>2σ (*I*)
Intensity data range Θ (°)	2.48–27.47	2.84–27.47
R_1[a]	0.0199	0.0172
wR_2[a]	0.0529	0.0408
GoF	1.058	1.094

[a]Definitions of indices: $R_1 = \Sigma(F_o - F_c)/\Sigma(F_o)$; $wR_2 = [\Sigma[w(F_o^2 - F_o^2)^2]/\Sigma[w(F_0^2)^2]]^{1/2}$.

the silane alcoholysis reaction to much more polar substrates than previously accessible. We anticipate that with more complex DMA soluble polyol and carbohydrate substrates bearing multiple hydroxyl of more differentiated reactivity, better overall selectivity towards silylations of a single hydroxyl function can be achieved in future studies. Increased yields of selectively silylated products may also be obtainable through the use of excess silane in order to account for reagent loss due to practically unavoidable traces of water in the hygroscopic solvent.

The similarity between the chemical and physical properties of DMF and DMA suggests that **1** would show very similar behaviour in DMA as observed by NMR results in DMF-d_7. Substitution of the labile solvent ligand in **1a** by either the alcohol or the silane, for the latter possibly in an η^2-fashion analogous to the mechanism proposed for $[IrH_2(PPh_3)(THF)_2]SbF_6$ by Luo and Crabtree (8), could start a sequence of reactions leading to the formation of the true catalyst. The composition and structure of the actual active species, however, remain elusive. An NMR scale reaction of **1** with triethylsilane in DMF-d_7 at ambient temperature resulted in complicated ^{1}H and ^{31}P spectra suggesting the formation of at least five different unidentified complexes in solution. Remarkably no signals were observable in the hydride region of the spectrum at this temperature. Upon subsequent addition of an equimolar amount of ethylene glycol to the NMR tube reaction mixture the normal silylation products were again observed.

Conclusion

The new dimeric complex $Ru_2(\mu\text{-}Cl)_2Cl_2(CO)_4(PMe_3)_2$ (**1**) forms an active silane alcoholysis catalyst in DMA. In contrast to the two other homogeneous catalysts systems investigated, $[IrH_2(PPh_3)(THF)_2]SbF_6$ and $RhCl(PPh_3)_3$, **1** does not suffer from coordinative inhibition in this solvent. The heterogeneous system consisting of Pd(0) generated in situ through reduction of PdX_2 (X = Cl$^-$, OAc$^-$) by the silane also is an active catalyst in DMA. The new complex *cis,cis,trans*-$RuCl_2(CO)_2(PMe)_2$ (**3**) isolated from the same reaction mixture as **1** is an active silane alcoholysis catalyst in nonpolar solvents, but completely inactive in DMA.

Experimental

General

All manipulation were performed under a dry argon atmosphere by standard Schlenk-tube techniques. NMR spectra were recorded on a Bruker Avance 400 MHz instrument and IR spectra on a BOMEM FT-IR. ^{1}H NMR spectra simulations were performed using the MEX program (21). For the VT NMR studies the probe temperatures of the NMR spectrometer were independently calibrated using an internal thermocouple. ^{31}P NMR spectra were recorded using a capillary containing 85% H_3PO_4 as the internal standard. GC analyses were performed on a HP 6850 gas chromatograph equipped with a flame ionization detector and integrator.

© 2001 NRC Canada

Mass spectra were obtained with a HP 5970-IN GC-MS spectrometer at the University of Guelph Laboratory Services Division or on a VARIAN Saturn 2000. GC-MS/MS were obtained in our own laboratory. Elemental analyses were performed by Guelph Chemical Laboratories.

Reagents were purchased from Aldrich, Strem Chemicals, Caledon Laboratories, or Fisher Scientific and used as received. Solvents and ethylene glycol were purified by standard techniques and stored under argon. DMA was dried by vacuum distillation from BaO (23) and subsequently stored over activated 4 Å molecular sieves. $[IrH_2(PPh_3)_2(THF)_2]SbF_6$ was synthesized according to the literature methods (8, 14).

Synthesis of $Ru_2(\mu\text{-}Cl)_2Cl_2(CO)_4(PMe_3)_2$ and *cis,cis,trans*-$RuCl_2(CO)_2(PMe_3)_2$

With the exception of the recrystallization procedure, this method is essentially the same as the previously published procedure; carbon monoxide was passed through a boiling solution of ruthenium trichloride dihydrate (0.87 g) in 2-methoxyethanol (25 mL) for 3.5 h. Trimethylphosphine (0.54 g) was added to the hot solution and carbon monoxide was passed through the boiling solution for a further 19 h. The solution had become brownish yellow. The solvent was evaporated under reduced pressure. The resulting greenish-white solid (yield 73%) was recrystallized from CH_2Cl_2–Et_2O giving dimeric species $Ru_2(\mu\text{-}Cl)_2Cl_2(CO)_4(PMe_3)_2Cl_2$ in 38% yield with respect to ruthenium. Subsequent evaporation of the remaining mother liquor and recrystallization of the remaining solid residue from EtOH–water gives the complex *cis,cis,trans*-$RuCl_2(CO)_2(PMe_3)_2$ in 34% yield. Total yield in ruthenium is 34 + 38 = 72%.

*$Ru_2(\mu\text{-}Cl)_2Cl_2(CO)_4(PMe_3)_2$ (**1**)*

For spectroscopic data, see Table 3. Anal. calcd. for $C_{10}H_{18}Cl_4O_4P_2Ru_2$: C 19.74, H 2.98; found: C 19.93, H 3.03.

*$RuCl_2(CO)_2(PMe_3)(O{=}C(CD_3)N(CD_3)_2)$ (**1a**)*

For spectroscopic data see Table 3.

cis,cis,trans-*$RuCl_2(CO)_2(PMe_3)_2$ (**3**)*

For spectroscopic data see Table 3. Anal. calcd. for $C_8H_{18}Cl_2O_2P_2Ru$: C 25.26, H 4.77; found: C 25.48, H 5.21.

X-ray crystal structure determinations

Colourless X-ray quality crystalline samples of both complexes (**1** and **3**) were obtained by slow crystal growth from saturated solutions of the respective solvent–cosolvent mixture at low temperature. Intensity data were collected on a Nonius CAD4 diffractometer. General data collection parameters are listed in Table 5.[6] Accurate cell dimension and crystal orientation matrices were obtained by a least-squares fit of the setting angles of 25 reflections in the ranges indicated in Table 5. Data were acquired using the $\omega - 2\Theta$ method over the ranges indicated in Table 5 and are corrected for Lorentz-polarization and absorption effects. The intensities of 3 standard reflections were measured every 120 reflections and showed 0.8% decay for **1** and no decay for **3**. For both structures the position of the ruthenium atoms were determined by the Patterson method and other nonhydrogen atoms were located by successive difference Fourier syntheses. The structures were refined anisotropically by full-matrix least-squares on F^2. The weighting scheme was $w = 1/[\sigma^2(F_o^2) + (aP)^2 + bP]$ where $P = (F_o^2 + 2F_c^2)/3$. Hydrogen atoms were clearly visible in difference maps and positioned on geometric grounds (C—H 0.96 Å). All calculations were performed using SHELX 97 (24) and PLATON (25) on a Pentium III computer running the LINUX 2.1 operating system.

O-silylation of ethylene glycol

The *O*-silylation reactions of ethylene glycol were conducted by three methods, each of which was found to be most practical depending on the catalyst system used.

Method 1

For catalyst $[IrH_2(PPh_3)_2(THF)_2]SbF_6$; a DMA (3 mL) solution of the Ir catalyst (0.075 mmol = 3 mol% in metal with respect to ethylene glycol) and ethylene glycol (2.5 mmol, 155 mg, 140 μL) was prepared in a three-neck round-bottomed flask fitted with a pressure-equilibrating addition funnel and an Schlenk stopcock. The apparatus was connected to a gas bubbler. A second DMA (3 mL) solution of Et_3SiH (1 eq. = 2.5 mmol, 291 mg, 399 μL or 2 eq. = 5.0 mmol, 582 mg, 798 μL) was prepared in the addition funnel. The silane solution was quickly added with stirring from the addition funnel to the three-neck round-bottomed flask containing the solution of the catalyst and ethylene glycol. The rate of reaction was qualitatively followed by monitoring the speed of the evolved hydrogen with time until hydrogen evolution had stopped indicating the end point of the reaction.

Method 2

For catalysts $RhCl(PPh_3)_3$, $Ru_2(\mu\text{-}Cl)_2Cl_2(CO)_4(PMe_3)_2$, *cis,cis,trans*-$RuCl_2(CO)_2(PMe_3)_2$, and $Co_2(CO)_8$; a DMA, (6 mL) solution of Et_3SiH (1 eq. = 2.5 mmol, 291 mg, 399 μL or 2 eq. = 5.0 mmol, 582 mg, 798 μL) and ethylene glycol (2.5 mmol, 155 mg, 140 μL) was prepared in the addition funnel. The mixed solution was added quickly from the addition funnel to the Schlenk flask containing catalyst (0.075 mmol or 0.0375 mmol for dimer **1** = 3 mol% of metal with respect to ethylene glycol). The rate of reaction was qualitatively followed by monitoring the speed of the evolved hydrogen with time until hydrogen evolution had stopped indicating the end point of the reaction.

Method 3

For catalysts $PdCl_2$ and $Pd(OAc)_2$; a DMA (6 mL) solution of Et_3SiH (1 eq. = 2.5 mmol, 291 mg, 399 μL or 2 eq. = 5.0 mmol, 582 mg, 798 μL) was prepared in an addition fun-

[6] CIF files containing all relevant data for the crystal structure determinations of **1** and **3**, as well as original kinetic data for Fig. 4, have been deposited with CISTI. The supplementary material may be purchased from the Depository of Unpublished Data, Document Delivery, CISTI, National Research Council Canada, Ottawa, ON K1A 0S2, Canada. For information on obtaining material electronically go to http://www.nrc.ca/cisti/irm/unpub_e.shtml. Crystallographic information has also been deposited with the Cambridge Crystallographic Data Centre. Copies of the data can be obtained, free of charge, on application to the Director, CCDC, 12 Union Road, Cambridge CB2 1EZ, U.K. (fax: 44-1223-336033 or e-mail: deposit@ccdc.cam.ac.uk).

© 2001 NRC Canada

nel. The silane solution was added quickly from the addition funnel to a three-neck round-bottomed flask containing the catalyst (0.075 mmol = 3 mol% of metal with respect to ethylene glycol). The system was allowed to equilibrate for 3 min. Ethylene glycol (2.5 mmol, 155 mg, 140 μL) was added via a syringe into the mixture. The rate of reaction was qualitatively followed by monitoring the speed of the evolved hydrogen with time until hydrogen evolution had stopped indicating the end point of the reaction.

Product analysis

The reaction products $Et_3SiOCH_2CH_2OH$, $Et_3SiOCH_2CH_2OSiEt_3$, as well as the side products Et_3SiOH and $Et_3SiOSiEt_3$, were authenticated by ^1H and ^{13}C NMR, and by matching their GC–MS spectra to their known fragmentation patterns available from the NIST compound database supplied with the MS spectrometer software. Quantitative analysis of the reaction mixtures was performed through multi-level calibration of the GC for ethylene glycol, triethylsilane, $Et_3SiOCH_2CH_2OH$, and $Et_3SiOCH_2CH_2OSiEt_3$ over the entire relevant concentration range using authentic compound samples and NMP as an internal standard.

$Et_3SiOCH_2CH_2OH$: ^1H NMR ($CDCl_3$, 298K) δ: 3.65 (m, 4H, $SiOCH_2CH_2OH$), 2.10 (br s, 1H, OH), 0.93 (t, $J_{H,H}$ = 8 Hz, 9H, $Si(CH_2CH_3)_3$), 0.59 (q, $J_{H,H}$ = 8 Hz, 6H, $Si(CH_2CH_3)_3$). ^{13}C NMR ($CDCl_3$, 298K) δ: 63.69, 63.65 (2 s, $SiOCH_2CH_2OH$), 6.67 (s, $Si(CH_2CH_3)_3$), 4.29 (s, $Si(CH_2CH_3)_3$).

$Et_3SiOCH_2CH_2OSiEt_3$: ^1H NMR($CDCl_3$, 298K) δ: 3.64 (s, 4H, $SiOCH_2CH_2OSi$), 0.92 (t, $J_{H,H}$ = 8 Hz, 9H, $Si(CH_2CH_3)_3$), 0.58 (q, $J_{H,H}$ = 8 Hz, 6H, $Si(CH_2CH_3)_3$). ^{13}C NMR ($CDCl_3$, 298K) δ: 64.18 (s, $SiOCH_2CH_2OSi$), 6.37 (s, $Si(CH_2CH_3)_3$), 4.34 (s, $Si(CH_2CH_3)_3$).

Acknowledgments

The authors thank Dr. Alex Bain for help with the MEX simulations and the Natural Sciences and Engineering Research Council of Canada (NSERC), the Canadian Foundation for Innovation (CFI), the Ontario Innovation Trust Fund (OIT), VARIAN Inc., as well as the University of Guelph, for funding.

References

1. M.P. Doyle, K.G. Higgins, V. Bagheri, R.J. Pieters, P.J. Lewis, and M.M Pearson. J. Org. Chem. **55**, 6082 (1990).
2. D.H. Barton and M.J. Kelly. Tetrahedron Lett. **33**, 5041 (1992).
3. T.C. Bedard and J.Y. Corey. J. Organomet. Chem. **428**, 315 (1992).
4. B.T. Gregg and A.R. Cutler. Organometallics, **13**, 1039 (1994).
5. M.J. Burn and R.G. Bergman. J. Organomet. Chem. **472**, 43 (1994).
6. C. Lorenz and U. Schubert. Chem. Ber. **128**, 1267 (1995).
7. S. Chang, E. Scharrer, and M. Brookhart. J. Mol. Catal. A: Chem. **130**, 107 (1998).
8. X.-L. Luo and R.H. Crabtree. J. Am. Chem. Soc. **111**, 2527 (1989).
9. U. Oehmichen and H. Singer. J. Organomet. Chem. **243**, 199 (1983).
10. A.J. Chalk. J. Chem. Soc. Chem. Commun. 847 (1970).
11. I. Ojima, T. Kogure, M. Nihonyanagi, H. Kono, and S. Inaba. Chem. Lett. 501, (1973).
12. R.J. Corriu and J.J.E. Moreau. J. Chem. Soc. Chem. Commun. 38, (1973).
13. R.J.P. Corriu and J.J.E. Moreau. J. Organomet. Chem. **114**, 135, (1976).
14. S.N. Blackburn, R.N. Haszeldien, and R.V. Parish. J. Organomet. Chem. **192**, 329 (1980).
15. L.H. Sommer and J.E. Lyons. J. Am. Chem. Soc. **91**, 7061 (1969).
16. J. M. Blackwell, K.L. Foster, V.H. Beck, and W.E. Piers. J. Org. Chem. **64**, 4887 (1999).
17. H. Singer, E. Hademer, U. Oehmichen, and P. Dixneuf. J. Organomet. Chem. **178**, C13 (1979).
18. C.F.J. Barnard, J.A. Daniels, J. Jeffrey, and R.J. Mawby. J. Chem. Soc. Dalton Trans. 953 (1976).
19. C.K. Johnson. Technical Report ORNL-5138. ORNL, 1976.
20. A.G. Orpen, L. Bramer, F.H. Allen, O. Kennard, D.G. Watson, and R. Taylor. J. Chem. Soc. Dalton Trans. S1 (1989).
21. A.D. Bain and G.J. Duns. J. Magn. Reson. Ser. A, **112**, 258 (1995).
22. R.H. Crabtree, P.C. Demou, D. Eden, J.M. Mihelcic, C.A. Parnell, J.M. Quirk, and G.E. Morris. J. Am. Chem. Soc. **104**, 6994 (1982).
23. M.A. Andrews. Organometallics, **8**, 2703 (1989).
24. G.M. Sheldrick. SHELXL 97. Program for crystal structure determination. Universität Göttingen, Göttingen. 1997.
25. A.L. Spek. PLATON. Program package for crystal structure analysis and display. University of Utrecht, Utrecht. 1999.

© 2001 NRC Canada

The life, death, and ROMP activity of ruthenium complexes containing the basic, chelating diphosphine bis(dicyclohexyl)-1,4-phosphinobutane

Dino Amoroso, Glenn P.A. Yap, and Deryn E. Fogg

Abstract: Reaction of $RuCl_2(PPh_3)_3$ with bis(dicyclohexyl)-1,4-phosphinobutane (dcypb) under N_2 affords access to a formerly elusive family of dcypb complexes based on the $RuCl_2(PP)$ core. Under Ar or vacuum atmosphere, decomposition occurs via Ru-promoted dehydrogenation of the dcypb ligand. While the N_2-stabilized species $[RuCl_2(dcypb)]_2(N_2)$ (**4a**) is easily handled under N_2 in nonchlorinated solvents, reaction with chlorinated solvents rapidly yields paramagnetic $Ru_2Cl_5(dcypb)_2$ (**5**). The N_2 ligand within **4a** is readily displaced under H_2 or CO atmosphere, yielding $Ru_2Cl_4(dcypb)_2(H_2)$ (**6**) or $RuCl_2(dcypb)(CO)_2$, the latter as a mixture of *ccc*-(**7**) and *tcc*-(**8**) isomers. Benzylidene derivative $RuCl_2(dcypb)(CHPh)$ (**1a**), prepared in situ by reaction of **4a** with $PhCHN_2$, proves exceptionally active in ring-opening metathesis polymerization (ROMP) of norbornene. The X-ray crystal structure of **5** is reported: triclinic, a = 13.390(2), b = 15.726(2), c = 19.524(2) Å, α = 77.325(2), β = 70.964(2), γ = 73.478(2)°, with space group $P\bar{1}$ and Z = 2.

Key words: ruthenium, alkylphosphine, dehydrogenation, carbene, metathesis, crystal structure.

Résumé : La réaction du $RuCl_2(PPh_3)_3$ avec le bis(dicyclohexyl)-1,4-phosphinobutane (dcypb), sous atmosphère d'azote, permet d'accéder à la famille antérieurement élusive de complexes de dcypb comportant un noyau $RuCl_2(PP)$. Sous atmosphère d'argon ou sous vide, il se produit une décomposition qui se produit par le biais d'une déshydrogénation du ligand dcypb provoquée par le Ru. Alors que l'on peut facilement manipuler l'espèce stabilisée par le N_2 $[RuCl_2(dcypb)]_2(N_2)$, **4a**, sous atmosphère d'azote, dans des solvants non chlorés, la réaction dans des solvants chlorés conduit à la formation de l'espèce paramagnétique $Ru_2Cl_5(dcypb)_2$, **5**. On peut facilement déplacer le ligand N_2 du composé **4a** sous atmosphère de H_2 ou de CO avec formation de $Ru_2Cl_4(dcypb)_2(H_2)$, **6**, ou de $RuCl_2(dcypb)(CO)_2$ qui existe sous la forme de mélange d'isomères *ccc*-(**7**) et *tcc*-(**8**). Le dérivé benzylidène, $RuCl_2(dcypb)(CHPh)$, **1a**, préparé in situ par réaction du composé **4a** avec $PhCHN_2$, est exceptionnellement actif dans la polymérisation par ouverture de cycle et métathèse du norbornène. On a déterminé la structure cristalline par diffraction des rayons X du composé **5**: triclinique, a = 13,390(2), b = 15,726(2) et c = 19,524(2)Å, α = 77,325(2), β = 70,964(2) et γ = 73,478(2)°, groupe d'espèce $P\bar{1}$ et Z = 2.

Mots clés : ruthénium, alkylphosphine, déshydrogénation, carbène, métathèse, structure cristalline.

[Traduit par la Rédaction]

Introduction

Enhanced catalytic activity is associated with use of electron-rich phosphine ligands in a range of reactions promoted by late transition metal complexes, including metathesis (1, 2) and hydrogenation (3, 4) catalysis. Complexes of chelating alkyldiphosphines remain little explored in such chemistry, relative to the ubiquitous aryldiphosphine derivatives. We recently described the first Ru–diphosphine catalysts to exhibit high activity in ring-opening metathesis polymerization (ROMP) without ligand loss (2). Benzylidene catalysts $RuCl_2(PP)(CHPh)$ (PP = $R_2P(CH_2)_4PR_2$; R = Cy (dcypb, 1,4-bis(dicyclohexylphosphino)butane) (**1a**), R = Ph (dppb, 1,4-bis(diphenylphosphino)butane) (**1b**)) were generated in situ by reaction of mixed-phosphine species $RuCl_2(PP)(PPh_3)$ (**2**) or dimeric $[RuCl_2(dppb)]_2$ with phenyldiazomethane. The inhibiting effect of free PPh_3 was explored within the $RuCl_2(dppb)(PPh_3)$–$[RuCl_2(dppb)]_2$ pair, but no route to the corresponding $[RuCl_2(dcypb)]_2$ precursor existed. Here we report a new route to PPh_3-free Ru complexes containing the chelating, basic diphosphine ligand dcypb, with insights into decomposition pathways that have until now hindered the broader deployment of such systems. The ROMP activity of the PPh_3-free system is described.

Received September 5, 2000. Published on the NRC Research Press Web site at http://canjchem.nrc.ca on July 11, 2001.

Dedicated to Professor Brian R. James on the occasion of his retirement, in honour of his outstanding contributions to catalysis and chemistry.

D. Amoroso, G.P.A. Yap, and D.E. Fogg.[1] Center for Catalysis Innovation and Research, Department of Chemistry, University of Ottawa, Ottawa, ON K1N 6N5, Canada.

[1]Corresponding author (telephone: (613) 562-5800 ext. 6057; fax: (613) 562-5170; e-mail: dfogg@science.uottawa.ca).

Experimental

Unless otherwise stated, all operations were performed under N_2 using standard Schlenk or drybox techniques. Dry, oxygen-free solvents were obtained using an Anhydrous Engineering solvent purification system, and stored over Linde 4 Å molecular sieves. $CDCl_3$ and C_6D_6 were dried over activated sieves (Linde 4 Å) and degassed by consecutive

 DOI: 10.1139/cjc-79-5/6-958 © 2001 NRC Canada

freeze-pump-thaw cycles. Phenyldiazomethane (5), dcypb (6), $RuCl_2(PPh_3)_3$ (**3**) (7), and *t*-$RuCl_2(dppe)_2$ (8) were prepared according to literature procedures. $RuCl_3 \cdot 3H_2O$ was purchased from Strem Chemicals. Norbornene was purchased from Aldrich and distilled from sodium under N_2. Hydrogen (Praxair, UHP grade) was passed through a Deoxo cartridge and Drierite column in series; CO (Praxair) was used as received.

^{31}P and ^{13}C NMR spectra were recorded on a Varian XL-300 spectrometer, ^1H NMR spectra on a Varian Gemini 200 or Bruker AMX-500 spectrometer. Peaks are reported in ppm, relative to 85% aq. H_3PO_4 (^{31}P) or the deuterated solvent (^1H, ^{13}C). Solid state NMR data were recorded on a Bruker ASX-200 MHz spectrometer, infrared spectra on a Bomem MB100 IR spectrometer. Microanalytical data were obtained using a PerkinElmer Series II CHNS/O instrument. Gel permeation chromatography (GPC) data were obtained with CH_2Cl_2 as eluent (flow rate 1.0 mL min^{-1}; samples 1–2 mg mL^{-1}) using a Wyatt DAWN light-scattering instrument equipped with Optilab DSP refractometer, HPLC system with a Waters model 515 pump, Rheodyne model 7725i injector with a 200 μL injection loop, and Waters Styragel HR3 column.

Preparation of $Ru_2Cl_4(dcypb)_2(N_2)$ (4a)

A green solution of **3** (500 mg, 0.52 mmol) and dcypb (259 mg, 0.57 mmol) in C_6H_6 (5 mL) was stirred at 21°C under N_2. Orange **4a** began to precipitate from solution within 1 h. The orange suspension was diluted with hexanes after 18 h and the product was filtered off, washed with hexanes (3 × 10 mL), and dried under a steady flow of N_2 for 24 h. Yield: 0.303 g (91%). FAB-MS (*m*/*z*): 1245 ([M – N_2]$^+$). IR (Nujol) (cm^{-1}): 2124 (N_2) (m). ^1H NMR ($CDCl_3$) δ: 0.7–3.1 (br, C*H*$_2$, Cy of dcypb). $^{31}P\{^1H\}$ NMR ($CDCl_3$) δ: 57.5 (d, $^2J_{P,P}$ = 39 Hz), 45.0 (d, $^2J_{P,P}$ = 27 Hz), 44.6 (d, $^2J_{P,P}$ = 39 Hz), 42.3 (d, $^2J_{P,P}$ = 27 Hz); (C_6D_6) δ: 60.1 (d, $^2J_{P,P}$ = 39 Hz), 49.1 (d, $^2J_{P,P}$ = 26 Hz), 45.3 (d, $^2J_{P,P}$ = 39 Hz), 37.4 (d, $^2J_{P,P}$ = 26 Hz). Solid-state $^{31}P\{^1H\}$ CP-MAS NMR (80.9 MHz) δ: 45–57 (br, unresolved), 43.6 (br), 41.2 (br). Anal. calcd. for $C_{56}H_{104}Cl_4N_2P_4Ru_2$: C 52.81, H 8.25, N 2.20; found: C 52.90, H 8.19, N 1.90.

Preparation of $Ru_2Cl_5(dcypb)_2$ (5)

Complex **4a** (40 mg, 0.04 mmol) was dissolved in $CDCl_3$ (0.5 mL) and the solution was monitored by $^{31}P\{^1H\}$ NMR. Resolution degraded perceptibly over ~30 min, and a broad singlet emerged at 50 ppm. On further reaction, S/N values decreased, and many new peaks could be discerned (46–63, 15–32 ppm). Slow evaporation deposited red crystals of **5**.

Decomposition of 4a under vacuum

(*i*) NMR-scale. A solution of **4a** (3.0 mg, 4.7 μmol Ru) in C_6D_6, with *t*-$RuCl_2(dppe)_2$ (2.3 mg, 2.35 μmol) as an internal standard, was freeze-pump-thaw degassed in a round-bottom Schlenk flask. $^{31}P\{^1H\}$ NMR spectra were measured after every second cycle of degassing. No NMR signals were discerned after six degassing cycles, though gas evolution was sustained over three further cycles. (*ii*) Large-scale. A suspension of **4a** (20 mg, 0.016 mmol Ru_2) in benzene (10 mL) was freeze-pump-thaw degassed until no signals were evident by NMR. Concentration and addition of cold hexanes afforded a dark grey-green solid, which was filtered off, washed with cold hexanes, and dried under a flow of Ar. Yield: 16 mg. IR (Nujol) (cm^{-1}): 1944 (Ru-H) (m-w), 1629 (C=C) (m-w). (*iii*) Prolonged exposure of solid **4a** to vacuum at 50°C resulted in a mixture of diamagnetic products (multiple ^{31}P NMR signals in the region from 75 to –15 ppm).

NMR-scale preparation of $Ru_2Cl_4(dcypb)_2(H_2)$ (6)

Stirring a suspension of **4a** (4 mg, 3 μmol Ru_2) in C_6D_6 (0.5 mL) under H_2 at room temperature afforded a homogeneous orange solution within 15 min. No starting material was spectroscopically observable after 30 min. ^1H NMR (C_6D_6) δ: 0.6–3.0 (br, C*H*$_2$, Cy of dcypb), –11.8 (br s, *H*$_2$). $^{31}P\{^1H\}$ NMR (C_6D_6) δ: 65.1 (d, $^2J_{P,P}$ = 25 Hz), 59.2 (d, $^2J_{P,P}$ = 40 Hz), 45.9 (d, $^2J_{P,P}$ = 25 Hz), 43.9 (d, $^2J_{P,P}$ = 40 Hz). Hydride T_1 (min) = 26 msec (300 K, 500 MHz).

Preparation of $RuCl_2(dcypb)(CO)_2$ (ccc-(7), tcc-(8))

A suspension of **4a** (27 mg, 39 μmol Ru_2) in THF (5 mL) was stirred under CO for 24 h, affording a clear yellow solution. The solution was concentrated and hexanes added to coprecipitate **7** and **8** as a yellow powder (1:4). Yield: 23 mg (88%). IR (Nujol) (cm^{-1}): 2052 (CO) (s, **7**), 2038 (s, **8**), 1976 (s, **8**), 1962 (s, **7**). ^1H NMR (C_6D_6) δ: 0.8–2.4 (br, C*H*$_2$, Cy of dcypb). $^{13}C\{^1H\}$ NMR (C_6D_6) δ: 198.7 (t, $^2J_{P,P(cis)}$ = 12 Hz, **7**), 193.5 (dd, $^2J_{P,P(trans)}$ = 113 Hz, $^2J_{P,P(cis)}$ = 11 Hz, **7**), 193.8 (dd, $^2J_{P,P(trans)}$ = 109 Hz, $^2J_{P,P(cis)}$ = 23 Hz, **8**). $^{31}P\{^1H\}$ NMR (C_6D_6) δ: 39.4 (d, $^2J_{P,P}$ = 22 Hz, **7**), 17.1 (d, $^2J_{P,P}$ = 22 Hz, **7**), 13.8 (s, **8**). Anal. calcd. for $C_{30}H_{52}Cl_2O_2P_2Ru$: C 53.09, H 7.72; found: C 53.39, H 7.93.

In situ polymerization of norbornene by 1a

Optimization of the procedure has been described (2). Blank polymerization experiments carried out without added Ru catalyst showed no ROMP over 24 h. In a representative catalytic procedure, $PhCHN_2$ (1.1 μL, 10.6 μmol) was added to an orange suspension of **4a** (6.6 mg, 10.6 μmol) in C_6D_6 (2 mL). Vigorous bubbling ensued, and all of the solids dissolved, forming a deep orange solution, which was immediately added to a stirred solution of norbornene (200 mg, 2.1 mmol) in $CDCl_3$ or C_6D_6 (5 mL). The progress of the reaction was monitored by removing aliquots for NMR analysis. (*i*) ROMP via **4a** + 2 $PhCHN_2$ in $CDCl_3$–C_6D_6: M_n 2.4 × 10^6, M_w/M_n = 1.4; (*ii*) via **2a** (prepared in situ by addition of 2 equiv PPh_3 to **4a**) + $PhCHN_2$ in $CDCl_3$–C_6D_6: M_n 2.4 × 10^6, M_w/M_n = 1.2; (*iii*) via **4a** + 2 $PhCHN_2$ in neat benzene: bimodal, M_n 1.9 × 10^6, M_w/M_n = 2.4; M_n 20 000, M_w/M_n = 3.8.

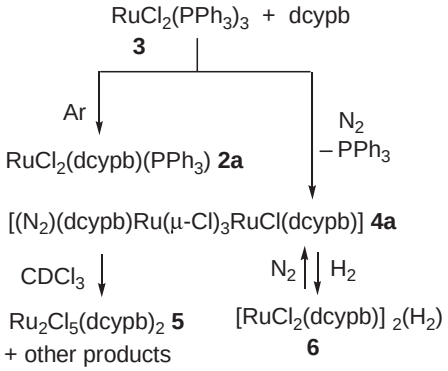
X-ray crystallographic analysis of 5

Crystal and data collection parameters for **5** are provided in Table 1.[2] Suitable crystals were selected, mounted on thin glass fibres using viscous oil, and cooled to the data collection temperature. Data were collected on a Bruker AX SMART 1k CCD diffractometer using 0.3° ω-scans at 0, 90,

[2] Copies of materials on deposit may be purchased from The Depository of Unpublished Data, Document Delivery, CISTI, National Research Council of Canada, Ottawa, ON K1A OS2, Canada. Tables of hydrogen atom coordinates and bond lengths and angles have also been deposited with the Cambridge Crystallographic Database, and can be obtained on request from the Director, Cambridge Crystallographic Data Centre, University Chemical Laboratory, 12 Union Road, Cambridge CB2 1EZ, U.K.

© 2001 NRC Canada

Scheme 1.

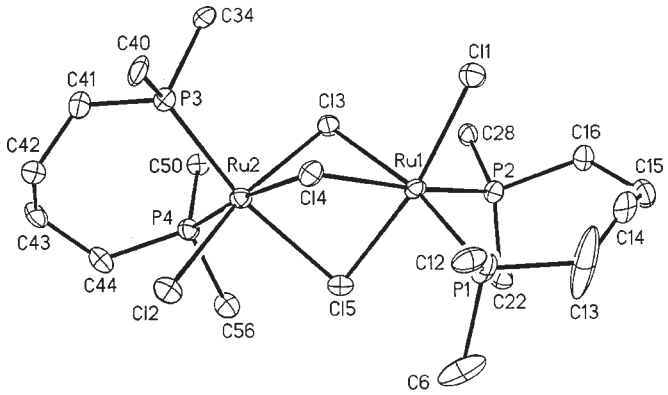


and 180° in ϕ. Unit-cell parameters were determined from 60 data frames collected at different sections of the Ewald sphere. Semi-empirical absorption corrections based on equivalent reflections were applied (9). No symmetry higher than triclinic was evident from the diffraction data. Solution in $P\bar{1}$ yielded chemically reasonable and computationally stable results of refinement. The structure was solved by direct methods, completed with difference Fourier syntheses and refined with full-matrix least-squares procedures based on F^2. A carbon atom, C(14), in one of the ligands was located conformationally disordered in two positions with roughly 50/50 site occupation distribution. The large anisotropic displacement parameters on C(13) suggest similar disorder. Attempts to model this disorder were unsuccessful, however, owing to insufficient resolution between the contributing atomic positions. A molecule of benzene and two molecules of chloroform were located in the asymmetric unit. The benzene molecule of crystallization was constrained as flat hexagon. All nonhydrogen atoms were refined with anisotropic displacement parameters. All hydrogen atoms were treated as idealized contributions. All scattering factors and anomalous dispersion factors are contained in the SHEXTL 5.10 program library (10).

Results and discussion

Treatment of **3** with dcypb in benzene under Ar yields the mixed-phosphine complex **2a** (11), which differs from its dppb analogue **2b** in undergoing no dimerization (with loss of PPh_3) in solution. The very high solubility of **2a** has so far prevented its isolation. In strong contrast is the reaction of **3** with dcypb under N_2 atmosphere, which affords a high-yield route to sparingly soluble $[(N_2)Ru(dcypb)(\mu\text{-}Cl)_3RuCl(dcypb)]$ (**4a**) (Scheme 1). This net displacement of triphenylphosphine ligand by N_2 has no precedent in the corresponding aryldiphosphine chemistry. The identity of **4a** is confirmed by NMR and IR spectroscopy and microanalysis. ^{31}P NMR analysis reveals four doublets for the inequivalent phosphine groups within **4a**, in a pattern similar to that earlier reported (12) for dppb analogue **4b**. The ^1H NMR spectrum of **4a** is less informative, consisting only of a series of overlapping multiplets between 0.7–3.1 ppm arising from the cyclohexyl protons and the methylene protons of the dcypb backbone. A strong IR band for ν(N≡N) is evident at 2124 cm^{-1}.

Fig. 1. ORTEP drawing of $Ru_2Cl_5(dcypb)_2$ (**5**). Thermal ellipsoids depicted at 30% probability level; cyclohexyl rings, hydrogen atoms, and solvate molecules omitted for clarity. A detailed structural representation is included in the Supplementary Material.



The solubility of **4a** is slightly improved in halogenated solvents such as CH_2Cl_2 or $CDCl_3$, but decomposition in these solvents yields the mixed-valence dimer $Ru_2Cl_5(dcypb)_2$ **5**.[3] James and co-workers (12, 13) have reported extensively on the synthesis, reactivity, and catalytic chemistry of such species, obtained via reaction of chelating diphosphines with $RuCl_3(PR_3)_2$ (R = Ph, *p*-tolyl). Attempts to prepare clean **5** on large scale by the reaction of **4a** with $CDCl_3$ or ethereal HCl, resulted in product mixtures, as judged by in situ ^{31}P NMR analysis prior to complete loss of the diamagnetic signals. Slow evaporation of $CDCl_3$ solutions under N_2 permitted isolation of crystals suitable for X-ray analysis. The molecular structure of **5** is shown in Fig. 1; crystal data and selected structural parameters appear in Tables 1 and 2, respectively.

Complex **5** adopts a triply chloride-bridged diruthenium structure, in which the coordination geometry at each metal center is distorted octahedral. The structure is unsymmetrical, with one of the octahedra being rotated by 120° about the Ru–Ru vector. A similar structure was earlier reported for $Ru_2Cl_5(P(n\text{-}Bu)_3)_4$ (14), whereas the only previous crystal structure of a chelating diphosphine derivative, $Ru_2Cl_5(chiraphos)_2$, exhibits a symmetrical ligand arrangement (13). Ruthenium—phosphorus and —chloride distances fall within the ranges reported, as do angles within the Ru-P-Cl skeleton. Chloride atoms *trans* to phosphorus display distinctly longer Ru—Cl bond distances (av. 2.49 Å) compared to those *trans* to Cl (av. 2.38 Å), as expected from the stronger *trans* influence of phosphine. The average bridging angle in **5** (83.7°) is nearly 15° larger than the ideal value of 70.5° for two regular face-sharing octahedra (14), indicating that the Ru centers are further apart than expected for a regular cofacial bioctahedron. The Ru—Ru distance of 3.278 Å is considerably longer than the upper limit associated with the presence of a metal–metal bond (2.95 Å) (13). As with the chiraphos and the $P(n\text{-}Bu)_3$ complexes, the crystallographic data do not permit assignment of formal oxidation states to the ruthenium atoms.

[3] Note added in proof: complex **5** was originally prepared via this route, and partially transformed into **6** by treatment with H_2 in DMA or CH_2Cl_2. Private communication from B.R. James, based on data contained in ref. 6.

© 2001 NRC Canada

Table 1. Crystal data and structure refinement for **5**.

Empirical formula	$C_{64}H_{112}Cl_{11}P_4Ru_2$
FW	1597.51
T (K)	203(2)
Wavelength (Å)	0.71073
Crystal system, space group	Triclinic, $P\bar{1}$
Unit cell dimensions	
a, b, c (Å)	13.390(2), 15.726(2), 19.524(2)
α, β, γ (°)	77.325(2), 70.964(2), 73.478(2)
Volume (Å^3)	3689.3(8)
Z, density$_{calcd.}$ (mg m^{-3})	2, 1.438
Absorption coefficient (mm^{-1})	0.932
F(000)	1662
Crystal size (mm)	0.10 × 0.10 × 0.03
Theta range for data collection (°)	1.11–20.81
Limiting indices	$-12 \le h \le 13$, $-15 \le k \le 15$, $0 \le l \le 19$
Reflections collected/unique ($R_{(int)}$ = 0.1237)	29133/7712
Completeness to θ = 28.83	99.7
Absorption correction	Semi-empirical from equivalents
Max. and min. transmission	0.928077 and 0.637019
Refinement method on F^2	Full-matrix least-squares
Data/restraints/parameters	7712/0/722
GoF on F^2	1.025
R^a	0.0533
$R_w{}^b$	0.1009

[a] $R = \Sigma||F_o| - |F_c||/\Sigma|F_o|$.
[b] $R_w = [\Sigma w\delta^2/\Sigma wF_o{}^2]^{1/2}$.

Table 2. Selected bond lengths (Å) and angles (°) for (**5**).

Bond lengths (Å)			
Ru(1)—P(1)	2.309(3)	Ru(2)—P(3)	2.323(2)
Ru(1)—P(2)	2.325(3)	Ru(2)—P(4)	2.348(3)
Ru(1)—Cl(5)	2.395(2)	Ru(2)—Cl(2)	2.360(3)
Ru(1)—Cl(1)	2.387(2)	Ru(2)—Cl(3)	2.373(2)
Ru(1)—Cl(3)	2.495(2)	Ru(2)—Cl(4)	2.466(2)
Ru(1)—Cl(4)	2.504(2)	Ru(2)—Cl(5)	2.505(2)
Bond angles (°)			
P(1)-Ru(1)-P(2)	95.14(9)	P(3)-Ru(2)-P(4)	93.75(9)
Cl(5)-Ru(1)-Cl(1)	168.81(8)	Cl(2)-Ru(2)-Cl(3)	168.58(9)
P(1)-Ru(1)-Cl(3)	169.32(9)	P(3)-Ru(2)-Cl(5)	168.60(9)
P(2)-Ru(1)-Cl(4)	172.19(9)	P(4)-Ru(2)-Cl(4)	173.97(9)

In aromatic solvents, **4a** is stable for weeks in solution under N_2. In contrast with the dppb systems, which exist in equilibrium with the "naked" dimers $[RuCl_2(PP)]_2$ **9** under N_2 (eq. [1], (12)), no peaks for $[RuCl_2(dcypb)]_2$ are observed.

[1] $$\underset{\mathbf{4}}{Ru_2Cl_4(PP)_2(N_2)} \rightleftharpoons \underset{\mathbf{9}}{Ru_2Cl_4(PP)_2} + N_2$$

The lability of the dinitrogen ligand is indicated, however, by its facile replacement under H_2 or CO atmosphere. Displacement of N_2 by dihydrogen is complete within 10 min at 1 atm H_2, as indicated by a pronounced shift in the location of the ^{31}P NMR doublets associated with the "L-end" of the complex (Table 3). The ^1H NMR spectrum reveals a singlet for bound H_2 at –11.8 ppm. The T_1 (min) value of 26 msec (300 K, 500 MHz) corresponds to an H—H distance of 0.89 Å, assuming rapid rotation of the dihydrogen ligand; this compares well with the value of 0.86 Å reported for **4b** (15). H_2-coordination is readily reversed under N_2 atmosphere. Under CO, mononuclear $RuCl_2(dcypb)(CO)_2$ is formed as a mixture of isomers, **7** and **8** (Scheme 2). The two are readily distinguished by $^{31}P\{^1H\}$ NMR; the phosphine groups of *all-cis*-**7** appear as a pair of doublets, whereas a singlet is found for *tcc*-**8**. Consistent with the proposed structures is the carbonyl region of the $^{13}C\{^1H\}$ NMR spectrum, as well as the IR data. The former shows a triplet and a doublet of doublets for **7**, but only a doublet of doublets for **8**. Two IR ν(CO) bands are seen for each complex.

Surprisingly, in view of the observed lability of the dinitrogen ligand in **4a**, no peaks for a dimer of type **9** were evident even under Ar atmosphere, or following freeze-pump-thaw (FPT) experiments carried out to shift the presumed equilibrium (eq. [1]) to the right. Sustained gas evolution was observed in NMR tubes subjected to successive FPT cycles (>20), but no new peaks were evident by $^{31}P\{^1H\}$ NMR, even at low temperature (183 K). Degassing experiments using *trans*-$RuCl_2(dppe)_2$ as internal standard were carried out in Schlenk vessels, in which the higher surface area permitted more efficient removal of dissolved gas. A steady decrease in concentration of **4a** is measured with increasing number of FPT cycles, signifying conversion of **4a** to a paramagnetic Ru product. Gas evolution is sustained after complete loss of the NMR signals, probably owing to paramagnetic broadening of signals for remaining **4a**. Observation of a large ^1H NMR singlet for dissolved H_2 at 4.2 ppm after each FPT cycle is consistent with Ru-promoted

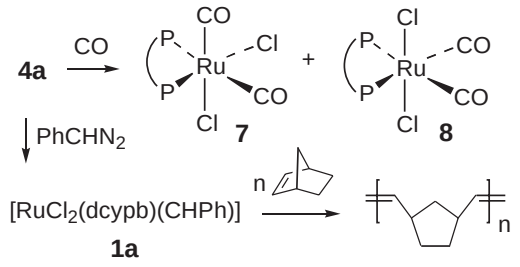
© 2001 NRC Canada

Table 3. $^{31}P\{^{1}H\}$ NMR data for $Ru_2Cl_4(PP)_2(L)$ complexes.

Complex	Chemical shifts (δ, ppm)	$^{2}J_{P,P}$ (Hz)
$Ru_2Cl_4(dcypb)_2(N_2)$ (**4a**)	60.1 (d), 45.3 (d); 49.1 (d), 37.4 (d)	40; 26
$Ru_2Cl_4(dppb)_2(N_2)$ (**4b**) (12)	54.4 (d), 53.5 (d); 46.6 (d), 36.8 (d)	45; 32
$Ru_2Cl_4(dcypb)_2(H_2)$ (**6**)	59.2 (d), 43.9 (d); 65.1 (d), 45.9 (d)	40; 25

Note: Measured at room temperature in C_6D_6, 121 MHz.

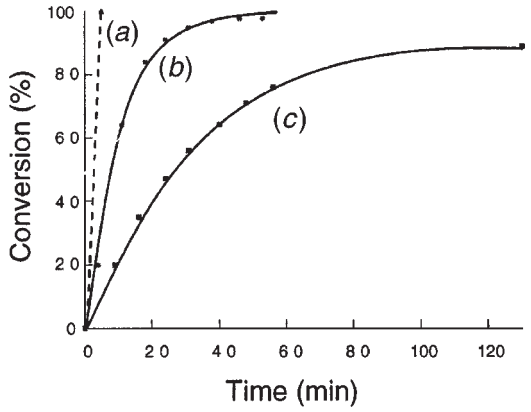
Scheme 2.



dehydrogenation of the cyclohexyl rings and (or) the dcypb backbone (catalytic dehydrogenation of the solvent itself is excluded by observation of this behaviour in benzene solvent). A ν(C=C) stretching band appears at 1629 cm^{-1} in the IR spectrum, as well as a signal at 1944 cm^{-1} assigned to Ru–H. No HCl was detected by GC-MS, and no precipitate formed on forcing the effluent gas through concentrated ammonia or NH_4PF_6 solutions, suggesting that HCl is not evolved in the reaction.

The utility of closely related Ru complexes in catalytic dehydrogenation of sp^3 C–H bonds has been established by Leitner and co-workers (16, 17). While forcing conditions were required for activation of cyclooctane, dehydrogenation of the cyclohexyl rings within complexes containing $Cy_2P(CH_2)_nPCy_2$ (n = 3, 4) was induced at 50°C, resulting in diamagnetic η^3-cyclohexenyl derivatives. Chaudret and co-workers (18–20) have likewise described intramolecular dehydrogenation of cyclohexyl rings within Ru–PCy_3 complexes at room temperature, affording Ru(II) complexes containing η^3- and (or) η^2-cyclohexenyl rings. A related process is almost certainly involved in dehydrogenation of **4a**, in which retention of both chloride ligands may be responsible for formation of a Ru(III) product. We do not exclude the possibility of concomitant attack on the four-carbon backbone; agostic interactions between Ru and bound dppb, culminating in deuterium incorporation into the backbone methylene groups, have been noted (21), while we have observed C–H bond activation within the dcypb backbone in related silylene chemistry (22). Confirmation of the identity of the dehydrogenation product(s) is hampered by paramagnetism and poor crystallinity. Attempts to probe the reaction by thermal gravimetric analysis are complicated by the observation of other diamagnetic products in solid-state degassing experiments. The high activity of these species toward activation of saturated C–H bonds under exceptionally mild conditions is notable; however, facile intramolecular attack may be attributed to the combination of steric bulk and high basicity in the dcypb ligand. The ease of such reactions in the absence of stabilizing donor ligands may account for prior difficulties in gaining access to this chemistry under Ar atmosphere. Use of N_2 as a labile donor to inhibit intramolecular attack opens up a potentially rich catalytic and coordination chemistry.

Fig. 2. ROMP activity of dcypb complexes. (*a*) **4a** + 2 $PhCHN_2$, $CDCl_3$-C_6D_6; (*b*) **2a** + 2 $PhCHN_2$, $CDCl_3$-C_6D_6; and (*c*) **4a** + 2 $PhCHN_2$, C_6D_6.



We recently described polymerization via $RuCl_2(PP)(CHPh)$ systems derived from **2**, in which high ROMP activity in norbornene polymerization was observed despite the presence of the catalyst poison PPh_3 (2). PPh_3-free **1a**, generated in situ by addition of $PhCHN_2$ to **4a** (Scheme 2), functions as a much more avid catalyst (Fig. 2). Thus, while ROMP of norbornene by the **2a**–$PhCHN_2$ system requires nearly an hour at substrate:catalyst ratios of 200:1, polymerization via **4a** is complete before the first NMR measurement can be taken (5 min, lower limit for the turnover frequency = 2400 h^{-1}). Despite the susceptibility of **4a** to decomposition by chlorinated solvent, mixed solvent systems, in which the catalyst was generated in C_6D_6 and subsequently added to a $CDCl_3$ solution of norbornene, showed much higher activity than ROMP in neat C_6D_6. Decreased metathesis activity in nonpolar solvents is characteristic of these Ru systems (1). The slow rate of polymerization in neat benzene permits competing decomposition via extrusion of the carbene as stilbene (a process characteristic of Ru–carbene complexes). Polymer polydispersities for reactions in benzene are consequently *higher* than those observed in the mixed solvent systems (PDI 3.8 vs. 1.2–1.4), and a bimodal molecular weight distribution is observed, indicating the presence of more than one ROMP-active species. The very rapid rate of polymerization in $CDCl_3$–C_6D_6 (Fig. 2*a*) suggests that decomposition of **1a** cannot compete with norbornene metathesis in this solvent system, and this is supported by the low polydispersity obtained.

Conclusions

The foregoing describes the first general route into the chemistry of chlororuthenium–phosphine complexes con-

© 2001 NRC Canada

taining the basic, bulky diphosphine, dcypb. Steric pressure, allied with high electron density, renders these species susceptible to decomposition by attack on solvent or on the dcypb ligands. Where such processes can be restrained, this heightened reactivity can be redirected and exploited in catalysis, as exemplified in the potent ROMP reactivity of the carbene derivative.

Acknowledgments

This work was supported by the Natural Sciences and Engineering Research Council of Canada (NSERC), the Canada Foundation for Innovation, and the Ontario Innovation Trust.

References

1. (*a*) E.L. Dias, S.T. Nguyen, and R.H. Grubbs. J. Am. Chem. Soc. **119**, 3887 (1997); (*b*) P. Schwab, R.H. Grubbs, and J.W. Ziller. J. Am. Chem. Soc. **118**, 100 (1996).
2. D. Amoroso and D.E. Fogg. Macromolecules, **33**, 2815 (2000).
3. M. Burk, J.P. Martinez, J.E. Feaster, and N. Cosford. Tetrahedron, **50**, 4399 (1994).
4. N.T. McManus and G.L. Rempel. J. Macromol. Sci. R. M. C. **C35**, 239 (1995).
5. X. Creary. *In* Organic syntheses. Vol. VII. *Edited by* J. P. Freeman. John Wiley & Sons, Toronto. 1990. p. 438.
6. D.E.K.Y. Chau. M.Sc. thesis. University of British Columbia. Vancouver, B.C. 1992.
7. P.S. Hallman, T.A. Stephenson, and G. Wilkinson. Inorg. Synth. **12**, 237 (1970).
8. J. Chatt and R.G. Hayter. J. Chem. Soc. 896 (1961).
9. R. Blessing. Acta Crystallogr. Sect. A: Fundam. Crystallogr. **A51**, 33 (1995).
10. G.M. Sheldrick. Bruker AXS, Madison, WI. 1997.
11. K.S. MacFarlane, A.M. Joshi, S.J. Rettig, and B.R. James. Inorg. Chem. **35**, 7304 (1996).
12. A.M. Joshi, I.S. Thorburn, S.J. Rettig, and B.R. James. Inorg. Chim. Acta, **198**–**200**, 283 (1992).
13. I.S. Thorburn, S.J. Rettig, and B.R. James. Inorg. Chem. **25**, 234 (1986), and refs. cited therein.
14. G. Chioccala and J.J. Daly. J. Chem. Soc. A. 1981 (1968).
15. A.M. Joshi and B.R. James. J. Chem. Soc. Chem. Commun. 1785 (1989).
16. C. Six, B. Gabor, H. Gorls, R. Mynott, P. Philipps, and W. Leitner. Organometallics, **18**, 3316 (1999).
17. W. Leitner and C. Six. Chem. Ber. **130**, 555 (1997).
18. S. Sabo-Etienne and B. Chaudret. Coord. Chem. Rev. **178**–**180**, 381 (1998).
19. B. Chaudret, P. Dagnac, D. Labroue, and S. Sabo-Etienne. New J. Chem. **20**, 1137 (1996).
20. M.L. Christ, S. Sabo-Etienne, and B. Chaudret. Organometallics, **14**, 1082 (1995).
21. M. Ogasawara and M. Saburi. Organometallics, **13**, 1911 (1994).
22. D. Amoroso, M. Haaf, G.P.A. Yap, R. West, and D.E. Fogg. Organometallics, accepted.

© 2001 NRC Canada

Intra- and inter-ion-pair protonic—hydridic bonding in polyhydridobis(phosphine)rhenates

Kamaluddin Abdur-Rashid, Alan J. Lough, and Robert H. Morris

Abstract. The hexahydridobis(phosphine)rhenate anions, $[ReH_6(PR_3)_2]^-$ (PR_3 = PCy_3, P-*i*-Pr_3, PPh_3, PMe_3) were generated by potassium hydride deprotonation of the neutral heptahydride conjugate acids ($ReH_7(PR_3)_2$), isolated as their $[K(18\text{-crown-6})]^+$ and $[K(1,10\text{-diaza-18-crown-6})]^+$ salts, and characterized by NMR and IR spectroscopy and elemental analyses. Structures from single crystal X-ray diffraction were obtained for the $[K(1,10\text{-diaza-18-crown-6})]^+$salts and these indicate the presence of short protonic—hydridic bonds involving the hydrides of the anions and the proton donor NH moieties of the cations. The structure of $[K(1,10\text{-diaza-18-crown-6})][ReH_6(P\text{-}i\text{-}Pr_3)_2]$ adopts a one-dimensional zigzag chain with alternating cations and anions connected and held together by inter-ion N-H$\cdots$H$_x$-Re interactions (x = 1 or 2). Short distances between the NH protons of the cations and hydrides of the anion ranging from 1.6 to 1.9 Å are estimated for this complex. A different kind of chain structure is observed for $[K(1,10\text{-diaza-18-crown-6})][ReH_6(PMe_3)_2]$ in which the combined effects of inter-ion protonic—hydridic bonding (N-H$\cdots$H$_x$-Re) and inter-ion electrostatic interactions (ReH$_x^-\cdots$K$^+\cdots$H$_x^-$Re), result in one-dimensional networks of alternating cations and anions, with the metals and hydrides occupying the interior and the organic moieties of the phosphine ligands and crown ether lining the exterior of cylindrical supramolecular assemblies. A combination of intra- and inter-ion protonic–hydridic and intra-ion-pair electrostatic interactions in $[K(1,10\text{-diaza-18-crown-6})][ReH_6(PPh_3)_2]$ result in the formation of discrete two-dimensional $\{[K(1,10\text{-diaza-18-crown-6})][ReH_6(PPh_3)_2]\}_4$ tetramers. The PCy_3 salt is disordered but appears to consist of isolated 1:1 ion pairs containing strong intra-ion-pair NH$\cdots$HRe bonding. The solid-state IR spectra of the $[K(1,10\text{-diaza-18-crown-6})]^+$ salts show low-frequency shifts for the NH bands relative to $[K(1,10\text{-diaza-18-crown-6})][BPh_4]$, and perturbed Re-H bands relative to those in the $[K(18\text{-crown-6})]^+$ salts. The magnitude of $\Delta\nu$NH is related to the basicity of the anion as indicated by the pK_α^{THF} of the conjugate acid form ($ReH_7(PR_3)_2$), which increases as $PPh_3 < < PMe_3 < P\text{-}i\text{-}Pr_3 < PCy_3$. Solution ^{1}H NMR, NOE, and T_1 relaxation measurements of $[K(1,10\text{-diaza-18-crown-6})][ReH_6(PPh_3)_2]$ indicate that these interactions also persist in toluene solutions of this compound.

Key words: rhenium, hydride, phosphine, hydrogen bonding, self-assembly.

Résumé : On a généré les anions hexahydrobis(phosphine)rhénate, $[ReH_6(PR_3)_2]^-$ (PR_3 = PCy_3, P-*i*-Pr_3, PPh_3, PMe_3) par une déprotonation à l'aide d'hydrure de potassium des acides conjugués, heptahydrure neutre, $ReH_7(PR_3)_2$; on les a isolés sous la forme de sels $[K(18\text{-couronne-6})]^+$ et $[K(1,10\text{-diaza-18-couronne-6})]^+$ et on les a caractérisés par RMN, spectroscopie infrarouge et analyses élémentaires. On a déterminé les structures des sels $[K(1,10\text{-diaza-18-couronne-6})]^+$ par diffraction des rayons X sur des cristaux uniques et celles-ci indiquent la présence de courtes liaisons proton—hydrure impliquant les hydrures des anions et les portions de NH donneur de proton des cations. Le structure $[K(1,10\text{-diaza-18-couronne-6})][ReH_6(P\text{-}i\text{-}Pr_3)_2]$ adopte la forme d'une chaîne monodimensionnelle en zigzag comportant, en alternance, des cations et des anions reliés et retenus ensemble par des interactions N-H$\cdots$H$_X$-Re entre les ions (x = 1 ou 2). On a évalué que les distances entre les protons NH des cations et les hydrures de l'anion sont courtes et qu'elles vont de 1,6 à 1,9 Å. On observe une structure différente pour la chaîne du $[K(1,10\text{-diaza-18-couronne-6})][ReH_6(PMe_3)_2]$ dans laquelle les effets combinés de la liaison interionique proton—hydrure, N-H$\cdots$H$_x$-Re, et des interactions électrostatiques interioniques, ReH$_X^-\cdots$K$^+\cdots$H$_X^-$Re, conduisent à des réseaux unidimensionnels de cations et d'anions en alternance alors que les atomes de métal et les atomes d'hydrure occupent l'intérieur et les portions organiques des ligands phosphines et que l'éther couronne recouvre la partie extérieure des assemblages supramoléculaires cylindriques. Dans le $[K(1,10\text{-diaza-18-couronne-6})][ReH_6(PPh_3)_2]$, une combinaison d'interactions électrostatiques intra- et inter-ion proton–hydrure et intra-paire d'ions conduit à la formation de tétramères individuels $\{[K(1,10\text{-diaza-18-couronne-6})][ReH_6(PPh_3)_2]\}_4$. Le sel de PCy_3 est désordonné, mais il semble être formé de paires d'ions 1:1 isolées qui contiennent de fortes liaisons NH$\cdots$HRe intra-paires d'ions. Les spectres infrarouges à l'état solide des sels de $[K(1,10\text{-diaza-18-couronne-6})]^+$ montrent que les bandes NH se déplacent faiblement vers de plus faibles fréquences par rapport au $[K(1,10\text{-diaza-18-couronne-6})][BPh_4]$ et que les bandes de Re-H sont perturbées par rapport à celles des sels de $[K(18\text{-couronne-6})]^+$. L'amplitude du $\Delta\nu$NH est liée à la basicité de l'anion, telle qu'indiquée par le pK_α^{THF} de la forme

Received September 29, 2000. Published on the NRC Research Press Web site at http://canjchem.nrc.ca on July 17, 2001.

This paper is dedicated to Brian James for his outstanding contributions to inorganic and organometallic chemistry.

K. Abdur-Rashid, A.J. Lough, and R.H. Morris.[1] Department of Chemistry, University of Toronto, 80 St. George St., Toronto, ON M5S 3H6, Canada.

[1]Corresponding author (telephone and fax: (416) 978-6962; e-mail: rmorris@chem.utoronto.ca).

 DOI: 10.1139/cjc-79-5/6-964 © 2001 NRC Canada

conjuguée de l'acide, $ReH_7(PR_3)_2$, qui augmente de $PPh_3 < < PMe_3 < P\text{-}i\text{-}Pr_3 < PCy_3$. L'EON en RMN du ^1H et les mesures des temps de relaxation T_1 du [K(1,10-diaza-18-couronne-6)][$ReH_6(PPh_3)_2$] indiquent que ces interactions persistent aussi dans les solutions de ce composé dans le toluène.

Mots clés : rhénium, hydrure, phosphine, liaison hydrogène, autoassemblage.

[Traduit par la Rédaction]

Introduction

Since the first reports of M-H···H-X protonic—hydridic or dihydrogen bonds (1–3), there have been numerous studies of this bonding between various hydrogen bond donors, X-H (X = O, N, C), and transition-metal hydride complexes (4–13) or main group hydride compounds (M = B, Ga) (14–19). These interactions have been verified by solution NMR, IR, single crystal X-ray, and neutron diffraction studies and theoretical calculations (20, 21) and have been shown to have similar structural, energetic, electronic, and spectroscopic characteristics to conventional X-H···Y hydrogen bonds, where X and Y are electronegative elements. Classical hydrogen bonds play crucial roles in various chemical, biological, and material systems (22). Similarly, it is becoming increasingly evident that this nonclassical hydrogen bonding represents more than just a unique and fascinating phenomenon; it can influence the chemical and physical characteristics and reactivity profiles of organometallic and main group metallohydride systems. For example, Haack et al. (23) reported an active catalyst for the asymmetric solvent-transfer hydrogenation of ketones that contains a RuH···HN interaction while Gatling and Jackson (19) recently highlighted the role of "dihydrogen bonds" in determining the stereoselective reactivity of aminoboranes.

Various research groups are currently investigating the use of these nonclassical hydrogen bonds for the systematic crystal engineering of organized molecular solids (6, 16, 17, 24–28). These protonic—hydridic bonds facilitate templated covalent bond formation during the pyrolysis of borohydride adducts of amines and aminoalcohols (28). Gladfelter's group (17) reported that these interactions are important in determining the solid-state structure of gallium hydride – amine adducts, such as cyclotrigallazane, and are significant in facilitating the formation of nanocrystalline gallium nitride during their thermal decomposition at elevated temperatures.

Some of our most recent studies involve the utilization of ion-pairing to facilitate and enhance protonic–hydridic interactions between transition-metal polyhydride anions $[MH_x(PR_3)_2]^-$, (M = Os, Ru, Ir) and potassium aza-crown cations to assemble novel and well-defined ionic structural motifs (6, 24, 25). Our choice of such systems was based on the expectation that the high basicity of anionic hydrides would make them better hydrogen bond acceptors compared to their neutral or cationic counterparts. In addition, an electrostatic contribution to the protonic—hydridic bond formation is expected, since the proton donor is a constituent of the cation. This has resulted in the first reports of one-dimensional chains held together by a combination of protonic–hydridic and electrostatic M-CO···K interactions in the solid-state structures of $[K(aza\text{-}18\text{-}crown\text{-}6)]^+$ salts of $[MH_3(XO)(P\text{-}i\text{-}Pr_3)_2]^-$ anions (M = Os, Ru, Re; X = C, N) (24), while one-dimensional chains held together by intermolecular protonic—hydridic bonds are observed in the $[K(1,10\text{-}diaza\text{-}18\text{-}crown\text{-}6)]^+$ salts of $[MH_x(P\text{-}i\text{-}Pr_3)_2]^-$ (M = Ir, × = 4; M = Os, Ru, x = 5) anions (6, 24, 25). The strength of the protonic–hydridic interactions in these salts, as verified by NMR and solution and solid-state IR studies, were shown to be related to the basicity of the anions (6, 24), which compliments previous studies that relates the strength of these interactions with the acidity of the proton donor species (7, 9, 29). An interesting observation was the spectacular increase in the activity of both the M—H (M = Os, Ru) and N—H bonds in solutions of these salts, leading to rapid and efficient deuteration of these two moieties upon exposure to D_2 gas (6). This observation has resulted in our subsequent development of novel ruthenium-based catalyst systems for the hydrogenation of nitriles, ketones, and imines (30, 31).

Our current study seeks to exploit and combine the synergistic effects of ion-pairing and intermolecular protonic—hydridic bonding to assemble and design novel supramolecular structural types. Furthermore, it is expected that reactivity studies involving these systems could help in identifying novel catalysts. Thus, we have extended our study to include salts of rhenium polyhydride anions. In a recently reported compilation of acidities of transition-metal hydrides and dihydrogen complexes in tetrahydrofuran (32), we found that the pK_α^{THF} of various cationic and neutral rhenium polyhydride acids are exceptionally sensitive to the nature of the ligands. The high polarizability of the Re—H bonds in rhenium polyhydride anions is expected to significantly influence the proton-accepting ability of the hydride ligands in the formation of protonic—hydridic bonded species, while steric congestion in the conjugate anions can be selectively controlled by an appropriate choice of phosphine ligands. In addition, the favorable electrostatic interactions that are known to exist between potassium crown-ether cations and the hydrides of rhenium polyhydride anions should also contribute another dimensionality in the formation of organized molecular assemblies (33–35). Here we report the synthesis, spectroscopic properties, and X-ray crystal structures of a series of hexahydridobis(phosphine)rhenate salts. This report demonstrates the subtle and related roles of ligand nucleophilicity and stereochemistry in determining the degree and types of intermolecular interactions and, hence, the molecular packing in the crystal lattice. The salts $K[ReH_6(PPh_3)_2]$, $[K(THF)_2][ReH_6(PPh_3)_2]$ (33), and [K(18-crown-6)][$ReH_6(PR_3)_2$], R = Ph, C_6H_4F, (34) were the only compounds of this type reported before this work.

Experimental section

General

All preparations and manipulations were carried out under H_2, N_2, or Ar atmospheres with the use of standard Schlenk, vacuum line, and glove box techniques in dry, oxygen-free

© 2001 NRC Canada

solvents. Tetrahydrofuran (THF), diethyl ether (Et_2O), and hexanes were dried and distilled from sodium benzophenone ketyl. Deuterated solvents were degassed and dried over activated molecular sieves. Potassium hydride, 18-crown-6, 1-aza-18-crown-6, 1,10-diaza-18-crown-6, trimethylphosphine, and rhenium metal (powder) were supplied by Aldrich Chemical Company. $ReOCl_3(P\text{-}i\text{-}Pr_3)_2$ and $ReOCl_3(PMe_3)_2$ were synthesized using a similar procedure as reported for the preparation of $ReOCl_3(PCy_3)_2$ (36), while the neutral heptahydrides, $ReH_7(PR_3)_2$, R = Cy (32, 36), *i*-Pr (37), Ph (32, 38), Me (39), were prepared using the simplified and modified procedure illustrated below for $ReH_7(PPh_3)_2$. NMR spectra were recorded on a Varian Unity-500 (500 MHz for ^1H) or on a Varian Gemini 300 MHz spectrometer (300 MHz for ^1H and 121.5 for ^{31}P). All ^{31}P spectra were recorded with proton decoupling and ^{31}P chemical shifts were measured relative to 85% H_3PO_4 as an external reference. ^1H chemical shifts were measured relative to partially deuterated solvent peaks but are reported relative to tetramethylsilane. T_1 measurements were made at 500 MHz using the inversion recovery method. The temperature of the probe was calibrated using the temperature dependence of the chemical shifts of MeOH. NOE measurements were also obtained at 500 MHz. Infrared spectra were obtained on a Nicolet 550 Magna-IR spectrometer. Microanalyses were performed by Guelph Chemical Laboratories Ltd. Although the samples were crystalline and spectroscopically pure, the carbon analyses were low in most cases.

Synthesis

$ReH_7(PPh_3)_2$

Diethyl ether (100 mL) was added to a mixture of $ReOCl_3(PPh_3)_2$ (1.0 g, 1.22 mmol) and $LiAlH_4$ (500 mg, 12.5 mmol) under an atmosphere of argon and the mixture was stirred for 1 h and then filtered. Ethanol was added slowly and dropwise to the filtrate, with thorough mixing between each addition until there was no further evolution of hydrogen gas. The resulting mixture was evaporated to dryness under vacuum, and the solids extracted with 4 × 10 mL of THF. The combined THF extract was concentrated to 5 mL and hexanes (20 mL) added, precipitating a white solid, which was filtered, washed with 2 × 3 mL of hexanes, then dried under vacuum. Yield = 602 mg, 70%. The purity of the compound was determined by comparing its ^1H and ^{31}P NMR spectra with those reported in the literature (32, 38).

*$[K(Q)][ReH_6(PR_3)_2]$ (Q = 18-crown-6 (**1**), 1,10-diaza-18-crown-6 (**2**)) (PR_3 = PCy_3 (**a**), P-i-Pr_3 (**b**), PPh_3 (**c**), PMe_3 (**d**))*

These salts were prepared using similar procedures as illustrated for $[K(18\text{-crown-6})][ReH_6(PPh_3)_2]$ (**1c**).

*$[K(18\text{-crown-6})][ReH_6(PPh_3)_2]$ (**1c**)*

THF (5 mL) was added to a mixture of $ReH_7(PPh_3)_2$ (300 mg, 0.42 mmol), KH (50 mg, 1.25 mmol), and 18-crown-6 (112 mg, 0.42 mmol). After stirring for 4 h, the mixture was filtered and the solids washed with 2 × 1.0 mL THF. Hexanes (15 mL) were added to the combined filtrate to precipitate a yellow solid that was filtered off, washed with hexanes and dried in vacuo. Yield = 398 mg, 93%. T_1 (^1H) (toluene-d_8, Re-H, 500 MHz, ms) 195 (295 K), 186 (288 K), 174 (274 K), 173 (267 K), 177 (260 K), 180 (253), 205 (240), 264 (225 K). IR (Nujol) (cm^{-1}): 1852, 1883, 1956 (νRe-H). ^1H NMR (toluene-d_8) (ppm): –6.91 (t, J_{HP} = 14.28 Hz, 6H, ReH), 3.18 (s, 24H, CH_2) 7.00–7.94 (m, 30H, Ph). ^{31}P NMR (ppm): 40.21.

*$[K(18\text{-crown-6})][ReH_6(PCy_3)_2]$ (**1a**)*

Yield = 86%. IR (Nujol) (cm^{-1}): 1717, 1826, 1880, 1935 (νRe-H). ^1H NMR (toluene-d_8) (ppm): –9.15 (t, J_{HP} = 16.47 Hz, 6H, ReH), 1.41–2.57 (m, 66H, Cy), 3.34 (s, 24H, CH_2). ^{31}P NMR (ppm): 48.30.

*$[K(18\text{-crown-6})][ReH_6(P\text{-}i\text{-}Pr_3)_2]$ (**1b**)*

Yield = 96%. ^1H NMR (toluene-D_8) (ppm): –9.45 (t, J_{HP} = 18.57 Hz, 6H, ReH), 1.48 (m, 36H, CH_3), 2.06 (m, 6H, CH), 3.23 ppm (s, 24H, CH_2). ^{31}P NMR (ppm): 71.34. IR (Nujol) (cm^{-1}): 1725, 1834, 1871, 1925, 1979 (νRe-H).

*$[K(18\text{-crown-6})][ReH_6(PMe_3)_2]$ (**1d**)*

Yield = 74%. IR (Nujol) (cm^{-1}): 1823, 1872, 1891, 1917, 1952 (νRe-H). ^1H NMR (toluene-d_8) (ppm): –7.98 (t, J_{HP} = 16.29 Hz, 6H, ReH), 1.98 (d, 18H, CH_3), 3.26 (s, 24H, CH_2). ^{31}P NMR (ppm): 38.23.

*$[K(1,10\text{-diaza-18-crown-6})][ReH_6(PCy_3)_2]$ (**2a**)*

Yield = 94%. IR (Nujol) (cm^{-1}): 1720, 1822, 1874, 1927 (νRe-H); 3336, 3276, 3178 (νN-H). ^1H NMR (toluene-d_8) (ppm): –9.23 (t, J_{HP} = 16.41 Hz, 6H, ReH), 1.37–3.38 (m, 92H, Cy, CH_2, NH). ^{31}P NMR (ppm): 48.02. Anal. calcd.: C 54.67, H 9.37, N 2.66; found: C 53.93, H 9.31, N 2.53.

*$[K(1,10\text{-diaza-18-crown-6})][ReH_6(P\text{-}i\text{-}Pr_3)_2]$ (**2b**)*

Yield = 96%. ^1H NMR (toluene-d_8) (ppm): –9.88 (t, J_{HP} = 18.87 Hz, 6H, ReH), 1.14 (m, 36H, CH_3), 1.74 (m, 6H, CH), 2.09 (qi, J_{HH} = 7.09 Hz, 2H, NH) 2.73 (m, 8H, CH2), 3.56–3.58 (m, 16H, CH_2). ^{31}P NMR(ppm): 70.8. IR (Nujol) (cm^{-1}): 1744, 1842, 1868, 1842, 1927, 1969 (νRe-H); 3186 (νN-H).

*$[K(1,10\text{-diaza-18-crown-6})][ReH_6(PPh_3)_2]$ (**2c**)*

Yield = 92%. ^1H T_1 (toluene-d_8, Re-H, 500 MHz, ms) 254 (316 K), 206 (302 K), 177 (288 K), 159 (274 K), 160 (267 K), 172 (260 K), 266 (245 K), 932 (231 K); (N-H, 500 MHz, ms) 710 (316 K), 581 (302 K), 486 (288 K), 420 (274 K), 433 (267 K), 422 (260 K), 413 (231 K). IR (Nujol) (cm^{-1}): 1837, 1853, 1868, 1889, 1940, 1961 (νRe-H); 3229 (νN-H). ^1H NMR (toluene-d_8) (ppm): –6.90 (t, J_{HP} = 14.41 Hz, 6H, ReH), 1.04 (qi, J_{HH} = 6.81 Hz, 2H, NH) 2.35 (m, 8H, CH_2), 3.15 (s, 8H, CH_2), 3.27 (s, 8H, CH_2) 7.00–7.88 (m, 30H, Ph). ^{31}P NMR (ppm): 40.21. Anal. calcd.: C, 56.62, H 6.14, N 2.75; found: C 56.36, H 6.40, N 2.77.

*$[K(1,10\text{-diaza-18-crown-6})][ReH_6(PMe_3)_2]$ (**2d**)*

Yield = 78%. IR (Nujol) (cm^{-1}): 1818, 1866, 1909, 1939 (νRe-H); 3214 (νN-H). ^1H NMR (toluene-d_8) (ppm): –7.99 (t, J_{HP} = 16.38 Hz, 6H, ReH), 1.85 (d, 18H, CH_3), 1.95 (qi, J_{HH} = 7.38 Hz, 2H, NH) 2.46 (m, 8H, CH_2), 3.41 (m, 16H, CH_2). ^{31}P NMR (ppm): 37.60.

© 2001 NRC Canada

Table 1. Summary of crystal data, details of intensity collection, and least-squares refinement parameters for **2b**, **2c**, and **2d**.

	2b	**2c**	**2d**
Empirical formula	$C_{48}H_{62}KN_2O_4P_2Re$	$C_{34}H_{82}KN_2O_5P_2Re$	$C_{18}H_{50}KN_2O_4P_2Re$
M_r	1018.24	886.26	645.84
Crystal size (mm)	0.35 × 0.32 × 0.24	0.35 × 0.29 × 0.34	0.35 × 0.30 × 0.30
Crystal class	Monoclinic	Triclinic	Orhorhombic
Space group	C_2/c	$P\bar{1}$	$P2(1)2(1)2(1)$
Temperature (K)	150.0	150.0	150
a (Å)	45.1564(14)	11.0923(3)	16.0727(2)
b (Å)	12.6205(2)	11.1891(2)	17.3373(2)
c (Å)	39.0307(12)	19.0602(4)	20.4311(3)
α (°)	90	103.500(1)	90
β	119.882(1)	91.982(1)	90
γ	90	108.607(1)	90
V (Å^3)	19286.3(9)	2164.69(8)	5693.3(1)
Z	16	2	8
D_{calc} (g cm^{-3})	1.403	1.360	1.507
μ (Mo Kα) (mm^{-1})	2.715	3.013	4.550
F (000)	8320	928	2624
Range θ collected (°)	4.08–26.37	4.17–26.33	4.09–26.36
No. of reflections	48 971	18 783	42 530
Independent reflections	19 405	8449	11 466
$R_1[I > 2\sigma(I)]$	0.0399	0.0311	0.0318
wR_2 (all data)	0.0781	0.0869	0.0844
Goodness of fit	1.018	1.083	1.054
Parameters refined	1082	423	507
Max peak in final ΔF map (e Å^{-3})	0.775	1.762	1.435

Note: Definition of R indices: $R_1 = \Sigma(F_o - F_c)/\Sigma(F_o)$; $wR_2 = [\Sigma[w(F_o^2 - F_c^2)^2]/\Sigma[w(F_o^2)^2]]^{1/2}$.

Deuteration studies

A weighed sample of the desired complex was dissolved in the required solvent in a NMR tube under an argon atmosphere. The tube was then fitted with an adapter, by which it was connected to a vacuum line. The sample was cooled to liquid nitrogen temperature, degassed and closed. After warming to room temperature, D_2 gas at 1 atm (1 atm = 101.325 kPa) pressure was allowed into the NMR tube, which was then flame-sealed.

Determination of pK_α^{THF}

The pK_α^{THF} of $ReH_7(P\text{-}i\text{-}Pr_3)_2$ was related to the pK_α^{THF} = 41 of $ReH_7(PCy_3)_2$ (32) by the following procedure: a mixture of $ReH_7(PCy_3)_2$ (20 mg, 0.027 mmol) and [K(18-crown-6)][$ReH_6(P\text{-}i\text{-}Pr_3)_2$] (22 mg, 0.027 mmol) was dissolved in THF-d_8 and allowed to reach acid–base equilibrium over a period of 6 h. The concentrations of the added compounds along with their respective conjugate species were determined by ^{1}H and gated–decoupled ^{31}P NMR (K = 0.16). The derived pK_α^{THF} value of $ReH_7(P\text{-}i\text{-}Pr_3)_2$ was used to determine the pK_α^{THF} of $ReH_7(PMe_3)_2$ using similar procedures.

X-ray structure analysis

Crystals were obtained by the slow diffusion of diethyl ether or hexanes into THF solutions of the complexes under a nitrogen atmosphere. Data were collected on a Nonius Kappa-CCD diffractometer using Mo Kα radiation (λ = 0.71073 Å). The CCD data were integrated and scaled using the DENZO-SMN software package and the structures were solved and refined using SHELXTL Ver.5.0. The crystallographic data for complexes **2b**, **2c**, and **2d** are listed in Table 1. The hydrides in **2c** were located and refined with isotropic thermal parameters.

Results and discussion

Synthesis of the complexes

Several procedures are available for the preparation of the neutral rhenium heptahydrides, $ReH_7(PR_3)_2$ (34, 36, 40); however, the modified method used in this study resulted in spectroscopically pure products and greater than 60% isolated yields. Addition of diethyl ether to a mixture of $ReOCl_3(PR_3)_2$ and $LiAlH_4$ gave a colorless solution after stirring at room temperature for several minutes. Removal of the excess $LiAlH_4$ and quenching the etheral solution with ethanol resulted in the generation of the heptahydrido complexes. $ReH_7(PCy_3)_2$ and $ReH_7(PPh_3)_2$ were isolated as white powders, while $ReH_7(P\text{-}i\text{-}Pr_3)_2$ and $ReH_7(PMe_3)_2$ were isolated as tan-coloured viscous oils. Incomplete removal of triphenylphosphine from $ReOCl_3(PMe_3)_2$ resulted in the formation of a small amount of $ReH_5(PMe_3)_2(PPh_3)$ as an impurity during the preparation of $ReH_7(PMe_3)_2$.

The anionic hydride salts, [K(Q)][$ReH_6(PR_3)_2$], were prepared in 75–98% yields by deprotonation of the neutral heptahydide conjugates using KH in the presence of the desired crown ether (Q) in THF under N_2 or Ar atmospheres. The presence of the crown ether resulted in

© 2001 NRC Canada

Table 2. Summary of selected ^{1}H NMR (toluene-d_8) and solid-state IR (Nujol) characteristics of the M-H and N-H units of $[K(Q)][ReH_6(PR_3)_2]$; Q = 18-crown-6 and 1,10-diaza-18-crown-6.

Complex	ν (N-H) (cm^{-1})	δ (N-H) (ppm)	δ (Re-H) (ppm)	pK_α^{THF}
[K(1,10-diaza-18-crown-6)]	3279	1.00[a]		
$[BPh_4]$	3284			
[K(18-crown-6)]			–9.15	41
$[ReH_6(PCy_3)_2]$ (**1a**)				
[K(1,10-diaza-18-crown-6)]	3178	—[b]	–9.23	
$[ReH_6(PCy_3)_2]$ (**2a**)	3276			
	3336			
[K(18-crown-6)]			–9.45	40
$[ReH_6(P\text{-}i\text{-}Pr_3)_2]$ (**1b**)				
[K(1,10-diaza-18-crown-6)]	3186	2.04	–9.88	
$[ReH_6(P\text{-}i\text{-}Pr_3)_2]$ (**2b**)				
[K(18-crown-6)]			–6.91	30
$[ReH_6(PPh_3)_2]$ (**1c**)				
[K(1,10-diaza-18-crown-6)]	3229	1.04	–6.90	
$[ReH_6(PPh_3)_2]$ (**2c**)				
[K(18-crown-6)]			–7.98	38
$[ReH_6(PMe_3)_2]$ (**1d**)				
[K(1,10-diaza-18-crown-6)]	3214	1.95	–7.99	
$[ReH_6(PMe_3)_2]$ (**2d**)				

[a]Determined in THF.
[b]Obscured by peaks of the PCy_3.

$$[1]\quad ReH_7(PR_3)_2 + KH + Q \xrightarrow[-H_2]{THF} [K(Q)][ReH_6(PR_3)_2]$$

a shorter reaction time than that reported for the preparation of $K[ReH_6(PPh_3)_2]$, using KH alone (33), which is quite likely due to an increase in the solubility of the otherwise insoluble KH in the presence of the crown ether. The excess KH was conveniently removed by filtration, and the polyhydride salt precipitated as its $[K(crown\text{-}ether)]^+$ salt by the addition of hexanes or diethyl ether. The contamination of $ReH_7(PMe_3)_2$ with some $ReH_5(PMe_3)_2(PPh_3)$ posed no problem in the reaction with KH since, under the reaction conditions, the heptahydride complex is selectively deprotonated. Another complication was the formation of small amounts of salts of the anionic dimer $[\{ReH_2(PMe_3)_2\}_2(\mu\text{-}H_3)]^-$, which could be avoided by carrying out the deprotonation reaction under a H_2 atmosphere. A full study of a series of these novel anionic dimers is currently underway and will be reported elsewhere in due course (41).

The hexahydrido rhenium salts, **1a**, **2a**, **1b**, **2b**, **1d**, and **2d** were isolated as colourless, air- and moisture-sensitive salts, which are soluble in THF, benzene, and toluene. Complexes **1c** and **2c** are yellow, only moderately air-sensitive as solids and display similar solubility characteristics as the other salts. All of these rhenium hexahydride salts are expected to exist as 1:1 ion-pairs in solution, as evidenced by their solubility in the aromatic solvents. The X-ray structures and solid-state IR spectra establish the presence of NH···HRe interactions in the $[K(1,10\text{-diaza-18-crown-6})]^+$ salts (see below).

Relative pK_α^{THF} values for the complexes

The pK_α^{THF} values for the neutral conjugate acids of the complexes used in this study were determined by neutral acid – anionic base reactions in THF-d_8 by means of quantitative ^{31}P and ^{1}H NMR spectroscopy. These pK_α^{THF} values are approximations to absolute, free ion pK_α^{THF} and are obtained by crudely correcting the observed K for 1:1 ion-pairing effects by use of the Fuoss equation (32). The pK_α^{THF} value of $ReH_7(P\text{-}i\text{-}Pr_3)_2$ was determined to be 40.2 by using eq. [3] and the previously reported value of 41 for the pK_α^{THF} of $ReH_7(PCy_3)_2$ (32). No correction ΔpK_d is required for ion pairing because the inter-ion distances are expected to be very similar.

$$[2]\quad ReH_7(PCy_3)_2 + [K(18\text{-crown-}6)][ReH_6(P\text{-}i\text{-}Pr_3)_2] \underset{}{\overset{K}{\rightleftharpoons}} [K(18\text{-crown-}6][ReH_6(PCy_3)_2] + ReH_7(P\text{-}i\text{-}Pr_3)_2$$

$$[3]\quad pK_\alpha^{THF}\{ReH_7(P\text{-}i\text{-}Pr_3)_2\} = pK_\alpha^{THF}\{ReH_7(PCy_3)_2\} - pK + \Delta pK_d$$

Similarly, from an equilibrium involving $ReH_7(P\text{-}i\text{-}Pr_3)_2$ and **1d** (K = 0.016), the pK_α^{THF} of $ReH_7(PMe_3)_2$ was determined to be 38.4. The pK_α^{THF} of $ReH_7(PPh_3)_2$ in THF was previously reported to be 30 (32). A comparison of the pK_α^{THF} values show that the acidities of the neutral heptahydride complexes are exceptionally susceptible to substituent effects of the phosphine ligands, with an unprecedented 11 pK_α^{THF} unit difference between the acid dissociation constants for $ReH_7(PCy_3)_2$ and $ReH_7(PPh_3)_2$. To date, these complexes represent some of the least acidic polyhydride complexes to have their pK_α^{THF} determined.

NMR spectra

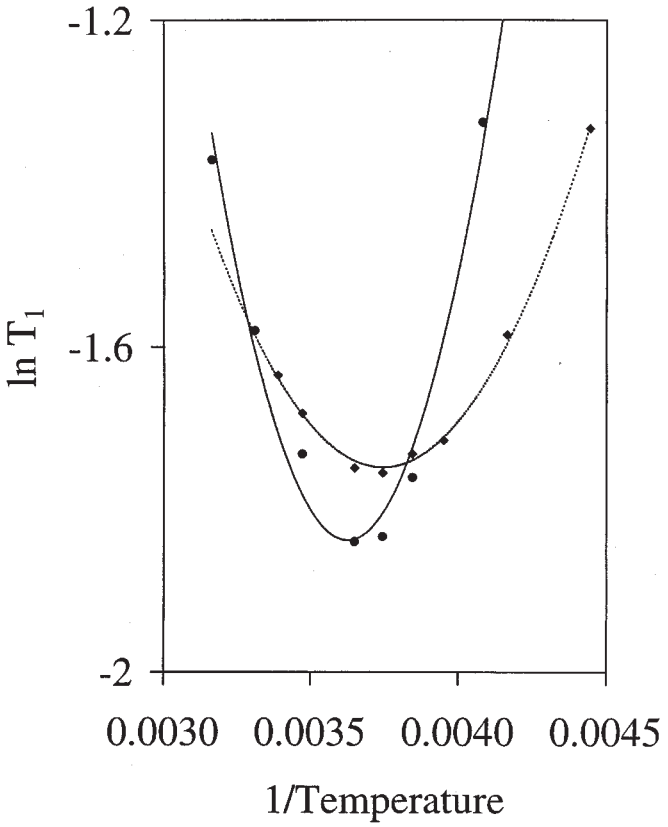
Selected ^{1}H NMR (hydride region) and solid–state IR (NH) characteristics for the rhenium hexahydride salts are listed in Table 2. The ^{1}H NMR chemical shift of the NH unit

© 2001 NRC Canada

Table 3. 500 MHz ^{1}H NMR T_1 values (hydride and NH) for [K(1,10-diaza-18-crown-6)] [$ReH_6(PPh_3)_2$] (**2c**) and [K(18-crown-6)][$ReH_6(PPh_3)_2$] (**1c**) in toluene-d_8.

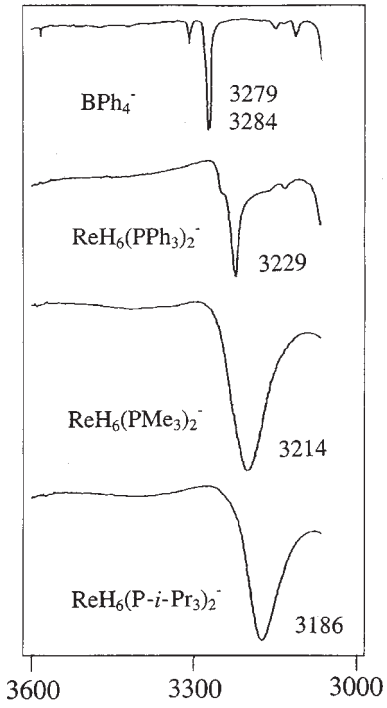
	T_1 (ms)		
	2c		**1c**
Temperature (K)	ReH_6	NH	ReH_6
316	254	710	
302	206	581	
295			195
288	177	486	186
274	159	420	174
267	160	433	173
260	172	422	177
253			180
245	266		
240			205
231	932	413	
225			264

Fig. 1. Plot of ln (^{1}H T_1 relaxation time) against 1/Temperature (1/K) for [K(1,10-diaza-18-crown-6)][$ReH_6(PPh_3)_2$] (●) and [K(18-crown-6)][$ReH_6(PPh_3)_2$] (◆) in toluene-d_8. [Complex] = 32 mM.



of [K(1,10-diaza-18-crown-6)]BPh_4 in THF-d_8 is also included in Table 2, since this salt is totally insoluble in toluene. The triplets in the hydride region of the ^{1}H NMR spectra of the salts are indicative of a fluxional process that makes all six hydrides chemically equivalent in the presumably dodecahedral structure. In general, the salts show increasingly high-field shifts for the hydride resonance with

Fig. 2. Solid-state (Nujol mull) IR spectra of [K(1,10-diaza-18-crown-6)]$^+$ (NH region) with the anions shown.



increasing basicity of the phosphine ligands, except for the PCy_3 complexes, which have chemical shifts at lower fields than the analogous P-*i*-Pr_3 complexes.

The hydride region of the ^{1}H NMR spectra of the PCy_3 and P-*i*-Pr_3 salts shows a slight up-field shift of the hydride resonance in the [K(1,10-diaza-18-crown-6)]$^+$ salts, relative to their [K(18-crown-6)]$^+$ analogues. Such changes were also observed in other protonic—hydridic bonded polyhydride compounds and are believed to be a characteristic feature of this phenomenon. A low-field shift in the resonance of the proton donor moiety is a characteristic feature of protonic—hydridic bonding (2, 6, 9, 25, 29, 42–45). Thus, the results in Table 2 clearly indicate that these interactions are present in the [K(1,10-diaza-18-crown-6)]$^+$ salts, the extent of which is obviously dependent on the nature of the tertiary phosphine ligands. Relative to δ NH of [K(1,10-diaza-18-crown-6)][BPh_4], Δδ NH of the polyhydride salts is in the order PPh_3 < PMe_3 < P-*i*-Pr_3, which is consistent with the trend observed for the change in the hydride chemical shift relative to the [K(18-crown-6)]$^+$ salts. The much smaller change for the PPh_3 complex may be due to shielding caused by the phenyl ring currents. The NH peak of **2a** is obscured by the peaks of the tricyclohexylphosphine protons.

Only **2c** has a resonance for the NH in the ^{1}H NMR spectrum that is free from overlap with those of the phosphine ligands. On this basis **2c** was chosen for a NOE difference experiment. Irradiation of the hydride resonance at –6.90 ppm resulted in a definite, but unquantified, NOE enhancement of the NH resonance at 1.04 ppm. Likewise, irradiation of the NH resonance resulted in enhancement of the hydride resonance. This clearly indicates the existence of dipolar interactions between the hydrides and NH moieties in solutions of this complex.

© 2001 NRC Canada

Fig. 3. Molecular structure and atomic numbering of [K(1,10-diaza-18-crown-6)] [$ReH_6(P\text{-}i\text{-}Pr_3)_2$] (**2b**).

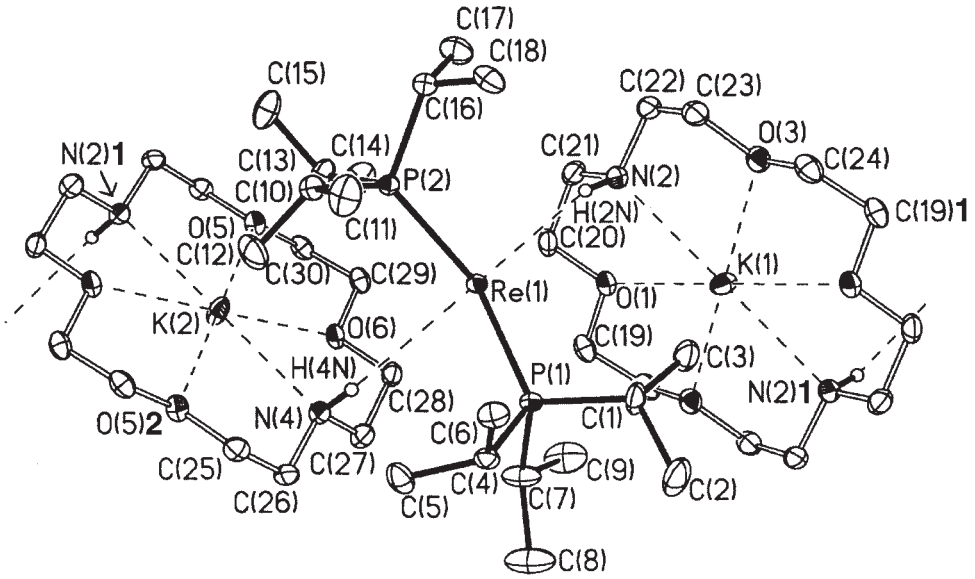


Table 4. Selected bond distances (Å) and angles (deg) for [K(1,10-diaza-18-crown-6)] [$ReH_6(P\text{-}i\text{-}Pr_3)_2$] (**2b**).

Bond distance (Å)			
Re(1)—P(1)	2.372(1)		
Re(1)—P(2)	2.352(1)		
K(1)—N(2)	2.826(4)	K(2)—N(4)	2.833(4)
K(1)—N(2)**1**	2.826(4)	K(2)—N(4)**2**	2.833(4)
K(1)—O(1)	2.876(3)	K(2)—O(5)	2.837(3)
K(1)—O(1)**1**	2.876(3)	K(2)—O(5)**2**	2.837(3)
K(1)—O(3)	2.836(3)	K(2)—O(6)	2.848(3)
K(1)—O(3)**1**	2.836(3)	K(2)—O(6)**2**	2.848(3)
Bond angles (deg)			
P(1)-Re(1)-P(2)	151.19(4)		
N(2)-K(1)-N(2)**1**	180.0	N(4)-K(2)-N(4)**2**	180.0

Spin lattice relaxation (T_1) is very sensitive to dipole–dipole interactions at short distances since the strength of the interaction is proportional to r^{-6}. Thus, T_1 measurements have been used to quantitatively determine the strength of protonic–hydridic interactions in neutral, cationic, and anionic protonic—hydridic bonded systems (2, 6, 9, 12, 24). Table 3 summarizes the ^1H T_1 times of the hydride and NH moieties in **1c** and **2c**, while Fig. 1 shows the plot of ln T_1 against inverse temperature for the hydride in each salt. This shows a lower hydride min T_1 in **2c** (156 ms, 500 MHz) relative to **1c** (172 ms, 500 MHz) indicating that there are small dipolar contributions from the NH moieties to the relaxation rate of the hydride nuclei. The min T_1 values are typical of classical rhenium polyhydride complexes with no short hydride–hydride distances (no dihydrogen ligands) (46). If a typical ReH···HN contact of 1.8 Å were present at all times, then we estimate that the minimum T_1 of **2c** should have been about 100 ms.[2] Therefore these protonic—hydridic-bonded ion pairs appear to be only a fraction of the total number of ion-pair structures in the toluene-d_8. However, the minimum T_1 of the hydride in **2c** occurs at a higher temperature (278 K) than in **1c**, which could be on account of the formation of intermolecular protonic—hydridic bonded aggregates of **2c** in solution. The minimum T_1 of the NH moiety of **2c** is 410 ms at 230 K, 500 MHz, which is significantly lower than the 548 ms at 189 K, 500 MHz reported for the NH in [K(diaza-18-crown-6)][$OsH_5(P\text{-}i\text{-}Pr_3)_2$] (6). This indicates that the average NH···HM distance is shorter for the rhenium compound than the osmium compound in solution. This also depends on differences in the dynamic behavior of the ion pairs.

Infrared spectra of the complexes

Changes in the IR stretching modes of both the proton donor and acceptor are characteristic of hydrogen bonding in general, including protonic—hydridic bonding. This allows the strength of this nonclassical hydrogen bond to be estimated using various empirical relationships (2, 6, 9, 43). The wavenumbers of the NH vibration modes for the series of [K(1,10-diaza-18-crown-6)]$^+$ salts in Nujol are listed in Table 2. Except for **2a**, the [K(1,10-diaza-18-crown-6)]$^+$ salts all show a decrease in the NH stretching mode relative to [K(1,10-diaza-18-crown-6)][BPh_4], in which there is no protonic–hydridic interaction. The IR spectrum of **2a** shows three ν NH bands at 3336, 3276, and 3178 cm^{-1}. This is unlike the trend observed for **2b**, **2c**, and **2d**, and may reflect the disordered structure of the ion pair detected by single crystal X-ray diffraction. The NH vibrational modes in **2b**, **2c**, and **2d** are broad singlets at 3229, 3214, and 3186 cm^{-1}, respectively, which are more intense and shifted to lower frequencies relative to those of [K(1,10-diaza-18-crown-6)][BPh_4] at 3284 and 3279 cm^{-1} (Fig. 2).

The broadening and shifting to lower frequency of the NH mode in these salts are indicative of protonic–hydridic inter-

[2] If we assume that **2c** has a structure with five hydrides with the same max relaxation rates at 500 MHz as **1c** (1/0.173 = 5.78 s^{-1}) and one hydride with an additional relaxation contribution from protonic—hydridic bonding at 1.8 Å (1/0.173 + 77.5/(1.8^2) = 29.7 s^{-1}) (46), then we calculate an averaged max relaxation rate of 5.78 × 5/6 + 29.7 × 1/6 = 9.77 s^{-1} which corresponds to a minimum T_1 of 102 ms.

© 2001 NRC Canada

Fig. 4. One-dimensional chain structure of [K(1,10-diaza-18-crown-6)][$ReH_6(P\text{-}i\text{-}Pr_3)_2$].

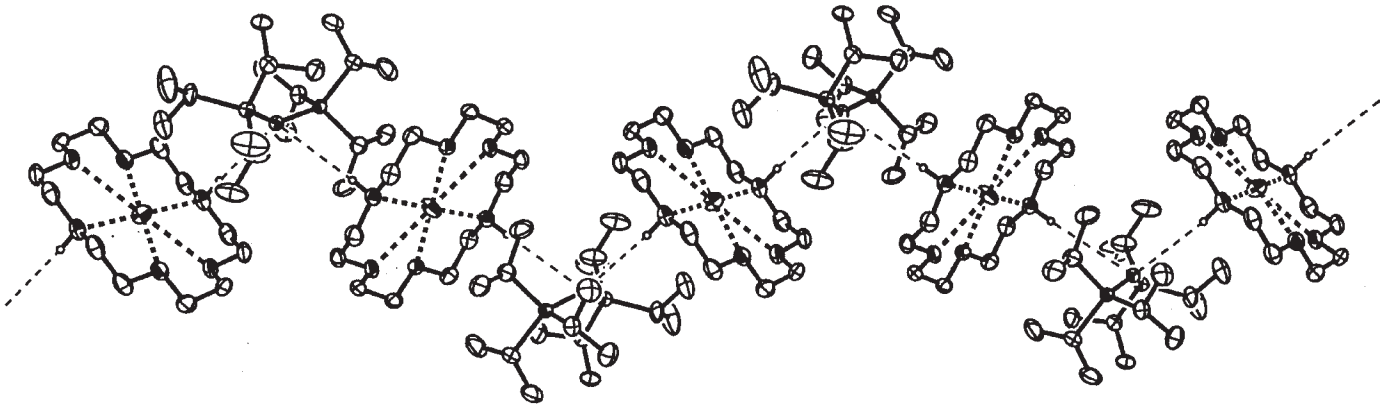
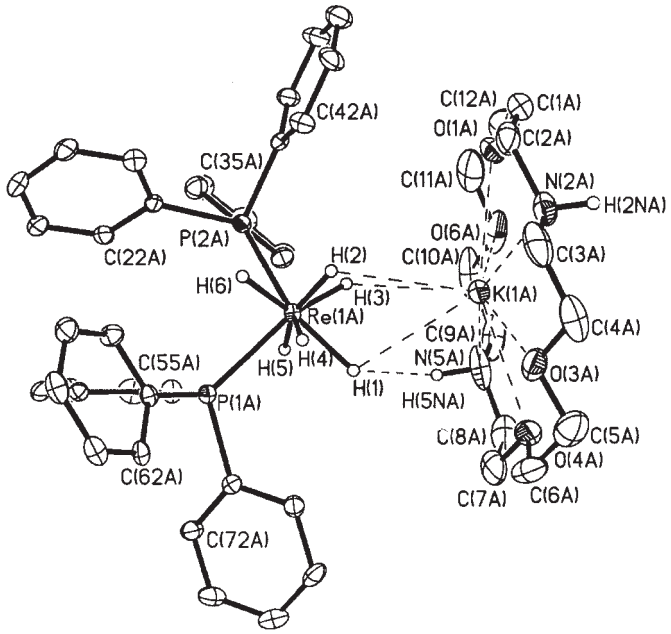


Fig. 5. Molecular structure and atomic numbering of [K(1,10-diaza-18-crown-6)][$ReH_6(PPh_3)_2$] (**2c**).



actions, the strength of which are in the order PPh_3 < PMe_3 < P-*i*-Pr_3. In addition, the intensities of the N-H vibrational modes in the salts differ immensely, and are in the order PPh_3 < PMe_3 < P-*i*-Pr_3; the same order as observed for Δν NH. Interestingly, the NH vibrational mode at 3178 cm^{-1} in **2a** is lower than any of the NH modes observed for **2b**, **2c**, and **2d**, and could possibly be due to a very strong intra-ion-pair protonic–hydridic interaction in this salt. Such a low NH vibrational mode would be consistent with the very low acidity of $ReH_7(PCy_3)_2$. Thus, the basicity and steric bulk of the ancillary phosphine ligands are obviously important factors in controlling and determining the extent of protonic–hydridic interactions in these salts.

The IR spectra of the hexahydride salts have lower ν ReH wavenumbers in the PCy_3 complex (1717 cm^{-1}) than for the PPh_3 complex (1884, 1853 cm^{-1}). A lower metal–hydride stretching frequency might be expected to be indicative of weaker metal—hydride bonding. This suggests that destabilization of the rhenium—hydride bonds in the anions is possibly a strong determinant in the acidity of the neutral conjugate species.

The formation of protonic—hydridic bonding in transition-metal complexes usually results in lower wavenumber and broad M-H vibrational modes. In general, the ν Re-H bands in the [K(1,10-diaza–18-crown-6)]$^+$ salts are much broader and more intense relative to those in the respective [K(18-crown-6)]$^+$ analogues. However, the presence of several Re-H bands and the overlapping of vibrational modes prevent correlation between the strength of the protonic—hydridic bond and Δν Re-H.

Deuteration studies

Complexes **2a**, **2b**, **2c**, and **2d** undergo H–D exchange upon exposure to an atmosphere of D_2 gas in toluene-d_8 and THF-d_8 solutions, with incorporation of deuterium in the NH moieties of the cations and hydride hydrogens of the anions. This is evidenced by a reduction in the intensities of the hydride and NH chemical shifts, and the observation of HD gas in the ^{1}H NMR spectra of the complexes. The reaction was invariably slow for all of complexes, requiring months for significant reduction in the intensities of the NH and hydride chemical shifts at room temperature. This prevented accurate comparisons of rates for the deuterium exchange process. On the other hand, no H–D exchange was observed for the series of [K(18-crown-6)]$^+$ salts over a similar time period. The observation of deuterium exchange in the [K(1,10-diaza-18-crown-6)]$^+$ salts is further evidence of close intermolecular contacts between the NH moieties of the cations and hydrides of the anions in solution of these salts.

Structure of the complexes

The crystal structures of the [K(1,10-diaza-18-crown-6)][$ReH_6(PR_3)_2$] salts were determined in this work. The structure of **2a** was disordered and contained several positional occupancies of the cation that prevented proper refinement. However, the anionic moiety in the unit cell crystallizes with *cis*-PCy_3 ligands, with a P-Re-P bond angle of 146.8°, while the potassium is shifted out of the plane of the cation, and is presumably electrostatically interacting with the undetected hydrides of the anion. The distance between the potassium of the cation and rhenium of the anion is 3.7 Å, which is similar to the 3.81 and 3.77 Å observed for the two units in **2c** (see below). Further discussion of this

© 2001 NRC Canada

Table 5. Selected bond distances (Å) and angles (deg) for [K(1,10-diaza-18-crown-6)] $[ReH_6(PPh_3)_2]$ (**2c**).

Bond distance (Å)			
Re(1A)—H(1)	1.68(4)	Re(1B)—H(7)	1.67(3)
Re(1A)—H(2)	1.48(4)	Re(1B)—H(8)	1.66(4)
Re(1A)—H(3)	1.61(4)	Re(1B)—H(9)	1.45(4)
Re(1A)—H(4)	1.37(4)	Re(1B)—H(10)	1.63(4)
Re(1A)—H(5)	1.48(4)	Re(1B)—H(11)	1.58(3)
Re(1A)—H(6)	1.60(4)	Re(1B)—H(12)	1.60(4)
Re(1A)—P(1A)	2.355(1)	Re(1B)—P(1B)	2.374(1)
Re(1A)—P(2A)	2.3757(1)	Re(1B)—P(2B)	2.357(1)
Re(1A)—K(1A)	3.808(1)	Re(1B)—K(1B)	3.770(1)
K(1A)—N(2A)	2.907(4)	K(1B)—N(2B)	2.885(4)
K(1A)—N(5A)	2.879(6)	K(1B)—N(5B)	2.885(4)
K(1A)—H(1)	3.08(4)	K(1B)—H(7)	3.01(4)
K(1A)—H(2)	2.88(4)	K(1B)—H(8)	2.96(4)
Bond angles (deg)			
P(1A)-Re(1A)-P(2A)	103.29(4)	P(1B)-Re(1B)-P(2B)	106.68(4)
N(2A)-K(1A)-N(5A)	154.8(1)	N(2B)-K(1B)-N(5B)	152.80(1)

Fig. 6. Tetrameric assembly of [K(1,10-diaza-18-crown-6)][$ReH_6(PPh_3)_2$]. Carbon atoms of the crown ether and phosphine ligands are omitted for clarity. An arbitrary numbering scheme has been used here.

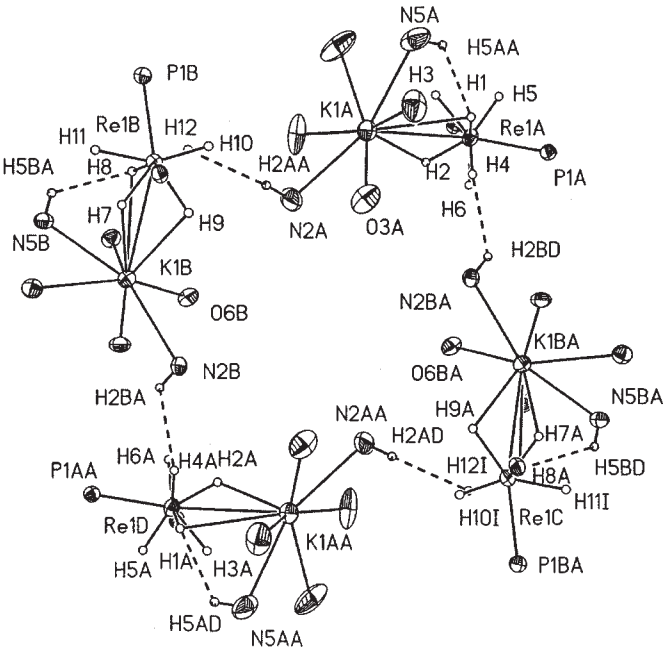
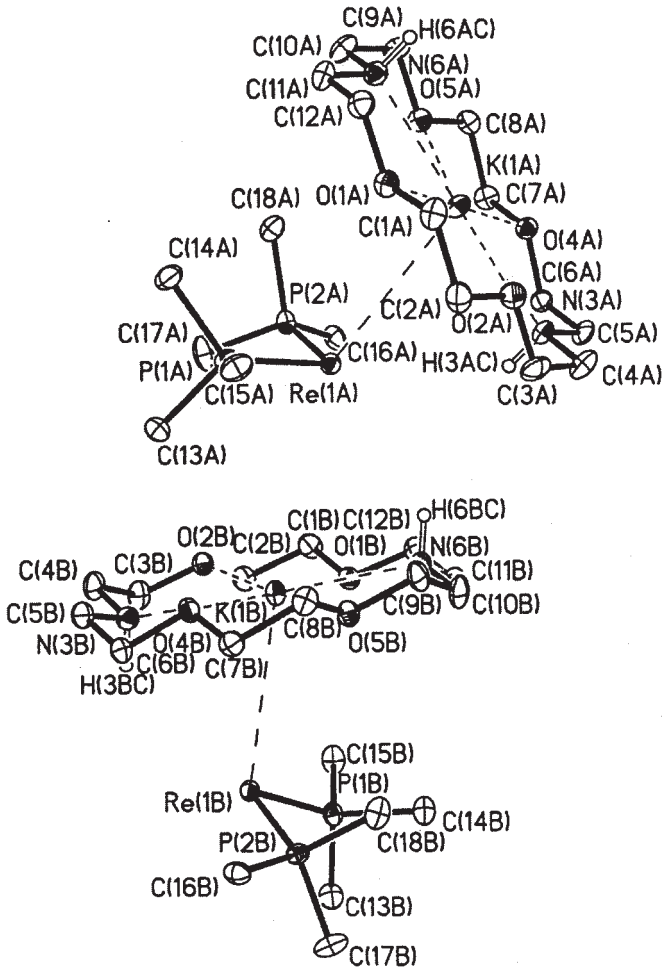


Fig. 7. Molecular structure and atomic numbering of [K(1,10-diaza-18-crown-6)][$ReH_6(PMe_3)_2$] (**2d**).



structure is not merited, on account of the extent of the disorder in the crystal structure.

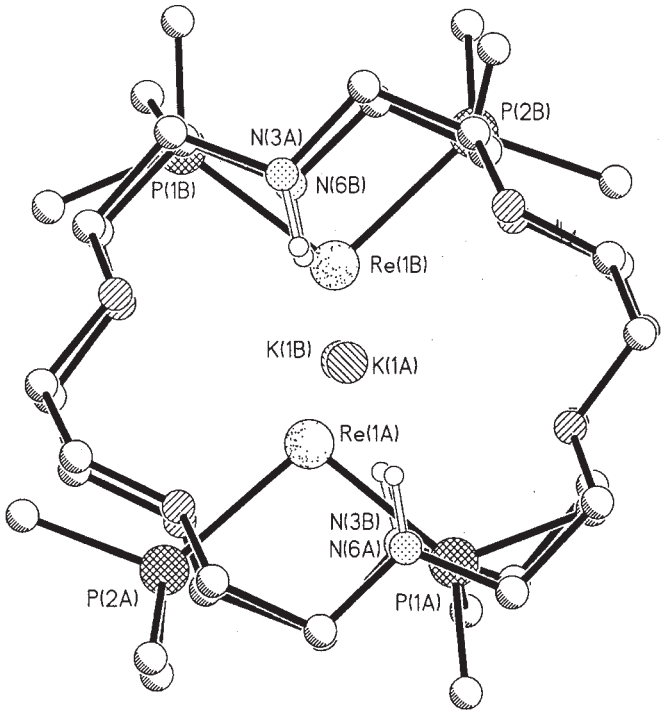
The crystal structure of **2b** is shown in Fig. 3 and includes the atomic numbering of all non-hydrogen atoms. Selected bond angles and bond lengths are listed in Table 4. The salt crystallizes with a THF molecule trapped in the crystal lattice which is not interacting with either the cation or anion. The hydrides of the anion were not located. The potassium is located on an inversion center in the cation. The P-Re-P bond angle is 151.19(4)°. The average Re—P bond distance is 2.362(1) Å which is longer than that observed in the isoelectronic $[MH_x(P\text{-}i\text{-}Pr_3)_2]^-$ anions (M = Ir, 2.261 Å; Os, 2.293 Å) (25). The cations are oriented so that the NH hydrogens are directed towards the rhenium of the anions, and are apparently interacting, through protonic—hydridic bonding, with the undetected hydrides.

© 2001 NRC Canada

Table 6. Selected bond distances (Å) and angles (deg) for [K(1,10-diaza-18-crown-6)][$ReH_6(PMe_3)_2$], **2d**.

Bond distance (Å)			
Re(1A)—P(1A)	2.342(1)	Re(1B)—P(1B)	2.340(2)
Re(1A)—P(2A)	2.333(1)	Re(1B)—P(2B)	2.335(1)
Re(1A)—K(1A)	3.881(1)	Re(1B)—K(1B)	3.860(1)
K(1A)—N(3A)	2.810(6)	K(1B)—N(3B)	2.828(6)
K(1A)—N(6A)	2.799(5)	K(1B)—N(6B)	2.802(5)
K(1A)—O(1A)	2.836(5)	K(1B)—O(1B)	2.811(5)
K(1A)—O(2A)	2.855(5)	K(1B)—O(2B)	2.849(5)
K(1A)—O(4A)	2.944(5)	K(1B)—O(4B)	2.941(5)
K(1A)—O(5A)	2.854(5)	K(1B)—O(5B)	2.867(5)
Bond angles (deg)			
P(1A)-Re(1A)-P(2A)	99.95(5)	P(1B)-Re(1B)-P(2B)	99.75(5)
N(3A)-K(1A)-N(6A)	177.4(2)	N(3B)-K(1B)-N(6B)	177.3(2)

Fig. 8. View of the asymmetric unit of [K(1,10-diaza-18-crown-6)][$ReH_6(PMe_3)_2$] showing the cylindrical assembly.



Unlike the linear one-dimensional chain structures observed for [K(1,10-diaza-18-crown-6)][$MH_x(P\text{-}i\text{-}Pr_3)_2$] (M = Ir, Os, Ru) (6, 25), the structure of the rhenium salt consist of zigzag chains of alternating cations and anions, since the NH moieties of the cations are interacting with hydrides on the same side of the anions and opposite to the two isopropylphosphine ligands. This is more clearly illustrated in Fig. 4.

The two NH moieties are approximately directly pointing towards the rhenium atom, with N-H-Re bond angles of 165 and 175°. If a typical N—H bond length of 1.0 Å is used, then the distances of the NH hydrogens of the cations from the rhenium atoms of the anions are 3.2 and 3.5 Å. Likewise, the distances of the nitrogen atoms from the rhenium atoms are 4.19 and 4.48 Å, respectively. These distances are equal or shorter than the corresponding distances of 3.4 Å (NH···Ru) and 4.37 Å (N···Ru) in [K(1,10-diaza-18-crown-6)][$RuH_5(P\text{-}i\text{-}Pr_3)_2$] (6), which is calculated to have a proton–hydride NH···HRu distance of 1.8 Å. These results indicate that short proton–hydride distances in the range of 1.6–1.9 Å are present in complex **2b**.

The molecular structure of **2c** consists of two similar structural units, each of which is comprised of two [K(1,10-diaza-18-crown-6)][$ReH_6(PPh_3)_2$] subunits, one of which is shown in Fig. 5. Selected bond lengths and angles are listed in Table 5. The two P-Re-P bond angles in each unit are 103.2° and 106.6°. The potassium is shifted 0.6 Å out of the best plane through the O_4N_2 ring towards the anion and is electrostatically bonded to three of the hydride ligands, with K—H bond lengths ranging from 2.81 to 3.01 Å. These distances are similar to the 2.63–2.92 Å reported in the crystal structure of [$K(THF)_2$][$ReH_6(PPh_3)_2$] (33).

The NH units of the cations are directed towards the hydrides of the anions to foster the formation of nonclassical hydrogen bonds. There are two types of NH···HRe interactions in the crystal structure (Fig. 6). One of these involves an intra-ion-pair protonic—hydridic bond between one of the NH moieties of the $[K(1,10\text{-diaza-18-crown-6})]^+$ cation and a hydride of its associated anion, with an NH···HRe bond distance of 2.3 Å. The other involves an inter-ion interaction between the other NH unit of the same cation and a hydride of the adjacent anion, with a similar NH···HRe bond distance of 2.3 Å. The N-H groups of the NH···HRe bonds are directed to a point beyond the Re—H bond in a similar fashion to the NH···HIr bonds in (pyridinethione)hydridoiridium(III) complexes (4–13). The two $[K(1,10\text{-diaza-18-crown-6})]^+$ cations interacting with each anion are oriented so that the N-Re-N bond angle subtended between the two NH moieties and the rhenium is 112.1°, while the angle between the best planes of the two cations is approximately 80°. The bonding arrangements and the relative orientation of the anions and cations result in the two structural units forming a two-dimensional tetrameric {[K(1,10-diaza-18-crown-6)][$ReH_6(PPh_3)_2$]}$_4$ assembly.

The structure of **2d** consists of two similar units, shown in Fig. 7 with appropriate atomic numbering. The metrical parameters are listed in Table 6. The two trimethylphosphine ligands in the anion are *cis* to each other with a P-Re-P bond angle of 99.91°. The crystal lattice consists of extended infinite one-dimensional chains of alternating and interpenetrating anions and cations, which are held together by a

© 2001 NRC Canada

Table 7. Comparison of selected solid-state properties of the complexes [K(1,10-diaza-18-crown-6)][$ReH_6(PR_3)_2$].

Phosphine	PMe_3	PPh_3	P-*i*-Pr_3	PCy_3
Tolman's cone angle (θ)	118	145	160	170
Re-P (Å)	2.34	2.36, 2.37	2.36	2.36
P-Re-P (°)	100	106.6, 103.2	151	147
N···Re (Å)	4.02	4.19	4.19	—
N′···Re′ (Å)[a]	4.12	4.20	4.48	—
K···Re (Å)	3.86	3.81	5.33	3.7
K···Re′ (Å)[b]	3.88	6.23	5.85	8.4
IR Δν NH (cm^{-1})[c]	67	52	95	103, 5

[a]N′ refers to the other nitrogen in the diazacrown while Re′ is the closest Re to this N′.
[b]Re′ is the next closest Re to this potassium ion.
[c]Shift to lower wavenumber from the ν NH of [K(1,10-diaza-18-crown-6)]BPh_4 (3281 cm^{-1}) that is not involved in H-bonding.

combination of inter-ion protonic–hydridic, N-H···H-Re, and Re-H_x···K^+···H_xRe, interactions.

The anion is oriented so that the two phosphine ligands are directed away from the cations, with the P-Re-P plane almost perpendicular to the plane containing the two NH moieties of neighboring cations and the rhenium of the anion. The N-Re-N angle between the NH moieties of the neighboring cations and the rhenium of the anion is 74.8°. This arrangement facilitates the most unhindered approach of the NH moieties and potassium of the two neighboring cations to the undetected hydrides of the anion. The potassium atom is only slightly out of the plane of the crown ether, with a N-K-N bond angle of 177.3°. The NH hydrogens of the cation are not directly pointed at the hydrides of the anion. This may be due to a steric imposition on the structure so as to accommodate both types of interactions. There is also the possibility of the formation of bifurcated bonding modes between the proton and two or more hydrides of the anion. The distances of the NH protons of the cations from the rhenium of the anion are 3.32 and 3.34 Å, while the distances of the respective nitrogen atoms from the rhenium are 4.02 and 4.12 Å. These distances indicate much closer approaches of the NH moieties to the anion than in any other [K(1,10-diaza-18-crown-6)]$^+$ polyhydride salt. The electrostatic interaction between the potassium atom and hydrides of the anions is obviously a very significant synergistic contributor to the extended molecular chain assembly. The Re-K distances of adjoining cations are 3.87 and 4.44 Å. If typical Re-H distances of 1.65 Å are assumed, then the estimated H^-···K^+ distances are 2.22 and 2.79 Å, which are much shorter than those observed in complexes **2b** and **2c**.

An interesting feature of the molecular structure of **2d** is the observation of an extended one-dimensional cylindrical supramolecular assembly when the molecular chain assembly is viewed along its axis. This is illustrated in Fig. 8. The cylindrical stacking is such that all the potassium atoms of the [K(1,10-diaza-18-crown)]$^+$ cations are superimposed, while the rhenium atoms of the anions are arranged in an alternating fashion on either side of the potassium atoms and are superimposed. The constituent atoms of the 1,10-diaza-18-crown-6 (C, N, O) are superimposed. The two sets of trimethylphosphine ligands on either side of the cations are also superimposed. The overall structure is such that the metal atoms and hydride ligands (undetected) occupy the interior, while the organic moieties of the crown-ether and phosphine ligands line the periphery of the supramolecular cylindrical structure.

Comparison of the solid-state properties

Table 7 lists selected properties of the complexes in the order of increasing size of the ligands according to the Tolman's cone angle θ (47). The usual increase in metal—phosphorus bond length with increase in θ is observed. The small P-Re-P angles for the PMe_3 and PPh_3 complexes may result from the strong interaction of the potassium with the hydrides; in each case there are short K···Re distances. The PCy_3 complex also appears to have a short K···Re distance but it maintains a larger angle between the bulky phosphine ligands apparently by a distortion of the crown, that is not well-defined because of the disorder in the structure. The structures (the first three, at least) have the common property of containing short Re···N distances (4.0–4.5 Å) to all of the nitrogens in the crowns. Clearly ReH···HN bonding is important in all cases when judged by these distances and the reduction in ν NH from the non-hydrogen-bonded value of approximately 3281 cm^{-1}. The P-*i*-Pr_3 structure is unique in that NH···HRe bonding is more important than K···HRe bonding. This is seen in the long, uniform 5.3 and 5.85 Å spacing between the K^+ and $ReH_6(P\text{-}i\text{-}Pr_3)_2^-$ centres.

Conclusions

Reaction of $ReH_7(PR_3)_2$ with KH in the presence of 18-crown-6 and 1,10-diaza-18-crown-6 resulted in the formation of [K(crown-ether)][$ReH_6(PR_3)_2$] salts. The solid-state structures of the [K(1,10-diaza-18-crown-6)]$^+$ salts vary with the size of the ligands. The disordered salt with large PCy_3 groups appears to consist of isolated 1:1 ion pairs with a strong intra-ion-pair NH···HRe bond. In contrast the P-*i*-Pr_3 salt has evenly spaced anions and cations in a chain held together by protonic—hydridic bonds. The salt with the smaller PPh_3 groups consists of 1:1 ion pairs with K···HRe and intra-ion-pair NH···HRe bonding with additional weaker, inter-ion-pair NH···HRe bonds that result in a unique ring structure of four ion pairs. The small $ReH_6(PMe_3)_2^-$ units allow close approach of the potassium and NH groups to form

© 2001 NRC Canada

chains held together by Re-$H_x^-\cdots K^+\cdots H_x^-$-Re and NH···HRe interactions.

Intermolecular protonic—hydridic bonding is also present in solutions of these salts, as illustrated by the ^{1}H NMR variable temperature T_1 and NOE measurements of [K(1,10-diaza-18-crown-6)][$ReH_6(PPh_3)_2$]. The strength of the protonic—hydridic bonds was qualitatively examined by the change in the NH stretching frequency of the cation as a function of the ancillary phosphine ligands of the anions, and was found to be in the order $PPh_3 < PMe_3 <$ P-*i*-Pr_3. The pK_α^{THF} of the neutral conjugate acids $ReH_7(PR_3)_2$, is in the order $PPh_3 << PMe_3 <$ P-*i*-$Pr_3 < PCy_3$. Thus the strength of the protonic–hydridic interactions is clearly dependent on the basicity of the anions. Even though $[ReH_6(PCy_3)_2]^-$ represents the most basic anion, there appear to be both strong and weak protonic—hydridic bonds on the basis of ν NH in the disordered solid-state structure of its [K(1,10-diaza-18-crown-6)]$^+$ salt.

Acknowledgements

This work was supported by a grant to R.H.M from the Natural Sciences and Engineering Research Council of Canada (NSERC). Dr. Timothy Burrow is gratefully acknowledged for assistance with the high-field NMR studies.

Supporting information

X-ray crystallographic tables (55 pages) for complexes **2b**, **2c**, and **2d** may be purchased from the Depository of Unpublished Data, Document Delivery, CISTI, National Research Council Canada, Ottawa, ON K1A 0S2, Canada (http://www.nrc.ca/cisti/irm/unpub_e.shtml for information on ordering electronically). Crystal data, data collection and refinement parameters, atomic coordinates, bond lengths and angles, and hydrogen coordinates have been deposited with the Cambridge Crystallographic Data Centre. Copies of the data can be obtained, free of charge, on application to the Director, CCDC, 12 Union Road, Cambridge CB2 1EZ, U.K. (Fax: 44-1223-336033 or e-mail: deposit@ccdc.cam.ac.uk).

References

1. R.C. Stevens, R. Bau, D. Milstein, O. Blum and, and T.F. Koetzle. J. Chem. Soc. Dalton Trans. 1429 (1990).
2. A.J. Lough, S. Park, R. Ramachandran, and R.H. Morris. J. Am. Chem. Soc. **116**, 8356 (1994).
3. J.C. Lee, Jr, A.L. Rheingold, B. Muller, P.S. Pregosin, and R.H. Crabtree. J. Chem. Soc. Chem. Comm. 1021 (1994).
4. R.H. Morris. Can. J. Chem. **74**, 1907 (1996).
5. W. Xu, A.J. Lough, and R.H. Morris. Can. J. Chem. **75**, 475 (1997).
6. K. Abdur-Rashid, D.G. Gusev, A.J. Lough, and R.H. Morris. Organometallics, **19**, 834 (2000).
7. R.H. Crabtree. J. Organomet. Chem. **557**, 111 (1998).
8. P. Desmurs, K. Kavallieratos, W.B. Yao, and R.H. Crabtree. New J. Chem. **23**, 1111 (1999).
9. E.S. Shubina, N.V. Belkova, A.N. Krylov, E.V. Vorontsov, L.M. Epstein, D.G. Gusev, M. Niedermann, and H. Berke. J. Am. Chem. Soc. **118**, 1105 (1996).
10. J.A. Ayllon, S.F. Sayers, B. Donnadieu, B. Chaudret, and E. Clot. Organometallics, **18**, 3981 (1999).
11. H.S. Chu, C.P. Lau, K.Y. Wong, and W.T. Wong. Organometallics, **17**, 2768 (1998).
12. L.M. Epstein and E.S. Shubina. Ber. Bunsen-Ges. Phys. Chem. Chem. Phys. **102**, 359 (1998).
13. S. Aime, R. Gobetto, and E. Valls. Organometallics, **16**, 5140 (1997).
14. T.B. Richardson, S. de Gala, and R.H. Crabtree. J. Am. Chem. Soc. **117**, 12875 (1995).
15. W.T. Klooster, T.F. Koetzle, P.E.M. Siegbahn, T.B. Richardson, and R.H. Crabtree. J. Am. Chem. Soc. **121**, 6337 (1999).
16. P.D. Godfrey, W.J. Grigsby, P.J. Nichols, and C.L. Raston. J. Am. Chem. Soc. **119**, 9283 (1997).
17. J.P. Campbell, J.-W. Hwang, J. Victor G. Young, R.B.V. Dreele, C.J. Cramer, and W.L. Gladfelter. J. Am. Chem. Soc. **120**, 521 (1998).
18. L.M. Epstein, E.S. Shubina, E.V. Bakhmutova, L.N. Saitkulova, V.I. Bakhmutov, A.L. Chistyakov, and I.V. Stankevich. Inorg. Chem. **37**, 3013 (1998).
19. S.C. Gatling and J.E. Jackson. J. Am. Chem. Soc. **121**, 8655 (1999).
20. P.L.A. Popelier. J. Phys. Chem. A, **102**, 1873 (1998).
21. Q. Liu and R. Hoffmann. J. Am. Chem. Soc. **117**, 10108 (1995).
22. G.M. Whitesides, E.E. Simanek, J.P. Mathias, C.T. Seto, D.N. Chin, M. Mammen, and D.M. Gordon. Acc. Chem. Res. **28**, 37 (1995).
23. K.J. Haack, S. Hashiguchi, A. Fujii, T. Ikariya, and R. Noyori. Angew. Chem. Int. Ed. Engl. **36**, 285 (1997).
24. D.G. Gusev, A.J. Lough, and R.H. Morris. J. Am. Chem. Soc. **120**, 13138 (1998).
25. K. Abdur-Rashid, D.G. Gusev, S.E. Landau, A.J. Lough, and R.H. Morris. J. Am. Chem. Soc. **120**, 11826 (1998).
26. R. Custelcean and J.E. Jackson. J. Am. Chem. Soc. **120**, 12935 (1998).
27. R. Custelcean and J.E. Jackson. Angew. Chem. Int. Ed. Engl. **38**, 1661 (1999).
28. R. Custelcean, M. Vlassa, and J.E. Jackson. Angew. Chem. Int. Ed. **39**, 3299 (2000).
29. J.A. Ayllon, C. Gervaux, S. Sabo-Etienne, and B. Chaudret. Organometallics, **16**, 2000 (1997).
30. K. Abdur-Rashid, A.J. Lough, and R.H. Morris. Organometallics, **19**, 2655 (2000).
31. K. Abdur-Rashid, A.J. Lough, and R.H. Morris. Organometallics, **20**, 1047 (2001).
32. K. Abdur-Rashid, T.P. Fong, B. Greaves, D. Gusev, J.G. Hinman, S.E. Landau, A.J. Lough, and R.H. Morris. J. Am. Chem. Soc. **122**, 9155 (2000).
33. D. Alvarez, E.G. Lundquist, J.W. Ziller, W.J. Evans, and K.G. Caulton. J. Am. Chem. Soc. **111**, 8392 (1989).
34. D. Baudry and M. Ephritikhine. J. Organomet. Chem. **311**, 189 (1986).
35. J.W. Bruno, J.C. Huffman, M.A. Green, and K.G. Caulton. J. Am. Chem. Soc. **106**, 8310 (1984).
36. E.H.K. Zeiher, D.G. DeWit, and K.G. Caulton. J. Am. Chem. Soc. **106**, 7006 (1984).
37. S.W. Carr, E.H. Fowles, X.L.R. Fontaine, and B.L. Shaw. J. Chem. Soc. Dalton Trans. 573 (1990).
38. D. Baudry, M. Ephritikhine, and H. Felkin. J. Organomet. Chem. **224**, 363 (1982).

© 2001 NRC Canada

39. D. Lyons and G. Wilkinson. J. Chem. Soc. Dalton Trans. 587 (1985).
40. X.L. Luo and R.H. Crabtree. J. Am. Chem. Soc. **112**, 4813 (1990).
41. J. Hinman, K. Abdur-Rashid, A.J. Lough, and R.H. Morris. Inorg. Chem. **40**, 2480 (2001).
42. J.C. Lee, E. Peris, A.L. Rheingold, and R.H. Crabtree. J. Am. Chem. Soc. **116**, 11 014 (1994).
43. E. Peris and E. Crabtree. J. Chem. Soc. Chem. Commun. 2179 (1995).
44. E. Peris, J.C. Lee, J.R. Rambo, O. Eisenstein, and R.H. Crabtree. J. Am. Chem. Soc. **117**, 3485 (1995).
45. B.P. Patel, J. Wessel, W. Yao, J.C. Lee, E. Peris, T.F. Koetzle, G.P.A. Yap, J.B. Fortin, J.S. Ricci, G. Sini, A. Albinati, O. Eisenstein, A.L. Rheingold, and R.H. Crabtree. New J. Chem. **21**, 413 (1997).
46. P.J. Desrosiers, L. Cai, Z. Lin, R. Richards, and J. Halpern. J. Am. Chem. Soc. **113**, 4173 (1991).
47. C.A. Tolman. Chem. Rev. **77**, 313 (1977).

© 2001 NRC Canada

A computational approach to seeking methylmercury(II) thiolate calix[4]arene hosts for both octasulfur and organosulfur compounds as guests

Stephan Knoblauch, H. Fred Koch, Catherine Polydore, and D. Max Roundhill

Abstract: Calculations have been carried out on the conformational preferences of calix[4]arene thiols and their methylmercury(II) derivatives. Calculations have also been carried out on host–guest combinations of methylmercury(II) ethanethiolate calix[4]arenes and 1,4-dithiacyclohexane, octasulfur, thiacyclopropane, and thiophene. For the 1,4-dithiacyclohexane, thiacyclopropane, and thiophene guests, calculations have been carried out for both 1:1 and 1:4 ratios of the methylmercury(II) ethanethiolate calix[4]arene to the sulfur containing guests. For octasulfur only the 1:1 host–guest ratio has been considered because it has four sulfurs that are conformationally arranged to bind to the four mercury(II) centers. The computational results generally show that host–guest formation is enthalpically favored over the separated molecules in cases where adducts with mercury-sulfur donor atom interactions are allowed to reach energy minima.

Key words: calixarene, methylmercury, octasulfur, organosulfur compounds.

Résumé : On a effectué des calculs théoriques sur les préférences conformationnelles des calix[4]arènethiols et de leurs dérivés méthylmercure(II). On a aussi effectué des calculs sur des combinaisons hôte–invité entre les dérivés méthylmercure(II) de calix[4]arèneéthanethiolates et le 1,4-dithiacyclohexane, l'octasoufre, le thiacyclopropane et le thiophène. Dans les cas où l'invité est le 1,4-dithiacyclohexane, l'octasoufre et le thiophène, on a effectué des calculs pour des rapports 1:1 et 1:4 de dérivés méthylmercure(II) de calix[4]arèneéthanethiolates et de molécules invitées contenant du soufre. Dans le cas de l'octasoufre, on n'a considéré que les résultats du rapport 1:1 en raison du fait que cette molécule comporte quatre atomes de soufre qui sont conformationnellement arrangés pour se lier aux quatre centres mercure(II). Pour les cas où les adduits comportant des interactions entre le mercure et l'atome donneur de soufre peuvent atteindre les énergies minimales, les résultats des calculs montrent que d'une façon générale, la formation d'une paire hôte–invité est enthalpiquement favorisée par rapport aux molécules séparées.

Mots clés : calixarène, méthylmercure, octasoufre, composés organosulfurés.

[Traduit par la Rédaction]

Introduction

Calixarenes are cyclic oligomers that have cavities that can occlude guest molecules. These calixarene molecules have a wide rim with *tert*-butyl substituents, and a narrow rim with phenol groups (1). The guest molecules can be uncharged organic compounds, anions, or metal cations that bind to selective functional groups. An alternate target is to prepare metallocalixarenes that can act as selective hosts for different classes of organic molecules, especially those that can interact with the metal centers (2). Although there are examples of metallacages that can act as hosts, there are few examples of such hosts being constructed from calixarenes (3–11).

One approach is to target metallocalixarenes with metals on either rim as selective hosts for elemental sulfur, organosulfur, or organonitrogen compounds. The discovery of hosts for these compounds is important because environmental concerns place ever more stringent requirements on removing sulfur, organosulfur compounds, and organonitrogen compounds from hydrocarbon mixtures. To remove trace quantities of these compounds from pure hydrocarbons, one approach is to use a host that will selectively bind them. One strategy therefore is to use size and shape selectivity to achieve this goal, but another is to use the coordination properties of the metals in the metallocages to bind the sulfur atoms in the targeted guest molecules. Since mercury(II) forms stable complexes with sulfur donor ligands, we have computationally targeted methylmercuric thiolate calix[4]arenes as hosts for sulfur and organosulfur compounds.

Results

Calculations were carried out on a DEC α computer system (433 MHz) using the SPARTAN Version 5.0.2 software

Received August 8, 2000. Published on the NRC Research Press Web site at http://canjchem.nrc.ca on July 11, 2001.

Dedicated to Professor Brian R. James on the occasion of his 65th birthday.

S. Knoblauch[1], H.F. Koch, C. Polydore, and D.M. Roundhill. Department of Chemistry and Biochemistry, Texas Tech. University, Lubbock, TX 79409-1061, U.S.A.

[1]Corresponding author (telephone: (806) 742-3067; fax: (806) 742-1289; e-mail: ULDMR@ttacs.ttu.edu).

 DOI: 10.1139/cjc-79-5/6-977 © 2001 NRC Canada

Table 1. Conformational energies of narrow rim 2-ethanethio calix[4]arenes (R = *tert*-butyl).

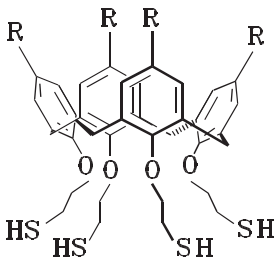
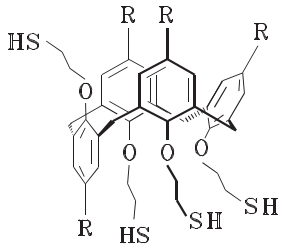
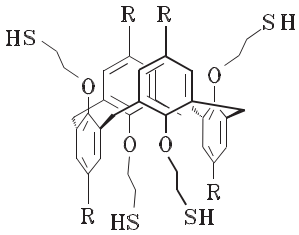
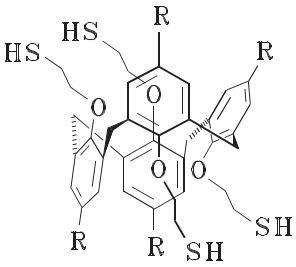
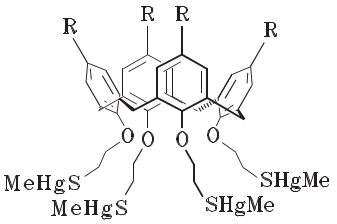
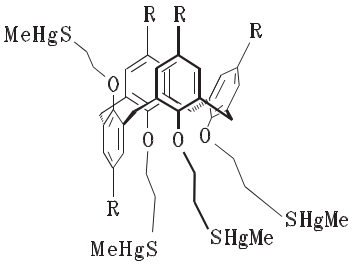
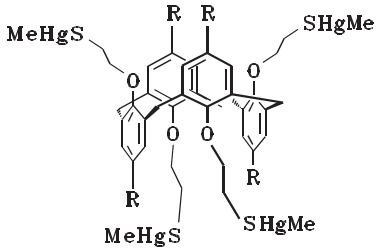
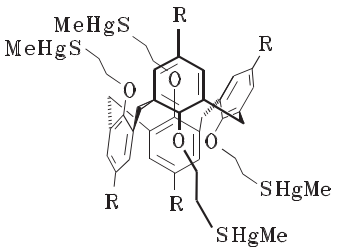
Compound	Energy (kcal mol^{-1})
 Cone u, u, u, u	–129
 Partial cone u, u, u, d	–104
 1, 3–Alternate u, d, u, d	–138
	–134

Table 2. Conformational energies of narrow rim 2-ethanethiomercuriomthyl calix[4]arenes (R = *tert*-butyl).

Compound	Energy (kcal mol^{-1})
 Cone u, u, u, u	–159
 Partial cone u, u, u, d	–89
 1, 3–Alternate u, d, u, d	–30
 1, 2–Alternate u, u, d, d	–115

package. This package was chosen because it has the algorithms available for metals such as mercury. All calculations were carried out using PM3 geometry optimization. All reasonable conformations were computationally searched before the one with the minimum energy was chosen. The enthalpies for the systems that we have investigated are collected in Tables 1–7. These chosen systems are the conformational preferences for the 2-ethanethiol narrow rim substituted calix[4]arene (10) and its methylmercury(II) de-

© 2001 NRC Canada

Table 3. Computational energies of separated organomercuric calix[4]arene hosts and cyclic sulfur guests (R = *tert*-butyl).

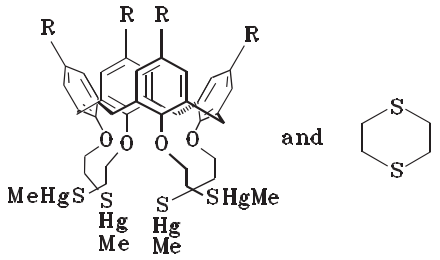
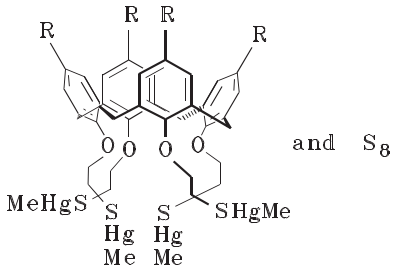
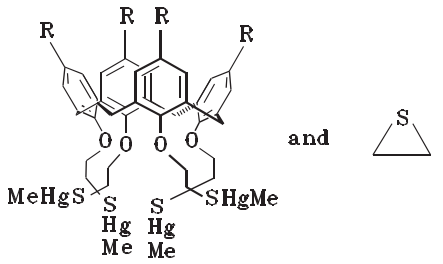
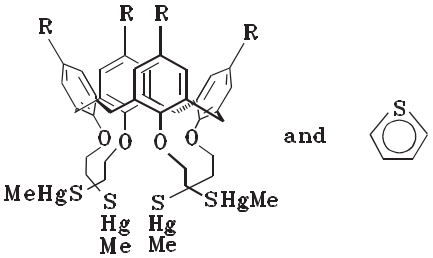
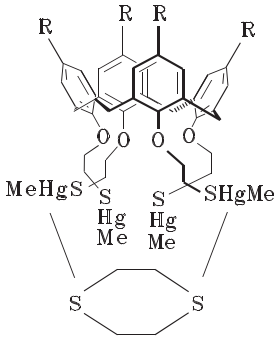
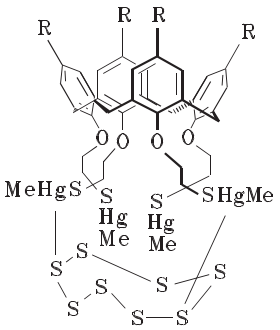
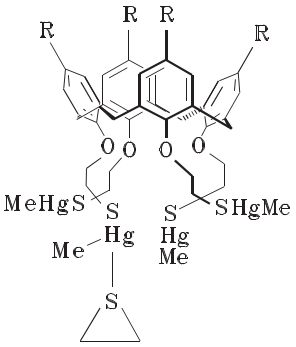
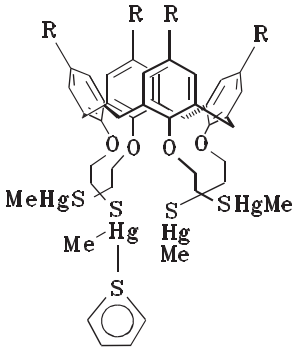
Compound	Energy (kcal mol^{-1})
	–93
	–91
	–60
	–107

Table 4. Computational energies of combined organomercuric calix[4]arene hosts and cyclic sulfur guests (R = *tert*-butyl).

Compound	Energy (kcal mol^{-1})
	–142
	–216
	–126
	–104

rivative. Other systems on which calculations have been carried out combine this methylmercury(II) calix[4]arene with 1,4-dithiahexane, octasulfur, thiacyclopropane, and thiophene. Pairwise calculations have been made for both the bound and unbound combinations among these compounds, and calculations have been carried out with both one and four organosulfur compounds associated with the methylmercury(II)-substituted calix[4]arene through mercury(II)–sulfur donor atom interactions. Conformational calculations have also been carried out on the simple calix[4]arene thiol (12) and its hypothetical methylmercury(II) derivative, along with the octasulfur adduct of the methylmercury(II) derivative. For comparison, calculations have also been carried out on the hypothetical derivatives having the thiol or methylmercury functionalities on the wide rim, and also on a host–guest octasulfur compound with this wide rim functionalized methylmercury(II)-

© 2001 NRC Canada

Table 5. Computational energies of organomercuric calix[4]arene hosts and a potential elemental sulfur guest.

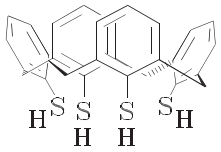
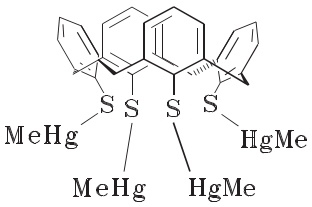
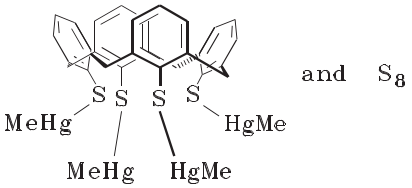
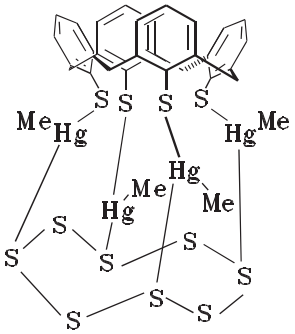
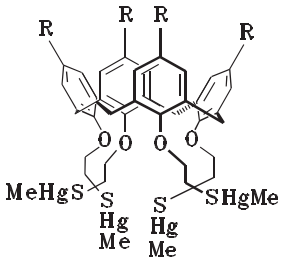
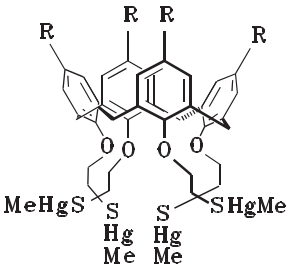
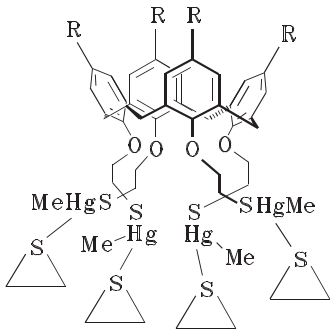
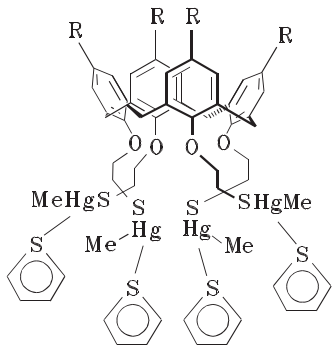
Compound	Energy (kcal mol^{-1})
	+117
	+177
 and S_8	+208
	+120

Table 6. Computational energies of organomercuric calix[4]arene hosts and multiple potential guests (R = *tert*-butyl).

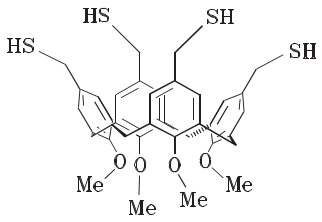
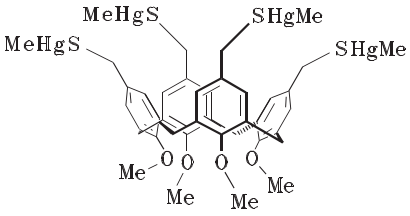
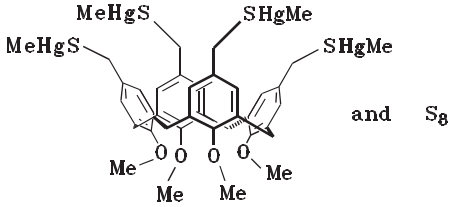
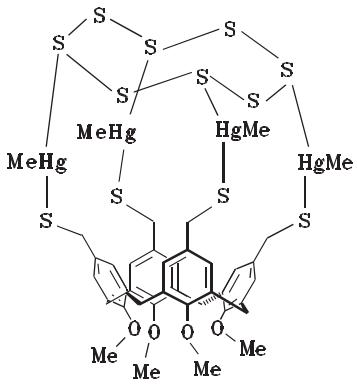
Compound	Energy (kcal mol^{-1})
 and 4 	–23
 and 4 	+84
	–58
	–18

substituted calix[4]arene. In each calculation the energy min is sought for each compound investigated. Nevertheless, we recognize that in molecules of this size and complexity with heavy metals present there are many conformational types possible, so we only consider large differences in energy as being significant, and we have made no attempt to rationalize small energy differences as we have sought the lowest energy conformation.

The results in Table 1 summarize the computational energies found for the cone (*u*, *u*, *u*, *u*), partial cone (*u*, *u*, *u*, *d*), 1,3-alternate (*u*, *d*, *u*, *d*), and 1,2-alternate (*u*, *u*, *d*, *d*) of the 2-ethanethiol-substituted calix[4]arenes. The computations on this particular molecule in some respects have been carried out as an evaluation of our method. As expected the calculations show that there are only small energy differences between the four different conformers. The highest energy is found for the partial cone conformation (–104 kcal mol^{-1}), with the other three conformers being very closely spaced in energy (–129 to –138 kcal mol^{-1}). This is not an unreasonable finding. The results in Table 2 are again conformational energies, but this time for the methylmercury(II) ethanethiolate-substituted calix[4]arene. Again computational energy differences are observed, but now the difference in energies between the conformers are considerably larger, ranging from –30 to –159 kcal mol^{-1}. These larger conformational energy values likely result from the steric interactions being greater

© 2001 NRC Canada

Table 7. Computational energies of wide rim substituted calix[4]arenes and their host–guest combinations.

Compound	Energy (kcal mol^{-1})
	–43
	+58
 and S_8	+164
	–115

for compounds with methylmercury groups than for hydrogens on sulfur, and also because there are many more electrons in the methylmercury(II) groups than hydrogen that will be affected by these interactions. These computational results suggest that the cone conformation (–159 kcal mol^{-1}) will be the most favored conformation, and that the 1,3-alternate will be the least favored. Because we find the cone conformation to be the most computationally favored, it is this conformer that we have used to compute the energies of the adducts with sulfur and organosulfur guests.

In computing the energies of the different host–guest combinations we have in each case made two sets of calculations. In the first case we calculate the energy of the system when the host and guest(s) are placed sufficiently far apart that there are no interactions between the two molecules. In the second case the host–guest molecules are initially placed sufficiently close that intermolecular attractions between mercury(II) and sulfur donor atoms can occur. During minimization the host–guest combination remain within their van der Waals radii. In each case we have carried out a sufficient number of iterations (usually of the order of 200–300) that minimization occurs. This strategy of carrying out pairwise calculations is employed because each computational pair involves systems that are isoelectronic with each other, and therefore direct comparisons can be made between the two systems. In Table 3 the computational data for the separated host–guest pairs are collected for the methylmercury(II) ethanethiolate calix[4]arene and a single 1,4-dithiacyclohexane, octasulfur, thiacyclopropane, or thiophene molecule, and in Table 4 the data are the results for the systems where these host–guest combinations interact. Since we anticipate that the largest interactions within these pairs will be between the mercury centers on the host and the electron pairs on sulfur on the guest, these are the configurations that we have allowed to minimize. For the energy differences between the separated and combined host–guest configurations we obtain the following values in kcal mol^{-1}, where a negative value corresponds to a lowering in energy upon host–guest adduct formation: 1,4-dithiacyclohexane (–49), octasulfur (–125), thiacyclopropane (–66), and thiophene (+3). The large decrease in energy resulting from interaction of the sulfur atoms of octasulfur with the four mercury(II) centers in the methylmercury(II) ethanethiolate calix[4]arene indicates that there is a very favorable host–guest interaction between the two. This favorability is a consequence of their being four mercury(II)–octasulfur interactions in the molecule, and that the octasulfur can maintain its preferred chair conformation in the bound host–guest system. The energy lowering upon forming a host–guest complex with either 1,4-dithiacyclohexane or thiocyclopropane is significantly smaller. In each case there are fewer mercury(II)–sulfur interactions than there are with octasulfur. The greater lowering in enthalpy for thiacyclopropane (–66) than for 1,4-dithiacyclohexane (–49) is interesting, especially since the latter has two mercury(II)–sulfur interactions. A possible explanation for this result is that the advantage of the additional mercury–sulfur interaction is counteracted by the raising of the conformational energy of the guest, since in the host–guest complex the 1,4-dithiacyclohexane is present in the boat conformer rather than in the energetically favored chair.

The simple calix[4]arene thiol with SH rather than OH groups on the narrow rim has been reported in the literature (13), and a series of host–guest molecules are also potentially available from this precursor. We have therefore computationally investigated the methylmercury(II) derivative of this precursor, along with its host–guest complex with octasulfur. The results of these calculations are collected in Table 5. Again we find that the host–guest complex has a lower energy than does the separated pair, with the energy lowering being 88 kcal mol^{-1}. This change is smaller than is observed with the previous system, which has an oxygen and the two additional methylene groups of the ethanethiolate moiety on the narrow rim. This reduced lowering of enthalpy upon host–guest formation with the shorter chain

© 2001 NRC Canada

system may be a consequence of this system having the mercury(II) centers closer to the calix[4]arene template, and therefore having less conformational flexibility to adapt to the steric requirements of the octasulfur guest molecule.

A further set of calculations have been carried out for thiacyclopropane and thiophene as a guest. In these calculations each methylmercury(II) host is associated with a single sulfur atom, which leads to a host:guest ratio of 1:4. Again, computational comparisons are made between the separated and complexed analogs (Table 6). For thiacyclopropane, the enthalpy decrease upon complexation of four molecules is 35 kcal mol^{-1}, and for four thiophene molecules the corresponding enthalpy decrease is 102 kcal mol^{-1}. Interestingly, the binding of four thiophenes results in a decrease in the enthalpy of the system, whereas the binding of a single thiophene results in a small enthalpy increase. Inspection of the two enthalpy minimized structures indicates that in the one with four bound thiophenes, the thiophene molecules are somewhat oriented in toward the calix[4]arene structure, possibly indicative of weak π-interactions between them. There is no indication of any π,π-interactions between the thiophene molecules themselves. A final set of calculations have been carried out on another hypothetical methylmercury(II) host. This host is similar to that shown in Tables 2–4, except that now these functionalities are present on the wide rim rather than on the narrow rim. These data are collected in Table 7. The host–guest combination with octasulfur show a decrease in enthalpy of 279 kcal mol^{-1} from the separated pair. Since this decrease is larger than is observed upon host–guest formation with the narrow rim substituted derivative (125 kcal mol^{-1}), it is suggestive that the wide-rim-substituted methylmercury(II) host may be a better one for an octasulfur guest than the narrow rim analog.

We suggest that this computational approach may have some validity in seeking hosts for octasulfur and organosulfur guests. We recognize that this approach has many limitations, and that the unfavorable entropic contribution will reduce the favorability of these host–guest adduct associations, and may even be sufficient to cause the free energies of host–guest formation to be positive. Clearly, experimental data will be required before approaches such as this one can be fully judged and evaluated.

Acknowledgements

We thank the Robert A. Welch Foundation and the U.S. Army Research Office for financial support. We thank Mario Rodriquez, Ekkehard Stehfest, and Greg Gellene for assistance.

References

1. C.D. Gutsche. Calixarenes revisited. *In* Monographs in supramolecular chemistry. *Edited by* J. Fraser Stoddart. The Royal Society of Chemistry, Cambridge, U.K. 1998.
2. D.M. Roundhill. Prog. Inorg. Chem. **43**, 533 (1995).
3. F.C.J.M. van Veggel, W. Verboom, and D.N. Reinhoudt. Chem. Rev. **94**, 279 (1994).
4. P.J. Stang and B. Olenyuk. Acc. Chem. Res. **30**, 502 (1997).
5. P.J. Stang. Chem. Eur. J. **4**, 19 (1998).
6. A.J. Stemmler, J.W. Kampf, and V.L. Pecoraro. Angew. Chem. Int. Ed. Engl. **35**, 2841 (1996).
7. Z. Zheng, C.B. Knobler, C.E. Curtis, and M.F. Hawthorne. Inorg. Chem. **34**, 432 (1995).
8. P.J. Stang, D.H. Cao, K. Chen, G.M. Gray, D.C. Muddiman, and R.D. Smith, Jr. Am. Chem. Soc. **119**, 5163 (1997).
9. D.C. Smith., Jr. Inorg. Chem. **37**, 1791 (1998).
10. X. Delaigue, J.M. Harrowfield, M.W. Hosseini, A. De Cian, J. Fischer, and N. Kyritsakis. J. Chem. Soc. Chem. Comm. 1579 (1994).
11. S. Knoblauch, O. M. Falana, J. Nam, D.M. Roundhill, H. Hennig, and K. Zeckert. Inorg. Chim. Acta, **300–302**, 328 (2000).
12. A.T. Yordanov, B.R. Whittlesey, and D.M. Roundhill. Inorg. Chem. **37**, 3526 (1998).
13. C.G. Gibbs and C.D. Gutsche. J. Am. Chem. Soc. **115**, 5338 (1993).

© 2001 NRC Canada

Synthesis, spectroscopic characterization, and structural studies of new Cu(I) and Cu(II) complexes containing organophosphorus ligands, and crystal structures of $(Ph_3P)_2Cu[S_2PMe_2]$, $(Ph_3P)_2Cu[(OPPh_2)_2N]$, $Cu[(OPPh_2)_2N]_2$, and $Cu[(OPPh_2)(SPPh_2)N]_2$

Anca Silvestru, Adina Rotar, John E. Drake, Michael B. Hursthouse, Mark E. Light, Sorin I. Farcas, Roland Rösler, and Cristian Silvestru

Abstract: The Cu(I) complexes, $(Ph_3P)_2CuL$ (L = $[S_2PMe_2]^-$, $[OSPR_2]^-$ (R = Me, Ph), $[(XPR_2)(YPR'_2)N]^-$ (X, Y, R, R′ = O, O, Ph, Ph; O, S, Ph, Ph; O, S, OEt, Ph; S, S, Me, Me)) and Cu(II) complexes, CuL_2 (L = $[(XPR_2)(YPR'_2)N]^-$ (X, Y, R, R′ = O, O, Ph, Ph; O, S, Ph, Ph)), have been prepared. The Cu(I) derivatives were characterized by multinuclear NMR spectroscopy and in two cases by X-ray crystallography. $(Ph_3P)_2Cu[S_2PMe_2]$ (**1**) crystallizes in the orthorhombic space group $P2_12_12_1$ (No. 19) with cell parameters a = 9.782(2), b = 17.808(4), c = 20.216(4) Å, V = 3521(6) Å^3 and Z = 4, and $(Ph_3P)_2Cu[(OPPh_2)_2N]$ (**4**) in the triclinic space group $P\bar{1}$ (No. 2) with cell parameters a = 9.8079(2), b = 12.9141(3), c = 22.5666(5) Å, α = 75.714(2), β = 79.465(2), γ = 68.2770(8)°, V = 2559.9(1) Å^3 and Z = 2. In both cases the phosphorus ligands are bidentate, thus resulting in monomeric molecules that contain tetrahedral CuP_2S_2 and CuP_2O_2 cores. The molecular structures of two of the Cu(II) derivatives were also determined. $Cu[(OPPh_2)_2N]_2$ (**8**) and $Cu[(OPPh_2)(SPPh_2)N]_2$ (**9**) crystallize in the triclinic space group $P\bar{1}$ (No. 2) with cell parameters a = 8.887(2), b = 10.739(2), c = 12.477(3) Å, α = 77.61(3), β = 76.15(5), γ = 79.46(3)°, V = 1118.3(4) Å^3 and Z = 1 for **8**, and a = 9.626(2), b = 14.151(3), c = 24.752(5) Å, α = 88.23(3), β = 79.93(3), γ = 89.77(3)°, V = 3181(1) Å^3 and Z = 3 for **9**. The molecule of $Cu[(OPPh_2)_2N]_2$ (**8**) has a planar CuO_4 core, while in $Cu[(OPPh_2)(SPPh_2)N]_2$ (**9**) both planar and tetrahedral copper cores are observed in a ratio of 1:2.

Key words: structure, copper, thiophosphinates, oxo- and thio-imidodiphosphinates.

Résumé : On a préparé les complexes suivants du Cu(I), $(Ph_3P)_2CuL$ (L = $[S_2PMe_2]^-$, $[OSPR_2]^-$ (R = Me, Ph), $[(XPR_2)(YPR'_2)N]^-$ (X, Y, R, R′ = O, O, Ph, Ph; O, S, Ph, Ph; O, S, OEt, Ph; S, S, Me, Me)) et du Cu(II), CuL_2 (L = $[(XPR_2)(YPR'_2)N]^-$ (X, Y, R, R′ = O, O, Ph, Ph; O, S, Ph, Ph)). On a caractérisé les dérivés du Cu(I) par spectroscopie RMN multinucléaire et, dans deux cas, par diffraction des rayons X. Les cristaux de $(Ph_3P)_2Cu[S_2PMe_2]$ (**1**) sont orthorhombiques, groupe d'espace $P2_12_12_1$ (No. 19) avec a = 9,782(2), b = 17,808(4) et c = 20,216(4) Å, V = 3521(6) Å^3 et Z = 4; ceux du $(Ph_3P)_3Cu[OPPh_2)_2N]$ (**4**) sont tricliniques, groupe d'espace $P\bar{1}$ (No. 2) avec a = 9,08079(2), b = 12,9141(3) et c = 22,5666(5) Å, α = 75,714(2), β = 79,465(2) et γ = 68,2770(8)°, V = 2559,9(1) Å^3 et Z = 2. Dans les deux cas, les ligands phosphorés sont bidentates ce qui conduit à des molécules monomères qui comportent des unités centrales CP_2S_2 et CP_2O_2 tétraédriques. On a aussi déterminé les structures moléculaires de deux des dérivés du Cu(II). Les cristaux de $Cu[(OPPh_2)_2N]_2$ (**8**) et de $Cu[(OPPh_2)(SPPh_2)N]_2$ (**9**) sont tous les deux tricliniques, groupe d'espace $P\bar{1}$ (No. 2) avec a = 8,887(2), b = 10,739(3) et c = 12,477(3) Å, α = 77,61(3), β = 76,15(5) et γ = 79,46(3)°, V = 1118,3(1) Å^3 et Z = 1, pour le composé **8**, et avec a = 9,626(2), b = 14,151(3) et c = 24,752(5) Å, α = 88,23(3), β = 79,93(3) et γ = 89,77(3)°, V = 3181(1) Å^3 et Z = 3, pour le composé **9**. La molécule de $Cu[(OPPh_2)_2N]_2$ (**8**) comporte une unité centrale de CuO_4 qui est plane alors que dans la molécule de $Cu[(OPPh_2)(SPPh_2)N]_2$ (**9**), on observe la

Received August 31, 2000. Published on the NRC Research Press Web site at http://canjchem.nrc.ca on July 11, 2001.

Dedicated to Professor Brian James on the occasion of his 65th birthday.

A. Silvestru, A. Rotar, R. Rösler, and C. Silvestru. Chemistry Department, "Babes-Bolyai" University, RO-3400 Cluj-Napoca, Romania.
J.E. Drake.[1] Chemistry and Biochemistry, University of Windsor, Windsor, ON N9B 3P4, Canada.
M.B. Hursthouse and M.E. Light. Department of Chemistry, University of Southampton, Highfield, Southampton SO17 1BJ, U.K.
S.I. Farcas. Institute for Isotopic and Molecular Technology, RO-3400 Cluj-Napoca 5, P.O. Box 700, Romania.

[1]Corresponding author (telephone: (519) 253-4232; fax: (519) 973-7098; e-mail: ak4@uwindsor.ca).

 DOI: 10.1139/cjc-79-5/6-983 © 2001 NRC Canada

présence d'unités de cuivre planes et tétraédriques dans un rapport de 1:2.

Mots clés : structure, cuivre, thiophosphinates, oxo- et thio-imidodiphosphinates.

[Traduit par la Rédaction]

Introduction

Relatively few copper complexes containing both neutral donors and *O*,*O*′-diorganodithiophosphato ligands have been structurally characterized (1, 2). For Cu(I) derivatives, the presence of the P-neutral ligand affords tetrahedral mononuclear $(Ph_3P)_2Cu[S_2P(OR)_2]$ (R = Et (3), $(OR)_2$ = $(OCH_2)_2CMe_2$ (4)) or dinuclear $[(Ph_3P)Cu\{S_2P(OEt)_2\}]_2$ (5) complexes. Polynuclear phosphine adducts of Cu(I) thiolates have also been reported (6, 7). Recent studies on neutral Cu(I) thiocarboxylates with triphenylphosphine demonstrate that complexes of different stoichiometry and structure can be obtained with small changes in the thio ligand. Thus, for example, using 1:1:1 stoichiometric ratios of CuCl:Na[S(O)CR]:PPh_3, the thioacetate anion gave the tetramer $[Cu\{S(O)CMe\}(PPh_3)]_4$, while for R = Ph a 4:4:3 complex $[Cu_4\{S(O)CPh\}_4(PPh_3)_3]$ was isolated. Attempts to prepare a 4:4:3 derivative for R = Me failed; only the tetrameric complex being isolated. Thioacetate and thiobenzoate ligands both gave products of 1:1:2 stoichiometry, but for R = Me the complex was a dimer $[Cu\{S(O)CMe\}(PPh_3)_2]_2$, whereas for R = Ph it was a monomer (8). In the absence of a neutral ligand, a polynuclear Cu(I) cluster complex, $[Cu\{S_2P(O\text{-}i\text{-}Pr)_2\}]_4$, has been isolated (9). On the other hand, the use of $[(XPR_2)_2N]^-$ (X = S, Se) ligands, which are characterized by flexible XPNPX skeletons and a larger X···X bite, resulted in the displacement of a coordinated triphenylphosphine, leading to trigonal, mononuclear Cu(I) complexes, $(Ph_3P)Cu[(XPR_2)_2N]$ (R = Ph, X = S (10), Se (11)). Reaction of Cu(II) salts with dithio ligands of the type $(SPR_2)(SPR'_2)NH$ resulted in polynuclear Cu(I) complexes such as trinuclear $[Cu\{(XPR_2)(YPR'_2)N\}]_3$ (R, R′ = *i*-Pr, *i*-Pr; *i*-Pr, Ph; *i*-Pr, OPh; OEt, OPh (12)) or tetranuclear $[Cu^I_4\{(SPPh_2)_2N\}_3][Cu^ICl_2]$ (R, R′ = Ph, Ph (13, 14)). By contrast, with *O*,*S*- and *O*,*O*-phosphorus ligands of the type $[OSPR_2]^-$ and $[(OPR_2)(YPR'_2)N]^-$, no Cu(I) complexes have been reported to date, and only one Cu(II) complex $Cu[\{OP(OPh)_2\}_2N]_2$ (15) has been reported. Therefore, we decided to examine the differences that result in copper complexes using related ligands when the organic groups and (or) the chalcogens attached to the phosphorus atoms are changed.

We report on the synthesis and spectroscopic characterization of new $(Ph_3P)_2CuL$ and CuL_2 complexes of anionic phosphorus ligands, as well as the crystal and molecular structures of two Cu(I) derivatives, $(Ph_3P)_2Cu[S_2PMe_2]$ and $(Ph_3P)_2Cu[(OPPh_2)_2N]$, along with two Cu(II) derivatives, $Cu[(OPPh_2)_2N]_2$ and $Cu[(OPPh_2)(SPPh_2)N]_2$.

Experimental

Materials

Starting materials were prepared according to published methods: $NaS_2PMe_2\cdot 2H_2O$ (16), $NaOSPMe_2\cdot 1.5H_2O$ (17), NH_4OSPPh_2 (18, 19), $Na[(OPPh_2)_2N]$ (20), $K[(OPPh_2)(SPPh_2)N]$ (21), $K[\{OP(OEt)_2\}(SPPh_2)N]$ (22), and $K[(SPMe_2)_2N]$ (23). All solvents were dried and distilled prior to use.

Physical measurements

The ^1H, ^{13}C, and ^{31}P NMR spectra were recorded on a Varian Gemini 300S instrument operating at 299.5, 75.4, and 121.4 MHz, respectively, using solutions in dried $CDCl_3$. The ^1H and ^{13}C and ^{31}P chemical shifts are reported in ppm relative to TMS and external H_3PO_4 85%, respectively. Electron spin resonance (ESR) measurements were performed at room temperature on a Radiopan SE/X-2543 9GHz ESR spectrometer, using a 100 kHz field modulation.

Preparation of $(Ph_3P)_2CuL$ compounds (1–7)

Typically, stoichiometric amounts of $(PPh_3)_2CuNO_3$ (0.54 g, 0.83 mmol) and $NaS_2PMe_2\cdot 2H_2O$ (0.15 g, 0.81 mmol) were placed in a round-bottom flask and solvent (CH_2Cl_2, ca. 20 mL) was added. The reaction mixture was stirred for 2 h at room temperature, followed by filtration to remove $NaNO_3$. Concentration under vacuum gave $(Ph_3P)_2Cu[S_2PMe_2]$ (**1**), as a colorless solid. Recrystallization from a CH_2Cl_2–*n*-hexane mixture gave crystals suitable for X-ray diffraction studies, yield 70% (0.35 g), mp 185–187°C. ^1H NMR δ: 1.77 (d, $^2J_{P,H}$ = 12.8 Hz, 6H, P-CH_3), 7.24 (t, $^3J_{H,H}$ = 7.2 Hz, 12H, P(C_6H_5)$_3$-*meta*), 7.34 (t, $^3J_{H,H}$ = 7.1 Hz, 6H, P(C_6H_5)$_3$-*para*), 7.45 (dd, $^3J_{H,H}$ = 8.5, $^3J_{P,H}$ = 9.2 Hz, 12H, P(C_6H_5)$_3$-*ortho*). ^{13}C NMR δ: 31.84 (d, $^1J_{P,C}$ = 48.2 Hz, P-*C*H_3), 128.40 (d, $^2J_{P,C}$ = 8.7 Hz, P(C_6H_5)$_3$-*ortho*), 129.44 (P(C_6H_5)$_3$-*para*), 134.11 (d, $^3J_{P,C}$ = 14.6 Hz P(C_6H_5)$_3$-*meta*). ^{31}P NMR δ: –4.1 (2P, *P*Ph_3), 60.7 (1P, *P*Me_2).

In the same fashion the following compounds were prepared:

$(Ph_3P)_2Cu[OSPMe_2]$ (**2**)*:* from $(PPh_3)_2CuNO_3$ (0.46 g, 0.70 mmol) and $NaOSPMe_2\cdot 1.5H_2O$ (0.11 g, 0.69 mmol) Recrystallization gave colorless crystals, yield 88% (0.44 g), mp 143–145°C. ^1H NMR δ: 1.54 (d, $^2J_{P,H}$ = 12.7 Hz, 6H, P-CH_3); 7.32 (m, 30H, P(C_6H_5)$_3$). ^{31}P NMR δ: –2.7 (2P, *P*Ph_3), 64.1 (1P, *P*Me_2).

$(Ph_3P)_2Cu[OSPPh_2]$ (**3**)*:* from $(PPh_3)_2CuNO_3$ (0.47 g, 0.72 mmol) and NH_4OSPPh_2 (0.18 g, 0.71 mmol). Recrystallization gave colorless crystals, yield 98% (0.49 g), mp 148–151°C. ^1H NMR δ: 7.22 (m, 36H, P(C_6H_5)$_3$, P-C_6H_5-*meta* + *para*), 7.75 (dd, $^3J_{H,H}$ = 6.9, $^3J_{P,H}$ = 12.6 Hz, 4H, P-C_6H_5-*ortho*). ^{13}C NMR δ: 127.60 (d, $^3J_{P,C}$ = 12.8 Hz, P-C_6H_5-meta), 128.45 (d, $^2J_{P,C}$ = 8.5 Hz, P(C_6H_5)$_3$-*ortho*), 129.60 (P(C_6H_5)$_3$-*para*, P-C_6H_5-*para*), 130.80 (d, $^2J_{P,C}$ = 9.9 Hz, P-C_6H_5-*ortho*), 134.00 (d, $^3J_{P,C}$ = 13.8 Hz, P(C_6H_5)$_3$-*meta*). ^{31}P NMR δ: –3.8 (2P, *P*Ph_3), 55.3 (1P, *P*Ph_2).

$(Ph_3P)_2Cu[(OPPh_2)_2N]$ (**4**)*:* from $(PPh_3)_2CuNO_3$ (0.38 g, 0.58 mmol) and $Na[(OPPh_2)_2N]$ (0.26 g, 0.59 mmol). Recrystallization gave colorless crystals, yield 84% (0.42 g), mp 168–170°C. ^1H NMR δ: 7.15 (m, 42H,

© 2001 NRC Canada

P(C_6H_5)$_3$, P-C_6H_5-meta + *para*), 7.68 (dd, $^3J_{H,H}$ = 7.4, $^3J_{P,H}$ = 11.1 Hz, 8H, P-C_6H_5-*ortho*). ^{13}C NMR δ: 127.43 (d, $^3J_{P,C}$ = 12.8 Hz, P-C_6H_5-meta), 128.17 (P(C_6H_5)$_3$-*ortho*), 129.10 (P(C_6H_5)$_3$-*para*), 129.28 (P-C_6H_5-*para*), 131.36 (d, $^2J_{P,C}$ = 9.2 Hz, P-C_6H_5-*ortho*), 134.13 (d, $^3J_{P,C}$ = 7.8 Hz, P(C_6H_5)$_3$-meta). ^{31}P NMR δ: –6.5 (2P, *P*Ph$_3$), 18.9 (2P, *P*Ph$_2$).

*(Ph$_3$P)$_2$Cu[(OPPh$_2$)(SPPh$_2$)N] (***5***):* from (PPh$_3$)$_2$CuNO$_3$ (0.34 g, 0.52 mmol) and K[(OPPh$_2$)(SPPh$_2$)N] (0.24 g, 0.50 mmol). Recrystallization gave colorless crystals, yield 94% (0.47 g), mp 170°C. ^{1}H NMR δ: 7.22 (m, 42H, P(C_6H_5)$_3$, P-C_6H_5-*meta* + *para*), 7.59 (ddd, $^3J_{H,H}$ = 7.0, $^4J_{H,H}$ = 1.1, $^3J_{P,H}$ = 12.1 Hz, 4H, P(O)-C_6H_5-*ortho*), 7.85 (ddd, $^3J_{H,H}$ = 7.5, $^4J_{H,H}$ = 1.4, $^3J_{P,H}$ = 13.5 Hz, 4H, P(S)-C_6H_5-*ortho*). ^{13}C NMR δ: 127.46 (d, $^3J_{P,C}$ = 11.4 Hz, P-C_6H_5-*meta*), 127.61 (d, $^3J_{P,C}$ = 10.9 Hz, P-C_6H_5-*meta*), 128.21 (d, $^2J_{P,C}$ = 8.0 Hz, P(C_6H_5)$_3$-*ortho*), 129.04 (P(C_6H_5)$_3$-*para*), 129.43 (P-C_6H_5-*para*), 129.54 (P-C_6H_5-*para*), 130.93 (d, $^2J_{P,C}$ = 10.3 Hz, P(O)-C_6H_5-*ortho*), 131.26 (d, $^2J_{P,C}$ = 9.1 Hz, P(S)-C_6H_5-*ortho*), 134.12 (d, $^3J_{P,C}$ = 15.2 Hz, P(C_6H_5)$_3$-*meta*). ^{31}P NMR δ: –5.7 (2P, *P*Ph$_3$), 18.1 (1P, *P*(O)Ph$_2$), 30.0 (1P, *P*(S)Ph$_2$).

*(Ph$_3$P)$_2$Cu-[{OP(OEt)$_2$}(SPPh$_2$)N] (***6***):* from (PPh$_3$)$_2$CuNO$_3$ (0.46 g, 0.71 mmol) and K[{OP(OEt)$_2$}(SPPh$_2$)N] (0.29 g, 0.71 mmol). Recrystallization gave colorless crystals, yield 92% (0.46 g), mp 160°C. ^{1}H NMR δ: 1.01 (t, $^3J_{H,H}$ = 6.9 Hz, 6H, P-O-CH$_2$C*H*$_3$), 3.67 (dq, $^3J_{H,H}$ = 6.9, $^3J_{P,H}$ = 7.1 Hz, 4H, P-O-C*H*$_2$CH$_3$), 7.24 (m, 36H, P(C_6H_5)$_3$, P-C_6H_5-*meta* + *para*), 7.90 (dd, $^3J_{H,H}$ = 7.4, $^3J_{P,H}$ = 13.4 Hz, 4H, P-C_6H_5-*ortho*). ^{31}P NMR δ: –5.2 (2P, *P*Ph$_3$), 4.4 (1P, *P*(OEt)$_2$), 34.2 (1P, *P*Ph$_2$).

*(Ph$_3$P)$_2$Cu[(SPMe$_2$)$_2$N] (***7***):* from (PPh$_3$)$_2$CuNO$_3$ (0.41 g, 0.63 mmol) and K[(SPMe$_2$)$_2$N] (0.15 g, 0.62 mmol). Recrystallization gave colorless crystals, yield 80% (0.40 g), mp 149–152°C. ^{1}H NMR δ: 1.81 (d, $^2J_{P,H}$ = 12.0 Hz, 12H, P-C*H*$_3$), 7.35 (m, 30H, P(C_6H_5)$_3$). ^{31}P NMR δ: –2.9 (2P, *P*Ph$_3$), 40.0 (2P, *P*Me$_2$).

Preparation of Cu[(OPPh$_2$)$_2$N]$_2$ (8)

Stoichiometric amounts of $CuCl_2 \cdot 2H_2O$ (0.095 g, 0.56 mmol) and K[(OPPh$_2$)$_2$N] (0.51 g, 1.12 mmol) were placed in a round-bottom flask and solvent (MeOH, ca. 20 mL) was added. The reaction mixture was stirred for 12 h at room temperature and the solvent was removed to dryness under vacuum. The blue-greenish residual solid was extracted twice with CH_2Cl_2 (ca. 20 mL) to remove KCl and unreacted starting materials. Concentration of the blue solution under vacuum then gave Cu[(OPPh$_2$)$_2$N]$_2$ (**8**) as a blue solid. Recrystallization from a CH_2Cl_2–*n*-hexane mixture gave crystals suitable for X-ray diffraction studies, yield 72% (0.36 g), mp 273 to 274°C. ESR (X band): $g_\perp$ = 2.017 ± 0.004, $g_\parallel$ = 2.086 ± 0.004, A = 140 ± 10 Gs, B = 30 ± 10 Gs.

Preparation of Cu[(OPPh$_2$)(SPPh$_2$)N]$_2$ (9)

Stoichiometric amounts of $CuCl_2 \cdot 2H_2O$ (0.092 g, 0.54 mmol) and K[(OPPh$_2$)(SPPh$_2$)N] (0.5 g, 1.06 mmol) were placed in a round-bottom flask and CH_2Cl_2 (20 mL) was added. The reaction mixture, which immediately turned brown, was stirred for 6 h at room temperature before KCl was filtered off to leave a brown solution. Concentration under vacuum gave Cu[(OPPh$_2$)(SPPh$_2$)N]$_2$ (**9**) as a dark brown solid. Recrystallization from a CH_2Cl_2–*n*-hexane mixture gave crystals suitable for X-ray diffraction studies, yield 66% (0.33 g), mp 90–91°C. ^{31}P NMR δ: 21.5 (1P), 23.5 (1P, *P*(O)Ph$_2$, *P*(S)Ph$_2$).

X-ray crystallographic analysis

Colourless, block crystals of (Ph$_3$P)$_2$Cu[S$_2$PMe$_2$] (**1**) and (Ph$_3$P)$_2$Cu[(OPPh$_2$)$_2$N] (**4**), a blue block crystal of Cu[(OPPh$_2$)$_2$N]$_2$ (**8**), and a dark brown block crystal of Cu[(OPPh$_2$)(SPPh$_2$)N]$_2$ (**9**) were mounted on glass fibres. Data for **1**, **4**, and **8** were collected on an Enraf Nonius KappaCCD area detector (ϕ scans and ω scans to fill Ewald sphere) at the University of Southampton EPSRC National Crystallography Service. For **9**, data collection and processing was carried out by G. Yapp, then at the University of Windsor, using a Siemens SMART/CCD system. Cell refinement (24) gave cell constants corresponding to orthorhombic (for **1**) and triclinic (for **4**, **8**, and **9**) cells whose dimensions are given in Table 1, along with other experimental parameters. An absorption correction was applied (25), which resulted in transmission factors ranging from 0.870 to 0.825 for **1**, 0.943 to 0.842 for **4**, 0.937 to 0.773 for **8**, and 0.927 to 0.861 for **9**.

The structures were solved by direct methods (26). All of the nonhydrogen atoms were treated anisotropically. Hydrogen atoms were included in idealized positions with isotropic thermal parameters set at 1.2 times that of the carbon atom to which they were attached. The data for **1** and **4** were of much better quality than that for **8**, and the positions of the higher residual peaks in the latter made no chemical sense. The final cycle of full-matrix least-squares refinement (27) was based on 8027 (**1**), 10601 (**4**), 3925 (**8**), and 9164 (**9**) observed reflections (4949 (**1**), 6343 (**4**), 3289 (**8**), and 7548 (**9**) for $F^2 > 4\sigma(F^2)$) and 399 (**1**), 613 (**4**), 269 (**8**), and 799 (**9**) variable parameters and converged (largest parameter shift was 0.001 times its esd). The absolute configuration parameter for **1** was –0.017(12). Selected distances and bond angles are given in Tables 2–5 and the molecules are displayed in the ORTEP diagrams in Figs. 1–4.[2]

Results and discussion

The preparation of the Cu(I) complexes ((Ph$_3$P)$_2$CuL) is achieved by the reaction of stoichiometric amounts of

[2] Supplementary material including the final atomic coordinates and equivalent isotropic thermal parameters for the nonhydrogen atoms, anisotropic thermal parameters for the nonhydrogen atoms, final fractional coordinates and thermal parameters for hydrogen atoms, and all bond distances and angles, have been deposited and may be purchased from the Depository of Unpublished Data, Document Delivery, CISTI, National Research Council of Canada, Ottawa, ON, Canada, K1A 0S2 (http://www.nrc.ca/cisti/irm/unpub_e.shtml). Tables of atomic coordinates for the structures reported in this paper have also been deposited with the Cambridge Crystallographic Data Centre. Copies of the data can be obtained, free of charge, on application to the Director, CCDC, 12 Union Road, Cambridge, CB2 1EZ, U.K. (fax: 44-1223-336033 or e-mail:deposit@ccdc.cam.ac.uk). Structure factor amplitudes are no longer being deposited and may be obtained directly from the author.

© 2001 NRC Canada

Table 1. Crystal data and structure refinement for $(Ph_3P)_2Cu(S_2PMe_2)$ (**1**), $(Ph_3P)_2Cu[(OPPh_2)_2N]$ (**4**), $Cu[(OPPh_2)_2N]_2$ (**8**), and $Cu[(OPPh_2)(SPPh_2)N]_2$ (**9**).

	1	**4**	**8**	**9**
Empirical formula	$C_{38}H_{36}P_3S_2Cu$	$C_{60}H_{50}NO_2P_4Cu$	$C_{48}H_{40}N_2O_4P_4Cu$	$C_{48}H_{40}N_2O_2P_4S_2Cu$
FW	713.24	1004.43	896.24	928.36
T (°C)	298(2)	298(2)	298(2)	298(2)
λ (Å)	0.71073	0.71073	0.71073	0.71073
Crystal system	Orthorhombic	Triclinic	Triclinic	Triclinic
Space group	$P2_12_12_1$	$P\bar{1}$	$P\bar{1}$	$P\bar{1}$
a (Å)	9.782(2)	9.8079(2)	8.887(2)	9.626(2)
b (Å)	17.808(4)	12.9141(3)	10.739(2)	14.151(3)
c (Å)	20.216(4)	22.5666(5)	12.477(3)	24.752(5)
α (°)		75.714(2)	77.61(3)	88.23(3)
β (°)		79.465(2)	76.15(3)	79.93(3)
γ (°)		68.2770(8)	79.46(3)	89.77(3)
Volume (Å^{-3})	3521.6(1)	2559.9(1)	1118.3(4)	3318(1)
Z	4	2	1	3
$\rho_{calcd.}$ (g cm^{-3})	1.345	1.303	1.331	1.394
μ (mm^{-1})	0.901	0.596	0.677	0.774
F(000)	1480	1044	463	1437
Crystal size (mm)	0.25 × 0.15 × 0.10	0.30 × 0.15 × 0.10	0.10 × 0.10 × 0.10	0.20 × 0.10 × 0.10
θ range for data collection (°)	3.05–27.89	3.00–27.47	3.21–25.03	1.64–23.24
Limiting indices	$-9 \le h \le 12$, $-18 \le k \le 23$, $-25 \le l \le 25$	$-12 \le h \le 12$, $-16 \le k \le 16$, $-22 \le l \le 28$	$-10 \le h \le 10$, $-12 \le k \le 12$, $-14 \le l \le 14$	$-10 \le h \le 10$, $-15 \le k \le 15$, $0 \le l \le 27$
Reflections collected	21154	16010	9925	9164
Independent reflections	8028 (R_{int} = 0.0623)	10601 (R_{int} = 0.0422)	3925 (R_{int} = 0.0428)	9164 (R_{int} = 0.0496)
Max. and min. transmissions	0.870 and 0.825	0.943 and 0.842	0.937 and 0.773	0.9266 and 0.8605
Refinement method	Full-matrix least-squares on F^2			
Data/restraints/ parameters	8027/0/399	10601/0/613	3925/0/269	9164/0/799
GoF on F^2	0.971	1.003	1.062	1.060
Final R indices [$F^2 > 4\sigma(F^2)$]	R_1 = 0.0455, wR_2 = 0.0788	R_1 = 0.0499, wR_2 = 0.0967	R_1 = 0.0702, wR_2 = 0.2010	R_1 = 0.0423, wR_2 = 0.1129
R indices (all data)	R_1 = 0.1059, wR_2 = 0.0937	R_1 = 0.1048, wR_2 = 0.1134	R_1 = 0.0806, wR_2 = 0.2129	R_1 = 0.0538, wR_2 = 0.1193
Largest diff. peak and hole (e Å^3)	0.220 and –0.279	0.412 and –0.419	2.305 and –0.477	0.708 and –0.312

© 2001 NRC Canada

Table 2. Selected bond lengths (Å) and angles (°) for $(PPh_3)_2CuS_2PMe_2$ (**1**).

Bond lengths (Å)			
Cu(1)—P(1)	2.2718(10)	Cu(1)—P(2)	2.2796(10)
Cu(1)—S(1)	2.4343(12)	Cu(1)—S(2)	2.4797(12)
S(1)—P(3)	1.997(2)	S(2)—P(3)	2.000(2)
Bond angles (°)			
P(1)-Cu(1)-P(2)	117.09(4)	P(1)-Cu(1)-S(1)	117.60(4)
P(2)-Cu(1)-S(1)	107.08(4)	P(1)-Cu(1)-S(2)	114.20(4)
P(2)-Cu(1)-S(2)	111.43(4)	S(1)-Cu(1)-S(2)	85.07(4)
P(3)-S(1)-Cu(1)	80.75(5)	P(3)-S(2)-Cu(1)	79.56(5)
C(1)-P(1)-Cu(1)	113.83(11)	C(19)-P(2)-Cu(1)	117.34(13)
C(7)-P(1)-Cu(1)	112.16(11)	C(25)-P(2)-Cu(1)	113.45(11)
C(13)-P(1)-Cu(1)	119.02(13)	C(31)-P(2)-C(19)	103.1(2)
S(1)-P(3)-S(2)	112.47(7)	C(37)-P(3)-C(38)	103.7(3)

Table 3. Selected bond lengths (Å) and angles (°) for $(Ph_3P)_2Cu[(OPPh_2)_2N]$ (**4**) and $Cu[(OPPh_2)_2N]_2$ (**8**).

4		**8**	
Bond lengths (Å)			
Cu(1)—O(1)	2.122(2)	Cu(1)—O(1)	1.917(3)
Cu(1)—O(2)	2.165(2)	Cu(1)—O(2)	1.918(3)
Cu(1)—P(1)	2.2554(7)	P(1)—O(1)	1.515(3)
Cu(1)—P(2)	2.2449(7)	P(2)—O(2)	1.508(3)
P(3)—O(1)	1.505(2)	P(1)—N(1)	1.579(3)
P(4)—O(2)	1.503(2)	P(2)—N(1)	1.575(4)
P(3)—N(1)	1.586(2)		
P(4)—N(1)	1.586(2)		
Bond angles (°)			
O(1)-Cu(1)-P(1)	103.55(5)	O(1)-Cu(1)-O(2)	94.67(13)
O(1)-Cu(1)-P(2)	109.51(5)	O(1)-Cu(1)-O(1)′	180.0
O(2)-Cu(1)-P(1)	106.91(5)	O(2)-Cu(1)-O(1)′	85.33(13)
O(2)-Cu(1)-P(2)	107.50(5)	P(1)-O(1)-Cu(1)	131.60(17)
P(1)-Cu(1)-P(2)	126.10(3)	O(1)-P(1)-N(1)	117.35(18)
O(1)-Cu(1)-O(2)	100.32(7)	P(1)-N(1)-P(2)	125.6(2)
P(3)-O(1)-Cu(1)	119.13(11)	O(2)-P(2)-N(1)	117.09(19)
O(1)-P(3)-N(1)	118.43(11)	P(2)-O(2)-Cu(1)	132.6(2)
P(3)-N(1)-P(4)	129.5(2)		
O(2)-P(4)-N(1)	118.56(12)		
P(4)-O(2)-Cu(1)	119.14(10)		

Note: Symmetry equivalent position ($-x + 2, -y + 1, -z + 2$) given by a prime.

$(Ph_3P)_2CuNO_3$ with the ammonium or alkali salt of the appropriate organophosphorus acid in CH_2Cl_2 as solvent, in accord with rxn. [1]

$$[1] \quad (Ph_3P)_2CuNO_3 + ML \rightarrow (Ph_3P)_2CuL + MNO_3$$

where L = (S_2PMe_2) (**1**), $(OSPR_2)$ (R = Me (**2**), Ph (**3**)), $[(XPR_2)(YPR'_2)N]$ (X, Y, R, R′ = O, O, Ph, Ph (**4**), O, S, Ph, Ph (**5**), O, S, OEt, Ph (**6**), S, S, Me, Me (**7**)).

All of the compounds are isolated in good yields as crystalline colorless solids and X-ray quality crystals are obtained for **1** and **4**. In previous reports, the use of $[(XPR_2)_2N]^-$ (X = S, Se) ligands was found to result in displacement of a coordinated triphenylphosphine and isolation of trigonal $(Ph_3P)Cu[(XPR_2)_2N]$ (R = Ph, X = S (10), Se (11)). By contrast, for all reactions (eq. [1]) investigated in this work, the isolated products are found to preserve two neutral phosphine ligands coordinated to the metal atom, even though similar reaction conditions were used. This suggests that changes in the organic groups and (or) chalcogens on phosphorus can influence the stoichiometry of the isolated Cu(I) adducts.

The $(Ph_3P)_2CuL$ derivatives are readily dissolved in chloroform, which is therefore used as the preferred solvent for recording NMR spectra. In all cases, both ^1H and ^{31}P NMR data are consistent with a 2:1 molar ratio between the neutral and anionic ligands. For $(Ph_3P)_2Cu[OSPR_2]$ (R = Me, Ph) derivatives, the magnitude of the ^{31}P chemical shifts is indicative of an *O*,*S*-bidentate coordination of the monothio ligand moieties δ: R = Me, 64.1 (PMe_2) (cf. $Me_2P(S)OMe$ 94.3 (28), $Me_2P(O)SMe$ 45.9 (29)), R = Ph 55.3 (PPh_2) (cf. $Ph_2P(S)OMe$ 83.5 (29), $Ph_2P(O)SMe$ 42.8 (29)). The ^{31}P chemical shifts assigned for the phosphorus atoms of the anionic ligand in the spectra of the Cu(I) imidodiphosphinato complexes $(Ph_3P)_2Cu[(XPR_2)(YPR'_2)N]$, are also consistent with a chelated ligand. This behavior suggests that tetrahe-

© 2001 NRC Canada

Table 4. Selected bond lengths (Å) and angles (°) for $Cu[(OPPh_2)(SPPh_2)N]_2$ (**9**).

9a		**9b**	
Bond lengths (Å)			
Cu(1)—O(1)	1.940(2)	Cu(2)—O(3)	1.940(2)
Cu(1)—O(2)	1.934(2)	Cu(2)—O(3)′	1.940(2)
Cu(1)—S(1)	2.2837(11)	Cu(2)—S(3)	2.3398(13)
Cu(1)—S(2)	2.2931(11)	Cu(2)—S(3)′	2.3398(13)
P(1)—O(1)	1.517(2)	P(5)—O(3)	1.517(3)
P(1)—N(1)	1.590(3)	P(5)—N(3)	1.583(3)
P(2)—N(1)	1.590(3)	P(6)—N(3)	1.595(3)
P(2)—S(1)	2.0311(14)	P(6)—S(3)	2.0216(15)
P(3)—O(2)	1.518(2)		
P(3)—N(2)	1.577(3)		
P(4)—N(2)	1.578(3)		
P(4)—S(2)	2.0344(14)		
Bond angles (°)			
O(1)-Cu(1)-S(1)	100.12(8)	O(3)-Cu(2)-S(3)	97.47(8)
O(1)-Cu(1)-S(2)	149.35(8)	O(3)-Cu(2)-S(3)′	82.53(8)
O(1)-Cu(1)-O(2)	88.91(11)	O(3)-Cu(2)-O(3)′	180
O(2)-Cu(1)-S(1)	140.59(8)	O(3)′-Cu(2)-S(3)	82.53(8)
O(2)-Cu(1)-S(2)	100.74(8)	O(3)′Cu(2)-S(3)′	97.47(8)
S(1)-Cu(1)-S(2)	90.76(5)	S(3)-Cu(2)-S(3)′	180
Cu(1)-O(1)-P(1)	130.10(15)	Cu(2)-O(3)-P(5)	125.37(16)
O(1)-P(1)-N(1)	117.42(15)	O(3)-P(5)-N(3)	117.45(15)
P(1)-N(1)-P(2)	125.53(19)	P(5)-N(3)-P(6)	120.93(19)
S(1)-P(2)-N(1)	117.69(12)	S(3)-P(6)-N(3)	115.43(12)
Cu(1)-S(1)-P(2)	106.06(6)	Cu(2)-S(3)-P(6)	104.19(5)
Cu(1)-O(2)-P(3)	132.82(15)		
O(2)-P(3)-N(2)	116.78(15)		
P(3)-N(2)-P(4)	132.57(19)		
S(2)-P(4)-N(2)	118.91(12)		
Cu(1)-S(2)-P(4)	107.00(5)		

Note: Symmetry equivalent position (*–x, –y, –z)* given by a prime.

dral structures similar to that established in the solid state for $(Ph_3P)_2Cu[S_2PMe_2]$ (**1**) and $(Ph_3P)_2Cu[(OPPh_2)_2N]$ (**4**) (see below), are preserved in solution. However, a recent report (8) demonstrates that the nature of the anionic ligand may result in significant structural modifications so that, in the solid state, $(Ph_3P)_2Cu[S(O)CPh]$ is mononuclear with only a weak intramolecular Cu···O interaction (2.439(2) Å), while $[(Ph_3P)_2Cu(OSCMe)]_2$ is dinuclear with different coordination modes for the monothiocarboxylato moieties (*S*-bridging and *O*,*S*-bridging).

The Cu(II) complexes, $Cu[(OPPh_2)(YPPh_2)N]_2$ (Y = O (**8**), S (**9**)), are obtained by reacting stoichiometric amounts of $CuCl_2 \cdot 2H_2O$ with the potassium salt of the imidodiphosphinato acid in organic solvent at room temperature, in accord with rxn. [2].

$$[2] \quad CuCl_2 \cdot 2H_2O + K[(OPPh_2)(YPPh_2)N] \rightarrow Cu[(OPPh_2)(YPPh_2)N]_2 + 2KCl + 2H_2O$$

Blue crystals of the dioxo derivative **8** are also formed directly in an NMR tube during evaporation in open atmosphere of a $CDCl_3$ solution of $(Ph_3P)_2Cu[(OPPh_2)_2N]$ (**4**) (*m*/*z* 896 (molecular ion), and identical spectroscopic properties as a pure sample of the same compound). In the EPR spectrum of **8**, the characteristic hyperfine structure for Cu(II) ions is observed. The hyperfine tensor exhibits axial symmetry with the strongest interaction for the case when the magnetic field is parallel to the deformation axis of the paramagnetic center. For the perpendicular orientation the splitting is too small and the four lines cannot be separated. The analysis of the spectrum was carried out with the axially symmetric spin Hamiltonian, the nuclear quadrupole interaction being neglected. The values of the hyperfine tensor *A* and *B* (parallel and perpendicular components to the tetragonal axis) and of the *g*-factors were calculated. The *g*-factors are consistent with a $|x^2 - y^2>$ ground state of the paramagnetic ion, while the magnitude of the *A* value suggests a relatively large electronic density at the Cu nucleus.

The brown crystals of the monothio derivative **9** are readily soluble in organic solvents, and the ^{31}P NMR spectrum of its $CDCl_3$ solution exhibited two broad resonance signals. A more detailed examination of its spectroscopic properties, both in solution and the solid state, is being undertaken.

Crystal structure of $(Ph_3P)_2Cu[S_2PMe_2]$ (1)

The dithiophosphinato derivative $(Ph_3P)_2Cu[S_2PMe_2]$ (**1**), is monomeric. Its molecular structure is displayed as an ORTEP diagram (Fig. 1), and important bond distances and bond angles are given in Table 2. The dithio ligand is essentially isobidentate (Cu(1)—S(1) 2.4343(12), Cu(1)—S(2) 2.4797(12) Å), resulting in approximately tetrahedral

© 2001 NRC Canada

Fig. 1. ORTEP plot of the molecule $(Ph_3P)_2Cu(S_2PMe_2)$ (**1**). The atoms are drawn with 50% probability ellipsoids.

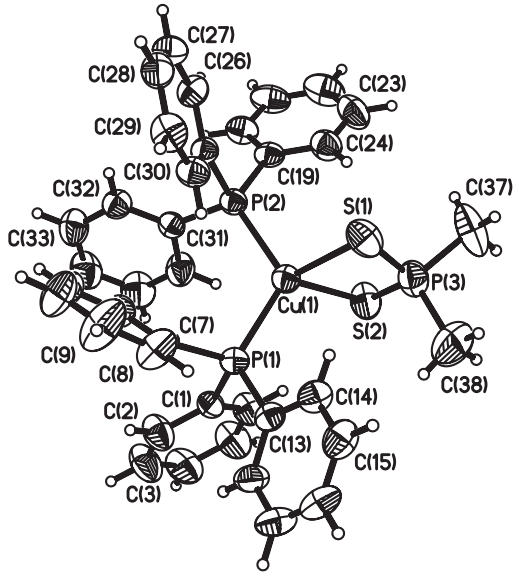
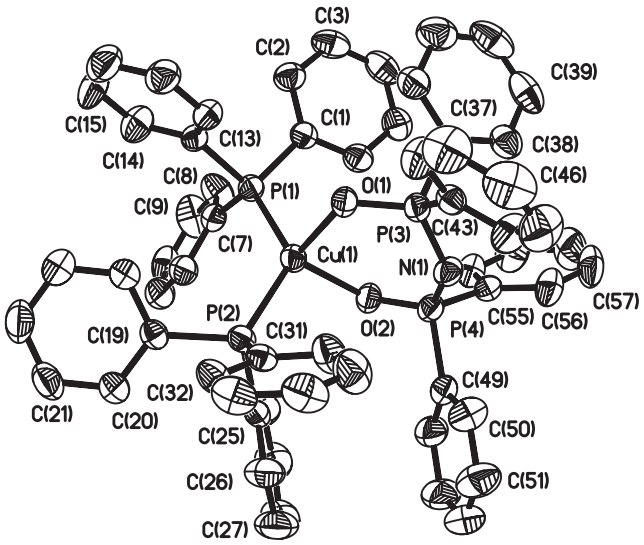


Fig. 2. ORTEP plot of the molecule $(Ph_3P)_2Cu[(OPPh_2)_2N]$ (**4**). The atoms are drawn with 50% probability ellipsoids. Hydrogen atoms are omitted for clarity.



CuP_2S_2 coordination (dihedral angle Cu(1)-P(1)-P(2) – Cu(1)-S(1)-S(2) 86.9°). The four-membered CuS_2P chelate ring is nonplanar but folded about the S(1)–S(2) axis (17.3°). The overall molecular structure is very similar to that of the related dithiophosphato derivative, $(Ph_3P)_2Cu[S_2P(OEt)_2]$ (3). The main difference is in the relative magnitudes of the phosphorus sulfur bond lengths (1.997(2), 2.000(2) Å in **1** vs. 1.967(2), 1.973(2) Å), reflecting the nature of the phosphorus ligands, which contain P–C or P–OC bonds.

Crystal structure of $(Ph_3P)_2Cu[(OPPh_2)_2N]$ (4)

The molecular structure of the Cu(I) imidodiphosphinate, $(Ph_3P)_2Cu[(OPPh_2)_2N]$ (**4**), is displayed as an ORTEP diagram (Fig. 2), and important bond distances and bond angles

Fig. 3. ORTEP plot of the molecule $Cu[(OPPh_2)_2N]_2$ (**8**). The atoms are drawn with 50% probability ellipsoids. Carbon atoms of the phenyl rings other than the ipso atoms and hydrogen atoms are omitted for clarity. Copper located at –1 symmetry center.

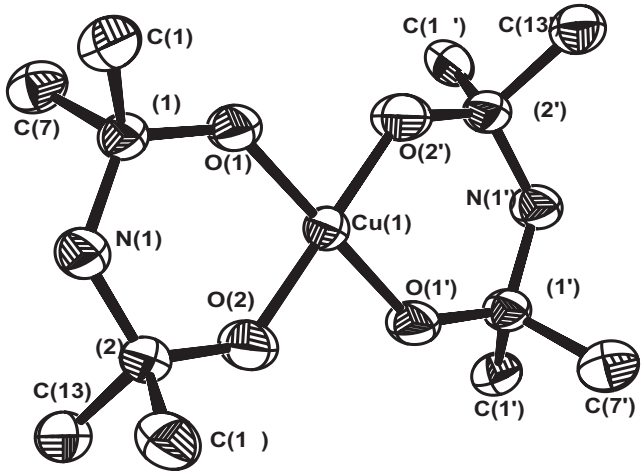
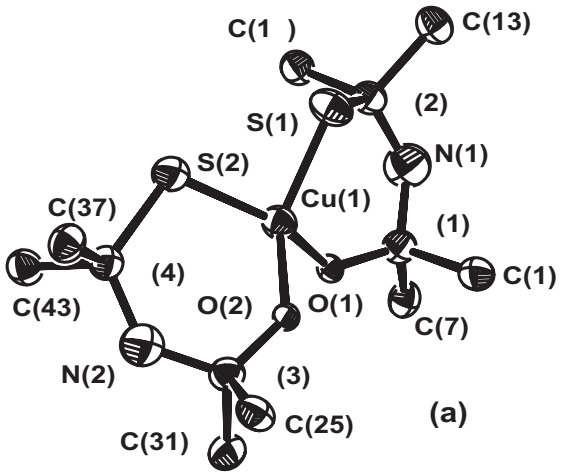
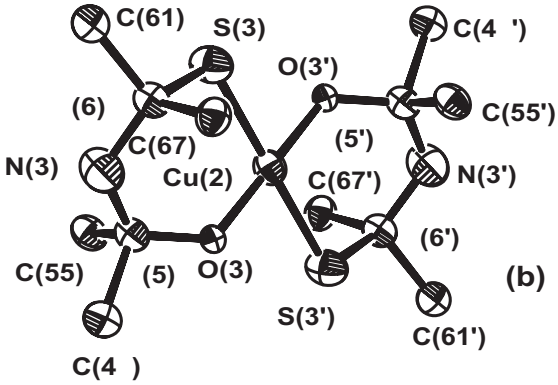


Fig. 4. ORTEP plot of the molecule $Cu[(OPPh_2)(SPPh_2)N]_2$ (**9**) showing the two copper environments: (*a*) tetrahedral, with Cu located at a general position; and (*b*) square planar, with Cu located at –1 symmetry center. The atoms are drawn with 50% probability ellipsoids. Carbon atoms of the phenyl rings other than the ipso atoms and hydrogen atoms are omitted for clarity.





© 2001 NRC Canada

are given in Table 3. This mononuclear compound contains a chelating dioxo ligand (Cu(1)—O(1) 2.122(2), Cu(1)—O(2) 2.165(2) Å), and the resulting tetrahedral CuP_2O_2 core is characterized by a dihedral angle Cu(1)-P(1)-P(2) – Cu(1)-O(1)-O(2) 88.1° close to that observed in **1**. The six-membered CuO_2P_2N chelate ring displays a twisted boat conformation being folded about the P(3)–O(2) axis (dihedral angle O(2)-Cu(1)-O(1)-P(3) – O(2)-P(4)-N(1)-P(3) 29.0°). Similar tetrahedral, mononuclear structures have also been reported for related β-diketonato derivatives, such as $(R_3P)_2Cu[(OCCF_3)_2C]$ (R = Ph (30), Cy (31)).

Crystal structure of $Cu[(OPPh_2)_2N]_2$ (8)

The crystal of the Cu(II) complex **8** contains discrete molecules of $Cu[(OPPh_2)_2N]_2$ displayed as an ORTEP diagram in Fig. 3. Both imidodiphosphinato ligands act as chelating units, leading to a distorted square planar CuO_4 core, with *trans*-O-Cu-O angles of 180° and *endocyclic*-O-Cu-O angles (94.67(13)°) larger than *exocyclic* (85.33 (13)°). Not only is the CuO_4 core planar (dihedral angle Cu(1)-O(1)-O(2) – Cu(1)-O(1′)-O(2′) 0°), but the whole spiro-bicyclic system is almost planar (deviations from the CuO_4 plane: P(1) –0.136, P(2) 0.076, N(1) –0.002 Å). The quasi-planarity of the six-membered CuO_2P_2N ring in **8** is in strong contrast to the twisted boat conformation observed in **4**, pointing out the high flexibility of the OPNPO skeleton. The Cu—O bond distances are considerably shorter in **8** (1.917(3), 1.918(3) Å) than in **4** (2.122(2), 2.165(2) Å), while the P—O and P—N distances are similar as are the O-P-N angles. However, the P-N-P and Cu-O-P angles are larger in **8** than in **4** (ca. 4 and 13°, respectively, (Table 3)), which is presumably required to achieve the planarity of the chelate ring. The overall structure is similar to that of the related derivative, $Cu[\{OP(OPh)_2\}_2N]_2$ (15), indicating that at least in this case, replacement of phenoxy by phenyl groups on phosphorus atoms does not result in significant structural changes.

Crystal structure of $Cu[(OPPh_2)(SPPh_2)N]_2$ (9)

The most interesting feature of the solid state structure of the monothio derivative, $Cu[(OPPh2)(SPPh_2)N]_2$ (**9**), is the presence of both tetrahedral (*a*) and square-planar (*b*) copper environments in a 2:1 ratio, as displayed as an ORTEP diagram in Fig. 4. Important bond distances and bond angles are given in Table 4.

The copper atom is in a special position in the square-planar molecule (Fig. 9*b*) to give the *trans*-CuO_2S_2 core (O(3)-Cu(2)-O(3′) and S(3)-Cu(2)-S(3′) of 180°) with the *endocyclic* O(3)-Cu(2)-S(3) angle (97.47(8)°) again larger than the *exocyclic* O(3)-Cu(2)-S(3′) (82.53(8)°). A similar coordination geometry is found in one of the two independent molecules of $Cu[(OCPh)(SCNEt_2)CH]_2$ (32) in which the crystals contain one molecule with a *trans*-arrangement of the square-planar CuO_2S_2 core and a second molecule with a *cis*-arrangement of the chalcogen atoms around the metal center. In contrast to the dioxo derivative **8**, the six-membered $CuOSP_2N$ ring in **9b** exhibits a twisted boat conformation which is folded about the P(6)–O(3) axis (dihedral angle O(3)-Cu(2)-S(3)-P(6) – O(3)-P(5)-N(3)-P(6) 44.3°).

The other molecule (Fig. 9a) exhibits tetrahedral distortion, with a dihedral angle Cu(1)-O(1)-S(1) – Cu(1)-O(2)-S(2) of 46.51°. The two $CuOSP_2N$ rings, which are not related by symmetry, also exhibit distorted boat conformations, but one ring is folded about the P(1)–S(1) axis (dihedral angle S(1)-Cu(1)-O(1)-P(1) – S(1)-P(2)-N(1)-P(1) 145.2°), while the other is folded about the Cu(1)–N(2) axis (dihedral angle Cu(1)-O(2)-P(3)-N(2) – Cu(1)-S(2)-P(4)-N(2) 26.5°). The P-N-P angles within the two chelate rings in **9a** are significantly different (125.53(19) and 132.57(19)°); both being larger than in **9b** (120.93(19)°).

The Cu—O, P—O, P—S, and P—N bond distances in the two independent molecules are similar (Table 4), but the Cu—S bond distances in the square-planar core of **9b** (2.3398(13) Å) are significantly longer than in the tetrahedral core of **9a** (2.2837(11), 2.2931(1) Å) or in the *trans*-$Cu[(OCPh)(SCNEt_2)CH]_2$ complex (*trans*-isomer 2.254(1) Å, *cis*-isomer 2.236(2), 2.244(2) Å).

Concluding comments

Previous reports have indicated that ligands such as $[(XPPh_2)_2N]^-$ (X = S, Se) tend to displace coordinated triphenylphosphine resulting in the isolation of trigonal $(Ph_3P)Cu[(XPR_2)_2N]$ species. By contrast, monomeric, tetrahedral Cu(I) complexes of the type $(Ph_3P)_2CuL$ (L = $[(XPR_2)(YPR'_2)N]^-$ (X, Y, R, R′ = O, O, Ph, Ph; O, S, Ph, Ph; O, S, OEt, Ph, S, S, Me, Me)), $[S_2PMe_2]^-$, $[OSPR_2]^-$ (R = Me, Ph) are formed by treatment of $(Ph_3P)_2CuNO_3$ with salts of the appropriate organophosphorus acid, regardless of the nature of the organophosphorus ligands. The presence of a tetrahedral Cu^IX_4 core is confirmed by the X-ray structures of $(Ph_3P)_2Cu[S_2PMe_2]$ (**1**) and $(Ph_3P)_2Cu[(OPPh_2)_2N]$ (**4**), and NMR studies indicate that the tetrahedral coordination environment at the Cu(I) atom is also preserved in solution.

For related Cu(II) complexes, $Cu[(OPPh_2)_2N]_2$ (**8**) has the expected planar CuO_4 core but, remarkably, the whole spiro-bicyclic system is almost planar. Even more surprising is the existence of copper in both planar and tetrahedral environments in the case of the monothio derivative $Cu[(OPPh_2)(SPPh_2)N]_2$ (**9**), with the planar and tetrahedral molecules being in a ratio of 1:2.

The conformations of the six-membered $CuOXP_2N$ (X = O, S) rings differ considerably in **1**, **4**, and **8**, providing further evidence of the high flexibility of the OPNPX skeleton.

Acknowledgment

J.E.D. wishes to thank the Natural Sciences and Engineering Research Council of Canada (NSERC) for financial support. M.B.H. thanks the U.K. Engineering and Physical Sciences Research Council for support of the X-ray facilities at Southampton.

References

1. I. Haiduc, D.B. Sowerby, and S.F. Lu. Polyhedron, **14**, 3389 (1995), and refs. therein.
2. I. Haiduc and D.B. Sowerby. Polyhedron, **15**, 2469 (1995).
3. M.G.B. Drew, G.A. Forsyth, M. Gasan, R.J. Hobson, and D.A. Rice. J. Chem. Soc. Dalton Trans. 1027 (1987).
4. U.N. Tripathi, R. Bohra, G. Srivastava, and R.C. Mehrotra. Polyhedron, **11**, 1187 (1992).
5. Q.H. Chen, S.F. Lu, X.Y. Huang, and J.Q. Huang. Jiegou Huaxue (J. Struct. Chem.), **13**, 102 (1994).

© 2001 NRC Canada

6. I.G. Dance, L.J. Fitzpatrick, and M.L. Scudder. J. Chem. Soc. Chem. Commun. 546 (1983).
7. I.G. Dance, M.L. Scudder, and L.J. Fitzpatrick. Inorg. Chem. **24**, 2547 (1985).
8. T.C. Deivaraj, G.X. Lai, and J.J. Vittal. Inorg. Chem. **39**, 1028 (2000).
9. S.L. Lawton, W.J. Rohrbaugh, and G.T. Kokotailo. Inorg. Chem. **11**, 612 (1972).
10. I Haiduc, R. Cea-Olivares, R.A. Toscano, and C. Silvestru. Polyhedron, **14**, 1067 (1995).
11. J. Novosad, M. Necas, J. Marek, P. Veltsistas, C. Papadimitriou, I. Haiduc, M. Watanabe, and J. D. Woollins. Inorg. Chim. Acta, **290**, 256 (1999).
12. D.J. Birdsall, A.M.Z. Slawin, and J.D. Woollins. Inorg. Chem. **38**, 4152 (1999).
13. O. Siiman, C.P. Huber, and M.L. Post. Acta Crystallogr. B: Struct Sci. **B34**, 2629 (1978).
14. O. Siiman. Inorg. Chem. **20**, 2285 (1981).
15. H. Richter, E. Fluck, H. Riffel, and H. Hess. Z. Anorg. Allg. Chem. **496**, 109 (1983).
16. R.G. Cavell, W. Byers, and E.D. Day. Inorg. Chem. **10**, 2710 (1971).
17. T.A. Mastryukova, A.E. Shipov, and M.I. Kabachnik. Zh. Obshch. Khim. **32**, 3579 (1962).
18. W.A. Higgins, R.W. Vogel, and W.G. Craig. J. Am. Chem. Soc. **77**, 1864 (1955).
19. C. Silvestru, I. Haiduc, K.H. Ebert, H.J. Breunig, and D.B. Sowerby. J. Organomet. Chem. **468**, 113 (1994).
20. R.O. Day, R.R. Holmes, A. Schmidpeter, K. Stoll, and L. Howe. Chem. Ber. **124**, 2443 (1991).
21. R. Rösler, J.E. Drake, C. Silvestru, J. Yang, and I. Haiduc. J. Chem. Soc. Dalton Trans. 391 (1996).
22. G. Balazs, J.E. Drake, C. Silvestru, and I. Haiduc. Inorg. Chim. Acta, **287**, 61 (1999).
23. C. Silvestru, R. Rösler, I. Haiduc, R. Cea-Olivares, and G. Espinosa-Perez. Inorg. Chem. **34**, 3352 (1995).
24. Z. Otwinowski and W. Minor. *In* Methods in enzymology. Vol. 276. *Edited by* C.W. Carter, Jr. and R.M. Sweet. Academic Press, New York. 1997. p. 307.
25. (*a*) R.H. Blessing. Acta Crystallogr. A: Fundam. Crystallogr. **A51**, 33 (1995); (*b*) J. Appl. Crystallogr. **30**, 421 (1997).
26. G.M. Sheldrick. Acta Crystallogr. A: Fundam. Crystallogr. **A46**, 467 (1990).
27. G.M. Sheldrick. SHELXL 97 and SHELXL 93. Program for crystal structure refinement. University of Gottingen, Germany. 1997.
28. G. Haegele, W. Kuchen, and H. Steinberger. Z. Naturforsch. **29b**, 349 (1974).
29. J.C. Tebby (*Editor*). CRC handbook of phosphorus-31 nuclear magnetic resonance data. Vol. 13. CRC Press, Boca Raton. 1991. p. 364.
30. M. Bartlett, and G.J. Palenik. Acta Crystallogr. A: Fundam. Crystallogr. **A25**, S173 (1969).
31. H.K. Shin, M.J. Hampden-Smith, E.N. Duesler, and T.T. Kodas. Can. J. Chem. **70**, 2954 (1992).
32. R. Richter, J. Sieler, E. Ludwig, E. Uhlemann, and L. Golic. Z. Anorg. Allg. Chem. **513**, 114 (1984).

© 2001 NRC Canada

The reduction of oxygen and hydrogen peroxide on dinuclear ruthenium phthalocyanine electrocatalytic surfaces

Mehrdad Ebadi, Christos Alexiou, and A.B.P. Lever

Abstract: The electrochemical properties of both mononuclear $L_2Ru^{II}Pc$ and dinuclear $[(THF)Rupc]_2$ species are described. The former is dominated by ring oxidation and reduction processes while the latter displays a series of metal localized processes. A Pourbaix diagram describes the various surfaces which can be generated by exposing a graphite electrode modified with $[(THF)Rupc]_2$ to aqueous buffer at different polarization over a wide range of pH. The behavior of these various surfaces towards the electrocatalytic reduction of both oxygen and hydrogen peroxide is described. Most importantly, three different regimes of hydrogen peroxide reduction are observed dependent on the nature of the modified electrode surface. At high pH the four electron reduction of oxygen to water is observed via a 2 + 2 mechanism.

Key words: phthalocyanine, ruthenium, ruthenium phthalocyanine, cyclic voltammetry, suface modified electrode, Pourbaix diagram, electrocatalysis, oxygen reduction, hydrogen peroxide reduction.

Résumé : On décrit les propriétés électrochimiques des espèces mononucléaires $L_2Ru^{II}Pc$ et dinucléaires $[(THF)Rupc]_2$. Les propriétés du premier sont dominées par des processus d'oxydation et de réduction du cycle alors que celles du deuxième présentent une série de processus métalliques localisés. Un diagramme de Pourbaix permet de décrire les diverses surfaces qui peuvent être générées lorsqu'on expose une électrode de graphite modifiée avec du $[(THF)Rupc]_2$ à divers tampons, à diverses polarisations et sur une grande plage de pH. On décrit le comportement de ces diverses surfaces vis-à-vis la réduction électrocatalytique de l'oxygène ainsi que du peroxyde d'hydrogène. Et, de façon plus importante, on observe trois régimes différents de réduction du peroxyde d'hydrogène suivant la nature de la surface de l'électrode modifiée. À des valeurs élevées de pH, on peut observer que la réduction de l'oxygène par quatre électrons pour donner de l'eau se fait par un mécanisme 2 + 2.

Mots clés : phtalocyanine, ruthénium, phtalocyanine de ruthénium, voltampérométrie cyclique, électrode à surface modifiée, diagramme de Pourbaix, électrocatalyse, réduction de l'oxygène, réduction du peroxyde d'hydrogène.

[Traduit par la Rédaction]

Introduction

There is intense interest in the use of metallophthalocyanine species in the design of chemical sensors (1). Metallophthalocyanines are especially important in this respect because of their rich redox behavior, the ability to use almost any metallic and some nonmetallic elements in the central cavity, their easy modification by substituting the ring, their intense color, and general medical inertness (2). An especially simple approach is to lay down a monolayer (or a few layers) of a metallophthalocyanine on a graphite surface thereby creating a metallophthalocyanine electrode and to measure the response of this electrode to perturbation by a redox active target (for examples using this approach, see refs. 3–18).

It is general practice to place these modified metallophthalocyanine (or metalloporphyrin) electrodes into an aqueous phase (in which the metallophthalocyanine surface is usually totally insoluble) and observe an electrocatalytic response to the target, often as a function of the pH of the aqueous phase (8, 15–17, 19–28). The nature of the surface of a metallophthalocyanine modified electrode will change as the polarization of the electrode changes or as the pH of the solution, in which it is immersed, changes. Clearly the catalytic activity must also change with the surface. If we observe an $M^{II/I}$ redox wave and suppose that M^I reduces molecular oxygen but M^{II} does not, then there is the rather obvious fact that polarized positive of the $M^{II/I}$ wave, there is no oxygen reduction, i.e., the surface is inactive, and close to, or negative of this $M^{II/I}$ wave, oxygen reduction proceeds, i.e., the surface is active. One might suppose that as one proceeds further negative of the $M^{II/I}$ wave, perhaps to a putative $M^{I/0}$ wave, activity would continue, however the surface will have changed, in this example, from predominantly M^I to predominantly M^0. The catalytic activity of the M^0 surface can be expected to be different from that of an M^I sur-

Received October 4, 2000. Published on the NRC Research Press Web site at http://canjchem.nrc.ca on July 14, 2001.

Dedicated to Professor Brian James on the occasion of his 65th birthday.

M. Ebadi, C. Alexiou, and A.B.P. Lever.[1] Department of Chemistry, York University, Toronto, ON M3J1P3, Canada.

[1]Corresponding author (telephone: (416) 736-2100, ext. 22309; fax: (416) 736-5936; e-mail: blever@yorku.ca).

 DOI: 10.1139/cjc-79-5/6-992 © 2001 NRC Canada

face and it does not follow that any catalytic activity will necessarily be retained as demonstrated here and elsewhere (16, 29, 30).

In this report we analyze the surface electrochemistry (31, 32) of dinuclear ruthenium phthalocyanine as a function of the polarization of the electrode and the pH of the aqueous phase in which it is immersed. The reactivity of oxygen and of hydrogen peroxide on the various surfaces is probed.

Dinuclear ruthenium phthalocyanine is of especial interest for study in this context because of the prior rather limited experience of oxygen activation by ruthenium porphyrins (33–35) coupled to the interest in generating a four electron oxygen reduction catalyst using cofacial dinuclear porphyrin species (19, 21, 27, 36–44). Although less directly relevant, there has also been interest recently in tetra-ruthenated metalloporphyrins (45) and in various carbido and nitrido bridged phthalocyanines and porphyrin–phthalocyanines (46–53).

Experimental

The buffer solutions were prepared by using 0.1 M $NaCH_3COO$, 0.1 M KH_2PO_4, and 0.15 M $KHCO_3$. The desired pH was obtained by addition of conjugate acids or 0.1 M NaOH solution and monitored with a pH meter. Nitrogen gas was used to remove dissolved oxygen in the solutions prior to the cyclic voltammetric (CV) experiment. Tetrahydrofuran (THF, Caledon) was distilled over sodium wire before use. Tetrabutylammonium hexafluorophosphate ($TBAPF_6$, Aldrich) was used without further purification. Oxygen and nitrogen gas (Praxair) were used as supplied.

Bis(dimethylsulfoxide)phthalocyaninatoruthenium(II) was prepared following a literature procedure (54). $RuCl_3$ (0.5 g) was added to phthalonitrile (5 g) and naphthalene (2 g). The solids were transferred into a test tube and heated to 275°C. After 1 h, the test tube was left to cool to room temperature and the crude product was Soxhlet extracted with MeOH (2 h) and hexane (24 h). The crude Rupc was then transferred into degassed DMSO (60 mL) and refluxed under nitrogen at 130°C. After three hours of heating the solution was left to cool to room temperature and violet $(DMSO)_2$Rupc was collected and washed with DMSO, followed by MeOH, and dried under vacuum at 70°C. Dissolving in the minimum amount of chloroform and reprecipitating the product by addition of DMSO leads to further purification of the $(DMSO)_2$Rupc. Yield 60%. The NMR and UV–vis spectra were consistent with the literature (54).

Bis(phthalocyaninato)diruthenium(II) $[Rupc]_2$ was prepared by the thermal decomposition of $(DMSO)_2$Rupc at 330°C under vacuo (ca. 1×10^{-5} torr) (54). The UV–vis spectrum (in THF, bands at 296 (s), 422 (w), 598 (vs), and 698 (m) nm.) is consistent with the previous literature (55).

Electrochemical measurements were performed with an RDE3 Pine potentiostat and an X-Y recorder. A basal plane pyrolytic graphite (bpg, Union Carbide) disc, sealed to a copper shaft with polyolefin heat shrinkable tubing was used as a working electrode in the surface CV experiments. The electrode was mounted on the shaft with the basal plane of the graphite exposed. The surface of the electrode was polished with 0.05 μm alumina powder, sonicated in doubly distilled water, and rinsed with acetone and water before each experiment. Exposing the polished bpg electrode to an oxygen-free THF solution of $[(THF)Rupc]_2$ (0.1 mM) modified the graphite electrode with a surface of $[(THF)Rupc]_2$. After 1 min of soaking, the electrode would be removed, rinsed with MeOH and doubly distilled water, and transferred to the cell. A saturated calomel electrode was used as a reference electrode in the surface experiments in water. Surface experiments using dichloromethane employed an AgCl/Ag electrode with ferrocene added as an internal standard. Due to the irreversibility of the ferrocenium/ferrocene couple, there was no additional check on the validity of the AgCl/Ag electrode.

In the solution CV experiments, a platinum disc sealed in glass was used as the working electrode and AgCl/Ag as the reference. The ferrocenium/ferrocene couple was used to reference the data to SCE (56). The platinum disc was polished with 0.3 μm alumina powder, rinsed, and sonicated in doubly distilled water before each experiment. A platinum wire was used as the counter electrode in both surface and solution CV experiments.

In O_2 reduction experiments, solutions were bubbled with pure gas for 20–30 min. The following parameters were used in our calculations: $D_{O_2} = 1.67 \times 10^{-5}$ ($cm^2\ s^{-1}$) (57), saturated $[O_2] = 1.1$ mM (58), and 0.01 $cm^2\ s^{-1}$ for the kinematic viscosity of water (59). A 2% solution of H_2O_2 was prepared in distilled water for hydrogen peroxide studies.

Results and discussion

Ruthenium phthalocyanine forms a series of octahedral mononuclear species of general formula $L_2Ru^{II}pc$ (13, 60–80). In addition, the dimeric $[Rupc]_2$ has been described. This is formed most readily by the thermal decomposition of $(DMSO)_2Ru^{II}pc$ (54, 55, 62, 81, 82) and contains a Ru—Ru bond of length 240 pm. The dinuclear species dissolves in coordinating solvents (sol) to generate the mononuclear $(sol)_2Ru^{II}pc$. It is also reactive towards oxygen generating, in solution, oligomeric pcRu-O-Rupc species (82, 83). $L_2Ru^{II}pc$ species may also be prepared by dissolving $[(THF)Rupc]_2$ in oxygen-free THF and adding a coordinating ligand, L. However the species in THF in the absence of oxygen and any coordinating ligands (L) is evidently the dimeric $[(THF)Rupc]_2$ complex. Under such conditions, its electronic spectrum and electrochemical properties differ significantly from those of an $L_2Ru^{II}pc$ species (84) dissolved in THF, e.g., as would be expected for $(THF)_2Ru^{II}pc$.

Electronic spectra and electrochemistry of the mononuclear $L_2Ru^{II}pc$ species

Thus, $L_2Ru^{II}pc$[2] species usually give rise to an electronic spectrum typical of a fourfold symmetric metallophthalocyanine species, having a single and intense Q band with vibrational satellites (85), albeit in some cases rather broader than usually observed (60, 61, 69, 73, 74, 86,

[2] The normal oxidation state of a phthalocyaninato anion is –2. For simplicity this is written as pc. However, the first ring oxidized species is written pc^{1-} while pc^{3-}…pc^{6-} refer to the successively one-electron reduced species, respectively.

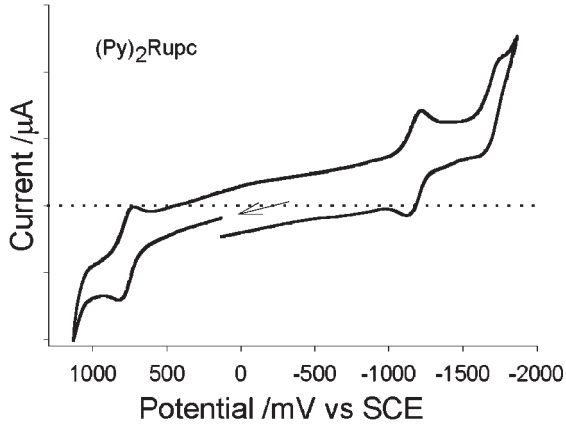
© 2001 NRC Canada

87). In THF, on the other hand, a solution of $[(THF)Rupc]_2$ gives an atypical spectrum exhibiting a Q band with a well-defined additional but weaker peak at lower energy (55).

Mononuclear $L_2Ru^{II}pc$ (L = coordinating neutral ligand such as DMSO, pyridine, carbon monoxide, imidazole, acetonitrile) are oxidized initially at the ring, at ca. 0.5–0.8 V vs. SCE, to generate $L_2Ru^{II}pc^{1-}$ species (Fig. 1, Table 1) (61, 74, 88–90). When L is a halide or nitrite anion (X) oxidation to $X_2Ru^{III}pc$ apparently occurs, near 0 V vs. SCE (69, 86, 87), but ring oxidized products are again obtained if L_2 is CO or X (X is a halide anion) (74).

Ring reduction to $L_2Ru^{II}pc^{3-}$ species for coordinating neutral ligands (L) is observed near –1.0 to –1.3 V vs. SCE. (74, 88, 90) such that the difference in ring oxidation and reduction potentials is in the range of ca. 1.8–2.0 V. The second reduction step to $L_2Ru^{II}pc^{4-}$ species occurs about 0.5 V to a more negative potential than the first (56, 88).

Fig. 1. The cyclic voltammogram of $(Py)_2Ru^{II}pc$. This solution was obtained by dissolving dimeric $[(THF)Rupc]_2$ into dichloromethane and adding 2% pyridine. Scan rate 100 mV s^{-1}, 0.1 M $TBAPF_6$.



Solution electrochemistry of the dinuclear $[(THF)Rupc]_2$

Dinuclear $[Rupc]_2$ dissolved in THF exhibits an electronic spectrum (Fig. 6, spectrum 1 of ref. 55) inconsistent with that for an $L_2Ru^{II}Pc$ species. Moreover, its previously unpublished electrochemical profile shown here (Fig. 2, Table 1) is completely different from that of a typical metallophthalocyanine species (56). Figure 2 displays the cyclic voltammogram of $[(THF)Rupc]_2$ in THF at –15°C. Four redox waves at 0.98 (wave I), 0.48 (wave II), –0.13 (wave III), and –0.55 (wave IV) vs. SCE are observed. By scanning the potential more negative than wave IV, an irreversible wave at –1.38 (wave V) is also observed. The peak currents of waves I–IV are linearly proportional to the square root of scan rate, characteristic of diffusion controlled redox processes. A weak wave observed around 0.8 V, absent from a freshly prepared solution, grows when oxygen is allowed into the electrochemical cell and evidently arises from an oxygenated impurity (55). These optical and electrochemical data clearly identify the solution species in THF as the dimeric species probably axially coordinated by solvent, i.e., $[(THF)Rupc]_2$.

To determine the number of electrons involved at each wave, a series of chronoamperometry experiments (91) were conducted (Fig. 3). In these experiments, an initial potential equal to the open circuit potential (open circuit potential lies between waves II and III) is applied to the working electrode. The potential is then stepped to a diffusion-controlled region of waves I–V and the current is recorded as a function of electrolysis time. Figure 3 shows the current functions ($i.t^{1/2}$) obtained from these chronoamperometry experiments. The magnitude of $i.t^{1/2}$ is used to determine the relative number of electrons involved in each redox wave, and is defined as:

$$[1] \qquad i.t^{1/2} = nFAC_oD_o{}^{1/2}\,\pi^{-1/2}$$

where A is the area of the electrode (cm^2), C_o is the concentration (mol cm^{-3}), and D_o is the diffusion coefficient ($cm\ s^{-1}$).

In Fig. 3, the current functions obtained for the reduction of $[(THF)Rupc]_2$ at a potential negative of wave III and positive of wave IV, are equal in magnitude (but opposite in sign) to those obtained for $[(THF)Rupc]_2$ oxidation at a potential positive of wave II and negative of wave I, suggesting an equal number of electrons are involved in these two waves. Using the data in Fig. 3, the relative number of electrons involved at each wave was determined to be one electron for each of waves II, III, and IV, and two electrons for waves I and V. The chronoamperometry results were reproducible for all the waves, with the exception of wave I where values between 2–3 were observed. Wave I lies close to the solvent limiting potential, which can result in overestimation of the number of electrons involved at this wave. The relative CV peak currents of waves I–IV are essentially the same suggesting that one electron is also involved at wave I. Attempts to obtain further information through spectroelectrochemical studies failed, as a result of the instability of the oxidation and reduction products on this longer time scale.

The first two reduction processes occurring between 0 and –0.5 V vs. SCE lie significantly positive of the ring reduction process noted above for monomeric $L_2Ru^{II}pc$ species. Due to the large ligand field strength of low spin octahedral d^6 Ru^{II} species, reduction to the Ru(I) species will occur at a significantly negative potential and this process has not been identified in six coordinate Ru^{II} phthalocyanine species.

However in four coordinate dinuclear species, lower lying empty orbitals will arise. Thus a molecular orbital description of the frontier orbitals in $[(THF)Rupc]_2$ has been presented (55). Coupling of the d orbitals of two d^6 ruthenium(II) moieties leads to a frontier description (81) $\sigma^2\pi^4\delta^2\delta^{*2}\pi^{*2}$ yielding a Ru=Ru double bond. The two reduction couples then reasonably are assigned to addition of electrons to the $d(\pi^*)$ level forming first the mixed valence Ru^I–Ru^{II} species and then subsequently the Ru^I–Ru^I species, possessing a single Ru–Ru bond. Correspondingly the two oxidation couples may refer to sequential loss of electrons from $d(\pi^{*2})$ yielding mixed valence Ru^{II}–Ru^{III} and finally Ru^{III}–Ru^{III}, which we note in passing, will have a triple bond. However, the magnitude of the potentials does not allow us to exclude the alternate possibility that phthalocyanine ring oxidation, commonly observed with mononuclear ruthenium phthalocyanines (60, 61, 69, 74,

© 2001 NRC Canada

Table 1. Summary of selected redox potentials ($E_{1/2}$, V) vs. SCE.

Complex	Conditions	Oxidation	Reduction[a]
$(DMSO)_2Rupc$	CH_2Cl_2–DMSO	0.78	–1.07, –1.57
$(Py)_2Rupc$	CH_2Cl_2–Py	0.77	–1.18, –1.70
$[(THF)Rupc]_2$	THF	0.98 (I), 0.48 (II)	–0.13 (III), –0.55 (IV), –1.38 (V)
$[(THF)Rupc]_2$	Surface pH = 1.97[b]		–0.005, –0.58
$[(THF)Rupc]_2$	Surface pH = 11.6[b]	–0.30	–0.63, –1.22
$[(THF)Rupc]_2$	Surface, CH_2Cl_2	0.84 (A), 0.30 (B)	–0.45 (C), –0.94 (D)

[a]Reduction processes for $L_2Ru^{II}Pc$ species are ring reduction processes. The first two reduction processes for $[(THF)Rupc]_2$ are metal localized, the third reduction is probably ring localized.
[b]Aqueous solution; the axial THF molecule may be replaced by water, or by hydroxyl ion in the basic medium.

Fig. 2. The cyclic voltammogram of $[(THF)Rupc]_2$ in THF. Scan rate 100 mV s^{-1}, 0.1 M $TBAPF_6$.

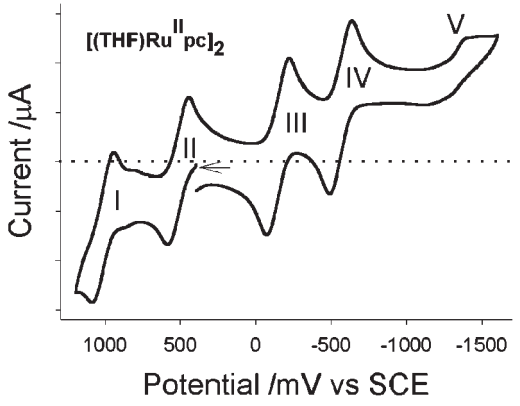
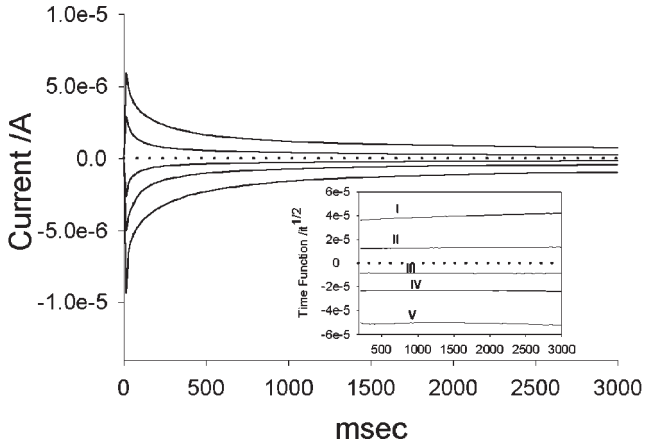


Fig. 3. Chronoamperometric current as a function of time following the potential step for $[(THF)Rupc]_2$ in THF, 0.1 M $TBAPF_6$. E(initial) = 200 mV vs. SCE. Potential was stepped to 1200, 650, –450, –950, and –1600 mV vs. SCE from the top curve down to the bottom, respectively. The top two represent oxidation processes and the bottom three reduction processes. Insert: the $i.t^{1/2}$ function plotted against time for the data in the main part of the figure.



92), is occurring here. Wave V is likely the ring reduction process, pc^{2-}/pc^{3-}. The electrochemical behaviour in THF, characteristically different from that of a mononuclear metallophthalocyanine species, is unequivocal proof of the existence therein of the dimeric $[(THF)Rupc]_2$.

In addition we note that in the solution chemistry of the monomer, the difference between the first oxidation process and the first reduction process is 1.8–2.0 V, while for the dimer in solution, the difference between first oxidation and *second* reduction is only about 1 V. This arises because in the former case, oxidation and reduction involve ring processes, while in the latter, they involve metal localized processes.

Surface electrochemistry of the dinuclear $[(THF)Rupc]_2$

When a basal plane pyrolytic graphite electrode is dipped into a THF solution of $[(THF)Rupc]_2$, a deposit is laid down to generate a modified ruthenium phthalocyanine electrode. The surface electrochemistry of this modified electrode is very reminiscent of the $[(THF)Rupc]_2$ solution electrochemistry discussed above. Thus if this electrode is exposed to dichloromethane, four waves are observed (Fig. 4, Table 1) with approximately the same potentials as observed for the solution species (Fig. 1, Table 1). There can be little doubt that waves A, B, C, and D correspond in assignment to those described above as I, II, III, and IV, respectively.

When this modified electrode is exposed to aqueous solution,[3] waves B, C, and D can be observed, depending on solution pH (Fig. 5). They are true surface processes whose current has a linear dependence on scan rate (91). The open circuit potential of this surface is just positive of wave B confirming that waves C and D are both reduction processes. These surface waves are dependent on the pH of the solution in which the electrode is immersed as shown in Figs. 5 and 6 shifting to more negative potentials with increasing pH and with a slope corresponding with a *n*-proton – *n*-electron system (91).

Further confirmation of the dimeric nature of the surface, and its inherent stability, is obtained by laying down the phthalocyanine layer on glass instead of bpg. If this layer is then dried and re-dissolved in THF, the majority species recovered, based on electronic spectroscopy, is again $[(THF)Rupc]_2$ contaminated with some incidental oxidation product.

Further, we also briefly explored the surface electrochemistry of $(DMSO)_2Rupc$. The first scan of such a surface (not shown) shows a single wave at –0.50 V at pH 1.8. This can be readily ascribed to the $Ru^{II}pc^{2-}/Ru^{II}pc^{3-}$ wave (seen in Fig. 1 at –1.2 V) shifted to –0.50 V under these acidic conditions. This is fully consistent with the previous literature concerning the pH dependence of the Mpc^{2-}/Mpc^{3-} wave (7,

[3]In the aqueous environment, the axial THF is probably replaced by water or hydroxide ion.

© 2001 NRC Canada

Fig. 4. Cyclic voltammogram of a surface modified $[(THF)Rupc]_2$/bpg electrode immersed in dichloromethane. Scan rate 100 mV s^{-1}, 0.1 M $TBAPF_6$.

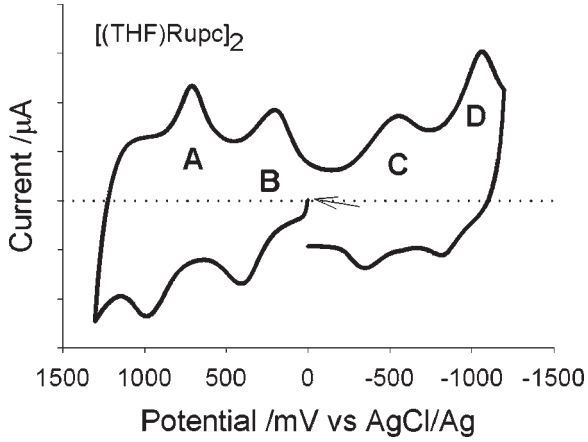
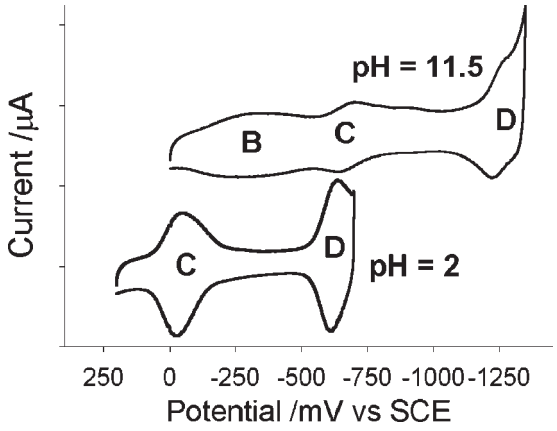


Fig. 5. Cyclic voltammograms for surface modified $[(THF)Rupc]_2$/bpg electrodes immersed in aqueous phosphate buffer at pH = 2.0 and 11.5 as indicated. Waves A and B are net reduction, while wave C is oxidation of the surface. Scan rate 100 mV s^{-1}.

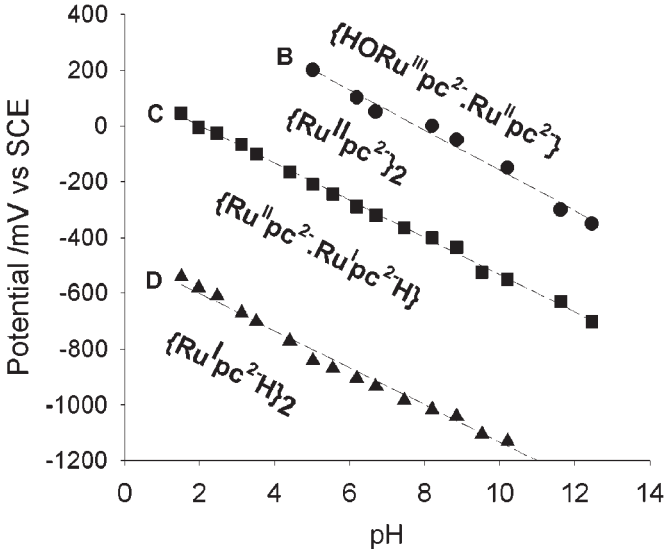


16, 93). The key conclusion is that a surface bound monomeric $L_2Ru^{II}pc$ species only displays a single reduction wave under conditions where $[(THF)Rupc]_2$ displays two waves.

A Pourbaix diagram for dimeric ruthenium phthalocyanine

By varying the pH at which cyclic voltammetric data are collected, a Pourbaix diagram (pH vs. potential) can be constructed (94). This diagram (Fig. 6) demonstrates an approximately –60 mV pH^{-1} dependence for all three waves. Previously the $Fe^{III/II}$ couple in Fepc and related species has been shown to be pH dependent because of the $HOFe^{III}pc/Fe^{II}pc$ couple (16, 28, 95). Wave B likely results from the similar process $[HORu^{III}pc{\cdot}Ru^{II}pc]/[Ru^{II}pc{\cdot}Ru^{II}pc]$. In the case of Fepc, there is usually a break in the *E* vs. pH line indicative of the pK_b of the $HOFe^{III}pc$ species. This is not evident here (nor with Cl_{16}Fepc (95)) indicating the very high Lewis acidity of the Ru^{III} centre. Waves C and D probably involve successive protonation at the aza bridge sites (96). Aside from displaying the potential at which waves B,

Fig. 6. A Pourbaix diagram indicating the pH dependence of waves B, C, and D, and indicating the nature of the surface modified regions (phosphate buffer).



C, and D can be observed as a function of pH, this diagram serves an especially useful purpose for surface electrochemistry. Assuming that just positive of wave B, the species on the electrode is $[HORu^{III}pc{\cdot}Ru^{II}pc]$ one can infer the nature of the surface formed upon subsequent 1-electron – 1-proton reduction, defined by the ca. –59 mV pH^{-1} slopes. Thus, in the range shown (Fig. 6), four different surface modified electrodes are effectively generated. We can then proceed to investigate the oxygen and hydrogen peroxide reduction chemistry on these various surfaces.

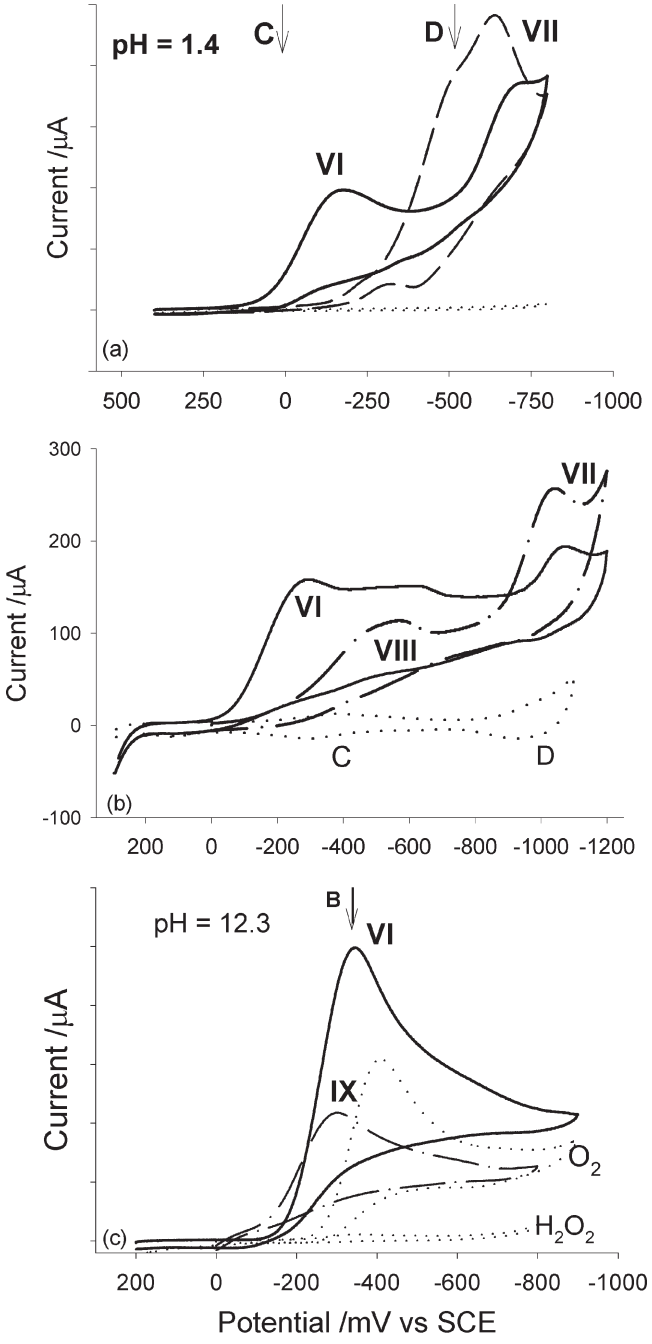
Oxygen and hydrogen peroxide electrocatalytic reduction

There is a long history of studies of the electrocatalytic reduction of oxygen and of hydrogen peroxide at phthalocyanine modified electrodes (3, 5, 7, 9, 11, 14, 15, 26, 28, 30, 93, 95, 97–126). Most research has been carried out with iron and cobalt phthalocyanines. Usually, oxygen is reduced in a two electron process to hydrogen peroxide, and with appropriately active phthalocyanines, this is often followed at more negative potentials by a further two electron reduction of hydrogen peroxide to water. The four electron reduction of water, which is more desirable from the viewpoint of fuel cell applications, has been observed in a number of cases involving iron, cobalt, rhodium, iridium, or platinum phthalocyanines (7, 17, 22, 98, 109, 112–115, 117, 118, 121, 122, 127–131). However, it is still a sought after process whose mechanistic details are yet poorly understood.

Dimeric ruthenium phthalocyanine exhibits new, hitherto unobserved, facets of oxygen and hydrogen peroxide reduction electrocatalysis due specifically to the variation in the active surface caused by the choice of polarization potential and the pH in which the electrode is immersed. Oxygen reduction (wave VI) occurs in a fairly narrow and flat potential range throughout the pH regime from 1–14 (Figs. 5 and 6). This is very similar to earlier studies (7, 11, 95, 126), except that in some of these studies there is a pronounced shift for the oxygen reduction wave to less negative potentials at very

© 2001 NRC Canada

Fig. 7. Comparison of oxygen and hydrogen peroxide reduction at a $[(THF)Rupc]_2$/bpg surface modified electrode. Phosphate buffer, scan rate 100 mV s^{-1}. Because of variation in concentration, the relative current between oxygen and hydrogen peroxide reduction is not meaningful. In all three graphs, the solid line is for oxygen reduction, peak labeled VI, and the hatched line is for hydrogen peroxide reduction, peaks VII, VIII, and IX. The blank bpg response is shown as a dotted line. Labels C and D define the positions of the $[(THF)Rupc]_2$/bpg reduction processes and B, the first oxidation process at the relevant pH locations shown as short vertical arrows: (*a*) pH 1.4; (*b*) H_2O_2 pH 6.2, O_2 pH 7.0; and (*c*) pH 12.3. The two dotted line curves refer to blank uncoated bpg responding to oxygen or hydrogen peroxide as labeled.



low pH, i.e., the process becomes pH dependent. This is absent in the current study at least down to pH 2. The oxygen reduction wave is followed at more negative potentials, up to pH 10, by one or two additional waves, which correspond with the subsequent reduction of hydrogen peroxide formed at the electrode from the initial two-electron reduction of dioxygen.

The identity of these additional waves due to hydrogen peroxide reduction is confirmed by independent studies of the $[(THF)Rupc]_2$/bpg electrode immersed in oxygen-free hydrogen peroxide. The same waves are generated (Fig. 7). Most unfortunately, the $[(THF)Rupc]_2$ surface is rather unstable in bulk hydrogen peroxide, with the second and subsequent scans revealing some decomposition. The very small amounts of hydrogen peroxide formed upon oxygen reduction, are reduced to water or diffuse away, such that the surface under an oxygen environment is quite stable and subsequent scans are very similar to the first scan. Above pH 10, there is no concomitant hydrogen peroxide reduction wave and we demonstrate below that water is then the primary product of a net four electron reduction of oxygen. Note that if a $[(THF)Rupc]_2$/bpg electrode is used to study oxygen reduction, and is subsequently placed into a deaerated aqueous solution, the original B, C, and D waves are recovered, indicating that the surface is stable to oxygen exposure (unlike the solution) (83).

In oxygen reduction studies at a surface modified electrode, the appearance of an additional wave due to subsequent hydrogen peroxide reduction is, of course, well known (3, 7, 17, 18, 26, 28, 102, 110, 120, 122, 124–126, 132). The striking observation with the $[(THF)Rupc]_2$ surface is the presence of three different potential regions for hydrogen peroxide reduction (waves VII–IX), depending on the active surface, which is correspondingly dependent on pH. We discuss first the reduction chemistry of hydrogen peroxide on these surfaces, since the oxygen reduction chemistry is related thereto. Because of the aforementioned decomposition in the presence of bulk hydrogen peroxide, the potentials of the waves noted below were derived from the oxygen reduction experiments except for pH > 10.

Hydrogen peroxide reduction at the $[(THF)Rupc]_2$/bpg modified electrode

Wave VII – low pH

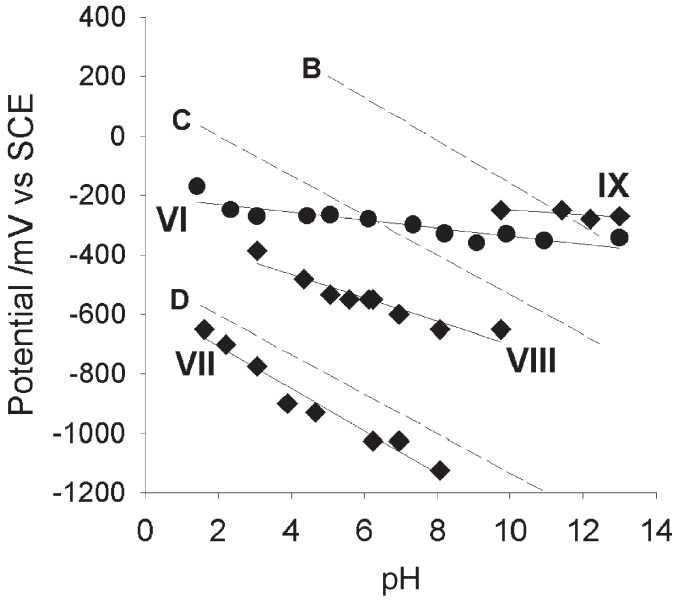
In the pH range 1–7, hydrogen peroxide is reduced at relatively negative potentials (wave VII), shifting to more negative potential with increasing pH (Fig. 8). This is a typical region observed in previous studies of hydrogen peroxide reduction at a metallophthalocyanine/graphite modified electrode (7, 8, 11, 126). Indeed the potential vs. pH correlation is almost coincident for $[(THF)Rupc]_2$ and for the cobalt crown phthalocyanine previously described (7). However, while in the cobalt crown phthalocyanine case, the linearity extends unbroken to higher pH, on the $[(THF)Rupc]_2$ surface, this more negative wave disappears from about pH 6 to be replaced by a second hydrogen peroxide reduction wave at less negative potential.

Wave VIII – near pH 7

In the pH range ca. 3–10 a hydrogen peroxide reduction wave (VIII) appears at ca. −400 to −650 mV, which is very

© 2001 NRC Canada

Fig. 8. A Pourbaix diagram indicating the pH dependence of waves B, C, and D, as well as oxygen reduction and the three regions of hydrogen peroxide reduction (phosphate buffer). The labels VI,VII, VIII, and IX correspond with the waves shown in Figs. 7*a–c*.



similar to the data observed for cobalt polytetraaminophthalocyanine (3). This wave VIII shifts slightly to more negative potentials with increasing pH (Fig. 8). In the range from about pH 3–8, both waves VII and VIII can be observed in the same voltammogram. Below pH 5 this wave is very weak appearing, if at all, only as an indistinct shoulder on the oxygen reduction wave. With bulk hydrogen peroxide at pH 1.4 there is a shoulder on the wave VII reduction process, near –500 mV, which may be associated with the wave VIII process, but the instability and lack of reproducibility of the surface in the presence of bulk hydrogen peroxide, makes this conjecture hard to confirm.

Wave IX – above pH 10.

Above about pH 10 a new, almost pH independent, hydrogen peroxide reduction wave (IX) appears near –300 mV (Fig. 6*c*). This wave was explored using bulk hydrogen peroxide in the cell, recording only the first voltammogram. The existence of this wave IX at a potential close to and indeed slightly positive of the oxygen reduction wave explains the absence of any additional hydrogen peroxide reduction wave appearing in the oxygen reduction experiment at pH 10 and above. Any hydrogen peroxide formed upon reduction of oxygen in this pH range would rapidly be reduced to water.

Oxygen reduction

The electrochemical reduction of oxygen has been explored in great detail for many years (133–135) and is, therefore, not presented in detail here. On a $[(THF)Rupc]_2$/bpg surface modified electrode, oxygen reduction occurs at a potential (wave VI) only slightly less positive than that observed on a bare bpg surface (Fig. 6). The process is essentially pH independent, consistent with many studies of oxygen reduction at a platinum electrode (133, 135). In the pH range where hydrogen peroxide reduction occurs at a significantly more negative potential than oxygen reduction, the well-documented two-electron reduction of oxygen to hydrogen peroxide is observed. Above pH 10, in the regime where oxygen reduction occurs at a similar potential or indeed negative of hydrogen peroxide reduction, the 2 + 2 electron reduction of oxygen directly to water is observed (Fig. 6). Thus, the formation of water above pH 10 is clearly associated with the ability of the surface to reduce hydrogen peroxide at a potential positive of that of oxygen reduction. Note that bare bpg does not reduce hydrogen peroxide within the limits noted in Fig. 6.

These observations are confirmed by conventional Koutecky–Levich plots (136, 137) for oxygen reduction generating straight lines (not shown) whose slopes in the mass transfer region at pH = 12.3 (slope = 2.18×10^4 $As^{-1/2}$) and pH = 2.3 (slope = 1.16×10^4 $As^{-1/2}$) correspond well with the theoretical values for $n = 4$ (slope = 2.43×10^4 $As^{-1/2}$) and $n = 2$ (slope = 1.13×10^4 $As^{-1/2}$), respectively. The linearity of the plot also indicates that oxygen reduction is first order with respect to dissolved O_2. More detailed analysis of the mechanism of oxygen reduction on $[(THF)Rupc]_2$/bpg is presented elsewhere (138).

Summary and conclusions

While oxygen reduction at the $[(THF)Rupc]_2$/bpg electrode has similar features to many other metallophthalocyanine modified electrodes, the hydrogen peroxide reduction is unique in displaying three independent regions of activity depending on pH. The simultaneous appearance within a narrow pH range of both waves VII and VIII is most noteworthy. The significance of this is as yet undetermined. It is possible that we are observing two sequential one-electron reductions of hydrogen peroxide to water, an observation which would be extremely unusual but may occur as consequence of the formation of stable hydroperoxyruthenium species on the surface. Certainly iron forms such electrochemically active species, of considerable importance in the biological field (139–144) and hydroperoxoiron species show complex electrochemical activity leading to cleavage of the peroxo bond and formation of oxo species (145). Thus similar and complex reactivity towards ruthenium centers can be anticipated. It is obvious from Fig. 5 that the three processes are electrocatalyzed by three different $[(THF)Rupc]_2$/bpg surfaces; in effect there are three different electrodes which respond necessarily in different ways to the bulk hydrogen peroxide. It is also highly probable that the various intermediate "H_2O_2" ruthenium species involve a varying number of bound protons.

It is unfortunate that the surface is unstable in the presence of bulk hydrogen peroxide, since this precludes a detailed electrochemical analysis to obtain information on reaction rates, order of reactant species, influence of film thickness, etc. A future study of perhalogenated $[(THF)Rupc]_2$ is planned in the expectation that such a surface should be much more stable. More detailed studies of the oxygen reduction process on the $[(THF)Rupc]_2$ electrode are available (138), but in view of the previous extensive lit-

© 2001 NRC Canada

erature on metallophthalocyanine electrocatalyzed oxygen reduction, such data are not presented here.

The intent of this paper was to demonstrate that through polarizing a modified electrode immersed in buffers of various pH, a range of different surface modified electrodes can be obtained and that the properties of these electrodes can vary dramatically. We have demonstrated here that the reactivities of variously reduced surfaces towards hydrogen peroxide are quite different. Elsewhere (29, 32) we shall demonstrate examples of where a surface, active towards reduction becomes totally inactive when polarized at more negative potentials even though the thermodynamic driving force must have increased, and then becomes active again at a further negative potential. The longer term application of this concept is to explore systems where the products of reduction of a target such as carbon dioxide will vary with polarization and pH as the surface chemistry is modified.

Acknowledgments

We thank the Natural Sciences and Engineering Research Council (NSERC) for financial support and the Johnson Matthey Company for a loan of Ruthenium trichloride.

References

1. A.B.P. Lever. J. Porphyr. Phthalocya. **3**, 488 (1999).
2. C.C. Leznoff and A.B.P. Lever (*Editors*). The phthalocyanines; properties and applications. Vol. 1–4. VCH, New York. 1989–1993.
3. Y.-H. Tse, P. Janda, H. Lam, J. Zhang, W.J. Pietro, and A.B.P. Lever. J. Porphyr. Phthalocya. **1**, 3 (1997).
4. J. Zhang, Y.H. Tse, W.J. Pietro, and A.B.P. Lever. J. Electroanal. Chem. **406**, 203 (1996).
5. Y.H. Tse, P. Seymour, N. Kobayashi, H. Lam, C.C. Leznoff, and A.B.P. Lever. Inorg. Chem. **30**, 4453 (1991).
6. M.R. Hempstead, A.B.P. Lever, and C.C. Leznoff. Can. J. Chem. **65**, 2677 (1987).
7. N. Kobayashi, P. Janda, and A.B.P. Lever. Inorg. Chem. **31**, 5172 (1992).
8. J. Zhang, W.J. Pietro, and A.B.P. Lever. Can. J. Chem. **73**, 1072 (1995).
9. D.Y. Hwang, J. Park, and S. Kim. Bull. Kor. Chem. Soc. **19**, 795 (1998).
10. C.-Q. Sun, G.-J. Liu, and H.-A. Zhang. Gaodeng Xuexiao Huaxue Xuebao **19**, 382 (1998).
11. S. Dong, B. Liu, J. Liu, and N. Kobayashi. J. Porphyr. Phthalocya. **1**, 333 (1997).
12. S. Komorsky-Lovric, M. Lovric, and F. Scholz. Mikrochim. Acta, **127**, 95 (1997).
13. M. Sekota and T. Nyokong. Electroanal. **9**, 1257 (1997).
14. J.H. Zagal, J. Pavez, L. Basaez, and M.J. Aguirre. Proc. Electrochem. Soc. **95**, 74 (1996).
15. S. Zecevic, B. Simic Glavaski, E. Yeager, A.B.P. Lever, and P.C. Minor. J. Electroanal. Chem. **196**, 339 (1985).
16. A.A. Tanaka, C. Fierro, D.A. Scherson, and E. Yeager. Mater. Chem. Phys. **22**, 431 (1989).
17. A.A. Tanaka, C. Fierro, D. Scherson, and E.B. Yaeger. J. Phys. Chem. **91**, 3799 (1987).
18. N. Kobayashi, K. Adachi, and T. Osa. Anal. Sci. **6**, 449 (1990).
19. E. Ngameni, Y. Le Mest, M. L'Her, J.P. Collman, N.H. Hendricks, and K. Kim. J. Electroanal. Chem. **220**, 247 (1987).
20. C.L. Ni, I. Abdalmuhdi, C.K. Chang, and F.C. Anson. J. Phys. Chem. **91**, 1158 (1987).
21. C.K. Chang and F.C. Anson. J. Phys. Chem. **91**, 1158 (1987).
22. D. Ozer, R. Parash, F. Brottman, U. Mor, and A. Bettelheim. J. Chem. Soc. Faraday Trans 1, **80**, 1139 (1984).
23. H.-Y. Liu, L. Abdalmudhi, C.K. Chang, and F.C. Anson. J. Phys. Chem. **89**, 665 (1985).
24. R.J.H. Chan, Y.O. Su, and T. Kuwana. Inorg. Chem. **24**, 3777 (1985).
25. M.F. Zipplies, W.A. Lee, and T.C. Bruice. J. Am. Chem. Soc. **108**, 4433 (1986).
26. H. Behret. Z. Physik. Chem **113**, 97 (1978).
27. Y.K. Choi, S. Jeon, J.K. Park, and K. H. Chjo. Electrochim. Acta, **42**, 1287 (1997).
28. A. Van der Putten, A. Elzing, W. Visscher, and E. Barendrecht. J. Electroanal. Chem. **221**, 95 (1987).
29. J.S. Chen and A.B.P. Lever. To be submitted.
30. J. Zagal, P. Bindra, and E. Yeager. J. Electrochem. Soc. **127**, 506 (1980).
31. A.B.P. Lever. Pure Appl. Chem. **70**, 755 (1998).
32. A.B.P. Lever. Abstracts of the 1st international conference on porphyrins and phthalocyanines. ICPP-1. Dijon. 2000. p. PLEN20.
33. S. Popovici, W. Leyffer, and R. Holze. J. Porphyr. Phthalocya. **3**, 265 (1999).
34. K. Kim. Part I. Electrocatalytic four-electron reduction of dioxygen by metalloporphyrins adsorbed on graphite. Part II. Synthesis, characterization and electrochemistry of diruthenium cofacial porphyrin dimers. Notes: (1987) 190 pp. Avail.: Univ. Microfilms Int. Order No. DA8707683 From: Diss. Abstr. Int. B 1987, 47, 124870.
35. D. Pang and Z. Wang. J. Electroanal. Chem. **340**, 35 (1992).
36. Y. Le Mest, M. L'Her, N.H. Hendricks, K. Kim, and J.P. Collman. Inorg. Chem. **31**, 835 (1992).
37. Y. LeMest, C. Inisan, A. Laouenan, M. LHer, J. Talarmin, M. ElKhalifa, and J.Y. Saillard. J. Am. Chem. Soc. **119**, 6095 (1997).
38. J.P. Collman, P. Denisevich, Y. Konai, M. Marrocco, C. Koval, and F.C. Anson. J. Am. Chem. Soc. **102**, 6027. (1980).
39. C.K. Chang. Adv. Chem. Ser. **173**, 162 (1979).
40. R.R.J. Durand, C.S. Bencosme, J.P. Collman, and F.C. Anson. J. Am. Chem. Soc **105**, 2710 (1983).
41. C.K. Chang, H.Y. Liu, and I. Abdalmuhdi. J. Am. Chem. Soc. **106**, 2725 (1984).
42. J.P. Collman, N.H. Hendricks, C.R. Leidner, E. Ngameni, and M. L'Her. Inorg. Chem. **27**, 387 (1988).
43. R. Guilard, S. Brandes, C. Tardieux, A. Tabard, M. L'Her, C. Miry, P. Gouerec, Y. Knop, and J.P. Collman. J. Am. Chem. Soc. **117**, 11721 (1995).
44. R. Karaman, S. Jeon, Ö. Almarsson, and T.C. Bruice. J. Am. Chem. Soc. **114**, 4899 (1992).
45. F.C. Anson, C. Shi, and B. Steiger. Acc. Chem. Res. **30**, 437 (1997).
46. G. Rossi, V.L. Goedken, and C. Ercolani. J. Chem. Soc. Chem. Commun. 46 (1988).
47. G. Rossi, M. Gardini, G. Pennesi, C. Ercolani, and V.L. Goedken. J. Chem. Soc. Dalton Trans. 193 (1989).
48. A.M. Paoletti, G. Pennesi, G. Rossi, and C. Ercolani. Inorg. Chem. **34**, 4780 (1995).
49. C. Ercolani, J. Jubb, G. Pennesi, U. Russo, and G. Trigiante. Inorg. Chem. **34**, 2535 (1995).

© 2001 NRC Canada

50. M.P. Donzello, C. Ercolani, K.M. Kadish, Z. Ou, and U. Russo. Inorg. Chem. **37**, 3682 (1998).
51. R. Caminiti, M.P. Donzello, C. Ercolani, and C. Sadun. Inorg. Chem. **37**, 4210 (1998).
52. C. Ercolani, S. Hewage, R. Heucher, and G. Rossi. Inorg. Chem. **32**, 2975 (1993).
53. C. Ercolani and B. Floris. Phthalocyanines: properties and applications. Vol 2. *Edited by* C.C. Leznoff and A.B.P. Lever. VCH Publishers, New York. 1992. p. 1.
54. W. Kobel and M. Hanack. Inorg. Chem **25**, 103 (1986).
55. A. Capobianchi, A.M. Paoletti, G. Pennesi, G. Rossi, R. Caminiti, and C. Ercolani. Inorg. Chem. **33**, 4635 (1994).
56. A.B.P. Lever, E.R. Milaeva, and G. Speier. Phthalocyanines: properties and applications. Vol. 3. VCH Publishers, New York. 1993. pp. 1–69.
57. I.O. Zaytsev and G.G Aseyev. (*Editors*) Properties of aqueous solutions of electrolytes. CRC Press, Boca Raton, FL, 1992.
58. K. Shigehara and F.C. Anson. J. Phys. Chem. **86**, 2776 (1982).
59. D.R. Lide. Handbook of chemistry and physics. CRC Press, Boca Raton, FL. 1997.
60. M. Weidemann, S. Sievertsen, and H. Homborg. Z. Anorg. Allg. Chem. **624**, 909 (1998).
61. D. Dolphin, B.R. James, A.J. Murray, and J.R. Thornback. Can. J. Chem. **58**, 1125 (1980).
62. H. Bertagnolli, A. Weber, W. Hoerner, T.S. Ertel, U. Reinoehl, M. Hanack, M. Hees, and R. Polley. Inorg. Chem. **36**, 6397 (1997).
63. A. Bulatov, S. Knecht, L.R. Subramanian, and M. Hanack. Chem. Ber. **126**, 2565 (1993).
64. U. Keppeler and M. Hanack. Chem. Ber **119**, 3363 (1986).
65. U. Keppeler, W. Kobel, H.U. Siehl, and M. Hanack. Chem. Ber **118**, 2095 (1985).
66. B.D. Berezin and G.V. Sennikova. Dokl. Acad. Nauk. SSSR **159**, 1127 (1964).
67. M.M. Doeff and D.A. Sweigart. Inorg. Chem. **20**, 1683 (1981).
68. M. Hanack, S. Knecht, and R. Polley. Chem. Ber. **128**, 929 (1995).
69. M. Czekalla, S. Sievertsen, and H. Homborg. Z. Anorg. Allg. Chem. **621**, 1205 (1995).
70. S. Sievertsen, M. Weidemann, O. Tsantzikrause, and H. Homborg. Z. Anorg. Allg. Chem. **621**, 1567 (1995).
71. G.E. Bossard, M.J. Abrams, M.C. Darkes, J.F. Vollano, and R.C. Brooks. Inorg. Chem. **34**, 1524 (1995).
72. D. Guez, D. Markovitsi, M. Sommerauer, and M. Hanack. Chem. Phys. Lett. **249**, 309 (1996).
73. M. Weidemann and H. Homborg. Z. Anorg. Allg. Chem. **622**, 1182 (1996).
74. M. Weidemann and H. Homborg. Z. Anorg. Allg. Chem. **622**, 1705 (1996).
75. T. Nyokong and J. Guthriestrachan. Inorg. Chim. Acta, **208**, 239 (1993).
76. M. Hanack and Y.-G. Kang. Chem. Ber. **124**, 1607 (1991).
77. M. Hanack and P. Vermehren. Chem. Ber. **124**, 1733 (1991).
78. M. Hanack, J. Osio-Barcina, E. Witke, and J. Pohmer. Synthesis – Stuttgart, 211 (1992).
79. M. Hanack, S. Knecht, and H.J. Schulze. J. Organomet. Chem. **445**, 157 (1993).
80. S. Omiya, M. Tsutsi, E.F. Meyer Jr, I. Bernal, and D.L. Cullen. Inorg. Chem. **19**, 134 (1980).
81. (*a*) R. Caminiti, M.P. Donzello, C. Ercolani, and C. Sadun. Inorg. Chem. **38**, 3027 (1999); (*b*) J. Hesschenbrouck, E. Solari, R. Scopelliti, C. Floriani and N. Re. J. Organomet. Chem. **596**, 77 (2000).
82. L. Alagna, A. Capobianchi, G. Pennesi, T. Prosperi, and G. Rossi. Journal De Physique IV, **7**, 1261 (1997).
83. A. Capobianchi, G. Pennesi, A.M. Paoletti, G. Rossi, R. Caminiti, C. Sadun, and C. Ercolani. Inorg. Chem. **35**, 4643 (1996).
84. A.B.P. Lever. Adv. Inorg. Chem. Radiochem. **7**, 27 (1965).
85. M.J. Stillman and T. Nyokong. Phthalocyanines: properties and applications. Vol. 1. VCH Publishers, New York. 1989. p. 133.
86. S. Sievertsen, M. Weidemann, H. Huckstadt, and H. Homborg. J. Porphyr. Phthalocya. **1**, 379 (1997).
87. S. Sievertsen, H. Schlehahn, and H. Homborg. Z. Naturforsch. **48B**, 50 (1993).
88. C. Alexiou and A.B.P. Lever. Unpublished observations.
89. M. Weidemann, H. Hückstädt, and H. Homborg. Z. Anorg. Allg. Chem. **624**, 846 (1998).
90. K. Dürr and M. Hanack. J. Porphyr. Phthalocya. **3**, 224 (1999).
91. A.J. Bard and L.R. Faulkner. Electrochemical methods; fundamentals and applications. John Wiley & Sons, New York. 1980.
92. M. Sekota and T. Nyokong. Polyhedron, **15**, 2901 (1996).
93. D. Schlettwein and T. Yoshida. J. Electroanal. Chem. **441**, 139 (1998).
94. M. Pourbaix. Atlas of electrochemical equilibria in aqueous solutions. Pergamon Press, Oxford. 1966.
95. M.N. Golovin, P. Seymour, K. Jayaraj, Y. Fu, and A.B. Lever. Inorg. Chem. **29**, 1719 (1990).
96. P.A. Bernstein and A.B.P. Lever. Inorg. Chim. Acta, **198/200**, 543 (1992).
97. J.B. Ouyang, K. Shigehara, A. Yamada, and F.C. Anson. J. Electroanal. Chem. **297**, 489 (1991).
98. A. Elzing, A. Van der Putten, W. Visscher, and E. Barendrecht. J. Electroanal. Chem. Interfacial Electrochem. **233**, 99 (1987).
99. A. Elzing, A. Van der Putten, W. Visscher, and E. Barendrecht. J. Electroanal. Chem. Interfacial Electrochem. **200**, 313 (1986).
100. F. Van den Brink, W. Visscher, and E. Barendrecht. J. Electroanal. Chem. Interfacial Electrochem. **157**, 283 (1983).
101. J.A.R. Van Veen and C. Visser. Electrochim. Acta, **24**, 921 (1979).
102. S. Kobayashi and Y. Nishiyama. J. Phys. Chem. **89**, 1167 (1985).
103. H. Behret, H. Binder, G. Sandstede, and G.G. Schere. J. Electroanal. Chem. **117**, 29 (1981).
104. J. Zagal, M. Paez, A.A. Tanaka, J.R. dos Santos, and C.A. Linkous. J. Electroanal. Chem. **339**, 13 (1992).
105. J. Zagal. Coord. Chem. Rev. **119**, 89 (1992).
106. J.B. Goodenough. J. Appl. Electrochem. **19**, 108 (1989).
107. C. Paliteiro, A. Hamnett, and J.B. Goodenough. J. Electroanal. Chem. Interfacial Electrochem. **160**, 359 (1984).
108. F. Van den Brink, W. Visscher, and E. Barendrecht. J. Electroanal. Chem. Interfacial Electrochem. **157**, 305 (1983).
109. O. Ikeda, S. Itoh, and H. Yoneyama. Bull. Chem. Soc. Jpn. **61**, 1428 (1988).
110. N. Kobayashi and W.A. Nevin. Appl. Organomet. Chem. **10**, 579 (1996).
111. P. Vasudevan, N. Phougat, and A.K. Shukla. Appl. Organomet. Chem. **10**, 591 (1996).
112. C. Paliteiro, A. Hamnett, and J.B. Goodenough. J. Electroanal. Chem. Interfacial Electrochem. **249**, 167 (1988).

© 2001 NRC Canada

113. T. Osaka, K. Naoi, T. Hirabayashi, and S. Nakamura. Bull. Chem. Soc. Jpn. **59**, 2717 (1986).
114. K. Oyaizu, A. Haryono, J. Natori, and E. Tsuchida. J. Chem. Soc. Faraday Trans. **94**, 3737 (1998).
115. V. Ivanovic, S. Zecevic, M. Avramov-Ivic, and B. Nikolic. J. Serb. Chem. Soc. **59**, 997 (1994).
116. R. Jiang and S. Dong. J. Electroanal. Chem. Interfacial Electrochem. **246**, 101 (1988).
117. C. Paliteiro and J.B. Goodenough. J. Electroanal. Chem. **239**, 273 (1988).
118. F. Van den Brink, W. Visscher, and E. Barendrecht. J. Electroanal. Chem. Interfacial Electrochem. **172**, 301 (1984).
119. R.K. Sen, J. Zagal, and E. Yeager. Inorg. Chem. **16**, 3379 (1977).
120. J.H. Zagal, M.J. Aguirre, L. Basaez, J. Pavez, L. Padilla, and A. Toro-Labbe. Proc. Electrochem. Soc. **95**, 89 (1996).
121. F. Van den Brink, W. Visscher, and E. Barendrecht. J. Electroanal. Chem. Interfacial Electrochem. **175**, 279 (1984).
122. A. Van der Putten, A. Elzing, W. Visscher, and E. Barendrecht. J. Electroanal. Chem. Interfacial Electrochem. **214**, 523 (1986).
123. K.A. Radyushkina, M.V. Merenkova, and M.R. Tarasevich. Elektrokhim. **29**, 514 (1993).
124. K.A. Radyushkina and M.R. Tarasevich. Russ. J. Electrochem. **34**, 92 (1998).
125. K.A. Radyushkina, M.V. Merenkova, M.R. Tarasevich, M.G. Gal'pern, S.V. Kudrevich, and I.G. Novozhilova. Elektrokhim. **28**, 1032 (1992).
126. P. Janda, N. Kobayashi, P. Auburn, H. Lam, C.C. Leznoff, and A.B.P. Lever. Can. J. Chem. **67**, 1109 (1989).
127. F. Coowar, O. Contamin, M. Savy, and G. Scarbeck. J. Electroanal. Chem. **246**, 119 (1988).
128. O. El Mouahid, C. Coutanceau, E.M. Belgsir, P. Crouigneau, J.M. Leger, and C. Lamy. J. Electroanal. Chem. **426**, 117 (1997).
129. D. Woehrle, D. Schlettwein, G. Schnurpfeil, G. Schneider, E. Karmann, T. Toshida, and M. Kaneko. Polym. Adv. Technol. **6**, 118 (1995).
130. A.L. Bouwkamp-Wijnoltz, W. Visscher, and J.A.R. Van Veen. Electrochim. Acta, **39**, 1641 (1994).
131. A. Elzing, A. Van der Putten, W. Visscher, and E. Barendrecht. J. Electroanal. Chem. Interfacial Electrochem. **233**, 113 (1987).
132. G.I. Zakharkin and M.P. Tarasevich. Elektrokhim. **11**, 1019 (1975).
133. D.T. Sawyer, A. Sobkowiak, and J.I. Roberts. Jr. Electrochemistry for chemists. John Wiley & Sons, New York. 1995.
134. A.E. Martell and D.T. Sawyer. Oxygen complexes and oxygen activation by transition metals. Plenum Press, New York. 1987.
135. D.T. Sawyer. Oxygen chemistry. Oxford University Press, Oxford. 1991.
136. J. Koutecky and V.C. Levich. Zh. Fiz. Khim. **32**, 1565 (1956).
137. J. Koryta and J. Dvorak. Principles of electrochemistry. John Wiley & Sons, New York. 1987.
138. M. Ebadi. Ph.D. thesis. York University, Toronto. 2000. in process.
139. W. Wonwoo Nam, H. Jung Han, S.-Y. Oh, Y.J. Lee, M.-H. Choi, S.-Y. Han, C. Kim, S.K. Woo, and W. Shin. J. Am. Chem. Soc. **122**, 8677 (2000).
140. M. Sono, M.P. Roach, E.D. Coulter, and J.H. Dawson. Chem. Rev. **96**, 2841 (1996).
141. P.R. Ortiz de Montellano. Cytochrome P450: structure, mechanism, and biochemistry. 2nd ed. Plenum Press, New York. 1995.
142. J.E. Erman, L.P. Hager, and S.G. Sligar. Adv. Inorg. Biochem. **10**, 71 (1994).
143. T. Ogihara, S. Hikichi, M. Akita, T. Uchida, T. Kitagawa, and Y. Moro-oka. Inorg. Chim. Acta, **297**, 162 (2000).
144. H. Shimada, S.G. Sligar, H. Yeom, and Y. Ishimura. Oxygenases and model systems. *Edited by* T. Funabiki. Kluwer Academic Publishers, Dordrecht, The Netherlands. 1997.
145. D.T. Sawyer, A. Sobkowiak, and J.I. Roberts Jr. Electrochemistry for chemists. 2nd ed. John Wiley & Sons, New York. 1995. p. 413.

© 2001 NRC Canada

The role of a hydroxycyclopentadienyl ruthenium dicarbonyl formate in formic acid reductions of carbonyl compounds catalyzed by Shvo's diruthenium catalyst

Charles P. Casey, Steven W. Singer, and Douglas R. Powell

Abstract: Addition of excess HCO_2H to $\{2,5\text{-}Ph_2\text{-}3,4\text{-}Tol_2(\eta^5\text{-}C_4CO)]Ru(CO)_2\}_2$ (**6**) at –20°C led to the formation of $[2,5\text{-}Ph_2\text{-}3,4\text{-}Tol_2(\eta^5\text{-}C_4COH)]Ru(CO)_2(\eta^1\text{-}OCHO)$ (**5**), a proposed intermediate in catalytic transfer hydrogenations developed by Shvo. Hydroxycyclopentadienyl formate **5** undergoes rapid reversible dissociation of HCO_2H at –20°C, and undergoes decarboxylation at 1°C to form a 1:10 mixture of $\{[2,5\text{-}Ph_2\text{-}3,4\text{-}Tol_2(\eta^5\text{-}C_4CO)]_2H\}Ru_2(CO)_4(\mu\text{-}H)$ (**3**):$[2,5\text{-}Ph_2\text{-}3,4\text{-}Tol_2(\eta^5\text{-}C_4COH)Ru(CO)_2H]$ (**4**). **5** does not reduce PhCHO below the temperature at which **5** is converted to hydride **4**. The catalytic production of benzyl alcohol from **5** and PhCHO in the presence of excess HCO_2H is not accelerated by higher concentrations of PhCHO, indicating that **5** does not directly reduce PhCHO. Formate complex **5** is the precursor of hydride **4** which transfers hydrogen to PhCHO. A crucial role for the CpOH proton in the decarboxylation of **5** was indicated by the much slower decarboxylation of the methoxycyclopentadienyl analog $[2,5\text{-}Ph_2\text{-}3,4\text{-}Tol_2(\eta^5\text{-}C_4COCH_3)]Ru(CO)_2(\eta^1\text{-}OCHO)$ (**7**). A mechanism for decarboxylation of **5** is proposed which involves reversible dissociation of formic acid to form the unsaturated dienone dicarbonyl ruthenium intermediate **C**, followed by simultaneous transfer of hydride to ruthenium from the formic acid carbon and of proton to the carbonyl of **C** from the formic acid OH group.

Key words: Shvo catalyst, ruthenium formate, decarboxylation.

Résumé : L'addition d'un excès de HCO_2H au complexe $\{2,5\text{-}Ph_2\text{-}3,4\text{-}Tol_2(\eta^5\text{-}C_4CO)][Ru(CO_2\}_2$ (**6**), à –20°C, conduit à la formation de $[2,5\text{-}Ph_2\text{-}3,4\text{-}Tol_2(\eta^5\text{-}C_4COH)]Ru(CO)_2(\eta^1\text{-}OCHO)$ (**5**), un intermédiaire présumé dans les hydrogénations par transfert catalytique développées par Shvo. Le formate d'hydrocyclopentadiényle, **5**, subit une dissociation réversible rapide en HCO_2H à –20°C et il subit une décarboxylation à 1°C conduisant à la formation d'un mélange 1:10 de $\{[2,5\text{-}Ph_2\text{-}3,4\text{-}Tol_2(\eta^5\text{-}C_4CO)]_2H\}Ru_2(CO)_4(\mu\text{-}H)$ (**3**) : $[2,5\text{-}Ph_2\text{-}3,4\text{-}Tol_2(\eta^5\text{-}C_4COH)Ru(CO)_2H]$ (**4**). Le composé **5** ne réduit pas le PhCHO en dessous de la température à laquelle ce composé est transformé en hydrure **4**. La vitesse de la production catalytique d'alcool benzylique à partir de **5** et de PhCHO, en présence d'un excès de HCO_2H n'est pas accélérée par des concentrations plus élevées de PhCHO; ce résultat indique que **5** ne réduit pas le PhCHO directement. Le complexe **5** à base de formate est le précurseur de l'hydrure **4** qui transfère de l'hydrogène au PhCHO. Un rôle crucial pour le proton du CpOH dans la décarboxylation du composé **5** est mis en évidence par la décarboxylation beaucoup plus lente de l'analogue méthyoxycyclopentadiényle, $[2,5\text{-}Ph_2\text{-}3,4\text{-}Tol_2(\eta^5\text{-}C_4COCH_3)]Ru(CO)_2(\eta^1\text{-}OCHO)$ (**7**). On propose un mécanisme de décarboxylation du composé **5**; il implique une dissociation réversible de l'acide formique conduisant à la formation de l'intermédiaire insaturé **C**, ruthénium dicarbonyle diénone, suivi par un transfert simultané d'hydrure du carbone de l'acide formique vers le ruthénium et du proton du groupe OH de l'acide formique vers le carbonyle de l'intermédiaire **C**.

Mots clés : catalyseur de Shvo, formate de ruthénium, décarboxylation.

[Traduit par la Rédaction]

Introduction

Recently, we began investigating Shvo's fascinating hydrogenation catalyst, $\{[2,3,4,5\text{-}Ph_4(\eta^5\text{-}C_4CO)]_2H\}Ru_2(CO)_4(\mu\text{-}H)$ (**1**), which catalyzes the reduction of a wide variety of unsaturated organic substrates (1). Shvo has proposed that $[2,3,4,5\text{-}Ph_4(\eta^5\text{-}C_4COH)Ru(CO)_2H]$ (**2**), a unique organometallic complex containing both acidic OH and hydridic

Received September 26, 2000. Published on the NRC Research Press Web site at http://canjchem.nrc.ca on July 14, 2001.

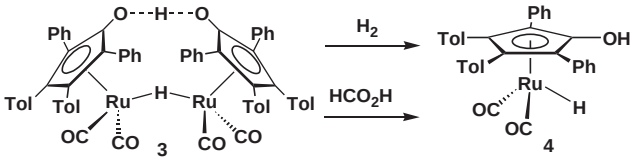
Dedicated to Brian James on the occasion of his 65th birthday in recognition of his insightful research on homogeneous catalysis of hydrogenation.

C.P. Casey,[1] S.W. Singer, and D.R. Powell. Department of Chemistry, University of Wisconsin-Madison, Madison, WI 53706, U.S.A.

[1]Corresponding author (telephone: (608) 262-0584; fax: (608) 265-4534; e-mail: casey@chem.wisc.edu).

 DOI: 10.1139/cjc-79-5/6-1002 © 2001 NRC Canada

Scheme 1.



RuH functions, is the active species in the reductions. Our long term interest in complexes containing acidic and hydridic hydrogens and their growing importance in homogeneous catalysis prompted us to initiate a detailed mechanistic study of Shvo's catalytic system (2, 3). Our studies of the tolyl-substituted analogs {[2,5-Ph_2-3,4-Tol_2(η^5-C_4CO)]$_2$H}$Ru_2(CO)_4$(μ-H) (**3**) and [2,5-Ph_2-3,4-Tol_2(η^5-C_4COH)$Ru(CO)_2H$] (**4**) (Scheme 1) provided persuasive evidence that **4** reduced carbonyls and imines by a concerted hydrogen transfer mechanism (4). Alkenes appear to be reduced by a very different mechanism, probably involving CO dissociation from **4** to form a reactive 16e species.

One puzzling aspect of the chemoselectivity of catalysis by **1** was that carbonyls were efficiently reduced by either H_2 or HCO_2H, but alkenes were reduced only by H_2 (5). Shvo's proposal that hydroxycyclopentadienyl hydride **2** was the common active species in all the catalytic reactions appeared to be at odds with the observation that chemoselectivity could be affected by the choice of the reducing agent used to generate **2**. We considered the possibility that the hydroxycyclopentadienyl ruthenium formate **B** might play a direct role in reductions catalyzed by **1** that use HCO_2H as the reducing agent. Shvo had proposed the intermediacy of formate **B** but had never observed it (Scheme 2). Formate complexes have also been proposed as important intermediates in transfer hydrogenation reactions where HCO_2H is the hydrogen source and in the transition-metal-catalyzed reductions of CO_2 (6).

We initiated studies of the interaction of HCO_2H with the Shvo catalytic system to answer three questions: (*i*) Are formate complexes formed? (*ii*) Do they reduce carbonyls and (or) alkenes? (*iii*) Are they converted to hydrides, and if so, how? Here, we report the low-temperature observation of a tolyl-substituted analog of hydroxycyclopentadienyl formate **B**, its failure to reduce benzaldehyde, and mechanistic studies of its decarboxylation. These studies afford insight into the decarboxylation of formate complexes and clarify the role of HCO_2H in Shvo's catalytic system.

Results

Observation of a hydroxycyclopentadienyl ruthenium formate

We previously reported that heating diruthenium hydride **3** with excess HCO_2H at 80°C in THF-d_8 for 10 min led to the formation of a solution of hydroxycyclopentadienyl ruthenium hydride **4** (4). A possible intermediate in this reaction is the hydroxycyclopentadienyl formate **5**. In an effort to observe this species directly, we monitored the reaction of excess HCO_2H with a suspension of the more reactive diruthenium complex {2,5-Ph_2-3,4-Tol_2(η^5-C_4CO)$Ru(CO)_2$}$_2$ (**6**) in THF-d_8 by ^{1}H NMR spectroscopy at room temperature (Scheme 3). After 5 min, two new tolyl resonances were observed at δ 2.16 and 2.18 in 1:2 ratio in addition to the tolyl resonance of **6** at δ 2.11. The resonance at δ 2.16 and a hydride resonance at δ –9.76 were assigned to hydroxycyclopentadienyl hydride **4**. The resonance at δ 2.18 and a characteristic (7) formate resonance at δ 7.76 were assigned to the hydroxycyclopentadienyl formate complex [2,5-Ph_2-3,4-Tol_2(η^5-C_4COH)]$Ru(CO)_2$(η^1-OCHO) (**5**). After 10 min, a 1:1 ratio of **4**:**5** was observed and a small hydride resonance at δ –18.25 indicated the formation of some diruthenium hydride **3**. After 30 min, the only species seen were a 1:1 ratio of **3**:**4**; all of diruthenium complex **6** was consumed and there was no evidence for remaining intermediate formate complex **5**. The ratio of **3**:**4** remained constant for 10 h at room temperature. The mixture was converted to a solution of **4** by heating for 10 min at 80°C.

The reaction was complicated by the low solubility of dimer **6** in THF-d_8; all solid material was not dissolved until after 30 min of reaction. To circumvent these solubility problems, the reaction was also studied in CD_2Cl_2, in which **6** is more soluble. HCO_2H (0.4 M) was injected into a CD_2Cl_2 solution of **6** (0.02 M) at room temperature and the reaction was immediately monitored by ^{1}H NMR spectroscopy. After 2 min, >95% of **6** was consumed, and the major product was formate **5**, identified by a formate resonance at δ 7.87 and a tolyl resonance at δ 2.23. Hydroxycyclopentadienyl hydride **4** and diruthenium hydride **3** were present in a 4:5 ratio. The tolyl methyl resonance of **3** overlaps the resonance of **5**, so the relative amounts of **3**, **4**, and **5** were estimated by comparison of the intensity of the formate resonance to that of the hydride resonances of **3** (δ –18.63) and **4** (δ –9.81). After 5 min, dimer **6** was completely consumed, there was no evidence for remaining formate intermediate **5**, and the major products were a 2.5:1 mixture of **3**:**4**. After 20 min, the ratio of products was steady at 2.5:1. The ratio of **3**:**4** slowly changed over time; after 10 h, the ratio of **3**:**4** was 4:1.

Clean conversion of ruthenium dimer 6 to hydroxycyclopentadienyl ruthenium formate 5 at –20°C

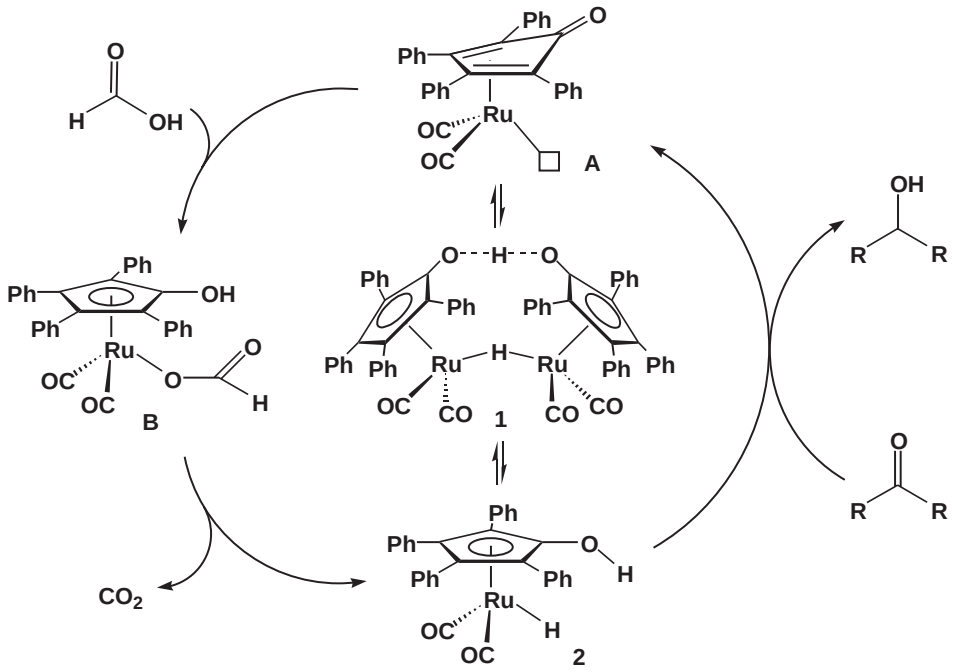
Since evidence for the transient formation of hydroxycyclopentadienyl ruthenium formate **5** from **6** and excess HCO_2H was obtained at room temperature, low-temperature studies were initiated in an effort to observe high concentrations of **5**. HCO_2H (0.2 M) was injected into an NMR tube containing a CD_2Cl_2 solution of **6** (0.03 M) at –78°C. The tube was inserted into an NMR probe precooled to –20°C and the reaction was followed by ^{1}H NMR spectroscopy. After 30 min, 5% **6** (tolyl methyl δ 2.06) remained and 95% of the material had been converted to **5** (tolyl methyl δ 2.20, formate hydrogen δ 7.47). No further change in the equilibrium ratio (K_{eq} = [**5**]^2/[**6**][HCO_2H]^2 $\approx$ 55) was seen over the next 30 min. In the ^{13}C NMR spectrum, the formate resonance of **5** was observed at δ 172. At concentrations $\geq$0.4 M HCO_2H, no resonances for dimer **6** were observed, consistent with the estimated equilibrium constant.

Isotope labeling evidence for reversible dissociation of HCO_2H from 5

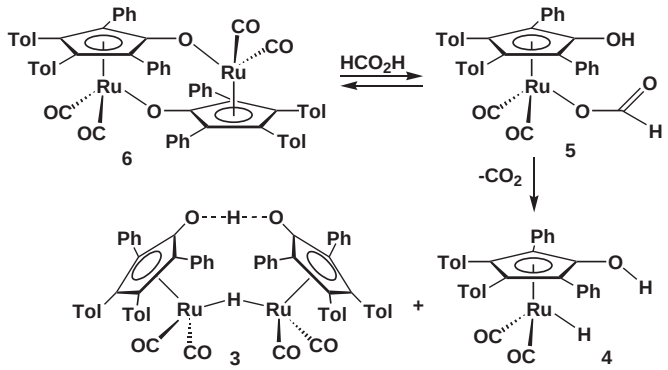
The observation of a steady ratio of **5**:**6** in the presence of excess HCO_2H requires an equilibrium process. Equilibration is readily explained by invoking dienone carbonyl inter-

© 2001 NRC Canada

Scheme 2.



Scheme 3.



mediate **C** which can either dimerize to form **6** or react with HCO_2H to give **5**, possibly via an intermediate formic acid complex **D** (Scheme 4).

Exchange of DCO_2H with **5** occurred rapidly at –20°C and is consistent with the intervention of intermediate **C**. A solution of deuterated formate complex was prepared by addition of DCO_2H (0.3 M) to a CD_2Cl_2 solution of **6** (0.03 M) at –20°C. After 30 min, the ^{1}H NMR spectrum showed >98% conversion to [2,5-Ph_2-3,4-Tol_2(η^5-C_4COH)]Ru(CO)$_2$(η^1-OCDO) (**5-d**); no formate ^{1}H NMR resonance was observed. The tube was cooled to –78°C and an equal amount of HCO_2H (0.3 M) was added. When the tube was replaced in the NMR spectrometer at –20°C, a formate resonance was seen at δ 7.75. The integrated intensity of this resonance relative to the tolyl methyl resonance of **5** at δ 2.20 was 0.5:6, indicating a 1:1 equilibrium mixture of **5**:**5-d**. Equilibration is rapid at –20°C.

Kinetics of decarboxylation of hydroxycyclopentadienyl ruthenium formate 5

The rate of decarboxylation of **5** generated from **6** and excess HCO_2H in CD_2Cl_2 at –20°C was measured by ^{1}H NMR spectroscopy at 1°C. The major product of the decarboxylation was diruthenium hydride **3** and hydroxycyclopentadienyl hydride **4** was the minor product (10:1 ratio). Duplicate kinetic runs on 0.06 M solutions of **5**, formed from **6** and 0.2 M HCO_2H, gave k_{obs} = 5.9 and 5.8 × 10^{-4} s^{-1}. Rates were slower in the presence of higher concentrations of HCO_2H. Duplicate runs on solutions of **5** prepared from **6** and 0.4 M HCO_2H gave k_{obs} = 3.2 and 4.2 × 10^{-4} s^{-1}. Duplicate runs on solutions of **5** prepared from **6** and 1.0 M HCO_2H gave k_{obs} = 2.0 and 1.7 × 10^{-4} s^{-1}.

Isotope effects on decarboxylation were investigated using 0.06 M solutions of **5-d** prepared by adding 0.2 M DCO_2H to CD_2Cl_2 solutions of **6** at –20°C. Duplicate kinetic runs on solutions of **5-d** at 1°C gave k_{obs} = 5.6 and 5.2 × 10^{-4} s^{-1}. The isotope effect on decarboxylation, $k_5/k_{5\text{-}d}$ = 1.1 ± 0.1, was negligible.

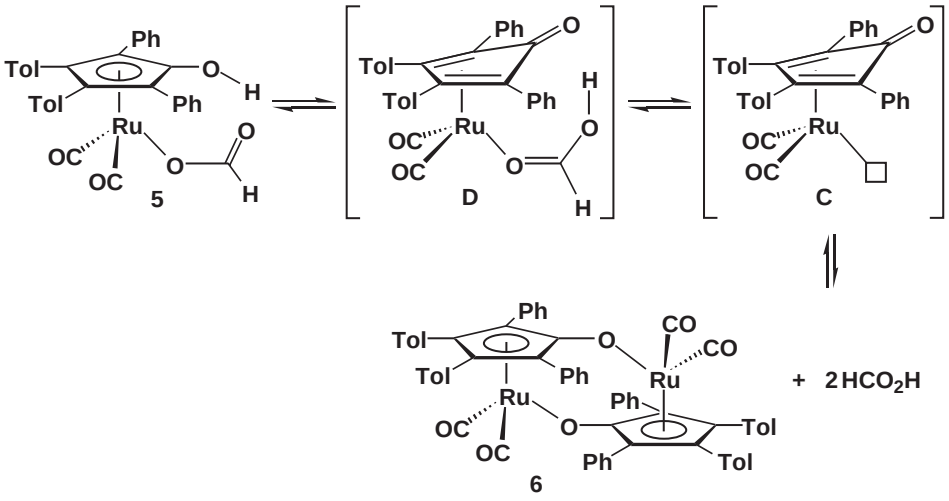
Previous studies on decarboxylation of CpFe(CO)$_2$(η^1-OCHO) had shown that reversible CO dissociation was the first step in the decarboxylation (8). To test whether CO dissociation was involved in the decarboxylation of **5**, the rate of decarboxylation of **5** under 1.4 atm (1 atm = 101.325 kPa) of ^{13}CO was measured in the presence of 0.2 M HCO_2H at 1°C. No inhibition of decarboxylation (k_{obs} = 5.7 × 10^{-4} s^{-1}) was observed and there was no incorporation of ^{13}CO into diruthenium hydride **3** or hydroxycylopentadienyl hydride **4** (10:1 ratio of products). The formation of [2,5-Ph_2-3,4-Tol_2(η^4-C_4CO)]Ru(CO)$_2$(^{13}CO) as a byproduct (<5%) of the decarboxylation was indicated by a characteristic tolyl methyl resonance at δ 2.25 in ^{1}H NMR.

Hydroxycyclopentadienyl ruthenium formate 5 does not reduce benzaldehyde

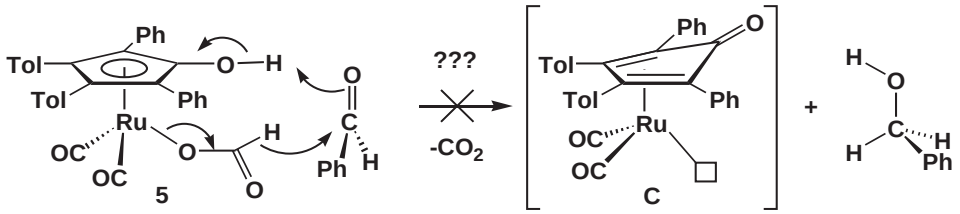
Shvo proposed that hydroxycyclopentadienyl hydride **4** is the active hydrogen transfer agent in all the reductions catalyzed by diruthenium hydride **3**. For reductions with HCO_2H, we wished to explore the possibility that the

© 2001 NRC Canada

Scheme 4.



Scheme 5.



hydroxycyclopentadienyl formate **5** might be the active reducing agent (Scheme 5) (Formic acid and formate salts are well-known reducing agents, see ref. 9).

We devised a method for producing **5** in the presence of benzaldehyde at low temperature patterned after our earlier observation that reaction of **4** with PhCHO in the presence of CF_3CO_2H leads to the formation of benzyl alcohol and [2,5-Ph_2-3,4-Tol_2(η^5-C_4COH)]Ru$(CO)_2$(η^1-O_2CCF_3). We have proposed that the hydroxycyclopentadienyl trifluoroacetate complex is formed by addition of CF_3CO_2H to the coordinatively unsaturated intermediate **C** generated by hydrogen transfer from **4** to PhCHO.

PhCHO (0.8 M) was added to a CD_2Cl_2 solution of **4** (0.03 M) containing HCO_2H (0.5 M) at –78°C and the solution was monitored by ^{1}H NMR spectroscopy at –29°C. Rapid disappearance ($t_{0.5} \approx 1$ min) of the δ –9.74 hydride resonance of **4** and rapid appearance of resonances for $PhCH_2OH$ and **5** were observed. No further reduction of PhCHO by **5** was observed even after the temperature was raised to –15°C. These observations indicate that **4** is a much more reactive reducing agent than **5**; indeed, no observation requires that **5** act as a hydride donor.

When the above solution was warmed to 0°C, the onset temperature for decarboxylation of **5**, the resonance for $PhCH_2OH$ began growing slowly. Upon further warming to 20°C, rapid catalytic reduction of PhCHO was observed, along with the appearance of characteristic NMR resonances for diruthenium hydride **3**. After 20 min, the ratio of **5** to **3** was 1:6, unreacted HCO_2H (0.06 mmol) and PhCHO (0.10 mmol) remained, and 10 equiv of benzyl alcohol had been produced.

The above experiment does not exclude the possibility that **5** may transfer hydrogen to substrates at a rate similar to that of decarboxylation. To test for this possibility, decarboxylation of **5** was carried out at 10°C in the presence of varying amounts of PhCHO. If the rate of hydrogen transfer from **5** to PhCHO is competitive with decarboxylation, the rate of $PhCH_2OH$ formation should increase at higher PhCHO concentration. The rate of formation of $PhCH_2OH$ (δ 4.68 in ^{1}H NMR) was monitored in solutions containing 0.4 M and 0.8 M PhCHO. Plots of the concentration of $PhCH_2OH$ vs. time were linear. (The constant rate of alcohol formation is due to the nearly constant concentrations of **5,** which is continually regenerated, and of benzaldehyde, which is present in excess.) The rate of formation of benzyl alcohol did not depend on the concentration of benzaldehyde ($k = 1.20 \times 10^{-1}$ s^{-1} for 0.4 M PhCHO, and $k = 1.16 \times 10^{-1}$ s^{-1} for 0.8 M PhCHO). Therefore, the hydroxycyclopentadienyl ruthenium formate **5** does not directly reduce benzaldehyde.

Synthesis of a methoxycyclopentadienyl ruthenium formate

Our studies of the reduction of carbonyls and imines by hydroxycyclopentadienyl ruthenium hydride **4** highlighted the crucial importance of the CpOH proton in promoting hydrogen transfer. The triethylsiloxy derivative of **4**, [2,5-Ph_2-3,4-Tol_2(η^5-$C_4COSiEt_3$)]Ru$(CO)_2$H, was unreactive towards carbonyls and imines under the same conditions that **4** was highly reactive (4). The possible role of the CpOH proton of **5** in decarboxylation and hydrogen transfer reactions prompted us to investigate the reactivity of its methoxy-substituted analog.

[2,5-Ph_2-3,4-Tol_2(η^5-C_4COCH_3)]Ru$(CO)_2$(η^1-OCHO) (**7**) was synthesized in a two-step procedure from dimer **6** (Scheme 6). Reaction of excess CH_3I with **6** in CH_2Cl_2 led to the isolation of the methyoxycyclopentadienyl ruthenium

© 2001 NRC Canada

Scheme 6.

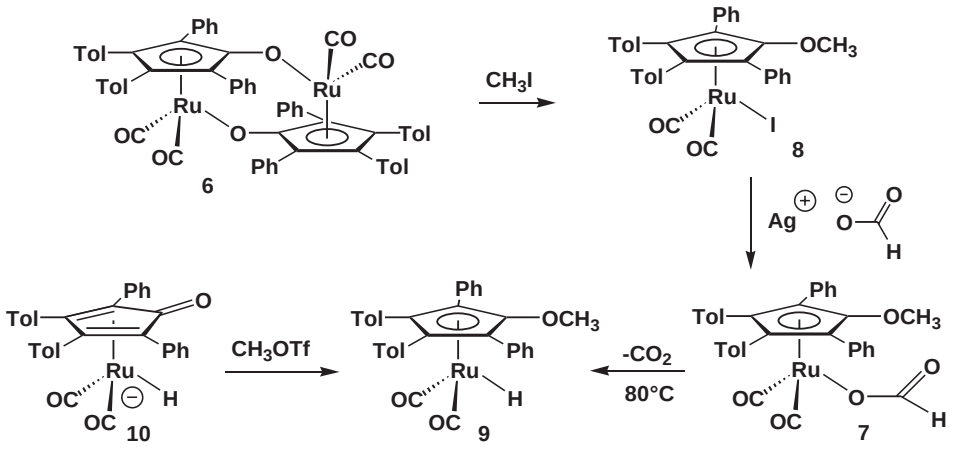
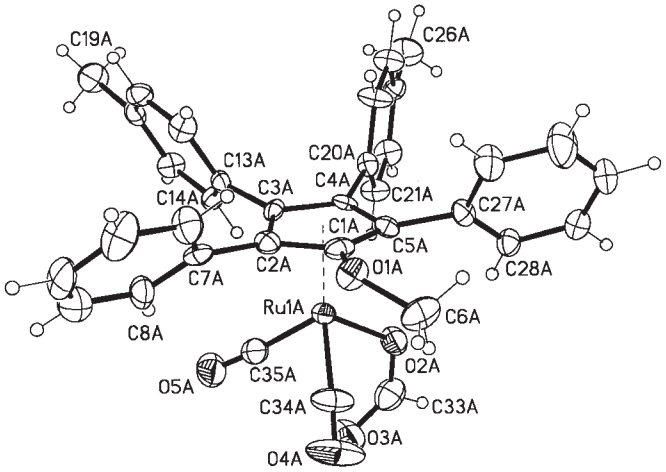


Fig. 1. X-Ray crystal structure of [2,5-Ph_2-3,4-Tol_2(η^5-C_4COCH_3)]Ru$(CO)_2$(η^1-OCHO) (**7**). Thermal ellipsoids are drawn at 50% probability.



iodide [2,5-Ph_2-3,4-Tol_2(η^5-C_4COCH_3)]Ru$(CO)_2$I (**8**) as a red powder in 67% yield. Following a procedure similar to that used for the synthesis of Pd(II) formates (10), reaction of **8** with a suspension of AgOCHO in CH_2Cl_2 gave the desired methoxycyclopentadienyl ruthenium formate **7** as an off-white powder in 56% yield. **7** was thermally stable in the solid state and solution at room temperature. Addition of excess DCO_2H to a CD_2Cl_2 solution of **7** resulted in no diminution of its formate ^{1}H NMR resonance (δ 7.81) after 24 h.

Complex **7** has spectroscopic features characteristic of a metal formate complex: an IR band at 1618 cm^{-1} assigned to the ν_{asym} (CO_2) absorption (11), a formate ^{1}H NMR resonance at δ 7.81, and a formate ^{13}C NMR resonance at δ 168.3. The X-ray crystal structure of **7** confirmed its structural assignment as an O-bound η^1-formate complex (Fig. 1). The unit cell contained three molecules per asymmetric unit and two of the molecules were disordered with respect to the position of the formate and the carbon monoxide ligands. In the ordered molecule, the O(2A)—C(33A) distance (1.27 Å) and C(33A)—O(4A) distance (1.23 Å) are similar to structurally characterized η^1-formate complexes (12). The Ru(1A)—O(1A) distance (2.30 Å) and C(1A)—O(1A) distance (1.35 Å) are characteristic of η^5 coordination of the CpOMe ligand.[2]

Very slow decarboxylation of methoxycyclopentadienyl ruthenium formate 7

The high thermal stability of **7** is remarkable in comparison to the rapid decarboxylation of **5** at room temperature. Decarboxylation of **7** required heating at 80°C in THF-d_8 (k_{obs} = 1.7 × 10^{-4} s^{-1}; $t_{0.5}$ = 67 min) (Scheme 6). The major product formed in 75% yield was the methoxycyclopentadienyl ruthenium hydride [2,5-Ph_2-3,4-Tol_2(η^5-C_4COCH_3)]Ru$(CO)_2$H (**9**), which was characterized by spectroscopy (RuH at δ –9.78 in ^{1}H NMR) and by independent synthesis from NEt_4[2,5-Ph_2-3,4-Tol_2(η^4-C_4CO)Ru$(CO)_2$H] (**10**) and excess CH_3OTf. The decarboxylation of **7** was not clean and produced small amounts of four unidentified side products. In an independent control experiment, **9** was stable for 1 h at 80°C in THF-d_8. When the decarboxylation was attempted under 1.7 atm (1 atm = 101.325 kPa) of ^{13}CO at 80°C and the formate ^{1}H NMR resonance of **7** was monitored, <5% decarboxylation was observed. Over the same time, the ^{13}C NMR resonance at δ 201 for the CO ligands of **7** grew relative to the aromatic resonances, indicating ^{13}CO incorporation into **7**.

Discussion

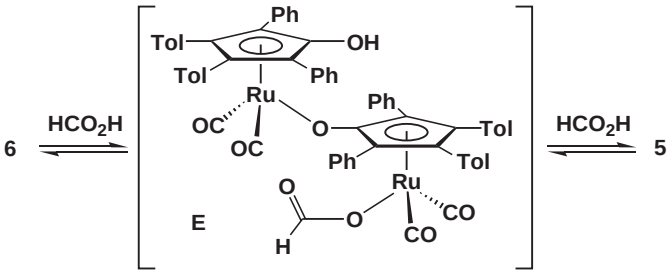
Direct observation of hydroxycyclopentadienyl ruthenium formate 5

Shvo had proposed the intermediacy of hydroxycyclopentadienyl ruthenium formate **B** in reductions catalyzed by **1** that use HCO_2H as the reducing agent (5*b*),

[2] Copies of material on deposit may be purchased from the Depository of Unpublished Data, Document Delivery, CISTI, National Research Council Canada, Ottawa, ON K1A 0S2, Canada (http:/www.nrc.ca/cisti/irm/unpubl_e.shtml for information on ordering electronically). Some of this supplementary material has also been deposited with the Cambridge Crystallographic Data Centre. Copies of the data can be obtained, free of charge, on application to the Director, CCDC, 12 Union Road, Cambridge CB2 1EZ, U.K. (Fax: 44-1223-336033 or e-mail: deposit@ccdc.cam.ac.uk).

© 2001 NRC Canada

Scheme 7.



but had never observed it. We have found that the hydroxycyclopentadienyl ruthenium formate **5** is readily formed by addition of excess HCO_2H to Ru dimer **6** at low temperature. The hydroxycyclopentadienyl formate is unstable and loses CO_2 at 0°C to form hydroxycyclopentadienyl ruthenium hydride **4**. In addition, **5** undergoes rapid exchange with DCO_2H at –20°C, presumably by reversible dissociation of formic acid and formation of the unsaturated dienone dicarbonyl intermediate **C**. The rapid decarboxylation of **5** is consistent with the failure to observe it under catalytic conditions.

Mays et al. (13) reported that scrambling of two symmetric Ru dimers analogous to **6** required heating at 52°C for 55 min. The rate of dissociation of dimer **6** at –20°C should be very slow while the reaction between **6** and HCO_2H has a half-life of about 15 min at this temperature. Since the rate of addition of HCO_2H to dimer **6** is much faster than dissociation of the dimer, the mechanism of formation of **5** must involve direct addition of HCO_2H to dimer **6**, instead of dissociation of **6** to dienone intermediate **C** followed by oxidative addition of HCO_2H. A possible mechanism proceeding through the diruthenium HCO_2H adduct **E** is outlined in Scheme 7.

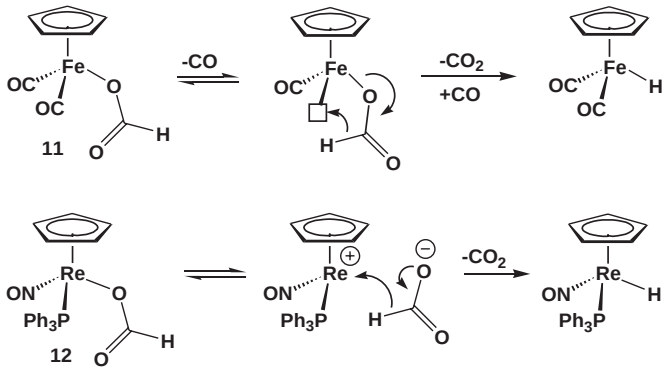
Hydroxycyclopentadienyl ruthenium formate 5 does not reduce benzaldehyde

At the beginning of this work, we hypothesized that the hydroxycyclopentadienyl formate **5** might be the active reducing agent in reductions of carbonyls by formic acid using the Shvo catalyst. This hypothesis seemed plausible since the formate anion has been demonstrated to act as a hydride donor in a number of organic reactions and has been shown to donate hydride directly to NAD^+ in reactions catalyzed by formate dehydrogenase (9, 14). However, we have obtained no evidence that **5** directly transfers hydrogen to carbonyls. The hydroxycyclopentadienyl formate **5** does not reduce benzaldehyde below the temperature at which it decarboxylates to give the hydroxycyclopentadienyl hydride **4**, which we have previously shown to reduce benzaldehyde very rapidly. Moreover, higher concentrations of PhCHO do not cause more rapid formation of benzyl alcohol from **5**. Therefore, the role of hydroxycyclopentadienyl formate **5** is to decarboxylate to **4** which is the active hydrogen transfer agent.

Mechanism of decarboxylation of hydroxycyclopentadienyl ruthenium formate 5

Two types of mechanism have been proposed for metal formate decarboxylations and both involve initial generation

Scheme 8.



of a vacant coordination site. Darensbourg et al. (8) showed that $CpFe(CO)_2(\eta^1\text{-OCHO})$ (**11**) exchanges ^{13}CO faster than it undergoes decarboxylation, and proposed a mechanism involving CO dissociation to give an unsaturated species, followed by β-hydride elimination concurrent with CO_2 formation (Scheme 8). Based upon kinetic studies and deuterium isotope effects, Merrifield and Gladysz (15) proposed that decarboxylation of $CpRe(NO)(PPh_3)(\eta^1\text{-OCHO})$ (**12**) proceeds by dissociation of formate ion to form a tight ion pair, followed by hydride transfer from the formate ion to the unsaturated rhenium cation. Our evidence suggests that the decarboxylation of **5** does not proceed by either type of mechanism.

The hydroxy group on the cyclopentadienyl ring of **5** plays a crucial role in the decarboxylation since **5** decomposes at temperatures 79° lower ($t_{0.5}$ = 19 min at 1°C) than the corresponding methoxycyclopentadienyl formate complex **7** ($t_{0.5}$ = 67 min at 80°C). CO inhibition of the decarboxylation of **7** and ^{13}CO exchange into **7** at 80°C provides persuasive evidence that CO dissociation is the initial step in the decarboxylation of **7**, just as it is in the case of iron formate **11**. However, since CO does not inhibit decarboxylation of **5** and since ^{13}CO does not exchange into **5** and is not incorporated into its decarboxylation products, it is clear that decarboxylation of **5** does not involve CO dissociation.

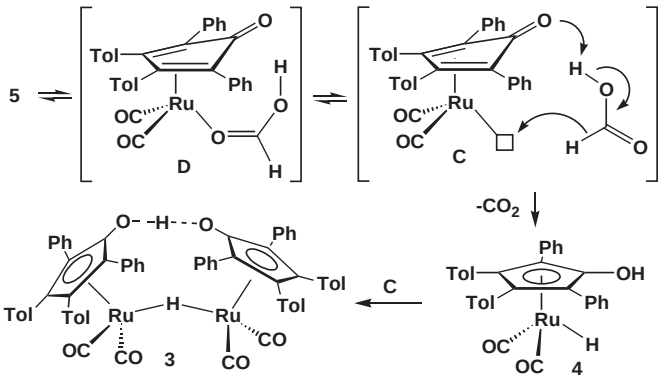
The huge difference in the rates of decarboxylation between **5** and **7** is also inconsistent with a simple ion pair mechanism as proposed by Merrifield and Gladysz (15) for rhenium formate **12**. If **5** decomposed by an ion-pair mechanism, then the same pathway should have been available to **7** and the compounds should have undergone decarboxylation at similar rates.

Any viable mechanism for the decarboxylation of **5** must account for: (*i*) the much faster decarboxylation of **5** compared to its CpOMe derivative **7**; (*ii*) the lack of CO inhibition of the rate of decarboxylation of **5**; (*iii*) the lack of ^{13}CO incorporation into **5** or its decarboxylation products; (*iv*) the rapid exchange of DCO_2H with **5**; (*v*) a negligible deuterium isotope effect on decarboxylation of $k_5/k_{5\text{-}d}$ = 1.1 ± 0.1; (*vi*) and slower decarboxylation at higher HCO_2H concentration.

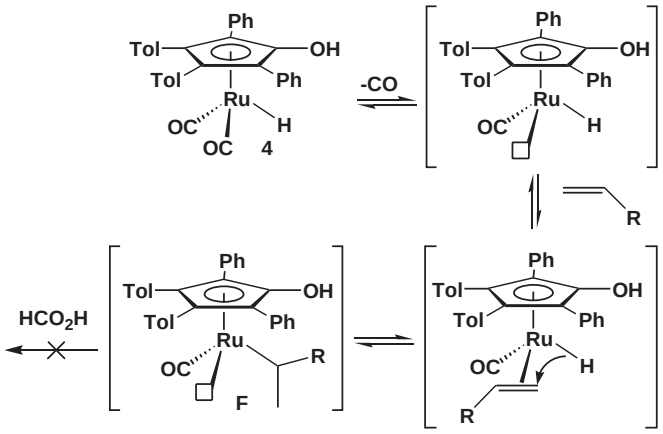
The mechanism shown in Scheme 9 provides an attractive explanation for these observations. The CpOH proton plays a special role in the formation of unsaturated dienone intermediate **C** and formic acid via a formic acid complex **D**. The

© 2001 NRC Canada

Scheme 9.



Scheme 10.



very rapid and reversible dissociation of formic acid from **D** explains DCO_2H exchange with **5**. The key step in the decarboxylation is a slower concerted transfer of hydride from the carbon of formic acid to ruthenium of **C** and of proton from the oxygen of formic acid to the dienone carbonyl of **C** that produces hydroxycyclopentadienyl hydride **4** and CO_2. The slower decarboxylation at higher formic acid concentration can be explained by stabilization of **5** by hydrogen bonding between formic acid and the formate ligand of **5** that must be broken up in the formation of **C** (16).[3]

A primary deuterium isotope effect would be expected for this mechanism. In other formate decarboxylations, k_H/k_D was 1.55 for the decarboxylation of rhenium formate **12** (15), 3.1 for the Rh-catalyzed transfer hydrogenation of itaconic acid with HCO_2H (17), and 2.2 for hydride transfer from HCO_2^- to NAD^+ catalyzed by formate dehydrogenase (13b). While the small to negligible isotope effect observed in the decarboxylation of **5** is troublesome, we have not been able to devise a satisfactory alternative mechanism.

Relevance to Shvo catalytic system

Our studies show how HCO_2H reduces carbonyl compounds in the Shvo catalytic system. Formic acid first reacts with ruthenium species to generate the transient hydroxycyclopentadienyl formate complex **5**. This formate complex is not itself a hydride transfer agent but it undergoes rapid decarboxylation to generate the hydroxycyclopentadienyl hydride **4**. This hydride then rapidly reduces carbonyl compounds. The unsaturated dienone dicarbonyl intermediate **C** generated in this process rapidly reacts with formic acid to regenerate **5** and continue the catalytic cycle or reacts with **4** to generate the diruthenium hydride complex **3**, which can slowly reenter the catalytic cycle by reaction with HCO_2H.

Our results also help explain why the Shvo system does not catalyze the reduction of alkenes by HCO_2H. We have shown that while hydroxycyclopentadienyl hydride **4** rapidly reduces aldehydes, it reduces alkenes only under a hydrogen atmosphere. We suggest that alkene reduction proceeds via CO dissociation from **4**, coordination of an alkene, and reversible hydride migration to give unsaturated alkyl intermediate **F**. H_2 addition to **F** leads to alkene reduction but HCO_2H interaction with intermediate **F** does not lead to alkane formation (Scheme 10). However, further experiments are needed to more fully understand the catalytic reactions of **4** with alkenes.

The much more rapid decarboxylation of hydroxycyclopentadienyl formate **5** than methoxycyclopentadienyl formate **7** highlights the crucial importance of an acidic proton in promoting decarboxylation. In related work on the hydrogenation of CO_2 to formic acid catalyzed by $[Rh(norbornadiene)(PMe_2Ph)_3]BF_4$ and by $Ru(PMe_3)_4H_2$, Tsai and Nicholas (18*a*) and Noyori and co-workers (18*b*) have independently proposed that the acidic proton of a coordinated water interacts with CO_2 to promote hydride addition to generate formate intermediates. Earlier we reported that the acidic CpOH proton of **4** is required for concerted hydride addition to carbonyl compounds (4). A deeper understanding of the role of acidic protons in mediating the formation and consumption of CO_2 by transition metal complexes should lead to more efficient catalysts for both transfer hydrogenation and CO_2 reduction.

Experimental

General methods

Manipulations of air and moisture sensitive compounds were performed in a nitrogen atmosphere glovebox or using standard high-vacuum line techniques. THF-d_8, toluene, and hexane were distilled from sodium–benzophenone. CH_2Cl_2 and CD_2Cl_2 were distilled from CaH_2. PhCHO (Amend) was distilled immediately before use. 96% HCO_2H (Aldrich) and 95% DCO_2H (Aldrich) were stored under nitrogen. Syntheses of $\{[2,5\text{-}Ph_2\text{-}3,4\text{-}Tol_2(\eta^5\text{-}C_4CO)]_2H\}Ru_2(CO)_4(\mu\text{-}H)$ (**3**), $[2,5\text{-}Ph_2\text{-}3,4\text{-}Tol_2(\eta^5\text{-}C_4COH)Ru(CO)_2H]$ (**4**), $\{2,5\text{-}Ph_2\text{-}3,4\text{-}Tol_2(\eta^5\text{-}C_4CO)]Ru(CO)_2\}_2$ (**6**), and $NEt_4[2,5\text{-}Ph_2\text{-}3,4\text{-}Tol_2(\eta^4\text{-}C_4CO)Ru(CO)_2H]$ (**10**) were previously described (4). AgOCHO was synthesized by the method of Yamamoto and co-workers (19). All other reagents were used as received.

[3] Puddephatt and co-workers observed slower $[Ru_2(\mu\text{-}CO)(CO)_4(\mu\text{-}dppm)_2]$ catalyzed decarboxylation of formic acid at higher HCO_2H concentrations. His proposed mechanism involved HCO_2^- in the rate determining step; higher concentration of formic acid was suggested to shift the equilibrium to a less reactive hydrogen bonded adduct $[(HCO_2)_2H]^-$.

© 2001 NRC Canada

^{1}H NMR were obtained on a Bruker AC 250, Bruker AC 300, or Varian Unity 500 spectrometer. ^{13}C NMR spectra were obtained on a Varian Unity 500 spectrometer operating at 125 MHz. IR spectra were measured on a Mattson Polaris FT-IR spectrometer. Mass spectra were determined on a VG AutoSpec M mass spectrometer. Elemental analysis was performed by Desert Analytics of Tucson, Arizona.

Addition of HCO_2H to 6 in THF-d_8

HCO_2H (6.8 μL, 0.18 mmol, 0.4 M) was added to a THF-d_8 solution of **6** (11 mg, 0.01 mmol, 0.02 M) at –78°C. The reaction was monitored by ^{1}H NMR spectroscopy at room temperature. Spectra were obtained at 5 min intervals for 35 min, until the solution was homogeneous and **6** had been completely consumed. After 10 h, the relative amounts of **3** and **4** were measured. During the reaction, the tube was periodically shaken to dissolve the remaining solid material.

Addition of HCO_2H to 6 in CD_2Cl_2

HCO_2H (6.3 μL, 0.17 mmol, 0.4 M) was added to a CD_2Cl_2 solution of **6** (12 mg, 0.01 mmol, 0.02 M) at –78°C. The homogeneous solution was monitored by ^{1}H NMR spectroscopy at room temperature. Spectra were obtained at 5 min intervals for 30 min, until **6** had been completely consumed. After 10 h, the relative amounts of **3** and **4** were measured.

[2,5-Ph_2-3,4-Tol_2(η^5-C_4COH)]Ru(CO)$_2$(η^1-OCHO) (5)

HCO_2H (3.2 μL, 0.08 mmol, 0.2 M) was added to a CD_2Cl_2 solution of **6** (13 mg, 0.01 mmol, 0.03 M) and the tube inserted into an NMR probe precooled to –20°C. After 30 min, the area ratio of the tolyl methyl resonances at δ 2.20 (**5**):δ 2.06 (**6**) was 20:1. For **5**, ^{1}H NMR (CD_2Cl_2, 500 MHz) δ: 2.20 (s, 6H, tolyl CH_3), 6.84 (AA′BB′, 8H, tolyl), 7.32 (m, 6H, phenyl), 7.42 (m, 4H, phenyl), 7.47 (s, OCHO). ^{13}C NMR (CD_2Cl_2,125 MHz) δ: 21.8 (tolyl CH_3), 87.9 (C 3,4 of Cp), 99.1 (C 2,5 of Cp), 126.7–138.7 (8 resonances aromatic), 147.0 (C1 of Cp), 172.0 (OCHO), 199.2 (CO). Four aliquots of 3.2 μL of HCO_2H were added at –78°C to the solution of **5** in CD_2Cl_2 containing 0.2 M HCO_2H. After the addition of each aliquot, the NMR tube was reinserted into the probe cooled to –20°C and a ^{1}H NMR spectrum was obtained. The ^{1}H NMR chemical shifts of the formate hydrogen of **5** changed by 0.36 ppm with concentration: [HCO_2H], δ **5**; 0.2 M, 7.47; 0.4 M, 7.67; 0.6 M, 7.76; 0.8 M, 7.80; 1.0 M, 7.83. Over the same concentration range, the formate hydrogen of free formic acid changed by 0.18 ppm from δ 7.92 to 8.10.

Exchange of [2,5-Ph_2-3,4-Tol_2(η^5-C_4COH)]Ru(CO)$_2$(η^1-OCDO) (5-d) with HCO_2H

DCO_2H (5.2 μL, 0.13 mmol, 0.3 M) was added to a CD_2Cl_2 solution of **6** (15 mg, 0.01 mmol, 0.03 M) at –78°C. The tube was placed in an NMR probe precooled to –20°C and the reaction monitored by ^{1}H NMR. After 30 min, >98% conversion to **5-d** was observed. No formate hydrogen resonance in the region between δ 7.50 and δ 8.00 was visible. The tube was removed and cooled to –78°C. HCO_2H (5μL, 0.12 mmol, 0.3 M) was added via syringe and the tube replaced in the spectrometer at –20°C. A formate resonance at δ 7.75 was observed in the ^{1}H NMR spectrum.

Kinetics of decarboxylation of 5

HCO_2H (3 μL, 0.1 mmol, 0.2 M) was added to a CD_2Cl_2 solution of **6** (15 mg, 0.01 mmol, 0.03 M) at –78°C. The tube was placed in an NMR probe precooled to –20°C and the reaction monitored by ^{1}H NMR as described above. The NMR tube was removed from the probe and cooled to –78°C. The NMR probe was warmed to 1 ± 0.5°C and the tube reinserted. Decarboxylation was monitored by the disappearance of the resonance for phenyl protons at δ 7.45 in the ^{1}H NMR spectrum. The reaction followed first order kinetics to >80% conversion. See *Results*.

Decarboxylation of 5 under ^{13}CO

HCO_2H (2.9 μL, 0.08 mmol, 0.2 M) was added to a CD_2Cl_2 solution of **6** (14 mg, 0.01 mmol, 0.03 M) at –78°C. The tube was placed in an NMR probe precooled to –20°C and the reaction monitored by ^{1}H NMR spectroscopy until **5** and **6** had reached equilibrium. The tube was removed from the probe, cooled to –78°C, degassed, and ^{13}CO (1 atm) (1 atm = 101.325 kPa) was added. The tube was placed in an NMR probe precooled to 1 ± 0.5°C and the rate of decarboxylation of **5** was measured as described above (k_{obs} = 5.7×10^{-4} s^{-1}, $t_{0.5}$ = 20 min).

Competition between 4 and 5 in PhCHO reduction

Diruthenium hydride **3** (12 mg, 0.01 mmol) in THF was degassed and placed under 1 atm (1 atm = 101.325 kPa) of H_2 at –78°C. The tube was sealed at –78°C and heated to 80°C for 8 h. THF was evaporated and CD_2Cl_2 was condensed in to dissolve the yellow, oily solid. The solution was cooled to –78°C and HCO_2H (10 μL, 0.26 mmol, 0.5 M) and PhCHO (30 μL, 0.29 mmol, 0.8 M) were added successively via syringe. The tube was placed in an NMR probe precooled to –29°C. The reaction was monitored at –29°C for 25 min, at –15°C for 10 min, at 0°C for 10 min, and at 21°C for 20 min. See *Results*.

Effect of PhCHO concentration on rate of benzyl alcohol formation

Two identical solutions of **5** were prepared by addition of HCO_2H (7.8 μL, 0.2 mmol, 0.5 M) to CD_2Cl_2 solutions of Ru dimer **6** (15 mg, 0.01 mmol, 0.025 M) at –78°C. Tubes containing the solutions were placed into an NMR probe precooled to –20°C and the reaction monitored by ^{1}H NMR until no **6** was observable in the ^{1}H NMR spectrum. The tubes were cooled to –78°C and 17 μL PhCHO (0.16 mmol, 0.4 M) was syringed into one tube and 34 μL PhCHO (0.32 mmol, 0.8 M) was syringed into the second tube. The tubes were placed in an NMR probe precooled to 10 ± 0.5°C and the rate of appearance of the ^{1}H NMR resonance for $PhCH_2OH$ (δ 4.68) was monitored for 40 min. Plots of the concentration of $PhCH_2OH$ were linear. For 0.4 M PhCHO, $k = 1.20 \times 10^{-1}$ s^{-1}; for 0.8 M PhCHO, $k = 1.16 \times 10^{-1}$ s^{-1}.

[2,5-Ph_2-3,4-Tol_2(η^5-C_4COCH_3)]Ru(CO)$_2$I (8)

Reaction of **6** (200 mg, 0.17 mmol) with CH_3I (400 μL, 6.40 mmol) in CH_2Cl_2 (10 mL) for 40 h at room temperature followed by evaporation of solvent under vacuum gave a red, oily solid. Chromatography on silica gel using 1:1 CH_2Cl_2:hexane afforded **8** as a red powder (167 mg, 67%), mp 195–202°C (dec). IR (CH_2Cl_2) (cm^{-1}): 2033 (s), 1988

© 2001 NRC Canada

(s). ^{1}H NMR (CD_2Cl_2, 300 MHz) δ: 2.21 (s, 6H, tolyl CH_3), 3.45 (s, OCH_3), 6.87 (AA′BB′, 8H, tolyl), 7.32 (m, 6H, phenyl), 7.53 (m, 4H, phenyl). ^{13}C NMR (CD_2Cl_2, 125 MHz) δ: 21.2 (tolyl CH_3), 62.9 (OCH_3), 88.0 (C3,4 of Cp), 102.4 (C2,5 of Cp), 126.8–138.8 (8 resonances, aromatic), 147.0 (C1 of Cp), 198.2 (CO). Anal. calcd. for $C_{34}H_{27}O_3RuI$: C 57.39, H 3.82; found: C 57.56, H 3.77.

[2,5-Ph_2-3,4-Tol_2(η^5-C_4COCH_3)]Ru(CO)$_2$(η^1-OCHO) (7)

A suspension of AgOCHO (150 mg, 0.87 mmol) in a solution of **8** (130 mg, 0.18 mmol) in CH_2Cl_2 (10 mL) was stirred for 18 h at room temperature until IR monitoring indicated complete consumption of **8**. The mixture was filtered to give a light green solution. Evaporation of solvent and chromatography of the resulting green solid on silica gel using 3:1 CH_2Cl_2:acetone gave **7**, as an off-white powder (75 mg, 56%), mp 130–135°C (dec). IR (CH_2Cl_2) (cm^{-1}): 2043 (s), 1993 (s), 1618 (m). ^{1}H NMR (CD_2Cl_2, 300 MHz) δ: 2.20 (s, 6H, tolyl CH_3), 3.46 (s, OCH_3), 6.84 (AA′BB′, 8H, tolyl), 7.32 (m, 6H, phenyl), 7.48 (m, 4H, phenyl), 7.81 (s, OCHO). ^{13}C NMR (CD_2Cl_2, 125 MHz) δ 21.2 (tolyl CH_3), 62.0 (OCH_3), 88.4 (C 3,4 of Cp), 102.5 (C 2,5 of Cp), 126.7–138.7 (8 resonances, aromatic), 143.7 (C1 of Cp), 168.3 (OCHO), 198.8 (CO). Anal. calcd. for $C_{35}H_{28}O_5Ru$: C 66.76, H 4.48; found: C 66.56, H 4.38.

Decarboxylation of 7

A THF-d_8 solution of **7** (0.03 M) containing ferrocene as an internal standard was heated at 80 ± 0.2°C. The disappearance of the ^{1}H NMR resonance for -OCHO (δ 7.68) was monitored at 20, 66, 119, and 194 min; $k_{obs} = 1.7 \times 10^{-4}$ s^{-1}, $t_{0.5}$ = 67 min. The major product was [2,5-Ph-3,4-Tol(η^5-C_4COCH_3)]Ru(CO)$_2$H (75%); four unidentified minor products were also observed.

Decarboxylation of 7 in the presence of ^{13}CO

A THF-d_8 solution of **7** (0.03 M) containing ferrocene as an internal standard was heated to 80 ± 0.2°C under ^{13}CO (1 atm added at –78°C (1 atm = 101.325 kPa)). The disappearance of the ^{1}H NMR resonance for -OCHO (δ 7.68) was monitored at 30, 60, and 120 min. ^{1}H NMR showed that <5% of **7** had reacted after 2 h. ^{13}C NMR showed dramatic growth of the CO resonance of **7** (δ 201) relative to aromatic resonances of **7**.

[2,5-Ph_2-3,4-Tol_2(η^5-C_4COCH_3)]Ru(CO)$_2$H (9)

Addition of CH_3OTf (250 μL, 2.2 mmol) to a suspension of NEt_4[2,5-Ph_2-3,4-Tol_2(η^4-C_4CO)Ru(CO)$_2$H] (**10**) (225 mg, 0.31 mmol) in toluene (10 mL) gave a green solution with a white precipitate. The solution was filtered and solvent evaporated under vacuum. The residue was dissolved in hexane (5 mL), filtered through a glass wool, and cooled to –30°C for 18 h to give **9** (40 mg, 22%) as a yellow precipitate. IR (CH_2Cl_2) (cm^{-1}): 2018 (s), 1958 (s). ^{1}H NMR (CD_2Cl_2, 300 MHz) δ: –9.80 (s, RuH), 2.21 (s, 6H, tolyl CH_3), 3.42 (s, 3H, OCH_3), 6.86 (d, ^3J = 8.4 Hz, 4H, tolyl), 6.96 (d, ^3J = 8.4 Hz, 4H, tolyl), 7.25 (m, 6H, phenyl), 7.37 (m, 4H, phenyl). ^{13}C NMR (CD_2Cl_2, 125 MHz) δ: 21.2 (tolyl CH_3), 66.9 (OCH_3), 94.9 (C 3,4 of Cp), 104.6 (C 2,5 of Cp), 127.9–137.5 (8 resonances, aromatic), 138.9 (C1 of Cp), 202.1 (CO). HR-MS (EI) calcd. for $C_{34}H_{28}O_3Ru$: 586.1075; found: 586.1029.

X-ray crystal structure determination of [2,5-Ph_2-3,4-Tol_2(η^5-C_4COCH_3)]Ru(CO)$_2$(η^1-OCHO) (7)

X-ray quality crystals were grown by slow evaporation of a CH_2Cl_2–hexane solution of **7**. A yellow plate-shaped crystal of dimensions 0.38 × 0.25 × 0.21 mm was selected for structural analysis. Intensity data for this compound were collected using a Bruker SMART ccd area detector mounted on a Bruker P4 goniometer using graphite-monochromated Mo Kα radiation (λ = 0.71073 Å). The sample was cooled to 133(2) K. The intensity data, which nominally covered 1.5 hemispheres of reciprocal space, were measured as a series of *f* oscillation frames each of 0.4° for 60 s per frame. The detector was operated in 512 × 512 mode and was positioned 5.00 cm from the sample. Coverage of unique data was 98.8% complete to 25.00 deg in θ. Cell parameters were determined from a nonlinear least-squares fit of 5158 peaks in the range $3.30 < \theta < 25.32°$. The first 50 frames were repeated at the end of data collection and yielded 459 peaks showing a variation of –0.15% during the data collection. A total of 30 480 data were measured in the range $3.28 < \theta < 25.00°$. The data were corrected for absorption by the empirical method (20) giving min and max transmission factors of 0.8084 and 0.8871. The data were merged to form a set of 15 000 independent data with R(int) = 0.0586.

The orthorhombic space group $P2(1)2(1)2(1)$ was determined by systematic absences and statistical tests and verified by subsequent refinement. The structure was solved by direct methods and refined by full-matrix least-squares methods on F^2 (21). Hydrogen atom positions were initially determined by geometry and were refined using a riding model. Non-hydrogen atoms were refined with anisotropic displacement parameters. A total of 1210 parameters were refined against 216 restraints and 15 000 data to give $wR(F^2) = 0.1067$ and $S = 1.010$ for weights of $w = 1/[\sigma^2 (F^2) + (0.0300P)^2 + 2.2000P]$, where $P = [F_o^2 + 2F_c^2]/3$. The final $R(F)$ was 0.0483 for the 11 005 observed, $[F > 4\sigma(F)]$, data. The largest shift/s.u. was 0.003 in the final refinement cycle. The final difference map had maxima and minima of 0.581 and –0.505 e $Å^{-3}$, respectively. The absolute structure was determined by refinement of the Flack parameter (22).

Acknowledgments

Financial support from the Department of Energy, Office of Basic Energy Sciences, is gratefully acknowledged. Steven Singer thanks the NIH (5T32 GM 08505) for support under a Chemistry Biology Interface Training Grant. Grants from NSF (CHE-9629688) and NIH (I S10 RR04981–01) for the purchase of NMR spectrometers, and from NSF (CHE-9105497) for the purchase of X-ray instruments are acknowledged.

References

1. Y. Shvo, D. Czarkie, and Y. Rahamim. J. Am. Chem. Soc. **108**, 7400 (1986).

© 2001 NRC Canada

2. (*a*) C.P. Casey, Y. Wang, R.S. Tanke, P.A. Hazin, and E.W. Rutter, Jr. New J. Chem. **18**, 43 (1994); (*b*) C.P. Casey. J. Organomet. Chem. **400**, 205 (1990).
3. (*a*) R. Noyori and S. Hashiguchi. Acc. Chem. Res. **30**, 97 (1997); (*b*) D.A. Alonso, P. Brandt, S.J.M. Nordin, and P.G. Andersson. J. Am. Chem. Soc. **121**, 9580 (1999); (*c*) M. Yamakawa, H. Ito, and R. Noyori. J. Am. Chem. Soc. **122**, 1466 (2000).
4. C.P. Casey, S.W. Singer, D.R. Powell, R.K. Hayashi, and M. Kavana. J. Am. Chem. Soc. J. Am. Chem. Soc. **123**, 1090 (2001).
5. (*a*) N. Menashe and Y. Shvo. Organometallics, **10**, 3885 (1991); (*b*) N. Menashe, E. Salant, and Y. Shvo. J. Organomet. Chem. **514**, 97 (1996); (*c*) Y. Blum, D. Czarkie, Y. Rahamim, and Y. Shvo. Organometallics, **4**, 1459 (1985).
6. (*a*) A. Behr. Angew. Chem. Intl. Ed. Engl. **27**, 661 (1988); (*b*) W. Leitner. Angew. Chem. Intl. Ed. Engl. **34**, 2207 (1995); (*c*) R. Noyori. Chem. Rev. **95**, 260 (1995).
7. D.J. Darensbourg and R.A. Kudaroski. Adv. Organomet. Chem. **22**, 129 (1983).
8. D.J. Darensbourg, M.B. Fischer, R.E. Schmidt, Jr., and B.J. Baldwin. J. Am. Chem. Soc. **103**, 1297 (1981).
9. M. Hudlicky. Reductions in organic chemistry. Am. Chem. Soc. 1996. Chap. 4. pp. 46–47.
10. M. Oshima, T. Sakamoto, Y. Maruyama, F. Ozawa; I. Shimizu, and A. Yamamoto. Bull. Chem. Soc. Jpn. **73**, 453 (2000).
11. C.C. Tso and A.R. Cutler. Inorg. Chem. **29**, 471 (1990).
12. (*a*) D.J. Darensbourg, C.S. Day, and M.B. Fischer. Inorg. Chem. **20**, 3577 (1981); (*b*) D.M. Grove, G. van Koten, H.C.J. Ubbels, A. Zoet, and A. Spek. J. Organomet. Chem. **263**, C10 (1984); (*c*) L.K. Fong, J.R. Fox, and N.J. Cooper. Organometallics, **6**, 223 (1987); (*d*) M.K. Whittesley, R.N. Perutz, and M.H. Moore. Organometallics, **15**, 5166 (1996); (*e*) H. Konno, A. Kobayashi, K. Sakamoto, F. Fagalde, N.E. Katz, H. Saitoh, and O. Ishitani. Inorg. Chim. Acta, **299**, 155 (2000).
13. M.J. Mays, M.J. Morris, P.R. Raithby, Y. Shvo, and D. Czarkie. Organometallics, **8,** 1162 (1989).
14. (*a*) M.H. O'Leary. Acc. Chem. Res. **21**, 450 (1988); (*b*) J.S. Blanchard and W.W. Cleland. Biochemistry, **19**, 3543 (1980); (*c*) J.D. Hermes, S.W. Morrical, M.H. O'Leary, and W.W. Cleland. Biochemistry, **23**, 5479 (1984).
15. J.H. Merrifield and J.A. Gladysz. Organometallics, **2**, 783 (1983).
16. Y. Gao, J.K. Kuncheria, H.A. Jenkins, R.J. Puddephatt, and G.P.A. Yap. J. Chem. Soc. Dalton Trans. 3212 (2000).
17. W. Leitner, J.M. Brown, and H. Brunner. J. Am. Chem. Soc. **115**, 152 (1993).
18. (*a*) J.-C. Tsai and K.M. Nicholas. J. Am. Chem. Soc. **114**, 5117 (1992); (*b*) P.G. Jessop, Y. Hsiao, T. Ikariya, and R. Noyori. J. Am. Chem. Soc. **118**, 344 (1996).
19. M. Oshima, I. Shimzu, A. Yamamoto, and F. Ozawa. Organometallics, **10**, 1221 (1991).
20. G.M. Sheldrick. SADABS. Program for empirical absorption of area detector data. University of Göttingen, Germany. 1996.
21. G.M. Sheldrick. SHELXTL Version 5 Reference Manual. Bruker-AXS, 6300 Enterprise Dr., Madison, WI 53719–1173, U.S.A. 1994.
22. H.D. Flack. Acta Crystallogr. Sect. A: Fundam. Crystallogr. **39**, 876 (1983).

© 2001 NRC Canada

Polymerization of 1-hexene catalyzed by Cp^*TiMe_3-$B(C_6F_5)_3$; a mechanistic and structural study

Michael C. Murray and Michael C. Baird

Abstract: Solutions of the Ziegler–Natta system Cp^*TiMe_3 – $B(C_6F_5)_3$ in toluene catalyze the polymerization of 1-hexene to mixtures of atactic poly-1-hexenes and complex oligomeric materials, which were characterized by ^1H and $^{13}C\{^1H\}$ NMR spectroscopy and gel permeation chromatography (GPC). The polymer molecular weights and the relative proportions of polymers and oligomers vary with temperature, monomer:catalyst ratios, and degree of dilution and may generally be rationalized in terms of a conventional Ziegler–Natta mechanism. The $^{13}C\{^1H\}$ NMR spectra of the polymers exhibit resonances suggesting significant degrees of 2,1-insertions during propagation, while experiments utilizing $Cp^*Ti(^{13}CH_3)_3$ verify that initiation in toluene involves predominantly via 1,2-insertion of the first monomer unit but that 2,1-insertions occur up to 15–20% of the time in CH_2Cl_2. NMR experiments involving $Cp^*Ti(^{13}CH_3)_3$ demonstrate that both methyl groups in the presumed active species $Cp^*TiMe_2^+$ are incorporated into polymer

Key words: titanium, polymers, polymerization, Ziegler–Natta.

Résumé : Des solutions dans le toluène du système de Ziegler–Natta Cp^*TiMe_3 – $B(C_6F_5)_3$ catalysent la polymérisation du hex-1-ène en mélanges de polyhex-1-ènes atactiques et à des matériaux oligomères que l'on a caractérisés par spectroscopie RMN du ^1H et du $^{13}C\{^1H\}$ et par chromatographie par perméation de gel (CPG). Les poids moléculaires et les proportions relatives des polymères et des oligomères varient avec la température, les rapports monomère/catalyseur et le degré de dilution et on peut généralement les rationaliser en fonction d'un mécanisme de Ziegler–Natta conventionnel. Les spectres RMN du $^{13}C\{^1H\}$ des polymères comportent des résonances qui suggèrent des degrés significatifs d'insertions 2,1 au cours de la propagation alors que des expériences à l'aide de $Cp^*Ti(^{13}CH_3)_3$ permettent de confirmer que l'initiation dans le toluène implique principalement une insertion 1,2 de la première unité de monomère mais que des insertions 2,1 se produisent dans 15 à 20 % des cas dans le CH_2Cl_2. Des expériences de RMN impliquant $Cp^*Ti(^{13}CH_3)_3$ démontrent les polymères incorporent les deux groupes méthyles présumément actifs des espèces $Cp^*TiMe_2^+$.

Mots clés : titane, polymères, polymérisation, Ziegler–Natta.

[Traduit par la Rédaction]

Introduction

The utilization of metallocenes of the type Cp'_2MR_2 (M = Ti, Zr, Hf; R = alkyl; Cp′ = substituted cyclopentadienyl) as homogeneous olefin polymerization catalyst precursors has received considerable attention in recent years, in large part because of the high degrees of stereoregularity and the narrow molecular weight distributions that are often possible (1). Activation is readily achieved by alkyl abstraction reactions involving, e.g., Lewis acid cocatalysts such as the borane $B(C_6F_5)_3$ (eq. [1]), which give the formally $14e^-$ cationic species $[Cp'_2MR]^+$; these are believed to be the actual catalysts.

[1] $$Cp'_2MR_2 + B(C_6F_5)_3 \rightarrow [Cp'_2MR]^+ + [BR(C_6F_5)_3]^-$$

Similar species are apparently formed on treating, for example, metallocene dihalides with the oligomeric methylalumoxane (MAO), and commercially viable processes are based on use of this cocatalyst. Of increasing importance is the utilization of such catalyst systems to prepare homo- and copolymers of α-olefins such as 1-hexene (2), of interest both from the perspective of understanding mechanisms of α-olefin polymerization and because of the high commercial importance of materials such as polyethylene-co-1-hexene (linear low-density polyethylene, LLDPE).

We (3) and others (4) have reported the analogous utilization of monocyclopentadienyl–titanium olefin polymerization systems, often based on activation of Cp^*TiMe_3 by $B(C_6F_5)_3$ (eq. [2]).

[2] $$Cp^*TiMe_3 + B(C_6F_5)_3 \rightarrow Cp^*TiMe_2(\mu\text{-}Me)B(C_6F_5)_3 \ (\mathbf{I})$$

Received August 8, 2000. Published on the NRC Research Press Web site at http://canjchem.nrc.ca on July 11, 2001.

Dedicated to Professor Brian James in recognition of his many contributions to organometallic chemistry and catalysis.

M.C. Murray and M.C. Baird.[1] Department of Chemistry, Queen's University, Kingston, ON K7L 3N6, Canada.

[1]Corresponding author (telephone: (613) 533-2614; fax: (613) 533-6669; e-mail: bairdmc@chem.queensu.ca).

 DOI: 10.1139/cjc-79-5/6-1012 © 2001 NRC Canada

Table 1. Polymer data.

Exp. No.	Volume of 1-hexene[a] (mL)	Cp^*TiMe_3 (mmol) (ratio hexane:Ti)	Temp (°C)	Time (h)	Conversion (%)	Activity (kg polymer per mol catalyst per h)	Comments[b]
1	3 (5)	0.06 (400:1)	–30	12	71		Bimodal: ~1/2 with $M_{W_P} \approx 145\,000$; ~1/2 with $M_{W_P} \approx 24\,000$; small amount of oligomers
2 (3)	3 (5)	0.06 (400:1)	–10	0.5	47	31.6	Bimodal: ~1/2 with $M_{W_P} \approx 110\,000$; ~1/2 with $M_{W_P} \approx 8\,000$; small amount of oligomers
3 (5)	3 (5)	0.18 (130)	–10	0.5	51	11.7	Mostly oligomers
4 (9)	3 (5)	0.06 (400:1)	0	0.5	23, 46	23.3	Bimodal: 1/2 with $M_{W_P} \approx 70\,000$–$100\,000$; 1/2 with $M_{W_P} \approx 10\,000$; small amount of oligomers
5 (11)	3 (5)	0.06 (400:1)	+21	0.5	37	24.9	Bimodal: ~1/2 with $M_{W_P} \approx 30\,000$–$45\,000$; ~1/2 with $M_{W_P} \approx 8\,000$; small amount of oligomers

[a]Value in parentheses represents volume of toluene (mL).
[b]M_{W_P} = most probable molecular weight (peak maximum), PD = polydispersity.

The active species $Cp^*TiMe_2(\mu\text{-}Me)B(C_6F_5)_3$ (**I**) behaves as a source of the $10e^-$ cationic complex $[Cp^*TiMe_2]^+$, which is an extremely active initiator for both Ziegler–Natta and carbocationic polymerization reactions (3, 4). Increasing attention has also recently been devoted to polymerization of α-olefins such as 1-hexene by mono- and non-cyclopentadienyl metal compounds (5). We have previously shown that **I** is an active initiator for the polymerization of 1-hexene (3*h*), and we provide here further details of this investigation. We also provide insight into the mechanisms by which this process occurs, and the unusual microstructures of the resulting polymers. The effects of temperature, catalyst, and monomer concentration on the yields, molecular weights, molecular weight distributions, and stereo- and regio-regularities of the materials produced are used to extract mechanistic insight into the polymerization processes.

Experimental

All operations were performed under purified argon using normal Schlenk techniques or a Vacuum Atmospheres Dry Lab. Solvents were purified by standard methods, and distilled and degassed before use. All 1D ^1H, ^{13}C, and $^{13}C\{^1H\}$ NMR spectra and 2D COSY and HMQC spectra were recorded using Bruker Avance 400 or 500 spectrometers in CD_2Cl_2 or $CDCl_3$ (polymers), chemical shifts being determined by reference to residual ^1H and ^{13}C solvent peaks. Calculations of ^{13}C chemical shifts were carried out utilizing commercial software (6). Gel permeation chromatography (GPC) experiments with the polymers were carried out at room temperature using a Waters Model 440 liquid chromatograph or a Waters Model 2690 with THF as eluent and polystyrene standards. The compounds Cp^*TiMe_3 (7*a*), $Cp^*Ti(^{13}CH_3)_3$ (3*c*), and $B(C_6F_5)_3$ (7*b*) were prepared as reported previously.

Purification of 1-hexene was effected by stirring over CaH_2 followed by vacuum distillation. In a typical polymerization run, a toluene solution of $B(C_6F_5)_3$ (31 mg, 0.06 mmol) was added to a stirred toluene solution of Cp^*TiMe_3 (14 mg, 0.06 mmol) and 1-hexene (3 mL, 24 mmol). The reaction was quenched after 30 min by the addition of MeOH, all of the volatile materials were removed under reduced pressure, and the resulting polymer residue was dissolved in hexanes (40 mL) and passed through 10 g of silica gel to remove the purple catalyst residue. The reaction flask and column were washed with hexanes (3 × 40 mL), the fractions were combined, and the solvent was removed under reduced pressure. The resulting polymer mixtures were analyzed by ^1H and $^{13}C\{^1H\}$ NMR spectroscopy and GPC. Fractionation of several samples was effected by reduced pressure trap-to-trap distillation of a low boiling oligomeric fraction. The high molecular weight polymer fractions were then analyzed by ^1H and $^{13}C\{^1H\}$ NMR spectroscopy and GPC; the low molecular weight fraction by ^1H and $^{13}C\{^1H\}$ NMR spectroscopy. Experimental conditions and results are outlined in greater detail in Table 1, where data are given for the polymeric materials obtained. The data given are, in most cases, averages of the results of two or more experiments, with the experimental errors as indicated. Conversions are given as percentages of the 1-hexene polymerized.

Results and discussion

Polymer syntheses and properties

Abstraction of a methyl ligand from Cp^*TiMe_3 by 1 equiv of the Lewis acid $B(C_6F_5)_3$ produces the polymerization initiator $Cp^*TiMe_2(\mu\text{-}Me)B(C_6F_5)_3$ (**I**, eq. [2]). In a typical polymerization run, a toluene solution of $B(C_6F_5)_3$ was added to a solution of Cp^*TiMe_3 in 1-hexene or in toluene–1-hexene; polymerization runs were carried out at various monomer:catalyst ratios, degrees of dilution, and temperatures, although it should be noted that those conducted at room temperature and above were not thermostatted effectively and generally became quite warm. In most of the polymerization runs, the viscosity of the solutions increased noticeably within minutes, indicating that extensive polymerization had occurred.

A summary of experimental data, conversions, and molecular weights for representative polymerization runs is pre-

© 2001 NRC Canada

Fig. 1. Number system for regioregular poly-1-hexene.

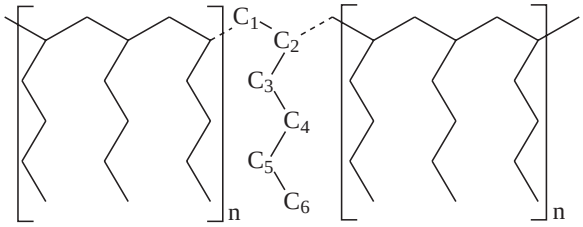
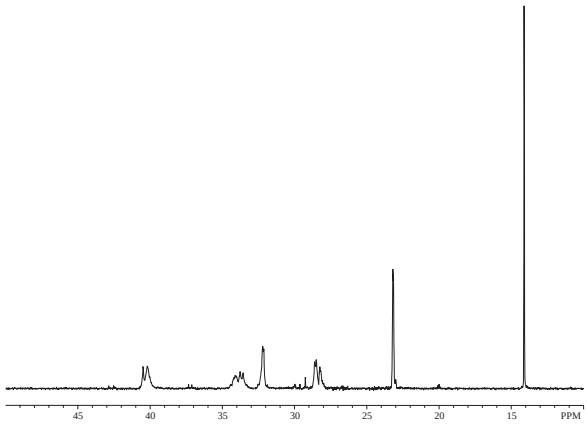


Fig. 2. $^{13}C\{^{1}H\}$ NMR spectrum of regioregular poly-1-hexene.

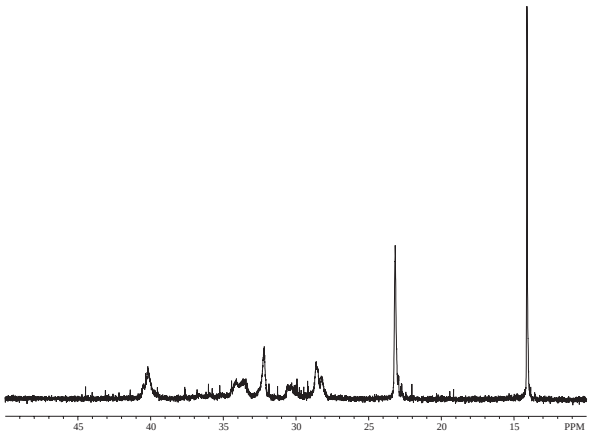


sented in Table 1. As we wished to acquire catalyst activity data, most of the polymerization runs were terminated after 0.5 h, although higher conversions were shown to be possible by allowing the reactions, in some cases, to proceed for longer periods of time. Experiment 1, for instance, was begun at –30°C but allowed to warm to +6°C over 12 h, and as can be seen, the conversion is relatively high although we cannot in fact reliably estimate the activity in this case. The catalyst system is very sensitive to trace impurities, especially Lewis bases and proton sources, and many of the runs were carried out several times to check for reproducibility.

As may be noted in Table 1, most experiments involved a monomer:catalyst ratio of 400:1 in 5 mL toluene. In most of these cases, bimodal distributions of polymers were obtained with a very high molecular weight fraction (M_w varying from $>10^5$ at low temperatures to 4.5×10^4 at room temperature) and a low molecular weight fraction ($M_w \leq 10^4$). In addition to these two polymer fractions, most reactions also produced small amounts of very low molecular weight liquid oligomers (0–25% of the total); these could be removed by trap-to-trap distillation, as described in the *Experimental* section. Although in some cases oligomers were the major product, they were little studied; however, consideration of the relative intensities of the olefinic resonances in the ^{1}H NMR spectra of several suggested that M_n ~250.

As is clear from Table 1 (expt. 2, 4, 5), there is a general inverse relationship between temperature and molecular weights of the high molecular weight fractions. This trend is consistent with earlier results on, e.g., the polymerization of propylene by **I** (3*k*) and of 1-hexene by metallocenes (2*f*), and presumably is to be attributed to an increased rates of propagation relative to rates of chain termination – transfer. Complementing these results, it was also found that decreasing the monomer:catalyst ratios to 130:1 and 44:1, i.e., by

Fig. 3. $^{13}C\{^{1}H\}$ NMR spectrum of crude poly–oligo-1-hexene.



factors of ~3 and ~9, respectively, resulted in drastically decreased molecular weights in the more monomer starved systems; similar behaviour has been reported for other systems (5*d*). Maintaining the monomer:catalyst ratio at 400:1 while diluting the reaction mixtures (15 mL toluene) also resulted in decreases in molecular weights; presumably the rate of (bimolecular) coordination of monomer to active site decreased relative to the rate of (unimolecular) chain termination via β-H elimination. Conversions of 1-hexene were lower at the lowest temperatures, presumably for kinetic reasons, and also at higher temperatures, presumably because of catalyst decomposition.

Following our preliminary communication (3*h*), similar catalyst activities and polymer molecular weights were reported for catalyst systems involving Cp^*TiCl_2(*O*-aryl) activated by MAO (4*o*). We note also that the highest catalytic activities of **I** for the polymerization of 1-hexene are comparable with those of some metallocene systems (2*g*, *m*, *o*, *r–t*, *v*), although lower than others (2*k*, *u*). We note that neither the bimodality of the poly-1-hexene distribution nor the proclivity under certain conditions to produce predominantly oligomers has been noted previously with other catalyst systems.

Polymer microstructures; modes of chain propagation

Although only very low conversions were obtained at temperatures below –30°C, the high molecular weight polymers thus formed appeared to be highly regioregular. The numbering system for regioregular poly-1-hexene is shown in Fig. 1, the $^{13}C\{^{1}H\}$ NMR spectrum of such a polymer in Fig. 2. As can be seen, the spectrum exhibits only the anticipated six resonances, centered at δ 14.1 (sharp s, C6), 23.3 (br s, C5), 28.5 (m, C4), 34 (m, C3), 32.2 (br s, C2), and 40.5 (m, C1). In contrast to the $^{13}C\{^{1}H\}$ NMR spectra of highly stereoregular isotactic (2*k*) and syndiotactic (2*u*) poly-1-hexenes, which exhibit uniformly narrow resonances, the C(1)–C(4) resonances of the polymers discussed here consisted of broad multiplets indicative of the presence of comparable amounts of most of the possible pentads. Thus the materials are atactic (8*b*).

The $^{13}C\{^{1}H\}$ NMR spectra of the poly-1-hexenes formed at –10°C and above exhibit not only the six primary resonances mentioned above, but also many additional resonances (Fig. 3), many narrow, some broad. In particular, we

© 2001 NRC Canada

Fig. 4. $^{13}C\{^1H\}$ NMR spectrum of purified oligo-1-hexene.

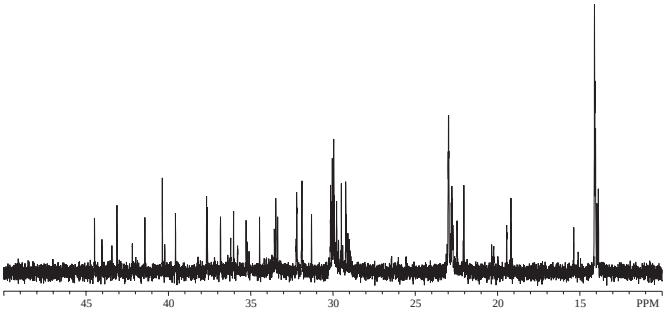
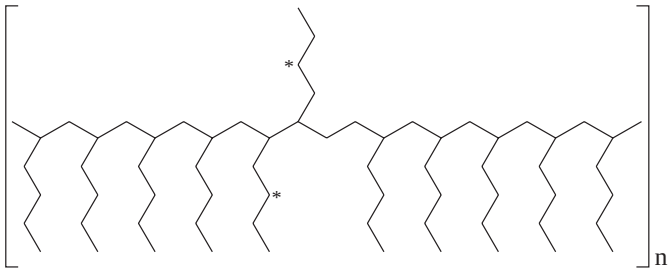


Fig. 5. Microstructure of regioirregular poly-1-hexene, showing tail-to-tail moiety.



note a rather intense, broad (1 ppm in width) resonance centered at δ ~30.5 and attributable to CH_2 groups on the basis of J-mod experiments, in addition to weaker broad resonances in the region δ 35–38, and many sharp, weaker resonances in the regions δ 19–24 and 28–45. Although we originally interpreted the sharp resonances in terms of regioirregularities in the polymer chain arising from 2,1-insertions (3*k*), in fact they are substantially removed on separation of oligomer from polymer and are present in the NMR spectra of oligomers (Fig. 4).

In contrast, the broad anomaly in the $^{13}C\{^1H\}$ NMR spectra of poly-1-hexene at δ ~30.5 remains in the polymer spectra after the low molecular weight oligomers have been removed, and must be interpreted in terms of unusual polymer microstructures since it has rarely been reported in the $^{13}C\{^1H\}$ NMR spectra of poly-1-hexenes reported elsewhere (2*o*, 8*a*). We can also rule out, on the basis of relative intensities, the possibility that it is to be attributed to end groups of some kind (2*o*, 8*a*), and we are left with the alternative that it is to be attributed to significant amounts of a main chain carbon microstructure that is not normally found in poly-1-hexene formed in a Ziegler–Natta process.

One such possibility is that the anomalous resonance involved 2,1-insertion of 1-hexene molecules followed by chain straightening via a series of reversible β-elimination and reinsertion processes, akin to the "chain walking" nickel(II) and palladium(II) catalyzed polymerizations of α-olefins (10). However, net 5,1-enchainments can be readily ruled out because a comparable number of methyl branches would result and the $^{13}C\{^1H\}$ NMR spectra are essentially devoid of the requisite methyl resonances at δ ~20 (6, 9), while similar 6,1-insertions may also be ruled out as HMBC and HSQC-TOCSY experiments indicate that one or more components of the resonance at δ ~30.5 exhibit spin–spin coupling to methyl group protons, at least a six bond coupling if the resonance is to be attributed to a "chain straightened" backbone methylene carbon atom (of course we cannot rule out the possibility that some of the resonances in the δ ~30.5 manifold are a result of 6,1-insertions.)

The other possibility is that the anomalous resonance at δ ~30.5 is indicative of a microstructure resulting from a 2,1-followed by a 1,2-insertion of 1-hexenes, i.e., involving tail-to-tail incorporation of two monomers (Fig. 5). There would result a poly-1-hexene chain that would contain -CH(Bu)CH_2CH_2CH(Bu)- units, and we find indeed that ^{13}C NMR chemical shift calculations predict (6), for the carbon atoms indicated by asterisks, a downfield shift of 1.3 ppm relative to "regular" C(4) carbon atom chemical shifts (δ ~28.5) (see also ref. 10*b*). Interestingly, 2,1-insertions are normally found to result in significant retardation of metallocene catalyzed polymerization of propylene (1*d*), the accepted rationale being that rates of propagation following a 2,1-insertion are low because of increased steric hindrance near the metal. However, the active sites of monocyclopentadienyl catalysts are much less sterically congested than are those of metallocenes, and it has been shown that rates of propagation with such systems are not severely lowered by 2,1-insertions during the polymerization of propylene by **I** (3*k*). For instance, up to 15% of the monomer incorporated involves 2,1-insertions during propylene polymerizations catalyzed by **I** (3*k*), much higher than the ~1% observed in metallocene systems (1*f*). Interestingly, 2,1-insertions have rarely been reported for metallocene catalyzed polymerizations of α-olefins larger than propylene.

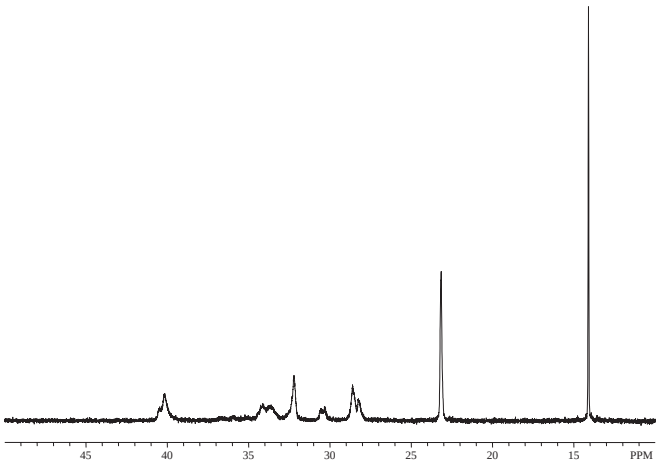
As will be shown below, experiments involving 1-hexene polymerization by Cp*Ti($^{13}CH_3$)$_2$(μ-Me)B(C_6F_5)$_3$ in CH_2Cl_2 confirm that a significant proportion of 2,1-insertions occurs during the initiation step. In addition, 2,1-insertions followed by β-H elimination are found to give the most predominant olefinic end group, identified by ^1H NMR spectroscopy, and thus, it is very reasonable that 2,1-insertions occur during the propagation step of 1-hexene polymerization by **I** in toluene. Other resonances are to be anticipated for the tail-to-tail structure shown in Fig. 6, and chemical shift calculations (6) suggest that some are obscured by the stronger "regular" resonances, but that others are to be seen as rather weak resonances in the region δ 35–38 of purified polymer (Fig. 6).

Oligomer microstructures

The $^{13}C\{^1H\}$ NMR spectra of the oligo-1-hexenes (Fig. 4) exhibit only very sharp resonances, consistent with assignments to low molecular weight materials. In addition, there are many as yet unassigned resonances that are not normally present in spectra of poly-1-hexene, a result in part of the low molecular weights of the materials since end group resonances would clearly be more evident. In addition, many isomers are possible, resulting from multiple β-H elimination reactions. However, unusual resonances such as those at δ ~20 and 12 may be indicative of methyl and ethyl branches arising from 5,1- and 4,1-insertions, respectively, (incomplete chain walking), while intense resonances at δ ~30 are consistent both with 6,1-enchainments (see above for discussion of mechanism) and with resonances of dimers and (or) trimers of 1-hexene (2*h*, *p*). Under those conditions which produce predominantly oligo-1-hexene, the observed conversions and product distributions require formation of up to 20

© 2001 NRC Canada

Fig. 6. $^{13}C\{^1H\}$ NMR spectrum of purified poly-1-hexene (partially) regioirregular.

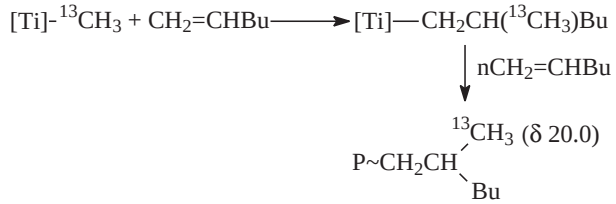


molecules of oligomer per catalyst site. Thus the resulting methyl branches do not arise solely via insertions of 1-hexene into the original Ti–Me bonds of the catalyst, but rather via the olefin incorporation–isomerization processes discussed above. In these cases, the rates of propagation must be low relative to the rates of isomerization, and we note that oligomer formation is indeed favoured when the monomer:catalyst ratio is low, i.e., under conditions where the system is starved of monomer. Also consistent with this hypothesis, we note that lower molecular weights are obtained under conditions of greater dilution even when the monomer:catalyst ratio is the normal (400:1). In these cases, the rates of the presumed bimolecular propagation process become less competitive than the rates of isomerization, an internal reorganization of the coordinated polymer chain.

Mechanisms of initiation by I

As is generally true for polymerization of α-olefins (1, 2, 5), the preferred mode of initiation in toluene is via 1,2-insertions into the Ti–Me bonds. Evidence for this is obtained from labelling experiments which were carried out using $Cp^*Ti(^{13}CH_3)_3$. In a typical experiment, a solution of $Cp^*Ti(^{13}CH_3)_3$ in toluene at 0°C was treated with a solution of 1.1 equiv of $B(C_6F_5)_3$ in 5 mL toluene, as above, and the $^{13}C\{^1H\}$ NMR spectrum was found to be identical to that shown in Fig. 3, except that it also exhibited a relatively strong resonance at δ ~20, consistent with terminal methyl branching formed as in eq. [3] (5*c*, *f*).

[3]



The crude poly-1-hexene was then fractionated, and the $^{13}C\{^1H\}$ NMR spectra of both fractions were found to exhibit relatively strong resonances at δ ~20, thus in both cases, it would seem that 1,2-insertion processes are involved in the initiation steps.

In a complementary NMR experiment carried out in CD_2Cl_2 at –50°C, a solution of $Cp^*Ti(^{13}CH_3)_3$ was treated with a solution of 1.1 equiv of $B(C_6F_5)_3$ in CD_2Cl_2, also at –50°C. ^1H and $^{13}C\{^1H\}$ NMR spectra of $Cp^*Ti(^{13}CH_3)_2(\mu\text{-}^{13}CH_3)B(C_6F_5)_3$ (3*c*) were observed; in addition, a small amount of free $[^{13}CH_3B(C_6F_5)_3]^-$ was also invariably formed, as evidenced by a broad resonance at δ ~10. This observation is consistent with an equilibrium between contact and solvent separated ion pairs (eq. [4]).

[4] $$Cp^*Ti(^{13}CH_3)_2(\mu\text{-}^{13}CH_3)B(C_6F_5)_3 \rightarrow [Cp^*Ti(^{13}CH_3)_2]^+ + [^{13}CH_3B(C_6F_5)_3]^-$$

On the addition of 0.1 mL of 1-hexene (1-hexene:Ti ratio = 13) in CD_2Cl_2 at –50°C, the $[^{13}CH_3B(C_6F_5)_3]^-$ resonance at δ ~10 increased in intensity and the resonance of **I** disappeared immediately as the 1-hexene coordinated to the titanium centre and displaced the borate ligand. Interestingly, there were observable no resonances of significant intensity attributable to Ti–$^{13}CH_3$ groups, implying that both of the original Ti–$^{13}CH_3$ groups were very quickly incorporated into polymer. As the sample warmed to room temperature, a weak methane resonance appeared at δ ~–4.2. The ^1H and $^{13}C\{^1H\}$ NMR spectra of polymer (containing only trace amounts of oligomers) exhibited, in addition to all of the expected polymer resonances, prominent resonances at δ ~20 and 10.5 in the $^{13}C\{^1H\}$ NMR spectrum. The former corresponds to type of ^{13}C labelled methyl end group discussed above, while the latter could be attributed to an ethyl end group, resulting from a 2,1-insertion process. These assignments were consistent with chemical shift comparisons with calculated ^{13}C chemical shifts (6, 9), the possibility that the resonance at δ ~10.5 were to be attributed to residual $[^{13}CH_3B(C_6F_5)_3]^-$ being ruled out because of an absence of the corresponding methyl resonance at δ ~0.44 in the ^1H NMR spectrum (3*m*).

An unambiguous demonstration of 2,1-insertion during initiation of 1-hexene polymerization has not, apparently, been previously reported. In addition, the catalyst system under consideration here seems to induce 2,1-insertions to a much greater extent than is the case for α-olefin polymerization by metallocenes (29). Comparisons of the relative integrations of the resonances at δ ~20 and 10.5 in an NOE suppressed $^{13}C\{^1H\}$ NMR spectrum showed that 2,1-insertions occur 15–20% of the time, quite consistent with the comparable number of 2,1-insertions during propylene polymerization catalyzed by **I** (3*k*).

As mentioned above, the $^{13}CH_3$ resonance of the Ti–$^{13}CH_3$ groups of **I** disappears immediately on interaction with 1-hexene in CD_2Cl_2, and no new resonances attributable to Ti–$^{13}CH_3$ groups are observed. This observation suggests that both methyl groups are very quickly involved in polymerization and that two polymer chains are probably growing simultaneously from the titanium, a process which seems not to have been demonstrated previously for other catalyst systems.

Mechanisms of chain termination – transfer

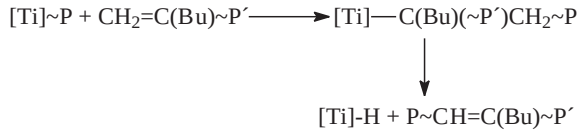
The ^1H NMR spectra of most samples of poly–oligo-1-hexenes exhibit resonances at δ ~4.66 and 4.72, ~5.3–5.5, and ~5.1, attributable, respectively, to vinylidene groups

© 2001 NRC Canada

RR′(C=CH_2), dialkyl-substituted alkenes (RCH=CHR′), and trialkyl-substituted alkenes (RCH=CHR′R″) (9). The vinylidene groups are formed via β-H elimination following a 1,2-insertion, a common but not the predominant mode of chain transfer during the polymerization of α-olefins by metallocene catalysts (2*f*).

Disubstituted alkenes may be formed via β-H elimination after a 2,1-insertion, a very important mode of chain transfer during the 1-hexene polymerization by metallocenes (2*f*). Presumably dialkyl-substituted alkenes RCH=CHR′ do not leave the inner coordination sphere of the titanium during the reversible β-H elimination steps, as **I** has been shown to be incapable of polymerizing cyclohexene (3*e*), and we find that **I** does not copolymerize ethylene with *cis*- or *trans*-2-butene although it does homopolymerize 1-hexene in the presence of a mixture of *cis*- and *trans*-2-butene.

Trialkyl-substituted olefins are presumably a result of the types of vinylidene insertion – β-H elimination processes shown in eq. [5], and have been postulated previously (2*n*, 11).



[5]

The ^{1}H NMR spectra also exhibit much weaker resonances at δ ~5.65, ~5.8 (total intensity 1), and ~4.95 (total intensity 2), suggestive of vinyl end groups (P~CH_2CH=CH_2) (9*a*), which would arise from the above mentioned "chain walking" after a 2,1-insertion followed by β-H elimination (10).

Upon separation of the crude poly–oligo-1-hexene mixture into oligo-1-hexene and poly-1-hexene fractions, there were noticeable differences between the NMR spectra of the two fractions. The olefinic region of the ^{1}H NMR spectrum of the poly-1-hexene exhibited only a strong resonance at δ ~5.45, attributed to disubstituted olefinic groups, and much weak resonances at δ 5.1 and 4.7, attributed to lesser amounts of trialkyl substituted internal alkenes and vinylidene groups, respectively. The relative amounts of the three different types of olefinic groups, and therefore, the relative importance of the chain transfer mechanisms leading to them are similar to findings during the polymerization of 1-hexene by metallocene catalysts (2*f*). The ^{1}H NMR spectra of purified oligo-1-hexene fractions exhibit the remainder of the olefinic peaks mentioned above.

Nature of the initiator(s)

As mentioned above, **I** functions as a precursor to the cationic, 10e$^-$ species $[Cp^*TiMe_2]^+$, which is believed to the true Ziegler–Natta catalyst in this system. Although $[Cp^*TiMe_2]^+$ has been long known to behave as a very effective catalyst for the polymerization of, e.g., ethylene and propylene (3*g*, *k*, *n*), this study is to our knowledge the first to demonstrate that both Ti–methyl groups are quickly transferred to growing polymer chains. In contrast, during the carbocationic polymerization of styrene initiated by the same cationic complex, the Ti–methyl bonds largely remain intact once chain growth begins (3*g*).

The fact that polymerization occurs at two sites on the titanium distinguishes **I** fundamentally from both metallocene-based Ziegler–Natta (1) and constrained geometry catalyst (1*g*) systems, which can contain only one active alkyl ligand *cis* to a vacant site. While it is not at all clear at this point why **I** can simultaneously form high and low molecular weight polymers in addition to oligomers, with each component often exhibiting relatively narrow molecular weight distributions ($M_w/M_n \approx 1.5$–3.0), clearly there is more than one initiator responsible for the polymerization of 1-hexene and other α-olefins by Cp^*TiMe_3 and $B(C_6F_5)_3$ (3*l*, 9*f*) and the bifunctionality of the system may be a factor. For instance, it is possible that chain propagation processes at the two sites do not proceed independently, but that the presence of one long chain or branching near the titanium changes drastically the relative rates of propagation and chain transfer at the other. It is also possible that β-H elimination to give a titanium hydride could be followed by association of two cationic titanium centres via a hydride bridge, again altering the relative rates of propagation and chain transfer of the system.

Acknowledgments

This research was made possible by financial assistance from Queen's University and the Natural Sciences and Engineering Research Council.

References

1. (*a*) P.C. Möhring and N.J. Coville. J. Organomet. Chem. **479**, 1 (1994); (*b*) V.K. Gupta, S. Satish, and I.S. Bhardwaj. J. Macromol. Sci. Rev. Macromolec. Chem. Phys. **C34**, 439 (1994); (*c*) H.H. Brintzinger, D. Fischer, R. Mülhaupt, B. Rieger, and R.M. Waymouth. Angew. Chem. Int. Ed. Eng. **34**, 1143 (1995); (*d*) M. Bochmann. J. Chem. Soc. Dalton Trans. 255 (1996); (*e*) W. Kaminsky and M. Arndt. Adv. Polymer Sci. **127**, 143 (1997); (*f*) J.C.W. Chien. *In* Topics in catalysis. Vol. 7. *Edited by* T.J. Marks and J.C. Stevens. J.C. Baltzer, Switzerland. 1999. p. 125; (*g*) A.L. McKnight and R.M. Waymouth. Chem. Rev. **9**8 2587. (1998)
2. (*a*) K. Soga and H. Yanagihara. Macromol. Chem. **189**, 2839 (1988); (*b*) T. Asanuma, Y. Nishimori, M. Ito, N. Uchikawa, and T. Shiomura. Polymer Bull. **25**, 567 (1991); (*c*) K. Soga, D.H. Lee, and Y. Morikawa. Polymer **33**, 2408 (1992); (*d*) T. Asanuma, Y. Nishimori, M. Ito, and T. Shiomura. Makromol. Chem. Rapid Commun. **14**, 315 (1993); (*e*) J.C.W. Chien, and B.M. Gong, J. Polym. Sci. **A31**, 1747 (1993); (*f*) G.N. Babu, R.A. Newmark, and J.C.W. Chien. Macromol. **27**, 3383 (1994); (*g*) H. Yasuda and E. Ihara. Tetrahedron, **15**, 4563 (1995); (*h*) C. Janiak, K.C.H. Lange, and P. Marquardt. Macromol. Chem. Rapid Commun. **16**, 643 (1995); (*i*) D. Coevoet, H. Cramail, and A. Deffieux. Macromol. Chem. Phys. **197**, 855 (1996); (*j*) H. Hagihara, T. Shiono, and T. Ikeda. Macromolecules, **31**, 3184 (1998); (*k*) Y. Yamaguchi, N. Suzuki, A. Fries, T. Mise, H. Koshino, Y. Ikegami, H. Ohmori, and A. Matsumoto. J. Poly. Sci.: Part A Polymer Chem. **37**, 283 (1999); (*l*) D. Coevoet, H. Cramail, and A. Deffieux. Macromol. Chem. Phys. **200**, 1208 (1999); (*m*) O. Henschke, J. Knorr, and A. Arnold. Pure. Appl. Chem **A53**, 473 (1998); (*n*) A. Yano, M. Sone, S. Hasegawa, M. Sato, and A. Akimoto. Macromol. Chem. Phys. **200**, 933 (1999); (*o*) H. Frauenrath, H. Keul, and H. Hoecker. Macromol. Rapid Commun. **19**, 391

© 2001 NRC Canada

(1998); (*p*) H.Q. Liu, A. Deffieux, and P. Sigwalt. Makromol. Chem. **192**, 2111 (1991); (*q*) W. Kaminsky, A.-M. Schauwienold, and F. Freidanck. J. Mol. Catal. **112**, 37 (1996); (*r*) N. Naga and K. Mizunuma. Macromol. Rapid Commun. **18**, 581 (1997); (*s*) N. Naga, T. Shiono, and T. Ikeda. Macromol. Chem. Phys. **200**, 1587 (1999); (*t*) E. Ihara, M. Nodono, K. Katsura, Y. Adachi, H. Yasuda, M. Yamahashira, H. Hashimoto, N. Kanehisa, and Y. Kai. Organometallics, **17**, 3945 (1998); (*u*) T. Asanuma, Y. Nishimori, M. Ito, N. Uchikawa, and T. Shiomura. Polym. Bull. **25**, 567 (1991); (*v*) N. Suzuki, T. Mise, Y. Yoshitaka, T. Chihara, Y. Ikegami, H. Ohmori, A. Matsumoto, and Y.J. Wakatsuki. J Organomet. Chem. **560**, 47 (1998).

3. (*a*) D.J. Gillis, M.-J. Tudoret, and M.C. Baird. J. Am. Chem. Soc. **115**, 2543 (1993); (*b*) D.J. Gillis, R. Quyoum, M.-J. Tudoret, Q. Wang, D. Jeremic, A.W. Roszak, and M.C. Baird. Organometallics, **15**, 3600 (1996); (*c*) Q. Wang, R. Quyoum, D.J. Gillis, D. Jeremic, and M.C. Baird. J. Organomet. Chem. **527**, 7 (1997); (*d*) F. Barsan and M.C. Baird, J. Chem. Soc. Chem. Commun. 1065 (1995); (*e*) D. Jeremic, Q. Wang, R. Quyoum, and M.C. Baird. J. Organomet. Chem. **497**, 143 (1995); (*f*) Q. Wang and M.C. Baird. Macromolecules, **28**, 8021 (1995); (*g*) Q. Wang, R. Quyoum, D.J. Gillis, M.-J. Tudoret, D. Jeremic, B.K. Hunter, and M.C. Baird. Organometallics, **15**, 693 (1996); (*h*) M.C. Murray and M.C. Baird. J. Mol. Cat. **128**, 1 (1998); (*i*) T.L. Tremblay, S.W. Ewart, M.J. Sarsfield, and M.C. Baird. J. Chem. Soc. Chem. Commun. 831 (1997); (*j*) M.J. Sarsfield, S.W. Ewart, T.L. Tremblay, A.W. Roszak, and M.C. Baird. J. Chem. Soc. Dalton Trans. 3097 (1997); (*k*) S.W. Ewart, M.J. Sarsfield, D. Jeremic, T.L. Tremblay, E.F. Williams, and M.C. Baird. Organometallics, **17**, 1502 (1998); (*l*) E.F. Williams, M.C. Murray, and M.C. Baird. Macromolecules, **33**, 261 (2000); (*m*) S.Y. Desjardins, A.A. Way, M.C. Murray, D. Adirim, and M.C. Baird. Organometallics, **17**, 2382 (1998); (*n*) S.W. Ewart, M.J. Sarsfield, E.F. Williams, and M.C. Baird. J. Organomet. Chem. **579**, 106 (1999).
4. (*a*) C. Pellecchia, P. Longo, A. Proto, and A. Zambelli. Makromol. Chem. Rapid Commun. **13**, 265 (1992); (*b*) C. Pellecchia, P. Longo, A. Proto, and A. Zambelli. Makromol. Chem. Rapid Commun. **13**, 277 (1992); (*c*) J.C.W. Chien, Z. Salajka, and S. Dong. Macromolecules, **25**, 3199 (1992); (*d*) A. Kucht, H. Kucht, S. Barry, J.C.W. Chien, and M.D. Rausch. Organometallics, **12**, 3075 (1993); (*e*) T.E. Ready, R.O. Day, J.C.W. Chien, and M.D. Rausch. Macromolecules, **26**, 5822 (1993); (*f*) A. Zambelli, C. Pellecchia, L. Oliva, P. Longo, and A. Grassi. A. Makromol. Chem. **192**, 223 (1991); (*g*) H. Kucht, A. Kucht, J.C.W. Chien, and M.D. Rausch. Appl. Organomet. Chem. **8**, 393 (1994); (*h*) C. Pellecchia, A. Immirzi, A. Grassi, and A. Zambelli. Organometallics, **12**, 4473 (1993); (*i*) J.C. Flores, J C.W. Chien, and M.D. Rausch. Organometallics, **13**, 4140 (1994); (*j*) J.C. Flores, J.S. Wood, J.C.W. Chien, and M.D. Rausch. Organometallics, **15**, 4944 (1996); (*k*) A. Grassi, A. Zambelli, and F. Laschi. Organometallics, **15**, 480 (1996); (*l*) J. Sassmannshausen and M. Bochmann. J. Organomet. Chem. **548**, 23 (1997); (*m*) C. Pellecchia, D. Pappalardo, L. Oliva, and A. Zambelli. J. Am. Chem. Soc. **117**, 6593 (1995); (*n*) Y.-X. Chen, P.-F. Fu, C.L. Stern, and T.J. Marks. Organometallics, **16**, 5958 (1997); (*o*) K. Nomura, N. Naga, M. Miki, and K. Yanagi. Macromolecules, **31**, 7588 (1998); (*p*) J.R. Park, T. Shiono, and K. Soga. Macromolecules **25**, 521 (1992); (*q*) C. Pellecchia, D. Pappalardo, and G.J. Gruter. Macromolecules, **32**, 4491 (1999).
5. (*a*) C.J. Schaverien. J. Mol. Catal. **90**, 177 (1994); (*b*) C.J. Schaverien. Organometallics, **13**, 69 (1994); (*c*) R.R. Schrock, R. Baumann, S.M. Reid, J.T. Goodman, R. Stumph, and W.M. Davis. Organometallics, **18**, 3649 (1999); (*d*) M. Aizenberg, L. Turculet, W.M. Davis, F. Schattenmann, and R.R. Schrock. Organometallics, **17**, 4795 (1998); (*e*) A. van der Linden, C.J. Schaverien, N. Meijboom, C. Ganter, and A.G. Orpen. J. Amer. Chem. Soc. **117**, 3008 (1995); (*f*) J.D. Scollard, D.H. McConville, J.J. Vittal, and N.C. Payne. J. Mol. Catal. **128**, 201 (1998).
6. ChemWindow 6 Spectroscopy. Bio-Rad Laboratories, Philadelphia, PA, U.S.A. 1999.
7. (*a*) M. Mena, P. Royo, R. Serrano, M.A. Pellinghelli, and A. Tiripicchio. Organometallics, **8**, 476 (1989); (*b*) A.G. Massey and A.J. Park. J. Organomet. Chem. **2**, 245 (1964).
8. (*a*) T. Asakura, K. Hirano, and M. Demura. Makromol. Chem. Rapid Commun. **12**, 215 (1991) ; (*b*) T. Asakura, M. Demura, and Y. Nishiyama. Macromolecules, **24**, 2334 (1991); (*c*) S. Nemes, and J. Borbély. Pure Appl. Chem. **A34**, 2355 (1997); (*d*) H.N. Cheng. Polym. Bull. **26**, 325 (1991).
9. (*a*) C.J. Pouchert and J. Behnke. The Aldrich library of ^{13}C and ^{1}H FT NMR spectra. 1st ed. Aldrich Chemical Company, Inc., U.S.A. 1993; (*b*) G.B. Galland, R.F. de Souza, R.S. Mauler, and F.F. Nunes. Macromolecules, **32**, 1620 (1999); (*c*) E.F. McCord, W.H. Shaw, and R.A. Hutchinson. Macromolecules, **30**, 246 (1997); (*d*) E.W. Hansen, R. Blom, and O.M. Bade. Polymer, **38**, 4295 (1997); (*e*) A. Jurkiewicz, N.W. Eilerts, and E.T. Hsieh. Macromolecules, **32**, 5471 (1999).
10. (*a*) C.M. Killian, D.J. Tempel, L.K. Johnson, and M. Brookhart. J. Amer. Chem. Soc. **118**, 11664 (1996); (*b*) L.K. Johnson, C.M. Killian, S.D. Arthur, J. Feldman, E.F. McCord, S.J. McLain, K.A. Kreutzer, M.A. Bennett, E.B. Coughlin, S.D. Ittel, A. Parthasarathy, D.J. Tempel, and M.S. Brookhart. (DuPont) PCT Int. Appl. WO 96/23 010. 1996.
11. (*a*) B. Folie and C.J. Ruff. Polym. Prepr. (Am. Chem. Soc. Div. Polym. Chem.) **39**, 201 (1998) ; (*b*) T.D. Shaffer, J.A.M. Canich, and K.R. Squire. Macromolecules, **31**, 5145 (1998).

© 2001 NRC Canada

Stereochemistry at carbon upon protonolysis of a late transition metal-alkyl bond: a reaction of relevance to catalytic enantioselective hydrogenation of olefins

Jason A. Wiles, Steven H. Bergens, and Victor G. Young, Jr.

Abstract: Reaction of [Ru((*R*)-BINAP)(H)(MeCN)$_n$(acetone)$_{3-n}$](BF$_4$) (where n = 0–3) (**2**) with 1 equiv of the olefin substrate methyl α-acetamidoacrylate (MAA) in acetone at room temperature immediately generated a mixture (72:28) of two diastereomers of the complex [Ru((*R*)-BINAP)(MeCN)(MAA(H))](BF$_4$) (**3**). The olefin–hydride insertion reaction between **2** and MAA to generate **3** was regioselective, with transfer of the hydride to the β-olefinic carbon and transfer of ruthenium to the α-carbon in both diastereomers of **3**. The two diastereomers of **3** differ by the absolute configuration at the α-carbon of MAA(H) (($S_{C\alpha}$)-**3** and ($R_{C\alpha}$)-**3**). The absolute configuration of the major (($S_{C\alpha}$)-**3**) diastereomer was determined by X-ray diffraction in conjunction with NMR spectroscopic data. Protonolysis of the ruthenium–carbon bond in **3** and in the methyl α-acetamidocinnamate (MAC) analog ([Ru((*R*)-BINAP)(MeCN)((*S*)-MAC(H))](BF$_4$) (($S_{C\alpha}$)-**4**)) by addition of 2 equiv HBF$_4$·Et$_2$O in CH$_2$Cl$_2$ at room temperature was not stereospecific and did not occur with β-hydride elimination from the methyl or benzyl groups.

Key words: ruthenium, BINAP, enantioselective, hydrogenation, catalysis.

Résumé : La réaction du [Ru((*R*)-BINAP(H)(MeCN)$_n$(acétone)$_{3-n}$](BF$_4$) (dans lequel n = 0–3) (**2**) avec un équivalent du substrat oléfinique α-acétamidoacétate de méthyle ("MAA"), dans l'acétone, à la température ambiante, conduit immédiatement à la formation d'un mélange (72:28) de deux diastéréomères du complexe [Ru((*R*)-BINAP(MeCN)("MAA"(H))](BF$_4$) (**3**). La réaction d'insertion oléfine–hydrure entre **2** et "MAA" pour générer **3** est régiosélective; dans les deux diastéréomères de **3**, le transfert de l'hydrure se portant sur le carbone oléfinique β et le transfert de ruthénium sur le carbone α. Les deux diastéréomères de **3** diffèrent par la configuration absolue au niveau du carbone en α du "MAA"(H) (($S_{C\alpha}$)-**3**) et (($R_{C\alpha}$)-**3**). On a déterminé la configuration absolue du produit principal, le diastéréomère (($S_{C\alpha}$)-**3**), par diffraction des rayons X alliée aux données de spectroscopie RMN. La protonolyse de la liaison ruthénium–carbone présente dans le composé **3** et dans son analogue α-acétamidocinnamate de méthyle ("MAC"), le [Ru((*R*)-BINAP(MeCN)((*S*)-"MAC"(H))](BF$_4$) (($S_{C\alpha}$)-**4**), a été réalisée par addition de deux équivalents de HBF$_4$·Et$_2$O, dans du CH$_2$Cl$_2$, à la température ambiante; cette réaction n'est pas stéréospécifique et elle ne se produit pas par le biais d'une élimination β à partir des groupes méthyle ou benzyle.

Mots clés : ruthénium, BINAP, énantiosélective, hydrogénation, catalyseur.

[Traduit par la Rédaction]

Introduction

The first reported use of ruthenium complexes as homogeneous catalysts for hydrogenation of olefins was a landmark paper published by James and co-workers (1) nearly 40 years ago. This paper, in part, laid the groundwork for James' further development of the first enantioselective catalytic hydrogenation using a ruthenium catalyst containing a chiral bis(phosphine) ligand (2). These papers helped found and inspire the development of ruthenium – chiral bis(phosphine) catalysts, the most versatile and widely used catalyst systems for the enantioselective hydrogenation of olefins and ketones.

The mechanisms for hydrogenations catalyzed by ruthenium–bis(phosphine)-halide complexes, as well as the chemistry of such compounds, have been extensively studied by James et al. (3). Mechanistic studies by James, Noyori, and others showed that hydrogenation of α,β-unsaturated acids (e.g., tiglic acid ((*E*)-CH$_3$CH=C(CH$_3$)CO$_2$H)) using Ru((*R*)-BINAP)(O$_2$CCH$_3$)$_2$ (**1**) as catalyst in MeOH proceeds by heterolytic cleavage of H$_2$ and subsequent protonolysis of a ruthenium(II)–alkyl bond (4). As the putative ruthenium(II)–alkyl intermediate occurred after the turnover-limiting step in the catalytic cycle, it was impossible to detect in solution, and the stereochemistry of this key enantio-determining step

Received September 1, 2000. Published on the NRC Research Press Web at http://canjchem.nrc.ca site on July 11, 2001.

Dedicated to Professor Brian James on the occasion of his 65th birthday.

J.A. Wiles and S.H. Bergens.[1] Department of Chemistry, University of Alberta, Edmonton, AB T6G 2G2, Canada. **V.G. Young, Jr.** X-ray Crystallographic Laboratory, 160 Kolthoff Hall, Chemistry Department, 207 Pleasant St. S.E., The University of Minnesota, Minneapolis, MN 55455, U.S.A.

[1]Corresponding author (telephone: (780) 492-9703; fax: (780) 492-8231; e-mail: steve.bergens@ualberta.ca).

 DOI: 10.1139/cjc-79-5/6-1019 © 2001 NRC Canada

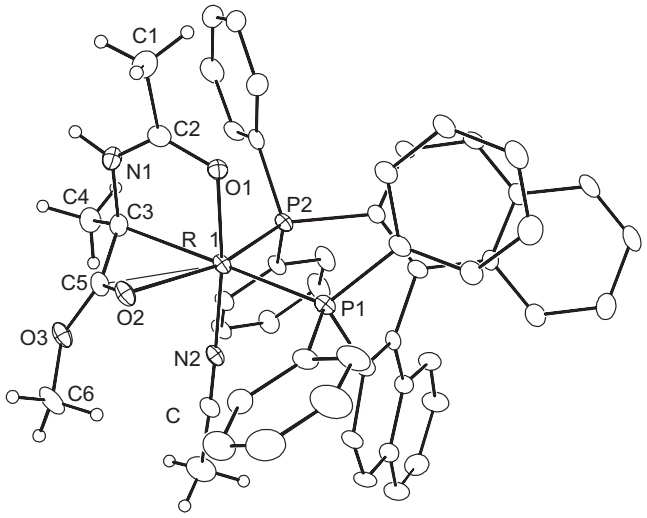
could not be directly observed. A comparison of NMR data for the isotopomers of $CH_3CHDCD(CH_3)CO_2H$ obtained from deuterations of tiglic acid in MeOD using **1** and using $RhCl(PPh_3)_3$ as a catalyst lead to the conclusion that protonolysis proceeded via retention of configuration at carbon (*4b*). Most catalytic hydrogenations of olefins that involve protonolysis (solvolysis) of a metal–carbon bond are believed to, or have been shown to, proceed via a net *syn*-addition of H_2 across the olefin; the presumed consequence of retention at carbon during the protonolysis. There are reported examples, however, for which direct protonolysis of Pt–C σ bonds through back-side attack was postulated to account for catalytic net *anti*-addition of deuterium to certain olefins using platinum–tin complexes as catalysts (5). We now report the first direct observations of protonolysis of the catalyst–alkyl bond in two putative diastereomeric intermediates for catalytic hydrogenation of olefins.

Results and discussion

Reaction of [Ru((*R*)-BINAP)(H)$(MeCN)_n(acetone)_{3-n}$](BF$_4$) (where n = 0–3) (**2**) (6) with 1 equiv of methyl α-acetamidoacrylate (MAA) in acetone at room temperature generated upon mixing (>99% by NMR analysis) a mixture of two species in a ratio of 72:28 (eq. [1]).

NMR spectroscopy, electrospray-ionization mass spectrometry (EI-MS), and microanalysis indicated that these species were two diastereomeric forms of the complex [Ru((*R*)-BINAP)(MeCN)(MAA(H))](BF$_4$) (**3**). Complex **3** resulted from olefin–hydride insertion between MAA and **2**. We previously reported the preparation, solid-state structure, and reactivity of a related complex formed by reaction between **2** and methyl α-acetamidocinnamate (MAC) in >99% diastereomeric excess (de), viz., [Ru((*R*)-BINAP)(MeCN)((*S*)-MAC(H))](BF$_4$) (($S_{C\alpha}$)-**4**) (6). In accord with ($S_{C\alpha}$)-**4**, the olefin–hydride insertion reaction between **2** and MAA was regioselective, with transfer of the hydride to the β-olefinic carbon in MAA and transfer of ruthenium to the α-carbon in both diastereomers of **3** (for similar regioselective insertion of MAA into Ru–H bonds of chiral clusters, see ref. 7). NMR

Fig. 1. Structure of ($S_{C\alpha}$)-**3** as determined by X-ray diffraction.[2,3]

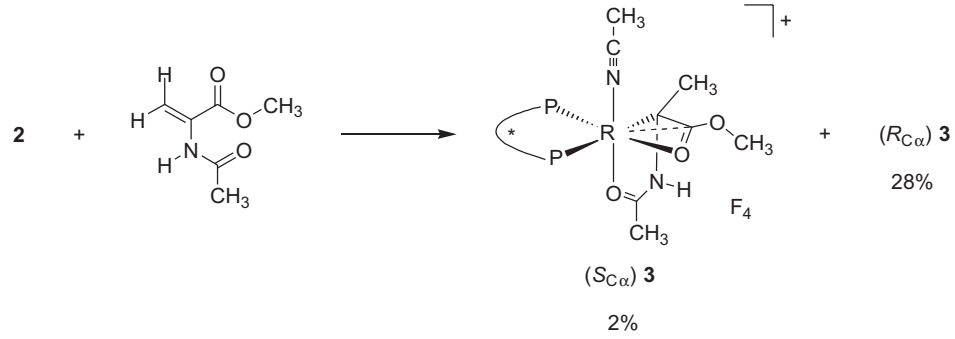


chemical shifts and coupling constants for both diastereomers of **3** parallel those previously found for ($S_{C\alpha}$)-**4**. For example, $^{13}C\{^1H\}$ NMR signals from the coordinated amido and the ester carbonyls, as well as from the α-carbon of **3** (that σ-bonded to ruthenium) are comparable to those of ($S_{C\alpha}$)-**4**. From these similarities, we conclude that the two diastereomers of **3** differ by the absolute configuration at the α-carbon of MAA(H) (($S_{C\alpha}$)-**3** and ($R_{C\alpha}$)-**3**). The absolute configuration of the major (72%) diastereomer was determined as follows.

Slow liquid–liquid diffusion of di-*n*-butyl ether into a 1,2-dimethoxyethane solution of **3** (72:28) at room temperature produced X-ray quality crystals.[2] Diffraction data was collected from two separate samples. In both cases, the molecular structure of the isolated species was of ($S_{C\alpha}$)-**3**, as shown in Fig. 1. The molecular structures of ($S_{C\alpha}$)-**3** and ($S_{C\alpha}$)-**4** are quite similar.

Both are best described as the enolates of MAA(H)$^-$ and MAC(H)$^-$ bonded to ruthenium through Cα (C3) and through

[1]



[2] Crystal data for ($S_{C\alpha}$)-**3**: $C_{52}H_{45}BF_4N_2O_3P_2Ru$, FW = 995.72, yellow plate, crystal size 0.40 × 0.25 × 0.13 mm, orthorhombic, $C222_1$, a = 21.4849(2), b = 29.7175(2), c = 18.8513(2) Å, V = 12036.1(2) Å^3, Z = 8, $\rho_{calcd.}$ = 1.099 g cm^{-3}, μ (Mo Kα) = 0.361 mm^{-1}, T = 173(2) K, λ (Mo Kα) = 0.71073 Å. Data were collected using a Siemens SMART Platform CCD diffractometer (θ range for data collection of 1.17 to 25.04°); 10589 independent reflections (8758 with $F_o^2 > 2\sigma(F_o^2)$) were measured. The structure was solved via direct methods (SHELXTL-V5.0). Full-matrix least-squares refinement on F^2 (SHELXTL-V5.0) yielded R_1 = 0.0480 ($F_o^2 > 2\sigma(F_o^2)$) and wR_2 = 0.1261 (all data). GoF on F^2 = 1.041.

© 2001 NRC Canada

the amido and ester carbonyl groups.[3] To determine if ($S_{C\alpha}$)-**3** was the major or minor diastereomer, the crystal used for one of the two structure determinations was dissolved at –78°C in CD_2Cl_2. The ^1H NMR spectrum revealed a 95:5 (major:minor) mixture of the diastereomers of **3** within the crystal.[4] These X-ray and NMR data show that the major diastereomer of **3** formed by reaction of MAA and **2** is ($S_{C\alpha}$)-**3**. As stated above, use of MAC results in almost exclusive formation of this diastereomer (($S_{C\alpha}$)-**4**).[5]

Crystals of the minor diastereomer suitable for X-ray diffraction could not be obtained. In an attempt to confirm that it was ($R_{C\alpha}$)-**3**, we effected the protolytic cleavage of the Ru–Cα bond with $HBF_4{\cdot}Et_2O$ in CH_2Cl_2 solution. Addition of 2 equiv $HBF_4{\cdot}Et_2O$ to a solution of **3** (72:28) in CH_2Cl_2 at room temperature followed by addition of excess MeCN (9.5 equiv) generates *N*-acetylalanine methyl ester ($MAA(H)_2$) and the known dicationic compound [Ru((*R*)-BINAP)$(MeCN)_4$]$(BF_4)_2$ (8). Protonolysis with retention of configuration at Cα of the mixture of ($S_{C\alpha}$)-**3** and ($R_{C\alpha}$)-**3** (72:28) will generate $MAA(H)_2$ in 44% (*R*) enantiomeric excess (ee) (72% (*R*)-$MAA(H)_2$ and 28% (*S*)-$MAA(H)_2$). The ee of the $MAA(H)_2$ isolated from the protonolysis was 44% (*S*); the protonolysis of the Ru–C bond in **3** occurred with apparent inversion of configuration at carbon.[6] This experiment was repeated twice.

Two control experiments showed that ($S_{C\alpha}$)-**3** and ($R_{C\alpha}$)-**3** do not interconvert in the absence of acid under these conditions. First, the compositions of 72:28 and 95:5 mixtures of these diastereomers did not change over several days in CH_2Cl_2 at room temperature. Second, exposure of **3** to D_2 (1 atm, 1 atm = 101.325 kPa) at room temperature does not result in H–D exchange at Cβ (Ru-Cα-C*H*$_3$). We previously showed that formation of the MAC analogue (($S_{C\alpha}$)-**4**) is reversible under these conditions using a similar experiment (6*b*). Specifically, exposure of ($S_{C\alpha}$)-**4** to D_2 (1 atm) resulted in H–D exchange at Cβ of MAC(H) (Ru-Cα-C*H*$_2$Ph) via β-hydride elimination and subsequent H–D exchange at the ruthenium-hydride. Thus, conversion between ($S_{C\alpha}$)-**3** and ($R_{C\alpha}$)-**3** did not occur to an appreciable extent prior to reaction with acid.

There is the possibility that reaction of **3** with $HBF_4{\cdot}Et_2O$ generated dicationic diastereomeric ruthenium(IV)–hydrido-alkyl complexes ($S_{C\alpha}$)-**3′** and ($R_{C\alpha}$)-**3′** by protonation at the ruthenium centre. These dicationic diastereomers could in principle interconvert via β-H elimination from the methyl group before elimination of $MAA(H)_2$. To investigate this possibility, we prepared **3**-d_1 (in which one β-H of Ru-Cα-C*H*$_3$ was replaced by deuterium, prepared by reaction of **2**-d_1 with MAA) and reacted it with 2 equiv $HBF_4{\cdot}Et_2O$. After treatment with MeCN and purification, the recovered $MAA(H)_2$ consisted of $MAA(H)_2$-β-d_1 as the sole isotopomer. β-H elimination at the methyl group of **3′**, face flip of the coordinated olefin, and olefin–hydride insertion is expected to cause some scrambling of deuterium between the α- and β-positions of $MAA(H)_2$. The absence of any such scrambling shows that if the dicationic diastereomers ($S_{C\alpha}$)-**3′** and ($R_{C\alpha}$)-**3′** do form, they do not interconvert via β-H elimination from the methyl group.

Although these experiments indicated that protonolysis of the ruthenium–carbon bonds in ($S_{C\alpha}$)-**3** and ($R_{C\alpha}$)-**3** proceeded by inversion, protonation of a sample enriched in ($S_{C\alpha}$)-**3** (95:5) using 2 equiv $HBF_4{\cdot}Et_2O$ yielded, after treatment with MeCN and purification, $MAA(H)_2$ in 44% ee (*S*). This is the same ee as that obtained from the 72:28 mixture of ($S_{C\alpha}$)-**3** and ($R_{C\alpha}$)-**3**, respectively, and it shows that the protonolysis is not stereospecific. This result is confirmed by protonolysis of ($S_{C\alpha}$)-**4**-d_1, the MAC derivative of ($S_{C\alpha}$)-**3**-d_1 (where one β-H of Ru-Cα-C*H*$_2$Ph was replaced by deuterium), prepared by reaction of **2**-d_1 with MAC (6*a*). Reaction of ($S_{C\alpha}$)-**4**-d_1 with 2 equiv $HBF_4{\cdot}Et_2O$ yielded, after treatment with MeCN and purification, $MAC(H)_2$-β-d_1 as the sole isotopomer in 12% ee (*R*). Thus, protonolysis of the ruthenium–carbon bond in ($S_{C\alpha}$)-**4**-d_1 is also not stereospecific, and it too does not involve β-H elimination from the benzyl group.

Conclusions

Our previous report of the MAC compound ($S_{C\alpha}$)-**4** was the first solid-state structure of a diastereomeric catalyst–substrate complex of the same absolute configuration as the major product enantiomer of an olefin hydrogenation. This report of the MAA compound ($S_{C\alpha}$)-**3** is the second; as such, it adds to the sparse knowledge base of the structures of these diastereomeric putative catalytic intermediates. Reaction of MAC with **2** favours almost exclusive formation of

[3] Selected bond lengths (Å) and angles (°) with estimated standard deviations for ($S_{C\alpha}$)-**3** are as follows: Ru(1)—N(2) 1.995(4), Ru(1)—P(1) 2.3525(13), Ru(1)—P(2) 2.2640(11), Ru(1)—O(1) 2.072(3), Ru(1)—O(2) 2.278(3), Ru(1)—C(3) 2.230(5), Ru(1)—C(5) 2.345(5), C(3)—C(4) 1.515(7) Å; C(5)-C(3)-C(4) 119.1(4), N(1)-C(3)-C(5) 112.1(4), N(1)-C(3)-C(4) 111.4(4), Ru(1)-C(3)-N(1) 101.4(4), Ru(1)-C(3)-C(4) 132.0(3), Ru(1)-C(3)-C(5) 76.1(3)°.

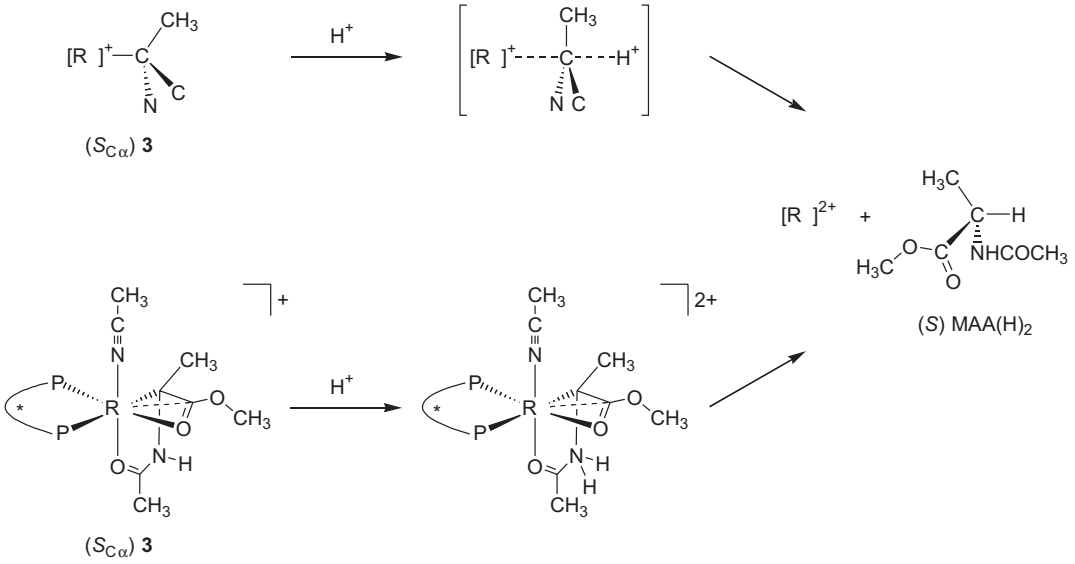
[4] We both dissolved the crystal and analyzed the resulting solution at low temperature to prevent any diastereomeric interconversion that may occur. This precaution was not necessary as ^{31}P NMR spectroscopic analysis of **3** (72:28 and 95:5 (major:minor) diastereomeric ratios) in acetone-d_6 over a range of temperatures from –80 to +25°C showed the ratios of diastereomers did not vary under these conditions. The 95:5 ratio observed in the crystal analyzed by X-ray diffraction was the same ratio found for the entire crop of crystals (bulk sample).

[5] As we reported previously, only ($S_{C\alpha}$)-**4** is observed in NMR spectra recorded at room temperature. Subsequent spectra recorded at low temperature show the presence (8%) of the other fluctional diastereomer, ($R_{C\alpha}$)-**4**. Selected NMR data (CD_2Cl_2, –40°C) for ($S_{C\alpha}$)-**4** and ($R_{C\alpha}$)-**4** (the asterisks denote resonances attributed to the minor diastereomer (($R_{C\alpha}$)-**4**): $^{13}C\{H\}$ NMR (100.6 MHz) δ: 36.1 (s, Ph*C*H$_2$CRu*), 37.8 (s, Ph*C*H$_2$CRu), 66.9 (dd, $^2J_{P(B),C}$ = 42.0 Hz, $^2J_{P(A),C}$ = 3.5 Hz, Ru*C*), 70.0 (dd, $^2J_{P(B'),C}$ = 42.0 Hz, $^2J_{P(A'),C}$ = 3.5 Hz, Ru*C**), 157.9 (br s, *C*O$_2$CH$_3$*), 159.7 (d, $J_{P(B),C}$ = 3.0 Hz, *C*O$_2$CH$_3$), 179.6 (d, $J_{P(B),C}$ = 7.0 Hz, NH*C*OCH$_3$), 179.9 (d, $J_{P(B'),C}$ = 7.0 Hz, NH*C*OCH$_3$*). $^{15}N\{H\}$ NMR INEPT (40.5 MHz) δ: 184.4 (dd, $^2J_{P(A),N}$ = 4.5 Hz, $^2J_{P(B),N}$ = 3.0 Hz, CH$_3$C*N*-Ru). The corresponding ^{15}N resonance for ($R_{C\alpha}$)-**4** was not observed; however, the $^{31}P\{^1H\}$ NMR spectrum of ($R_{C\alpha}$)-**4** prepared using $CH_3C^{15}N$ displayed $^2J_{P(A'),N}$ = 4.5 Hz and $^2J_{P(B'),N}$ = 3.0 Hz. $^{31}P\{H\}$ NMR (161.9 MHz) δ: 32.9 (d, $^2J_{P,P}$ = 23.5 Hz, 1P, P(B)), 40.1 (d, $^2J_{P,P}$ = 24.0 Hz, 1P, P(B′)*), 55.2 (d, $^2J_{P,P}$ = 24.0 Hz, 1P, P(A′)*), 59.4 (d, $^2J_{P,P}$ = 23.5 Hz, 1P, P(A)).

[6] The ee of $MAA(H)_2$ was spectroscopically (^1H NMR) determined using a chiral shift reagent ((+)-Eu(tfc)$_3$) after separation from [Ru((*R*)-BINAP)$(MeCN)_4$]$(BF_4)_2$ by colum chromatography (Florisil–EtOAc). The absolute configuration of the major enantiomer was determined by comparison to authentic (*S*)-$MAA(H)_2$.

© 2001 NRC Canada

Scheme 1.



($S_{C\alpha}$)-**4** as major diastereomer (6). The methyl analogue generated using MAA favours the same absolute configuration as major diastereomer (($S_{C\alpha}$)-**3**), but with a weaker bias (72:28). The protonolysis of these compounds under the described conditions is not stereospecific, and it does not proceed via β-H elimination from the benzyl or methyl groups. Although the lack of observable β-H elimination from the benzyl or methyl groups implies that equilibration of the diastereomers does not occur during the protonolysis, such equilibration may still occur via protonation at the amido nitrogen followed by β-H elimination to form an iminium. These experiments and labeling studies are moot on this point because of rapid proton exchange between the amido group and $HBF_4{\cdot}Et_2O$.

Another explanation for this lack of stereospecificity is that two pathways operate in parallel for the protonolysis. One pathway, resulting in retention at carbon, is protonation at ruthenium followed by elimination of alkane. We note that although there are few examples, all reported electrophilic abstractions of alkyl or vinyl ligands from early or late transition-metal centres by protonolysis occur with retention of configuration at carbon (9). The other pathway, resulting in inversion at carbon, is electrophilic attack at the back side of the Ru–C σ-bond (Scheme 1). Such a possibility has been suggested to account for inversion of configuration at carbon for alkyl abstraction from zirconium complexes by boranes (10), and as discussed in the introduction, for the observed net *anti*-addition of H_2 in certain hydrogenations of olefins (5).

Another explanation for this lack of stereospecificity is prior protonation of a substrate lone pair followed by intramolecular proton transfer. Similar processes have been reported in the literature (cleavage of a Fe–C σ-bond via protonation at nitrogen has been observed, see ref. 11). Scheme 1 shows such a pathway involving protonation of the amido group of MAA(H), followed by a suprafacial intramolecular proton delivery to C(3) with inversion of stereochemistry (intramolecular proton delivery and its role in the reversal of stereochemistry has appeared in the literature, see ref. 12).

Further experimentation (such as low-temperature NMR studies) is required to investigate the stereochemical course of these protonation reactions and their relevance to catalytic hydrogenation of olefins. These results do show, however, that protonolysis of a catalyst–carbon bond is a complicated process, one that should not be assumed a priori to proceed with strict retention.

Experimental

General considerations

All reactions were conducted under an atmosphere of dry Ar (Praxair, 99.998%) using standard Schlenk and glovebox techniques. NMR spectra were recorded using a Bruker AM-400 (^1H at 400.1 MHz, ^2H at 61.4 MHz, ^{13}C at 100.6 MHz, ^{15}N at 40.5 MHz, and ^{31}P at 161.9 MHz) spectrometer. The chemical shifts for ^1H, ^2H, and ^{13}C are reported in parts per million (δ) relative to external TMS and were referenced to residual solvent signals. The chemical shifts for ^{15}N and ^{31}P are reported in parts per million (δ) relative to external liquid NH_3 and external 85% H_3PO_4, respectively. NMR abbreviations used: broad (br), singlet (s), doublet (d), doublet of doublets (dd), doublet of doublet of doublets (ddd), triplet (t), quartet (q), doublet of quartets (dq), doublet of triplets (dt), and multiplet (m). Electron-impact high-resolution mass spectrometry (EI-HRMS) of *N*-acetylalanine methyl ester ($MAA(H)_2$) was performed on a Kratos MS50 spectrometer. Mass spectrometric analysis of **3** (MeCN solution) was performed on a Micromass ZabSpec Hybrid Sector-TOF spectrometer using positive-mode electrospray ionization (ESI-MS (pos)). Calculated *m*/*z* values refer to the isotopes ^{12}C, ^1H, ^{14}N, ^{16}O, ^{31}P, and ^{102}Ru. Microanalyses were performed at the University of Alberta Microanalysis Laboratory.

© 2001 NRC Canada

Materials

Argon gas (Praxair, 99.998%) was dried by passage through a column containing 3 Å molecular sieves and phosphorus pentoxide before use. Dihydrogen gas (Praxair, 99.99%) was passed through an Alltech Oxy-Trap to remove trace amounts of oxygen before use. Dideuterium gas (Aldrich, 99.8%; Praxair, 99.7%) was used as received. All protiated solvents (Anachemia, Caledon, and Fisher Scientific) and deuterated solvents (99.5–99.9% D, Cambridge Isotope Laboratories) were distilled from appropriate drying agents (13) under an atmosphere of argon gas before use except absolute ethanol (200 proof), which was used as received. Unless stated otherwise, all reagents were used as received from Aldrich. [Ru((*R*)-BINAP)(H)(MeCN)$_n$(acetone)$_{3-n}$](BF$_4$) (where n = 0–3) (**2**), **2**-d_1, methyl α-acetamidoacrylate (MAC), [Ru((*R*)-BINAP)(MeCN)((*S*)-MAC(H))](BF$_4$) (($S_{C\alpha}$)-**4** and ($S_{C\alpha}$)-**4**-d_1) were prepared as described previously (6). The ee and absolute configuration of the MAC(H)$_2$-β-d_1 generated from protonolysis of ($S_{C\alpha}$)-**4**-d_1 was determined as described previously (6). Methyl α-acetamidoacrylate (MAA) was purified by column chromatography on neutral alumina (acetone) before use. (*rac*)-MAA(H)$_2$ and (*S*)-MAA(H)$_2$ were prepared by the esterification of (*rac*)-*N*-acetylalanine and (*S*)-*N*-acetylalanine, respectively, using diazomethane (14).

Syntheses

All glassware and syringes were successively treated with ethanolic ammonium hydroxide solution, acetone, and oven-dried before use. Organometallic products were isolated in a glovebox filled with dinitrogen gas and were stored at –30°C for prolonged periods.

3 *and* **3**-d_1

[Ru((*R*)-BINAP)(1–3;5,6-η-C$_8$H$_{11}$)(MeCN)](BF$_4$) (6) (323.9 mg, 0.338 mmol) was partially dissolved in acetone (15.0 mL) under an atmosphere of Ar and subjected to 3 freeze-pump-thaw cycles. The reactor was backfilled with H$_2$ (20 psig, 1 psig = 6.894 kPa) at room temperature and vigorously shaken for 10 min. The resulting orange solution was subjected to 3 freeze-pump-thaw cycles and backfilled with Ar. To this solution at room temperature was added an acetone solution (5.0 mL) of MAA (48.3 mg, 0.338 mmol). The resulting amber solution was shaken for 1 min and the solvent was removed under reduced pressure to give a yellow solid. Dropwise addition of Et$_2$O (80 mL) to a CH$_2$Cl$_2$ (2.0 mL) solution of the product afforded a yellow powder. The product was collected by filtration and washed with Et$_2$O (3 × 10 mL) to yield 310.7 mg (92%) of **3**. NMR spectroscopic analysis showed that the product contained a diastereomeric mixture of ($S_{C\alpha}$)-**3** and ($R_{C\alpha}$)-**3** (72:28). An in situ reaction monitored by NMR spectroscopy displayed the same ratio of diastereomers. The method used for the preparation of **3**-d_1 was the same as that for **3** with substitution of D$_2$ for H$_2$. ESI-MS (pos) *m*/*z*: 909.2 ([M – BF$_4$]$^+$) (exact mass calcd. for C$_{52}$H$_{45}$N$_2$O$_3$P$_2$Ru, 909.2). NMR spectroscopic data for **3** (the asterisks denote resonances attributed to the minor diastereomer (($R_{C\alpha}$)-**3**): ^{1}H NMR (400.1 MHz, (CD$_3$)$_2$CO, 25°C) δ: 1.17 (d, $^4J_{P,H}$ = 5.0 Hz, 3H, RuC-C*H*$_3$*), 1.61 (d, $^4J_{P,H}$ = 5.0 Hz, 3H, RuC-C*H*$_3$), 1.83 (s, 3H, C*H*$_3$CN), 1.92 (s, 3H, C*H*$_3$CN*), 2.04 (s, 3H, NHCOC*H*$_3$), 2.17 (s, 3H, NHCOC*H*$_3$*), 3.77 (s, 3H, CO$_2$C*H*$_3$*), 3.85 (s, 3H, CO$_2$C*H*$_3$), 6.4–8.1 (aromatic), 8.38 (br s, 1H, N*H*COCH$_3$), 9.02 (br s, 1H, N*H*COCH$_3$*). ^{1}H NMR (400.1 MHz, (CD$_3$)$_2$CO, –40°C) δ: 0.99 (d, $^4J_{P,H}$ = 5.0 Hz, 3H, RuC-C*H*$_3$*), 1.55 (d, $^4J_{P,H}$ = 5.0 Hz, 3H, RuC-C*H*$_3$), 1.84 (s, 3H, C*H*$_3$CN), 1.89 (s, 3H, C*H*$_3$CN*), 2.03 (s, 3H, NHCOC*H*$_3$), 2.17 (s, 3H, NHCOC*H*$_3$*), 3.74 (s, 3H, CO$_2$C*H*$_3$*), 3.82 (s, 3H, CO$_2$C*H*$_3$), 6.4–8.1 (aromatic), 8.69 (br s, 1H, N*H*COCH$_3$), 9.28 (br s, 1H, N*H*COCH$_3$*). ^{13}C{^{1}H} NMR (100.6 MHz, CD$_2$Cl$_2$, 25°C) δ: 4.2 (s, *C*H$_3$CN-Ru*), 4.5 (s, *C*H$_3$CN-Ru), 17.4 (br s, RuC-*C*H$_3$*), 18.8 (s, RuC-*C*H$_3$), 19.7 (s, NHCO*C*H$_3$*), 20.4 (s, NHCO*C*H$_3$), 52.6 (s, CO$_2$*C*H$_3$*), 52.9 (s, CO$_2$*C*H$_3$), 63.3 (dd, $^2J_{P,C(trans)}$ = 44.0 Hz, $^2J_{P,C(cis)}$ = 4.0 Hz, Ru*C*), 66.4 (br d, $^2J_{P,C(trans)}$ = 43.0 Hz, Ru*C**), 126–142 (overlapping aromatic and CH$_3$*C*N), 161.5 (d, $J_{P,C}$ = 3.0 Hz, overlapping ($S_{C\alpha}$)-**3** and ($R_{C\alpha}$)-**3**, *C*O$_2$CH$_3$), 179.3 (d, $J_{P,C}$ = 7.0 Hz, NH*C*OCH$_3$), 179.9 (d, $J_{P,C}$ = 7.0 Hz, NH*C*OCH$_3$*). ^{13}C{^{1}H} NMR (100.6 MHz, CD$_2$Cl$_2$, –40°C) δ: 4.1 (s, *C*H$_3$CN-Ru*), 4.3 (s, *C*H$_3$CN-Ru), 16.9 (s, RuC-*C*H$_3$*), 18.2 (s, RuC-*C*H$_3$), 19.5 (s, NHCO*C*H$_3$*), 20.1 (s, NHCO*C*H$_3$), 52.4 (s, CO$_2$*C*H$_3$*), 52.6 (s, CO$_2$*C*H$_3$), 63.0 (dd, $^2J_{P,C(trans)}$ = 43.5 Hz, $^2J_{P,C(cis)}$ = 4.0 Hz, Ru*C*), 66.8 (dd, $^2J_{P,C(trans)}$ = 44.5 Hz, $^2J_{P,C(cis)}$ = 3.0 Hz Ru*C**), 124–141 (overlapping aromatic and CH$_3$*C*N), 159.1 (s, *C*O$_2$CH$_3$*), 160.1 (s, *C*O$_2$CH$_3$), 178.6 (d, $J_{P,C}$ = 7.0 Hz, NH*C*OCH$_3$), 179.1 (d, $J_{P,C}$ = 6.5 Hz, NH*C*OCH$_3$*). ^{15}N NMR INEPT (40.5 MHz, (CD$_3$)$_2$CO, 25°C) δ: 183.1 (dd, $^2J_{P(A),N}$ = 4.5 Hz, $^2J_{P(B),N}$ = 3.0 Hz, CH$_3$C*N*-Ru), 184.8 (dd, $^2J_{P(A),N}$ = 4.0 Hz, $^2J_{P(B),N}$ = 3.0 Hz, CH$_3$C*N*-Ru*). ^{15}N NMR INEPT (40.5 MHz, (CD$_3$)$_2$CO, –40°C) δ: 181.9 (br apparent t, $^2J_{P(A),N}$ = $^2J_{P(B),N}$ = 3.5 Hz, CH$_3$C*N*-Ru), 183.5 (br, CH$_3$C*N*-Ru*). ^{31}P{^{1}H} NMR (161.9 MHz, (CD$_3$)$_2$CO, 25°C) δ: 33.8 (d, $^2J_{P,P}$ = 22.0 Hz, 1P, P(B)), 38.8 (br d, $^2J_{P,P}$ = 21.0 Hz, 1P, P(B′)*), 58.5 (br d, $^2J_{P,P}$ = 21.0 Hz, 1P, P(A′)*), 59.7 (d, $^2J_{P,P}$ = 22.0 Hz, 1P, P(A)). ^{31}P{^{1}H} NMR (161.9 MHz, (CD$_3$)$_2$CO, –40°C) δ: 33.4 (d, $^2J_{P,P}$ = 23.0 Hz, 1P, P(B)), 38.7 (d, $^2J_{P,P}$ = 22.0 Hz, 1P, P(B′)*), 57.1 (d, $^2J_{P,P}$ = 22.0 Hz, 1P, P(A′)*), 59.4 (d, $^2J_{P,P}$ = 23.0 Hz, 1P, P(A)). Anal. calcd. for C$_{52}$H$_{45}$BF$_4$N$_2$O$_3$P$_2$Ru: C 62.72, H 4.56, N 2.81; found: C 62.35, H 4.88, N 2.64.

Protonations of **3** *and* **3**-d_1

To a stirred solution of ($S_{C\alpha}$)-**3** and ($R_{C\alpha}$)-**3** (72:28) (101.0 mg, 0.101 mmol) in CD$_2$Cl$_2$ (0.50 mL) at room temperature was added a solution of HBF$_4$·Et$_2$O (54% w/w in Et$_2$O, 28.0 μL, 0.203 mmol). The originally orange colored solution immediately turned red in color upon addition of HBF$_4$·Et$_2$O. After stirring for 15 min, CD$_3$CN (50.0 μL, 0.957 mmol) was added to the reaction mixture to generate a yellow colored solution. Analysis of the reaction mixture by ^{1}H and ^{31}P NMR spectroscopy indicated that exclusive formation of MAA(H)$_2$ and [Ru((*R*)-BINAP)(CD$_3$CN)$_4$](BF$_4$)$_2$ occurred. The solution was evaporated to dryness and the residue was thoroughly washed with EtOAc (3 × 5 mL) and the wash was passed through a column of Florisil™ (0.5 cm × 7.0 cm). The clear, colorless eluent was evaporated to dryness to give pure MAA(H)$_2$. Protonation of **3**-d_1 exclusively liberated MAA(H)$_2$-β-d_1, as determined by ^{1}H and ^{2}H NMR spectroscopy (^{1}H NMR (400.1 MHz, CDCl$_3$, 25°C) δ: 1.39 (dt, $^3J_{H,H}$ = 7.0 Hz, $^3J_{H,D}$ = 2.0 Hz, 2H, CHC*H*$_2$D (Hβ)), 2.02 (s, 3H, NHCOC*H*$_3$), 3.76 (s, 3H,

© 2001 NRC Canada

CO_2CH_3), 4.60 (apparent q, $^3J_{H,H}$ = 7.0 Hz, 1H, C*H*CH_2D (Hα)), 6.05 (br s, 1H, N*H*$COCH_3$). $^2H\{^1H\}$ NMR (61.4 MHz, $CHCl_3$, 25°C) δ: 1.39 (s, $CHCH_2D$)). The enantiomeric excess (ee) and absolute configuration (44% (*S*)) of purified $MAA(H)_2$ and $MAA(H)_2$-β-d_1 were determined as follows. The ee was spectroscopically determined (^1H NMR) using a chiral lanthanide shift reagent (europium tris[3-(trifluoromethylhydroxymethylene)-(+)-camphorate] ((+)-Eu(tfc)$_3$)) in $CDCl_3$. Sufficient shift reagent was added (0.2–0.4 equiv) to separate the methoxy signals (ca. 4 ppm) of the two enantiomers of $MAA(H)_2$ (low-field enantiomer (*R*), high-field enantiomer (*S*)). That these were signals of the enantiomers of $MAA(H)_2$ was confirmed by repeating the experiment using (*rac*)-$MAA(H)_2$. The ratio of these methoxy signals was used to quantify the ee. The absolute configuration of the major enantiomer of the product was determined by addition of authentic (*S*)-$MAA(H)_2$ to the samples and subsequently determining the ee via NMR spectroscopy as described above. Addition of (*S*)-$MAA(H)_2$ caused the intensity of the high-field ((*S*)-enantiomer) methoxy signal to increase.

Deuteriolysis of **3**

In a 5-mm NMR tube, ($S_{C\alpha}$)-**3** and ($R_{C\alpha}$)-**3** (72:28) (10.3 mg, 0.0103 mmol) were dissolved in CD_2Cl_2 (0.50 mL) at room temperature under Ar. The headspace of the NMR tube was thoroughly purged with D_2 and the tube was vigorously shaken. Monitoring the reaction over a 30-min period by ^1H NMR spectroscopy showed the generation of $MAA(H)_2$-α-d_1 (10%) and no detectable incorporation of deuterium in the two diastereomers of **3** (($S_{C\alpha}$)-**3** and ($R_{C\alpha}$)-**3**).

Crystal structure determination of ($S_{C\alpha}$)-3

Slow liquid-liquid diffusion of di-*n*-butyl ether into a 1,2-dimethoxyethane solution of **3** (72:28) at room temperature produced X-ray quality crystals. The structure was determined as described in the supplementary material.[7] Crystal data for ($S_{C\alpha}$)-**3**: $C_{52}H_{45}BF_4N_2O_3P_2Ru$, FW = 995.72, yellow plate, crystal size 0.40 × 0.25 × 0.13 mm, orthorhombic, $C222_1$, a = 21.4849(2), b = 29.7175(2), and c = 18.8513(2) Å, V = 12036.1(2) Å^3, Z = 8, $\rho_{calcd.}$ = 1.099 g cm^{-3}, μ (Mo Kα) = 0.361 mm^{-1}, T = 173(2) K, λ (Mo Kα) = 0.71073 Å. Data were collected using a Siemens SMART Platform CCD diffractometer (θ range for data collection of 1.17–25.04°); 10589 independent reflections (8758 with $F_o^2 > 2\sigma(F_o^2)$) were measured. The structure was solved via direct methods (SHELXTL-V5.0). Full-matrix least-squares refinement on F^2 (SHELXTL-V5.0) yielded R_1 = 0.0480 ($F_o^2 > 2\sigma(F_o^2)$) and wR_2 = 0.1261 (all data). GoF on F^2 = 1.041. Selected bond lengths (Å) and angles (°) with estimated standard deviations for ($S_{C\alpha}$)-**3** are as follows: Ru(1)—N(2) 1.995(4), Ru(1)—P(1) 2.3525(13), Ru(1)—P(2) 2.2640(11), Ru(1)—O(1) 2.072(3), Ru(1)—O(2) 2.278(3), Ru(1)—C(3) 2.230(5), Ru(1)—C(5) 2.345(5), C(3)—C(4) 1.515(7) Å; C(5)-C(3)-C(4) 119.1(4), N(1)-C(3)-C(5) 112.1(4), N(1)-C(3)-C(4) 111.4(4), Ru(1)-C(3)-N(1)101.4(3), Ru(1)-C(3)-C(4) 132.0(3), Ru(1)-C(3)-C(5)76.1(3)°.

Acknowledgments

We sincerely appreciate the technical support and helpful discussions provided by Mr. G. Bigam, Mrs. G. Aarts, and Dr. T. Nakashima of the University of Alberta High Field NMR Laboratory. We also thank the Natural Sciences and Engineering Research Council of Canada (NSERC) and the University of Alberta for financial support.

References

1. J. Halpern, J.F. Harrod, and B.R. James. J. Am. Chem. Soc. **83**, 753 (1961).
2. (*a*) B.R. James, D.K.W. Wang, and R. Voigt. J. Chem. Soc. Chem. Comm. 574 (1975); (*b*) B.R. James, A. Pacheco, S.J. Rettig, I.S. Thorburn, R.G. Ball, and J.A. Ibers. J. Mol. Catal. **41**, 147 (1987).
3. (*a*) L.R. Dinelli, A.A. Batista, K. Wohnrath, M.P. de Araujo, S.L. Queiroz, M.R. Bonfadini, G. Oliva, O.R. Nascimento, P.W. Cyr, K.S. McFarlane, and B.R. James. Inorg. Chem. **38**, 5341 (1999); (*b*) N.D. Jones, K.S. MacFarlane, M.B. Smith, R.P. Schutte, S.J. Rettig, and B.R. James. Inorg. Chem. **38**, 3956 (1999); (*c*) N.D. Jones, K.S. MacFarlane, M.B. Smith, R.P. Schutte, S.J. Rettig, and B.R. James. Inorg. Chem. **38**, 3956 (1999); (*d*) K.S. MacFarlane, S.J. Rettig, Z. Liu, and B.R. James. J. Organomet. Chem. **557**, 213 (1998); (*e*) K.S. MacFarlane, I.S. Thorburn, P.W. Cyr, E.K.-Y. Chau, S.J. Rettig, and B.R. James. Inorg. Chim. Acta, **270**, 130 (1998); (*f*) S.L. Queiroz, A.A. Batista, G. Oliva, M.T.D.P. Gambardell, R.H.A. Santos, K.S. McFarlane, S.J. Rettig, and B.R. James. Inorg. Chim. Acta, **267**, 209 (1998); (*g*) B.R. James. Catal. Today, **37**, 209 (1997); (*h*) D.E. Fogg and B.R. James. Inorg. Chem. **36**, 1961 (1997); (*i*) K.S. MacFarlane, A.M. Joshi, S.J. Rettig, and B.R. James. Inorg. Chem. **35**, 7304 (1996); (*j*) D.E.K.Y. Chau and B.R. James. Inorg. Chim. Acta, **240**, 419 (1995); (*k*) D.E. Fogg, S.J. Rettig, and B.R. James. Can. J. Chem. **73**, 1084 (1995); (*l*) D.E. Fogg and B.R. James. Inorg. Chem. **34**, 2557 (1995); (*m*) A.A. Batista, E.A. Polato, S.L. Queiroz, O.R. Nascimento, B.R. James, and S.J. Rettig. Inorg. Chim. Acta, **230**, 111 (1995); (*n*) A.M. Joshi, K.S. MacFarlane, and B.R. James. J. Organomet. Chem. **488**, 161 (1995); (*o*) D.E. Fogg, B.R. James, and M. Kilner. Inorg. Chim. Acta, **222**, 85 (1994); (*p*) A.M. Joshi, I.S. Thorburn, S.J. Rettig, and B.R. James. Inorg. Chim. Acta, **200**, 283 (1992); (*q*) T.W. Dekleva, A.M. Joshi, I.S. Thorburn, B.R. James, S.V. Evans, and J. Trotter. Israel J. Chem. **30**, 343 (1990); (*r*) A.M. Joshi and B.R. James. J. Chem. Soc. Chem. Comm. **22**, 1785 (1989); (*s*) C. Hampton, W.R. Cullen, B.R. James, and J.-P. Charlan. J. Am. Chem. Soc. **110**, 6918 (1988); (*t*) C. Hampton, T.W. Dekleva, B.R. James, and W.R. Cullen. Inorg. Chim. Acta, **145**, 165 (1988); (*u*) I.S. Thorburn, S.J. Rettig, and B.R. James. Inorg. Chem. **25**, 234 (1986); (*v*) B.R. James and D.K.W. Wang. Can. J. Chem.

[7] Supplementary material may be purchased from the Depository of Unpublished Data, Document Delivery, CISTI, National Research Council Canada, Ottawa, ON K1A 0S2, Canada. For information on obtaining material electronically go to http://www.nrc.ca/cisti/irm/unpub_e.shtml. Crystallographic information has also been deposited with the Cambridge Crystallographic Data Centre. Copies of the data can be obtained, free of charge, on application to the Director, CCDC, 12 Union Road, Cambridge CB2 1EZ, U.K. (fax: 44-1223-336033 or e-mail: deposit@ccdc.cam.ac.uk).

© 2001 NRC Canada

58, 245 (1980); (*w*) B.R. James and D.K.W. Wang. Inorg. Chim. Acta, **19**, L17 (1976) and refs. cited therein.
4. (*a*) M.T. Ashby and J. Halpern. J. Am. Chem. Soc. **113**, 589 (1991); (*b*) T. Ohta, H. Takaya, and R. Noyori. Tetrahedron Lett. **31**, 7189 (1990). Subsequent mechanistic investigations of α,β-unsaturated carboxylic acids have appeared: (*c*) M. Shaharuzzaman, J. Braddock-Wilking, J.S. Chickos, C.N. Tam, R.A.G.D. Silva, and T.A. Keiderling. Tetrahedron: Asymmetry, **9**, 1111 (1998); (*d*) C.-C. Chen, T.-T. Huang, C.-W. Lin, C. Rong, A.C.S. Chan, and W.T. Wong. Inorg. Chim. Acta, **270**, 247 (1998); (*e*) A.C.S. Chan, C.C. Chen, T.K. Yang, J.H. Huang, and Y.C. Lin. Inorg. Chim. Acta, **234**, 95 (1995); (*f*) J.M. Brown, M. Rose, F.I. Knight, and A. Wienand. Recl. Trav. Chim. Pays-Bas. **114**, 242 (1995); (*g*) J.M. Brown. Chem. Soc. Rev. 25 (1993); (*h*) M. Saburi, H. Takeuchi, M. Ogasawara, T. Tsukahara, Y. Ishii, T. Ikariya, T. Takahashi, and Y. Uchida. J. Organomet. Chem. **428**, 155 (1992).
5. F. van Rantwijk and H. van Bekkum. J. Mol. Catal. **1**, 383 (1975/76) and refs. cited therein.
6. (*a*) J.A. Wiles and S.H. Bergens. Organometallics, **18**, 3709 (1999); (*b*) J.A. Wiles and S.H. Bergens. Organometallics, **17**, 2228 (1998); (*c*) J.A. Wiles, S.H. Bergens, and V.G. Young. J. Am. Chem. Soc. **119**, 2940 (1997).
7. *a*) D. Mani, H.-T. Schacht, A.K. Powell, and H. Vahrenkamp. Chem. Ber. **122**, 2245 (1989); (*b*) D. Mani, H.-T. Schacht, A.K. Powell, and H. Vahrenkamp. Organometallics, **6**, 1360 (1987). Structures of other α-metallated amino acids have been reported: (*c*) B. Kayser, C. Missling, J. Knizek, H. Nöth, and W. Beck. Eur. J. Inorg. Chem. 375 (1998); (*d*) B. Kayser, H. Nöth, M. Schmidt, W. Steglich, and W. Beck. Chem. Ber. **129**, 1617 (1996).
8. K. Mashima, T. Hino, and H. Takaya. J. Chem. Soc. Dalton Trans. 2099 (1992).
9. (*a*) E.J. O'Connor, M. Kobayashi, H.G. Floss, and J.A. Gladysz. J. Am. Chem. Soc. **109**, 837 (1987); (*b*) W.N. Rogers and M.C. Baird. J. Organomet. Chem. **182**, C65 (1979); (*c*) M.D. Fryzuk and B. Bosnich. J. Am. Chem. Soc. **101**, 3043 (1979); (*d*) S. Komiya, T. Ito, M. Cowie, A. Yamamoto, and J.A. Ibers. J. Am. Chem. Soc. **98**, 3874 (1976); (*e*) J. Schwartz and J.A. Labinger. Angew. Chem. Int. Ed. Eng. **15**, 333 (1976); (*f*) M.P. Periasamy and H.M. Walborsky. J. Am. Chem. Soc. **97**, 5930 (1975); (*g*) J.A. Labinger, D.W. Hart, W.E. Seibert III, and J. Schwartz. J. Am. Chem. Soc. **97**, 3851 (1975); (*h*) J.F. Normant, G. Cahiez, C. Chuit, and J. Villieras. J. Organomet. Chem. **77**, 269 (1974); (*i*) B.E. Mann, B.L. Shaw, and N. Tucker. J. Chem. Soc. Chem. Commun. 1333 (1970).
10. (*a*) R.E.V.H. Spence, W.E. Piers, Y. Sun, M. Parvez, L.R. MacGillivray, and M.J. Zaworotko. Organometallics, **17**, 2459 (1998); (*b*) X. Yang, C.L. Stern, and T.J. Marks. J. Am. Chem. Soc. **116**, 10015 (1994).
11. Y.-R. Hu, T.W. Leung, S.-C. H. Su, A. Wojcicki, M. Calligaris, and G. Nardin. Organometallics, **4**, 1001 (1985).
12. H.E. Zimmerman and A. Ignatchenko. J. Am. Chem. Soc. **120**, 12992 (1998).
13. (*a*) J. Leonard, B. Lygo, and G. Procter. Advanced practical organic chemistry. 2nd ed. Chapman & Hall, London. 1995; (*b*) Experimental organometallic chemistry: a practicum in synthesis and characterization. *Edited by* A.L. Wayda and M.Y. Darensbourg. ACS Symposium Series 357, American Chemical Society, Washington, DC. 1987.
14. (*a*) J. Leonard, B. Lygo, and G. Procter. Advanced practical organic chemistry. 2nd ed. Chapman & Hall, London. 1995. pp. 103–106; (*b*) B.D. Vineyard, W.S. Knowles, M.J. Sabacky, G.L. Bachman, and D.J. Weinkauff. J. Am. Chem. Soc. **99**, 5946 (1977).

© 2001 NRC Canada

Transition metal phthalocyanine and porphyrin complexes as catalysts for the polymerization of alkenes

Gregory S. Long, Benjamin Snedeker, Kyle Bartosh, Michelle L. Werner, and Ayusman Sen

Abstract: Vanadium phthalocyanine and porphyrin complexes, in conjunction with methylaluminoxane (MAO) or $EtAlCl_2$ cocatalyst, have been found to catalyze the homopolymerization of ethene. In addition, the copolymerization of ethene with propene and 1-decene was achieved with the vanadium phthalocyanine complex and MAO. Nickel phthalocyanine complex was also found to catalyze the polymerization of ethene in the presence of MAO. However, only dimerization was observed when $EtAlCl_2$ was used as the cocatalyst.

Key words: phthalocyanine, porphyrin, polymerization, copolymerization, ethene, propene, 1-decene.

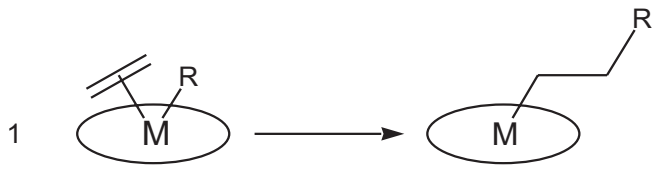
Résumé : On a observé que l'utilisation de complexes de vanadium avec la phtalocyanine et la porphyrine, en association avec du méthylaluminoxane (MAO) ou du $EtAlCl_2$ comme cocatalyseurs, permet de catalyser l'homopolymérisation de l'éthène. De plus, il a été possible de réaliser une copolymérisation de l'éthène avec du propène et du déc-1-éne avec le complexe de vanadium avec la phtalocyanine en présence de MAO. On a aussi observé que, en présence de MAO, le complexe de nickel avec la phtalocyanine catalyse la polymérisation de l'éthène. Toutefois, on n'a observé qu'une dimérisation en présence de $EtAlCl_2$ comme cocatalyseur.

Mots clés : phtalocyanine, porphyrine, polymérisation, copolymérisation, éthène, propène, déc-1-ène.

[Traduit par la Rédaction]

Introduction

The catalytic insertion polymerization and copolymerization of simple alkenes, such as ethene and 1-alkenes, is of intense academic and industrial interest. Highly active alkene polymerization catalysts based on: (*i*) metallocenes derived from early transition metals; and (*ii*) late transition-metal diimine complexes, have been developed. These and related developments in the area have been reviewed recently (1, 2). To our knowledge, similar alkene polymerization catalysts based on metal complexes with flat phthalocyanine and porphyrin ligands have not been reported. Metal-catalyzed alkene polymerization requires the insertion of a precoordinated alkene into a metal—carbon bond *cis* to it and, a priori, it is not clear that that an alkene and an alkyl group can occupy *cis*-coordination positions in metal phthalocyanine and porphyrin complexes (see eq. [1]).



Herein, we demonstrate that metal phthalocyanine and porphyrin complexes can, indeed, be effective catalysts for alkene polymerizations. The metal complexes employed are shown in Fig. 1.

Received September 12, 2000. Published on the NRC Research Press Web site at http://canjchem.nrc.ca on July 19, 2001.

Dedicated to Professor Brian James, a friend.

G.S. Long, B. Snedeker, K. Bartosh, M.L. Werner, and A. Sen.[1] Department of Chemistry, The Pennsylvania State University, University Park, PA 16802, U.S.A.

[1]Corresponding author (telephone: (814) 863-2460; fax: (814) 863-8403; e-mail: asen@chem.psu.edu).

Experimental

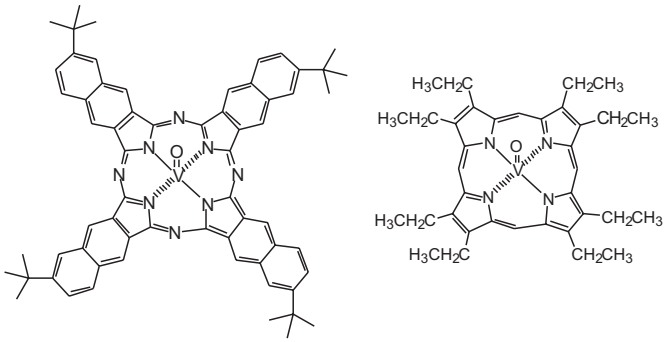
General procedures and materials

All reactions were prepared in an inert atmosphere (N_2) drybox. Polymerizations utilizing ethene were performed in a 125 mL Parr stainless steel autoclave equipped with a glass liner unless otherwise noted. Ambient temperature NMR analyses were performed on a Bruker DPX300 or DRX400 NMR, using $CDCl_3$ as the solvent unless otherwise noted. All high-temperature NMR analyses were performed on a Bruker DPX300 NMR at 120°C in 1,2-dichlorobenzene or 1,1,2,2-tetrachloroethane using d_6-DMSO or d_2-1,1,2,2-tetrachloroethane as lock solvents, respectively.

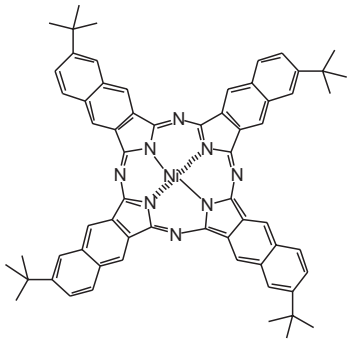
All complexes and reagents were used as supplied from Aldrich Chemical Company. Ethene and propene were used as supplied from MG Industries. Methylaluminoxane (MAO, 30 wt% solution in toluene) was used as supplied from Albemarle Chemicals, Inc. Solvents were dried over CaH_2,

 DOI: 10.1139/cjc-79-5/6-1026 © 2001 NRC Canada

Fig. 1. Structures of phthalocyanine and porphyrin complexes utilized.



(**A**) (**B**)



(**C**)

distilled, and freeze–thaw degassed three times prior to use in the inert atmosphere drybox.

GC analysis for butene was performed on a HP5890 series II gas chromatograph with a J & W Scientific DB-5 column, 30 m × 0.530 mm i.d. and 0.50 μm film thickness, run at 30°C for 10 min.

Synthesis of polyethene using vanadium phthalocyanine and porphyrin compounds A and B

To a glass-lined autoclave was added **A** or **B** (10 μmol), 10 mL chlorobenzene, and either 100 equiv MAO (90 mg of 30 wt% solution in toluene, 1 mmol) or 30 equiv $EtAlCl_2$ (218 mg of 1 M solution in hexanes, 0.3 mmol). The vessel was sealed and pressurized to 700 psi with ethene and stirred at 50°C for 4 h. The vessel was cooled and the remaining ethene pressure was released slowly. Methanol (10 mL) was added to the reaction mixture to quench the remaining reactive aluminum species and precipitate any insoluble product. Solid product was collected by vacuum filtration, washed with 10 mL methanol, and dried in vacuo.

Copolymerization of ethene and propene with vanadyl 2,11,20,29-tetra-*tert*-butyl-2,3-naphthalocyanine (A)

To a glass-lined autoclave was added **A** (10.0 mg, 10 μmol), 10 mL chlorobenzene, and 100 equiv MAO (90 mg of 30 wt% solution in toluene, 1 mmol). The vessel was sealed and charged with 5.2 g propene in an acetone – dry ice cooling bath. The autoclave was subsequently pressurized to 700 psi with ethene and stirred at 120°C for 20 h. The vessel was cooled and the unreacted gaseous monomer mixture was released slowly. Methanol (10 mL) was added to the reaction mixture to quench the remaining reactive aluminum species and precipitate any insoluble product. Product was collected by vacuum filtration, washed with 10 mL methanol, and dried in vacuo to yield 0.58 g rubbery solid.

Copolymerization of ethene and 1-decene with vanadyl 2,11,20,29-tetra-*tert*-butyl-2,3-naphthalocyanine (A)

To a glass-lined autoclave was added **A** (10.0 mg, 10 μmol), 10 mL chlorobenzene, 100 equiv MAO (90 mg of 30 wt% solution in toluene, 1 mmol), and 1 g 1-decene. The vessel was sealed and pressurized to 700 psi with ethene and stirred at 120°C for 20 h. The vessel was cooled and the remaining ethene pressure was released slowly. Methanol (10 mL) was added to the reaction mixture to quench the remaining reactive aluminum species and precipitate any insoluble product. Product was collected by vacuum filtration, washed with 10 mL methanol, and dried in vacuo to yield 3.32 g rubbery solid.

Synthesis of butene using nickel(II) chloride

To a glass-lined autoclave was added nickel(II) chloride (6.5 mg, 50 μmol), 10 mL chlorobenzene, and either 30 equiv $EtAlCl_2$ (1.1 g of 1 M solution in hexenes) or 100 equiv MAO (450 mg of 30 wt% solution in toluene, 5 mmol). The vessel was sealed and pressurized to 700 psi with ethene and stirred at 50°C for 1 h. The vessel was cooled and the gas containing ethene and butene was released slowly, with samples taken for GC analysis. Methanol (10 mL) was added to the reaction mixture to quench the remaining reactive aluminum species. Butene was quantified by GC.

Synthesis of butene and polyethene using nickel(II) 2,11,20,29-tetra-*tert*-butyl-2,3-naphthalocyanine (C)

To a glass-lined autoclave was added **C** (49.8 mg, 50 μmol), 10 mL chlorobenzene, and either 30 equiv $EtAlCl_2$ (1.1 g of 1 M solution in hexanes) or 100 equiv MAO (450 mg of 30 wt% solution in toluene, 5 mmol). The vessel was sealed and pressurized to 700 psi with ethene and stirred at 50°C for 1 h. The vessel was cooled and the gas containing ethene and butene was released slowly, with samples taken for GC analysis. Methanol (10 mL) was added to the reaction mixture to quench the remaining reactive aluminum species and (or) to precipitate insoluble polyethene. The solid product was isolated and dried under vacuum.

Results and Discussion

Homopolymerization of ethene by vanadium compounds

Table 1 summarizes our results of ethene homopolymerization by vanadyl naphthalocyanine and porphyrin complexes, **A** and **B**, respectively. Control experiments indicated that neither the vanadium complexes nor the aluminum cocatalysts were by themselves active for ethene polymerization under the reaction conditions. The vanadyl naphthalocyanine complex **A** appears to be more productive than **B**, given the low solubility of **A** in the volume of solvent used in this system. Although alkylation of the solvent

© 2001 NRC Canada

Table 1. Polymerization of ethene by vanadium compounds.[a]

Compound (10 μmol)	Cocatalyst (equiv)	Solvent (10 mL)	Yield (g)	Activity (kg (mol cat)$^{-1}$ h^{-1})
A	$EtAlCl_2$ (30)	Chlorobenzene	0.90	22.5
A	MAO (100)	Chlorobenzene	1.00	25.0
A	MAO (100)	Toluene	1.21	30.2
B	$EtAlCl_2$ (30)	Chlorobenzene	0.12	3.0
B	MAO (100)	Chlorobenzene	1.17	29.2

[a]Reaction conditions: 125 mL glass-lined stainless autoclave, 700 psi ethene, 50°C, 4 h.

Table 2. Copolymerization of ethene and 1-alkenes with vanadyl naphthalocyanine (**A**).[a]

Comonomer (g)	Cocatalyst (equiv)	Temperature (°C)	Yield (g)	Comonomer incorporation (%)[b]
Propene (5.2)	MAO (100)	120	0.58	13
1-Decene (1)	MAO (100)	50	1.05	Trace
1-Decene (1)	MAO (100)	120	3.32	7.4

[a]Standard conditions: 125 mL glass-lined stainless autoclave, 10 μmol **A**, 10 mL chlorobenzene, 700 psi ethene, 20 h.
[b]As determined by ^{1}H NMR spectroscopy.

Table 3. Polymerization and dimerization of ethene by nickel(II) compounds.[a]

Compound	Cocatalyst (equiv)	Solid product (g)	Butene (g)	Activity (kg (mol cat)$^{-1}$ h^{-1})
$NiCl_2$	$EtAlCl_2$ (30)	None	Trace	—
$NiCl_2$	MAO (100)	None	1.45	29.0
C	$EtAlCl_2$ (30)	None	1.01	20.2
C	MAO (100)	0.32	Trace	6.5

[a]Reaction conditions: 125 mL glass-lined stainless autoclave, 10 mL chlorobenzene, 700 psi ethene, 50°C, 1 h.

occurs when toluene is used in conjunction with $EtAlCl_2$, toluene is an acceptable (if not better) solvent when MAO is used as the cocatalyst, as can be seen in Table 1. The solid product formed is linear polyethene. This is confirmed by the observation of a singlet at 1.2 ppm in the ^{1}H NMR spectrum. The absence of a significant methyl resonance also rules out branching. Differential scanning calorimetry (DSC) also confirmed a linear structure with a T_m above 130°C.

Copolymerization of ethene and 1-alkenes by vanadyl naphthalocyanine (A)

Homopolymerization attempts with alkenes other than ethene were unsuccessful. However, it was possible to copolymerize 1-alkenes with ethene (Table 2). Interestingly, significant incorporation of 1-alkene is only observed at higher reaction temperatures and with MAO as the cocatalyst. Comonomer incorporation was confirmed and quantified by ^{1}H NMR spectroscopy, which showed larger methyl peak integrations compared to linear polyethene and the appearance of methine and nonmain-chain methylene proton resonances. The decrease of product crystallinity compared to linear polyethene also supported copolymer formation, with typical peak T_m values decreasing from greater than 130°C for linear polyethene to approximately 123°C for the ethene–propene copolymer and just below 130°C with ethene–1-decene product; the DSC peak for the latter was significantly broader than the DSC peak of linear polyethene.

Polymerization and oligomerization of ethene by nickel compounds

Perhaps the clearest influence of the macrocyclic ligand can be seen in reactions involving nickel compounds. As shown in Table 3, both the nature of the alkylating agent and the presence of the naphthalocyanine ligand has a strong effect on the reaction with ethene. Thus, with MAO as the alkylating agent, ethene is selectively dimerized by $NiCl_2$ but polymerized by the naphthalocyanine complex, **C**. Interestingly, compound **C** catalyzes the dimerization rather than polymerization of ethene when $EtAlCl_2$ is used as the alkylating agent. Control experiments indicated that neither $NiCl_2$ nor **C** alone was capable of ethene polymerization–dimerization.

Conclusion

It is clear from the above results that metal complexes with flat phthalocyanine and porphyrin ligands are indeed effective catalysts for the polymerization of ethene. The failure of the same catalyst to homopolymerize higher alkenes and the relatively low incorporation of the latter alkenes in copolymerization with ethene can be ascribed to unfavorable steric interactions between the ligand and the alkyl substituent on the monomer.

The observed alkene polymerization by metal phthalocyanine and porphyrin complexes raises a number of

© 2001 NRC Canada

interesting mechanistic questions. First, is the polymerization proceeding in accordance with the mechanism shown in eq. [1]? In principle, this is possible for the vanadium complexes since the ligands are 8-e^- donors leaving the vanadium center with multiple coordination unsaturation. However, the observed activity of the nickel phthalocyanine complex is less easily explained. The Ni(II) complex is a 16-e^- system, with only one coordination position open. Upon alkylation an anionic alkyl species should form and, for polymerization–dimerization to proceed, the ethene has to directly insert into the nickel-alkyl bond *without* prior coordination to the metal center. Such a step has little precedence in alkene polymerization (1, 2). The *complete* decoordination of the phthalocyanine ligand does not appear likely since product formation was not observed when ethene was exposed to a 1:1:30 mixture of $NiCl_2$, aluminum phthalocyanine, and $EtAlCl_2$ (also see Table 3). The combination of aluminum(III) phthalocyanine chloride and MAO was also found to be inactive.

Another interesting issue concerning the reactivity of the nickel phthalocyanine complex is the dramatic change in product selectivity as a function of the alkylating agent (Table 3). In most alkene polymerization systems, MAO is a better cocatalyst than $EtAlCl_2$ because of the ability of the former to function both as an alkylating agent, as well as a strong Lewis acid that is capable of creating a vacant coordination site on the (transition) metal by ligand abstraction (1, 2). In the nickel phthalocyanine complex, following alkylation, there is no ligand present that can be easily removed by a Lewis acid (the decoordination of one of the coordinated nitrogens on the phthalocyanine rings is possible but not very likely).

Studies are currently underway to address the above and related mechanistic questions.

Acknowledgements

This research was supported by a grant from the U.S. Department of Energy, Office of Basic Energy Sciences (DE-FG02–84ER13295). Methylaluminoxane was graciously donated by Albemarle Chemicals, Inc. The authors would like to thank Dr. Ian Harrison of the PSU Polymer Science Department of the use of the DSC equipment and Dr. Shengsheng Liu for his assistance in its use.

References

1. (*a*) G.W. Coates. Chem. Rev. **100**, 1223 (2000); (*b*) G.G. Hlatky. Coord. Chem. Rev. **181**, 243 (1999); (*c*) H.H. Brintzinger, D. Fischer, R. Mulhaupt, B. Rieger, and R.M. Waymouth. Angew. Chem. Int. Ed. Engl. **34**, 1143 (1995).
2. (*a*) S.D. Ittel and L.K. Johnson. Chem. Rev. **100**, 1169 (2000); (*b*) G.J.P. Britovsek, V.C. Gibson, and D.F. Wass. Angew. Chem. Int. Ed. Engl. **181**, 429 (1999).

© 2001 NRC Canada

A novel coordination mode for a pyridylphosphine ligand. X-ray structures of $[RuCl_2(NO)L]$ (I) and $[RuCl_2(NO)L]\cdot DMSO$ (II) (L = $[(2\text{-py})_2PC_2H_4POO(2\text{-py})_2]^-$)

Alzir A. Batista, Salete L. Queiroz, Peter C. Healy, Robbie W. Buckley, Sue E. Boyd, Susan J. Berners-Price, Eduardo E. Castellano, and Javier Ellena

Abstract: The ruthenium(II) complex, $[RuCl_2(NO)L]$ (**I**), (L = $[(2\text{-py})_2PC_2H_4PO_2(2\text{-py})]^-$) was obtained from recrystallization of $RuCl_3NO$(d2pype) (d2pype = $(2\text{-py})_2PC_2H_4P(2\text{-py})_2$) in the presence of HNO_3, crystallizing in the monoclinic space group $P2_1$ (no. 4), with a = 8.012(4) Å, b = 14.454(4) Å, c = 9.353(3) Å, β = 105.77(3)°, and Z = 2. Crystals of the DMSO solvate of the complex (**II**) were obtained from $(CD_3)_2SO$ solution, crystallizing in the monoclinic space group $P2_1/c$ (no.14) with a = 9.7080(2) Å, b = 22.2920(5) Å, c = 11.5230(3) Å, β = 92.0450(10)°, and Z = 4. In both complexes, the geometry about the ruthenium atom is a distorted octahedron mainly as a result of the tridentate [*P*,*N*,*O*]-bonding mode of L. The ν (NO) bands at 1875 cm^{-1} in both complexes are consistent with the linear disposition of the NO group and the Ru atom as is observed in the X-ray crystal structure (Ru-N1-O1 angle = 178.5(4)°).

Key words: pyridylphosphine, nitrosyl, ruthenium complex, X-ray structure.

Résumé : La recristallisation du $RuCl_3NO$(d2pype) (d2pype = $(2\text{-(py)}_2PC_2H_4P(2\text{-py})_2$) en présence de HNO_3 conduit à la formation du complexe de ruthénium(II), $[RuCl_2(NO)L]$ (**1**), (L = $[(2\text{-py})_2PC_2H_4P(2\text{py})_2)]^-$) qui cristallise dans le groupe d'espace $P2_1$ (no. 4), avec a = 8,012(4) Å, b = 14,454(4) Å et c = 9,353(3) Å, β = 105,77(3)° et Z = 2. Les cristaux du produit de solvatation du complexe par le DMSO (2) ont été obtenus à partir d'une solution de $(CD_3)_2SO$; ils cristallisent dans le groupe d'espace $P2_1/c$ (no.14) avec a = 9,7080(2) Å, b = 22,2920(5) Å et c = 11,5230(3) Å, β = 92,0450(10)° et Z = 4. Dans les deux complexes, la géométrie autour de l'atome de ruthénium est un octaèdre déformé en raison principalement du mode de liaison tridentate [*P*,*N*,*O*] de L. Les fréquences des bandes NO, à 1875 cm^{-1}, dans les deux complexes sont en accord avec une disposition linéaire du groupe NO et de l'atome de Ru; c'est ce qui est observé dans la structure cristalline obtenue par diffraction des rayons X alors que l'angle Ru-N1-O1 est de 178,5(4)°.

Mots clés : pyridylphosphine, nitrosyle, complexe du ruthénium, structure cristalline par diffraction des rayons X.

[Traduit par la Rédaction]

Introduction

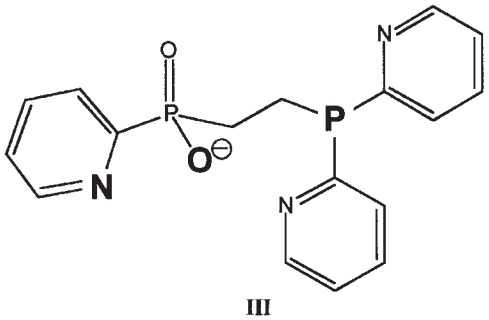
Pyridylphosphines are very attractive ligands for coordination chemistry. Their importance in inorganic medicinal chemistry has been demonstrated (1) and they have been utilized in the development of potential homogeneous catalysts for use in aqueous media (2–7). At a more fundamental level, they are of interest because of the variety of coordination modes which they demonstrate. Indeed, pyridylphosphine metal complexes have been observed (for *P*-coordinated see ref. 8; for *P*,*N*-coordinated see ref. 9; for *N*,*N*′-coordinated see ref. 10; for *N*,*N*′,*N*″-coordinated see ref. 11; for *P*,*N*,*N*′-coordinated see ref. 12; for *P*,*P*,*N*-coordinated see ref. 7) in which the ligand binds via the P atom, via the phosphorus and one pyridyl group (*P*,*N*), via two pyridyl groups (*N*,*N*′; PPh(py) and $P(py)_3$), via three pyridyl groups (*N*,*N*′,*N*″; $P(py)_3$) and via the phosphorus and two pyridyl groups (*P*,*N*,*N*′, $PPh(py)_2$ and $P(py)_3$).

Received October 3, 2000. Published on the NRC Research Press Web site at http://canjchem.nrc.ca on July 13, 2001.

Dedicated to Professor Brian James on the occasion of his 65th birthday.

A.A. Batista.[1] Departamento de Química, Universidade Federal de São Carlos, CP 676, 13565–905, São Carlos, SP, Brazil.
S.L. Queiroz, P.C. Healey, R.W. Buckley, S.E. Boyd, and S.J. Berners-Price. School of Science, Griffith University, Brisbane, Queensland 4111, Australia.
E.E. Castellano and J. Ellena. Instituto de Física de São Carlos, Universidade de São Paulo, São Carlos, Brazil.

[1]Corresponding author (telephone: +55-16-260-8285; fax: +55-16-260-8350 e-mail: alzir@dq.ufscar.br).



III

 DOI: 10.1139/cjc-79-5/6-1030 © 2001 NRC Canada

Recently, a new coordination mode was reported for pyridylphosphines. In the complex $RuCl_2((2\text{-py})_2P(CH(CH_2)_3CH)P(2\text{-py})_2)PPh_3$, the ligand has a *P,P,N*-bonding mode, with either a *mer*- or *fac*-arrangement of the three P donor atoms (7). Adding to the increasing coordination possibilities of this intriguing and versatile class of ligands, we report here the X-ray structure determination of the complexes $[RuCl_2(NO)L]$ (**I**) (L = $[(2\text{-py})_2PC_2H_4PO_2(2\text{-py})]^-$), and its DMSO solvate (**II**) in which the ligand, **III**, acts as an unusual tridentate [*P,N,O*] ligand.

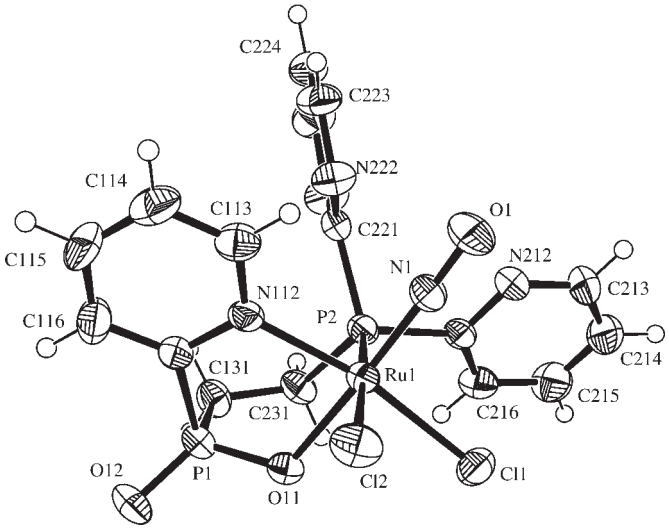
Experimental

Infrared spectra were recorded as CsI pellets on a Bomem-Michelson 102 instrument. ^{31}P, ^1H, and $^1H\{^{31}P\}$ NMR spectra (^{31}P 161.9 MHz) were obtained in DMSO-d_6 solutions at room temperature with a Varian Unity 400 spectrometer. ^1H NMR chemical shifts are reported in ppm, relative to residual DMSO (taken as δ 2.49 ppm). ^{31}P NMR chemical shifts are reported relative to external H_3PO_4 (85%) (taken as 0 ppm). Spectral assignments were confirmed by analysis of absolute value, gradient selected, COSY, NOESY (τ_{mix} = 800 ms), and ^{31}P HMBC (J_{PH} = 20 Hz) experiments conducted on the solution. Pulse sequences were as supplied in the Varian VNMR6.1B NMR package. The numbering scheme adopted for the reporting of the ^1H NMR data parallels the numbering scheme used for the attached ^{13}C atoms in the X-ray structure of the complex (Fig. 1). Coupling constants are recorded as absolute values, in Hz. Elemental analyses were performed at the Department of Chemistry, Federal University of São Carlos, São Carlos (SP), Brazil.

Reagent grade solvents were distilled from $Na(Et_2O)$, $CaH_2(CH_2Cl_2)$, $Mg–I_2(MeOH)$ under Ar. $RuCl_3\cdot 3H_2O$ and perdeuterated dimethylsulfoxide were used as supplied (Aldrich). 1,2-Bis(di-2-pyridylphosphino)ethane (d2pype) and $RuCl_3NO$ were prepared according to published procedures (2, 13).

$RuCl_3NO$(d2pype) was obtained from the reaction of $RuCl_3NO$ (100 mg, 0.42 mmol) with d2pype (170 mg, 0.42 mmol) in 5 mL of CH_2Cl_2. The mixture was stirred for 2 h under Ar at room temperature. The volume of the solution was then reduced and the resultant yellow precipitate collected by filtration and washed with methanol and ether and dried under vacuum. Yield: 0.245 g, 91%. Anal. calcd. $C_{22}H_{20}Cl_3N_5OP_2Ru$ (%): C 41.30, H 3.15, N 10.95; found: C 41.00, H 3.22, N 11.00. Crystals of **I** (yield 15%), of reddish color, were obtained by slow evaporation of a CH_2Cl_2 – diethyl ether solution of the crude product $RuCl_3NO$(d2pype) (to increase the solubility of the yellow solid two drops of HNO_3 were added to this solution). ^1H NMR (400 MHz, DMSO-d_6, 298 K) δ: 8.77 (dd, 1H, *J* = 6.3, 1.3, *H*113), 8.71 (ddd, 1H, *J* = 4.8, 1.6, 1.3, *H*213), 8.54 (ddd, 1H, *J* = 4.8, 1.7, 1.1, *H*223), 8.05 (ddd, 1H, *J* = 7.6, 7.6, 1.3, *H*115), 7.96 (m, 1H, *H*215), 7.93 (m, 1H, *H*216), 7.79 (m, 1H, *H*226), 7.76 (m, 1H, *H*225), 7.70 (m, 2H, *H*114, *H*116), 7.52 (ddd, 1H, *J* = 7.2,4.8, 1.7, *H*214), 7.39 (ddd, 1H, *J* = 7.2, 4.8, 1.6, *H*224), 3.3 (m, 2H, CH_2[2]), 2.58 (m, 1H, CH_2), 2.18 (ddd, 1H, *J* = 17, 12, 5, CH_2). ^{31}P NMR (161.9 MHz, DMSO-d_6, 298 K) δ: 33.8 (d, $^3J_{PP}$ = 22.2 Hz, (2-Py)*P*OO), 26.0 (d, (2-Py)$_2$*P*Ru). Anal. calcd. $C_{17}H_{16}Cl_2N_4O_3P_2Ru$: C 36.58, H 2.89, N 10.04; found: C 36.42, H 3.00, N 10.02. Crystals of **II** (of reddish color) were obtained from a perdeuterated DMSO solution of **I** on standing.

Fig. 1. ORTEP view of the asymmetric unit of $[RuCl_2(NO)(2\text{-py})_2PC_2H_4P{=}O,O^-(2\text{-py})]$ (**I**), showing the atom labelling and the 50% probability ellipsoids.



X-ray crystallographic analyses

$[RuCl_2(NO)L]$

All measurements were made on a Rigaku AFC7R rotating anode diffractometer with graphite monochromated Mo Kα (λ = 0.71070 Å) radiation. The final unit cell parameters were based on 25 reflections with $18.4 \le 2\theta \le 19.4$. The data were processed using the teXsan package (14) and corrected for Lorentz and polarization effects. The structure was solved by heavy atom Patterson techniques, expanded by using Fourier techniques and refined by full-matrix least-squares on |*F*|s (14).

$[RuCl_2(NO)L]\cdot DMSO$

All measurements were made on an Enraf–Nonius κCCD diffractometer with graphite monochromated Mo Kα (λ = 0.71070 Å) radiation. The final unit cell parameters were based on all reflections. The structure was solved by direct methods with SHELXS-97 (15). The Fourier map obtained showed all non-hydrogen atoms. The model was refined by full-matrix least-squares procedure on F^2 by means of SHELXL-97 (16). The DMSO solvent molecule presents some degree of disorder, which was modeled with two positions for the sulfur atom with their occupation factors adding to one.

The hydrogen atoms of the aromatics rings and CH_2 groups were set to isotropic, with a thermal parameter 20% greater than the equivalent isotropic displacement parameter of the carbon atom to which each one is bonded; this percentage was set to 50% for the hydrogen atoms of the methyl groups. All the hydrogen atoms were stereochemically positioned and

[2] Resonances coincide with the H_2O resonance.

© 2001 NRC Canada

Table 1. Crystal data and structure refinement.

Compound	**I**	**II**
Empirical formula	$C_{17}H_{16}Cl_2N_4O_3P_2Ru$	$C_{19}H_{22}Cl_2N_4O_4P_2RuS$
Formula weight	558.3	636.38[a]
Temperature (K)	293(2)	293(2)
Wavelength (Å)	0.71070	0.71070
Crystal system	Monoclinic	Monoclinic
Space group	$P2_1$ (no. 4)	$P2_1/c$ (no. 14)
Unit cell dimensions		
a (Å)	8.012(4)	9.7080(2)
b (Å)	14.454(4)	22.2920(5)
c (Å)	9.353(3)	11.5230(3)
β (°)	105.77(3)	92.045(1)
Volume (Å^3)	1042.3(7)	2492.1(1)
Z	2	4
Density (calculated) (mg m^{-3})	1.779	1.696
Absorption coefficient (mm^{-1})	1.189	1.090
F(000)	556	1280
Crystal size (mm^3)	0.50 × 0.30 × 0.10	0.03 × 0.16 × 0.06
θ range for data collection (°)	2.64–25.02	1.83–27.56
Index ranges	0, 9; 0, 17; –11, 10	–12, 11; –28, 28; –14, 14
Reflections collected	2077	38 959
Independent reflections	1936 (R(int) = 0.0210)	5735 (R(int) = 0.0843)
Max and min transmission	0.942 and 0.765	0.984 and 0.711
Refinement method	Full-matrix least-squares on F	Full-matrix least-squares on F^2
Computing[b]	TeXsan (15)	SHELXS-97 (15), SHELXL-97 (16), COLLECT (17), Denzo-SMM (18)
Absorption correction	ψ-scan (19)	Multiscan (20)
Data, parameters	1936, 262	5735, 310
Goodness-of-fit	1.501	1.129
Final R indices [$I > 2\sigma(I)$]	R = 0.024, Rw = 0.024	$R1$ = 0.054, $wR2$ = 0.149
R indices (all data)	R = 0.028, Rw = 0.024	$R1$ = 0.075, $wR2$ = 0.174

[a] For non-deuterated DMSO.
[b] Data collection, data processing, structure solution, and structure refinement, respectively.

refined with the riding model. All non-H atoms were refined anisotropically.

Crystal data, data collection procedures, structure determination methods, and refinement results are summarized in Table 1. Complete tables of crystallographic data, hydrogen atom coordinates, anisotropic thermal parameters, bond lengths and angles, torsion angles, intermolecular contacts, and least-squares planes have been deposited as supplementary material.[3]

Results and discussion

The single crystal structure determinations of the two complexes are consistent with the formation of discrete molecular complexes separated by normal van der Waals interactions. In spite of their different crystal symmetry and the presence of a solvent molecule in one the structures, the molecular structures of the complexes in both crystal forms are essentially identical, as can be seen by comparing the bond lengths and angles reported in Table 2. For this reason we shall refer to the unsolvated form to discuss the molecular geometry of the complex. The molecular structure of the complex is both interesting and unexpected. For the reaction of $RuCl_3NO$ with the d2pype ligand, one would expect a complex with formula $RuCl_3NO$(d2pype-*P,P′*), with the phosphorous atoms coordinated *trans* to the chlorine atoms as a bidentate ligand, as obtained for the dppm, dppe, and dppp diphosphine ligands (13, 21), with the further possibility of coordination of pyridyl nitrogen through displacement of one chloride anion (7, 12). In this case however, as can be seen in the X-ray structure (Fig. 1), one of the phosphorus atoms of the d2pype ligand has been oxidized to a phosphinate (R_2POO^-) with loss of one pyridyl group. This affords a rare example of a tridentate [*P,N,O*] ligand (22) that coordinates to the ruthenium atom through the unoxidized phosphorus atom, a nitrogen atom from the pyridyl group attached to the oxidized phosphorus and the deprotonated hydroxyl group on the oxidized phosphorus, the latter displacing one chloride anion from the coordination sphere.

While the mechanism for the formation of this ligand and complex remains speculative at this stage, we (23) have shown previously in studies on compounds of bidentate phosphine ligands with silver(I) salts that coordination of bidentate phosphine ligands can be via a single phosphorous

[3] Supplementary material may be purchased from the Depository of Unpublished Data, Document Delivery, CISTI, National Research Council Canada, Ottawa, ON K1A OS2, Canada). Tables of bond lengths and angles have also been deposited with the Cambridge Crystallographic Data Centre and can be obtained, free of charge, on request from the Director, C CDC, 12 Union Road, Cambridge, CB2 1EZ, U.K. (Fax: +44-1223-336-033, e-mail: deposit@ccdc.cam.ac.uk).

© 2001 NRC Canada

Table 2. Selected bond lengths (Å) and angles (°).

Bond lengths	**I**	**II**		**I**	**II**
Ru(1)—Cl(1)	2.369(1)	2.360(1)	P(2)—C(211)	1.818(4)	1.821(4)
Ru(1)—Cl(2)	2.425(2)	2.433(1)	P(2)—C(221)	1.834(5)	1.834(5)
Ru(1)—P(2)	2.345(2)	2.346(1)	P(2)—C(231)	1.824(5)	1.807(5)
Ru(1)—O(11)	2.024(3)	2.032(3)	O(1)—N(1)	1.159(6)	1.137(5)
Ru(1)—N(1)	1.728(4)	1.740(4)	N(112)—C(111)	1.357(6)	1.347(6)
Ru(1)—N(112)	2.105(3)	2.088(3)	N(112)—C(113)	1.349(6)	1.347(6)
P(1)—O(11)	1.538(3)	1.544(3)	N(212)—C(211)	1.344(6)	1.342(7)
P(1)—O(12)	1.467(4)	1.470(3)	N(212)—C(213)	1.324(6)	1.333(6)
P(1)—C(111)	1.818(5)	1.824(5)	N(222)—C(221)	1.327(7)	1.325(6)
P(1)—C(131)	1.798(6)	1.824(5)	N(222)—C(223)	1.335(7)	1.341(7)
Bond angles					
Cl(1)-Ru(1)-Cl(2)	90.64(5)	91.29(5)	N(1)-Ru(1)-N(112)	95.1(2)	95.9(2)
P(2)-Ru(1)-Cl(1)	88.43(5)	87.71(4)	N(112)-Ru(1)-P(2)	93.5(1)	94.1(1)
P(2)-Ru(1)-Cl(2)	175.17(5)	175.03(4)	N(112)-Ru(1)-Cl(1)	169.6(1)	169.1(1)
O(11)-Ru(1)-Cl(1)	87.19(8)	87.36(9)	N(112)-Ru(1)-Cl(2)	86.6(1)	86.0(1)
O(11)-Ru(1)-Cl(2)	88.7(1)	87.93(1)	C(211)-P(2)-Ru(1)	112.0(2)	113.2(2)
O(11)-Ru(1)-P(2)	86.6(1)	87.16(9)	C(221)-P(2)-Ru(1)	113.4(2)	115.6(2)
O(11)-Ru(1)-N(112)	82.7(1)	82.0(1)	C(231)-P(2)-Ru(1)	111.6(2)	109.9(2)
N(1)-Ru(1)-Cl(1)	95.0(1)	94.8(1)	C(211)-P(2)-C(221)	103.1(2)	104.1(2)
N(1)-Ru(1)-Cl(2)	93.5(2)	94.6(1)	C(231)-P(2)-C(211)	107.4(2)	107.5(2)
N(1)-Ru(1)-P(2)	91.3(2)	90.3(1)	C(231)-P(2)-C(221)	108.9(2)	106.1(2)
N(1)-Ru(1)-O(11)	176.9(2)	176.6(2)	O(11)-P(1)-C(111)	111.0(2)	100.5(2)
O(11)-P(1)-C(131)	106.6(2)	106.3(2)	O(1)-N(1)-Ru(1)	178.5(4)	178.0(4)
O(12)-P(1)-O(11)	118.0(2)	118.0(2)	C(111)-N(112)-Ru(1)	116.6(3)	117.1(3)
O(12)-P(1)-C(111)	111.9(2)	111.2(2)	C(113)-N(112)-Ru(1)	123.8(3)	123.2(3)
O(12)-P(1)-C(131)	113.9(2)	112.0(2)	C(111)-N(112)-C(113)	119.3(3)	119.7(4)
C(111)-P(1)-C(131)	105.0(2)	107.8(2)	C(213)-N(212)-C(211)	116.8(4)	116.1(5)
P(1)-O(11)-Ru(1)	117.7(2)	116.7(2)	C(221)-N(222)-C(223)	116.9(5)	116.8(5)

atom and that the noncoordinated phosphine in these complexes can undergo oxidation to the phosphine oxide. It seems reasonable to assume in the present circumstances that at least a small concentration of a $RuCl_3NO$(d2pype) complex exists in solution with the d2pype ligand coordinated to the ruthenium ion via one phosphorus atom only and that the presence of the strong oxidizing acid HNO_3 has oxidized the noncoordinated P atom. It is worth noting that, while the elimination of a pyridyl group and oxidation of the phosphorus to the phosphinate has not been observed previously for pyridyl phosphines, autoxidation of alkyl phosphines to phosphinates and phosphate esters, via a proposed radical chain mechanism, has been observed (24).

The geometry around the ruthenium atom in **I** (Fig. 1) is a distorted octahedron, the distortion mainly due to the tridentate mode of bonding by the ligand L.

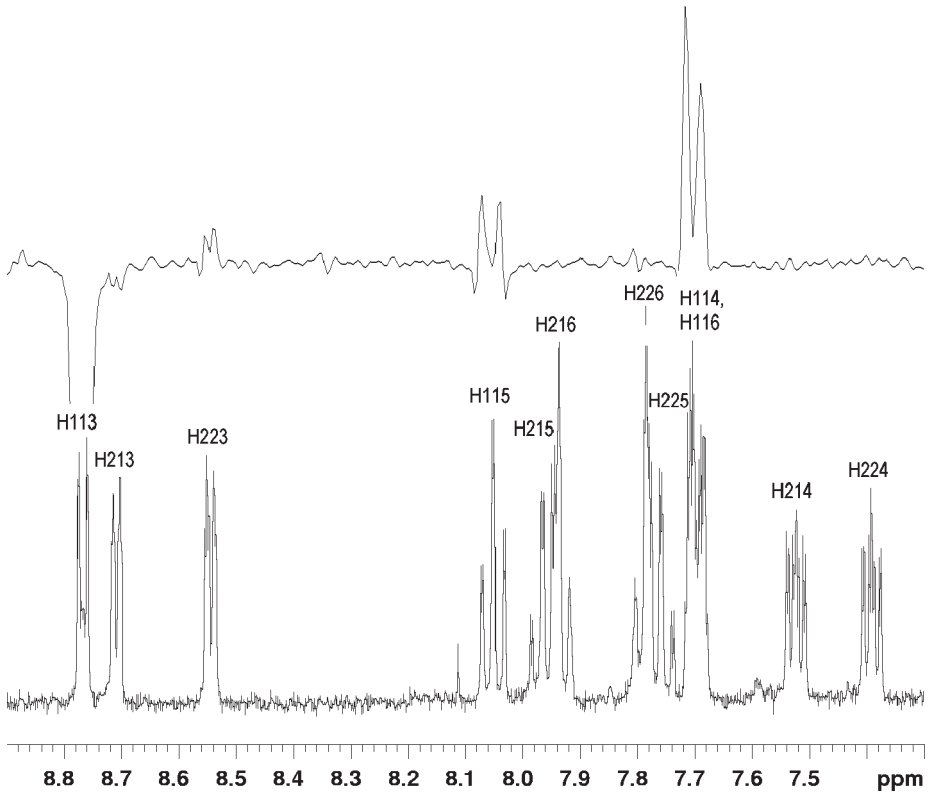
Bond lengths (Table 2) are consistent with a *trans* influence of the coordinated phosphorus atom, P2. The Ru—Cl2 bond (2.425(2) Å) *trans* to P2 is significantly longer than the Ru—Cl1 bond (2.369(1) Å) *trans* to N112. In addition, the Ru—NO bond length (1.728(4) Å), for which the nitrogen atom is *trans* to the oxygen (O^-), is shorter than the Ru—NO distance for which the nitrogen is *trans* to phosphorus or chlorine in the $RuCl_3$(dppb)NO and $[RuCl_5(NO)]^{2-}$ complexes (1.748(8) Å and 1.738(2) Å, respectively) (21, 25). This reflects the $P > Cl^- > O^-$ order in the *trans* influence series (26). The Ru—P2 distance (2.345(2) Å) is similar to other monodentate coordinated P atoms (22, 27). The Ru—O bond length in the present complex (2.024(3) Å) also lies within the range of similar bond lengths reported in the literature (22). The short metal—nitrogen bond (Ru—NO, 1.728(4) Å) and the NO bond length of 1.159(6) Å, longer than in the free NO^+ group (1.06 Å) (28) by almost 0.1 Å, consistent with significant π-bonding between the ruthenium and the nitrogen atom of the NO^+ ligand. The P=O bond length (1.467(4) Å) is not significantly different from that found for triphenylphosphine oxide (1.46(1) Å) (29) and dppbO (1.482(2) Å) (30). The other bond lengths in the complex are similar to those found in the literature (8–13, 31). The observed Ru-N-O bond angle for **I** (178.5(4)°) shows that these atoms are almost colinear in the complex. The angles involving the phosphorus atoms (Table 2) show that these atoms are in tetragonal environments, as expected.

It is interesting that the complex adopts a stable "closed" environment because of the favourable, intramolecular, donor–acceptor interactions occurring between the N atoms of the noncoordinated pyridyl rings and the NO^+ group. This is evidenced in the pyridyl—nitrosyl distances O1—N212 (3.360(7) Å) and O1—N222 (3.138(7) Å). The coordination geometry of the coordinated pyridyl function completes the closed structure (N222—N212 = 3.610(7) Å and H113—N222 = 2.870(7) Å).

The IR of a CsI disk of **I** shows a strong, sharp band at 1875 cm^{-1} corresponding to ν (NO^+) (13, 21, 32). The IR data previously observed for *fac*-[$RuCl_3$(NO)(dppm)] and

© 2001 NRC Canada

Fig. 2. Aromatic region of the ^{1}H NMR (400 MHz, DMSO-d_6, 298 K) spectrum of **I**. The upper trace shows the corresponding region of a row extracted from a GNOESY experiment (τ_{mix} = 800 ms) conducted on the same sample. Cross relaxation occuring between nuclei located on different pyridyl residues is evidenced by the cross peak correlating the resonances at δ 8.77 and δ 8.54.



mer-[$RuCl_3(NO)(AsPPh_3)_2$], in which the nitrosyls are *trans* to chlorine atoms, have their ν (NO) bands at 1867 and 1869 cm^{-1}, respectively, (13, 21, 33). Medium bands at 1570, 1447, and 1424 cm^{-1} correspond, respectively, to C=N(py) and C=C stretching vibrations of the aromatic rings (32, 34). A medium band at 1284 cm^{-1} and a strong one at 1231 cm^{-1} belong to the P=O and P-O, respectively, (32). Other bands typical of the aromatic rings are present in the spectrum between 500–1000 cm^{-1}.

^{31}P and ^{1}H NMR data recorded for complex **I** (Fig. 2) suggest that the structure of the complex in solution is not substantially different from that observed in the solid state.

The lack of symmetry in the complex renders all resonances inequivalent. The spin system was therefore readily assigned, either directly by inspection or by analysis of standard two-dimensional experiments. As expected, the ^{1}H NMR spectroscopic properties of the two noncoordinated pyridyl groups were quite similar and distinct from those of the *N*-coordinated pyridyl. The relative arrangement of these two pyridyls, with respect to their relative individual proximities to the *N*-coordinated pyridyl, was evidenced by weak cross peaks in the NOESY matrix between δ 8.77 and 8.54 ppm (Fig. 2), which are indicative of nOe transfer occurring between *H*113 and *H*223. This suggests that on average these protons are separated by a distance <5 Å, consistent with the X-ray data which positions these protons 3.324 Å apart. No other significant inter-pyridyl nOes were present in the spectrum.

Conclusion

Coordinated pyridylphosphine ligand in the presence of a strong oxidizing acid can be oxidated to a phosphinate, with loss of one pyridyl group. Surprisingly, the $RuCl_2(NO)(2\text{-}py)_2PC_2H_4$ $POO(2\text{-}py)_2$ (where the phosphine is a tridentate [*P,N,O*] ligand), is chemically very stable and does not react with strongly coordinating ligands such as DMSO. ^{31}P NMR data recorded for complex **I** in $(CD_3)_2SO$ suggest that the structure of the complex in solution is not substantially different from that observed in the solid state. A $(CD_3)_2SO$ solution of complex **I** produces only the solvated species (complex **II**). The sharp band at 1875 cm^{-1} in the IR spectrum shows that complex **I** is of the {Ru^{II}-NO^+} type.

References

1. S.J. Berners-Price, R.J. Bowen, P. Galettis, P.C. Healy, and M.J. McKeage. Coord. Chem. Rev. **185**, 823 (1999).
2. R.J. Bowen, A.C. Garner, S.J. Berners-Price, I.D. Jenkins, and R.E. Sue. J. Organomet. Chem. **554**, 181 (1998).
3. (*a*) Z.-Z. Zhang and H. Cheng. Coord. Chem. Rev. **147**, 1 (1996); (*b*) G.R. Newkome. Chem. Rev. **93**, 2067 (1993).
4. G. Franció, R. Scopelliti, C.G. Arena, G. Bruno, D. Dormmí, and F. Faraone. Organometallics, **17**, 338 (1998).
5. (*a*) D. Drommi, F. Nicolò, C.G. Arena, G. Bruno, F. Faraone, and R. Gobetto. Inorg. Chim. Acta, **221**, 109 (1994); (*b*) S. Gladiali, L. Pinna, C.G. Arena, E. Rotondo, and F. Faraone. J. Mol. Catal. **66**, 183 (1991).

© 2001 NRC Canada

6. Z.-Z. Zhang, H.-P. Xi, W.-J. Zhao, K.-Y. Jiang, R.-J. Wang, H.-G. Wang, and Y. Wu. J. Organomet. Chem. **454**, 221 (1993).
7. N.D. Jones, K.S. MacFarlane, M.B. Smith, R.P. Schutte, S.J. Rettig, and B.R. James. Inorg. Chem. **38**, 3956 (1999).
8. (*a*) C.J.L. Lock and M.A. Turner. Acta Crystallogr. Sect. C: Cryst. Struct. Chem. **C43**, 2096 (1987); (*b*) J.P. Farr, M.M. Olmstead, F.E. Wood, and A.L. Balch. J. Am. Chem. Soc. **105**, 792 (1983); (*c*) A. Maisonnet, J.P. Farr, M.M. Olmstead, C.T. Hunt, and A.L. Balch. Inorg. Chem. **21**, 3961 (1982); (*d*) J.P. Farr, M.M. Olmstead, and A.L. Balch. Inorg. Chem. **21**, 6654 (1982); (*d*) J.P. Farr, M.M. Olmstead, and A.L. Balch. J. Am. Chem. Soc. **102**, 6654 (1980).
9. (*a*) M.M. Olmstead, A. Maisonnat, J.P. Farr, and A.L. Balch. Inorg. Chem. **20**, 4060 (1981); (*b*) D. Drommi, F. Nicolò, C.G. Arena, G. Bruno, F. Faraone, and R. Gobetto. Inorg. Chim. Acta, **221**,109 (1994); (*c*) K. Kurtev, D. Ribola, R.A. Jones, D.J. Cole-Hamilton, and G. Wilkinson. J. Chem. Soc. Dalton Trans. 55 1980; (*d*) N.D. Jones, K.S. MacFarlane, M.B. Smith, R.P. Schutte, S.J. Rettig, and B.R. James. Inorg. Chem. **38**, 3956 (1999).
10. (*a*) P. Espinet, P. Gómez-Elipe, and F. Villafañe. J. Organomet. Chem. **450**, 145 (1993); (*b*) M.G. Ehrlich, F.R. Fronczek, S.F. Watkins, G.R. Newkome, and D.C. Hager. Acta Crystallogr. Sect. C: Cryst. Struct. Commun. **C40**, 78 (1984).
11. (*a*) R. Gregorzik, J. Wirbser, and H. Vahrenkamp. Chem. Ber. **125**, 1575 (1992); (*b*) F.R. Keene, M.R. Snow, P.J. Stephenson, and E.R.T Tiekink. Inorg. Chem. **27**, 2040 (1988); (*c*) R.K. Boggess and D.A. Zatko. J. Coord. Chem. **4**, 217 (1975).
12. R.P. Schutte, S.J. Rettig, A.M. Joshi, and B.R. James. Inorg. Chem. **36**, 5809 (1997).
13. A.A. Batista, C. Pereira, S.L. Queiroz, L.A.A. Oliveira, R.H.A. Santos, and M.T.P. Gambardella. Polyhedron, **16**, 927 (1997).
14. teXsan. Crystal structure analysis package. Molecular Structure Corp., The Woodlands, Texas. 1997.
15. G.M. Sheldrick. SHELXS-97. Program for crystal structure resolution. University of Göttingen, Göttingen, Germany. 1997.
16. G.M. Sheldrick. SHELXL-97. Program for crystal structures analysis. University of Göttingen, Göttingen, Germany. 1997.
17. Z. Otwinowski and W. Minor. COLLECT. Nonius BV, Delft, The Netherlands. 1997.
18. HKL Denzo and Scalepack. C.W. Carter, Jr. and R.M. Sweet (*Editors*). *In* Methods in enzymology. 276. Academic Press, New York. pp. 307–326.
19. A.C.T. North, D.C. Phillips, and F.S. Mathews. Acta Crystallogr. Sect. A: Cryst. Phys. Diffr. Theor. Gen. Crystallogr. **A24**, 351 (1968).
20. R.H. Blessing. Acta Crystallogr. **A51**, 33 (1965).
21. A.A. Batista, C. Pereira, K. Wohnrath, S.L. Queiroz, R.H.A. Santos, and M.T.P. Gambardella. Polyhedron, **18**, 2079 (1999).
22. P. Bhattacharyya, M.L. Loza, J. Parr, and A.M.Z. Slawin. J. Chem. Soc. Dalton Trans. 2917 (1999).
23. D. Affandi, S.J. Berners-Price, Effendy, P.J. Harvey, P.C. Healy, B.E. Ruch, and A.H. White. J. Chem. Soc. Dalton Trans. 1411 (1997).
24. (*a*) S.J. Berners-Price, R.E. Norman, and P.J. Sadler. J. Inorg. Biochem. **31**, 197 (1987); (*b*) S.A. Buckler. J. Am. Chem. Soc. **84**, 3093 (1962).
25. J.T. Veal and D.J. Hodgson. Inorg. Chem. **11**, 1420 (1972).
26. J.E. Huheey. Inorganic chemistry. 3rd ed. Harper and Row, New York. 1983. p. 540.
27. M. Maji, M. Hossian, M. Chatterjee, S.K. Chattopadadhyay, V.G. Puranik, P. Chakrabarti, and S. Ghosh. Polyhedron, **18**, 3739 (1999).
28. J.D. Lee. A new concise inorganic chemistry. 3rd ed. Van Nostrand Reinhold Co. Ltd., New York. 1977. p. 215.
29. G. Bandoli, G. Bartololozzo, D.A. Clements, V. Croatto, and C. Panattoni. J. Chem. Soc. A, 2778 (1970).
30. M.R.M. Fontes, G. Oliva, J. Zukerman-Schpector, S.L. Queiroz, and A.A. Batista. Acta Crystallogr. Sect. C: Cryst. Struct. Commun. **C47**, 2699 (1991).
31. M.P. Felicissimo and A.A. Batista. XXXIII Int. Conf. on Coord. Chem. (Book of Abstracts), Florence, Italy. 1998. p. 467.
32. K. Nakamoto. Infrared and Raman spectra of inorganic and coordination compounds. Part B. 5th ed. John Wiley and Sons, Inc., New York. 1997. p. 84.
33. D.H.F. Souza, G. Oliva, A. Teixeira, and A.A. Batista. Polyhedron, **14**(8), 1031 (1995).
34. I.A. Setyawati, S.J. Rettig, and C. Orvig. Can. J. Chem. **77**, 2033 (1999).

© 2001 NRC Canada

Reactions of SO_2 with *trans*-Ir(CO)(Cl)(TPPTS)$_2$ in water

Allen A. Bowden and Jim D. Atwood

Abstract: Reaction of SO_2 with *trans*-Ir(CO)(Cl)(TPPTS)$_2$ in water mirrors the nature of SO_2 dissolved in water. At low pH (pH = 1) where SO_2 exists as the hydrated species $SO_2 \cdot H_2O$, only Ir(CO)(Cl)(SO_2)(TPPTS)$_2$ forms. At higher pH (pH = 6) where HSO_3^- dominates, no SO_2 complex is observed and a hydride, Ir(CO)(Cl)(H)(OH)(TPPTS)$_2$, is the primary product. A mixture of SO_2 and O_2 does not lead to an iridium sulfate or show any evidence of the dioxygen adduct upon reaction in water with *trans*-Ir(CO)(Cl)(TPPTS)$_2$, in contrast to the analogous reaction in organic solvents. In water, only the SO_2 complex, Ir(CO)(Cl)(SO_2)(TPPTS)$_2$, is observed prior to decomposition. The contrasts to the PPh_3 analogues in organic solvents provide further insight to water as a solvent for organometallic complexes.

Key words: iridium(I), sulfur dioxide, water soluble, TPPTS.

Résumé : La réaction du SO_2 avec le *trans*-Ir(CO)(Cl)(TPPTS)$_2$ dans l'eau est un miroir de la nature du SO_2 dissous dans l'eau. À faible pH (pH = 1), alors que le SO_2 existe sous la forme d'espèces hydratées $SO_2 \cdot H_2O$, il ne se forme que du Ir(CO)(Cl)(SO_2)(TPPTS)$_2$. À des pH plus élevés (pH = 6), alors que l'anion HSO_3^- prédomine, on n'observe pas de formation de complexe avec le SO_2 et le produit primaire est un hydrure, Ir(CO)(Cl)(H)(OH)(TPPTS)$_2$. Un mélange de SO_2 et de O_2 ne conduit pas à la formation d'un sulfate d'iridium; de plus, on ne détecte aucune indication de formation d'un adduit avec le dioxygène lors de la réaction dans l'eau du *trans*-Ir(CO)(Cl)(TPPTS)$_2$ et ceci est en opposition avec la réaction analogue dans les solvants organiques. Dans l'eau, on n'observe que la formation du complexe avec le SO_2, Ir(CO)(Cl)(SO_2)(TPPTS)$_2$, avant sa décomposition. Le contraste avec les analogues PPh_3 dans les solvants organiques permet de comprendre le mécanisme d'action de l'eau comme solvant pour les complexes organométalliques.

Mots clés : iridium(I), bioxyde de soufre, soluble dans l'eau, TPPTS.

[Traduit par la Rédaction]

Introduction

Addition reactions of small molecules to square-planar iridium(I) complexes have been extensively studied since Vaska's initial investigations began in 1961 with O_2 addition to *trans*-Ir(CO)Cl(PPh_3)$_2$ (1). These complexes have been used as models for intermediates in catalytic cycles (2) with a wide variety of reactants forming stable adducts with Vaska's complex and derivatives (3). One of the main advantages of these complexes is that triphenylphosphine can be easily substituted by a different phosphine ligand and thus the effect of changing the electronic and steric environment around the metal center can be monitored. For example, studies on O_2 binding have increased the understanding of steric and electronic factors in dioxygen coordination (4). In addition the recent development of water-soluble phosphines such as the trisulfonated triphenylphosphine derivative, TPPTS (TPPTS = P(*m*-$C_6H_4SO_3Na)_3$), means that water-soluble square-planar metal complexes can be made and hence the effect of carrying out these reactions in water can be investigated.

This manuscript examines the reactions of *trans*-Ir(CO)Cl(TPPTS)$_2$ (**1**) with sulfur dioxide at various pHs. There have been very few modeling studies in water, thus, investigation of these reactions increases understanding of the various interactions of organometallic complexes in water. SO_2 reactions are of further interest due to environmental problems and the hope that a metal complex may lead to a route for removal of SO_2 from waste streams (5).

Received September 5, 2000. Published on the NRC Research Press Web site at http://canjchem.nrc.ca on July 13, 2001.

Dedicated to Professor Brian James on the occasion of his 65th birthday.

A.A. Bowden and J.D. Atwood.[1] Department of Chemistry, University at Buffalo, The State University of New York, Buffalo, NY 14260–3000, U.S.A.

[1]Corresponding author (fax: (716) 645-6963; e-mail: jatwood@acsu.buffalo.edu).

Experimental

Materials

$IrCl_3 \cdot 3H_2O$ was purchased from Johnson Matthey. Anhydrous SO_2(g) was purchased from Matheson. Deuterated solvents were purchased from Cambridge Isotope Lab, Aldrich Chemical Co., or MSD labs. Carbon monoxide was purchased from Praxair. All were used without further purification. Compound (**1**) was prepared as previously described (6). The water used was triply distilled and deionized. Solvents were used as received without further purification. Control of pH was effected with Baker DILUT-IT buffers.

 DOI: 10.1139/cjc-79-5/6-1036 © 2001 NRC Canada

Table 1. Summary of ^{31}P NMR and IR spectroscopic data.

Complex	^{31}P NMR (D_2O)	IR (cm^{-1})		^{1}H NMR (D_2O)
		H_2O	KBr	
trans-Ir(CO)Cl(TPPTS)$_2$ (**1**)	26.2 (s, br)	1986	1967	—
Ir(CO)Cl(O_2)(TPPTS)$_2$ (**2**)	6.5 (s)	2040	2008	—
Ir(CO)Cl(SO_2)(TPPTS)$_2$ (**3**)	10.9 (s)	2043	2017	—
[Ir(CO)(OH_2)(TPPTS)$_2$]$^+$ (**4**)	29.8 (s)	—	—	—
(H)Ir(CO)Cl(OH)(TPPTS)$_2$ (**5**)	2.0 (s)	—	—	–13.26 (t) $J_{P\text{-}H}$ = 13.0 Hz
trans-Ir(CO)(OH)(TPPTS)$_2$ (**6**)	29.5 (s)	—	—	—
(H)Ir(CO)(Cl)$_2$(TPPTS)$_2$ (**7**)	2.5 (s)	2067	—	–15.8 (t) $J_{P\text{-}H}$ = 11.0 Hz

Instrumentation

Infrared spectra were recorded on a Mattson Polaris Fourier transform spectrophotometer, in the range 2200–400 cm^{-1}. Solution spectra were recorded using a 0.1 mm CaF_2 solution cell. Solid-state spectra were recorded as KBr discs. All spectra are reported in wavenumbers (cm^{-1}) and summarized in Table 1.

NMR spectra, both ^1H and ^{31}P, were recorded on a Varian VXR-400 spectrometer. For ^1H NMR spectra, residual solvent peaks were used as an internal reference. The aromatic proton signals were not assigned. An external sample of 85% H_3PO_4 in D_2O was used as a reference for the ^{31}P NMR spectra; this was assigned a shift of 0.0 ppm. ^{31}P NMR spectra are proton decoupled. Spectra recorded in H_2O used a sealed capillary containing D_2O for the lock. All chemical shifts (δ) are reported in ppm and all coupling constants (J) in Hz. ^{31}P NMR spectra are summarized in Table 1.

Reactions

NMR scale reactions with O_2 and SO_2 used pressures of 600 mmHg (1mmHg = 133.322 Pa). The reactions with mixtures of O_2 and SO_2 used 300 mmHg (1mmHg = 133.322 Pa) of each gas.

Reaction of *trans*-Ir(CO)(Cl)(TPPTS)$_2$ with SO_2

1 (0.1 g, 0.067 mmol) was dissolved in H_2O (10 mL) and then SO_2 was passed over the solution for 5 min. The solution immediately turned bright green and the IR spectrum indicated a single CO stretch at 2043 cm^{-1} that was assigned to the SO_2 complex, Ir(CO)Cl(SO_2)(TPPTS)$_2$ (**3**). Additionally a ^{31}P NMR spectrum, recorded using an internal D_2O standard, indicated a single product at 10.9 (s) ppm. Isopropanol was added to precipitate this product as a green solid. After the solid was vacuum dried an IR spectrum was recorded in KBr indicating **1** and **3**. This suggests that the addition of SO_2 is reversible. Precipitated solid: (KBr) ν_{CO} = 1980 cm^{-1} (**1**) (59%), ν_{CO} = 2017 cm^{-1} (**3**) (41%).

1 (25 mg, 0.017 mmol) was dissolved in D_2O and placed under an atmosphere of SO_2 (570 mmHg (1 mmHg = 133.322 Pa)). The solution immediately turned bright green. The initial ^{31}P NMR spectrum taken after 10 min revealed a single peak for **3**. The solution was left for several weeks under an SO_2 atmosphere, at which point a new, unassigned peak was observed at 44 ppm. Despite the acidic nature of the solution, the ^1H NMR spectrum showed no hydride signal. After several months, the peak at 44 ppm dominated and the solution was colorless. ^{31}P NMR (D_2O), 10 min: 10.9 (s) (**3**); several weeks: 44.1 (s) (23%), 10.9 (s) (**3**) (77%).

The procedure was repeated using d^6-DMSO. As with the reaction in D_2O a bright green solution formed within 10 min. Analysis by ^{31}P NMR spectroscopy showed the chemical shift for the product was similar to that for the reaction in D_2O. In this solvent there was also a peak observed at around 44 ppm after several weeks but in greatly reduced amounts (2% vs. 23% in D_2O). ^{31}P NMR (d^6-DMSO) 10 min 11.2 (s) (**3**); several weeks: 43.4 (s) (2%), 11.2 (s) (83%).

Results and discussion

Coordination of SO_2 to Ir(I) complexes has been extensively studied for many years (7–9). Coordination is reversible with a pyramidal SO_2 along the z axis. The reaction of SO_2 with *trans*-Ir(CO)(Cl)(TPPTS)$_2$ in water is very similar producing a single complex which, by comparison to previously published data (7, 8), could be identified as the SO_2 complex, Ir(CO)Cl(SO_2)(TPPTS)$_2$. The solid state IR data were very close to those for the analogous PPh_3 complex. The KBr spectrum for the TPPTS complex had a CO stretch at 2017 cm^{-1} compared to 2013 cm^{-1} for the equivalent PPh_3 complex (7). In addition, further support for the formation of this complex comes from the ^{31}P NMR data. The chemical shift for Ir(CO)Cl(SO_2)(P(*p*-tolyl)$_2$)$_2$ in d^8-toluene is reported at 10.3 (s) ppm, compared to 10.9 (s) ppm for the TPPTS complex in D_2O (8). The characterization data provide strong support for formation of Ir(CO)(Cl)(SO_2)(TPPTS)$_2$ although the product could not be isolated pure because of reversible SO_2 loss typical for such complexes (7–9).

The exclusive formation of the SO_2 complex is pH dependent. When SO_2 is added to water (pH $\cong$ 1.0) the composition is essentially hydrated SO_2 (10). In fact $SO_2 \cdot H_2O$ is the dominant species until the pH reaches about 1.5. As pH increases, the concentration of HSO_3^- increases. At pH 4 it is the major species in solution. Finally, above pH 6.5, SO_3^{2-} is the major species.

When the reaction of SO_2 with *trans*-Ir(CO)(Cl)(TPPTS)$_2$ was carried out at pH 2 there were some differences in the ^{31}P NMR spectrum from the solution with no pH control. Although the solution was still the characteristic green color of the SO_2 complex, there were two additional minor prod-

© 2001 NRC Canada

Table 2. Products of the reactions of SO_2 with *trans*-$Ir(CO)(Cl)(TPPTS)_2$ at different pHs.

pH	Product(s)
1 (Unbuffered)	**3**
2	**3** (81%), **5** (5%), 14% of unknown product with ^{31}P NMR at 17.4 (s) ppm
4	**3** (br) and **5** in equal amounts
6	**5**

ucts, one of which was shown by ^1H NMR spectrum to contain a hydride. As pH was increased, the amount of SO_2 complex decreased and the hydride-containing product **5** continued to grow as shown by a new resonance in the ^{31}P NMR spectrum at 1.9 (s) ppm together with the hydride signal in the ^1H NMR spectrum. At pH 6 there were more significant changes, the solution was a dark yellow color and the ^{31}P NMR spectrum showed the amount of hydride containing product had greatly increased. There was no signal for the SO_2 complex at this pH. The ^1H NMR spectrum confirmed that the new complex contained an iridium-hydride resonance at –13.3 ppm. These changes with pH are summarized in Table 2.

The identity of complex **5** would most likely be the six-coordinate species, $Ir(CO)Cl(H)(OH)(TPPTS)_2$. The characterization for this complex (^{31}P NMR = 1.9 ppm, ^1H NMR = –13.3 (t)) is similar to those for HCl addition (^{31}P NMR = 2.5 ppm, ^1H NMR = –15.8 (t)) and HBF_4 or H_2SO_4 addition (^{31}P NMR = 7.4, ^1H NMR = –14.8 (t)), but more similar in ^{31}P NMR shift to the neutral HCl addition product. The solution is considerably less acidic for formation of $Ir(CO)(Cl)(H)(OH)(TPPTS)_2$ than for the other hydride complexes.

An alternative could involve HSO_3^- coordination to iridium. There are very few examples of HSO_3^- coordination to metal centers. These can be formed by either insertion of SO_2 into a metal hydroxy bond (9) or hydrolysis of bound -SO_3R (11). One example was prepared from the reaction between *trans*-$Ir(CO)(OH)(P(p\text{-tolyl})_3)_2$ and SO_2. The product formed was assigned to $(HO_2SO)Ir(CO)(SO_2)(P(p\text{-tolyl})_3)_2$ (9).

Oxidation of SO_2 to sulfate has been shown to occur upon reaction of SO_2 with $Ir(CO)(Cl)(O_2)(PPh_3)_2$ (12). In water, the analogous reaction does not occur.

$$[1] \qquad Ir(CO)(Cl)(O_2)(TPPTS)_2{}^2 + SO_2 \rightarrow [\mathbf{A}] \rightarrow Ir(CO)(Cl)(SO_2)(TPPTS)_2$$

Instead a species **A** is formed quickly in high yield (eq. [1]). **A** can be precipitated by addition of isopropanol; **A** has a CO stretch at 2078 cm^{-1} and a ^{31}P NMR at –9.8 (s) ppm. If **A** is left in solution or redissolved in H_2O it rearranges to the SO_2 complex, $Ir(CO)(Cl)(SO_2)(TPPTS)_2$. We cannot unequivocally identify **A**, however the simplest suggestion involves SO_2 coordinated to the Ir(III) complex as a planar molecule. Planar coordination of SO_2 is preferred when the metal is in a higher oxidation state (14). The coordination site could be opened by Cl^- dissociation, expected to occur readily in aqueous solution. When the dioxygen is eliminated (several hours in solution) the SO_2 changes to the pyramidal geometry favored for Ir(I) (9).

The THF reaction between *trans*-$Ir(CO)Cl(PPh_3)_2$ and H_2SO_4 (15) formed a single product, $Ir(CO)Cl(SO_4)(PPh_3)_2$, via an unidentified hydride species. The ^1H NMR spectrum for reaction of H_2SO_4 with *trans*-$Ir(CO)(Cl)(TPPTS)_2$ in H_2O showed two hydrides, one of these (–15.8 (t) ppm) corresponds to the HCl addition product $Ir(CO)(Cl)_2(H)(TPPTS)_2$ (**7**) prepared independently and, in combination with the ^{31}P NMR data, confirms the presence of this complex.[3] The chemical shifts in the ^{31}P NMR (7.5 (s) ppm) and the IR spectra (ν_{CO} = 2060 $cm^{-1)}$ suggest that the other hydride complex (–14.8 (t) ppm, $J_{P\text{-}H}$ = 11 Hz) is the six-coordinate cation, $Ir(CO)(Cl)(H)(OH_2)(TPPTS)_2]^+HSO_4^-$. There was no evidence for formation of a sulfate complex.

A shift of the CO stretching mode to higher frequency in H_2O as compared to solid state (KBr) or DMSO solution was previously attributed to hydrogen bonding of water along the *z* axis of a square-planar complex (16). A similar shift is observed for three complexes reported in this manuscript, $Ir(CO)(Cl)(SO)_2(TPPTS)_2$, $Ir(CO)(Cl)(O_2)(TPPTS)_2$, and $Ir(CO)(Cl)_2(H)(TPPTS)_2$ indicating that the shift to higher frequency (30 cm^{-1}) in water is not limited to a specific geometry for the metal center.

Conclusions

The reaction with SO_2 in strongly acidic solution is the same as with similar square-planar complexes in organic solution. A single product is formed with data consistent for formation of square pyramidal $Ir(CO)Cl(SO_2)(TPPTS)_2$. The SO_2 is bound reversibly. There are significant differences when the pH is altered, as the pH increases a new product forms, $Ir(CO)Cl(H)(OH)(TPPTS)_2$, until at pH 6 it is the only complex present.

Acknowledgement

We are grateful to the Department of Energy, BES, Grant no. ER 13775 for support of this research.

References

1. L. Vaska and J.W. DiLuzio. J. Am. Chem. Soc. **83**, 2784 (1961).
2. J.D. Atwood. Coord. Chem. Rev. **83**, 93 (1988), and refs. therein.
3. (*a*) R.F. Heck. J. Am. Chem. Soc. **86**, 2796 (1964); (*b*) L. Vaska and J. DiLuzio. J. Am. Chem. Soc. **83**, 1262 (1961); **83**, 2784 (1961); (*c*) J. Chatt and B.L. Shaw. J. Chem. Soc. 5075 (1962); (*d*) L. Vaska. Science (Washington, D.C.), **140**, 809 (1963).

[2] The dioxygen complex was prepared as follows: **1** (100 mg, 0.067 mmol) was dissolved in deareated distilled water and O_2 was passed over the solution for 2 h. The IR spectrum of the solution indicated the presence of a single product, $Ir(CO)Cl(O_2)(TPPTS)_2$ (**2**). A sample of this solution was also analyzed by ^{31}P NMR showing a single peak at 6.5 ppm. IR ν_{CO}: 2040 cm^{-1} in H_2O; 2010 cm^{-1} in DMSO; 2008 cm^{-1} in KBr, $Ir(CO)Cl(O_2)(PPh_2(m\text{-}C_6H_4SO_3Na))_2$ characterization (13). IR (KBr) ν_{CO} = 2012 cm^{-1}, ^{31}P NMR (2-methoxyethanol–D_2O) = 12.8 (s) ppm.

[3] Characterization data for $Ir(CO)(Cl)_2(H)(TPPTS)_2$: ν_{CO} = 2066 cm^{-1}; ^{31}P NMR = 2.5 (s) ppm; ^1H NMR = –15.8(t, $J_{P\text{-}H}$ = 11.0 Hz).

© 2001 NRC Canada

4. H.J. Lawson and J.D. Atwood. J. Am. Chem. Soc. **111**, 6223 (1989).
5. (*a*) R.R. Ryan, P.G. Eller, and D.C. Moody. Inorg. Chem. **15**, 2442 (1976); (*b*) R.R. Ryan and D.C. Moody. J. Chem. Soc. Chem. Commun. 503 (1976); (*c*) J.E. Boyqs, C.M. Crain, and J.E. Whiteford. J. Phys. Chem. **61**, 482 (1957).
6. D.P. Paterniti, P.J. Roman Jr., and J.D. Atwood. Organometallics, **16**, 3371 (1997).
7. L. Vaska. Acc. Chem. Res. **1**, 335 (1968).
8. S.L. Randall, C.A. Miller, T.S. Janik, M.R. Churchill, and J.D. Atwood. Organometallics, **13**, 141 (1994).
9. C.A. Miller, C.H. Lake, M.R. Churchill, and J.D. Atwood. Organometallics, **14**, 5442 (1995).
10. F.A. Cotton and G. Wilkinson. Advanced inorganic chemistry. 5th ed. Wiley-Interscience, New York. 1988. pp. 519–520.
11. C.A. Poffenberger and A. Wojcicki. Inorg. Chem. **19**, 3795 (1980).
12. (*a*) R.W. Horn, E. Weissberger, and J.P. Collman. Inorg. Chem. **9**, 2367 (1970); (*b*) J.M. Ritchey, D.C. Moody, and R.R. Ryan. Inorg. Chem. **22**, 2276 (1983).
13. J. Kovacs, T.D. Todd, J.H. Reibenspies, F. Joó, and D.J. Darensbourg. Organometallics, **19**, 3963 (2000).
14. (*a*) W.A. Schenk. Angew Chem. Int. Ed. Engl. **26**, 98 (1987); (*b*) G.J. Kubas. Inorg. Chem. **18**, 182 (1979); (*c*) R.R. Ryan, G.J. Kubas, D.C. Moody, and P.G. Eller. Struct. Bonding (Berlin), **8**, 48 (1981).
15. J. Valentine, D. Valentine, and J.P. Collman. Inorg. Chem. **10**, 219 (1971).
16. D.P. Paterniti, P.J. Roman Jr., and J.D. Atwood. Organometallics, **16**, 3371 (1997).

© 2001 NRC Canada

Synthesis of sulfated mono- and ditertiary phosphines, complex chemistry and catalysis

H. Gulyás, A. Dobó, and J. Bakos

Abstract: Cyclic and bicyclic sulfates have been prepared from commonly available alcohols. Nucleophilic cleavage of the cyclic sulfates affords a new type of water-soluble mono- and ditertiary phophines bearing -OSO_3Li groups in distinguished positions in the molecular framework. Both phosphines have amphiphilic character. Reactions of the chiral **2** and the dppp analogue **5** with $[Rh(COD)Cl]_2$ and $Pt(PhCN)_2Cl_2$ provide novel zwitterionic complexes. Rhodium complexes of **2** and **5** have been successfully applied in liquid biphasic hydroformylation of styrene and octene-1. When the rhodium complex of **5** was used as catalyst in hydroformylation of styrene, less then 4 ppm rhodium could be detected in the organic phase.

Key words: cyclic sulfates, water soluble phosphines, amphiphilic character, Rh complexes, Pt complexes, hydroformylation.

Résumé : On a préparé des sulfates cycliques et bicycliques à partir d'alcools disponibles facilement. Le clivage nucléophilique des sulfates cycliques conduit à la formation d'un nouveau type de phosphines mono- et ditertiaires, solubles dans l'eau, portant des groupes -OSO_3Li dans des positions définies du squelette moléculaire. Les deux types de phosphines présentent un caractère amphiphilique. Les réactions du $[Rh(COD)Cl]_2$ et du $Ph(PhCN)_2Cl_2$ avec composé chiral **2** et de son analogue à la dppp, **5**, conduisent à la formation de nouveaux complexes zwitterioniques. On a pu appliquer avec succès les complexes **2** et **5** du rhodium à l'hydroformylation biphasique liquide du styrène et de l'oct-1-ène. Quand on a utilisé le complexe de rhodium **5** comme catalyseur dans l'hydroformylation du styrène, on n'a détecté que quatre ppm de rhodium dans la phase organique.

Mots clés : sulfates cycliques, phosphines solubles dans l'eau, caractère amphiphilique, complexes du rhodium, complexes du platine, hydroformylation.

[Traduit par la Rédaction]

Introduction

Much effort has been directed toward the synthesis of new catalytic species with recent focus on water-soluble catalysts (for recent reviews see ref. 1). Transition-metal complexes can easily be rendered water soluble by incorporating polar substituents (2) e.g., -SO_3Na, -CO_2Na, -OH, -PMe_3^+, -NMe_3^+, -$PO(ONa)_2$, and polyethers.

Recently we introduced a novel route to a new class of water-soluble phosphines (3). We have reasoned that this methodology will be of particular interest since: (*i*) a wide range of starting compounds (e.g., diol, triol, tetrol) is available; (*ii*) the synthesis is simple; and (*iii*) provides an easy access to a series of amphiphilic or water-soluble phosphines. Water solubility of these phosphines is provided by the -OSO_3Li group.

Salts of sulfuric acid hemiesters are known to be excellent detergents. For example sodium dodecylsulfate is used in many aqueous organometallic catalytic systems to improve the catalytic activity and (or) selectivity of the reaction (4). In our case the sulfate group is attached to the ligand itself, rendering it not only water-soluble, but also amphiphilic. To our knowledge, only a very few ligands with amphiphilic properties have been reported (5). These ligands are expected to increase the activity of organic–aqueous biphasic catalytic systems by improvement of the miscibility of the two liquid phases (6). Also quite few ligands are known, where the coordinating functional group is not affected by the group providing the water solubility (7). In these molecules the -PPh_2 unit is remote enough from the -OSO_3Li function so that the electronic nature of the -PPh_2 group will be unaffected.

Hemilabile ligands have recently come into focus. Weak coordination of a functional group can stabilize certain conformations of the catalytically active complex and improve the selectivity of a reaction (8). Another advantage of a

Received September 5, 2000. Published on the NRC Research Press Web site at http://canjchem.nrc.ca on July 14, 2001.

Dedicated to Professor Brian James on the occasion of his 65th birthday.

H. Gulyás. Research Group for Petrochemistry, Hungarian Academy of Science, H-8201 Veszprém, P.O. Box 158, Hungary.
A. Dobó. Central Research Institute for Chemistry of the Hungarian Academy of Sciences H-1025 Budapest, Pusztaszeri u. 59-67, Hungary.
J. Bakos.[1] Department of Organic Chemistry, University of Veszprém, H-8201 Veszprém, P.O. Box 158, Hungary.

[1]Corresponding author (telephone: (36) 88 422022/4355; fax: (36) 88 427492; e-mail: bakos@almos.vein.hu).

 DOI: 10.1139/cjc-79-5/6-1040 © 2001 NRC Canada

weakly coordinating functional group is that it can be easily replaced by the substrate resulting in an increase in the activity of the catalyst. A hard sulfate group is not expected to have strong coordination ability toward soft metal centers, but its labile coordination should not be overlooked.

We report here detailed synthetic route for the preparation of mono- and ditertiary phosphines. Complex formation and catalytic application of the model compounds are presented.

Experimental

General information

Synthesis of the phosphines and their complexes were carried out under a purified argon atmosphere using standard Schlenk-type techniques. Tetrahydrofuran (THF), diethyl ether (Et_2O), toluene, and benzene were distilled from sodium benzophenone ketyl under argon. Methylene chloride (CH_2Cl_2) and pyridine were distilled from CaH_2 and methanol (MeOH) was distilled from $Mg(OMe)_2$ under argon. Water (H_2O) was distilled twice under argon. Deuterated methanol and water (CD_3OD and D_2O) were deoxygenated by bubbling with argon for 10 min. Deuterated chloroform ($CDCl_3$) was deoxygenated by distillation under argon. Pentaerythritol was purchased from Aldrich and used as received. (2*R*,4*R*)-2,4-Pentanediol was prepared by the slightly modified literature method (9). GC analyses were performed using a Hewlett–Packard 5830A gas chromatograph (SPB-1 30 m column, film thickness (0.1 μm), N_2 carrier gas (2 mL min^{-1})). Optical rotations were obtained using a Schmidt Haensch 21245 polarimeter. Nuclear magnetic resonance spectra were recorded on a Varian Unity 300 and Bruker DRX-500 spectrometer using $CDCl_3$, CD_3COCD_3, D_2O, and CD_3OD as solvents. The ^1H and ^{13}C NMR chemical shifts are referenced to internal or external standard $SiMe_4$, and to residual portio-solvent peaks (i.e., $CHCl_3$). The ^{31}P NMR spectra were recorded with 85% H_3PO_4 as an external standard. The ^{195}PtNMR (64 MHz) chemical shift is given in ppm relative to Na_2PtCl_6 as an external standard. Positive chemical shifts are downfield from the standard. Adjustments of pH were performed using an OP-211/1 Laboratory Digital pH Meter. Rhodium content of the organic phase was determined by atom absorption using a PerkinElmer 5100 PC atom absorption spectrometer, electrothermal atomization HGA 600, AS 70 autosampler, and GEM software. Fast atom bombardment (FAB) mass spectrometric measurements were performed using a VG-ZAB-2SEQ reverse geometry instrument operating at an accelerating voltage of 8 kV. A cesium ion gun producing 30 keV ions was utilized for ion bombardment. Glycerol was used as the FAB matrix.

Catalysis

Two-phase hydroformylation reactions of styrene and 1-octene with rhodium complexes of **2** and **5** were carried out in a 20 mL stainless steel autoclave. The catalysts were made in situ. Mixing the water, toluene, alkene, phosphine, and $[Rh(COD)Cl]_2$ resulted in an orange emulsion which was transferred into the autoclave under argon atmosphere. The autoclave was pressurized with CO–H_2 and then placed in a heating mantle preheated to the desired reaction temperature. The autoclave was shaken at a frequency of 180 min^{-1}, 75 deg from the upright position, with a horizontal amplitude of 3 cm. The reaction was monitored by the change in pressure.

Leaching of rhodium was determined as follows: The toluene phase was separated. 0.5 mL of cH_2SO_4 and 1 mL of cH_2O_2 were added. Further 5x1mL of cH_2O_2 was added during one week. All volatiles were evaporated from the homogenous solution. 10 mL of deionised water and 0.1 g of Na_2SO_4 were added. Analysis was undertaken on a Perkin Elmer 5100 PC atom absorption spectrometer in conjunction with a series of rhodium standards.

Cyclic sulfates

Cyclic sulfate **1** was prepared using the general literature method described by Gao and Sharpless (10).

Synthesis of (4*R*,6*R*)-4,6-dimethyl-2,2-dioxide-1,3,2-dioxathiane (1)

Thionyl chloride (4.6 mL, 0.064 mol) was added, via a dropping funnel, to (2*R*,4*R*)-2,4-pentanediol (5.5 g, 0.053 mol) in 50 mL CCl_4. The resulting light brown solution was refluxed for 1 h to complete the sulfite formation. HCl was removed under reduced pressure (the water aspirator was adjusted to a quite gentle flow). CH_3CN (50 mL), $NaIO_4$ (16 g, 0.075 mol), and $RuCl_3$ hydrate (0.008 g, 0.032 mmol, 40% ruthenium) were added to the solution. The resulting brown mixture was cooled to 0°C and 75 mL of water was added slowly. The mixture turned orange within 5 min. The reaction was allowed to stir at ambient temperature for 1 h. The mixture was then diluted with Et_2O (400 mL). The organic phase was separated, washed with water (20 mL), saturated $NaHCO_3$ solution (2 × 20 mL), and brine (20 mL). After being dried over $MgSO_4$ the solution was filtered through a pad of SiO_2 to remove the ruthenium. The solvent was removed in vacuum. Recrystallization of the product from Et_2O–hexane yielded a white crystalline solid (8.85 g, 82%), mp 34 to 35°C. $[\alpha]_D^{24}$ = 37.5° (c 5.02, $CHCl_3$). ^1H NMR (300.15 MHz, $CDCl_3$) δ: 1.64 (d, J_{HCCH} = 6.6 Hz, 6H, CH_3), 2.03 (t, J_{HCCH} = 5.6 Hz, 2H, CH_2), 5.03 ppm (pseudo-sext due to signal overlap, 2H, CH). ^{13}C NMR (75.42 MHz, $CDCl_3$) δ (ppm): 20.0 (s, CH_3), 35.5 (s, CH_2), 80.3 (s, CH).

Synthesis of 2,4,8,10-tetraoxa-3,9-dithiaspiro[5.5]undecane 3,9-dioxide (3)

A solution of $SOCl_2$ (17.5 mL, 0.24 mol) in pyridine (20 mL) was added dropwise to a solution of pentaerythritol (13.6 g, 0.1 mol) in pyridine (250 mL). The reaction mixture was stirred for 3 h. The solvent, remaining $SOCl_2$, and most of the pyridine–hydrochloride were removed under reduced pressure. The brownish-white solid residue was washed with water, $NaHCO_3$ solution, water again, and with diethyl ether. After drying, the product was obtained as a white, microcrystalline solid (19.3 g, 85%), mp 152°C. ^1H NMR (500.13 MHz, CD_3COCD_3) δ: 3.929 (d, J_{HCH} = 12.0 Hz, 1H, CH_2), 3.934 (d, J_{HCH} = 12.0 Hz, 1H, CH_2), 4.406 (d, J_{HCH} = 12.1 Hz, 1H, CH_2), 4.411 (d, J_{HCH} = 12.1 Hz, 1H, CH_2, 4.61 (d, J_{HCH} = 12.1 Hz, 2H, CH_2), 4.94 ppm (d, J_{HCH} = 12.3 Hz, 2H, CH_2). ^{13}C NMR (75.42 MHz, CD_3COCD_3) δ (ppm): 35.68 (s, C), 59.95 (s, CH_2), 59.99 (s, CH_2).

© 2001 NRC Canada

Synthesis of 2,4,8,10-tetraoxa-3,9-dithiaspiro[5.5]undecane 3,3,9,9-tetraoxide (4)

$NaIO_4$ (54.3 g, 0.25 mol) and $RuCl_3$ hydrate (27.2 mg, 0.107 mmol, 40% ruthenium) were added to the bicyclic sulfite **3** (19.3 g, 0.085 mol) in 400 mL of CH_3CN. Water (240 mL) was added slowly to the brown suspension. The mixture turned orange and a considerable amount of white solid precipitated. The reaction was stirred further for 1.5 h. The white solid was filtered and washed exhaustively with water. The white residue was dried at ambient temperature and extracted with hot acetone. Removal of the solvent under reduced pressure yielded a white, microcrystalline solid (17.6 g, 68% calculated for pentaerythritol), mp 280–282°C. ^{1}H NMR (300.15 MHz, CD_3COCD_3) δ (ppm): 5.01 (s, 8H, CH_2). ^{13}C NMR (75.42 MHz, CD_3COCD_3) δ (ppm): 34.30 (s, C), 74.4 (s, CH_2).

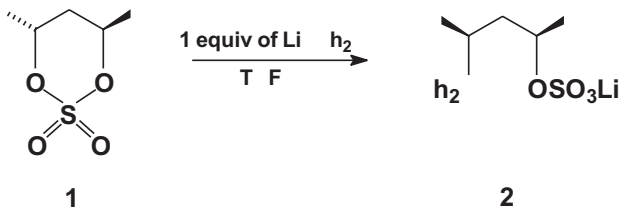
Synthesis of (2*R*,4*S*)-4-(diphenylphosphino)-pent-2-yl sulfate lithium salt (2)-butyl sulfate lithium salt

(4*R*,6*R*)-4,6-Dimethyl-2,2-dioxide-1,3,2-dioxathiane (**1**) (2.0 g, 0.012 mol) in THF (15 mL) was added to $LiPPh_2$·dioxane adduct (4.4 g, 0.016 mol) in THF (50 mL) at 0°C, meanwhile the bright red color turned light brown. The mixture was stirred at ambient temperature for 1 h. The THF was removed under reduced pressure, then deoxygenated water (40 mL) and Et_2O (20 mL) were added. The aqueous phase was separated and washed with Et_2O (20 mL) again. The pH of the solution was adjusted to 7.0 using diluted H_2SO_4 solution. The water was removed under reduced pressure, then CH_2Cl_2 (20 mL) was added. Li_2SO_4 was removed by filtration. Evaporation of the solvent under vacuum yielded a white, solid foam (3.1 g, 72%). FAB-MS$^-$: 351 (M – Li$^+$). ^{1}H NMR (300.15 MHz, $CDCl_3$) δ (ppm): 0.84 (dd, J_{PCCH} = 15.1 Hz, J_{HCCH} = 6.6 Hz, 3H, CH_3), 1.01 (d, J_{HCCH} = 6.0 Hz, 3H, CH_3), 1.02 (overlapped by the signal of CH_3, 1H, diastereotopic CH_2), 1.57 (br m, 1H, diastereotopic CH_2), 2.55 (br s, 1H, C*H*-PPh_2), 4.49 (br m, 1H, C*H*-OSO_3Li), 6.91 (br m, 6H, Ar), 7.23 (br m, 4H, Ar). ^{31}P NMR (121.42 MHz, $CDCl_3$) δ (ppm): 1.13. ^{13}C NMR (125.77 MHz, D_2O) δ: 17.99 (d, J_{PCC} = 14.7 Hz, *C*H_3-CH-PPh_2), 23.40 (s, *C*H_3-CH-OSO_3Li), 27.37 (d, J_{PC} = 6.9 Hz, CH_3-*C*H-PPh_2), 42.63 (d, J_{PCC} = 15.8 Hz, *C*H_3-CH-OSO_3Li), 77.71 (d, J_{PCCC} = 12.3 Hz, CH_3-*C*H-OSO_3Li), 131.03 (s, Ar), 131.50 (d, J_{PCC} = 6.3 Hz, Ar), 135.99 (d, J_{PCC} = 17.6 Hz, Ar), 138.41 (d, J_{PCC} = 32.7 Hz, Ar).

Preparation of 1,3-bis(diphenylphosphino)-2,2-bis(lithiumsulfatemethyl)-propane (5)

2,4,8,10-Tetraoxa-3,9-dithiaspiro[5.5]undecane 3,3,9,9-tetraoxide (**4**) (3.0 g, 0.012 mol) in THF (20 mL) was added to $LiPPh_2$·dioxane adduct (8.4 g, 0.035 mol) in THF (60 mL) at 0°C, meanwhile the red color of the reaction mixture faded. The mixture was stirred at ambient temperature for 1 h. The THF was removed under reduced pressure, then deoxygenated water (40 mL) and Et_2O (20 mL) were added. After separation of the phases, the aqueous phase was washed with Et_2O (20 mL) again. The pH of the solution was adjusted to 7.0 using a diluted H_2SO_4 solution. The water was removed under reduced pressure, then CH_2Cl_2 (20 mL) and CH_3OH (6 mL) were added. Li_2SO_4 was removed by filtration. The solvent was evaporated in vacuum

Scheme 1.



to give a white solid foam (5.42 g, 73%). FAB-MS$^-$: 637 (M – Li$^+$). ^{1}H NMR (500.13 MHz, D_2O) δ (ppm): 2.28 (s, 4H, CH_2), 3.89 (s, 4H, CH_2), 6.89 (m, 8H, Ar), 6.95 (t, J_{HCCH} = 7.1 Hz, 4H, Ar), 7.09 (m, 8H, Ar). ^{31}P NMR (202.45 MHz, D_2O) δ (ppm): –28.9. ^{13}C NMR (125.77 MHz, D_2O) δ (ppm): 33.05 (m, CH_2), 42.20 (t, J_{PCC} = 12.1 Hz, C), 71.62 (m, CH_2), 128.98 (d, J_{PCCC} = 3.8 Hz, Ar), 129.29 (s, Ar), 133.15 (d, J_{PCC} = 21.4 Hz, Ar), 138.35 (d, J_{PC} = 7.5 Hz, Ar).

Results and discussion

Preparation of cyclic sulfates

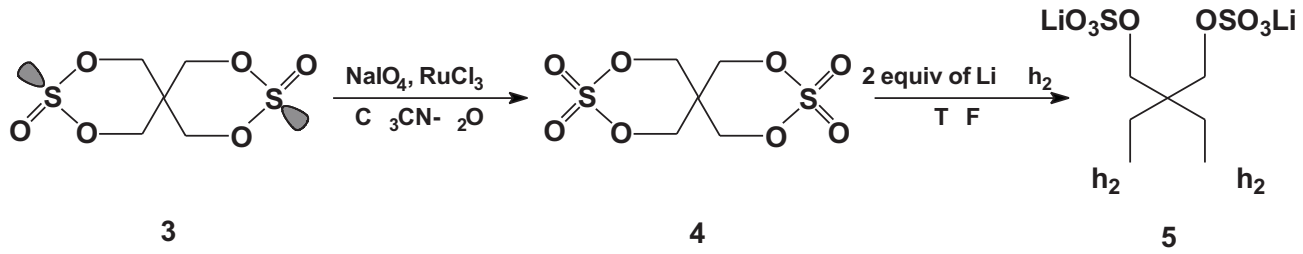
Cyclic sulfate of (2*R*,4*R*)-2,4-pentanediol (**1**) (Scheme 1) was obtained by a simple one pot reaction following the procedure developed for 1,2-cyclic sulfates by Gao and Sharpless (10). The synthesis involves the treatment of diols with thionyl chloride followed by ruthenium-catalyzed oxidation. Sulfate **1** could be obtained in this way with high yield (82%).

The bicyclic sulfate of pentaerythritol (**4**) could not be prepared by the general literature method. Pentaerythritol and $SOCl_2$ react with negligible reaction rate in CCl_4, which is the recommended solvent for the sulfite formation. Obviously, this fact is due to the poor solubility of the tetrol in CCl_4. Although, upon addition of dioxane to the CCl_4, the bicyclic sulfate could be isolated after the oxidation step, the yield was still very poor (17%).

To gain the product in a satisfying yield, a different procedure has been developed for the synthesis of **4** (Scheme 2). (*i*) The formation of sulfite and the oxidation were carried out in consecutive manner by the isolation of the intermediate sulfite **3**. Reaction of pentaerythritol and $SOCl_2$ in pyridine provided the corresponding bicyclic sulfite **3** with good yield (85%). Even though this spiro-compound is a known molecule of great practical importance (11), its stereochemistry has not been discussed in the literature in details. In a double chair conformation this molecule should have a C_2 axis as the only symmetry element, but its ^{1}H NMR spectrum exhibits a more complex picture. Details of the stereochemical investigation of the bicyclic sulfite will be presented in a subsequent publication. (*ii*) Racemic bicyclic sulfite was dissolved in CH_3CN. $NaIO_4$ and a catalytic amount of $RuCl_3 \cdot 3H_2O$ were added. Slow addition of water to this mixture initiated the oxidation. The crude product was precipitated from the reaction mixture spontaneously. The modified procedure afforded the bicyclic sulfate ester **4** in a 68% overall yield after purification.

© 2001 NRC Canada

Scheme 2.



3 4 5

Preparation, stability, and characterization of the novel phosphines

The monotertiary phosphine **2** has been prepared by the nucleophile cleavage of the cyclic sulfate of (2*R*,4*R*)-2,4-pentanediol **1** with $LiPPh_2$ in THF (Scheme 1). Nucleophilic attack occurred with complete inversion at the stereogenic center.

The bicyclic sulfate ester **4** reacts smoothly with 2 equivalents of $LiPPh_2$ to give the new water-soluble "sulfated" phosphine **5**, which has two hydrophilic tails attached to the bridgehead carbon atom (Scheme 2). It is interesting to note that the ditertiary phosphine **5** is a structural analogue of the well-known ligands dppp (1,3-(diphenylphosphino)propane) and dpppts (tetrasulfonated dppp). Both dppp and dpppts have important catalytic applications (12).

Although it is known that an ionic sulfate group can act as a leaving group (13), it was clear that its anionic nature renders it kinetically much less reactive than a $ROSO_2OR'$. The negative charge decreases the polarity of C—O bond, and the electrostatic repulsion between the "leaving group" and an anionic attacking group also increases the activation energy of the substitution. Accordingly, no replacement of the $-OSO_3Li$ was experienced in THF at ambient temperature, even when an excess of $LiPPh_2$ was used. The sulfated phosphines proved to be stable in hot, neutral, or slightly basic aqueous solution also. For example, when the aqueous solution of **5** was heated at 80°C for 1 h, or the aqueous solution of **2** was heated at 90°C, pH = 10 for several hours no appreciable amount of decomposition or hydrolysis could be detected.

NMR and FAB-MS data are in agreement with the formula in the case of both phosphines. Both phosphines feature amphiphilic character. For example, at ambient temperature solubility of **2** is 490 g L^{-1} in H_2O and 290 g L^{-1} in CH_2Cl_2. For a comparison, the water solubility of TPPMS (monosulfonated triphenylphosphine) having about the same size and one sulfonate group is 12 g L^{-1} (14). Ditertiary phosphine **5** with two sulfated tails attached to the bridgehead carbon atom has a great water solubility and is also soluble in a number of organic solvents (alcohols, THF).

Characterization of Rh(I) and Pt(II) complexes

Rh(I) and Pt(II) complexes are often applied catalysts in homogenous catalysis (15). To study the coordination features of the new phosphines, reactions of **2** and **5** with $[Rh(COD)Cl]_2$ (COD = 1,5-cyclooctadiene) and $Pt(PhCN)_2Cl_2$ were carried out. Reactions were monitored by ^{31}PNMR spectroscopy since the coordination shifts and metal–phosphorus coupling constants are diagnostic features for the identification of the products.

Coordination chemistry of the ligands with rhodium

The monotertiary phosphine **2** was reacted with $[Rh(COD)Cl]_2$ at a 2:1 phosphorus:Rh ratio in CD_3OD and D_2O (Scheme 3). In both solvents two complexes were formed and some of the ligand remained uncoordinated. The ^{31}P NMR spectrum (CD_3OD) exhibited resonances at 36.8 ppm (d, $J_{Rh\text{-}P}$ = 147 Hz) and 30.4 ppm (d, $J_{Rh\text{-}P}$ = 147 Hz). The coordination shifts ($\Delta\delta = \delta_{complex} - \delta_{free\ ligand}$) are 29.5 and 35.9 ppm, respectively. Relative intensity of the two doublets (signal at 30.4 ppm compared to the signal at 36.8 ppm) was 0.3. The broad signals were indicative of a dynamic equilibrium between the complexes and the free ligand, which was more significant in D_2O than in CD_3OD. For example doublet character of the signal at 30.4 ppm was not perceptible in D_2O.

We presumed that $[Rh(COD)Cl]_2$ was cleaved by 2 equiv of the phosphine to give complex **I**, but the substitution of chloride leading to complex **II** did not take place completely. To prove our hypothesis, the experiment was repeated in CD_3OD saturated with KCl. Under these conditions, chloride substitution didn't take place at all, which resulted in the disappearance of the doublet at 30.4 ppm and an increase in the intensity of the signal of the free ligand.

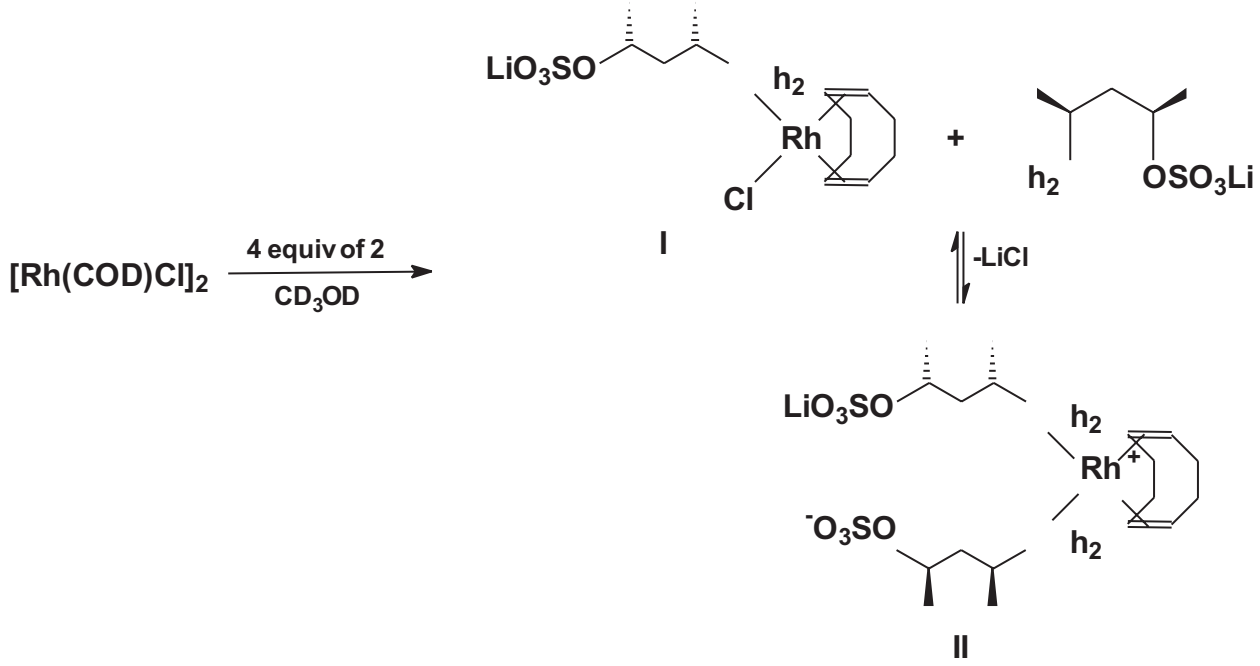
When ligand **2** was reacted with $[Rh(COD)Cl]_2$ at a 1:1 or lower phosphorus:Rh ratio in CD_3OD the doublet at 30.4 ppm was absent from the spectrum again. When phosphorus:Rh ratio was increased to 4, the relative intensity of the two signals (30.4 vs. 36.8 ppm) was found to increase to 0.66, and a new species appeared at about 50 ppm. All signals were broad probably as a result of an exchange between the free and coordinated phosphine. Doublet character of the signal at 36.8 ppm and multiplicity of the new resonance were not observable. Finally, $[Rh(COD)Cl]_2$ was treated with $AgNO_3$ in CD_3OD to obtain $[Rh(COD)(CD_3OD)_2]NO_3$. This complex, with two weakly coordinating ligands, was reacted with 2 equiv of the phosphine. Now the spectrum displayed only a doublet at 30.4 ppm.

These results clearly indicate that the doublet at 36.8 ppm belongs to the complex **I**, and the other doublet at 30.4 ppm can be assigned to the complex **II**. Chemical shifts are consistent with the proposed structures. Since chloride is expected to be a weaker σ-donor and a stronger π-acceptor ligand than phosphine **2**, electron density of the central atom should be larger in **II** than in **I** resulting a more downfield resonance for complex **I**.

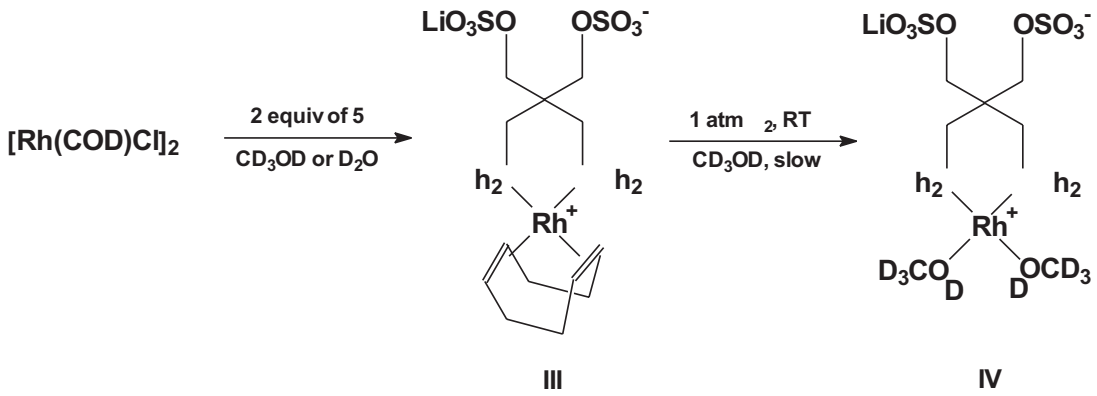
When chelating phosphine **5** was reacted in a 2:1 ratio with $[Rh(COD)Cl]_2$ in CD_3OD or D_2O–EtOAc, complex **III** formed as the only species (Scheme 4). ^{31}P NMR data of **III** (δ 13.9 ppm (d, J_{RhP} = 141 Hz), in CD_3OD or D_2O) do not significantly differ from that of the analogue complex of

© 2001 NRC Canada

Scheme 3.



Scheme 4.



dppp (16). MS-FAB$^+$ and MS-FAB$^-$ spectra of the complex showed parent ions [M + Li^+] (*m*/*z* = 855) and [M – Li^+] (*m*/*z* = 848). A zwitterionic structure for the complex is suggested in which one of the -OSO_3^- groups of the ligand acts as a counterion for the rhodium.

When H_2 was bubbled into the solution of **III**, a minor amount (13% based on ^{31}P NMR) of complex **IV** arose (δ 37.5 ppm (d, J_{RhP} = 187 Hz) in CD_3OD). The relative resistance of **III** against oxidative addition of H_2 is not surprising. Analogous complexes behave in a similar way as described in the literature (16). Complexes containing NBD (NBD = 2,5-bicyclo[2.2.1]heptadiene) instead of COD tends to react with hydrogen without difficulty, since NBD is easily saturated under a hydrogen atmosphere (17).

Coordination chemistry of the ligands with Pt(II)

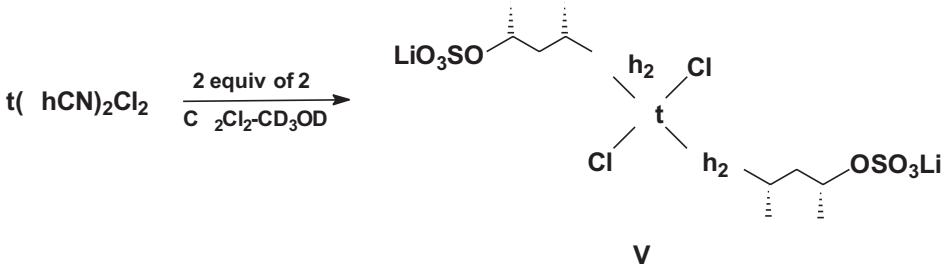
When amphiphilic phosphine **2** was reacted in a 2:1 ratio with $Pt(PhCN)_2Cl_2$ in CH_2Cl_2 or in a mixture of CH_2Cl_2 and MeOH, complex **V** formed exclusively. ^{31}P NMR spectrum of the complex is characteristic of a square-planar, *dsp*^{2} hybrid PtP_2X_2 species (δ 27.7 (s, $J_{Pt\text{-}P}$ = 2544 Hz) in CD_3OD). The value of $J_{Pt\text{-}P}$ clearly indicates the presence of two phosphine ligands *trans* to each other (Scheme 5).

Compound **5** forms three complexes when reacted in a 1:1 ratio with $Pt(PhCN)_2Cl_2$ in a mixture of CH_2Cl_2–D_2O. Complex **VI** (δ –1.8 ppm (s, $J_{Pt\text{-}P}$ = 3467 Hz), in D_2O), **VII** (δ –3.0 ppm (s, $J_{Pt\text{-}P}$ = 2215 Hz), in D_2O), and **VIII** (δ –6.8 ppm (s, $J_{Pt\text{-}P}$ = 3438 Hz), in D_2O) are generated in a 1:0.81:0.73 ratio (Scheme 6). ^{31}P NMR data clearly indicated that both of the phosphorus on the chelating ligand are coordinated and that they are equivalent (i.e., the other two coordination sites should be occupied by the same species in each complex). The coupling values of $J_{Pt\text{-}P}$ of **VI** and **VIII** suggested chloride or solvent coordination *trans* to the phosphorus, whereas $J_{Pt\text{-}P}$ of **VII** is characteristic of Pt(II) phosphine complexes with phosphorus atoms *trans* to each other.

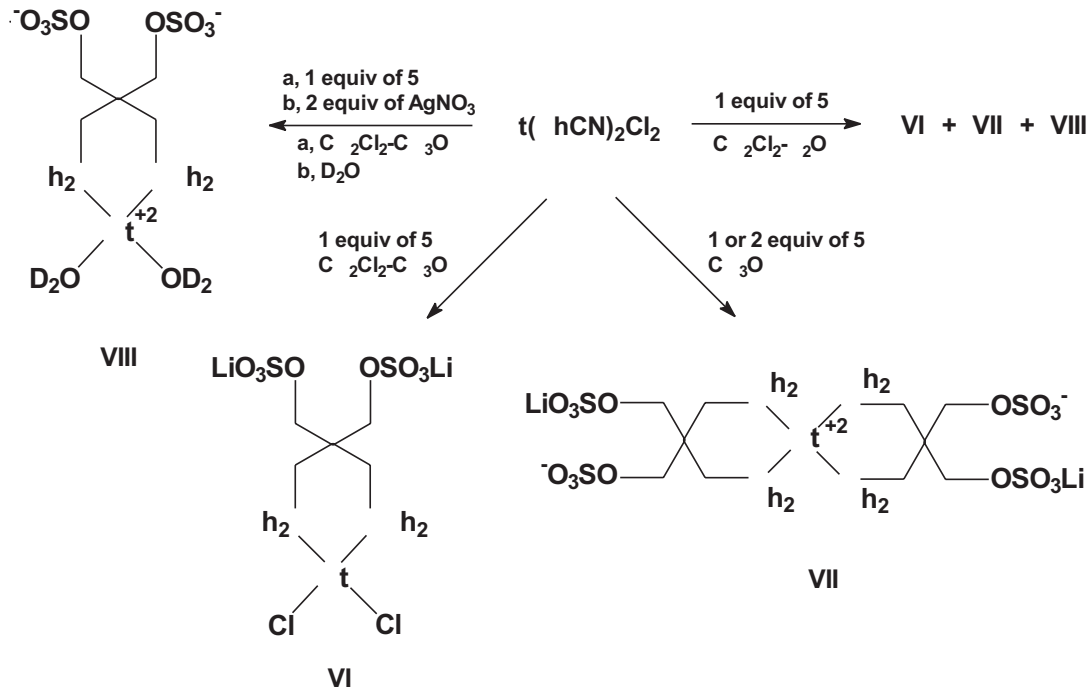
Complex **VII** could be obtained as the only product from the reaction mixture when the experiment was carried out in

© 2001 NRC Canada

Scheme 5.



Scheme 6.



CD_3OD at a 1:1 or 1:2 ligand:metal ratio. Some of the starting complex remained unreacted when a 1:1 ligand to platinum ratio was used. Based on the ^{31}P NMR data and the experimental evidence, either a dimeric or a monomeric square-planar PtP_4 structure could be imagined for complex **VII**. The $^{195}Pt\{^1H\}$-NMR spectrum clearly showed the presence of four equivalent phosphorus atoms coordinating to the platinum (δ –5011 ppm (q, $J_{Pt\text{-}P}$ = 2215 Hz), in D_2O) (Fig. 1). This fact confirms the square-planar, zwitterionic PtP_4 structure, in which two OSO_3^- groups act as counter ions for the central atom. Further evidence of the structure was obtained by FAB-MS spectroscopy. The parent ion [M – Li^+] was detected and the measured isotopic distribution showed nice agreement with the simulated one (Fig. 2). Note that the formation of **VII** as a single product even at a 1:1 ligand-to-metal ratio under the conditions above is probably due to the poor solubility of the precursor in MeOH and as a consequence an excess of the ligand was present in the solution.

To inhibit the substitution of chlorides either by a second phosphine ligand or solvent, the ligand was dissolved in MeOH and was added to a CH_2Cl_2 solution of the precursor [$Pt(PhCN)_2Cl_2$] in a 1:1 ratio (Scheme 6). In this case only one complex was formed which was assumed to be complex **VI** based on ^{31}P NMR data (CD_3OD, δ –1.5 ppm (s, $J_{Pt\text{-}P}$ = 3445 Hz), in CD_3OD). The slight difference in the spectroscopic data is probably due to the different nature of the solvent.

Dichloro-complex **VI** could be transformed into the aqua complex **VIII** by treatment with $AgNO_3$ in H_2O (D_2O) or with CF_3SO_3Ag in a THF–H_2O (D_2O) solvent mixture. A negligible amount of **VII** was also formed in both cases. Since the NMR data of the complex **VIII** are independent of the applied silver salt, strong coordination of NO_3^- or $CF_3SO_3^-$ can be excluded. The broad resonances of complex **VIII** were indicative of an exchange of H_2O molecules in the coordination sphere.

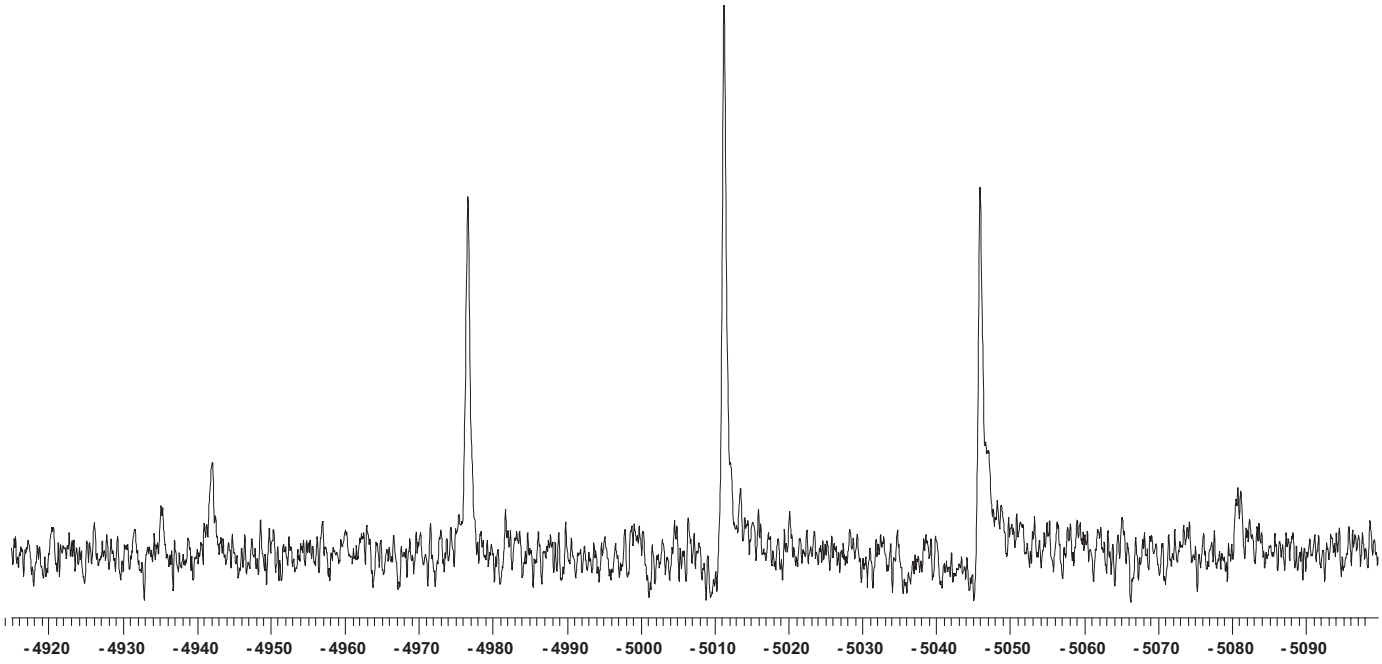
Hydroformylation of styrene and octene-1

Rhodium complexes of **2** and **5** were used for hydroformylation of styrene and octene-1 (Scheme 7). Both systems proved to be suitable catalysts for hydroformylation (Table 1).

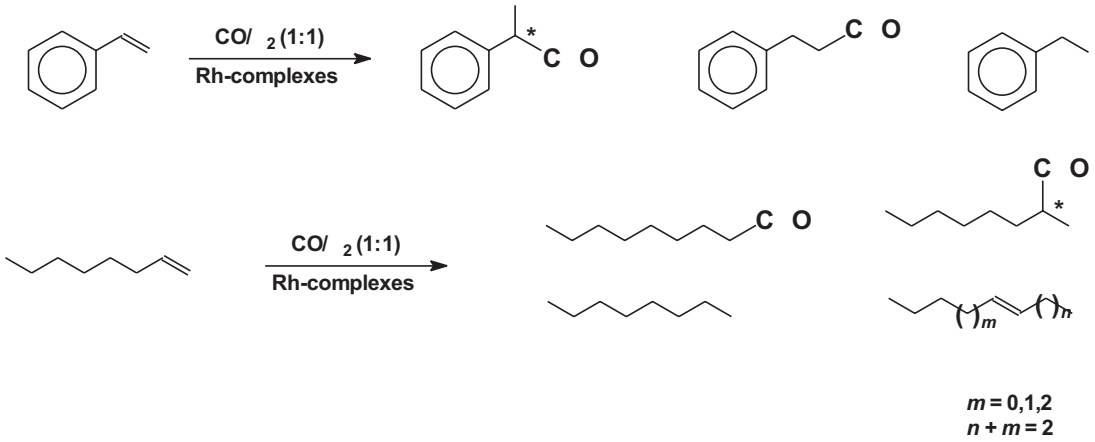
Ligands **2** and **5** gave complete chemoselectivity toward hydroformylation of styrene: no hydrogenation of the substrate was observed.

© 2001 NRC Canada

Fig. 1. ^{195}Pt NMR spectrum of the complex **VII**.



Scheme 7.



Up to 90% regioselectivity towards the more valuable branched aldehyde was observed when **2** was used as the ligand. At the same time, though, no optical induction was detected. It is not surprising, since optically active monodentate ligands usually provide very poor enantioselectivity even in relatively apolar medium. Additionally, the enantiomeric excess of the chiral products obtained in aqueous media is generally much lower than in organic solvents (17). An explanation for the lower enantiomeric excess could be the partial racemization via an enol intermediate, which is known to proceed swiftly in protic media (18). The evaluation of the suitability of the chiral ligand **2** for other asymmetric catalysis is in progress.

The rhodium complex of **5** gives a lower regioselectivity (81%) in a toluene–H_2O two-phase system. An important finding was that after separation of the phases, less than 4 ppm of the rhodium with respect to the amount of the rhodium catalyst employed was detected in the colorless organic phase. The aqueous phase could be recycled. The decrease in activity is probably due to the partial oxidation of the phosphine and a small loss of the catalyst during phase separation. In the absence of organic solvent, the regioselectivity toward the branched aldehyde increased to 86%.

No hydrogenation side product was observed in the hydroformylation of octene-1 either, although both ligands allow a moderate isomerization of the substrate (Table 2). Both ligands provide rather low selectivity under the applied conditions toward the more valuable normal aldehyde. Increasing the ligand **2**:rhodium ratio from 2 to 4 led to a slight increase in selectivity to *n*-aldehyde, but the activity

© 2001 NRC Canada

Table 1. Hydroformylation of styrene.

Ligand	Subst./Rh	Solvent	*T* (°C)	*t* (h)	Conv. (%)	Selectivity b/n (%)
2[a]	250	PhMe–H_2O	60	3	100	90/10
5[b, c]	300	PhMe–H_2O	80	4	100	81/19
5[d]	300	PhMe–H_2O	80	12	95	81/19
5[e]	300	PhMe–H_2O	80	12	84	79/21
5[f]	300	H_2O	80	10	87	86/14

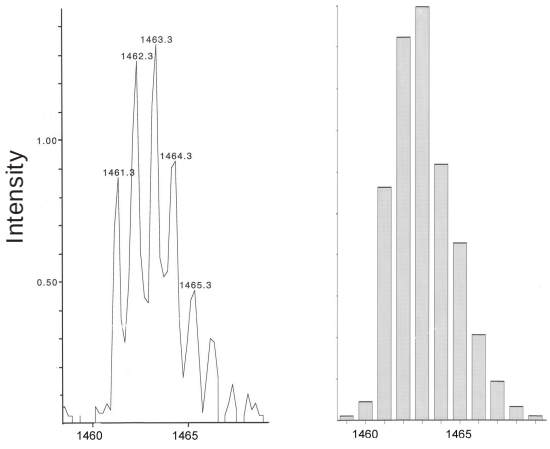
Note: Conditions: catalyst: $[Rh(COD)Cl]_2$ + ligand; initial pressure: 70 bar ($CO:H_2$ = 1:1); P/Rh = 2.2; water (3mL); toluene (3 mL) (if used).
[a][Rh] = 1.0×10^{-2} M.
[b][Rh] = 2.2×10^{-2} M.
[c]Less than 4 ppm rhodium could be detected in the organic phase.
[d]First recycling of the aqueous phase.
[e]Second recycling of the aqueous phase.
[f][Rh] = 2.9×10^{-2} M.

Table 2. Hydroformylation of octene-1.

							Select. (%)			
Ligand	Subst./Rh	P/Rh	Solvent	*T* (°C)	*t* (h)	Conv. (%)	isom[a]	n-ald	b-ald[b]	n/b
2[c]	250	2.05	H_2O	60	6	100	2.6	53.7	43.7 (4.7)	1.23
2[c]	250	2.20	PhMe–H_2O	60	6	100	2.8	53.4	43.8 (5.3)	1.21
2[c]	250	4.00	PhMe–H_2O	60	8	79	7.1	59.1	33.8 (-)	1.75
5[d]	300	2.40	PhMe–H_2O	80	5	99	5.8	46.7	47.5 (11.5)	0.98
5[d]	300	2.40	H_2O	80	17	85	16.0	53.5	30.5(0.3)	1.75

Note: Conditions: catalyst: $[Rh(COD)Cl]_2$ + ligand; initial pressure: 70 bar ($CO:H_2$ = 1:1), 3.5 mL of water, 3.5 mL of toluene (when used).
[a]Percentage of 2-, 3-, 4-octenes formed.
[b]Percentage of 2-ethylheptanal and 2-propylhexanal formed.
[c][Rh] = 1.5×10^{-2} M.
[d][Rh] = 2.9×10^{-2} M.

Fig. 2. Measured and simulated isotopic distribution of the parent ion of the complex **VII** (FAB-MS^-:M – Li^+).



decreased. The complex modified with **5** provided the highest normal:branched ratio in a substrate–water two-phase system, but a considerable amount of isomerized octenes was formed.

Conclusions

We have discovered a versatile route for the synthesis of water-soluble mono- and ditertiary phosphines. The starting materials are readily available, and the transformations highly selective. The synthetic route is sufficiently flexibile to allow fine tuning of the structure of water-soluble ligands. Reaction of **2** with $[Rh(COD)Cl]_2$ resulted in an equilibrium of Rh(COD)Cl(**2**) and zwitterionic $Rh(COD)(\mathbf{2})_2$ complexes, meanwhile **5** gave the zwitterionic Rh(COD)(**5**) complex as the only product. Treatment of **2** with $Pt(PhCN)_2Cl_2$ gave the square-planar *trans*-$PtCl_2(\mathbf{2})_2$ complex. Reaction of **5** with $Pt(PhCN)_2Cl_2$ in a D_2O–CH_2Cl_2 two-phase system provided three complexes, which could be identified as $PtCl_2(\mathbf{5})$, and zwitterionic complexes $Pt(\mathbf{5})_2$ and $Pt(D_2O)_2(\mathbf{5})$.

Rhodium complexes of **2** and **5** could be successfully applied as catalysts for hydroformylation of styrene and octene-1. The use of **2** in the hydroformylation of styrene resulted in high regioselectivity toward the branched aldehyde (up to 90%), however, no optical induction was observed. When the rhodium complex of **5** was applied as a catalyst in the biphasic hydroformylation of styrene, only 4 ppm of rhodium could be detected in the organic phase.

The application of these sulfated phosphines in other biphasic and aqueous transition-metal catalyzed reactions is being studied.

Acknowledgements

Financial support from Hungarian National Science Foundation (OTKA T 032 004) is gratefully acknowledged. We are grateful to Mr. Béla Édes for skillful assistance in the synthetic and catalytic experiments.

References

1. Recent reviews see: (*a*) F. Joó and Á. Kathó. J. Mol. Catal. A: Chem. **116**, 3 (1997); (*b*) B. Cornils, W.A. Herrmann, and

© 2001 NRC Canada

R.W. Eckl. J. Mol. Catal. A: Chem. **116**, 27 (1997); (*c*) I.T. Horváth and F. Joó. Aqueous organometallic chemistry and catalysis. Kluwer Academic Publishers, Dordrecht. 1995.
2. (*a*) W.A. Herrmann and C.W. Kohlpainter. Angew. Chem. Int. Ed. Engl. **32**, 1524 (1993); (*b*) P. Kalck and F. Monteil. Adv. Organometal. Chem. **34**, 219 (1992); (*c*) M. Barton and J.M. Atwood. J. Coord. Chem. **24**, 43 (1991); (*d*) M.J. Russel. Platinum Met. Rev. **32**, 179 (1988).
3. H. Gulyás, P. Árva, and J. Bakos. Chem. Commun. 2385 (1997).
4. (*a*) G. Oehme, E. Paetzold, and R. Selke. J. Mol. Catal. **71**, L1 (1992); (*b*) A. Kumar, G. Oehme, J.P. Roque, M. Schwarze, and R. Selke. Angew. Chem. **106**, 2272 (1994); (*c*) S. Trinkhaus, R. Kadyrov, R. Selke, J. Holz, L. Götze, and A. Börner. J. Mol. Catal. A: Chem. **144**, 15 (1999), and refs. therein.
5. (*a*) H. Ding, B.E. Hanson, T. Bartik, and B. Bartik. Organometallics, **13**, 3761 (1994); (*b*) D.J. Bauer, J. Fischer, S. Kuchen, K.P. Langhans, O. Stelzer, and N. Werferling. Z. Naturforsch. B: Chem. Sci. **49**, 1511 (1994); (*c*) T. Okano, N. Harada, and J. Kiji. Chem. Lett. **6**, 1057 (1994); (*d*) E. Valls, J. Suades, B. Donadieu, and R. Mathieu. Chem. Commun. 771 (1996); (*e*) M.S. Goedheijt, B.E. Hanson, J.N.H. Reek, P.C.J. Kamer, and P.W.N.M. van Leeuwen. J. Am. Chem. Soc. **122**, 1650 (2000).
6. B. Fell and G. Papandogianakis. J. Mol. Catal. **66**, 143 (1991).
7. (*a*) H. Ding, B.E. Hanson, and J. Bakos. Angew. Chem. Int. Ed. Engl. **34**, 1645 (1995); (*b*) H. Ding, J. Kang, B.E. Hanson, and C.W. Kohlpaintner. J. Mol. Catal. A: Chem. **124**, 21 (1997).
8. (*a*) N. Nomura, J. Jin, H. Park, and T.V. RajanBabu. J. Am. Chem. Soc. **120**, 459 (1998); (*b*) M. Nandi, J. Jin, and T.V. RajanBabu. J. Am. Chem. Soc. **120**, 459 (1998), and refs. therein.
9. (*a*) K. Ito, T. Harada, A. Tai, and Y. Izumi. Chem. Lett. 1049 (979); (*b*) K. Ito, T. Harada, A. Tai. Bull. Chem. Soc. Jpn. **53**, 3367 (1980).
10. Y. Gao and K.B. Sharpless. J. Am. Chem. Soc. **110**, 7538 (1988).
11. (*a*) A. Guenther, T. Koenig, W.D. Habicher, and K. Schwetlick. Polym. Degrad. Stab. **55**, 209 (1997); (*b*) Polym. Degrad. Stab. **60**, 385 (1998); Polym. Degrad. Stab. **64**, 115 (1999).
12. (*a*) E. Drent, J.A.M. van Broekhoven and M.J. Doyle. J. Organomet. Chem. **417**, 235 (1991); (*b*) E. Drent. Pat. Appl. EP 121 965 (1984) (to Shell); (*c*) G. Verspui, G. Papadogianakis, and R.A. Sheldon. Chem. Commun. 401 (1998).
13. M.J. Burk, A. Pizzano, J.A. Martin, L.M. Liable-Sands, and A.L. Rheingold. Organometallics, **19**, 250 (2000), and refs. therein.
14. B. Salvesen and J. Bjerrum. Acta Chem. Scand. **16**, 735 (1962).
15. B. Cornils and W.A. Herrmann. Applied homogeneous catalysis with organometallic compounds. Wiley–VCH, Weinheim. 1996.
16. (*a*) D.A. Slack, J. Greveling, and M.C. Baird. Inorg. Chem. **18**, 3125 (1979); (*b*) D. Heller, S. Borns, W. Baumann, and R. Selke. Chem. Ber. **129**, 85 (1996).
17. (*a*) I. Tóth, I. Guo, and B.E. Hanson. J. Mol. Catal. A: Chem. **116**, 217 (1997); (*b*) R.W. Eckl, T. Priermeier, and W.A. Herrmann. J. Organometal. Chem. **532**, 243 (1997); (*c*) M.D. Miquel-Serrano, A.M. Masdeu-Bulto, C. Claver, and D. Sinou. J. Mol. Catal. A: Chem. **143**, 49 (1999).
18. I. Tóth and B.E. Hanson. J. Mol. Catal. **71**, 365 (1992).

© 2001 NRC Canada

Scope and limitations of ruthenium-catalyzed metathesis of simple polymer-bound alkenes

Peter G. Breed, James A. Ramsden, and John M. Brown

Abstract: Synthetic procedures for the preparation of two types of functional resin are described, both based on 2% cross-linked polystyrene with a high density (>60%) of side-chains and terminated by a primary alcohol. In the first case the C_{11} side-chain is linked to the polymer through a sulfide, and in the second an ether linkage is employed to incorporate a $(CH_2CH_2O)_4$ unit. In both cases the resins have ^{13}C NMR spectra that are informative in the chain terminus region without special operating conditions. Model intermolecular metathesis reactions were carried out on allylcarbamic acid *tert*-butyl ester and various alkenes with Grubbs' catalyst. On the basis of these experiments, gel-phase metathesis was successfully demonstrated between a polymer-bound allyl ether and simple symmetrical disubstituted alkenes, monitoring the extent of reaction by ^{13}C NMR. These reactions did not go to completion even with recycling and some evidence for competing interchain metathesis is presented, based on the increased broadening and reduced mobility of the ensuing polymer.

Key words: alkene metathesis, ruthenium, gel-phase, ^{13}C NMR.

Résumé : On décrit des méthodes de synthèse de deux types de résines fonctionnelles qui comportent toutes les deux du polystyrène réticulé à 2%, une densité élevée (>60%) de chaînes latérales et qui se terminent par un alcool primaire. Dans le premier cas, la chaîne latérale en C_{11} est liée au polymère par un sulfure et, dans le deuxième cas, on utilise une liaison éther pour incorporer une unité $(CH_2CH_2O)_4$. Dans les deux cas, les spectres RMN du ^{13}C des résines fournissent de l'information sur la région terminale de la chaîne sans nécessiter de conditions spéciales. Utilisant le catalyseur de Grubb, on a effectué des réactions modèles de métathèse intermoléculaire avec l'ester *tert*-butylique de l'acide allylcarbamique et divers alcènes. Sur la base des résultats de ces expériences et faisant appel à la RMN du ^{13}C pour suivre le déroulement de la réaction, on a pu mettre en évidence la métathèse en phase gel entre un oxyde d'allyle lié au polymère et des alcènes simples disubstitués de façon symétrique. Ces réactions ne sont pas complètes, même si on fait du recyclage; de plus, en se basant sur une augmentation de l'élargissement des signaux et sur la mobilité réduite du polymère qui en résulte, on présente des données qui mettent en évidence l'existence de réactions compétitives de métathèse interchaînes.

Mots clés : métathèse d'alcène, ruthénium, phase gel, RMN du ^{13}C.

[Traduit par la Rédaction]

Introduction

With the rapid development of solid-phase organic synthesis in response to the demands of combinatorial chemistry and high-throughput screening (1), suitable reaction types have been appraised. Desirable qualities include the ability to separate the polymer-bound product from reagents, solvents, and other reaction components, appropriate reactivity for the required functional transformation, and above all quantitative conversion so that the product is a coherent species. On this basis homogeneous catalysis seems ideal where applicable, since the solution phase catalyst may be separated from the medium by a simple filtration, and the reaction rate controlled by catalyst concentration. In addition, all the efforts that have been channeled into catalyst specificity applied to chemo-, regio-, and stereo-control may be brought to bear in solid-phase reactions. In some cases, the application of catalysis to solid-phase reactions has been routinely successful (e.g., in Suzuki coupling) (2) but in others it has proved more difficult to reproduce the stereoselectivity of solution-phase results across the board (e.g., in Sharpless dihydroxylation) (3).

As in any other area of synthesis, progress in solid-phase synthesis depends on methods for the analysis of product purity. Although considerable strides have been made in direct on-bead assay by IR (4), NMR (5), and other techniques (6), it remains a challenge for the discipline. This is especially the case when reactions are conducted on resin phases where the loading of reacting sites is low, as in the case of the popular Wang resin (typically 0.5 mmol g^{-1}) (7), Argogel (typically 0.43 mmol g^{-1}) (8), and Tentagel (typically 0.2 mmol g^{-1}) (9). This provided a basis for the synthesis of polystyrene resins with a high level of functionality, based on a readily accessible precursor. The use of 2% cross-linked 63% chloromethylated polystyrene (Fluka) provided

Received September 12, 2000. Published on the NRC Research Press Web site at http://canjchem.nrc.ca on July 11, 2001.

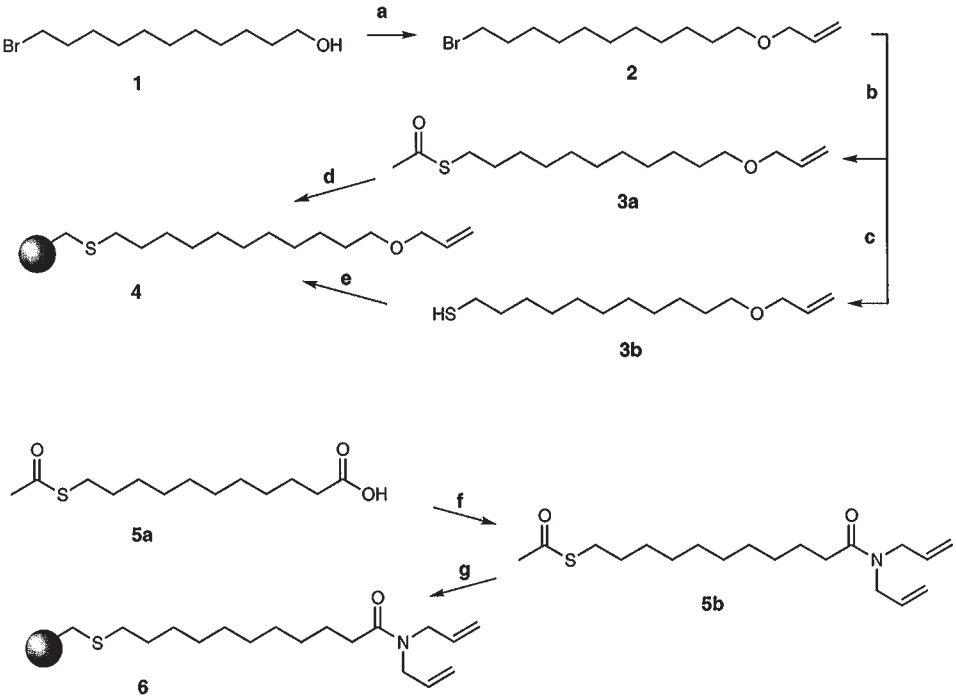
Dedicated to Professor Brian James, a pioneer of ruthenium organometallic chemistry.

P.G. Breed, J.A. Ramsden, and J.M. Brown.[1] Dyson Perrins Laboratory, University of Oxford, South Parks Rd. Oxford OX1 3QY, U.K.

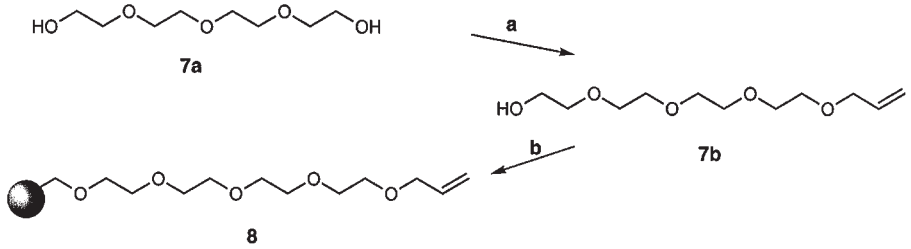
[1]Corresponding author (telephone: 44 1865 275 642; fax: 44 1865 275674; e-mail: bjm@ermine.ox.ac.uk).

 DOI: 10.1139/cjc-79-5/6-1049 © 2001 NRC Canada

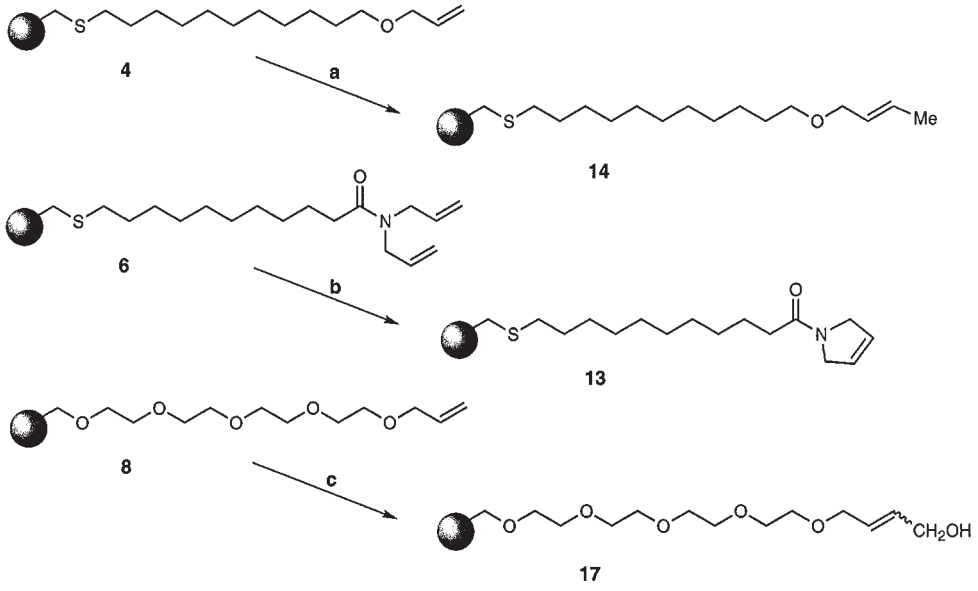
Scheme 1. (*a*) NaH, allyl bromide, THF, reflux 18 h, 76%; (*b*) $KSC(O)CH_3$, DMF, 18 h, RT, 74%; (*c*) NaOH, MeOH, H_2O, reflux 25 min, 49%; (*d*) PS, NaOMe, THF–DMF (1:3), 50°C, 60 h, 98%; (*e*) NaH, PS, THF, 60°C, 14 h, quant.; (*f*) $SOCl_2$ then $(C_3H_5)_2NH$, C_7H_8, 69%; (*g*) NaOMe, THF, 1 h, then PS, THF, 55°C, 18 h, quant.



Scheme 2. Polymer synthesis in the polyoxyethylene series: (*a*) Na, allyl bromide, 18 h at RT, then 100°C, 50%; (*b*) PS, NaH, THF, 60°C, 18 h, 90% conversion.

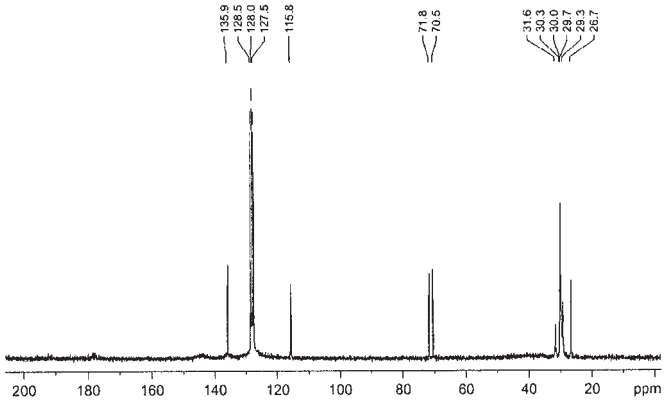


Scheme 3. Examples of successful polymer-phase metatheses: (*a*) of polymer **4** with but-2-ene (50% in CH_2Cl_2, 3 mol% catalyst, sealed tube, ambient, 84 h), quantitative; (*b*) of polymer **6** (CH_2Cl_2, 10 mol% catalyst, 48 h), quantitative; (*c*) of polymer **8** with *Z*-but-2-en-1,4-diol (40% in diglyme, 3 mol% catalyst), 83–87% with reexposure to the catalyst.



© 2001 NRC Canada

Fig. 1. MAS ^{13}C NMR spectrum of polymer **4** suspended in benzene-d_6.



polymers that were suitable for our purpose based on the criteria of mechanical stability and solvent-swelling properties, where the loading is in the 2 to 3 mmol g^{-1} region (for an alternative dendrimer-based approach to high–loading polystyrene, see ref. 10). Methods for the incorporation of side-chains, and the ease of obtention of good quality ^{13}C NMR spectra that reveal signals from the terminal region of the side-chain have already been reported (11).

In the present paper the application of alkene metathesis to solid-phase chemistry is described, using high-loading resins. In prior work, Bletcher and co-workers (12) demonstrated that Tentagel or polystyrene bound dialkenes could be subjected to efficient Ru-complex catalyzed intramolecular metathesis leading from 70 to >90% of the ring-closed product based on isolation by cleavage from the resin. In addition intermolecular metathesis between polymer-bound terminal alkenes and disubstituted alkenes was similarly shown to occur in 46 to >95% yield. A contemporary study employed solid-phase metathesis for the simultaneous cyclization and release of the product from the polymer (13). The high reactivity of norbornene in ring-opening metathesis has been exploited with styrene as the solution coreactant (14); the reverse strategy with vinylpolystyrene and norbornene leads to ring opening methathesis polymerization (ROMP) in the solid state and results in a support with a far higher density of functional sites than the original (15). The significance of solid-phase reactions has been recognized in recent reviews on alkene metathesis by Grubbs and others (16).

Results and discussion

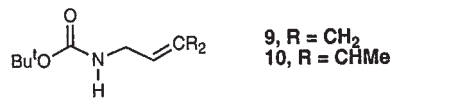
Polymer synthesis

For the preparation of sulfide-linked polymers, the synthetic route of Scheme 1 was adopted. Commercially available 11-bromoundecanol (**1**) was converted into its allyl ether **2**, which was in turn converted into the *S*-thioester **3a** by S_N2 displacement. Hydrolysis then produced the thiol **3b**. Two strategies were adapted for the polymer linkage step; either the thiolate anion was generated in situ from **3a**, or directly from the thiol. In both cases the reaction with 63% chloromethylated polystyrene (2% crosslinked) gave polymer **4** quantitatively within experimental error. Although most use was made of standard ^{13}C NMR spectra in the characterization of polymers, magic angle spinning (MAS) was occasionally also used, and Fig. 1 records the spectrum of **4** swollen in C_6D_6. For initial studies of metathesis, a related synthesis was conducted. 11-Acetylthioundecanoic acid (**5a**) (17) was converted into the corresponding diallylamide **5b** via the corresponding acid chloride, and then attached to polymer in the manner described for **3a**, again the reaction to form polymer **6** was quantitative as judged by weight gain and ^{13}C NMR results.

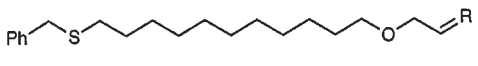
The related synthesis of O-linked polymers is shown in Scheme 2. The allyl ether **7b** of tetraethylene glycol **7a** was prepared, and its Na salt was reacted with PS for 18 h at 60°C in THF. These conditions, the result of some optimization efforts, produced polymer **8** in 90% yield, with characteristic ^{13}C NMR fingerprint.

Metathesis experiments

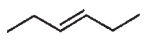
Conditions suitable for cross-metathesis of a terminal alkene **9** with *Z*-but-2-ene were established first. In these and subsequent reactions the "standard" Grubb's catalyst (bis(tricyclohexylphosphine)benzylidineruthenium(IV) dichloride) was utilized. It was found that employing a 100-fold excess of *Z*-but-2-ene in CH_2Cl_2 at ambient temperature with 2 mol% catalyst gave complete reaction to form a *Z*:*E* mixture (1:3) of the disubstituted alkene **10**. Applying these exact conditions to the metathesis of polymer **4** did not result in observable metathesis or significant change in weight. At first the thiolate residue was suspected, and hence, monomer **11** was synthesized. This was shown to be reactive under the conditions of metathesis, giving **12** as an *E*/*Z* mixture in 85% yield. Furthermore, the intramolecular metathesis of polymer **6** to give the corresponding pyrroline **13** occurred smoothly, although 10% Ru catalyst and a reaction time of 48 h were required. It was noted that although the product polymer gave a good ^{13}C NMR spectrum corresponding to complete loss of starting material and the formation of cyclopentene, it appeared dark green-black under a microscope, despite intensive washings with a variety of solvents.



9, R = CH_2
10, R = CHMe



11, R = CH_2
12, R = CHMe



15



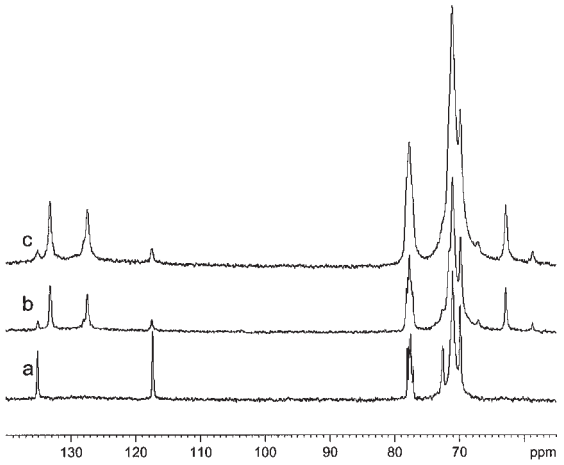
16a R = TBDMSi
16b R = H
16c R = Me
16d R = $CH_2OCH_2CH_2OMe$

This appeared to indicate some catalyst decomposition and irreversible reaction with the polymer.

On the basis of this set of experiments there appeared to be two further explanations for the failure of polymer cross-metathesis; firstly that the concentration of reagent and (or) catalyst in the polymer interstices was intrinsically low, and

© 2001 NRC Canada

Fig. 2. (*a*) Polymer **8** swollen in $CDCl_3$, 125 MHz; (*b*) after one cycle of metathesis with *Z*-but-2-en-1,4-diol to give predominantly **17**; (*c*) after two cycles of metathesis. Note the broadening of both resin and solvent (78 ppm) resonances.



secondly that the polymer environment led to a lowered reactivity. The first of these possibilities was tested in part by changing the reaction conditions, conducting metathesis of polymer **4** in CH_2Cl_2:*Z*-but-2-ene (1:1) in a sealed tube with 3 mol% catalyst. After 3.5 days at ambient temperature, workup gave a polymer whose ^{13}C NMR spectrum indicated complete reaction to form an *E*:*Z* isomeric mixture of the butenyl ether **14** (Scheme 3). This success could not, however, be duplicated with other alkenes and cross-metathesis of polymer **4** with either *E*-hex-2-ene (**15**) or the bis-TBDMS ether of *Z*-but-2-en-1,4-diol **16a** failed.

Appraisal of the results at this stage suggested that the reactivity of polymer **4** in metathesis was substantially lower than expected from the model experiments. One possibility was that the polarity of the polymer medium was lower than that of the solution because of the high density of hydrocarbon chains. This could lead to both unfavourable partition and lower reactivity of the catalyst in the polymer phase. For these reasons further metathesis experiments were carried out with the polymeric allyl ether **8**. Since the initial experiments failed completely for alkenes other than *Z*-but-2-ene, the polyether polymer **8** was reacted first with *Z*-but-2-en-1,4-diol **16b**. Under a variety of conditions slow metathesis was observed, but the ^{13}C NMR of the product **17** always showed some unreacted starting material. A single run with the corresponding ether **16c** went to completion, however. For the diol, best results were obtained when the solvent was diglyme (83%, 3 mol% catalyst, 168 h) Less successful experiments were conducted in CH_2Cl_2 (63%, 18 h) and THF (30%, 18 h). The presence of 10% of MeOH appeared to slow the turnover rate in CH_2Cl_2 even though it makes the partly immiscible diol fully soluble. In DMSO, DMF, or MeCN turnover was not observed, although there is some swelling of the polymer in these solvents. No discernable reaction took place in water (18).

Since only 83% yield was observed under the most favourable conditions, the polymer **17**, thus formed, was resubjected to the same reaction conditions. This, however, led to a rather small enhancement of the overall yield (83–87%). At the same time it was noted that the ^{13}C NMR resonances of the polymer became broader after each cycle (Fig. 2). This indicates that a change in the morphology of the polymer takes place during metathesis. The simplest interpretation is that crosslinking takes place within the bead by interchain metathetical reactions. Indeed an additional 1 to 2% of linkages would be expected to make a profound difference to the mobility of polymer-bound chains and thus affect the ^{13}C NMR line-widths. At this level there should be detectable additional signals in the NMR spectrum and there was an unassigned shoulder at 127.5 ppm in the spectra of samples of polymer **17**. This was close to, but not coincident with, the alkene carbon resonance of model compound **16d** at 129 ppm, taken in the presence of polymer **8** to best simulate the signal environment of the trace impurity in **17**.

In summary these experiments demonstrate the feasibility of metathesis reactions on the pendant side-chains of high-loading polystyrene resins, and the feasibility of monitoring the product directly by ^{13}C NMR. Under the conditions described, the utility is limited because of the low on-polymer reactivity and the lack of quantitative reaction (a prerequisite for successful solid-state combinatorial chemistry) with any but the most simple alkene reactants.

Experimental

General

Reactions involving air-sensitive reagents were performed under a dry argon atmosphere, using standard vacuum line techniques in Schlenk glassware. Solvents were deoxygenated where necessary by repeated freeze-thaw-freeze cycles, in which the solvent was frozen using liquid nitrogen, and allowed to warm until fully molten in vacuo or by pump-fill degassing, in which case the solvent was cooled to near freezing, usually using a dry ice – acetone bath, evacuated, and refilled with argon while swirling using a Whirlimixer™ to facilitate complete gas exchange. Transfers were carried out using stainless steel cannula wire or by syringe. For reactions using resin bound substates, "Swirler" refers to a Büchi Rotavapor M and "Bubbler" refers to a designed piece of glassware where the resin was supported on a glass sinter in solvent and agitated by argon passage.

Solvents were purchased from Rathburns, Fisons, Ultrafine, Aldrich, or Prolabo and dried immediately before use by distillation from standard drying agents (19). Merrifield resin was purchased from Fluka, and was 2% crosslinked with divinylbenzene (~4.3 mmol Cl per g resin) 200–400 mesh. Flash chromatography was performed using Fluorochem Silca gel 60, 40–63 μm, 550 $m^2\ g^{-1}$, or with commercial Biotage apparatus; KP-Sil™ 90 g cartridges (32–63 μm, 60 Å, 500–550 $m^2\ g^{-1}$ silica). Melting points were recorded by the author on a Reichert–Koffler block apparatus and are uncorrected. Infrared spectra were recorded on PerkinElmer 1750 or PerkinElmer Paragon 1000 FT spectrometers. ^1H and ^{13}C NMR spectra were recorded on Varian Gemini 200 (200 MHz), Bruker AM 200 (200 MHz), Bruker WH 300 (300 MHz), Bruker DPX 400 (400 MHz), Bruker AMX 500 (500 MHz), or Bruker AM 500 (500 MHz) spectrometers. MAS spectra were recorded on a Bruker MSL 200 (50.3 MHz) spectrometer. Polymer samples to be analyzed were prepared by placing an appropriate amount of polymer (usually ~120–130 mg) in a 5 mm

© 2001 NRC Canada

NMR tube and small amounts of solvent until the polymer was fully swollen and 2–4 mm of excess solvent remained. The tube was then vibrated either using a sonicator, whirlimixer, or by gently tapping the tube on a wooden surface until no air bubbles were visible and the suspension appeared homogeneous. The samples were then allowed to settle for a minimum of 10 min before being place in the spectrometer. For MAS samples by swelling the polymer in the solvent and transferring to a sinter. The excess solvent was removed by brief suction (~30 s) the sample was then transferred to the rotor. Unless otherwise stated operations were performed at room temperature.

Synthesis of polymers and their precursors

*Preparation of 3-(11-bromo-undecyloxy)propene (**2**)*

Sodium hydride (2.24 g, 60% in paraffin, 56 mmol) was washed with pentane (3 × 10 mL) and then suspended in THF (80 mL) and allyl bromide (10.4 mL, 120 mmol). 11-Bromoundecanol (10 g, 40 mmol) in THF (50 mL) was added dropwise. The solution was heated under reflux for 18 h. The solvent was removed in vacuo, the residue was dissolved in water (100 mL) and extracted with dichloromethane (1 × 125 mL, 1 × 100 mL). The combined organic extracts were washed with water (100 mL), dried over magnesium sulfate, and the solvent was removed in vacuo. The product was further purified by column chromatography (SiO_2, pentane–toluene, 2:1) and Kugelrohr distilled (150°C, 4 mbar) to give a colourless oil (8.86 g, 76%). IR (thin film) (cm^{-1}): 3080 (m, C=C-H_2, str), 2928 (s, C-H_2, str), 2856 (s, C-H_2, str), 1728 (m), 1647 (w, C=C, str), 1464 (s, C-H, def), 1346 (s, CH_3, def), 1254 (m), 1106 (s, C-O, str), 996 (m, -CH=CH_2, def), 922 (s, -CH=CH_2, def), 722 (w, CH_2, rocking), 645 (m, C-Br). ^{1}H NMR (500 MHz, $CDCl_3$) δ: 5.92 (ddt, J = 17.2, 10.6, 5.2 Hz, 1H, $H_{2'}$), 5.27 (dq, J = 17.2, 1.6 Hz, 1H, $H_{3'a}$), 5.17 (dq, J = 10.4, 1.3 Hz, 1H, $H_{3'b}$), 3.96 (dt, J = 6.8, 1.3 Hz, 2H, $H_{1'}$), 3.42 (t, J = 7.0 Hz, 2H, H_1 or H_{11}), 3.41 (t, J = 7.1 Hz, 2H, H_{11} or H_1), 1.85 (tt, J = 7.5, 7.0 Hz, 2H, H_{10}), 1.58 (tt, J = 7.0, 7.0 Hz, 2H, H_2), 1.43–1.26 (m, 14H, H_{3-9}). ^{13}C NMR (125 MHz, $CDCl_3$) δ: 135.1 ($C_{2'}$), 116.6 ($C_{3'}$), 71.7 ($C_{1'}$), 70.5 (C_1), 34.0 (C_{11}), 32.8 (C_{10}), 29.7, 29.5, 29.4, 29.4, 28.7, 28.1 ($C_{2,4-9}$), 26.1 (C_3).

Preparation of thioacetic acid S*-(11-allyloxy-undecyl) ester (**3a**)*

To a solution of potassium thioacetate (5.71 g, 50 mmol) in dimethylformamide (50 mL) was added 3-(11-bromo-undecyloxy)propene (27.28 g, 25 mmol). The solution was stirred for 18 h, then added to water (350 mL). This solution was then extracted with ether (3 × 100 mL, 2 × 50 mL). The combined ether extracts were washed with potassium carbonate solution (100 mL, 10%) and saturated potassium carbonate (2 × 100 mL), dried over sodium carbonate, and the solvent was removed in vacuo. The product was further purified by column chromatography (SiO_2, pentane–dichloromethane, 1:1) to give the product as a colourless oil (5.29 g, 74%). CI-MS (NH_4) *m/z* (%): 287 ($[M + H]^+$, 38), 245 ($[M + H - CH3CO]^+$, 39), 227 ($[M + H - CH_2CHCH_2OH]^+$, 27), 187 ($[M - CH_3CO - OCH_2CH{=}CH_2]^+$, 100). HRMS calcd.: 287.2045; found: 287.2047. IR (thin film) (cm^{-1}): 3369 (w, COC-H_3, str), 3079 (m, C=C-H_2, str), 2924 (s, C-H_2, str), 2853 (s, C-H_2, str), 1694 (s, C=O, str), 1647 (w, C=C, str), 1464 (s, C-H, def), 1429 (m, C-H, def), 1353 (s, CH_3, def), 1262 (m), 1107 (s, C-O, str), 998 (m, -CH=CH_2, def) 954, 923 (s, -CH=CH_2, def), 801 (w), 722 (w, CH_2, rocking), 672 (w), 627. ^{1}H NMR (500 MHz, $CDCl_3$) δ: 5.92 (ddt, J = 17.2, 10.8, 5.5 Hz, 1H, $H_{2'}$), 5.27 (dq, J = 17.2, 1.4 Hz, 1H, $H_{3'a}$), 5.16 (dq, J = 10.8, 1.4 Hz, 1H, $H_{3'b}$), 3.96 (dt, J = 5.6, 1.4 Hz, 2H, $H_{1'}$), 3.42 (t, J = 6.7 Hz, 2H, H_1), 2.86 (t, J = 7.4 Hz, 2H, H_{11}), 2.32 (s, 3H, H_{13}), 1.67–1.52 (m, 4H, H_2, H_{10}), 1.34–1.26 (m, 14H, H_{3-9}). ^{13}C NMR (125 MHz, $CDCl_3$) δ: 196.0 (C_{12}), 135.1 ($C_{2'}$), 116.6 ($C_{3'}$), 71.7 ($C_{1'}$), 70.5 (C_1), 30.58 (C_{11}), 29.7, 29.5, 29.4, 29.1, 29.1, 28.9 ($C_{2,4-10,13}$), 26.1(C_3).

*Preparation of poly[1-(11-allyloxy-undecylsulfanylmethyl)-4-vinyl benzene-co-vinyl-benzene-co-divinyl-benzene] (**4**)*

From thioacetic acid S*-(11-allyloxy-undecyl)ester:* To a suspension of sodium methoxide (730 mg, 13.5 mmol) in THF (5 mL) was added dropwise, via cannula, a solution of thioacetic acid *S*-(11-allyloxy-undecyl)ester (3.22 g, 11.25 mmol) in THF (5 mL). After 1 h, THF (10 mL) was added, followed by dimethylformamide (30 mL). This solution was added via cannula to a flask containing Merrifield resin (1.74 g, 4.3 mmol g^{-1}) and this suspension was swirled at 50°C for 60 h The suspension was then transferred to a sinter and washed with dichloromethane (3 × 50 mL), dimethylformamide (3 × 50 mL), dichloromethane (3 × 50 mL), water (50 mL), methanol (50 mL), dichloromethane (3 × 50 mL), dimethylformamide (3 × 50 mL), dichloromethane (3 × 50 mL), and pentane (3 × 50 mL). Drying in vacuo gave the product as a colourless opaque tacky polymer (3.28 g, 98%). IR (KBr disk) (cm^{-1}): 3082 (vw, C=C-H_2, str) 3058 (vw, C=C-H_2, str), 3024 (w, Ar-H, str), 2924 (s, C-H_2, str), 2852 (m, C-H_2, str), 1723 (w) 1702 (w), 1647 (w, C=C, str), 1604 (w, ar), 1510 (m, ar), 1494 (w), 1452 (m, C-H, def), 1421 (w, C-H, def), 1347 (m), 1271 (w), 1239 (w), 1137 (vw), 1104 (s, C-O, str), 1018 (vw), 997 (w, -CH=CH_2, def), 920 (s, -CH=CH_2, def), 827 (m, para Ar, C-H bnd), 760 (m, Ph), 700 (s, Ph). ^{13}C MAS NMR (50.3 MHz, C_6D_6) δ: 135.9 ($C_{2'}$), 115.8 ($C_{3'}$), 71.8 ($C_{1'}$), 70.5 (C_1), 30.3, 30.0, 29.7, 29.3, 26.7 (C_{2-11}).

*Through isolation of the intermediate 11-allyloxy-undecane-1-thiol (**3b**):* Thioacetic acid *S*-(11-allyloxy-undecyl) ester (4.29 g, 15 mmol) in methanol (50 mL) was placed in round-bottom flask, and a solution of sodium hydroxide (2.40 g, 60 mmol) in water (3.8 mL) – methanol (10 mL) was added via cannula. The solution was heated at reflux for 25 min, then poured into phosphate buffer (pH 5.5, 100 mL). The solution was extracted with dichloromethane (2 × 100 mL, 1 × 25 mL). The combined extracts were washed with water (1 × 100 mL), and solvent was removed in vacuo. The product was further purified by column chromatography (SiO_2, pentane–toluene, 1:1) to give 11-allyloxy-undecane-1-thiol as a colourless oil (1.784 g, 49%). CI-MS (NH_4) *m/z* (%): 262 ($[M + NH_4]^+$, 22). ^{1}H NMR (500 MHz, $CDCl_3$) δ: 5.91 (ddt, J = 17.3, 10.6, 5.5 Hz, 1H, $H_{2'}$), 5.26 (dq, J = 17.3, 1.6 Hz, 1H, $H_{3'a}$), 5.16 (dq, J = 10.3, 1.5 Hz, 1H, $H_{3'b}$), 3.95 (dt, J = 5.5, 1.5 Hz, 2H, $H_{1'}$), 3.41 (t, J = 6.6 Hz, 2H, H_1), 2.51 (q, J = 7.3 Hz, 2H, H_{11}), 1.75 (br s, 1H, SH), 1.63–1.54 (m, 4H, H_2, H_{10}), 1.40–1.22 (m, 14H, H_{3-9}). ^{13}C NMR

© 2001 NRC Canada

(125 MHz, $CDCl_3$) δ: 135.0 ($C_{2'}$), 116.6 ($C_{3'}$), 71.7 ($C_{1'}$), 70.5 (C_1), 34.0 (C_{10}), 29.7, 29.5, 29.4, 29.0, 28.3 ($C_{2,4-9}$), 26.1 (C_3), 24.6 (C_{11}). Sodium hydride (288 mg, 60% in paraffin, 7.2 mmol) was washed with pentane (3 × 10 mL) and suspended in THF (10 mL). Merrifield resin (1.047 g, 4.5 mmol) was added washing into flask with THF (20 mL), followed by 11-allyloxy-undecane-1-thiol (1.650 g, 6.75 mmol), rinsing the syringe with THF (15 mL). Upon addition of the thiol, effervescence was observed. The suspension was swirled at 60°C overnight. Water (10 mL) was added, and the suspension was swirled for 10 min. The suspension was transferred to a sinter and washed with dichloromethane (25 mL), water (25 mL), dichloromethane (3 × 25 mL), and ethanol (25 mL), and then dried in vacuo to give the product as a colourless tacky polymer (1.993 g, quant.).

*Preparation of (11-allyloxy-undecylsulfanylmethyl)benzene (**11**)*

Sodium hydride (180 mg, 60% in paraffin, 4.5 mmol) was washed with pentane (3 × 5 mL) and suspended in THF (6 mL). *S*-Benzylisothiouronium chloride (405 mg, 2 mmol) was added and the mixture was heated at reflux for 150 min. THF (10 mL) was added and the mixture was heated at reflux for 4 h. 3-(11-Bromo-undecyloxy)propene (583 mg, 2 mmol) was added and the mixture was heated at reflux for 18 h. After cooling, toluene (20 mL) and water (10 mL) were added and the THF was removed in vacuo. Toluene (40 mL) was added and the mixture was washed with water (3 × 30 mL). The combined water washings were extracted with toluene (20 mL), and the combined toluene extracts were dried over sodium sulfate. The product was isolated by column chromatography (SiO_2, dichloromethane–pentane, 1:1) giving the product as a pale yellow oil (466 mg, 69%). CI-MS (NH_4) *m*/*z* (%): 335 ($[M + H]^+$, 100). HRMS calcd.: 335.2409; found: 335.2410. ^{1}H NMR (500 MHz, $CDCl_3$) δ: 7.31 (s, 2H, H_{15} or H_{14}), 7.30 (s, 2H, H_{14} or H_{15}), 7.27–7.20 (m, 1H, H_{16}), 5.92 (ddt, *J* = 17.2, 10.4, 5.6 Hz, 1H, $H_{2'}$), 5.27 (dq, *J* = 17.2, 1.7 Hz, 1H, $H_{3'a}$), 5.17 (ddt, *J* = 10.4, 1.9, 1.3 Hz, 1H, $H_{3'b}$), 3.96 (dt, *J* = 5.64, 1.4 Hz, 2H, $H_{1'}$), 3.70, (s, 2H, H_{12}), 3.42 (t, *J* = 6.7 Hz, 2H, H_1), 2.40, (t, *J* = 7.4 Hz, 2H, H_{11}), 1.62–1.51 (m, 4H, H_2, H_{10}), 1.38–1.20 (m, 14H, H_{3-9}). ^{13}C NMR (125 MHz, $CDCl_3$) δ: 138.6 (C_{13}), 135.1 ($C_{2'}$), 128.8 (C_{15}), 128.4 (C_{14}), 126.8 (C_{16}), 116.7 ($C_{3'}$), 71.8 ($C_{1'}$), 70.5 (C_1), 36.2 (C_{12}), 31.3 (C_{11}), 29.7, 29.5, 29.5, 29.2, 28.8 ($C_{2,4-10}$), 26.1 (C_3).

Preparation of thioacetic acid S*-(10-diallylcarbamoyl decyl) ester (**5b**)*

To a solution of 11-acetylsulfamyl-undecanoic acid (1.820 g, 7 mmol) in toluene (10 mL) was added thionyl chloride (2 mL, 27 mmol), and the mixture was heated at reflux for 2 h. The solvent was removed in vacuo. The acid chloride was dissolved in toluene (10 mL), and diallylamine (5 mL, 40 mmol) was added. The mixture was stirred for 1 h before the addition of saturated sodium hydrogen carbonate (20 mL). Dichloromethane (100 mL) was then added; the solution was washed with saturated sodium hydrogen carbonate (50 mL) and phosphate buffer (pH 5.5, 50 mL), then dried over magnesium sulfate. The product was further purified by column chromatography (SiO_2, pentane – ethyl acetate, 5:1) to give the product as a pale yellow oil (1.569 g, 69%). CI-MS (NH_4) *m*/*z* (%): 340 ($[M + H]^+$, 100), 298 ($[M - C_3H_5]^+$, 14). HRMS calcd.: 340.2310; found: 340.2309. ^{1}H NMR (500 MHz, $CDCl_3$) δ: 5.84–5.70 (m, 2H, $H_{2'}$), 5.25–5.05 (m, 2H, $H_{3'}$), 3.98 (br d, *J* = 5.8 Hz, 2H, $H_{1'a}$), 3.86 (br d, *J* = 4.5 Hz, 2H, $H_{1'b}$), 2.85 (t, *J* = 2.4 Hz, 2H, H_{11}), 2.32 (s, 3H, H_{13}), 2.30 (t, *J* = 7.6 Hz, 2H, H_2), 1.63 (q, *J* = 7.3 Hz, 2H, H_3 or H_{10}), 1.55 (q, 7.4 Hz, 2H, H_{10} or H_3), 1.37–1.22 (m, 16H, H_{4-9}). ^{13}C NMR (125 MHz, $CDCl_3$) δ: 196.0 (C_{12}), 173.2 (C_1), 133.4 ($C_{2'a}$), 133.0 ($C_{2'b}$), 117.0 ($C_{3'a}$), 116.5 ($C_{3'b}$), 49.1 ($C_{1'a}$), 47.8 ($C_{1'b}$), 32.9 (C_2), 30.6 (C_{11}), 29.4, 29.4, 29.4, 29.1, 29.0, 28.8 ($C_{4-10,\ 13}$), 25.3 (C_3).

*Preparation of poly-[*N,N*-diallyl-11-(4-vinyl-benzyl sulfanylundecanoic acid amide)-co-vinyl-benzene-co-divinyl-benzene] (**6**)*

To sodium methoxide (194 mg, 3.6 mmol) was added a solution of thioacetic acid *S*-(10-diallylcarbamoyl decyl) ester (1.018 g, 3 mmol) in THF (2 mL). The solution was stirred for 1 h, then a small aliquot removed and analyzed by ^{1}H NMR, which showed complete deacetylation. The solvent was then removed in vacuo, the solid was redissolved in THF (10 mL), and the solution was added via cannula to a flask containing Merrifield resin (465 mg, 4.3 mmol g^{-1}) swollen in THF (5 mL). The suspension was swirled at 55°C for 18 h, then transferred to a sinter and washed with dichloromethane (2 × 40 mL), water (40 mL), dimethylformamide (4 × 40 mL), and dichloromethane (5 × 40 mL), then dried in vacuo yielding the product as a colourless polymer (1.019 g, quant.). IR (KBr disk) (cm^{-1}): 3081 (w, C=C-H_2, str), 3024 (w, C=C-H or Ar-H, str), 2921 (s, C-H, str), 2852 (m, C-H, str), 1701 (m, C=O, str), 1654 (s, C=C, str), 1636 (s, C=C, str), 1458 (m, C-H, def), 1420 (m, C-H, str), 1213 (br, m), 1113 (w), 1016, 989 (m, -CH=CH_2, def), 912 (m, -CH=CH_2, def), 824 (m), 761 (m, Ph), 698 (m, Ph). ^{13}C NMR (125 MHz, $CDCl_3$) δ: 173.2 (C_1), 133.5, 133.0 ($C_{2'}$), 117.1, 116.5 ($C_{3'}$), 49.2, 47.8 ($C_{1'}$), 33.0 (C_2), 31.7, 29.4 (C_{4-11}), 25.3 (C_3).

*Preparation of 2-(2-(1-(2-allyloxy-ethoxy)-ethoxy)-ethoxy)-ethanol (**7**) (20)*

A 500 mL round-bottom flask was charged with sodium (5.93 g, 0.257 mol) and tetraethylene glycol (200 g). The solution was stirred at 80°C for 18 h. The solution was allowed to cool to room temperature, then 3-bromopropene (23 mL, 0.266 mol) was added dropwise over 15 min. The solution was warmed to 70°C for 90 min and 100°C for 60 min. The solution was allowed to cool to room temperature and added to a mixture of saturated sodium chloride (400 mL) and water (200 mL). The aqueous solution was extracted with dichloromethane (2 × 200 mL, 4 × 50 mL). The combined extracts were extracted with water (2 × 200 mL, 11 × 100 mL), however TLC showed that some product remained in the dichloromethane layer. The solvent was reduced in vacuo to 150 mL and the solution was further extracted with water (2 × 150 mL). The solvent was then totally removed in vacuo, and the oil was redissolved in ether (500 mL) and extracted with water (5 × 100 mL). Sodium chloride was added to the combined water extracts until the solution was saturated. The solution was extracted with dichloromethane (3 × 150 mL, 6 × 100 mL), and the combined extracts were

© 2001 NRC Canada

reduced in vacuo to 500 mL. The solution was dried over sodium sulfate and solvent was removed in vacuo. The oil was then fractional distilled using a 5 inch Vigreux column, and the fraction at 102–112°C at 0.03–0.04 mm Hg (1 mm Hg = 133.32 kPa) was collected. TLC showed this to be a mixture consisting mainly of the desired product, but contained small amounts of tetraethyleneglycol diallyl ether and tetraethylene glycol. The oil was redissolved in saturated sodium chloride (300 mL), and extracted with ether (2 × 200 mL, 5 × 100 mL). The combined extracts were dried over magnesium sulfate, and solvent was removed in vacuo. The oil was triturated with pentane (2 × 50 mL). Solvent was removed in vacuo giving a colourless oil (30.76 g, 50%), which contained a slight trace of the diallyl ether of tetraethyleneglycol, bp 102–112°C, 0.03–0.04 mm Hg ((lit. (21) 99–101°C, 0.2 mm Hg). CI-MS (NH_4) *m/z* (%): 235 ($[M + H]^+$, 100). ^{1}H NMR (500 MHz, $CDCl_3$) δ: 5.87 (ddt, *J* = 17.2, 10.3, 5.7 Hz, 1H, $H_{2'}$), 5.22 (dq, *J* = 17.2, 1.6 Hz, 1H, $H_{3'a}$), 5.13 (dm, *J* = 10.3 Hz, 1H, $H_{3'b}$) 3.98 (dm, *J* = 5.6 Hz, 2H, $H_{1'}$), 3.68–3.54 (m, 8H, $H_{1–8}$), 2.81 (br s, 1H, OH). ^{13}C NMR (125 MHz, $CDCl_3$) δ: 134.7 ($C_{2'}$), 116.8 ($C_{1'}$), 72.5 (C_7), 72.0 ($C_{1'}$), 70.5, 70.5, 70.5, 70.2 ($C_{2–7}$), 69.3 (C_1), 61.6 (C_8).

*Preparation of poly[1-(2-(2-(1-(2-allyloxy-ethoxy)-ethoxy)-ethoxy)-ethoxy methyl)-4-vinyl benzene-co-vinyl-benzene-co-divinyl-benzene] (**8**)*

Merrifield resin (1.164 g, 4.3 mmol g^{-1}), sodium hydride (800 mg, 60% in paraffin, 20 mmol), THF (20 mL), and 2-(2-(1-(2-allyloxy-ethoxy)-ethoxy)-ethoxy)-ethanol (**7**) (4.686 g, 20 mmol) were placed in 50 mL round-bottom flask, and swirled at 60°C for 18 h. The suspension was transferred to a sinter with THF, and washed with DMF (3 × 30 mL), water (3 × 30 mL), methanol (3 × 30 mL), tetraethyleneglycol dimethyl ether (3 × 30 mL), methanol (3 × 30 mL), and dichloromethane (3 × 30 mL) and dried in vacuo giving the product as colourless opaque tacky polymer (2.056 g, 90%). ^{13}C MAS NMR (50.3 MHz, $(CD_3)_2SO$) δ: 134.1 ($C_{2'}$), 115.1 ($C_{3'}$), 71.1 ($C_{1'}$), 70.0 ($C_{2–8}$), 69.1 (C_1).

Experimental for metathesis reactions

Diallylcarbamic acid *tert*-butyl ester (21, 22), 2,5-dihydropyrrole-1-carboxylic acid *tert*-butyl ester (23), and allyl-carbamic acid *tert*-butyl ester (23) were prepared by literature procedures.

Preparation of but-2-enylcarbamic acid-tert-*butyl ester (**10**) (24)*

Bis(tricyclohexylphosphine)benzylidineruthenium(IV) dichloride (27.4 mg, 1 mol%) and allylcarbamic acid-*tert*-butyl ester (**9**) (524 mg, 3.33 mmol) were placed in a Schlenk tube fitted with a dry ice condenser. Dichloromethane (65 mL) was added via cannula. *Z*-2-Butene was condensed into a Schlenk tube cooled in a dry ice – acetone bath, and 3.5 mL was transferred into the tube using a dry ice cooled syringe. The solution was stirred for 6 h, the condenser was then removed, a needle was inserted into the septum, and the solution was left overnight. The solvent was then removed in vacuo and the product was isolated by column chromatography (SiO_2, pentane – ethyl acetate, 2:1) to give the product as brown oil (510 mg, 89%). A small quantity of the two isomers was partially separated by preparative GLC (Peg 20M, 15%, 175°C). ^{1}H NMR (500 MHz, $CDCl_3$) δ (*Z*)-isomer: 5.60 (dqd, *J* = 10.4, 6.7, 1.0 Hz, 1H, H_2), 5.42 (dtd, *J* = 10.4, 7.0, 1.0 Hz, 1H, H_3), 4.48 (br s, 1H, NH), 3.78 (br s, 2H, H_4), 1.67 (dd, *J* = 6.7, 0.9 Hz, 3H, H_1), 1.45 (s, 9H, H_7); (*E*)-isomer: 5.60 (dq, *J* = 14.7, 7.0, 1H, H_2), 5.45 (dt, *J* = 14.7, 6.3 Hz, 1H, H_3), 4.54 (br s, 1H, NH), 3.66 (br s, 2H, H_3), 1.67 (d, *J* = 7.0 Hz, 3H, H_1), 1.45 (s, 9H, H_7). ^{13}C NMR (125 MHz, mixed isomers, $CDCl_3$) δ: 155.8 (C_{5Z}), 155.7 (C_{5E}), 127.6 (C_{3E}), 127.5 (C_{2E}), 127.2 (C_{3Z}), 126.7 (C_{2Z}), 79.1 (C_6), 42.5 (C_{4E}), 37.3 (C_{4Z}), 28.4 (C_7), 17.6 (C_{1E}), 12.9 (C_{1Z}).

General procedure for screening of metathesis of allyl-carbamic acid tert-*butyl ester (**9**)*

Allyl-carbamic acid *tert*-butyl ester (78.6 mg, 0.5 mmol) and bis(tricyclohexylphosphine)benzylidineruthenium(IV) dichloride (8.2 mg, 10 μmol) were placed in a Schlenk tube and degassed. In a separate Schlenk tube dichloromethane (10 mL) and the alkene (5 mmol) were degassed. The liquid was transferred via cannula to the first Schlenk tube. The reactions were followed both by TLC and (or) by removing aliquots (0.5 mL), removing the solvent in vacuo, and analyzing by ^{1}H NMR.

Pent-2-enyl-carbamic acid tert-*butyl ester (25):* Using *E*-2-hexene; ^{1}H NMR (500 MHz, $CDCl_3$) δ: 5.63 (dtt, *J* = 15.3, 6.2, 1.3 Hz, 1H, H_3), 5.43 (dt, *J* = 15.3, 5.9 Hz, 1H, H_4), 4.55 (br s, 1H, NH), 3.68 (br t, 2H, H_5), 2.02 (qddd, *J* = 7.3, 6.2, 1.5, 1.2, 2H, H_2), 1.44 (s, 9H, H_8), 0.97 (td, *J* = 7.4, 1.2, 3H, H_1). ^{13}C NMR (125 MHz, $CDCl_3$) δ: 155.7 (C_6), 134.6 (C_4), 125.3 (C_3), 79.1 (C_7), 42.5 (C_5), 28.4 (C_8), 25.2 (C_2), 13.4 (C_1).

*4-*tert-*Butoxycarbonylamino-but-2-enyl)-carbamic acid* tert-*butyl ester:*

Bis(tricyclohexylphosphine)benzylidineruthenium(IV) dichloride (97 mg, 2 mol%) and allyl-carbamic acid *tert*-butyl ester (1.00 g, 5.92 mmol) were placed in a Schlenk tube. Chloroform (50 mL) was added via cannula and the solution was stirred at 50°C for 3 days. More bis(tricyclohexylphosphine)benzylidineruthenium(IV) dichloride (97 mg, 2 mol%) was added and the solution was stirred for a further 3 days at 50°C. The solvent was removed in vacuo and the stereoisomeric products were separated by chromatography on a Biotage apparatus (ethyl acetate – pentane, 1:4). ^{1}H NMR (500 MHz, $CDCl_3$) *E*-isomer δ: 5.55 (br s, 2H, H_1), 4.88 (br s, 2H, NH), 3.77 (br s, 4H, H_2), 1.44 (s, 18H, H_1). ^{13}C NMR (125 MHz, $CDCl_3$) δ: 155.7 (C_3), 128.4 (C_1), 79.4 (C_4), 41.9 (C_2), 28.4 (C_5). ^{1}H NMR (500 MHz, $CDCl_3$) *Z*-isomer δ: 5.61 (br s, 2H, H_1), 4.63 (br s, 2H, NH), 3.72 (br s, 4H, H_2), 1.44 (s, 18H, H_5). ^{13}C NMR (125 MHz, $CDCl_3$) δ: 155.9 (C_3), 128.9 (C_1), 79.4 (C_4), 37.1 (C_2), 28.4 (C_5).

*Preparation of 11-(but-2-enyloxy-undecyl)-sulfanylmethylbenzene (**12**)*

Bis(tricyclohexylphosphine)benzylidineruthenium(IV) dichloride (8.2 mg, 2 mol%) was placed in a Schlenk tube fitted with a dry ice condenser. *Z*-2-butene was condensed into a Schlenk tube cooled in a dry ice – acetone bath, and 0.5 mL was transferred into the tube using a dry ice cooled syringe.

© 2001 NRC Canada

11-(Allyloxy-undecylsulfanylmethyl)benzene (0.5 mmol, 167 mg) in dichloromethane (10 mL) was added via cannula, and the solution was stirred for 5.5 h. The solvent was removed in vacuo and the product was further purified by column chromatography (SiO_2, dichloromethane–pentane, 1:1) yielding the product as a yellow oil (134 mg, 85%). CI-MS (NH_4) *m*/*z* (%): 349 ($[M + H]^+$, 100), 293 ($[M - C_4H_7]^+$, 2). HRMS calcd.: 349.2565; found: 349.2575. ^{1}H NMR (500 MHz, $CDCl_3$) δ: 7.31 (s, 2H, H_{14} or H_{15}), 7.30 (s, 2H, H_{15} or H_{14}), 7.27–7.20 (m, 1H, H_{16}), 5.75–5.53 (m, 2H, $H_{2'}$ and $H_{3'}$), 4.02 (ddt, *J* = 6.6, 1.5, 1.0 Hz, 2H, $H_{1'Z}$), 3.88 (dt, 6.2, 1.2 Hz, 2H, $H_{1'E}$), 3.70 (s, 2H, H_{12}), 3.41 (t, *J* = 6.9 Hz, 2H, H_{1Z}), 3.39 (t, *J* = 6.9 Hz, 2H, H_{1E}), 2.40 (t, *J* = 7.6 Hz, 2H, H_{11}), 1.71 (ddt, *J* = 6.5, 1.6, 1.2 Hz, 3H, $H_{4'E}$), 1.66 (ddt, *J* = 6.8, 1.7, 0.9 Hz, 3H, $H_{4'Z}$), 1.61–1.51 (m, 4H, H_2 and H_{10}), 1.40–1.14 (m, 14H, H_{3-9}). ^{13}C NMR (125 MHz, $CDCl_3$) δ: 138.7 (C_{13}), 129.2 ($C_{2'E}$), 128.8 (C_{15}), 128.4 (C_{14}), 127.8 ($C_{3'E}$), 127.5 ($C_{2'Z}$), 127.1 ($C_{3'Z}$), 126.8 (C_{16}), 71.5 (C_{1E}), 70.4 (C_{1Z}), 70.3 ($C_{1'E}$), 66.0 (C_{1Z}), 36.3 (C_{12}), 31.4 (C_{11}), 29.8, 29.5, 29.5, 29.2, 28.9 ($C_{2,4-10}$), 26.2 (C_3), 17.7 ($C_{4'E}$), 13.2 ($C_{4'Z}$).

*Preparation of poly[1-(2,5-dihydro-pyrrol-1-yl)-11-(4-vinyl benzyl sulfanyl)-undec-1-one-co-vinyl-benzene-co-divinyl-benzene] (**6**)*

Bis(tricyclohexylphosphine)benzylidineruthenium(IV) dichloride (26 mg, 31 μmol) and resin **75** (150 mg, 312 μmol) were placed in a round-bottom flask and dichloromethane (6 mL) was added. The suspension was swirled under argon for 48 h, before being transferred to a sinter with dichloromethane, and washed with dichloromethane (3 × 25 mL), dimethylformamide (3 × 25 mL), and various combinations of ethanol, methanol, dimethylformamide, pentane, toluene, acetonitrile, and dimethylsulfoxide. However no washing solvent, or combination successfully removed the dark-green colour from the bead. The polymer was finally washed with dichloromethane (3 × 25 mL), and dried in vacuo, giving the product as a dark green polymer (142 mg, 92%). IR (KBr disc) (cm^{-1}): 3081 (w), 3055 (w), 3024 (m), 2926 (s), 2848 (m), 1944 (br, m), 1719 (s), 1702 (s), 1654 (s), 1648 (s), 1420 (m), 1263 (m), 1198 (m), 1107 (m), 1069 (w), 997 (m), 917 (m), 823 (s), 737 (s), 695 (m, Ph), 669 (s). ^{13}C NMR (125 MHz, $CDCl_3$) δ: 171.8 (C_1), 126.0 ($C_{2'}$), 53.5 ($C_{1'a}$), 52.9 ($C_{1'b}$), 34.5, 33.2, 29.44, 26.3, 25.0 (C_{2-11}).

*Preparation of poly-[11-but-2-enyloxy-undecyl sulfanyl methyl-(4-vinyl benzene)-co-vinyl-benzene-co-divinyl-benzene] (**14**)*

*From metathesis of resin **4** with Z-2-butene:* Resin **4** (200 mg, 2.27 mmol g^{-1}) was placed in a thick walled glass tube (12 mm bore) and washed down with THF. The solvent was removed by blowing argon over the suspension until no solvent was visible outside the polymer. The polymer was then dried in vacuo. The tube was then cooled in a dry ice – acetone bath. *Z*-2-Butene was condensed into a Schlenk tube cooled in a dry ice – acetone bath, and 0.6 mL was transferred into the tube using a dry ice cooled syringe. Bis(tricyclohexylphosphine)benzylidineruthenium(IV) dichloride (11.2 mg, 3 mol%) in dichloromethane (0.6 mL) was then added to the tube. The bottom of the tube was cooled in liquid nitrogen before sealing. The tube was left at room temperature for 84 h. The lower half of the tube was then cooled in liquid nitrogen and the upper part was broken. The polymer was transferred to a sinter with dichloromethane and washed with dimethylformamide (3 × 25 mL), dichloromethane (3 × 25 mL), and pentane (3 × 25 mL), and dried in vacuo yielding the pale orange product polymer (206 mg, 94%). IR (thin film) (cm^{-1}): 3052 (w, C-H, str), 3023 (m, Ar-H or C=C-H, str), 2926 (s, C-H, str), 2850 (m, C-H, str), 1720 (m), 1702 (m), 1603 (m, Ar-H, def), 1509 (m, Ar-H, def), 1492 (m, Ar-H, def), 1440 (m, C-H, def), 1420 (m, C-H, def), 1364 (w, C-H_3, def), 1312 (w), 1260 (m), 1212 (w), 1180 (w, C-O, str), 1144 (w), 1108 (m, C-O, str), 1066 (w), 1018 (w), 965 (m, (E)-H-C=C-H, def), 908 (w), 823 (m, para Ar, C-H bnd), 759 (m, Ph, bnd), 747 (m), 698 (m, Ph, bnd), 672 (w), 661 (m). ^{13}C NMR (125 MHz, $CDCl_3$) δ: 128.9 ($C_{2'}$), 127.6 ($C_{3'}$), 71.2 (C_1), 70.0 ($C_{1'}$), 31.2, 29.3, 25.8 (C_{2-11}), 17.6 ($C_{4'E}$), 13.0 ($C_{4'Z}$).

From Resin-OH and crotyl bromide: Potassium hydride (35% in mineral oil) was placed in a preweighed Schlenk tube and washed with pentane (3 × 10 mL). The residual pentane was removed in vacuo to give (120 mg, 3.0 mmol). The Schlenk tube was cooled in dry ice – acetone bath, and solution of 18-crown-6 (555 mg, 2.1 mmol) in THF (22 mL) was added slowly via cannula. Resin-OH (12) was placed in the swirler, and the potassium hydride solution was added via cannula. As the suspension warmed to room temperature effervescence was observed. The suspension was allowed to warm to room temperature and swirled for 30 min. Crotyl bromide (1.0 mL, 10 mmol) was added and the suspension was swirled overnight, then transferred to a sinter with dichloromethane, and washed with dimethylformamide (3 × 30 mL), dichloromethane (30 mL), and pentane (30 mL), then dried in vacuo to give the product as a colourless tacky polymer (521 mg, 18% (by ^{13}C NMR)).

*General procedure for screening of metathesis of resin **8** and various alkenes*

Resin **8** (150 mg, 0.32 mmol) and bis(tricyclohexylphosphine)benzylidineruthenium(IV) dichloride (7.8 mg, 3 mol%) were loaded into a small Schlenk tube with a small magnetic follower. The contents of the Schlenk tube were degassed. The alkene and solvent were placed in a separate Schlenk tube, degassed, and added via cannula. The suspension was stirred slowly for the stated amount of time, then transferred to a sinter with a solvent (usually dichloromethane) and washed with some of the following solvents: dichloromethane, dimethylformamide, methanol, pentane, tetraglyme, THF, and dried in vacuo For the cross-metathesis product with *Z*-but-2-en-1,4-diol. ^{13}C NMR (125 MHz, $CDCl_3$) δ: 133.2 ($C_{3'}$), 127.4 ($C_{2'}$), 70.9 ($C_{3'}$), 69.8, 67.2 (C_{1-8}), 62.8 ($C_{1'}$), 58.6 ($C_{4'}$).

References

1. (*a*) C.L. Kingsbury, S.J. Mehrman, and J.M. Takacs. Curr. Org. Chem. **3**, 497 (1999); (*b*) B.A. Lorsbach and M.J. Kurth. Chem. Rev. **99**, 1549 (1999); (*c*) R.C.D. Brown. J. Chem. Soc. Perkin Trans. 1, 3293 (1998).
2. (*a*) S. Chamoin, S. Houldsworth, C.G. Kruse, W.I. Bakker, and V. Snieckus. Tetrahedron Lett. **39**, 4179 (1998); (*b*) S.R. Piettre and S. Baltzer. Tetrahedron Lett. **38**, 1197 (1997);

© 2001 NRC Canada

(*c*) R. Frenette and R.W. Friesen. Tetrahedron Lett. **35**, 9177 (1994); (*d*) R. Franzén. Can. J. Chem. **78**, 957 (2000).
3. R. Riedl, R. Tappe, and A. Berkessel. J. Am. Chem. Soc. **120**, 8994 (1998).
4. B. Yan, J.B. Fell, and G. Kumaravel. J. Org. Chem. **61**, 7467 (1996).
5. (*a*) R. Warrass and G. Lippens. J. Org. Chem. **65**, 2946 (2000); (*b*) T. Wehler and J. Westman. Tetrahedron Lett. **37**, 4771 (1996); (*c*) R. Jelinek, A.P. Valente, K.G. Valentine, and S.J. Opella. J. Magn. Reson. **125**, 185 (1997); (*d*) Y.R. de Miguel, N. Bampos, K.M. Nalin de Silva, J.K.M. Sanders, and S.A. Richards. Chem. Commun. 2267 (1998); (*e*) G. Lippens, M. Bourdonneau, C. Dhalluin, R. Warrass, T. Richert, C. Seetharaman, C. Boutillon, and M. Piotto. Curr. Org. Chem. **3**, 147 (1999).
6. S.R. McAlpine and S.L. Schreiber. Chem. Eur. J. **5**, 3528 (1999).
7. S.S. Wang. J. Org. Chem. **40**, 1235 (1975).
8. M. Grotli, C.H. Gotfredsen, J. Rademann, J. Buchardt, A.J. Clark, J.O. Duus, and M. Meldal. J. Comb. Chem. **2**, 108 (2000).
9. R. Quarrell, T.D.W. Claridge, G.W. Weaver, and G. Lowe. Mol. Diversity, **1**, 223 (1996).
10. A. Basso, B. Evans, N. Pegg, and M. Bradley. Tetrahedron Lett. **41**, 3763 (2000).
11. (*a*) J.M. Brown and J.A. Ramsden. Chem. Commun. 2117 (1996); (*b*) I.P. Thomas, J.A. Ramsden, T.Z. Kovacs, and J.M. Brown. Chem. Commun. 1507 (1999).
12. M. Schuster, J. Pernerstorfer, and S. Blechert. Angew. Chem. Int. Ed. Engl. **35**, 1979 (1996)
13. J.H. van Maarseveen, J.A.J. den Hartog, V. Engelen, E. Finner, G. Visser, and C.G. Kruse. Tetrahedron Lett. **37**, 8249 (1996).
14. (*a*) G.D. Cuny, J.R. Cao, A. Sidhu, and J.R. Hauske. Tetrahedron, **55**, 8169 (1999); (*b*) J.U. Peters and S. Blechert. Synlett, 348 (1997).
15. A.G.M. Barrett, S.M. Cramp, and R.S. Roberts. Org. Lett. **1**, 1083 (1999).
16. (*a*) M. Schuster and S. Blechert. Angew. Chem. Int. Ed. Engl. **36**, 2037 (1997); (*b*) R.H. Grubbs and S. Chang. Tetrahedron, **54**, 4413 (1998); (*c*) T. Naota, H. Takaya, and S.I. Murahashi. Chem. Rev. **98**, 2599 (1998).
17. (*a*) F.S. Varveri, J. Nikokavouras, A.E. Mantaka-Marketou, and M. Micha-Screttas. Monatsh. Chem. **120**, 967 (1989); (*b*) R.N. Reddie. Synth. Commun. **17**, 1129 (1987).
18. T.A. Kirkland, D.M. Lynn, and R.H. Grubbs. J. Org. Chem. **63**, 9904 (1998).
19. D.D. Perrin, W.L.F. Armarego, and D.R. Perrin. Purification of laboratory reagents. Pergamon Press, Oxford. 1988.
20. R. Riemschnieder and H.J. Koetzsch. Monatsh. Chem. **90**, 787 (1959).
21. G.C. Fu, S.T. Nguyen, and R.H. Grubbs. J. Am. Chem. Soc. **115**, 9856 (1993).
22. B.A. Johns and C.R. Johnson. Tetrahedron Lett. **39**, 749 (1998).
23. T. Horiuchi, T. Ohta, E. Shirakawa, K. Nozaki, and H. Takaya. J. Org. Chem. **62**, 4285 (1997).
24. (*a*) M.A. Walters and A.B. Hoem. J. Org. Chem. **59**, 2645 (1994); (*b*) H. Nemoto, H.N. Jimenez, and Y. Yamamoto. J. Chem. Soc. Chem. Commun. 1304 (1990).
25. J.C. Anderson, D.C. Siddons, S.C. Smith, and M.E. Swarbrick. J. Chem. Soc. Chem. Commun. 1835 (1995).

© 2001 NRC Canada

Proton- and lanthanide-coordinating properties of the tetraaza macrocycle (EDDA–KA)$_2$ in aqueous solution

Bin Song, Glen S. Kurokawa, Shuang Liu, and Chris Orvig

Abstract: The new potentially multidentate ligand (EDDA–KA)$_2$ has been prepared and its acid–base properties determined. Its coordination properties with three lanthanide ions (La^{3+}, Gd^{3+}, and Lu^{3+}) and Fe^{3+} have been studied in aqueous solution (I = 0.16 M NaCl, 25°C) by potentiometric pH, spectrophotometric, and ^{1}H NMR titrations. In total, eight pK_a values could be determined by these diverse methods. From the ^{1}H NMR titrations, all the deprotonation steps could be determined and assigned (in groups). Strong hydrogen bonding among two nitrogen atoms and one oxygen atom on the pyrone ring was observed, and the corresponding pK_a values were estimated to be 13.2 and 14.0. By comparison with similar systems, an equilibrium constant for the formation of the hydrogen bond was estimated, $K_I = 10^{4.4}$. Eight stability constants in total were determined for various protonation states of the La^{3+} and Gd^{3+} complexes, but for Lu^{3+} only the last four constants were obtained. The species distribution diagram showed that [M(EDDA–KA)$_2$-4H]$^{2-}$ predominated in the range $5 \le pH \le 9$ and [M(EDDA–KA)$_2$-6H]$^{4-}$ predominated in the region $9 \le pH \le 11$. In the former complex, two strong hydrogen bonds anchored the macrocycle and Ln^{3+} was coordinated with the four carboxylate groups; in the latter, the two hydrogen bonding protons were absent and the metal ion might also bind to the nitrogens on the macrocycle. The stability of Gd^{3+}–(EDDA–KA)$_2$ is lower than the analogous Gd^{3+} complexes of DOTA, DTPA, and DTPA–BMA.

Key words: acidity constants, stability constants, La^{3+}, Gd^{3+}, Lu^{3+}, Fe^{3+}, amino carboxylate chelator.

Résumé : On a préparé le nouveau ligand (EDDA–KA)$_2$ qui est potentiellement multidentate et on a déterminé ses propriétés acide–base. Faisant appel à des titrages spectrophotométriques, à l'aide de pH potentiométrique ou de la RMN du ^{1}H et opérant en solutions aqueuses (I = 0,16 M NaCl, 25°C) on a étudié ses propriétés de coordination avec trois ions de la série des lanthanides (La^{3+}, Gd^{3+} et Lu^{3+}) ainsi qu'avec le Fe^{3+}. Au total, on a ainsi déterminer huit valeurs de pK_a par ces diverses méthodes. Sur la base des titrages par RMN du ^{1}H, on a pu déterminer toutes les étapes de déprotonation et les attribuer (en groupes). On a observé de fortes liaisons hydrogènes entre deux atomes d'azote et un atome d'oxygène sur la pyrone; on a évalué que les valeurs correspondantes des pK_a sont 13,2 et 14,0. Par comparaison avec d'autres systèmes semblables, on a évalué que la constante d'équilibre pour la formation de la liaison hydrogène est $K_I = 10^{4,4}$. On a déterminé un total de huit constantes de stabilité pour les divers états de protonation des complexes de La^{3+} et Gd^{3+}; toutefois, dans le cas du Lu^{3+}, on n'a déterminer que les quatre dernières constantes. Le diagramme de distribution des espèces montre que [M(EDDA–KA)$_2$-4H]$^{2-}$ est l'espèce prédominante à des pH allant de 5 à 9 et que [M(EDDA–KA)$_2$-6H]$^{4-}$ est l'espèce prédominante à des pH allant de 9 à 11. Dans le premier complexe, deux liaisons hydrogènes fortes permettent d'ancrer le macrocycle et le Ln^{3+} est coordiné aux quatre groupes carboxylates; dans le dernier complexe, les deux protons formant la liaison hydrogène sont absents et l'ion métallique pourrait aussi se lier aux azotes du macrocycle. La stabilité du Gd^{3+}–(EDDA–KA)$_2$ est inférieure à celles des complexes analogues du Ga^{3+} avec DOTA, DTPA et DTPA–BMA.

Mots clés : constantes d'acidité, constantes de stabilité, La^{3+}, Gd^{3+}, Lu^{3+}, Fe^{3+}, agent de chélation aminocarboxylate.

[Traduit par la Rédaction]

Introduction

Aminocarboxylate compounds are widely used as chelators for a variety of transition-metal and lanthanide ions; some of these complexes are used in vivo as diagnostic probes, such as magnetic resonance imaging (MRI) contrast agents (1-3).

Received October 2, 2000. Published on the NRC Research Press Web site at http://canjchem.nrc.ca on July 17, 2001.

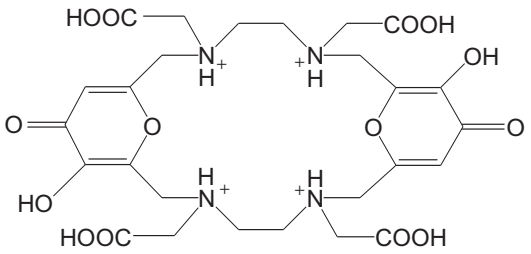
Dedicated to Professor Brian R. James on the occasion of his 65th birthday.

B. Song, G.S. Kurokawa, and C. Orvig.[1] Medicinal Inorganic Chemistry Group, Department of Chemistry, University of British Columbia, 2036 Main Mall, Vancouver, BC V6T 1Z1, Canada.
S. Liu. DuPont Pharmaceuticals, Medical Imaging R&D, 331 Treble Cove Road, 500-3, No. Billerica, MA 01862-2987, U.S.A.

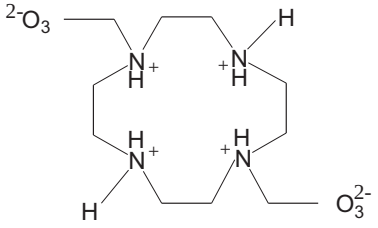
[1]Corresponding author (telephone: (604) 822-4449; fax: (604) 822-2847; email: orvig@chem.ubc.ca).

 DOI: 10.1139/cjc-79-5/6-1058 © 2001 NRC Canada

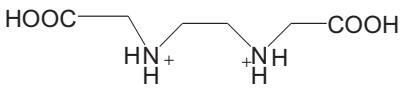
Scheme 1.



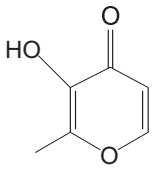
$H_4(EDD -)_2^{4+}$



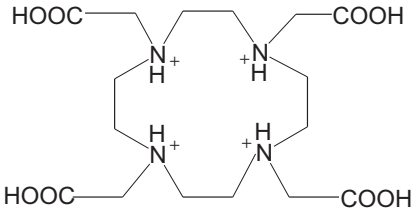
$H_4(DO2)$



$H_2(EDD)^{2+}$



M to



$H_4(DOT)^{4+}$

The solution chemistry of these ligands is of critical importance — the results evince the structures of the complexes in solution and the species distribution as a function of concentration, L:M ratio, and pH, information of direct relevance to the function of these compounds in vivo. The aqueous chemistry of lanthanide ions (Ln^{3+}) is dominated by their oxophilicity (4, 5) with the strongest binding ligands containing carboxylato or phosphonato oxygen donors. Amines alone are poor donors for Ln^{3+} in water; however, incorporated into aminocarboxylates they form quite stable Ln(III) complexes. There are numerous reports of stability constants for Ln(III) complexes of aminocarboxylate derivatives including EDTA analogues (e.g., DTPA (6)) and macrocycles (e.g., DOTA (7)). Replacing the carboxylate group with other functional groups, for example hydroxyl or pyridine (8), has been tried to alter the coordination ability of the aminocarboxylates.

In this study, we have prepared a rather unusual macrocylic amino carboxylate compound $(EDDA–KA)_2$ (see Scheme 1), measured its acidity constants, and studied its aqueous complexation with La^{3+}, Gd^{3+}, and Lu^{3+}. $(EDDA–KA)_2$ is unusual in that the insertion of a pyrone ring between the two EDDA molecules renders the proton and metal ion binding properties of, and hydrogen-binding in, $(EDDA–KA)_2$ very different from its parent ligand EDDA and from the structurally similar compound DOTA.

Experimental section

Materials

EDDA was from Sigma, kojic acid was from Lancaster, and paraformaldehyde was from Fisher Scientific. Atomic absorption standard solutions of La^{3+} and Lu^{3+} were purchased from Sigma, while that of Gd^{3+} was from Aldrich. NaOH (1 M) solution used as titer was from Fisher Scientific, and its concentration was established with potassium biphthalate from Anachemia Canada Inc. Standard buffer solutions (pH = 4.00 and 7.00), NaCl for controlling the ionic strength of the solution, and HCl(aq) were also purchased from Fisher Scientific. Water used in the experiments was deionized (Barnstead D8902 and D8904 cartridges) and distilled (Corning MP-1 Megapure still) and depleted in CO_2 by boiling under Ar for about 30 min. D_2O, NaOD, and DCl were purchased from Cambridge Isotope Laboratories.

Instrumentation

Potentiometric measurements were carried out with an automatic titration system consisting of a Metrohm 713 pH meter equipped with Metrohm 6.0233.100 electrode, a model 665 Metrohm Dosimat autoburet (5 mL burette, absolute error ±0.015 mL, accuracy ±0.005 mL), water-jacketed titration vessels, and a Julabo UC circulating bath. Both pH meter and autoburet were controlled by an IBM compatible PC and the titration was controlled by a locally written QBasic program. UV spectra were recorded with a HP 8453 spectrophotometer and the ^1H NMR spectra were obtained at 200MHz on a Bruker AC-200 instrument.

Preparation of $(EDDA–KA)_2$

To a suspension of EDDA (1.75 g, 10 mmol) in 90% ethanol (180 mL) was added paraformaldehyde (0.8 g, 27 mmol), and kojic acid (3.0 g, 10 mmol). The reaction mixture was heated to reflux for 48 h. The mixture was then cooled to room temperature, and the resulting solid was col-

© 2001 NRC Canada

lected by filtration, washed with ethanol, and dried under vacuum overnight. This crude product was suspended in 20 mL water with stirring, and the resulting solution was slowly titrated with 5 M NaOH to pH ~ 10. After clarification of this solution by filtration, concentrated HCl was then added dropwise to the filtrate until the pH of the mixture was 3.0; after stirring the resulting suspension for 1 h, the solid was collected by filtration, washed with ethanol, and dried under vacuum overnight. The yield was ≥90%. ^{1}H NMR (D_2O) δ: 6.50 (s, 2 H), 4.45 (s, 4 H), 3.92 (s, 4 H), 3.78 (s, 4 H), 3.42 (t, 4 H), 3.32 (s, 4 H), 2.90 (t, 4 H). ^{13}C NMR (D_2O, 150 MHz) δ: 182.9, 176.0, 168.5, 167.5, 153.9, 148.1, 61.8, 56.1, 52.8, 50.9, 48.6, 47.6. MS (EI, 70 eV) *m*/*z* (relative intensity, assignment): 625 (12, $[M + H]^+$), 609 (24, $[M + H\text{-}O]^+$), 313 (100, $[M + 2H]^{2+}$), 297 (27, $[M + 2H\text{-}O]^{2+}$), 177 (20). Elemental anal. calcd. for (EDDA–KA)$_2$·1.5H_2O (%): C 47.93, H 5.41, N 8.60; found: C 47.93, H 5.31, N 8.56.

Potentiometric pH titrations

The acidity constants for (EDDA–KA)$_2$ were determined by titrating 50 mL aq 5.6 mM HCl (I = 0.16 M NaCl, 25°C) in the presence of 0.3 mM to 0.4 mM (EDDA–KA)$_2$ under Ar with 3 mL 0.11 M NaOH. The constants were calculated on an IBM compatible computer containing a Pentium II processor using a curve-fit procedure (a Newton–Gauss nonlinear-least-squares program) and the data within the range $2.3 \le pH \le 10.3$. This corresponded to about 67% neutralization for the equilibrium $[H_2(EDDA–KA)_2]^{2+}$–$[H(EDDA–KA)_2]^+$ and about 99% neutralization for the equilibrium $[(EDDA–KA)_2\text{-}3H]^{3–}$–$[(EDDA–KA)_2\text{-}4H]^{4–}$. The direct pH meter readings were used to calculate the acidity constants (the pH meter was calibrated with standard buffer solutions pH = 4.00 and pH = 7.00 every day before the titrations); i.e., these constants are the so-called practical, mixed, or Brønsted constants (9). Their negative logarithms, given for aqueous solutions at I = 0.16 M (NaCl) and 25°C, may be converted into the corresponding concentration constants by subtracting 0.02 log unit (9). This conversion term contains both the junction potential of the glass electrode and the hydrogen ion activity (9, 10). The final results of the acidity constants were determined from the average of 19 independent titrations.

The stability constants of La^{3+}, Gd^{3+}, and Lu^{3+} with (EDDA–KA)$_2$ were determined under the same conditions as for the acidity constants, except that Na^+ was partly replaced by the respective metal ion (I = 0.16 M, 25°C). The ligand to M^{3+} ratios used in these experiments were slightly greater than 1:1. The calculations were carried out by a similar curve-fitting procedure using a Newton–Gauss nonlinear least-square program in the range $2 < pH < 10$. The final results come from the average of at least eight independent titrations for each metal ion.

UV titrations

A series of 0.04 mM (EDDA–KA)$_2$ solutions were prepared, and the pH of each solution was adjusted at 25°C and the ionic strength was kept at 0.16 with 1.6 M NaCl; the UV spectrum of each solution was then recorded at 25°C. At a given wavelength, the absorption and the corresponding pH could be fitted with a curve-fit procedure using a Newton–Gauss nonlinear-least-squares program; pK_a values could be calculated from this fitting. The lowest pH taken in the experiments was 1.6, corresponding to about 28% neutralization for the equilibrium $[H_2(EDDA–KA)_2]^{2+}$–$[H(EDDA–KA)_2]^+$, and the highest pH was 13.5, about 28% neutralization for the equilibrium $[(EDDA–KA)_2\text{-}5H]^{5–}$–$[(EDDA–KA)_2\text{-}6H]^{6–}$. In addition to the potentiometric pK_a values, pK_a values in the high pH range ($13 \le pH \le 14$) were also obtained. The results obtained by this method came from the avg of five independent experiments.

^{1}H NMR titrations

(EDDA–KA)$_2$ (0.085 g, 0.13 mmol) was dissolved in 16 mL D_2O and 0.05 mL 30% NaOD. The pH meter reading value pH* of this solution was 13.4 and the concentration was about 0.09 M. About 0.5 mL of the solution was taken as an aliquot for ^{1}H NMR measurement and the pH of the remaining solution was adjusted to 13.24 with concentrated DCl solution and another 0.5 mL of solution removed as a second aliquot. The above procedure was continued until a series of solutions with different pH values was obtained and a series of NMR spectra were recorded. The chemical shifts of each signal at each pH were used to evaluate the acidity constants. The calculation was carried out on an IBM-compatible computer with a Pentium II processor by a curve-fit procedure using a Newton–Gauss nonlinear-least-squares program with data over the pD range $1.8 \le pD \le 13.8$, corresponding to about 20% neutralization for the equilibrium $[H_2(EDDA–KA)_2]^{2+}$–$[H(EDDA–KA)_2]^+$ and about 24% neutralization for the equilibrium $[(EDDA–KA)_2\text{-}5H]^{5–}$–$[(EDDA–KA)_2\text{-}6H]^{6–}$. During the calculation, the pH meter reading values pH* were converted to pD by adding 0.4 log unit (11). The pK_a values obtained in D_2O could be converted to the corresponding values in H_2O by eq. [1] (12). The results obtained by NMR were from three independent series of experiments.

$$[1] \qquad pK_a\ (H_2O) = (pK_a\ (D_2O) - 0.45)/1.015$$

Results and discussion

Synthesis of (EDDA–KA)$_2$

It is known that kojic acid undergoes Mannich reactions with primary or secondary amines in the presence of excess paraformaldehyde (13, 14). The aminomethylation occurs at the *ortho* position to the enolic hydroxyl group at room temperature. The hydroxymethyl group at C6 (the *para* position of the enolic hydroxyl group) is relatively unreactive towards amines. In this study, however, we found that kojic acid reacted with ethylenediamine-*N*,*N*′-diacetic acid (EDDA) in the presence of formaldehyde to form a novel macrocyclic chelant (EDDA–KA)$_2$. The reaction was carried out in 90–95% ethanol under reflux for 48 h (Scheme 2).

The Mannich reaction proceeds through two pathways (15) and is usually a result of a complex series of equilibria, related to the nature of the reactants and reaction conditions. EDDA reacts with paraformaldehyde first, to form a substituted five-membered imidazolidine intermediate (Scheme 2), which undergoes rapid electrophilic reaction at the *ortho* position of the enolic hydroxyl group to give the initial EDDA–KA adduct. Because of the *N*-substitution, the amine N atom is more basic and the carboxylate proton is shifted to

© 2001 NRC Canada

Scheme 2.

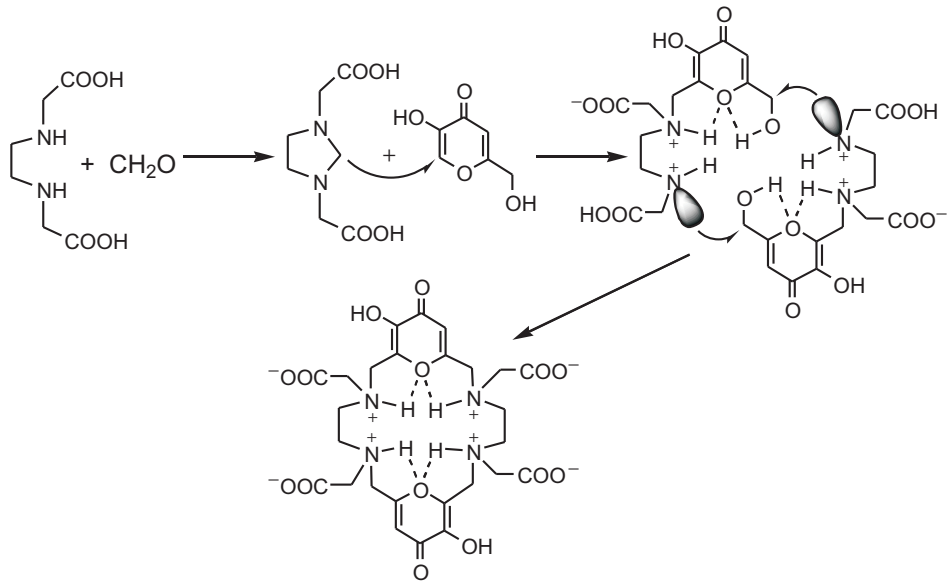


Table 1. Logarithms of the literature acidity constants and the corresponding estimated values for $H_4(EDDA–KA)_2)^{4+}$.

Compound	pK_a (-COOH)	pK_a (N-H)	pK_a (-OH)	Conditions	Reference
$H_2(EDDA)^{2+}$	1.28, 2.30	6.49, 9.44	—	0.20 M $NaClO_4$, 37°C	16
$H_2(EDDA)^{2+}$	—	6.55, 9.62	—	0.1 M KNO_3, 25°C	17
$H_4(DOTA)^{2+}$		3.95, 4.85		0.1 M KCl, 25°C	18
		9.69, 11.14			
Maltol	—	—	8.40	0.16 M NaCl, 25°C	19
$H_4(EDDA–KA)_2)^{4+}$	1–2, 2–3	4–5, 9–11	8–9	n/a	Estimated

the amine N atom to form a zwitterion. The N-H group forms a strong hydrogen bond with the pyrone O atom, rendering the 6-hydroxymethyl group more reactive towards the remaining amine N atom (Scheme 2) of another EDDA–KA adduct thus dimerizing and causing the relative orientation of the two pyrone groups in $(EDDA–KA)_2$.

Acidity constants

These were determined by three different methods — potentiometry, UV spectrophotometry, and ^1H NMR spectroscopy. From the structure of $(H_4(EDDA–KA)_2)^{4+}$ (Scheme 1), one can deduce that ten protons in total may be ionisable from the fully protonated 4+ species, i.e., four protons from the carboxylate groups, four protons from the nitrogen atoms, and two protons from the pyrone OH groups. According to the corresponding acidity constants of EDDA, DOTA, and maltol, listed in Table 1 with structures in Scheme 1, initial guesses of the pK_a values for $[H_4(EDDA–KA)_2]^{4+}$ could be made and these values are listed in the last row of Table 1. This was a necessary process because of the complexity of the protonation problem in $(EDDA–KA)_2$.

It is surprising that only six acidity constants were determined in the range $2 \le pH \le 11$. From low to high, the pK_a values are: 1.95 ± 0.12, 2.60 ± 0.08, 3.19 ± 0.04, 3.80 ± 0.03, 7.42 ± 0.04, 8.24 ± 0.04. As was estimated in Table 1, the first two protons are released mainly from the two carboxylate groups, with pK_a values lower than 2. Therefore, eight more deprotonation steps should have been observed in the range $2 \le pH \le 11$. Another discrepancy between the potentiometrically measured pK_a values and the estimated ones is that, in the range $6 \le pH \le 10$ only two pK_as were determined whereas there should be four pK_as according to the estimation.

To ascertain if there were more deprotonation steps in the range pH > 12, UV spectrophotometric titrations were undertaken; however, with this method only three groups of pK_a values were determined. It was impossible to separate the four pK_as in the range $2 \le pH \le 4$ and the two pK_as in the range $7 \le pH \le 9$ with the absorbance vs. pH fitting; only the avgs of the pK_as were obtained in these two pH ranges.

Since the UV absorption of the compound is associated with the n-π^* transition of the pyrone ring and, in the range $7 \le pH \le 9$, the absorption band has a significant red shift with increasing pH, it is reasonable to assign the deprotonation(s) in this pH range to the OH group(s) of the pyrone ring. The important result obtained by this method is that in the region $12 \le pH \le 14$, there is an absorbance change with pH and a pK_a value can be determined. As discussed above, it is impossible from the fitting to quantify the number of deprotonation steps in this pH range.

The pK_a values of the three groups measured by this UV spectrophotometric method, i.e., $2 \le pH \le 4$, $7 \le pH \le 9$ and pH > 13 are 3.00, 7.93, and 13.64, respectively (Table 2). Whereas the averages of pK_as from potentiometric titration in the first two pH ranges are 2.89 and 7.83. The results from the two different methods agree, and evince their reli-

© 2001 NRC Canada

Table 2. Comparison of the acidity constants of $(EDDA–KA)_2$ measured by potentiometric, UV spectrophotometric, and NMR titrations (I = 0.16 M NaCl, 25°C).

Method	pK_a ($2 \le pH \le 4$)	pK_a ($7 \le pH \le 9$)	pK_a ($13 \le pH \le 14$)
Potentiometric	2.89 ± 0.18[a]	7.83 ± 0.08[b]	—
Spectrophotometric	3.00 ± 0.20	7.93 ± 0.08	13.6 ± 0.4
NMR	—	7.76 ± 0.10	13.5 ± 0.3

[a] The average of the first four pK_a values measured potentiometrically.
[b] The average of the last two pK_a values measured potentiometrically.

Fig. 1. ^1H NMR spectrum of $(EDDA–KA)_2$ in D_2O, pD = 12.0; signals at $5 > \delta > 4.5$ are from H_2O.

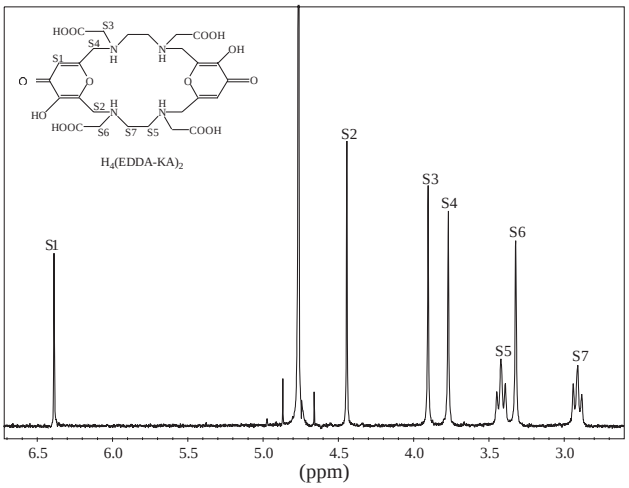
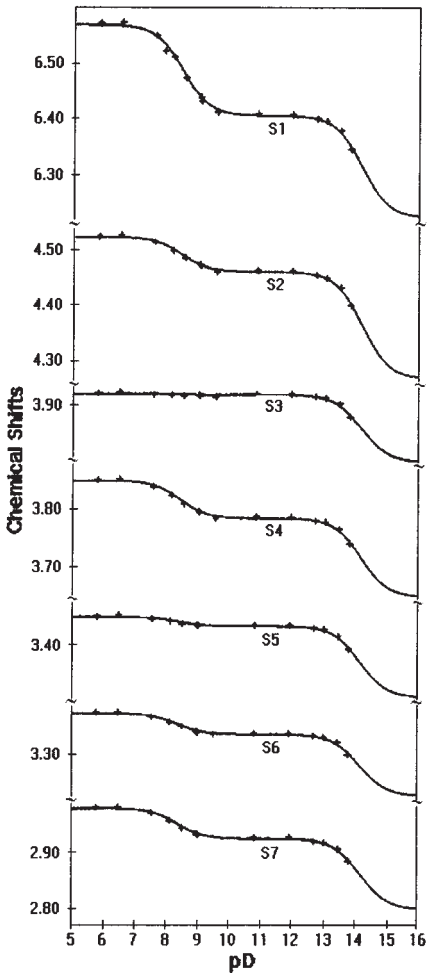


Fig. 2. NMR chemical shifts vs. pD for $(EDDA–KA)_2$; the points represent the experimental results and the lines are the best fit using the determined acidity constants in Table 2.



ability. It should be noted, however, that because the highest pH taken in the UV experiment was 13.5, it is difficult to determine an accurate value for the last pK_a by spectrophotometry (hence the large error limit).

The third method used in determining the acidity constants of the complicated system $(H_4(EDDA–KA)_2)^{4+}$ was ^1H NMR spectroscopy, a powerful technique since it provides structural information about sites of deprotonation over a given pH range.

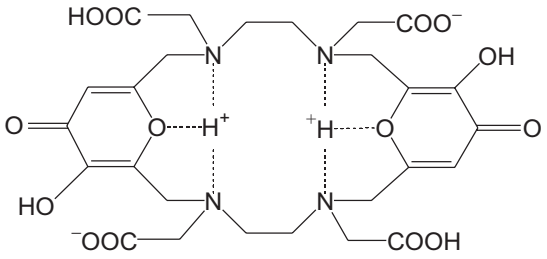
The ^1H NMR spectrum of $(EDDA–KA)_2$ at pD = 12 is shown in Fig. 1. The signal at about 6.4 ppm (S1) clearly belongs to the methine hydrogen atom on the pyrone ring and the 2 triplets (S5 and S7) belong to the methylene hydrogen atoms between the two nitrogen atoms. The other assignments were made according to the chemical shift changes of each signal with pH. Figure 2 shows the chemical shift changes with pH for all seven signals. That S1 has the largest shift in the range $6 \le pD \le 9$ proves that, in this pH range, the two pyrone OH groups deprotonate, in agreement with the UV spectrophotometric study. With this in mind, the other signals could be assigned; for example, S3 was assigned to the CH_2 group farthest from the OH, and S7 to the CH_2 closer to the OH residue than the S5 CH_2. All the assignments are shown in Fig. 1.

From separate experiments, it was determined that in the low pD range, $1 \le pD \le 4$, most of the signals had large chemical shift changes, but the fitting was poor because of precipitation (vide supra). Some deprotonations at the nitrogen atoms occurred in this pD range. From the potentiometric pH titrations it was known that there were four deprotonation steps in this pD range; therefore, two of the protons could be assigned to the ammonium groups and the other two protons to the carboxylate groups.

The fittings in Fig. 2 also reveal the corresponding acidity constants which are listed in the last row of Table 2. Since the highest pD in the NMR experiment was only 13.8, the pK_a result in the range $13 \le pD \le 14$ has correspondingly large error limits. It is clear that the NMR experiment is in good agreement with the results obtained from the other two methods. The result for the final pK_a value in the range $13 \le pH \le 14$ should be the average of the result from the UV and NMR titrations, that is (13.64 + 13.5)/2 = 13.6 ± 0.4. As we know from the structure of the substance, there are always two protons which have the same chemical environment, so

© 2001 NRC Canada

Scheme 3.



there should be two pK_a values in this pH range. It is difficult to estimate how much these two deprotonation steps influence each other and therefore it is difficult to resolve the two acidity constants from the above result. If we suppose that there is no interdependence between the two deprotonation steps, according to statistics, the two pK_a values should lie at least 0.6 log unit apart (20). Comparing with the result for the two OH groups, however, two protons far away from each other have pK_a values separated by about 0.8 log unit — still larger than the statistical estimation. Therefore we use $1 \times 10^{0.8}$ as the lower limit of the difference of the two constants in the range $13 \le pH \le 14$. In this way two pK_a values: $pK^{H}_{(L-4H)} = 13.2 \pm 0.4$ and $pK^{H}_{(L-5H)} = 14.0 \pm 0.4$ were obtained. These values are necessary for the evaluation of the stability constants of $(EDDA–KA)_2$ with metal ions.

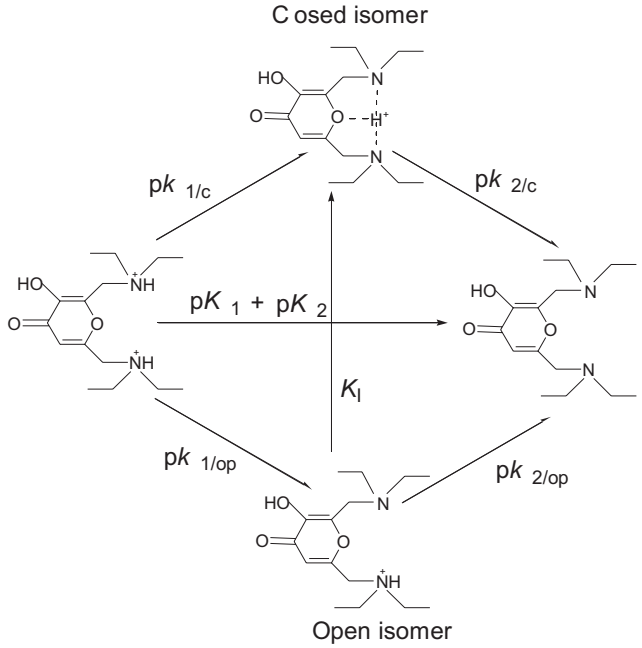
Solution structure of $(EDDA–KA)_2$ and its deprotonation steps

From the above results with the three different methods, a clear picture can be elucidated of how $[H_4(EDDA–KA)_2]^{4+}$ is deprotonated step-by-step in aqueous solution under these experimental conditions. Starting in acid solution, the first two protons are released from the two carboxylate groups in $[H_4(EDDA–KA)_2]^{4+}$ with pK_a < 1; these two acidity constants must be lower than the corresponding values in EDDA (vide infra). In the second deprotonation step, two ammonium nitrogen atoms are deprotonated and two strong hydrogen bonds are thus formed with a proton shared among two nitrogen atoms and one oxygen atom (Scheme 3). A neutral species is now formed, with the lowest solubility in aqueous solution of all the species; hence the precipitation in the range $2.8 \le pH \le 3.0$ and the dissolution if either acid or base is added to the solution. The pK_a values for these first two ammonium deprotonations are 1.95 and 2.60. Subsequently, the other two carboxylate groups are deprotonated with pK_a values 3.19 and 3.80. In the range $7 \le pH \le 9$, both UV and NMR spectra have proven that deprotonation occurs at the OH groups on the pyrone ring with pK_a values 7.42 and 8.24.

Lastly, with pK_a values as high as 13.2 and 14.0, the two strong hydrogen bonds are finally deprotonated. These last two $(EDDA–KA)_2$ pK_a values can be understood because the strong four centre hydrogen bonds must be very stable; however, why are the other two protons on the ammonium nitrogen atoms so acidic (pK_a values 1.95 and 2.60)?

In our previous studies, factors affecting the acidity constants in similar systems have been discussed in detail (21). Among the factors, a charge effect (coulombic), a polar effect, a statistical effect, and intramolecular hydrogen bonding are normally important. It is known that intramolecular hydrogen bonding between two nitrogen atoms is very weak because nitrogen is a poor hydrogen bond acceptor (22); however, oxygen is an excellent hydrogen bond acceptor. Thus, in $(EDDA–KA)_2$, the intramolecular hydrogen bond among the two nitrogen atoms and one oxygen atom is so strong, with an average pK_a value 13.6 (Table 2).

Scheme 4.



Scheme 4 illustrates the microscopic deprotonation behaviour of the ammonium N atoms and the formation of the intramolecular hydrogen bonds in $(EDDA–KA)_2$. Because of the high symmetry of the molecule, in each step, two protons (Scheme 3) are involved and the average of the acidity constants are used in this discussion. In Scheme 4, the macro acidity constant pK_{a2} has been determined but pK_{a1} and K_I are unknown. To calculate these two constants, at least two micro acidity constants should be known.

In Table 1, the two acidity constants for EDDA (average of literature values) pK_{a1} = 6.52 and pK_{a2} = 9.53 are listed (16,17). For en (1,2-diaminoethane), the corresponding values are pK_{a1} = 7.19 and pK_{a2} = 9.99 (25°C, 0.16 M KCl) (23). The difference (–1.13) between (pK_{a1} + pK_{a2}) of EDDA and (pK_{a1} + pK_{a2}) of en reflects the effect of the two carboxyl groups in EDDA; we can therefore estimate for each constant an average effect of 0.56 pK unit. Since the micro acidity constants for the open isomer of en are known (p$k_{a1/op}$ = 7.40 and p$k_{a2/op}$ = 9.78) (21), the corresponding values for EDDA can be estimated by deducting 0.56 from the value for en, i.e. p$k_{a1/op}$ = 6.84 and p$k_{a2/op}$ = 9.22. (Here we suppose that the stability of the intramolecular hydrogen bond in each system is identical, a reasonable assumption because the two molecules are structurally similar and it is known that the intramolecular hydrogen bond between two amine N atoms is very weak (21, 22). Another assumption is that p$k_{a1/op}$ and p$k_{a2/op}$ for $(EDDA–KA)_2$ and for EDDA are the same. By comparing the structure of the two compounds,

© 2001 NRC Canada

Table 3. Stability constants of La^{3+}, Gd^{3+}, and Lu^{3+} with $(EDDA–KA)_2$ as measured by potentiometric pH titration (I = 0.16 M NaCl, 25°C).

Stability constant	La^{3+}	Gd^{3+}	Lu^{3+}
$\log K^{M}_{MHL}$	3.0 ± 0.5	3.0 ± 0.5	—
$\log K^{M}_{ML}$	3.4 ± 0.2	3.6 ± 0.2	—
$\log K^{M}_{M(L-H)}$	3.42 ± 0.17	3.7 ± 0.2	—
$\log K^{M}_{M(L-2H)}$	3.83 ± 0.14	3.90 ± 0.10	—
$\log K^{M}_{M(L-3H)}$	6.26 ± 0.08	6.80 ± 0.09	6.1 ± 0.2
$\log K^{M}_{M(L-4H)}$	7.62 ± 0.06	8.81 ± 0.10	8.26 ± 0.14
$pK^{M}_{M(L-4H)}$	9.41 ± 0.15	9.04 ± 0.07	9.4 ± 0.3
$pK^{M}_{M(L-5H)}$	9.6 ± 0.2	9.36 ± 0.10	9.6 ± 0.3
$\log K^{M}_{M(L-5H)}$	11.4 ± 0.3	13.0 ± 0.3	12.1 ± 0.4
$\log K^{M}_{M(L-6H)}$	15.8 ± 0.4	17.6 ± 0.3	16.5 ± 0.4

one can see that this assumption should be no problem. In Scheme 4, $pk_{a1/op}$ = 6.84, $pk_{a2/op}$ = 9.22 and pK_{a2} = 13.6; thus, pK_{a1} can be easily calculated according to eq. [2].

$$[2] \quad pK_{a1} = pk_{a1/op} + pk_{a2/op} - pK_{a2} = 6.84 + 9.22 - 13.6 = 2.46$$

This value is very close to the average of our experimentally measured two values averaging 2.28 at low pH range ((1.95 + 2.60)/2), whereas $k_{a1/cl}$ can be calculated from K_{a1} and $k_{a1/op}$ (24) (eq. [3]).

$$[3] \quad k_{a1/cl} = K_{a1} - k_{a1/op} = 1 \times 10^{-2.46} - 1 \times 10^{-6.84} = 1 \times 10^{-2.46}$$

That is, $pk_{a1/cl}$ = 2.46. These calculations suggest that the deprotonations of the first two ammonium residues in $(EDDA–KA)_2$ have low pK_as because of intramolecular hydrogen bonding.

Now the formation constant K_I of the intramolecular hydrogen bond in $(EDDA–KA)_2$ can be evaluated from $pk_{a1/cl}$ and $pk_{a1/op}$ as in eq. [4].

$$[4] \quad \log K_I = pk_{a1/op} - pk_{a1/cl} = 6.84 - 2.46 = 4.38 \approx 4.4$$

As soon as K_I is known, the degree of formation of the intramolecular hydrogen bond can be evaluated according to eq. [5].

$$[5] \quad \text{Closed\%} = [K_I/(K_I + 1)] \times 100\%$$

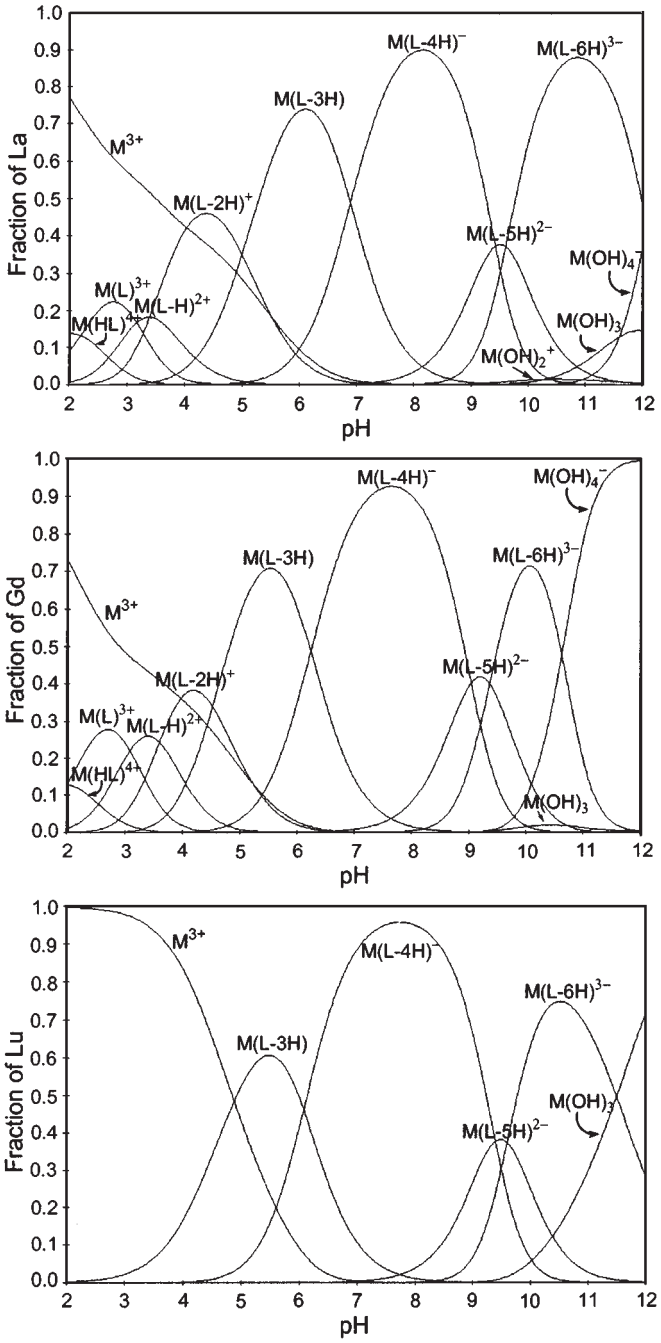
In the case of $(EDDA–KA)_2$, $\log K_I = 4.4$, $K_I = 2.4 \times 10^4$, closed% ≈ 100%. These values give us some quantitative ideas about how strong is the intramolecular hydrogen bond, and it is!

Stability constants of $(EDDA–KA)_2$ with La^{3+}, Gd^{3+}, and Lu^{3+}

Since there are 11 protonation states in pH-dependent equilibrium in solution for $(EDDA–KA)_2$, it is theoretically possible for a given metal ion to form 10 metal complexes, differing only the number of protons included in the complex. As described above, if $(EDDA–KA)_2$ is used to express the neutral ligand, the 10 possible complexes for M^{3+} are: $[MH_3(EDDA–KA)_2]^{6+}$, $[MH_2(EDDA–KA)_2]^{5+}$, $[MH(EDDA–KA)_2]^{4+}$, $[M(EDDAKA)_2]^{3+}$, $[M(EDDA–KA)_2\text{-}H]^{2+}$, $[M(EDDA–KA)_2\text{-}2H]^{+}$, $[M(EDDA–KA)_2\text{-}3H]$, $[M(EDDA–KA)_2\text{-}4H]^{-}$, $[M(EDDA–KA)_2\text{-}5H]^{2-}$, $[M(EDDA–KA)_2\text{-}6H]^{3-}$. Just as the first two pK_as were too low to be determined, the first three stability constants for species $[MH_3(EDDA–KA)_2]^{6+}$ and $[MH_2(EDDA–KA)_2]^{5+}$, cannot be measured in the range $2 \le pH \le 10$. Therefore, only the last eight species exist and the corresponding stability constants may be determined.

Using potentiometric pH titrations, eight complexes in the range $2 \le pH \le 10$ could be determined and fit to the experimental data with eight log K values for each of the three

Fig. 3. Species distribution diagram for the La^{3+}, Gd^{3+}, and Lu^{3+}–$(EDDA–KA)_2$ systems (M^{3+}:L = 1:1.1).



© 2001 NRC Canada

Table 4. Hydrolysis constants of La^{3+}, Gd^{3+}, and Lu^{3+} used in the calculation of the stability constants $M(EDDA–KA)_2$ (25). (I = 0.16 M NaCl, 25°C).

Hydrolysis constant	La^{3+}	Gd^{3+}	Lu^{3+}
$pQ_{11}(M^{3+} + H_2O = M(OH)^{2+} + H^+)$	8.5	8.0	8.7
$pQ_{12}(M^{3+} + 2H_2O = M(OH)_2^+ + 2H^+)$	17.2	16.4	17.5[a]
$pQ_{13}(M^{3+} + 3H_2O = M(OH)_3 + 3H^+)$	27.5	25.2	25.8[a]
$pQ_{14}(M^{3+} + 4H_2O = M(OH)_4^- + 4H^+)$	39.1	34.4	—

[a]Because of lack of data for Lu^{3+}, these values are the corresponding values for Yb^{3+}.

metal ions studied. The results are summarized in Table 3; according to the stability constants, species distribution diagrams were calculated and are given in Fig. 3.

The log K^M_{MHL} data in Table 3 have large error limits because these are estimated values. For Lu^{3+}, the first four constants could not be obtained from the fitting, possibly because the corresponding constants were too small to be determined. Hydrolysis is a big problem in determining the stability constants of lanthanide complexes in aqueous solution (25). In the data fitting, the hydrolysis species $M(OH)_y$ (y = 1–4) were included with constants listed in Table 4. It is clear from the fitting that hydrolysis must be included for all three metal ions studied.

The $pK^H_{M(L-4H)}$ and $pK^H_{M(L-5H)}$ values in Table 3 represent the deprotonation of two hydrogen bonded protons from each metal ion complex. These constants can be directly fit and are independent of the pK_a values of the ligand. Because of the presence of the metal ion, the protons were more easily released from the complex than they were from the ligand itself. This acidifying effect can be quantified with ΔpK values, that is the difference between the pK_a values of ligand and the corresponding pK_a values of the complexes. The calculated ΔpK values are: $\Delta pK_{L-4H} = pK^H_{(L-4H)} - pK^H_{M(L-4H)}$ = 3.8 (La^{3+}), 4.2 (Gd^{3+}), 3.8 (Lu^{3+}); $\Delta pK_{L-5H} = pK^H_{(L-5H)} - pK^H_{M(L-5H)}$ = 4.4 (La^{3+}), 4.6 (Gd^{3+}), 4.4 (Lu^{3+}). The error limits of these values are 0.4; for different metal ions, the values are the same within the error limits. In line with similar acidities of these three ions, there are increases in acidity of the complexes by three to five log units.

The stability constants of the coordinated complexes can be evaluated from the acidity constants of the ligand and the $pK^H_{M(L-4H)}$ and $pK^H_{M(L-5H)}$ values according to the following equations:

$$[6] \quad \log K^M_{M(L-5H)} = pK^H_{M(L-4H)} + \log pK^M_{M(L-4H)} - pK^H_{M(L-4H)}$$

$$[7] \quad \log K^M_{M(L-6H)} = pK^H_{(L-5H)} + \log K^M_{M(L-5H)} - K^H_{M(L-5H)}$$

The results are given in the last two rows in Table 3. Because the error limits for $pK^H_{(L-4H)}$ and $pK^H_{(L-5H)}$ are quite large, the results for log $K^M_{M(L-5H)}$ and log $K^M_{M(L-6H)}$ also have larger error limits than the corresponding $pK^H_{M(L-4H)}$ and $pK^H_{M(L-5H)}$ values.

Structure of the metal ion complexes

Before comparing the stability constants of the La^{3+}, Gd^{3+}, and Lu^{3+} complexes, let us first consider the structures of the complexes in solution. We have discussed the stepwise deprotonation of the ligand and the strong four center intramolecular hydrogen bonds which are stable in the range $3 \le pH \le 12$. In the presence of a metal ion, these hydrogen bonds will break, and the proton will be released at a lower pH because any coordination of the metal ion will make the proton on the ligand more acidic (26). Since for each metal complex the corresponding pK_a values ($pK^H_{M(L-4H)}$ and $pK^H_{M(L-5H)}$, e.g. for Gd^{3+}, 9.04 and 9.36) are still larger than are the acidity constants (7.42 and 8.24) of the pyrone OH groups, we can be sure that the deprotonation occurred at the hydrogen bonding amine residue and not at the pyrone OH. This means that, for all other complex species in solution except the fully deprotonated species $[M(L-6H)]^{3-}$, the four center intramolecular hydrogen bonds among the amine residues and the pyrone oxygens are still present. Where is the metal ion located then in these species, in which the amine residues are occupied by the intramolecular hydrogen bonds? In the case of $M(L-H)^{2+}$ and $M(L-2H)^+$, only carboxylate groups are deprotonated; hence, the metal ion can coordinate with these groups. In [M(L-3H)] and $[M(L-4H)]^-$, the OH group(s) on the pyrone ring is (are) deprotonated; therefore it is also possible for the metal ion to coordinate to the pyrone ring to form a five-membered chelate.

To locate the metal ion in the [M(L-3H)] and $[M(L-4H)]^-$ complexes, several UV and NMR experiments with the La^{3+} system were undertaken. The NMR spectra of $La(EDDA–KA)_2$ are very similar to those of the ligand itself, i.e. seven signals were observed although the signals are somewhat broader. This suggests that the symmetry of the compound does not change upon lanthanum coordination. From the potentiometric titrations, no $La_2(EDDA–KA)_2$ is known to form; if the metal ion binds at only one pyrone, the molecular symmetry would be lowered. The NMR studies also showed that signal S1 (related to methine hydrogen atom on the pyrone ring) in the NMR spectra of $La(EDDA–KA)_2$ had almost same chemical shift as in $(EDDA–KA)_2$ at the same given pH (e.g., pH = 8.0 and 10.4). These results suggest that the metal ion coordinates at the carboxylate groups rather than at the pyrone in the species [M(L-3H)] and $[M(L-4H)]^-$. Similar results were obtained by UV spectrophotometric titration. A blue shift of the spectrum was not observed when La^{3+} was added to a $(EDDA–KA)_2$ solution at pH 9.0; if the metal ion coordinated at the pyrone, the positive charge of the metal ion would have caused a blue shift in the spectrum of the ligand, just like hydrogen does.

Comparing the stability of the complexes of La^{3+}, Gd^{3+}, and Lu^{3+}

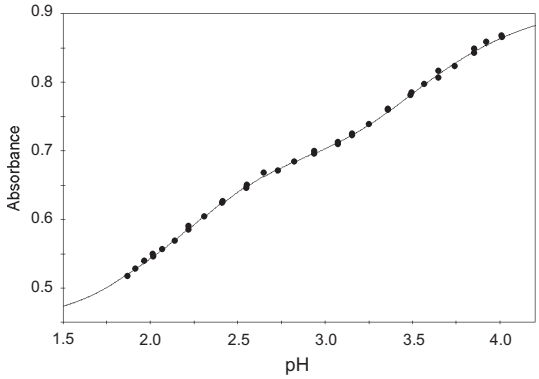
Comparing the stability constants listed in Table 3, it can be seen that regardless of the protonation state in the complexes, the stabilities for the three complexes are always $La^{3+} \cong Lu^{3+} < Gd^{3+}$. This result is quite at odds with the order of the stabilities of La^{3+}, Gd^{3+}, and Lu^{3+} complexes of other similar ligands. In Table 5, the stability constants of La^{3+}, Gd^{3+}, and Lu^{3+} with five oxygen–nitrogen donor ligands are listed; it is evident that for each ligand there is a stability order $La^{3+} < Gd^{3+} < Lu^{3+}$. Therefore, the discrepancy of the stability constants of $(EDDA–KA)_2$ must be caused by its structure.

© 2001 NRC Canada

Table 5. Stability constants of La^{3+}, Gd^{3+} and Lu^{3+} with EDDA, EDTA, oxalic acid, DO2P, and DOTA.

Stability constant	La^{3+}	Gd^{3+}	Lu^{3+}	Conditions	Ref.
log K_1 (M^{3+} + $EDDA^{2-}$ = $M(EDDA)^+$)	7.04	8.13	9.09	I = 0.1 M KNO_3, 25°C	27
log β_2 (M^{3+} + $2EDDA^{2-}$ = $M(EDDA)_2^-$)	11.77	14.21	17.57	I = 0.1 M KNO_3, 25°C	27
log K (M^{3+} + $EDTA^{4-}$ = $M(EDTA)^-$)	15.19	16.82	19.14	I = 0.1 M KCl, 25°C	28
log β_2 (M^{3+} + $2ox^{2-}$ = $M(ox)_2^-$)	7.9	8.68	9.2	I = 1.0 M $NaClO_4$, 25°C	29, 30
log K (M^{3+} + $DO2P^{4-}$ = $M(DO2P)^-$)	16.0	18.2	19.3	I = 0.1 M KNO_3, 25°C	31
log K (M^{3+} + $DOTA^{4-}$ = $M(DOTA)^-$)	21.7	24.0	29.2	I = 0.1 M KCl, 25°C	32, 33

Fig. 4. Fit of the absorbance vs. pH data for the Fe^{3+}–$(EDDA–KA)_2$ system. The points are from the titration data and the curve is the best fit using the values discussed in the text.



In $(EDDA–KA)_2$, the pyrone rings not only make the macrocycle larger in size, but also inhibit changes of the molecular conformation. A smaller metal ion like Lu^{3+} may not fit the macrocycle so well and only a few of the atoms on the macrocycle might actually coordinate the metal ion; whereas the larger Gd^{3+} and La^{3+} may bind with more atoms on the macrocycle and may also coordinate to the four carboxylate groups with a structure similar to that of $Ln(DOTA)^-$ (34). Hence, the order of the stability of the complexes of these two metal ions with $(EDDA–KA)_2$ would be the same as with other similar ligands (Table 5). The absolute values of log $K^{M}_{M(L-6H)}$ for the complexes of $(EDDA–KA)_2$ (Table 3) are still much smaller than the corresponding values of log $K^{M}_{M(L-4H)}$ for $Ln(DOTA)^-$ (Table 5), even for Gd^{3+} and La^{3+}, meaning that the coordination of the atoms on the macrocycle is weaker in $[Ln(EDDA–KA)_2]^-$ than that in $Ln(DOTA)^-$. That the values for $[Ln(EDDA–KA)_2]^-$ (Ln = Gd^{3+}, log $K^{M}_{M(L-6H)}$ = 17.6; La^{3+}, log $K^{M}_{M(L-6H)}$ = 15.8) are only slightly larger than the corresponding values of $Ln(EDTA)^-$ (Ln = Gd^{3+}, log $K^{M}_{M(EDTA)}$ = 16.82; La^{3+}, log $K^{M}_{M(EDTA)}$ = 15.19) means that the macrocycle, including four nitrogen atoms and two oxygen atoms, has a coordination ability on a par with the two nitrogen atoms in EDTA. This suggests that the metal ion might only coordinate with some of the atoms on the macrocycle in $[Ln(EDDA–KA)_2]^-$.

To avoid toxicity with MRI agents, a most important point is the stability of the complex at physiological pH, i.e., pH = 7.4. The conditional stability constant K^{*}_{ML} (eq. [8]) is often used to compare the relative thermodynamic stabilities of different chelators at pH 7.4 (3).

$$[8] \quad K^{*}_{ML} = K_{ML}/(1 + K_1[H] + K_1K_2[H]^2 + \ldots + K_1K_2 \ldots K_n[H]^n)$$

K_1, K_2, … K_n are the stepwise protonation constants of the ligand. However, for $(EDDA–KA)_2$, this is not a good idea because the stepwise stability constants (K_{MHL}, K_{MH2L}, … $K_{MHn\text{-}1L}$) are not included in eq. [8], whereas at pH 7.4, the predominant species is $[M(EDDA–KA)_2\text{-}4H]^-$ for this system (Fig. 3). This problem can be avoided by comparing pM values of the chelators at pH 7.4 (35). For Gd^{3+}–$(EDDA–KA)_2$, a value 6.82 was obtained (calculated for pH = 7.4 with $[L]_{tot} = [M]_{tot} = 1 \times 10^{-6}$ M). Comparing with other chelators (e.g. DOTA 11.93, DTPA 12.02, DTPA–BMA 10.38) (35),[2] this value is really too small for practical application; the result implies that Gd^{3+}–$(EDDA–KA)_2$ is not stable enough to be a MRI contrast agent.

The selectivity of $(EDDA–KA)_2$ is also not good. Although the ligand coordinates to Ca^{2+} very weakly (the stability constant measured for $[Ca(EDDA–KA)_2\text{-}4H]^{2-}$ is 2.5 and the formation of $[Ca(EDDA–KA)_2\text{-}6H]^{4-}$ was not observed by potentiometric titration), the coordination of $(EDDA–KA)_2$ to Cu^{2+} is quite strong and the corresponding pM value is 7.3. As the selectivity of a chelator to Gd^{3+} and Cu^{2+}, Zn^{2+}, and Ca^{2+} reflects the toxicity of the Gd^{3+} complex (36), this result implies that Gd^{3+}–$(EDDA–KA)_2$ would not be selective enough to be a good MRI contrast agent.

Coordination of Fe^{3+} to $(EDDA–KA)_2$

We also tried to measure the stability constants of the $Fe(III)(EDDA–KA)_2$ complexes under the same conditions as the stability constants of lanthanide complexes were measured. Because of the strong tendency to hydrolyze of Fe^{3+} (25), it was not possible to determine the constants at pH > 4. A strong color change was observed in the range $2 \leq pH \leq 4$ when the ligand and Fe^{3+} were mixed, and the stability constants for the complexes formed in the low pH range could be determined spectrophotometrically.

A series of absorbances measured at different pH values can be fitted in a manner similar to that used to fit the potentiometric data by taking into account the species Fe^{3+}, $[Fe(EDDA–KA)_2\text{-}H]^{2+}$, $[Fe(EDDA–KA)_2\text{-}2H]^+$, and $[H_2(EDDA–KA)_2]^{2+}$, $[H(EDDA–KA)_2]^+$, $(EDDA–KA)_2$, $[(EDDA–KA)_2\text{-}H]^-$, $[(EDDA–KA)_2\text{-}2H]^{2-}$. This does mean that the deprotonation of the pyrone OH group was ignored and that only the coordination of the carboxylate groups was included in the model. This is clearly a reasonable model for pH < 4 and the good fit (Fig. 4) bears this out. The results

[2] The values are calculated by using the stability constants given in refs. 18 and 35 for pH 7.4 with [L] = [M] = 1×10^{-6} M. The results are different from the results given in ref. 35 because of the different conditions.

© 2001 NRC Canada

obtained for the stability constants are log K = 3.43 ± 0.12 and log K = 4.11 ± 0.06, which are quite close to the corresponding results listed in Table 3 for La^{3+} and Gd^{3+}. Further complexation clearly happens, but it cannot prevent the hydrolysis of Fe^{3+}. It is reasonable from this limited study to suppose that the stability constants with Fe^{3+} have values similar to those for $(EDDA–KA)_2$ with La^{3+} and Gd^{3+}.

Conclusions

The acidity constants determined suggest that there are two strong four center intramolecular hydrogen bonds in $(EDDA–KA)_2$ in the range $3 \leq pH \leq 12$. The strong hydrogen bonds make the last two deprotonation steps difficult, with very high pK_a values; the first two protons are released from the fully protonated amine groups easily. For $[M(EDDA–KA)_2\text{-}5H]^{2–}$ and $[M(EDDA–KA)_2\text{-}6H]^{3–}$, the metal ion may also coordinate with the nitrogens or pyrone oxygens, whereas for all other species, the metal ion only coordinated with the four carboxlate groups in aqueous solution. That the stability of the complex $[Lu(EDDA–KA)_2\text{-}6H]^{3–}$ is lower than the corresponding Gd^{3+} complex may be because Lu^{3+} is too small to fit into the macrochelate ring of the ligand. On the stability and selectivity point of view, the Gd–$(EDDA–KA)_2$ complex will not be a good MRI contrast agent.

Acknowledgements

This work was supported by the Natural Sciences and Engineering Research Council of Canada (NSERC) and by Du Pont Pharmaceuticals Inc.

References

1. R.B. Lauffer. Chem. Rev. **87**, 901 (1987).
2. G.R. Choppin and K.M. Schaab. Inorg. Chim. Acta, **252**, 299 (1996).
3. P. Caravan, J.J. Ellison, T.J. McMurry and R.B. Lauffer. Chem. Rev. **99**, 2293 (1999).
4. G.R. Choppin. Pure Appl. Chem. **27**, 23 (1971).
5. T. Moeller. *In* The Lanthanides. Vol. 4. *Edited by* T. Moeller. Pergamon, Oxford. 1973. pp. 1.
6. A.D. Watson. J. Alloys Compd. **207**, 14 (1994).
7. K. Kumar, T. Jin, X. Wang, J.F. Desreux, and M.F. Tweedle. Inorg. Chem. **33**, 3823 (1994).
8. P. Caravan, P. Mehrkhodavandi, and C. Orvig. Inorg. Chem. **36**, 1316 (1997).
9. H. Sigel, A.D. Zuberbühler, and O. Yamauchi. Anal. Chim. Acta, **255**, 63 (1991).
10. H.M. Irving, M.G. Miles, and L.D. Pettit. Anal. Chim. Acta, **38**, 475 (1967).
11. P.K. Glasoe and F.A. Long. J. Phys. Chem. **64**, 188 (1960).
12. R.B. Martin. Science (Washington, D.C.), **139**, 1198 (1963).
13. J.J. Molenda, M.A. Basinger, T.P. Hanusa, and M.M. Jones. J. Inorg. Biochem. **55**, 131 (1994).
14. M.K. Patel, R. Fox, and P.D. Taylor. Tetrahedron, **52**, 1835 (1996).
15. M. Tramontini and L. Angiolini. Tetrahedron, **46**, 1791 (1990).
16. T. Nozaki and T. Hashimoto. Nippon Kagaku Kaishi, 1794 (1973).
17. G. Degischer and G. Nancollas. Inorg. Chem. **9**, 1259 (1970).
18. E. Clarke and A.E. Martell. Inorg. Chim. Acta, **190**, 27 (1991).
19. P. Caravan, L. Gelmini, N. Glover, F.G. Herring, H. Li, J.H. McNeill, S.J. Rettig, I.A. Setyawati, E. Shuter, Y. Sun, A.S. Tracey, V.G. Yuen, and C. Orvig. J. Am. Chem. Soc. **117**, 12 759 (1995).
20. B. Song, G. Feldmann, M. Bastian, B. Lippert, and H. Sigel. Inorg. Chim. Acta, **235**, 99 (1995).
21. B. Song, P. Mehrkhodavandi, P. Buglyó, Y. Mikata, Y. Shinohara, K. Yoneda, S. Yano, and C. Orvig, J. Chem. Soc. Dalton Trans. 1325 (2000).
22. G.A. Jeffrey and W. Saenger. Hydrogen bonding in biological structures. Springer–Verlag, Berlin, Heidelberg. 1991.
23. M. Branca, G. Micera, T. Kiss, and M. Sinibaldi, J. Chem. Res. Synop., 392 (1990).
24. B. Song, G. Oswald, M. Bastian, H. Sigel, and B. Lippert. Metal-Based Drugs, **3**, 131 (1996).
25. C.F. Baes, Jr. and R.E. Mesmer. The hydrolysis of cations. R.E. Krieger Publishing Company, Malabar, Florida. 1986.
26. B. Song, J. Zhao, R. Griesser, C. Meiser, H. Sigel and B. Lippert. Chem. Eur. J. **5**, 2374 (1999).
27. L. Thompson. J. Inorg. Nucl. Chem. **24**, 1083 (1962).
28. R. Betts and O. Dahlinger. Can. J. Chem. **37**, 91 (1959).
29. T. Sekine. J. Inorg. Nucl. Chem. **26**, 1463 (1964).
30. S. Lyle and S. Naqvi. J. Inorg. Nucl. Chem. **29**, 2441 (1967).
31. L. Burai, J. Ren, Z. Kovacs, E. Briicher, and A.D. Sherry. Inorg. Chem. **37**, 69 (1998).
32. E. Clarke and A.E. Martell. Inorg. Chim. Acta, **190**, 37 (1991).
33. M. Lochin, J. Desreux, and E. Merciny. Inorg. Chem. **25**, 2646 (1986).
34. S. Aime, M. Botta, and G. Ermondi. Inorg. Chem. **31**, 4291 (1992).
35. C. Paul-Roth and K.N. Raymond. Inorg. Chem. **34**, 1408 (1995).
36. W.P. Cacheris, S.C. Quay, and S.M. Rocklage. Magn. Reson. Imaging, **8**, 467 (1990).

© 2001 NRC Canada

Aggregation studies of benzoporphyrin derivative

David Delmarre, Noboru Hioka, Ron Boch, Ethan Sternberg, and David Dolphin

Abstract: The photophysical properties of a ring B benzoporphyrin derivative 1,3-diene dimethylester were investigated in solution (water–DMSO mixtures). At low proportions of water in DMSO, the diester obeys Beer's law at all pH values and ionic strengths investigated. For solvent systems containing more than 30% water, the extent of deviation from Beer's law as a function of porphyrin concentration is attributed to formation of porphyrin dimers. Dimerization equilibrium constants (*K*d) have been determined in different percentage of solvent mixtures, using absorption and fluorescence spectroscopies, and were found to exhibit a linear correlation between log (*K*d) and the inverse of the dielectric constant (log (*K*d) = 24.6 – 1060.4 × $1/\varepsilon_{mix}$). This equation permits the calculation of *K*d in mixtures of water–DMSO.

Key words: porphyrins, dimerization, aggregation, fluorescence, benzoporphyrin derivative, photodynamic therapy, photosensitizers.

Résumé : Opérant en solution (mélanges DMSO–eau), on a étudié les propriétés photophysiques d'un diester méthylique 1,3-diénique du cycle B d'une benzoporphyrine. À des concentrations faibles d'eau dans le DMSO, le diester obéit à la loi de Beer, à tous les pH et à toutes les forces ioniques étudiées. Pour les systèmes de solvant contenant plus de 30% d'eau, on observe une déviation par rapport à la loi de Beer qui varie avec la concentration en porphyrine; cette déviation est attribuée à la formation de dimères de la porphyrine. On a déterminé les constantes d'équilibre de la dimérisation (*K*d) à divers pourcentages de mélanges de solvant en faisant appel aux spectroscopies d'absorption et de fluorescence et on a trouvé qu'il existe une corrélation linéaire entre log (*K*d) et l'inverse de la constante diélectrique (log (*K*d) = 25,6 – 1060,04 × $1/\varepsilon_{mél}$). Cette équation permet de calculer la valeur de *K*d dans des mélanges d'eau–DMSO.

Mots clés : porphyrine, dimérisation, agrégation, fluorescence, dérivé de la benzoporphyrine, thérapie photodynamique, photosensibilisateur.

Introduction

Porphyrins are versatile molecules. They possess interesting redox behaviour, affinity towards metals and biological functions. They are also amenable to modifications of their peripheral substituents. An interesting aspect of porphyrin chemistry concerns their use as photosensitizers for photodynamic therapy (PDT) (1–3). Photodynamic therapy involves administration of a photosensitizer that accumulates with some selectivity in the target tissues. Tissue is then irradiated with visible light to initiate the generation of oxidants which then go on to generate damage. This treatment has been tested against cancer, age-related macular degeneration (AMD), psoriasis (4, 5), arthritis, and viral infections (6, 7). The first generation of porphyrins used in PDT, Photofrin®, has been approved in Canada, Europe, Japan, and the U.S.A. for the treatment of several different cancers (8).

We have focussed our attention on benzoporphyrin derivatives (9) since these compounds are structurally related to BPDMA verteporfin (**1**), which is QLT Inc.'s second generation PDT drug (recently approved in North America and Europe, as Visudyne®, for the treatment of age-related macular degeneration), to investigate the aggregation processes in aqueous–organic solvents.

In general, porphyrins have a high tendency to aggregate and it is known that the aggregation state determines their photophysical properties (10–12), as well the binding properties to biological targets (13). This later point may be detrimental to the success of a prospective drug since whereas the large hydrophobicity of dimers or higher aggregates may increase the affinity for target tissues aggregation reduces the production of singlet oxygen and thus the efficiency of the PDT treatment.

Received October 10, 2000. Published on the NRC Research Press Web site at http://canjchem.nrc.ca on July 14, 2001.

Dedicated to Professor Brian James on the occasion of his 65th birthday.

D. Delmarre, R. Boch, E. Sternberg, and D. Dolphin.[1] University of British Columbia, Department of Chemistry, 2036 Main Mall, Vancouver, BC V6T 1Z1, Canada.
N. Hioka. Universidade Estadual de Maringa, Brazil.

[1]Corresponding author (telephone: (604) 822-4571; fax: (604) 822-9678; email: ddolphin@qltinc.com).

Materials and methods

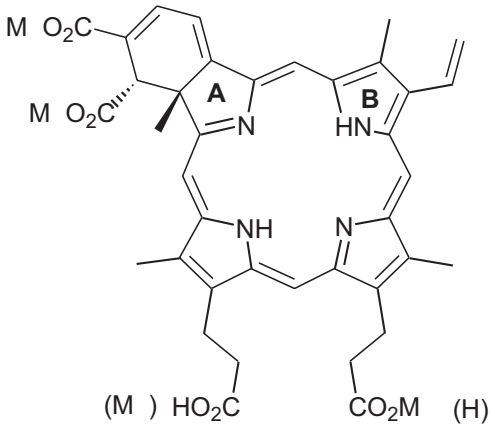
Reagents

All reagents and solvents are analytical grade and were used without further purification.

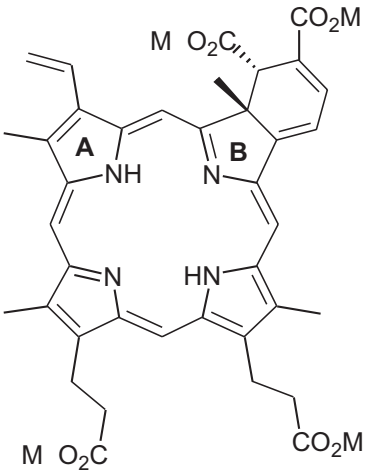
Methods

Compound **2** was synthesized according to the published method (14). Metallation of the porphyrin with zinc and

 DOI: 10.1139/cjc-79-5/6-1068 © 2001 NRC Canada



1



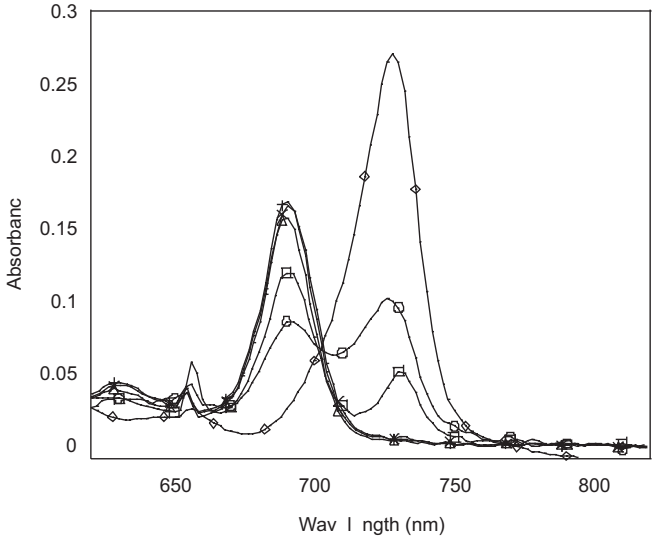
2

nickel was achieved according to Adler et al. (15). Buffers used were potassium phosphate or potassium phthalate. The ionic strength was kept at 0.1 using KCl. The water–dimethylsulfoxide (DMSO) mixtures were prepared by volume. In static fluorescence experiments all samples were excited at 430 nm (Soret band) and emission recorded in the 600–800 nm region.

Apparatus

Visible spectra were obtained using Hewlett–Packard 8452A Diode Array and Cary 50 spectrophotometers with cuvettes of 1.0 cm optical length. Static fluorescence measurements were performed using an Aminco Bowman Series 2 luminescence spectrometer. The excited-state lifetimes were measured at 25°C with a multifrequency (0.1–200 MHz) phase-modulation fluorometer described elsewhere (16). The samples were excited at 442 nm with a liconix He-Cd laser and DCM (4-dicyanomethylene-2-methyl-6-p-dimethylamino-styryl-4H-pyran) in DMSO was used as a reference (τ = 2.130 ns). The emission wavelength was selected by means of a cut-off filter (GG475).

Fig. 1. Absorption spectra of compound **2** in various H_2O–DMSO mixtures ($c = 5 \times 10^{-6}$ mol L^{-1}) for 0% water (+), 20% water (X), 30% water (△), 40% water (□), 50% water (○), 60% water (◇).



Results and discussion

Absorption spectroscopy

The tetraester porphyrin (**2**) in pure DMSO exhibits a major band at 692 nm attributed to the monomeric form. Figure 1 shows changes in the spectra of the diester at different ratios of water–DMSO mixtures. For ratios below 30% water, small changes in the absorption spectra were observed. Increasing the water concentration to 30% (or higher) caused a new band (red shift) to appear at 724 nm while the peak at 692 nm decreased in intensity. For a 60% concentration of water the spectral peak at 692 nm is absent with only one band at 724 nm present. This new band can be attributed to dimers of porphyrins and the presence of an isosbestic point at 700 nm is in agreement with this analysis. Experiments performed at various water:DMSO ratio mixtures and at various diester concentration reveal in the same way, the isosbestic point and dimer peak. The absorbance values at 692 nm against porphyrin concentration for increasing proportion of water:DMSO ratios are shown in Fig. 2. When the solvent ratio is below 30% water, a linear correlation between the absorbance and concentration of porphyrin is obtained. Behaviour according to Beer's law indicates that only monomer is present under these conditions. For ratios above 30% water, deviations from linearity are observed. In these cases the data can be fitted by assuming an equilibrium between monomer and dimer which can be expressed as:

$$M + M \underset{}{\overset{Kd}{\rightleftharpoons}} D$$

where *K*d is the dimerization constant and D and M are respectively the dimer and the monomer forms; *K*d can be expressed as:

[1] $\quad Kd = [D] / [M]^2$

© 2001 NRC Canada

Fig. 2. Absorbance at 692 nm as a function of the concentration of the porphyrin: 0% water (+), 20% water (X), 30% water (△), 40% water (□), 50% water (○), 60% water in DMSO (◇). Lines represent calculated values derived using a linear regression or eq. [3].

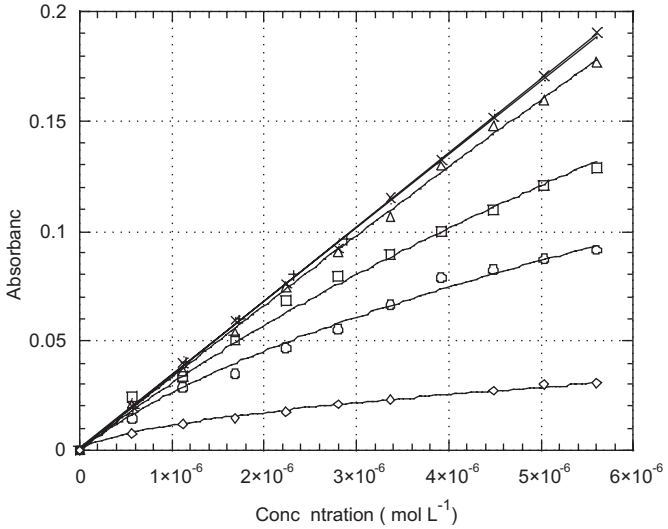
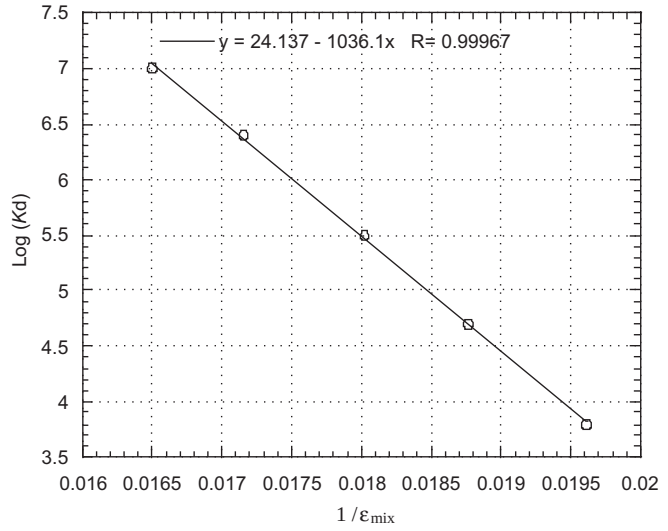


Fig. 3. Log (*K*d) as a function of $1/\varepsilon_{mix}$ at T = 25°C.



The total concentration of the porphyrins [Po] can be expressed as

[2] $[Po] = [M] + 2[D]$

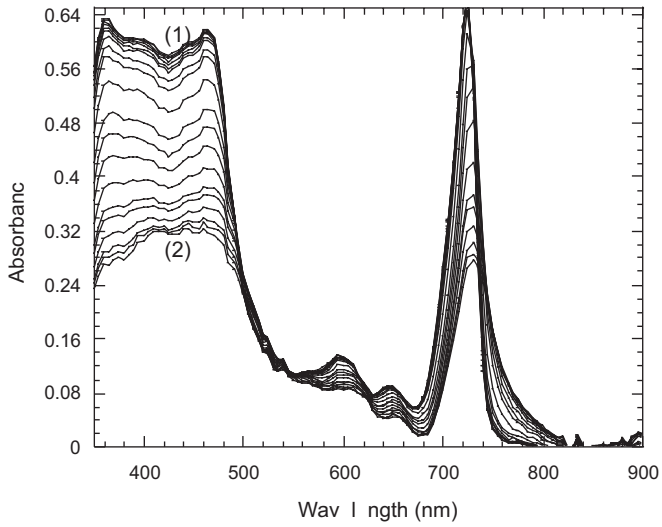
Absorbance for the monomers may be expressed as

[3] $$A_M = ((1 + 8 \times K\mathrm{d} \times [Po])^{0.5} - 1) \times \varepsilon_M / (4 \times K\mathrm{d})$$

where ε_M is the absortivity of the monomer.

A similar equation can be developed for the dimer band. These equations assume that: (*i*) there is negligible overlap between the absorption bands of the dimer and the monomer which is true for the present case; (*ii*) the ε_M does not change with solvent composition and ε_M = 33 800 mol^{-1} L cm^{-1} obtained from experiments involving 0–20% water was used for all cases.

Fig. 4. Effect of temperature on the absorption spectra of compound **2** in 66% water, 33% DMSO: (*a*) T = 25°C, (*b*) T = 85°C.



As shown in Fig. 2, for solvent mixtures above 30% water, the data were fitted by eq. [3] or by an equation based on the dimer band (not shown), and for each case the *K*d was calculated. The calculated values of the logarithm equilibrium constant, from the data in Fig. 2, are 3.8, 4.7, 5.5, 6.4, and 7 at water mixtures in DMSO of 30, 40, 50, 60, and 66%, respectively, at 25°C.

Although **2** is a hydrophobic molecule, it still has a small dipolar moment, thus dipole–dipole interactions can provide a correlation between *K*d and the dielectric constant of the solvent (ε_{mix}).

The free energy (ΔG) in an equilibrium has two components, the non-electrostatic (ΔG_{nE}) and the electrostatic which is a function of 1/ε. Therefore,

[4] $$\Delta G = \Delta G_{nE} + A/\varepsilon$$

where A contains several terms. ΔG is given by:

[5] $$\Delta G = -RT \ln K$$

Rearranging eqs. [4] and [5], gives

[6] $$\log K = C - (A / (2.3RT)) \times 1/\varepsilon$$

In this case, C and A are set as constants. The dielectric constant of the different mixtures (ε_{mix}) can be approximated by a linear relation as:

[7] $$\varepsilon_{mix} = x_{DMSO} \times \varepsilon_{DMSO} + x_{H_2O} \times \varepsilon_{H_2O}$$

Where x is the molar fraction of each component and ε_{DMSO} = 46.6 and ε_{H_2O} = 78.3 at 25°C (17).

Figure 3 represents the logarithm of the equilibrium constant as a function of the theoretical $1/\varepsilon_{mix}$ (18). A linear relationship can be observed between log (*K*d) and $1/\varepsilon_{mix}$ which indicates that the dimerization process for the diester in water–DMSO solvents obey the dipole–dipole interaction model for the dielectric effect. The equation log (*K*d) = 24.6 – 1060.4 × $1/\varepsilon_{mix}$ can be used to calculate the equilibrium constant as a function of water percentage in DMSO, as shown in Fig. 4.

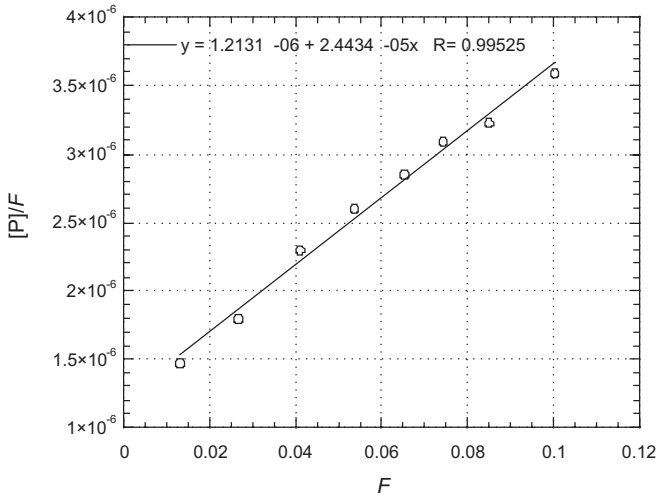
© 2001 NRC Canada

Table 1. Summary of the photophysical properties of compound **2** in different solvent mixtures.

% Water	Absorption λ_Q (nm)	log $(Kd)_{abs}$	Emission λ_{em} (nm)	Life-time (ns) / χ_r^2	*Q*f	log $(Kd)_{em}$
0	692	—	700	6 ± 0.1 / 1.03	0.04	—
20	691	—	701	—	0.04	—
30	692–724[a]	3.8	700	6 ± 0.3 / 4.7	0.035	—
40	692–723[a]	4.7	699	—	0.03	—
50	691–724[a]	5.5	698	—	0.01	5.6
60	725	6.4	698	—	—	—
66	724	7	698	—	—	6.9

[a]Monomer and dimer peaks.

Fig. 5. Relationship of fluorescence intensity to total porphyrin concentration in a mixture of 66% water – 33% DMSO according to eq. [10] for compound **2**. Symbols show experimental results: the straight line is calculated by using linear regression analysis.



Parameters other than the solvent sometimes can be influential in aggregation. In particular, the pH and the ionic strength. The effects of pH (3–8) and ionic strength (1×10^{-3} to saturating concentration of 1×10^{-1} M) with KCl were investigated and found to have no influence on the aggregation process.

Furthermore, no changes were observed when the temperature was increased from 25°C to 85°C of the diester in pure DMSO. However, in a mixture of 66% water in DMSO, an increase in temperature promotes a red shift from 724 to 736 nm coupled to decreasing intensity and broadening (Fig. 4). The Soret band similarly undergoes a decrease. This shift of the band probably indicates the formation of bigger aggregates or reorganization of the solvent. After addition of detergent a blue shift is observed from 736 to 690 nm which indicates the return to the monomeric form.

Emission spectroscopy

The fluorescence properties of the diester **2** were studied over the concentration range 1×10^{-9} to 1×10^{-7} mol L^{-1} in various mixtures of water–DMSO. In all solvents the emission spectrum of the diester consists of a single band with a maximum centered at 700 nm. No new band or shift were observed by adding water (19–22).

Table 2. Summary of the absorption properties of compound **2** and metallated compound with nickel.

	DMSO (nm)	Water–DMSO (66–33%) (nm)
Compound **1**	692	724
Compound **3**	673	690
Compound **3** + piperidine	665	665

Using time resolved fluorescence in pure DMSO revealed a unique species with a life-time of 6 ± 0.1 ns (χ_r^2 = 1.03) which was determined by the Maximum Entropy Method (MEM) as described by Livesey and Brochon (23) and Brochon (24).

Introducing small quantities of water does not change the life-time, but χ_r^2 is not seen to increase. For 30% water χ_r^2 was found to be 4.7. Introducing a second or a third exponential neither improved or decreased χ_r^2. These high χ_r^2 values mean that new nonfluorescent species are being formed. These results agree with the literature that porphyrin dimers do not fluoresce (3).

The fluorescence quantum yields (*Q*f) were determined using ZnTPP in toluene as reference. The *Q*f values were obtained under air-saturated conditions, listed in Table 1; these were estimated from eq. [3]:

$$[8] \qquad Qf^S = (n^S/n^R)^2(F^S \times A^R)/(A^S \times F^R) \times Qf^R$$

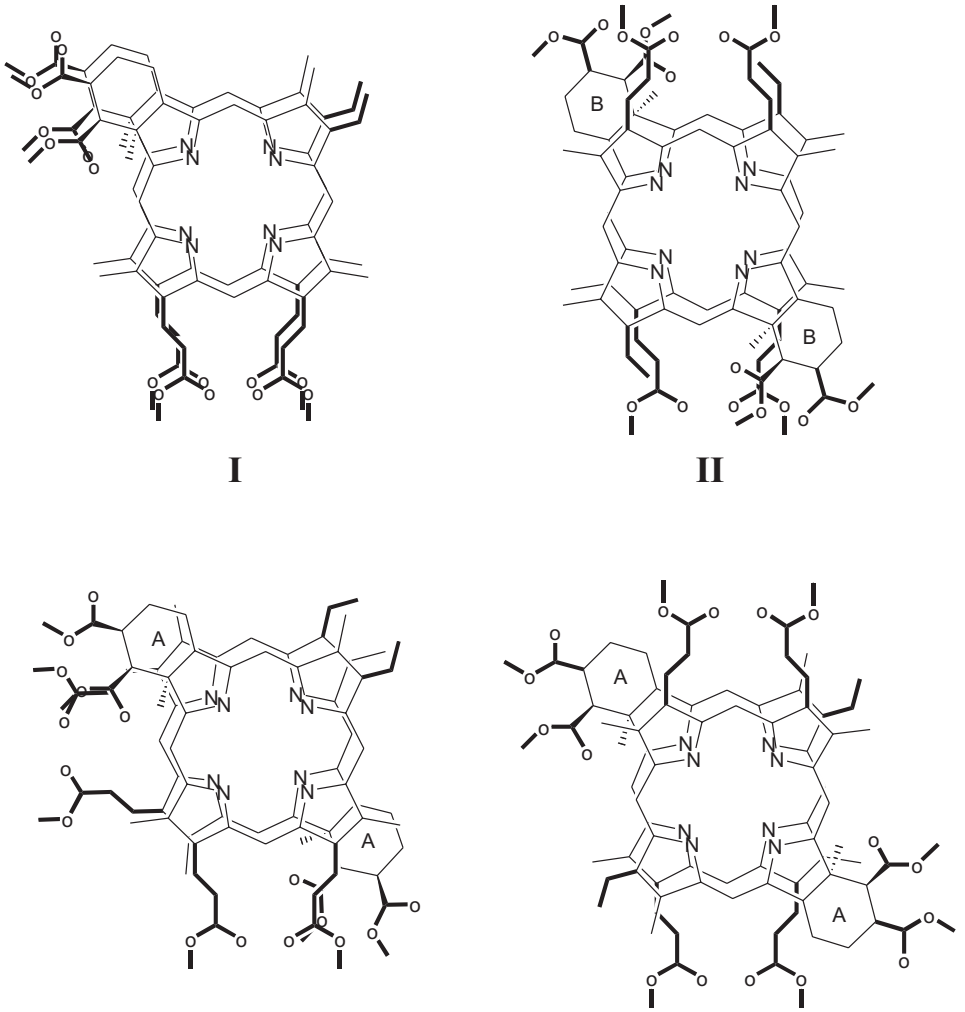
Where Qf^R is the quantum yield of ZnTPP in toluene (*Q*f = 0.033), *A* is the absorbance at the excitation, *F* is the integrated area of the emission spectra, and *n* is the refractive index of the solution. The symbols S and R refer to the sample and reference, respectively. Table 1 shows a decrease of *Q*f as the percentage of water increases. Once again, these results indicate the presence of dimeric forms of the diester in solvent mixtures with high water content.

For solvent mixtures containing less than 20% water, the integrated fluorescence intensity (*F*) data shows that for an increase in diester concentration (1×10^{-9} to 1×10^{-7} mol L^{-1}), a linear correlation between *F* and the concentration of diester is observed (not shown). However, the fluorescence intensity was found to increase in a nonlinear fashion with the concentration of the diester for solvent mixtures above 20% of water.

The plot of the integrated fluorescence intensity over the concentration range can also be used to calculate the dimerization constant *K*d according to Margalit et al. (25).

© 2001 NRC Canada

Fig. 6. Possible conformations for A–A and B–B dimers.



This model assumes that dimerization is the dominant aggregation process and only the monomeric species present in solution fluoresces. This was previously determined by time-resolved fluorescence experiments.

Taking eqs. [1] and [2], the total porphyrin concentration [Po] can be expressed as

$$[9] \qquad [Po] = [M] + 2Kd[M]^2$$

Using the second hypothesis and experimental conditions where absorbance at the excitation wavelength is lower than 0.1, we can assume a direct proportionality between the emitted fluorescence intensity F and concentration of the monomer.

If a is the constant of proportionality, eq. [9] can be written

$$[10] \qquad [Po]/F = a + 2a^2KdF$$

The constant of dimerization can be obtained using the values for the slope and intercept of the plot of [Po]/F vs. F (Fig. 5).

The logarithm of the constant of dimerization for 66% water solution is 6.9 and for 50% water solution is 5.6. Using the previous equation obtained from absorption spectroscopy (log (Kd) = 24.6 – 1060.4 × $1/\varepsilon_{mix}$), the calculated log Kd were 7 and 5.5, respectively, for 66% and 50% water. These values are in good agreement with the absorption results. Table 1 shows a summary of these results.

Structure of the dimer

Usually porphyrin dimers show a blue shift (26) in the Q-band relative to the monomeric form. For diester **2**, a red shift was observed from 692, to give a new sharp, more intense band at 724 nm, probably corresponding to a stacked structure similar to a "deck of cards" (J-aggregate) (27). This type of aggregate was observed for binding of tetracationic porphyrins with DNA (28–34) and for the self aggregation of *meso*-tetra(4-sulfonatophenyl)porphyrin (29–31). To confirm this observation, the metallated (nickel) porphyrin diester (**3**) was prepared. In pure DMSO, this metallated porphyrin shows a maximum Q-band at 673 nm

© 2001 NRC Canada

and no fluorescence. Upon adding water to the solution, a red shift was observed as a result of the porphyrin dimerization.

Adding excess piperidine to the nickelated diester in pure DMSO promoted the complexation of nickel by two piperidine molecules (Ni porphyrins are well known to accept two axial ligands). This compound exhibited a band at 665 nm which was invariant upon addition of water; a dimer peak was not observed. In this case, the piperidine ligand prevent the aggregation process by steric effects. Table 2 summarizes the results.

The same type of experiment was completed with zinc complex and once again no dimer was observed, even in the absence of amine. Presumably this is due to axial complexation of water ligands.

If both hydrophobic and dipolar (electrostatic) interactions account for the formation of this unique dimer, then why is an inverse correlation with dielectric constant seen when no dependence on ionic strength was observed? We suggest below a structure for the dimer in which the dipoles of the monomer cancel each other out. If this occurs, then electrostatic interactions will be smaller. Since we could only work between 1×10^{-3} to 1×10^{-1} M KCl this may have been too low an ionic strength to see an effect.

So far we have seen none of this specific dimerization with any A-ring derivatives of benzoporphyrin derivatives, such as **1**. However, all of the B-ring derivatives of **2** that we have studied show this specific dimerization. Does this difference between A- and B-ring systems suggest the nature of the dimer? If we simply superimpose two molecules of an A-ring derivative directly one on top of each other (as shown in Fig. 6, (I)) we might anticipate that while the net dipoles are aligned the hydrophobic interactions of both the porphyrins and "benzo" rings should be maximized (the same would be true for two B-ring molecules superimposed in this manner). However, this is unlikely since the trans conformation of the benzo ring substituents prevents close approach of these parts of the molecule and consequently the molecules as a whole.

If however, two B-ring molecules are superimposed in a head-to-tail fashion (Fig. 6, (II)) close approach of the two porphyrin rings is possible. Molecular simulation (MM+ force field optimized by Polack-Ribiere, see ref. 32) suggests that the closest approach of the benzo rings in a head-to-head fashion is ~5.4 Å whereas in a head-to-tail arrangement the porphyrin rings can approach to ~2.7 Å to each other. In addition, the dipoles of the two molecules can cancel each other (even the eight ester groups can take up conformations to achieve this). Moreover, even the two vinyl groups can have hydrophobic interactions with the propionate side chains. When, on the other hand two A-ring molecules are superimposed in this fashion (Fig. 6, (III and IV)) the dipoles cannot cancel and there is less opportunity for the esters to align dipoles or for the vinyl groups to have any hydrophobic interactions. Thus, the face-to-face, head-to-tail conformation depicted in Fig. 6 for the B-ring derivatives seems to be the structure which best explains the observation described above and at the same time may explain why B-ring derivatives form these specific dimers while A-ring derivatives do not.

Conclusion

These results demonstrate that the BPD B-ring derivative **2** in water–MSO undergoes self-aggregation. The red shift observed in the absorption spectra is most likely a consequence of dimer formation consisting of two head-to-tail stacked molecules of the diester. This tendency may be partially explained by both favorable hydrophobic interactions between the aromatic moieties of the porphyrin systems, whose contribution would increase as the percentage of water in DMSO increases and to favorable dipolar interactions in this conformation. The special pair at the reaction centers of plants and photosynthetic bacteria (where dimerization is aided by Mg··· side chain interaction) also show similar red-shifted sharp absorption bands (33). In this case, the nature of the dimer has been elucidated by X-ray crystallography (34). The dimerization constants obtained from absorption and fluorescence spectroscopy are in good agreement and follow the equation $\log (K\mathrm{d}) = 24.6 - 1060.4 \times 1/\varepsilon_{mix}$ which permits the calculation of *K*d in water–DMSO at various composition ratios. Metallated porphyrins with ligands in axial positions can prevent the dimerization process and could be used as a drug for PDT.

Acknowledgement

We gratefully acknowledge Professor Bernard Valeur and Jean-Pierre Lefevre for the life-time measurements in the Laboratory of Photophysics and Photochemistry Supramolecular and Macromolecular (ENS Cachan, France). Also we express our gratitute to the Brazilian grant agency CNPq for the support of Noboru Hioka. This work was supported by a CRD grant from the Natural Sciences and Engineering Research Council of Canada (NSERC).

References

1. A.M. Richter, E. Waterfield, A.K. Jain, E.D. Sternberg, D. Dolphin, and J.G. Levy. Photochem. Photobiol. **52**, 495 (1990).
2. B. Aveline, T. Hasan, and R. Redmond. Photochem. Photobiol. **59**, 328 (1994).
3. B. Aveline. T. Hasan, and R. Redmond. Photochem. Photobiol. **59**, 328 (1994).
4. H. Lui and R.R. Anderson. Dermatol. Clinics, **11**, 1 (1993).
5. J.G. Levy, A. Chan, and H.A. Strong. SPIE **2625**, 86 (1995).
6. J. North, H. Neyndorff, and J.G. Levy. J. Photochem. Photobiol. B. **17**, 99 (1993).
7. J. North, H. Neyndorff, D. Kimg, and J.G. Levy. Blood Cells, **18**, 129 (1992).
8. E. Sternberg and D. Dolphin. Curr. Med. Chem. **3**, 239 (1996).
9. A.M. Richter, E. Waterfield, A.K. Jain, E. Sternberg, D. Dolphin, and J. Levy. Photochem. Photobiol. **3**, 495 (1990).
10. T.J. Dougherty, J.E. Kaufman, A. Goldfarb, K.R. Weishaupt, D.G. Boyle, and M. Mittelman. Cancer Res. **38**, 2628 (1978).
11. T.J. Dougherty and R.E. Thoma. *In* Lasers in photomedicine and photobiology. *Edited by* R. Pratesi and C.A. Sacchi. Springer–Verlag, Berlin. 1980. p. 67.
12. F. Richelli. J. Photochem. Photobiol. B, **29**, 109 (1995).
13. A.M. Richter, E. Waterfield, A.K. Jain, B. Allison, E.D. Sternberg, D. Dolphin, and J.G. Levy. Br. J. Cancer, **63**, 87 (1991).

© 2001 NRC Canada

14. E.D. Sternberg, D. Dolphin, A. Tovey, A.M. Richter, and J.G. Levy. U.S. Patent 5 880 145, 1999.
15. A.D. Adler, F.R. Longo, K. Kampas, and J. Kim. J. Inorg. Nucl. Chem. **32**, 2443 (1970).
16. J. Pouget, J. Mugnier, and B. Valeur. J. Phys. E. Sci. Instr. **22**, 855 (1989).
17. John A. Dean (*Editor*). Lange's handbook of chemistry. 12th ed. McGraw–Hill Book Co., New York, U.S.A., 1979. p. 5.
18. K.B. Wiberg. Physical organic chemistry. 2nd ed. John Wiley and Sons, Inc., New York. 1966. p. 261.
19. R.F. Khairutdinov and N. Serpone. J. Phys. Chem. B, **103**, 761 (1999).
20. W.I. White. *In* The porphyrins. *Edited by* D. Dolphin. Vol. 5. Academic Press, New York. 1978. p. 303.
21. C.D. Tail, D. Holden, and M. Gouterman. Chem. Phys. Lett. **100**, 268 (1983).
22. G.J. Smith. Photochem. Photobiol. **41**, 123 (1985).
23. A.K. Livesey and J.C. Brochon. Biophys. J. **52**, 693 (1987).
24. J.C. Brochon. *In* Methods in enzymology. *Edited by* M.L. Johnson and L. Brands. Vol. 240. Academic Press, San Diego. 1994. Chap. 13.
25. R. Margalit, N. Shaklai, and S. Cohen. Biochem. J. **209**, 547 (1983).
26. M.R. Wasielewski, M.P. Niemczyk, and W.A Sveck. Tetrahedron Lett. **23**, 3215 (1982).
27. D.C. Barber, R.A. Freitag-Beeston, and D.G. Whitten. J. Phys. Chem. **95**, 4074 (1991).
28. R.F. Pasternack, C. Bustamante, P.J.Collings, A. Gianetto, and E. Gibbs. J. Am. Chem. Soc. **115**, 5393 (1993).
29. N. Micali, A. Romeo, R. Lauceri, R. Purrello, F. Mallamace, and L. Monso Scolaro. J. Phys. Chem. B, **104**, 9416 (2000).
30. N. Micali, F. Mallamace, A. Romeo, R. Purrello, and L. Monso Scolaro. J. Phys. Chem. B, **104**, 5897 (2000).
31. K. Kano, K. Fukuda, H. Wakami, R. Nishiyabu, and R.F. Pasternack. J. Am. Chem. Soc. **122**, 7494 (2000).
32. Hyperchem Pro. Release 5.11. Hypercube, Inc. Gainsville, Florida. 1999.
33. T.P. Causgrove, P. Cheng, D.C. Brune, and R.E. Blankenship. J. Phys. Chem. **97**, 5519 (1993).
34. J. Deishemhofer and H. Michel. Crystallogr. Mol. Biol. **126**, 421 (1987).

© 2001 NRC Canada

Titanocene(III) catalyzed homogeneous hydrosilation–hydrogenation of pyridines

John F. Harrod, Ronghua Shu, Hee-Gweon Woo, and Edmond Samuel

Abstract: The homogeneous catalytic hydrosilation–hydrogenation of pyridines is observed in the presence of Cp_2TiMe_2 (Cp = η^5-C_5H_5) and CpCp*$TiMe_2$ (Cp* = η^5-C_5Me_5) as catalysts and using $PhSiH_3$ or $PhMeSiH_2$ as the source of Si-H. Under appropriate conditions, and with appropriate ring-substitution, good yields of the *N*-silyldihydropyridine or *N*-silyltetrahydropyridine products are be obtained. Although complete saturation is not achieved with organosilane alone, carrying out the reaction under moderate H_2 pressures can give excellent yields of *N*-silylpiperidines. Under moderate pressures of H_2, $[Cp_2TiH]_2$ catalyzes rapid H–D exchange between H_2 and the 2- and 6-positions of C_5D_5N. Under the same conditions, only traces of hydrogenation are observed. This, together with the regioselectivity of 3-picoline hydrosilation–hydrogenation, leads to the conclusion that the key step in the reaction is probably addition of Ti-Si to C=N.

Key words: hydrosilation, hydrogenation, pyridines, dimethyltitanocene, catalysis.

Résumé : Lorsqu'on utilise du $PhSiH_3$ ou du $PhMeSiH_2$ comme source de Si-H, en présence de Cp_2TiMe_2 (Cp = η^5-C_5H_5) ou de CpCp*$TiMe_2$ (Cp* = η^5-C_5Me_5) comme catalyseurs, on peut observer une hydrosilation–hydrogénation catalytique homogène des pyridines. Dans des conditions appropriées et en présence de substituants appropriés, il est possible d'obtenir de bons rendements de *N*-silyldihydropyridines ou de *N*-silyltétrahydropyridines. Même si l'on n'arrive pas à obtenir une saturation complète avec l'organosilane seul, les réactions effectuées sous des pressions modérées d'hydrogène peuvent conduire à d'excellents rendements des *N*-silylpipéridines. Sous des pressions modérées d'hydrogène, le $[Cp_2TiH]_2$ catalyse un échange rapide de H–D entre le H_2 et les positions 2 et 6 du C_5H_5N. Dans les mêmes conditions, on n'observe que de traces d'hydrogénation. Ce résultat et la régiosélectivité de l'hydrosilation/hydrogénation de la 3-picoline nous amènent à conclure que l'étape clé de la réaction est probablement l'addition de Ti-Si sur la double liaison C=N.

Mots clés : hydrosilation, hydrogénation, pyridines, diméthyltitanocène, catalyse.

[Traduit par la Rédaction]

Introduction

Many catalytic and stoichiometric reactions of titanocene derivatives with Group 14 hydrides have been reported. These include the dehydropolymerization of silanes (1) and germanes (2), cross-dehydrocoupling of silanes with alcohols (3), amines (4), hydrazines (5), and acetylenes (6), hydrosilation of ketones (7), esters (8), imines (9), and olefins (10), reductive cyclization of eneones (11), and polymerization of acetylenes (12).

Catalytic hydrosilation of a variety of unsaturated substrates has been widely used for functionalization of silicon compounds (13) and polymers (14, 15) and in organic synthesis (7–10, 16–18). A large class of substrates, which have to date resisted attempts at homogeneous catalytic hydrosilation, are the highly resonance stabilized aromatics such as benzene, pyridine, pyrrole, and thiophene. In this paper we report the use of titanocene derivatives as catalysts for the first examples of homogeneously catalyzed hydrosilation–hydrogenation of pyridines.[3]

Received August 8, 2000. Published on the NRC Research Press Web site at http://canjchem.nrc.ca on July 19, 2001.

Dedicated to Professor Brian James on the occasion of his 65th birthday.

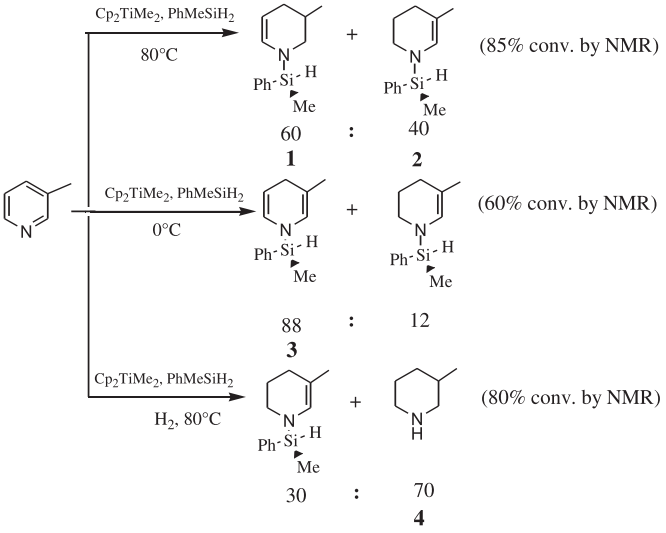
J.F. Harrod,[1] R. Shu, and H.-G. Woo.[2] Chemistry Department, McGill University, Montreal, QC H3A 2K6, Canada.
E. Samuel. UMR 7576 CNRS, Ecole Nationale Supérieure de Chimie de Paris, 11 rue Pierre et Marie Curie, 75231 Paris CEDEX 05, France.

[1]Corresponding author (telephone: (514) 398-6911; fax: (514) 398-3797; e-mail: harrod@chemistry.mcgill.ca).
[2]Present address: Department of Chemistry, Chonnam University, Chonnam, Republic of Korea.

[3]A preliminary communication of this work has appeared, see ref. 19. Crystallographic data for **9a** and **10** (excluding structure factor tables) may be purchased from the Depository of Unpublished Data, Document Delivery, CISTI, National Research Council Canada, Ottawa, ON K1A 0S2, Canada. For information on obtaining material electronically go to http://www.nrc.ca/cisti/irm/unpub_e.shtml. Crystallographic information has also been deposited with the Cambridge Crystallographic Data Center as supplementary publication nos. CCDC 102516 (**9a**) and CCDC 102515 (**10**). Copies of the data are available free of charge from CCDC, 12 Union Road, Cambridge CB21EZ, U.K. (fax: +44 1223-336-033; e-mail: deposit@ccdc.cam.ac.uk).

 DOI: 10.1139/cjc-79-5/6-1075 ©2001NRCCanada

Fig. 1. Reactions of 3-picoline.

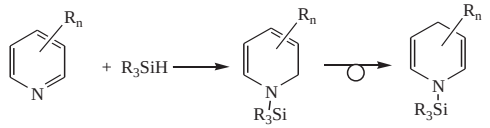


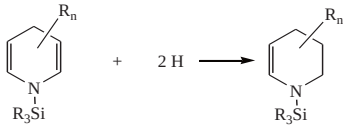
Results

Hydrosilation of pyridines in the presence of titanocene-derived catalysts

To our knowledge, pyridine is the only example of an aromatic substrate that has been successfully hydrosilated. A number of platinum group metals catalyze the addition of Me_3SiH to pyridine, with palladium being particularly effective (20). However, there is no report in the literature of a homogeneous catalytic hydrosilation of pyridine.

In the present work, both Cp_2TiMe_2 (Cp = η^5-C_5H_5) and CpCp*$TiMe_2$ (Cp* = η^5-C_5Me_5) were found to catalyze the hydrosilation–hydrogenation of pyridine, and a number of its derivatives, with $PhMeSiH_2$. Depending on the conditions, the reaction results in the addition of either Si-H, or Si-H and 2 additional atoms of H to the aromatic nucleus (eqs. [1] and [2]). The addition of more hydrogen to the primary diene product is expected in view of the known high catalytic activity of Cp_2TiMe_2 for hydrogen transfer from Si-H to certain olefinic substrates (21).

[1] 

[2] 

When the reaction is carried out at 80°C in the presence of Cp_2TiMe_2 with pyridine, or 4-picoline, the *N*-silyldihydropyridine intermediate is not observed, presumably because its hydrogenation occurs too rapidly. Under the same conditions 3,5-lutidine gives the *N*-silyl-1,4-dihydropyridine as the principal product, while 3,4-lutidine does not react.

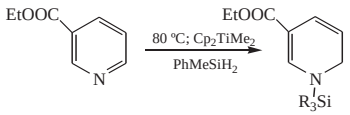
Even in the presence of a large excess of silane, the third double bond is not saturated, but reactions of pyridine, or 4-picoline, under a moderate pressure of H_2 (15–20 atm, 1 atm = 133.322 Pa) do result in complete saturation to give the respective *N*-silylpiperidines as the major products. Reaction of 3,5-lutidine under H_2 pressure gives substantial conversion to the *N*-silyl-1,2,3,4-tetrahydrolutidine, but none of the fully saturated product is produced.

The behavior of 3-picoline varies dramatically, depending on the reaction conditions. The three main reactions are summarized in Fig. 1. At 80°C, in the absence of H_2, the two *N*-silyltetrahydropyridine isomers, **1** and **2**, are the principal products. Under H_2, the **1**-isomer is fully saturated, while the **2**-isomer is unreactive.

Lowering the temperature both slows down the reaction steps and modifies the regioselectivity with respect to **1** and **2**. As the temperature is lowered, the rate of step [2] slows relative to step [1], resulting in ever-increasing amounts of the *N*-silyl-1,4-dihydro-3-picoline (**3**) relative to the tetrahydro-3-picolines, **1** and **2**. At the same time, the ratio of **1** to **2** progressively increases, until at 0°C **1** is no longer detectable. The influences of temperature on the products of the 3-picoline reaction are summarized in Table 1.

In general, the presence of a substituent at the 2- or 6-position shuts down the ring hydrosilation reaction. Thus, no hydrosilation was detected in reactions of $PhMeSiH_2$ with 2-picoline, 2,6-lutidine, 2-cyanopyridine, or 2,2′-bipyridine. An exception to this rule is quinoline, which undergoes reaction in the absence of additional H_2 to give a 3:1 mixture of *N*-phenylmethylsilyl-1,2,3,4-tetrahydroquinoline and *N*-phenylmethylsilyl-1,4-dihydroquinoline. Under moderate H_2 pressure, the only product isolated is *N*-phenylmethylsilyl-1,2,3,4- tetrahydroquinoline.

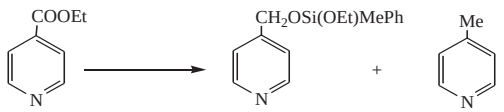
Hydrosilation of ethyl nicotinate (eq. [3]) gives a near-quantitative yield of *N*-phenylmethylsilyl-1,6-dihydro-3-carboethoxypyridine (**5**). The high selectivity for reduction

[3] 

5

of the pyridine ring rather than the ester group is surprising, given the known high reactivity of esters towards hydrosilation under similar conditions (8). It should also be noted that the apparent regioselectivity in this case (1,6-addition) differs from that seen with 3-picoline and 3,5-lutidine (1,4-addition). However, given the high catalytic activity of the dimethyltitanocene–silane system for double bond migration (10), these products are more likely to be thermodynamically, rather than kinetically, determined.

An interesting reversal of selectivity is observed with ethyl isonicotinate (eq. [4]). In this case, the ester function is preferentially reduced, and no ring-hydrosilated products are observed. The major product (ca. 80%) under our standard conditions is **6**, in which the ester has been reduced to the alkoxide level. A significant amount (20%) of 4-picoline is also produced.

[4] 

6

© 2001 NRC Canada

Table 1. Percentages of the products from hydrosilation–hydrogenation of 3-picoline under various reaction conditions.

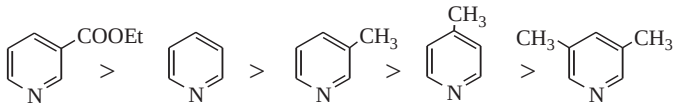
Temperature (°C)	*N*-(phenylmethylsilyl)-4-dihydro-3-picoline (**3**)	*N*-(phenylmethylsilyl)-2,3,4-tetrahydro-3-picoline (**1**)	*N*-(phenylmethylsilyl)-4,5,6-tetrahydro-3-picoline (**2**)
0	88	ND[a]	12
24	85	ND	15
50	27	17.2	56
60	19	27	49
80	3	57	39
80[b]	ND	ND	30

Note: All reactions run under standard concentration conditions of Cp_2TiMe_2:3-picoline:$PhMeSiH_2$ = 1:10:15. Concentrations determined by integration of ^1H NMR spectra.

[a]ND: not detected.

[b]Under 200 psi H_2, isolated yield. The blance of product in this case (70%) is 3-methylpiperidine (**4**).

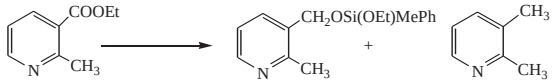
Scheme 1.



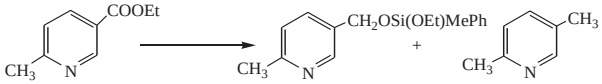
Relative rate	50	:	20	:	7	:	3	:	1
pK_a			5.58		5.70		5.99		6.15

Ring hydrosilation of ethyl nicotinate can be suppressed by substitution at the ring 2-, or 6-position. Thus, both ethyl 2-methyl- and ethyl 6-methyl-nicotinate hydrosilate exclusively at the ester function (eqs. [5] and [6]). Again, in both cases there is significant reduction to the alkoxide level products, **7** and **8**, and the respective lutidines. In the case of ethyl 2-methyl-nicotinate, the lutidine is the major product. No ring reduction products were detected by NMR spectrocopy. In all of the nicotinate and isonicotinate reactions, conversion of the reactant is quantitative by NMR.

[5]



[6]



Cp_2TiMe_2 is ineffective for the hydrosilation–hydrogenation of pyridine with $PhSiH_3$, or Ph_2SiH_2, because of competing Si-H–SiH dehydrocoupling reactions. The resulting oligophenylsilanes then hydrosilate the pyridine to give an intractable mixture of products. Neither *N*-silyldihydropyridine nor *N*-silylpiperidine products were detected by NMR in any of the $PhSiH_3$ reactions. The effectiveness of $PhMeSiH_2$ is due to its slower rate of homodehydrocoupling. With a CpCp*$TiMe_2$ catalyst the rate of dehydrocoupling of $PhSiH_3$ is relatively much slower than hydrosilation as compared to the Cp_2TiMe_2 catalyst, and successful hydrosilation can be achieved with this combination of reactants.

A reaction of CpCp*$TiMe_2$ with pyridine and $PhSiH_3$ (molar ratio of 1:2:4, respectively) at room temperature for four days gave 85% conversion of the pyridine to a mixture of *N*-(phenylsilyl)-1,2,3,4-tetrahydropyridine and *N*-(phenylmethylsilyl)-1,2,3,4-tetrahydropyridine. NMR spectroscopy showed the product also contained CH_4, $PhMeSiH_2$, and $PhMe_2SiH$, the usual products arising from methyl transfer reactions from the catalyst precursor (1*b*). The two *N*-silyl-tetrahydropyridine derivatives were present in a ratio of 4:1 and were the only observable pyridine-derived products. No CpCp*Ti species were detectable by NMR spectroscopy in the product. A similar reaction using $PhMeSiH_2$ instead of $PhSiH_3$ proceeded much more slowly to give the *N*-phenylmethylsilyl- and *N*-phenyldimethylsilyl-tetrahydropyridine products.

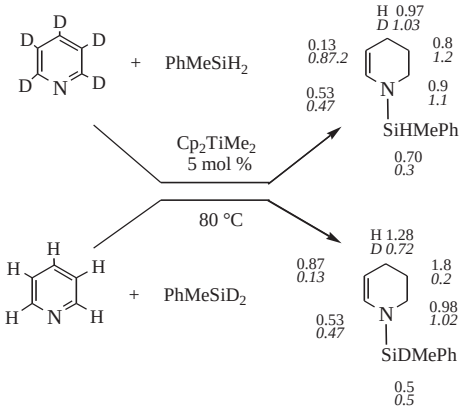
Influence of ring substitution on the rate of hydrosilation

The rates of reaction of some of the hydrosilations described above were qualitatively measured from the initial slopes of reactant concentration vs. time plots. The qualitative rate order from the reactants studied is shown in Scheme 1.

This sequence shows that the rate of ring hydrosilation correlates inversely with the basicity of the pyridine. Although no complexity constant data are available for this particular system, the first formation constant with alkyl pyridines for the later transition-metal consistently correlates with the basicity of the pyridine (22). There is no reason to believe that the case would be otherwise with the titanocene(III) system, and it is reasonable to infer that the

© 2001 NRC Canada

Fig. 2. Results of H–D exchange experiments with pyridine.



rate is higher the more weakly bound the pyridine is to the Ti center for the examples studied.

Experiments involving H–D exchange

^{1}H NMR spectra of reactions of pyridine-d_5 with $PhMeSiH_2$, and of unlabeled pyridine with $PhMeSiD_2$ in the presence of Cp_2TiMe_2, revealed extensive H–D exchange between unreacted pyridine and unreacted silane. The amount of exchange at the 2- and 6-positions of the recovered pyridine was much greater than at the other positions.

After hydrosilation–hydrogenation in these reactions had gone to completion, the recovered *N*-silyltetrahydropyridines showed minor, irregular H–D exchange at all positions of the reduced pyridine ring, with the 6-position clearly showing a higher extent of exchange than the others. The data for the two complementary exchange experiments are summarized in Fig. 2. It should be noted that the estimated errors in these NMR-determined values are about ±10%. Given the obvious complexity of the reactions leading to these products, and the likelihood of kinetic isotope effects, no real significance can be attributed to the small amounts of scrambling observed.

A reaction of Cp_2TiMe_2, pyridine-d_5, and $PhMeSiD_2$ gave *N*-(phenylmethyldeuterosilyl)-2,3,4-tetradeuteropyridine-d_5. Neither unreacted $PhMeSiD_2$, nor the small amount of $PhMe_2SiD$ produced by Me transfer from Cp_2TiMe_2 to silicon, showed any evidence of H incorporation into the Ph or Me groups. There was also no NMR evidence for migration of D to the Cp rings nor for transfer of D to, or from, toluene solvent.

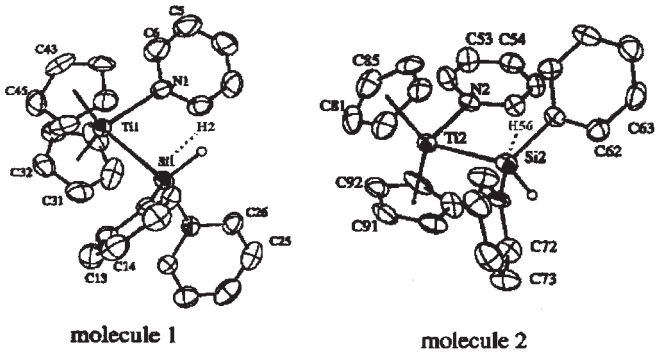
Reactions of pyridine with H_2

Given the activity of the titanocene system for the hydrosilation of the pyridine ring, its activity for hydrogenation was also studied. A preprepared $[Cp_2TiH]_2$ catalyst (20) proved to be weakly active for hydrogenation of pyridine (~5% conversion to piperidine after 24 h at 80°C under 400 psi H_2, 1 psi = 6.894 kPa). However, under these conditions, pyridine-d_5 underwent essentially complete exchange of H with the D at the 2- and 6-positions of the unreacted pyridine.

Titanocene(III) (silyl)pyridine and pyridyl complexes

Complexes of the general type $Cp_2Ti(SiHRR')(py)$ (**9**) (R = H, alkyl, or aryl; R′ = alkyl or aryl; py = pyridine or substituted pyridine) can be easily prepared by precipitation from mixtures of the appropriate pyridine and $[Cp_2Ti(SiHRR')]_2$ in toluene (1*b*). The same compound precipitates in a one-pot reaction of Cp_2TiMe_2, $RR'SiH_2$, and the appropriate pyridine in toluene (19). The products are generally purple, air-sensitive, microcrystalline solids with low solubility in hydrocarbon solvents.

Fig. 3. The two conformers of **9a** in the solid state. The ORTEP thermal ellipsoids are shown at the 30% probability level (19).



Crystals suitable for structure determination by X-ray diffraction analysis were obtained for the case py = pyridine and R = R′ = Ph, **9a**. The monoclinic crystals contain eight formula units of **9a** and two disordered molecules of pyridine solvent in the unit cell. The eight molecules of **9a** are present as two conformers, molecule 1 and molecule 2, as shown in Fig. 3 (19).

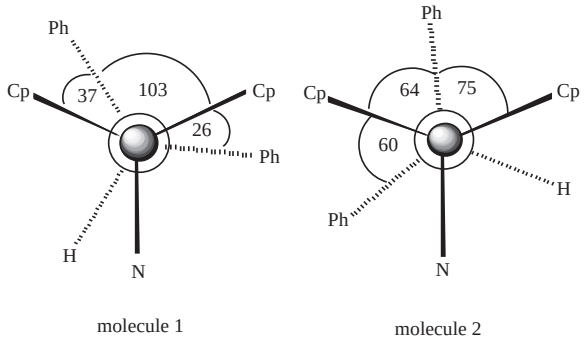
The structure of **9a** can be compared to the analogous Me_3P complex (23). The Ti—Si bond lengths of the two conformers of **9a** are within the range observed for $Cp_2Ti(SiR_3)(PMe_3)$ complexes. However, the Si-Ti-N bond angles of the two conformers of **9a** are quite different from each other and significantly larger (87.2(2)° for molecule 1 and 91.4(2)° for molecule 2) than those in the Me_3P complexes with $SiHPh_2$ (84.8(1)°), SiH_2Ph, and SiHPhMe (both 80.9(1)°) ligands (23). The fact that the angles between the Si-Ti-N planes and the pyridine ring planes of the two conformers are quite different (28.8(4)° for molecule 1 and 14.8(3)° for molecule 2) suggests that steric effects are largely responsible for these differences.

Molecule 2 is close to a gauche configuration (Fig. 4) and, hence, intramolecular contacts are minimized. On the other hand, molecule 1 is constrained, presumably by lattice forces, to a conformation that is much closer to eclipsed. In both conformers there is a close contact between Si and the *ortho*-hydrogen, H(2) (2.83 Å, molecule 1), or H(56) (2.82 Å, molecule 2), which is responsible for the tilting of the pyridine ring. These calculated distances are much shorter than the calculated contact radius sum (3.3 Å) and probably represent a minimum approach that can be tolerated without some distortion of the molecule. In molecule 1, the smaller Si(1)-Ti(1)-N(1) angle increases the encroachment of the Si on H(2), forcing a larger tilting of the pyridine ring plane. There are also important changes in the orientations of the phenyl groups to accommodate the differing steric interactions in the two conformers.

Compounds **9** with R and (or) R′ = alkyl are more soluble, and more prone to decomposition, than those where R and R′ = Ph or H. Thus, reactions of $PhMeSiH_2$, or *n*-$BuMeSiH_2$,

© 2001 NRC Canada

Fig. 4. Projections of molecules 1 and 2 along the Ti–Si bond.



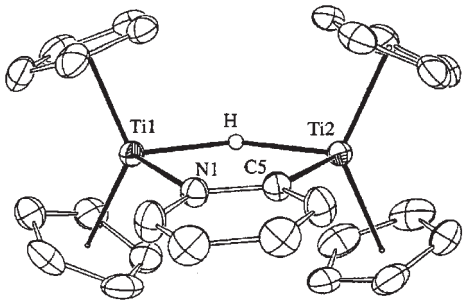
with Cp_2TiMe_2 in the presence of pyridine initially give purple solutions of **9**, but these solutions rapidly darken at room temperature and eventually precipitate dark brown crystals of a new compound, **10**.

The structure of **10** (Fig. 5) closely resembles those of several other hydride-bridged bimetallic titanocene complexes whose structures have been reported. $Cp_2Ti(\mu\text{-}H)(\mu\text{-}HSiHPh)TiCp_2$ (**11**) (1*b*), $Cp_2Ti(\mu\text{-}H)(\mu\text{-}PCy_2)TiCp_2$ (**12**) (24), and $CpTi(\mu\text{-}H)(\mu\text{-}\eta^5,\eta^5\text{-}C_{10}H_8)(\mu\text{-}Cl_2AlEt_2)TiCp$ (25) all have the motif of two titanocene-derived units connected by one hydride bridge and one formally uninegative ligand bridging through a lone pair. The Ti—H bond distances in **10** (1.92(2) and 1.91(2) Å) are not significantly different from those of **11** (1.97(4) Å) and **12** (2.01(5) and 2.00(5) Å). Similarly, the Cp—Ti distances (2.09(1) Å) and Cp-Ti-Cp angles (131.8(2) and 132.7(3)°) in **10** are also close to the corresponding values in **11** (2.053(3) to 2.081(4) Å; 130.6(1) and 131.1(1)°) (R = H, R′ = Ph) and **12**. The Ti(1)—C(5) length (2.205(2) Å) is the same as the Ti(2)—N length, as a result of the C–N disorder. This length is close to the lengths (2.18 to 2.19 Å) found for other sp^2-C ligands bound to titanocene (26), and the same as the Ti—N distance (2.202(2) Å) in a dimeric titanocene(III) pyrazole complex (2.206(4) Å) (27). It is slightly longer than the Ti—N length in titanocene(II)bipyridyl (2.14(2) Å) (28). In the similar monometallic species $Cp^*_2Sc(\eta^2\text{-}N,C\text{-}C_5H_4N)$ (29) and $[Cp_2Zr(\eta^2\text{-}N,C\text{-picolyl})(PMe_3)]^+$ (30) the M—C bonds are slighly longer than the M—N bonds.

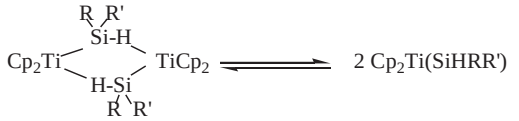
The mechanism of the formation of 9 and 10

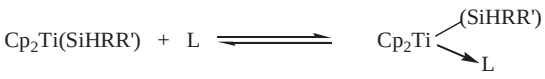
The Cp_2TiMe_2 catalyzed silane dehydrocoupling reaction of $PhMeSiH_2$ is almost completely suppressed in the presence of pyridine, 3- and 4-methylpyridine, or 3,5-lutidine. 2,6-Lutidine has no influence on the dehydrocoupling reaction, behaving essentially as an inert solvent. In the latter case, no complex **9** could be detected (by EPR spectroscopy), or isolated. It is, therefore, likely that the formation of **9** blocks the activity of those titanocene species responsible for the dehydrocoupling reaction. These results provide strong evidence in support of the equilibria shown in eqs. [7] and [8]. In the absence of a donor ligand L, the equilibrium in eq. [7] shifts to the left to give the Si-H bridged bimetallic complex (23a). In the presence of a strong donor ligand, such as a pyridine, or trimethylphosphine, the equilibrium in eq. [8] shifts to the right to produce the ligated, monometallic titanocene(III) silyl complexes. The influence

Fig. 5. The structure of **10**. The ORTEP thermal ellipsoids are shown at the 30% probability level (19)

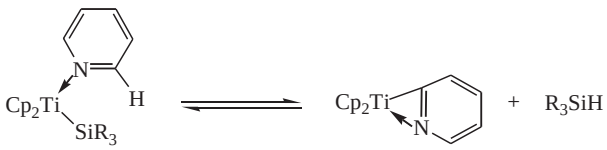


of the steric bulk of both the silyl and the donor ligands on the equilibria is very evident. As mentioned above, with bulkier donor ligands, such as 2,6-dimethylpyridine or triphenylphosphine, formation of the ligated silyl complex is inhibited and the equilibria shift towards the left. Bulkier silyl groups can also prevent the formation of a ligated complex.

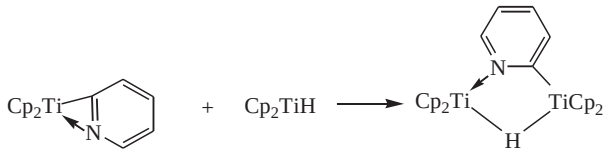
[7] 

[8] 

The formation of **10** could take place through a number of plausible routes. One would be the prior formation of $Cp_2Ti(\eta^2\text{-}N,C\text{-pyridyl})$ (**13**) by the 1,3-silane elimination reaction shown in eq. [9], followed by reaction with Cp_2TiH (eq. [10]). Reaction [9] is strongly favored by the close approach of the Si to the proximal pyridine C-H hydrogen, revealed in the structure of **10**. In such a mechanism, the activation energy would be relatively low, since the Ti could move from $\eta^1\text{-}N$ coordination to $\eta^2\text{-}N,C$ coordination with relatively little sacrifice in energy. A similar process was previously proposed by Klei and Teuben (30) for the decomposition of $Cp_2Ti(alkyl)(py)$ complexes, and this type of coordination has been demonstrated for a number of metals (31, 32). However, **13** has not been thoroughly structurally characterized. *ortho*-Metallations of pyridine by other early transition metals have also been reported (33–35). The reaction mechanism seems to be similar in all of these systems.

[9] 

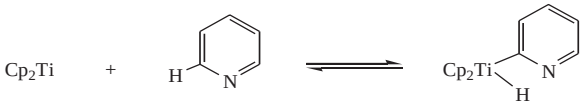
13

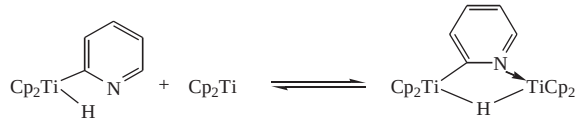
[10] 

© 2001 NRC Canada

Another mechanism analogous to eq. [9], but involving Cp_2TiH(pyridine) (**14**), rather than $Cp_2Ti(SiR_3)$(pyridine), is also plausible. Attempts to detect **14** during hydrosilation reactions, or during the synthesis of **10**, were unsuccessful. This is not surprising since **14**, generated at –20°C by reaction of $[Cp_2TiH]_2$ (21) with pyridine, decomposes rapidly on warming to room temperature. The product of this decomposition exhibits an EPR signal (g = 1.9905), which is very close to that reported for the putative $Cp_2Ti(\eta^2$-*N*,*C*-$MeC_5H_3N)$ (30). It is possible that both of these intramolecular eliminations participate in the production of **10**. Although there is little doubt that the hydride route occurs rapidly in the absence of any silyl ligands, the same cannot be said for the silyl route, since primary and secondary titanocene silyls are known to decompose to produce titanocene hydrides.

A third plausible mechanism for the production of **10** is reaction of a molecule of a Cp_2TiH(pyridyl) complex (**14**) with Cp_2Ti. The former complex could be produced by a concerted oxidative addition of a pyridine C-H bond to Cp_2Ti, as shown in eqs. [11] and [12]. A similar process was proposed earlier to explain the formation of **11** (1*b*). We have also previously suggested that Cp_2Ti could be produced as a transient intermediate in the reactions of Cp_2TiMe_2 with silanes. It is possible that the pyridine competes more effectively for the titanocene intermediate than the less reactive secondary silanes, resulting in the formation of a hydrido(pyridyl), rather than a silyl(pyridine) product. The more reactive silanes (phenylsilane and diphenylsilane) could compete more effectively than the pyridine for titanocene.

[11] 

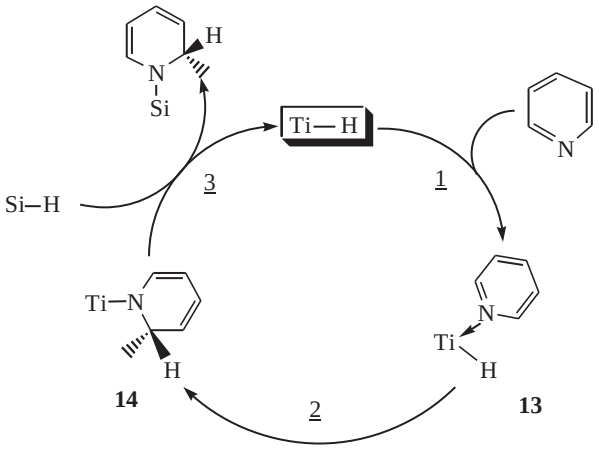
[12] 

The mechanism of the hydrosilation–hydrogenation of pyridines

The results described above indicate that the reactions proceed first by hydrosilation, followed by hydrogenation. The diene resulting from the initial hydrosilation step is expected to be a good substrate for titanocene-catalyzed hydrogenation by the by-product H_2 from dehydrocoupling reactions, or by direct titanium-mediated transfer of H from Si-H, since such cohydrogenation is commonly used in titanocene catalyzed dehydrocoupling reactions (10, 36).

The isolation of complexes **9** supports the assumption that Cp_2Ti^{III}(silyl)(py) complexes are intermediates, or at least catalytic precursors, in the hydrosilation–hydrogenation reactions. On the other hand, the deuterium–proton exchanges between substrates, or between substrates and H_2, clearly indicate the participation of undetected hydride species as well. Isotope exchange between Si-H and the 2- and 6-positions of pyridine substrates can be accounted for by assuming that eq. [9] is reversible. There are a number of other

Fig. 6. A Ti-H based catalytic cycle.



examples of such *ortho*-metallations of pyridine, involving Ti^{III} and other transition metal ions (27, 34, 35). Exchanges at other positions of the ring are expected to occur by conventional reversible β-hydride addition–elimination cycles as further hydrogenation of the *N*-silyldihydropyridine proceeds. However, the results summarized in Fig. 2 show there is relatively little H–D scrambling in the product other than at the 6-position.

The hydrosilation of pyridines is a special case of imine hydrosilation. Willoughby and Buchwald (9) proposed a plausible mechanism for ketimine hydrosilation involving a classical hydrometallation. The pyridine analogue of this mechanism is illustrated in Fig. 6. In this figure the catalytic cycle is carried by a Ti-H species and silylation occurs by a σ-bond metathesis between Si-H and Ti-N.

Since very little direct hydrogenation of pyridine occurs with these catalysts, it is unlikely that the initial step involves addition of a Ti-H bond to the C=N bond of pyridine. An alternative mechanism involves a cycle in which it is Ti-Si that carries the catalysis, as shown in Fig. 7. This is supported to some degree by the regioselectivities observed with 3-picoline as the substrate. If there is a methyl group at the 3-position of the pyridine, steric hindrance will induce the bulky Cp_2Ti group to move to the 6-position rather than the 2-position, as illustrated in Fig. 8. This is indeed the regioselectivity observed in the lower temperature regime (see Table 1). At higher temperatures, the relative rate of the higher activation energy process of migration of the Cp_2Ti towards the 2-position will increase, as observed. In the case of the Ti-H mechanism, there would be little steric preference for the migration of H to the 2- or the 6-position.

There is ample evidence for both M–H addition and M–Si addition occurring in later transition metal catalyzed olefin hydrosilation (37). M–H addition will normally be faster than M–Si addition. However, β-hydrogen elimination can also be so fast, particularly in the present case where it involves rearomatization, that formation of product is frustrated. In such a situation, the slower M–Si addition can lead to product if the reverse process is also relatively slow.

The minor amounts of H–D scrambling observed in the isotopic labeling experiments show that the hydrogen transfer steps following hydrosilation are essentially irreversible. The larger amount of scrambling at the 6-position in these

© 2001 NRC Canada

Fig. 7. A Ti-Si based catalytic cycle.

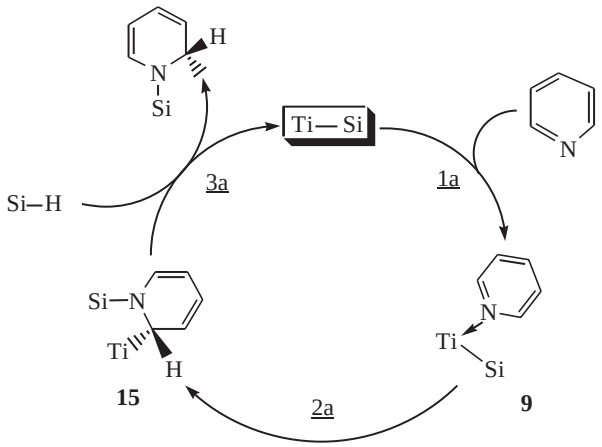
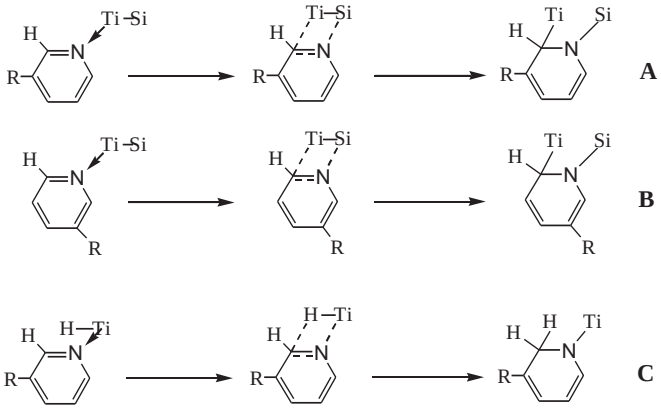


Fig. 8. The two alternative reaction coordinates for C=N insertion into the Ti–Si bond. At 25°C **a**:**b** > 15; at 50°C **a**:**b** = 3.



experiments cannot be attributed to an *ortho*-metalation, such as eq. [9], since this would also cause a similar amount of scrambling at the 2-position. The apparent absence of scrambling at the 2-position requires that the rate of the initial addition of Si-H to N=C be faster than the process that leads to isotope exchange at the 2- and 6-positions of the *unreacted* pyridine. Also, the enhanced exchange at the 6-position of the hydrosilated–hydrogenated product most likely results from an unproductive β-hydride addition–elimination reaction of the eneamine, due to stabilization of the double bond through conjugation to the N.

Once the hydrosilation step has occurred, the nature of the final observed products is determined by the outcome of a complicated set of reactions, including double bond migrations and hydrogenations, effected by reversible β-hydride addition–elimination reactions. The degree to which the products from the alkyl-substituted pyridines are kinetically, or thermodynamically, determined is the subject of continuing study.

The resistance of the enamine products to complete saturation could be due to the stabilization of one of the critical intermediates in the hydrogenation cycle by intramolecular *N*-coordination, or simply because of the unusual stability of the double bond through conjugation to the N lone pair. Blocking of the reaction at the diene level in the case of 3,5-lutidine appears to be the consequence of the much lower reactivity of a trisubstituted double bond towards hydrogenation in this system. In the case of the 3-picoline reaction, a similar lowering of reactivity explains the resistance of **2** to hydrogenation.

The influence of ring substitution on rate.

The reactivity order for the series of substituted pyridines shown above correlates with the basicity of the pyridine. Since the stability of complexes **9** should increase with the basicity of the pyridine, we conclude that tight binding of the pyridine to the Ti has a negative effect on reaction rates, presumable by increasing the activation energy of step 2*a* in Fig. 7. If binding becomes too weak, as in the case of substrates with substituents at the 2- or 6-positions, then reaction is also inhibited.

The dramatic reversal of chemical selectivity between ethyl nicotinate and ethyl isonicotinate may also be due to the fact that the ester group in the 4-position lowers the binding of the N to Ti, relative to binding of the ester function, to the point that ester reduction is the dominant reaction. With the ester group in the 3-position the absence of conjugation between the ester and N leaves the N sufficiently basic, which is the preferred coordination site.

Conclusions

Titanocene derivatives show an exceptional activity for the catalytic hydrosilation of pyridines and, to date, are the only known homogeneous catalysts for this reaction. The reactions show interesting variations in the level of reduction and regioselectivity of the substrate, depending on the ring substitution and the reaction conditions. The ability of the catalyst to effect hydrogenation in the presence of H_2 allows the synthesis of dihydro- and tetrahydro-pyridines, and piperidines in reasonable yields using a single catalyst system. An unusual chemical selectivity is observed with nicotinic and isonicotinic esters. In the former case, only reduction of the ring occurs, while in the latter exclusive reduction of the ester is observed. These results illustrate the extreme sensitivity of the reactions to electronic and steric effects.

The initial step in the reaction appears to be the addition of a Ti–Si species across the C=N bond of the pyridine to give an *N*-silyldihydropyridine. A further two hydrogen atoms can be transferred to give the tetrahydropyridine, but complete reduction only occurs in the presence of H_2.

We are continuing to study the reactions of prochiral pyridines in the presence of chiral titanocene catalysts.

Experimental

All manipulations were performed under an atmosphere of argon, using standard Schlenk techniques. Dry, oxygen-free solvents were employed throughout. Glassware was flame-dried, or oven-dried, before use.

Elemental analyses were performed by Galbraith Laboratories, Inc., and by Oneida Research Services, Whitesboro, New York. $LiAlD_4$, $LiAlH_4$, *n*-BuLi, and Cp_2TiCl_2 (Aldrich) were used as received. Pyridine-d_5 (Aldrich) was dried over

© 2001 NRC Canada

4 Å molecular sieves. Pyridine and alkyl pyridines (Aldrich) were distilled over calcium hydride before use. Quinoline (Aldrich) was distilled under reduced pressure before use. Organosilanes and deuterated organosilanes were prepared from the corresponding chlorosilanes (Hüls America) by reduction with $LiAlH_4$ ($LiAlD_4$) (38). Cp_2TiMe_2 (39) and $CpCp^*TiMe_2$ (40) were prepared according to literature procedures.

Manipulation of air-sensitive crystals was performed either in standard Schlenk apparatus, or in a Braun LabMaster 130 inert-atmosphere glove-box equipped with a catalytic purifier and an Ar atmosphere circulation system. Both H_2O and O_2 were maintained at <2 ppm.

^1H and ^{13}C NMR spectra were recorded on a Varian Unity 500 FT spectrometer operating at 499.9 MHz for ^1H and 125.7 MHz for ^{13}C. ^1H spectra were referenced to C_6H_5D in C_6D_6 (δ 7.15). ^{13}C NMR spectra were referenced to C_6D_6 (δ 128.0). Silicon NMR spectra were recorded in C_6D_6 on a Varian XL-300 spectrometer operating at 59.9 MHz and employing a DEPT pulse sequence (41). The structures of all organic products were confirmed using COSY and HQMC methods. An external standard of tetramethylsilane was used.

Mass spectra were recorded on a KRATOS MS25RFA spectrometer equipped with a KRATOS DS90 data system.

Preparation of $Cp_2Ti(SiHPh_2)(py)$ (9a)

This complex was prepared using a modification of the method for the preparation of titanocene(silyl)trimethylphosphine complexes (22). Typically, Cp_2TiMe_2 (75 mg, 0.36 mmol) was added to a solution of diphenylsilane (0.17 mL, 0.72 mmol) and pyridine (0.5 mL, 6.20 mmol.) in *n*-hexane–toluene (6 mL, 5:1 v/v). In the course of 4 h, the solution turned dark brown and then deep violet. After a further 16 h at room temperature, the solution was stored at –20°C for 2 days to yield small, dark violet needles of **9** (yield: 146 mg, 92%). Anal. calcd. for $C_{28.25}H_{27.25}N_{1.25}SiTi$: C 73.72, H 5.97, N 3.81, Si 6.10, Ti 10.40; found: C 72.83, H 5.99, N 3.22, Si 5.98, Ti 10.26. The instability of this compound in solution precluded recrystalization and X-ray data were obtained on crystals isolated directly from the reaction. The X-ray structure showed the presence of 0.25 molecules of lattice pyridine per molecule of **9** (19).

Preparation of $Cp_2Ti(\mu\text{-}H)(1\kappa N,2\kappa C\text{-pyridyl})TiCp_2$ (10)

Cp_2TiMe_2 (120 mg, 0.58 mmol) was added to a solution of phenylmethylsilane (0.24 mL, 1.73 mmol) and pyridine (1.0 mL, 12.4 mmol) in *n*-hexane–toluene (6:1 v/v, 7.0 mL). After standing for 2 h without stirring, the solution had turned deep violet in color. On standing for a further 24 h at room temperature, the solution slowly turned dark brown. It was then kept at 5°C for 1 day to yield dark brown plates suitable for X-ray analysis (yield: 83 mg, 56%). Anal. calcd. for $C_{27.5}H_{27.5}N_{1.5}Ti_2$: C 69.56, H 5.84, N 4.42, Ti 20.18; anal. calcd. for $C_{26}H_{26}Ti_2N$: C 68.98, H 5.79, N 3.22, Ti 22.01; found: C 66.27, H 5.12, N 3.04, Ti 22.33. The X-ray structure of these crystals showed the presence of 0.5 molecules of lattice pyridine per molecule of **10** (19). The poor elemental analysis resulted in part from loss of lattice pyridine from the crystal during vacuum drying of the sample. EPR: (toluene, 220 K): g_{iso} = 1.984, A_{Ti} = 12 G.

The ^1H NMR spectrum of a saturated solution of **10** in toluene-d_8 at room temperature consisted of two very broad, unresolved, paramagnetically shifted peaks at δ 31.6 (20H, Cp) and 15.6 (4H, pyridyl). No resonance assignable to the bridging hydride was detected.

Catalytic hydrosilation–hydrogenation reactions of pyridines

Synthesis of N-*(phenylmethylsilyl)-2,3,4-tetrahydropyridine*

$PhMeSiH_2$ (3.5 mL, 25.6 mmol) and pyridine (1.0 mL, 12.5 mmol) were added to Cp_2TiMe_2 (0.13 g, 0.7 mmol, 6 mol% catalyst based on pyridine). After a while, the solution color changed to dark blue, then purple accompanied by gas evolution. The mixture was stirred at 80°C. After 12 h an ^1H NMR spectrum of the dark-brown-purple reaction mixture showed that >95% of the pyridine had reacted to give a yield of ca. 80% of *N*-(phenylmethylsilyl)-2,3,4-tetrahydropyridine. The crude product was distilled under vacuum to give 1.29 g (50% isolated yield) *N*-(phenylmethylsilyl)-2,3,4-tetrahydropyridine as a colorless liquid (bp 57°C, 0.12 mm Hg). EI-MS *m/z* (%): 203 (M^+, 100), 188 ([M – $CH_3]^+$ 18.5), 121 ([M – $C_5H_8N]^+$, 76.6). ^1H NMR (300 MHz, benzene-d_6, 22°C) δ: 0.28 (d, *J* = 3.3 Hz, 3H, $SiCH_3$), 1.57 (m, 2H, $NCH_2CH_2CH_2CH$=CH), 2.00 (m, 2H, $NCH_2CH_2CH_2CH$=CH), 2.99 (m, 2H, $NCH_2CH_2CH_2CH$=CH), 4.62 (m, 1H, $NCH_2CH_2CH_2CH$=CH), 5.01 (q, *J* = 3.3 Hz, 1H, SiH), 6.28 (dt, ^3J = 7.8 Hz, ^4J = 3.0 Hz, 1H, $NCH_2CH_2CH_2CH$=CH), 7.2 and 7.5 (2m, 5H, C_6H_5). $^{29}Si\{^1H\}$ NMR (59.9 MHz, benzene-d_6, 22°C) δ: –9.1.

Synthesis of N-*(phenylmethylsilyl)piperidine*

$PhMeSiH_2$ (5.0 mL, 36.5 mmol), pyridine (2.0 mL, 24.7 mmol), and Cp_2TiMe_2 (0.36 g, 1.72 mmol) were thoroughly mixed and sealed in a glass lined, stirred autoclave. The conditions were set at 80°C and 250 psi H_2. After 24 h, *N*-(phenylmethylsilyl)-piperidine (2.0 g, 40% based on pyridine) was isolated by vacuum distillation as a pale yellow liquid (bp 54–56°C, 0.01 mm Hg).^1H NMR (500 MHz, benzene-d_6, 22°C) δ: 0.29 (d, *J* = 3.0 Hz, 3H, $SiCH_3$), 1.27 (m, 4H, $NCH_2CH_2CH_2CH_2CH_2$), 1.40 (q, *J* = 5.5 Hz, 2H, $NCH_2CH_2CH_2CH_2CH_2$), 2.8 (m, 4H, NCH_2CH_2 $CH_2CH_2CH_2$), 5.02 (quart, *J* = 3.0Hz, 1H, SiH), 7.22 and 7.58 (2m, 5H, C_6H_5). $^{29}Si\{^1H\}$ NMR (59.9 MHz, benzene-d_6, 22°C) δ: –10.5. COSY and HMQC NMR experiments were in conformity with the structure assignment.

Reactions of C_5H_5N with $PhMeSiD_2$ and C_5D_5N with $PhMeSiH_2$

$PhMeSiD_2$ (0.44 mL, 3.2 mmol) and pyridine (0.09 mL, 1.0 mmol) were added to Cp_2TiMe_2 (23 mg, 0.11 mmol, 10 mol% catalyst per pyridine). After a while, the solution color changed from orange to dark blue, then to purple accompanied by gas evolution. The mixture was stirred at 80°C. After 12 h an ^1H NMR spectrum indicated that *N*-(phenylmethylsilyl)-2,3,4-tetrahydropyridine(H/D) had been produced in 94% yield, based on pyridine. After exposure to dry air to oxidize the catalyst, the ^1H and ^2H NMR spectra were recorded without further purification.

A reaction between $PhMeSiH_2$ (0.89 mL, 6.5 mmol) and pyridine-d_5 (0.35 mL, 4.32 mmol) was carried out in the

© 2001 NRC Canada

presence of Cp_2TiMe_2 (45 mg, 0.22 mmol, 5 mol%). The mixture was stirred at 80°C for 8 h and then distilled under vacuum to give 0.19 g (20% isolated yield, bp 57°C, 0.12 mm Hg) of *N*-(phenylmethylsilyl)-2,3,4-tetrahydropyridine(H/D) as a colorless liquid

Reaction of Cp_2TiMe_2, pyridine-d_5, and $PhMeSiD_2$ under H_2

$PhMeSiD_2$ (0.30 mL, 2.2 mmol), and pyridine-d_5 (0.12 mL, 1.4 mmol) were added to Cp_2TiMe_2 (0.15 g, 0.36 mmol). The reaction mixture was stirred at room temperature under H_2 (1 atm). After three days, the dark-brown solution was fractionally distilled to give 0.18 g of *N*-(phenylmethylsilyl)-2,3,4-tetrahydropyridine(H/D) as a colorless liquid.

Reaction of 3-picoline, Cp_2TiMe_2, and $PhMeSiH_2$

$PhMeSiH_2$ (3.56 mL, 26 mmol), 3-picoline (1.8 mL, 18.4 mmol), and Cp_2TiMe_2 (0.40 g, 1.8 mmol) were added to a Schlenk tube and stirred at 80°C. After six days, the dark brown–purple reaction mixture was distilled under vacuum (yield 1.3 g, bp 84–86°C, 0.02 mm Hg). NMR showed the product to be a mixture of **1** and **2** (in a ratio of 3:2, respectively). **1**: ^{1}H NMR (500 MHz, benzene-d_6, 22°C) δ: 0.72 (m, 3H, $NCH_2C(H)(CH_3)CH_2CH{=}CH$), 1.64 (m, 1H, $NCH_2C(H)(CH_3)CH_2CH{=}CH$), 2.04, 1.71 (m, 2H, $NCH_2C(H)(CH_3)CH_2CH{=}CH$), 2.98, 2.60 (m, 2H, $NCH_2C(H)(CH_3)CH_2CH{=}CH$), 4.57 (m, 1H, $NCH_2C(H)(CH_3)CH_2CH{=}CH$), 4.99 (quart, J = 3.5 Hz, 1H, SiH), 6.22 (t, J = 8.5 Hz, 1H, $NCH_2C(H)(CH_3)CH_2CH{=}CH$), 7.2, 7.5 (m,$C_6H_5$). EI-MS *m*/*z* (%): 217 ([M^+], 100), 202 ([M – $C_7H_9Si]^+$, 50), 121 ([M – $C_9H_{10}N]^+$, 26). **2**: ^{1}H NMR (500 MHz, benzene-d_6, 22°C) δ: 0.28 (d, J = 3.4 Hz, 3H, $SiCH_3$), 1.54 (m, 2H, $NCH{=}C(CH_3)CH_2CH_2CH_2$), 1.61 (d, J = 1.0 Hz, 3H, $NCH{=}C(CH_3)CH_2CH_2CH_2$), 1.85 (t, J = 6.25 Hz, 2H, $NCH{=}C(CH_3)CH_2CH_2CH_2$), 2.91 (m, 2H, $NCH{=}C(CH_3)CH_2CH_2CH_2$), 5.02 (quart, J = 3.4 Hz, 1H, SiH), 6.08 (m, 1H, $NCH{=}C(CH_3)CH_2CH_2CH_2$), 7.2 and 7.5 (2m, 5H, C_6H_5).

Reaction of 3-picoline, Cp_2TiMe_2, and $PhMeSiH_2$ under H_2

$PhMeSiH_2$ (3.56 mL, 26 mmol), 3-picoline (1.8 mL, 18.4 mmol), and Cp_2TiMe_2 (0.40 g, 1.8 mmol, 10 mol%) were added to a 50 mL stirred pressure bomb and heated at 80°C under hydrogen (200 psi). After four days the product was shown by ^{1}H NMR to be mainly a mixture of **2** and **4**, in a ratio of 3:7. The mixture was fractionally distilled under vacuum to give 1.0 g of pure **2** (bp 84–86°C, 0.02 mm Hg).

Synthesis of N*-(phenylmethylsilyl)-2,3,4-tetrahydro-4-picoline*

A mixture of $PhMeSiH_2$ (3.56 mL, 26 mmol), 4-picoline (1.8 mL, 18.4 mmol), and Cp_2TiMe_2 (0.40 g, 1.8 mmol) was stirred at 80°C for six days and then distilled under vacuum to give *N*-(phenylmethylsilyl)-2,3,4-tetrahydro-4-picoline as a colorless liquid (2.1 g, 53% isolated yield based on 4-picoline, bp 85–87°C, 0.15 mm Hg). EI-MS *m*/*z* (%): 217 (M^+, 37), 202 ([M – $CH_3]^+$, 100), 121 ([M – $C_5H_8N]^+$, 37). ^{1}H NMR (200 MHz, benzene-d_6, 22°C) δ: 0.30 (d, J = 3.3 Hz, 3H, $SiCH_3$), 1.0 (d, J = 6.8 Hz, 3H, $NCH_2CH_2CH(CH_3)CH{=}CH$), 1.6, 1.3 (m, 2H, $NCH_2CH_2CH(CH_3)CH{=}CH$), 2.28 (m, 1H, $NCH_2CH_2CH(CH_3)CH{=}CH$), 3.02 (m, 2H, $NCH_2CH_2CH(CH_3)CH{=}CH$), 4.56 (dd, ^3J = 7.8 Hz, $^3J'$ = 3.0 Hz, 1H $NCH_2CH_2CH(CH_3)CH{=}CH$), 5.04 (quartet, J = 3.3 Hz, 1H, SiH), 6.26 (dd, ^3J = 7.8 Hz, ^4J = 1.8 Hz, 1H, $NCH_2\ CH_2CH(CH_3)CH{=}CH$), 7.2 and 7.5 (2m, 5H, C_6H_5).

Preparation of N*-(phenylmethylsilyl)-2,3,4-tetrahydroquinoline*

$PhMeSiH_2$ (6.0 mL, 43.2 mmol) and quinoline (3.3 mL, 28.8 mmol) were added to Cp_2TiMe_2 (0.60 g, 2.88 mmol, 10 mol%) in a stirred autoclave under 200 psi of H_2 at 80°C. After 48 h, *N*-(phenylmethylsilyl)-2,3,4-tetrahydroquinoline was vacuum distilled as a yellowish liquid (4.0g, 54% isolated yield, bp 160°C, 0.02 mm Hg). EI-MS *m*/*z* (%): 253 ([M^+], 100), 132 ([M – $C_7H_9Si]^+$, 38.3), 121 ([M – $C_9H_{10}N]^+$, 42.1). ^{1}H NMR (200 MHz, benzene-d_6, 22°C) δ: 0.44 (d, J = 3.4 Hz, 3H, $SiCH_3$), 1.55 (m, 2H, $NCH_2CH_2CH_2$), 2.60 (t, J = 6.6 Hz, 2H, $NCH_2CH_2CH_2$), 3.11 (m, 2H, $NCH_2CH_2CH_2$), 5.37 (quart, J = 3.4 Hz, 1H, SiH), 6.7–7.2 and 7.5–7.7 (2m, 4H, CH on the phenylene ring). ^{29}Si NMR (59.9 MHz, benzene-d_6) δ: –12.6 ppm.

Reaction of quinoline, Cp_2TiMe_2, and $PhMeSiH_2$

$PhMeSiH_2$ (2.0 mL, 14.4 mmol) and quinoline (1.1 mL, 9.6 mmol) were added to Cp_2TiMe_2 (0.20 g, 0.96 mmol, 10 mol%) and stirred at 80°C for 36 h. *N*-(Phenylmethyl-silyl)-2,3,4-tetrahydroquinoline and *N*-(phenylmethylsilyl)-2-dihydro-quinoline were formed in a ratio of 3:1, respectively. ^{1}H NMR *(N*-(phenylmethylsilyl)-2-dihydro-quinoline) (200 MHz, benzene-d_6, 22°C) δ: 0.38 (d, J = 3.3 Hz, 3H $SiCH_3$), 3.48 (m, 2H, $NCH_2CH{=}CH$), 4.71 (m, 1H, $NCH_2CH{=}CH$), 6.22 (d, ^2J = 7.7 Hz, 1H, $NCH_2CH{=}CH$). ^{29}Si NMR (59.9 MHz, benzene-d_6): –10.6. A small amount of 1,2,3,4-tetrahydroquinoline was also detected in the mixture: ^{1}H NMR (500 MHz, benzene-d_6, 22°C) δ: 1.57 (m, 2H, $NCH_2CH_2\ CH_2$), 2.51 (t, J = 6.3 Hz, 2H, $NCH_2CH_2CH_2$), 2.76 (t, J = 5.54 Hz, 2H, NCH_2), 3.0 (br s, 1H, NH), 6.22 (d, J = 8.0 Hz, 1H), 6.62 (t, J = 7.0 Hz, 1H), 6.85 (d, J = 7.0 Hz, 1H), 6.95 (t, J = 7.0 Hz, 1H).

Reaction of 3,5-lutidine and $PhMeSiH_2$

$PhMeSiH_2$ (3.56 mL, 26 mmol), 3,5-lutidine (2.1 mL, 18.4 mmol), and Cp_2TiMe_2 (0.31 g, 1.41 mmo, 8 mol%) were mixed a Schlenk tube. After a while the solution turned dark blue, then violet, progressively accompanied by gas evolution. The violet solution was stirred at 80°C for 8 days, and then distilled under vacuum. Analysis of the crude product by ^{1}H NMR showed a complete conversion of the lutidine and a 70% yield of *N*-(phenylmethylsilyl)-4-dihydro-3,5-lutidine. Fractional distillation yielded the pure dihydropyridine (2.5 g, 60% yield, bp 80–90°C, 0.02 mm Hg). FAB-MS (NBA) *m*/*z*: 229 [M^+]. ^{1}H NMR (500 MHz, benzene-d_6, 22°C) δ: 0.25 (d, J = 3.0 Hz, 6H $NCH{=}C(CH_3)CH_2C(CH_3){=}CH$), 2.69 (s, 2H, $NCH{=}C(CH_3)CH_2C(CH_3){=}CH$), 4.99 (quartet, J = 3.0 Hz, 1H, SiH), 5.87 (s, 2H, $NCH{=}C(CH_3)CH_2C(CH_3){=}CH$), 7.2 and 7.5 (2m, 5H, C_6H_5). ^{29}Si NMR (59.9 MHz, benzene-d_6, 22°C) δ: –8.0.

© 2001 NRC Canada

Reaction of ethyl nicotinate and $PhMeSiH_2$ in the presence of Cp_2TiMe_2

$PhMeSiH_2$ (0.45 mL, 3.3 mmol) and ethyl nicotinate (0.3 mL, 2.2 mmol) were added to Cp_2TiMe_2 (40 mg, 0.20 mmol). After a while, the solution color changed from orange to dark blue, then purple, accompanied by gas evolution. The mixture was stirred at 80°C for 3 h, at which point an ^1H NMR spectrum of the product showed that conversion of ethyl nicotinate was complete and ethyl *N*-(phenylmethylsilyl)-1,6-dihydronicotinate was produced in 90% yield. EI-MS *m*/*z* (%): 274 ($[M + 1]^+$, 3.6), 196 ($[M - C_6H_5]^+$, 4.4). ^1H NMR (200 MHz, benzene-d_6, 22°C) δ: 0.06 (d, J = 3.5 Hz, 3H, $SiCH_3$), 0.97 (t, J = 7.2 Hz, 3H, OCH_2CH_3), 3.32 (m, 2H, NCHC(OEt)CHCHCH_2), 4.06 (t, J = 7.2 Hz, 2H, OCH_2CH_3), 4.60 (dt, J = 8.0 Hz, J' = 3.4 Hz, 1H, NCH=C(OEt)CH=CHCH$_2$), 4.72 (q, J = 3.5 Hz, 1H, SiH), 5.58 (dm, J = 8.0 Hz, 1H, NCH=C(OEt)CH=CHCH$_2$), 7.48 (s, 1H, NCH=C(OEt)CH=CHCH$_2$).

Reaction of ethyl isonicotinate with $PhMeSiH_2$ in the presence of Cp_2TiMe_2

$PhMeSiH_2$ (0.26 mL, 1.91 mmol) and ethyl isonicotinate (0.13 mL, 0.95 mmol) were added to Cp_2TiMe_2 (10 mg, 0.05 mmol). The solution color became dark blue then brown over the course of 3 h. It was then stirred at 80°C for a further 36 h. Near-quantitative conversion the ethyl nicotinate to a mixture of 4-picoline and the silylether **6** (ratio 1:5) was observed by ^1H NMR. ^1H NMR (200 MHz, benzene-d_6, 22°C) δ: 0.35 (s, 3H, $SiCH_3$), 1.15 (t, 3H, OCH_2CH_3), 3.7 (q, 2H, OCH_2CH_3), 4.61 (m, 2H, CH_2O), 6.8–8.5 (m, 9H, PhH and the H on the pyridine ring).

Reactions of ethyl 2-methylnicotinate and methyl 6-methylnicotinate with $PhMeSiH_2$ in the presence of Cp_2TiMe_2

Ethyl 2-methylnicotinate and $PhMeSiH_2$ were reacted under the same conditions as ethyl isonicotinate and similar color changes occurred during the raction. The mixture was stirred at room temperature for 24 h. Quantitative conversion to 2,3-lutidine and **7** (ratio 2:3) was observed in 5 h by ^1H NMR. ^1H NMR of **7** (200 MHz, benzene-d_6, 22°C) δ: 0.35 (s, 3H, $SiCH_3$), 1.15 (t, 3H, OCH_2CH_3), 2.40 (s, 3H, Me on the ring), 3.7 (q, 2H, OCH_2CH_3), 4.60 (m, 2H, CH_2O), 6.7–8.6 (m, 8H, PhH and H's on the pyridine ring).

Under similar conditions, methyl 6-methylnicotinate gave a quantitative conversion to 2,6-lutidine and **8** (ratio of 1:4) by ^1H NMR. ^1H NMR for **8** (200 MHz, benzene-d_6, 22°C) δ: 0.37 (s, 3H, $SiCH_3$), 2.50 (s, 3H, Me on the ring), 3.40 (s, 3H, OCH_3), 4.65 (m, 2H, CH_2O), 6.6–8.0 (m, 8H, PhH and H's on the pyridine ring)].

Relative rates of reaction of pyridine, 3-picoline, 4-picoline, 3,5-lutidine, and ethyl nicotinate with Cp_2TiMe_2 and $PhMeSiH_2$

In separate Schlenk reactors, pyridine (0.35 mL, 4.6 mmol), 3-picoline (0.45 mL, 4.6 mmol), 4-picoline (0.45 mL, 4.6 mmol), 3,5-lutidine (0.48 mL, 4.6 mmol), and ethyl nicotinate (0.67 mL, 4.6 mmol) were added to a mixture of Cp_2TiMe_2 (0.09 g, 0.43 mmol) and $PhMeSiH_2$ (0.89 g, 6.5 mmol) together with 50 μL of $SiEt_4$ (in the case of pyridine 0.13 mL of C_6D_6 was also added). The mixtures were stirred at room temperature. NMR samples were extracted periodically by syringe. The conversions were calculated based on the comparison of integrals.

Reaction of pyridine-d_5 with H_2 catalyzed by Cp_2Ti-H

Pyridine-d_5 (0.30 mL, 3.94 mmol) was added to a solution of Cp_2Ti-H (50 mg, 0.28 mmol in 1 mL toluene-d_8, containing a known concentration of Me_4Si as calibrant) in a miniature stirred pressure reactor. The mixture was held at 400 psi H_2 and 80°C for 10 h. Analysis by ^1H NMR showed <10% of the pyridine was hydrogenated, but >90% of the D at the 2- and 6-positions was exchanged with H.

Reaction of $CpCp^*TiMe_2$, pyridine, and $PhSiH_3$

A 5 mm NMR tube was charged with $PhSiH_3$ (30 μL, 0.24 mmol), $CpCp^*TiMe_2$ (20 mg, 0.07 mmol), pyridine (11 μL, 0.14 mmol), and benzene-d_6 (0.4 mL). After thorough mixing, the solution was left to stand at room temperature. It very slowly turned green and after 4 days the ^1H NMR spectrum only showed resonances assignable to the following compounds: *N*-(phenylsilyl)-2,3,4-tetrahydropyridine; ^1H NMR (200 MHz, benzene-d_6, 22°C) δ: 1.52 (m, 2H, $NCH_2CH_2CH_2CH$=CH), 1.92 (m, 2H, $NCH_2CH_2CH_2CH$=CH), 2.96 (m, 2H, $NCH_2CH_2CH_2$ CH=CH), 4.99 (s, 2H, SiH_2), 6.22 (m, 1H, $NCH_2CH_2CH_2CH$=CH), 6.64 (m, 1H, $NCH_2CH_2CH_2CH$=CH), 7.14 (m, 3H, *m*-, *p*-C_6H_5), 7.42 (m, 2H, *o*-C_6H_5). *N*-(phenylmethylsilyl)-2,3,4-tetrahydropyridine, $PhMeSiH_2$, $PhMe_2SiH$, and CH_4. The *N*-(phenylsilyl)-2,3,4-tetrahydropyridine and *N*-(phenylmethylsilyl)-2,3,4-tetrahydropyridine formed in a ratio of 4:1. No CpCp*Ti species were observed in the NMR spectra, probably because of paramagnetism.

Acknowledgments

Financial support from the NSERC of Canada and the Fonds FCAR du Québec are gratefully acknowledged.

References

1. (*a*) C. Aitken, J.F Harrod, and E. Samuel. J. Organomet. Chem. **279**, C11 (1985); (*b*) C. Aitken, J.F. Harrod, and E. Samuel. J. Am. Chem. Soc. **108**, 4059 (1986); (*c*) L.S. Chang and J.Y. Corey. Organometallics, **6**, 1595 (1987); (*d*) L.S. Chang and J.Y. Corey. Organometallics, **8**, 1885 (1989); (*e*) J.Y. Corey, X-H. Zhu, T.C. Bedard, and L.D. Lange. Organometallics, **10**, 924 (1991).
2. C. Aitken, J.F. Harrod, A. Malek, and E. Samuel. J. Organomet. Chem. **349**, 285 (1988).
3. T.C. Bedard and J.Y. Corey. J. Organometal. Chem. **428**, 315 (1992).
4. H.Q. Liu and J.F. Harrod. Organometallics, **11**, 822 (1992).
5. J. He, H. Liu, J.F. Harrod, and R. Hynes. Organometallics, **13**, 336 (1994).
6. H.Q. Liu and J. F. Harrod. Can. J. Chem. **68**, 1100 (1990).
7. (*a*) S. Xin and J.F Harrod. J. Organometal. Chem. **499**, 181 (1995); (*b*) S. Xin and J.F. Harrod. Can. J. Chem. **73**, 999 (1995); (*c*) M.B. Carter, B. Schiott, A. Gutiérrez, and S.L. Buchwald. J. Am. Chem. Soc. **116**, 11670 (1994).
8. (*a*) S.C. Berk, K.A. Kreutzer, and S.L. Buchwald. J. Am. Chem. Soc. **113**, 5093 (1991); (*b*) M.T. Reding and S.L. Buchwald. J. Org. Chem. **60**, 7884 (1995).

© 2001 NRC Canada

9. C.A. Willoughby and S.L. Buchwald. J. Am. Chem. Soc. **116**, 11631 (1994).
10. J.F. Harrod and S.S. Yun. Organometallics, **6**, 1381 (1987).
11. N.M. Kablaoui and S.L. Buchwald. J. Am. Chem. Soc. **118**, 3182 (1996).
12. T. Grasczyk and J.F. Harrod. J. Polymer Sci. Part A, **32**, 3183 (1994).
13. Comprehensive handbook on hydrosilylation. *Edited by* B. Marciniec. Pergamon Press, New York. 1992.
14. Comprehensive handbook on hydrosilylation. *Edited by* B. Marciniec. Pergamon Press, New York. 1992. pp. 184–192 and 215–217.
15. A.W. van der Made, P.W.N.M. van Leeuwen, J.C. de Wilde, and R.A.C. Brandes. Adv. Mat. **5**, 466 (1993).
16. H. Brunner, H. Nishiyama, and K. Itoh. *In* Catalytic asymmetric synthesis. *Edited by* I. Ojima. VCH Publishers, New York. 1993. p. 303.
17. I. Ojima, Z. Li, and J. Zhu. *In* The chemistry of organic silicon compounds. Vol. 2. *Edited by* Z. Rappoport and Y. Apeloig. John Wiley & Sons, New York. 1998. p. 1687.
18. E. Campi and P. Perlmutter. *In* Advanced asymmetric synthesis. *Edited by* G.R. Stephenson. Chapman and Hall, London. 1996. Chap. 10.
19. L. Hao, J.F. Harrod, A.-M. Lebuis, Y. Mu, R. Shu, E. Samuel, and H.-G. Woo. Angew. Chem. Int Ed. Engl. **37**, 3126 (1998).
20. (*a*) N.C. Cook and J.E. Lyons. J. Am. Chem. Soc. **87**, 3283 (1965); (*b*) **88**, 3396 (1966).
21. (*a*) J. E. Bercaw and H.H. Brintzinger. J. Am. Chem. Soc. **91**, 730 (1969); (*b*) J.E. Bercaw, R.H. Marvich, H.G. Bell, and H.H. Brintzinger. J. Am. Chem. Soc. **94**, 1219 (1972).
22. (*a*) Critical stability constants. Vol. 5 (1st supplement). *Edited by* A.E. Martell and R.M.Smith. Plenum Press, New York. 1982. pp 219–231; (*b*) Stability constants of metal ion complexes, IUPAC data deries No. 22, Part B, organic ligands. *Compiled by* D.D. Perrin. Pergamon Press, New York. 1979.
23. (*a*) E. Samuel, Y. Mu, J.F. Harrod, Y. Dromzee, and Y. Jeannin. J. Am. Chem. Soc. **112**, 3435 (1990); (*b*) J. Britten, Y. Mu, J.F. Harrod, J. Polowin, M.C. Baird, and E. Samuel. Organometallics, **12**, 2672 (1993).
24. S. Xin, H-G. Woo, J.F. Harrod, E. Samuel, and A-M. Lebuis. J. Am. Chem. Soc. **119**, 5307 (1997).
25. L.J. Guggenberger and F.N. Tebbe. J. Am. Chem Soc. **95**, 7870 (1973).
26. V.V. Bhide, M.F. Ferona, A. Djebli, and W.J. Youngs. Organometallics, **9**, 1766 (l990).
27. B.F. Fieselmann and G.D. Stucky. Inorg. Chem. **17**, 2074 (1978).
28. M.E. Thompson, S.M. Baxter, A.R. Bulls, B.J. Burger, M.C. Nolan, B.D. Santarsiero, W.P. Schaefer, and J.E. Bercaw. J. Am. Chem. Soc. **109**, 203 (1987).
29. R.F. Jordan, D.F. Taylor, and N.C. Baenziger. Organometallics, **9**, 1546 (1990).
30. (*a*) E Klei and J.H. Teuben. J. Organomet. Chem. **214**, 53 (1981); (*b*) E. Klei and J.H. Teuben. J. Chem. Soc. Chem. Commun. 659 (1978).
31. K.H. den Haan, Y. Wielstra, and J.H. Teuben. Organometallics, **6**, 2053 (1987).
32. (*a*) L.C. Francesconi, D.R. Corbin, D.N. Hendrickson, and G.D. Stucky. Inorg. Chem. **17**, 2078 (1978); (*b*) **18**, 3074 (1979); (*c*) **20**, 2059 (1981).
33. R. Jungst, D. Sekutiwski, J. David, M. Luly, and G.D. Stucky. Inorg. Chem. **16**, 1645 (1977).
34. A.M. McPherson, B.F. Fieselmann, D.L. Lichtenberger, G.L. McPherson, and G.D. Stucky. J. Am. Chem. Soc. **101**, 3425 (1979).
35. (*a*) W.A. Howard and G. Parkin. J. Am. Chem. Soc. **116**, 606 (1994); (*b*) W.A. Howard and G. Parkin. Organometallics, **12**, 2363 (1993); (*c*) W.A. Howard and G. Parkin. J. Organomet. Chem. **472**, C1 (1994); (*d*) M.J. Carney, P.J. Walsh, F.J. Hollander, and R.G. Bergman. Organometallics, **11**, 761 (1992).
36. J.Y. Corey, J.L. Huhmann, and X.-H. Zhu. Organometallics, **12**, 112 (1993).
37. (*a*) M. Eisen. *In* The chemistry of organosilicon compounds. Vol. 2/3. *Edited by* Z. Rappoport and Y. Apeloig. John Wiley & Sons, Chichester. 1998. p. 2037; (*b*) I. Ojima and J. Zhu. *In* The chemistry of organosilicon compounds. Vol. 2/2. *Edited by* Z. Rappoport and Y. Apeloig. John Wiley & Sons, Chichester. 1998. p. 1704; (*c*) J.F. Harrod and A.J. Chalk. *In* Organic syntheses via metal carbonyls. Vol. II. *Edited by.* I. Wender and P. Pino. John Wiley & Sons, New York. l977. p. 673; (*d*) M.A. Schroeder and M.S. Wrighton. J. Organomet. Chem. **128**, 345 (1977); (*e*) A.N. Nesmeyanov, R. Kh. Friedlina, E.C. Chukovskaya, R.G. Petrova, and A.B. Belyavsky. Tetrahedron, **17**, 61 (1962).
38. R.A. Benkeser, H. Landesman, and D.J. Foster. J. Am. Chem. Soc. **74**, 648 (1952).
39. E. Samuel and M.D. Rausch. J. Am. Chem. Soc. **95**, 6263 (1973).
40. G. J. Erskine, D. A.Wilson, and J. D. McCowan, J. Organomet. Chem. **114**, 119 (1976).
41. E.A. Williams and J.D. Cargioli. *In* Annual reports on NMR spectroscopy.Vol. 15. *Edited by* G.A. Webb. Academic Press, New York. 1983. p. 235.

© 2001 NRC Canada

REVIEW / SYNTHÉSE

The Heck reaction in the production of fine chemicals

Johannes G. de Vries

Abstract. An overview is given of the use of the Heck reaction for the production of fine chemicals. Five commercial products have been identified that are produced on a scale in excess of 1 ton/year. The herbicide Prosulfuron™ is produced via a Matsuda reaction of 2-sulfonatobenzenediazonium on 3,3,3-trifluoropropene. The sunscreen agent 2-ethylhexyl *p*-methoxy-cinnamate has been produced on pilot scale using Pd/C as catalyst. Naproxen™ is produced via the Heck reaction of 2-bromo-6-methoxy-naphthalene on ethylene, followed by carbonylation of the product. Monomers for coatings are produced via a Heck reaction on 2-bromo-benzocyclobutene. A key step in the production of the antiasthma agent Singulair™ is the use of the Heck reaction of methyl 2-iodo-benzoate on allylic alcohol (**18**) to give ketone (**20**). The high cost of palladium has spurred much research aimed at the development of more active palladium catalysts. Ligandless catalysts are very attractive for production, but work only on reactive substrates. Palladacycles are much more stable than Pd–phosphine complexes and can be used at higher temperatures. The same effect has been reached with pincer ligands. Bulky ligands lead to coordinatively unsaturated Pd-complexes, which are highly active for the Heck reaction. Recycle of palladium catalysts is also very important to reduce cost. Immobilization of catalysts by attaching ligands to solid support is not very useful, because of leaching and reduced activity. In ligandless Heck reactions the catalyst can be precipitated on carriers such as silica, dicalite, or celite. This material can be restored to its original activity by treatment with I_2 or Br_2.

Key words: homogeneous catalysis, palladium, arylation, olefination, ligandless, catalyst recycle.

Résumé : On présente une revue de l'utilisation de la réaction de Heck dans la production de produits chimiques fins. On a identifié cinq produits commerciaux qui sont produits sur une échelle supérieure à une tonne par année. L'herbicide Prosulfuron® est produit par le biais d'une réaction de Matsuda du 2-sulfonatobenzènediazonium sur le 3,3,3-trifluoropropène. L'agent solaire 4-méthoxycinnamate de 2-éthylhexyle a été produit à l'échelle pilote à l'aide d'un catalyseur de Pd/C. Le Naproxen® est produit par le biais d'une réaction de Heck du 2-bormo-6-méthoxynaphtalène sur l'éthylène, suivie d'une carbonylation du produit. Des monomères de couches protectrices sont produits par le biais d'une réaction de Heck sur le 2-bromobenzocyclobutène. Une étape clé dans la production de l'agent antiasthmatique Singulair® est l'utilisation de la réaction de Heck du 2-iodobenzoate de méthyle sur l'alcool allylique **18** pour obtenir la cétone **20**. Le prix élevé du palladium a provoqué beaucoup de recherches dans le but de développer des catalyseurs du palladium qui soient plus actifs. Les catalyseurs sans ligands sont très attrayants pour la production, mais ils ne sont utiles qu'avec des substrats réactifs. Les cycles palladiés sont beaucoup plus stables que les complexes Pd/phosphine et ils peuvent être utilisés à des températures plus élevées. On peut obtenir le même effet avec des ligands en forme de pinces. Les ligands encombrés conduisent à des complexes à coordination insaturée du Pd qui sont très actifs pour la réaction de Heck. Le recyclage des catalyseurs de palladium est important afin de minimiser les coûts. L'immobilisation des catalyseurs en attachant des ligands à un support solide n'est pas très utile en raison du lessivage et de la réduction de l'activité. Dans les réactions de Heck sans ligand, il est possible de précipiter le catalyseur sur des porteurs, comme la silice, la dicalite ou la célite; ce matériel peut être ramené à son activité originale par traitement avec du I_2 ou du Br_2.

Mots clés : catalyse hétérogène, palladium, arylation, oléfination, sans ligand, recyclage du catalyseur.

[Traduit par la Rédaction]

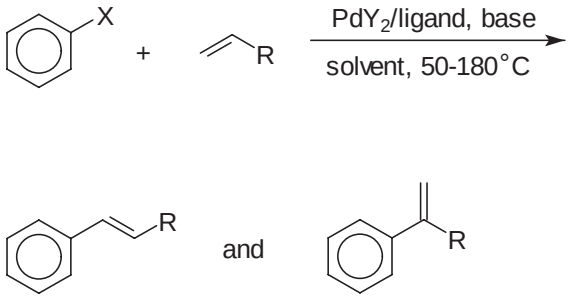
Received October 13, 2000. Published on the NRC Research Press Web site at http://www.canjchem.nrc.ca on July 14, 2001.

Dedicated to Brian James, a great scientist and a superb lecturer with a keen sense of humour, on the occasion of his 65th birthday.

J.G. de Vries. DSM-Research, Life Sciences-Chemistry & Catalysis, P.O. Box 18, 6160 MD Geleen, The Netherlands. (Telephone: +31-46-4761572; fax: +31-46-4767604. e-mail: hans-jg.vries-de@dsm-group.com).

 DOI: 10.1139/cjc-79-5/6-1086 © 2001 NRC Canada

Scheme 1. The Heck reaction.



X = I, Br, Cl, COCl, OSO_2R, SO_2Cl, N_2^+X, C(O)OC(O)Ar, SiR_2OH
Y = Cl, OAc

Introduction

Fine chemicals are produced on a scale of roughly between 1 and 10 000 tons per year. They comprise pharmaceuticals, agrochemicals, polymer additives, flavours and fragrances, food and feed additives, and chemical intermediates to name the most important classes. With relatively few exceptions, fine chemicals are produced via stoichiometric chemistry as this is easily scaled up and does not need specialized equipment. Unfortunately, these production methods also lead to relatively large amounts of waste (1).

Use of homogeneous catalysis has a number of obvious advantages (1–3): (*i*) less waste; (*ii*) lower cost, in particular if shortcuts in total syntheses can be achieved; (*iii*) high chemo- and regioselectivity, easily tuned by the ligands; (*iv*) asymmetric catalysis for the single step production of enantiopure fine chemicals.

If a product grows to a large volume, use of catalysis in a second-generation process becomes attractive because low cost is essential. Prime examples are Ibuprofen™ (carbonylation) (5), Naproxen™ (Heck reaction and carbonylation) (6), malonate esters (carbonylation) (7), and Metolachlor™ (asymmetric hydrogenation) (8).

The lack of homogeneous catalysis in first generation processes is very apparent in the production of pharmaceuticals. This is related to the limited duration of patent protection inducing a very strong time-to-market incentive. Because of this it is not possible to drastically change complex synthesis routes. Fortunately, there is an increasing interest in the use of homogeneous catalysis among medicinal chemists.

The history of homogeneous catalysis fine chemicals was initially largely dominated by asymmetric catalysis, particularly enantioselective hydrogenations (9). Recently, palladium catalysed aromatic substitution reactions have been used increasingly for the production of fine chemicals. In the past few years, five new processes based on the use of the Heck reaction have been reported.

The Heck reaction

The Heck arylation reaction (Scheme 1), invented independently by Mizoroki and Heck (10) in 1970 establishes a bond between olefins and aromatic rings. Initially, reports only mentioned the use of aryl bromides and iodides as arylating agent. Later, variants were developed using aromatic triflates (11), aroyl chlorides (12), aryl sulfonyl chlorides (13), aromatic diazonium salts (14) (the Matsuda reaction), aroyl anhydrides (15), aryl chlorides (16–20), and arylsilanols (21). Consequently, the number of commercially available aromatic substrates is very high. The diazonium salts work at room temperature or below and thus are suitable for reactions with thermally labile olefins. In situ preparation of the diazonium salt from the aniline during the Heck reaction has also been reported (22). The variant using aromatic anhydrides only produces the aromatic acid as side product, which can be recycled. In addition it does not need phosphine ligands or a base (15). Hence, this reaction is salt free.

Most heteroaromatic halides and pseudohalides can be used in the Heck reaction, though sometimes substrates with halide *ortho*- to the heteroatom cause problems (10).

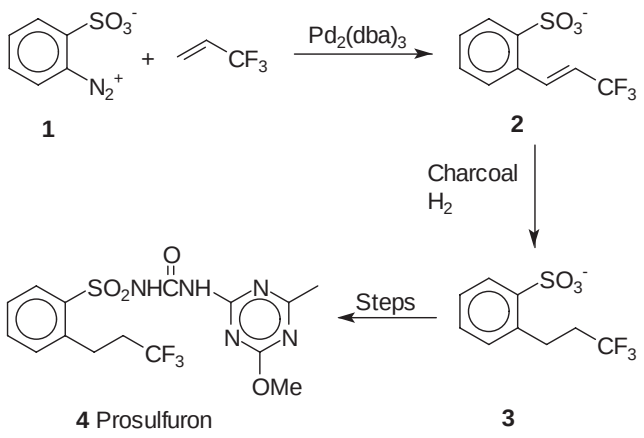
The Heck reaction works best with alkenes containing electron-withdrawing groups and in most cases gives the β-arylated products exclusively. Olefins with electron-donating groups give rise to mixtures of α- and β-arylated products. If palladium complexes with bidentate ligands are used the regioselectivity can be determined by the choice of leaving groups. Noncoordinating anions like triflate lead mainly to the α-arylated products, whereas halides predominantly give the β-products (10*e*). Simple olefins may suffer from Pd-catalyzed isomerization reactions leading to mixtures. Acetylenes may also be used and are generally more reactive than olefins (10).

Pd-catalysts are used with very few exceptions, usually $PdCl_2$ or $Pd(OAc)_2$ alone or in combination with Ph_3P or *o*-Tol_3P (2 or 3 equiv). Almost all Heck reactions require the presence of a base, which is often triethylamine. The combination $Pd(OAc)_2$, $MHCO_3$ (M = Na, K), KOAc or K_2HPO_4 with a phase transfer salt is also often used (Jeffery conditions) (10*f*). The ligand, the counter ion, the base, the phase transfer salt, and the solvent all have a profound influence on the rate and the selectivity of the reaction; many of these effects are related to the oxidation state and the coordination chemistry of the catalyst (23). It is also possible to use heterogeneous palladium catalysts such as Pd/C (24). Palladium clusters have also shown to be active (25); in fact Pd-clusters seem to form in most phosphine free Heck reactions. There is an ongoing debate whether the clusters themselves are catalytically active or if it is a monomeric soluble form of Pd that is the active catalyst (10*i*, 26). Obviously, to increase activity it is of importance to keep the size of these nanoclusters small. This can be achieved by the addition of tetraalkylammonium salts (Jeffery conditions) (10*f*) or with weakly binding polymers (27) or dendrimers (28). In most cases the active species is based on Pd(0), though it can be anionic (23). Proposals have also been advanced for Pd(II)–Pd(IV) cycles (29–31).

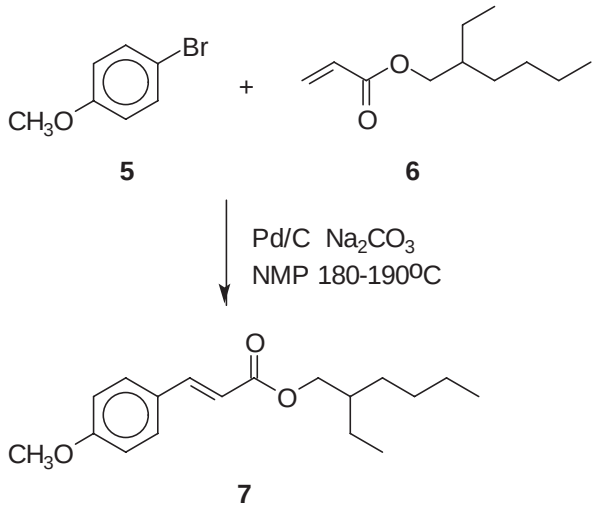
Typical solvents for the Heck reaction are dipolar nonprotic solvents like DMF and NMP. An asymmetric variant

© 2001 NRC Canada

Scheme 2. Synthetic scheme for the production of the herbicide Prosulfuron™.



Scheme 3. Sunscreen agent via the Heck reaction.



of the Heck reaction has been developed (32). The scope of this transformation has been limited thus far.

Use of the Heck reaction for the production of fine chemical intermediates

The herbicide Prosulfuron™

The first reported example of industrial use of the Heck reaction was for the production of Prosulfuron™, a new and highly active herbicide, by Ciba–Geigy (now Novartis) (33). In this instance, the Matsuda variant was used to great advantage as the substrate also contains a sulfonate group. The 2-sulfonatobenzenediazonium, which was prepared by diazotization of the aniline, is a neutral compound and relatively stable. The Heck reaction of this betaine on 3,3,3-trifluoropropene was performed at 15°C in HOAc using $Pd_2(dba)_3$ (0.5–1 mol%) as catalyst (Scheme 2). It was not necessary to isolate the Heck product. After addition of some active carbon to deposit the palladium on, the double bond was hydrogenated. Not only was the catalyst used in two consecutive steps, this method also allowed the catalyst to be reclaimed by filtration in 95% yield. The reaction is performed in a single reactor without isolation of the intermediates. The average yield per step is in excess of 90%.

Sunscreen agent via a ligandless Heck reaction

Companies producing bromine and aromatic bromides are of course in an excellent position to apply the Heck reaction. This advantage is not limited to the raw material position, but also involves the ability to recycle the bromide salts that are formed as waste. Because of the presence of large deposits of bromide, Israel has a flourishing organobromide industry. This has lead to the development of a new process for the production of 2-ethylhexyl *p*-methoxy-cinnamate, the most common UV-B sunscreen (34). The process involves the Heck reaction of *p*-bromoanisole with 2-ethylhexyl acrylate (Scheme 3). In this process, palladium on carbon is used as the catalyst without any ligands. This has the disadvantage of relatively low reactivity as compared to most homogeneous catalysts, necessitating a reaction temperature of 190°C. Also, as a result of the high reaction temperature some diarylation is found, mainly the 3,3′-isomer in up to 4%. Presumably, some palladium dissolves during the reaction, but after consumption of the starting materials all palladium precipitates, allowing easy catalyst recovery. The reaction mixture can contain up to 15% of water, which actually has an accelerating effect. This process, which was developed at the IMI institute for R & D in Israel, has been used on pilot scale to produce several tons of sunscreen agent in yields ranging from 75–92%.

Naproxen™ via Heck reaction and hydroxycarbonylation

Another producer of organobromine compounds, Albemarle, developed a new process for the production of Naproxen™, based on the Heck reaction of 2-bromo-6-methoxynaphthalene with ethylene, followed by carbonylation to Naproxen™ (Scheme 4) (6, 35, 36). The bromide already was an intermediate for the existing production of Naproxen™ and hence was available at a low price (37).

The key to the commercial success was finding a catalyst for the Heck reaction that was sufficiently active. This was accomplished by screening ligands based on their steric and electronic properties. From these results it was found that a phosphine ligand with steric and electronic properties in the middle of those screened would be optimal. These properties were found in neomenthyldiphenylphosphine. Because of the high activity of the catalyst it was possible to use a substrate:catalyst ratio of between 2000 and 3000 with the reaction going to completion at 95–105°C within a few hours. An ethylene pressure of around 3 kPa was used. This process is run on a scale of 500 tons per year. The bromide is recycled.

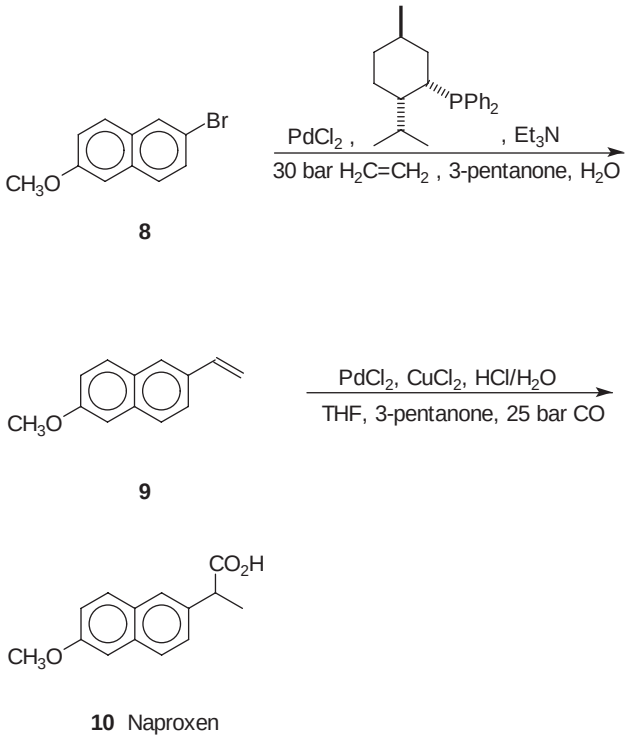
The hydroxycarbonylation process is catalyzed by a mixture of $PdCl_2$, $CuCl_2$ and HCl.

Monomers for coatings of electronic components

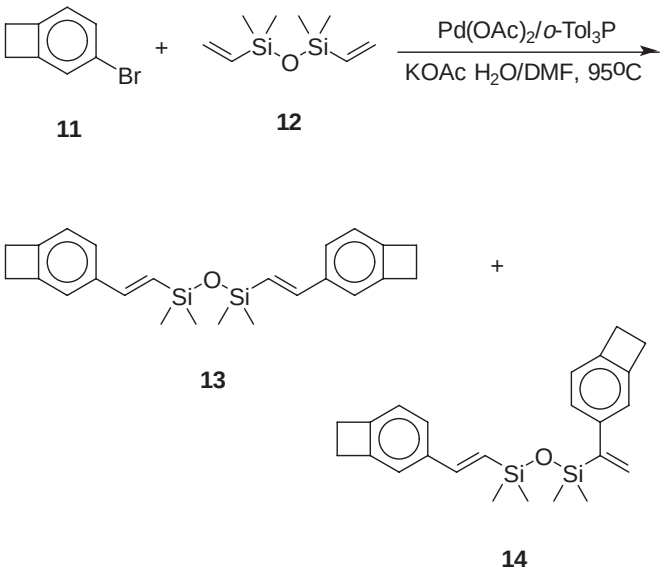
The mild conditions of the Heck reaction are also highly suitable for making carbon—carbon bonds with aromatic compounds that are thermally labile. This was the key to success in the production of benzocyclobutene-containing monomers. These are used to form coatings (known as

© 2001 NRC Canada

Scheme 4. Naproxen™ via Heck reaction and hydroxycarbonylation.



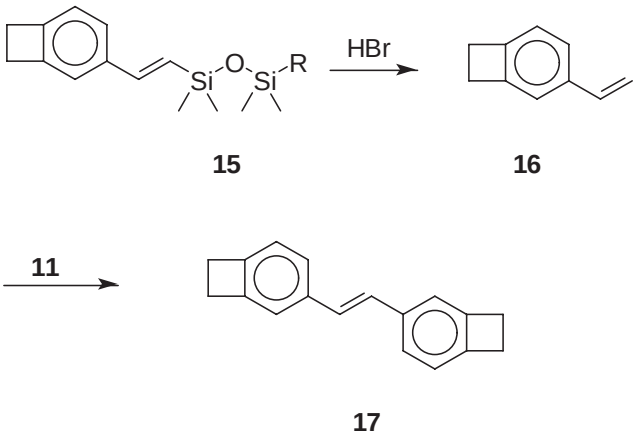
Scheme 5. Monomers for coatings via the Heck reaction.



Cyclotene™) for electronic components. The benzocyclobutene groups form *ortho*-quinone-dimethanes upon heating to 180°C, which may react with the double bond introduced by the Heck reaction, thus leading to cross-linking by Diels–Alder reaction.

The monomers are formed by Heck reaction of 4-bromobenzocyclobutene with tetramethyldivinyldisiloxane catalyzed by $Pd(OAc)_2$–*o*-Tol_3P in DMF–H_2O using KOAc as base (Scheme 5) (38). The optimal catalyst for this reaction

Scheme 6. Mechanism of formation of the stilbene side product.



was found after screening a range of phosphorus ligands at 95°C. Tri-*ortho*-tolylphosphine gave the best results of the commercially available ligands in terms of product yield (83%). No correlation was found between ligand parameters on one hand, and conversion of bromide, yield of product, or regioselectivity on the other hand. The ligand parameters used were cone angle for bulkiness and pK_a for electronic properties.

A major side product (3–11%) in these reactions is the stilbene (**17**), which is formed by desilylation of the initially formed monoarylated disiloxane (**15**) followed by Heck reaction on the vinyl group (Scheme 6). Initial results using Et_3N as base gave much higher yields of this side product.

This Heck reaction is performed by Dow on a scale of several tons per year.

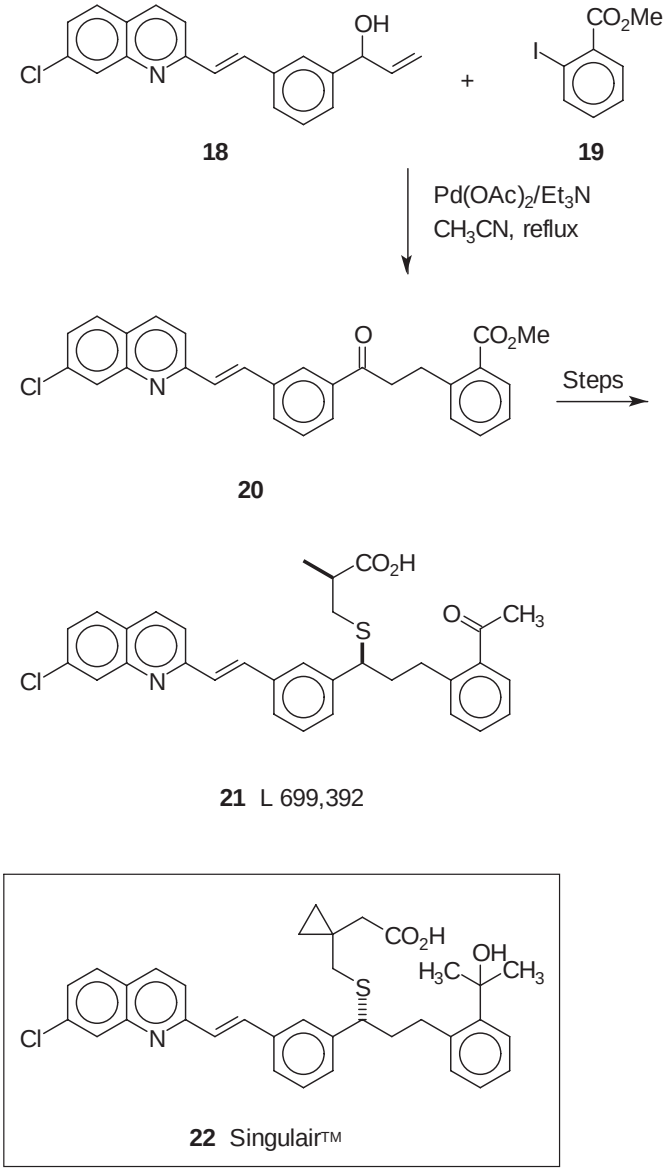
The Heck reaction as the key step in the production of an antiasthma agent

An important aspect of the attractiveness of the Heck reaction is the ability to form carbon—carbon bonds without the use of strongly basic reagents such as Grignards and lithiated carbon nucleophiles. Hence, the functional group tolerance of the Heck reaction is very wide allowing its use in the latter stages of a total synthesis. This aspect is very important in the production of Merck's LTD_4 antagonist Singulair™ (**22**) (39) that has been introduced on the market as an antiasthma agent. A synthesis has been published for the closely related L-699 392 (**21**) (Scheme 7) (40). The key step in the synthesis is the Heck reaction of methyl 2-iodobenzoate with allylic alcohol (**18**). Because of the high reactivity of these substrates it was possible to use ligandless $Pd(OAc)_2$ as catalyst with Et_3N as base in CH_3CN as solvent. With 1 mol% of catalyst the reaction is complete in 1 h. A minor by-product was formed via arylation of the 2-position. However, the product could be obtained in pure form by crystallization.

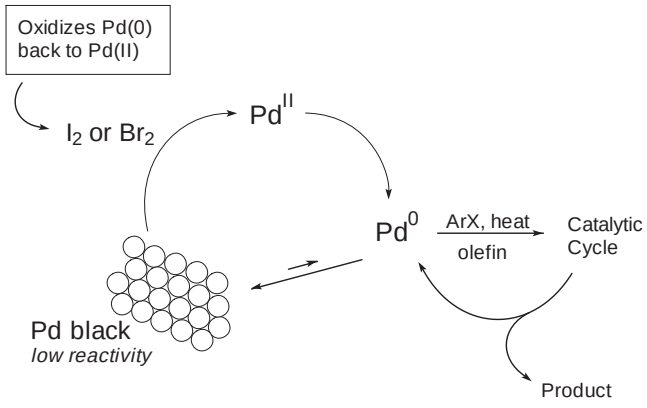
In this variant, reaction on the allylic alcohol leads to the formation of a ketone, because β-hydride elimination of the palladium–alkyl intermediate leads to the preferential formation of the enol.

© 2001 NRC Canada

Scheme 7. The Heck reaction in the production of antiasthma agents.



Scheme 8. A practical catalyst recycle for ligandless Heck reactions.



Development aspects

A major aspect in the development of a homogeneous catalyzed reaction is the cost of the catalyst. This in turn is strongly dependent on two important parameters: (*i*) The activity of the catalyst expressed as turnover frequency (TOF: mol of product/mol of catalyst h); (*ii*) The stability of the catalyst expressed as total turnover number (this might include recycling; TON = mol of product/mol of catalyst).

For this reason, much effort has been put into the development of new, more active, and more stable palladium catalysts. The palladacycle developed by Herrmann et al. (17) is a good example. Because of its increased stability, the catalyst can be used at higher temperatures, thus producing higher reaction rates. In addition, unreactive arylating agents like aryl chlorides can be used. More variations on this theme are the use of bulky phosphite (18, 41) or phosphoramidite ligands (42), carbene ligands (43, 44), and pincer ligands (31, 45). Another interesting, cheap, and very active class of catalysts are the palladacycles based on aromatic compounds with side chains containing N (41, 46), O (47), or S (48, 49). The more active catalysts also have allowed the use of chloroarenes as arylating agents, which is tremendously important because of the much wider commercial availability and the lower costs of these compounds (16–20).

Separation of the product can sometimes be hampered by the presence of a phosphine ligand. Therefore, ligandless Heck reactions are preferred where possible, as shown in three of the above five cases.

Because of the steadily rising cost of palladium, catalyst recovery and recycle has become a major issue. Recovery is easy in the case of the ligandless Heck reactions as the catalyst precipitates completely once all the substrate has been used up. If ligands are used this can be a problem, though sometimes water-soluble ligands can be used to allow for two-phase catalysis (50–53). Ionic liquids have also been reported as an aid in catalyst recycle (54–56). The recovered catalyst is usually returned to the catalyst manufacturer for reclaiming as catalyst activity is greatly diminished. Recycling methods based on the immobilization of ligands are usually flawed, as the instability of the palladium complexes will invariably lead to leaching (10*i*). In addition, reactivity is usually severely compromised. Immobilization of ligandless palladium has some merit (57). Even though leaching occurs extensively, the palladium precipitates on the support at the end of the reaction. However, these catalysts are usually less active.

Recently, a new method for catalyst recycle was reported from our laboratories (58, 59). In this method, $Pd(OAc)_2$ is used as ligandless catalyst. At the end of the reaction, the catalyst precipitates in >99% as Pd(0) on an inexpensive carrier material like silica, dicalite, or celite. This catalyst is about 10 times less active than the $Pd(OAc)_2$ that is used initially. However, full catalytic activity can be restored by the addition of a few equivalents of I_2 or Br_2 (Scheme 8). These halogens oxidize Palladium(0) to Pd(II) which is then reduced again during the next cycle to form highly active catalytic species.

© 2001 NRC Canada

Conclusion

The Heck reaction is finding increasing use for the production of fine chemicals on a scale of 1–500 tons per year. At least five published cases are known of products that have been produced on a scale of more than 1 ton using the Heck reaction. Advantages when compared to more classical methods such as Friedel–Crafts chemistry are superb functional group tolerance, mild conditions, less waste, and sometimes a shorter route than the original stoichiometric route. This has spurred renewed activity in the area of development of new, faster and more stable catalysts. Catalyst recycle is particular easy with ligandless catalysts, where treatment of the precipitated Pd with I_2 leads to full regeneration of activity.

Acknowledgements

We thank the Dutch Ministry of Economics Affairs for a subsidy under the EET program (EETK97107). I thank David Hyett for correcting the manuscript.

References

1. R.A. Sheldon. J. Mol. Catal. A: Chem. **107**, 75 (1996).
2. J.G. de Vries. *In* Encyclopedia of Catalysis. *Edited by* I.T. Horváth. John Wiley and Sons, New York. to appear in 2001.
3. B. Cornils and W.A. Herrmann (*Editors*). Vol 1 and 2. Applied homogeneous catalysis with organometallic compounds. VCH, Weinheim. 1996.
4. M. Beller and C. Bolm (*Editors*). Transition metals for organic synthesis — Building blocks and fine chemicals. Wiley-VCH, Weinheim. 1998.
5. M. Beller. Applied homogeneous catalysis with organometallic compounds. Vol 1. *Edited by* B. Cornils and W.A. Herrmann. VCH, Weinheim. 1996. p. 148.
6. J. McChesney. Spec. Chem. **6**, 98 (1999).
7. (*a*) P. Pollak. *In* Ullmann's encyclopedia of industrial chemistry. Vol A 16. *Edited by* B. Elvers, S. Hawkins, and G. Schulz. VCH, Weinheim. 1990. p. 63; (*b*) P. Pollak and G. Romeder. *In* Kirk-Othmer's encyclopedia of chemical technology. 4th ed. Vol 15. *Edited by* J.I. Kroschwitz and M. Howe-Grant. John Wiley and Sons, New York. 1995. p. 928.
8. F. Spindler, B. Pugin, H.-P. Jalett, H.-P Buser, U. Pittelkow, and H.-U. Blaser. *In* Catalysis of organic reactions. *Edited by* R.E. Malz, Jr. Chem. Ind. (London), **68**, 153 (1996).
9. H.U. Blaser, F. Spindler, and M. Studer. Appl. Catal. A, accepted for publication.
10. (*a*) R.F. Heck. Org. React. (N.Y.), **27**, 345 (1982); (*b*) R.F. Heck. *In* Comprehensive organic synthesis. Vol 4. *Edited by* B.M. Trost and I. Fleming. Pergamon Press, Oxford. 1991. p. 833; (*c*) A. de Meijere and F.E. Meyer. Angew. Chem. Int Ed. Engl. **33**, 2379 (1995); (*d*) J. Tsuji. Palladium reagents and catalysts — Innovations in organic synthesis. Wiley, Chichester, U.K. 1995; (*e*) W. Cabri and I. Candiani. Acc. Chem. Res. **28**, 2 (1995); (*f*) T. Jeffery. *In* Advances in metal-organic chemistry. Vol 5. *Edited by* L.S. Liebeskind. JAI Press, Inc., Greenwich, Connecticut. 1996. p. 153; (*g*) S. Bräse and A. de Meijere. In Metal-catalyzed cross-coupling reactions. *Edited by* F. Diederich and P.J. Stang. Wiley–VCH, Weinheim. 1998. p. 99; (*h*) M. Beller, T.H. Riermeier, and G. Stark. *In* Transition metals for organic synthesis — Building blocks and fine chemicals. Vol 1. *Edited by* M. Beller and C. Bolm. Wiley-VCH, Weinheim. 1998. p. 208; (*i*) I.P. Beletskaya and A.V. Cheprakov. Chem. Rev. **100**, 3009 (2000).
11. K. Ritter. Synthesis, 735 (1993).
12. H.-U. Blaser and A. Spencer. J. Organomet. Chem. **233**, 267 (1982).
13. M. Miura, H. Hashimoto, K. Itoh, and M. Nomura. J. Chem. Soc. Perkin Trans.1, 2207 (1990).
14. K. Kikukawa and T. Matsuda. Chem. Letters, 159 (1977).
15. M.S. Stephan, A.J.J.M. Teunissen, G.K.M. Verzijl, and J.G. de Vries. Angew. Chem. Int. Ed. Engl. **37**, 662 (1998).
16. M. Portnoy, Y. Ben-David, I. Rousso, and D. Milstein. Organometallics, **13**, 3465 (1994).
17. W.A. Herrmann, C. Brossmer, C.-P. Reisinger, T.H. Riermeier, K. Öfele, and M. Beller. Chem. Eur. J. **3**, 1357 (1997).
18. M. Beller and A. Zapf. Synlett. **7**, 792 (1998).
19. M.T. Reetz, G. Lohmer, and R. Schwickardi. Angew. Chem. Int. Ed. Engl. **37**, 481 (1998).
20. A.P. Littke and G.C. Fu. J.Org.Chem. **64**, 10 (1999).
21. K. Hirabayashi, Y. Nishihara, A. Mori, and T. Hiyama. Tetrahedron Lett. **39**, 7893 (1998).
22. M. Beller, H. Fischer, and K. Kühlein. Tetrahedron Lett. **35**, 8773 (1994).
23. C. Amatore and A. Jutand. Acc. Chem. Res. **33**, 314 (2000).
24. V.M. Wall, A. Eisenstadt, D.J. Ager, and S.A. Laneman. Platinum Met. Rev. **43**, 138 (1999).
25. M.T. Reetz, R. Breinbauer, and K. Wanninger. Tetrahedron Lett. **37**, 4499 (1996).
26. M.T. Reetz and E. Westermann. Angew. Chem. Int. Ed. Engl. **39**, 165 (2000).
27. S. Klingelhöfer, W. Heitz, A. Greiner, S. Oestreich, S. Förster, and M. Antonietti. J. Am. Chem. Soc. **119**, 10116 (1997).
28. S. Mecking, R. Thomann, H. Frey, and A. Sunder. Macromolecules, **33**, 3958 (2000).
29. M. Beller, H. Fischer, W.A. Herrmann, K. Öfele, and C. Brossmer. Angew. Chem. Int. Ed. Engl. **34**, 1848 (1995).
30. B.L. Shaw. New J.Chem. 77 (1998).
31. M. Ohff, A. Ohff, M.E. van der Boom, and D. Milstein. J. Am. Chem. Soc. **119**, 11687 (1997).
32. M. Shibasaki, C.D.J. Boden, and A. Kojima. Tetrahedron, **53**, 7371 (1997).
33. P. Baumeister, W. Meyer, K. Oertle, G. Seifert, U. Siegrist, and H. Steiner. *In* Heterogeneous catalysis and fine chemicals IV. *Edited by* H.U. Blaser, A. Baiker, and R. Prins. Elsevier Science bv., Amsterdam. 1997. p. 37.
34. A. Eisenstadt. *In* Catalysis of organic reactions. *Edited by* F.E. Herkes. Chemical Industries **75.** Chemical Industries, 1998. p. 415.
35. R.W. Lin, R. Herndon, R.H. Allen, K.C. Chockalingham, G.D. Focht, and R.K. Roy. World Patent WO 98/30529 (1998) to Albemarle Corporation.
36. T.-C. Wu. U.S. Patent 5 315 026 (1994) and U.S. Patent 5 536 870 (1996), both to Albemarle Corporation.
37. P.J. Harrington and E. Lodewijk. Org. Process Res. Dev. **1**, 72 (1997).
38. R.A. DeVries, P.C. Vosejpka, and M.L. Ash. *In* Catalysis of organic reactions. *Edited by* F.E. Herkes. Chemical Industries, **75**, 1998. p. 467.
39. G. Higgs. Chem. Ind. 827 (1997).
40. I. Shinkai, A.O. King, and R.D. Larsen. Pure Appl. Chem. **66**, 1551 (1994).
41. D.A. Albisson, R.B. Bedford, and P.N. Scully. Tetrahedron Lett. **39**, 9793 (1998).
42. G.P.F. van Strijdonck, M.D.K. Boele, P.C.J. Kamer, J.G. de Vries, and P.W.N.M. van Leeuwen. Eur. J. Inorg. Chem. 1073 (1999).
43. W.A. Herrmann, M. Elison, J. Fischer, C. Koecher, and G.R.J. Artus. Angew. Chem. Int. Ed. Engl. **107**, 2602 (1995).

© 2001 NRC Canada

44. D.S.G. McGuiness, J. Melinda, K.J. Cavell, B.W. Skelton,and A.H. White. J. Organomet. Chem. **565**, 165 (1998).
45. F. Miyazaki, K. Yamaguchi, and M. Shibasaki. Tetrahedron Lett. **40**, 7379 (1999).
46. M. Ohff, A. Ohff, and D. Milstein. Chem. Commun. 357 (1999).
47. I.P. Beletskaya, A.N. Kashin, N.B. Karstedt, and A.V. Chuchurjukin. Poster at OMCOS 10, Versailles, France. 1999.
48. D.E. Bergbreiter, P.L. Osburn, and Y.-S. Liu. J. Am. Chem. Soc. **121**, 9531 (1999).
49. A.S. Gruber, D. Zim, G. Ebeling, A.L. Monteiro, and J. Dupont. Org. Lett. **2**, 1287 (2000).
50. A.L. Casalnuovo and J.C. Calabrese. J. Am. Chem. Soc. **112**, 4324 (1990).
51. J.-P. Genêt, E. Blart, and M. Savignac. Synlett. 715 (1992).
52. B.M. Bhanage, F.G. Zhao, M. Shirai and M. Arai. Tetrahedron Lett. **39**, 9509 (1998).
53. M. Beller, J.G.E. Krauter, and A. Zapf. Angew. Chem. Int. Ed. Engl. **36**, 772 (1997).
54. A.J. Carmichael, M.J. Earle, J.D. Holbrey, P.B. McCormac, and K.R. Seddon. Org. Lett. **1**, 997 (1999).
55. V.P.W. Boehm and W.A. Herrmann. Eur. J. Chem. **6**, 1017 (2000).
56. L. Xu, W. Chen, and J. Xiao. Organometallics, **19**, 1123 (2000).
57. F.Zhao, B.M. Bhanage, M. Shirai, and M. Arai. Chem. Eur. J. **6**, 843 (2000).
58. F.J. Parlevliet, A.H.M. de Vries, and J.G. de Vries. Dutch Patent Application 1 015 520 (2000).
59. J.G. de Vries. Lecture at 12th ISHC, Stockholm, Sweden. (2000).

© 2001 NRC Canada

2000 Macromolecular Science and Engineering Award Lecture

The versatility of azobenzene polymers

Almeria Natansohn and Paul Rochon

Abstract: The well-known *trans–cis–trans* photoisomerization of azobenzenes produces at least three different kinds of motion in the polymer materials to which the azobenzenes are bound. The first is a photoinduced motion of the azobenzene groups only, and they can align in a selected position with respect to the light polarization. The second is a macroscopic motion of huge amounts of polymeric material, producing surface deformation, and the third is a reorganization of smectic domains in liquid crystalline polymers. These motions and their consequences are briefly discussed in relation to the polymer structure and some possible photonic applications are mentioned.

Key words: photoinduced orientation, azobenzene polymers, surface gratings, photonics, thermochromism, photochromism, photorefractivity, photoinduced chirality and switching.

Résumé : La photoisomérisation bien connue *trans-cis-trans* des azobenzènes donne lieu à au moins trois types différents de mouvements dans les matériaux polymères auxquels ils sont liés. Le premier est un mouvement photoinduit impliquant uniquement les groupes azobenzène et ils peuvent s'aligner dans une position choisie par rapport à la polarisation de la lumière. Le deuxième est un mouvement macroscopique de grandes quantités de matériau polymère qui provoque une déformation de la surface et le troisième est une réorganisation dans les domaines smectiques des polymères à l'état de cristal liquide. On discute brièvement de ces mouvements et de leurs conséquences en relation avec la structure du polymère et on fait état de quelques applications photoniques possibles.

Mots clés : orientation photoinduite, polymères azobenzène, réseaux de surface, photonique, thermochromie, photochromie, photoréfractivité, chiralité photoinduite, inversion de chiralité.

[Traduit par la Rédaction]

Introduction

Azobenzenes have been known and studied for a very long time. Their initial use was as dyestuff for a variety of things. Azobenzene photoisomerization is also very well-known and has been reviewed in a reference book (1). When the azobenzene group is incorporated into a polymer, its photoisomerization can have a wide range of unexpected possible consequences. These have also been reviewed (2).

About 15 years ago, Todorov et al. (3) noted yet another unexpected phenomenon related to the photoisomerization of some azobenzene groups when dissolved into a polymer matrix. The azobenzenes photoisomerize under polarized laser illumination and eventually orient perpendicular to the laser polarization, producing dichroism and birefringence in the polymer film. Around 1987, a few papers from Ringsdorf and Wendorff's laboratories in Germany rediscovered the same phenomenon in liquid crystalline polymers containing azobenzene groups. These groups were now the mesogens *and* the photoactive moieties (4). At about the same time, Ichimura et al. (5), in Japan, proposed the "command surfaces" concept, where the azobenzene was the "commander" and liquid crystalline Langmuir–Blodgett films were the "soldiers" which would align with the *trans* or with the *cis* azobenzene, and the switching was initiated by illumination. Although all these papers appeared before the review by Kumar and Neckers (2), they were too recent then to be included there.

By 1991, at the time we got involved in this type of research, the field practically exploded with papers coming from many research groups all over the world. A consistent trait of these reports was that most were unaware of both the pioneering work done in this field and of the work done at the same time by other groups. This was certainly true in our case. The findings were unexpected, exciting, and raised enormous possibilities for reversible optical memory and photonic applications. In the last 10 years, the research activity has grown exponentially, and there still is no review covering all these new implications of azobenzene photoisomerization in polymer structures. Here, we mention some very useful reviews: one by us in 1993 (6) covering most of the literature to date; one reviewing surface gratings research done mainly in Tripathy's group (7), and a more

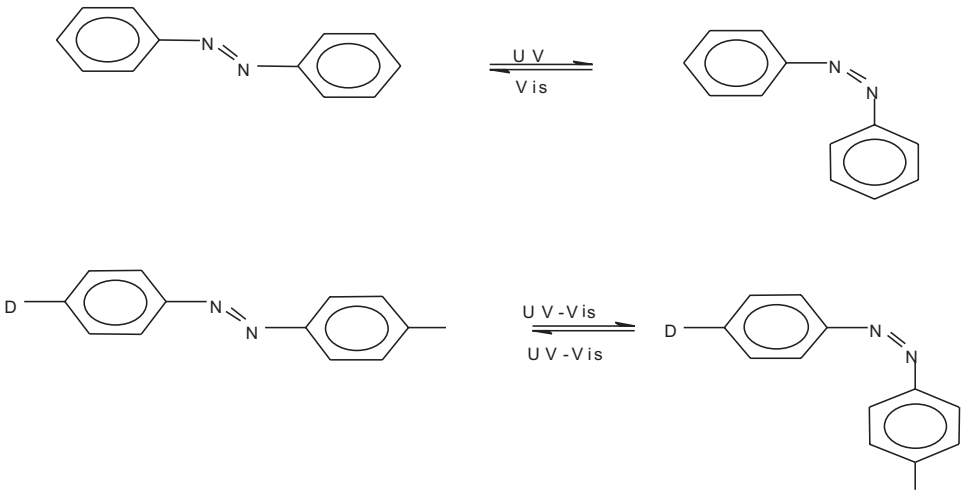
Received March 6, 2001. Published on the NRC Research Press Web site at http://canjchem.nrc.ca on August 6, 2001.

A. Natansohn.[1] Department of Chemistry, Queen's University, Kingston, ON K7L 3N6, Canada.
P. Rochon. Department of Physics, Royal Military College, Kingston, ON K7K 5L0, Canada.

[1]Corresponding author (telephone: 613-533-2008; fax: 613-533-6669; e-mail: natansoh@chem.queensu.ca).

 DOI: 10.1139/cjc-79-7-1093 © 2001 NRC Canada

Fig. 1. Azobenzene photoisomerization; without substituents (up), with donor–acceptor substituents (down).



recent one covering photoalignment in liquid crystalline polymers (8). The best review available, covering both photoinduced birefringence and surface relief gratings, belongs to Delaire and Nakatani (9).

This article is not intended to review the state of the art on photoinduced motions in polymers triggered by azobenzene photoisomerization. We are working on a review on this subject, and — as expected — the task is huge and challenging. In this article, we will give a summary of our own involvement in this area of research and we will point out what we believe are our contributions. This is a wonderful area of research, in our experience almost anything we start studying reveals new and exciting findings. It also has helped us, and others, challenge some very basic concepts of polymer science.

Azobenzene photoisomerization

One can think of azobenzene as a photochromic material, because it has two isomers, *cis* and *trans*, that absorb at different wavelengths. The max absorbance depends on the substituents, but for the unsubstituted azobenzene the *trans* isomer has a max absorbance at 313 nm and the *cis* isomer at 436 nm (1). In principle, one could use light to switch between the two isomers and "store" information until switched back. In practice, this is not possible, for two reasons. First, the color change is not noticeable, because of the much lower absorptivity of the *cis* isomer. Second, the *cis* isomer is very unstable and it cannot be conserved ("stored") for more than a few hours. With donor–acceptor substituents, the *trans* and *cis* absorbances become superimposed, thus such azobenzenes are not photochromic anymore. The *cis* lifetime is also much shorter. Thus, donor–acceptor substituted azobenzenes will switch back and forth between the *trans* and *cis* isomers for as long as they are illuminated at the absorbing wavelength. The schematic illustration of azobenzene photoisomerization is shown in Fig. 1.

Motions induced by photoisomerization

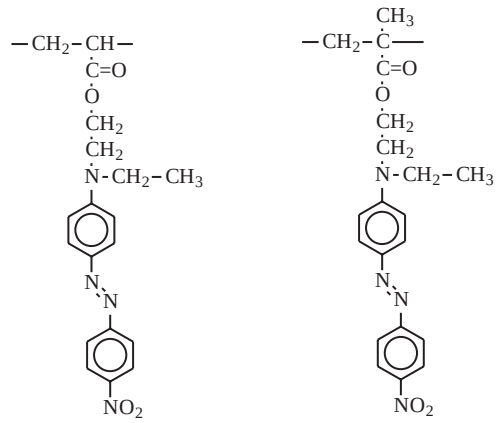
While the azobenzene (azo) group is subjected to continuous laser illumination at low intensities (normally a few mW cm^{-2}), photoisomerization occurs at a very high rate. Although the details are not yet well understood, the quantum yields are high (1) and the switching time is believed to be shorter than picoseconds. Even when the azobenzenes are not bound on a polymer chain, but just dispersed in it as a solid solution, this constant *trans–cis–trans* photoisomerization activity results in the azobenzene group moving around and slightly changing its position. This type of motion is expected, especially when the azo group is not bound to the polymer. This was the case for the first report of photoinduced birefringence (3). When the azobenzene group is bound, the presence of a flexible spacer, separating the rather rigid, but mobile azo group, from the rigid and entangled polymer backbone, was believed to be required. This spacer would "decouple" the azo motion from the backbone, allowing it to move around. This was the basis for the liquid crystalline polymer research (4). The longer the spacer between the azo group and the backbone, the more "freedom" the azo groups would have, but this longer spacer and the presence of the mesogenic azo groups would also provide liquid crystalline properties to the resulting polymer. At that time it was believed that liquid crystallinity was a required condition to allow the azo group freedom to move. Working with polymers with shorter spacers (two methylene units, see Fig. 2), we were very surprised to discover (10, 11) that this kind of motion can occur well below the glass transition temperature (*T*g) of the material. In fact, the liquid crystallinity requirement was unnecessary, as we and then many other research groups demonstrated.

Yet another, much more surprising type of movement happens while photoisomerization takes place. If the laser light intensity is modulated and hits the surface of the polymer film at different intensities, a massive movement of the polymer material may accompany the photoisomerization. The motions are thus not limited to the azo rigid group, but involve many polymer chains, because the volumes affected by this kind of movement are of the order of up to cubic microns. This extremely surprising finding was reported almost at the same time by our group (12) and by Tripathy's group (13).

Finally (although other surprises may still await discovery), another novel type of movement in polymer materials

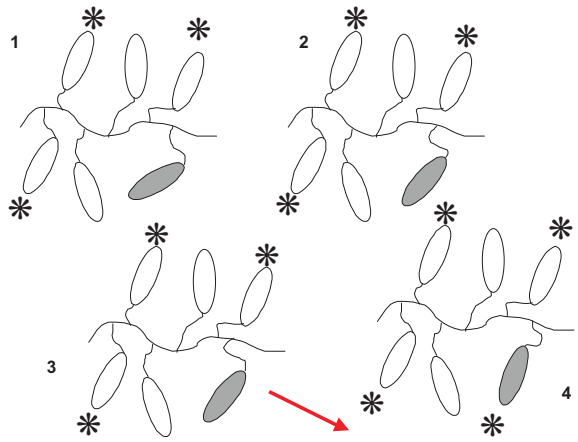
© 2001 NRC Canada

Fig. 2. Poly(4′-[[[(2-acryloyloxy)ethyl]ethyl]amino]-4-nitroazobenzene) (pDR1A) and poly(4′-[[[(2-methacryloyloxy)ethyl]ethyl]amino]-4-nitroazobenzene) (pDR1M), the first two high-*T*g amorphous polymers investigated in our group.



pDR1A pDR1M

Fig. 3. A random distribution of the azo groups in a hypothetical 6-*mer* chain. The groups with an asterisk are already perpendicular to the light polarization direction (represented by the arrow). The azo group shown at the lower right side of the chain goes through a series of isomerizations until it reaches the inert alignment.

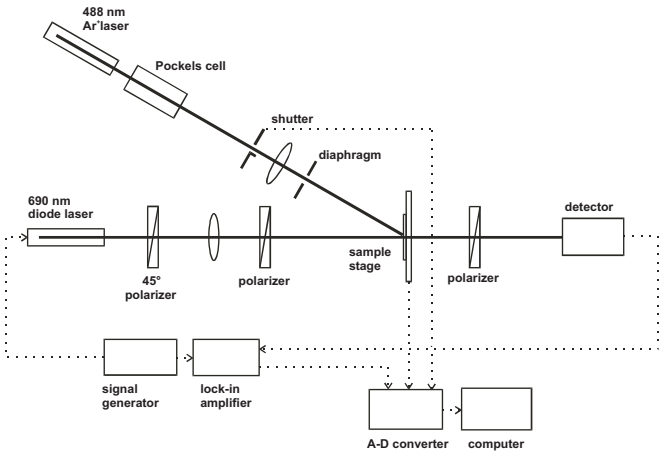


containing azobenzene groups is a reorientation of whole smectic (liquid crystalline) domains in polymers. If subjected to circularly polarized light, for example, the domains will rearrange from a disordered state to a supramolecular helical ordered state of the same handedness as the incoming light. This can be observed by measuring optical rotation or circular dichroism (14, 15). Some more details about these three kinds of unexpected motions will be given in the following subchapters.

Photoinduced birefringence

Regarding the first type of motion, involving solely the azobenzene groups and leaving the main chain almost inert, an interesting consequence occurs when linearly polarized light is being used. In an amorphous, high-*T*g polymer film containing azobenzene groups, these groups tend to be randomly distributed. When the film is prepared by spin coating, which happens in most cases, the rotation of the stage produces a preferred orientation within the plane of the film. This preferred orientation can be destroyed by heating the film above *T*g. Heating randomizes all preorientation and allows any trapped solvent to escape. Illuminating such a film with linearly polarized light activates the photoisomerization of the azo groups having a component of their dipole parallel to the polarization direction of the light. In other words, any azobenzene group that happens to lie perpendicular to the light polarization will not photoisomerize. The azo groups that do isomerize will also move slightly in the process, and if at the end of a photoisomerization cycle they happen to fall perpendicular to the light polarization, they will also become inert to light. This means that the concentration of the azo groups lying perpendicular to the light polarization will steadily increase and eventually reach a saturated value. A possible schematic illustration of the phenomenon is shown in Fig. 3. A portion of an azo polymer chain containing six structural units is shown in four stages of illumination. The polarization of the light is shown in the figure as an arrow. The azo groups already perpendicular to the light polarization, thus inert to the process, are marked with asterisks. The emphasis is on the motion of the "gray" chromophore, that isomerizes and moves slightly between 1 and 4, when it happens to fall in the position perpendicular to the light polarization. Thus, at the end of the schematic process represented here, the number of chromophores aligned perpendicular to the light polarization has increased from three to four. It is possible to measure this alignment of the azo groups either as dichroism or as birefringence. A typical set-up for measuring birefringence is illustrated in Fig. 4.

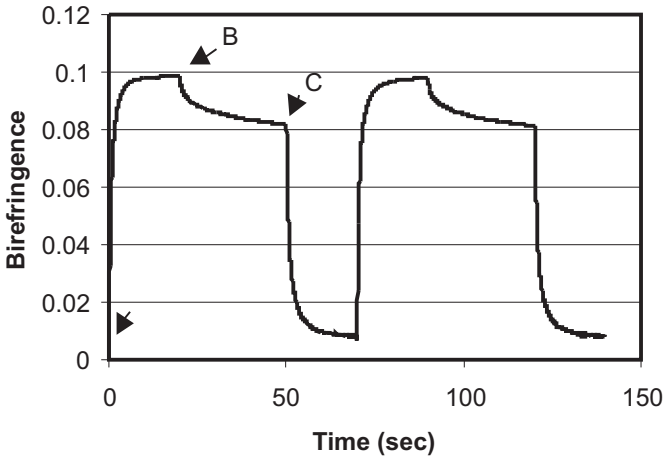
Fig. 4. A typical set-up to measure photoinduced birefringence in azo polymers. The 488 nm laser is used as a pump and the 690 nm laser is used as a probe.



Thus, starting with a sample with no preferred orientation of the azo groups, after illumination one obtains a birefringent sample. Using a laser on a random sample, the illuminated spot is now birefringent. Upon turning the laser off, the photostationary state, containing some *cis* isomers, relaxes to a stable state in which the orientation (and birefringence) is conserved to a significant level (typically between 60 and 95%, depending on the material). The most exciting aspect of the phenomenon, that was pointed out by

© 2001 NRC Canada

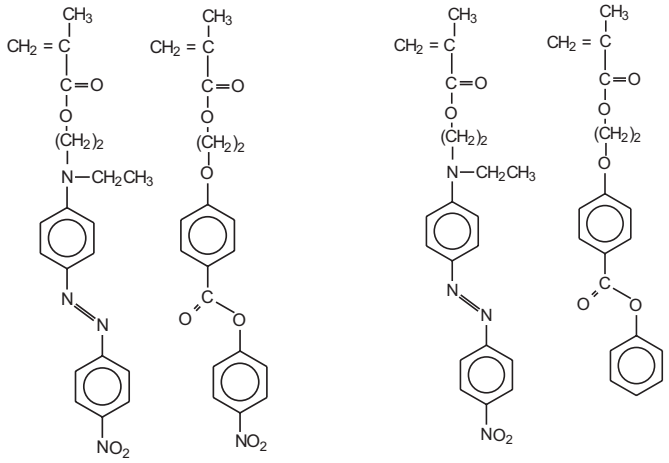
Fig. 5. Typical repeated measurement of photoinduced birefringence on a sample of pDR1M. Linearly polarized light is turned *on* at point A and the photoinduced birefringence starts growing and reaches a saturated level. At point B the light is turned off and some relaxation occurs. At point C, circularly polarized light is turned *on* and the photoinduced birefringence is erased.



our group for the first time (11), is that illumination with circularly polarized light will restore the preferred random orientation of the azobenzene groups, thus "erasing" the birefringence. A typical birefringence measurement is shown in Fig. 5, where birefringence is induced, allowed to relax, and then erased, twice. This cycle is very reproducible and can be repeated tens of thousands of times on the same spot on the polymer film before photobleaching starts occuring (16).

A lot of research was dedicated in our group to investigating the levels of birefringence, the rates of photoinducing it, the rates of relaxation and — especially — the relation between the polymer structure and the photoinduced birefringence. We have investigated various azobenzene groups as chromophores, and linked them into polymer structures by various means, for example as side groups (with different types and lengths of spacers) or within the main chain. We have varied the concentration of the azobenzene groups in the polymer film, by synthesizing copolymers and preparing blends with various comonomers and polymers, respectively. It is not possible to review or even to summarize this work here, but good overviews can be found in a book chapter (17) and in a "research news" article in *Advanced Materials* (18). We would like to mention here the most significant (and surprising) result in photoinduced birefringence obtained by our group. This was the existence of cooperative motions well below the polymer glass transition temperature. Cooperative motion is well-known and understood in ordered systems. When some of the groups (like azobenzenes) in such a system are subjected to motion (in this case photoinduced motion), the thermodynamic drive to form ordered phases coerces any other group to move in concert. Figure 6 illustrates two pairs of comonomers studied for cooperative motion. For the pair on the left, both comonomers contain rigid-rod structures of comparable polarity, one is an azobenzene and one is an ester. Copolymers with compositions varying between 0 and 100% azobenzene structural units were synthesized and their photoinduced motion ana-

Fig. 6. Two pairs of comonomers to demonstrate cooperative motion in amorphous high-*T*g copolymers.



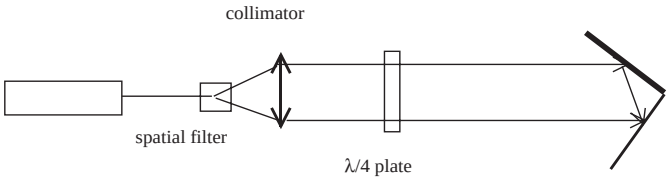
lyzed both by optical (19) and by spectroscopic (20) means. Both methods clearly indicate that the azobenzene group not only changes its own orientation when irradiated with polarized light, but it also moves the ester group in concert. The cooperative motion of the ester group is very powerful, it can be estimated that — of the overall photoinduced birefringence — almost 45% can be due to the ester group. What drives the ester group to move? These copolymers are not semicrystalline or liquid crystalline, thus it is difficult to imagine a steric factor being the determining one. Both the ester and azo groups are polar, and their relative orientation within the copolymer film insures electrical neutrality of the film. If some groups are moved (the azo groups are being moved by the polarized light), then the equilibrium dipolar distribution is altered, and the ester group may be moving to restore this equilibrium. To check this assumption, the pair of comonomers on the right in Fig. 6 was synthesized, and — again — a series of copolymers covering the whole possible range of compositions was prepared. These copolymer films were also subjected to the photoinduced birefringence procedure, and the results were indeed different. Even though there still was some cooperative motion of the nonpolar ester groups, this cooperative motion was minimal. We could then conclude that polarity is the main driving force behind cooperative motion in amorphous azo copolymers well below their *T*g. This conclusion also helped solve some long-standing disagreements in the literature (21).

Surface relief gratings

About 1993, in an effort to compare our azobenzene polymers with the new photorefractive polymers reported in the current literature, we started trying to produce volume holographic gratings, to measure their diffraction efficiency. By using a mirror set-up (Fig. 7) and thus an interference pattern, we expected to produce volume polarization gratings of alternating orientation domains in the polymer films. We expected to be able to measure diffraction efficiencies of about 1%, which was at that time the state-of-the-art level for photorefractive polymers. Much to our surprise, our very first experiment produced a grating with 20% diffraction efficiency. It took us some time to realize that the gratings — now visible with the naked eye — were due to a certain de-

© 2001 NRC Canada

Fig. 7. Set-up for gratings inscription.



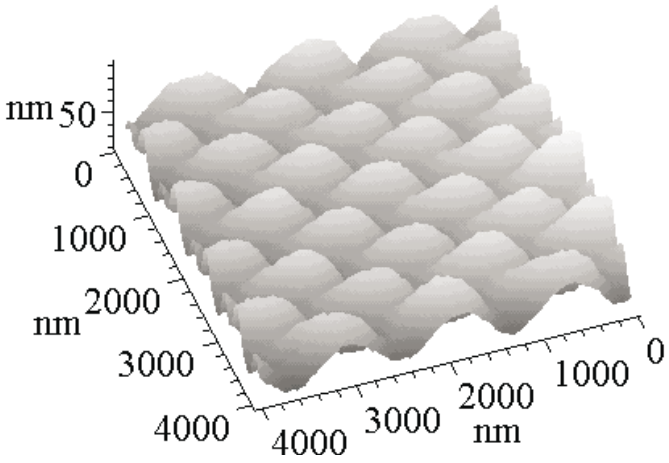
formation of the surface of the film. Also, these gratings were not optically erasable, but it was possible to write on top of them, while keeping the initial ones still there. Atomic force microscopy showed that the corrugation achieved only with light on polymer films of high *T*g was as deep as hundreds of nanometers, even to the micron level (12) (Fig. 8).

The explanation for these phenomena, also reported by groups in the U.S. and Denmark, is the second kind of motion mentioned in the *Photoinduced motions* part of this article. The actual mechanism for the unusual phenomenon is still under investigation; currently four possible mechanisms are proposed (22–26). There is a wide range of possible application of these gratings in photonic devices, some of them mentioned in one of our articles (18).

Photorefractivity

If one thinks in terms of photonic devices, photoinduced birefringence can produce reversible waveguides, while surface relief gratings can act as couplers of the light in and out of these photoinscribed waveguides. Thus, on a simple polymer film, one could inscribe a "photonic printed circuit" using light only. Another necessary function would be switching. If our polymers would also be photorefractive as can be verified by the two-beam coupling procedure (27), then switching can be done electronically. The requirements for photorefractivity in a polymer are: (*i*) the possibility to modulate the refractive index with an electric field; (*ii*) photoconduction; and (*iii*) the presence of charge traps. Our azo-based polymers already fulfill the first condition, since the azo groups we are using have nonlinear optical (NLO) properties based on their delocalized electronic structure. Such azo polymers were amongst the first to be used in NLO materials, mainly for second harmonic generation (28). The presence of charge traps is usually taken for granted in any polymer material, thus the only condition needed for our polymers to exhibit photorefractive properties is photoconduction. This is relatively easy to accomplish if one replaces the amine end of the azobenzene chromophore with a carbazole or a tetramethyldiaminobiphenyl (TPD) moiety, which are very well-known photoconductive groups. Figure 9 shows the structure of a few polymers designed to fulfill all the required properties for photorefractivity. These polymers are either side-chain methacrylates (29, 30), or very stable polyimides with carbazole within the main chain (31), or TPD-based polyesters.[2] None of these polymers have optimal photorefractive properties. Nevertheless, they are the first polymers mentioned in the literature to contain all the required structural attributes for photorefractivity within a single structural unit *and* show the possibility to combine three photonic "functions" (waveguiding, coupling, and switching).

Fig. 8. AFM pictures of two superimposed gratings successively inscribed on the same piece of film.



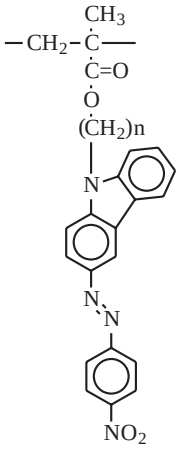
Photoinduced liquid crystalline phases

Studies of the surface relief gratings are very active worldwide, on the one hand because of the still intriguing mechanism of formation and control, on the other hand because of the wide area of possible applications. In collaboration with Professor Pietsch's group (Potsdam, Germany), we obtained some other unexpected results. Professor Pietsch was using SAXS to monitor the disappearance of the surface relief gratings while subjecting the polymer sample to various temperature programs. Amazingly, it was found that when light is used in situ together with heating, and after the surface grating starts disappearing (as confirmed by atomic force microscopy), a volume density grating is being formed below the surface where the relief grating was present. The density grating has a similar diffraction efficiency, but it is not "visible" by surface analysis. This means that below the surface of the polymer film, a dense phase is formed and alternates with a less dense phase. The periodicity of the buried structure is identical to the initial periodicity of the surface deformation induced by light. Interestingly, such a density grating can be obtained in a polymer film of pDR1M (see Fig. 2), but it does not form in a film of a very similar polymer, without the donor–acceptor substitution at the azobenzene ring. The explanation suggested for this phenomenon (32) is the formation of a liquid crystalline phase (the dense phase) where the peaks of the surface gratings existed before heating. Figure 10 schematically illustrates the formation of the buried density grating. PDR1M is an amorphous polymer, and the presence of a photo- and thermally induced novel liquid crystalline phase has still to be demonstrated. If true, this would be the only instance (to our knowledge) of a photoinduced liquid crystalline phase in an otherwise amorphous polymer. Photoinduced isotropization, at temperatures just below clearing, is very well-known and studied. Photoinduced ordering, to the order level of a liquid crystal, was only known in materials that do have a crystalline or liquid crystalline phase and need the light energy to provide thermodynamic ordering.

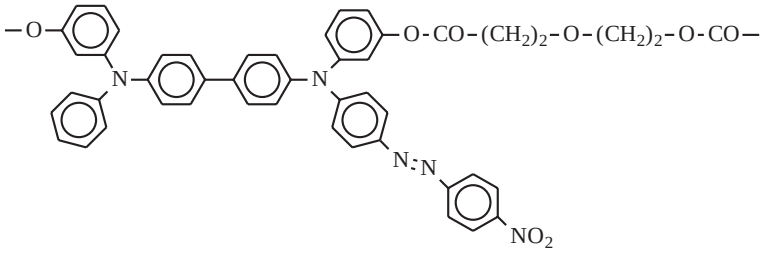
[2] G. Iftime, F. Lagugné Labarthet, A. Nathansohn, P. Rochon, and K. Murti. Submitted.

© 2001 NRC Canada

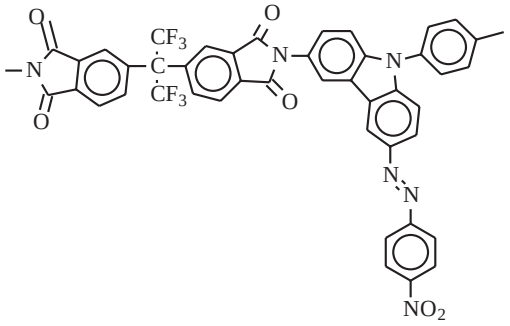
Fig. 9. A few photorefractive polymers.



pnCARBA

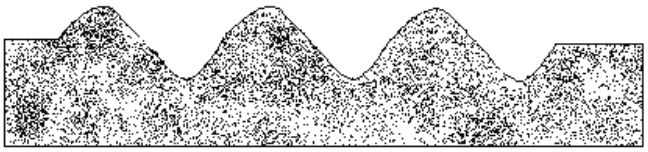


Azo-TPD-PC



pI

Fig. 10. Schematics of formation of the buried lateral grating in a pDR1M film. The top shows the gratings before being heated, the bottom is the same film, after heating and illumination, with the grating now buried inside the film.



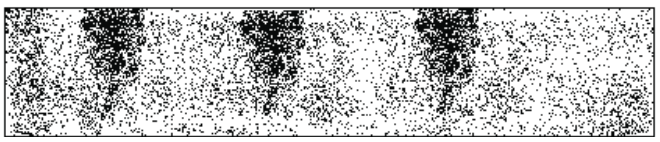
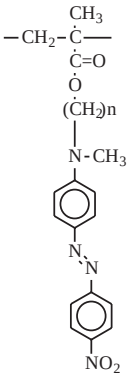


Fig. 11. A series of liquid crystalline azo polymers.



pnMAN

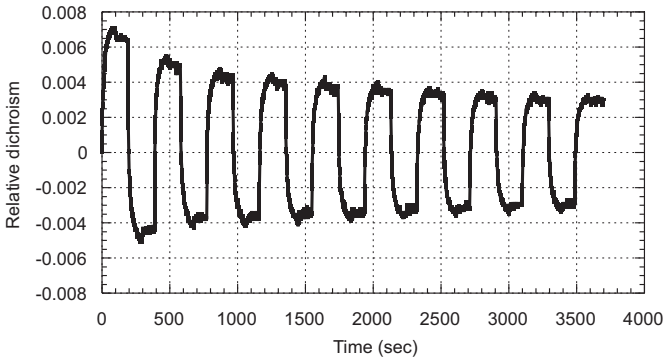
Thermo- and photochromism

This brings us back full circle, into studying liquid crystalline polymers, after having dedicated most of our time to high-*T*g amorphous materials. Photoinduced orientation in liquid crystalline polymers was reported — as we already mentioned — in 1987 (4). Since these materials have an intrinsic tendency to order, the levels of photoinduced birefringence can be much higher than in amorphous polymers (33). Of course, the obvious disadvantage of such materials is that erasing the photoinduced birefringence is not simple, for exactly the same reason it is so easy to obtain high degrees of order. Surface gratings formation in liquid crystalline azo polymers has also been studied (34).

We decided to study, systematically, a series of liquid crystalline polymers consisting of our most investigated mesogen (amino-nitro-substituted azobenzene), a methacrylate backbone and a spacer of variable length (different number of methylene units). The general formula of the series is given in Fig. 11. A subtle difference between p2MAN and pDR1M, for example, is the substituent at the nitrogen atom of the chromophore. While our "workhorse" had an ethyl group, because it was prepared from the dye Disperse Red 1, the liquid crystalline polymer equivalent

© 2001 NRC Canada

Fig. 12. Circular dichroism switching in p4MAN by irradiation with right circularly polarized light and then with left circularly polarized light.



(and the other members of this series) has a methyl. The difference allows better packing of the chromophores, and they become mesogens. P2MAN is liquid crystalline, while pDR1M has no known thermotropic phase. All pnMAN polymers exibit a glassy state, followed by a smectic range. The transition temperatures (glassy–smectic and smectic–isotropic) depend on the spacer length.

As usual, and as we have already became accustomed to, there were plenty of surprises to uncover when we investigated photoinduced motions in this series. First, these polymers show thermochromic and photochromic behavior (35). Both depend on the spacer length, with the polymers being divided into two major types. The first, with the spacer length roughly up to nine methylene groups, forms amorphous reddish films upon spin coating. The color changes *irreversibly* to orange after heating the films above their *T*g. In the smectic phase, however, the film become cloudy and the color is again more red than orange. The second type, polymers with spacers longer than nine methylene groups, form orange films upon spin coating, and their color changes *reversibly* to red upon heating. In both cases, the orange color is more stable, and it has been assigned to an antiparallel pairing of the donor–acceptor substituted azo chromophores. The color change is — of course — accompanied by an absorbance shift in the electronic spectra.

When an orange film of a shorter spacer polymer film is irradiated with linearly polarized light, the color changes again to red. This change is irreversible if the sample is kept in the dark. The explanation for this photochromic effect is as follows. In an orange film, the chromophores are mostly paired in an antiparallel fashion. Linearly polarized light induced isomerization and reorientation of the azobenzene group, thus breaking the pairs. Isolated chromophores, which are a result of illumination, absorb preferentially at higher wavelengths, thus the film color changes from orange to red. The change is very specific and the contrast is good enough to allow the use of masks for "writing" on the polymer films.

The main question that still needs to be answered is how general is the thermo- and photochromism phenomenon. Obviously, this requires a spacer that is long enough to allow independent motion of the mesogen–chromophore and produce the antiparallel pairing. Does this mean that only polymers having a liquid crystalline phase undergo this pairing? We still don't have the answer to this question, but research is in progress.

Photoinduced chirality and switching

The other major surprise offered by the pnMAN series was its behavior when illuminated with circularly polarized light in the smectic phase. This is the third type of motion mentioned in the *Photoinduced motions* part of this article. A polymer film in its smectic phase consists of a multitude of smectic domains of various sizes and arrangements. Since the films were obtained by spin coating, it is reasonable to assume that most of the azobenzene mesogens are in the film plane, because of the centrifugal force of film formation. Thus, the smectic layers should be perpendicular to the film surface and each domain should have a slightly different orientation of these layers. The incoming circularly polarized light will be affected by the first smectic layer on the film surface, which will change its polarization to slightly elliptic. The now slightly elliptic light penetrating through to the second smectic domain will now change the overall orientation of this domain towards becoming perpendicular to the long axis of the ellipse. This, in turn will make the light more elliptical and the next domain will be affected even more than the second, and so on. Thus, circularly polarized light illuminated on the smectic film will move the successive domains on the vertical axis more and more in the direction of the handedness of the light. In other words, right circularly polarized light will photoinduce a right-handed helical organization of the smectic domains as the light penetrates the film. From a polymer with no chiral center in its structure, one can obtain a helical supramolecular arrangement just by illumination (15). This is clearly seen in the circular dichroism spectrum of the material after illumination. Prior to illumination the material shows no circular dichroism.

The fact that chirality can be induced in achiral azo smectic polymer films had been previously reported (14, 36–38). Only recently, the relation between the handedness of the circularly polarized light and the handedness of the photoinduced supramolecular helix has been clarified (15, 37). These findings raise many more questions than they answer. Some obvious ones are: Is the smectic phase a requirement for this phenomenon? Does the polarity of the mesogen play any role? What is the nature of the photoinduced helix? Needless to say, research is in progress in our group and in other groups worldwide.

The most interesting aspect of this phenomenon, though, is the fact that circularly polarized light of the opposite handedness can unwind the photoinduced supramolecular helix, to again produce an achiral material. This means that addressing these materials with circularly polarized light of opposite handedness actually operates like an optical switch, as illustrated in Fig. 12. There is a slight decrease of the circular dichroism value after a few cycles; this is due to the tendency of the circularly polarized light to align the chromophores perpendicular to its polarization, i.e., in the direction of propagation of light. When the chromophores are perpendicular to the film surface, they do not contribute to the circular dichroism spectrum. The initial value for dichroism can be recovered after heating the film above its isotropization temperature, thus the dichroism decrease is not a photobleaching effect.

© 2001 NRC Canada

Possible photonic applications

There are many possible photonic applications of the phenomena reported here. Reversible optical storage, either digital or holographic, is the most obvious one. This application is very attractive, since the writing procedure is relatively fast and extremely easy, the long term stability is excellent, and erasing is again a very simple and efficient procedure. Digital storage can be performed point by point, which allows flexibility for the process, while holographic storage can be envisaged on a three-dimensional scale, because of the possibility to store more than one image on the same polymer film by rotating the film upon exposure.

Even more attractive is the possibility to build a whole photonic device on a simple polymer film. The first type of photoinduced motion allows writing lines, as well as points, and these lines can act as waveguides, confining an optical signal within them. Surface gratings can act as couplers of light in and out of these waveguides, and photorefractivity allows switching of the light signals between two different paths optically written on the polymer film.

Apart from these two major possibilities, photonic filters, polarization separators, shape recognition, liquid crystal orientation and switching, and many, many other possible photonic applications exist. Some of them were reviewed in ref. 18.

Conclusions

The recent discoveries in azobenzene photoisomerization and the motions that it induces in a variety of polymer materials are extremely exciting, both from a fundamental understanding of materials and from a practical point of view, as there is a huge potential for photonic applications. This area of research is only about 15-years-old, and the most interesting discoveries are probably still awaiting us.

Acknowledgments

A. N., Canada Research Chair in Polymer Chemistry, thanks the CRC Program of the Government of Canada. We acknowledge funding for this research by the Natural Sciences and Engineering Research Council of Canada (NSERC), Department of Defence, Canada, and the Office of Naval Research, U.S.A. This research was performed by a series of very talented and industrious young scientists, working as students and postdoctoral associates. We are extremely grateful for their collaboration.

References

1. H. Rau. *In* Photochemistry and photophysics. Vol. II. *Edited by* J.K. Rabek. CRC Press, Inc, Boca Raton, Florida. 1990. p. 119.
2. G.S. Kumar and D.C. Neckers. Chem. Rev. **89**, 1915 (1989).
3. T. Todorov, L. Nikolova, and N. Tomova. Appl. Opt. **23**, 4309 (1984).
4. M. Eich, J. Wendorff, B. Reck, and H. Ringsdorf. Makromol. Chem. **8**, 59 (1987).
5. K. Ichimura, Y. Suzuki, T. Seki, A. Hosoki, and K. Aoki. Langmuir, **4**, 1214 (1988).
6. S. Xie, A. Natansohn, and P. Rochon. Chem. Mater. **5**, 403 (1993).
7. N.K. Viswanathan, D.Y. Kim, S. Bian, J. Williams, W. Liu, L. Li, L. Samuelson, J. Kumar, and S. Tripathy. J. Mater. Chem. **9**, 1941 (1999).
8. K. Ichimura. Chem. Rev. **100**, 1847 (2000).
9. J.A. Delaire and K. Nakatani. Chem. Rev. **100**, 1817 (2000).
10. P. Rochon, J. Gosselin, A. Natansohn, and S. Xie. Appl. Phys. Lett. **60**, 4 (1992).
11. A. Natansohn, P. Rochon, J. Gosselin, and S. Xie. Macromolecules, **25**, 2268 (1992).
12. P. Rochon, E. Batalla, and A. Natansohn. Appl. Phys. Lett. **66**, 136 (1995).
13. D.Y. Kim, S.K. Tripathy, L. Li, and J. Kumar. Appl. Phys. Lett. **66**, 1166 (1995).
14. L. Nikolova, T. Todorov, M. Ivanov, F. Andruzzi, S. Hvilsted, and P.S. Ramanujam. Opt. Mater. (Amsterdam), **8**, 255 (1997).
15. G. Iftime, F. Lagugné Labarthet, A. Natansohn, and P. Rochon. J. Am. Chem. Soc. **122**, 12 646 (2000).
16. A. Natansohn and P. Rochon. *In* Progress in Pacific polymer science. Vol. 3. *Edited by* K.P. Ghiggino. Springer–Verlag, Berlin, Heidelberg. 1994. p. 295.
17. A. Natansohn and P. Rochon. *In* ACS Symposium Series: Photonic and optoelectronic polymers. Vol. 672. *Edited by* K.J. Wynne and S.A. Jenekhe. American Chemical Society, Washington, D.C. 1997. p. 236.
18. A. Natansohn and P. Rochon. Adv. Mater. (Weinheim, Ger.), **11**, 1387 (1999).
19. X. Meng, A. Natansohn, C. Barrett, and P. Rochon. Macromolecules, **29**, 946 (1996).
20. T. Buffeteau, A. Natansohn, P. Rochon, and M. Pézolet. Macromolecules, **29**, 8783 (1996).
21. A. Natansohn, P. Rochon, X. Meng, C. Barrett, T. Buffeteau, S. Bonenfant, and M. Pézolet. Macromolecules, **31**, 1155 (1998).
22. C.J. Barrett, A.L. Natansohn, and P.L. Rochon. J. Phys. Chem. **100**, 8836 (1996).
23. C.J. Barrett, P.L. Rochon, and A.L. Natansohn. J. Chem. Phys. **109**, 1505 (1998).
24. T.G. Pedersen and P.M. Johansen. Phys. Rev. Lett. **79**, 2470 (1997).
25. P. Lefin, C. Fiorini and J.M. Nunzi. Pure Appl. Opt. **7**, 71 (1998).
26. J. Kumar, L. Li, X. L. Jiang, D.Y. Kim, T.S. Lee, and S. Tripathy. Appl. Phys. Lett. **72**, 2096 (1998).
27. W.E. Moerner and S.M. Silence. Chem. Rev. **94**, 127 (1994).
28. D.M. Burland, R.D. Miller, and C.A. Walsh. Chem. Rev. **94**, 31 (1994).
29. M.S. Ho, C. Barrett, J. Paterson, M. Esteghamatian, A. Natansohn, and P. Rochon. Macromolecules, **29**, 4613 (1996).
30. C. Barrett, B. Choudhury, A. Natansohn, and P. Rochon. Macromolecules, **31**, 4845 (1998).
31. J.P. Chen, F. Lagugné Labarthet, A. Natansohn, and P. Rochon. Macromolecules, **32**, 8572 (1999).
32. U. Pietsch, P. Rochon, and A. Natansohn. Adv. Mater. **12**, 1129 (2000).
33. S.J. Zilker, T. Bieringer, D. Haarer, R.S. Stein, J.W. v. Egmond, and S.G. Kostromine. Adv. Mater. **10**, 855 (1998).
34. P.S. Ramanujam, M. Pedersen, and S. Hvilsted. Appl. Phys. Lett. **74,** 3227 (1999).
35. F. Lagugné Labarthet, S. Freiberg, C. Pellerin, M. Pézolet, A. Natansohn, and P. Rochon. Macromolecules, **33**, 6815 (2000).
36. I. Naydenova, L. Nikolova, P.S. Ramanujam, and S. Hvilsted. J. Opt. A: Pure Appl. Opt. **1**, 438 (1999).
37. M. Ivanov, I. Naydenova, T. Todorov, L. Nikolova, T. Petrova, N. Tomova, and V. Dragostinova. J. Mod. Opt. **47,** 861 (2000).
38. L. Nikolova, L. Nedelchev, T. Todorov, T. Petrova, N. Tomova, V. Dragostinova, P.S. Ramanujam, and S. Hvilsted. Appl. Phys. Lett. **77**, 657 (2000).

© 2001 NRC Canada

A fluorescent host–guest complex of cucurbituril in solution: a molecular Jack O'Lantern

Brian D. Wagner, Shannon J. Fitzpatrick, Monica A. Gill, Andrew I. MacRae, and Natasa Stojanovic

Abstract: Fluorescence enhancement of a probe molecule in solution by the container molecule cucurbituril (CB) is reported for the first time. The fluorescence of the probe 2-anilinonaphthalene-6-sulfonate (2,6-ANS) in aqueous Na_2SO_4 solution is found to increase by a maximum factor of 5.0 upon addition of cucurbituril. This fluorescence enhancement is the result of the formation of a host–guest inclusion complex, in which the guest 2,6-ANS is incorporated inside the cavity of the host, cucurbituril. Measurement of the enhancement as a function of cucurbituril concentration yielded a value of the equilibrium constant (K) of 52 ± 10 M^{-1}. It is proposed that the mode of inclusion involves the phenyl group of the 2,6-ANS, because of the relatively small size of the cucurbituril cavity. It is further proposed that the observed enhancement is a result of loss of rotational mobility of the phenyl ring relative to the naphthyl fluorophore of 2,6-ANS upon inclusion of the phenyl ring. Since the name cucurbituril is derived from the Latin word for "pumpkin," this fluorescent host–guest complex is referred to as a "molecular Jack O'Lantern," with the 2,6-ANS serving as the candle.

Key words: host–guest chemistry, fluorescence, cucurbituril, inclusion compounds.

Résumé : On a provoqué pour la première fois une augmentation de la fluorescence d'une molécule sonde, en solution, à l'aide la molécule de cucurbiturile. On a trouvé que, en solution aqueuse de Na_2SO_4, l'addition de cucurbiturile provoque une augmentation (facteur maximal de 5,0) de la fluorescence de la sonde 2,6-ANS. L'augmentation de la fluorescence résulte de la formation d'un complexe d'inclusion hôte/invité dans lequel le 2,6-ANS invité est incorporé dans la cavité du cucurbiturile qui agit comme hôte. Des mesures de l'augmentation en fonction de la concentration de cucurbiturile ont permis de déterminer que la valeur de la constante d'équilibre, K, est de 52 ± 10 M^{-1}. Il est suggéré que, en raison de la taille relativement faible de la cavité du cucurbiturile, le mode d'inclusion implique le groupe phényle du 2,6-ANS. On suggère de plus que l'augmentation observée résulte d'une perte de mobilité rotationnelle du noyau phényle par rapport au fluorophore naphtyle du 2,6-ANS lors de l'inclusion du noyau phényle. Puisque le nom cucurbiturile est dérivé du mot latin pour "citrouille," on réfère à ce complexe fluorescent hôte/invité comme à une "lanterne moléculaire" dans laquelle le 2,6-ANS sert de chandelle.

Mots clés : chimie hôte/invité, fluorescence, cucurbiturile, composés d'inclusion.

[Traduit par la Rédaction]

Introduction

In this paper we report the first observation of fluorescence enhancement of a guest molecule in solution by the host molecule cucurbituril (CB). Cucurbituril (1–3) is an interesting cage compound consisting of a C,N σ-framework, as shown in Fig. 1. It was first prepared by Behrend et al. (4) in 1905, but was not characterized until the work of Mock and co-workers (5) in 1981. The most interesting feature of this molecule is that it contains a rigid and well-defined internal cavity, which has a diameter of ca. 5.5 Å with two opposing portals of diameter ca. 4.0 Å lined with carbonyl groups. The presence of this internal cavity makes cucurbituril a potential host molecule for the encapsulation of smaller guest molecules. This potential for forming supramolecular host–guest inclusion complexes is the reason for the growing interest in the properties and applications of this molecule. Specific host–guest inclusion complexes of other container molecules (6), such as cyclodextrins (7) and calixarenes (8), have found various useful applications, including improved trace analysis techniques and molecular recognition. Those of cucurbituril also have the potential for practical applications; this potential is as yet completely unexplored.

The host abilities of cucurbituril have now been well-demonstrated. Cucurbituril has been shown to form host–guest inclusion complexes with a wide range of guest molecules, including alkylammonium ions (9), alkali metal cations (10), amino acids and alcohols (11), tetrahydrofuran (12), and aromatic molecules such as organic dyes (13) and toluene (14). It has also shown to be proficient at forming rotaxanes, threading onto various types of molecules containing alkyl chains (15).

All of these previous studies on the host–guest inclusion complexes of cucurbituril have been performed using NMR (9, 12), UV–vis spectroscopy (10, 13), or calorimetry (11, 14). However, there have been no reports of fluorescence

Received February 5, 2001. Published on the NRC Research Press Web site at http://canjchem.nrc.ca on July 27, 2001.

B.D. Wagner,[1] S.J. Fitzpatrick, M.A. Gill, A.I. MacRae, and N. Stojanovic. Department of Chemistry, University of Prince Edward Island, Charlottetown, PE C1A 4P3, Canada.

[1]Corresponding author (telephone: (902) 628-4351; fax: (902) 566-0632; e-mail: bwagner@upei.ca).

 DOI: 10.1139/cjc-79-7-1101 © 2001 NRC Canada

Fig. 1. Structures of (*a*) cucurbituril and (*b*) 2,6-ANS.

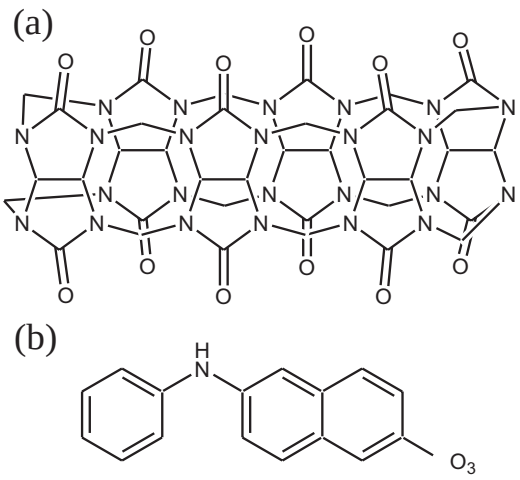
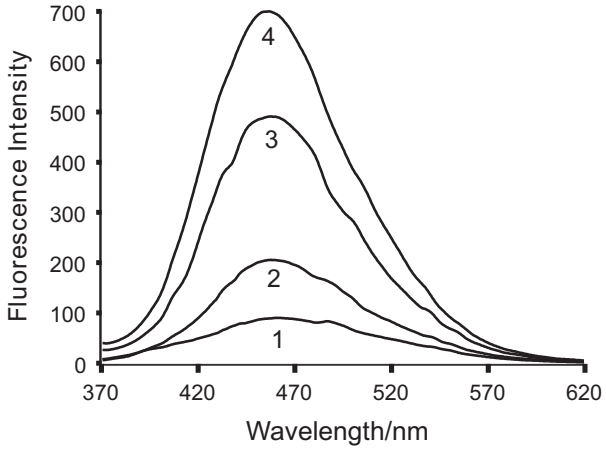


Fig. 2. The fluorescence spectrum of 2,6-ANS (2.0×10^{-5} M) in Na_2SO_4 solution (0.20 M) in the presence of: (*a*) 0 mM; (*b*) 4 mM; (*c*) 20 mM; and (*d*) 48 mM cucurbituril.



studies of the host–guest inclusion complexes of cucurbituril in solution. In fact, none of the guests previously shown to be encapsulated by cucurbituril have been shown to undergo fluorescence enhancement when incorporated into the cucurbituril cavity. This is in marked contrast to the inclusion complexes of cyclodextrins for example that have been extensively investigated by fluorescence spectroscopy (16). This technique has proven to be an extremely sensitive and informative method for studying such host–guest inclusion phenomena. Furthermore, enhancement of guest fluorescence leads to the potential application of cucurbituril as a molecular sensor for specific guests, since the observation of increased fluorescence provides a simple and sensitive means for detecting the presence of the guest. In the work described in this paper, we report the results for a fluorescent probe, which is not only encapsulated by cucurbituril, but also exhibits significant enhancement of its fluorescence upon encapsulation.

In a previous attempt to observe fluorescence enhancement by cucurbituril in solution using the highly polarity-sensitive fluorescent probe 1-anilinonaphthalene-8-sulfonate (1,8-ANS), a fluorescent precipitate was obtained (17). This interesting solid, also reported by Buschmann and Wolff (18), proved to be a lattice-inclusion compound, rather than the expected host–guest inclusion compound (17). In the present work, the fluorescence enhancement in solution of the related probe 2-anilinonaphthalene-6-sulfonate (2,6-ANS, shown in Fig. 1) is described. This probe was chosen for two reasons. First, its fluorescence is also extremely sensitive to the polarity of its local environment (19, 20), and thus, should show changes to its fluorescence upon inclusion within cucurbituril. Second, it has a more streamlined shape than 1,8-ANS, with less steric crowding between the two groups on the naphthalene; this should allow it to be included more easily into the relatively small cavity of cucurbituril.

Experimental

Materials

The synthesis and characterization of the cucurbituril (CB) used has been previously described (17). The sample used was found to contain 30.0% H_2O (by drying for 4 h in a vacuum oven at 140°C and 10 torr (1 torr = 133.322 kPa)) and 2.0% H_2SO_4 (by NaOH titration) by mass; these values were taken into account in the preparation of cucurbituril solutions of specific concentrations. Na_2SO_4, K_2SO_4, Na_2HPO_4, and NaH_2PO_4 were obtained from Fisher Scientific and used as received. High purity 2,6-ANS was obtained from Molecular Probes and used as received.

Spectroscopic measurements

All absorption and fluorescence measurements were performed on solutions in 1 cm^2 quartz cuvettes. Absorption spectra were measured on a Cary 50 Bio UV–vis spectrophotometer. Fluorescence spectra were measured on a Photon Technologies International LS-100 luminescence spectrometer.

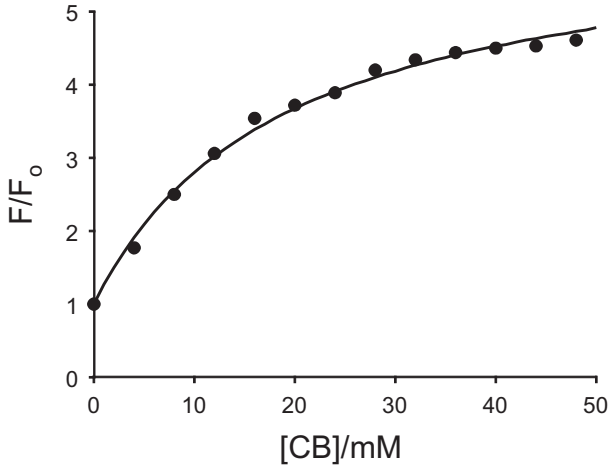
Solutions were made in 0.20 M aqueous Na_2SO_4 (necessary for significant CB solubility), with [2,6-ANS] = 2.0×10^{-5} M. At the excitation wavelength used (330 nm), there was a small absorption by the host cucurbituril, increasing the absorbance from 0.32 in the absence of CB to 0.41 at the highest [CB]. Blank solutions containing CB only were found to exhibit emission (although at much lower levels than the solutions also containing 2,6-ANS, ranging from 10 to 26%). For this reason, the fluorescence of these blank solutions was measured at the same [CB] as for the 2,6-ANS solutions, and the measured integrated fluorescence subtracted from that of the solutions containing guest. The fluorescence enhancement (F/F_o) was determined quantitatively by taking the ratio of integrated area under the fluorescence spectrum in the presence (F, corrected for CB emission as described above) and absence (F_o) of cucurbituril.

Results and discussion

When cucurbituril (CB) was added to a solution of 2,6-ANS, the fluorescence of the solution was found to increase significantly, i.e., fluorescence enhancement was observed, as shown in Fig. 2 (it should be noted that the spectra in Fig. 2 have not been corrected for the emission of the CB reference solutions). Figure 3 shows a plot of the fluores-

© 2001 NRC Canada

Fig. 3. Observed fluorescence enhancement (F/F_0) of 2,6-ANS (2.0×10^{-5} M) in Na_2SO_4 solution (0.20 M) as a function of cucurbituril concentration.



cence enhancement F/F_0 (corrected for CB emission) as a function of [CB]. This plot clearly shows that the enhancement increases sharply with [CB] at lower concentrations, then levels off at an enhancement of ca. 5.0. This behavior is indicative of the formation of a 1:1 host–guest complex, ANS + CB $\rightleftharpoons$ ANS:CB, for which (21):

$$[1] \qquad F/F_0 = 1 + (F_\infty/F_0 - 1)\frac{[\mathrm{CB}]_0 K}{(1 + [\mathrm{CB}]_0 K)}$$

where F_∞/F_0 is the enhancement when every guest molecule is complexed, and K is the association constant (K = [ANS:CB]/[ANS][CB]). This can be tested by plotting a reciprocal-reciprocal plot of F_0/F vs. 1/[CB]; this plot will be nonlinear if higher-order complexes are formed. In this case, the plot was linear (R = 0.997) confirming simple 1:1 host–guest complexation. Nonlinear least-squares fitting of the data to eq. [1] gave a value of $K = 52 \pm 10$ M^{-1} and $F_\infty/F_0 = 6.1 \pm 0.7$; this fit is shown as the solid line in Fig. 3.

Other salt solutions were also used, and gave similar results for the enhancement and K. In 0.20 M K_2SO_4, $K = 44 \pm 11$ M^{-1} and $F_\infty/F_0 = 6.0 \pm 0.6$. This result is of interest, since it has been proposed that cucurbituril is soluble in aqueous salt solutions as a result of coordination of the cation to the carbonyls along the upper and lower rims of the molecule (12). The lack of a significant effect of changing the counterion from Na^+ to K^+ suggests that the coordinated cation does not interfere with the interaction between the host cucurbituril and the 2,6-ANS guest. In a Na_2HPO_4–NaH_2PO_4 buffer solution (pH = 6.80), $K = 36 \pm 12$ M^{-1} and $F_\infty/F_0 = 6.7 \pm 1.0$. These similar values (within experimental error) in the buffered vs. unbuffered Na salt solutions is also significant, as it indicates that acid content is unimportant in the formation of this inclusion complex. This observation is important because there is a small amount (2%) of sulfuric acid contained in our CB sample as a result of the synthesis procedure.

It is interesting to compare these results to those reported for 2,6-ANS in α-cyclodextrin (α-CD) and its hydroxypropylated derivative (HP-α-CD) (22), which has a slightly larger cavity size (5.7 vs. 5.0 Å), but with a much larger opening (5.7 vs. 4.0 Å). The fit values of F_∞/F_0 were reported to be 22 in α-CD and 58 in HP-α-CD, compared with the value of 6.1 in CB. Thus, the CD's provide significantly higher enhancement for 2,6-ANS than does CB. The values of K were reported to be ≤20 M^{-1} in α-CD and 110 M^{-1} in HP-α-CD, compared with the value of 52 M^{-1} in CB. Thus, 2,6-ANS forms a stronger complex with CB than with α-CD, but weaker than that with HP-α-CD.

These results can also be compared with values of K for similar CB inclusion complexes obtained by other techniques. In particular, inclusion complexes of a number of aromatic dyes, with shapes and sizes similar to 2,6-ANS, have been previously studied. In the case of phenol blue, a value of K = 93 M^{-1} was determined in aqueous HCl solution by measuring dye stabilization by the host (23). This value was much larger than that found for β-CD. In the case of methyl orange, a value of K = 58 M^{-1} was obtained in water:formic acid solution by UV–vis spectroscopy (13), with a slightly higher value of K = 69 M^{-1} found for β-CD. These values of the association constant are very similar to that of 52 M^{-1} obtained by fluorescence in this work.

From a consideration of the size of the cucurbituril cavity and opening, and the size and shape (substitution at each end of the naphthalene ring) of 2,6-ANS, it seems most likely that it is the anilino group that is becoming included within the CB cavity, rather than the naphthalene fluorophore itself. This proposal is supported by three pieces of experimental evidence: (*i*) the values of K for this complex and for those with the organic dyes described above, which only contain phenyl groups, are very similar. (*ii*) Although significant enhancement of the 2,6-ANS fluorescence is observed, there is only a very small accompanying blue shift in the spectrum (≤3 nm). This value would be expected to be much larger if the naphthalene fluorophore was experiencing a less polar environment due to inclusion into the CB cavity, for example, a significant blue shift is clearly seen in both 1,8-ANS (15–55 nm) (24) and 2,6-ANS (28–40 nm) (22) in various cyclodextrins. (*iii*) Although the enhancement observed is significant, it is much lower than that observed in the cyclodextrins, as described above, in which inclusion is more likely to involve the naphthalene moiety rather than the phenyl group. We propose that in the CB inclusion complex, the enhancement is not a result of decreased polarity from inclusion of the naphthalene ring, but instead a result of decreased rotational freedom of the included phenyl ring. It has been established that in aqueous solution, charge transfer followed by energy transfer is the major nonradiative decay pathway for 2,6-ANS (19, 20). However, for this to occur, there is a required twisting of the phenyl ring relative to the naphthalene ring in the S_1 state. If the phenyl group is included in the massive CB cage, this ability to twist would be greatly reduced, resulting in moderately enhanced fluorescence but no spectral shift.

Although this fluorescence data does not provide direct evidence that a true host–guest inclusion complex has formed, the significant enhancement observed, as well as its dependence on cucurbituril concentration, does provide compelling indirect evidence that such an inclusion complex is indeed formed, since interfacial interactions would not be expected to be particularly strong between these two molecules. If a linear analog of CB could be obtained, then it

© 2001 NRC Canada

could be determined conclusively whether the presence of the cavity is required to observe enhancement. It should be noted that glycoluril itself (the building block of cucurbituril) is insoluble in aqueous solution, and thus its effect on 2,6-ANS cannot be investigated. Direct evidence for inclusion, as well as the specific mode of inclusion, could of course be obtained from X-ray crystallography, if single crystals of the CB:2,6-ANS complex could be obtained. We are currently working on this approach to conclusively determine the structure of the CB:2,6-ANS complex.

This observed inclusion of 2,6-ANS in CB in solution, as indicated by the significant 2,6-ANS fluorescence enhancement, is in marked contrast to the previously reported interaction of 1,8-ANS with CB, in which a lattice inclusion solid compound formed, with no inclusion of the 1,8-ANS molecule inside the CB cavity (17). This difference must be attributable to the steric interactions between the nearby sulfonate and phenyl groups in 1,8-ANS. These steric interactions are absent in 2,6-ANS, since the two groups are at opposite ends of the naphthalene ring and point in opposing directions. This significant difference in the guest structure allows for the inclusion of the phenyl group in the case of 2,6-ANS in CB, but prevents its inclusion in the case of 1,8-ANS. The reasons why a lattice inclusion precipitate is formed in the latter case were discussed previously (17).

Since the name cucurbituril is derived from the Latin for pumpkin, we describe this unique fluorescent inclusion complex as a *molecular Jack O'Lantern*, with the fluorescent 2,6-ANS serving as the candle inside the hollow pumpkin of cucurbituril. In our proposed structure, the "candle" is partly hanging outside of the "pumpkin." In future work, we hope to find a fluorescent guest that not only is small enough to fit completely inside the CB cavity but also is sensitive enough to show enhanced fluorescence, and also absorbs at a wavelength well above the absorption band of cucurbituril. In this way, the candle will be completely inside the pumpkin, providing a better example of a molecular Jack O'Lantern. Finding such a probe is expected to be quite challenging, especially since small probes tend to absorb at short wavelengths.

Conclusions

Fluorescence enhancement of the probe 2,6-ANS by cucurbituril has been observed in solution. In comparison to α-CD, the cyclodextrin most similar in cavity size, cucurbituril was found to bind 2,6-ANS more strongly, but resulted in a significantly smaller fluorescence enhancement. This observed enhancement indicates that the formation of a host–guest inclusion complex of 2,6-ANS into the cavity of cucurbituril occurs in solution. This is in contrast to previously reported results for the related probe 1,8-ANS, which formed a lattice inclusion solid with cucurbituril. This work shows that not only is cucurbituril a good receptor for guest molecules, but also, like cyclodextrins, it can enhance guest fluorescence, and thus has the potential to be useful in fluorescent molecular sensor design.

Acknowledgments

Financial support for this work was provided by the Natural Sciences and Engineering Research Council of Canada (NSERC) and by the UPEI Senate Committee on Research.

References

1. W.L. Mock. Top. Curr. Chem. **175**, 1 (1995).
2. P. Cintas. J. Inclus. Phenom. Mol. **17**, 205 (1994).
3. W.L. Mock. *In* Comprehensive supramolecular chemistry. Vol. 2. *Edited by* F. Vögtle. Pergamon Press, Oxford, U.K. 1996. pp. 477.
4. R. Behrend, E. Meyer, and F. Rusche. Liebigs Ann. Chem. **339**, 1 (1905).
5. W.A. Freeman, W. L. Mock, and N.-Y. Shih. J. Am. Chem. Soc. **103**, 7367 (1981).
6. D.J. Cram and J.M. Cram. Container molecules and their guests. The Royal Society of Chemistry, Cambridge, U.K. 1997.
7. S. Li and W.C. Purdy. Chem. Rev. **92**, 1457 (1992).
8. D. Diamond and M.A. McKervey. Chem. Soc. Rev. **25**, 15 (1996).
9. W.L. Mock and N.-Y. Shih. J. Org. Chem. **48**, 3618 (1983).
10. R. Hoffman, W. Knoche, C. Fenn, and H.-J. Buschmann. J. Chem. Soc. Faraday Trans. **90**, 1507 (1994).
11. H.-J. Buschmann, K. Jansen, and E. Schollmeyer. Thermochim. Acta, **317**, 95 (1998).
12. Y.-M. Jeon, J. Kim, D. Whang, and K. Kim. J. Am. Chem. Soc. **118**, 9790 (1996).
13. H.-J. Buschmann and E. Schollmeyer. J. Inclus. Phenom. Mol. **29**, 167 (1997).
14. D.A. Dantz, C. Menschke, H.-J. Buschmann, and E. Schollmeyer. Supramol. Chem. **9**, 79 (1998).
15. D. Whang, K.-M. Park, J. Heo, P. Ashton, and K. Kim. J. Am. Chem. Soc. **120**, 4899 (1998).
16. P. Bortolus and S. Monti. *In* Advances in photochemistry. *Edited by* D.C. Neckers, D.H. Volman, and G. von Bünau. John Wiley & Sons. 1996. pp. 1.
17. B.D. Wagner and A.I. MacRae. J. Phys. Chem. B **103**, 10114 (1999).
18. H.-J. Buschmann and T. Wolff. J. Photochem Photobiol. A, **121**, 99 (1999).
19. E.M. Kosower, H. Dodiuk, K. Tanizawa, M. Ottolenghi, and N. Orbach. J. Am. Chem. Soc. **97**, 2167 (1975).
20. E.M. Kosower, H. Dodiuk, and H. Kanety. J. Am. Chem. Soc. **100**, 4179 (1978).
21. A. Muñoz de la Peña, F. Salinas, M.J. Gómez, M.I. Acedo, and M. Sánchez Peña. J. Inclus. Phenom. Mol. **15**, 131 (1993).
22. B. D. Wagner and S. J. Fitzpatrick. J. Incl. Phenom. Macro. **38**, 467 (2000).
23. H.-J. Buschmann and E. Schollmeyer. J. Incl. Phenom. Mol. **14**, 91 (1992).
24. B. D. Wagner and P. J. MacDonald. J. Photochem. Photobiol. A, **114**, 151 (1998).

© 2001 NRC Canada

A convenient and selective route to a *trans*-difunctionalized macrocyclic hexadentate N_4O_2 ligand

Hongyan Luo, Robin D. Rogers, and Martin W. Brechbiel

Abstract: The synthesis and characterization of a novel difunctionalized tetraaza macrocycle, 1,8-bis(2-hydroxybenzyl)-1,4,8,11-tetraazacyclotetradecane (abbreviated H_2bcyclamb), is described. The diprotic hexadentate ligand N_4O_2 was conveniently synthesized in two steps by the cyclic condensation reaction of 1,4,8,11-tetraazacyclotetradecane (abbreviated cyclam) and salicylaldehyde, followed by $NaBH_4$ reduction of the cyclic hexahydropyrimidine condensate. The difunctionalization was selective and is the first procedure of *trans*-difunctionalization of a tetraazamacrocycle, without generating mono-, tri-, or tetra-functionalized products, with only 1,8-difunctionalized product being isolated, and with the convenience of the functionalization occurring as a result of deprotection. The *trans*-arrangement of the two functional groups in H_2bcyclamb was verified by X-ray crystallographic studies of the copper(II) complex $[Cu(H_2bcyclamb)](OAc)_2\cdot 2H_2O$. The crystal is monoclinic, $P2_1/c$, with a = 10.0931(2), b = 13.8820(1), c = 10.8752(1) Å, β = 106.332(1)°, V = 1462.26(3) Å^3. The structure of $[Cu(H_2bcyclamb)](OAc)_2\cdot 2H_2O$ also shows the metal ion in an elongated octahedral geometry.

Key words: 1,8-difunctionalized, cyclam, copper(II) complex.

Résumé : On décrit la synthèse et la caractérisation d'un nouveau tétraazamacrocycle bifonctionnel, le 1,8-bis(2-hydroxybenzyl)-1,4,8,11-tétraazacyclotétradécane (abrév.: H_2bcyclamb). On a facilement synthétisé, en deux étapes, le ligand diprotique hexadentate N_4O_2 par le biais d'une réaction de condensation cyclique du 1,4,8,11-tétraazacyclotétradécane (abrév.: cyclam) et du salicylaldéhyde, suivie d'une réduction par le $NaBH_4$ de l'hexahydropyrimidine cyclique provenant de la condensation. La bifonctionnalisation s'est faite de façon sélective et il s'agit de la première réaction de bifonctionnalisation *trans* d'un tétraazamacrocycle, sans génération de produits mono-, tri- et tétrafonctionnalisés; seul le produit résultant de la 1,8-bifonctionnalisation est isolé grâce au fait que la fonctionnalisation se produit à la suite d'une déprotection. L'arrangement *trans* des deux groupes fonctionnels du H_2bcyclamb a été confirmé par des études de diffraction des rayons X du complexe de cuivre(II), $[Cu(H_2bcyclamb)](OAc)_2\cdot 2H_2O$. Les cristaux sont monocliniques, groupe d'espace $P2_1/c$, avec a = 10,0931(2), b = 13,8820(1) et c = 10,8752(1) Å, β = 106,332(1)° et V = 1462,26(3) Å^3. La structure cristalline du $[Cu(H_2bcyclamb)](OAc)_2\cdot 2H_2O$ montre aussi que l'ion métallique se trouve dans une géométrie octaédrique allongée.

Mots clés : 1,8-bifonctionnalisé, cyclame, complexe de cuivre(II).

[Traduit par la Rédaction]

Introduction

Tetraaza macrocycles are widely used as building frameworks for chelates that retain the advantage of the macrocyclic effect inherited from the tetraaza parents (1–3). One of the current efforts involves introducing pendant donating sites to two of the nitrogen atoms on the framework. The goal of this effort has been to expand the coordination sphere from the square-plane provided by the parent tetraazamacrocycle to an octahedral environment, so as to meet the geometric preference of metal centers with six-coordinate tendencies. The coordination chemistry of difunctionalized tetraaza chelates has been summarized recently (4). We have been interested in developing *trans-N,N″*-difunctionalized tetraaza macrocyclic chelates with two 2-hydroxybenzyl groups that provide an N_4O_2 donor-set as an extension of our ongoing studies on the use of bifunctional tetraaza macrocyclic chelates for the sequestration of radioisotopes for medical applications (5–9). While this would provide a six-coordinate environment with two phenolic donors, we have also envisioned this class of compound as a potential intermediate to eight coordinate ligands of mixed donor character. Additionally, the 2-hydroxybenzyl groups could either be retained in such a case, or serve as protecting groups that could serve to permit sequential introduction of two other sets of *trans* arranged sets of metal binding groups

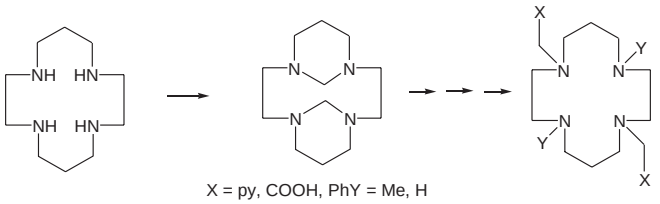
Received January 9, 2001. Published on the NRC Research Press Web site at http://canjchem.nrc.ca on July 27, 2001.

H. Luo and M.W. Brechbiel.[1] Radioimmune & Chemistry Section, Radiation Oncology Branch, NCI, NIH, Bethesda, MD 20892, U.S.A.
R.D. Rogers.[2] Department of Chemistry, The University of Alabama, Tuscaloosa, AL 35487, U.S.A.

[1]Corresponding author (telephone (301) 496-0591; fax: (301) 402-1923; e-mail: martinwb@box-m.nih.gov).
[2]Author to whom correspondence about crystallography may be addressed.

 DOI: 10.1139/cjc-79-7-1105 © 2001 NRC Canada

Scheme 1.



(10). In this communication, we present our progress in this regard.

Technically, placing pendant groups on only two of the four equivalent nitrogen atoms on tetraaza frameworks has been more difficult to accomplish than alkylating only one, three, or all four nitrogens. The difficulties result in part from the possible generation of regioisomers and from complications arising from the possible presence of mono-, tri-, and (or) tetra-substituted products that co-occur with the desired disubstituted product (11). Furthermore, unlike for mono- or tetra-functionalization, using a large excess of one of the reactants is not applicable for maximizing production of the desired disubstituted product. Direct *N*,*N*″-difunctionalization of tetraazamacrocycles by haloalkylation has been attempted, but tedious chromatography for isolation of the desired product was necessary and contributed to low yields (15–35%) (12).

N,*N*″-Difunctionalization of tetraazamacrocycles has been accomplished indirectly in several cases via protected *N*,*N*″-diprotected tetraazamacrocycles by tosylation (11, 13, 14), carbamylation (15, 16), or sulfomethylation (17, 18). This was made possible as a result of the achieved isolation of only one predominant regioisomer of *N*,*N*″-diprotected tetraazamacrocycles under carefully chosen conditions, such as reaction solvents, temperature, pH, or slow, careful addition of reagents (11, 14, 16, 18–20). However, in many of the examples, other regioisomers of diprotected (11, 18), triprotected (14), or tetraprotected (16) species were also found to be present (19). A stepwise route to *trans*-dialkylated derivatives of tetrazamacrocycles by haloalkylation under 3- or 4-nitrogen-bridged protection provided by one silicon-, carbon-, or other heteroatom-containing group was reported (21, 22). This route, however, has not found application in preparation of *N*,*N*″-difunctionalized tetraaza macrocyclic chelates, presumably due to inconvenience as compared to the other routes.

Protection via formation of hexahydropyrimidine (aminal) provides another route to produce *N*,*N*″-difunctionalized cyclam-based macrocyclic chelates (cyclam = 1,4,8,11-tetraazacyclotetradecane) (23–26). The intermediates of the protected cyclam, were prepared either by cyclic condensation of the tetraaza and dichloromethane (23, 26) or formaldehyde (27) (Scheme 1). The intermediates were either reacted with a haloalkane followed by hydrolysis (24) or reduction (23), or hydrogenation followed by a reaction with haloalkane (25). *trans*-*N*,*N*″-Difunctionalized tetraazamacrocyclic products have been prepared via this route recently for 2-pyridyl (3 steps) (26), aminoalkyl, and carboxymethyl functional groups (4 steps) (25).

In the previously described hexahydropyrimidine route, the aldehyde was used only as a protecting group, i.e., the corresponding fragment was either removed or reduced to a methyl group that was not an essential part of the donor character of the chelating moiety and the two remaining secondary amines were converted to tertiary amines that are usually less coordinating than the secondary counter-part. Thus, the hexahydropyrimidine route could be further explored, since there are possibilities to provide an efficient introduction of additional donor groups by using aldehydes that bear donating functional groups. Salicylaldehyde and other aldehyde derivatives have been used to provide a convenient and selective functionalization route to unsymmetric acyclic chelates from *N*-monoalkylated or *N*,*N*′-dialkylated diamines (28). We report herein application of this chemistry to the regioselective preparation of a *trans*-*N*,*N*″-macrocyclic hexadentate $N_4O_2^{2-}$ ligand from cyclam (Scheme 2), and the synthesis and characterization of the corresponding Cu(II) complex unequivocally confirming the structure of this ligand.

In the present study, cyclam and two equivalents of salicylaldehyde were reacted, affording a sole, bisaminal or bis(hexahydropyrimidine) analog, 15,16-bis(2-hydroxyphenyl)-1,4,8,11-tetraazatricyclo[9.3.1.1^{4,8}]hexadecane in moderate yields.[3] The hexahydropyrimidine rings were then selectively cleaved upon borohydride reduction to yield the 1,8-disubstituted cyclam-based N_4O_2 ligand, 1,8-bis(2-hydroxybenzyl)-1,4,8,11-tetraazacyclotetradecane (abbreviated H_2bcyclamb or **3**, Scheme 2).[4] Satisfactory analytical data for **2** and **3** were obtained.[5] In this case, salicylaldehyde functions both as a protecting agent and as a source of a functional potential donor via a phenol group. The two 2-hydroxybenzyl groups are available to function as pendant

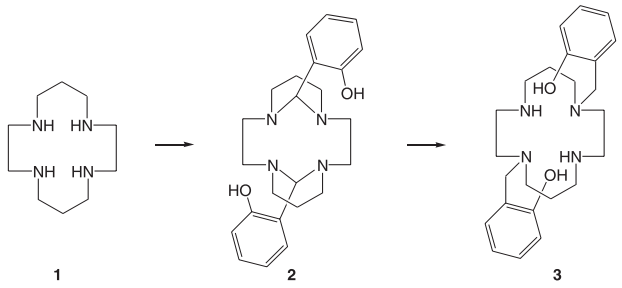
[3] To cyclam (1.75 g, 8.7 mmol) in MeOH (15 mL) was added salicylaldehyde (3.13 g, 25.6 mmol) in MeOH (15 mL) in a round-bottom flask. The mixture was heated at reflux for 4 h, then concentrated to a yellow solid. The solid was recrystallized from MeCN and an off-white crystalline product was obtained after storage at −4°C for 2 days. The product was filtered off, washed with Et_2O (2 × 15 mL), then dried in vacuo overnight (yield: 2.55 g, 71%). CI-MS *m*/*z*: 409 ([M + 1]$^+$). $^{13}C\{^1H\}$ NMR ($CDCl_3$, 125.708 MHz) δ: 158.2, 128.8, 127.9, 123.7, 118.4, 118.2 (minor, Me*C*N), 117.3, 50.9, 49.5, 45.0, 29.6 (minor, *Me*CN), 19.9 (br). Anal. calcd. for $C_{24}H_{32}N_4O_2 \cdot 0.45MeCN$: C 70.04, H 7.87, N 14.60; found: C 70.03, H 8.31, N 14.81.

[4] To **2** (1.53 g, 3.74 mmol) in MeOH (70 mL) was added $NaBH_4$–Al_2O_3 (wt. 10%, 2.12 g, ~5.7 mmol) in small portions. The mixture was heated at reflux for 6 h, evaporated to near dryness at low pressure, treated with 10% NH_4OAc (100 mL), and then extracted with $CHCl_3$ (2 × 150 mL). The organic phase was dried over Na_2SO_4 and then concentrated to a yellow residue, which was treated with cold acetone. A white powder was isolated from the yellow solution. The powder was filtered out, washed with acetone (5 mL), and air dried. The yield was 0.596 g (39%, based on **2**). CI-MS *m*/*z*: 413 ([M + 1]$^+$). $^{13}C\{^1H\}$ NMR ($CDCl_3$, 127.7 MHz) δ: 158.0, 131.4, 129.3, 125.0, 118.3, 117.4, 54.3, 53.2, 51.2, 49.2, 46.6, 24.6. Anal. calcd. for $C_{24}H_{32}N_4O_2 \cdot 0.45H_2O$: C 66.67, H 8.90, N 12.96; found: C 66.48, H 8.56, N 12.81.

[5] NMR spectra were recorded on Varian Gemini 300 spectrometer, with δ referenced to the internal TMS. CI-MS and FAB-MS were recorded with a Finnigan 3000 and Extrel 4000 with positive ion detection, respectively. Elemental analyses were performed by Galbraith Laboratories Inc. Knoxville, TN 37921-1750.

© 2001 NRC Canada

Scheme 2.

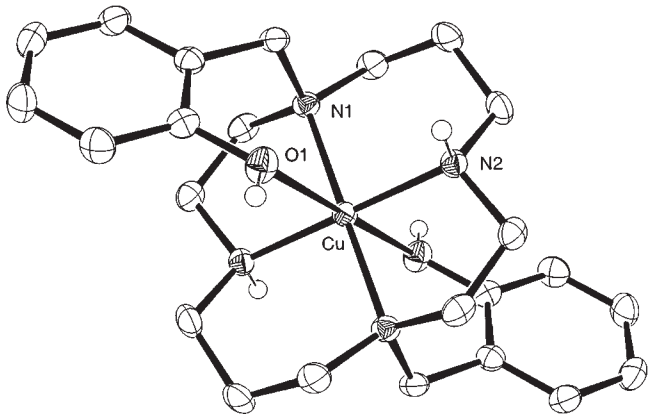


donating groups as soon as the deprotection is done. Thus, the new route is different from the previous hexahydropyrimidine route, with the overall reaction being shortened significantly and with the product retaining two of the secondary amine N-atoms (24, 25).

The efficiency of the procedure (2 steps) reported herein for *trans*-difunctionalization of tetraaza **1** is an improvement from the currently known conditionally selective procedures for tetraazamaclocycles-based *trans*-N_4O_2 ligands (usually 4 or more steps) (11, 14, 18–20, 25). In contrast to haloalkylation routes, the overall reaction is concise and selective. In fact, it is the first procedure of *trans*-difunctionalization of a tetraaza macrocycle that does not generate mono-, tri-, or tetra-functionalized products, with only 1,8-difunctionlized product being isolated, and it is also coupled with the convenience of the functionalization occurring as a result of the deprotection. This efficiency was ensured by use of a stoichiometric cyclic condensation[6] and subsequent clean cleavage of the cyclic condensate. Formation of the *trans*-difunctionalized product in our case was exclusive, presumably due to the steric control of the reductive ring opening (deprotection) process, which prevented the formation of a *cis*-difunctionalized product. Regioselectivity was not observed in the reduction of an analogous condensate, 1,4,8,11-tetraazatricyclo[9.3.1.$1^{4,8}$]-hexadecane, which lacked the bulky character of the 2-hydroxybenzyl substituent on the bridging carbon atoms (25). The X-ray crystal structure of the Cu(II) complex from **3** confirms unequivocally the assignment of *trans*-difunctionalization for **3**. Thus, synthesis of a *trans*-difunctionalized tetraaza ligand was accomplished both conveniently and regioselectively.

Examples of Cu(II) complexes of cyclic N_4O_2 ligands with two *trans*-arranged difunctional groups have appeared in the past decade (13, 29–33). The known cyclic N_4O_2 com-

Fig. 1. ORTEP drawings of $[Cu(H_2bcyclamb)]^{2+}$; 50% probability thermal ellipsoids are shown. Hydrogen atoms attached to carbon atoms are excluded for clarity. Selected bond distances (Å) and bond angles (°): Cu—N(1) 2.046(2), Cu—N(2) 2.013(2), Cu—O 2.651(2) Å; N(1)-Cu-N(2) 93.01(8), N(1)-Cu-N(1a) 180.0, N(1)-Cu-N(2a) 86.99(8), N(2)-Cu-N(2a) 180.0, O(1)-Cu-N(1) 85.4(1), O(1)-Cu-N(2) 88.8(1), O(1)-Cu-N(1a) 94.6(1), O(1)-Cu-N(2a) 91.2(1), O(1)-Cu-O(1a) 180.0°.



plexes of Cu(II) with solved structures were all functionalized with acetate functional groups. A reaction of **3** with $Cu(OAc)_2 \cdot H_2O$ was carried out. The mixture of the two reactants was dissolved in methanol–chloroform (1:1) upon heating to boiling. The solution was filtered immediately and permitted to evaporate slowly. Pink solids, isolated after several days, were dried in vacuo and identified as $[Cu(H_2bcyclamb)](OAc)_2 \cdot 1/3H_2O$ by microanalysis and mass spectrometry.[7] A crystal from the mother liquor was suitable for crystallographic studies and the structure of $[Cu(H_2bcyclamb)](OAc)_2 \cdot 2H_2O$ was solved.[8] An ORTEP drawing of the molecular structure is shown in Fig. 1.

trans-Difunctionalized N_4O_2 chelates are superior to their *cis* counterparts in formation of six-coordinate copper(II) complexes, because, in the latter case, not all donor sites will be coordinated to the metal due to strain or steric effects (29, 33). Given that a lengthened octahedron is preferred for the coordination geometry of the Cu(II) complex cation owing to the Jahn–Teller effect, the *trans*-difunctionalized N_4O_2 chelate permits expansion of the coordination sphere accordingly with the two pendant donor sites, while the coordination of the Cu-N_4 fragment remains intact. In this specific case, the Cu—N bonds are 2.013(2) and 2.046(2) Å, which are close to the values of 2.005(2) and 2.062(2) Å found in

[6] A slight excess of aldehyde was used to ensure that there was no 1:1 condensation product.

[7] FAB-MS *m/z*: 474 ($[Cu(H_2bcyclamb) - 1]^+$). Anal. calcd for $C_{28}H_{42}N_4O_6Cu \cdot 1/3H_2O$: C 56.03, H 7.17, N 9.33; found: C 56.05, H 7.40, N 9.21.

[8] The crystals are monoclinic, space group $P2_1/c$, with cell parameters and calculated volume of: a = 10.0931(2), b = 13.8820(1), c = 10.8752(1) Å, β = 106.332(1)°, V = 1462.26(3) Å^3. For Z = 2 and FW = 630.23 the calculated density of $[Cu(H_2bcyclamb)](OAc)_2 \cdot 2H_2O$ is 1.431 g cm^{-3}. Preliminary examination and data collection were performed with Mo Kα radiation. A total of 9006 reflections were collected on a Siemens SMART diffractometer, and 3387 were unique (R(int) = 0.036) and 2553 were considered observed ($I > 2\sigma(I)$). Refinement of the structure utilized all 3387 unique reflections. The structure was solved using the program SHELXTL 5 and was refined by full-matrix least-squares methods to 0.0401 and 0.0772 for R and wR, respectively, (calculated on observed reflections only). A complete set of data may be purchased from the Depository of Unpublished Data, Document Delivery, CISTI, National Research Council Canada, Ottawa, ON K1A 0S2, Canada. For information on obtaining material electronically go to http://www.nrc.ca/cisti/irm/unpub_e.shtml. Crystallographic information has also been deposited with the Cambridge Crystallographic Data Centre (No. 162851). Copies of the data can be obtained, free of charge, on application to the Director, CCDC, 12 Union Road, Cambridge CB2 1EZ, U.K. (fax: 44-1223-336033 or e-mail: deposit@ccdc.cam.ac.uk).

© 2001 NRC Canada

the carboxylic congener (13) and comparable to the value of 2.02 Å observed in the Cu(II)—cyclam (34). At a distance of 2.651(2) Å, the two phenolic oxygen atoms are coordinated to the metal center without deprotonation, as found in some cases with carboxylic analogs (13, 29). It is known, however, that neutral Cu(II) complexes can be formed when a base is added during complexation with diprotic *trans*-difunctionalized N_4O_2 chelates (13, 30–32). Thus, formation of neutral Cu(II) complexes with this chelate may be possible if increased basic conditions are employed.

Our new N_4O_2 chelate with two phenolic functional groups on cyclam is complementary to the difunctionalized cyclam that is dominated with carboxylic groups. Since this novel chelate is stable in aqueous solution and common organic solvents, in contrast to the known carboxylic counterpart that was found to be lactamized in aqueous solution (13), this chelate has potential in complexing metallic isotopes such as ^{64}Cu and ^{67}Cu in radiopharmaceutical applications. In addition, as demonstrated here and in other reports, one could instead employ aldehyde derivatives to react with the tetraazamacrocycle (27, 35). Hence, this general method appears suitable for generation of numerous structural derivatives that maintain the hexadentate metal coordination sphere based on cyclam.[9,10] Furthermore, the new hexadentate N_4O_2 chelate itself can also be used in synthesis of octadentate chelates based on tetraaza macrocycles, wherein a variety of other donor groups could be introduced at the two remaining secondary nitrogens.

In conclusion, we have developed a convenient route to a new type of diprotic hexadentate N_4O_2 chelate based on cyclam with two 2-hydroxybenzyl pendant groups. The new route to this *trans*-difunctionalized hexadentate (N_4O_2) ligand was not only simple and efficient, as featured by just two convenient steps, but also regioselective. The *trans*-difunctionalized cyclam with two phenolic pendant donor sites are complementary to the current difunctionalized cyclam community. This expected *trans*-difunctionalized structure of the chelate was confirmed by X-ray crystallography. Work remains underway to investigate the coordination chemistry of this chelate, preparation of further derivatives based upon this chelate, and their potential radiopharmaceutical chemistry.

Acknowledgments

We thank Mr. Noel Wittaker and Mr. Wesley White for their service in mass spectrometry and NMR spectroscopy, respectively, on our samples.

References

1. K.P. Wainwright. Coord. Chem. Rev. **166**, 35 (1997).
2. P.V. Bernhardt and G.A. Lawrance. Coord. Chem. Rev. **104**, 297 (1990).
3. R.D. Hancock, H. Maumela, and A.S. Desousa. Coord. Chem. Rev. **148**, 315 (1996).
4. M. Meyer, V. Dahaoui-Gindrey, C. Lecomte, and L. Guilard. Coord. Chem. Rev. **180**, 1313 (1998).
5. J.W.M. Bulte, C.C. Wu, M.W. Brechbiel, R.A. Brooks, J. Vymazal, M. Holla, and J.A. Frank. Invest. Radiol. **33**, 841 (1998).
6. L.L. Chappell, B.E. Rogers, M.B. Khazaeli, M.S. Mayo, D.J. Buchsbaum, and M.W. Brechbiel. Bioorg. Med. Chem. **7**, 2313 (1999).
7. E. Dadachova, L.L. Chappell, and M.W. Brechbiel. Nucl. Med. Biol. **26**, 977 (1999).
8. E. Horak, F. Hartmann, K. Garmestani, C.C. Wu, M.W Brechbiel, O.A. Gansow, N.F. Landolfi, and T.A. Waldmann. J. Nucl. Med. **38**, 1944 (1997).
9. D.E. Milenic, M. Roselli, M.W. Brechbiel, C.G. Pippin, T.J. McMurray, J.A. Carrasquillo, D. Colcher, R. Lambrecht, O.A. Gansow, and J. Schlom. Eur. J. Nucl. Med. **25**, 471 (1998).
10. T. Johnson and M. Quibell. Tetrahedron Lett. **35**, 463 (1994).
11. I.M. Helps, D. Parker, J.R. Morphy, and J. Chapman. Tetrahedron, **45**, 219 (1989).
12. M. Di Vaira, F. Mani, N. Nardi, P. Stoppioni, and A. Vacca. J. Chem. Soc. Dalton Trans. 2679 (1996).
13. J. Chapman, G. Ferguson, J.F. Gallagher, M.C. Jennings, and D. Parker. J. Chem. Soc. Dalton Trans. 345 (1992).
14. I.M. Helps, D. Parker, J. Chapman, and G. Ferguson. J. Chem. Soc. Chem. Commun. 1094 (1988).
15. J. Huskens, D.A. Torres, Z. Kovacs, J.P. Andre, C.F.G.C. Geraldes, and A.D. Sherry. Inorg. Chem. **36**, 1495 (1997).
16. Z. Kovacs and A. D. Sherry. Synthesis, 759 (1997).
17. J.M. Weeks, M.R. Taylor, and K.P. Wainwright. J. Chem. Soc. Dalton Trans. 317 (1997).
18. J. Van Westrenen and A.D. Sherry. Bioconjugate Chem. **3**, 524 (1992).
19. A. Dumont, V. Jacques, Q.X. Peng, and J.F. Desreux. Tetrahedron Lett. **35**, 3707 (1994).
20. Z. Kovacs and A.D. Sherry. J. Chem. Soc. Chem. Commun. 185 (1995).
21. P.L. Anelli, M. Murru, F. Uggeri, and M. Virtuani. J. Chem. Soc. Chem. Commun. 1317 (1991).
22. A. Roignant, I. Gardinier, H. Bernard, J.J. Yaouanc, and H. Handel. J. Chem. Soc. Chem. Commun. 1233 (1995).
23. G. Royal, V. Dahaoui-Gindrey, S. Dahaoui, A. Tabard, R. Guilard, P. Pullumbi, and C. Lecomte. Eur. J. Org. Chem. 1971 (1998).
24. C. Bucher, G. Royal, J.M. Barbe, and R. Guilard. Tetrahedron Lett. **40**, 2315 (1999).
25. A. Comparone and T.A. Kaden. Helv. Chim. Acta, **81**, 1765 (1998).
26. R. Guilard, A.G. Bessmertnykh, and I.P. Beletskaya. Synlett, 1190 (1997).
27. R.W. Alder, E. Heilbronner, E. Honegger, A.B. McEwen, R.E. Moss, E. Olefirowicz, P.A. Petillo, R.B. Sessions, G.R. Weisman, J.M. White, and Z.Z. Yang. J. Am. Chem. Soc. **115**, 6580 (1993).
28. H.Y. Luo, J.M. Lo, P.E. Fanwick, J.G. Stowell, and M.A. Green. Inorg. Chem. **38**, 2071 (1999).
29. H. Aneetha, Y.H. Lai, S.C. Lin, K. Panneerselvam, T.H. Lu, and C.S. Chung. J. Chem. Soc. Dalton Trans. 2885 (1999).
30. L.Q. Chen, L.K. Thompson, J.N. Bridson, J. Xu, S.S. Ni, and R.P. Guo. Can. J. Chem. **71**, 1805 (1993).

[9] Preliminary results affirmed that cyclam reacted with two equivalents of 2-pyridinecarboxaldehyde in a similar fashion and yielded the expected condensate with satisfactory analytical results. Reduction of this intermediate yielded the desired product as verified by FAB-MS. The details of synthesis and coordination chemistry of the potential $N_4N'_2$-chelate will be reported elsewhere.

[10] During the preparation of this manuscript, routes to *cis*-bis(pyridylmethyl) and *trans*-bis(pyridylmethyl) functionalized cyclam were reported starting from cyclam (3 steps), or the corresponding macrocyclic dioxotetraamine (2 steps) (36).

© 2001 NRC Canada

31. K.Y. Choi, I.H. Suh, J.G. Kim, Y.S. Park, S.I. Jeong, I.K. Kim, C.P. Hong, and S.N. Choi. Polyhedron, **18**, 3013 (1999).
32. J. Costa, R. Delgado, M.G.B. Drew, and V. Felix. J. Chem. Soc. Dalton Trans. 1063 (1998).
33. Y.J. Lin, X.M. Ye, B. Hao, L.J. Song, J.D. Xu, and S.S. Ni. Jiegou Huaxue (Chin. J. Struct. Chem.), **15**, 362 (1996).
34. P.A. Tasker and L. Sklar. J. Cryst. Mol. Struct. **5**, 329 (1975).
35. G.R. Weisman, C.H. Suzzy, H. Ho, and V. Johnson. Tetrahedron Lett. **21**, 335 (1980).
36. A.E. Goeta, J.A.K. Howard, D. Maffeo, H. Puschmann, J.A.G. Williams, and D.S. Yufit. J. Chem. Soc. Dalton Trans. 1873 (2000).

© 2001 NRC Canada

An efficient route to 5-iodo-1-methylimidazole: synthesis of xestomanzamine A

Francis B. Panosyan and Ian W.J. Still

Abstract: An efficient and practical route to C-5 functionalized *N*-methylated imidazoles is reported. 5-Iodo-1-methylimidazole was synthesized in four steps from imidazole, with complete regiospecificity, in 73% overall yield. The synthesis of xestomanzamine A, a marine natural product isolated in 1995 from an Okinawan sponge of *Xestospongia* sp., has been achieved using 5-iodo-1-methylimidazole in a modified Grignard reaction with a β-carboline ester moiety, in an overall yield of 59% based upon imidazole and 53% based upon tryptamine.

Key words: xestomanzamine A, 5-iodo-1-methylimidazole, methyl β-carboline-1-carboxylate.

Résumé : On propose une méthode efficace et pratique de préparer des imidazoles *N*-méthylés et fonctionnalisés en C-5. On a synthétisé le 5-iodo-1-méthylimidazole en quatre étapes à partir de l'imidazole, avec une régiospécificité complète et un rendement global de 73%. Faisant appel à une réaction de Grignard modifiée entre le 5-iodo-1-méthylimidazole et un ester de la β-carboline, on a réalisé la synthèse de la xestomanzamine A, un produit naturel marin isolé en 1995 à partir de l'éponge d'Okinawa *Xestospongia* sp.; le rendement global est de 59% à partir de l'imidazole et de 53% sur la base de la tryptamine.

Mots clés : xestomanzamine A, 5-iodo-1-méthylimidazole, β-carboline-1-carboxylate de méthyle.

[Traduit par la Rédaction]

Introduction

There has recently been intensive interest in the biological activity of naturally occurring marine alkaloids (for a recent review of marine natural products, see ref. 1). The very prolific β-carboline class of alkaloids has been the focus of particular attention (2, 3). Many of these alkaloids are isolated from sponges and two such compounds are xestomanzamine A (**1**) and its 3,4-dihydro analogue xestomanzamine B (**2**). These cytotoxic constituents of an Okinawan sponge (*Xestospongia* sp.) were first isolated in 1995 (4), and one synthesis of xestomanzamine A has been reported (5). This synthesis required at least eight steps from indole-3-carboxaldehyde, as well as a key coupling reaction with a 5-lithiated 1-methylimidazole, itself requiring three steps for its preparation, which proceeds in a yield of less than 50%. We have developed a considerably shorter, more efficient route to xestomanzamine A, which we now describe.

Results and discussion

A likely biosynthetic route to xestomanzamine A would probably involve condensation of tryptophan **3** with the *N*-methylated histidine-derived aldehyde **4** to produce the tetrahydro-β-carboline[2] intermediate **5**. Decarboxylation, and a series of oxidative steps would then lead to **2** and finally to **1**, Scheme 1. We decided to adopt a similar strategy in our approach but with the initial construction of the β-carboline unit in the form of the 1-carboxylate ester **6**. We then planned to carry out a modified Grignard reaction, using a 5-halo-1-methylimidazole **7**, to lead directly to xestomanzamine A, Scheme 2.

Before we began our approach to **7b** and **7c** we attempted, without success, to form the Grignard reagent from the commercially available 5-chloro-1-methylimidazole **7a**. While the analogous 5-bromo- and 5-iodoimidazoles are not, at first sight, difficult synthetic targets, one well documented complication in imidazole chemistry is the rapid equilibration of 4- and 5-imidazolyl anions to their much more stable 2-imidazolyl anion counterpart (6, 7). Thus, lithiation of *N*-methylimidazole, followed by bromination or iodination, was ruled out. Attempts to carry out regioselective bromination of *N*-methylimidazole with a variety of reagents, including NBS, pyridinium tribromide, 2,4,4,6-tetrabromo-2,5-cyclohexadienone, and dibromotriphenylphosphorane were also unsuccessful. Some conversion (20%) of *N*-methylimidazole to **7b** was achieved using 2,3-dibromo-5,5-dimethylhydantoin (DBDMH) in THF at 0°C (8). The low yield obtained, however, combined with a report (9) of the low reactivity of 5- and 4-bromo-1-methylimidazoles towards magnesium, convinced us to turn our attention to the synthesis of the iodo compound **7c**.

The synthesis of 5-iodo-1-methylimidazole was attempted by the strategy used by Balaban and Pyman (10) and, more recently, by Garegg and Samuelsson (11). We planned to carry out iodination of imidazole at all three carbons, selective deiodination and then regiospecific methylation to afford 5-iodo-1-methylimidazole **7c**, Scheme 3.

Received February 22, 2001. Published on the NRC Research Press Web site at http://canjchem.nrc.ca on July 27, 2001.

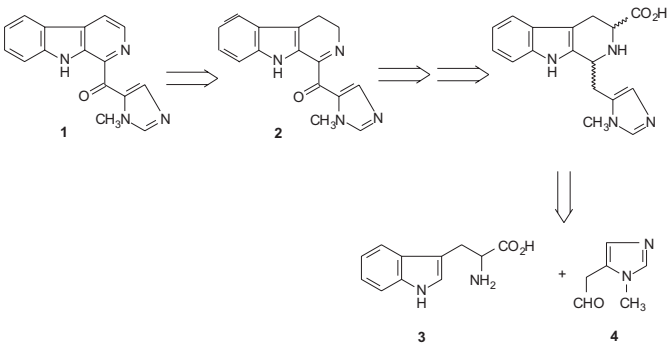
F.B. Panosyan and I.W.J. Still.[1] Department of Chemistry, University of Toronto at Mississauga, Mississauga, ON L5L 1C6, Canada.

[1]Corresponding author (telephone: (905) 828-5354; fax: (905) 828-5425; e-mail: istill@utm.utoronto.ca).

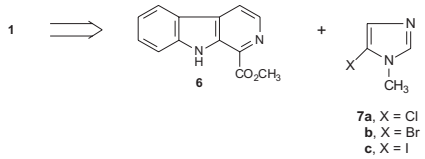
[2]IUPAC name is 1,2,3,4-tetrahydro-9*H*-pyrido[3,4-*b*]indole.

 DOI: 10.1139/cjc-79-7-1110 © 2001 NRC Canada

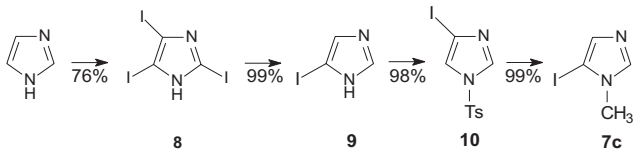
Scheme 1.



Scheme 2.



Scheme 3.



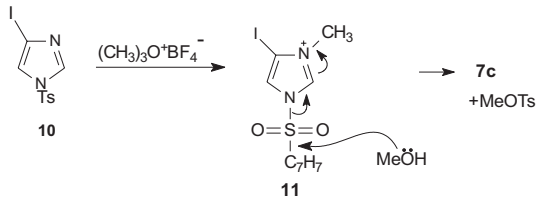
In our hands, the conversion of imidazole to the triiodiomidazole **8** was best achieved with iodine in an aqueous solution of sodium hydroxide, in the presence of potassium iodide (12). 2,4,5-Triiodoimidazole **8** separated from the solution upon neutralization with acetic acid, in 76% yield.

The next step was the selective deiodination of **8** to 4(5)-iodoimidazole **9**. The use of sodium sulfite by Balaban and Pyman (10) for the analogous bromo-series has been extended to the selective deiodination reaction of **8** (13). This reaction, in our hands, afforded **9** in 99% yield, by using 30% ethanol in water as the refluxing solvent, instead of water, to avoid complete deiodination. The ^{1}H NMR spectrum of the reduction product **9** showed the expected signals at δ 7.62 and 7.18, indicative of H(2) and H(4)-(5), respectively.

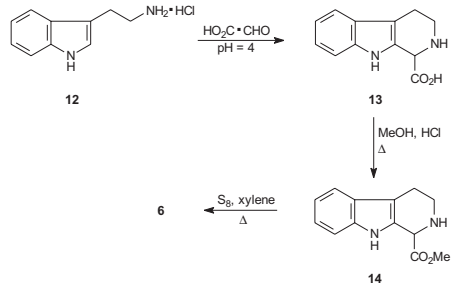
Numerous attempts to regioselectively methylate **9** to produce the desired **7c** were to no avail, under a variety of pH conditions and using both methyl iodide and dimethyl sulfate as methylating agents. Finally, we were able to take advantage of a highly selective two-step procedure that involves the initial, regioselective tosylation (14) of **9** to produce 4-iodo-1-tosylimidazole **10** in 98% yield. This selectivity may be rationalized on steric grounds, although the formation of **10** as a result of a thermodynamic equilibration of two initially formed regioisomers cannot be ruled out.

The final conversion of **10** into the desired 5-iodo-1-methylimidazole **7c** was achieved using trimethyloxonium

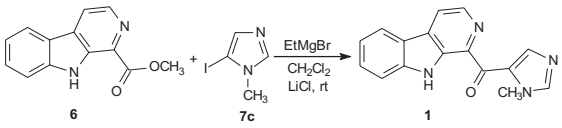
Scheme 4.



Scheme 5.



Scheme 6.



tetrafluoroborate, followed by a methanol quench, in a modification of a recent report by Lindel and Hochgürtel (15). This reaction afforded **7c** in 99% yield. The ^{1}H NMR spectrum had three singlet peaks at δ 3.62, 7.13, and 7.62, for the methyl, H(4), and H(2) protons, respectively. These values were in excellent agreement with the reported literature values (12) for 5-iodo-1-methylimidazole.

This very successful, regioselective methylation at N(3) of **10** using trimethyloxonium tetrafluoroborate presumably proceeds via the 5-iodo-1-methyl-3-tosylimidazolium salt **11**, which is not isolated, Scheme 4.

The sequence of reactions leading to **7c** from imidazole (Scheme 3) does not carry the disadvantages associated with many earlier methods for the synthesis of 5-iodo-1-methylimidazole; namely, low yields, poor reproducibility, and tedious purification methods. The overall yield for the four-step synthesis of **7c** from imidazole was 73%.

The synthesis of the β-carboline ester **6** was much more straightforward, Scheme 5. The initial 1,2,3,4-tetrahydro-β-carboline derivative **13** was obtained through a Pictet–Spengler condensation of tryptamine hydrochloride **12** with glyoxylic acid, forming **13** as a white solid, in 80% yield. The Pictet–Spengler reaction is known to proceed under mildly acidic conditions. This reaction was initiated by the addition of a concentrated solution of potassium hydroxide to solubilize the reagents, and then the pH was adjusted to about 4 with glacial acetic acid. Purification of **13** was readily achieved by simply stirring the product briefly in methanol at 0°C and then filtering. The acid showed the IR bands at ν 3343 (NH) and 1616 (bonded C=O) cm^{-1}, as expected for this compound (16).

© 2001 NRC Canada

Fischer esterification of **13** with methanol gave methyl 1,2,3,4-tetrahydro-β-carboline-1-carboxylate **14**, as its hydrochloride salt (17). The synthesis of **6** was completed by dehydrogenation of **14**, after careful neutralization of the salt with 2,2,6,6-tetramethylpiperidine, using sulfur in refluxing xylene, in 87% yield. The ester showed a carbonyl band in the IR at ν 1678 cm^{-1}, which is attributed to strong intramolecular hydrogen bonding with the indole NH.

Our initial attempt to complete the synthesis of xestomanzamine A was carried out by addition of a solution of EtMgBr and 5-iodo-1-methylimidazole **7c** in THF to a solution of the β-carboline methyl ester **6** in THF, in the presence of excess lithium chloride (17). The indole NH present in **6** was first deprotonated with the addition of one equivalent of EtMgBr, prior to the addition of **7c**. Xestomanzamine A was obtained, but in very low yield. A mild procedure has been reported for metal–halogen exchange with *N*-protected 4-iodoimidazoles (18), using EtMgBr in CH_2Cl_2. Repeating the reaction in CH_2Cl_2 again afforded xestomanzamine A, this time in greatly improved yield. We speculate that the use of dichloromethane may give the Grignard organomagnesium intermediate greater covalent character, thus making the imidazol-5-yl carbanionoid less sensitive to equilibration with its imidazol-2-yl counterpart, Scheme 6.

It was noticed during these initial attempts that the addition of EtMgBr to **7c** produced a white precipitate prior to addition to the β-carboline ester. Grignard reagents are known to exist in equilibrium with the corresponding binary organomagnesium compounds. At low temperatures, and when there is a solvent-induced precipitation of the magnesium salt, there is a shift of the equilibrium towards the organomagnesium species $MgAr_2$. We, thus, decided to direct the equilibrium towards the Grignard reagent ArMgX by warming the solution of EtMgBr and **7c** briefly, prior to addition to the β-carboline methyl ester **6**. In this way the yield of xestomanzamine A was increased finally to 81%.

The physical data (mp, IR, ^1H and ^{13}C NMR), which we obtained for xestomanzamine A, are in excellent agreement with those reported for the natural product (4).

Our four-step preparation of 5-iodo-1-methylimidazole in excellent overall yield provides ready access to a synthetic intermediate with the potential to facilitate the synthesis of other natural products with the *N*-substituted, C-5 functionalized imidazole substructure (19). The efficient total synthesis of xestomanzamine A (**1**) has been achieved through a modified Grignard reaction of **7c** with the β-carboline ester **6**, involving a total of four steps from tryptamine (53% overall yield) and five steps from imidazole (59% overall yield).

Experimental

Methanol was dried over magnesium. Xylenes and dichloromethane were distilled over calcium hydride. Tetrahydrofuran and diethyl ether were dried over sodium benzophenone ketyl. Molecular sieves (3 Å) were activated by heating in a furnace to 500°C for 3 h. All glassware for anhydrous reactions was dried overnight prior to use and these reactions were carried out under argon. TLC were run on Merck silica gel 60 F_{254} plates, with detection by means of a 254 nm UV visualizer. Melting points were recorded on a capillary melting point apparatus and are uncorrected. IR spectra reported were recorded on a Nicolet FT-IR spectrophotometer in the form of KBr disks, unless specified otherwise. The ^1H NMR spectra (200 MHz) and ^{13}C NMR spectra (125 MHz), unless specified otherwise, were obtained in $CDCl_3$ with an internal standard of TMS.

2,4,5 Triiodoimidazole (8)

Modification of a described procedure (11): a solution of iodine (45.0 g, 0.18 mol) in 20% aqueous potassium iodide (300 mL) was added dropwise to a stirred solution of imidazole (7.06 g, 0.1 mol) in 2 M sodium hydroxide (600 mL) at room temperature and the resulting mixture was stirred overnight. Addition of acetic acid until the mixture was neutral gave a white precipitate, which was filtered off, washed with water, and air dried to give a product sufficiently pure to continue in the next step: (35.4 g, 76%): mp 186–190°C, lit. (11) mp 190–192°C.

4(5)-Iodoimidazole (9)

Modification of a described procedure (13): triiodoimidazole (1.0 g, 2.24 mmol) and sodium sulfite (4.2 g, 33.3 mol) were heated at reflux in 30% ethanol in water solution (50 mL) for 24 h. The ethanol was removed under reduced pressure. The remaining solution was filtered and the filtrate extracted with diethyl ether (3 × 15 mL). The organic extracts were combined, dried (Na_2SO_4), and concentrated under reduced pressure to afford the pure product **9** as a white solid (0.43 g, 99%): mp 136 to 137°C, lit. (13) mp 137 to 138°C. ^1H NMR δ 7.18 (s, 1H), 7.62 (s, 1H). ^1H NMR (DMSO-d_6) δ 7.31 (s, 1H), 7.65 (s, 1H).

4-Iodo-1-*p*-toluenesulfonylimidazole (10)

Compound **10** was prepared from **9** based upon the procedure of Cliff and Pyne (14). White solid (98%): mp 146 to 147°C (EtOH), lit. (14) mp 146 to 147°C; ^1H NMR δ 2.46 (s, 3H), 7.37 (s, 1H), 7.40 (d, J = 8.5 Hz, 2H), 7.83 (d, J = 8.5 Hz, 2H), 7.88 (s, 1H).

5-Iodo-1-methylimidazole (7c)

To a solution of **10** (0.94 g, 2.81 mmol) in dry CH_2Cl_2 (30 mL) was added trimethyloxonium tetrafluoroborate (0.46 g, 3.11 mmol). After the mixture was stirred at room temperature for 24 h, methanol (15 mL) was added. The solvent was removed under reduced pressure and the residue was acidified with 1% HCl and extracted with CH_2Cl_2 (2 × 15 mL). The aqueous solution was then basified with 5% $NaHCO_3$ solution and extracted with CH_2Cl_2 (3 × 15 mL). The organic extracts from the basified solution were combined, dried (Na_2SO_4), and the solvent removed under reduced pressure to afford the white product **7c** (0.58 g, 99%): mp 106 to 107°C, lit. (12) mp 102 to 103°C. ^1H NMR δ 3.62 (s, 3H), 7.13 (s, 1H), 7.62 (s, 1H).

1,2,3,4-Tetrahydro-β-carboline-1-carboxylic acid (13)

Tryptamine hydrochloride **12** (1.95 g, 9.91 mmol) was dissolved in water (30 mL) while heating. Glyoxylic acid monohydrate (1.10 g, 11.95 mmol) in water (10 mL) was added to this solution, followed by the dropwise addition of potassium hydroxide (0.65 g, 11.58 mmol) in water (10 mL). The pH was adjusted to 4.0 with HOAc and the mixture al-

© 2001 NRC Canada

lowed to stir at room temperature for 2 h. The solution was then chilled and vacuum filtered, giving an impure yellow solid. The solid was dried under vacuum and suspended in methanol at 0°C, then quickly filtered by suction to afford the pure white product (1.99 g, 80%): mp 210 to 211°C, lit. (20) mp 205–208°C. IR (cm^{-1}): 3343 (NH), 1616 (C=O).

Methyl 1,2,3,4-tetrahydro-β-carboline-1-carboxylate (hydrochloride salt) (14)

The carboxylic acid **13** (4.50 g, 20.80 mmol) was stirred in dry methanol (100 mL), while dry HCl gas was bubbled through the mixture for approximately 2 min. The solid dissolved giving a golden yellow solution. The mixture was then brought to reflux through 3 Å sieves in a Soxhlet apparatus for 3 h under argon. Most of the methanol (70 mL) was removed under reduced pressure. The precipitate formed was collected by suction filtration, washed with cold toluene (30 mL), and dried under vacuum, giving the ester hydrochloride as yellow crystals (5.23 g, 94%): mp 205–208°C, lit. (21) mp 212–214°C. IR (cm^{-1}): 3384 (NH), 1757 (C=O). ^{1}H NMR (DMSO-d_6) δ 3.00 (t, J = 6.0 Hz, 2H), 3.54 (t, J = 6.2 Hz, 2H), 3.88 (s, 3H), 5.70 (s, 1H), 7.05–7.20 (m, 2H), 7.44–7.52 (m, 2H), 10.30 (s, 2H), 11.17 (s, 1H).

Methyl β-carboline-1-carboxylate (6)

The ester hydrochloride **14** (4.00 g, 15.02 mmol), precipitated sulfur (1.13 g, 35.15 mmol), and 2,2,6,6-tetramethylpiperidine (2.40 g, 17.03 mmol) were heated at reflux in dry xylenes (200 mL) for 5 h giving a brown solution. Evolution of H_2S could be detected with lead acetate paper. The solution was allowed to cool slowly overnight, forming brown needles. The xylene was removed under reduced pressure and the residual solids were placed in a Soxhlet thimble and extracted with acetone (100 mL) for 3 h. The acetone extracted the ester **6** from the reaction mixture while leaving the insoluble 2,2,6,6-tetramethylpiperidine hydrochloride in the Soxhlet thimble. The acetone was removed under reduced pressure giving a brown solid. Purification of the solid by column chromatography (ethyl acetate) gave **6** as a pale yellow solid (2.94 g, 87%): mp 165 to 166°C, lit. (22) mp 166°C. IR (cm^{-1}): 3378 (NH), 1678 (C=O). ^{1}H NMR δ 4.14 (s, 3H), 7.35–7.63 (m, 3H), 8.15–8.19 (m, 2H), 8.60 (d, J = 4.8 Hz, 1H), 9.90 (s, 1H).

Xestomanzamine A (1)

Ethylmagnesium bromide (1 M in hexane) (0.5 mL, 0.50 mmol) was added dropwise to a solution of 5-iodo-1-methylimidazole **7c** (0.104 g, 0.50 mmol) in dichloromethane (15 mL) under argon at 0°C. After completing the addition, the mixture was warmed briefly with a heat gun to complete the dissolution and then allowed to stir for 1 h at room temperature. In another flask, to a stirring solution of β-carboline ester **6** (0.104 g, 0.46 mmol) and lithium chloride (0.2 g, 4.7 mmol) in dichloromethane (20 mL) under argon at 0°C, ethylmagnesium bromide (1 M in hexane) (0.5 mL, 0.50 mmol) was added dropwise with a syringe. After completion of stirring (1 h), the solution of **7c** and ethylmagnesium bromide was added by cannula dropwise to the β-carboline ester solution at 0°C. The temperature of the reaction flask was allowed to reach 25°C and the mixture was stirred for 24 h. The mixture was quenched (5% $NaHCO_3$) and extracted with dichloromethane (3 × 25 mL). The organic extracts were combined and dried (Na_2SO_4). The dichloromethane was removed under reduced pressure and the resulting solid was purified by column chromatography (ethyl acetate–methanol, 95:5) to give the final product **1** as a yellow solid (0.103 g, 81%): mp 184 to185°C, lit. (4) mp 185 to 186°C. IR (Nujol) (cm^{-1}): 3419, 1606, 1214, 1127 (lit. (4) IR (KBr pellet) (cm^{-1}): 3427, 1612, 1211, 1128). ^{1}H NMR δ 4.11 (s, 3H), 7.35 (dd, J = 7.9, 6.4 Hz, 1H), 7.55 (dd, J = 7.5, 6.4 Hz, 1H), 7.60 (d, J = 7.5 Hz, 1H), 7.69 (s, 1H), 8.17 (d, J = 4.9 Hz, 1H), 8.20 (d, J = 7.9 Hz, 1H), 8.60 (d, J = 4.9 Hz, 1H), 8.94 (s, 1H) (lit. (4) ^{1}H NMR ($CDCl_3$) δ 4.05 (s, 3H), 7.30 (dd, J = 8.2, 6.2 Hz, 1H), 7.55 (dd, J = 7.3, 6.2 Hz, 1H), 7.57 (d, J = 7.3 Hz, 1H), 7.66 (s, 1H), 8.09 (d, J = 5.0 Hz, 1H), 8.12 (d, J = 8.2 Hz, 1H), 8.55 (d, J = 5.0 Hz, 1H), 8.93 (s, 1H)). ^{13}C NMR δ 184.4, 143.8, 143.4, 141.0, 138.2, 136.7, 136.6, 131.7, 129.8, 129.3, 121.8, 120.9, 120.7, 118.6, 111.9, 35.3 (lit.(4) ^{13}C NMR ($CDCl_3$) δ 184.2, 143.6, 143.3, 140.8, 137.9, 136.5, 136.4, 131.5, 129.7, 129.6, 121.7, 120.6, 120.5, 118.4, 111.8, 35.2.

Note added in proof: After this work had been accepted for publication we became aware of a related report on the synthesis of xestomanzamines A and B: B.E.A. Burm, P. Blokker, E. Jongmans, E. van Kampen, M.J. Wanner, and G.-J. Koomen. Heterocycles, **55**, 495 (2001).

Acknowledgment

We thank the Natural Sciences and Engineering Research Council of Canada (NSERC) for partial support of this research.

References

1. (*a*) D.J. Faulkner. Nat. Prod. Rep. **17**, 1 (2000); (*b*) D.J. Faulkner. Nat. Prod. Rep. **17**, 7 (2000) and earlier annual reviews on this topic.
2. B.J. Baker. *In* Alkaloids: chemical and biological perspectives. Vol. 10. *Edited by* S.W. Pelletier. Elsevier, Oxford. 1996. p. 358.
3. B.E. Love. Org. Prep. Proced. Int. **28**, 1 (1996).
4. M. Kobayashi, Y.-J. Chen, S. Aoki, Y. In, T. Ishida, and I. Kitagawa. Tetrahedron, **51**, 3727 (1995).
5. P. Molina, P.M. Fresneda, and S. Garcia-Zafra. Tetrahedron Lett. **37**, 9353 (1996).
6. M.P. Groziak and L. Wei. J. Org. Chem. **56**, 4296 (1991).
7. B. Iddon, A.K. Peterson, J. Becher, and N.J. Christensen. J. Chem. Soc. Perkin Trans. 1, 1475 (1995).
8. C. Chassaing, A. Haudrechy, and Y. Langlois. Tetrahedron Lett. **38**, 4415 (1997).
9. A.R. Katritzky, J.J. Slawinski, F. Brunner, and S. Gorun. J. Chem. Soc. Perkin Trans. 1, 1139 (1989).
10. (*a*) I.E. Balaban and F.L. Pyman. J. Chem. Soc. 947 (1922); (*b*) I.E. Balaban and F.L. Pyman. J. Chem. Soc. 1564 (1924).
11. P. Garegg and B. Samuelsson. Synthesis, 813 (1979).
12. B. Iddon and B.L. Lim. J. Chem. Soc. Perkin Trans. 1, 735 (1983).
13. M.S.R. Naidu and H.B. Bensusan. J. Org. Chem. **33**, 1307 (1968).
14. M.D. Cliff and S.G. Pyne. J. Org. Chem. **60**, 2378 (1995).
15. T. Lindel and M. Hochgürtel. J. Org. Chem. **65**, 2806 (2000).

© 2001 NRC Canada

16. B.T. Ho and K.E. Walker. Org. Synth. **51**, 136 (1971).
17. I.W.J. Still and J. McNulty. Heterocycles, **29**, 2057 (1989).
18. R.M. Turner, S.D. Lindell, and S.V. Ley. J. Org. Chem. **56**, 5739 (1991).
19. F.B. Panosyan. M.Sc. thesis. University of Toronto. 2000.
20. J. Gynther. Acta Chem. Scand. Ser. B, **B42**, 433 (1988).
21. K.L. Rinehart Jr., J. Kobayashi, G.C. Harbour, J. Gilmore, M. Mascal, T.G. Holt, L.S. Shield, and F. Lafargue. J. Am. Chem. Soc. **109**, 3378 (1987).
22. H. Achenbach and K. Biemann. J. Am. Chem. Soc. **87**, 4177 (1965).

© 2001 NRC Canada

Synthesis and antifungal properties of benzylamines containing boronate esters

Christopher M. Vogels, Liliya G. Nikolcheva, David W. Norman, Heather A. Spinney, Andreas Decken, Mark O. Baerlocher, Felix J. Baerlocher, and Stephen A. Westcott

Abstract: Addition of 3-$H_2NC_6H_4$Bpin (pin = 1,2-$O_2C_2Me_4$) to a series of aldehydes and 4-(4,4,5,5-tetramethyl-1,3,2-dioxaborolan-2-yl)acetophenone afforded the corresponding benzylideneamines in moderate to high yields. Hydroboration of these imines with catecholborane (HBcat, cat = 1,2-$O_2C_6H_4$) at room temperature gives, upon aqueous workup, the corresponding borylamines. An X-ray diffraction study was carried out on imine **1h** derived from 9-anthraldehyde and 3-$H_2NC_6H_4$Bpin. Crystals of **1h** were triclinic, a = 9.6793(4) Å, b = 10.7397(4) Å, c = 11.5353(4) Å, α = 105.1890(10)°, β = 97.3030(10)°, γ = 102.1480(10)°, Z = 2 with space group $P\bar{1}$ and crystals of *N*-[3-(4,4,5,5-tetramethyl-1,3,2-dioxaborolan-2-yl)phenyl]-4-methoxybenzylamine **2c** were orthorhombic, a = 8.6612(4) Å, b = 10.3794(4) Å, c = 20.6033(9) Å, Z = 4 with space group $P2_12_12_1$. Amines have been tested for their antifungal properties against *Aspergillus niger* and *Aspergillus flavus*.

Key words: benzylamines, boronate esters, aminoboron, hydroboration, antifungal.

Résumé : L'addition de 3-$H_2NC_6H_4$Bpin (pin = 1,2-$O_2C_2Me_4$) à une série d'aldéhyde et à la 4-(4,4,5,5-tétraméthyl-1,3,2-dioxaborolan-2-yl)acétophénone conduit aux benzylidèneamines correspondantes avec des rendements qui vont de bons à excellents. L'hydroboration de ces imines avec du catécholborane (HBcat, cat = 1,2-$O_2C_6H_4$), à la température ambiante, fournit les borylamines correspondances après extraction. Une étude par diffraction des rayons X a été réalisée sur l'imine **1h** provenant du 9-anthraldéhyde et du 3-$H_2NC_6H_4$Bpin. Les cristaux de **1h** sont tricliniques, groupe d'espace $P\bar{1}$, avec a = 9,6793(4) Å, b = 10,7397(4) Å et c = 11,5353(4) Å, α = 105,1890(10)°, β = 97,3030(10)° et γ = 102,1480(10)° et Z = 2; les cristaux de *N*-[3-(4,4,5,5-tétraméthyl-1,3,2-dioxaboralan-2-yl)phényl]-4-méthoxybenzylamine, **2c**, sont orthorhombiques, groupe d'espace $P2_12_12_1$, avec a = 8,661(4) Å, b = 10,3794(4) Å et c = 20,6033(9) Å et Z = 4. Les amines ont été évaluées pour leur activité antifongique contre *Aspergillus niger* et *Aspergillus flavus*.

Mots clés : benzylamines, esters de l'acide boronique, aminobore, hydroboration, antifongique.

[Traduit par la Rédaction]

Introduction

The bioinorganic chemistry of boron is an area of growing interest (1–10). For example, boron-containing amino acids are among the most potent inhibitors of the serine proteases chymotrypsin and subtilisin (10). Serine proteases are a diverse group of proteolytic enzymes whose numerous physiological functions include digestion, growth, differentiation, cell signalling and migration, immunological defence, and apoptosis. Proteases are also vital in the generation of most disease processes. Much effort has therefore focused on the synthesis of boron-containing amino acid and peptide derivatives for possible applications as enzyme inhibitors. Although aminoboronic acid derivatives have significant biological activity and are useful synthetic intermediates in organic chemistry (11,12), synthetic routes to these compounds are scarce and involve complicated procedures. As a result, relatively few examples of aminoboron compounds have been studied (13–19). As part of our program to develop synthetically attractive routes to aminoboron compounds, we have prepared a series of boronated benzylamines derived from the reaction of 3-$H_2NC_6H_4$Bpin (pin = 1,2-$O_2C_2Me_4$) with various aldehydes and the boron-containing ketone 4-(4,4,5,5-tetramethyl-1,3,2-dioxaborolan-2-yl)acetophenone and tested these compounds for their antifungal properties. Results are reported herein.

Received October 20, 2000. Published on the NRC Research Press Web site at http://canjchem.nrc.ca on July 30, 2001.

C.M. Vogels, L.G. Nikolcheva, D.W. Norman, H.A. Spinney, M.O. Baerlocher, and S.A. Westcott.[1] Department of Chemistry, Mount Allison University, Sackville, NB E4L 1G8, Canada.
F.J. Baerlocher. Department of Biology, Mount Allison University, Sackville, NB E4L 1G7, Canada.
A. Decken.[2] Department of Chemistry, University of New Brunswick, Fredericton, NB E3B 5A3, Canada.

[1]Corresponding author (telephone: (506) 364-2351; fax: (506) 364-2313; e-mail: swestcott@mta.ca).
[2]Corresponding author for crystallography (telephone: (506) 453-4875; fax: (506) 453-4981; e-mail: adecken@unb.ca).

Experimental

Reagents and solvents used were obtained from Aldrich Chemicals. NMR spectra were recorded on a JEOL JNM-

 DOI: 10.1139/cjc-79-7-1115 © 2001 NRC Canada

GSX270 FT NMR spectrometer. ^{1}H NMR chemical shifts are reported in ppm and referenced to residual protons in deuterated solvent at 270.05 MHz. ^{11}B NMR chemical shifts are referenced to external $F_3B{\cdot}OEt_2$ at 86.55 MHz. ^{13}C NMR chemical shifts are referenced to solvent carbon resonances as internal standards at 67.80 MHz. Multiplicities are reported as (s) singlet, (d) doublet, (t) triplet, (q) quartet, (quint) quintet, (m) multiplet, (br) broad, and (ov) overlapping. Infrared spectra were obtained using a Mattson Genesis II FT-IR spectrometer and reported in cm^{-1}. Melting points were measured uncorrected with a Mel-Temp apparatus. Microanalyses for C, H, and N were carried out at Desert Analytics (Tucson, Arizona).

Transesterification

Protection of the starting boronic acids (10.0 mmol) with 1 equiv of pinacol was carried out in methylene chloride in the presence of 10 g of activated molecular sieves (type 4A). The reactions were allowed to proceed for 5 days at which point the sieves were removed by suction filtration and the product isolated upon removal of the solvent under vacuum.

2-(4,4,5,5-Tetramethyl-1,3,2-dioxaborolan-2-yl)benzaldehyde (2-FPBpin)

Yield: 68% of a yellow oil; bp 97°C. IR (Nujol): 2920, 2856, 1699, 1595, 1462, 1379, 1257, 1146, 860, 764, 666. ^{1}H NMR (in $CDCl_3$) δ 10.54 (s, 1H), 7.95 (d, J = 8 Hz, 1H), 7.87 (d, J = 8 Hz, 1H), 7.58 (m, 2H), 1.35 (s, 12H). ^{13}C NMR δ 194.4, 141.1, 135.3, 132.8, 130.6, 130 (br, C-B), 127.7, 84.2, 24.6. ^{11}B NMR δ 31.7 (br).

3-(4,4,5,5-Tetramethyl-1,3,2-dioxaborolan-2-yl)benzaldehyde (3-FPBpin)

Yield: 77% of a white solid; mp 49°C. IR (Nujol): 2970, 2880, 1710, 1605, 1460, 1361, 1194, 1144, 965, 702. ^{1}H NMR (in $CDCl_3$) δ 10.05 (s, 1H), 8.31 (s, 1H), 8.08 (d, J = 8 Hz, 1H), 8.00 (d, J = 8 Hz, 1H), 7.54 (t, J = 8 Hz, 1H), 1.37 (s, 12H). ^{13}C NMR δ 192.6, 140.7, 137.3, 135.8, 131.3, 130 (br, C-B), 128.4, 84.3, 24.9. ^{11}B NMR δ 31.2 (br). Anal. calcd. for $C_{13}H_{17}O_3B$: C 67.28, H 7.38; found: C 67.38, H 7.28.

4-(4,4,5,5-Tetramethyl-1,3,2-dioxaborolan-2-yl)benzaldehyde (4-FPBpin)

Yield: 71% of a pale yellow solid; mp 50°C. IR (Nujol): 2972, 2880, 1711, 1460, 1361, 1144, 858, 651. ^{1}H NMR (in $CDCl_3$) δ 10.05 (s, 1H), 7.98 (d, J = 8 Hz, 2H), 7.88 (d, J = 8 Hz, 2H), 1.37 (s, 12H). ^{13}C NMR δ 192.9, 138.8, 135.5, 135 (br, C-B), 128.8, 84.5, 25.1. ^{11}B NMR δ 31.1 (br). Anal. calcd. for $C_{13}H_{17}O_3B$: C 67.28, H 7.38; found: C 67.56, H 7.25.

4-(4,4,5,5-Tetramethyl-1,3,2-dioxaborolan-2-yl)acetophenone

Yield: 97% of a pale yellow solid; mp 60–62°C. IR (Nujol): 2941, 2858, 1691, 1556, 1508, 1460, 1360, 1265, 1215, 1144, 1093, 1016. ^{1}H NMR (in $CDCl_3$) δ 7.91 (m, 4H), 2.60 (s, 3H), 1.35 (s, 12H). ^{13}C NMR δ 197.9, 138.7, 134.7, 130 (br, C-B), 127.0, 83.9, 26.5, 24.6. ^{11}B NMR δ 31.2 (br). Anal. calcd. for $C_{14}H_{19}O_3B$: C 68.32, H 7.78; found: C 68.28, H 7.86.

Preparation of imines

Imines were prepared by combining the starting aldehyde (or ketone) with 1 equiv of 3-$H_2NC_6H_4$Bpin in methylene chloride and 10 g of activated molecular sieves (type 4A). After 3–5 days the sieves were removed by suction filtration and the imine was obtained following removal of the solvent under vacuum. Imine **1j** was isolated following crystallization from hot hexane.

1a

Yield: 81% of an off-white solid; mp 70°C. IR (Nujol): 2925, 1629, 1573, 1452, 1377, 1353, 1140, 1069, 963, 906, 801, 755. ^{1}H NMR (in $CDCl_3$) δ 8.52 (s, 1H), 7.91 (m, 2H), 7.68 (m, 2H), 7.49 (m, 3H), 7.40 (m, 2H), 1.37 (s, 12H). ^{13}C NMR δ 160.6, 151.7, 136.5, 132.6, 131.5, 129.0, 129 (br, C-B), 128.9, 128.8, 126.2, 125.0, 84.1, 25.1. ^{11}B NMR δ 31.5 (br).

1b

Yield: 79% of a bright yellow solid; mp 111°C. IR (Nujol): 2925, 2856, 1708, 1628, 1602, 1525, 1461, 1360, 1319, 1147, 1075, 967, 908, 852, 705. ^{1}H NMR (in $CDCl_3$) δ 8.61 (s, 1H), 8.35 (d, J = 8 Hz, 2H), 8.09 (d, J = 8 Hz, 2H), 7.76 (d, J = 8 Hz, 1H), 7.67 (s, 1H), 7.48–7.38 (ov m, 2H), 1.37 (s, 12H). ^{13}C NMR δ 157.6, 150.5, 149.5, 141.9, 133.7, 130 (br, C-B), 129.6, 129.0, 126.1, 125.2, 124.2, 84.3, 25.1. ^{11}B NMR δ 31.2 (br).

1c

Yield: 92% of a white solid; mp 92°C. IR (Nujol): 2968, 2893, 1705, 1620, 1605, 1572, 1510, 1456, 1352, 1248, 1140, 1026, 831, 706. ^{1}H NMR (in $CDCl_3$) δ 8.43 (s, 1H), 7.85 (d, J = 8 Hz, 2H), 7.64 (ov m, 2H), 7.39 (ov m, 2H), 6.99 (d, J = 8 Hz, 2H), 3.87 (s, 3H), 1.36 (s, 12H). ^{13}C NMR δ 162.2, 159.7, 151.8, 132.1, 130.6, 130 (br, C-B), 129.4, 128.6, 126.2, 124.9, 114.2, 83.9, 55.4, 25.0. ^{11}B NMR δ 31.6 (br).

1d

Yield: 85% of a pale yellow solid; mp 98°C. IR (Nujol): 2959, 1609, 1561, 1456, 1370, 1314, 1150, 1070, 964, 853, 791, 705. ^{1}H NMR (in $CDCl_3$) δ 8.79 (s, 1H), 7.70 (d, J = 8Hz, 1H), 7.59 (s, 1H), 7.41 (t, J = 8 Hz, 1H), 7.29 (d, J = 8 Hz, 1H), 6.92 (s, 2H), 2.53 (s, 6H), 2.32 (s, 3H), 1.37 (s, 12H). ^{13}C NMR δ 161.1, 152.8, 139.9, 138.8, 132.1, 130.8, 130 (br, C-B), 129.9, 128.7, 126.5, 124.3, 84.1, 25.0, 21.4, 21.3. ^{11}B NMR δ 32.1 (br).

1e

Yield: 82% of an off-white solid; mp 145°C. IR (Nujol): 2935, 2858, 1626, 1591, 1562, 1462, 1414, 1375, 1352, 1267, 1140, 1111, 1070, 962, 916, 856, 818, 706. ^{1}H NMR (in $CDCl_3$) δ 9.21 (s, 1H), 8.16 (d, J = 8 Hz, 1H), 7.85 (d, J = 8 Hz, 1H), 7.76 (s, 1H), 7.69 (m, 1H), 7.55–7.40 (ov m, 4H), 1.38 (s, 12H), 1.33 (s, 12H). ^{13}C NMR δ 162.6, 162.4, 151.5, 135.3, 132.1, 130.8, 130.1, 130 (br, C-B), 128.7, 127.0, 126.4, 125.4, 84.0, 83.8, 24.9, 24.8. ^{11}B NMR δ 31.3 (br).

1f

Yield: 86% of an off-white solid; mp 219°C. IR (Nujol): 2935, 2858, 1630, 1599, 1572, 1462, 1377, 1348, 1140, 964,

© 2001 NRC Canada

852, 706. ^{1}H NMR (in $CDCl_3$) δ 8.53 (s, 1H), 8.28 (s, 1H), 8.07 (d, *J* = 8 Hz, 1H), 7.93 (d, *J* = 8 Hz, 1H), 7.69 (d, *J* = 8 Hz, 1H), 7.64 (s, 1H), 7.48 (t, *J* = 8 Hz, 1H), 7.45–7.33 (ov m, 2H), 1.36 (s, 24H). ^{13}C NMR δ 160.4, 151.5, 137.6, 135.9, 135.6, 132.2, 130.9, 129.7 (br, C-B), 128.6, 128.2, 126.1, 124.8, 84.0, 24.9. ^{11}B NMR δ 31.5 (br).

1g

Yield: 92% of an off-white solid; mp 208°C. IR (Nujol): 2971, 2910, 1710, 1623, 1608, 1511, 1465, 1355, 1271, 1142, 1087, 964, 855, 702. ^{1}H NMR (in $CDCl_3$) δ 8.52 (s, 1H), 7.90 (s, 4H), 7.70 (d, *J* = 8 Hz, 1H), 7.64 (s, 1H), 7.42–7.36 (ov m, 2H), 1.36 (s, 24H). ^{13}C NMR δ 160.6, 151.5, 138.7, 135.3, 132.7, 132 (br, C-B), 129 (br, C-B), 128.8, 128.2, 126.2, 125.1, 84.1, 25.1. ^{11}B NMR δ 31.5 (br).

1h

Yield: 81% of an off-white solid; mp 209°C. IR (Nujol): 2969, 2889, 1606, 1572, 1462, 1413, 1354, 1268, 1141, 1066, 965, 852, 739, 705. ^{1}H NMR (in $CDCl_3$) δ 9.70 (s, 1H), 8.76 (d, *J* = 8 Hz, 2H), 8.55 (s, 1H), 8.06 (d, *J* = 8 Hz, 2H), 7.85 (s, 1H), 7.80 (d, *J* = 8 Hz, 1H), 7.59–7.48 (ov m, 6H), 1.39 (s, 12H). ^{13}C NMR δ 159.8, 152.0, 132.6, 131.1, 130.5, 130.4, 130 (br, C-B), 128.9, 128.7, 127.2, 127.1, 126.1, 125.3, 124.9, 124.7, 83.9, 24.8. ^{11}B NMR δ 31.4 (br).

1i

Yield: 89% of an off-white solid; mp 176°C. IR (Nujol): 2974, 2881, 1628, 1575, 1484, 1424, 1358, 1321, 1145, 1073, 965, 909, 856, 807, 708. ^{1}H NMR (in $CDCl_3$) δ 8.56 (s, 2H), 8.39 (s, 1H), 8.04 (d, *J* = 8 Hz, 2H), 7.73–7.69 (ov m, 4H), 7.55 (t, *J* = 8 Hz, 1H), 7.45–7.36 (ov m, 4H), 1.37 (s, 24H). ^{13}C NMR δ 159.6, 151.3, 137.0, 132.7, 131.2, 130 (br, C-B), 129.5, 129.3, 128.8, 126.3, 124.9, 84.0, 25.0. ^{11}B NMR δ 31.0 (br).

1j

Yield: 37% of a pale yellow solid; mp 149–152°C. IR (Nujol): 2916, 2856, 1630, 1460, 1375, 1321, 1273, 1207, 1142, 1095, 1016. ^{1}H NMR (in $CDCl_3$) δ 7.96–7.86 (ov m, 4H), 7.55 (d, *J* = 8 Hz, 1H), 7.36 (t, *J* = 8 Hz, 1H), 7.25 (s, 1H), 6.92 (d, *J* = 8 Hz, 1H), 2.22 (s, 3H), 1.37 (s, 12H), 1.34 (s, 12H). ^{13}C NMR δ 165.6, 151.0, 141.9, 134.7, 131 (br, C-B), 129.7, 128.4, 126.3, 125.3, 122.3, 83.8, 24.9, 17.6. ^{11}B NMR δ 30.9 (br).

Synthesis of amines

Catecholborane (1.2 mmol) in 5 mL of toluene was added dropwise to a stirred solution of the imine (1.0 mmol) in 10 mL of toluene under an atmosphere of dinitrogen. The reaction was allowed to proceed for 24 h at which point water (5 mL) was added. The organic phase was extracted and the corresponding amine was isolated by flash chromatography through alumina followed by removal of solvent. Conversely, formation of the amine could also be achieved by reduction of the imine with 3 equiv of $NaBH_4$ in 10 mL of methanol, followed by an organic extraction with Et_2O and filtration.

2a

Yield: 78% of a white solid; mp 86°C. IR (Nujol): 3416, 2969, 2885, 1602, 1582, 1515, 1447, 1353, 1320, 1274, 1143, 1073, 965, 863, 706. ^{1}H NMR (in $CDCl_3$) δ 7.36–7.31 (ov m, 5H), 7.18–7.15 (ov m, 3H), 6.73 (m, 1H), 4.35 (s, 2H), 1.33 (s, 12H). ^{13}C NMR δ 147.5, 139.3, 130 (br, C-B), 128.6, 128.5, 127.4, 127.1, 123.9, 119.1, 115.3, 83.5, 48.1, 24.7. ^{11}B NMR δ 31.8 (br). Anal. calcd. for $C_{19}H_{24}NO_2B$: C 73.79, H 7.84, N 4.53; found: C 73.80, H 7.59, N 4.73.

2b

Yield: 58% of a yellow solid; mp 125°C. IR (Nujol): 3418, 2971, 2883, 1599, 1579, 1518, 1459, 1342, 1140, 846, 709. ^{1}H NMR (in $CDCl_3$) δ 8.19 (d, *J* = 8 Hz, 2H), 7.53 (d, *J* = 8 Hz, 2H), 7.19–7.12 (ov m, 3H), 6.64 (m, 1H), 4.48 (s, 2H), 1.33 (s, 12H). ^{13}C NMR δ 147.5, 147.1, 146.7, 130 (br, C-B), 128.9, 127.8, 124.6, 123.8, 119.4, 115.3, 83.8, 47.5, 24.8. ^{11}B NMR δ 32.3 (br). Anal. calcd. for $C_{19}H_{23}N_2O_4B$: C 64.41, H 6.56, N 7.91; found: C 64.75, H 6.40, N 8.16.

2c

Yield: 80% of an off-white solid; mp 105°C. IR (Nujol): 3398, 2974, 2875, 1604, 1579, 1512, 1462, 1363, 1236, 1138, 1086, 1026, 847, 706. ^{1}H NMR (in $CDCl_3$) δ 7.31 (d, *J* = 8 Hz, 2H), 7.22 (ov m, 2H), 7.17 (s, 1H), 6.91 (d, *J* = 8 Hz, 2H), 6.76–6.71 (m, 1H), 4.29 (s, 2H), 3.82 (s, 3H), 1.35 (s, 12H). ^{13}C NMR δ 158.8, 147.6, 131.4, 130 (br, C-B), 128.9, 128.7, 124.0, 119.2, 115.5, 114.0, 83.7, 55.3, 47.8, 24.8. ^{11}B NMR δ 32.6 (br). Anal. calcd. for $C_{20}H_{26}NO_3B$: C 70.81, H 7.74, N 4.13; found: C 71.17, H 7.88, N 4.42.

2d

Yield: 70% of a white solid; mp 126°C. IR (Nujol): 3397, 2967, 2883, 1603, 1581, 1511, 1464, 1376, 1273, 1142, 1086, 857, 707. ^{1}H NMR (in $CDCl_3$) δ 7.26–7.17 (ov m, 2H), 7.11 (m, 1H), 6.89 (s, 2H), 6.77 (m, 1H), 4.21 (s, 2H), 2.33 (s, 6H), 2.29 (s, 3H), 1.35 (s, 12H). ^{13}C NMR δ 148.0, 137.5, 137.2, 132.4, 130 (br, C-B), 129.0, 128.7, 123.7, 118.2, 115.6, 83.7, 42.4, 24.8, 20.9, 19.4. ^{11}B NMR δ 33.0 (br). Anal. calcd. for $C_{22}H_{30}NO_2B$: C 75.20, H 8.62, N 3.99; found: C 74.89, H 8.59, N 4.08.

2e

Yield: 78% of a white solid; mp 138°C. IR (Nujol): 3429, 2943, 2868, 1603, 1581, 1518, 1452, 1377, 1350, 1142, 964, 852, 706. ^{1}H NMR (in $CDCl_3$) δ 7.85 (d, *J* = 8 Hz, 1H), 7.38–7.33 (ov m, 2H), 7.25 (t, *J* = 8 Hz, 1H), 7.18–7.16 (ov m, 3H), 6.75 (m, 1H), 4.55 (s, 2H), 1.33 (s, 12H), 1.32 (s, 12H). ^{13}C NMR δ 147.8, 145.7, 136.1, 130.9, 129 (br, C-B), 128.5, 128.3, 128 (br, C-B), 126.4, 123.6, 119.6, 115.8, 83.6, 83.4, 48.2, 24.8. ^{11}B NMR δ 31.9 (br). Anal. calcd. for $C_{25}H_{35}NO_4B_2$: C 68.99, H 8.12, N 3.22; found: C 69.27, H 8.06, N 3.39.

2f

Yield: 74% of a white solid; mp 166°C. IR (Nujol): 3361, 2970, 2868, 1606, 1583, 1522, 1460, 1363, 1144, 1090, 964, 852, 708. ^{1}H NMR (in $CDCl_3$) δ 7.78 (s, 1H), 7.70 (d, *J* = 8 Hz, 1H), 7.44 (d, *J* = 8 Hz, 1H), 7.30 (t, *J* = 5 Hz, 1H), 7.15–7.10 (ov m, 3H), 6.67 (m, 1H), 4.29 (s, 2H), 1.31 (s, 12H), 1.29 (s, 12H). ^{13}C NMR δ 147.5, 138.7, 134.0, 133.6, 130.6, 129 (br, C-B), 128.7, 128.0, 123.9, 119.3, 115.4, 83.8, 83.6, 48.3, 24.8. ^{11}B NMR δ 31.4 (br). Anal. calcd. for

© 2001 NRC Canada

$C_{25}H_{35}NO_4B_2$: C 68.99, H 8.12, N 3.22; found: C 69.27, H 8.10, N 3.37.

2g

Yield: 68% of a white solid; mp 131°C. IR (Nujol): 3402, 2972, 2870, 1608, 1579, 1518, 1446, 1360, 1275, 1144, 1092, 962, 856, 706. ^{1}H NMR (in $CDCl_3$) δ 7.79 (d, *J* = 8 Hz, 2H), 7.35 (d, *J* = 8 Hz, 2H), 7.16–7.14 (ov m, 3H), 6.65 (m, 1H), 4.31 (s, 2H), 1.31 (s, 24H). ^{13}C NMR δ 147.5, 142.8, 135.1, 129 (br, C-B), 128.7, 127 (br, C-B), 126.8, 124.0, 119.3, 115.4, 83.7, 48.3, 24.9. ^{11}B NMR δ 31.7 (br). Anal. calcd. for $C_{25}H_{35}NO_4B_2$: C 68.99, H 8.12, N 3.22; found: C 69.18, H 7.98, N 3.69.

2h

Yield: 69% of a white solid; mp 205°C. IR (Nujol): 3392, 2968, 2864, 1599, 1581, 1512, 1429, 1350, 1323, 1277, 1140, 966, 852, 731, 708. ^{1}H NMR (in $CDCl_3$) δ 8.57 (s, 1H), 8.38 (d, *J* = 8 Hz, 2H), 8.15 (d, *J* = 8 Hz, 2H), 7.65–7.55 (ov m, 4H), 7.45–7.35 (ov m, 3H), 7.00 (m, 1H), 5.27 (s, 2H), 1.48 (s, 12H). ^{13}C NMR δ 147.8, 131.5, 130.4, 129.5, 129.1, 129 (br, C-B), 128.8, 127.8, 126.4, 125.1, 124.2, 124.1, 118.3, 115.8, 83.7, 40.9, 24.8. ^{11}B NMR δ 33.2 (br). Anal. calcd. for $C_{27}H_{28}NO_2B$: C 79.21, H 6.91, N 3.42; found: C 79.27, H 7.05, N 3.46.

2i

Yield: 70% of a white solid; mp 60°C. IR (Nujol): 3392, 2973, 2883, 2841, 1604, 1581, 1510, 1462, 1377, 1144, 1076, 964, 852, 785, 704. ^{1}H NMR (in $CDCl_3$) δ 7.33 (s, 1H), 7.30–7.24 (ov m, 3H), 7.18–7.14 (ov m, 6H), 6.69 (m, 2H), 4.31 (s, 4H), 1.33 (s, 24H). ^{13}C NMR δ 147.7, 140.0, 130 (br, C-B), 129.0, 128.9, 126.9, 126.6, 124.2, 119.4, 115.6, 83.8, 48.4, 25.0. ^{11}B NMR δ 31.7 (br). Anal. calcd. for $C_{32}H_{42}N_2O_4B_2$: C 71.12, H 7.85, N 5.19; found: C 70.93, H 8.06, N 5.29.

2j

Yield: 31% of a white solid; mp 170°C. IR (Nujol): 3361, 2927, 2856, 1610, 1581, 1523, 1462, 1375, 1360, 1317, 1270, 1240, 1211, 1140. ^{1}H NMR (in $CDCl_3$) δ 7.78 (d, *J* = 8 Hz, 2H), 7.39 (d, *J* = 8 Hz, 2H), 7.10–7.03 (ov m, 3H), 6.48 (m, 1H), 4.56 (q, *J* = 8 Hz, 1H), 4.04 (br s, 1H), 1.51 (d, *J* = 8 Hz, 3H), 1.33 (s, 24H). ^{13}C NMR δ 148.5, 146.6, 135.1, 129 (br, C-B), 128.6, 127 (br, C-B), 125.3, 123.6, 120.4, 115.3, 83.6, 53.4, 24.8, 24.7. ^{11}B NMR δ 31.9 (br). Anal. calcd. for $C_{26}H_{37}NO_4B_2$: C 69.52, H 8.30, N 3.12; found: C 70.09, H 8.21, N 3.23.

Biological testing

New boron compounds were tested for antifungal activity against pure cultures of *Aspergillus niger* and *Aspergillus flavus* supplied by Ward's Natural Science Ltd. (St. Catharines, Ontario, Canada). Cultures were maintained on Sabouraud dextrose agar (20, 21). Eight agar plugs (10 mm diameter) were cut from a 5–8 day-old colony and homogenized in distilled, sterilized water (4 mL). From this suspension, 0.5 mL was transferred aseptically to a Petri plate with Sabouraud dextrose agar (15 mL) and spread evenly over the entire surface. Each plate was provided with four evenly spaced paper disks (7 mm Whatman Number 1 filter paper) containing the boron compound (0, 25, 50, and 100 μg respectively). Each compound was applied to the disks as a solution (50 mg compound per 10 mL of acetone) where control disks were treated with neat acetone (20 μL). Test plates with fungal homogenates were incubated at 20°C for 48 h. Four replicate plates were used for each test. Antifungal activity was taken by the diameter of the clear zone surrounding the disk.

X-ray crystallography

Crystals of **1h** and **2c** were grown from methylene chloride solutions cooled to 5°C. Single crystals were mounted using a glass fibre and Paratone-N oil and frozen in the cold stream of the goniometer. Data were collected on a Bruker AXS P4/SMART 1000 diffractometer using ω and φ scans with a scan width of 0.3° and 30 s exposure times. The detector distance was 4 cm. The data were reduced (SAINT) and corrected for absorption (SADABS). The structures were solved by direct methods and refined by full-matrix least-squares on F^2(SHELXTL). All non-hydrogen atoms were refined anisotropically. Hydrogen atoms were located in Fourier difference maps and refined isotropically. Crystallographic data are summarized in Table 1 and atomic coordinates, thermal parameters, and bond lengths and angles have been deposited as supporting information.[3]

Results and discussion

We have found that attempts to prepare imines from 3-aminophenylboronic acid (3-$H_2NC_6H_4B(OH)_2$) proved exceedingly difficult owing to the ease with which boronic acids form insoluble anhydrides (6). However, protection of the boronic acid groups can be accomplished by transesterification with pinacol ($HOCMe_2CMe_2OH$) to afford quantitative formation of the organic soluble aminoboronate ester 3-$H_2NC_6H_4$Bpin (pin = 1,2-$O_2C_2Me_4$) (22). Reactions of this amine with aldehydes proceed smoothly to give the corresponding boron-containing aldimines **1a**–**i** in moderate to high yields (Fig. 1). This methodology provides an easy and general route to imines derived from aniline and benzaldehyde derivatives where the boronate ester functionality can be selectively incorporated into either or both of the aryl groups. Imines containing boronate esters are important intermediates in organic chemistry and have been used recently to prepare a number of pharmacologically important compounds (23–27). For instance, Whiting and co-workers (23) have recently used imine intermediates containing boronate esters to make enantio-enriched γ-phenyl-γ-amino alcohols. Incorporation of the boronate ester functionality in these cases is accom-

[3] Supplementary material may be purchased from the Depository of Unpublished Data, Document Delivery, CISTI, National Research Council Canada, Ottawa, ON K1A 0S2, Canada (http://www.nrc.ca/cisti/irm/unpub_e.shtml for information on ordering electronically). Crystallographic data have been deposited with the Cambridge Crystallographic Data Centre (CCDC nos. 160253 and 160254). Copies of the data can be obtained, free of charge, on application to the Director, CCDC, 12 Union Road, Cambridge CB2 1EZ, U.K. (Fax: 44-1223-336033 or e-mail: deposit@ccdc.cam.ac.uk).

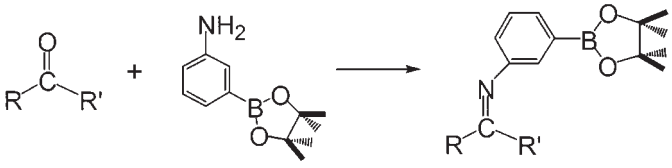
© 2001 NRC Canada

Table 1. Crystallographic data collection parameters for **1h** and **2c**.

Complex	**1h**	**2c**
Formula	$C_{27}H_{26}BNO_2$	$C_{20}H_{26}BNO_3$
FW	407.30	339.23
Crystal system	Triclinic	Orthorhombic
Space group	$P\bar{1}$	$P2_12_12_1$
a (Å)	9.6793(4)	8.6612(4)
b (Å)	10.7397(4)	10.3794(4)
c (Å)	11.5353(4)	20.6033(9)
α (deg)	105.1890(10)	90
β (deg)	97.3030(10)	90
γ (deg)	102.1480(10)	90
V (Å^3)	1110.01(7)	1852.20(14)
Z	2	4
ρ_{calcd} (g cm^{-3})	1.219	1.217
Crystal size (mm^3)	0.125 × 0.250 × 0.275	0.150 × 0.275 × 0.350
Temperature (K)	173(1)	173(1)
Radiation	Mo Kα (λ = 0.71073)	Mo Kα (λ = 0.71073)
μ (mm^{-1})	0.075	0.080
Total reflections[a]	12 380	20 702
Total unique relections	7720	6618
No. of variables	384	331
R_{int}	0.0140	0.0188
θ range (deg)	1.86–32.50	1.98–32.50
Largest difference		
Peak/hole (e Å^{-3})	0.407/–0.155	0.374/–0.132
R^a	0.0476	0.0382
R_w	0.1301	0.0901
GoF	0.924	0.969

[a] $R = \Sigma||F_o| - |F_c||\Sigma|F_o|$; $R_w = (\Sigma[w(F_o^2 - F_c^2)^2/\Sigma[wF_o^4])^{1/2}$.

Fig. 1. Synthesis of boronated benzylideneamines.



1

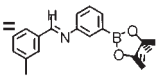
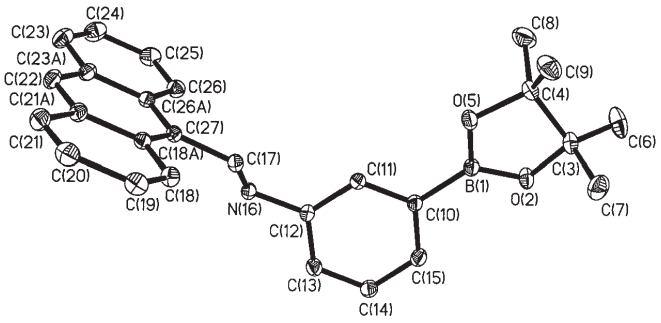
a: R = C_6H_5, R' = H
b: R = 4-$C_6H_4NO_2$, R' = H
c: R = 4-C_6H_4OMe, R' = H
d: R = 2,4,6-$C_6H_2Me_3$, R' = H
e: R = 2-C_6H_4Bpin, R' = H
f: R = 3-C_6H_4Bpin, R' = H
g: R = 4-C_6H_4Bpin, R' = H
h: R =  R' = H
i: R =  R' = H
j: R = 4-C_6H_4Bpin, R' = Me

Fig. 2. Molecular structure of **1h** with ellipsoids drawn at the 30% probability level. Hydrogen atoms were omitted for clarity.



plished by deprotonation of acetophenone-derived imines followed by alkylation with ICH_2Bpin at low temperatures. Reduction of these imines is subsequently achieved with BH_3 reagents. Likewise, boronated imines have been used in Suzuki–Miyaura cross-coupling reactions in the synthesis of 4-substituted phenylalanine derivatives (24). Carborane imines have also been prepared lately for use in boron neutron capture therapy (28).

In this study, we have found that aldimines **1a**–**i** show a signal for the N=CH methine proton between δ 8.50 and 9.70 ppm in the ^{1}H NMR spectra and a resonance at ca. 160 ppm in the ^{13}C NMR spectra corresponding to this sp^2 carbon. A broad peak at around 30 ppm in the ^{11}B NMR spectra is observed for all aldimines, indicating that the boron atom lies in a three-coordinate C-Bpin environment (29). This result is somewhat surprising for the 2-FPBpin derivative **1e** as it suggests no significant intramolecular interac-

© 2001 NRC Canada

Table 2. Selected bond lengths (Å) and angles (°) for **1h** and **2c**.

Compound **1h**		Compound **2c**	
Bond lengths (Å)			
B(1)—O(2)	1.358(1)	B(1)—O(2)	1.368(1)
B(1)—O(5)	1.365(1)	B(1)—O(5)	1.367(1)
B(1)—C(10)	1.554(1)	B(1)—C(10)	1.554(1)
O(2)—C(3)	1.465(1)	O(2)—C(3)	1.466(1)
C(4)—O(5)	1.462(1)	C(3)—C(4)	1.5651(1)
C(10)—C(15)	1.397(1)	C(4)—O(5)	1.469(1)
C(10)—C(11)	1.400(1)	C(10)—C(11)	1.392(1)
C(11)-C(12)	1.392(1)	C(11)—C(12)	1.404(1)
C(12)—C(13)	1.394(1)	C(12)—N(16)	1.385(1)
C(12)—N(16)	1.423(1)	N(16)—C(17)	1.451(2)
C(13)—C(14)	1.387(1)	C(17)—C(18)	1.511(2)
C(14)—C(15)	1.390(1)	C(18)—C(19)	1.392(2)
N(16)—C(17)	1.277(1)	C(19)—C(20)	1.380(2)
C(17)—C(27)	1.473(1)	C(20)—C(21)	1.396(2)
		C(21)—O(24)	1.370(1)
		O(24)—C(25)	1.425(1)
Bond angles (°)			
O(2)-B(1)-O(5)	113.71(8)	O(5)-B(1)-O(2)	113.51(8)
O(2)-B(1)-C(10)	124.75(8)	O(5)-B(1)-C(10)	123.68(9)
O(5)-B(1)-C(10)	121.52(7)	O(2)-B(1)-C(10)	122.81(9)
B(1)-O(2)-C(3)	106.72(7)	B(1)-O(2)-C(3)	107.37(8)
B(1)-O(5)-C(4)	107.57(7)	B(1)-O(5)-C(4)	107.10(7)
C(15)-C(10)-B(1)	121.97(8)	C(11)-C(10)-C(15)	118.78(9)
C(11)-C(10)-B(1)	119.71(8)	C(11)-C(10)-B(1)	119.49(8)
C(11)-C(12)-N(16)	122.28(8)	C(15)-C(10)-B(1)	121.73(9)
C(13)-C(12)-N(16)	118.50(8)	N(16)-C(12)-C(11)	118.56(9)
C(17)-N(16)-C(12)	117.41(7)	C(13)-C(12)-C(11)	117.77(9)
N(16)-C(17)-C(27)	123.36(8)	C(12)-N(16)-C(17)	122.63(10)
C(19)-C(18)-C(18A)	121.47(8)	N(16)-C(17)-C(18)	110.29(10)
C(26A)-C(27)-C(17)	121.68(7)	C(23)-C(18)-C(19)	117.86(10)
C(18A)-C(27)-C(17)	117.78(7)	C(23)-C(18)-C(17)	119.78(12)
		C(20)-C(19)-C(18)	121.52(10)
		O(24)-C(21)-C(22)	124.23(9)
		O(24)-C(21)-C(20)	115.83(10)
		C(21)-O(24)-C(25)	116.96(8)

tion exists between the boron atom and the imine nitrogen (30). Yet we have found that imines derived from 2-FPBpin and ethylene diamine show considerable interaction in both solution and in the solid state.[4] An X-ray diffraction study on **1h** was carried out to verify the formation of imines in these reactions. The molecular structure of **1h** is shown in Fig. 2 and crystallographic data given in Table 1. Selected bond distances and angles are shown in Table 2 and atomic coordinates are provided in Table 3. The imine C(17)—N(16) bond distance of 1.277(1) Å is comparable to azomethine compounds derived from salicylaldehyde and phenylboronic acid (25). The B—O bond distances (avg = 1.361(1) Å) are also typical for three-coordinate Bpin groups (22) and significantly shorter than those observed in chelate complexes with diphenylborinic acid (ca. 1.5 Å), where the boron atom is four-coordinate (31). Interestingly, **1h** is distorted from planarity as the anthracene ring is twisted 87.3° away from the N(16)–arene plane.

Diboronated imines will be of special interest as potential enzyme inhibitors as the corresponding amines contain two boron groups that may enhance specific binding to biomolecules. Along with aldimines **1e**–**g** we have prepared the diboronated ketimine derivative **1j** from a condensation reaction of 3-$H_2NC_6H_4$Bpin with 4-(4,4,5,5-tetramethyl-1,3,2-dioxaborolan-2-yl)acetophenone. Although the methyl group for this compound shows a peak at δ 2.22 ppm in the ^{1}H NMR spectra, two different pinacol resonances are observed at 1.37 and 1.34 ppm, suggesting slightly different environments for the Bpin groups. The ^{11}B NMR spectra for **1j**, however, shows only one peak at δ 30.9 ppm as the two different boron resonances could not be differentiated.

Reduction of imines **1a**–**j** using $NaBH_4$ in methanol gave selective formation of the corresponding benzylamines **2a**–**j** in low to moderate yields. Related benzylaminoboronic acids have been reported previously (32). Indeed, benzazaborole derivatives have been prepared by condensation of 2-

[4] L.G. Nikolcheva, C.M. Vogels, A. Decken, S.A. Westcott. Unpublished results.

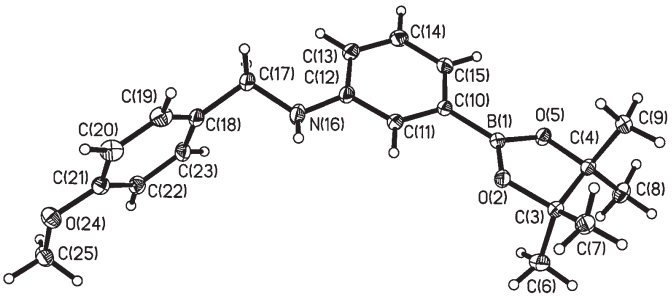
© 2001 NRC Canada

Table 3. Atomic coordinates ($\times 10^4$) and equivalent isotropic displacement parameters ($Å^2 \times 10^3$) for **1h**.

	x	*y*	*z*	*U*(eq)
B(1)	2413(1)	8553(1)	9366(1)	25(1)
O(2)	1830(1)	9096(1)	10 326(1)	31(1)
C(3)	2460(1)	8731(1)	11 373(1)	30(1)
C(4)	2938(1)	7461(1)	10 749(1)	31(1)
O(5)	3165(1)	7667(1)	9577(1)	34(1)
C(6)	1342(1)	8519(2)	12 155(1)	54(1)
C(7)	3713(2)	9909(1)	12 082(1)	49(1)
C(8)	1770(2)	6174(1)	10 459(1)	53(1)
C(9)	4335(1)	7343(2)	11 409(1)	46(1)
C(10)	2301(1)	8907(1)	8141(1)	24(1)
C(11)	2675(1)	8100(1)	7128(1)	24(1)
C(12)	2675(1)	8427(1)	6037(1)	23(1)
C(13)	2275(1)	9577(1)	5949(1)	28(1)
C(14)	1904(1)	10 390(1)	6945(1)	31(1)
C(15)	1908(1)	10 057(1)	8031(1)	28(1)
N(16)	3028(1)	7606(1)	4991(1)	25(1)
C(17)	4085(1)	7097(1)	5169(1)	24(1)
C(18)	7098(1)	7411(1)	5076(1)	28(1)
C(18A)	6022(1)	6378(1)	4172(1)	23(1)
C(19)	8529(1)	7564(1)	5048(1)	33(1)
C(20)	8987(1)	6718(1)	4092(1)	35(1)
C(21)	8002(1)	5738(1)	3199(1)	32(1)
C(21A)	6490(1)	5522(1)	3209(1)	26(1)
C(22)	5480(1)	4498(1)	2312(1)	29(1)
C(23A)	4013(1)	4252(1)	2342(1)	27(1)
C(23)	3002(1)	3141(1)	1455(1)	36(1)
C(24)	1580(1)	2873(1)	1504(1)	41(1)
C(25)	1084(1)	3708(1)	2437(1)	36(1)
C(26)	2006(1)	4784(1)	3295(1)	30(1)
C(26A)	3516(1)	5107(1)	3287(1)	24(1)
C(27)	4529(1)	6179(1)	4181(1)	23(1)

Note: *U*(eq) is defined as one-third of the trace of the orthogonalized U^{ij} tensor.

Fig. 3. Molecular structure of **2c** with ellipsoids drawn at the 30% probability level. Hydrogen atoms were omitted for clarity.



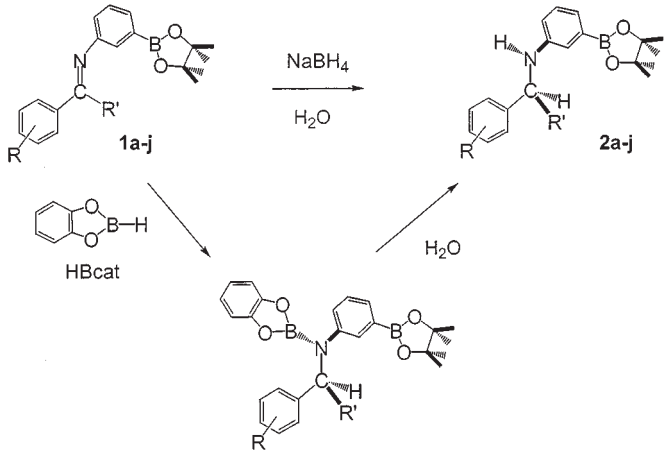
(aminomethyl)benzene boronic acids (33–35). Protection of the boronic acid group by transesterification with pinacol, however, inhibits such intramolecular cyclizations from occurring in the case of **2e**. Formation of amines **2a**–**j** in these reactions is monitored by disappearance of the imine N=CH resonance in the ^{1}H NMR spectra with concomitant formation of a peak at around δ 4.3 ppm corresponding to a benzylic CH_2 resonance. Once again, the ^{11}B NMR spectra show broad peaks around δ 30 ppm, suggesting no significant intramolecular or intermolecular N → B interaction is occurring in these complexes. An X-ray diffraction study was carried out on **2c** to confirm this result. The molecular structure of **2c** is shown in Fig. 3 and selected bond distances and angles are given in Table 2. Atomic coordinates are provided in Table 4. As expected, the N(16)—C(17) bond distance of 1.451(2) Å in **2c** is significantly longer than the double bond observed for **1h**. The B—O bond distances are once again typical for three-coordinate Bpin environments at B(1)—O(5) 1.367(1) and B(1)—O(2)

Table 4. Atomic coordinates ($\times 10^4$) and equivalent isotropic displacement parameters ($Å^2 \times 10^3$) for **2c**.

	x	*y*	*z*	*U*(eq)
B(1)	8800(1)	2734(1)	1477(1)	26(1)
O(2)	9301(1)	3805(1)	1801(1)	30(1)
C(3)	10 808(1)	4156(1)	1530(1)	29(1)
C(4)	10 761(1)	3500(1)	846(1)	27(1)
O(5)	9692(1)	2423(1)	952(1)	29(1)
C(6)	12 021(2)	3595(1)	1984(1)	43(1)
C(7)	10 924(2)	5609(1)	1518(1)	38(1)
C(8)	12 286(1)	2957(1)	608(1)	40(1)
C(9)	10 030(1)	4338(1)	325(1)	34(1)
C(10)	7365(1)	1945(1)	1694(1)	26(1)
C(11)	6720(1)	2168(1)	2302(1)	28(1)
C(12)	5437(1)	1474(1)	2529(1)	30(1)
C(13)	4769(1)	574(1)	2110(1)	36(1)
C(14)	5396(1)	345(1)	1501(1)	38(1)
C(15)	6699(1)	1007(1)	1293(1)	33(1)
N(16)	4957(1)	1662(1)	3163(1)	40(1)
C(17)	3431(1)	1300(2)	3389(1)	53(1)
C(18)	3371(1)	1329(1)	4121(1)	39(1)
C(19)	2542(1)	2259(1)	4462(1)	42(1)
C(20)	2472(1)	2252(1)	5131(1)	41(1)
C(21)	3266(1)	1308(1)	5479(1)	30(1)
C(22)	4106(1)	371(1)	5151(1)	32(1)
C(23)	4140(1)	390(1)	4477(1)	39(1)
O(24)	3135(1)	1374(1)	6141(1)	38(1)
C(25)	4089(2)	530(1)	6511(1)	40(1)

Note: *U*(eq) is defined as one-third of the trace of the orthogonalized U^{ij} tensor.

Fig. 4. Reduction of boronated benzylideneamines.



© 2001 NRC Canada

Table 5. Boron compounds tested for antifungal activity.

Entry	Compound	Dose (μg/disk)	Diameter of clear zone (mm)	
			A. niger	*A. flavus*
1	PhC(O)H	100	0	0
2	2-FPBA	25	16.2	13.4
3	2-FPBpin	25	12.0	9.4
4	3-$H_2NC_6H_4B(OH)_2$	100	0	0
5	**2b**	100	3.0	4.5
6	**2c**	100	9.0	6.3
7	**2e**	100	0	0

Note: Each compound was introduced onto a small paper disk which was placed in a culture medium. The diameter of the clear zone (the area where fungus — *A. niger* or *A. flavus* — did not grow) around each disk indicated antifungal activity.

1.368(1) Å. No significant interaction between the boron and nitrogen atoms is observed.

Interestingly, reduction of the imines could also be carried out using the gentle hydroboration reagent, catecholborane (HBcat, cat = 1,2-$O_2C_6H_4$). Reactions proceed to give the corresponding *N*-borylamine products where the hydride has added to the imine carbon and the electron deficient boryl group (BR_2) is bound to the electron rich nitrogen atom (Fig. 4). Interestingly, the ^{11}B NMR spectra for these multiply borated intermediates show broad overlapping peaks around δ 30 and 21 ppm corresponding to the C-Bpin and N-Bcat resonances, respectively. Addition of catecholborane to these bulky imines usually requires reaction times of up to 2 h. Subsequent addition of water to the *N*-borylamine intermediates afforded the benzylamines **2a**–**j** along with boric acid. Unfortunately, we were unable to affect hydroborations of these imines using pinacolborane (HBpin), even when a metal catalyst was employed (36, 37). This result is not surprising as HBpin is a significantly less reactive borane than HBcat (38).

Recent studies have shown that related heterocyclic boron compounds show appreciable antifungal activity (39–41). We therefore decided to examine these new benzylamine derivatives for their antifungal activities (42). Selected results for these compounds are shown in Table 5. Benzaldehyde was tested as a control and, as expected, showed no antifungal behaviour against either *A. niger* or *A. flavus*. Remarkably, both 2-formylphenylboronic acid (2-FPBA, Entry 2) and 2-FPBpin (Entry 3) showed considerable fungitoxicity, with the unprotected boronic acid showing slightly enhanced activity over the pinacolated derivative. These data suggest that the boron groups are responsible for the observed toxicities. Unfortunately, no activity was observed with the analogous 3- and 4-boronated derivatives (3- and 4-FPBpin) or the amine control, 3-$H_2NC_6H_4B(OH)_2$ (Entry 4). Of all the benzylamine derivatives tested, only **2b** (Entry 5) and **2c** (Entry 6) showed any appreciable activity. Higher doses of the amine, as compared with the aldehyde derivatives (100 vs. 25 μg/disk), were required. Somewhat surprising is the observation that the amine derived from 2-FPBpin (**2e**) showed no toxicity even at these higher doses (Entry 7). Further work is therefore being conducted to further our understanding of the role boron plays in fungitoxicity. The results of which will be reported in due course.

Conclusion

We have prepared a number of new imines containing boronate ester groups via condensation reactions with 3-$H_2NC_6H_4$Bpin (pin = 1,2-$O_2C_2Me_4$) and readily available aldehydes. A novel diboronated ketimine derived from 3-$H_2NC_6H_4$Bpin and 4-(4,4,5,5-tetramethyl-1,3,2-dioxaborolan-2-yl)acetophenone was also prepared. Reduction of these imines with catecholborane generated the corresponding amines, upon aqueous workup. This methodology provides an easy and efficient route to secondary benzylamines containing boronate esters where the boron functionality can be selectively incorporated into either or both of the amine aryl rings. We have also found that several of these boron containing compounds display antifungal behaviour against both *A. niger* and *A. flavus*.

Acknowledgements

Thanks are gratefully extended to the Natural Sciences and Engineering Research Council of Canada (NSERC), the Research Corporation (Cottrell College Science Award), the University of New Brunswick, and Mount Allison University for financial support. We also wish to thank Dan Durant, Roger Smith, and Jackie Jacob for their expert technical assistance, Dr. Hilary Jenkins (St. Mary's University) for the generous gift of 9-anthraldehyde, and anonymous reviewers for helpful comments.

References

1. C. Morin. Tetrahedron, **50**, 12 521 (1994).
2. V.S. Stroll, B.T. Eger, R.C. Hynes, V. Martichonok, J.B. Jones, and E.F. Pai. Biochemistry, **37**, 451 (1998).
3. Z.-Y. Zhang and B.D. Smith. J. Am. Chem. Soc. **120**, 7141 (1998).
4. G.S. Weston, J. Blázquez, F. Baquero, and B.K. Shoichet. J. Med. Chem. **41**, 4577 (1998).
5. D. Bao, W.P. Huskey, C.A. Kettner, and F. Jordan. J. Am. Chem. Soc. **121**, 4684 (1999).
6. V. Martichonok and J.B. Jones. J. Am. Chem. Soc. **118**, 950 (1996).
7. E. Skordalakes, R. Tyrell, S. Elgendy, C.A. Goodwin, D. Green, G. Dodson, M.F. Scully, J.-M.H. Freyssinet, V.V. Kakkar, and J.J. Deadman. J. Am. Chem. Soc. **119**, 9935 (1997).

© 2001 NRC Canada

8. J.D. Cox, N.N. Kim, A.M. Traish, and D.W. Christianson. Nat. Struct. Biol. **6**, 1043 (1999).
9. Z.-Q. Tian, B.B. Brown, D.P. Mack, C.A. Hutton, and P.A. Bartlett. J. Org. Chem. **62**, 514 (1997).
10. C.A. Kettner and A.B. Shenvi. J. Biol. Chem. **259**, 15106 (1984).
11. N. Miyaura and A. Suzuki. Chem. Rev. **95**, 2457 (1995).
12. S. Sakuma, M. Sakai, R. Itooka, and N. Miyaura. J. Org. Chem. **65**, 5951 (2000).
13. H. Eggert, J. Frederiksen, C. Morin, and J.C. Norrild. J. Org. Chem. **64**, 3846 (1999).
14. R.J. Snow, W.W. Bachovchin, R.W. Barton, S.J. Campbell, S.J. Coutts, D.M. Freeman, W.G. Gutheil, T.A. Kelly, C.A. Kennedy, D.A. Krolikowski, S.F. Leonard, C.A. Pargellis, L. Tong, and J. Adams. J. Am. Chem. Soc. **116**, 10 860 (1994).
15. C.S. Brosz, J.C. Calabrese, and C.A. Kettner. Tetrahedron: Asymmetry, **8**, 1435 (1997).
16. C.J. Ward, P. Patel, P.R. Ashton, and T.D. James. Chem. Commun. 229 (2000).
17. J.J.S. Lamba and J.M. Tour. J. Am. Chem. Soc. **116**, 11 723 (1994).
18. A. Dicko, M. Montury, and M. Baboulene. Synth. Commun. **18**, 459 (1988).
19. J.M. Jego, B. Carboni, and M. Vaultier. J. Organomet. Chem. **435**, 1 (1992).
20. E. Block, R. DeOrazio, and M. Thiruvazhi. J. Org. Chem. **5**9 2273 (1994).
21. F.J. Baerlocher, R.F. Langler, M.U. Frederiksen, N.M. Georges, and R.D. Witherell. Aust. J. Chem. **52**, 167 (1999).
22. C.M. Vogels, H.L. Wellwood, K. Biradha, M.J. Zawortko, and S.A. Westcott. Can. J. Chem. **77**, 1196 (1999), and refs. therein.
23. H.E. Sailes, J.P. Watts, and A. Whiting. Tetrahedron Lett. **41**, 2457 (2000).
24. F. Firooznia, C. Gude, K. Chan, N. Marcopulos, and Y. Satoh. Tetrahedron Lett. **40**, 213 (1999).
25. H. Höpfl, M. Sánchez, N. Farfán, and V. Barba. Can. J. Chem. **76**, 1352 (1998).
26. M.P. Hughes and B.D. Smith. J. Org. Chem. **62**, 4492 (1997).
27. M.P. Groziak, A.D. Ganguly, and P.D. Robinson. J. Am. Chem. Soc. **116**, 7597 (1994).
28. I.B. Sivaev, A.B. Bruskin, V.V. Nesterov, M. Yu. Antipin, V.I. Bregadze, and S. Sjöberg. Inorg. Chem. **38**, 5887 (1999).
29. H. Nöth and B. Wrackmeyer. *In* Nuclear magnetic resonance spectroscopy of boron compounds. Springer–Verlag, Berlin. 1978.
30. H. Höpfl, M. Sánchez, V. Barba, N. Farfán, S. Rojas, and R. Santillan. Inorg. Chem. **37**, 1679 (1998).
31. J. Grünefeld, W. Kliegel, S.J. Rettig, and J. Trotter. Can. J. Chem. **77**, 439 (1999).
32. A.M. Genaev, S.M. Nagy, G.E. Salnikov, and V.G. Shubin. Chem. Comm. 1587 (2000).
33. P.T. Hawkins and A.U. Blackham. J. Org. Chem. **32**, 597 (1967).
34. H.E. Dunn, J.C. Catlin, and H.R. Synder. J. Org. Chem. **33**, 4483 (1968).
35. M. Lauer and G. Wulff. J. Organomet. Chem. **256**, 1 (1986).
36. I. Beletskaya and A. Pelter. Tetrahedron, **53**, 4957 (1997).
37. R.T. Baker, J.C. Calabrese, and S.A. Westcott. J. Organomet. Chem. **498**, 109 (1995).
38. S. Pereira and M. Srebnik. Tetrahedron Lett. **37**, 3283 (1996).
39. T. Pandey and R.V. Singh. Main Group Met. Chem. **23**, 345 (2000).
40. T. Pandey and R.V. Singh. Synth. React. Inorg. Met. Org. Chem. **30**, 855 (2000), and refs. therein.
41. T. Pandey and R.V. Singh. Met. Based Drugs, **7**, 7 (2000).
42. F.J. Baerlocher, M.O. Baerlocher, C.L. Chaulk, R.F. Langler, and S.L. MacQuarrie. Aust. J. Chem. **53**, 399 (2000).

© 2001 NRC Canada

Reduction of hexaammineruthenium(III) ions by a series of tris(polypyridyl)chromium(II) ions — Revisiting the $Cr(NN)_3^{3+/2+}$ self-exchange rate

K. Omar Zahir

Abstract: The kinetics of the outer-sphere oxidation of $Cr(NN)_3^{2+}$ ions (NN = 2,2′-bipyridine, 1,10-phenanthroline, and their substituted analogs) by hexaammineruthenium(III) was studied using laser flash photolysis. The $Cr(NN)_3^{2+}$ ions were generated via the reductive quenching of the $*Cr(NN)_3^{3+}$ excited states by oxalate ions or by H_2edta^{2-}. The second-order rate constants were found to vary with the driving force of the reaction. The rate constants increase from $(7.1 \pm 0.5) \times 10^6$ M^{-1} s^{-1} for $Cr(5\text{-Clphen})_3^{2+}$ to $(2.6 \pm 0.2) \times 10^8$ M^{-1} s^{-1} for $Cr(4,7\text{-Me}_2\text{phen})_3^{2+}$. The self-exchange rate constant for the couple ($Cr(NN)_3^{3+/2+}$) was calculated by applying Marcus cross relation to present and other known reactions of $Cr(NN)_3^{n+}$ ions, where $n = 3$ or 2 with various reactants and is estimated to be $(6 \pm 4) \times 10^7$ M^{-1} s^{-1}.

Key words: tris(polypyridyl)chromium(II)/(III) self-exchange rate, hexaammineruthenium(III), oxidation of $Cr(NN)_3^{2+}$.

Résumé : Faisant appel à la photolyse éclair au laser, on a étudié la cinétique de l'oxydation dans la couche externe d'ions $Cr(NN)_3^{2+}$ (NN = 2,2′-bipyridine, 1,10-phénanthroline et leurs analogues substitués) par l'hexaammineruthénium(III). Les ions $Cr(NN)_3^{2+}$ ont été générés par le biais d'un piégeage réducteur des états excités $*Cr(NN)_3^{3+}$ par des ions oxalate ou par du H_2edta^{2-}. On a trouvé que les constantes de vitesse du deuxième ordre varient avec l'affinité de la réaction. Les constantes de vitesse augmentent de $(7{,}1 \pm 0{,}5) \times 10^6$ M^{-1} s^{-1} pour le $Cr(5\text{-Clphen})_3^{2+}$ à $(2{,}6 \pm 0{,}2) \times 10^8$ M^{-1} s^{-1} pour le $Cr(4,7\text{-Me}_2\text{phen})_3^{2+}$. On a calculé la constante de vitesse d'autoéchange du couple $Cr(NN)_3^{3+}/2+$ en appliquant la relation croisée de Marcus à ces réactions et à d'autres réactions connues d'ions $Cr(NN)_3^{n+}$ ($n = 3$ ou 2) avec divers réactifs et on l'a évaluée à $(6 \pm 4) \times 10^7$ M^{-1} s^{-1}.

Mots clés : vitesse d'autoéchange tris(polypyridyl)chrome(II)/(III), hexaammineruthénium(III), oxydation de $Cr(NN)_3^{2+}$.

[Traduit par la Rédaction]

Introduction

Over the past 20 years, considerable attention has been directed at studying the electron and energy transfer reactions of transition-metal excited states particularly that of polypyridyl complexes of ruthenium(II) and chromium(III) ions ($*M(NN)_3^{n+}$) (1, 2). This interest in these excited states derives in part from their possible use in solar energy conversion (3, 4). An additional reason for this interest is that the rates of electron transfer reactions of these complexes can be used to test the theoretical models of electron transfer reactions (5, 6). Most of such studies, however, have been focused on $Ru(NN)_3^{*2+/3+}$ systems and with the exception of $Cr(bpy)_3^{2+}$ (bpy = 2,2′-bipyridine), few studies involving the electron transfer reactions of $Cr(NN)_3^{2+}$ complexes have been reported.

The difficulty in studying the oxidation of $Cr(NN)_3^{2+}$ has been partly due to the instability of the $Cr(NN)_3^{2+}$ ion. However, such studies have now become possible due to the availability of a laser flash photolysis method which involves irreversible quenching of the ^2E excited states of $Cr(NN)_3^{3+}$ to generate $Cr(NN)_3^{2+}$ ions (7). This method, which consists of using H_2edta^{2-} or oxalate ions as the quencher of the $*Cr(NN)_3^{3+}$ excited states, is an excellent way of producing $Cr(NN)_3^{2+}$ ions with a quantum yield of 2, and has been employed to study electron transfer reactions of $Cr(NN)_3^{2+}$ with dioxygen (7), Co(III) amine complexes (8), and SO_2 (9).

No experimental determination of the rate of $Cr(NN)_3^{3+/2+}$ self-exchange reaction has been made, and in the few cases where Marcus cross relation was used to examine the self-exchange reaction, it led to a wide range of values (5, 10–12). A better estimation of this intrinsic parameter is essential if $Cr(NN)_3^{3+/2+}$ systems are to be applied to test the theoretical models of electron transfer reactions. We have now employed the above mentioned method of generating $Cr(NN)_3^{2+}$ to study the kinetics of the reduction of $Ru(NH_3)_6^{3+}$ by a series of $Cr(NN)_3^{2+}$ ions. Both sets of reaction partners are inert to substitution requiring that the reaction proceeds through an outer-sphere mechanism. The self-exchange rate constant for the $Ru(NH_3)_6^{3+/2+}$ couple has been experimentally determined (13–15), and the standard free energy changes for the reactions between $Ru(NH_3)_6^{3+}$ and $Cr(NN)_3^{2+}$ are well-known. The results from the present study and others available in the literature on the cross-reaction between $Cr(NN)_3^{2+}$ and various oxidants are then subjected to Marcus cross relation to estimate the rate constant for the self-exchange reactions for $Cr(NN)_3^{3+/2+}$.

Received November 29, 2000. Published on the NRC Research Press Web site at http://canjchem.nrc.ca on July 30, 2001.

K.O. Zahir. Department of Chemistry, California State University at Northridge, Northridge, CA 91330–8262, U.S.A. (Telephone: (818) 677-2089; fax: (818) 677-4068; e-mail: omar.zahir@csun.edu).

 DOI: 10.1139/cjc-79-7-1124 © 2001 NRC Canada

Experimental

Materials

Tris(polypyridine)chromium(III) complexes were prepared according to the published procedures (5, 16, 17), and their purity was checked by comparison of the UV–vis spectra, emission spectra, and lifetime values. Hexaammineruthenium(III) chloride was prepared and purified according to the published procedures (14). Sodium oxalate (T.J. Baker) and disodium ethylenediaminetetraacetate (Na_2H_2edta) (Fischer) were used as received. Sodium chloride was used to adjust the ionic strength of the solutions at 0.1 M.

Kinetic data

The kinetic data were obtained using a homebuilt laser flash photolysis system that was based on literature design (18). The excitation of the $Cr(NN)_3^{3+}$ complexes was carried out at either 423 or 452 nm by a 300 ns pulse from a modified Model DL-1200 PhaseR dye laser. The quenching of the $*Cr(NN)_3^{3+}$ excited states by oxalate ions or H_2edta^{2-} was monitored at 728 nm. The formation and then subsequent disappearance of $Cr(NN)_3^{2+}$ were monitored at 440 nm for NN (5-Clphen), 430 nm (phen), 480 nm (5-Mephen), 440 nm (4,7-Me_2phen), and 560 nm (bpy) (11). The kinetic studies were carried out under an oxygen-free atmosphere using Argon gas. Pseudo-first-order conditions with more than 10-fold excess of ruthenium(III) complex were maintained. The absorbance–time data for the loss of $Cr(NN)_3^{2+}$ (typically 6–8 μM) collected in each experiment were analyzed by a nonlinear least-squares analysis of exponential absorbance–time curves.

Results and discussion

Kinetics of the Cr(II)–Ru(III) reactions

Under the experimental conditions employed, the formation of $Cr(NN)_3^{2+}$ was very rapid. The details of this quenching process were discussed elsewhere (7). Control experiments were carried out to investigate whether any competitive quenching of $*Cr(NN)_3^{3+}$ by $Ru(NH_3)_6^{3+}$ occurs. Under our experimental conditions, no significant quenching of $*Cr(NN)_3^{3+}$ by $Ru(NH_3)_6^{3+}$ took place and the formation of $Cr(NN)_3^{2+}$ was the only quenching pathway that was operative. The loss of $Cr(NN)_3^{2+}$ due to its reaction with $Ru(NH_3)_6^{3+}$ is rapid, and proceeds as shown in eq. [1].

$$[1] \quad Cr(NN)_3^{2+} + Ru(NH_3)_6^{3+} \rightarrow Cr(NN)_3^{3+} + Ru(NH_3)_6^{2+}$$

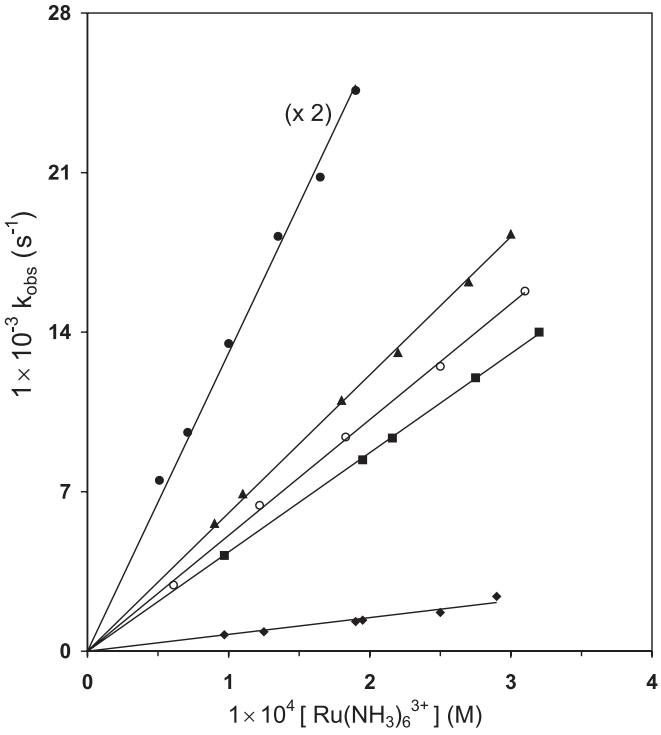
For a given complex, the kinetic data were the same regardless of which quencher (H_2edta^{2-} or oxalate ions) were used to generate $Cr(NN)_3^{2+}$. The rate law for the reaction described in eq. [1] can be written as

$$[2] \quad -d[Cr(NN)_3^{2+}]/dt = k_{12}[Cr(NN)_3^{2+}][Ru(NH_3)_6^{3+}]$$

$$[3] \quad k_{obs} = k_{12}[Ru(NH_3)_6^{3+}]$$

Here k_{12} is the second-order rate constant for the oxidation of $Cr(NN)_3^{2+}$ by $Ru(NH_3)_6^{3+}$. The kinetic data for rxn. [1] is plotted in Fig. 1 which shows that k_{obs} increases linearly with an increase in the concentration of $Ru(NH_3)_6^{3+}$ complex. As the plots in Fig. 1 pass through the origin for all the Cr(II) complexes studied, it is suggested that eq. [1] is the sole pathway for the disappearance of $Cr(NN)_3^{2+}$ and eqs. [2] and [3] are applicable. The values of the second-order rate constant (k_{12}) were obtained from the slopes of such plots, and a summary of the cross-reaction rate constants (k_{12}) for rxn. [1] is presented in Table 1. The slowest reaction was observed with $Cr(5\text{-Clphen})_3^{2+}$ which has the smallest $\Delta°E$ value of 0.21 V, and for $Cr(4,7\text{-}Me_2phen)_3^{2+}$ which has the largest $\Delta°E$ value among all the Cr(II) complexes studied, the value of k_{12} obtained was the largest.

Fig. 1. Plot of k_{obs} (the observed rate constant for the reduction of $Ru(NH_3)_6^{3+}$ complex by $Cr(NN)_3^{2+}$ complexes) vs. $[Ru(NH_3)_6^{3+}]$ at ambient temperature. The data are shown for NN = 4,7-Me_2phen (circles), 5-Mephen (triangle), phen (open circles), bpy (squares), and 5-Clphen (diamonds).



Estimation of the self-exchange rate for the $Cr(NN)_3^{2+/3+}$ couple using Marcus cross relation

Considering that both partners in rxn. [1] are substitutionally inert, it is expected that rxn. [1] proceeds via an outer-sphere electron transfer mechanism. Marcus cross relation (eq. [4]) has been successfully utilized to evaluate the self-exchange reaction of many redox couples (13, 19, 20).

$$[4] \quad k_{12} = (k_{11}k_{22}K_{12}f_{12})^{1/2}$$

$$\log f_{12} = (\log K_{12})^{1/2}/[4 \log (k_{11}k_{22}/Z^2)]$$

Here, k_{12} is the rate constant for the cross-reaction, k_{11} and k_{22} are the self-exchange rates for the two partners, and K_{12} is the equilibrium constant for the cross-reaction. The results from the present study and other systems for which kinetic and thermodynamic data are available were subjected to such treatment to estimate the rate constant for the $Cr(NN)_3^{3+/2+}$ self-exchange reaction (eq. [5]) and the results are presented in Table 1.

© 2001 NRC Canada

Table 1. Summary of experimental rate constants (M^{-1} s^{-1}) for outer-sphere electron transfer between $Cr(NN)_3^{n+}$ complexes and various reactants and estimation of the $Cr(NN)_3^{3+/2+}$ self-exchange rate constant.

Reactants ($Cr(NN)_3^{2+}$–X) or X-$Cr(NN)_3^{3+}$)	log K_{12}	k_{12} (M^{-1} s^{-1})[a]	k_{11} (X) (M^{-1} s^{-1})	k_{22} Cr(NN) (M^{-1} s^{-1})
$Cr(5\text{-Clphen})_3^{2+}$–$Ru(NH_3)_6^{3+}$	3.74[b]	7.1×10^{6}[a]	3×10^{3}[c]	9×10^{6}
$Cr(bpy)_3^{2+}$–$Ru(NH_3)_6^{3+}$	5.26[b]	4.3×10^{7}[a]	3×10^{3}[c]	1×10^{7}
$Cr(phen)_3^{2+}$–$Ru(NH_3)_6^{3+}$	5.60[b]	4.9×10^{7}[a]	3×10^{3}[c]	1×10^{7}
$Cr(5\text{-Mephen})_3^{2+}$–$Ru(NH_3)_6^{3+}$	5.93[b]	5.7×10^{7}[a]	3×10^{3}[c]	7×10^{6}
$Cr(4,7\text{-Me}_2\text{phen})_3^{2+}$–$Ru(NH_3)_6^{3+}$	8.47[b]	2.6×10^{8}[a]	3×10^{3}[c]	2×10^{6}
$Cr(5\text{-Clphen})_3^{2+}$–$O_2$	0.20	2.3×10^{5}[d]	4.5×10^{2}[e,f]	1×10^{8}
$Cr(bpy)_3^{2+}$–O_2	1.69	6.0×10^{5}[d]	4.5×10^{2}[e,f]	2×10^{7}
$Cr(phen)_3^{2+}$–O_2	2.03	1.5×10^{6}[d]	4.5×10^{2}[e,f]	6×10^{7}
$Cr(5\text{-Mephen})_3^{2+}$–$O_2$	2.37	2.2×10^{6}[d]	4.5×10^{2}[e,f]	6×10^{7}
$Cr(4,7\text{-Me}_2\text{phen})_3^{2+}$–$O_2$	4.90	2.8×10^{7}[cd]	4.5×10^{2}[e,f]	1×10^{7}
$Cr(bpy)_3^{2+}$–$Co(en)_3^{3+}$	1.69	2.2×10^{3}[g]	7.7×10^{-5}[h]	1×10^{9}
	1.69	3.8×10^{2}[i]	7.7×10^{-5}[h]	4×10^{7}
$Cr(bpy)_3^{2+}$–$Co(bpy)_3^{3+}$	9.64	1.1×10^{8}[g]	18[j]	1×10^{7}
$Cr(bpy)_3^{2+}$–$Co(phen)_3^{3+}$	10.5	1.3×10^{8}[g]	45[k]	1×10^{6}
$Cr(bpy)_3^{2+}$–$Co(NH)_6^{2+}$	5.34	2.5×10^{2}[i]	1×10^{-6}[h]	4×10^{6}
$Cr(bpy)_3^{2+}$–Fe^{3}+	16.9	7.3×10^{8}[l]	4.2[m]	5×10^{5}
$Cr(bpy)_3^{2+}$–$Co([14]aneN_4)^{3+}$	11.5	4.4×10^{7}[n]	8×10^{-4}[o]	8×10^{8}
$Co(sep)_3^{2+}$–$Cr(5\text{-Mephen})_3^{3+}$	1.76	2.0×10^{5}[p]	5.1[q]	2×10^{8}
V^{2+}–$Cr(bpy)_3^{3+}$	0.0	4.2×10^{2}[r]	3×10^{-3}[s]	6×10^{7}

[a]Present work, obtained from the plots of k_{obs} vs. [$Ru(NH)_6^{3}$+], error limit ± 10%.
[b]Using the °*E* for $Ru(NH)_6^{3}$+ as 0.051 V, and $Cr(NN)_3^{3+}$/2+ as 0.17 V (5-Clphen), 0.26 V (bpy), 0.28 V (phen), 0.30 V (5-Mephen), and 0.45 V (4,7-Me_2phen) (ref. 5, 10, and 11).
[c]Reference 13.
[d]Reference 7.
[e]Reference 23 (experimental value).
[f]A value of 10 M^{-1} s^{-1} has been estimated for O_2–O_2^- self-exchange rate using Marcus cross relation (7).
[g]Reference 8.
[h]Reference 24.
[i]Reference 21.
[j]Reference 13.
[k]Reference 20.
[l]Reference 22.
[m]Reference 13.
[n]Reference 9.
[o]Reference 25.
[p]Reference 5.
[q]Reference 26.
[r]Reference 19.
[s]Reference 20.

[5] $$Cr(NN)_3^{2+} + Cr(NN)_3^{3+} \longrightarrow Cr(NN)_3^{3+} + Cr(NN)_3^{2+}$$

The data in Table 1 shows that the calculated values of $Cr(NN)_3^{3+/2+}$ exchange rate span over a large range. However, out of the 18 reactions examined, the majority of the estimated values fell in the range 1×10^7 to 1×10^8 M^{-1} s^{-1}. In an earlier study (12), a value of 4×10^9 M^{-1} s^{-1} was estimated for the cross-reaction of $Cr(bpy)_3^{2+}$ with $Cr(5,6\text{-diMephen})_3^{3+}$ in 0.1 M HCl – 90% methanol. In another study, an exchange rate of 1×10^9 M^{-1} s^{-1} was estimated from the rate constant for the reaction of $Co(sepulcrate)^{2+}$ with $Cr(5\text{-Mephen})_3^{3+}$ (5). On the other hand, a much lower value of 1×10^5 M^{-1} s^{-1} was estimated for the reduction of Fe^{3+} by $Cr(NN)_3^{2+}$ ions under acidic conditions (11).

At this point, it would also be interesting to examine the ground-state self-exchange rate ($Cr(NN)_3^{3+/2+}$) in the light of the excited state self-exchange rate ($Cr(NN)_3^{2+}$) (eq. [6]).

[6] $$*Cr(NN)_3^{3+} + Cr(NN)_3^{2+} \rightarrow Cr(NN)_3^{2+} + *Cr(NN)_3^{3+}$$

Here $*Cr(NN)_3^{3+}$ is the ^2E excited states of $Cr(NN)_3^{3+}$. Considering that the two pairs of reactants in the ground and excited state reactions (eqs. [5] and [6]) are very similar in size and charge type, it is expected that the solvent reorganization barrier and the work terms will be same for the two reactions. Assuming that both the reactions are adiabatic, they would differ only in their inner-sphere barrier. As the inner-sphere barrier for the ground- and the excited-state exchange reactions are the same, the $Cr(NN)_3^{3+/2+}$ and

© 2001 NRC Canada

$Cr(NN)_3^{*3+/2+}$ exchange reactions should be expected to proceed at similar rates. In earlier estimates of the excited-state self-exchange rate ($Cr(NN)_3^{2+}$), values of 1×10^8 M^{-1} s^{-1} (5) and 4×10^7 M^{-1} s^{-1} (10) were reported.[1] These estimated values for the excited-state exchange reaction fall in the middle of the range of values estimated in the present study for the ground-state self-exchange reaction, $Cr(NN)_3^{3+/2+}$. We conclude that the most likely value for the ground state self-exchange reaction ($Cr(NN)_3^{3+/2+}$) is very similar to the values of 1×10^8 M^{-1} s^{-1} or 4×10^7 M^{-1} s^{-1} estimated for the excited-state exchange reaction ($Cr(NN)_3^{2+}$).

For the few cases in Table 1 where significantly different values were obtained for the ground-state exchange reaction, it is suspected that such a discrepancy may be due to the uncertainties in the parameters used for the calculations or due to other contributing factors. For example, the value of 5×10^5 M^{-1} s^{-1} obtained for the $Cr(NN)_3^{2+}$–Fe^{3+} cross-reaction is certainly low, perhaps due to the reported non-adiabaticity of the Fe(II)/(III) couple or because of the large driving force of this reaction which might place it in the Marcus inverted region. For the $Cr(NN)_3^{2+}$–$Co(en)_3^{3+}$ reaction, two values have been reported for the cross-reaction which are almost an order of magnitude different from each other. One of the values (4×10^7 M^{-1} s^{-1}) is within the range for the majority of the values, whereas the other value (1×10^9 M^{-1} s^{-1}) appears to be too large.

The data in Table 1 shows that the majority of the reactions gave values for the ground-state exchange reaction that are relatively closely clustered, and are also in the same range as the excited-state self-exchange rate. Based on these results, we propose an average value of $(6 \pm 4) \times 10^7$ M^{-1} s^{-1} for the $Cr(NN)_3^{3+/2+}$ self-exchange reaction. This value by no means can be considered as the true value for that reaction, however, it is perhaps the best estimate so far as it is based on a relatively larger body of data and the parameters used to calculate the self-exchange reaction of the $Cr(NN)_3^{3+/2+}$ couple using Marcus cross relation are known with higher certainty.

Acknowledgment

This work was supported by the Office of Research and Sponsored Projects at California State University, Northridge. The author is thankful to Dr. James H. Espenson and Dr. Albert Haim for some useful discussion and for their valuable input.

References

1. N. Sutin. Adv. Chem. Ser. **254** 231 (1998).
2. (*a*) K. Kalyanasundaram. Coord. Chem. Rev. **46**, 161 (1982); (*b*) M.A. Jamieson, N. Serpone, and M.Z. Hoffman. Coord. Chem. Rev. **39**, 121 (1981).
3. B.S. Brunschwig and C. Creutz. Proc. DOE Sol. Photochem. Res. Conf. 19th, 1995.
4. W.D.K. Clark and N. Sutin. J. Am. Chem. Soc. **99**, 4676 (1977); (*a*) P.J. DeLaive, J.-T. Lee, H. Abruna, H.W. Sprintscnik, T.J. Meyer, and D.J. Whitten. Adv. Chem. Ser. **168**, 28 (1978).
5. N. Sutin. Adv. Chem. Phys. **106**, 7 (1999).
6. (*a*) D.K. Liu, B.S. Brunschwig, C. Creutz, and N. Sutin. J. Am. Chem. Soc. **108**, 1749 (1986); (*b*) B.S. Brunschwig and N. Sutin. J. Am. Chem. Soc. **100**, 7568 (1978).
7. K. Zahir, J.H. Espenson, and A. Bakac. J. Am. Chem. Soc. **110**, 5059 (1988).
8. K. Zahir, J.H. Espenson, and A. Bakac. Inorg. Chem. **27**, 3144 (1988).
9. C.A. Simmons, A. Bakac, and J.H. Espenson. Inorg. Chem. **28**, 581 (1989).
10. N. Serpone, M.A. Jamieson, M.S. Henry, M.Z. Hoffman, F. Bolleta, and M. Maestri. J.Am. Chem. Soc. **101**, 2907 (1979).
11. N. Serpone, M.A. Jamieson, S.S. Emmi, P.G. Fuochi, Q.G. Mulazzani, and M.Z. Hoffman. J. Am. Chem. Soc. **103**, 1091 (1981).
12. G.J. Ferraudi and J.F. Endicott. Inorg. Chim. Acta, **37**, 219 (1979)
13. R.A. Marcus and N. Sutin. Biochim. Biophys. Acta, **811**, 265 (1985).
14. T.J. Meyer and H. Taube. Inorg. Chem. **7**, 2369 (1968).
15. B.S. Brunschwig, C. Creutz, D.H. Macartney, T.K. Sham, and N. Sutin. Faraday Discuss. Chem. Soc. **74**, 113 (1982).
16. E. Konig and S.J. Herzog. J. Inorg. Nucl. Chem. **32**, 585, (1970).
17. R. Srinam, M.Z. Hoffman, M.A. Jamieson, and N. Serpone. J. Am. Chem. Soc. **102**, 1754 (1980).
18. J.D. Melton, J.H. Espenson, and A. Bakac. Inorg. Chem. **25**, 4104 (1986).
19. R.A. Marcus. Pure Appl. Chem. **69**, 13 (1997); N. Sutin. *In* Encyclopedia of science and technology. *Edited by* T. Martin. McGraw–Hill Publishing, New York. 2000.
20. M.Chou, C. Creutz, and N. Sutin. J. Am. Chem. Soc. **99**, 5615 (1977).
21. A.M. Zwickel and H. Taube. Faraday Discuss. Chem. Soc. **29**, 42 (1982)
22. A. Bakac, K. Zahir, and J.H. Espenson. Inorg. Chem. **27**, 315 (1988).
23. J. Lind, A. Shen, G. Merrenyi, and B.O. Jonsson. J. Am. Chem. Soc. **111**, 7654 (1989).
24. K. Zahir, W. Bottcher, and A. Haim. Inorg. Chem. **24**, 1966 (1984).
25. J.F. Endicott, B. Durham, M.D. Glick, T.J. Anderson, J.M. Kuszaj, and W.G. Balakrishnan. J. Am. Chem. Soc. **103**, 1431 (1981).
26. I.I. Creaser, J. MacB. Harrofield, A.J. Herlt, A.M. Sargeson, and J. Springborg. J. Am. Chem. Soc. **99**, 3181 (1977).

[1] In another study, the rate constant for the $*Cr(NN)_3^{3+}$–$Cr(NN)_3^{2+}$ exchange reaction was estimated to be 3×10^5 M^{-1} s^{-1} (10) and has been considered too low by others.

© 2001 NRC Canada

Kinetic study of the proton transfer reaction between 1-nitro-1-(4-nitrophenyl)alkanes and TBD and MTBD bases in acetonitrile solvent

Iwona Grześkowiak, Włodzimierz Gałęzowski, and Arnold Jarczewski

Abstract: The rates of proton transfer reactions between C-acids of the series of nitroalkanes with increasing bulk of R = H, Me, Et, *i*-Pr substituent as: 4-nitrophenylnitromethane (**0**), 1-(4-nitrophenyl)-1-nitroethane (**1**), 1-(4-nitrophenyl)-1-nitropropane (**2**), 2-methyl-1-(4-nitrophenyl)-1-nitropropane (**3**) and 1,5,7-triazabicyclo[4.4.0]dec-5-ene (TBD), 7-methyl-1,5,7-triazabicyclo[4.4.0]dec-5-ene (MTBD) have been measured in acetonitrile at pseudo-first-order conditions. The product of the proton transfer reaction with MTBD in acetonitrile is dissociated into free ions while that of the TBD reaction is composed of a comparable amount of ions and ion pairs. The second-order rate constants (k_{2H}) for these bases of almost equal strength in acetonitrile (pK_a = 24.70, 24.97 for MTBD and TBD) and C-acids **1**, **2**, and **3** are: 317, 86, 7.6 dm^3 mol^{-1} s^{-1}; and 15 200, 5300, 1100 dm^3 mol^{-1} s^{-1}, respectively. The appropriate primary deuterium kinetic isotope effects (k_H/k_D) are 12.5, 10.8, 6.9; and 9.9, 11.2, 12.6. The influence of steric hindrance brought by reacting C-acids and bases is discussed. The different structure of the transition states and the products as mono- and double-hydrogen bonded complexes for these series of C-acids and MTBD and TBD bases is manifested by a distinct reaction mechanism which we attempt to explain.

Key words: proton transfer, kinetic study, C-acids, organic bases, acetonitrile, kinetic isotope effects.

Résumé : Opérant dans l'acétonitrile, dans des conditions de pseudo-premier ordre, on a mesuré les vitesses des réactions de transferts de proton entre le 1,5,7-triazabicyclo[4.4.0]déc-5-ène (TBD) et le 7-méthyl-1,5,7-triazabicyclo[4.4.0]déc-5-ène (MTBD) et les C-acides d'une série de nitroalcanes comportant des substituants R = H, Me, Et, *i*-Pr de plus en plus volumineux, comme les 4-nitrophénylnitrométhane, **0**, 1-(4-nitrophényl)1-nitroéthane, **1**, 1-(4-nitrophényl)-1-nitropropane, **2**, 2-méthyl-1-(4-nitrophényl)-1-nitropropane, **3**. Le produit de la réaction de transfert avec le MTBD dans l'acétonitrile est dissocié en ions libres alors que celui de la réaction avec le TBD est composé de quantités comparables d'ions et de paires d'ions. Les constantes de vitesse du deuxième ordre, k_{2H}, pour ces bases de force pratiquement égales dans l'acétonitrile (pK_a = 24,70 pour le MTBD et 24,97 pour le TBD) avec les C-acides **1**, **2** et **3** sont 317, 86 et 7,6 dm^3 mol^{-1} s^{-1} et de 15 200, 5300 et 1100 dm^3 mol^{-1} s^{-1} respectivement pour le MTBD et le TBD. On discute de l'influence de l'empêchement stérique qui se développe entre les C-acides et les bases. Les différentes structures des états de transition et des produits sous les formes de complexes avec une seule ou deux liaisons hydrogènes pour les C-acides et les bases MTBD et TBD se manifestent par des mécanismes de réactions distincts que l'on essaye d'expliquer.

Mots clés : transfert de proton, étude cinétique, C-acides, bases organiques, acétonitrile, effets isotopiques cinétiques.

[Traduit par la Rédaction]

Introduction

In our previous papers (1–4), we found that the proton transfer reaction from nitroalkanes differing by the bulk of R substituents and also by the types of electron withdrawing group, but having very similar acidity in acetonitrile, showed significant differences in the kinetic behavior particularly in the presence of a common BH^+ cation. Generally, the products of reactions of these systems of C-acids and strong guanidine and amidine bases in acetonitrile are at least 97% dissociated into free ions as indicated by conductometric measurements (4, 5). The reason why this went undetected in earlier spectrophotometric studies, in which the Benesi–Hildebrand formalism was applied, has been already explained in detail (1, 4, 5). Then a general indication for kinetic experiments of the proton transfer reactions, in particular those of not very large equilibrium constants, was to carry out measurements in BH^+–B buffer solutions to maintain reversible pseudo-first-order conditions (5, 6). However, large concentrations of BH^+ cation caused an anion association that was manifested by a blue shift in electronic spectra (6). Also in some cases the unexpected negative salt effect was observed (2). In our previous paper (1), a general equation for the rates of proton transfer reac-

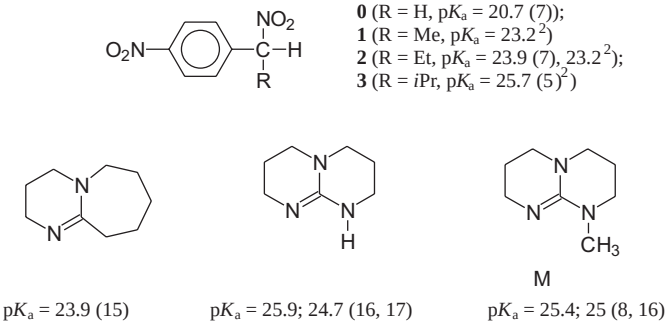
Received December 15, 2000. Published on the NRC Research Press Web site at http://canjchem.nrc.ca on August 3, 2001.

I. Grześkowiak, W. Gałęzowski, and A. Jarczewski.[1]
Faculty of Chemistry, A. Mickiewicz University, Grunwaldzka 6, 60–780 Poznań, Poland.

[1]Corresponding author (telephone: 00-4861-8291-479; fax: 00-4861-8658-008; e-mail: arnold@main.amu.edu.pl).

 DOI: 10.1139/cjc-79-7-1128 © 2001 NRC Canada

Scheme 1. C-acids and bases used in the experiments.



tions between C-acids and strong organic bases with a product existing in two forms, ions and ion pairs, was derived and its applicability tested for a number of the reaction systems. We found that this equation is fulfilled for most reaction systems, which is visible from the parallel plots of k_{obs} vs. base concentration for different [BH^+] concentrations (1). The reactions between C-acids **1**, **2** (7), and **3** (5) and MTBD base, that has a negligible homoconjugation constant (8) and very large basicity (9), show considerable decrease of second-order rate constants with the concentration of $MTBDH^+$ (1). The extent of this reduction increased with the bulk of alkyl substituent in the C-acid. This negative salt effect is rather unusual, since for reactions with transition state more polar than substrates, normally the increase of the rate constants with ionic strength is observed (10). The most reasonable explanation of this effect was to assume the mechanism including the pyramidal carbanion as an intermediate (11–13).

In this paper the results of kinetic and equilibrium experiments with the systems of reaction of proton transfer between C-acids **0**, **1**, **2**, and **3** and strong cyclic bases (TBD and MTBD in acetonitrile (MeCN)) are reported. It was interesting to study the different reactivity of TBD and MTBD bases and to compare these results with those obtained previously in THF solvent (2).

We also wanted to learn if the same pattern of reactivity with varying steric hindrance in the C-acid would be held in a polar medium as we already found a weak dependence of KIE values on this factor as well as steric hindrance of reactants (1–4). This prompted us to verify if the position of nitro groups (14) of reacting C-acids provided the predominant contribution in formation of the transition state (Scheme 1).

Experimental

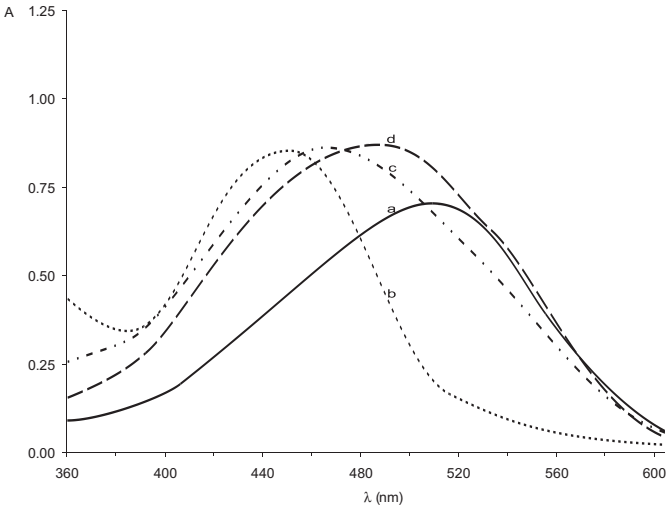
Acetonitrile, the spectroscopic grade solvent from Romil, was stored over CaH_2, distilled over P_2O_5 and finally, fractionally distilled over CaH_2. The middle fraction was collected and stored under a nitrogen atmosphere, free from moisture and CO_2.

C-acids

4-Nitrophenylnitromethane (**0**) (4 and refs. cited therein), 1-(4-nitrophenyl)-1-nitroethane (**1**), 1-(4-nitrophenyl)-1-nitropropane (**2**), 2-methyl-1-(4-nitrophenyl)-1-nitropropane (**3**) were prepared according to procedures already published (4). The melting points and spectra after recrystallization from ethanol were in accordance with the literature.

The deuterated analogues of **1**, **2**, and **3** were prepared as previously described (4).

Fig. 1. Spectra for reactions of 1-(4-nitrophenyl)–1-nitropropane (**2**) (2.5×10^{-5} M) with TBD (1×10^{-3} M) and MTBD (1×10^{-3} M) in MeCN and THF solvents. Curves: (a) **2** with MTBD in MeCN, λ_{max} = 514 nm; (*b*) **2** with TBD in THF, λ_{max} = 450 nm; (*c*) **2** with TBD in MeCN, λ_{max} = 460 nm; (d) as c traces of oxygen present, red intermediate, λ_{max} = 488 nm.



Bases

1,5,7-Triazabicyclo[4.4.0]dec-5-ene (TBD) and 7-methyl-1,5,7-triaza-bicyclo[4.4.0]dec-5-ene (MTBD), commercial products from Aldrich, were used without further purification. The purity of the bases was satisfactory as tested by NMR and titration methods (16). The results of titration of base solutions were consistent with gravimetric concentrations within 1%.

The product of reaction of nitroalkanes with TBD in MeCN in an inert atmosphere (argon) was indefinitely stable. However, in the presence of atmospheric oxygen the band at ~460 nm slowly disappeared (Fig. 1*c*), which was accompanied by the appearance of a new band, very similar to nitronate ion (Fig. 1*a*), at $\lambda_{max} \cong 488$ nm (red intermediate) (Fig. 1*d*). This step of the reaction could be turned over to 460 nm, characteristic for the mixture of nitronate ions and ion pairs by saturation of the reaction mixture with argon. Repeated delivery of traces of atmospheric oxygen caused the appearance of the red intermediate until the concentration of the oxygen was not large or the exposure of the reaction to it was not long enough. In other words, the isosbestic point for the reaction of TBD could be observed in between anions – hydrogen bonded ion pairs and the red intermediate λ_{max} = 475 nm, (Fig. 1*c*, *d*) as far as the final product — ketone λ_{max} = 270 nm (not shown in Fig. 1) — is not formed. This caused the loss of the isosbestic point, indicating irreversibility of the reaction step to ketone (Scheme 2).

[2] W. Galezowski, M. Stanczyk, and A. Jarczewski. Unpublished results.

© 2001 NRC Canada

Addition of water to the ion pair, product protected with argon, did not cause visible appearance in the spectrum of the red intermediate. This eliminates the possibility that the atmospheric moisture facilitates dissociation of the ion pair. Then we presume that the red species is an oxidation product of the ion pair, to ketone (Scheme 2). The attempts to isolate or characterize this product, λ_{max} = 488 nm, by NMR spectrometry failed, possibly due to its very low concentration which eventually turns to ketone. We were unable to produce a larger concentration of this even by bubbling the air through concentrated solution of the ion-pair product in MeCN. The red oxidation intermediate absorbing at λ_{max} = 488 nm is not visible for the MTBD reaction where the double hydrogen bonded complex cannot be formed. The control experiments show that the presence of air had no effect on the reaction of MTBD with nitroalkanes when ion association to the mono-hydrogen-bonded complex was forced by a massive amount of BH^+ cation (6). Then, under aerobic conditions, we did not observe a slow increase in absorbtion band at λ_{max} = 488 nm. Moreover, in anaerobic conditions the initial product of the MTBD reaction shows λ_{max} = 514 nm band characteristic for nitronate anion excluding the possible "red intermediate". So we presume that the red species is characteristic only for the reaction of TBD.

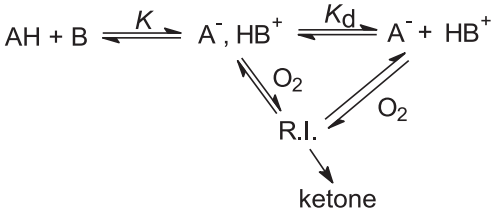
The slow follow up oxidation of TBD product had no effect on the results of our proton transfer kinetic measurements, however, further experiments in a longer observation period, towards the careful identification of this red species that could be erroneously considered as free nitronate anion, seem to be necessary. Leffek and Matinopoulos-Scordou (18) already observed similar complicity for the reaction of ethyl bis(4-nitrophenyl)acetate with TMG in THF solvent. They suggested the reaction pathway via three colored species: carbanion (λ_{max} = 513 nm), presumably a radical anion (λ_{max} = 665 nm), and finally dinitrobenzophenone (λ_{max}= 292 nm). A similar type of reaction sequence has been noted for the base-catalyzed autooxidation of substituted esters (19), however there were no further suggestions why this particular carbanion is susceptible to oxidation in the presence of excess base and an electron acceptor as atmospheric oxygen present in the reaction system.

The working solutions of C-acids and bases were prepared freshly before each kinetic or equilibrium experiment and kept under argon, to protect the system against atmospheric CO_2, O_2, and moisture. Kinetic measurements were performed using a stopped flow spectrophotometer made by Applied Photophysics. The values of k_{obs} were measured for typically five concentrations of base in a large excess over C-acid [2.5×10^{-5} M] to ensure pseudo-first-order kinetics (Tables 1 and 2). The second-order rate constants k_f were obtained by the least-squares calculation. The activation parameters were evaluated from these by means of the method of the least-squares fit to the transition-state theory equation.

Electronic absorption spectra were completed on a Hewlett-Packard 8452A diode array spectrophotometer using a thermostated cell holder. All spectra were recorded at 25°C.

The value of spectrophotometric equilibrium constant K of 0.352 for the reaction between **3** and MTBD in acetonitrile was calculated using the following equation: $K = f^2[BH^+][A^-]/[B][AH]$. $[A^-]$ was found from the absorbance at λ = 600 nm, where the absorption of the ion pair is negligible, [AH] was calculated as a difference of an analytical C-acid's concentration and the sum of ($[A^-]$ + [ion pair]). The K_d used for calculation of [ion pair] is 0.0024 (6).

Scheme 2. Equilibrium between nitronate anions and hydrogen-bonded ion pairs for the reaction of TBD and C-acids: **0**, **1**, **2**, **3** in MeCN. (AH (C-acids **0**–**3**), B (TBD base), A^-HB^+ (hydrogen-bonded ion pair), R.I. (red intermediate), ketone).



The proton transfer for these systems of reactions is complete in the concentration ranges shown in Tables 1 and 2.

The conductometric titration of **3** with TBD in MeCN was carried out at 25°C. Initial concentration of **3** was 2×10^{-2} M. The conductometric cell was protected against moisture, CO_2, and O_2 with argon. The measurements were completed using a Tesla BM–484 semiautomatic conductivity bridge operating at 1592 Hz with a conventional, calibrated cell with platinum electrode. The cell constant was 0.8744 cm^{-1} (5).

Results and discussion

The reaction of a series of C-acids with different steric hindrance (Scheme 1) with MTBD in acetonitrile gives colored nitronate anions of λ_{max} = 508, 514, and 515 nm for **1**, **2**, and **3** respectively (Fig.1*a*) while the spectrum of TBD product is a sum of the two spectra for free nitronate anions and ion pairs (Fig. 1*c*) (6). The λ_{max} = 460 nm for ion pairs and nitronate anions (Fig. 1*c*), for reaction of **2** with TBD in MeCN, is close to that of λ_{max} = 450 nm found in THF (Fig. 1*b*), where the dissociation of the ion-pair product is meaningless (2). Generally, the same pattern of the products is observed for C-acids **1**–**3** including 4-nitrophenylnitromethane (**0**), which could be considered as the least hindered compound in this series.

Then the mechanism of reaction could be illustrated by Scheme 2.

This observation is general for C-acids **0**–**3**. Thus, the dissociation constant measured for TBD with **0** was $K_d = 0.81 \times 10^{-4}$ M while with MTBD the corresponding value was 100 times larger ($K_d = 1.15 \times 10^{-2}$ M) (6). The rough conductometric K_d value for the ion-pair product of **3** with TBD was $K_d = 5 \times 10^{-4}$ M, $\Lambda_o = 151.6 \pm 0.1$ ohm^{-1} cm^2 mol^{-1} while with MTBD the corresponding value was $K_d = 2 \times 10^{-3}$ M (6).

The range of the base concentration was chosen to minimize the contribution of the reverse reaction to the observed rate constant k_{obs} so the plots of k_{obs} vs. [B] concentration cross the origin within the standard deviation (Fig. 2). Then the values of the rate constant for the backward reaction (k_b) could be omitted. This enabled us to perform the kinetic measurements of these proton transfer reactions in the absence of BH^+–B buffer (1, 5, 6).

© 2001 NRC Canada

Table 1. Rate constants for proton–deuteron transfer reactions of 1-(4-nitrophenyl)-1-nitroethane (**1**), 1-(4-nitrophenyl)-1-nitropropane (**2**), and 2-methyl-1-(4-nitrophenyl)-1-nitropropane (**3**) with TBD base in acetonitrile solvent.

C-acid	°C	10^3[TBD] (M)	k_{obs} (s^{-1})	k_2 (M^{-1} s^{-1})	k_{2H}/k_{2D}
1 (H)	10	1–5	8.57–50.50	10 400 ± 300	
	15	1–5	10.21–52.24	10 900 ± 500	
	25	1–5	14.51–74.77	15 200 ± 200	
	35	1–5	19.35–96.81	19 700 ± 400	
1 (D)	10	1–5	0.85–4.82	984 ± 33	10.5 ± 0.4
	15	1–5	0.85–4.93	1190 ± 130	9.1 ± 1.0
	25	1–5	1.49–7.54	1540 ± 70	9.9 ± 0.5
	35	1–5	2.13–11.54	2360 ± 30	8.4 ± 0.2
2 (H)	10	1–5	3.03–15.34	3090 ± 80	
	15	1–5	3.35–19.18	3970 ± 60	
	25	1–5	4.82–25.73	5300 ± 120	
	35	1–5	6.42–34.30	6890 ± 180	
2 (D)	10	1–5	0.24–1.28	263 ± 8	11.8 ± 0.5
	15	1–5	0.28–1.48	308 ± 24	12.9 ± 1.0
	25	1–5	0.48–2.34	473 ± 15	11.2 ± 0.4
	35	1–5	0.73–3.59	714 ± 7	9.6 ± 0.3
3 (H)	10	1–5	0.74–3.87	757 ± 32	
	15	1–5	0.81–4.02	760 ± 56	
	25	1–5	1.07–5.55	1120 ± 30	
	35	1–5	1.36–7.52	1530 ± 50	
3 (D)	10	1–5	0.04–0.21	45 ± 4	16.8 ± 1.7
	15	1–5	0.05–0.25	53 ± 3	14.3 ± 1.3
	25	1–5	0.08–0.44	89 ± 3	$12.6 \pm 0.5_5$
	35	1–5	0.09–0.62	137 ± 7	11.2 ± 0.7

Table 2. Rate constants for proton–deuteron transfer reactions of 1-(4-nitrophenyl)-1-nitroethane (**1**), 1-(4-nitrophenyl)-1-nitropropane (**2**), and 2-methyl-1-(4-nitrophenyl)-1-nitropropane (**3**) with MTBD base in acetonitrile solvent.

C-acid	°C	10^2[MTBD] (M)	10^2 k_{obs} (s^{-1})	k_2 (M^{-1} s^{-1})	k_{2H}/k_{2D}
1 (H)	10	1–5	155.7–883.0	181 ± 3	
	15	1–5	190.5–995.4	204 ± 3	
	25	1–5	275.2–1552.0	317 ± 9	
	35	1–5	394.9–2215.0	454 ± 7	
1 (D)	10	1–5	10.73–54.18	11.3 ± 0.8	16.0 ± 1.2
	15	1–5	13.38–82.01	17.1 ± 0.4	11.9 ± 0.3
	25	1–5	22.37–121.80	25.3 ± 0.7	12.5 ± 0.5
	35	1–5	35.11–199.80	40.9 ± 0.7	11.1 ± 0.3
2 (H)	10	1–5	38.99–248.30	52 ± 2	
	15	1–5	46.80–280.40	59 ± 1	
	25	1–5	73.23–419.70	86 ± 3	
	35	1–5	110.30–594.60	119 ± 6	
2 (D)	10	1–5	2.79–20.02	4.3 ± 0.2	12.1 ± 0.7
	15	1–5	3.09–27.77	5.3 ± 0.3	11.1 ± 0.7
	25	1–5	6.28–38.46	7.9 ± 0.4	10.8 ± 0.7
	35	1–5	9.92–61.82	12.7 ± 0.8	9.3 ± 0.8
3 (H)	10	1–5	2.59–16.62	3.5 ± 0.1	
	15	1–5	3.30–20.90	4.4 ± 0.1	
	25	1–5	5.30–35.73	7.6 ± 0.1	
	35	1–5	8.45–54.58	11.7 ± 0.3	
3 (D)	10	1–5	0.21–1.69	$0.4 \pm 0.0_5$	8.8 ± 1.2
	15	1–5	0.25–2.73	0.6 ± 0.1	7.3 ± 1.1
	25	1–5	0.48–4.85	1.1 ± 0.1	6.9 ± 0.6
	35	1–5	0.94–7.83	1.7 ± 0.1	6.9 ± 0.4

© 2001 NRC Canada

Fig. 2. Rate constants k_{obs} for proton transfer reaction between 2-methyl-1-(4-nitrophenyl)-1-nitropropane **3** [2.5×10^{-5}] M and MTBD [B] M in MeCN at 10, 15, 25, 35 C°.

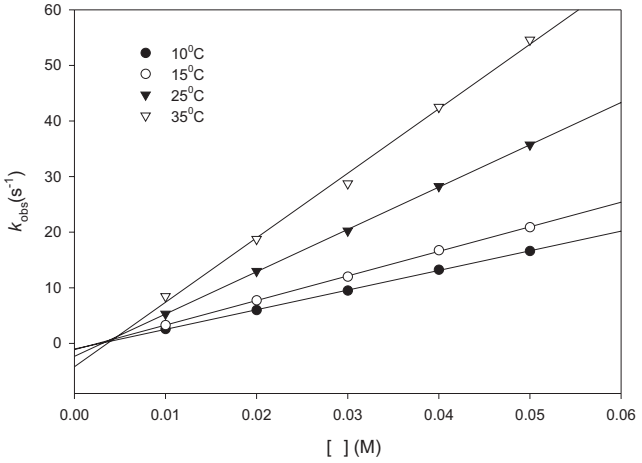


Table 3. Rate constants and KIE for proton transfer reactions between 1-nitro-1-(4-nitrophenyl) alkanes and DBU, TBD, and MTBD bases in MeCN, THF, and CB solvents at 25°C.

	DBU		TBD		MTBD	
R	k_{2H}[a]	k_H/k_D	k_{2H}	k_H/k_D	k_{2H}	k_H/k_D
MeCN solvent						
1	1820[b]	12.1[b]	15 200	9.9	317	12.5
2	496[b]	12.6[b]	5300	11.2	86	10.8
3	43[b]	13[b]	1120	12.6	7.6	6.9
THF solvent						
1	800[c]	11.4[c]	19000[d]	9.7[d]	161[d]	10.9[d]
2	219[c]	12.1[c]	6780[d]	12.1[d]	46.3[d]	10.1[d]
3	7.8[c]	9.7[c]	875[d]	14.8[d]	3[d]	8.5[d]
CB solvent						
1	1660[c]	12.4[c]				
2	356[c]	11.7[c]				
3	14.6[c]	9.4[c]				

Note: $D^{25}_{MeCN} = 35.94$; $D^{25}_{THF} = 7.58$; $D^{25}_{CB} = 5.62$.
[a]k_{2H} (dm^3 mol^{-1} s^{-1}).
[b]Data from ref. 4.
[c]Data from ref. 3.
[d]Data from ref. 2.

Then observed values of rate constants were a function of base concentration [B], according to following equation,

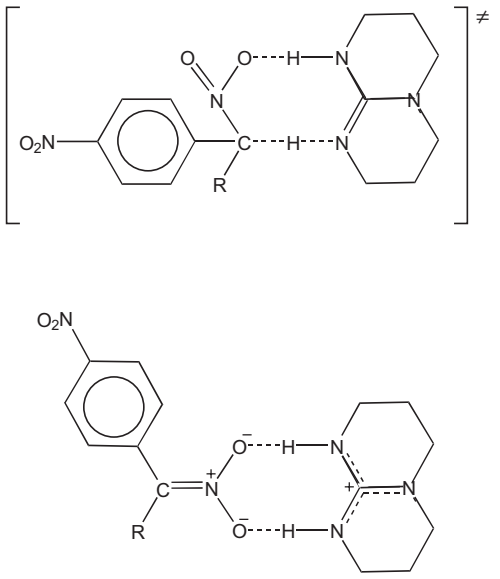
$$[1] \qquad k_{obs} = k_2[B]$$

where k_{obs} (s^{-1}) is the observed rate constant, k_2 (dm^3 mol^{-1} s^{-1}) is the rate constant of the forward reaction, and [B] is the base concentration.

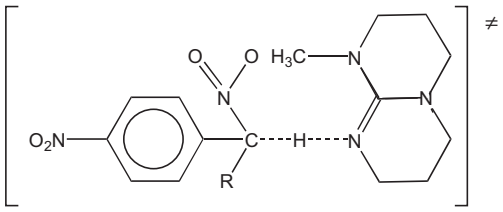
The rate constants k_2 were calculated using k_{obs} values collected in Tables 1 and 2. The errors quoted for proton k_{2H} and deuteron k_{2D} transfer reactions are standard deviations.

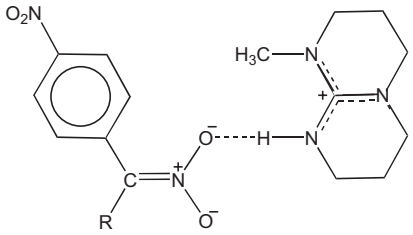
Rate constants k_{2H} for the reactions of C-acids **1**–**3** and TBD base (Table 1) decrease by one order of magnitude along with growing bulk of R substituents (15 200, 5300, and 1100 dm^3 mol^{-1} s^{-1}). A similar relation is observed for the reaction of more hindered base MTBD (Table 2), although for much smaller rate constants (317, 86, and 7.6 dm^3 mol^{-1} s^{-1}) due to different structure of the transition state which is not stabilized by two hydrogen bonds as occurred for the TBD reaction (20, 21) (Scheme 3).

Scheme 3. Structures of the transition state and the product for the proton transfer between C-acids: **0**–**3** and TBD and MTBD bases in acetonitrile solvent.



Reaction product





Reaction product

The ratios k_{TBD}/k_{MTBD} varied considerably with the structure of C-acid and were 4–7, 26, and 55 for deprotonation of diarylmethanes (16), ethyl bis(4-nitrophenyl)acetate (22), and dimethyl(4-nitrophenyl)malonate (23), respectively. These ratios evaluated for reactions of **1**–**3** in THF were

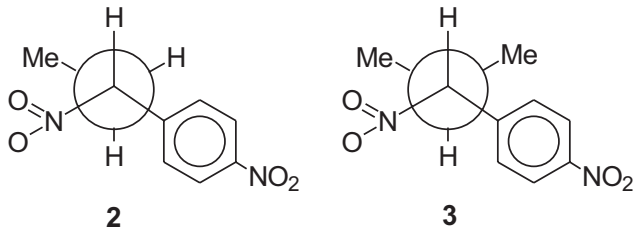
© 2001 NRC Canada

Table 4. Activation parameters for the proton and deuteron transfer reactions from 1-(4-nitrophenyl)-1-nitroethane (**1**), 1-(4-nitrophenyl)-1-nitropropan (**2**), and 2- methyl-1-(4-nitrophenyl)-1-nitropropane (**3**) to nitrogen bases: DBU, TBD, and MTBD in acetonitrile solvent at 25°C.

	DBU (4)			TBD			MTBD		
R	$\Delta H^{\neq a}$	$\Delta S^{\neq b}$	$\Delta H^{\neq}_D - \Delta H^{\neq}_H$	$\Delta H^{\neq}$	$\Delta S^{\neq}$	$\Delta H^{\neq}_D - \Delta H^{\neq}_H$	$\Delta H^{\neq}$	$\Delta S^{\neq}$	$\Delta H^{\neq}_D - \Delta H^{\neq}_H$
H- transfer									
1	15.4 ± 0.6	–131.0 ± 2.0		17.2 ± 1.9	–107.4 ± 6.5		25.1 ± 1.6	–113.0 ± 5.5	
2	17.8 ± 0.7	–134.0 ± 2.0		20.2 ± 1.7	–106.1 ± 5.8		22.1 ± 1.0	–133.9 ± 3.6	
3	19.9 ± 0.5	–147.0 ± 2.0		19.4 ± 3.0	–121.5 ± 10.3		33.2 ± 1.0	–117.0 ± 3.2	
D- transfer									
1	22.4 ± 0.6	–128.0 ± 2.0	7.0 ± 0.8	22.1 ± 2.2	–109.4 ± 7.3	4.9 ± 2.9	33.3 ± 2.0	–106.4 ± 10.1	8.2 ± 2.6
2	25.2 ± 0.5	–130.0 ± 2.0	7.4 ± 0.9	27.0 ± 1.2	–103.3 ± 4.1	6.8 ± 2.1	28.8 ± 1.4	–131.1 ± 4.6	6.7 ± 1.7
3	27.5 ± 0.2	–142.8 ± 0.5	7.6 ± 0.5	30.7 ± 1.6	–104.8 ± 5.3	11.3 ± 3.4	40.5 ± 3.6	–109.1 ± 12.3	7.3 ± 3.7

[a] $\Delta H^{\neq}$ (kJ mol^{-1}).
[b] $\Delta S^{\neq}$ (J mol^{-1} deg^{-1}).

Scheme 4. Low-energy conformers of 1-(4-nitrophenyl)-1-nitropropane (**2**) and 2-methyl-1-(4-nitrophenyl)-1-nitropropane (**3**).



much larger (118, 146, and 287, respectively (2)). The influence of position of nitro groups in nitro-substituted diarylmethanes on the k_{TBD}/k_{MTBD} = 4–7 is distinct as was estimated before by kinetic methods (16). This effect is not as large as for the present system of reactions where k_{TBD}/k_{MTBD} = 48–150 depending on the structure of C-acids **1**–**3** (Tables 1 and 2).

Generally, along with the growing bulk of the R substituent, significant reduction of the rate constants is observed which is consistent with earlier observations made by Bordwell and co-workers (24, 25). This indicates that the steric factors play an important role, and is similar with the results reported by other authors for the case of presence of different crowding in the vicinity of the reaction center (26–30). This relation is consistent with increased steric inhibition to planarity in the carbanion and most of all different structure of the complex of the transition state (2).

The KIEs' values are moderately large, but almost invariable ranging from 10–13 for TBD base, with the tendency to be larger for more hindered C-acids: 9.9, 11.2, 12.6 for **1**, **2**, and **3**, respectively (Table 1).

The unusual KIE values are obtained for the reaction with MTBD (Table 2) where they are declining with the increase of bulk of the R substituent: 12.5, 10.8, 6.9. Usually the steric hindrance causes an increase of KIE due to either desolvation of the transition state or a steeper energy barrier (4, 30). However, just the reverse effect was already found that steric hindrance in both the base and C-acid may in fact reduce the KIE (3, 4, 26).

The rate constants and KIE are insensitive to the polarity of the solvent (Table 3). One can expect much faster ionogenic reaction in polar MeCN than nonpolar CB. The fastest reaction in this set of C-acids has been observed for TBD both in MeCN and THF while for MTBD the rates are two orders of magnitude smaller. Then we presume that the charge separation in two different hydrogen-bonded complexes of transition state for TBD and MTBD reactions (Scheme 3) is not advanced. This is manifested by the meaningless influence of polarity of the solvent, also suggesting an uncoupled mechanism (31).

The different mechanism for the reactions of **1**–**3** with TBD and MTBD is reflected in the values of activation parameters collected in Table 4.

The large, negative $\Delta S^{\neq}$ values close to –110 J mol^{-1} K^{-1} for TBD and MTBD are characteristic for ionogenic mechanism of reaction. There is a distinct increase in $\Delta H^{\neq}$ together with the bulk of R in the sequence of C-acids for reaction with DBU. The largest value of enthalpy of activation ($\Delta H^{\neq}$) has been found for the most hindered reaction between **3** and MTBD (Table 4). There is a significant difference between the $\Delta H^{\neq}$ found for TBD and MTBD reactions with **3** ($\Delta H^{\neq}_{TBD}$ = 19.4 and $\Delta H^{\neq}_{MTBD}$ = 33.2 kJ mol^{-1}) indicating a different mechanism for the latter reaction. The simultaneous increase of enthalpy of activation ($\Delta H^{\neq}$) and negative values of entropy of activation ($\Delta S^{\neq}$) along with increasing steric hindrance of reactants cause a rise in free enthalpy of activation ($\Delta G^{\neq}$) of 6.7 and 9.3, for TBD and MTBD, respectively. Hence, the lack of a compensating effect suggests that restriction of free motion within the active complex rather than desolvation of the transition state determine the changes of the entropy of activation.

The reactions with TBD and MTBD show different patterns of the effect of steric hindrance on KIE. The KIE values grow with steric hindrance for the TBD reaction while with DBU and MTBD, the reverse effect was observed (Table 3). In the case of the TBD reaction, the double hydrogen bond determines the structure of the transition state (Scheme 3) (2, 23). By means of PM3 level computation, with the assumption of the T.S. structure (Scheme 3), it was proved that generally for reaction of C-acids **1**–**3** with TBD base, the HCNO dihedral angle in the T.S. complex decreases along with the bulk of R substituent in the C-acid.

The reaction with MTBD proceeds with different structures of T.S. complexes (Scheme 3). The PM3 calculation level applied for the most stable conformer of **3** with

© 2001 NRC Canada

antiperiplanar positions of the hydrogen atoms with MTBD base show three energetically equivalent T.S. complexes with the Me group of the base located in between NO_2 and $PhNO_2$, $PhNO_2$ and *i*-Pr, NO_2 and *i*-Pr (Scheme 4). The same computation applied for C-acid **2** with MTBD indicated the lowest energy conformer for T.S. complex with the Me group of the base located between $PhNO_2$ and Me groups (Scheme 4).

In this case, the HCNO angle is small, i.e. the nitro group is almost coplanar with the proton transfer axis. For the least hindered C-acid **1**, the Me group of the MTBD base is always located between NO_2 and $PhNO_2$. The MTBD transition states are characterized by a larger level of energy, than in the case of TBD, which is in good agreement with a little larger values of enthalpy of activation (Table 4).

Thus, the reaction of MTBD proceeds with different structures of transition state than the TBD reaction (Scheme 3), where along with growing bulk of substituent R in C-acid, a decrease in HCNO angle is found. Hence, the conclusion can be drawn, that the smaller the angle the larger is KIE.

The results of this work indicate two factors influencing KIE values. The additional stabilization of the transition state by a hydrogen bond, such as in TBD reactions, seems to increase KIE. Steric hindrance in C-acid, which affects the HCNO angle in the transition state of the TBD reaction, also increases KIE.

The above conclusions could be summarized in a statement that, for the reactions of nitroalkanes with guanidine bases, the KIE values increase when the structure of the transition state is less product-like.

In conclusion, we claim that the KIE values are greatly influenced by the factor resulting from the structure of the complex of transition state which is formed with hydrogen bonds between a base and oxygen atom of nitro groups of reacting C-acid. The further study of this problem seems to be advisable.

Acknowledgements

We gratefully acknowledge the financial support from a KBN grant No. 7 T09A 074 21.

References

1. W. Galezowski, I. Grzeskowiak, and A. Jarczewski. Can. J. Chem. **77**, 1042 (1999).
2. W. Galezowski, I. Grzeskowiak, and A. Jarczewski. J. Chem. Soc. Perkin Trans. 2, 1607 (1998).
3. W. Galezowski and A. Jarczewski. Can. J. Chem. **68**, 2242 (1990).
4. W. Galezowski and A. Jarczewski. J. Chem. Soc. Perkin Trans. 2, 1647 (1989).
5. W. Galezowski and A. Jarczewski. Can. J. Chem. **70**, 935 (1992).
6. W. Galezowski, M. Stanczyk, I. Grzeskowiak, and A. Jarczewski. J. Chem. Soc. Perkin Trans. 2, 2647 (1996).
7. W. Galezowski, M. Stanczyk, and A. Jarczewski. Can. J. Chem. **75**, 285 (1997).
8. W. Galezowski, A. Jarczewski, M. Stanczyk, B. Brzezinski, F. Bartl, and G. Zundel. J. Chem. Soc. Faraday Trans. 1, **93**, 2515 (1997).
9. R. Schwesinger, J. Willaredt, H. Schlemper, M. Keller, D. Schmitt, and H. Fritz. Chem. Ber. **127**, 2235 (1994).
10. C.L. Perrin and J. Pressing. J. Am. Chem. Soc. **93**, 5705 (1971).
11. F.G. Bordwell and W.J. Boyle, Jr. J. Am. Chem. Soc. **97**, 3447 (1975).
12. F.G. Bordwell, W.J. Boyle, Jr., and K.C. Yee. J. Am. Chem. Soc. **87**, 3879 (1970).
13. A.J. Kresge. Can. J. Chem. **52**, 1897 (1974).
14. F. Terrier, L. Xiao, P.G. Farrell, D. Moscowitz. J. Chem. Soc. Perkin Trans. 2, 1259 (1992).
15. K.T. Leffek, P. Pruszynski, and K. Thanapaalasingham. Can. J. Chem. **67**, 590 (1989).
16. G. Schroeder, B. Leska, A. Jarczewski, B. Nowak-Wydra, and B. Brzezinski. J. Mol. Struct. **344**, 77 (1995).
17. R. Schwesinger. Chimia, **39**, 269 (1985).
18. K.T. Leffek and A.E. Matinopoulos-Scordou. J. Chem. Soc. Perkin Trans. 2, 1099 (1979).
19. N. Rabjohn and C.A. Harbert. J. Org. Chem. **35**, 3240 (1950).
20. E. van Aken, H. Wynberg, and F. Van Bolhuis. J. Chem. Soc. Chem. Commun. 629 (1992).
21. P.H. Boyle, M.A. Convery, A.P. Davis, G.D. Hosken, and B.A. Murray. J. Chem. Soc. Chem. Commun. 239 (1992).
22. G. Schroeder, B. Brzezinski, B. Leska, B. Gierczyk, and A. Jarczewski. Bull. Pol. Acad. Sci. Chem. **44**, 45 (1996).
23. G. Schroeder, B. Brzezinski, A. Jarczewski, E. Grech, and P. Milart. J. Mol. Struct. **384**, 127 (1996).
24. F.G. Bordwell and H.E. Fried. Tetrahedron Lett. 1121 (1977).
25. F.G. Bordwell, J.E. Bartmess, and J.A. Hautala. J. Org. Chem. **43**, 3107 (1978).
26. N. Sugimoto, M. Sasaki, and J. Osugi. J. Chem. Soc. Perkin Trans. 2, 655 (1984).
27. N. Sugimoto and M. Sasaki. J. Chem. Soc. Faraday Trans. 1, **81**, 1441 (1985).
28. K.T. Leffek and P. Pruszynski. Can. J. Chem. **66**, 1454 (1988).
29. M. Hojatti and K.T. Leffek. Can. J. Chem. **62**, 2653 (1984).
30. E.S. Lewis and L.H. Funderburk. J. Am. Chem. Soc. **89**, 2322 (1967).
31. J.L. Kurz and L.C. Kurz. J. Am. Chem. Soc. **94**, 4451 (1972).

© 2001 NRC Canada

Equilibrium geometry, vibrational frequencies, and heat of formation of HOBr, $HBrO_2$, and $HBrO_3$ isomers

Cristina Maria P. Santos, Roberto B. Faria, Juan O. Machuca-Herrera, and Sérgio de P. Machado

Abstract: The equilibrium geometries, vibrational frequencies, heat capacity, and heat of formation for compounds of general formula $HBrO_x$ were calculated by DFT (BP and pBP methods) with DN* and DN** numerical basis sets. The comparison of our HOBr calculated results with the HOBr experimental values points out that the BP and pBP methods are as good as other ab initio and DFT methods related in the literature employing extended basis sets. The calculated $HBrO_x$ total energy and heat of formation values, at 0 and 298.15 K, present the following order: HOBr < HBrO; HOOBr < HOBrO < $HBrO_2$; HOOOBr < $HOBrO_2$ < HOOBrO < $HBrO_3$. The $HBrO_x$ heat of formation was calculated using isodesmic and homodesmic reactions and the results show that, in general, the use of these reactions gives similar results.

Key words: HOBr, $HBrO_2$, $HBrO_3$, DFT, numerical basis.

Résumé : Utilisant des ensembles de base numériques DN* et DN**, on a déterminé les géométries d'équilibre, les fréquences vibrationnelles, les capacités calorifiques et les chaleurs de formation de composés de formule générale $HBrO_x$ à l'aide de calculs DFT (méthodes BP et pBP). La comparaison des valeurs que nous avons calculées pour HOBr avec les valeurs expérimentales correspondantes suggère que les méthodes BP et pBP sont aussi bonnes que d'autres méthodes ab initio et DFT apparentées de la littérature qui font appel à des ensembles de base élargis. Les valeurs calculées, à 0 K et à 298,15 K, pour l'énergie totale et la chaleur de formation des $HBrO_x$ sont dans l'ordre suivant: HOBr < HBrO < ; HOOBr < HOBrO < $HBrO_2$; HOOOBr < $HOBrO_2$ < HOOBrO < $HBrO_3$. La chaleur de formation des $HBrO_x$ a été calculée à l'aide de réactions isodesmiques et homodesmiques et les résultats montrent que, en général, l'utilisation de ces réactions conduit à des résultats semblables.

Mots clés : HOBr, $HBrO_2$, $HBrO_3$, DFT, ensembles de base numériques.

[Traduit par la Rédaction]

Introduction

Halogen compounds are involved in the mechanisms of ozone depletion in the stratosphere and underlying troposphere (1, 2). These reactions occur in catalytic cycles including free radicals as well halogen oxides and some of them connect bromine and chlorine chemistry to the destruction of the ozone layer (3). In addition to the very well known effect of chlorine compounds, Barrie et al. (4) have shown that a lower level of ozone can be related to a high concentration of the bromine compounds in the atmosphere. These authors associated the ozone depletion to the photochemistry of bromoform ($CHBr_3 + h\nu \rightarrow Br\cdot + CHBr_2\cdot$) and to catalytic reactions involving BrO_x radicals. Related to a global impact on the ozone layer, the bromine species has been responsible for 40% and 25% of the ozone loss over Arctic and Antarctica regions, respectively, during the winter (5, 6). Other experimental results (7–9) have suggested that the reaction $BrO\cdot + HO_2\cdot \rightarrow HOBr + O_2$ proceeds faster than had been supposed before by Cox and Sheppard (10). Elrod et al. (11) proposed a temperature dependence for this reaction and also determined HBr and O_3 as another possible products. More recently, McElroy et al. (12) associated the enhanced concentrations of bromine species in the atmosphere to catalytic reactions involving bromine monoxide, originated from the sea salt accumulated on the snow pack.

With all this bromine chemistry being proposed, we have decided to use the HOBr to verify the ability of theoretical methods and basis set to calculate the equilibrium geometry, vibrational frequencies, and heat of formation of compounds involving hydrogen, oxygen, and bromine atoms. This choice was made considering that the HOBr contains three elements related with catalytic cycles of ozone depletion, presents several theoretical results in the literature, and has known experimental values.

In this study, we employed the BP and pBP density functional models with numerical basis set using the Spartan 5.0. The comparison of the calculated HOBr results with experimental values have shown that these theories are as good as

Received January 18, 2001. Published on the NRC Research Press Web site at http://canjchem.nrc.ca on July 30, 2001.

C.M.P. Santos, R.B. Faria,[1] J.O. Machuca-Herrera, and S. de P. Machado. Departamento de Química Inorgânica, Instituto de Química, Universidade Federal do Rio de Janeiro, Caixa Postal 68563, Rio de Janeiro, RJ, 21945–970, Brazil.

[1]Corresponding author (telephone: 55 21 562-7148; fax: 55 21 290-4746; e-mail: faria@iq.ufrj.br).

 DOI: 10.1139/cjc-79-7-1135 © 2001 NRC Canada

other ab initio and DFT methods employing extended basis sets. Based on these HOBr results, we applied BP and pBP models to forecast the equilibrium geometry, vibrational frequencies, and the thermodynamic properties for all HOBr, $HBrO_2$, and $HBrO_3$ isomers.

Several theoretical studies have been done for the HOBr and the HBrO isomers. McGrath and Rowland (13), based on Gaussian-2 theory, determined the ideal gas heat of formation of HOBr. Lee (14) used the CCSD(T) level of theory, with a triple ζ-polarized basis set, for the determination of equilibrium structures, vibrational frequencies, quadratic force fields, dipole moments, and IR intensity of HOBr, HBrO, and other triatomic bromine compounds. Francisco et al. (15), using 962(d)/6-311G(d,p) basis, reported MP2, CISD, CCSD(T), and MRCISD optimized geometries and total energies for the HOBr ground state. These authors also calculated the vibrational frequencies by MP2, CISD, and CCSD(T) methods. Ying and Zhao (16) employed MP2 and B3LYP models with a basis set including polarization functions (6-311G(d,p)) and polarization and diffuse functions (6-311++G(d,p)) to obtain HOBr geometry and vibrational frequencies. Equilibrium geometry and harmonic frequencies for HOBr using CCSD(T) method with pseudo+TZ2P basis were determinated by Füsti-Molnár et al. (17). The HOBr and HBrO equilibrium geometries were determinated by Li and Francisco (18) using the CCSD(T) method with 6-31G, 6-311G (2d,2p), 6-311G (2df,2p), and 6-311G(3df,3pd) basis sets while the vibrational frequencies were calculated only by the 6-31G and 6-311G(3df,3pd) basis sets.

For the $HBrO_2$ isomers, only four theoretical works were found. Lee (19) using CCSD(T) level of theory, with the TZ2P basis set, calculated the equilibrium geometries, dipole moments, harmonic vibrational frequencies, and rotational constants for the HOOBr, HOBrO, and $HBrO_2$ molecules. Based on the isodesmic reaction HOOBr + HOH →HOOH + HOBr, where the same number of bond types is maintained on the reactants' and on the products' side, Lee (19) also determinated the heat of formation of the $HBrO_2$ isomers. Guha and Francisco (20) made the same determinations employing various density functional methods (BLYP, SVW, and B3LYP) with the 6-311++G (3df,3pd) basis set. The energies for the $HBrO_2$ isomers were calculated using the G2 and CCSD(T) methods based on the geometries forecasted by the B3LYP theory with 6-311++G(3df,3pd) basis set. More recently, Guha and Francisco (21, 22) studied the isomerization pathways for the $HBrO_2$ isomers. The geometries, vibrational frequencies, and relative energies were obtained for the $HBrO_2$ isomers and their transition states using the QCISD method with 6-31G(d), 6-311G(d,p), and 6-311G(2d, 2p) basis sets (21). Also using the QCISD method, they determined the equilibrium geometry, vibrational frequencies, and relative energies for the HOOBr → HOBrO isomerization transition state (22).

The $HBrO_3$ isomers were studied by Guha and Francisco (23, 24). In the first work, these authors determined the equilibrium geometries, vibrational frequencies, and relative energies for the HOOOBr, $HOBrO_2$, HOOBrO, and $HBrO_3$ molecules using ab initio (MP2, CISD, and CCSD(T)) and DFT (B3LYP) methods, with TZ2P and 6-311++G(3df,3pd) basis sets. The HOOOBr heat of formation was calculated based on the isodesmic reaction HOOOBr + 2HOH → 2HOOH + HOBr. In the second work, they determinated the geometries, vibrational spectra, and relative energies for the HOOOBr and HOOBrO isomers using the quadratic configuration interaction method (QCISD) with 6-31G(d,p), 6-311G(d,p), and 6-311G(2d,2p) basis sets.

The density functional methods employed in this work present a basic difference to the other methods because it employs numerical basis sets (25) and not the more common Gaussian basis sets. Comparisons of bond distances and dipole moments calculated using numerical and Gaussian basis sets suggest that DN* and DN** numerical basis sets perform similar to 6-31G(d) and to 6-311G(d,p) basis sets, respectively (25). Because of this, numerical basis sets have been employed recently on studies involving rare gas dimers (26), heterocycle compounds (27, 28), and annelated oxirenes (29) and has been claimed as performing as good as some of the most sophisticated Gaussian basis sets (29). In addition, comparisons between numerical and their similar Gaussian basis sets has shown that the relative computational time are greater for the Gaussian basis sets than for the numerical basis sets making the last more attractive (25).

Computational methods

All calculations were done using SPARTAN (Wavefunction Inc., Irvine, California), Version 5.0, on a RISC 6000 workstation, using the density functional method (DFT). In doing this, two different nonlocal DFT models were used. These models are based on nonlocal corrections added to the local density model as proposed by Becke (30) and Perdew (31). In the Becke–Perdew (BP) model, a new potential, comprising a local part and a gradient correction (32), is used in place of the local potential in the self-consistent field (SCF) procedure. This gradient correction needs to be recalculated at every SCF iteraction. In the perturbative Becke–Perdew (pBP) model, an alternative computational approach is used and the gradient correction is introduced only after the convergence based on the local potential alone has been achieved. Both DN* and DN** numerical basis sets employed in DFT calculations describe the inner shell of each atomic orbital by a single function and the valence shell by a pair of functions and include a set of five *d*-type polarization functions for all atoms except hydrogen. The DN** is identical to DN* except for the fact that it includes *p*-type polarization functions for hydrogen atoms.

The zero-point vibrational energy (*ZPVE*) and vibrational thermal energy (E_{vib}) were obtained directly from the program, based on eqs. [1] and [2].

$$[1] \qquad ZPVE = 0.5 N_A h \Sigma \nu_i$$

$$[2] \qquad E_{vib} = RT \Sigma [(h\nu_i/kT)/(e^{h\nu_i/kT} - 1)$$

Where N_A is Avogadro's number, h is the Planck constant, ν_i is the fundamental vibrational frequency, k is the Boltzmann constant, R is the perfect gas constant, and T is the temperature in kelvin scale (33).

© 2001 NRC Canada

Table 1. Equilibrium geometries (Å), total energies (hartree), and vibrational frequencies (cm^{-1}) for the HOBr and HBrO isomers.

Parameters	BP/DN*	BP/DN**	pBP/DN*	pBP/DN**	Experimental
HOBr					
H-O	0.987	0.977	0.992	0.983	0.961[a]
O-Br	1.888	1.888	1.889	1.889	1.834[a]
HOBr	101.5°	101.4°	101.8°	101.7°	102.3°[a]
E_T	–2650.313	–2650.320	–2650.312	–2650.319	—
$\nu_{O\text{-}Br}$	595	595	593	591	626[b], 620[c]
δ_{HOBr}	1167	1164	1152	1138	1164[b], 1162[c]
$\nu_{H\text{-}O}$	3592	3678	3548	3633	3590[b], 3614[d]
HBrO					
H-Br	1.512	1.495	1.528	1.509	—
Br-O	1.716	1.744	1.742	1.744	—
HBrO	106.8°	107.1°	107.3°	107.1°	—
E_T	–2650.224	–2650.227	–2650.223	–2650.226	—
$\nu_{Br\text{-}O}$	697	693	702	697	—
δ_{HBrO}	783	787	776	777	—
$\nu_{H\text{-}Br}$	2022	2070	1956	2009	—

[a]Reference 39.
[b]Reference 40.
[c]Reference 41.
[d]Reference 42.

Results and discussion

HOBr — geometry, vibrational frequencies, and C_p^0

The calculated equilibrium geometries, total energies, and vibrational frequencies for the HOBr isomer can be found in Table 1. The calculated equilibrium geometry has the expected angular geometry (C_S symmetry). The comparison of BP and pBP geometries with the experimental values shows that the O—Br bond length is more difficult to reproduce than the H—O bond length. Despite the closer proximity of all calculated equilibrium geometry values with the experimental ones, the CCSD(T)/pseudo+TZ2P used by Füsti-Molnár et al. (17) (H—O = 0.965 Å, O-Br = 1.834 Å, HOBr = 102.3°) is slightly better than all other results in the literature.

The comparison of calculated vibrational frequencies related in the literature with the experimental values shows that H—O stretching is the most difficult to reproduce, being generally overestimated, in some cases by more than 200 cm^{-1}. Based on this, our DFT results can be considered in good agreement with the experimental values, mainly for HOBr bend and HO stretch frequencies. From these results, we can say that BP and pBP methods with DN* and DN** numerical basis sets are a good option to forecast vibrational frequencies for bromine compounds.

The HOBr heat capacity (C_p°) was calculated based on the summation, at 298.15 K, of the vibrational ($C_{p\ vib.}^\circ$), translational ($C_{p\ trans.}^\circ$), and rotational ($C_{p\ rot.}^\circ$) contributions, as shown by eqs. [3]–[5], respectively (33). The molecule was considered a rigid rotor and an harmonic oscillator.

$$[3] \qquad C_{p\ vib.}^\circ = R\Sigma\{(h\nu_i/kT)^2[(e^{h\nu_i/kT})/(e^{h\nu_i/kT} - 1)^2]\}$$

$$[4] \qquad C_{p\ trans.}^\circ = 5/2R$$

$$[5] \qquad C_{p\ rot.}^\circ = 3/2R$$

Both HOBr heat capacity values (C_p°) obtained by BP and pBP methods (at 298.15 K) are very close to the 9.2 cal mol^{-1} K^{-1}, in agreement with the McGrath and Rowland (13) result of 9.18 cal mol^{-1} K^{-1}.

HBrO — geometry, vibrational frequencies, and C_p^0

For the HBrO isomer, with angular geometry (C_S symmetry), the results are also listed on Table 1. The DFT results show this isomer at approximately 0.09 hartree higher than HOBr, in agreement with Lee (14) whocalculated this difference as 0.1 hartree. For vibrational frequency, our DFT values are closer to the CCSD results (18).

Considering that CCSD methods has calculated HOBr geometry in good agreement with the experimental values and supposing that the same tendencies will be maintained for the HBrO, the geometries obtained by these methods (14, 18) should be the most probable. Otherwise, based on the fact that DFT methods gave a good set of results for the HOBr vibrational frequencies, we can be confident of the following prevision for the HBrO isomer: $\nu_{Br\text{-}O} \cong 700$ cm^{-1}, $\delta_{HOBr} \cong 780$ cm^{-1}, and $\nu_{H\text{-}Br} \cong 2000$ cm^{-1}.

HOBr and HBrO heat of formation

The HOBr heat of formation was calculated using eq. [7], based on the same isodesmic reaction (rxn. [6]) employed by McGrath and Rowland (13).

$$[6] \qquad HOBr + ClO\cdot \rightarrow HOCl + BrO\cdot$$

$$[7] \qquad \Delta H_f^\circ\ (HOBr) = \Delta H_f^\circ\ (HOCl) + \Delta H_f^\circ\ (BrO\cdot) - \Delta H_f^\circ\ (ClO\cdot) - \Delta H_r$$

The ΔH_r (heat of reaction) was obtained from the calculated values for all species in rxn. [6]. The experimental ΔH_f° values for the species in the right side in eq.[7] were obtained from *NIST–JANAF Thermochemical Tables* (34).

© 2001 NRC Canada

Table 2. Heat of reaction and HOBr and HBrO heats of formation employing different reactions (at 298.15 K).[a]

Method/basis set	Reaction	ΔH_r (kcal mol^{-1})	ΔH_f° (HOBr) (kcal mol^{-1})	ΔH_f° (HBrO) (kcal mol^{-1})
BP/DN*	[6]	9.864 (9.875)	–21.9 (–19.3)	31.43 (34.05)
	[11]	8.111 (8.401)	–12.6 (–10.3)	40.76 (42.99)
	[12]	–1.426 (–1.541)	–12.9 (–10.3)	40.45 (43.03)
	[13]	0.610 (0.733)	–13.3 (–10.7)	40.02 (42.59)
BP/DN**	[6]	10.303 (10.316)	–22.3 (–19.7)	33.36 (35.97)
	[11]	9.437 (9.755)	–13.9 (–11.7)	41.81 (44.01)
	[12]	–0.930 (–1.038)	–13.4 (–10.8)	42.32 (44.90)
	[13]	0.246 (0.362)	–13.7 (–11.1)	42.02 (44.59)
pBP/DN*	[6]	2.311 (2.320)	–14.3 (–11.7)	38.93 (41.55)
	[11]	8.087 (8.358)	–12.5 (–10.3)	40.74 (42.99)
	[12]	–1.405 (–1.527)	–12.9 (–10.3)	40.38 (42.97)
	[13]	0.659 (0.788)	–13.2 (–10.7)	40.02 (42.59)
pBP/DN**	[6]	2.686 (2.695)	–14.7 (–12.1)	40.81 (43.44)
	[11]	9.508 (9.822)	–13.9 (–11.7)	41.58 (43.78)
	[12]	–1.039 (–1.155)	–13.3 (–10.7)	42.27 (44.85)
	[13]	0.293 (0.416)	–13.6 (–11.0)	41.91 (44.48)
Experimental (35)		—	–13.59 (–11.09)[b]	—
Experimental (36)		—	–14.3 (–11.8)	—
Benson's value (37)		—	–19[c]	—
Experimental (38)		—	–9[c]	—

[a]Values in parenthesis are at 0 K.
[b]Values corrected considering ΔH_f^0(OH) of 9.175 kcal mol^{-1} (at 0 K) and 9.318 kcal mol^{-1} (at 298.15 K) (34).
[c]Values at 300 K.

At 298.15 K,

$$[8] \quad \Delta H_r = \Delta E + \Delta ZPVE + \Delta E_{vib} + \Delta E_{rot} + \Delta E_{trans} + \Delta nRT$$

where ΔE is the electronic energy calculated by the quantum mechanical program and Δn is the change in the number of mol. In eq. [8], each term was obtained from the difference between the calculated values for products and reactants. Considering that for rxn. [6] Δn is equal to zero and $\Delta E_{rot} = \Delta E_{trans} = \Delta n(3/2)RT$ for angular molecules ($\Delta E_{rot} = \Delta nRT$ and $\Delta E_{trans} = \Delta n(3/2)RT$ for linear molecules), the expression above becomes

$$[9] \quad \Delta H_r = \Delta E + \Delta ZPVE + \Delta E_{vib}$$

At 0 K, the heat of reaction is given by

$$[10] \quad \Delta H_r = \Delta E + \Delta ZPVE$$

Considering only isodesmic rxn. [6], it can be seen in Table 2 that ΔH_f°(HOBr) values, calculated by BP and pBP methods, at 298.15 K, are close to –22 and –14.5 kcal mol^{-1}, respectively. This 7.5 kcal mol^{-1} difference between these two values can be attributed to the 8.0 kcal mol^{-1} difference found between the total energy values obtained for ClO· using the BP and pBP methods. It was a surprise that such a difference was not observed for BrO·. In addition, the pBP values are very close to the McGrath and Rowland (13) result of –14.2 kcal mol^{-1}, that was obtained using Gaussian-2 theory. These pBP and G2 values are in good agreement with the experimental Ruscic and Berkowitz's value (35) (at 298 K) of –13.59 ± 0.42 kcal mol^{-1} and Lock and co-workers's (36) value of –14.3 ± 1 kcal mol^{-1}. The Ruscic and Berkowitz value presented here was corrected for the more recent ΔH_f° (OH) of 9.175 kcal mol^{-1} (at 0 K) and 9.318 kcal mol^{-1} (at 298.15 K) listed in the *NIST–JANAF Thermochemical Tables* (34). Benson's (37) and Monks and co-workers's (38) values are very different to these mentioned results. Based on the proximity of the Ruscic and Berkowitz (35) and Lock et al. (36) experimental values, we consider these two results as the more reliable. Consequently, we can say that the pBP theory results are in good agreement with the most reliable experimental results.

At 0 K, our pBP HOBr heat of formation values, determined using rxn. [6], are very close to the G2 value (13) of –11.7 ± 1.6 kcal mol^{-1} and the experimental values (35, 36) of –11.09 ± 1 kcal mol^{-1} (corrected for the OH heat of formation of 9.175 kcal mol^{-1}) and –11.8 ± 1 kcal mol^{-1}.

From the comparison of our results and the experimental values we conclude that the pBP level of theory, with DN* or DN** numerical basis set, gives good results for calculations of thermodynamic properties of HOBr based on isodesmic rxn. [6]. As can be seen from the small difference of 0.4 kcal mol^{-1} between the results using DN* and DN**, the polarization on hydrogen included in the DN** basis set did not make a significant difference for the description of HOBr and HOCl molecules used in isodesmic rxn. [6]. Otherwise, the BP model was not able to handle the ClO· radical and turned the ΔH_f° (HOBr) calculated value far from the more reliable experimental results.

The HBrO heat of formation presented on Table 2 was obtained based on the calculated relative energy to HOBr. Considering only the pBP theory and isodesmic rxn. [6] we can

© 2001 NRC Canada

Table 3. Equilibrium geometries (Å) and total energies (hartree) for $HBrO_2$ isomers.

Parameters	BP/DN*	BP/DN**	pBP/DN*	pBP/DN**
HOOBr				
H-O	0.992	0.983	0.999	0.989
O-O	1.408	1.409	1.405	1.407
O-Br	1.975	1.975	1.99	1.988
HOO	101.9°	101.9°	102.5°	102.3°
BrOO	111.8°	111.8°	111.6°	112.1°
HOOBr	87.6°	88.8°	89.3°	89.4°
E_T	–2725.493	–2725.450	–2725.491	–2725.498
HOBrO				
H-O	0.99	0.98	0.995	0.986
O-Br	1.926	1.926	1.93	1.93
Br-O_t	1.708	1.708	1.709	1.708
HOBr	102.6°	102.4°	102.9°	102.7°
$OBrO_t$	111.8°	111.8°	112.1°	112.0°
$HOBrO_t$	81.0°	81.7°	81.0°	81.6°
E_T	–2725.478	–2725.486	–2725.477	–2725.484
$HBrO_2$				
H-Br	1.570	1.551	1.588	1.568
Br-O	1.683	1.684	1.685	1.687
HBrO	99.7°, 100.1°	99.6°, 100.2°	100.3°, 100.3°	99.6°, 100.0°
OBrO	115.9°	115.8°	115.6°	116.2°
E_T	–2725.394	–2725.397	–2725.393	–2725.396

Table 4. Vibrational frequencies (cm^{-1}) for $HBrO_2$ isomers.

Parameters	BP/DN*	BP/DN**	pBP/DN*	pBP/DN**
HOOBr				
τ_{HOOBr}	266	267	263	262
δ_{OOBr}	473	477	464	469
ν_{O-Br}	530	532	520	526
ν_{O-O}	867	871	865	870
δ_{HOO}	1385	1380	1356	1345
ν_{H-O}	3482	3568	3413	3512
HOBrO				
τ_{HOBrO}	224	224	222	222
δ_{OBrOt}	380	396	385	386
ν_{Br-O}	504	504	500	500
ν_{Br-Ot}	785	785	784	785
δ_{HOBr}	1072	1060	1064	1039
ν_{H-O}	3560	3649	3509	3595
$HBrO_2$				
$Br_{umbrella}$	271	252	253	278
δ_{OBrO}	752	749	734	742
$\nu_{Br-O(sym)}$	768	766	755	761
δ_{HBrO}	793	772	765	776
$\nu_{Br-O(asym)}$	837	835	831	831
ν_{H-Br}	1724	1761	1663	1703

state that the ΔH_f° (HBrO) is close to 40 kcal mol^{-1} (at 298 K).

Isodesmic and homodesmic reactions

As can be noticed in Table 2, the HOBr heat of formation values obtained by the BP model using rxn. [6] are significantly lower than the values obtained using the pBP model. This posed a question to us about the validity of the employment of isodesmic reactions involving open shell molecules. In this way, we have decided to try other reactions to calculate the HOBr heat of formation. In these reactions called homodesmic after Lee (14), the number of bonds of the same type was conserved but not necessarily between the same atoms. In Table 2 we also present the HOBr heat of formation calculated by the homodesmic rxns. [11]–[13].

[11] $HOBr + HCl \rightarrow HOCl + HBr$

[12] $HOBr + Cl_2 \rightarrow HOCl + BrCl$

[13] $HOCl + Br_2 \rightarrow HOBr + BrCl$

As can be seen in Table 2, all calculated HOBr heat of formations using homodesmic rxns. [11]–[13] are very close to each other and close to the more reliable experimental values in a range of 2 kcal mol^{-1}.

$HBrO_2$ isomers — relative energies, geometry, vibrational frequencies, and C_p^0

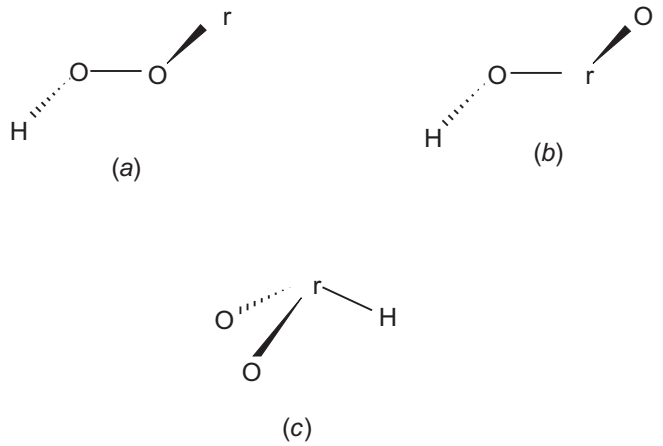
The equilibrium geometry energy values obtained in this work provided the following order: HOOBr < HOBrO < $HBrO_2$. This stability order is the same found by Lee (19) and Guha and Francisco (20). The average energy values for HOOBr, HOBrO, and $HBrO_2$ are equal to –2725.483 hartree, –2725.481 hartree, and –2725.395 hartree, respectively, and agree well with the Guha and Francisco (20) values that used BLYP and B3LYP theories.

The calculated equilibrium geometries, total energies, and vibrational frequencies are presented in Tables 3 and 4 for all $HBrO_2$ isomers. The $HBrO_2$ isomers have their calculated structures presented in Fig. 1.

For the HOOBr, our pBP/DN* O—O value is equal to the value calculated by Guha and Francisco (20, 21) using the B3LYP/6-311++G(3df,3pd) and QCISD/6-311G(d,p), but

© 2001 NRC Canada

Fig. 1. Calculated structures for $HBrO_2$ isomers: (*a*) HOOBr, (*b*) HOBrO, and (*c*) $HBrO_2$. See Table 3 for geometrical parameters.



our H—O and Br—O bond lengths are longer. Angle values are in close agreement with the BLYP and B3LYP methods (20), both with the 6-311++G basis set. In general, our calculated vibrational frequencies are in good agreement with other calculated values (19–21). The calculated HOOBr heat capacity points to a value of 12.8 cal mol^{-1} K^{-1}.

For the HOBrO isomer our average calculated dihedral angle of 81.3° is very close to the other calculated results (19–22). Our H—O, Br—O_t, and Br—O bond length values are in good agreement with those calculated by the BLYP (20) and QCISD (21) methods. The HOBr and $OBrO_t$ angles are in concordance with the values presented on the literature (19–21). For the vibrational frequency our calculated BP and pBP torsion values (τ) are smaller than CCSD(T) and B3LYP methods (19, 20) but agree very well with BLYP and QCISD methods (20, 21). The $\nu_{Br\text{-}O}$ and the $\nu_{Br\text{-}Ot}$ values are in good agreement with the CCSD(T) (19) and BLYP (20) methods, respectively. Our $\nu_{H\text{-}O}$ average value of 3578 cm^{-1} is closer with the BLYP (20) result than the other calculated values. Our OBrO and HOBr bend values are in agreement with the CCSD(T) (19) and BLYP (20) values, respectively. All HOBrO heat capacity determinated in this work point to a value of 13.5 cal mol^{-1} K^{-1}, being independent of the method or basis set employed.

The $HBrO_2$ isomer with C_1 symmetry, presents the H—Br and Br—O bond lengths and the HBrO and OBrO angles in agreement with the values obtained by Guha and Francisco (20, 21). Our calculated vibrational frequencies are very close to the BLYP (20) values. The predicted BP and pBP $HBrO_2$ heat capacity value is 12.5 cal mol^{-1} K^{-1}.

$HBrO_2$ isomers — heat of formation

As $\Delta n = 0$, the eqs. [9] and [10] can be used to obtain all the heat of reaction (ΔH_r) values. Table 5 presents the heat of reaction and the HOOBr, HOBrO, and $HBrO_2$ heats of formation obtained by the use of the rxns. [14] and [16]. The HOBrO and $HBrO_2$ values were obtained from their calculated relative energies to the HOOBr isomer.

For isodesmic rxn. [14], we have

[14] HOOBr + HOH → HOOH + HOBr

[15] ΔH_f° (HOOBr) = ΔH_f° (HOOH) + ΔH_f° (HOBr) − ΔH_f° (HOH) − ΔH_r

In eq. [15], the HOOH and HOH ΔH_f° experimental values were taken from *NIST–JANAF Thermochemical Tables* (34). For the HOBr heat of formation we have used the values of –11.46 kcal mol^{-1}, at 0 K, and –13.97 kcal mol^{-1}, at 298.15 K that was an average of the Ruscic and Berkowitz (35) and Lock et al. (36) values. The Ruscic and Berkowitz value was corrected for the more recent ΔH_f° (OH), as cited above.

For homodesmic rxn. [16], we have

[16] HOOBr + HOH + Cl_2 → HOOH + HOCl + BrCl

[17] ΔH_f° (HOOBr) = ΔH_f° (HOOH) + ΔH_f° (HOCl) + ΔH_f° (BrCl) − ΔH_f° (HOH) − ΔH_f° (Cl_2) − ΔH_r

All the HOOH, HOCl, BrCl, HOH, and Cl_2 ΔH_f° experimental values were taken from *NIST–JANAF Thermochemical Tables* (34).

At 0 K, the HOOBr heat of formation values were determinated for the first time by Guha and Francisco (20) using isodesmic rxn. [14]. Our BP and pBP values using isodesmic rxn. [14] and homodesmic rxn. [16] agree very well with their BLYP/6-311++G (3df,3pd) value (20) of 5.2 kcal mol^{-1}. The CCSD(T)/TZ2P (19), G2/6-311++G(3df,3pd) (20), and B3LYP/6-311++G(3df,3pd) (20) values of 10.5 kcal mol^{-1}, 7.8 kcal mol^{-1}, and 8.1 kcal mol^{-1} are in agreement with each other but are higher than our values.

Based on rxns. [14] and [16], the BP and pBP HOBrO heat of formation values (see Table 5), at 0 K, are very close to the B3LYP/6-311++G(3df,3pd) value (20) of 13.8 kcal mol^{-1} and the CCSD(T)/TZ2P value (19) of 14.7 kcal mol^{-1}. Otherwise, the G2 value (20) of 10.7 kcal mol^{-1} and the BLYP value (20) of 8.6 kcal mol^{-1} are lower than our calculated values.

At 0 K, the $HBrO_2$ isomer heat of formation, using rxns. [14] and [16] and the DN* basis set, show values in good agreement with the CCSD(T)/TZ2P (19) of 64.3 kcal mol^{-1} and B3LYP/6-311++G(3df,3pd) (20) of 65.3 kcal mol^{-1}. The inclusion of polarization on hydrogen by the use of the DN** basis set increases the heat of formation of this isomer by, approximately, 3 kcal mol^{-1}.

$HBrO_3$ isomers — relative energies, geometry, vibrational frequencies, and C_p^0

The equilibrium geometry energy values obtained in this work provided the following order: HOOOBr < $HOBrO_2$ < HOOBrO < $HBrO_3$. The pBP and BP methods indicate that the HOOOBr is more stable (0.014 hartree and 0.016 hartree, respectively), than the $HOBrO_2$. This order is not in agreement with the Guha and Francisco results (23) which gave $HOBrO_2$ more stable than the HOOOBr by 0.001 hartree. The $HBrO_3$ isomers' equilibrium geometry, total energies, and vibrational frequencies are presented on Tables 6 and 7. The Fig. 2 presents the structures of all calculated $HBrO_3$ isomers.

© 2001 NRC Canada

Table 5. Heats of reaction and HOOBr, HOBrO, and $HBrO_2$ heats of formation employing different reactions (at 298.15 K).[a]

Methods	Reaction	ΔH_r (kcal mol^{-1})	$\Delta H_f°$ (HOOBr) (kcal mol^{-1})	$\Delta H_f°$ (HOBrO) (kcal mol^{-1})	$\Delta H_f°$ ($HBrO_2$) (kcal mol^{-1})
BP/DN*	[14]	9.503 (9.777)	1.75 (4.84)	9.77 (13.42)	58.46 (64.32)
	[16]	7.984 (8.240)	2.94 (6.02)	10.96 (14.60)	59.64 (65.50)
BP/DN**	[14]	8.603 (8.773)	2.65 (5.85)	10.09 (13.85)	61.24 (67.33)
	[16]	7.556 (7.709)	3.36 (6.55)	10.80 (14.55)	61.95 (68.03)
pBP/DN*	[14]	9.592 (9.852)	1.66 (4.77)	9.57 (13.16)	57.63 (63.53)
	[16]	8.053 (8.296)	2.87 (5.96)	10.77 (14.35)	58.83 (64.72)
pBP/DN**	[14]	8.743 (8.932)	2.51 (5.69)	9.69 (13.41)	60.92 (67.00)
	[16]	7.579 (7.752)	3.34 (6.51)	10.53 (14.22)	61.82 (67.82)

[a]Values at 0 K are presented between parenthesis.

Table 6. Equilibrium geometries (Å) and total energies (hartree) for $HBrO_3$ isomers.

Parameters	BP/DN*	BP/DN**	pBP/DN*	pBP/DN**
HOOOBr				
H-O	0.993	0.984	0.999	0.984
O-O_a	1.517	1.517	1.538	1.517
O-O_b	1.306	1.306	1.293	1.295
O_b-Br	2.085	2.085	2.114	2.116
HO_aO	99.9°	100.1°	99.8°	99.2°
O_aOO_b	111.5°	111.4°	112.1°	110.9°
BrO_bO	114.6°	114.6°	115.0°	112.7°
O_aOO_bBr	82.4°	82.5°	83.6°	81.0°
HO_aOO_b	41.3°	41.3°	42.2°	41.2°
E_T	–2800.686	–2800.694	–2800.683	–2800.690
$HOBrO_2$				
H-O	0.993	0.983	0.999	0.989
Br-O	1.936	1.935	1.943	1.944
Br-O_t	1.667, 1.659	1.667, 1.659	1.668, 1.661	1.667, 1.662
HOBr	101.0°	101.0°	102.6°	102.6°
$OBrO_t$	104.4°, 101.2°	104.4°, 101.3°	105.4°, 103.1°	105.4°, 103.0°
O_tBrO_t	112.8°	112.8°	111.8°	111.8°
$HOBrO_t$	–77.4°, –14.7°	–77.3°, –14.7°	–90.7°, 26.6°	–90.7°, 26.6°
E_T	–2800.670	–2800.678	–2800.669	–2800.676
HOOBrO				
H-O	0.991	0.981	0.997	0.988
O-O	1.410	1.411	1.406	1.409
O-Br	2.055	2.055	2.081	2.065
Br-O_t	1.717	1.716	1.715	1.717
HOO	101.9°	102.0°	103.0°	102.0°
OOBr	112.7°	112.7°	113.9°	112.4°
$OBrO_t$	112.9°	112.9°	115.3°	111.7°
HOOBr	86.4°	86.4°	86.9°	87.4°
$OOBrO_t$	83.7°	83.5°	76.4°	80.5°
E_T	–2800.662	–2800.668	–2800.656	–2800.666
$HBrO_3$				
H-Br	1.54	1.523	1.554	1.538
Br-$O_{a,b}$	1.648	1.649	1.65	1.65
Br-O_c	1.649	1.649	1.65	1.65
$HBrO_{a,b}$	102.6°	102.7°	102.9°	102.9°
$HBrO_c$	102.8°	102.8°	102.9°	102.9°
O_aBrO_b	114.8°	114.8°	114.6°	114.6°
O_bBrO_c	115.6°	115.5°	115.4°	115.4°
E_T	–2800.557	–2800.560	–2800.555	–2800.558

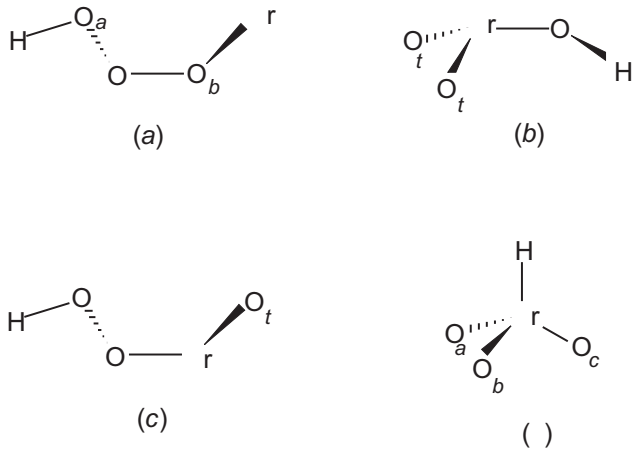
© 2001 NRC Canada

Table 7. Vibrational frequencies (cm^{-1}) for $HBrO_3$ isomers.

Parameters	BP/DN*	BP/DN**	pBP/DN*	pBP/DN**
HOOOBr				
τ_{OOOBr}	124	125	125	121
δ_{OOBr}	182	190	196	184
τ_{HOOO}	335	333	333	319
$\nu_{O\text{-}Br}$	462	461	442	437
δ_{OOO}	466	467	466	463
$\nu_{O\text{-}O(sym)}$	663	661	642	645
$\nu_{O\text{-}O(asym)}$	972	972	1006	1011
δ_{HOO}	1316	1317	1269	1268
$\nu_{H\text{-}O}$	3513	3592	3469	3538
$HOBrO_2$				
$Br_{umbrella}$	289	297	257	256
δ_{OBrOt}	339	341	325	325
$\nu_{Br\text{-}O}$	485	495	480	477
$\nu_{Br\text{-}Ot(sym)}$	812	813	811	812
$\nu_{Br\text{-}Ot(asym)}$	863	863	858	858
δ_{HOBr}	1042	1063	1269	1003
$\nu_{H\text{-}O}$	3528	3617	3469	3561
HOOBrO				
τ_{OOBrO}	97	95	48	71
δ_{OBrO}	180	179	163	182
δ_{OOBr}	227	228	224	230
H_{wag}	399	399	392	403
$\nu_{Br\text{-}O(sym)}$	515	511	489	533
$\nu_{Br\text{-}O(asym)}$	771	772	772	770
$\nu_{O\text{-}O}$	885	882	884	882
δ_{HOO}	1376	1359	1346	1341
$\nu_{H\text{-}O}$	3505	3597	3437	3536
$HBrO_3$				
δ_{OBrO}	289, 296	291, 308	292, 308	293, 308
$Br_{umbrella}$	352	361	361	361
$\nu_{Br\text{-}O(sym)}$	778, 781	780, 791	766, 773	766, 774
δ_{HBrO}	789	799	781	780
$\nu_{Br\text{-}O(asym)}$	883	883	884	884
$\nu_{H\text{-}Br}$	1921	1948	1867	1897

For the HOOOBr, the BP, and pBP H—O_a, O—O_a, and Br—O_b bond lengths are slightly higher than the literature values (23, 24). The O—O_b values are smaller than the B3LYP (23) and QCISD (24) results. The BrOOO dihedral angle that conferred the lower energy is 82.4°, in good agreement with the QCISD/6-311G(d,p) value of 82.2° (24). The BP and pBP HO_aO angles are smaller than other literature values (23, 24) and the O_aOO_b and BrO_bO angles are close to the B3LYP result (23). For vibrational frequencies, the BrOOO torsion is lower than the value of 131 cm^{-1} determinated by Guha and Francisco (23, 24) and the HOOO torsion is lower than the values of 395 cm^{-1} and 437 cm^{-1} obtained using B3LYP (23) and QCISD (24) methods, respectively. The symmetric $\nu_{O\text{-}O}$ values are slightly higher than the B3LYP (23) and QCISD (24) methods. The $\nu_{O\text{-}H}$ values are lower than the Guha and Francisco values of 3713 cm^{-1} and 3726 cm^{-1} (23, 24). The OO_bBr, O_aOO_b, and HO_aO bend values are lower than B3LYP (23) and QCISD (24) results. Based on vibrational frequencies, the HOOOBr heat capacity was estimated as equal to 17.5 cal mol^{-1} K^{-1}.

Fig. 2. Calculated structures for $HBrO_3$ isomers: (*a*) HOOOBr, (*b*) $HOBrO_2$, (*c*) HOOBrO, and (*d*) $HBrO_3$. See Table 6 for geometrical parameters.



For the $HOBrO_2$ isomer there is only the Guha and Francisco results using the B3LYP method (23). Comparing it with our results, we find that our bond length values and $OBrO_t$ angles are slightly higher and the HOBr angle is slightly lower than the B3LYP results (23). Generally, the BP and pBP methods gave vibrational frequency values lower than the calculated by Guha and Francisco (23). The average of the calculated heat capacity has a value of 17.7 cal mol^{-1} K^{-1}.

The HOOBrO isomer bond lengths and angles values are in agreement with the QCISD results (24). For vibrational frequencies, the OOBrO torsion has scattered values considering all mentioned methods. The BP and pBP asymmetric $\nu_{Br\text{-}O}$ are higher than the values of 481 cm^{-1} and 476 cm^{-1} obtained by B3LYP (23) and QCISD (24) methods, respectively; $\nu_{O\text{-}O}$, $\nu_{O\text{-}H}$, and symmetric $\nu_{Br\text{-}O}$ are lower than the values obtained by these same methods. The bend values are slightly lower than those in the literature (23, 24). The HOOBrO heat capacity obtained has an average value of 17.6 cal mol^{-1} K^{-1}.

The $HBrO_3$ isomer presents HBr and BrO bond lengths slightly higher than B3LYP values (23) and BP and pBP HBrO angles in good agreement with the Guha and Francisco result of 103.4° (23). All BP and pBP vibrational frequencies have lower values when compared to the Guha and Francisco results (23). The $HBrO_3$ heat capacity calculated values are close to 16.0 cal mol^{-1} K^{-1}.

$HBrO_3$ isomers — heat of formation

As $\Delta n = 0$, the eqs. [9] and [10] were used to obtain the ΔH_r. The heat of reaction and all $HBrO_3$ heats of formation are presented in Table 8 together with other literature results. The $HOBrO_2$, HOOBrO, and $HBrO_3$ heats of formation were obtained based on relative energies.

The calculation of the HOOOBr heat of formation was made using two reactions. For isodesmic rxn. [18], we have

[18] $\quad HOOOBr + 2HOH \rightarrow 2HOOH + HOBr$

[19] $\quad \Delta H_f^\circ\,(HOOOBr) = 2 \times \Delta H_f^\circ\,(HOOH) + \Delta H_f^\circ\,(HOBr) - 2 \times \Delta H_f^\circ\,(HOH) - \Delta H_r$

© 2001 NRC Canada

Table 8. Heats of reaction and HOOOBr, $HOBrO_2$, HOOBrO, and $HBrO_3$ heats of formation (in kcal mol^{-1} at 298.15 K)[a] employing different reactions.

Methods	Reactions	ΔH_r	ΔH_f° (HOOOBr)	ΔH_f° ($HOBrO_2$)	ΔH_f° (HOOBrO)	ΔH_f° ($HBrO_3$)
BP/DN*	[18]	27.74 (28.64)	8.73 (12.06)	18.41 (21.71)	24.30 (27.52)	87.74 (91.55)
	[20]	26.22 (27.10)	9.92 (13.24)	19.60 (22.89)	25.49 (28.70)	88.93 (92.73)
BP/DN**	[18]	27.05 (27.74)	9.42 (12.96)	19.09 (22.60)	25.57 (28.98)	91.10 (95.13)
	[20]	26.00 (26.68)	10.13 (13.66)	19.80 (23.30)	26.28 (29.68)	91.81 (95.83)
pBP/DN*	[18]	27.63 (28.48)	8.84 (12.22)	17.95 (21.25)	25.72 (28.89)	87.36 (91.22)
	[20]	26.09 (26.92)	10.05 (13.42)	19.16 (22.45)	26.93 (30.09)	88.57 (92.42)
pBP/DN**	[18]	27.07 (27.82)	9.40 (12.88)	17.92 (21.33)	25.12 (28.49)	90.49 (94.49)
	[20]	25.91 (26.64)	10.23 (13.70)	18.75 (22.15)	25.95 (29.31)	91.32 (95.31)
G1 (23)		—	(13.2)	(6.5)	(25.8)	(72.2)
G2 (23)		—	(13.6)	(5.7)	(26.2)	(71.6)
B3LYP/ 6-311++G(3df,3pd) (23)	[18]	—	(18.1)	(17.2)	(33.0)	(86.7)
CCSD(T)/ 6-311++G(3df,3pd)// B3LYP/ 6-311++G(3df,3pd) (23)	[18]	—	(18.2)	(12.6)	(32.8)	(78.1)
CCSD(T)/ 6-311++G(3df,3pd)// CCSD(T)/TZ2P (23)	[18]	—	(18.1)	(12.4)	(32.7)	(77.9)

[a]Values at 0 K are presented between parenthesis.

For the homodesmic rxn. [20], we have

[20] $HOOOBr + 2HOH + Cl_2 \rightarrow 2HOOH + HOCl + BrCl$

[21] $\Delta H_f^\circ(HOOOBr) = 2 \times \Delta H_f^\circ(HOOH) + \Delta H_f^\circ(HOCl) + \Delta H_f^\circ(BrCl) - 2 \times \Delta H_f^\circ(HOH) - \Delta H_f^\circ(Cl_2) - \Delta H_f^\circ$

The BP and pBP HOOOBr heats of formation were calculated using eq. [19] and eq. [21], with the calculated ΔH_r and the experimental ΔH_f°obtained from the *NIST–JANAF Thermochemical Tables* (34).

As can be seen in Table 8, our results for the heats of formation of the $HBrO_3$ isomers are not sensitive to the method or basis set used. At 0 K, the heats of formation for the isomers HOOOBr, $HOBrO_2$, HOOBrO, and $HBrO_3$ can be considered close to 13 kcal mol^{-1}, 22 kcal mol^{-1}, 29 kcal mol^{-1}, and 93 kcal mol^{-1}, respectively. Otherwise, the results of Guha and Francisco (23), reproduced in this table for comparison purposes, show that the heat of formation values for these isomers are very dependent of the method and basis used as has been noticed for $HClO_3$ isomers (43). This dependence of the method and basis used can be understood as a special difficulty posed by these halogen compounds. For the HOOBrO isomer, our results are in the middle of the Guha and Francisco results calculated by several methods and not too far from the values of 32.7 kcal mol^{-1} and 32.8 kcal mol^{-1} obtained by the highest basis set calculations. For HOOOBr, our results are close to G1 and G2 values. For the $HOBrO_2$ and $HBrO_3$ isomers, our results are significantly higher than the other results.

In this way, we calculated the HOOOBr isomer as the most stable isomer, in disagreement with Guha and Francisco (23) results that indicate $HOBrO_2$ as the most stable isomer. Considering the basis size and the methods used by these authors, the $HOBrO_2$ should be the most stable isomer. It means that the BP and pBP methods using DN* or DN** basis sets have some difficulty in handling the very special kind of chemical bond that is present between the oxygen atoms in the HOOOBr isomer.

Conclusions

Relative energy, equilibrium geometry, vibrational frequencies, heat capacity, and heat of formation of several compounds of general formula $HBrO_x$ were calculated by BP and pBP models, using numerical basis sets.

The comparison of the BP and pBP HOBr results with the HOBr experimental results has shown a good agreement and suggests that these methods and basis sets can be a good option to forecast properties of inorganic bromine compounds. The comparison of our calculated HOBr values with other very reliable calculation methods support this conclusion, too.

The HOBr heat of formation results obtained by the use of homodesmic and isodesmic reactions gave similar results, with the exception for the BP method considering a isodesmic reaction containing ClO· species. In addition, the calculated HOBr heat of formation values support the experimental values of Ruscic and Berkowitz (35) and Lock et al. (36).

The density functional theories when applied for HBrO, $HBrO_2$, and $HBrO_3$, isomers give the total energy orders: HOBr < HBrO; HOOBr < HOBrO < $HBrO_2$; HOOOBr < $HOBrO_2$ < HOOBrO < $HBrO_3$. For the HOOOBr and $HOBrO_2$ isomers, the calculated stability order is exchanged in relation to the order reported by Guha and Francisco (23, 24) suggesting that the BP and pBP methods using the DN* or DN** basis set have some difficulty in handling the O—O—O bond present in HOOOBr. Otherwise, as the $HBrO_2$ isomers' energy order is the same calculated by the most sophisticated methods and basis sets, this suggests that

© 2001 NRC Canada

the methods and basis set used in this work can handle the peroxide bond correctly.

The calculated equilibrium geometry, vibrational frequencies, and heat capacity are in agreement with other methods as has been observed for HOBr.

No clear tendency was observed for the results obtained by BP and pBP models, nor by the use of the DN* or DN** basis sets. In addition, the use of homodesmic and isodesmic reactions gave, in most of the cases, very similar results.

Note

During the submission of this paper a theoretical work by Guha and Francisco on isomerization pathways for $HBrO_3$ isomers has appeared (44). The results presented in this paper show that the $HOBrO_2$ isomer is the most stable based only on the total energy calculated by the QCISD method using several different basis sets and the geometry obtained by QCISD/6-311G(2d,2p). No heat of formation results were presented.

Acknowledgments

This work was supported by the Fundação de Amparo à Pesquisa do Rio de Janeiro (FAPERJ), Fundação José Bonifácio (FUJB), Fundação Coordenação de Aperfeiçoamento de Pessoal de Nível Superior (CAPES), and Conselho Nacional de Desenvolvimento Científico e Tecnológico (CNPq).

References

1. M.J. Molina and F.S. Rowland. Nature (London), **249**, 810 (1974).
2. S.C. Wofsy, M.B. McElroy, and Y.L. Yung. Geophys. Res. Lett. **2**, 215 (1975).
3. Y.L. Yung, J.P. Pinto, R.T. Watson, and S.P. Sander. J. Atmos. Sci. **37**, 339 (1980).
4. L.A. Barrie, J.W. Bottenheim, R.C. Schnell, P.J. Crutzen, and R.A. Rasmunssen. Nature (London), **334**, 138 (1988).
5. R.J. Salawitch, M.B. McElroy, J.H. Yatteau, S.C. Wofsy, M.R. Schoeberl, L.R. Lait, P.A. Newman, K.R. Chan, M. Lowenstein, J.R. Podolske, S.E. Srahan, and M.H. Profitt. Geophys. Res. Lett. **17**, 561 (1990).
6. J.G. Anderson, D.W. Toohey, and W.H. Brune. Science (Washington, D.C.), **39**, 251 (1991).
7. G. Poulet, M. Pirre, F. Maguin, R. Ramaroson, and G. Le Bras. Geophys. Res. Lett. **19**, 2305 (1992).
8. I. Bridier, B. Veyret, and R. Lesclaux. Chem. Phys. Lett. **201**, 563 (1993).
9. M. Larichev, F. Maguin, G. Le Bras, and G. Poulet. J. Phys. Chem. **99**, 15911 (1995).
10. R.A. Cox and D.W. Sheppard. J. Chem. Soc. Faraday Trans. 2, **78**, 1383 (1982).
11. M.J. Elrod, R.F. Meads, J.B. Lipson, J.V. Seeley, and M.J. Molina. J. Phys. Chem. **100**, 5808 (1996).
12. C.T. McElroy, C.A. McLinden, and J.C. McConnell. Nature (London), **397**, 338 (1999).
13. M.P. McGrath and F.S. Rowland. J. Phys. Chem. **98**, 4773 (1994).
14. T.J. Lee. J. Phys. Chem. **99**, 15 074 (1995).
15. J.S. Francisco, M.R. Hand, and I.H. Williams. J. Phys. Chem. **100**, 9250 (1996).
16. L. Ying and X. Zhao. J. Phys. Chem. A, **101**, 3569 (1997).
17. L. Füsti-Molnár, P.G. Szalay, and G.G. Balint-Kurti. J. Chem. Phys. **110**, 8448 (1999).
18. Z. Li and J.S. Francisco. J. Chem. Phys. **111**, 5780 (1999).
19. T.J. Lee. Chem. Phys. Lett. **262**, 559 (1996).
20. S. Guha and J.S. Francisco. J. Phys. Chem. A, **101**, 5347 (1997).
21. S. Guha and J.S. Francisco. Chem. Phys. **247**, 387 (1999).
22. S. Guha and J.S. Francisco. Chem. Phys. Lett. **319**, 650 (2000).
23. S. Guha and J.S. Francisco. J. Phys. Chem. A, **102**, 2072 (1998).
24. S. Guha and J.S. Francisco. J. Phys. Chem. A, **103**, 8000 (1999).
25. W.J. Hehre and L. Lou. A guide to density functional calculations in Spartan. Wavefunction, Inc., Irvine, California. 1997.
26. T.D. Fridgen and J.M. Parnis. J. Chem. Phys. **109**, 2162 (1998).
27. W.J. Hehre, F. Freeman, and A. Phornvoranunt. J. Mol. Struct. **492**, 225 (1999).
28. F. Freeman and W.J. Hehre. J. Mol. Struct. **529**, 225 (2000).
29. E. Lewars. Can. J. Chem. **78** (2), 297 (2000).
30. A.D. Becke. Phys. Rev. A: At. Mol. Opt. Phys. **38**, 3089 (1988).
31. J.P. Perdew. Phys. Rev. B: Condens. Matter, **33**, 8822 (1986).
32. L. Fan and T. Ziegler. J. Chem. Phys. **94**, 6057 (1991).
33. G. Herzberg. Molecular spectra and molecular structure. Vol. II. Krieger Publishing Company, Malabar, Florida. 1991.
34. M.W. Chase Jr. NIST–JANAF thermochemical tables. 4th ed. J. Phys. Chem. Ref. Data. Monograph no. 9. 1998. Part I and II.
35. B. Ruscic and J. Berkowitz. J. Chem. Phys. **101**, 7795 (1994).
36. M. Lock, R.J. Barnes, and A. Sinha. J. Phys. Chem. **100**, 7972 (1996).
37. S.W. Benson. Thermochemical kinetics. 2rd ed. John Wiley, New York. 1976.
38. P.S. Monks, L.J. Stief, M. Krauss, S.C. Kuo, and R.B. Klemm. J. Chem. Phys. **100**, 1902 (1994).
39. Y. Koga, H. Takeo, S. Kondo, M. Sugie, C. Matsumura, G.A. McRae, and E.A. Cohen. J. Mol. Spectrosc. **138**, 467 (1989).
40. G.A. Mc Rae and E.A. Cohen. J. Mol. Spectrosc. **139**, 369 (1990).
41. I. Schwager and A. Arkell. J. Amer. Chem. Soc. **22**, 6006 (1967).
42. E.A. Cohen, G.A. McRae, T.L. Tan, R.R. Friedl, J.W.C. Johns, and M. Noel. J. Mol. Spectrosc. **173**, 55 (1995).
43. J.S. Francisco and S.P. Sander. J. Phys. Chem. **100**, 573 (1996).
44. S. Guha and J.S. Francisco J. Phys. Chem. A, **104**, 9321 (2000).

© 2001 NRC Canada

Using secondary alpha deuterium kinetic isotope effects to determine the stereochemistry of an E2 reaction; the stereochemistry of the E2 reaction of 1-chloro-2-phenylethane with potassium *tert*-butoxide in *tert*-butyl alcohol

Peter James Smith, David A.J. Crowe, and Kenneth Charles Westaway

Abstract: Isotopic labelling studies have shown that the E2 reaction of 1-chloro-2-phenylethane with potassium *tert*-butoxide in *tert*-butyl alcohol occurs via an anti-periplanar stereochemistry. This demonstrates that the different secondary alpha deuterium kinetic isotope effects found for the high and low base concentrations and in the presence of 18-crown-6 ether are because of changes in transition state structure that occur when the form of the reacting base changes rather than to a change in the stereochemistry of the reaction.

Key words: E2 reaction, stereochemistry, secondary alpha deuterium kinetic isotope effects, transition state.

Résumé : Des études de marquage isotopique ont permis de démontrer que la réaction E2 du 1-chloro-2-phényléthane avec *tert*-butylate de potassium dans l'alcool *tert*-butylique se produit avec une stéréochimie antipériplanaire. Cette observation démontre que les divers effets isotopiques cinétiques secondaires du deutérium en alpha qui ont été observés à des concentrations élevées et faibles de base et en présence de l'éther 6-couronne-18 sont dus à des changements dans la structure de l'état de transition qui se produisent lorsqu'il se produit un changement dans la forme de la base qui réagit plutôt que la stéréochimie de la réaction.

Mots clés : réaction E2, stéréochimie, effets isotopiques cinétiques secondaires du deutérium en alpha, état de transition.

[Traduit par la Rédaction]

Introduction

The stereochemistry of E2 elimination reactions has been investigated for some time (1–5). An E2 reaction can occur with an anti-periplanar (the dihedral angle between the abstracted β-hydrogen and the leaving group is 180°, Fig. l*a*) or a syn-periplanar (the dihedral angle between the leaving group and abstracted β-hydrogen is 0°, Fig. l*b*) stereochemistry. Although theoretical calculations (3, 6) indicate that the anti-periplanar stereochemistry is favoured, not all E2 reactions follow the anti-periplanar pathway. For example, syn-periplanar E2 reactions are observed in rigid cyclic systems where a β-hydrogen and the leaving group are coplanar (2, 7). Syn-periplanar E2 eliminations are also observed when the less rigid, but rotationally restricted, 1,2-dihaloacenaphthalenes (8) and 2,3-dihalo-2,3-dihydrobenzofurans (9) react with alkoxide ions.

Received November 30, 2000. Published on the NRC Research Press Web site at http://canjchem.nrc.ca on August 3, 2001.

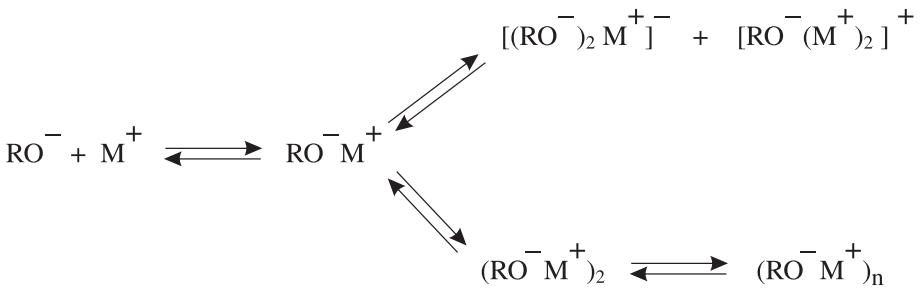
P.J. Smith and D.A.J. Crowe. Department of Chemistry, University of Saskatchewan, Saskatoon, SK S7N 0W0, Canada. **K.C. Westaway.**[1] Department of Chemistry and Biochemistry, Laurentian University, Sudbury, ON P3E 2C6, Canada.

[1]Corresponding author (fax: (705) 675-4844; e-mail: kwestawa@nickel.laurentian.ca).

Changes in the form of the abstracting base can also affect the stereochemistry of an E2 reaction. Bartsch and Zavada (5) state that alkoxide ions exist as dissociated ions, ion pairs, several different complex ions, or ion-pair aggregates connected by a series of equilibria (eq. [1]).

The amount of association increases as (*i*) the cation is made smaller, i.e., going from cesium to lithium; (*ii*) the alkoxide ion is made larger, i.e., the base is changed from methoxide ion to *tert*-butoxide ion; and (*iii*) when a less polar solvent is used and the strength of the base is increased, e.g., the solvent is changed from ethanol to *tert*-butyl alcohol (10–12). Surprisingly, 18-crown-6 ether does not affect the degree of association (13), although a 1:1 K^+–18-crown-6 ether complex does form in potassium *tert*-butoxide – *tert*-butyl alcohol (l4). Zavada et al. (15) found a greater percentage of syn-periplanar dehydrohalogenation of 5-decyl halides with the associated base (potassium *tert*-butoxide in benzene) than when the base was the dissociated ion (potassium *tert*-butoxide in *tert*-butyl alcohol). Bartsch and Lee (2) also found the amount of syn-elimination from *endo*-2-bicyclo[2.2.1]heptyl bromide and 2,4,6-triisopropylbenzenesulfonate was significantly higher with the associated base (potassium *tert*-butoxide in triglyme) than when 18-crown-6 ether was present. The higher proportion of syn-elimination with the associated base may occur because the counter ion in the associated base stabilizes the partial charge on the leaving group in the syn-periplanar E2 transition state (Fig. 2).

 DOI: 10.1139/cjc-79-7-1145 © 2001 NRC Canada

[1] 

Zavada et al. (15) also reported that the amount of syn-elimination increased as the electronegativity of the leaving group increased from bromo to fluoro in the E2 reactions of 5-decyl halides. Several workers (16–18) have suggested that Elcb-like E2 reactions (with poor leaving groups) occur with the syn-periplanar stereochemistry rather than the anti-periplanar stereochemistry that is found for E2 reactions, which have good leaving groups and central transition states.

Smith and Westaway (19) reported that the syn-periplanar E2 elimination from 2-phenylethyldimethylamine oxide had a large secondary alpha deuterium kinetic isotope effect of 1.34, whereas a small secondary alpha deuterium kinetic isotope effect of 1.02 was found for the anti-periplanar E2 reaction of 2-phenylethyltrimethylammonium ion with ethoxide ion in ethanol. Although both reactions had extensive C_β–H and C_α–N bond rupture in their transition states, there is obviously a very different amount of C=C bond formation in the two transition states, i.e., large in the anti-periplanar transition state and small in the syn-periplanar transition state. This led to the suggestion that one might be able to use the magnitude of the secondary alpha deuterium isotope effect to determine the stereochemistry of the E2 elimination reaction. Recently, different secondary alpha deuterium kinetic isotope effects have been found when different concentrations of base (potassium *tert*-butoxide in *tert*-butyl alcohol) were used in the E2 reaction of 1-chloro-2-phenylethane. The different isotope effects could arise because (*i*) the structure of the E2 transition state changes and (or) (*ii*) because the stereochemistry of the reaction changes when different concentrations of base (different bases) are used. This study was undertaken to determine whether the change in the secondary alpha deuterium isotope effect was due to a change in the stereochemistry of the E2 reaction between 1-chloro-2-phenylethane and *tert*-butoxide ion.

Results and discussion

The secondary alpha deuterium kinetic isotope effects observed for the E2 reaction of 1-chloro-2-phenylethane at different base (potassium *tert*-butoxide in *tert*-butyl alcohol) concentrations (eq. [2]) are presented in Table 1. The results show that a smaller secondary alpha deuterium isotope effect of 1.032 ± 0.004 is found for the 1-chloro-2-phenylethane E2 reaction at low base concentrations (between 0.036 and 0.228 M), while a larger isotope effect of 1.050 ± 0.005 is observed at higher concentrations of base (>0.36 M) and at low base concentrations in the presence of 18-crown-6 ether.[2] The 1-chloro-2-phenylethane at low base concentrations were thought to react via the normal anti-periplanar stereochemistry. The larger secondary alpha deuterium kinetic isotope effects found for the E2 reaction of 1-chloro-2-phenylethane at high base concentrations and in the presence of the crown ether could be observed because (*i*) the stereochemistry of the reaction changed to syn-periplanar and (or) (*ii*) the transition state structure changes when the form of the abstracting base changes. At low concentrations of base and in the presence of 18-crown-6 ether, the abstracting base is undoubtedly the free ion. At high concentrations of base, the abstracting base would be one or more of the ion pair, the triple ion, or an ion aggregate. Changing the form of the abstracting base could alter the stereochemistry of the E2 reaction (Fig. 1) and (or) cause a change in the structure of the transition state altering the magnitude of the alpha deuterium kinetic isotope effect. This study was undertaken to determine if the change in the secondary alpha deuterium kinetic isotope effect was due to a change in the stereochemistry of the E2 reaction or due to a change in the structure of the E2 transition state.

The diastereomers of 1-chloro-2-phenyl-1,2-d_2 ethane were synthesized via the scheme shown in Fig. 3. An NMR analysis of the β-bromostyrene showed that the starting material for the synthesis consisted of 75% of the (*E*)-isomer and 25% of the (*Z*)-isomer. A spinning-band distillation of the β-bromostyrene gave samples of isomeric purity ranging from 75 to 88% of the (*E*)-isomer. However, it was not possible to obtain a pure sample of the (*E*)-isomer, so the synthesis was carried out on three different mixtures of β-bromostyrene isomers. These stereospecific syntheses led to the *threo*-(*RS*,*SR*) and *erthyro*-(*SR*,*RS*) 1-chloro-2-phenyl-1,2-d_2 ethanes. The *threo* diastereomers were formed from the (*E*)-isomer of the β-bromostyrene and the *erythro* diastereomers from the (*Z*)-isomer of β-bromostyrene. These mixtures of diastereomers were reacted at both low and high concentrations of base, i.e., where the different secondary al-

[2] $$C_6H_5CH_2CL_2\text{-}Cl + (CH_3)_3CO^- \xrightarrow{(CH_3)_3COH} C_6H_5CH{=}CL_2 + (CH_3)_3COH + Cl^-$$

$$L = H, D$$

[2] A student t-test showed that the secondary alpha deuterium kinetic isotope effects at "high base" concentrations and in the presence of 18-crown-6 ether are different from those at the "low base" concentrations at the 99% confidence level.

© 2001 NRC Canada

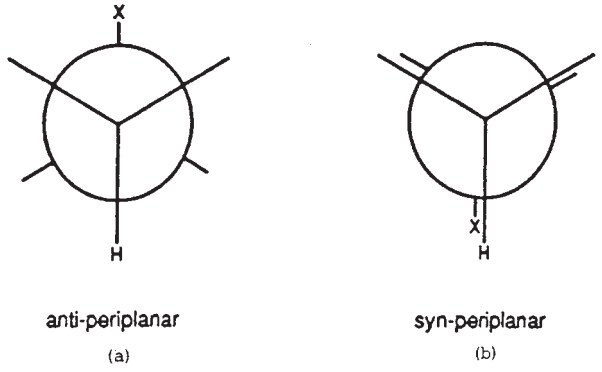
Table 1. The secondary alpha deuterium kinetic isotope effects for the E2 reaction between 1-chloro-2-phenylethane or 1-chloro-2-phenyl-1,1-d_2 ethane and potassium *tert*-butoxide in *tert*-butyl alcohol at 40°C.

[Base] (M)	[18-C-6] (M)	$(k_H/k_D)_\alpha$
0.0364		1.026 ± 0.016[a]
0.0736		1.029 ± 0.005
0.0736		1.034 ± 0.009
0.0832		1.035 ± 0.011
0.100		1.035 ± 0.009
0.2284		1.032 ± 0.009
Avg.		1.032 ± 0.004[b]
0.3640		1.044 ± 0.009
0.3860		1.055 ± 0.006
Avg.		1.050 ± 0.008[b]
0.0118	0.01311	1.056 ± 0.014
0.00662	0.006482	1.047 ± 0.018
0.00627	0.00690	1.047 ± 0.010
Avg.		1.050 ± 0.005[b]

[a]The error in the isotope effects is $1/k_D[(\Delta k_H)^2 + (k_H/k_D)^2 \times (\Delta k_D)^2]^{1/2}$, where Δk_H and Δk_D are the standard deviations for the average rate constants for the reactions of the nondeuterated and deuterated substrates, respectively.

[b]Standard deviation. The student t-test indicated that the secondary alpha deuterium kinetic isotope effects at "high base" concentrations and in the presence of 18-crown-6 are different from those at "low base" concentrations at the 99% confidence level.

Fig. 1. The anti-periplanar (*a*) and syn-perplanar (*b*) stereochemistry for an E2 reaction.



pha deuterium kinetic isotope effects were observed. All the possible E2 products, formed when the different diastereomers of the 1-chloro-2-phenyl-1,2-d_2 ethanes react with *tert*-butoxide ion in *tert*-butyl alcohol, are presented in Fig. 4. The *threo* diastereomers produce compounds I and II when the elimination occurs via the anti-periplanar stereochemistry, whereas compounds III and IV would be formed if the elimination occurred via the syn-periplanar stereochemistry. The *erythro* compounds on the other hand, form products III and IV when the elimination occurs with an anti-periplanar stereochemistry and compounds I and II when it occurs by the syn-periplanar pathway. Thus, if the E2 reaction occurs only via the anti-periplanar pathway, the %(I + II) and the %(III + IV) should be the same as the %(*E*)-isomer and the %(*Z*)-isomer, respectively, in the starting material, i.e., all of

Fig. 2. A syn-periplanar E2 reaction with the counter ion in the ion-pair assisting the removal of the leaving group.

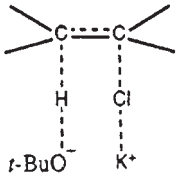
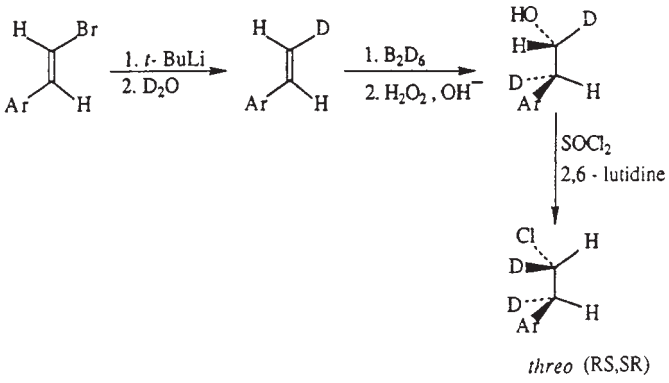


Fig. 3. The stereospecific synthesis of the 1-chloro-2-phenylethane diastereomers.



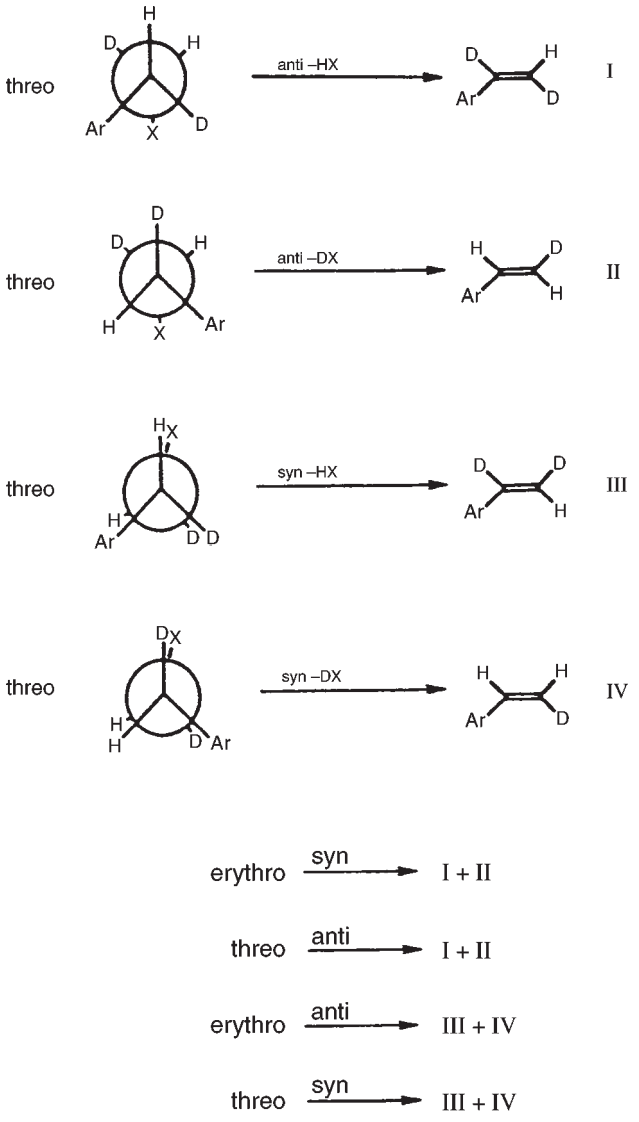
the *threo* isomer (made from the (*E*)-isomer in the synthesis) will form products I and II while the *erthyro* isomers (made from the (*Z*)-isomer in the synthesis) will form products III and IV. If the elimination occurs by the syn-periplanar pathway, the %(I + II) and the %(III + IV) should be opposite the %(*E*)-isomer and the %(*Z*)-isomer, respectively, in the starting material, i.e., the *threo* isomer will only form III and IV while the *erthyro* isomer will produce only I and II. Finally, if the stereochemistry of the elimination reaction is partly syn- and partly anti-, the %(I + II) and the %(III + IV) will be intermediate between the above values.

The stereochemistry of the E2 reactions of the 1-chloro-2-phenyl-1,2-d_2 ethane diastereomers was determined by isolating the products and analyzing them by NMR spectroscopy. The chemical shifts and coupling constants for all of the possible products formed from a syn- and an anti-periplanar elimination are shown in Table 2. The %(I + II) and the %(III + IV) obtained when the 1-chloro-2-phenyl-1,2-d_2 ethane diastereomers were reacted with potassium *tert*-butoxide in *tert*-butyl alcohol concentrations ranging from 0.062–0.23 M (where the secondary alpha deuterium kinetic isotope effect was 1.032) and ranging from 0.36–0.39 M (where the isotope effect was 1.050) are presented in Table 3. The %(I + II) and the %(III + IV) are, within experimental error, identical to the %(*E*)- and %(*Z*)-isomers, respectively, in the starting material in every case. This clearly indicates that (*i*) the E2 reaction of of 1-chloro-2-phenylethane occurs 100% via the anti-periplanar pathway at all concentrations of *tert*-butoxide ion and (*ii*) the change in the secondary alpha deuterium kinetic isotope effect is not due to a change in the stereochemistry of the reaction but must be due to a change in the structure of the E2 transition state.

It is worth noting that the method of determining the stereochemistry of the E2 reactions was tested by reacting

© 2001 NRC Canada

Fig. 4. The E2 products formed from anti- and syn-periplanar elimination of the possible deuterated 1-chloro-2-phenylethane diastereomers.



the 1-chloro-2-phenyl-1,2-d_2 ethane with ethoxide ion in ethanol. These reactions were investigated because they were expected to react via an anti-periplanar stereochemistry. This stereochemistry was expected because (*i*) the substrates are acyclic (3, 6); (*ii*) ion pairing is much less likely in the more polar solvent ethanol than in *tert*-butyl alcohol (10); and (*iii*) because the leaving group in these reactions is at least as good as the trimethylammonium leaving group (16, 18) Bourns and Frosst (20) used to demonstrate that the E2 reaction of 2-phenylethyltrimethylammonium bromide with ethoxide ion in ethanol occurred with an anti-periplanar stereochemistry. The %(I + II) and the %(III + IV) was identical, within experimental error, to the %(*E*)- and the %(*Z*)-isomers, respectively, in the starting material. Thus, the results indicate that this E2 reaction in ethoxide ion and ethanol proceeds with an anti-periplanar stereochemistry and confirm that the stereochemical test is valid.

The results clearly show that the E2 reaction of 1-chloro-2-phenylethane with *tert*-butoxide ion in *tert*-butyl alcohol occurs with an anti-periplanar stereochemistry. Therefore, the different secondary alpha deuterium kinetic isotope effects found at different concentrations of base are not due to a change in stereochemistry, but reflect differences in the structure of the E2 transition state. It is also obvious that the change in the secondary alpha deuterium kinetic isotope effect (transition state structure) must result from changes in the form of the reacting base.

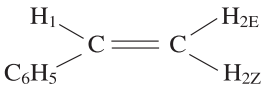
Although the reactive form of the base might be the triple ion or an ion pair aggregate at the highest potassium *tert*-butoxide concentrations (0.3–0.4 M) used in this study, it seems more likely, for two reasons, that the ion pair or a solvated ion pair is the reacting base. Zavada and co-workers (13) reported that the ion pair is the dominant form of the base in 0.1–0.5 M potassium *tert*-butoxide–*tert*-butyl alcohol. This, coupled with the first order dependance of the rate on *tert*-butoxide ion, suggests that the ion pair is the reacting base when the base concentration is 0.3–0.4 M and the larger secondary alpha deuterium kinetic isotope effect is observed.

Conversely, at low base concentrations (<0.23 M) in the absence of 18-crown-6 ether, the reacting base is almost certainly the free ion. However, it seems likely that the reaction does not occur via a simple E2 mechanism under these conditions. Zavada et al. (4) demonstrated that 5-decyl bromide reacts with potassium *tert*-butoxide in *tert*-butyl alcohol by two competing mechanisms; a simple E2 reaction and a reaction where a *free* (dissociated) K^+ ion complexes with the leaving group and provides electrophilic catalysis for its removal (Fig. 5). The reaction was first order in base indicating that the complexing reaction was kinetically indistinguishable from the uncomplexed reaction (21). If the complexing mechanism is operative at low base concentrations, the reaction occurs with a stronger base (the negative charge on the oxygen of the *free tert*-butoxide ion would be greater than that on the oxygen of the ion pair, the reactant at high base concentrations). Also, the low base concentration reaction with the free *tert*-butoxide ion has a better leaving group (the complexed chloride ion leaving group would be a weaker base than the uncomplexed chloride ion). The More O'Ferrall energy surface diagram predicts (*i*) that changing to a better leaving group would not change the amount of C_α–X bond rupture in the transition state but that (*ii*) changing to a stronger base would lead to an E2 transition state with less C_α–X bond rupture. The net effect of these two changes in the reactants should lead to a transition state with less C_α–X bond rupture. This would produce the smaller secondary alpha deuterium kinetic isotope effect that is observed.

Finally, the larger secondary alpha deuterium kinetic isotope effect in the reaction with the crown ether at low base concentrations, suggests that C_α–X bond rupture is more advanced in the transition state when 18-crown-6 ether is used. 18-Crown-6 ether forms a 1:1 complex with potassium ions (13). This means the potassium ion is no longer available to assist in the removal of the leaving group, i.e., that there is a poorer leaving group. Since the More O'Ferrall energy surface diagram suggests that changing to a poorer leaving group leads to a transition state with a longer C_α–X bond, a

© 2001 NRC Canada

Table 2. The NMR spectra of the possible E2 products from (*RS,SR*) *threo*-1-chloro-2-phenyl-1,2-d_2 ethane.



	Chemical shifts (ppm)			Coupling constants (Hz)	
Compound	H_1	H_{2E}	H_{2Z}	$H_{1,2E}$	$H_{1,2Z}$
(*Z*)-Styrene-1,2-d_2 (I)		5.22 (t)		1.7	
(*E*)-Styrene-2-*d* (II)	6.71		5.74 (d)		17.4
(E)-Styrene-1,2-d_2 (III)			5.73 (t)		2.8
(*Z*)-Styrene-2-*d* (IV)	6.71	5.23 (d)		11.0	

Table 3. The product distribution of the E2 reaction between 1-chloro-2-phenyl-1,2-d_2 ethane and potassium *tert*-butoxide in *tert*-butyl alcohol at 40°C.

[Base]	Product distribution (%)				Anti-periplanar
(M)	I	II	III	IV	elimination (I + II) (%)
TEST I: the starting material was 77% (*E*), 23% (*Z*)					
0.430	59.4	19.7	16.6	4.3	79[a]
0.310	63.6	13.6	17.4	5.5	77
0.124	64.5	14.0	18.5	3.0	79
0.103	57.1	20.7	18.2	4.0	78
0.062	60.6	15.2	20.6	3.6	76
Avg.					78 ± 1.3[b]
TEST II: the starting material was 83% (*E*), 17% (*Z*)					
1.035	68.1	15.3	11.7	4.8	83[a]
0.124	70.7	12.6	11.1	5.6	83
Avg.					83 ± 0.0[b]
TEST III: the starting material was 88% (*E*), 12% (*Z*)					
0.865	71.8	16.4	6.1	5.7	88[a]
0.0865	71.1	16.4	7.1	5.4	88
Avg.					88 ± 0.0[b]

[a]The rest of the elimination product is the %(III + IV), i.e., 21% for Test I.
[b]Standard deviation.

larger secondary alpha deuterium kinetic isotope effect would be expected in the 18-crown-6 ether reactions. This is, in fact, what is observed.

Conclusion

Obviously, the magnitude of the secondary alpha deuterium kinetic isotope effects cannot be used to determine the stereochemistry of an E2 reaction. Rather, the changes in the secondary alpha deuterium isotope effect in these E2 reactions are due to changes in the structure of the transition state that occur when the form of the reacting base is altered.

Experimental

General

NMR spectra were determined in solution in chloroform-*d* on a Bruker AM300 instrument. All the chemical shifts are reported in ppm from tetramethylsilane. The UV spectra were measured on a Hewlett Packard HP8451A diode array spectrophotometer. An NMR analysis showed that both the 1, 1-d_2, and the 1,2-d_2 1-chloro-2-phenylethanes were 99% deuterated at the appropriate positions.

Preparation of reagents

1-Chloro-2-phenylethane

2-Phenylethanol was prepared using the method of Amundsen and Nelson (22). Ethyl phenylacetate (5.9 g, 0.036 mol) in anhyd ether (10 mL) was added slowly to a stirred mixture of lithium aluminum hydride (1.4 g, 0.038 mol) in anhyd ether (60 mL). The mixture was heated at reflux for 7 h and allowed to cool. Sulphuric acid (10%, 50 mL) was added slowly. The organic layer was separated, washed with water, dried over anhyd magnesium sulphate, and the ether removed on a rotary evaporator. The 2-phenylethanol was used in the next step without further purification. ^{1}H NMR δ 7.22–7.38 (m, 5H), 3.86 (t, J = 6.6 Hz, 2H), 2.87 (t, J = 6.6 Hz, 2H), 1.39 (br s, 1H).

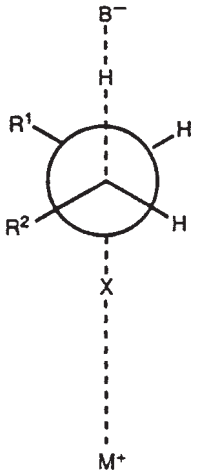
The 1-chloro-2-phenylethane was prepared by adding a mixture of 2-phenylethanol (1 g, 0.0082 mol) and 2,6-lutidine (0.9 g, 0.0082 mol) dropwise to a stirred solution of thionyl chloride (1.2 g, 0.010 mol) in toluene (2 mL). Two drops of water were added to break up the solid that formed and the reaction was stirred for 30 min at 40°C. Cold water was added slowly and the toluene separated as an upper layer. The toluene layer was washed successively with water, 10% sodium bicarbonate solution, and water, then dried over anhyd sodium sulphate and the solvent removed on a rotary evaporator. Distillation gave 1.0 g (0.0071 mol, 87%) of 1-chloro-2-phenylethane bp 47–50°C, 1.5 mm Hg (lit. (23) 34°C, 1 mm of Hg). ^{1}H NMR δ 7.20–7.35 (m, 5H), 3.71 (t, J = 7.5 Hz, 2H), 3.06 (t, J = 7.5 Hz, 2H).

1-Chloro-2-phenyl-1,2-d_2 *ethane diastereomers*

*(*E*)-Styrene-*β*-*d*:* (*E*)-Styrene-β-*d* was prepared using the method described by Tao and Saunders (24). (*E*)-β-Bromostyrene (Aldrich) (1.0 g, 5.5 mmol) in dry ether (7 mL) (heated at reflux over and distilled from sodium) was cooled to –78°C and *tert*-butyl lithium in pentane (1.7 M, 4.9 mL) (Aldrich) was added slowly. The mixture was stirred for 30 min at –78°C, then deuterium oxide (>99.9% d_2) (0.22 g, 11 mmol) was added dropwise with stirring. The reaction mixture was warmed to room temperature and water (10 mL) was added. The organic layer was separated and the aqueous layer was extracted once with

© 2001 NRC Canada

Fig. 5. An anti-periplanar E2 elimination from a free *tert*-butoxide ion and a metal-complexed leaving group.



ether. The combined organic layers were dried over anhyd magnesium sulphate and the solvent was removed on a rotary evaporator at room temperature. The crude yield of (*E*)-styrene-β-*d* was 0.56 g (96%). If the product was not used immediately, it was stored as an ether solution to minimize isomerization and (or) polymerization.

NMR spectroscopy showed that the β-bromostyrene consisted of 75% of the (*E*)-isomer, the rest being (Z). Several attempts to separate the isomers were made, spinning-band distillation being the most successful. Several batches of styrene-β-*d* were made, with degrees of isomeric purity ranging from 75 to 88% of the (*E*)-isomer. In each case, the isomeric constitution of the styrene-β-*d* determined by NMR was the same as that of the β-bromostyrene used for the synthesis.

erythro-*2-Phenyl-1,2*-d_2 *ethanol:* The procedure used by Dohner and Saunders (25) was followed. Deuteroborane, generated by the addition of boron trifluoride etherate (4.75 mL, 0.029 mol) to a solution of sodium borodeuteride (>98% d_4) (0.921 g, 0.022 mol) in tetrahydrofuran (200 mL) at 0°C, was added dropwise to (*E*)-styrene-β-*d* (0.56 g, 0.005 mol) in tetrahydrofuran (5 mL) in a 50 mL three-necked round-bottom flask equipped with a nitrogen inlet, a nitrogen outlet, and a dropping funnel. After the reaction mixture had been stirred for 3 h at room temperature, water (0.8 mL), sodium hydroxide (4 mL, 3 M), and hydrogen peroxide (4 mL of a 30% solution) were added. This mixture was stirred for 4 h and then extracted with ether (3 × 30 mL). The combined ether extracts were washed with an aqueous ferrous sulphate solution, then with water, and dried over anhyd magnesium sulphate. Evaporation of the ether and distillation at 49–50°C at 1.5 mm yielded 0.55 g (88%) of the product. ^{1}H NMR δ 7.22–7.38 (m, 5H), 3.84 (d, J = 4.5 Hz, 1H), 2.85 (d, J = 4.5 Hz, 1H), 1.39 (br s, 1H).

threo-*1-Chloro-2-phenyl-1,2*-d_2 *ethane:* This was prepared from *erythro*-2-phenyl-1,2-d_2 ethanol using the method and quantities described for 1-chloro-2-phenylethane.[3] ^{1}H NMR δ 7.20–7.35 (m, 5H), 3.71 (m, 1H), 3.06 (d, 1H). ^{13}C NMR δ 138.0, 128.8, 128.6, 126.9, 44.6 (t, J = 23 Hz), 38.8 (t, J = 20 Hz).

Potassium tert-*butoxide in* tert-*butyl alcohol*

tert-Butyl alcohol was dried over 3 Å molecular sieve beads for at least 24 h, then refluxed over and distilled from powdered 3 Å molecular sieves under a dry nitrogen atmosphere (26). Sufficient potassium (typically, 8 g of potassium in 1 to 2 g chunks) was added to dry *tert*-butyl alcohol (200 mL) through which dry, high purity nitrogen was being bubbled. The mixture was left until all the potassium had reacted. The base solution was stored under dry nitrogen in the refrigerator and aliquots were removed under dry nitrogen and diluted with dry *tert*-butyl alcohol for kinetic studies. When the base had been diluted for kinetic studies, its concentration was determined by titrating it in CO_2-free distilled water with 0.01 N sulphuric acid (BDH Volumetric) to a bromocresol green endpoint. A blank sample containing only CO_2-free distilled water and indicator normally reached the end point with the first drop of sulphuric acid. Although every attempt was made to keep the potassium *tert*-butoxide solution free of air and water, some of the *tert*-butoxide ion was inevitably destroyed by reaction with water or carbon dioxide. Thus, second order rate constants measured with different batches of the base were not reproducible to better than ±10%.

Kinetic measurements

Two different methods were used. For reactions where the base concentration was 0.01 M or less, the reaction was carried out and monitored in a 1 cm cuvette in the spectrophotometer cell. Because of the significant absorption of *tert*-butoxide ion in the 200–250 nm range at base concentrations >0.01 M, the reactions were carried out in a constant temperature bath and aliquots of the reaction mixture were quenched before measurement of the spectrum. All the rate constants were measured under pseudo first-order conditions with the base being at least twenty times more concentrated than the substrate in the reaction mixture. No attempt was made to control the ionic strength.

Water-bath method

The potassium *tert*-butoxide solution was made by pipetting the required volume of the stock (1 M) base solution into a dry 200 mL volumetric flask and making up the volume with dry *tert*-butyl alcohol. Approximately 22 mL of this solution was transferred into each, of up to seven, 25 mL dry, volumetric reaction vessels fitted with serum caps. The solutions were temperature equilibrated in the constant temperature bath for at least 30 min and filled up to the mark with the base solution. To one of the reaction ves-

[3] A referee expressed concern about the formation of a phenonium ion, which would alter the stereochemistry of this step of the synthesis. This reaction was done in toluene and since phenonium ions have only been found in good ionizing solvents such as HOAc or formic acid, (27) it is difficult to envisage it forming it this reaction. More important, the phenonium ion intermediate can be ruled out because there was no evidence of the rearranged product when this reaction was used in the synthesis of the 1-chloro-2-phenyl-1,1-d_2 ethane that was to measure the secondary alpha deuterium KIE. A referee also questioned the stereochemistry of the chlorosulfite ester reaction. However, March (28) reports that this reaction proceeds with inversion of configuration.

© 2001 NRC Canada

sels was added 1 mL of temperature-equilibrated dry *tert*-butyl alcohol and the solution was titrated to determine the base concentration.

The reactions were started by adding 1 mL of a temperature equilibrated solution of the substrate (approximately 5×10^{-5} M, but accurately known) in dry *tert*-butyl alcohol to the reaction vessel with a calibrated syringe. At intervals of several minutes, 1 mL aliquots of the reaction mixture were withdrawn with a syringe and quenched in 20 mL of the appropriate concentration of hydrochloric acid in distilled 95% ethanol. The quenched aliquot was diluted to 25 mL with 95% ethanol and the UV spectrum was recorded. Best results were obtained by measuring against a reference sample of ethanol or quenching solution, subtracting the absorbance at a point on the baseline of the product spectrum from the absorbance at λ_{max} for the product. Ten aliquots were normally taken from each vessel over two half-lives.

After ten or more half-lives, samples were taken and quenched to obtain a value for the product absorbance when the reaction was complete (OD_∞). The pseudo first-order rate constant was obtained from the slope of the plot of ln ($OD_\infty - OD_t$) vs time (t).

Cuvette method

The base solution was prepared by diluting the stock base solution using the method described above. If required, 18-crown-6 was first weighed into a 50 mL volumetric flask and 3 mL of the base solution were pipetted into each of seven oven dried cuvettes with tightly fitting stoppers. The cuvettes were left in the thermostated cell holder in the spectrophotometer for at least 20 min to allow them to reach thermal equilibrium. One cell was used as the reference. The reactions were started by adding between 5–10 μL of substrate solution (typically 5×10^{-3} M in *tert*-butyl alcohol) to the cuvette using a syringe and inverting the cuvette several times to ensure mixing.

The computer-controlled spectrophotometer measured absorbencies for the samples at predetermined intervals over at least two half lives. Rate constants were obtained from between 25–40 data points using either the above OD_∞ method or from Guggenheim plots.

Secondary alpha deuterium kinetic isotope effects

When the water bath method was used to determine the secondary alpha deuterium kinetic isotope effect, the rate constants for six reactions were determined simultaneously in the same constant temperature bath; three reactions used the deuterated substrate and three used the nondeuterated substrate. When the cuvette method was used, the rate was determined for three deuterated and three nondeuterated substrates simultaneously in the thermostated cell holder. The secondary alpha deuterium kinetic isotope effect was obtained by dividing the average rate constants for the nondeuterated and deuterated substrates.

Determination of the elimination stereochemistry

A stock potassium *tert*-butoxide solution was diluted in a volumetric flask with dry *tert*-butyl alcohol, temperature equilibrated in a constant temperature bath, and filled to the mark with dry *tert*-butyl alcohol. This stock solution was at least twenty times more concentrated than the substrate. The required amount (approximately 20 mg) of the 1-choro-2-phenyl-1,2-d_2 ethane diastereomers was weighed into the reaction vessel and temperature equilibrated. The reaction was started by quickly adding the base solution to the reaction vessel. After ten half-lives (>99.9% reaction) the reaction was quenched by adding cold water and the organic products were extracted three times with pentane. After the combined pentane extracts had been washed with water and dried over anhyd magnesium sulphate, the pentane was removed at room temperature in a rotary evaporator. An NMR analysis of the residue in 1 mL of chloroform-*d* gave the composition of the product.

Acknowledgment

The authors gratefully acknowledge the financial support provided by the Natural Sciences and Engineering Research Council of Canada (NSERC).

References

1. H. Matsuda, T. Hamatani, S. Matsubara, and M. Schlosser. Tetrahedron, **44**, 2865 (1988).
2. R.A. Bartsch and J.G. Lee. J. Org. Chem. **55**, 5247 (1990).
3. M.J.S. Dewar and Y.-C. Yuan. J. Am. Chem. Soc. **112**, 2095 (1990).
4. J. Zavada, M. Pankova, and A. Vitek. Coll. Czech. Chem. Commun. **55**, 695 (1990).
5. R.A. Bartsch and J. Zavada. Chem. Rev. **80**, 453 (1980).
6. (*a*) G.A. Stuart and H. Eyring. J. Chem. Ed. **35**, 550 (1958); (*b*) A.F. Thomas and B. William. Tetrahedron Lett. 1309 (1965); (*c*) K. Fukui and H. Fujimoto. Tetrahedron Lett. 4303 (1965).
7. W.H. Saunders, Jr. and A.F. Cockerill. *In* Mechanisms of elimination reactions. Wiley Interscience, New York. 1973.
8. E. Baciocchi, R. Ruzziconi, and G.V. Sebastiani. J. Org. Chem. **47**, 3237 (1982).
9. E. Baciocchi, R. Ruzziconi, and G.V. Sebastiani. J. Am. Chem. Soc. **105**, 6114 (1983).
10. J. H. Exner and E.C. Steiner. J. Am. Chem. Soc. **96**, 1782 (1974).
11. V. Pechanec, O. Kocian, and J. Zavada. Coll. Czech. Chem. Commun. **47**, 3405 (1982).
12. V. Fiandanese, C.V. Maffeo, C. Marchese, and F. Naso. J. Chem. Soc. Perkin Trans. 2, 221 (1975).
13. V. Pechanec, O. Kocian, V. Halaska, M. Pankova, and J. Zavada. Coll. Czech. Chem. Commun. **46**, 2166 (1981).
14. V. Pechanec, O. Kocian, and J. Zavada. Coll. Czech. Chem. Commun. **48**, 1144 (1983).
15. J. Zavada, M. Pankova, and M. Svoboda. Coll. Czech. Chem. Comm. **41**, 3778 (1976).
16. C. Ingold. Proc. Chem. Soc. London, 265 (1962).
17. N.T. Anh. J. Chem. Soc. Chem. Commun. 1089 (1968).
18. D.S. Bailey and W.H. Saunders, Jr. J. Am. Chem. Soc. **92**, 6904 (1970).
19. P.J. Smith and K.C. Westaway. Can. J. Chem. **65**, 2149 (1987).
20. A.N. Bourns and A.C. Frosst. Can. J. Chem. **48**, 133 (1970).
21. J. Zavada, M. Pankova, and A. Vitek. Coll. Czech. Chem. Commun. **46**, 3247 (1981).
22. L.H. Amundsen and L.S. Nelson. J. Am. Chem. Soc. **73**, 242 (1951).
23. R.L. Huang and S. Singh. J. Chem. Soc. 891 (1958).

© 2001 NRC Canada

24. Y.T. Tao and W.H. Saunders, Jr. J. Am. Chem. Soc. **105**, 3183 (1983).
25. B.R. Dohner and W.H. Saunders, Jr. Can. J. Chem. **64**, 1026, (1986).
26. D.R. Burfield and R.H. Smithers. J. Org. Chem. **48**, 2420 (1983).
27. J. March. *In* Advanced organic chemistry: reactions, mechanisms, and structure. 4th ed, John Wiley & Sons, New York. 1992. pp. 317–319.
28. J. March. *In* Advanced organic chemistry: reactions, mechanisms, and structure. 4th ed, John & Sons, New York. 1992. p. 327.

© 2001 NRC Canada

Original disymmetric bolaforms bearing at least one sulfobetaine head; synthesis and surface properties

Souad Souirti and Michel Baboulène

Abstract: We describe a simple and efficient method for the synthesis of disymmetric bolaforms bearing at least one sulfobetaine head. In this process, we could introduce successively on α,ω-bis(dialkylamino) alkane a sulfobetaine head and a cationic, a sulfobetaine, or a carboxybetaine head, in excellent yield. This is the first synthesis of disymmetric sulfobetaine bolaforms. The method is easily generalized to various types of head functional groups. The wide range of bolaforms produced by this method has been exploited to study their surface properties and to determine the respective roles of the polar heads and the lengths of the spacers (*n*) on self-aggregation in aqueous media. A critical micellar concentration (cmc) was observed with the compounds with a spacer of 12 carbon atoms (*n* = 12). Micellization appeared to be consistent with a "wicket-like" conformation, which did not appear to form with the *n* = 8 compounds.

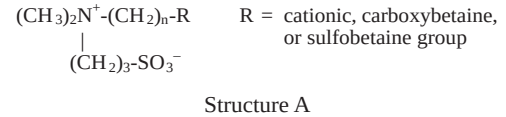
Key words: disymmetric bolaform, sulfobetaine, carboxybetaine, cationic amphiphile, synthesis, surface properties.

Résumé : Nous décrivons une simple et efficace méthode d'accés à des dissymmétriques bolaformes ayant au moins une tête sulfobétaine. Dans ce procédé nous pouvons introduire successivement sur les azotes d'un α,ω-bis(dialkylamino) alkane une tête sulfobétaine et une tête cationique ou sulfobétaine ou carboxybétaine avec d'excellents rendements. C'est la première synthèse de sulfobétaines bolaformes dissymétriques. La méthode décrite est facilement généralisable à diverses têtes polaires. La diversité des bolaformes ainsi obtenus permet d'aborder, à partir d'une étude tensiométrique, leurs propriétés de surface et de discuter du rôle des têtes polaires et de la distance entre les deux têtes (*n*) dans le mode d'aggrégation de ces composés en milieu aqueux. Les composés avec *n* = 12 se prêtent à la détermination d'une concentration micellaire critique (cmc). Leur micellisation semble en accord avec une conformation " en boucle" qui ne se retrouve pas pour les composés avec *n* = 8.

Mots clés : bolaforme disymmétrique, sulfobétaine, carboxybétaine, amphiphile cationique, synthèse, paramètres de surface.

Introduction

There have been a large number of descriptions of the synthesis of amphiphilic molecules, which self-aggregate into vesicles, as these compounds have a variety of application in chemistry and biochemistry (1, 2). Among the numerous families of surfactants, a novel architecture represented by the bolaform structure has been developed (3). Bolaforms are molecules bearing two polar heads separated by a hydrophobic chain of variable length. This structure lends itself to a modular synthesis of derivatives with different chains and polar heads. However, despite numerous reports on bolaforms, to our knowledge there are no descriptions of bolaforms with betaine heads. We have currently been investigating bolaforms derived from betaine (4). The encouraging preliminary results prompted us to examine derivatives with a sulfobetaine head. These compounds find applications as detergents and in cosmetics (5). Recently, Spencer et al. (6) have reported the inhibitory action of *N,N′*-bis[dimethylammonium-1-(4-butylsulfonyl)]dodecane, a sulfobetaine surfactant, on squalene synthetase. Nevertheless, the amphiphilic character of this compound was not conjured up, and we also know the importance of organized molecular systems into biological applications. Consequently, the bolaform structure open new perspectives for the surfactant chemistry. For this purpose, knowledge of the surface properties and comprehension of the process of vesicle formation will also require a number of derivatives for studying the self-aggregation behaviour. The interest of different polar heads at the ends of the hydrophobic chain is an added interest for such investigations.



Structure A

We present here a simple and general method for preparation of original disymmetric bolaforms bearing a sulfobetaine head with the other head being either cationic

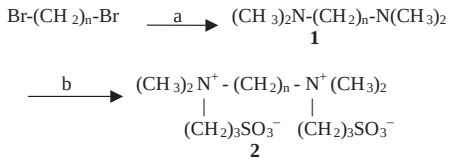
Received November 13, 2000. Published on the NRC Research Press Web site at http://canjchem.nrc.ca on August 3, 2001.

S. Souirti and M. Baboulène.[1] Laboratoire des Interactions Moléculaires et Réactivités Chimiques et Photochimiques, UMR (CNRS 5623) Université Paul Sabatier 118 route de Narbonne, 31062 Toulouse cédex 06 France.

[1]Corresponding author (telephone: 33 61 55 62 72; fax: 33 61 25 17 33; e-mail: mbab@ramses.ups-tlse.fr).

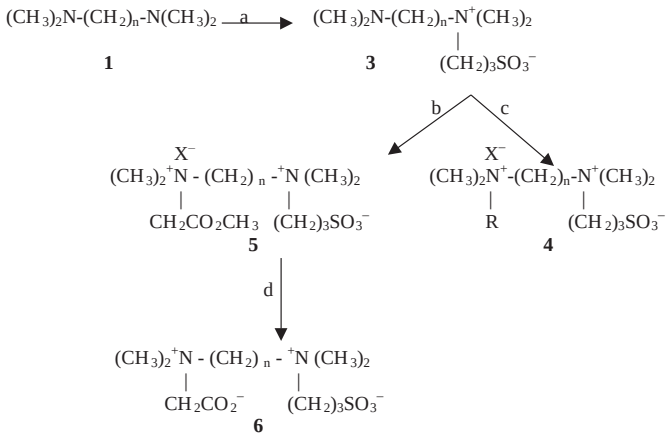
 DOI: 10.1139/cjc-79-7-1153 © 2001 NRC Canada

Scheme 1.



a: $HN(CH_3)_2$, ethanol/water, reflux;
b: 1,3-propane sultone, acetonitrile, reflux

Scheme 2.



a: 1,3-propane sultone, acetone, 15–20°C;
b: $BrCH_2CO_2C_2H_5$, methanol, reflux; *c*: RX, methanol, reflux, *d*: resin Amberlist™ OH^-, methanol, 20°C, 3 h.

or a betaine (structure A). The surface properties of the compounds prepared was then examined.

Synthesis

The sulfobetaine structure is readily produced by condensation of an amine with an alkylsultone (7). We employed this method using α,ω-bis(dialkylamino) alkane **1** according to Scheme 1.

This condensation reaction is quantitative. The sulfobetaines **2** are readily recovered with a high degree of purity by filtration because of the absence of by-products and the crystalline nature of the product. However, if the reaction mixture is heated, the reaction does not stop at the monocondensation product, but we did succeed in obtaining a quantitative yield of the monocondensed product **3** by using a large excess of sultone at a temperature of 15–20°C (Scheme 2). We have envisaged to take advantage of this particular reactivity. The compounds **3**, which are readily isolated in a pure state, can be utilized as intermediates in the synthesis of the disymmetric bolaforms (Scheme 2). The insertion of the second polar head is simple and easily generalized to various types of head.

Table 1 lists typical results that illustrate the possibilities of these novel synthons. This process should not be difficult to carry out on an industrial scale.

The bolaforms prepared were characterized from their IR and NMR spectra. It should be noted that the deshielding

Table 1. Yield and melting points of bolaforms prepared.

	n	R	X	Yield (%)	mp (°C)
2a	8	—	—	95	210
2b	12	—	—	96	218
3a	8	—	—	98	199
3b	12	—	—	98	230
4a	8	CH_3	I	95	225
4b	12	CH_3	I	95	222
4c	8	$C_{12}H_{25}$	Br	87	120
4d	12	$C_{12}H_{25}$	Br	87	105
4e	8	C_2H_5	Br	82	115
4f	12	C_2H_5	Br	80	125
5a	8	—	—	88	188–190
5b	12	—	—	83	170
6a	8	—	—	78	230
6b	12	—	—	75	260

Note: Calculated from Gibbs' equation (8).

observed on the chemical shifts of the $N\text{-}CH_3$ and $N\text{-}CH_2$ groups are consistent with quaternization of the nitrogen atom. Furthermore, the disymmetry of the polar heads was indicated by the differentiation of the ^{13}C NMR peaks of the $N\text{-}CH_3$ groups, which was further support for the proposed structures.

Surface properties

The surfactant properties of these novel bolaforms were studied by measuring interfacial tension (γ) in water, and calculated using the Gibbs' equation (8). The data are illustrated in Figs. 1 and 2 and listed in Table 2.

All compounds tested led to a marked reduction in interfacial tension at the air–water interface (30–35 mN m^{-1}). However, this action was found to depend on the concentration of the particular compound as a function of polar head and length of spacer. The compounds with $n = 12$ exhibited a break in the interfacial tension vs. concentration plots. This property of micellization occurred at relatively low values of critical micelle concentration (cmc), which shows promise for industrial applications.

We noted that the cmc value was strongly dependent on the nature of the polar head. The carboxy-sulfobetaine bolaform **6b** (cmc = 5.5 mM) was a better surfactant than the symmetrical sulfobetaine **2b** (cmc = 8.2 mM) or the carboxybetaine analogs (cmc = 6.7–8 mM (4)). On the other hand, the passage of carboxy-sulfobetaine **6b** to ammonium-sulfobetaine **5b** led to an increase in cmc (cmc = 18 mM). This can be accounted for by the stronger repulsion of the polar heads enhanced by steric interactions. Our findings are in line with those described for cationic bolaforms (12–18 mM (9)). Furthermore, these results were in accordance with those of the general literature; a spacer with $n = 8$ does not permit micellization. By contrast, we noted that introduction of a long alkyl chain onto the nitrogen atom led to a decrease in the cmc value. This was attributed to an increased hydrophobicity. For example, compound **4c** micellized at low concentration (cmc = 5 mM) despite the short spacer ($n = 8$), which is not generally compatible with micellization (9). The surfactants **4c** and **4d**, thus, represent

© 2001 NRC Canada

Fig. 1. Plots of interfacial tension (obtained by tensiometry) vs. log [bolaform] at 25°C in water.

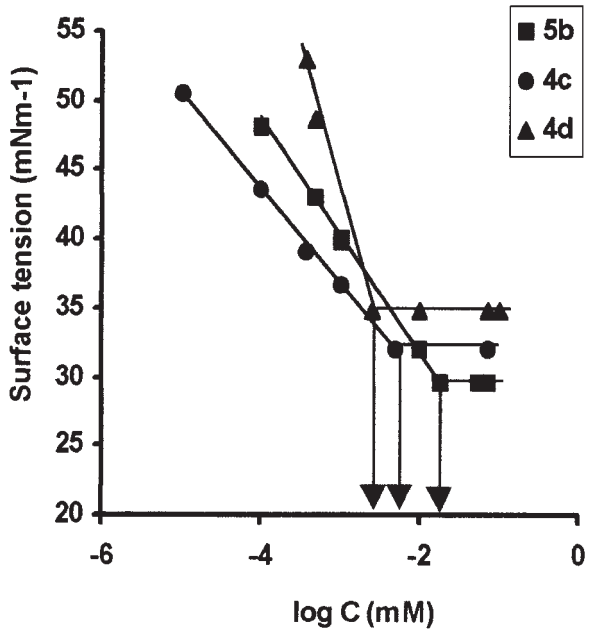
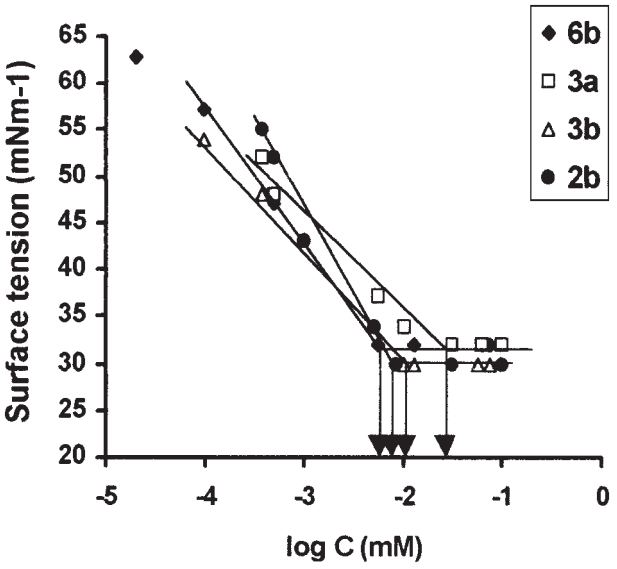


Fig. 2. Plots of interfacial tension (obtained by tensiometry) vs. log [bolaform] at 25°C in water.



a new family of surfactants as a hybrid between bolaforms and gemini surfactants (10). The synthesis proposed here is in keeping with the general pattern of the current research on the access to new potential surfactants. It was noteworthy that the presence of an iodine atom on the cationic head of the bolaforms **4a** and **4b** prevented micellization (at the concentrations studied = 10^{-1} M) even with a -$(CH_2)_{12}$- spacer (comparison **4b** and **4f**).

A number of comments can be made on the surface areas as calculated from the Gibbs' equation (8). The betaine bolaforms **6b** and **2b** occupy a space at the interface that is the arithmetic sum of the surface areas of the two polar heads (11, 12). These results are consistent with the length and flexibility of the spacer, which indicates that these surfactants adopt a " wicket-like" conformation at the air–water interface. By contrast, the calculated surface areas of the head of the disymmetric bolaforms **4d** (A = 188 Å^2) and **4f** (A = 167 Å^2) is slightly superior as the arithmetic sum of the calculated surface areas of the two polar heads (A ~ 130 Å^2) suggests the "wicked-like" conformation undergoes a flattening at the air–water interface. The presence of the methyl acetate group in compound **5b** (A = 252 Å^2) led significantly to flattening out of the molecule at the interface. A same arrangement was proposed for the bolaforms with a spacer n = 8 (see **4c**, A = 275 Å^2). This influence of the length of the hydrophobic chain was also demonstrated by comparison of the molecular areas of compounds **3a** with **3b**. This linear arrangement would be consistent with a more extended occupation of the interface. This type of molecular organization has been described for non-ionic (13) and cationic bolaforms.[2] On the other hand, it can envisage that these structures lead to a vesicular self-association. Further interpretations will have to await the results of light scattering and electron microscopic studies (in progress).

Table 2. Surface parameters of compounds in water at 25°C.

	γ (mN m^{-1})[a]	cmc (mM)	Γ (mol m^{-2})[a]	A (Å^2)[a]
2a	30[c]	—	—	—
2b	30	8.2	1.81×10^{-6}	91.56
3a	32	30	1.32×10^{-6}	125
3b	30	10	2.16×10^{-6}	77.6
4a	30.8[b]	—	—	—
4b	29.8[b]	—	—	—
4c	32	5	6.02×10^{-7}	275
4d	34.8	2.4	8.83×10^{-7}	188
4e	32[b]	—	—	—
4f	33	70	10×10^{-7}	167
5a	34[b]	—	—	—
5b	29.5	18	6.5×10^{-7}	252
6a	30[b]	—	—	—
6b	32	5.5	1.8×10^{-6}	92.26

[a] γ = interfacial tension by the stirrup detachment method.; Γ = superficial excess; A = area of the polar head.
[b] Obtained at [C] = 1×10^{-1} M.

Conclusion

We describe here a convenient route to disymmetric bolaforms bearing at least one sulfobetaine head, which could be scaled up for industrial applications. The method lends itself to a modular synthesis enabling preparation of a variety of derivatives with different polar heads and different spacers. To our knowledge, this is a first synthesis of sulfobetaine disymmetric bolaforms.

Our preliminary results on the surface properties of these bolaforms are encouraging, as they all led to a marked reduction in interfacial tension at the air–water interface at low concentrations. This surfactant action suggests that, by comparison with the well-known activity of other betaine surfactants, these bolaforms have potential applications as

[2] I. Rico-Lattes personal communication.

© 2001 NRC Canada

corrosion inhibitors. The role of the disymmetric head structure and the length of the spacers were demonstrated in micellar self-aggregation behaviour. Self-organization into vesicles is currently under investigation. Comprehension of their physicochemical properties will be facilitated by this convenient route to a wide range of derivatives of original disymmetric bolaform structure.

Experimental

General

Reagents were of commercial quality and were used without purification. IR spectra (ν, cm^{-1}) were recorded on a PerkinElmer 683 spectrophotometer. ^1H and ^{13}C NMR spectra (δ, ppm) were obtained on Bruker AC 80 or Bruker AC 200 instruments. Surface active properties were calculated using Gibbs' equation with the data obtained from measurements carried out Prolabo No. 3 tensima.

Typical procedure for the synthesis of compounds 1

A solution of dimethylamine (33% of ethanol) (3×10^{-2} mol) and dibromoalkane (1×10^{-2} mol) were added to a solution of sodium carbonate (2×10^{-2} mol) in ethanol (60 mL) and water (15 mL). The reaction mixture was heated at reflux and stirred for 24 h. Then the resulting compound was isolated by evaporating of the solvent under reduced pressure. The crude product washed with water (1×10 mL) was extracted with EtO_2.The organic phase was dried on anhyd Na_2SO_4 and evaporated in vacuo. The crude oil was purified by distillation.

*1,8-bis(*N,N- *dimethylamino)octane (**1a**)*

Yield: 98%. Colourless oil, bp 60°C, 0.06 mm Hg. ^1H NMR (200 MHz, $CDCl_3$) δ 1.1 (m, 12H, $(CH_2)_6$), 2.3 (t, 4H, NCH_2), 1.9 (s, 12H, NCH_3). ^{13}C NMR (200 MHz, $CDCl_3$) δ 27.2–28.3 ($(CH_2)_6$), 45.2 (NCH_3), 59.7 (NCH_2). Anal calcd. for $C_{12}H_{28}N_2$ (200.37): C 71.86, H 13.97, N 13.97; found: C 71.66, H 14.15, N 14.13.

*1,12-bis(*N,N-*dimethylamino)dodecane (**1b**)*

Yield: 98%. Colourless oil, bp 80–82°C, 0.05 mm Hg. ^1H NMR (200 MHz, $CDCl_3$) δ 1.1 (m, 20H, $(CH_2)_{10}$), 2.1 (t, 4H, NCH_2), 1.9 (s, 12H, NCH_3). ^{13}C NMR (200 MHz, $CDCl_3$) δ 27.4–28.5 ($(CH_2)_{10}$), 45.4 (NCH_3), 59.9 (NCH_2). Anal calcd. for $C_{16}H_{36}N_2$ (256.47): C 74.86, H 14.03, N 10.92; found: C 74.73, H 13.90, N 11.62.

Typical procedure for the synthesis of compounds 2

Compounds **2** were prepared by the addition of diamine **1** (1×10^{-2} mol) to 1,3-propane sultone (2.2×10^{-2} mol) in anhyd acetonitrile (100 mL). The solution was stirred at reflux for 4 h, then cooled and filtered. After crystallization from methanol–acetone (1:9), pure compounds **2** were obtained as solid, which decomposed during melting point determination.

*1,8-bis(*N,N- *dimethylammonio*-N-*propyl-1-sulfonate)octane (**2a**)*

Yield: 95%. White powder, mp 210°C. IR (KBr) (cm^{-1}): 1480 (C-N^+), 1040 (S=O). ^1H NMR (200 MHz, D_2O) δ 1.2 (m, 12H, $(CH_2)_6$), 1.9 (qt, 4H, CH_2-C-SO_3), 2.9 (t, 4H, CH_2SO_3), 3.0 (s, 12H, NCH_3), 3.2 (t, 4H, CH_2N), 3.4 (t, 4H, CH_2N). ^{13}C NMR (200 MHz, D_2O) δ 20.7–31.1 ($(CH_2)_6$), 49.8 (CH_2-C-SO_3), 53.1 (NCH_3), 64.4 (NCH_2), 66.7 (CH_2SO_3). Anal calcd. for $C_{18}H_{40}N_2O_6S_2$ (444.64): C 48.62, H 9.07, N 6.30, S 14.42; found: C 48.96, H 9.30, N 5.94, S 13.97.

*1,12-bis(*N,N- *dimethylammonio*-N-*propyl-1-sulfonate)dodecane (**2b**)*

Yield: 95%. White powder, mp 215°C. IR (KBr) (cm^{-1}): 1480 (C-N^+), 1040 (S=O). ^1H NMR (200 MHz, D_2O) δ 1.2 (m, 20H, $(CH_2)_{10}$), 2.2 (qt, 4H, CH_2-C-SO_3), 2.6 (t, 4H, CH_2SO_3), 3.0 (s, 12H, NCH_3), 3.2 (t, 4H, CH_2N), 3.3 (t, 4H, CH_2N). ^{13}C NMR (200 MHz, D_2O) δ 20.7–31.1 ($(CH_2)_{10}$), 49.8 (CH_2-C-SO_3), 53.1 (NCH_3), 64.4 (NCH_2), 66.8 (CH_2SO_3). Anal calcd. for $C_{22}H_{48}N_2O_6S_2$ (500.75): C 52.77, H 9.66, N 5.29, S 12.8; found: C 52.13, H 9.42, N 5.39, S 12.23.

Typical procedure for the synthesis of compounds 3

Sulfobetaine **3** was prepared by the addition of α,ω-bis(*N*,*N*-dimethylamino) alkane (1×10^{-2} mol) to a stirred solution of 1,3-propane sultone (2×10^{-3} mol) in anhyd acetone (50 mL). The reaction mixture was stirred at room temperature for 3 h, cooled, and filtered. The amphiphilic product was purified by recrystallization from methanol–ether (1:9), and dried in vacuo over phosphorus pentoxide.

*1-(*N,N-*dimethylammonio*-N-*propyl-1-sulfonate)-8-(*N′,N′-*dimethylamino)octane (**3a**)*

Yield: 98%. White powder, mp 198–200°C. IR (KBr) (cm^{-1}): 1480 (C-N^+), 1040 (S=0). ^1H NMR (80 MHz, D_2O) δ 1.2 (m, 12H, $(CH_2)_6$), 2.0–2.2 (m, 10H, NCH_2, NCH_3, CH_2-C-SO_3), 2.7–3.2 (m, 12H, N^+CH_3, N^+CH_2, $CH_2SO_3^-$). ^{13}C NMR (200 MHz, D_2O) δ 20.7–31.6 ($(CH_2)_6$), 46.5 (NCH_3), 49.8 (CH_2-C-SO_3), 53.2 (N^+CH_3), 61.4 (NCH_2), 64.5 (N^+CH_2), 66.7 ($CH_2SO_3^-$). Anal. calcd. for $C_{15}H_{34}N_2O_3S$ (322.5): C 55.86, H 10.63, N 8.69, S 9.94; found: C 55.50, H 10.46, N 8.46, S 9.62.

*1-(*N,N-*dimethylammonio*-N-*propyl-1-sulfonate)-12-(*N′,N′-*dimethylamino)dodecane (**3b**)*

Yield: 98%. White powder, mp 230°C. IR (KBr) (cm^{-1}): 1480 (C-N^+), 1040 (S=0). ^1H NMR (80 MHz, D_2O) δ 1.2 (m, 20H, $(CH_2)_{10}$), 1.9–2.2 (m, 10H, NCH_2, NCH_3, CH_2-C-SO_3^-), 2.9–3.2 (m, 12H, N^+CH_3, N^+CH_2, CH_2-$CH_2SO_3^-$). ^{13}C NMR (200 MHz, D_2O) δ 20.7–31.6 ($(CH_2)_{10}$), 46.5 (NCH_3), 49.8 (CH_2-C-SO_3), 53.2 (N^+CH_3), 61.4 (NCH_2), 64.5 (N^+CH_2), 66.7 ($CH_2SO_3^-$). Anal. calcd. for $C_{19}H_{49}N_2O_3S$ (378.61): C 60.27, H 11.18, N 7.40, S 8.47; found: C 59.93, H 11.02, N 7.07, S 8.54.

Typical procedure for the synthesis of compounds 4

A mixture of sulfobetaine **3** (1×10^{-2} mol) and of haloalkane (1×10^{-2} mol) in absolute MeOH (50 mL) was heated at reflux for 4 h. After removing the solvent in vacuo, the residual oil was purified by trituration with anhyd ether, and then evaporated in vacuo and dried over phophorus pentoxide.

© 2001 NRC Canada

*1-(*N,N-*dimethylammonio*-N-*propyl-1-sulfonate)-8-(*N′-*trimethylammonium iodid)octane* ***(4a)***

Yield: 95%. Yellow powder, mp 225°C. IR (KBr) (cm^{-1}): 1480 (C-N^+), 1040 (S=0). ^1H NMR (80 MHz, D_2O) δ 1.2 (m, 12H, $(CH_2)_6$), 2.1 (qt, 2H, CH_2-C-SO_3^-), 3.0–3.5 (m, 23H, NCH_3, NCH_2, $CH_2SO_3^-$). ^{13}C NMR (200 MHz, D_2O) δ 20.0–31.0 ($(CH_2)_6$), 49.9 (CH_2-C-SO_3), 53.2 and 55.5 (NCH_3), 66.3 ($NCH_2(SO_3)$), 66.7 ($CH_2SO_3^-$), 69.4 ($NCH_2(I)$). Anal. calcd. for $C_{16}H_{37}IN_2O_3S$ (464.45): C 41.38, H 8.03, N 6.03, S 6.91; found: C 40.93, H 8.34, N 5.95, S 6.95.

*1-(*N,N-*dimethylammonio*-N-*propyl-1-sulfonate)-12-(*N′-*trimethylammonium iodid)dodecane* ***(4b)***

Yield: 95%. Yellow powder, mp 222°C. IR (KBr) (cm^{-1}): 1480 (C-N^+), 1040 (S=0). ^1H NMR (80 MHz, D_2O) δ 1.2 (m, 20H, $(CH_2)_{10}$), 2.1 (qt, 2H, CH_2-C-SO_3^-), 2.8–3.2 (m, 23H, NCH_3, NCH_2, $CH_2SO_3^-$). ^{13}C NMR (200 MHz, D_2O) δ 26.7–31.1 ($(CH_2)_{10}$), 49.8 (CH_2-C-SO_3), 53.2 and 55.3 (NCH_3), 64.4 ($NCH_2(SO_3)$), 66.7 ($CH_2SO_3^-$), 69.3 (N^+CH_2). Anal. calcd. for $C_{20}H_{45}IN_2O_3S$ (520.56), C 46.15, H 8.71, N 5.38, S 6.16; found: C 45.96, H 8.93, N 5.18, S 6.00.

*1-(*N,N-*dimethylammonio*-N-*propyl-1-sulfonate)-8-(*N′,N′-*dimethyl*-N′-*dodecylammonium bromid)octane* ***(4c)***

Yield: 87%. White powder, mp 120°C. IR (KBr) (cm^{-1}): 1480 (C-N^+), 1040 (S=0). ^1H NMR (80 MHz, D_2O) δ 0.8 (t, 3H, CH_3-C_{11}), 1.3 (m, 32H, $(CH_2)_{10}$, $(CH_2)_6$), 2.1 (qt, 2H, CH_2-C-SO_3^-), 2.6–3.3 (m, 22H, NCH_3, NCH_2, $CH_2SO_3^-$). ^{13}C NMR (200 MHz, D_2O) δ 16.6 (C-CH_3), 20.8–34.6 ($(CH_2)_6$, $(CH_2)_{10}$), 49.9 (CH_2-C-SO_3), 53.5 and 54.4 (NCH_3), 64.5 and 66.3 (NCH_2), 66.7 ($CH_2SO_3^-$), 69.4 (N^+CH_2). Anal. calcd. for $C_{27}H_{59}BrN_2O_3S{\cdot}H_2O$ (550.63): C 58.84, H 11.07, N 5.08, S 5.81; found: C 58.95, H 10.95, N 4.80, S 6.00.

*1-(*N,N-*dimethylammonio*-N-*propyl-1-sulfonate)-12-(*N′,N′-*dimethyl*-N′-*dodecylammonium bromid)dodecane* ***(4d)***

Yield: 85%. White powder, mp 105°C. IR (KBr) (cm^{-1}): 1480 (C-N^+), 1040 (S=0). ^1H NMR (80 MHz, D_2O) δ 0.8 (t, 3H, CH_3-C_{11}), 1.3 (m, 40H, $(CH_2)_{10}$, $(CH_2)_{10}$), 2.1 (qt, 2H, CH_2-C-SO_3^-), 3.0–3.3 (m, 22H, NCH_3, NCH_2, $CH_2SO_3^-$). ^{13}C NMR (200 MHz, D_2O) δ 16.6 (C-CH_3), 20.6–34.4 ($(CH_2)_{10}$), 49.9 (CH_2-C-SO_3), 53.5 and 54.4 (NCH_3), 64.2 and 66.1 (NCH_2), 66.3 ($CH_2SO_3^-$). Anal. calcd. for $C_{31}H_{61}BrN_2O_3S{\cdot}H_2O$ (645.85): C 57.59, H 9.75, N 4.33, S 4.95; found: C 55.79, H 10.05, N 4.42, S 4.55.

*1-(*N,N-*dimethylammonio*-N-*propyl-1-sulfonate)-8-(*N′,N′-*dimethyl*-N′-*ethylammonium bromid) octane* ***(4e)***

Yield: 82%.White powder, mp 115°C. ^1H NMR (80 MHz, D_2O) δ 1.1 (t, 3H, CH_3), 1.5 (m, 12H, $(CH_2)_6$), 2.1 (qt, 2H, CH_2-C-SO_3), 2.9–3.1 (m, 14H, N-CH_3, CH_2SO_3), 3.3 (m, 8H, NCH_2), 3.5 (t, 2H, NCH_2-C-S). ^{13}C NMR (200 MHz, D_2O) δ 10.13 (CH_3), 21.0–31.0 $(CH_2)_6$, 47.8 (CH_2-C-S), 52.4 (NCH_3), 52.2 (CH_3N-S), 62.0, 63.7, 65.8 (NCH_2), 66.5 (CH_2S). Anal. calcd. for $C_{17}H_{39}BrN_2O_3S{\cdot}H_2O$ (449.49): C 45.43, H 9.19, N 6.23, S 7.13; found: C 45.62, H 9.05, N 5.98, S 7.35.

*1-(*N,N-*dimethylammonio*-N-*propyl-1-sulfonate)-12-(*N′,N′-*dimethyl*-N′-*ethylammonium bromid)dodecane* ***(4f)***

Yield: 80%.White powder, mp 125°C. ^1H NMR (80 MHz, D_2O) δ 1.1 (t, 3H, CH_3), 1.3 (m, 16H, $(CH_2)_8$), 2.2 (qt, 2H, CH_2-C-SO_3), 2.9–3.2 (m, 14H, N-CH_3, CH_2SO_3), 3.3 (m, 8H, NCH_2), 3.6 (t, 2H, NCH_2-C-S). ^{13}C NMR (200 MHz, D_2O) δ 10.03 (CH_3), 20.7–31.1 ($(CH_2)_8$), 49.8 (CH_2-C-S), 52.4 (NCH_3), 53.2 (CH_3N-S), 62.0, 64.48, 66.1 (NCH_2), 66.6 (CH_2S). Anal. calcd. for $C_{21}H_{47}BrN_2O_3S{\cdot}H_2O$ (505.60): C 49.88, H 9.77, N 5.54, S 4.08; found: C 50.02, H 9.94, N 5.28, S 4.42.

Typical procedure for the synthesis of compounds 5

A mixture of monosulfonate **3** (1×10^{-2} mol) and bromoacetate (2×10^{-2} mol) in anhyd methanol (40 mL) was heated at reflux under agitation for 6 h. The solvent was evaporated in vacuo. The residual oil was precipitated by ether and purified by washed successively with ether and acetone.

*1-(*N,N-*dimethylammonio*-N-*propyl-1-sulfonate)-8-(*N′,N′-*dimethyl*-N′-*ethylacetate ammonium bromid)octane* ***(5a)***

Yield: 88%. White powder, mp 185–190°C. IR (KBr) (cm^{-1}): 1470–1460 (C-N^+), 1040 (S=0), 1640 (C=O). ^1H NMR (80 MHz, D_2O) δ 1.3 (m, 8H, $(CH_2)_4$), 1.7 (m, 4H, CH_2-C-N), 2.1 (qt, 2H, CH_2-C-SO_3^-), 2.6–3.5 (m, 20H, NCH_3, NCH_2, $CH_2SO_3^-$), 3.8 (s, 3H, OCH_3), 4.2 (s, 2H, CH_2CO_2). ^{13}C NMR (200 MHz, D_2O) δ 20.8–34.6 ($(CH_2)_6$), 50.0 (CH_2-C-SO_3), 53.3 and 54.3 (NCH_3), 56.0 (OCH_3), 63.8 and 64.5 (NCH_2), 66.8 ($CH_2SO_3^-$), 68.5 (CH_2CO_2), 168.4 (CO_2). Anal. calcd. for $C_{18}H_{39}BrN_2O_5S$ (475.48): C 45.47, H 8.27, N 5.89, S 6.74; found: C 45.30, H 8.97, N 5.91, S 6.86.

*1-(*N,N-*dimethylammonio*-N-*propyl-1-sulfonate)-12-(*N′,N′-*dimethyl*-N′-*ethylacetate ammonium bromid)dodecane* ***(5b)***

Yield: 83%. White powder, mp 170°C. IR (KBr) (cm^{-1}): 1460 (C-N^+), 1040 (S=0), 1640 (C=O). ^1H NMR (80 MHz, D_2O) δ 1.26 (m, 16H, $(CH_2)_8$), 1.7 (m, 4H, CH_2-C-N), 2.1 (qt, 2H, CH_2-C-SO_3^-), 3.0–3.2 (m, 22H, NCH_3, NCH_2, $CH_2SO_3^-$), 3.8 (s, 3H, OCH_3), 4.2 (s, 2H, CH_2CO_2). ^{13}C NMR (200 MHz, D_2O) δ 20.8–31.2 ($(CH_2)_{10}$), 50.0 (CH_2-C-SO_3), 53.3 and 54.4 (NCH_3), 56.0 (OCH_3), 63.7 and 64.6 (NCH_2), 68.5 ($CH_2SO_3^-$), 68.7 (CH_2CO_2), 168.4 (CO_2). Anal. calcd. for $C_{22}H_{47}BrN_2O_5S$ (531.59): C 49.71, H 8.91, N 5.27, S 6.03; found: C 49.67, H 9.03, N 4.98, S 6.02.

Typical procedure for the synthesis of compounds 6

A mixture of compound **5** (1×10^{-2} mol) in methanol and anion-exchange resin (OH^-) (amberlist IRA 400) (25 g) was stirred for 3 h at room temperature. Then, the mixture was filtered and evaporated in vacuo. The residual oil was triturated from ether, and recrystallized from ether–methanol (9:1).

*1-(*N,N-*dimethylammonio*-N-*propyl-1-sulfonate)-8-(*N′,N′-*dimethylammonio*-N′-*acetate)octane* ***(6a)***

Yield: 78%. White powder, mp 230°C. IR (KBr) (cm^{-1}): 1480 (C-N^+), 1200 and 1050 (S=0), 1650–1630 (C=O). ^1H NMR (200 MHz, D_2O) δ 1.4 (m, 8H, $(CH_2)_4$), 1.8 (m, 4H, CH_2-C-N), 2.2 (qt, 2H, CH_2-C-SO_3^-), 2.9 (t, 2H, CH_2SO_3), 3.0 and 3.1 (s, 12H, NCH_3), 3.4–3.6 (m, 6H, NCH_2), 3.8 (s, 2H, CH_2CO_2). ^{13}C NMR (200 MHz, D_2O) δ 20.8–30.4 ($(CH_2)_6$), 49.9 (CH_2-C-SO_3), 53.2 and 53.9 (NCH_3), 64.5 (NCH_2), 66.8 ($CH_2SO_3^-$), 68.6 (CH_2CO_2), 171.9 (CO_2). Anal. calcd. for $C_{17}H_{36}N_2O_5S{\cdot}H_2O$ (396.54): C 51.44,

© 2001 NRC Canada

H 9.58, N 7.06, S 8.06; found: C 51.24, H 9.71, N 6.97, S 8.44.

*1-(*N,N-*dimethylammonio*-N-*propyl-1-sulfonate)-12-(*N′,N′-*dimethylammonio*-N′-*acetate)dodecane (**6b**)*

Yield: 75%. White powder, mp 260°C. IR (KBr) (cm^{-1}): 1480 (C-N^+), 1200 and 1050 (S=0), 1650–1630 (C=O). ^{1}H NMR (200 MHz, D_2O) δ 1.3 (m, 16H, $(CH_2)_8$), 1.7 (m, 4H, CH_2-C-N), 2.2 (qt, 2H, CH_2-C-SO_3^-), 2.3 (t, 2H, CH_2SO_3), 3.0 and 3.2 (s, 12H, NCH_3), 3.4–3.6 (m, 6H, NCH_2), 3.7 (s, 2H, CH_2CO_2). ^{13}C NMR (200 MHz, D_2O) δ 20.7–30.4 ($(CH_2)_{10}$), 49.8 (CH_2-C-SO_3), 53.2 and 53.8 (NCH_3), 64.4 (NCH_2), 67.1 ($CH_2SO_3^-$), 68.6 (CH_2CO_2), 171.8 (CO_2). Anal. calcd. for $C_{21}H_{44}N_2O_5S\cdot H_2O$ (454.65): C 55.43, H 10.11, N 6.15, S 7.03; found: C 55.42, H 10.43, N 5.82, S 7.28.

References

1. N. Kimizuka, T. Wakiyama, H. Miyauchi, T. Yoshimi, M. Tokuhiro, and T. Kunitake. J. Am. Chem. Soc. **118**, 5808 (1996) and refs. cited therein.
2. G.H. Escamilla. *In* Advances in dendrinic macromolecules. Vol 2. *Edited by* JAJ Press Inc. 1995. pp. 157–190.
3. J.H. Fuhrhop and J. Mathieu. J. Chem. Soc. Chem. Commun. 144 (1983).
4. S. Souirti and M. Baboulène. in press.
5. XXIX CED annual Meeting. Barcelona. 1999. May.
6. T.A. Spencer, T.J. Onofrey, R.O. Cann, J.S. Russel, L.E. Lee, D.E. Blanchard, A. Castro, P. Gu, G. Jiang, and I. Schechter. J. Org. Chem. **64**, 807 (1999).
7. E.J. Fendler, C.L. Day, and J.H. Fendler. J. Phys. Chem. **76**, 1460 (1972).
8. J.W. Gibbs. The collected works of J.W. Gibbs. Vol 1. Longmans and Green, London. 1928. p. 119.
9. F.M. Menger and S. Wreen. J. Phys. Chem. **78**, 1387 (1974).
10. S. Bhattacharya and S. De. J. Chem. Soc. Chem. Commun. 651 (1995).
11. Y. Chevalier, S. Brunel, and P. Le Perchec. J. Chim. Phys. - Chim. Biol. **92**, 1025 (1995).
12. J.B. Le Toumelin and M. Baboulène. Langmuir, **12**, 2128 (1996).
13. S. Franceschi, N. de Viguerie, M. Rivière, and A. Lattes. New. J. Chem. **23**, 447 (1999) and refs. cited therein.

© 2001 NRC Canada

Elimination, ring-contraction, and fragmentation reactions of 1-thioflavanone 1-oxides

László Somogyi

Abstract: Epimeric thioflavanone sulfoxides (**2b**) were selectively transformed into thioflavone (**1a**), thioaurone (**3a**), and di(2-cinnamoylphenyl) disulfide (**4**). Disulfide **4** can be recyclized into thioaurones (**3a**–**c**) and thioflavanones (**2a**, **5**) with heterolysis of the S—S bond. The 3-*p*-anisylidene sulfoxide analog of **2b** (**6**) transforms, with fragmentation, into 4′-methoxythioaurone **3b**.

Key words: chalcone, ring contraction, sulfoxides, thioaurones, thioflavonoids.

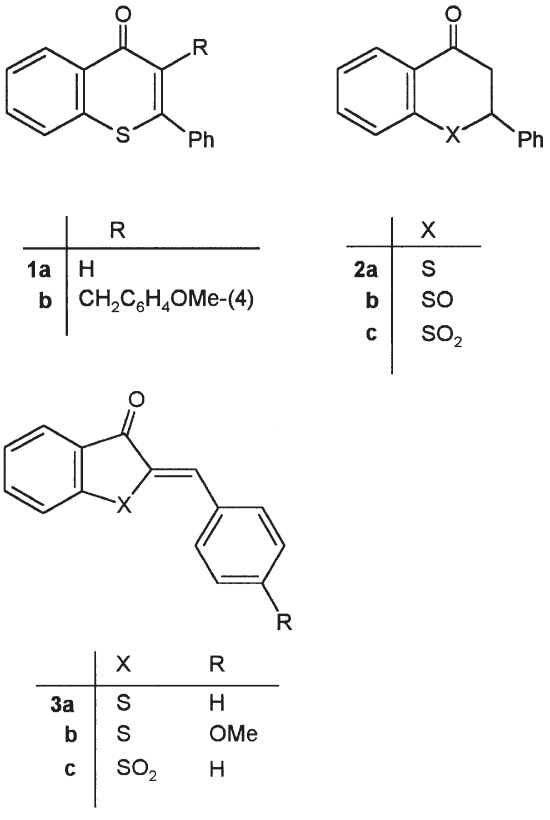
Résumé : On a réalisé la transformation sélective des sulfoxydes épimères de la thioflavanone (**2b**) en thioflavone (**1a**), thioaurone (**3a**) et en disulfure de di(2-cinnamoylphényle) (**4**). Le disulfure **4** peut être recyclisé en thioaurones (**3a**–**b**) et en thioflavanones (**2a**, **5**) avec hétérolyse de la liaison S—S. Le sulfoxyde de 3-*p*-anisylidène analogue de **2b** (**6**) subit une fragmentation et se transforme en 4′-méthoxythioaurone (**3b**).

Mots clés : chalcone, contraction de cycle, sulfoxydes, thioaurones, thioflavonoïdes.

[Traduit par la Rédaction]

Introduction

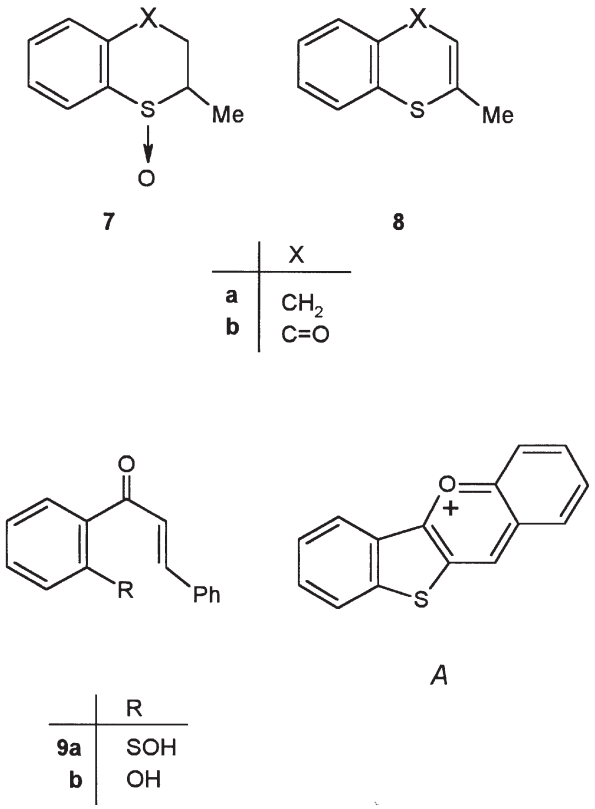
In the course of our efforts for the synthesis of 1-thioflavone derivatives, dehydrogenation of the dihydrobenzothiopyran (thioflavan) ring became necessary. Several methods useful in flavonoid chemistry have been successfully adopted (1, 3*c*) for thioflavanones, however, in some cases these methods were found either ineffective or, just the opposite; destructively drastic. Due to the greater variability of the electronic states of sulfur as compared to that of oxygen, additional methods, e.g., treatment (2) with PCl_5, or ceric ammonium nitrate (CAN) oxidation (3*a*–*c*) of thioflavanone (**2a**), and also alkali-mediated (2, 3*b*) or Pummerer-type transformation (3*b*) of sulfoxides (e.g., **2b**, in ca. 50% yield) have been successfully applied for the dehydrogenation. The PCl_5, CAN, or alkali-mediated transformations may have severe limitations when sensitive functional groups are present. As to the Pummerer-type transformation, 2-methyl-1-thiochroman 1-oxides (**7a**, **b**) have been transformed (3*d*) into the corresponding thiochromenes (**8a**, **b**) in nearly quantitative yields by treatment with acetic anhydride. However, due to the different electronic properties of the Me and Ph groups, the sulfoxides **2b** and 6-Me-**2b** undergo also ring-contraction reaction photochemically (4*b*, 4*d*), thermally (1), or upon treatment with I_2–DMSO (1) to give thioaurones (**3a**, 5-Me-**3a**) merely in 14–70% yields. Because of the relatively poor yields and the competing formation of **1a** and **3a**, we decided to find a selective conversion of thioflavanone 1-oxide (**2b**) into **1a** or **3a**.



Received December 19, 2000. Published on the NRC Research Press Web site at http://canjchem.nrc.ca on August 3, 2001.

L. Somogyi. Department of Organic Chemistry, University of Debrecen, P.O. Box 20, H-4010 Debrecen, Hungary. (Fax: + 36 (52) 453-836).

 DOI: 10.1139/cjc-79-7-1159 © 2001 NRC Canada

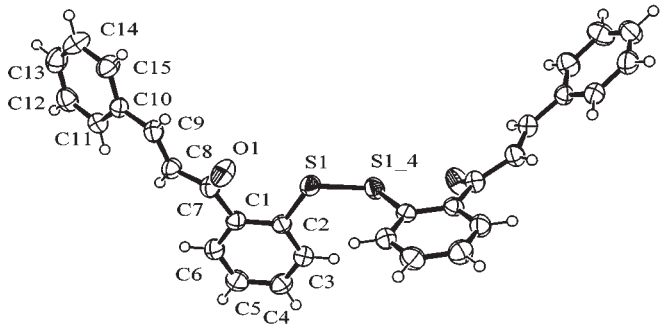


Results and discussion

The conversions of thioflavanone 1-oxide (**2b**) into either thioflavone (**1a**) or thioaurone (**3a**) proceed with loss of the elements of water, which are consumed by Ac_2O. The initial steps of these elimination reactions are, however, different. The Pummerer-type reactions of sulfoxides involve (3*e*, 3*f*) transient formation of sulfur and sulfur-stabilized carbonium cations. Accordingly, reaction conditions favouring the activation of the acyl moiety of the anhydrides may be advantageous for the formation of thioflavone, which starts with an electrophilic attack at the sulfoxide group exerted by the proton of the acid catalyst, or by the acetyl cation generated from Ac_2O by protonolysis or by the electrophilic acetyl moiety of Ac_2O being activated by the strong nucleophile (15) 4-dimethylaminopyridine (DMAP) (see Scheme 1). Thus, treatment of sulfoxide **2b** with Ac_2O–(TsOH), Ac_2O–DMPA, or TFAA–Et_3N afforded **1a** in excellent yields (>80% for the pure product, see Table 1).

The methylene group of 1-(thio)benzopyran-4-ones is activated by the neighboring carbonyl and -XCH(Ph)- groups (X = O, S, SO, SO_2), so this is the reactive site of the molecule when treated with bases. Thus, the deprotonated C-3 creates a bond to the electron-deficient sulfur, and then the transiently generated thiiranium (4) species is stabilized by ring contraction and loss of proton to give 2-benzylidenebenzo[*b*]thiophen-3(2*H*)-one (thioaurone **3a**, see Scheme 1). Accordingly, treatment of sulfoxide **2b** with Ac_2O in the presence of NaOAc, which behaved as a strong base in this medium, afforded thioaurone (**3a**) almost quantitatively (see Table 1).

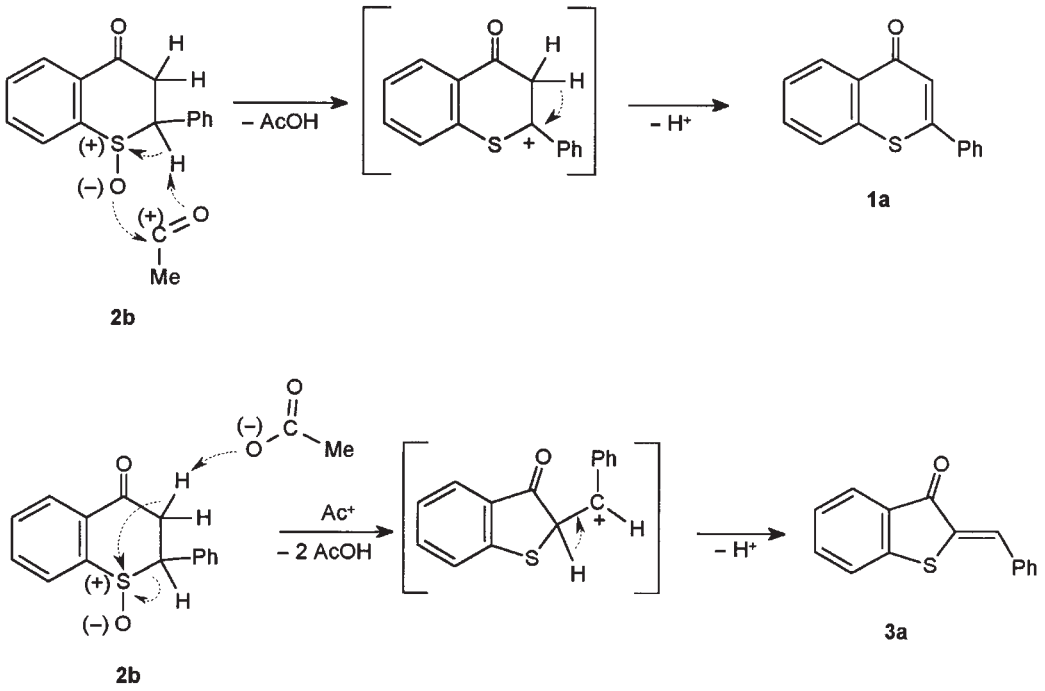
Fig. 1. ORTEP drawing of compound **4** with 50% of the thermal ellipsoids.



On varying the acid or base character of the additives, treatment of sulfoxide **2b** with Ac_2O–Et_3N or $(EtCO)_2O$–Et_3N, and also with 1,3-diisopropylcarbodiimide (DIC, see Table 1), gave a new high-melting yellow product sparingly soluble in most of the common organic solvents. (In the reaction of **2b** with DIC a considerable amount of thioflavanone 1,1-dioxide **2c** was also produced, see Table 1). At room temperature, the Ac_2O–Et_3N-mediated transformation of the *equatorial* (1,2-*trans*) sulfoxide epimer (5) **2b** afforded this product in a yield half times higher than the *axial* (1,2-*cis*) (3*c*, 5) compound (see Table 1). One the basis of C, H, and S analyses (see footnotes of Table 1) and the nonanalyzable 200 MHz ^{1}H NMR spectrum, a $C_{15}H_{11}OS$ (FW = 239.31) elemental composition was first suggested for the new compound with some uncertainty, as the hydrogen content was concerned. The product was, however, quite different in all respects (color, mp, TLC, solubility, IR, ^{1}H NMR and EI-mass spectra, etc.) from **1a** and **3a**, respectively, ($C_{15}H_{10}OS$, FW = 238.3) or **2a** ($C_{15}H_{12}OS$, FW = 240.3). Eventually, the MALDI-TOF spectrometry (see also Table 1, footnotes) indicated a $C_{30}H_{22}O_2S_2$ (FW = 478.61) composition. X-Ray diffraction analysis of this new compound revealed the open-chain disulfide structure **4** (see Fig. 1) with an S—S bond distance of 2.053 Å. (Previously, photolysis of thiochroman-4-one 1-oxides has been reported (4*d*) to give o-hydroxyaralkyl disulfides in 6–8% yields via thiyl radicals). The *trans*-chalcone structure of compound **4** was corroborated by the J = 15.77 Hz coupling of the vinylene hydrogens at δ = 7.90 and 7.77 ppm in the 500 MHz ^{1}H NMR spectrum. Disulfide **4** was presumably produced from sulfoxide **2b** via a 2-cinnamoylbenzenesulfenic acid intermediate (**9a**). This step of the ring-opening of **2b** seems to be similar to the well-known base-mediated formation of 2′-hydroxychalcones (e.g., **9b**) from flavanones, however, sulfenic acids (3*g*) are generally highly unstable. Decomposition of pseudopeptidic sulfoxides via β-elimination to sulfenic acids (followed by bimolecular recombination to thiolsulfinates RS(O)SR) and the corresponding alkene has been reported most recently (16). Upon treatment with trihaloacetic anhydride [$(CX_3CO)_2O$, X = F, Cl] in a Pummerer-like reaction, thiolsulfinates are known (17) to transform into disulfides and sulfinyl carboxylates [$RS(O)OCOCX_3$] which latter gives adducts readily with olefins.

© 2001 NRC Canada

Scheme 1.



Before performing the MALDI-TOF MS and X-ray measurements discussed above to lead to the identification of the disulfide-structure for **4**, EI-MS (see footnotes of Table 1) and HR-MS experiments were carried out with the *m*/*z* = 240 ion (M = 240.0599 Da). However, neither these mass spectral studies nor the 200 and 360 MHz ^{1}H NMR spectra (each containing superimposed signals in the "aromatic" region; δ = 8.16–7.42 ppm) gave convincing evidence for the structure of the new compound. The fragment *m*/*z* = 237 (base peak in the EI-MS) could be attributed to the formation of the benzo[*b*]thieno-[3,2-*b*]pyrylium ion (*A*), whose perchlorate has been previously prepared (7) by the condensation of 1-thia-3-indanone with salicylic aldehyde in AcOH–$HClO_4$. The same fragment was observed in the EI-MS of 1,2-*cis*-**2b** (3*c*, 5) and **3a** as a base peak, but with lesser intensity for the 1,2-*trans*-**2b**, (5) and not at all in the spectrum of thioflavone (**1a**) where *m*/*z* = 238 [$M^{+\cdot}$] was the base peak (5).

Since the reaction of other sulfoxides with active methylene compounds in the presence of dehydrating agents (Ac_2O, P_4O_{10}, DCC) has been reported (6) to furnish sulfonium ylides, a possible formation of 1,2- or 1,3-sulfur ylides similar to the thiiranium intermediate mentioned above was considered. Therefore, the reactivity of the sparingly soluble new compound **4** (at that time with uncertain structure) was also examined (see Table 2). Thus, treatment with Ac_2O–H_2SO_4 afforded thioflavone (**1a**) and thioaurone (**3a**) in poor yields. Similarly, when reacted with the I_2–DMSO couple or (in contrast to the transformation of **2b** in acid medium) with hot AcOH or cold sulfuric acid again **3a** was formed, and the reaction with CAN resulted in thioaurone 1,1-dioxide (**3c**). Interestingly, upon treatment with 4-methoxybenzaldehyde–piperidine (which is known to transform **2a** into **5**), compound **4** underwent transformation into 4′-methoxythioaurone (**3b**) and 3-(4-methoxybenzylidene)thioflavanone (**5**, see Scheme 2). Cleavage of the S—S bond, exhibiting acid–base properties can be effected by both nucleophiles or bases and electrophiles (3*g*).

The aforementioned anisaldehyde–piperidine-mediated recyclization of **4** into the thiaindanone and thiobenzopyranone derivatives **3b** and **5** can be explained by the heterolysis of the S—S bond followed by cyclization into **3a** and **2a** (see Scheme 3), and their subsequent transformation with the aldehyde into **3b** and **5**, respectively. Indeed, treatment of thioaurone **3a** with 4-anisaldehyde in piperidine at 150°C for 1.5 h afforded ca. 65% of **3b**. Compound **3b** was also formed in good yield in a fragmentation reaction upon treatment of 3-(4-methoxybenzylidene)thioflavanone 1-oxide (**6**) with Ac_2O–TsOH (see Table 1). Recently, deprotection–cyclization of 4-methoxybenzyl-protected 2′-mercaptochalcones into thioflavanones has been reported (14).

Experimental

Melting points (uncorrected): Kofler block. Solutions were concentrated under reduced pressure in a rotary evaporator (<50°C, bath). TLC: Kieselgel 60 F_{254} (Merck, Alurolle). IR(KBr discs): PerkinElmer 16 PC-FT spectrometer. ^{1}H NMR: 200 MHz, Bruker WP 200 SY and 500 MHz, Bruker DRX 500 spectrometers. MS: VG-7035 GC–MS–DS (EI, 70 eV, direct insertion technique); high-resolution spectrometry (EI, 70 eV, resolution 10 000, accuracy ±5 ppm, direct insertion), AEI MS-902; MALDI-TOF measurements, Bruker BIFLEX III^{TM} mass spectrometer (19 kV acceleration voltage with pulsed ion extraction (PIE^{TM}); detection of the positive ions, reflection mode (20 kV); laser desorption, nitrogen laser (337 nm, 1 ns pulse width) operating at 4 Hz, 100–120 shots were summed; external linear calibration, with poly(ethylene glycol) (M_n = 1450, MWD = 1.02). Solu-

© 2001 NRC Canada

Table 1. Transformation of sulfoxides **2b** and **6**.[a]

Substrate (mmol)	Agents (mmol)		Reaction temperature (°C)[b] (time (h))	Work-up[c]	Product	% Yield crude (pure)[d]	Mp (°C) (solvent)	Lit. mp (°C) (solvent)
2b (1)	Ac_2O (53)	TsOH[e]	100 (24)	B, C	**1a**	95.3 (76.9)	125 (2-PrOH–hexane)	125[f] (EtOH)
2b[g] (5.5)	Ac_2O (148)	DMAP[h] (8.25)	Room temp. (72)	B, D	**1a**	(80)[i]	125 (2-PrOH)	125[f] (EtOH)
2b[g] (3)	TFAA[j,k] (63)	Et_3N[k,l] (14.4)	Room temp. (2)	A	**1a**	85[d]	124.5[m]	125[f] (EtOH)
2b[n] (2)	Ac_2O (53)	NaOAc[o] (10)	105 (4)	E, F	**3a**	99.5[p] (75)	132 (MeOH)	134 to 134.5 [q] (EtOH)
2b[r] (6)	Ac_2O (159)	Et_3N[l] (29)	Room temp. (22)	A	**4**[s]	41[d] (39.4)	229–230[m], 238–240[t]	
2b[u] (6)	Ac_2O (159)	Et_3N[l] (29)	Room temp. (19)	A	**4**[s]	65.3[d] (53)	228–230[m], 238[v]	
2b[u] (2)	$(EtCO)_2O$ (55)	Et_3N[l] (7.2)	Room temp. (24)	A	**4**[s]	52.6[d] (41)	226–227[m], 236–237[t]	
2b[r] (3)	DIC[w,x] (7)		Room temp. (24)	B, G, H	**4**[s]	26[d]	238[m]	
				I	**2c**[y]	(40)	155.5 (2-PrOH)	155 to 156[z] (2-PrOH)
6[aa] (2)	Ac_2O (74)	TsOH[e]	100 (24)	B, C, D, F	**3b**	80 (68)	158 to 159 (2-PrOH)	158 to 159[q] (EtOH)

[a]For general methods see *Experimental*. [b]Bath. [c]See *Experimental*. [d]Without work-up of mother liquors. [e]4-Toluenesulfonic acid, a catalytic amount. [f]Reference 2. [g]1,2-*cis*. [h]4-Dimethylaminopyridine. [i]After purification by column chromatography (silica gel 60, 0.063–0.2 mm, 110 g, $r \sim 4.8$ cm, $l = 12$ cm, $CHCl_3$). [j]Trifluoroacetic anhydride. [k]CAUTION! The agents should be mixed carefully with ice–salt cooling. [l]Dried with and distilled from P_4O_{10}. [m]Crude product. [n]Either 1,2-*cis* or *trans*. [o]Anhydrous. [p]Contaminated by a small amount of **1a** when obtained from 1,2-*trans*-**2b** and by a somewhat larger one starting from the 1,2-*cis* diastereomer. [q]Reference 12. [r]The 1,2-*cis* isomer. [s]MALDI-TOF-MS (*m*/*z*): 584.98 [M + $^{107}Ag^+$] (calcd. 585.01). EI-MS *m*/*z* (%): 240(12), 239(20), 238(63), 237(100), 208(6), 178(3), 165(10), 149(3), 136(23), 134(16). IR (KBr) ν (cm^{-1}): 1650 (s), 1588 (s), 1574 (s), 1496 (w), 1454 (m), 1448 (m), 1338 (s). ^1H NMR ($[CD_3]_2SO$, 500.13 MHz) at 700 K δ: 7.90 and 7.77 (each d, 1H, $J = 15.77$ Hz; 2 *trans H*-vinylene). Anal. calcd. for $C_{30}H_{22}O_2S_2$ (478.61) (%): C 75.28, H 4.63, S 13.40; found (%): C 75.20, H 4.85, S 13.41. For the stereostructure of the molecule see Fig. 1. [t]From DMF with addition of some water to the hot solution. [u]The 1,2-*trans* isomer. [v]Recrystallized from Ac_2O. [w]1,3-Diisopropylcarbodiimide. [x]In the presence of anhydrous benzene (5 mL) with or without addition of anhyd Et_3N (21 mmol). [y]Identical (TLC, $CHCl_3$–EtOAc (95:5)) with an authentic specimen. [z]Reference 3*a*: 155°C or 156 to 157°C (from 2-PrOH); ref. 3*c*: 155 to 156°C (from 2-PrOH). [aa]Prepared according to ref. 13.

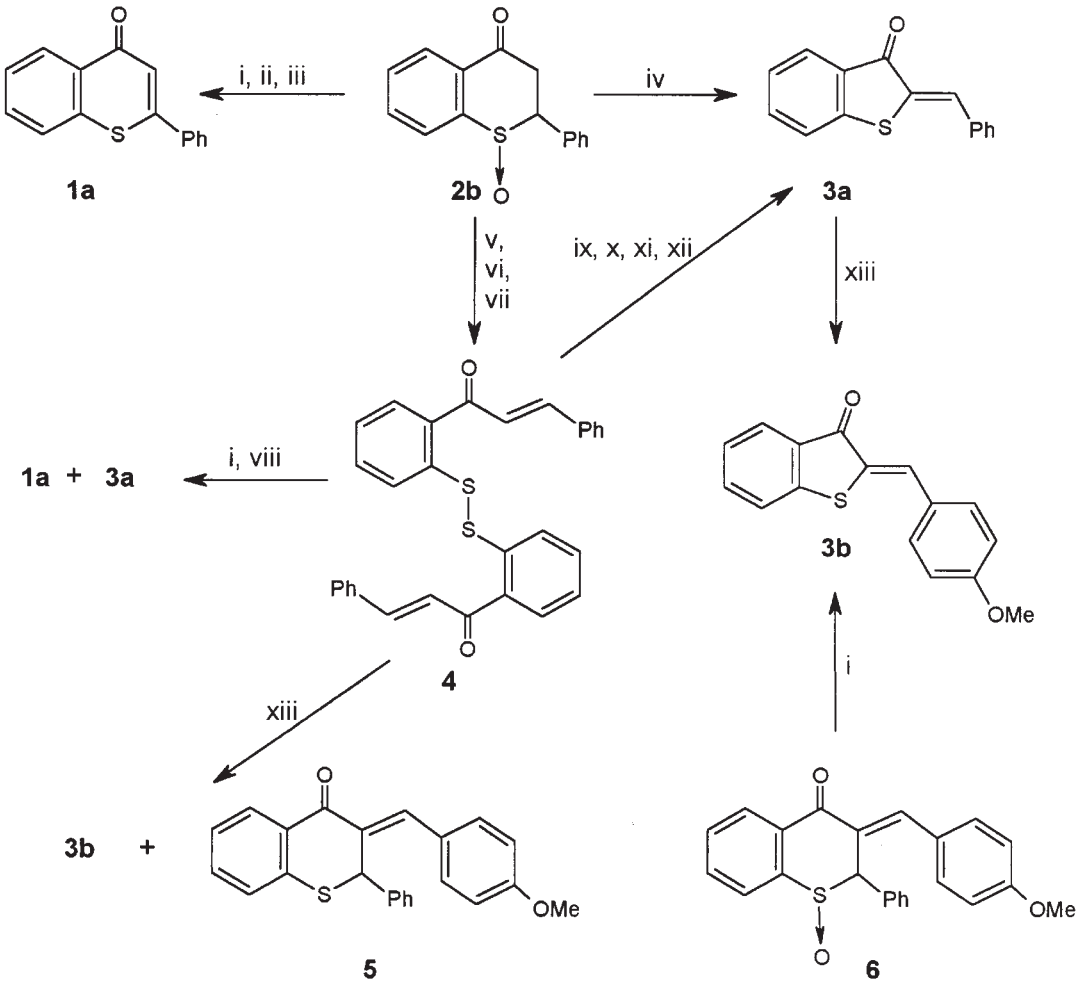
Table 2. Transformation of disulfide **4** into thioflavone (**1a**) and thioaurones **3a**, **b**, **c**.[a]

Substrate (mmol)	Agents (mmol)		Reaction temperature (°C)[b] (time (h))	Work-up[c]	Product	% Yield crude (pure)[d]	Mp (°C) (solvent)	Lit. mp (°C) (solvent)
4 (1.75)	Ac_2O (265)	H_2SO_4[e] (12.6)	Room temp. (20)	E, J, F	**1a**	(9)	124 (2-PrOH)	125[f] (EtOH)
					3a	(12)	133 to 134 (2-PrOH)	134 to 134.5[g] (EtOH)
4 (0.5)	AcOH[h] (873)		Bp (21)	B, D, K	**3a**	(50)	133 to 134 (2-PrOH)	134 to 134.5[g] (EtOH)
4 (0.5)	H_2SO_4[e] (18)		Room temp. (0.083)	E, J, K	**3a**	49 (43)	134 (2-PrOH)	134 to 134.5[g] (EtOH)
4 (0.125)	I_2 (0.25)	DMSO (35.2)	100 (24)	B, L, K	**3a**	(42)	132 to 133 (2-PrOH)	134 to 134.5[g] (EtOH)
4 (3)	4-MBA[i] (6.9)	$C_5H_{11}N$[j] (4.6)	152 (1.2)	B, C, K	**3b**[k]	50[d] (34)	159.5 (2-PrOH)	158 to 159[g] (EtOH)
4 (1.5)	CAN[l] (13.7)		75 (3[m] + 2.5)	B, D, F	**3c**[n]	(23)	160 (2-PrOH)	156–158 (EtOH)[o], 164 to 165 (Me_2CO–CH_2Cl_2)[p]

[a]For general methods see *Experimental*. [b]Bath. [c]See *Experimental*. [d]Without work-up of mother liquors. [e]Concentrated (96%). [f]Reference 2. [g]Reference 12. [h]99 to 100%. [i]4-Methoxybenzaldehyde. [j]Piperidine. [k]Besides, 3-(4-methoxybenzylidene)thioflavanone (**5**, mp 131°C (from 2-PrOH), ref. 11: 132°C (from MeOH)) could be isolated in 3% yield. [l]$(NH_4)_2Ce(NO_3)_6$, in the presence of MeCN (200 mL) and H_2O (20 mL). [m]Input. [n]IR (KBr) ν (cm^{-1}): 1708 (C=O), 1296 and 1156 (SO_2); ref. 13: 1708, 1294, and 1156 cm^{-1}. [o]Reference 3*b*. [p]Reference 13.

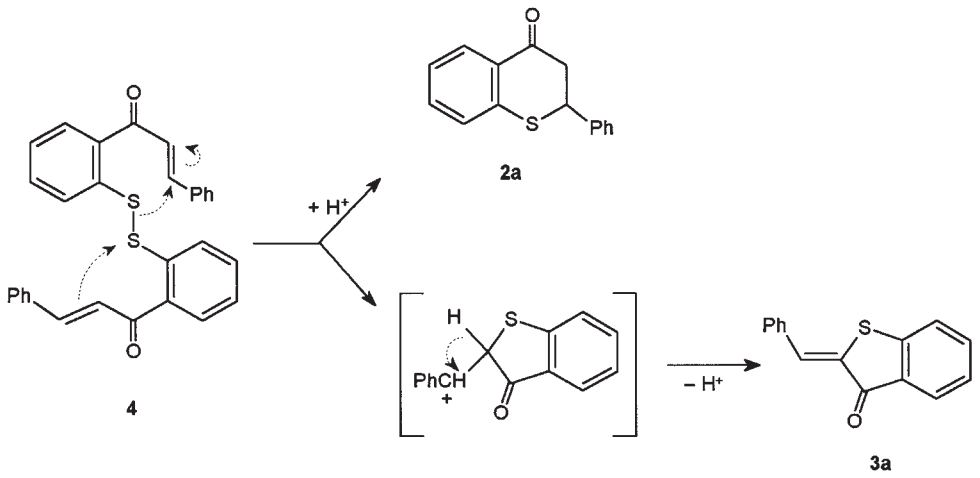
© 2001 NRC Canada

Scheme 2.



(i) Ac_2O/TsOH; (ii) Ac_2O/DMAP; (iii) TFAA/Et_3N; (iv) Ac_2O/NaOAc; (v) Ac_2O/Et_3N; (vi) $(EtCO)_2O$/Et_3N;(vii) 1,3-Diisopropylcarbodiimide/PhH; (viii) Ac_2O/H_2SO_4, room temp.; (ix) AcOH, reflux; (x) H_2SO_4, room temp.; (xi) I_2/DMSO; (xii) $PhI(OAc)_2$/AcOH, reflux; (xiii) 4-Methoxybenzaldehyde/piperidine (see also Tables 1 and 2).

Scheme 3.



© 2001 NRC Canada

tions for preparation of samples: 1,8-dihydroxy-9(10*H*)-anthracenone matrix–THF (20 mg mL^{-1}), AgTFA–THF (5 mg mL^{-1}) to enhance the cationization; 0.5 μL of the mixture of solutions analyte (1 mg **4** mL^{-1} CH_2Cl_2) – matrix – AgTFA in 10:50:1 v/v ratio was deposited onto the sample plate (stainless steel) and allowed to air-dry). X-ray diffraction analysis (for yellow plate crystals (0.48 × 0.39 × 0.1 mm) of $C_{30}H_{22}O_2S_2$, grown from Ac_2O, M = 478.6, orthorhombic, a = 10.387(1) Å, b = 12.298(1) Å, c = 18.471(1) Å, V = 2359.7 $Å^3$, Z = 8, space group: *Pbcn*, ρ_{calc} = 1.347 g cm^{-3}): Enraf–Nonius MACH3 diffractometer; data were collected at 293(1) K, Mo Kα radiation λ = 0.71073 Å, ω-2Θ motion, Θ_{max} = 27.8°, 2222 reflections of which 1612 were unique with $I > 2\sigma(I)$; decay: 4%. The structure was solved using the SIR-92 software (8) and refined on F^2 using SHELX-97 program (9); publication material was prepared with the WINGX-97 suite (10); R(F) = 0.039 and $wR(F^2)$ = 0.094 for 2222 reflections, 154 parameters.

General method for the preparation and work-up of the reaction mixtures

The substrate was added to a mixture of the reagents and allowed to react, if necessary with stirring, as indicated in Tables 1 and 2. The reaction mixtures were processed:

(A) The product was filtered off from the cold reaction mixture; (B) The reaction mixture was concentrated; (C) The residue was triturated with MeOH and (or) water to give a crude product; (D) A $CHCl_3$ solution of the residue was washed with (when DMAP was used at first with aq. $KHSO_4$) aq. $NaHCO_3$ and water, dried ($MgSO_4$), treated with fuller's earth and charcoal and then concentrated; (E) The cold reaction mixture was poured into ice water; (F) The crude product was purified by column chromatography (eluent, $CHCl_3$); (G) The residue was triturated with hexane to give a crude product; (H) The crude product was triturated with $CHCl_3$ and the undissolved material was filtered off; (I) The material dissolved in the filtrate was purified by column chromatography (eluent, $CHCl_3$); (J) The mixture was extracted with $CHCl_3$ and processed as in (D); (K) Crystallization from the solvent indicated in Table 1 or 2; (L) A $CHCl_3$ solution of the residue was washed with a necessary amount of aq. $Na_2S_2O_3$ and water, dried ($MgSO_4$), treated with charcoal and then concentrated.

*3-(4-Methoxybenzyl)thioflavone (**1b**)*

According to the known method (11), a mixture of anisaldehyde (8.753 g, 98%, 63 mmol), thioflavanone (**2a**, 14.418 g, 60 mmol), and piperidine (2.5 mL, 25.28 mmol) was heated at 152°C (bath) for 2.5 h (instead of the 1 h reported), cooled and treated with MeOH to give crude (6.311 g, 29.3%, mp 123–126°C) or recrystallized 3-(4-methoxybenzylidene)thioflavanone (**5**, 5.572 g, 25.9%), mp 133–133.5°C (from 2-PrOH); ref. 11: 132°C (from MeOH), yield 52.2%. The mother liquor of the crude product **5** was concentrated and the residue triturated with EtOAc (10 mL) to give, after successive addition of hexane (30 mL), crude (2.623 g, 12.2%) or recrystallized colorless **1b** (2.245 g, 10.4%), mp 148.5°C (from 2-PrOH). IR (KBr) (cm^{-1}) ν: 1618 (C=O). ^{1}H NMR ($CDCl_3$, 360 MHz) δ 8.57–8.55 (m, 1 H, 5-H), 7.60–7.36 (m, 8 H, 6,7,8-H and Ph), 6.96–6.93 (d-shaped m, 2 H, 2″, 6″-H) 6.73–6.69 (m, 2 H, 3″, 5″-H), 3.94 (s, 2 H, CH_2), 3.73 (s, 3 H, OMe). Anal. calcd. for $C_{23}H_{18}O_2S$ (%): C 77.07, H 5.06; found (%): C 77.26, H 5.08.

Acknowledgements

The author is indebted to Prof. L. Szilágyi, D.Sc. (Department of Organic Chemistry, University of Debrecen) for the 500 MHz ^{1}H NMR spectrum of **4**, to Z. Dinya, Ph.D. (Department of Organic Chemistry) for the EI-MS (VG-7035), and also to Á. Gömöry and K. Vékey, Ph.D. (Chemical Research Center, Hungarian Academy of Sciences, Budapest) for the high-resolution mass spectra (AEI MS-902), as well as to S. Kéki, Ph.D. (Department of Applied Chemistry) for the MALDI-TOF MS. A. Cs. Bényei, Ph.D. (Laboratory for X-ray Diffraction Analysis, University of Debrecen) is thanked for the X-ray diffraction analysis supported by a Tempus JEP (Grant No. 9252–95) and the Hungarian Scientific Research Fund (OTKA Grant No. D25136 and M28249). The author is greatly obliged to the Hungarian Scientific Research Fund (for a grant, OTKA T025016).

References

1. L. Somogyi. Synth. Commun. **29**, 1857 (1999), and refs. cited therein.
2. F. Arndt, W. Flemming, E. Scholz, V. Löwensohn, G. Källner, and B. Eistert. Ber. Dtsch. Chem. Ges. **58**, 1612 (1925).
3. (*a*) R. Bognár, J. Bálint and M. Rákosi. Liebigs Ann. Chem. 1529 (1977); (*b*) J. Bálint. Ph.D. Dissertation, Kossuth Lajos University, Debrecen, Hungary, 1978. (Synthesis of thioflavonoids: oxidative and reductive transformations, reactions with oxo reagents) (in Hungarian)); (*c*) L. Somogyi. Liebigs Ann. Chem. 959 (1994); (*d*) R.B. Morin, D.O. Spry, and R.A. Mueller. Tetrahedron Lett. 849 (1969); (*e*) J.P. Marino. Sulfur-containing cations. *In* Topics in sulfur chemistry. Vol. 1. *Edited by* A. Senning. Georg Thieme Publishers, Stuttgart. 1976. pp. 1–110; (*f*) S. Oae. Sulfoxides sulfilimines. *In* Organic chemistry of sulfur. *Edited by* S. Oae. Plenum Press, New York and London. 1977. pp. 383–471; (*g*) L. Field. Disulfides and polysulfides. *In* Organic chemistry of sulfur. *Edited by* S. Oae. Plenum Press, New York and London. 1977. pp. 303–382.
4. (*a*) H. Kwart and E.R. Evans. J. Org. Chem. **31**, 413 (1966); (*b*) R.A. Archer and B.S. Kitchell. J. Am. Chem. Soc. **88**, 3462 (1966), and refs. cited therein; (*c*) H. Hofmann and G. Salbeck. Angew. Chem. **81**, 424 (1969); Angew. Chem. Int. Ed. Engl. **8**, 456 (1969); (*d*) I.W.J. Still, P.C. Arora, M.S. Chauhan, M.-H. Kwan, and M.T. Thomas. Can. J. Chem. **54**, 455 (1976); (*e*) P.J. Cox, N.E. MacKenzie and R.H. Thomson. Tetrahedron Lett. **22**, 2221 (1981); (*f*) N.E. MacKenzie and R.H. Thomson. J. Chem. Soc. Perkin Trans. 1, 395 (1982); (*g*) A.T. Hudson and M.J. Pether. J. Chem. Res. (S), 56 (1983); J. Chem. Res. (M), 0664 (1983); (*h*) D.F. Rane, R.E. Pike, M.S. Puar, J.J. Wright, and A.T. McPhail. Tetrahedron, **44**, 2397 (1988); (*i*) C.D. Gabbutt, J.D. Hepworth, B.M. Heron, and M. Kanjia. Tetrahedron, **50**, 827 (1994); (*j*) C.D. Gabbutt, J.D. Hepworth, and B.M. Heron. Tetrahedron, **50**, 7865 (1994).
5. A.C. Bényei and L. Somogyi. Phosphorus, Sulfur and Silicon, **143**, 191 (1998).
6. (*a*) H. Nozaki, Z. Morita, and K. Kondo. Tetrahedron Lett. 2913 (1966); (*b*) H. Nozaki, D. Tunemoto, Z. Morita, K. Nakamura, K. Watanabe, M. Takaku, and K. Kondo. Tetrahe-

© 2001 NRC Canada

dron, **23**, 4279 (1967); (*c*) A.F. Cook and J.G. Moffatt. J. Am. Chem. Soc. **90**, 740 (1968).
7. G.N. Dorofeenko, V.I. Volbushko, V.I. Dulenko, and E.N. Kornilova. Khim. Geterotsikl. Soedin. 1181 (1976); Chem. Abstr. **86**, 43 592n (1977).
8. A. Altomare, G. Cascarano, C. Giacovazzo, and A. Guagliardi. J. Appl. Crystallogr. **26**, 343 (1993).
9. G.M. Sheldrick. SHELXL-97. Universität Göttingen, Germany. 1997.
10. L.J. Farrugia. WINGX-97 system. University of Glasgow, U.K. 1996.
11. A. Lévai, Á Szöllosi, and G. Tóth. Acta Chim. Hung. **128**, 359 (1991); Chem. Abstr. **115**, 158 908e (1991).
12. N. Kucharczyk and V. Horák. Coll. Czech. Chem. Commun. **33**, 92 (1968).
13. W. Adam, D. Golsch, L. Hadjiarapoglou, A. Lévai, C. Nemes, and T. Patonay. Tetrahedron, **50**, 13113 (1994).
14. (*a*) M.T. Konieczny, B. Horowska, A. Kunikowski, J. Konopa, K. Wierzba, Y. Yamada, and T. Asao. J. Org. Chem. **64**, 359 (1999); (*b*) A.W. Taylor and D.K. Dean. Tetrahedron Lett. **29**, 1845 (1988).
15. (*a*) E.F.V. Scriven. Chem. Soc. Rev. **12**, 129 (1983); (*b*) M. Fieser, R.L. Danheiser, and W. Roush. Fieser and Fieser's reagents for organic synthesis **9**, 178 (1981). J. Wiley and Sons, New York.
16. J.-M. Poudrel and P. Karuso. Tetrahedron Lett. **41**, 6185 (2000).
17. T. Morishita, N. Furukawa, and S. Oae. Tetrahedron, **37**, 3115 (1981).

© 2001 NRC Canada

Détermination de la stabilité du complexonate peu soluble à partir des données pH-métriques

Igor Povar

Résumé : Nous avons élaboré une méthode de détermination du produit de solubilité du complexonate avec une composition connue à partir seulement des valeurs d'équilibre du pH, étant donnée la composition initiale du mélange hétérogène (le lot *a*). Pour la détermination de la constante de stabilité en solution, ce lot des données est complété par l'information sur la solubilité du précipité. Nous avons montré que, dans l'absence de réactions de formation des complexes dans la solution, on peut évaluer les concentrations d'équilibre, celles-ci résiduaires des composantes du précipité, sur la base du lot *a*. On tire la conclusion sur la possibilité de l'application de la méthode élaborée pour le test et la standartisation des électrodes ion-sélectives. On discute les qualités et les défauts de la méthode élaborée. Par ailleurs, les valeurs des constantes d'équilibre et des concentrations d'équilibre et les concentrations résiduaires pour une série de systèmes réels, que nous avons calculées à partir des données expérimentales connues, s'accordent bien avec celles des tables obtenues dans les mêmes conditions.

Mots clés : méthode potentiométrique, système hétérogène, complexonate peu soluble, complexone, concentration d'équilibre, produit de solubilité, constante de stabilité, réaction d'hydrolyse.

Abstract: A new method has been developed for the determination of the solubility product of complexonate of known composition; because of the initial composition of the heterogeneous mixture (lot *a*), it uses only the equilibrium values of the pH. For the determination of the stability constant in solution, these data have been completed with information on the solubility of the precipitate. We have shown that, on the basis of lot *a* and in the absence of reactions of formation of complexes in solution, it is possible to evaluate the equilibrium constants, since they are residuals of the compositions of the precipitate. We conclude on the possibility of applying this method to the test and standardization of ion-selective electrodes. The qualities and defect of the method are discussed. Otherwise, the values for the equilibrium constants and the equilibrium as well as the residual concentrations that we have calculated for a series of real systems from known experimental data are in good accord with those reported in tables under the same conditions.

Key words: potentiometric method, heterogeneous system, slightly soluble complexonate, complexone, equilibrium concentration, solubility product, stability constant, hydrolysis reaction.

[Journal Translation]

Introduction

Les produits de solubilité (K_S) de même que les constantes de stabilité des complexonates peu solubles dans un système « phase solide – solution saturée » sont utilisés à la résolution de plusieurs importantes tâches de la chimie analytique (1–3).

À présent les caractéristiques quantitatives d'équilibre des systèmes hétérogènes, y compris les produits de solubilité, sont déterminées par les méthodes physico-chimiques, parmi lesquelles la plus efficace est la méthode potentiométrique (4–6). Une des méthodes les plus sévères de la détermination de K_S est la méthode de la mesure de l'activité de tous les ions formant le précipité. Cependant cette méthode est liée à certaines suppositions et admissions, inévitables à la mesure de l'activité des ions du précipité. En plus, la question de la création des électrodes ion-sélectives stables et reproduites est décidée pour un petit nombre des ions.

L'une des méthodes d'étude des équilibres chimiques hétérogènes la plus souvent utilisée reste la méthode classique de solubilité. Dans le cadre de cette méthode lors de l'étude des équilibres chimiques dans le système « complexonate peu soluble (la phase solide) – solution saturée (la phase liquide) », on obtient deux lots de données expérimentales : (*i*) la dépendance de la solubilité (*S*) de concentrations initiales des constituants dans la solution et (*ii*) la mesure de *S*, accompagnée de la détermination d'une ou de quelques fonctions supplémentaires de la composition de la solution, le plus souvent du pH. Dans le second cas une certaine partie d'information sur les concentrations initiales devient fréquemment superflue, et c'est pourquoi une partie des données n'est parfois pas présentée. Du moment où toutes les constantes sont connues, la connaissance des concentrations analytiques (les concentrations résiduelles) des constituants du sédiment dans la solution saturée est largement suffisante pour calculer les concentrations d'équilibre et du produit de solubilité (4).

Reçu le 31 août 2000. Publié sur le site Web des Presses scientifiques du CNRC http://revcanchim.cnrc.ca le 6 août 2001.

I. Povar.[1] Institut de Sciences Réales de l'Université d'État de Moldova, Chisinau, République de Moldova.

[1]Adresse actuelle : Institut de Chimie, Académie de Sciences de Moldova, 3, rue Academiei, 2028 Chisinau, République de Moldova (courriel : ipovar@hotmail.com).

 DOI: 10.1139/cjc-79-7-1166 © 2001 CNRC Canada

Suite à l'analyse de la solubilité des complexonates, les auteurs (3) ont constaté la régularité suivante. Pour les ligands comme les anions d'EDTA et ses analogues, la formation des complexonates peu solubles protonés (type I) est plus caractéristique avec la composition générale $M'_1M_xH_yL_{z(S)}$ (7–10) (ici et plus bas, la quantité de l'eau hydratée en précipité n'est pas indiquée), où M'_1 est le cation du métal alcalino-terreux, $x = 0, 1, 2$, en fonction des valeurs de charges de l'ion du métal M et du ligand L. Par ailleurs, les complexones avec la plus petite dentantité forment des complexonates peu solubles $M'_x\ ML_{(S)}$ (type II) (11). Il convient de remarquer que les mesures de la solubilité sont caractérisées par une plus grande durée et un grand volume du travail en comparaison avec d'autres méthodes de la détermination des constantes de l'équilibre (4).

Nous avons élaboré auparavant une méthode potentiométrique de la détermination du produit de solubilité des acides peu solubles (y compris des complexones) de composition connue, qui est basée sur les données de pH de leurs solutions saturées. L'essence de la méthode consiste en un compte sévère de l'influence du pH pour le procès de la formation du complexonate peu soluble. La valeur du pH peut influencer soit directement, dans le cas de la formation du complexonate protonés ou hydroxocomplexes mixtes, soit indirectement, quand les ions de H^+ ou de OH^- figurent dans la réaction de protonation du ligand-complexone, qui sont les bases conjuguées des acides faibles. Cette méthode a été utilisée pour la détermination de K_S des complexones peu solubles, comme le EDTA et les autres.

Le but de ce travail est l'élaboration de la méthode potentiométrique de la détermination du produit de solubilité des complexonates peu solubles des deux types, ainsi que de leurs constantes de stabilité en solution à partir des données sur la solubilité en combinaison avec des mesures du pH.

La méthode peut être utilisée même si la phase solide ne contient pas d'ions de H^+ ou de OH^- (complexonates du type II). Dans ce cas, il est nécessaire qu'au moins l'un des constituants du complexonate neutre participe aux réactions d'hydrolyse ou de protonation (protolyse).

Partie théorique

D'abord, nous examinerons le système hétérogène contenant un complexonate protoné peu soluble ayant la composition $M'_1M_xH_yL_{z(S)}$ (du type I) en qualité de phase solide. Dans la phase liquide, nous considérerons une série d'équilibres coexistants. En fonction de valeurs de pH dans la solution aqueuse, peuvent se former des complexes protonés MH_xL normaux (moyens) ML et même des hydroxocomplexes mixtes $M(OH)_xL$. À l'augmentation du rapport ligand/métal, la formation des complexonates avec la composition ML_2 et ML_3 est possible. Dans le cas général, le lot complet des équilibres indiqués peut être représenté sous forme des équations (pour la simplicité les charges on laisse passer) :

$$[1]\qquad M'_lM_xH_yL_{z(S)} = lM' + xM + yH + zL,$$

$$K_S = [M']^l[M]^x[H]^y[L]^z$$

$$[2]\qquad M + (n-m)H + mH_2O + kL = MH_n(OH)_mL_k,$$

$$\beta_{1n(m)k} = \frac{[MH_n(OH)_mL_k]}{([M][H]^{n-m}[L]^k)}$$

$$[3]\qquad M + iH_2O = M(OH)_i + iH, \quad K_i = [M(OH)_i][H]^i/[M]$$

$$[4]\qquad L + jH = H_jL, \quad K_j = [H_jL]/([H]^j[L])$$

Les équations [3] et [4] incluent les réactions possibles d'hydrolyse de l'ion métallique et celles de protolyse de l'anion du complexonate. On indique aussi les constantes d'équilibre correspondantes. Le système d'équations du bilan des matériaux dans ce système hétérogène peut être écrit sous la forme (12, 13) :

$$\begin{aligned} C^0_M &= C_M + x[M'_lM_xH_yL_z]_{(S)} \\ [5]\qquad C^0_L &= C_L + z[M'_lM_xH_yL_z]_{(S)} \\ C^0_H &= C_H + y[M'_lM_xH_yL_z]_{(S)} \end{aligned}$$

où C^0_M et C^0_L sont les concentrations initiales en ion métallique et en ligand dans le mélange hétérogène; C^0_H (C^0_{OH}) représente la concentration en excès des ions d'hydrogène (d'hydroxyde) ($C^0_H = -C^0_{OH}$). Dans les équations [5] par C_i nous avons noté les concentrations résiduaires des ions et par $[M'_lM_xH_yL_z]_{(S)}$, le nombre de moles du précipité par litre de solution. Il est à signaler, que les équations du type [5] ne se réalisent exactement que pour les solutions diluées, quand le volume du mélange hétérogène est pratiquement égal au volume de la phase liquide (14). Dans le cas du déroulement des réactions [2] à [4], les concentrations résiduaires des ions sont exprimées par les relations :

$$[6]\qquad C_M = \sum_{i=0}[M(OH)_i] + \sum_{n=1}\sum_{m=0}\sum_{k=0}[MH_n(OH)_mL_k]$$

$$[7]\qquad C_L = \sum_{j=0}[H_jL] + \sum_{n=1}\sum_{m=0}\sum_{k=0}k[MH_n(OH)_mL_k]$$

$$[8]\qquad C^0_H = [H] - [OH] + \sum_{j=1}j[H_jL] - \sum_{i=1}i[M(OH)_i] + \sum_{n=1}\sum_{m=0}\sum_{k=0}(n-m)[MH_n(OH)_mL_k]$$

En excluant le terme $[M'_lM_xH_yL_z]_{(S)}$ du système d'équations [5], nous obtenons

$$[9]\qquad zC^0_M - xC^0_L = z\sum_{i=0}[M(OH)_i] - x\sum_{j=0}[H_jL] + \sum_{n=1}\sum_{m=0}\sum_{k=0}(z-ky)[MH_n(OH)_mL_k$$

$$[10]\qquad yC^0_M - xC^0_H = \sum_{i=0}(y+ix)[M(OH)_i] - x\sum_{j=1}j[H_jL] - x[H] + x[OH] + \sum_{n=1}\sum_{m=0}\sum_{k=0}(y-x(n-m))[MH_n(OH)_mL_k]$$

En exprimant les concentrations d'équilibre des espèces dans les équations [6] à [10] par les constantes d'équilibre [2] à [4], nous obtenons (si $i = 0$, alors $K_0 = 1$) :

© 2001 CNRC Canada

$$[11]\quad C_M = [M]\alpha_M + \sum_{n=1}\sum_{m=0}\sum_{k=0}\beta_{1n(m)k}[M][H]^{n-m}[L]^k$$

$$[12]\quad C_L = [L]\alpha_L + \sum_{n=1}\sum_{m=0}\sum_{k=0}k\beta_{1n(m)k}[M][H]^{n-m}[L]^k$$

$$[13]\quad C_H = [H] - K_W[H]^{-i} + [L]\varphi_L - [M]\varphi_M + \sum_{n=1}\sum_{m=0}\sum_{k=0}(n-m)\beta_{1n(m)k}[M][H]^{n-m}[L]^k$$

$$[14]\quad zC_M^0 - xC_L^0 = z[M]\alpha_M - x[L]\alpha_L + \sum_{n=1}\sum_{m=0}\sum_{k=0}(z-ky)\beta_{1n(m)k}[M][H]^{n-m}[L]^k$$

$$[15]\quad yC_M^0 - xC_H^0 = \sum_{i=0}(y+ix)K_i[M][H]^{-i} - x[H] + x[OH] - x\varphi_L + \sum_{n=1}\sum_{m=0}\sum_{k=0}(y-x(n-m))\beta_{1n(m)k}[M][H]^{n-m}[L]^k$$

Dans les équations mentionnées plus haut, la notation (13) a été utilisée :

$$\alpha_M = \sum_{i=o}K_i[H]^{-i} \qquad \alpha_L = \sum_{j=o}K_j[H]^j$$

$$\varphi_M = \sum_{i=o}iK_i[H]^{-i} \qquad \varphi_L = \sum_{j=1}jK_j[H]^j$$

En mesurant la solubilité du complexonate $M'_1M_xH_yL_{z(S)}$ en fonction du pH, donc et de C_H^0 alors $zC_M^0 = xC_L^0 = const$ et $C_L = zS$. Il faut mentionner que $pH = -\log a_{H+} = -\log [H^+]\gamma_{H+}$, où γ_{H+} est le coefficient d'activité du proton. En partant des données S(pH), à condition que les constantes d'équilibre [2] à [4] soient connues, sur la base de la solution du système d'équations [11] et [12] avec deux inconnues [M] et [L], nous pouvons déterminer le produit de solubilité du complexonate peu soluble. Si la solubilité est mesurée en eau, alors pour le calcul il faut utiliser l'équation [13], puisque dans ce cas $C_H = yS$. Alors nous parvenons au système d'équations [11] à [13], grâce auquel nous pouvons, en principe, calculer la constante de stabilité β de l'un des complexonates en solution. Ainsi, on peut être sûr que la quantité obtenue β sur la base d'une seule mesure, S(pH) n'aura qu'un caractère approximatif.

Nous admettons qu'en qualité de données expérimentales nous avons des concentrations initiales des constituants du précipité dans le mélange hétérogène C_i^0 et leurs concentrations résiduaires dans la solution C_i, de même que le pH du mélange. À la variation du rapport des concentrations en C_M^0 et en C_L^0, existe une corrélation évidente entre la solubilité S et les concentrations résiduaires C_i. Si $C_M^0 < C_L^0$, alors $C_M = xS$, $C_L > zS$. Par contre, si $C_M^0 > C_L^0$, alors $C_L = zS$ et $C_M > xS$. Dans le cas d'un lot complet de données C_i^0, C_i et pH, nous pouvons utiliser les équations [11] à [15], les trois desquelles sont indépendantes. À l'analyse des ces équations nous pouvons tirer les conclusions suivantes. Sur la base du système d'équations [14] et [15] et des constantes d'équilibre de table [2] à [4], nous calculons les concentrations d'équilibre de l'ion métallique et du complexone à l'aide de la corrélation [1] — la quantité K_S. Ainsi, le produit de solubilité peut être déterminé seulement sur la base des valeurs du pH de la solution saturée, connaissant la composition initiale du mélange préparé. En résolvant le système de trois équations indépendantes arbitraires, par exemple, {[11], [14], [15]} ou {[11], [12], [15]}, on obtient la constante de stabilité de l'une des espèces solubles du complexonate. Pour atteindre ce but, il faut mesurer encore la concentration de l'un des constituants du précipité ou sa solubilité.

Si dans la solution saturée la formation des complexes est absente, alors les équations [14] et [15] se simplifient, ayant la forme suivante :

$$[16]\quad zC_M^0 - xC_L^0 = z[M]\alpha_M - x[L]\alpha_L + \sum_{n=1}\sum_{m=0}\sum_{k=0}(z-ky)\beta_{1n(m)k}[M][H]^{n-m}[L]^k$$

$$[17]\quad yC_M^0 - xC_H^0 = \sum_{i=0}(y+ix)K_i[M][H]^{-i} - x[H] + x[OH] - x\varphi_L + \sum_{n=1}\sum_{m=0}\sum_{k=0}(y-x(n-m))\beta_{1n(m)k}[M][H]^{n-m}[L]^k$$

La solution du système des équations [16] et [17] donne les résultats suivants :

$$[18]\quad [M] = \frac{\{C_M^0(qx-y) + x([OH]-[H])\}\alpha_L + \varphi_L C_M^0(z-nx)}{z\varphi_L\alpha_M - \alpha_L\sum_{i=0}(y+ix)K_i[H]^{-i}}$$

$$[19]\quad [L] = \frac{C_M^0(nx-z) + z[M]\alpha_M}{x\alpha_L}$$

Ainsi, si les valeurs de C_i^0 et de pH de la solution sont connues, la solution du système d'équations [16] et [17] permet de déterminer les concentrations d'équilibre [M] et [L]. À l'aide de la relation

$$C_i = [i] \times \alpha_i$$

on calcule les concentrations résiduaires des constituants « i » du précipité (ou sa solubilité).

On examine aussi le cas de formation du complexonate moyen peu soluble (du type II) de composition $M'_xML_{(S)}$:

$$[20]\quad M'_xML_{(S)} = xM' + L + M, \qquad K_S = [M']^x[M][L]$$

Nous examinerons le lot des réactions [2] à [4] en solution. Les équations du bilan des matériaux dans la solution [11] à [13] (ici $C_H^0 = C_H$) sont complétées par les relations

$$C_M^0 = C_M + [M'_xML_{(S)}], \qquad C_L^0 = C_L + [M'_xML_{(S)}]$$

La différence entre la deuxième et la première est :

$$[21]\quad C_L^0 - C_M^0 = [L]\alpha_L - [M]\alpha_M + \sum_{n=1}\sum_{m=0}\sum_{k=0}(k-1)\beta_{1n(m)k}[M][H]^{n-m}[L]^k$$

Comme dans le cas précédent, à condition de connaître la composition initiale du mélange (C_i^0) et des valeurs du pH en solution saturée, on peut calculer la quantité K_S [20] sur la base des équations [13] et [20] et des constantes

© 2001 CNRC Canada

Tableau 1. Les résultats de l'analyse (7, 15) et de nos calculs des produits de solubilité $pK_S = -\log K_S$ dans les systèmes $Y(NO_3)_3$–H_5L–H_2O (L^{5-}–oedta) (**A**) et $Y(NO_3)_3$–H_5L–H_2O (L^{5-}–gph) (**B**), $C_Y° = 0{,}01$ mol L^{-1}, $t = 25°C$, $n = C_L°/C_Y°$.

n	$[H^+] \times 10^2$ (mol L^{-1})	I (mol L^{-1})	pK_S
(A) Système (7)			
0,90	2,51	0,034	35,15
1,00	2,73	0,030	34,95
1,10	2,82	0,032	34,49
1,20	2,90	0,033	34,20
1,40	3,08	0,036	33,86
1,60	3,25	0,034	33,64
Valeur moyenne 34,38 ± 0,59			
34,65 ± 0,24 (7)			
(B) Système (15)			
0,90	2,27	0,032	27,35
1,00	2,96	0,032	28,12
1,25	2,94	0,029	27,11
1,50	2,95	0,031	26,55
1,80	2,96	0,033	26,16
Valeur moyenne 27,06 ± 0,75			
27,02 ± 0,35 (15)			

d'équilibre des réactions [2] à [4]. Si on mesure encore la solubilité du précipité ou la concentration résiduaire de l'ion métallique ou du ligand, alors, sur la base du système de trois équations indépendantes [13], [17], [11] ou [12], on détermine la constante de stabilité de l'espèce chimique fixée du complexonate.

Donc, pour la détermination du produit de solubilité du complexonate dans tous les deux cas il est suffisant de connaître la composition initiale du mélange et la valeur d'équilibre du pH de la solution. Pour la détermination de la constante de stabilité du complexe, ce lot minimum des paramètres doit être complété par des données sur la solubilité de la phase solide. Il faut mentionner que la possibilité de cette minimisation n'a jamais été remarquée.

Résultats du calcul et discussion

Comme illustration de la mise en œuvre du moyen proposé de la détermination des constantes d'équilibre, nous ferons l'analyse de deux types du système « complexonate peu soluble – solution saturée[2]».

Les données expérimentales pour les systèmes examinés ici ont été obtenues par les auteurs (7, 8, 15) par la méthode des concentrations résiduelles (ou de la solubilité) à la concentration initiale constante du sel $Y(NO_3)_3$, $C_Y° = 0{,}01$ mol L^{-1}, en changeant le rapport des concentrations $n = C_L^0/C_Y^0$. Après l'acquisition de l'état de l'équilibre, la phase liquide était séparée de la phase solide par le filtrage. La détermination des concentrations résiduelles de l'yttrium et des ligands était faite selon la méthode spécialement élaborée (7, 8, 15). À la base de la méthode se trouve la détermination spectrophotométrique des ions de l'yttrium en forme de complexe avec l'arsenazo III et la détermination du ligand selon la réduction de l'absorption du complexe de l'yttrium avec un autre indicateur, le bleu de thymol.

La valeur du pH était mesurée avec une électrode en verre, et la concentration d'équilibre des ions de l'hydrogène était trouvée en utilisant le coefficient de l'activité calculée selon l'équation de Davies (16).

Type I. Les complexonates $YH_2L_{(S)}$ (L^{5-}–oxyéthylidènediphosphonate, oedph; le système A) et $YH_2A_{(S)}$ (A^{5-}–glycine–bis-méthylphosphonate, gph; le système B)

Les données expérimentales connues pour ces systèmes (7, 15) sont réunies au tableau 1. Les deux ligands représentent des anions de l'acide penta-basique. Les constantes de protonation des ligands ($I_1 = 0{,}1$) (3, 17) ont été recalculées à force ionique $I_2 = 0{,}03$ à l'aide de l'équation élargie de Davies (16) :

$$[22] \quad \log K_2 = \log K_1 + 0{,}509 \sum_i v_i Z_i^2 \left[\frac{\sqrt{I_2} - \sqrt{I_1}}{(1+\sqrt{I_1})(1+\sqrt{I_2})} \right]$$

La concentration de l'ion d'hydrogène a été calculée par Tereshin et al. (7) en utilisant le coefficient d'activité, à l'aide de l'équation de Devis (16). La composition des deux précipités est exprimée par la formule $MH_2L_{(S)}$. Les expériences ont été effectuées en milieu fortement acide, où l'hydrolyse de l'ion de l'yttrium ($\alpha_y = 1$) n'a pas lieu. Les auteurs (7, 15) ont démontré que la réaction de complexation de l'yttrium avec des complexones en solution dans les conditions examinées n'a pas lieu. D'après les données présentées par les auteurs (7, 15), $nC_M^0 = C_L^0$ et $C_H^0 = 5C_L^0 = 5nC_M^0$. Pour ces systèmes, les équations du bilan [14] et [15] prennent la forme :

$$[23] \quad C_M^0 - C_L^0 = [M] - [L]\alpha_L,$$

$$2C_M^0 - C_H^0 = 2[M] - [H] - \varphi_L[L]$$

où

$$\alpha_L = 1 + \sum_{j=1}^{5} K_j [H]^j, \quad \varphi_L = \sum_{j=0}^{5} j K_j [H]^j$$

En utilisant l'équation [23] on trouve immédiatement que

$$[24] \quad [M] = [L]\alpha_L + C_M^0(1-n)$$

et

$$[25] \quad [L] = \frac{[H] - 3nC_M^0}{2 + K_1[H] - K_3[H]^3 - 2K_4[H]^4 - 3K_5[H]^5}$$

Déterminant [M] et [L] à l'aide des équations [24] et [25], on calcule K_S :

$$MH_2L_{(S)} = M + 2H + L, \; K_S = [M][H]^2[L].$$

Comme on peut voir au tableau 1, nos résultats du calcul de K_S coïncident bien avec les valeurs des produits de solubilité, déterminées par les auteurs (7) sur la base des concen-

[2] Il faut remarquer que le choix des données expérimentales nécessaires n'était pas évident, puisque habituellement les auteurs n'indiquent pas le lot complet de données. Dans la littérature nous n'avons trouvé que trois ouvrages (7, 8, 15), dans lesquels sont indiqués tous les paramètres expérimentaux figurant aux équations de comtes [18] et [19].

© 2001 CNRC Canada

Tableau 2. Les résultats de l'analyse (8) et de nos calculs des concentrations d'équilibre de l'ion de l'yttrium dans les systèmes $Y(NO_3)_3$–H_4L–H_2O, (L^{4-}–abdph), $C_Y°$= 0,01 mol L^{-1}, t = 25°C, $n = C_L°/C_Y°$.

L'analyse et le compte du travail (8)						Le compte du présent travail
n	I (mol L^{-1})	z/x	y/x	$[H^+] \times 10^2$ (mol L^{-1})	$[Y^{3+}] \times 10^3$ (mol L^{-1})	$[Y^{3+}] \times 10^3$ (mol L^{-1})
0,5	0,043	0,92	1,39	1,15	5,10	5,13
0,7	0,040	1,02	1,60	1,54	4,03	4,00
0,9	0,036	1,06	0,62	2,96	1,83	1,87
1,0	0,032	1,09	1,09	2,94	0,99	1,04
1,25	0,029	1,15	1,66	2,92	0,26	0,26
1,8	0,031	1,81	3,84	3,29	0,35	0,39
2,5	0,031	2,49	6,38	3,55	0,12	0,13
2,8	0,031	2,84	7,73	3,55	0,25	0,25

Tableau 3. Les résultats de l'analyse (8) et de nos calculs des concentrations résiduelles du ligand dans les systèmes $Y(NO_2)_3$–H_4L–H_2O, (L^{4-}abdph), $C_Y°$= 0,01 mol L^{-1}, t = 25°C, $n = C_L°/C_Y°$.

L'analyse et le compte du travail (8)						Le compte du présent travail
n	I (mol L^{-1})	z/x	y/x	$[H^+] \times 10^2$ (mol L^{-1})	$C_L \times 10^3$ (mol L^{-1})	$C_L \times 10^3$ (mol L^{-1})
0,5	0,043	0,92	1,39	1,15	0,51	0,52
0,7	0,040	1,02	1,60	1,54	0,88	0,88
0,9	0,036	1,06	0,62	2,96	0,36	0,38
1,0	0,032	1,09	1,09	2,94	0,21	0,23
1,25	0,029	1,15	1,66	2,92	1,28	1,29
1,8	0,031	1,81	3,84	3,29	0,53	0,62
2,5	0,031	2,49	6,38	3,55	0,39	0,42
2,8	0,031	2,84	7,73	3,55	0,32	0,32

trations résiduaires en ion de l'yttrium et en ligand. En même temps, nos calculs ont confirmé la supposition que, dans les conditions examinées, les complexes de la composition YH_iL en solution ne se forment pas.

Ainsi, cette méthode peut être appliquée pour le contrôle de l'authenticité et la justesse du modèle de l'équilibre défini plus tôt (la composition, la stabilité et les constantes de la formation des espèces chimiques).

Complexonate $YHL_{(S)}$ (L^{4-}–aminobenzylidène-diphosphonate, abdph)

Dans le système $Y(NO_3)_3$–H_4L–H_2O le précipité $YHL_{(S)}$ se forme à C_Y^0 = 0,01 mol L^{-1} seulement pour $n = C_L^0/C_Y^0 = 1$ (8). Dans le domaine $1 < n \leq 3,4$ la formation du précipité d'une composition variable a été établie, où le rapport du ligand à l'yttrium augmente jusqu'à la valeur 3,35, et où, en qualité des phases individuelles, se contiennent des précipités de $YHL_{(S)}$ et d'acide. Par example, pour n = 2,5 la composition du précipité s'exprime avec la formule $YH_7L_{2,5}$ = YHL + 1,5H_4L (tableaux 2 et 3). À la température ambiante, la valeur mesurée $[H^+]$ de la solution saturée, contenant le précipité, est à 2,94 × 10^{-2} mol L^{-1}. Pour cette valeur basse de $[H^+]$, la formation des complexes en solution est absente, $\alpha_Y = 1$ et α_L est calculé par la relation :

$$\alpha_L = 1 + \sum_{j=1} K_j [H]^j$$

où les constantes K_j recalculées ici à force ionique I indiquée au tableau 2 selon l'équation [22] ont été empruntées de (20) : log K_1 = 10,29; log K_2 = 18,46; log K_3 = 23,75 et log K_4 = 25,35 (I = 0,1 mol L^{-1}, t = 25 ± 0,1°C).

Pour n = 1, les équations [18] et [19] se réduisent à ($q = 4 \times n = 4$) :

$$[26] \quad [Y] = C_Y = \frac{(3C_Y^0 - [H])\alpha_L}{K_2[H]^2 + 2K_3[H]^3 + 3K_4[H]^4 - 1},$$

$$[L] = \frac{C_L}{\alpha_L} = \frac{[Y]}{\alpha_L}$$

Alors le produit de solubilité pour la réaction

$$YHL_{(S)} = Y^{3+} + H^+ + L^{4-}$$

est égal

$$K_S = [Y][H][L] = \alpha_L [H] \frac{(3C_Y^0 - [H])^2}{K_2[H]^2 + 2K_3[H]^3 + 3K_4[H]^4 - 1} = 5,29 \times 10^{-29}$$

où

$$pK_S = -\log K_S = 28,28$$

La valeur obtenue coïncide pratiquement avec celle de la moyenne géométrique pK_S = 28,3, calculée dans (8) sur la base de C_Y et C_L.

© 2001 CNRC Canada

Tableau 4. Les résultats de l'analyse (11) et des nos calculs des constantes d'équilibre dans le système La^{3+}–nitryletriacétate–H_2O à 25°C et I = 0,1 (H, Na)ClO_4.

$C_H^\circ \times 10^3$ (mol L^{-1})	$S \times 10^3$ (mol L^{-1})	p[H]	$pK_S = -\log K_s$	$\log \beta_1$
52,43	5,68	1,426	14,48	10,69
43,69	4,88	1,506	14,41	10,65
34,93	4,22	1,612	14,26	10,45
21,84	1,81	1,750	14,69	10,92
17,47	1,62	1,853	14,55	10,78
1,97	0,41	2,789	14,36	10,57
Valeur moyenne	$p\overline{K}_s = 14{,}5 \pm 0{,}2$			
	$\log \overline{\beta}_1 = 10{,}7 \pm 0{,}2$			

Les équations [18] et [19] permettent aussi de vérifier la sûreté et la concordance des données expérimentales obtenues avant sur les concentrations de l'équilibre et celles résiduaires (ou la solubilité), seulement sur la base de la valeur d'équilibre du pH de la solution, connaissant la composition initiale du mélange. Les valeurs de la concentration d'équilibre de l'ion de l'yttrium [Y^{3+}] et la concentration résiduelle du ligand [L^{4-}], mesurées par les auteurs (8), ainsi que les résultats de nos comptes sont présentés aux tableaux 2 et 3. La coïncidence satisfaisante reçue entre les données de comptes seulement à la base des données du pH et les données expérimentales confirme la justesse des équations [18], [19] et [26].

Par example, pour n = 1,25, les auteurs (8) ont donné les valeurs suivantes [Y^{3+}] = 0,26 × 10^{-3} mol L^{-1} et C_L = 1,29 × 10^{-3} mol L^{-1}. Le calcul d'après [26] donne le résultat suivant : [Y^{3+}] = 0,26 × 10^{-3} mol L^{-1} et C_L= 1,28 × 10^{-3} mol L^{-1}, qui s'accorde bien avec les valeurs obtenues auparavant (8).

Donc, la méthode proposée ici de la détermination des concentrations d'équilibre des ions du complexe peu soluble peut être utilisée pour le contrôle et la standartisation des nouvelles électrodes ion-selectives. Pour cela, il est nécessaire de choisir un tel système hétérogène, pour qui les constantes de l'équilibre des réactions secondaires [3] et [4] ainsi que la composition de la phase solide formée sont connues exactement.

Type II. Complexonate $LaL_{(S)}$ (L^{L3-}–nitryletriacétate, nta)

Dans le travail (11) la solubilité du sel LaL × $nH_2O_{(S)}$ a été étudiée en fonction de p[H] = –log [H] en deux milieux à I = const : (*i*) en mélange $HClO_4$ et $NaClO_4$ et (*ii*) en milieu $NaClO_4$. Les valeurs K_S et β_1 ont été calculées à l'aide des équations

$$[27] \quad S = (K_S \alpha)^{1/2} + \beta_1 K_S$$

$$K_S = [La][L], \quad \beta_1 = [LaL]/K_S$$

au moyen de la détermination des paramètres de la relation linéaire $S(\alpha_L^{1/2})$ par la méthode des moindres carrés. Toutefois, une telle méthode a des restrictions. Comme la solubilité du sel en milieu acide augmente d'habitude très fortement, la condition I = *const* n'est pas satisfaite et les valeurs sont mesurées avec une précision différente. En plus, l'équation [27] a été déduite sur la base des suppositions :

$$(i) \ \alpha_L \approx \sum_{j=1} K_j [H]^j$$

et

$$(ii) \ S \approx [ML]$$

juste dans le cas de la formation des espèces protonées très stables ([L] ≅ 0) et des complexonates stables ([M] ≅ 0).

Tableau 5. Les données de table et celles calculées des constantes d'équilibre dans le système La^{3+}–nitryletriacétate–H_2O à 25°C et I = 0,1 (H, Na)ClO_4.

$\log \beta_1$	pK_S	Référence
10,7 ± 0,2	14,4 ± 0,2	(11)
10,7 ± 0,2	14,5 ± 0,2	le travail présent

En milieu acide la solubilité du nitryletriacétate de lanthane se fait à 25°C environ 10^{-3} mol L^{-1} (tableau 2). L'anion L^{3-} forme trois espèces protonées (18, 19) :

$$L^{3-} + H^+ = HL^{2-} \quad \log K_{HL} = 9{,}73$$

$$L^{3-} + 2H^+ = H_2L^- \quad \log K_{H_2L} = 12{,}22$$

$$L^{3-} + 3H^+ = H_3L \quad \log K_{H_3L} = 14{,}11$$

Les complexonates protonés de lanthane ne se forment pas (3). L'espèce cationique H_4L^+ prédomine en solutions aqueuses à pH < 0,8.

Pour ce système, les équations [11] à [13] ont la formule ($C_M = C_L = S$) :

$$[28] \quad S = [M] + [ML], \quad S = [L]\sum_{j=0}^{3} K_j [H]^j + [ML]$$

$$C_H^0 = [H] + [L]\sum_{j=1} jK_j [H]^j = [H] + [L]\varphi_L$$

Delà, on obtient

$$[29] \quad [L] = (C_H^0 - [H])/\varphi_L$$

$$[M] = [L]\alpha_L = C_H^0 - [H])\alpha_L/\varphi_L$$

Ensuite, on détermine K_S à l'aide de l'équation [29].

Des équations [28] et [29], on trouve

$$[30] \quad [ML] = S - [M] = S - (C_H^0 - [H])\alpha_L/\varphi_L$$

La résolution des équations [27] à [30] donne l'expression du calcul de la constante de stabilité en phase aqueuse

$$[31] \quad \beta_1 = \frac{S\varphi_L^2 - \alpha_L (C_H^0 - [H])\varphi_L}{\alpha_L (C_H^0 - [H])^2}$$

Au tableau 4, sont réunis les résultats des mesures, exécutées en (11), de même que les valeurs $\log \beta_1$ et $pK_S = -\log K_S$, calculées par les équations [31] et [27] à [29]. Leurs valeurs s'accordent avec les données (11) (tableau 5). Elles confirment la justesse des suppositions du travail (11) pour ce système.

© 2001 CNRC Canada

Conclusion

L'exigence préliminaire nécessaire pour l'utilisation du procédé élaboré est la réalisation des conditions suivantes : (*i*) les coefficients d'activité se maintiennent constants; (*ii*) la composition de la phase solide connue d'avance doit rester constante; (*iii*) les constantes d'équilibre utilisées dans les calculs doivent être exactes et sûres; (*iv*) dans le cas $C_H^0 \cong$ [H], il est impossible d'obtenir des résultats fidèles sur la base des équations, qui contiennent la différence des quantités $C_H^0 -$ [H].

Les avantages de l'approche proposée sur la détermination K_S par comparaison avec la méthode (11) consistent dans le fait qu'on n'exige pas la connaissance de la valeur de *S*, qui est déterminée d'habitude avec une précision plus petite que celle obtenue par la mesure potentiométrique du pH. (À présent on peut mesurer le pH avec la reproductivié de ± 0,005 unités (18), en utilisant les électrodes en verre de haute qualité. En plus, par un choix soigneux et un maintien des conditions de l'expérience la reproductivité peut être augmentée encore par un ordre de grandeur (20)). En même temps l'équation du type [31] donne la solution exacte de la valeur de la constante de stabilité β_1, sans recourir à la méthode itérative du calcul ou au traitement graphique des résultats.

La méthode donnée peut aussi être utilisée, comme on l'a montré ci-dessus, pour la vérification de la justesse des valeurs de table des constantes d'équilibre obtenues auparavant.

La réalisation des expériences doit être adéquate aux équations utilisées. À cet égard, nous prêterons attention à la nécessité de satisfaire à une haute précision et exactitude au cours de la préparation des solutions, puisque dans les formules de calcul figurent les concentrations initiales des constituantes du précipité. Les relations déduites ne sont justes que dans les conditions de la précipitation de l'un des composés considérés. Si deux et plusieurs précipités différents se forment, autrement dit, si nous obtenons un précipité de composition variable à la suite du mélange de quelques substances individuelles dans un rapport différent, les équations perdent leur sens.

Considérant les particularités de la méthode donnée à la présentation des données expérimentales, il faut indiquer non seulement la force ionique, la température et la méthode de la mesure, mais encore les concentrations initiales de tous les composants ajoutés au système. La méthode élaborée peut être utilisée largement, puisque un grand nombre des réactions d'équilibre passant dans les systèmes hétérogènes examinés répondent très sensiblement aux changements du pH de la solution (4). Cette méthode, naturellement, peut aussi être appliquée pour des complexes avec d'autres ions multifonctionels.

Reconnaissance

L'auteur exprime la gratitude au critique (rédacteur) scientifique, dont quelles remarques et les conseils ont permis d'améliorer considérablement la qualité de l'article.

Références

1. L. Saran, E. Cavalheiro et E.A. Neves. Talanta, 42, 2027 (1995).
2. J. Karhu, L. Harju et A. Ivasca. Anal. Chim. Acta, **380**, 105 (1999).
3. N.M. Dyatlova, V.Y. Temkina et K.J. Popov. Complexones et complexonates des métaux. Moscou, Khimia. 1988 (en russe).
4. M. Beck et I. Nagypal. Chemistry of complex equilibria. Budapest, Academiai Kiado. 1989.
5. K.E. Heusler. Electrochim. Acta, **41**, 411 (1996).
6. M. Trojanowicz, P.W. Alexander et D.B. Hibbert. Anal. Chim. Acta, **370,** 267 (1998).
7. G.S. Tereshin et L.K. Kharitonova. Zh. Neorg. Khim. **19**, 1264 (1974).
8. G.S. Tereshin, L.K. Kharitonova et V.N. Goryatcheva. Koord. Khim. **8**, 1189 (1977).
9. T.J. Janjic, L.B. Pfendt et M.B. Celap. J. Inorg. Nucl. Chem. **41**, 1019 (1975).
10. K. Yoshitani. Bull. Chem. Soc. Jpn. **58**, 1646 (1985).
11. N.A. Skorik, V.N. Kumok et V.V. Serebrennikov. Zh. Neorg. Khim. **12**, 3381 (1967).
12. I.G. Povar. Russ. J. Inorg. Chem. **41**, 1167 (1996).
13. I.G. Povar. J. Anal. Chem. **53**, 1113 (1998).
14. E.N. Beresnev. Méthode des concentrations résiduaires. Moscou, Nauka. 1992 (en russe).
15. G.S. Tereshin, L.K. Kharitonova, L.V. Krinitskaya et T.P. Korabelnikova. Zh. Neorg. Khim. **19**, 1131 (1974).
16. C.W. Davies. Ion Association. Butterworths, London. 1962. p. 41.
17. S. Westerback, K. Rajan et A. Martell. J. Am. Chem. Soc. **87**, 2567 (1965).
18. A.E. Martell et R.M. Smith. Critical stability constants. Vol. 1–5. Plenum Press, New York. 1972–1982.
19. M.J. Kabatchnik, R.P. Lastovsky et T.Y. Medved. Dokl. Akad. Nauk. SSSR, **177**, 582 (1967).
20. F.J.C. Rossotti et P.J. Whewell. J. Chem. Soc. Dalton, 1223 (1977).

© 2001 CNRC Canada

Synthetic dyes: simple and original ways to 4-substituted flavylium salts and their corresponding vitisin derivatives

Christine Roehri-Stoeckel, Emmanuel Gonzalez, André Fougerousse, and Raymond Brouillard

Abstract: Flavylium salts substituted at the 4-position have been prepared according to a Grignard reaction of some flavones with appropriate alkyl- and aryl-magnesium bromides. Among these compounds, 4-methyl flavylium salts were gently reacted with aromatic aldehydes, affording new anthocyanidin pigments, some of which are of the vitisin family. These are the first examples of chemically synthesized vitisidins (aglycones of vitisins). Compared to the more common flavylium salts, they demonstrate a large bathochromic shift (from about 100–200 nm), thus providing blue-violet and green colours, so difficult to obtain with anthocyanidins in general.

Key words: 4-substituted flavylium chlorides, vitisin aglycones, blue-violet and green anthocyanidin pigments.

Résumé : Nous avons développé la synthèse de sels de flavylium substitués en position 4. Ils ont été obtenus par réaction de bromures d'alkyle et d'aryle magnésium avec des flavones. Les chlorures de flavylium substitués en position 4 par un groupement méthyle réagissent, dans des conditions douces, avec des aldéhydes aromatiques conduisant à de nouveaux pigments anthocyanidiques dont certains appartiennent à la famille des vitisines. Il s'agit ici de la première synthèse chimique de vitisidines. La bande d'absorption de ces nouveaux pigments subit un effet bathochrome (de 100 à 200 nm) par rapport aux sels de flavylium les plus connus. Ils produisent des couleurs bleu-violet et vertes, que l'on n'observe quasiment jamais avec les anthocyanidines les plus communes.

Mots clés : chlorures de flavylium substitués en position 4, aglycones de vitisines, pigments anthocyanidiques bleu-violet et verts.

Introduction

Flavylium salts (2-phenyl-benzopyrilium salts) are the aglycones of the large natural family of molecules known as anthocyanins. These pigments are ubiquitous in higher plant flowers and fruits (1, 2). The chemistry of these compounds has been reviewed (3–5). To prepare them, two synthetic approaches have been largely used. One is the condensation reaction of 2-hydroxybenzaldehydes with acetophenones; the other uses reductive or oxidative reagents, which are applied to various kinds of flavonoid compounds.

In the present work, flavones and Grignard reagents are the starting compounds (6, 7). They could be made to react, leading to the formation of 4-substituted flavylium salts (Scheme 1). Flavylium salts bearing a substituent at the 4-position are important compounds since they are known to be less sensitive to nucleophiles, especially water, and they give only minor amounts of the colourless pseudobases (8). Indeed, a detailed investigation of the structures usually appearing in slightly acidic aqueous media, shows that the presence of a substituent at C-4 enlarges the pH domain where the flavylium cationic form exists to approximately pH 5, with at the same time significant amounts of quinonoidal bases being formed. Compared to common 3-deoxyanthocyanidins (aglycones), 4-substituted flavylium salts feature characteristic hypsochromic spectral shifts. A strong absorption also occurs in the near-UV range (370–390 nm).

Moreover, 4-methylflavylium derivatives are also interesting because of the exceptionally high acidity of the methyl group attached to the electrophilic C-4 carbon atom. This unique feature allows them to react with aromatic aldehydes for instance, to give new flavylium dyes, which are characterized by unusually large bathochromic shifts in the visible range (maxima of absorption situated between 500 and 750 nm). By increasing the length of the aldehyde conjugated chain (9, 10), the maximum of absorption evolves towards the near-IR region. For instance, in methanol, going from **8** to **10** results in a 80 nm bathochromic shift. Kanitz et al. (11), have described an analogous type of reactivity for the 2-alkylbenzopyrilium cations with aromatic aldehydes in the preparation of varied polymethine dyes. Within the same frame of research, other 2-(arylalkenyl)-benzopyrilium perchlorates could also be prepared (12, 13).

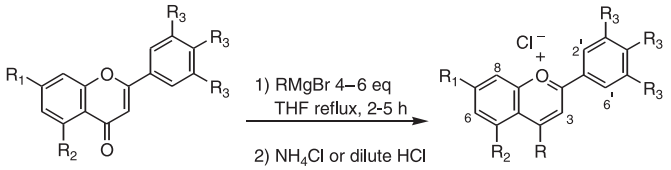
Received May 19, 2000. Published on the NRC Research Press Web site at http://canjchem.nrc.ca on August 3, 2001.

C. Roehri-Stoeckel, E. Gonzalez, A. Fougerousse, and R. Brouillard.[1] Laboratoire de Chimie des Polyphénols, UMR 7509 du CNRS, Université Louis Pasteur, 4, rue Blaise Pascal, 67008 Strasbourg, France.

[1]Corresponding author (telephone: 33 (0)3 90 24 13 42; fax: 33 (0)3 90 24 13 41; e-mail: brouil@chimie.u-strasbg.fr).

 DOI: 10.1139/cjc-79-7-1173 © 2001 NRC Canada

Scheme 1.



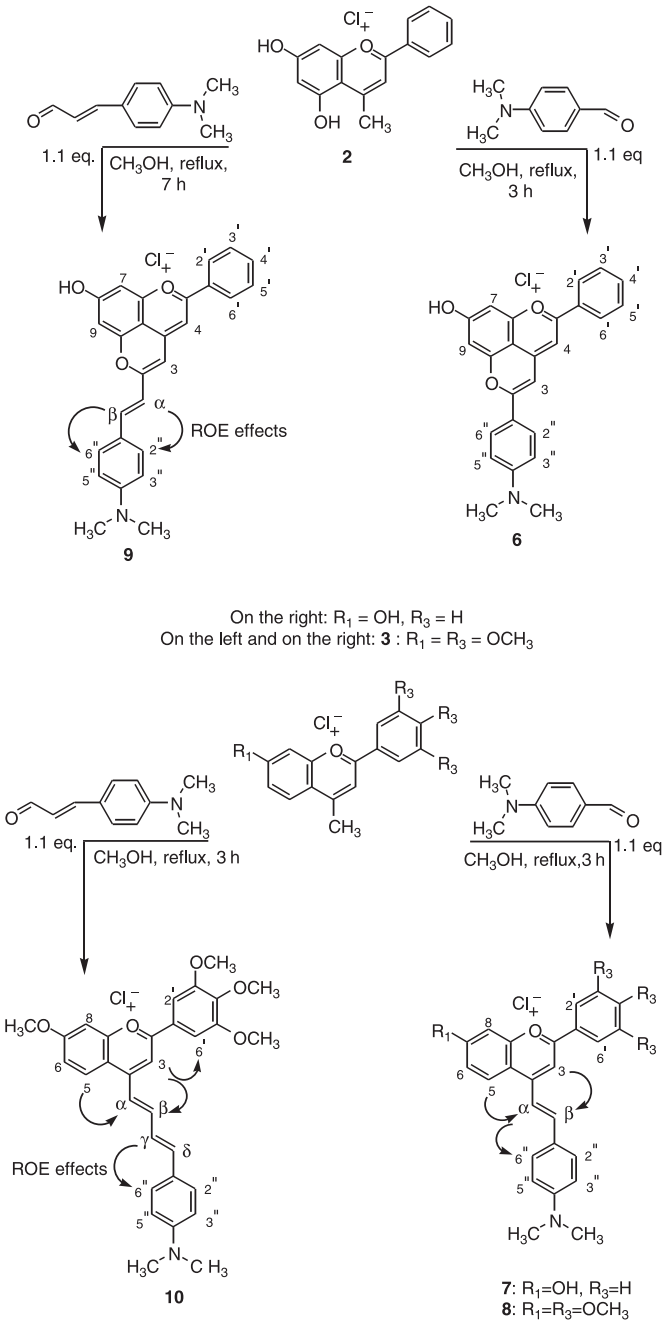
1 : R = phenyl, R_1=OH, R_2=OH, R_3=H
2 : R = methyl, R_1=OH, R_2=OH, R_3=H
3 : R = methyl, R_1=OCH_3, R_2=H, R_3=OCH_3
4 : R = 4-fluoro-phenyl, R_1=OH, R_2=OH, R_3=H
5 : R = phenyl, R_1=OCH_3, R_2=H, R_3=OCH_3

Results and discussion

Reaction of 5,7-dihydroxyflavone or chrysin, with an excess of phenylmagnesium bromide in THF under reflux conditions, followed by hydrochloric acid hydrolysis, afforded **1** (Scheme 1). Compound **2** was obtained in the same way, replacing phenylmagnesium bromide with methylmagnesium bromide. In this case, however, hydrolysis using saturated ammonium chloride, instead of hydrochloric acid, was necessary to have the flavylium salt precipitated. Nevertheless, this is not the most suitable work-up since the remaining magnesium salt also precipitates in that medium. Therefore, to remove the undesirable magnesium salt, several washings were applied to the crude precipitate. Compound **3** was prepared from the 7,3′,4′,5′-tetramethoxyflavone and methylmagnesium bromide. It could not be obtained readily by just pouring the mixture into saturated ammonium chloride. For this compound, the following procedure proved to be useful: the chromenol intermediate was extracted from the saturated ammonium chloride solution using ethylacetate, and then concentrated under reduced pressure. The corresponding residue was then dissolved in acidified methanol (hydrochloric acid 12 M, three drops) and stirred for one more hour. In particular, we observed that for the flavone itself, or for nonhydroxylated flavones, the corresponding flavylium cations were more difficult to obtain. A mixture of the chromenol and its parent flavylium form was obtained, even in fairly acidic solutions. Compound **4** was prepared like **2**, and **5** like **1**.

The condensation reactions of 4-*N*,*N*-dimethylaminobenzaldehyde and 4-*N*,*N*-dimethylaminocinnamaldehyde were performed using **2**, **3**, and 7-hydroxy-4-methylflavylium chloride (previously prepared in our laboratory following known procedures (3)) (Scheme 2). Concerning the stereochemistry of double bonds, in all cases, ^{1}H NMR coupling constants indicated an *E* configuration. With **7** and **10**, rotating Overhauser enhancement (ROE) ^{1}H NMR spectra feature through space interactions between protons H(5) and Hα, H(6″) and Hα (in the case of **7**), and H(6″) and Hγ (in the case of **10**). Another through space interaction relates proton β to H(3). These data (represented by arrows on Scheme 2) pointed out a s-*cis* conformation. Very interestingly, addition of 4-*N*,*N*-dimethylaminobenzaldehyde to **2**

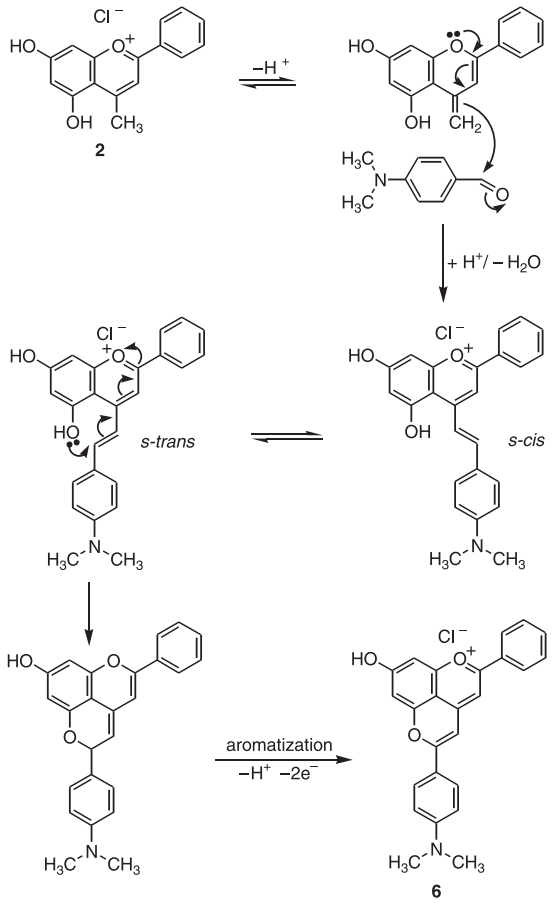
Scheme 2.



led to an adduct rapidly transforming into a more stable cyclic structure showing a lowering of the visible absorption maximum compared to the first formed open structures (Scheme 3). Also in this case, immediately after mixing the reagents under reflux conditions, the solution turned green then slowly evolved towards purple. In all the other cases, with the exception of **9**, the solution remained green. The kinetic course of the transformation of **2** into **6** was monitored by UV–vis absorption spectrometry using a diluted sample made of **2** and 4-*N*,*N*-dimethylaminobenzaldehyde. Spectral features characteristic of three different structures could be registered as a function of time (Fig. 1). Using identical conditions, except for the nature of the aldehyde, the rate of formation of **9** was shown to be lower than that of **6**, probably

© 2001 NRC Canada

Scheme 3.

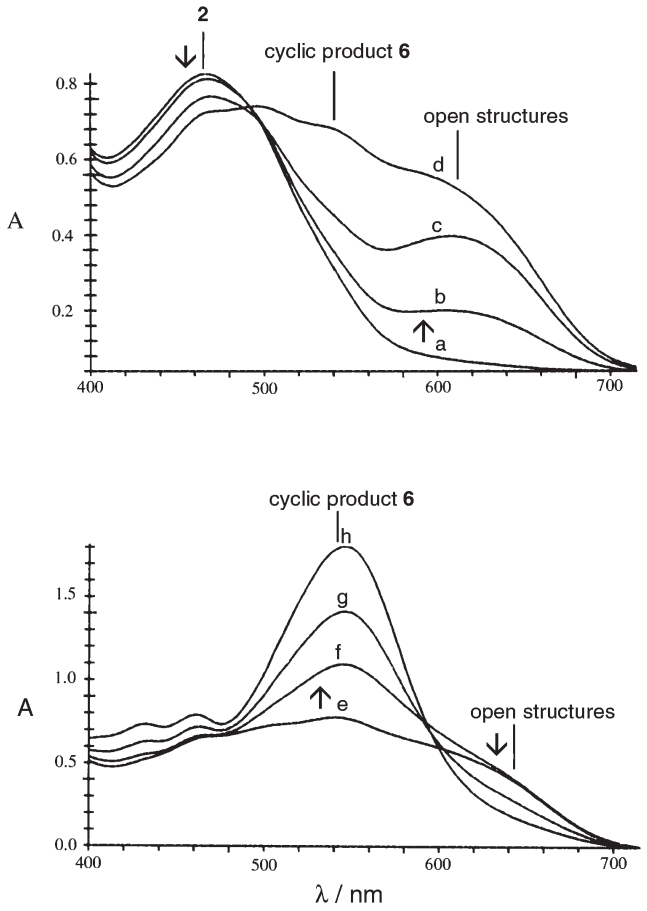


because of the difference in the energy of activation between the s-*cis* and the s-*trans* tautomers. HPLC chromatograms were very helpful to monitor the progress of the reaction until completion (Fig. 2). Compounds **6** and **9** are colourants similar to the vitisins, a new family of pigments recently isolated from red wine (14–17). Vitisins are bisflavylium cations characterized by two mesomeric forms.

Conclusion

New 3-deoxyanthocyanidins were prepared using flavones and alkyl- or aryl-magnesium bromides leading to 4-substituted flavylium salts shown to feature more stable colours than the corresponding nonsubstituted flavylium analogs. Compounds **1**–**5** were obtained in one step in excellent yields. Moreover, 4-methyl-flavylium cations could be made to react with aromatic aldehydes, under mild conditions, furnishing compounds **6**–**10** characterized by an unusual visible absorption range from 500 to 700 nm; common anthocyanins only absorbing light in the 500–550 nm range. Increasing the length of the aldehyde conjugated chain or changing the aldehyde structure could afford flavylium chlorides absorbing in the near-IR region. Now, we know how to produce the basic red, blue, and yellow colours, with a unique family of dyes: the 3-deoxyanthocyanidins. Moreover, among these dyes, the vitisin aglycones of **6** and **9** could be interesting especially in the field of human health, in relation to what is known as the "French Paradox" (18).

Fig. 1. UV–vis absorption evolving bands of the transformation of **2** into **6** (in methanol under reflux conditions). Uppert part: (*a*) *t* = 0; (*b*) *t* = 1 h; (*c*) *t* = 3 h; (*d*) *t* = 6 h. Lower part: (*e*) *t* = 10 h; (*f*) *t* = 14 h; (*g*) *t* = 18 h; (*h*) *t* = 22 h.



Indeed, the "French Paradox" tells us that wine polyphenols are responsible of the surprisingly low rate of cardiovascular diseases in the French population. It should be kept in mind that wine anthocyanins and tanins (polyphenols) evolve during wine ageing giving rise to new wine pigments, among which, vitisins are probably an important class. These type of pigments are not to be found in grapes and this is why pigments **6** and **9**, although not natural, may be useful drugs to combat heart disorders.

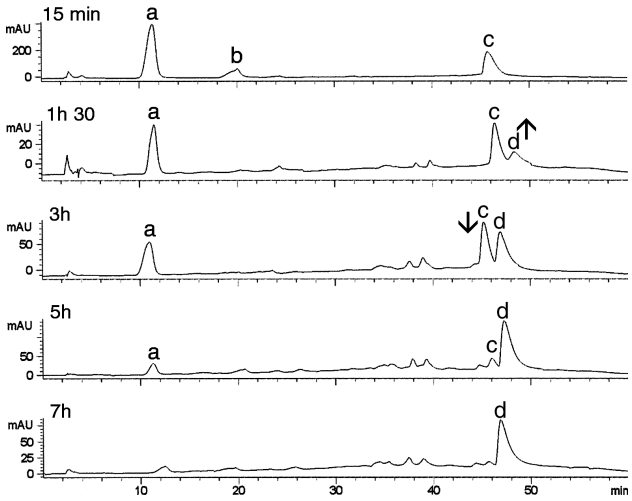
Experimental

General

Methyl-, phenyl-, and 4-fluorophenyl-magnesium bromides, as well as chrysin, 4-*N*,*N*-dimethylaminobenzaldehyde, and 4-*N*,*N*-dimethylaminocinnamaldehyde are commercial reagents. 7-Hydroxy-4-methylflavylium chloride and 7,3′,4′,5′-tetramethoxyflavone were synthesized in our laboratory according to previously published procedures (3, 19). Tetrahydrofuran (THF) was dried over sodium and benzophenone. Reactions implying alkyl- and aryl-magnesium bromides were performed under a nitrogen controlled atmosphere. Merck Silica gel (0.063–0.200 mm, 70–230 mesh) was used for column chromatography. HPLC pigment purity was checked by HPLC (Spectra Physics apparatus equipped

© 2001 NRC Canada

Fig. 2. HPLC monitoring of the condensation reaction between *N,N*-dimethylaminocinnamaldehyde (*a*) and 5,7-dihydroxy-4-methylflavylium chloride (*b*). Intermediate open structures (*c*); final stable cyclic form **9** (*d*). Reaction was at completion after 7 h in methanol under reflux conditions.



with a Hewlett Packard diode-array detector), with a reversed phase Merck C-18 LiChrospher column (5 μm, 125 × 4 mm). Binary elution systems were **A** (47.5 CH_3CN – 47.5 H_2O – 5 HCOOH) and **B**: (95 H_2O – 5 HCOOH). A flow rate of 0.5 mL min^{-1} was used with a linear 30 min gradient from 30 to 90% **A**, reaching 100% **A** at 50 min and going back to 30% **A** at 60 min. Compounds **9** and **10** were eluted with 100% **A**. Detection wavelengths (nm) are as follows: 280, 360, 470, 540, and 598.

UV–vis spectra were recorded from a diode-array spectrometer fitted with a 1 cm quartz cell. Hydrochloric acid (0.1 M) or methanolic solutions were used to measure wavelengths (nm) of maximum of absorption. Mass spectrometry analyses are of three different types: electronic impact (EI), positive electrospray ionization (ES^+), and positive fast atom bombardment (FAB^+). ^1H NMR spectra were recorded either from a 200 or a 500 MHz apparatus. Chemical shifts (δ, ppm) are related to internal standards as follows: TMS (δ_H = 0.00), CD_3OD (δ_H = 3.35). Coupling constants *J* are expressed in Hertz (Hz). Compound **6** ^1H NMR signals were assigned by COSY experiments and **7**, **9**, and **10** ^1H NMR signals by COSY and ROESY experiments.

Syntheses

*5,7-Dihydroxy-4-phenylflavylium chloride or 5,7-dihydroxy-2,4-diphenyl-1-benzopyrilium chloride (**1**)*

A solution of chrysin (400 mg, 1.57 mmol) in dry THF (15 mL) was dropwise added to 9.5 mL (6 eq.) of a 1 M phenylmagnesium bromide solution in THF.

Method A: the mixture was heated at reflux for 2 h and stirred 2 more hours at room temperature. Acidified water (150 mL of 12 M hydrochloric acid, a few drops) were then added to the mixture. After evaporation of THF, a red precipitate appeared. Filtration gave **1** (546 mg, 99%). MW = 350.5. HR-MS [M^+] calcd. for $C_{21}H_{15}O_3$: 315.1021; found: 315.1022. UV–vis (HCl 0.1 M with 1% methanol) λ (nm) (ε, M^{-1} cm^{-1}): 388 (18 600 ± 200), 454 (10 000 ± 100). ^1H NMR (200 MHz, CD_3OD) δ 8.38 (dd, *J* = 1.5, 7.5 Hz, 2H, H2′, H6′), 8.00 (s, 1H, H3), 7.79–7.54 (m, 8H, H3′, H4′, H5′, H2″, H3″, H4″, H5″, H6″), 7.10 (d, *J* = 2 Hz, 1H, H6 or H8), 6.65 (d, *J* = 2 Hz, 1H, H6 or H8).

*5,7-Dihydroxy-4-methylflavylium chloride or 5,7-dihydroxy-4-methyl-2-phenyl-1-benzopyrilium chloride (**2**)*

A solution of chrysin (5,7-dihydroxyflavone) (1.08 g, 4.25 mmol) in dry THF (30 mL) was dropwise added to 9 mL (6 eq.) of a 3 M methylmagnesium bromide solution in THF.

Method B: after heating at reflux for 2 h, the mixture was poured into a saturated ammonium chloride solution (100 mL). A red precipitate was formed, then filtered, and finally washed with tap water (150 mL); 800 mg of **2** was obtained (yield 65%). MW = 288.5. ES^+-MS: 253. UV–vis (HCl 0.1 M with 1% methanol) λ (nm) (ε, M^{-1} cm^{-1}): 378 (12 800 ± 200), 436 (9 000 ± 200). ^1H NMR (200 MHz, CD_3OD) δ 8.40 (dd, *J* = 1.5, 7.5 Hz, 2H, H2′, H6′), 8.16 (s, 1H, H3), 7.83–7.76 (m, 3H, H3′, H4′, H5′), 7.04 (d, *J* = 2 Hz, 1H, H-6 or H8), 6.77 (d, *J* = 2 Hz, 1H, H6 or H8) (the methyl protons exchange with solvent deuterium atoms (20)).

*7,3′,4′,5′-Tetramethoxy-4-methylflavylium chloride or 7-methoxy-4-methyl-2-(3,4,5-trimethoxyphenyl)-1-benzopyrilium chloride (**3**)*

7,3′,4′,5′-Tetramethoxyflavone (400 mg, 1.17 mmol) in anhydrous THF (15 mL) was dropwise added to 1.6 mL (4 eq.) of a 3 M methylmagnesium bromide solution in THF.

Method C: after heating at reflux for 2 h, the mixture was poured into saturated ammonium chloride (50 mL). Extraction with ethyl acetate gave a residue, which was treated with acidified methanol after removal of the ethyl acetate. The solution was then stirred for 1 h and finally concentrated under vacuum to give a red solid **3** (yield 418 mg, 95%). MW = 376.5. HR-MS [M^+] calcd. for $C_{20}H_{21}O_5$: 341.1389; found: 341.1417. UV–vis (HCl 0.1 M with 1% methanol) λ (nm) (ε, M^{-1} cm^{-1}): 444 (28 200 ± 500). ^1H NMR (200 MHz, CD_3OD) δ 8.68 (s, 1H, H3), 8.43 (d, *J* = 9 Hz, 1H, H5), 8.03 (d, *J* = 2 Hz, 1H, H8), 7.84 (s, 2H, H2′, H6′), 7.59 (dd, *J* = 2, 9 Hz, 1H, H6), 4.22 (s, 3H, OCH_3-C(7)), 4.08 (s, 6H, OCH_3-C(3′), OCH_3-C(5′)), 4.00 (s, 3H, OCH_3-C(4′)) (the methyl proton exchange with solvent deuterium atoms).

*5,7-Dihydroxy-4-(4-fluorophenyl)flavylium chloride or 5,7-dihydroxy-4-(4-fluorophenyl)-2-phenyl-1-benzopyrilium chloride (**4**)*

Compound **4** (470 mg, yield: 70%) was obtained by heating at reflux for 5 h, 10 mL (6 eq.) of a 1 M fluorophenylmagnesium bromide solution and chrysin (430 mg, 1.69 mmol) in anhydrous THF. Work-up followed method B. MW = 368.5. HR-MS [M^+] calcd. for $C_{21}H_{14}FO_3$: 333.0927; found: 333.0934. UV–vis (HCl 0.1 M with 1% methanol) λ (nm) (ε, M^{-1} cm^{-1}): 386 (19 100 ± 300), 454 (10 000 ± 300). ^1H NMR (200 MHz, CD_3OD) δ 8.39 (dd, *J* = 1.5, 7.5 Hz, 2H, H2′, H6′), 7.95 (s, 1H, H3), 7.82–7.28 (m, 7H, H3′, H4′, H5′, H2″, H3″, H5″, H6″), 7.03 (d, *J* = 2 Hz, 1H, H6 or H8), 6.61 (d, *J* = 2 Hz, 1H, H6 or H8).

© 2001 NRC Canada

*7,3′,4′,5′-Tetramethoxy-4-phenylflavylium chloride or 7-methoxy-2-(3,4,5-trimethoxyphenyl)-4-phenyl-1-benzopyrilium chloride (**5**)*

Compound **5** (330 mg, yield: 64%) was obtained by heating at reflux for 4 h, 7,3′,4′,5′-tetramethoxyflavone (400 mg, 1.17 mmol) and 4.7 mL (4 eq.) of a 1 M phenylmagnesium bromide solution in dry THF. Work-up followed method A. MW = 438.5. HR-MS [M^+] calcd. for $C_{25}H_{23}O_5$: 403.1545; found: 403.1553. UV–vis (HCl 0.1 M with 1% methanol) λ (nm) (ε, M^{-1} cm^{-1}): 364 (15 100 ± 300), 458 (30 000 ± 800). ^{1}H NMR (400 MHz, CD_3OD) δ 8.67 (s, 1H, H3), 8.21 (d, *J* = 9 Hz, 1H, H5), 8.13 (d, *J* = 2 Hz, 1H, H8), 7.94 (m, 2H, H2″, H6″), 7.92 (s, 2H, H2′, H6′), 7.85–7.77 (m, 3H, H3″, H4″, H5″), 7.59 (dd, *J* = 2, 9 Hz, 1H, H6), 4.25 (s, 3H, OCH_3-C(7)), 4.09 (s, 6H, OCH_3-C(3′), OCH_3-C(5′)), 4.02 (s, 3H, OCH_3-C(4′)).

*8-Hydroxy-5-phenyl-2-(4-(*N,N*)-dimethylamino)phenyl-1,6-dioxaphenalene chloride (**6**)*

A solution of 5,7-dihydroxy-4-methylflavylium chloride (**2**) (576 mg, 2 mmol) and 4-*N*,*N*-dimethylaminobenzaldehyde (328 mg, 1.1 eq.) in methanol (30 mL) was heated at reflux for 3 h. The initially red solution rapidly turned green, then purple. The progress of the reaction was monitored using HPLC. The solvent was removed under vacuum and the precipitate washed with a 50:50 mixture of diethyl ether and ethyl acetate; 470 mg (yield 56%) of **6** was obtained after recrystallization in ethanol. MW: 417.5. HR-MS [M^+] calcd. for $C_{25}H_{20}NO_3$: 382.1443; found: 382.1443. UV–vis (methanol with 5% HCl 0.1 M) λ (nm) (ε, M^{-1} cm^{-1}): 548 (46 500 ± 500). ^{1}H NMR (500 MHz, CD_3OD) δ 7.97 (d, *J* = 7.5 Hz, 2H, H2′, H6′), 7.78 (d, *J* = 9 Hz, 2H, H2″, H6″), 7.61 (m, 1H, H4′), 7.53 (m, 2H, H3′, H5′), 7.25 (s, 1H, H4 or H3), 7.18 (s, 1H, H4 or H 3), 6.89 (d, *J* = 2 Hz, 1H, H9 or H7), 6.83 (d, *J* = 2 Hz, 1H, H9 or H7), 6.62 (d, *J* = 9 Hz, 2H, H3″, H5″), 3.00 (s, 6H, $2CH_3$).

*4-[4-(4-(*N,N*-Dimethylamino)phenyl)ethenyl]-7-hydroxyflavylium chloride or 4-[4-(4-(*N,N*-dimethylamino)phenyl)ethenyl]-7-hydroxy-2-phenyl-1-benzopyrilium chloride (**7**)*

Compound **7** was synthesized from 7-hydroxy-4-methylflavylium chloride (400 mg, 1.47 mmol) and 4-*N*,*N*-dimethylaminobenzaldehyde (240 mg, 1.1 eq.) in the same way as **6**. A green precipitate was obtained (yield, 500 mg, 84%). MW: 403.5. HR-MS [M^+] calcd. for $C_{25}H_{22}NO_2$: 368.1650; found: 368.1654. UV–vis (methanol with 5% HCl 0.1 M) λ (nm) (ε, M^{-1} cm^{-1}): 640 nm (80 000 ± 1000). ^{1}H NMR (500 MHz, CD_3OD) δ 8.42 (d, *J* = 15 Hz, 1H, Hβ), 8.39 (d, *J* = 9 Hz, 1H, H5), 8.25 (d, *J* = 7.5 Hz, 2H, H2′, H6′), 8.14 (s, 1H, H3), 7.87 (d, *J* = 9 Hz, 2H, H2″, H6″), 7.76 (d, *J* = 15 Hz, 1H, Hα), 7.72–7.61 (m, 3H, H3′, H4′, H5′), 7.07 (d, *J* = 9 Hz, 1H, H6), 6.97 (s, 1H, H8), 6.86 (d, *J* = 9 Hz, 2H, H3″, H5″), 3.17 (s, 6H, $2CH_3$).

*4-[4-(4-(*N,N*-Dimethylamino)phenyl)ethenyl]-3′,4′,5′,7-tetramethoxyflavylium chloride or 4-[4-(4-(*N,N*-dimethylamino)phenyl)ethenyl]-7-methoxy-2-(3,4,5-trimethoxyphenyl)-1-benzopyrilium chloride (**8**)*

Compound **8** was prepared from **3** (180 mg, 0.48 mmol) and 4-*N*,*N*-dimethylaminobenzaldehyde (78 mg, 1.1 eq.) in the same manner as **6**. A green precipitate was obtained (yield, 196 mg, 80%). MW: 507.5. HR-MS [M^+] calcd. for $C_{29}H_{30}NO_5$: 472.2124; found: 472.2125. UV–vis (methanol with 5% HCl 0.1 M) λ (nm) (ε, M^{-1} cm^{-1}): 652 (78 600 ± 800). ^{1}H NMR (200 MHz, CD_3OD) δ 8.69 (d, *J* = 15 Hz, 1H, Hβ), 8.47 (d, *J* = 9 Hz, 1H, H5), 8.25 (s, 1H, H3), 7.95 (d, *J* = 9 Hz, 2H, H2″, H6″), 7.72 (d, *J* = 15 Hz, 1H, Hα), 7.58 (s, 2H, H2′, H6′), 7.51 (d, *J* = 2 Hz, 1H, H8), 7.28 (dd, *J* = 2, 9 Hz, 1H, H6), 6.92 (d, *J* = 9 Hz, 2H, H3″, H5″), 4.08 (s, 3H, OCH_3-C(7)), 4.06 (s, 6H, OCH_3-C(3′), OCH_3-C(5′)), 3.95 (s, 3H, OCH_3-C(4′)), 3.29 (s, 6H, $2CH_3$).

*8-Hydroxy-5-phenyl-2-[2-(4-(*N,N*)-dimethylamino)phenyl]-ethenyl-1,6-dioxaphenalene chloride (**9**)*

Compound **9** was obtained by heating at reflux in methanol 5,7-dihydroxy-4-methylflavylium chloride (550 mg, 1.9 mmol) and 4-*N*,*N*-dimethylaminocinnamaldehyde (367 mg, 1.1 eq.). The progress of the reaction was monitored by HPLC. The solution rapidly became green then turned purple. After refluxing the mixture for 7 h, the reaction was stopped. Once the methanol was evaporated, the residue was washed with a 50:50 mixture of diethyl ether and ethyl acetate and with a 50:50 mixture of chloroform and ethyl acetate giving 750 mg of a black purple solid (yield 89%). MW: 443.5. HR-MS [M^+] calcd. for $C_{27}H_{22}NO_3$: 408.1600; found: 408.1600. UV–vis (methanol with 5% HCl 0.1 M) λ (nm) (ε, M^{-1} cm^{-1}): 628 (19 100 ± 300). ^{1}H NMR (500 MHz, CD_3OD) δ 7.99 (d, *J* = 7.5 Hz, 2H, H2′, H6′), 7.67–7.54 (m, 4H, H3′, H4′, H5′, Hβ), 7.36 (d, *J* = 9 Hz, 2H, H2″, H6″), 7.26 (s, 1H, H4), 6.96 (d, *J* = 2 Hz, 1H, H7 or H9), 6.93 (d, *J* = 2 Hz, 2H, H7 or H9), 6.73 (s, 1H, H3), 6.69 (d, *J* = 15 Hz, 1H, Hα), 6.54 (d, *J* = 9 Hz, 2H, H3″, H5″), 2.94 (s, 6H, $2CH_3$).

*4-[4-(4-(*N,N*-Dimethylamino)phenyl)-butadienyl]-3′,4′,5′,7-tetramethoxyflavylium chloride or 4-[4-(4-(*N,N*-dimethylamino)phenyl)-butadienyl]-7-methoxy-2-(3,4,5-trimethoxyphenyl)-1-benzopyrilium chloride) (**10**)*

Compound **10** was obtained by heating at reflux in methanol for 3 h **3** (150 mg, 0.40 mmol) with 4-*N*,*N*-dimethylaminocinnamaldehyde (77 mg, 1.1 eq.). After the methanol was evaporated, the green residue was purified over silica gel (elution: MeOH–CH_2Cl_2, 5:95) and gave 160 mg of **10** (yield, 75%). MW: 533.5. HR-MS [M^+] calcd. for $C_{31}H_{32}NO_5$: 498.2280; found: 498.2291. UV–vis (methanol with 5% HCl 0.1 M) λ (nm) (ε, M^{-1} cm^{-1}): 730 (66 600 ± 900). ^{1}H NMR (500 MHz, CD_3OD with TFA) δ 8.62 (dd, *J* = 12, 15 Hz, 1H, Hβ), 8.39 (d, *J* = 9 Hz, 1H, H5), 8.38 (s, 1H, H3), 7.72 (d, *J* = 9 Hz, 2H, H2″, H6″), 7.65 (s, 2H, H2′, H6′), 7.61 (d, *J* = 15 Hz, 1H, Hδ), 7.59 (d, *J* = 2 Hz, 1H, H8), 7.53 (d, *J* = 15 Hz, 1H, Hα), 7.45 (dd, *J* = 12, 15 Hz, 1H, Hγ), 7.34 (dd, *J* = 2, 9 Hz, 1H, H6), 7.10 (d, *J* = 9 Hz, 2H, H3″, H5″), 4.07 (s, 3H, OCH_3-C(7)), 4.03 (s, 6H, OCH_3-C(3′), OCH_3-C(5′)), 3.92 (s, 3H, OCH_3-C(4′)), 3.21 (s, 6H, $2CH_3$).

References

1. T. Goto and T. Kondo. Angew. Chem. Int. Ed. Engl. **30**, 17 (1991).
2. R. Brouillard and O. Dangles. *In* The flavonoids: Advances in research since 1986. *Edited by* J.B. Harborne. Chapman and Hall, London. 1993. pp. 565–588.

© 2001 NRC Canada

3. J.G. Sweeny and G.A. Iacobucci. Tetrahedron, **37**, 1481 (1981).
4. G.A. Iacobucci and J.G. Sweeny. Tetrahedron, **39**, 3005 (1983).
5. M. Elhabiri, P. Figuereido, A. Fougerousse, and R. Brouillard. Tetrahedron Lett. **36**, 4611 (1995).
6. B.S. Kirkiacharian, A. Danan, and P.G. Koutsourakis. Synthesis, 879, (1991).
7. V. Srjvastava, S. Ray, and M.M. Singh. Indian J. Chem. Sect. B: Org. Chem. Incl. Med. Chem. **32B**, 569 (1993).
8. R. Brouillard. Phytochemistry, **22**, 1311 (1983).
9. H. Nakazumi, S. Watanabe, S. Kado, and T. Kitao. Chem. Lett. 1039 (1989).
10. N.A. Orlova, T.N. Gerasimova, and V.V. Shelkovnikov. Chem. Heterocycl. Compd. **33**, 1400 (1997).
11. A. Kanitz, H. Hartmann, and P. Czerney. J. Prakt. Chem. **340**, 34 (1998).
12. P. Czerney, U-W. Grummt, and W. Günther. J. Prakt. Chem. **340**, 214 (1998).
13. A.I. Tolmachev, N.A. Derevyanko, A.A. Ishchenko, M.A. Kudinova, I. Yu. Kargapolova, N.A. Orlova, and T.N. Gerasimova. Chem. Heterocycl. Compd. **34**, 444 (1998).
14. H. Fulcrand, P.J.C. dos Santos, P. Sarni-Manchado, V. Cheynier, and J. Favre-Bonvin. J. Chem. Soc. Perkin Trans. 1, 735 (1996).
15. J. Bakker and C.F. Timberlake. J. Agric. Food Chem. **45**, 35 (1997).
16. J. Bakker, P. Bridle, T. Honda, H. Kuwano, N. Saito, N. Terahara, and C.F. Timberlake. Phytochemistry, **44**, 1375 (1997).
17. H. Fulcrand, C. Benabdeljalil, J. Rigaud, V. Cheynier, and M. Moutounet. Phytochemistry, **47**, 1401 (1998).
18. S. Renaud and M. de Lorgeril. Lancet, **339**, 1523 (1992).
19. T.S. Wheeler (*Editor*). *In* Organic syntheses coll. Vol. 4. John Wiley & Sons, New York. 1963. pp. 478–481.
20. H. Jolibois, F. Theobald, J. Vebrel, A. Laarif, and C. Devin. J. Chem. Res-S. 746 (1986).

© 2001 NRC Canada

Photochemical behaviour of 1,4-dichlorobenzene in aqueous solution

Laurence Meunier, Jean-François Pilichowski, and Pierre Boule

Abstract: Several photoproducts were identified in the direct photolysis of 1,4-dichlorobenzene (1,4-DCB) in air-saturated aqueous solution, namely 4-chlorophenol, hydroquinone, hydroxybenzoquinone, and 2,5-dichlorophenol. In the absence of oxygen the latter is not formed and phenol was detected, but the unexpected formations of 4,4′-dichlorobiphenyl, 2,4′,5-trichlorobiphenyl, and a terphenyl derivative are observed. Mechanisms are proposed to explain the formations of identified photoproducts. The phototransformation of 1,4-DCB may be photoinduced by NO_3^- or Fe^{III} salts. The main primary product is 2,5-dichlorophenol, which results from a hydroxylation without dechlorination. Some other products have been identified in particular 4-chlorophenol and 2,5-dichlorobenzoquinone in the case of Fe^{III} salts.

Key words: 1,4-dichlorobenzene, photolysis, aqueous solution, induced phototransformation.

Résumé : Plusieurs photoproduits ont été identifiés lors la photolyse du 1,4-dichlorobenzène (1,4-DCB) en solution aqueuse aérée : le 4-chlorophénol, l'hydroquinone, la benzoquinone et le 2,5-dichlorophénol. En absence d'oxygène ce dernier ne se forme pas, mais il apparaît du phénol et surtout on observe la formation de 4,4′-dichlorobiphényle, de 2,4′,5-trichlorobiphényle et d'un dérivé de type terphényle. Des mécanismes réactionnels sont proposés pour expliquer la formation des divers produits identifiés. La phototransformation du 1,4-DCB peut aussi être photoinduite par des ions nitrate ou des sels ferriques. Le principal produit initialement formé est le 2,5-dichlorophénol qui résulte d'une hydroxylation sans déchloration. Quelques autres produits ont été identifiés en particulier le 4-chlorophénol et la 2,5-dichlorobenzoquinone dans le cas des sels ferriques.

Mots clés : 1,4-dichlorobenzène, photolyse, solution aqueuse, transformation photoinduite.

Introduction

1,4-Dichlorobenzene (1,4-DCB) is produced in very large amounts and its use is very popular in many homes. Most often it is used without any precaution as an insect repellant or to eliminate bad smells. It is included in the list of Priority Substances to be assessed under the Canadian Environmental Protection Act (1). Its LD_{50} (500 mg kg^{-1} orally in rats) (2) is a little lower than that of chlorophenols (3). Special attention was focussed on the population exposure in Ontario (1), and its physico-chemical and biological properties were the subject of many studies (4).

The photochemical behaviour of chlorobenzenes in water is interesting since photochemical pathways depend on the solvent and very little is known about the transformation of 1,4-DCB in water. To our knowledge, the direct photolysis of 1,4-DCB in water was briefly reported by Boule et al. (5). The main initial photoreaction was assumed to be photohydrolysis leading to 4-chlorophenol, but products (hydroquinone and hydroxybiphenyls) resulting from secondary reactions were also detected by fluorescence even at low conversions. The quantum yield of disappearance was evaluated at 0.010. The yield of formation of the triplet state in methanol was evaluated at 0.95 by Alfassi and Previtali (6). The same authors measured the rate constant of disappearance of the triplet state in methanol ($[3.0 \pm 0.4] \times 10^5$ s^{-1}) that corresponds to a lifetime equal to 3.3 μs.

It may be assumed that the mechanism of this reaction is similar to the mechanism of monochlorobenzene transformation into phenol, which was the subject of some controversies. According to Previtali and Ebbesen (7), the main reaction observed when monochlorobenzene is photolyzed in pure water is the transformation into phenol, but the reduction into benzene is also detected. These reactions are assumed to result from two competitive pathways: a singlet state photosubstitution reaction with the radical cation as an intermediate, and a homolytic C—Cl bond cleavage in both excited singlet and triplet states. On the other hand, Tissot et al. (8) observed a quantitative transformation into phenol, which was attributed to the photohydrolysis of a polarized short-lived triplet state that was not directly observed. The transformation of monochlorobenzene induced by hydroxyl radicals was reported by Merga et al. (9). The major prod-

Received December 15, 2000. Published on the NRC Research Press Web site at http://canjchem.nrc.ca on August 3, 2001.

L. Meunier, J.-F. Pilichowski, and P. Boule.[1] Laboratoire de Photochimie Moléculaire et Macromoléculaire, Université Blaise Pascal (Clermont-Ferrand) UMR CNRS 6505 F-63177 Aubière cedex France.

[1]Corresponding author (telephone: 33 (0) 4 73 40 71 76; fax: 33 (0) 4 73 40 77 00; e-mail: Pierre.Boule@univ-bpclermont.fr).

 DOI: 10.1139/cjc-79-7-1179 © 2001 NRC Canada

ucts are the three isomeric chlorophenols. This reaction implies the intermediate formation of an $OH^{\bullet}$ adduct. No results were reported about the transformation of monochloro- or dichlorobenzenes induced by excitation of photoinducers such as nitrate ions or ferric salts that produce hydroxyl radicals under irradiation.

The aim of the present work is to study the mechanism of the direct phototransformation of 1,4-DCB in pure water. The reactions induced by excitation of nitrate ions and Fe^{III} salts are also considered.

Experimental

Reactants and analytical standards

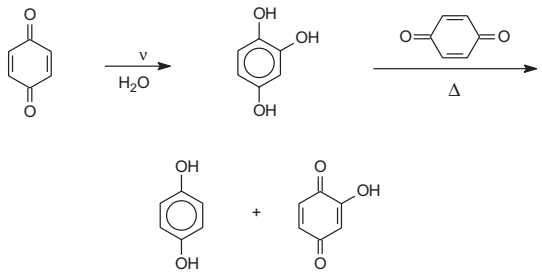
1,4-Dichlorobenzene (99+%) from Aldrich was used without further purification. The following compounds were used as analytical standards: 4-chlorophenol 99+% (Aldrich), 2,5-dichlorophenol >98% (Fluka), hydroquinone >99.5% (Merck), benzoquinone 99% (Merck), 2,5-dichlorohydroquinone (Kodak). Potassium nitrate, used as photochemical inducer, was obtained from Prolabo RP Normapur, while ferric perchlorate nonahydrate (>97%) was purchased from Fluka.

2,5-Dichlorobenzoquinone was obtained by oxidation of 2,5-dichlorohydroquinone by ferric perchlorate in excess. The mixture was heated at 60°C overnight. 2,5-Dichlorohydroquinone was quantitatively transformed and the reaction mixture was directly used for the calibration of HPLC.

4′-Chlorophenyl-*p*-benzoquinone was synthesized from 4-chloroaniline and *p*-benzoquinone. The procedure, which was proposed by Brassard and L'Ecuyer (10) and reported by Carlson and Miller (11), involves the diazotation of 4-chloroaniline. The crude product was recrystallized from an ethanol–acetone mixture. Its structure was supported by mass spectrometry results ((70 eV) *m*/*z*: 218–220, main fragment at 183).

4′-Chloro-2,5-dihydroxybiphenyl-(4′-chlorophenylhydroquinone) (4′-$ClPhQH_2$) was obtained by reduction of previous compound by sodium dithionite ($Na_2S_2O_4$). The crude product was purified by HPLC. Its formula was supported by mass spectrometry results (*m*/*z*: 220–222, main fragment at 185).

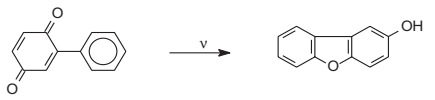
Hydroxybenzoquinone was obtained by irradiation of benzoquinone in solution. Actually, irradiation leads to two main products, hydroquinone and hydroxybenzoquinone, in approximately equal amounts (12).



[1]

From the HPLC evaluation of benzoquinone transformed and hydroquinone formed, it is possible to deduce an approximate value of the concentration of hydroxybenzoquinone present.

2-Hydroxydibenzofuran was obtained by photocyclization of phenylbenzoquinone in aqueous solution. Phenylbenzoquinone was provided by Eastman. The reaction is quantitative by irradiation at 365 nm (13):



[2]

Solutions were prepared with water purified with Milli-Q device and controlled by its resistivity (>18 MΩ cm).

Irradiations

Direct phototransformation of 1,4-DCB was studied by irradiating aqueous solutions at 254 nm in a quartz reactor with a low pressure mercury lamp (germicidal lamp). Reactor and lamp were located on both focal axes of a cylindrical mirror with an elliptic base. The number of photons received was evaluated at 7.09×10^{15} photons cm^{-3} s^{-1} using uranyl oxalate as a chemical actinometer (14).

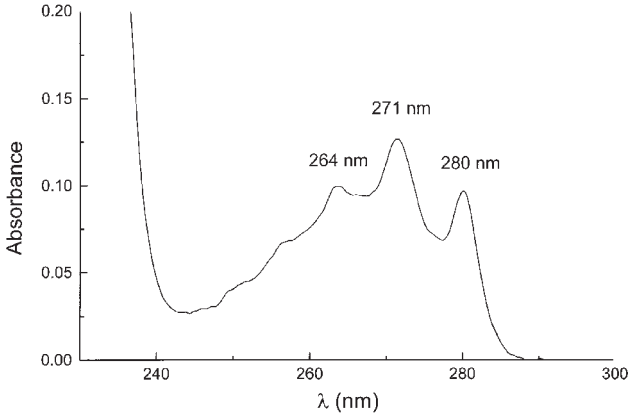
This device is appropriate for the analysis of products since incident photon flow is relatively intense. However it is not appropriate for the determination of quantum yields since the optical path is not well defined and it is not possible to calculate the percentage of light absorbed. For determination of quantum yields solutions were irradiated in quasi-parallel beam using one germicidal lamp. The incident photon flow was evaluated at 1.33×10^{14} photons cm^{-3} s^{-1} using potassium ferrioxalate as the chemical actinometer (14), since it is much more sensitive than uranyl oxalate.

To study the photochemical degradation induced by excitation of nitrate ions solutions were irradiated with 6 fluorescent lamps Duke GL20E. These lamps emit light not only between 275 and 350 nm with a maximum near 310 nm but also on the mercury lines located at 365, 405, and 436 nm. Wavelengths shorter than 290 nm were cut off using a Pyrex reaction chamber. The number of photons received in the range 290–350 nm was roughly evaluated at 6×10^{15} photons cm^{-3} s^{-1} by uranyl oxalate. It is difficult to obtain an accurate value since the actinometer absorbs a low percentage of photons emitted on mercury lines.

Reactions photoinduced by excitation of Fe^{III} were studied by irradiating solutions with three Mazda MAW125 lamps. These lamps consist of filtered medium pressure mercury arc. Actually, according to the spectrum given by the manufacturer, they emit about 87% of photons at 365 nm, about 6% at 334 nm, and 3% at 313 nm. Emission at 313 nm is perhaps lower after use, therefore, direct excitation of 1,4-DCB is completely excluded. The reactor in Pyrex was placed along the central axis of the device and the solution maintained at room temperature by a cooling jacket. With this device the photon flow received by the solution was evaluated at 1.2×10^{16} photon cm^{-3} s^{-1} using Aberchrome 540 as the actinometer (15), because uranyl oxalate is not sufficiently absorbing at this wavelegth and potassium ferrioxalate is too sensitive for this device.

© 2001 NRC Canada

Fig. 1. UV spectrum of an aqueous solution of 1,4-dichlorobenzene (1,4-DCB) (4.0×10^{-4} M).



Deoxygenation

To control the influence of oxygen on the formation of photoproducts some solutions were deoxygenated. Argon bubbling cannot be used with diluted solutions because of the high vapor pressure of 1,4-DCB. Water contained in the photochemical reactor in the presence of some crystals of 1,4-DCB was deoxygenated by argon bubbling before dissolution of the reactant. After closing the reactor with a septum, the water was magnetically stirred to dissolve the 1,4-DCB. The concentration was evaluated from HPLC according to a reference solution of known concentration.

Analyses

The UV spectra were recorded on Cary 3 (Varian) spectrophotometer. Irradiated solutions were analysed by HPLC on Waters 996 equipped with a photodiode array detector or on Merck L-6200 equipped with fluorescent detection. In both cases the column was C_{18} 250 mm × 4 mm, and the eluent water–methanol (30:70 or 25:75, v/v).

Several photoproducts were identified by GC–MS on Hewlett-Packard 5989 equipped with a capillary column Machery Nagel Optima 5 (25 m × 0.25 mm i.d.). Products were detected by electronic impact (70 ev) mass spectrometry (EI-MS). Nuclear magnetic resonance (NMR) spectra were obtained on samples dissolved in acetone-d_6 (internal reference) with a Bruker AC400 spectrometer. ^{1}H and H–H COSY (2D) classical sequences were used.

The formation of chloride ions in irradiated solutions was measured with a specific electrode after calibration with standard aqueous solutions of NaCl.

Isolation of photoproducts V and VI

About 100 mL of a deoxygenated solution of 1,4-DCB almost saturated was irradiated for 30 min with 6 low pressure mercury lamps. This process was repeated 20 times. The irradiated solutions were filtered to remove remaining crystals of 1,4-DCB and purged with nitrogen to completely eliminate unreacted 1,4-DCB from the solution. The products were extracted with ether and, after evaporation, isolated by HPLC (Column C_{18}, eluent water–methanol (25:75 v/v)).

Table 1. Formation of H^+ and Cl^- in a solution of 1,4-DCB (4.5×10^{-4} M) irradiated at 254 nm.

1,4-DCB converted	$[H^+]$	$[Cl^-]$
2.7×10^{-4} M (59%)	$(3.6 \pm 0.2) \times 10^{-4}$	$(4.0 \pm 0.2) \times 10^{-4}$

Results

Physico-chemical properties of 1,4-DCB

1,4-DCB is a white crystalline solid. According to the Handbook of Chemistry and Physics, its density at 20°C is 1.2475. It is often classified as insoluble in water. Nevertheless, its solubility is sufficient to record its UV spectrum in aqueous solution. The solubility was evaluated by comparing the UV spectrum of an aqueous saturated solution with the spectrum of a solution of known concentration in a mixture MeOH–H_2O (5:95 v/v), and it was evaluated at $(4.8 \pm 0.3) \times 10^{-3}$ M (i.e., 71 ppm), which is in good agreement with literature data (74–80 ppm (4)). It was checked that the molar absorption coefficient of 1,4-DCB is not influenced by low percentage of MeOH.

The UV spectrum of 1,4-DCB is given in Fig.1. The absorption band has several maxima located at 264, 271, and 280 nm. The corresponding molar absorption coefficients were evaluated at 246, 310, and 236 M^{-1} cm^{-1} respectively. No absorption was detected at $\lambda > 290$ nm.

Direct photolysis at 254 nm

Air-saturated solutions

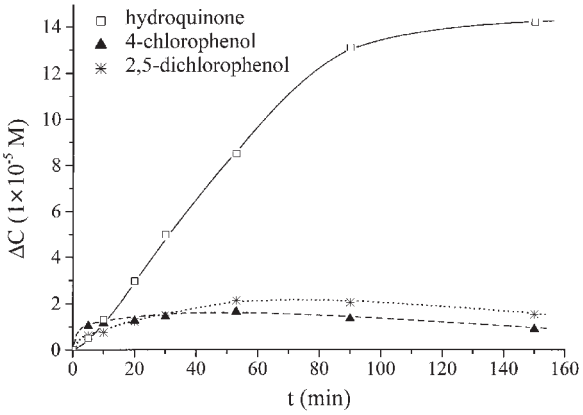
A solution (4.7×10^{-4} M) was irradiated for a few hours at 254 nm. The quantum yield, calculated by HPLC measurement of the amount of 1,4-DCB transformed, was determined to be $\phi = 0.050 \pm 0.01$. This value is significantly higher than the previous evaluation (0.01) (5). The significant increase of absorbance during the irradiation complicates the evaluation of absorbed light and, consequently, the calculation of the quantum yield.

The disappearance of 1,4-DCB can be compared with the formation of H^+ and Cl^- evaluated from the pH decrease and specific electrode measurements, respectively (Table 1). It was experimentally proved that the relative formation of H^+ and Cl^- increases with increasing conversion, which may be related to the elimination of the second chlorine atom in a secondary reaction.

The main products identified on the HPLC chromatogram are hydroquinone (**II**), 4-chlorophenol (**III**), 2,5-dichlorophenol (**IV**), and hydroxybenzoquinone (**I**). Their formations were quantified using commercial compounds (Fig. 2) except for hydroxybenzoquinone, which was only qualitatively identified. It was noted that the formation of 2,5-dichlorophenol is twice as high in oxygen-saturated solution as compared to the air-saturated solution. The major product initially formed is 4-chlorophenol, but it does not accumulate and its formation reached a stationary concentration after a few minutes. This phenomenon is related with a short delay observed in the formation of hydroquinone, which is due to the high transformation quantum yield of 4-chlorophenol, higher than 0.6 according to Grabner et al. (16). Therefore, it was not possible to establish an accurate

© 2001 NRC Canada

Fig. 2. Quantification of the main photoproducts identified in an air-saturated aqueous solution of 1,4-DCB (3.7×10^{-4} M) irradiated at 254 nm (one germicidal lamp).

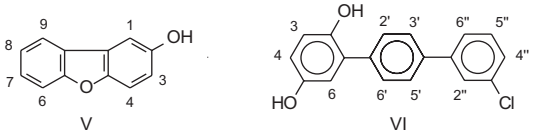


initial mass balance. To prove that 4-chlorophenol cannot accumulate in the solution, 4-chlorophenol (1.4×10^{-5} M) was added to a solution of 1,4-DCB (8.9×10^{-5} M), and after 10 min irradiation the concentration of 4-chlorophenol was only 1.2×10^{-6} M.

The phototransformation of 1,4-DCB was also observed in solutions irradiated in the range 275–350 nm, along with the formation both of hydroxybenzoquinone and trace amounts of hydroquinone. 4-Chlorophenol and 2,5-dichlorophenol are formed in a first stage as it appears in Fig. 2, but do not accumulate in these conditions due to the fact they absorb at longer wavelengths than 1,4-DCB.

Deoxygenated solutions

Solutions of 1,4-DCB (3.7×10^{-4} M), deoxygenated as reported in *Experimental* section, were irradiated at 254 nm. The formation of 2,5-dichlorophenol was not observed, but two unexpected photoproducts **V** and **VI** appeared on the HPLC chromatogram. These two products were not observed in irradiated diluted solutions (6.7×10^{-5} M). They were isolated as described in the *Experimental* section and identified by MS and ^{1}H NMR spectroscopy, respectively, as 2-hydroxydibenzofuran (2-HDBF) and 3″-chloro-2,5-dihydroxy-*p*-terphenyl (CDTP):



V VI

*Product **V**:* MS *m*/*z* (%): 184 ($M^{\bullet+}$, 100), 128. ^{1}H NMR (CD_3COCD_3) δ 8.37 (s, OH), 8.00 (dd, *J* = 7.0, 1.3 Hz, H6), 7.55 (dd, *J* = 7.9, 0.9 Hz, H9), 7.47 (dt, *J* = 7.9, 1.3 Hz, H8), 7.47 (d, *J* = 2.5 Hz, H1), 7.44 (d, *J* = 8.8 Hz, H4), 7.33 (dt, *J* = 7.5, 0.9 Hz, H7), 7.01 (dd, *J* = 8.8, 2.5 Hz, H3).

The identification of **V** was corroborated by its typical UV spectrum (maxima at 251, 289, 310–320 nm) and by comparison of its HPLC retention time with those of an authentic sample of 2-HDBF obtained by photolysis of phenylbenzoquinone.

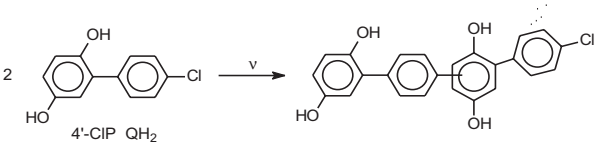
*Product **VI**:* MS *m*/*z* (%): 296 ($M^{\bullet+}$, 100), 298 ($M^{\bullet+}$, 33), consistent with $C_{18}H_{13}ClO_2$. ^{1}H NMR (CD_3COCD_3) δ 7.83 (s, OH), 7.82 (s, OH), 7.72 (t, *J* = 1.9 Hz, H2″), 7.70 (s, 4H, H2′, 3′, 5′, 6′), 7.67 (m, H6″), 7.49 (t, *J* = 7.9 Hz, H5″), 7.39 (m, H4″), 6.86 (d, *J* = 3.0 Hz, H6), 6.84 (d, *J* = 8.75 Hz, H3), 6.69 (dd, *J* = 8.75, 3.0 Hz, H4).

It was deduced from the H–H COSY spectrum that the four protons 2′, 3′, 5′, and 6′ are fortuitously equivalent and generate a single absorption (δ = 7.70 ppm) without any apparent coupling constant.

Three other photoproducts were identified as phenol (*m*/*z* = 94), 4,4′-dichlorobiphenyl (*m*/*z* = 222, 224, 226) and 2,4′,5-trichlorobiphenyl (*m*/*z* = 256, 258, 260) from GC–MS analysis of the crude product of phototransformation after evaporation of water.

The formations of 2-HDBF and terphenyl derivative were also observed in deoxygenated solutions of 1,4-DCB irradiated between 275 and 350 nm. Some complementary experiments were carried out to explain the formation of 2-HDBF in deoxygenated solution. (*i*) A deoxygenated solution of hydroquinone (6.7×10^{-4} M) and 1,4-DCB ($c \approx 4 \times 10^{-3}$ M) was irradiated in the range 290–350 nm. In these conditions the excitation of 1,4-DCB is negligible compared to the excitation of hydroquinone. It was observed that 2-HDBF appears as one of the main photoproducts. (*ii*) 4′-Chloro-2,5-dihydroxybiphenyl (4′-$ClPhQH_2$), synthesized as described in the *Experimental* section, was irradiated in the range 290–350 nm in various conditions. 2-HDBF was the main photoproduct on HPLC chromatogram of a deoxygenated dilute solution ($c \approx 6 \times 10^{-5}$ M) irradiated for a few minutes. This reaction was not observed in the presence of oxygen and it is a minor pathway when the concentration of 4′-$ClPhQH_2$ is as high as 1.4×10^{-3} M. In relatively concentrated solutions irradiation leads to the formation of an insoluble product identified as an adduct resulting from elimination of HCl between two molecules (CI-MS *m*/*z* = 404, 405 [M + 1], and 433 [M + 29]).

[3]



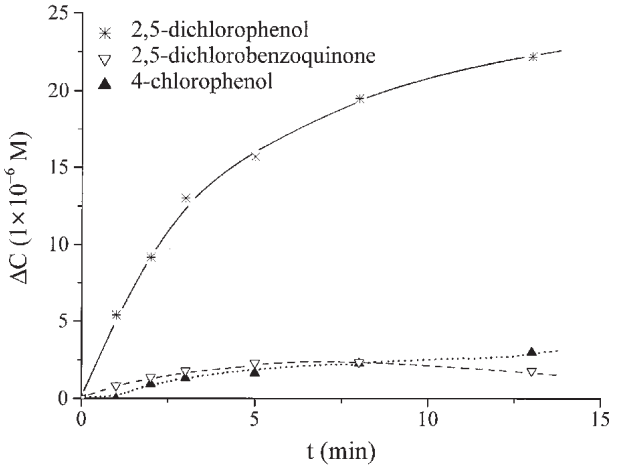
Reactions induced by excitation of nitrate ions or ferric ions

Nitrate ions absorb at wavelengths shorter than 340 nm with a maximum at 302 nm (molar absorption coefficient ε = 7.2 M^{-1} cm^{-1} at 302 nm), hence, when solutions are irradiated in the range 290–350 nm, NO_3^- is excited without excitation of 1,4-DCB.

An air-saturated solution of 1,4-DCB (3.3×10^{-4} M) and KNO_3 (1×10^{-2} M) was irradiated between 290 and 350 nm. The incident photon flow was roughly 6×10^{15} photons cm^{-3} s^{-1} (see *Experimental* section), but the solution absorbs only a fraction of this energy (probably less than 20%). The main photoproduct detected on the HPLC chromatogram of a solution irradiated for 165 min was 2,5-dichlorophenol. The formation of 4-chlorophenol was also observed, but in such minor amounts that it could not be quantified. Nitrate ions

© 2001 NRC Canada

Fig. 3. Quantification of the main photoproducts identified in an air-saturated aqueous solution of 1,4-DCB (3.6×10^{-4} M) irradiated at 365 nm in the presence of ferric salts (1×10^{-3} M).



are converted into nitrite. 2,5-Dichlorophenol presents a kinetics of formation of primary photoproduct.

The mass balance was not expected to be very good since irradiations were long and in a range where most of photoproducts, such as 2,5-dichlorophenol, 4-chlorophenol, hydroquinone, benzoquinone (not quantified but necessarily formed from 4-chlorophenol), absorb.

Ferric salts absorb at longer wavelengths than nitrate ions and can be excited at 365 nm without excitation of 1,4-DCB. In our experimental conditions, only quinones are expected to absorb at this wavelength. However, it can be noted that the lamps used for the irradiation have a minor emission at 313 nm (about 3% of photons) and at 334 nm (about 6%). A solution of 1,4-DCB (2.6×10^{-4} M) with added ferric salt (1×10^{-3} M) was irradiated under these conditions. The main photoproducts detected by HPLC are 2,5-dichlorophenol, 2,5-dichlorobenzoquinone, and 4-chlorophenol. These products present a kinetics of primary photoproducts (Fig. 3). A small amount of benzoquinone was also detected at 250 nm.

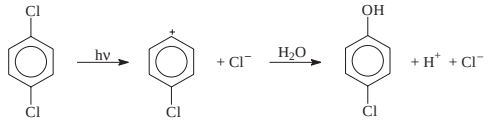
The absence of hydroquinone and 2,5-dichlorohydroquinone result from their oxidation by Fe^{III}, as it was checked that Fe^{III} easily oxidizes these two compounds into 1,4-benzoquinone and 2,5-dichloro-1,4-benzoquinone, respectively.

Discussion and mechanisms

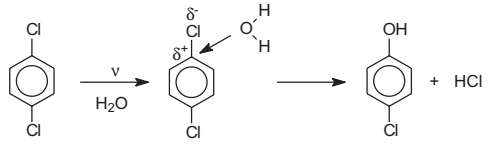
Direct photolysis

Formation of 4-chlorophenol and hydroquinone

In previous work the main initial reaction was assumed to be a photohydrolysis leading to the formation of 4-chlorophenol (5). This mechanism is most likely since it also agree with the phototransformation of monochlorobenzene and several other chloroaromatic derivatives, such as 3-chlorophenol (17), 3-chloroaniline, and one derivative used as a pesticide (18). The intermediate formation of a carbocation may be suggested (eq. [4]),

[4] 

but a concerted mechanism is more likely since, in the case of 3-chlorophenol and 3-chloroaniline, no transient was observed in laser flash photolysis (eq. [5]).

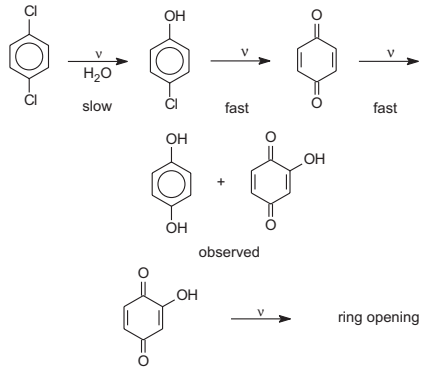
[5] 

Photohydrolysis may be assumed to occur either from the excited singlet state or from the triplet state. The triplet state is more likely for the following reasons: (*i*) Alfassi and Previtali (6) experimentally proved that the yield of formation of 1,4-DCB triplet state is about 0.95 in methanol; (*ii*) the photohydrolysis of monochlorobenzene can be sensitized by acetone-d_6 (19); and (*iii*) the photohydrolysis of monohalogenophenols can also be sensitized (20).

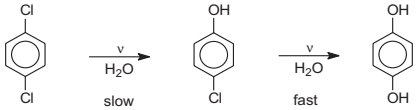
4-Chlorophenol does not accumulate much since it absorbs at the irradiation wavelengths and its quantum yield of disappearance is high. It does, however, accumulate a little better when solutions are irradiated at 254 nm as compared to 275–350 nm, because it absorbs more at longer wavelengths when compared to 1,4-DCB. According to the concentration of oxygen, it is transformed into hydroquinone (20–22). The reaction involves the intermediate formation of a carbene (20, 23). *p*-Benzoquinone cannot be observed when solutions are irradiated at 254 nm since it has a strong absorption band at 245 nm and it is easily phototransformed into hydroquinone (12). Thus, the formation of hydroquinone in air-saturated solutions is attributed to the following sequence controlled by the first step (eq. [6]), whereas in the absence of oxygen hydroquinone is formed by photohydrolysis (eq. [7]) (21).

© 2001 NRC Canada

[6]



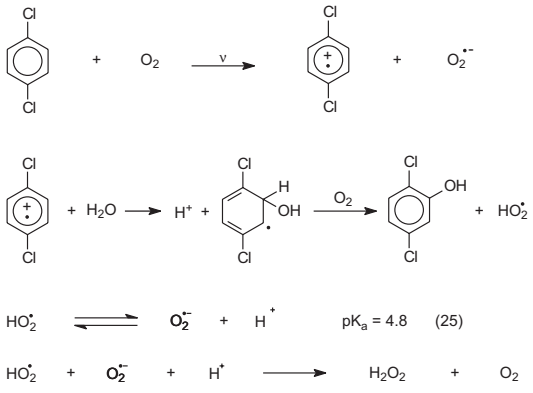
[7]



Formation of 2,5-dichlorophenol

The formation of 2,5-dichlorophenol is not negligible when 1,4-DCB is irradiated in pure water. It was not observed in the absence of oxygen, which is not surprising since it implies the oxidation of the ring. It can be explained either by the photoionization of the excited singlet state or by the oxidation of triplet state by oxygen or by the oxidation of the ground state by singlet oxygen resulting from the deactivation of 1,4-DCB. The latter may be ruled out because the rate of deactivation of singlet oxygen in water is 5×10^5 s^{-1} (24) and the rate of reaction of 1,4-DCB is ca. 1.7×10^5 M^{-1} s^{-1} or lower, since it is 1.7×10^5 with 9,10-dichloroanthracene in $CHCl_3$ (24). With a concentration of 1,4-DCB equal to 4.7×10^{-4} M, the rate of reaction of $^1O_2$ is expected to be ca. 6000 times lower than the rate of deactivation. In contrast, both other mechanisms are consistent with experimental results. If the formation of 2,5-dichlorophenol results from the photoionization of the singlet state, the effect of oxygen is explained by a competition between the trapping of ejected electron by oxygen and the recombination electron–cation. On the other hand the oxidation of the triplet state of 1,4-DCB by oxygen is consistent with the lifetime of the triplet state. It can be noted that the lifetime of the triplet state of 1,4-DCB is most likely shorter in water than in methanol (3.3 μs according to ref. 6), since Previtali and Ebbesen (7) reported that the triplet state of monochlorobenzene is about 10 times shorter in water than in methanol.

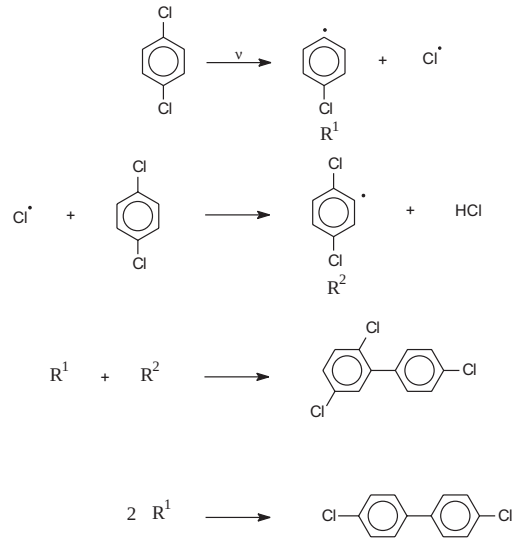
[8]



In a second stage, 2,5-dichlorophenol may be formed by $OH^\bullet$ radicals resulting from the excitation of H_2O_2.

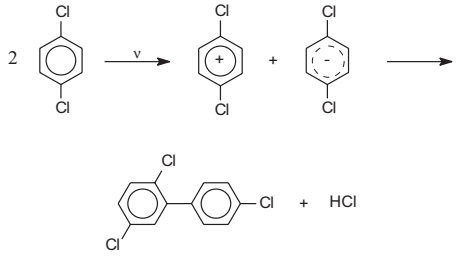
In the absence of oxygen the formation of 4,4′-dichlorobiphenyl and 2,4′,5-trichlorobiphenyl may be explained by the C–Cl bond homolysis in the triplet state:

[9]



However, the charge transfer from the triplet state, disregarded in the case of monochlorobenzene (7), cannot be excluded here since the triplet state has a high yield of formation (0.95) and a longer lifetime (6).

[10]

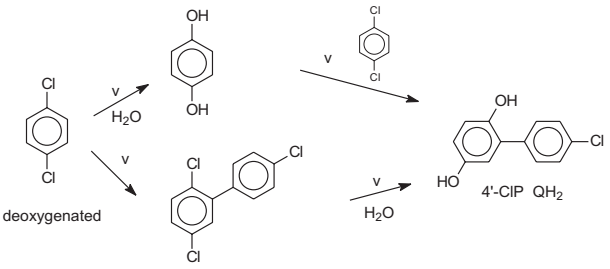


Formation of 2-hydroxydibenzofuran (2-HDBF) and 3″-chloro-2,5-dihydroxy-p-terphenyl (CDTP)

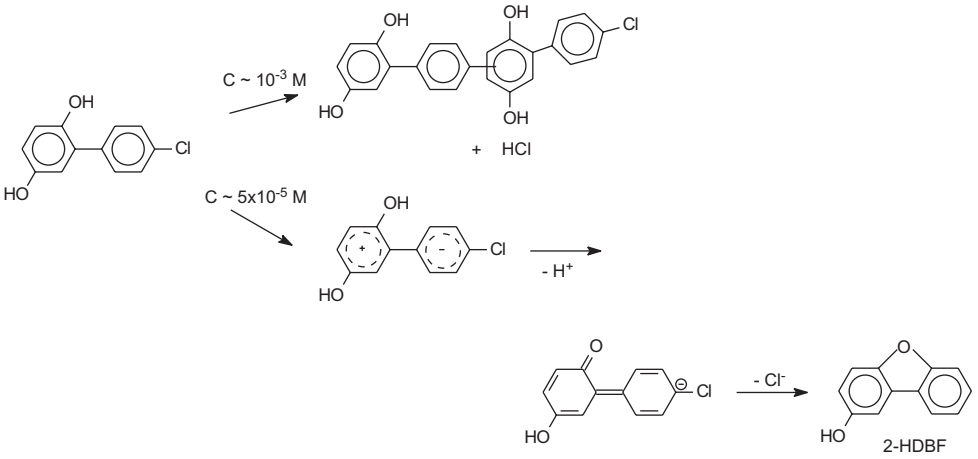
It was previously reported that phenylbenzoquinone photocyclizes with a high yield into 2-HDBF (13). In our experimental conditions it is difficult to explain the intermediate formation of phenylbenzoquinone. In addition, the following features can be noted: (*i*) the formation of 2-HDBF was observed when a deoxygenated solution of hydroquinone is excited in the presence of 1,4-DCB; (*ii*) the excitation of a deoxygenated mixture hydroquinone and 4-chlorophenol leads to the formation of 2,4′,5-trihydroxybiphenyl (20); (*iii*) 2,4′,5-trichlorobiphenyl is expected to be photohydrolyzed into 4′-chloro-2,5-dihydroxybiphenyl (4′-$ClPhQH_2$) (other products are not excluded); and (*iv*) it was observed (present work) that 4′-$ClPhQH_2$ irradiated in diluted deoxygenated solution leads to the formation of 2-HDBF. Therefore, the formation of 2-HDBF may be attributed to an internal charge transfer in excited 4′-$ClPhQH_2$. In relatively concentrated solutions an intermolecular charge transfer leads to the formation of a four-ring adduct (eq. [11*b*]).

© 2001 NRC Canada

[11a]

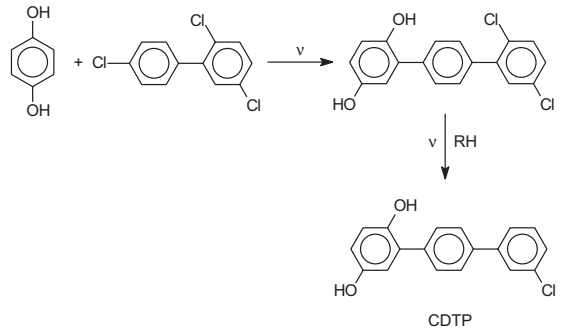


[11b]



The formation of CDTP may be explained similarly by the addition of hydroquinone on 2,4′,5-trichlorobiphenyl followed by a reductive elimination of one chlorine atom.

[12]



Induced phototransformation

The excitation of nitrate ions or ferric salts leads to the formation of hydroxyl radicals:

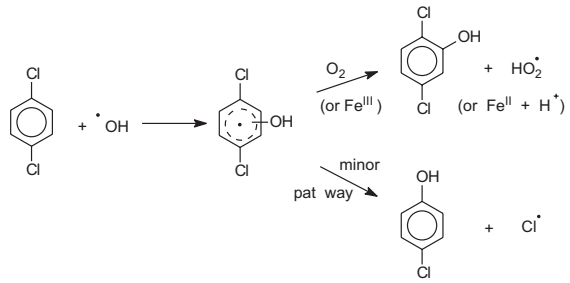
[13]

$$NO_3^- + H_2O \xrightarrow{v} {}^{\bullet}NO_2 + {}^{\bullet}OH + {}^{-}OH \quad (26)$$

$$Fe^{III}\text{–}OH \xrightarrow{v} Fe^{II} + {}^{\bullet}OH \quad (27)$$

The formation of 4-chlorophenol and 2,5-dichlorophenol result from the hydroxylation of the ring with or without dechlorination:

[14]



Hydroquinone observed in the case of excitation of nitrate ions may result from the further photohydrolysis of 4-chlorophenol or from the substitution of Cl by $OH^{\bullet}$. In the case of the excitation of Fe^{III}, hydroquinone and 2,5-dichlorohydroquinone cannot be observed since they are oxidized by Fe^{III}. The observed formation of benzoquinone and 2,5-dichlorobenzoquinone result from this oxidation.

Acknowledgments

The authors thank Ministère de la Recherche et de la Technologie (MRT) and Centre National de la Recherche Scientifique (CNRS) for their financial supports. They are grateful to M. Renard and D. Harakat for their assistance in mass spectrometry.

References

1. M.E. Meek, M. Giddings, and R. Gomes. Environ. Carcin. Eco. R. **12**, 277 (1994) and refs. cited therein.

© 2001 NRC Canada

2. Merck Index. 11th ed. Merck & Co. Inc., Rahway, New Jersey, U.S.A. 1989. p. 482.
3. Merck Index. 11th ed. Merck & Co. Inc., Rahway, New Jersey, U.S.A. 1989. p. 332.
4. R.J. Lewis. Sax's dangerous properties of industrial materials. Report 13. 8th ed. Van Nostrand Reinhold, New York. 1993. p. 128.
5. P. Boule, A. Tissot, and J. Lemaire. Chemosphere, **14**, 1789 (1985).
6. Z.B. Alfassi and C.M. Previtali. J. Photochem. **30**, 127 (1985).
7. C.M. Previtali and T.W. Ebbesen. J. Photochem. **30**, 259 (1985).
8. A. Tissot, P. Boule, and J. Lemaire. Chemosphere, **13**, 381 (1984).
9. G. Merga, H.-P. Schuchmann, B.S. Madhava Rao, and C. von Sonntag. J. Chem. Soc. Perkin Trans. 2, 1097 (1996).
10. P. Brassard and P. L'Ecuyer. Can. J. Chem. **36**, 700 (1958).
11. B.W. Carlson and L.L. Miller. J. Am. Chem. Soc. **107**, 479 (1985).
12. A. Rossi, G. Guyot, and P. Boule. C.R. Ac. Sci. Paris **303**, Série II, 1179 (1986).
13. M. Sarakha, A. Rossi, G. Guyot, and P. Boule. C.R. Ac. Sci. Paris **307**, Série II, 739 (1988).
14. J.F. Rabek. Experimental methods in photochemistry and photophysics. The University Press, Belfast, 1982. pp. 944–949.
15. (*a*) H.G. Heller and J.R. Langan. J. Chem. Soc. Perkin Trans. 2, 341 (1981); (*b*) Z. Guo, G. Wang, Y. Tang, and X. Song. J. Photochem. Photobiol. A, **88**, 31 (1995) and refs. cited therein.
16. G. Grabner, C. Richard, and G. Köhler. J. Am. Chem. Soc. **116**, 11470 (1994).
17. P. Boule G. Guyon, and J. Lemaire. Chemosphere, **11**, 1179 (1982).
18. B. David, M. Lhote, V. Faure, and P. Boule. Water Res. **32**, 2451 (1998).
19. A. Tissot, P. Boule, and J. Lemaire. Chemosphere, **13**, 381 (1984).
20. K. David-Oudjehani and P. Boule. New J. Chem. **19**, 199 (1995).
21. K. Oudjehani and P. Boule, J. Photochem. Photobiol. A, **68**, 363 (1992).
22. A-P.Y. Durand and R.G. Brown. Chemosphere, **31**, 3595 (1995).
23. A-P.Y. Durand, R.G. Brown, D. Worral, and F. Wilkinson. J. Photochem. Photobiol. A, **96**, 35 (1996).
24. F. Wilkinson and J.G. Brummer. J. Phys. Chem. Ref. Data, **10**, 810 (1981).
25. B.H.J. Bielski, D.E. Cabelli, R.L. Arudi, and A.B. Ross. J. Phys. Chem. Ref. Data, **14**, 1041 (1985).
26. M. Daniels, R.V. Meyers, and E.V. Belardo. J. Phys. Chem. **72**, 389 (1968).
27. B.C. Faust and J. Hoigné. J. Atm. Env. **24A**, 79 (1990).

© 2001 NRC Canada

Dimeric and polymeric [Eu(tta)$_3$L] complexes (tta = thenoyltrifluoroacetonato, L = 4,4′-bipyridine, *trans*-1,2-bis(4-pyridyl)ethylene, 4,4′-bipyridine-*N*,*N*′-dioxide)

Corey Seward and Suning Wang

Abstract: The reaction of Eu(tta)$_3$ (tta = thenoyltrifluoroacetonato) with 4,4′-bipyridine (bipy), *trans*-1,2-bis(4-pyridyl)ethylene (bipyete), and 4,4′-bipyridine-*N*,*N*′- dioxide (bipyo) yielded three distinct complexes [Eu(tta)$_3$(bipy)(H$_2$O)] (**1**), [Eu(tta)$_3$(bipyete)(CH$_3$OH)]·CH$_3$OH·bipyete (**2**), and [Eu(tta)$_3$(bipyo)]·CH$_3$OH (**3**), respectively. Compounds **1** and **2** have a hydrogen-bond linked dimer structure, while **3** has a one-dimensional chain structure linked by coordination bonds, which further forms two-dimensional arrays, resulting in an intercalation lattice that hosts methanol guest molecules. In solution compounds **1** and **2** emit a red color, characteristic of Eu(III), when irradiated by UV light, while compound **3** has no emission either in solution or the solid state.

Key words: europium complexes, luminescence, structure, 4,4′-bipyridine, 1,2-bis(4-pyridyl)ethylene, 4,4′-bipyridine-*N*,*N*′-dioxide.

Résumé : Les réactions de Eu(tta)$_3$ (tta = thénoyltrifluoroacéténato) avec la 4,4′-bipyridine (bipy), le *trans*-1,2-bis(4-pyridyl)éthylène (bipyete) et le *N*,*N*′-dioxyde de la 4,4′-bipyridine (bipyo) conduisent à trois complexes distincts qui sont respectivement [Eu(tta)$_3$(bipy)(H$_2$O)] (**1**), [Eu(tta)$_3$(bipyete)(CH$_3$OH)]·CH$_3$OH·bipyete (**2**) et [Eu(tta)$_3$(bipyo)]·CH$_3$OH (**3**). Les composés **1** et **2** comportent une structure dimère reliée par des liaisons hydrogènes alors que la structure du composé **3** est une chaîne unidimensionnelle avec des liaisons de coordination qui forme ensuite des arrangements bidimensionnels qui conduit à un réseau d'intercalation qui agit comme hôte pour les molécules de méthanol invitées. En solution, lorsqu'ils sont soumis à une irradiation par de la lumière UV, les composés **1** et **2** donnent lieu à l'émission d'une couleur rouge caractéristique de Eu(III) alors que le composé **3** ne donne lieu à aucune émission en solution ou à l'état solide.

Mots clés : complexes d'europium, luminescence, structure, 4,4′-bipyridine, 1,2-bis(4-pyridiyl)éthylène, *N*,*N*′-dioxyde de la 4,4′-bipyridine.

[Traduit par la Rédaction]

Introduction

Thenoyltrifluoroacetonato europium(III) complexes of the general formula Eu(tta)$_3$L (tta = thenoyltrifluoroacetonato and L = a neutral chelate, e.g., 1,10-phenanthroline) have attracted much attention recently because some of them have been demonstrated to be promising red emitters in electroluminescent devices (1). The tta ligand is one of the best ligands known for activating red emission of Eu(III) ions (2). Because of the poor volatility of Eu(tta)$_3$L complexes, the electroluminescent devices that use them as emitters are often fabricated by doping into a polymer matrix (1). Linking the Eu(tta)$_3$ units together by bridging ligands could lead to polynuclear species that may facilitate the direct thin-film formation of Eu(III) compounds by spin-coating without using a polymer matrix. Recently we have demonstrated the utility of the 4,4′-bipyridine ligand and the roles of polynuclear species in promoting luminescent film formation of Tb(III) benzoate compounds by spin-coating processes (3). In addition to 4,4′-bipyridine (bipy), *trans*-1,2-bis(4-pyridyl)ethylene (bipyete) and 4,4′-bipyridine-*N*,*N*′-dioxide are also known to be good bridging ligands for metal ions (4, 5). Therefore, we examined the utility of bipy, bipyete, and bipyo as bridiging ligands for the formation of luminescent polynuclear complexes containing the Eu(tta)$_3$ unit. Three novel Eu(III) complexes have been isolated and characterized, which show distinct structural features and luminescent properties. The detail is described herein.

Received March 1, 2001. Published on the NRC Research Press Web site at http://canjchem.nrc.ca on August 3, 2001.

C. Seward and S. Wang.[1] Department of Chemistry, Queen's University, Kingston, ON K7L 3N6, Canada.

Corresponding author (fax: (613) 545-6669 e-mail: wangs@chem.queensu.ca.).

Experimental

All syntheses were carried out in a fumehood, in air, at room temperature. Chemicals were purchased from Aldrich and used without further purification. Methanol was purchased from Caledon and used without further purification.

 DOI: 10.1139/cjc-79-7-1187 © 2001 NRC Canada

The hydration content of 4,4′-bipyidine-*N*,*N*′-dioxide was determined to be 1.5 by thermogravometric analysis (TGA) using a PerkinElmer TGA7 Thermogravometric Analyzer. Elemental analyses were performed by Canadian Microanalytical Service, Ltd., Delta, British Columbia. Excitation and emission spectra were recorded on a Photon Technologies International QuantaMaster Model C-60 spectrometer.

Synthesis of $[Eu(tta)_3(bipy)(H_2O)]$ (1)

A solution of europium chloride hexahydrate (0.183 g, 0.5 mmol) in a minimum amount of methanol was added to a solution of thenoyltrifluoroacetone (Htta) (0.333 g, 1.5 mmol) dissolved in a minimum amount of methanol in a 20 mL vial. The pale yellow solution was neutralized with a saturated solution of sodium hydroxide in methanol. Methanol (8 mL) was layered carefully upon this solution, and a solution of 4,4′-bipyridine (0.156 g, 1.0 mmol) in a minimum amount of methanol was added dropwise. The reaction vial was allowed to diffuse slowly, and then the solvent was allowed to evaporate slowly at ambient temperatures, yielding yellow block crystals of **1** in 93% yield. Anal. calcd. for $C_{34}H_{22}F_9N_2O_7S_3Eu$: C 41.26, H 2.24, N 2.83; found: C 41.71, H 2.19, N 3.03.

Synthesis of $[Eu(tta)_3(bipyete)(CH_3OH)]\cdot CH_3OH\cdot$bipyete (2)

Europium chloride hexahydrate (0.5 g, 1.365 mmol), Htta (0.910 g, 4.094 mmol), and sodium hydroxide (0.164 g, 4.094 mmol) were dissolved in methanol (10 mL) with stirring. The solution was filtered into a 40 mL vial, and methanol (8 mL) was carefully layered upon it. A solution of *trans*-1,2-bis(4-pyridyl)ethylene (0.497 g, 2.73 mmol) in methanol (10 mL) was then added dropwise. The reaction vial was allowed to diffuse slowly, then to evaporate slowly at ambient temperatures, yielding pale yellow plates of **2** in 31% yield. Anal. calcd. for $C_{50}H_{40}F_9N_4O_8S_3Eu$: C 48.28, H 3.24, N 4.50; found: C 48.24, H 2.84, N 4.43.

Synthesis of $[Eu(tta)_3(bipyo)]\cdot$MeOH (3)

Europium chloride hexahydrate (0.125 g, 0.34 mmol), Htta (0.227 g, 1.02 mmol), and sodium hydroxide (0.040 g, 1.02 mmol) were dissolved in methanol (10 mL). Methanol (10 mL) was carefully layered upon the solution. A solution of 4,4′-bipyridine-*N*,*N*′-dioxide·1.5hydrate (0.128 g, 0.595 mmol) in methanol (10 mL) was added dropwise. The reactants were allowed to diffuse slowly, then the solvent was allowed to evaporate slowly at ambient temperatures, affording pale yellow needles of **3** in 39% yield. Anal. calcd. for $C_{35}H_{24}F_9N_2O_9S_3Eu$: C 40.59, H 2.34, N 2.70; found: C 39.98, H 2.16, N 2.70.

X-ray crystallography analysis

Single crystals of **1**–**3** were obtained from methanol solutions, and mounted on glass fibres. Data were collected on a Bruker SMART CCD 1000 diffractometer with graphite-monochromated Mo Kα radiation, operated at 50 kV and 35 mA at 23°C for **1** and **2**, and at 25°C for **3**. The 2θ ranges were 3.82–50.02, 3.64–45.02, and 2.22–46.60° for **1**, **2**, and **3**, respectively. No significant decay was observed. Data were processed on a Pentium PC using Bruker AXS SHELXTL software package (version 5.1) (6). The structures were solved by direct methods. One of the C_5H_3S rings in each structure displays a small degree of rotational disorder but could not be modeled. Some of the CF_3 groups that display a typical rotational disorder have been modeled and refined successfully. Metal, sulfur, oxygen, fluorine, nitrogen, and most carbon atoms were refined anisotropically. The positions of hydrogen atoms were calculated, and their contributions in structural factor calculations were included. Crystal data are summarized in Table 1.[2]

Results and discussion

Syntheses and structures

Compounds **1**–**3** were obtained from methanol solution by a "one-pot" reaction of $EuCl_3\cdot 6H_2O$ with Htta and the bridging ligand bipy, bipyete, or bipyo in the presence of NaOH. Although similar reaction conditions were employed for the three compounds, compounds **1**–**3** have distinct compositions and structures. Compound **1** $[Eu(tta)_3(bipy)(H_2O)]$ has one bipy ligand and one aqua ligand, compound **2** $[Eu(tta)_3(bipyete)(CH_3OH)]\cdot CH_3OH\cdot$bipyete has one coordinated bipyete ligand, one free bipyete, one coordinated methanol ligand, and one non-coordinate methanol ligand, and compound **3** $[Eu(tta)_3(bipyo)]\cdot CH_3OH$ has one bipyo ligand and one non-coordinate methanol molecule.

Compound **1** was synthesized initially with the intention to produce bipy linked polynuclear Eu(III) compounds. X-ray crystal structural analysis, however, revealed that compound **1** has a dimeric structure in the solid state. As shown in Fig. 1, only one nitrogen donor from each bipy ligand is coordinated to the Eu(III) center. The remaining nitrogen donor forms a hydrogen bond with the aqua ligand as indicated by the N(2A)···O(7) distance of 2.74(1) Å. The two bipy ligands are nearly eclipsed with the shortest atomic separation distance between the two ligands being 3.63(2) Å. The Eu(III) center is eight-coordinated with an approximate square antiprism geometry, commonly observed in lanthanide complexes. The separation distance between the two Eu(III) centers is 13.367 Å and the N(1)-Eu(1)-O(7) angle is 76.5(5)°. All three C_4H_3S rings are oriented away from the bipy ligands (i.e., adopting the pseudo "*fac*" geometry), perhaps to minimize the interactions between bipy and tta ligands. The failure of bipy to link $Eu(tta)_3$ units together by coordination bonds to form polynuclear species is somewhat surprising since bipy is a well-known ligand to act as a bridge between two metal ions. One possible explanation is the geometric (i.e., N-Eu-N bond angle) restriction that

[2] Crystallographic information may be purchased from the Depository of Unpublished Data, Document Delivery, CISTI, National Research Council Canada, Ottawa, ON K1A 0S2, Canada. For information on obtaining material electronically go to http://www.nrc.ca/cisti/irm/unpub_e.shtml. Crystallographic information has also been deposited with the Cambridge Crystallographic Data Centre. Copies of the data can be obtained, free of charge, on application to the Director, CCDC, 12 Union Road, Cambridge CB2 1EZ, U.K. (fax: 44-1223-336033 or e-mail: deposit@ccdc.cam.ac.uk).

© 2001 NRC Canada

Table 1. Crystal data.

Compound	**1**	**2**	**3**
Formula	$C_{34}H_{22}F_9N_2O_7S_3Eu$	$C_{50}H_{40}F_9N_4O_8S_3Eu$	$C_{35}H_{24}F_9N_2O_9S_3Eu$
FW (g mol^{-1})	989.68	1244.01	1035.70
Crystal system	Monoclinic	Monoclinic	Triclinic
Space group	$P2_1/n$	$P2_1/c$	$P\bar{1}$
a (Å)	12.981(4)	15.259(9)	10.8130(12)
b (Å)	18.067(6)	17.555(9)	10.8971(14)
c (Å)	16.933(8)	20.592(11)	18.628(2)
α (°)	90	90	95.161(2)
β (°)	94.44(2)	108.33(6)	94.963(2)
γ (°)	90	90	111.134(2)
V (Å^3)	3960(3)	5236(5)	2022.3(4)
Z	4	4	2
$\rho_{calcd.}$ (g cm^{-3})	1.660	1.578	1.701
Crystal size (mm)	0.1 × 0.4 × 0.3	0.05 × 0.5 × 0.3	0.2 × 0.2 × 0.4
Absorp. coeff. (mm^{-1})	1.832	1.405	1.801
T (K)	296(2)	296(2)	298(2)
No. unique reflections	6984	6837	5744
No. reflections used	6984	6837	5744
No. parameters used	517	694	533
R_{int}	0.1613	0.0597	0.0491
R_1 [$I > 2\sigma(I)$]	0.0997	0.0736	0.0624
wR_2 [$I > 2\sigma(I)$]	0.2435	0.1721	0.1591
$2\theta_{max}$ (°)	50.02	45.02	46.60
GoF	1.019	1.022	0.945

would force the bipy ligand to bend if the bipy ligand were bridging two Eu(III) ions by coordination bonds.

To increase the flexibility of the bridging ligand, we replaced bipy with a longer bridging ligand *trans*-1,2-bis(4-pyridyl)ethylene, resulting in compound **2**, $[Eu(tta)_3(bipyete)(CH_3OH)]\cdot CH_3OH\cdot bipyete$.

The structure of **2**, shown in Fig. 2, resembles that of **1**. The bipyete ligand is bound to the Eu(III) center by one nitrogen atom only. A methanol molecule is coordinated to the Eu(III) center, which forms a hydrogen bond with N(2A) atom, as indicated by N(2A)···O(7) distance of 2.68(1) Å. The N(1)-Eu(1)-O(7) angle of 73.5(3)° is slightly less than the corresponding angle in **1**. The Eu(1)···Eu(1A) separation distance of 15.583 Å is much longer than that in **1**, which is not surprising since the bipyete ligand contains an extra CH=CH unit with respect to 4,4′-bipy. In contrast to the structure of **1**, two of the C_4H_3S rings are oriented away from bipyete, while the third one is oriented toward the bipyete ligands. The two bipyete ligands are planar and are nearly eclipsed with the shortest atomic separation distance between them being 3.483 Å. There is a non-coordinating bipyete molecule in the lattice, which forms a hydrogen bond with a non-coordinating methanol solvent molecule. The non-coordinating bipyete molecule stacks with coordinated bipyete ligands in the crystal lattice as shown by the crystal packing diagrams in Fig. 3. The shortest atomic separation distance between the coordinate and non-coordinate bipyete ligands is 3.405 Å. The planarity of the bipyete ligand, attributable to the conjugation of the pyridyl portion with the ethylene portion, forces the bipyete ligand to coordinate to the Eu(III) center in a similar linear fashion as observed for the 4,4′-bipy in **1**, which is again believed to be responsible for the formation of the hydrogen-bond linked dimer structures of **2**.

The third bridging ligand we investigated was 4,4′-bipyrdine-*N*,*N*′-dioxide (bipyo). Long et al. (5*a*) have shown recently that bipyo is capable of linking lanthanide ions together by coordination bonds. Because of the geometry of the lone pairs of electrons from the oxygen atoms, the bipyo ligand has been found to bind to two metal ions in a nonlinear fashion, with the two metal ions being either *trans* or *cis* with respect to the bipyridyl unit (5). Hence, we anticipated that the bipyo ligand may be able to link two $Eu(tta)_3$ units together by coordination bonds. Indeed, as shown by the structure of compound **3** in Fig. 4, the bipyo ligand functions as a bridging ligand by binding to two Eu(III) centers through the two oxygen atoms, thus resulting in the formation of a one-dimensional coordination polymer. Each Eu(III) center in **3** is eight-coordinate with an approximate square antiprism geometry. The arrangement of the three tta ligands in **3** has a similar pseudo "*fac*" geometry as observed in **2**. The $Eu(tta)_3$ units are all arranged in a *cis*-fashion, relative to the bipyo chains. The O(7)-Eu(1)-O(8A) angle of 67.4(2)° is much less than the corresponding angles observed in **1** and **2**, and the Eu···Eu separation distance within the one-dimensional chain is 12.276 Å. An interesting feature of **3** is that the one-dimensional chains are coupled in an approximate face-to-face fashion to form a two-dimensional layered array. The shortest nonhydrogen atom separation distance between two neighbouring layers is

© 2001 NRC Canada

Table 2. Selected bond lengths (Å) and angles (°).

Bond lengths (Å)		Bond angles (°)			
Compound 1					
Eu(1)—O(1)	2.335(11)	O(1)-Eu(1)-O(5)	144.8(4)	O(4)-Eu(1)-O(7)	141.3(4)
Eu(1)—O(5)	2.346(11)	O(1)-Eu(1)-O(3)	80.0(5)	O(2)-Eu(1)-O(7)	83.9(5)
Eu(1)—O(3)	2.368(13)	O(5)-Eu(1)-O(3)	82.1(4)	O(6)-Eu(1)-O(7)	70.1(4)
Eu(1)—O(4)	2.379(10)	O(1)-Eu(1)-O(4)	118.3(4)	O(1)-Eu(1)-N(1)	73.4(4)
Eu(1)—O(2)	2.398(11)	O(5)-Eu(1)-O(4)	83.1(4)	O(5)-Eu(1)-N(1)	72.7(4)
Eu(1)—O(6)	2.406(10)	O(5)-Eu(1)-O(2)	144.4(4)	O(3)-Eu(1)-N(1)	74.2(4)
Eu(1)—O(7)	2.429(13)	O(3)-Eu(1)-O(2)	112.4(5)	O(4)-Eu(1)-N(1)	139.3(5)
Eu(1)—N(1)	2.621(12)	O(4)-Eu(1)-O(2)	72.7(4)	O(2)-Eu(1)-N(1)	141.4(4)
		O(1)-Eu(1)-O(6)	138.7(4)	O(6)-Eu(1)-N(1)	123.9(4)
		O(3)-Eu(1)-O(6)	138.1(4)	O(7)-Eu(1)-N(1)	76.5(5)
		O(4)-Eu(1)-O(6)	75.0(4)	O(1)-Eu(1)-O(7)	80.3(5)
		O(2)-Eu(1)-O(6)	77.8(4)	O(5)-Eu(1)-O(7)	100.5(5)
				O(3)-Eu(1)-O(7)	148.3(4)
Compound 2					
Eu(1)—O(3)	2.350(8)	O(3)-Eu(1)-O(5)	81.1(3)	O(5)-Eu(1)-O(7)	74.7(3)
Eu(1)—O(5)	2.349(9)	O(3)-Eu(1)-O(1)	113.4(3)	O(1)-Eu(1)-O(7)	144.2(3)
Eu(1)—O(1)	2.356(9)	O(5)-Eu(1)-O(1)	138.2(3)	O(6)-Eu(1)-O(7)	112.0(3)
Eu(1)—O(6)	2.365(8)	O(3)-Eu(1)-O(6)	144.8(3)	O(2)-Eu(1)-O(7)	144.9(3)
Eu(1)—O(2)	2.378(9)	O(1)-Eu(1)-O(6)	76.9(3)	O(4)-Eu(1)-O(7)	80.0(3)
Eu(1)—O(4)	2.420(8)	O(3)-Eu(1)-O(2)	75.9(3)	O(3)-Eu(1)-N(1)	141.0(3)
Eu(1)—O(7)	2.442(8)	O(5)-Eu(1)-O(2)	76.7(3)	O(5)-Eu(1)-N(1)	117.5(3)
Eu(1)—N(1)	2.603(9)	O(6)-Eu(1)-O(2)	76.8(3)	O(1)-Eu(1)-N(1)	76.7(3)
		O(5)-Eu(1)-O(4)	145.1(3)	O(6)-Eu(1)-N(1)	73.1(3)
		O(1)-Eu(1)-O(4)	74.1(3)	O(2)-Eu(1)-N(1)	139.2(3)
		O(6)-Eu(1)-O(4)	141.9(3)	O(4)-Eu(1)-N(1)	76.6(3)
		O(2)-Eu(1)-O(4)	114.7(3)	O(7)-Eu(1)-N(1)	73.5(3)
		O(3)-Eu(1)-O(7)	79.9(3)		
Compound 3					
Eu(1)—O(4)	2.358(8)	O(4)-Eu(1)-O(6)	74.0(3)	O(4)-Eu(1)-O(8A)	146.8(2)
Eu(1)—O(6)	2.357(7)	O(4)-Eu(1)-O(5)	109.7(3)	O(6)-Eu(1)-O(8A)	82.1(3)
Eu(1)—O(5)	2.367(7)	O(4)-Eu(1)-O(2)	77.2(3)	O(5)-Eu(1)-O(8A)	83.5(3)
Eu(1)—O(2)	2.374(7)	O(6)-Eu(1)-O(2)	76.5(2)	O(2)-Eu(1)-O(8A)	75.0(3)
Eu(1)—O(1)	2.377(7)	O(5)-Eu(1)-O(2)	143.7(3)	O(1)-Eu(1)-O(8A)	106.4(3)
Eu(1)—O(7)	2.390(7)	O(4)-Eu(1)-O(1)	80.7(3)	O(7)-Eu(1)-O(8A)	67.4(2)
Eu(1)—O(8A)	2.412(7)	O(6)-Eu(1)-O(1)	142.1(3)	O(6)-Eu(1)-O(3)	118.9(3)
Eu(1)—O(3)	2.403(7)	O(5)-Eu(1)-O(1)	144.8(3)	O(5)-Eu(1)-O(3)	75.5(2)
		O(4)-Eu(1)-O(7)	143.5(3)	O(2)-Eu(1)-O(3)	137.2(3)
		O(6)-Eu(1)-O(7)	140.1(3)	O(1)-Eu(1)-O(3)	76.9(3)
		O(5)-Eu(1)-O(7)	79.6(2)	O(7)-Eu(1)-O(3)	78.2(2)
		O(2)-Eu(1)-O(7)	116.7(2)	O(8A)-Eu(1)-O(3)	142.3(3)
		O(1)-Eu(1)-O(7)	73.8(3)		

~5.4 Å. Furthermore, methanol solvents are situated in the channels between the layers as shown in Fig. 5. The methanol molecule (O(9)) forms a hydrogen bond with O(7) atom of the bipyo ligand as evident by the O(7)···O(9) distance of 2.967 Å. The extended structure of **3** can be, therefore, considered as a two-dimensional intercalation (7) host material for methanol guest molecules. TGA experiments indicated the methanol molecules in **3** could be driven out of the host lattice by heating to 65°C, but the readsorption of methanols to the crystal lattice appears to be irreversible.

Luminescence

$Eu(tta)_3$ and $Eu(tta)_3(phen)$ are well-known to have a bright red luminescence, attributed to the efficient activation of the emission from the Eu(III) center by the tta ligand (1, 2, 8). It is, therefore, not surprising to observe red luminescence from compounds **1** and **2** in solution. The emission spectra of both compounds are identical and dominated by an intense and narrow emission band at $\lambda = 613$ nm due to the $5D_0 \rightarrow 7F_2$ transition, as shown in Fig. 6. The UV–vis spectra and excitation bands of **1** and **2** in solution (CH_2Cl_2 or THF) are from the ligands and resemble those of $Eu(tta)_3$ and $Eu(tta)_3(Phen)$ (2, 8). Therefore, we believe that the observed red luminescence from **1** and **2** is due to an *indirect* excitation process or energy transfer process facilitated by the tta ligand. The free ligands, 4,4′-bipy and 4,4′-bipyete, have an emission band at 381 and 386 nm, respectively. Their excitation bands (321 nm and 327 nm, respectively)

© 2001 NRC Canada

Fig. 1. A diagram showing the molecular structure of **1** with 50% thermal ellipsoids and labeling schemes. For clarity, hydrogen atoms and fluorine atoms are omitted. All carbon atoms are shown as isotropic spheres.

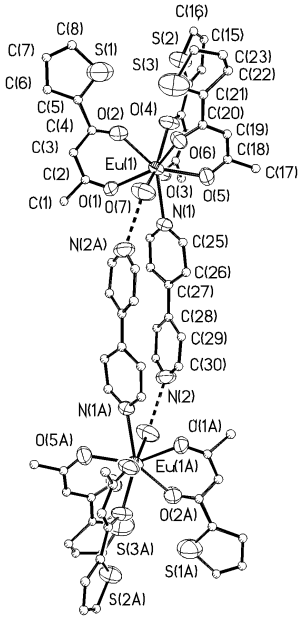
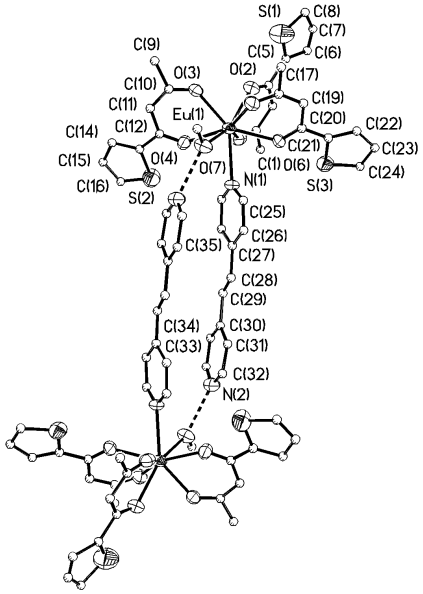


Fig. 2. A diagram showing the molecular structure of **2** with 50% thermal ellipsoids and labeling schemes. For clarity, hydrogen atoms and fluorine atoms are omitted. All carbon atoms are shown as isotropic spheres.



overlap with part of the excitation bands of **1** and **2** (at ~ 300–350 nm region). The fact that no emission bands that match those of free 4,4′-bipy or 4,4′-bipyete were observed in the spectra of **1** and **2** indicates that these ligands are also likely involved in the energy transfer process to the Eu(III) center

Fig. 3. A diagram showing the π-stacking between coordinate and non-coordinate bipyete ligands in **2**.

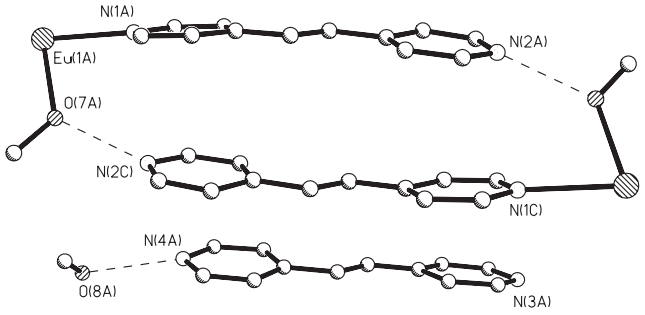
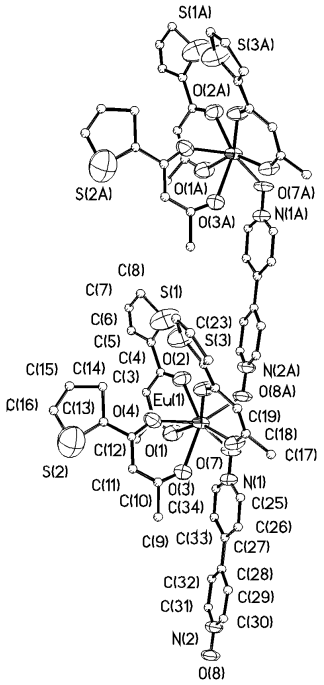


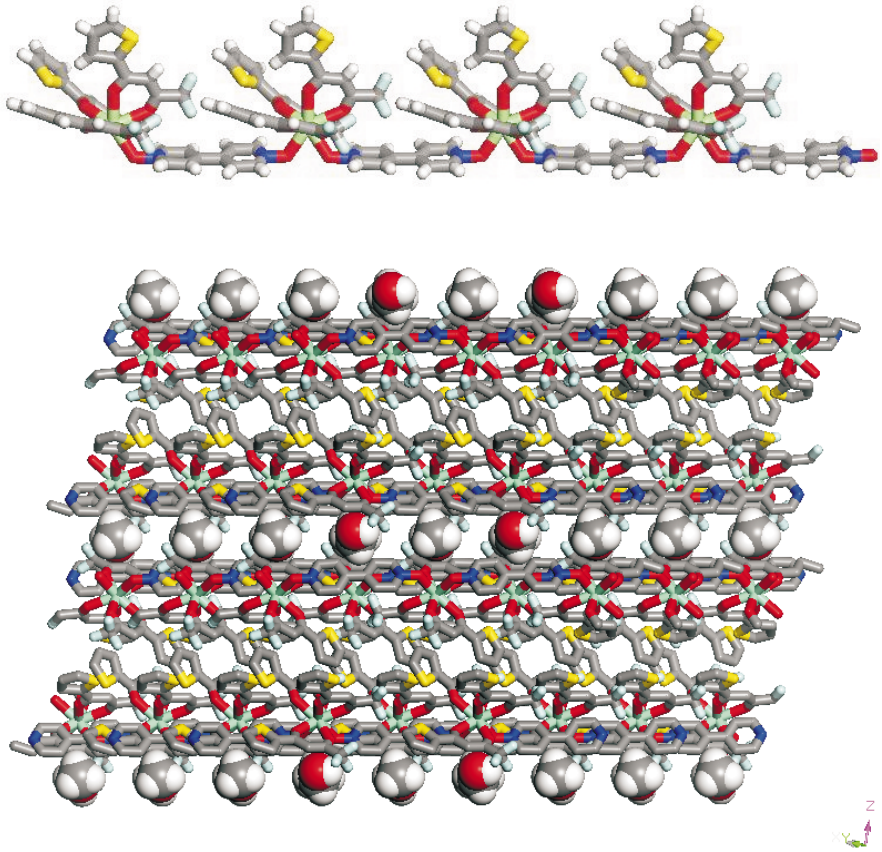
Fig. 4. A diagram showing the structure of **3** with 50% thermal ellipsoids and labeling schemes. For clarity, hydrogen atoms and fluorine atoms are omitted. All carbon atoms are shown as isotropic spheres.



and that they are likely still bound to the Eu(III) center in solution. Because of the insolubility of compound **3**, its' luminescent property in solution was not investigated. In the solid state, only compound **1** shows a bright red luminescence (Fig. 6*b*), while **2** has a very weak emission that is barely above the noise level, and **3** has no emission at all. The excitation band of **1** in the solid state has a maximum similar to that in solution, but is much broader than the solution excitation band. The broad excitation band of **1** is characteristic of ligands, not the Eu(III) ion. Therefore, the red emission of **1** in the solid state can also be attributed to an *indirect* excitation process. It is, however, somewhat surprising that **2** displays only very weak luminescence in the solid state. The crystal structural analysis shows that there is a π-stacking among the coordinated and non-coordinated bipyete

© 2001 NRC Canada

Fig. 5. Top: A diagram showing the one-dimensional chain of **3**. Orange: oxygen, dark blue: nitrogen, yellow: sulfur, green: europium, light blue: fluorine, gray: carbon. Bottom: A diagram showing the layered lattice and the intercalation of methanol solvent molecules in **3** between the chains. The methanol solvent molecules are highlighted using space-filling representation while the one-dimensional chains are presented as ball and sticks.



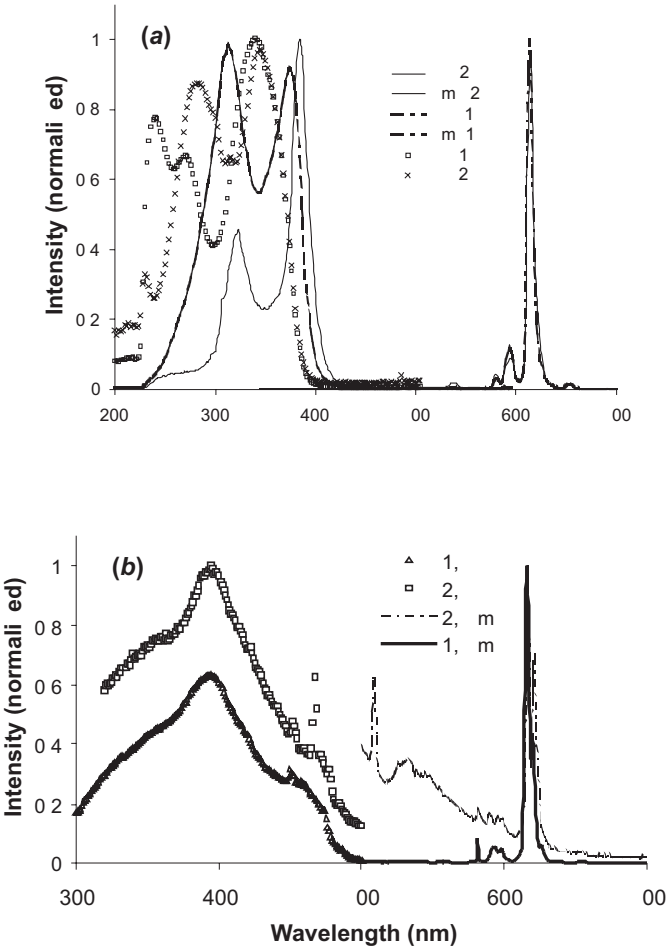
ligands and no π-stacking between the tta ligands in the crystal lattice. It is, therefore, possible that the absence of luminescence of **2** in the solid state is related to the π-stacking of the bipyete ligands, which may interfere with the energy transfer process. Although luminescent quenching via π-stacking has been well-documented previously (9), the relationship between the π-stacking of bipyete ligands in the crystal lattice and the very low emission intensity of Eu(III) emission of **2** in the solid state is yet to be understood.

The absence of luminescence of **3** in the solid state appears to be caused by bipyo ligands. The mixture of $Eu(NO_3)_3$ with bipyo ligands in a methanolic solution shows no luminescence at all, indicating that the bipyo ligand by itself is not capable of activating the emission from Eu(III). Addition of bipyo ligands to a bright red luminescent solution containing $Eu(tta)_3(phen)$ resulted in a complete quenching of red emission from the Eu(III) center, which supports the hypothesis that the absence of emission from **3** is indeed caused by the bipyo ligand. The free bipyo ligand has a weak blue emission band in solution (λ = 400 nm) and the solid state (λ = 484 nm). The excitation band (λ = 416 nm in the solid state) of bipy overlaps with that of the tta ligand in **1**, **2**, and $Eu(tta)_3(phen)$. It is, therefore, likely that the bipyo ligand interferes with the energy transfer process from the tta ligand to the Eu(III) center, thus quenching the Eu(III) emission in **3**.

Because compound **1** is a bright red emitter in solution and the solid state, we attempted to use it as a red emitter in electroluminescent devices. Thin films of compound **1** can be achieved by spin-casting the solution of **1** in toluene and THF to a polymer substrate (PVK). Alternatively, compound **1** can be doped into PVK, and then spin-casted into thin films. The photoluminescent spectra of the films of **1** are similar to that of compound **1** in solution and the solid state. Two-layer devices with the structure of ITO/PVK/**1**/(Mg/Ag) and three-layer devices with the structure of ITO/PVK/**1**/PBD/(Mg/Ag) were fabricated using the same procedure reported previously, where PVK and PBD (2-(4-biphenylyl)-5-(4-*tert*-butylphenyl)-1,3,4-oxadiazole) are used as a hole transport and an electron transport layer, respectively. However, no electroluminescence was observed from any of the devices fabricated. There are many possible causes for the failure of the EL devices. The most likely cause is the mismatch of the host layers, thereby preventing efficient energy transfer to the Eu(III) center. Modification of the hole transport and electron transport materials in the devices may be the key for obtaining electroluminescence from **1**. However, suitable hole transport and electron trans-

© 2001 NRC Canada

Fig. 6. (*a*) UV–vis, excitation and emission spectra of **1** amd **2** in solution (1.0×10^{-4} M in CH_2Cl_2); and (*b*) excitation and emission spectra of **1** and **2** in the solid state.



port materials for Eu(III) films obtained by spin-casting are still rather rare, which limits our current study on electroluminescent properties of **1**.

In summary, we have demonstrated that bipy and bipyete ligands are capable of linking $Eu(tta)_3$ units together to form red luminescent dinuclear complexes by both coordination and hydrogen bonds, and bipyo can link $Eu(tta)_3$ units together by coordination bonds to form a novel one-dimensional chain structure and in turn an intercalation lattice that can host methanol molecules. However, the bipyo ligand is not capable of activating red emission from Eu(III) centers and effectively quenches the red emission from the $Eu(tta)_3$ unit. The application of compound **1** as a red emitter in electroluminescent devices requires further investigation.

Acknowledgments

We thank the Natural Sciences and Engineering Research Council of Canada (NSERC) and the Xerox Research Center of Canada (XRCC) for financial support. We thank Dr. Nanxing Hu at XRCC for assistance in the attempted electroluminescent device fabrication.

References

1. (*a*) R.A. Campos, I.P. Kovalev, Y. Guo, N. Wakili, and T. Skotheim. J. Appl. Phys. **80**, 7144 (1996); (*b*) J. Kido and K. Nagai. J. Alloys Comp. **192**, 30 (1993); (*c*) X. Zhang, R. Sun, Q. Zheng, T. Kobayashi, and W. Li. Appl. Phys. Lett. **71**, 2596 (1997); (*d*) J. Kido, K. Nagai, Y. Okamoto, and T. Skotheim. Chem. Lett. 1267 (1991); (*e*) T. Sano, M. Fujita, T. Fujii, Y. Hamada, K. Shibata, and K. Kuroki. Jpn. J. Appl. Phys. **34**, 1883 (1995).
2. R.A. Gudmundsen, O.J. Marsh, and E. Matovich. J. Chem. Phys. **39**, 272 (1963).
3. C. Seward, N.X. Hu, and S. Wang. J. Chem. Soc. Dalton Trans. 134 (2001).
4. (*a*) M. Fujita, Y.J. Kwon, S. Washizu, and K. Ogura. J. Am. Chem. Soc. **116**, 1151 (1994); (*b*) R.W. Gable, B.F. Hoskins, and R. Robson. J. Chem. Soc. Chem. Commun. 1677 (1990); (*c*) J. Lu, C. Yu, T. Niu, T. Paliwala, G. Crisci, F. Somosa, and A.J. Jacobson. Inorg. Chem. **37**, 4637 (1998); (*d*) J. Lu, T. Paliwala, S.C. Lim, C. Yu, T. Niu, and A.J. Jacobson. Inorg. Chem. **36**, 923 (1997); (*e*) P.J. Stang, N.E. Persky, and J. Manna. J. Am. Chem. Soc. **119**, 4777 (1997); (*f*) S. Roche, C. Haslam, H. Adams, S.L. Heath, and J.A. Thomas. Chem. Commun. 1681 (1998); (*g*) O.M. Yaghi and H. Li. J. Am. Chem. Soc. **117**, 10401 (1995); (*h*) P. Losier and M.J. Zaworotko. Angew. Chem. Int. Ed. Engl. **35**, 2779 (1996); (*i*) S. Subramanian and M.J. Zaworotko. Angew. Chem. Int. Ed. Engl. **34**, 2127 (1995).
5. (*a*) D.L. Long, A.J. Blake, N.R. Champness, and M. Schröder. Chem. Commun. 1369 (2000); (*b*) D.L. Long, A.J. Blake, N.R. Champness, and M. Schröder. Chem. Commun. 2273 (2000); (*c*) M.J. Plater, M.R. St. J. Foreman, and A.M.Z. Slawin. Inorg. Chim. Acta, **303**, 132. (2000); (*d*) R.K. Agarwal and J. Prakash. Polyhedron, **10**, 2809 (1991).
6. SHELXTL NT: crystal structure analysis package. Version 5.10. Bruker AXS Inc. Madison, WI. 1999.
7. D.W. Bruce and D. O'Hare (*Editors*). Inorganic materials. John Wiley & Sons, Chichester. 1995.
8. (*a*) H. Winston, O.J. Marsh, C.K. Suzuki, and C.L. Telk. J. Chem. Phys. **39**, 267 (1963); (*b*) S.B. Meshkova, N.V. Rusakova, Z.M. Topilova, M.O. Lozinskii, and L.K. Kudryavtseva. Koord. Khim. **18**, 210 (1992).
9. (*a*) J. Kim, D.T. McQuade, S.K. McHugh, and T.M. Swager. Angew. Chem. Int. Ed. Engl. **39**, 3868 (2000) and refs. therein; (*b*) S. Bevers, S. Schutte, and L.W. McLaughlin. J. Am. Chem. Soc. **122**, 5905 (2000); (*c*) K. Shirai, M. Matsuoka, and K. Fukunishi. Dyes Pigm. **42**, 95 (1999); (*d*) M. Balon, P. Guardado, M.A. Munoz, and C. Carmona. Biospectroscopy, **4**, 185 (1998); (*e*) J.S. Hinzmann, R.L. McKenna, T.S. Pierson, F. Han, F.J. Kezdy, and D.E. Epps. Chem. Phys. Lipids, **62**, 123 (1992).

© 2001 NRC Canada

Synthesis, structure, and reactivity of diamidophosphine complexes of yttrium and the lanthanides

Michael D. Fryzuk, Peihua Yu, and Brian O. Patrick

Abstract: The reaction of the dilithiodiamidophosphine ligand precursor $PhP(CH_2SiMe_2NPh)_2Li_2(THF)_2$([NPN]$Li_2(THF)_2$) with $LnCl_3(THF)_3$ (Ln = Y, Sm, Ho, Yb, Lu; THF = tetrahydrofuran) in refluxing toluene generates the mononuclear complexes [NPN]LnCl(THF) in good yield. The molecular structures have been shown to be five-coordinate in the solid state and in solution. Attempts to prepare alkyl derivatives have only met with partial success; the reaction of MeMgCl with [NPN]YCl(THF) generates the partially characterized mixed-metal derivative [NPN]YMe_2MgCl. The reaction with $LiAlH_4$ results in complete ligand exchange and the formation of the tetranuclear lithium aluminum hydride derivative {[NPN]$AlH_2Li(THF)$}$_2$. Reduction of the lutetium derivative with KC_8 and naphthalene generated the dinuclear naphthalene-bridged species {[NPN]Lu}$_2$(μ-η^4:η^4-$C_{10}H_8$) wherein each Lu centre engages in η^4-coordination to opposite sides of the arene moiety. X-ray crystallography was used to characterize the four complexes.

Key words: lanthanides, yttrium, mixed-donor ligands, aluminum, lithium, naphthalene.

Résumé : La réaction du précurseur de ligand dilithiodiamidophosphine $PhP(CH_2SiMe_2NPh)_2Li_2(THF)_2$([NPN]$Li_2(THF)_2$) avec du $LnCl_3(THF)_3$ (Ln = Y, Sm, Ho, Yb, Lu; THF = tétrahydrofurane), dans du toluène au reflux, génère des complexes mononucléaires [NPN]LnCl(THF) avec de bons rendements. Il a été démontré que, à l'état solide ainsi qu'en solution, les structures moléculaires sont pentacoordinées. Les essais effectués en vue de préparer des dérivés alkylés n'ont donné que des succès partiels; la réaction du MeMgCl avec le [NPN]YCl(THF) conduit à la formation du dérivé métallique mixte [NPN]YMe_2MgCl, qui a été partiellement caractérisé. La réaction avec le $LiAlH_4$ donne lieu à un échange complet de ligands et à la formation de l'hydrure de lithium et d'aluminium tétranucléaire {[NPN]$AlH_2Li(THF)$}$_2$. La réduction du dérivé du lutécium avec du KC_8 et du naphtalène génère l'espèce dinucléaire ponté par du naphtalène, {[NPN]Lu}$_2$(μ-η^4:η^4-$C_{10}H_8$) dans lequel chaque centre Lu est engagé dans une coordination η^4 avec les côtés opposés de la portion arène. On a fait appel à la diffraction des rayons X pour caractériser quatre des complexes.

Mots clés : lanthanides, yttrium, ligands à donneurs mixtes, aluminium, lithium, naphtalène.

[Traduit par la Rédaction]

Introduction

Early transition metal complexes with formally d^0 electronic configurations have been prominent as catalyst precursors for the polymerization of α-olefins (1). While the cyclopentadienyl ancillary ligand provided the initial surge of activity, recent reports have focused on nonmetallocene systems, and in particular, multidentate amido ligands (2–4). Our strategy for ligand design has centred on the combination of two vastly different donor types in a chelate array in an effort to allow access to a variety of different oxidation states at the metal centre. Several new multidentate ligands based on varying the number of amide and phosphine moieties have been developed in our lab (5–7). Herein we report on the preparation of a series of lanthanide complexes [NPN]LnCl(THF) that incorporate a tridentate ligand containing one phosphine and two amido donors ([NPN] = [$PhP(CH_2SiMe_2NPh)_2$]; Ln = Y (**1**), Sm (**2**), Ho (**3**), Yb (**4**), Lu (**5**)).

Received January 30, 2001. Published on the NRC Research Press Web site at http://canjchem.nrc.ca on August 10, 2001.

M.D. Fryzuk,[1] P. Yu, and B.O. Patrick.[2] Department of Chemistry, University of British Columbia, 2036 Main Mall, Vancouver, BC V6T 1Z1, Canada.

[1]Corresponding author (telephone: (604) 822-2897; fax: (604) 822-2847; e-mail: fryzuk@chem.ubc.ca).
[2]UBC X-ray crystallographic service.

Experimental

All experimental manipulations were carried out under an atmosphere of purified dinitrogen rigorously excluding air and moisture using standard Schlenk or glovebox techniques (Vacuum Atmospheres HE-553-2 glovebox equipped with a MO-40-2H purification system and a −40°C freezer). Solvents were purified according to conventional procedures and were freshly distilled prior to use. Unless otherwise stated, ^1H and $^{31}P\{^1H\}$ NMR spectra were recorded on a Bruker AC-200 instrument operating at 200 and 81.0 MHz, respectively.

The compounds $LnCl_3(THF)_3$ (8), [NPN]$Li_2(THF)_2$ (9), and KC_8 (10) were prepared as described in the literature.

 DOI: 10.1139/cjc-79-7-1194 © 2001 NRC Canada

MeMgCl (solution in THF), $LiAlH_4$, and naphthalene were purchased from Aldrich.

Elemental analyses were performed in the microanalysis laboratory of this department by Mr. P. Borda.

Preparation of [NPN]LnCl(THF) (Ln = Y, Sm, Ho, Yb, Lu)

General procedure for **1**–**5**: at room temperature, toluene (100 mL) was added to a mixture of $[NPN]Li_2(THF)_2$ (1.18 g, 2 mmol) and $LnCl_3(THF)_3$ (2 mmol) and the resulting slurry was heated under reflux overnight. After cooling to room temperature, the mixture was filtered through Celite. The solvent was evaporated to dryness and the residue washed with hexane and dried under vacuum, yielding **1** (0.97 g, 70%), **3** (0.96 g, 68%), **5** (1.12 g, 71%) as white powders, **2** (1.15 g, 75%) as a yellow powder, and **4** (1.18 g, 74%) as an orange powder.

*[NPN]YCl(THF) (**1**)*

EI-MS *m*/*z* (%): 593 ($[M - Cl]^+$, 10), 558 ($[M - THF]^+$, 100). ^1H NMR (C_6D_6, 200 MHz, 298 K) δ: 7.92 (m, 2H, PPh *p*-H), 7.40 (m, 4H, NPh *o*-H), 7.15 (m, 6H, NPh *m*-H and PPh *m*-H), 6.80 (m, 2H, NPh *p*-H), 2.93 (m, 4H, THF), 1.60 (m, 2H, PCH_2Si), 1.00 (m, 2H, PCH_2Si), 0.76 (m, 4H, THF), 0.30 and 0.24 (s, 12H total, $SiCH_3$). $^{31}P\{^1H\}$ NMR (C_6D_6, 81 MHz, 298 K) δ: –27.17 (d, $J_{P,Y}$ = 77.1 Hz). Anal. calcd. for $C_{28}H_{39}ClN_2OPSi_2Y$: C 53.29, H 6.23, N 4.44; found: C 53.56, H 6.26, N 4.43.

*[NPN]SmCl(THF) (**2**)*

EI-MS *m*/*z* (%): 623 ($[M - THF]^+$, 100), 558 ($[M - THF - Cl]^+$, 15). ^1H NMR (C_6D_6, 200 MHz, 298 K) δ: 6.42 (m, 1H, PPh *p*-H), 6.05 (m, 6H, NPh *m*-H and PPh *m*-H), 5.76 (m, 4H, NPh *o*-H), 4.80 (m, 2H, NPh *p*-H), 4.42 (m, 2H, PCH_2Si), 2.35 and 2.21 (s, 12H total, $SiCH_3$), 2.60 (m, 2H, PCH_2Si), 1.13 (m, 4H, THF), 0.05 (m, 4H, THF). Anal. calcd. for $C_{28}H_{39}ClN_2OPSi_2Sm$: C 48.56, H 5.68, N 4.04; found: C 48.85, H 5.75, N 4.01.

*[NPN]HoCl(THF) (**3**)*

EI-MS *m*/*z* (%): 634 ($[M - THF]^+$, 100), 599 ($[M - THF - Cl]^+$, 25). Anal. calcd. for $C_{28}H_{39}ClN_2OPSi_2Ho$: C 47.56, H 5.50, N 3.96; found: C 47.72, H 5.63, N 3.87.

*[NPN]YbCl(THF) (**4**)*

EI-MS *m*/*z* (%): 643 ($[M - THF]^+$, 100), 607 ($[M - THF - Cl]^+$, 18). Anal. calcd. for $C_{28}H_{39}ClN_2OPSi_2Yb$: C 47.02, H 5.50, N 3.92; found: C 47.22, H 5.60, N 3.86.

*[NPN]LuCl(THF) (**5**)*

EI-MS *m*/*z* (%): 644 ($[M - THF]^+$, 100), 558 ($[M - THF - Cl]^+$, 20). ^1H NMR (C_6D_6, 200 MHz, 298 K) δ: 7.90 (m, 2H, PPh *o*-H), 7.41 (m, 4H, NPh *o*-H), 7.15 (m, 6H, NPh *m*-H and PPh *m*-H), 6.81 (m, 2H, NPh *p*-H), 2.98 (m, 4H, THF), 1.58 (m, 2H, PCH_2Si), 0.97 (m, 2H, PCH_2Si), 0.69 (m, 4H, THF), 0.32 and 0.25 (s, 12H total, $SiCH_3$). $^{31}P\{^1H\}$ NMR (C_6D_6, 81 MHz, 298 K) δ: –22.70 (s). Anal. calcd. for $C_{28}H_{39}ClN_2OPSi_2Lu$: C 46.89, H 5.48, N 3.91; found: C 46.63, H 5.90, N 4.02.

Methylation of [NPN]YCl(THF) using MeMgCl

To a suspension of [NPN]YCl(THF) (**1**) (0.63 g, 1 mmol) in toluene (30 mL) was added MeMgCl (0.7 mL, 3.0 M in THF, 2.1 mmol) at room temperature, and the mixture was stirred overnight. After removal of the volatiles, the residue was extracted with hexane–toluene (1:1, 2 × 5 mL), and the mixture was filtered through Celite. Upon cooling to –30°C a white crystalline product formulated as $[NPN]YMe_2MgCl(THF)$ (**6**) could be obtained in 50% yield (0.34 g). ^1H NMR (C_6D_6, 200 MHz, 298 K) δ: 7.68 (m, 2H, PPh *o*-H), 7.50 (m, 6H, NPh *m*-H and PPh *m*-H), 7.12 (m, 1H, PPh *p*-H), 6.97 (m, 4H, NPh *o*-H), 6.85 (m, 2H, NPh *p*-H), 2.61 (m, 4H, THF), 1.18 (m, 2H, PCH_2Si), 1.06 (m, 2H, PCH_2Si), 0.71 (m, 4H, THF), 0.45 and –0.02 (s, 12H total, $SiCH_3$), –0.14 (m, 3H, Me), –0.62 (m, 3H, Me). $^{31}P\{^1H\}$ NMR (C_6D_6, 81 MHz, 298 K) δ: –46.5(s). Anal. calcd. for $C_{30}H_{45}ClN_2OPSi_2MgY$: C 52.55, H 6.68, N 4.08; found: C 52.98, H 6.59, N 4.02.

Reaction of [NPN]YCl(THF) with $LiAlH_4$; synthesis of $\{[NPN]AlH(\alpha\text{-}H)Li(THF)\}_2$ (7)

To a stirred mixture of [NPN]YCl(THF) (**1**) (1.26 g, 2 mmol) and $LiAlH_4$ (0.1 g, 2.6 mmol) was added THF (50 mL) at –78°C. After warming to room temperature, the mixture was stirred overnight. After removal of the precipitate by filtration, the solvent was evaporated to dryness under vacuum, the white residue was extracted with toluene (2 × 15 mL), and the mixture filtered through Celite. Partial removal of the volatiles and cooling to –30°C to yield (0.58 g, 54%) compound **7** as colorless crystals. ^1H NMR (C_6D_6, 200 MHz, 298 K) δ: 7.75 (m, 2H, PPh *o*-H), 7.05 (m, 10H, NPh *o*-H and *m*-H, and PPh *m*-H), 6.81 (m, 2H, NPh *p*-H), 3.61 (m, 4H, THF), 1.68 (m, 2H, PCH_2Si), 1.25 (m, 4H, THF), 0.95 (m, 2H, PCH_2Si), 0.52 and –0.21 (s, 12H total, $SiCH_3$). $^{31}P\{^1H\}$ NMR (C_6D_6, 81 MHz, 298 K) δ: –36.01 (q, $J_{P,Li}$ = 66.4 Hz). Anal. calcd. for $C_{28}H_{41}N_2OPSi_2AlLi$: C 61.97, H 7.61, N 5.16; found: C 61.68, H 7.24, N 5.30.

Reaction of [NPN]LuCl(THF) with KC_8 and naphthalene ($C_{10}H_8$); preparation of $\{[NPN]Lu\}_2(\mu\text{-}\eta^4\text{:}\eta^4\text{-}C_{10}H_8)$ (8)

To a mixture of [NPN]LuCl(THF) (**5**) (1.43 g, 2 mmol), KC_8 (0.27 g, 2 mmol), and naphthalene (0.128 g, 1 mmol) was added toluene at –78°C, leading the immediate development of a purple colour. The mixture was warmed to room temperature and stirred overnight to generate a dark purple colour. After filtration, the volatiles were removed under vacuum, the residue was washed with hexane (3 × 15 mL), and then the remaining solid was recrystallized from toluene. Compound **8** was obtained as dark red crystals by slowly evaporating the solvent at room temperature. Yield 35% (0.47 g). ^1H NMR (C_6D_6, 200 MHz, 298 K) δ: 7.25 (m, 4H, PPh *o*-H), 7.02 (m, 20H, NPh *o*-H and *m*-H, and PPh *m*-H), 6.78 (m, 4H, NPh *p*-H), 4.12 (m, 4H, $C_{10}H_8$), 2.51 (m, 4H, $C_{10}H_8$), 1.24 (m, 4H, PCH_2Si), 0.65 (m, 4H, PCH_2Si), 0.21 and 0.02 (s, 24H total, $SiCH_3$). $^{31}P\{^1H\}$ NMR (C_6D_6, 81 MHz, 298 K) δ: –9.1 (s). ^{13}C NMR (C_6D_6, 75.45 MHz, 298 K) δ: 159.7 (m, ipso-C_6H_5N), 131.6 (m, *o*-C_6H_5N), 129.6 (s, *m*/*p*-C_6H_5N), 122.9 (m, ipso-C_6H_5P), 120.6 (m, *o*-C_6H_5P), 105.8 (m, ipso-$C_{10}H_8$), 104.4 (s, *m*/*p*-C_6H_5P), 89.8

© 2001 NRC Canada

Table 1. Crystallographic data for **1**, **4**, **7**, and **8**.

	1	**4**	**7**	**8**
Chemical formula	$C_{28}H_{39}ClN_2OPSi_2Y$	$C_{28}H_{39}ClN_2OPSi_2Yb$	$C_{63}H_{90}N_4O_2P_2Si_4Al_2Li_2$	$C_{58}H_{70}N_4P_2Si_4Lu_2$
FW	631.13	715.27	1177.56	1347.44
Crystal Size (mm)	0.40 × 0.25 × 0.10	0.30 × 0.20 × 0.20	0.35 × 0.20 × 0.12	0.30 × 0.25 × 0.10
Crystal system	Monoclinic	Monoclinic	Triclinic	Triclinic
Space group	$P2_1/n$ (No. 14)	$P2_1/n$ (No. 14)	$P\bar{1}$ (No. 2)	$P\bar{1}$ (No. 2)
T (°C)	–100	–100	–100	–100
λ (Å)	0.71069	0.71069	0.71069	0.71069
a (Å)	15.3199(7)	15.1656(5)	12.8490(9)	10.033(1)
b (Å)	12.0338(5)	12.0402(3)	16.146(2)	11.2951(4)
c (Å)	17.432(1)	17.5551(6)	19.415(2)	13.711(1)
α (°)			68.498(2)	98.892(1)
β (°)	100.906(3)	101.027(3)	121.518 (2)	96.494(2)
γ (°)			66.523(2)	109.255(2)
V (Å^3)	3155.7(2)	3146.3(2)	3355.5(5)	1426.5(2)
Z	4	4	2	1
$D_{calcd.}$ (g cm^{-3})	1.328	1.510	1.165	1.568
F(000)	1312	1436	1260	674
μ (cm^{-1})	20.84	32.07	2.05	36.21
$2\theta_{max.}$ (°)	55.8	55.8	55.9	56.8
GoF	0.93	0.97	1.37	1.23
R_1[a]	0.028	0.025	0.039	0.027
wR_2[b]	0.077	0.074	0.107	0.074

[a] $R_1 = (|F_o - F_c|/ \Sigma|F_o|[I > 3\sigma(I)]$.
[b] $wR_2 = [\Sigma w(F_o^2 - F_c^2)^2/\Sigma wF_o^4]^{1/2}$ (all data).

(s, CH, $C_{10}H_8$), 31.9 (s, CH, $C_{10}H_8$), 22.9 (s, $SiCH_2P$), 14.8 (s, $(CH_3)_2Si$). Anal. calcd. for $C_{58}H_{70}N_4P_2Si_4Lu_2$: C 51.71, H 5.20, N 4.16; found: C 51.58, H 5.34, N 4.30.

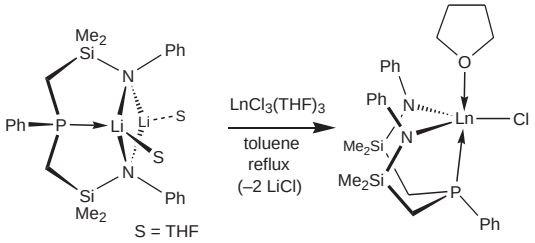
X-ray crystallography

Single crystals of compounds **1**, **4**, **7**, and **8** suitable for X-ray diffraction studies were selected and mounted on a glass fiber using Paratone oil. The crystallographic data appear in Table 1.[3] All measurements were made on a Rigaku/ADSC CCD area detector at 173 K, with graphite monochromated Mo Kα radiation (λ = 0.71069 Å), performing 2θ–ω scans. The structures of **1**, **4**, and **7** were solved by direct methods using SIR97 (11) and **8** by the Patterson method (12) and refined by full-matrix least-squares methods on F^2 for all data. Unless otherwise stated, all nonhydrogen atoms were refined anisotropically. All hydrogen atoms were included in the model at geometrically calculated positions with C—H distances of 0.98 Å and the isotropic thermal parameter for each H atom (B_H) is equal to 1.2 times B_{iso} of the atom to which it is bonded. Unmodified statistical weights ($w = 1/\sigma^2(F_o^2)$) were employed for all structures. The coordinated THF molecules in **1** and **4** were found to be disordered and were subsequently refined isotropically in two separate orientations.

Results and discussion

A series of complexes of the formula [NPN]LnCl(THF) ([NPN] = $[PhP(CH_2SiMe_2NPh)_2]$; Ln = Y (**1**), Sm (**2**), Ho (**3**), Yb (**4**), Lu (**5**)) were prepared in high yield (>70%) by reaction of $[NPN]Li_2(THF)_2$ with $LnCl_3(THF)_3$ in molar ratio of 1:1 in toluene under reflux (eq. [1]).

[1]



Ln = Y **1**
Ln = Sm **2**
Ln = Ho **3**
Ln = Yb **4**
Ln = Lu **5**

Using THF as the solvent led to lower yields of the products. Compounds **1**–**5** are moisture sensitive, moderately soluble in toluene and Et_2O, but very soluble in THF. The

[3] Supplementary material may be purchased from the Depository of Unpublished Data, Document Delivery, CISTI, National Research Council Canada, Ottawa, ON K1A 0S2, Canada. For information on obtaining material electronically go to http://www.nrc.ca/cisti/irm/unpub_e.shtml. Crystallographic information has also been deposited with the Cambridge Crystallographic Data Centre. Copies of the data can be obtained, free of charge, on application to the Director, CCDC, 12 Union Road, Cambridge CB2 1EZ, U.K. (Fax: 44-1223-336033 or e-mail: deposit@ccdc.cam.ac.uk).

© 2001 NRC Canada

Fig. 1. Molecular structure of [NPN]YCl(THF) (**1**).

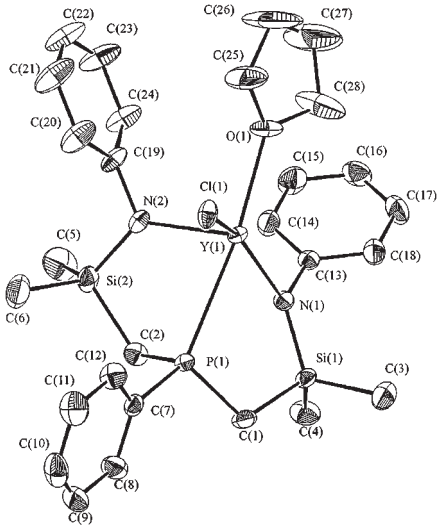
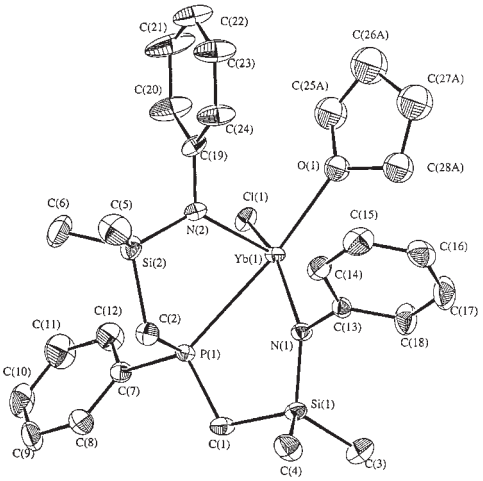


Fig. 2. Molecular structure of [NPN]YbCl(THF) (**4**).



compounds were characterized by elemental analyses, mass spectrometry, and ^{1}H and ^{31}P NMR spectroscopy where possible. The most intense peaks observed in the mass spectra correspond to the fragments [NPN]LnCl ($[M - THF]^+$) and [NPN]Ln ($[M - THF - Cl]^+$). Although the Sm(III), Ho(III), and Yb(III) derivatives (**2**, **3**, and **4**, respectively) are paramagnetic, the samarium derivative [NPN]SmCl(THF) (**2**) exhibited ^{1}H NMR signals (although no ^{31}P NMR resonance could be detected); no diagnostic signals could be detected in both the ^{1}H and ^{31}P NMR spectra for compounds **3** and **4**. For complexes **1** and **5**, the ^{1}H NMR spectra each show two signals due to coordinated THF at ca. 2.9 and 0.7 ppm, respectively. More importantly, both diamagnetic derivatives **1** and **5** show very symmetrical NMR patterns in solution suggestive of at least C_s symmetry; for example, only two environments for the silylmethyl protons ($SiMe_2$) are observed and the phenyl groups attached to nitrogen are equivalent.

The molecular structures of **1** and **4** were determined by X-ray crystallography and are shown in Figs. 1 and 2, respectively; selected bond distances and angles are given in Tables 2 and 3. These two derivatives are isostructural and isomorphous in the solid state. Both compounds display

Table 2. Selected bond distances (Å) and angles (°) for compound **1**.

Bond distances (Å)			
Y(1)—Cl(1)	2.7561(6)	Y(1)—P(1)	2.9276(6)
Y(1)—N(1)	2.260(2)	Y(1)—N(2)	2.240(2)
Y(1)—O(1)	2.350(2)	P(1)—C(7)	1.826(2)
N(1)—C(13)	1.407(3)	N(2)—C(19)	1.421(3)
Bond angles (°)			
Cl(1)-Y(1)-O(1)	91.54(5)	Cl(1)-Y(1)-P(1)	90.82(2)
Cl(1)-Y(1)-N(2)	94.95(5)	Cl(1)-Y(1)-N(1)	145.98(5)
O(1)-Y(1)-N(2)	94.39(7)	O(1)-Y(1)-N(1)	113.35(6)
N(1)-Y(1)-N(2)	105.30(7)	P(1)-Y(1)-O(1)	171.44(5)
P (1)-Y(1)-N(1)	68.09(5)	P(1)-Y(1)-N(2)	77.20(5)
Y(1)-N(2)-C(19)	117.6(1)	Y(1)-N(1)-C(13)	103.8(1)
Y(1)-P(1)-C(2)	95.06(8)	Y(1)-P(1)-C(1)	109.46(8)
Y(1)-P(1)-C(7)	135.45(8)	C(1)-P(1)-C(2)	103.5(1)

Table 3. Selected bond distances (Å) and angles (°) for compound **4**.

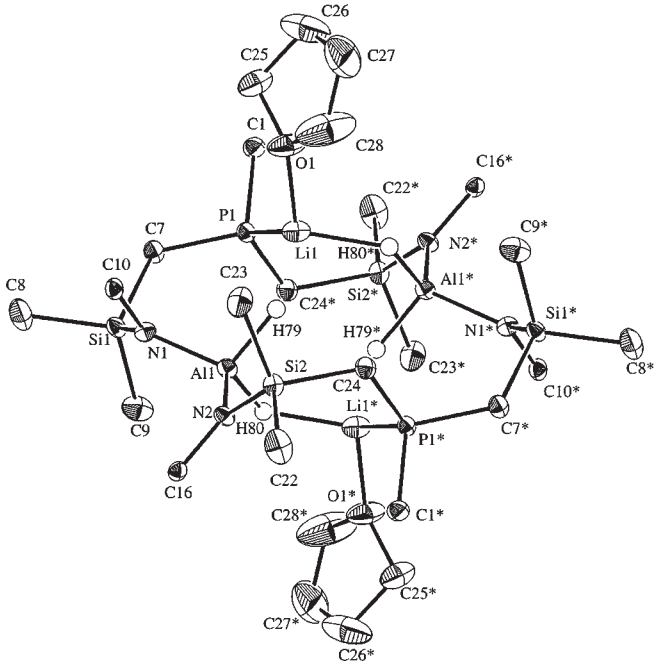
Bond distances (Å)			
Yb(1)—Cl(1)	2.7188(9)	Yb(1)—P(1)	2.8809(9)
Yb(1)—N(1)	2.213(3)	Yb(1)—N(2)	2.199(3)
Yb(1)—O(1)	2.325(3)	P(1)—C(7)	1.825(4)
N(2)—C(19)	1.421(5)	N(1)—C(13)	1.412(5)
Bond angles (°)			
Cl(1)-Yb(1)-O(1)	92.67(7)	Cl(1)-Yb(1)-P(1)	90.62(3)
Cl(1)-Yb(1)-N(2)	95.70(8)	Cl(1)-Yb(1)-N(1)	147.55(8)
O(1)-Yb(1)-N(2)	91.9(1)	O(1)-Yb(1)-N(1)	111.2(1)
N(1)-Yb(1)-N(2)	104.7(1)	P(1)-Yb(1)-O(1)	170.01(8)
P(1)-Yb(1)-N(1)	69.68(8)	P(1)-Yb(1)-N(2)	78.38(8)
Yb(1)-N(1)-C(13)	107.6(2)	Yb(1)-N(2)-C(19)	118.3(2)
Yb(1)-P(1)-C(1)	108.8(1)	Yb(1)-P(1)-C(2)	95.7(1)
Yb(1)-P(1)-C(7)	135.3(1)	C(1)-P(1)-C(2)	103.6(2)

five-coordinate environments around the central metals with the coordinated THF occupying the position opposite to the phosphorus atom. Overall, the geometries around each central metal are very similar and can be described as distorted square pyramidal by defining the base of the pyramid by P(1), O(1), N(1), and Cl(1), with N(2) in the apical position. This rather unsymmetrical geometry observed in the solid state cannot account for the solution data; in fact, the solution data are more consistent with a trigonal bipyramidal structure wherein the two amide donors and the chloride occupy the equatorial plane with the phosphine and THF moieties are apical resulting is C_s molecular symmetry. Presumably the small structural differences between the solid state and in solution are a result of crystal packing in the former.

The Y—Cl (2.7561(6) Å) bond distance in **1** is longer than that reported for the mononuclear diamido complex [DADMB]YCl(THF)$_2$ (Y—Cl 2.574(2) Å), while Y—N (average 2.250 Å) and Y—O (2.350(2) Å) in compound **1** are comparable to those in compound [DADMB]YCl(THF)$_2$ (DADMB = [6,6′-Me_2-(C_6H_3)$_2$](2,2′-$NSiMe_2$-*t*-Bu)$_2$) (average Y—N 2.250 Å, average Y—O 2.376 Å) (2). The bond distances Yb—Cl (2.710 Å), Yb—N (average 2.212 Å), and

© 2001 NRC Canada

Fig. 3. Molecular structure of $\{[NPN]AlH(\mu\text{-}H)Li(THF)\}_2$ (**7**). For clarity the Ph groups at N and P are omitted.



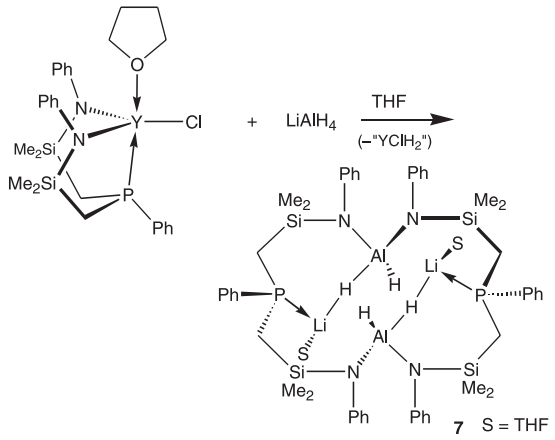
Yb—P (2.881 Å) in compound **4** can be compared to other Yb(III) phosphine complexes; for example, in $Cp^*_2YbCl(dmpm)$, the Yb—Cl bond distance of 2.532 Å is considerably shorter than that found in **4**, while the Yb—P bond length in **4** is slightly shorter than 2.941 Å found in the aforementioned permethylytterbocene derivative (13). The Yb(II) derivative $[(Me_2Si)_2N]_2Yb(dmpe)$ shows Yb—N and Yb—P bond distances of 2.331 and 3.012 Å, respectively, which are both longer than that found in **4** (14).

Attempts to generate metal–carbon bonds by metathesis of the remaining chloride ligands of [NPN]LnCl(THF) have not met with success. Generally mixtures of products are obtained upon addition of RLi (R = Me, CH_2SiMe_3) to [NPN]YCl(THF) (**1**). However, it was found that the addition of MeMgCl to **1** did result in the formation of an adduct of the empirical formula $[NPN]YMe_2MgCl$ (**6**). This material is clearly not the expected product, [NPN]YMe(THF). The proposed formulation of **6** is from elemental analyses; while ^1H and ^{31}P NMR spectroscopy could be obtained, a definitive structure has so far eluded us, as have suitable crystals for single crystal X-ray diffraction studies. From the solution NMR data, it is clear that phosphorus is not bound to Y (no coupling between yttrium-89 and phosphorus-31) and there are two metal–methyl environments. Further speculation on the structure of **6** must await additional data.

Attempts to prepare a hydride of the general formula $\{[NPN]YH(THF)\}_x$ by the reaction of **1** with $LiAlH_4$ in THF instead resulted in ligand transfer from yttrium to aluminum and the production in reasonable yield of the air-, moisture-, and slightly light-sensitive dinuclear aluminate **7** (eq. [2]).

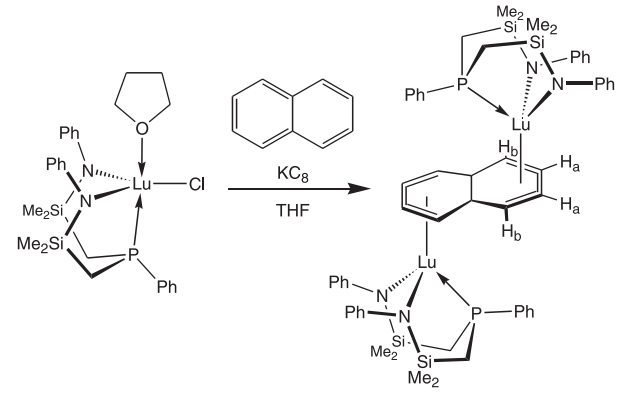
The molecular structure of **7** was determined by X-ray crystallography. As shown in Fig. 3, the Al atoms are each coordinated by two amido donors and two hydrides in a distorted tetrahedral coordination mode. Selected bond distances and angles are given in Table 4. The Li atoms are each coordinated by three atoms (P, O, H) and the angles of P-Li-O (113.7(3)°), P-Li-H (109.5°), and O-Li-H (105.2°) are in agreement with those expected for pseudo-tetrahedral geometries. The average Al—N (1.85 Å), Al—H (1.57 Å), and Li—H (1.84 Å) distances are comparable to those in the related disilylamido aluminate, $[(Me_3Si)_2N]_2Al(\mu\text{-}H)_2Li\cdot 2Et_2O$ (Al—N 1.86, Al—H 1.58, and Li—H 1.93 Å) (15). Stoichiometry requires that $YClH_2(THF)_x$ also be generated; however, the identity of the yttrium side-product was not pursued.

[2]



Recently, we have reported the formation of yttrium and lutetium complexes with polycyclic aromatic compounds that were formulated as $\{[P_2N_2]Ln\}_2(\mu\text{-}\eta^4\text{:}\eta^4\text{-}C_{10}H_8)$ by reducing $\{[P_2N_2]LnCl\}_2$ (Ln = Y, Lu) using KC_8 in the presence of aromatic compounds such as naphthalene and anthracene (16). A similar reaction of [NPN]LuCl(THF) with KC_8 and naphthalene resulted in the generation of $\{[NPN]Lu\}_2(\mu\text{-}\eta^4\text{:}\eta^4\text{-}C_{10}H_8)$ (**8**) in moderate yield (eq. [3]).

[3]



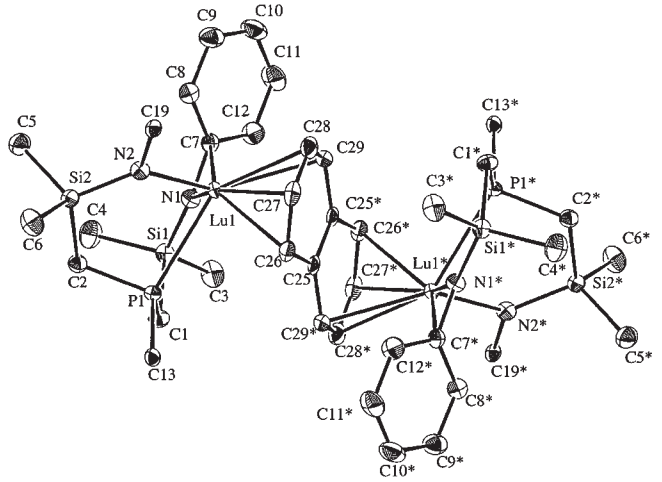
Exactly analogous transformations are also evident for the reaction of the holmium and yttrium analogues, although these reactions were not examined in detail. While the lutetium reaction provides proof of concept for this process for some of the lanthanides, it is interesting to note that this kind of reductive process completely fails to provide any kind of isolable product for the samarium and ytterbium derivatives **2** and **4**, despite the fact that divalent states are known for these particular lanthanide elements; it is not

© 2001 NRC Canada

Table 4. Selected bond distances (Å) and angles (°) for compound **7**.

Bond distances (Å)			
P(1)—Li(1)	2.575(4)	Li(1)—O(1)	1.904(5)
Al(1)—N(1)	1.847(2)	Al(1)—N(2)	1.863(2)
Al(1)—H(79)	1.55	Al(1)—H(80)	1.56
Li(1)—H(80)	1.84		
Bond angles (°)			
H(79)-Al(1)-H(80)	107.0	N(1)-Al(1)-N(2)	116.80(8)
H(79)-Al(1)-N(1)	108.4(5)	H(79)-Al(1)-N(2)	101.0
H(80)-Al(1)-N(2)	111.5	H(80)-Al(1)-N(1)	111.3
P(1)-Li(1)-O(1)	113.7(3)	P(1)-Li(1)-H(80)	109.5
H(80)-Li(1)-O(1)	105.2		

Fig. 4. Molecular structure of $\{[NPN]Lu\}_2(\mu\text{-}\eta^4\text{:}\eta^4\text{-}C_{10}H_8)$ (**8**). For clarity the Ph groups at N(2) and P(1) are omitted.



clear if reduction to a putative "Ln(II)[NPN]" species complicates these latter reactions. The ^{1}H NMR spectroscopic data of **8** show only two sets of signals for the $C_{10}H_8$ moiety, which indicate that the bridging naphthalene unit is symmetrically bound. In addition, only one signal for its $^{31}P\{^1H\}$ NMR spectrum also demonstrates equivalent phosphine donors on both Lu(III) centers.

The crystal structure of **8** has been determined and is shown in Fig. 4. Selected bond distances and angles are given in Table 5. The conformation of **8** is very similar to that of compound $\{[P_2N_2]Y\}_2(\mu\text{-}\eta^4\text{:}\eta^4\text{-}C_{10}H_8)$. Each [NPN]Lu unit binds in an η^4 fashion on the opposite sides of the different rings of the naphthalene unit. The naphthalene moiety is distorted slightly with elongated bond lengths, and its rings become nonplanar (16). The average Lu—C (2.59 Å) π-bond distances in compound **8** is found similar to the average π-bond distance of Lu—C(Cp) (2.63 Å) in compound $(C_5H_5)_2$Lu-*t*-Bu(THF) (17). It is interesting to note that the short distance between Lu(1) and C(7) (2.75 Å) appears to indicate a η^2-N,C interaction of the amide in solid state. However, the ^{13}C NMR spectrum shows no evidence of any asymmetry and both ipso carbons resonate at 159.7 ppm, a shift typical for uncoordinated NPh linkages (2).

Table 5. Selected bond distances (Å) and angles (°) for compound **8**.

Bond distances (Å)			
Lu(1)—P(1)	2.7538(8)	Lu(1)—C(7)	2.755(3)
Lu(1)—N(1)	2.214(3)	Lu(1)—N(2)	2.174(3)
Lu(1)—C(26)	2.551(3)	Lu(1)—C(27)	2.614(4)
Lu(1)—C(28)	2.612(4)	Lu(1)—C(29)	2.605(3)
C(25)—C(26)	1.438(5)	C(26)—C(27)	1.426(5)
C(28)—C(29)	1.450(5)	C(27)—C(28)	1.372(5)
C(25)*—C(29)	1.414(5)	C(25)—C(25)*	1.451(6)
Bond angles (°)			
P(1)-Lu(1)-N(1)	72.49(7)	P(1)-Lu(1)-N(2)	80.49(8)
N(1)-Lu(1)-N(2)	113.0(1)	C(7)-Lu(1)-N(1)	30.4(1)
P(1)-Lu(1)-C(26)	85.40(8)	C(7)-Lu(1)-N(2)	115.4(1)
P(1)-Lu(1)-C(27)	113.16(9)	P(1)-Lu(1)-C(28)	141.25(9)
P(1)-Lu(1)-C(29)	135.52(7)	N(1)-Lu(1)-C(26)	129.0(1)
N(1)-Lu(1)-C(28)	130.8(1)	N(1)-Lu(1)-C(27)	151.1(1)
N(1)-Lu(1)-C(29)	99.5(1)	N(1)-Lu(1)-C(26)	129.0(1)
C(7)-Lu(1)-C(28)	106.6(1)	C(7)-Lu(1)-C(27)	95.9(1)
C(7)-Lu(1)-C(29)	80.7(1)	C(7)-Lu(1)-C(26)	136.9(1)
N(2)-Lu(1)-C(26)	107.6(1)	N(2)-Lu(1)-C(27)	95.9(1)
N(2)-Lu(1)-C(28)	108.4(1)	N(2)-Lu(1)-C(29)	138.6(1)
Lu(1)-N(1)-C(7)	96.7(2)	Lu(1)-C(7)-N(1)	53.0(2)
C(25)-C(25)*-C(29)	118.7(4)	C(25)*-C(25)-C(26)	117.4(4)
C(26)-C(25)-C(29)*	123.9(4)	C(25)-C(26)-C(27)	120.8(3)
C(26)-C(27)-C(28)	119.7(3)	C(27)-C(28)-C(29)	119.5(3)

Conclusions

The results of this study indicate that the NPN ligand system can be incorporated onto certain Group 3 and lanthanide derivatives to generate five-coordinate, mononuclear complexes. However, these materials are not especially versatile as starting materials for entry into organometallic chemistry as most of the attempts to generate metal–carbon bonds result in mixtures of complexes. The only successful transformation so far is the incorporation of naphthalene under reducing conditions to give a bridging naphthalene unit. Since incorporation of alkyl species has proven difficult, it is likely that the use of these ligand systems with Group 3 and the lanthanides as catalyst precursors for polymerization of α-olefins will not be optimal.

Acknowledgment

Funding was provided by the Natural Sciences and Engineering Research Council of Canada (NSERC).

References

1. H.H. Brintzinger, D. Fischer, R. Mulhaupt, B. Rieger, and R. Waymouth. Angew. Chem. Int. Ed. Engl. **34**, 1143 (1995).
2. T.I. Gountchev and T.D. Tilley. Organometallics, **18**, 2896 (1999).
3. R.R. Schrock. Acc. Chem. Res. **30**, 9 (1997).
4. G.J.P. Britovsek, V.C. Gibson, and D.F. Wess. Angew. Chem. Int. Ed. Engl. **38**, 429 (1999).
5. M.D. Fryzuk, J.B. Love, S.J. Rettig, and V.G. Young. Science, **275**, 1445 (1997).
6. M.D. Fryzuk, J.B. Love, and S.J. Rettig, Organometallics, **17**, 846 (1998).

© 2001 NRC Canada

7. J.D. Cohen, M.D. Fryzuk, T.M. Loehr, M. Mylvaganam, and S.J. Rettig. Inorg. Chem. **37**, 112 (1998).
8. K.H. den Haan, J.L. de Boer, J.H. Teuben, A.L. Spek, B. Kojic-Prodic, G.R. Hays, and R. Huis. Organometallics, **5**, 1726 (1986).
9. M.D. Fryzuk, S.A. Johnson, and S.J. Rettig. J. Am. Chem. Soc. **120**, 11024 (1998).
10. A. Fürstner, and D.N. Jumbam. Tetrahedron, **48**, 5991 (1992).
11. A. Altomare, M.C. Burla, G. Cammalli, M. Cascarano, C. Giacovazzo, A. Guagliardi, A.G.G. Moliterni, G. Polidori, and A. Spagna. J. Appl. Crystallogr. **32**, 115 (1999).
12. P.T. Beurskens, G. Admiraal, G. Beurskens, W.P. Bosman, S. Garcia-Granda, R.O. Gould, J.M.M. Smits, and C. Smykalla. The DIRDIF program system, technical report of the crystallography laboratory. University of Nijmegen, The Netherlands. 1992.
13. T.D. Tilley, R.A. Andersen, and A. Zalkin. Inorg. Chem. **22**, 856 (1983).
14. T.D. Tilley, R.A. Andersen, and A. Zalkin. J. A. Chem. Soc. **104**, 3725 (1982).
15. A. Heine and D. Stalke. Angew. Chem. Int. Ed. Engl. **31**, 854 (1992).
16. M.D. Fryzuk, L. Jafarpour, F.M. Kerton, J.B. Love, and S.J. Rettig. Angew. Chem. Int. Ed. Engl. **39**, 767 (2000).
17. W.J. Evans, A.L. Wayda, W.E. Hunter, and J.L. Atwood. J. Chem. Soc. Chem. Commun. 292 (1981).

© 2001 NRC Canada

Tetrazole ethers from lignin model phenols: synthesis, crystal structures, and photostability

Andy Z. Lu, Thomas Q. Hu, David A. Osmond, Brian O. Patrick, and Brian R. James

Abstract: The phenolic OH moiety in lignin is one of the key functional groups responsible for the photo-induced yellowing of mechanical wood pulps and papers. To evaluate new protective groups for the stabilization of lignin phenols, the model compounds, 2-methoxy-4-propylphenol (**1**) and 4-hydroxy-3-methoxyacetophenone (**2**) were reacted with 5-chloro-1-phenyl-1*H*-tetrazole to give the corresponding tetrazole ethers **1′** and **2′**, respectively, that were then studied for their photostability. The synthesis of these ethers was more efficient than that of alkyl ethers because of less hydrolysis of the alkylating agent under the reaction conditions. Compounds **1′** and **2′** were fully characterized, including X-ray crystal structure analyses. Crystals of **1′** and **2′** were monoclinic of space groups $P2_1/c$ and $P2_1/a$, respectively. For **1′**: a = 9.8679(6), b = 16.708(1), c = 10.2841(6) Å, β = 109.732(5)°, Z = 4. For **2′**: a = 7.7212(2), b = 27.350(5), c = 14.569(3) Å, β = 101.30(2)°, Z = 8. The structures were solved by direct methods and refined by full-matrix least-squares procedures to R = 0.039 (R_w = 0.046) for 2029 reflections with $I \geq 3\sigma(I)$ (for **1′**), and to R = 0.055 (R_w = 0.073) for 3634 reflections with $I \geq 3\sigma(I)$ (for **2′**). Compound **2′** was much more photostable than the precursor phenol on exposure to strong fluorescent light, while **1′** was only slightly more stable than the precursor phenol.

Key words: alkylation, ethers, lignin model compounds, methylation, phenols, yellowing inhibition.

Résumé : Le groupe OH de la portion phénolique de la lignine est l'un des groupes fonctionnels clés responsables du jaunissement photoinduit des pâtes et papiers mécaniques dérivés du bois. Dans le but d'évaluer de nouveaux groupes protecteurs pour la stabilisation des phénols des lignines, on a fait réagir des composés modèles, le 2-méthoxy-4-propylphénol (**1**) et la 4-hydroxy-3-méthoxyacétophénone (**2**), avec le 5-chloro-1-phényl-1*H*-tétrazole pour obtenir respectivement les éthers correspondants **1′** et **2′** du tétrazole dont on a alors étudié la photostabilité. La synthèse de ces éthers s'avère plus efficace que celle des oxydes d'alkyles en raison d'une plus faible hydrolyse de l'agent alkylant dans les conditions réactionnelles. On a caractérisé complètement les éthers **1′** et **2′**, y compris par diffraction des rayons X. Les cristaux des composés **1′** et **2′** sont monocliniques, groupes d'espaces $P2_1/c$ et $P2_1/a$, respectivement. Pour **1′**, a = 9,8679(6), b = 16,780(1) et c = 10,2841(6) Å, β = 109,732(5)° et Z = 4. Pour **2′**, a = 7,7212(2), b = 27,350(5) et c = 14,569(3) Å, β = 101,30(2)° et Z = 8. Les structures ont été résolues par des méthodes directes et affinées par des procédures des moindres carrés (matrice complète) jusqu'à des valeurs de R = 0,039 (R_w = 0,046) pour 2029 réflexions avec $I \geq 3\sigma(I)$ (pour **1′**) et de R = 0,055 (R_w = 0,073) pour 3634 réflexions avec $I \geq 3\sigma(I)$ (pour **2′**). Lorsqu'on le soumet à une forte lumière fluorescente, le composé **2′** est beaucoup plus photostable que son précurseur phénolique alors que le composé **1′** n'est que légèrement plus stable que son précurseur phénolique.

Mots clés : alkylation, éthers, composés modèles pour la lignine, méthylation, phénols, inhibition du jaunissement.

[Traduit par la Rédaction]

Introduction

Canada is the world's largest producer of mechanical wood pulps. In 1998, Canada produced about 10 million tonnes of such pulps, accounting for one third of the total world production (1). Mechanical wood pulps, produced in 90–98% yields because of the retention of practically all the cellulose, hemicelluloses, and lignin in wood, have high opacity and are good materials for making printing papers; however, such papers turn yellow and lose brightness rapidly when exposed to light and this limits their main use to the production of short-life paper products such as newsprint and telephone directories (2).

Lignin is a random, three-dimensional biopolymer of substituted phenylpropane units. The light-induced yellowing of mechanical wood pulps and papers is due to the oxidation of lignin phenoxy radicals to yellow *o*-quinones (3, 4). One important source of the phenoxy radicals is lignin phenols that can produce the radicals via direct photolysis (5), or H-atom abstraction from the phenolic-OH by photoexcited lignin carbonyl groups (6) or singlet oxygen (7).

Received March 2, 2001. Published on the NRC Research Press Web site at http://canjchem.nrc.ca on August 15, 2001.

A.Z. Lu, B.O. Patrick, and B.R. James.[1] Chemistry Department, The University of British Columbia, Vancouver, BC V6T 1Z1, Canada.
T.Q. Hu[2] **and D.A. Osmond.** Pulp and Paper Research Institute of Canada, Vancouver Laboratory, 3800 Wesbrook Mall, Vancouver, BC V6S 2L9, Canada.

[1]Corresponding author (telephone: (604) 822-6645; fax: (604) 822-2847; e-mail: brj@chem.ubc.ca).
[2]Corresponding author (telephone: (604) 222-3200; fax: (604) 222-3207; e-mail: thu@paprican.ca).

 DOI: 10.1139/cjc-79-8-1201 © 2001 NRC Canada

Fig. 1. ORTEP diagram of **1′**, showing 50% probability thermal ellipsoids.

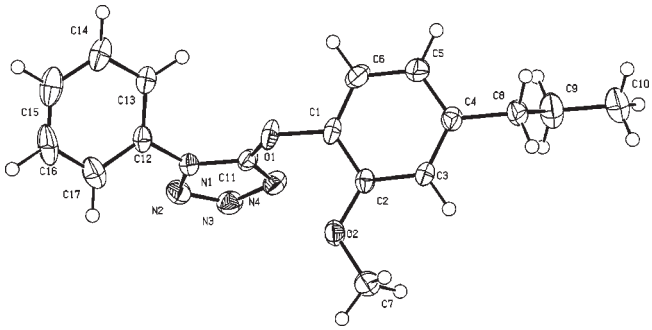
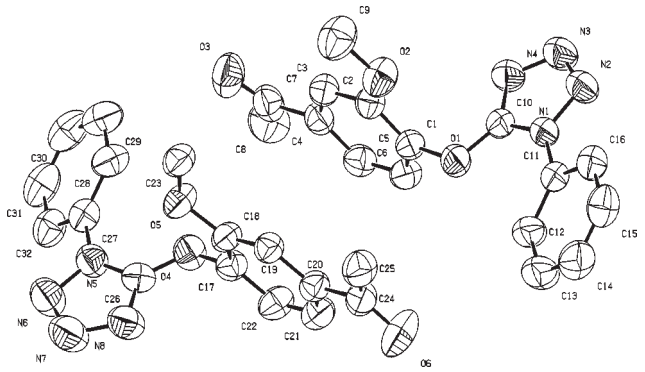


Fig. 2. ORTEP diagram of **2′**, showing two molecules in the asymmetric unit; 50% probability thermal ellipsoids are shown.



Alkylation of lignin phenols with the extremely toxic dimethylsulfate (8) has been shown to retard the photoreactivity of the lignin phenols in wood, newspapers, and groundwood pulps (5, 9), but a large excess of the reagent (in weight, greater than that of the oven-dried pulp) (9, 10) is required because of its rapid hydrolysis in the aqueous alkaline conditions needed. Other less toxic reagents such as olefin oxides (11) and diazomethane (12) have been studied for the alkylation of lignin phenols. Propylene- and butylene-oxides effect only partial protection of lignin phenols and give lower brightness stabilization (vs. dimethylsulfate) of groundwood mechanical pulps (11). Diazomethane is less effective than propylene-oxide in improving the brightness stability of spruce thermomechanical pulp (12), and its generation and alkylation require an anhydrous environment.

We have tested 5-chloro-1-phenyl-1*H*-tetrazole, a nontoxic and nonvolatile alkylating reagent, for the alkylation and possible stabilization of lignin phenols. This paper describes the reaction of this reagent with the lignin model phenols, 2-methoxy-4-propylphenol (**1**) and 4-hydroxy-3-methoxyacetophenone (**2**), and the structural and photostability studies of the ether products (**1′** and **2′**, respectively).

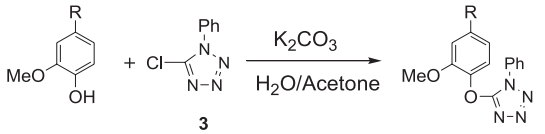
Results and discussion

Alkylation of lignin model phenols with 5-chloro-1-phenyl-1*H*-tetrazole (3)

5-Chloro-1-phenyl-1*H*-tetrazole (**3**) is a water-insoluble alkylating reagent available commercially and readily synthesized from sodium azide and *N*-phenyldichloroazomethine (13, 14). It has been used to alkylate simple phenols in dry acetone to give tetrazole ethers that can then be hydrogenolyzed to give simple arenes (15, 16). None of the literature examples, however, involved the use of an aqueous reaction medium or substrates resembling the structures of lignin phenols.

Treatment of **1** with 1 equiv. of **3** and 2 equiv. of K_2CO_3 in 1:1 v/v H_2O–acetone (pH 13.3) at 60°C for 18 h gave the purified tetrazole ether **1′** in 62% yield (eq. [1]). The structure of **1′** was established by ^{1}H NMR, MS, elemental analysis, and an X-ray crystal structure (Fig. 1). Similarly **2** gave **2′** in 39% yield, eq. [1] (Fig. 2). Both **1′** and **2′** are new compounds; no attempt was made to optimize the yields. Under the conditions used (pH 13.3), it is expected that other OH groups (aliphatic hydroxyl groups in lignin and those in carbohydrates) would react much slowly with **3** than the lignin phenolic-OH groups, if such a treatment were to be applied to mechanical wood pulps.

[1]



R = ^{n}Pr (**1**); C(O)Me (**2**) R = ^{n}Pr (**1'**); C(O)Me (**2'**)

The structures of **1′** and **2′** reveal expected bond lengths and angles. Within the tetrazole rings the double bonds between N(2)—N(3) and between N(4)—C(11) (or N(4)—C(10)) are characterized by bond lengths of 1.286–1.306 Å, while N(1)—N(2) and N(3)—N(4) have single bond lengths of 1.358–1.376 Å. The N(1)—C(12) lengths are 1.432 and 1.431 Å, and at the newly formed ether O-atom, the O(1)—C(tetrazole) bonds are 1.331 and 1.327 Å in **1′** and **2′**, respectively, which are shorter than the O(1)—C(phenyl) lengths of 1.417 and 1.418 Å. Within the tetrazole ring, the smallest angles are at N(1), N(2), and N(4) (106.9, 106.0, and 104.2° in **1′**, and 106.3, 107.0, and 104.2° in **2′**), while those at N(3) and C(10 or 11) are all in the 111.1–111.8° range. Differences in corresponding torsion angles of **1′** and **2′** likely result from crystal packing effects; for example, the N(2)-N(1)-C(12)-C(13) angle in **1′** is –124.1°, whereas the N(2)-N(1)-C(11)-C(12) angle in **2′** is –155.7°.

Compound **2** was more difficult to alkylate than **1**, and this was shown by monitoring the conversions of the phenols using GC with 3,4-dimethoxy-1-ethylbenzene added as an internal reference to the reaction medium. For example, the conversions of **1** at 60°C were 42 (6 h), 62 (18 h), and 75% (23 h), vs. corresponding values of 12, 39, and 50% for conversions of **2**. The lower reactivity of **2** is attributed to the lower nucleophilicity of its phenolate anion resulting from the delocalization of the anionic charge by the electron-withdrawing α-carbonyl group. A very low reactivity of lignin model phenols possessing α-carbonyl groups toward alkylation by ethylene oxide has been reported previously (17).

We also compared the alkali-induced hydrolysis of **3** (to give the 5-hydroxy derivative) with that of the easily handled α-butylene oxide (to give 1,2-dihydroxybutane) in H_2O–acetone (1:1 v/v) at 60°C with a 2:1 molar ratio of K_2CO_3 to the

© 2001 NRC Canada

Fig. 3. %ISO brightness vs. fluorescent light exposure time for the paper sheets impregnated with solvent (S) and models **1**, **1′**, and **1″**.

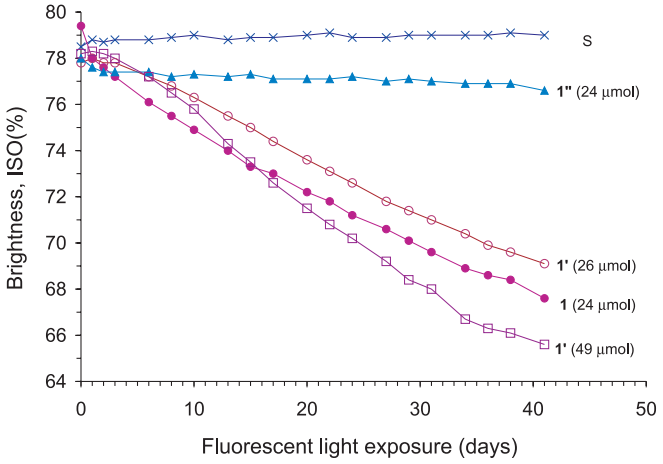
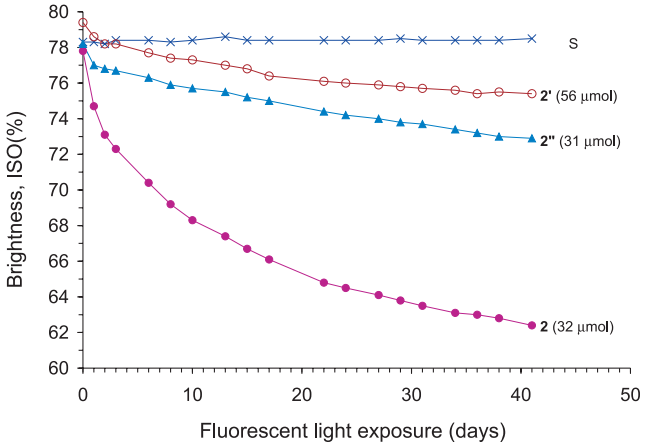


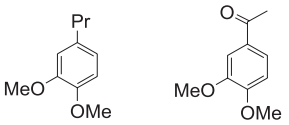
Fig. 4. %ISO brightness vs. fluorescent light exposure time for the paper sheets impregnated with solvent (S) and models **2**, **2′**, and **2″**.



alkylating reagent. We found that **3** was more stable toward alkali-induced hydrolysis than α-butylene oxide (12 and 43% hydrolysis of **3** after 6 and 21 h, respectively, vs. 33 and 77% hydrolysis for the butylene oxide). Data for α-butylene oxide were obtained by GC analyses of samples withdrawn from a single reaction using toluene as an internal reference; those for **3** were obtained from gravimetric determinations of **3** recovered from two reactions. The higher stability towards alkali-induced hydrolysis of **3** is likely responsible for the efficient synthesis of **1′** using just one equivalent of **3**.

Photostability of the tetrazole ethers

To study the photostability of the tetrazole ethers **1′** and **2′**, their corresponding phenols **1** and **2**, as well as the methylated derivatives **1″** and **2″** in a solid-state, cellulosic environment, we first deposited the compounds in filter paper sheets made from pure cellulose. The sheets were soaked with 0.10 M solutions of the compounds in methyl cellosolve, $MeOCH_2CH_2OH$ (one sheet per compound), and a control sheet (soaked with methyl cellosolve only) was also prepared to allow for the estimation of incorporated methyl cellosolve. The tetrazole ethers **1′** and **2′** had about twice the affinity for the filter papers as the precursor phenols or the methylated derivatives: the amounts absorbed were 24, 49, and 24 μmol for **1**, **1′**, and **1″**, and 32, 56, and 31 μmol for **2**, **2′**, and **2″**, respectively. Another sheet was soaked with a 0.06 M solution of **1′** to give a sheet impregnated with 26 mol of **1′**.



1'' 2''

Next, the model compound-impregnated filter sheets were subjected to an accelerated yellowing experiment using "cool white" fluorescent lamps as the light source. The lamps have a similar broadband spectrum to normal office fluorescent lamps with the maximum spectral output at ~570 nm, but have about nine times the intensity. They were used to simulate paper use in an office environment. Figures 3 and 4 show the plots of %ISO brightness vs. fluorescent light exposure time of the sheets impregnated with the solvent (S), **1**, **1′**, and **1″** and with the solvent (S), **2**, **2′**, and **2″**, respectively. At a higher impregnation (49 μmol), tetrazole ether **1′** was slightly more stable than the precursor phenol **1** (24 μmol) at the early stage of light-induced yellowing but less stable at the later stage. At similar impregnation, **1′** (26 μmol) was more stable than **1** throughout the exposure time, but it was less stable than the methylated derivative **1″** (Fig. 3). For example, after 41 days the %ISO brightness for **1′** has dropped from 77.8 to 69.1 (8.7 brightness point loss), while values for **1** and **1″** changed from 79.4 to 67.5 (11.9 brightness point loss) and from 78.2 to 76.6 (1.6 brightness point loss), respectively. These data represent a brightness stabilization (yellowing inhibition) of only 27% when the phenolic group in **1** was protected as the tetrazole ether, but a brightness stabilization of 86% when the phenolic group was protected as the methyl ether. The percent brightness stabilization is defined as [(change in brightness of reference sample – change in brightness of treated sample) / change in brightness of reference sample] × 100% (18).

The tetrazole ether **2′** was much more stable than the precursor phenol **2** and the methylated derivative **2″** on exposure to the fluorescent light (Fig. 4). For example, after 41 days, the %ISO brightness for **2** and **2″** have dropped from 77.8 to 62.4 (15.4 brightness point loss) and from 78.2 to 72.9 (5.3 brightness point loss), respectively. The %ISO brightness for **2′** changed only from 79.4 to 75.4 (4.0 brightness point loss), even though the amount of **2′** in the sheet was close to double that of **2** and **2″** (a lower impregnation value for the same sample will always give a lower brightness loss, see Fig. 3). These data represent a brightness stabilization of 74% when the phenolic group in **2** was protected as the tetrazole ether, compared to a brightness stabilization of 66% when protected as the methyl ether. The tetrazole ethers **1′** and **2′** are both white as powders. The more light-induced yellowing of **1′** than **2′** likely indicates

© 2001 NRC Canada

more cleavage of the tetrazole ether bond in **1′** under light exposure; whether the increased yellowing of **1′** is due to a colour-forming reaction from the cleaved tetrazole group, the cleaved phenol, or both, is unclear.

The above photostability data show that effective photostabilization of lignin phenols by conversion to tetrazole ethers is favored by the presence of an α-carbonyl at the C(1) position of the lignin aromatic ring. In softwood lignins, the number of free phenols is probably <20 per 100 phenylpropane units (19). Among such phenols, only one has been estimated to have a C(1) α-carbonyl group, the majority having an α-hydroxyl group (19). As the α-hydroxyl group and alkyl group (such as the Pr substituent in **1**) have similar electronic properties, e.g., the Hammett σ_{para} values for -CH(OH)CH_3 and *n*-Pr are –0.07 and –0.15, respectively, (20), conversion of the hydroxyl group to an α-carbonyl group may be necessary to obtain significant lignin photostabilization by conversion of the lignin phenols to tetrazole ethers. 2,3-Dichloro-5,6-dicyano-1,4-benzoquinone (DDQ) can oxidize the α-hydroxyl to the α-carbonyl group in lignin model compounds (21) and lignin (22), but a reagent more compatible with wood pulp reactions is needed, and catalytic, oxidative-dehydrogenations are being considered by us. The success of **3** in photostabilizing the acetophenone derivative (**2**), via the formation of **2′**, has also prompted us to introduce a sulfonate group in to the phenyl ring of **3** to give a water-soluble derivative. Future papers will describe our efforts in these areas of research.

Conclusions

The protection of the phenolic hydroxyl groups in lignin model compounds, 2-methoxy-4-propylphenol (**1**) and 4-hydroxy-3-methoxyacetophenone (**2**), as the tetrazole ethers can be achieved in aqueous alkaline media using 5-chloro-1-phenyl-1*H*-tetrazole (**3**) as the alkylating agent; **3** is nontoxic and more stable toward alkali-induced hydrolysis than other alkylating agents such as α-butylene oxide. The tetrazole ether **2′** from **2** is much more photostable than the precursor phenol on exposure to strong fluorescent light, while the tetrazole ether **1′** from **1** is only slightly more stable than the precursor phenol. Photostablization of lignin phenols by conversion to tetrazole ethers seems to require conversion of the α-hydroxyl to α-carbonyl groups, which is unlikely to be commercially viable.

Experimental

General procedures

All chemicals were purchased from Aldrich unless otherwise specified. Reactions were carried out under Ar and monitored by GC and (or) TLC. GC was performed on a Hewlet-Packard model 5890 using a 25 m × 0.2 mm Carbowax column (80°C for 2 min, then an increase to 220°C at a rate of 10°C per min, and a final time of 8 min at 220°C). TLC was performed on Al-backed, precoated silica gel plates (E. Merck, type 5554). ^{1}H NMR spectra were recorded in $CDCl_3$ using $SiMe_4$ as the internal standard on a Bruker AC-200 spectrometer. Mass spectra were determined on a Kratos-AEI model MS 50 spectrometer operating at 70 eV. 2-Methoxy-4-propylphenol (**1**) and 1,2-dimethoxy-4-propylbenzene (**1″**) were prepared from the hydrogenation of eugenol and 4-allyl-1,2-dimethoxybenzene over Pd/C, respectively, (23). The residual light yellow colors in **1**, **1″**, and 4-hydroxy-3-methoxyacetophenone (**2**) (Aldrich) were removed by filtration of their solutions in CH_2Cl_2 through Celite–activated charcoal–Florisil–silica (1:5:5:1).

Synthesis of 2-methoxy-4-propylphenyl-1′-phenyl-5′-tetrazole ether (1′)

To **1** (0.399 g, 2.4 mmol) in distilled water (5 mL) and acetone (5 mL) in a 25 mL flask equipped with a condenser and a magnetic stirring bar was added K_2CO_3 (0.663 g, 4.8 mmol) and 5-chloro-1-phenyl-1*H*-tetrazole (**3**) (0.433 g, 2.4 mmol). The mixture was stirred at 60°C overnight (ca. 18 h), cooled to room temperature (~20°C), acidified with 1 N HCl solution, and then extracted with Et_2O (4 × 30 mL). The combined ether extract was dried over anhydrous $MgSO_4$ for 20 min before being filtered. Removal of the filtrate solvent under reduced pressure gave 0.620 g of crude **1′** as a light-yellow solid (83% crude yield). Purification by column chromatography on silica gel using hexane:ethyl acetate (9:1 and then 1:1) as eluent, followed by recrystallization from MeOH, gave 0.463 g of **1′** as white crystals (62% yield). Crystals suitable for X-ray analysis were obtained at –20°C from a diluted MeOH solution of **1′**. EI-MS *m/z* (%): 310 (M^+, 42), 240 (58), 165 (85), 117 (100). ^{1}H NMR δ: 0.95 (t, 3H, CH_2CH_3), 1.63 (m, 2H, CH_2CH_3), 2.60 (t, 2H, CH_2CH_2), 3.75 (s, 3H, OCH_3), 6.80–7.90 (m, 8H, aromatic). Anal. calcd. for $C_{17}H_{18}N_4O_2$: C 65.79, H 5.85, N 18.05; found: C 66.08, H 5.85, N 18.19.

Synthesis of 3-methoxy-4-(1′-phenyl- 5′-tetrazol)-oxyacetophenone (2′)

Identical to the preparation of **1′**, **2** (0.407 g, 2.4 mmol) was reacted with **3** (0.433 g, 2.4 mmol) and K_2CO_3 (0.663 g, 4.8 mmol) in H_2O–acetone (1:1, 10 mL) to give 0.290 g of **2′** as a light-yellow crystalline solid (39% yield). Filtration of a CH_2Cl_2 solution of this solid through Celite–activated charcoal–Florisil–silica (1:5:5:1) gave **2′** as colorless crystals. EI-MS *m/z* (%): 310 (M^+, 12), 240 (13), 198 (10), 165 (34), 117 (100). ^{1}H NMR δ: 2.62 (s, 3H, OCH_3), 3.86 (s, 3H, C(O)CH_3), 7.40–7.90 (m, 8H, aromatic). Anal. calcd. for $C_{16}H_{14}N_4O_3$: C 61.93, H 4.55, N 18.06; found: C 61.94, H 4.56, N 17.80.

X-ray crystallographic analyses of 1′ and 2′

A needle crystal of **1′** (~ 0.45 × 0.25 × 0.20 mm) and a plate crystal of **2′** (~ 0.40 × 0.10 × 0.50 mm) were each mounted in a glass fibre. Measurements were made on a Rigaku ADSC CCD area detector with graphite monochromated Mo Kα (for **1′**) or Cu Kα (for **2′**) radiation. For **1′**, cell constants and an orientation matrix for data collection, derived from 6295 reflections, corresponded to a monoclinic cell, space group $P2_1/c$ (No. 14), FW = 310.35 with dimensions: a = 9.8679(6), b = 16.708(1), c = 10.2841(6) Å, β = 109.732(5)°, V = 1596.0(2) Å^3, Z = 4, ρ_{calc} = 1.37 g cm^{-3}; absent reflection: $h0l$: ($l \neq 2n$), $0k0$: ($k \neq 2n$). The data were collected at –100 ± 1°C to a max 2θ value of 55.8° in 0.50° oscillations with 15.0 s exposures. A sweep of data was done using Φ oscillations from 0.0 to 190.0° at χ = 0°, and a second sweep was performed using ω oscillations between

© 2001 NRC Canada

–19.0 and 23.0° at $\chi = 90.0°$. The crystal to detector distance was 40.64 mm. The detector swing angle was –5.52°. Of the 13144 reflections which were collected, 3407 were unique (R_{int} = 0.052); equivalent reflections were merged. Data were collected and processed using the d*TREK program (MSC). The linear absorption coefficient (μ) for Mo Kα radiation is 0.9 cm^{-1}, and the data were corrected for Lorentz and polarization effects.

For **2′**, the unit-cell parameters for the monoclinic cell were refined by least-squares on setting angle values for 22 reflections (86.69° < 2θ < 98.43°). Crystal data at 21°C are: space group = $P2_1/a$ (No. 14), FW = 310.31, a = 7.7212(2), b = 27.350(5), c = 14.569(3) Å, β = 101.30(2)°, V = 3017(1) $Å^3$, Z = 8, ρ_{calc} = 1.37 g cm^{-3}; absent reflection: $h0l$: ($h \neq 2n$), $0k0$: ($k \neq 2n$). Data collection and reduction were as described earlier (23) with some modifications: the diameter of the incident beam collimator was 1.0 mm; of the 6933 reflections that were collected, 6448 were unique (R_{int} = 0.056); over the course of data collection, the standards increased by 6.8% and a linear correction factor was applied to the data to account for this phenomenon; for Cu Kα radiation μ is 7.7 cm^{-1}, and a correction for secondary extinction was applied (coefficient = 3.3×10^{-6}).

The structures were solved using the methods cited earlier (23). Compound **2′** crystallizes with two molecules in the asymmetric unit, and these are related by a pseudocentre of inversion, with only the orientation of the MeO substituent breaking any true symmetry. The final cycle of full-matrix least squares refinement for **1′** was based on 3286 observed reflections ($I > 0.00\ \sigma(I)$) and 208 variable parameters, and converged (largest parameter shift was 0.00 times its esd) with unweighted (R) and weighted (R_w) agreement factors of 0.072 and 0.106, respectively. For **2′**, there were correspondingly 6299 observed reflections, 416 variable parameters, and agreement factors of 0.101 and 0.170. R is defined as $\Sigma||F_o| - |F_c||/\Sigma|F_o|$, and R_w as $(\Sigma(F_o^2 - F_c^2)^2/\Sigma_w(F_o^2)^2)^{1/2}$. For **1′**, R = 0.039 (R_w = 0.046) for the 2029 reflections with $I \geq 3\sigma(I)$; for **2′**, the corresponding R and R_w values are 0.055 and 0.073, respectively, for 3634 reflections. The standard deviation of an observation of unit weight was 1.15 (for **1′**) and 2.35 (for **2′**). The max and min peaks on the final difference Fourier map corresponded to 0.34 and –0.32 e $Å^{-3}$, respectively, for **1′**, and 0.33 and –0.35 e $Å^{-3}$ for **2′**.

Final atomic coordinates and equivalent isotropic thermal parameters (B_{eq}), bond lengths, bond angles, anisotropic thermal parameters, torsion angles, intermolecular contacts (out to 3.60 Å), and least-square planes are included as supplementary materials.[3]

Impregnation of a model compound into a filter paper sheet

A 5.0 × 6.3 cm Whatman (No. 1) filter paper (~275 mg) was conditioned at 23°C and 50% humidity for 2 days, weighed, and soaked in a 0.10 or 0.06 M compound solution in methyl cellosolve ($MeOCH_2CH_2OH$) or just methyl cellosolve alone for 10 min. The sheet was removed, air-dried for 10 min, and conditioned at 23°C and 50% humidity for 20 h and weighed again. The amount of impregnated model compound was calculated by subtracting the amount of methyl cellosolve incorporated into the sheet (2.4 ± 0.1 mg) from the weight difference of the conditioned sheet before and after impregnation with the model compound. Using 0.10 M solutions, the amounts of model compounds impregnated were 24, 49, and 24 μmol (i.e., 3.9, 15.2, and 4.3 mg) for **1**, **1′**, and **1″**, respectively, and 32, 56, and 31 μmol (i.e., 5.3, 17.5, and 5.5 mg) for **2**, **2′**, and **2″**, respectively. Using a 0.06 M solution, the amount of **1′** impregnated was 26 μmol (i.e., 8.1 mg).

Accelerated fluorescent light-induced yellowing experiments

The accelerated, fluorescent light-induced yellowing experiments were performed in a light-box (LuzChem Research Inc.) equipped with 8 F8T5CW fluorescent lamps (Albrite Lighting Ltd.) which have a max output at ~570 nm and a light intensity of ~1500 foot-candle. The irradiation was performed in the 23°C temperature and 50% humidity room, and the brightness (%ISO) of the sheets monitored in a Technibrite Micro TB-1C instrument. ISO (International Standardization Organization) brightness of a paper is a measurement of the directional reflectance of light at 457 nm of the paper in an Elrepho instrument, calibrated to be 100% for MgO and 0% for a dark black background (24). The higher the %ISO brightness, the whiter (less yellow) the paper.

Acknowledgments

We thank Alexandra Kwong for her assistance with the yellowing experiments and Dr. Cyril Heitner for discussions. We also thank the Natural Sciences and Engineering Research Council of Canada (NSERC) for partial financial support to A.Z. Lu via the Mechanical and Chemimechanical Pulps Network and a research grant.

References

1. H. Matussek and V. Stefan. Pulp and paper international fact and price book. Miller Freeman, Brussels. 1998. p. 260.
2. C.J. Biermann. Handbook of pulping and papermaking. 2nd ed. Academic Press, San Diego, C.A. 1996. p. 62.
3. G.J. Leary. J. Pulp Paper Sci. **26**, J154 (1994) and refs. therein.
4. C. Heitner. *In* Photochemistry of lignocellulosic materials. *Edited by* C. Heitner and J.C. Scaiano. ACS Symposium Series 531. The American Chemical Society, Washington, D.C. 1993. p. 3 and refs. therein.
5. G.J. Leary. Tappi J. **51**, 257 (1968).
6. K.P. Kringstad and S.Y. Lin. Tappi J. **53**, 2296 (1970).
7. G. Brunow and M. Sivonen. Pap. Puu-Pap. Tim. **23**, 215 (1975).
8. The Merck index — an encyclopedia of chemicals, drugs, and biologicals. 12th ed. Merck & Co., Inc. New Jersey. 1996.

[3] Supplementary material may be purchased from the Depository of Unpublished Data, Document Delivery, CISTI, National Research Council Canada, Ottawa, ON K1A 0S2, Canada. For information on obtaining material electronically go to http://www.nrc.ca/cisti/irm/unpub_e.shtml. Crystallographic information has also been deposited with the Cambridge Crystallographic Data Centre (CCDC No. 164995 and 164996). Copies of the data can be obtained, free of charge, on application to the Director, CCDC, 12 Union Road, Cambridge CB2 1EZ, U.K. (fax: 44-1223-336033 or e-mail: deposit@ccdc.cam.ac.uk).

© 2001 NRC Canada

9. D.H. Andrews and R.P. Singh. Can. Patent 810 571 (1966).
10. J.A. Schmidt and C. Heitner. J. Wood Chem. Tech. **11**, 397 (1991).
11. R.P. Singh. Tappi J. **49**, 281 (1966).
12. U. Tschirner and C.W. Dence. Paper and Timber, **4**, 338 (1988).
13. J.C. Kauer and W.A. Sheppard. J. Org. Chem. **32**, 3580 (1967).
14. J.A.C. Alves and R.A. Johnstone. Synthetic Commun. **27**, 2645 (1997).
15. W.J. Musliner and J.W. Gates, Jr. J. Am. Chem. Soc. **88**, 4217 (1966).
16. C.F. Barfknecht, R.V. Smith, and V.D. Reif. Can. J. Chem. **48**, 2138 (1970).
17. H. Ishikawa, T. Oki, and F. Fujita. J. Japan Wood Res. Soc. 85 (1961).
18. A.J. Ragauskas. Tappi J. **76**, 153 (1993).
19. E. Alder. Wood Sci. Technol. **11**, 169 (1977).
20. D.D. Perrin, B. Dempsey, and E.P. Serjeant. pK_a Prediction for organic acids and bases. Chapman and Hall, New York. 1981. Table A-1.
21. H.D. Becker and E. Alder. Acta Chem. Scand. **15**, 218 (1961).
22. E. Alder, H.D. Becker, T. Ishihara, and A. Stamvik. Holzforschung, **20**, 3 (1966).
23. T.Q. Hu, B.R. James, S.J. Rettig, and C.-L. Lee. Can. J. Chem. **75**, 1234 (1997).
24. TAPPI test methods, T452 om-92. Tappi Press, Atlanta. 1996.

© 2001 NRC Canada

Electrical conductivity, speeds of sound, and viscosity of aqueous ammonium nitrate solutions

Abdul Wahab and Sekh Mahiuddin

Abstract: Density, electrical conductivity, speeds of sound, and viscosity of aqueous ammonium nitrate solutions were measured as functions of concentration (m, mol kg^{-1}) ($0.1599 \leq m \leq 20.42$) and temperature (T, K) ($273.15 \leq T \leq 323.15$). Experimental values are consistent with the reported data. Variation of isotherms of electrical conductivity, isentropic compressibility, and structural relaxation time with concentration evoke structural information on the ion solvation in aqueous ammonium nitrate solution at different concentration regions. The primary hydration numbers of ammonium nitrate were estimated at a particular concentration at which the isentropic compressibility isotherms converge. The existence of free hydrated ions, resulting from strong ion solvent interactions in dilute to 9.1 mol kg^{-1}, the solvent-separated ion-pairs resulting from the relative competition between the ion–solvent and the ion–ion interactions in 9.1 to 12.0 mol kg^{-1}, and the solvent-shared ion-pairs beyond 12.0 mol kg^{-1} resulting from a decrease in the number of solvent molecules, govern the transport process.

Key words: electrical conductivity, speeds of sound, viscosity, ammonium nitrate, hydration number.

Résumé : On a mesuré les densités, conductivités électriques, vitesses du son et viscosités de solutions aqueuses de nitrate d'ammonium en fonction de la concentration (m, mol kg^{-1}) ($0{,}1599 \leq m \leq 20{,}42$) et de la température ($T$, K) ($273{,}15 \leq T \leq 323{,}15$). Les valeurs expérimentales sont en accord avec les données rapportées dans la littérature. Les variations dans les isothermes de la conductivité électrique, de la compressibilité isentropique et du temps de relaxation structurale en fonction de la concentration fournit des indications structurales sur la solvatation de l'ion en solution aqueuse de nitrate d'ammonium dans les diverses régions de concentration. On a évalué les nombres d'hydratation primaires du nitrate d'ammonium à une concentration donnée, celle à laquelle les isothermes de compressibilité isentropiques convergent. L'existence d'ions hydratés libres observée dans la région de concentration de diluée à 9,1 mol kg^{-1} résulte de fortes interactions ion solvant, celle des paires d'ions séparés par le solvant observée dans la région de concentration allant de 9,1 mol kg^{-1} à 12,0 mol kg^{-1} résulte de la compétition relative entre d'une part l'ion et le solvant et d'autre part les paires d'ions séparés par le solvant et enfin celle des paires d'ions qui se partagent le solvant observées dans la région de concentration allant au-delà de 12,0 mol kg^{-1} résulte d'un nombre trop faible de molécules de solvant pour gouverner le processus de transport.

Mots clés : conductivité électrique, vitesses du son, viscosité, nitrate d'ammonium, nombre d'hydratation.

[Traduit par la Rédaction]

Introduction

The solvation structure of ions in different concentration regions in water and nonaqueous media have been of immense importance to the technologist and theoretician because of the different interactions and equilibria involved. The existence of ions, solvated ions, ion-pairs (solvent-separated, solvent-shared, and contact ion-pairs), and free solvent depends on the concentration region (1).

The reported hydration number of NH_4^+ is varied from 4 to 11 (2). On the other hand, NH_4^+ with same molar mass, equivalent partial molar volume, and tetrahedral structure as that of water fits in the water cage (3). The hydration number of H_3O^+ is reported as 4 (2). Therefore, the primary hydration number of NH_4^+ should be around 4. X-ray (4) and neutron (5) diffractions of aqueous ammonium nitrate have been reported in the concentration region of ~12–18 mol kg^{-1}. X-ray studies showed that NO_3^- is only hydrated, whereas neutron diffraction studies suggested the formation of ion-pairs within the reported concentration region. Recent ab initio simulation (6) of NH_4^+ in water medium predicted that five molecules of water are coordinated to NH_4^+. The simulation studies (6) also reveal that out of five water molecules, four water molecules are directly attached to NH_4^+ through strong hydrogen bonding interactions resulting in rigid structure, whereas the fifth water molecule is mobile and is exchanged with one of the four water molecules.

Among the many approaches (2), the acoustic method (7–9) seems to be an alternative proposition for studying the solvent structure around ions. Earlier we reported (10–12) that if both cation and anion are hydrated a rigid structure is formed and the isentropic compressibility isotherms converge at a particular concentration, which is characteristic of

Received December 11, 2000. Published on the NRC Research Press Web site at http://canjchem.nrc.ca on August 17, 2001.

A. Wahab and S. Mahiuddin.[1] Material Science Division, Regional Research Laboratory, Jorhat-785 006, Assam, India.

[1]Corresponding author (fax: +91-376-370011; e-mail: mahirrljt@yahoo.com).

 DOI: 10.1139/cjc-79-8-1207 © 2001 NRC Canada

Table 1. Least-squares fitted values of the constant parameters of the density equation, $\rho = a - b(T - 273.15\ \text{K})$, for aqueous ammonium nitrate solutions.

m (mol kg^{-1})	a (kg m^{-3})	b (kg m^{-3} K^{-1})	Std dev in ρ (kg m^{-3})
0.1599	1014.5 ± 0.5	0.4813 ± 0.0115	0.06
0.1972	1014.4 ± 0.5	0.4538 ± 0.0112	0.04
0.2399	1015.8 ± 0.2	0.4453 ± 0.0463	0.07
0.5749	1025.3 ± 0.3	0.3993 ± 0.0073	0.17
0.6503	1027.6 ± 0.4	0.4288 ± 0.0094	0.08
0.9973	1039.4 ± 0.3	0.4439 ± 0.0070	0.14
1.189	1043.1 ± 0.7	0.4267 ± 0.0159	0.09
1.269	1051.1 ± 0.2	0.4659 ± 0.0057	0.09
1.501	1052.4 ± 0.2	0.4398 ± 0.0047	0.10
1.975	1067.0 ± 0.3	0.4972 ± 0.0059	0.10
1.989	1066.7 ± 0.2	0.4617 ± 0.0048	0.10
2.393	1076.3 ± 0.5	0.5135 ± 0.0114	0.10
2.422	1077.2 ± 0.2	0.5014 ± 0.0048	0.10
2.505	1078.1 ± 0.2	0.4725 ± 0.0060	0.15
2.913	1090.3 ± 0.2	0.5179 ± 0.0049	0.09
2.990	1091.0 ± 0.3	0.5395 ± 0.0724	0.05
3.009	1091.5 ± 0.2	0.5003 ± 0.0053	0.12
3.100	1094.1 ± 0.1	0.5251 ± 0.0023	0.04
3.214	1096.1 ± 0.6	0.5229 ± 0.0135	0.10
3.885	1111.7 ± 0.1	0.5475 ± 0.0029	0.05
4.009	1113.1 ± 0.3	0.5289 ± 0.0083	0.18
4.093	1115.2 ± 0.9	0.5525 ± 0.0195	0.09
4.338	1121.2 ± 0.1	0.5602 ± 0.0019	0.03
4.653	1126.5 ± 0.6	0.5504 ± 0.0126	0.09
4.695	1127.4 ± 0.2	0.5366 ± 0.0047	0.09
4.974	1134.0 ± 0.1	0.5776 ± 0.0030	0.05
5.947	1154.3 ± 0.1	0.5906 ± 0.0020	0.03
6.536	1163.2 ± 0.2	0.6025 ± 0.0038	0.06
6.999	1170.5 ± 0.1	0.6065 ± 0.0022	0.04
7.483	1176.6 ± 0.2	0.5999 ± 0.0038	0.07
7.888	1175.9 ± 1.1	0.5808 ± 0.0223	0.10
8.733	1195.6 ± 0.1	0.6110 ± 0.0030	0.06
8.654	1192.6 ± 0.5	0.5992 ± 0.0106	0.08
8.938	1197.7 ± 0.2	0.6037 ± 0.0037	0.06
10.25	1214.5 ± 0.1	0.6299 ± 0.0031	0.06
11.17	1224.0 ± 0.6	0.6177 ± 0.0129	0.09
11.93	1233.8 ± 0.2	0.6267 ± 0.0038	0.06
13.66	1249.8 ± 0.6	0.6223 ± 0.0122	0.09
14.19	1257.1 ± 0.1	0.6550 ± 0.0032	0.06
17.23	1281.2 ± 0.8	0.6403 ± 0.0174	0.10
20.42	1304.2 ± 0.9	0.6305 ± 0.0192	0.14

an electrolyte. On the other hand, the existence and equilibria of hydrated ions and different ion-pairs (solvent-separated ion-pair, solvent-shared ion-pair, and contact ion-pair) in a wide concentration region have an influence on the viscosity and the electrical conductivity. Therefore, in this paper, we report the electrical conductivity, speeds of sound, and viscosity of aqueous ammonium nitrate solutions as functions of concentration and temperature.

Experimental

Ammonium nitrate (>99.5%, Qualigens Fine Chemicals, India) was recrystallized twice from double-distilled water and then kept under vacuum desiccator over P_2O_5. Double-distilled water was used to prepare solutions. All solutions were prepared by mass with ±0.2% uncertainty.

Densities (ρ, kg m^{-3}) of all solutions were measured accurately to ±0.1 kg m^{-3} by using a single-stem graduated pycnometer. The pycnometer was calibrated by using double-distilled water.

Electrical conductivities (κ, S m^{-1}) were measured by employing precision component analyzer 6425 (Wayne Kerr) with an accuracy of ±0.1%. Uncertainty in conductivity was within ±0.4 S m^{-1}. The conductivity cell was calibrated by using 0.1 mol kg^{-1} KCl solution (13). The cell constant was found to be 173 m^{-1} with negligible temperature coefficient.

Viscosities (η, mPa s) were measured with the help of a Schott-Geräte AVS 310 unit equipped with micro-Ubbelohde viscometer. Two viscometers were used depending on the magnitude of the viscosity of solutions. The viscometers were calibrated by using double-distilled water and were found to be 0.009595 and 0.013103 mm^2 s^{-2}. Average of five efflux times was taken to calculate viscosity. The uncertainty in efflux time was ±0.05 s.

Speeds of sound (u, m s^{-1}) in aqueous ammonium nitrate solutions were measured with an accuracy of ±0.1 m s^{-1} by using a variable path-interferometer (multifrequency ultrasonic interferometer, M-83, Mittal Enterprises, New Delhi) at 2 MHz. Details of measurements are given elsewhere (10–12, 14).

All the measurements were made as functions of concentration (m, mol kg^{-1}) ($0.1599 \le m \le 20.42$) and temperature (T, K) ($273.15 \le T \le 323.15$). Thermostat type CT–1520 (Schott-Geräte), RSL 6D (Lauda), or F32 HP (Julabo) was used to maintain the temperature of the solution to ±0.02 K.

Results and discussion

Densities were found to be a linear function of temperature and are given in Table 1. An isotherm of ρ vs. m at 298.15 K, as an example, is illustrated in Fig. 1 along with the reported values (15–18). Experimental density values at 298.15 K were comparable within ±0.4% with the literature values. Values of speeds of sound, electrical conductivity, and viscosity are given in Tables 1S-3S (*Supplementary materials*), respectively.[2]

Isotherms of η vs. m and κ vs. m at three different temperatures are shown in Figs. 2 and 3, respectively. The present viscosities were compared with the reported values (15, 16, 18) at 298.15 K. It was found that the measured viscosities are comparable within ±1% with the reported values (15, 16, 18) up to 6 mol kg^{-1}. Beyond this concentration the measured viscosities are ~4.3% higher than that of Campbell and Kartzmark (16) and ~2.6% than that of Campbell et al. (18). On the other hand, viscosity values of Campbell et al. (18) are ~2.7% higher than that of Campbell and Kartzmark (16).

[2] Supplementary material may be purchased from the Depository of Unpublished Data, Document Delivery, CISTI, National Research Council Canada, Ottawa, ON K1A 0S2, Canada. For information on obtaining material electronically go to http://www.nrc.ca/cisti/irm/unpub_e.shtml.

© 2001 NRC Canada

Fig. 1. Variation of density with concentration of aqueous ammonium nitrate solutions at 298.15 K.

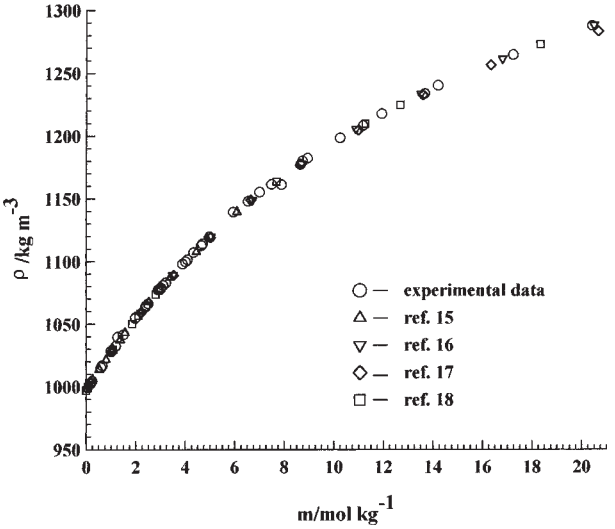
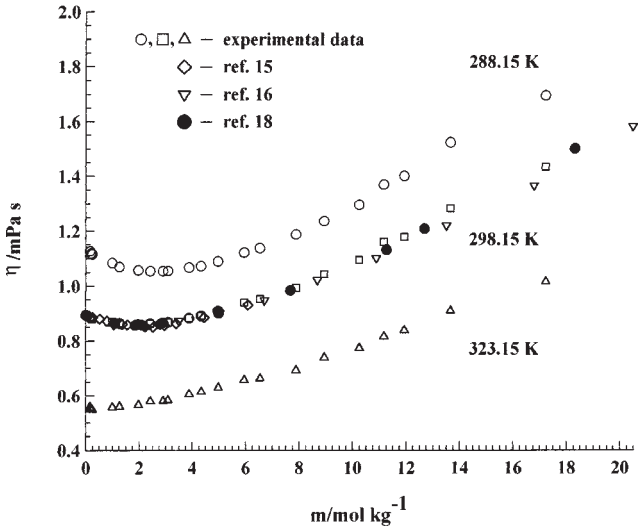


Fig. 2. Plots of viscosity vs. concentration of aqueous ammonium nitrate solutions at three different temperatures.



The deviation in electrical conductivity values between ours and that of Campbell and Kartzmark (16) and Wishaw and Stokes (19) was ~9% in the concentration range of ~2–5 mol kg^{-1} and is gradually reduced to ~1% in the higher concentration range. We could not compare the speeds of sound data because of the lack of reported values.

The isentropic compressibilities (κ_s, Pa^{-1}), of aqueous ammonium nitrate solutions were calculated from the following relation:

$$[1] \qquad \kappa_s = 1/u^2\rho$$

where u is the speeds of sound and ρ is the density of the solutions. Isotherms of κ_s vs. m at three temperatures are plotted in Fig. 4. In earlier papers (11, 12), we reported an isothermal equation of the following form:

$$[2] \qquad \kappa_s = a_1 + b_1 m + c_1 m^d$$

Fig. 3. Isotherms of electrical conductivity of aqueous ammonium nitrate solutions at three different temperatures. Symbols are experimental and reported values and solid lines are calculated from eq. [4].

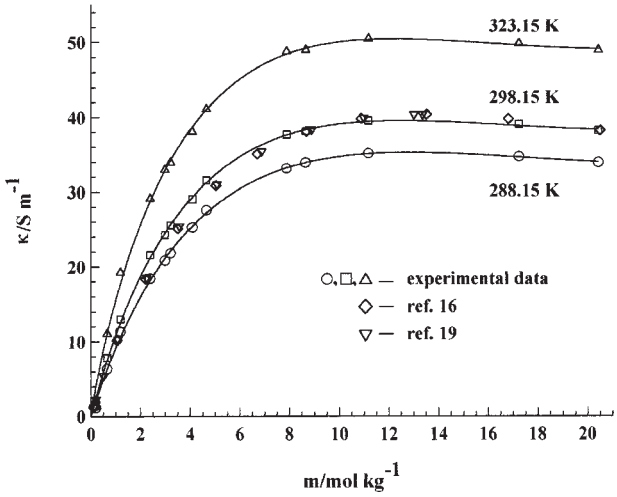
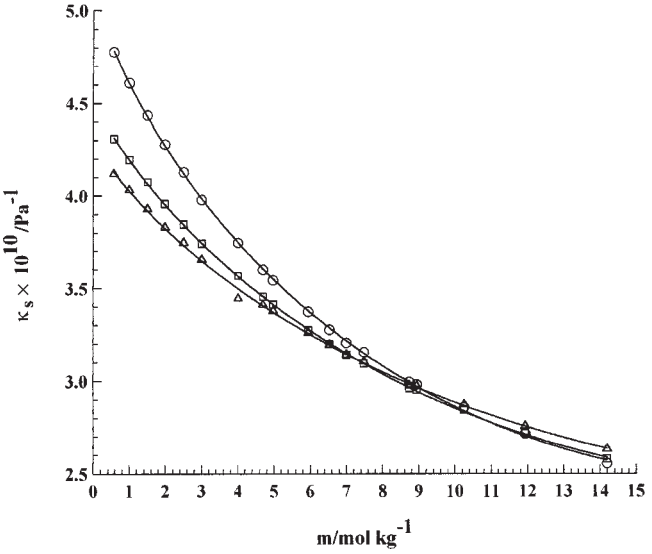


Fig. 4. Plots of isentropic compressibility vs. concentration of aqueous ammonium nitrate solutions at: 273.15 (○), 298.15 (□), and 323.15 (Δ) K.



to fit the isentropic compressibilities. In eq. [2], a_1, b_1, and c_1 are the temperature-dependent parameters, d is the adjustable parameter, and m is the concentration in mol kg^{-1}. The best-fit values of the parameters in eq. [2] are collected in Table 2. Surprisingly, as it is apparent from Table 2 and Fig. 4, eq. [2] can reproduce the isentropic compressibilities within ±0.7%, except for 4.009 mol kg^{-1} at 323.15 K, where the reproducibility was ±1.6%.

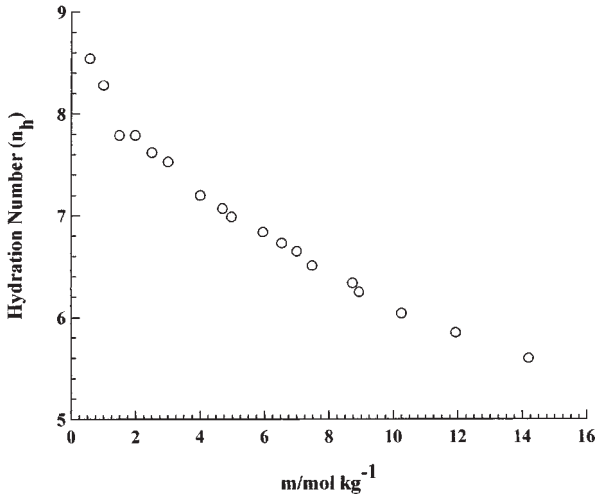
Considering the temperature range of our study, we consider qualitatively that the isentropic compressibility isotherms converge at 9.1 mol kg^{-1} (Fig. 4). At this concentration all the available water molecules are involved in the primary hydration shell of ammonium nitrate with $\kappa_{s,h}$ = 2.960 × 10^{-10} Pa^{-1}, $\kappa_{s,h}$ is the isentropic compressibility of the primary hydration shell of the solute at 9.1 mol kg^{-1}. The

© 2001 NRC Canada

Table 2. Least-squares fitted values of the parameters of eq. [2] for isentropic compressibility for aqueous ammonium nitrate solutions.

T (K)	a_1 (1×10^{10}) (Pa^{-1})	b_1 (1×10^{10}) (Pa^{-1} kg mol^{-1})	c_1 (1×10^{10}) (Pa^{-1} kg^d mol^{-d})	d	Std dev in κ_s (1×10^{12})
273.15	5.096 ± 0.018	–1.614 ± 0.540	1.125 ± 0.527	1.09 ± 0.04	0.98
278.15	4.946 ± 0.018	–1.333 ± 0.4256	0.8838 ± 0.4110	1.10 ± 0.04	0.86
283.15	4.800 ± 0.128	–1.253 ± 4.108	0.8407 ± 3.987	1.10 ± 0.37	2.72
288.15	4.689 ± 0.016	–0.7360 ± 0.1701	0.3682 ± 0.1565	1.18 ± 0.05	0.80
293.15	4.601 ± 0.017	–0.7271 ± 0.2075	0.3784 ± 0.1926	1.16 ± 0.06	0.77
298.15	4.516 ± 0.014	–0.5959 ± 0.1254	0.2940 ± 0.1133	1.20 ± 0.05	0.61
303.15	4.441 ± 0.013	–0.4718 ± 0.0780	0.1760 ± 0.0669	1.25 ± 0.06	0.59
308.15	4.423 ± 0.014	–1.460 ± 0.877	1.138 ± 0.868	1.06 ± 0.04	0.97
313.15	4.342 ± 0.010	–0.4034 ± 0.0536	0.1359 ± 0.0449	1.27 ± 0.05	0.50
318.15	4.314 ± 0.013	–0.4226 ± 0.0801	0.1586 ± 0.0690	1.24 ± 0.07	0.62
323.15	4.309 ± 0.027	–0.7426 ± 0.6026	0.4620 ± 0.5800	1.11 ± 0.11	1.48

Fig. 5. Variation of hydration number of aqueous ammonium nitrate solutions at 298.15 K.



$\kappa_{s,h}$ of ammonium nitrate is lower than that of sodium nitrate ($\kappa_{s,h} = 3.04 \times 10^{-10}$ Pa^{-1}) (20) and lithium nitrate ($\kappa_{s,h} = 3.34 \times 10^{-10}$ Pa^{-1}) (11) and much lower than that of free water ($\kappa_s = 4.477 \times 10^{-10}$ Pa^{-1}). These results indicate stronger ion–solvent interactions in ammonium nitrate solutions at 9.1 mol kg^{-1} than in the above cited nitrate salt solutions.

The hydration numbers (n_h) of ammonium nitrate were calculated from the reported relation (10, 11)

$$[3] \qquad n_h = [\kappa_{s,\phi} - \kappa_{s,h}V_\phi]/[V_1(\kappa_{s,h} - \kappa_{s,1})]$$

In eq. [3], $\kappa_{s,\phi}$ is the conventional apparent molal isentropic compressibility (21), V_ϕ is the apparent molal volume, V_1 is the molar volume of the solvent, and $\kappa_{s,1}$ is the isentropic compressibility of the solvent. The apparent molal volume at infinite dilution was found to be 4.72×10^{-6} m^3 mol^{-1} and is in good agreement with the reported values (22) at 298.15 K, which suggests the reliability of the experimental density values.

The calculated hydration numbers from eq. [3] are depicted in Fig. 5. The primary hydration number of ammonium nitrate at 9.1 mol kg^{-1} was found to be 6.2 and is in good agreement with the water molecules per mol of solute (6.1) at that concentration. Solubility data (23) suggested a structural transition at around 42% (~9.05 mol kg^{-1}) in aqueous ammonium nitrate solution. On the other hand, the phase diagram constructed based on the available data in the literature (24–26) showed that the eutectic point appears at 0.145 mol fraction (~9.4 mol kg^{-1}). These concentrations (~9.05 and 9.4 mol kg^{-1}) are in good agreement with the concentration (~9.1 mol kg^{-1}) at which the isentropic compressibility isotherms converge (Fig. 4).

To distribute the total primary hydration number (6.2) of ammonium nitrate into its ionic hydration number, we require the primary hydration number of either NH_4^+ or NO_3^- as a reference. For aqueous ammonium nitrate, contradictory primary hydration numbers of NH_4^+ have been reported in the literature (2, 4, 5). It has also been reported that NH_4^+ and H_2O have same molar mass and equivalent molar volumes and both have a tetrahedral structure (3). Therefore, NH_4^+ can fit in the water structure. The primary hydration number for NH_4^+ may be equivalent to 4, which is the same as that for H_3O^+ (2).

X-ray (4) and neutron (5) diffraction have been employed to study the hydration of NH_4^+ and NO_3^- in 8.0 mol L^{-1} (~13.5 mol kg^{-1}) and 12.0 and 15.0 mol kg^{-1} ammonium nitrate solutions, respectively. X-ray diffraction studies revealed the hydration of NO_3^-, whereas neutron diffraction studies showed the ion-pair formation and the water molecules are weakly hydrogen bonded to both NH_4^+ and NO_3^-. From Fig. 4, it may be noted that at 9.1 mol kg^{-1} the primary hydration shell of ammonium nitrate is just saturated and beyond this concentration overlap of cation and anion occurs leading to the formation of ion-pairs due the strong and predominant ion–ion interactions. Recent ab initio simulation (6) of ammonium ion in water showed that there are five water molecules coordinated to NH_4^+, with four of them are directly hydrogen bonded to each proton of NH_4^+ in the tetrahedral cage. The remaining water molecule is mobile and is exchangeable with one of the four water molecules directly attached to NH_4^+.

The variation of electrical conductivity isotherms of aqueous ammonium nitrate solutions as depicted in Fig. 3 show that the conductivity maximum (κ_{max}) occurs at ~12 mol kg^{-1}. To quantify the concentration at which κ_{max} appears, the Casteel–Amis equation (27):

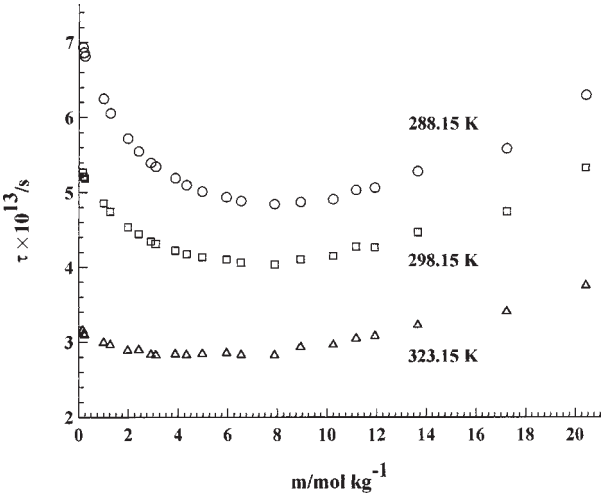
$$[4] \qquad \kappa = \kappa_{max}\ (m/\mu)^a\ \exp\ [b(m - \mu)^2\text{-}a(m - \mu)/\mu]$$

© 2001 NRC Canada

Table 3. Least-squares fitted values of the parameters of eq. [4] for conductivity of aqueous ammonium nitrate solutions.

T (K)	κ_{max} (S m^{-1})	a	b (1×10^{-3}) (kg^2 mol^{-2})	μ (mol kg^{-1})	Std dev in κ (S m^{-1})
288.15	35.26	0.9520	0.1476	12.77	0.40
298.15	39.52	0.9421	0.1684	12.41	0.42
323.15	50.40	0.8751	0.1673	12.12	0.76

Fig. 6. Variation of structural relaxation time with concentration of aqueous ammonium nitrate solutions at three different



has been used to fit the conductivity data, and the least-squares fitted values of the parameters in eq. [4] are collected in Table 3. In eq. [4], μ is the concentration (mol kg^{-1}) at which conductivity becomes maximum (κ_{max}), m is the concentration (mol kg^{-1}), and a and b are the empirical parameters. Equation [4] can reproduce the conductivity data within ±3% except in the low concentration region. From Table 3, it is apparent that the maximum conductivity appears at 12.43 ± 0.34 mol kg^{-1}, beyond this concentration conductivity values decrease by 3.0–3.8% within the temperature range of the present study.

From Figs. 3 and 4 it may be argued that up to 9.1 mol kg^{-1} free hydrated NH_4^+ and NO_3^- exist, and in the concentration range 9.1–12.0 mol kg^{-1} solvent-separated ion-pairs are formed. Beyond 12.0 mol kg^{-1}, transition to the solvent-shared ion-pairs occurs as a result of a decrease in the number of available water molecules in comparison to hydration number (Fig. 5). To support our views we have plotted shear relaxation time ($\tau = 4\eta\kappa_s/3$) vs. m (mol kg^{-1}) at three different temperatures (Fig. 6). It is apparent that τ decreases up to ~7–9 mol kg^{-1} then increases with concentration. The shallow minimum at m_{min} in τ vs. m isotherms is more pronounced at low temperatures, because at low temperatures the hydrogen bond of water is reinforced significantly (28), which is further broken by NH_4^+. The structure breaking effect of NH_4^+ causes the τ values to decrease up to ~7–9 mol kg^{-1}. Beyond ~7–9 mol kg^{-1}, the NH_4^+ and NO_3^- are set for ion association due to a decrease in the number of available water molecules around them resulting in the increase in τ values with concentration. Small deviation in τ vs. m isotherms at ~7–9 mol kg^{-1} at higher temperatures may be attributed to breaking–loosening of hydrogen bonds in bulk water and water in the secondary hydration sphere of ions due to the thermal vibrations.

In the preceding section we obtained 6.2 as the total primary hydration number of ammonium nitrate. Considering the primary hydration number of NH_4^+ as 4.0 (6), the primary hydration number of NO_3^- is estimated to be 2.2. The estimated primary hydration number of NO_3^- in aqueous ammonium nitrate is less than 3–6 water molecules around NO_3^- (2). To fulfil the minimum primary hydration number of NO_3^- in aqueous ammonium nitrate solution, NO_3^- may share water molecules involved in the primary hydration sphere of NH_4^+ leading to the formation of solvent-separated ion-pairs.

Acknowledgements

Financial assistance from the Department of Science and Technology, New Delhi, and gift of the RLS 6D thermostat from Deutsche Gesellschaft für Technische Zusammenarbeit (GTZ) GmbH, Germany are gratefully acknowledged. Authors express their gratitude to the Director of the laboratory for the facilities and interest in this work.

References

1. Y. Marcus. *In* Ion solvation. John Wiley & Sons, Chichester, U.K. 1986.
2. H. Ohtaki and T. Radnai. Chem. Rev. **93**, 1157 (1993).
3. P.M. Vollmar. J. Chem. Phys. **39**, 2236 (1963).
4. R. Caminity, G. Licheri, G. Piccaluga, and G. Pinna. J. Chem. Phys. **68**, 1967 (1978).
5. P.A.M. Walker, D.G. Lawrence, and G.W. Neilson. J. Chem. Soc. Faraday Trans. 1, **85**, 1365 (1989).
6. F. Brugé, M. Bernasconi, and M. Parrinello. J. Am. Chem. Soc. **121**, 10883 (1999).
7. J.Ó.M. Bockris and P.P.S. Saluja. J. Phys. Chem. **76**, 2140 (1972).
8. H. Endo and O. Nomoto. J. Chem. Soc. Faraday Trans. 2, **77**, 217 (1981).
9. G. Onori. J. Chem. Phys. **89**, 510 (1988).
10. N. Rohman, N.N. Dass, and S. Mahiuddin. J. Chem. Eng. Data. **44**, 465 (1999).
11. N. Rohman, S. Mahiuddin, and N.N. Dass. J. Chem. Eng. Data. **44**, 473 (1999).
12. N. Rohman, N.N. Dass, and S. Mahiuddin. Aust. J. Chem. **53**, 463 (2000).
13. Y.C. Wu, W.F. Koch, and K.W. Pratt. J. Res. Natl. Inst. Stand. Technol. **96**, 191 (1991).
14. N. Rohman, A. Wahab, N.N. Dass, and S. Mahiuddin. Fluid Phase Equilibr. **178**, 277 (2001).
15. F.H. Getman. J. Am. Chem. Soc. **30**, 721 (1908).

© 2001 NRC Canada

16. A.N. Campbell and E.M. Kartzmark. Can. J. Res. **28B**, 43 (1950).
17. A.N. Campbell and E.M. Kartzmark. Can. J. Res. **28B**, 161 (1950).
18. A.N. Campbell, A.P. Gray, and E.M. Kartzmark. Can. J. Chem. **31**, 617 (1953).
19. B.F. Wishaw and R.H. Stokes. J. Am. Chem. Soc. **76**, 2065 (1954).
20. N. Rohman. Ph.D. thesis, Dibrugarh University, Dibrugarh, India. 2000.
21. M.J. Blandamer. J. Chem. Soc. Faraday Trans. **94**, 1057 (1998).
22. A. Roux, G.M. Musbally, G. Perron, J.E. Desnoyers, P.P. Singh, E.M. Woolley, and L.G. Hepler. Can. J. Chem. **56**, 24 (1978).
23. J.W. Mellor. *In* A comprehensive treatise on inorganic and theoretical chemistry. Vol. 2. Longmans, Green and Co., London. 1956. p. 839.
24. E.W. Washburn (*Editor*). International critical tables of numerical data: Physics, chemistry, and technology. Vol. 4. McGraw-Hill Book Comp. Inc., New York. 1929. p. 217.
25. S.T. Bowden. *In* The phase rule and phase reactions. Macmillan and Co. Limited, London. 1950. p. 233.
26. A.S. Negi and S.C. Anand. *In* A text book of physical chemistry. Wiley Eastern Limited, New Delhi. 1986. p. 447.
27. J.F. Casteel and E.S. Amis. J. Chem. Eng. Data. **17**, 55 (1972).
28. H. Hase, K. Ishioka, Y. Miyatake, M. Kobayashi, and M. Kobayashi, J. Phys. Chem. **95**, 8541 (1991).

© 2001 NRC Canada

Effect of kinetic synergist on transport of copper(II) through a liquid membrane containing P_{507} in kerosene

Dingsheng He, Ming Ma, Hui Wang, and Pandeng Zhou

Abstract: A new kinetic synergism system for copper(II) transport through a bulk liquid membrane containing mono(2-ethyhexyl)-2-ethyhexyl phosphate and Manoxol OT (OT) was examined. The influence of stripping agent, anion, pH in feed phase, and carrier concentration were investigated. The kinetics of Cu(II) transport could be analyzed in the formalism of two consecutive irreversible first-order reactions, considering both extraction and stripping. The pseudo-first-order apparent rate constants of interfacial reactions in membrane transport are determined by altering the temperature. The activation energy values are 38.1 kJ mol^{-1} for extraction and 32.8 kJ mol^{-1} for stripping. The experiments demonstrated that Manoxol OT is a good kinetic synergist for Cu(II) transport through liquid membranes in this study. The kinetic synergism of OT for extraction of Cu^{2+} ions is analyzed.

Key words: copper ions, kinetic synergist, liquid membrane.

Résumé : On a étudié un nouveau système de synergie cinétique pour le transport du cuivre(II) à travers une membrane formée d'une masse liquide contenant du phosphate de mono(2-éthylhexyle)-2-éthylhexyle ainsi que du Manoxol OT (OT). On a examiné l'influence de l'agent de redissolution, le pH de la phase insérée et la concentration du porteur. On peut analyser la cinétique du transport du Cu(II) dans un formalisme de deux réactions irréversibles et consécutives du premier ordre appliquées à l'extraction et à la redissolution. Les constantes apparentes de pseudo-premier ordre des réactions interfaciales dans le transport à travers la membrane ont été déterminées en modifiant la température. Les valeurs de l'énergie d'activation sont de 38,1 kJ mol^{-1} pour l'extraction et de 32,8 kJ mol^{-1} pour la redissolution. Les expériences réalisées au cours de cette étude ont démontré que le Manoxol OT est un bon agent de synergie cinétique pour le transport du Cu(II) à travers des membranes liquides. On a analysé la synergie cinétique du OT pour l'extraction des ions Cu^{2+}.

Mots clés : ions cuivres, synergie cinétique, membrane liquide.

[Traduit par la Rédaction]

Introduction

In metal recovery, liquid membranes play an attractive role in separation science (1, 2). This is shown in references to the broad applications for copper recovery by liquid membranes (3). The separating power of liquid membranes is directly related to the efficiency of the carrier molecules present in the membrane. Mono(2-ethyhexyl)-2-ethyhexyl phosphate (HEH(EHP), P_{507}) is an acidic extractant most in use. Although P_{507} has been used in extraction separation of Co(II) and Ni(II) ions, little work has been reported on its use as a carrier in a liquid membrane for transport of Cu(II). This aspect assumes particular importance because of the problem of separation of Cu(II) from other valuable metal ions such as Co(II), Ni(II), and Mn(II). In extraction of Cu(II) with liquid membrane containing P_{507} as the carrier, the rate of mass transfer is very slow. To promote the rate of mass transfer and to devise an efficient liquid membrane system for the extraction of Cu(II) with P_{507}, a kinetic synergist (Manoxol OT, $C_{20}H_{37}O_7SNa$, abbreviation OT or NaA) is added to the membrane. Manoxol OT is a surfactant and used as a kinetic synergist for the extraction of Cu(II) with oxime (4), but in liquid membranes, where extraction and stripping can take place simultaneously, the kinetic synergism system composed of OT and acidic phosphoric extractor has scarcely been investigated. In this paper, the permeation rate of Cu(II) ions through a liquid membrane containing P_{507} and OT in kerosene has been studied as a function of different transport conditions. The pseudo-first-order apparent rate constants were determined between the membrane and feed solution interface or stripping solution interface. When the temperature was altered, the kinetics of coupled transport of Cu(II) ions through a liquid membrane containing P_{507} and OT is analyzed, considering both extraction and stripping behavior. To date, the effect of the kinetic synergist (OT) on transport of Cu(II) ions through liquid membrane containing an acidic extractor as carrier is little reported in the literature.

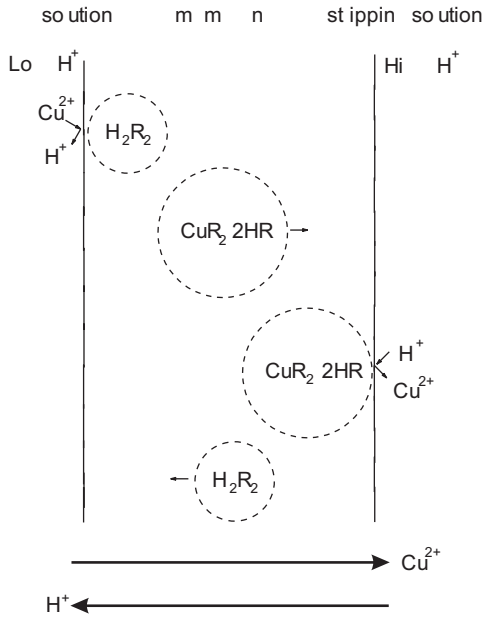
Received September 15, 2000. Published on the NRC Research Press Web site at http://canjchem.nrc.ca on August 21, 2001.

D. He,[1] M. Ma, H. Wang, and P. Zhou. Department of Chemistry Hunan Normal University, Changsha, 410081, P.R. China.

[1]Corresponding author (telephone: 0731-887 1952; fax: +86 731-568 0000; e-mail: mming@public.cs.hn.cn).

 DOI: 10.1139/cjc-79-8-1213 © 2001 NRC Canada

Fig. 1. Schematic description of counter-transport.



Theoretical section

Copper(II) sulfate pentahydrate ($CuSO_4 \cdot 5H_2O$) was used in this study. The extraction reaction on feed side-membrane interface is (5):

[1] $$Cu^{2+}_{aq} + 2H_2R_{2org} = CuR_2 \cdot 2HR_{org} + 2H^+_{aq}$$

The stripping reaction on the stripping side membrane interface is:

[2] $$CuR_2 \cdot 2HR_{org} + 2H^+_{aq} = Cu^{2+}_{aq} + 2H_2R_{2org}$$

where H_2R_2 is dimerized from HEH(EHP) (an acidic extractant). According to ref. 6, the mechanism of coupled transport of Cu(II) ions through a liquid membrane is a counter-transport. The schematic description is summarized in Fig. 1.

In the experiments, the variation of Cu(II) concentration with time was directly measured in both the donor (c_d, M) and the acceptor (c_a, M). The corresponding change in the membrane (c_m, M) was established from the material balance. For practical reasons, mol fractions are used

[3] $$R_d = \frac{n_d}{n_{do}} \quad R_m = \frac{n_m}{n_{do}} \quad R_a = \frac{n_a}{n_{do}}$$

where n_{do} is the initial mol of Cu(II) ions in the donor phase at $t = 0$ and n_d, n_m, and n_a are the mol of Cu(II) ions in the donor, membrane, and acceptor phases (at $t = t$), respectively. Obviously, we have $R_d + R_m + R_a = 1$. Our experimental results (as shown in the later sections) reveal that R_d decreases monoexponentially with time, and R_a follows a monotonically increasing sigmoid-type curve, while the time evolution of R_m presents a maximum. These results suggest that the transport of Cu(II) ions obeys the kinetic laws of two consecutive irreversible first-order reactions according to the kinetic scheme (7, 8):

[4] $$d \xrightarrow{k_1} m \xrightarrow{k_2} a$$

where d, m, and a stand for Cu(II) ions in the donor, membrane, and acceptor phases, respectively. It was found that the presence of the important proton gradient drives the whole transport process to completion without any back leakage of Cu(II) ions. Therefore, the above kinetic scheme may be described by the following eqs. (7):

[5] $$\frac{dR_d}{dt} = -k_1 R_d = J_d$$

[6] $$\frac{dR_m}{dt} = k_1 R_d - k_2 R_m$$

[7] $$\frac{dR_a}{dt} = k_2 R_m = J_a$$

where J stands for flux and $k_1$and k_2 are the pseudo-first-order apparent rate constants of the interfacial rxns. [1] and [2].

When $k_1 \neq k_2$, integrating the above differential equations gives

[8] $$R_d = \exp(-k_1 t)$$

[9] $$R_m = \frac{k_1}{k_2 - k_1}[\exp(-k_1 t) - \exp(-k_2 t)]$$

[10] $$R_a = 1 - \frac{1}{k_2 - k_1}[k_2 \exp(-k_1 t) - k_1 \exp(-k_2 t)]$$

It can be seen that R_d vs. t yields a decreasing monoexponential curve, whereas the time variation of both R_m and R_a is biexponential. The actual numerical analysis was carried out by nonlinear curve fitting.

According to eq. [9], R_m increases at first, then decreases with time, i.e., it has a max when $dR_m/dt = 0$.

[11] $$t_{max} = \frac{\ln (k_1/k_2)}{k_1 - k_2}$$

[12] $$R_m^{max} = \left(\frac{k_1}{k_2}\right)^{-k_2/(k_1 - k_2)}$$

Experimental

Materials

All the reagents, including $CuSO_4 \cdot 5H_2O$, H_2SO_4, HCl, $Na_2SO_4 \cdot 10H_2O$, used in the present work were of analytical grade. They were supplied by Hunan Chemical Reagent Corporation. P_{507} is a commercial extractant and is product of Shanghai Organic Chemistry Institute. OT is L.R. grade.

Stock solution of Cu(II) was prepared by dissolving $CuSO_4 \cdot 5H_2O$ in deionized water and was analyzed by $Na_2S_2O_3$ titration using starch as the indicator. The Cu(II) feed solution was prepared by taking a known amount of the Cu(II) stock solution and diluting it with water to a given extent after adding a calculated amount of the desired CH_3COOH and CH_3COONa.

The stripping solution was prepared by taking the required amount of HCl and diluting it with deionized water to a known volume.

© 2001 NRC Canada

Fig. 2. Apparatus used for coupled transport of Cu^{2+} through liquid membrane: (*a*) stripping phase; (*b*) feed phase; (*m*) membrane phase.

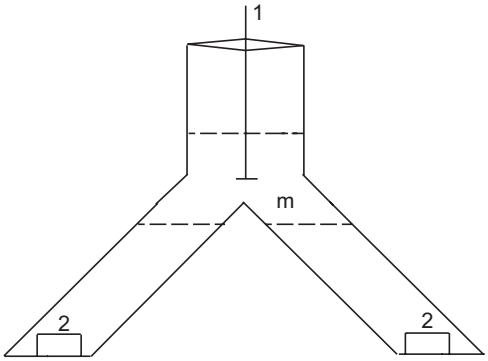
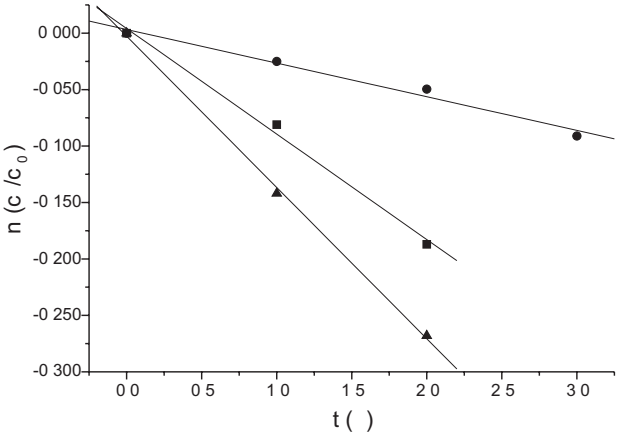


Fig. 3. Plot of ln of Cu(II) ions in feed phase through SLM vs. time. (■) 9.4×10^{-6} M OT; (●) 0.08 M P_{507}; (▲) 0.08 M P_{507} + 9.4×10^{-6} M OT (stripping phase = 2 M HCl).



HEH(EHP) solution was prepared by taking the calculated amount of extractant and diluting it with kerosene. Distilled kerosene (185–225°C) was obtained by washing commercial kerosene with concentrated sulfuric acid and then distilling it.

A microporous polypropylene membrane was used as a solid support. The film was obtained from the Hunan Plastic Research Institute. It was a 0.02 mm thick film with a nominal porosity of 51% and an effective pore size of 0.03 μm.

All the experiments were carried out using the deionized water saturated with kerosene.

Transport experiments of bulk liquid membrane (BLM)

The transport experiments were carried out using a thermostat (T = 30 ± 0.1°C) as presented in Fig. 2. The aqueous feed solution (40.00 mL) consisted of 1.57×10^{-3} M Cu^{2+}, pH = 4.35 (CH_3COONa–CH_3COOH), I = 0.5. The feed solution was put in the left side (*b*) of the vessel and stirred at 650 rpm. The stripping solution, which consisted of 2 M HCl (40.00 mL), was located in the right side (*a*) of the vessel and was stirred at 650 rpm. The membrane phase (30.00 mL) containing HEH(EHP) in kerosene was added to the top of the water solution and stirred at 650 rpm. The interface surfaces were as follows: $S_{feed\text{-}membrane} = S_{membrane\text{-}stripping\ phase} = 5.90\ cm^2$.

Fig. 4. Plot of R_d vs. time at different carrier concentrations: (●) 0.04; (■) 0.08; (▲) 0.12; (○) 0.16; (□) 0.20 M. Membrane = 7.5×10^{-4} M OT + different carrier concentration, stripping phase = 2 M HCl, feed phase = 1.57×10^{-3} M Cu^{2+}, pH = 4.35 (CH_3COOH–CH_3COONa), I = 0.5, T = 32 ± 0.1°C.

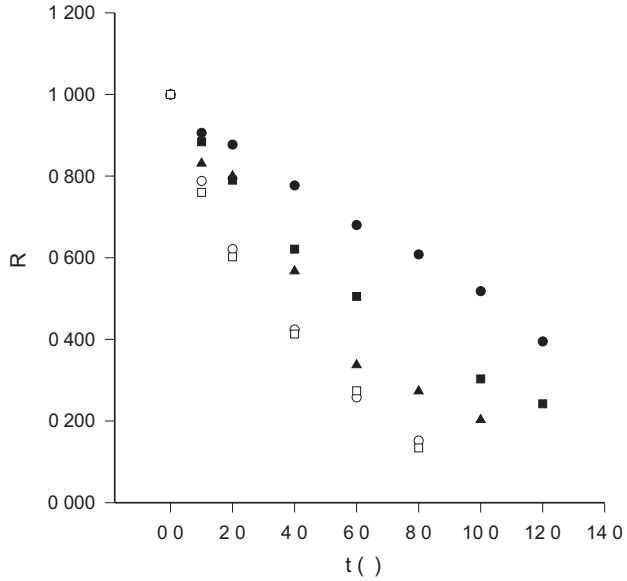
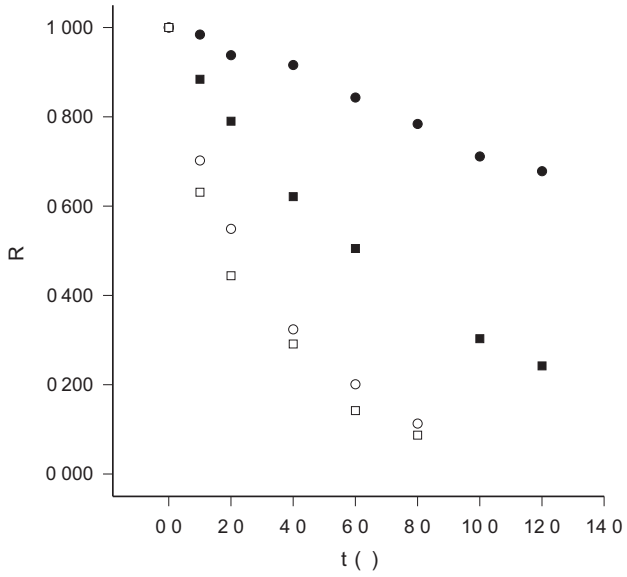


Fig. 5. Plot of R_d vs. time at different pH in feed solution. Membrane = 0.08 M P_{507} + 7.5×10^{-4} M OT, stripping phase = 2 M HCl, feed phase = 1.57×10^{-3} M Cu^{2+}, I = 0.5, T = 32 ± 0.1°C. pH (CH_3COOH–CH_3COONa) in feed phase (●) 3.80; (■) 4.35; (○) 4.81; (□) 5.47.



Transport experiments of supported liquid membrane (SLM)

The experiments were performed at 30 ± 0.1°C with a simple diffusion cell. The diffusion cell consisted of two Perspex half cells. The two half cells were separated by a membrane with an area of 18 cm^2. The membrane was impregnated with the carrier dissolved in kerosene and clamped between the two half cells. The aqueous feed solu-

© 2001 NRC Canada

Table 1. Effect of OT in organic phase on extraction percentage of copper(II) (%).

	Time (min)							
	0	0.5	1.0	3.0	5.0	10.0	15.0	30.0
0.08 M P_{507}	0	60.8 ± 0.8	62.7 ± 0.5	63.2 ± 0.4	64.0 ± 0.2	64.0 ± 0.5	64.5 ± 0.8	64.0 ± 0.3
0.08 M P_{507} + 7.5 × 10^{-4} M OT	0	63.1 ± 0.8	64.3 ± 0.5	64.0 ± 0.5	64.0 ± 0.6	63.9 ± 0.4	64.4 ± 0.3	64.3 ± 0.3
7.5 × 10^{-4} M OT	0	1.4 ± 0.2	2.7 ± 0.8	1.6 ± 1.0	1.4 ± 0.5	1.9 ± 0.2	0	

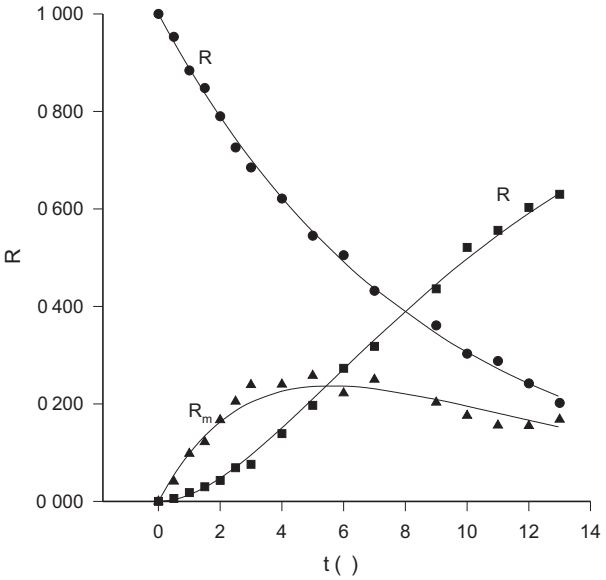
Note: Phase ratio = 1:1, T = 28–30°C, pH in feed solution = 4.35.

Table 2. Effect of P_{507} concentration on interfacial tension between feed phase and membrane or stripping phase and membrane

	P_{507} (M)				
	0.04	0.08	0.12	0.16	0.20
$\sigma_{\text{feed-membrane}}$ (mN m^{-1})	15.10	13.10	11.84	11.18	10.57
$\sigma_{\text{stripping-membrane}}$ (mN m^{-1})	17.64	16.63	16.22	15.40	15.70

Note: Membrane at different P_{507} concentration in kerosene, feed phase = 1.57 × 10^{-3} M Cu^{2+}, pH = 4.35 (CH_3COOH–CH_3COONa), I = 0.5, stripping phase = 2 M HCl.

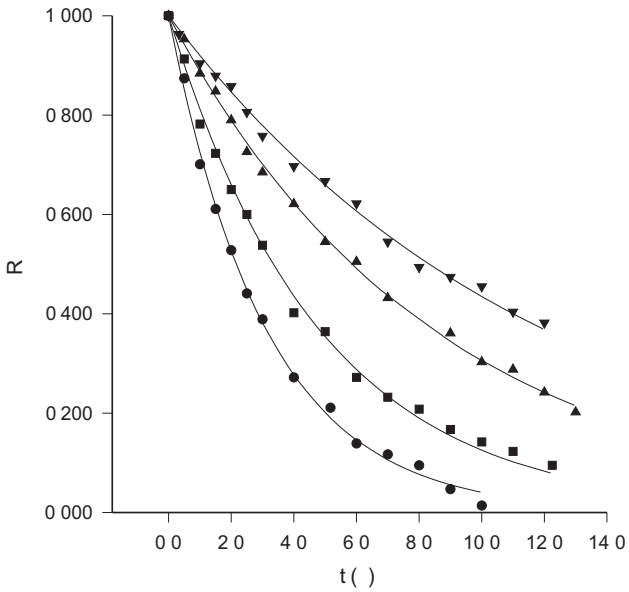
Fig. 6. Time dependence of R_d in feed phase, R_m in membrane phase, and R_a in stripping phase. Membrane = 0.08 M P_{507} + 7.5 × 10^{-4} M OT–kerosene, T = 32°C. Theoretical curves calculated from eqs. [8]–[10]: (●) R_d; (▲) R_m; (■) R_a.



tion (140 mL) consisted of 1.57 × 10^{-3} M Cu^{2+}, pH = 4.35. The stripping solution (140 mL) consisted of 2 M HCl. The stirring rates are 650 rpm in donor and acceptor phases.

In transport experiments, the samples were taken out from the feed solution and stripping solution at scheduled time intervals and analyzed for copper content using spectrophotometry. The experimental results reported are the arithmetic mean of two independent experiments. Some experimental results are given by doing a repeated number of experiments. The reproducibility is very good. The fluxes obtained were reproducible within ca. ±10%.

Fig. 7. Time evolution of R_d during coupled transport. Membrane = 0.08 M P_{507} + 7.5 × 10^{-4} M OT–kerosene. Theoretical curves calculated from eq. [8]: (▼) T = 22; (▲) T = 32; (■) T = 41; (●) T = 50°C.



Determination of interfacial tension

Interfacial tension was measured by the drop volume method (9). All measurements were carried out in a water bath at 30 ± 0.1°C. The instrument for determination of interfacial tension was first corrected using the known interfacial tension of a benzene–water system. A good agreement between experiments and literatures was shown.

Results and discussion

Effect of OT on extraction of Cu(II)

Extraction experiments

To witness kinetic synergism of OT for extraction of Cu(II) ions with P_{507}, solvent extraction experiments were devised. The results are shown in Table 1. The experimental data in Table 1 reveal that the extraction equilibrium time is 1 min when trace OT was added to the organic phase containing P_{507}, while it was 5 min when the organic phase merely contained P_{507}. This indicates that trace OT can accelerate the extraction of Cu(II) ions when it is added to the organic phase only containing P_{507}. Because there is a close fraction extracted in the presence and absence of OT, Table 1 also shows that OT is a kinetic synergist.

© 2001 NRC Canada

Table 3. Effect of temperature on kinetic parameters transport of Cu(II) ions through liquid membrane.

T (°C)	k_1 (1×10^2) (h^{-1})	k_{2a} (1×10^2) (h^{-1})	k_{2m} (1×10^2) (h^{-1})	t_{max} (h)	R_m^{max}	J_d^{max} (1×10^2) (h^{-1})	J_a^{max} (1×10^2) (h^{-1})
22	8.33 ± 0.06	14.55 ± 0.24	14.77 ± 0.29	8.97	0.271	–3.95	3.95
32	11.84 ± 0.07	25.65 ± 0.28	25.80 ± 0.46	5.60	0.238	–6.10	6.10
41	20.76 ± 0.18	35.34 ± 0.44	36.06 ± 0.63	3.65	0.275	–9.73	9.73
50	32.09 ± 0.27	48.44 ± 0.67	48.50 ± 0.84	2.52	0.295	–14.30	14.30

Note: Membrane = 0.08 M P_{507} + 7.5×10^{-4} M OT, feed phase = 1.57×10^{-3} M Cu^{2+}, pH = 4.35 (CH_3COOH–CH_3COONa), I = 0.5, stripping phase = 2 M HCl.

Fig. 8. Time evolution of R_m during coupled transport. Membrane = 0.08 M P_{507} + 7.5×10^{-4} M OT–kerosene. Theoretical curves calculated from eq. [9]: (▼) T = 22; (▲) T = 32; (■) T = 41; (●) T = 50°C.

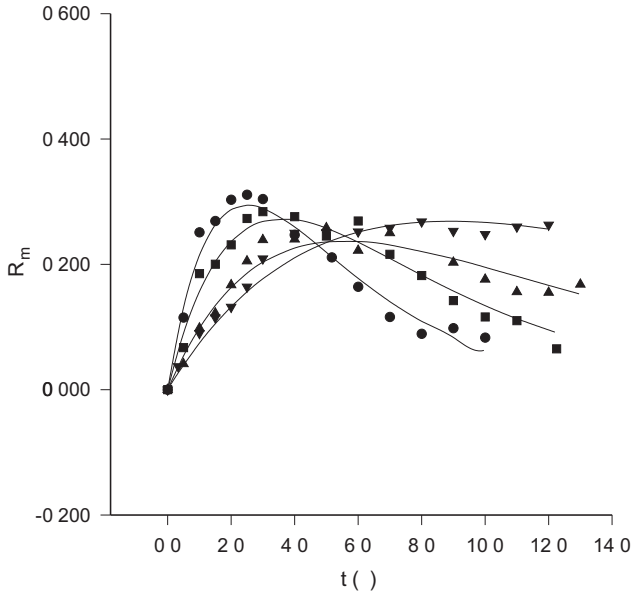
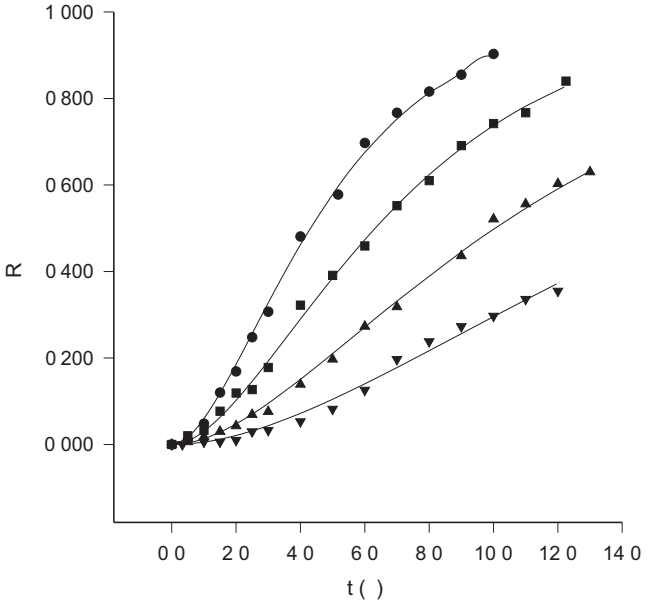


Fig. 9. Time evolution of R_a during coupled transport. Membrane = 0.08 M P_{507} + 7.5×10^{-4} M OT–kerosene. Theoretical curves calculated from eq. [10]: (▼) T = 22; (▲) T = 32; (■) T = 41; (●) T = 50°C.



Experiments of SLM

Figure 3 shows that Manoxol OT can raise the membrane entrance flux. The experiments of SLM and extraction verify that OT is a kinetic synergist for extraction of Cu(II) in the study.

Experiments of bulk liquid membrane

Effect of stripping agent on transport of Cu(II)

When the feed solution and membrane were as above and the stripping phase contained either 2 M HCl, 2 M HNO_3, and 1 M H_2SO_4, the values of R_d are 0.386, 0.512, and 0.434, respectively, after transport of 8 h. Consequently, HCl is used as the stripping agent in later experiments.

Effect of anion in feed on transport of Cu(II)

To compare the relative effectiveness of the various anions in promoting Cu(II) ion transport, experiments on the effect of the anion on transport of Cu(II) ions through liquid membranes were devised. When the composition of the membrane and stripping phase was as above and the feed solution contained either 0.5 M Na_2SO_4 and 0.5 M CH_3COONa, the values of R_d are 0.551 and 0.386, respectively, after transport of 8 h. These experiments indicate that the transport of Cu(II) ions is promoted by CH_3COO^- in the feed solution.

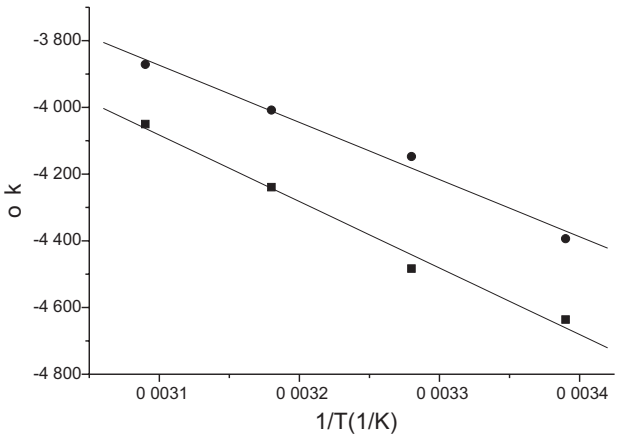
Effect of carrier concentration

The transport experiments were accomplished at five different carrier concentrations: 0.04, 0.08, 0.12, 0.16, and 0.20 M. It is quite clear from Fig. 4 that the flux of Cu(II) increases with an increase in the concentration up to 0.16 M carrier in the membrane, and beyond 0.16 M carrier, the flux has no distinct increase up to 0.2 M carrier in membrane.

In a lower carrier concentration, the interface between the feed phase and membrane is not saturated by the carrier. Therefore, the flux increases with an increase in the carrier concentration. Table 2 indicates the variation of interfacial tension with carrier concentration in the membrane. The experimental result indicates that the carrier molecule has a weak surface activity and that the adsorption of carrier molecules at the interface between the feed solution and the membrane or stripping solution and membrane increases with an increase in carrier concentration. The conclusion explains the fact that the fluxes of the Cu(II) ions increase with an increase in carrier concentration.

© 2001 NRC Canada

Fig. 10. Arrhenius plot of log k (k, s^{-1}) vs. $1/T$ (T, K): (■) log k_1 ~ $1/T$; (●) log k_2 ~ $1/T$.



In addition, a blank experiment was performed in which the membrane contained no carrier. No detectable movement of the Cu(II) ions through the liquid membrane was found in the blank experiment.

Effect of pH in the aqueous feed solution

The effect of pH in the feed solution on the transport of Cu(II) ions was investigated. The experiments were accomplished at four different pH values, 3.80, 4.35, 4.81, and 5.47. It is shown in Fig. 5 that the flux of Cu(II) ions increases with an increase in values of pH of the feed solution. This reveals the importance of protons in the feed phase for coupled transport of Cu(II) ions. According to the principle of shift of chemical equilibrium, if the amounts of protons in the feed phase decrease, rxn. [1] will shift to the right. The variation of fluxes with pH in the feed solution is therefore explained.

Effect of temperature on transport of Cu(II) ions

The effect of temperature on the transport of Cu(II) ions across the bulk liquid membrane was examined at 295, 305, 314, and 323 K. The experimental results are collected in Table 3 and Figs. 6–9. It is quite obvious that k_{1d} and k_{2a} increase with an increase in the temperature. In all cases, $k_{1d} < k_{2a}$ at every temperature. An Arrhenius-type plot is followed perfectly in Fig. 10. The activation energy values are 38.1 kJ mol^{-1} for extraction and 32.8 kJ mol^{-1} for stripping.

Figures 6–9 indicate the time evolution of the concentration of Cu(II) transported in the feed, membrane and stripping phase, respectively.

A good agreement between the theoretical curves and the experimental points is shown in Figs. 6–9. The experimental results in Table 2 indicate that the carrier molecules have weak surface activity and can be adsorbed at the interface. This is beneficial to the extraction reaction at the feed-membrane interface. The results suggest that the Cu(II) ions transport could be described by the kinetic laws of two consecutive irreversible first-order reactions disregarding diffusion processes (as shown in eq. [4]).

Analysis of kinetic synergic mechanism

OT is an ionic surfactant. It is absorbed at the interface between kerosene and the feed phase when OT is dissolved in kerosene. The ionic reaction between OT and Cu^{2+} in the feed solution is faster than the complex reaction between P_{507} and Cu^{2+} ions. According to ref. 10, Cu^{2+} ions in the feed solution can preferentially react with OT at the interface in the following manner:

[13] $Cu^{2+}_{aq} + 2HA \text{ (or } NaA)_{interface} \rightarrow CuA_{2\ intrface} + 2H^+ \text{ (or } Na^+)_{aq}$

HA is an acid of OT. Because the ionic associated substance, CuA_2, is not as stable as a P_{507}–Cu^{2+}coordination compound, the exchange reaction between CuA_2 and P_{507} can take place at the interface.

Fig. 11. Plot of pH vs. equilibrium time of releasing H^+ in extraction reaction: (●) curve (*a*), 1.6 mL 0.1 M P_{507}–kerosene, feed phase = 35 mL 1.57×10^{-3} M Cu^{2+}, pH = 4.35 (no CH_3COOH–CH_3COONa); (■) curve (*b*), 1.6 mL (0.1 M P_{507} + 2.3×10^{-5} M OT (HA)), feed phase is the same as curve (*a*); (▲) curve (*c*), 1.6 mL (0.1 M P_{507} + 4.6×10^{-5} M CuA_2), feed phase is the same as curve (*a*).

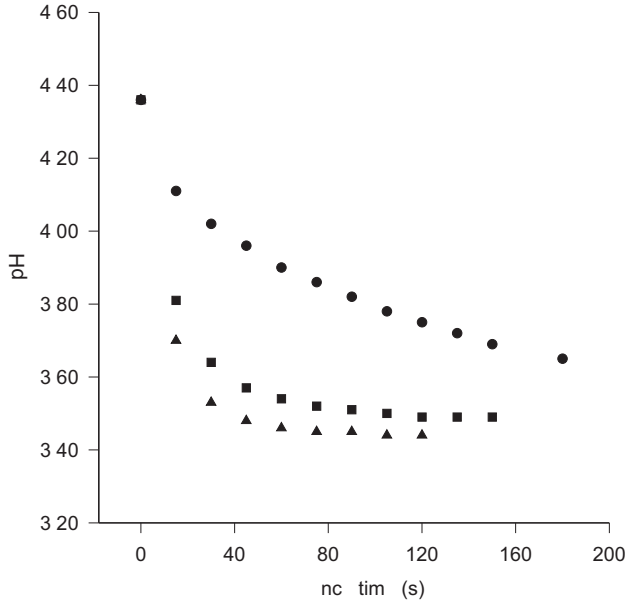
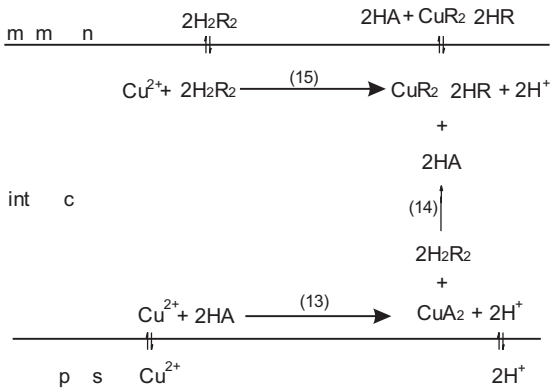


Fig. 12. Schematic description of extraction of Cu^{2+} ions in presence of OT.



© 2001 NRC Canada

[14] $CuA_{2interface} + 2H_2R_{2interface} = CuR_2 \cdot 2HR_{interface} + 2HA_{interface}$

The total reaction for rxns. [13] and [14] is as follows:

[15] $Cu^{2+}_{aq} + 2H_2R_{2org} \rightarrow CuR_2 \cdot 2HR_{org} + 2H^{+}_{aq}$

Reaction [14] is a key reaction for understanding the kinetic synergism of OT for rxn. [15]. To verify that rxn. [14] is faster than rxn. [15], extraction experiments were devised. First, according to eq. [15], a feed solution of Cu(II) ions and 0.1 M P_{507}–kerosene was mixed and shaken. The pH in the feed solution was determined at different times with a pH meter. The time of releasing H^+ ions for eq. [15] was ascertained. If rxn. [15] is in the equilibrium, the pH value in feed phase does not change. Then, the equilibrium time is given. If the equilibrium time of releasing H^+ ions is longer, eq. [15] takes place at a slower rate. Second, the trace copper salt (CuA_2) for OT was added in 0.1 M P_{507}–kerosene. According to eq. [14], the extraction experiment is repeated with the same feed solution of Cu(II) ions. The equilibrium time of releasing H^+ ions for eq. [14] is also determined. By comparison with the equilibrium times of releasing H^+ ions for eqs. [14] and [15], we know which reaction of eqs. [14] and [15] is faster.

Figure 11 indicates that the equilibrium times are 135, 90 and 60 s for curves (*a*), (*b*), and (*c*), respectively. The experimental result verifies that rxn. [14] is faster than rxn. [15] and that OT can accelerate the extraction of Cu^{2+} ions. The kinetic synergism of OT for extraction of Cu^{2+} ions is achieved through rxns. [13] and [14]. The schematic description of the extraction is shown in Fig. 12.

Conclusion

Cu(II) ions can be effectively transported through a liquid membrane containing P_{507} and OT in kerosene. The experiments confirmed that OT is a good kinetic synergist for transport of Cu(II) ions when it is added in liquid membranes containing P_{507} in kerosene. The pseudo-first-order apparent rate constants of the interfacial reactions of extraction and stripping are determined on the basis of a scheme implying two consecutive irreversible first-order reactions.

References

1. A.A. Elhassadi and D.D. Do. Separ. Sci. Technol. **34**, 461 (1999).
2. D.E. Barnes and G.D. Marshall. Separ. Sci. Technol. **30**, 751 (1995).
3. J. Vander-Linden and R.F. De. Ketelaere. J. Membrane Sci. **139**, 125 (1998).
4. Second study group 203. Organic chemistry (Chinese). **1**, 1 (1979).
5. S. Jinglan, S. Sixiu, and G. Zili. J. Shandong University, **3**, 70 (1983).
6. P.R. Danesi. Separ. Sci. Technol. **19**, 857 (1984–85).
7. D. He, M. Ma, and Z. Zhao. J. Membrane Sci. **169**, 53 (2000).
8. D. He, M. Ma, X. Hua-Zeng, and Q. Xie. Chinese J. Applied Chem. **17**, 47 (2000).
9. Z.G. Xi. Physical chemistry of surfactants. Peking University Press, Beijing. 1984. pp. 13 and 14.
10. Z. Cheng. Nonferrous Metal, **4**, 36 (1981).

© 2001 NRC Canada

One-pot sol-gel synthesis of sulfated ZrO_2–SiO_2 catalysts for alcohol dehydration

Quan Zhuang and Jack M. Miller

Abstract: Sulfated ZrO_2–SiO_2 catalysts were synthesized by one-pot sol-gel method using ammonium sulfate, zirconium propoxide, and tetraethyl orthosilicate as precursors. The catalysts were characterized by N_2 adsorption and DRIFTS. On calcining the gel at elevated temperature, the ammonium sulfate decomposed, giving a sulfated zirconia–silica catalyst. By adding ammonium sulfate to the sol-gel synthesis system, the surface area, pore size, and pore volume of the resultant catalyst were increased. The one-pot sol-gel synthesized catalyst with an optimum loading of SO_4^{2-} 14 mol% showed significantly higher catalytic activity, with a selectivity of 100%, for isopropanol dehydration when compared to the impregnated catalyst. The one-pot sol-gel synthesis method is an effective way to prepare sulfated zirconia catalyst.

Key words: sulfated zirconia, sol-gel synthesis, acid catalyst, alcohol dehydration, N_2 adsorption, DRIFT.

Résumé : On a synthétisé des catalyseurs de ZrO_2–SiO_2 sulfatés par une méthode monotope sol-gel utilisant du sulfate d'ammonium, du propylate de zirconium et de l'orthosilicate de tétraéthyle comme précurseurs. On a caractérisé les catalyseurs par adsorption de N_2 et DRIFTS. Par calcination du gel à température élevée, il y a décomposition du sulfate d'ammonium qui conduit au catalyseur de zircone–silice sulfaté. L'addition de sulfate d'ammonium au système de synthèse sol-gel, il y a augmentation de l'aire de la surface, de la taille des pores et du volume des pores du catalyseur qui en résulte. Pour la réaction de déshydratation de l'isopropanol, l'activité catalytique du catalyseur du catalyseur obtenu par synthèse monotope sol-gel, avec un contenu optimal de 14 mol% de SO_4^{2-}, est beaucoup plus élevée que celle du catalyseur imprégné et sa sélectivité est de 100%. La méthode de synthèse monotope sol-gel est une voie efficace pour préparer un catalyseur de zircone sulfatée.

Mots clés : zircone sulfatée, synthèse sol-gel, catalyseur acide, déshydratation d'alcools, adsorption de N_2, DRIFTS.

[Traduit par la Rédaction]

Introduction

Sulfated zirconia is an important catalyst for fuel and energy industry because of its high activity for the isomerization of light hydrocarbons at lower temperature (1). Cosmo Oil of Japan and UOP have jointly commercialized an industrial production process for light naphtha isomerization by use of a proprietary sulfated zirconia catalyst.[1] It has been reported that after sulfation, the zirconia surface becomes strongly acidic (2), or even superacidic (3), because it may show a Hammett function value ($-H_0$) of larger than 12. Usually zirconia is sulfated as follows: in the preparation stage, the zirconium hydroxyl gel is treated with a sulfuric acid or ammonium sulfate solution (4). Also it can be prepared by impregnation with ca. 0.5–1.0 M sulfuric acid or ammonium sulfate on zirconia (5). In either case the catalyst should be calcined at 450–550°C, otherwise no strong- or super-acidity will be observed (6). Tanabe et al. (7) and Yamaguchi (8) have reported that incorporating a small amount of silica into the catalyst may increase the surface area and the thermal stability.

In recent years, there have been extensive studies on sol-gel synthesis of oxides, because it may provide specific properties to the oxide, which cannot be obtained by the conventional coprecipitation preparation method (9). Under appropriate synthesis condition, such as metal alkoxide concentration, pH, the type of complexing agent, the amount of hydrolyzing water, drying techniques, the textural properties of the oxide can be precisely controlled. Since the advent of this method, it has stimulated more and more interests in its application in the field of catalytic materials research. The sol-gel synthesis method can be used to prepare both catalysts and catalyst supports (10). With the sol-gel synthesis method, if the precursor (metal salt or complex) of an active component (a metal or metal oxide) in a supported catalyst is added to the preparation solution, a supported catalyst can be obtained after hydrolysis, gelation, drying, and calcining. This is the so-called one-step or one-pot synthesis of a catalyst (11, 12), which is simple and convenient for preparing catalysts in some cases.

Supported sulfate catalysts are commercially available for alcohol dehydration in laboratories (13). It is also being applied in industry (14).

In this paper, we report our attempt to prepare the sulfated zirconia–silica catalyst by the one-pot sol-gel synthesis method using ammonium sulfate, zirconium(IV) propoxide, and tetraethyl orthosilicate as precursors. Its catalytic perfor-

Received July 20, 2000. Published on the NRC Research Press Web site at http://canjchem.nrc.ca on August 22, 2001.

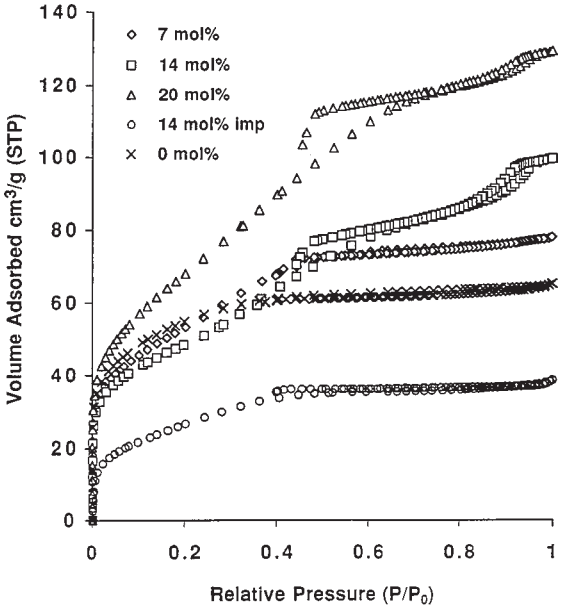
Q. Zhuang and J.M. Miller.[2] Department of Chemistry, Brock University, St. Catharines, ON L2S 3A1, Canada.

[1]Q.Z. was a research scientist at Cosmo Research Institute, Cosmo Oil Co.

[2]Corresponding author (telephone: (905) 688-5550 ext. 3789; fax: (905) 684-2277; e-mail: jmiller@brocku.ca).

 DOI: 10.1139/cjc-79-8-1220 © 2001 NRC Canada

Fig. 1. N_2 adsorption isotherms of the catalysts with different SO_4^{2-} content (based on synthetic concentrations).



mance was evaluated for isopropanol dehydration, which is known as an acid-catalyzed reaction. N_2 adsorption and DRIFTS were employed to characterize the catalysts.

Experimental

One-pot sol-gel synthesis of the catalysts

n-Butanol was obtained from Caledon Laboratories, all other chemicals were obtained from Aldrich and used as received.

A series of sulfated ZrO_2–SiO_2 (molar ratio, 75:25) with sulfur contents up to 20 mol% were synthesized by the one-pot sol-gel method. Briefly, ammonium sulfate, zirconium propoxide, and tetraethyl orthosilicate were used as the precursors and 2,4-pentanedione (H-acac) as the complexing agent (9).[3] The appropriate amounts of zirconium propoxide and tetraethyl orthosilicate were dissolved in the solvent, *n*-butanol. The solution was heated to 60°C under stirring to thoroughly mix the components, then it was cooled down to room temperature, and H-acac was added. The alkoxides in the solution were hydrolyzed over night by adding an aqueous solution of ammonium sulfate. A yellowish transparent gel was obtained, which was dried at 100°C to remove the solvent and then calcined at 500°C for 3 h in air to remove the organics. The total concentration of the alkoxides in *n*-butanol solution was 0.8 M. The molar ratio of the complexing agent to the alkoxides was 0.5. The molar ratio of hydrolyzing water to alkoxide was 11:1. A reference catalyst was also prepared by impregnating a sol-gel synthesized ZrO_2–SiO_2 (75:25) with 1 M ammonium sulfate solution. The slurry was evaporated to dryness under stirring and then calcined at 500°C for 1 h.[4]

Characterization of the catalysts

N_2 adsorption analysis was measured by using a Coulter SA 3100 instrument at –196°C. Samples were degassed under vacuum at 200°C for 1 h immediately prior to N_2 adsorption analysis. From the isotherm, Brunauer–Emmett–Tellar (BET) surface area, pore volume, and pore size distribution were calculated by using the Barret, Joyner, and Halenda (BJH) method (15).

DRIFTS spectra were acquired using a Spectra Tech DRIFTS accessory (The Collector) in an ATI Mattson Research Series FT-IR spectrometer equipped with a Michelson interferometer, a helium–neon laser, a KBr beam splitter, a DTGS (deuterated triglycerol sulfate) detector with a spectra range of 4000–400 cm^{-1}, and a standard high-intensity source. The diffuse-reflectance FT-IR were recorded under vacuum after evacuating the samples at 100°C for 30 min. The sample chamber was designed to be used in situ on the collector DRIFTS accessory. Five hundred scans were collected.

Isopropanol dehydration evaluation

The catalytic activity evaluation of the catalysts for isopropanol dehydration was performed using a continuous flow fixed-bed micro reactor made of Pyrex glass.[3] The inner diameter of the reactor was 6 mm, its length was 25 cm. With each reaction, 200 mg fresh catalyst was put into the middle of the reactor. A thermocouple was placed just below the catalyst bed to monitor the reaction temperature, which was manipulated by a temperature controller. Before the reaction, the catalyst was heated to the reaction temperature under a flow of N_2. The reactions were performed at temperature range of 100–160°C at 1 atm (1 atm = 103.325 kPa). The reactant, isopropanol, was introduced into the reactor by a N_2 bubbler, which was kept at a constant temperature (16).[3] The flow rate of N_2 was 100 mL min^{-1}, giving a weight hour space velocity (WHSV) of the reactant as 1.8 h^{-1}. The products were analyzed by an on-line PerkinElmer Sigma 3B gas chromatograph, employing a Porapaq R column, 800/100 mesh, 6 ft × 0.125 in, with a thermal conductivity detector (TCD). To analyze all of the products in the exit stream from the reactor, the GC column was heated by programming from 150 to 220°C for 15 min.[3] The main product was propylene, with minimal amounts of diisopropylether as the byproduct. The activities were stablized in ca. 20 min. After that time, two consecutive analyses were carried out, which were within 5%. An average is reported throughout the *Discussion* section.

Results and discussion

Figure 1 shows the N_2 adsorption isotherms of the catalysts. The catalysts showed type IV isotherms, some with H2 hysteresis (15). By adding the $(NH_4)_2SO_4$ into the sol-gel synthesis solutions, the N_2 adsorption of the resultant catalysts increased, especially at the intermediate and high relative pressure range. The pore size distributions of the catalysts are displayed in Fig. 2. It can be seen that the textural structure of the catalysts were mesoporous. As the

[3] Q. Zhuang and J.M. Miller. Submitted.
[4] The sulfate concentrations reported for the catalysts are based on synthetic concentrations in the uncalcined materials, not on analysis after calcining.

© 2001 NRC Canada

Fig. 2. Pore size distributions of the catalysts with different SO_4^{2-} content (based on synthetic concentrations).

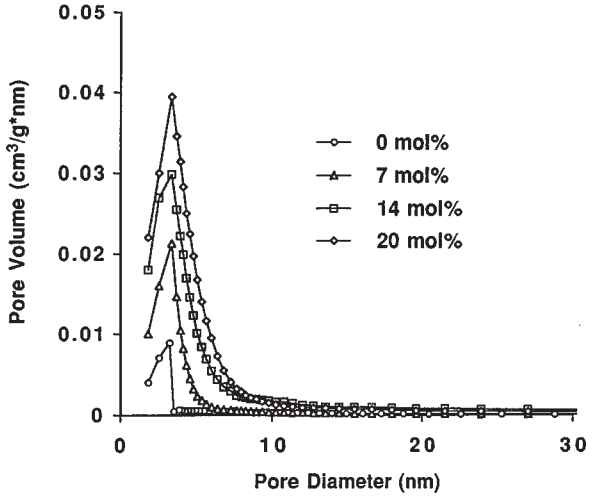


Table 1. Surface area (SA) and pore volume of the catalysts.

SO_4^{2-} mol% in catalyst[a]	SA (m^2 g^{-1})	Pore volume (cm^3 g^{-1})
0 (0)	198.2	0.10
7 (1.9)	191.2	0.12
14 (3.8)	183.2	0.15
20 (5.4)	248.1	0.20
14 impre	97.4	0.06

[a]Value in parentheses represents S wt% in catalyst, based on synthesis.

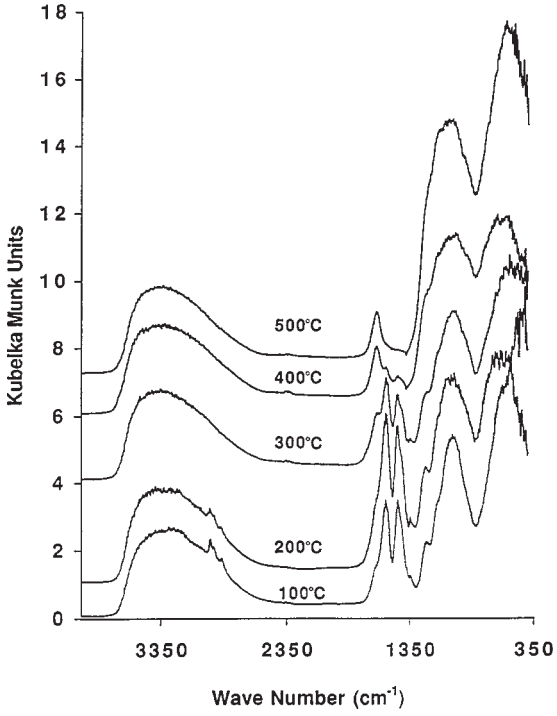
amount of $(NH_4)_2SO_4$ was increased in the one-pot synthesis solution, both of the pore size and pore volume of the catalysts increased.

The surface area and pore volume of the catalyst are summarized in Table 1. By adding $(NH_4)_2SO_4$ to the sol-gel synthesis solution, the pore volume of the resultant catalysts significantly increased, and it even could be doubled at SO_4^{2-} 20 mol%. But only at higher $(NH_4)_2SO_4$ contents, did the surface area of the catalyst increase. Usually, from the N_2 adsorption isotherm, the contribution to the surface area comes mainly from the low relative pressure adsorption, while the pore volume contribution comes from the intermediate and high relative pressure adsorption. The addition of $(NH_4)_2SO_4$ to the gel mainly increased the N_2 adsorption at the intermediate and higher relative pressure range, thus showing in the increase of the pore volume.

It has been reported that SO_4^{2-} can form bridge structures between zirconium atoms in a sulfated zirconia catalyst (17). In the synthesis of the catalysts by the one-pot sol-gel method, the $(NH_4)_2SO_4$ is probably incorporated into the gel in a similar way, which may affect the structure of the gel. After drying and calcining, this kind of textural structure might be partly retained in the framework of the catalyst, resulting in large pore size and pore volume.

It can be seen from Table 1, with the impregnated catalyst (SO_4^{2-} 14 mol%), its surface area and pore volume decreased to ca. half of those of the ZrO_2–SiO_2 support. This was caused by the interaction of the acidic solution of $(NH_4)_2SO_4$ with the ZrO_2–SiO_2 gel, causing a shrinkage in the porous structure.

Fig. 3. DRIFTS spectra of the catalysts, SO_4^{2-} 14 mol% (synthesis level), after calcining at different temperatures.



The DRIFT spectra of the catalyst with SO_4^{2-} 14 mol% after calcining at different temperatures are shown in Fig. 3. The absorption peaks at 1050 cm^{-1} can be assigned to the Si-O-Zr vibration (18). The small shoulder peaks at 1224 and 1346 cm^{-1} are from the asymmetric stretching of S=O. The unresolved absorption peaks at 2700–3700 cm^{-1} are due to the hydrogen-bonded OH, and possibly some adsorbed water (with the bending peaks at 1631 cm^{-1}) on the catalyst surface. The peak at ca. 618 cm^{-1} is due to the vibration of zirconia (18). The absorption peaks at 2800–3000 cm^{-1} are assigned to the residual organics in the gel. When calcined at higher temperatures, these peaks were totally eliminated. At ca. 1559 and 1460 cm^{-1}, two peaks were observed and are assigned to the vibration of N—H (19). As the calcining temperature was increased to 200°C, these two peaks increased. This is principally due to the release of the organics and the evolution of the porous structure of the gel, which enabled more N-H groups migrating to the surface to be well distributed or dispersed. When the calcining temperature was further increased, the N—H absorption peaks decreased and finally disappeared. This was possibly caused by the decomposition of $(NH_4)_2SO_4$ and elimination of NH_3.

Figure 4 shows the catalytic activities of the one-pot sol-gel synthesized catalysts with different SO_4^{2-} content. As the SO_4^{2-} content was increased, the activity increased first, then decreased, giving an optimum content of SO_4^{2-} at 14 mol%. This was due to both the loading and the dispersion of SO_4^{2-} in the catalyst. As SO_4^{2-} content in the catalyst was increased, the activity increased. However, when the SO_4^{2-} content was increased over a certain value, its dispersion decreased. Therefore, the activity decreased too.

Figure 5 shows the activities and selectivities of two catalysts with SO_4^{2-} content of 14 and 17 mol%, respectively, under different temperatures. Two perspectives can be ob-

© 2001 NRC Canada

Fig. 4. The catalytic activities of the catalysts with different SO_4^{2-} content for isopropanol dehydration (140°C, 1 atm, WHSV = 1.8 h^{-1}).

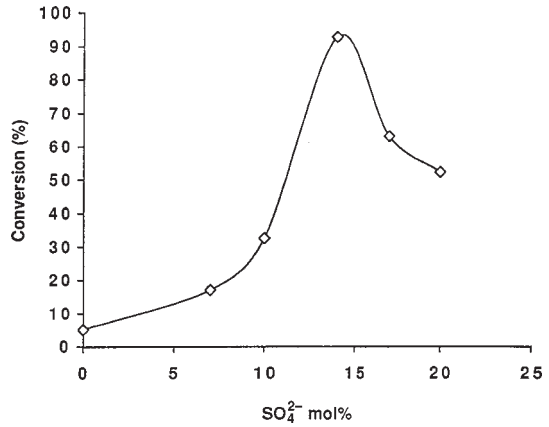
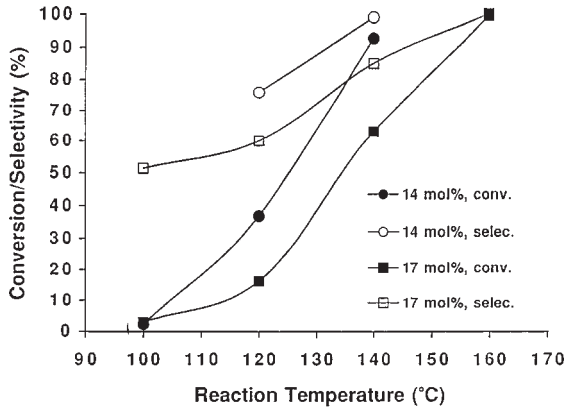


Fig. 5. The activity and selectivity of SO_4^{2-}–ZrO_2–SiO_2, 14 and 17 mol% vs. reaction temperature.



tained from the experimental results. First, at higher temperature, hence higher conversion, the selectivity was higher and could reach 100%. Second, with a catalyst of higher activity, its selectivity was also higher.

The byproduct, diisopropyl ether, seems to be formed by a consecutive reaction between isopropanol and propylene. When the conversion was higher, less isopropanol is available, thus giving a higher selectivity (20).

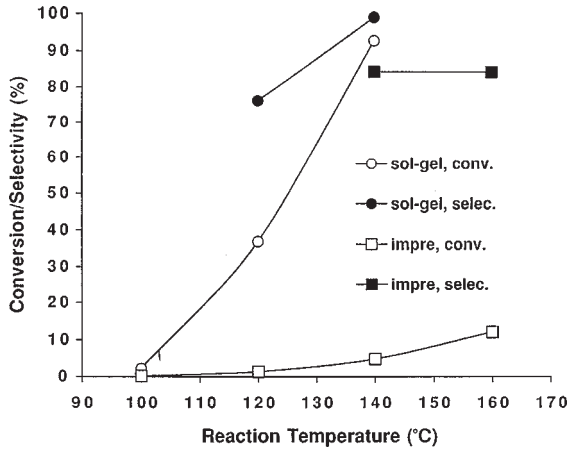
Figure 6 shows the catalytic performance of the one-pot sol-gel synthesized and the impregnated catalysts. The one-pot sol-gel synthesized catalyst was far more active and selective than the impregnated catalyst.

The activity of the present catalyst for isopropanol dehydration was higher than the solid acid catalyst TiO_2–SiO_2 (TiO_2–SiO_2 50 wt%, 3% conversion at 140°C).[3] It can be pointed out that a strong solid acid catalyst can be obtained by the one-pot sol-gel synthesis method using $(NH_4)_2SO_4$ as one of the starting materials.

Conclusions

The one-pot sol-gel synthesis method by using $(NH_4)_2SO_4$ as starting material is effective for preparing sulfated zirconia catalyst. By adding $(NH_4)_2SO_4$ to the sol-gel preparing solution, the surface area, pore size, and pore volume of the

Fig. 6. The activity and selectivity of SO_4^{2-}–ZrO_2–SiO_2, 14 mol%, prepared by one-pot sol-gel method and impregnation vs. reaction temperature.



resultant catalysts were increased. After calcining, the $(NH_4)_2SO_4$ decomposed, giving a sulfated catalyst with relatively higher pore size and pore volume. The optimum loading of SO_4^{2-} with the one-pot sol-gel synthesized catalyst was 14 mol%, showing much higher catalytic activity, with a selectivity of 100%, for isopropanol dehydration than the impregnated catalyst.

References

1. X. Song and A. Sayari. Catal. Rev. Sci. Eng. **38**, 329 (1996).
2. M. Hino and K. Arata. J. Chem. Soc. Chem. Commun. 851 (1980).
3. M. Misono and T. Okuhara. CHEMTECH. **Nov.**, 23 (1993).
4. D.A. Ward and E.I. Ko. J. Catal. **150**, 18 (1994).
5. B.H. Davis, R.A. Keogh, and R. Srinivanson. Catal. Today, **20**, 219 (1994).
6. F.R. Chen, G. Coudurier, J.F. Joly, and J.C. Vedrine. J. Catal. **143**, 616 (1993).
7. K. Tanabe, H. Hatori, and T. Yamaguchi. Crit. Rev. Surf. Chem. **1**, 1 (1990).
8. T. Yamaguchi. Appl. Catal. **61**, 1 (1990).
9. J.M. Miller and L.J. Lakshmi. J. Phys. Chem. B, **102**, 6465 (1998).
10. M. Schneider and A. Biker. Catal. Rev.-Sci. Eng. **37**, 515 (1995).
11. J.M. Miller, D. Wails, J.S. Hartman, and J.L. Belelie. J. Chem. Soc. Faraday Trans. **93**, 2439 (1997).
12. R.D. Gonzalez, T. Lopez, and R. Gomez. Catal. Today, **35**, 293 (1997).
13. Aldrich catalogue of fine chemicals. Synth. Commun. **22**, 159 (1992).
14. M. Misono and N. Nojiri. Appl. Catal. **64**, 1 (1990).
15. S.J. Gregg, and K.S.W. Sing. Adsorption, surface area, and porosity. Academic Press, London. 1982
16. S. Srinivasan, C.R. Narayanan, A. Biaglow, R. Gorte, and A.K. Datye. Appl. Catal. A, **132**, 271 (1995).
17. B.A. Morrow, R.A. McFarlane, M. Lion, and J.C. Lavalley. J. Catal. **107**, 232 (1987).
18. T. Lopez, J. Navarrete, R. Gomez, O. Novaro, F. Figueras, and H. Armendariz. Appl. Catal. A, **125**, 217 (1995).
19. K. Nakamoto. Infrared and Raman spectra of inorganic and coordination compounds. 5th ed. John Wiley & Sons, New York. 1997.
20. Q. Zhuang and J.M. Miller. Appl. Catal. A, **209**, L1 (2001).

© 2001 NRC Canada

Sol-gel synthesis of ternary phosphate–ZrO_2–SiO_2 catalysts for alcohol dehydration

Quan Zhuang and Jack M. Miller

Abstract: Phosphate–ZrO_2–Si_2O catalysts were synthesized by sol-gel method using tributyl phosphite, zirconium propoxide, and tetraethyl orthosilicate as precursors. They were characterized by N_2 adsorption, ^{31}P CP MAS NMR, and DRIFTS. At lower P content, monomeric phosphates were formed on the surface of the catalysts, which were mainly responsible for the isopropanol dehydration activity. At higher P content, polyphosphates were formed, and thus, the dehydration activity decreased. An optimum P content for dehydration activity was found to be at 10 mol%.

Key words: sol-gel synthesis, ternary oxides, phosphate, acid catalyst, alcohol dehydration, ^{31}P CP MAS NMR, N_2 adsorption, DRIFTS.

Résumé : On a synthétisé des catalyseurs phosphate–ZrO_2–SiO_2 par la méthode sol-gel utilisant du phosphite de triéthyle, du propylate de zirconium et de l'orthosilicate de tétraéthyle comme précurseurs. On les a caractérisés par adsorption de N_2, RMN CP MAS du ^{31}P et DRIFTS. À des teneurs faibles en P, il se forme des phosphates monomères à la surface des catalyseurs qui se sont avérés responsables pour activité de déshydratation de l'isopropanol. À des teneurs en P plus élevées, il se forme des polyphosphates et il en résulte une diminution de l'activité de déshydratation. On a déterminé que la teneur optimale en P pour l'activité de déshydratation est de 10 mol%.

Mots clés : synthèse sol-gel, oxydes ternaires, phosphate, catalyseur acide, déshydratation des alcools, RMN CP MAS du ^{31}P, adsorption du N_2, DRIFTS.

[Traduit par la Rédaction]

Introduction

Recently, phosphorus-containing oxides have been synthesized by various methods to obtain inorganic materials with new porous structures and (or) new properties. Among them, SAPO and AIPO types have been reported as having uniform porous structure, showing molecular sieve function, as well as catalytic activity, for some reactions due to the surface acidity (1, 2). Meanwhile, supported phosphoric acid catalysts prepared by impregnation have been widely used as catalysts for catalyzing olefin hydration (3), alkylation (4), dehydration (5–7), and dimerization (4).

On the other hand, there have been extensive studies on sol-gel synthesis of oxides, because it may provide specific properties to the oxide that cannot be obtained by the conventional coprecipitation preparation (8). Under appropriate synthesis conditions, such as metal alkoxide concentration, pH, the type of complexing agent, the amount of hydrolyzing water, drying technique, the textural properties of the oxide can be controlled. Since the advent of this method, it has stimulated more and more interest in its application in the field of catalytic materials research. The sol-gel synthesis method can be used to prepare both catalyst and catalyst support (9).

In this paper, we report our attempt to prepare the ternary phosphate–zirconia–silica catalysts by the sol-gel synthesis method using tributyl phosphite, zirconium(IV) propoxide, and tetraethyl orthosilicate as precursors. Its catalytic performance was evaluated for isopropanol dehydration, and N_2 adsorption, DRIFTS, and ^{31}P CP MAS NMR were employed to characterize the catalysts.

Received July 20, 2000. Published on the NRC Research Press Web site at http://canjchem.nrc.ca on August 22, 2001.

Q. Zhuang and J.M. Miller.[1] Department of Chemistry, Brock University, St. Catharines, ON L2S 3A1, Canada.

[1]Corresponding author (telephone: (905) 688-5550 ext. 3789; e-mail: jmiller@brocku.ca).

[2]Q. Zhuang and J.M. Miller. Submitted.

Experimental

Sol-gel synthesis of the catalysts

n-Butanol was obtained from Caledon Laboratories, all other chemicals were obtained from Aldrich and used as received.

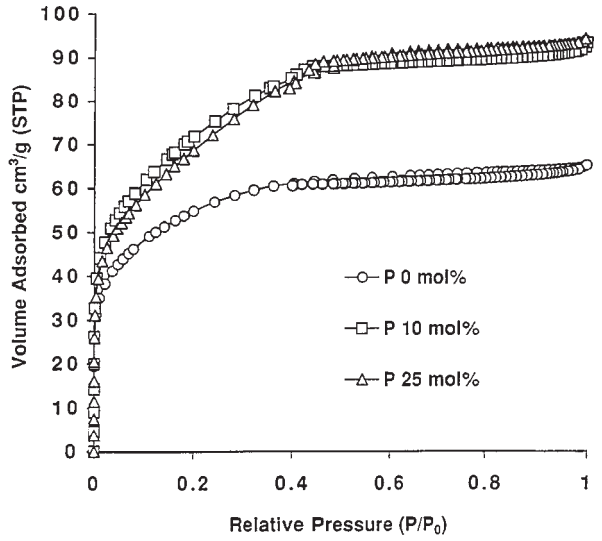
A series of P–ZrO_2–SiO_2 (Zr:Si molar ratio was fixed at 75:25) catalysts with P contents of up to 25 mol% were synthesized by the sol-gel method. Briefly, tributyl phosphite (density 0.925 g mL^{-1}), zirconium propoxide (70%, density 1.044 g mL^{-1}), and tetraethyl orthosilicate (98%, density 0.93 g mL^{-1}) were used as the precursors and 2,4-pentanedione (H-acac) as the complexing agent (8).[2] The appropriate amounts of zirconium propoxide and tetraethyl orthosilicate were desolved in the solvent, *n*-butanol (density 0.81 g mL^{-1}). The solution was heated to 60°C under stirring to mix the components thoroughly, then it was cooled down to room temperature. Tributyl phosphite and H-acac were added and the solution was stirred for 30 min. Then the alkoxides in the solution were hydrolyzed over night by adding water. A yellowish transparent gel was obtained, which

 DOI: 10.1139/cjc-79-8-1224 © 2001 NRC Canada

Table 1. Reagent amounts (g) used in the catalyst P–ZrO_2–SiO_2 preparation.

	P mol%					
Reagent	0	5	10	15	20	25
Tributyl phosphite	0.00	3.00	6.00	9.00	12.00	15.00
Zirconium propoxide	84.14	79.94	75.73	71.52	67.31	63.11
Teraethyl orthosilicate	12.74	12.10	11.47	10.83	10.19	9.56
n-Butanol	166.63	167.82	169.04	170.60	171.43	172.61
2,4-Pentanedione	12.00	12.00	12.00	12.00	12.00	12.00
H_2O	47.50	47.50	47.50	47.50	47.50	47.50

Fig. 1. N_2 adsorption isotherms of the catalysts (concentrations based on synthesis).



was dried at 100°C to remove the solvent and then calcined at 500°C for 3 h to remove the organics. The total concentration of the alkoxides in *n*-butanol solution was 0.8 M. The molar ratio of the complexing agent to the alkoxides was 1:2. The molar ratio of hydrolyzing water to alkoxide was 11:1. Table 1 shows the reagent amounts used in the catalyst preparation.[3]

Characterization of the catalysts

N_2 adsorption analysis was measured by using a Coulter SA 3100 instrument at –196°C. Samples were degassed under vacuum at 200°C for 1 h immediately prior to N_2 adsorption analysis. From the isotherm, the Brunauer–Emmett–Tellar (BET) surface area, pore volume, and pore size distribution were calculated by using the Barret, Joyner, and Halenda (BJH) method (10).

CP MAS NMR experiments were carried out on a Bruker Avance DPX 300 multinuclear FT NMR instrument. A standard bore Bruker MAS/CP MAS probe with 4 mm zirconia rotors was used. ^{31}P NMR spectra were obtained at 121.50 MHz using cross polarization with proton decoupling during acquisition and referenced to $(NH_4)_3PO_4$ (chemical shift = 0 ppm). Samples were spun at 8 kHz. A 1 ms cross-polarization contact time was used with a 4 s recycle delay between the pulses. 124 FIDs were accumulated with a spectral window of 36 kHz. Prior to recording the spectra, the samples were degassed at 100°C for 30 min in a flow of helium and immediately transferred into the zirconia rotors for the NMR measurements.

DRIFTS spectra were acquired using a Spectra Tech DRIFTS accessory (The Collector) in an ATI Mattson RS-1 FT-IR spectrometer equipped with a Michelson interferometer, a helium–neon laser, a KBr beam splitter, a DTGS (deuterated triglycerol sulfate) detector with a spectra range of 4000–400 cm^{-1}, and a standard high-intensity source. The diffuse-reflectance FT-IR were recorded at 100°C under vacuum after evacuating the samples at 100°C for 30 min. The sample chamber was designed to be used in situ on the collector DRIFTS accessory.

Isopropanol dehydration evaluation

The catalytic activity evaluation of the catalysts for isopropanol dehydration was performed using a continuous flow fixed-bed micro reactor made of Pyrex glass.[2] The inner diameter of the reactor was 6 mm, its length was 25 cm. With each reaction, 200 mg of fresh catalyst was put into the middle of the reactor. A thermocouple was placed just below the catalyst bed to monitor the reaction temperature, which was manipulated by a temperature controller. Before each reaction, the catalyst was heated to the reaction temperature under a flow of N_2. The reactions were performed at the temperature range of 150–230°C at 1 atm (1 atm = 101.325 kPa). The reactant, isopropanol, was introduced into the reactor by a N_2 bubbler, which was kept at 23°C (11).[2] The flow rate of N_2 was 100 mL min^{-1}, giving a weight hour space velocity (WHSV) of the reactant as 1.8 h^{-1}. The products were analyzed by an on-line PerkinElmer Sigma 3B gas chromatograph, employing a Porapaq R column, 800/100 mesh, 6 ft × 0.125 in, with a thermal conductivity detector (TCD). To analyze all of the products in the exit stream from the reactor, the GC column was heated by programming from 150 to 220°C for 15 min.[2] The activities were stablized in ca. 20 min. After that time, two consecutive analyses were carried out, which were within 5%. An average is reported throughout the *Discussion* section. The main product was propylene, with trace amounts of diisopropyl ether as by-product, with selectivity close to 100%.

Results and discussion

Figure 1 shows the N_2 adsorption isotherms of the catalysts. The catalysts display type IV isotherms (10). By add-

[3] The mol% of phosphorous quoted throughout is based on the synthesis concentrations, not analysis of the calcined catalysts.

© 2001 NRC Canada

Fig. 2. Pore size distributions of the catalysts (concentrations based on synthesis).

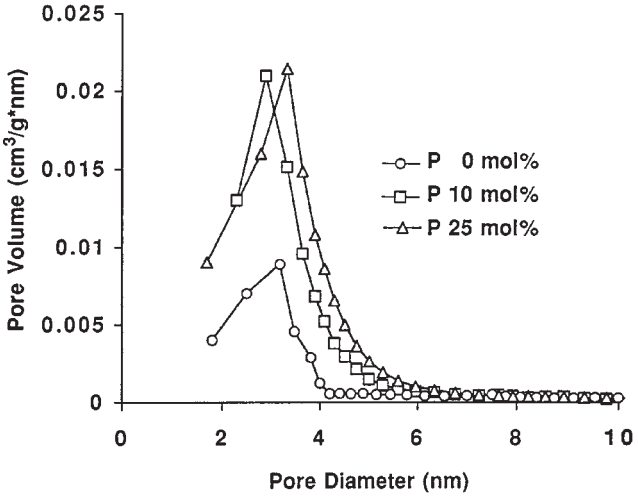


Fig. 3. ^{31}P CP MAS NMR spectra of the catalyst, P 10 mol%, after treating at 100, 233, 366, and 500°C, respectively (downward).

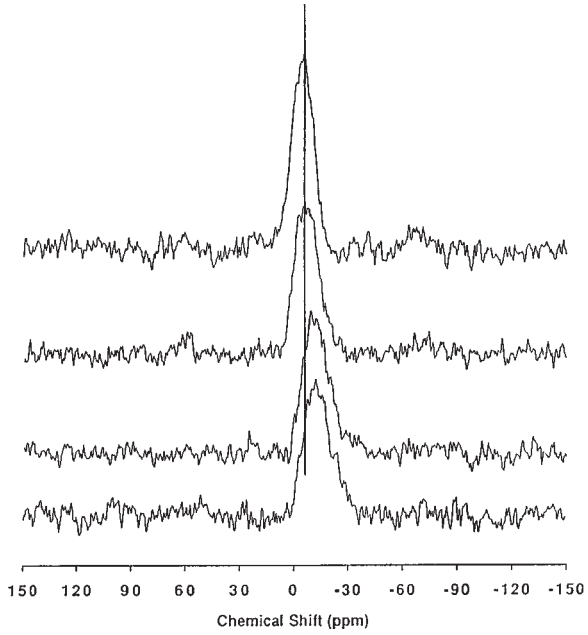


Table 2. ^{31}P CP MAS data of the catalyst P–ZrO_2–SiO_2 (P 10 mol%) after calcining at different temperatures.

T (°C)	^{31}P chemical shift (ppm)
100	–4.1
233	–5.4
366	–8.2
500	–11.5

Fig. 4. ^{31}P CP MAS NMR spectra of the catalysts after calcining at 500°C, P content: 5, 10, 15, 20, and 25 mol% (upward), with concentrations based on synthesis.

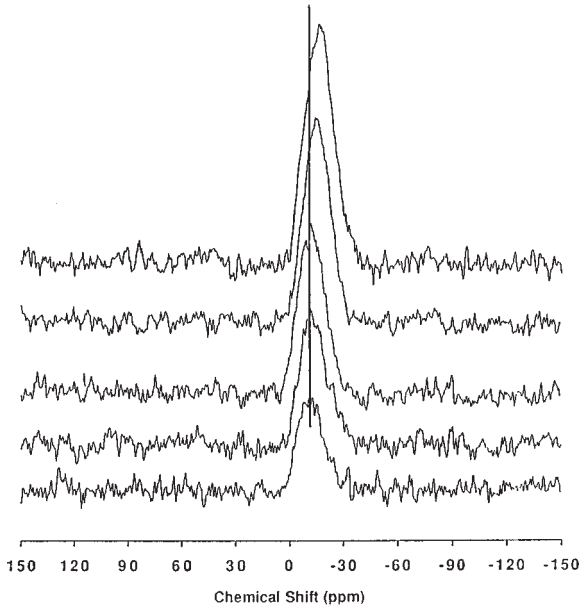


Table 3. ^{31}P CP MAS data of the catalysts P–ZrO_2–SiO_2 with different P content after calcining at 500°C.

P mol%	^{31}P chemical shift (ppm)
5	–10.4
10	–11.5
15	–12.0
20	–14.7
25	–14.7

Note: P concentrations are based on synthesis, not analysis.

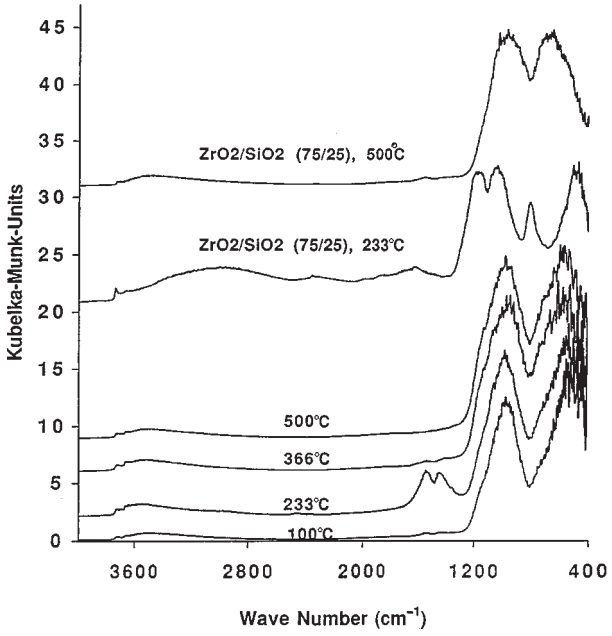
ing phosphorus in the form of tributyl phosphite into the sol-gel synthesis solutions, the N_2 adsorption of the resultant catalysts increases, especially at the intermediate and high relative pressure range. The pore size distributions of the catalysts are displayed in Fig. 2. It can be seen that the textural structure of the catalysts are mesoporous. As the amount of P is increased in the synthesis solution, the pore size distribution broadens to the larger pore diameter side, and the total pore volume of the catalysts increases. From P 0.0 to 25 mol%, the surface area increases from 180 to 250 $m^2\ g^{-1}$ and the pore volume from 0.10 to 0.14 $cm^3\ g^{-1}$.

To evaluate the evolution process of the ternary P–ZrO_2–SiO_2 catalysts, ^{31}P CP MAS NMR spectra of the catalyst with P 10 mol% calcined at different temperatures were acquired and the results are shown in Table 2 and Fig. 3. As the calcining temperature is increased, the chemical shift of ^{31}P NMR resonance shifts up field, from –4.1 ppm after being heat treated at 100°C to –11.5 ppm with the sample treated at 500°C. The intensities of the ^{31}P NMR peaks decrease when increasing the temperature of heat treatment. The ^{31}P NMR resonance peaks at the above chemical shift ranges are due to the monomeric phosphates (2, 12). It is well-known that P(III) can be easily oxidized to P(V) (13). Thus in our system, after heat treating the gel in air, the P(III) from tributyl phosphites is oxidized to P(V) in the form of phosphates.

Figure 4 and Table 3 show the ^{31}P NMR spectra of the catalysts with different P contents after calcining at 500°C. It can be seen that when the P content in the catalyst is increased, the intensity of the ^{31}P resonance increases, with an

© 2001 NRC Canada

Fig. 5. DRIFTS spectra of the catalyst after calcining at different temperatures (P 10 mol%).



upfield shift (from –10.4 ppm with P 5 mol% to –14.7 ppm with P 25 mol%). These changes are caused by partial formation of polyphosphates when the P contents in the catalysts are increased.

The DRIFT spectra of the catalyst with P 10 mol% after calcining at different temperatures were measured, and the results are shown in Fig. 5 together with the DRIFT spectra of ZrO_2:SiO_2 (75:25) calcined at 233 and 500°C, respectively. The absorption peaks at ~980 cm^{-1} are assigned to Si—OH stretching and Zr-O-Si modes of ZrO_2–SiO_2 (14). Nogami (15) reported that the peaks at 500–600 cm^{-1} are due to the polyhedra ZrOx. It can be seen that in our catalysts these ZrOx polyhedra exist. The absorption at ~3730 cm^{-1} is caused by the vibration of Si—OH. The peaks at ~3500 cm^{-1} are ascribed to the hydrogen-bonded hydroxyl band (16, 17). As shown in the ^{31}P CP MAS NMR results, after calcining, the phosphorus species in the gel gradually change to the phosphate, and hence, the new absorption peaks at ~3650 cm^{-1} could be reasonably assigned to the OH groups affiliated to the phosphates, which are acidic. The peaks at 1540 and 1445 cm^{-1} appear after increasing the calcining temperature to 233°C. On further increasing the calcining temperature, they disappear. Since we could not observe these peaks with pure ZrO_2–SiO_2 system, they must be related with some specific intermediate organic phosphorous species being formed, which then migrate to the surface and decompose during the evolution of the structure of the final catalysts on heat treatment at higher temperature (18). The phosphorus-containing gel is yellow, whereas ZrO_2–SiO_2 is nearly white and tributyl phosphite is colorless, indicating that at the gel stage the two materials have different structures. This can be seen from their DRIFTs spectra after calcining at 233°C. On heat treating at higher temperature (500°C) the frameworks of the two materials are similar, because they show similar DRIFTs spectra. The phosphates

Fig. 6. The catalytic activities of the catalysts with different P content for isopropanol dehydration (210°C, 1 atm, WHSV = 1.8 h^{-1}) (concentration based on synthesis).

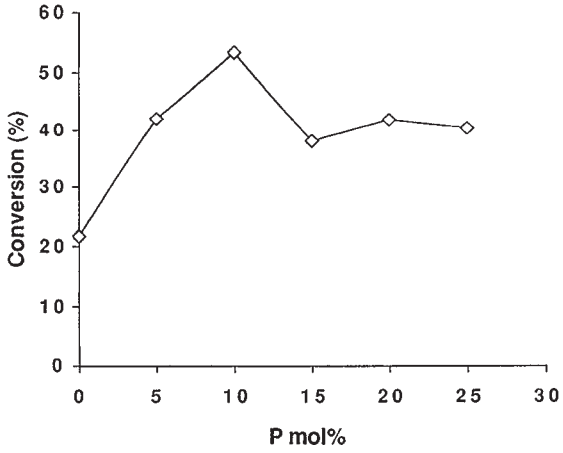
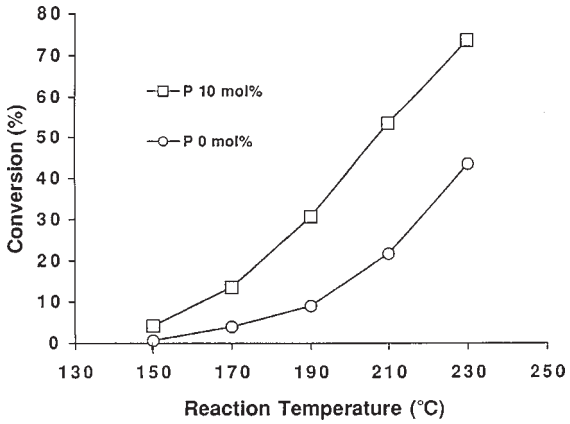


Fig. 7. The activity (as conversion) of P–ZrO_2–SiO_2, P 0.0 and 10 mol% vs. reaction temperature.



may have only weak interaction with the framework of ZrO_2–SiO_2.

Figure 6 shows the catalytic activities of the sol-gel synthesized catalysts with different P content for isopropanol dehydration. As the P content is increased, the activity increases first, then decreases, and then levels off, giving an optimum content of P at 10 mol%. It is clear that the dehydration activity of the catalysts are due to the acidity of the phosphates on the surface (3). As the P content in the catalysts is increased, some of the monomeric phosphates change to polyphosphates as evidenced by the results of ^{31}P NMR characterization. This may explain the decline of the activity of the catalysts with higher P content.

Figure 7 shows the activities of the two catalysts without P and with 10 mol% of P, respectively, under different temperatures. Under the tested reaction temperature range, the activity of the P containing catalyst is higher than the catalyst without P.

Conclusions

By sol-gel method, phosphate–ZrO_2–SiO_2 catalysts were synthesized. The ^{31}P CP MAS NMR spectra revealed that at lower P content, monomeric phosphates were formed on the

© 2001 NRC Canada

surface of the catalysts, which were mainly responsible for the isopropanol dehydration activity. When P content was increased, polyphosphates were formed, causing the decrease of the activity. The optimum P content was 10 mol%.

References

1. Q. Gao, B.M. Weckhuysen, and R.A. Schoonheydt. Micropor. Mesopor. Mat. **27**, 75 (1999).
2. J. Quartararo, M. Guelton, M. Rigole, J. Amoureux, C. Fernandez, and J. Grimblot. J. Mater. Chem. **9**, 2637 (1999)
3. C.M. Fougret, M.P. Atkins, and W.F. Holderich. Appl. Catal. A, **181**, 145 (1999).
4. K. Tanabe and W.F. Holderich. Appl. Catal. A, **181**, 399 (1999).
5. J.N. Armor. Appl. Catal. A, **78**, 141 (1991).
6. W.F. Holderich. Stud. Surf. Sci. Catal. **75**, 127 (1993).
7. Y. Kita, K. Kishino, and K. Nakagawa. Nippon Kagaku Kaishi, **3**, 269 (1996).
8. J.M. Miller and L.J. Lakshmi. J. Phys. Chem. B, **102**, 6465 (1998).
9. M. Schneider and A. Biker. Catal. Rev. Sci. Eng. **37**, 515 (1995).
10. S.J. Gregg and K.S.W. Sing. Adsorption, surface area and porosity. Academic Press, London. 1982.
11. S. Srinivasan, C.R. Narayanan, A. Biaglow, R. Gorte, and A.K. Datye. Appl. Catal. A, **132**, 271 (1995).
12. E.C. DeCario, J.C. Edwards, T.R. Scalzo, D.A. Storm, and J.W. Bruno. J. Catal. **132**, 498 (1991).
13. F.A. Cotton, G. Wilkinson, C.A. Murillo, and M. Bochmann. Advanced inorganic chemistry. 6th ed. John Wiley & Sons, New York. 1999.
14. D.M. Pickup, G. Mountjoy, G.W. Wallidge, R.J. Newport, and M.E. Smith. Phys. Chem. Chem. Phys. **1**, 2527 (1999).
15. M. Nogami. J. Non-Cryst. Solids, **69**, 415 (1985).
16. S.W. Lee and R.A. Condrate, Sr. J. Mater. Sci. **23**, 2951 (1988).
17. M. Andriarainarivelo, R. Corriu, D. Leclercq, P.H. Mutin, and A. Vioux. J. Mater. Chem. **6**, 1665 (1996).
18. K. Nakamoto. Infrared and Raman spectra of inorganic and coordination compounds. 5th ed. John Wiley & Sons, New York. 1997.

© 2001 NRC Canada

Stereoselective addition of acetone to the C=N bond of [4.3.0] boron heterobicycles

Victor Barba, Damian Cuahutle, Rosa Santillan, and Norberto Farfán

Abstract: The reaction of *N*-salicylidene-2-aminophenolate (SAP-H_2) derivatives with phenyl boronic acid afforded five new boron bicyclic species in moderate yields, as confirmed by an X-ray study of the boron heterocycle derived from 2-amino-4-chlorophenol. The results also showed that the boron complexes derived from Schiff bases undergo an acetolysis reaction to give the corresponding dioxazaborocines containing all substituents on the same side also in good yields. The structure of one of the addition products was established by X-ray analysis showing that, in the solid state, it exists as a dimeric structure formed by hydrogen bonds.

Key words: borocines, tridentate ligands, imines, boronic acids.

Résumé : La réaction de dérivés du *N*-salicylidène-2-aminophénolates (SAP-H_2) avec l'acide phénylboronique conduit, avec des rendements modérés, à la formation de cinq nouvelles espèces bicycliques du bore dont la structure a été confirmée par diffraction des rayons X sur l'hétérocycle contenant du bore dérivé du 2-amino-4-chlorophénol. Les résultats montrent aussi que les complexes du bore dérivés des bases de Schiff subissent une réaction d'acétolyse conduisant à la formation, avec de bons rendements, des dioxazaborocines correspondantes comportant tous les substituants sur le même côté. La structure de l'un des produits d'addition a été déterminée par une étude par diffraction des rayons qui a montré que, à l'état solide, il existe sous la forme d'une structure dimère formées par des liaisons hydrogènes.

Mots clés : borocines, ligands tridentates, imines, acides boroniques.

[Traduit par la Rédaction]

Introduction

The addition reaction of nucleophiles to the C=N bond of imines or imine derivatives is a well-known procedure that provides reactive iminium salts, nitrones, acylimines, and sulfonimine when the electrophilicity of the carbon atom of the C=N bond is increased by *N*-alkylation (1), *N*-oxidation (2), *N*-acylation (3), or *N*-sulfonation (4). Moreover, the use of organometallic reagents results in a more efficient addition of the nucleophilic species to the imine owing to an increased polarization of the C=N bond (5–7). These reactions are very interesting because the use of chiral imines allows asymmetric synthesis of amines (8) whereby the selectivity and efficiency of a nucleophilic addition of an organometallic reagent to the C=N bonds are assisted by the presence of stoichiometric amounts of an external chiral auxiliary (8, 9).

In contrast, boron reagents are highly electrophilic so that coordination of the nitrogen atom to the boron could polarize the C=N bond and increase the ability of a nucleophilic species to react with the carbon atom in this group. We have prepared several boron compounds derived from tridentate Schiff bases and arylboronic acids (10–17); these complexes form bicyclic or macrocyclic structures showing intramolecular N–B dative bonds where the polarization of the C=N is increased.

Continuing our investigations on boronates, herein we described the formation of five new bicyclic boron complexes (**2a**–**e**) derived from iminodiphenols (**1a**–**e**) and phenylboronic acid. These derivatives contain a C=N bond that is polarized by coordination of the nitrogen atom to the boron atom forming a N–B dative bond. The polarization of this bond was evidenced by acetolysis of the imine group of the boron compounds to produce dioxazaborocines **4a**–**e** showing all substituents on the same side with very high diastereoselectivity.

Results and discussion

Tridentate ligands **1a**–**e** were synthesized by condensation of salicylaldehyde with the corresponding aminophenol derivative. The reaction was carried out under reflux of methanol for 30 min to give the corresponding imines in good yields. The ^{1}H NMR spectra of compounds **1a**–**e** present a single signal between 8.07 and 9.10 ppm, typical of an imine proton.

Treatment of **1a**–**e** with 1 equivalent of phenylboronic acid in the presence of THF gives boronates **2a**–**e** (Scheme 1) via elimination of 2 equivalents of water. From this reaction, boronate **2c** was obtained in crystalline form allowing determination of its X-ray crystal structure, which showed that upon coordination the ligand adopts a geometry

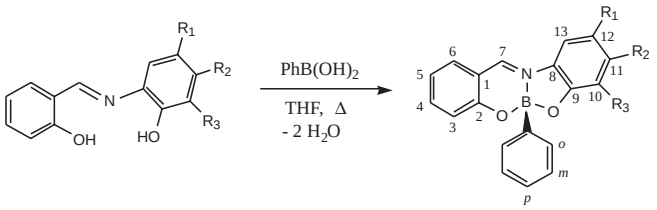
Received February 20, 2001. Published on the NRC Research Press Web site at http://canjchem.nrc.ca on August 24, 2001.

V. Barba, D. Cuahutle, R. Santillan, and N. Farfán.[1] Depto. de Química, Centro de Investigación y de Estudios Avanzados del IPN, Apdo. Postal 14–740, 07000 México D. F., México.

[1]Corresponding author (telephone: +52 57 47 37 21; fax: +52 57 47 71 13; e-mail: jfarfan@mail.cinvestav.mx).

 DOI: 10.1139/cjc-79-8-1229 © 2001 NRC Canada

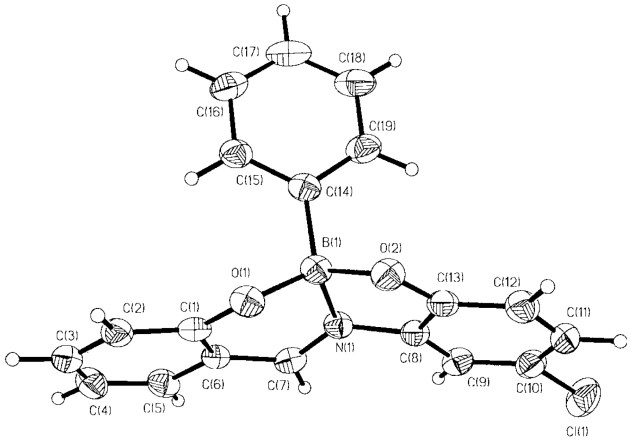
Scheme 1.



1a–f **2a–f**

	R_1	R_2	R_3
a:	NO_2	H	H
b:	Me	H	H
c:	Cl	H	H
d:	Me	H	Me
e:	H	Me	H
f:	H	H	H

Fig. 1. ORTEP diagram of the molecular structure of compound **2c.**



that leads to a highly delocalized system with enhanced stability, as described in previous studies (16, 17). Compounds **2a**–**e** were obtained as pale yellow-orange solids and were characterized by elemental analysis, mass spectrometry, IR, and ^{1}H, ^{13}C, and ^{11}B NMR spectrometry. Formation of similar [4.3.0] heterobicyclic systems using an ONO donor ligand has been described previously for elements, such as phosphorus (18), manganese (19), vanadium (20–22), and molybdenum (23–25). The mass spectra of compounds **2a**–**e**, showing the molecular ion $[M]^+$ and a base peak corresponding to the loss of the phenyl group, is in agreement with previous results (26).

The C=N stretching band in the IR spectra is shifted to higher wavenumbers by $\Delta\bar{\nu}$ = 4–8 cm^{-1} upon complex formation as shown in other boron compounds (10–17). The ^{1}H NMR data show that the signal corresponding to the azomethine group is shifted to lower field in the boron complexes as compared to the free ligands ($\Delta\delta \approx 0.6$ ppm). The same effect is observed in the ^{13}C NMR spectra where the signal for C-7 is observed between 147.9 and 152.0 ppm for compounds **2a**–**c** and **2e**, whereas the same signal in ligands **1a**–**c** and **1e** appears between 161.3 and 165.3 ppm. The only exception was compound **2d**, which shows a similar shift (162.9 ppm) to the free ligand (162.3 ppm). The ^{11}B NMR chemical shifts are indicative of tetra-coordinated species (δ = +8.6, +11.0, +9.0, +7.5, and +8.0 for **2a**–**e**, respectively) (27).

The X-ray analysis for **2c** (Fig. 1) established the [4.3.0] heterobicyclic structure; details of the crystal data and summary of collection parameters are given in Table 1 and selected bond distances and bond angles are compared in Table 2.[2] The value for the intramolecular N—B donor-acceptor bond length for boronate **2c** is 1.591(6) Å, which is shorter than the unsubstituted boronate **2f** (1.613(5) Å) (17) and in accordance with the N—B dative bond distances for boronates, which are in the range from 1.586(2) to 1.681(5) Å (28).

The N(1)—C(7) bond length (Table 2) is significantly longer in **2c** (1.284(5) Å) as compared to **2f** (1.249(4) Å), indicating a weaker N–B dative bond in **2c**. The bond angles around the boron atom in **2c** are in the range of 99.8(4)–113.7(4)°. The lowest value corresponds to the O(2)-B(1)-N(1) bond angle in the five-membered heterocycle, whereas the largest corresponds to the O(1)-B(1)-C(Ph) bond angle; the values are similar to those found in compound **2f**.

The environment of the boron atom can be evaluated by the tetrahedral character (THC) (28) showing a large distortion (74%), due to high strain in the five-membered heterocycle. The ring strain of the two heterocycles is perhaps best expressed by torsion angles of 33.4° for the O(1)-B(1)-N(1)-C(7) in the six-membered ring and –20.2° in the O(2)-B(1)-N(1)-C(8) of the five-membered ring.

When the reaction of **1d** was carried out in ethanol under reflux, the monomeric structure **3** was formed (Scheme 2). In this case the solvent reacts through an intermediate, which results from reaction of the phenolic group of the ligand with a hydroxyl group from phenylboronic acid, as proposed in Scheme 3. The formation of type IV boronates can be explained based on the observation that six-membered boron heterocycles (type II) are more stable than five-membered ones (type III), as indicated by the formation of compound **3** where the hydroxyl group attached to the boron atom is substituted by an OCH_2CH_3 group.

The X-ray crystal structure of **3** (Fig. 2) consists of discrete molecules with strong intramolecular hydrogen bonds between the ethoxy moiety and phenolic fragment as can be inferred from the O(3)···O(2) bond distance (2.615 Å). Selected bond lengths of **3** are summarized in Table 2 and compared with the corresponding data for boronate **2c**. It can be seen that significant differences in the N—B, B—O, N(1)—C(8), and N(1)—C(7) bond lengths are found; the longer distances are found for **3**. For example the N—B bond for **3** is 1.621(2) Å), whereas the N—B bond for **2c** is 1.591(6) Å.

The bond angles around the boron atoms for **3** and **2c** are very similar; however, the THC value is larger for **3** (77%) indicating that the annular tension produced by formation of a five-membered ring distorts the tetrahedral geometry.

[2] Suplementary material may be purchase from: The Depository of Unpublished Data, Document delivery, CISTI, National Research Council of Canada, Ottawa, ON K1A 0S2, Canada (DUD No. 3298). This data has also been deposited with the Cambridge Crystallographic Data Center, CCDC No. 149208 for **3**, 149209 for **4d**, and 149210 for **2c**. Copies of this information may be obtained free of charge from The Director, CCDC, 12 Union Road, Cambridge, CB2 1EZ, U.K. (fax: +44-1223-336-033; e-mail: deposit@ccdc.cam.ac.uk or www: http://www.ccdc.cam.ac.uk).

© 2001 NRC Canada

Table 1. Experimental crystallographic data for compounds **2c**, **3**, and **4d**.

Compound	**2c**	**3**	**4d**
Formula	$C_{19}H_{13}BClNO_2$	$C_{23}H_{24}BNO_3$	$C_{24}H_{24}BNO_3$
Crystal size (mm)	0.36 × 0.24 × 0.24	0.56 × 0.37 × 0.36	0.50 × 0.50 × 0.30
FW (g mol^{-1})	333.56	373.24	385.25
Space group	$P2_1/a$	$C2/c$	$P\bar{1}$
Cell parameters			
a (Å)	7.8837(6)	22.928(5)	7.744(2)
b (Å)	14.5561(13)	9.227(2)	10.886(2)
c (Å)	13.6979(12)	21.482(4)	12.645(3)
α (°)	90.00	90.00	81.81(3)
β (°)	95.595(7)	117.86(3)	79.92(3)
γ (°)	90.00	90.00	85.59(3)
V (Å^3)	1564.4(2)	4017.9(14)	1037.4(4)
Z	4	8	2
μ (mm^{-1})	0.255	0.080	0.080
$\rho_{calcd.}$ (g cm^{-3})	1.416	1.234	1.233
Data collection[a]			
Total reflections	2317	7337	3847
Unique reflections	2180	3788	3636
R_{merge}	0.058	0.067	0.033
Refinement			
R / R_w (F)[b]	0.0425 / 0.1109	0.0412 / 0.1064	0.0416 / 0.1181
R / R_w (F^2) (all data)	0.1558/ 0.1634	0.1008 / 0.1291	0.1149 / 0.1507
No. of variables	270	349	358
GoF	0.870	0.975	1.008
$\Delta\rho_{min}$ (e Å^{-3})	–0.207	–0.147	–0.156
$\Delta\rho_{max}$ (e Å^{-3})	0.193	0.157	0.212

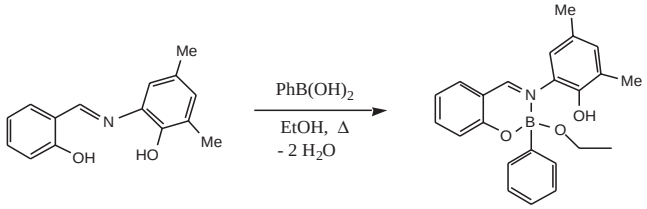
[a] T = 295 K, Enraf-Nonius CAD4 diffractometer, Mo Kα (λ = 0.71073) radiation.
[b] $R = \Sigma||F_o| - |F_c||/\Sigma|F_o|$, $R_w = [\Sigma w(|F_o| - |F_c|)^2/\Sigma w|F_o|^2]^{1/2}$.

Table 2. Selected bond lengths and bond angles of compounds **2c**, **3**, and **4d**.

	2c	**3**	**4d**
Bond lengths (Å)			
N(1)—B(1)	1.591(6)	1.621(2)	1.677(3)
N(1)—C(8)	1.412(6)	1.443(2)	1.465(3)
N(1)—C(7)	1.284(5)	1.292(2)	1.505(3)
O(1)—B(1)	1.456(6)	1.472(2)	1.456(3)
O(1)—C(1)	1.348(5)	1.338(2)	1.354(3)
O(2)—B(1)	1.486(6)	1.456(3)	1.484(3)
O(2)—C(13)[a]	1.356(5)	1.429(3)	1.357(3)
B(1)—(C_{Ph})[b]	1.611(7)	1.602(3)	1.592(4)
Bond angles (°)			
O(1)-B(1)-N(1)	107.0(4)	107.5(2)	107.5(2)
O(1)- B(1)-O(2)	112.2(4)	111.5(2)	111.9(2)
O(1)-B(1)-(C_{Ph})[b]	113.7(4)	109.1(2)	111.9(2)
O(2)-B(1)-N(1)	99.8(4)	101.4(2)	100.0(2)
O(2)-B(1)-(C_{Ph})[b]	111.7(4)	115.2(2)	113.0(2)
N(1)-B(1)-(C_{Ph})[b]	111.6(4)	111.7(2)	111.8(2)
C(1)-O(1)-B(1)	116.8(3)	122.0(2)	123.3(2)
B(1)-O(2)-C(13)[a]	107.8(3)	116.9(2)	110.4(2)
C(7)-N(1)-C(8)	129.4(4)	117.7(2)	114.3(2)
C(7)-N(1)-B(1)	121.8(4)	120.2(2)	113.9(2)
C(8)-N(1)-B(1)	107.9(3)	122.1(2)	103.1(2)

[a] C(9) for **4d** and C(22) for **3**.
[b] C_{Ph} = ipso carbon of the phenyl group.

Scheme 2.



Evidence for the formation of boronate **3** was also obtained from the NMR spectra. The ^{1}H NMR spectrum shows a single signal at 8.17 ppm, which is shifted to lower field compared with **2a**–**e**. However, the ^{13}C NMR spectrum shows the signal corresponding to C-7 at δ = 163.8, which is at lower field in comparison with boronates **2a**–**e**. The tetracoordination of the boron atom can be seen from the ^{11}B NMR spectrum, where a value of +7.0 ppm has been measured.

The dioxazaborocines **4a**–**e** were obtained in moderate yields (45–89%) by aldol condensation, resulting in the acetolysis of boronates **2a**–**e** after 6 h of heating at reflux (Scheme 4). The lowest yield corresponds to complex **2a** containing a NO_2 group that produces an electron-withdrawing effect.

Exclusive formation of the diastereoisomer containing the CH_3COCH_2 and NH groups in a *cis* configuration supports the proposal of a six-membered transition state. It is impor-

© 2001 NRC Canada

Scheme 3.

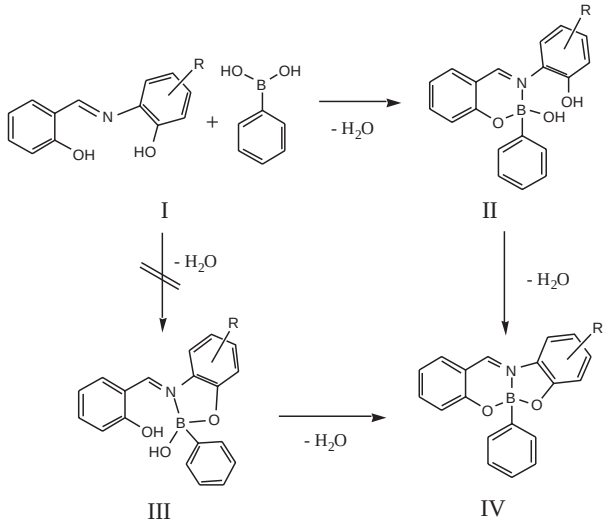
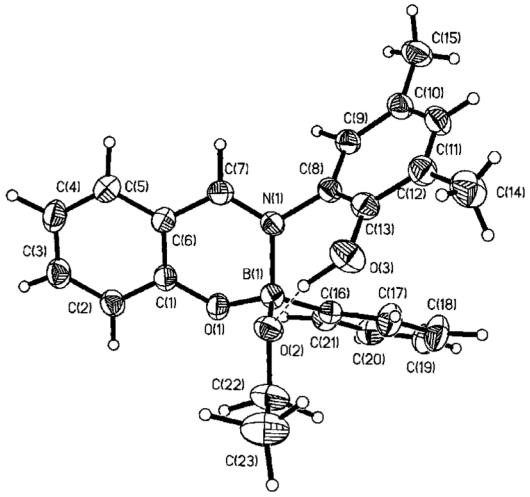


Fig. 2. ORTEP diagram of the molecular structure of compound **3**.



tant to notice that the fusion of the [4.3.0] heterobicyclic system is also *cis*, in contrast to the dioxazaborocines described by Woodgate (29), which provide a *cis–trans* diasteromeric mixture of [4.4.0] heterobicycles, although the major product also has a *cis* fusion. As a matter of fact, our results are in accordance with the results found in [3.3.0] dioxazaborocines that provide a *cis* fusion (30, 31).

The spectroscopic data allowed complete characterization for **4a**–**e**. The IR spectra showed the absence of the C=N group and appearance of a new band between 1702–1706 cm^{-1} corresponding to the C=O group, and the mass spectra showed the molecular ion for the boronates.

The NMR spectra show a singlet corresponding to the NH group between 8.07 and 9.02 ppm. In solution, there is no evidence for hydrogen bonding involving this group although it is present in the solid state (vide infra), as shown for **4d**. The -CH_2-CH- fragment gives rise to an AMX system at δ = 2.83–3.71 due the existence of stereogenic centers. The ^{11}B NMR spectra of **4a**–**e** show a broad signal between 7.6 and 12.0 ppm, characteristic for tetra-

Scheme 4.

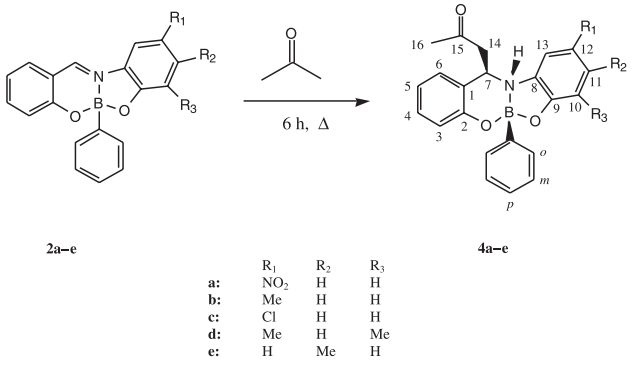
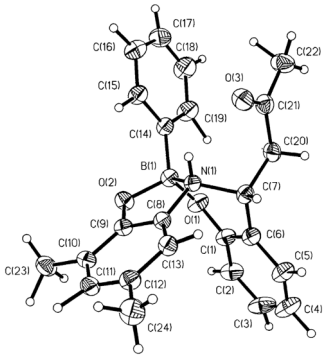


Fig. 3. ORTEP diagram of the molecular structure of compound **4d**.



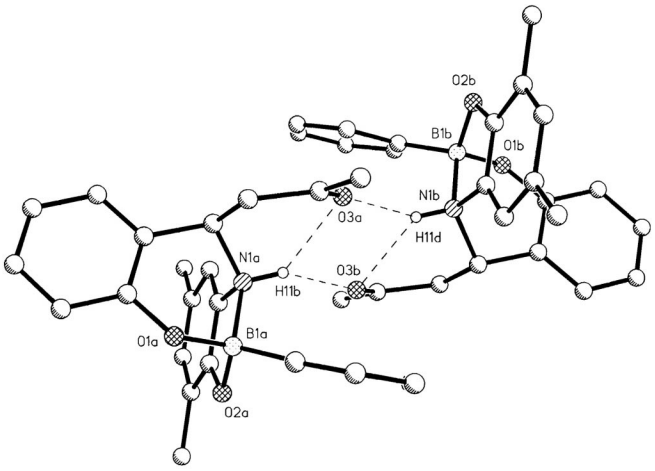
coordinated boron atoms bonded to two oxygen atoms, one nitrogen atom, and one carbon atom.

A crystal suitable for X-ray diffraction was obtained for compound **4d** and the molecular structure is shown in Fig. 3. Details of the crystal data and summary of data collection parameters are given in Table 1 and selected bond distances and angles are listed in Table 2. The N—B bond length (1.677(3) Å) is larger than that of **2c** and **3** and similar boronates described in the literature (10–17, 28). The difference in these values may be partially attributed to an increase in bond distance on going from an sp^2 to sp^3 hybridization on the nitrogen atom. The B—O distance is shorter in the six-membered (1.456(3) Å) than in the five-membered heterocycle (1.484(3) Å) due to higher annular tension in the five-membered ring. The angles around the boron atom are approximately tetrahedral in the range between 100.0(2)° (O(2)-B(1)-N(1)) and 113.0(2)° (O(2)-B(1)-(C_{Ph})) and are similar to the boronates described previously (10–17) showing a THC value of 75%.

Figure 3 shows that the boron–phenyl moiety, the -CH_2COCH_3 fragment, and the hydrogen attached to the nitrogen atom have a *cis* disposition. The molecular packing reveals the interaction present at the oxygen and hydrogen atoms forms a dimeric structure in the solid state. The molecular structure of this compound is evident in Fig. 4 whereby the centrosymmetric structure is formed by relatively strong hydrogen bonds that result in the formation of the four-membered heterocycle ring through inter- and intramolecular interactions. The H(11b)···O(3a) intramolecular distance of 2.20 Å is slightly shorter than the

© 2001 NRC Canada

Fig. 4. ORTEP diagram showing the dimeric form for **4d** by hydrogen bonding.



H(11b)···O(3b) intermolecular distance of 2.28 Å. The H(11b)—N(1a) distance (0.89 Å) is in accordance with this type of bond (32). These results allow the conclusion that the additional stabilization of the molecule is achieved owing to the inter- and intramolecular hydrogen bonding that leads to the dimeric structure.

Conclusions

In conclusion, boron complexes derived from tridentate ligands are readily formed leading in all cases to [4.3.0] heterobicyclic structures containing dative N–B bonds as evidenced by the X-ray analysis of compound **2c**. The use of different solvents leads to other heterocycles, as was shown by formation of compound **3**. Furthermore, it was shown that coordination of the nitrogen atom to boron is responsible for the polarization of the C=N bond and the facile and stereoselective reaction with nucleophiles such as acetone, leading to the products having all substituents in a *cis* configuration. The stereochemistry of the NH, phenyl, and carbonyl groups in **4d** is responsible for the dimeric structure formed in the solid state.

Experimental

Reagents and instrumentation

All starting materials were commercially available. Solvents were used without further purification, but single crystals were grown from spectrophotometric grade solvents.

NMR spectra were recorded in $CDCl_3$ and DMSO-d_6 solutions on Bruker Avance DPX 300 and Jeol GSX-270 spectrometers. Chemical shifts (ppm) are relative to $(CH_3)_4Si$ for ^1H and ^{13}C and $BF_3{\cdot}OEt_2$ for ^{11}B. Coupling constants are quoted in Hz. Infrared spectra were recorded on a PerkinElmer 16F-PC FT-IR spectrophotometer. Mass spectra were recorded on a Hewlett-Packard 5989A spectrometer. Melting points were obtained on a Gallenkamp MFB-595 equipment and are uncorrected. Midwest Microlab, LLC, Indianapolis, IN 46250 performed elemental microanalyses.

General procedure for the preparation of ligands 1a–e

To prepare the tridentate ligands **1a–e**, equimolar quantities of the corresponding aminophenol and salicylaldehyde were heated at reflux in methanol for 30 min. The solvent and the water formed during the reaction were removed by a Dean–Stark trap to yield a solid, which was washed with chloroform and used without further purification. The preparation of **1b** has been published (33).

*[2-(2-Hydroxybenzyliden)amino]-4-nitrophenol (**1a**)*

Compound **1a** was prepared from 2-amino-4-nitrophenol (1.0 g, 6.49 mmol) and salicylaldehyde (0.79 g, 6.49 mmol). The product was obtained as an orange solid (yield: 1.1 g, 4.26 mmol, 66%), mp 228–231°C. MS (70 eV) *m*/*z* (%): 258 (M^+, 100), 241 (19), 211 (53), 165 (23), 128 (8), 119 (9), 77 (20). IR (KBr) (cm^{-1}): 3448, 2918, 2850, 1624, 1522, 1336, 1278, 1140. ^1H NMR (300 MHz, DMSO-d_6) δ: 9.10 (s, 1H, H7), 8.27 (d, *J* = 2.7 Hz, 1H, H13), 8.07 (dd, *J* = 8.9, 2.7 Hz, 1H, H11), 7.69 (d, *J* = 7.7 Hz, 1H, H6), 7.42 (td, *J* = 7.7, 1.3 Hz, 1H, H4), 7.20 (d, *J* = 8.9 Hz, 1H, H10), 6.98 (t, *J* = 7.7 Hz, 1H, H5), 6.96 (d, *J* = 7.7 Hz, 1H, H3). ^{13}C NMR (75 MHz, DMSO-d_6) δ: 165.3 (C7), 161.4 (C2), 158.6 (C12), 140.8 (C9), 136.6 (C8), 134.4 (C4), 133.6 (C6), 124.6 (C11), 120.2 (C1), 119.9 (C5), 117.6 (C3), 117.2 (C10), 116.2 (C13).

*[2-(2-Hydroxybenzyliden)amino]-4-methylphenol (**1b**)*

Compound **1b** was prepared from 2-amino-4-methylphenol (1.01 g, 8.18 mmol) and salicylaldehyde (1.0 g, 8.18 mmol). The product was obtained as dark red crystals (yield: 1.79 g, 7.85 mmol, 95%), mp 162–165°C. MS (70 eV) *m*/*z* (%): 227 (M^+, 60), 227 (100), 197 (19), 134 (70), 106 (12), 77 (40). IR (KBr) (cm^{-1}): 3854, 2914, 1634, 1624, 1598, 1524, 1488, 1466, 1294, 1282, 1230, 1192, 1160, 1144, 764, 590. ^1H NMR (300 MHz, DMSO-d_6) δ: 8.95 (s, 1H, H7), 7.60 (dd, *J* = 7.7, 1.6 Hz, 1H, H6), 7.38 (td, *J* = 7.7, 1.6 Hz, 1H, H4), 7.18 (d, *J* = 1.6 Hz, 1H, H13), 6.97 (dd, *J* = 7.7, 1.6 Hz, 1H, H3), 6.95 (t, *J* = 7.7 Hz, 1H, H5), 6.93 (d, *J* = 8.2 Hz, 1H, H10), 6.86 (d, *J* = 8.2 Hz, 1H, H11), 2.25 (s, 3H, Me). ^{13}C NMR (75 MHz, DMSO-d_6) δ: 161.3 (C7), 160.7 (C2), 148.8 (C9), 134.4 (C8), 132.7 (C4), 132.2 (C6), 128.4 (C12), 128.2 (C11), 119.7 (C1), 119.5 (C13), 118.6 (C5), 116.6 (C3), 116.2 (C10), 20.0 (Me).

*[2-(2-Hydroxybenzyliden)amino]-4-chlorophenol (**1c**)*

Compound **1c** was prepared from 2-amino-4-chlorophenol (0.56 g, 3.95 mmol) and salicylaldehyde (0.48 g, 3.95 mmol). The product was obtained as an orange solid (yield: 0.83 g, 3.35 mmol, 85%), mp 221–223°C. MS (70 eV) *m*/*z* (%): 249 ($[M + 2]^+$, 34), 247 (M^+, 100), 238 (11), 154 (73), 127 (26), 99 (20), 77 (37), 51 (48). IR (KBr) (cm^{-1}): 3068, 3044, 2918, 2850, 1630, 1618, 1592, 1524, 1426, 1350, 1288, 1236, 1200, 1184, 1138, 898, 766. ^1H NMR (300 MHz, DMSO-d_6) δ: 8.99 (s, 1H, H7), 7.62 (dd, *J* = 7.8, 1.4 Hz, 1H, H6), 7.47 (d, *J* = 2.5 Hz, 1H, H13), 7.37 (td, *J* = 7.8, 1.6 Hz, 1H, H4), 7.15 (dd, *J* = 7.6, 2.5 Hz, 1H, H11), 6.96 (d, *J* = 7.8 Hz, 1H, H3), 6.95 (t, *J* = 7.8 Hz, 1H, H5), 6.94 (d, *J* = 7.6 Hz, 1H, H10). ^{13}C NMR (75 MHz, DMSO-d_6) δ 163.7 (C7), 161.5 (C2), 151.0 (C9), 137.1 (C8), 134.1 (C4), 133.4 (C6), 128.2 (C11), 123.5 (C12),

© 2001 NRC Canada

120.3 (C1), 120.1 (C13), 119.8 (C3), 118.6 (C5), 117.6 (C10).

*[2-(2-Hydroxybenzyliden)amino]-4,6-dimethylphenol (**1d**)*

Compound **1d** was prepared from 6-amino-2,4-dimethylphenol (0.53 g, 3.89 mmol) and salicylaldehyde (0.47 g, 3.89 mmol). The product was obtained as a brown solid (yield: 0.83 g, 3.44 mmol, 88%), mp 159 to 160°C. MS (70 eV) *m*/*z* (%): 241 (M^+, 97), 148 (99), 121 (28), 91 (43), 77 (65), 55 (59), 43 (100). IR (KBr) (cm^{-1}): 3568, 3054, 3018, 2990, 2888, 2850, 1616, 1522, 1462, 1302, 1232, 1204, 1180, 1138, 760. ^{1}H NMR (300 MHz, DMSO-d_6) δ: 8.88 (s, 1H, H7), 7.66 (dd, *J* = 8.5, 1.5 Hz, 1H, H6), 7.38 (td, *J* = 8.5, 1.5 Hz, 1H, H4), 6.96 (s, 1H, H13), 6.85 (s, 1H, H11), 6.92–6.97 (m, 2H, H3, H5), 2.22 (s, 3H, *Me*-C10), 2.18 (s, 3H, *Me*-C12). ^{13}C NMR (75 MHz, DMSO-d_6) δ: 162.3 (C7), 161.2 (C2), 147.4 (C9), 137.0 (C8), 133.6 (C4), 133.0 (C6), 130.7 (C11), 129.2 (C10), 126.6 (C12), 120.7 (C1), 119.6 (C3), 117.7 (C5), 117.4 (C13), 21.1 (*Me*-C12), 17.2 (*Me*-C10).

*[2-(2-Hydroxybenzyliden)amino]-5-methylphenol (**1e**)*

Compound **1e** was prepared from 2-amino-5-methylphenol (0.50 g, 4.09 mmol) and salicylaldehyde (0.48 g, 4.09 mmol). The product was obtained as an orange solid (yield: 0.89 g, 3.91 mmol, 96%), mp 154–156°C. MS (70 eV) *m*/*z* (%): 227 (M^+, 100), 226 (80), 198 (7), 134 (56), 107 (20), 77 (35). IR (KBr) (cm^{-1}): 3568, 2916, 2360, 1634, 1624, 1526, 1488, 1464, 1292, 1282, 1232, 1190, 1144, 764, 590. ^{1}H NMR (300 MHz, DMSO-d_6) δ: 8.67 (s, 1H, H7), 7.42 (d, *J* = 7.6 Hz, 1H, H6), 7.40 (td, *J* = 7.6, 1.6 Hz, 1H, H4), 7.05 (d, *J* = 7.7 Hz, 1H, H13), 7.03 (d, *J* = 7.7 Hz, 1H, H12), 7.01 (s, 1H, H10), 6.97 (d, *J* = 7.6 Hz, 1H, H3), 6.93 (t, *J* = 7.6 Hz, 1H, H5), 2.33 (s, 3H, Me). ^{13}C NMR (75 MHz, DMSO-d_6) δ: 163.8 (C7), 160.7 (C2), 147.8 (C9), 135.6 (C8), 133.8 (C4), 132.9 (C6), 130.6 (C11), 129.5 (C12), 119.8 (C5), 119.5 (C1), 118.9 (C13), 117.4 (C3), 115.8 (C10), 20.9 (C*Me*).

General method for the preparation of compounds 2a–e

An equimolecular amount of phenylboronic acid was added to a solution of the tridentate ligand in THF (usually about 10 mL for 2 to 3 mmol). The mixture was heated at reflux for 30 min and the water removed with a Dean–Stark trap. The solid obtained was collected by filtration under vacuum and washed with small amounts of benzene and hexane.

*2-Phenyl-4′-nitrobenzo[*d*]benzo[*h*]-6-aza-1,3-dioxa-2-boracyclonon-6-ene (**2a**)*

Compound **2a** was prepared from **1a** (0.26 g, 1.00 mmol) and phenylboronic acid (0.12 g, 1.00 mmol). The product was obtained as a yellow solid (yield: 0.30 g, 0.87 mmol, 87%), mp 236–238°C. MS (70 eV) *m*/*z* (%): 344 (M^+, 16), 268 (15), 267 (100), 221 (60), 193 (8), 77 (11), 51 (10). IR (KBr) (cm^{-1}): 3420, 2918, 2850, 1646, 1628, 1610, 1550, 1506, 1466, 1456, 1334, 1300, 1182, 1154, 914. ^{1}H NMR (300 MHz, $CDCl_3$) δ: 8.54 (s, 1H, H7), 8.42 (d, *J* = 2.3 Hz, 1H, H13), 8.32 (dd, *J* = 8.0, 2.3 Hz, 1H, H11), 7.65 (td, *J* = 7.5, 1.4 Hz, 1H, H4), 7.48 (dd, *J* = 7.5, 1.8 Hz, 1H, H6), 7.16 (d, *J* = 7.5 Hz, 1H, H3), 7.13–7.30 (m, 6H, H10, H-*o*, -*m*, -*p*), 7.03 (td, *J* = 7.5, 1.4 Hz, 1H, H5). ^{13}C NMR (75 MHz, $CDCl_3$) δ: 163.8 (C2), 158.3 (C12), 152.0 (C7), 140.2 (C9), 139.9 (C4), 132.5 (C6), 131.2 (C-*o*), 130.9 (C8), 128.7 (C-*p*), 127.9 (C-*m*), 124.6 (C11), 121.3 (C5), 120.8 (C3), 119.1 (C1), 114.8 (C13), 111.9 (C10). ^{11}B NMR (96 MHz, $CDCl_3$) δ: +8.6 ($h_{1/2}$ = 152 Hz). Anal. calcd. for $C_{19}H_{13}BN_2O_4$: C 66.28, H 3.78, N 8.14; found: C 65.98, H 3.91, N 8.54.

*2-Phenyl-4′-methylbenzo[*d*]benzo[*h*]-6-aza-1,3-dioxa-2-boracyclonon-6-ene (**2b**)*

Compound **2b** was prepared from **1b** (0.26 g, 1.00 mmol) and phenylboronic acid (0.12 g, 1.00 mmol). The product was obtained as a yellow solid (yield: 0.27 g, 0.86 mmol, 87%), mp 219 to 220°C. MS (70 eV) *m*/*z* (%): 313 (M^+, 9), 268 (1), 236 (100), 165 (1), 102 (2), 77 (6). IR (KBr) (cm^{-1}): 2918, 2850, 1628, 1608, 1552, 1496, 1456, 1303, 1256, 1188, 1174, 1126, 958, 940, 812, 764, 752, 704. ^{1}H NMR (300 MHz, $CDCl_3$) δ: 8.29 (s, 1H, H7), 7.56 (td, *J* = 7.7, 1.6 Hz, 1H, H4), 7.37 (dd, *J* = 7.7, 1.6 Hz, 1H, H6), 7.34 (dd, *J* = 7.3, 1.5 Hz, 2H, H-*o*), 7.27 (d, *J* = 1.6 Hz, 1H, H13), 7.23 (d, *J* = 7.7 Hz, 1H, H3), 7.14–7.20 (m, 4H, H11, H-*m*, -*p*), 7.02 (d, *J* = 8.3 Hz, 1H, H10), 6.95 (td, *J* = 7.7, 1.6 Hz, 1H, H5), 2.37 (s, 3H, Me). ^{13}C NMR (75 MHz, $CDCl_3$) δ: 157.9 (C2), 157.1 (C9), 148.3 (C7), 138.1 (C4), 133.7 (C-*p*), 131.7 (C6, C-*o*), 130.7 (C8), 129.5 (C12), 128.2 (C11), 127.8 (C-*m*), 120.7 (C5), 120.6 (C3), 119.7 (C1), 115.6 (C13), 115.2 (C10), 21.4 (C*Me*). ^{11}B NMR (96 MHz, $CDCl_3$) δ: +11.0 ($h_{1/2}$ = 161 Hz). Anal. calcd. for $C_{20}H_{16}BNO_2$: C 76.68, H 5.11, N 4.47; found C 76.55, H 5.23, N 4.53.

*2-Phenyl-4′-chlorobenzo[*d*]benzo[*h*]-6-aza-1,3-dioxa-2-boracyclonon-6-ene (**2c**)*

Compound **2c** was prepared from **1c** (0.28 g, 1.14 mmol) and phenylboronic acid (0.14 g, 1.14 mmol). The product was obtained as a yellow solid (yield: 0.29 g, 0.87 mmol, 76%). Crystals suitable for X-ray diffraction were obtained when the reaction was performed in a 1:1 mixture of methylene chloride–hexane at room temperature without stirring, mp 227–229°C. MS (70 eV) *m*/*z* (%): 335 ($[M + 2]^+$, 4), 333 (M^+, 12), 256 (100), 221 (12), 192 (2), 77 (16), 51 (16). IR (KBr) (cm^{-1}): 2918, 1628, 1608, 1550, 1468, 1454, 1378, 1264, 1226, 1192, 1176, 1018, 958, 816, 756. ^{1}H NMR (300 MHz, DMSO-d_6) δ: 8.31 (s, 1H, H7), 7.63 (td, *J* = 8.1, 1.5 Hz, 1H, H4), 7.43 (d, *J* = 8.1 Hz, 2H, H-*o*), 7.40 (dd, *J* = 8.1, 1.5 Hz, 1H, H6), 7.04 (d, *J* = 8.1 Hz, 1H, H3), 7.10–7.30 (m, 6H, H10, H11, H13, H-*m*, -*p*), 6.96 (t, *J* = 8.1 Hz, 1H, H5). ^{13}C NMR (75 MHz, DMSO-d_6) δ: 158.1 (C2), 157.6 (C9), 150.1 (C7), 139.0 (C4), 132.6 (C8), 132.0 (C6), 131.6 (C12), 131.6 (C-*o*), 128.5 (C-*p*), 128.0 (C-*m*), 124.5 (C11), 121.0 (C3), 120.8 (C5), 119.4 (C10), 116.4 (C1), 115.8 (C13). ^{11}B NMR (96 MHz, $CDCl_3$) δ: +9.0 ($h_{1/2}$ = 570 Hz). Anal. calcd. for $C_{19}H_{13}BClNO_2$: C 68.37, H 3.90, N 4.20: found C 67.93, H 3.99, N 4.22.

*2-Phenyl-2,4-dimelthylbenzo[*d*]benzo[*h*]-6-aza-1,3-dioxa-2-boracyclonon-6-ene (**2d**)*

Compound **2d** was prepared from **1d** (0.38 g, 1.59 mmol) and phenylboronic acid (0.19 g, 1.59 mmol). The product was obtained as an orange solid (yield: 0.35 g, 1.08 mmol,

© 2001 NRC Canada

68%), mp 185–187°C. MS (70 eV) *m*/*z* (%): 327 (5), 250 (100), 220 (2), 165 (1), 117 (2), 77 (14), 51 (8). IR (KBr) (cm^{-1}): 1624, 1554, 1490, 1478, 1460, 1390, 1374, 1326, 1304, 1288, 1270, 1258, 1244, 1228, 1198, 1152, 764. ^1H NMR (270 MHz, $CDCl_3$) δ: 8.24 (s, 1H, H7), 8.16 (d, *J* = 8.0 Hz, 1H, H6), 7.60 (td, *J* = 8.0, 1.7 Hz, 1H, H4), 7.28–7.46 (m, 3H, H-*o*, -*p*), 7.15 (d, *J* = 8.0 Hz, 1H, H3), 7.06–7.12 (m, 2H, H-*m*), 6.91 (t, *J* = 8.0 Hz, 1H, H5), 6.94 (s, 1H, H11), 6.51 (s, 1H, H13), 2.41 (s, 3H, CH_3-C10), 2.17 (s, 3H, CH_3-C12). ^{13}C NMR (68 MHz, $CDCl_3$) δ: 162.9 (C7), 161.1 (C2), 139.2 (C9), 135.3 (C6), 133.8 (C8), 132.4 (C10), 132.2 (C11), 131.3 (C-*o*), 130.9 (C12), 130.8 (C4), 127.6 (C-*p*), 127.1 (C-*m*), 122.5 (C13), 120.2 (C3), 119.3 (C5), 115.4 (C1), 20.4 (*Me*-C12), 17.2 (*Me*-C10). ^{11}B NMR (87 MHz, $CDCl_3$) δ: +7.5 ($h_{1/2}$ = 395 Hz). Anal. calcd. for $C_{21}H_{18}BNO_2$: C 77.06, H 5.51, N 4.28; found C 77.34, H 5.17, N 4.51.

*2-Phenyl-3′-methylbenzo[*d*]benzo[*h*]-6-aza-1,3-dioxa-2-boracyclonon-6-ene (**2e**)*

Compound **2e** was prepared from **1e** (0.5 g, 2.20 mmol) and phenylboronic acid (0.27 g, 2.20 mmol). The product was obtained as an orange solid (yield: 0.59 g, 1.88 mmol 85%), mp 227–229°C. MS (70 eV) *m*/*z* (%): 313 (M^+, 20), 312 (100), 313 (68), 268 (2), 235 (8), 208 (16), 164 (24), 131 (10), 104 (28), 77 (9). IR (KBr) (cm^{-1}): 2916, 2850, 2344, 1630, 1526, 1506, 1488, 1464, 1282, 1232, 1190, 1144, 824. ^1H NMR (270 MHz, $CDCl_3$) δ: 8.25 (s, 1H, H7), 7.52 (td, *J* = 7.7, 1.5 Hz, 1H, H4), 7.34 (dd, *J* = 7.7, 1.5 Hz, 1H, H6), 7.31 (dd, *J* = 7.1, 1.5 Hz, 2H, H-*o*), 7.22 (s, 1H, H10), 7.20 (d, *J* = 7.7 Hz, 1H, H3), 7.11 (d, *J* = 8.1 Hz, 1H, H12), 7.07–7.16 (m, 3H, H-*m*, -*p*), 6.98 (d, *J* = 8.1 Hz, 1H, H13), 6.92 (td, *J* = 7.7, 1.5 Hz, 1H, H5), 2.33 (s, 3H, Me-C11). ^{13}C NMR (68 MHz, $CDCl_3$) δ: 157.5 (C2), 156.9 (C9), 147.9 (C7), 137.8 (C4), 133.4 (C12), 131.3 (C6, C-*o*), 130.4 (C8), 129.1 (C11), 127.8 (C-*p*), 127.4 (C-*m*), 120.4 (C3), 120.3 (C5), 119.3 (C1), 115.2 (C10), 114.8 (C13), 21.0 (*Me*-C11). ^{11}B NMR (87 MHz, $CDCl_3$) δ: +8.0 ($h_{1/2}$ = 64 Hz). Anal. calcd. for $C_{20}H_{16}BNO_2$: C 76.68, H 5.11, N 4.47; found C 76.47, H 5.19, N 4.49.

*2-Ethoxy-2-phenyl-3-(2-hydroxy-3,5-dimethyl)phenyl-benzo[*e*]-3-aza-1-oxa-2-boracyclohex-3-ene (**3**)*

Compound **3** was prepared from **1d** (0.25 g, 1.04 mmol) and phenylboronic acid (0.13 g, 1.04 mmol) in ethanol (30 mL). The mixture was heated at reflux for 2 h using a Dean Stark trap and then cooled to room temperature. After standing overnight, red crystals are obtained (yield: 0.21 g, 0.56 mmol, 54%), which were collected by filtration and dried, mp 205 to 206°C. MS (15 eV) *m*/*z* (%): 373 (10), 327 (100), 250 (8), 165 (5), 115 (13), 77 (46), 51 (18). IR (KBr) (cm^{-1}): 2918, 2845, 1632, 1622, 1530, 1482, 1462, 1236, 1192, 1144, 824, 756. ^1H NMR (300 MHz, $CDCl_3$) δ: 8.17 (s, 1H, H7), 7.72 (d, *J* = 7.1 Hz, 1H, H6), 7.63 (td, *J* = 7.1, 1.5 Hz, 1H, H4), 7.36–7.43 (m, 3H, H-*o*, -*p*), 7.14 (d, *J* = 7.1 Hz, 1H, H3), 7.11 (td, *J* = 7.8, 1.6 Hz, 2H, H-*m*), 7.03 (s, 1H, H11), 6.97 (td, *J* = 7.1, 1.5 Hz, 1H, H5), 6.82 (s, 1H, H13), 3.71 (q, *J* = 6.8 Hz, 2H, -OCH_2-), 2.23 (s, 3H, CH_3-C10), 2.02 (s, 3H, CH_3-C12), 1.23 (t, *J* = 6.8 Hz, 3H, -CH_2CH_3). ^{13}C NMR (75 MHz, $CDCl_3$) δ: 163.8 (C7), 161.4 (C2), 146.3 (C9), 139.1 (C8), 133.9 (C6), 133.0 (C4), 132.9 (C11), 132.6 (C-*o*), 132.3 (C10), 131.1 (C12), 128.2 (C-*m*), 127.3 (C-*p*), 120.1 (C5), 119.9 (C3), 117.6 (C13), 116.5 (C1), 58.8 (OCH_2), 18.8 (CH_2CH_3), 17.8 (CH_3-C12), 16.2 (CH_3-C10). ^{11}B NMR (96 MHz, $CDCl_3$) δ: +7.0 ($h_{1/2}$ = 154 Hz). Anal. calcd. for $C_{23}H_{24}BNO_3$: C 73.99, H 6.43, N 3.75; found: C 73.85, H 6.10, N 3.59.

General method for the preparation of compounds 4a–e

A small quantity of compounds **4a**–**e** was dissolved in 40 mL of acetone and the mixture was heated at reflux for 6 h. The water and part of the solvent were separated with a Dean–Stark trap. The solution was allowed to stand overnight at room temperature, the solid obtained was collected by filtration under vacuum, and washed with small amounts of acetone.

*7-(2-Ketopropyl)-2-phenyl-4′-nitrobenzo[*d*]benzo[*h*]-6-aza-1,3-dioxa-2-boracyclononane (**4a**)*

Compound **4a** was obtained from **2a** (0.50 g, 1.45 mmol). A yellow solid was formed and collected by filtration (yield: 0.26 g, 0.65 mmol, 45%), mp 215–217°C. MS (15 eV) *m*/*z* (%): 402 (M^+, 24), 344 (25), 268 (21), 267 (100), 221 (28), 193 (7), 77 (9). IR (KBr) (cm^{-1}): 3140, 2938, 2850, 1702, 1510, 1322, 1276, 1222, 1036, 1008, 960, 768. ^1H NMR (300 MHz, DMSO-d_6) δ: 9.02 (s, 1H, NH), 7.50 (d, *J* = 8.0 Hz, 2H, H-*o*), 7.25 (t, *J* = 8.0, 3H, H-*m*, -*p*), 7.17 (t, *J* = 7.3 Hz, 1H, H4), 7.14 (d, *J* = 7.3 Hz, 1H, H6), 7.10 (s, 1H, H13), 7.07 (d, *J* = 7.3 Hz, 1H, H3), 6.88 (d, *J* = 8.2 Hz, 1H, H11), 6.79 (t, *J* = 7.3 Hz, 1H, H5), 6.69 (d, *J* = 8.2 Hz, 1H, H10), 4.79 (dd, *J* = 9.3, 3.2 Hz, 1H, H7), 3.32 (dd, *J* = 18.7, 9.3 Hz, 1H, H14a), 3.20 (dd, *J* = 18.7, 3.2 Hz, 1H, H14b), 2.01 (s, 3H, H16). ^{13}C NMR (75 MHz, DMSO-d_6) δ: 207.1 (C15), 159.7 (C2), 153.4 (C12), 138.9 (C9), 135.5 (C4), 133.2 (C-*o*), 131.2 (C6), 129.2 (C8), 128.6 (C-*p*), 127.5 (C-*m*), 123.8 (C11), 119.8 (C1), 117.3 (C3), 116.3 (C5), 114.1 (C13), 112.3 (C10), 48.8 (C7), 46.9 (C14), 30.2 (C16). ^{11}B NMR (96 MHz, DMSO-d_6) δ: +12.0 ($h_{1/2}$ = 432 Hz). Anal. calcd. for $C_{22}H_{19}BN_2O_5$: C 65.67, H 2.24, N 6.96; found C 65.39, H 2.51, N 6.69.

*7-(2-Ketopropyl)-2-phenyl-4′-methylbenzo[*d*]benzo[*h*]-6-aza-1,3-dioxa-2-boracyclononane (**4b**)*

Compound **4b** was obtained from **2b** (0.50 g, 1.60 mmol). A yellow solid was formed and collected by filtration (yield: 0.49 g, 1.32 mmol, 83%), mp 243–245°C. MS (15 eV) *m*/*z* (%): 371 (M^+, 12), 327 (22), 237 (25), 236 (100), 235 (41), 77 (13). IR (KBr) (cm^{-1}): 3146, 2918, 1704, 1504, 1490, 1314, 1280, 1244, 1226, 966, 760, 750, 708. ^1H NMR (300 MHz, DMSO-d_6) δ: 8.66 (s, 1H, NH), 7.59 (dd, *J* = 7.4, 1.7 Hz, 2H, H-*o*), 7.30 (td, *J* = 7.4, 1.7 Hz, 3H, H-*m*, -*p*), 7.22 (td, *J* = 7.3, 1.2 Hz, 1H, H4), 7.12 (d, *J* = 1.8 Hz, 1H, H13), 7.09 (dd, *J* = 7.3, 1.2 Hz, 1H, H6), 6.92 (dd, *J* = 8.2, 1.8 Hz, 1H, H11), 6.86 (dd, *J* = 7.3, 1.2 Hz, 1H, H3), 6.78 (td, *J* = 7.3, 1.2 Hz, 1H, H5), 6.72 (d, *J* = 8.2 Hz, 1H, H10), 4.66 (dd, *J* = 11.7, 2.7 Hz, 1H, H7), 3.71 (dd, *J* = 19.7, 11.4 Hz, 1H, H14a), 2.88 (dd, *J* = 19.7, 2.7 Hz, 1H, H14b), 2.25 (s, 3H, CH_3-C12), 2.04 (s, 3H, H16). ^{13}C NMR (75 MHz, DMSO-d_6) δ: 209.9 (CO), 157.0 (C2), 156.4 (C9), 131.5 (C-*o*), 131.2 (C4), 130.7 (C11), 128.3 (C-*m*), 128.2 (C12), 128.1 (C8), 127.9 (C-*p*), 127.7 (C6), 122.9 (C1), 121.0 (C5), 120.9 (C3), 120.8 (C13), 113 (C10), 59.9 (C7),

© 2001 NRC Canada

46.0 (C14), 30.4 (C16), 21.2 (*C*H_3-C12). ^{11}B NMR (96 MHz, DMSO-d_6) δ: +9.2 ($h_{1/2}$ = 221 Hz). Anal. calcd. for $C_{23}H_{22}BNO_3$: C 74.39, H 5.93, N 3.77; found C 74.53, H 6.04, N 3.79.

*7-(2-Ketopropyl)-2-phenyl-4′-chlorobenzo[*d*]benzo[*h*]-6-aza-1,3-dioxa-2-boracyclononane (**4c**)*

Compound **4c** was obtained from **2c** (0.50 g, 1.50 mmol). A yellow solid was formed and collected by filtration (yield: 0.40 g, 1.02 mmol, 69%), mp 236–238°C. MS (15 eV) *m*/*z* (%): 393 ([M + 2]$^+$, 1), 391 (M$^+$, 9), 333 (11), 315 (6), 313 (20), 258 (38), 256 (100), 231 (23), 229 (65), 147 (6), 145 (7). IR (KBr) (cm^{-1}): 3138, 2916, 2850, 1702, 1502, 1490, 1310, 1282, 1246, 1226, 954, 760, 750, 708. ^{1}H NMR (300 MHz, DMSO-d_6) δ: 9.04 (s, 1H, NH), 7.55 (d, *J* = 8.0 Hz, 2H, H-*o*), 7.28 (t, *J* = 8.0, 3H, H-*m*, -*p*), 7.12 (s, 1H, H13), 7.10 (t, *J* = 7.1 Hz, 1H, H4), 7.08 (d, *J* = 7.1 Hz, 1H, H6), 6.96 (d, *J* = 7.1 Hz, 1H, H3), 6.85 (d, *J* = 8.3 Hz, 1H, H11), 6.71 (t, *J* = 7.1 Hz, 1H, H5), 6.69 (t, *J* = 8.3 Hz, 1H, H10), 4.85 (dd, *J* = 9.5, 3.6 Hz, 1H, H7), 3.28 (dd, *J* = 18.6, 9.5 Hz, 1H, H14a), 3.23 (dd, *J* = 18.6, 3.6 Hz, 1H, H14b), 1.99 (s, 3H, H16). ^{13}C NMR (75 MHz, DMSO-d_6) δ: 207.3 (C15), 155.0 (C2), 143.6 (C9), 138.2 (C4), 134.6 (C-*o*), 132.4 (C12), 130.5 (C6), 128.9 (C8), 128.2 (C-*p*), 127.6 (C-*m*), 123.6 (C11), 119.7 (C1), 115.6 (C5), 115.2 (C3), 114.4 (C13), 110.4 (C10), 49.2 (C7), 47.9 (C14), 30.7 (C16). ^{11}B NMR (96 MHz, DMSO-d_6) δ: +10.8 ($h_{1/2}$ = 548 Hz). Anal. calcd. for $C_{22}H_{19}BClNO_3$: C 67.43, H 4.85, N 3.58; found C 67.49, H 4.84, N 3.69.

*7-(2-Ketopropyl)-2-phenyl-2′,4′-dimethylbenzo[*d*]benzo[*h*]-6-aza-1,3-dioxa-2-boracyclononane (**4d**)*

Compound **4d** was obtained from **2d** (0.50 g, 1.52 mmol). Orange crystals were formed and collected by filtration (yield: 0.48 g, 1.25 mmol, 82%), mp 197 to 198°C. MS (15 eV) *m*/*z* (%): 385 (M$^+$, 4), 327 (8), 307 (18), 250 (100), 223 (98), 163 (7), 77 (9), 43 (19). IR (KBr) (cm^{-1}): 3170, 2922, 1706, 1502, 1488, 1324, 1282, 1242, 1222, 1032, 1000, 962, 760, 748, 708. ^{1}H NMR (300 MHz, DMSO-d_6) δ: 8.70 (s, 1H, NH), 7.55 (d, *J* = 7.4 Hz, 2H, H-*o*), 7.23–7.33 (m, 3H, H-*m*, -*p*), 7.12 (t, *J* = 7.6 Hz, 1H, H4), 7.02 (s, 1H, H13), 6.92 (d, *J* = 7.6 Hz, 1H, H6), 6.87 (d, *J* = 7.6 Hz, 1H, H3), 6.74 (s, 1H, H11), 6.70 (t, *J* = 7.6 Hz, 1H, H5), 4.74 (dd, *J* = 7.5, 2.7 Hz, 1H, H7), 3.52 (dd, *J* = 14.6, 7.5 Hz, 1H, H14a), 3.02 (dd, *J* = 14.6, 2.7 Hz, 1H, H14b), 2.16 (s, 3H, CH_3-C12), 2.02 (s, 3H, CH_3-C10), 1.99 (s, 3H, H16). ^{13}C NMR (75 MHz, DMSO-d_6) δ: 205.0 (C15), 155.7 (C2), 154.7 (C9), 131.9 (C-*o*), 130.9 (C11), 129.3 (C4), 128.8 (C6), 128.3 (C8), 127.2 (C-*m*, -*p*), 126.2 (C10), 124.8 (C12), 120.5 (C1), 119.7 (C5), 119.4 (C3), 118.9 (C13), 58.3 (C7), 46.4 (C14), 30.3 (C16), 20.2 (Me-C12), 14.9 (Me-C10). ^{11}B NMR (96 MHz, DMSO-d_6) δ: +7.9 ($h_{1/2}$ = 1803 Hz). Anal. calcd. for $C_{24}H_{24}BNO_3$: C 74.81, H 6.23, N 3.64; found C 74.83, H 6.34, N 3.69.

*7-(2-Ketopropyl)-2-phenyl-3′-methylbenzo[*d*]benzo[*h*]-6-aza-1,3-dioxa-2-boracyclononane (**4e**)*

Compound **4e** was obtained from **2e** (0.50 g, 1.60 mmol). A yellow solid was formed and collected by filtration (yield: 0.45 g, 1.21 mmol, 76%), mp 235–237°C. MS (15 eV) *m*/*z* (%): 371 (M$^+$, 8), 327 (14), 239 (34), 236 (100), 235 (25), 77 (7). IR (KBr) (cm^{-1}): 3180, 2916, 1704, 1512, 1492, 1316, 1280, 1238, 1030, 976, 758. ^{1}H NMR (300 MHz, DMSO-d_6) δ: 8.82 (s, 1H, NH), 7.55 (d, *J* = 7.5 Hz, 2H, H-*o*), 7.30–7.35 (m, 3H, H-*m*, -*p*), 7.23 (t, *J* = 7.4 Hz, 1H, H4), 7.14 (s, 1H, H10), 7.11 (d, *J* = 7.4 Hz, 1H, H6), 7.07 (d, *J* = 8.0 Hz, 1H, H12), 6.93 (d, *J* = 8.0 Hz, 1H, H13), 6.88 (d, *J* = 7.4 Hz, 1H, H3), 6.68 (d, *J* = 7.4 Hz, 1H, H5), 4.64 (dd, *J* = 11.8, 2.6 Hz, 1H, H7), 3.67 (dd, *J* = 18.9, 11.8 Hz, 1H, H14a), 2.83 (dd, *J* = 18.9, 2.6 Hz, 1H, H14b), 2.17 (s, 3H, CH_3-C12), 2.00 (s, 3H, H16). ^{13}C NMR (75 MHz, DMSO-d_6) δ: 208.6 (CO), 158.6 (C2), 157.3 (C9), 133.2 (C4), 132.6 (C11), 132.1 (C8), 131.6 (C-*o*), 129.7 (C12), 128.8 (C-*m*), 127.5 (C-*p*), 126.8 (C6), 121.0 (C1), 120.1 (C5), 119.7 (C3), 114.8 (C10), 113.2 (C13), 60.2 (C7), 45.3 (C14), 30.2 (C16), 20.8 (Me-C12). ^{11}B NMR (96 MHz, DMSO-d_6) δ: +7.6 ($h_{1/2}$ = 255 Hz). Anal. calcd. for $C_{23}H_{22}BNO_3$: C 74.39, H 5.93, N 3.77: found C 74.53, H 6.31, N 3.68.

Instrumentation

The X-ray diffraction studies were determined on an Enraf-Nonius CAD4 diffractometer (λ (Mo Kα) = 0.71073 Å, graphite monochromator, *T* = 293 K, ω-2θ scan) and the crystals were mounted in LINDEMAN tubes. Absorption correction was not necessary, corrections were made for Lorentz and polarization effects. Solution and refinement: direct methods (SHELXS 86) for structure solution and SHELXS 97 (34) software package for refinement and data output. Hydrogen atoms were determined by difference Fourier maps and their positions as well as one overall isotropic thermal parameter were refined.

Acknowledgments

Financial support from the Consejo Nacional de Ciencia y Tecnologia (CONACyT, México) is acknowledged. The authors wish to thank Guillermo Uribe for NMR spectra.

References

1. N.J. Leonard and J.V. Paukstelis. J. Org. Chem. **28**, 3021 (1963).
2. R. Bonnett, V.M. Clark, and A. Todd. J. Chem. Soc. 2102 (1959).
3. H. Böhme, S. Ebel, and K. Hartke. Chem. Ber. **98**, 1463, (1965).
4. M. Ueda and N. Miyaura. J. Organomet. Chem. **595**, 31 (2000).
5. T. Ichiyanagi, S. Kuniyama, M. Shimizu, and T. Fujisawa. Chem. Lett. 1033 (1998).
6. H. Nakamura, K. Nakamura, and Y. Yamamoto. J. Am. Chem. Soc. **120**, 4242 (1998).
7. H. Nakamura, H. Iwama, and Y. Yamamoto. J. Am. Chem. Soc. **118**, 6641 (1996).
8. R. Bloch. Chem. Rev. **98**, 1407 (1998) and refs cited therein.
9. Y. Takaya, M. Ogasawara, T. Hayashi, M. Sakai, and N. Miyaura. J. Am. Chem. Soc. **120**, 5579 (1998).
10. H. Höpfl and N. Farfán. J. Organomet. Chem. **547**, 71 (1997).
11. H. Höpfl and N. Farfán. Can. J. Chem. **76**, 1853 (1998).
12. H. Höpfl, M. Sánchez, V. Barba, N. Farfán, S. Rojas, and R. Santillan. Inorg. Chem. **37**, 1679 (1998).
13. V. Barba, D. Cuahutle, M.E. Ochoa, R. Santillan, and N. Farfán. Inorg. Chim. Acta, **303**, 7 (2000).

© 2001 NRC Canada

14. N. Farfán, H. Höpfl, V. Barba, M.E. Ochoa, R. Santillan, E. Gómez, and A. Gutiérrez. J. Organomet. Chem. **581**, 70 (1999).
15. V. Barba, R. Luna, D. Castillo, R. Santillan, and N. Farfán. J. Organomet. Chem. **604**, 273 (2000).
16. N. Farfán, R. Santillan, and H. Höpfl. Main Group Chem. **7**, 3 (1999).
17. H. Höpfl, M. Sánchez, N. Farfán, and V. Barba. Can. J. Chem. **76**, 1352 (1998).
18. C.Y. Wong and R. McDonald. Inorg. Chem. **35**, 325 (1996).
19. S. Dutta and A. Chakravorty. Polyhedron, **13**, 1811 (1994).
20. K. Ramesh, T.K. Lal, and R.N. Mukherjee. Polyhedron, **11**, 3083 (1992).
21. M.J. Clague, N.L. Keder, and A. Butler. Inorg. Chem. **32**, 4754 (1993).
22. S. Dutta, P. Basu, and A. Chakravorty. Inorg. Chem. **32**, 5343 (1993).
23. J. Topich and J.T. Lyon. Polyhedron, **3**, 55 (1984).
24. J. Topich. Inorg. Chem. **20**, 3704 (1981).
25. J.U. Mondal, F.A. Schultz, T.D. Brennan, and W.R. Scheidt. Inorg. Chem. **27**, 3950 (1988).
26. E. Hohaus, K.D. Klöppel, B. Paschold, and H.R. Schulten. Z. Anorg. Allg. Chem. **493**, 41 (1982).
27. H. Nöth and B. Wrackmeyer. NMR — basic principles and progress. Vol. 14. Springer–Verlag, Berlin. 1978.
28. H. Höpfl. J. Organomet. Chem. **581**, 129 (1999).
29. P.D. Woodgate, G.M. Horner, N.P. Maynard, and C.E.F. Rickard. J. Organomet. Chem. **592**, 180 (1999).
30. C.D. Davies, S.P. Marsden, and E.S. Stokes. Tetrahedron Lett. **8**, 1 (2000).
31. C.D. Farthing, and S.P. Marsden. Tetrahedron Lett. **8**, 5 (2000).
32. A. Bondi. J. Phys. Chem. **68**, 441 (1964).
33. M. Kabak, A. Elmali, and Y. Elerman. J. Molec. Struc. **477**, 151 (1999).
34. G.M. Sheldrick. Program for crystal structure determination. University of Göttingen, Germany. 1997.

© 2001 NRC Canada

Synthesis and decarboxylation of Δ^2-cephem-4,4-dicarboxylic acids

Saul Wolfe, Stephen Ro, Chan-Kyung Kim, and Zheng Shi

Abstract: Penicillin V was converted in 14 steps into Δ^2-cephems having hydrogen at C-3, hydrogen or methyl at C-2, and two methoxycarbonyl, two benzyloxycarbonyl, or one methoxycarbonyl and one benzyloxycarbonyl substituent at C-4. Deprotection of these Δ^2-cephem-4,4-dicarboxylic acid esters by alkaline hydrolysis (in the case of methyl esters) or hydrogenolysis (in the case of benzyl esters) led in all cases to rapid decarboxylation of the Δ^2-cephem-4,4-dicarboxylic acid or Δ^2-cephem-4,4-dicarboxylic acid monoester. With hydrogen at C-2, hydrolysis of the dimethyl ester with 1 equiv of base produced a Δ^2-cephem. With 2 equiv of base, and with all compounds having methyl at C-2, hydrolysis or hydrogenolysis afforded 4α-substituted-Δ^2-cephems.

In contrast, simpler benzyl or methyl acetamidomalonates could be deprotected without difficulty to afford stable malonic acids. Reasons for the differences in ease of decarboxylation were examined using semiempirical (AM1) and ab initio (3-21G) molecular orbital calculations. The decarboxylation barriers of unionized cephem or acetamido malonic acids were found to be high (35–40 kcal mol^{-1}). Although the monoanion of acetamidomalonic acid retained a high barrier, the epimeric monoanions of a Δ^2-cephem malonic acid decarboxylated with barriers of only 2 kcal mol^{-1}.

Key words: mercaptoazetidinone, bromomalonate esters, MO calculations, sulfoxides, hydrogenolysis.

Résumé : On a transformé la pénicilline V en quatorze étapes en Δ^2-céphèms portant un hydrogène en C-3, un hydrogène ou un méthyle en C-2 et deux méthoxycarbonyles, deux benzoyloxycarbonyles ou un méthoxycarbonyle et un benzoyloxycarbonyle comme substituants en C-4. Le déprotection de ces esters de Δ^2-céphem-4,4-dicarboxylique par hydrolyse alcaline (dans le cas des esters méthyliques) ou par hydrogénolyse (dans les cas des esters benzyliques) conduit dans tous les cas à une décarboxylation rapide de l'acide Δ^2-céphem-4,4-dicarboxylique ou de son monoester. L'hydrolyse de l'ester diméthylique du produit portant un hydrogène en C-2 à l'aide d'un équivalent de base conduit à un Δ^2-céphem. Avec deux équivalents de base ainsi qu'avec tous les composés portant un groupe méthyle en C-2, l'hydrolyse ou l'hydrogénolyse conduit à des Δ^2-céphems portant un substituant en position 4α.

Par ailleurs, il est possible de déprotéger sans difficulté les acétamidomalonates de benzyle ou de méthyle plus simples pour obtenir des acides maloniques stables. Faisant appel à des calculs d'orbitales moléculaires semi-empiriques (AM1) et ab initio, on a étudié les différences dans la facilité de ces décarboxylations. On a trouvé que les barrières à la décarboxylation des acides céphems dicarboxyliques et des acétamidomaloniques non ionisés sont relativement élevées (35-40 kcal/mol). Même si la barrière est encore élevée pour le monoanion de l'acide acétamidomalonique, les monoanions épimères d'un acide Δ^2-céphem malonique se décarboxylent avec une barrière qui n'est que d'environ 2 kcal mol^{-1}.

Mots clés : mercaptoazétidinone, esters de l'acide bromomalonique, calculs OM, sulxoydes, hydrogénolyse.

[Traduit par la Rédaction]

Introduction

The antibacterial activity of the Δ^2-cephem-4α-carboxylic acid **1** is 100 times less than that of the Δ^3-cephem **2** (1). Since cephalosporins undergo $\Delta^3 \rightleftarrows \Delta^2$ equilibration in solution to give mixtures in which the 4α-carboxy-Δ^2-isomers (**3a**) usually predominate (2), there is a resultant loss of activity, and the origin of this loss of activity has received considerable attention (3).

The cephalosporin receptor is a serine peptidase whose active site hydroxyl group is acylated by the β-lactam ring (4). Most workers accept that this chemical reaction proceeds by deprotonation of the serine OH, coupled to nucleophilic addition of the resulting anion to the β-lactam carbonyl group (5). In terms of this mechanism, the decrease in antibacterial activity that accompanies the isomerization to **3a** would be a consequence of the decreased susceptibility of the β-lactam carbonyl group of a Δ^2-cephem towards nucleophilic attack. Indeed **1** is most readily obtained by *alkaline hydrolysis* of the methyl ester of **2** (6).

Received January 29, 2001. Published on the NRC Research Press Web site at http://canjchem.nrc.ca on August 22, 2001.

S. Wolfe,[1] S. Ro, C.-K. Kim,[2] and Z. Shi. Department of Chemistry, Simon Fraser University, Burnaby, BC V5A 1S6, Canada.

[1]Corresponding author (telephone: (604) 291-5972; fax: (604) 291-5973; e-mail: swolfe@sfu.ca).
[2]On leave from Department of Chemistry, Inha University, Inchon, 402–751, Korea.

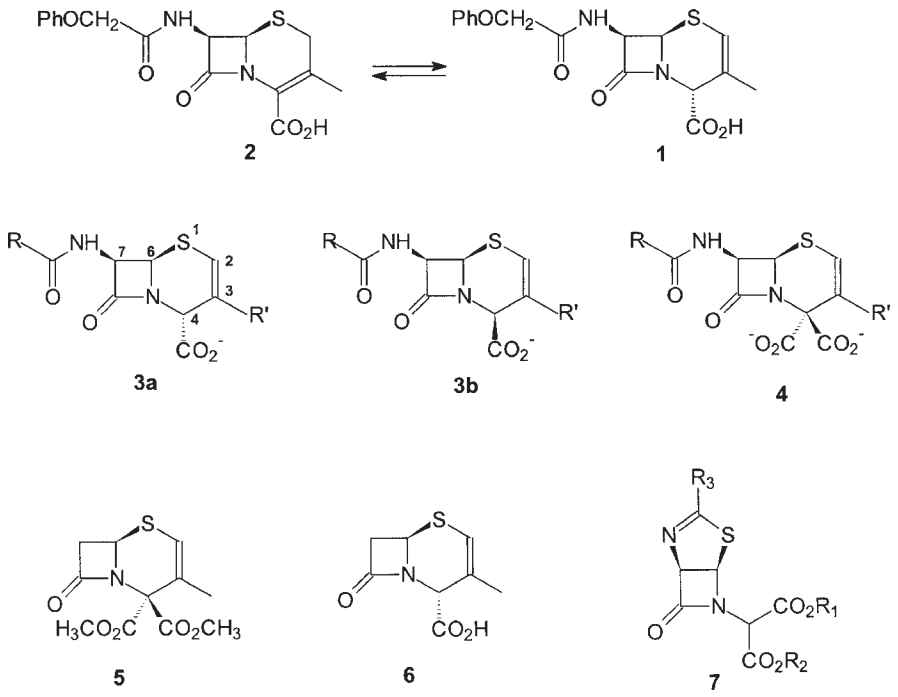
 DOI: 10.1139/cjc-79-8-1238 © 2001 NRC Canada

However, in the case of an exocellular peptidase from *Streptomyces* R61, which has been studied in some detail (7), including a crystal structure (8), the catalytic efficiencies towards 6-aminopenicillanic acid, cephaloglycine and penicillin G are 0.2, 22, and 13 000, respectively, but the corresponding second-order rate constants for alkaline hydrolysis of the β-lactam rings of these compounds are 0.15, 0.90, and 0.50 M^{-1} s^{-1} (7). The absence of any correlation between the trends in the enzymatic and nonenzymatic rate constants is not consistent with the claim that the acyl-enzyme is formed by nucleophilic addition to the β-lactam carbonyl group.

In a different approach to the problem, following an examination of the crystal structures of active and inactive β-lactam compounds, Cohen (9) proposed that **3a** are inactive as a consequence of a misfit with the receptor, and suggested that their 4β-carboxy epimers (**3b**) would exhibit a better fit, with restored activity. However, the activity of a Δ^2-cephem-4β-carboxylic acid proved to be less than that of its 4α-epimer (10).

Independently, structure-activity studies and calculations by Wolfe and Hoz (11) led to the proposal that **3a** react more rapidly than Δ^3-cephems with the hydroxyl group of the peptidase receptor, but are less effectively complexed; in addition, in agreement with Cohen, it was suggested that epimerization to **3b** would lead to improved complexation with the receptor, at the expense of an inherent decrease in reactivity with the serine hydroxyl group.

These findings led to the idea that the presence of the 4β-carboxyl group in a Δ^2-cephem-4,4-dicarboxylic acid such as **4** might allow effective complexation to the peptidase, and the concurrent presence of the 4α-carboxyl group might enhance the rate of the acylation step, the two effects together leading to enhanced antibacterial activity in a Δ^2-cephem. The work reported here was undertaken to test this idea. Although it was known that the malonate **5** had yielded only the decarboxylated product **6** following alkaline hydrolysis and acidification (12), that reaction mixture was maintained at pH 2 for 1 h prior to the isolation of the product. It was hoped that decarboxylation could be avoided in the present work by the elimination of an extended acidic treatment following the deprotection of a Δ^2-cephem-4,4-dicarboxylic acid diester.



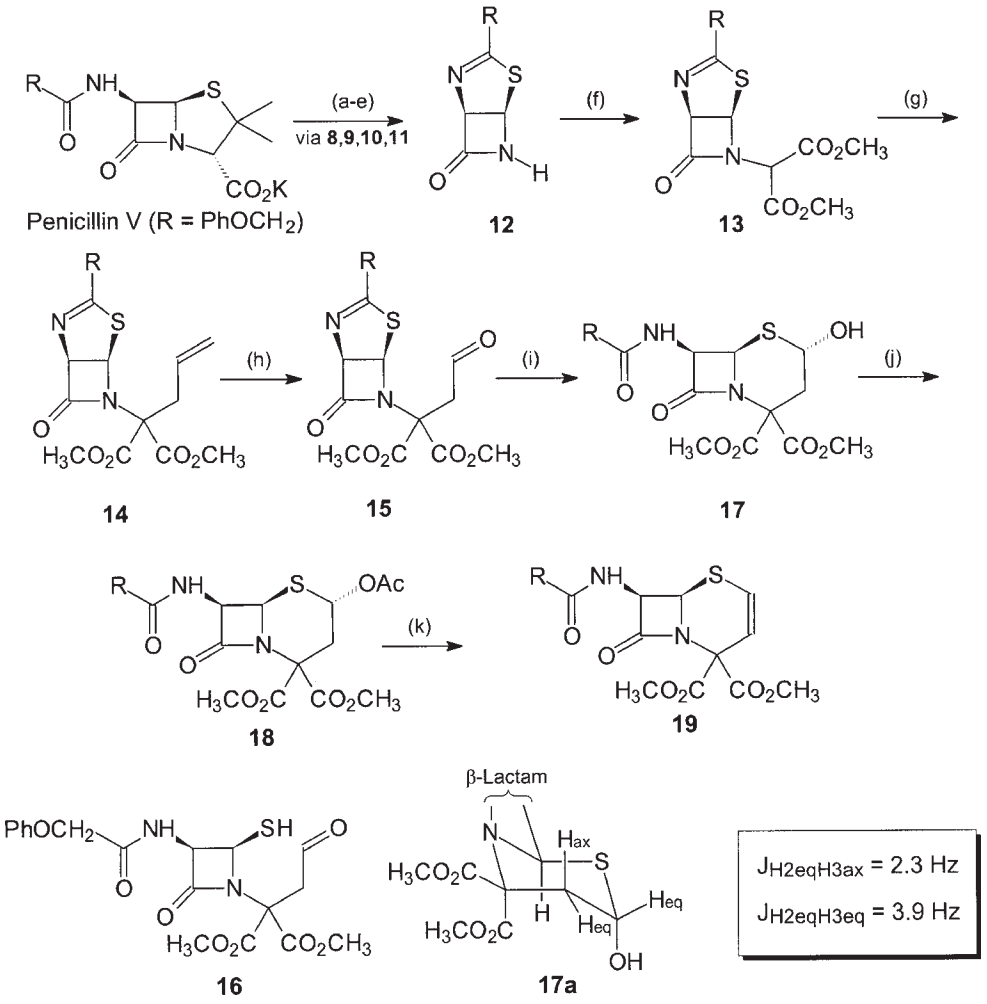
Syntheses of substrates

Malonyl-substituted thiazoline-azetidinones of type **7** have often been reported in the literature (13), usually as intermediates in syntheses requiring the attachment of an acetate chain to the β-lactam nitrogen. By virtue of its acidic α-proton, **7** also serves as a potential branch point for the construction of a new ring. The conversion of penicillin V into the Δ^2-cephem **19** is summarized in Scheme 1. Scheme 2 summarizes a different sequence leading to the 2-methyl-Δ^2-cephems **24**.

In Scheme 1, dimethyl bromomalonate, prepared by irradiating a solution of bromine and dimethyl malonate, was reacted with the thiazoline azetidinone **12** (14) in the presence of benzyl trimethylammonium hydroxide (Triton B) to give **13** in 50% yield. Coupling with allyl bromide in the presence of Triton B or sodium hydride produced **14** which, upon ozonolysis and treatment with dimethyl sulfide afforded an aldehyde (**15**) in quantitative yield. Exposure of this aldehyde to 3% perchloric acid in a 1:1 solution of dichloromethane–acetone (15), led to hydrolysis to the mercaptoazetidinone **16**, followed by cyclization to the hydroxycepham **17** in 94% from **14**.

© 2001 NRC Canada

Scheme 1. Reagents and conditions: (*a*) CH_3I, DMF; (*b*) AcOH, H_2O_2, CH_2Cl_2; (*c*) $P(OMe)_3$, $MgSO_4$, toluene; (*d*) Et_3N; (*e*) $KMnO_4$, $MgSO_4$, EtOH; (*f*) Triton B, $BrCH(CO_2CH_3)$, DMF, –50 to 20°C; (*g*) Triton B or NaH, allyl bromide; (*h*) O_3, CH_2Cl_2-CH_3OH, –78°C, then Me_2S; (*i*) $HClO_4$, CH_2Cl_2–acetone; (*j*) Ac_2O, H_2SO_4, AcOH; (*k*) pTsOH, toluene, Δ.



The configuration at C-2 and the conformation of the six-membered ring of **17** (see **17a**) were evident from the ^1H NMR spectrum, which showed J_{H2H3} and $J_{H2H3'}$ = 2.3 and 3.9 Hz, respectively. The axial orientation of the hydroxyl group is evidence of an S-C-O Edward–Lemieux effect (16).

The dehydration of **17** was unexpectedly difficult and was best achieved in 52% yield by acetylation to **18**, followed by heating with *p*-toluenesulfonic acid in refluxing toluene.

In Scheme 2, the dimethyl malonate **14** and its dibenzyl ester and mixed methyl benzyl ester analogs, prepared by the reaction of **12** with the appropriate bromomalonate followed by allylation, were treated with iodine in a mixture of methylene chloride and water to give the 2β-substituted iodomethylcephams **20** (13). In each case, the configuration at C-2 and the conformation shown in **20a** could be assigned on the basis of a positive NOE between H_2 and H_6, and from H_2H_3 coupling constants of 1.9 and 12.2 Hz.

At this point, the synthetic plan called for dehydrohalogenation of **20** to **23**, and isomerization to **24**. However, exposure of **20** to sodium hydride or 1,8-diazabicyclo[5.4.0]undec-7-ene (DBU) or Triton B produced complex mixtures. To circumvent the possibility that this was the result of participation by sulfur in the elimination of iodide, the iodomethylcephams were first oxidized to the sulfoxides **21** using sodium periodate in aqueous methanol. Dehydrohalogenation with DBU now proceeded smoothly to give the exomethylene sulfoxides **22**, which afforded the exomethylene cephams **23** following reduction with phosphorus tribromide. Isomerization to **24** was achieved using trifluoroacetic acid.

In the case of the epimeric methyl benzyl esters (R_1 = Me, R_2 = CH_2Ph), which were formed in a 1:1 ratio in the coupling with **12**, separation was achieved at the stage of the exomethylene sulfoxide **22**. Since 2D-NOESY experiments were inconclusive in allowing configurations to be assigned to the epimers of **22**–**24**, the technique of aromatic solvent-induced shifts (ASIS) (17) was applied to **24**. Changing the solvent from deuterated chloroform to benzene leads to an upfield chemical shift of atoms or groups on the convex (α) face of the molecule, because the V-shaped bicyclic ring system blocks access of the solvent to the concave (β) face.

As seen in Table 1, except for H_3, the change from chloroform to benzene leads to an upfield shift of the protons. The data suggest that epimer A has the benzyl ester on the α face and that epimer B has the methyl ester on the α face.

To corroborate these conclusions, ASIS measurements were performed on a compound of known stereochemistry, the methyl ester of penicillin V. In deuterated chloroform,

© 2001 NRC Canada

Scheme 2. Reagents and conditions: (*a*) Triton B, DMF, –50 to 20°C; (*b*) Triton B or NaH, allyl bromide; (*c*) I_2, CH_2Cl_2–H_2O; (*d*) $NaIO_4$, MeOH–H_2O; (*e*) DBU, CH_2Cl_2; (*f*) PBr_3, DMF, 0°C; (*g*) TFA, CH_2Cl_2, 0°C.

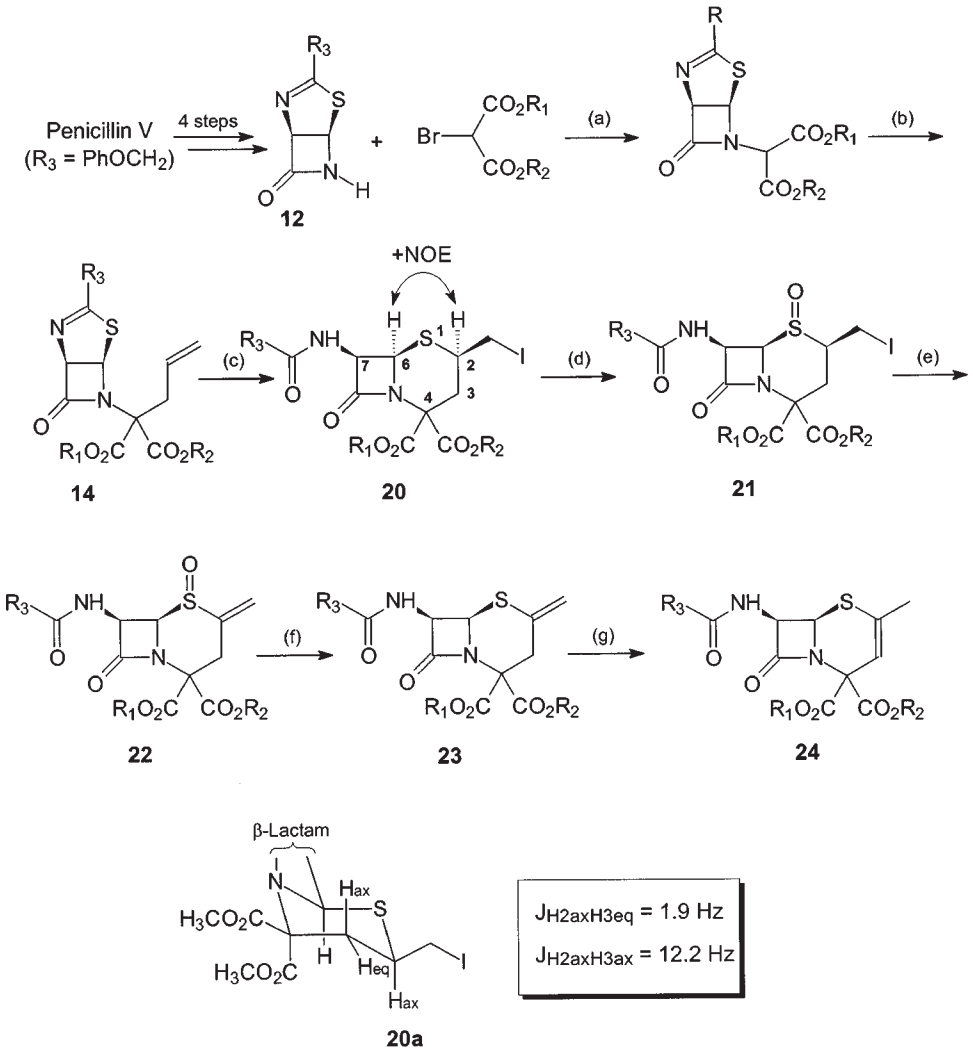
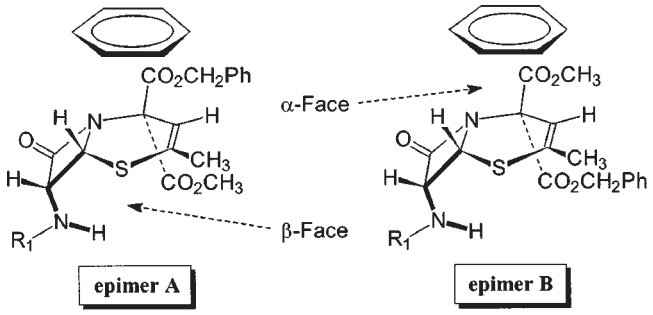


Table 1. Chemical shifts (δ) of epimer A and epimer B of **24**.



	Epimer A		Epimer B		Δ ($CDCl_3$–C_6D_6, ppm)	
Proton	$CDCl_3$	C_6D_6	$CDCl_3$	C_6D_6	Epimer A	Epimer B
H_3	5.85	6.02	5.86	6.05	–0.17	–0.18
H_6	5.31	5.18	5.33	5.13	0.13	0.20
H_7	5.77	5.61	5.80	5.58	0.17	0.22
$PhOCH_2$	4.56	3.99	4.56	4.03	0.57	0.53
4-CO2CH_3	3.77	3.52	3.74	3.23	0.26	0.50
4-CO_2CH_2PH	5.24	4.99	5.27	5.27	0.25	–0.03

© 2001 NRC Canada

the ester methyl group, which occupies the convex face of the molecule, is found at 3.76 ppm. In deuterated benzene the chemical shift is 3.20 ppm, a difference of 0.56 ppm. The corresponding difference in epimer B is 0.50 ppm.

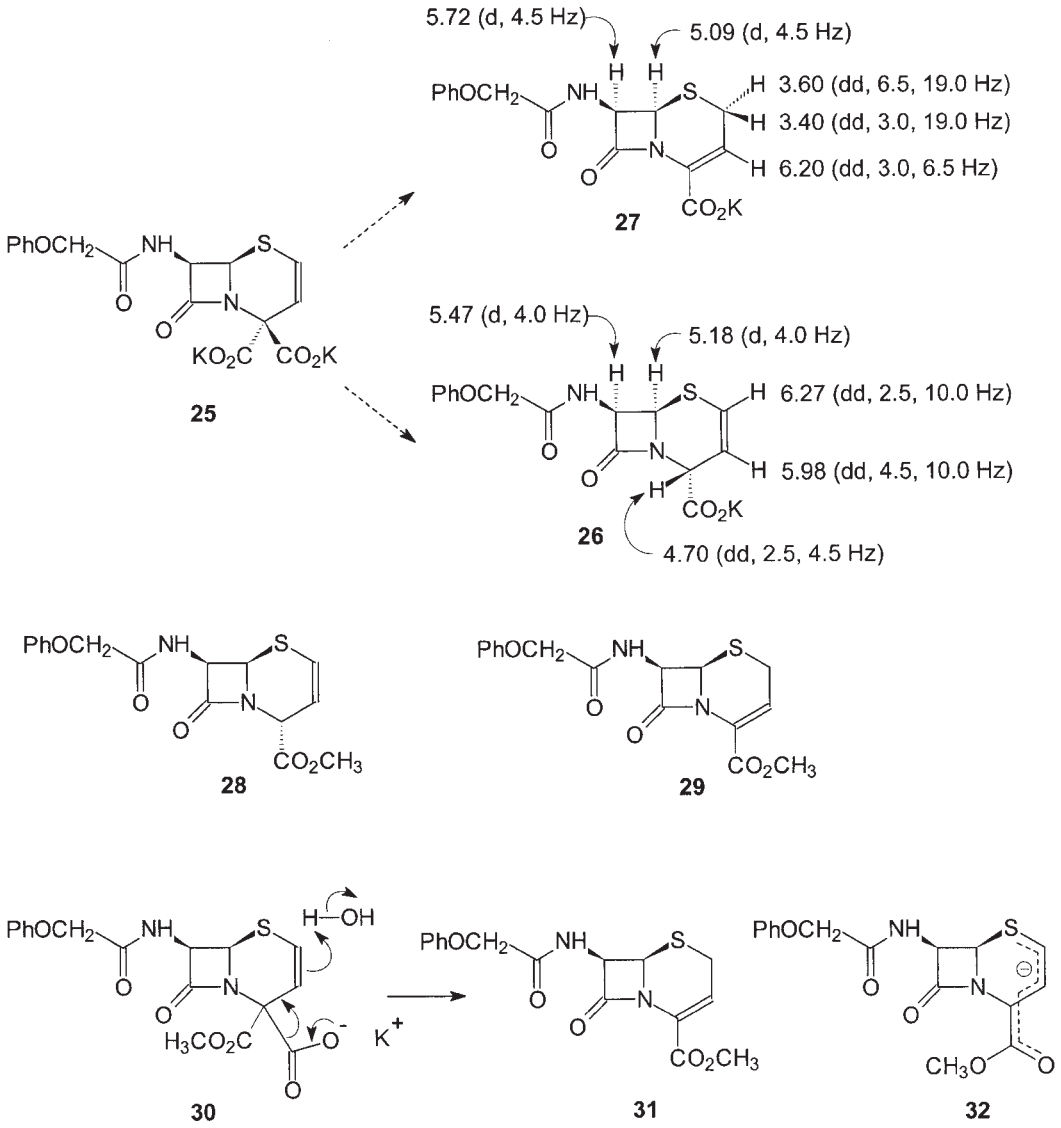
Deprotection of the Δ^2-cephem-4,4-dicarboxylic acid esters

Alkaline hydrolysis of 19

In an initial set of experiments, **19** was treated at –8°C with 2 equiv of potassium hydroxide in aqueous pyridine, and the solvent was then removed under reduced pressure below 30°C. This afforded a product that exhibited significant antibacterial activity against a penicillin-sensitive strain of *Staphylococcus aureus*. However, the product was not the malonate salt **25**. As seen in **26** and **27**, the ^{1}HMR spectrum (in D_2O) was that of a mixture of *decarboxylated* Δ^2- and Δ^3-cephems. Cephems of type **27**, having hydrogen at C-3, are known to be active, and one of these, ceftizoxime, is a widely used antibiotic (18).

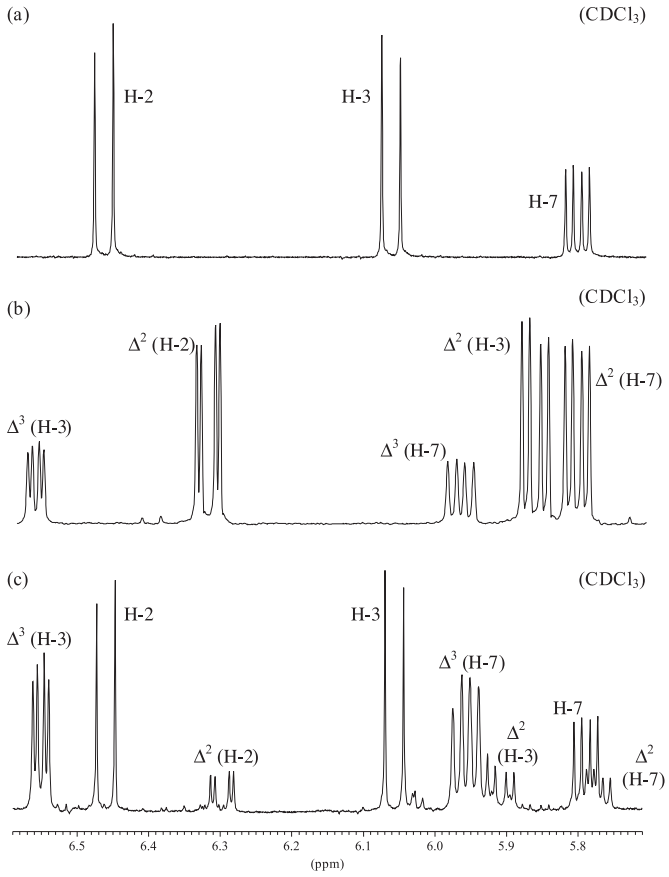
Following these initial experiments, subsequent hydrolyses were performed with a minimum of manipulation: reaction mixtures were acidified, and the products quickly extracted into an appropriate organic solvent and esterified with diazomethane. Using this protocol, the reaction of **19** with *2* equiv of potassium hydroxide produced a 7:1 mixture of decarboxylated Δ^2- and Δ^3-cephem esters (**28** and **29**, respectively). However, *1* equiv of potassium hydroxide reversed the **28**:**29** ratio to 1:4 (see Fig. 1).

These results suggest that a carboxylate anion **30**, formed in the first hydrolysis step, undergoes rapid decarboxylation concerted with a shift of the double bond, as depicted in **30** → **31**. Subsequently, C-2 deprotonation of **31**, leading, via **32**, to the more stable Δ^2-isomer **28**, competes with the hydrolysis of the second ester.



© 2001 NRC Canada

Fig. 1. (*a*) The 5.5–6.6 ppm region in the ^{1}H NMR spectrum of **1**; (*b*) spectrum of a mixture of **28** and **29**; (*c*) after exposure of **19** to 1 equiv of KOH in aqueous pyridine.



Alkaline hydrolysis of 24 ($R_1 = R_2 = Me$)

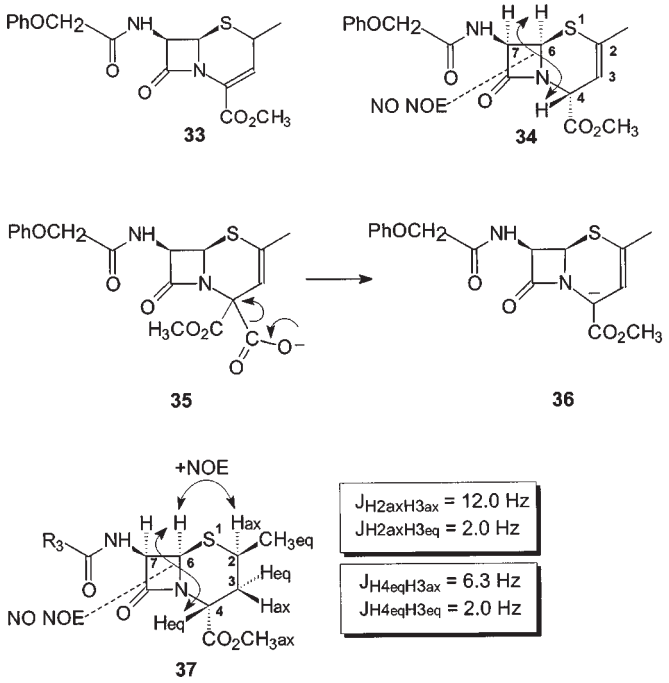
The foregoing analysis suggested that the introduction of an electron-releasing C-2-methyl group, as in **24**, might affect the results of alkaline hydrolysis in two ways: preferably, the concerted decarboxylation pathway that is presumed to cause the lability of the Δ^2-cephem-4,4-dicarboxylic acid would become disfavoured; alternatively, if this is not the case and the initial product is again a Δ^3-ester (**33**), this ester should resist isomerization of the double bond, because C-2 deprotonation leading to the more stable Δ^2-ester **34** would be disfavoured.

In the event, the hydrolysis of the dimethyl ester (**24**, $R_1 = R_2 = Me$) with either 1 or 2 equiv of potassium hydroxide in aqueous pyridine, followed by the usual work-up, afforded the *same* product in each case, the Δ^2-cephem **34**.

The simplest explanation of these results is that the carboxylate anion **35** decarboxylates rapidly to **36**. Although the concerted decarboxylation pathway leading initially to the Δ^3-isomer is disfavoured, the presence of the C-2-methyl group leads to direct decarboxylation to the Δ^2-isomer as the predominant pathway. An alternative explanation is that, despite our expectations regarding the kinetic acidity of **33**, under alkaline conditions the introduction of the C-2-methyl group somehow *enhances* the $\Delta^3 \rightarrow \Delta^2$ rearrangement. This point was addressed using the dibenzyl ester **24** ($R_1 = R_2 = CH_2Ph$).

Hydrogenolysis of 24 ($R_1 = R_2 = CH_2Ph$)

Experiments were performed using 10% palladium on carbon, in aqueous ethanol containing 2 equiv of sodium bicarbonate (Method A), and in aqueous acetic acid (pH 4 to 5) (Method B). Products were isolated by filtration through Celite, followed by evaporation or lyophilization and conversion to the methyl ester. This led, in ethanol, to the Δ^2-ester **34** as the sole product (>90%). In acetic acid, the products were **34** and the *cepham* **37**, whose stereochemistry was elucidated from the H_2H_3 coupling constants, a positive NOE between H_2 and H_6 and the absence of an NOE between H_4 and H_6.



Thus, in contrast to the C-2-unsubstituted diester **19**, which, following the exposure of one carboxyl group, decarboxylates with rearrangement of the double bond, in the case of the C-2-methylated esters there is rapid decarboxylation *without rearrangement of the double bond*.

Hydrogenolysis of the epimeric methyl benzyl esters 24 (R_1, R_2 = Me, CH_2Ph)

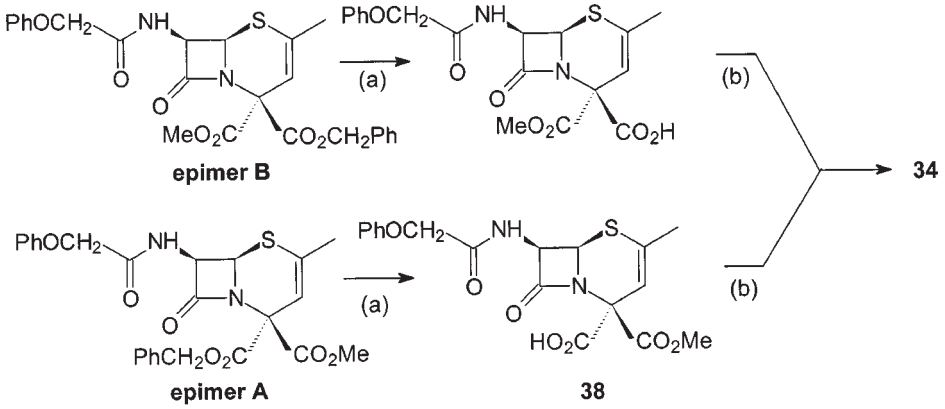
As summarized in Scheme 3, hydrogenolysis using Method B resulted in decarboxylation with the formation of **34** in both cases. Carbanion **36** is implicated as an intermediate in these reactions since the decarboxylation of **38** proceeds with inversion of configuration at C-4. The pK_1 of malonic acid is 2.85 at 298 K (19), so that in aqueous acetic acid the Δ^2-cephem-4,4-dicarboxylic acid **38** would be fully ionized.

Preparation and deprotection of acetamidomalonate esters

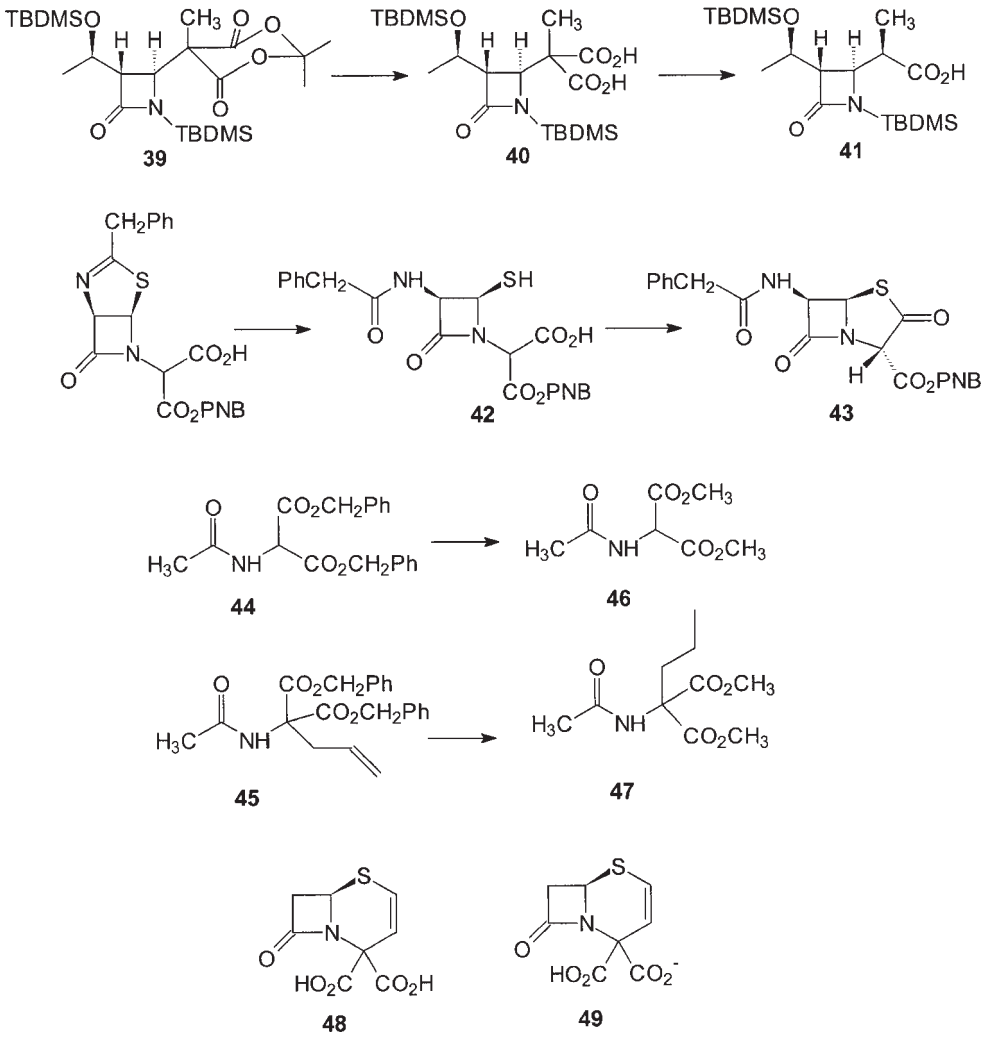
There are numerous examples of stable β-lactam-containing malonic acids (20). The Meldrum acid derivative **39** hydrolyzes under basic conditions to give the malonic acid **40**, whose decarboxylation to **41** requires refluxing ethyl acetate in the presence of formic acid. The malonic

© 2001 NRC Canada

Scheme 3. Reagents and conditions: (*a*) H_2, Pd/C, HOAc–H_2O; (*b*) CH_2N_2, CH_2Cl_2–EtOH, 0°C.

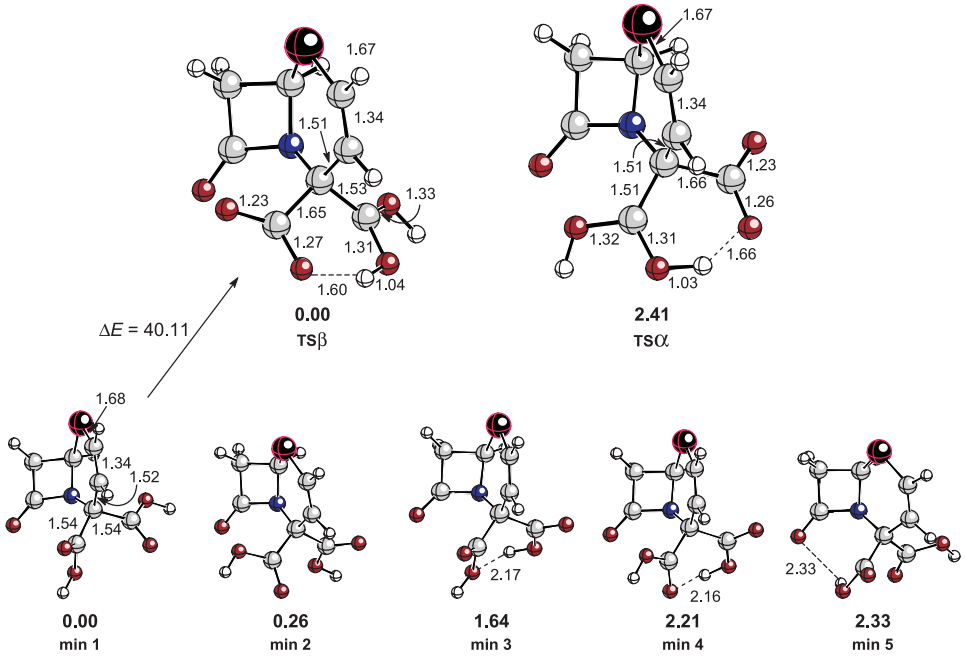


acid **42** can be isolated and converted to the penam **43**. Based on these precedents, the rapid decarboxylation observed in all cases following deprotection of **19** and **24** was unexpected. In an effort to understand this result, the dibenzyl acetamidomalonates **44** and **45** were synthesized (see *Experimental*) and subjected to hydrogenolysis followed by esterification with diazomethane. The products, isolated in 81% and 82% yields, respectively, were the dimethyl malonates **46** and **47**. Subsequent experiments established that the malonic acid precursors of **46** and **47** could be maintained at room temperature for at least 24 h without noticeable decomposition.



© 2001 NRC Canada

Fig. 2. Neutral decarboxylation of **48** (AM1 calculations). **Min 1**–**min 5** are the five lowest energy structures of the diacid; TSα and TSβ are the transition structures for α- and β-decarboxylation. Energies are in kcal mol^{-1}, relative to **min 1** and TSβ.



Theoretical considerations

The reasons for the differences in ease of decarboxylation were examined using semiempirical and ab initio molecular orbital calculations. With AM1 (21), calculations on 4,4-dicarboxy-Δ^2-cephem (**48**) yielded 5 minima corresponding to torsion within the carboxyl groups. The most stable structure (**min 1**) and the least stable structure (**min 5**) differ in energy by 2.3 kcal mol^{-1} (Fig. 2). The two most stable structures (**min 1** and **min 2**) have the *Z*-conformation (22). The next two (**min 3** and **min 4**) have one carboxyl group in the *Z*-conformation and other in the *E*-conformation. The least stable structure (**min 5**) has both carboxyl groups in the *E*-conformation.

The transition structures **TS**α and **TS**β, calculated for the decarboxylation of the α- and β-carboxyl groups of **48** are included in Fig. 2. The β-decarboxylation barrier, corresponding to decarboxylation from the concave face of the molecule, is lower by 2.4 kcal mol^{-1}.

The transition structures are late, as proton transfer is almost complete. The barrier, calculated from **min 1** is 40.1 kcal mol^{-1}. In Bach's high level ab initio calculations (23), malonic acid was found to have a decarboxylation barrier of 33.2 kcal mol^{-1}. The experimental barrier is 30.8 kcal mol^{-1} (23). Since the calculated neutral barriers are high, the facile decarboxylations observed experimentally cannot be attributed to the decarboxylation of a 4,4-dicarboxy-Δ^2-cephem or its monoester.

On the other hand, the α- and β-decarboxylation barriers of the monoanions **49** (Fig. 3) are vanishingly small (2.04 and 2.08 kcal mol^{-1}, respectively).

Figures 4 and 5 show the results of ab initio (3-21G) calculations of the decarboxylation barriers of acetamidomalonic acid (35.2 kcal mol^{-1}) and its monoanion (26.3 kcal mol^{-1}). The barrier decreases in the anion, but does not become vanishingly small. It is noteworthy that the monoanion of phenylmalonic acid decarboxylates 3 to 4 times faster than the undissociated acid (24).

The calculations are consistent with experiment: the undissociated cephem and acetamidomalonic acids have comparable (high) decarboxylation barriers, which disappear in the case of the cephem monoanions. Since these anions would be fully formed at pH > 3 in water solvent, it does not appear possible to test the prediction that 4,4-dicarboxy-Δ^2-cephems will have significant antibacterial activity.

Experimental

General

All reactions were performed under dry nitrogen using oven-dried (140°C, 24 h) glassware. The glassware was allowed to cool in a desiccator under vacuum and assembled cold, capped with rubber septa, and evacuated with dry nitrogen gas. Solvents were distilled prior to use and dried, as necessary, by literature procedures (25). Diazomethane was prepared by treatment of a cold solution of *N*-methyl-*N*-nitrosotoluene-4-sulfonamide (DIAZALD) in 95% ethanol with 1.0 mL portions of 12.5 M sodium hydroxide. Both ^{1}H and ^{13}C nuclear magnetic resonance (NMR) spectra were recorded on a Bruker Model AMX 400 Spectrometer operating at 400.1 MHz and 100.6 MHz, respectively. Chemical shifts (δ) are reported in parts per million (ppm) relative to tetramethylsilane (TMS) in an appropriate deuterated solvent. Infrared (IR) spectra were obtained on a Bomen–Hartmann–Braun spectrometer (1% KBr or 1% solution). High-resolution mass spectra refer to either direct inlet electron impact (EI) measurements or chemical ionization (CI) measurements, using isobutane, and were provided by Dr. G. Eigendorf at the University of British Columbia. Low-

© 2001 NRC Canada

Fig. 3. Decarboxylation of the monoanions of **48** (AM1 calculations). Energies are in kcal mol^{-1}; bond lengths are in Å. Net atomic charges are shown in parentheses.

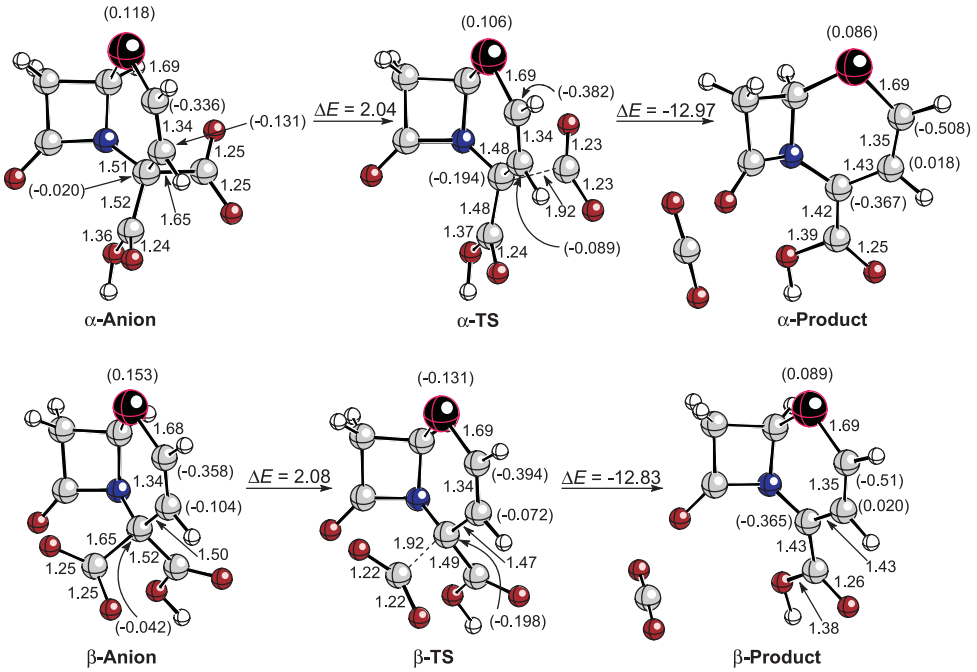


Fig. 4. Decarboxylation of acetamidomalonic acid (3-21G calculations). Energies are in kcal mol^{-1}; bond lengths are in Å.

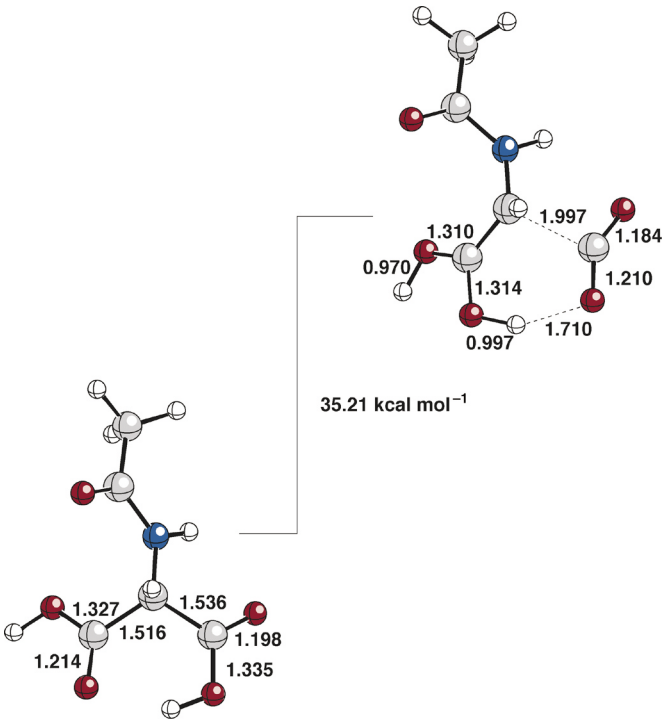
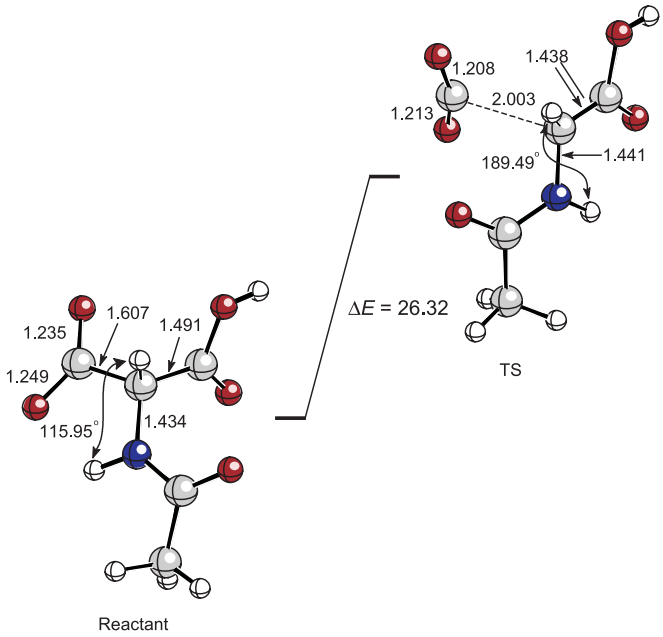


Fig. 5. Decarboxylation of the monoanion of acetamidomalonic acid (3-21G calculations). Bond lengths are in Å; bond angles are in deg.



resolution mass spectra refer to direct inlet EI measurements or CI measurements, using isobutane, or fast-atom bombardment (FAB), employing xenon gas, on a Kratos MS50 Spectrometer operated at 70 eV by G. Owens at Simon Fraser University. Melting points (mp) were determined on a Fisher–Johns apparatus, and are uncorrected. Optical rotations were obtained using a Rudolph automatic polarimeter. Analytical thin-layer chromatography was carried out on precoated Merck Silica gel 60 F-254 plates with aluminium backing. Spots were observed under short-wavelength ultraviolet light, or were visualized with iodine vapour, ninhydrin, or ceric sulfate. Flash column chromatography was carried out on Merck Silica gel 60 (230–400 Mesh), according to the method of Still et al. (26), unless stated otherwise, using only distilled solvents under dry nitrogen gas. Elemental analyses were performed by M.K. Yang on a

© 2001 NRC Canada

Carlo Erba model 1106 elemental analyzer at Simon Fraser University.

Penicillin V methyl ester (8)

Methyl iodide (14.0 mL, 31.9 g, 225 mmol) was added dropwise, with stirring, to a suspension of penicillin V (77.0 g, 198 mmol) in dimethylformamide (400 mL). Stirring was continued at room temperature for 17 h. The solvent was then removed under reduced pressure, and the residual oil was diluted with dichloromethane (300 mL), washed successively with water (4 × 150 mL), and saturated sodium chloride (300 mL), dried over magnesium sulfate and evaporated to give the product as an orange oil (72.3 g, 94%), which crystallized upon trituration with ether; mp 60 to 61°C. $[\alpha]_D^{20}$ +124.1° (c 0.137, $CHCl_3$). Mass spectrum (CI, *m*/*z*): 365 (M+1). IR (KBr) (cm^{-1}): 3366, 1786, 1744, 1701. ^1H NMR ($CDCl_3$): 7.35 (4H, t, Ar + NH), 7.05 (1H, t, Ar), 6.94 (1H, d, Ar), 5.75 (1H, dd, 4.3, 9.3 Hz, H-6), 5.59 (1H, d, 4.3 Hz, H-5), 4.57 (1H, d, 15.1 Hz, CHH), 4.55 (1H, d, 15.1 Hz, CHH), 4.47 (1H, s, H-3), 3.78 (3H, s, ester CH_3), 1.60 (3H, s, CH_3), 1.49 (3H, s, CH_3). ^{13}C NMR ($CDCl_3$): 172.96 (acetamido C=O), 168.04 (β-lactam C=O), 167.87 (ester C=O), 157.11, 129.86, 122.47, 114.20 (aromatic), 70.57 (C-3), 67.85 (C-5), 67.38 ($PhOCH_2$), 64.79 (C-2), 58.23 (C-6), 52.35 (CO_2CH_3), 31.91 (CH_3), 26.91 (CH_3). Anal. calcd. for $C_{17}H_{20}N_2O_5S$: C 56.03, H 5.53, N 7.69; found: C 55.75, H 5.55, N 7.59.

Penicillin V methyl ester sulfoxide (9)

Hydrogen peroxide (34.0 mL of 50%, 17.0 g, 500 mmol) was added, with stirring during 1 h, to a solution of penicillin V methyl ester (72.3 g, 198 mmol) in dichloromethane (800 mL) and glacial acetic acid (92 mL). Stirring was continued for 17 h, and the yellow solution was then washed successively with saturated sodium bicarbonate (2 × 200 mL), water (2 × 200 mL), and saturated sodium chloride (400 mL), dried over magnesium sulfate and evaporated. The resulting yellow foam crystallized upon treatment with hot methanol (150 mL). The product was collected and washed with cold methanol (40 mL) to give 76.4 g (78%) of the methyl ester of penicillin V sulfoxide; mp 118–120°C (lit. (27) mp 121.5 to 122.5°C). $[\alpha]_D^{20}$ +202.7° (c 0.148, $CHCl_3$). Mass spectrum (CI, *m*/*z*): 381 (M+1). IR (KBr) (cm^{-1}): 3380, 1802, 1757, 1694, 1065. ^1H NMR ($CDCl_3$): 8.26 (1H, d, 10.4 Hz, NH), 7.29 (2H, m, Ar), 7.01 (1H, t, Ar), 6.94 (2H, d, Ar), 6.09 (1H, dd, 4.6, 10.5 Hz, H-6), 5.04 (1H, d, 4.6 Hz, H-5), 4.68 (1H, s, H-3), 4.53 (2H, s, $PhOCH_2$), 3.82 (3H, s, ester CH_3), 1.73 (3H, s, 2-CH_3), 1.22 (3H, s, shows nOe with H-5 at 5.04 ppm, 2-CH_3). ^{13}C NMR ($CDCl_3$): 173.08 (acetamido C=O), 168.30 (β-lactam, ester C=O), 157.20, 129.72, 122.26, 115.02 (aromatic), 76.57 (C5), 75.32 (C2), 67.29 ($PhOCH_2$), 66.55 (C-3), 55.67 (C-6), 52.91 (ester CH_3), 19.44 (CH_3), 18.73 (CH_3). Anal. calcd. for $C_{17}H_{20}N_2O_6S$: C 53.67, H 5.30, N 7.36; found: C 53.30, H 5.30, N 7.36.

Rearrangement of penicillin V sulfoxide

Trimethylphosphite (70.0 mL, 73.6 g, 593 mmol) was added to a mixture of penicillin V methyl ester sulfoxide (53.0 g, 139 mmol) and anhydrous magnesium sulfate (33.0 g, 274 mmol) in benzene (1100 mL). The reaction mixture was refluxed overnight, with stirring, and then cooled and filtered through Celite. The filtrate was concentrated under reduced pressure, using a Javex trap, to afford a yellow oil having a crude weight of 68 g (140%). Purification by column chromatography, using ethyl acetate – hexanes (1:1), afforded **10** as a white solid (43.9 g, 87%), mp 56–58°C. $[\alpha]_D^{20}$ –165.6° (c 0.157, $CHCl_3$). Mass spectrum (CI, *m*/*z*): 347 (M+1). IR (KBr) (cm^{-1}): 1765, 1738. ^1H NMR ($CDCl_3$): 7.28 (2H, t, Ar), 7.00 (1H, t, Ar), 6.93 (2H, d, Ar), 6.01 (1H, dt, 1.2, 4.1 Hz, H-3), 5.93 (1H, d, 4.2 Hz, H-4), 5.10 (1H, q, 1.4 Hz, allylic H), 4.97 (1H, dd, 1.4, 14.6 Hz, C*H*H), 4.92 (1H, br s, =CH*H*), 4.91 (1H, dd, 1.4, 14.6 Hz, C*H*H), 4.84 (1H, br s, =CH*H*), 3.76 (3H, s, ester CH_3), 1.75 (3H, br s, CH_3). ^{13}C NMR ($CDCl_3$): 173.23 (thiazoline N=C), 169.30 (ester C=O), 165.02 (β-lactam C=O), 157.73, 129.64, 121.97, 114.84 (aromatic), 134.67 (*C*H_2=CH), 117.46 (CH_2=*C*CH_3), 92.25 (C-3), 67.78 ($PhOCH_2$), 67.21 (C-4), 58.86 (*C*HCO_2CH_3), 52.52 (CO_2CH_3), 21.52 (CH_2=C*C*H_3). Anal. calcd. for $C_{17}H_{18}N_2O_4S$: C 58.94, H 5.24, N, 8.09; found: C 59.27, H 5.26, N 7.78.

Isomerization of 10

Triethylamine (8.5 mL, 61 mmol) was added dropwise, with stirring, to a solution of **10** (48.3 g, 140 mmol) in dichloromethane (270 mL). The solution was stirred for 3 h, and the solvent was then evaporated under reduced pressure. The residue crystallized from warm methanol to give 30.1 g (62%) of **11**, mp 64–66°C. $[\alpha]_D^{20}$ +24.4° (c 0.205, $CHCl_3$). Mass spectrum (CI, *m*/*z*): 347 (M+1). IR (KBr) (cm^{-1}): 1759, 1723, 1643, 1597. ^1H NMR ($CDCl_3$): 7.26 (2H, m, Ar), 6.99 (1H, t, Ar), 6.94 (2H, d, Ar), 6.06 (1H, dt, 1.2, 4.0 Hz, H-3), 5.87 (1H, d, 4.0 Hz, H-4), 4.99 (1H, dd, 1.2, 14.3 Hz, C*H*H), 4.93 (1H, dd, 1.2, 14.3 Hz, CH*H*), 3.75 (3H, s, ester CH_3), 2.22 (3H, s, =CCH_3), 1.76 (3H, s, =CCH_3). ^{13}C NMR ($CDCl_3$): 172.09 (thiazoline N=C), 163.76 (β-lactam C=O), 163.37 (ester C=O), 157.74, 129.67, 122.03, 114.86 (aromatic), 155.79 (NC=C$(CH_3)_2$), 118.72 (N*C*=C$(CH_3)_2$), 92.70 (C-3), 69.51 (C-4), 67.74 ($PhOCH_2$), 51.90 (CO_2CH_3), 23.77, 21.88 (C=C(*C*$H_3)_2$). Anal. calcd. for $C_{17}H_{18}N_2O_4S$: C 58.94, H 5.24, N 8.09; found: C 59.25, H 5.20, N 8.10.

Thiazoline azetidinone (12)

A solution of potassium permanganate (12.2 g, 77 mmol) and magnesium sulfate (8.41 g, 70 mmol) in water (480 mL) was added during 80 min to a solution of **11** (30.1 g, 87 mmol) in 95% ethanol (600 mL). Additional potassium permanganate (5 × 3.6 g, 114 mmol) was subsequently added every 10 min. The solvent was then removed under reduced pressure, and the brown residue was shaken with ethyl acetate (720 mL) and water (360 mL), and filtered. The organic layer was separated and the aqueous phase was extracted with ethyl acetate (3 × 100 mL). The combined organic extracts were washed with saturated sodium chloride (1000 mL), dried over magnesium sulfate, and evaporated. The residue was treated with hot ethyl acetate to give **12** as yellowish-white crystals (15.9 g, 78%), mp 157 to 158°C (lit. (27) mp 157 to 158°C). $[\alpha]_D^{20}$ +121.4° (c 0.14, $CHCl_3$). Mass spectrum (CI, *m*/*z*): 235 (M+1). IR (KBr) (cm^{-1}): 3216, 1757, 1719. ^1H NMR ($CDCl_3$): 7.29 (2H, m, Ar), 7.02

© 2001 NRC Canada

(1H, t, Ar), 6.98 (2H, d, Ar), 6.34 (1H, br s, NH), 6.08 (1H, dd, 0.9, 3.9 Hz, H-3), 5.33 (1H, d, 3.9 Hz, H-4), 5.02 (1H, dd, 0.9, 14.3 Hz, C*H*H), 4.93 (1H, dd, 0.9, 14.3 Hz, CH*H*). ^{13}C NMR ($CDCl_3$): 172.12 (thiazoline N=C), 164.36 (β-lactam C=O), 157.79, 129.69, 122.08, 114.92 (aromatic), 94.83 (C-3), 68.00 ($PhOCH_2$), 62.86 (C-4). Anal. calcd. for $C_{11}H_{10}N_2O_2S$: C 56.39, H 4.30, N 11.96; found: C 56.01, H 4.31, N 11.57.

Dimethyl bromomalonate (28)

Bromine (1.8 mL, 5.58 g, 35 mmol) was added dropwise with stirring, during 60 min, to a solution of dimethyl malonate (3.46 mL, 4.0 g, 35 mmol) in carbon tetrachloride (15 mL), with irradiation by a 150 W bulb mounted beneath the reaction vessel. When the evolution of gas had ceased, water (50 mL) was added and the phases were separated. The aqueous layer was extracted with chloroform (2 × 40 mL) and the combined organic extracts were washed successively with saturated sodium bicarbonate (2 × 75 mL) and saturated sodium chloride (100 mL), dried over magnesium sulfate, and evaporated. The residue was distilled, and the fraction boiling at 105–108°C and 11 torr (1 torr = 133.322 Pa) was collected as a colourless oil (5.02 g, 62%). ^{1}H NMR ($CDCl_3$): 4.85 (1H, s, CH), 3.83 (6H, s, CH_3).

Dibenzyl malonate

Concentrated sulfuric acid (0.2 mL of 96%, 0.2 g, 1.96 mmol) was slowly added to a suspension of malonic acid (20.1 g, 193 mmol) and benzyl alcohol (47.0 mL, 49.1 g, 454 mmol) in toluene (70 mL). Employing a Dean–Stark trap, the mixture was heated to reflux for 2 h, and approximately 7 mL of water were removed. The solution was cooled, diluted with ethyl acetate (100 mL), and washed successively with saturated sodium bicarbonate (2 × 100 mL), water (2 × 100 mL) and saturated sodium chloride (100 mL), dried over magnesium sulfate, and evaporated. The residue was distilled, and the fraction boiling at 188°C and 0.2 torr (1 torr = 133.322 Pa) was collected as a colourless oil (50.0 g, 91%). Mass spectrum (EI, *m*/*z*): 285 (M). IR (neat) (cm^{-1}): 1745. ^{1}H NMR ($CDCl_3$): 7.35–7.32 (10H, m, Ar), 5.18 (4H, s, benzyl CH_2), 3.48 (2H, s, malonyl CH_2).^{13}C NMR ($CDCl_3$): 166.18 (ester C=O), 135.34, 128.59, 128.41, 128.27 (aromatic), 67.26 ($PhCH_2O$), 41.61 ($COCH_2CO$).

Dibenzyl bromomalonate (20*a*, 29)

With irradiation by a 250 W bulb mounted beside the reaction vessel, bromine (6.5 mL, 20.2 g, 126 mmol) was added dropwise during 2 h, with stirring, to a solution of dibenzyl malonate (19.6 g, 69.0 mmol) in carbon tetrachloride (51 mL). Water (50 mL) was then added and the layers were separated. The aqueous layer was extracted with dichloromethane (2 × 40 mL) and the combined organic extracts were washed successively with saturated sodium bicarbonate (2 × 75 mL) and saturated sodium chloride (100 mL), dried over magnesium sulfate, and evaporated. The oily residue (22.0 g) was purified by column chromatography using ethyl acetate – hexanes (1:8) to yield 6.91 g (28%) of the product as a colourless oil, which solidified in the freezer as white crystals, mp 26 to 27°C. IR (neat) (cm^{-1}): 1744. ^{1}H NMR ($CDCl_3$): 7.36–7.30 (10H, m, Ar), 5.22 (4H, s, benzyl CH_2), 4.92 (1H, s, CH). ^{13}C NMR ($CDCl_3$): 164.28 (ester C=O), 134.58–128.29 (aromatic), 68.72 ($PhCH_2O$), 42.20 ($COCHBrCO$). Anal. calcd. for $C_{17}H_{15}O_4Br$: C 56.22, H 4.16; found: C 55.84, H 4.09.

Benzyl methyl bromomalonate

Dimethyl malonate (10 mL, 11.56 g, 87.5 mmol), in methanol (70 mL), was treated with a solution of potassium hydroxide (4.89 g, 87.2 mmol) in methanol (70 mL). The solution was stirred for 24 h, then refrigerated overnight. The white crystals were filtered, rinsed with cold methanol, and dried to give 9.72 g (65%) of potassium methyl malonate, mp 160–162°C (dec). Mass spectrum (CI, *m*/*z*): 103 (M+1-(K+CH_3)). IR (KBr) (cm^{-1}): 1738, 1728. ^{1}H NMR (D_2O): 3.56 (3H, s, CH_3), 3.15 (2H, s, CH_2). ^{13}C NMR (D_2O): 176.78 (carboxyl C=O), 174.80 (ester C=O), 55.36 (CO_2CH_3). Anal. calcd. for $C_4H_5O_4K$: C 30.76, H 3.23; found: C 30.69, H 3.19.

Benzyl bromide (3.8 mL, 5.46 g, 31.9 mmol) was added to a suspension of potassium methyl malonate (5.63 g, 32.7 mmol) in dimethylformamide (80 mL). The mixture was stirred for 22 h, diluted with ethyl acetate (150 mL), washed with water (3 × 150 mL), dried over magnesium sulfate, and evaporated to give benzyl methyl malonate as a colourless oil (6.47 g, 97%). IR (neat) (cm^{-1}): 1755, 1732. Mass spectrum (CI, *m*/*z*): 209 (M+1). ^{1}H NMR ($CDCl_3$): 7.36 (5H, m, Ar), 5.19 (2H, s, $PhCH_2$), 3.74 (3H, s, CH_3), 3.44 (2H, s, malonyl CH_2). ^{13}C NMR ($CDCl_3$): 166.83 (ester C=O), 166.31 (ester C=O), 135.42, 128.60, 128.42, 128.25 (aromatic), 67.18 (CO_2CH_2Ph), 52.41 (CO_2CH_3), 41.30 (malonyl CH_2). Anal. calcd. for $C_{11}H_{12}O_4$: C 46.01, H 3.86; found: C 46.03, H 3.88.

With irradiation by a 150 W Westinghouse reflector spotlight mounted underneath the reaction vessel, bromine (2.7 mL, 8.38 g, 52.4 mmol) was added dropwise during 60 min, with stirring, to a solution of benzyl methyl malonate (11.0 g, 52.8 mmol) in carbon tetrachloride (40 mL). Once the evolution of gas had ceased, water (40 mL) was added and the phases were separated. The aqueous layer was extracted with chloroform (2 × 40 mL) and the combined organic extracts were washed with saturated sodium bicarbonate (2 × 120 mL) and saturated sodium chloride (120 mL), dried over magnesium sulfate, and evaporated. The residue was purified by column chromatography using ethyl acetate – hexanes (30:70) to give the product as a colourless oil (10.3 g, 68%). Mass spectrum (CI, *m*/*z*): 287, 289 (M+1). IR (neat) (cm^{-1}): 1767, 1746. ^{1}H NMR ($CDCl_3$): 7.36 (5H, m, Ar), 5.25 (2H, s, $PhCH_2$), 4.89 (1H, s, malonyl CH), 3.80 (3H, s, CH_3). ^{13}C NMR ($CDCl_3$): 164.97 (ester C=O), 164.38 (ester C=O), 134.68, 128.89, 128.74, 128.33 (aromatic), (CO_2CH_2Ph), 53.92 (CO_2CH_3), 42.02 (malonyl CH).

Coupling of 12 with dimethyl bromomalonate

A solution of **12** (4.45 g, 19 mmol) in dimethylformamide (40 mL) was cooled to –55°C and Triton B (15.0 mL of a 40% methanolic solution, 6.36 g, 38 mmol) was added dropwise. Stirring was continued for 30 min, and a solution of dimethylbromomalonate (4.85 g, 23 mmol) in dimethylformamide (20 mL) was then added dropwise. Stirring was continued overnight, and the mixture was

© 2001 NRC Canada

warmed to room temperature. Ethyl acetate (450 mL), saturated sodium chloride (110 mL), and 1.0 M hydrochloric acid (50 mL) were added, and the organic phase was separated, washed with water (2 × 120 mL) and saturated sodium chloride (150 mL), dried over magnesium sulfate, and evaporated under reduced pressure. The residue was purified by column chromatography using ethyl acetate – hexanes (2:3) to give **13** (3.33 g, 50%). $[\alpha]_D^{20}$ –88.2° (c 0.17, $CHCl_3$). IR (neat) (cm^{-1}): 1782, 1755, 1748, 1682. Mass spectrum (EI, *m*/*z*): 364 (M). ^{1}H NMR ($CDCl_3$): 7.29 (2H, t, Ar), 7.00 (1H, t, Ar), 6.92 (2H, d, Ar), 6.09 (1H, dt, 1.2, 4.2 Hz, H-3), 6.00 (1H, d, 4.2 Hz, H-4), 5.12 (1H, s, CH), 4.98 (1H, dd, 1.2, 14.3 Hz, PhOC*H*H), 4.89 (1H, dd, 1.2, 14.3 Hz, PhOCH*H*), 3.82 (3H, s, CH_3), 3.72 (3H, s, CH_3). ^{13}C NMR ($CDCl_3$): 172.99 (thiazoline N=C), 165.12 (β-lactam C=O), 164.29 (ester C=O), 157.78, 129.64, 122.02, 114.86 (aromatic), 93.17 (C-3), 68.10 (C-4), 67.90 ($PhOCH_2$), 60.29 (malonyl CH), 55.96 (CO_2CH_3), 53.40 (CO_2CH_3). Anal. calcd. for $C_{16}H_{16}N_2O_6S$: C 52.74, H 4.43, N 7.69; found: C 52.39, H 4.36, N 7.85.

Coupling of 12 with dibenzyl bromomalonate

Triton B (15.4 mL of a 40% methanolic solution, 6.52 g, 39 mmol) was slowly added at –55°C to a solution of the azetidinone (4.4 g, 19 mmol) in dimethylformamide (40 mL). The red solution was stirred for 30 min at –55°C and then treated dropwise with a solution of the bromomalonate (7.1 g, 20 mmol) in dimethylformamide (20 mL). When the addition was complete the reaction mixture was warmed to 0°C and stirring was continued for 2.5 h. Ethyl acetate (450 mL), saturated sodium chloride (110 mL), and 1.0 M hydrochloric acid (50 mL) were added and the organic phase was separated, washed with water (2 × 120 mL) and saturated sodium chloride (150 mL), dried over magnesium sulfate, and evaporated under reduced pressure. The residue crystallized from hot ethyl acetate – hexanes (1:2) to yield 4.8g (49%) of the product as yellow crystals, mp 90–92°C. $[\alpha]_D^{20}$ –71.8° (c 0.209, $CHCl_3$). Mass spectrum (FAB, *m*/*z*): 516 (M). IR (KBr) (cm^{-1}): 1768, 1744. ^{1}H NMR (acetone-d_6): 7.36 –7.29 (12H, m, Ar), 6.97 (3H, m, Ar), 6.14 (1H, dt, 1.2, 4.1 Hz, H-3), 6.03 (1H, d, 4.1 Hz, H-4), 5.32 (1H, s, CH), 5.24 (2H, s, benzyl CH_2), 5.19 (2H, s, benzyl CH_2), 4.96 (1H, dd, 1.2, 14.4 Hz, C*H*H), 4.76 (1H, dd, 1.2, 14.4 Hz, CH*H*). ^{13}C NMR ($CDCl_3$): 172.90 (thiazoline N=C), 164.50 (β-lactam C=O), 164.40 (ester C=O), 163.73 (ester C=O), 157.79, 134.43–114.86 (aromatic), 93.12 (C-3), 68.55 (CO_2CH_2Ph), 68.11 (C-4), 67.86 ($PhOCH_2$), 56.49 ($NCH(CO_2CH_2Ph)_2$). Anal. calcd. for $C_{28}H_{24}N_2O_6S$: C 65.10, H 4.68, N 5.42; found: C 64.81, H 4.62, N 5.48.

Coupling of 12 with the mixed bromomalonate

To a solution of the thiazoline azetidinone (4.01 g, 17.1 mmol), cooled to –55°C in dimethylformamide (40 mL), were added dropwise with stirring Triton B (13.5 mL of a 40% methanolic solution, 5.70 g, 34.1 mmol), followed by a solution of the bromomalonate (5.4 g, 16.9 mmol) in dimethylformamide (15 mL). When the addition was complete, the reaction mixture was warmed to –40°C and stirring was continued for 1 h. The cooling bath was then removed and stirring was continued for an additional 22 h. Ethyl acetate (200 mL) was added and the solution was washed successively with 0.1 M hydrochloric acid (200 mL), water (3 × 200 mL), and saturated sodium chloride (200 mL), dried over magnesium sulfate, and evaporated. Purification by column chromatography using ethyl acetate – hexanes (1:1) gave the product as a light yellow, viscous oil (5.45 g, 75%). Mass spectrum (CI, *m*/*z*): 365 ((M+1)-$PhCH_2$). IR (neat) (cm^{-1}): 1784, 1761, 1748. ^{1}H NMR ($CDCl_3$): isomer A: 7.32 (8H, m, Ar), 6.91 (2H, m, Ar), 6.08 (1H, dt, 1.2, 4.1 Hz, H-3), 5.98 (1H, d, 4.1 Hz, H-4), 5.25 (1H, d, 12.3 Hz, PhC*H*H), 5.22 (1H, d, 12.3 Hz, PhCH*H*), 5.15 (1H, s, malonyl CH), 4.97 (1H, dd, 1.2, 14.3 Hz, PhOC*H*H), 4.86 (1H, dd, 1.2, 14.3 Hz, PhOCH*H*), 3.69 (3H, s, CH_3); isomer B: 7.32 (8H, m, Ar), 7.01 (2H, m, Ar), 6.09 (1H, dt, 1.2, 4.1 Hz, H-3), 5.99 (1H, d, 4.1 Hz, H-4), 5.18 (2H, s, $PhCH_2$), 5.17 (1H, s, malonyl CH), 4.91 (1H, dd, 0.8, 14.3 Hz, PhOC*H*H), 4.68 (1H, 1.3, 14.3 Hz, PhOCH*H*), 3.80 (3H, s, CH_3). ^{13}C NMR ($CDCl_3$): 173.02, 172.93 (thiazoline N=C, both isomers), 165.08, 164.55, 164.40, 164.32, 164.25, 163.79 (β-lactam C=O, ester C=O, both isomers), 157.74, 134.45–114.84 (aromatic, both isomers), 93.15, 93.10 (C-3, both isomers), 68.52, 68.47 (CO_2CH_2Ph, both isomers), 68.09, 68.03 (C-4, both isomers), 67.85, 67.80 ($PhOCH_2$, both isomers), 56.23, 56.13 (malonyl CH, both isomers). Anal. calcd. for $C_{22}H_{20}N_2O_6S \cdot 0.5H_2O$: C 58.79, H 4.71, N 6.23; found: C 58.95, H 4.55, N 6.41.

Allylation of 13

The dimethyl ester (3.32 g, 9.53 mmol) was dissolved in dimethylformamide (33 mL), the solution was cooled to 0°C, and a 40% methanolic solution of Triton B (5.6 mL, 2.06 g, 12.3 mmol) was added dropwise during 20 min. Allyl bromide (2.5 mL, 3.5 g, 29 mmol) was then added in one portion. The reaction mixture was stirred at 0°C for 2 h and diluted with ethyl acetate (100 mL). The organic layer was washed successively with water (3 × 100 mL) and saturated sodium chloride (100 mL), dried over sodium sulfate, and evaporated to give an orange oil. Chromatography on silica gel using ethyl acetate – hexanes (3:7) gave **14** as a viscous pale yellow oil (3.47 g, 94%). $[\alpha]_D^{20}$ –21.1° (c 0.285, $CHCl_3$). Mass spectrum (EI, *m*/*z*): 404 (M). IR (neat) (cm^{-1}): 3401, 1778, 1755, 1748, 1678. ^{1}H NMR ($CDCl_3$): 7.30 (2H, t, Ar), 7.00 (1H, t, Ar), 6.94 (2h, d, Ar), 6.01 (1H, d, 4.2 Hz, H-4), 5.92 (1H, dt, 1.2, 4.2 Hz, H-3), 5.71 (1H, ddt, 7.2, 10.1, 17.4 Hz, C*H*=CH_2), 5.19–5.10 (2H, m, CH=CH_2), 4.99 (1H, dd, 1.2, 14.3 Hz, PhOC*H*H), 4.89 (1H, dd, 1.2, 14.3 Hz, PhOCH*H*), 3.80 (3H, s, CH_3), 3.76 (3H, s, CH_3), 3.10 (1H, ddt, 1.1, 7.2, 14.4 Hz, C*H*HCH=CH_2), 3.04 (1H, ddt, 1.1, 7.2, 14.4 Hz, CH*H*CH=CH_2). ^{13}C NMR ($CDCl_3$): 172.87 (thiazoline N=C), 166.67 (β-lactam C=O), 166.21 (ester C=O), 164.15 (ester C=O), 157.84, 129.63, 121.97, 114.87 (aromatic), 131.17 (CH=*C*H_2), 120.29 (*C*H=CH_2), 90.84 (C-3), 70.04 (C-4), 68.80 (malonyl CH), 67.95 ($PhOCH_2$), 53.46 (CO_2CH_3), 53.37 (CO_2CH_3), 38.18 (CH_2CH=CH_2). Anal. calcd. for $C_{19}H_{20}N_2O_6S$: C 56.43, H 4.98, N 6.93; found: C 56.39, H 4.92, N 6.91.

Allylation of the dibenzyl ester

Sodium hydride (0.658 g of a 60% suspension in mineral oil, 16.5 mmol) was added in portions at 0°C to a solution of the dibenzyl ester (4.05 g, 7.84 mmol) in

© 2001 NRC Canada

dimethylformamide (60 mL). The mixture was stirred for 20 min at 0°C, warmed to room temperature, recooled to 0° and treated, during 15 min, with allyl bromide (1.6 mL, 2.2 g, 18 mmol). The ice bath was removed after an additional 20 min, and the bright red reaction mixture was stirred for 16 h. Water (500 mL) was added and the mixture was extracted with dichloromethane (4 × 50 mL). The combined organic extracts were washed with water (3 × 100 mL) and saturated sodium chloride (200 mL), dried over magnesium sulfate, and evaporated to yield a yellow oil (2.4 g). Purification by column chromatography using ethyl acetate – hexanes (1:1) gave the product as a bright yellow viscous oil (1.5 g, 34%). $[\alpha]_D^{20}$ –26.9° (c 0.557, $CHCl_3$). Mass spectrum (CI, *m*/*z*): 557 (M+1). IR (CH_2Cl_2) (cm^{-1}): 1777, 1750. ^1H NMR ($CDCl_3$): 7.34–7.26 (12H, m, Ar), 7.00 (1H, t, Ar), 6.90 (2H, d, Ar), 5.92 (1H, d, 4.2 Hz, H-4), 5.84 (1H, dt, 1.2, 4.2 Hz, H-3), 5.66 (1H, ddt, 7.0, 8.5, 10.0 Hz, =CH), 5.16 (2H, s, benzyl CH_2), 5.11 (2H, s, benzyl CH_2), 5.07–5.04 (2H, m, $=CH_2$), 4.82 (1H, dd, 1.2, 14.2 Hz, PhOC*H*H), 4.52 (1H, dd, 1.2, 14.2 Hz, PhOCH*H*), 3.10 (1H, ddt, 1.0, 7.0, 14.0 Hz, allyl C*H*H), 3.07 (1H, ddt, 1.0, 7.0, 14.0 Hz, allyl CH*H*). ^{13}C NMR ($CDCl_3$): 172.83 (thiazoline N=C), 165.90 (β-lactam C=O), 165.53 (ester C=O), 164.17 (ester C=O), 134.60 (CH=*C*H_2), 157.82, 134.48–114.88 (aromatic), 120.46 (*C*H=CH_2), 90.76 (C-3), 70.14 (C-4), 68.83 (NCCH=CH_2), 68.43 (PhCH_2O), 67.83 (PhOCH_2), 38.16 (*C*H_2CH=CH_2). Anal. calcd. for $C_{31}H_{28}N_2O_6S$: C 66.89, H 5.07, N 5.03; found: C 67.20, H 5.37, N 5.19.

Allylation of the mixed ester

The azetidinone (4.35 g, 10.2 mmol) was dissolved in dimethylformamide (35 mL), the solution was cooled to 0°C, and 40% methanolic Triton B (6.0 mL, 2.21 g, 13.2 mmol) was added dropwise over 20 min, with stirring. Then allyl bromide (2.6 mL, 3.63 g, 30.0 mmol) was added and stirring was continued for 2 h at 0°C. Ethyl acetate (150 mL) was added and the solution was washed with water (3 × 150 mL) and saturated sodium chloride (150 mL), dried over sodium sulfate, and evaporated to give an orange oil. Chromatography on silica gel using ethyl acetate – hexanes (1:1) gave the product as a yellow oil (3.94 g, 83%). IR (neat) (cm^{-1}): 1778, 1755, 1746. ^1H NMR ($CDCl_3$): isomer A: 7.29 (8H, t, Ar), 6.91 (2H, t, Ar), 5.98 (1H, d, 4.1 Hz, H-4), 5.90 (1H, dt, 1.1, 4.2 Hz, H-3), 5.70 (1H, ddt, 6.5, 10.0, 17.0 Hz, CH_2C*H*=CH_2), 5.21 (2H, s, PhCH_2), 5.15–5.06 (2H, m, $CH_2CH=C$*H*$_2$), 4.93 (1H, dd, 1.1, 14.3 Hz, PhOC*H*H), 4.79 (1H, dd, 1.2, 14.3 Hz, PhOCH*H*), 3.73 (3H, s, CH_3), 3.14–3.01 (2H, m, C*H*$_2$CH=CH_2). Isomer B: 7.33 (8H, t, Ar), 7.00 (2H, t, Ar), 5.95 (1H, d, 4.2 Hz, H-4), 5.86 (1H, dt, 1.1, 4.2 Hz, H-3), 5.68 (1H, ddt, 6.5, 10.0, 17.0 Hz, CH_2C*H*=CH_2), 5.17 (2H, s, PhCH_2), 5.15–5.06 (2H, m, $CH_2CH=C$*H*$_2$), 4.86 (1H, dd, 1.0, 14.3 Hz, PhOC*H*H), 4.61 (1H, dd, 1.3, 14.2 Hz, PhOCH*H*), 3.69 (3H, s, CH_3), 3.14–3.01 (2H, C*H*$_2$CH=CH_2). ^{13}C NMR ($CDCl_3$): 172.93, 172.87 (thiazoline N=C, both isomers), 166.50, 166.124, 165.99, 165.58, 164.23, 164.12 (β-lactam C=O, ester C=O, both isomers), 157.78, 131.04–128.34, 127.60–121.94, 114.84 (aromatic, both isomers), 134.67, 134.53 (CH=*C*H_2, both isomers), 120.45, 120.41 (*C*H=CH_2, both isomers), 90.77 (C-3, both isomers), 70.11, 70.03 (CO_2CH_2Ph, both isomers), 68.86, 68.71 (malonyl C, both isomers), 68.39 (C-4, both isomers), 67.86, 67.80 (PhOCH_2, both isomers), 53.41, 53.31 (CO_2CH_3, both isomers), 38.23, 38.02 (*C*H_2CH=CH_2). Anal. calcd. for $C_{25}H_{24}N_2O_6S$: C 62.49, H 5.03, N 5.83;. Found: C 62.28, H 5.17, N 5.78.

Conversion of 14 into the hydroxycepham 17

A solution of **14** (8.14 g, 20.1 mmol) in dichloromethane (100mL) and methanol (50 mL) was cooled to –78°C, and treated with ozone at a rate of 1.5 L min^{-1} until a blue colour persisted. Excess ozone was purged using nitrogen gas, and the reaction was quenched with dimethyl sulfide (12.3 mL, 10.4 g, 167.5 mmol). The cooling bath was then removed and the solution was allowed to warm to room temperature. Evaporation of the solvent afforded a yellow syrup (9.0 g). This was dissolved in a mixture of dichloromethane (150 mL) and acetone (150 mL), and treated with 3% perchloric acid (25 mL, 0.75 g, 7.47 mmol). The mixture was stirred for 90 min and then diluted with ethyl acetate (300 mL), washed with saturated sodium chloride (6 × 100 mL), dried over magnesium sulfate, and evaporated to give a yellow oil. Purification by column chromatography using ethyl acetate – hexanes (1:1) yielded **17** (8.0 g, 94%). $[\alpha]_D^{20}$ +217.7° (c 0.40, $CHCl_3$). Mass spectrum (CI, *m*/*z*): 407 ((M+1)-H_2O). IR (KBr) (cm^{-1}): 3480, 3341, 1778, 1753, 1680. ^1H NMR ($CDCl_3$): 7.38 (1H, d, 9.3 Hz, NH), 7.31 (2H, t, Ar), 7.01 (1H, t, Ar), 6.92 (2H, d, Ar), 5.77 (1H, dd, 4.6, 9.3 Hz, H-7), 5.55 (1H, d, 4.6 Hz, H-6), 5.35 (1H, 2.3, 3.9, H2), 4.52 (2H, s, PhOCH_2), 3.85 (3H, s, CH_3), 3.81 (3H, s, CH_3), 2.78 (1H, dd, 3.9, 14.4 Hz, H-3), 2.53 (1H, dd, 2.3, 14.4 Hz, H-3). ^{13}C NMR ($CDCl_3$): 168.91 (acetamido C=O), 167.83 (β-lactam C=O), 165.04 (ester C=O), 163.76 (ester C=O), 156.94, 129.76, 122.36, 114.84 (aromatic), 70.71 (C-2), 67.11 (PhOCH_2), 61.70 (C-7), 59.01 (C-6), 54.63 (C-4), 53.94 (CO_2CH_3), 53.47 (CO_2CH_3), 35.62 (C-3). Anal. calcd. for $C_{18}H_{20}N_2O_8S$: C 50.94, H 4.75, N 6.60; found: C 50.58, H 4.89, N 6.16.

Dehydration of 17

A solution of **17** (200 mg, 0.47 mmol) in acetic anhydride (1.4 mL, 1.5 g, 14.8 mmol) was treated, with stirring, with a 1% w/v solution of sulfuric acid in acetic acid (0.3 mL, 3 mg, 0.03 mmol). After 2.5 h, sodium acetate hexahydrate (750 mg, 3.9 mmol) was added and stirring was continued overnight. Ethyl acetate (50 mL) was added and the organic layer was washed successively with water (2 × 50 mL) and saturated sodium bicarbonate (50 mL), dried over magnesium sulfate, and evaporated to give a pale yellow oil. A solution of this oil in toluene (150 mL) was treated with *p*-toluenesulfonic acid monohydrate (70 mg, 0.37 mmol), and the mixture, protected from moisture by a calcium chloride drying tube, was refluxed overnight. The solvent was then evaporated under reduced pressure. The residue was purified by column chromatography using ethyl acetate – hexanes (3:2) to give the 4,4-dimethoxycarbonyl-Δ^2-cephem **19** as a yellow foam (489 mg, 52%). $[\alpha]_D^{20}$ +400.0° (c 0.26, $CHCl_3$). Mass spectrum (CI, *m*/*z*): 407 (M+1). IR (KBr) (cm^{-1}): 3310, 1786, 1748, 1690. ^1H NMR ($CDCl_3$): 7.39 (1H, d, 9.0 Hz, NH), 7.33 (2H, t, Ar), 7.04 (1H, t, Ar), 6.94 (2H, d, Ar), 6.47 (1H, d, 10.4 Hz, H-2), 6.07 (1H, d, 10.4 Hz, H-3), 5.81 (1H, dd, 4.2, 9.0 Hz, H-7), 5.31 (1H, d, 4.2 Hz, H-6), 4.56 (2H, s, PhOCH_2), 3.87 (3H, s, CH_3), 3.84 (3H, s, CH_3).

© 2001 NRC Canada

^{13}C NMR ($CDCl_3$): 168.58 (acetamido C=O), 166.07 (β-lactam C=O), 164.28 (ester C=O), 163.23 (ester C=O), 157.10, 129.82, 122.48, 114.96 (aromatic), 122.20 (C-2), 115.18 (C-3), 67.37 ($PhOCH_2$), 63.67 (C-4), 59.67 (C-7), 55.08 (C-6), 54.00 (CO_2CH_3), 53.66 (CO_2CH_3). Anal. calcd. for $C_{18}H_{18}N_2O_7S$: C 53.20, H 4.46, N 6.89; found: C 53.38, H 4.66, N 6.55.

Conversion of the allylated dimethyl ester to 20 (R_1 = R_2 = Me)

A solution of the dimethyl ester (3.38 g, 8.70 mmol) in a mixture of dichloromethane (123 mL) and water (61 mL) was treated in two portions during 30 min with iodine (2.45 g, 9.65 mmol). The purple reaction mixture was stirred at room temperature for 5.5 h, and the reaction was then quenched with 1% sodium sulfite (50 mL). The organic layer was washed successively with water (2 × 150 mL) and saturated sodium chloride (150 mL), dried over magnesium sulfate, and evaporated to give a yellow foam. Purification by column chromatography using ethyl acetate – hexanes (1:1) afforded a white foam (3.24 g, 68%). $[\alpha]_D^{20}$ +177.8° (c 0.135, $CHCl_3$). Mass spectrum (CI, *m*/*z*): 423 ((M+1)-I). IR (KBr) (cm^{-1}): 3318, 1780, 1748, 1690. ^{1}H NMR ($CDCl_3$): 7.32 (3H, t, Ar + NH), 7.03 (1H, t, Ar), 6.93 (2H, d, Ar), 5.82 (1H, dd, 4.6, 9.5 Hz, H-7), 5.39 (1H, d, 4.6 Hz, H-6), 4.54 (2H, s, $PhOCH_2$), 3.86 (3H, s, CH_3), 3.85 (3H, s, CH_3), 3.28 (1H, dd, 5.4, 10.3 Hz, C*H*HI), 3.18 (1H, dd, 8.0, 10.3 Hz, CH*H*I), 2.95 (1H, m, H-2), 2.74 (1H, dd, 1.9, 14.1 Hz, H-3), 2.03 (1H, dd, 12.2, 14.1 Hz, H-3). Anal. calcd. for $C_{19}H_{21}IN_2O_7S$: C 41.62, H 3.86, N 5.11; found: C 41.81, H 3.86, N 5.02.

Conversion of the allylated dibenzyl ester to 20 (R_1 = R_2 = CH_2Ph)

Iodine (1.35 g, 5.3 mmol) was added in three portions over 30 min to a biphasic solution of the dibenzyl ester (2.8 g, 5.0 mmol) in dichloromethane (70 mL) and water (35 mL). The mixture was stirred for 3 h, additional dichloromethane (98 mL) was added, and the organic layer was then separated and washed successively with saturated sodium bicarbonate (200 mL), 0.01 M sodium sulfite (200 mL), water (200 mL), and saturated sodium chloride (200 mL), dried over magnesium sulfate, and evaporated. Chromatography using ethyl acetate – hexanes (1:1) gave 2.63 g (74%) of the iodomethylcepham as a yellow foam. $[\alpha]_D^{20}$ +162.5° (c 0.39, $CHCl_3$). Mass spectrum (CI, *m*/*z*): 439 ((M+1)-I-CO_2CH_2Ph). IR (KBr) (cm^{-1}): 3318, 1780, 1746, 1688. ^{1}H NMR ($CDCl_3$): 7.34–7.23 (13H, m, Ar + NH), 7.03 (1H, t, Ar), 6.94 (2H, d, Ar), 5.82 (1H, dd, 4.6, 9.6 Hz, H-7), 5.40 (1H, d, 4.6 Hz, H-6), 5.27 (1H, d, 12.0 Hz, benzyl C*H*H), 5.20 (1H, d, 11.9 Hz, benzyl CH*H*), 5.17 (1H, d, 12.0 Hz, benzyl C*H*H), 5.09 (1H, d, 11.9 Hz, benzyl CH*H*), 4.53 (2H, s, $PhOCH_2$), 3.20 (1H, dd, 5.3, 10.2 Hz, C*H*HI), 3.08 (1H, dd, 8.1, 10.2 Hz, CH*H*I), 2.84 (1H, m, shows nOe with H-6 at 5.40 ppm, H-2), 2.71 (1H, dd, 1.9, 14.1 Hz, H-3), 2.03 (1H, dd, 12.3, 14.1 Hz, H-3). ^{13}C NMR ($CDCl_3$): 168.42 (acetamido C=O), 166.33 (β-lactam C=O), 164.36 (ester C=O), 163.86 (ester C=O), 157.09, 134.46, 134.32, 129.82, 128.97, 128.80, 128.62, 128.56, 122.45, 114.99 (aromatic), 69.05, 68.58 (CO_2CH_2Ph), 67.33 ($PhOCH_2$), 66.16 (C-4), 58.88 (C-7), 58.28 (C-6), 38.72 ($CHCH_2I$), 37.31 (C-2), 5.95 (C-3). Anal. calcd. for $C_{31}H_{29}N_2IO_2S$: C 53.15, H 4.17, N 4.00; found: C 53.15, H 4.02, N 3.89.

Conversion of the allylated methyl benzyl ester to 20 (R_1 = Me, R_2 = CH_2Ph)

Iodine (1.64 g, 6.46 mmol) was added in two portions over 30 min to a solution of the mixed ester (both diastereomers) (2.75 g, 5.90 mmol) in a biphasic mixture of dichloromethane (83 mL) and water (41 mL). The purple solution was stirred at room temperature for 5 h, the reaction was quenched with 1% sodium sulfite (50 mL), and the organic layer was then washed successively with water (2 × 80 mL) and saturated sodium chloride (80 mL), dried over magnesium sulfate, and evaporated. Purification by column chromatography using ethyl acetate – hexanes (1:1) afforded the product as a white foam (3.34 g, 94%). Mass spectrum (CI, *m*/*z*): 363 ((M+1)-(I+CO_2CH_2Ph)).IR (KBr) (cm^{-1}): 3310, 1778, 1748, 1688. ^{1}H NMR ($CDCl_3$): isomer A: 7.41–7.29 (8H, m, Ar + NH), 7.03 (1H, t, Ar), 6.93 (2H, d, Ar), 5.80 (1H, dd, 4.6, 9.6 Hz, H-7), 5.38 (1H, d, 4.6 Hz, H-6), 5.25 (2H, s, $PhCH_2$), 4.53 (2H, s, $PhOCH_2$), 3.78 (3H, s, CH_3), 3.19 (1H, dd, 5.3, 10.3 C*H*HI), 3.09 (1H, dd, 8.0, 10.3 Hz, CH*H*I), 2.81 (1H, m, H-2), 2.70 (1H, dd, 1.9, 14.1 Hz, H-3), 2.00 (1H, dd, 12.2, 14.1 Hz, H-3). Isomer B: 7.41–7.30 (8H, m, Ar + NH), 7.04 (1H, t, Ar), 6.93 (2H, d, Ar), 5.84 (1H, dd, 4.6, 9.6 Hz, H-7), 5.39 (1H, d, 4.6 Hz, H-6), 5.28 (1H, d, 12.1 Hz, PhC*H*H), 5.17 (1H, d, 12.1 Hz, PhCH*H*), 4.54 (2H, s, $PhOCH_2$), 3.74 (3H, s, CH_3), 3.27 (1H, dd, 5.4, 10.3 Hz, C*H*HI), 3.18 (1H, dd, 7.8, 10.3 Hz, CH*H*I), 2.96 (1H, m, H-2), 2.73 (1H, dd, 1.8, 14.0 Hz, H-3), 2.04 (1H, dd, 12.4, 14.0 Hz, H-3). ^{13}C NMR ($CDCl_3$): 168.44 (acetamido C=O), 166.34 (β-lactam C=O), 164.40 (ester C=O), 164.29 (ester C=O), 157.09, 134.44, 129.81, 129.05, 128.83, 128.65, 122.45, 114.99 (aromatic), 68.60 (CO_2CH_2Ph), 67.33 ($PhOCH_2$), 65.96 (C-4), 58.88 (C-7), 58.23 (C-6), 53.74 (CO_2CH_3), 38.71 (CH_2I), 37.28 (C-2), 5.98 (C-3). Anal. calcd. for $C_{25}H_{25}N_2IO_7S$: C 48.09, H 4.04, N 4.49; found: C 48.41, H 4.02, N 4.29.

Synthesis of 21 (R_1 = R_2 = Me)

A solution of the iodomethylcepham (3.24 g, 5.91 mmol) in methanol (250 mL) was treated dropwise with stirring, during 15 min, with a solution of sodium periodate (1.34 g, 6.27 mmol) in methanol (28 mL) and water (28 mL). When the addition was complete, the mixture was heated to 35°C, and stirring was continued for 2.0 h. A white precipitate was removed by filtration, and washed with ethyl acetate (200 mL). The combined filtrates were washed successively with water (200 mL) and saturated sodium chloride (200 mL), dried over magnesium sulfate, and evaporated to give a brown foam. Column chromatography using ethyl acetate – hexanes (2:3) gave the sulfoxide as a pale yellow foam (1.19 g, 36%). Mass spectrum (CI, *m*/*z*): 437 ((M+1)-I). ^{1}H NMR ($CDCl_3$): 8.05 (1H, d, 10.6 Hz, NH), 7.30 (2H, t, Ar), 7.01 (1H, t, Ar), 6.93 (2H, d, Ar), 6.12 (1H, dd, 4.8, 10.6 Hz, H-7), 4.85 (1H, d, 4.7 Hz, H-6), 4.55 (2H, s, $PhOCH_2$), 3.89 (3H, s, CH_3), 3.86 (3H, s, CH_3), 3.46 (1H, dd, 7.2, 10.7 Hz, C*H*HI), 3.26 (1H, dd, 8.0, 10.7 Hz, CH*H*I), 2.86 (1H, dd, 12.7, 14.7 Hz, H-3), 2.68 (1H, m, H-2), 2.30 (1H, dd, 2.0, 14.7 Hz, H-3).

© 2001 NRC Canada

Synthesis of 21 (R_1 = R_2 = CH_2Ph)

A solution of sodium periodate (44.0 mg, 0.21 mmol) in 50% methanol (0.7 mL) was added dropwise at 55°C to a solution of the iodomethylcepham (113.6 mg, 0.16 mmol) in methanol (7 mL). When the addition was complete, more 50% methanol (2 mL) was added, and the solution was stirred at 60°C for 2 h and then diluted with water (20 mL). Extraction with dichloromethane (4 × 10 mL), drying over magnesium sulfate and evaporation, followed by column chromatography using ethyl acetate – hexanes (1:1) yielded the β-sulfoxide (53.7 mg, 62%). Mass spectrum (CI, *m*/*z*): 455 ((M+1)-I-CO_2CH_2Ph). IR (KBr) (cm^{-1}): 3381, 1788, 1746, 1692, 1082. ^{1}H NMR ($CDCl_3$): 8.07 (1H, d, 10.5 Hz, NH), 7.34–7.23 (12H, m, Ar), 7.03 (1H, t, Ar), 6.92 (2H, d, Ar), 6.11 (1H, dd, 4.8, 10.5 Hz, H-7), 5.29 (1H, d, 12.0 Hz, benzyl C*H*H), 5.21 (1H, d, 11.8 Hz, benzyl CH*H*), 5.19 (1H, d, 12.0 Hz, benzyl C*H*H), 5.11 (1H, d, 11.8 Hz, benzyl CH*H*), 4.85 (1H, d, 4.8 Hz, H-6), 4.54 (2H, s, $PhOCH_2$), 3.38 (1H, dd, 7.6, 10.7 Hz, C*H*HI), 3.16 (1H, dd, 7.9, 10.7 Hz, CH*H*I), 2.84 (1H, dd, 12.7, 14.7 Hz, β-H-3), 2.52 (1H, m, H-2), 2.23 (1H, dd, 1.8, 14.7 Hz, α-H-3). ^{13}C NMR ($CDCl_3$): 168.65 (acetamido C=O), 166.30 (β-lactam C=O), 163.95 (ester C=O), 162.97 (ester C=O), 157.18, 134.38, 134.21, 129.91, 129.80, 129.72, 129.17, 128.90, 128.74, 128.66, 128.63, 128.58, 128.49, 128.36, 122.38, 122.28, 115.00, 114.92 (aromatic), 69.31 (CO_2CH_2Ph), 69.26 (C-6) 68.85 (CO_2CH_2Ph), 67.23 ($PhOCH_2$), 65.21 (C-4), 58.97 (C-7), 55.36 (C-2), 24.96 ($CHCH_2I$), 1.16 (C-3).

Synthesis of 21 (R_1 = Me, R_2 = CH_2Ph)

A solution of the mixed iodomethylcephams (2.83 g, 4.71 mmol) in methanol (200 mL) was treated, during 15 min, with a solution of sodium periodate (1.32 g, 6.17 mmol) in 50% methanol (46 mL). The reaction mixture was heated to 35°C and stirred for 2.5 h. A white precipitate was then removed by filtration and washed with ethyl acetate (200 mL). The filtrate was washed successively with water (200 mL) and saturated sodium chloride (200 mL), dried over magnesium sulfate, and evaporated to give a brown foam. Column chromatography using ethyl acetate – hexanes (1:1) yielded the mixed sulfoxides as a pale yellow foam (1.52 g, 52%). Mass spectrum (CI, *m*/*z*): 378 ((M+1)-(I+CO_2CH_2Ph)). IR ($CHCl_3$) (cm^{-1}): 3364, 1782, 1748, 1692. ^{1}H NMR ($CDCl_3$): isomer A: 8.04 (1H, d, 10.6 Hz, NH), 7.40–7.26 (7H, m, Ar), 7.00 (1H, t, Ar), 6.92 (2H, d, Ar), 6.10 (1H, dd, 4.8, 10.6 Hz, H-7), 5.26 (2H, s, $PhCH_2$), 4.81 (1H, d, 4.8 Hz, H-6), 4.54 (2H, s, $PhOCH_2$), 3.81 (3H, s, CH_3), 3.36 (1H, dd, 7.7, 10.7 Hz, C*H*HI), 3.11 (1H, dd, 7.8, 10.7 Hz, CH*H*I), 2.81 (1H, dd, 12.7, 14.8 Hz, H-3), 2.22 (1H, dd, 2.0, 14.8 Hz, H3), 2.48 (1H, m, H-2). Isomer B: 8.08 (1H, d, 10.6 Hz, NH), 7.40–7.26 (7H, m, Ar), 7.00 (1H, t, Ar), 6.92 (2H, d, Ar), 6.13 (1H, dd, 4.8, 10.6 Hz, H-7), 5.30 (1H, d, 11.9 Hz, PhC*H*H), 5.23 (1H, d, 11.9 Hz, PhCH*H*), 4.87 (1H, d, 4.8 Hz, H-6), 4.54 (2H, s, $PhOCH_2$), 3.76 (3H, s, CH_3), 3.46 (1H, dd, 7.4, 10.7 Hz, C*H*HI), 3.26 (1H, dd, 8.0, 10.7 Hz, CH*H*I), 2.87 (1H, dd, 12.7, 14.1 Hz, H-3), 2.28 (1H, dd, 1.8, 14.7 Hz, H-3), 2.69 (1H, m, H-2).

Dehydroiodination of 21 (R_1 = R_2 = Me)

1,8-Diazabicyclo[5.4.0]undec-7-ene (0.26 mL, 0.27 g, 1.74 mmol) was added to a solution of the sulfoxide (814 mg, 1.44 mmol) in dichloromethane (30 mL). The solution was stirred for 1.0 h, and then washed successively with 0.5 M hydrochloric acid (50 mL) and water (50 mL), dried over sodium sulfate, and evaporated. Purification by column chromatography using ethyl acetate – hexanes (3:2) gave the exomethylene compound as a white foam (226 mg, 36%). $[\alpha]_D^{20}$ +136.8° (c 0.095, $CHCl_3$). Mass spectrum (CI, *m*/*z*): 437 (M+1). IR (KBr) (cm^{-1}): 3370, 1786, 1750, 1694. ^{1}H NMR ($CDCl_3$): 8.21 (1H, d, 10.8 Hz, NH), 7.30 (2H, t, Ar), 7.01 (1H, t, Ar), 6.93 (2H, d, Ar), 6.05 (1H, dd, 4.7, 10.8 Hz, H-7), 5.93 (1H, s, CH=C*H*H), 5.65 (1H, s, CH=CH*H*), 4.80 (1H, d, 4.7 Hz, H-6), 4.55 (2H, s, $PhOCH_2$), 3.90 (3H, s, CH_3), 3.88 (1H, d, 14.3 Hz, H-3), 3.82 (3H, s, CH_3), 2.75 (1H, d, 14.3 Hz, H-3). ^{13}C NMR ($CDCl_3$): 168.56 (acetamido C=O), 166.29 (β-lactam C=O), 164.00 (ester C=O), 163.58 (ester C=O), 157.23, 129.69, 122.19, 114.93 (aromatic), 144.42 (C-2), 122.64 (C=*C*H_2), 71.40 (C-6), 67.21 ($PhOCH_2$), 66.60 (C-4), 59.34 (C-7), 54.06 (CO_2CH_3), 53.63 (CO_2CH_3), 27.59 (C-3). Anal. calcd. for $C_{19}H_{20}N_2O_8S\cdot H_2O$: C 50.22, H 4.88, N 6.16; found: C 49.91, H 4.86, N 5.87.

Dehydroiodination of 21 (R_1 = R_2 = CH_2Ph)

1,8-Diazabicyclo[5.4.0]undec-7-ene (0.40 mL, 0.41 g, 2.7 mmol) was added dropwise to a solution of the sulfoxide (0.44 g, 0.61 mmol) in dichloromethane (20 mL). The solution was stirred for 40 min and 0.5 M hydrochloric acid (20 mL) was then added. The organic layer was separated and washed successively with water (20 mL), saturated sodium bicarbonate (20 mL), and saturated sodium chloride (20 mL), dried over magnesium sulfate, and evaporated. Chromatography using ethyl acetate – hexanes (1:1) gave 0.19 g (52%) of the product as a white foam, mp 55–57°C. $[\alpha]_D^{20}$ +166.7° (c 0.072, $CHCl_3$). Mass spectrum (CI, *m*/*z*): 454 ((M+1)-CO_2CH_2Ph). IR (KBr) (cm^{-1}): 3362, 1788, 1748, 1694, 1044. ^{1}H NMR ($CDCl_3$): 8.23 (1H, d, 10.6 Hz, NH), 7.35–7.23 (12H, m, Ar), 7.00 (1H, t, Ar), 6.92 (2H, d, Ar), 6.03 (1H, dd, 4.7, 10.6 Hz, H-7), 5.71 (1H, s, =C*H*H), 5.31 (1H, d, 12.0 Hz, benzyl C*H*H), 5.24 (1H, s, benzyl CH*H*), 5.21 (1H, s, benzyl C*H*H), 5.12 (1H, s, =CH*H*), 5.03 (1H, d, 12.0 Hz, benzyl CH*H*), 4.81 (1H, d, 4.7 Hz, H-6), 3.84 (1H, d, 14.2 Hz, H-3), 2.66 (1H, d, 14.2 Hz, H-3). ^{13}C NMR ($CDCl_3$): 168.54 (acetamido C=O), 165.54 (β-lactam C=O), 164.18 (ester C=O), 163.00 (ester, C=O), 157.24, 134.43, 129.69, 129.12, 128.88, 128.80, 128.68, 128.65, 128.58, 122.18, 114.94 (aromatic), 143.87 (C-2), 122.77 (=CH_2), 71.33 (C-6), 69.24 (CO_2CH_2Ph), 68.52 (CO_2CH_2Ph), 67.21 ($PhOCH_2$), 66.52 (C-4), 59.28 (C-7), 27.49 (C-3). Anal. calcd. for $C_{31}H_{28}N_2O_8S$: C 62.91, H 4.98, N 5.10; found: C 63.25, H 4.79, N 4.76.

Dehydroiodination of 21 (R_1 = Me, R_2 = CH_2Ph)

1,8-Diazabicyclo[5.4.0]undec-7-ene (0.4 mL, 0.41 g, 2.67 mmol) was added to a solution of the mixed sulfoxides (1.27 mg, 2.07 mmol) in dichloromethane (42 mL). The solution was stirred for 1.5 h and then washed successively with 0.5 M hydrochloric acid (50 mL) and water (50 mL), dried over sodium sulfate, and evaporated. Purification by column chromatography using ethyl acetate – hexanes (1:1) afforded two compounds (514 mg, 49%): epimer B (R_f 0.25,

© 2001 NRC Canada

308 mg) and epimer A (R_f 0.14, 207 mg). Epimer A: $[\alpha]_D^{20}$ +123.8° (c 0.84, $CHCl_3$). IR (KBr) (cm^{-1}): 3363, 1789, 1749, 1695. ^1H NMR ($CDCl_3$): 8.21 (1H, d, 10.6 Hz, NH), 7.39–7.27 (7H, m, Ar), 7.00 (1H, t, Ar), 6.94 (2H, d, Ar), 6.02 (1H, dd, 4.7, 10.6 Hz, H-7), 5.70 (1H, s, C=C*H*H), 5.29 (1H, d, 11.7 Hz, PhC*H*H), 5.17 (1H, d, 11.7 Hz, PhCH*H*), 5.10 (1H, br s, C=CH*H*), 4.78 (1H, d, 4.7 Hz, H-6), 4.54 (2H, s, $PhOCH_2$), 3.85 (3H, s, CH_3), 3.83 (1H, br d, 14.2 Hz, H-3), 2.74 (1H, d, 14.2 Hz, H-3). ^{13}C NMR ($CDCl_3$): 168.57 (acetamido C=O), 166.20 (β-lactam C=O), 164.08 (ester C=O), 162.95 (C=O), 157.24, 134.48, 129.70, 129.02, 128.66, 128.57, 122.19, 114.94 (aromatic), 144.34 (C-2), 122.74 (C=*C*H_2), 71.40 (C6), 69.17 (CO_2CH_2Ph), 67.21 ($PhOCH_2$), 66.78 (C-4), 59.34 (C-7), 53.50 (CO_2CH_3), 27.57 (C-3). Anal. calcd. for $C_{25}H_{24}N_2O_8S$: C 58.59, H 4.72, N 5.47; found: C 58.44, H 4.77, N 5.17. Epimer B: $[\alpha]_D^{20}$ +122.7° (c 0.073, $CHCl_3$). IR (KBr) (cm^{-1}): 3364, 1786, 1750, 1694. ^1H NMR ($CDCl_3$): 8.24 (1H, d, 10.6 Hz, NH), 7.37–7.26 (7H, m, Ar), 7.01 (1H, t, Ar), 6.94 (2H, d, Ar), 6.06 (1H, dd, 4.6, 10.6 Hz, H-7), 5.92 (1H, s, C=C*H*H), 5.64 (1H, br s, C=CH*H*), 5.40 (1H, d, 12.0 Hz, PhC*H*H), 5.22 (1H, d, 12.0 Hz, PhCH*H*), 4.83 (1H, d, 4.6 Hz, H-6), 4.55 (2H, s, $PhOCH_2$), 3.89 (1H, br d, 14.3 Hz, H-3), 3.71 (3H, s, CH_3), 2.74 (1H, d, 14.3 Hz, H-3). ^{13}C NMR ($CDCl_3$): 168.55 (acetamido C=O), 165.58 (β-lactam C=O), 164.09 (ester C=O), 163.55 (C=O), 157.21, 134.52, 129.68, 129.19, 129.00, 128.82, 122.17, 114.91 (aromatic), 143.86 (C-2), 122.69 (C=*C*H_2), 71.29 (C-6), 68.55 (CO_2CH_2Ph), 67.18 ($PhOCH_2$), 66.32 (C-4), 59.27 (C-7), 53.93 (CO_2CH_3), 27.41 (C-3). Anal. calcd. for $C_{25}H_{24}N_2O_8S{\cdot}0.5H_2O$: C 57.57, H 4.86, N 5.37; found: C 57.62, H 4.76, N 5.27.

Reduction of 22 (R_1 = R_2 = Me)

A solution of the sulfoxide (175 mg, 0.40 mmol) in dimethylformamide (10 mL) was cooled to 0°C, and treated with phosphorus tribromide (75 μL, 114 mg, 0.42 mmol). The reaction mixture was stirred for 30 min at 0°C, poured onto ice (20 g), and extracted with ethyl acetate (2 × 20 mL). The organic layer was washed successively with water (2 × 40 mL) and saturated sodium chloride (40 mL), dried over anhydrous sodium sulfate, and evaporated. Chromatography using ethyl acetate – hexanes (1:1) afforded the exomethylene cepham as a white foam (171 mg, 95%). $[\alpha]_D^{20}$ +305.9° (c 0.085, $CHCl_3$). IR (KBr) (cm^{-1}): 3370, 1782, 1751, 1688. ^1H NMR ($CDCl_3$): 7.41 (1H, d, 9.3 Hz, NH), 7.33 (2H, t, Ar), 7.04 (1H, t, Ar), 6.94 (2H, d, Ar), 5.75 (1H, dd, 4.4, 9.3 Hz, H-7), 5.48 (1H, d, 0.9 Hz, C=C*H*H), 5.41 (1H, d, 4.4 Hz, H-6), 5.41 (1H, d, 0.9 Hz, C=CH*H*), 4.55 (2H, s, $PhOCH_2$), 3.87 (3H, s, CH_3), 3.82 (3H, s, CH_3), 3.03 (1H, d, 14.0 Hz, H-3), 2.99 (1H, dt, 0.9, 14.0 Hz, H-3). ^{13}C NMR ($CDCl_3$): 168.49 (acetamido C=O), 166.39 (β-lactam C=O), 164.74 (esters C=O), 157.12, 129.79, 122.37, 114.94 (aromatic), 132.58 (C2), 121.39 (C=*C*H_2), 67.31 ($PhOCH_2$), 66.54 (C-4), 58.92 (C-7), 57.91 (C-6), 53.86 (CO_2CH_3), 53.50 (CO_2CH_3), 39.46 (C-3). Anal. calcd. for $C_{19}H_{20}N_2O_7S{\cdot}0.25H_2O$: C 53.70, H 4.86, N 6.59; found: C 53.63, H 5.08, N 6.70.

Reduction of 22 (R_1 = R_2 = CH_2Ph)

Phosphorus tribromide (0.046 mL, 0.13 g, 0.48 mmol) was added, with stirring, at 0°C to a solution of the exomethylene sulfoxide (0.14 g, 0.24 mmol) in dimethylformamide (5.4 mL). Stirring was continued for 1 h and the mixture was then poured onto ice (60 g) and extracted with ethyl acetate (3 × 40 mL). The organic extract was washed successively with water (4 × 40 mL) and saturated sodium chloride (100 mL), dried over anhydrous sodium sulfate, and evaporated to give the product as a yellow foam. Chromatography on Brockmann neutral alumina (40–200 mm mesh) and elution with ethyl acetate – hexanes (1:1) gave a white foam (0.13 g, 97%). $[\alpha]_D^{20}$ +206.1° (c 0.165, $CHCl_3$). IR (KBr) (cm^{-1}): 3414, 1783, 1747, 1690. ^1H NMR ($CDCl_3$): 7.40 (1H, d, 9.5 Hz, NH), 7.34–7.24 (12H, m, Ar), 7.03 (1H, t, Ar), 6.93 (2H, d, Ar), 5.74 (1H, dd, 4.4, 9.5 Hz, H-7), 5.41 (1H, d, 4.4 Hz, H-6), 5.37 (1H, s, =C*H*H), 5.27 (1H, d, 12.0 Hz, benzyl C*H*H), 5.20 (1H, 7.6 Hz, benzyl CH*H*), 5.18 (1H, d, 7.6 Hz, benzyl C*H*H), 5.09 (1H, d, 12.0 Hz, benzyl CH*H*), 5.15 (1H, s, =C*H*H), 4.54 (2H, s, $PhOCH_2$), 3.01 (1H, d, 14.0 Hz, H-3), 2.97 (1H, dt, 0.5, 14.0 Hz, H-3). ^{13}C NMR ($CDCl_3$): 168.40 (acetamido C=O), 165.68 (β-lactam C=O), 164.74 (ester C=O), 164.08 (ester C=O), 157.13, 134.52, 129.80, 128.82, 128.67, 128.60, 128.54, 122.44, 115.00 (aromatic), 132.25 (C-2), 121.46 (=CH_2), 68.93 (CO_2CH_2Ph), 68.31 (CO_2CH_2Ph), 67.40 ($PhOCH_2$), 66.68 (C-4), 58.91 (C-7), 57.89 (C-6), 39.40 (C-3). Anal. calcd. for $C_{31}H_{28}N_2O_7S{\cdot}H_2O$: C 63.04, H 5.12, N 4.74; found: C 62.89, H 4.96, N 4.99.

Reduction of 22 (R_1 = Me, R_2 = CH_2Ph) (epimer A)

A solution of the exomethylene sulfoxide (epimer A) (135 mg, 0.26 mmol) in dimethylformamide (6 mL) was cooled to 0°C and treated with phosphorus tribromide (53 μL, 151 mg, 0.56 mmol). The solution was stirred for 20 min at 0°C and then poured onto ice (10 g) and extracted with ethyl acetate (2 × 20 mL). The organic layer was washed successively with water (3 × 40 mL) and saturated sodium chloride (40 mL), dried over sodium sulfate, and evaporated. Purification by chromatography using ethyl acetate – hexanes (1:1) afforded a white foam (120 mg, 79%). IR (KBr) (cm^{-1}): 3302, 1786, 1748, 1692. ^1H NMR ($CDCl_3$): 7.41 (1H, d, 9.4 Hz, NH), 7.37–7.29 (7H, m, Ar), 7.03 (1H, t, Ar), 6.93 (2H, d, Ar), 5.74 (1H, dd, 4.4, 9.4 Hz, H-7), 5.43 (1H, s, C=C*H*H), 5.40 (1H, d, 4.4 Hz, H-6), 5.36 (1H, d, 12.1 Hz, PhC*H*H), 5.34 (1H, s, C=CH*H*), 5.18 (1H, d, 12.1 Hz, PhCH*H*), 4.54 (2H, s, $PhOCH_2$), 3.72 (3H, s, CH_3), 3.02 (1H, d, 14.1 Hz, H-3), 2.99 (1H, d, 14.1 Hz, H-3). ^{13}C NMR ($CDCl_3$): 168.45 (acetamido C=O), 166.31 (β-lactam C=O), 164.10 (ester C=O), 164.00 (ester C=O), 157.16, 134.62, 129.80, 128.54, 128.63, 128.36, 122.42, 115.02 (aromatic), 132.63 (C-2), 121.00 (C=*C*H_2), 68.84 (CO_2CH_2Ph), 67.41 ($PhOCH_2$), 66.77 (C-4), 58.95 (C-7), 57.87 (C-6), 53.31 (C-3), 39.40 (C-3). Anal. calcd. for $C_{25}H_{24}N_2O_7S$: C 60.47, H 4.87, N 5.64; found: C 60.50, H 4.84, N 5.50.

Reduction of 22 (R_1 = Me, R_2 = CH_2Ph) (epimer B)

A solution of the exomethylene sulfoxide (epimer B) (135 mg, 0.26 mmol) in dimethylformamide (6 mL) was cooled to 0°C and treated with phosphorus tribromide (53 μL, 151 mg, 0.56 mmol). The solution was stirred for 20 min at 0°C and then poured onto ice (10 g) and extracted

© 2001 NRC Canada

with ethyl acetate (2 × 20 mL). The organic layer was washed successively with water (3 × 40 mL) and saturated sodium chloride (40 mL), dried over anhydrous sodium sulfate, and evaporated. Purification by chromatography using ethyl acetate – hexanes (1:1) afforded a white foam (115 mg, 76%). Mass spectrum (CI, *m*/*z*): 362 ((M+1)-CO_2CH_2Ph). IR (KBr) (cm^{-1}): 3333, 1782, 1750, 1690. ^1H NMR ($CDCl_3$): 7.39 (1H, d, 9.4 Hz, NH), 7.38–7.29 (7H, m, Ar), 7.03 (1H, t, Ar), 6.93 (2H, d, Ar), 5.72 (1H, dd, 4.4, 9.4 Hz, H-7), 5.39 (1H, d, 4.4 Hz, H-6), 5.38 (1H, d, 0.8 Hz, C=C*H*H), 5.23 (1H, d, 12.0 Hz, PhC*H*H), 5.22 (1H, d, 12.0 Hz, PhCH*H*), 5.17 (1H, d, 0.8 Hz, C=CH*H*), 4.53 (2H, s, $PhOCH_2$), 3.79 (3H, s, CH_3), 2.99 (1H, d, 14.0 Hz, H-3), 2.95 (1H, dt, 0.8, 14.0 Hz, H-3). ^{13}C NMR ($CDCl_3$): 168.43 (acetamido C=O), 165.73 (β-lactam C=O), 164.75 (ester C=O), 164.65 (ester C=O), 157.15, 134.58, 129.80, 128.90, 128.70, 128.62, 122.41, 114.99 (aromatic), 132.23 (C-2), 121.71 (C=*C*H_2), 68.34 (CO_2CH_2Ph), 67.39 ($PhOCH_2$), 66.49 (C-4), 58.95 (C-7), 57.93 (C-6), 53.70 (CO_2CH_3), 39.36 (C-3). Anal. calcd. for $C_{25}H_{24}N_2O_7S$: C 60.47, H 4.87, N 5.64; found: C 60.47, H 4.87, N 5.39.

Isomerization of 23 (R_1 = R_2 = Me)

The exomethylenecepham (150 mg, 0.36 mmol) was dissolved in dichloromethane (5 mL), the solution was cooled to 0°C, and trifluoroacetic acid (4.0 mL, 2.70 g, 51.9 mmol) was added with stirring. Stirring was continued for 45 min at 0°C, and the solvent was then removed under reduced pressure. Column chromatography using ethyl acetate – hexanes (1:1) gave the 2-methyl-Δ^2-cephem as a white foam (122 mg, 81%). $[\alpha]_D^{20}$ +187.5° (c 0.08, $CHCl_3$). IR (KBr) (cm^{-1}): 3306, 1786, 1748, 1688. ^1H NMR ($CDCl_3$): 7.39 (1H, d, 9.0 Hz, NH), 7.32 (2H, t, Ar), 7.04 (1H, t, Ar), 6.94 (2H, d, Ar), 5.85 (1H, q, 1.4 Hz, H-3), 5.79 (1H, dd, 4.2, 9.0 Hz, H-7), 5.31 (1H, d, 4.2 Hz, H-6), 4.57 (2H, s, $PhOCH_2$), 3.86 (3H, s, CH_3), 3.83 (3H, s, CH_3), 2.01 (3H, d, 1.4 Hz, CH_3). ^{13}C NMR ($CDCl_3$): 168.70 (acetamido C=O), 166.39 (β-lactam C=O), 164.68 (ester C=O), 163.59 (ester C=O), 157.13, 129.82, 122.45, 114.98 (aromatic), 132.58 (C-2), 110.65 (C-3), 67.34 ($PhOCH_2$), 64.40 (C4), 59.49 (C-7), 56.13 (C-6), 53.90 (CO_2CH_3), 53.54 (CO_2CH_3), 24.34 (CH_3). Anal. calcd. for $C_{19}H_{20}N_2O_7S$: C 54.28, H 4.79, N 6.66; found: C 54.33, H 4.87, N 6.77.

Isomerization of 23 (R_1 = R_2 = CH_2Ph)

Trifluoroacetic acid (3 mL) was added dropwise, with stirring at 0°C, to a solution of the exomethylene cepham (0.13 g, 0.23 mmol) in dichloromethane (3 mL). The solution was stirred for 40 min and then evaporated to afford the 2-methyl-Δ^2-cephem (0.13 g, 100%) as a yellow foam. $[\alpha]_D^{20}$ +227.8° (c 0.18, $CHCl_3$). Mass spectrum (CI, *m*/*z*): 439 ((M+1)-(CO_2CH_2Ph)). IR ($CHCl_3$) (cm^{-1}): 3418, 1788, 1748, 1696. ^1H NMR ($CDCl_3$): 7.35–7.22 (13H, m, Ar + NH), 7.04 (1H, t, Ar), 6.93 (2H, d, Ar), 5.87 (1H, 1.3 Hz, H-3), 5.78 (1H, q, 4.2, 9.1 Hz, H-7), 5.33 (1H, d, 4.2 Hz, H-6), 5.24 (1H, d, 12.2 Hz, benzyl C*H*H), 5.21 (1H, d, 12.3 Hz, benzyl CH*H*), 5.18 (1H, d, 12.2 Hz, benzyl C*H*H), 5.11 (1H, d, 12.3 Hz, benzyl CH*H*), 1.99 (3H, d, 1.3 Hz, CH_3). ^{13}C NMR ($CDCl_3$): 168.50 (acetamido C=O), 165.63 (β-lactam C=O), 163.99 (ester C=O), 163.75 (ester C=O), 157.10, 134.56, 129.82, 128.65, 128.53, 128.10, 122.44, 114.96 (aromatic), 132.91 (C-2), 110.48 (C-3), 68.99 (CO_2CH_2Ph), 68.36 (CO_2CH_2Ph), 67.32 ($PhOCH_2$), 64.66 (C-4), 59.44 (C-7), 56.26 (C-6), 24.30 (CH_3). Anal. calcd. for $C_{31}H_{28}N_2O_7S$: C 64.71, H 5.01, N 5.35; found: C 65.02, H 4.93, N 4.89.

Isomerization of 23 (R_1 = Me, R_2 = CH_2Ph) (isomer A)

A solution of the exomethylenecepham (isomer A) (77 mg, 0.13 mmol) in dichloromethane (5 mL) was cooled to 0°C, treated with trifluoroacetic acid (1.7 mL, 2.52 g, 22.1 mmol), stirred for 45 min, and then evaporated to dryness. Column chromatography using ethyl acetate – hexanes (1:1) gave a white foam (63 mg, 88%). $[\alpha]_D^{20}$ +227.6° (c 0.145, $CHCl_3$). IR (KBr) (cm^{-1}): 3422, 1788, 1748, 1692, 1686. ^1H NMR ($CDCl_3$): 7.39–7.30 (8H, m, Ar + NH), 7.04 (1H, t, Ar), 6.94 (2H, d, Ar), 5.86 (1H, q, 1.3 Hz, H-3), 5.77 (1H, dd, 4.2, 9.1 Hz, H-7), 5.34 (1H, d, 16.4 Hz, PhC*H*H), 5.31 (1H, d, 4.2 Hz, H-6), 5.14 (1H, d, 16.4 Hz, PhCH*H*), 4.56 (2H, s, $PhOCH_2$), 3.74 (3H, s, CH_3), 1.99 (3H, d, 1.2 Hz, CH_3). ^{13}C NMR ($CDCl_3$): 168.64 (acetamido C=O), 165.66 (β-lactam C=O), 164.57 (ester C=O), 163.64 (ester C=O), 157.10, 134.68, 129.82, 128.68, 128.15, 122.45, 114.96 (aromatic), 68.33 (CO_2CH_2Ph), 67.31 ($PhOCH_2$), 64.51 (C-4), 59.48 (C-7), 56.15 (C-6), 53.75 (CO_2CH_3), 24.31 (CH_3). Anal. calcd. for $C_{25}H_{24}N_2O_7S$: C 60.47, H 4.87, N 5.64; found: C 60.21, H 4.73, N 5.78.

Isomerization of 23 (R_1 = Me, R_2 = CH_2Ph) (isomer B)

The exomethylenecepham (isomer B) (46 mg, 0.08 mmol) was dissolved in dichloromethane (5 mL), and the solution was cooled to 0°C and treated with trifluoroacetic acid (1.0 mL, 1.48 g, 13.0 mmol). The solution was stirred at 0°C for 45 min, and then evaporated. Purification by column chromatography using ethyl acetate – hexanes (1:1) gave a white foam (42 mg, 91%). $[\alpha]_D^{20}$ +253.9° (c 0.086, $CHCl_3$). IR (KBr) (cm^{-1}): 3412, 1788, 1748, 1692. ^1H NMR ($CDCl_3$): 7.38–7.30 (8H, m, Ar + NH), 7.04 (1H, t, Ar), 6.93 (2H, d, Ar), 5.87 (1H, q, 1.3 Hz, H-3), 5.79 (1H, dd, 4.1, 9.0 Hz, H-7), 5.35 (1H, d, 12.1 Hz, PhC*H*H), 5.33 (1H, d, 4.1 Hz, H-6), 5.20 (1H, d, 12.1 Hz, PhCH*H*), 4.56 (2H, s, $PhOCH_2$), 3.74 (3H, s, CH_3), 2.00 (3H, d, 1.2 Hz, CH_3). ^{13}C NMR ($CDCl_3$): 168.27 (acetamido C=O), 166.01 (β-lactam C=O), 163.73 (ester C=O), 163.45 (ester C=O), 156.86, 134.44, 129.55, 128.28, 128.10, 122.18, 114.72 (aromatic), 132.55 (C-2), 110.35 (C-3), 68.60 (CO_2CH_2Ph), 67.09 ($PhOCH_2$), 64.33 (C-4), 59.19 (C-7), 55.99 (C-6), 53.13 (CO_2CH_3), 24.06 (CH_3). Anal. calcd. for $C_{25}H_{24}N_2O_7S$: C 60.47, H 4.87, N 5.64; found: C 59.92, H 4.96, N 5.69.

Diazotization of dibenzyl malonate (30)

Anhydrous potassium carbonate (6.58 g, 47.6 mmol) was added to a solution of dibenzyl malonate (4.50 g, 15.8 mmol) in acetone (45 mL). The mixture was stirred for 15 min, cooled to 0°C, and a solution of benzenediazonium chloride, prepared by addition of a solution of sodium nitrite (1.10 g, 16 mmol) in water (13.2 mL) to a solution of aniline hydrochloride (2.07 g, 16.0 mmol) in 1.0 M hydrochloric acid (16.2 mL), was added dropwise. The ice bath was removed and stirring was continued at room temperature for 10 min. The reaction mixture was then poured onto crushed

© 2001 NRC Canada

ice and extracted with ethyl acetate (3 × 100 mL), dried over magnesium sulfate, and evaporated to afford a red oil which slowly solidified in the freezer. Trituration with anhydrous methanol produced yellow needles (5.21 g, 85%), mp 47–49°C. Mass spectrum (CI, *m/z*): 389 (M+1). IR (KBr) (cm^{-1}): 1726, 1530. ^1H NMR ($CDCl_3$): 7.42–7.13 (15H, m, Ar), 5.34 (2H, s, benzyl CH_2), 5.33 (2H, s, benzyl CH_2), 3.48 (1H, s, NH). ^{13}C NMR ($CDCl_3$): 163.17 (ester C=O), 163.04 (ester C=O), 141.80–115.73 (aromatic), 66.74 (CO_2CH_2Ph). Anal. calcd. for $C_{23}H_{20}N_2O_4$: C 71.12, H 5.19, N 7.21; found: C 71.17, H 4.97, N 7.10.

Dibenzyl acetamidomalonate

Zinc dust (7.23 g, 110.6 mg-atoms) was added to a solution of the diazo compound (6.50 g, 16.7 mmol) in acetic anhydride (29.0 mL, 31.4 g, 307.4 mmol) and glacial acetic acid (116 mL). The mixture was stirred at room temperature for 1 h, at 40°C for 20 min, and then filtered. The insoluble material was rinsed with glacial acetic acid (10 mL) and the combined filtrates were treated with water to the cloud point. The product was allowed to crystallize, collected, and recrystallized from absolute ethanol to give dibenzyl acetamidomalonate (1.97 g, 35%) as white needles, mp 107–109°C. Mass spectrum (CI, *m/z*): 342 (M+1). IR (KBr) (cm^{-1}): 3299, 1753, 1657. ^1H NMR ($CDCl_3$): 7.32 (6H, m, Ar), 7.25 (4H, m, Ar), 6.54 (1H, s, 7.0 Hz, NH), 5.29 (1H, d, 7.0 Hz, CH), 5.20, 5.16 (4H, ABq, 18.7 Hz, benzyl CH_2), 2.07 (3H, s, CH_3). ^{13}C NMR ($CDCl_3$): 169.66 (acetyl C=O), 166.17 (ester C=O), 134.72–128.19 (aromatic), 68.18 (CO_2CH_2Ph), 56.55 ($CH_3CONHCH$), 22.71 (CH_3CO). Anal. calcd. for $C_{19}H_{19}NO_5$: C 66.85, H 5.61, N 4.10; found: C 66.65, H 5.59, N 4.25.

Dibenzyl allyl acetamidomalonate

A solution of dibenzyl acetamidomalonate (38.1 mg, 0.112 mmol) in acetone (4.0 mL) was treated with anhydrous potassium carbonate (40.5 mg, 0.293 mmol) and sodium iodide (23.9 mg, 0.159 mmol). The mixture was stirred for 10 min, and allyl bromide (0.02 mL, 28.0 g, 0.231 mmol) was added. The mixture was then refluxed, with stirring, for 19 h, cooled, and ethyl acetate (10 mL) and water (2 mL) were added. The organic layer was separated, washed successively with 5% hydrochloric acid (10 mL), water (10 mL) and saturated sodium chloride (10 mL), dried over magnesium sulfate, and evaporated to give an oil which slowly solidified. Crystallization using hot ethyl acetate – hexanes afforded white needles (30.9 mg, 82%), mp 81 to 82°C. Mass spectrum (CI, *m/z*): 382 (M+1). IR (KBr) (cm^{-1}): 3231, 1744, 1642. ^1H NMR ($CDCl_3$): 7.30 (6H, m, Ar), 7.24 (4H, m, Ar), 6.75 (1H, s, NH), 5.48 (1H, ddt, 7.4, 10.2, 16.9 Hz, =CH), 5.16, 5.10 (4H, ABq, 12.2 Hz, benzyl CH_2), 5.02 (1H, ddt, 1.0, 1.0, 10.2 Hz, =C*H*H), 4.97 (1H, ddt, 1.0, 1.0, 16.9 Hz, =CH*H*), 3.10 (2H, ddd, 1.0, 1.0, 7.4 Hz, allyl CH_2), 2.01 (3H, s, CH_3). ^{13}C NMR ($CDCl_3$): 169.00 (acetyl C=O), 167.44 (ester C=O), 134.94, 128.57, 128.52, 128.30 (aromatic), 131.08 ($CH_2CH=CH_2$), 119.96 ($CH_2CH=CH_2$), 68.14 (CO_2CH_2Ph), 66.51 (CH_3CONHC), 37.05 ($CH_2CH=CH_2$), 22.92 (CH_3CONH). Anal. calcd. for $C_{22}H_{23}NO_5$: C 69.28, H 6.08, N 3.67; found: C 69.23, H 6.08, N 4.40.

Hydrolysis of 19

A

A solution of **19** (79 mg, 0.19 mmol) in pyridine (12 mL) was cooled to –8°C and 0.99 M potassium hydroxide (0.4 mL, 22.2 mg, 0.40 mmol, 2.1 mol equiv) was added, with stirring. Stirring was continued for 2.5 h, and the solvent was then removed under reduced pressure. The residue was dissolved in water (20 mL) and the solution was extracted with ethyl acetate (2 × 20 mL). The organic layer was dried and evaporated to give unreacted diester (4 mg). The aqueous layer was acidified to pH 4 with 0.1 N hydrochloric acid and extracted with ethyl acetate (2 × 10 mL). The extract was dried over anhydrous sodium sulfate and evaporated to give a 7:1 mixture (by ^1H NMR) of 4-carboxy-Δ^2- and 4-carboxy-Δ^3-cephems.

Δ^2-Cephem: ^1H NMR (acetone-d_6): 8.17 (1H, d, 8.7 Hz, NH), 7.30 (2H,m, Ar), 7.00 (3H, m, Ar), 6.50 (1H, dd, 2.5, 10.4 Hz, H-2), 5.97 4.1 Hz, H-6), 4.94 (1H, d, 2.5, 4.4 Hz, H-4), 4.64 (2H, s, $PhOCH_2$).

Δ^3-Cephem: ^1H NMR (acetone-d_6): 8.00 (1H, d, 9.2 Hz, NH), 7.28 (2H, m, Ar), 6.94 (3H, m, Ar), 6.58 (1H, dd, 2.6, 6.4 Hz, H-3), 5.94 (1H, dd, 4.9, 9.2 Hz, H-7), 5.15 (1H, d, 4.9 Hz, H-6), 4.70 (2H, s, $PhOCH_2$), 3.65(1H, dd, 2.6, 19.1 Hz, SC*H*H), 3.51 (1H, dd, 6.4, 19.1 Hz, SCH*H*).

A solution of the mixed 4-carboxy-Δ^2- and 4-carboxy-Δ^3-cephems in dichloromethane (10 mL) was cooled to 0°C and diazomethane was added, followed after 5 min by one drop of acetic acid. The solvent was evaporated and the residue was purified by preparative layer chromatography, using ethyl acetate – hexanes (1:1), to give a 7:1 mixture of Δ^2- and Δ^3-esters (8 mg).

Δ^2-Ester: Mass spectrum (CI, *m/z*): 349 (M+1). IR (KBr) (cm^{-1}): 3408, 1784, 1751, 1697. ^1H NMR ($CDCl_3$): 7.40 (1H, d, 9.2 Hz, NH), 7.32 (2H, t, Ar), 7.04 (1H, t, Ar), 6.93 (2H, d, Ar), 6.32 (1H, dd, 2.5, 10.4 Hz, H-2), 5.87 (1H, dd, 4.3, 10.4 Hz, H-3), 5.81 (1H, dd, 4.2, 9.2 Hz, H-7), 5.23 (1H, d, 4.2 Hz, H-6), 4.95 (1H, dd, 2.5, 4.3 Hz, H-4), 4.5 (2H, s, $PhOCH_2$). ^{13}C NMR ($CDCl_3$): 168.50 (acetamido C=O), 167.55 (β-lactam C=O), 164.37 (ester C=O), 156.97, 129.79, 122.40, 114.82 (aromatic), 119.65 (C-2), 113.35 (C-3), 67.20 ($PhOCH_2$), 60.03 (C-7), 53.32 (C-6), 53.04 (CO_2CH_3), 49.33 (C-4). Anal. calcd. for $C_{16}H_{16}N_2O_5S\cdot0.25H_2O$: C 54.46, H 4.71, N 7.84; found: C 54.21, H 4.90, N 7.44.

Δ^3-Ester: Mass spectrum (CI, *m/z*): 349 (M+1). ^1H NMR ($CDCl_3$): 7.28 (1H, d, 9.4 Hz, NH), 7.31 (2H, t, Ar), 7.04 (1H, t, Ar), 6.93 (2H, d, Ar), 6.56 (1H, dd, 2.5, 6.3 Hz, H-3), 5.97 (1H, dd, 5.0, 9.4 Hz, H-7), 5.00 (1H, d, 5.0 Hz, H-6), 4.57 (2H, s, $PhOCH_2$), 3.60 (1H, dd, 2.5, 19.2 Hz, SC*H*H), 3.42 (1H, dd, 6.4, 19.2 Hz, SCH*H*).

B

A solution of **19** (80 mg, 0.23 mmol) in pyridine (1 mL) was cooled to –8°C, and 0.99 M potassium hydroxide (0.2 mL, 0.20 mmol, 0.9 mol equiv) was added, with stirring. Stirring was continued for 2.5 h, and the solvent was then removed under reduced pressure. The residue was dis-

© 2001 NRC Canada

solved in water (10 mL) and the solution was extracted with ethyl acetate (2 × 25 mL). The organic layer was dried and evaporated to give unreacted diester (3 mg). The aqueous layer was acidified to pH 4 with 0.1 N hydrochloric acid and extracted with ethyl acetate (2 × 10 mL). The extract was dried over sodium sulfat and evaporated to give a 5.4:1 Δ^3:Δ^2 mixture of 4-carboxycephems. A solution of this mixture in dichloromethane (10 mL) was cooled to 0°C and treated with diazomethane. After 5 min, one drop of acetic acid was added, and the solvent was evaporated. The residue was purified by preparatory layer chromatography, using ethyl acetate – hexanes (1:1), to give a 5.4:1 Δ^2:Δ^3 mixture of 4-methoxycarbonylcephems (7 mg).

C

A solution of **19** (24 mg, 0.06 mmol) in acetonitrile (4 mL) and water (2 mL) was cooled to –5°C, and treated, with stirring, with 0.99 M potassium hydroxide (1.2 mL, 6.7 mg, 0.12 mmol). Stirring was continued for 1.5 h, and the solvent was then evaporated under reduced pressure. The residue was dissolved in water (20 mL) and the solution was extracted with ethyl acetate (2 × 20 mL). The organic layer was dried and evaporated to give unreacted diester (4 mg). The aqueous layer was acidified to pH 4 with 0.1 N sulfuric acid and extracted with ethyl acetate (2 × 10 mL). The extract was dried over sodium sulfate and evaporated to give the 4-carboxy-Δ^2-cephem. A solution of this compound in dichloromethane (10 mL) was cooled to 0°C and treated with diazomethane. After 5 min, one drop of acetic acid was added and the solvent was then removed. The residue was purified by preparatory layer chromatography using ethyl acetate – hexanes (1:1) to give the Δ^2-ester (5 mg, 29%).

Deprotection of 24

A

A solution of the dimethyl ester (19 mg, 0.045 mmol) in pyridine (0.24 mL) was cooled to 0°C and treated with 1 M potassium hydroxide (0.048 mL, 1.9 mg, 0.045 mmol, 1 mol equiv). Stirring was continued for 2.5 h, and the solvent was then removed under reduced pressure. The residue was dissolved in water (20 mL) and this solution was extracted with ethyl acetate (2 × 20 mL). The organic layer was evaporated and dried to give unreacted diester (7 mg). The aqueous layer was acidified to pH 4 with 0.1 N hydrochloric acid and extracted with ethyl acetate (2 × 10 mL). The extract was dried over sodium sulfate and evaporated. The residue was dissolved in dichloromethane (7 mL), cooled to 0°C, and diazomethane was added. After 30 min, one drop of acetic acid was added, and the solvent was removed. Column chromatography of the residue, using ethyl acetate – hexanes (2:3), afforded the 4-methoxycarbonyl-Δ^2-ester. $[\alpha]_D^{20}$ +424.2° (c 0.165, $CHCl_3$). Mass spectrum (CI, *m*/*z*): 363 (M+1). HR-MS-CI calcd. for $C_{17}H_{18}N_2O_5S$: 363.1015 (M+1); found: 363.1018 (M+1). IR ($CHCl_3$) (cm^{-1}): 3412, 1778, 1751, 1694. ^1H NMR ($CDCl_3$): 7.36–7.30 (3H, m, Ar + NH), 7.04 (1H, t, Ar), 6.94 (2H, d, Ar), 5.81 (1H, dd, 4.1, 9.2 Hz, H-7), 5.62 (1H, dq, 1.3, 2.7 Hz, =CH), 5.23 (1H, dd, 0.4, 4.1 Hz, H-6), 4.96 (1H, ddq, 0.4, 2.0, 2.7 Hz, shows nOe with H-3 and CH_3 at 5.62 and 1.96 ppm, respectively, allyl CH), 1.96 (3H, dd, 1.3, 2.0 Hz, CH_3). ^{13}C NMR ($CDCl_3$): 168.52 (acetamido C=O), 168.37 (ester C=O), 164.74 (β-lactam C=O), 157.13, 129.82, 122.44, 114.96 (aromatic), 130.07 (C-2), 108.68 (C-3), 67.36 ($PhOCH_2$), 59.97 (C-7), 54.57 (C-6), 52.84 (ester CH_3), 50.07 (C-4), 24.28 (CH_3).

B

To a solution of the dibenzyl ester (26.5 mg, 0.046 mmol) in 95% ethanol (6.0 mL) and water (3.0 mL) were added sodium bicarbonate (8.9 mg, 0.106 mmol) and 10% palladium on carbon (82.3 mg). The apparatus was flushed thrice with nitrogen and thrice with hydrogen, and then stirred rapidly under hydrogen for 25 min. The mixture was filtered through Celite and the Celite was rinsed with water (3 × 5 mL). The filtrate was concentrated under reduced pressure to remove ethanol, and then lyophilized to give a white solid (16.9 mg). This material, in dimethylformamide (0.2 mL), was treated with methyl iodide (5.5 μL, 12.5 mg, 0.088 mmol). The mixture was stirred for 2.5 h and then diluted with dichloromethane (5 mL), washed successively with water (3 × 5 mL) and saturated sodium chloride (5 mL), dried over magnesium sulfate, and evaporated to give the methyl ester of 2-methyl-Δ^2-cephem V (3.5 mg, 91%).

C

To a solution of the dibenzyl ester (34.3 mg, 0.056 mmol) in glacial acetic acid (7.5 mL) and water (3.6 mL) was added 10% palladium on carbon (71.2 mg). The apparatus was purged in the usual manner and the mixture was stirred rapidly under hydrogen for 20 min and then centrifuged. The pellet was suspended in ice-cold 68% acetic acid (5.0 mL) and centrifuged again. The combined supernatants were lyophilized, and the white residue, in a mixture of absolute ethanol (2.0 mL) and dichloromethane (5.0 mL), was treated with diazomethane. The solution was stirred for 2 h and the solvent was then removed under reduced pressure. Chromatography of the residue using ethyl acetate – hexanes (1:1) gave two products, the 4-methoxycarbonyl-Δ^2-cephem (R_f 0.50, 4.3 mg, 21%) as a white solid, mp 125 to 126°C, and the 4-methoxycarbonyl-Δ^2-cepham (R_f 0.44, 1.5 mg, 2%) as a colourless film. $[\alpha]_D^{20}$ +160.0° (c 0.050, $CHCl_3$). Mass spectrum (CI, *m*/*z*): 365 (M+1). HR-MS-CI calcd. for $C_{17}H_{20}N_2O_5S$: 365.1171 (M+1); found: 365.1164. IR ($CHCl_3$) (cm^{-1}): 3414, 1778, 1751, 1694. ^1H NMR ($CDCl_3$): 7.31 (3H, m, Ar + NH), 7.05 (1H, t, Ar), 6.96 (2H, d, Ar), 5.76 (1H, dd, 4.5, 9.7 Hz, H-7), 5.27 (1H, d, 4.5 Hz, H-6), 4.80 (1H, dd, 2.0, 6.2 Hz, H-4), 4.55 (2H, s, $PhOCH_2$), 3.78 (3H, s, ester CH_3), 3.06 (1H, ddq, 2.0, 6.3, 6.8 Hz, $CHCH_3$), 2.25 (1H, ddd, 2.0, 2.0, 14.1 Hz, α-H-3), 1.69 (1H, ddd, 6.3, 12.0, 14.1 Hz, β-H-3), 1.25 (3H, d, 6.8 Hz, CH_3). ^{13}C NMR ($CDCl_3$): 169.75 (acetamido C=O), 168.36 (ester C=O), 165.39 (β-lactam C=O), 157.83, 129.78, 122.40, 115.03 (aromatic), 67.43 ($PhOCH_2$), 59.13 (C-7), 56.25 (C-6), 52.68 (ester CH_3), 50.26 (C-4), 34.86 (C-2), 31.81 (C-3), 21.34 (CH_3).

D

To a solution of isomer A (46 mg, 0.093 mmol) in glacial acetic acid (10 mL) and water (4.7 mL) was added 10% palladium on carbon (103 mg). The apparatus was purged in the

© 2001 NRC Canada

usual manner and the mixture was stirred rapidly under hydrogen for 20 min and then centrifuged. The pellet was suspended in ice-cold 67% acetic acid (5.0 mL) and centrifuged again. The combined supernatants were lyophilized, and the white residue, in a mixture of absolute ethanol (2.0 mL) and dichloromethane (5.0 mL), was treated with diazomethane. The solution was stirred for 2 h and the solvent was then removed under reduced pressure. Chromatography using ethyl acetate – hexanes (1:1) gave the 4-methoxycarbonyl-Δ^2-cephem (23.3 mg).

E

To a solution of isomer B (46 mg, 0.093 mmol) in glacial acetic acid (10 mL) and water (4.7 mL) was added 10% palladium on carbon (110 mg). The apparatus was purged in the usual manner and the mixture was stirred rapidly under hydrogen for 20 min and then centrifuged. The pellet was suspended in ice-cold 68% acetic acid (5.0 mL) and centrifuged again. The combined supernatants were lyophilized, and the residue, in a mixture of absolute ethanol (2.0 mL) and dichloromethane (5.0 mL), was treated with diazomethane. The solution was stirred for 2 h and the solvent was then removed under reduced pressure. Chromatography using ethyl acetate – hexanes (1:1) afforded the Δ^2-cephem (8.8 mg) and the cepham (7.0 mg).

Deprotection of model malonates

A

To a solution of dibenzyl acetamidomalonate (29.9 mg, 0.088 mmol) in glacial acetic acid (4.1 mL) and water (2.6 mL) was added 10% palladium on carbon (119.8 mg). The apparatus was flushed thrice with nitrogen, thrice with hydrogen and the mixture was then stirred rapidly under hydrogen for 55 min and centrifuged. While the supernatant was cooled in an ice bath, the pellet was suspended in ice-cold 61% acetic acid (4 mL) and centrifuged again. The combined supernatants were lyophilized to give acetamidomalonic acid as a fluffy white solid. An ice-cold solution of this material in a mixture of dichloromethane (1.8 mL) and 95% ethanol (0.3 mL) was treated, in 10 min intervals, with diazomethane, bubbled in from a DIAZALD reaction mixture using a stream of dry nitrogen. The solvent was removed under reduced pressure and the residue, in ethyl acetate, was filtered through a short layer of silica gel. Crystallization from hot methanol gave dimethyl acetamidomalonate as white needles (13.5 mg, 81%), mp 126–128°C. Mass spectrum (EI, *m*/*z*): 189 (M). IR (KBr) (cm^{-1}): 3304, 1750, 1740, 1651. ^{1}H NMR ($CDCl_3$): 6.47 (1H, d, 7.0 Hz, NH), 5.21 (1H, d, 7.0 Hz, CH), 3.82 (6H, s, ester CH_3), 2.08 (3H, s, acetamido CH_3). ^{13}C NMR ($CDCl_3$): 169.61 (acetamido C=O), 166.81 (ester C=O), 56.14 ($CH_3CONHCH$), 53.33 (CO_2CH_3), 22.68 (CH_3CONH). Anal. calcd. for $C_7H_{11}NO_5$: C 44.45, H 5.86, N 7.40; found: C 44.35, H 5.79, N 7.41.

B

To a solution of dibenzyl allylacetamidomalonate (32.5 mg, 0.0852 mmol) in glacial acetic acid (4.2 mL) and water (2.7 mL) was added 10% palladium catalyst (116.3 mg). The mixture was purged thrice with nitrogen and thrice with hydrogen and then stirred under hydrogen for 1 h and centrifuged. The pellet was suspended in 61% acetic acid (4.0 mL), centrifuged again, and the combined supernatants were lyophilized to give the malonic acid. This was dissolved in a mixture of dichloromethane (1.8 mL) and 95% ethanol (0.3 mL), the solution was cooled in an ice bath, and excess diazomethane was introduced in a stream of dry nitrogen. The solution was stirred for 2 h, evaporated, and the residue, in ethyl acetate (2 mL), was flushed through a short column of silica gel. Evaporation and crystallization from ethyl acetate – hexanes afforded dimethyl *n*-propyl acetamidomalonate as white needles (19.2 mg, 82%) mp 127 to 128°C. Mass spectrum (CI, *m*/*z*): 232 (M+1). IR (KBr) (cm^{-1}): 3273, 1748, 1642. ^{1}H NMR ($CDCl_3$): 6.77 (1H, br s, NH), 3.77 (6H, s, ester CH_3), 2.29 (2H, m, CH_2), 2.03 (3H, s, acetamido CH_3), 1.12 (2H, m, CH_2), 0.90 (3H, t, 7.3 Hz, CH_3). ^{13}C NMR ($CDCl_3$): 168.89 (acetamido C=O), 168.75 (ester C=O), 66.62 ($CH_3CONHC(CO_2CH_3)_2$), 53.30 (CO_2CH_3), 34.52 ($CH_3CONHCCH_2CH_2CH_3$), 22.96 (CH_3CONH), 17.08 ($CH_3CONHCCH_2CH_2CH_3$), 13.74 ($NHCCH_2CH_2CH_3$). Anal. calcd. for $C_{10}H_{17}NO_5$: C 51.94, H 7.41, N 6.06; found: C 52.13, H 7.44, N 5.88.

Acknowledgements

This research was supported by the Natural Sciences and Engineering Research Council of Canada (NSERC). The authors thank Dr. Raymond Bowers, Dr. Blair Johnston, Avtar Sundher, Jason Galpin, and Marie-Claire Wilson for preliminary synthetic studies related to this project.

References

1. S. Wolfe. Can. J. Chem. **72**, 1014 (1994).
2. S. Mobashery and M. Johnston. J. Org. Chem. **51**, 4723 (1986), and refs. cited therein.
3. J.-M. Frère, J.A. Kelly, D. Klein, and J.-M. Ghuysen. Biochem. J. **203**, 223 (1982), and refs. cited therein.
4. J.-M. Frére, M. Nguyen-Distèche, J. Coyette, and B. Joris. *In* The chemistry of β-lactams. *Edited by* M.I. Page. Blackie Academic and Professional, London. 1992. p. 148.
5. E.J. Lietz, H. Truher, D. Kahn, M.L. Hokenson, and A.L. Fink. Biochemistry, **39**, 4971 (2000), and refs. cited therein; M. Hata, Y. Fujii, M. Ishii, T. Hoshino, and M. Tsuda. Chem. Pharm. Bull. **48**, 447 (2000), and refs. cited therein.
6. R.B. Morin, B.G. Jackson, R.A. Mueller, E.R. Lavagnino, W.B. Scanlon, and S.L. Andrews. J. Am. Chem. Soc. **96**, 1401 (1969); g.V. Kaiser, R.D.G. Cooper, R.E. Koehler, C.F. Murphy, J.A. Webber, I.G. Wright, and E.M. Van Heyningen. J. Org. Chem. **35**, 2430 (1970).
7. J.M. Frère and B. Joris. CRC Crit. Rev. Microbiol. **11**, 299 (1985).
8. J.A. Kelly, J.R. Knox, P.C. Moews, G.J. Hine, J.B. Bartolone, H. Zhao, B. Joris, J.M. Frère, and J.M. ghuysen. J. Biol. Chem. **260**, 6449 (1985).
9. N.C. Cohen. J. Med. Chem. **26**, 259 (1983).
10. N.C. Cohen, I. Ernest, H. Fritz, H. Fuhrer, G. Ribs, R. Scartazzini, and P. Wirz. Helv. Chim. Acta, **70**, 1967 (1987).
11. S. Wolfe and T. Hoz. Can. J. Chem. **72**, 1044 (1994).
12. K. Kühlein and H. Jensen. Liebigs Ann. Chem. 369 (1974).
13. A.G. Long. *In* Recent advances in the chemistry of β-lactam antibiotics. *Edited by* J. Elks. Spec. Pub. Roy. Soc. Chem., London. 1976. p. 214.

© 2001 NRC Canada

14. R.D.G. Cooper and F.L. José. J. Am. Chem. Soc. **92**, 2575 (1970).
15. M. Narisada, H. Onoue, M. Ohtani, F. Watanabe, T. Okada, and W. Nagata. Tetrahedron Lett. 1755 (1978).
16. S. Wolfe, B.M. Pinto, V. Varma, and R.Y.N. Leung. Can. J. Chem. **68**, 1051 (1990); S. Wolfe and Z. Shi. Isr. J. Chem. **40**, 343 (2000).
17. R.D.G. Cooper, P.V. DeMarco, J.C. Cheng, and N.D. Jones. J. Am. Chem. Soc. **91**, 1408 (1969); R.D.G. Cooper, P.V. DeMarco, and D.O. Spry. J. Am. Chem. Soc. **91**, 1528(1969); D.H.R. Barton, F. Comer, and P.G. Sammes. J. Am. Chem. Soc. **91**, 1529 (1969).
18. H.C. Neu. Rev. Infect. Dis. **5**, S319 (1983).
19. E.P. Serjeant and B. Dempsey. Ionization constants of organic acids in aqueous solution. IUPAC Chem. Data Ser. **23**, 42 (1979).
20. (*a*) L. Ghosez, J. Marchand-Brynaert, J. Vekemans, and S. Bogdan. Tetrahedron, **39**, 2493 (1983); (*b*) W.-B. Choi, H.R.O. Churchill, J.E. Lynch, A.S. Thompson, G.R. Humphrey, R.P. Volante, P.J. Reider, and I. Shinkai. Tetrahedron Lett. **35**, 2275 (1994).
21. M.J.S. Dewar, E.G. Zoebisch, E.F. Healy, and J.J.P. Stewart. J. Am. Chem. Soc. **107**, 3902 (1985).
22. K.B. Wiberg and K.E. Laidig. J. Am. Chem. Soc. **110**, 1872 (1988).
23. R.D. Bach and C. Canepa. J. Org. Chem. **61**, 6346 (1996).
24. G.A. Hall, Jr. and E.S. Hanrahan. J. Phys. Chem. **69**, 2402 (1965).
25. D.D. Perrin and W.L.F. Armarego. *In* Purification of laboratory chemicals. 3rd ed. Pergamon Press, London. 1988.
26. W.C. Still, M. Kahn, and A. Mitra. J. Am. Chem. Soc. **43**, 2923 (1978).
27. R.D.G. Cooper and F.L. José. J. Am. Chem. Soc. **94**, 1021 (1972).
28. C.S. Palmer and P.W. McWherter. Org. Synth. Coll. **1**, 245 (1950).
29. M. Cossement, J. Marchant-Brynaert, S. Bogdan, and L. Ghosez. Tetrahedron Lett. **24**, 2563 (1983).
30. B.E. Hoogenboom, P.J. Ihrig, A.N. Langsjoen, C.J. Linn, and S.D. Mulder. J. Chem. Ed. **68**, 689 (1991).

© 2001 NRC Canada

Generation, electrocyclic ring opening, and unprecedented conversion of a 3-acylaminoazetinone into *cis*-3,4-disubstituted azetidinones

Saul Wolfe, Stephen Ro, and Zheng Shi

Abstract: An attempt to synthesize the nucleus of cefaclor by insertion of an appropriately functionalized rhodium carbene into a β-lactam N—H bond leads instead to attack at sulfur, followed by fragmentation into a four-membered thietanone and a four-membered 3-acylaminoazetinone. The azetinone undergoes electrocyclic ring opening, with a calculated half-life of 11 s at 40°C, to a *trans*-disubstituted vinyl isocyanate, but can be trapped by saturated, unsaturated allylic and benzylic alcohols to form 3,4-disubstituted azetidinones in which the *cis*- isomer predominates.

Key words: rhodium carbene, torquochemical, azetinone, mercaptoazetidinone.

Résumé : Un essai de synthèse du noyau cefaclor, par insertion d'un carbène de rhodium fonctionnalisé de façon appropriée dans une liaison N—H d'un β-lactame, conduit plutôt à une attaque au niveau du soufre, suivie d'une fragmentation en une thiétanone à quatre chaînons et à une 3-acétylaminoazétinone à quatre chaînons. L'azétinone subit une ouverture de cycle électrocyclique, avec un temps de demi-vie de 11 s à 40°C, qui conduit à un isocyanate de vinyle *trans*-disubstitué; on peut toutefois la piéger à l'aide d'alcools saturés, insaturés et benzyliques qui avec formation d'azétidinones 3,4-disubstituées dans lesquelles l'isomère *cis* prédomine.

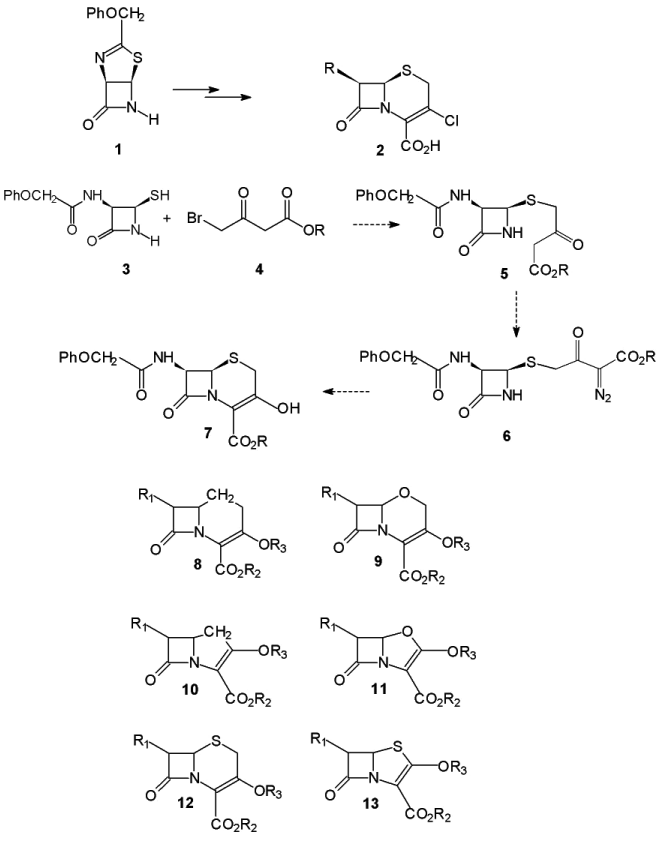
Mots clés : carbène de rhodium, torquochimique, azétinone, mercaptoazétidinone.

[Traduit par la Rédaction]

Introduction

The thiazoline azetidinone **1** (Cooper's compound), which is readily accessible from penicillin V (1), is a useful starting material for the partial synthesis of unnatural β-lactam-containing compounds (2). The work reported here began with the idea that **1** might serve as a precursor of the 3-chloro-Δ^3-cephem nucleus (2), which is a desirable synthetic target (3) because of the orally effective broad-spectrum antibacterial properties of cefaclor (**2**, R = D-PhCH(NH_2)CONH) (4).

It was thought that hydrolysis of **1** to the mercaptoazetidinone **3** (5), followed by reaction with a γ-bromoacetoacetate (**4**), diazotization of **5** (6), and cyclization of **6** via N—H insertion using rhodium acetate (7), would lead to a 3-hydroxycephem **7**, the precursor of **2**. Significantly, although this plan appeared to have ample precedent in the numerous reports of carbenoid insertion into β-lactam N—H bonds to produce carbacephems (**8**) (8), oxacephems (**9**) (9), carbapenems (**10**) (10), and oxapenems (**11**) (11), there were no reported examples of the successful application of this methodology to syntheses of cephems (**12**) or penems (**13**). A reason for this absence of (published) activity soon became clear.



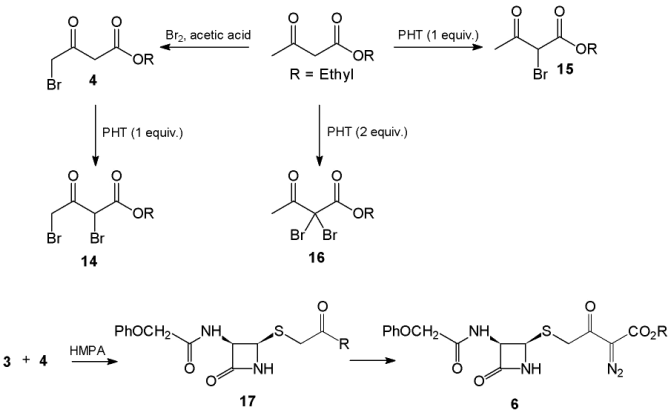
Received January 29, 2001. Published on the NRC Research Press Web site at http://canjchem.nrc.ca on August 21, 2001.

S. Wolfe,[1] S. Ro, and Z. Shi. Department of Chemistry, Simon Fraser University, Burnaby, BC V5A 1S6, Canada.

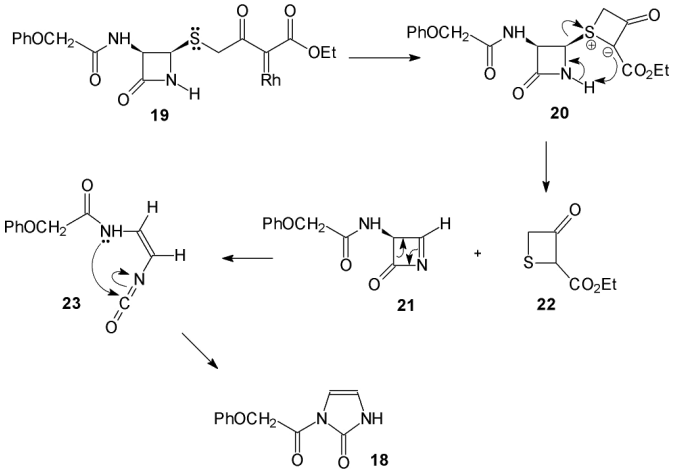
[1]Corresponding author (telephone: (604) 291-5972; fax: (604) 291-5973; e-mail: swolfe@sfu.ca).

 DOI: 10.1139/cjc-79-8-1259 © 2001 NRC Canada

Scheme 1.



Scheme 2.



Serendipitous formation and electrocyclic ring opening of an acylaminoazetinone

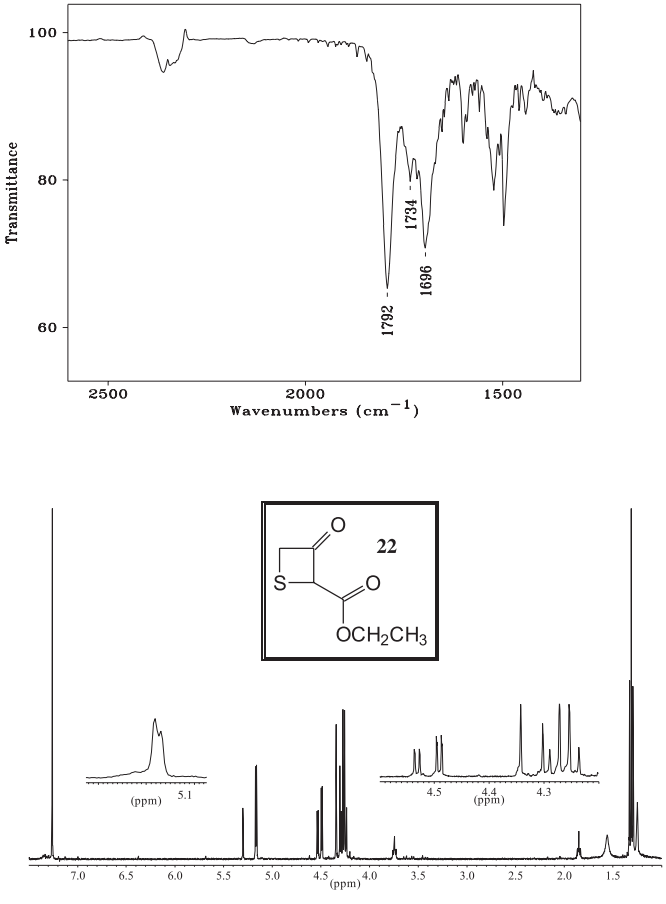
The synthesis of **6** is summarized in Scheme 1. Bromination of ethyl acetoacetate in acetic acid produced the γ-bromide **4** (R = Et), which was converted to the α,γ-dibromide **14** with 1 equiv of pyrrolidone hydrotribromide (PHT) (12). With 1 and 2 equiv of PHT, ethyl acetoacetate gave, successively, the α-bromide **15** and the α,α-dibromide **16**. Following Osborne (13), who reported that **3** reacts with ethyl bromoacetate in hexamethylphosphoramide solvent (HMPA) to give **17** (R = OEt), stirring of **3** with **4** in HMPA afforded **17** (R = CH_2CO_2Et) in 53% yield. The same product was obtained from the α,γ-dibromide **14**. Diazo transfer to **17** (R = CH_2CO_2Et) to form **6** (mp 135–137°C) proceeded reproducibly in 70–75% yield using *p*-carboxybenzenesulfonyl azide and triethylamine in acetonitrile (14).[2]

Refluxing of **6** with rhodium acetate in benzene did not lead to **7**. Instead, a compound $C_{11}H_{10}N_2O_3$ was isolated as an oil, whose IR and ^{1}H NMR spectra showed the presence of $PhOCH_2$- and -CH=CH-, and the absence of a β-lactam ring. The structure considered initially was *N*-phenoxyacetylimidazolone (**18**), whose formation could be rationalized in terms of Scheme 2, which proposes attack of the metallocarbenoid **19** on sulfur to form the neutral sulfonium ylide **20** (16). Fragmentation of **20** into the neutral acylaminoazetinone **21** ($C_{11}H_{10}N_2O_3$) and the neutral thietanone **22**, ring opening of **21** to the *cis*-vinyl isocyanate **23** (17), and cyclization of **23** would lead to **18** (18).

Support for this mechanistic proposal was sought through a search for **22** among the products, and by an independent synthesis of the putative imidazolone **18**. Refluxing of **6** with rhodium acetate in methylene chloride afforded, in 32% yield, a fragrant oil $C_6H_8O_3S$, identified as **22** on the basis of its IR and ^{1}H NMR spectra (Fig. 1). In subsequent experiments, conducted in refluxing benzene, both the presumed imidazolone **18** (68%) and **22** were isolated as products.

The synthesis of **18** is summarized in Scheme 3. Reaction of aminoacetaldehyde diethyl acetal with potassium cyanate gave the ureidoacetal **24** (19) which, when refluxed with phenoxyacetyl chloride in acetonitrile containing 4 Å molecular sieves, underwent acylation and cyclization to **18**, a crystalline compound that melted with decomposition at 82°C and liquefied completely at 89°C. It was immediately apparent, from the isolation of a crystalline compound and from the IR and NMR spectra, that **18** was different from the rhodium acetate product; the latter exhibited, inter alia, a

Fig. 1. The IR and ^{1}H NMR spectra of **22**.



[2] For other diazo transfer reagents and conditions, see ref. 15.

© 2001 NRC Canada

Scheme 3.

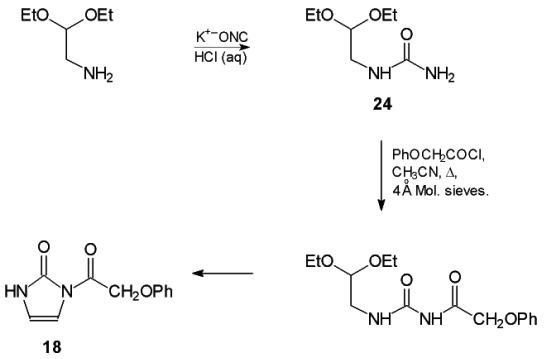
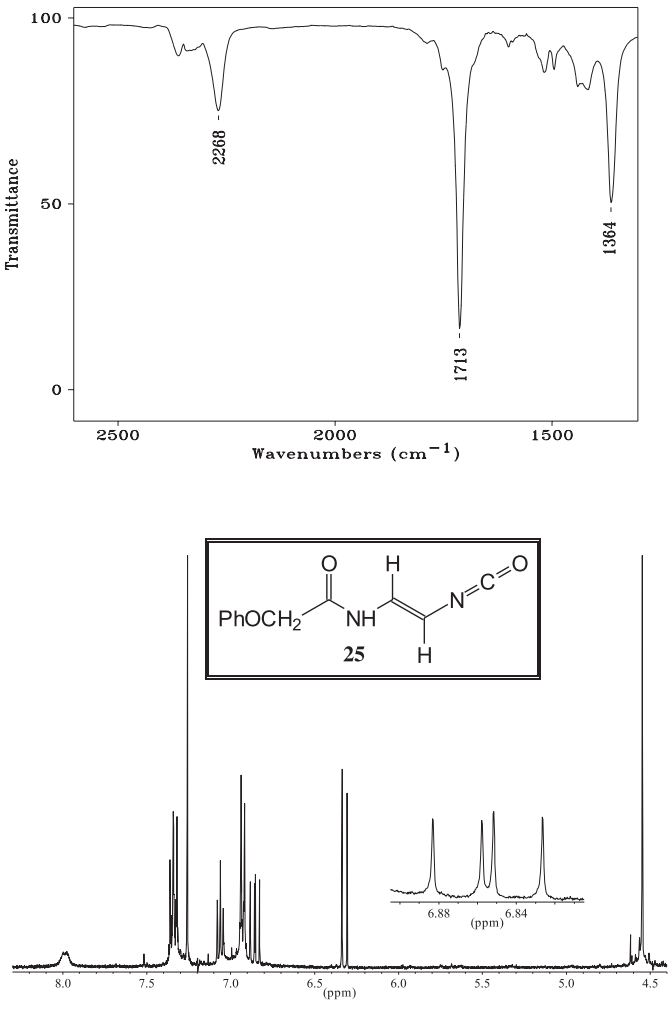
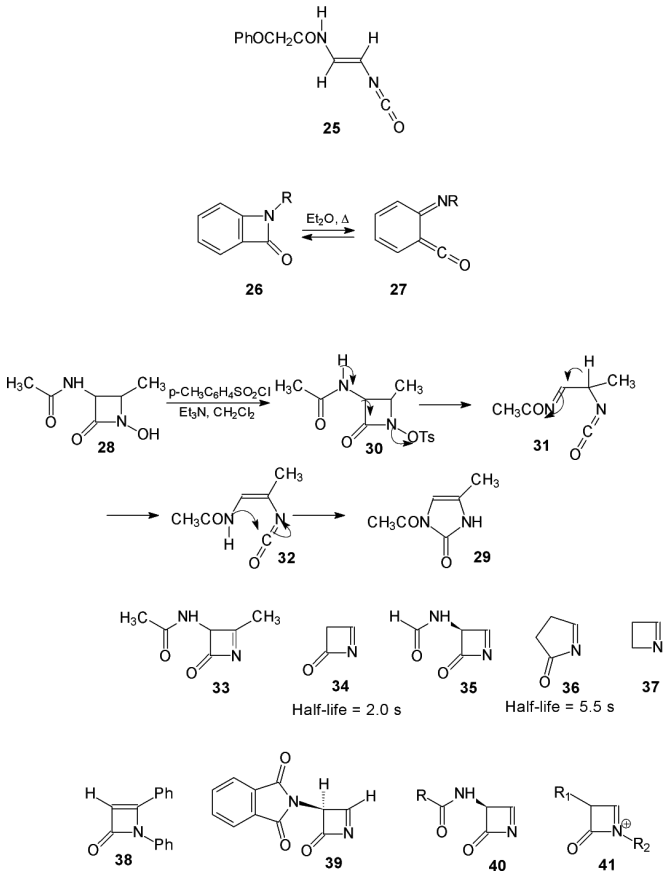


Fig. 2. The IR and ^{1}H NMR spectra of **25**.



carbonyl stretch at 1713 cm^{-1}, while **18** showed peaks at 1732 and 1559 cm^{-1}.

A closer examination of the spectra of the rhodium acetate product (Fig. 2) then revealed a possible isocyanate absorption at 2268 cm^{-1} in the IR, previously (and erroneously) assigned by us to carbon dioxide, a possible isocyanate carbon at 123.33 ppm (20) in the ^{13}C NMR, previously interpreted as an aromatic carbon, and a 12.5 Hz H-C=C-H coupling constant in the ^{1}H NMR, which is compatible with the presence of a *trans*-double bond (21). All of these observations are consistent with the *trans*-substituted vinyl isocyanate **25** as the structure of the rhodium acetate product. This corresponds to the less-hindered torquochemical (22) sense of conrotatory ring opening of the putative azetinone **21**.

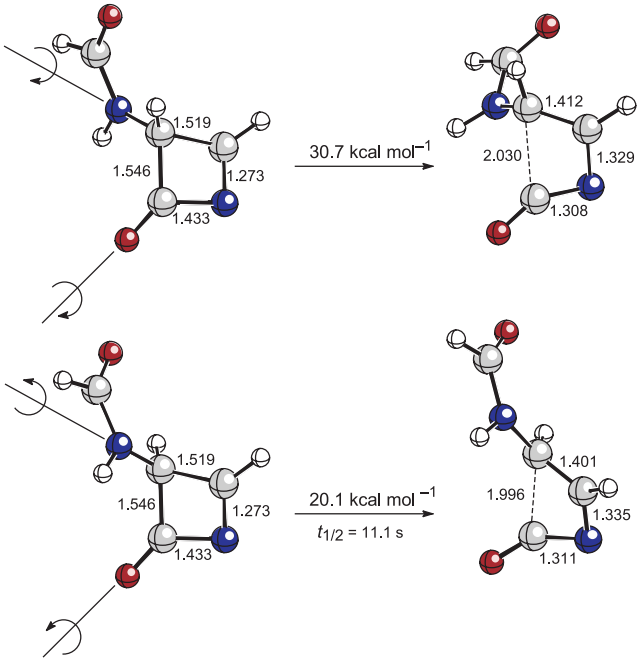


There is precedent for such an electrocyclic reaction in the behaviour of the benzoazetinones **26**, which equilibrate with iminoketenes **27** (23). In related work, Li and Miller (24) have reported that tosylation of the 1-hydroxy-2-azetidinone **28** leads to the imidazolone **29**, possibly via intermediates **30**–**32**. The cyclization **32** → **29** is analogous to **23** → **18** but, in view of ref. 23 and the present findings, it can be proposed that the precursor of **32** is the azetinone **33**, whose preferred mode of electrocyclic ring opening leads to a *trans*-relationship between the methyl and acylamino groups.

The *tert*-butyl- and adamantyl-substituted benzoazetinones **26** exhibit carbonyl stretching bands at 1812 and 1825 cm^{-1}, respectively, (23). The calculated (HF/6-31G*) C=O stretch of the parent azetinone **34** is at 1895 cm^{-1}, and the calculated (6-31G*) C=O stretch of the acylaminoazetinone **35** is at 1889 cm^{-1} (see *Experimental*). Since no IR peak higher than 1800 cm^{-1} can be detected during the reaction of **6** with rhodium acetate, the acylaminoazetinone **21** is presumed to have an extremely short lifetime. In retrospect, this is not surprising: **34** has a half-life of 2.0 ± 0.5 s at 35°C (25), the homologous 1-pyrrolin-5-one **36** has a half-life of 5.5 ± 0.5 s (25), and at-

© 2001 NRC Canada

Fig. 3. Conrotatory ring opening of a 3-acylaminoazetinone (6-31G*//6-31G* calculations). Upper: reactant and transition structure leading to the *Z*-isomer. Lower: reactant and transition structure leading to the *E*-isomer.



tempts to synthesize 1-azetine (**37**) lead instead to 2-azabutadiene (26).

Figure 3 shows the transition structures of the two conrotatory modes of electrocyclic ring opening of the acylaminoazetidinone **35**, calculated at the MP2/6-31G*//6-31G* level (27). The pathway leading to the *trans*-substituted vinyl isocyanate is 10 kcal mol^{-1} lower in energy. From the calculated 20.1 kcal mol^{-1} barrier and the Eyring equation, the estimated half-life of **35** is 11 s at 40°C.

An unprecedented result — Trapping the 3*S*-acylaminoazetinone with alcohols leads to *cis*-disubstituted azetidinones

Substituted 2-azetin-4-ones (**38**) are isolable and, in some cases, crystalline compounds (28). In contrast, with the exception of the phthalimido compound **39**, claimed in the patent literature (29), 1-azetin-4-ones (**40**) and 1-azetidinium cations (**41**) are known only as the often-proposed but never-observed intermediates in C-4-substitution reactions of 2-azetidinones (30). With compounds containing a C-3-substituent, all previous work involving the generation and capture of these putative intermediates has led (31) to *trans*-3,4-disubstituted azetidinones. In contrast, *cis*-3-phenoxyacetamido-4-alkoxyazetidinones have now been found to be produced as the major isomers (32) when saturated, unsaturated, and aromatic alcohols are included in reaction mixtures containing **6** and rhodium acetate.

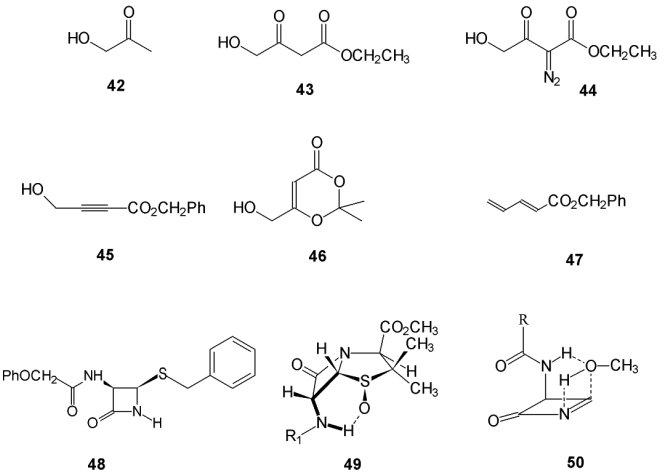
Table 1 summarizes the results of these trapping experiments. The yields shown in this table refer to isolated yields of pure *cis*- and (or) *trans*-isomers.

Table 1. Reaction of **6** with rhodium acetate in methylene chloride in the presence of RXH to form 3-phenoxyacetylamino-4-XR-substituted azetidinones.

RXH	Temperature (°C)	Yield of *cis*-isomer	Yield of *trans*-isomer
EtOH	20	15	nd[a]
IpOH	20	41	12
$PhCH_2OH$	40	70	22
$Me_2C{=}CHCH_2OH$	40	69	24
$HC{\equiv}CCH_2OH$	40	26	12
$CH_2{=}CHCH_2OH$	40	36	14
Furfuryl alcohol	40	50	nd
$PhCH_2SH$	40	12	4

[a]Not detected.

More complex alcohols, including hydroxyacetone (**42**), ethyl γ-hydroxyacetoacetate (**43**) (33), ethyl α-diazo-γ-hydroxyacetoacetate (**44**), benzyl 4-hydroxy-2-propynoate (**45**) (34), and 6-hydroxymethyl-1,3-dioxin-4-one (**46**) (35) did not react with the azetinone. In the case of **43**, the product was the 4-ethoxyazetidinone, presumably via prior lactonization, with liberation of ethanol, under the reaction conditions. Benzylamine, *N*-benzylamine, and benzyl pentadienoate (**47**) (36) also did not react. Benzyl mercaptan gave the *cis*-benzyl sulfide **48** in low yield (Table 1).



Theoretical considerations

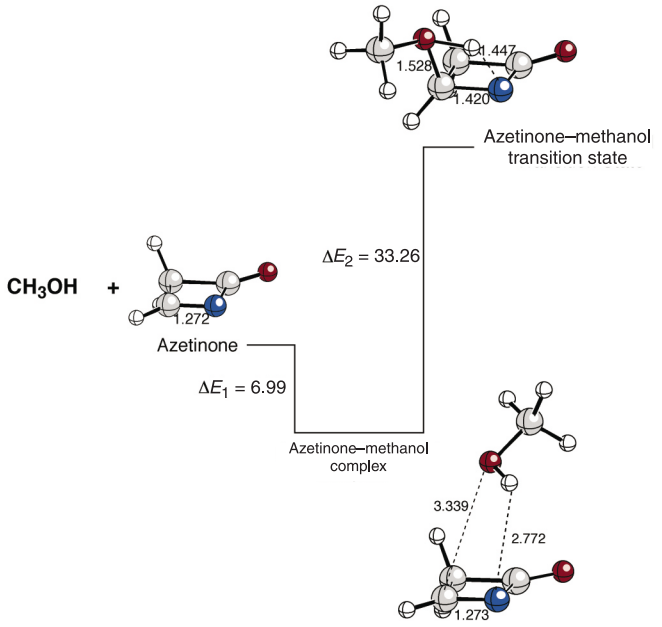
The oxidation of penicillins leads to *S*-sulfoxides **49**, in which the sulfoxide oxygen occupies the concave (β) face, and is *syn* to the acylamino side chain (37). The evidence strongly suggests (37) that the oxidant is delivered to the more hindered face of the bicyclic system by hydrogen bonding to the amide N—H.

In the present work, using no more than a two-fold excess of an alcohol in the relatively nonpolar solvent methylene chloride, the alcohol is delivered *syn* to the acylamino group of the putative 3-acylaminoazetinone. With the earlier oxidation experiments as a precedent, the chair-like hydrogen-bonded transition state **50** could be proposed to account for the trapping results. This idea was pursued computationally.

Figure 4 summarizes the results of 3-21G calculations of the four-centred *cis*-addition of methanol to the parent

© 2001 NRC Canada

Fig. 4. *cis*-Addition of methanol to 1-azetin-4-one (3-21G calculations). Energy differences are in kcal mol^{-1}; bond lengths are in Å.



azetinone. Figure 5, which is more interesting, shows the 6-31G* transition structures for the four-centred addition of methanol *syn* and *anti* to the acylamino group of an acylamino-substituted azetinone. The *syn* structure shows no evidence of the intramolecular hydrogen bond postulated in **50**. Nevertheless, based on single point MP2/6-31G* calculations, the energy of this structure is 2.03 kcal mol^{-1} lower than that of the *anti*. In addition, the developing C···O bond is rather short, suggesting a product-like transition state. If this were the case, the *products* of the addition might also show a *syn*-preference. This is indeed the case; as seen in Fig. 6, the *gauche* conformation of MeO-CH_2CH_2-NHCHO is significantly more stable than the *anti*. Finally, the calculated MP2/6-31G*//6-31G* barrier for the *syn* addition of Fig. 5 is 20.6 kcal mol^{-1}, almost the same as that shown in Fig. 3 for the electrocyclic ring opening (20.1 kcal mol^{-1}).

Experimental

3-Phenoxyacetamido-4-mercapto-2-azetidinone (3)

A 40% aqueous solution of *p*-toluenesulfonic acid hydrate (13 mL) was added to a solution of the thiazoline azetidinone **1** (5.03 g, 21.5 mmol) in a mixture of dichloromethane (100 mL) and acetone (100 mL). The mixture was stirred for 2 h, and the mercaptoazetidinone was then collected by filtration and dried in vacuo. A second crop was recovered by evaporation of the filtrate and trituration with a minimum amount of water (4.93 g, 91%), mp 138–140°C (lit. (38) 133–135°C). MS (CI, *m*/*z*): 219 ((M + 1)-H_2S). IR (KBr) (cm^{-1}): 3283, 3210, 1761, 1659. ^{1}H NMR (DMSO-d_6): 8.93 (1H, d, 9.3 Hz, NH), 8.79 (1H, s, NH), 7.29 (2H, t, Ar), 6.98 (3H, m, Ar), 5.32 (1H, dd, 4.7, 9.3 Hz, H-3), 5.00 (1H, 4.7, 10.2 Hz, H-4), 4.61 (1H, d, 15.1 Hz, C*H*H), 4.58 (1H, d, 15.1 Hz, CH*H*), 3.19 (1H, d, 10.3 Hz, SH). ^{13}C

Fig. 5. Transition structures for the four-centered *cis*-addition of methanol *syn* (left) and *anti* (right) to 3-formylamino-1-azetin-4-one. Geometries have been optimized at 6-31G*. Relative energies refer to single point MP2/6-31G* calculations at the 6-31G* optimized geometries.

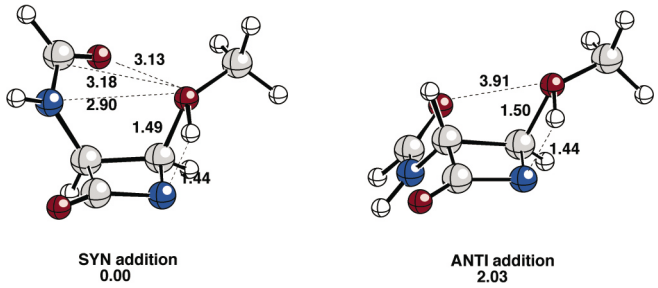
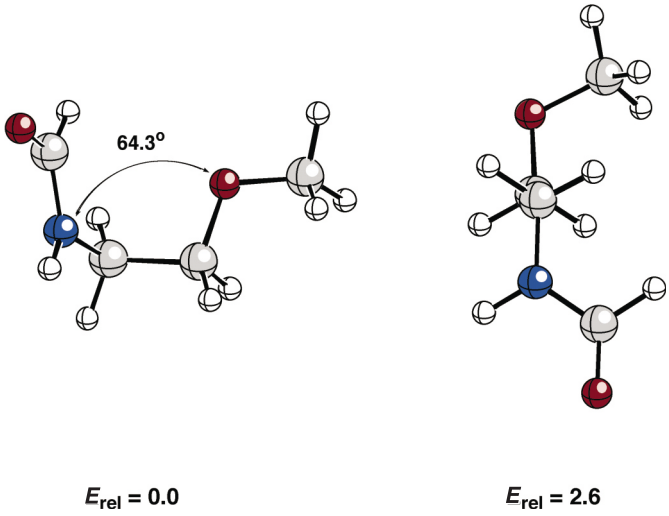


Fig. 6. The gauche effect in MeO-CH_2CH_2-NHCHO (MP2/6-31G*//6-31G*) calculations. The gauche conformation is 2.6 kcal mol^{-1} more stable than the *anti*.



NMR (DMSO-d_6): 166.59 (acetamido C=O), 161.90 (β-lactam C=O), 157.33, 129.47, 121.46, 114.86 (aromatic), 150.11 (C-3), 124.76 (C-4), 66.35 ($PhOCH_2$). Anal. calcd. for $C_{11}H_{12}N_2O_3S$: C 52.37, H 4.79, N 11.10; found: C 52.24, H 5.00, N 11.30.

Ethyl γ-bromoacetoacetate (4) (39)

A solution of bromine (1.4 mL, 4.34 g, 27.1 mmol) in glacial acetic acid (4 mL) was added dropwise, with stirring at 0°C, to a solution of ethyl acetoacetate (3.2 mL, 3.3 g, 25.1 mmol) in glacial acetic acid (9 mL). After the addition was complete, the ice bath was removed and stirring was continued overnight. The yellow solution was then diluted with ether (30 mL) and washed successively with water (3 × 30 mL), saturated sodium bicarbonate (4 × 40 mL), water (40 mL), and saturated sodium chloride (40 mL), dried over magnesium sulfate, and evaporated to afford the product as a yellowish-green liquid (3.99 g, 76%). The compound was characterized spectroscopically, and used directly in the next step. MS (CI, *m*/*z*): 209 (M + 1, for ^{79}Br), 211 (M + 1, for ^{81}Br). IR (KBr) (cm^{-1}): 1744, 1726. ^{1}H NMR ($CDCl_3$): 4.20 (2H, q, 7.1 Hz), 4.05 (2H, s), 3.70 (2H, s), 1.29 (3H, t,

© 2001 NRC Canada

7.1 Hz). ^{13}C NMR ($CDCl_3$): 194.44 (acetyl C=O), 166.52 (ester C=O), 61.73 (ester methylene), 46.05 (C-4), 33.66 (C-2), 14.03 (methyl).

Ethyl α,γ-dibromoacetoacetate (14)

A solution of ethyl γ-bromoacetoacetate (12.5 mg, 0.060 mmol) in tetrahydrofuran (0.2 mL) was treated with a solution of pyrrolidone hydrotribromide (20.5 mg, 0.060 mmol) in tetrahydrofuran (0.7 mL). Stirring was continued for 3 h, and the solids were then removed by filtration. The filtrate was diluted with ethyl acetate (5 mL), washed successively with water (5 mL) and saturated sodium chloride, dried over magnesium sulfate, and evaporated to afford the product as a yellow oil (15.8 mg, 91%). ^{1}H NMR ($CDCl_3$): 5.17 (1H, s), 4.30 (2H, q, 7.2 Hz), 1.31 (3H, t, 7.2 Hz). IR (neat) (cm^{-1}): 1748, 1728.

Ethyl α-bromoacetoacetate (15)

A solution of pyrrolidone hydrotribromide (49.5 mg, 0.099 mmol) in tetrahydrofuran (0.8 mL) was added dropwise to a solution of ethyl acetoacetate (0.012 mL, 12.3 mg, 0.095 mmol) in tetrahydrofuran (0.4 mL). After 30 min, the reaction mixture was diluted with ether (4 mL) and maintained overnight at –5°C. The mixture was then filtered and the filtrate was evaporated to dryness. The residue was dissolved in ethyl acetate (5 mL), and this solution was washed successively with saturated sodium bicarbonate (5 mL) and water (5 mL), dried over magnesium sulfate, and evaporated to afford the product as a colourless oil. ^{1}H NMR ($CDCl_3$): 4.77 (1H, s), 4.30 (2H, q, 7.3 Hz), 2.45 (3H, s), 1.32 (3H, t, 7.3 Hz).

Ethyl α,α-dibromoacetoacetate (16)

A solution of pyrrolidone hydrotribromide (77.1 mg, 0.158 mmol) in tetrahydrofuran (0.9 mL) was added dropwise, with stirring, to a solution of ethyl acetoacetate (0.011 mL, 10.9 mg, 0.084 mmol) in tetrahydrofuran (0.3 mL). The mixture was stirred for 3 h and the filtrate was then diluted with ethyl acetate (5 mL), washed successively with saturated sodium bicarbonate (50 mL), water (50 mL), and saturated sodium chloride (50 mL), dried over magnesium sulfate, and evaporated to give the product (12.2 mg, 51%). ^{1}H NMR ($CDCl_3$): 4.38 (2H, q, 7.2 Hz), 2.60 (3H, s), 1.35 (3H, t, 7.2 Hz).

Coupling of 3 with ethyl bromoacetate

Ethyl bromoacetate (3.4 μL, 5.1 mg, 0.03 mmol) was added to a solution of **3** (6.5 mg, 0.03 mmol) in hexamethylphosphoric triamide (0.06 mL). The solution was stirred for 23 h. Ethyl acetate (10 mL) was then added and the resulting solution was washed successively with water (2 × 10 mL) and saturated sodium chloride (10 mL), dried over magnesium sulfate, and evaporated. The residue was crystallized from chloroform–ether to give **2**, 5.8 mg (66%) (13). ^{1}H NMR ($CDCl_3$): 7.44 (1H, d, 8.9 Hz, NH), 7.24 (2H, t, Ar), 7.03 (1H, t, Ar), 6.94 (2H, t, Ar), 6.65 (1H, br s, NH), 5.62 (1H, dd, 4.5, 8.9 Hz, H-3), 5.14 (1H, d, 4.5 Hz, H-4), 4.57 (2H, s, $PhOCH_2$), 4.17 (2H, q, 7.2 Hz, ester CH_2), 3.27 (1H, d, 11.5 Hz, SC*H*H), 3.24 (1H, d, 11.5 Hz, SCH*H*), 1.27 (3H, t, 7.2 Hz, ester CH_3). ^{13}C NMR ($CDCl_3$): 170.32 (acetamido C=O), 168.84 (ester C=O), 165.35 (β-lactam C=O), 157.22, 129.81, 122.41, 114.92 (aromatic), 67.44 ($PhOCH_2$), 62.03 (C4), 61.93 ($CO_2CH_2CH_3$), 60.44 (C-3), 32.91 (SCH_2CO), 14.05 ($CO_2CH_2CH_3$).

Coupling of 3 with 4

Ethyl γ-bromoacetoacetate (2.01 g, 9.64 mmol) was added dropwise with stirring during 15 min to a solution of **3** (2.14 g, 8.49 mmol) in hexamethylphosphoric triamide (30 mL). The pale yellow solution was stirred for 24 h, diluted with ethyl acetate (50 mL) and washed successively with water (3 × 50 mL) and saturated sodium chloride (50 mL), dried over magnesium sulfate, and evaporated. The resulting foam (**5**) crystallized upon trituration with anhydrous ether, 1.84 g (57%), mp 106–108°C. $[\alpha]_D^{20}$ +69.6° (c 0.115, chloroform). MS (EI, *m*/*z*): 380 (M). HR-MS-EI calcd. for $C_{17}H_{20}N_2O_6S$: 380.1042 (M); found: 380.1044. IR (KBr) (cm^{-1}): 3304, 1762, 1735, 1701, 1675. ^{1}H NMR ($CDCl_3$): 7.38 (1H, d, 8.7 Hz, NH), 7.32 (2H, t, Ar), 7.04 (1H, t, Ar), 6.96 (2H, d, Ar), 6.66 (1H, s, NH), 5.56 (1H, dd, 4.7, 8.7 Hz, H-3), 5.00 (1H, d, 4.7 Hz, H-4), 4.58 (1H, d, 15.2 Hz, PhOC*H*H), 4.57 (1H, d, 15.2 Hz, PhOCH*H*), 4.19 (2H, q, 7.2 Hz, ester CH_2), 3.66 (1H, d, 16.0 Hz, SC*H*H), 3.54 (1H, d, 16.0 Hz, SCH*H*), 3.48 (1H, d, 15.5 Hz, COC*H*HCO), 3.45 (1H, d, 15.5 Hz, COCH*H*CO), 1.28 (3H, t, 7.2 Hz, ester CH_3). ^{13}C NMR ($CDCl_3$): 198.00 (C=O), 168.85 (acetamido C=O), 166.93 (ester C=O), 165.16 (β-lactam C=O), 157.20, 129.82, 122.41, 114.97 (aromatic), 67.41 (PhOCH), 61.89 (C-4), 61.59 ($CO_2CH_2CH_3$), 60.60 (C-3), 47.07 ($COCH_2CO$), 40.46 (SCH_2CO), 14.06 ($CO_2CH_2CH_3$). Anal. calcd. for $C_{17}H_{20}N_2O_6S\cdot0.5H_2O$: C 52.43, H 5.44l N 7.19; found: C 52.37, H 5.15, N 7.61.

***p*-Carboxybenzenesulfonyl azide**

A suspension of the potassium salt of *p*-carboxybenzenesulfonic acid (10.00 g, 41.6 mmol) in chlorosulfonic acid (14.0 mL) was heated for 3 h at 100°C. The reaction mixture was then cooled to room temperature and cautiously poured onto ice (40 g). The white precipitate was collected, air dried, dissolved in acetone (125 mL), and treated with a solution of sodium azide (3.11 g, 47.8 mmol) in water (20 mL). After warming at 40°C for 2.5 h, with addition of water as necessary to maintain one phase, the solution was immersed in ice, water was added to the cloud point, and crystallization was allowed to proceed. The crystals were collected, triturated with ether (50 mL), and dried to give the product (4.89 g, 52%), mp 177–179°C (lit. (40) mp 180°C (dec)). MS (EI, *m*/*z*): 227 (M). IR (KBr) (cm^{-1}): 3100–2554, 2151, 1703, 1377. ^{1}H NMR ($CDCl_3$, triethylamine salt): 10.06 (1H, br s, NH), 8.23 (2H, d, 8.8 Hz, Ar), 7.91 (2H, d, 8.8 Hz, Ar), 2.61 (6H, q, 7.2 Hz, CH_2), 1.05 (9H, t, 7.2 Hz, CH_3). ^{13}C NMR ($CDCl_3$, triethylamine salt): 170.49 (carboxylate), 143.98, 139.09, 130.49, 126.93 (aromatic), 45.26 (CH_3CH_2N), 8.71 (CH_3CH_2N).

Diazo transfer to 5

p-Carboxybenzenesulfonyl azide (845 mg, 3.72 mmol) was added to a solution of the azetidinone (1.29 g, 3.39 mmol) in acetonitrile (28 mL). The suspension was stirred in an ice bath while triethylamine (1.4 mL, 1.02 g, 10.04 mmol) was added dropwise. The suspension dissolved

© 2001 NRC Canada

initially and, after 10 min, a precipitate reappeared. The ice bath was removed and the mixture was stirred for 3 h and then filtered. The filtrate was evaporated and the yellow residue, in dichloromethane (80 mL), was washed with saturated sodium bicarbonate (2 × 80 mL) and water (80 mL), dried over magnesium sulfate, and evaporated. Trituration with ethyl acetate – ether (1:5) and cooling overnight at 5°C afforded **6** as a pale yellow solid (0.98 g, 71%), mp 135–137°C. $[\alpha]_D^{20}$ +55.0° (c 0.109, chloroform). MS (CI, *m*/*z*): 161, 219. IR (KBr) (cm^{-1}): 3310, 3192, 2145, 1765, 1719, 1663, 1645. ^1H NMR ($CDCl_3$): 7.38 (1H, d, 11.9 Hz, NH), 7.34 (2H, m, Ar), 7.03 (1H, t, Ar), 6.94 (2H, d, Ar), 6.48 (1H, br s, NH), 5.62 (1H, ddd, 1.0, 4.7, 9.1 Hz, H-3), 5.13 (1H, d, 4.7 Hz, H-4), 4.56 (2H, s, $PhOCH_2$), 4.28 (2H, dq, 7.1, 7.2 Hz, nonequivalent protons of ester methylene), 4.02 (1H, d, 14.5 Hz, SC*H*H), 3.61 (1H, d, 14.5 Hz, SCH*H*), 1.31 (3H, t, 7.1 Hz, ester CH_3). ^{13}C NMR ($CDCl_3$): 188.02 (acetyl C=O), 168.68 (acetamido C=O), 165.39 (β-lactam C=O), 161.40 (ester, C=O), 157.21, 129.81, 122.40, 114.99 (aromatic), 67.44 ($PhOCH_2$), 61.99 (C4), 61.58 ($CO_2CH_2CH_3$), 60.35 (C-3), 36.97 (SCH_2CO), 14.26 ($CO_2CH_2CH_3$). Anal. calcd. for $C_{17}H_{18}N_4O_6S\cdot0.5H_2O$: C 49.15, H 4.61, N 13.49; found: C 48.90, H 4.51, N 12.55.

Rhodium(II) acetate (41)

A solution of rhodium(III) chloride trihydrate (126.3 mg, 0.48 mmol) and sodium acetate trihydrate (259.1 mg, 1.90 mmol) in absolute ethanol (2.5 mL) and glacial acetic acid (2.5 mL) was heated at 105°C for 1.5 h. The green reaction mixture was then cooled and filtered. Recrystallization from hot methanol and drying at 35°C in vacuo yielded emerald green crystals (87.1 mg, 33%). IR (KBr) (cm^{-1}): 1588, 1439, 1433. ^1H NMR (acetone-d_6): 1.74 (s). Anal. calcd. for $Rh_2C_8H_{12}O_8$: C 21.74, H 2.74; found: C 21.98, H 2.86.

Reaction of 6 with rhodium acetate — Isolation and characterization of the thietanone 22

Rhodium(II) acetate (5.1 mg, 0.015 mmol) was added to a solution of **6** (20 mg, 0.049 mmol) in dichloromethane (2 mL). The solution was stirred for 23 h and then flushed through a 5-cm column of silica gel, using dichloromethane, to give unreacted diazoketone (5 mg) and **22** as a colourless, fragrant film (2.5 mg, 32%). MS (CI, *m*/*z*): 161 (M + 1). HR-MS-CI calcd. for $C_6H_8O_3S$: 161.0262 (M + 1); found: 161.0267. IR (CH_2Cl_2) (cm^{-1}): 1792, 1694. ^1H NMR ($CDCl_3$): 5.16 (1H, d, 3.6 Hz, CH), 4.52 (1H, dd, 3.6, 6.2 Hz, C*H*H), 4.33 (1H, d, 16.2 Hz, CH*H*), 4.26 (2H, q, 7.1 Hz), 1.31 (3H, t, 7.1 Hz). ^{13}C NMR ($CDCl_3$): 189.40 (ring C=O), 166.35 (ester C=O), 69.76 (ring CH), 62.49 (ester CH_2), 54.31 (ring CH_2), 14.03 (ester methyl).

Reaction of 6 with rhodium acetate — Isolation and characterization of 25

Rhodium(II) acetate (0.5 mg, 0.001 mmol) was added to a suspension of **6** (9.8 mg, 0.024 mmol) in benzene (1.1 mL). The mixture was immediately immersed in an oil bath preheated to 85°C. The red solution was stirred for 2.5 h, cooled, diluted with water (5.0 mL), and extracted with dichloromethane (2 × 5 mL). The organic extract was washed with saturated sodium chloride (10 mL), dried over magnesium sulfate, and evaporated under reduced pressure at 25°C. The residue was dried under high vacuum (3.6 mg, 68%). HR-MS-CI calcd. for $C_{11}H_{10}N_2O_3$: 219.0762 (M + 1); found: 219.0766. IR (CH_2Cl_2) (cm^{-1}): 3410, 2268, 1713. ^1H NMR ($CDCl_3$): 7.99 (1H, d, 10.1 Hz, NH), 7.34 (2H, m, Ar), 7.07 (1H, t, Ar), 6.94 (2H, d, Ar), 6.86 (1H, dd, 10.1, 12.5 Hz, =C*H*-NH), 6.32 (1H, d, 12.5 Hz, C*H*=CH-NH), 4.55 (2H, s, $PhOCH_2$). ^{13}C NMR ($CDCl_3$) (^{13}C–^1H 2D-COSY): 166.47 (C=O), 157.59, 130.60, 123.33, 115.47 (aromatic), 121.55 (NH*C*HCHN=C=O), 108.06 (NHCH*C*HN=C=O), 67.96 ($PhOCH_2CONH$).

Ureidoacetaldehyde diethyl acetal (24)

Aminoacetaldehyde diethyl acetal (3.3 mL, 3.02 g, 22.7 mmol) was mixed with 5 g of crushed ice, cooled to 0°C, and 5 N hydrochloric acid (4.5 mL, 0.82 g, 22.5 mmol) (cooled to –40°C), was added quickly, followed by a solution of potassium cyanate (2.54 g, 31.3 mmol) in water (6.0 mL). The mixture was stirred vigorously for 15 min at 0°C and then refluxed for 3 h and cooled. The product crystallized upon scratching with a glass rod (2.8 g, 70%), mp 102–104°C (lit. (19) mp 107 to 108°C). MS (CI, *m*/*z*): 177 (M + 1). IR (KBr) (cm^{-1}): 3383, 3210, 1657. ^1H NMR ($CDCl_3$): 5.53 (1H, s, NH), 4.90 (2H, br s, NH_2), 4.48 (1H, t, 5.2 Hz, CH), 3.69 (2H, dq, 7.0, 9.3 Hz, ester CHH), 3.54 (2H, dq, 7.0, 9.3 Hz, ester C*H*H), 3.28 (2H, dd, 5.6, 5.6 Hz, CH_2NH), 1.19 (6H, t, 7.0 Hz, CH_3). ^{13}C NMR ($CDCl_3$): 159.10 (NCON), 101.70 (OCHO), 62.98 (methyl), 43.45 ($NHCH_2$), 15.29 (CH_2O). Anal. calcd. for $C_7H_{16}N_2O_3$: C 47.71, H 9.15, N 15.90; found: C 47.59, H 8.90, N 15.73.

***N*-Phenoxyacetylimidazolone (18)**

Phenoxyacetyl chloride (0.03 mL, 37 mg, 0.20 mmol) was added to a solution of ureidoacetaldehyde diethyl acetal (35 mg, 0.20 mmol) in acetonitrile (2.0 mL), to which activated 4 Å molecular sieves (10 mg) had been added. The mixture was stirred at room temperature for 30 min and then refluxed for 5 h, cooled, and filtered. The filtrate was evaporated and the residue was purified by column chromatography using ethyl acetate – hexanes (1:1). Crystallization from ethyl acetate – hexanes gave material melting at 82–89°C. MS (EI, *m*/*e*): 218 (M). HR-MS-EI calcd. for $C_{11}H_{10}N_2O_3$: 218.0686 (M); found: 218.0691. IR (KBr) (cm^{-1}): 1732, 1694. ^1H NMR ($CDCl_3$): 9.34 (1H, br s, NH, coupled to =CH at 6.33), 7.29 (2H, m, Ar), 7.00 (3H, m, Ar + C*H*=CHNH), 6.44 (1H, dd, 2.4, 3.3 Hz, =C*H*-NH), 5.32 (2H, s, $PhOCH_2$). ^{13}C NMR ($CDCl_3$): 166.71 (phenoxyacetyl C=O), 158.05 (imidazolone C=O), 152.21, 129.54, 121.84, 115.138 (aromatic), 114.83 (CONHCH*C*HN), 111.93 (CONH*C*HCHN), 68.02 ($PhOCH_2$).

Trapping of the azetinone

(i) With ethanol

Rhodium(II) acetate (3.0 mg, 0.007 mmol) was added to a solution of the diazoketone (37.9 mg, 0.09 mmol) and ethanol (0.01 mL, 7.9 mg, 0.20 mmol) in dichloromethane (5 mL). The red solution was stirred for 20 h and then evaporated. The residue was chromatographed, using a dichloromethane – ethyl acetate elution gradient, to yield the

© 2001 NRC Canada

thietanone and *cis*-3-phenoxyacetamido-4-ethoxy-2-azetidinone as a colourless film (3.7 mg, 15%). $[\alpha]_D^{20}$ –12.1° (c 0.165, chloroform). MS (CI, *m*/*z*): 265 (M + 1). HR-MS-CI calcd. for $C_{13}H_{16}N_2O_4$: 265.1188 (M + 1); found: 265.1185. IR ($CHCl_3$) (cm^{-1}): 3412, 1790, 1691. ^1H NMR ($CDCl_3$): 7.32 (3H, m, Ar + NH), 7.03 (1H, t, Ar), 6.92 (2H, d, Ar), 6.54 (1H, br s, NH), 5.52 (1H, ddd, 1.4, 3.9, 9.5 Hz, H-3), 5.17 (1H, d, 3.9 Hz, H-4), 4.59 (1H, d, 15.1 Hz, PhOC*H*H), 4.53 (1H, d, 15.1 Hz, PhOCH*H*), 3.61 (1H, dq, 7.0, 14.0, OC*H*H), 3.48 (1H, dq, 7.0, 14.0 Hz, OCH*H*), 1.17 (3H, t, 7.0 Hz, CH_3). ^{13}C NMR ($CDCl_3$): 168.30 (acetamido C=O). 167.24 (β-lactam C=O), 157.63, 129.80, 122,32, 114.85 (aromatic), 81.09 (C4), 67.47 ($PhOCH_2$), 64.61 (OCH_2CH_3), 59.76 (C-3), 14.92 (OCH_2CH_3).

(ii) With isopropanol

Rhodium(II) acetate (1 mg, 0.002 mmol) was added to a solution of the diazoketone (14.1 mg, 0.035 mmol) and 2-propanol (0.003 mL, 2.4 mg, 0.039 mmol) in dichloromethane (1 mL). The red solution was stirred overnight under nitrogen and then evaporated. The residue was chromatographed using dichloromethane to elute the thietanone and a blue film, which decolourized upon washing with water to afford a white solid. Fractional crystallization from ethyl acetate – pentane afforded the *cis*-isomer as white crystals (4.0 mg, 41%), mp 93–95°C, and the *trans*-isomer (1.2 mg, 12%). *cis*-Isomer: $[\alpha]_D^{20}$ +29.3° (c 0.205, chloroform. MS (CI, *m*/*z*): 279 (M + 1). HR-MS-EI calcd. for $C_{14}H_{18}N_2O_4$: 278.1267 (M); found: 278.1266. IR (KBr) (cm^{-1}): 3410, 1792, 1690. ^1H NMR ($CDCl_3$): 7.38 (1H, d, 9.6 Hz, NH), 7.32 (2H, m, Ar), 7.03 (1H, t, Ar), 6.93 (2H, d, Ar), 6.60 (1H, br s, NH), 5.54 (1H, ddd, 1.4, 3.9, 9.6 Hz, H-3), 5.27 (1H, d, 3.9 Hz, H-4), 4.60 (1H, d, 15.1 Hz, PhOC*H*H), 4.54 (1H, d, 15.1 Hz, PhOCH*H*), 3.77 (1H, septet, 6.2 Hz, CH), 1.19 (3H, d, 6.2 Hz, methyl), 1.12 (3H, d, 6.2 Hz, methyl). ^{13}C NMR ($CDCl_3$): 168.22 (acetamido C=O), 167.57 (β-lactam C=O), 154.93, 129.81, 122.29, 114.85 (aromatic), 79.76 (C4), 71.90 (isopropyl CH), 67.44 ($PhOCH_2$), 59.89 (C-3), 22.59, 22.25 (isopropyl methyls). *trans*-Isomer: ^1H NMR ($CDCl_3$) 7.32 (2H, m Ar), 7.09 (1H, d, 7.6 Hz, N*H*), 7.04 (1H, t, Ar), 6.92 (2H, d, Ar), 6.33 (1H, br s, N*H*), 5.22 (1H, d, 1.2 Hz, H-4), 4.54 (2H, s, $PhOCH_2$), 4.59 (1H, dd, 1.2, 7.6 Hz, H-3), 3.87 (1H, sept, 5.6 Hz, Ip H), 1.23 (3H, d, 5.6 Hz, Me), 1.21 (3H, d, 5.6 Hz, Me).

(iii) With benzyl alcohol

A solution of the diazoketone (19.7 mg, 0.048 mmol) and benzyl alcohol (0.011 mL, 11.5 mg, 0.106 mmol) in dichloromethane (2.6 mL) was stirred briefly with rhodium (II) acetate (3.1 mg, 14 mol%), and then immersed in a preheated oil bath at 50°C. The red solution was refluxed for 28 h and evaporated to give a red residue with a fragrant odour. The residue was chromatographed, using dichloromethane (20 mL) to elute the thietanone, followed by dichloromethane – ethyl acetate (1:1) to isolate a crystalline *cis*-benzyloxyazetidinone (15.9 mg, 70%), mp 128–131°C, and an oily *trans*-benzyloxyazetidinone (5 mg, 22%). *cis*-Isomer: $[\alpha]_D^{20}$ +26.7° (c 0.15, chloroform). MS (CI, *m*/*z*): 327 (M + 1). IR (CH_2Cl_2) (cm^{-1}): 3414, 1792, 1692. ^1H NMR ($CDCl_3$): 7.39 (1H, d, 9.6 Hz, NH), 7.32–7.26 (7H, m, Ar), 7.02 (1H, t, Ar), 6.87 (2H, d, Ar), 6.65 (1H, br s, NH), 5.51 (1H, ddd, 1.4, 3.9, 9.6 Hz, H-3), 5.26 (1H, d, 3.9 Hz, H-4), 4.57 (2H, s, $PhOCH_2$), 4.53 (1H, d, 15.0 Hz, benzyl C*H*H), 4.50 (1H, d, 15.0 Hz, benzyl CH*H*). ^{13}C NMR ($CDCl_3$): 168.57 (acetamido C=O), 168.05 (β-lactam C=O), 138.61, 130.44, 129.25, 128.55, 128.51, 122.55, 115.83 (aromatic), 81.61 (C-4), 70.82 (OCH_2Ph), 68.13 ($PhOCH_2$), 60.68 (C-3). Anal. calcd. for $C_{18}H_{18}N_2O_4 \cdot H_2O$: C 62.78, H 5.85, N 8.13; found: C 62.25, H 5.41, N 7.92. *trans*-Isomer: ^1H NMR ($CDCl_3$): 7.36–7.30 (8H, m, Ar + NH), 7.04 (1H, m, Ar), 6.92 (2H, d, Ar), 6.91 (1H, d, 7.1 Hz, NH), 6.83 (1H, br s, NH), 5.27 (1H, d, 1.0 Hz, H-4), 4.95 (1H, dd, 1.0, 7.1 Hz, H-3), 4.87 (1H, d, 11.8 Hz, OC*H*HPh), 4.70 (1H, d, 11.8 Hz, OCH*H*Ph), 4.67 (1H, d, 14.9 Hz, PhOC*H*H), 4.63 (1H, d, 14.9 Hz, PhOCH*H*).

(iv) With dimethallyl alcohol

A solution of the diazoketone (181 mg, 0.45 mmol) and 3-methyl-2-butenol (0.12 mL, 102 mg, 1.2 mmol) in dichloromethane (34 mL) was stirred with rhodium(II) acetate (20 mg, 0.05 mmol) and placed in a preheated oil bath at 50°C. The red solution was refluxed for 11 h and the solvent was then removed. The residue was chromatographed, using dichloromethane (100 mL), to isolate the thietanone, followed by dichloromethane – ethyl acetate (1:1) to yield the *cis*- and *trans*-disubstituted azetidinones as blue solids. These was dissolved in dichloromethane (20 mL), and the solutions were washed with water (20 mL), dried over magnesium sulfate, and evaporated to give the crystalline *cis*-disubstituted azetidinone (94 mg, 69%), mp 79–83°C, and the *trans*-disubstituted azetidinone (33 mg, 24%). *cis*-Isomer: $[\alpha]_D^{20}$ –8.6° (c 0.116, chloroform). MS (CI, *m*/*z*): 305 (M + 1). HR-MS-CI calcd. for $C_{16}H_{20}N_2O_4$: 305.1502 (M + 1); found: 305.1504. IR (CH_2Cl_2) (cm^{-1}): 3412, 1790, 1692. ^1H NMR ($CDCl_3$): 7.32 (3H, m, Ar + NH), 7.03 (1H, t, Ar), 6.93 (2H, d, Ar), 6.49 (1H, br s, NH), 5.49 (1H, ddd, 1.2, 3.8, 9.4 Hz, H-3), 5.25 (1H, m, OCH_2CH=), 5.18 (1H, d, 3.8 Hz, H-4), 4.57 (1H, d, 15.0 Hz, PhOC*H*H), 4.52 (1H, d, 15.0 Hz, PhOCH*H*), 4.06 (1H, dd, 6.9, 11.5 Hz, OC*H*HCH=), 4.00 (1H, dd, 6.9, 11.5 Hz, OCH*H*CH=), 1.76 (3H, s, methyl), 1.64 (3H, s, methyl). ^{13}C NMR ($CDCl_3$): 168.31 (acetamido C=O), 167.20 (β-lactam C=O), 157.25, 129.77, 122.29, 114.91 (aromatic), 138.69 (OCH_2CH=*C*), 119.46 (OCH_2CH=C), 80.67 (C4), 67.45 ($PhOCH_2$), 65.63 (OCH_2CH=), 59.80 (C3), 25.70 (methyl), 18.03 (methyl). *trans*-Isomer: MS (CI, *m*/*z*): 305 (M + 1). IR (CH_2Cl_2) (cm^{-1}): 1786, 1696. ^1H NMR ($CDCl_3$): 7.32 (2H, t, Ar), 7.16 (1H, d, 7.6 Hz, NH), 7.04 (1H, t, Ar), 6.91 (2H, d, Ar), 6.54 (1H, br s, NH), 5.34 (1H, m, OCH_2CH=), 5.13 (1H, d, 1.2 Hz, H-4), 4.65 (1H, 1.2, 7.6 Hz, H-3), 4.53 (2H, s, $PhOCH_2$), 4.18 (1H, dd, 7.3, 11.3 Hz, OC*H*HCH=), 4.11 (1H, dd, 7.3, 11.3 Hz, OCH*H*CH=), 1.76 (3H, s, methyl), 1.70 (3H, s, methyl). ^{13}C NMR ($CDCl_3$): 169.01, 165.70, 157.08, 138.69, 129.74, 122.18, 114.73, 119.58, 83.94, 67.12, 65.14, 63.64, 25.71, 18.01. Anal. calcd. for $C_{16}H_{20}N_2O_4$: C 63.14, H 6.62, N 9.20; found: C 63.37, H 6.68, N 8.98.

(v) With propargyl alcohol

A solution of **6** (20.2 mg, 0.050 mmol) and propargyl alcohol (0.006 mL, 5.8 mg, 0.10 mmol), in dichloromethane (2.4 mL), was stirred with rhodium(II) acetate (2 mg, 0.005 mmol) and placed in a preheated oil bath at 50°C. The

© 2001 NRC Canada

red solution was refluxed for 15 h, and the solvent was then evaporated. The red residue was chromatographed, using dichloromethane, to isolate the thietanone, followed by dichloromethane – ethyl acetate (1:1) to give the products as blue solids. These were dissolved in dichloromethane (10 mL) and washed successively with water (10 mL) and saturated sodium chloride (10 mL), dried over magnesium sulfate, and evaporated to give the *cis*-isomer (4.3 mg, 26%) and the *trans*-isomer (2 mg, 12%). *cis*-Isomer: $[\alpha]_D^{20}$ –29.4° (c 0.340, chloroform). MS (CI, *m*/*z*): 275 (M + 1). HR-MS-CI calcd. for $C_{14}H_{14}N_2O_4$: 275.1032 (M + 1); found: 275.1035. IR ($CHCl_3$) (cm^{-1}): 3420, 3306, 2402, 1790, 1690. ^{1}H NMR ($CDCl_3$): 7.32 (3H, m, Ar + NH), 7.03 (1H, t, Ar), 6.93 (2H, m, Ar), 6.79 (1H, br s, NH), 5.55 (1H, ddd, 1.4, 4.0, 9.6 Hz, H-3), 5.36 (1H, d, 4.0 Hz, H-4), 4.56 (1H, d, 15.1 Hz, PhOC*H*H), 4.53 (1H, d, 15.1 Hz, PhOCH*H*), 4.23 (1H, dd, 2.4, 16.2 Hz, OC*H*H), 4.18 (1H, dd, 2.4, 16.2 Hz, OCH*H*), 2.50 (1H, t, 2.4 Hz, (C=C-H). ^{13}C NMR ($CDCl_3$): 168.45 (acetamido C=O), 166.94 (β-lactam C=O), 157.21, 129.78, 122.34, 114.95 (aromatic), 81.02 (C-4), 78.35 (OCH_2C=CH), 75.93 (OCH_2C=*C*H), 67.44 ($PhOCH_2$), 59.96 (C-3), 56.50 (OCH_2C=CH). *trans*-Isomer: ^{1}H NMR ($CDCl_3$): 7.35–7.30 (3H, m, Ar + NH), 7.05 (1H, t, Ar), 6.93 (2H, d, Ar), 6.50 (1H, br s, NH), 5.31 (1H, d, 1.1 Hz, H-4), 4.66 (1H, dd, 1.1, 7.2 Hz, H-3), 4.54 (2H, s, $PhOCH_2$), 4.37 (1H, dd, 1.2, 2.4 Hz, OC*H*HC=CH), 4.36 (1H, dd, 1.2, 2.4 Hz, OCH*H*C=CH), 2.49 (1H, t, 2.4 Hz, OCH_2C=CH).

(vi) With allyl alcohol

To **6** (14.7 mg, 0.036 mmol) and allyl alcohol (0.006 mL, 5.1 mg, 0.81 mmol), in dichloromethane (2.6 mL) was added rhodium(II) acetate (2 mg, 0.005 mmol). The mixture was immersed in a preheated oil bath at 50°C and refluxed for 11 h. The solvent was then removed and the red residue chromatographed using dichloromethane, to elute the thietanone, followed by dichloromethane – ethyl acetate (1:1) to give the products as blue films. These were dissolved in dichloromethane (10 mL) and the solutions were washed successively with water (10 mL) and saturated sodium chloride (10 mL), dried over magnesium sulfate, and evaporated to give the *cis*-isomer (3.6 mg, 36%) and the *trans*-isomer (1.4 mg, 14%) as colourless oils. *cis*-Isomer: $[\alpha]_D^{20}$ –14.3° (c 0.070, $CHCl_3$). MS (CI, *m*/*z*): 277 (M + 1). HR-MS-CI calcd. for $C_{14}H_{16}N_2O_4$: 277.1188 (M + 1); found: 277.1189. IR ($CHCl_3$) (cm^{-1}): 3418, 1788, 1692. ^{1}H NMR ($CDCl_3$): 7.37 (3H, m, Ar + NH), 7.03 (1H, m, Ar), 6.92 (2H, m, Ar), 6.55 (1H, br s, NH), 5.87 (1H, ddt, 5.6, 10.4, 17.2 Hz, =CH), 5.53 (1H, ddd, 1.4, 3.9, 9.6 Hz, H-3), 5.33 (1H, dq, 1.4, 17.2 Hz, =C*H*H), 5.22 (1H, dq, 1.4, 10.4 Hz, =CH*H*), 5.21 (1H, d, 3.9 Hz, H-4), 4.58 (1H, d, 15.1 Hz, PhOC*H*H), 4.53 (1H, d, 15.1 Hz, PhOCH*H*), 4.22 (1H, ddt, 1.4, 5.6, 12.7 Hz, OC*H*H), 4.13 (1H, ddt, 1.4, 5.6, 12.7 Hz, OCH*H*). ^{13}C NMR ($CDCl_3$): 168.90 (acetamido C=O), 168.40 (β-lactam C=O), 157.25, 129.87, 122.33, 115.00 (aromatic), 133.19 (OCH_2CH=CH_2), 118.28 (OCH_2CH=*C*H_2), 81.01 (C-4), 70.06 (OCH_2CH=CH_2), 67.46 ($PhOCH_2$), 59.88 (C-3). *trans*-Isomer: ^{1}H NMR ($CDCl_3$): 7.33 (2H, t, Ar), 7.12 (1H, d, 7.0 Hz, NH), 7.04 (1H, t, Ar), 6.91 (2H, d, Ar), 6.47 (1H, br s, NH), 5.93 (1H, m, OCH_2C*H*=CH), 5.33 (1H, dq, 1.4, 3.0, 16.7 Hz, CH=C*H*H), 5.25 (1H, dq, 1.4, 2.6, 10.4 Hz, CH=CH*H*), 5.16 (1H, d, 1.2 Hz, H-4), 4.67 (1H, dd, 1.2, 7.4 Hz, H-3), 4.53 (2H, s, $PhOCH_2$), 4.22 (1H, ddt, 1.4, 5.4, 12.7 Hz, OC*H*HCH=CH_2), 4.12 (1H, ddt, 1.4, 6.1, 12.7 Hz, OCH*H*CH=CH_2).

(vii) With furfuryl alcohol

A solution of **6** (31 mg, 0.076 mmol) and furfuryl alcohol (0.014 mL, 0.162 mmol) in dichloromethane (4 mL) was heated to reflux under nitrogen and rhodium(II) acetate (5 mg, 0.01 mmol) was added. Refluxing was continued for 14 h, and the solvent was then removed. The residue was chromatographed on silica gel; elution with 7:3 ethyl acetate:hexanes gave 12.1 mg (50%) of the *cis*-product. ^{1}H NMR ($CDCl_3$): 7.39–7.29 (4H, m, Ph + furfuryl + NH), 7.03 (1H, t, Ph), 6.92 (2H, d, Ph), 6.34 (2H, d, 1.4 Hz, furfuryl), 6.32 (1H, br s, NH), 5.51 (1H, ddd, 1.3, 3.9, 9.6 Hz, H-3), 5.28 (1H, d, 3.9 Hz, H-4), 4.57 (1H, d, 13.2 Hz, OC*H*H), 4.54 (1H, d, 14.9 Hz, PhOC*H*H), 4.52 (1H, d, 13.2 Hz, OCH*H*), 4.50 (1H, d, 14.9 Hz, PhOCH*H*).

With hydroxyacetone (42)

To bromoacetone (2.06 g, 15.1 mmol), in dimethylformamide (80 mL), was added sodium formate (2.11 g, 31.00 mmol). The solution was stirred for 6 h, diluted with ethyl acetate (100 mL), washed successively with water (2 × 100 mL) and saturated sodium chloride (100 mL), dried over magnesium sulfate, and evaporated at room temperature to give the formate ester (900 mg, 59%). IR (neat) (cm^{-1}): 1726, 1678. ^{1}H NMR (100 MHz, $CDCl_3$): 8.16 (1H, s, aldehyde CHO), 4.76 (2H, s, OCH_2), 2.20 (3H, s, CH_3).

The formate ester (900 mg, 8.82 mmol), in absolute ethanol (10 mL), was stirred for 72 h with *p*-toluenesulfonic acid hydrate (5 mg, 0.03 mmol). The solution was evaporated at room temperature and the residue was chromatographed, using dichloromethane–ether (3:7), to give **42** as a pale yellow oil. MS (EI, *m*/*z*): 73 (M – 1), 74 (M). HR-MS-EI calcd. for $C_3H_6O_2$: 74.0368 (M); found: 74.0369. IR (neat) (cm^{-1}): 3424, 1724. ^{1}H NMR ($CDCl_3$): 4.25 (2H, s), 3.12 (1H, br s), 2.18 (3H, s). ^{13}C NMR ($CDCl_3$): 206.91 (C=O), 68.67 (CH2), 25.18 (CH_3).

Hydroxyacetone (6.9 mg, 0.093 mmol) was dried azeotropically with chloroform, and added to a solution of **6** (20.5 mg, 0.051 mmol) in dichloromethane (3 mL). The solution was stirred, rhodium(II) acetate (2.0 mg, 0.005 mmol) was added, and the mixture was refluxed for 16 h with continuous monitoring by TLC. Although **22** was produced, no β-lactam-containing product was detected. The same result was obtained when the reaction was repeated at room temperature.

With ethyl γ-hydroxyacetoacetate (43)

Sodium formate (2.82 g, 41.5 mmol) was added to a solution of ethyl γ-bromoacetoacetate (**4**) (4.33 g, 20.7 mmol) in dimethylformamide (80 mL). The solution was stirred rapidly for 2 h and then diluted with ethyl acetate (200 mL), washed successively with water (2 × 200 mL), and saturated sodium chloride (200 mL), dried over magnesium sulfate, and evaporated to afford the formate ester as a bright yellow oil (2.83 g, 78%). ^{1}H NMR (100 MHz, $CDCl_3$): 8.16 (1H, s, aldehyde CHO), 4.91 (2H, s, OCH_2CO), 4.26 (2H, q, 7.1 Hz,

© 2001 NRC Canada

ester CH_2), 3.53 (2H, s, $COCH_2CO$), 1.30 (3H, t, 7.1 Hz, ester CH_3). This oil was dissolved in absolute ethanol (100 mL) and stirred for 20 h with *p*-toluenesulfonic acid hydrate (232.3 mg, 1.2 mmol). The solvent was evaporated and the residue, in ethyl acetate (50 mL), was washed successively with water (50 mL) and saturated sodium chloride (50 mL), dried over magnesium sulfate, and evaporated. Purification of the product by column chromatography using ethyl acetate – hexanes (3:7) gave **43** as a yellow oil (1.14 g, 48%). MS (CI, *m*/*z*): 147 (M + 1). IR (neat) (cm^{-1}): 3472, 1732, 1626. ^1H NMR ($CDCl_3$): 4.38 (2H, d, 5.0 Hz, $HOCH_2CO$), 4.20 (2H, q, 7.2 Hz, ester CH_2), 3.49 (2H, s, $COCH_2CO$), 3.01 (1H, br. t, 5.0 Hz, $HOCH_2$), 1.28 (3H, t, 7.2 Hz, ester CH_3). ^{13}C NMR ($CDCl_3$): 202.29 (hydroxyacetyl C=O), 166.33 (acetate C=O), 68.49 ($HOCH_2COCH_2$), 61.74 ($CO_2CH_2CH_3$), 45.38 ($HOCH_2COCH_2CO_2CH_2CH_3$), 13.98 ($CH_2CO_2CH_2CH_3$). Anal. calcd. for $C_6H_{10}O_4$: C 49.31, H 6.90; found: C 49.21, H 6.81.

To a solution of **6** (18.4 mg, 0.045 mmol), in dichloromethane (4.0 mL), were added ethyl γ-hydroxyacetoacetate (14.5 mg, 0.099 mmol) (dried azeotropically with chloroform (3×)), and rhodium(II) acetate (3 mg, 0.007 mmol). The solution was refluxed for 7 h and then evaporated. The residue was subjected to chromatography using a dichloromethane – ethyl acetate gradient to yield **22** and a white solid identical to the product from trapping with ethanol.

With ethyl γ-hydroxy-α-diazoacetoacetate (44)

To ethyl γ-hydroxyacetoacetate (0.59 g, 4.04 mmol), in acetonitrile (10 mL), was added *p*-carboxybenzenesulfonyl azide (1.04 g, 4.57 mmol) followed, during 10 min at 0°C, by triethylamine (1.7 mL, 1.2 g, 2.20 mmol). The pale yellow solution was stirred at 0° for an additional 15 min and DBU (0.6 mL, 0.61 g, 4.01 mmol) was added to precipitate a yellow solid. After an additional 3 h of stirring at 0°, the mixture was filtered and the filtrate was evaporated. The residue was dissolved in ethyl acetate (50 mL) and the solution was washed successively with water (2 × 50 mL), saturated sodium bicarbonate (50 mL) and saturated sodium chloride (50 mL), dried over magnesium sulfate, and evaporated to give a red oil (309 mg). Purification by column chromatography, using ethyl acetate – hexanes (2:3), gave **44** as a yellow oil (178.5 mg, 26%). MS (CI, *m*/*z*): 173 (M + 1). IR (neat) (cm^{-1}): 3488, 2986–2911, 2145, 1721, 1659. ^1H NMR ($CDCl_3$): 4.61 (2H, d, 5.1 Hz, $HOCH_2$), 4.28 (2H, q, 7.1 Hz, ester CH_2), 3.40 (1H, 5.1 Hz, OH), 1.33 (3H, t, 7.1 Hz, ester CH_3). ^{13}C NMR ($CDCl_3$): 191.79 (hydroxyacetyl C=O), 160.82 (acetate C=O), 66.97 ($HOCH_2CO$), 61.97 ($CO_2CH_2CH_3$), 14.31 ($CO_2CH_2CH_3$). Anal. calcd. for $C_6H_8N_2O_4$: C 41.87, H 4.68, N 16.27; found: C 42.51, H 4.88, N 15.83.

To a solution of **6** (17.8 mg, 0.044 mmol) in dichloromethane (2.8 mL), was added ethyl γ-hydroxy-α-diazoacetoacetate (14.8 mg, 0.086 mmol) (dried azeotropically with chloroform (3×)). The solution was stirred, rhodium(II) acetate (3 mg, 0.007 mmol) was added, and the mixture was refluxed for 10 h. Although the thietanone **22** was detected, no β-lactam-containing product was found. The same result was obtained when the reaction was repeated at room temperature.

With benzyl 4-hydroxyprop-2-ynoate (45)

A solution of 3,4-dihydro-2*H*-pyran (28.0 mL, 25.82 g, 0.307 mol) in dichloromethane (100 mL) was cautiously added, at 0°C, to a solution of propargyl alcohol (16.5 mL, 15.90 g, 0.283 mol) and *p*-toluenesulfonic acid hydrate (159 mg, 0.089 mmol) in dichloromethane (80 mL). The solution was stirred for 2 h at 25° and then washed successively with water (100 mL), saturated sodium bicarbonate (100 mL), and saturated sodium chloride (100 mL), dried over magnesium sulfate, and evaporated. Purification by vacuum distillation afforded tetrahydro-2-(2-propynyloxy)pyran as a colourless oil (32.9 g, 83%), bp 63–65°C/9 torr (1 torr = 133.322 Pa). MS (CI, *m*/*z*): 141 (M + 1). IR (cm^{-1}): 3293, 2118. ^1H NMR ($CDCl_3$): 4.80 (1H, t, 3.3 Hz, OCHO), 4.27 (1H, dd, 2.4, 15.7 Hz, OC*H*HC=CH), 4.21 (1H, d, 2.4, 15.7 Hz, OCH*H*C=CH), 3.82 (1H, m, CH_2*H*HCHO), 3.49 (1H, m, CH_2CH*H*OCHO), 2.40 (1H, t, 2.4 Hz, C=C-H), 1.84–1.72 (6H, m, $OCH_2CH_2CH_2CH_2CH$). ^{13}C NMR ($CDCl_3$): 96.85 (OCHO), 79.81 (OCH_2C=CH), 73.90 (OCH_2C=*C*H), 61.97 ($OCH_2CH_2CH_2CH_2CH$), 53.97 (OCH_2C=CH), 30.22 ($OCH_2CH_2CH_2CH_2CH$), 25.35 ($OCH_2CH_2CH_2CH_2CH$), 19.00 ($OCH_2CH_2CH_2CH_2CH$).

A solution of the tetrahydropyranyl ether (2.06 g, 14.73 mmol) in tetrahydrofuran (15 mL), was treated, at –78°C, with a 2.5 M solution of *n*-butyllithium in hexane (5.9 mL, 0.94 g, 14.75 mmol). The resulting yellow solution was stirred for 1.5 h at –78°, and benzyl chloroformate (2.0 mL, 2.39 g, 14.01 mmol), in a solution of tetrahydrofuran (2.0 mL) and hexamethylphosphoramide (3.5 mL), was then added dropwise. The reaction mixture was warmed to –65° for 2 h and then to room temperature during 7.0 h, cooled to 0°, and treated with water (30 mL). The mixture was diluted with ether (60 mL) and the organic phase was separated and washed successively with water (60 mL) and saturated sodium chloride (60 mL), dried over magnesium sulfate, and evaporated. Purification by column chromatography using ethyl acetate – hexanes (1:9) afforded the tetrahydropyranyl ether of **45** as a colourless oil. ^1H NMR (100 MHz, $CDCl_3$): 7.39 (5H, s, Ar), 5.32 (1H, s, OCHO), 5.17 (2H, s, benzyl CH_2), 4.82 (2H, s, OCH_2C=CH), 3.93–3.47 (2H, m, $OCHOCH_2CH_2$), 1.73 (6H, m, $OCH_2CH_2CH_2CH_2$). A portion of this oil (50 mg, 0.18 mmol), in dry methanol (3.8 mL), was treated with trifluoroacetic acid (0.07 mL, 104 mg, 0.91 mmol). The solvent was evaporated after 30 min, and the product was purified by column chromatography using ethyl acetate – hexanes (1:4) to yield **45** as white crystals (12 mg, 35%), mp 102–104°C. MS (CI, *m*/*z*): 191 (M + 1). IR (KBr) (cm^{-1}): 3468, 1742. ^1H NMR (100 MHz, $CDCl_3$): 7.41 (5H, s, Ar), 5.21 (1H, br s, OH), 5.09 (2H, s, benzyl CH_2), 4.70 (2H, s, $HOCH_2$). ^{13}C NMR ($CDCl_3$): 178.86 (ester C=O), 173.15 ($HOCH_2C$=*C*CO_2CH_2Ph), 133.83, 129.19, 128.93, 128.01 (aromatic), 89.87 ($HOCH_2C$=C), 74.57 ($HOCH_2C$=C), 67.88 (CO_2CH_2Ph). Anal. calcd. for $C_{11}H_{10}O_3 \cdot 0.25H_2O$: C 67.86, H 5.44; found: C 67.83, H 5.28.

Rhodium(II) acetate (1 mg, 0.002 mmol) was added to a solution of **6** (12.0 mg, 0.030 mmol) and **45** (8.5 mg, 0.045 mmol) (dried azeotropically with chloroform (3×)), in dichloromethane (2.5 mL). The red solution was refluxed for 10 h while being monitored by TLC. Purification by column chromatography, using a dichloromethane – ethyl acetate

© 2001 NRC Canada

elution gradient, afforded **22** and unreacted **45**. The same result was obtained when the reaction was repeated at room temperature.

With 6-hydroxymethyl-2,2-dimethyl-4*H*-1,3-dioxin-4-one (46)

To 2,2,6-trimethyl-4*H*-1,3-dioxin-4-one (0.93 mL, 1.01 g, 7.12 mmol) in carbon tetrachloride (25 mL), were added *N*-bromosuccinimide (1.26 g, 7.08 mmol) and benzoyl peroxide (3 mg, 0.012 mmol). The mixture was heated to reflux with a heat gun and irradiated for 60 min with a 500 W Photoflood No. 2 bulb mounted beside the flask. The mixture was then cooled to 0°, filtered, and the filtrate was evaporated. The residue, in hexanes (20 mL), was washed successively with water (20 mL), saturated sodium bicarbonate (20 mL), water (20 mL), and saturated sodium chloride (20 mL), dried over magnesium sulfate, and evaporated to give 6-bromomethyl-2,2-dimethyl-4*H*-1,3-dioxin-4-one (300 mg, 19%) as a pale yellow oil. ^{1}H NMR (100 MHz, $CDCl_3$): 5.55 (1H, s, =CH), 3.90 (2H, s, $BrCH_2$), 1.74 (6H, s, CH_3).

A solution of this bromide in dimethylformamide (3.5 mL) was treated with sodium formate (206.5 mg, 3.04 mmol). The solution was stirred for 5 h and was then diluted with ether (25 mL), washed successively with water (25 mL) and saturated sodium chloride (25 mL), dried over magnesium sulfate, and evaporated to give the formate ester as a yellow oil. A solution of this compound in dry methanol (9.0 mL) was cooled to 0°, and a solution of anhydrous potassium carbonate (198.5 mg, 1.44 mmol) in water (2.3 mL) was added during 10 min. The solvent was evaporated after an additional 30 min of stirring. The residue, in dichloromethane (20 mL), was washed successively with 0.2 M hydrochloric acid (20 mL), water (20 mL), and saturated sodium chloride (20 mL), dried over magnesium sulfate, and evaporated. The product was purified by column chromatography using ethyl acetate – hexanes (3:7) to yield **46** as a yellow oil (37.9 mg). MS (CI, *m*/*z*): 159 (M + 1). IR (neat) (cm^{-1}): 3418, 1713. ^{1}H NMR ($CDCl_3$): 5.56 (1H, t, 1.2 Hz, =CH), 4.19 (2H, d, 1.2 Hz, $HOCH_2$), 2.35 (1H, br s, OH), 1.70 (6H, s, CH_3). ^{13}C NMR ($CDCl_3$): 169.85 (C=O), 161.02 (CO*C*H=C), 107.06 (H_3CCCH_3), 92.37 ($HOCH_2CCH$), 60.99 ($HOCH_2C$), 25.01 (CH_3). Anal. calcd. for $C_7H_{10}O_4 \cdot 0.5H_2O$: C 50.30, H 6.63; found: C 50.71, H 6.49.

To a solution of **6** (10.1 mg, 0.025 mmol) in dichloromethane (2.3 mL) was added **46** (11.1 mg, 0.059 mmol), which had been dried azeotropically with chloroform (3×). The resulting solution was stirred, rhodium(II) acetate (2 mg, 0.005 mmol) was added, and the mixture was refluxed for 9 h while being monitored by TLC. Although the thietanone **22** was formed, no β-lactam-containing product was isolated after evaporation of the solvent and chromatography of the residue. The same result was obtained when the reaction was repeated at room temperature.

With benzyl *trans*-2,4-pentadienoate (47)

To finely ground *trans*-2,4-pentadienoic acid (39.8 mg, 0.41 mmol), in dry dimethylformamide (6.0 mL), was added anhydrous potassium carbonate (56.3 mg, 0.41 mmol). The mixture was stirred for 10 min, and benzyl bromide (0.05 mL, 71.9 g, 0.42 mmol) was then added, with stirring, over a 5 min period. Additional dimethylformamide (5.0 mL) was added after 3 h, and the solution was stirred for 18 h, diluted with ethyl acetate (20 mL), and washed successively with water (4 × 20 mL) and saturated sodium chloride (20 mL), dried over magnesium sulfate, and evaporated to give a yellow oil (30.5 mg). Purification by column chromatography using ethyl acetate – hexanes (1:7) gave **47** as a colourless oil (13.8 mg, 18%). MS (CI, *m*/*z*): 189 (M + 1). HR-MS-CI calcd. for $C_5H_6O_2$: 189.0915 (M + 1); found: 189.0921. IR (neat) (cm^{-1}): 1716, 1642, 1600. ^{1}H NMR ($CDCl_3$): 7.40–7.26 (6H, m, Ar + H-3), 6.46 (1H, ddt, 0.6, 7.0, 10.0 Hz, H-4), 5.96 (1H, dd, 0.6, 15.4 Hz, H-2), 5.62 (1H, dt, 0.6, 17.0 Hz, =C*H*H), 5.50 (1H, dt, 0.6, 10.0 Hz, =CH*H*), 5.20 (2H, s, benzyl CH_2). ^{13}C NMR ($CDCl_3$): 166.57 (ester C=O), 145.10 (CH_2=*C*H-CH), 136.18, 128.56, 128.40), 125.57 (*C*H_2=CH-CH), 121.97 (CH_2=CH-CH-*C*H), 66.23 (CH-CH-CO_2CH_2Ph).

The ester (11.1 mg, 0.059 mmol) was dried azeotropically with chloroform and added to a solution of **6** (17.2 mg, 0.042 mmol) in dichloromethane (5.0 mL). The solution was stirred, rhodium(II) acetate (3 mg, 0.007 mmol) was added, and the mixture was refluxed for 4.5 h. Other than the thietanone **22** and unreacted **47**, isolated after chromatography using dichloromethane followed by dichloromethane – ethyl acetate (1:1), no β-lactam-containing product was detected. The same result was obtained when the reaction was repeated at room temperature.

With benzyl mercaptan

To a solution of **6** (48.9 mg, 0.12 mmol) and benzyl mercaptan (0.025 mL, 26.5 mg, 0.213 mmol), in dichloromethane (3 mL), was added rhodium acetate (6.3 mg, 0.014 mmol). The mixture was heated to reflux for 9 h, cooled to room temperature, diluted with dichloromethane (10 mL), and washed with water (2 × 13 mL). The dichloromethane layer was dried over sodium sulfate, evaporated, and purified by column chromatography using ethyl acetate – hexanes (2:1) to give the *cis*-benzyl sulfide (5.0 mg, 12%) and the *trans*-benzyl sulfide (1.5 mg, 4%). *cis*-Isomer: ^{1}H NMR ($CDCl_3$): 7.41–7.27 (8H, m, Ar + NH), 7.03 (1H, t, Ar), 6.94 (2H, d, Ar), 6.60 (1H, br s, NH), 5.58 (1H, dd, 4.6, 9.1 Hz, H-3), 4.91 (1H, d, 4.6 Hz, H-4), 4.55 (1H, d, 15.0 Hz, PhOC*H*H), 4.51 (1H, d, 15.0, PhOCH*H*), 3.72 (1H, d, 13.7 Hz, SC*H*HPh), 3.69 (1H, d, 13.7 Hz, SCH*H*Ph). *trans*-Isomer: ^{1}H NMR ($CDCl_3$): 7.35–7.27 (7H, m, Ar), 7.03 (1H, t, Ar), 7.01 (1H, d, 7.7 Hz, NH), 6.90 (2H, d, Ar), 5.59 (1H, br s, NH), 4.82 (1H, d, 2.3 Hz, H-4), 4.60 (1H, dd, 2.3, 7.7 Hz, H-3), 4.50 (2H, s, $PhOCH_2$), 3.90 (1H, d, 13.8 Hz, SC*H*HPh), 3.89 (1H, d, 13.8 Hz, SCH*H*Ph).

Theoretical

Calculations were performed using Gaussian 98 (42). Stationary points were optimized fully at the level indicated, and characterized by frequency analysis. For the calculations of C=O stretching frequencies of azetinones, calculated frequencies were scaled by 0.89 (43).

Acknowledgements

This research was supported by the Natural Sciences and Engineering Research Council of Canada (NSERC). The au-

© 2001 NRC Canada

thors thank Marie-Claire Wilson for valuable experimental assistance.

References

1. R.D.G. Cooper and F.L. José. J. Am. Chem. Soc. **92**, 2575 (1970).
2. S. Wolfe, S. Ro, C.-K. Kim, and Z. Shi. Can. J. Chem. **79**, 1238 (2001).
3. S. Kukolja and R.R. Chauvette. *In* Chemistry and biology of β-lactam antibiotics. Vol. 1. *Edited by* R. B. Morin and M. Gorman. Academic Press, Inc., New York. 1982. p. 93; S. Kukolja. *In* Recent advances in the chemistry of β-lactams. *Edited by* J. Elks. Spec. Pub. Roy. Soc. Chem., London. 197, p. 180; Y. Hamashima, K. Ishikura, H. Ishitobi, H. Itani, T. Kubota, K. Minami, M. Murakami, W. Nagata, M. Narisada, Y. Nishitani, T. Okada, H. Onoue, H. Satoh, Y. Sendo, T. Tsuji, and M. Yoshioka. *In* Recent advances in the chemistry of β-lactams. *Edited by* J. Elks. Spec. Pub. Roy. Soc. Chem. London. 1976. p. 243; R.K. Thaper, Y. Kumar, and J.-M. Khanna. Synth. Comm. **25**, 883 (1995); H. Tanaka, S. Sumida, Y. Kameyama, K. Sorajo, I. Wada, and S. Torii. Bull. Chem. Soc. Jpn. **69**, 3651 (1996); H. Tanaka, R. Kikuchi, and S. Torii. Bull. Chem. Soc. Jpn. **69**, 1391 (1996); H. Tanaka, S. Sumida, Y. Nishioka, N. Kobayashi, Y. Tokumaru, Y. Kameyama, and S. Torii. J. Org. Chem. **62**, 3610 (1997).
4. D.A. Preston. Int. Congr. Symp. Ser. R. Soc. Med. **188**, 3 (1992).
5. M. Narisada, H. Onoue, M. Ohtani, F. Watanabe, T. Okada, and W. Nagata. Tetrahedron Lett. 1755 (1978).
6. M. Regitz. Angew. Chem. Int. Ed. Engl. **6**, 733 (1967); M. Regitz. Synthesis, 351 (1972).
7. R.J. Ponsford and R. Southgate. J. Chem. Soc. Chem. Commun. 846 (1979); R.W. Ratcliffe, T.N. Salzmann, and B.G. Christensen. Tetrahedron Lett. **21**, 31 (1980).
8. C.C. Bodurow, B.D. Boyer, J. Brennan, C.A. Bunnell, J.E. Burks, M.A. Carr, C.W. Doecke, T.M. Eckrich, J.W. Fisher, J.P. Gardner, B.J. Graves, P. Hines, C. Hoying, B.G. Jackson, M.D. Kinnick, C.D. Kochert, J.S. Lewis, W.D. Luke, L.L. Moore, J.M. Morin, Jr., R.L. Nist, D.E. Prather, D.L. Psarks, and W.C. Vladuchick. Tetrahedron Lett. **30**, 2321 (1989); D.A. Evans and E.B. Sjogren. Tetrahedron Lett. **26**, 3787 (1985).
9. S. Yamamoto, H. Itani, H. Takahashi, T. Tsuji, and W. Nagata. Tetrahedron Lett. **25**, 4545 (1984); D. Habich and W. Hartwig. Tetrahedron, **40**, 3667 (1984).
10. T. Kametani, S.-P. Huang, T. Nagahara, and M. Ihara. J. Chem. Soc. Perkin Trans. 1, 2282 (1981).
11. G. Brooks, T.T. Howarth, and E. Hunt. J. Chem. Soc. Chem. Commun. 642 (1981).
12. D.V.C. Awang and S. Wolfe. Can. J. Chem. **49**, 706 (1969).
13. N.F. Osborne. J. Chem. Soc. Perkin Trans 1, 146 (1980).
14. J.B. Hendrickson and W.A. Wolf. J. Org. Chem. **33**, 3610 (1968); M. Regitz, J. Hocker, and A. Liedhegener. Org. Syn. Coll. Vol V. 179 (1973); T. Curphey. Org. Prep. Proced. Int. **13**, 112 (1981).
15. M. Regitz and F. Menz. Chem. Ber. **101**, 2622 (1968); M. Regitz and J. Rtter. Chem. Ber. (1992); J.C. Lee and J.Y. Yuk. Synth. Commun. **25**, 1511 (1995); D.F. Taber, Y. You, and Y. Song. J. Org. Chem. **60**, 1093 (1995); D.F. Taber, D.M. Gleave, R.J. Herr, K. Moody, and M.J. Hennessy. J. Org. Chem. **60**, 2283 (1995).
16. S. Oida, A. Yoshida, and E. Ohki. Heterocycles, **14**, 1999 (1980); T. Kametani, N. Kanaya, T. Mochizuki, and T. Honda. Heterocycles, **19**, 1023 (1982); H. Fliri, C.-P. Mak, K. Prasad, G. Schulz, and P. Stttz. Heterocycles, **20**, 205 (1983); H.M.L. Davies and L.V.T. Crisco. Tetrahedron Lett. **28**, 371 (1987); C.J. Moody and R.J. Taylor. Tetrahedron Lett. **29**, 6005 (1988); A. Padwa and M.D. Weingarten. Chem. Rev. **96**, 223 (1996); S. Sengupta and S. Mondal. Tetrahedron Lett. **41**, 2965 (2000).
17. R.L. Danheiser, S.K. Gee, and H. Sard. J. Am. Chem. Soc. **104**, 7670 (1982). E.N. Marvell. *In* Thermal electrocyclic reactions. *Edited by* H. H. Wasserman. Academic Press, New York. 1980. p. 146.
18. J. Marchand-Brynaert and L. Ghosez. Bull. Soc. Chim. Belg. **94**, 1021 (1985).
19. R. Duschinsky and L.A. Dolan. J. Am. Chem. Soc. **68**, 2350 (1946).
20. R.M. Silverstein, G.C. Bassler, and T.C. Morril. Spectrometric identification of organic compounds. 5th ed. John Wiley, New York. 1991. p. 264.
21. R.M. Silverstein, G.C. Bassler, and T.C. Morrill. Spectrometric identification of organic compounds. 5th ed. John Wiley, New York. 1991. p. 221.
22. E. Piers and K.A. Ellis. Tetrahedron Lett. **34**, 1875 (1993); K. Nakamura and K.N. Houk. J. Org. Chem. **60**, 686 (1995).
23. R.A. Olofson, D.S. Morrison, and A. Banerji. J. Org. Chem. **49**, 2653 (1984).
24. X. Li and M.J. Miller. Tetrahedron Lett. **36**, 1617 (1995).
25. F. Gavina, A.M. Costero, and M.R. Andreu. J. Org. Chem. **55**, 434 (1990)
26. J.C. Guillemin, J.M. Denis, and A. Lablache-Combier. J. Am. Chem. Soc. **103**, 468 (1981).
27. W.J. Hehre, L. Radom, P. v R. Schleyer, and J.A. Pople. Ab initio molecular orbital theory. Wiley, New York. 1986.
28. R.A. Olofson, R.K. Vander Meer, D.H. Hoskin, M. Bernheim, S. Stournas, and D.S. Morrison. J. Org. Chem. **49**, 3367 (1984); I.R. Dunkin, M.A. Lynch, R. Withnell, A.J. Boulton, and N. Henderson. J. Chem. Soc. Chem. Commun. 1777 (1989); B. Liu and A.G. Wee. Heterocycles, **36**, 445 (1993).
29. J.C. Sheehan. U.S. Patents 3 487 070, 3 487 071, 3 487 072, 3 487 074, 3 487 079, 3 487 090. 1969.
30. S. Wolfe and M.P. Goeldner. Tetrahedron Lett. 5131 (1973); K. Clauss, D. Grimm, and G. Proessel. Liebigs Ann. Chem. 539 (1974); A. Suarato, P. Lombardi, C. Galliani, and G. Franceschi. Tetrahedron Lett. 4059 (1978); C.L. Branch and M.J. Pearson. J. Chem. Soc. Perkin Trans. 1, 2268 (1979); T. Kobayashi, N. Ishida, and T. Hiraoka. J. Chem. Soc. Chem. Commun. 736 (1980); M.D. Bachi, A. Gross, and F. Frolow. J. Org. Chem. **47**, 765 (1982); M. Aratani, K. Sawada, and M. Hashimoto. Tetrahedron Lett. **23**, 3921 (1982); P.J. Reider, R. Rayford, and E.J.J. Grabowski. Tetrahedron Lett. **23**, 379 (1982); P.J. Reider and E.J.J. Grabowski. Tetrahedron Lett. **23**, 2293 (1982); D. Planchenault, R. Wisedale, T. Gallagher, and N.J. Hales. J. Org. Chem. **62**, 3438 (1997); S.R. Martel, D. Planchenault, R. Wisedale, T. Gallagher, and N.J. Hales. Chem. Commun. 1897 (1997).
31. C.L. Branch and M.J. Pearson. J. Chem. Soc. Perkin Trans. 1, 2208 (1979).
32. K.D. Barrow and T.M. Spotswood. Tetrahedron Lett. 3325 (1965); S. Wolfe and W.S. Lee. Chem. Comm. 242 (1968); A. Vigerani and G.G. Gallo. J. Heterocycl. Chem. **4**, 583 (1987).
33. S. Yamamoto, H. Itani, H. Takahashi, T. Tsuji, and W. Nagata. Tetrahedron Lett. **25**, 4545 (1984).
34. R.A. Earl and L.B. Townsend. Org. Synth. **60**, 81 (1981).
35. M. Sato, J.-I. Sakai, K. Takayama, S. Kobayashi, M. Suzuki, and C. Kaneko. Chem. Pharm. Bull. **38**, 94 (1990).
36. Y. Ueda and S.C. Maynard. Tetrahedron Lett. **26**, 6309 (1985); A.I. Meyers, T.J. Sowin, S. Scholz, and Y. Ueda. Tetrahedron

© 2001 NRC Canada

Lett. **28**, 5103 (1987); T.J. Sowin and A.I. Meyers. J. Org. Chem. **53**, 4154 (1988).
37. R.D.G. Cooper, L.D. Hatfield, and D.O. Spry. Acc. Chem. Res. **6**, 32 (1973).
38. M. Narisada, H. Onoue, M. Ohtani, and F. Watanabe. Tetrahedron Lett. 1755 (1978).
39. W.D. Kumler. J. Am. Chem. Soc. **60**, 857 (1938); F. Krohnke and H. Timmler. Ann. Chem. **69**, 614 (1936).
40. J.B. Hendrickson and W.A. Wolfe. J. Org. Chem. **33**, 3610 (1968).
41. P. Legzdins, R.W. Mitchell, G.L. Rempel, J.D. Ruddick, and G. Wilkinson. J. Chem. Soc. A, 3322 (1970).
42. Gaussian 98, Revision A.6. M.J. Frisch, G.W. Trucks, H.B. Schlegel, G.E. Scuseria, M.A. Robb, J.R. Cheeseman, V.G. Zakrzewski, J.A. Montgomery, Jr., R.E. Stratmann, J.C. Burant, S. Dapprich, J.M. Millam, A.D. Daniels, K.N. Kudin, M.C. Strain, O. Farkas, J. Tomasi, V. Barone, M. Cossi, R. Cammi, B. Mennucci, C. Pomelli, C. Adamo, S. Clifford, J. Ochterski, G.A. Petersson, P.Y. Ayala, Q. Cui, K. Morokuma, D.K. Malick, A.D. Rabuck, K. Raghavachari, J.B. Foresman, J. Cioslowski, J.V. Ortiz, B.B. Stefanov, G. Liu, A. Liashenko, P. Piskorz, I. Komaromi, R. Gomperts, R.L. Martin, D.J. Fox, T. Keith, M.A. Al-Laham, C.Y. Peng, A. Nanayakkara, C. Gonzalez, M. Challacombe, P.M.W. Gill, B. Johnson, W. Chen, M.W. Wong, J.L. Andres, M. Head-Gordon, E.S. Replogle, and J.A. Pople. Gaussian, Inc., Pittsburgh Pennsylania. 1998.
43. A.P. Scott and L. Radom. J. Phys. Chem. **100**, 16 502 (1996).

© 2001 NRC Canada

A topochemical rearrangement with multiple inversions of configuration

Saul Wolfe, Yih-Huang Hsieh, Raymond J. Batchelor, Frederick W.B. Einstein, and Ian D. Gay

Abstract: Crystalline 2-benzyloxypyridine-1-oxide rearranges slowly at room temperature to crystalline 1-benzyloxy-2-pyridone. No intermediates are detected when the process is followed by solid-state ^{13}C NMR. The crystal structure of the pyridine-1-oxide strongly suggests that a topochemically controlled intramolecular process, in which the benzyl group migrates with retention of configuration, is not feasible. On the other hand, although somewhat disfavoured by initial solid-state O···C···O angles significantly less than the ideal 180°, intermolecular topochemically controlled processes can be envisaged that lead, with multiple inversions of configuration, either to net retention of configuration or to net inversion of configuration in the benzyl group. In contrast to the 50–80% inversion observed in solution, in the solid state only inversion is observed experimentally when chirally labelled α-deuteriobenzyloxypyridine-1-oxide is allowed to rearrange.

Key words: X-ray crystallography, solid-state ^{13}C NMR, benzyl-α-D-alcohol, 2-benzyloxypyridine-1-oxide, 1-benzyloxy-2-pyridone.

Résumé : Le 1-oxyde de 2-benzyloxypyridine à l'état cristallin se réarrangement lentement, à la température ambiante, pour conduire à la 1-benzyloxypyrid-2-one. Lorsqu'on a suivi cette transformation par RMN du ^{13}C à l'état solide, on n'a pas pu détecter d'intermédiaires. La structure cristalline du 1-oxyde de pyridine suggère fortement qu'il n'est pas possible de suggérer l'existence d'un processus intramoléculaire contrôlé de façon topochimique dans lequel le groupe benzyle migrerait avec rétention de configuration. Par ailleurs, même s'il est légèrement défavorisé à l'état solide par des angles initiaux O···C···O inférieurs à la valeur idéale de 180°, il est possible d'envisager des processus intermoléculaires contrôlés de façon topichimique qui conduiraient après de multiples inversions de configuration à une rétention ou à une inversion nette de configuration dans le groupe benzyle. Par opposition aux degrés d'inversion de 50 à 80% observés expérimentalement en solution, le réarrangement du 1-oxyde de l'α-deutérobenzyloxypyridine à l'état solide ne donne lieu qu'à de l'inversion.

Mots clés : diffraction des rayons X, RMN du ^{13}C à l'état solide, alcool α-D-benzylique, 1-oxyde de 2-benzyloxypyridine, 1-benzyloxypyrid-2-one.

[Traduit par la Rédaction]

We recently reported (1) that the Tieckelmann reaction, the conversion of a 2-alkoxypyridine-1-oxide (**1**) into a 1-alkoxy-2-pyridone (**2**) (2), is not an intramolecular [1*s*,4*s*] sigmatropic rearrangement (3), as some workers had previously believed (4), but a two-step intermolecular process. In the first step (see Fig. 1), an alkyl group R* is transferred, with inversion of configuration, from one molecule of **1** to the *N*-oxide of a second molecule, to form the anion of 2-hydroxypyridine-*N*-oxide (**3**) and a 1,2-dialkoxypyridinium cation (**4**). In the second step, the nature of which depends upon the alkyl group and the solvent, one of the alkyl groups of **4** is transferred, also with inversion of configuration, to one of the oxygens of **3**. The product is then formed, without crossover and with net retention of configuration, by a double inversion of one alkyl group, or with crossover and net inversion of configuration, by single inversions of two alkyl groups.

Although four channels are, in principle, possible for the second step, only two have so far been observed. Based on kinetic studies, crossover experiments and measurement of the secondary H/D isotope effect, in dimethylformamide (DMF) at 140°C **1** (R = methyl) reacts exclusively via channel A. In the case of **1** (R = benzyl), crossover experiments and kinetic and stereochemical studies showed that channels A and B compete in DMF at 140°C, with channel A comprising about 80% of the reaction. In chloroform at 140°C, channels A and B compete equally.

Ollis and co-workers (5) have made the interesting observation that **5** undergoes quantitative Tieckelmann rearrangement to **6** in the solid state during 13 months at –15°C. The topochemical nature (6) of this reaction was not examined, but there are numerous related examples of intermolecular methyl transfer which proceed under topochemical control in the solid state (7). In each case, the crystal structure exhibits an intermolecular X···CH3···Y angle close to linearity

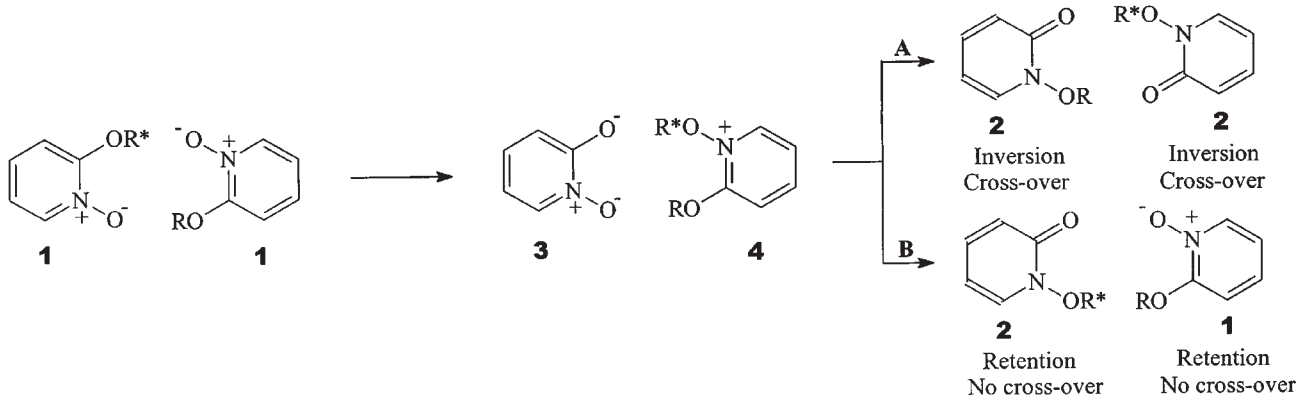
Received January 29, 2001. Published on the NRC Research Press Web site at http://canjchem.nrc.ca on August 22, 2001.

S.Wolfe,[1] Y.-H. Hsieh, R.J. Batchelor, F.W.B. Einstein, and I.D. Gay. Department of Chemistry, Simon Fraser University, Burnaby, BC V5A 1S6, Canada.

[1]Corresponding author (telephone: (604) 291-5972; fax: (604) 291-5973; e-mail: swolfe@sfu.ca).

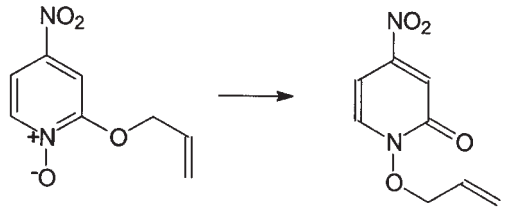
 DOI: 10.1139/cjc-79-8-1272 © 2001 NRC Canada

Fig. 1. Rearrangement of **1** (R = benzyl) to **2** (R = benzyl) with net inversion of configuration in the benzyl group (channel A) or with net retention of configuration in the benzyl group (channel B).

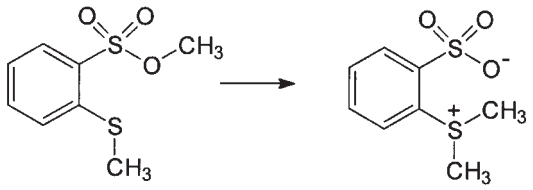


and an X···Y distance of 4 to 5 Å, and the reaction occurs exclusively, or is much faster, in the solid state than in solution or in the melt.

There is also an example of an intermolecular solid state rearrangement that is observable within 1 week at 40°C, but which, because of the molecular packing in the crystal, cannot proceed under topochemical control (8). This is the celebrated reaction **7** → **8** which, as a paradigm of linear methyl transfer (9), had previously been found to be intermolecular in solution (10). To account for the non-topochemical nature of the solid state reaction, Venugopalan et al. (8) have suggested that intermolecular methyl transfer can take place at defects such as microcavities, surfaces, and other irregularities in the ordered crystal arrangement.



5 **6**



7 **8**

2-Methoxypyridine-1-oxide (**1**, R = methyl) is reported to crystallize in two forms (11): anhydrous needles, mp 78 to 79°C, and hydrated prisms, mp 66.5 to 67.5°C. In our hands, despite considerable effort, only a hydrate, mp 73–76°C, was observed (1), as needles from ethyl acetate, and as tabular prisms after boiling in toluene, followed by cooling. The tabular prisms were employed for the determination of the crystal structure. Figure 2 shows a portion of this crystal structure, including relevant geometrical parameters. The molecules in the set that includes **A**, **B**, and **C** are mutually related by simple translations in the *x*-direction, as are the molecules of the crystallographically distinct set that includes **D** and **E**. The figure displays an edge-viewed cross section of a sheet structure, two-dimensionally extended parallel to the *xy*-plane, which is the result of the formation of chains cross-linked by hydrogen bonds from water molecules to nitroxide oxygen atoms.

Since the methyl group is positioned *anti* to the C—N bond,[2] Fig. 2 strongly suggests that an intramolecular transfer of this group in the solid state is improbable. However, there are several potential pathways for an intermolecular, topochemically controlled Tiekelmann rearrangement: for example, a transfer of methyl groups from **A** to **B** and from **B** to **C** would convert **B** to product. Alternatively, a transfer of methyl groups from **A** to **D** and from **D** to **B**, or from **A** to **D** and **D** to **E**, etc., would convert **D** to product. The relevant O···O distances in the crystal, which range from 4.322(2)–4.451(2) Å, are close to the calculated gas phase value of 4.32 Å for the bimolecular complex, shown in Fig. 5 of ref. 1; however, the O···C···O angles in the crystal, which range from 107.5(2)–121.6(2)°, deviate substantially from linearity and from the calculated gas phase angle of 174.2°, also shown in Fig. 5 of ref. 1. This is one possible reason for our inability to observe an intermolecular solid-state reaction (9). A second is that, in the solid, each nitroxide oxygen is hydrogen-bonded to one or two water molecules, and it is known that the solvation of a nucleophile by just one water molecule greatly reduces the rate of an intermolecular *gas-phase* S_N2 reaction (12).

A distinction between these possibilities became possible when one of us (Y.H.) discovered that a sample of crystalline 2-benzyloxypyridine-1-oxide (**1**, R = benzyl), which had been maintained at room temperature for some time, had undergone partial rearrangement to **2** (R = benzyl).

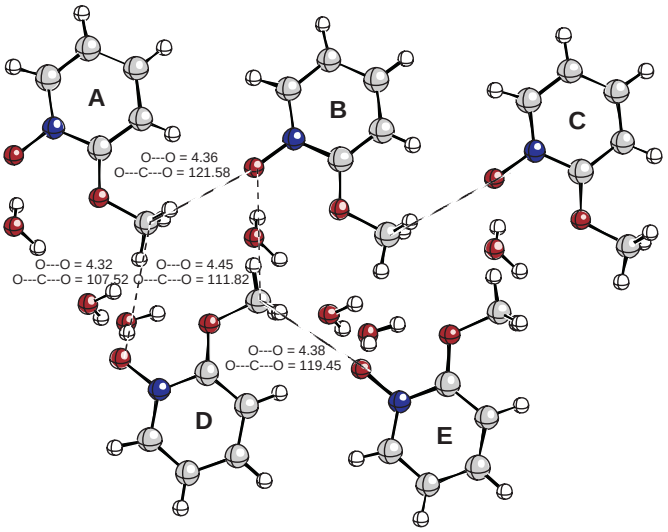
Figure 3 shows a portion of the crystal structure of **1** (R = benzyl).

It can be seen that, except for the absence of water molecules and the substitution of a phenyl group for one of the methyl hydrogens, there is a similar arrangement of the mol-

[2] The N-C-O-C torsion angles are 178.9(2)° and –178.5(3)°.

© 2001 NRC Canada

Fig. 2. A portion of the crystal structure of **1** (R = methyl), showing intermolecular O···O distances and O···C···O angles.



ecules of the methyl and benzyl compounds. Consequently, the possibilities for intermolecular topochemical rearrangement are also similar.

Referring to Fig. 3, molecules **A**, **D**, **B**, **E**, and **C** are sequentially related by a 2_1-screw operation. There is a second crystallographically unique molecule in the structure which shows a closely similar arrangement about an alternate screw axis. One can visualize numerous combinations of relatively small rotations of molecules and (or) internal rotations about CH_2—O, CH_2—C, or C^{ring}—O bonds which would produce the 180° angle required for the concerted transfer of a benzyl group, with inversion of configuration. For example: (*i*) transfer from **A** to **B** and **B** to either **C** or **E**, or from **A** to **D** and **D** to either **B** or **E** could produce **2** (R = benzyl) with net inversion of configuration in the benzyl group; alternatively, (*ii*) transfer from **A** to **D**, with inversion of configuration, followed by counterclockwise rotation of **A**, and return of the benzyl group to **A** with inversion of configuration will produce **2** with net retention of configuration in the benzyl group.

Figure 4 shows a portion of the crystal structure of **2** (R = benzyl).

Molecules, related by simple translations in *x*, are shown, and the nearest approaches between neighbouring NO and methylene groups are indicated. The N-O-C-C dihedral angle is 175.4(5)°. It is noteworthy that the much smaller intermolecular C-C···O-N torsion angles listed in Fig. 3 permit neither (*i*) nor (*ii*) above to produce this conformation initially, so that subsequent conformational rearrangement of **2** (R = benzyl) within the host crystal of **1** (R = benzyl) may be expected to lead to degradation of the crystal as the solid-state reaction proceeds.

The foregoing analyses of the two crystal structures permit the following tentative predictions: (*i*) the initial step of a solid-state Tieckelmann rearrangement of **1** (R = methyl, benzyl) will be slow, because of the substantial deviation of the entering and leaving groups from linearity; (*ii*) in the case of **1** (R = methyl), rearrangement is slowed further by

Fig. 3. The crystal structure of **1** (R = benzyl), showing intermolecular O···O distances and O···C···O angles.

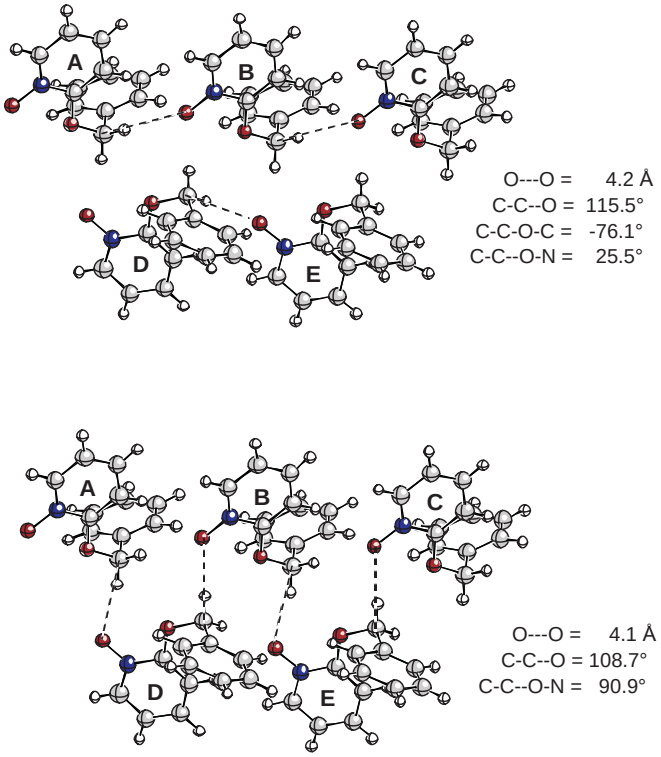
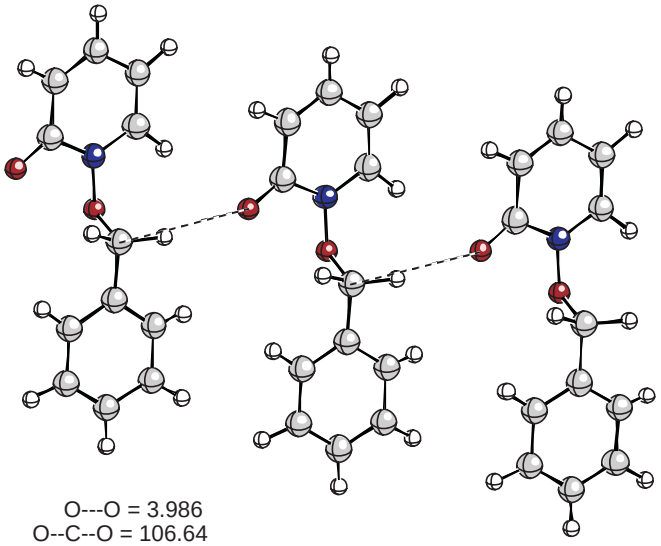


Fig. 4. The crystal structure of **2** (R = benzyl).

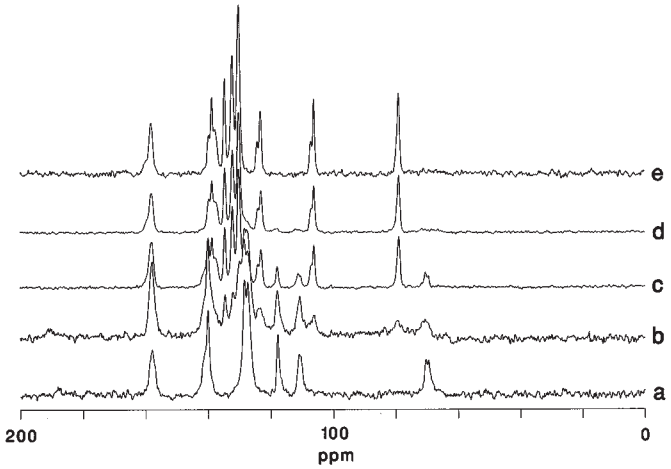


the presence of the water molecules;[3] (*iii*) depending on the nature of the intramolecular and intermolecular librations in the crystal, the solid-state rearrangement of **1** (R = benzyl) could potentially produce **2** with net inversion of configuration, or with net retention of configuration; (*iv*) since the antiperiplanar N-O-C-C conformation of **2** (R = benzyl) can probably not be accommodated within the host lattice of **1** (R = benzyl), the reaction likely proceeds at domain boundaries or packing defects and will be accompanied by a loss

[3] The intermolecular RCH_2···O distances are from 0.15–0.36 Å larger in **1** (R = methyl, hydrate) than in **1** (R = benzyl).

© 2001 NRC Canada

Fig. 5. (*a*) The solid-state ^{13}C NMR spectrum of a fresh sample of **1** (R = benzyl); (*b*) the spectrum after 10 months; (*c*) the spectrum after 25 months; (*d*) the spectrum after 36 months; (*e*) the spectrum of an authentic sample of **2** (R = benzyl).



of crystallinity. Indeed, the crystal of **1** (R = benzyl) used for the X-ray structure determination decayed on a time scale of months; remeasurement of selected reflections showed that all had dropped to 28% of their original intensities after 130 days.

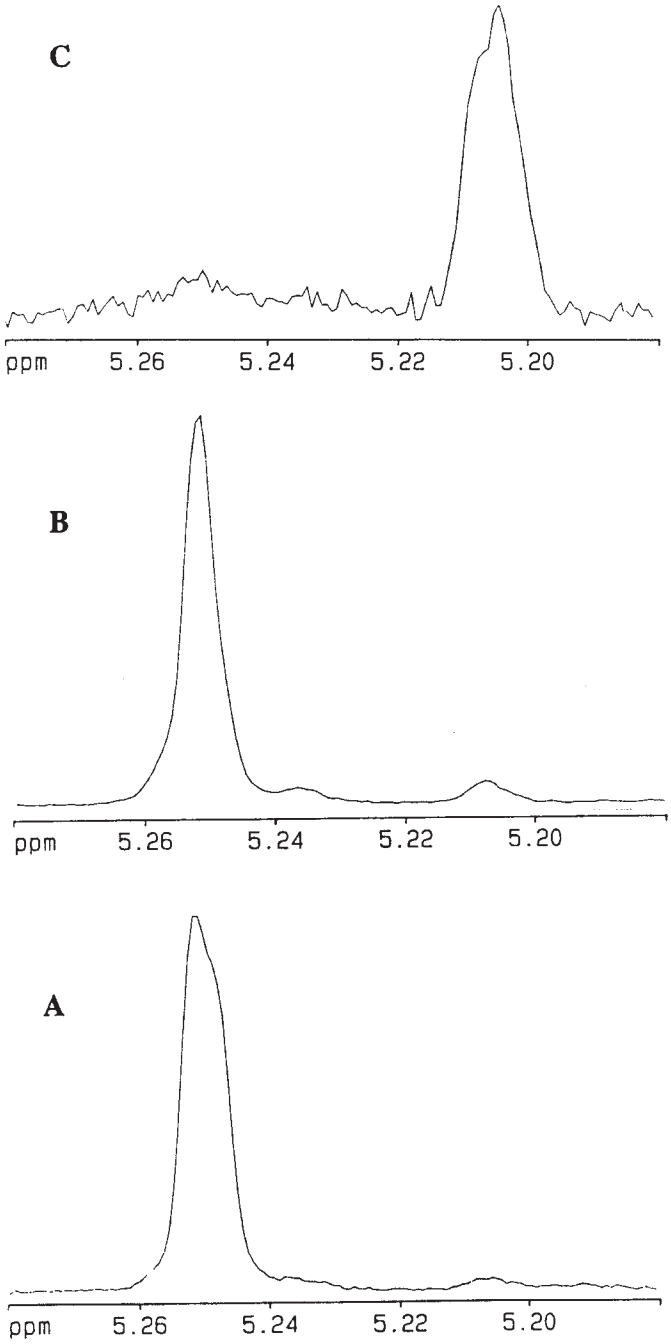
The conversion of **1** to **2** (R = benzyl) was also followed at room temperature by solid-state ^{13}C NMR, and was also found to occur on a time scale of months. Figure 5 shows: (a) the spectrum of a fresh sample of **1**; (*b*) the spectrum after 10 months; (*c*) the spectrum after 25 months; (*d*) the spectrum after 36 months; (*e*) the spectrum of an authentic sample of **2**. While not all carbon resonances are resolved in the solid, the occurrence of the reaction is easily seen from the decay of the peaks at 70, 110, and 118 ppm, and the growth of peaks at 79, 106, 132, and 135 ppm. There is a steady conversion of **1** to **2**, and no peaks corresponding to intermediates are observed. Unfortunately, **1** has a long spin-lattice relaxation time, necessitating a repolarization delay of 90 s. This makes it impractical to signal average to a significantly better signal-to-noise ratio than shown. Consequently the presence of intermediates at levels up to a few percent of the total cannot be excluded.

Assuming that the rearrangement occurs in more than one step, with each step slow for the reasons already stated, transient formation of **3** and **4** can be expected, but these would only have been observable in the initial stages of the reaction.

To determine the stereochemical course of the rearrangement, a sample of optically active 2-(α-deuteriobenzyloxy)-pyridine-1-oxide was synthesized as described previously (1, 13), carefully crystallized from ethyl acetate, and allowed to stand for 11 months. At this time the rearrangement was found to be 85% complete. The reactant and product were separated, benzyl alcohol was released from each, by treatment with sodium methoxide in the case of **1**, and by treatment with zinc and acetic acid in the case of **2**, and the alcohols were converted to their Mosher esters (1, 14) for determination of their ^{1}H NMR spectra.

Figure 6 shows the deuterium-decoupled ^{1}H NMR spectra of the benzyl protons of the Mosher esters of: (A) the benzyl-α-d-alcohol employed to prepare the initial sample of **1**; (B) the benzyl-α-D-alcohol recovered from **1** following rearrangement; (C) the benzyl-α-D-alcohol recovered from **2** following rearrangement. Samples (A) and (B) are identical; sample (C) is the epimer of (A).

Fig. 6. Deuterium-decoupled ^{1}H NMR spectra of the benzyl protons of the Mosher esters of: (*a*) chirally labelled benzyl-α-D-alcohol; (*b*) chirally labelled benzyl-α-D-alcohol recovered from **1** (R = benzyl), after partial rearrangement to **2**; (*c*) chirally labelled benzyl-α-D-alcohol recovered from **2** after partial rearrangement.



It follows that the solid-state rearrangement of **1** (R = benzyl) proceeds with essentially complete inversion of configuration, in contrast to the 50–80% inversion observed in

© 2001 NRC Canada

solution. Based on our earlier examination of Fig. 3, it can be concluded that the topochemical rearrangement is an intermolecular process that proceeds by transfer of a benzyl group from **A** to **B** and **B** to **C**, etc., or by transfer from **A** to **D**, **D** to **B**, **B** to **E**, and **E** to **C**, etc., with inversion of configuration in every step.

Experimental

NMR Studies

The sample used for NMR experiments was supplied as a powder of fine crystals. This was loosely packed into a segment of 5 mm NMR tubing, and remained in this tube over the course of all measurements. The sample had a tendency to "clump" over time, and was occasionally stirred with a spatula and repacked. During the whole course of the NMR experiments, the sample was exposed to the atmosphere, and was maintained at ambient laboratory temperature, 23 ± 5°C. Probe temperatures during NMR experiments were also within this range.

Solid-state ^{13}C NMR spectra were recorded at 37.56 MHz on a 3.5T instrument. ^{1}H–^{13}C cross-polarization was used, with a contact time of 2 ms and a relaxation delay of 90 s. The sample was spun at the magic angle at 2.4 kHz; at this speed and field, small spinning sidebands are seen for the *sp* carbons. These were suppressed, in the spectra shown, by a phase-cycled TOSS pulse sequence. Proton decoupling fields of 50–85 kHz were used, the higher fields giving a slight improvement in line width. Resonances were referred to TMS using solid adamantane as a secondary standard, taking the shift of the high-frequency line to be 38.56 ppm.

Stereochemical studies

Full details of the synthesis of chirally deuterated **1**, of the recovery of benzyl-α-D-alcohol from **1** and **2**, of the conversion of these alcohols to Mosher esters, and of the NMR analyses of these esters can be found in ref. 1.

X-ray crystallography

One large crystal of **1** (hydrate, R = methyl)[4] (obtained from toluene solution and believed to be anhydrous) was exposed to a dry nitrogen atmosphere in a crystallographic glove box while it was cleaved to produce the fragment used for crystallographic analysis. When the crystal was exposed to the dry atmosphere it appeared to begin to liquefy. Nonetheless a fragment was successfully sealed in a capillary tube, after which time it ceased to "melt" while the remaining fragments liquefied completely. It seems likely that the sample was undergoing dehydration in the glove box to produce a lower melting substance or mixture. Full-matrix least-square refinement, on *F*, of 254 parameters for 1558 data ($I_o > 2.5\ \sigma(I_o)$) included independent coordinates for all atoms, anisotropic displacement parameters for the non-hydrogen atoms, and a single isotropic thermal parameter for each of the following three groups of hydrogen atoms: those on the C_5N-rings, those of the methyl groups, and those of the water molecules.

A crystal of **1** (R = benzyl)[5] obtained from ethyl acetate solution was mounted on a glass fiber using epoxy adhesive. While less than 1% decays of the intensity standards were observed during data acquisition, remeasurement of three of the stronger reflections showed a systematic decay over a period of 130 days, by which time the net intensities had all dropped to 28% of their original values. This net loss of intensity appeared to apply equally to all the reflections tested. A peak search at the end of that time revealed only reflections indexed on the original cell and orientation. Full-matrix least-squares refinement, on *F*, of 273 parameters for 1728 data ($I_o > 2.5\sigma(I_o)$) included independent coordinates and anisotropic displacement parameters for the non-hydrogen atoms. Hydrogen atoms were riding in calculated positions (C—H, 0.95 Å) and were initially assigned isotropic thermal parameters proportionate to the equivalent isotropic parameter of the respective carbon atoms. Subsequently, all hydrogen atom isotropic thermal parameters were constrained to have equivalent shifts.

A fragment cleaved from a crystal of **2** (R = benzyl)[6] obtained from hexane solution was mounted on a glass fiber using epoxy adhesive. Full-matrix least-squares refinement, on *F*, of 138 parameters for 570 data ($I_o > 2.5\sigma(I_o)$) was conducted analogously to that of **1** (R = benzyl).

All data were acquired at room temperature using an Enraf–Nonius CAD-4F diffractometer and with graphite-monochromatized Mo K_α radiation. Complex scattering factors for neutral atoms (15) were used in the calculation of structure factors. The programs used for data reduction, structure solution, and graphical output were from the NRCVAX Crystal Structure System (16). The program suite CRYSTALS (17) was employed in the refinement. Full details of the X-ray crystallographic structure determinations have been deposited as hardcopy and in CIF format.[7]

Acknowledgement

This research was supported by the Natural Sciences and Engineering Research Council of Canada (NSERC).

[4] Crystal structure of **1-Me-hydrate**: colourless prism, $C_6H_7NO_2 \cdot 1.5H_2O$, triclinic, space group $P\bar{1}$, $Z = 4$, $a = 6.5109(8)$ Å, $b = 6.8620(13)$ Å, $c = 17.4633(23)$ Å, $\alpha = 79.511(13)°$, $\beta = 88.944(11)°$, $\gamma = 73.374(12)°$, $V = 734.64$ Å^3, $T = 293$ K, $R_F = 0.028$, $GoF = 1.49$.

[5] Crystal structure of **1-Bz**: colourless prism, $C_{12}H_{11}NO_2$, monoclinic, space group $P2_1/a$, $Z = 8$, $a = 16.4480(20)$ Å, $b = 6.3356(7)$ Å, $c = 20.941(3)$ Å, $\beta = 111.597(9)°$, $V = 2029.0$ Å^3, $T = 293$ K, $R_F = 0.041$, $GoF = 1.86$.

[6] Crystal structure of **2-Bz**: colourless prism, $C_{12}H_{11}NO_2$, orthorhombic, space group $Pc2_1b$,; $Z = 4$, $a = 5.8898(5)$ Å, $b = 13.0782(14)$ Å, $c = 13.3848(12)$ Å, $\nu = 1031.00$ Å^3, $T = 293$ K, $R_F = 0.040$, $GoF = 1.59$.

[7] Full details of the crystallographic structure determinations, displacement ellipsoid plots of the molecular structures, and a diagram of the extended H-bonding in **1-Me-hydrate**, tables of crystallographic details, atomic coordinates, distances and angles, anisotropic displacement parameters, and least-squares planes are available as supplementary data, and may be purchased from the Depository of Unpublished Data, Documentary Delivery, CISTI, National Research Council Canada, Ottawa, ON K1A 0S2, Canada (http:\\www.nrc.ca\cisti\irm\unpub_e.shtml for information on ordering electronically). The CIF file is also available. Tables of crystallographic details, atomic coordinates, and distances and angles have also been deposited with the Cambridge Crystallographic Data Centre. Copies of the data can be obtained free of charge, on application to the Director, CCDC, 12 Union Road, Cambridge CB2 1EZ, U.K. (Fax: 44-1223-336033 or e-mail: Structure factors are no longer being deposited and may be obtained from the author.

© 2001 NRC Canada

References

1. S. Wolfe, K. Yang, N. Weinberg, Z. Shi, Y.-H. Hsieh, R.D. Sharma, S. Ro, and C.-K. Kim. Chem. Eur. J. **4**, 886 (1998).
2. (*a*) F.J. Dinan and H Tieckelmann. J. Org. Chem. **29**, 1650 (1964); (*b*) J.E. Litster and H. Tieckelmann. J. Am. Chem. Soc. **90**, 4361 (1968).
3. R.B. Woodward and R. Hoffmann. Angew. Chem. Intl. Ed. Engl. **8**, 781 (1969).
4. I. Hoppe. Ph.D. Dissertation, University of Göttingen, Göttingen, Germany, 1971; U. Schöllkopf and I. Hoppe. Tetrahedron Lett. 4527 (1970); U. Schöllkopf and I.Hoppe. Liebigs Ann. Chem. **765**, 153 (1972); D. Alker, S. Mageswaran, W.D. Ollis, and H. Shahriari-Zavareh. J. Chem. Soc. Perkin Trans. 1. 1631 (1990); D. Alker, W.D. Ollis, and H. Shahriari-Zavareh. J. Chem. Soc. Perkin Trans. 1. 1637 (1990); W.J. le Noble and M.R. Daka. J. Am. Chem. Soc. **100**, 5961 (1978).
5. D. Alker, W.D. Ollis, and H. Shahriari-Zavareh. J. Chem. Soc. Perkin Trans. 1. 1623 (1990).
6. M.D. Cohen and G.M.J Schmidt. J. Chem. Soc. 1996 (1964).
7. (*a*) C.N. Sukenik, J.A.P. Bonapace, N.S. Mandel, P.-Y. Lau, G. Wood, and R.G.Bergman. J. Am. Chem. Soc. **99**, 851 (1977); (*b*) J.D. Dunitz. Pure Appl. Chem. **63**, 177 (1991); (*c*) M. Dessolin, O. Eisenstein, M. Golfier, T. Prangw, and P. Sautet. J. Chem. Soc. Chem. Commun. 132 (1992); (*d*) J.D. Dunitz. Acta Crystallogr. Sect. B: Struct. Sci. **B51**, 619 (1995); (*e*) M. Smrčina, S. Vyskočil, V. Hanuš, M. Polášek, V. Langer, B.G.M. Chew, D.B. Zax, H. Verrier, K. Harper, T.A. Claxton, and P. Kočovsky. J. Am. Chem. Soc. **118**, 487 (1996); S. Vyskočil, M. Smrčina, and V. Langer. Abstr. ACS Nat. Meet. 220th. 2000. No. 507.
8. P. Venugopalan, K. Venkatesan, J. Klausen, E. Novotny-Bregger, C. Leumann, A. Eschenmoser, and J.D. Dunitz. Helv. Chim. Acta, **74**, 662 (1991).
9. S. Wolfe, C.-K. Kim, K. Yang, N. Weinberg, and Z. Shi. Can. J. Chem. **76**, 359 (1998).
10. L. Tenud, S. Farook, J. Seibl, and A. Eschenmoser. Helv. Chim. Acta, **53**, 2059 (1970).
11. J.N. Gardner and A.R. Katritzky. J. Chem. Soc. 4375 (1957).
12. M. Henchman, J.F. Paulson, and P.M. Hierl. J. Am. Chem. Soc. **105**, 5569 (1983); D.K. Bohme and A.B. Raksit. J. Am. Chem. Soc. **106**, 3447 (1984); P.M. Hierl, A.F. Ahrens, M. Henchman, A.A. Viggiano, and J.F. Paulson. J. Am. Chem. Soc. **108**, 3142 (1986); R.A.J. O'Hair, G.E. Davico, J. Hacaloglu, T.T. Dang, C.H. DePuy, and V.M. Bierbaum. J. Am. Chem. Soc. **116**, 3609 (1994); P.M. Hierl, J.F. Paulson, and M.J. Henchman. J. Phys. Chem. **99**, 15 655 (1995).
13. G.E. Keck, K.H. Tarbet, and L.S. Geraci. J. Am. Chem. Soc. **115**, 8467 (1993); G.E. Keck and D. Krishnamurthy. J. Org. Chem. **61**, 7638 (1996).
14. D.E. Ward and C.K. Rhee. Tetrahedron Lett. **49**, 7165 (1991).
15. International tables for X-ray crystallography. Vol. IV. *Edited by* J.A. Ibers and W.C. Hamilton. Kynoch Press, Birmingham, U.K. 1975. p. 99.
16. E.J. Gabe, Y. LePage, J.-P. Charland, F.L. Lee, and P.S. White. J. Appl. Crystallogr. **22**, 384 (1989).
17. D.J. Watkin, C.K. Prout, J.R. Carruthers, P.W. Betteridge, and R.I. Cooper. CRYSTALS. Issue 11. Chemical Crystallography Laboratory, University of Oxford, Oxford. 1999.

© 2001 NRC Canada

The ozonolysis of *ortho*-xylene and its relevance to the history of the benzene problem

Saul Wolfe and Zheng Shi

Abstract: Using B3LYP density functional theory in conjunction with the 6-311++G** basis set, the relative rates of the initial rate-determining attack of ozone upon the carbon—carbon bonds of *o*-xylene are found to be 4,5- ≅ 3,4- > 2,3- > 1,2-. With the assumption that the final products glyoxal (G), methylglyoxal (M), and dimethylglyoxal (D) are determined by the site of the initial attack, and taking statistical factors into account, the ratio G:M:D is calculated to be 3:2:1. This is close to the value found experimentally, and identical to the result predicted by the contention that two nearly equivalent Kekulé–Pauling valence bond (resonance) structures of *o*-xylene exist and each localized carbon—carbon double bond of these structures is oxidized at the same rate. Although Frontier Molecular Orbital theory also predicts a 3:2:1 ratio of G:M:D, this theory incorrectly predicts that the initial attack of ozone will take place at the 1,2- and 4,5- bonds, with 1,2-attack slightly preferred. These results are discussed in relation to a recent historical analysis of the benzene problem, and it is concluded that since the products of ozonolysis of *o*-xylene are determined by the relative energies of the transition states leading to the four possible primary ozonides, these transition states should be the focus of theory.

Key words: Kekulé structure, resonance, frontier orbital theory, density functional theory, kinetics.

Résumé : Faisant appel à la théorie de la densité fonctionnelle B3LYP en relation avec l'ensemble de base 6-311++G**, on a trouvé que les vitesses relatives des attaques initiales, qui déterminent la vitesse de la réaction de l'ozone sur les doubles liaisons carbone-carbone du 1,2-diméthybenzène varient dans l'ordre 4,5- ≅ 3,4- > 2,3- > 1,2-. Si on fait l'hypothèse que les produits finaux, glyoxal (G), méthylglyoxal (M) et diméthylglyoxal (D) sont déterminés par le site de l'attaque initiale, et tenant compte des facteurs statistiques, le rapport G:M:D calculé est égal à 3:2:1. Cette valeur se rapproche de la valeur expérimentale et elle est identique à la valeur que l'on peut prédire en se basant sur l'existence de deux structures de Kekulé–Pauling pratiquement équivalentes pour le 1,2-diméthylbenzène à partir desquelles les doubles liaisons carbone-carbone localisées seraient oxydées à la même vitesse. Même si la théorie des orbitales frontières conduit aussi à une prédiction d'un rapport G:M:D de 3:2:1, cette théorie conduit à la prédiction incorrecte que l'attaque initiale de l'ozone se fera au niveau des liaisons 1,2- et 4,5-, avec une légère préférence pour l'attaque 1,2. On discute de ces résultats en relation avec une analyse historique récente du problème du benzène et on en conclut que, puisque les produits d'ozonolyse du 1,2-diméthylbenzène sont déterminés par les énergies relatives des états de transition conduisant aux quatre ozonides primaires possibles, la théorie devrait être orientée vers l'étude de ces états de transition.

Mots clés : structure de Kekulé, résonance, théorie des orbitales frontières, théorie de la densité fonctionnelle, cinétique.

[Traduit par la Rédaction]

Introduction

In an absorbing two-part account of the history of the benzene problem, Brush (1) has drawn attention to the title reaction, which at one time (2 (ref. 1*a*, footnotes)) was thought to lend experimental support to Kekulé's oscillation theory (3) and its reformulation by Pauling (4). In Pauling's terminology, *o*-xylene is a resonance hybrid of the two nearly equivalent valence-bond (VB) structures **1** and **2**, and complete ozonolysis, followed by decomposition of the ozonide, should yield methylglyoxal (**3**) and glyoxal (**4**) in the ratio 2:1 from **1**, butanedione (**5**) and **4** in the ratio 1:2 from **2**, and an overall **3**:**4**:**5** ratio of 2:3:1.

To test Kekulé's theory, Levene and Cole (5) examined the ozonolysis of *o*-xylene in acetic anhydride at –30°C. After treatment of the ozonide with ice, they identified the *p*-nitrophenylosazones of **3**, **4**, and **5** among the products. Since the total yield of these products was less than 2%, and their proportions had not been determined, the reaction was reexamined by Haaijman and Wibaut (6) using chloroform as the solvent and work-up with sodium bisulfite or hydroxylamine. In addition to copious amounts of formic acid, acetic acid, and oxalic acid, Haaijman and Wibaut obtained dimethylglyoxime, methylglyoxime, and glyoxime in a total yield of 19–26% of the theoretical, based on *o*-xylene, and in the proportions 19–24% dimethylglyoxime (≡**5**), 32–37% methylglyoxime (≡**3**), and 42–47% glyoxime (≡**4**).

Received January 29, 2001. Published on the NRC Research Press Web site at http://canjchem.nrc.ca on August 22, 2001.

S. Wolfe[1] and Z. Shi. Department of Chemistry, Simon Fraser University, Burnaby, BC V5A 1S6, Canada.

[1]Corresponding author (telephone: (604) 291-5972; fax: (604) 291-5973; e-mail: swolfe@sfu.ca).

 DOI: 10.1139/cjc-79-8-1278 © 2001 NRC Canada

Fig. 1. The HOMO–LUMO (FMO) treatment of the attack of ozone upon the 4,5-bond (channel *a*) of *ortho*-xylene.

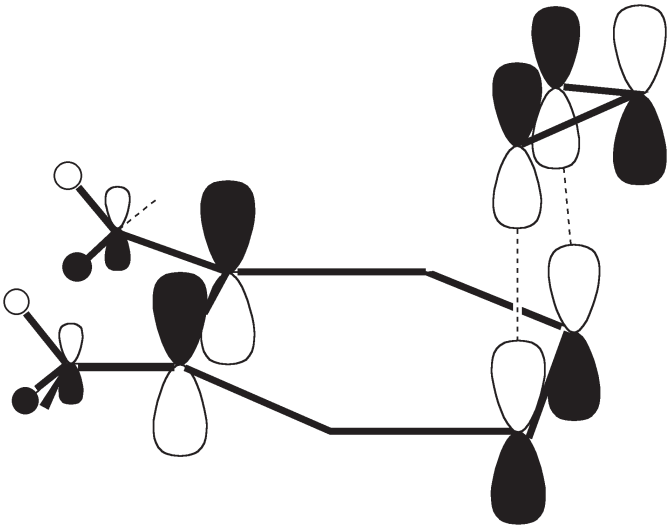
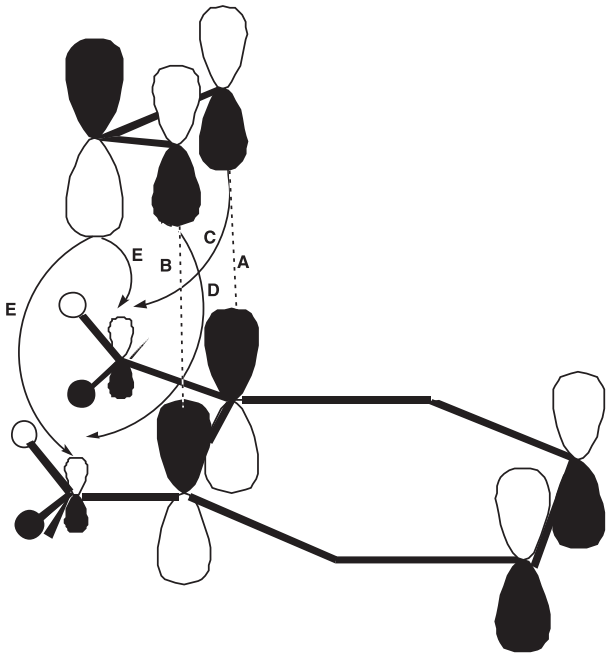


Fig. 2. The HOMO–LUMO (FMO) treatment of the attack of ozone upon the 1,2-bond (channel *b*) of *ortho*-xylene.



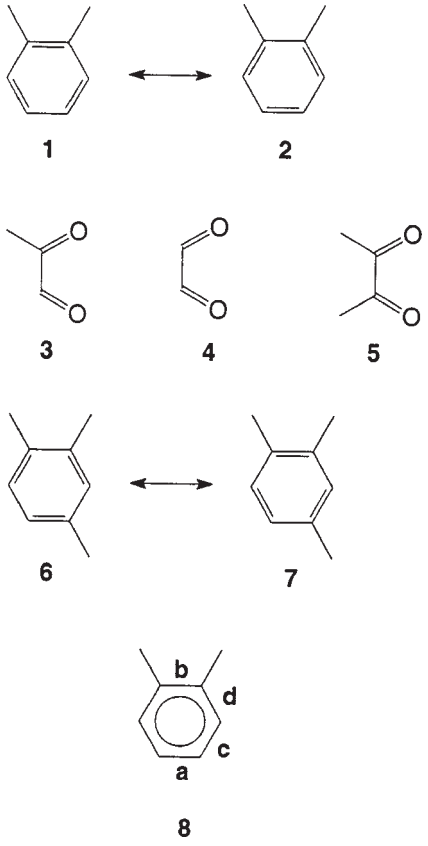
These relative yields are close to the predicted values, but Haaijman and Wibaut could not yet reach a definitive conclusion, because the degree of steric hindrance by the methyl groups was uncertain and the experiment had afforded only one-quarter of the theoretical yield of the products. Accordingly, they also examined the ozonolysis of 1,2,4-trimethylbenzene. In this case, if the compound is written as a hybrid of **6** and **7**, the products would still be **3**, **4**, and **5**, but in the new proportions 4:1:1. Although the total yield of **3**–**5** was reduced to 11–13%, the relative amounts, 66.2% (**3**), 14.2% (**4**), and 17.9% (**5**), were in excellent agreement with the theoretical prediction. Haaijman and Wibaut concluded that "it is certain that *o*-xylene reacts with ozone according to the two canonical structures proposed by Kekulé."

The current status of this conclusion is examined in some detail by Brush (1), in an analysis of how the VB treatment of benzene, including reference to the ozonolysis of *o*-xylene, eventually came to be superseded by the "superior" (7) molecular orbital (MO) method. Nonetheless, Brush concludes, although the (Levene–Cole) experiment "has … dropped out of the textbooks," one could still ask "how MO explains (the result)." "I do not doubt that a modern quantum chemist could provide such an explanation if necessary, but so far I have not found one in print."

The present work was stimulated by the foregoing remarks.

Results and discussion

The application of qualitative FMO (frontier molecular orbital) theory (8) to the problem requires several assumptions: (*i*) the initial attack of ozone to form a 1,2,3-trioxolane, the primary ozonide, is both rate-determining and product-determining (9). For example, referring to structure **8**, initial attack at bond *a* is equivalent to initial attack at bond *d*, and leads to the same result as the complete ozonolysis of **2**. Likewise, initial attack at bond *b* is equivalent to attack at bond *c*, and leads to the same result as the complete ozonolysis of **1**; (*ii*) since ozonolysis is an oxidative process, the rate-determining electron transfer takes place between the *o*-xylene donor and the ozone acceptor so that the principal focus is on the interaction between the HOMO of xylene and the LUMO of ozone; (*iii*) in its nodal character the LUMO of ozone (**9**) resembles ψ_3 of the Hückel treatment of allyl. Calculations at all levels (extended Hückel,



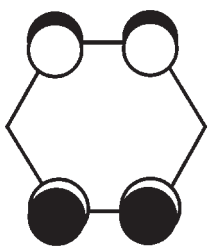
© 2001 NRC Canada

semiempirical, ab initio) confirm this point; (*iv*) the attachment of two methyl groups removes the degeneracy of the *E*-type π-MOs of benzene (**10ab**) and produces a $^2B_1$ π-HOMO (**11**) and a $^2A_2$ π-NHOMO (**12**) (**11** and **12** refer to 6-31G* calculations (10)). Since, from photoelectron spectroscopy (11), the energy difference between **11** and **12** is 0.52 eV (11.99 kcal), **11** is employed in the analysis.

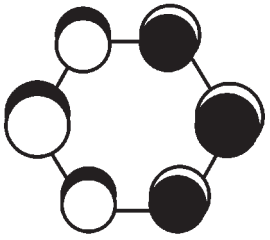
It is immediately apparent, upon inspection of **11**, that the FMO treatment predicts the initial attack of ozone to take place primarily at *a* and at *b*, since overlap with the ozone LUMO is possible only at these sites. From (*i*) above, it follows that, if the coefficients at *a* and *b* are the same, the qualitative MO and qualitative VB treatments are equivalent. However, upon closer examination, this first-order MO treatment seems to be incomplete, because the coefficients at *a* and *b* are not the same. Calculations at all levels (extended Hückel, semiempirical, ab initio) find the *p*-atomic orbital coefficients at *b* to be slightly larger than those at *a*.



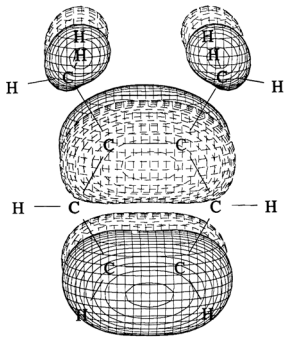
9



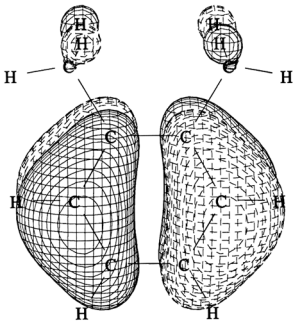
10a



10b



11



12

Figures 1 and 2 show the origin of **11** schematically, and also the primary and secondary overlaps in the HOMO–LUMO interactions associated with reaction at *a* and at *b*; **11** is formed from the out-of-phase interaction between **10a** and **13**, the *E*′ combination of two π-type methyl group orbitals. Since **10a** lies higher than **13**, **10a** makes the larger contribution to the HOMO, as depicted in the figures.



13

Figure 1, which refers to attack at *a*, is straightforward. Figure 2, which depicts attack at *b*, requires comment. The primary HOMO–LUMO overlap is shown in the dotted lines A and B. If this were the only criterion, the larger coefficients at the ring carbons of *b* would permit the prediction that attack at *b* is slightly preferred over attack at *a*. However, Fig. 2 also exhibits secondary overlap, shown by the curved arrows C, D, and E. Whether this secondary overlap is rate-enhancing or rate-retarding is difficult to predict from qualitative considerations alone, because C and D are out-of-phase (retarding), and E is in-phase (enhancing). Thus, at this level of treatment, Haaijman and Wibaut's "steric hindrance by the methyl groups" may or may not exist. A more rigorous analysis is necessary.

Figure 3 is the 6-31G* (10) HOMO of *cis*-2-butene. The out-of-phase relationship between π_{cc} and π_{Me} is reminiscent of that seen in **11**. Figure 4 shows the 6-311++G** transition structures calculated using Gaussian 98 (12) for the attack of ozone *syn* to the methyl groups and *anti* to the methyl groups. Geometrical parameters of interest are the C···O distances (Å) and the attack and tilt angles (deg). These angles are defined as explained in Fig. 5, where **a** is the C-C=C-C (*anti*) or H-C=C-H (*syn*) plane, **b** is the O_3 plane, and **c** is the plane that includes C=C and the termini of ozone. The attack angle is the angle between planes **a** and **c**; the tilt angle is the angle between planes **a** and **b**. In the *syn* attack the attack angle is 105.8°, the tilt angle is 46.0°, and the C···O distances are 2.36 Å; the corresponding parameters for *anti* attack are 78.2 and 21.4°, and 2.19 Å. These geometries suggest that *syn* attack is significantly more encumbered. The relative unimportance of interaction E is reflected in the free energies of the *syn* and *anti* transition structures: the *anti* structure is lower by 1.911 kcal mol^{-1}, corresponding to k_{anti}/k_{syn} = 25 at 298 K. If the attack of ozone at *b* of *o*-xylene were to be similarly retarded relative to attack at *a*, the FMO treatment would then predict attack at *a* to be the dominant reaction channel. This would be equivalent to the bizarre assertion that only VB structure **2** is oxidized. At this (second-order) level, the HOMO–LUMO FMO treatment has, therefore, failed. A possible reason for this failure is that FMO theory assumes a reactant-like transition state, but ozonolysis of an aromatic compound will proceed via a high energy product-like transition state which is not properly patterned by the HOMO of the reactant. This point was pursued by examination of the transition structures for attack at *a*, *b*, *c*, and *d* of *o*-xylene.

The calculations were performed (12) at the Hartree–Fock (HF) level with the 6-311++G** basis set (HF/6-311++G**//HF/6-311++G**), and also using density functional theory (DFT) with the B3LYP functional (13) and the same basis set (B3LYP/6-311++G**//B3LYP/6-311++G**). For the calculation of the free energies at 243 K and at 298 K, vibrational frequencies were scaled using the 298 K scaling

© 2001 NRC Canada

Fig. 3. The 6-31G* HOMO of *cis*-2-butene.

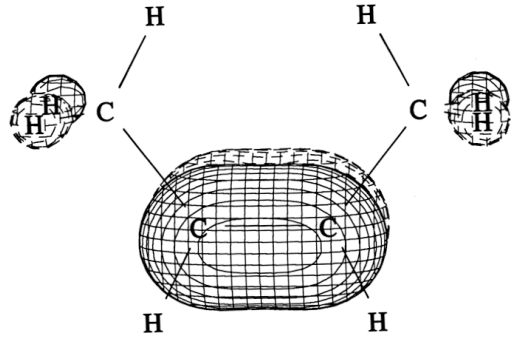
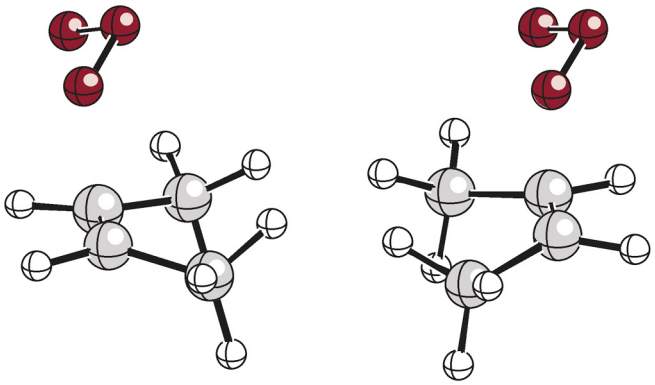


Fig. 4. The 6-311++G** transition structures for the attack of ozone *syn* (left) and *anti* (right) to the methyl groups of *cis*-2-butene.



Attack angle	105.8
Tilt angle	46.0
C---O	2.36

Attack angle	78.2
Tilt angle	21.4
C---O	2.19

factors recommended in ref. 14: for HF calculations: ΔH_{vib}, 0.8951; ΔS_{vib}, 0.9021; for DFT calculations: ΔH_{vib}, 0.9989; ΔS_{vib}, 1.0015. Tables 1 and 2 summarize the results for 298 K and 243 K, respectively, and Fig. 6 shows the DFT transition structures of the four reaction channels.

Since each channel begins from the same reactants, the free energy differences can be equated to $\Delta\Delta G^{\ddagger}$. This allows the relative rates to be calculated.

As expected from the *cis*-2-butene calculations, channel *b* is the least favourable and, at 298 K, reaction via this channel is 25 times slower than reaction via channel *a*. On the other hand, channel *c*, which leads to the same products as channel *b*, is kinetically competitive with channel *a*. Neither the unimportance of channel *b* nor the importance of channel *c* was predicted by qualitative FMO theory.

From the free energies of the four transition structures the relative proportions of **3**, **4**, and **5** can be calculated. The rates of formation are:

[1] $V_3 = 2V_b + 2V_c$

[2] $V_4 = 2V_a + V_b + V_c + 2V_d$

[3] $V_5 = V_a + V_d$

Fig. 5. Definitions of the attack and tilt angles in the transition structures of the reaction of ozone with *cis*-2-butene.

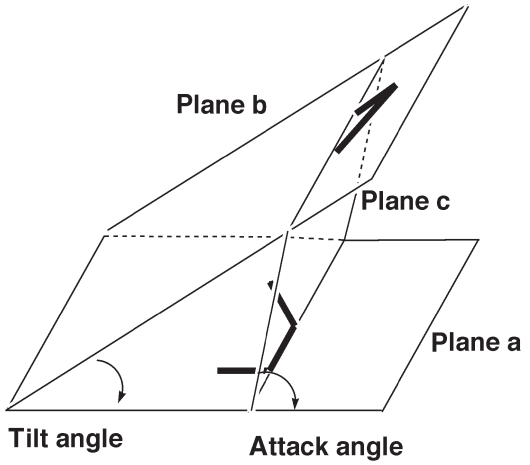
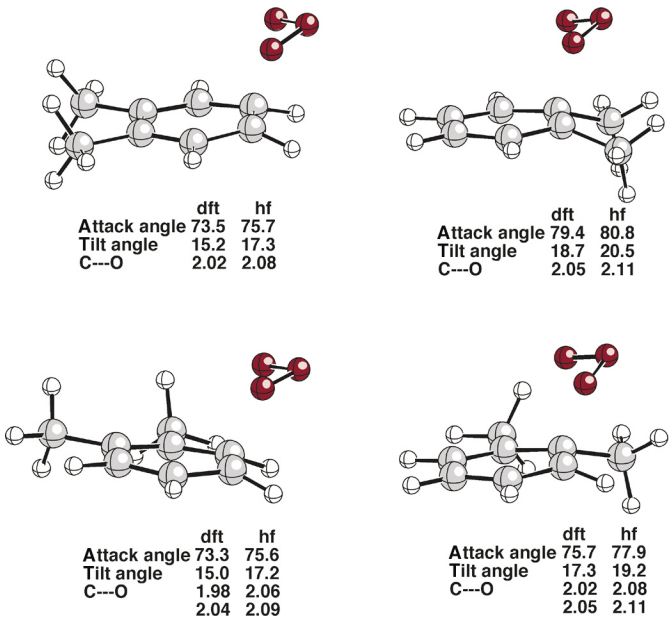


Fig. 6. The B3LYP/6-311++G** transition structures for the attack of ozone at *a*, *b*, *c*, and *d* of **8**.



	dft	hf
Attack angle	73.5	75.7
Tilt angle	15.2	17.3
C---O	2.02	2.08

	dft	hf
Attack angle	79.4	80.8
Tilt angle	18.7	20.5
C---O	2.05	2.11

	dft	hf
Attack angle	73.3	75.6
Tilt angle	15.0	17.2
C---O	1.98	2.06
	2.04	2.09

	dft	hf
Attack angle	75.7	77.9
Tilt angle	17.3	19.2
C---O	2.02	2.08
	2.05	2.11

where V_a, V_b, V_c, and V_d are the rates of the initial steps of channels *a*–*d*. Assuming second-order kinetics (15),

[4] $V_a = k_a[O_3][\text{xylene}]$

[5] $V_b = k_b[O_3][\text{xylene}]$

[6] $V_c = k_c[O_3][\text{xylene}]$

[7] $V_d = k_d[O_3][\text{xylene}]$

With the introduction of the statistical factors $n_a = n_b = 2$ and $n_c = n_d = 4$,

[8] $k_a = n_a(\kappa T/h)e^{-\Delta G_a^{\ddagger}/RT}$

[9] $k_b = n_b(\kappa T/h)e^{-\Delta G_b^{\ddagger}/RT}$

[10] $k_c = n_c(\kappa T/h)e^{-\Delta G_c^{\ddagger}/RT}$

[11] $k_d = n_d(\kappa T/h)e^{-\Delta G_d^{\ddagger}/RT}$

© 2001 NRC Canada

Table 1. Absolute[a] and relative[b] free energies of the four transition structures TS_a, TS_b, TS_c, and TS_d at 298 K, from HF[c] and DFT[c] calculations, with and without scaling of vibrational frequencies.

	HF		DFT	
	Scaled	Unscaled	Scaled	Unscaled
TS_a	–533.00925(0.00)	–532.99129(0.00)	–536.30386(0.00)	–536.30367(0.00)
TS_b	–533.00662(1.65)	–532.99129(1.69)	–536.30119(1.68)	–536.30098(1.69)
TS_c	–533.00859(0.42)	–530.99075(0.34)	–536.30371(0.10)	–536.30365(0.02)
TS_d	–533.00838(0.54)	–532.99036(0.58)	–536.30297(0.56)	–536.30276(0.57)

[a]In atomic units (1 au = 627.5 kcal mol^{-1}).
[b]In parentheses, in kcal mol^{-1}.
[c]See text.

Table 2. Absolute[a] and relative[b] free energies of the four transition structures TS_a, TS_b, TS_c, and TS_d at 243 K, from HF[c] and DFT[c] calculations, with and without scaling of vibrational frequencies.

	HF		DFT	
	Scaled	Unscaled	Scaled	Unscaled
TS_a	–533.00117(0.00)	–532.98301(0.00)	–536.29542(0.00)	–536.29522(0.00)
TS_b	–532.99873(1.53)	–532.98053(1.55)	–536.29288(1.59)	–536.29269(1.59)
TS_c	–533.00033(0.52)	–530.98228(0.46)	–536.29520(0.14)	–536.29500(0.14)
TS_d	–533.00045(0.45)	–532.98226(0.47)	–536.29466(0.48)	–536.29466(0.48)

[a]In atomic units (1 au = 627.5 kcal mol^{-1}).
[b]In parentheses, in kcal mol^{-1}.
[c]See text.

Table 3. Ozonolysis of *o*-xylene: calculated percentages of **3**, **4**, and **5** from eqs. [12] and [13], the percentages predicted by the resonance description of *o*-xylene, and the experimental result of ref. 6.

	HF				DFT					
	Scaled		Unscaled		Scaled		Unscaled			
	243 K	298 K	243 K	298 K	243 K	298 K	243 K	298 K	**1** ↔ **2**	Experimental
3	19.1	24.6	21.3	27.0	31.1	33.1	31.1	35.5	33.3	32–37
4	57.1	54.4	56.0	53.2	51.1	50.1	51.1	48.9	50.0	42–47
5	23.8	21.0	22.7	19.8	17.8	16.8	17.8	15.6	16.7	19–24

The calculated product ratios are then as follows:

$$[12]\quad \mathbf{3}/\mathbf{5} = V_3/V_5 = \frac{2V_b + 2V_c}{V_a + V_d} = \frac{2k_b + 4k_c}{k_a + 2k_d} = \frac{2e^{-\Delta G_b^{\ddagger}/RT} + 4e^{-\Delta G_c^{\ddagger}/RT}}{e^{-\Delta G_a^{\ddagger}/RT} + 2e^{-\Delta G_d^{\ddagger}/RT}}$$

$$[13]\quad \mathbf{4}/\mathbf{5} = V_4/V_5 = \frac{2V_a + V_b + V_c + 2V_d}{V_a + V_d} = \frac{2k_a + k_b + k_c + 2k_d}{k_a + k_d} = \frac{2e^{-\Delta G_a^{\ddagger}/RT} + e^{-\Delta G_b^{\ddagger}/RT} + 2e^{-\Delta G_c^{\ddagger}/RT} + 4e^{-\Delta G_d^{\ddagger}/RT}}{e^{-\Delta G_a^{\ddagger}/RT} + 2e^{-\Delta G_d^{\ddagger}/RT}}$$

The percentages of **3**, **4**, and **5** calculated using eq. [12] and [13] are collected in Table 3 for two temperatures (–30°C and 25°C), two computational procedures (HF and DFT), and with and without scaling of vibrational frequencies. Table 3 also includes the percentages of **3**–**5** predicted by the resonance description 1 ↔ 2, and the experimental results of Haaijman and Wibaut (6). The scaled DFT results are in almost exact agreement with the resonance prediction.

Concluding remarks

The present work leads to the conclusions that ozone reacts at equal rates at the unsubstituted 3,4- and 4,5- bonds of *o*-xylene (channels *a* and *c* of **8**) and that the 3:2:1 product ratio is determined by these kinetics. Although a 3,4-double bond is present in canonical structure **1** and a 4,5-double bond is present in canonical structure **2**, the resonance interpretation makes no distinction between the 1,2- and 3,4- reactivities of **1**, or between the 2,3- and 4,5- reactivities of **2**. Consequently, the ozonolysis experiment cannot be regarded as confirmation of the existence of localized double bonds in *o*-xylene. Likewise, although FMO theory also leads to a 3:2:1 product ratio, it does this by the incorrect prediction that these products are formed solely via channels *a* and *b*. In short, since the products of ozonolysis of *o*-xylene are determined by the relative energies of the transition states leading to the four possible primary ozonides, these transition states should be the focus of any theory.

© 2001 NRC Canada

Acknowledgement

This work was supported by the Natural Sciences and Engineering Research Council of Canada (NSERC).

References

1. (*a*) S.G. Brush. Stud. Hist. Phil Sci. Part A, **30**, 21 (1999); (*b*) **30**, 263 (1999).
2. S.G. Brush. Stud. Hist. Phil Sci. Part A, **30**, 168 (1999); **30**, 171 (1999).
3. A. Kekulé. Bull. Soc. Chim. Fr. **1**, 98 (1865); Ann. Chem. **137**, 129 (1866).
4. L. Pauling and G.W. Wheland. J. Chem. Phys. **1**, 362 (1933).
5. A.A. Levene and A.G. Cole. J. Am. Chem. Soc. **54**, 338 (1932).
6. P.W. Haaijman and J.B. Wibaut. Rec. Trav. Chim. Pays–Bas, **60**, 842 (1941).
7. J. McMurry. Organic chemistry. Brooks/Cole Publishing Company, Monterey, California. 1984. p. 456.
8. K. Fukui. Angew. Chem. Int. Ed. Engl. **21**, 801 (1982).
9. J.M. Anglada, R. Crehuet, and J.P. Bofill. Chem. Eur. J. **5**, 1809 (1999), and refs. cited therein.
10. W.J. Hehre, L. Radom, P. v R. Schleyer, and J.A. Pople. Ab initio molecular orbital theory. Wiley, New York. 1986.
11. K. Kesper, N. Münzel, W. Pietzuch, H. Specht, and A. Schweig. J. Mol. Struct: THEOCHEM. **200**, 375 (1989).
12. Gaussian 98, Revision A.6. M.J. Frisch, G.W. Trucks, H.B. Schlegel, G.E. Scuseria, M.A. Robb, J.R. Cheeseman, V.G. Zakrzewski, J.A. Montgomery, Jr., R.E. Stratmann, J.C. burant, S. Dapprich, J.M. Millam, A.D. Daniels, K.N. Kudin, M.C. Strain, O. Farkas, J. Tomasi, V. Barone, M. Cossi, R. Cammi, B. Mennucci, C. Pomelli, C. Adamo, S. Clifford, J. Ochterski, G.A. Petersson, P.Y. Ayala, Q. Cui, K. Morokuma, D.K. Malick, A.D. Rabuck, K. Raghavachari, J.B. Foresman, J. Cioslowski, J.V. Ortiz, B.B. Stefanov, G. Liu, A. Liashenko, P. Piskorz, I. Komaromi, R. Gomperts, R.L. Martin, D.J. Fox, T. Keith, M.A. Al-Laham, C.Y. Peng, A. Nanayakkara, C. Gonzalez, M. Challacombe, P.M.W. Gill, B. Johnson, W. Chen, M.W. Wong, J.L. Andres, M. Head-Gordon, E.S. Replogle, and J.A. Pople. Gaussian, Inc. Pittsburgh, Pennsylvania. 1998.
13. C. Lee, W. Yang, and R.G. Parr. Phys. Rev. B: Condensed Matter, **B37**, 785 (1988); A.D. Becke. Phys. Rev. A: At. Mol. Opt. Phys. **A38**, 3098 (1988); A.D. Becke. J. Chem. Phys. **97**, 9173 (1992); A. Becke. J. Chem. Phys. **98**, 5648 (1993); P.J. Stephens, F.J. Devlin, C.F. Chablowski, and M.J. Frisch. J. Phys. Chem. **98**, 11 623 (1994).
14. A.P. Scott and L. Radom. J. Phys. Chem. **100**, 16 502 (1996).
15. P.S. Bailey. Ozonation in organic chemistry. Vol. 1. Academic Press, New York. 1978; C.S. Kan, F. Su, J.G. Calvert, and J.H. Shaw. J. Phys. Chem. **85**, 2359 (1981); R.L. Kuczkowski. 1,3-Dipolar cycloadditions. *Edited by* A. Padwa. Wiley, New York. 1984; D. Johnson, A.R. Rickard, C.D. McGill, and G. Marston. Phys. Chem. Chem. Phys. **2**, 323 (2000).

© 2001 NRC Canada

A comprehensive computational examination of transannular Diels–Alder reactions of unsubstituted C14 trienes — Barriers, template effects, and the Curtin–Hammett principle

Saul Wolfe, Anthony V. Buckley, and Noham Weinberg

Abstract: A combination of MM3-level molecular mechanics calculations and PM3-level semiempirical molecular orbital calculations has been employed, in conjunction with an algorithm for the comprehensive conformational analysis of cyclic compounds, to obtain 1202 unique 1,3,9-cyclotetradecatriene conformations, distributed over the six possible geometrical isomers, and 70 unique transannular Diels–Alder transition structures leading to the six possible stereoisomeric tricyclic olefins. A kinetic analysis that takes into account all minima of a given geometrical isomer and all transition structures leading to the same tricyclic product leads to a free energy of activation that is almost the same as the free energy difference between the lowest minimum and the lowest transition structure (the Curtin–Hammett principle). A substantial template effect, mainly entropic in origin, is found when the transannular reactions are compared to the Diels–Alder reactions of the cognate 2,4-hexatrienes with the 2-butenes. Although the cyclization of the *trans-cis-trans* triene favours the *cis-anti-cis* over the *trans-anti-trans* product by more than 20 kcal mol^{-1}, the situation is reversed in the acyclic reaction. A cyclic triene that can cyclize directly to a *trans-anti-trans* tricycle can therefore be proposed.

Key words: molecular models, Deslongchamps, Takahashi, *trans-anti-trans* tricycle, MM3, PM3, transition states.

Résumé : On a fait appel à des calculs de mécanique moléculaire au niveau MM3 et des calculs d'orbitales moléculaires semi-empiriques au niveau PM3, en association avec un algorithme pour l'analyse conformationnelle détaillée des composés cycliques pour obtenir 1202 conformations uniques du cyclotétradéca-1,3,9-triène distribuées sur six isomères géométriques possibles ainsi que 70 structures de transition de réactions de Diels–Alder transannullaires conduisant aux six oléfines tricycliques stéréoisomères possibles. Une analyse cinétique qui tient compte de tous les minima d'un isomère géométrique donné et de toutes les structures de transition conduisant au même produit tricyclique conduit à une énergie libre d'activation qui est pratiquement la même que la différence d'énergie libre entre le minimum le plus bas et la structure de transition de plus basse énergie (principe de Curtin–Hammett). On a observé un effet de gabarit important, principalement d'origine entropique, quand on compare les réactions transannulaires aux réactions de Diels–Alder d'hexa-2,4-dienes connus avec des but-2-ènes. Même si la cyclisation du triène *trans-cis-trans* favorise la formation du produit *cis-anti-cis* par rapport à celle du produit *trans-anti-trans* par plus de 20 kcal mol^{-1}, la situation est inversée dans la réaction acyclique. Il est donc possible de proposer un triène cyclique qui se cycliserait directement en un tricycle *trans-anti-trans*.

Mots clés : modèles moléculaires, Deslongchamps, Takahashi, tricycle *trans-anti-trans*, MM3, PM3, états de transition.

[Traduit par la Rédaction]

Introduction

Although the use of molecular models to rationalize or predict relative stabilities of isomers and results of chemical reactions has a long and rich history (1), there are pitfalls. A model "at best merely *abstracts* a few particular and selected molecular properties" (2), "does not provide an adequate picture of molecular motion" (3), and, in general, assumes fixed bond angles and low barriers to rotation about single bonds "in contrast to the real situation of relatively easily deformable bond angles and substantial barriers to rotation about single bonds" (4).

The recent research of Deslongchamps (5) and Takahashi (6) and their co-workers into a transannular Diels–Alder approach to steroid synthesis illustrates both the predictive capabilities and also some of the limitations of molecular models. For the reaction **1** → **2**, in the general case (R ≠ H), there are eight geometrical isomers of **1** and eight diastereomers of **2**. Examination of Dreiding models of analogs of **1** having R = Me and $m = n = 4$ (5*b*) allowed Deslongchamps and co-workers to predict the relationship between the geometry of **1** and the stereochemistry of **2**. These predictions were accompanied by comprehensive ex-

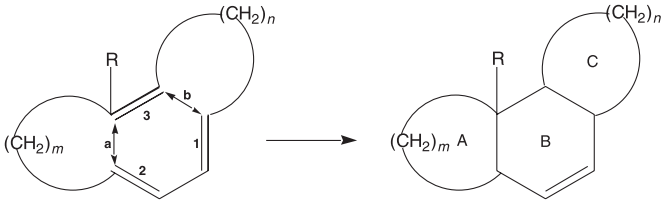
Received January 29, 2001. Published on the NRC Research Press Web site at http://canjchem.nrc.ca on August 22, 2001.

S. Wolfe,[1] A.V. Buckley, and N. Weinberg. Department of Chemistry, Simon Fraser University, Burnaby, BC V5A 1S6, Canada.

[1]Corresponding author (telephone: (604) 291-5972; fax: (604) 291-5973; e-mail: swolfe@sfu.ca).

 DOI: 10.1139/cjc-79-8-1284 © 2001 NRC Canada

perimental studies in which cyclization temperatures ranging from 80–365°C and products sometimes different from the predicted were observed. Although closer inspection of models permitted rationalization of unexpected results, it was evident that a more rigorous kinetic analysis, based on appropriate computations, was necessary, and several such studies, involving a limited treatment of the conformational space of reactants and transition structures, have been reported (5*d*, 5*e*, 5*g*, 6*c*).



1 **2**

There is no doubt that the experimental and theoretical treatment of transannular Diels–Alder reactions is in good hands. Nonetheless, some questions remain. For example: (*i*) How many minima and how many transannular Diels–Alder transition structures (TS) exist for each geometrical isomer of **1**? (*ii*) For a given geometrical isomer, do different TS lead to different products? (*iii*) For a given geometrical isomer which minimum produces the lowest energy TS? (*iv*) If there are many minima and many TS, what are the reaction barriers? (*v*) Is the Curtin–Hammett principle (7) relevant? (*vi*) Is there a template effect and, if so, what is its origin? (*vii*) Is a *trans-anti-trans* product directly accessible by a transannular Diels–Alder reaction?

In the present work we attempt to answer these questions for the case of the C14 triene **1**, R = H, m = *n* = 4, by a combination of MM3-level molecular mechanics calculations (8) and PM3-level semiempirical molecular orbital calculations (9), in conjunction with an efficient algorithm for the comprehensive conformational analysis of cyclic compounds (10).

Strategy

Application of the procedure of ref. 10 to 100 000 probe C14 triene structures produced 38 552 closed rings; MM3 minimization of 10 000 of these rings afforded 1370 minima. These were reoptimized, using PM3, to give 1172 *unique* minima (no imaginary frequencies), distributed as follows (double bond geometries are designated C or T, and in the order 1–2–3 shown in **1**): CCC 191, CCT 142, TTC 95, TTT 95, CTC (≡TCC) 350, CTT (≡TCT) 299. The 1172 PM3 structures were then subdivided further into those having s-*cis* or s-*trans* conformations, defined according to the diene dihedral angles: s-*cis* = 0–90°, s-*trans* = 90–180°. The distribution of PM3 minima at this stage is summarized in Table 1.

As a prelude to the calculation of transannular Diels–Alder transition structures, the Gibbs free energies of the 1172 minima were computed at 298 K, using PM3 within the Gaussian 94 (11) and Gaussian 98 (12) programme systems. Then, taking into account the bond lengths found in PM3 transition structures of cognate acyclic Diels–Alder reactions

Table 1. Distribution of PM3 conformational and geometrical isomers of the C14 triene **1**, R = H, *m* = *n* = 4.

Geometrical Isomer (1–2–3)[a]	s-*cis*[a]	s-*trans*[a]
CCC	107	84 (1)
CCT	69	73 (1)
TTC	57 (2)	38
TTT	48 (2)	47
TCC ≡ CTC	130 (9)	169 (3)
TCT ≡ CTT	157 (8)	193 (4)

[a]See text for definitions.

Table 2. Numbers of transition structures and stereochemistry of the tricyclic products of transannular Diels–Alder reactions of geometrical isomers of the C14 triene **1**, R = H, *m* = *n* = 4.

Isomer (1–2–3)[a]	Number of TS	Products
CCC	11	*cis-syn-cis*
CCT	4	*cis-anti-cis*
	3	*cis-anti-trans*
TTC	7	*trans-syn-trans*
	5	*cis-syn-cis*
TTT	4	*trans-anti-cis*
TCC ≡ CTC	16	*trans-syn-cis*
	2	*cis-syn-cis*
TCT ≡ CTT	8	*cis-anti-cis*
	5	*trans-anti-cis*
	5	*trans-anti-trans*

[a]See text for definitions.

(see later), the 568 s-*cis* conformations (**A**) were submitted for transition structure search according to the following protocol: (*i*) **a** and **b** bond lengths (see **1**) of 2.2 Å were imposed on each structure, and all other geometrical parameters were optimized; (*ii*) the **a** and **b** bond lengths of **B**, the structures from (*i*), were reduced to 1.6 Å, and the structures were minimized without constraint to yield **C**, stereo and conformational isomers of the tricyclic products **2**; (*iii*) the quadratic synchronous transit method of Schlegel and coworkers (13, 14) was applied to **A**, **B**, and **C** to yield a total of 70 unique stationary points having a single imaginary frequency; (*iv*) the free energies of these transition structures were calculated at 298 K; (*v*) using the reaction path following method of Gonzalez and Schlegel (15), the intrinsic reaction coordinates (IRC) connecting transition structures to their monocyclic precursors and tricyclic products were calculated. This process yielded an additional 30 monocyclic minima, identified in parentheses in Table 1, to make a total of 1202.

Results

Transannular Diels–Alder reactions

Table 2 summarizes the results. In two cases, CCC and TTT, a single tricyclic product is predicted. In three cases, CCT, TTC, and CTC, two tricyclic products are predicted. The CTT isomer can cyclize in three ways. However, although each of the 11 possible cyclization pathways can be found with the aid of Dreiding models, it is clear from Figs. 1–6 that only in the case of the TTC isomer would more than one transannular Diels–Alder product be

© 2001 NRC Canada

Fig. 1. Transannular cyclization of the CCC triene.

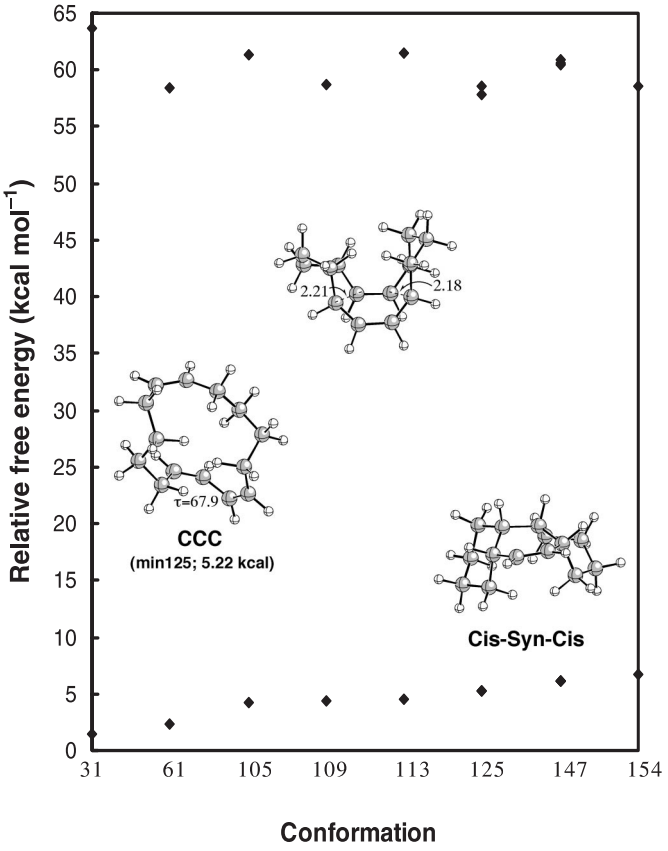
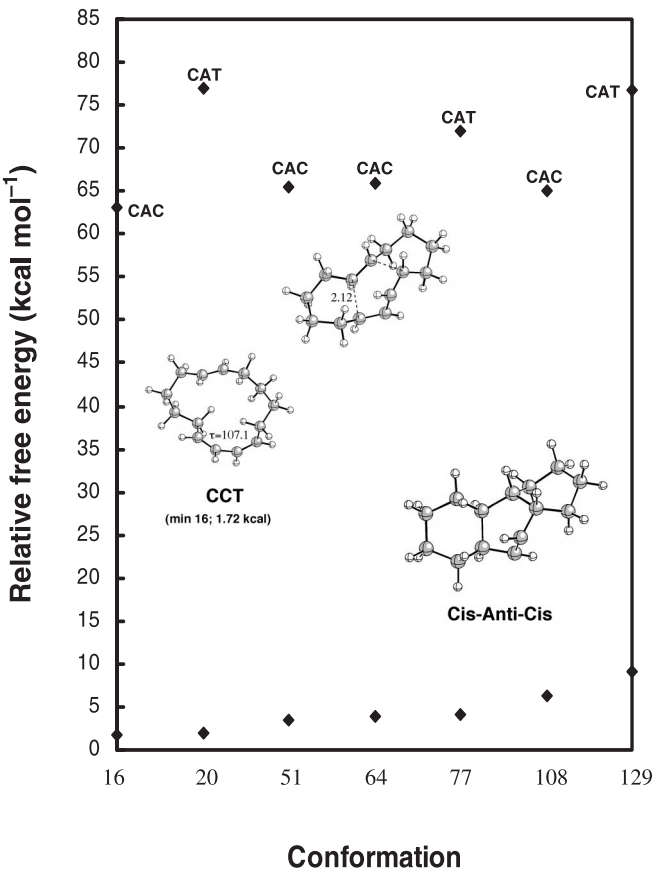


Fig. 2. Transannular cyclization of the CCT triene.



kinetically feasible. This follows from the Curtin–Hammett principle (7), which states, in part (16): "the product composition … is controlled … by the difference in standard free energies … of the respective transition states."

The figures show the free energy of each TS and the free energies of the minima that are IRC-linked to these TS, all relative to the most stable minimum. The figures also provide the ordering of these minima relative to the lowest energy monocyclic minimum, and the stereochemistry of the tricyclic isomer that is produced from each TS. The structures shown in the figures are the TS having the lowest free energy at 298 K, and the minimum and product that are linked to this TS. For example, according to Fig. 1, which refers to the CCC isomer, each of the 11 transannular Diels–Alder TS, whose free energies are ca 58–64 kcal mol^{-1} higher than the free energy of the lowest minimum, cyclizes to the *cis-syn-cis* (CSC) isomer. The 11 TS are linked to minima 31, 61, 105, 109, 113, 125, 147, and 154, of the total of 192 (Table 1), which are, in turn, ca 2–8 kcal mol^{-1} less stable than the most stable minimum. The TS of lowest free energy is derived from minimum 125, whose free energy is 5.22 kcal mol^{-1} higher than that of the most stable minimum. This minimum can be seen in Fig. 7, which shows the free energy and diene dihedral angles of the most stable conformation of each monocyclic isomer.

Cognate acyclic Diels–Alder reactions

The transannular reactions just discussed have acyclic counterparts in the reactions of the *cis*,*cis*-, *cis*,*trans*- and *trans*,*trans*-2,4-hexadienes with *cis*- and *trans*-2-butene, to form the stereoisomeric 3,4,5,6-tetramethylcyclohexenes. Figures 8–10 show the PM3 transition structures of, respectively, the *cis*,*cis*-diene with *cis*- (CCC) and *trans*-2-butene (CCT), the *trans*,*trans*-diene with *cis*- (TTC) and *trans*-2-butene (TTT) and the *cis*,*trans*-diene with *cis*- (CTC) and *trans*-2-butene (CTT). The numbers included in the figures are the **a** and **b** bond lengths (Å) and the relative free energies at 298 K.

As seen in Fig. 8, there are two CCC TS, one, corresponding to *endo* approach of the dienophile, which leads to the *trans-syn-trans* olefin and the other, corresponding to *exo* approach of the dienophile, which leads to the *cis-syn-cis* olefin. The *endo* TS, which minimizes Me–Me repulsive interactions, is 3.91 kcal mol^{-1} more stable, but is not accessible in the corresponding transannular reaction (Fig. 1). This reaction is calculated to lead exclusively to the *cis-syn-cis* isomer, with a prohibitively high barrier (vide infra).

Figure 8 also shows two CCT TS, one leading to the *trans-anti-cis* olefin, and the other, less stable by 8.95 kcal mol^{-1} because of the presence of two Me–Me eclipsing interactions, leading to the *cis-anti-cis* olefin, which has an improbable *trans*-double bond. In the transannular reaction (Fig. 2), the *cis-anti-cis* TS is more stable, despite the formation of a *trans*-olefin, because of the ring strain (not shown) required to achieve the *cis-anti-trans* TS. In each case (TS 20, 77, and 129), one of the C···C bond lengths is at least 2.30 Å.

As seen in Fig. 9, in the case of the TTC reaction, *exo* approach of the dienophile, leading to the *trans-syn-trans* ole-

© 2001 NRC Canada

Fig. 3. Transannular cyclization of the TTC triene.

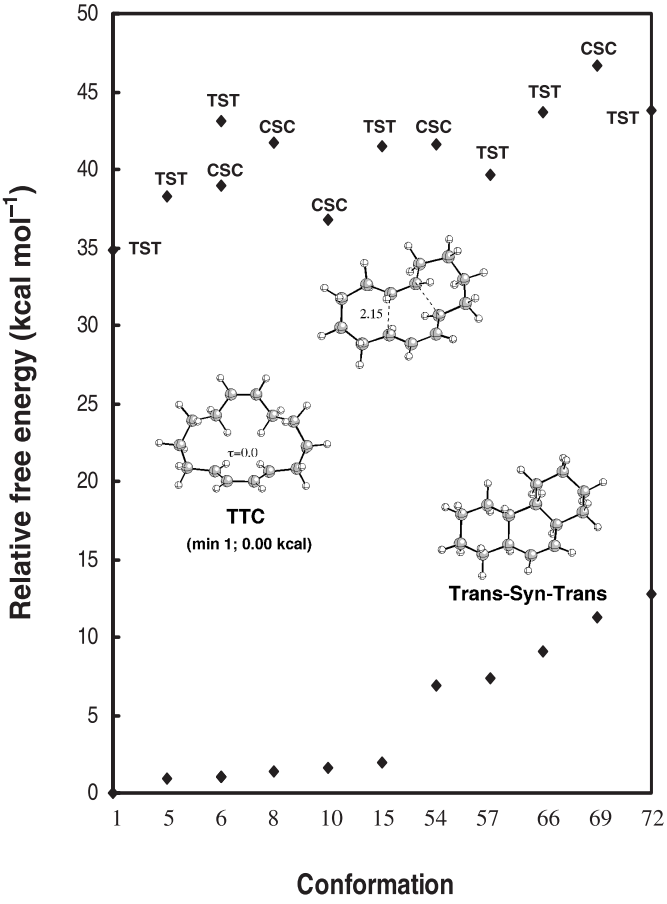
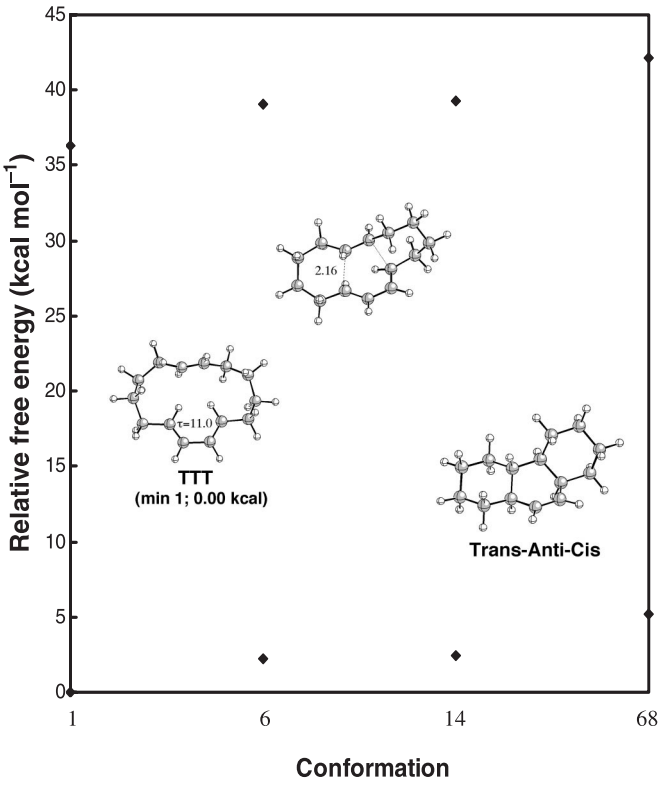


Fig. 4. Transannular cyclization of the TTT triene.



fin, is 1.55 kcal mol^{-1} more stable than *endo* approach, leading to the *cis-syn-cis* olefin. A similar difference is seen in the transannular reaction (Fig. 3).

In the case of the TTT reaction, leading exclusively to the *trans-anti-cis* olefin, Figs. 4 and 9 show very similar C···C bond lengths and diene dihedral angles, presumably because of the absence of strain in the four-carbon bridges of the transannular reaction.

In the case of the TCC reaction (Fig. 10), both *endo* and *exo* approach of the dienophile lead to the same olefin, with the *endo* approach slightly preferred. In the transannular reaction (Fig. 5), the most stable TS (from min 239) is the result of *exo* approach, and *endo* approach is seen only in the very high energy TS (not shown) from minima 32, 110, 115, 138, and 184.

The TCT reaction (Figs. 6 and 10) leads to *trans-anti-trans* and *cis-anti-cis* olefins (all *trans-anti-cis* TS of the transannular reaction lead to *trans*-double bonds in ring B). It is very significant that *the TCT reaction can produce a trans-anti-trans isomer* and that the TS of the acyclic reaction is *more stable* than the *cis-anti-cis* TS. In the transannular reaction, the situation is reversed by more than 20 kcal mol^{-1}! The explanation is that separation of the diene and the dienophile by four-carbon bridges does not allow the *favoured trans-anti-trans* TS to be achieved. Since the *trans-anti-trans* stereochemistry is the preferred result of a transannular Diels–Alder reaction (5), a synthetic strategy that might yield this isomer directly would appear to require a TCT geometry in the macrocycle and separation of the diene and dienophile components by bridges containing more than four atoms. We shall return to this point.

Table 3. Mean free energies of activation ($\Delta G_b^{\ddagger}$) and Curtin–Hammett free energies of activation ($\Delta G_{CH}^{\ddagger}$) (kcal mol^{-1}) of transannular Diels–Alder reactions of geometrical isomers of the C14 triene **1**, R = H, $m = n = 4$.

Isomer	Product	$\Delta G_{CH}^{\ddagger}$	$\Delta G_b^{\ddagger}$
CCC	*cis-syn-cis*	57.84	58.77
CCT	*cis-anti-cis*[a]	63.17	63.92
	cis-anti-trans	71.89	72.68
TTC	*trans-syn-trans*	34.88	35.57
	cis-syn-cis	36.75	37.43
TTT	*trans-anti-cis*	36.36	36.92
TCC	*cis-syn-trans*	45.21	45.95
	cis-syn-cis[a]	62.17	62.75
TCT	*cis-anti-cis*	45.89	46.68
	trans-anti-cis[a]	61.88	62.63
	trans-anti-trans	66.71	67.37

[a]Ring B has a *trans* double bond.

Discussion

General

The following additional observations are made upon inspection of Figs. 1–6: (*i*) in two cases (TTC and TTT) the most stable TS is produced from the most stable minimum; (*ii*) in one case (CCC) minimum 125 is linked to two, and minimum 147 is linked to three different TS; (*iii*) in two cases (CTC and CTT) the same TS is linked to more than

© 2001 NRC Canada

Table 4. A comparison of the Curtin–Hammett thermodynamic parameters ($\Delta H^{\ddagger}_{CH}$, $T\Delta S^{\ddagger}_{CH}$, and $\Delta G^{\ddagger}_{CH}$) of transannular Diels–Alder reactions of geometrical isomers of the C14 triene **1**, R = H, m = *n* = 4 with the thermodynamic parameters ($\Delta H^{\ddagger}$, $T\Delta S^{\ddagger}$, and $\Delta G^{\ddagger}$) of cognate acyclic Diels–Alder reactions (T = 298 K).

	Cyclic			Acyclic			
Reactant(s)	$\Delta H^{\ddagger}_{CH}$	$T\Delta S^{\ddagger}_{CH}$	$\Delta G^{\ddagger}_{CH}$	$\Delta H^{\ddagger}$	$T\Delta S^{\ddagger}$	$\Delta G^{\ddagger}$	Product[a]
CCC	54.02	–3.82	57.84	54.61	–16.24	70.85	*cis-syn-cis*
				52.24	–14.69	66.93	*trans-anti-trans*
CCT	68.24	–3.65	71.89	53.92	–17.24	71.16	*cis-anti-trans*
TTC	32.01	–2.78	34.88	37.19	–16.27	53.46	*trans-syn-trans*
	33.77	–2.98	36.75	38.51	–16.50	55.01	*cis-syn-cis*
TTT	30.90	–5.46	36.36	37.01	–16.83	53.84	*trans-anti-cis*
TCC	41.12	–4.09	45.21	42.92	–15.60	58.52	*trans-syn-cis*
				42.81	–16.07	58.88	*cis-syn-trans*
TCT	41.05	–4.84	45.89	44.63	–16.28	60.90	*cis-anti-cis*
	62.79	–3.92	66.71	41.81	–17.33	59.14	*trans-anti-trans*

[a]Reactions leading to a *trans* double bond are not included.

Fig. 5. Transannular cyclization of the TCC triene.

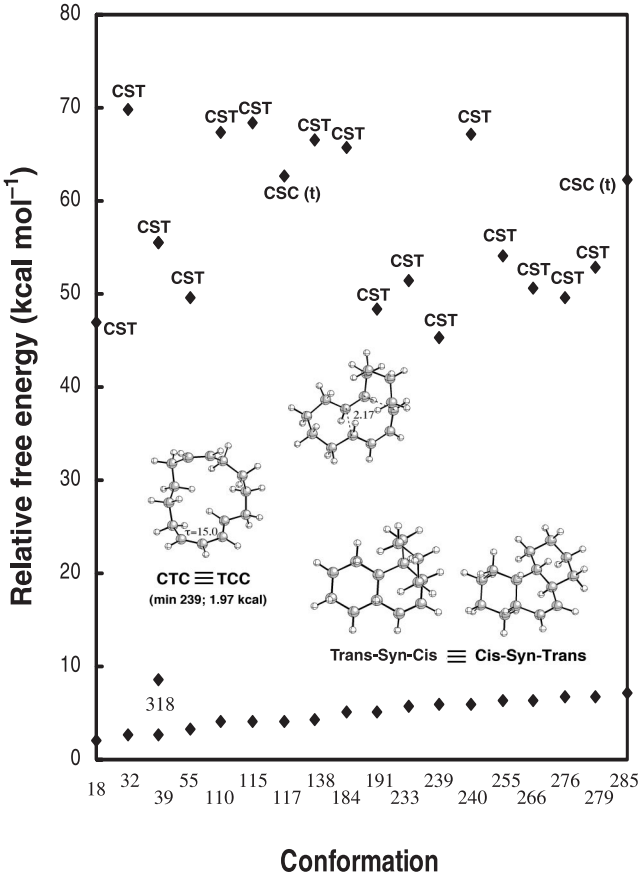
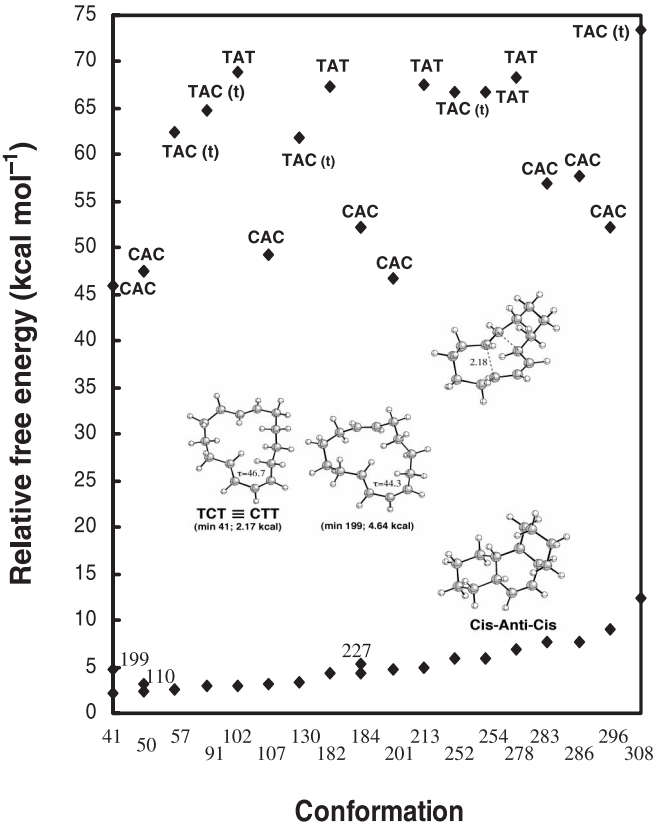


Fig. 6. Transannular cyclization of the TCT triene.



one minimum (39 and 318 in the CTC; 41 and 199, 50 and 110, 184 and 227 in the CTT); (*iv*) as already noted, the *cis-anti-cis* tricycle of Fig. 2, the *cis-syn-cis* tricycle of Fig. 5 and the *trans-anti-cis* tricycle of Fig. 6 have an improbable *trans* double bond in ring B.

Cyclization barriers and the generalized Curtin–Hammett principle

Consider a molecule A, which has *n* stable rapidly interconverting conformations A_i (i = 1,…,*n*), some of which, A^{r}_{t} (t = 1,…,*m*), can be transformed into a product *P* via *m* different transition states $A^{\ddagger}_{t}$. The partial rates for the *m* channels are given by eq. [1],

$$[1] \qquad V_t = k_t\,[A^{r}_{t}]$$

where

$$[2] \qquad k_t = (\kappa T/h)e^{-\Delta G^{\ddagger}_{t}/RT}$$

are the partial rate constants, and

© 2001 NRC Canada

Fig. 7. The lowest minima of the six C14 trienes.

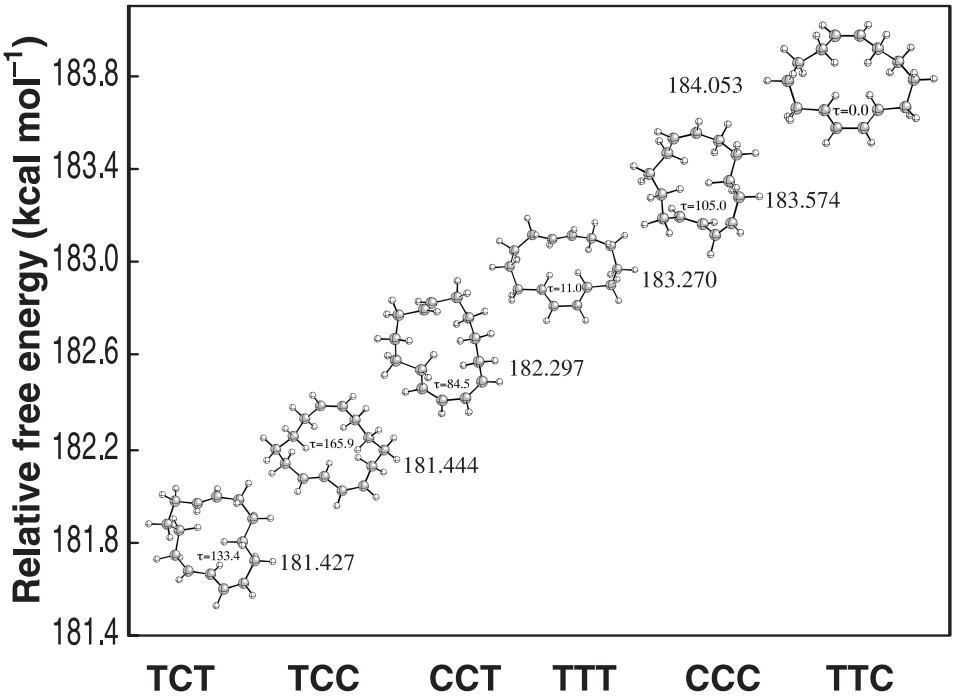


Fig. 8. Transition structures for the intermolecular CCC and CCT reactions.

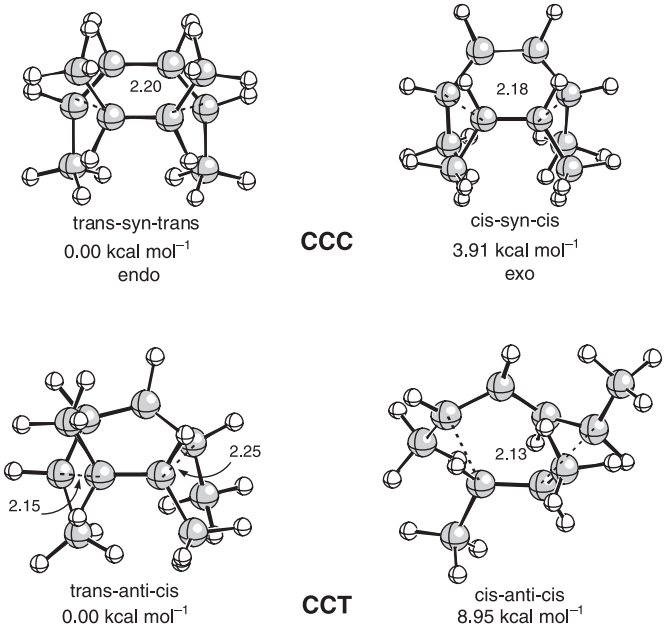
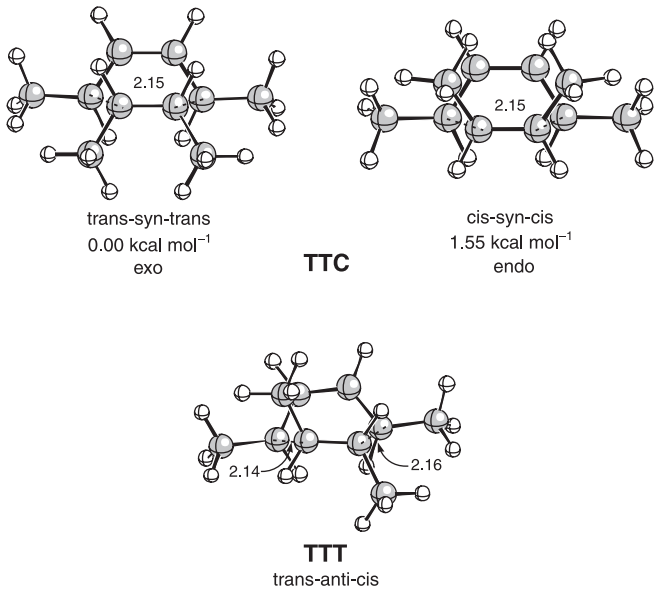


Fig. 9. Transition structures for the intermolecular TTC and TTT reactions.



$$[3] \qquad [A_t^r] = \frac{e^{-G_t/RT}}{\sum_{i=1}^{n} e^{-G_t/RT}}[A]$$

are the concentrations of reactive conformations related to the overall concentration [*A*] through appropriate Boltzmann factors.

The overall rate ν is the sum of the partial rates

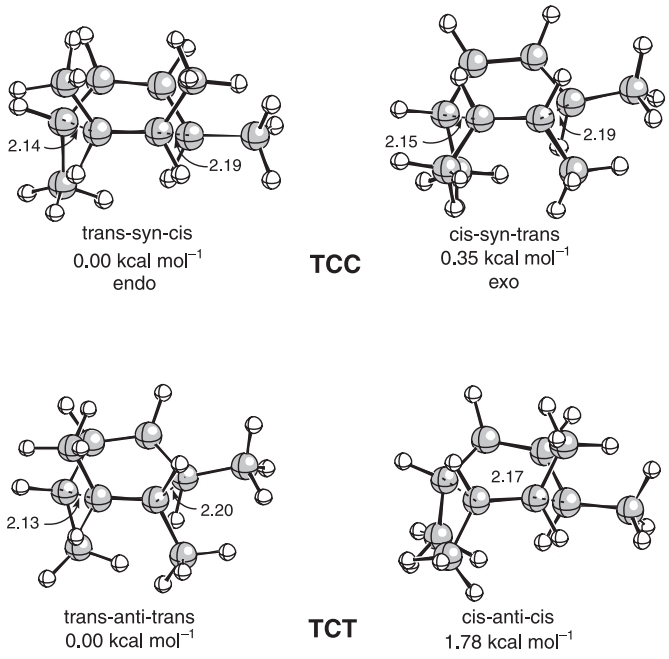
$$[4] \qquad \nu = \sum_{t=1}^{m} \nu_t$$

and, from eq. [1]–[4],

$$[5] \qquad \nu = \frac{\kappa T}{h} \frac{\sum_{t=1}^{m} e^{-G_t^{\ddagger}/RT}}{\sum_{i=1}^{n} e^{-G_i/RT}}[A]$$

© 2001 NRC Canada

Fig. 10. Transition structures for the intermolecular TCC and TCT reactions.



Since the overall rate ν is

[6] $$\nu = k[A]$$

the overall rate constant k is given by eq. [7],

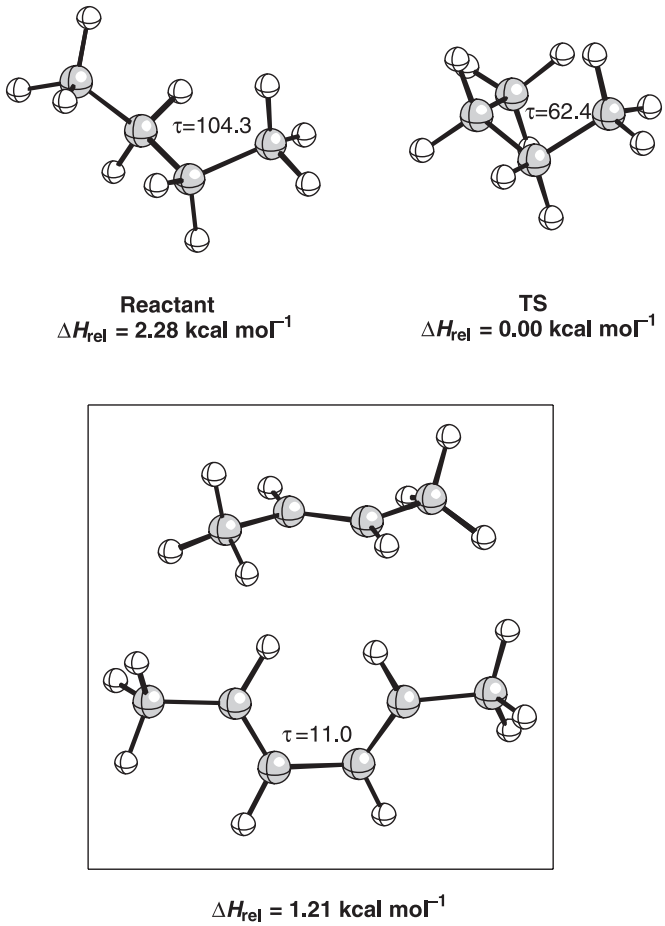
[7] $$k = \frac{\kappa T}{h} \frac{\sum_{t=1}^{m} e^{-G_t^{\ddagger}/RT}}{\sum_{i=1}^{n} e^{-G_i/RT}}$$

and the corresponding mean standard Gibbs free energy of reaction is

[8] $$\Delta G_b^{\ddagger} = -RT \ln \left[\frac{\sum_{t=1}^{m} e^{-G_t^{\ddagger}/RT}}{\sum_{i=1}^{n} e^{-G_i/RT}} \right]$$

Table 3 summarizes the $\Delta G_b^{\ddagger}$, calculated at 298 K from eq. [8], for each of the transannular Diels–Alder reactions of the present work. This table also includes the Curtin–Hammett barriers ($\Delta G_{CH}^{\ddagger}$), defined (7) *as the free energy difference between the lowest minimum and the lowest TS*. It can be seen that the $\Delta G_b^{\ddagger}$ values, which take into account *all* of the minima and *all* of the TS leading to the same product, are not very different from the Curtin–Hammett barriers. Consequently, although equations analogous to eq. [8] can be derived for $\Delta H_b^{\ddagger}$ and $\Delta S_b^{\ddagger}$, the analysis of template effects that follows in the next section was based on $\Delta H_{CH}^{\ddagger}$, and $\Delta S_{CH}^{\ddagger}$, defined as differences in enthalpy and entropy between the lowest minima and lowest TS.

Fig. 11. Analysis of ground-state destabilization in the cyclization of the TTT isomer.



Template effects

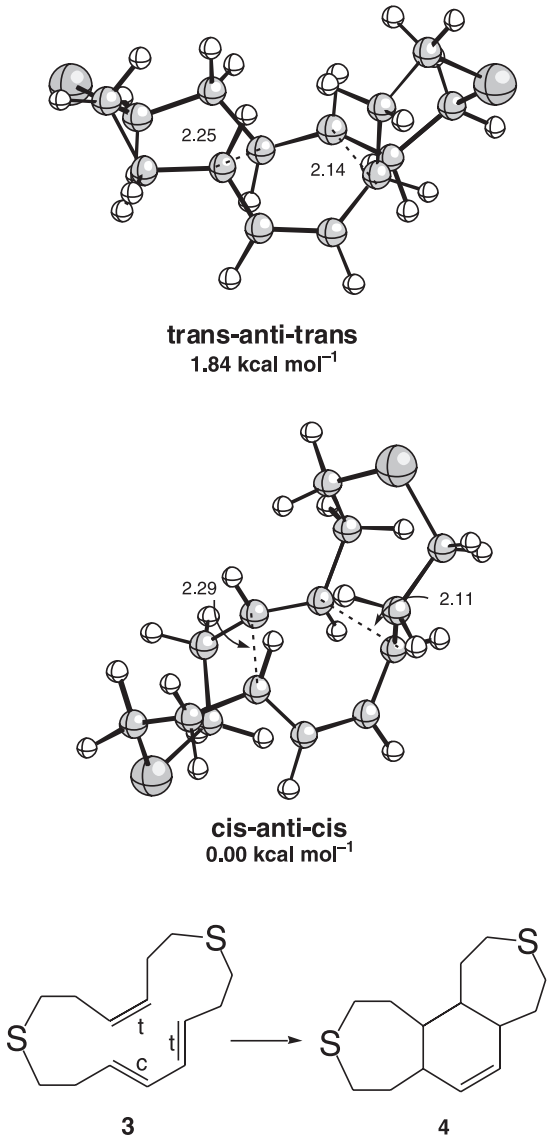
Table 4 compares, for T = 298 K, the Curtin–Hammett free energies of activation of the transannular Diels–Alder reactions (from Table 3), and the enthalpic and entropic contributions to these free energies, with the corresponding quantities for the acyclic Diels–Alder reactions of Figs. 8–10. The latter data were obtained with the assumption that the initial thermodynamic parameters are the sum of the diene and dienophile parameters, i.e., that the reaction coordinate is repulsive between reactants and TS.

There is a significant template effect. With the exception of the very unfavourable CCT reaction, which produces a *trans* double bond, and the TCT reaction that leads to the *trans-anti-trans* product, all transannular reactions have substantially lower free energies of activation than their acyclic counterparts. Since the transannular reactions are unimolecular and the acyclic reactions are bimolecular, there is a uniformly large entropic contribution to the template effect. Interestingly, in the most favourable TTC and TTT transannular reactions there is also a significant enthalpic contribution to the template effect.

This effect appears to be caused by ground-state destabilization in the transannular reactions, as is summarized in Fig. 11. The structure shown at the bottom of the figure is obtained by truncation of the lowest TTT minimum (Figs. 4 and 7) to the corresponding acyclic reactant com-

© 2001 NRC Canada

Fig. 12. Two transition structures for the transannular Diels–Alder cyclization of the triene **3** to the olefin **4**.



plex. The truncated structure is destabilized enthalpically relative to the separated reactants by 1.2 kcal mol^{-1}. The structures at the upper left and upper right of the figure are obtained by truncation of the four-carbon chains of the TTT minimum and TS to the corresponding conformations of *n*-butane. The reduction of the two C-C-C-C dihedral angles, from 104.3° in the minimum to 62.4° in the TS, reduces the ring strain by a total of 4.56 kcal mol^{-1}. The total ground-state destabilization (5.77 kcal mol^{-1}) is close to the $\Delta\Delta H^{\ddagger}$ value of 6.11 kcal mol^{-1} seen in Table 4.

Is cyclization to a *trans-anti-trans* product feasible?

It was suggested earlier that the inherently more favourable reaction channel leading to the *trans-anti-trans* stereochemistry cannot be achieved by a cyclic TCT triene in which the diene and dienophilic components are separated by four atoms. Inspection of Dreiding models suggested that the addition of a fifth atom to these bridges, as in the dithia compound **3** (Fig. 12) would overcome the problem. A very cursory examination of the cyclization of **3** to **4** produced one TS leading to the *cis-anti-cis* product and one TS leading to the *trans-anti-trans* product. In contrast to Fig. 6, in which every *trans*-anti-*trans* TS is destabilized by at least 20 kcal mol^{-1}, the free energy difference between the two structures of Fig. 12 is only 1.84 kcal mol^{-1}. A comprehensive examination of the cyclization of the TCT isomer of **3** is currently in progress.

Acknowledgements

This research was supported financially by the Natural Sciences and Engineering Research Council of Canada (NSERC). The authors thank Dr. J.I. Seeman for a helpful discussion on the subject of the Curtin–Hammett principle and Professor Chan-Kyung Kim for assistance with one of the calculations.

References

1. (*a*) A. Walton. Molecular and crystal structure models. Ellis Horwood, New York. 1978; (*b*) O.B. Ramsay. Stereochemistry. Heyden and Sons, London. 1981; (*c*) C. Trindle. Croat. Chim. Acta, **57**, 1231 (1984).
2. K. Mislow. Introduction to stereochemistry. W.A. Benjamin, New York. 1966. p. 42.
3. C.J. Suckling, K.E. Suckling, and C.W. Suckling. Chemistry through models. Cambridge University Press, London. 1978. pp. 175–176.
4. E.L. Eliel and S.H. Wilen. Stereochemistry of organic compounds. John Wiley, New York. 1994. p. 41.
5. (*a*) K. Baettig, C. Dallaire, R. Pitteloud, and P. Deslongchamps. Tetrahedron Lett. **28**, 5249 (1987); **28**, 5253 (1987); **28**, 5255 (1987); (*b*) S. Lamothe, A. Ndibwami, and P. Deslongchamps. Tetrahedron Lett. **29**, 1639, (1988); **29**, 1641 (1988); (*c*) A. Marinier and P. Deslongchamps. Can. J. Chem. **70**, 2350 (1992); (*d*) A. Ndibwami, S. Lamothe, P. Soucy, S. Goldstein, and P. Deslongchamps. Can. J. Chem. **71**, 714 (1993); (*e*) Y.L. Dory, P. Soucy, M. Drouin, and P. Deslongchamps. J. Am. Chem. Soc. **117**, 518 (1995); (*f*) L. Barriault, S.G. Ouellet, and P. Deslongchamps. Tetrahedron, **53**, 14 937 (1997); (*g*) M. Couturier, Y.L. Dory, D. Fortin, A. Rouillard, and P. Deslongchamps. Tetrahedron, **54**, 10 089 (1998); (*h*) R. Lavoie, A. Toró, and P. Deslongchamps. Tetrahedron, **55**, 13 037 (1999); (*i*) R. Lavoie, S.G. Ouellet, C. Dallaire, Y.L. Dory, A. Toró, and P. Deslongchamps. Tetrahedron, **56**, 5509 (2000); (*j*) E. Marsault, A. Toro, P. Nowak, and P. Deslongchamps. Tetrahedron, **57**, 4243 (2001).
6. (*a*) T. Takahashi, K. Shimizu, T. Doi, and J. Tsuji. J. Am. Chem. Soc. **110**, 2674 (1988); (*b*) T. Takahashi, Y. Sakamoto, and T. Doi. Tetrahedron Lett. **33**, 3519 (1992); (*c*) T. Sakamoto, H. Yamada, and T. Takahashi. Synlett. 231 (1995).
7. J.I. Seeman. Chem. Rev. **83**, 83 (1983).
8. N.L. Allinger, Y.H. Yuh, and J.-H. Lii. J. Am. Chem. Soc. **111**, 8551 (1989).
9. J.J.P. Stewart. J. Comput. Chem. **10**, 209, (1989); **10**, 221 (1989).
10. N. Weinberg and S. Wolfe. J. Am. Chem. Soc. **116**, 9860 (1994).
11. Gaussian 94 (Revision D.1). M.J. Frisch, G.W. Trucks, H.B. Schlegel, P.M.W. Gill, B.G. Johnson, M.A. Robb, J.R.

© 2001 NRC Canada

Cheeseman, T.A. Keith, G.A. Petersson, J.A. Montgomery, K. Raghavachari, M.A. Al-Laham, V.G. Zakrzewski, J.V. Ortiz, J.B. Foresman, J. Cioslowski, B.B. Stefanov, A. Nanayakkara, M. Challacombe, C.Y. Peng, P.Y. Ayala, W. Chen, M.W. Wong, J.L. Andres, E.S. Replogle, R. Gomperts, R.L. Martin, D.J. Fox, J.S. Binkley, D.J. Defrees, J. Baker, J.P. Stewart, M. Head-Gordon, C. Gonzales, and J.A. Pople. Gaussian, Inc., Pittsburgh, PA. 1995.

12. Gaussian 98, Revision A.6. M.J. Frisch, G.W. Trucks, H.B. Schlegel, G.E. Scuseria, M.A. Robb, J.R. Cheeseman, V.G. Zakrzewski, J.A. Montgomery, Jr., R.E. Stratmann, J.C. burant, S. Dapprich, J.M. Millam, A.D. Daniels, K.N. Kudin, M.C. Strain, O. Farkas, J. Tomasi, V. Barone, M. Cossi, R. Cammi, B. Mennucci, C. Pomelli, C. Adamo, S. Clifford, J. Ochterski, G.A. Petersson, P.Y. Ayala, Q. Cui, K. Morokuma, D.K. Malick, A.D. Rabuck, K. Raghavachari, J.B. Foresman, J. Cioslowski, J.V. Ortiz, B.B. Stefanov, G. Liu, A. Liashenko, P. Piskorz, I. Komaromi, R. Gomperts, R.L. Martin, D.J. Fox, T. Keith, M.A. Al-Laham, C.Y. Peng, A. Nanayakkara, C. Gonzalez, M. Challacombe, P.M.W. Gill, B. Johnson, W. Chen, M.W. Wong, J.L. Andres, M. Head-Gordon, E.S. Replogle, and J.A. Pople. Gaussian, Inc. Pittsburgh PA. 1998.
13. C. Peng and H.B. Schlegel. Isr. J. Chem. **33**, 449 (1994).
14. C. Peng, P.Y. Ayala, H.B. Schlegel, and M.J. Frisch. J. Comput. Chem. **17**, 49 (1996).
15. C. Gonzales and H.B. Schlegel. J. Chem. Phys. **90**, 2154 (1989); J. Chem. Phys. **94**, 5523 (1990).
16. N.S. Zefirov. Russ. J. Org. Chem. **33**, 138 (1997).

© 2001 NRC Canada

ADDITIONS AND CORRECTIONS/AJOUTS ET CORRECTIONS

Additions and corrections: Solution multinuclear (^{31}P,^{111}Cd,^{77}Se) magnetic resonance studies of cadmium complexes of heterocyclic aromatic thiones and the structure of [tetrakis(2(1*H*)-pyridinethione)cadmium] nitrate, $[Cd(C_5H_5NS)_4](NO_3)_2$

Umarani Rajalingam, Philip A.W. Dean, and Hilary A. Jenkins[1]

Re: Can. J. Chem. **78**, 590 (2000).
To be consistent with the way in which the data are presented: in the title for Table 3, $[CdL_n(SePCy_3)_{4-n}]^{2+}$ should be replaced with $[CdL_{4-n}(SePCy_3)_n]^{2+}$, and in the title for Table 4, $[CdL_n(SPCy_3)_{4-n}]^{2+}$ should be replaced with $[CdL_{4-n}(SPCy_3)_n]^{2+}$.

[1]Current address: Department of Chemistry, Saint Mary's University, Halifax, Nova Scotia B3H 3C3, Canada.

 DOI: 10.1139/cjc-79-8-1293 © 2001 NRC Canada

ADDITIONS AND CORRECTIONS/AJOUTS ET CORRECTIONS

Additions and corrections: Expoxide of a ketene acetal. The first 2,2-dialkoxyoxirane to be isolated

Małgorzata Dawid, Paul C. Venneri, and John Warkentin

Ref.: Can. J. Chem. **79**, 110 (2001).

After this paper was published we became aware of an earlier report (M.S. Newman and E. Kilbourn. J. Org. Chem. **35**, 3186 (1970)) concerning a 2,2-dialkoxyoxirane. Our claim, that we were the first to isolate such a compound, is therefore not correct.

 DOI: 10.1139/cjc-79-8-1294 © 2001 NRC Canada

National Research Council Canada
Ottawa, Canada K1A 0R6

Conseil national de recherches Canada
Ottawa, Canada K1A 0R6

Postage paid at Ottawa
Publications mail
Registration No. 1240447

Port payé à Ottawa
Poste-publication
Enregistrement n° 1240447

Canadian Journal of Chemistry

Volume 79, Number 9, September 2001

Revue canadienne de chimie

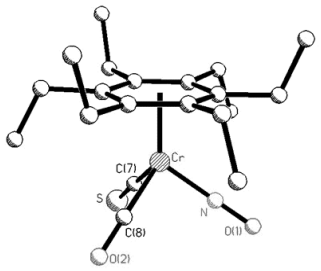
Volume 79, numéro 9, septembre 2001

2000 Alcan Award Lecture

Adventures in organometallic NMR: steric restraints, slowed rotations, and skeletal rearrangements

Michael J. McGlinchey

1295–1309



An analysis of the hydration thermodynamics of the CONH group

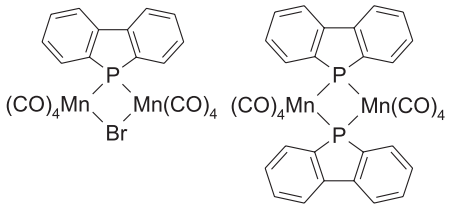
Giuseppe Graziano

1310–1320

Synthesis and characterization of manganese complexes of the dibenzophospholyl ligand

Andreas Decken, Melanie A. Neil, and Frank Bottomley

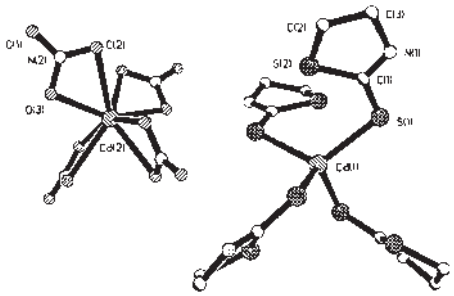
1321–1329



Cadmium complexes of thiones. Part II.[1] A synthetic, solution, and solid-state MAS $^{111/113}$Cd NMR study of cadmium complexes of 1,3-thiazolidine-2-thione, and the structures of [tetrakis(1,3-thiazolidine-2-thione)cadmium] trifluoromethanesulfonate ($[Cd(C_3H_5NS_2)_4](CF_3SO_3)_2$) and [tetrakis(1,3-thiazolidine-2-thione)cadmium][tetrakis(nitrato-*O,O′*)cadmate] ($[Cd(C_3H_5NS_2)_4][Cd(O_2NO)_4]$)

Umarani Rajalingam, Philip A.W. Dean, Hilary A. Jenkins, Michael Jennings, and James M. Hook

1330–1337



Continued on inside back cover / Suite au verso

Canada

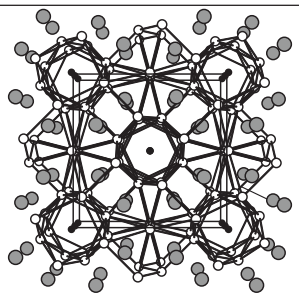
Printed in Canada by / Imprimé au Canada par
University of Toronto Press Inc.
Typesetting by / Typographie par
NRC Research Press / Presses scientifiques du CNRC

0008-4042(200109)79:9;1-3

$Ti_5Si_{1.3}Sb_{1.7}$ — The first titanium silicide antimonide, forming a crystal structure not found in either binary system

Holger Kleinke

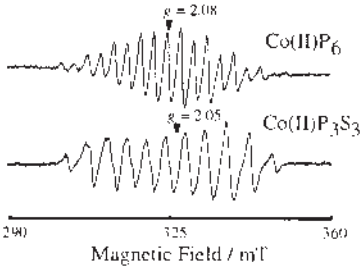
1338–1343



New low-spin Co(II) complexes with novel tripodal 1,1,1-tris(dimethylphosphinomethyl)ethane ligand: electron transfer kinetics and spectroscopic characterization of $Co(II)P_6$ and $Co(II)P_3S_3$ ions in aqueous solution

Satoshi Iwatsuki, Kenji Obeyama, Nobuyoshi Koshino, Shigenobu Funahashi, Kazuo Kashiwabara, Takayoshi Suzuki, and Hideo D. Takagi

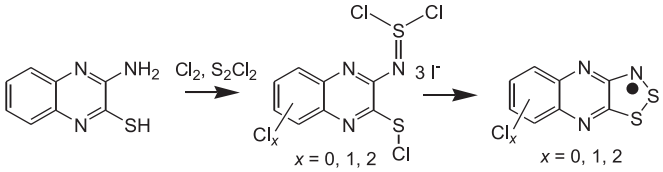
1344–1351



Quinoxaline-1,2,3-dithiazolyls — Synthesis, EPR characterization, and redox chemistry

A. Wallace Cordes, James R. Mingie, Richard T. Oakley, Robert W. Reed, and Hongzhou Zhang

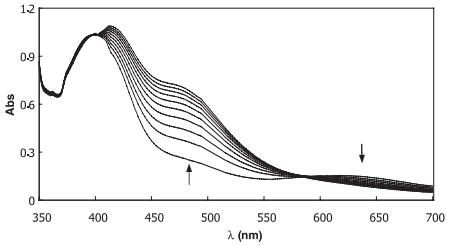
1352–1359



Synthesis, characterization, and thermodynamics of tertiary phosphine cobalt(III) Schiff-base complexes

Mozaffar Asadi and Ali Hossein Sarvestani

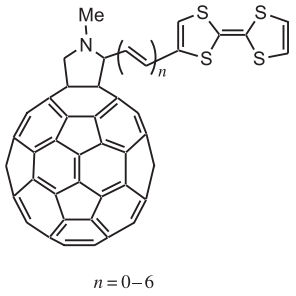
1360–1365



Calculations on the electronic structure and nonlinear second-order susceptibilities of fulleropyrrolidine–tetrathiafulvalene(C_{60}PY–TTF) based on donor–bridge–acceptor dyads

Wei Fu, Hong-Xing Zhang, Ji-Kang Feng, and Wei Li

1366–1375



Concluded on facing page / Suite et fin à la page précédente

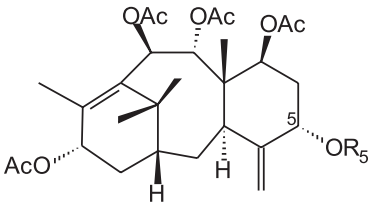
^{1}H NMR studies of proton transfer equilibria in hydrogen bonds — the role of the entropy

Roland Langner and Georg Zundel

1376–1380

Reanalysis of the biotransformation of 4(20),11(12)-taxadiene derivatives

Di-An Sun, Françoise Sauriol, Orval Mamer, and Lolita O. Zamir

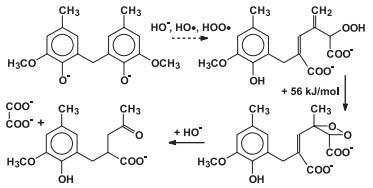


R_5 = OAc: **1**
R_5 = Cinn: **2**

1381–1393

Alkaline oxidative degradation of diphenylmethane structures — Activation energy and computational analysis of the reaction mechanism

Lubo Jurasek, Lívia Krištofová, Yujun Sun, and Dimitris S. Argyropoulos



1394–1401

The Canadian Journal of Chemistry is affiliated with the Canadian Society for Chemistry and publishes papers in all areas of chemistry.

La Revue canadienne de chimie est affiliée à la Société canadienne de chimie et publie des articles dans tous les domaines de la chemie.

2000 Alcan Award Lecture

Adventures in organometallic NMR: steric restraints, slowed rotations, and skeletal rearrangements

Michael J. McGlinchey

Abstract: The structures and NMR fluxionality of a wide variety of organometallic complexes (including tetrahedral cluster cations and systems of the type $(C_nR_n)ML_3$, where R = Et, Ph) are discussed. Barriers to tripodal and peripheral substituent rotations are reported, and the relevance of correlated rotations to molecular machines is outlined. Haptotropic shifts in (cyclopenta[*def*]phenanthrenyl)ML_n and (cyclopenta[*l*]phenanthrenyl)ML_n complexes are rationalized in terms of the aromatic character of the transition states. Likewise, the barriers to silatropic shifts in polyindenylsilanes can be correlated with the aromaticity of the intermediate isoindenes. Finally, the use of cobalt clusters to control cyclohexane ring conformations is described.

Key words: NMR ring currents, fluxionality, correlated rotations, molecular rearrangements, haptotropic shifts.

Résumé : Les structures et la non-rigidité à l'échelle de temps de la RMN d'une grande variété de complexes organométalliques (dont des clusters tétraédriques cationiques et des systèmes du type $(C_nR_n)ML_3$ dans lesquels R = Et, Ph) sont discutées. Les barrières de rotation des substituants tripodes et périphériques sont données et le rapport entre les rotations concertées et les machines moléculaires est souligné. Les déplacements haptotropiques dans les complexes (cyclopenta[*def*]phénanthrényl)ML_n et (cyclopenta[*l*]phénanthrényl)ML_n sont rationalisés en termes du caractère aromatique des états de transition. De la même manière, les barrières des déplacements silatropiques dans les polyindénylsilanes sont corrélées avec l'aromaticité des intermédiaires isoindènes. Enfin, l'utilisation de clusters de cobalt pour contrôler la conformation de cyclohexanes est décrite.

Mots clés : courants de cycle en RMN, non-rigidité, rotations concertées, réarrangements moléculaires, déplacements haptotropiques.

Prologue

At the outset, I wish to acknowledge Alcan for their continued support of the inorganic chemistry community in Canada, and also to thank CSC for administering the awards program that provides recognition and encouragement to researchers and teachers whose activities cover a wide spectrum of the enormous enterprise we call Chemistry.

Since arriving at McMaster 28 years ago, my graduate and undergraduate thesis students, postdoctoral collaborators, and I have worked in a number of apparently diverse areas. These have encompassed the use of metal vapours as synthetic reagents (1–6), the chemistry of metal π-complexes (7–12), NMR spectroscopic studies of transition metal nuclei, such as ^{45}Sc (13), ^{47,49}Ti (14), ^{61}Ni (15), ^{91}Zr (16), hitherto unexplored in organometallic systems (17), syntheses and fluxional behaviour of metal hydrides (18), metal clusters (19–32), organometallic derivatives of natural products (33), and the stabilization of short-lived intermediates such as benzyl anions (34) or cations (35, 36), silyl cations (37), trimethylenemethane (38), and tetramethylenebenzene (39). More recently, we have focused our attention on the migrations of organometallic moieties across polycyclic surfaces and on the molecular dynamics of sterically hindered molecules.

In this brief overview, I shall attempt to show how several of these seemingly very disparate topics in fact followed a common thread as our research progressed in a semiorderly fashion.

Received February 20, 2001. Published on the NRC Research Press Web site at http://canjchem.nrc.ca on September 20, 2001.

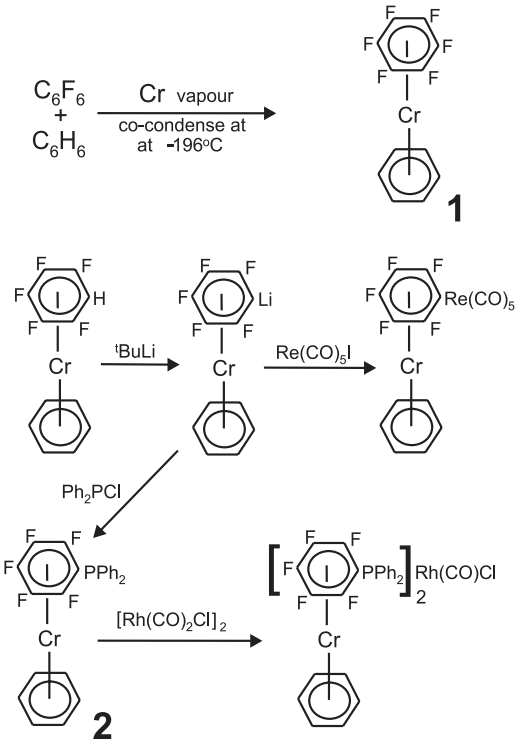
M.J. McGlinchey. Department of Chemistry, McMaster University, Hamilton, ON L8S 4M1, Canada (fax: (905) 522-2509; e-mail: mcglinc@mcmaster.ca).

Metal vapours, ring currents, and diamagnetic anisotropy

In 1972, the chemistry of metal vapours was still very much in its infancy (40); in those days researchers built their own relatively unsophisticated equipment from glass-sewer piping and resistance-heated ceramic crucibles — a far cry from today's commercially available metal evaporators with their electron gun technology (41). Nevertheless, one could vaporize metals such as chromium (1–6), nickel (42), or

 DOI: 10.1139/cjc-79-9-1295 © 2001 NRC Canada

Scheme 1. Synthetic routes to $(C_6F_5X)Cr(C_6H_6)$ sandwich complexes.



germanium (43), cocondense them onto a liquid nitrogen cooled surface with a potential ligand, and generate novel organometallics. Typically, we were able to prepare synthetically useful quantities of previously unavailable sandwich complexes, as illustrated in Scheme 1.

Parenthetically, one should note the topicality of the sandwich complex $(C_6F_6)Cr(C_6H_6)$ (**1**) whose sixfold symmetry was remarkably reminiscent of the Star Wars "tie fighters" that were in vogue at that time.

The NMR spectra of these new systems revealed a number of surprising facets, such as the clear inter-ring $J_{H,F}$ couplings in $(C_6F_6)Cr(C_6H_6)$ (**1**) shown in Fig. 1 (4), or the magnitude of the $J_{F,F}$ values in $(C_6F_5X)Cr(C_6H_6)$ sandwiches, as exemplified by the phosphine complex **2** (44). Typically, in fluoroarenes, the coupling between *ortho* fluorines is ≈20 Hz, while *meta* couplings are normally approximately 4 Hz; in the sandwich complexes, the corresponding $^3J_{F,F}$ and $^4J_{F,F}$ values are in the ranges of 90–110 and 40–50 Hz, respectively. These very marked changes wrought upon the ^{19}F chemical shifts and fluorine–fluorine coupling constants within the pentafluorophenyl rings upon complexation to a $(C_6H_6)Cr$ moiety made us reflect upon the possible influence of the metal on the aromatic ring current.

We, therefore, sought a sensitive probe with which to monitor changes in the aromatic ring current, but which was also sufficiently distant from the metal as to be unaffected by it directly. The classic work of Cram and co-workers (45) had demonstrated that protons positioned directly above an aromatic system, as in the alkyl chain of a cyclophane, were markedly shielded. Our idea was then to synthesize a metal complex of a cyclophane, and to compare the chemical shifts of the protons above the ring in both the free and the

Fig. 1. ^{19}F and ^1H NMR spectra of $(C_6F_6)Cr(C_6H_6)$ (**1**); each resonance is a septet because of inter-ring coupling.

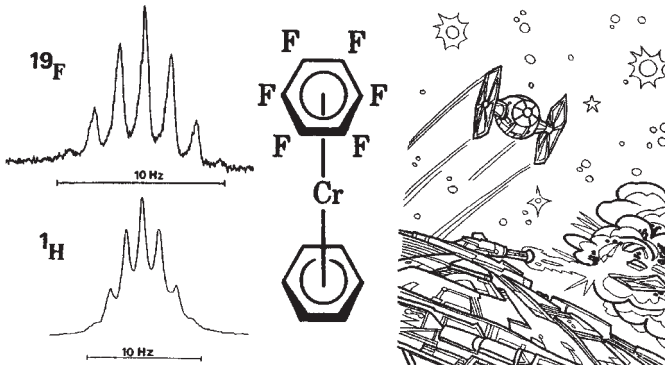
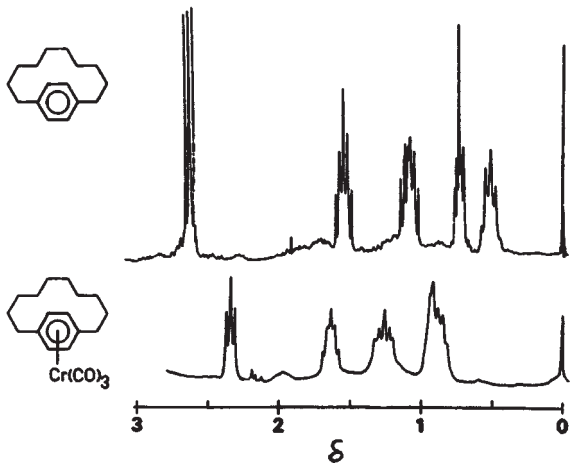


Fig. 2. 220 MHz ^1H NMR spectra of [10]paracyclophane (**3**) and its $Cr(CO)_3$ complex **4**.



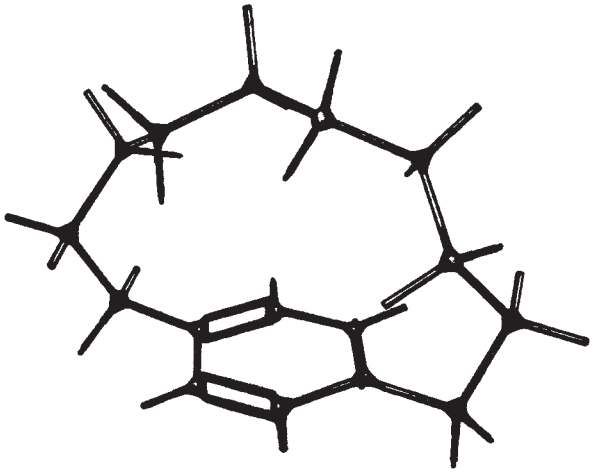
complexed systems. At that time (1975), a 220 MHz spectrometer was considered a high-field instrument, and fortunately, we were able to acquire ^1H NMR spectra of [10]paracyclophane (**3**) and of its $Cr(CO)_3$ complex (**4**) and they are shown in Fig. 2 (46).

It is evident that, in the complex, those protons positioned in the shielding cone of the ring current (β, γ, δ, and ε methylene groups) are now less shielded; in contrast, the α-methylene protons, which lie in the deshielding region, have now moved to lower frequency. Our conclusion was that the aromatic ring current had been attenuated upon complexation. Since that time, several researchers have investigated this phenomenon, with occasionally confusing results (47). Interestingly, while some authors have raised the possibility that complexation of an arene to a chromium tricarbonyl unit actually renders the system *antiaromatic* (48), very recent NICS calculations do not support this view (49).

Returning to the mid-1970s, a crucial criterion to be satisfied when evaluating ring current contributions to proton chemical shifts was, of course, a reliable molecular geometry. Since [10]paracyclophane is a liquid, we chose to take advantage of the molecular modeling programs that were just being developed, notably by Allinger at the University of Georgia. The experimentally measured chemical shifts for

© 2001 NRC Canada

Fig. 3. Fieser molecular model of [10]paracyclophane used to calculate proton positions relative to the arene ring centre, and hence to evaluate ring current shifts.

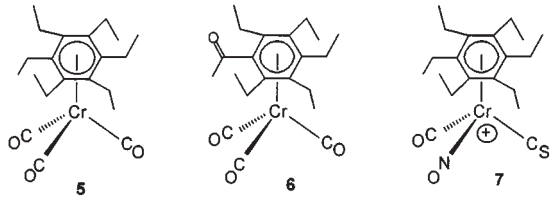


the methylene groups of [10]paracyclophane, in conjunction with the calculated geometry (shown in Fig. 3 as a Fieser model) revealed that the standard Waugh–Fessenden–Johnson–Bovey ring-current model (50, 51) had serious inadequacies.

This semiclassical model and the ring-current tables derived from it have been used many thousands of times since their inception, and presumably, the majority of users have never considered its rather flimsy theoretical underpinnings. In brief, Waugh and Fessenden (50) attributed the entire 1.5 ppm chemical shift difference between the protons in benzene and the vinylic protons in 1,3-cyclohexadiene to the ring current effect. They then calculated the effect of an *in-plane* six-electron current on a benzene proton. Since this calculation predicted too large a deshielding (2.78 ppm), the in-plane current was split into two loops, one above and the other below the ring plane, until the desired 1.5 ppm deshielding was achieved; this occurred at a loop separation of 1.28 Å, and since that time, constant use has bestowed an imprimatur on this decidedly empirical model. The present status of NMR studies on cyclophanes, and of the relevance of ring current calculations, has recently been comprehensively reviewed (52).

In 1975, Barfield et al. (53) showed that one could not ignore the anisotropic contributions of the ring carbons to the chemical shifts of protons proximate to arene rings. This approach required a knowledge of the ^{13}C NMR tensor elements of the ring carbons and such data are, in principle, obtainable from measurements in the solid state. Fortuitously for us, the leading pioneer in this area, John Waugh at MIT, graciously agreed to measure the ^{13}C NMR tensor elements of a series of (arene)$Cr(CO)_3$ complexes, where the arene was C_6H_6, C_6Me_6, and C_6Et_6.

These experiments yielded a number of fascinating results: (*i*) the major change in tensor elements upon complexation occurs for σ_{22}, the radial element, which is shielded by approximately 50 ppm; this would induce a field along each carbon–hydrogen axis and may account for the large upfield (low frequency) shift always observed for the aromatic protons when an arene is coordinated to a $Cr(CO)_3$ moiety; (*ii*) in the solid-state spectrum of $(C_6Et_6)Cr(CO)_3$ (**5**), the isotropic chemical shifts of the ring carbons, methylene carbons, and methyl carbons are all doubled. This observation suggested to us that the sixfold symmetry of the hexaethylbenzene (HEB) ligand had been broken such that the ethyls projected alternately above and below the plane of the arene ring, and raised the possibility that such a slowing of the ethyl rotations might be detectable in a solution spectrum of **5** at a sufficiently low temperature.



5 **6** **7**

When I wrote the first draft of the manuscript to be published jointly with John Waugh (54), I somewhat whimsically referred to HEB as "*a hexapodous ligand with tentacular ethyl groups*"; fortunately my distinguished coauthor pointed out that I was mixing not only Latin and Greek, but also arms and legs! However, the paper also makes some serious points that still have relevance today. As is well-known, there have been many attempts to relate NMR chemical shifts to a variety of molecular properties, and we offered the following comment: "one would hope that, as more data become available, theories relating substituent parameters to isotropic shifts of carbon or fluorine nuclei in free or π-complexed aromatic systems will be superseded by correlations with appropriate tensor elements". It is gratifying to note that such data are now commonly available, and that Canadian scientists such as R.E. Wasylishen (55) have become prominent in this field.

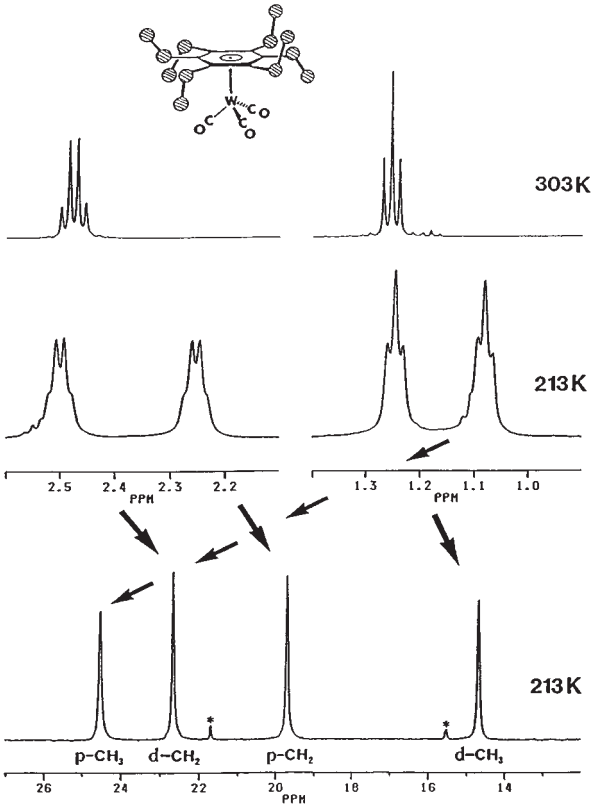
Molecular propellers and bevel gears

With the goal of determining the barrier to ethyl rotations in $(HEB)M(CO)_3$, where M = Cr, Mo, W, their variable-temperature ^1H and ^{13}C NMR spectra were recorded in CD_2Cl_2 and it was shown that this fluxional process could indeed be slowed on the NMR time scale (46*b*, 56), as illustrated in Fig. 4. Moreover, the proposed structure with alternating proximal and distal ethyl groups was confirmed X-ray crystallographically by Mislow and co-workers (57).

The question that now arose concerned the barrier to tripodal rotation and whether it was correlated with the ethyl rotations; that is, does this system function as a molecular analogue of a bevel gear? Clearly, one must construct a molecule in which the ethyl and tripodal rotations can be monitored independently, and we were able to accomplish this in two ways. Firstly, replacement of one ethyl group by an acetyl substituent, as in **6**, breaks the threefold symmetry such that, at low temperature, the slowed tripodal rotation yields a ^{13}C NMR spectrum in which the carbonyl environments are split in a 2:1 ratio (58); the barrier to tripodal rotation was evaluated as 9.5 ± 0.5 kcal mol^{-1}. More elegantly, perhaps, the ^{13}C NMR spectrum of the chiral cation $[(C_6Et_6)Cr(CO)(CS)(NO)]^+$ (**7**) exhibits at low temperature six ring-carbon environments, six methylene signals, and six methyl resonances, as shown in Fig. 5 (59). Simulation of

© 2001 NRC Canada

Fig. 4. Variable-temperature 400 MHz ^{1}H and 100 MHz ^{13}C NMR spectra of $(C_6Et_6)W(CO)_3$ showing the slowed interconversion of proximal and distal ethyls.

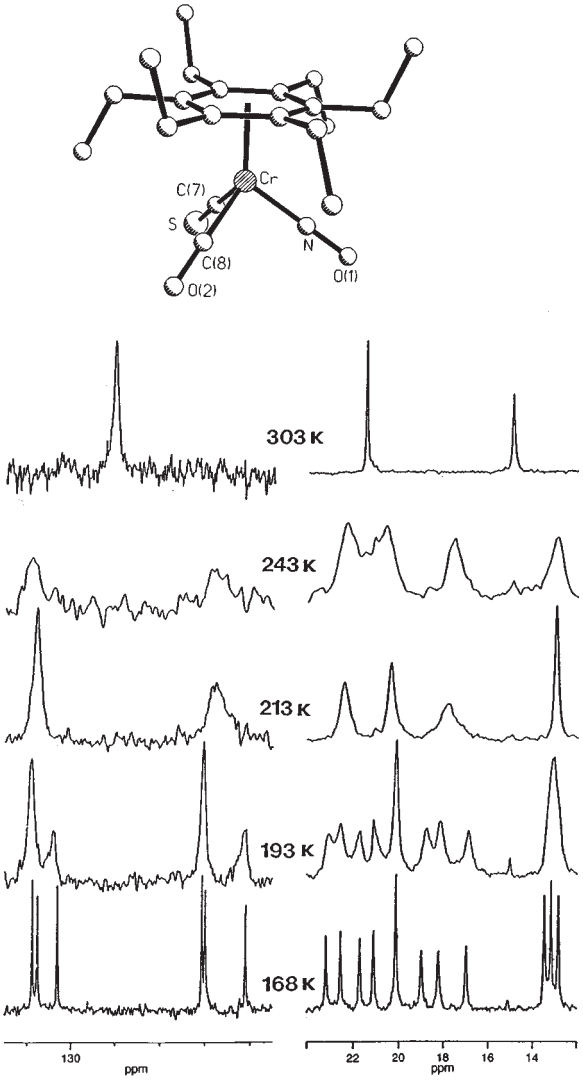


these spectra yield values of 9.5 ± 0.5 and 11.5 ± 0.5 kcal mol^{-1} for the tripodal and ethyl rotation barriers, respectively, showing that these two processes are not correlated. Subsequently, in a beautiful series of papers, Siegel and Kilway (60) used subtle stereochemical arguments to verify these conclusions.

At first sight, one might suspect that increasing the bulk of the tripodal substituents might enhance the steric interactions between themselves and the ethyl substituents, thus favoring the development of a molecular bevel gear. However, the $(HEB)Cr(CO)_2L$ system has other conformations available to it, and replacement of a carbonyl group by ligands with increasingly larger cone angles merely results in loss of the alternating proximal–distal arrangement of ethyl groups (61). Likewise, this phenomenon is also found in the $(HEB)RuCl_2L$ series, where the ethyl substituents have been shown to adopt the 3:3, 4:2, 5:1, or 6:0 conformations,[1] several of which are depicted in Fig. 6, thus demonstrating that placing too much steric pressure on a system can cause it to respond so as to frustrate one's plans.

In light of the conformational variability of hexaethylbenzene, it was deemed necessary to incorporate aryl substituents that, in principle, could not simply rotate away from the potential steric hindrance. Since we had already been working with metal complexes containing pentaphenylcyclopentadienyl or hexaphenylbenzene ligands (62), we chose to extend this study to include larger C_nPh_n systems.

Fig. 5. Variable-temperature 125 MHz ^{13}C NMR spectra of $[(C_6Et_6)Cr(CO)(CS)(NO)]^+$ (**7**) showing slowed ethyl and tripodal rotation on the NMR time scale.



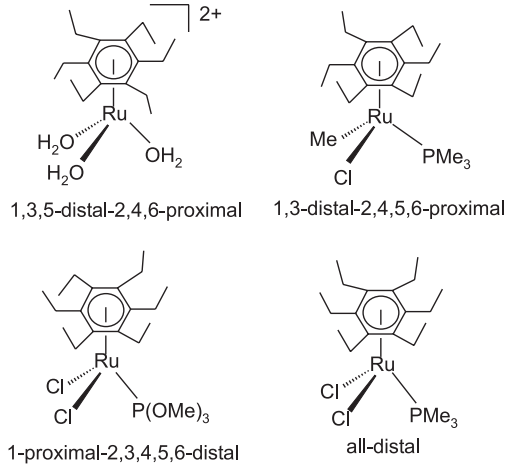
The peripheral phenyls in $(C_5Ph_5)ML_n$ complexes adopt a propeller-like geometry with dihedral angles (θ) of approximately 50° relative to the central ring; this represents a compromise between the sterically inaccessible fully coplanar geometry (θ = 0°) and the minimally hindered orientation (θ = 90°) whereby all conjugation is lost. In the series $[C_5Ph_5]^-$, C_6Ph_6, $[C_7Ph_7]^+$, the increasing radius of the central ring is counterbalanced by the changing angle between the peripheral phenyls, which decreases from 72 to 60 to 51.4°. Interestingly, however, the most crowded of these systems, i.e., $[C_7Ph_7]^+$, responds not merely by orienting the phenyls such that the average θ value is approximately 80° but also by allowing the central seven-membered ring to fold into a gentle boat conformation (63), as in Fig. 7.

As noted above, pentaphenyl-cyclopentadienyl complexes give rise to propeller structures and, when the ML_n unit is asymmetric as in $(C_5Ph_5)Fe(CO)(HC{=}O)(PMe_3)$ (**8**), the stereogenic metal centre combined with the helicity of the

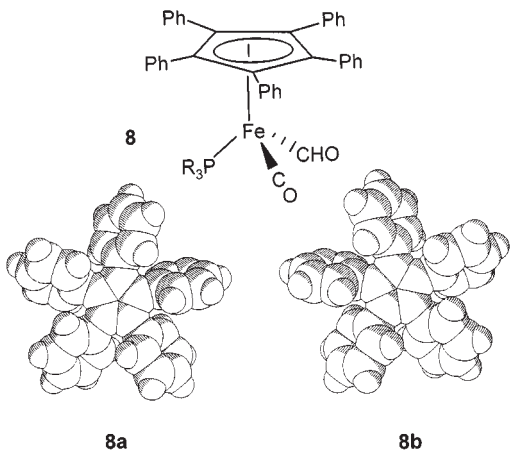
[1] (*a*) P.E. Lock. Unpublished results from this laboratory; (*b*) unpublished results cited in: M.A. Bennett. Coord. Chem. Rev. **166**, 225 (1997).

© 2001 NRC Canada

Fig. 6. X-ray crystallographically determined structures of $[(C_6Et_6)Ru(H_2O)_3]^{2+}$, $(C_6Et_6)RuCl(Me)[PMe_3]$, $(C_6Et_6)RuCl_2[P(OMe)_3)]$, and $(C_6Et_6)RuCl_2(PMe_3)$.

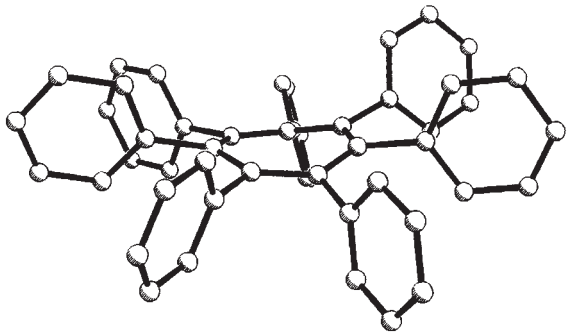


propeller (clockwise or anticlockwise) gives rise to diastereomers. However, oscillation of the peripheral phenyl rings interconverts diastereomers **8a** and **8b**. To follow the dynamics of such systems, and to determine whether the rotations of the peripheral aryl substituents and of the ML_n moiety are correlated, one must incorporate independent probes for both processes.

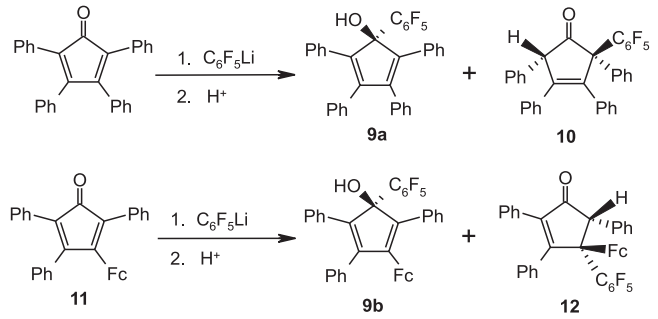


We have shown in a straightforward fashion that, in **8**, the barrier to tripodal rotation is ≈8.7 kcal mol^{-1}; this is readily accomplished since the five central-ring carbon environments become different when the process is slowed on the NMR time scale (62*a*). Slowed peripheral aryl rotation would render the proximal and distal ring edges inequivalent, but severe peak overlap, even on a 500 MHz spectrometer, makes such a determination an extremely difficult task. Our goal, therefore, was to synthesize complexes of the type $[C_5Ph_4(C_6F_5)]ML_n$, which would not only avoid the problem of extensive ^{1}H NMR peak overlap in the aromatic region, but also take advantage of the much larger ^{19}F chemical shift range.[2] However, this also requires the availability of $C_5Ph_4(C_6F_5)OH$ (**9a**) as a starting material. This

Fig. 7. X-ray crystal structure of the $[C_7Ph_7]^+$ cation showing the nonplanarity of the central ring.



Scheme 2. Reactions of substituted cyclopentadienones with pentafluorophenyllithium (Fc = ferrocenyl).



apparently trivial synthesis remains a challenge: treatment of tetracyclone with C_6F_5Li yields **9a** in poor yields, although sufficient for an X-ray crystallographic characterization (64). The major product is **10**, the result of a 1,6-addition process (see Scheme 2). Interestingly, with 3-ferrocenyl-2,4,5-triphenylcyclopentadienone (**11**), the principal site of nucleophilic attack is at the ferrocenyl-bearing ring carbon to give **12**, and the alcohol **9b** is only a minor product.

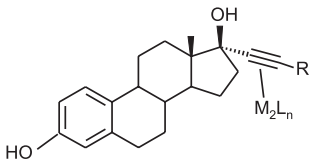
Current extensions of these concepts involve the use of arenes possessing peripheral substituents that are even more sterically demanding, and particular goals at present include hexanaphthylbenzene as well as systems of the type C_6Ph_5R, where R is an (η^5- or η^6-indenyl)ML_n moiety.

Steroids, terpenes, and metal-stabilized cluster cations

Concomitant with our studies concerning correlated motions of molecular fragments, we have investigated a wide range of fluxional processes. We have already discussed some examples of rotational fluxionality; let us now turn our attention to systems exhibiting translational stereochemical nonrigidity. As part of a 20-year collaboration with Professor Gérard Jaouen in Paris, a series of studies on the biochemical activity of organometallic derivatives of hormonal steroids (65–75) had led us inevitably into the world of chirality and other aspects of stereochemistry. In particular,

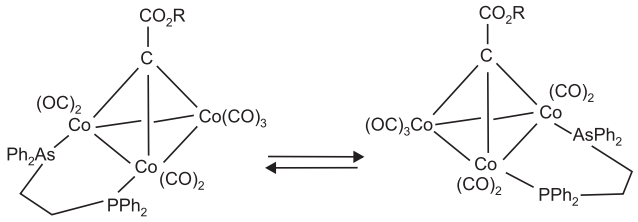
[2] Very recently, restricted rotation of a pentafluorophenyl ring in $[(C_5H_2(C_6F_5)_3]_2Fe$ has been reported: M.P. Thornberry, C. Slebodnick, P.A. Deck, and F.R. Fronczek. Organometallics, **19**, 5352 (2000).

© 2001 NRC Canada



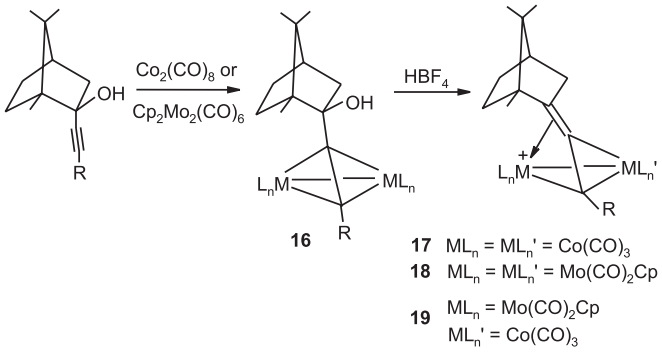
13a $M_2L_n = Co_2(CO)_6$
13b $M_2L_n = Mo_2(CO)_4Cp_2$

Scheme 3. Fluxional processes in arphos-tricobalt clusters.



14a R = Me
14b R = $CHMe_2$
15 R = menthyl

Scheme 4. Cobalt and molybdenum cluster cations derived from camphor.



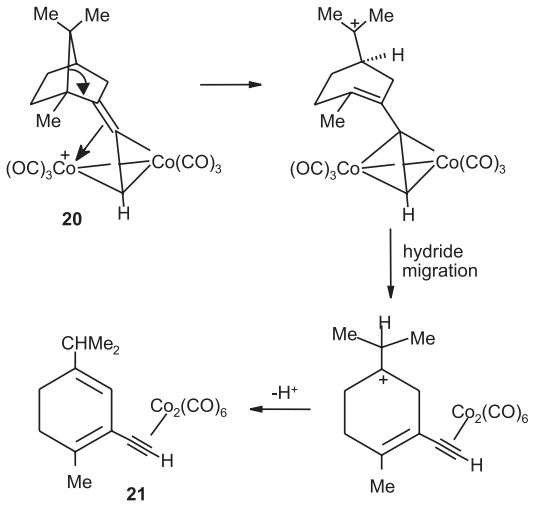
16

17 $ML_n = ML_n' = Co(CO)_3$
18 $ML_n = ML_n' = Mo(CO)_2Cp$
19 $ML_n = Mo(CO)_2Cp$, $ML_n' = Co(CO)_3$

17α-alkynylestradiol derivatives (**13**) that are complexed to a dimetallic fragment such as $Co_2(CO)_6$ or $(C_5H_5)_2Mo_2(CO)_4$ (66) show a remarkable ability to bind to specific receptor sites that are of crucial importance to the detection and possible treatment of breast cancer. Lack of space does not permit us to discuss this and other fascinating applications (76, 77) of bio-organometallic chemistry, but the interested reader may wish to consult the reviews describing the pioneering work of Jaouen and Vessières (78).

Metal complexes of steroids are, of course, chiral but we decided to invert the emphasis of the project in that one could also use such ligands to impose chirality onto a cluster so as to reveal hitherto hidden fluxional processes. For example, the tricobalt cluster $MeO_2C\text{-}CCo_3(CO)_7$(*arphos*) (**14a**) exists as a racemic mixture and resists all attempts to separate the enantiomers, implying the existence of a low-energy process that interconverts them (Scheme 3). Replacement of the methyl by an isopropyl group, as in **14b**, generates diastereotopic methyl environments whose NMR resonances undergo exchange with a barrier of ≈13 kcal mol^{-1} (79). A more elegant approach is to use a chiral substituent (either steroidal or terpenoid) at which point the two diastereomers of **15** yield different ^{31}P NMR resonances; it was subsequently demonstrated that the rapid interconversion of the enantiomers of **14** (or the diastereomers of **15**) occurs by migration of the Ph_2As terminus of the *arphos* ligand between two cobalt vertices with concomitant scrambling of the carbonyls (79, 80).

Scheme 5. Ring-opening of a dicobalt-bornyl cluster cation.



20 **21**

As noted previously, the dicobalt alkynyl-estradiol complex **13a** attaches itself strongly to hormonal receptor sites, and it was suspected that this binding was related to the ability of the metal cluster fragment to stabilize a cationic charge on the a carbon atom — a phenomenon that had been brilliantly exploited in synthetic studies by Nicholas (81, 82). We chose to take advantage of this effect to investigate the bornyl cation because of its pivotal role in the long-running controversy over the structures of classical vs. nonclassical cations (see ref. 83, with comments by P.V.R. Schleyer).

Treatment of camphor with an alkynyl anion yields, upon hydrolysis, the *endo* alkynol, which readily forms bimetallic complexes **16** containing cobalt or molybdenum vertices; upon protonation with HBF_4 these precursors yield the corresponding cations **17**–**19** (Scheme 4) (84, 85). The molybdenum-containing cluster cations **18** and **19** have been crystallographically characterized (86) and possess normal carbon—carbon bond lengths and angles — not surprisingly, since the charge is primarily located on the metal. This contrasts with Laube's now classic studies on the purely organic cations which strongly support a nonclassical formulation (87).

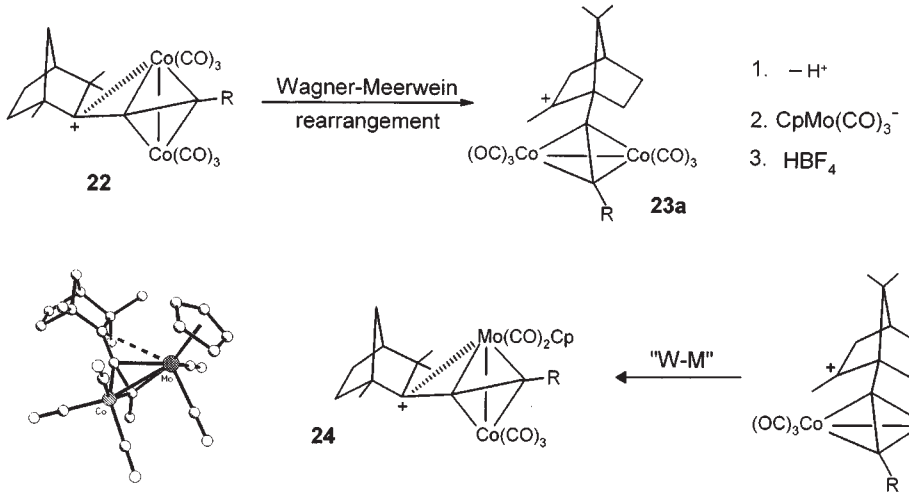
In contrast, the dicobalt cation **20** is readily identified by its NMR spectrum at –40°C but, when allowed to warm to room temperature, it undergoes a ring-opening that leads ultimately to the cluster-complexed alkynylcyclohexadiene, **21** (Scheme 5).[3]

Very different behaviour is exhibited by the corresponding fenchyl cation **22**, which readily undergoes a Wagner–Meerwein shift to place the dicobalt-alkynyl substituent at the bridgehead position in **23a**. Moreover, upon replacement

[3] J.H. Kaldis. Unpublished results from this laboratory.

© 2001 NRC Canada

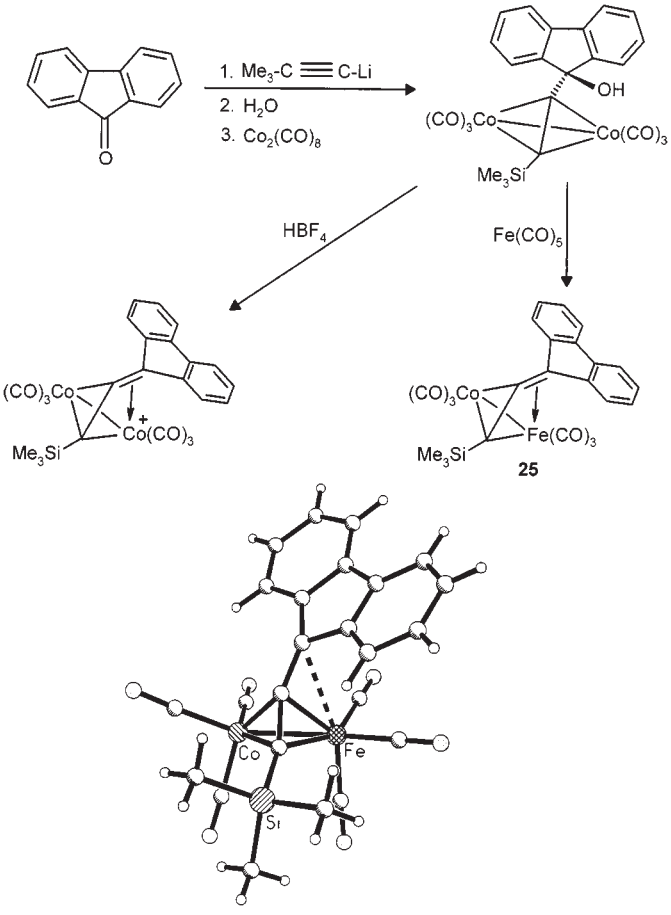
Scheme 6. Wagner–Meerwein skeletal rearrangements of metal-stabilized fenchyl cations.



of a tricarbonylcobalt vertex by an isolobal dicarbonyl(cyclopentadienyl)molybdenum group, as in **23b**, subsequent reprotonation reverses the sense of the original Wagner–Meerwein rearrangement so as to regenerate the fenchyl skeleton in which the cationic site is stabilized by complexation to an *exo* molybdenum vertex in **24** (Scheme 6) (88). Evidently, the direction of terpenoid rearrangements can be subtly controlled by an appropriate choice of stabilizing metal centre.

The outstanding ability of metal clusters to stabilize carbocations (89, 90) suggested that it might be possible to prepare hitherto unavailable species such as the antiaromatic fluorenyl, indenyl, and cyclopentadienyl cations which possess 12π-, 8π-, and 4π-electrons, respectively. In the event, these predictions were justified, and treatment of the appropriate ketones with an alkynyl anion, complexation to a dicobalt hexacarbonyl unit, and protonation yielded the hoped-for cluster-stabilized cations that were readily identified by NMR spectroscopy (91). Moreover, replacement of a $[Co(CO)_3]^+$ vertex by the isolobal neutral $Fe(CO)_3$ moiety gave the corresponding mixed-metal species that could be characterized by X-ray crystallography, and the structure of the fluorenyl cluster **25** is shown in Scheme 7.

Scheme 7. Cobalt- or iron-stabilized antiaromatic fluorenyl cations.



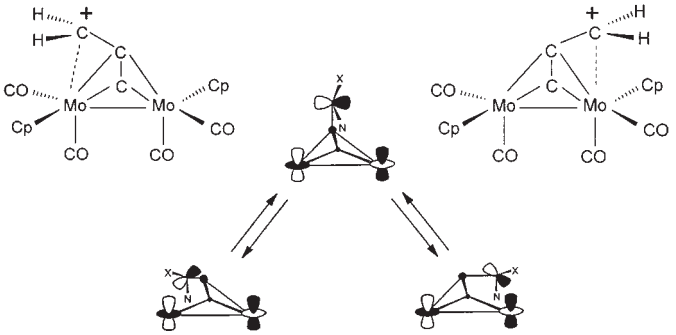
Rearrangement pathways: a combined NMR, X-ray crystallographic, and calculational approach

Fluxional behaviour of cluster-stabilized propargyl cations

The availability of a reasonably large number of structurally characterized metal-cluster stabilized propargyl cations of the type $[Cp_2Mo_2(CO)_4(RC{\equiv}C\text{-}CR'R'')]^+$, together with the corresponding variable-temperature NMR data, allowed us to establish a viable trajectory for the fluxional process that exchanges the cationic site between metal vertices, as illustrated in Scheme 8. Molecular orbital calculations at the extended Hückel level yielded an energy hypersurface from which the lowest energy trajectory for cation migration could be extracted (92); as shown in Fig. 8, the favoured structure places the cationic carbon close to one metal vertex and rotated so as to optimize the overlap between the vacant *p*-orbital on carbon with the filled *d*-orbital on the metal. In the transition state, the CH_2 group is oriented orthogonally with respect to the metal–metal vector so as to maintain

© 2001 NRC Canada

Scheme 8. Antarafacial migration of an α-methylene group between metal centres in a tetrahedral dimolybdenum-cluster cation; note how the *exo*- (X) and *endo*- (N) substituents maintain their relative positions.



overlap with an out-of-phase combination of metal *d*-orbitals.

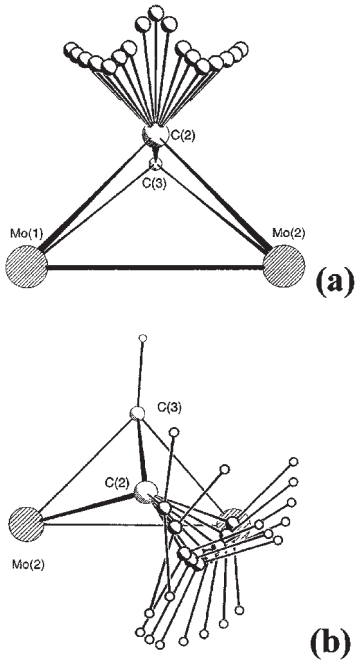
Now, an examination of the known X-ray structures of the $[Cp_2Mo_2(CO)_4(RC{\equiv}C\text{-}CR'R'')]^+$ cluster cations reveals that for those possessing a primary cationic site (R′ = R″ = H), the Mo···C$^+$ distance is ≈2.45 Å; for secondary cations (R′ = alkyl, aryl, ferrocenyl; R″ = H), this value increases to 2.55–2.65 Å, while for tertiary cations the Mo···C$^+$ distance can exceed 2.75 Å. As originally proposed by Bürgi and Dunitz (93), an appropriately selected set of X-ray crystal structures can provide a series of snapshots of a reaction pathway, and in the present case we can readily see how the experimental data can be mapped onto the calculated trajectory.

NMR measurements had already established that for clusters possessing a primary, secondary, or tertiary cationic site, respectively, the migration barrier falls from ≈20 to approximately 11 kcal mol^{-1}. Taken together, the molecular orbital calculations and the NMR and X-ray experimental data provide a coherent and relatively complete picture of the molecular dynamics of these metal-stabilized cationic systems.

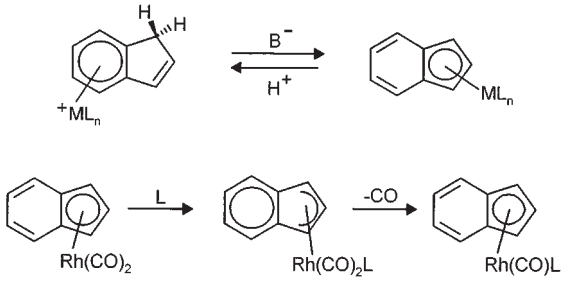
Haptotropic shifts across polycyclic surfaces

The capacity to carry out catalytic processes on surfaces may be related to the ability of the reacting species to migrate across the surface towards each other. It is therefore of considerable interest to understand the factors that come into play when organometallic moieties are placed onto a hydrocarbon surface and allowed to find their most favored sites of attachment. It has long been known that deprotonation of (η^6-indene)ML_n species, where ML_n = $Cr(CO)_3$, $Mo(CO)_3$, $(C_9H_7)Fe^+$, $(C_5Me_5)Rh^{2+}$, $(C_5Me_5)Ir^{2+}$, or $(C_2H_4)_2Rh^+$, results in migration of the metal fragment onto the five-membered ring, as in Scheme 9 (94); similar behaviour has been reported in the corresponding fluorenyl systems (95). These η^6 to η^5 processes are reversed on protonation, and such rearrangements are known as haptotropic shifts. A second phenomenon that is relevant to this observation is the so-called indenyl effect whereby ligand substitution in, for example (η^5-indenyl)$Rh(CO)_2$, proceeds approximately 1×10^8 times more rapidly than for the corresponding η^5-cyclopentadienyl system. This has been interpreted in terms of a slippage of the organometallic moiety into an η^3-structure, thus leading to a low-energy transition state possessing 6π-aromatic character (96).

Fig. 8. (*a*) EHMO-calculated trajectory of the α-carbon during the migration process; (*b*) calculated trajectory of the CH_2 fragment as it migrates between metal vertices (note the twisting motion as it approaches a molybdenum atom).



Scheme 9. Haptotropic shifts and ligand substitution reactions in (indenyl)ML_n systems.

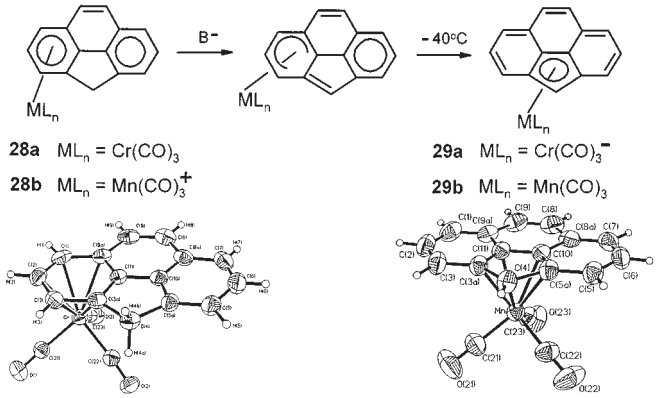


The possibility of combining these two concepts, whereby one might facilitate haptotropic shifts by providing a low-energy pathway with enhanced aromatic character, seemed to us to be attractive option. To this end, we chose to investigate the organometallic chemistry of cyclopenta[*def*]-phenanthrene (**26**) and of cyclopenta[*l*]phenanthrene (**27**). The $Cr(CO)_3$ and $Mn(CO)_3^+$ derivatives of **26** were readily preparable and, upon deprotonation, underwent facile η^6 to η^5 rearrangement (97). Figure 9 shows the X-ray crystal structures of (η^6-cyclopenta[*def*]phenanthrene)$Cr(CO)_3$ (**28a**) and of (η^5-cyclopenta[*def*]phenanthrenyl)$Mn(CO)_3$ (**29b**), which represent the before and after situations, respectively.

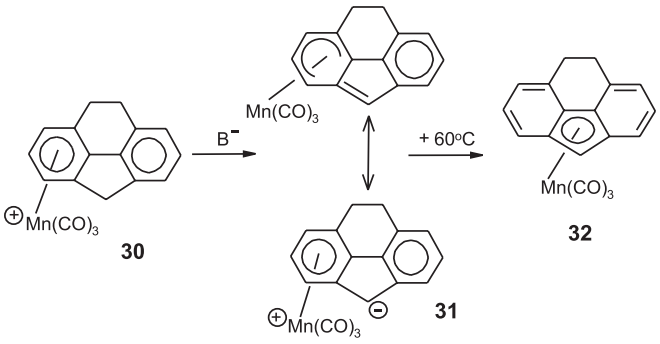
In contrast, as depicted in Scheme 10, hydrogenation of the C(4)—C(5) linkage to form [(η^6-4,5-dihydrocyclopenta[*def*]-phenanthrene)$Mn(CO)_3]^+$ (**30**) allowed the isolation of the zwitterionic intermediate, **31**, which only underwent the η^6 to η^5 haptotropic shift to give **32** when heated at 60°C for 1 h. These observations are readily explained in terms of the favored migration trajectory in which, as shown by EHMO

© 2001 NRC Canada

Fig. 9. Facile haptotropic shifts in the (cyclopenta[*def*]-phenanthrenyl)ML_n system.



Scheme 10. The barrier toward haptotropic shifts is markedly increased in (4,5-dihydrocyclopenta[*def*]-phenanthrenyl)$Mn(CO)_3$ (**30**).



calculations, the metal does *not* follow the least-motion pathway (98). (While there is no doubt that Density Functional Theory gives much more reliable quantitative results, we can carry out an EHMO calculation on such a hypersurface in just a few hours, and this guides our synthetic strategies.) Traversal of the common bond between the six-membered and five-membered rings is a symmetry-forbidden process (99). Instead the organometallic fragment takes a more circuitous route, shown in Fig. 10*a*, which allows the development of a 10π naphthalene-type transition state, as illustrated in Fig. 10*b*. It is evident that loss of the C(4)—C(5) double bond, as in **30**, disrupts the potential aromaticity of the transition state and raises the barrier for haptotropic shifts.

Let us compare these results with those for a series of (η^5-cyclopenta[*l*]phenanthrenyl)ML_n complexes (**33**) where ML_n = $Mn(CO)_3$, $TiCl_3$, $Fe(C_5H_5)$, or $Rh(C_2H_4)_2$, for which protonation does *not* effect a haptotropic shift.[4] Indeed, their behaviour is much more reminiscent of the known reactivity of the corresponding (η^5-cyclopentadienyl)ML_n complexes; typically, protonation of **33** where ML_n = $Rh(C_2H_4)_2$, yields 1-butene, and follows the classic pattern established by Cramer (100) for $(C_5H_5)Rh(C_2H_4)_2$. Molecular orbital calculations reveal that migration onto the central six-membered ring is greatly disfavored since it would disrupt the aromatic

Fig. 10. (*a*) Calculated migration pathway of a $Mn(CO)_3$ fragment during an η^6 to η^5 haptotropic shift, via (*b*) an aromatic naphthalene-type transition state.

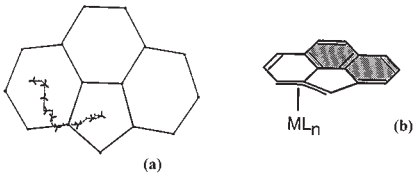
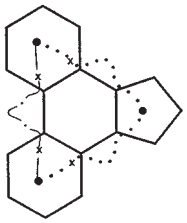


Fig. 11. Calculated migration pathways for haptotropic shifts in the (cyclopenta[*l*]phenanthrenyl)ML_n system (**33**) where ML_n = $Fe(C_5H_5)$; transition states are marked with an X.



character of all the peripheral rings. The energetically most viable pathways for haptotropic shifts between peripheral η^5 and η^6 sites are shown in Fig. 11 and again follow a circuitous route around the periphery of the ligand.

Attempts to prepare η^6-derivatives of **27** have thus far been thwarted by the propensity of the free ligand to undergo a [1,5]-hydrogen shift to generate the dibenzoisoindene, **34** that in turn reacts in a Diels–Alder fashion with its progenitor to yield the dimer **35**, as in Scheme 11 (101).

Sigmatropic shifts across polycyclic surfaces

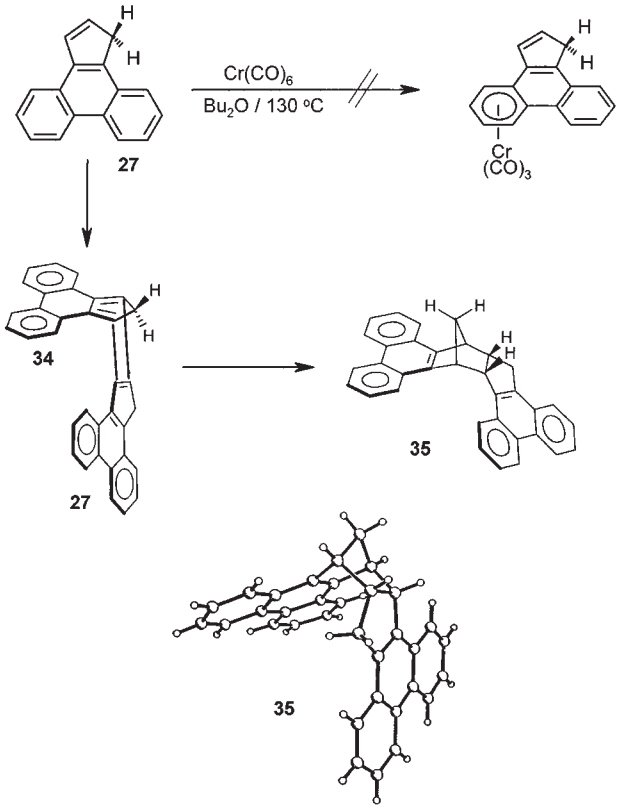
The haptotropic migrations described already are controlled by the interactions between the frontier orbitals of the organometallic fragment (which are primarily of metal *d*-character) and the π-manifold of the polycyclic hydrocarbon (99). However, it has long been known that σ-bonded groups, attached through either a main group or transition element, can undertake circumambulations with activation energies appropriate for study by variable-temperature NMR techniques. The classic mechanistic work in this area was the pioneering study by Cotton and co-workers (102), in which the 1,2-shift of a σ-$Fe(CO)_2(\eta^5$-$C_5H_5)$ fragment over a cyclopentadienyl ring, as in **36a**, was first elucidated and the barrier evaluated as 10.7 kcal mol^{-1}. (This can be reformulated in Woodward–Hoffmann terms as a [1,5]-suprafacial sigmatropic shift.) A crucial component in the original argument (103) was the nonfluxional character of the indenyl analogue, (η^1-C_9H_7)$Fe(CO)_2(\eta^5$-$C_5H_5)$ (**37a**) since a migration of the iron atom to the adjacent carbon would require the intermediacy of an isoindene **38a** with consequent loss of aromaticity (Scheme 12). We shall return to this point presently.

The ease of migration of silyl groups, for example in trimethylsilylcyclopentadiene, **36b** was elegantly demon-

[4] S.S. Rigby. Unpublished results from this laboratory.

© 2001 NRC Canada

Scheme 11. Diels–Alder trapping of the dibenzoisoindene **34**.

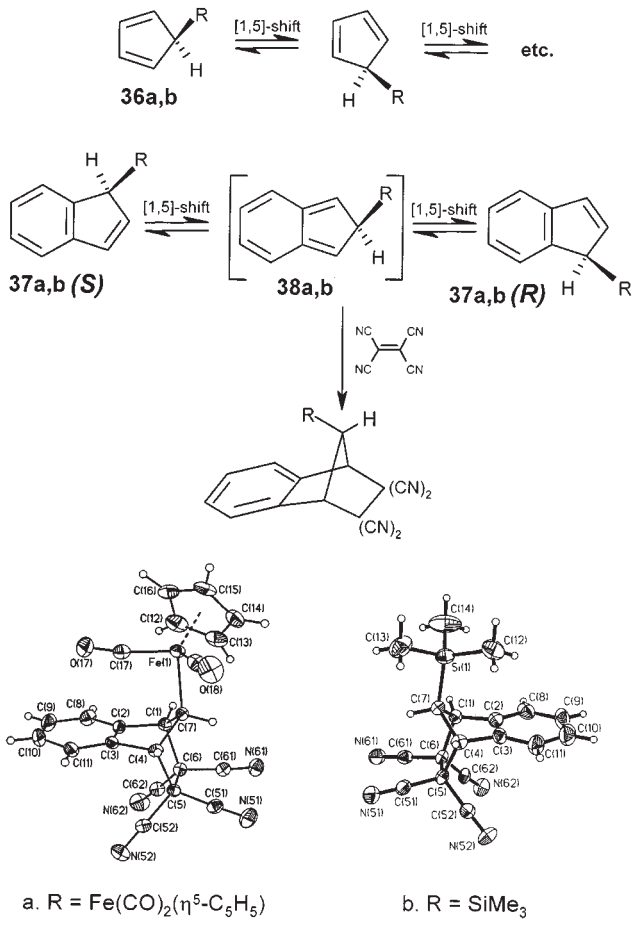


strated by Davison and co-workers (104) who also showed that the corresponding trimethylsilylindene, **37b** was likewise fluxional. However, in the latter case, there was a substantially increased activation energy (≈25 rather than 15 kcal mol^{-1}) reflecting the decrease in aromatic character in the transition state. Subsequent work by McMaster and Stobart (105) using a chiral (Me)(Ph)(*i*-Pr)Sn substituent confirmed the symmetry-allowed nature of the sigmatropic shift process. Moreover, the isoindenes **38a** and **38b** have each been intercepted by reaction with tetracyanoethylene, and the resulting Diels–Alder adducts characterized by X-ray crystallography (106, 107).

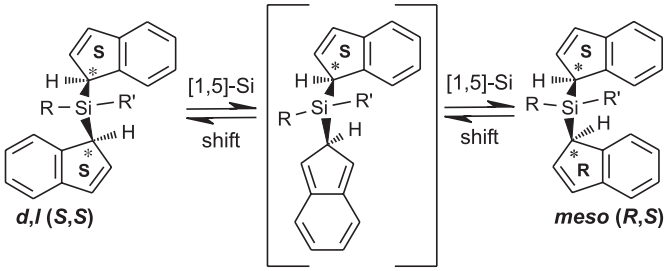
Our own involvement in this project arose as the result of our interest in the stereochemical requirements of ansa-metallocenes, which have been intensively studied as Ziegler–Natta catalysts (108). Bis(1-indenyl)dimethylsilane exists in both *meso* and *d*,*l* forms, which are separable (109), but can interconvert via the series of [1,5]-silatropic shifts depicted in Scheme 13 (110).

The corresponding tris(1-indenyl)silanes raise considerably the sterochemical complexity of the system, which now exists in four forms: two pairs of enantiomers that are, of course, diastereomeric with respect to each other (Scheme 14). The complete story would take too long to relate; suffice it to say that the eight magnetically inequivalent vinylic C(2) sites can be mapped onto the eight vertices of a cube. More interestingly, the network of exchanging allylic hydrogen environments at C(1) and vinylic hydrogens at C(3) can be mapped onto the sixteen vertices of a tesseract (hypercube), while the edges of this four-dimensional object represent symmetry-allowed [1,5]-suprafacial sigmatropic

Scheme 12. [1,5]-Sigmatropic shifts in (*a*) Fe- or (*b*) Si-substituted indenes.



Scheme 13. Interconversion of *meso*- and *d*,*l*-bis-(1-indenyl)dimethylsilanes via a series of [1,5]-silatropic shifts.



shifts (107). Such apparently complex interconversions of stereoisomers are now routinely resolvable by means of modern two-dimensional NMR techniques at the high magnetic fields currently available (106).

Returning briefly to the question of the nonfluxional behaviour of $(\eta^1\text{-}C_9H_7)Fe(CO)_2(\eta^5\text{-}C_5H_5)$ (**37a**), the original difficulty arose as the result of its thermal instability whereby loss of the two carbonyls above ≈80°C yields benzoferrocene (103). Nowadays, however, a simple two-dimensional exchange experiment (EXSY) clearly shows (Fig. 12) that the proton environments at C(1) and at C(3) are indeed interconverting and, as anticipated for a system

© 2001 NRC Canada

Scheme 14. Silatropomers of tris(1-indenyl)silane.

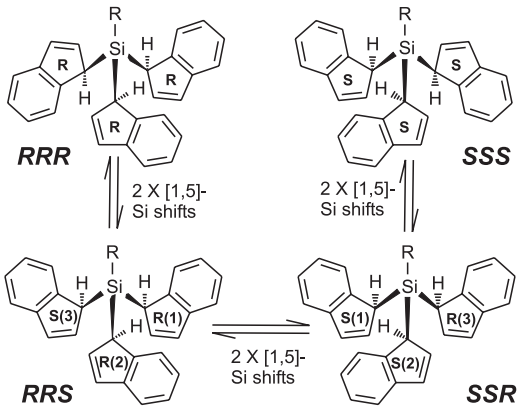
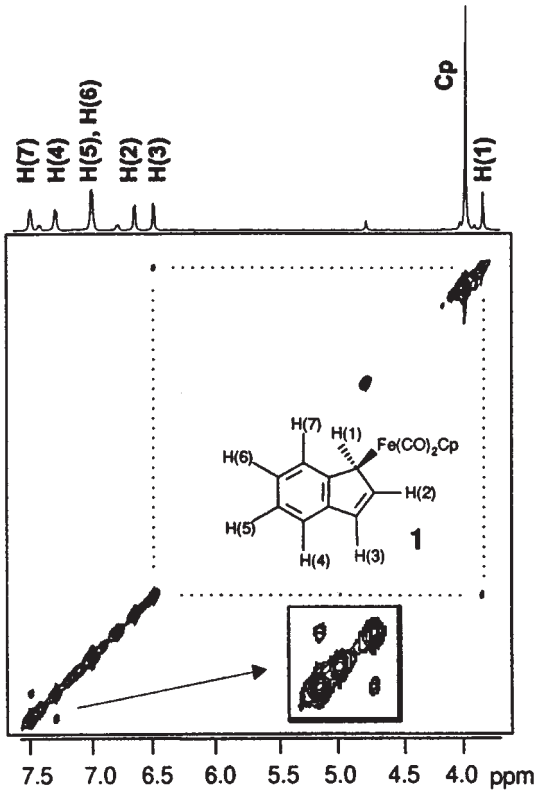


Fig. 12. 2D-EXSY ^{1}H NMR spectrum showing exchange between C(1) and C(3) sites in **37a**.

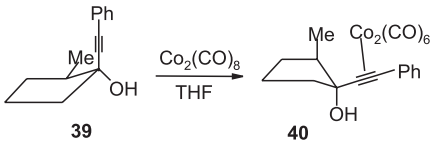


passing through an isoindene structure, the measured barrier of ≈25 kcal mol^{-1} is substantially higher than for the cyclopentadienyl complex **36a** (106).

Cobalt clusters as stereochemical switches

As a final comment, we note that metal clusters can affect the course of a chemical reaction not merely through their electronic properties but rather by the enhanced stereochemical requirements of a bulky substituent. Some years ago, we reported that complexation of a dicobalt hexacarbonyl moiety onto the alkyne linkage of 2-methyl-1-phenylethynylcyclopentanol (**39**) brought about a conformational ring flip such that the acetylenic unit moved from its original pseudo-axial site into the less-hindered pseudo-equatorial position in the cluster **40**, as shown in Scheme 15 (112).

Scheme 15. Complexation-induced ring flip in an alkynylcyclopentanol.



We have very recently extended these ideas to the alkynylcyclohexanol system, and have shown that it is possible to control the ring conformation.[5] The most spectacular examples involve the *trans*- and *cis*-isomers of 1,4-bis(triphenylsilylethynyl)cyclohexane-1,4-diol (**41** and **42**), respectively. In the *trans*-isomer, addition of a $Co_2(CO)_6$ fragment to each of the axial alkyne substituents causes a ring flip such that both cluster units now occupy equatorial sites in **43** (Fig. 13). However, in the *cis*-isomer, the molecule chooses to alleviate the steric strain imposed by the incorporation of two bulky groups by adopting a well-defined twist-boat conformation, **44**, illustrated in Fig. 14. These molecules, as well as a series of related alkyne clusters, have all been characterized by X-ray crystallography, and the resulting modifications in their chemical reactivity are now being investigated.

Closing remarks

In this report, I have tried to show how our research goals have progressed from the purely synthetic to a fuller understanding of the molecular dynamics of a wide range of organometallic systems. With the techniques and instrumentation currently available, one can establish not merely the energetics of fluxional processes but also the precise pathways by which they occur. Moreover, by gaining an understanding of the electronic and steric factors involved, a certain degree of control may be attained. As we learn the rules of the game, we see that the possibility of designing and building molecular machines is becoming a more viable objective.

Acknowledgments

During the course of my time in Canada, I have had the privilege of working with a superb group of undergraduates, graduate students, and postdoctoral collaborators, many of whom are cited in the references. It has also been my good fortune to have interacted with a number of outstanding scientists, some of whom are or were my own colleagues at McMaster, especially Alex Bain, Brian Sayer, and Don Hughes for their NMR expertise, Jim Britten and Colin Lock for X-ray crystal structure determinations, and also Michael Baird (Queen's) as well as my long-time collaborator Gérard Jaouen in Paris. I have learned much from numerous conver-

[5] N.M. Deschamps. Unpublished results from this laboratory.

© 2001 NRC Canada

Fig. 13. Interconversion of chair conformers of *trans*-1,4-bis(triphenylsilyl-ethynyl)cyclohexan-1,4-diol upon incorporation of $Co_2(CO)_6$ moieties.

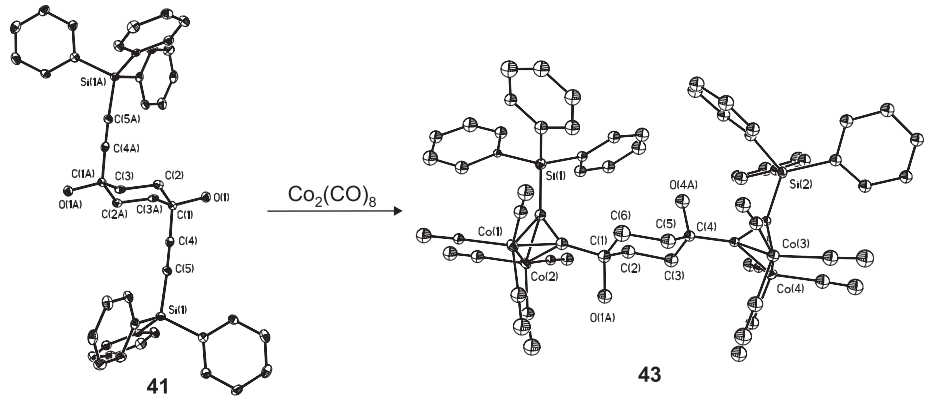
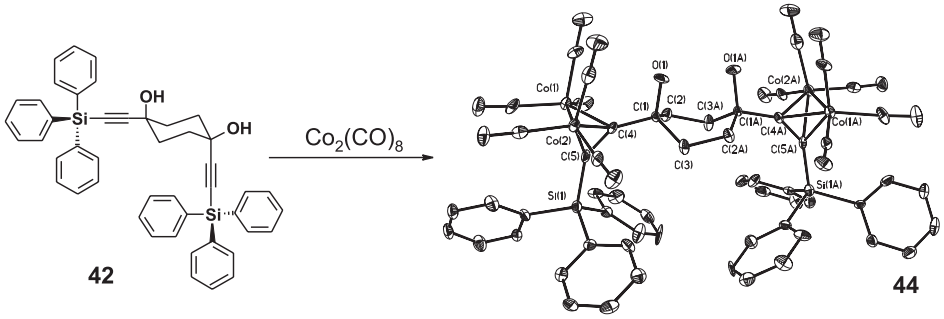


Fig. 14. Interconversion of boat and chair conformers of *cis*-1,4-bis(triphenylsilyl-ethynyl)cyclohexan-1,4-diol upon incorporation of $Co_2(CO)_6$ moieties.



sations with Tom Albright (Houston), Jean-Yves Saillard (Université de Rennes), and Jay Siegel (UC, San Diego); I am grateful for their profound and insightful comments whenever I sought their counsel. Finally, I acknowledge the generous hospitality of Bruno Chaudret and his colleagues at the Laboratoire de Chimie de Coordination in Toulouse where this account was written.

Financial support for our work has been provided by the Natural Sciences and Engineering Research Council of Canada (NSERC), the Petroleum Research Fund (administered by the American Chemical Society), Atomic Energy of Canada Limited, the Province of Ontario, and McMaster University.

References

1. P.S. Skell, D.L. Williams-Smith, and M.J. McGlinchey. J. Am. Chem. Soc. **95**, 3337 (1973).
2. M.J. McGlinchey and T.-S. Tan. Can. J. Chem. **52**, 2439 (1974).
3. T.-S. Tan and M.J. McGlinchey. J. Chem. Soc. Chem. Commun. 155 (1976).
4. M.J. McGlinchey and T.-S. Tan. J. Am. Chem. Soc. **98**, 2271 (1976).
5. A. Agarwal, M.J. McGlinchey, and T.-S. Tan. J. Organomet. Chem. **141**, 85 (1977).
6. Nguyen Hao and M.J. McGlinchey. J. Organomet. Chem. **165**, 225 (1979).
7. S. Top, G. Jaouen, and M.J. McGlinchey. J. Chem. Soc. Chem. Comm. 643 (1980).
8. M. Mlekuz, P. Bougeard, B.G. Sayer, M.J. McGlinchey, C.A. Rodger, M.R. Churchill, J.W. Ziller, S.-K. Kang, and T.A. Albright. Organometallics, **5**, 1656 (1986).
9. B. Mailvaganam, B.E. McCarry, B.G. Sayer, R.E. Perrier, R. Faggiani, and M.J. McGlinchey. J. Organomet. Chem. **335**, 213 (1987).
10. (*a*) H.K. Gupta, P.E. Lock, and M.J. McGlinchey. Organometallics, **16**, 3628 (1997); (*b*) H.K. Gupta, P.E. Lock, D.W. Hughes, and M.J. McGlinchey. Organometallics, **16**, 4355 (1997).
11. L.C.F. Chao, H.K. Gupta, D.W. Hughes, J.F. Britten, S. Rigby, A.D. Bain, and M.J. McGlinchey. Organometallics, **14**, 1139 (1995).
12. H.K. Gupta, N. Rampersad, M. Stradiotto, and M.J. McGlinchey. Organometallics, **19**, 184 (2000).
13. P. Bougeard, M. Mancini, B.G. Sayer, and M.J. McGlinchey. Inorg. Chem. **24**, 93 (1985).
14. B.G. Sayer, D.G. Bickley, N. Hao, G. Dénès, C. Detellier, and M.J. McGlinchey. J. Magn. Reson. **50**, 50 (1982).
15. Nguyen Hao, M.J. McGlinchey, B.G. Sayer, and G.J. Schrobilgen. J. Magn. Reson. **46**, 158 (1982).
16. (*a*) B.G. Sayer, G. Dénès, N. Hao, D.G. Bickley, and M.J. McGlinchey. Inorg. Chim. Acta, **48**, 53 (1981); (*b*) B.G. Sayer, J.I.A. Thompson, N. Hao, T. Birchall, D.R. Eaton, and M.J. McGlinchey. Inorg. Chem. **20**, 3748 (1981).
17. D.G. Bickley, M.J. McGlinchey, and G.J. Schrobilgen. Can. Chem. News, **36**, 19 (1984).
18. D.R. Eaton, K.A. Moffat, M.J. McGlinchey, and R.J. Buist. J. Am. Chem. Soc. **106**, 8110 (1984).

© 2001 NRC Canada

19. M.J. McGlinchey, M. Mlekuz, P. Bougeard, B.G. Sayer, A. Marinetti, J.-Y. Saillard, and G. Jaouen. Can. J. Chem. **61**, 1319 (1983).
20. M. Mlekuz, P. Bougeard, M.J. McGlinchey, and G. Jaouen. J. Organomet. Chem. **253**, 117 (1983).
21. J.-F. Halet, J.-Y. Saillard, R. Lissillour, M.J. McGlinchey, and G. Jaouen. Inorg. Chem. **24**, 218 (1985).
22. J.-F. Halet, G. Jaouen, M.J. McGlinchey, and J.-Y. Saillard. Actual. Chimique, **April**, 23, (1985).
23. M. Mlekuz, P. Bougeard, B.G. Sayer, M.J. McGlinchey, S. Peng, A. Marinetti, J.-Y. Saillard, and G. Jaouen. Organometallics, **4**, 1123 (1985).
24. M. Mlekuz, P. Bougeard, B.G. Sayer, M.J. McGlinchey, R. Faggiani, C.J.L. Lock, and G. Jaouen. Organometallics, **4**, 2046 (1985).
25. J.-F. Halet, J.-Y. Saillard, R. Lissillour, M.J. McGlinchey, and G. Jaouen. Organometallics, **5**, 139 (1986).
26. M. Mlekuz, M.F. D'Agostino, J.W. Kolis, and M.J. McGlinchey. J. Organomet. Chem. **303**, 361 (1986).
27. M.F. D'Agostino, M. Mlekuz, J.W. Kolis, B.G. Sayer, C.A. Rodger, J.-F. Halet, J.-Y. Saillard, and M.J. McGlinchey. Organometallics, **5**, 2345 (1986).
28. R.A. Gates, R.E. Perrier, B.G. Sayer, M.F. D'Agostino, and M.J. McGlinchey. Organometallics, **6**, 1181 (1987).
29. M.F. D'Agostino, M. Mlekuz, and M.J. McGlinchey. J. Organomet. Chem. **345**, 371 (1988).
30. M.F. D'Agostino and M.J. McGlinchey. Polyhedron, **7**, 807 (1988).
31. R.A. Gates, M.F. D'Agostino, K.A. Sutin, M.J. McGlinchey, T.S. Janik, and M.R. Churchill. Organometallics, **8**, 20 (1990).
32. M.F. D'Agostino, C.S. Frampton, and M.J. McGlinchey. Organometallics, **10**, 1383 (1991).
33. (*a*) D.T. Clark, K.A. Sutin, and M.J. McGlinchey. Organometallics, **8**, 155 (1989); (*b*) B. Mailvaganam, R.E. Perrier, B.G. Sayer, B.E. McCarry, R.A. Bell, and M.J. McGlinchey. J. Organomet. Chem. **354**, 325 (1988).
34. (*a*) G. Jaouen, S. Top, and M.J. McGlinchey. J. Organomet. Chem. **195**, C5 (1980); (*b*) G. Jaouen, S. Top, B.G. Sayer, and M.J. McGlinchey. J. Am. Chem. Soc. **105**, 6426 (1983).
35. S. Top, G. Jaouen, and M.J. McGlinchey. J. Chem. Soc. Chem. Commun. 1110 (1980).
36. P.A. Downton, B.G. Sayer, and M.J. McGlinchey. Organometallics, **11**, 3281 (1992).
37. (*a*) R. Ruffolo, A. Decken, L. Girard, H.K. Gupta, M.A. Brook, and M.J. McGlinchey. Organometallics, **13**, 4328 (1994); (*b*) R. Ruffolo, M.A. Brook, and M.J. McGlinchey. Organometallics, **17**, 4992 (1998).
38. L. Girard, M.C. Baird, M.J. Chetcuti, and M.J. McGlinchey. J. Organomet. Chem. **478**, 179 (1994).
39. L. Girard, A. Decken, A. Blecking, and M.J. McGlinchey. J. Am. Chem. Soc. **116**, 6427 (1994).
40. (*a*) P.S. Skell, J.J. Havel, and M.J. McGlinchey. Acc. Chem. Res. **6**, 97 (1973); (*b*) P.S. Skell and M.J. McGlinchey. Angew. Chem. Int. Ed. Engl. **14**, 195 (1975).
41. (*a*) M.J. McGlinchey. Synthesis of organometallic compounds using metal atoms. *In* The chemistry of the metal-carbon bond. *Edited by* F.R. Hartley and S. Patai. John Wiley & Sons, New York. 1982. pp. 539–574; (*b*) P.L. Timms and T.W. Turney. Adv. Organomet. Chem. **15**, 53 (1977); (*c*) J.R. Blackborrow and D. Young. Metal vapor synthesis in organometallic chemistry. Springer–Verlag, Berlin. 1979.
42. N. Hao, J.F. Sawyer, B.G. Sayer, and M.J. McGlinchey. J. Am. Chem. Soc. **101**, 2203 (1979).
43. M.J. McGlinchey and T.-S. Tan. Inorg. Chem. **14**, 1209 (1975).
44. R. Faggiani, N. Hao, C.J.L. Lock, B.G. Sayer, and M.J. McGlinchey. Organometallics, **2**, 96 (1983).
45. (*a*) D.J. Cram and H.U. Daeniker. J. Am. Chem. Soc. **76**, 2743 (1954). (*b*) D.J. Cram and J.M. Cram. Acc. Chem. Res. **4**, 204 (1971), and refs. therein.
46. (*a*) A. Agarwal, J.A. Barnes, J.L. Fletcher, M.J. McGlinchey, and B.G. Sayer. Can. J. Chem. **55**, 2575 (1977); (*b*) J.L. Fletcher. Ph.D. thesis, McMaster University. 1977.
47. (*a*) C.S. Keller. Tetrahedron Lett. 2361 (1978); (*b*) C. Elschenbroich, B. Spangenberg, and H. Mellinghof. Chem. Ber. **117**, 3165 (1984); (*c*) N. Mori and M. Takamori. Magn. Reson. Chem. **24**, 151 (1986); (*d*) L.W. Jenneskens, W.H. deWolf, and F. Bickelhaupt. J. Organomet. Chem. **390**, 171 (1990); (*e*) R.H. Mitchell, P. Zhou, S. Venugopalan, and T.W. Dingle. J. Am. Chem. Soc. **112**, 7812 (1990); (*f*) A.Z. Kreindlin, V.S. Kaganovich, P.V. Petrovsky, and M.I. Rybinskaya. Russ. Chem. Bull. **42**, 1405 (1993).
48. D.V. Simion and T.S. Sorensen. J. Am. Chem. Soc. **118**, 7345 (1996).
49. P.v.R. Schleyer, B. Kiran, D.V. Simion, and T.S. Sorensen. J. Am. Chem. Soc. **122**, 510 (2000).
50. J.S. Waugh and R.W. Fessenden. J. Am. Chem. Soc. **79**, 846 (1957); **80**, 6697 (1958).
51. C.E. Johnson, Jr. and F.A. Bovey. J. Chem. Phys. **29**, 1012 (1958).
52. L. Ernst. Progr. Nucl. Mag. Res. Sp. **37**, 47 (2000).
53. M. Barfield, D.M. Grant, and D. Ikenberry. J. Am. Chem. Soc. **97**, 6956 (1975).
54. M.M. Maricq, J.S. Waugh, J.L. Fletcher, and M.J. McGlinchey. J. Am. Chem. Soc. **100**, 6902 (1978).
55. S. Kroeker, R.E. Wasylishen, and J.V. Hanna. J. Am. Chem. Soc. **121**, 1582 (1999), and refs. therein.
56. M.J. McGlinchey, P. Bougeard, B.G. Sayer, R. Hofer, and C.J.L. Lock. J. Chem. Soc. Chem. Commun. 789 (1984).
57. G. Hunter, D.J. Iverson, K. Mislow, and J.F. Blount. J. Am. Chem. Soc. **102**, 5942 (1980).
58. P.A. Downton, B. Mailvaganam, C.S. Frampton, B.G. Sayer, and M.J. McGlinchey. J. Am. Chem. Soc. **112**, 27 (1990).
59. B. Mailvaganam, C.S. Frampton, B.G. Sayer, S. Top, and M.J. McGlinchey. J. Am. Chem. Soc. **113**, 1177 (1991).
60. (*a*) K.V. Kilway and J.S. Siegel. J. Am. Chem. Soc. **113**, 2332 (1991); (*b*) K.V. Kilway and J.S. Siegel. J. Am. Chem. Soc. **114**, 255 (1992).
61. (*a*) M.J. McGlinchey. Adv. Organomet. Chem. **34**, 285 (1992); (*b*) J.R. Hamon, J.-Y. Saillard, A. LeBeuze, M.J. McGlinchey, and D. Astruc. J. Am. Chem. Soc. **104,** 7549 (1982); (*c*) J.F. Blount, G. Hunter, and K. Mislow. J. Chem. Soc. Chem. Commun. 170 (1984); (*d*) G. Hunter, J.F. Blount, J.R. Damewood, Jr., D.J. Iverson, and K. Mislow. Organometallics, **1**, 448 (1981); (*e*) D.J. Iverson, G. Hunter, J.F. Blount, J.R. Damewood, Jr., and K. Mislow. J. Am. Chem. Soc. **103**, 6073 (1981); (*f*) G. Hunter, J.R. Weakley, and W. Weissensteiner. J. Chem. Soc. Dalton Trans. 1545 (1987); (*g*) W.A. Hermann, W.R. Thiel, and E. Herdtweck. Polyhedron, **7**, 2027 (1988); (*h*) R.H. Dubois, M.J. Zaworotko, and P.S. White. J. Organomet. Chem. **362**, 155 (1989).
62. (*a*) L. Li, A. Decken, B.G. Sayer, M.J. McGlinchey, P. Bregaint, J.-R. Hamon, and C. Lapinte. Organometallics, **13**, 682 (1994); (*b*) B. Mailvaganam, B.G. Sayer, and M.J. McGlinchey. J. Organomet. Chem. **395**, 177 (1990).
63. (*a*) S. Brydges, J.F. Britten, L.C.F. Chao, H.K. Gupta, M.J. McGlinchey, and D.L. Pole. Chem. Eur. J. **4**, 1199 (1998); (*b*) H.K. Gupta, S. Brydges, and M.J. McGlinchey. Organometallics, **18**, 115 (1999).

© 2001 NRC Canada

64. H.K. Gupta, M. Stradiotto, D.W. Hughes, and M.J. McGlinchey. J. Org. Chem. **65**, 3652 (2000).
65. S. Top, G. Jaouen, A. Vessières, J.-P. Abjean, D. Davoust, C.A. Rodger, B.G. Sayer, and M.J. McGlinchey. Organometallics, **4**, 2143 (1985).
66. M. Savignac, G. Jaouen, C. A. Rodger, R.E. Perrier, B.G. Sayer, and M.J. McGlinchey. J. Org. Chem. **51**, 2328 (1986).
67. R.E. Perrier and M.J. McGlinchey. Can. J. Chem. **66**, 3003 (1988).
68. R.M. Moriarty, Y.-Y. Ku, U.S. Gill, R. Gilardi, R.E. Perrier, and M.J. McGlinchey. Organometallics, **8**, 960 (1989).
69. S. Top, M. Gunn, G. Jaouen, J. Vaissermann, J.-C. Daran, and M.J. McGlinchey. Organometallics, **11**, 1201 (1992).
70. R.E. Perrier, C.S. Frampton, and M.J. McGlinchey. J. Organomet. Chem. **435**, 357 (1992).
71. S. Tondu, G. Jaouen, M.F. D'Agostino, K.L. Malisza, and M.J. McGlinchey. Can. J. Chem. **70**, 1743 (1992).
72. G. Jaouen, S. Top, A. Vessières, B.G. Sayer, C.S. Frampton, and M.J. McGlinchey. Organometallics, **11**, 4061 (1992).
73. D. Osella, G. Dutto, G. Jaouen, A. Vessières, P.R. Raithby, L. De Benedetto, and M.J. McGlinchey. Organometallics, **12**, 4545 (1993).
74. S. Top, H. El Hafa, A. Vessières, J. Quivy, J. Vaissermann, D.W. Hughes, M.J. McGlinchey, J.-P. Mornon, E. Thoreau, and G. Jaouen. J. Am. Chem. Soc. **117**, 8372 (1995).
75. D. Osella, G. Dutto, C. Nervi, M.J. McGlinchey, A. Vessières, and G. Jaouen. J. Organomet. Chem. **533**, 97 (1997).
76. K.L. Malisza, S. Top, J. Vaissermann, B. Caro, M.-C. Sénéchal-Tocquer, D. Sénéchal, J.-Y. Saillard, S. Triki, S. Kahlal, J.F. Britten, M.J. McGlinchey, and G. Jaouen. Organometallics, **14**, 5273 (1995).
77. A. Gorfti, M. Salmain, G. Jaouen, M.J. McGlinchey, A. Bennouna, and A. Mousser. Organometallics, **15**, 142 (1996).
78. (*a*) G. Jaouen and A. Vessières. Pure Appl. Chem. **61**, 565 (1989); (*b*) G. Jaouen, A. Vessières, and I.S. Butler. Acc. Chem. Res. **26**, 361 (1993).
79. K.A. Sutin, J.W. Kolis, M. Mlekuz, P. Bougeard, B.G. Sayer, M.A. Quilliam, R. Faggiani, C.J.L. Lock, M.J. McGlinchey, and G. Jaouen. Organometallics, **6**, 439 (1987).
80. D.T. Clark, K.A. Sutin, R.E. Perrier, and M.J. McGlinchey. Polyhedron, **7**, 2297 (1988).
81. K.M. Nicholas. Acc. Chem. Res. **20**, 207 (1986).
82. A.J.M. Caffyn and K.M. Nicholas. *In* Comprehensive organometallic chemistry II. Vol 12. *Edited by* G. Wilkinson, F.G.A. Stone, and E.W. Abel. Pergamon Press, Oxford, U.K. 1995. Chap. 7.1. pp. 685–702.
83. H.C. Brown. The nonclassical ion problem. Plenum Press, New York. 1977.
84. M.F. D'Agostino, C.S. Frampton, and M.J. McGlinchey. Organometallics, **9**, 2972 (1990).
85. M.F. D'Agostino, C.S. Frampton, and M.J. McGlinchey. J. Organomet. Chem. **394**, 145 (1990).
86. M. Gruselle, H. El Hafa, M. Nikolski, G. Jaouen, J. Vaissermann, L. Li, and M.J. McGlinchey. Organometallics, **12**, 4917 (1993).
87. T. Laube. Angew. Chem. Int. Ed. Eng. **26**, 560 (1987).
88. M. Kondratenko, M. Gruselle, H. El Hafa, J. Vaissermann, G. Jaouen, and M.J. McGlinchey. J. Am. Chem. Soc. **117**, 6907 (1995).
89. M.J. McGlinchey, L. Girard, and R. Ruffolo. Coord. Chem. Rev. **143**, 331 (1995).
90. H. El Amouri and M. Gruselle. Chem. Rev. **96**, 1077 (1996).
91. J.A. Dunn, R. Ruffolo, S.S. Rigby, M.A. Brook, and M.J. McGlinchey. Organometallics, **18**, 3372 (1999).
92. L. Girard, P.E. Lock, H. El Amouri, and M.J. McGlinchey. J. Organomet. Chem. **478**, 189 (1994).
93. H.-B. Bürgi and J.D. Dunitz. Acc. Chem. Res. **16**, 153 (1983).
94. (*a*) A.N. Nesmeyanov, N.A. Ustynyuk, L.G. Makarova, S. Andre, Yu.A. Ustynyuk, L.N. Novikova, and Yu.N. Luzikov. J. Organomet. Chem. **154**, 45 (1978); (*b*) P.M. Treichel and J.W. Johnson. J. Organomet. Chem. **88**, 207 (1975); (*c*) C. White, J. Thompson, and P.M. Maitlis. J. Chem. Soc. Dalton Trans. 1654 (1977); (*d*) A. Salzer and C. Täschler. J. Organomet. Chem. **291**, 261 (1984); (*e*) D.T. Clark, M. Mlekuz, B.G. Sayer, B.E. McCarry, and M.J. McGlinchey. Organometallics, **6**, 2201 (1987).
95. (*a*) K.M. Nicholas, R.C. Kerber, and E.I Steifel. Inorg. Chem. **10**, 1519 (1971); (*b*) P.M. Treichel and J.W. Johnson. Inorg. Chem. **16**, (1977) 749; (*c*) P.M. Treichel and J.W. Johnson. J. Am. Chem. Soc. **99**, 1427 (1977); (*d*) P.M. Treichel, K.P. Fivizzani, and K.J. Haller, Organometallics, **1**, 931 (1982).
96. R.H. Crabtree. The organometallic chemistry of the transition metals. 2nd ed. John Wiley & Sons, New York. 1993. pp. 91 to 92, and refs. therein.
97. A. Decken, J. Britten, and M.J. McGlinchey. J. Am. Chem. Soc. **115**, 7275 (1993).
98. (*a*) A. Decken, S.S. Rigby, L. Girard, A.D. Bain, and M.J. McGlinchey. Organometallics, **16**, 1308 (1997); (*b*) M.J. McGlinchey, L. Girard, and A. Decken. *In* The synergy between dynamics and reactivity at clusters and surfaces. NATO ASI Series. Series C. Vol. 465. *Edited by* L.J. Farrugia. Kluwer Academic Publishers, Dordrecht, The Netherlands. 1995. pp. 203–216.
99. T.A. Albright, P. Hofmann, R. Hoffmann, C.P. Lillya, and P.A. Dobosh. J. Am. Chem. Soc. **105**, 3396 (1983).
100. R. Cramer. J. Am. Chem. Soc. **87**, 4717 (1965).
101. S.S. Rigby, M. Stradiotto, S. Brydges, D.L. Pole, S. Top, A.D. Bain, and M.J. McGlinchey. J. Org. Chem. **63**, 3735 (1998).
102. M.J. Bennett, F.A. Cotton, A. Davison, J.W. Faller, S.J. Lippard, and S.M. Morehouse. J. Am. Chem. Soc. **88**, 4371 (1966).
103. F.A. Cotton, A. Musco, and G. Yagupsky. J. Am. Chem. Soc. **89**, 6136 (1967).
104. (*a*) P.E. Rakita and A. Davison. Inorg. Chem. **8**, 1164 (1969); (*b*) P.E. Rakita and A. Davison. Inorg. Chem. **9**, 289 (1970); (*c*) A. Davison and P.E. Rakita. J. Organomet. Chem. **23**, 407 (1970); (*d*) R.B. Larrabee and B.F. Dowden. Tetrahedron Lett. 915 (1970); (*e*) A.J. Ashe, III. Tetrahedron Lett. 2105 (1970); (*f*) A.J. Ashe, III. J. Am. Chem. Soc. **92**, 2105 (1970).
105. A.D. McMaster and S. Stobart. J. Chem. Soc. Dalton Trans. 2275 (1982).
106. M. Stradiotto, D.W. Hughes, A.D. Bain, M.A. Brook, and M.J. McGlinchey. Organometallics, **16**, 5563 (1997).
107. M. Stradiotto, S.S. Rigby, D.W. Hughes, M.A. Brook, A.D. Bain, and M.J. McGlinchey. Organometallics, **15**, 5645 (1996).
108. R.L. Halterman. Chem. Rev. **92**, 965 (1992).
109. Y. Chen, M.D. Rausch, and J.C.W. Chien. Organometallics, **12**, 4607 (1993).
110. S. Rigby, L. Girard, A.D. Bain, and M.J. McGlinchey. Organometallics, **14**, 3798 (1995).
111. (*a*) S.S. Rigby, H.K. Gupta, N.H. Werstiuk, A.D. Bain, and M.J. McGlinchey. Polyhedron, **14**, 2787 (1995); (*b*) S.S. Rigby, H.K. Gupta, N.H. Werstiuk, A.D. Bain, and M.J. McGlinchey. Inorg. Chim. Acta, **251**, 355 (1996); (*c*) M. Stradiotto, M.A. Brook, and M.J. McGlinchey. Inorg. Chem. Commun. **1**, 105 (1998); (*d*) M. Stradiotto, M.A. Brook, and

© 2001 NRC Canada

M.J. McGlinchey. New J. Chem. **23**, 317 (1999); (*e*) M. Stradiotto, P. Hazendonk, A.D. Bain, M.A. Brook, and M.J. McGlinchey. Organometallics, **19**, 590 (2000); (*f*) M. Stradiotto, M.A. Brook, and M.J. McGlinchey. J. Chem. Soc. Perkin Trans. 2, 611 (2000); (*g*) M. Stradiotto and M.J. McGlinchey. Coord. Chem. Rev. in press (2001).

112. K.L. Malisza, L. Girard, D.W. Hughes, J.F. Britten, and M.J. McGlinchey. Organometallics, **14**, 4676 (1995).

© 2001 NRC Canada

An analysis of the hydration thermodynamics of the CONH group

Giuseppe Graziano

Abstract: The hydration thermodynamics of the CONH group play a fundamental role for the stability of the native conformation of globular proteins, but cannot be measured in a direct manner. The values of the thermodynamic functions have to be extracted from experimental measurements on model compounds using group additivity approaches. The estimates determined by Makhatadze and Privalov in the temperature range 5–100°C are used in the present study in view of their qualitative reliability. They are analyzed by means of a suitable approach that couples scaled particle theory calculations with the application of the modified Muller's model. It results that the negative entropy change is caused by the excluded volume effect for cavity creation, exaggerated in liquid water by the small size of water molecules themselves; the negative enthalpy change is determined by the H-bond energetics, formation of CONH–water H-bonds, and reorganization of water–water H-bonds. The negative heat capacity change, a striking feature of CONH hydration thermodynamics, is because the H-bonds in the hydration shell of the CONH group are less broken than those in bulk water in the temperature range examined.

Key words: peptide group, hydration, excluded volume effect, H-bonds, two-state model, negative heat capacity change.

Résumé : La thermodynamique de l'hydratation du groupe CONH joue un rôle fondamental dans la stabilité de la conformation de base des protéines globulaires, mais elle ne peut être mesurée directement. Les valeurs des fonctions thermodynamiques ont été extraites de mesures expérimentales sur des composés modèles en faisant appel à l'approche de l'additivité des groupes. Pour notre étude, compte tenu de leur fiabilité qualitative, on a utilisé les évaluations de Makhatadze et Privalov dans la plage de température allant de 5 à 100°C ans. On les a analysées à l'aide d'une approche appropriée qui met à profit des calculs de la théorie des particules graduées avec l'application du modèle modifié de Müller. On en déduit que: le changement négatif d'entropie est provoqué par l'effet de volume exclu pour la création de la cavité, exagéré dans l'eau liquide par la faible taille des molécules d'eau elles-mêmes; le changement négatif d'enthalpie est déterminé par les énergies impliquées dans les liaisons hydrogènes, la formation de liaisons hydrogènes CONH–eau et la réorganisation des liaisons hydrogènes eau–eau. Le changement négatif de capacité calorifique, une caractéristique importante dans la thermodynamique de l'hydratation du CONH, résulte du fait que, dans la plage de températures étudiée, les liaisons hydrogènes dans la couche d'hydratation du groupe CONH sont moins brisées que celles dans l'eau dans son ensemble.

Mots clés : groupe peptidique, hydratation, effet de volume exclu, liaisons hydrogènes, modèle à deux états, changement négatif de capacité calorifique.

[Traduit par la Rédaction]

Introduction

The structural organization of globular proteins is strongly influenced by the interactions of their constituent groups with water (1, 2). Consequently, it is important to gain a molecular level understanding of the hydration of proteins and their basic groups (3, 4). Among the latter, the CONH group is a fundamental unit and the hydration of this group is the focus of the present investigation. Very recently, the solvation thermodynamics of the peptide group has been investigated theoretically for its role in determining helix propensities (5). However, such approaches did not consider the temperature dependence of the thermodynamic functions, which is a central topic of the present study.

Following the Ben-Naim's analysis (6), hydration is defined as the transfer of a molecule from a fixed position in the ideal gas phase to a fixed position in water. The thermodynamics of this process do not include the effects due to the difference in the molar volume available to the solute molecule in the two phases (they are related to the translational degrees of freedom of the solute particle). Such effects are automatically excluded by using the molar concentration scale in the analysis of transfer experiments (6). Clearly, the Ben-Naim's definition of hydration accounts solely for the changes in thermodynamic functions due to the interactions of the solute molecule with water because there are no interactions in the ideal gas phase (i.e., what hydration is really about).

The optimum situation for a theoretical study would be to contrast the results of calculations against real experimental data. However, it is not possible to obtain real data for the

Received January 8, 2001. Published on the NRC Research Press Web site at http://canjchem.nrc.ca on August 14, 2001.

G. Graziano. Dipartimento di Chimica, Università di Napoli "Federico II", Complesso Universitario di Monte S.Angelo, Via Cinthia, 45 – 80126 Napoli, Italy and Facoltà di Scienze, Università del Sannio, Via Port'Arsa, 11 – 82100 Benevento, Italy (telephone: 39 081 674263; fax: 39 081 674199; e-mail: graziano@chemistry.unina.it and graziano@unisannio.it).

 DOI: 10.1139/cjc-79-9-1310 © 2001 NRC Canada

CONH group in a direct manner. The contribution of the CONH group to the changes in thermodynamic functions upon hydration has to be singled out by applying approaches based on the assumption of group additivity (7). Since this assumption is not strictly correct, especially when molecules contain polar groups (8), the estimates of the hydration thermodynamics for the CONH group existing in the literature have to be considered qualitatively correct, but not quantitatively exact. Notwithstanding, we would like to show that a suitable theoretical approach can rationalize well established and striking features of the CONH hydration thermodynamics.

In particular, the negative heat capacity change associated with the hydration of the CONH group completely contrasts with the positive values associated with the hydration of nonpolar moieties (9). The latter, as emphasized in previous works (10, 11), originate in the strong temperature dependence of H-bond reorganization among water molecules in the hydration shell. We would like to show that the difference in the sign of the heat capacity change is due to the physical characteristics of H-bond reorganization around the two chemically diverse classes of solutes. Specifically, the H-bonds in the hydration shell of nonpolar groups prove to be *more* broken than those in bulk water, whereas the H-bonds in the hydration shell of the CONH group are *less* broken than those in the bulk. Finally, the approach developed by Sharp and Madan (12–14) to calculate the hydration heat capacity change of both nonpolar and polar solutes is analyzed and contrasted against that devised in the present article.

Theory section

Adopting the standard state proposed by Ben-Naim (6), all the entropy change associated with solvation (i.e., gas to liquid transfer) is due to solvent reorganization since the solute molecule is in a fixed position, and its internal degrees of freedom are assumed to be unchanged on transfer (15). A liquid solvent, however, is a condensed phase in which each molecule occupies a finite volume. These simple and geometrical facts imply that insertion of a solute molecule gives rise to an excluded volume effect for the solvent molecules (10, 15). Since the molecular hard cores are impenetrable, solute insertion reduces the number of spatial configurations accessible to solvent molecules. This is a general effect common to all solvents. In response to volume exclusion, solvent molecules reorganize further providing another contribution to the entropy change (15). For water the latter contribution is clearly associated with a reorganization of H-bonds. Therefore, the hydration entropy change is given by:

$$[1] \qquad \Delta S^{\bullet} = \Delta S_x + \Delta S^h$$

where ΔS_x is the contribution due to the excluded volume effect and ΔS^h is the contribution attributable to the reorganization of H-bonds. Computer simulations have shown that the excluded volume effect is independent of the H-bonding potential when the density is fixed (16) and is essentially a geometric effect related to the size of solvent molecules. These findings support the validity of eq. [1]. Estimates for ΔS_x can be simply calculated from the Gibbs energy cost of cavity creation:

$$[2] \qquad \Delta S_x = -\Delta G_c/T$$

because ΔG_c is exactly related to the excluded volume effect and is a measure of the probability that the region of space, which a solute molecule would exclude to solvent molecules, is observed to have no solvent occupants when the solute is absent (17). On the other hand, ΔS^h can be evaluated in a hybrid manner by the difference $\Delta S^{\bullet} - \Delta S_x$.

The hydration enthalpy change of nonpolar compounds is given by the sum of two terms: the solute–water van der Waals interaction energy and the enthalpy contribution due to H-bond reorganization among water molecules in the hydration shell (9, 15). However, for the hydration of the CONH group, in view of its H-bonding capability, a correct separation of the solute–water interactions from the water–water ones is practically impossible. As a consequence, we do not try to separate anything and assume that the hydration enthalpy change is entirely due to H-bond contributions:

$$[3] \qquad \Delta H^{\bullet} = \Delta H^h$$

where ΔH^h takes into account both the formation of H-bonds between the CONH group and water molecules and the reorganization of H-bonds among the water molecules in the hydration shell (i.e., the van der Waals contribution is absorbed into the H-bonding energetics). Adopting this definition for ΔH^h, it is not possible to link ΔH^h and ΔS^h by means of the enthalpy–entropy compensation relationship (18), because they refer to different processes.

By combining eqs. [1] and [3], the hydration Gibbs energy change is:

$$[4] \qquad \Delta G^{\bullet} = \Delta H^h - T(\Delta S_x + \Delta S^h)$$

It is the sum of three contributions (*i*) the negative entropy change due to the excluded volume effect for cavity creation; (*ii*) the negative enthalpy change due to H-bond contributions, formation of CONH–water H-bonds, and reorganization of water–water H-bonds; and (*iii*) the entropy change due to water–water H-bond reorganization.

Finally, on the basis of eq. [3], the hydration heat capacity change is:

$$[5] \qquad \Delta C_p^{\bullet} = (\partial \Delta H^h/\partial T) = \Delta C_p^h$$

It arises from the temperature dependence of H-bond energetic contributions in the hydration shell of the CONH group.

The purpose of the present work is to analyze with such an approach the hydration of the CONH group over the temperature range 5–100°C. It will be shown that the H-bond energetics can be reproduced quite well by means of the modified Muller's model (15), which is briefly outlined below.

Modified Muller's model

Muller devised a model to calculate the contributions to hydration thermodynamics of nonpolar solutes arising from H-bond reorganization (19). By extending an earlier model developed by Angell (20), he considered that water molecules, in the bulk as well as in the hydration shell, exist in equilibrium between two H-bonding states. The lower state can be viewed as an intact H-bond, and the upper state as a

© 2001 NRC Canada

broken H-bond. The model has been modified by Lee and Graziano (15) to take into account the possibility that both the lower and upper states change passing from the bulk to the hydration shell. Accordingly, the H-bond contributions to the hydration heat capacity, enthalpy and entropy changes are given by:

$$[6] \quad \Delta C_p^h = (n^h/RT^2)[(\Delta H_{hs}^\circ)^2 f_{hs}(1 - f_{hs}) - (\Delta H_b^\circ)^2 f_b(1 - f_b)]$$

$$[7] \quad \Delta H^h = n^h[\Delta H_U - (1 - f_{hs})\Delta H_{hs}^\circ + (1 - f_b)\Delta H_b^\circ]$$

$$[8] \quad \Delta S^h = n^h[\Delta S_U - (1 - f_{hs})\Delta S_{hs}^\circ + (1 - f_b)\Delta S_b^\circ - R\Delta F]$$

where f_{hs} and f_b represent the fraction of broken H-bonds in the hydration shell and in the bulk, respectively; and in eq. [8], $\Delta F = F_{hs} - F_b$, with $F_b = f_b \ln f_b + (1 - f_b) \ln (1 - f_b)$, and F_{hs} similarly defined for the hydration shell: these are the "mixing" entropies characteristic of all the mixture models (21).

These equations contain seven parameters: ΔH_b° and ΔS_b° are the differences in enthalpy and entropy, respectively, between the two states in the bulk; ΔH_{hs}° and ΔS_{hs}° have the same meaning for the hydration shell; n^h is the number of H-bonds in the hydration shell; ΔH_U and ΔS_U are the differences in enthalpy and entropy, respectively, between the upper states in the hydration shell and those in the bulk. All these parameters are assumed to be temperature independent.

It must noted that, even though liquid water is known to have a continuum of energy levels, experimental evidence for the existence of two H-bonding states came from spectroscopic measurements, showing isobestic points in both IR and Raman spectra as a function of temperature (22). Recently, Hayward and Haymet (23), by performing molecular dynamics simulations on a realistic central force water model, have shown that the distribution of pairwise H-bond energies is a bimodal function (i.e., the total interaction energy between neighboring water pairs minus the van der Waals contribution). The strict geometric requirements for H-bond formation imply the existence of two distinguishable molecular distributions, not single configurations, that may be labeled intact and broken H-bonds. In addition, the physical reliability of the modified Muller's model has been validated by Dill and co-workers (24) using Monte Carlo simulations and the Mercedes-Benz model for water.

Clearly, the parameter values have to be determined in a robust manner to use the model (also see the *Appendix* section). By using the difference in heat capacity between liquid water and steam, and Pauling's estimate that $f_b = 0.15$ at 0°C (25), Muller calculated $\Delta H_b^\circ = 9.8$ kJ mol^{-1} and $\Delta S_b^\circ = 21.6$ J K^{-1} mol^{-1} (19). These estimates are close to those determined by Walrafen et al. (26), analyzing Raman spectra of liquid water in a large temperature range. This implies that the f_b values are reliable, since $f_b = K_b/(1 + K_b)$, where $K_b = \exp[-(\Delta H_b^\circ/RT) + (\Delta S_b^\circ/R)]$ is the thermodynamic constant governing the rupture equilibrium of H-bonds in the bulk. Therefore, two such parameter estimates are retained in the present work.

To evaluate n^h, we assume that each of the water molecules in the hydration shell of the CONH group is involved, on the average, in two H-bonds belonging to the hydration shell. Thus, $n^h = 2N_{H_2O}$, where N_{H_2O} is the number of water molecules in the hydration shell. This assumption differs from that used for nonpolar compounds by Muller ($n^h = (3/2)N_{H_2O}$) (19), but it is dictated by the need to also take into account the H-bonds formed by the CONH group with water molecules, because we have considered $\Delta H^\bullet = \Delta H^h$. This is the fundamental point to apply the modified Muller's model to a polar group that forms H-bonds with water molecules. The value of N_{H_2O} for the CONH group is estimated from the results of a Monte Carlo study of *N*-methylacetamide (NMA) in TIP4P water (27). Jorgensen and Swenson (27) found that there are 21 water molecules in the first hydration shell of NMA: 18 surround the two methyl groups and 3 are H-bonded to the CONH group (i.e., 2 at the carbonyl oxygen and 1 at the hydrogen on nitrogen). The latter number is reliable in view of the electronic structure of the peptide group, and therefore, $N_{H_2O} = 3$ for the CONH group.

The four remaining parameters cannot be fixed a priori, but are related to each other by eqs. [6]–[8]. Therefore, the model is under determined and a set of models are generated, each corresponding to a specific value of one selected parameter. The independent parameter selected is ΔH_U, and the other three parameters, namely ΔH_{hs}°, ΔS_{hs}°, and ΔS_U, are calculated using the values of ΔC_p^h, ΔH^h, and ΔS^h at 25°C in eqs. [6]–[8], as outlined in detail in ref. 15. The only difference with respect to the treatment in ref. 15 is that the compensation relation $\Delta H^h = T\Delta S^h$ is not considered at all in the present calculations. It should also be noted that, according to the devised procedure, the value of ΔS^h serves only to estimate ΔS_U, because, for each selected ΔH_U, ΔH_{hs}° and ΔS_{hs}° are determined from the values of ΔC_p^h and ΔH^h at 25°C.

When all the seven parameters are known, eqs. [6]–[8] allow the calculation of ΔC_p^h, ΔH^h, and ΔS^h at any temperature. The physical reliability of the different models is tested by comparing the ΔC_p^h values calculated with those of $\Delta C_p^\bullet$ over the whole temperature range. We use this procedure because the heat capacity change proves to be the more sensitive probe of the H-bonding situation in the hydration shell.

Scaled particle theory calculations

The Gibbs energy cost of cavity creation in water is calculated as a function of temperature by means of the following equation from scaled particle theory (SPT) (28, 29):

$$[9] \quad \Delta G_c = RT[K_0 + K_1(\sigma_2/\sigma_1) + K_2(\sigma_2/\sigma_1)^2 + K_3(\sigma_2/\sigma_1)^3]$$

where $K_0 = -\ln (1 - \xi)$, $K_1 = u = 3\xi/(1 - \xi)$, $K_2 = u(u + 2)/2$, $K_3 = \xi P v_1/RT$. In these relations R is the gas constant, ξ is the volume packing density of pure solvent, which is defined as the ratio of the physical volume of a mol of solvent molecules over the molar volume of the solvent, v_1 (i.e., $\xi = \pi\sigma_1^3 N_{av}/6v_1$), σ_1 and σ_2 are the hard-sphere diameters of the solvent and solute molecules, respectively, and P is the pressure.

© 2001 NRC Canada

Table 1. Thermodynamic data for the hydration process of the CONH group referred to the Ben-Naim standard state; they come from the last rows of Table IV in ref. 4, in which they were normalized per square angstrom of ASA of the peptide group.

T (°C)	$\Delta C_p^\bullet$ (J K^{-1} mol^{-1})	$\Delta H^\bullet$ (kJ mol^{-1})	$\Delta S^\bullet$ (J K^{-1} mol^{-1})	$\Delta G^\bullet$ (kJ mol^{-1})
5	–72.8	–58.2	–31.2	–49.5
25	–63.4	–59.6	–35.9	–48.9
50	–54.6	–61.1	–40.7	–48.0
75	–53.6	–62.5	–44.7	–46.9
100	–52.2	–63.8	–48.4	–45.8

Concerns about the treatment of pressure in SPT calculations have been raised by various authors (30, 31). Pierotti (29) pointed out that, contrary to most comments in the literature, SPT, as applied to real solutions, does not refer specifically to hard-sphere fluids, but to fluids whose density and pressure are determined by the actual intermolecular potential and whose molecules have "effective" spherical hard cores. This implies that the experimental value of P rather than the theoretical value of the hard-sphere fluid should be preferred in SPT calculations. We adopt this view and consider P = 1 atm (1 atm = 101.325 kPa), the hydrostatic pressure over liquid water, in all calculations.

It is well known that the results of SPT calculations depend strongly upon the values selected for σ_1 and σ_2 (31, 32). For this reason great care is needed to select the hard-sphere diameters by resorting to all relevant and reliable experimental data. For water, we use σ = 2.75 and 2.80 Å, both of which are close to the distance between two H-bonded water molecules, as revealed by the location of the first peak in the oxygen–oxygen radial distribution function of liquid water (33–35). Clearly, there is uncertainty in the size to be assigned to the CONH group, which is not a sphere. The physical or van der Waals volume of the CONH group, obtained by considering a system of interlocking spheres with radii equal to the van der Waals radii of the involved atoms, amounts to 18–20 cm^3 mol^{-1} (36), which would correspond to a sphere with a diameter of 3.8–4.0 Å. On the other hand, the analysis of experimental measurements in terms of group additivity has led to the following estimates for the partial molar volume of the CONH group at 25°C in water: 20 (37), 19.3 (38), 22.3 (8), 20.6 (39), and 19.8 (40) cm^3 mol^{-1}. As a consequence, we select two different values for the hard-sphere diameter of the CONH group, σ = 3.5 and 4.0 Å, which should span the right size range of the peptide group. In this regard, it should be noted that the hard-sphere diameter of ethylene, which is structurally similar to the peptide group, amounts to 4.07 Å (41).

In performing calculations, the hard-sphere diameters of water and CONH group are considered temperature independent. The temperature dependence of ΔG_c, apart from the RT factor, originates from that of the experimental water density, which is accurately known in a wide temperature range (42).

Experimental data

Makhatadze and Privalov (3, 4), by analyzing the hydration thermodynamics of small model compounds using the molar concentration scale and the group additivity principle, determined $\Delta H^\bullet$ = –(59.6 ± 1.3) kJ mol^{-1}, $\Delta G^\bullet$ = –(48.9 ± 2.5) kJ mol^{-1}, and $\Delta S^\bullet$ = –(35.9 ± 9.4) J K^{-1} mol^{-1} at 25°C for the CONH group. Such estimates for the hydration thermodynamics of the peptide group appear reliable. Indeed, Cabani et al. (8), in their outstanding analysis of hydration thermodynamic functions in terms of group additivity, determined $\Delta H^\bullet$ = –59.9 kJ mol^{-1} at 25°C, and using their hydration Gibbs energy data for the components of the CONH group, one obtains $\Delta G^\bullet$ = –48.7 kJ mol^{-1} at 25°C. Furthermore, for the peptide group, Wadso and co-workers (43) obtained $\Delta H^\bullet$ = –(58 ± 4) kJ mol^{-1}, and the vapor pressure data on NMA of Wolfenden (44), corrected for the contribution of the two methyl groups, gave $\Delta G^\bullet$ = –49.8 kJ mol^{-1}, always at 25°C.

However, to obtain a complete characterization of the hydration process, the temperature dependence of the thermodynamic functions $\Delta H^\bullet$, $\Delta S^\bullet$, and $\Delta G^\bullet$ has to be known. This is readily obtained by determining $\Delta C_p^\bullet$ in a large temperature range. Makhatadze and Privalov (45) measured, by means of differential scanning calorimetry (DSC), the partial molar heat capacity of triglycine, tetraglycine, and pentaglycine, then, by subtracting the heat capacity of the molecule in the gas phase, they obtained the hydration heat capacity changes in a large temperature range. Moreover, Makhatadze and Privalov (3, 45) dissected such values by means of a group additivity approach to single out the $\Delta C_p^\bullet$ contribution of the CONH group; such values are listed in the second column of Table 1. They obtained that $\Delta C_p^\bullet$ is negative and decreases in magnitude in the range 5–100°C; in particular, it amounts to –63.4 J K^{-1} mol^{-1} at 25°C. In this respect, Cabani et al. (8) determined $\Delta C_p^\bullet$ = –89.7 J K^{-1} mol^{-1} for the CONH group at 25°C, while the recent measurements of the partial molar heat capacities of several tripeptides by Hedwig and co-workers (46) should lead to a value of about –70 J K^{-1} mol^{-1} at room temperature. In addition, the CONH contribution to the heat capacity change associated with the dissolution into water of solid cyclic dipeptides and with the transfer of liquid *N*-alkylamides to water was found to be –(60 ± 6) (47) and –(65 ± 5) J K^{-1} mol^{-1} (48), respectively, at 25°C.

Makhatadze and Privalov (3, 4) used their $\Delta C_p^\bullet$ estimates to calculate $\Delta H^\bullet$, $\Delta S^\bullet$, and $\Delta G^\bullet$ in the range 5–100°C, starting from the values at 25°C. These data are collected in Table 1 and are analyzed using the approach devised above to try to reach a molecular level understanding of the hydration thermodynamics of the CONH group.

Results

The values of ΔG_c for the CONH group, calculated by means of SPT at the different temperatures, and the corre-

© 2001 NRC Canada

Table 2. Gibbs energy cost of cavity creation and entropy contributions as a result of the excluded volume effect and the reorganization of H-bonds associated with the hydration of the peptide group.

	T (°C)	ξ	ΔG_c (kJ mol^{-1})	ΔS_x (J K^{-1} mol^{-1})	ΔS^h (J K^{-1} mol^{-1})
σ_{H_2O} = 2.75 Å	5	0.364	18.1	–65.1	33.9
σ_{CONH} = 3.5 Å	25	0.363	19.2	–64.4	28.5
	50	0.360	20.5	–63.4	22.7
	75	0.355	21.5	–61.8	17.1
	100	0.349	22.3	–59.8	11.4
σ_{H_2O} = 2.75 Å	5	0.364	22.4	–80.5	49.3
σ_{CONH} = 4.0 Å	25	0.363	23.9	–80.2	44.3
	50	0.360	25.5	–78.9	38.2
	75	0.355	26.7	–76.7	32.0
	100	0.349	27.6	–74.0	25.6
σ_{H_2O} = 2.80 Å	5	0.384	19.6	–70.5	39.3
σ_{CONH} = 3.5 Å	25	0.383	20.9	–70.1	34.2
	50	0.380	22.3	–69.0	28.3
	75	0.375	23.3	–66.9	22.2
	100	0.368	24.1	–64.6	16.2
σ_{H_2O} = 2.80 Å	5	0.384	24.4	–87.7	56.5
σ_{CONH} = 4.0 Å	25	0.383	26.0	–87.2	51.3
	50	0.380	27.7	–85.7	45.0
	75	0.375	29.0	–83.3	38.6
	100	0.368	29.9	–80.1	31.7

Note: ΔG_c is estimated by means of SPT; ΔS_x is calculated as $\Delta S_x = -\Delta G_c/T$ and ΔS^h is calculated as $\Delta S^h = \Delta S^\bullet - \Delta S_x$.

sponding values of ΔS_x, obtained according to eq. [2], are listed in the third and fourth columns of Table 2. The work of cavity creation proves to be large and positive and increases with temperature, as already pointed out and discussed (10, 11). The values of ΔS_x are negative, little dependent on temperature, and larger than those of $\Delta S^\bullet$ in the whole range 5–100°C, regardless of the σ values used for water and the peptide group. The excluded volume effect is responsible for the negative hydration entropy of the CONH group. This finding is in line with the analysis of the hydration thermodynamics of noble gases, aliphatic and aromatic hydrocarbons, and aliphatic alcohols (11, 15, 49). The excluded volume effect is so large in water because it is exaggerated by the small size of water molecules themselves (10, 16). This is the physical origin of the fact that the hydration entropy change, at room temperature, is always negative regardless of the chemical nature of the group considered, polar or nonpolar. Indeed, Cabani et al. (8) suggested that the entropy does not appear to be the proper function to distinguish the hydration of polar from nonpolar groups.

Having determined ΔS_x in the 5–100°C temperature range, we can obtain estimates for ΔS^h by means of eq. [1]; the values are listed in the fifth column of Table 2. They are positive and decrease on raising temperature, regardless of the σ values used for water and the peptide group. The reorganization of H-bonds causes an increase in entropy, probably related to an increase in the configurational disorder of water molecules.

The situation for the hydration enthalpy change can be highlighted as follows. Jorgensen and Swenson (27) determined that the energetic interactions of NMA in TIP4P water, at room temperature, amount to –116 kJ mol^{-1}. By correcting for the contribution of the two methyl groups (50), one would obtain that the energetic interactions of the CONH group with water amount to –96 kJ mol^{-1}. This estimate is significantly larger than the $\Delta H^\bullet$ value at 25°C (–59.6 kJ mol^{-1}), because it does not take into account the enthalpy contribution due to the reorganization of water molecules upon CONH insertion. To make H-bonds with the CONH group, water molecules have to reorient, decreasing the net number of or the strength of some of the water–water H-bonds. The point is that there is no clear-cut way to separate the CONH–water contribution from the water–water contribution to $\Delta H^\bullet$. For this reason we assume in eq. [3] that all of $\Delta H^\bullet$ is due to H-bond reorganization.

We can now proceed in the application of the modified Muller's model. By fixing $n^h = 6$ and ΔH_U in the range –10–0 kJ mol^{-1}, and using $\Delta C_p^h = \Delta C_p^\bullet = -63.4$ J K^{-1} mol^{-1}, $\Delta H^h = \Delta H^\bullet = -59.6$ kJ mol^{-1}, and $\Delta S^h = \Delta S^\bullet - \Delta S_x = 44.3$ J K^{-1} mol^{-1} at 25°C, we have calculated the parameters ΔH_{hs}°, ΔS_{hs}°, and ΔS_U. They are collected in Table 3 (we recall that the choice of the ΔS^h value at 25°C is not really important because it only affects ΔS_U). Then, the values of f_{hs} and ΔC_p^h in the range 5–100°C have been computed for each choice of ΔH_U. The f_{hs} estimates are listed in Table 4 together with those of f_b, whereas the ΔC_p^h estimates are listed in Table 5 together with the $\Delta C_p^\bullet$ values.

To select the modified Muller's model closer to reality, we have compared the calculated ΔC_p^h functions with the $\Delta C_p^\bullet$ data. The comparison indicates that none of the models exactly reproduces the temperature dependence of $\Delta C_p^\bullet$; this is

© 2001 NRC Canada

Table 3. Parameter values of the modified Muller's model for the peptide group CONH calculated as a function of ΔH_U, by assuming for bulk water the parameter values determined by Muller himself (19), $n^h = 2$ $N_{H_2O} = 6$, and at 25°C, $\Delta C_p^h = \Delta C_p^\bullet = -63.4$ J K^{-1} mol^{-1}, $\Delta H^h = \Delta H^\bullet = -59.6$ kJ mol^{-1} and $\Delta S^h = \Delta S^\bullet - \Delta S_x = 44.3$ J K^{-1} mol^{-1}.

ΔH_U (kJ mol^{-1})	f_{hs} at 25°C (%)	ΔH°_{hs} (kJ mol^{-1})	ΔS°_{hs} (J K^{-1} mol^{-1})	ΔS_U (J K^{-1} mol^{-1})
0	2.4	18.2	30.3	23.0
–2.0	3.1	16.2	25.7	18.2
–4.0	4.0	14.3	21.5	13.7
–6.0	5.4	12.4	17.8	9.5
–8.0	7.7	10.5	14.6	5.7
–10.0	11.6	8.7	12.4	2.4

Table 4. Percentage values of f_{hs}, the fraction of broken H-bonds in the hydration shell, for different ΔH_U choices; $f_{hs}[-10]$ means the values of f_{hs} for $\Delta H_U = -10.0$ kJ mol^{-1}.

T (°C)	f_b	$f_{hs}[-10]$	$f_{hs}[-8]$	$f_{hs}[-6]$	$f_{hs}[-4]$	$f_{hs}[-2]$	$f_{hs}[0]$
5	16.3	9.3	5.8	3.9	2.7	2.0	1.5
25	20.5	11.6	7.7	5.4	4.0	3.1	2.4
50	25.9	14.7	10.3	7.8	6.1	5.0	4.2
75	31.3	17.9	13.2	10.5	8.7	7.5	6.7
100	36.3	21.1	16.3	13.5	11.7	10.6	9.8

Note: The percentage values of f_b, the fraction of broken H-bonds in the bulk, are reported for comparison purposes.

Table 5. Estimates of ΔC_p^h for different ΔH_U choices; $\Delta C_p^h[-10]$ means the values of ΔC_p^h for $\Delta H_U = -10.0$ kJ mol^{-1}.

T (°C)	$\Delta C_p^\bullet$	$\Delta C_p^h[-10]$	$\Delta C_p^h[-8]$	$\Delta C_p^h[-6]$	$\Delta C_p^h[-4]$	$\Delta C_p^h[-2]$	$\Delta C_p^h[0]$
5	–72.8	–61.7	–65.3	–68.0	–71.6	–74.3	–76.8
25	–63.4	–63.4	–63.4	–63.4	–63.4	–63.4	–63.4
50	–54.6	–61.2	–56.5	–51.6	–46.5	–41.1	–35.4
75	–53.6	–56.1	–47.0	–37.2	–26.2	–14.1	–0.5
100	–52.2	–49.3	–36.7	–22.3	–5.6	13.8	36.3

Note: The values of $\Delta C_p^\bullet$ are reported for comparison purposes. All the heat capacity values are in J K^{-1} mol^{-1}.

obviously related to the simplicity of the modified Muller's model. A satisfactory agreement, however, occurs for $\Delta H_U = -8.0$ kJ mol^{-1}; ΔC_p^h shows a monotonous decrease in magnitude as a function of temperature similar to that of $\Delta C_p^\bullet$, even though the steepness becomes too large beyond 75°C. Adopting the choice $\Delta H_U = -8.0$ kJ mol^{-1}, the two-state equilibrium of H-bonds in the hydration shell of the CONH group is characterized by $\Delta H^\circ_{hs} = 10.5$ kJ mol^{-1}, $\Delta S^\circ_{hs} = 14.6$ J K^{-1} mol^{-1}, and $\Delta S_U = 5.7$ J K^{-1} mol^{-1}, so that $f_{hs} = 0.077$ at 25°C. In contrast, the two-state equilibrium of H-bonds in the bulk is characterized by $\Delta H^\circ_b = 9.8$ kJ mol^{-1} and $\Delta S^\circ_b = 21.6$ J K^{-1} mol^{-1} so that $f_b = 0.205$ at 25°C. Therefore, as emphasized by the values reported in Table 4, the H-bonds in the hydration shell of the CONH group appear to be less broken than those in the bulk (remember that the hydration shell H-bonds are both the CONH–water and water–water H-bonds).

This happens because they are enthalpically stronger, $\Delta H^\circ_{hs} > \Delta H^\circ_b$, and their rupture causes a smaller entropy gain, $\Delta S^\circ_{hs} < \Delta S^\circ_b$ (i.e., it is expected for the large negative charge density on the carbonyl group and the positive charge density on the nitrogen atom). Furthermore, the hydration shell of the CONH group corresponds to a potential energy well of –8.0 kJ per mol of H-bond, accounting for the strong energetic interactions of the peptide group with water molecules. The entropy change plays a pivotal role in the two-state equilibrium, but it is difficult to attach a clear physical meaning to quantities like ΔS°_{hs} and ΔS°_b. In general, they should be a measure of the broken state degeneracy. As a consequence, the finding $\Delta S^\circ_{hs} < \Delta S^\circ_b$ can be explained by saying that the broken state of H-bonds has a lower degeneracy in the deep energy well around the CONH group than in bulk water (i.e., the strong energetic interactions not involved in the two-state equilibrium restrict the orientations available to interacting partners). Finally, the functions ΔH^h and $\Delta S_x + \Delta S^h$ calculated with the modified Muller's model characterized by $\Delta H_U = -8.0$ kJ mol^{-1} agree well with the values of $\Delta H^\bullet$ and $\Delta S^\bullet$ in the range 5–100°C (results not shown).

Discussion

Edsall (51) was the first, in 1935, to point out that $\Delta C_p^\bullet$ is large and positive for the hydration of nonpolar compounds, but negative for the hydration of polar ones. The microscopic determinants of this difference, however, have not been definitely assessed. A simple two-state model, such as that proposed by Gill et al. (52) to calculate $\Delta C_p^\bullet$ for nonpolar compounds, cannot produce negative values (i.e., consider that only one of the two terms in the square brack-

© 2001 NRC Canada

ets of eq. [6] would be present). Muller's model, however, can produce both positive and negative values of the heat capacity change by distinguishing the two-state equilibrium in the hydration shell from that in the bulk (19). In fact, eq. [6] shows that negative values of ΔC_p^h could arise in two limiting ways (*i*) if $f_{hs} = f_b$, which would require $\Delta H_{hs}^\circ < \Delta H_b^\circ$; or (*ii*) if $\Delta H_{hs}^\circ = \Delta H_b^\circ$, which would require $f_{hs} < f_b$. Actually, our calculations indicate that negative values of ΔC_p^h, with a temperature dependence similar to that of $\Delta C_p^\bullet$, are obtained with $\Delta H_{hs}^\circ > \Delta H_b^\circ$ and $f_{hs} << f_b$ (i.e., $\Delta S_{hs}^\circ < \Delta S_b^\circ$). In other words, the physical origin of the negative heat capacity change is in the fact that the H-bonds in the hydration shell of the CONH group are more intact than those in the bulk, over the whole temperature range of 5–100°C. This scenario is entirely different from that existing in the hydration shell of nonpolar compounds (10, 11, 15), where the H-bonds are always more broken than those in the bulk, leading to large positive ΔC_p^h values that decrease in a continuous manner with temperature. Therefore, the application of the modified Muller's model leads to the conclusion that (*i*) in the hydration shell of nonpolar solutes, $\Delta H_{hs}^\circ > \Delta H_b^\circ$ and $\Delta S_{hs}^\circ > \Delta S_b^\circ$ so that $f_{hs} > f_b$; (*ii*) in the hydration shell of the peptide group, $\Delta H_{hs}^\circ > \Delta H_b^\circ$ and $\Delta S_{hs}^\circ < \Delta S_b^\circ$ so that $f_{hs} << f_b$.

These results are a reflection of the different structural organization of water around the CONH group and nonpolar moieties. Monte Carlo simulations of NMA in water (27) showed that the carbonyl oxygen – water oxygen radial distribution function has a sharp peak at 3 Å with a small area, characteristic of the geometric restrictions proper of H-bonds; whereas the methyl – water oxygen radial distribution function has a broad peak centered near 4 Å with a large area, reflecting the existence of a disordered clathrate cage of water molecules around nonpolar groups.

Recently, Makhatadze et al. (53) pointed out that the temperature dependence of $\Delta C_p^\bullet$ for the CONH group depends on the model compounds from which it is singled out. Specifically, $\Delta C_p^\bullet$ would be always negative in the range 5–100°C, but it would increase with temperature more rapidly than the data reported in the second column of Table 1. In this regard, it should be noted that the modified Muller's models characterized by $\Delta H_U = -6.0$ or -4.0 kJ mol^{-1} give rise to a more pronounced temperature dependence of ΔC_p^h. Because these two models are characterized by $\Delta H_{hs}^\circ > \Delta H_b^\circ$ and $f_{hs} << f_b$ (see Tables 3–5), the emerging picture of the hydration shell does not qualitatively change, confirming that the H-bonds are substantially more intact than in the bulk.

An intriguing feature of the hydration thermodynamics of the CONH group is the following: $\Delta H^\bullet$ becomes more negative on increasing temperature because $\Delta C_p^\bullet$ is always negative. In other words, the CONH hydration is more exothermic at 100°C than at 25°C, even though the difference is small, amounting to only 4.2 kJ mol^{-1}. This finding is counterintuitive and difficult to grasp, but a better understanding can be reached. Since $\Delta H^\bullet = \Delta H^h$, we analyzed eq. [7] when $\Delta H_U = -8.0$ kJ mol^{-1}. A large contribution to ΔH^h comes from ΔH_U because, when multiplied times $n^h = 6$, it provides –48.0 kJ mol^{-1} at all temperatures. Passing to the other two terms, it emerges that $(1 - f_{hs})\Delta H_{hs}^\circ$ is larger in magnitude than $(1 - f_b)\Delta H_b^\circ$ over the whole temperature range: 9.7 kJ mol^{-1} vs. 7.8 kJ mol^{-1} at 25°C, and 8.8 kJ mol^{-1} vs. 6.2 kJ mol^{-1} at 100°C. Therefore according to eq. [7], the balance between the rupture of H-bonds in the bulk and the formation of H-bonds in the hydration shell is always exothermic; but it is slightly more exothermic at 100°C than at 25°C because f_{hs} increases with temperature less rapidly than f_b (i.e., $f_{hs} = 0.077$ at 25°C and 0.163 at 100°C, whereas $f_b = 0.205$ at 25°C and 0.363 at 100°C, see Table 4). This seems to be a clear and reliable explanation of the strange temperature dependence of $\Delta H^\bullet$.

A final point deserves attention. The value $N_{H_2O} = 3$ selected to perform the calculations with the modified Muller's model for the CONH group is different from the estimate that is obtained from the ratio of cavity surface areas (i.e., $N_{H_2O} \approx 6$). This is an important topic. For polar groups it is not correct to consider linear relationships of the hydration thermodynamic functions vs. the accessible surface area (ASA) (54), because the number of H-bonded water molecules does not depend on ASA, but on the chemical nature and charge density of the polar group itself (55). The breakdown of linear relationships between thermodynamic functions and ASA for the hydration of polar compounds has carefully been pointed out by Karplus and co-workers (56). Also this feature can be accounted for by our treatment, as demonstrated by the reliability of the functions calculated.

Relationship with the approach by Sharp and Madan

Sharp and Madan developed an interesting approach to calculate the hydration heat capacity change for charged, nonpolar, and polar solutes, by a combination of the random network model (RNM) of water and Monte Carlo simulations (12–14).

The random network model developed by Sceats and Rice (57), is based on the idea that liquid water retains much of the tetrahedral H-bonding network of ice, even with a randomly distorted connectivity. The fundamental assumption of RNM is that all H-bonds in liquid water are intact but they may be stretched and bent to an extent that depends on temperature and pressure. The existence of broken H-bonds in liquid water is not explicitly recognized. The basic elements of RNM are the following three structural parameters: (*i*) the mean H-bond length (*d*) corresponding practically to the position of the first peak in the oxygen–oxygen radial distribution function of water; (*ii*) the standard deviation in H-bond length (*s*); (*iii*) the root-mean-square value of the H-bond angle θ, which is defined as the smallest O···O-H angle formed by two neighboring water molecules.

Henn and Kauzmann (58) extended the RNM and provided an accurate function for the Helmholtz free energy of pure liquid water from which the thermodynamic properties were derived over a wide temperature range. Sharp and Madan used such a function to obtain explicit expressions for the heat capacity in terms of the H-bond structural parameters, with contributions mainly from H-bond stretching and bending (12–14). By setting d_0, s_0, and θ_0 as the average H-bond structural parameters for bulk water, the presence of a solute will modify such values for the water molecules in the hydration shell, leading to a change in heat capacity

$$[10] \quad \Delta C_p^h = C_p(d,s,\theta) - C_p(d_0,s_0,\theta_0)$$

where ΔC_p^h is the heat capacity change per H-bond perturbed by the solute. Sharp and Madan calculated the net

© 2001 NRC Canada

hydration heat capacity change by summing overall the H-bonds perturbed by the solute. In this manner they assumed that the reorganization of H-bonds among the water molecules in the hydration shell of the solute is the fundamental determinant of $\Delta C_p^\bullet$.

Performing Monte Carlo simulations in TIP4P water at constant temperature and pressure, Sharp and Madan determined the probability distribution function of the H-bond angle θ for bulk water and for the water molecules in the first hydration shell of various solutes (12–14). The distribution function of bulk water proves to be bimodal with a large peak centered at θ ≈ 12° and a small peak centered at θ ≈ 52°, producing an overall root-mean-square value of 29° (i.e., the area of the first peak is about four times larger than that of the second one). In addition, the linear H-bonds are slightly shorter than the bent ones. Therefore, bulk water consists of two H-bond populations: a predominantly linear population and a small but significant population of slightly longer and more bent H-bonds. The distribution function of θ for water molecules in the hydration shell of solutes is always bimodal, but (*i*) nonpolar groups cause a small increase of the peak at 12° and a corresponding decrease of the peak at 52°; and (*ii*) cations and polar groups cause a decrease of the peak at 12° and an increase of the peak at 52°. As a consequence, the overall root-mean-square value of θ is 22–24° for nonpolar solutes, and about 50° for cations and polar groups. Such changes are the main determinants of the heat capacity increase due to nonpolar solutes, and of the heat capacity decrease due to cations and polar groups (see eq. [3] in ref. 13).

In qualitative agreement with experimental data, Sharp and Madan obtained negative ΔC_p^h values for cations and positive ΔC_p^h values for nonpolar solutes, and interpreted their results with a demonstrative two-state model: H-bonds in the hydration shell of nonpolar groups are less distorted than those in the bulk because the perturbation is weak, whereas the opposite is true for those around cations because the perturbation is strong (see Fig. 4 of ref. 13). Clearly, it is very difficult to contrast such interpretation against that resulting from the application of the modified Muller's model because it is not at all clear the relationship existing between the distortion of H-bonds and the two states, broken and intact, postulated by Muller for H-bonds. In geometric terms one might argue that the H-bond between two water molecules is broken when θ is around 50°. Nevertheless, we note that Sharp and Madan computed the H-bond length and angle only for the pairs of water molecules that were H-bonded (i.e., those for which the oxygen—oxygen distance was less than or equal to 3.4 Å; this cutoff value corresponds to the first minimum in the oxygen–oxygen radial distribution function of liquid water). Clearly, such a procedure mainly probed intact H-bonds and neglected broken ones, introducing a significant bias in the analysis of Monte Carlo simulations.

Furthermore, the results reported in Table 3 of ref. 12, Fig. 2 of ref. 13, and Table 2 of ref. 14 indicate unequivocally that the calculated estimates of ΔC_p^h amount roughly to 50% of the experimental $\Delta C_p^\bullet$ values (i.e., for methane ΔC_p^h = 124 J K^{-1} mol^{-1} vs. $\Delta C_p^\bullet$ = 209 J K^{-1} mol^{-1}; for *n*-butane ΔC_p^h = 208 J K^{-1} mol^{-1} vs. $\Delta C_p^\bullet$ = 383 J K^{-1} mol^{-1}; for ethanol ΔC_p^h = 100 J K^{-1} mol^{-1} vs. $\Delta C_p^\bullet$ = 197 J K^{-1} mol^{-1}; for NMA ΔC_p^h = 75 J K^{-1} mol^{-1} vs. $\Delta C_p^\bullet$ = 167 J K^{-1} mol^{-1}; for K^+ ΔC_p^h = –34 J K^{-1} mol^{-1} vs. $\Delta C_p^\bullet$ = –72 J K^{-1} mol^{-1}; all such values are at 25°C). Therefore, the Sharp and Madan approach significantly underestimates the hydration heat capacity change for all the solutes studied and cannot be considered entirely satisfactory. In addition we raise the following general concerns.

(*i*) The hydration enthalpy change for a nonpolar solute is given by (10, 11):

$$[11] \quad \Delta H^\bullet = E_a + \Delta H^h$$

where E_a is the average solute–water interaction energy (mainly from van der Waals interactions in the case of nonpolar solutes), and ΔH^h is the enthalpy change due to the H-bond reorganization among the water molecules in the hydration shell. According to the theoretical calculations by different research groups (50, 59–62), E_a is a large negative quantity and $|E_a| > \Delta H^\bullet$ for all the nonpolar solutes considered (i.e., according to Jorgensen's calculations (50), for propane E_a = –27.6 kJ mol^{-1} vs. $\Delta H^\bullet$ = –21.0 kJ mol^{-1}; for neopentane E_a = –36.0 kJ mol^{-1} vs. $\Delta H^\bullet$ = –22.8 kJ mol^{-1}; for *n*-pentane E_a = –41.8 kJ mol^{-1} vs. $\Delta H^\bullet$ = –26.0 kJ mol^{-1}; all the values are at 25°C). This means that the reorganization of H-bonds in the hydration shell of nonpolar solutes is an endothermic process at room temperature ($\Delta H^h > 0$) and cannot lead to a net gain of H-bonds or to an increase in the population of linear and short H-bonds. To have $\Delta H^h > 0$, the H-bonds in the hydration shell should be more broken or more bent than those in bulk water. This is a general result (see the work by Levy and co-workers (62) for a recent and detailed analysis), but entirely neglected by Sharp and Madan in their approach, which is solely devoted toward the calculation of the hydration heat capacity change (i.e., it does not consider the other thermodynamic functions).

In addition, careful computer simulations by Laidig and Daggett (63), Mancera (64*a*), and Chau and Mancera (64*b*), using very reliable models of liquid water, have unequivocally found $f_{hs} > f_b$ for the hydration shell of nonpolar solutes over a large temperature range, lending support to the physical picture emerging from the application of the modified Muller's model. In particular, it is astonishing that the results of Mancera and of Sharp and Madan on the same system, namely methane in TIP4P water, are at odds. In all probability the inconsistency is because Mancera searched for both broken and intact H-bonds, whereas Sharp and Madan searched for intact H-bonds exclusively.

(*ii*) In the case of polar solutes it is necessary to distinguish the charged species from the neutral ones because they interact differently with the surrounding water molecules and cause different perturbations of the H-bonding network. In fact, according to the Sharp and Madan approach, urea causes a very weak perturbation of the H-bonding network of water (65), in marked contrast with the behavior of cations such as K^+ and Cs^+. Charged species have strong electrostatic interactions with the dipole moment of water molecules, but do not form direct H-bonds, whereas polar but neutral species form direct H-bonds with water molecules. Specifically the CONH group forms three H-bonds with water and the contribution of such H-bonds to $\Delta H^\bullet$ and $\Delta C_p^\bullet$ should be taken into account in view of their expected importance. Instead Sharp and Madan have considered

© 2001 NRC Canada

solely the H-bonds among water molecules in the hydration shell of the various solutes: the role played by the direct solute–water H-bonds in the case of polar molecules such as NMA and ethanol was completely neglected. This is a serious failure in our opinion. On the contrary, the approach devised in the present article, by recognizing that the hydration enthalpy change originates from both the formation of direct CONH–water H-bonds and the reorganization of water–water H-bonds, tries to account for the contribution of both of them to $\Delta C_p^{\bullet}$.

(*iii*) Sharp and Madan calculated solely the values of ΔC_p^h at 25°C, but entirely neglected the temperature dependence of the hydration heat capacity change. This point is very important and cannot be eluded. As the modified Muller's model calculations emphasize for both nonpolar and polar solutes (11, 15), the temperature dependence of ΔC_p^h is the fundamental feature to select the model closer to reality. Many different models can reproduce the $\Delta C_p^{\bullet}$ values at 25°C, but very few of them show the qualitatively correct temperature dependence of the heat capacity change. This implies that the temperature dependence of the calculated ΔC_p^h function is a necessary test to verify the general validity of the Sharp and Madan approach. However, such a test has not been performed yet.

Even though the Sharp and Madan approach may appear more appealing from a theoretical point of view, we believe that our treatment merits attention for the physical reliability of obtained results and for its usefulness in trying to establish a clear molecular picture of the heat capacity change upon hydration of both polar and nonpolar solutes.

Conclusion

We have shown that a simple theoretical approach, combining SPT and the modified Muller's model, is able to explain in a reliable manner most features of the CONH hydration thermodynamics in the 5–100°C temperature range. The negative entropy change is caused by the excluded volume effect related to the creation in liquid water of a cavity suitable to host the solute. More important, the negative heat capacity change is because the H-bonds in the hydration shell of the peptide group, both CONH–water and water–water H-bonds, are significantly more intact than those in bulk water. Such a conclusion may have a wide-ranging impact both in solution thermodynamics and in the field of protein folding.

Acknowledgements

Work supported by a P.R.I.N. grant from the Italian Ministry for University, and Scientific and Technological Research (M.U.R.S.T., Rome). The comments from the two referees and the hints from the Editor have been invaluable in shaping the final form of the manuscript.

References

1. W. Blokzijl and J.B.F.N. Engberts. Angew. Chem. Int. Ed. Engl. **32**, 1545 (1993).
2. (*a*) M. Oobatake and T. Ooi. Prog. Biophys. Mol. Bio. **59**, 237 (1993); (*b*) G. Graziano, F. Catanzano, A. Riccio, and G. Barone. J. Biochem. **122**, 395 (1997).
3. (*a*) G.I. Makhatadze and P.L. Privalov. J. Mol. Biol. **232**, 639 (1993); (*b*) P.L. Privalov and G.I. Makhatadze. J. Mol. Biol. **232**, 660 (1993).
4. G.I. Makhatadze and P.L. Privalov. Adv. Protein Chem. **47**, 307 (1995).
5. (*a*) S. Shimizu and K. Shimizu. J. Am. Chem. Soc. **121**, 2837 (1999); (*b*) F. Avbelj, P. Luo, and R.L. Baldwin. Proc. Natl. Acad. Sci. U.S.A. **97**, 10786 (2000).
6. A. Ben-Naim. Solvation thermodynamics. Plenum Press, New York. 1987.
7. (*a*) J.J. Savage and R.H. Wood. J. Solution Chem. **5**, 733 (1976); (*b*) K.A. Dill. J. Biol. Chem. **272**, 701 (1997).
8. S. Cabani, P. Gianni, V. Mollica, and L. Lepori. J. Solution Chem. **10**, 563 (1981).
9. G. Graziano and G. Barone. J. Am. Chem. Soc. **118**, 1831 (1996).
10. B. Lee. Biopolymers, **31**, 993 (1991).
11. (*a*) G. Graziano. Biophys. Chem. **82**, 69 (1999); (*b*) Phys. Chem. Chem. Phys. **1**, 1877 (1999); (*c*) Phys. Chem. Chem. Phys. **1**, 3567 (1999); (*d*) J. Phys. Chem. B, **104**, 9249 (2000).
12. (*a*) B. Madan and K.A. Sharp. J. Phys. Chem. **100**, 7713 (1996); (*b*) Biophys. Chem. **78**, 33 (1999).
13. K.A. Sharp and B. Madan. J. Phys. Chem. B, **101**, 4343 (1997).
14. B. Madan and K.A. Sharp. J. Phys. Chem. B, **101**, 11237 (1997).
15. B. Lee and G. Graziano. J. Am. Chem. Soc. **118**, 5163 (1996).
16. (*a*) B. Madan and B. Lee. Biophys. Chem. **51**, 279 (1994); (*b*) S.R. Durell and A. Wallqvist. Biophys. J. **71**, 1695 (1996); (*c*) M. Ikeguchi, S. Shimizu, S. Nakamura, and K. Shimizu. J. Phys. Chem. B, **102**, 5891 (1998).
17. (*a*) B. Lee. J. Chem. Phys. **83**, 2421 (1985); (*b*) G. Graziano. J. Phys. Soc. Jpn. **69**, 1566 (2000).
18. B. Lee. Biophys. Chem. **51**, 271 (1994).
19. (*a*) N. Muller. J. Solution Chem. **17**, 661 (1988); (*b*) Acc. Chem. Res. **23**, 23 (1990).
20. C.A. Angell. J. Phys. Chem. **75**, 3698 (1971).
21. H.S. Frank and F. Franks. J. Chem. Phys. **48**, 4746 (1968).
22. (*a*) J.D. Worley and I.M. Klotz. J. Chem. Phys. **45**, 2868 (1966); (*b*) G.E. Walrafen. J. Chem. Phys. **47**, 114 (1967); (*c*) D.E. Hare and C.M. Sorensen. J. Chem. Phys. **93**, 6954 (1990).
23. J.A. Hayward and A.D.J. Haymet. J. Chem. Phys. **114**, 3713 (2001).
24. K.A.T. Silverstein, A.D.J. Haymet, and K.A. Dill. J. Chem. Phys. **111**, 8000 (1999).
25. L. Pauling. The nature of the chemical bond. 3rd ed. Cornell University Press, Ithaca, New York. 1960.
26. G.E. Walrafen, M.R. Fisher, M.S. Hokmabadi, and W.H. Yang. J. Chem. Phys. **85**, 6970 (1986).
27. W.L. Jorgensen and C.J. Swenson. J. Am. Chem. Soc. **107**, 1489 (1985).
28. H. Reiss. Adv. Chem. Phys. **9**, 1 (1966).
29. R.A. Pierotti. Chem. Rev. **76**, 717 (1976).
30. (*a*) R.O. Neff and D. McQuarrie. J. Phys. Chem. **77**, 413 (1973); (*b*) S. Shimizu, M. Ikeguchi, S. Nakamura, and K. Shimizu. J. Chem. Phys. **110**, 2971 (1999).
31. K.E.S. Tang and V.A. Bloomfield. Biophys. J. **79**, 2222 (2000).
32. (*a*) E. Wilhelm and R. Battino. J. Chem. Phys. **56**, 563 (1972); (*b*) M. Lucas. J. Phys. Chem. **80**, 359 (1976); (*c*) N. Morel-Desrosiers and J.P. Morel. Can. J. Chem. **59**, 1 (1981).
33. (*a*) A.H. Narten and H.A. Levy. J. Chem. Phys. **55**, 2263 (1971); (*b*) W.E. Thiessen and A.H. Narten. J. Chem. Phys. **77**, 2656 (1982).

© 2001 NRC Canada

34. (*a*) A.K. Soper and M.G. Phillips. Chem. Phys. **107**, 47 (1986); (*b*) A.K. Soper, F. Bruni, and M.A. Ricci. J. Chem. Phys. **106**, 247 (1997).
35. J.M. Sorenson, G. Hura, R.M. Glaeser, and T. Head-Gordon. J. Chem. Phys. **113**, 9149 (2000).
36. (*a*) F.M. Richards. J. Mol. Biol. **82**, 1 (1974); (*b*) Y. Harpaz, M.Gerstein, and C. Chothia. Structure, **2**, 641 (1994).
37. E.J. Cohn and J.T. Edsall. Proteins, amino acids, and peptides. Hafner, New York. 1965.
38. A.K. Mishra and J.C. Ahluwalia. J. Phys. Chem. **88**, 86 (1984).
39. M. Iqbal and R.E. Verral. J. Phys. Chem. **91**, 967 (1987).
40. M. Hackel, G.R. Hedwig, and H.J. Hinz. Biophys. Chem. **73**, 163 (1998).
41. E. Wilhelm and R. Battino. J. Chem. Phys. **55**, 4012 (1971).
42. G.S. Kell. J. Chem. Eng. Data, **20**, 97 (1975).
43. P. Starzewski, I. Wadso, and W. Zielenkiewicz. J. Chem. Thermodyn. **16**, 331 (1984).
44. R. Wolfenden. Biochemistry, **17**, 201 (1978).
45. G.I. Makhatadze and P.L. Privalov. J. Mol. Biol. **213**, 375 (1990).
46. M. Hackel, H.J. Hinz, and G.R. Hedwig. J. Mol. Biol. **291**, 197 (1999).
47. K.P. Murphy and S.J. Gill. J. Mol. Biol. **222**, 699 (1991).
48. G. Barone, P. Del Vecchio, C. Giancola, and G. Graziano. Int. J. Biol. Macromol. **17**, 251 (1995).
49. (*a*) B. Lee. Biopolymers, **24**, 813 (1985); (*b*) G. Graziano. Can. J. Chem. **76**, 437 (1998); (*c*) J. Chem. Soc. Faraday Trans. **94**, 3345 (1998); (*d*) Can. J. Chem. **78**, 1233 (2000).
50. W.L. Jorgensen, J. Gao, and C. Ravimohan. J. Phys. Chem. **89**, 3470 (1985).
51. J.T. Edsall. J. Am. Chem. Soc. **57**, 1506 (1935).
52. S.J. Gill, S.F. Dec, G. Olofsson, and I. Wadso. J. Phys. Chem. **89**, 3758 (1985).
53. G.I. Makhatadze, M.M. Lopez, and P.L. Privalov. Biophys. Chem. **64**, 93 (1997).
54. (*a*) B. Lee and F.M. Richards. J. Mol. Biol. **55**, 379 (1971); (*b*) C. Chothia. Nature (London), **248**, 338 (1974); (*c*) J.A. Reynolds, D.B. Gilbert, and C. Tanford. Proc. Natl. Acad. Sci. U.S.A. **71**, 2925 (1974); (*d*) S.F. Dec and S.J. Gill. J. Solution Chem. **14**, 417 (1985); (*e*) D. Eisenberg and A.D. Wilcox. Nature (London), **319**, 199 (1986).
55. P.A. Karplus. Protein Sci. **6**, 1302 (1997).
56. T. Lazaridis, G. Archontis, and M. Karplus. Adv. Protein Chem. **47**, 426 (1995).
57. (*a*) M.G. Sceats and S.A. Rice. J. Chem. Phys. **72**, 3236, 3248, 3260 (1980); (*b*) S.A. Rice and M.G. Sceats. J. Phys. Chem. **85**, 1108 (1981).
58. A.R. Henn and W. Kauzmann. J. Phys. Chem. **93**, 3770 (1989).
59. (*a*) L.R. Pratt and D. Chandler. J. Chem. Phys. **67**, 3683 (1977); (*b*) S. Garde, A.E. Garcia, L.R. Pratt, and G. Hummer. Biophys. Chem. **78**, 21 (1999).
60. (*a*) F. Floris and J. Tomasi. J. Comp. Chem. **10**, 616 (1989); (*b*) F. Floris, J. Tomasi, and J.L. Pascual Ahuir. J. Comp. Chem. **12**, 784 (1991).
61. B. Guillot and Y. Guissani. J. Chem. Phys. **99**, 8075 (1993).
62. E. Gallicchio, M.M. Kubo, and R.M. Levy. J. Phys. Chem. B, **104**, 6271 (2000).
63. K.E. Laidig and V. Daggett. J. Phys. Chem. **100**, 5616 (1996).
64. (*a*) R.L. Mancera. J. Chem. Soc. Faraday Trans. **94**, 3549 (1998); J. Phys. Chem. B, **103**, 3774 (1999); (*b*) P.L. Chau and R.L. Mancera. Mol. Phys. **96**, 109 (1999).
65. (*a*) F. Vanzi, B. Madan, and K. Sharp. J. Am. Chem. Soc. **120**, 10748 (1998); (*b*) K. Sharp, B. Madan, E. Manas, and J.M. Vanderkooi. J. Chem. Phys. **114**, 1791 (2001).
66. K.A.T. Silverstein, A.D.J. Haymet, and K.A. Dill. J. Am. Chem. Soc. **122**, 8037 (2000).
67. D. Eisenberg and W. Kauzmann. The structure and properties of water. Oxford University Press, Oxford. 1969.

Appendix

An important point is the robustness of the results obtained with the modified Muller's model to changes in the parameters selected for bulk water. Very recently, Dill and co-workers (66) claimed that the *correct* values of ΔH_b° and ΔS_b° are those that best fit the configurational heat capacity of water as a function of temperature. The configurational heat capacity of water is not an experimental quantity, but it was calculated theoretically by Eisenberg and Kauzmann (67), subtracting the contributions due to molecular translations, rotations, and vibrations from the experimental heat capacity of bulk water in the whole liquid range (i.e., the configurational heat capacity should contain only the contributions due to the H-bonding network). Adopting this procedure, one obtains ΔH_b° = 8.0 kJ mol^{-1} and ΔS_b° = 20.1 J K^{-1} mol^{-1}, so that f_b = 0.312 at 25°C. Such estimates correspond exactly to those determined originally by Angell (20), are significantly different from those of Muller (i.e., ΔH_b° = 9.8 kJ mol^{-1} and ΔS_b° = 21.6 J K^{-1}mol^{-1}), and lead to a larger fraction of broken H-bonds in bulk water at all temperatures.

The *correct* values of ΔH_b° and ΔS_b° have been used to perform another complete set of calculations with the modified Muller's model for the peptide group, adopting the same procedure described in the text. Namely, we fixed n^h = 6 and ΔH_U in the range –10–0 kJ mol^{-1}, and used $\Delta C_p^h = \Delta C_p^\bullet$ = –63.4 J K^{-1} mol^{-1}, $\Delta H^h = \Delta H^\bullet$ = –59.6 kJ mol^{-1}, and $\Delta S^h = \Delta S^\bullet - \Delta S_x$ = 44.3 J K^{-1} mol^{-1} at 25°C. The calculated parameters ΔH_{hs}°, ΔS_{hs}°, and ΔS_U are collected in Table A1, whereas the calculated values of f_{hs} and ΔC_p^h, in the temperature range 5–100°C, for each choice of ΔH_U, are listed in Tables A2 and A3, respectively. A look at such tables soon emphasizes that the main conclusion of the work is robust: to have negative values of ΔC_p^h that decrease in magnitude in a continuous manner with temperature, f_{hs} has to be significantly smaller than f_b at all temperatures. The models closer to reality seem to be those characterized by ΔH_U in the range of –10 to –6 kJ mol^{-1}, which are qualitatively very similar to those obtained with the bulk parameters of Muller.

© 2001 NRC Canada

Table A1. Parameter values of the modified Muller's model for the CONH group calculated as a function of ΔH_U, by assuming for bulk water the parameter values selected originally by Angell (20), $n^h = 2N_{H_2O} = 6$, and, at 25°C, $\Delta C_p^h = \Delta C_p^\bullet = -63.4$ J K^{-1} mol^{-1}, $\Delta H^h = \Delta H^\bullet = -59.6$ kJ mol^{-1}, and $\Delta S^h = \Delta S^\bullet - \Delta S_x = 44.3$ J K^{-1} mol^{-1}.

ΔH_U (kJ mol^{-1})	f_{hs} at 25°C (%)	ΔH°_{hs} (kJ mol^{-1})	ΔS°_{hs} (J K^{-1} mol^{-1})	ΔS_U (J K^{-1} mol^{-1})
0	2.4	15.8	22.0	19.3
–2.0	3.1	13.8	17.8	14.8
–4.0	4.3	11.9	14.0	10.7
–6.0	6.1	10.0	10.9	7.0
–8.0	9.5	8.2	8.7	4.0
–10.0	16.5	6.5	8.2	1.9

Table A2. Percentage values of f_{hs}, the fraction of broken H-bonds in the hydration shell, for different ΔH_U choices, by assuming for bulk water the parameter values selected originally by Angell (20).

T (°C)	f_b	f_{hs}[–10]	f_{hs}[–8]	f_{hs}[–6]	f_{hs}[–4]	f_{hs}[–2]	f_{hs}[0]
5	26.5	14.1	7.7	4.7	3.1	2.1	1.5
25	31.2	16.5	9.5	6.1	4.2	3.1	2.4
50	36.8	19.5	12.0	8.2	6.0	4.7	3.8
75	41.9	22.3	14.5	10.4	8.1	6.7	5.7
100	46.4	25.0	17.0	12.8	10.4	9.0	8.0

Note: The notation corresponds to that in Table 4 of the text. The percentage values of f_b, the fraction of broken H-bonds in the bulk, are reported for comparison purposes.

Table A3. Estimates of ΔC_p^h for different ΔH_U choices, by assuming for bulk water the parameter values selected originally by Angell (20).

T (°C)	$\Delta C_p^\bullet$	ΔC_p^h[–10]	ΔC_p^h[–8]	ΔC_p^h[–6]	ΔC_p^h[–4]	ΔC_p^h[–2]	ΔC_p^h[0]
5	–72.8	–67.4	–70.4	–73.1	–75.5	–77.6	–79.6
25	–63.4	–63.4	–63.4	–63.4	–63.4	–63.4	–63.4
50	–54.6	–56.2	–52.9	–49.5	–46.0	–42.2	–38.3
75	–53.6	–48.4	–42.3	–35.8	–28.6	–20.6	–11.7
100	–52.2	–40.8	–32.6	–23.4	–12.8	–0.5	13.8

Note: The notation corresponds to that in Table 5 of the text. The values of $\Delta C_p^\bullet$ are reported for comparison purposes. All the heat capacity values are in J K^{-1} mol^{-1}.

© 2001 NRC Canada

Synthesis and characterization of manganese complexes of the dibenzophospholyl ligand

Andreas Decken, Melanie A. Neil, and Frank Bottomley

Abstract: Manganese carbonyl complexes bearing dibenzophospholyl (DBP) and 1-phenyldibenzophosphole (Ph-DBP) ligands have been prepared. Reaction of Li-DBP with $Mn(CO)_5Br$ gave $(\mu_2\text{-DBP})(\mu_2\text{-Br})Mn_2(CO)_8$, while reaction of bis(1,1′-dibenzophospholyl) and $Mn_2(CO)_{10}$ yielded $(\mu_2\text{-DBP})_2Mn_2(CO)_8$. The phosphine adducts $(Ph\text{-DBP})Mn_2(CO)_9$ and $(Ph\text{-DBP})_2Mn_2(CO)_8$ were obtained by reaction of Ph-DBP and $Mn_2(CO)_{10}$. The ligands are σ-bonded through the phosphorus atom in all complexes. The compounds were characterized by ^1H, ^{13}C, and ^{31}P NMR and IR spectroscopy, mass spectrometry, and X-ray diffraction.

Key words: dibenzophospholyl, dibenzophosphole, manganese, heterocycle.

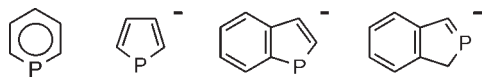
Résumé : On a préparé des complexes de manganèse-carbonyle portant des ligands dibenzophopholyle (DBP) et 1-phényldibenzophosphole (Ph-DBP). La réaction du Li-DBP avec du $Mn(CO)_5Br$ conduit à la formation de $(\mu_2\text{-DBP})(\mu_2Br)Mn_2(CO)_8$ alors que la réaction du bis(1,1′-dibenzophospholyl) avec le $Mn_2(CO)_{10}$ conduit à la formation du $(\mu_2\text{-DBP})_2Mn(CO)$. Par réaction avec du Ph-DBP et du $Mn_2(CO)_{10}$, on a obtenu les adduits phosphinés (Ph-DBP)Mn(CO) et (Ph-DBP)Mn(CO). Dans tous ces complexes, les ligands sont liés à l'atome de phosphore par une liaison σ. Les composés ont été caractérisés par spectroscopie IR, par RMN du ^1H, ^{13}C et ^{31}P, par spectrométrie de masse et par diffraction des rayons X.

Mots clés : dibenzophospholyle, dibenzophosphole, manganèse, hétérocycle.

[Traduit par la Rédaction]

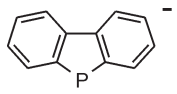
Introduction

Aromatic heterocycles containing phosphorus have been of much interest as ligands in transition metal complexes (1–4), especially in view of their potential applications in catalysis (5–7). Early studies focused on complexes of phosphinine and phospholyl, in part because ligands **1** and **2** were readily accessible. However, benzannelated phospholyl ligands such as **3** and **4** have recently emerged as interesting alternatives (8–14).



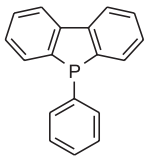
1 **2** **3** **4**

Their hydrocarbon analogues primarily bind through the π-electron system, but **1**–**4** can also ligate metals through the phosphorus lone pair, resulting in complexes containing ligands with σ-, π-, and mixed-bonding modes. Phospholyls display a high degree of aromaticity (15–20), but the hapticity as a ligand is controlled by substituents and the metal to which they are coordinated. The degree of aromaticity of benzannelated phospholyls has not been established, but both σ- and π-bonding have been found in complexes containing **3** and **4**. Such diversity can also be expected in complexes of dibenzophospholyl (DBP, **5**), although very little is known about the ligating abilities of this ligand.



5

We are exploring the chemistry of DBP with emphasis on the differences between its modes of coordination and those of the fluorenyl analogue, and of ligands **2**–**4**. In light of the facile synthesis and high stability of the fluorenyl complexes $(\eta^1\text{-}C_{13}H_9)Mn(CO)_5$ and $(\eta^5\text{-}C_{13}H_9)Mn(CO)_3$ (21–25),[2] we began with the preparation of manganese carbonyl complexes of the dibenzophospholyl anion **5**, and of 1-phenyldibenzophosphole (Ph-DBP, **6**).



6

The characterization, structures, and properties of the products are reported here.

Received April 25, 2001. Published on the NRC Research Press Web site at http://canjchem.nrc.ca on September 12, 2001.

A. Decken,[1] M.A. Neil, and F. Bottomley. Department of Chemistry, University of New Brunswick, P.O. Box 45222, Fredericton, NB E3B 6E2, Canada.

[1]Corresponding author (telephone: (506) 453-4875; fax: (506) 453-4981; e-mail: adecken@unb.ca).

[2]A. Decken, A. MacKay, M. Brown, and F. Bottomley. Unpublished results.

 DOI: 10.1139/cjc-79-9-1321 © 2001 NRC Canada

Experimental

General considerations

All reactions were carried out under an atmosphere of argon utilizing standard Schlenk techniques. Solvents were dried and distilled according to standard procedures (26). Melting points were measured in open glass capillaries using a Gallenkamp melting point apparatus and are uncorrected. ^{1}H, ^{13}C, and ^{31}P NMR spectra were recorded on a Varian Unity 400 spectrometer operating at 399.99, 100.6, and 161.31 MHz, respectively. The ^{1}H and ^{13}C NMR spectra were referenced relative to tetramethylsilane and the ^{31}P NMR spectra were referenced relative to external triphenylphosphine (δ = –6.0). Electron impact (EI) and fast atom bombardment (FAB) mass spectrometry experiments were performed on a Kratos MS-50 mass spectrometer, with 3-nitrobenzyl alcohol as the FAB matrix and helium as the bombarding gas. Infrared spectra were obtained on a Bruker IFS 25 instrument. Unless otherwise stated, all reagents were obtained from commercial suppliers and used without further purification. Manganese pentacarbonylbromide (27), 1-phenyldibenzophosphole (28), and bis(1,1′-dibenzophospholyl) (29) were prepared according to literature procedures. Lithium shavings were obtained from lithium rods (99% under mineral oil). Flash chromatography was carried out using Merck silica gel (330–400 mesh). Elemental analyses were preformed by Galbraith Laboratories, Knoxville, Tennesee.

Preparation of (μ_2-dibenzophospholyl)-(μ_2-bromo)-dimanganese-octacarbonyl (7)

To a solution of 1-phenyldibenzophosphole (0.45 g, 1.73 mmol) in THF (5 cm^3) was added lithium shavings (10-fold excess) and the mixture stirred overnight at room temperature. The solution was decanted and aluminum trichloride (0.077 g, 0.58 mmol) added, resulting in a dark brown-red solution (29, 30). The mixture was added dropwise to a solution of $Mn(CO)_5Br$ (1.898 g, 6.9 mmol) in THF (20 cm^3) producing a dark orange solution. After stirring overnight at room temperature, the solvent was removed under vacuum and the crude product purified by flash chromatography using a 1:1 mixture of ether:hexane to give **7** as an orange solid. Yield: 0.72 g, 1.20 mmol, 69%, mp 250°C (dec.). FAB-MS *m/z* (%): 596 (0.2) $[C_{20}H_8{}^{79}BrPMn_2O_8]^+$ ($[M]^+$); 484 (4) $[C_{16}H_8{}^{79}BrMn_2O_4P]^+$, $[(C_{12}H_8P)Mn_2(CO)_4{}^{79}Br]^+$; 349 (4) $[C_{14}H_8Mn_2O_2P]^+$, $[(C_{12}H_8P)Mn_2(CO)_2]^+$; 238 (5) $[C_{12}H_8PMn]^+$; 183 (18) $[C_{12}H_8P]^+$. IR (KBr disk) (cm^{-1}) ν_{CO}: 1968 (s, br), 2001 (s, br), 2057 (m-s). ^{1}H NMR (acetone-d_6) δ: 8.95 (dd, *J* = 8.0, 8.0 Hz, 2H), 8.21 (d, *J* = 8.0 Hz, 2H), 7.77 (m, 2H), 7.66 (dd, *J* = 8.0, 8.0 Hz, 2H). ^{13}C NMR ($CDCl_3$) δ: 215.28 (d, $J_{P,C}$ = 13 Hz, CO), 212.80 (d, $J_{P,C}$ = 18 Hz, CO), 208.08 (d, $J_{P,C}$ = 9 Hz, CO), 144.94 (d, $J_{P,C}$ = 25 Hz), 141.45 (d, $J_{P,C}$ = 6 Hz), 129.53 (s), 129.30 (s), 127.76 (s), 121.86 (s). ^{31}P{^{1}H} NMR ($CDCl_3$) δ: –42. Anal. calcd. for $C_{20}H_8BrO_8PMn_2$: C 40.20, H 1.35; found: C 39.66, H 1.46.

Compound **7** (0.15 g, 0.25 mmol) in xylenes (5 cm^3) was heated to reflux. Within 10 min the colour of the solution changed from orange to yellow and a yellow precipitate formed. After 1 h the mixture was cooled to room temperature, the precipitate separated by filtration and washed with hexane to give a bright yellow solid. The solid was identified as **11** by IR, ^{1}H NMR, and mass spectrometry and by unit cell determination of single crystals grown by vapour diffusion of CH_2Cl_2–hexanes at –23°C (see below). Yield: 0.082 g, 0.12 mmol, 96%. The remaining solution was concentrated to dryness under vacuum and the resulting orange-brown solid identified as $(\mu_2\text{-}Br)_2Mn_2(CO)_8$ based on IR spectroscopy (31) and mass spectrometry. Yield: 0.054 g, 0.11 mmol, 88%. EI-MS$^+$ *m/z* (%): 436 (0.4) $[C_6{}^{79}Br_2Mn_2O_6]^+$, $[Mn_2(CO)_6{}^{79}Br_2]^+$; 408 (23) $[C_5{}^{79}Br_2Mn_2O_5]^+$, $[Mn_2(CO)_5{}^{79}Br_2]^+$; 380 (8) $[C_4{}^{79}Br_2Mn_2O_4]^+$, $[Mn_2(CO)_4{}^{79}Br_2]^+$; 352 (2) $[C_3{}^{79}Br_2Mn_2O_3]^+$, $[Mn_2(CO)_3{}^{79}Br_2]^+$; 324 (4) $[C_2{}^{79}Br_2Mn_2O_2]^+$, $[Mn_2(CO)_2{}^{79}Br_2]^+$; 296 (84) $[C^{79}Br_2Mn_2O]^+$, $[Mn_2(CO)^{79}Br_2]^+$; 268 (6) $[{}^{79}Br_2Mn_2]^+$; 166 (36) $[C_2Mn_2O_2]^+$, $[Mn_2(CO)_2]^+$; 158 (100) $[{}^{79}Br_2]^+$.

Preparation of (1-phenyldibenzophosphole)-dimanganese-nonacarbonyl (9) and di(1-phenyldibenzophosphole)-dimanganese-octacarbonyl (10)

To a solution of dimanganese decacarbonyl (1.56 g, 4 mmol) in xylenes (25 cm^3) was added a solution of 1-phenyldibenzophosphole (1.04 g, 4 mmol) in xylenes (25 cm^3). The mixture was heated at reflux for 3 h, cooled to room temperature, and the insoluble materials removed by filtration. The filtrate was concentrated to dryness via trap-to-trap distillation under vacuum. Products **9** and **10** were separated by column chromatography using hexanes. Yield of yellow **9**: 0.43 g, 0.69 mmol, 17%, mp 179–181°C. EI-MS$^+$ *m/z* (%): 510 (13) $[C_{23}H_{13}PMn_2O_5]^+$, $[(C_{18}H_{13}P)Mn_2(CO)_5]^+$; 482 (19) $[C_{22}H_{13}PMn_2O_4]^+$, $[(C_{18}H_{13}P)Mn_2(CO)_4]^+$; 427 (52) $[C_{22}H_{13}PMnO_4]^+$, $[(C_{18}H_{13}P)Mn(CO)_4]^+$; 405 (64) $[C_{16}H_8PMn_2O_4]^+$, $[(C_{12}H_8P)Mn_2(CO)_4]^+$; 399 (25) $[C_{21}H_{13}PMnO_3]^+$, $[(C_{18}H_{13}P)Mn(CO)_3]^+$; 371 (49) $[C_{20}H_{13}PMnO_2]^+$, $[(C_{18}H_{13}P)Mn(CO)_2]^+$; 343 (9) $[C_{19}H_{13}PMnO]^+$, $[(C_{18}H_{13}P)Mn(CO)]^+$; 334 (23) $[C_8Mn_2O_8]^+$, $[Mn_2(CO)_8]^+$; 315 (81) $[C_{18}H_{13}PMn]^+$; 260 (96) $[C_{18}H_{13}P]^+$; 183 (95) $[C_{12}H_8P]^+$. IR (KBr disk) (cm^{-1}) ν_{CO}: 1918 (m), 1944 (m), 1972 (vs), 1987 (sh), 2014 (sh), 2084 (w). ^{1}H NMR (C_6D_6) δ: 7.69 (dd, *J* = 7.2, 6.8 Hz, 2H), 7.50 (m, 2H), 7.35 (d, *J* = 6.8 Hz, 2H), 7.0 (m, 4H), 6.82 (m, 3H). ^{13}C NMR ($CDCl_3$) δ: 222.98 (br, CO), 141.09 (d, $J_{P,C}$ = 10 Hz), 139.46 (d, $J_{P,C}$ = 49 Hz), 134.63 (d, $J_{P,C}$ = 39 Hz), 131.39 (s), 130.65 (d, $J_{P,C}$ = 13 Hz), 130.48 (s), 130.41 (d, $J_{P,C}$ = 8 Hz), 129.18 (d, $J_{P,C}$ = 3 Hz), 129.07 (d, $J_{P,C}$ = 3 Hz), 122.06 (d, $J_{P,C}$ = 6 Hz). ^{31}P{^{1}H} NMR ($CDCl_3$) δ: 65.

Yield of yellow **10**: 0.45 g, 0.52 mmol, 13%, mp 209–211°C. EI-MS$^+$ *m/z* (%): 427 (5) $[C_{22}H_{13}PMnO_4]^+$, $[(C_{18}H_{13}P)Mn(CO)_4]^+$; 362 (33) $[C_9Mn_2O_9]^+$, $[Mn_2(CO)_9)]^+$; 278 (100) $[C_6Mn_2O_6]^+$, $[Mn_2(CO)_6)]^+$; 260 (18) $[C_{18}H_{13}P]^+$; 183 (17) $[C_{12}H_8P]^+$. IR (Nujol mull) (cm^{-1}) ν_{CO}: 1970 (w), 1992 (vs), 2016 (w), 2090 (vw). ^{1}H NMR (C_6D_6) δ: 7.84 (dd, *J* = 7.6, 7.2 Hz, 2H), 7.65 (m, 2H), 7.43 (d, *J* = 7.6 Hz, 2H), 7.04 (m, 4H), 6.83 (m, 3H). ^{13}C NMR ($CDCl_3$) δ: 225.11 (br, CO), 141.08 (d, $J_{P,C}$ = 10 Hz), 140.52 (d, $J_{P,C}$ = 48 Hz), 133.57 (s), 130.89 (s), 130.72 (d, $J_{P,C}$ = 13 Hz), 130.47 (d, $J_{P,C}$ = 11 Hz), 129.96 (s), 128.96 (d, $J_{P,C}$ = 2 Hz), 128.86 (d, $J_{P,C}$ = 3 Hz), 121.80 (d, $J_{P,C}$ = 6 Hz). ^{31}P{^{1}H} NMR ($CDCl_3$) δ: 68.

Solutions of **9** and **10** in refluxing xylenes decomposed over a period of 12 h to yield 1-phenyldibenzophosphole (**6**) as shown by ^{31}P and ^{1}H NMR.

© 2001 NRC Canada

Preparation of bis(μ_2-dibenzophospholyl)-dimanganese-octacarbonyl (11)

A solution of dimanganese decacarbonyl (0.28 g, 0.710 mmol) in xylenes (10 cm^3) was added dropwise to a solution of bis(1,1′-dibenzophospholyl) (0.26 g, 0.710 mmol) in xylenes (10 cm^3) to give a yellow mixture. This was heated to reflux, becoming very dark brown in colour. Within 30 min a yellow solid precipitate formed. After 1.5 h the orange-brown mixture was slowly cooled to room temperature. The solvent was decanted and the solid washed with hexane (40 cm^3) to give **11** as a bright yellow solid. Yield: 0.39 g, 0.27 mmol, 78%, mp 240°C (dec.). EI-MS^+ *m/z* (%): 588 (86) $[C_{28}H_{16}P_2Mn_2O_4]^+$, $[(C_{12}H_8P)_2Mn_2(CO)_4]^+$; 560 (73) $[C_{27}H_{16}P_2Mn_2O_3]^+$, $[(C_{12}H_8P)_2Mn_2(CO)_3]^+$; 476 (100) $[C_{24}H_{16}P_2Mn_2]^+$, $[(C_{12}H_8P)_2Mn_2]^+$; 421 (74) $[C_{24}H_{16}P_2Mn]^+$, $[(C_{12}H_8P)_2Mn]^+$; 366 (86) $[C_{24}H_{16}P_2]^+$, $[(C_{12}H_8P)_2]^+$; 238 (18) $[C_{12}H_8PMn]^+$; 183 (90) $[C_{12}H_8P]^+$. IR (KBr disk) (cm^{-1}) ν_{CO}: 1970 (s), 1998 (s), 2058 (s). ^{1}H NMR (acetone-d_6) δ: 8.89 (m, 2H), 8.33 (d, *J* = 7.6 Hz, 2H), 7.84 (dd, *J* = 7.6, 7.6 Hz, 2H), 7.74 (dd, *J* = 7.6, 7.6 Hz, 2H). ^{13}C NMR (acetone-d_6, HMQC and HMBC) δ: 146, 142, 129, 129, 127, 122. ^{31}P NMR (acetone-d_6, HMBC) δ: –83. Anal. calcd. for $C_{32}H_{16}O_8P_2Mn_2$: C 54.86, H 2.30; found: C 54.36, H 2.34.

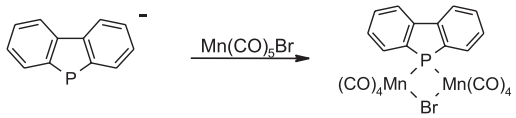
Heating **11** in refluxing xylenes or decane for 3 h yielded only intractable decomposition products.

X-ray diffraction experiments

Crystals suitable for diffraction studies were grown at –23°C by vapour diffusion of CH_2Cl_2–hexanes (**7**, **8**, **11**), CH_2Cl_2–methanol (**9**), or ether–pentane (**10**). Single crystals of **7** and **9** were mounted in thin-walled glass capillaries. Data were collected on a Rigaku AFC5R diffractometer using ω – 2θ scans at 16° per min to a max of 6 scans, ±*h*, –*k*, and ±*l* being collected in each case. Absorption corrections were made using ψ-scans. Crystal decay was not observed for **9** and a decay of 4% was corrected for **7**. Crystals of **8** and **11** were mounted on thin-glass fibers using epoxy cement, and crystals of **10** were coated with Paratone-N oil, mounted on a glass fiber, and frozen in the cold nitrogen stream of the goniometer. Data were collected on a Bruker AXS P4/SMART 1000 diffractometer using ω and ϕ scans with a scan width of 0.3° and 30 s exposure times. A hemisphere of data was collected at a detector distance of 4 cm. Crystal decay was not observed. The data were reduced (SAINT) (32) and corrected for absorption (SADABS) (33).

All structures were solved by direct-methods and refined by full-matrix least-squares on F^2 (SHELXTL) (34). All non-hydrogen atoms were refined anisotropically. Hydrogen atoms were located and refined isotropically where possible. Calculated positions and refinement based on a riding model were employed for **8** and **9** as well as the solvent molecule in **10**. Crystallographic data are summarized in Table 1 and selected interatomic distances and angles are presented in Tables 2–6 in the *Discussion* section.[3]

Scheme 1.



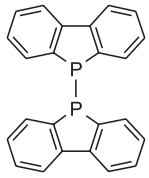
5 **7**

Results

Synthesis and properties

Compound **7** was formed by the reaction between Li-DBP and $Mn(CO)_5Br$ in THF at room temperature (Scheme 1).

The yields of **7** increased when $Mn(CO)_5Br$ was in excess, reaching a max at a $Mn(CO)_5Br$:Li-DBP ratio of 4:1; ratios below 2:1 yielded predominantly bis(1,1′-dibenzophospholyl) (**8**) as well as **7**.



8

Complexes **9** and **10** were obtained by heating at reflux a solution of **6** and $Mn_2(CO)_{10}$ in xylenes (Scheme 2).

Compound **11** was obtained by heating at reflux a solution of **8** and $Mn_2(CO)_{10}$ in xylenes (Scheme 3).

The products were characterized by elemental analysis, IR and NMR spectroscopies, and mass spectrometry, and X-ray diffraction. The complexes were either orange (**7**) or yellow (**9**–**11**) diamagnetic, crystalline solids. They were mildly air sensitive, but indefinitely stable under an inert atmosphere, both in solution and in the solid state. Compound **11** was insoluble in nonpolar hydrocarbons and only sparingly soluble in polar organic solvents. The remaining complexes were soluble in polar organic solvents, but sparingly soluble in nonpolar hydrocarbons. Compound **7** gave **11** and $(\mu_2\text{-Br})_2Mn_2(CO)_8$ when heated in refluxing xylenes (Scheme 4).

Compounds **9** and **10** decomposed slowly in refluxing xylenes to give **6** as the only product containing phosphorus, while **11** yielded only intractable decomposition products on prolonged heating in refluxing xylenes or decane.

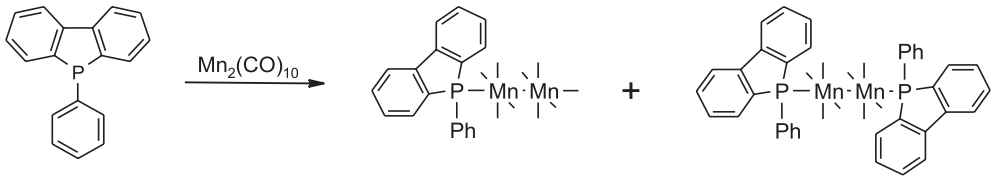
Discussion

Summarizing the results, reaction of the DBP anion **5** with $Mn(CO)_5Br$ yielded the complex $(\mu_2\text{-DBP})(\mu_2\text{-Br})Mn_2(CO)_8$ (**7**), and reaction of bis(1,1′-dibenzophospholyl) (**8**) with

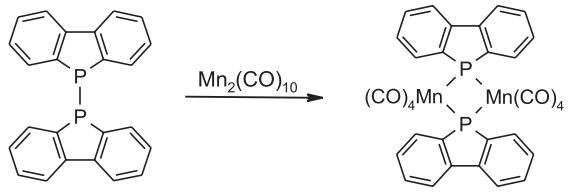
[3] Tables of crystallographic data, atomic coordinates, interatomic distances and angles, anisotropic displacement parameters, and hydrogen atom coordinates have been deposited. Copies may be purchased from the Depository of Unpublished Data (DUD No. 4304), Document Delivery, CISTI, National Research Council Canada, Ottawa, ON, Canada K1A 0S2 (http://www.nrc.ca/cisti/irm/unpub_e.shtml for information on ordering electronically). Crystallographic data for the structures has been deposited with the Cambridge Crystallographic Data Centre (CCDC 161701 (**7**), 161702 (**8**), 161703 (**9**), 161704 (**10**), and 161705 (**11**)). Copies of the data can be obtained on request from: The Director, Cambridge Crystallographic Data Centre, University Chemical Laboratory, 12 Union Road, Cambridge, CB2 1EZ, U.K. (fax: 44-1223-336033 or e-mail: deposit@ccdc.cam.ac.uk).

© 2001 NRC Canada

Scheme 2.



Scheme 3.



Scheme 4.

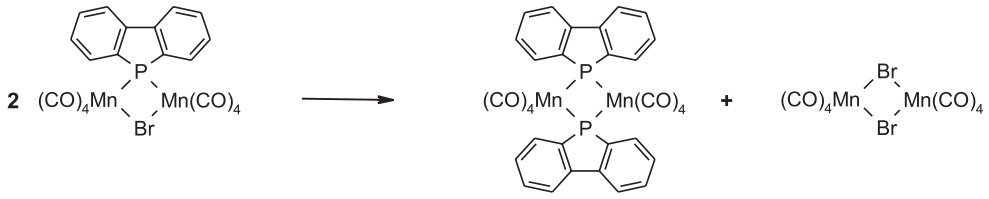


Fig. 1. View of **7**, thermal ellipsoids at the 30% probability level.

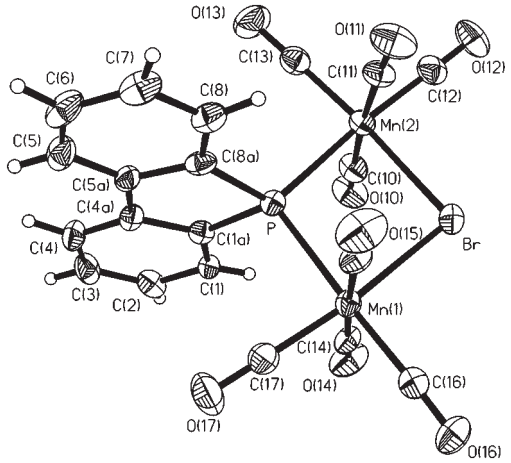
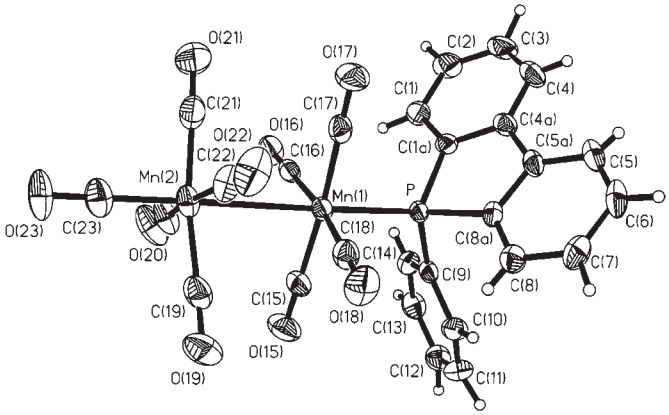


Fig. 2. View of **9**, thermal ellipsoids at the 30% probability level.



$Mn_2(CO)_{10}$ gave $(\mu_2\text{-DBP})_2Mn_2(CO)_8$ (**11**). The phosphine adducts $(Ph\text{-DBP})Mn_2(CO)_9$ (**9**) and $(Ph\text{-DBP})_2Mn_2(CO)_8$ (**10**) were obtained when Ph-DBP (**6**) was reacted with $Mn_2(CO)_{10}$. In all of the complexes the manganese was σ-coordinated by the phosphorus atom of the ligand. There was no involvement of the ligand's π-electrons. In contrast, the fluorenyl complex $(\eta^5\text{-}C_{13}H_9)Mn(CO)_3$ was prepared by reaction of the fluorenide anion with $Mn(CO)_5Br$ (21)[2], while η^5-phospholyl complexes were obtained by reaction of either 1-phenylphospholes or bis(1,1′-phospholyls) with $Mn_2(CO)_{10}$ (35–39).

The related phosphindolyl ligands **3** and **4** can act as π-donors (8, 29, 40) and it seemed reasonable that DBP could behave as a π-donor ligand as well. However, it appears that increasing benzannelation of the phospholyl skeleton decreases the ability of the ligand to bind in an η^5-fashion. Coordination of a metal to the central five-membered ring in DBP would result in a very unfavourable loss of local aromaticity in the six-membered rings. This effect is reduced for the phosphindolyl ligands **3** and **4** because of the lower degree of benzannelation and is absent for the phospholyl ligand **2** because it is not benzannelated. This argument is supported by the observation

© 2001 NRC Canada

Fig. 3. View of **10**, thermal ellipsoids at the 30% probability level. Hydrogen atoms have been omitted for clarity.

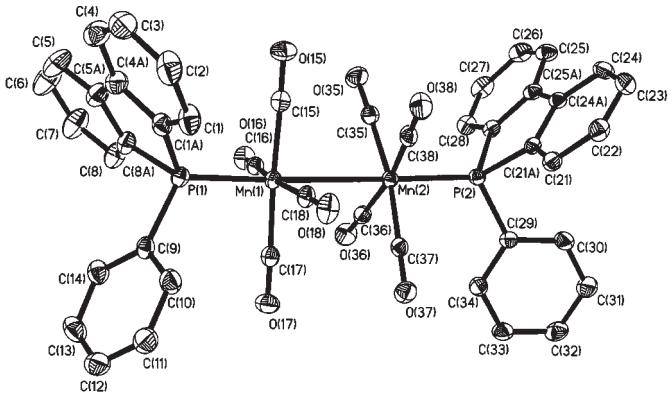
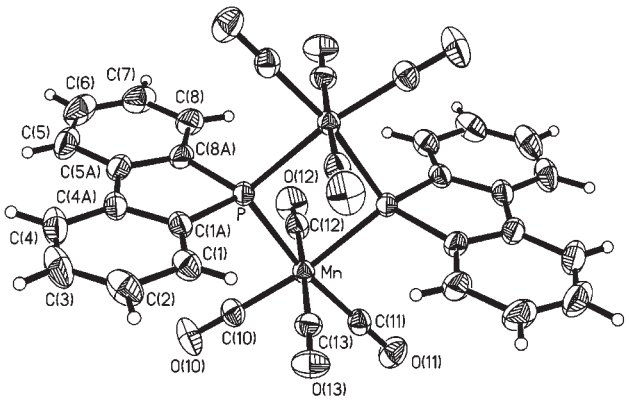
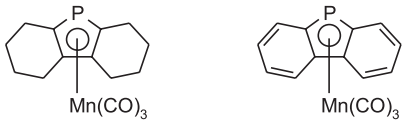


Fig. 4. View of **11**, thermal ellipsoids at the 30% probability level.



that the phosphindolyl ligand **3** (BP) can form (η^5-BP)$_2$Sm(THF)$_2$, whereas DBP gave (η^1-DBP)$_2$Sm(THF)$_4$ (29).

Local aromaticity in the six-membered rings is absent in the hydrogenated ligand DBP-H$_8$, for which the π-complex (η^5-DBP-H$_8$)Mn(CO)$_3$ (**12**) is known (39). There was no evidence for (η^5-DBP)Mn(CO)$_3$ (**13**) even as an intermediate in the reaction of **5** and Mn(CO)$_5$Br to give **7**.



12 **13**

Ligands **2**–**4** normally coordinate through their π-electrons and complexes containing bridging phospholyl ligands, as found in (μ_2-DBP)(μ_2-Br)Mn$_2$(CO)$_8$ (**7**) and (μ_2-DBP)$_2$Mn$_2$(CO)$_8$ (**11**) are rare. It was proposed on the basis of IR spectroscopy that (μ_2-BP)(μ_2-Br)Mn$_2$(CO)$_8$, a product of the reaction of Mn(CO)$_5$Br with **3**, contains a bridging phospholyl ligand (35). The only analogues of **7** that have been crystallographically analyzed are Cu and Ag complexes of **4** (10–13). The closest analogue to **11** is (μ_2-BP)$_2$Mn$_2$(CO)$_8$, isolated as a by-product from the reaction of Mn(CO)$_5$Br with **3** (35). Complexes in which the μ_2-DBP ligand has been authenticated are limited to (μ_2-DBP)$_2$Mo$_2$(CO)$_8$ and (μ_2-DBP)$_2$Mo$_2$(H-DBP)(CO)$_7$ (41).

The addition of a P—P bond across an Mn—Mn bond, as is the case in the reaction of **8** with Mn$_2$(CO)$_{10}$ to yield the bridged complex (μ_2-DBP)$_2$Mn$_2$(CO)$_8$ (**11**) is unusual for phospholyl compounds, but was observed for diphosphines, as in the reaction between Ph$_2$P—PPh$_2$ and Mn$_2$(CO)$_{10}$, which gave (μ_2-PPh$_2$)$_2$Mn$_2$(CO)$_8$ (42). The thermal rearrangement of **7** to yield **11** and (μ_2-Br)$_2$Mn$_2$(CO)$_8$ is surprising. An associative bimolecular mechanism is unlikely because the steric bulk of the DBP ligand would prohibit formation of the requisite dimer. The reaction most probably proceeds by breaking the Mn—P and Mn—Br bonds, followed by recombination of the resulting radicals. The reaction is quantitative and driven by the insolubility of **11**.

Molecular structures

A thermal ellipsoid plot of **7** is shown in Fig. 1 and selected interatomic distances and angles are presented in Table 2. The phosphorus atom is tetrahedrally coordinated and the manganese atoms adopt a distorted octahedral geometry. The four-membered Mn$_2$PBr ring forms a planar parallelogram with almost equal P—Mn distances (2.374(2) and 2.370(2) Å) and Mn—Br distances (2.536(1) and 2.548(2) Å). Obtuse angles are found at the bromine (93.12(5)°) and phosphorus atoms (102.20(7)°) and acute angles at the manganese centers (average, 82.34(6)°). The DBP skeleton is planar and almost orthogonal to the Mn$_2$PBr ring (torsion angle, 87.6°). The Mn···Mn distance is 3.692 Å and therefore no direct Mn–Mn interaction is present. Few compounds containing the (μ_2-PR$_2$)(μ_2-X)Mn$_2$(CO)$_8$ unit have been structurally characterized; their metric parameters compare well with those for **7** (43–45).

Thermal ellipsoid plots of **9** and **10** are depicted in Figs. 2 and 3, and interatomic distances and angles are presented in Tables 3 and 4, respectively. Both **9** and **10** contain six-coordinate manganese and four-coordinate phosphorus. The Ph-DBP ligand is axial in both complexes, as is common in Mn$_2$(CO)$_{10-n}$(PR$_3$)$_n$ (n = 1, 2) derivatives for steric reasons (46). The carbonyl groups of the Mn(CO)$_4$ units are staggered in both molecules. The Ph-DBP ligands adopt orientations in which the P–Ph tensors are staggered with respect to the carbonyl ligands on the nearest metal atom. In the disubstituted complex **10**, the Ph-DBP ligands are oriented such that the two phenyl groups are in a *cis*-conformation. The geometry of the Ph-DBP ligands in **9** and **10** are similar to other Ph-DBP metal complexes (47).

A thermal ellipsoid plot of **11** is shown in Fig. 4 and selected interatomic distances and angles are presented in Table 5. Compound **11** crystallizes in the monoclinic space group *C*2/*c* with four molecules per unit cell. The molecule is symmetric and as a result the Mn$_2$P$_2$ ring is planar, the two DBP ligands reside in the same plane and are orthogonal to the Mn$_2$P$_2$ ring. In the four-membered ring, the angles at phosphorus are 102.12(2)° and thus identical to that found in **7**, while the angles at the manganese centers in **11** are 77.88(2)°, compared to 82.34(6)° in **7**. The Mn$_2$P$_2$ ring exhibits two sets of Mn—P distances: 2.3670(4) and 2.3718(5) Å. These are comparable to those

© 2001 NRC Canada

Table 1. Crystal data and structure refinement for **7**–**11**.

	7	**8**	**9**	**10**·C_5H_{12}	**11**
Empirical formula	$C_{20}H_8BrO_8PMn_2$	$C_{24}H_{16}P_2$	$C_{27}H_{13}O_9PMn_2$	$C_{49}H_{38}O_8P_2Mn_2$	$C_{32}H_{16}O_8P_2Mn_2$
FW	597.02	366.31	622.22	926.61	700.27
Crystal size (mm)	0.06 × 0.18 × 0.20	0.10 × 0.28 × 0.28	0.10 × 0.40 × 0.45	0.05 × 0.30 × 0.35	0.08 × 0.20 × 0.33
Colour and habit	Orange plate	Pale yellow plate	Yellow plate	Yellow plate	Yellow plate
T (K)	296(1)	293(2)	296(1)	173(1)	298(2)
Wavelength (Å)	0.71073	0.71073	0.71073	0.71073	0.71073
Crystal syst.	Triclininc	Monoclinic	Triclinic	Monoclinic	Monoclinic
Space group	$P\bar{1}$	$P2_1/n$	$P\bar{1}$	$P2_1/c$	$C2/c$
a (Å)	8.473(2)	11.1868(7)	8.9431(9)	16.3376(8)	13.5769(7)
b (Å)	8.688(2)	5.6227(3)	12.1250(9)	18.2764(9)	11.0368(5)
c (Å)	15.324(3)	13.9311(8)	13.727(1)	14.9229(7)	19.5242(9)
α (°)	86.19(3)	90	69.098(6)	90	90
β (°)	79.45(3)	100.595(1)	71.976(7)	105.350(1)	94.139(1)
γ (°)	87.89(3)	90	78.037(8)	90	90
Volume (Å^3)	1106.2(4)	861.33(9)	1314.4(2)	4296.9(4)	2918.0(2)
Z	2	2	2	4	4
Abs. coeff. (mm^{-1})	3.064	0.257	1.074	0.717	1.028
θ range (°)	2.57–28.00	2.15–29.99	1.64–24.37	1.71–27.50	2.09–30.00
No. of reflns. collected	7748	8059	4488	34 720	13 975
No. of indep. reflns./R(int)	4565/0.1212	2508/0.0212	4262/0.0451	9880/0.0387	4264/0.0225
Min/max transmision	0.678/1.000	0.778/1.000	0.69/1.00	0.776/0.928	0.791/0.928
Data/restraints/parameters	4561/0/314	2508/0/150	4261/0/354	9880/0/654	4264/0/231
S (GoF) on F^2 [a]	0.995	1.054	1.066	0.927	0.915
$R_1(I > 2\sigma(I))$[b]	0.0422	0.0355	0.049	0.0414	0.0312
wR_2 (all data)[c]	0.081	0.1063	0.1596	0.0979	0.075
Largest diff. peak/hole (e Å^{-3})	0.392/–0.399	0.463/–0.157	0.653/–0.568	0.680/–0.476	0.397/–0.164

[a] $S = [\sum w(F_o^2 - F_c^2)^2/(n-p)]^{1/2}$. [b] $R_1 = \sum||(F_o| - |F_c||/\sum|F_o|$. [c] $wR_2 = [\sum w(F_o^2 - F_c^2)^2/\sum[wF_o^4])^{1/2}$, where $w^{-1} = \sigma^2(F_o^2) + (aP)^2 + bP$, and $P = (\max(F_o^2, 0) + 2F_c^2)/3$. For **7**, $a = 0.10$, $b = 0$; for **8**, $a = 0.0672$, $b = 0$; for **9**, $a = 0.085$, $b = 1.85$; for **10**, $a = 0.0509$, $b = 0$; for **11**, $a = 0.042$, $b = 0$.

Table 2. Selected bond distances (Å) and angles (°) for **7**.

Bond distances (Å)		Bond angles (°)	
Br—Mn(1)	2.536(1)	Mn(1)-Br-Mn(2)	93.12(5)
Br—Mn(2)	2.548(2)	P-Mn(1)-Br	82.43(6)
Mn(1)—P	2.374(2)	P-Mn(2)-Br	82.24(6)
Mn(2)—P	2.370(2)	Mn(2)-P-Mn(1)	102.20(7)
P—C(1A)	1.816(6)	C(1A)-P-C(8A)	89.7(3)
P—C(8A)	1.820(6)	C(4A)-C(1A)-P	112.1(4)
C(1A)—C(4A)	1.393(7)	C(1A)-C(4A)-C(5A)	113.4(5)
C(4A)—C(5A)	1.460(8)	C(8A)-C(5A)-C(4A)	113.0(5)
C(5A)—C(8A)	1.407(7)	C(5A)-C(8A)-P	111.7(4)

Table 3. Selected bond distances (Å) and angles (°) for **9**.

Bond distances (Å)		Bond angles (°)	
Mn(1)—P	2.2480(13)	P-Mn(1)-Mn(2)	178.37(4)
Mn(1)—Mn(2)	2.9198(10)	C(23)-Mn(2)-Mn(1)	178.4(2)
P—C(9)	1.816(5)	C(9)-P-C(8A)	104.6(2)
P—C(8A)	1.819(4)	C(9)-P-C(1A)	104.1(2)
P—C(1A)	1.821(4)	C(8A)-P-C(1A)	90.7(2)
C(1A)—C(4A)	1.387(7)	C(9)-P-Mn(1)	115.00(14)
C(4A)—C(5A)	1.479(7)	C(8A)-P-Mn(1)	120.0(2)
C(5A)—C(8A)	1.410(7)	C(1A)-P-Mn(1)	118.8(2)
		C(4A)-C(1A)-P	111.4(4)
		C(1A)-C(4A)-C(5A)	113.9(4)
		C(8A)-C(5A)-C(4A)	112.9(4)
		C(5A)-C(8A)-P	111.1(4)

© 2001 NRC Canada

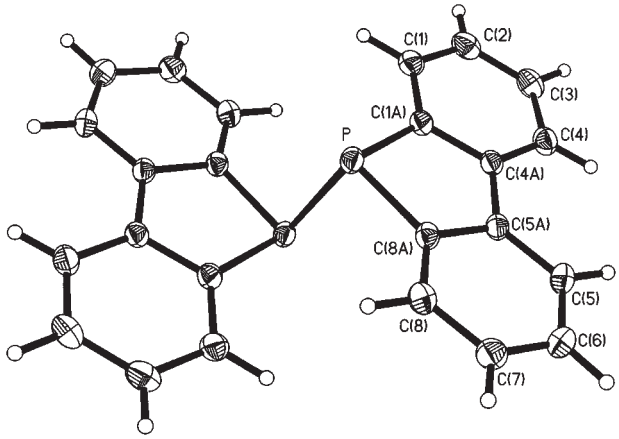
Table 4. Selected bond distances (Å) and angles (°) for **10**.

Bond distances (Å)		Bond angles (°)	
Mn(1)—P(1)	2.2223(7)	P(2)-Mn(2)-Mn(1)	176.96(2)
Mn(1)—Mn(2)	2.8937(5)	C(8A)-P(1)-C(1A)	91.27(13)
Mn(2)—P(2)	2.2309(7)	C(8A)-P(1)-C(9)	105.11(12)
P(1)—C(8A)	1.813(3)	C(1A)-P(1)-C(9)	104.07(11)
P(1)—C(1A)	1.819(3)	C(8A)-P(1)-Mn(1)	119.22(9)
P(1)—C(9)	1.823(3)	C(1A)-P(1)-Mn(1)	116.56(9)
C(1A)—C(4A)	1.400(4)	C(9)-P(1)-Mn(1)	116.85(8)
C(4A)—C(5A)	1.465(4)	C(4A)-C(1A)-P(1)	111.27(19)
C(5A)—C(8A)	1.421(4)	C(1A)-C(4A)-C(5A)	113.2(2)
P(2)—C(21A)	1.816(2)	C(8A)-C(5A)-C(4A)	114.1(2)
P(2)—C(28A)	1.827(2)	C(5A)-C(8A)-P(1)	110.1(2)
P(2)—C(29)	1.834(2)	C(21A)-P(2)-C(28A)	90.20(11)
C(21A)—C(24A)	1.400(3)	C(21A)-P(2)-C(29)	102.64(11)
C(24A)—C(25A)	1.472(3)	C(28A)-P(2)-C(29)	103.63(11)
C(25A)—C(28A)	1.402(3)	C(21A)-P(2)-Mn(2)	117.04(8)
		C(28A)-P(2)-Mn(2)	118.25(8)
		C(29)-P(2)-Mn(2)	120.12(8)
		C(24A)-C(21A)-P(2)	111.95(17)
		C(21A)-C(24A)-C(25A)	113.1(2)
		C(28A)-C(25A)-C(24A)	113.5(2)
		C(25A)-C(28A)-P(2)	111.21(17)

Table 5. Selected bond distances (Å) and angles (°) for **11**.

Bond distances (Å)		Bond angles (°)	
Mn—P′	2.3670(4)	P-Mn-P′	77.882(15)
Mn—P	2.3718(5)	C(1A)-P-C(8A)	90.19(8)
P—C(1A)	1.8240(15)	C(1A)-P-Mn′	117.52(5)
P—C(8A)	1.8243(15)	C(8A)-P-Mn′	116.42(5)
C(1A)—C(4A)	1.406(2)	C(1A)-P-Mn	115.63(5)
C(4A)—C(5A)	1.460(3)	C(8A)-P-Mn	115.78(6)
C(5A)—C(8A)	1.389(2)	Mn-P-Mn′	102.118(15)
		C(4A)-C(1A)-P	110.69(12)
		C(1A)-C(4A)-C(5A)	113.95(14)
		C(8A)-C(5A)-C(4A)	113.48(14)
		C(5A)-C(8A)-P	111.65(13)

Fig. 5. View of **8**, thermal ellipsoids at the 30% probability level.



© 2001 NRC Canada

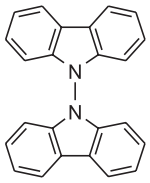
Table 6. Selected bond distances (Å) and angles (°) for **8**.

Bond distances (Å)		Bond angles (°)	
P—P′	2.2501(6)	C(1A)-P-C(8A)	89.42(6)
P—C(1A)	1.8238(13)	C(1A)-P-P′	97.82(4)
P—C(8A)	1.8241(13)	C(8A)-P-P′	97.82(4)
C(1A)—C(4A)	1.4091(17)	C(4A)-C(1A)-P	112.25(9)
C(4A)—C(5A)	1.4646(18)	C(1A)-C(4A)-C(5A)	112.88(11)
C(5A)—C(8A)	1.4049(17)	C(8A)-C(5A)-C(4A)	113.23(11)
		C(5A)-C(8A)-P	112.22(9)

in related bis(μ_2-phosphido)-dimanganese-octacarbonyls (48). The Mn···Mn distance is 3.686 Å, precluding a direct Mn–Mn interaction.

Compounds containing P—P bonds, such as bis(1,1′-dibenzophospholyl) (**8**) are of current interest (49–51). A thermal ellipsoid plot of **8** is shown in Fig. 5 and selected interatomic distances and angles are presented in Table 6.

Compound **8** crystallizes in the monoclinic space group $P2_1/n$ with two molecules per unit cell, each molecule lying on an inversion center. As a result the two DBP ring systems are coplanar. This is in contrast to the homologue 9,9′-bicarbazyl (**14**) where the two ring systems make a torsion angle of 72° (52). The difference in the torsion angles of **8** and **14** is explained by the decrease in repulsive H···H interactions as a consequence of the longer P—P (2.2501(6) Å) vs. N—N (average, 1.370 Å) distance.



14

The P—P distance in **8** is similar to other hindered diphosphines which range from 2.244(2) to 2.260(2) Å (53–55). Diphosphines with sterically less demanding substituents display shorter P—P bond lengths (2.190(1)–2.217(1) Å) (49, 56–59).

Acknowledgments

Professor T. Stanley Cameron (Dalhousie University) is thanked for the diffraction data for **7** and **9**, Dr. Larry Calhoun (UNB) for assistance with the NMR experiments, and Mr. Gilles Vautour (UNB) for mass spectrometry. We are grateful to the Natural Sciences and Engineering Research Council of Canada (NSERC) for financial support of this work.

References

1. F. Mathey. Coord. Chem. Rev. **137**, 1 (1994).
2. F. Mathey. Chem. Rev. **88**, 429 (1988).
3. F. Mathey and P.L. Floch. Coord. Chem. Rev. **179**–**180**, 771 (1988).
4. F. Mathey. New J. Chem. **11**, 585 (1987).
5. C. Janiak, U. Versteeg, K.C.H. Lange, R. Weimann, and E. Hahn. J. Organomet. Chem. **501**, 219 (1995).
6. S.J. Brown, X. Gao, D.G. Harrison, L. Koch, R.E.v.H. Spence, and G.P.A. Yap. Organometallics, **17**, 5445 (1998).
7. C. Janiak, K.C.H. Lange, U. Versteeg, D. Lentz, and P.H.M. Budzelaar. Chem. Ber. **129**, 1517 (1996).
8. D. Gudat, S. Häp, L. Szarvas, and M. Nieger. Chem. Commun. 1637 (2000).
9. D. Gudat, M. Nieger, and M. Schrott. Chem. Ber. **128**, 259 (1995).
10. D. Gudat, M. Schrott, and M. Nieger. J. Chem. Soc. Chem. Commun. 1541 (1995).
11. D. Gudat, M. Schrott, V. Bajorat, M. Nieger, S. Kotila, R. Fleischer, and D. Stalke. Chem. Ber. **129**, 337 (1996).
12. D. Gudat, A.W. Holderberg, N. Korber, M. Nieger, and M. Schrott. Z. Naturforsch. B, **54**, 1244 (1999).
13. D. Gudat, M. Schrott, V. Bajorat, M. Nieger, S. Kotila, R. Fleischer, and D. Stalke. Chem. Ber. **129**, 337 (1996).
14. D. Gudat. Coord. Chem. Rev. **163**, 71 (1997).
15. T. Clark, A. Elvers, F.W. Heinemann, M. Hennemann, M. Zeller, and U. Zenneck. Angew. Chem. Int. Ed. **39**, 2087 (2000).
16. A. Dransfeld, L. Nyulaszi, and P.v.R. Schleyer. Inorg. Chem. **37**, 4413 (1998).
17. B. Goldfuss and P.v.R. Schleyer. Organometallics, **16**, 1543 (1997).
18. B. Goldfuss, P.v.R. Schleyer, and F. Hampel. Organometallics, **15**, 1755 (1996).
19. F. Mathey. J. Organomet. Chem. **475**, 25 (1994).
20. G. Keglevich, Z. Böcskei, G.M. Kesertii, K. Ujszászy, and L.D. Quin. J. Am. Chem. Soc. **119**, 5095 (1997).
21. R.B. King and A. Efraty. J. Organomet. Chem. **23**, 527 (1970).
22. A.I. Yarmolenko, S.V. Kukharenko, L.N. Novikova, N.A. Ustynyuk, F.M. Dolgushin, A.I. Yanovsky, Yu.T. Struchkov, T.A. Kraftaeva, Yu.F. Oprunenko, and V.V. Strelets. Izv. Akad. Nauk. Khim.+ **45**, 199 (1996).
23. P.M. Treichel and J.W. Johnson. J. Chem. Soc. Chem. Commun. 688 (1976).
24. P.M. Treichel and J.W. Johnson. Inorg. Chem. **16**, 749 (1977).
25. N.E. Kolobova, V.I. Zolanovic and I.A. Lobanova. Izv. Akad. Nauk. Khim.+ 1651 (1980).
26. D.D. Perrin, W.L.F. Armarego, and D.R. Perrin. Purification of laboratory chemicals. Pergamon Press, New York. 1980.
27. E.W. Abel and G. Wilkinson. J. Chem. Soc. 1501 (1959).
28. S. Affandi, R.L. Green, B.T. Hsieh, M.S. Holt, J.H. Nelson, and E.C. Alyea. Syn. React. Inorg. Met. **17**, 307 (1987).
29. F. Nief and L. Ricard. J. Organomet. Chem. **464**, 149 (1994).
30. E.H. Braye, I. Caplier, and R. Saussez. Tetrahedron, **27**, 5523 (1971).
31. E.W. Abel and I.S. Butler. J. Chem. Soc. Faraday Trans. **63**, 45 (1967).

© 2001 NRC Canada

32. SAINT 6.02. Bruker AXS, Inc. Madison, Wisconsin, U.S.A. 1997–1999.
33. G.M. Sheldrick. SADABS, Bruker AXS, Inc. Madison, Wisconsin, U.S.A. 1999.
34. G.M. Sheldrick. SHELXTL 5.1. Bruker AXS, Inc. Madison, Wisconsin, U.S.A. 1997.
35. F. Nief, C. Charrier, F. Mathey, and M. Simalty. Phosphorus Sulfur, **13**, 259 (1982).
36. B. Deschamps, L. Ricard, and F. Mathey. Organometallics, **18**, 5688 (1999).
37. C. Charrier, H. Bonnard, and F. Mathey. J. Org. Chem. **47**, 2376 (1982).
38. E.W. Abel, N. Clark, and C. Towers. J. Chem. Soc. Dalton Trans. 1552 (1979).
39. F. Mathey and D. Thavard. Can. J. Chem. **56**, 1952 (1978).
40. E. Niecke, M. Nieger, and P. Wenderoth. Angew. Chem. Int. Ed. Engl. **33**, 353 (1994).
41. K. Maitra, V.J. Catalano, and J.H. Nelson. Bull. Soc. Chim. Fr. **134**, 471 (1997).
42. R.G. Hayter. J. Am. Chem. Soc. **86**, 823 (1964).
43. U. Flörke. Z. Kristallogr. **211**, 908 (1996).
44. U. Flörke and H.-J. Haupt. Acta Crystallogr. C, **53**, 876 (1997).
45. U. Flörke and H.-J. Haupt. Acta Crystallogr. C, **53**, 1799 (1997).
46. (*a*) H. Masuda, T. Taga, T. Sowa, T. Kawamura, and T. Yonezawa. Inorg. Chim. Acta, **101**, 45 (1985); (*b*) J.J. Hunt, E.N. Duesler, and R.T. Paine. J. Organomet. Chem. **320**, 307 (1987); (*c*) K. Henrick, M. McPartlin, J.A. Iggo, A.C. Kemball, M.J. Mays, and P.R. Raithby. J. Chem. Soc. Dalton Trans. 2669 (1987); (*d*) T.S.A. Hor, H.S.O. Chan, K.-L. Tan, L.-T. Phang, and Y.K. Yan. Polyhedron, **10**, 2437 (1991); (*e*) J. Münchenberg, A.K. Fischer, H. Thönnessen, P.G. Jones, and R. Schmutzler. J. Organomet. Chem. **529**, 361 (1997); (*f*) U. Flörke and H.-J. Haupt. Z. Kristallogr. New Cryst. Struct. **213**, 267 (1998); (*g*) U. Flörke and H.-J. Haupt. Z. Kristallogr. **191**, 153 (1990); (*h*) M.R. Churchill and A. Holladay. Cryst. Struct. Commun. **10**, 1263 (1981).
47. (*a*) J.F. Gallagher, E.C. Alyea, and G. Ferguson. Croat. Chem. Acta, **72,** 243 (1999); (*b*) N. Gul and J.H. Nelson. Organometallics, **18**, 709 (1999); (*c*) H. Zhang, J. Jiang, N. Yang, H. Dang, and B.K. Teo. J. Cluster Sci. **9**, 547 (1998); (*d*) S. Attar, V.J. Catalano, and J.H. Nelson. Organometallics, **15**, 2932 (1996); (*e*) J.M. Kessler, J.H. Nelson, J.S. Frye, A. DeCian, and J. Fischer. Inorg. Chem. **32**, 1048 (1993); (*f*) G.A. Bowmaker, H.J. Clase, N.W. Alcock, J.M. Kessler, J.H. Nelson, and J.S. Frye. Inorg. Chim. Acta, **210**, 107 (1993); (*g*) T.K. Miyamoto, Y. Matsuura, K. Okude, H. Ichida, and Y. Sasaki. J. Organomet. Chem. **373**, C8 (1989); (*h*) S. Affandi, J.H. Nelson, N.W. Alcock, O.W. Howarth, E.C. Alyea, and G.M. Sheldrick. Organometallics, **7**, 1724 (1988); (*i*) Y. Matsuura, K. Okude, H. Ichida, T.K. Miyamoto, and Y. Sasaki. Acta Cryst. C, **48**, 357 (1992); (*j*) S. Attar, N.W. Alcock, G.A. Bowmaker, J.S. Frye, W.H. Bearden, and J.H. Nelson. Inorg. Chem. **30**, 4166 (1991); (*k*) S. Attar, W.H. Bearden, N.W. Alcock, E.C. Alyea, and J.H. Nelson. Inorg. Chem. **29**, 425 (1990).
48. (*a*) U. Flörke, O. Krampe, and H.-J. Haupt. Acta Crystallogr. C, **54**, 918 (1998); (*b*) H. Masuda, T. Taga, K. Machida, and T. Kawamura. J. Organomet. Chem. **331**, 239 (1987); (*c*) B. Deppisch, H. Schäfer, D. Binder, and W. Leske. Z. Anorg. Allg. Chem. **519**, 53 (1984); (*d*) U. Flörke and H.-J. Haupt. Acta Crystallogr. C, **49**, 374 (1993); (*e*) H. Vahrenkamp. Chem. Ber. **111**, 3472 (1978).
49. J.K. Vohs, P. Wei, J. Su, B.C. Beck, S.D. Goodwin, and G.H. Robinson. J. Chem. Soc. Chem. Commun. 1037 (2000).
50. D. C. Pestana and P.P. Power. J. Am. Chem. Soc. **111**, 6887 (1989).
51. A.H. Cowley, A. Decken, N.C. Norman, C. Krüger, F. Lutz, H. Jacobsen, and T. Ziegler. J. Am. Chem. Soc. **119**, 3389 (1997).
52. G. Boyer, R.M. Claramunt, J. Elguero, M. Fathalla, C. Foces-Foces, C. Jaime, and A.L. Llamas-Saiz. J. Chem. Soc. Perkin Trans. 2, 757 (1993).
53. S.G. Baxter, A.H. Cowley, R.E. Davis, and P. Riley. J. Am. Chem. Soc. **103**, 1699 (1981).
54. S.S. Al-Juaid, P.B. Hitchcock, R.M. Matos, and J.F. Nixon. J. Chem. Soc. Chem. Commun. 267 (1993).
55. G. Becker, W. Golla, J. Grobe, K.W. Klinkhammer, D. Le Van, A.H. Maulitz, O. Mundt, H. Oberhammer, and M. Sachs. Inorg. Chem. **38**, 1099 (1999).
56. R. Richter, J. Kaiser, J. Sieler, H. Hartung, and C. Peter. Acta Crystallogr. B, **33**, 1887 (1977).
57. A. Dashti-Mommertz and B. Neumüller. Z. Anorg. Allg. Chem. **625**, 954 (1999).
58. O. Mundt, H. Riffel, G. Becker, and A. Simon. Z. Naturforsch. B, **43**, 952 (1988).
59. R.A. Alder, C. Ganter, C.J. Harris, andA.G. Orpen. J. Chem. Soc. Chem. Commun. 1170 (1992).

© 2001 NRC Canada

Cadmium complexes of thiones. Part II.[1] A synthetic, solution, and solid-state MAS $^{111/113}$Cd NMR study of cadmium complexes of 1,3-thiazolidine-2-thione, and the structures of [tetrakis(1,3-thiazolidine-2-thione)cadmium] trifluoromethanesulfonate ($[Cd(C_3H_5NS_2)_4](CF_3SO_3)_2$) and [tetrakis(1,3-thiazolidine-2-thione)cadmium][tetrakis(nitrato-*O,O′*)cadmate] ($[Cd(C_3H_5NS_2)_4][Cd(O_2NO)_4]$)

Umarani Rajalingam, Philip A.W. Dean, Hilary A. Jenkins, Michael Jennings, and James M. Hook

Abstract: Treatment of $Cd(O_3SCF_3)_2$ with the stoichiometric quantity of 1,3-thiazolidine-2-thione (tztH) allows isolation of $[Cd(tztH)_4](O_3SCF_3)_2$ (**1**). When tztH:Cd ≥ 2 the reaction of $Cd(NO_3)_2{\cdot}4H_2O$ with tztH leads to $[Cd(tztH)_4][Cd(O_2NO)_4]$ (**2**). The structures of both **1** and **2** have been determined by single crystal X-ray analysis. Colourless crystals of **1** are orthorhombic, space group *Fdd*2, with eight molecules per unit cell (Z = 8) of dimensions a = 20.139(3), b = 23.332(5), c = 14.214(3) Å. Those of **2** are tetragonal, space group $I\bar{4}$, with four molecules per unit cell (Z = 4) of dimensions a = 13.8853(11), c = 8.077(2) Å. The discrete homoleptic cation $[Cd(tztH)_4]^{2+}$ is characterized for the first time in **1** and **2**. The cations are of point group symmetry C_2 and S_4 in **1** and **2**, respectively. In both cases the ligands are S-bound, and the CdS_4 kernel is a squashed tetrahedron. In **2**, the eight-coordinate anion $[Cd(O_2NO)_4]^{2-}$ is characterized for the second time. ^{113}Cd CP MAS NMR data are reported for solid **1** and **2**, and also for solids produced by fusing $Cd(NO_3)_2{\cdot}4H_2O$ with different molar ratios amounts of tztH, and by fusing $Cd(O_3SCF_3)_2$ with six mol equivalents of tztH. In the $Cd(NO_3)_2{\cdot}4H_2O$:tztH mixtures, species identified include unreacted cadmium salt **2** ($[Cd(tztH)_4](NO_3)_2$) and possibly $Cd(tztH)_3(NO_3)_2$. $[Cd(tztH)_4](NO_3)_2$ becomes the major species only when a significant excess of tztH is used. In the mixtures with tztH:Cd > 4, neither $Cd(NO_3)_2{\cdot}4H_2O$ nor $Cd(O_3SCF_3)_2$ form complexes containing more than four tztH ligands. Reduced-temperature ^{111}Cd NMR data are reported for $Cd(ClO_4)_2{\cdot}6H_2O$:tztH mixtures in MeOH. Species identified are $Cd(tztH)_w^{2+}(solv)$ (w = 0–3).

Key words: 1,3-thiazolidine-2-thione, cadmium complexes, X-ray analysis, ^{113}Cd CP MAS NMR, solution ^{111}Cd NMR, tetrakis(1,3-thiazolidine-2-thione)cadmium(2+) cation, tetrakis(nitrato-*O,O′*)cadmate(2–) anion.

Résumé : Le traitement du $Cd(O_3SCF_3)_2$ avec une quantité stoechiométrique de 1,3-thiazolidine-2-thione (tztH) permet d'isoler le $[Cd(tztH)_4](O_3SCF_3)_2$ (**1**). Quand le tztH:Cd ≥ 2, la réaction du $CD(NO_3)_2{\cdot}4H_2O$ avec la tztH conduit à la formation de $[Cd(tztH)_4][Cd(O_2NO)_4]$ (**2**). Les structures des composés **1** et **2** ont été déterminées par diffraction des rayons X par un cristal unique. Les cristaux incolores du composé **1** sont orthorhombiques, groupe d'espace *Fdd*2, avec a = 20,139(3), b = 23,332(5) et c = 14,214(2) Å et Z = 8. Ceux du composé **2** sont orthogonaux, groupe d'espace $I\bar{4}$, avec a = 13,8853(11) et c = 8,077(2) Å et Z = 4. Dans les composés **1** et **2**, on a pu caractériser pour la première fois le cation homoleptique individuel $[Cd(tztH)_4]^{2+}$. Les cations sont respectivement de symétries ponctuelles C_2 et S_4.

Received January 16, 2001. Published on the NRC Research Press Web site at http://canjchem.nrc.ca on September 12, 2001.

Umarani Rajalingam,[2] Philip A.W. Dean,[3] Hilary A. Jenkins,[4] and Michael Jennings. Department of Chemistry, University of Western Ontario, London, ON N6A 5B7, Canada.
James M. Hook.[3] NMR Facility, University of New South Wales, Sydney 2052, Australia.

[1]Reference 2 is regarded as Part I.
[2]Present address: Urecoats Industries Inc., 4100 North Powerline Business Park, Pompano Beach, FL 33073, U.S.A.
[3]Corresponding authors (P.A.W. Dean: telephone: (519) 661-2111 ext 6331; fax: (519) 661-3022; e-mail: pawdean@uwo.ca; J.M. Hook: telephone: 61 2 9385-4689; fax: 61 2 9385-6141; e-mail: j.hook@unsw.edu.au).
[4]Present address: Department of Chemistry, Saint Mary's University, Halifax, NS B3H 3C3, Canada.

 DOI: 10.1139/cjc-79-9-1330 © 2001 NRC Canada

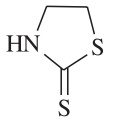
Dans chacun des cas, les ligands sont liés au soufre et le noyau CdS_4 est de forme tétraédrique aplatie. Dans le composé **2**, l'anion octacoordiné $[Cd(O_2NO)_4]^{2-}$ a été caractérisé pour la deuxième fois. On rapporte les données RMN du ^{113}Cd par la méthode CP MAS pour les composés solides **1** et **2** ainsi que pour les solides obtenus par fusion du $Cd(NO_3)_2 \cdot 4H_2O$ avec des rapports molaires divers de tztH ainsi que par la fusion du $Cd(O_3SCF_3)_2$ avec six équivalents molaires de tztH. Dans les mélanges $Cd(NO_3)_2 \cdot 4H_2O$:tztH, les espèces identifiées comprennent le sel de cadmium qui n'a pas réagi, **2**, $[Cd(tztH)_4](NO_3)_2$ et possiblement du $Cd(tztH)_3(NO_3)_2$. Le $[Cd(tztH)_4](NO_3)_2$ ne devient l'espèce majeure que lorsqu'on utilise un excès significatif de tztH. Dans les mélanges où la tztH:Cd > 4, ni le $Cd(NO_3)_2 \cdot 4H_2O$ ni le $Cd(O_3SCF_3)_2$ ne forment de complexes comportant plus de quatre ligands tztH. On rapporte les données relatives à la RMN du ^{111}Cd à température réduite pour des mélanges de $Cd(ClO_4)_2 \cdot 6H_2O$:tztH dans le MeOH. Les espèces identifiées sont les $Cd(tztH)_w^{2+}$ (solv) (w = 0–3).

Mots clés : 1,3-thiazolidine-2-thione, complexes du cadmium, diffraction des rayons X, RMN du ^{113}Cd par CP MAS, cation tétrakis(1,3-thiazolidine-2-thione)cadmium(2+), anion tétrakis(nitrato-*O,O′*)cadmate(2–).

[Traduit par la Rédaction]

Introduction

NMR spectroscopic and structural studies of complexes containing Cd—S bonds have been of long-standing interest in one of our laboratories (1*a–g* and refs. therein). Very recently we have extended this chemistry to include a structural and NMR spectroscopic study of complexes of cadmium with pyridine- and quinoline-thiones (2). In the present paper, we have extended our study of complexes of thiones to those of the heterocyclic ligand 1,3-thiazolidine-2-thione (tztH). Although tztH is known to have an interesting chemistry as a ligand (3), relatively few complexes of this ligand with cadmium have been reported (4–8), and there are no structural or metal NMR data available for homoleptic complexes of tztH with cadmium.



tztH

We provide here structural and solid-state ^{113}Cd NMR data for two salts containing the $[Cd(tztH)_4]^{2+}$ cation. One is an unexpected double salt, and in light of its occurrence, we have also explored the solid-state metal NMR data of mixtures obtained by fusing together tztH and $Cd(NO_3)_2 \cdot 4H_2O$ or $Cd(O_3SCF_3)_2$ (abbreviated $Cd(trif)_2$). Fusion of tztH and $Cd(NO_3)_2 \cdot 4H_2O$ was used earlier (7) to prepare a compound of formula $Cd(tztH)_4(NO_3)_2$.

Experimental

Methods and materials

All manipulations were carried out under an atmosphere of dry N_2(g) in a glove box or with a vacuum–N_2(g) manifold or under Ar(g) in a glove bag. Analar grade solvents (MeCN, $CHCl_3$, CH_2Cl_2, Me_2CO, Et_2O, toluene) were dried over 3 Å molecular sieves and deoxygenated using Ar(g) prior to use.

Before use, thiazolidine-2-thione (tztH) (Aldrich) was recrystallized from ethanol, and $Cd(NO_3)_2 \cdot 4H_2O$ (BDH) and $Cd(ClO_4)_2 \cdot 6H_2O$ (Alfa; both deliquescent) were both dried to a constant hydration state under vacuum in the heated port of the glove box. The literature method was used for the synthesis of anhyd $Cd(trif)_2$ (9). The metal triflate, nitrate, and perchlorate were weighed out in the glove box.

*Synthesis of $[Cd(tztH)_4](CF_3SO_3)_2$ (**1**)*

1,3-Thiazolidine-2-thione (1.19 g, 10.0 mmol) was dissolved in a solution of $Cd(trif)_2$ (1.02 g, 2.48 mmol) in 30 mL of MeCN:CH_2Cl_2 (3:1). At this stage, a 5 mL-portion of the mixture was diluted with another 10 mL of MeCN:CH_2Cl_2, then kept in a freezer (–15°C) for the production of single crystals for X-ray diffraction. The remaining solution was also kept in the freezer and from it, after a few days, was isolated 0.64 g of colourless crystals. These were washed with cold diethyl ether and dried in vacuum. Allowing the filtrate to again stand in the freezer for several days resulted in a further 0.31 g of product. The total prorated yield was 52%, mp 145 to 146°C. Anal. calcd. for $C_{14}H_{20}F_6N_4O_6S_{10}Cd_2$: C 18.95, H 2.27, N 6.31; found: C 19.75, 20.00, H 2.13, 2.25, N 6.08, 6.19. An X-ray analysis of **1** reveals no occluded solvent, and also there was no trace of any Cd-containing impurity in its solid-state ^{113}Cd NMR spectrum (see below).

*Synthesis of $[Cd(tztH)_4][Cd(NO_3)_4]$ (**2**)*

Solutions of $Cd(NO_3)_2 \cdot 4H_2O$ (0.525 g, 1.70 mmol) in MeCN (8 mL) and tztH (0.801 g, 6.72 mmol) in MeCN (10 mL) were mixed at room temperature. After 30 min, colourless crystals were separated by filtration and potential data crystals for X-ray analysis were taken, after which, the bulk was washed with ice cold diethyl ether and vacuum dried. Yield: 1.079 g (67.7%). Anal. calcd. for $C_{12}H_{20}N_8O_{12}S_8Cd_2$: C 15.19, H 2.12, N 11.80; found: C 15.32, 15.14, H 1.55, 1.59, N 11.74, 11.65. The crystals melt in the range 145.8 to 146.4°C, turning yellow with bubbling.

Compound **2** (identified by elemental microanalysis) was also formed from mixtures containing $Cd(NO_3)_2 \cdot 4H_2O$:tztH = 1:2.

Fused tztH:$Cd(NO_3)_2$ and tztH:$Cd(trif)_2$ mixtures

A weighed amount of the thione was added to a tube that contained a teflon-coated magnetic stirrer bar and was topped with a ground-glass socket. In the glove box, the appropriate metal salt was weighed into a tipping tube (10) having the matching ground-glass cone. In the glove bag, the two halves were joined. Then the thione was melted and the metal salt was tipped in with stirring to produce a homoge-

© 2001 NRC Canada

Table 1. Crystal data and structure refinement for $[Cd(tztH)_4](CF_3SO_3)_2$ (**1**) and $[Cd(tztH)_4][Cd(NO_3)_4]$ (**2**).

	1	**2**
Formula	$C_{14}H_{20}F_6N_4O_6S_{10}Cd$	$C_6H_{10}N_4O_6S_4Cd$
FW	887.34	474.82
Crystal system	Orthorhombic	Tetragonal
Space group	*Fdd*2	$I\bar{4}$
a (Å)	20.139(3)	13.8853(11)
b (Å)	23.332(5)	13.8853(11)
c (Å)	14.214(3)	8.077(2)
V (Å^3)	6679(2)	1557.3(4)
Z	8	4
$\rho_{calcd.}$ (g cm^{-3})	1.765	2.025
Crystal size (mm)	0.40 × 0.40 × 0.30	0.40 × 0.30 × 0.30
T (K)	294(2)	294(2)
Radiation	Mo Kα (λ = 0.71073 Å)	Mo Kα (λ = 0.71073 Å)
μ (cm^{-1})	13.48	19.67
Data collection method	ω-scans	ω-scans
θ range (°)	1.96–25.00	2.07–24.97
Total unique reflections measured	1664	999
Total observed reflections	1337[a]	972[a]
Data/restraints/parameters	1664/13/181	997/0/96
Final max Δ/σ	0.602	0.002
Max res. density/hole (e Å^3)	0.533, –0.453	0.258, –0.188
R[b]	0.0501	0.0180
R_w[b]	0.1195[c,d]	0.0453[d,e]
GoF[f]	1.024	1.032

[a] $I > 2\sigma(I)$
[b] $R = \Sigma(F_o - F_c)/\Sigma F_o$ and $R_w = [\Sigma w(F_o^2 - F_c^2)^2/\Sigma w F_o^4]^{1/2}$
[c] $w = 1/[\sigma^2(F_o^2) + (0.1011p)^2 + 21.7378p]$
[d] $p = (F_o^2 + 2F_c^2)/3$
[e] $w = 1/[\sigma^2(F_o^2) + (0.0216p)^2 + 0.1363p]$
[f] GoF = $[\Sigma w(F_o^2 - F_c^2)^2/(n - p)]^{1/2}$, where *n* is the number of reflections and *p* is the number of parameters refined.

neous mixture. The mixture was cooled to solidify it, finely ground in the glove bag, and used for the solid state NMR measurements, either directly or after repeated washings with toluene (3 × 5 mL of toluene per 0.6 g of $Cd(NO_3)_2 \cdot 4H_2O$) followed by drying and regrinding.

NMR spectra

Proton-decoupled solution 63.59 MHz ^{111}Cd NMR spectra were measured at UWO, using a Varian XL-300 spectrometer system, a typical acquisition time of 0.6 s, and inverse-gated decoupling to avoid the negative Overhauser effect (in the more usual ^{113}Cd region, artifacts were present in the frequency range of interest; no primary isotope effect is expected between ^{111}Cd and ^{113}Cd NMR spectra). The spectra were measured with samples in protiated solvents in 10 mm o.d. NMR tubes and a preshimmed field. A ^{2}H field-frequency lock was not used since the field drift was negligible. The samples were referenced to external $Cd(ClO_4)_2$(aq) (0.1 M) at ambient probe temperature (294 ± 2 K). Concentrations of samples in 10 mm o.d. NMR tubes were prepared on the basis of mass of sample per volume of solvent. For variable temperature NMR spectra, 30 min was allowed for thermal equilibration at each temperature.

Solid-state ^{113}Cd NMR spectra were acquired at UNSW using a Bruker MSL-300 spectrometer operating at 66.549 MHz with a Bruker WB-4BL double air-bearing cross-polarization probe. Samples of ca. 100 mg of the cadmium complexes were packed into 4 mm o.d. rotors made from partially stabilized zirconia and subjected to magic-angle spinning (MAS) at 2–8 kHz. Spectra were acquired at ambient probe temperature (292 K) using single-contact cross-polarization (CP) experiments with high-power ^{1}H decoupling during acquisition. Isotropic signal positions were found by comparing spectra acquired at two different MAS rates. After some experimentation, the following parameters were found to be optimal: pulse width, 3.3 μs (90°); contact time, 20 ms; recycle time, 60 s; acquisition time, 10–30 ms. Free induction decays were acquired and zero-filled to 8K prior to Fourier transformation. Usually 64–256 scans were sufficient for good signal to noise. The Hartman–Hahn match was set using $CdSO_4 \cdot 8H_2O$, which was also used as a secondary external reference that gives two signals (δ_{Cd} = –64.6 and –77.4) relative to 0.1 M $Cd(ClO_4)_2$(aq) (11).

All simulations of the MAS spectra were carried out using the Bruker Winfit program and gave the following parameters: the principle components δ_{11}, δ_{22}, δ_{33} with $\delta_{11} > \delta_{22} > \delta_{33}$; $\delta_{iso} = 1/3(\delta_{11} + \delta_{22} + \delta_{33})$. From these parameters, the span, $\Omega = |\delta_{33} - \delta_{11}|$, and the skew, $\kappa = 3(\delta_{iso} - \delta_{22})/\Omega$ (12), could be derived. The values of δ have an estimated error of ±1 ppm.

X-ray structure determinations

Crystals of **1** and **2** were obtained during their syntheses (see *Experimental* section). The data crystals were mounted

© 2001 NRC Canada

Table 2. Atomic coordinates (1×10^4) and equivalent isotropic displacement parameters (1×10^3, Å^2) for **1**.

Atom	*x*	*y*	*z*	U_{eq}
Cd(1)	5000	0	–4151(1)	56(1)
S(1)	3992(2)	196(2)	–5174(3)	70(1)
S(2)	4804(2)	1241(1)	–5636(2)	65(1)
S(3)	4753(2)	–898(1)	–3233(2)	64(1)
S(4)	3901(2)	–52(2)	–2167(3)	82(1)
N(1)	4033(5)	760(4)	–6776(8)	63(2)
N(2)	4234(5)	–1012(4)	–1533(8)	66(3)
C(1)	4248(6)	703(5)	–5922(9)	55(3)
C(2)	4703(7)	1598(5)	–6748(11)	76(3)
C(3)	4277(8)	1217(6)	–7340(12)	84(4)
C(4)	4310(5)	–690(4)	–2261(8)	46(3)
C(5)	3518(9)	–286(7)	–1093(12)	96(5)
C(6)	3876(7)	–777(6)	–698(10)	81(4)
O(21a)	–198(7)	1998(6)	3595(9)	61(4)
O(22a)	–648(10)	2633(7)	4758(18)	107(7)
O(23a)	–13(11)	1724(9)	5363(15)	127(7)
S(24a)	–358(3)	2043(2)	4652(4)	62(1)
C(25a)	–1129(13)	1672(9)	4615(15)	89(7)
F(26a)	–1298(10)	1540(8)	5494(14)	118(6)
F(27a)	–1065(12)	1172(9)	4153(19)	139(7)
F(28a)	–1581(13)	1984(12)	4110(20)	174(9)
O(21b)	–435(10)	2583(7)	5054(13)	50(5)
O(22b)	88(9)	1974(9)	3939(19)	74(6)
O(23b)	–1174(19)	2400(20)	3910(40)	187(19)
S(24b)	–563(4)	2140(4)	4324(7)	65(2)
C(25b)	–1080(30)	1590(30)	4780(30)	800(300)
F(26b)	–1396(14)	1384(13)	4020(20)	113(8)
F(27b)	–1566(12)	1817(10)	5327(19)	97(6)
F(28b)	–730(20)	1110(20)	4920(40)	201(16)

Note: U_{eq} is defined as one third of the trace of the orthogonalized U_{ij} tensor.

Table 3. Atomic coordinates (1×10^4) and equivalent isotropic displacement parameters (1×10^3, Å^2) for **2**.

Atom	*x*	*y*	*z*	U_{eq}
Cd(1)	10000	10000	10000	30(1)
S(1)	10353(1)	8486(1)	8358(1)	38(1)
S(2)	11669(1)	9932(1)	6674(1)	40(1)
N(1)	11837(2)	8123(2)	6427(4)	35(1)
C(1)	11306(2)	8771(2)	7149(4)	28(1)
C(2)	12772(3)	9498(3)	5701(6)	44(1)
C(3)	12573(3)	8457(3)	5266(6)	50(1)
Cd(2)	10000	5000	7500	31(1)
N(2)	9237(2)	6434(2)	9628(4)	36(1)
O(1)	8778(2)	7006(2)	10460(5)	64(1)
O(2)	10015(2)	6087(2)	10084(5)	52(1)
O(3)	8902(2)	6161(2)	8224(4)	39(1)

Note: U_{eq} is defined as one third of the trace of the orthogonalized U_{ij} tensor.

Table 4. Bond lengths (Å) and angles (°) for **1**.

Bond lengths (Å)	
Cd(1)—S(1)	2.540(3)
Cd(1)—S(3)	2.519(3)
S(1)—C(1)	1.671(13)
S(2)—C(1)	1.731(12)
S(2)—C(2)	1.797(15)
S(3)—C(4)	1.715(12)
S(4)—C(4)	1.704(11)
S(4)—C(5)	1.796(16)
N(1)—C(1)	1.297(17)
N(1)—C(3)	1.422(17)
N(2)—C(4)	1.288(14)
N(2)—C(6)	1.494(19)
C(2)—C(3)	1.494(19)
C(5)—C(6)	1.47(2)
Bond angles (°)	
S(1)-Cd(1)-S(1A)	110.09(18)
S(1)-Cd(1)-S(3)	106.78(10)
S(1)-Cd(1)-S(3A)	107.74(10)
S(3)-Cd(1)-S(3A)	117.62(15)
C(1)-S(1)-Cd(1)	104.2(4)
C(1)-S(2)-C(2)	93.2(6)
C(4)-S(3)-Cd(1)	106.5(4)
C(4)-S(4)-C(5)	90.5(7)
C(1)-N(1)-C(3)	119.3(11)
C(4)-N(2)-C(6)	118.7(10)
N(1)-C(1)-S(1)	124.4(10)
N(1)-C(1)-S(2)	111.2(9)
S(1)-C(1)-S(2)	124.4(8)
C(3)-C(2)-S(2)	106.6(9)
N(1)-C(3)-C(2)	109.1(13)
N(2)-C(4)-S(3)	122.8(8)
N(2)-C(4)-S(4)	113.0(9)
S(3)-C(4)-S(4)	124.2(7)
C(6)-C(5)-S(4)	110.6(11)
N(2)-C(6)-C(5)	102.7(11)

Note: Symmetry transformation used to generate equivalent atoms: $-x + 1, -y, z$.

in glass capillaries, and data were collected on a Siemens P4 diffractometer using XSCANS software. Crystal data and refinement parameters for **1** and **2** are listed in Table 1, while final positional parameters and equivalent isotropic thermal parameters for the two compounds are given in Tables 2 and 3. Selected interatomic distances and angles appear in Tables 4 and 5, for **1** and **2**, respectively.[5] In both cases, unit cell parameters were calculated from 25 centred high-angle reflections in the range $15 < 2\theta < 25$.

For **1**, systematic absences were consistent with the uniquely determined space group *Fdd*2, borne out by successful solution of the structure. The data were processed, semiempirical absorption corrections based on φ-scan data were applied, and full-matrix least-squares refinement on F^2 was performed using direct methods and the SHELXTL 5.03

[5] Supplementary material may be purchased from: The Depository of Unpublished Data (DUD No. 3304), Document Delivery, CISTI, National Research Council of Canada, Ottawa ON, Canada, K1A 0S2. These data have also been deposited with the Cambridge Crystallographic Data Center, and can be obtained from: The Director, Cambridge Crystallographic Data Center, University Chemical Laboratory, 12 Union Road, Cambridge, CB2 1EZ, U.K.

© 2001 NRC Canada

Table 5. Bond lengths (Å) and angles (°) for **2**.

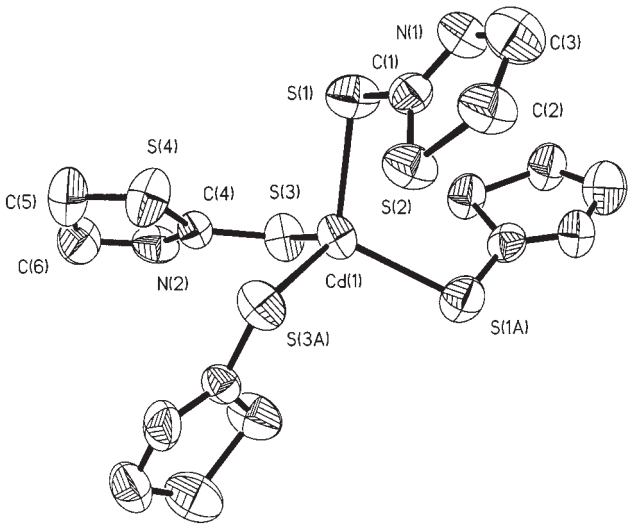
Bond lengths (Å)	
Cd(1)—S(1)	2.5329(9)
S(1)—C(1)	1.692(3)
S(2)—C(1)	1.732(3)
S(2)—C(2)	1.824(4)
N(1)—C(1)	1.302(5)
N(1)—C(3)	1.462(5)
C(2)—C(3)	1.513(6)
Cd(2)—O(2)	2.575(4)
Cd(2)—O(3)	2.294(3)
N(2)—O(1)	1.220(5)
N(2)—O(2)	1.239(4)
N(2)—O(3)	1.283(5)
Bond angles (°)	
S(1)-Cd(1)-S(1*A*)	105.91(2)
S(1)-Cd(1)-S(1*C*)	116.85(5)
C(1)-S(1)-Cd(1)	105.04(12)
C(1)-S(2)-C(2)	91.8(2)
C(1)-N(1)-C(3)	117.7(3)
N(1)-C(1)-S(1)	122.7(3)
N(1)-C(1)-S(2)	112.3(3)
S(1)-C(1)-S(2)	125.0(2)
C(3)-C(2)-S(2)	105.2(3)
N(1)-C(3)-C(2)	106.4(3)
O(2)-Cd(2)-O(2*D*)	131.06(10)
O(2)-Cd(2)-O(2*F*)	71.7(2)
O(2)-Cd(2)-O(3)	52.22(9)
O(2)-Cd(2)-O(3*D*)	126.97(11)
O(2)-Cd(2)-O(3*E*)	79.14(11)
O(2)-Cd(2)-O(3*F*)	101.52(10)
O(3)-Cd(2)-O(3*D*)	93.72(4)
O(3)-Cd(2)-O(3*F*)	150.5(2)
O(1)-N(2)-O(2)	123.1(4)
O(1)-N(2)-O(3)	119.3(3)
O(2)-N(2)-O(3)	117.6(3)
N(2)-O(2)-Cd(2)	88.8(2)
N(2)-O(3)-Cd(2)	101.1(2)

Note: Symmetry transformations used to generate equivalent atoms: *A*: $-y + 2, x, -z + 2$; *B*: $y, -x + 2, -z + 2$; *C*: $-x + 2, -y + 2, z$; *D*: $-y + 3/2, x - 1/2, -z + 3/2$; *E*: $y + 1/2, -x + 3/2, -z + 3/2$; *F*: $-x + 2, -y + 1, z$.

program package (13). The cation is located on a twofold axis, while the anion is at a general position. All non-hydrogen atoms of the cation were refined with anisotropic thermal parameters. There was disorder of the anion over two positions; the occupancies were 0.6 and 0.4 for the *a* and *b* anions, respectively. In the anions, all atoms were refined isotropically. The largest residual electron density peak (0.53 e $Å^{-3}$) was associated with S(24). In the final stages of refinement, $R = 5.01$ and $R_w = 11.95$.

For **2**, systematic absences were consistent with the space groups *I*4, *I*4/*m*, and $I\bar{4}$. The acentric option ($I\bar{4}$) resulted in chemically reasonable and computationally stable results. Processing of the data, application of absorption corrections, and refinement were carried out as for **1**. All non-hydrogen atoms were refined with anisotropic thermal parameters. The largest residual electron density peak (0.258 e $Å^{-3}$) was associated with the Cd cation. In the final stages of refinement, $R = 1.80$ and $R_w = 4.53$.

Fig. 1. A view of the cation in $[Cd(tztH)_4](trif)_2$ (**1**). Non-hydrogen atoms are shown as 50% probability thermal ellipsoids.



Results and discussion

Crystal structure of $[Cd(tztH)_4](trif)_2$ (1)

The crystal structure of **1** consists of discrete cations and anions, the anions being disordered. The structure of the cation is shown in Fig. 1. Selected bond distances and angles are given in Table 4.

In the cations, the ligands behave as S-donors. In an earlier study (6) it was suggested on the basis of IR spectroscopy that N-bonding of tztH occurred exclusively in this cation. However, tztH acts as a monodentate S-donor in catena-$CdCl_2$(tztH) (8). In **1**, the cation has C_2 point group symmetry. The Cd—S bond distances are 2.540(3) and 2.519(3) Å and are similar to the 2.5163(7) Å found for $[Cd(Py2SH)_4]^{2+}$ (Py2SH = 2-(1*H*)-pyridinethione) as the nitrate salt (2), but are shorter than the 2.605(2) Å found for catena-$CdCl_2$(tztH), in which the Cd atoms are six-coordinate (8).

The S-Cd-S angles range from 117.62(15) to 106.78(10)°. The CdS_4 kernel exhibits flattening along the C_2 axis, with S(1)-Cd-S(1A) and S(3)-Cd-S(3A) angles being larger than the other four S–Cd–S angles. A more regular flattening of the same type is observed for $[Cd(Py2SH)_4](NO_3)_2$ (1).

The Cd-S-C angles fall within the range observed for corresponding M-S-C angles in the literature (8, 14). Coordination produces relatively little change in the geometry of the ligand compared with that for the free ligand (15), as is commonly observed (8, 14). The atoms S(1)-C(1)-N(1)-S(2)-C(3) and S(3)-C(4)-N(2)-S(4)-C(6) lie in planes (mean deviations 0.008 and 0.022 Å, respectively). The atoms C(2) and C(5) (at the "flap" of the envelope conformation of their five-membered rings) lie out of their respective planes by 0.145 and 0.301 Å, respectively. The torsion angles Cd(1)-S(1)-C(1)-N(1) and Cd(1)-S(3)-C(4)-N(2) are 148.8 and –163.3°, respectively.

© 2001 NRC Canada

Fig. 2. A view of the cation and anion in $[Cd(tztH)_4][Cd(O_2NO)_4]$ (**2**). Non-hydrogen atoms are shown as 50% probability thermal ellipsoids.

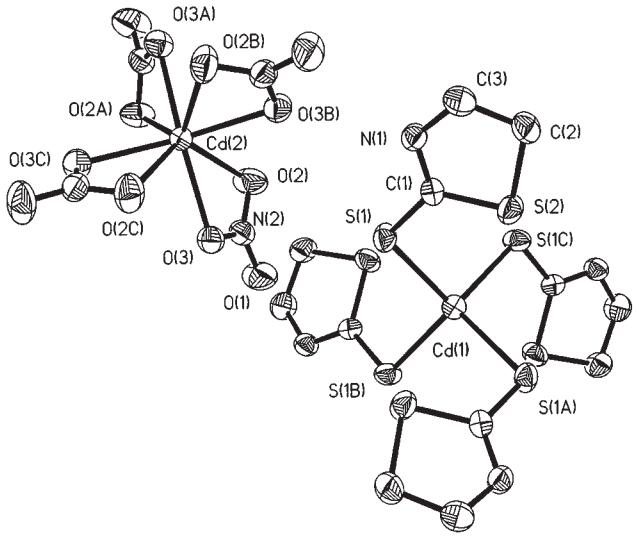
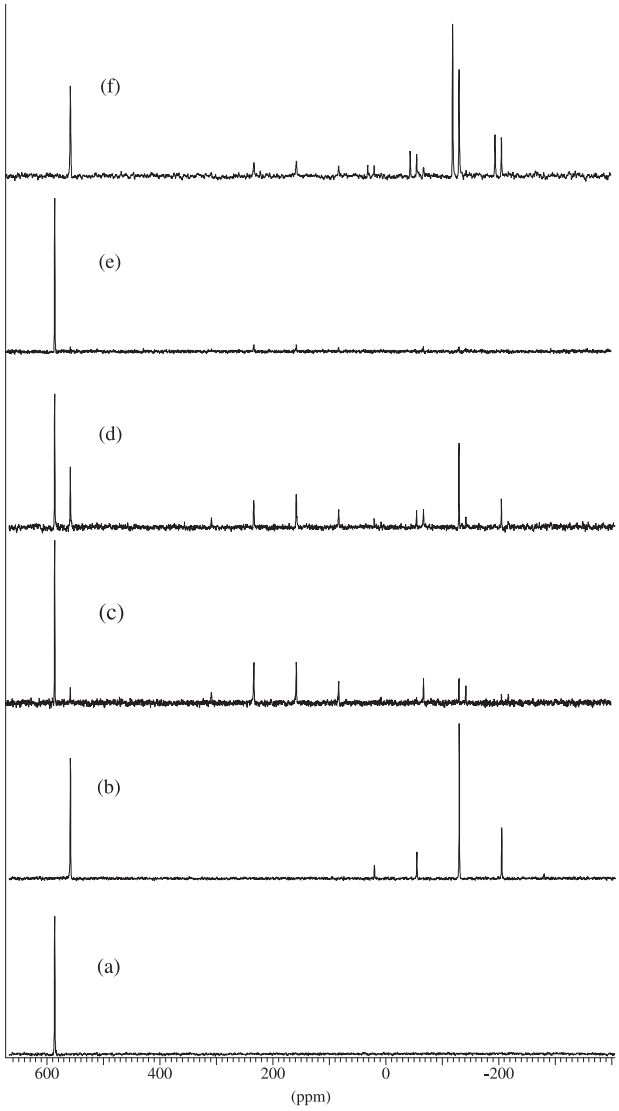


Fig. 3. ^{113}Cd CP MAS NMR spectra of **1**, **2**, and solids produced by fusion of $Cd(NO_3)_2{\cdot}4H_2O$ and tztH (see text). Spectrum of: (*a*) **1**; (*b*) **2**; (*c*) unwashed 1:4 $Cd(NO_3)_2{\cdot}4H_2O$:tztH mixture; (*d*) toluene-washed 1:4 $Cd(NO_3)_2{\cdot}4H_2O$:tztH mixture; (*e*) unwashed 1:6 $Cd(NO_3)_2{\cdot}4H_2O$:tztH mixture; (*f*) unwashed 1:2 $Cd(NO_3)_2{\cdot}4H_2O$:tztH mixture.



Crystal structure of $[Cd(tztH)_4][Cd(O_2NO)_4]$ (2)

This salt is comprised of discrete $[Cd(tztH)_4]^{2+}$ cations and $[Cd(O_2NO)_4]^{2-}$ anions. Figure 2 shows the ions, and selected bond distances and angles are presented in Table 5. Both ions have point group symmetry S_4. In the cation, the ligand is again S-bound. The Cd—S distance (2.5329(9) Å) is the same as the long Cd—S distance found in **1**. The CdS_4 kernel exhibits a tetragonal compression, the two independent S-Cd-S angles being 105.91(2) and 116.85(5)°. There is a strong resemblance to the distortion found for the CdS_4 kernel of $[Cd(Py2SH)_4](NO_3)_2$, which has been discussed in detail (2). The Cd-S-C angle of 105.04(12)° falls between the values observed for **1**, while the overall ligand geometry is similar to those in **1**: S(1)-C(1)-N(1)-S(2)-C(3) are planar (mean deviation, 0.033 Å), with C(2) out of plane by 0.367 Å. The Cd(1)-S(1)-C(1)-N(1) torsion angle is 163.1°.

Within the $[Cd(O_2NO)_4]^{2-}$ anions, the nitrate anions are bonded in an anisobidentate manner, with Cd(2)—O(2) and Cd(2)—O(3) being 2.575(4) and 2.294(3) Å, respectively. The O(2)-Cd(2)-O(3) bite angle is 52.22(9)°. The $[Cd(O_2NO)_4]^{2-}$ anion has been described once previously; it occurs in $[CdL^4(NO_3)_2][Cd(O_2NO)_4]$ (**3**, L^4 = 1,5,9,13-tetramethyl-1,5,9,13-tetra-azacyclohexadecane) (16). In **2**, the arrangement of the O-atoms in the anion is S_4-dodecahedral (17). The Cd—O bond distances and the O-Cd-O bite angle for $[Cd(O_2NO)_4]^{2-}$ in **2** are similar to those found for $[Cd(5)(O_2NO)_4]^{2-}$ in **3** (in ligand **1**, Cd—O = 2.55(2) and 2.27(2) Å, bite angle = 52.4(5)°; in ligand **2**, Cd—O = 2.60(2) and 2.27(2) Å, bite angle = 51.5(6)°), despite the lower symmetry of the latter. (The anion $[Cd(4)(O_2NO)_4]^{2-}$ in **3** appears to be still less symmetrical, though some disorder was evident. It is noteworthy that in this latter anion the individual ligands appear to be more symmetrically bound than in **2** or the corresponding $[Cd(5)(O_2NO)_4]^{2-}$ anion.) The anisobidenticity of the nitrate ligands in $[Cd(O_2NO)_4]^{2-}$ in **2**, where Δr (Cd—O) is 0.280(5) Å, is smaller than for homologous $[Zn(O_2NO)_4]^{2-}$ (as its Ph_4As^+ salt), where Δr (Zn—O) is 0.47(1) and 0.57(1) Å (18), but larger than in isoelectronic $Sn(O_2NO)_4$, in which Δr (Sn—O) varies from 0.00(1) to 0.06(1) Å (19).

Cadmium NMR spectra of 1 and 2

At 293 K exchange-averaged ^{111}Cd NMR spectra are observed for mixtures of $Cd(NO_3)_2{\cdot}4H_2O$ and tztH, e.g., δ_{Cd} increases monotonically from –95 to +125 as tztH:Cd is increased from 0 to 7.5 in a solution having 0.1 mol of Cd per L in MeOH. Presumably mixtures of species of the general type $[Cd(tztH)_w(NO_3)_x(MeOH)_y(H_2O)_z]^{2-x}$ (abbreviated $Cd(tztH)_w^{2+}(solv)$) are being formed in these mixtures. Unfortunately, poor solubility precludes reduced temperature solution NMR studies. Complexes of tztH with $Cd(ClO_4)_2$ are more soluble (and also more soluble than the corresponding triflates), and incremental addition of tztH to

© 2001 NRC Canada

Table 6. Solid-state ^{113}Cd NMR spectra of **1**, **2**, and species found in fused mixtures of $Cd(NO_3)_2 \cdot 4H_2O$ and tztH.

Substrate	δ_{iso}	δ_{11}, δ_{22}, δ_{33}	Ω	κ	Assignment
1	586	622, 582, 558[a]	61	+0.2	$[Cd(tztH)_4]^{2+}$
2	557[b]				$[Cd(tztH)_4]^{2+}$
	–131	12, –202, –202	214	+1	$[Cd(O_2NO)_4]^{2-}$
$Cd(NO_3)_2 \cdot 4H_2O$:tztH	586				$[Cd(tztH)_4]^{2+}$ [c]
mixtures[d]	558				$[Cd(tztH)_4]^{2+}$ [e]
	–131	12, –202, –202	214	+1	$[Cd(O_2NO)_4]^{2-}$ [f]
	83	271, 271, –294	565	–1	$Cd(tztH)_3(NO_3)_2$(?)
	–119	8, –183, –183	191	+1	$Cd(NO_3)_2 \cdot 4H_2O$

Note: See text for description of Ω and κ and Fig. 3.
[a] δ_{11}, δ_{22}, δ_{33} found at very low spinning speeds (925 Hz).
[b] This signal was isotropic down to a spinning speed of 1600 Hz.
[c] In $[Cd(tztH)_4](NO_3)_2$.
[d] In solid mixtures after fusion.
[e] In $[Cd(tztH)_4][Cd(O_2NO)_4]$.

$Cd(ClO_4)_2$ (0.07 mol L^{-1} of solvent) allowed observation of slow-exchange ^{111}Cd NMR spectra for several new species $Cd(tztH)_w^{2+}$(solv) in MeOH at 189 K: δ_{Cd} = –14, 73, 153, and 453 for w = 0, 1, 2, and 3, respectively (the complex with w = 4 is poorly soluble).

Neither **1** nor **2** were soluble enough in noncoordinating solvents for the measurement of their metal NMR spectra in solution, so the ^{113}Cd NMR spectra of the solids were measured. The ^{113}Cd CP MAS NMR spectrum of solid **1** showed a single line with δ_{Cd} (isotropic) = 586, having very low span (Fig. 3*a* and Table 6). This spectrum is clearly that of the $[Cd(tztH)_4]^{2+}$ cation, with its CdS_4 kernel, as found in the structural determination. For comparison, the solution ^{113}Cd NMR chemical shifts of $[Cd(Py2SH)_4]^{2+}$ (in which the 2-(1*H*-pyridinethione) is S-bound) and $[Cd(SPh)_4]^{2-}$ have been reported as 603 and ~590 ppm, respectively, (1*e*, 1*g*, 2). The ^{113}Cd CP MAS NMR spectrum of solid **2** consists of two resonances (Fig. 3*b*): the first has δ_{Cd} (isotropic) = 557, with no evidence of anisotropy, and can again be assigned to $[Cd(tztH)_4]^{2+}$. The change in δ_{Cd} of the $[Cd(tztH)_4]^{2+}$ cation on changing from **1** to **2** (29 ppm) is the same order of magnitude as found for other cadmium complexes when the counterion is changed, e.g., 23 ppm for $CdCl_4^{2-}$ when the cation is changed from thiaminium (as the monohydrate) to Et_4N^+ (20). Such changes are due to a combination of small changes in geometry of the cadmium complex and the change in its crystallographic environment. The second signal observed for solid **2**, δ_{Cd}(isotropic) = –131, has a spectrum consistent with axial symmetry: it must be due to the $[Cd(O_2NO)_4]^{2-}$ anion. For comparison, δ_{Cd} = –100 (20) for the distorted dodecahedral CdO_8 kernel (comprised of O-atoms from both NO_3^- and H_2O) found in $Cd(NO_3)_2 \cdot 4H_2O$ (21).

A compound described as $[Cd(tztH)_4](NO_3)_2$ has been synthesized by reaction of the metal salt with a small excess of the molten ligand, followed by repeated washing with toluene (6). In our studies, during which either MeCN or Me_2CO was used as solvent, **2** was isolated even from mixtures that contained significantly more than two equivalents of tztH. Therefore, we thought it worthwhile to scrutinize the solid products of the reaction of $Cd(NO_3)_2 \cdot 4H_2O$ and molten tztH using ^{113}Cd CP MAS NMR. The results of this study are summarized in Table 6. Typical spectra are included in Fig. 3. While there is some variability, probably reflecting the efficiency of stirring, the spectra of 1:4 Cd:tztH mixtures (e.g., Fig. 3*c*) typically show a signal at 586 ppm, which by comparison with the solid-state spectrum of **1** can be assigned to $[Cd(tztH)_4](NO_3)_2$, and also a pair of signals at 558 and –131 ppm that can be assigned to **2**. In addition, the signal of an axially symmetric species is observed at 83 ppm ($\delta_{11} = \delta_{22}$ = 271, δ_{33} = –294). We tentatively assign this spectrum to $Cd(tztH)_3(NO_3)_2$, since its intensity increases relative to that of **2** as the tztH:Cd ratio of the fused mixtures is increased (Fig. 3). Washing 1:4 fusion mixtures with toluene changes the ratio of species present but in our hands does not produce pure $[Cd(tztH)_4](NO_3)_2$ as indicated by the solid-state NMR spectrum (e.g., Fig. 3*d*). Increasing the relative amount of tztH in the fusion mixture to 1:6 (Fig. 3*e*) or higher increases the amount of $[Cd(tztH)_4](NO_3)_2$, as expected, and we conclude that a significant excess of tzt over the required 1:4 ratio must have been used in the literature synthesis of this compound. A mixture produced by fusion of a mixture in which Cd:tztH = 1:2 leads to a further species, although **2** and the possible $Cd(tztH)_3(NO_3)_2$ persist also (Fig. 3*f*). The new species has δ_{Cd} = –119, δ_{11} = 8, $\delta_{22} = \delta_{33}$ = –183. The isotropic chemical shift and the span (Ω) of the new species are very close to those of $Cd(NO_3)_2 \cdot 4H_2O$ (20, 22), and therefore, this spectrum is assigned to the nitrate itself.

After $Cd(trif)_2$ has been fused with six mol equivalents of tztH, the only ^{113}Cd NMR signal observed for the solidified mixture is a signal at 586 ppm that by comparison with the spectrum of pure **1** can be assigned to $[Cd(tztH)_4]^{2+}$. Thus Cd(II), as the nitrate or triflate, does not bind more than four tztH ligands even when the metal salt is fused with excess tztH. In contrast, CdS_6 kernels have been reported in complexes of Cd(II) with the thiocarbonyl S-donors *N*,*N*-dimethylthioformamide (23)[6] and thiourea (24). The CdS_6 kernel also occurs in various tris- (chelate) complexes of

[6] $Cd(trif)_2$ forms a 1:4 complex in the solid state (23*b*).

© 2001 NRC Canada

Cd(II) with the anions of dithioacids (25); these have ^{113}Cd chemical shifts of ca. 200 ppm, more shielded than, and therefore distinct from, those observed in the present paper.

Acknowledgments

This work was funded in part by the Natural Sciences and Engineering Research Council of Canada (NSERC).

References

1. (*a*) P.A.W. Dean, J.J Vittal, D.C. Craig, and M.L. Scudder. Inorg. Chem. **37**, 1661 (1998); (*b*) J.J. Vittal and P.A.W. Dean. Inorg. Chem. **35**, 3089 (1996); (*c*) P.A.W. Dean, N.C. Payne, J.J. Vittal, and Y. Wu. Inorg. Chem. **32**, 4632 (1993); (*d*) P.A.W. Dean and J.J. Vittal. *In* Metallothioneins. *Edited by* M. J. Stillman, C.F. Shaw, III, and K.T. Suzuki. VCH, New York. 1992. Chap. 14; (*e*) G.K. Carson and P.A.W. Dean. Inorg. Chim. Acta, **66**, 37 (l982); (*f*) P.A.W. Dean. Can. J. Chem. **59**, 322l (l98l); (*g*) G.K. Carson, P.A.W. Dean, and M.J. Stillman. Inorg. Chim. Acta, **56**, 59 (l98l); **108**, 71 (1985).
2. U. Rajalingam, P.A.W. Dean, and H.A. Jenkins. Can. J. Chem. **78**, 590 (2000).
3. E.S. Raper. Coord. Chem. Rev. **61**, 161 (1985); **129**, 109 (1994).
4. D. De Filippo, F. Devillanova, C. Preti, and G. Verani. J. Chem. Soc. A, 1465 (1971).
5. G. Columbini and C. Preti. J. Inorg. Nucl. Chem. **87**, 1159 (1975).
6. C. Preti and G. Tosi. J. Chem. Soc. Dalton Trans. 685 (1976).
7. K. Geetharani and D.N. Sathyanarayana. Indian J. Chem. A, **14A**, 170 (1976).
8. M. Kubiak and T. Glowiak. Acta Crystallogr. C, **C41**, 1580 (1985).
9. G.R. Hedwig and A.J. Parker. J. Am. Chem. Soc. **96**, 6589 (1974).
10. W.L. Jolly. The synthesis and characterization of inorganic compounds. Prentice Hall, New Jersey. 1970. p. 493.
11. G.S.H. Lee, K.J. Fisher, A.M. Vassallo, J.V. Hanna, and I.G. Dance. Inorg. Chem. **32**, 66 (1993).
12. R.K. Harris. Solid State Nucl. Mag. **2**, 285 (1993).
13. SHELXTL reference manual. Version 5.03. Siemens Energy and Automation, Inc., Analytical Instrumentation, Wisconsin. 1996.
14. (*a*) M. Kubiak and T. Glowiak. Acta Crystallogr. B, **38**, 2031 (1982); Acta Crystallogr. C, **43**, 641 (1987); (*b*) Z. Baoguang, L. Xioyun, and Y. Yunhua. Wuli Huaxue Xuebao, **1**, 289, (1985); Chem. Abstr. **103**, 62 963v (1985); (*c*) S.K. Hadjikakou, P. Aslanidis, P. Karagiannidis, D. Mentzafos, and A. Terzis. Polyhedron, **10**, 935 (1991); (*d*) A.R. Norris, A. Palmer, and A.L. Beauchamp. J. Crystallogr. Spectrosc. **20**, 23 (1990); (*e*) M. Maekawa, S. Kitagawa, Y. Nozaka, M. Munakata, and T. Kuroda-Sowa. Anal. Sci. **9**, 887 (1993); Chem. Abstr. **120**, 20 5046n (1993); (*f*) S. Ramaprabhu, E.A.C. Lucken, and G. Bernardinelli. J. Chem. Soc. Dalton Trans. 115 (1995); (*g*) P. Aslanidis, S.K. Hadjikakou, P. Karagiannidis, and P.J. Cox. Inorg. Chim. Acta, **271**, 243 (1998); (*h*) M. Cannas, G. Carta, G. Marongiu, and E.F. Trogu. Acta Crystallogr. B, **30**, 2252 (1974); (*i*) W.S. Sheldrick and C.Landgrafe. Inorg. Chim. Acta, **208**, 145 (1993); (*j*) W. Xu, A.J. Lough, and R.H. Morris. Inorg. Chem. **35**, 1549 (1996).
15. E.S. Raper, R.E. Oughtred, and I.W. Nowell. Inorg. Chim. Acta, **77**, L89 (1083).
16. N.W. Alcock, E.H. Curzon, P. Moore, and C. Pierpoint. J. Chem. Soc. Dalton Trans. 605 (1984).
17. J.L. Hoard and J.V. Silverton. Inorg. Chem. **2**, 235 (1963).
18. C. Bellitto, L. Gastaldi, and A.G. Tomlinson. J. Chem. Soc. Dalton Trans. 989 (1976).
19. C.D. Garner, D. Sutton, and S.C. Wallwork. J. Chem. Soc. A, 1949 (1967).
20. P.G. Mennitt, M.P. Shatlock, V.J. Bartuska, and G.E. Maciel. J. Phys. Chem. **85**, 2087 (1981).
21. B. Matković, B. Ribar, B. Zelenko, and S.W. Petersen. Acta Crystallogr. **21**, 719 (1966).
22. P. DuBois Murphy and B.C. Gerstein. J. Am. Chem. Soc. **103**, 3282 (1981).
23. C.M.V. Stålhandske, I. Persson, M. Sandström, and E. Kamienska-Piotrowicz. Inorg. Chem. **36**, 3174 (1997); **36**, 3167 (1997).
24. R. Petrova, O. Angelova, and J. Macicek. Acta Crystallogr. C, **53**, 565 (1997).
25. J. Sola, P. Gonzáles-Duarte, J. Sanz, I. Casals, T. Alsina, I. Sobrados, A. Alvarez-Larena, J.-F. Piniella, and X. Solans. J. Am. Chem. Soc. **115**, 10018 (1993), and refs. therein.

© 2001 NRC Canada

$Ti_5Si_{1.3}Sb_{1.7}$ — The first titanium silicide antimonide, forming a crystal structure not found in either binary system

Holger Kleinke

Abstract: $Ti_5Si_xSb_{3-x}$ can be prepared by melting mixtures of Ti, Si, and $TiSb_2$. The ternary phase with $x = 1.32(5)$ crystallizes in the W_5Si_3 type (space group *I*4/*mcm*, $Z = 8$, for $x = 1.32(5)$: $a = 1034.6(2)$, $c = 515.2(1)$ pm), while Ti_5Sb_3 and Ti_5Si_3 adopt the Yb_5Sb_3 type and the Mn_5Si_3 type, respectively. The Si and Sb atoms share two sites in $Ti_5Si_{1.32(5)}Sb_{1.68}$: one site is located within a linear chain with short interatomic bonds, which is almost exclusively occupied by Si (i.e., 92(1)% Si and 8% Sb), whereas the second site, being occupied by 80(2)% Sb and 20% Si, shows no significant interactions between the main group elements. Band structure calculations reveal the new silicide antimonide being metallic as a consequence of partly filled Ti *d* states. The structure is mainly stabilized by bonding Ti—Sb, Ti—Si, and Si—Si interactions.

Key words: titanium, silicide, antimonide, crystal structure, electronic structure, structure and bonding.

Résumé : On peut préparer le $Ti_5Si_xSb_{3-x}$ par fusion de mélanges de Ti, Si et $TiSb_2$. La phase ternaire dans laquelle $x =$ 1,32(5) cristallise comme le W_5Si_3 (groupe d'espace *I*4/*mcm* et $Z = 8$ pour $x = 1,32(5)$ avec $a = 1034,6(2)$ et $c =$ 515,2(1) pm) alors que les Ti_5Sb_3 et Ti_5Si_3 cristallisent plutôt comme le Yb_5Sb_3 et Mn_5Si_3, respectivement. Les atomes de Si et de Sb occupent deux sites dans le $Ti_5Si_{1,32(5)}Sb_{1,68}$: un site se trouve dans une chaîne linéaire avec de courtes liaisons interatomiques occupées presque exclusivement par du Si (soit 92(1)% de Si et 8% de Sb) alors que le deuxième site, occupé par 80(2)% de Sb et 20% de Si ne présente pas d'interactions significatives entre les éléments du groupe principal. Des calculs de structure de bande révèlent que le nouveau siliciure antimoniure est métallique en raison d'un remplissage partiel des états *d* du Ti. La structure est stabilisée principalement par des interactions de liaison Ti—Sb, Ti—Si et Si—Si.

Mots clés : titane, siliciure, antimoniure, structure cristalline, structure électronique, structure et liaison.

[Traduit par la Rédaction]

Introduction

The concept of mixing closely related metal atoms, such as niobium and tantalum, was used for the synthesis of a variety of hitherto unknown sulfides crystallizing in unprecedented structure types. The earliest examples include $Nb_{4.92}Ta_{6.08}S_4$ (1), $Nb_{6.74}Ta_{5.26}S_4$ (2), $Nb_{1.72}Ta_{3.28}S_2$ (3), and $Nb_{0.95}Ta_{1.05}S$ (4), whose structures exhibit mixed Nb and Ta occupancies in different ratios on the crystallographically independent metal atom sites. The three criteria for the so-called DFSO materials (DFSO = differential fractional site occupancies) developed on these findings were: (*i*) the metal atom sites are occupied by mixtures of two different metal atoms; (*ii*) these occupancies vary from site to site; and (*iii*) the crystal structure does not occur in any of the two corresponding binary systems (5, 6). DFSO-stabilized materials are not limited to sulfides or to metals of the same group only, as the discovery of some phosphides and antimonides of this kind revealed (e.g., $(Zr,Nb)_{11}P_4$ (7), $(Hf,Mo)_2P$ (8), $(Hf,Nb)_{10}Ni_3P_5$ (9), $(Zr,V)_{13}Sb_{10}$ (10), $(Zr,V)_{11}Sb_8$ (11), $(Hf,Ti)_7Sb_4$ (12), and (Zr,Ti)Sb (13)). In most cases, the different site preferences of the different metal atoms were investigated and well-understood. Related to the DFSO topic are the articles covering the phosphides $Zr_{2.7}Hf_{11.3}P_9$ (14) and ZrHfP (15), where Zr atoms of the parent phosphides $Zr_{14}P_9$ (16) and Zr_2P (17), respectively, were in part replaced by Hf atoms in an ordered way.

Although the DFSO concept was used for the syntheses of several new metal-rich compounds, which mostly enriched our knowledge of possible crystal structures, the transfer to using different anionic components just started. In the structures of the mixed chalcogenides $(Nb,Ta)_9(S,Te)_5$ (18), $Ta_5(S,Te)_2$ (19), $Ta_5(Se,Te)_3$ (20), $Ta_5(S,Se)_2$ (21), $Ta_9(S,Se)_4$ (21), and $Ta_6(S,Te)_4$ (22), the lighter (and smaller) chalcogen atoms generally prefer the smaller voids. The discovery of the first two antimonide-selenides $Zr_2(Sb,Se)$ (23) and $Zr_7(Sb,Se)_4$ (24), both published most recently, suggests a wider range of possible mixed occupancies. The latter two compounds, exhibiting different mixed occupancies, have no counterpart in the binary Zr-Sb and Zr-Se systems, and can thus be considered as *anionic* DFSO compounds. The same holds true for $Zr(Si,Sb)_2$, (ZrSiS structure), wherein the two main group positions are occupied by: (*i*) a Si–Sb mixture;

Received March 22, 2001. Published on the NRC Research Press Web site at http://canjchem.nrc.ca on September 12, 2001.

H. Kleinke. Department of Chemistry, University of Waterloo, Waterloo, ON N2L 3G1, Canada. (telephone: (519) 888-4567 ext. 3577; fax: (519) 746-0435; e-mail: kleinke@uwaterloo.ca).

 DOI: 10.1139/cjc-79-9-1338 © 2001 NRC Canada

and (*ii*) an Sb atom (25). The mixed-halide zirconium cluster compounds, though representing a different kind of chemistry, belong to the same category in that sense that new structures were achieved by using different anionic constituents (26, 27). Excluding so-called solid solutions like $CoGe_xP_{1-x}$ (28), only a few compounds with anionic sites occupied by mixtures of elements of the fourth and fifth main group were reported (e.g., $Hf_{27}(Si,P)_{16}$ (29)). In a further expansion of the DFSO concept, we report here on the second silicide antimonide exhibiting mixed Si–Sb occupancies, which complies to the criteria of anionic DFSO compounds.

Experimental section

Synthesis

The binary antimonide $TiSb_2$ was prepared first to minimize weight loss arising from vaporization of elemental antimony during the process of arc-melting. $TiSb_2$ was synthesized in a solid–liquid reaction of the elements in the stoichiometric 1:2 ratio at 650°C in an evacuated fused silica tube. Thereafter, titanium, $TiSb_2$, and silicon in the ratio of 4:1:1 were ground, thoroughly mixed, and then pressed to a pellet. In the final reaction step, the pellet was arc-melted twice under a flow of argon on a water-cooled copper hearth. The powder X-ray diffraction pattern obtained from the ground sample gave no evidence of the formation of any binary titanium silicide or antimonide, but pointed towards the existence of $Ti_3Si_xSb_{1-x}$ (Cr_3Si type like Ti_3Sb (30)). Therefore, energy dispersive analyses of X-rays, performed by using a scanning electron microscope with an additional EDX device, were carried out on selected crystals. No impurity atoms were detected; the standardless EDX analyses yielded an averaged Ti:Si:Sb ratio of 5:1.0(2):1.7(2).

Crystal structure

A small crystal of prismatic shape was selected under an optical microscope for the data collection using a diffractometer with an area detector system. After correcting for Lorentz and polarization effects, a numerical absorption correction was applied. The systematic extinction of $l = 2n + 1$ for all *0kl* reflections (in addition to the integral extinctions, namely $h + k + l = 2n + 1$) restricted the possible space groups to *I*4*/mcm*, *I*4*cm*, and $I\bar{4}c2$. The structure solution and refinement in the centrosymmetric space group *I*4*/mcm* were successful and converged smoothly (programs SHELXS and SHELXL (31)). Refinements in the acentric space groups *I*4*cm* and $I\bar{4}c2$ did not lead to any improvements of the *R* values or different ordering, but resulted in strong correlations instead.

The structure solution straightforward gave the four atomic positions as known from the W_5Si_3 structure type. Identifying the one Si site of the W_5Si_3 type with two short distances to two symmetry equivalent Si sites of 258 pm (E1) as Si and the other one (E2) as Sb, yielded the formula Ti_5SiSb_2 with very different displacement parameters of the E positions (namely U_{eq}(E1) = 50(20) pm^2; U_{eq}(E2) = 188(7) pm^2). Refining both E sites as being mixed occupied by Si and Sb improved the residual factors significantly (e.g., $R(F_o)$ decreased from 0.0565 to 0.0428) and yielded uniform displacement parameters. In the sum, full occupancy of each site was assumed for this refinement. The refined Si:Sb ratios were 92(1):8 for E1 and 20(2):80 for E2, giving a refined formula of $Ti_5Si_{1.32(5)}Sb_{1.68}$. Crystallographic details can be found in Table 1. Positional and equivalent displacement parameters and occupancy factors are given in Table 2.

Table 1. Crystallographic data for $Ti_5Si_{1.32(5)}Sb_{1.68}$.

Chemical formula: $Ti_5Si_{1.32(5)}Sb_{1.68}$
Formula weight: 481.87 g mol^{-1}
a = 1034.6(2) pm
c = 515.2(1) pm
V = 551.5(2) 1 × 10^6 pm^3
Z = 8
Space group: *I*4*/mcm* (No. 140)
T = 22°C
λ = 71.069 pm
ρ_{calcd} = 5.795 g cm^{-3}
μ = 151.1 cm^{-1}
$R(F_o)^a$ = 0.043; $R_w(F_o^2)^b$ = 0.088

$^a R(F_o) = \Sigma||F_o| - |F_c|| / \Sigma|F_o|$.
$^b R_w(F_o^2) = [\ \Sigma[w(F_o^2 - F_c^2)^2] / \Sigma[w(F_o^2)^2]]^{1/2}$.

Electronic structure

The band structure calculations were performed on hypothetical Ti_5SiSb_2. The structural parameters were taken from the refinements on $Ti_5Si_{1.32(5)}Sb_{1.68}$, using Si parameters for E1 and Sb parameters for E2. Within the self-consistent TB–LMTO–ASA program (TB–LMTO–ASA = tight binding – linear muffin tin orbitals – atomic spheres approximation) (32, 33), the density functional theory (34) is used with the local density approximation (LDA). The integration in *k* space was performed by an improved tetrahedron method (35) on a grid of 1331 *k* points in the irreducible section of the first Brillouin zone.

The Mulliken overlap populations (MOPs) (36), serving as an indicator for relative bond orders, were calculated for all interatomic distances using the Extended Hückel approximation (37–39) on hypothetical Ti_5SiSb_2 by solving the eigenvalue problem on 80 *k* points of the first Brillouin zone. The silicon and antimony parameters were used as published before (40), while the ionization potentials of titanium were optimized by charge iteration on Ti_5SiSb_2, with the Slater exponents and coefficients taken from standard sources (40). All parameters are summarized in Table 3, and a list of the distances and MOPs is presented in Table 4.

Results and discussion

Crystal structure

$Ti_5Si_{1.32(5)}Sb_{1.68}$ crystallizes in the W_5Si_3 structure type (Fig. 1), whereas Ti_5Sb_3 (41) and Ti_5Si_3 (42) occur in different structure types, namely in the Yb_5Sb_3 and the Mn_5Si_3 type, respectively. With both E sites being mixed occupied by different ratios of Si and Sb, this silicide antimonide can be classified as a typical DFSO-stabilized material.

Several binary compounds M_5E_3 (M = transition metal atom; E = main group element) are reported to adopt the W_5Si_3 structure type (43). Here, E is almost exclusively an

© 2001 NRC Canada

Table 2. Atomic positions, equivalent displacement parameters, and occupancy factors of $Ti_5Si_{1.32(5)}Sb_{1.68}$.

Atom	Site	*x*	*y*	*z*	U_{eq} (pm^2)	Occupancy
Ti(1)	4*b*	0	1/2	1/4	184(12)	1
Ti(2)	16*k*	0.0753(2)	0.2134(2)	0	176(9)	1
E(1)	4*a*	0	0	1/4	210(20)	0.92(1) Si + 0.08 Sb
E(2)	8*h*	0.1634(1)	0.3365(1)	0	158(5)	0.80(2) Sb + 0.2 Si

Table 3. Parameters used for extended Hückel calculations.

Orbital	H_{ii} (eV)	ζ_1	c_1	ζ_2	c_2
Ti, 4*s*	–7.77	1.50			
Ti, 4*p*	–4.11	1.50			
Ti, 3*d*	–8.04	4.55	0.4391	1.600	0.7397
Si, 3*s*	–17.30	4.63			
Si, 3*p*	–9.2	1.43			
Sb, 5*s*	–18.80	2.32			
Sb, 5*p*	–11.70	2.00			

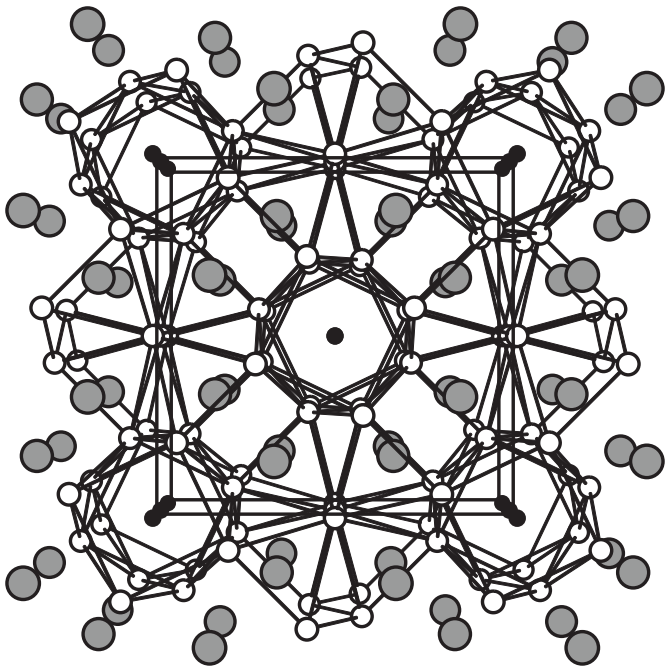
Table 4. Interatomic distances (*d*) and Mulliken overlap populations (MOP) for $Ti_5Si_{1.32(5)}Sb_{1.68}$.

Bond	*d* (pm)	MOP	
Ti(1)—Ti(1)	257.60(5)	0.352	2*x*
Ti(1)—E(2)	271.7(1)	0.352	4*x*
Ti(1)—Ti(2)	332.5(2)	0.089	8*x*
E(2)—E(2)	361.2(1)	–0.004	2*x*
E(1)—E(1)	257.60(5)	0.342	2*x*
Ti(2)—E(1)	267.2(2)	0.267	2*x*
Ti(2)—E(2)	275.2(2)	0.336	1*x*
Ti(2)—E(2)	277.9(2)	0.318	1*x*
Ti(2)—Ti(2)	301.1(2)	0.179	2*x*
Ti(2)—E(2)	301.5(1)	0.174	2*x*
Ti(2)—Ti(2)	309.2(3)	0.160	1*x*
Ti(2)—Ti(2)	327.4(2)	0.090	2*x*
Ti(2)—Ti(2)	331.1(3)	0.074	2*x*

element of the third or fourth main group. In general, pnictides and chalcogenides are unlikely to form the W_5Si_3 type because of the short E—E distances therein. Exceptions are a vanadium arsenide, where defects in the As chain are explainable by either an As deficiency or mixed V and As occupancies (44), and the tellurides $A_xK_4Te_3$ (A = Ca, Sr) (45) which can be considered as electron-precise compounds $(A^{2+})_{0.5}(K^{1+})_4(Te^{1-})(Te^{2-})_2$, each Te^{1-} forming two one-electron-two-center bonds. Also, ternary antimonides $Zr_5M_xSb_{3-x}$ (M = Fe, Co, Ni; $x \approx 0.5$) (46) and $Hf_{10}M_xSb_{6-x}$ (M = V, Cr, Mn, Fe, Co, Ni, Cu; $0.8 \leq x \leq 1.5$ for M = Fe) (47) are known to crystallize in ternary variants of the W_5Si_3 type. Therein, the linear E1 chain consists of different mixtures of M and Sb atoms; the M:Sb ratio may vary between 3:1 and 2:3, whereas the second E site (E2) is exclusively occupied by Sb atoms — in contrast to the situation in $Ti_5Si_{1.32(5)}Sb_{1.68}$.

Probably the compound most similar to $Ti_5Si_{1.3}Sb_{1.7}$ is the isostructural niobium silicide stannide "Nb_5SiSn_2". In this case, the site occupancies have not been investigated, i.e., both the E1 and E2 site exhibited negative displacement parameters when identified as silicon and tin, respectively, as

Fig. 1. Projection of the structure of $Ti_5Si_{1.32(5)}Sb_{1.68}$ along [0 0 1]. Symbols: Ti (white circles), E1 (black circles), E2 (gray circles). Only Ti—Ti bonds are shown.



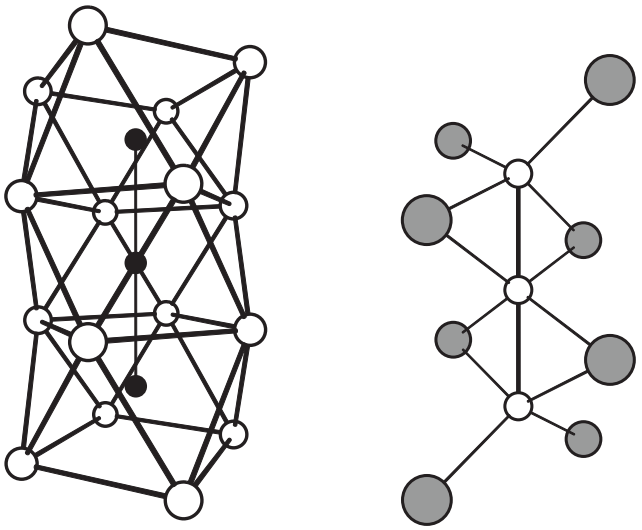
obtained from a Guinier powder pattern (48). Another related compound is V_4SiSb_2, which forms a defect variant of the W_5Si_3 structure: the metal position on site 4*k* is unoccupied, and Si and Sb occupy, without mixing, the 4*a* and 8*h* sites, respectively, (49). Thus, the Si atom in V_4SiSb_2 corresponds to the E1 site in $Ti_5Si_{1.3}Sb_{1.7}$, and the Sb atom to the E2 site.

The structure of $Ti_5Si_{1.3}Sb_{1.7}$ can be described based on two (interconnected) different columns running parallel to the tetragonal *c* axis. These two columns are interconnected by numerous Ti—Sb and Ti—Ti bonds. One column consists of face-condensed E1-centered Ti_8 square antiprisms. The other column comprises edge-sharing Ti-centered $E2_4$ tetrahedra, a condensation which results in a linear Ti chain with short interatomic distances = *c*/2 = 258 pm, by symmetry equidistant to the E1—E1 contacts in the linear E1 chain (Fig. 2).

As often found in metal-rich compounds, numerous valence electrons remain available for the formation of homoatomic bonds between the transition metal atoms Ti. Here, one short and several intermediate Ti—Ti bonds (namely, 258 and 301–333 pm) occur, resembling the Ti—Ti bond lengths in Ti_5Si_3 (258 and 314–320 pm). Elemental titanium crystallizes in the hexagonal closed packing (Mg type) with interatomic distances of 289 and 295 pm, and

© 2001 NRC Canada

Fig. 2. Column of face-condensed E1-centered Ti_8 square antiprisms (left) and of edge-condensed Ti-centered $E2_4$ tetrahedra (right). Symbols: Ti (white circles), E1 (black circles), E2 (gray circles).



Ti_5Sb_3 comprises several Ti—Ti distances starting at 284 pm.

The Ti—E distances are in the expected range, indicating strong bonding heteroatomic interactions. Note that E1 comprises primarily Si atoms and E2 mainly Sb atoms. The Ti—E1 distance of 267 pm is slightly larger than the sum of the Pauling single bond radii of $r_{Ti} + r_{Si}$ = 132 pm + 117 pm = 249 pm (50), which makes it comparable to the Ti—Si bonds observed in Ti_5Si_3 (Mn_5Si_3 structure, 257–280 pm). Similarly, the Ti—E2 distances range from 272 to 302 pm, while the Ti—Sb contacts in Ti_5Sb_3 are between 271 and 295 pm ($r_{Ti} + r_{Sb}$ = 132 pm + 139 pm = 271 pm).

The site preferences of Si and Sb are mostly ruled by size differences, and maybe also — to a smaller extent — by the different preferences to form homoatomic bonds. As a consequence of the parallel running equidistant E1 and Ti chains, the E1—E1 and Ti—Ti distances of 258 pm are considered to be a compromise; the 258 pm are somewhat short for a Ti—Ti bond, but too long for a strong Si—Si bond. Using Pauling's equation $d(n) = d(1) - 60$ pm $\times \log n$ (with n = Pauling bond order; $d(1) = 2r_{Si}$ = 234 pm), the bond order is estimated to be 0.40, smaller than the bond order of 1/2 expected based on the geometry of the chain (10, 11, 13, 51–53). The latter contributes — in addition to entropy effects — to the (minor) incorporation of Sb into the E1 chain, since the Sb atom is significantly larger than a Si atom (r_{Si} = 117; r_{Sb} = 139 pm). On the other hand, the E2 site mainly comprises Sb atoms, because an edge-condensation of Ti-centered Si_4 tetrahedra would unambiguously lead to unreasonably short Ti—Ti contacts.

Electronic structure

The band structure of the structure model Ti_5SiSb_2 is shown in the left part of Fig. 3, emphasizing via the *fat band representation* (54) the Si-based bands. The symmetry lines are chosen according to Bradley and Cracknell (55). The bands lowest in energy have Sb 5*s* character, followed by the two Si 3*s* bands with high dispersion. The latter results from the Si—Si bonds running parallel to [0 0 1]. Three-dimensional metallic properties are predicted based on the band structure, for several Ti-based bands cross the Fermi level along Z–Γ and X–P, i.e., parallel to the c^* axis, as well as along Γ–X (parallel to a^*), which leads to three-dimensional metallic conductivity because of the tetragonal symmetry. Small shifts of the Fermi level, e.g., arising from different Si:Sb ratios, cannot change the metallic character.

As depicted in the atomic projections of the densities of states (right part of Fig. 3), the region around the Fermi level E_F is dominated by Ti states. Basically all Sb *s* and *p* states occur more than 2 eV below E_F, as does the main part of the Si states. In the latter case, however, the antibonding Si states appear well above E_F (+3 eV).

Assuming a bond order of 1/2 for the Si—Si bond, a tentative assignment of oxidation states yields $(Ti^{1.8+})_5Si^{3-}(Sb^{3-})_2$. This assumption is supported by the differences in the electronegativities (EN) (EN(Ti) < EN(Si) < EN(Sb), e.g., Allred–Rochow: 1.32 < 1.74 < 1.82) and the absence of any bonds between the main group elements, except of the one in the linear E1 chain, and the presence of the Ti—Ti bonds. The Mulliken charges obtained for Ti_5SiSb_2 of +0.26 for Ti, –0.25 for Si, and –0.53 for Sb confirm the trend.

In the crystal orbital Hamiltonian populations (COHPs), the densities of states are weighted according to the bonding and antibonding contributions, comparable to the crystal orbital overlap populations known from the Extended Hückel theory (56). The COHPs, shown in Fig. 4, reveal that only a few antibonding states, namely in the Si—Si bond, are filled in the structure model of Ti_5SiSb_2. The heteroatomic Ti—Si and Ti—Sb interactions are optimized, for the Fermi level falls right between the bonding and antibonding states. On the other hand, the Ti—Ti interactions could use more valence electrons to fill more bonding states, i.e., to become stronger.

A more detailed look at the Mulliken overlap populations (Table 4) reveals that all Ti—Ti bonds < 333 pm are significantly bonding with MOPS > 0.07, though the shortest one stands out in this group with MOP = 0.35. These values may be compared to the Ti—Ti bonds in metallic titanium, in the structure of which the bonds of 289 and 295 pm exhibit MOPs of 0.23 and 0.22, respectively. Correspondingly, the bonding character of the Ti—Si, Ti—Sb, and Si—Si interactions is reflected in reasonably large positive overlap populations, as well.

Conclusion

The hitherto unknown titanium silicide antimonide $Ti_5Si_{1.32(5)}Sb_{1.68}$ has been successfully synthesized and characterized by single-crystal investigation, energy dispersive analyses of X-rays, and electronic structure calculations. In contrast to the binary compounds Ti_5Si_3 (Mn_5Si_3 type) and Ti_5Sb_3 (Yb_5Si_3 type), $Ti_5Si_{1.32(5)}Sb_{1.68}$ occurs in the W_5Si_3 structure type. While the Ti atoms occupy the W sites, the Si and Sb atoms fill in mixed occupancies, but in different ratios, the two Si sites of the W_5Si_3 structure. The Si atoms prefer the smaller site with two short homoatomic interactions. Thus, the possibility of Si and Sb atoms sharing one crystallographic position, has been used here for the first

© 2001 NRC Canada

Fig. 3. Left: band structure of the structure model Ti_5SiSb_2, emphasizing the Si-based bands. Right: densities of states (DOS) with the different atomic contributions.

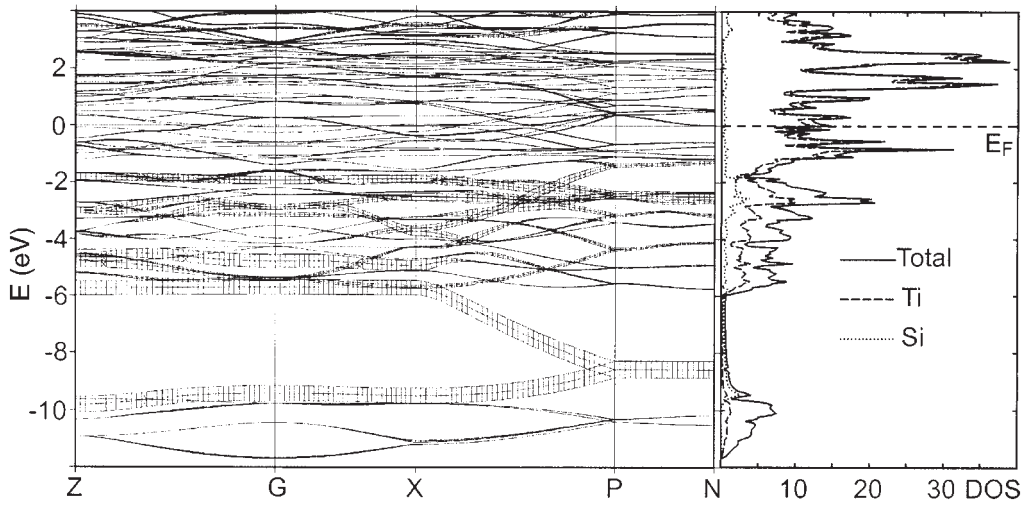
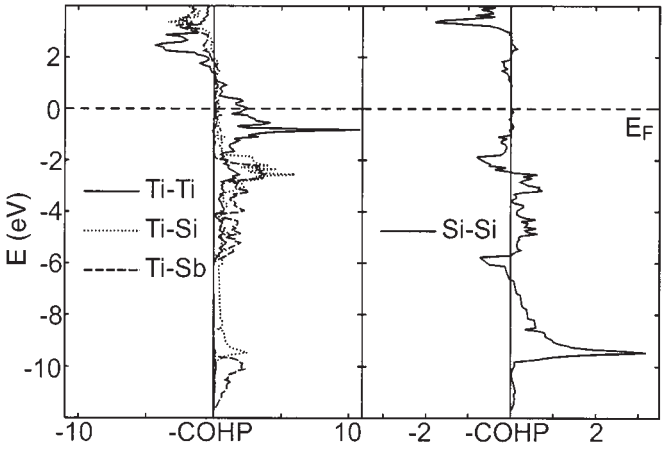


Fig. 4. Cumulated crystal orbital Hamiltonian populations (COHPs).



time to create a new compound with a structure not found in either binary system.

$Ti_5Si_{1.32(5)}Sb_{1.68}$ is a metallic conductor, independent of the exact Si:Sb ratio. The structure is stabilized by heteroatomic Ti—Si and Ti—Sb interactions, and additionally by (pseudo)homoatomic Ti—Ti and Si—Si bonds, while Sb—Sb interactions are negligible.

Acknowledgments

Financial support from Materials and Manufacturing Ontario (MMO) and Natural Sciences and Engineering Research Council of Canada (NSERC) is appreciated.

Supplementary material

Supplementary material (anisotropic displacement parameters (pm^2) for $Ti_5Si_{1.32(5)}Sb_{1.68}$) may be purchased from the Depository of Unpublished Data, Document Delivery, CISTI, National Research Council Canada, Ottawa, ON K1A 0S2, Canada (http://www.nrc.ca/cisti/irm/unpub_e.shtml for information on ordering electronically).

References

1. X. Yao and H.F. Franzen. J. Solid State Chem. **86**, 88 (1990).
2. X. Yao and H.F. Franzen. Z. Anorg. Allg. Chem. **598**/**599**, 353 (1991).
3. X. Yao and H.F. Franzen. J. Am. Chem. Soc. **113**, 1426 (1991).
4. X. Yao and H.F. Franzen. J. Alloys Compd. **183**, 7 (1992).
5. X. Yao, G.A. Marking, and H.F. Franzen. Ber. Bunsen-Ges. **96**, 1552 (1992).
6. H.F. Franzen and M. Köckerling. Prog. Solid State Chem. **23**, 265 (1995).
7. G.A. Marking and H.F. Franzen. Chem. Mater. **5**, 678 (1993).
8. J. Cheng and H.F. Franzen. J. Solid State Chem. **121**, 362 (1996).
9. H. Kleinke and H.F. Franzen. J. Am. Chem. Soc. **119**, 12 824 (1997).
10. H. Kleinke. J. Chem. Soc. Chem. Commun. 2219 (1998).
11. H. Kleinke. J. Mater. Chem. **9**, 2703 (1999).
12. H. Kleinke. Inorg. Chem. **38**, 2931 (1999).
13. H. Kleinke. J. Am. Chem. Soc. **122**, 853 (2000).
14. H. Kleinke and H.F. Franzen. J. Solid State Chem. **136**, 221 (1998).
15. L. Zeng and H.F. Franzen. J. Alloys Compd. **270**, 119 (1998).
16. L.-E. Tergenius, B.I. Noläng and T. Lundström. Acta Chem. Scand. Ser. A, **5A**, 693 (1981).
17. P.-J. Ahlzén and S. Rundqvist. Z. Kristallogr. **189**, 117 (1989).
18. T. Degen and B. Harbrecht. Angew. Chem. Int. Ed. Engl. **34**, 1089 (1995).
19. T. Degen and B. Harbrecht. Angew. Chem. Int. Ed. Engl. **34**, 2703 (1995).
20. M. Conrad and B. Harbrecht. Z. Anorg. Allg. Chem. **623**, 742 (1997).
21. B. Harbrecht, T. Degen, and M. Conrad. J. Alloys Compd. **246**, 37 (1997).
22. S. Debus and B. Harbrecht. Z. Anorg. Allg. Chem. **626**, 173 (2000).
23. H. Kleinke, D. Evans, and B. Harbrecht. Z. Kristallogr. Supplem. **16**, 43 (1999).
24. H. Kleinke and B. Harbrecht. Z. Anorg. Allg. Chem. **625**, 1873 (1999).
25. R. Lam and A. Mar. J. Solid State Chem. **134**, 388 (1997).

© 2001 NRC Canada

26. M. Köckerling, R.-Y. Qi, and J.D. Corbett. Inorg. Chem. **35**, 1437 (1996).
27. M. Köckerling. Inorg. Chem. **37**, 380 (1998).
28. A.M. Mills, R. Lam, and A. Mar. Can. J. Chem. **76**, 1588 (1998).
29. C.-C. Huang, J. Neuhausen, and W. Tremel. J. Chem. Soc. Chem. Commun. 17 (2000).
30. S. Ramakrishnan and G. Chandra. Phys. Lett. **100A**, 441 (1984).
31. G.M. Sheldrick. SHELXS 86. University of Göttingen, Göttingen, Germany. 1986; G.M. Sheldrick. SHELXL 93. University of Göttingen, Göttingen, Germany. 1993.
32. O.K. Andersen. Phys. Rev. **B12**, 3060 (1975).
33. H.L. Skriver. The LMTO method. Springer, Berlin. 1984.
34. U. van Barth and L. Hedin. J. Phys. C: Solid State Phys. **C4**, 2064 (1971).
35. P.E. Blöchl, O. Jepsen, and O.K. Andersen. Phys. Rev. B: Condens. Matter, **B49**, 16 223 (1994).
36. R.S. Mulliken. J. Chem. Phys. **23**, 2343 (1955).
37. R. Hoffmann. J. Chem. Phys. **39**, 1397 (1963).
38. M.-H. Whangbo and R. Hoffmann. J. Am. Chem. Soc. **100**, 6093 (1978).
39. M.-H. Whangbo, R. Hoffmann, T. Hughbanks, M. Kertesz, S. Wijeyesekera, C. Wilker, C. Zheng, M. Evian. EHMACC: A program for extended Hückel molecular and crystal calculations. Department of Chemistry, Cornell University, Ithaca, New York and Department of Chemistry North Carolina State University, Raleigh, North Carolina. 1987. M. Köckerling. PC Adaption: Institut für Synthesechemie, Gesamthochschule Duisburg, 1997.
40. E. Clementi and C. Roetti. At. Nucl. Data Tables, **14**, 177 (1974).
41. R. Berger. Acta Chem. Scand. Ser. A, **A31**, 889 (1977).
42. T. Kajitani, T. Kawase, K. Yamada, and M. Hirabayashi. Trans. Jpn. Inst. Met. **27**, 639 (1986).
43. P. Villars. Pearson's handbook. Desk ed. American Society for Metals, Materials Park, Ohio. 1997.
44. R. Berger. Acta Chem. Scand. Ser. A, **31A**, 223 (1977).
45. I. Schewe-Miller and P. Böttcher. J. Alloys Compd. **183**, 98 (1992).
46. Y.-U. Kwon, S.C. Sevov, and J.D. Corbett. Chem. Mater. **2**, 550 (1990).
47. H. Kleinke, C. Ruckert, and C. Felser. Eur. J. Inorg. Chem. 315 (2000).
48. R. Horyn and K. Lukaszewicz. Bull. Acad. Pol. Sci. Ser. Sci. Chim. **18**, 59 (1970).
49. P. Wollesen and W. Jeitschko. J. Alloys Compd. **243**, 67 (1996).
50. L. Pauling. The nature of the chemical bond. 3rd ed. Cornell University Press, Ithaca, New York. 1948.
51. H. Kleinke, M. Waldeck, and P. Gütlich. Chem. Mater. **12**, 2219 (2000).
52. H. Kleinke. J. Solid State Chem. **159**, 134 (2001).
53. G.A. Papoian and R. Hoffmann. Angew. Chem. Int. Ed. **39**, 2408 (2000).
54. O. Jepsen and O.K. Andersen. Z. Phys. **97**, 25 (1995).
55. C.J. Bradley and A.P. Cracknell. The mathematical theory of symmetry in solids. Clarendon Press, Oxford. 1972.
56. R. Dronskowski and P. Blöchl. J. Phys. Chem. **97**, 8617 (1993).

© 2001 NRC Canada

New low-spin Co(II) complexes with novel tripodal 1,1,1-tris(dimethylphosphinomethyl)ethane ligand: electron transfer kinetics and spectroscopic characterization of $Co(II)P_6$ and $Co(II)P_3S_3$ ions in aqueous solution

Satoshi Iwatsuki, Kenji Obeyama, Nobuyoshi Koshino, Shigenobu Funahashi, Kazuo Kashiwabara, Takayoshi Suzuki, and Hideo D. Takagi

Abstract: Substitution-inert Co(II) complexes with tripodal 1,1,1-tris(dimethylphosphinomethyl)ethane were produced in aqueous solution by the controlled-potential electrolysis. EPR studies indicated that the $Co(II)P_6$ and $Co(II)P_3S_3$ species are in the low-spin $t_{2g}^6e_g^1$ state. The analyses of the absorption spectra of the Co(II) species in solution indicated significant Jahn–Teller distortion in $Co(II)P_6$ and $Co(II)P_3S_3$ ions as expected for the low-spin d^7 electronic configuration, while less distortion was observed for the $Co(II)S_6$ ion. Kinetic studies of the redox reactions involving these Co(III/II) species confirmed that the electron self-exchange reactions for the $Co(III/II)P_6$ and $Co(III/II)P_3S_3$ couples are relatively fast ($k_{ex} \sim 1 \times 10^4$ dm^3 mol^{-1} s^{-1}), which is consistent with the results for other low-spin – low-spin Co(III/II) couples. It was concluded that the nephelauxetic effect of the P-donor atom stabilizes the low-spin state in Co(II), and that the rather rapid electron exchange rates for these Co(III/II) couples were explained by the lack of the spin reorganization process required for the ordinary low-spin – high-spin Co(III/II) couples.

Key words: cobalt(III/II), spin state, EPR study, kinetics, electron transfer.

Résumé : Faisant appel à l'électrolyse à potentiel contrôlé, en solution aqueuse, on a préparé des complexes de Co(II) comportant du 1,1,1-tris(diméthylphosphinométhyl)éthane tripodal et qui sont inertes vis-à-vis des substitutions. Des études de RPE indiquent que les espèces $Co(II)P_6$ et $Co(II)P_3S_3$ se trouvent dans un état $t_{2g}^6e_g^1$ de faible spin. Comme on pouvait s'y attendre pour la configuration électronique d^7 de faible spin, les analyses des spectres d'absorption des espèces Co(II) en solution mettent en évidence l'existence d'une distorsion importante de Jahn–Teller dans les ions $Co(II)P_6$ et $Co(II)P_3S_3$; on a toutefois observé moins de distorsion pour l'ion $Co(II)S_6$. Les études cinétiques des réactions redox impliquant ces espèces Co(III/II) ont confirmé que les réactions d'auto-échanges électroniques des couples $Co(III/II)P_6$ et $Co(IIII/II)P_3S_3$ sont relativement rapides ($k_{éc} \sim 1 \times 10^4$ dm^3 mol^{-1} s^{-1}) et ces observations sont en accord avec les résultats obtenus avec d'autres couples Co(III/II) de faible spin – faible spin. On en conclut que l'effet néphélauxétique de l'atome de P-donneur stabilise l'état de faible spin dans Co(II) et que les vitesses d'échanges électroniques relativement rapides observées pour ces couples Co(III/II) peuvent être expliquées par l'absence de processus de réorganisation de spin requis pour les couples Co(III/II) ordinaires de faible spin – spin élevé.

Mots clés : cobalt(III/II), état de spin, étude RPE, cinétique, transfert d'électron.

[Traduit par la Rédaction]

Introduction

The Co(III/II) electron transfer reactions have been intensively studied to identify the cause of sluggishness in low-spin – high-spin Co(III/II) couples, and various reaction mechanisms have been postulated to explain such specific behaviors (1–6). For the deeper understanding of the electron transfer reactions of Co(III/II), it seems essential to synthesize new stable Co(III) and Co(II) complexes and examine their reactivities. Kashiwabara and co-workers (7–13) intensively explored various Co(III) complexes with multidentate ligands possessing phosphorus atoms as donors. This research was carried out to examine the electronic states and structures of the new type of Co(III/II) couples stable in aqueous solution.

Among the low-spin Co(II) complexes, only bis(1,4,7-trithiacyclononane)cobalt(II) and some other encapsulated

Received February 2, 2001. Published on the NRC Research Press Web site at http://canjchem.nrc.ca on September 14, 2001.

S. Iwatsuki, K. Obeyama, N. Koshino, S. Funahashi, K. Kashiwabara, and D. Takagi.[1] Department of Chemistry, Graduate School of Science, Nagoya University, Chikusa, Nagoya, 464–8602 Japan.
T. Suzuki. Department of Chemistry, Graduate School of Science, Osaka University, Toyonaka, Osaka, 560-0043 Japan.

[1]Corresponding author (telephone and fax: +81-52-789-5473; e-mail: htakagi@chem4.chem.nagoya-u.ac.jp).

 DOI: 10.1139/cjc-79-9-1344 © 2001 NRC Canada

Table 1. Redox potentials and self-exchange rate constants (k_{ex}) for the selected redox couples in aqueous solution.

Redox couple	Spin state of Co(II)[a]	E^0 (V) vs. NHE	k_{ex} (dm^3 mol^{-1} s^{-1})
$[Co(ttcn)_2]^{3+/2+}$	Low-spin	0.42[b]	1.3×10^{5}[b]
$[Co(mmtp)(ttcn)]^{3+/2+}$	Low-spin	–0.11[c]	6×10^{4}[c]
$[Co(mmtp)_2]^{3+/2+}$	Low-spin	–0.26[c]	2×10^{4}[c]
$[Co(azacapten)]^{3+/2+}$	Low-spin	0.01	2.2×10^{4}[e]
$[Co(phen)_3]^{3+/2+}$	High-spin	0.37[d]	12[e]
$[Co(bpy)_3]^{3+/2+}$	High-spin	0.315[d]	5.7[e]
$[Co(sep)]^{3+/2+}$	High-spin	–0.30[d]	5.1[e]
$[Co(en)_3]^{3+/2+}$	High-spin	–0.18[e]	7.7×10^{-5}[e]
$[Co(diamsar)]^{3+/2+}$	High-spin	–0.32	0.4[e]
$[Co(tacn)_2]^{3+/2+}$	High-spin	–0.41	0.19[e]
$[Co(NH_3)_6]^{3+/2+}$	High-spin	0.06[e]	2×10^{-7}[e]
$[Ru(NH_3)_6]^{3+/2+}$		0.07[e]	8.2×10^{2}[f]

[a]At room temperature.
[b]Reference 19.
[c]This work.
[d]J.F. Endicott, K. Kumar, T. Ramasami, and F.P. Rotzinger. Prog. Inorg. Chem. **30**, 141 (1983).
[e]Reference 14.
[f]T.J. Meyer and H. Taube. Inorg. Chem. **7**, 2369 (1968).

complexes such as the 8-methyl-1,3,13,16-tetraaza-6,10,19-trithiabicyclo[6.6.6]eicosane (azacapten) complex have been kinetically analyzed (14–16). This is partly because some of the low-spin cobalt(II) are thermodynamically unstable (17), while others are substitution labile in solution. The redox potentials for selected Co(III/II) couples are listed in Table 1, in which it is seen that the standard redox potentials for some low-spin – low-spin couples are relatively higher than those for the ordinary low-spin – high-spin couples. However, several species such as tris(1,10-phenanthroline)cobalt(III/II) and tris(2,2′-bipyridine)cobalt(III/II) couples exhibit rather high redox potentials although Co(II) in these complexes are in the high-spin state at room temperature, indicating that the redox potentials of these complex ions are determined not only by the energy levels of HOMO for Co(II) and LUMO of Co(III) but also by the solvation free-energy difference between Co(II) and Co(III) species in relation to the size of the ions in each oxidation state and specific solute–solvent interactions such as the hydrogen bonding. Therefore, the redox potentials of Co(III/II) couples cannot be a good measure for the ligand-field strength and the relevant spin states of the redox couple. In other words, structural analyses of both Co(III) and Co(II) species in solution, by means of rather classical but very reliable EPR and UV–vis spectroscopy, is essential for the understanding of the structure–reactivity relation in the Co(III/II) systems.

From the kinetic point of view, it has been indicated that the electron self-exchange rate constants between the low-spin Co(III) and the high-spin Co(II) species are rather slow compared with those between low-spin Co(III) and low-spin Co(II) species (14). The necessity of extra reorganization energy for the multi-spin process has been generally accepted for the explanation of such a difference in the self-exchange rate constants. For example, it has been reported that the spin reorganization of the octahedral d^7 Co(II) in the high-spin state ($t_{2g}^5 e_g^2$) during the activation process of the electron exchange reaction requires as much as 103 kJ mol^{-1} for the $[Co(NH_3)_6]^{3+/2+}$ couple (1).[2] In this case, a kind of pre-equilibrium between the high-spin Co(II) and the low-spin Co(II) states exists before the electron transfer (ET) process.

[1] $\quad Co(II)^*[hs] \rightleftarrows Co(II)^*[ls]$

(<103 kJ mol^{-1} in the case of hexaammine complex)

[2] $\quad Co(III)[ls] \rightleftarrows Co(III)[hs]$

(<259 kJ mol^{-1} in the case of hexaammine complex)

[3] $\quad Co(II)^*[ls] + Co(III)[ls] \rightleftarrows Co(III)^*[ls] + Co(II)[ls]$

[4] $\quad Co(II)^*[hs] + Co(III)[hs] \rightleftarrows Co(III)^*[hs] + Co(II)[hs]$

The lower energy process (eq. [1]) is taken to be the preferred pathway. However, recent analyses of magnetic moment and microwave absorption of various Co(II) species in solution indicate that such a low spin – high spin equilibrium is extremely rapid (it requires only several nanoseconds) and the spin-equilibrium constant is not as large as it was originally suggested: the slow ET rates in such a reaction system has been attributed to the large inner-sphere reorganization in the low-spin Co(II) ($t_{2g}^6 e_g^1$) species, which is suppose to exhibit significant Jahn–Teller distortion (5). More recent studies by Swaddle and co-workers (3) support the explanations by Beattie et al. (4, 5).

It is a very difficult task to find inert low-spin Co(III) – high-spin Co(II) redox couples suitable for the measurements of both reduction and oxidation cross reactions in solution: many of these couples possess rather low redox potentials and the high-spin Co(II) species are very labile. The latter reason prevents us from precise investigations of the nature of the reactions involving Co(II) complexes in more detail. We have started to investigate the reactivity of a series of Co(III/II)–P_nS_{6-n} and –P_nN_{6-n} (P_nS_{6-n} and P_nN_{6-n} represent multidentate ligands with n = 0–6). In this article, we report new types of low-spin Co(II) species stable in aqueous solution. The structures of $Co(II)P_6$ and $Co(II)P_3S_3$ in solution were analyzed by the spectrophotometric and EPR methods. The oxidation and reduction reactions of these complexes were studied at ambient pressure.

[2]The estimated free energy difference between two different spin states in this article is erroneous as they used the reorganization parameter (for the vertical transition) instead of multiplying by 1/4. Therefore, the energy difference between the two spin states are smaller than the values shown in eqs. [1] and [2].

© 2001 NRC Canada

Experimental

Materials

$[Co(mmtp)_2](BF_4)_3$ (mmtp = tris(1,1,1-dimethylphosphinomethyl)ethane) was synthesized and purified by the previously reported method (13, 18). $[Co(mmtp)(ttcn)](BF_4)_3$ was synthesized from the trichloride salt of the mono-mmtp complex with ttcn (ttcn = 1,4,7-trithiacyclononane) (12, 13). $[Co(ttcn)_2](ClO_4)_3$ and $[Co(ttcn)_2](ClO_4)_2$ were synthesized by the literature method (19). $[Ru(NH_3)_6]Cl_3$ and $[Co(sep)]Cl_3$ (sep = 1,3,6,8,10,13,16,19-octaazabicyclo[6.6.6]eicosane) were obtained from Aldrich.

Measurements

A BAS100BW electrochemical analyzer (Bioanalytical Systems) was used for the measurements of cyclic voltammograms and for the controlled-potential electrolyses. JASCO V-560 and Shimadzu UV-1600 spectrophotometers were used to record the absorption spectra in solution. A Hitachi U-3400 UV–vis–near-IR spectrophotometer with the integration sphere was used for recording the absorption spectra of solid samples. A JES-RE IX X-band spectrometer was used for the measurements of EPR spectra of Co(II) species in solution. A Unisoku stopped-flow apparatus equipped with a controlled-potential electrolysis chamber (20) was used for the kinetic measurements. Sample solutions for kinetic measurements were prepared with twice-distilled water and degassed by Ar. All measurements were carried out under Ar atmosphere. The ionic strength of the sample solutions was adjusted by potassium chloride. The electrochemical measurements were carried out by using a thermostated cell (25°C) with a glassy carbon working electrode, a platinum wire counter electrode, and a Ag/AgCl reference electrode. Potassium chloride was used as the supporting electrolyte.

Results and discussion

Electrochemical measurements

The redox potentials of $[Co(ttcn)_2]^{3+/2+}$, $[Co(mmtp)(ttcn)]^{3+/2+}$, and $[Co(mmtp)_2]^{3+/2+}$ couples are summarized in Table 1. The peak separations for these couples are typically 69 mV and the ratios of the anodic and cathodic peak currents were 1:0.996, indicating that the signals are reversible. The E^0 value for $[Co(mmtp)(ttcn)]^{3+/2+}$ was closer to that for the $[Co(mmtp)_2]^{3+/2+}$ couple, rather than that for $[Co(ttcn)_2]^{3+/2+}$. Therefore, it seems that Co(II) oxidation state is destabilized by the substitution of one ttcn ligand for mmtp. The crystallographic data for the $[Co(mmtp)_2]^{3+}$ species (13) indicates that the Co—P bond is elongated because of the strong *trans* influence and probably by the steric hindrance of the rather bulky phosphine ligand.[2] The same argument may even be possible for the bond lengths between slightly larger Co(II) centers and the P-donor atoms, because of the strong σ-donicity of the P-atom and (or) the Jahn–Teller distortion expected for the low-spin d^7 configuration (see following discussion for the spin states of $Co(II)P_6$ and $Co(II)P_3S_3$). It seems that the thermodynamic stability of the Co(II) species in solution is somewhat lowered by the consecutive substitution of ttcn by the mmtp ligand. However, a spectroelectrochemical study of these complexes revealed that the Co(II) species produced by the controlled-potential electrolyses were substitution inert: reoxidation of the reduced solution either by peroxodisulfate salt or by electrolysis reproduced the original Co(III) species (yield > 95% after ca. 1 h).

EPR measurements

Aqueous solutions of $[Co(mmtp)_2]^{2+}$ and $[Co(mmtp)(ttcn)]^{2+}$ were prepared by the controlled-potential electrolyses at –550 and –500 mV vs. Ag/AgCl, respectively. The EPR spectra of these solutions at room temperature are shown in Fig. 1. A multiplet caused by the coupling with ^{59}Co (I = 7/2) and ^{31}P (I = 1/2) were observed at g_{iso} = 2.08 and 2.05 for $[Co(mmtp)_2]^{2+}$ and $[Co(mmtp)(ttcn)]^{2+}$, respectively, which may be compared with the value (g_{iso} = 2.10) estimated for low-spin $[Co(ttcn)_2]^{2+}$ in aqueous solution. It has been reported (21) that the g_{iso} value observed for the metal ions depends on the ligand-field strength: the g_{iso} value decreases to a value close to that for the free electron upon increasing the ligand-field strength. Therefore, the g_{iso} values obtained for the $[Co(mmtp)_2]^{2+}$ and $[Co(mmtp)(ttcn)]^{2+}$ complexes indicate that these complexes are in the low-spin electronic state and the ligand field of phosphine is larger than or comparable to that of thioether, which is consistent with the spectrophotometric observations described in the following section. The values of the g_{iso} parameter indicate that the ligand field increases in the order of $P_3S_3 > P_6 > S_6$.

Absorption spectra

The absorption spectra of the $[Co(ttcn)_2]^{3+}$, $[Co(mmtp)(ttcn)]^{3+}$, and $[Co(mmtp)_2]^{3+}$ species are shown in Fig. 2, and the energies corresponding to the two *d–d* transitions are summarized in Table 2, in which the 10*Dq* values as well as the Racah *B* parameter were calculated by the following equations (22, 23):

$$[5] \quad E\,(^1A_{1g} \rightarrow {}^1T_{1g}) = 10Dq - C \text{ or } E\,(^1A_{1g} \rightarrow {}^1T_{2g}) = 10Dq + 16B - C, \text{ where } C = 4B$$

It seems that the ligand-field strength of the P-atom is, as expected, rather large and is comparable to that of the S-atom in the thioether ligands. On the other hand, the nephelauxetic effect of the P-atom is larger than or compara-

[2] The previously reported analysis for the crystal structure of $[Co(mmtp)_2][Co(CN)_6]\cdot nH_2O$ (n = 2.25) was found to be erroneous. The space group $Pca2_1$ (No. 29) was incorrectly assigned, and the corrected one is *Pcam* (No. 57, $b\bar{a}c$ setting). Using the absorption-corrected intensity data (supplied by Professor Ohba), the structure was reanalyzed. It was found that four Co atoms (Co(A), Co(B), Co(C), and Co(D)) are located at the positions having their site symmetry of .2., ..*m*, $\bar{1}$, and ..*m*, respectively. Five O-atoms corresponding to the hydrated water were observed, and two of them were located on a crystallographically plane of symmetry. Thus, the analysis indicated that the number of hydrated water (n in the above formula) is 4, which is consistent with the elemental analysis. The details of the structural analysis and the parameter obtained are deposited in supplementary. We have also found that the bis(mmtp)rhodium(III) analog ($[Rh(mmtp)_2][Co(CN)_6]\cdot 4H_2O$) is isomorphorous to this cobalt(III) complex (T. Suzuki, unpublished work).

© 2001 NRC Canada

Fig. 1. EPR spectra of Co(II) produced by the controlled-potential electrolyses in aqueous solution at room temperature: (*a*) $[Co(mmtp)_2]^{2+}$, hyperfine coupling constants were estimated as 2.87 mT with Co(II) and as 5.74 mT with P by the simulation; (*b*) $[Co(mmtp)(ttcn)]^{2+}$, hyperfine coupling constants were estimated as 4.2 mT with Co(II) and as 5.45 mT with P by the simulation.

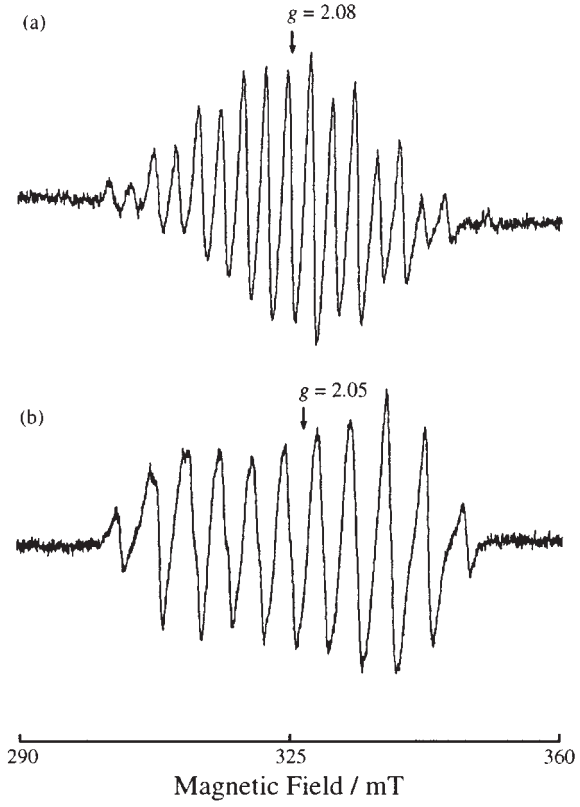
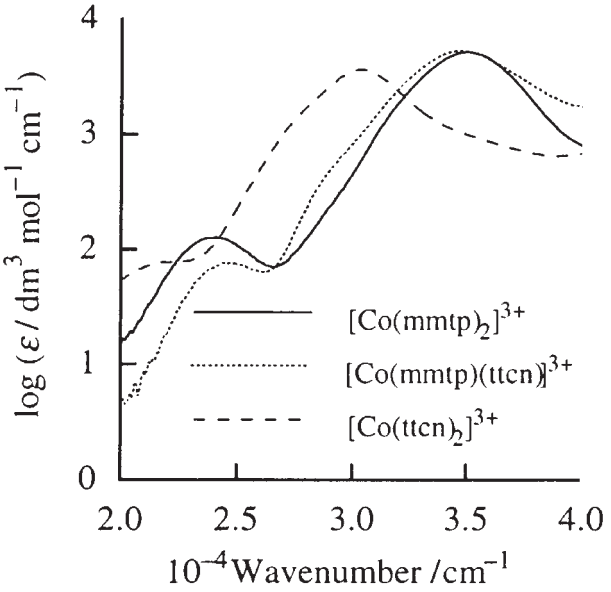


Fig. 2. Absorption spectra of Co(III) species in aqueous solution.



ble to that for the S-atom. These results indicate that the σ-donicity of the mmtp ligand is as large as that for ttcn, and the covalency of the Co—P bonds is as large as or larger than that for the Co—S bonds, probably through the strong π-interaction between the central Co(III) and the P-atom, coupled with the rather large σ-interaction.

In Fig. 3, the absorption spectra of $[Co(mmtp)_2]^{2+}$ and $[Co(mmtp)(ttcn)]^{2+}$ in aqueous solution are shown. The spectroelectrochemical analyses of $[Co(mmtp)_2]^{2+}$ and $[Co(mmtp)(ttcn)]^{2+}$ produced by the controlled-potential electrolyses revealed that $[Co(mmtp)_2]^{2+}$ and $[Co(mmtp)(ttcn)]^{2+}$ ions in aqueous solution exhibited only one or two absorption maxima in the visible region (λ = 678 nm (ε = 38 $dm^3\ mol^{-1}\ cm^{-1}$) and 924 nm (ε = 43), and λ = 638 nm (ε = 41), respectively). The absorption spectrum of $[Co(ttcn)_2]^{2+}$ in acetonitrile was reported by Wieghardt et al. (λ = 730 nm (ε = 11) and 560 nm (sh)) (19). However, their assignment of these two peaks ($^4T_{1g} \rightarrow {}^4T_{2g}$ and $^4T_{1g} \rightarrow {}^4A_{2g}$, respectively) was wrong as this complex is in the low-spin state (19, 24). It should be noted that one of the coordination axes of the Co(II) center with the low-spin d^7 electronic configuration may be elongated by the Jahn–Teller distortion, which causes splitting of the e_g level (Fig. 4); the ^2E_g ground term for the octahedral field splits into $^2A_{1g}$ (ground state) and $^2B_{1g}$ (excited state). The crystal structure of $[Co(ttcn)_2](ClO_4)_2$ indicates that the Jahn–Teller distortion is not very large (25). Therefore, the $^2A_{1g} \rightarrow {}^2B_{1g}$ transition should be observed at a much lower energy region. The absorption spectrum for $[Co(ttcn)_2](ClO_4)_2$ reported in this study is identical to that reported by Wieghardt et al. (19). It is plausible that the absorption spectrum in solution and that in the solid state may be different, as the fluxionality of the ttcn complexes has been observed even in the Pt(II) complex (26). Moreover, it is possible that the Jahn–Teller distortion may be enhanced in solution to produce a square-planar or square-pyramidal conformation. To examine the structure of $[Co(ttcn)_2]^{2+}$ in solution, we measured the diffuse reflectance spectrum of solid $[Co(ttcn)_2](ClO_4)_2$, which is shown in Fig. 5. In the solid state, $[Co(ttcn)_2](ClO_4)_2$ exhibits one broad absorption band in which two separate peaks at 474 (21 000 cm^{-1}) and 561 nm (18 000 cm^{-1}) was observed. The very broad band starting at ca. 1000 nm indicates that the absorption in the 730 nm region observed in solution also exists in the solid state but it is not well-resolved in the reflectance spectrum. This observation indicates that the structure of $[Co(ttcn)_2]^{2+}$ in the crystal is retained in solution. Therefore, the absorption at λ = 730 nm (ε = 11) and 560 nm (sh) are assigned to either $^2A_{1g}(^2E_g) \rightarrow {}^2_aT_{1g}$ or $^2A_g(^2E_g) \rightarrow {}^2_aT_{2g}$. In such a case, the 10*Dq* value is estimated as ca. 13 700 cm^{-1} (12, 19), and the structure of $[Co(ttcn)_2]^{2+}$ is identical both in the solid state and in solution: the Jahn–Teller splitting is not very large.

On the other hand, the absorption spectra of $[Co(mmtp)(ttcn)]^{2+}$ and $[Co(mmtp)_2]^{2+}$ ions in solution are very different from that for the $[Co(ttcn)_2]^{2+}$ ion. The absorption bands at 631 nm for $[Co(mmtp)(ttcn)]^{2+}$ and at 678 nm for $[Co(mmtp)_2]^{2+}$ may be assigned to the $^2A_{1g}(^2E_g) \rightarrow {}^2_aT_{1g}$ transition. However, we could not observe the absorption corresponding to the $^2A_{1g}(^2E_g) \rightarrow {}^2_aT_{2g}$, and $^2A_{1g}(^2E_g) \rightarrow {}^2_bT_{1g}$ transitions in such a case. On the other hand, a new band at 924 nm appeared for the latter complex. It has been reported (27) that severely distorted $[Co(NO_2)_6]^{4-}$ exhibits a

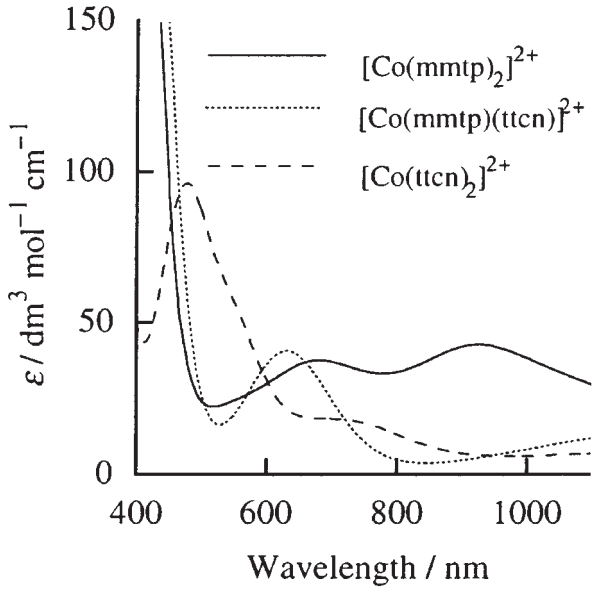
© 2001 NRC Canada

Table 2. Absorption bands and ligand-field parameters for Co(III) complexes in aqueous solution.

	$^1A_{1g} \rightarrow {}^1T_{1g}$ (cm^{-1})	$^1A_{1g} \rightarrow 1T_{2g}$ (cm^{-1})	$10Dq$ (cm^{-1})	B (cm^{-1})
$[Co(mmtp)_2]^{3+}$	2.41×10^4	[a]		
$[Co(mmtp)(ttcn)]^{3+}$	2.46×10^4	2.92×10^4	2.57×10^4	292
$[Co(ttcn)_2]^{3+}$	2.11×10^4	2.74×10^4	2.26×10^4	397

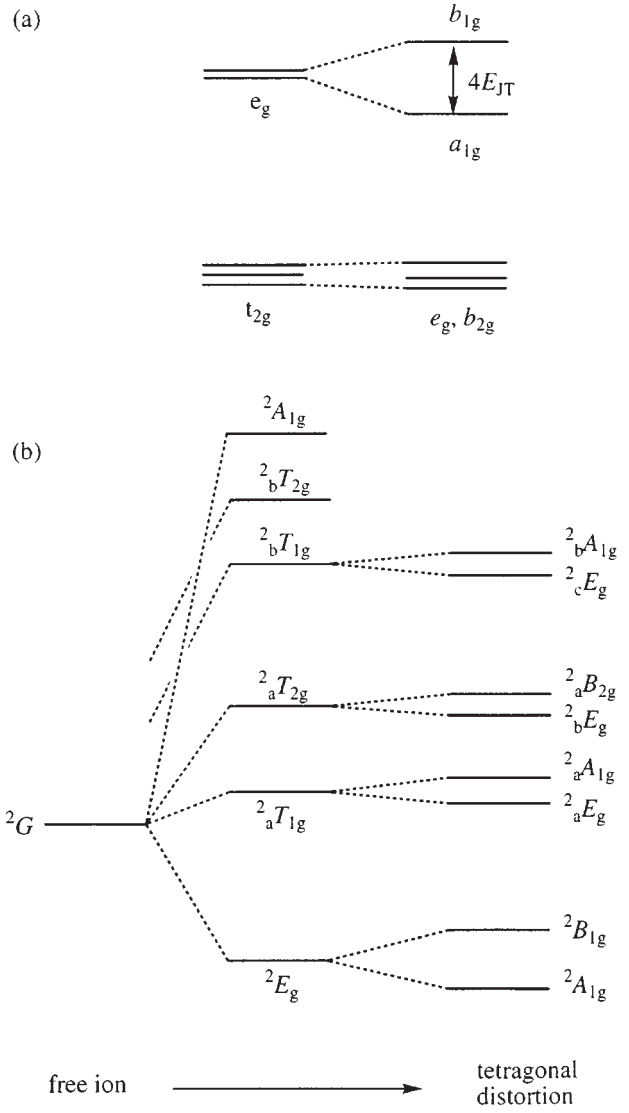
[a]Not observed.

Fig. 3. Absorption spectra of $[Co(mmtp)_2]^{2+}$, $[Co(mmtp)(ttcn)]^{2+}$, and $[Co(ttcn)_2]^{2+}$ in aqueous solution.



low-energy absorption band at ca. 1000 nm, which was assigned to the $^2A_{1g} \rightarrow {}^2B_{1g}$ transition from which the Jahn–Teller stabilization energy ($4E_{JT}$) was estimated as 8400 cm^{-1}. It is plausible that the Jahn–Teller distortion in $[Co(mmtp)_2]^{2+}$ is very large: the distortion may be comparable to that for the NO_2^- complexes. By assuming that the absorption bands at 678 and 924 nm correspond to the $^2A_{1g} \rightarrow {}^2_aT_{1g}$ and $^2A_{1g} \rightarrow {}^2B_{1g}$ transitions, respectively, the $10Dq$ and E_{JT} values are estimated as 14 700 and 2700 cm^{-1} for the $[Co(mmtp)_2]^{2+}$ complex. It is reasonable to consider, then, the absorption bands for the $^2A_{1g} \rightarrow {}^2_aT_{2g}$, and $^2A_{1g} \rightarrow {}^2_bT_{2g}$ transitions are located at energies higher than 500 nm. The absorption spectrum for the $[Co(mmtp)(ttcn)]^{2+}$ complex seems to possess the nature of both $[Co(ttcn)_2]^{2+}$ and $[Co(mmtp)_2]^{2+}$: an absorption at 631 nm and a broad band at 1100 nm region. The former band may be assigned to the $^2A_{1g} \rightarrow {}^2_aT_{1g}$ transition, while the latter band corresponds to the $^2A_{1g} \rightarrow {}^2B_{1g}$ transition: the Jahn–Teller distortion decreases in the order of $[Co(mmtp)_2]^{2+} > [Co(mmtp)(ttcn)]^{2+} >> [Co(ttcn)_2]^{2+}$. The higher-energy absorption bands corresponding to the $^2A_{1g} \rightarrow {}^2_aT_{2g}$, and $^2A_{1g} \rightarrow {}^2_bT_{1g}$ transitions are located at wavelength region shorter than 500 nm. Therefore, we conclude that the coordination by P-atom causes large tetragonal distortion from the octahedral symmetry because of the Jahn–Teller effect and (or) the strong *trans* influence of the P-donor, together with the steric effect originating from the bulky dimethylphosphine group.

Fig. 4. Ligand-field splitting expected for low-spin d^7 electronic configuration. (*a*) Splitting of the *d*-orbitals caused by the tetragonal distortion; and (*b*) the correlation diagram for the low-spin d^7 configuration.

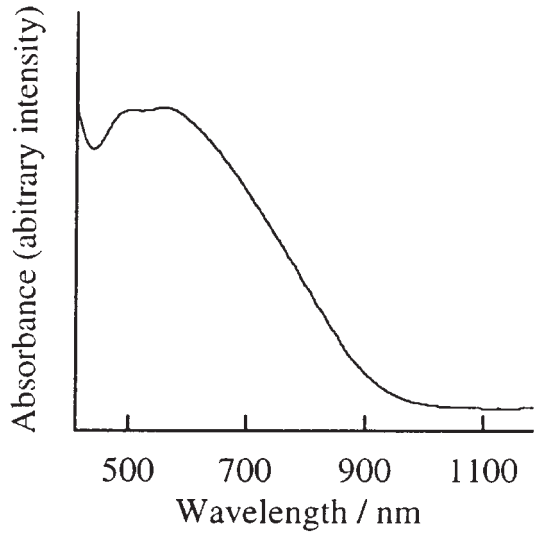


Kinetic studies

The oxidation reactions of Co(II) by $[Ru(NH_3)_6]^{3+}$ and the reduction reactions of Co(III) by $[Co(sep)]^{2+}$ ion were studied with the ionic strength of 0.1 mol dm^{-3} at various temperatures. The change in the absorption at 300 nm was used for the measurements of oxidation reactions, while the absorption change at 415 nm region was used to monitor reduction reactions. Pseudo-first- order conditions, [Co(II)] << [Ru(III)] and [Co(III)] >> $[Co(sep)^{2+}]$, were used. Kinetic

© 2001 NRC Canada

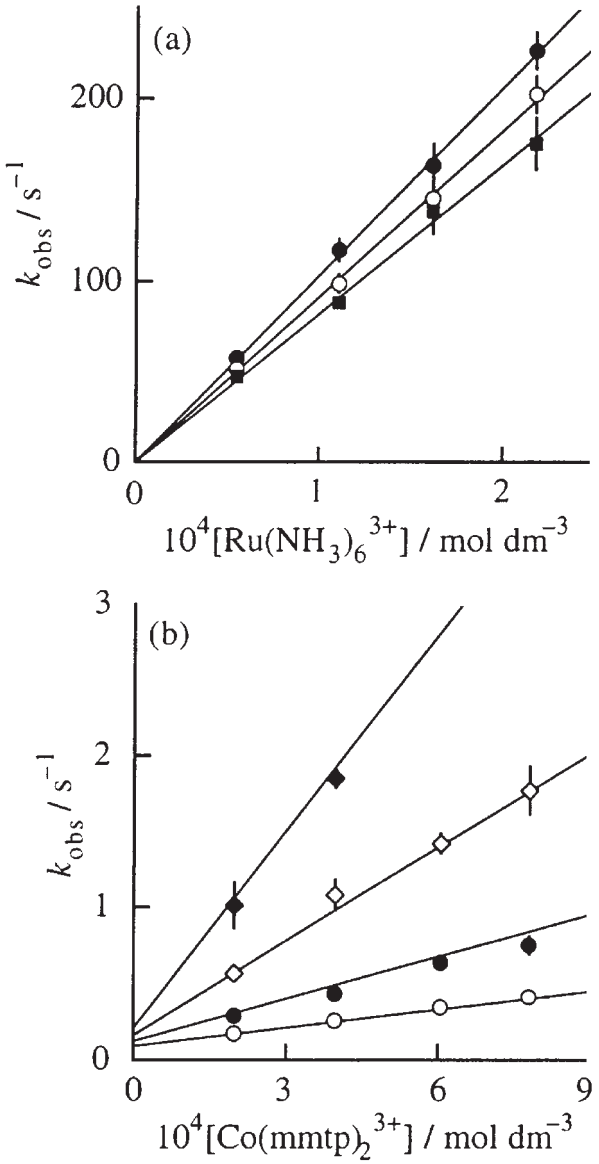
Fig. 5. Diffuse reflectance spectrum of solid $[Co(ttcn)_2](ClO_4)_2$.



traces fit first-order curves for more than three half-lives. The plots of the apparent first-order rate constant against the concentration of the excess reagent were linear (Fig. 6),[3] and the second-order rate constants were calculated from the slopes of the plots. For the reduction reaction of $[Co(mmtp)_2]^{3+}$ by $[Co(sep)]^{2+}$ (Fig. 6*b*), completion of the reactions was not expected under the experimental conditions (the potential difference between these two couples is merely 50 mV). The intercepts that appear in Fig. 6*b* are, therefore, taken as the evidence of the back reaction. However, no significant deviation from the pseudo-first-order kinetics was observed for these reactions up to three half-lives as mentioned above. The addition of excess $[Co(sep)]^{3+}$ to the reaction mixture did not alter the observed pseudo-first-order rate constant, either. Therefore, we decided that the second-order rate constants estimated from the slopes of the plots in Fig. 6*b* are fairly reliable. However, it was not fruitful to estimate the equilibrium constant for this reaction because of the significant errors in estimating the values of the intercepts. Instead, we directly estimated the rate constant for the back reaction, the results of which are also listed in Table 3. The second-order rate constants and related activation parameters are summarized in Table 3.

The electron self-exchange rate constants for the $[Co(mmtp)_2]^{3+/2+}$ and $[Co(mmtp)(ttcn)]^{3+/2+}$ couples were estimated by the Marcus cross relation (28, 29) as 2×10^4 and 6×10^4 dm^3 mol^{-1} s^{-1} from the oxidation and reduction cross reactions of the $[Co(mmtp)_2]^{3+/2+}$ and $[Co(mmtp)(ttcn)]^{3+/2+}$ couples, respectively. The difference in the self-exchange rate constants estimated from the oxidation and reduction cross reactions is taken to be within the acceptable errors inherent in the Marcus cross relation. The value of k_{ex} ($\sim 1 \times 10^4$ dm^3 mol^{-1} s^{-1}) is comparable to those for the other low-spin – low-spin Co(III/II) couples with encapsulated N_3S_3 and S_6 ligands (30, 31), while the self-exchange rate constant for the $[Co(ttcn)_2]^{3+/2+}$ couple (ca. 1×10^5 dm^3 mol^{-1} s^{-1}) is slightly larger than this value (16, 23, 32).

Fig. 6. Dependence of the first-order rate constant (k_{obs}) for the redox reactions of $[Co(mmtp)_2]^{3+/2+}$ couple on the concentration of excess reagent: (*a*) oxidation reaction of $[Co(mmtp)_2]^{2+}$ with $[Ru(NH_3)_6]^{3+}$ at: (■) 5, (○) 15, and (●) 25°C; and (*b*) reduction reaction of $[Co(mmtp)_2]^{3+}$ with $[Co(sep)]^{2+}$ at: (○) 15, (●) 25, (◇) 35, and (◆) 45°C.



The kinetic studies concerning the low-spin – high-spin Co(III/II) couples have, in many cases, been limited to the observations of the reduction reactions of Co(III), because of the lability of high-spin Co(II) species. Moreover, the very low redox potentials of such low-spin – high-spin Co(III/II)

[3] Supplementary material, including redox tables and X-ray crystallographic data, may be purchased from the Depository of Unpublished Data (DUD No. 3306), Document Delivery, CISTI, National Research Council Canada, Ottawa, ON K1A 0S2, Canada. For information on obtaining material electronically go to http://www.nrc.ca/cisti/irm/unpub_e.shtml. Crystallographic information has also been deposited with the Cambridge Crystallographic Data Centre. Copies of the data can be obtained, free of charge, on application to the Director, CCDC, 12 Union Road, Cambridge, CB2 1EZ, U.K. (fax: 44-1223-336033 or e-mail: deposit@ccdc.cam.ac.uk).

© 2001 NRC Canada

Table 3. Second-order rate constants and activation parameters for the redox reactions of Co(III/II).

	k_{12} (dm^3 mol^{-1} s^{-1})	$\Delta H^{\ddagger}$ (kJ mol^{-1})	$\Delta S^{\ddagger}$ (J K^{-1} mol^{-1})	k_{ex} (dm^3 mol^{-1} s^{-1})[a]
$[Co(mmtp)_2]^{2+}$ + $[Ru(NH_3)_6]^{3+}$	1.03×10^6	5.5 ± 0.4	–111 ± 1	1.0×10^4
$[Co(mmtp)_2]^{3+}$ + $[Co(sep)]^{2+}$	9.26×10^2	58.3 ± 0.1	7.5 ± 0.1	2.3×10^4
	(1.23×10^2)[b]	(18.2 ± 0.2)[b]	(–144 ± 1)[b]	(2.2×10^4)[b]
$[Co(mmtp)(ttcn)]^{2+}$ + $[Ru(NH_3)_6]^{3+}$	3.85×10^5	13.6 ± 0.9	–93 ± 3	9.6×10^4
$[Co(mmtp)(ttcn)]^{3+}$ + $[Co(sep)]^{2+}$	8.20×10^3	56.9 ± 0.2	–33.7 ± 0.1	2.2×10^4

Note: I = 0.10 mol dm^{-3} (KCl), T = 25°C.
[a]Self-exchange rate constant of Co(III/II) couples.
[b]Values obtained from the reverse reaction.

couples made it impossible to find suitable reducing reagents, that is the necessity of prereduction of the species made it difficult to precisely determine the concentration of the reducing reagents. Therefore, the kinetic studies with excess reductants and the kinetic studies of the oxidation reactions of such Co(III/II) couples are scarce, although such a study is essential to examine the mechanisms postulated to date, including the gating phenomenon. Recently several nonconcerted ET reactions have been reported in which the innersphere reorganization process takes place before the very fast outersphere ET with minimal outersphere reorganizations (33–36).

In this study, self-exchange rate constants for the low-spin – low-spin Co(III/II)–S_6, –P_3S_3, and –P_6 complexes were estimated. The self-exchange rate constants for these couples decreased in the following order: $[Co(ttcn)_2]^{3+/2+}$ > $[Co(mmtp)(ttcn)]^{3+/2+}$ > $[Co(mmtp)_2]^{3+/2+}$. Spectroelectrochemical analyses indicated that the Jahn–Teller distortion of the Co(II) species increases in this order. Therefore, it seems that the electron transfer reactions involving low-spin – low-spin Co(III/II) couples follow the norm of the ordinary outersphere ET regime: the degree of the innersphere reorganization that is related to the Jahn–Teller distortion in the $t_{2g}^6 e_g^1$ Co(II) state may govern the rate of electron transfer. Although the Co(II) species investigated in this study are in the low-spin electronic state, it is suggested that the investigation of a series of inert Co(II) with multidentate P_nS_{6-n} and P_nN_{6-n} ligands provides some inert low-spin Co(II) and spin-crossover Co(II) species.

Conclusion

In this study, we reported the characteristics and kinetic behavior of new low-spin cobalt(II) species electrochemically generated in solution. The ligand field of the P-donor is comparable to or larger than that of the S-donor because of the significant covalent character of the Co(II)—P bonds: the nephelauxetic parameter is smaller for Co—P than that for Co—S. However, large Jahn–Teller distortion in the $Co(II)P_6$ complex causes the relatively slow electron self-exchange rate constant for the Co(III/II)–P_6 couple compared with the Co(III/II)–S_6 couple.

Acknowledgment

This research was partly supported by the Grants-in-Aid for Scientific Research (Grant Nos. 05 453 042, 07 554 061, 07 504 003, 10 440 193, and 11 640 562) from the Ministry of Education, Science, and Culture of Japan and by the Kurata Foundations (Hitachi Corporation).

References

1. H.C. Stynes and J.A. Ibers. Inorg. Chem. **10**, 2304 (1971).
2. R.D. Shalders and T.W. Swaddle. Inorg. Chem. **34**, 4815 (1995).
3. P.D. Metelski, Y.-S. Fu, K. Khan, and T.W. Swaddle. Inorg. Chem. **38**, 3103 (1999).
4. J.K. Beattie and H. Elsbernd. Inorg. Chim. Acta, **240**, 641 (1995).
5. J.K. Beattie, R.A. Binstead, M.T. Kelso, P. Del Favero, T.G. Dewey, and D.H. Turner. Inorg. Chim. Acta, **235**, 245 (1995).
6. J.F. Endicott and T. Ramasami. J. Phys. Chem. **90**, 3740 (1986).
7. T. Ohishi, K. Kashiwabara, and J. Fujita. Bull. Chem. Soc. Jpn. **56**, 3441 (1983).
8. T. Ohishi, K. Kashiwabara, and J. Fujita. Bull. Chem. Soc. Jpn. **60**, 583 (1987).
9. I. Kinoshita, K. Kashiwabara, and J. Fujita. Bull. Chem. Soc. Jpn. **54**, 2683 (1981).
10. T. Ohishi, K. Kashiwabara, J. Fujita, S. Ohba, T. Ishii, and Y. Saito. Bull. Chem. Soc. Jpn. **59**, 385 (1986).
11. H. Matsui, M. Kita, K. Kashiwabara, and J. Fujita. Bull. Chem. Soc. Jpn. **66**, 1140 (1993).
12. K. Kashiwabara, M. Kita, J. Fujita, S. Kurachi, and S. Ohba. Bull. Chem. Soc. Jpn. **67**, 2145 (1994).
13. T. Ando, M. Kita, K. Kashiwabara, J. Fujita, S. Kurachi, and S. Ohba. Bull. Chem. Soc. Jpn. **65**, 2748 (1992).
14. A.G. Lappin. Redox mechanisms in inorganic chemistry. Ellis Horwood, New York. 1994.
15. I.I. Creaser, A.M. Sargeson, and A.W. Zanella. Inorg. Chem. **22**, 4022 (1983).
16. H. Doine (Takagi) and T.W. Swaddle. Inorg. Chem. **30**, 1858 (1991).
17. A. Yamasaki, Y. Mihara, and S. Fujiwara. Inorg. Chim. Acta, **26**, L32 (1978).
18. G.M. Whiteside, C.P. Casey, and J.K. Krieger. J. Am. Chem. Soc. **93**, 1379 (1971).
19. K. Wieghardt, H.J. Kuppers, and J. Weiss. Inorg. Chem. **24**, 3067 (1985).
20. Y. Kuchiyama, N. Kobayashi, and H.D. Takagi. Inorg. Chim. Acta, **227**, 31 (1998).
21. R.S. Drago. Physical methods in inorganic chemistry. Reinhold Publishing, New York. 1965.
22. A.B.P. Lever. Inorganic electronic spectroscopy. Elsevier, New York. 1968.
23. S. Chandrasekhar and A. McAuley. Inorg. Chem. **31**, 480 (1992).

© 2001 NRC Canada

24. P. Urbaniak, A. Grzejdziak, and J. Dziegiec. Russ. J. Coord. Chem. **21**, 772 (1995).
25. W.N. Setzer, C.A. Ogle, G.S. Wilson, and R.S. Glass Inorg. Chem. **22**, 266 (1983).
26. M. Matsumoto, M. Itoh, S. Funahashi, and H.D. Takagi. Can. J. Chem. **77**, 1638 (1999).
27. Von G. Backes and D. Reinen. Z. Anorg. Allg. Chem. **418**, 217 (1975).
28. N. Sutin. Prog. Inorg. Chem. **30**, 442 (1983).
29. B.S. Brunschwig, C. Creutz, D. Macartney, T.–K. Sham, and N. Sutin. Faraday Discuss. **74**, 113 (1982).
30. R.V. Dubs, L.R. Gahan, and A.M. Sargeson. Inorg. Chem. **22**, 2523 (1983).
31. P. Osvath, A.M. Sargeson, B.W. Skelton, and A.H. White. J. Chem. Soc. Chem. Commun. 1036 (1991).
32. H. Kuppers, K. Wieghardt, S. Steenken, B. Nuber, and J. Weiss. Z. Anorg. Allg. Chem. **573**, 43 (1989).
33. N. Koshino, Y. Kuchiyama, H. Ozaki, S. Funahashi, and H.D. Takagi. Inorg. Chem. **38**, 3352 (1999).
34. N. Koshino, Y. Kuchiyama, S. Funahashi, and H.D. Takagi. Can. J. Chem. **77**, 1498 (1999).
35. N.E. Meager, K.L. Juntunen, M.J. Heeg, C.A. Salhi, L.A. Ochrymowycz, and D.B. Rorabacher. J. Am. Chem. Soc. **114**, 10411 (1992).
36. M. Matsumoto, H. Kodama, S. Funahashi, and H.D. Takagi. Inorg. React. Mech. **2**, 19 (2000).

© 2001 NRC Canada

Quinoxaline-1,2,3-dithiazolyls — Synthesis, EPR characterization, and redox chemistry

A. Wallace Cordes, James R. Mingie, Richard T. Oakley, Robert W. Reed, and Hongzhou Zhang

Abstract: Oxidation of quinoxalineaminothiol with SCl_2 or S_2Cl_2/Cl_2 affords a series of compounds based on the quinoxaline-1,2,3-dithiazole framework QDTA. Under highly oxidizing conditions, the 1,2,3-dithiazolyl ring is opened to afford the acyclic dichlorosulfimino-sulfenyl chlorides Cl_x-QDTA-Cl_3 (x = 0, 1, 2). Reduction of these "trichloro" compounds leads to ring closure. For x = 2, reduction using S_2Cl_2 affords the dithiazolylium chloride [Cl_2-QDTA][Cl]. For all values of x, reduction with iodide ion (3 mol equiv) affords the corresponding dithiazolyl radical [Cl_x-QDTA]. The radicals can be isolated in good yield in crude form, but attempts to purify them by vacuum sublimation lead to thermal degradation. The radicals have nonetheless been fully characterized by EPR spectroscopy, and the assignments of the observed hyperfine coupling constants cross-matched with those obtained by computation at the B3LYP/6-31G** level. The structures of the trichloro compounds Cl_x-QDTA-Cl_3 (x = 1, 2) have been confirmed by X-ray crystallography. Crystal data: Cl-QDTA-Cl_3, monoclinic, space group $C2/c$, a = 30.561(5) Å, b = 4.9764(9) Å, c = 22.247(4) Å, β = 131.822(14)°, V = 2521.4(8) Å^3, Z = 8, $R(F)$ = 0.043, and $R_w(F)$ [$I \geq \sigma(I)$] = 0.049; Cl_2-QDTA-Cl_3, orthorhombic, space group $Pnma$, a = 18.627(12) Å, b = 6.848(4) Å, c = 10.926(7) Å, V = 1393.7(15) Å^3, Z = 4, $R(F)$ = 0.047, and $R_w(F)$ [$I \geq 3\sigma(I)$] = 0.060.

Key words: thiazyl radicals, molecular conductors, EPR spectroscopy, quinoxaline, DFT calculations.

Résumé : L'oxydation du quinoxalineaminothiol avec du SCl_2 ou du S_2Cl_2/Cl_2 conduit à la formation d'une série de produits dérivés du squelette quinoxaline-1,2,3-dithiazole (QDTA). Dans des conditions d'oxydation extrêmes, le cycle 1,2,3-dithiazolyle s'ouvre pour conduire à la formation de chlorures de dichlorosulfimine-sulfényles, Cl_x-QDTA-Cl_3 (x = 0, 1, 2). La réduction de ces composés "trichloro" conduit à une fermeture de cycle. Lorsque x = 2, la réduction à l'aide de S_2Cl_2 conduit à la formation du chlorure de dithiazolylium [Cl_2-QDTA][Cl]. Pour toutes les valeurs de x, la réduction à l'aide de l'ion iodure (trois équivalents) conduit à la formation du radical dithiazolyle correspondant [Cl_x-QDTA]. Les radicaux ont été isolés avec de bons rendements à l'état brut, mais les essais en vue de leur purification par sublimation sous vide à conduit à leur dégradation thermique. On a toutefois pu faire une caractérisation complète des radicaux par spectroscopie RPE et les attributions des constantes de couplage hyperfins observées correspondent bien à celles qui peuvent être faites sur la base de calculs au niveau B3LYP/6-31G**. Les structures des composés Cl_x-QDTA-Cl_3 (x = 1, 2) ont été confirmées par diffraction des rayons X. Les données cristallographiques: Cl-QDTA-Cl_3, monoclinique, groupe d'espace $C2/c$, a = 30,561(5) Å, b = 4,9764(9) Å et c = 22,247(4) Å, β = 131,822(14)°, V = 2521,4(8) Å^3, Z = 8, $R(F)$ = 0,043 et $R_w(F)$ [$I \geq \sigma(I)$]] = 0,049; Cl_2-QDTA-Cl_3, orthorhombique, groupe d'espace $Pnma$, a = 18,627(12) Å, b = 6,848(4) Å et c = 10,926(7) Å, V = 1393,7(15) Å^3, Z = 4, $R(F)$ = 0,047 et $R_w(F)$ [$I \geq 3\sigma(I)$] = 0,060.

Mots clés : radicaux thiazyles, conducteurs, spectroscopie RPE, quinoxaline, calculs DFT.

[Traduit par la Rédaction]

Introduction

During the last decade, research into the design of neutral radical conductors has developed along two slightly different paths, one searching for materials comprised of purely carbon-based π-frameworks, the other exploring radicals with heterocyclic (non-carbon based) systems. The two approaches share common challenges, including the requirement for materials in which: (*i*) solid state dimerization is suppressed; and (*ii*) intermolecular charge transfer is energetically facile. Several variations of the phenalenyl radical, the archetypal model behind the organic radical conductor concept (1), have recently been developed to address these issues, with encouraging results (2–4). In the heterocyclic arena several structural databases have been established, first on 1,2,3,5-dithiadiazolyls (DTDAs) **1** (5), and more recently on 1,3,2- and 1,2,3-dithiazolyls (DTAs) **2** (6–9) and **3** (10–12). Cyclic thioaminyls have also been pursued (13). While the initial focus of this work was on how to inhibit dimerization, the importance of the energetics of charge

Received April 23, 2001. Published on the NRC Research Press Web site at http://canjchem.nrc.ca on September 17, 2001.

A.W. Cordes. Department of Chemistry and Biochemistry, University of Arkansas, Fayetteville, AR 72701, U.S.A.
J.R. Mingie, R.T. Oakley,[1] R. Reed, and H. Zhang. Department of Chemistry, University of Waterloo, Waterloo, ON N2L 3G1, Canada.

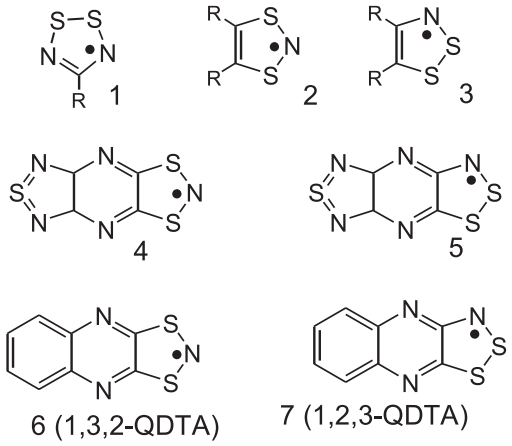
[1]Corresponding author (telephone: (519) 888-4582; fax: (519) 746-0435; e-mail: oakley@sciborg.uwaterloo.ca.).

 DOI: 10.1139/cjc-79-9-1352 © 2001 NRC Canada

Table 1. Computed (B3LYP/6-31G**) ion energetics (in eV) for radicals **1**–**7**.

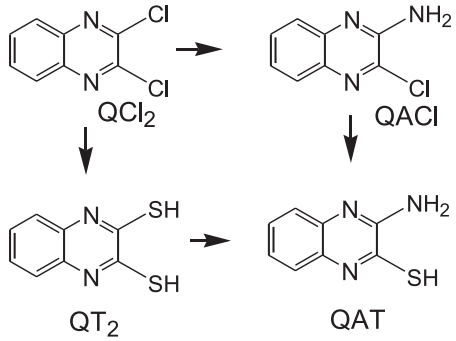
Compound	IP	EA	ΔH_{disp}	χ
1	7.82	1.02	6.81	4.42
2	6.77	–0.41	7.18	3.15
3	7.01	0.34	6.67	3.68
4	7.60	2.14	5.46	4.87
5	7.81	2.57	5.23	5.19
6	6.95	1.33	5.63	4.14
7	7.24	1.93	5.32	4.60

transfer is now well-recognized (14), and efforts to understand and control molecular ionization potentials (IP), electron affinities (EA), and the corresponding solution redox potentials (15) are being vigorously pursued.



With this latter end in mind we prepared and characterized the 1,3,2- and 1,2,3-dithiazolyls **4** (8) and **5** (11). The thiadiazolopyrazine (TDP) substituent on these radicals is extremely electron withdrawing, and causes an increase in both the molecular IP and EA relative to those of simple (monocyclic) DTAs. More importantly the substitution causes a dramatic decrease in the disproportionation enthalpy ΔH_{disp} (ΔH_{disp} = IP – EA) of the radical and, insofar as the gas-phase ΔH_{disp} can be related to the coulombic barrier to charge transfer in the solid state, the observed trend is encouraging. Structural analysis on **4** revealed that the radical does not dimerize (at room temperature), but the molecular spins remain isolated, and the material can be considered as a Mott–Hubbard (16) insulator. By contrast, molecules of **5** dimerize in the solid state, but magnetic and conductivity measurements indicate that the free spins present as defects serve as carriers of charge (11). As a continuation of this work, i.e., the development of structure and (or) property relationships in heterocyclic radicals, we wished to compare the two quinoxaline based systems **6** and **7**. The 1,3,2-compound **6** has been known for some time (17), although its solid-state structure and magnetic properties were reported only recently (7). By contrast the 1,2,3-compound **7** was hitherto unknown. Herein, we report the synthesis and characterization of a series of derivatives based on this "1,2,3-QDTA" skeleton.

Scheme 1.



Results and discussion

Ion energetics

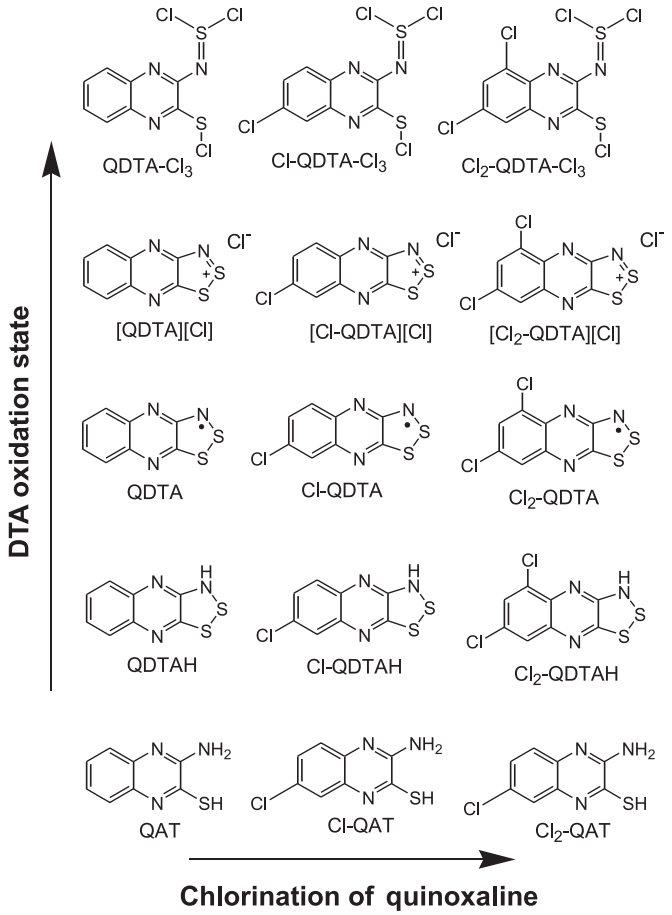
As noted above, one of the crucial factors in the design of neutral radical conductors is the requirement for materials with low disproportionation energies (ΔH_{disp}) (8, 11, 14, 15). Within the parlance of Pearson (18), we seek soft radicals, i.e., molecules which exhibit a low absolute hardness parameter η (where η = (IP – EA)/2). At the outset of this work, we set about exploring by computation, within an ab initio context, the ion energetics of series of 1,3,2- and 1,2,3-dithiazolyls. In Table 1 we provide the computed (B3LYP/6-31G**) IP and EA values for a range of such compounds. The results refine earlier (largely MNDO) estimates, and confirm that a simple 1,2,3,5-DTDA radical **1** has a lower ΔH_{disp} value, it is softer than a simple 1,3,2- or 1,2,3-DTA **2** or **3**. While on this basis both **2** and **3** systems appear to be less effective than **1**, the properties of the latter cannot be modified appreciably by substitution (the radical SOMO is nodal at the substituted carbon). By contrast the fusion of electron-withdrawing groups onto either of the DTA frames **2** or **3** leads to marked changes in ion energetics; both the IPs and EAs are increased. Accordingly the radicals become far more electronegative, i.e., χ = (IP + EA)/2 increases, but because the change in EA outpaces the change in IP, the radical disproportionation energy ΔH_{disp} (ΔH_{disp}= IP – EA) is decreased; in essence the radicals become softer. The most powerful electron sink that we have found is the TDP group, but the radicals so produced (**4** and **5**) are extremely electronegative. The quinoxaline residue affords slightly harder, but less electronegative systems, i.e., **6** and **7**. Having fully characterized the electrochemical properties, EPR, and solid-state properties of **4**, **5**, and **6** (1,3,2-QDTA), radical **7** (1,2,3-QDTA), therefore, became a desirable target for synthesis.

Synthesis

Quinoxalineaminothiol (QAT), the preferred starting material for the synthesis of QDTA **7**, is potentially accessible by a number of routes (Scheme 1) (19). The first involves the conversion of dichloroquinoxaline QCl_2 to the corresponding aminochloro derivative QACl, followed by thiation of the latter with sodium sulfide. However, while the first step is straightforward, the second provides only a low yield (10%) of QAT. The alternative pathway, involving the amination

© 2001 NRC Canada

Scheme 2.



of the intermediate dithiol QT_2, which is easily accessible from QCl_2, affords QAT in much higher overall yields.

Cyclization of QAT to a 1,2,3-dithiazole by treatment with sulfur chlorides proved to be a far more complex process than we had anticipated. Elaboration of the overall sequence of events is facilitated by reference to the manifold of oxidation states and compounds illustrated in Scheme 2.[2] Broadly speaking the nature of the product is a function of the oxidizing power of the sulfur chloride employed. Based on our experience with **5**, we were aware that sulfur monochloride would only produce an imide, e.g., QDTAH. It was therefore not surprising to find that reaction of QAT with S_2Cl_2, in stoichiometric amounts or in excess, afforded an insoluble orange powder exhibiting υ(NH) stretching bands in its IR spectrum. Sulfur dichloride proved to be a stronger but less selective oxidant. Thus, when heated at reflux in acetonitrile with excess SCl_2, QAT was oxidized directly to the open chain dichlorosulfimino-chlorosulfenyl or "trichloro" derivative Cl-QDTA-Cl_3. Attempts to prevent oxidation of the benzene ring were, for a long time, unsuccessful. Eventually, and somewhat to our surprise, we discovered that treatment of QAT with chlorine gas, followed by the addition of excess sulfur monochloride (at room temperature), gave rise to the precipitation of yellow crystals of QDTA-Cl_3. Attempts to recrystallize this material for analytical purposes were always thwarted by its partial conversion, upon dissolution in CH_3CN, into Cl-QDTA-Cl_3. That the quinoxaline ring was unsubstituted was confirmed by hydrolysis of the compound and recovery of QAT.

Cl-QDTA-Cl_3 is relatively resistant to further oxidation; indeed, it is conveniently recrystallized from acetonitrile saturated with chlorine gas. However, when Cl-QDTA-Cl_3 is heated at reflux in acetonitrile with excess sulfur monochloride, a dark orange crystalline precipitate of the salt [Cl_2-QDTA][Cl] (as a CH_3CN solvate) is produced. In essence the open chain trichloro unit is closed to a dithiazolylium cation, while the quinoxaline ring is further chlorinated. [Cl_2-QDTA][Cl] was then easily oxidized with chlorine to the corresponding trichloro derivative Cl_2-QDTA-Cl_3.

With the set of three trichloro compounds in hand, we explored their reactions with reducing agents. While Cl_2-QDTA-Cl_3 was easily reduced with a stoichiometric amount of iodide ion or excess S_2Cl_2 to Cl_2-QDTA-Cl, reduction of Cl-QDTA-Cl_3 required a more careful choice of reducing agent. Eventually, we found that hexamethyldisilane reacts with Cl-QDTA-Cl_3 to afford what we believe to be to [Cl-QDTA][Cl]. However, attempts to recrystallize this material led to its conversion to an insoluble solid exhibiting υ(NH) stretching bands and which, upon hydrolysis, afforded the dichlorinated aminothiol Cl_2-QAT. An analogous sequence of events was encountered upon reduction of QDTA-Cl_3. We interpret these observations in terms of the susceptibility of the dithiazolylium salts [QDTA][Cl] and [Cl-QDTA][Cl] to rearrange, with chlorination of the quinoxaline ring, to an imide (Scheme 3).

In our attempts to generate the radical oxidation states QDTA, Cl-QDTA, and Cl_2-QDTA we explored a variety of reducing agents (KI, Bu_4NI, Ph_3Sb, Zn), solvents (CH_3CN, SO_2), and starting oxidation states (Cl_x-QDTA-Cl_3 or [Cl_x-QDTA][Cl]). The most reliable method involved the use of potassium iodide in CH_3CN or SO_2 (see *Experimental* section). All three radicals could be isolated in crude form, as black crystalline solids, but purification for analytical purposes was extremely inefficient. Vacuum sublimation of the products from the crude matrix, the preferred purification method for heterocyclic radicals, inevitably led to decomposition and low recovery of sublimed product (<10%). Curiously, once isolated, the sublimed material could be resublimed with little or no loss.

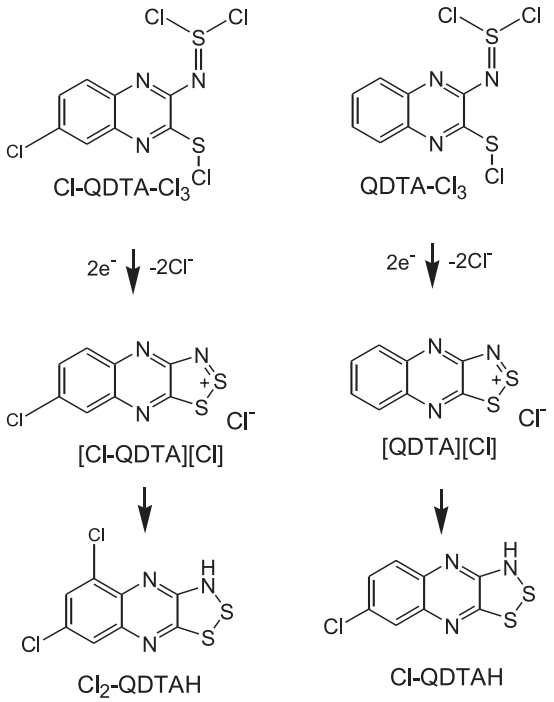
Crystal structures

The initial intent of this work was to characterize the structure and transport properties of the 1,2,3-QDTA radical in the solid state. However, the lability of this material, and its chlorinated derivatives Cl_x-QDTA (x = 1, 2), militated against the isolation of the material in sufficient quantity and quality to allow single crystal X-ray analysis. Nonetheless we were able to establish the crystal structures of the two trichloro derviatives (Cl_x-QDTA-Cl_3). These determinations

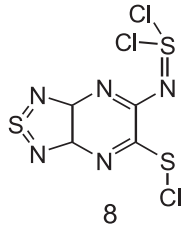
[2] The trichloro compounds depicted in Scheme 2 are identified by means of general formulas, e.g., Cl_x-Q-Cl_3; the degree of chlorination of the quinoxaline residue is indicated by the value of x. The dithiazole derivatives are labelled [Cl_x-QDTA][Cl] (cationic state), [Cl_x-QDTA] (radical state), [Cl_x-QDTAH] (imide state). The corresponding aminothiols are labelled Cl_x-QAT.

© 2001 NRC Canada

Scheme 3.



confirmed the presence of the dichlorosulfimino-sulfenyl chloride functional group in both compounds, and also established unequivocally the position(s) of chlorination on the benzene ring in the QDTA framework. Crystal data for these two compounds is provided in Table 2[3], and a summary of pertinent intramolecular structural features is given in Table 3. ORTEP drawings of the two molecules, showing atom numbering, are given in Fig. 1. In Cl-Q-Cl_3, the quinoxaline framework is planar to within 0.018 Å, with the N-1 and S-2 atoms lying, respectively, –0.058 and +0.016 Å from this plane. In Cl_2-Q-Cl_3, all the atoms save Cl-1 lie on a crystallographic mirror plane. The structural features of the dichlorosulfimino-sulfenyl chloride unit are very similar, with a short (localized) N=S double bond, and mirror the trends observed in compound **8** (11).



8

EPR spectra

The X-band EPR spectra of the three quinoxaline-based 1,2,3-DTA radicals, recorded at ambient temperature on samples dissolved in oxygen-free CH_2Cl_2, are shown in Figs. 2–4. The spectra are extremely complex; in the case of 1,2,3-QDTA **7** itself, coupling is observed to all three nitrogens as well as all four protons. In the chlorinated derivatives, some simplification is achieved by virtue of a reduction in the proton count, and $^{35/37}$Cl coupling is negligible. Nonetheless, extraction of hyperfine coupling required full spectral simulation; these are also shown in Figs. 2–4. The observed hyperfine coupling constants drawn from these simulations are summarized in Table 4 along with computed values at the B3LYP/6-31G** level; the latter served as an aid in making assignments. The correspondence between the observed and computed a_N values is relatively good (the latter being consistently about 15% higher), so that absolute assignments are relatively unequivocal. Such is not the case for the various a_H values. While we have been able, in all cases, to observe the expected number of ^{1}H couplings, the computed a_H values are several times larger than those derived experimentally. Thus, while we are relatively confident with the matches shown in Table 4 for H_1 and H_3, those for H_2 and H_4 are less certain.

Experimental

Quinoxalineaminothiol (QAT) was prepared by the conversion of commercially available (Aldrich) dichloroquinoxaline into quinoxalinedithiol (QT_2) (19), followed by the treatment of the latter with aqueous ammonia; the crude product was purified by recrystallization from benzonitrile. Sulfur monochloride, potassium iodide, and dichloroquinoxaline were obtained commercially (Aldrich), and used as received. Chlorine gas and sulfur dioxide gas (Matheson) were also used directly. The solvents dichloroethane (Fisher) and acetonitrile (Fisher HPLC grade) were dried by distillation from P_2O_5. All reactions were carried out under an atmosphere of nitrogen. Melting points are uncorrected. Elemental analyses were performed by MHW Laboratories, Phoenix, Arizona. Infrared spectra were recorded (at 2 cm^{-1} resolution on Nujol mulls) on a Nicolet Avatar FT-IR spectrometer. Low resolution mass spectra (70 eV, EI, DEI and CI, DCI, FAB) were run on a Finnigan 4500 quadrupole mass spectrometer (at McMaster University) and a VG 7070 mass spectrometer (at the University of Waterloo).

Preparation of QDTA-Cl_3

A gentle stream of chlorine gas was passed over a slurry of QAT (1.0 g, 5.64 mmol) in 10 mL of acetonitrile held at 0°C (ice bath) for 10 min. Within 60 s of initiating the chlorine flow, a solution of excess S_2Cl_2 (ca. 1.0 g) in 5 mL of CH_3CN was added dropwise to the mixture. After 5 min, the chlorine flow was halted, and the flocculent yellow solid filtered off under nitrogen, washed with 2 × 5 mL acetonitrile saturated with chlorine, and dried in vacuo. The crude (moisture-sensitive) product, QDTA-Cl_3 (0.845 g, 2.70 mmol, 48%) was used directly in all subsequent reactions. Attempts to purify this compound by recrystallization

[3] Copies of material on deposit may be purchased from the Depository of Unpublished Data, Document Delivery, CISTI, National Research Council Canada, Ottawa, ON K1A OS2, Canada. Tables of crystal data, data collection, refinement parameters, interatomic distances and angles, and atomic positional parameters reported in this paper have been deposited with the Cambridge Crystallographic Data Centre. Copies of this data can be obtained, free of charge, on application to the Director, CCDC, 12 Union Road, Cambridge CB2 1EZ, U.K. (fax: 44-1223-336033 or e-mail: deposit@ccdc.cam.ac.uk).

© 2001 NRC Canada

Table 2. Crystal, data collection, and refinement parameters.

	Cl-QDTA-Cl_3	Cl_2-QDTA-Cl_3
Formula	$C_8H_3Cl_4N_3S_2$	$C_8H_2Cl_5N_3S_2$
FW	347.06	381.51
a (Å)	30.561(5)	18.627(12)
b (Å)	4.9764(9)	6.848(4)
c (Å)	22.247(4)	10.926(7)
β (deg)	131.822(14)	—
V (Å^3)	2521.4(8)	1393.7(15)
D(calcd) (g cm^{-3})	1.83	1.82
Space group	*C*2/*c*	*Pnma*
Z	8	4
λ (Å)	0.7107	0.7107
Temperature (K)	293	293
Linear abs. coeff. (mm$^{-1)}$	1.24	1.32
$R(F)$, $R_w(F)^a$ [$I > n\sigma(I)$]	0.043, 0.049 (n = 1)	0.047, 0.060 (n = 3)

$^aR = [\Sigma||F_o| - |F_c||]/[\Sigma|F_o|]$; $R_w = \{[\Sigma w||F_o| - |F_c||^2]/[\Sigma(w|F_o|^2)]\}^{1/2}$.

Table 3. Summary of bond lengths (Å) in Cl-QDTA-Cl_3, Cl_2-QDTA-Cl_3, and **8**.

	Cl-QDTA-Cl_3	Cl_2-QDTA-Cl_3	**8**
(N)S—Cl	2.09(3)[a]	2.091(3)	2.0784(11)
N—S	1.498(4)	1.531(9)	1.516(3)
(S)N—C	1.400(5)	1.394(13)	1.403(5)
(C)S—Cl	1.993(2)	1.995(4)	1.990(2)
C—S	1.766(4)	1.719(10)	1.754(4)

Note: esds are in parentheses.
[a]Range over two values.

led to its partial conversion to Cl-QDTA-Cl_3, but the integrity of the quinoxaline skeleton was confirmed by hydrolysis of QDTA-Cl_3 to QAT. IR (1600–400 cm^{-1}): 1329 (s), 1292 (w), 1228 (m), 1161 (m), 1113 (m), 1017 (w), 903 (w), 805 (w), 754 (vs), 714 (w), 698 (w), 625 (vw), 593 (vw), 553 (vw), 539 (s), 458 (s).

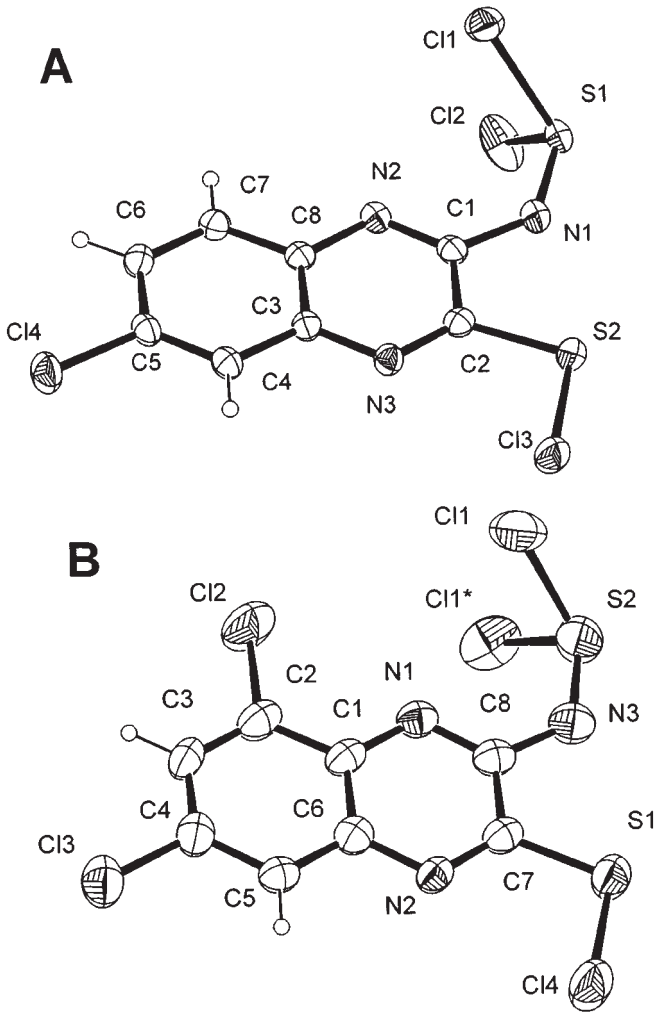
Preparation of Cl-QDTA-Cl_3

Excess (4 mL) of SCl_2 was added to a slurry of QAT (1.00 g, 5.64 mmol) in 30 mL of CH_3CN at room temperature. The mixture was stirred for 1 h during which time it changed color from red to yellow. The canary yellow precipitate was filtered off, washed with 2 × 10 mL portions of CH_3CN, and dried in vacuo; (1.3 g, 3.75 mmol, 66%). The product Cl-QDTA-Cl_3 (0.500 g, 1.44 mmol) was recrystallized from acetonitrile containing 2 mL of SCl_2 (to enhance the solubility of the compound). On cooling, lustrous yellow needles were formed: dec > 85°C. IR (1600–400 cm^{-1}): 1599 (m), 1556 (w), 1525 (w), 1481 (m), 1426 (w), 1320 (s), 1280 (w), 1211 (m), 1145 (m), 1119 (s), 1067 (m), 1015 (m), 964 (w), 926 (m), 878 (m), 830 (s), 710 (m), 651 (w), 622 (m), 588 (m), 557 (m), 521 (w), 494 (w), 457 (m), 425 (m). Anal. calcd. for $C_8H_3Cl_4N_3S_2$: C 27.68, H 0.87, N 12.11; found: C 27.92, H trace, N 12.07.

Preparation of Cl_2-QDTA-Cl_3

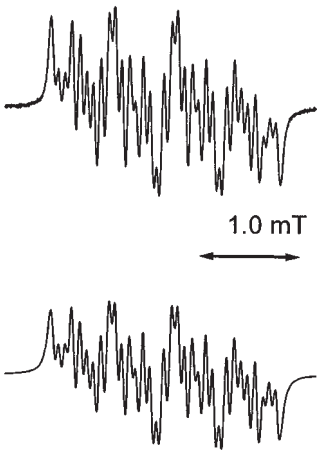
Excess S_2Cl_2 (4 mL) was added to a slurry of QAT (2.00 g, 11.3 mmol) in 60 mL of acetonitrile. The mixture was warmed gently to produce a red precipitate. Chlorine gas was then passed over the solid until a bright yellow precipitate was produced. Following the addition of more S_2Cl_2 (4 mL) the mixture was heated at reflux for 0.5 h. As the mixture reached the boiling point the solid dissolved to give

Fig. 1. ORTEP drawings (30% probability ellipsoids) of Cl-Q-Cl_3 (above) and Cl_2-Q-Cl_3 (below). In Cl_2-Q-Cl_3, atoms Cl1 and Cl1* are related by a mirror plane.



© 2001 NRC Canada

Fig. 2. X-band EPR spectrum (above) of 1,2,3-QDTA **7**, g = 2.0079, in CH_2Cl_2, and simulation (below) with L:G = 0.01, LW = 0.058 mT. Derived coupling constants are provided in Table 4.



a dark red-brown solution. The mixture was then cooled to room temperature and exposed to a flow of chlorine gas to form the final product. The yellow precipitate was filtered off under nitrogen, washed with chlorinated acetonitrile, and dried in vacuo. The product Cl_2-QDTA-Cl_3 (2.83 g, 7.42 mmol, 66%) was recrystallized from chlorinated acetonitrile a yellow needles, mp 120°C. IR (1600–400 cm^{-1}): 1590 (m), 1529 (w), 1334 (w), 1304 (s), 1281 (w), 1216 (m), 1191 (m), 1137 (s), 1082 (m), 1029 (m), 864 (s), 807 (s), 785 (m), 676 (m), 634 (m), 586 (m), 577 (m), 534 (m), 468 (s), 433 (m). Anal. calcd. for $C_8H_2Cl_5N_3S_2$: C 25.19, H 0.53, N 11.01; found: C 25.30, H trace, N 10.93.

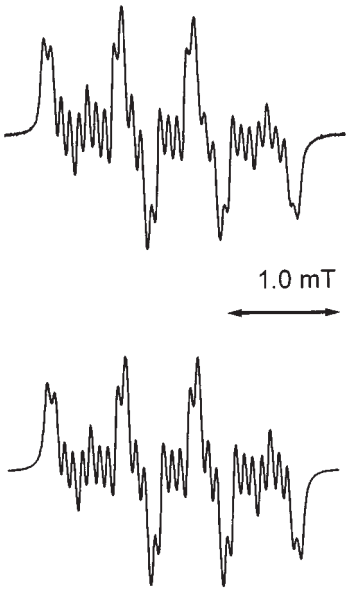
Preparation of [Cl_2-QDTA][Cl]·CH_3CN

Excess S_2Cl_2 (4 mL) was added to a slurry of Cl-Q-Cl_3 (1.50 g, 4.32 mmol) in 50 mL of CH_3CN. As the mixture was heated to reflux the solid dissolved to give a dark red-brown solution. After half an hour at reflux the solution was allowed to cool to room temperature. The orange brown crystalline solid which precipitated on cooling was filtered off, washed with 2 × 10 mL portions of CH_3CN, and dried in vacuo. The product [Cl_2-QDTA][Cl]·CH_3CN (1.25 g, 3.55 mmol, 82%) was recrystallized from acetonitrile containing a few drops of SCl_2. Infrared and elemental analysis confirmed that the compound (dec > 85°C) was solvated with 1 mol of acetonitrile. MS *m/z*: 274 (M^+, 100%). IR (1600–400 cm^{-1}): 2247 (w), 1661 (w), 1589 (m), 1537 (w), 1299 (w), 1276 (m), 1191 (m), 1091 (m), 1004 (m), 878 (m), 858 (m), 808 (w), 791 (w), 715 (m), 612 (m), 584 (w), 544 (w), 451(m). Anal. calcd. for $C_{10}H_5Cl_3N_4S_2$: C 34.15, H 1.43, N 15.93; found: C 33.89, H 1.20, N 15.98.

Characterization data for Cl_x-QAT (x = 0, 1, 2)

Hydrolysis of any of the dithiazoles described above with 10% aq NaOH afforded an orange solution which, upon treatment with glacial acetic acid, yielded a yellow precipitate of the corresponding quinoxaline aminothiol. These compounds can be recrystalllized from hot benzonitrile as yellow flakes. The following characterization data apply. QAT (starting material): dec > 250°C. IR (cm^{-1}): 3392 (s), 3274 (m), 3110 (w), 1636 (s), 1612 (w), 1592 (w), 1486 (m), 1136 (m), 1087 (s), 940 (w), 853 (m), 838 (w), 750 (w), 724 (w), 604 (s), 444 (w). Anal. calcd. $C_8H_7N_3S$: C 54.22, H 3.98, N 23.71; found: C 54.16, H 4.13, N 23.62. Cl-QAT: dec > 250°C. IR (cm^{-1}): 3413 (m), 3273 (w), 3117 (m), 1625 (s), 1587 (m), 1416 (m), 1353 (m), 1334 (m), 1232 (w), 1134 (m), 1101 (s), 1077 (m), 929 (m), 857 (m), 81 (s), 666 (w), 628 (m), 479 (m), 456 (s). Anal. calcd. for $C_8H_6ClN_3S$: C 45.39, H 2.86, N 19.85; found: C 46.66, H 3.10, N 19.96. Cl_2-QAT: dec > 250°C. IR (cm^{-1}): 3425 (m), 3286 (w), 3214 (w), 3117 (w), 1639 (w), 1599 (w), 1358 (m), 1241 (w), 1208 (w), 1110 (s), 975 (w), 846 (s), 681 (s), 657 (w), 587 (m), 541 (w), 439 (m). Anal. calcd. for $C_8H_5Cl_2N_3S$: C 39.04, H 2.05, N 17.07; found: C 38.88, H 1.94, N 16.96.

Fig. 3. X-band EPR spectrum (above) of Cl-QDTA, g = 2.0082, in CH_2Cl_2, and simulation (below) with L:G = 0.03, LW = 0.041 mT. Derived coupling constants are provided in Table 4.



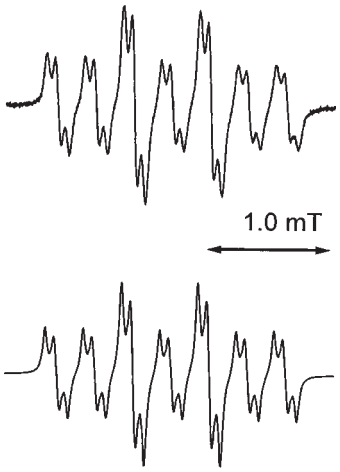
Generation of radicals Cl_x-QDTA (x = 0, 1, 2)

The same basic procedure was used for all three radicals. Three mol equiv of finely powdered and oven dried (100°C) potassium iodide were added to a slurry of Cl_x-Q-Cl_3 (ca. 1.0 g) in 10 mL of acetonitrile at room temperature. The mixture was then stirred for 20 min at room temperature, and the black solid (a mixture of Cl_x-QDTA and KCl) was filtered off, washed with cold acetonitrile, and dried in vacuo. The radicals were separated from the KCl matrix by gradient sublimation at 110–60°C per 1 × 10^{-2} torr (1 torr = 133.322 Pa). Overall recovery of the radicals was, however, extremely low; yields were generally <10% based on the amount of Cl_x-Q-Cl_3 used.

QDTA: dec > 150°C. IR (1600–400 cm^{-1}): 1582 (w), 1537 (vw), 1340 (w), 1323 (w), 1223 (m), 1140 (s), 1066 (m), 949 (m), 873 (w), 845 (w), 786 (w), 753 (s, br), 639 (w), 590 (w), 577 (w), 491 (w), 427 (w). Insufficient quantity of this material was obtained in a pure (sublimed) form for elemental analysis; but the integrity of the quinoxaline skeleton was confirmed by hydrolysis to QAT (vide supra). The radical itself was characterized by its EPR spectrum.

© 2001 NRC Canada

Fig. 4. X-band EPR spectrum (above) of Cl_2-QDTA, g = 2.0094, in CH_2Cl_2, and simulation (below) with L/G = 0.01, LW = 0.028 mT. Derived coupling constants are provided in Table 4.



Cl-QDTA: dec > 163°C. IR (1600–400 cm^{-1}): 1589 (w), 1533 (w), 1343 (w), 1304 (w), 1278 (w), 1199 (w), 1137 (w), 1077 (m), 943 (w), 906 (m), 814 (m), 792 (m), 664 (m), 649 (m), 596 (m), 577 (m), 513 (m), 458 (w), 484 (m), 435 (m). Anal. calcd. for $C_8H_3ClN_3S_2$: C 39.92, H 1.26, N 17.47; found: C 40.12, H 1.38, N 17.27.

Cl_2-QDTA: dec > 158°C. EI-MS (*m/z*): 274 (M^+, 100%), 228 ($[M - NS]^+$, 34%), 210 (10%), 158 (31%). IR (1600–400 cm^{-1}): 1588 (w), 1527 (w), 1303 (m), 1277 (m), 1195 (m), 1087 (m), 966 (m), 922 (m), 860 (m), 782 (w), 656 (w), 607 (w), 575 (w), 486 (w). Anal. calcd. for $C_8H_2Cl_2N_3S_2$: C 34.92, H 0.73, N 15.27; found: C 35.12, H 0.90, N 15.09.

X-ray measurements

X-ray data were collected at 293 K on ENRAF-Nonius CAD-4 and Rigaku Mercury CCD diffractometers with monochromated Mo K_α radiation. Crystals were mounted on glass fibers with silicone and data were collected using θ/2θ (Cl-QDTA-Cl_3) and ω (Cl_2-QDTA-Cl_3) scans. The structures were solved using direct methods and refined by full-matrix least-squares which minimized $\Sigma w(\Delta F)^2$.

EPR spectra

X-band EPR spectra were recorded (on radicals dissolved in degassed CH_2Cl_2) on a Bruker EMX-200 spectrometer; hyperfine coupling constants were obtained by spectral simulation using Simfonia (20) and WinSim (21). Lorentzian:Gaussian (L:G) ratios and line widths (LW) used in the simulations are provided in the figure captions.

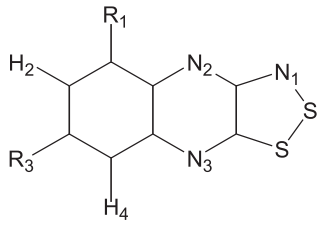
Density functional calculations

Adiabatic ionization potentials and electron affinities were calculated by means of ΔSCF calculations run on Pentium II workstations using the B3LYP-DFT method, as contained in the Gaussian 98W suite of programs (22). Geometries were optimized using the 6-31G** basis set, within the constraints of C_s (planar) symmetry; frequency calculations were not performed. Elsewhere (23), we have noted that the release of

Table 4. Observed and calculated[a] hyperfine coupling constants (in mT) in QDTA, Cl-QDTA, and Cl_2-QDTA radicals.[b]

	QDTA	Cl-QDTA	Cl_2-QDTA
N_1	0.653 (0.760)	0.639 (0.746)	0.618 (0.730)
N_2	0.301 (0.355)	0.309 (0.359)	0.308 (0.361)
N_3	0.006 (–0.071)	0.040 (–0.067)	0.039 (–0.061)
H_1	0.137 (0.351)	0.145 (0.356)	
H_2	0.070 (–0.286)	0.072 (–0.282)	0.72 (–0.287)
H_3	0.218 (0.510)		
H_4	0.004 (–0.388)	0.21 (–0.398)	0.19 (–0.396)
Cl_1[c]			— (0.023)
Cl_3[c]		— (0.048)	— (0.048)

[a]The calculated (B3LYP/6-31G**) coupling constants are shown in parentheses.
[b]The atom numbering scheme is provided below.
[c]Coupling constants refer to the ^{35}Cl isotope.



QDTA, $R_1 = R_3 = H$
Cl-QDTA, $R_1 = H$, $R_3 = Cl$
Cl_2-QDTA, $R_1 = R_3 = Cl$

planarity in 1,2,3-dithiazole anions can lead to S—N bond cleavage (a prediction echoed by electrochemical experiments). The present electron affinity results should therefore be viewed as estimates only.

Summary and conclusions

The development of cyclic and heterocyclic π-radicals suitable for applications as conductive molecular materials requires the pursuit of highly delocalized systems with favorable ion energetics, i.e., a low ΔH_{disp}. In this regard, the 1,2,3-QDTA systems investigated here represent appealing targets. However, from a synthetic standpoint, the construction of a 1,2,3-dithiazole ring on a quinoxaline framework is by no means trivial. The oxidizing conditions that successfully allow the synthesis of the ternary radical **5** by cyclization of an aminothiol are, in the present case, sufficiently harsh to cause chlorination of the benzene residue of the quinoxaline framework. This leads to a rich array of partially chlorinated derivatives, both cyclic and acyclic. We have nonetheless been able to isolate and characterize, by EPR spectroscopy, three 1,2,3-QDTA radicals. The EPR spectra of these radicals reveal a high degree of spin delocalization, similar to that observed in **5**, and much more so than observed in corresponding 1,3,2-system **6**.

While all the QDTA radicals reported here are stable indefinitely at room temperature, attempts to purify them by vacuum sublimation, and hence investigate their transport properties, have been thwarted by their tendency to thermally decompose. We attribute this instability to the delocalization of spin density onto the benzene residue, with a consequent tendency for the radicals to associate via C—C linkages, and thence rearrange. In the light of the present results, the thermal stability of **5** is remarkable, and empha-

© 2001 NRC Canada

sizes the importance of heteroatoms in suppressing radical coupling.

Acknowledgements

We thank the Natural Sciences and Engineering Research Council of Canada (NSERC) and the State of Arkansas, for financial support in the form of operating and equipment grants. We also acknowledge the Arkansas Science and Technology Authority for support of the X-ray facilities.

References

1. (*a*) R.C. Haddon. Nature (London), **256**, 394 (1975); (*b*) R.C. Haddon. Aust. J. Chem. **28**, 2333 (1975); (*c*) R.C. Haddon. Aust. J. Chem. **28**, 2343 (1975).
2. K. Goto, T. Kubo, K. Yamamoto, K. Nakasuji, K. Sato, D. Shiomi, T. Takui, M. Kubota, T. Kobayashi, K. Yakusi, and J. Ouyang. J. Am. Chem. Soc. **121**, 1619 (1999).
3. P.A. Koutentis, Y. Chen, Y. Cao, T.P. Best, M.E. Itkis, L. Beer, R.T. Oakley, A.W. Cordes, C.P. Brock, and R.C. Haddon. J. Am. Chem. Soc. **123**, 3864 (2001).
4. (*a*) X. Chi, M.E. Itkis, B.O. Patrick, T.M. Barclay, R.W. Reed, R.T. Oakley, A.W. Cordes, and R.C. Haddon. J. Am. Chem. Soc. **121**, 10395 (1999); (*b*) X. Chi, M. E. Itkis, K. Kirschbaum, A.A. Pinkerton, R.T. Oakley, A.W. Cordes, and R.C. Haddon. J. Am. Chem. Soc. **123**, 4041 (2001).
5. A.W. Cordes, R.C. Haddon, and R.T. Oakley. Adv. Mater. **6**, 798 (1994).
6. T.M. Barclay, A.W. Cordes, R.H. de Laat, J.D. Goddard, R.C. Haddon, D.Y. Jeter, R.C. Mawhinney, R.T. Oakley, T.T.M. Palstra, G.W. Patenaude, R.W. Reed, and N.P.C. Westwood. J. Am. Chem. Soc. **119**, 2633 (1997).
7. T.M. Barclay, A.W. Cordes, N.A. George, R.C. Haddon, R.T. Oakley, G.W. Patenaude, R.W. Reed, and H. Zhang. J. Chem. Soc. Chem. Commun. 873 (1997).
8. T.M. Barclay, A.W. Cordes, N.A. George, R.C. Haddon, M.E. Itkis, M.S. Mashuta, R.T. Oakley, G.W. Patenaude, R.W. Reed, J.F. Richardson, and H. Zhang. J. Am. Chem. Soc. **120**, 352 (1998).
9. S. Brownridge, H. Du, S.A. Fairhurst, R.C. Haddon, H. Oberhammer, S. Parsons, J. Passmore, M.J. Schriver, L.H. Sutcliffe, and N.P.C. Westwood. J. Chem. Soc. Dalton Trans. 3365 (2000).
10. T.M. Barclay, L. Beer, A.W. Cordes, R.T. Oakley, K.E. Preuss, N.J. Taylor, and R.W. Reed. Chem. Commun. 531 (1999).
11. T.M. Barclay, A.W. Cordes, R.C. Haddon, M.E. Itkis, R.T. Oakley, R.W. Reed, and H. Zhang. J. Am. Chem. Soc. **121**, 969 (1999).
12. (*a*) J.M. Rawson, and G.D. McManus. Coord. Chem. Rev. **189**, 135 (1999). (*b*) T. Torroba. J. Prakt. Chem. (Weinheim, Ger.), **341**, 99 (1999).
13. V. Benin and P. Kaszynski. J. Org. Chem. **65**, 8086 (2000).
14. (*a*) P. Kaszynski. J. Phys. Chem. A, **105**, 7626 (2001); (*b*) P. Kaszynski. J. Phys. Chem. A, **105**, 7615 (2001).
15. R.T. Boeré and T.L. Roemmele. Coord. Chem. Rev. **210**, 369 (2000).
16. N.F. Mott. *In* Metal-insulator transitions. Taylor and Frances, London. 1990.
17. G. Wolmershäuser and G. Kraft. Chem. Ber. **123**, 881 (1990).
18. (*a*) R.G. Pearson. Struct. Bonding (Berlin), **80**, 2 (1993); (*b*) R.G. Pearson. J. Chem Educ. **64**, 561 (1988).
19. H. Saikachi and S. Tagami. Chem. Pharm. Bull. **9**, 941 (1961).
20. WinEPR Simfonia. Bruker Instruments, Inc., Billerica, Massachusetts.
21. D.R. Duling. J. Magn. Reson. Ser. B, **104B**, 105 (1994).
22. Gaussian 98, Revision A.6. M.J. Frisch, G.W. Trucks, H.B. Schlegel, G.E. Scuseria, M.A. Robb, J.R. Cheeseman, V.G. Zakrzewski, J.A. Montgomery, Jr., R.E. Stratmann, J.C. Burant, S. Dapprich, J.M. Millam, A.D. Daniels, K.N. Kudin, M.C. Strain, O. Farkas, J. Tomasi, V. Barons, M. Cossi, R. Cammi, B. Mennucci, C. Pomelli, C. Adamo, S. Clifford, J. Ochterski, G.A. Petersson, P.Y. Ayala, Q. Cui, K. Morokuma, D.K. Malick, A.D. Rabuck, K. Raghavachari, J.B. Foreman, J. Cioslowski, J.V. Ortiz, B.B. Stefanov, G. Liu, D.J. Fox, T. Keith, M.A. Al-Laham, C.Y. Peng, A. Nanayakkara, M.W. Wong, J.L. Andres, C. Gonzalez, M. Head-Gordon, E.S. Repogle, and J.A. Pople. Gaussian, Inc., Pittsburgh, Pennsylvania. 1998.
23. T.M. Barclay, A.W. Cordes, J.D. Goddard, R.C. Mawhinney, R.T. Oakley, K.E. Preuss, and R.W. Reed. J. Am. Chem. Soc. **119**, 12 136 (1997).

© 2001 NRC Canada

Synthesis, characterization, and thermodynamics of tertiary phosphine cobalt(III) Schiff-base complexes

Mozaffar Asadi and Ali Hossein Sarvestani

Abstract: [Co(5-nitroSalen)(PBu_3)]$ClO_4 \cdot H_2O$ and [Co(Salpd)(PBu_3)]$ClO_4 \cdot H_2O$ were synthesized and characterized. The stability constants and the thermodynamic parameters were measured spectrophotometrically for 1:1 adduct formation of [CoL(PBu_3)]$ClO_4 \cdot H_2O$, (L = Salen, 5-nitroSalen, Salpd), and [Co(Salen)(PMe_2Ph)]$ClO_4 \cdot H_2O$ as acceptors with $P(OR)_3$ (R = Me, Et, *i*-Pr) as donors, in acetonitrile solvent and in constant ionic strength (I = 0.01 M) and at various temperatures. The trend of the reactivity of cobalt(III) Schiff-base complexes with PBu_3 axial ligand toward a given donor is as follows: 5-nitroSalen > Salen > Salpd.

Also, the following reactivity trend of the donors toward a given cobalt(III) Schiff-base complex is in the operation: $P(O\text{-}i\text{-}Pr)_3 > P(OEt)_3 > P(OMe)_3$.

Key words: cobalt(III) Schiff-base complexes, thermodynamic parameters, trialkylphosphite, adduct complexes, stability constants.

Résumé : On a effectué la synthèse et on a caractérisé les complexes suivants: [Co(5-nitroSalen)(PBu_3)]$ClO_4 \cdot H_2O$ et [Co(Salpd)(PBu_3)]$ClO_4 \cdot H_2O$. Faisant appel à des méthodes spectrophotométriques, on a mesuré les constantes de stabilité et les paramètres thermodynamiques pour la formation d'adduits 1:1 entre les complexes accepteurs [CoL(PBu_3)]$ClO_4 \cdot H_2O$ dans lesquels L = Salen, 5-nitroSalen et Salpd et [Co(Salen)(PMe_3Ph)]$ClO_4 \cdot H_2O$ et les $P(OR)_3$ (dans lesquels R = Me, Et, *i*-Pr) comme accepteurs, dans l'acétonitrile comme solvant, à force ionique constante (I = 0,01 M) et à diverses températures. La tendance de la réactivité des complexes des bases de Schiff du cobalt(III) avec le ligand PBu_3 axial est donnée par la séquence suivante: 5-nitroSalen > Salen > Salpd.

Du côté des donneurs vis-à-vis d'un complexe donné d'une base de Schiff du cobalt(III), la tendance est exprimée par la séquence suivante: $P(O\text{-}i\text{-}Pr)_3 > P(OEt)_3 > P(OMe)_3$.

Mots clés : complexes de bases de Schiff avec le cobalt(III), paramètres thermodynamiques, trialkylphosphite, adduits de complexes, constantes de stabilité.

[Traduit par la Rédaction]

Introduction

Many Co(III)–Salen tertiary phosphine complexes have been suggested as models for the vitamine B_{12} coenzyme (1–3). The properties of these Salen complexes were examined with the aim to gain an insight into the chemistry of the related biological molecules. Some extensive works have been done on these models (4–8). Recently the kinetics of ligand replacement reactions of the axial H_2O in the *trans*-$[Co(en)_2(H_2O)(Me)]^{2+}$ complex have been studied by Hamza et al. (9). The equilibrium of the adduct formation of $[Co(Salen)X]^+$ (X = tertiary phosphines) with NO_2^- has been studied. It was shown that the equilibrium constants decrease according to the following trend: $PPh_3 < PEtPh_2 < PBu_3$ (10). The formation constants for some $[Co(Salen)(PR_3)_2]^+$ were examined in acetonitrile and in ethanol 95% (11).

In this work, the new complexes [Co(5-nitroSalen)(PBu_3)]$ClO_4 \cdot H_2O$ and [Co(Salpd)(PBu_3)]$ClO_4 \cdot H_2O$ were synthesized and characterized. Thermodynamics of cobalt(III) Schiff-base complexes of the types [CoL(PBu_3)]$ClO_4 \cdot H_2O$, where L = Salen, 5-nitroSalen, Salpd, and [Co(Salen)(PMe_2Ph)]$ClO_4 \cdot H_2O$ as acceptors with ($P(OR)_3$, R = Me, Et, *i*-Pr) as donors, in acetonitrile solvent have been examined. By comparing the spectral and the thermodynamical properties of the synthesized complexes, we aimed to investigate the effects of different electronic and steric situations.

Received February 14, 2001. Published on the NRC Research Press Web site at http://canjchem.nrc.ca on September 19, 2001.

M. Asadi[1] and A.H. Sarvestani. Chemistry Department, College of Sciences, Shiraz University, Shiraz 71545, I.R. Iran.

[1]Corresponding author (telephone: 0098 711 2 224 829; fax: (0711) 2 220 027; e-mail: asadi@chem.susc.ac.ir).

Experimental

Materials

Salicylaldehyde, 5-nitrosalicylaldehyde, 1,2-ethylenediamine, 1,3-propanediamine, cobalt(II) acetate tetrahydrate, tributylphosphine, trialkylphosphites, tetraethylammonium perchlorate, dimethylphenylphosphine, and acetonitrile were purchased from Merck, Fluka, or Aldrich.

 DOI: 10.1139/cjc-79-9-1360 © 2001 NRC Canada

Table 1. The stability constants (K, L mol^{-1}) for [Co(Salen)-(PBu_3)]$ClO_4 \cdot H_2O$ with various $P(OR)_3$ in acetonitrile solvent.

Temperature (°C)	$P(OMe)_3$	$P(OEt)_3$	$P(O\text{-}i\text{-}Pr)_3$
20	348.9 ± 0.0	1640.0 ± 0.2	2098.7 ± 0.4
25	301.5 ± 0.0	1446.4 ± 0.1	1712.1 ± 0.3
30	279.8 ± 0.0	1126.0 ± 0.2	1595.7 ± 0.2
35	250.0 ± 0.0	948.4 ± 0.1	1340.0 ± 0.1
40	236.4 ± 0.0	852.1 ± 0.1	1135.6 ± 0.0

Note: λ = 460 nm.

Table 2. The stability constants (K, L mol^{-1}) for [Co(Salen)-(PMe_2Ph)]$ClO_4 \cdot H_2O$ with various $P(OR)_3$ in acetonitrile solvent.

Temperature (°C)	$P(OMe)_3$	$P(OEt)_3$	$P(O\text{-}i\text{-}Pr)_3$
20	1611.1 ± 0.3	5580.3 ± 3.5	11 525.1 ± 7.7
25	1189.0 ± 0.1	4992.3 ± 2.1	9 924.2 ± 5.9
30	1069.3 ± 0.1	4018.3 ± 1.2	8 698.4 ± 3.2
35	889.7 ± 0.1	3198.3 ± 1.3	7 577.8 ± 3.4
40°C	724.9 ± 0.1	2378.1 ± 0.8	6 577.1 ± 2.6

Note: λ = 470 nm.

Table 3. The stability constants (K, L mol^{-1}) for [Co(5-nitroSalen)-(PBu_3)]$ClO_4 \cdot H_2O$ with various $P(OR)_3$ in acetonitrile solvent.

Temperature (°C)	$P(OMe)_3$	$P(OEt)_3$	$P(O\text{-}i\text{-}Pr)_3$
20	474.6 ± 0.0	6482.0 ± 1.3	6604.4 ± 1.6
25	398.3 ± 0.0	4701.8 ± 0.5	5707.6 ± 1.4
30	368.8 ± 0.0	2965.8 ± 0.2	4641.1 ± 1.0
35	346.6 ± 0.0	2595.3 ± 0.1	3791.5 ± 0.1
40	299.4 ± 0.1	2042.9 ± 0.4	3300.6 ± 1.3

Note: λ = 450 nm.

Table 4. The stability constants (K, L mol^{-1}) for [Co(Salpd)-(PBu_3)]$ClO_4 \cdot H_2O$ with various $P(OR)_3$ in acetonitrile solvent.

Temperature (°C)	$P(OMe)_3$	$P(OEt)_3$	$P(O\text{-}i\text{-}Pr)_3$
20	243.6 ± 0.0	1125.7 ± 0.2	875.4 ± 0.1
25	228.5 ± 0.0	920.0 ± 0.1	783.1 ± 0.1
30	204.1 ± 0.0	756.0 ± 0.0	606.1 ± 0.0
35	190.0 ± 0.0	681.2 ± 0.0	524.7 ± 0.0
40	171.0 ± 0.0	552.9 ± 0.0	438.9 ± 0.0

Note: λ = 470 nm.

Instrumentation

The UV–vis spectra were recorded by a Jusco V-530 spectrophotometer. The NMR spectra were recorded by a Bruker Avance DPX 250 MHz spectrometer, and IR spectra were recorded by a PerkinElmer 781 IR spectrophotometer.

Synthesis of the complexes

The ligands Salen, 5-nitroSalen, and Salpd were prepared according to the literature (12). The [Co(Salen)-(PBu_3)]$ClO_4 \cdot H_2O$ and [Co(Salen)(PMe_2Ph)]$ClO_4 \cdot H_2O$ complexes were prepared by the methods described previously (10, 11).

The general procedure for the synthesis of the [Co(5-nitroSalen)(PBu_3)]$ClO_4.H_2O$ and [Co(Salpd)(PBu_3)]$ClO_4.H_2O$ is as follows: to a refluxing solution of Salpd (0.57 g, 2.01 mmol) or 5-nitroSalen (0.71 g, 2.01 mmol) in methanol (70 mL), were added $Co(OAC)_2 \cdot 4H_2O$ (0.50 g, 2.01 mmol) and tributylphosphine (0.5 mL, 2.01 mmol). The reaction mixture was refluxed for 1 h. The formed Co(II) complex was oxidized by blowing air into the solution for 2 h, and the solution was filtered. To the filtrate, an appropriate amount of sodium perchlorate (0.30 g, in 10 mL water) was added. The green crystals were formed after 24 h. The crystals were washed with some methanol, recrystallized in acetone–ethanol (95%), and dried in vacuum at 65°C.

*[*N,N′*-bis(salicylidene)-1,3-diaminopropanato]tri*-n-*butylphosphineCo(III) perchlorate monohydrate*

Yield: 70%. ^{1}H NMR ($CDCl_3$) δ: 0.76–0.81 (t, 9H, CH_3), 1.25–1.30 (m, 18H, CH_2), 2.75 (w, 2H, H_2O), 3.86–3.96, 4.22–4.28 (m, 6H, $CH_2CH_2CH_2$), 6.55–6.61 (t, 2H, ArH), 6.90–6.93 (d, 2H, ArH), 6.98–7.01 (d, 2H, ArH), 7.11–7.17 (t, 2H, ArH), 7.65 (s, 2H, CH=N). Anal. calcd. for $C_{29}H_{45}ClN_2O_7PCo$: C 52.86, H 6.88, N 4.25; found: C 53.49, H 6.69, N 4.61.

*[*N,N′*-bis(5-nitrosalicylidene)aza-1,2-diaminoethanato]tri*-n-*butylphosphineCo(III) perchlorate monohydrate*

Yield: 85%. ^{1}H NMR (DMSO-d_6) δ: 0.73–0.79 (t, 9H, CH_3), 1.21–1.26 (m, 9H, CH_2), 1.45–1.49 (m, 9H, CH_2), 2.51 (s, 2H, H_2O), 4.03 (s, 4H, CH_2CH_2), 7.15–7.19 (d, 2H, ArH), 8.15–8.20 (d, 2H, ArH), 8.51 (s, 4H, ArH, CH=N). Anal. calcd. for $C_{28}H_{41}ClN_4O_{11}PCo$: C 45.77, H 5.62, N 7.62; found: C 45.43, H 5.59, N 7.80.

Thermodynamic studies

The adduct complexes were obtained from the reaction of the acceptors with the donors, according to the eq. [1]:

$$[1] \qquad [CoLX]^+ + P(OR)_3 \longleftrightarrow [CoLX(P(OR)_3)]^+$$

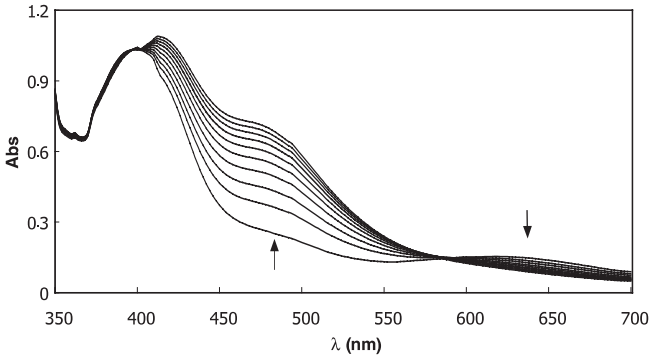
where L = Salen, Salpd, and 5-nitroSalen, X = PBu_3 and PMe_2Ph (only for Salen), R = Me, Et, and *i*-Pr.

A solution from each complex with a concentration at about 1×10^{-4} M and a constant ionic strength (I = 0.01 M) by tetraethylammonium perchlorate was prepared. From this solution, 2.5 mL was transferred into the thermostated cell compartment of the UV–vis instrument which was kept at constant temperature (±0.1°C) by circulating water and was titrated by the phosphite. The titration was done by adding aliquots of the phosphite with a Hamilton syringe (μL). The donors' concentrations were varied one- to three-fold in excess.

The absorption measurements were carried out at a fixed wavelength where the difference in absorption between the substrate and the product was the largest after the equilibrium was assessed. These fixed wavelengths for the systems are listed in Tables 1–4. The adduct formed shows an absorption different from the acceptor, while the donors show no absorption at those wavelengths.

© 2001 NRC Canada

Fig. 1. Spectrophotometric titration of $[Co(Salen)(PMe_2Ph)]^+$ with $P(O\text{-}i\text{-}Pr)_3$ in acetonitrile (I = 0.01 M Et_4NClO_4, T = 30°C).



Results and discussion

The characterization of the complexes

The new complexes $[Co(5\text{-nitroSalen})(PBu_3)]ClO_4 \cdot H_2O$ and $[Co(Salpd)(PBu_3)]ClO_4 \cdot H_2O$ were identified by elemental analysis, IR, NMR, and electronic spectra. The other complexes were identified only by IR, NMR, and electronic spectra.

Spectral characterization

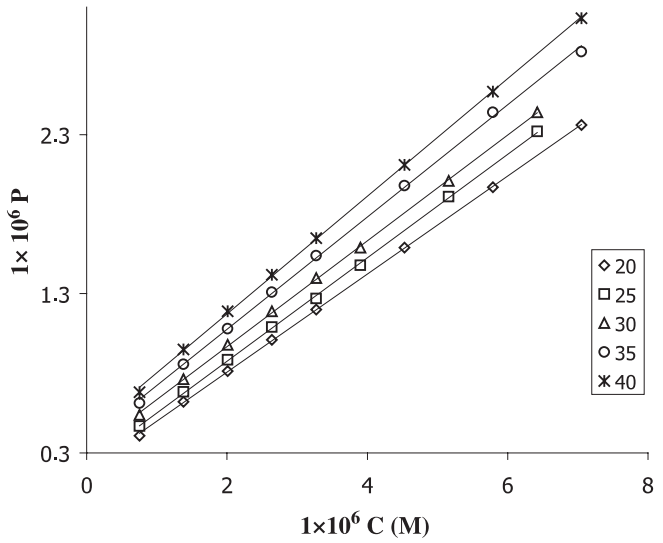
IR spectra: The absence of the coordinated water in all the studied complexes was confirmed by the absence of the absorption band around 3100 cm^{-1} (10). The absorption band around 1625–1640 cm^{-1} is related to the azomethane group, and the aromatic double bonds appeared at 1600–1605 cm^{-1} (13).

Electronic spectra: The electronic spectra, of all the studied complexes, show an absorption at 600–700 nm in non-coordinated solvent, that indicate the five-coordinated structure for them. All complexes show an intensive absorption band at 370–400 nm. This band did not reallychange in all the reactions studied. The absorption band at 600–700 nm vanished and the six-coordinated product species showed an absorption band at 400–500 nm (10). All measurements for the thermodynamic studies were carried out in this range. As an example, the variation of the electronic spectra for $[Co(Salen)(PMe_2Ph)]^+$, titrated with the $P(O\text{-}i\text{-}Pr)_3$, is shown in Fig. 1. The isosbestic points for this system show that there is only one reaction in equilibrium. The same is valid for other systems.

The ^1H NMR spectra: The ^1H NMR spectral data have been presented in the *Experimental* section. The NMR spectra of these complexes are consistent with the suggest formulation and show that the cobalt in these complexes is low-spin. The interesting point in the NMR of these complexes is the aromatic proton signals that are resolved in four groups in the ^1H NMR. For example, in $[Co(Salpd)(PBu_3)]^+$ these signals arranged from δ = 6.55 to 7.17 in the form of triplet, doublet, doublet, and triplet, that are related to the protons in the positions of 5, 3, 6, and 4 to the azomethane group, respectively. In the complex of $[Co(5\text{-nitroSalen})(PBu_3)]^+$, because of the NO_2 group, the aromatic proton signals shifted to the low field in such a way that the proton in the position 6 to the azomethane overlaps with the azomethane proton at δ = 8.51.

Fig. 2. The linear plot for $[Co(Salen)(PBu_3)]^+$ with $P(OEt)_3$ system at various temperatures (T = 20–40°C).

$P = \dfrac{C_A^\circ C_D^\circ}{A - A_A^\circ - A_D^\circ}$, $C = (C_A^\circ C_D^\circ)$.



Thermodynamic interpretations

The equilibrium constants of the various cobalt(III) Schiff base complexes studied were calculated by using Ketelaar et al.'s (14) equation

$$[2] \qquad \frac{C_A^\circ C_D^\circ}{A - A_A^\circ - A_D^\circ} = \frac{1}{(\varepsilon_C - \varepsilon_A - \varepsilon_D)}\left[\frac{1}{K} + (C_A^\circ + C_D^\circ)\right]$$

where C_A° and C_D° are the initial concentrations of the acceptor and the donor, respectively. A is the optical density of the solution including the acceptor and the donor; A_A° and A_D° are the optical densities of the pure acceptor and the pure donor in the solution of concentration C_A° and C_D°; ε_C, ε_A, and ε_D are the molar extinction coefficients of the complex, the acceptor, and the donor, respectively. K is the stability constant of the formed complex and the cell optical path length is 1 cm. A plot of $(C_A^\circ C_D^\circ/(A - A_A^\circ - A_D^\circ))$ vs. $(C_A^\circ + C_D^\circ)$ should produce a straight line if only the 1:1 complex is formed, while a mixture of 1:1 and 1:2 or only 1:2 complex in a system would lead to a curve. The stability constants of the studied cobalt(III) Schiff base complexes were calculated from the ratio of the slope to the intercept by the least-squares method using Excel 5 computer software. The K measurements were repeated at least twice and were reproducible. The linear plots for $[Co(Salen)(PBu_3)]^+$ with $P(OEt)_3$ at various temperatures are shown in Fig. 2, which signifies that only 1:1 complex is formed. Similar plots are obtained for other systems.

The thermodynamic parameters of the studied cobalt(III) Schiff base complexes were calculated by use of the well-known van't Hoff eq. [3]:

$$[3] \qquad \ln K = \frac{-\Delta H^\circ}{RT} + \frac{\Delta S^\circ}{R}$$

© 2001 NRC Canada

Table 5. The thermodynamic parameter values $\Delta H°$, $\Delta S°$, and $\Delta G°$ for $[Co(Salen)(PBu_3)]ClO_4 \cdot H_2O$ with various $P(OR)_3$ in acetonitrile solvent.

$P(OR)_3$	$\Delta H°$ (kJ mol^{-1})	$\Delta S°$ (J K^{-1} mol^{-1})	$\Delta G°$ (kJ mol^{-1})[a]
$P(OMe)_3$	–14.8 ± 1.1	–1.9 ± 3.7	–14.2 ± 2.2
$P(OEt)_3$	–25.6 ± 1.2	–25.9 ± 4.0	–17.7 ± 2.4
$P(O\text{-}i\text{-}Pr)_3$	–22.6 ± 1.3	–13.7 ± 4.4	–18.6 ± 2.6

[a]At 30°C.

Table 6. The thermodynamic parameter values $\Delta H°$, $\Delta S°$, and $\Delta G°$ for $[Co(Salen)(PMe_2Ph)]ClO_4 \cdot H_2O$ with various $P(OR)_3$ in acetonitrile solvent.

$P(OR)_3$	$\Delta H°$ (kJ mol^{-1})	$\Delta S°$ (J K^{-1} mol^{-1})	$\Delta G°$ (kJ mol^{-1})[a]
$P(OMe)_3$	–28.8 ± 2.3	–37.3 ± 7.6	–17.6 ± 4.6
$P(OEt)_3$	–34.3 ± 0.3	–44.2 ± 0.9	–20.9 ± 0.6
$P(OIpr)_3$	–21.3 ± 0.4	+5.5 ± 1.2	–22.8 ± 0.8

[a]At 30°C.

Table 7. The thermodynamic parameter values $\Delta H°$, $\Delta S°$, and $\Delta G°$ for $[Co(Salpd)(PBu_3)]ClO_4 \cdot H_2O$ with various $P(OR)_3$ in acetonitrile solvent.

$P(OR)_3$	$\Delta H°$ (kJ mol^{-1})	$\Delta S°$ (J K^{-1} mol^{-1})	$\Delta G°$ (kJ mol^{-1})[a]
$P(OMe)_3$	–13.7 ± 0.7	–1.0 ± 2.3	–13.4 ± 1.4
$P(OEt)_3$	–26.3 ± 1.3	–31.3 ± 4.3	–16.7 ± 2.6
$P(OIpr)_3$	–26.5 ± 1.6	–34.1 ± 5.4	–16.1 ± 3.2

[a]At 30°C.

Table 8. The thermodynamic parameter values $\Delta H°$, $\Delta S°$, and $\Delta G°$ for $[Co(5\text{-nitroSalen})(PBu_3)]ClO_4 \cdot H_2O$ with various $P(OR)_3$ in acetonitrile solvent.

$P(OR)_3$	$\Delta H°$ (kJ mol^{-1})	$\Delta S°$ (J K^{-1} mol^{-1})	$\Delta G°$ (kJ mol^{-1})[a]
$P(OMe)_3$	–16.8 ± 1.1	–6.1 ± 3.6	–14.9 ± 2.2
$P(OEt)_3$	–44.6 ± 1.8	–79.5 ± 6.0	–20.1 ± 3.6
$P(OIpr)_3$	–27.3 ± 1.2	–19.9 ± 3.9	–21.3 ± 2.4

[a]At 30°C.

where K is the stability constant, R is the gas constant, and T is the temperature in kelvin scale. Thermodynamic parameters of the studied cobalt(III) Schiff base complexes were obtained from the linear plots of ln K vs. $1/T$. The values of $\Delta H°$ and $\Delta S°$ were obtained from the slope and the intercept, respectively, by using the Excel computer program.

The stability constants and the thermodynamic parameters data are collected in Tables 1–8. The stability constants are given for the formation of 1:1 adducts only.

The acceptor property of cobalt(III) Schiff base complexes

It was suggested (15) that when Co(III) ion is chelated in a macrocycle having delocalized electronic structure, the complex loses its transition character and might become kinetically labile. The extent to which this happens is likely to be strongly dependent on the structure of the planar chelating system acting as acceptor of the donated charge. It can be concluded that in the ground state, the thermodynamic effects and even the kinetic *trans*-effects are mainly due to the charge donation to the cobalt atom via the σ-bond (2). Therefore the equatorial Schiff base ligands and the strong σ-donors like phosphines in the axial position can affect the stability of six- or five-coordinated cobalt(III) Schiff base complexes. The phosphine axial ligand *trans*-effect on the thermodynamics of the five-coordinated Co(III) Schiff base complexes has been well-studied (10, 11), but the *cis*-effect appears to be far less evident in this literature. We tried to find the steric and the electronic effects of some Schiff bases on the thermodynamic parameters of five-coordinated Co(III) Schiff base complexes. The steric effect of the axial phosphine ligands and the entering ligands were also studied. The thermodynamic aspect of the influence of the equatorial Schiff bases' ligands can be clearly seen from Tables 1, 3, and 4, and show the trend of Salpd < Salen < 5-nitroSalen, irrespective of the nature of the axial ligand. These results are in agreement with the trend of nucleophilicity of the cobalt atom in the Schiff base complexes toward the electrophiles.

The electronic effect of the equatorial Schiff base ligands

The electron-withdrawing property of the substituent groups on the Schiff base can influence the ability of the acceptor property of the complexes. The presence of an NO_2 withdrawing group causes 5-nitroSalen to become a weaker Schiff base than the unsubstituted Salen. Therefore, the cobalt atom in the $[Co(5\text{-nitroSalen})(PBu_3)]^+$ complex has more acceptor property than $[Co(Salen)(PBu_3)]^+$ and forms more stable complexes with donors (Tables 1 and 3).

The steric effect of the equatorial Schiff base ligands

By increasing the steric interactions of the Schiff base, the five-coordinate complex becomes more stable and the formation constant of this type decreases with an increase in steric interactions. Therefore, the five-coordinated $[Co(Salpd)(PBu_3)]^+$ complex has less acceptor ability than $[Co(salen)(PBu_3)]^+$ (Tables 1 and 4).

The effect of the axial ligand

The steric effect of the axial ligand is more important than the equatorial (10, 11). The stability constants for the PMe_2Ph axial ligand with lower steric interactions are more larger than PBu_3 (Tables 1 and 2). The difference between the nucleophilicity of the phosphites in the $[Co(Salen)(PMe_2Ph)]^+$ is better seen because of the decrease in steric interactions (Table 2).

Effect of the donors

In this work, we have examined three donors, $P(OMe)_3$, $P(OEt)_3$, and $P(O\text{-}i\text{-}Pr)_3$. The phosphite complexes are often similar to the phosphines but the phosphites tend to be more basic and less sterically hindered (16).

In addition to the electronic property, the phosphites have an important steric factor that is demonstrated by the Tolmane cone angle. The cone angles (degrees) for these phosphites are 107, 109, and 130°, for $P(OMe)_3$, $P(OEt)_3$, and $P(O\text{-}i\text{-}Pr)_3$, respectively (17). The steric interaction is increased with an increase in cone angle.

In the Salen and 5-nitroSalen complexes, the stability constants were increased by increasing Tolmane cone angles of the phosphites, which is in contrast to what is expected;, therefore, it seems that the electronic effect of the phosphites is more important than the steric effect toward the given acceptor (Tables 1–3), and there is an increasing tendency for the

© 2001 NRC Canada

adduct formation in the order $P(OMe)_3 < P(Oet)_3 < P(O\text{-}i\text{-}Pr)_3$. By increasing the steric interactions in the Salpd complex, the stability constant is decreased when the Tolmane cone angle increased (Table 4) and this order changes to $P(OMe)_3 < P(O\text{-}i\text{-}Pr)_3 < P(OEt)_3$.

The lower stability constant of the trimethylphosphite may be attributed to a "keto–enol" type of rearrangement to produce a phosphoryl linkage (18), but the triethylphosphite do not show this property (19).

Thermodynamic parameters

The heat of formation

The $\Delta H°$ value and its sign, is dependent on two factors: one of these factors, is the solvation effect and the other one is the heat of formation of the complex (20). The solvation effect for five- and six-coordinated complexes is not that different due to the same charge, although it seems that the five-coordinated complex is better solvated. The solvation effect for the donors is related to the interaction of solvent with the phosphites and this contribution for $\Delta H°$ can be positive after the equilibrium. In all cases, $\Delta H°$ values are negative, and it shows that the complex-formation contribution of $\Delta H°$ values is more important (Tables 5–8). For example, the heat of formations of $P(OMe)_3$ toward the acceptors are related to the stability constants for these systems (Tables 5–8).

Concerning the electronic effect contribution, the $\Delta H°$ values for $[Co(5\text{-nitroSalen})(PBu_3)]^+$ are more negative than the $[Co(Salen)(PBu_3)]^+$, and it shows that the complex formation in 5-nitroSalen is more important (Tables 5 and 8).

Concerning the steric effect of the equatorial Schiff base ligand on heat of formation, the $\Delta H°$ values for $[Co(Salpd)(PBu_3)]^+$ are nearly the same as $[Co(Salen)(PBu_3)]^+$. It can be due to the second factor, and there is some positive value from the solvation effect for $[Co(Salen)(PBu_3)]^+$, especially with $P(OEt)_3$ and $P(O\text{-}i\text{-}Pr)_3$ (Tables 5 and 7). The steric effect of the axial ligand is important and the enthalpy change values show this effect (Tables 5 and 6).

For a given acceptor, the solvation effect is different for the donors. $\Delta H°$ values for the triisopropylphosphite are less negative than triethylphosphite and these are in contrast to the stability constants. For example, the heat of formation for $[Co(Salen)(PMe_2Ph)]^+$ is smaller than the others, although the complex formation is the greatest. This is repeated for $[Co(Salen)(PBu_3)]^+$ and $[Co(5\text{-nitroSalen})(PBu_3)]^+$, and it seems that this donor is better solvated, and it reduces the overall enthalpy (Tables 1–8). The importance of this factor is better seen in the entropy.

The entropy

The $\Delta S°$ value and its sign, is also dependent on two factors: one of these factors is the difference in the number of the particles of the initial substances and the product complexes. The second factor is the liberation of the solvent molecules from the solvation shells (20). Concerning the first factor, the entropy change is decreased while the second factor is increased, but the net entropy change in most cases is negative, and it shows that the first factor is more important. The entropy change for trimethyl- and triethylphosphite properly decreases with increasing stability constant and indicates that the first factor is more important (Tables 5–8). For example, the entropy changes of $P(OMe)_3$ toward the acceptors are related to the stability constants for these systems and with increasing complex formation, the entropy change is decreased. The more negative entropy change for $P(OMe)_3$ in Table 6 is related to the higher stability constant for this system. The entropy change for triisopropylphosphite is governed by the second factor i.e., the libration of the solvent molecules, and it is less negative and is sometimes positive, although the stability constants are larger than the others. For example, the entropy change for $[Co(Salen)(PMe_2Ph)]^+$ complex with $P(O\text{-}i\text{-}Pr)_3$ is positive (Table 6), although the complex formation is the highest.

Conclusion

In this work, efforts were made to provide a quantitative measure of Schiff base effect on the acceptor property of Co(III) in some cobalt(III) Schiff base complexes, such as $[Co(Salen)(PBu_3)]^+$, $[Co(Salen)(PMe_2ph)]^+$, $[Co(5\text{-nitroSalen})(PBu_3)]^+$, and $[Co(Salpd)(PBu_3)]^+$, through adduct formation with $P(OMe)_3$, $P(OEt)_3$, and $P(O\text{-}i\text{-}Pr)_3$ in acetonitrile. The stability constants and the thermodynamic parameters obtained have showed the following trend of acceptor property of theSchiff-base complexes: 5-nitroSalen > Salen > Salpd.

Acknowledgements

We are grateful to Shiraz University Research Council for their financial support. Thanks are also given to B. Hemattinejhad for writing the modified computer program.

References

1. G. Costa, A. Puxeduu, and G. Tauzher. Inorg. Nucl. Chem. Lett. **4**, 319 (1968).
2. G. Costa, A. Puxeduu, and G. Tauzher. Inorg. Chem. Acta, **3**, 41 (1969).
3. A. Bigotto, G. Costa, G. Mestroni, G. Pellizer, A. Puxeddu, E. Reisenhofer, L. Stefani, and G. Tauzher. Inorg. Chem. Acta Rev. 41 (1970).
4. N. Bresciani-Pahor, M. Forcolin, L.G. Marzilli, L. Randaccio, M.F. Summers, and P.J. Toscano. Coord. Chem. Rev. **1**, 63 (1985).
5. L.G. Marzilli, F.M. Summers, E. Zangrando, N. Bresciani-Pahor, and L. Randaccio. J. Am. Chem. Soc. **108**, 4830 (1986).
6. L. Randaccio, N. Bresciani-Pahor, E. Zangrando, and L.G. Marzilli. Chem. Soc. Rev. **18**, 225 (1989).
7. M.S. Polson, L. Hansen, and L.G. Marzilli. Inorg. Chem. **36**, 307 (1997).
8. J. Halpern. Science (Washington, D.C.), **227**, 869 (1985).
9. M.S.A. Hamza, C. Ducker-Benfer, and R. van Eldik. Inorg. Chem. **39**, 3777 (2000).
10. G. Tauzher, G. Mestroni, A. Puxeddu, R. Costanzo, and G. Costa. J. Chem. Soc. A, 2504 (1971).
11. C.W. Smith, G.W. Van Loon, and M.C. Barid. Can. J. Chem. **54**, 1875 (1976).
12. J. Kjeld, C. van Bommel, W. Verboom, H. Kooijman, A.L. Spek, and N.D. Reinhoudt. Inorg. Chem. **37**, 4197 (1998).
13. N.S. Biradar, G.V. Karajagi, T.M. Aminabhavi, and W.E. Rudzinski. Inorg. Chem. Acta, **82**, 211 (1984).
14. J.A.A. Ketelaar, C. van DeStolpe, A. Coulsmit, and W. Dzcubes. Rec. Trav. Chim. Pays–Bas, **71**, 1104 (1952).

© 2001 NRC Canada

15. E.B. Fleischer, S. Jacobs and L. Mestichelli. J. Am. Chem. Soc. **90**, 2527 (1968).
16. F.A. Cotton, G. Wilkinson, C.A. Murillo, and M. Bochmann. Advanced inorganic chemistry. John Wiley and Sons, Inc., New York. 1999. p. 440.
17. T.L. Brown and K.J. Lee. Coord. Chem. Rev. **89,** 128 (1993).
18. K.F. Purcell and J.C. Kotz. *In* Inorganic chemistry. *Edited by* W.B. Saunders Company, London. 1977. p. 496.
19. M.S. Kharasch, R.A. Mosher, and I.B. Dorf. J. Org. Chem. **25**, 1000 (1960).
20. S. Ahrland. Helv. Chim. Acta, **50**, 306 (1967).

© 2001 NRC Canada

Calculations on the electronic structure and nonlinear second-order susceptibilities of fulleropyrrolidine–tetrathiafulvalene(C_{60}PY–TTF) based on donor–bridge–acceptor dyads

Wei Fu, Hong-Xing Zhang, Ji-Kang Feng, and Wei Li

Abstract: The semiempirical INDO calculations were carried out to investigate the charge-transfer interaction and to evaluate the second-order nonlinear susceptibilities for a series of fulleropyrrolidine–tetrathiafulvalene(C_{60}PY–TTF) dyads, C_{60}PY, and C_{60}PY-$(CH{=}CH)_n$-TTF (n = 0–6). The equilibrium geometries, electronic structures, and UV–vis spectra of these C_{60}PY–TTFs D–B–A dyads were determined by using ZINDO methods. On the basis of electronic spectra, we calculated the β for the dyads using the ZINDO-SOS expression, and found that these dyads have relatively large β. The calculated values of β are 48.78, 62.34, 97.90, 123.24, 183.78, 189.43, 193.45, 195.82 × 10^{-30} esu for C_{60}PY and C_{60}PY-$(CH{=}CH)_n$-TTF (n = 0–6), respectively, which shows the enhancing effect when TTF is introduced. The β significantly increases as n increases from 0–3; and it tends to be saturated in the end.

Key words: ZINDO-SOS, CI, structure, spectra, C_{60}PY–TTF.

Résumé : On a effectué des calculs semi-empiriques INDO dans le but d'étudier l'interaction de transfert de charge et pour évaluer les susceptibilités non linéaires du deuxième ordre, β, d'une série de dyades fulléropyrrolidine–tétrathiafulvalène (C_{60}PY–TTH), le C_{60}PY et des C_{60}PY-$(CH{=}CH)_n$-TTF (n = 0 à 6). Utilisant des méthodes ZINDO, on a déterminé les géométries d'équilibre, les structures électroniques et les spectres UV–vis des dyades C_{60}PY–TTF D–B–A. Sur la base des spectres électroniques et faisant appel à une expression ZINDO-SOS, on a calculé la valeur β pour les dyades et on a trouvé que ces dyades ont des valeurs de β relativement élevées. Les valeurs calculées pour β sont respectivement de 48,78, 62,34, 97,90, 123,24, 183,78, 189,43, 193,45, 195,82 × 10^{-30} esu pour le C_{60}PY et les C_{60}PY-$(CH{=}CH)_n$-TTF (n = 0 à 6); ces valeurs mettent en relief une augmentation de la valeur de β à l'introduction du TTF et une augmentation progressive de β lorsque n passe de 0 à 3 alors que la valeur devient alors saturée.

Mots clés : ZINDO-SOS, CI, structure, spectre, C_{60}PY–TTF.

[Traduit par la Rédaction]

Introduction

Over the past two decades, interest has increased tremendously in nonlinear optical phenomena because of potential applications both in scientific and technological areas (1–4). Growing attention has been paid to the design and synthesis of novel organic molecules with large second-order optical nonlinearities for the sake of their possible applications in optical signal processing, optical computing, and telecommunications (5). Recent results suggested that molecule-based organic nonlinear optical (NLO) materials possess many superior NLO characteristics, such as ultrafast response times, low dielectric constants, good processability characteristics, and enhanced nonresonant NLO response (6). The existence of a donor–π-acceptor (D–π-A) structure in a molecule has been identified as the most prominent molecular feature in the search for high molecular second-order NLO susceptibilities (β) (7–9). A variety of hyperpolarizable D–π-A organic molecules containing various acceptor units (7–9) such as nitro, cyano (10), sulfonyl, polycyanovinyl (11–13), babituric acid (14), or dianonium salts (15) and donor units (6–8) mainly diarylamines, alkoxyaryl groups, ferrocene (16, 17), 1,3-dithionle ring (10–13), or the TTF (18–20) have frequently been reported. In spite of these varieties of chromophores used, seeking more efficient donors, acceptors, and conjugating moieties still tempts researchers for the NLO compounds (21, 22).

Fullerenes, in particular the readily available C_{60} and C_{70}, are famous highly spherical delocalized π electron systems, that are expected to be excellent and potential electron acceptors in artificial photosynthesis influencing substantially the electron transfer process because of their symmetrical shape, large size, properties of the π-conjugated electron system, and high electron affinity (2.7 ± 0.1 eV) (23–25). Associating with appropriate electron donors through π-conjugated bridges, efficient NLO fullerene compounds are hopefully to be developed.

Received April 16, 2001. Published on the NRC Research Press Web site at http://canjchem.nrc.ca on September 20, 2001.

W. Fu,[1] H.-X. Zhang, J.-K. Feng, and W. Li. State Key Laboratory of Theoretical and Computational Chemistry, Institute of Theoretical Chemistry, Jilin University, Changchun, P.R. China, 130023.

[1]Corresponding author (fax: 086-431-8923907; e-mail: fengjikang@263.net).

 DOI: 10.1139/cjc-79-9-1366 © 2001 NRC Canada

Among the electron donors in NLO compounds, TTF dyads are intriguing candidates due to their high conjugation and strong ability to donate electrons. Some conventional organic TTF compounds exhibit satisfactory second-order NLO properties (19, 20). Thus, at an initial qualitative level, the relatively large nonlinear optical responses of the TTF-derived chromophores are anticipated; they are reminiscent of traditional organic π-chromophoric units, in that TTF donor is linked through a π-conjugated moiety with a C_{60}-type acceptor. In fact, C_{60}PY-(CH=CH)$_n$-TTF (n = 0, 1) have been synthesized (26) and weak electron transfer from TTF to C_{60} has been observed. We expect that C_{60}PY–TTF dyads may have good NLO properties, which stimulates the present theoretical investigation.

The semiempirical INDO (intermediate neglect of differential overlap) calculations were carried out to investigate the charge-transfer interaction and to evaluate the β for a series of C_{60}PY–TTF dyads as shown in Fig. 1. The equilibrium geometry, electronic structure, and UV–vis spectra of these C_{60}PY–TTFs based on D–B–A dyads are determined by using ZINDO methods. The UV–vis spectra results were calculated by the INDO-CI method. On the basis of electronic spectra, the β values for the dyads were evaluated by using the ZINDO-SOS expression. The results show that the calculated values of β are 48.78, 62.34, 97.90, 123.24, 183.78, 189.43, 193.45, 195.82 × 10^{-30} esu for C_{60}PY and C_{60}PY-(CH=CH)$_n$-TTF (n = 0–6), indicating the significant increase when TTF was introduced.

Theoretical method

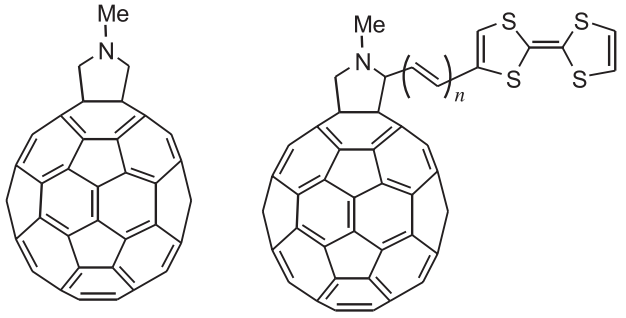
A quantitative description of molecular NLO response is derived from a power series expansion of the molecular polarization upon interaction with an oscillating external electromagnetic field (eq. [1]).

$$[1] \qquad P_i = \sum_j \alpha_{ij} E_j + \sum_{j\geq k} \beta_{ijk} E_j E_k + \sum_{j\geq k\geq l} \gamma_{ijkl} E_j E_k E_l + \ldots$$

Here, P_i is the molecular polarization induced along the ith axis, E_j is the jth component of the applied electric field, α is the linear polarizability, β is the first hyperpolarizability or the second-order susceptibility, and γ is the second hyperpolarizability or the third-order susceptibility. α, β, and γ describe the responsivity of the molecule to an electromagnetic perturbation and are constants for a given molecular geometry and external electromagnetic field. The β and γ are responsible for second- and third-harmonic generation respectively.

Several theoretical approaches for accurate calculation of β have been developed. Ab initio CPHF computations are numerically more accurate and precise, however, the results are not easily amenable to chemical interpretation and require substantial allocations of computational resources. Computationally intensive methods such as coupled Hartree–Fock (27), derivative Hartree–Fock (28), and correlated wave (29) ab initio procedures are applicable to molecules of only limited size (30). In contrast, the semiempirical-SOS method permit a basic understanding of origin of the NLO response in a chemical sense, by identifying the molecular excited states primarily responsible for NLO response within the SOS formalism. The

Fig. 1. A series of C_{60}PY–TTF dyads.



1 **2**: n=0, **3**: n=1, **4**: n=2, **5**: n=3, **6**: n=4 **7**: n=5 **8**: n=6

ZINDO-SOS method is of proven reliability in the description of molecular nonlinear optical properties (31*a–f*), many successful studies (17, 23, 25, 30, 32*a–c*) demonstrated that the ZINDO-SOS-derived nonlinear optical responses to be in agreement with the experiment. The second-order susceptibilities (25, 33*a–c*) and third-order susceptibilities (23, 32*c*, 34*a–c*) of dozens of molecules have been reported in our previous work. The sum-over-states (SOS) expression for the individual components of the second-order susceptibility tensor has been given from perturbation theory (35, 36):

$$[2] \qquad \beta_{ijk} + \beta_{ikj} = \frac{1}{4h^2} \left\{ \sum_{\substack{n\neq n' \\ n\neq g \\ n'\neq g}} (r^j_{gn'} r^k_{n'n} + r^k_{gn} r^i_{n'n} r^j_{gn}) \times \right.$$

$$\left(\frac{1}{(\omega_{n'g} - \omega)(\omega_{ng} + \omega)} + \frac{1}{(\omega_{n'g} + \omega)(\omega_{ng} - \omega)} \right) +$$

$$(r^i_{gn} r^j_{nn} r^k_{gn} + r^i_{gn'} r^k_{nn} r^j_{gn}) \times$$

$$\left(\frac{1}{(\omega_{n'g} - 2\omega)(\omega_{ng} - \omega)} + \frac{1}{(\omega_{n'g} + 2\omega)(\omega_{ng} + \omega)} \right) +$$

$$(r^j_{gn'} r^k_{n'n} r^i_{gn} + r^k_{gn'} r^j_{n'n} r^i_{gn}) \times$$

$$\left(\frac{1}{(\omega_{n'g} - \omega)(\omega_{ng} - 2\omega)} + \frac{1}{(\omega_{n'g} + \omega)(\omega_{ng} + 2\omega)} \right) +$$

$$4 \sum_n \left\{ \left[r^j_{gn} r^k_{gn} \Delta r^i_n (\omega^2_{ng} - 4\omega^2) + \right. \right.$$

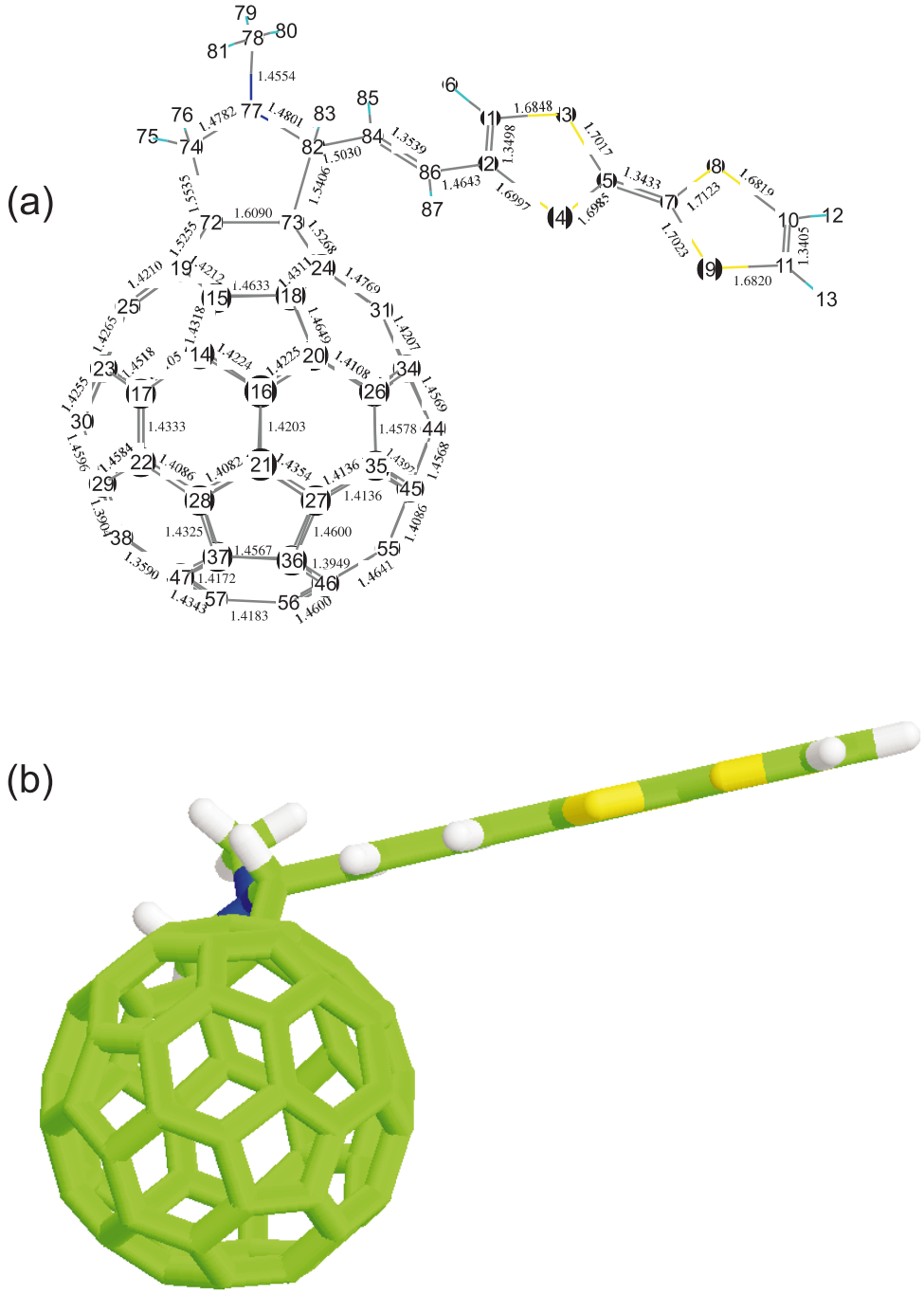
$$\left. r^i_{gn} (r^k_{gn} \Delta r^j_n + r^j_{gn} \Delta r^k_n)(\omega^2_{ng} + 2\omega^2) \right] \times$$

$$\left. \left. \left(\frac{1}{(\omega^2_{ng} - \omega^2)(\omega^2_{ng} - 4\omega^2)} \right) \right\} \right\}$$

Where the summations are over the complete sets of eigenstates $|n>$ and $|n'>$ of the unperturbed molecular system. The quantities $r^i_{gn'}$ and $r^i_{nn'}$ are matrix elements of the ith components of the dipole operator between the unperturbed ground and excited states and between the two excited

© 2001 NRC Canada

Fig. 2. (*a*) Optimized geometry of molecule **3**; and (*b*) the optimized lateral view of molecule **3**.



states, respectively; $\Delta r_n^i = r_{nn}^i - r_{gg}^i$ is the difference between the excited-state and ground-state energies. Although all 27 components of the β tensor can be computed, only the vector component in the dipolar direction (β_μ) is sampled by electric field-induced second-harmonic generation (EFISH) experiments. β_μ is given by

$$[3] \qquad \beta_\mu = (\mu_x\beta_x + \mu_y\beta_y + \mu_z\beta_z)/(\mu_x^2 + \mu_y^2 + \mu_z^2)^{1/2}$$

where

$$[4] \qquad \beta_i = \beta_{iii} + 1/3\sum_{i\neq j}(\beta_{jii} + \beta_{iji} + \beta_{iij}) \qquad i, j \in (x, y, z)$$

The all-valence ZINDO technique (37) was employed to provide the transition dipole moments and the transition energies needed in the SOS expressions (eq. [2]). Standard parameters and basis functions were used. In the computation of a series of C_{60}PY–TTF dyads, the 290 low-energy transitions between SCF and MECI electronic configurations were chosen to undergo CI mixing. The 290 states were found to be sufficient for effective convergence of the SOS procedure.

© 2001 NRC Canada

Table 1. Calculated and observed spectra of C_{60} and a series of C_{60}PY–TTF dyads.

1		**2**		**3**		**4**		**5**		**6**		**7**		**8**		C_{60cal} (32*c*)	
λ	*f*	λ	*f*	λ	*f*	λ	*f*	λ	*f*	λ	*f*	λ	f	λ	*f*	λ	*f*
Calculated																	
599.5	0.0077	639.0	0.0049	700.3	0.0059	722.7	0.0071	724.3	0.0078	725.6	0.0079	726.0	0.0078	728.4	0.0085	543.5	0.00
		592.2	0.0037	605.9	0.0125	611.6	0.0231	638.8	0.0436	635.6	0.0434	640.1	0.0437	640.1	0.0435	538.2	0.00
429.2	0.0152	430.9	0.0136	436.6	0.0192	439.0	0.0226	434.3	0.0126	436.4	0.0142	437.2	0.0165	431.0	0.0171		
247.1	0.8516	247.6	0.5075	245.6	0.7425	249.6	0.7477	249.8	0.6999	249.7	0.6678	245.6	0.7514	244.9	0.7486	250.4	3.41
236.8	1.0504	239.5	0.6506	239.5	0.2203	239.9	0.1758	237.5	0.1701	237.6	0.2255	239.7	0.3544	239.8	0.4543	236.1	3.75
213.7	3.0046	213.0	4.5079	214.7	4.7937	216.6	4.6612	219.4	4.6776	219.6	4.6789	218.9	4.8954	218.7	5.3217	213.3	21.87
Experimental																	
430 (42)		430 (26)														256 (strong)	
250																227 (shoulder)	
215 (strong)																211 (strong)	

Results and discussion

Geometric structure

By using the INDO/2 (included in ZINDO package) method, the geometries of dyads **1**–**8** (shown in Fig.1) were optimized. The same method has previously been employed to obtain the equilibrium geometry of C_{60} where R_{6-6} = 1.3979 Å and R_{5-6} = 1.4507 Å (32*c*) compared with R_{6-6} = 1.40 Å, R_{5-6} = 1.45 Å in the NMR experiment (38). The optimized structure for C_{60}PY–TTF is shown in Fig. 2 with molecule **3** as an example and its bond lengths are comparable with that of C_{60}. A pyrrolidine ring is fused with a 6,6-ring junction of C_{60} (see Fig. 2*a*). By the addition reaction, the C_{72}—C_{73} bond becomes a single bond with 1.6090 Å of bond length compared with 1.614 Å in ((3,4-dimethoxyphenyl)methano) fullerene (39). The single bond (C_{72}—C_{73}) has a bond order of 0.9539 from the INDO/2 calculation. C_{72}—C_{73} is protruded from C_{60} sphere (see Fig. 2*a*), which causes all the surrounding C—C bonds to be stretched. For example, the C_{72}—C_{19} bond distance is 1.5255 Å, the C_{73}—C_{24} distance is 1.5268 Å, and in the pyrrolidine portion C_{74}—C_{72} is 1.5535 Å and C_{82}—C_{73} is 1.5406 Å. For the other bond in the C_{60} part, as it is farther and farther from the C_{72}—C_{73} bond, its bond length changes less and less compared with that of C_{60}. For molecule **3**, the calculated eight C—S bonds distances are between 1.68–1.72 Å, compared with C—S 1.714 Å (40) for tetrahydrothiophene. For the pyrrolidine part, the calculated C_{74}—N_{77}, C_{82}—N_{77}, and C_{78}—N_{77} distances are 1.4782, 1.4801, and 1.4554 Å, respectively, (see Fig. 2*a*), which are comparable with 1.467 Å of the N—C standard single bond (41). The INDO calculation showed that the distance from C_{35} to the center of the C_{60} sphere is 3.698 Å, longer than 3.5477 Å in the original C_{60}, calculated at the same level.

The lateral figures of molecule **3** are shown in Fig. 2*b*, which indicates that the TTF fragment and methine bridge are coplanar.

UV–vis spectra

The calculated wavelength and oscillator strength of the UV absorptions for dyads **1**–**8** are listed in Table 1 with the experimental values and the results of C_{60} listed for comparison. Figure 3 shows a brief diagram for the calculated absorption of molecule **3** as an example. The UV–vis spectra of dyads **1**–**8** retains the main electronic feature of C_{60}. For both series of C_{60}PY–TTF dyads and C_{60} spectra, the UV region absorption is dominant. For these C_{60}PY–TTF dyads, there are three strong absorption peaks near 213–219, 236–240, and 247–250 nm corresponding to those of 213, 236, and 250 nm for C_{60} (32*c*), and in consistence with 211, 227, and 256 nm for the experiment (43), respectively. From molecule **2**–**8**, the 213–219 nm absorption tends to red-shift and the oscillator strength increases. In the latter molecular orbital analyses of molecule **4**, we can find that the absorption band, which has strong oscillator strength that will certainly enhance the second-order nonlinearity, originates from the mixing of TTF with C_{60}PY.

Because of the interaction between the C_{60}PY and TTF parts, the weak absorptions above 410 nm become significant for the C_{60}PY–TTF dyads, while there are no absorptions in the original C_{60} over the 410 nm region. The

© 2001 NRC Canada

Fig. 3. The UV–vis spectrum of molecule **3**.

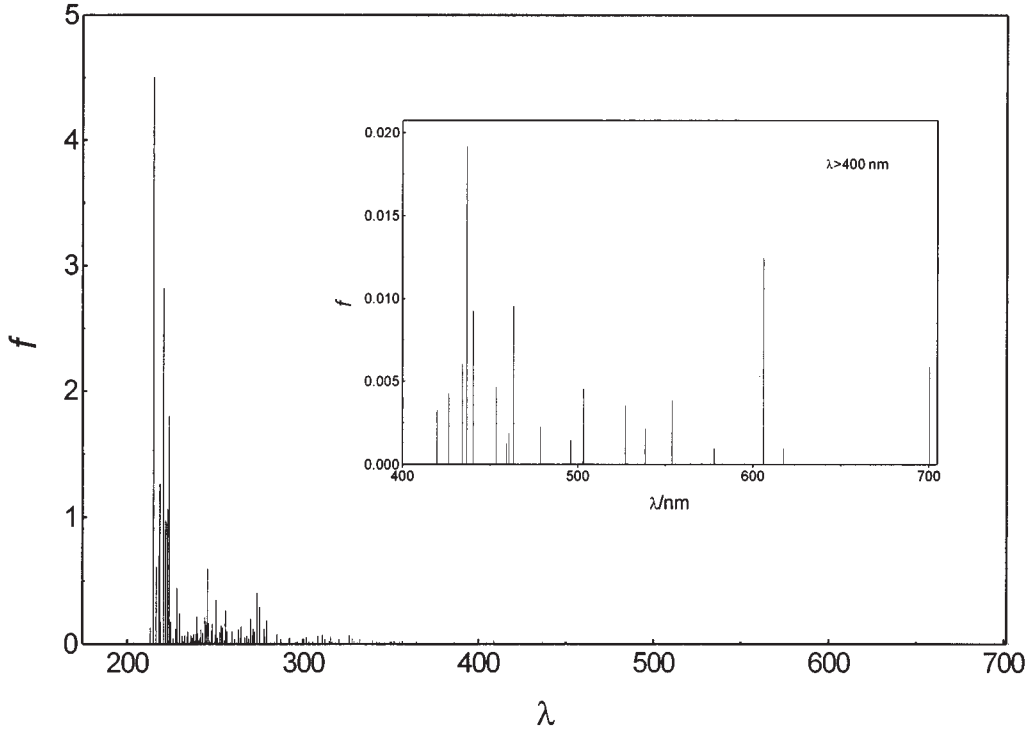
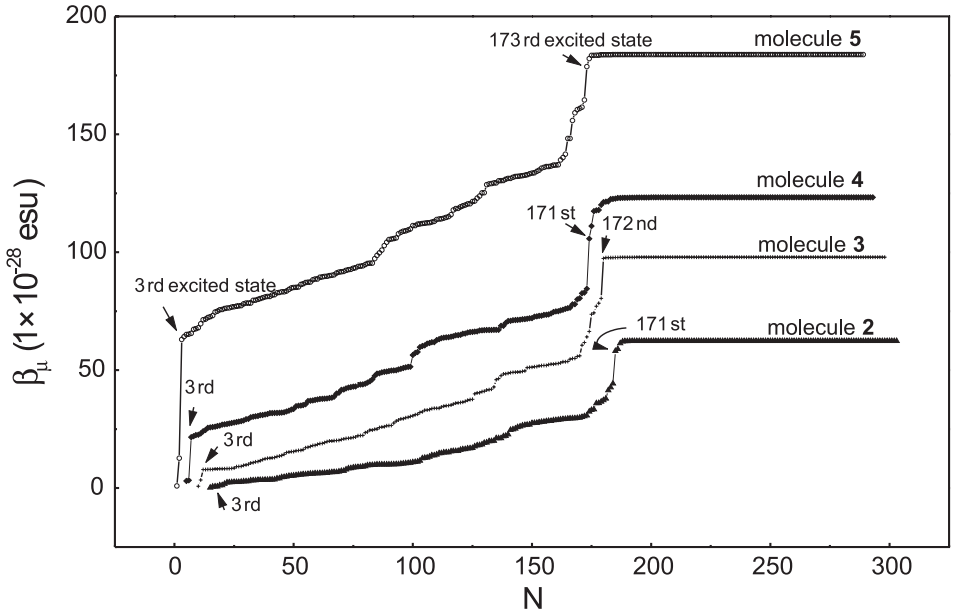


Fig. 4. β values plotted against numbers of excited states for molecules **2**–**5**.



characteristic absorption peaks of C_{60}PY–TTF dyads are in the region over 410 nm, and shown in Table 1. For molecule **3**, the absorption band over 410 nm was amplified and inserted in Fig. 3. There are three new absorption bands at 700–730 nm (except molecule **1** at 599.5 nm and molecule **2** at 639.0 nm), 592–640 nm, and 429–431 nm. Among them, the 429–431 nm absorption band owns relatively large oscillator strength and is consistent with the observed band in the 430 nm region for molecules **1**–**3**.

The lowest energy absorptions at 599.5, 639.9, 700.3, 722.7, 724.3, 725.6, 726.0, and 728.4 nm for dyads **1**–**8** comes from the electron transitions from HOMO to LUMO and relate with the forbidden absorption of C_{60} at 558.3 nm (35). The addition of pyrrolidine destroys the spherical conjugated π-electron structure of C_{60} and makes the *Ih* symmetry of C_{60} broken, so the forbidden absorption in C_{60} appears and shifts to 599.5 nm in C_{60}PY. When the TTF fragment is introduced, the 639.0 nm absorption significantly red-shifts

© 2001 NRC Canada

Table 2. The μ (De), β (1×10^{-30} esu), and β_0 (1×10^{-30} esu) for a series of C_{60}PY–TTF dyads.

Molecule	μ (De)	β (ω = 1.064 μm)	β_0
1	2.86	48.78	28.88
2	3.07	62.34	48.69
3	4.44	97.90	72.56
4	5.15	123.24	98.87
5	5.76	183.78	144.57
6	5.99	189.43	148.96
7	6.15	193.45	152.15
8	6.26	195.82	152.77
C_{60}–AN_{cal} (25)		32.17	
C_{60}–AN_{exp} (44)		67 ± 20	

(700.3 nm) further. As the length of the methine bridge *n* increases (from 1 to 6), this absorption red-shifts from 700.3 to 728.4 nm and the oscillator strength increases also. We analyzed the component of this absorption band and found that the methine bridge and TTF fragment play important roles for molecules **3**–**8** but not for molecule **2**. Therefore, the lowest energy absorption of molecules **3**–**8** gets more significant red-shift than molecule **2** due to the charge transfer from the C_{60} part to the methine bridge. The 592–640 nm absorption originates from the charge transfer from TTF to C_{60}, which is illustrated in the latter discussion section of NLO properties, and this absorption band significantly contributes to the second-order susceptibility. The 429–431 nm absorption corresponds to the observed band in the 430 nm region for molecules **1**–**3**. Taking molecule **3** as a representative, the absorption at 429–431 comes from the transition from HOMO-4 to LUMO+8. The component on the C_{60} part is dominant for HOMO-4 and LUMO+8. Therefore, this absorption comes from the electron transfer on the three-dimensional conjugative sphere of C_{60}.

NLO properties

On the basis of the optimized geometric structures and electronic spectra, the nonlinear second-order optical susceptibilities β_{ijk} and β_μ were calculated by using the ZINDO-SOS method.

In the SOS expression (eq. [2]) for β, the summation is over the complete sets of eigenstates $|n>$, $|m>$, and $|q>$ of the unperturbed system. They have to be truncated in practical calculations (17) for feasibility. In eq. [2], the dominator of each term includes ω_{ng} and $\omega_{n'g}$. When *n* and *n*′ increase, the energy differences between the ground state and the excited states will increase, i.e., the denominator will increase more and more. It means the contribution for β will become less important when *n* and *n*′ reach a certain value. Li et al. (25) demonstrated that 197 excited states were found to be sufficient for effective convergence for C_{60} (35). We considered that the series of C_{60}PY–TTF dyads are more complicated than C_{60}, so it is necessary to include 290 configurations in the calculations of β. Figure 4 illustrates the relationship between the number of the excited states involved and the values of β_μ (ω = 1.064 μm), which indicates that β_μ converges when the number of excited states exceed 190. The converged β_μ is simplified as β. The values of β relate to ω, the laser field frequency. ω is taken at 1.064 μm located at the nonresonant region (see the discussion about dispersion in the latter section). The converged values of β are listed in Table 2 where the β_0 corresponds to ω = 0. The calculated (25) and experimental (44) values of C_{60}–aniline (C_{60}–AN) are listed in Table 2 for comparison. Table 2 also shows that $\beta_8 \sim \beta_7 \sim \beta_6 \sim \beta_5 > > \beta_4 > \beta_3 > \beta_2 > \beta_1$. As we expected, the inclusion of TTF makes β increase significantly compared with C_{60}–pyrrolidine, then enhances the second-order NLO response. In accordance with the traditional organic chromophore designing guidelines, the greater electron delocalization in the C_{60}PY–TTF structures leads to the larger second-order NLO responses. For example, as the length of the bridge in the C_{60}PY–TTF molecules increases (see dyads **2**–**8**), the calculated response increases from 62.34 to 97.90, 123.24, 183.78, 189.43, 193.45, and 195.82×10^{-30} esu for β, respectively. It shows that β trends to be saturated as $n > 3$, which is in accordance with the effect of conjugation length on β for many traditional organic push–pull π-conjugated molecules (30, 34, 45).

Figure 4 illustrates the β accumulations up to 290 excited states for molecules **2**–**5**. While molecules **6**–**8** have the same characteristics as molecule **5**. As shown in Fig. 4, the first several excited states and the excited states around the 171st make main contributions to β.

In 1975, Oudar (2, 3) developed the famous two-level approximation as shown below

$$[5] \qquad \beta_\mu = \frac{3e^2\hbar}{2m} \frac{Wf\Delta\mu}{[W^2 - (2\hbar\omega)^2][W^2 - (\hbar\omega)^2]}$$

Where ω is the frequency of the laser field, $W = \hbar\omega_n$ is the transition energy from ground state to a specific excited state *n*, *f* is the oscillator strength of the transition, and Δμ is the difference of dipole moments between the excited state and ground state. Equation [5] clearly indicates the contribution of an excited state to β.

In the low-lying excited states, the third excited state plays important roles as shown in Fig. 4. The third excited state for molecules **2**–**5** lies at 592.2, 605.9, 611.6, and 638 nm with oscillator strength of 0.0037, 0.0125, 0.0231, and 0.0436, respectively, that comes from the electron transfer from HOMO-2 to LUMO. From eq. [5], the contribution of the third excited states to β should follow the order **5** > **4** > **3** > **2**, even though the contribution for molecule **2** is too small to notice due to the small oscillator strength, which shows clearly in Fig. 4. The component on the C_{60} part is dominant for the LUMO orbitals of the above four molecules. The HOMO-2 orbital is shown in Fig. 5 which demonstrates that the component on the C_{60} part is dominant for the HOMO-2 orbital of molecule **2** but the HOMO-2 orbitals of molecules **3**–**5** contain a significant contribution of methine bridge, while molecule **5** also contains the contribution from the TTF fragment. Maybe this is why the absorption peak generated from the third excited state red-shifts (Table 1) from molecule **2** to **5**. According to the two-level approximation formula (eq. [5]), the contribution of the third excited state to β is 0.129, 5.896, 20.248, and 58.818×10^{-30} esu for molecules **2**–**5**, respectively. The difference in Mulliken charge (ΔQ) between the ground state and the third excited

© 2001 NRC Canada

Fig. 5. The HOMO-2 orbital of molecules **2**–**5**.

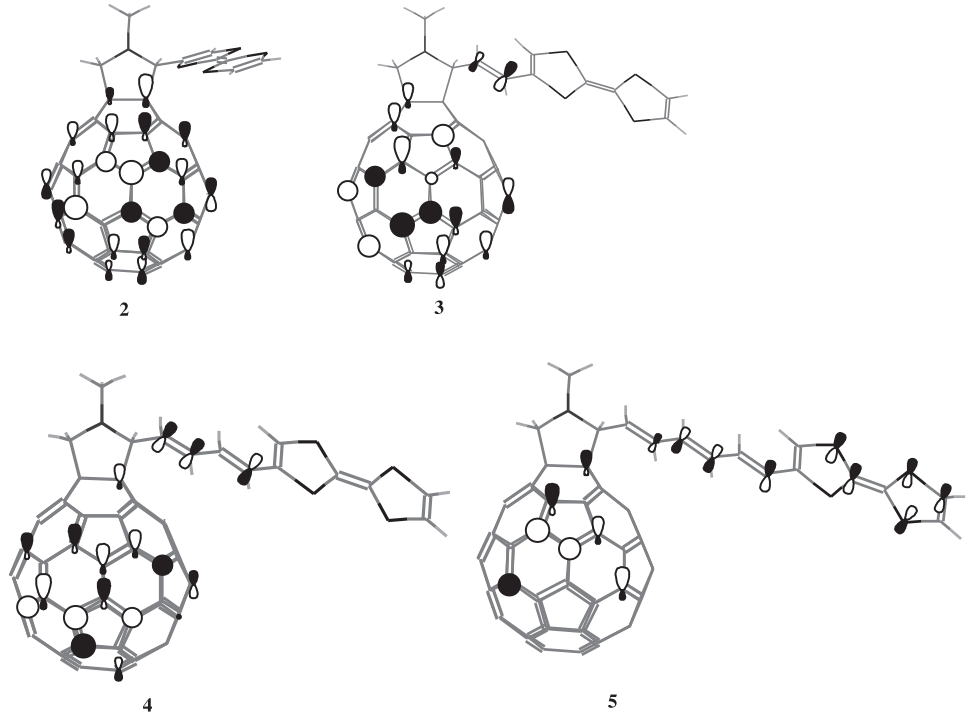
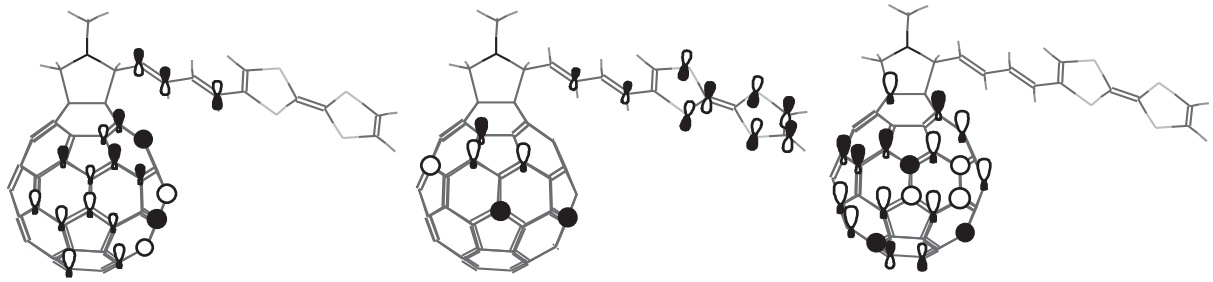


Fig. 6. Frontier orbital of molecule **4**.



state is listed in Table 3 for molecules **2**–**5** which indicates the charge transfer increase from molecule **2** to **5**, consistent with the traditional point of view that the larger charge transfer enhances. We noticed that the contribution to β from the low-lying excited band for molecule **5** is much more considerable, because of the relatively strong charge transfer from TTF to C_{60} through the methine bridge for molecule **5** (as shown in Table 3). Molecules **6**–**8** are similar to molecule **5**, since they have the similar excited state structure and transition properties in both low-lying and high-lying excited states, with molecule **5**.

Now let us examine the 171st, 172nd, 171st, and 173rd excited states which induce absorption at 213.0, 214.7, 216.6 and 219.4 nm in the high-energy excited band of molecules **2**–**5**, respectively, that evidently contribute to β. We have analyzed the component of these absorptions and found that they are similar. Taking molecule **4** as an example, the 216.6 nm absorption of molecule **4** comes from the mixing of electron transition from HOMO-11 to LUMO+11; HOMO-10 to LUMO+3, LUMO+4, LUMO+5, LUMO+11; and HOMO-5 to LUMO+12. The weight of these six transitions is 5.8, 25.6, 8.9, 10.2, 12.9, and 6.9%, respectively. Among them, the component on the C_{60} part is dominant for HOMO-10, LUMO+3, LUMO+4, LUMO+5, LUMO+11, and LUMO+12 orbitals, while the HOMO-5 orbital contains the contribution of the ethylene bridge and the HOMO-11 orbital contains the contribution of the TTF fragment. The LUMO+11, HOMO-5, and HOMO-11 orbitals are shown in Fig. 6, which shows that the transition from HOMO-11 to LUMO+11 is equivalent to the electron transfer from TTF to C_{60}, and the other transitions are equivalent to the electron transfer on the three-dimensional conjugation sphere of C_{60}; they were regarded as the source of the second-order NLO susceptibility. In the molecules involved, these absorptions are very strong and do have much larger oscillator strength than other absorptions. With reference to the two-level approximation (eq. [5]), these excited states should overwhelmingly contribute to β and the same conclusion is indicated in Fig. 4.

As mentioned above, the important excited state that evidently contributes to β for molecule **2**–**5**, contains not only the low-lying excited states but also the high-lying excited

© 2001 NRC Canada

Fig. 7. Molecules **3**, **9**, and **10**.

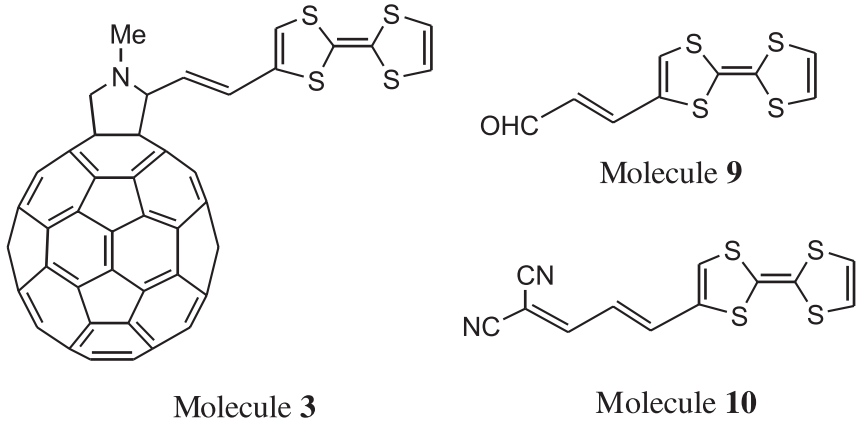


Fig. 8. β values plotted against numbers of excited states for molecule **10.**

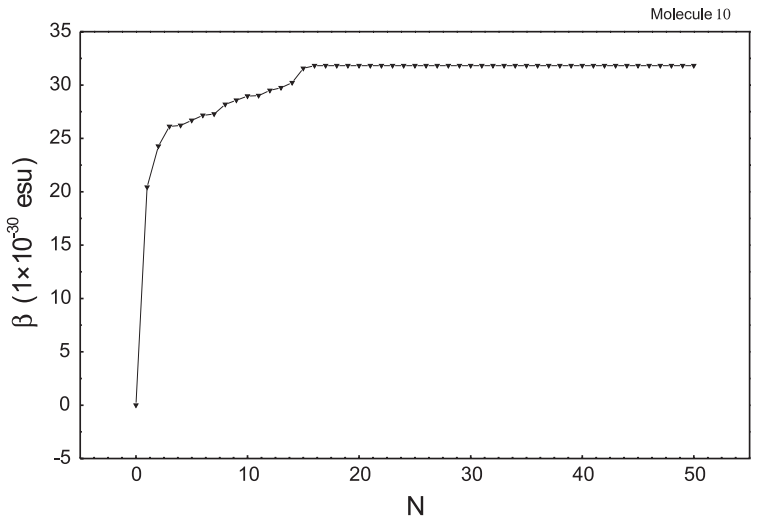


Table 3. ΔQ between the ground state and the third excited state.

Molecule:	**2**	**3**	**4**	**5**
The number of methine bridges (*n*):	0	1	2	3
ΔQ_{C60}	–0.035	–0.056	–0.106	–0.338
ΔQ_{TTF}	0.018	0.031	0.069	0.299

ones. The contribution of the low-lying excited states increase as the number of methine bridges increase from 0 to 3, therefore, $\beta_5 > \beta_4 > \beta_3 > \beta_2$. The calculated results indicate that the contribution of low-lying excited states on β of molecule **6**–**8** is similar to that of molecule **5**. Therefore, $\beta_8 \sim \beta_7 \sim \beta_6 \sim \beta_5$, showing a saturation phenomenon of the π-conjugation length. In the conventional π-conjugated push–pull polyenes, one anticipates an enhancement in the β value with an increase in π-conjugation length between the electron-donation and electron-withdrawing groups. The relationship between the π-conjugation bridge length and NLO response has been discussed in several publications (46–49).

It is known from above analyses that the series of C_{60}PY–TTF dyads have different sources of NLO response compared with conventional push–pull organic conjugation molecules. As usual, the low-energy excited state controls the NLO response of the molecule for conventional push–pull organic conjugation molecules. In most cases, the first excited state inducing the transition from HOMO to LUMO controls the NLO response of molecule and there is no strong absorption in high-energy excited states, so β will soon converge with the number of excited state increasing. But there are strong absorptions for C_{60}PY–TTF dyads in the high-lying excited states that significantly contribute to β. The contribution to β in low-energy excited states increases as the number of ethylene bridges increase. The significant charge transfer will take place when $n > 3$ (n is the number of ethylene bridges). Unfortunately, only molecule **2** and **3** ($n = 0$, $n = 1$) were synthesized in the experiment and weak electronic transfer was observed in the IR region, which is in accordance with our calculated results.

To compare the differences between C_{60}PY–TTF dyads and conventional organic compounds, with -CHO and two-cyanovinyl groups substituting C_{60} in C_{60}PY–TTF dyads, we designed molecules **9** and **10** (see Fig. 7) and calculated their UV–vis spectra and β using the ZINDO-SOS method.

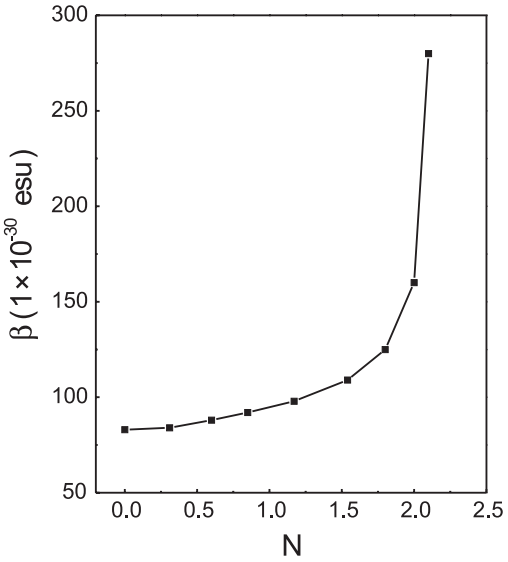
© 2001 NRC Canada

Table 4. The UV–vis spectra and β (1×10^{-30} esu) of molecules **3**, **9**, and **10**.

Molecule	λ_{cal}	λ_{exp} (20)	β (ω = 1.064 μm)[a]	β_0[a]	$\mu\beta_0$[a]	$\mu\beta_0$[b]	$\mu\beta_0$[b]	$\mu\beta_{0exp}$[c]
3			97.9	72.56	322.17			
9	471	486	10.23	8.61	39.17	10.9	34	35
10	615	633	31.81	28.32	188.95	35.0	175	234

[a]Calculated by ourselves by ZINDO-SOS method.
[b]As described in ref. 20 by FF–PM3 method.
[c]As described in ref. 20 by EFISH experiment.

Fig. 9. The relationship between β and different electric field frequencies for molecule **3**.



The calculated and observed values of these molecules are listed in Table 4.

Table 4 shows that the spectra and β of molecules **9** and **10** are in accordance with observed values and calculated values by Lucas et al. (20). This indicates that the ZINDO method is applicable to the TTF system. Figure 8 shows the β accumulation with excited states up to 50 for molecule **10**. It can be seen that the first excited state that induces the 615 nm absorption controls the NLO response and the β converges after 20 excited states. It confirms our analyses. Lucas et al. (20) showed that molecules **9** and **10** are considered excellent NLO materials with big β. Table 4 also lists the β of molecule **3**, which has a similar structure to molecules **9** and **10** and has a higher β than that of molecules **9** and **10**.

Taking molecule **3** for example, we have examined the dispersions of the β (see Fig. 9). Figure 9 displays the calculated dispersion curve for β (–2ω; ω, ω) of molecule **3** as a function of frequency (ω). The calculated data can be extrapolated to zero static quantity β (0; 0,0). We take ω = 1.064 μm (1.17 eV) in all calculations, and it is in the nonresonant area.

Conclusion

The semiempirical INDO calculations were carried out to investigate the charge-transfer interaction and to evaluate the second-order susceptibilities (β) for a series of C_{60}PY–TTF dyads. The calculated values of β are 48.78, 62.34, 97.90, 123.24, 183.78, 189.43, 193.45, 195.82 × 10^{-30} esu for C_{60}PY and C_{60}PY-(CH=CH)$_n$-TTF (n = 0–6), respectively, which shows a dramatic increase when TTF was introduced. The second-order NLO response not only comes from the contribution of the low-lying excited states but also comes from that of the high-lying ones. The NLO properties of C_{60}PY–TTF dyads can mainly be attributed to the result of electron transfer on the three-dimensional conjugation sphere of C_{60} and the electron transfer from TTF and the methine bridge to the C_{60} part. Finally, we compared the result of C_{60}PY–TTF dyads with conventional organic compounds, which were similar to the structure of C_{60}PY–TTF dyads, and found that the second-order nonlinear optical susceptibilities of C_{60}PY–TTF dyads were much higher.

Acknowledgments

This work is supported by the National Natural Science Foundation of China.

References

1. K.C. Rustagi and J. Ducuing. Opt. Commun. **10**, 258 (1974).
2. J.L. Ourdar and D.S. Chemla. J. Chem. Phys. **66**, 2664 (1977).
3. J.L. Ourdar. J. Chem. Phys. **67**, 446 (1977).
4. F. Meyers, S.R. Marder, B.M. Pierce, and J.L. Bredas. J. Am. Chem. Soc. **116**, 10 703 (1994).
5. V.P. Rao, A.K.-Y. Jen, K.Y. Wong, and K.J. Drost. Tetrahedron Lett. **34**, 1747 (1993).
6. M. Gonzalez, N. Martin, J.L. Segura, J. Garun, and J. Aorduna, Tetrahedron Lett. **39**, 3269 (1998).
7. M.S. Wong, C. Bossard, F. Pan, and P. Gunter. Adv. Mater. **8**, 677 (1996).
8. N.J. Long. Angew. Chem. Int. Ed. Engl. **34**, 21 (1995).
9. L.R. Dalton, A.W. Harper, R. Ghosn, W.H. Steier, M. Ziari, H. Fetterman, Y. Shi, R.V. Mustacich, A.K.-Y. Jen, and K.J. Shea. Chem. Mater. **7**, 1060 (1995).
10. W. Fu, J.K. Feng, K.Q. Yu, A.M. Ren, M. Cui, Y.X. Li, and C.C. Sun. Chin. J. Chem. **18**, 175 (2000).
11. J. Garin, J. Orduna, J.I. Ruperez, R. Alcala, B. Villacampa, C. Sanchez, N. Martin, J.L. Segura, and M. Gonzalez. Tetrahedron Lett. **39**, 3577 (1998).
12. G. Scheibe, W. Seiffert, G. Molneicher, C. Jutz, and H.J. Springer. Tetrahedron Lett. 5053 (1966).
13. N. Martin, L. Sanchez, C. Seoane, E. Orti, P.M. Viruela, and R. Viruela. J. Org. Chem. **63**, 1268 (1998).
14. R.C. Bong, T.J. Jong, and J.L. Seung. J. Chem. Soc. Perkin Trans. 2, 2141 (1996).
15. S.H. Kang, Y.-M. Jeon, K. Kim, S. Houbrechts, E. Hendrickx, and A. Persoons. J. Chem. Soc. Chem. Commun. 635 (1995).

© 2001 NRC Canada

16. Y. Qian, Y.M. Sun, J.Z Liu, and J.Y. Wu. Acta Chim. Sinica. **56**, 340 (1998).
17. D.R. Kanis, M.A. Ratner, and T.J. Marks. J. Am. Chem. Soc. **114**, 10 338 (1992).
18. M. Gonzalez, N. Martin, and L. Jose. Tetrahedron Lett. **39**, 3269 (1998).
19. M.H. Herranz, N. Martin, L. Sanchez, and J. Garin. Tetrahedron, **54**, 11 651 (1998).
20. A.I. de Lucas, N. Martin, L. Sanchez, and C. Seoane. Tetrahedron, **54**, 4655 (1998).
21. G.J. Ashwell, G. Jefferies, D.G. Hamilton, D.E. Lynch, M.P.S. Roberts, and C.R. Brown. Nature (London), **375**, 385 (1995).
22. C.M. Whitaker, E.V. Patterson, K.L. Kott, and R.J. McMahon. J. Am. Chem. Soc. **118**, 9699 (1996).
23. J. Li, J.K. Feng, and C.C. Sun. Int. J. Quantum Chem. **52**, 673 (1994).
24. S.H. Yang, C.L. Pettiette, J. Conceical, O. Cheshnovsky, and R.E. Smalley. Chem. Phys. Lett. **139**, 233 (1987).
25. J. Li, J.K. Feng, and C.C. Sun. J. Phys. Chem. **98**, 8636 (1994).
26. N. Martin, L. Sanchez, C. Seoane, R. Andreu, J. Garin, and J. Orduna. Tetrahedron Lett. **37**, 5979 (1996).
27. S.P. Karna, P.N. Prasad, and M. Dupuis. J. Chem. Phys. **94**,1171 (1991).
28. C.E. Dykstra and P.J. Jasien. Chem. Phys. Lett. **109**, 388 (1984).
29. J.E. Rice, R.D. Amos, S.M. Colwell, N.C. Handy, and J. Sanz. J. Chem. Phys. **93**, 8828 (1990).
30. D.R. Kanis, M.A. Ratner, and T.J. Marks. Chem. Rev. **94**, 195 (1994).
31. (*a*) J. Zyss, I. Ledoux, S. Volkov, V. Chernyak, S. Mukamel, G.P. Bartholomew, and G.C. Bazan. J. Am. Chem. Soc. **122**, 11 956 (2000); (*b*) M. Rumi, J.E. Ehrlich, A.A. Heikal, J.W. Perry, S. Barlow, Z. Hu, M.M. Dianne, T.C. Parker, H. Röckel, S. Thayumanavan, S.R. Marder, D. Beljonne, and J.-L. Brėdas. J. Am. Chem. Soc. **122**, 9500 (2000); (*c*) S.R. Marder, W.E. Torruellas, and M.B. Desce. Science (Washington, D.C.), **276**, 1233(1999); (*d*) M. Albota, D. Beljonne, J.L. Brėdas, J.E. Ehrlich, J.-Y. Fu, A.A. Heikal, S.E. Hess, T. Kogej, M.D. Levin, S.R. Marder, D.M. Maughon, J.W. Perry, H. Röckel, M. Rumi, G. Subramaniam, W.W. Webb, X.L. Wu, and C. Xu. Science (Washington, D.C.), **281**, 1653 (1998); (*e*) S.D. Bella, I.L. Fragala, M.A. Ratner, and T.J. Marks. J. Am. Chem. Soc. **115**, 682 (1993); (*f*) A. Ulman, C.S. Willand, W. Kohler, D.R. Tobello, D.J. Williams, and L. Handley. J. Am. Chem. Soc. **112**, 7083 (1990).
32. (*a*) M. Fanti, G. Orlandi, and F. Zerbetto. J. Am. Chem. Soc. **117**, 6101 (1995); (*b*) J.L. Brédas, C. Adant, P. Tackx, and A. Persoons. Chem. Rev, **94**, 243 (1994); (*c*) J. Li, J.K. Feng, and C.C. Sun. Chem. Phys. Lett. **203**, 560 (1993).
33. (*a*) W. Fu, J.K. Feng, G.B. Pan, and X. Zhang. Theor. Chem. Acc. **106**, 241 (2001); (*b*) J.K. Feng, X.S. Gao, and C.C. Sun. Chin. Sci. Bull. **35**, 2022 (1990); (*c*) X.L. Gao, J.K. Feng, and C.C. Sun. Int. J. Quantum Chem. **42**, 1747 (1992).
34. (*a*) W. Fu, J.K. Feng, and G.B. Pan. THEOCHEM. **545**, 157 (2001); (*b*) W. Fu, J.K. Feng, A.M. Ren, M. Cui, H.W. Jin, J.H. Wang, and Y.Q. Shen. Chem. J. Chin. Univ. **21**, 771 (2000); (*c*). J.K. Feng, X.L. Gao, and C.C. Sun. Acta Chim. Sin. **50**, 111 (1992).
35. (*a*) B.J. Orr and T.F. Ward. Mol. Phys. **20**, 513 (1971); (*b*) C.C. Teng and A.F. Garito. Phys. Rev. Lett. **50**, 350 (1983).
36. D.M. Bishop. Adv. Quant. Chem. **25**, 1. (1994).
37. J. Ridley and M.C. Zerner. Theor. Chim. Acta, **32**, 111 (1973).
38. C.S. Yannoni, P.P. Bernier, D.S. Bethune, G. Meijer, and J.R. Salem. J. Am. Chem. Soc. **113**, 3190 (1991).
39. J. Osterodt, M. Nieger, and F. Vögtle. J. Chem. Soc. Chem. Commun. 1607 (1994).
40. CRC Handbook of chemistry and physics. 74th ed. *Edited by* David R. Lide and H.P.R. Frederikse. pp. 9–40.
41. CRC Handbook of chemistry and physics. 74th ed. David R. Lide and H.P.R. Frederikse. pp. 9–37.
42. M. Maggini and G. Scorrano. J. Am. Chem. Soc. **115**, 9798 (1993).
43. H. Ajie, M.M. Alvarez, S.J. Anz, R.D. Beck, F. Diederich, K. Fostiropoulos, D.R. Huffman, W. Krätschmer, Y. Rubin, K.E. Schriver, D. Sensharma, and R.L. Whetten. J. Phys. Chem. **94**, 8630 (1990).
44. Y. Wang and L. Cheng. J. Phys. Chem. **96**, 1530 (1992).
45. W. Fu, J.K. Feng, K.Q. Yu, A.M. Ren, and C.C. Sun. Chin. J. Chem. **18**, 820 (2000).
46. X.L. Gao, J.K. Feng, and C.C. Sun. Int. J. Quantum Chem. **42**,1747 (1992).
47. M. Jain and J. Chandrasekhar. J. Phys. Chem. **97**, 4044 (1993).
48. C. Dehu, F. Meyers, and J.L. Brédas. J. Am. Chem. Soc. **115**, 6198 (1993).
49. M. Barzoukas, A. Fort, C. Serbutoviez, L. Oswald, and J.F. Nicoud. Chem. Phys. **153**, 457 (1991).

© 2001 NRC Canada

^{1}H NMR studies of proton transfer equilibria in hydrogen bonds — the role of the entropy

Roland Langner and Georg Zundel

Abstract: The influence of the entropy on the proton transfer equilibria AH···B ⇄ A$^-$···H$^+$B in the dimethylphosphinic acid (DMP)-*N*-base and in the methanesulfonic acid (MSA)-*N*-oxide hydrogen bonds is studied by ^{1}H NMR spectroscopy as a function of the ΔpK_a, i.e., the pK_a of the base minus the pK_a of the acid. It is shown that with increasing ΔpK_a the proton transfers to the N-oxide acceptor. In the DMP + N-base family of systems, first the double-minimum proton potentials ($\Delta H = 0$) occurs and only with further increasing ΔpK_a do the POH···N ⇄ PO$^-$···H$^+$N equilibria become symmetrical ($\Delta G = 0$). ΔG and ΔH are connected by the Gibbs–Helmholtz equation, $\Delta G = \Delta H - T\Delta S$. Hence, the reason of this effect is the large negative interaction entropy term (ΔS_I) arising from the large order around the polar structure, which shifts the equilibria strongly to the left-hand side. With the MSA-*N*-oxide hydrogen bonds a single-minimum proton potential was found. The minimum shifts with increasing ΔpK_a from the donor to the acceptor of the O···H$^+$···N hydrogen bonds. It is shown that with increasing ΔpK_a the proton potential becomes on average symmetrical, whereas the proton is still largely on the left-hand side. This result is also explained by the large negative interaction entropy due to the order of the environment if the proton is at the acceptor B.

Key words: entropy, hydrogen bonds, infrared, spectroscopy, proton transfer.

Résumé : Utilisant la spectroscopie RMN du ^{1}H en fonction du ΔpK_a, c'est-à-dire du pK_a de la base moins le pK_a de l'acide, on a étudié l'influence de l'entropie sur l'équilibre de transfert de proton AH···B ⇄ A$^-$···H$^+$B dans les liaisons hydrogènes entre l'acide diméthylphosphinique (DMP) et le N d'une base et entre l'acide méthanesulfonique (MSA) et un azote, sous la forme d'oxyde d'azote. On a montré qu'une augmentation du ΔpK_a conduit à un transfert de proton vers l'oxyde d'azote qui agit comme accepteur. Dans la famille de systèmes DMP + N-base, on observe au début un double-minimum des potentiels de protons ($\Delta H = 0$); l'équilibre POH···N ⇄ PO$^-$···H$^+$N ne devient symétrique ($\Delta G = 0$) qu'en augmentant le ΔpK_a encore plus. Les ΔG et ΔH sont liés par l'équation de Gibbs–Helmholtz, $\Delta G = \Delta H - T\Delta S$. On peut en conclure que cet effet est causé par un terme d'entropie d'interaction négative, ΔS_I, qui est très élevé et qui découle d'un ordre très important autour de la structure polaire qui déplace fortement l'équilibre vers la gauche. Avec les liaisons hydrogènes MSA – oxyde d'azote on n'a observé qu'un seul minimum. Les minima se déplacent avec une augmentation des ΔpK_a du donneur vers l'accepteur des liaisons hydrogènes O···H$^+$···N. On a montré qu'avec une augmentation du ΔpK_a, le potentiel des protons prend déjà une forme moyenne qui est symétrique même si le proton est encore principalement vers la gauche. On peut aussi expliquer ce résultat par la présence d'une entropie d'interaction fortement négative qui résulte de l'environnement si le proton se trouve au niveau de l'accepteur B.

Mots clés : entropie, liaisons hydrogènes, infrarouge, spectroscopie, transfert de proton.

[Traduit par la Rédaction]

Introduction

Acid-base equilibria (AH···B ⇄ A$^-$···H$^+$B) play an important role with all proton transfer processes. According to Huyskens et al. (1, 2), families of systems in which proton transfer occurs are characterized according to the following definitions: (*i*) all systems of a family have the same hydrogen bond donor (AH) and all acceptors (B) are also similar molecules; they only differ with regard to the pK_a of B; or (*ii*) the acceptor (B) is always the same and the donors (AH) are similar molecules, which differ only in their pK_a values. The ΔpK_a is defined as pK_a of the acceptor (B) minus the pK_a of the donor (AH) (1, 2).

The pK_a values of the donor and acceptor groups can be in the region of –2 to 10, i.e., such equilibria occur with very acidic as well as with strongly basic systems (3, 4). In systems with higher pK_a of the donors and acceptors, double-minimum proton potentials are present in the AH···B ⇄ A$^-$···H$^+$B hydrogen bonds. In systems with lower pK_a, broad flat single-minima occur in the A···H$^+$··B bonds (4). The enthalpy of the proton transfer process is represented by ΔH. When $\Delta H = 0$, both wells of the double-minimum proton potential are energetically equivalent. The free enthalpy of the proton transfer process is represented by ΔG. When $\Delta G = 0$, the nonpolar and the polar proton limiting structures have the same weight.

Received April 2, 2001. Published on the NRC Research Press Web site at http://canjchem.nrc.ca on September 20, 2001.

R. Langner and G. Zundel.[1,2] Institute of Physical Chemistry, University of Munich, Butenandstraβe 5–13, D-81377 Munich, Germany.

[1]Present address: Bruno Walter Straβe 2, A-5020 Salzburg, Austria.

[2]Corresponding author: (fax: ++43 (0) 662-642311-76; e-mail: georg_zundel@gmx.at).

 DOI: 10.1139/cjc-79-9-1376 © 2001 NRC Canada

In this study we investigate the importance of the interaction entropy (ΔS_I) for equilibria with either a typical double-minimum or a typical broad flat single-minimum proton potential family. The double-minimum family (6) are the dimethylphosphinic acid (DMP, pK_a = 3.8) + N-base systems with POH···N ⇄ PO$^-$···H$^+$N hydrogen bonds, and the broad flat single-minimum proton potential systems are the methanesulfonic acid (MSA, pK_a = –1.92) + N-oxide systems with SO···H$^+$···ON hydrogen bonds (7, 8). In the following, we compare the shape of the proton potential (double-minimum or broad flat single-minimum) with the position of the proton transfer equilibrium (50% proton transfer, i.e., symmetrical distribution of the proton in the hydrogen bonds).

Experimental

The chemicals of the highest available purity were purchased from Fluka or Aldrich. Dimethylphosphinic acid was synthesized as described by Reinhardt et al. (9). Diethylphosphinic anhydride was synthesized by heating dimethylphosinyl chloride with dimethylphosphinic acid ethyl ester under release of ethyl chloride (10). While the first component was obtained by chlorination of the acid with phosphorous pentachloride, the second component was obtained by a conversion of the acid chloride with sodium ethoxide. Diethylbenzylamine was synthesized by nucleophilic aliphatic substitution of benzyl chloride with diethylamine in boiling acetonitrile (11).

The methanesulfinic acid (0.9% water) was dried with a well-defined amount of its anhydride; a 3% excess of anhydride was added to avoid water traces arising from the complex preparation.

The N-oxides were dissolved several times in dry ethanol, followed by removal of the solvent. The bases were recrystallized from dry ethanol.

2,6-Dichloropyridine-*N*-oxide, 2,5-dichlorophyridine-*N*-oxide, 3,5-dichloropyridine-*N*-oxide, 2-chloropyridine-*N*-oxide, 3-chloropyridine-*N*-oxide, and 3-bromopyridine-*N*-oxide were synthesized by direct *N*-oxidation of the substituted pyridine with peroxotrifluoracetic acid with heating (12, 13). 2-Cyanopyridine-*N*-oxide was synthesized by the same procedure, using peroxoacetic acid (12, 13). 4-Chloropyridine-*N*-oxide was synthesized by the reaction of 4-nitropyridine-*N*-oxide with a tenfold excess of acetylchloride with ice cooling, followed by hydrolysis with ice water (14). 4-Dimethylaminopyridine-*N*-oxide was synthesized by nucleophilic aromatic substitution of 4-chloropyridine-*N*-oxide with an aqueous solution of dimethylamine in an autoclave at 150°C (14). Triethylamine-*N*-oxide was synthesized by direct *N*-oxidation of triethylamine with hydrogen peroxide (15). All preparations and transfers of the solutions were performed in a water-free glove box.

Results and discussion

The shape of the proton potential can be determined considering the wavenumber dependence of the intensity of the IR continua (4). The IR continua that extends from 3000 cm^{-1} toward smaller wavenumbers demonstrate that double-minimum proton potentials are present, whereas IR continua in the region 1600–600 cm^{-1} prove the existence of broad flat single-minimum proton potentials in the hydrogen bonds.

The dimethylphoshinic acid + N-base family of systems

Considering the shape and wavenumber distribution, as well as the intensity of the IR continua, it was shown in ref. 4 that on average the dimethylphosphinic acid + 1-methylmorpholine system displays a largely symmetrical double-minimum proton potential for the OH···N ⇄ O$^-$···H$^+$N hydrogen bonds. The ΔpK_a value of the system when ΔH = 0 amounts to 4.3 (4).

The position of the proton transfer equilibria can be determined from the IR bands (5, 6) or by NMR spectroscopy (5). With this family of systems the IR bands are often strongly masked by the IR continua, therefore, we determined the equilibria using NMR spectroscopy (Table 1). Figure 1 shows the NMR results as a function of the ΔpK_a value. The δ_{HB} values scatter strongly,and therefore, it seems that no precise information can be obtained. An analysis of the data shows, however, that a systematic course is found if one considers only the systems with N-bases having a relatively low and comparable shielding screening of the nitrogen atoms (systems 1, 4, 7, 8, 11–13, 16), indicating that the chemical shift of the proton is also influenced by sterical effects. The points of these systems (black squares) are on straight lines with a cross section at ΔpK_a = 6.5 ± 0.5. Thus, in these DMP + N-base systems 50% proton transfer occurs at ΔpK_a = 6.5 ± 0.5.

In ref. 6 we have seen that with this family of systems the double-minimum proton potential is on average symmetrical (ΔH = 0) with the DMP + 1-methylmorpholine system. The ΔpK_a of this system is 4.3 ± 0.5. Thus, with this family of systems both wells are energetically equivalent with the ΔpK_a = 4.3 ± 0.5 system. As shown above, with this family of systems only 50% proton transfer ($\Delta G°$ = 0) is found with ΔpK_a = 6.5 ± 0.5. Thus, with increasing ΔpK_a of the N-bases (ΔpK_a = 4.3 ± 0.5) the double-minimum proton potential becomes on average symmetrical (ΔH = 0), whereas the 50% proton transfer, i.e., symmetry with regard to the proton transfer equilibrium (ΔG = 0), is reached with ΔpK_a = 6.5 ± 0.5, i.e., with a system with a N-base with higher pK_a.

This result can easily be explained considering the Gibbs–Helmholtz equation. The quantities in this equation can be split (16):

$$-\Delta G = \ln K_{PT} = -\frac{\Delta H_0 + \Delta H_I}{RT} + \frac{\Delta S_0 + \Delta S_I}{R}$$

Herewith the intrinsic quantities ΔH_0 and ΔS_0 describe the behavior of the systems in gas phase. The extrinsic terms ΔH_I and ΔS_I take into account the influence of the environment. In the case of the AH···B ⇄ A$^-$···H$^+$B equilibria in liquids, Onsager's reaction field (17, 18) strongly influences the position of these equilibria. The solvate structure becomes more or less ordered and this order increases the weight of the polar structure A$^-$···H$^+$B. This order results in the large negative entropy values, shifting the equilibria strongly to the left-hand side.

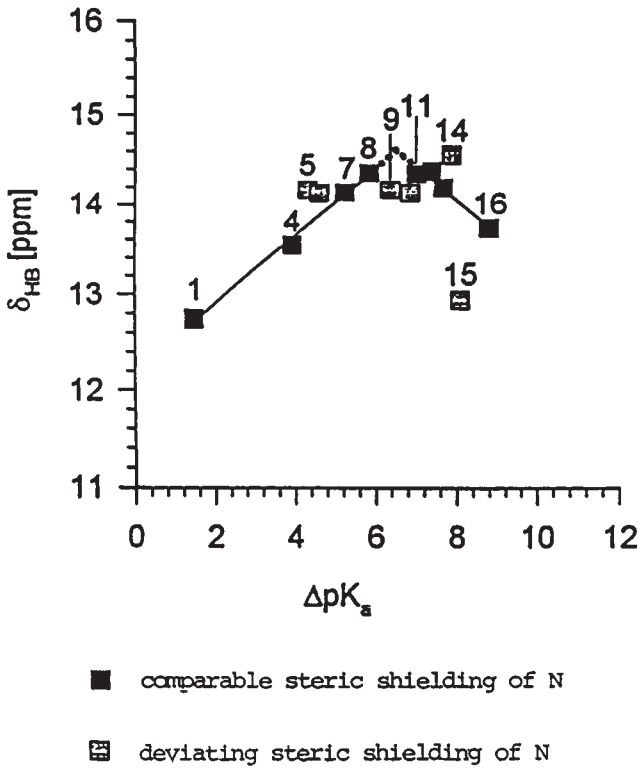
If ΔH = 0, the proton potential is on average symmetrical, i.e., both wells of the double-minimum proton potential are energetically equivalent. The negative ΔS value, however, causes the equilibria be to strongly shifted to the left-hand

© 2001 NRC Canada

Table 1. Complexes of DMP + amine (1:1).

Number	Bases	ΔpK_a	δ_{HB} (ppm)
1	DMP + cyanmethyldiethylamine	1.47	12.74
2	DMP + 1-methylbenzimidazole	2.46	(13.82)
3	DMP + 1,2-dimethylbenzimidazole	3.47	14.36
4	DMP + cyanethyldimethylamine	3.92	13.53
5	DMP + 1-methylmorpholine	4.30	14.16
6	DMP + 1-ethylmorpholine	4.59	14.12
7	DMP + triallylamine	5.23	14.13
8	DMP + dimethylbenzylamine	5.83	14.35
9	DMP + diethylbenzylamine	6.36	14.21
10	DMP + tri-*n*-butylamine	6.85	13.97
11	DMP + 1-methylpiperidine	7.00	14.34
12	DMP + diethylmethylamine	7.38	14.37
13	DMP + triethylamine	7.67	14.18
14	DMP + chinuclidine	7.87	14.55
15	DMP + 1,2,2,6,6-pentamethylpiperidine	8.11	12.93
16	DMP + 1,8-diazabicyclo[5.4.0]undec-7-en	8.82	13.72
17	DMP + 1,3,4,6,7,8-hexahydro-1-methyl-2*H*-pyrimido-[1,2-*a*]-pyrimidine	9.92	11.35

Fig. 1. Chemical shift of the hydrogen-bonded proton as a function of the ΔpK_a value of the DMP + N-base 1:1 complexes. For numbering of systems see Table 1. At 20°C (0.1 M in $CDCl_3$): (■) comparable sterical screening of *N*; (▤) deviating sterical screening of *N* (see text).



side. Thus, with increasing ΔpK_a, initially the proton potential becomes on average symmetrical ($\Delta H = 0$) and with further increasing ΔpK_a the proton transfer equilibrium becomes symmetrical ($\Delta G = 0$). The large interaction entropy term (ΔS_I) arising from the strong order of the solvent around the polar structure is responsible for this effect.

The methanesulfonic acid + N-oxide family of systems

We have considered a family of systems with double-minimum proton potentials. In the following we discuss a family with single-minimum proton potentials: the methanesulfonic acid (MSA) + N-oxide family of systems. All systems studied are summarized in Table 2. The pK_a value of methanesulfonic acid is –1.92 (19). In ref. 8 we have shown that single-minimum proton potentials are present in the $SO\cdots H^+\cdots ON$ hydrogen bonds of these systems. In the case of small ΔpK_a values a relatively narrow single-minimum is present at the donor. With increasing pK_a of the N-oxide, i.e., upon increasing ΔpK_a, this minimum not only shifts in the direction of the acceptor but also becomes very broad and flat. The systems now show large proton polarizability. In system 5 (MSA + 3,5-dichloropyridine-*N*-oxide) the IR continuum is most intense and extends the most toward smaller wavenumbers. From ref. 8 it is known that this system is the system with the most symmetrical proton potential and the largest proton polarizability. The ΔpK_a of this systems amounts to 0.98. The NMR results in Fig. 2 show, however, that the hydrogen-bonded proton is most deshielded in system 11 (MSA + 4-chloropyridine-*N*-oxide). Hence, in the system with the $\Delta pK_a = 2.25$ the hydrogen-bonded proton is equally distributed between the donor and the acceptor. Thus, also with this family of systems, upon increasing the ΔpK_a, first the proton potential becomes on average symmetrical and at systems with higher ΔpK_a values the proton is equally distributed between the donor and the acceptor.

This result is also explained by entropy (*S*). With increasing the ΔpK_a the structures become more polar, and hence, their environments become more ordered. Thus, the amount of the negative entropy increases, shifting the proton in the direction of the donor.

© 2001 NRC Canada

Table 2. Complexes of MSA + (*R*)-pyridine-*N*-oxide (1:1).

Number	Bases	ΔpK_a	δ_{HB} (ppm)
1	MSA + 2,6-dichloropyridine-*N*-oxide	–1.18	14.48
2	MSA + 2-cyanopyridine-*N*-oxide	–0.16	15.06
3	MSA + 2,5-dichloropyridine-*N*-oxide	–0.10	15.40
4	MSA + 4-nitropyridine-*N*-oxide	0.17	15.40
5	MSA + 3,5-dichlorophyridine-*N*-oxide	0.98	16.21
6	MSA + 2-chloropyridine-*N*-oxide	1.11	16.34
7	MSA + 4-acetylpyridine-*N*-oxide	1.45	—
8	MSA + 4-carbomethoxypyridine-*N*-oxide	1.51	16.70
9	MSA + 3-brompyridine-*N*-oxide	1.76	16.69
10	MSA + 3-chloropyridine-*N*-oxide	1.79	16.74
11	MSA + 4-chloropyridine-*N*-oxide	2.25	16.81
12	MSA + pyridine-*N*-oxide	2.71	—
13	MSA + 4-phenylpyridine-*N*-oxide	2.75	16.75
14	MSA + 4-methylpyridine-*N*-oxide	3.21	16.51
15	MSA + 4-methoxypyridine-*N*-oxide	5.80	14.40
16	MSA + 4-dimethylaminopyridine-*N*-oxide	5.80	14.40
17	MSA + 1-ethylmorpholine-*N*-oxide	—	12.39
18	MSA + triethylamine-*N*-oxide	7.05	12.32

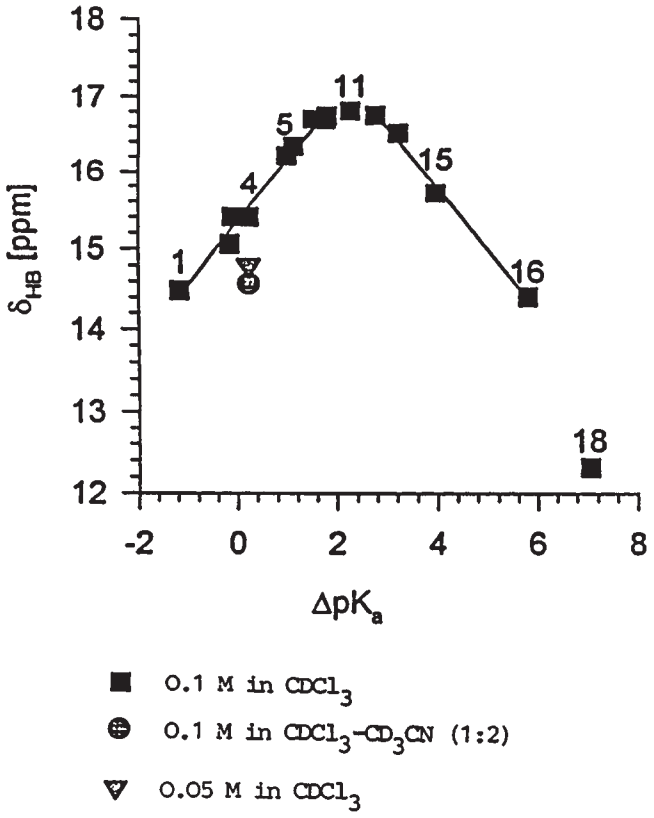


Fig. 2. Chemical shift of the hydrogen-bonded proton as a function of the ΔpK_a value of the MSA + *N*-oxide 1:1 complexes. For numbering of systems see Table 2. At 20°C (0.1 M in $CDCl_3$): (■) 0.1 M in $CDCl_3$; (⊜) 0.1 M in $CDCl_3$–CD_3CN (1:2); (▽) 0.5 M in $CDCl_3$.

Conclusions

With increasing the ΔpK_a of the dimethylphosphinic acid-*N*-oxide systems the double-minimum proton potential first becomes symmetrical ($\Delta H = 0$) and then with further increasing the ΔpK_a the $OH\cdots ON \rightleftarrows O^-\cdots H^+ON$ equilibrium becomes symmetrical ($\Delta G = 0$). The large negative interaction entropy term (ΔS_I) is responsible for this result, which is caused by the large order of the solvent around the polar structure.

A similar result is obtained for the family of the methanesulfonic acid-*N*-oxide systems. In these systems very strong $O^-\cdots H^+\cdots ON$ hydrogen bonds with single-minimum proton potential are present. With increasing the ΔpK_a the proton potential first becomes symmetrical, very broad, and flat. With further increasing the ΔpK_a the distribution of the proton in the hydrogen bonds becomes symmetrical. Again, the entropy interaction is responsible for this effect.

References

1. P. Huyskens and Th. Zeegers-Huyskens. J. Chem. Phys. **61**, 81 (1964).
2. P. Huyskens and G. Fernandez. Ind. Chim. Belg. **38**, 1237 (1973).
3. R. Lindemann. J. Chem. Soc. Faraday Trans. 2, **73**, 788 (1977).
4. R. Langner and G. Zundel. J. Phys. Chem. A, **102**, 6635 (1998).
5. G. Zundel. *In* Advances in chemical physics. Vol. 11. John Wiley & Sons, Chicago. 2000. pp. 1–218.
6. G. Zundel. *In* The hydrogen bond — recent developments in theory and experiments. Vol. 2. *Edited by* P. Schuster, G. Zundel, and C. Sandorfy. Elsevier, Amsterdam. 1976. Chap. 15.
7. R. Langner and G. Zundel. J. Phys. Chem. A, **99**, 12214 (1995).
8. R. Langner and G. Zundel. J. Chem. Soc. Faraday Trans. **94**, 1805 (1998).
9. H. Reinhardt, D. Bianchi, and D. Mölle. Chem. Ber. **90**, 1656 (1957).
10. G.M. Kosolapoff and R.M. Watson. J. Am. Chem. Soc. **73**, 5466 (1951).

© 2001 NRC Canada

11. R. Hemmer and W. Lürken. *In* Methoden der Organischen Chemie (Houben Weyl). Vol. E16d. *Edited by* D. Klamann and G. Thieme. Verlag, Stuttgart. 1992. p. 665.
12. A. Albini and S. Pietra. Heterocyclic N-oxides. CRC-Press, Boca Raton. 1991.
13. R.A. Abramovich and E.M. Smith. *In* Heterocyclic compounds. Vol. 14. *Edited by* R.A. Abramovitch. John Wiley & Sons, New York. 1974. Part 2. p. 1.
14. A.R. Katritzky, E.W. Randall, and L.E. Sutton. J. Chem. Soc. 1769 (1957).
15. H. Freytag. *In* Methoden der Organischen Chemie (Houben Weyl). Vol. 11. *Edited by* E. Müller and G. Thieme. Verlag, Stuttgart. 1958. Part 2. p. 190.
16. J. Fritsch and G. Zundel. J. Phys. Chem. **88**, 6295 (1984).
17. L. Onsager. J. Am. Chem. Soc. **58**, 1436 (1936).
18. J. Maleki. *In* Molecular interactions. *Edited by* H. Ratajczak and W.J. Orville-Thomas. John Wiley & Sons, London. 1982. Chap. 4.
19. A.K. Covington and R. Tompson. J. Solution Chem. **3**, 603 (1974).

© 2001 NRC Canada

Reanalysis of the biotransformation of 4(20),11(12)-taxadiene derivatives

Di-An Sun, Françoise Sauriol, Orval Mamer, and Lolita O. Zamir

Abstract: Reanalysis of the biotransformation of 4(20),11(12)-taxadiene derivatives by *Absidia coerulea* ATCC 10738a unravelled additional unprecedented rearrangement reactions. 5α,7β,9α,10β,13α-pentaacetoxy-4(20),11(12)-taxadiene (**1**) was converted to 10 new minor taxane derivatives in addition to the previously reported C-1, C-14-hydroxylations and C-15-hydroxylated *abeo*-taxane. In addition, 2-deacetoxytaxinine J (**2**) was successfully metabolized with the same fungi.

Key words: natural products, terpenes and terpenoids, microorganism, oxygenation, rearrangement.

Résumé : Une étude approfondie de la biotransformation des dérivatifs du 4(20),11(12)-taxadiene par *Absidia coerulea* ATCC 10738a a décelé des produits additionnels provenant de réarrangement chimiques. Le 5α,7β,9α,10β,13α-pentaacetoxy-4(20),11(12)-taxadiene (**1**) a été converti en 10 nouveaux dérivés de taxane minoritaires en plus des hydroxylations en C-1, C-14 et de la formation d'un 15-hydroxy-*abeo*-taxane déjà publiés. De plus, le métabolisme du 2-deacetoxytaxinine J (**2**) par le même microorganisme est décrit.

Mots clés : produits naturels, terpènes et terpénoides, microorganisme, hydroxylations, réarrangements chimique.

Introduction

Continuing investigation of the biotransformation of taxane derivatives has shown that a minor variation in the structure can lead to substantially different products (1–16). Substitution patterns of 4(20),11(12)-taxadiene derivatives as well as incubation conditions led to different metabolites. It was reported (4) that a C-5 cinnamoyl group in taxanes, such as 2-deacetoxytaxinine J, taxinine J, taxinine, prevented their metabolism with various microorganisms. We have recently found (17) that when 2-deacetoxytaxinine J is deacetylated at C-7, C-9, and C-10, it is readily biotransformed despite the presence of the C-5-cinnamoyl group. Differently substituted taxanes were metabolized to a taxane with a C10-C11 double bond or unprecedented 1(15→11)*abeo*-taxanes (18). The microbial transformation of 5α,7β,9α,10β,13α-pentaacetoxy-4(20),11(12)-taxadiene with *Absidia coerulea* was reported (4) to give high yields of C-1 (39%) and C-14 (26%) hydroxylation products. In addition, these authors (4) found that 2-deacetoxytaxinine J, which differs from the previous substrate by a cinnamoyl on C-5 instead of an acetyl, could not be metabolized by 25 collected fungi including *A. coerulea* (12).

In this publication, we have reevaluated the metabolism of 5α,7β,9α,10β,13α-pentaacetoxy-4(20),11(12)-taxadiene and found additional products, some of them with unprecedented or rare functionalities, albeit in very low yields. In addition, we succeeded in hydroxylating 2-deacetoxytaxinine J at C-1 (7% yield) and at C-14 (12% yields) with *A. coerulea* ATCC 10738a along with two minor products.

Received April 12, 2001. Published on the NRC Research Press Web site at http://canjchem.nrc.ca on September 20, 2001.

D.-A. Sun and L.O. Zamir.[1] Human Health Research Center, INRS-Institut Armand-Frappier, Université du Québec, 531 boul. des Prairies, Laval, QC H7V 1B7, Canada.
F. Sauriol. Department of Chemistry, Queen's University, Kingston, ON K7L 3N6, Canada.
O. Mamer. Biomedical Mass Spectrometry Unit, McGill University, 1130 Pine Avenue West, Montréal, QC H3A 1A3, Canada.

[1]Corresponding author at McGill Centre for Translational Research in Cancer, Sir Mortimer B. Davis-Jewish General Hospital, 3755 Cote Ste. Catherine Rd., Suite D-127, Montréal, QC H3T 1E2, Canada (telephone: (450) 687-5010 ext. 4260; fax: (450) 686-5501 / (514) 481-2797; e-mail: lolita.zamir@inrs-iaf.uquebec.ca).

Results and discussion

Substrates, fungi, incubation conditions

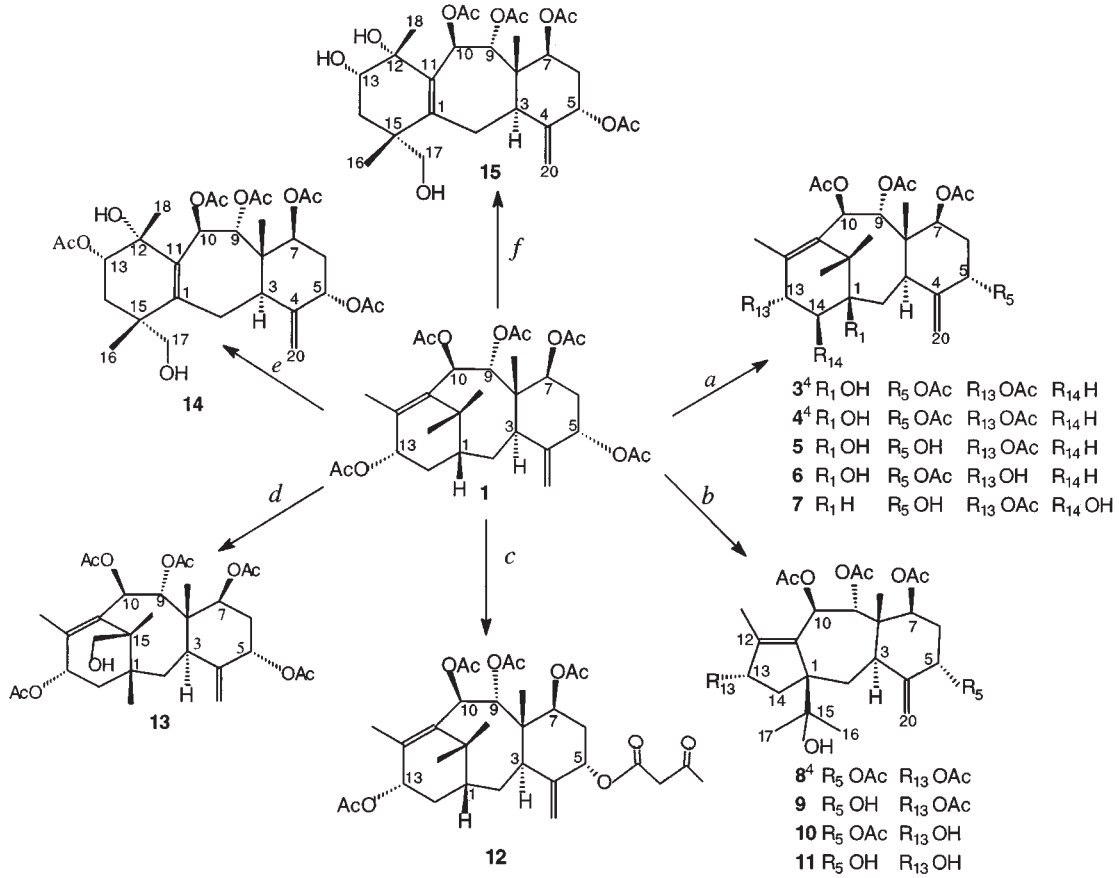
The substrate **1** (4, 19, 20) was obtained by semisynthesis from 2-deacetoxytaxinine J (21) by decinnamoylation (22) followed by acetylation. The fungi used in this work was obtained from ATCC and might slightly differ from the Chinese strain used by previous workers (4, 6, 7). The media used for the growth of the culture is also different (6, 7). The isolation and purification of the taxanes obtained from incubation of the substrates **1** and 2-deacetoxytaxinine J (**2**) with *A. coerulea* ATCC 10738a involved chromatographic techniques (flash and thin layer) as well as preparative HPLC.

Characterization of taxanes 3–7 (Scheme 1)

As expected from previous results (4), incubation of the substrate **1** with *A. coerulea* ATCC 10738a led to C-1-hydroxylation, taxane **3**, C-14-hydroxylation, taxane **4** as well as the *abeo*-taxane **8**. Their NMR and mass spectra data

 DOI: 10.1139/cjc-79-9-1381 © 2001 NRC Canada

Scheme 1. Microbial transformation products and yields of taxane **1** by fungi *A. coerulea* ATCC 10738a. (*a*) Yield (%): taxane **3** (9.9), taxane **4** (7), taxane **5** (1.4), taxane **6** (0.3), taxane **7** (0.2). *(b)* Yield (%): taxane **8** (3.1), taxane **9** (0.1), taxane **10** (0.2), taxane **11** (0.3). *(c)* Yield (%): taxane **12** (0.8). *(d)* Yield: taxane **13** (0.2). *(e)* Yield: taxane **14** (0.4). *(f)* Yield (%): taxane **15** (0.1).



were identical to the literature values (4). In addition, taxanes **5**–**7** were isolated. The ^{1}H NMR data of taxanes **5** and **3** (4) are very similar except for the chemical shift of H-5. The chemical shift of H-5 in taxane **5** is shielded compared to taxane **3** (4.27 vs. 5.36 ppm), suggesting the presence of an acetoxy group in **3**. The respective FAB-HRMS data for both compounds confirm that indeed taxane **5** is 7β,9α,10β,13α-tetraacetoxy-1β,5α-dihydroxy-14(20),11(12)-taxadiene. Similarly, taxane **6** differs from **3** (4) only in H-13, which is attached to an OH instead of an acetoxy group. The structure of **6** is therefore 5α,7β,9α,10β-tetraacetoxy-1β,13α-dihydroxy-4(20),11(12)-taxadiene. The NMR data of taxane **7** differ from the known taxane **4** (4) only in H-5. Here too, we see a deacetylation at C-5 (H-5 of **7** 4.27 ppm whereas 5.36 ppm for **4**). The structure of taxane **7** is 7β,9α,10β,13α-tetraacetoxy-5α,14β-dihydroxy-4(20),11(12)-taxadiene.

Characterization of 11(15→1)*abeo*-taxanes 8–11 (Scheme 1)

The 11(15→1)*abeo*-taxanes isolated were easily characterized because they differed from the known compound **8** (4) by a deacetylation at C-5 (taxane **9**), C-13 (taxane **10**), and at C-5 and C-13 (taxane **11**). The NMR data as well as the FAB-HRMS confirm these results. The structure of taxane **9** is therefore 7β,9α,10β,13α-tetraacetoxy-5α-hydroxy-11(15→1)*abeo*-4(20),11(12)-taxadiene. The structure of taxane **10** is 5α,7β,9α,10β-tetraacetoxy-13α-hydroxy-11(15→1)*abeo*-4(20),11(12)-taxadiene and of taxane **11** is 7β,9α,10β-triacetoxy-5α,13α-dihydroxy-11(15→1)*abeo*-4(20),11(12)-taxadiene.

Characterization of taxane 12 with an unprecedented β-keto-butyrate substitution at C-5 (Scheme 1, Table 1)

The only difference between taxane **12** and taxane **1** is the replacement of an acetoxy group by the unusual O-CO-CH_2-CO-CH_3. This group is indicated by the presence of two deshielded proton resonances (3.65 and 3.47 ppm, J = 15.6 Hz) correlated to a single carbon (49.8 ppm) and an extra methyl singlet appearing at a shift characteristic of a methyl next to a ketone (2.30 ppm). The methylene protons shows HMBC correlations to two carbonyls: an ester and a ketone (165.7, 200.1), while the methyl group shows correlation to the ketone carbon. The positioning of that group at 5 is supported by the observation of long range NOE between the methyl-18 and the methylene protons. Such NOE is always observed between cinnamoyl group and methyl-18 due to the U-shape of the molecule. The other evidence is that all the protons of taxane **12** appear at very similar shifts from those of taxane **1** with the exception of H-5, which has a 0.08 ppm downshift of 5.46 ppm from 5.38 ppm of the taxane **1**.

© 2001 NRC Canada

Table 1. ^{1}H and ^{13}C NMR data for **12**.

Position	δ ^{1}H NMR multiplicity[a] (*J* (Hz))	δ ^{13}C NMR[b]	HMBC	NOESY[c]
1	1.87 o, m	40.4		2b (s), 9 (s), 14a (s), 16 (w), 17 (s), 19 (m)
2a	1.90 o, m	27.4		2b (s)
2b	1.76 m			2a/1 (s), 20b (s)
3	2.88 br d (5.3)	37.8		7 (s), 14b (s), 18 (w), 19 (w)
4	—	—		
5	5.46 br s	75.6		6a (w), 6b (m), 20a (s)
6a	2.02 m	34.0		5 (w), 6b (s), 7 (w)
6b	1.84 m			5 (m), 6a (s), 19 (s)
7	5.52 dd (11.5, 4.7)	69.9		3 (s), 6b (s), 10 (s), 18 (m)
8	—	46.1		
9	5.90 d (11.0)	76.7	7, 8, 10, 19, 169.7	1/2a (m), 17 (s), 19 (m)
10	6.21 d (11.0)	71.4	9, 11, 12, 15, 168.8	7 (s), 18 (s)
11	—	—		
12	—	137.1		
13	5.94 br t (≈ 9.2)	70.4		10 (w), 14a (m), 16 (s), 17 (m), 18 (w)
14a	2.65 dt (14.1, 9.8, 9.8)	31.1	12	1/2a (s), 13 (s), 14b (s), 16 (w)
14b	1.0			3 (m), 14a (s)
15	—	39.4		
16	1.13 s	31.1	1, 11, 15, Me	1/2a (w), 13 (s), 14a (w), 17 (s)
17	1.62 s	27.4	1, 11, 15, Me	1/2b (s), 9 (s), 16 (s)
18	2.14 s	15.1	11, 12, 13	3 (w), 7 (s), 10 (s), 13 (w), Ac(3.65) (w)
19	0.84 s	13.3	3, 7, 8, 9	9 (s), 2a/1 (s), 6b (s)
20a	5.31 s	116.1		5 (s), 20b (s)
20b	4.98 s		3	2b (s), 20a (s)
OAc	2.10 s	21.2	169.8	
	2.06 s	20.9	169.5	
	2.02 s	20.4	169.8	
	1.97 s	20.6	168.9	
CO		165.7		
CH_2-	3.65 d (15.6)	49.8	200.1, 165.7	18 (w), OAc (2, 10) (w)
CO	3.47 d (15.6)	200.1		18 (w), OAc (2, 10) (w)
Me	2.30 s	30.2	200.1	

[a]Multiplicity: br (broad), s (singlet), d (doublet), t (triplet), m (multiplet), o (overlapping). The precision of the coupling constants is ±0.25 Hz.
[b]The ^{13}C NMR chemical shifts were extracted from the HSQC and HMBC (for quaternary carbons) experiments (±0.2 ppm).
[c]NOESY intensities are marked as strong (s), medium (m), or weak (w).

Characterization of 16-hydroxylated taxane 13 (Scheme 1, Table 2)

The original four methyls in taxane **1** have been replaced by three methyl singlets and two doublet resonances at 3.70 ppm (11.6 Hz, 1H) and 3.19 ppm (11.6 Hz, 1H), suggesting the insertion of an oxygen in one of the methyls. The appearance of a resonance at 70.0 ppm in the ^{13}C NMR data of taxane **13** confirmed this structure. This new carbon is correlated to those two protons in the HSQC experiment confirming the presence of a CH_2OH group. To assign unambiguously which methyl was hydroxylated, the HMBC experiment was used. This experiment shows that the most deshielded methyl (2.25 ppm) can be assigned to methyl-18 as we observe correlations to the usual C-11, C-12, and C-13. In HMBC, we further note that the methyl appearing at 1.72 ppm can be assigned to methyl-17 as we observe correlations to C-1, C-11, and C-15. This methyl is further correlated to the new hydroxylated carbon (at 70 ppm) confirming that the hydroxylation took place on methyl-16. A correlation between the proton-16 at 3.19 ppm with carbon-11 further confirm the assignment. The NOESY experiment unambiguously determined that the hydroxylation is at 16. Indeed H-13 has a correlation with H-16a and H-16b as well as with H-18. It is interesting to note that this unprecedented hydroxylation on C-16 follows a report in our laboratory of a C-17-hydroxylation (18).

Characterization of taxanes 14 and 15 with an unusual core skeleton (Scheme 1)

The structure of the taxanes **14** and **15** has a very unusual rearranged core. Their structures were determined unambiguously using the usual 2D NMR approach as described below.

*Taxane **14** (Table 3)*

At first, the spectrum of taxane **14** is not that different from the one obtained for regular taxanes. We note the presence of three methyl singlets (more shielded than usual), an *exo*-methylene from H-20, the usual H-7 and H-5 coupled to the methylene protons H-6*a* and H-6*b* and the pair of doublets for H-9 and H-10 coupled together. On the A-ring, H-13 is coupled to the methylene assigned to H-14, as expected. The presence of an extra CH_2OH group is deduced from the

© 2001 NRC Canada

Table 2. ^{1}H and ^{13}C NMR data for **13**.

Position	δ ^{1}H NMR multiplicity[a] (*J* (Hz))	δ ^{13}C NMR[b]	HMBC	NOESY[c]
1	1.99 o, m	35.7		
2a	1.90 o, m	26.7		
2b	1.82 o, m			
3	2.93 d (5.9)	38.0		7 (s), 14b (m), 18 (w)
4	—	—		
5	5.39 br s	74.6		6b (w), 20a (s)
6a	1.95 o, m	34.3		
6b	1.80 o, m			
7	5.55 dd (5.0, 11.4)	69.7		3 (s), 10 (s), 18 (s)
8	—	45.5		
9	5.91 d (11.2)	76.7	7, 8, 10, 170.1	2a (w), 17 (s), 19 (m)
10	6.14 d (11.2)	72.0	9, 11, 12, 15	7 (m), 18 (s)
11	—	131.7		
12	—	138.8		
13	5.84 br t (9.5)	70.1		16a (s), 16b (m), 18 (w)
14a	2.62 dt (14.5, 10.6, 10.6)	30.9		1 (w), 13 (w), 14b (s)
14b	1.064 dd (14.5, 7.4)			1 (w), 3 (s), 13 (w), 14a (s)
15	—	45.5		
16a	3.70 d (11.6)	70.0		13 (s), 16b (s), 17 (w)
16b	3.19 d (11.6)		11	13 (m), 16a (s), 17 (m)
17	1.72 s	23.0	1, 11, 15, 16	1 (m), 9 (s), 16a (w), 16b (s)
18	2.25 s	15.1	11, 12, 13	3 (w), 7 (w), 10 (s)
19	0.86 s	13.3	3, 7, 8, 9	2b/6b (w), 9 (m), 20b (w)
20a	5.29 s	115.8	5	5 (m), 20b (s)
20b	4.97 s			2b/6b (m), 20a (s)
OAc	2.18 s	21.5	169.6	
	2.07 s	21.2	170.3	
	2.06 s	20.8	169.3	
	2.03 s	20.8	170.1	
	1.97 s	21.0	169.8	

[a]Multiplicity: br (broad), s (singlet), d (doublet), t (triplet), m (multiplet), o (overlapping). The precision of the coupling constants is ±0.25 Hz.
[b]The ^{13}C NMR chemical shifts were extracted from the HSQC and HMBC (for quarternary carbons) experiments (±0.2 ppm).
[c]NOESY intensities are marked as strong (s), medium (m), or weak (w).

appearance of two protons (3.45 (d), 11.0 Hz and 3.20 (d) 11.0 Hz) correlated to a single carbon in the HSQC experiment (68.4 ppm). The most striking evidence that we are dealing with a very different structure derives from the HMBC experiment. The methyl appearing at 1.00 ppm can be assigned to methyl-19 as it is correlated to the usual C-3, C-7, C-8, and C-9. The greatest surprise came from the other two methyls, as neither of them is correlated to two olefinic carbons as would be expected from methyl-18.

Both of these methyls are correlated to different olefinic carbons. The methyl appearing at 1.15 ppm has been assigned to methyl-18 on the basis of its correlation to the hydroxylated C-13. This methyl is also correlated to an oxygenated quaternary carbon (C-12, 70.8 ppm) and to an olefinic quaternary carbon at 134.7 ppm. The other methyl, appearing at 1.09 ppm shows correlation to C-15 quaternary carbon (at 43.4 ppm), C-14 methylene carbon, the new CH_2OH group (68.4 ppm), and to another quaternary olefinic carbon (at 145.6 ppm). The 134.7 ppm olefinic carbon is also correlated to H-9, H-10, and H-2a, while the other olefinic carbon (145.6 ppm) is correlated to H-2a, H-10, and to the protons from the extra CH_2OH group. Such observations are only compatible with an olefinic double bond at the junction of ring A and B as shown on the structure in Scheme 1. The extra CH_2OH group is then assigned to C-17. The presence of an OH group on C-17 was confirmed by the observation of a coupling between the two H-17 protons and a hydroxyl group in an earlier spectrum.

The stereochemistry of that unusual compound can be deduced from the coupling constants and the NOESY experiment. A possible model is shown in Fig. 1. We will first consider the stereochemistry of rings B and C. The very large coupling constant observed between H-2a and H-3 (11.1 Hz) can be explained by a trans diaxial orientation of these two protons. The axial orientation of methyl-19 at the junction of ring B and C is confirmed by the strong NOE observed between H-2a and Me-19. The axial methyl 19 also has NOE with the axial proton H-6b and the equatorial proton H-9 (*cis* respect to Me-19). The lack of NOE between H-10 and Me-19 indicates a *trans* relationship between these two groups, which suggests that H-10 has a *trans* equatorial orientation. The *trans* diequatorial orientation of H-9 and

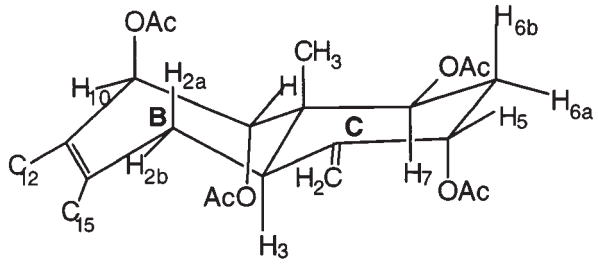
© 2001 NRC Canada

Table 3. ^{1}H and ^{13}C NMR data for **14**.

Position	δ ^{1}H NMR multiplicity[a] (*J* (Hz))	δ ^{13}C NMR[b]	HMBC	NOESY[c]
1	—	145.6		
2a	2.65 dd (11.1, 14.2)	23.4	1, 8, 11	2b (s), 19 (m), 20b (w)
2b	2.2 o, m			2a (s), 3 (m), 16 (m), 17a (m), 20b (m)
3	2.79 d (11.1)	35.9		2a (m), 2b (m), 7 (s), 17a (w)
4	—			
5	5.33 br s	74.1		6a (s), 20a (s), 6b (w)
6a	2.10 o, m	31.6		6b (s), 5/7 (w)
6b	1.74 m			6a (s), 5 (w), 19 (s)
7	5.32 o, dd (11.2, 5.0)	70.1		
8		45.7		
9	5.14 d (6.6)	68.6	3, 10, 11, 169.1	10 (s), 19 (s)
10	5.84 d (6.6)	67.4	1, 8, 9, 11, 12, 169.1	9 (s), 18 (s)
11	—	134.7		
12	—	70.8		
13	4.84 dd (3.6, 12.3)	73.6		14b (w), 18 (m), 16 (m)
14a	2.27 t (12.4)	32.1		14b (s)
14b	1.50 dd (3.6, 12.4)		12, 13, 15	13 (s), 14a (s), 16 (m)
15	—	43.4		
16	1.09 s	21.2	1, 14, 15, 17	2b (s), 13 (s), 17a (m), 17b (m), 14b (s)
17a[d]	3.45 d (11.0)	68.4	1, 14, 16	17b (s), 16 (s), 2b (s), 3 (m)
17b	3.20 d (11.0)		1, 14	17a (s),16 (s)
18	1.15 s	23.3	11, 12, 13	10 (s), 13 (s)
19	1.00 s	10.7	3, 7, 8, 9	2a (s), 6b (s), 9 (s)
20a	5.27 s	113.4	5	5 (s), 20b (s)
20b	4.93 s		3, 5	2b (s), 20a (s)
OAc	2.11 s	21.1		
	2.09 s	21.1		
	2.07 s	21.1		
	2.01 s	20.9		
	1.98 s	20.9		

[a]Multiplicity: br (broad), s (singlet), d (doublet), t (triplet), m (multiplet), o (overlapping). The precision of the coupling constants is ±0.25 Hz.
[b]The ^{13}C NMR chemical shifts were extracted from the HMQC and HMBC (for quaternary carbons) experiments (±0.2 ppm).
[c]NOESY intensities are marked as strong (s), medium (m), or weak (w).
[d]The shifts and *J* value of 17a and 17b in another spectra are 3.45 dd (10.7, 3.2) and 3.2 dd (10.7, 7.3), respectively. In that spectra, the OH-17 is located at 1.46 dd (7.3, 3.2).

Fig. 1. Stereochemistry of the unusual taxane skeleton of **14** and **15**.



H-10 is supported by a smaller coupling between these two protons (6.6 Hz). The H-7 on the C-ring is in the axial orientation as can be deduced from the large coupling (11.2 Hz) with one of its H-6 neighbours. Due to the small couplings observed for H-5 with the neighboring methylenic protons H-6a/H-6b, this proton must be in the equatorial orientation. The NOE observed between H-3 and H-7 confirms their *cis*-α-orientation. For the A-ring, the NOE observed between the H-3α and the H-17a proton (3.45 ppm) suggests that the C-17 methylene group is in the α-orientation. The large NOE between the proton at position 13 (4.84 ppm) and the β-Me-16 supports a β-orientation. Finally methyl-18 is probably also β because of its large NOE with β-H-13. The NOE between methyl-18 and H-10 can be interpreted as an interaction between these pseudoequatorial Me-18 and H-10, which are spatially close.

*Taxane **15** (Table 4)*

This taxane is very similar to the previous one, the main difference being in the chemical shift observed for H-13, which is much more shielded (3.72 ppm) than in taxane **14** (4.84 ppm). This difference has been attributed to the fact that H-13 is now substituted by an OH group instead of an acetoxy.

Biotransformation of 2-deacetoxytaxinine J (Scheme 2)

We were surprised that the incubation of 2-deacetoxytaxinine J (**2**) with *A. coerulea* ATCC 10738a led to three products. Indeed, it had been reported that 2-deacetoxytaxinine J could not be metabolized by a Chinese species of *A. coerulea* (4).

In metabolite **16** (Table 5), H-1 (at 1.85 ppm) has disappeared and H-14a has a different pattern. It is now coupled to two protons instead of three (H-14a at 2.55 ppm dd,

© 2001 NRC Canada

Table 4. ^{1}H and ^{13}C NMR data for **15**.

Position	δ ^{1}H NMR multiplicity (*J* (Hz))[a]	δ ^{13}C NMR[b]
1	—	
2a	2.63 dd (10.4, 14.7)	23.5
2b	2.11 o, m	
3	2.76 d (10.1)	36.6
4	—	
5	5.33 t	74.3
6a	2.11 o, m	31.6
6b	1.72 m	
7	5.28 o, dd (5.2, 11.4)	70.2
8	—	
9	5.18 d (6.2)	69.3
10	5.61 d (6.2)	69.2
11	—	
12	—	
13	3.72 dd (4.0, 12.1)	72.2
14a	1.96 o, m	36.3
14b	1.65 m	
15	—	
16/18/19	1.02 s	22.7
17a	3.46 d (10.9)	68.5
17b	3.20 d (10.9)	
18/17/19	1.16 s	21.2
19/17/18	1.13 s	11.4
20a	5.27 s	113.6
20b	4.95 s	
OAc	2.11 s	21.1
	2.06 s × 2	20.9
	1.976 s	20.8

[a]Multiplicity: br (broad), s (singlet), d (doublet), t (triplet), m (multiplet), o (overlapping). The precision of the coupling constants is ±0.25 Hz.
[b]The ^{13}C NMR chemical shifts were extracted from the HSQC.

9.8 Hz, 14.9 Hz). Moreover, the chemical shift of H-14b is 1.52 ppm instead of 0.98 ppm for 2-deacetoxytaxinine J **2**. The most convincing evidence for the oxygenation at C-1 is the additional quaternary carbon at 75.6 ppm obtained from HMBC, where H-14ab, H-16, and H-17 correlate to this carbon. This value is in accordance with other C-1 β-hydroxylations (4, 18). The structure for taxane **16** is therefore 1-β-hydroxy-2-deacetoxytaxinine J. High resolution mass spectra confirmed the elemental composition of the sodiated quasimolecular ion of taxane **16**.

*Taxane **17** (Table 6)*

In the ^{1}H NMR data of taxane **17**, the resonances corresponding to 14a and 14b have disappeared, while an oxygen-bearing methine signal appeared at 3.52 ppm. Confirmation was obtained by the resonance at 79.2 ppm in the ^{13}C NMR (Table 6). The stereochemistry of the 14-hydroxyl group was determined to be β by the NOESY experiment. Indeed, H-14 correlated with H-3 and H-7 correlates with H-3. High resolution mass spectra confirmed the elemental composition of the sodiated quasimolecular ion of taxane **17**.

*Taxane **18** (Table 7)*

The ^{1}H NMR data of taxane **18** showed the presence of an *abeo*-taxane with four C-methyls (0.91, 1.11, 1.30, 1.95 ppm) and four acetyls (1.51, 1.97, 1.99, 2.07 ppm). The 11(15→1)-*abeo*-taxane structure was confirmed by the newly introduced carbon at 62.6 ppm and the carbon at 75.4 ppm which are attributed to C-1 and C-15, respectively. Additional HMBC correlations of the protons of Me-16/Me-17 (1.11 and 1.30 ppm) with C-1 (62.6 ppm) and C-15 (75.4 ppm), and Me-16/Me-17 (27.0 and 24.9 ppm) support this structure. The positioning of the other groups are very similar to the starting material; ie, a *trans*-cinnamoyl on C-5 and four acetyls on C-7, C-9, C-10, and C-13. The relative stereochemistry of taxane **18** was determined from the NOESY experiment. High resolution mass spectra confirmed the elemental composition of the sodiated quasimolecular ion of taxane **18**.

Taxane **19** is easily characterized as 13-deacetyl-2-deacetoxytaxinine J by comparison with the NMR data of the substrate 2-deacetoxytaxinine J. The detailed NMR data are described in the *Experimental* section. High resolution mass spectra confirmed the elemental composition of the sodiated quasimolecular ion of taxane **19**.

Experimental

Instrumentation

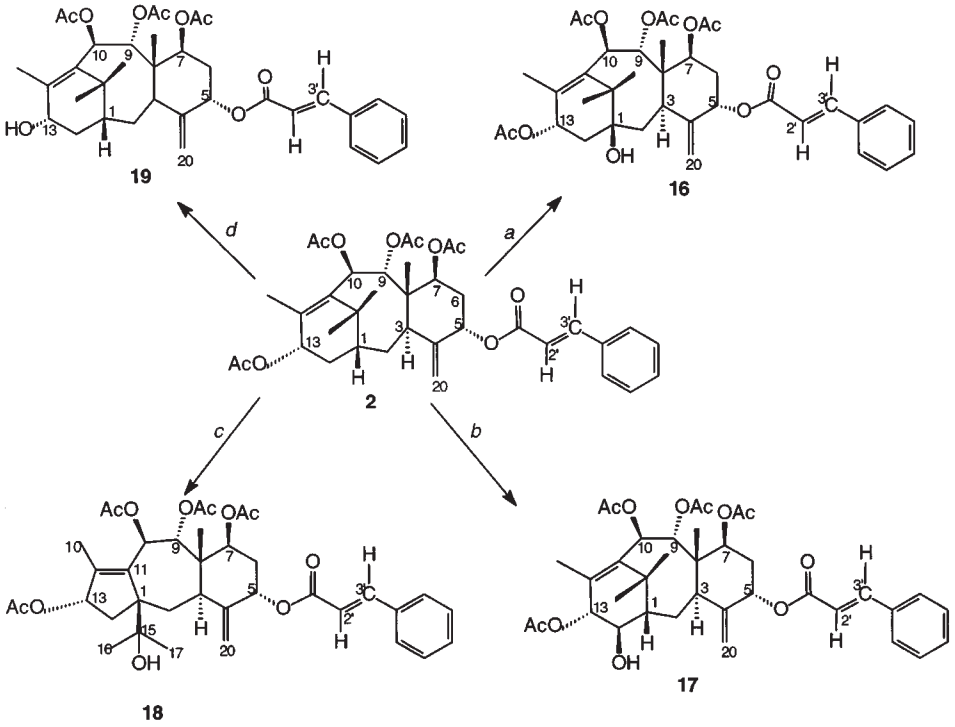
Flash chromatography was performed on Silica gel 60 (230–400 mesh EM Science). Thin layer chromatography was conducted on Silica Gel 60 F254 precoated TLC plates (0.25 mm, EM Science). The compounds were visualized on TLC plates with 10% sulfuric acid in ethanol and heating on a hot plate. Na_2SO_4 was the drying agent used in all work up procedures. Analytical HPLC was performed on a Waters 600 FHU delivery system coupled to a PDA 996 detector. Preparative and semipreparative HPLC were carried out on a Waters Delta Prep 3000 instrument coupled to a UV 486 Tunable Absorbance detector set at 227 nm (Waters, Montreal, Quebec, Canada). Analytical HPLC was performed with two Whatman partisil 10 ODS-2 analytical columns (4.6 × 250 mm) in series. Semipreparative HPLC was performed with two Whatman partisil 10 ODS-2 Mag-9 semipreparative columns (9.4 × 250 mm) in series. Preparative HPLC was performed with one partisil 10 ODS-2 MAG-20 preparative column (22 × 500 mm). The products were eluted with a 50 min linear gradient of acetonitrile (25–100%) in water at a flow rate of 18 mL min^{-1} (preparative HPLC) and 3 mL min^{-1} (semipreparative HPLC). All the reagents and solvents were of the best available commercial quality and were used without further purification.

NMR and mass spectrometry measurement

All the NMR data were obtained at room temperature on a Bruker Avance-500 spectrometer operating at 500.13 MHz for proton and at 125.77 MHz for carbon-13. The solvent $CDCl_3$ was used as an internal reference (7.25 ppm for proton and 77.0 ppm for carbon-13). The various 2D spectra were acquired and processed using standard procedures. For phase-sensitive 2D experiments (NOESY and HSQC), the data were acquired using the TPPI phase mode. The NOESY experiment was obtained using a mixing time of 0.3 s and a

© 2001 NRC Canada

Scheme 2. Microbial transformation products and yields of 2-deacetoxxytaxinine J by fungi *A. coerulea* ATCC 10738a. (*a*) Yield (%): taxane **16** (6.9). (*b*) Yield (%): taxane **17** (11.5). (*c*) Yield (%): taxane **18** (3.3). (*d*) Yield (%): taxane **19** (0.5).



relaxation delay of 1 s. The intensity of the cross-peaks in the NOESY experiment is designated as strong (s), medium (m), and weak (w). Positive ion fast atom bombardment mass spectra (FAB-MS) were obtained with a Vacuum Generators ZAB-HS double-focussing instrument using a xenon beam having 8 kV energy at 1 mA equivalent neutral current. Low-resolution mass spectra were obtained in glycerol. Samples were dissolved in 0.2 μL DMSO before addition of 0.5 μL glycerol. FAB-HRMS was similarly obtained in glycerol–DMSO at a resolving power of 12 000.

Substrates

The substrate 5α,7β,9α,10β,13α-pentaacetoxy-4(20),11-taxadiene (**1**) (19, 20) was prepared from the acetylation of 2-deacetoxydecinnamoyltaxinine J (23–25). 2-Deacetoxydecinnamoyltaxinine J (**2**) was obtained from the cleavage of the cinnamoyl side chain of 2-deacetoxytaxinine J (**1**), following the procedure of Bathini et al. (22).

Since a detailed NMR data of the substrates are not available in the literature, we are reporting them here for comparison with the biotransformation products.

1

^{1}H NMR (500 MHz, $CDCl_3$) δ: 0.83 (s, 3H, Me-19), 1.02 (dd, *J* = 14.6, 8.9, 1H, H-14b), 1.12 (s, 3H, Me-16), 1.61 (s, 3H, Me-17), 1.72 (o m, 1H, 2b), 1.78 (o m, 1H, 6b), 1.86 (o m, 1H, 2b), 1.86 (o m, 1H, H-1), 1.91 (ddd, *J* = 14.5, 4.9, 2.6, 1H, H-6), 1.96 (s, 3H, Ac), 2.01 (s, 3H, Ac), 2.04 (s, 3H, Ac), 2.05 (s, 3H, Ac), 2.17 (s, 3H, Ac), 2.18 (d, *J* = 0.7, 3H, Me-18), 2.64 (dt, *J* = 14.4, 9.7, 9.7, 1H, H-14a), 2.89 (br d, *J* = 5.9, 1H, H-3), 4.94 (s, 1H, H-20b), 5.27 (s, 1H, H-20a), 5.37 (dd, *J* = 3.4, 2.4, 1H, H-5), 5.54 (dd, *J* = 11.7, 5.41 1H, H-7), 5.89 (o d, *J* = 11.1, 1H, H-9), 5.92 (o t, *J* = ~9.0, H-13), 6.24 (d, *J* = 11.2, 1H, H-10). ^{13}C NMR (125 MHz, $CDCl_3$) δ: 40.4 (C-1), 27.4 (C-2), 37.5 (C-3), 146.6 (C-4), 74.7 (C-5), 34.1 (C-6), 70.0 (C-7), 46.2 (C-8), 76.7 (C-9), 71.6 (C-10), 134.6 (C-11), 137.3 (C-12), 70.7 (C-13), 31.4 (C-14), 39.5 (C-15), 31.1 (C-16), 27.5 (C-17), 14.9 (C-18), 13.3 (C-19), 115.7 (C-20).

2

^{1}H NMR (500 MHz, $CDCl_3$) δ: 0.86 (s, 3H, Me-19), 0.97 (dd, *J* = 14.7, 7.0, 1H, H-14b), 1.08 (s, 3H, Me-16), 1.61 (s, 3H, Me-17), 1.70 (s, Ac-13), 1.76 (br dd, *J* = 15.0, 5.0, 1H, 2b), 1.84 (o m, 1H, 6b), 1.84 (o m, 1H, H-1), 1.87 (o m, 1H, 2b), 1.93 (ddd, *J* = 14.5, 5.1, 2.5, 1H, H-6), 1.98 (s, 3H, Ac-10), 2.02 (s, 3H, Ac-9), 2.06 (s, 3H, Ac-7), 2.33 (s, 3H, Me-18), 2.71 (dt, *J* = 1.6, 9.8, 9.8, 1H, H-14a), 3.01 (br d, *J* = 5.0, 1H, H-3), 5.01 (d, *J* = 1.1, 1H, H-20b), 5.56 (t, *J* = 2.8, 1H, H-5), 5.67 (dd, *J* = 11.4, 5.0, 1H, H-7), 5.79 (br dd, *J* = ~9.6, ~7.8, 1H, H-13), 5.93 (d, *J* = 11.2, 1H, H-9), 6.29 (d, *J* = 11.2, 1H, H-10), 6.56 (d, *J* = 16.0, 1H, CH=α), 7.39 (o m, 3H, *m*- and *p-Ph*), 7.48 (m, 2H, *o-Ph*), 7.76 (d, *J* = 916.1, 1H, CH=β). ^{13}C NMR (125 MHz, $CDCl_3$) δ: 40.2 (C-1), 27.3 (C-2), 37.5 (C-3), 146.4 (C-4), 74.8 (C-5), 34.6 (C-6), 70.0 (C-7), 46.3 (C-8), 76.7 (C-9), 71.7 (C-10), 135.0 (C-11), 137.2 (C-12), 70.6 (C-13), 31.9 (C-14), 39.4 (C-15), 31.2 (C-16), 27.2 (C-17), 15.3 (C-18), 13.2 (C-19), 116.0 (C-20), 166.1 (C=O-1′), 118.4 (CH=α), 145.7 (=CH Ph-β), 134.1 (Ph-C1), 128.1 (*o*-Ph), 129.0 (*m*-Ph), 130.6 (*p*-Ph), 21.0 and 170.7 (Ac-13), 21.0 and 169.2 (Ac-10), 20.8 and 170.2 (Ac-9), 21.5 and 169.8 (Ac-7).

Microorganism

Absidia coerulea ATCC 10738a was purchased from American Type Culture Collection (ATCC).

© 2001 NRC Canada

Table 5. ^{1}H and ^{13}C NMR data for **16**.

Position	δ ^{1}H NMR multiplicity[a] (*J* (Hz))	δ ^{13}C NMR[b]	HMBC	NOESY[c]
1	—	75.6		
2a	2.00 m	36.7		2b (w), 17 (w), 19 (w)
2b	1.85 m		4	2a (s), 14b (m), 19 (s), 20b (s)
3	2.96 br d (5.5)	40.85	1, 2, 8, 19	7 (s), 10 (w), 14b (s), 18 (s)
4	—	145.2		
5	5.59 br s (2.7)	74.3	3, 4, 20, 165.8	6 (s), 20a (s)
6	1.99–1.85 m	34.1		
7	5.66 dd (5.0, 11.4)	69.4	6, 8, 19, 169.5	3 (s), 6 (s), 10 (s), 18 (s,s)
8	—	46.2		
9	5.94 o, d (11.2)	75.8	170.0	
10	6.30 d (11.2)	71.0	8, 9, 11, 12, 15, 168.8	7 (s), 18 (m)
11	—	134.6		
12	—	138.90		
13	5.95 o, m	70.9	170.0	14a (m), 18 (m), 2a (m), 16 (s), 17 (s)
14a	2.55 dd (9.8, 14.8)	41.2	1, 2, 12, 13	9/13 (s), 14b (s), 16 (m) 2b (w), 3 (m), 14a (s)
14b	1.52 dd (6.7, 14.8)			
15	—	43.2		
16	1.17 s	27.0	1, 11, 15, Me	9/13 (s), 14a (m), 17 (s)
17	1.61 s	21.5	1, 11, 15, Me	9/13 (s), 2a (s), 16 (s)
18	2.32 s	14.9	11, 12, 13	3 (s), 7 (s), 9/13 (m), 10 (s), o-Ph (w)
19	0.88 s	12.9	3, 7, 8, 9	9/13 (s), 20b (m), 3 (m), 2a (s), 2b/6 (s)
20a	5.41 s	115.9	3, 4, 5, 8	5 (s), 20b (s)
20b	5.08 s		3, 4, 5, 8	2b/6 (s), 19 (m), 20a (s)
OAc	2.06 s	21.2	169.6	
	2.03 s	20.4	169.9	*o*-Ph (s), *m*-Ph (w)
	1.99 s	20.6	168.9	
	1.72 s	20.5	170.3	
O-CO	—	165.8	—	
=CH-α	6.54 d (16.0)	117.8	C1(Ph), 165.8	18 (w), 1.72 (w), o-Ph (w)
=CH-β	7.76 d (16.0)	145.4	C1(Ph), *o*-Ph, 165.8	
Ph	—	133.6	—	
o	7.48 m	127.8		
m	7.39 m	128.9		
p	7.39 m	130.3		

[a]Multiplicity: br (broad), s (singlet), d (doublet), t (triplet), m (multiplet), o (overlapping). The precision of the coupling constants is ±0.25 Hz.
[b]The ^{13}C NMR chemical shifts were extracted from the HSQC and HMBC (for quaternary carbons) experiments (±0.2 ppm).
[c]NOESY intensities are marked as strong (s), medium (m), or weak (w).

Incubation, biotransformation procedure

General

Cultures were grown in potato dextrose (24 g L^{-1}, DIFCO laboratories) broth, and was incubated at 25°C and 125 rpm, unless otherwise indicated. The *A. coerulea* ATCC 10738a was first preserved on silica gel and kept in a 4°C cold room to prevent mutation (26). The seed culture was prepared by the addition of several grains of silica gel that absorbed the fungus to 30 mL of medium in a 125 mL Erlermeyer flask. The culture was incubated for 3 days. At preparative scale, to a 2000 mL flask, containing 1000 mL potato dextrose broth, was added a small fraction of the above fungus seed (homogenized before use). The flasks were at first cultured for 3 days. Then to the flasks was added the substrate dissolved in DMSO and continued culturing for another 14 days. At the end of the incubation, the culture was homogenized and extracted with CH_2Cl_2. The CH_2Cl_2 extract was further purified. Culture controls with the same medium and substrate but without fungi were performed at the same conditions.

*For 5α,7β,9α,10β,13α-pentaacetoxy-4(20),11-taxadiene (**1**)*

To each of the three 2 L flasks containing 1 L of medium, was added 160 mg substrate (dissolved in 3 mL DMSO). After 14 days incubation, the culture was extracted with CH_2Cl_2 (500 mL × 3 for 1 L culture). The CH_2Cl_2 crude residue was 509 mg. The extract was first applied to a silica gel flash chromatography column (31 g), eluted with CH_2Cl_2 (300 mL), CH_2Cl_2–MeOH (400:1, 200:1, 150:1; 100:1, 100:1.5, 100:2, 100:3, 100:20 each 300 mL), and ninety 30 mL fractions were obtained. The fractions were combined into 14 fractions based on the TLC. Each of the above fractions were separated by preparative HPLC and finally the following compounds were obtained: **3** (48.8 mg, 9.9%), **4** (33.6 mg, 7%), **5** (6.3 mg, 1.4%), **6** (1.2 mg, 0.3%), **7** (0.7 mg, 0.2%), **8** (15.3 mg, 3.1%), **9** (0.3 mg, 0.1%), **10** (0.9 mg, 0.2%), **11** (1.4 mg, 0.3%), **12** (4.5 mg, 0.8%), **13**

© 2001 NRC Canada

Table 6. ^{1}H and ^{13}C NMR data for **17**.

Position	δ ^{1}H NMR multiplicity[a] (*J* (Hz))	δ ^{13}C NMR[b]	HMBC	NOESY[c]
1	1.79 o, m	50.0		
2a	2.10 m	26.1		
2b	1.90 m			
3	2.77 br d (5.7)	38.5	8, 19	7 (s), 14 (s), 18 (s)
4	—	145.7		
5	5.39 br t (2.7)	74.8	3, 4, 20, 166.0	H(1.88) (w), 20a (w)
6	1.93–1.84 m	34.6		
7	5.62 o, dd (5.2, 11.4)	69.9	6, 8, 19, 169.9	3 (s), 18 (s), CHα (s)
8	—	46.5		
9	5.94 d (11.1)	76.4	8, 10, 11, 19, 170.1	17 (s), 19 (s), H(1.88) (w)
10	6.27 d (11.1)	71.6	8, 9, 11, 12, 15, 169.2	18 (s), 7/13 (s)
11	—	137.7		
12	—	135.0		
13	5.65 o, m	81.3	11, 12, 14, 173.3	14 (m), 16 (s), 18 (m)
14	3.52 d (4.6)	79.2	1, 2, 13, 15	3 (s), 13 (m), OAc (1.79) (s), H(2.05) (s)
15	—	—		
16	1.18 s	31.2	1, 11, 15, Me	13 (s), 17 (s), OAc (1.79) (m)
17	1.66 s	27.3	1, 11, 15, Me	2/6/1 (s), 9 (s), 16 (s)
18	2.33 s	15.3	11, 12, 13	3 (m), 10 (s), 13 (s), 16 (w), CHα (s), OAc (1.79) (w)
19	0.86 s	13.0	3, 7, 8, 9	2/6/1 (s), 9 (s), 20b (m)
20a	5.39 s	116.3	3, 4, 5, 8	5 (m), 20b (s)
20b	5.05 s		3, 4, 5	20a (s), H(2.04) (s), 19 (w)
OAc	1.79 s	20.9	173.3 (13)	
	1.99 s	21.0	169.2 (10)	
	2.03 s	20.8	170.1 (9)	
	2.06 s	21.4	169.9 (7)	
O-CO	—	166.0	—	
=CH-α	6.51 d (16.0)	118.3	C=O, C-β, C-1(ph)	Ph(*o*) (w), 18 (w), H(1.80) (w)
=CH-β	7.76 d (16.0)	145.9	C=O, C-α, C-1(ph),	
Ph	—	134.1	—	
o	7.49 m	128.1		
m	7.40 m	129.0		
p	7.40 m	130.7		

[a]Multiplicity: br (broad), s (singlet), d (doublet), t (triplet), m (multiplet), o (overlapping). The precision of the coupling constants is ±0.25 Hz.
[b]The ^{13}C NMR chemical shifts were extracted from the HSQC and HMBC (for quaternary carbons) experiments (±0.2 ppm).
[c]NOESY intensities are marked as strong (s), medium (m), or weak (w).

(0.5 mg, 0.2%), **14** (1.9 mg, 0.4%), **15** (0.5 mg, 0.1%). The substrate (**1**) was also recovered (193.5 mg, 40.3%).

*For 2-deacetoxytaxinine J (**2**)*

To each of the four 2 L flasks containing 1 L of medium, was added 150 mg of substrate (in 3 mL DMSO). After 14 days incubation, the culture was extracted with CH_2Cl_2 (500 mL × 3 for 1 L culture). The CH_2Cl_2 extract obtained (912 mg) was first applied to a silica gel flash chromatography column (40 g), eluted with CH_2Cl_2 (300 mL), CH_2Cl_2–MeOH (300:1, 200:1, 100:1, 100:2, 100:3, 100:20 each 300 mL), and seventy 30 mL fractions were obtained. The fractions were combined into six fractions based on the TLC. Each of the above fractions was separated by preparative HPLC and the following compounds were obtained: **16** (42.5 mg, 6.9%), **17** (70.9 mg, 11.5%), **18** (20 mg, 3.3%), **19** (2.5 mg, 0.5%), and 346.5 mg (57.8%) of the substrate **2**, was recovered.

Compound data

The data for **3**, **4**, and **8** are given here since they are only partially reported (4).

3: $[\alpha]_D^{22}$ –1.3° (*c* 1.33, $CHCl_3$). FAB-HRMS calcd. for $C_{30}H_{42}O_{11}Na$ ($[M + Na]^+$): 601.2625; found: 601.2624. ^{1}H NMR (500 MHz, $CDCl_3$) δ: 0.84 (s, Me-19), 1.2 (s, Me-16), 1.57 (dd, *J* = 14.9, 7.2 Hz, 1H, H-14b), 1.60 (s, Me-17), 1.77 (ddd, *J* = 14.8, 11.5, 3.3 Hz, 1H, H-6b), 1.80 (d, *J* = 15.0 Hz, 1H, H-2b), 1.90 (ddd, *J* = 14.8, 4.8, 3.3 Hz, 1H, H-6a), 1.97 (s, Ac), 2.00 (o m, 1H, H-2a), 2.01 (s, Ac), 2.04 (s, Ac), 2.06 (s, Ac), 2.16 (s, Ac), 2.17 (s, Me-18), 2.48 (dd, *J* = 14.9, 9.6 Hz, 1H, H-14a), 2.84 (d, *J* = 5.6 Hz, 1H, H-3), 5.00 (s, 1H, H-20b), 5.30 (s, 1H, H-20a), 5.39 (t, *J* = 3.3 Hz, 1H, H-5), 5.52 (dd, *J* = 11.5, 4.8 Hz, 1H, H-7), 5.90 (d, *J* = 11.2 Hz, 1H, H-9), 6.08 (t, *J* = 8.3 Hz, 1H, H-13), 6.24 (d, *J* = 11.2 Hz, 1H, H-10). ^{13}C NMR (125 MHz, $CDCl_3$) δ: 13.2 (C-19), 14.9 (C-18), 20.8 (OCOMe-13), 20.9 (OCOMe-10), 21.4 (OCOMe-9), 21.4(OCOMe-7), 21.8 (OCOMe-5), 22.1

© 2001 NRC Canada

Table 7. ^{1}H and ^{13}C NMR data for **18**.

Position	δ ^{1}H NMR multiplicity[a] (*J* (Hz))	δ ^{13}C NMR[b]	HMBC	NOESY[c]
1	—	62.6		
2a	2.33 dd (9.0, 14.5)	29.1	1, 8, 15	2b (s), 9 (s), 19 (m)
2b	1.47 d (14.5)			2a (s), 3 (s), 14b (s), 20b (s)
3	2.70 d (9.0)	38.9	1, 2, 7, 8, 19	2b (s), 5 (w), 7 (s), 10 (w), 14b (s)
4	—	145.1		
5	5.53 br s	74.1	165.3	6a (s), 6b (s), 20a (s)
6a	2.01 m	34.2		
6b	1.93 m			
7	5.63 dd (5.2, 11.1)	69.8	6, 8, 19, 169.5	3 (s), 6a (s), 10 (s)
8	—	44.9		
9	5.92 br s	*76.9*		2a (s), 19 (s)
10	6.37 br s	69.2		3 (s), 7 (s), 18 (s), Ac(1.5) (w), Ph-*o* (s)
11	—	136.9		
12	—	146.0		
13	5.41 t (7.0)	79.3		14a (s), 16 (s), 18 (s)
14a	2.47 dd (7.3, 14.0)	44.4	11, 12, 15	13 (s), 14b (s)
14b	1.17 dd (7.3, 14.0)			
15	—	75.4		
16	1.11 s	27.0	1, 15, Me	13 (w), Me-17 (w)
17	1.30 s	24.9	1, 15, Me	2a (w), 2b (w), 14a (s), Me-16 (w)
18	1.95 s	11.8	11, 12, 13	13 (w), 10 (w), Ph-o (s)
19	0.91 s	12.9	3, 7, 8, 9	2a (w), 5 (w), 6a (s), 9 (s)
20a	5.34 s	114.6	3, 4, 5, 8	5 (s), 20b (s)
20b	4.92 s		3, 4, 5	2b (s), 20a (s), 19 (w)
OAc	1.51 s	20.5	170.8	
	1.97 s	20.8	167.8	
	1.99 s	20.8	169.7	
	2.07 s	21.3	169.8	
O-CO	—	165.5		
=CH-α	6.38 d (16.0)	118.2	165.5, C1(Ph)	See H-10
=CH-β	7.68 d (16.0)	145.2	C=O, C-1, C-*o*, C-α	
Ph	—	134.3		
o	7.50 m	128.1		
m	7.37 m	129.0		
p	7.37 m	130.5		

[a]Multiplicity: br (broad), s (singlet), d (doublet), t (triplet), m (multiplet), o (overlapping). The precision of the coupling constants is ±0.25 Hz.

[b] The ^{13}C NMR chemical shifts were extracted from the HSQC and HMBC (for quaternary carbons) experiments (±0.2 ppm). Some of the carbons are very broad, indicating that a conformational exchange is going on.

[c]NOESY intensities are marked as strong (s), medium (m), or weak (w).

(C-17), 27.3 (C-16), 34.0 (C-6), 37.1 (C-2), 41.1 (C-14), 41.2 (C-3), 43.8 (C-15), 46.4 (C-8), 69.7 (C-7), 70.9 (C-13), 71.2 (C-10), 74.6 (C-5), 76.2 (C-1), 76.2 (C-9), 115.9 (C-20), 134.3 (C-11), 139.4 (C-12), 145.8 (C-4), 169.1 (OCOMe-10), 169.7 (OCOMe-5), 169.8 (OCOMe-7), 170.2 (OCOMe-9), 170.2 (OCOMe-13).

4: $[\alpha]_D^{22}$ –10.2° (*c* 1.45, $CHCl_3$). FAB-HRMS calcd. for $C_{30}H_{42}O_{11}Na$ ($[M + Na]^+$): 601.2625; found: 601.2625. ^{1}H NMR (500 MHz, $CDCl_3$) δ: 0.82 (s, 3H, Me-19), 1.22 (s, 3H, Me-16), 1.65 (s, 3H, Me-17), 1.76 (ddd, *J* = 14.5, 11.8, 4.0 Hz, 1H, H-6b), 1.80 (o m, 1H, H-1), 1.90 (o m, 1H, H-6a), 1.97 (s, 3H, Ac-10), 2.0–1.9 (o m, 2H, H-2), 2.01 (s, 3H, Ac-9), 2.04 (s, 3H, Ac-7), 2.15 (s, 6H, Ac-5, Ac-13), 2.19 (d, *J* = 1.1 Hz, 3H, Me-18), 2.67 (br d, *J* = 6.0 Hz, 1H, H-3), 3.57 (d, *J* = 5.3 Hz, 1H, H-14), 4.98 (s, 1H, H-20b), 5.28 (s, 1H, H-20a), 5.36 (dd, *J* = 3.4, 2.3 Hz, 1H, H-5), 5.48 (dd, *J* = 11.6, 5.0 Hz, 1H, H-7), 5.81 (dq, *J* = 5.3, 1.1 Hz, 1H, H-13), 5.90 (d, *J* = 11.1 Hz, 1H, H-9), 6.21 (d, *J* = 11.1 Hz, 1H, H-10). ^{13}C NMR (125 MHz, $CDCl_3$) δ: 50.7 (C-1), 26.3 (C-2), 38.7 (C-3), 146.1 (C-4), 74.7 (C-5), 34.0 (C-6), 69.9 (C-7), 46.3 (C-8), 76.4 (C-9), 71.5 (C-10), 137.2 (C-11), 135.1 (C-12), 81.1 (C-13), 78.6 (C-14), 39.6 (C-15), 31.0 (C-16), 27.6 (C-17), 15.0 (C-18), 13.1 (C-19), 116.0 (C-20), 21.8 (OCOMe-13), 21.4 (OCOMe-5), 21.4 (OCOMe-7), 20.8 (OCOMe-9), 20.9 (OCOMe-10), 172.7 (OCOMe-13), 169.6 (OCOMe-5), 169.9 (OCOMe-7), 170.2 (OCOMe-9), 169.2 (OCOMe-10).

5: $[\alpha]_D^{22}$ –58.5° (*c* 0.28, $CHCl_3$). FAB-HRMS calcd. for $C_{28}H_{40}O_{10}Na$ ($[M + Na]^+$): 559.2519; found: 559.2520. ^{1}H NMR (500 MHz, $CDCl_3$) δ: 0.81 (s, 3H, Me-19), 1.06 (s,

© 2001 NRC Canada

3H, Me-16), 1.55 (s, 3H, Me-17), 1.55 (o m, 1H, H-14b), 1.66 (ddd, *J* = 13.7, 11.5, 3.6 Hz, 1H, H-6b), 1.78 (d, *J* = 15.5 Hz, 1H, H-2b), 1.95 (ddd, *J* = 13.7, 5.0, 2.2 Hz 1H, H-6a), 1.98 (s, 3H, Ac-10), 2.02 (s, 3H, Ac-9), 2.03 (o m, 1H, H-2a), 2.04 (s, 3H, Ac-7), 2.06 (s, 3H, Ac-13), 2.18 (d, *J* = 1.1 Hz, 3H, Me-18), 2.57 (dd, *J* = 15.4, 9.9 Hz, 1H, H-14a), 3.15 (br d, *J* = 5.5 Hz, 1H, H-3), 4.31 (d, *J* = 2.6 Hz, 1H, H-5), 4.89 (s, 1H, H-20b), 5.20 (s, 1H, H-20a), 5.66 (dd, *J* = 11.4, 5.2 Hz, 1H, H-7), 5.82 (d, *J* = 11.1 Hz, 1H, H-9), 5.90 (dd, *J* = 9.9, 4.1 Hz, 1H, H-13), 6.27 (d, *J* = 11.1 Hz, 1H, H-10). ^{13}C NMR (125 MHz, $CDCl_3$) δ: 75.4 (C-1), 36.6 (C-2), 39.3 (C-3), 150.7 (C-4), 73.2(C-5), 35.9 (C-6), 69.5 (C-7), 47.0 (C-8), 76.1 (C-9), 71.7 (C-10), 135.5 (C-11), 139.4 (C-12), 70.8 (C-13), 41.5 (C-14), 43.1 (C-15), 28.2 (C-16), 20.4 (C-17), 15.8 (C-18), 12.6 (C-19), 112.8 (C-20), 21.0 (OCOMe-13), 21.4 (OCOMe-7), 20.8 (OCOMe-9), 21.0 (OCOMe-10), 169.9 (OCOMe-13), 169.7 (OCOMe-7), 170.3 (OCOMe-9), 169.2 (OCOMe-10).

***6**:* $[\alpha]_D^{22}$ +73.3° (*c* 0.03, $CHCl_3$). FAB-HRMS calcd. for $C_{28}H_{40}O_{10}Na$ ($[M + Na]^+$): 559.2519; found: 559.2518. ^{1}H NMR (500 MHz, $CDCl_3$) δ: 0.83 (s, 3H, Me-19), 1.02 (s, 3H, Me-16), 1.55 (s, 3H, Me-17), 1.61 (o dd, *J* = 15.3, 4.7 Hz, 1H, H-14b), 1.76 (ddd, *J* = 14.6, 11.7, 3.6 Hz, 1H, H-6b), 1.81 (d, *J* = 15.5 Hz, 1H, H-2b), 1.95 (o m, 1H, H-6a), 1.99 (s, 3H, Ac-10), 2.01 (o m, 1H, H-2a), 2.03 (s, 3H, Ac-9), 2.05 (s, 3H, Ac-7), 2.11 (s, 3H, Ac-5), 2.31 (br s, 3H, Me-18), 2.62 (dd, *J* = 15.3, 10.0 Hz, 1H, H-14a), 2.89 (br d, *J* = 5.8 Hz, 1H, H-3), 4.66 (br dd, *J* = 10.0, 5.0 Hz, 1H, H-13), 5.04 (d, *J* = 1.5 Hz, 1H, H-20b), 5.33 (s, 1H, H-20a), 5.39 (dd, *J* = 3.6, 2.4 Hz, 1H, H-5), 5.54 (dd, *J* = 11.8, 5.2 Hz, 1H, H-7), 5.84 (d, *J* = 11.1 Hz, 1H, H-9), 6.24 (d, *J* = 11.1 Hz, 1H, H-10). ^{13}C NMR (125 MHz, $CDCl_3$) δ: 12.8 (C-19), 15.9 (C-18), 20.4 (C-17), 20.6 (OCOMe-9), 20.7 (OCOMe-10), 21.1 (OCOMe-5), 21.1 (OCOMe-7), 27.9 (C-16), 33.8 (C-6), 36.6 (C-2), 41.5 (C-3), 43.1 (C-15), 45.2 (C-14), 46.6 (C-8), 68.9 (C-13), 69.5 (C-7), 71.8 (C-10), 75.0 (C-5), 75.4 (C-1), 76.0 (C-9), 134.1 (C-11), 143.1 (C-12), 145.5 (C-4), 115.8 (C-20), 169.1 (OCOMe-10), 169.7 (OCOMe-7), 169.9 (OCOMe-5), 170.1 (OCOMe-9).

***7**:* $[\alpha]_D^{22}$ –104.7° (*c* 0.05, $CHCl_3$). FAB-HRMS calcd. for $C_{28}H_{40}O_{10}Na$ ($[M + Na]^+$): 559.2519; found: 559.2518. ^{1}H NMR (500 MHz, $CDCl_3$) δ: 0.79 (s, 3H, Me-19), 1.09 (s, 3H, Me-16), 1.61 (s, 3H, Me-17), 1.66 (ddd, *J* = 13.7, 11.6, 3.5 Hz, 1H, H-6b), 1.78 (br m, 1H, H-1), 1.91 (o m, 2H, H-2), 1.92 (o m, 1H, H-6a), 1.98 (s, 3H, Ac-10), 2.02 (s, 3H, Ac-9), 2.05 (s, 3H, Ac-7), 2.13 (s, 3H, Ac-13), 2.24 (d, *J* = 1.0 Hz, 3H, Me-18), 2.92 (br d, *J* = 5.0 Hz, 1H, H-3), 3.51 (d, *J* = 3.4 Hz, 1H, H-14), 4.27 (t, *J* = 2.8 Hz, 1H, H-5), 4.84 (s, 1H, H-20b), 5.15 (s, 1H, H-20a), 5.44 (br dq, *J* = 3.4, 1.5 Hz, 1H, H-13), 5.62 (dd, *J* = 11.6, 4.9 Hz, 1H, H-7), 5.83 (d, *J* = 10.9 Hz, 1H, H-9), 6.25 (d, *J* = 10.9 Hz, 1H, H-10). ^{13}C NMR (125 MHz, $CDCl_3$) δ: 12.2 (C-19), 15.7 (C-18), 20.5 (OCOMe-9), 20.7 (OCOMe-10), 20.8 (OCOMe-13), 21.1 (OCOMe-7), 25.7 (C-2), 26.3 (C-17), 31.7 (C-16), 35.8 (C-6), 36.4 (C-3), 39.2 (C-15), 46.8 (C-8), 49.1 (C-1), 69.6 (C-7), 71.9 (C-10), 73.0 (C-5), 76.3 (C-9), 79.5 (C-14), 81.9 (C-13), 112.6 (C-20), 135.7 (C-12), 137.5 (C-11), 169.1 (OCOMe-10), 169.5 (OCOMe-7), 170.1 (OCOMe-9), 172.5 (OCOMe-13).

***8**:* $[\alpha]_D^{22}$ –35.1° (*c* 0.43, $CHCl_3$). FAB-HRMS calcd. for $C_{30}H_{42}O_{11}Na$ ($[M + Na]^+$): 601.2625; found: 601.2624. ^{1}H NMR (500 MHz, $CDCl_3$) δ: 0.86 (s, Me-19), 1.11 (s, Me-16), 1.20 (dd, *J* = 13.9, 7.9 Hz, 1H, H-14b), 1.30 (s, Me-17), 1.40 (d, *J* = 14.5 Hz, 1H, H-2b), 1.83 (ddd, *J* = 15.2, 11.6, 3.6 Hz, 1H, H-6b), 1.91 (s, Me-18), 1.95 (s, Ac), 1.96 (o m, 1H, H-6a), 1.97 (s, Ac), 2.00 (s, Ac), 2.04 (s, Ac), 2.05 (s, Me), 2.32 (dd, *J* = 14.5, 9.6 Hz, 1H, H-2a), 2.47 (dd, *J* = 13.9, 7.3 Hz, 1H, H-14a), 2.63 (br m, 1H, H-3), 4.85 (s, 1H, H-20b), 5.24 (s, 1H, H-20a), 5.35 (dd, *J* = 3.6, 2.2 Hz, 1H, H-5), 5.50 (dd, *J* = 11.6, 5.3 Hz, 1H, H-7), 5.52 (o, t, *J* = 7.3 Hz 1H, H-13), 5.85 (br d, *J* = 10.4 Hz, 1H, H-9), 6.34 (d, *J* = 10.4 Hz, 1H, H-10). ^{13}C NMR (125 MHz, $CDCl_3$) δ: 11.7 (C-18), 12.9 (C-19), 20.8 (OCOMe), 20.8 (OCOMe), 21.0 (OCOMe), 21.2 (OCOMe), 21.4 (OCOMe), 24.8 (C-17), 27.0 (C-16), 29.0 (C-2), 33.8 (C-6), 38.4 (C-3), 44.1 (C-14), 44.8 (C-8), 62.8 (C-1), 69.2 (C-10), 69.7 (C-7), 74.1 (C-5), 75.3 (C-15), 76.9 (C-9), 79.3 (C-13), 114.2 (C-20), 136.7 (C-11), 145.3 (C-4), 146.6 (C-12), 167.5 (OCOMe), 169.2 (OCOMe), 169.3 (OCOMe), 169.5 (OCOMe), 170.2 (OCOMe).

***9**:* $[\alpha]_D^{22}$ –356.7° (*c* 0.03, $CHCl_3$). FAB-HRMS calcd. for $C_{28}H_{40}O_{10}Na$ ($[M + Na]^+$): 559.2519; found: 559.2518. ^{1}H NMR (500 MHz, $CDCl_3$) δ: 0.85 (br s, 3H, Me-19), 1.10 (s, 3H, Me-16), 1.30 (o m, 1H, H-14b), 1.30 (s, 3H, Me-17), 1.44 (br d, *J* = 14.1 Hz, 1H, H-2b), 1.79 (ddd, *J* = 14.4, 11.2, 3.5 Hz, 1H, H-6b), 1.90 (br s, 3H, Me-18), 1.95 (o m, 1H, H-6a), 1.96 (s, 3H, Ac-9), 1.98 (s, 3H, Ac), 2.03 (s, 3H, Ac), 2.05 (s, 3H, Ac-7), 2.48 (dd, *J* = 14.1, 9.3 Hz, 1H, H-2a), 2.48 (dd, *J* = 14.1, 7.2 Hz, 1H, H-14a), 2.82 (d, *J* = 9.3 Hz, 1H, H-3), 4.33 (dd, *J* = 3.5, 1.6 Hz, 1H, H-5), 4.76 (s, 1H, H-20b), 5.11 (s, 1H, H-20a), 5.46 (t, *J* = 7.2 Hz, 1H, H-13), 5.56 (dd, *J* = 11.2, 5.1 Hz, 1H, H-7), 5.80 (br d, *J* = 9.8 Hz, 1H, H-9), 6.32 (br d, *J* = 9.8 Hz, 1H, H-10). ^{13}C NMR (125 MHz, $CDCl_3$) δ: 63.0 (C-1), 29.0 (C-2), 37.2 (C-3), 72.5 (C-5), 35.7 (C-6), 69.4 (C-7), 45.0 (C-8), 76.8 (C-9), 69.4 (C-10), 136.3 (C-11), 146.2 (C-12), 79.6 (C-13), 43.9 (C-14), 75.3 (C-15), 26.8 (C-16), 24.8 (C-17), 11.8 (C-18), 12.7 (C-19), 111.5 (C-20), 21.0 (OCOMe), 21.1 (OCOMe-7), 20.6 (OCOMe), 20.6 (OCOMe), 170.8 (OCOMe), 169.6 (OCOMe-7), 169.5 (OCOMe), 167.5 (OCOMe).

***10**:* $[\alpha]_D^{22}$ –163.9° (*c* 0.07, $CHCl_3$). FAB-HRMS calcd. for $C_{28}H_{40}O_{10}Na$ ($[M + Na]^+$): 559.2519; found: 559.2518. ^{1}H NMR (500 MHz, $CDCl_3$) δ: 0.86 (s, 3H, Me-19), 1.05 (s, 3H, Me-16), 1.18 (dd, *J* = 14.2, 7.3 Hz, 1H, H-14b), 1.29 (s, 3H, Me-17), 1.41 (d, *J* = 14.1 Hz, 1H, H-2b), 1.83 (ddd, *J* = 14.6, 11.1, 4.0 Hz, 1H, H-6b), 1.96 (s, 3H, Ac-10), 1.97 (o m, 1H, H-6a), 1.98 (s, 3H, Ac), 2.01 (s, 3H, Me-18), 2.03 (s, 3H, Ac), 2.05 (s, 3H, Ac-7), 2.32 (dd, *J* = 14.1, 9.4 Hz, 1H, H-2a), 2.39 (dd, *J* = 14.2, 7.3 Hz, 1H, H-14a), 2.68 (d, *J* = 9.4 Hz, 1H, H-3), 4.51 (t, *J* = 7.3 Hz, 1H, H-13), 4.86 (s, 1H, H-20b), 5.24 (s, 1H, H-20a), 5.34 (dd, *J* = 4.0, 2.2 Hz, 1H, H-5), 5.50 (dd, *J* = 11.1, 5.1 Hz, 1H, H-7), 5.81 (br d, *J* = 10.0 Hz, 1H, H-9), 6.33 (d, *J* = 10.0 Hz, 1H, H-10). ^{13}C NMR (125 MHz, $CDCl_3$) δ: 62.8 (C-1), 29.0 (C-2), 38.6 (C-3), 145.5 (C-4), 73.9 (C-5), 33.8 (C-6), 69.6 (C-7), 44.8 (C-8), 77.0 (C-9), 69.9 (C-10), 134.3 (C-11), 149.7 (C-12), 76.9 (C-13), 47.3 (C-14), 75.1 (C-15), 26.8 (C-16), 24.7 (C-17), 11.4 (C-18), 12.6 (C-19), 113.9 (C-20), 21.0

© 2001 NRC Canada

(OCOMe), 21.1 (OCOMe-7), 20.6 (OCOMe), 20.6 (OCOMe-10), 169.6 (OCOMe-7), 169.9 (OCOMe), 169.5 (OCOMe), 167.7 (OCOMe-10).

11: $[\alpha]_D^{22}$ –95.8° (*c* 0.08, $CHCl_3$). FAB-HRMS calcd. for $C_{26}H_{38}O_9Na$ ($[M + Na]^+$): 517.2414; found: 517.2413. ^1H NMR (500 MHz, $CDCl_3$) δ: 0.84 (s, 3H, Me-19), 1.04 (s, 3H, Me-16), 1.22 (o m, 1H, H-14b), 1.29 (s, 3H, Me-17), 1.44 (d, *J* = 14.4 Hz, 1H, H-2b), 1.78 (ddd, *J* = 14.3, 11.7, 3.6 Hz, 1H, H-6b), 1.96 (s, 3H, Ac-10), 1.96 (d, *J* = 1.1 Hz, 3H, Me-18), 1.96 (o m, 1H, H-6a), 1.98 (s, 3H, Ac-9), 2.05 (s, 3H, Ac-7), 2.32 (dd, *J* = 14.4, 9.3 Hz, 1H, H-2a), 2.44 (dd, *J* = 14.2, 7.4 Hz, 1H, H-14a), 2.75 (d, *J* = 9.3 Hz, 1H, H-3), 4.36 (dd, *J* = 3.6, 2.0 Hz, 1H, H-5), 4.41 (t, *J* = 7.4 Hz, 1H, H-13), 4.77 (s, 1H, H-20b), 5.49 (dd, *J* = 11.7, 4.1 Hz, 1H, H-7), 5.79 (br, 1H, H-9), 6.25 (d, *J* = 10.4 Hz, 1H, H-10), 5.11 (s, 1H, H-20a). ^{13}C NMR (125 MHz, $CDCl_3$) δ: 62.8 (C-1), 28.9 (C-2), 37.7 (C-3), 72.5 (C-5), 35.9 (C-6), 69.7 (C-7), 45.3 (C-8), 77.1 (C-9), 69.8 (C-10), 134.5 (C-11), 150.0 (C-12), 77.3 (C-13), 47.3 (C-14), 75.4 (C-15), 26.8 (C-16), 24.7 (C-17), 11.7 (C-18), 12.6 (C-19), 111.6 (C-20), 21.1 (OCOMe-7), 20.6 (OCOMe-9), 20.6 (OCOMe-10), 170.1 (OCOMe-7), 169.7 (OCOMe-9), 168.0 (OCOMe-10).

12: $[\alpha]_D^{22}$ –15.8° (*c* 0.08, $CHCl_3$). FAB-HRMS calcd. for $C_{32}H_{44}O_{11}K$ ($[M + K]^+$): 643.2521; found: 643.2519. ^1H NMR (500 MHz, $CDCl_3$): see Table 1. ^{13}C NMR (125 MHz, $CDCl_3$): see Table 1.

13: $[\alpha]_D^{22}$ –289.5° (*c* 0.06, $CHCl_3$). FAB-HRMS calcd. for $C_{30}H_{42}O_{11}Na$ ($[M + Na]^+$): 601.2625; found: 601.2624. ^1H NMR (500 MHz, $CDCl_3$): see Table 2. ^{13}C NMR (125 MHz, $CDCl_3$): see Table 2.

14: $[\alpha]_D^{22}$ –34.3° (*c* 0.13, $CHCl_3$). FAB-HRMS calcd. for $C_{30}H_{42}O_{12}Na$ ($[M + Na]^+$): 617.2574; found: 617.2573. ^1H NMR (500 MHz, $CDCl_3$): see Table 3. ^{13}C NMR (125 MHz, $CDCl_3$): see Table 3.

15: $[\alpha]_D^{22}$ –48° (*c* 0.03, $CHCl_3$). FAB-HRMS calcd. for $C_{28}H_{40}O_{11}Na$ ($[M + Na]^+$): 575.2468; found: 575.2468. ^1H NMR (500 MHz, $CDCl_3$): see Table 4. ^{13}C NMR (125 MHz, $CDCl_3$): see Table 4.

16: $[\alpha]_D^{22}$ –14.9° (*c* 0.48, $CHCl_3$). FAB-HRMS calcd. for $C_{37}H_{46}O_{11}Na$ ($[M + Na]^+$): 689.2938; found: 689.2941. ^1H NMR (500 MHz, $CDCl_3$): see Table 5. ^{13}C NMR (125 MHz, $CDCl_3$): see Table 5.

17: $[\alpha]_D^{22}$ –9.9° (*c* 1.71, $CHCl_3$). FAB-HRMS calcd. for $C_{37}H_{46}O_{11}Na$ ($[M + Na]^+$): 689.2938; found: 689.2939. ^1H NMR (500 MHz, $CDCl_3$): see Table 6. ^{13}C NMR (125 MHz, $CDCl_3$): see Table 6.

18: $[\alpha]_D^{22}$ –39.8° (*c* 0.25, $CHCl_3$). FAB-HRMS calcd. for $C_{37}H_{46}O_{11}Na$ ($[M + Na]^+$): 689.2938; found: 689.2941. ^1H NMR (500 MHz, $CDCl_3$): see Table 7. ^{13}C NMR (125 MHz, $CDCl_3$): see Table 7.

19: $[\alpha]_D^{22}$ –94.9° (*c* 0.10, $CHCl_3$). FAB-HRMS calcd. for $C_{35}H_{44}O_9Na$ ($[M + Na]^+$): 631.2883; found: 631.2880. ^1H NMR (500 MHz, $CDCl_3$) δ: 0.85 (s, 3H, Me-19), 0.96 (s, 3H, Me-17/Me-16), 1.09 (dd, *J* = 15.1, 5.4 Hz, 1H, H-14b), 1.55 (s, 3H, Me-16/Me-17), 1.78 (o m, 1H, H-2b), 1.79 (o m, 1H, H-1), 1.82 (o ddd, *J* = 15.0, 11.6, 3.7 Hz, 1H, H-6b), 1.90 (dd, *J* = 13.4, 5.5 Hz, 1H, H-2a) 1.98 (s, 3H, Ac), 2.03 (s, 3H, Ac), 2.05 (s, 3H, Ac), 2.06 (o m, 1H, H-6a), 2.39 (s, 3H, Me-18), 2.82 (dt, *J* = 15.1, 9.1 Hz, 1H, H-14a), 3.05 (d, *J* = 5.5 Hz, 1H, H-3), 4.53 (br s, 1H, H-13), 5.00 (s, 1H, H-20b), 5.34 (s, 1H, H-20a), 5.52 (br s, 1H, H-5), 5.63 (dd, *J* = 11.6, 5.2 Hz, 1H, H-7), 5.86 (d, *J* = 11.0 Hz, 1H, H-9), 6.26 (d, *J* = 11.0 Hz, 1H, H-10), 6.68 (d, *J* = 15.9 Hz, 1H, H-2′), 7.38 (m, 3H, H-Ph-*m*,*p*), 7.53 (m, 2H, H-Ph-*o*), 7.70 (d, *J* = 15.9 Hz, 1H, H-3′). ^{13}C NMR (125 MHz, $CDCl_3$) δ: 170.2 (OCOMe-9), 169.7 (OCOMe-7), 169.2 (OCOMe-10), 146.6 (C-4), 145.9 (C-3′), 141.7 (C-12), 134.5 (Ph-C_1), 134.2 (C-11), 130.3 (Ph-*m*/*p*), 128.8 (Ph-*p*/*m*), 128.1 (Ph-*o*), 117.6 (C-2′), 115.7 (C-20), 76.7 (C-9), 75.0 (C-5), 72.2 (C-10), 69.8 (C-7), 68.0 (C-13), 46.4 (C-8), 39.8 (C-1), 38.9 (C-15), 37.7 (C-3), 36.2 (C-14), 34.0 (C-6), 31.6 (C-16/17), 27.0 (C-2), 26.5 (C-17/16), 21.2 (OCOMe-7), 20.8 (OCOMe-10), 20.6 (OCOMe-9), 16.0 (C-18), 12.9 (C-19).

Conclusion

Biotransformation reactions are still difficult to predict. In this work, we have seen that different results can be obtained by slight variations of the source of microorganisms or incubation conditions. Further experiments are in progress in our laboratory to correlate functional groups of a specific taxane with fungal chemical reactions.

Acknowledgments

We thank the Natural Sciences and Engineering Research Council of Canada (NSERC), the Cancer Research Society, and the Canadian Breast Cancer Research Initiative for support of this work via operating grants to Lolita O. Zamir. La Fondation Armand-Frappier and the Institut National de la Recherche Scientifique are acknowledged for a predoctoral fellowship to Di-An Sun. We thank Dr. Li Zhicao (Zhongling (Huizhou) High Science and Technology, Co. Ltd.) for a generous gift of 2-deacetoxytaxinine J isolated from *Taxus yunnanensis.*

References

1. S. Hu, D.A. Sun, and A.I. Scott. Tetrahedron Lett. **41**, 1703 (2000).
2. R.N. Patel. Ann. Rev. Microbiol. **98**, 361 (1998).
3. D. Lee, K.-C. Kim, and M.-J. Kim. Tetrahedron Lett. **39**, 9039 (1998).
4. S. Hu, D.A. Sun, X. Tian, and Q. Fang. Tetrahedron Lett. **38**, 2721 (1997).
5. S. Hu, X. Tian, W. Zhu, and Q. Fang. Biocatal. Biotransform. **14,** 241 (1997).
6. S. Hu, X. Tian, W. Zhu, and Q. Fang. J. Nat. Prod. **59**, 1006 (1996).
7. S. Hu, X. Tian, W. Zhu, and Q. Fang. Tetrahedron, **52**, 8739 (1996).
8. R.L. Hanson, J.M. Howell, B.B. Brzozowski, S.A. Sullivan, R.N. Patel, and L.J. Szarka. Biotechnol. Appl. Biochem. **26**, 153 (1997).
9. H. Xu, K.D. Cheng, W.S. Fang, P. Zhu, and C. Meng. Chin. Chem. Lett. **8**, 1055 (1997).

© 2001 NRC Canada

10. R. Zocher, W. Weckwerth, C. Hacker, B. Kammer, T. Hornbogen, and D. Ewald. Biochem. Biophys. Res. Commun. **229**, 16 (1996).
11. J.Z. Zhang, L.H. Zhang, D.A. Sun, J.Q. Gu, and Q.C. Fang. Chin. Chem. Lett. **7**, 1091 (1996).
12. V.K. Nanduri, R.L. Hanson, T.L. LaPorte, R.Y. Ko, R.N. Patel, and L.J. Szarka. Biotechnol. Bioeng. **48**, 547 (1995).
13. R.N. Patel, A. Banerjee, J.M. Howell, C.G. McNamee, D. Brzozowski, V.K. Nanduri, J.K. Thothathil, and L.J. Szarka. Ann. N. Y. Acad. Sci. 166 (1995).
14. R.N. Patel, A. Banerjee, R.Y. Ko, J.M. Howell, W.-S. Li, F.T. Comezoglu, R.A. Partyka, and L.J. Szarka. Biotechnol. Appl. Biochem. **20**, 23 (1994).
15. R. Brieva, J.Z. Crich, and C.J. Sih. J. Org. Chem. **58**, 1068 (1993).
16. R.L. Hanson, J.M. Wasylyk, V.K. Nanduri, D.L. Cazzulino, R.N. Patel, and L.J. Szarka. J. Biol. Chem. **269**, 22 145 (1994).
17. D.A. Sun, F. Sauriol, O. Mamer, and L.O. Zamir. Biorg. Med. Chem. **9**, 793 (2001).
18. D.A. Sun, A. Nikolakakis, F. Sauriol, O. Mamer, and L.O. Zamir. Biorg. Med. Chem. **9**, 1985 (2001).
19. D.P. Della Casa de Marcano and T.G. Halsall. J. Chem. Soc. Chem. Commun. 1282 (1969).
20. M.K. Yeh, J.S. Wang, L.P. Liu, and F.C. Chen. J. Chin. Biochem. Soc. **35**, 304 (1988).
21. V.S. Parmar, A. Jha, K.S. Bisht, P. Taneja, S.K. Singh, A. Kumar, A. Poonam, R. Jain, and C.E. Olsen. Phytochemistry, **50**, 1267 (1999).
22. Y. Bathini, R.G. Micetich, and M. Daneshtalab. Synth. Commun. **24**, 1513 (1994).
23. L. Barboni, P. Gariboldi, G. Appendino, R. Enriu, B. Gabberta, and E. Bombardelli. Liebigs Ann. Chem. 345 (1995).
24. W.M. Chen, P.L. Zhang, and J.Y. Zhou. Yaoxue Xuebao, **29**, 207 (1994).
25. S.K. Chattopadhyay and R.P. Sharma. Phytochemistry, **39**, 935 (1995).
26. D.D. Perkins. Can. J. Microbiol. **8**, 591 (1962).

© 2001 NRC Canada

Alkaline oxidative degradation of diphenylmethane structures — Activation energy and computational analysis of the reaction mechanism

Lubo Jurasek, Lívia Krištofová, Yujun Sun, and Dimitris S. Argyropoulos

Abstract: A diphenylmethane model compound (2,2′-methylenebis[6-methoxy-4-methylphenol]) and residual kraft lignin were treated with alkaline hydrogen peroxide. Kinetic data for the disappearance of the model and the diphenylmethane structures in the residual lignin was collected. The activation energies for the degradation were found to be similar (54 ± 11 kJ mol^{-1} for the model and 58 ± 5 kJ mol^{-1} for the residual lignin). A comparison of the activation energies with the data of a previous study on a biphenyl model compound (3,3′-dimethoxy-5,5′-dimethyl-[1,1′-biphenyl]-2,2′-diol) showed a substantially higher activation energy for the degradation of the latter. Pathways for the degradation of 2,2′-methylenebis[6-methoxy-4-methylphenol] were proposed and the intermediates subjected to computational analysis using a semiempirical method (PM3). The results suggest that initially a common pathway exists, resulting in 2-[2-hydroxy-3-methoxy-5-methyl-phenylmethyl]-4-methyl-2,4-hexadienedioic acid. Then the pathway branches into three, resulting in three major degradation products. The main driving force of the reactions is the formation of radical sites after reaction with hydroxyl radicals and subsequent radical coupling with perhydroxyl radicals to form peroxides. All the reactions on the pathways are exothermic except for the transformations of peroxides into dioxetanes. The dioxetanes cleave exothermically resulting in ring cleavage and fragmentation. The computed data permitted for the rationalization as to why the diphenylmethane structures appear to be more labile than biphenyl structures under alkaline oxidative conditions.

Key words: activation energy, alkaline oxidative degradation, computational chemistry, lignin, reaction mechanism.

Résumé : On a traité le 2,2′-méthylènebis[6-méthoxy-4-méthylphénol], un diphénylméthane modèle ainsi que de la lignine kraft résiduelle avec du peroxyde d'hydrogène en milieu alcalin. On a recueilli des données cinétiques relatives à la disparition du modèle et des structures diphénylméthane dans la lignine résiduelle. On a trouvé que les énergies d'activation pour la dégradation sont semblables (54 ± 11 kJ mol^{-1} pour le modèle et 58 ± 5 kJ mol^{-1} pour la lignine résiduelle). Une comparaison de ces énergies d'activation avec les données obtenues au cours d'une étude antérieure sur le 3,3′-diméthoxy-5,5′-diméthyl-[1,1′-biphényl]-2,2′-diol, un biphényle modèle, montre que l'énergie d'activation pour la dégradation de ce dernier est beaucoup plus élevée. Des voies réactionnelles sont proposées pour la dégradation du 2,2′-méthylènebis[6-méthoxy-4-méthylphénol] et on a soumis les intermédiaires à une analyse par calculs à l'aide d'une méthode semi-empirique (PM3). Les résultats suggèrent qu'initialement il existe une voie commune conduisant à la formation de l'acide 2-[2-hydroxy-3-méthoxy-5-méthyl-phénylméthyl]-4-méthylhexa-2,4-dièneedioïque. La réaction continuerait suivant trois voies qui conduiraient à trois produits différents. La force motrice principale des réactions est la formation de sites radicalaires après réaction avec des radicaux hydroxyles et le couplage radicalaire subséquent avec des radicaux perhydroxyles qui conduit à la formation de peroxydes. Toutes les réactions de chacune des voies réactionnelles sont exothermiques à l'exception des transformations des peroxydes en dioxétanes. Les dioxétanes se clivent d'une façon exothermique en provoquant des ouvertures de cycles et des fragmentations. Les données calculées permettent de rationaliser pourquoi, dans des conditions oxydantes en milieu alcalin, que les structures de type diphénylméthane semblent plus labiles que celles du type biphényle.

Mots clés : énergie d'activation, dégradation oxydante en milieu alcalin, chimie théorique, lignine, mécanisme réactionnel.

[Traduit par la Rédaction]

Introduction

Lignin is known to resist total degradation even under the severe conditions of kraft pulping, and only bleaching causes a substantial removal of residual kraft lignin from the fibre. Residual kraft lignin contains a significant amount of chromophoric structures such as biphenyl, diphenylmethane, α-5, and stilbene units (1–4). The process of formation of condensed structures in lignin during various alkaline pulping processes has been recently investigated (4), using quan-

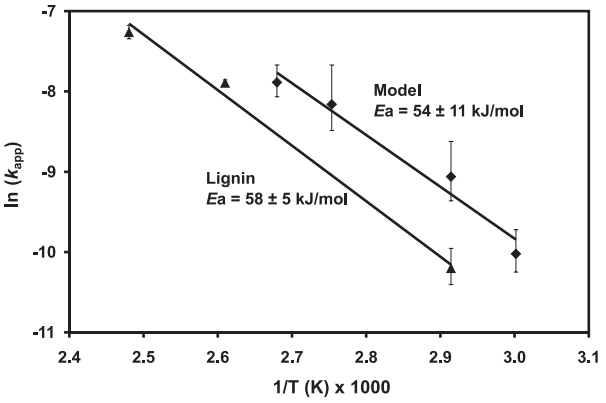
Received January 28, 2001. Published on the NRC Research Press Web site at http://canjchem.nrc.ca on September 21, 2001.

L. Jurasek, L. Krištofová, Y. Sun, and D.S. Argyropoulos.[1] Paprican and Pulp and Paper Research Centre, Department of Chemistry, McGill University, 3420 University Street, Montréal, QC H3A 2A7, Canada.

[1]Corresponding author (telephone: (514) 398-6178; fax: (514) 398-8254; e-mail: dargyr@po-box.mcgill.ca).

 DOI: 10.1139/cjc-79-9-1394 © 2001 NRC Canada

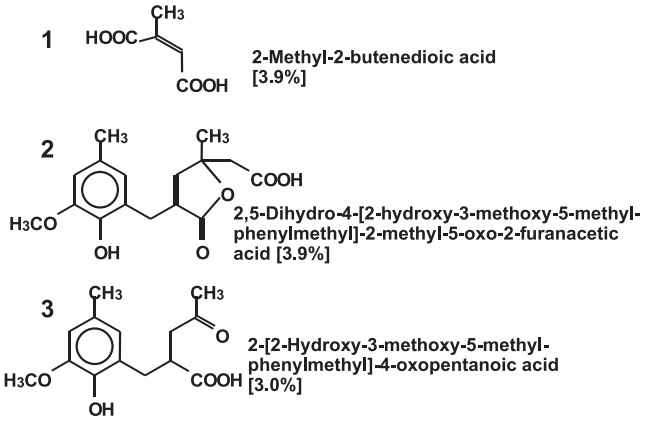
Fig. 1. Comparison of activation energies for the alkaline oxidative degradation of diphenylmethane structures in residual kraft lignin and in the model compound MMMP.



titative ^{31}P NMR spectroscopy. The cleavage of alkyl–aryl ether linkages during the kraft cook leads to the formation of new free phenolic hydroxyls and, consequently, their content in residual lignin as well as in soluble lignin increases during the cook (5). These cleavages lead to an enhancement of the content of condensed structures. Thus, it has been shown recently (4) that kraft pulping of milled wood lignin led to an increased content of stable biphenyl moieties, which eventually became an integral part of the residual kraft lignin structure. After Brunow and co-workers' (6) discovery of dibenzodioxocins in lignin, studies of their degradation under alkaline and kraft pulping conditions have shown conversion of dibenzodioxocins into phenolic alkylated biphenyl-type units within residual kraft lignin (7). Unlike biphenyl structures, which are present in native lignins and accumulate in residual lignin as other structures degrade, the diphenylmethane moieties are formed de novo by condensation of aromatic rings during soda or kraft pulping (4, 8), and analyses have shown that residual lignin in unbleached kraft pulp contains about 20% of diphenylmethane units (9).

Residual lignin can be degraded by a variety of bleaching reactions using either chlorine compounds or chlorine-free chemistry. Interest in minimizing the content of chlorinated compounds in mill effluents prompted, among other measures, the development of totally chlorine-free (TCF) bleaching based on oxygen chemistry. One of the variants of TCF bleaching is an alkaline hydrogen peroxide treatment. The chemistry of this process has been studied earlier and reactions with both anions and radicals have been considered (10–12). The aromatic rings appear stable to hydroperoxide anions (13) but react with hydroxyl radicals (10), which are believed to be the principal species responsible for the oxidative degradation of lignin (14). An alternative mechanism has been proposed (15) for 2,2′-methylenebis[6-methoxy-4-methylphenol] (MMMP, protonated compound **4**) degradation, which involves a nucleophilic attack by hydroperoxide anion. Hydrogen peroxide reacts with lignin in two ways: (*i*) peroxyl anions (HOO^-) nucleophilically attack and eliminate lignin chromophores — these reactions are rapid and occur at low temperatures; (*ii*) hydroxyl radicals ($HO^{\cdot}$), superoxide radical anions ($OO^{\cdot -}$), or perhydroxyl radicals ($HOO^{\cdot}$), formed through the decomposition of hydrogen peroxide, oxidatively degrade phenolic structures into carboxylic acids. The radical reactions require higher temperature but lead to the scission of C—C bonds, fragmentation, and dissolution of lignin, and thus, to its removal from fibre.

Scheme 1. Degradation products of MMMP according to Sun et al. (18). The yields are in square brackets. These products may be formed by three different routes named butenedioate, furanacetate, and oxopentanoate pathways.



In our previous report (16) on the mechanism of alkaline oxidative degradation of a biphenyl-type model compound (3,3′-dimethoxy-5,5′-dimethyl-[1,1′-biphenyl]-2,2′-diol), we determined the activation energies for the degradation process and proposed various pathways. In the present effort, we focus on an analogous diphenylmethane model compound (MMMP) and on diphenylmethane structures in residual kraft lignin.

Results and discussion

Activation energy

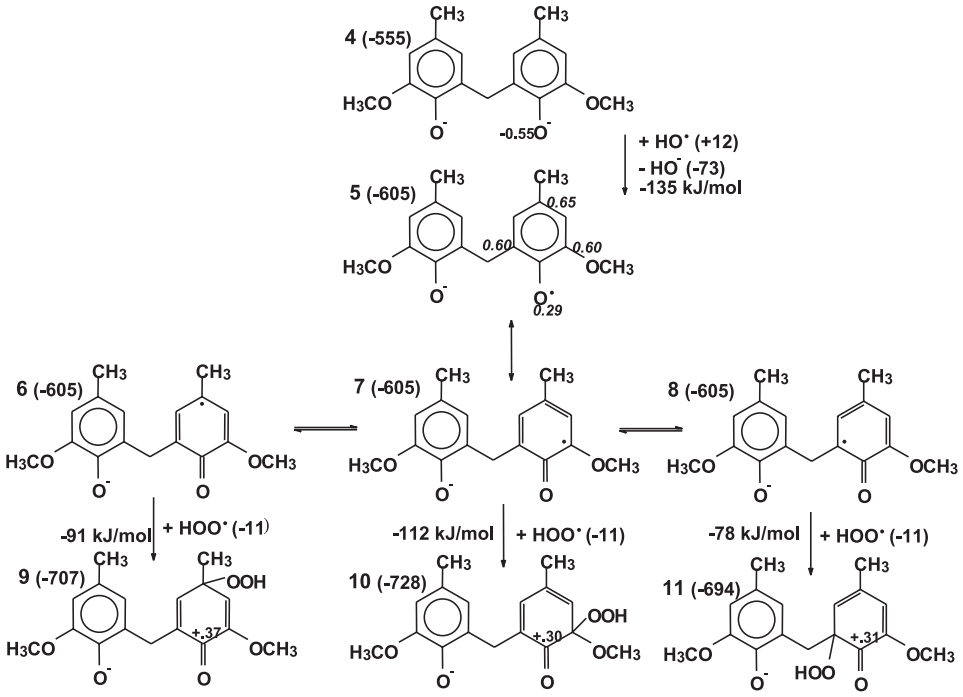
The activation energy for the degradation of MMMP was determined to be 54 ± 11 kJ mol^{-1}, while that for the degradation of diphenylmethane structures in residual kraft lignin was 58 ± 5 kJ mol^{-1} (Fig. 1). The finding that the activation energies are not significantly different suggests that the reaction mechanisms of the degradation may be similar and that MMMP might mimic the behaviour of diphenylmethane structures in lignin. A comparison with our previous study (16) on the activation energy (117 kJ mol^{-1}) for the oxidative degradation of a biphenyl model compound (2,2′-dihydroxy-3,3′-dimethoxy-5,5′-dimethyl-[1,1′-biphenyl]-2,2-diol) shows a substantial difference. Thus, we are finding, in agreement with a previous report (17), that biphenyl structures are more stable in an alkaline oxidative environment and a higher temperature is needed to degrade them effectively. While the activation energies of MMMP and diphenylmethane moieties in lignin are very similar, the apparent rate constants (k_{app} in Fig. 1) are approximately three times lower for lignin than for MMMP.

Proposed mechanism of the oxidative degradation of diphenylmethane structures

The products of degradation of 2,2′-methylenebis[6-methoxy-4-methylphenol] (MMMP) under conditions similar to those used in this work were analyzed previously (18) and the main compounds were identified as shown in

© 2001 NRC Canada

Scheme 2. First part of the common pathway starting with the anion **4** of the model compound (MMMP) leading (via radical mechanisms) to peroxide **10**. Heats of formation of the compounds are given in brackets in kJ mol^{-1}. All reactants were taken into account and computed heats of reactions are shown next to the arrows. Partial charges (underlined) and electron spin densities (in italics) are indicated on some atoms.



Scheme 1. The abundance of the three products was approximately equal (3 to 4%), and none are predominant. It should be noted that the yields reported by Sun et al. (18) and quoted here are based on the starting compound. However, the reaction mixture in which the products were identified still contained 53.3% of unreacted material. Thus, the respective yield figures for compounds **1**–**3** should be quoted as 8.4, 8.4, and 6.4%, respectively. The reaction mixture also contained a number of minor products accounting altogether for 36.6% of the converted material. To these products we should also add oxalic acid, which is accounted for by one of our pathways and was subsequently found upon reinspection of the lab records in a 4% yield. Therefore, approximately 40% of the converted material was accounted for as products.

In this work we have made an attempt to devise the simplest reaction pathways explaining the formation of the products determined previously (18). Our efforts were guided by the results of the computations as well as by previously published pathways for oxidative degradation of similar compounds (11–14). The results of this effort suggest the existence of a common initial pathway leading to the formation of an intermediate dicarboxylic compound (2-[2-hydroxy-3-methoxy-5-methyl-phenylmethyl]-4-methyl-2,4-hexadienedioate) (compound **14**). From this intermediate, the pathway branches into three, each of which leads to formation of one of the three main degradation products. We will now describe the proposed pathways in some detail.

The common initial pathway

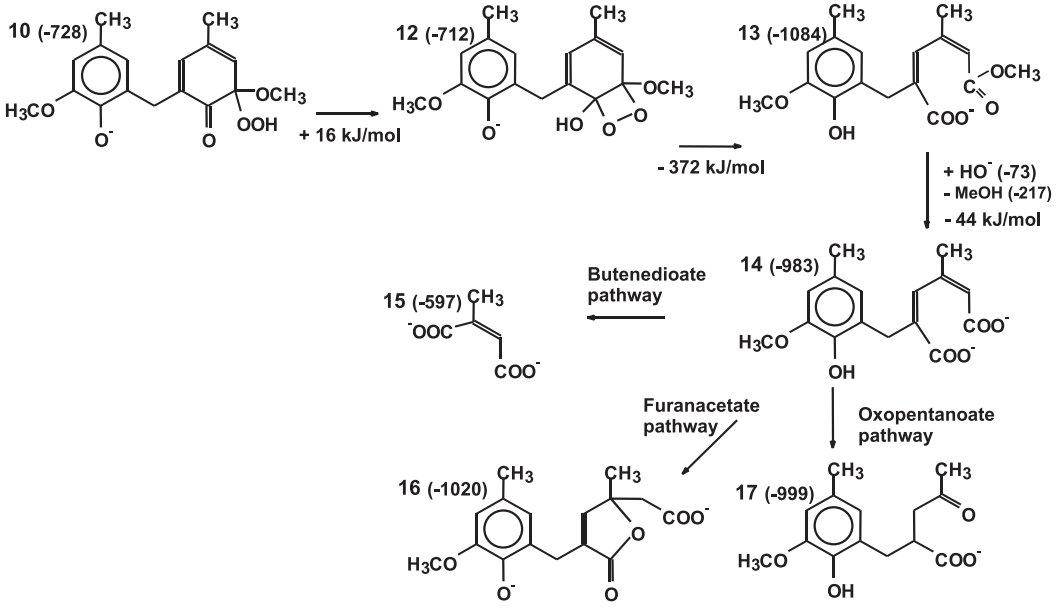
The oxidative degradation of MMMP is initiated by an electrophilic attack by hydroxyl radicals (Scheme 2). The phenolate groups of the MMMP dianion (**4**) have been computed as the most electronegative sites and therefore, likely points of an attack by electrophilic hydroxyl radicals. The charges on the phenolate groups (–0.55) are more negative than the corresponding groups on an analogous biphenyl model compound investigated previously (17) (charge –0.53), which could contribute to the higher reactivity of MMMP as compared to an analogous biphenyl compound.

The resulting phenoxy radical **5** (Scheme 2), shows high electron spin densities (0.65, 0.60, and 0.60) in three positions on the ring suggesting the three resonant structures **6**, **7**, and **8**, respectively. Any one of these three radical sites could couple with the perhydroxyl radical present in the reaction mixture but one of the resulting peroxides (**10**) is most favorable thermodynamically (heat of formation –728 kJ mol^{-1}, compared with –707 and –694 kJ mol^{-1} of the other two peroxides, **9** and **11**). Therefore, it is reasonable to assume that peroxide **10** is the predominant intermediate. The computed heats of formation of all reactants leading to **10** indicate exothermic reactions, which supports the proposed pathway. We have also attempted to compute the products derived from the other two peroxides (**9** and **11**) but found no feasible pathways leading to the experimentally identified products.

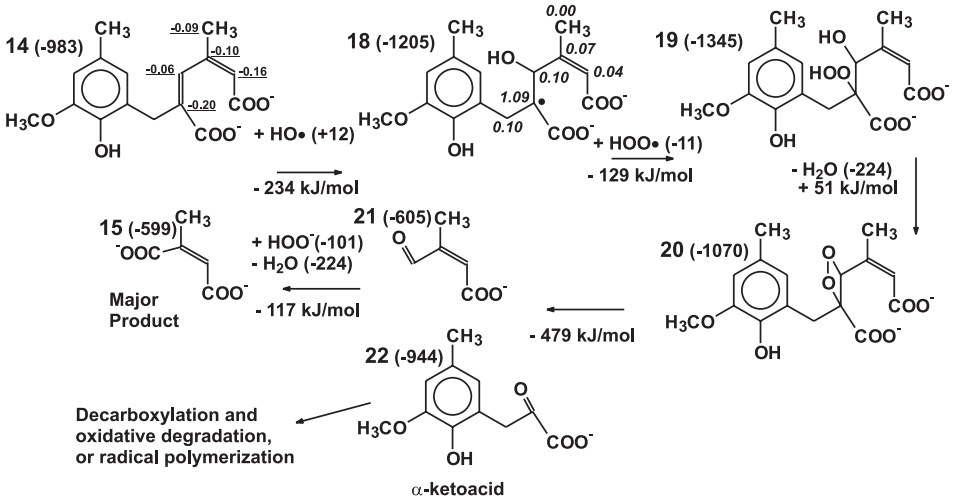
In analogy with our previous study (16), we assume that perhydroxyl radical rather than superoxide radical anion is the reactive species involved in the radical coupling reactions. Couplings with superoxide radical anions gave us products with unreasonably high values of heats of formation. However, our computations were done in vacuo and we plan to address this question again in future using solvated intermediates.

© 2001 NRC Canada

Scheme 3. Second part of the common pathway starting with peroxide **10** and leading to a dicarboxylic intermediate (**14**). The intermediate is a point from which three pathways branch off and lead to the anions **15**–**17** of the main products (**1**–**3**) described by Sun et al. (18). See Scheme 2 for the explanation of symbols.



Scheme 4. The butenedioate branch pathway starts with the dicarboxylic intermediate **14** and proceeds via radical reactions toward a dianion **15** of the degradation product **1**, determined by Sun et al. (18). See Scheme 2 for the explanation of symbols.



The favorable peroxide intermediate **10** is predicted to undergo further degradation as shown in Scheme 3. The peroxide transforms into a dioxetane (**12**) by an endothermic reaction calculated to consume 16 kJ mol^{-1}. The required heat of reaction is similar to that reported for an analogous reaction of the biphenyl model compound studied previously (15 kJ mol^{-1}) (16). The possible meaning of the endothermic reactions for considering the thermodynamic barriers will be discussed later in this section.

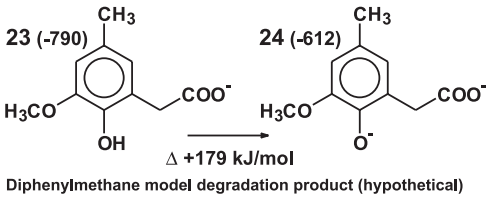
Following the formation of the dioxetane **12**, we predict that a highly exothermic C—C scission (formation of **13**) followed by demethylation yields a dicarboxylic intermediate (2-[2-hydroxy-3-methoxy-5-methylphenylmethyl]-4-methyl-2,4-hexadienedioate) **14**. The intermediate provides a branching point for the forthcoming three pathways named butenedioate, furanacetate, and oxopentanoate pathways, respectively, according to the anions **15**–**17**, of the experimentally proven (18) final products **1**–**3**, respectively. We will now discuss the subsequent concurrent pathways.

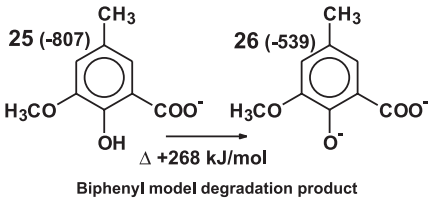
The butenedioate pathway

The pathway is outlined in Scheme 4. The degradation of the intermediate **14** is believed to be initiated by another attack by a hydroxyl radical. Such attack usually occurs at a strongly electronegative site but to substantiate the degradation of the aliphatic chain leading to the formation of one of the final products (**15**), we must assume that the attack by hydroxy radical (and the ensuing radical addition) occurs at a carbon atom with a small negative charge (computed as

© 2001 NRC Canada

Scheme 5. Computations of ionization states of two analogous degradation products (**23** and **25**) suggest preferential ionization of the phenolic hydroxyl of the hypothetical product **23**. See Scheme 2 for the explanation of symbols.

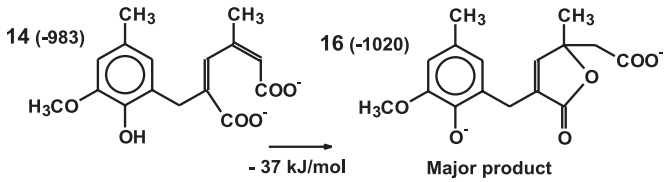




–0.06). The radical addition results in a radical (**18**) with high spin density (1.09) at the site of coupling reaction with a perhydroxyl radical. The coupling results in the formation of a peroxide (**19**). Both the radical addition and coupling reactions are exothermic according to the computations. However, for the peroxide to form the dioxetane (**20**), the computations suggest that 51 kJ mol^{-1} heat has to be supplied.

The dioxetane **20** then cleaves exothermically to yield a product (**21**), which upon exothermic oxidation with hydroperoxyl anion, leads to the formation of **15** — an anion of one of the major products (**1**), determined experimentally (18). The degradation of **20** also leads to the formation of an α-keto acid (**22**). An analogous reaction with a biphenyl model compound computed previously (16), led (after decarboxylation and oxidation of an analogous α-keto acid) to the formation of 2-hydroxy-3-methoxy-5-methylbenzoic acid, the main product of the biphenyl model compound degradation. However, no analogous aromatic acid was found among the degradation products of MMMP. Scheme 5 illustrates an attempt to explain this apparent discrepancy. Compound **22** (Scheme 4) may yield the hypothetical intermediate (**23**) (Scheme 6), after decarboxylation and oxidation analogous to that proposed previously (16) for the formation of of 2-hydroxy-3-methoxy-5-methylbenzoic acid (its phenolate anion (**25**) is shown in Scheme 5). However, computations of heats of formation shown in Scheme 5 suggest that the hypothetical product (**23**), compared to **25**, is more likely to yield a phenolate anion (**24**), which would then become subject of an attack by hydroxyl radicals and could undergo further degradation or polymerization reactions. This could explain why the hypothetical intermediate (**23**) is not found among the MMMP degradation products (18). Alternatively, Scheme 5 suggests that the analogous biphenyl model degradation product (**25**) produces a phenolate much less readily. It is therefore unlikely to undergo further degradation reactions and is present among the biphenyl model degradation products (18). It should be noted that in the reactions shown in Scheme 5, the hydrogen ions have been omitted and therefore, the differences in the heats of formation do not indicate the heats of ionization.

Scheme 6. Furanacetate branch pathway starting with the common dicarboxylic intermediate **14** and results in an anion (**16**) of a major degradation product (**2**), determined by Sun et al. (18). See Scheme 2 for the explanation of symbols.



The furanacetate pathway

This branch pathway (Scheme 6) consists of exothermic lactonization of the dicarboxylic intermediate (**14**), yielding an anion (**16**) of the furanacetic acid product **2** (Scheme 1).

The oxopentanoate pathway

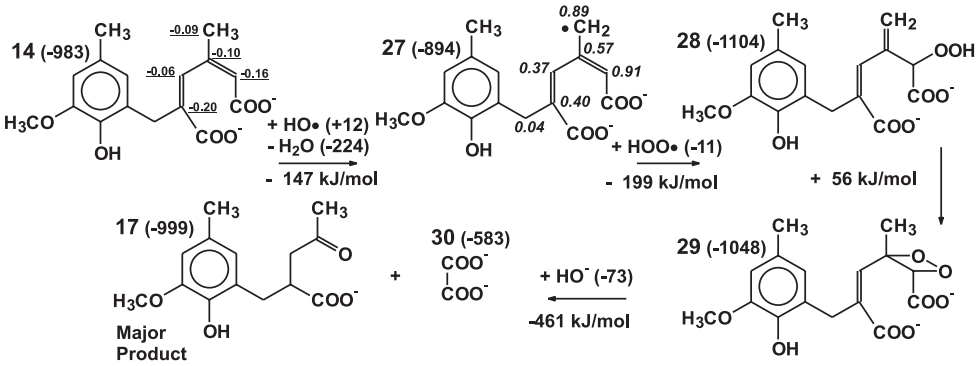
This pathway is the third of the branching pathways. Its course is outlined in Scheme 7. As the previous two it also starts from the dicarboxylic intermediate **14**. Computational investigation of several variants of this pathway led to this scheme judged to be thermodynamically most favourable. We presume that an exothermic reaction with a hydroxyl radical leads to hydrogen abstraction from the intermediate **14**, resulting in a benzylic radical species (**27**), with high spin density (0.91) at the site of coupling reaction with a perhydroxyl radical. This exothermic reaction yields a peroxide (**28**). Transformation of **28** into a dioxetane structure (**29**) is predicted to be an endothermic reaction (+56 kJ mol^{-1}). The dioxetane **29** then undergoes an exothermic C—C scission and yields an anion (**17**) of a major degradation product (**3**), identified previously (18). A byproduct of the scission is predicted to be oxalate **30**, originally not noticed (18) due to a very low gas chromatography response factor. A review of the analytical data (unpublished) revealed the presence of about 2% of oxalic acid among the reaction products, in agreement with this prediction.

Alternative radical reactions

In addition to the pathways described above, we explored other reactions as alternatives. Thus, hydrogen abstraction from the diphenylmethyl carbon of MMMP rather than formation of a phenoxy radical was considered as a likely reaction leading to the formation of a stable diphenylmethane radical. However, we could not derive the experimental products (Scheme 1) from this intermediate. Possible alternatives to hydrogen abstraction reactions in Scheme 7 could be hydroxyl radical additions to unsaturated structures. We have computed two such scenarios and were able to arrive at the determined products but the computed reactions appeared thermodynamically less favourable (the barriers were +84 and +115 kJ mol^{-1}). It is interesting to note that Sun et al. (18) reported a low yield (0.5%) of a 1-hydroxylated derivative of compound **2**. This derivative is probably a product of a hydroxyl radical addition reaction. We also computed an alternative to Scheme 4, based on hydrogen abstraction from an unsaturated carbon. Although the alterna-

© 2001 NRC Canada

Scheme 7. The oxopentanoate branch pathway starting with the common intermediate **14** and leading, via radical reactions, to an anion (**17**) of the major product **3**, determined by Sun et al. (18). See Scheme 2 for the explanation of symbols.



tive yielded a barrier marginally lower (+50 instead of +51 kJ mol^{-1}) we did not consider it likely.

There is little doubt that, in addition to reactions proposed in Schemes 2–7, various alternative reactions take place during the oxidative degradation of the diphenylmethane structures. However, the outcome of these reactions may have been either a condensation or conversion of the substrate to carbonate, explaining why the overall yields of the reaction products were not quantitative (see Scheme 1 and a discussion of the yields).

Barriers on the reaction pathways

In our previous investigation (16) of a biphenyl-type model compound, we concluded from our computations that the only endothermic steps on the degradation pathway are transformation reactions of peroxides into corresponding dioxetanes. It should also be noted that *all* such transformations were computed as endothermic. It is significant that the same rule can be extended to all pathways presented in this work on MMMP. Consideration of reaction barriers in this case is somewhat complicated by the branching of the pathway. However, the common initial pathway (Schemes 2 and 3) has one endothermic step (+16 kJ mol^{-1}, Scheme 3) after which there is no barrier to the end of the furanacetate branch (Scheme 6). Therefore, this barrier could be the one controlling the disappearance of MMMP. In comparison, the disappearance of the biphenyl compound encounters a much greater barrier further down the pathway (+94 kJ mol^{-1}) (16). The activation energy for the disappearance of MMMP is also lower (54 ± 11 kJ mol^{-1}) than the previously determined activation energy (117 kJ mol^{-1}) for the biphenyl model (16).

Significant endothermic steps have been computed on the other two branch pathways, butenedioate and oxopentanoate (+51 and +56 kJ mol^{-1}, respectively; see Schemes 4 and 7). These values are similar to the experimentally determined activation energy for the disappearance of the model compound MMMP. It is tempting to speculate that the activation energy reflects these barriers. Thus it seems that not only the disappearance of MMMP but also the formation of the degradation products encounters lower energy barriers than those observed for the degradation pathway of the analogous biphenyl model (16).

Experimental

Materials

MMMP used in this work was synthesized according to Kratzl and Virhopper (19). 3,4-Dimethoxyphenol (97%) was used for GC–FID quantification; 2-chloro-4,4,5,5-tetramethyl-1,3,2-dioxaphospholane (95%) was used as a phosphitylation reagent; magnesium sulphate (99.99%), sodium hydroxide (99.99%), and potassium iodide (99.9%) were purchased from Aldrich. Distilled water used in this study was treated with a NANO pure Analytical Deionization System (Barnstead).

Activation energy

The degradation of 2,2′-methylenebis[6-methoxy-4-methylphenol] (MMMP; an anion of this compound (**4**) is shown in Scheme 2) was carried out in dilute alkali with hydrogen peroxide at four different temperatures (60, 70, 90, and 100°C) for various intervals (5–60 min). The pH of the starting reaction mixture was 12.4. Under the most extreme conditions (100°C for 45 min), the pH dropped to about 10.2 after the reaction. The molar excess of hydrogen peroxide over MMMP was high enough to maintain residual hydrogen peroxide at >15% of the original amount under all conditions of the kinetic study. The amount of unreacted MMMP was identified using GC–FID analyses; the lowest recorded yield was 28% of the original amount.

A similar set of reactions with residual kraft lignin was carried out at 70, 110, and 130°C for 15–90 min. Phenolic hydroxyl groups in the diphenylmetane structures were assayed using quantitative ^{31}P NMR spectroscopy. These structures show a ^{31}P chemical shift signal in the interval 142.7–144.0 ppm. The original amount of these groups was 0.243 mmol g^{-1} and dropped to about 10% of this at the most extreme treatment conditions (90 min at 110°C).

From the reaction rates measured at various conditions, we calculated apparent reaction constants (k_{app}) and determined their errors from the errors of the corresponding plots. The activation energies for the oxidative degradation of: (*i*) MMMP; and (*ii*) diphenylmethane structures in residual kraft lignin, were calculated from the kinetic data using the Arrhenius equation (20). The errors of the E_a estimates were calculated using averages of the errors of the ln (k_{app}) data.

© 2001 NRC Canada

Treatment of 2,2′-methylenebis[6-methoxy-4-methylphenol]

MMMP was oxidized with hydrogen peroxide as a function of time and temperature using a 40-mL glass-lined steel bomb reactor. The molar ratio of MMMP to hydrogen peroxide and sodium hydroxide was 1:6:4, respectively. To approximately 100 mg of MMMP in the glass liner we added 20 mL of deionized water, 1.23 mg of magnesium sulphate in solution, and 58.4 mg of sodium hydroxide in solution. The mixture was heated and stirred for 5 min to solubilize the ingredients. After cooling, 190 μl of 30% aqueous hydrogen peroxide was added and the whole transferred into a glass liner and covered with a glass lid. The reactor was sealed and placed in a preheated oil bath, and kept there for the specified time. At the end of the reaction, the reactor was rapidly cooled and 2 mL of the reaction mixture was withdrawn for measurement of the residual hydrogen peroxide. The pH of the solution after reaction (9.5–11.8) was adjusted to about 2 with 1 N hydrochloric acid. The mixture was then lyophilized and the solids extracted three times with approximately 5 mL of ethyl acetate. Before weighing the solute, the extract was placed into a preweighed vial, allowed to dry at room temperature, and then desiccated in vacuo for 2 days.

Treatment of residual kraft lignin

The procedure was similar to that used for the model compound. Residual kraft lignin from black spruce kraft pulp (50 mg, i.e., 0.273 mmol of C9 units), free of metal, was suspended in 1 mL of deionized water and 1 mL of 1 N sodium hydroxide was added. The pH of the suspension was 13.4. Hydrogen peroxide (65 μl, 30% in water) was then added at the molar ratio of lignin C9 units to hydrogen peroxide, equal to 1:2.3. At the end of the reaction period, the mixture was acidified to pH 2. The precipitated degraded lignin was then lyophilized and brought to constant weight.

Gas chromatography with flame ionization detection (GC–FID)

The analyses were carried out on a Hewlett–Packard 5890A gas chromatograph equipped with a DB-5 capillary column. The injection port temperature was 250°C and the oven temperature was raised from 70°C to 250°C with a gradient of 15°C min^{-1}. One mL of pyridine was added to the dry product and the vial was immediately closed and shaken until all dissolved. Fifty μl were transferred to a new vial and 0.3 mL of pyridine and 100 μL of internal standard solution was added. The internal standard was 3,4-dimethoxyphenol (1.004 mg in 100 μL). *N*,*O*-Bis(trimethylsilyl)acetamide was added as a silylation reagent. The GC response factor relative to the internal standard was determined as follows: accurately measured amounts of the internal standard and diphenylmethane were mixed well in pyridine. Then the sample was silylated and the resulting solution injected. The integrated areas from GC were compared to determine the response factor.

Quantitative ^{31}P NMR analysis

Lignin samples were analyzed for the content of diphenylmethane structures using a previously published method (21).

Computational methods

All compounds listed in the various schemes have been subjected to computational analysis of the geometry-optimized structures. The optimization was done using the third parametrization semiempirical method (PM3) (22, 23) after subjecting the structures to simulated annealing and preliminary optimization with a molecular mechanics method (MM+) derived from the method of Allinger (24). All computational methods were used as implemented by HyperChem Professional, Version 5.11 (HyperCube, Inc.). The details of the computational protocol were the same as described previously (16). The values of heats of formation, charges on individual atoms, and electron spin densities (α–β atomic orbital electron populations) were computed on the optimized structures.

Conclusions

The activation energy for the alkaline oxidative degradation of the diphenylmethane model compound (2,2′-methylenebis[6-methoxy-4-methylphenol]) (MMMP) and diphenylmethane structures in residual lignin is similar (54 ± 11 and 58 ± 5 kJ mol^{-1}, respectively), supporting the relevance of MMMP to represent diphenylmethane moieties of kraft lignins.

The critical steps in the degradation sequence may be the aromatic ring cleavage and the scission of the newly formed aliphatic side chain.

Both aromatic and aliphatic scission mechanisms may be similar and might consist of the following steps: (*i*) formation of radical sites by reactions with hydroxyl radicals; (*ii*) radical coupling reactions of the radical sites with perhydroxyl radicals, resulting in formation of peroxides; (*iii*) transformation of peroxides into dioxetanes; (*iv*) scission of the dioxetane structures.

MMMP is more easily degraded (as reported by Johansson and Ljunggren (17)) than the corresponding biphenyl model for these main reasons: (*i*) the activation energy for the disappearance of MMMP is lower; (*ii*) the critical endothermic reactions on the MMMP degradation pathway require less energy; (*iii*) the initial electrophilic attack by a hydroxyl radical is facilitated by the more electronegative phenolic hydroxyl oxygen; (*iv*) the course of the degradation of the diphenylmethane structures branches into at least three pathways thus providing multiple ways for the structure to degrade; (*v*) carboxylic acid group formation during the degradation of the diphenylmethane moieties provides less protection for the residual aromatic structures due to the greater distance from the phenolic hydroxyl.

The above conclusions from the model compounds can probably be extended to the biphenyl and diphenylmethane structures in lignin.

Acknowledgements

We wish to thank Dr. Peter McGarry (Paprican) for valuable comments and suggestions. Professor Leif Eriksson (Department of Quantum Chemistry, Uppsala University, Sweden) kindly provided us with advice on computation methods.

© 2001 NRC Canada

References

1. Z.-H. Jiang and D.S. Argyropoulos. J. Pulp Paper Sci. **25**, 25 (1999).
2. T. Eriksson and J. Gierer. J. Wood Chem. Technol. **5**, 53 (1985).
3. A. Granata and D.S. Argyropoulos. J. Agric. Food Chem. **43**, 1538 (1995).
4. B. Ahvazi, G. Pageau, and D.S Argyropoulos. Can. J. Chem. **76**, 506 (1998).
5. K. Toven. Int. Symp. Wood Pulping Chem. 10th. 1999. Vol. II, 340 (1999).
6. P. Karhunen, P. Rummakko, J. Sipila, J. Brunow, and I. Kilpelalnen. Tetrahedron Lett. **36**, 169 (1995).
7. P. Karhunen, J. Mikkola, A. Pajunen, and G. Brunow. Nord. Pulp Pap. Res. J. **14**, 123 (1999).
8. D.S. Argyropoulos and S.B. Menachem. Lignin. *In* Advances in biochemical engineering/biotechnology. Vol. 57. *Edited by* K.E. Erickson. Springer–Verlag, Berlin, Heidelberg. 1997. pp. 127–158.
9. Y.Z. Lai, M. Funaoka, and H.T. Chen. Int. Symp. Wood Pulping Chem. 7th. 1993. 308 (1993).
10. J. Gierer and F. Imsgard. Svensk. Papperstidn. **80**, 510 (1977).
11. C.W. Bailey and C.W Dence. Tappi J. **52**, 491 (1969).
12. G. Gellerstedt, K. Gustafsson, and E.-L. Lindfors Nord. Pulp Paper Res. J. **1**, 14 (1986).
13. J. Gierer. Holzforschung, **51**, 34 (1997).
14. J. Gierer, E. Yang, and T. Reitberger. Holzforschung, **46**, 495 (1992).
15. H. Xu and Y.Z. Lai. J. Wood Chem. Technol. **17**, 223 (1997).
16. L. Jurasek, Y. Sun, and D.S. Argyropoulos. A detailed study of the alkaline oxidative degradation of a residual kraft lignin model compound. *In* Fundamentals and catalysis of oxidative delignification processes. *Edited by* D.S. Argyropoulos. ACS Books Series 785. American Chemical Society, Washington, D.C. 2001. pp. 130–148.
17. E. Johansson and S. Ljunggren. J. Wood Chem. Technol. **14**, 507 (1994).
18. Y. Sun, M. Fenster, A. Yu, R.M. Berry, and D.S. Argyropoulos. Can. J. Chem. **77**, 667 (1999).
19. K. Kratzl and F.W. Virhopper. Monatsh. Chem. **102**, 425 (1971).
20. S.R. Radel and M.H. Navidi. Chemistry. 2nd ed. West Publishing Company, St. Paul, Minnesota. 1994. pp. 663–668.
21. B.C. Ahvazi and D.S. Argyropoulos. Nord. Pulp Paper Res. J. **12**, 282 (1997).
22. J.J.P. Stewart. J. Comput. Chem. **10**, 209 (1989*a*).
23. J.J.P. Stewart. J. Comput. Chem. **10**, 221 (1989*b*).
24. N.L. Allinger. J. Am. Chem. Soc. **99**, 8127 (1977).

© 2001 NRC Canada

Canadian Journal of Chemistry

Author Index
Volume 79, 2001

Revue canadienne de chimie

Index des auteurs
Volume 79, 2001

Abdur-Rashid, K., 964
Adams, H., 731, 760
Agustinho, S.C.M., 760
Akim, L.G., 201
Albinati, A., 693
Albrecht, M., 709
Alexiou, C., 992
Alguindigue, S.S., 809
Alper, H., 587
Amoroso, D., 958
Angelici, R.J., 578
Aresta, M., 570
Argyropoulos, D.S., 201, 1394
Armstrong, D.A., 405
Asadi, M., 70, 1360
Ashby, M.T., 809
Askalany, A.H., 42
Atwood, J.D., 1036
Aylward, W.M., 1
Baboulène, M., 1153
Bachmann, P., 519
Baerlocher, M.O., 1115
Baerlocher, F.J., 1115
Bailey, A.J., 792
Baines, K.M., 461
Baird, M.C., 1012
Baker, P.K., 263
Bakhmutov, V.I., 479
Bakhmutova, E.V., 479
Bakos, J., 725, 1040
Balakrishnan, V.K., 157
Balch, A.L., 922
Balci, M., 35
Ball, J.M., 304
Barba, V., 1229
Barthazy, P., 904
Bartosh, K., 1026
Bartosz-Bechowski, H., 752
Basickes, L., 854
Batchelor, R.J., 938, 1272
Batista, A.A., 1030
Battaglia, L., 621
Beagley, P., 731
Belchior, J.C., 211
Belkova, N.V., 479
Bennett, M.A., 655
Benson, G.C., 388
Bényei, A.C., 635
Bergens, S.H., 1019
Berges, J., 405
Bergman, R.G., 525
Berners-Price, S.J., 1030
Bertotti, M., 679
Besenyei, G., 649, 688
Bhattacharyya, S., 938
Bianchini, C., 479
Blanco, C.A., 448
Blaser, H.-U., 566
Boch, R., 1068
Bond, A.M., 613
Bonilla, R.J., 719
Bottomley, F., 1321
Boule, P., 1179
Bourgeois, M.-J., 257
Bowden, A.A., 1036
Boyd, S.E., 1030
Braga, J.P., 211
Brechbiel, M.W., 1105
Breed, P.G., 1049
Broggini, D., 904
Brouillard, R., 1173
Brown, J.M., 1049
Brown, M.A., 463
Bruce, D.W., 472
Buchanan, G.W., 195
Buckley, A.V., 1284
Buckley, R.W., 1030
Buncel, E., 157
Bunn, A.G., 854
Burford, N., 342
Butler, D.C.D., 472
Cadoret, J., 626
Cai, Z.-S., 29
Calderazzo, F., 495
Cameron, T.S., 342
Campagnole, M., 257
Cantin, A.M., 377
Cao, D., 455
Cao, S., 272
Carpenter, B.E., 291, 857
Casagrande, B., 566
Casey, C.P., 1002
Castellano, E.E., 1030
Catellani, M., 742
Centoducatte, R., 121
Chapados, C., 13
Chen, L., 29
Chen, Y.-T., 221, 455
Chim, J.L.C., 607
Choi, H.Y., 337
Chomka, K., 760
Chow, A., 437
Chung, M.-K., 949
Ciunik, Z., 752, 868
Claver, C., 560
Cole-Hamilton, D.J., 472
Colodette, J.L., 201
Cooper, L., 490
Cordes, A.W., 1352
Coulter, K.R., 930
Cowan, J.J., 792
Cromer, M., 370
Crowe, D.A.J., 1145
Cserépi-Szűcs, S., 725
Cuahutle, D., 1229
Cugini, F., 742
Das, P.K., 809
Dave, V., 461
Davies, P., 731
Davies, S.C., 490
Dawid, M., 110, 1294
de Almeida Santos, R.H., 679
de Blois, S., 13
de Castro, E.V.R., 121
de Vries, J.G., 1086
Dean, P.A.W., 1293, 1330
Decken, A., 1115, 1321
Delaude, L., 529
Delmarre, D., 1068
del Rio, I., 560
Demchenko, A.P., 358
Demonceau, A., 529
den Reijer, C.J., 693
Dibenedetto, A., 570
Dileo, C., 570
Dilworth, J.R., 490
Dobó, A., 1040
Dolphin, D., 1068
dos Santos Silva, H.A., 679
Dotta, P., 693
Drake, J.E., 983

© 2001 NRC Canada

Drew, M.G.B., 263
Durran, S.E., 780
Duś, D., 868
Dust, J.M., 157
Duval, P.B., 536
Dworschak, R.G., 437
Dyson, P.J., 705
Ebadi, M., 992
Einstein, F.W.B., 938, 1272
Ellena, J., 1030
Ellis, D.J., 705
Elzner, S., 593
Emmett, M.R., 546
Englert, U., 495
Ens, W., 437
Epstein, L.M., 479
Escher, E., 377
Evans, D.S., 263
Fabbri, D., 670
Fackler, J.P., Jr., 896
Fang, Q., 174
Farcas, S.I., 983
Farfán, N., 1229
Faria, R.B., 1135
Feng, J.-K., 1366
Ferguson, G., 949
Fish, R.H., 888
Fitzpatrick, S.J., 1101
Fleischer, M.A., 75
Fogg, D.E., 958
Fornika, R., 642
Fougerousse, A., 1173
Franco, D.W., 679
Fryzuk, M.D., 536, 1194
Fu, W., 1366
Funahashi, S., 1344
Gaisberger, B., 394
Gałęzowski, W., 1128
Gao, H., 578
Gao, Y., 915
Gay, I.D., 1272
Gelbrich, T., 780
Geletti, Y.V., 792
Gill, M.A., 1101
Gillis, H.A., 80
Gladiali, S., 670
Gömöry, Á., 725
Gonzalez, E., 1173
Görls, H., 642
Graziano, G., 105, 1310
Greaney, M., 546
Griffith, W.P., 598
Grundwald-Wyspiańska, M., 775
Grześkowiak, I., 1128
Guliński, J., 775
Gulyás, H., 1040
Gupta, R.N., 418
Haines, R.I., 54
Harrod, J.F., 1075
Hartman, J.S., 426
Harvey, P.D., 552
Hassan, A.A., 42
He, D., 1213
He, S., 510
He, W., 127
Healy, P.C., 1030
Hegedüs, C., 725
Hemscheidt, T., 418
Hendrickson, C.L., 546
Henry, B.R., 279
Herraiz-Sierra, I., 448
Hidai, M., 632
Hill, C.L., 792
Hill, J.M., 817
Hioka, N., 1068
Hiyama, T., 593
Hnatiw, J.B., 304
Holly, S., 649
Hook, J.M., 1330
Horikawa, Y., 388
Hou, Z., 29
Hsieh, Y.-H., 1272
Hu, T.Q., 1201
Huang, Y., 719
Hughes, D.L., 490
Hursthouse, M.B., 780, 983
Hutchings, D.R., 54
Iwatsuki, S., 1344
Jablonski, C., 463
Jafarpour, L., 626
James, B.R., 1201
James, S.L., 709
Jamshid, K.A., 70
Jan, D., 529
Jarczewski, A., 1128
Jenkins, H.A., 1293, 1330
Jennings, M., 1330
Jennings, M.C., 915
Jensen, C.M., 823
Jessop, P.G., 719
Jezierski, A., 570
Jiang, M.H., 174
Jiang, X., 127
Joó, F., 635
Jorge, F.E., 121
Jurasek, L., 1394
Kashiwabara, K., 1344
Kenawy, I., 42
Kessler, M., 642
Khan, M.A., 830
Khomutov, O.G., 183
Kim, C.-K., 1238
Kinal, A., 35
King, J.F., 461
Kirby, C.W., 296
Kleinke, H., 1338
Kliegel, W., 226
Klymchenko, A.S., 358
Knoblauch, S., 977
Koch, H.F., 977
Kodess, M.I., 183
Konkol, M., 490
Koshino, N., 1344
Koteva, K.P., 377
Kovács, J., 635
Krisdhasima, V., 848
Krištofová, L., 1394
Krüger, C., 642
Kurokawa, G.S., 1058
Lam, K.C., 342
Langner, R., 1376
Lau, M.-K., 607
Laurenczy, G., 635
Le, N., 238
LeBlanc, D.J., 342
Lee, D.W., 823
Lee, J., 830
Lee-Ruff, E., 114
Legzdins, P., 502
Leitner, W., 642
Lemes, N.H.T., 211
Lemieux, R.U., 238
Leung, W.-H., 607
Lever, A.B.P., 992
Lewandowski, M., 775
Leznoff, C.C., 878
Li, H.L., 328
Li, W., 1366
Li, Y.-N., 29
Light, M.E., 780, 983
Lightfoot, P., 472
Lin, H.-K., 221, 455
Ling, C.-C., 238
Liu, S., 1058
Long, G.S., 1026
Loop, I., 183
López-de-Luzuriaga, J.M., 896
Lord, G., 337
Lork, E., 183
Lough, A.J., 964
Lu, A.Z., 1201
Lu, B.C.-Y., 388
Lu, J., 127
Lu, X., 319, 364
Lubell, W.D., 94
Lubkowitz, G., 226
Lucas, R.J., 54
Luo, H., 1105

© 2001 NRC Canada

Ma, M., 1213
Macdonald, C.L.B., 342
Machado, S.P., 1135
Machuca-Herrera, J.O., 1135
MacRae, A.I., 1101
Magnuson, K., 823
Mahajan, D., 848
Mahiuddin, S., 1207
Małecka, E., 775
Małgorzata, D., 1294
Mamer, O., 1381
Mann, B.E., 760
March, R.E., 124
Marciniec, B., 775
Markó, L., 725
Marshall, A.G., 546
Martin, M., 519
Martinez, H.E., 50
Martinsson, A., 938
Masi, D., 479
Max, J.-J., 13
McAuley, A., 930
McComb, M.E., 437
McDonald, R., 291
McGarvey, B.R., 679
McGlinchey, M.J., 1295
Medici, S., 670
Meilleur, D., 552
Mele, G., 587
Menzek, A., 35
Merkley, N., 312
Meunier, L., 1179
Mezzetti, A., 904
Miller, D., 54
Miller, J.M., 1220, 1224
Mingie, J.R., 1352
Mitchell, T.R.B., 655
Mizobe, Y., 632
Moineau, C., 587
Montaudon, E., 257
Morales-Morales, D., 823
Mori, V., 679
Morlay, C., 370
Morris, R.H., 964
Mouginot, Y., 370
Moulik, S.P., 1
Murray, M.C., 1012
Nâdasdi, L., 635
Narracci, M., 570
Natansohn, A., 1093
Neil, M.A., 1321
Neszmélyi, A., 649
Netherton, M.R., 461
Neugebauer, W.A., 377
Ng, F.T.T., 817
Niesyty, K., 752
Nikolcheva, L.G., 1115
Noels, A.F., 529
Nolan, S.P., 626
Noll, B.C., 922
Norman, D.W., 1115
North, M.R., 75
Nozaki, K., 593
Oakley, R.T., 1352
Obeyama, K., 1344
Okajima, T., 22
Oleschuk, R.D., 437
Olmstead, M.M., 922
Opolski, A., 868
Orvig, C., 1058
Osmond, D.A., 1201
Ozturk, T., 358
Palepu, R., 1
Pampaloni, G., 495
Pan, P., 131
Panosyan, F.B., 1110
Papp, G., 635
Park, D.K., 337
Park, Y.S., 337
Párkányi, L., 649
Parvez, M., 857
Pashkevich, K.I., 183
Passarelli, V., 495
Patrick, B.O., 1194, 1201
Perez-Encabo, A., 448
Perreault, H., 437
Peruzzini, M., 479
Petryk, M.W.P., 279
Phillips, A.D., 342
Phillips, S., 922
Piers, W.E., 291, 857
Pilichowski, J.-F., 1179
Pincock, J.A., 63
Pinna, F., 621
Pirri, G., 670
Pivovarenko, V.G., 358
Pokriefke, J.O., 226
Polydore, C., 977
Pope, M.T., 802
Povar, I., 1166
Powell, D.R., 830, 1002
Power, W.P., 296
Pregosin, P.S., 693
Preston, K.R., 437
Pruchnik, F.P., 868
Puddephatt, R.J., 915
Pulacchini, S., 670
Qian, K., 546
Qian, X., 272
Qian, Y., 127
Queiroz, S.L., 1030
Quickenden, T.I., 80
Rabion, A., 888
Rajalingam, U., 1293, 1330
Ramnauth, J., 114
Ramos, J.F., 50
Ramsden, J.A., 1049
Rastegar, M.F., 195
Rauk, A., 405
Redón, R., 823
Reed, R.W., 1352
Reid, D.L., 319
Rettig, S.J., 226, 502, 536, 857, 930
Rheingold, A.L., 342
Richards, R.L., 490
Richardt, P.J.S., 613
Richter-Addo, G.B., 830
Rifai, S., 63
Riggio, R., 50
Ro, S., 1238, 1259
Robertson, V., 949
Rocha, R.C., 145
Rochon, P., 1093
Rodgers, R.P., 546
Roehri-Stoeckel, C., 1173
Rogers, R.D., 1105
Rojas, A., 448
Röschenthaler, G.-V., 183
Rösler, R., 983
Rotar, A., 983
Roundhill, D.M., 977
Samonte, J.L., 802
Samuel, E., 1075
Sanders, J.R., 490
Santillan, R., 1229
Santos, C.M.P., 1135
Saraçoglu, N., 35
Sarvestani, A.H., 1360
Sauriol, F., 1381
Sayer, B.G., 418
Scheffer, J.R., 349
Schlaf, M., 949
Seino, H., 632
Sen, A., 1026
Serni, G., 495
Sevenard, D.V., 183
Seward, C., 1187
Shehetta, I., 42
Sheldon, R.A., 688
Shi, Y.-L., 328
Shi, Z., 1238, 1259, 1278
Shibahara, F., 593
Shoemaker, J.A.W., 426
Shu, R., 1075
Shubina, E.S., 479
Siebenhaar, B., 566
Silvestru, A., 983
Silvestru, C., 983

© 2001 NRC Canada

Simal, F., 529
Simándi, L.I., 649
Singer, S.W., 1002
Six, C., 642
Slawin, A.M.Z., 780
Smith, D.C., Jr., 626
Smith, K.M., 502
Smith, M.B., 780
Smith, P.J., 1145
Smith, S., 760
Snedeker, B., 1026
Sobota, P., 490
Solar, S., 394
Somogyi, L., 1159
Song, B., 1058
Song, G., 272
Song, H., 29
Song, J.H., 337
Souirti, S., 1153
Spek, A.L., 709
Spenser, I.D., 418
Spey, S., 760
Spinney, H.A., 1115
Spirlet, M.R., 529
Spohr, U., 238
Sproull, R.D., 848
Squires, C., 760
Standing, K.G., 437
Staples, R.J., 896
Stark, L., 342
Starosta, R., 868
Stefanova, R., 63
Sternberg, E., 1068
Stevens, E.D., 626
Stevens, M.R., 655
Still, I.W.J., 1110
Stojanovic, N., 1101
Strukul, G., 621
Studer, M., 566
Stynes, D.V., 795
Su, X.-C., 221, 455
Suchozak, B., 878
Sun, D.-A., 1381
Sun, H.-W., 221
Sun, Y., 1394
Suriaatmaja, M., 598
Suzuki, T., 1344
Swaddle, T.W., 75, 841
Symons, M.C.R., 124
Szöllősy, Á., 725
Takagi, F., 632
Takagi, H.D., 1344
Tellers, D.M., 525
Thomas, C.A., 719
Tiefenthaler, D., 742
Toma, H.E., 145
Tommasi, I., 570
Tracey, A.S., 938
Tregloan, P.A., 613
Trotter, J., 226
Trzeciak, A.M., 752
van Koten, G., 709
van Leeuwen, P.W.N.M., 560
vanLoon, G.W., 157
van Zyl, W.E., 896
Veilleux, A., 13
Veldman, N., 709
Venneri, P.C., 110, 312, 1294
Verspui, G., 688
Vialemaringe, M., 257
Vincent, J.-M., 888
Vittori, O., 370
Vogels, C.M., 1115
Vorontsov, E.V., 479
Wagner, B.D., 1101
Wahab, A., 1207
Walsh, D., 342
Wang, C., 174
Wang, H., 1213
Wang, R., 495
Wang, S., 1187
Wang, Z., 328, 388, 823
Wang, X.M., 174
Warkentin, J., 110, 312, 319, 364, 1294
Wayland, B.B., 854
Wedd, A.G., 613
Wei, L., 94
Wei, Q.-L., 29
Weinberg, N., 1284
Weinstock, I.A., 792
Welton, T., 705
Werner, H., 519
Werner, M.L., 1026
Westaway, K.C., 1145
Westcott, S.A., 1115
White, C., 731
White, J.M., 613
Wietrzyk, J., 868
Wiles, J.A., 1019
Williams, I.D., 607
Willis, A.C., 655
Withers, S.G., 510
Wojdat, E., 868
Wolfe, S., 1238, 1259, 1272, 1278, 1284
Wong, A.W., 510
Wong, W.-T., 607
Woo, H.-G., 1075
Wu, B.-X., 29
Xie, Y., 127
Yachandra, V.K., 888
Yan, P., 127
Yap, G.P.A., 195, 857, 958
Yi, G.-B., 830
Young, V.G., Jr., 1019
Yu, P., 1194
Yu, W.T., 174
Yung, C., 823
Zahir, K.O., 1124
Zamir, L.O., 1381
Zanobini, F., 479
Zhang, H., 1352
Zhang, H.-X., 1366
Zhao, G.-H., 221
Zhao, R., 131
Zhao, X., 174
Zhao, X.-Z., 29
Zhou, J., 841
Zhou, P., 1213
Zhou, Y.F., 174
Zhou, Z.-F., 221, 455
Zhu, S.-R., 221, 455
Zhuang, Q., 1220, 1224
Ziolkowski, J., 570
Ziólkowski, J.J., 752
Znamirowski, M., 437
Zobi, F., 795
Zundel, G., 1376

© 2001 NRC Canada

PREVIEW / APERÇU

Forthcoming special issues / Numéros spécials à paraître

November 2001	In honour of Professor Victor Snieckus
June 2002	In honour of Professor J. Bryan Jones
August 2002	In honour of Professor Ray Lemieux
November 2002	In honour of Professor Tris Chivers
June 2003	In honour of Professor Don Arnold

Forthcoming articles / Articles à paraître

2000 Maxxam Award Lecture - Unified theory of extraction	J. Pawliszyn
An experimental and theoretical approach to phosphonodithioato complexes: molecular orbital analysis by hybrid-DFT and EHT calculations on *trans*-bis[*O*-alkyl-phenylphosphonodithioato]Ni^{II} and vibrational assignments	M.C. Aragoni, M. Arca, F.A. Devillanova, J.R. Ferraro, F. Isaia, F. Lelj, V. Lippolis, and G. Verani
Binding of anti-inflammatory drug indomethacin with cyclodextrin and DNA; solubility, spectroscopic, and voltammetric studies	I.S. Shehatta and M.S. Ibrahim
Disquac predictions on thermodynamic properties of ternary and higher multicomponent mixtures. Part II. Results for HE of ternary mixtures containing nonpolar components, or one polar, two polar compounds, or one alcohol and hydrocarbons or CCl_4	J.A. Gonzalez, J. Carmona, N. Riesco, I.G. de la Fuente, and J.C. Cobos
Geometric and solvent effects on intramolecular phenolic hydrogen abstraction by carbonyl *n*, π^* and π, π^* triplets	E.C. Lathioor and W.J. Leigh
Interaction of human serum albumin with oxovanadium ions studied by FT-IR spectroscopy, gel and capillary electrophoresis	M. Purcell, J.F. Neault, H. Malonga, H. Arakawa, and H.A. Tajmir-Riahi
Oxidative coupling of naphtho-9-crown-3 ether: X-ray crystal structure and solution and solid-state NMR analysis of the dimer	G.W. Buchanan, M.F. Rastegar, G.P.A. Yap, A. Moghimi, and M. Ghandi
Regioselective upper rim functionalizations of calix[4]arene by diphenylphosphino groups	J. Gagnon, M. Vézina, M. Drouin, and P.D. Harvey
Solubility of nonpolar gases in 2,2,2-trifluoroethanol and 1,1,1,3,3,3-hexafluoropropan-2-ol at several temperatures and 101.33 kPa partial pressure of gas	M.A. Sánchez, A.M. Mainar, J.I. Pardo, M.C. López, and J.S. Urieta
Solubility predictions for crystalline nonelectrolyte solutes dissolved in organic solvents based upon the Abraham General Solvation Model	W.E. Acree, Jr. and M.H. Abraham
Synthesis of chloro-(2-methylimidazole)ruthenium(III) complexes and their aqueous solution chemistry: the crystal structure of $[2\text{-MeImH}]_2[RuCl_5 2\text{-MeIm}]$	C. Anderson
Tests for aromaticity applied to the pentalenoquinones: a computational study	C. Delamere, C. Jakins, and E. Lewars
The metal template effect on *O*-alkylation of tetrahydroxy[3.1.3.1]metacyclophane with 4-(chloromethyl)pyridine to afford tetrakis[(4-pyridylmethyl)oxy]-[3.1.3.1]metacyclophanes and their conformational studies	T. Yamato, K. Kumamaru, and H. Tsuzuki

© 2001 NRC Canada

National Research Council Canada
Ottawa, Canada K1A 0R6

Conseil national de recherches Canada
Ottawa, Canada K1A 0R6

Postage paid at Ottawa
Publications mail
Registration No. 1240447

Port payé à Ottawa
Poste-publication
Enregistrement n° 1240447

Canadian Journal of Chemistry

Revue canadienne de chimie

Volume 79, Number 10, October 2001

Volume 79, numéro 10, octobre 2001

2000 Maxxam Award Lecture
Unified theory of extraction

Janusz Pawliszyn

1403–1414

Interaction of human serum albumin with oxovanadium ions studied by FT-IR spectroscopy and gel and capillary electrophoresis

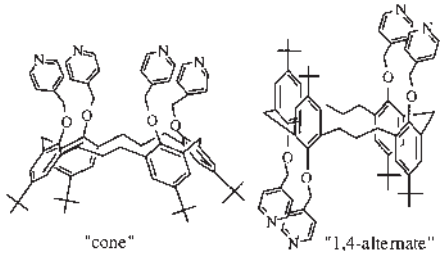
M. Purcell, J.F. Neault, H. Malonga, H. Arakawa, and H.A. Tajmir-Riahi

1415–1421

The metal template effect on *O*-alkylation of tetrahydroxy[3.1.3.1]metacyclophane with 4-(chloromethyl)pyridine to afford tetrakis-[(4-pyridylmethyl)oxy][3.1.3.1]metacyclophanes and their conformational studies

Takehiko Yamato, Kenji Kumamaru, and Hirohisa Tsuzuki

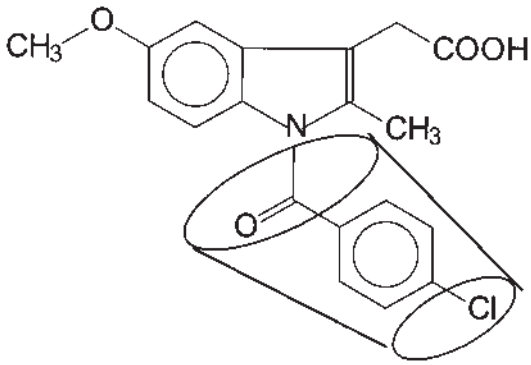
1422–1430



Binding of anti-inflammatory drug indomethacin with cyclodextrin and DNA: solubility, spectroscopic, and voltammetric studies

I.S. Shehatta and M.S. Ibrahim

1431–1438



Continued on inside back cover / Suite au verso

Canada

Printed in Canada by / Imprimé au Canada par
University of Toronto Press Inc.
Typesetting by / Typographie par
NRC Research Press / Presses scientifiques du CNRC

000 -4042 200110 79 10 1-

Regioselective upper-rim functionalizations of calix[4]arene by diphenylphosphino groups

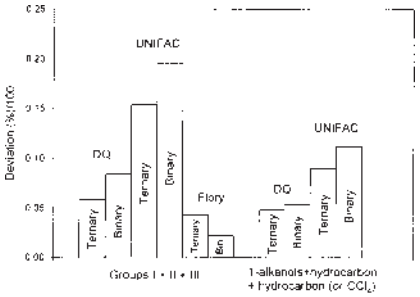
Jonathan Gagnon, Martin Vézina, Marc Drouin, and Pierre D. Harvey

1439–1446

DISQUAC predictions on thermodynamic properties of ternary and higher multicomponent mixtures. II. Results for H^E of ternary mixtures containing nonpolar components, or one polar compound, two polar compounds, or one alcohol and hydrocarbons, or CCl_4

Juan Antonio Gonzalez, Javier Carmona, Nicolas Riesco, Isaias Garcia de la Fuente, and Jose Carlos Cobos

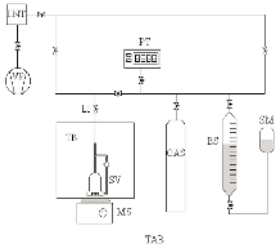
1447–1459



Solubility of nonpolar gases in 2,2,2-trifluoroethanol and 1,1,1,3,3,3-hexafluoropropan-2-ol at several temperatures and 101.33 kPa partial pressure of gas

Miguel Angel Sánchez, Ana María Mainar, Juan Ignacio Pardo, María Carmen López, and José Santiago Urieta

1460–1465



Solubility predictions for crystalline nonelectrolyte solutes dissolved in organic solvents based upon the Abraham general solvation model

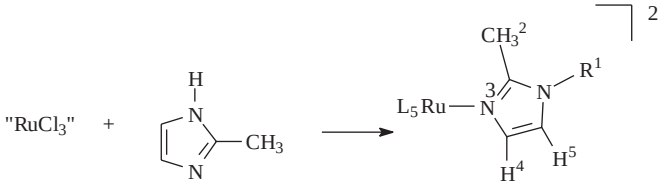
William E. Acree, Jr. and Michael H. Abraham

1466–1476

Synthesis of chloro(2-methylimidazole)ruthenium(III) complexes and their aqueous solution chemistry, and the crystal structure of $[2\text{-MeImH}]_2[RuCl_5\text{2-MeIm}]$

Craig Anderson

1477–1482

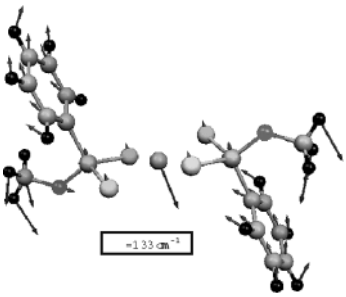


Concluded on facing page / Suite et fin à la page précédente

An experimental and theoretical approach to phosphonodithioato complexes: molecular orbital analysis by hybrid-DFT and EHT calculations on *trans*-bis[*O*-alkyl-phenylphosphonodithioato]Ni^{II} and vibrational assignments

M. Carla Aragoni, Massimiliano Arca, Francesco A. Devillanova, John R. Ferraro, Francesco Isaia, Francesco Lelj, Vito Lippolis, and Gaetano Verani

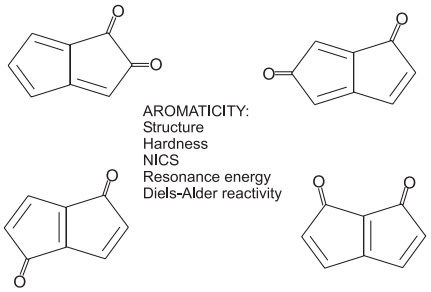
1483–1491



Tests for aromaticity applied to the pentalenoquinones — A computational study

C. Delamere, C. Jakins, and E. Lewars

1492–1504



Oxidative coupling of naphtho-9-crown-3 ether: X-ray crystal structure and solution and solid-state NMR analysis of the dimer

G.W. Buchanan, M.F. Rastegar, G.P.A. Yap, A. Moghimi, and M. Ghandi

1505–1510

Author Index **AI-1**

Index des auteurs **AI-1**

The Canadian Journal of Chemistry is affiliated with the Canadian Society for Chemistry and publishes papers in all areas of chemistry.

La Revue canadienne de chimie est affiliée à la Société canadienne de chimie et publie des articles dans tous les domaines de la chemie.

2000 Maxxam Award Lecture

Unified theory of extraction

Janusz Pawliszyn

Abstract: The sample preparation step in an analytical process typically consists of extraction of components of interest from a sample matrix. This procedure can vary in degree of selectivity, speed, and convenience depending on the approach and conditions used as well as on geometric configurations of the extraction phase and conditions. Optimization of this process aids enhancement in performance of the overall analysis. Proper design of the extraction devices and procedures facilitates rapid and convenient on-site implementation, coupling to separation–quantification, and (or) automation. The key to rational choice, optimization, and design is an understanding of fundamental principles governing mass transfer of analytes in multiphase systems. There is a tendency to divide extraction techniques according to random criteria. In this article, common principles among different extraction techniques are emphasized and a unified approach based on convolution of mathematical functions describing individual steps is presented. This approach considers gas, solvent, liquid polymer, and solid surfaces as extraction phases and air, water, and solids as sample matrices. The parameters that affect the kinetics of extraction techniques are emphasized resulting in new calibration strategies and novel geometric designs.

Key words: separations, extractions, microextractions, mass transfer, multiphase equilibria.

Résumé : Dans un processus analytique, l'étape de préparation de l'échantillon consiste généralement en une extraction des composants recherchés d'une matrice d'échantillon. Dépendant de l'approche et des conditions utilisées ainsi que des configurations géométriques de la phase d'extraction et des conditions, le degré de sélectivité de cette procédure peut varier considérablement. L'optimisation de ce processus permet d'augmenter la performance de l'analyse globale. Une mise au point appropriée des procédures et des appareils d'extraction permet d'accélérer et de rendre plus commode leur réalisation sur place ainsi que le couplage séparation/quantification et/ou automation. La clé pour un choix rationnel, une optimisation et une mise au point est une compréhension des principes fondamentaux qui gouvernent le transfert de masse des analytes dans des systèmes multiphases. Il y a une tendance à diviser les techniques d'extraction à l'aide de critères aléatoires. Dans cet article, on fait ressortir des principes communs aux diverses techniques d'extraction et on présente une approche unifiée basée sur des fonctions mathématiques de convolution qui décrivent les étapes individuelles. Cette approche considère les gaz, les solvants, les polymères liquides et les surfaces solides comme des phases d'extraction et l'air, l'eau et les solides comme des matrices d'échantillon. On identifie les paramètres qui affectent la cinétique des techniques d'extraction en raison de nouvelles stratégies de calibration et de nouvelles configurations géométriques.

Mots clés : séparations, extractions, microextractions, transfert de masse, équilibre multiphase.

[Traduit par la Rédaction]

Introduction

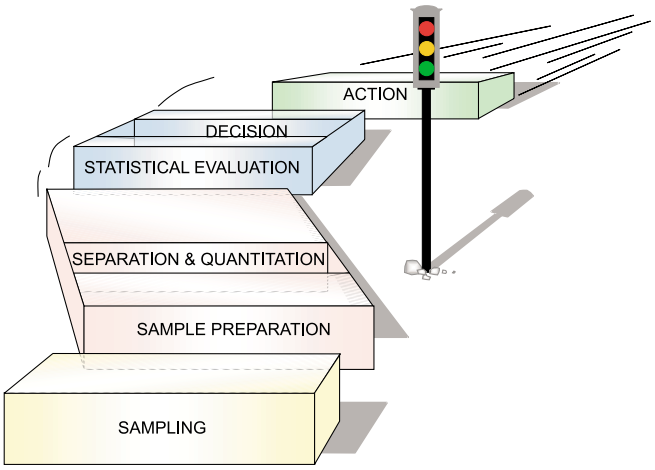
The analytical procedure for complex samples consists of several steps typically including sampling, sample preparation, separation, quantitation, statistical evaluation, and decision making (see Fig. 1**)**. Each step is critical for obtaining correct and informative results. The sampling step includes deciding where to get samples that properly define the object or problem being characterized and choosing a method to obtain samples in the right amounts. The objective of the sample preparation step is to isolate the components of interest from a sample matrix, because most analytical instruments cannot handle the matrix directly. Sample preparation involves extraction procedures and can also include "clean up" procedures for very complex "dirty" samples. This step must also bring the analytes to a suitable concentration level for detection and therefore sample preparation methods typically include enrichment. During the separation step of the analytical process, the isolated complex mixture containing target analytes is divided into its constituents, typically by means of a chromatographic or electrophoretic techniques. Quantitation is the determination of amounts of the identified compounds. The identification can be based on a retention time combined with selective detection; more frequently, however, more specific instruments, namely mass spectrometers, are used to eliminate possible errors in quantification due to interferences by confirming identity of analytes. Statistical evaluation of the results provides an es-

Received March 21, 2001. Published on the NRC Research Press Web site at http://canjchem.nrc.ca on October 2, 2001.

J. Pawliszyn. Department of Chemistry, University of Waterloo, Waterloo, ON N2L 3G1, Canada. (fax: (519) 746-0435; e-mail: janusz@uwaterloo.ca).

 DOI: 10.1139/cjc-79-10-1403 © 2001 NRC Canada

Fig. 1. Steps in analytical process.



timate of the target compound concentration in the sample being analyzed. The data will then support appropriate decisions, which might include a move to take another sample for further investigation of the object or problem.

It is important to note, as emphasized by Fig. 1, that steps in an analytical method follow one after another, and a subsequent step cannot begin until the preceding one has been completed. Therefore, the slowest step determines the overall speed of the analytical process, and improving the speed of a single step may not result in a throughput increase. To increase the throughput of analysis, all steps need to be considered. Also, errors performed in any preceding step, including sampling, will result in the overall poor performance of the procedure.

There have been major breakthroughs in the development of improved instrumentation, which involve miniaturization of analytical devices and hyphenation of different steps into one system. It is recognized that an ideal instrument would perform all the analytical steps without human intervention, preferably directly on the site where an investigated system is located rather than moving the sample to laboratory, as is a common practice in many cases at the present time. This approach would eliminate errors and time associated with sample transport and storage and,therefore, result in more accurate, precise, and faster analytical data. Although such a device has not yet been built, today's sophisticated instruments, such as the gas chromatograph–mass spectrometer (GC–MS) or the liquid chromatograph–mass spectrometer (LC–MS), can separate and quantify complex mixtures and automatically apply chemometric methods to statistically evaluate results. It is much more difficult to hyphenate sampling and sample preparation steps, primarily because the current state of the art in sample preparation techniques employs multi-step procedures involving organic solvents. These characteristics make it difficult to develop a method that integrates sampling and sample preparation with separation methods, for the purposes of automation. The result is that over 80% of analysis time is currently spent on sampling and sample preparation steps for complex samples.

One of the reasons for slow progress in the area of sample preparation is that the fundamentals of extraction involving natural, frequently complex, samples are much less developed and understood compared to more physicochemically simpler systems used in separation and quantification steps such as chromatography and mass spectrometry. This situation creates a feeling that rational design and optimization of extraction systems is not possible. Therefore development of sample preparation procedures is frequently considered to be "art" not "science".

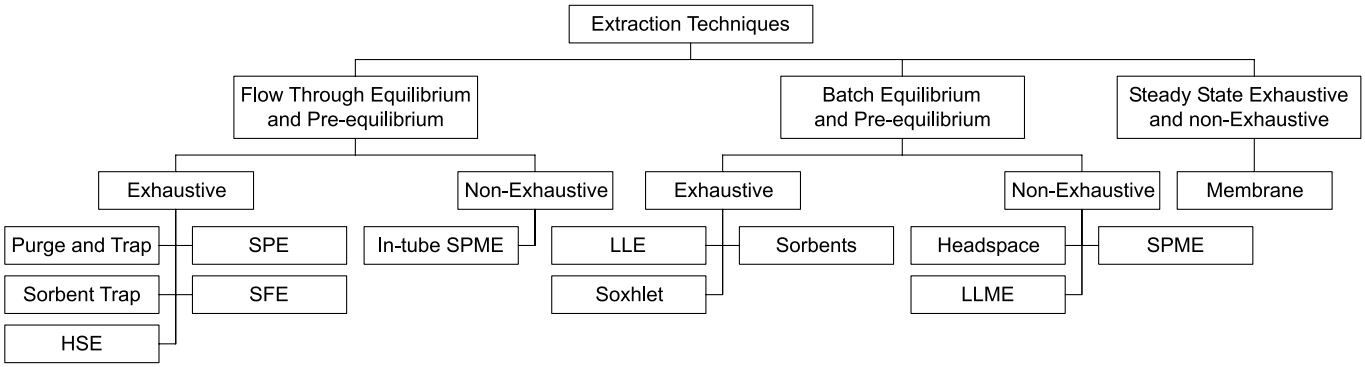
This situation creates a tendency by practitioners and regulatory agencies to prefer exhaustive vs. nonexhaustive techniques (see Fig. 2) even though this choice results frequently in labour intensive and costly procedures. The main objective of the exhaustive techniques is to completely remove all analytes from a sample matrix and transfer them to the extraction phase. The fundamental advantage of exhaustive methods is that in principle they do not require calibration since the vast majority of analytes are transferred to the extraction phase. This objective is accomplished by application of overwhelming volumes of extraction phase. To reduce the amounts of solvents and time required to accomplish exhaustive removal, batch equilibrium techniques (for example, liquid–liquid extractions) are frequently replaced by flow-through techniques. For example, a sorbent bed can be packed with extraction phase dispersed on a supporting material and when sample is passed through analytes are retained on the bed. Large volumes of sample can be passed through a small cartridge and the flow through a well-packed bed facilitates rapid mass transfer. The extraction procedure is followed by reextraction of analytes into small volume of solvent resulting in high enrichment. This strategy is used in sorbent trap techniques and solid phase extraction (SPE) (1). Alternatively, the sample (typically a solid sample) can be packed in the bed and the extraction phase can be used to remove and transport the analytes to the collection point. In supercritical fluid extraction (SFE), compressed gas is used to wash analytes from the sample matrix, while in-purge and trap-atmospheric pressure inert gas performs the same function. In dynamic solvent extraction, such as a Soxhlet, the solvent continuously removes the analytes from the matrix at the boiling point of the solvent. In more recent hot solvent extraction techniques, smaller volumes of organic solvent are used to accomplish higher enrichment at the same time, because of increased solvent capacity and eluting capability at high temperatures and pressures (2).

Alternatively nonexhaustive approaches can be designed based on equilibrium, pre-equilibrium and permeation principles (3). Equilibrium nonexhaustive techniques are fundamentally analogues to the equilibrium exhaustive techniques, however, the capacity of the extraction phase is smaller, and in most cases is not sufficient to remove the majority of analytes from the sample matrix. This is caused by use of a small volume of the extracting phase relative to sample volume (microextraction, such as solvent microextraction or solid phase microextraction (SPME)) (4) or a low K value, for example as is typically encountered in gaseous headspace techniques (5).

Pre-equilibrium conditions are accomplished by breaking the contact between the extraction phase and the sample matrix before the point of equilibrium with the extracting phase has been reached. The devices that are used are frequently identical to the microextraction systems, however, extraction

© 2001 NRC Canada

Fig. 2. Classification of sample preparation techniques.



times are shorter. In permeation techniques, such as membrane extraction, continuous steady state transport of analytes through the extraction phase is accomplished by simultaneous reextraction of analytes.

As the above discussion and as Fig. 2 indicates, there is a fundamental similarity among extraction techniques used in the sample preparation process. In all techniques, the extraction phase is in contact with the sample matrix, and analytes are transported between the phases. For exhausitve techniques, the phase ratio is higher and geometries are more restrictive compared to nonexhaustive approaches to ensure the quantitative transfer of analytes. The thermodynamics of the process is defined by the extraction phase – sample matrix distribution constant. It would be instructive to consider in more detail the kinetics of processes occurring at the extraction phase – sample matrix interface, since this defines the time of the analytical procedure. In many cases, the analytes are reextracted from the extraction phase, but this step is not discussed here since this process is analogues and much simpler in principle compared to removing analytes from a more complex sample matrix. The main objective of this article is to outline the common fundamental principles among various extraction techniques to facilitate a better understanding of selection criteria for appropriate techniques, device geometries, and operational conditions.

Theory

The fundamental thermodynamic principle common to all chemical extraction techniques involves distribution of analyte between the sample matrix and the extraction phase. When liquid is used as the extraction medium then the distribution constant (K_{es})

$$[1] \qquad K_{es} = a_e/a_s = C_e/C_s$$

defines the equilibrium conditions and ultimate enrichment factors achievable in the technique, where a_e and a_s are the activities of analytes in the extraction phase and matrix, correspondingly, which can be approximated by the appropriate concentrations. For solid extraction phase adsorption, equilibria can be explained by the following equation:

$$[2] \qquad K^s_{es} = S_e/C_s$$

where S_e is solid extraction phase surface concentration of adsorbed analytes. The above relationship is similar to eq. [1], with the exception that extraction phase concentration is replaced with surface concentration. The S_e term in the numerator indicates that the sorbent surface area available for adsorption must also be considered. This complicates the calibration at equilibrium conditions because of displacement effects and the nonlinear adsorption isotherm (6). The above equations can be used to calculate the amount of analyte in the extraction phase at equilibrium conditions (4). For example, for equilibrium liquid-microextraction techniques and large sample, including direct extraction from the investigated system, the appropriate expression is very simple

$$[3] \qquad n = K_{es}V_eC_s$$

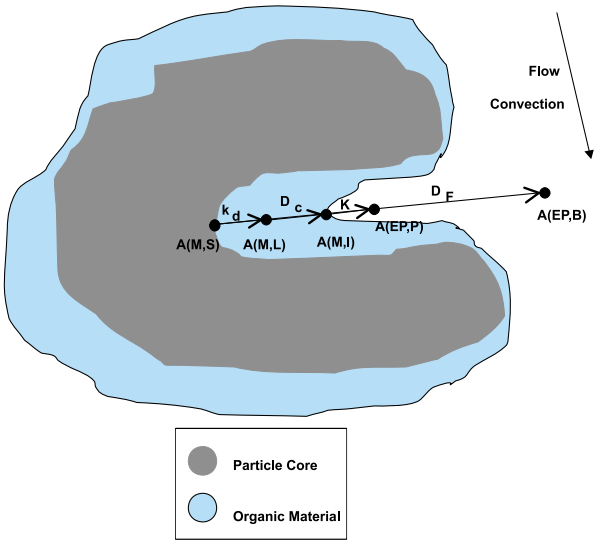
where K_{es} is the extraction phase – sample matrix distribution constant, V_e is the volume of the extraction phase, and C_s is the concentration of the sample. However, in practice kinetic factors, defined by the dissociation constants, diffusion coefficient, and agitation condition, frequently determine the amount of extracted analytes since the overall rates are slow and therefore extraction amounts for limited time experiments do not reach equilibrium values.

The most challenging extractions occur when a solid is present as a part of the sample matrix. This case will be considered as the most general example of extraction since it involves a number of fundamental processes occurring during the extraction. If we assume that a matrix particle consists of an organic layer on an impermeable but porous core and the analyte is adsorbed onto the pore surface, the extraction process can be modelled by considering several basic steps as shown in Fig. 3. To remove the analyte from the extraction vessel, the compound must first be desorbed from the surface (Fig. 3, A(M,S)), then it must diffuse through the organic part of the matrix (A(M,I)) to reach the matrix–fluid interface (A(M,L)). At this point the analyte must be solvated by the extraction phase (A(EP,P)) and then it must diffuse through the static extraction phase present inside the pore to reach the portion of the extraction phase influenced by convection, to be transported through the interstitial pores of the matrix and eventually to reach the bulk of the extraction phase (A(EP,B)). The simplest way to design a kinetic model for this problem is to adopt equations developed by engineers to investigate mass transport through porous media (7, 8).

For the purpose of this discussion we consider the efficient and frequently applied experimental arrangement for removing solid-bound semivolatile analytes, involving the use of a piece of stainless-steel tubing as the extraction ves-

© 2001 NRC Canada

Fig. 3. Processes involved in extraction of heterogeneous samples containing porous solid particles. The terms in the figure are discussed in the text.



sel. The sample is typically placed inside the tubing and a linear-flow restrictor is attached at the end of the vessel to maintain the pressure. During the process, the extraction phase continuously removes analytes from the matrix, which are then transferred to the collection vessel after the expansion of the fluid. This leaching process is very similar to chromatographic elution with packed columns, particularly to the frontal method. The main difference is that in sample preparation analytes are dispersed in the matrix at the beginning of the experiment, whereas in chromatographic frontal analysis a long plug is introduced into the column at the initial stage of the separation process. The principal objective of the extraction is to remove analytes from the vessel in the least amount of time, requiring elution conditions under which the analytes are unretained. In chromatography, on the other hand, the ultimate goal is to separate components of the sample, which requires retention of analytes in the column. Another major difference is that the packing matrix is usually well-characterized in chromatography, but in sample preparation it is often unknown.

One way to develop a mathematical model for this extraction approach is to establish the mass balance equation for the system after carefully considering of the individual mass transfer steps, occurring during the extraction process (see Fig. 3), and specific boundary conditions (9). Extensive investigations on similar topics have already been conducted by engineers, who have studied the mass transfer in porous media (7), and chromatographers (8). In these studies the relationship between various matrix parameters and flow conditions on the elution profile were described mathematically, and verified experimentally. In chromatography this relationship is usually described as contributions from each of the mass transfer steps to the height equivalent to a theoretical plate (HETP). The overall performance of the system can be defined as the sum of the relevant individual components judiciously selected to reflect the most significant individual steps present in the elution process. For the purpose of this discussion, this approach is adopted to develop a model for extraction kinetics in flow-through techniques.

The effect of slow desorption kinetics of analytes from the matrix on the elution profile, can be described as the contribution to the HETP (8), h_{RK}:

$$[4] \qquad h_{RK} = \frac{2ku_e}{(1+k)^2(1+k_o)k_d}$$

where k is the partition ratio, k_d is the dissociation rate constant of the analyte–matrix complex of reversible process, k_o is the ratio of the intraparticulate void volume to the interstitial void space and is expressed as:

$$[5] \qquad k_o = \frac{\varepsilon_i(1-\varepsilon_e)}{\varepsilon_e}$$

where ε_i is intraparticulate porosity and ε_e is interstitial porosity; u_e is the interstitial linear extraction phase velocity expressed as:

$$[6] \qquad u_e = u(1 + k_o)$$

where $u = L/t_0$ is chromatographic linear velocity, L is the length of the extraction vessel, and t_0 is time required to remove one void volume of the extraction phase from the vessel. Chromatographic and interstitial linear velocities are identical if matrix particles have low porosity. This analysis can be extended to elution through a matrix having multiple adsorption sites characterized by different dissociation rate constants by using the approach described by Giddings (10).

The diffusion of the analyte in the liquid or swollen solid part of the matrix is important when polymeric materials are extracted or the matrix has substantial organic content. Its contribution can be expressed as h_{DC}:

$$[7] \qquad h_{DC} = \frac{2}{3}\frac{k}{(k+1)^2}\frac{d_c^2}{D_s}u_e$$

where d_c is the thickness of the matrix component permeable to analyte and D_s is the diffusion coefficient of the analyte in the sample matrix.

The analytes migrate in and out of a pore structure of the matrix during the elution. This can be described as resistance to mass transfer in the fluid associated with the porous nature of the environmental matrices, which gives rise to the following HETP component, h_{DP}:

$$[8] \qquad h_{DP} = \frac{\theta(k_o + k + kk_o)^2 d_p^2 u_e}{30\,k_o(1+k_o)^2(1+k)^2 D_p}$$

where θ is tortuosity factor for the porous particle and D_p is the diffusion coefficient of the analyte in the material filling the pores, which in most practical cases will be an extraction phase, and therefore D_p=D_e, where D_e is the diffusion coefficient of the analyte in the extraction phase. This contribution can be quite important considering the relatively large particle size (about 1 mm) of environmental matrices and becomes particularly important when the pores are filled with dense organic material, such as humic matter rather than the extraction phase.

In the flowing bulk of the fluid an analyte experiences resistance to mass transfer associated with eddy diffusion (ran-

© 2001 NRC Canada

dom paths of the analytes through the vessel filled with the particles), which is given by h_{ED}:

$$[9] \qquad h_{ED} = 2\lambda d_p$$

where λ is a structural parameter and is close to 1 for spherical matrix particles. This contribution to band broadening is the most important factor in HPLC separations and it is expected to remain significant in extractions because of matrices typically having large particle sizes.

In addition, we should also consider analyte diffusion along the axis of the vessel (longitudinal diffusion) which can be defined as h_{LD}:

$$[10] \qquad h_{LD} = \frac{\gamma_M D_e}{u_e}$$

where γ_M is the obstruction factor, which characterize the structure of the matrix. This component is expected to be small. The analyte concentration profile generated during the experiment as a function of time $C(x,t)$ can be represented using the equation that describes the dispersion of a plug of finite width (9):

$$[11] \qquad \frac{C(x,t)}{C_o} = \frac{1}{2}\left\{ ERF\left(\frac{\frac{L}{2} - x - \frac{ut}{1+k}}{\sigma\sqrt{2}} \right) + ERF\left(\frac{\frac{l}{2} + x + \frac{ut}{1+k}}{\sigma\sqrt{2}} \right) \right\}$$

where L is the length of the vessel, C_0 is the initial concentration of analyte in the extraction vessel, and σ is the mean square root dispersion of the band expressed as:

$$[12] \qquad \sigma = \sqrt{Ht\frac{u}{1+k}}$$

where H is equivalent to the HETP in chromatographic systems and is a sum of the contributions discussed above ($H = h_{RK} + h_{DC} + h_{DP} + h_{ED} + h_{LD}$). The mass of analyte eluted from the vessel during a given extraction time t can be calculated from the following equation:

$$[13] \qquad \frac{m(t)}{m_o} = \frac{\int_{-\infty}^{-\frac{1}{2}L} C(x,t)\mathrm{d}x}{C_s L}$$

where, $m(t)$ is the extracted mass of analyte and m_o is the total amount of analyte in the vessel at the beginning of the experiment. We will refer to this function as the time elution profile emphasizing the similarity of the extraction process in this simple case to chromatographic elution.

The above discussion applies only to the situation when the analytes are initially present in a fluid phase, which in flow through techniques corresponds to elution of uniform spikes from the extraction vessel or when weakly adsorbed native analytes are removed from an organic-poor matrix such as sand. In the other words, the above relationships are suitable for systems in which the partitioning equilibrium between the matrix and extraction fluid is reached quickly compared to the fluid flow. They are also suitable to model static – dynamic extractions, under good solubility conditions ($k = 0$), in which the sample is initially exposed to the static extraction phase (vessel is capped) for a time required to achieve equilibrium condition prior to elution by fluid flow. If dynamic extraction is performed from the beginning of extraction, then in the majority of practical cases the system is not expected to achieve the initial equilibrium conditions. This is because of slow mass transport between the matrix and the fluid (for example, slow desorption kinetics or slow diffusion in the matrix). The expected relationship between amount of analyte removed from the vessel versus time can be obtained in this case by convoluting the function describing the rate of mass transfer between the phases $F(\tau)$ with the elution time profile $m/m_o(t)$ derived above (eq. [13]) (11):

$$[14] \qquad \int_{\tau=0}^{\tau=1} \frac{m(t-\tau)}{m_o} F(\tau)\mathrm{d}\tau$$

The resulting function describes a process where elution and the mass transfer between the phases occur simultaneously. In this discussion we will refer to this function as the extraction time profile to emphasize the point that in a majority of extraction cases these two processes are expected to be combined. $F(\tau)$ describes the kinetics of the process, which defines the release rate of analyte from the sample matrix and can include, for example, the matrix–analyte complex dissociation rate constant, the diffusion coefficient, the time constant that describes swelling of the matrix that will facilitate removal of analyte, or a combination of the above. Detailed discussion and applications of this model to describe and (or) investigate processes in supercritical fluid extraction have been described in detail elsewhere (12, 13).

Discussion

The above conclusion can be stated in more general way. Convolution among functions describing individual processes occurring during the extraction, describes the overall extraction process and represents a unified way to describe the kinetics of these processes. The exact mathematical solution to the convolution integral is frequently difficult to obtain, but graphical representation of the solution can be calculated using Fourier transform or numerical approaches. Frequently it is possible to incorporate mathematical functions that describe a combination of the unit processes. In the example of the flow-through system discussed above, the elution function describes the effect of porosity and analyte affinity towards the extraction matrix on the extraction rate. It should be emphasized that the convolution approach considers all processes equivalently. In practice, however, a small number and frequently just one unit process controls the overall rate of extraction.

Determination of the limiting step is not possible by qualitative agreement with the mathematical model since the effect on recovery of most of the unit processes has an

© 2001 NRC Canada

exponential decay nature. To properly recognize them, quantitative agreement and (or) effect of extraction parameters needs to be examined. Identification of the limiting process provides valuable insight on the most effective approach to optimization of the extraction.

In heterogeneous samples for example, the release of solid-bound analytes from sample matrix, through a reversal of chemisorption or inclusion, frequently controls the extraction rate. By recognizing this fact, extraction parameters can be changed to increase the extraction rates. For example, dissociation of the chemisorbed analytes can be accomplished either by using high temperature or by application of catalysts. Recognition of this fact lead to the development of high-temperature supercritical fluid extraction (14), followed by the evolution of both the hot-solvent extraction (15) and microwave extraction approach, with more selective energy focusing at the sample matrix – extraction phase interface (16). There is also an indication that milder conditions can be applied by taking advantage of the catalytic properties of the extraction phase or additives (17). However, to realize this opportunity more research needs to be performed to gain more insight about the nature of interactions between analytes and matrices. The benefits are not only improved speed, but also selectivity resulting from application of appropriate conditions. This strategy of simultaneous extraction and clean-up has been applied successfully to a very difficult case of extraction of polychlorinated dibenzo-*p*-dioxins from fly ash (18).

If the extraction rate is controlled by mass transport of analytes in the pores of the matrix, than the process can be successfully enhanced by application of sonic and microwave energy, which induce convection even in the small dimensions of the pore. Frequently, diffusion through the whole or portion of sample matrix containing natural or synthetic polymeric material controls the extraction rate (19). In this case, swelling the matrix and increasing temperature results in increased diffusion coefficients and therefore increased extraction rates.

For homogeneous samples and flowing fluid extraction phase the description of the extraction process is much simpler and can be based directly on the chromatographic theory for liquid stationary phases. Let us consider another case of the flow-through system where the extraction phase is dispersed as a thin layer inside the extraction bed and the sample flows through the cartridge. The bed can be constructed of a piece of fused silica capillary, internally coated with a thin film of extracting phase (a piece of open tubular capillary GC column; in-tube SPME) (20), or the bed may be packed with extracting phase dispersed on an inert supporting material (SPE cartridge). In these geometric arrangements, the concentration profile along the *x*-axis, of the tubing containing the extracting phase as a function of time (*t*), can be described by adopting the expression for dispersion of a concentration front:

$$[15] \quad C(x,t) = 0.5C_s\left(1 - erf\frac{x - \frac{ut}{1+k}}{\sigma\sqrt{2}}\right)$$

where u_s is linear velocity of the sample through the tube, and k is the partition ratio defined as:

$$[16] \quad k = K_{es}\frac{V_e}{V_v}$$

where K_{es} is a extraction phase – sample matrix distribution constant, V_e is the volume of the extracting phase, and V_v is a void volume of the tubing containing the extracting phase. σ is the mean square root dispersion of the front defined as:

$$[17] \quad \sigma = \sqrt{Ht\frac{u}{1+k}}$$

where H is equivalent to the HETP (height equivalent to theoretical plate) in chromatographic systems. This can be calculated as a sum of individual contributions to the front dispersion. These contributions are dependent on the particular geometry of the extracting system as discussed previously in the theory section of this article.

Equation [15] indicates that the front of analyte migrates through the capillary–bed with speed proportional to the linear velocity of the sample and inversely related to the partition ratio. For the in-tube SPME and short capillaries with a small dispersion, the minimum extraction time for in-tube SPME at equilibrium conditions can be assumed to be similar to the time required for the centre of the band to reach the end of the capillary

$$[18] \quad t_e = \frac{L\left(1 + K_{es}\frac{V_e}{V_v}\right)}{u}$$

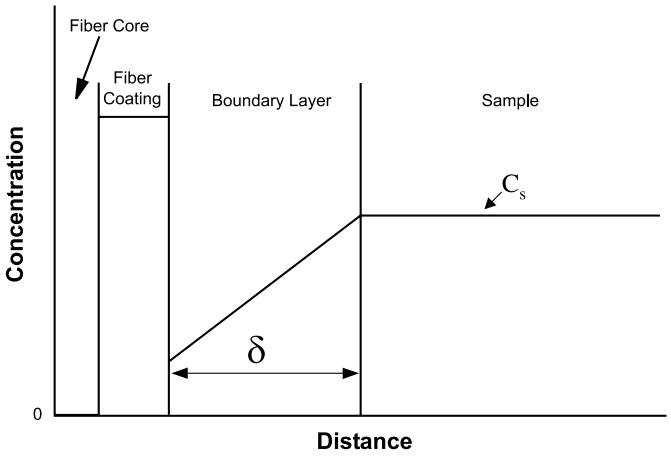
where L is the length of the capillary holding the extraction phase. For packed bed extractors typical for SPE techniques, analogous equations can be developed. In that case, the calculated time corresponds to the maximum extraction time before breakthrough occurs. As expected, the extraction time is proportional to the length of the capillary and inversely proportional to the linear flow rate of the sample. Extraction time also increases with an increase in the extraction phase – sample distribution constant and with the volume of the extracting phase but decreases with an increase of the void volume of the capillary.

Coupling equations for systems involving convection caused by flow through a tube as discussed above, are frequently not available for other means of agitation and other geometric configurations. In these cases the most successful approach is to consider the boundary layer formed at the interface between the sample matrix and the extraction phase. Independent of the agitation level, fluid contacting a fibre's surface is always stationary, and as the distance from the fibre surface increases, the fluid movement gradually increases until it corresponds to bulk flow in the sample. To model mass transport, the gradation in fluid motion and convection of molecules in the space surrounding the fibre surface can be simplified as a zone of a defined thickness in which no convection occurs, and perfect agitation occurs in the bulk of the fluid everywhere else. This static layer zone is called *Prandtl* boundary layer (see Fig. 4) (21).

A precise understanding of the definition and thickness of the boundary layer in this sense is useful. The thickness of

© 2001 NRC Canada

Fig. 4. Boundary layer model of the mass transfer kinetics between extraction phase and sample matrix.



the boundary layer (δ) is determined by both the rate of convection (agitation) in the sample and an analyte's diffusion coefficient. Thus, in the same extraction process, the boundary layer thickness will be different for different analytes. Strictly speaking, the boundary layer is a region where analyte flux is progressively more dependent on analyte diffusion and less on convection, as the extraction phase is approached. For convenience however, analyte flux in the bulk of the sample (outside of the boundary layer) is assumed to be controlled by convection, whereas analyte flux within the boundary layer is assumed to be controlled by diffusion. δ is defined as the position where this transition occurs or the point at which convection towards the extraction phase is equal to diffusion away. At this point, analyte flux from δ towards the extraction phase (diffusion controlled) is equal to the analyte flux from the bulk of the sample towards δ, controlled by convection.

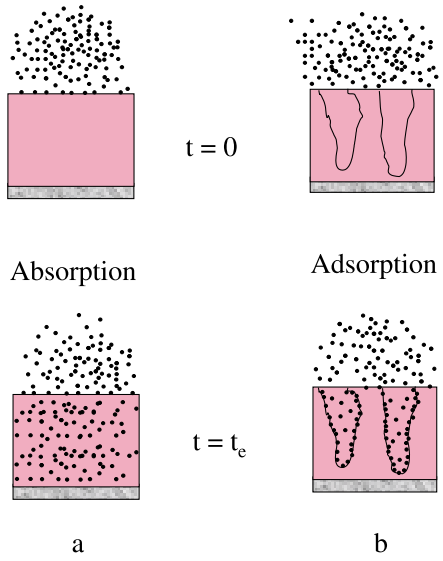
In many cases when the extraction phase is well-dispersed, forming a thin coating, the diffusion of analytes through the boundary layer controls the extraction rate. The equilibration time (t_e) can be estimated as time required to extract 95% of the equilibrium amount and calculated for these cases from the equation below (4):

$$[19] \quad t_e = B\frac{\delta a K_{es}}{D_s}$$

where a is the extraction phase thickness, D_s is the analyte's diffusion coefficient in the sample matrix, and K_{es} is the analyte's distribution constant between the extraction phase and the sample matrix. B is a geometric factor referring to the geometry of the supporting material upon which the extraction phase is dispersed on. The boundary layer thickness can be calculated for given convection conditions using engineering principles and it is discussed in more detail later. Equation [19] can be used to predict equilibration times when the extraction rate is controlled by diffusion in the boundary layer, which is valid for thin extraction phase coatings (a < 200 microns) and high distribution constants (K_{es} > 100).

The properties of the extraction phase should be carefully optimized. These include both bulk physicochemical properties, such as polarity, and physical properties. The discussion

Fig. 5. Extraction using (*a*) absorptive and (*b*) adsorptive extraction phases immediately after exposure of the phase to the sample (t = 0) and after completion of the extraction ($t = t_e$).



to this point has been limited to extraction by liquid phases. These exhibit wide linear dynamic ranges associated with linear absorption isotherms. They also facilitate gentle sample preparation since chemisorbtion and catalytic properties, frequently associated with solid surfaces, are absent. No loss or modification of the analyte occurs during extraction and (or) desorbtion. Despite these attractive properties of liquid extraction media, solid phases are frequently used because of their superior selectivity and sensitivity for some groups of compounds. There is a substantial difference in performance between liquid and solid coatings (Fig. 5). In the case of liquid coatings, the analytes partition into the extraction phase, where the molecules are solvated by the coating molecules. The diffusion coefficient in the liquid coating allows the molecules to penetrate the whole volume of the coating within a reasonable extraction time if the coating is thin (see Fig. 5*a*). In the case of solid sorbents the coating has a well-defined crystalline structure, which if dense, substantially reduces the diffusion coefficients within the structure. Therefore within the experimental time, sorption occurs only on the porous surface of the coating (see Fig. 5*b*). During extraction by solid phase, compounds with poor affinity towards the phase are frequently displaced at longer extraction times by analytes characterized by stronger binding or those present in the sample at high concentrations. This effect is associated with the fact that there is only a limited surface area available for adsorption. If this area is substantially occupied then a competition effect occurs (6) and the equilibrium amount extracted can vary with concentrations of both the target and the other analytes. On the other hand, in the case of extraction with liquid phases, partitioning between the sample matrix and extraction phase occurs. In this case, equilibrium extraction amounts vary only if the bulk coating properties are modified by the extracted components, which only occurs when the amount extracted is a substantial portion (a few percent) of the extraction phase. This is rarely observed, since extraction–enrichment techniques are typi-

© 2001 NRC Canada

cally used to determine trace contamination, samples however cannot be neglected as a possible course of nonlinearity, when quantifying very complex matrices.

The only way to overcome this fundamental limitation of porous coatings is, as the above figure suggests, to use an extraction time much less than the equilibrium time, so that the total amount of analytes accumulated onto the porous coating is substantially below the saturation value. When performing such experiments, not only it is critical to precisely control extraction times, but also convection conditions since they determine the thickness of the diffusion layer. One way of eliminating the need for compensation of differences in convection is to normalize (use consistent) agitation conditions. For example, the use of mechanical stirring in the laboratory at a well-defined rotation rate or fans for field air monitoring, will ensure consistent convection (22, 23). The short-time exposure measurement described above has an advantage associated with the fact that the rate of extraction is defined by diffusivity of analytes through the boundary layer of the sample matrix and the corresponding diffusion coefficients, rather than by distribution constants. This situation was illustrated in Fig. 6 for cylindrical geometry of the extraction phase dispersed on the supporting rod.

The analyte concentration in the bulk of the matrix can be considered constant when a short sampling time is used and there is a constant supply of an analyte via convection. These assumptions are true for most cases of sampling, where the volume of sample is much greater then than the volume of the interface and the extraction process does not affect the bulk sample concentration. In addition, the solid coating can be treated as a perfect sink. The adsorption binding is instantaneous and essentially irreversible. The analyte concentration on the coating surface is far from saturation and can be assumed to be negligible for short sampling times and relatively low analyte concentrations in a typical sample. The analyte concentration profile can be assumed to be linear from C_s to C_0. In addition, the initial analyte concentration on the coating surface (C_0) can be assumed to be equal to zero when extraction begins. Diffusion of analytes inside the pores of a solid coating controls mass transfer from *b* to *d*.

The function describing the mass of extracted analyte with sampling time can be derived using the analogy of the heat transfer problem, (24) which results in the following equation:

$$[20] \qquad n(t) = \frac{AD_s}{\delta}\int_0^t C_s(t)\mathrm{d}t$$

where *n* is the mass of extracted analyte over sampling time (*t*) in ng, D_s is the gas-phase molecular diffusion coefficient, *A* is the surface area of the sorbent, δ is the thickness of the boundary layer surrounding the extraction phase, B_1 is a geometric factor, and C_s is analyte concentration in the bulk of the sample. It can be assumed that the analyte concentration is constant for very short sampling times and therefore eq. [20] can be further reduced to:

$$[21] \qquad n(t) = \frac{D_s A}{\delta} C_s t$$

where *t* is the sampling time (25).

It can be seen from eq. [21] that the amount of extracted mass is proportional to the sampling time, the D_s for each analyte, and bulk sample concentration and is inversely proportional to δ. This is consistent with the fact that an analyte with a greater D_s will cross the interface and reach the surface of the fibre coating faster. Values of D_s for each analyte can be found in the literature or estimated from physicochemical properties (25). This relationship allows for quantitative analysis. Equation [21] can be modified to estimate the analyte concentration in the sample for rapid sampling with solid sorbents.

$$[22] \qquad C_s = \frac{n\delta}{B_1 D_s A t}$$

The amount of extracted analyte (*n*) can be estimated from the detector response.

The thickness of the boundary layer (δ) is a function of sampling conditions. The most important factors affecting δ are geometric configuration of the extraction phase, sample velocity, temperature, and D_s for each analyte. The effective thickness of the boundary layer can be estimated for the coated fibre geometry (see Fig. 6) using eq. [23], adapted from heat transfer theory (21)

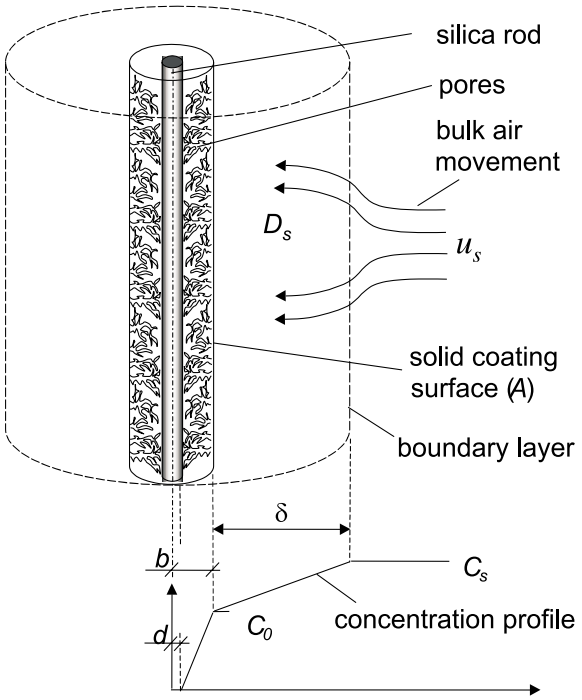
$$[23] \qquad \delta = 9.52\frac{d}{\mathrm{Re}^{0.62}\, Sc^{0.38}}$$

where *Re* is the Reynolds number ($Re = 2u_s d/\nu$): u_s is the linear sample velocity, ν is the kinematic viscosity of matrix, *Sc* is the Schmidt number ($Sc = \nu/D_s$), and *d* is the fibre diameter. The effective thickness of the boundary layer in eq. [23] is a surrogate (or average) estimate and does not take into account changes of the thickness that may occur when the flow separates and (or) a wake is formed. Equation [23] indicates that the thickness of the boundary layer will decrease with an increase of the linear sample velocity (Fig. 6). Similarly, when sample temperature (T_g) increases, the kinematic viscosity also increases. Since the kinematic viscosity term is present in the numerator of *Re* and in the denominator of *Sc*, the overall effect on δ is small. A reduction of the boundary layer and an increase of the mass transfer rate for an analyte can be achieved in at least two ways, i.e., by increasing the sample velocity and by increasing the sample temperature. However, the temperature increase will reduce the solid sorbent efficiency. As a result, the sorbent coating may not be able to adsorb all molecules reaching the surface and therefore stop to behave as a zero sink for all analytes.

Equations [19] and [21] indicate that use of the headspace above the sample as an intermediate phase might be an interesting approach to accelerate extraction for analytes characterized by high Henry constants. When a thin extraction phase is used, the initial extraction rate and, hence, the extraction time is controlled by the diffusion of analytes through the boundary layer present in the sample matrix. The presence of a gaseous headspace facilitates rapid transport into the extraction phase because of the high diffusion coefficients. To increase the transport from the sample matrix into the headspace the system can be designed to produce a large sample–headspace interface. This can be accomplished by using large diameter vials with good agita-

© 2001 NRC Canada

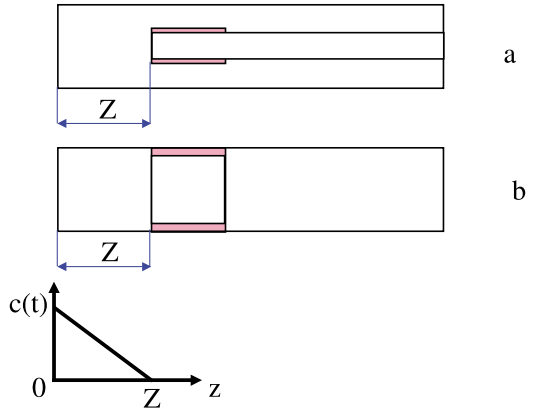
Fig. 6. Schematic of the diffusion based calibration model. The terms are defined in the text.



tion, purge, or even spray systems. At room temperature only volatile analytes are transported through the headspace. For low volatility compounds, heating of the sample is a good approach, if loss in magnitude of the distribution constant can be accepted. The ultimate approach is to heat the sample and cool the extraction phase at the same time. Heating of the sample does not only increases the Henry constant, but also induces convection of the headspace due to density gradients associated with temperature gradients present in the system, resulting in a higher mass transport rates. The cooling of the sorbent increases its capacity. Collection of analytes can be performed in the same vial (26) or can be separated in space similarly as in the purge and trap technique. In the heating-cooling experiments, both kinetic and thermodynamic factors are addressed simultaneously. Headspace approaches are also interesting since adverse affects associated with presence of solids, oily or high molecular weight interferences, which can cause fouling of the extraction phase, are eliminated.

Consideration of different arrangements of the extraction phase is always beneficial. For example, extension of the boundary layer by a protective shield that restricts convection would result in time weighted average (TWA) measurement of analyte concentration (see eq. [21]). Various diffusive samplers have been developed based on this principle. For example, when the extracting phase in SPME device is not exposed directly to the sample, but is contained in a protective tubing (needle) without any flow of the sample through it (see Fig. 7), the diffusive transfer of analytes occurs through the static sample (gas phase or other matrix), trapped in the needle. The system can consist either of an externally coated fibre with extraction phase withdrawn into the needle (Fig. 7*a*) or internally coated needle (Fig. 7*b*).

Fig. 7. SPME–TWA approaches based on the (*a*) in-needle fibre and (*b*) in-needle coating.



These geometric arrangements represent a very powerful method, capable of generating a response proportional to the integral of the analyte concentration over time and space (when the needle is moved through space) (27). In these cases, the only mechanism of analyte transport to the extracting phase is diffusion through the matrix contained in the needle. During this process, a linear concentration profile (shown in Fig. 7) is established in the tubing between the small needle opening, characterized by surface area A and the distance Z between the needle opening and the position of the extracting phase. The amount of analyte extracted (dn) during time interval (dt), can be calculated by considering Fick's first law of diffusion (4)

$$[24] \qquad \mathrm{d}n = AD\frac{\mathrm{d}c}{\mathrm{d}z}\mathrm{d}t = AD\frac{\Delta C(t)}{Z}\mathrm{d}t$$

where $\Delta C(t)/Z$ is an expression of the gradient established in the needle between the needle opening and the position of the extracting phase (Z), $\Delta C(t) = C(t) - C_Z$, where $C(t)$ is a time dependent concentration of analyte in the sample in the vicinity of the needle opening, and C_Z is the concentration of the analyte in the gas phase in the vicinity of the coating. C_Z is close to zero for a high extraction phase – matrix distribution constant capacity, therefore, $\Delta C(t) = C(t)$. The concentration of analyte at the coating position in the needle (C_Z) will increase with integration time, but it will be kept low compared to the sample concentration because of the presence of the extraction phase. Therefore, the accumulated amount over time can be calculated as:

$$[25] \qquad n = D\frac{A}{Z}\int C_s(t)d$$

As expected, the extracted amount of analyte is proportional to the integral of the sample concentration over time, the diffusion coefficient of analyte in the matrix filling the needle (D), in the area of the needle opening (A), and inversely proportional to the distance of the coating position in respect of the needle opening (Z). It should be emphasized that eqs. [24] and [25] are valid only in a situation where the amount of analyte extracted onto the sorbent is a small fraction (below RSD of the measurement, typically 5%) of the equilibrium amount in respect to the lowest concentration in the sample. To extend integration times, the coating can be

© 2001 NRC Canada

placed further into the needle (larger Z), the opening of the needle can be reduced by placing an additional orifice (smaller A), or a higher capacity sorbent can be used. The first two solutions will result in low measurement sensitivity. An increase of sorbent capacity presents a more attractive opportunity. It can be achieved by either increasing the volume of the coating or its affinity towards the analyte. An increase of the coating volume will require an increase of the device size. The optimum approach to increased integration time is to use sorbents characterized by large coating – gas distribution constants. If the matrix filling the needle is other then sample matrix then an appropriate matrix–sample distribution constant should be added to numerator in eq. [25] as discussed below in the case of membrane extraction.

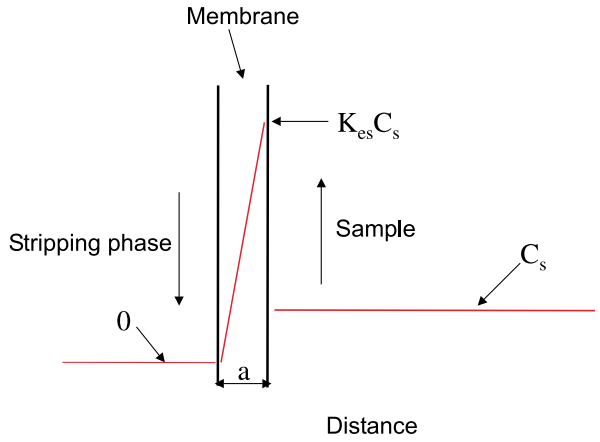
The capacity of the extraction phase for the difficult to extract analytes such as polar or ionic species is frequently enhanced by introducing a derivatization step. The objective of this approach is frequently not only to convert the native analytes into less polar analytes that are extracted more efficiently, but also to frequently label them for better detection and (or) chromatography. The most interesting implementation of this approach is simultaneous extraction–derivatization. In this technique, the derivatization reagent is present in the extraction phase during the extraction. The major advantage of this approach is that two steps are integrated into one. There are two limiting cases describing the combination between extraction and derivatization. The first occurs when mass transfer to the fibre is slow compared to the reaction rate. In this case eq. [18], as discussed above, describes the accumulation rate of analytes in the extraction phase.

In the second limiting case, the situation is reversed in that the reaction rate is slow compared to the transport of analytes to the extraction phase. In the other words, at any time during the extraction, the extraction phase is at equilibrium with the analyte remaining in a well-agitated sample, resulting in uniform reaction rate throughout the coating. This is a typical case for thinly dispersed extraction phase, since the equilibration time for well-agitated conditions is very short compared to a typical reaction rate constant. The accumulation rate of the product in the extraction phase (n/t) can then be defined by:

$$[26] \qquad n = V_e k_r K_{es} \int C_s(t)\mathrm{d}t$$

where C_s is the initial concentration of analyte in the sample and k_r is chemical reaction rate constant. In the other words, when the sample is of large volume, such as direct sampling in the field, the reaction and accumulation of analyte in the extraction phase proceeds with the same rate as long as reagent is present in an excess amount. It is worth noting that the rate is also proportional to the extraction phase – sample matrix distribution constant. If the concentration varies during the accumulation, the collected amount corresponds to the integral over concentration and time, similarly as discussed above in the case of time weighted average sampling. For limited sample volume, however, the concentration of analyte in the sample phase decreases with time as it is partitioned into the coating and converted to product, resulting in a gradual decrease of the rate. The time required to exhaustively extract analytes from a limited volume can be estimated using experimental parameters (4).

Fig. 8. Membrane extraction at good sample agitation and stripping conditions. The terms are defined in the text.



For continuous monitoring applications, extraction using membrane is an attractive approach. Permeation through membrane is a specific extraction process where the sorbtion into and desorbtion out of the extraction phase occurs simultaneously (see Fig. 8). The sample (donor phase) is in contact with one side of the membrane where extraction into membrane material occurs, while permeated analytes are removed by the stripping phase (acceptor). For membrane extraction with good flow (agitation) conditions at both acceptor and donor sites and efficient stripping, the rate of mass transport through the membrane is controlled by the diffusion of analytes through the membrane material. The concentration gradient which facilitates transport across the membrane is formed by the difference in analyte concentration between the sample side ($K_{es}C_s$) and the stripping phase (0). The mass transfer rate through the membrane (n/t) can be estimated at steady state conditions using the following equation (28):

$$[27] \qquad n/t = B_2 A D_e K_{es} C_s/a$$

Where A is the surface area of the membrane, D_e is the diffusion coefficient in the membrane material, K_{es} is the membrane material – sample matrix distribution constant, a is a thickness of the membrane, and B_2 is a geometric factor defined by the shape of the membrane. The permeation rate through the membrane is proportional to both the diffusion coeficient (D_e) and the distribution constant (K_{es}). D_e determines the rate of analyte migration through the membrane and K_{es} the magnitude of the concentration gradient generated in the membrane. This information can be used to calibrate the extraction process a priori if these parameters are obtained from tables or experimental data (29).

The concentration of unknown can be calculated by converting the eq. [27]:

$$[28] \qquad C_s = \frac{an}{B_2 A D_e K_{es} t}$$

The membrane material – sample matrix distribution constant K_{es} determines the sensitivity of membrane extraction (see eq. [27]) indicating that the membrane, although a

© 2001 NRC Canada

physical barrier, is also a concentrating medium, analogous to the extraction phase in other configurations. However the concentration in the stripping gas phase are lower compared to the sample since the gradient needs to exist in the membrane to generate diffusive mass transfer through the membrane material (see Fig. 8). Therefore, incorporating sorbent after the membrane would allow concentration of the extract and therefore sensitive analysis (29). When the membrane is in direct contact with the aqueous phase then the mass transfer through the boundary layer surrounding the membrane could contribute to the overall mass transfer in the system. Therefore, for analytes characterized by a high Henry constant, it is important to consider headspace membrane extraction arrangement.

Conclusions

Reliance on physicochemical constants in calibration might appear unconventional or even make some researchers uncomfortable. However as the theory indicates, these constants define the extraction process and there is an opportunity to take advantage of this fact. Physicochemical constants can be frequently estimated from simple experiments or calculated by considering the molecular structures of analytes, extraction phase, and matrix, which adds to attractiveness of this approach. For equilibrium microextraction techniques the extraction phase – sample matrix distribution constant is used to quantify the concentration of analytes in the sample matrix (see eq. [2]). For extraction approaches controlled by the mass transfer in the boundary layer, calibration can be based on the diffusion coefficient in the sample matrix at constant extraction time under well-defined agitation conditions. When the derivatization reaction kinetics controls the extraction rate, the rate constant can provide a means for calibration. In some cases, as in membrane extraction, a combination of constants defines the extraction rate and can be used for calibration. The major argument against using this approach is that physicochemical constants are affected by many experimental parameters, such as temperature and matrix conditions. However, the impact of temperature change can be compensated for and therefore direct calibration for simple matrices is possible (30). For more complex matrices, internal standard or standard addition calibration, applied routinely in exhaustive techniques to monitor recoveries, can be used to compensate for matrix variations (31). In future research, correlations between distribution constants and simple measurements such as turbidity and pH may be found to account for matrix variations and therefore eliminate the need for internal calibration. The advantages of nonexhaustive extraction are its fundamental simplicity and fewer geometric restrictions, which facilitate a number of interesting on-site implementations by integrating the sampling and sample preparation steps. Additionally, more information can be obtained about the investigated system. For example, it is possible to speciate and determine distribution of analyte in multiphase systems since the extraction process does not disturb the equilibria naturally present in the system. Therefore, different forms of an analyte are extracted and quantified according to their corresponding distribution constants and (or) diffusion coefficients.

A better understanding of the fundamentals of the extraction processes facilitates exploration of new opportunities, which makes sample preparation a more vital and scientifically exciting part of the analytical process. The focus in this discussion has been on chemical extraction, purposely neglecting extraction approaches involving mechanical principles, which would introduce an additional level of complexity, although these would be interesting to explore in future development of the technology.

Acknowledgments

Support for this work was provided from Natural Sciences and Engineering Research Council of Canada (NSERC), Varian, and Restek.

References

1. E.M. Thurman and M.S. Mills. Solid phase extraction. John Wiley & Sons, New York. 1998.
2. J. Dean. Extraction methods for environmental analysis. John Wiley & Sons, New York. 1998.
3. A. Handley. Extraction methods in organic analysis. Sheffield Academic Press, Sheffield, U.K. 1999.
4. J. Pawliszyn. Solid phase microextraction. Wiley–VCH, New York. 1997.
5. B.V. Ioffe and A.G. Vitenberg. Headspace analysis and methods in gas chromatography. John Wiley & Sons, New York. 1984.
6. T. Gorecki, X. Yu, and J. Pawliszyn. Analyst, **124**, 643 (1999).
7. F.A.L. Dullien. Porous media. Academic Press, San Diego. 1992.
8. C. Horvath and H.J. Lin. J. Chromatogr. **149**, 43 (1978).
9. J. Crank. Mathematics of diffusion. Clarendon Press, Oxford. 1989.
10. J.C. Giddings. Anal. Chem. **35**, 1999 (1963).
11. J.A. Cadzow, and H.F. Van Landingham. Signals, systems, and transforms. Prince Hall, New Jersey. 1985.
12. K.D. Bartle, A.A. Clifford, S.B. Hawthorne, J.J. Langenfeld, D.J. Miller, and R. Robinson. J. Supercrit. Fluids, **3**, 143 (1990).
13. J. Langenfeld, S. Hawthorne, D. Miller, and J. Pawliszyn. Anal. Chem. **67**, 1727 (1995).
14. J. Langenfeld, S. Hawthorne, D. Miller, and J. Pawliszyn. Anal. Chem. **65**, 338 (1993).
15. B.E. Richter, B.A. Jones, J.L. Ezzell, N.L. Porter, N. Avdalovic, and C. Pohl. Anal. Chem. **68**, 1033 (1996).
16. J.R.J. Pare, J.M.R. Belanger, K. Li, and S.S. Stafford. J. Microcolumn Sep. **7**, 37 (1995).
17. N. Alexandrou and J. Pawliszyn. Anal. Chem, **61**, 2770 (1989).
18. Z. Miao, Z. Zhang, and J. Pawliszyn. J. Microcolumn Sep. **6**, 459 (1994).
19. K.D. Bartle, T. Boddington, A.A. Clifford, and N. Cotton. Anal. Chem. **63**, 2371 (1991).
20. R. Eisert and J. Pawliszyn. Critical Rev. Anal. Chem. **27**, 103 (1997).
21. A.D. Young. Boundary layers. BSP Professional Books, Oxford. 1989.
22. F. Augusto, J. Koziel, and J. Pawliszyn. Anal. Chem. **73**, 481 (2001).
23. K. Sukola, J. Koziel, F. Augusto, and J. Pawliszyn. Anal. Chem. **73**, 13 (2001).

© 2001 NRC Canada

24. H.S. Carslaw and J.C. Jaeger. Conduction of heat in solids. Clarendon Press, Oxford. 1986.
25. J. Koziel, M. Jia, and J. Pawliszyn. Anal. Chem. **72**, 5178 (2000).
26. Z. Zhang and J. Pawliszyn. Anal. Chem. **67**, 34 (1995).
27. M. Chai and J. Pawliszyn. Environ. Sci. Technol. **29**, 693 (1995).
28. Y. Luo, M. Adams, and J. Pawliszyn. Anal. Chem. **70**, 19 (1998).
29. Y. Luo and J. Pawliszyn Anal. Chem. **72**, 1064 (2000).
30. P. Martos and J. Pawliszyn. Anal. Chem. **69**, 206 (1997).
31. C. Grote and K. Levsen. *In* Applications of solid phase microextraction. *Edited by* J. Pawliszyn. Royal Society of Chemistry, Cambridge, U.K. 1999. Chap. 12.

© 2001 NRC Canada

Interaction of human serum albumin with oxovanadium ions studied by FT-IR spectroscopy and gel and capillary electrophoresis

M. Purcell, J.F. Neault, H. Malonga, H. Arakawa, and H.A. Tajmir-Riahi

Abstract: Some oxovanadium compounds have shown potential to inhibit RNase activity, while at the same time not inhibiting DNase activity. Some vanadyl complexes also inhibit protein synthesis in rabbit reticulocytes, but induce activation of protein–tyrosine kinase. To gain an insight into the interaction of oxovanadium ions with proteins, the present study was designed to examine the bindings of $VOSO_4$ and $NaVO_3$ salts with human serum albumin (HSA) in aqueous solution at physiological pH with metal ion concentrations of 0.0001 to 1 mM and HSA (fatty acid free) concentration of 2% w/v. Gel and capillary electrophoresis (CE) and Fourier transform infrared (FT-IR) spectroscopic methods were used to determine the metal ion binding mode, association constant, and the secondary structure of the protein in the presence of the oxovanadium compounds. Gel electrophoresis results showed that a maximum of 20 vanadyl cations (VO^{2+}) are bound per HSA molecule with strong ($K_1 = 7.0 \times 10^7$ M^{-1}) and weak ($K_2 = 6.5 \times 10^5$ M^{-1}) bindings. Similarly, capillary electrophoresis showed two major bindings for vanadyl cation with $K_1 = 1.2 \times 10^8$ M^{-1} and $K_2 = 8.5 \times 10^5$ M^{-1}, whereas vanadate (VO_3^-) has only a weak binding affinity ($K = 6.0 \times 10^3$ M^{-1}) with HSA molecule. The VO_3^- binds mainly to the lysine ε-amino NH_3^+ groups, while VO^{2+} binds possibly to the histidine nitrogen atom and the N-terminal of the α-amine residue. Infrared spectroscopic analysis showed metal ion binding results in major protein secondary structural changes from that of the α-helix (55.0 to 43–44%) to the β-sheet (22.0 to 23–26%), β-antiparallel (12.0 to 13–16%), and turn (11.0 to 17–18%), at high metal ion concentration. The observed spectral changes indicate a partial unfolding of the protein structure, in the presence of oxovanadium ions.

Key words: oxovanadium, protein, binding mode, binding constant, secondary structure, electrophoresis, FT-IR spectroscopy.

Résumé : Certains composés de l'oxovanadium présentent du potentiel pour inhiber l'activité de la RNase tout en n'inhibant pas la DNase. Certains complexes de vanadyle inhibent aussi la synthèse des protéines dans les réticulocytes de lapins tout en induisant une activation de la kinase de la protéine-tyrosine. Ce travail a été entrepris dans le but de mieux comprendre les interactions entre les ions oxovanadium et les protéines et, à cette fin, on a mesuré la fixation de sels de $VOSO_4$ et de $NaVO_3$ avec l'albumine de sérum humain (ASH; ne contenant pas d'acide gras libre) à une concentration de 2% w/v, en solution aqueuse, au pH physiologique et en présence d'ions métalliques à des concentrations allant de 0,0001 à 1 mM. On a fait appel à l'électrophorèse capillaire et sur gel ainsi qu'à des méthodes de spectroscopie infrarouge à transformation de Fourier (FT-IR) pour déterminer le type de fixation des ions métalliques, les constantes d'association et les structures secondaires de la protéine en présence de composés oxovanadium. Les résultats d'électrophorèse sur gel montrent qu'un maximum de 20 cations vanadyles (VO^{2+}) sont liés à la molécule d'ASH avec des fixations fortes ($K_1 = 7{,}0 \times 10^7$ M^{-1}) et faibles ($K_2 = 6{,}5 \times 10^5$ M^{-1}). De la même manière, l'électrophorèse capillaire met en évidence deux fixations principales pour l'ion vanadyle avec $K_1 = 1{,}2 \times 10^8$ M^{-1} et $K_2 = 8{,}5 \times 10^5$ M^{-1} alors qu'on n'observe qu'une seule fixation faible ($K_1 = 6{,}0 \times 10^3$ M^{-1}) d'ASH avec le vanadate (VO_3^-). L'anion VO_3^- si lie principalement aux groupes NH_3^+, ε-amino, de la lysine alors que le cation VO^{2+} se lierait vraisemblablement avec l'atome d'azote de l'histidine et le N-terminal du résidu d'acides aminés. L'analyse par spectroscopie infrarouge montre que la fixation des ions métalliques provoque des changements importants dans la structure secondaire de la protéine qui, à concentration d'ion métallique élevée, passe de 55 à 43–44% de α-hélice, de 22,0 à 23–26% de feuillet-β, de 12,0 à 13–16% de β-antiparallel et de 11,0 à 17–18%. Les changements spectraux observés indiquent que, en présence d'ions oxovanadium, la structure de la protéine se déplie légèrement.

Mots clés : oxovanadium, protéine, mode de fixation, constante de fixation, électrophorèse, spectroscopie FT-IR.

[Traduit par la Rédaction]

Received April 10, 2001. Published on the NRC Research Press Web site at http://canjchem.nrc.ca on October 2, 2001.

M. Purcell, J.F. Neault, H. Malonga, H. Arakawa,[1] and H.A. Tajmir-Riahi.[2] Department of Chemistry-Biology, University of Québec at Trois-Riviéres, C.P. 500, TR, QC G9A 5H7, Canada.

[1]Dr. H. Arakawa was on sabbatical leave from Hokkaido Institute of Technology, Sapporo, Japan.
[2]Correponding author (telephone: (819) 376-5052 ext. 3310; fax: (819) 376-5084; e-mail: tajmirri@uqtr.uquebec.ca).

 DOI: 10.1139/cjc-79-10-1415 © 2001 NRC Canada

Introduction

Vanadium enters cells as vanadate (VO_3^-), where it is reduced to the vanadyl cation (VO^{2+}) at physiological pH (1–3). These metal ions bind to a variety of biological molecules including proteins, amino acids, nucleic acids, phosphates, and phospholipids and alter their structural properties (2–6). Some of oxovanadium complexes have shown potential to inhibit RNase activity by acting as a transition analogue, while at the same time not inhibiting DNase activity. The activation of cytosolic protein–tyrosine kinase by vanadate ions has been studied and the effects of these cations on the biological actions of insulin were reviewed (7, 8). Similarly, the inhibition effect of vanadyl cations on the activity of Na-, K-ATPase has been investigated (9). The association constants of vanadium complexes formed with different ligands show strong affinity for coordination to both nitrogen and oxygen donor groups (10). Recently, on the basis of the electron spin echo envelope modulation, coordination of the vanadyl cation to nitrogen atoms of Lys ε-amine or the terminal α-amine of a protein or peptide has been demonstrated (11). To better understand the biochemical role of vanadium with respect to its ability to promote and (or) inhibit enzymatic effects in biological systems (3, 11–13), the structural analyses of vanadium–protein complexes, including the metal ion binding sites, the binding constants, and the effects of metal ion coordination on the secondary structure of the protein, are of major biological importance. Thus, the present study is designed to examine, in vitro, the complexation of oxovanadium ions with human serum albumin (HSA).

Human serum albumin (HSA) represents an important and the most abundant protein constituent of blood plasma and serves as a protein storage component. Recently, the three-dimensional structure of HSA was determined through X-ray crystallographic measurements (14). This globular protein, which has many important physiological functions, consists of a single polypeptide chain of 585 amino acids (15, 16). HSA contributes considerably to colloid osmotic blood pressure and realizes the transport and distribution of many molecules and metabolites such as fatty acids, amino acids, hormones, cations and anions, and many diverse drugs. It also makes possible to bind and carry through the bloodstream many drugs that are poorly soluble in water (16). It has been shown that the distribution, the free concentration, and the metabolism of various drugs can be significantly altered as a result of their bindings to HAS (17). Therefore, the interaction of oxovanadium ions with HSA has major biochemical importance.

We now report the gel and capillary electrophoresis as well as Fourier transform infrared (FT-IR) spectroscopic results on the interaction of $VO^{2+}$and VO_3^- with HSA, in aqueous solutions at physiological pH, using various concentrations of oxovanadium ions with a constant concentration of HSA. Spectroscopic evidence regarding the cation binding mode, the association constant, and the secondary structure of the protein are provided here. To our knowledge, our structural information provides the first spectroscopic evidence of a vanadium–HSA interaction that helps elucidation of the nature of this biologically important complexation both in vitro and in vivo.

Materials and methods

Materials

Human serum albumin (HSA) fraction V (fatty acid free) was purchased from Sigma. Hydrated crystalline $VOSO_4$ and $NaVO_3$ salts were from Aldrich and recrystallized from water. D_2O (99.8%D) was from Aldrich. Other chemicals were of reagent grade and used without further purification.

Preparation of stock solution

Human serum albumin (HSA, fatty acid free) was dissolved in Na–phosphate buffer (0.1 M, pH 7.2) containing NaCl (50 mM) to attain the concentration of 4% w/v. The $VOSO_4$ and $NaVO_3$ (0.0002–2 mM) solutions were prepared in double-distilled water. For the samples to be analyzed by FT-IR spectroscopy, a solution of the vanadium salt was added dropwise to the protein solution with constant stirring to ensure the formation of homogeneous solution and to attain the desired metal ion concentrations of 0.0001, 0.001, 0.01, 0.1, and 1 mM with a final protein concentration of 2% w/v. The pH or pD of the solution was adjusted to 6.8–7.5 by the addition of NaOH–NaOD (0.1 M) or HCl–DCl (0.1 M).

Gel electrophoresis

Polyacrylamide gel electrophoresis was performed at room temperature in the buffer system of Laemmli (18), using miniature slab gels (Hoefer Scientific Instruments) containing 8% acrylamide. The gels were stained with Coomassie brilliant blue and scanned with a LKB 2400 Ultro Scan XL laser densitometer. The polypeptide content of the band was evaluated by integration of the peak and molecular weight was estimated from the low molecular weight standards from Bio-Rad. The absorbance of the laser beam at 633 nm was recorded, and the relationship between staining intensity and protein concentration was confirmed to be linear. HSA was diluted in H_2O to attain a final concentration of 1.5 μM and mixed with oxovanadium ions to attain final concentrations of 0.0001–1 mM. The denaturating conditions were optimised to ensure the integrity of the oxovanadium–HSA complexes formed during the migration.

Capillary electrophoresis

P/ACE System MDQ (Beckman) with PDA (photodiode array) detector was used in this study. Uncoated fused silica capillary of 75 μm i.d. and 57 cm length was used. The capillary was initially conditioned by washing with 1 N sodium hydroxide for 30 min, followed by a 15 min wash with 0.1 M sodium hydroxide. Then, it was extensively rinsed with deionized water and the running buffer before use. Samples were injected using a voltage of 10 kV for 5 s. Electrophoresis was carried out at 25 kV for 12 min using normal polarity. All runs were carried out 25°C in a run buffer of Tris–HCl (20 mM, pH 7.2). The electropherograms were monitored at 220 nm. Stock solutions of HSA (1.0% w/v) were prepared in Tris–HCl (8 mM, pH 7.2), and $VOSO_4$ (0.2 mM) and $NaVO_3$ (4 mM) were prepared in deionized water. The capillary inlet and outlet vials were replenished after every run. The VO^{2+} and VO_3^- binding experiments were performed in Tris–HCl (4 mM, pH 7.2) containing a constant concentration of HSA (0.1% w/v) and

© 2001 NRC Canada

various concentrations of VO^{2+} (10^{-6} to 10^{-1} mM) and VO_3^- (10^{-1} to 2 mM). Each sample was allowed to equilibrated for 30 min before injection.

Data analysis

The binding constants for the VO^{2+}–HSA and VO_3^-–HSA complexes were determined by capillary electrophoresis using Scatchard analysis (19–21). The average number (R_f) of oxovanadium ions bound per one binding site of the HSA was determined from the change of the peak height using the following equation:

$$[1] \qquad R_f = (H - H_o)/(H_s - H_o)$$

where H is the change of the peak height measured for added oxovanadium ion concentration, and H_o and H_s correspond to the peak heights of the free HSA and the oxovanadium ion saturated, respectively. Using the equation for binding constant

$$[2] \qquad K_b = [\text{oxovanadium ion} - \text{HSA}]/[\text{HSA}][\text{oxovanadium ion}]$$

the experimental oxovanadium ion binding constants (K_b) were then computed by fitting the experimental values of R_f and the oxovanadium ion concentrations to eq. [3].

$$[3] \qquad R_f = K_b[\text{oxovanadium ion}]/(1 + K_b[\text{oxovanadium ion}])$$

The last equation gives a convenient form for Scatchard analysis:

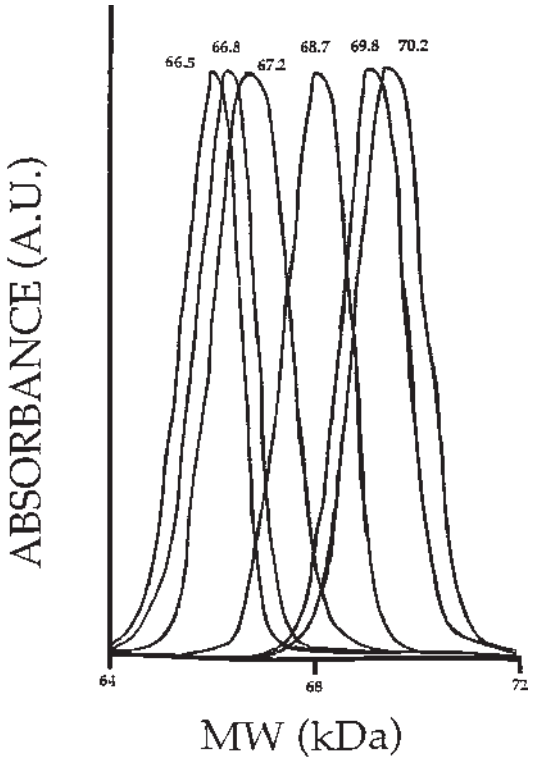
$$[4] \qquad R_f/[\text{oxovanadium ion}] = K_b - K_b R_f$$

The binding constants of VO^{2+}–HSA were also determined by polyacrylamide gel electrophoresis by the same procedure of the capillary electrophoresis except that R_f was calculated from the mobility of each sample, and the logarithmic form of eq. [4] was used instead of eq. [4].

FT-IR spectroscopic measurements

Infrared spectra were recorded on a BOMEMDA3–0.02 Fourier transform infrared spectrometer equipped with a nitrogen cooled HgCdTe detector and a KBr beam splitter. Solution spectra were recorded using AgBr windows with a resolution of 2 cm^{-1} and 100–500 scans. The subtraction of H_2O from protein solution was carried out as reported in our previous reports (22, 23). The difference spectra [(protein solution + vanadium ion solution) – (protein solution)] were generated using the polypeptide antisymmetric and symmetric C—H stretching bands (24), located at 2900–2800 cm^{-1} as internal standard. The protein C—H stretching vibrations exhibit no spectral changes upon metal ion interaction and are, therefore, canceled on spectral subtraction. The accuracy of this method of subtraction was tested by using several control samples with the same protein or metal ion concentrations, which resulted in the formation of a flat baseline. However, a similar absorption scale was used for the spectra of the free protein and its oxovanadium complexes as well as for the difference spectra produced. This method allowed us to obtain meaningful spectral differences between the free protein and its vanadium complexes at different metal ion concentrations. These spectral differences were then used, to characterize the nature of the metal–protein interaction.

Fig. 1. Densitometric profile showing the positions of the vanadyl–HSA complexes from the polyacrylamide gel electrophoresis. Vanadyl–HSA at: 70.2 (1 mM), 69.8 (0.1 mM), 68.7 (0.01 mM), 67.2 (0.001 mM), and 66.8 kDa (0.0001 mM) and HSA free at 66.5 kDa (the maximum error, based on two experiments is 0.3 kDa).



Determination of the secondary structure of the protein

Determination of the secondary structure of HSA and its vanadium complexes was carried out on the basis of the procedure described by Byler and Susi (25). The secondary structure of the protein was determined from the shape of the amide I band, located at 1650–1660 cm^{-1}. Fourier self-deconvolution and second-derivative resolution enhancement were applied to increase the spectral resolution in the region of 1700–1600 cm^{-1}. The second-derivative curves were produced using a point convolution of 11 or 13. The resolution enhancement resulting from self-deconvolution and the second derivative is such that the number and the position of the bands to be fitted are determined. To quantify the area of the different components of the amide I contour, revealed by self-deconvolution and second derivative, a least-square iterative curve-fitting was used to fit the Lorentzian line shapes to the spectra between 1700–1600 cm^{-1}. Before curve-fitting was done, a straight baseline passing through the ordinates at 1700 and 1600 cm^{-1} was subtracted. The baseline is then modified again by the least-square curve-fitting, which allowed for a horizontal baseline to be adjusted, as an additional parameter, to obtain the best fit. It is known that no meaningful curve-fitting can be performed by simple examination of the original infrared spectra, which is why the self-

© 2001 NRC Canada

Fig. 2. Plots for $VOSO_4$ concentrations vs. molecular weights of VO^{2+}–HSA complexes and the number of vanadyl cations bound to HSA.

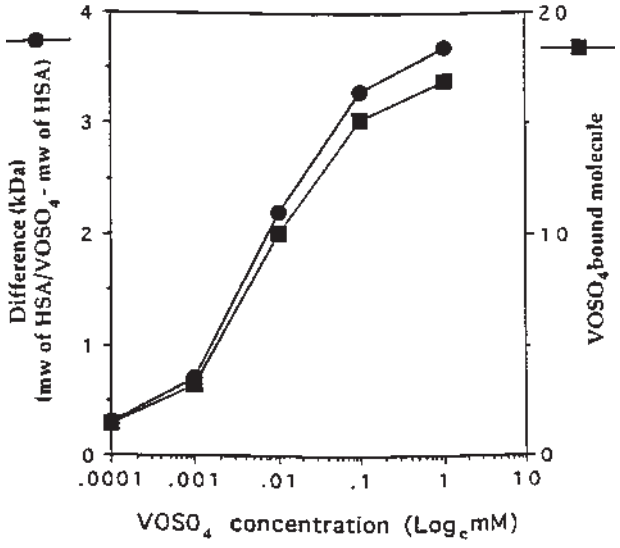
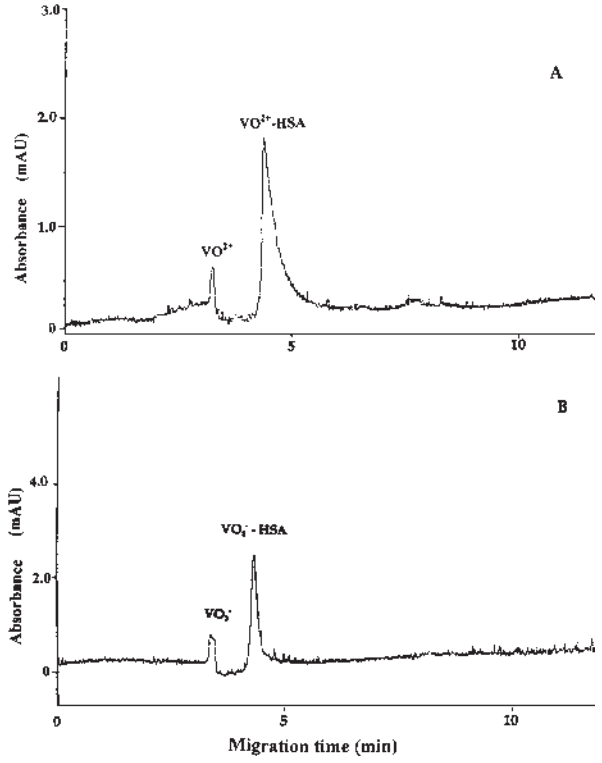
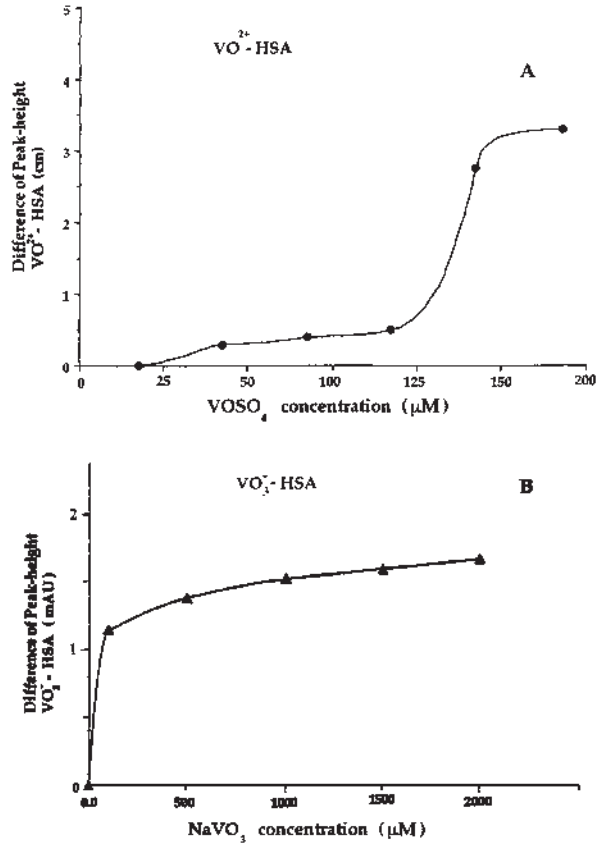


Fig. 3. Electropherograms showing mixtures containing constant concentration (0.1% w/v) of HSA and (*a*) 0.001 mM of $VOSO_4$ and (*b*) 0.1 mM of $NaVO_3$ at 220 nm. The capillary electrophoresis was performed at 25 kV in a run buffer of Tris–HCl (20 mM, pH 7.2).



deconvolution procedure has to be carried out first. The curve-fitting was done using 25 simulations. The results of curve-fitting were analysed as follows: each Lorentzian band is assigned to a secondary structure according to the frequency of its maximum; α-helix (1658–1650 cm^{-1}), β-sheet (1615–1640 cm^{-1}), turn (1666–1673 cm^{-1}), random coil (1641–1645 cm^{-1}), and β-antiparallel (1680–1692 cm^{-1}). The area of all the band components assigned to a given conformation are then summed and divided by the total area. The number obtained is taken as the proportion of the polypeptide chain in that conformation. These assignments are consistent with the previous values determined theoretically (24) and experimentally (25). The accuracy of this method was tested on several proteins of the known conformational contents (through X-ray diffraction analysis), such as cytochrome c (α-helix 49%) and RNase A (α-helix 27%) (26, 27), which resulted in 2 to 3% differences. The data treatments of protein conformational analysis are also reported in our recent publication (28).

Fig. 4. Plots for oxovanadium ions concentrations vs. difference of peak heights in (*a*) VO^{2+}–HSA and (*b*) VO_3^-–HSA complexes from free HSA. Incubation of constant concentration (0.1% w/v) of HSA and various concentrations of oxovanadium ions were carried out in Tris–HCl (4 mM, pH 7.2) and the mixtures were subjected to the capillary electrophoresis.



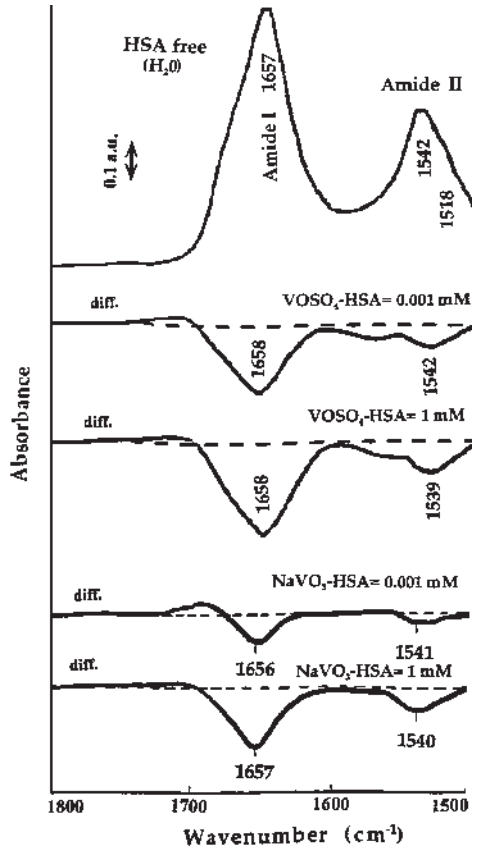
Results and discussion

Gel electrophoresis

To study the nature of vanadium–HSA complexation, polyacrylamide gel electrophoresis was performed. The results obtained from the gel electrophoresis and densitometric measurements are presented in Fig. 1, which clearly show complexation between the VO^{2+} and HSA in aqueous solution. A peak was observed at 66.5 kDa corresponding to the free HSA and the other peaks at 66.8, 67.2, 68.7, 69.8, and

© 2001 NRC Canada

Fig. 5. FT-IR spectra (top first curve) and difference spectra [(protein solution + metal ion solution) – (protein solution)] (bottom four curves) of the free human serum albumin (HSA) and its vanadium complexes in aqueous solution at physiological pH with different metal ion concentrations in the region of 1800–1500 cm^{-1}. The baseline is shown as broken lines.

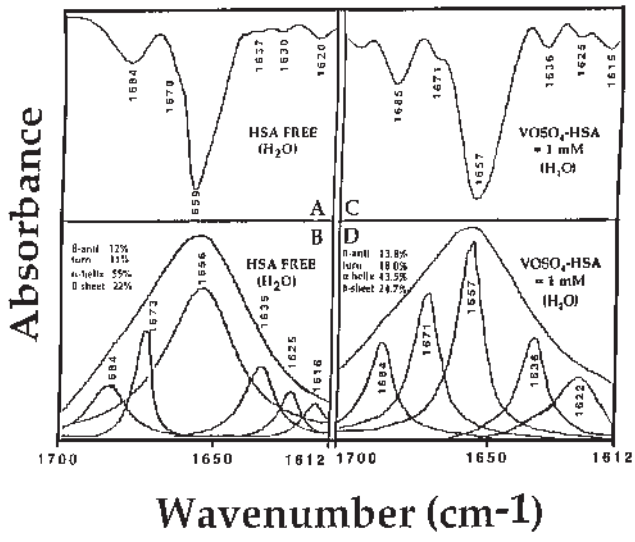


70.2 kDa are vanadyl protein complexes formed with cation concentrations of 0.0001, 0.001, 0.01, 0.1, and 1 mM, respectively. Figure 2 shows the relationship between vanadyl cation concentrations and the increase of molecular weight relative to free HSA. These results indicate that five distinct complexes are formed with cation–protein molar ratios of 1.5:1, 3.5:1, 10:1, 15:1, and 20:1. We thus suggest that about 1.5–20 vanadyl cations are bound per HSA molecule.

Capillary electrophoresis

In recent years, capillary electrophoresis was used to determine the binding constants of metal–protein complexes (29). The bindings of vanadyl cations and vanadate anions to HSA were also studied by capillary electrophoresis. The mixtures containing various concentrations of oxovanadium ions and constant concentration of HSA were subjected to the capillary electrophoresis. The electropherograms were monitored at 220 nm in a run buffer of Tris–HCl (20 mM, pH 7.2). As shown in Fig. 3, vanadyl cation and VO^{2+}–HSA (Fig. 3*a*) and vanadate anion and VO_3^-–HSA (Fig. 3*b*) were separated by the present condition. Figure 4*a* shows that binding of vanadyl cation to HSA occurred at two steps, since the increase of peak height of VO^{2+}–HSA reached plateaus at vanadyl concentrations of 0.1 and 10 μM. On the contrary, the binding of vanadate anion to HSA occurred at

Fig. 6. Second derivative resolution enhancement and curve-fitted amide I region (1700–1612 cm^{-1}) and secondary structure determination of the free HSA (curves *a* and *b*) and its vanadyl complexes (curves *c* and *d*) in aqueous solution with 1 mM cation concentration.



one step and the peak height of the VO_3^-–HSA reached plateau at vanadate concentration of 100 μM. To estimate the binding constants of the VO^{2+}–HSA and VO_3^-–HSA, Scatchard analysis (19) was performed by using data of R_f (the number of oxovanadium ions bound per one binding site of HSA) and R_f/concentrations of oxovanadium ions. The Scatchard plot for the VO^{2+}–HSA showed a biphasic slope indicating two distinct cation binding site and the binding constants were estimated to be 1.2×10^8 and 8.5×10^5 M^{-1}, respectively. In contrast, the plot for the VO_3^-–HSA showed a monophasic slope and the binding constant was estimated to be 6.0×10^3 M^{-1}.

Furthermore, based on the mobility of each VO^{2+}–HSA complex on the polyacrylamide gel, Scatchard plot for R_f vs. (R_f/concentrations of vanadyl cations) was performed. This analysis showed that vanadyl cation has a strong and a weak binding site. The binding constants for the two sites were calculated to be 7.0×10^7 and 6.5×10^5 M^{-1}, respectively. It should be noted that the binding nature of the VO^{2+}–HSA complexes observed from capillary electrophoresis are almost the same pattern as that of the gel electrophoresis. No binding constant was calculated for the VO_3^-–HSA from gel electrophoresis, due to a weak anion–protein interaction.

Metal cations such as Ni^{2+} and Cu^{2+} show strong affinity towards HSA with the binding constants ranging from 10^5 to 10^6 M^{-1} (17). HSA has two major strong binding sites (30). The first is the cysteine residue in position 34 (site V), which is able to bind Au^+, Ag^+, Hg^{2+}, and Cd^{2+} cations. The second is the so-called amino terminal (site VI), a binding site with high affinity for Ni^{2+} and Cu^{2+} cations, where the key feature is a histidine residue in the third position of the peptide chain (31). The vanadyl cation was shown to have strong affinity towards the imidazole nitrogen atom of histidine residues (11). Furthermore, recent structural analysis of the active site of vanadium chloroperoxidase showed that vanadyl cation binds directly to the nitrogen atom of

© 2001 NRC Canada

Table 1. Secondary structure determination for the free HSA and its $VOSO_4$ and $NaVO_3$ complexes (HSA–$VOSO_4$ (HSA–$NaVO_3$)) in H_2O at physiological pH with different metal ion concentrations.

Amide I components (cm^{-1})	HSA free (%)	0.001 mM (%)	0.01 mM (%)	0.1 mM (%)	1 mM (%)
1692–1680 β-Antiparallel	12.0 ± 1	12.0 (12.6)	12.5 (12.9)	14.0 (13.6)	13.8 (13.8)
1673–1666 Turn	11.0 ± 1.0	15.0 (11.5)	17.0 (11.9)	17.0 (15.8)	17.0 (17.8)
1658–1650 α-Helix	55.0 ± 3.0	50.0 (53.3)	45.5 (52.4)	43.5 (47.6)	43.5 (43.4)
1641–1645 Random*	11.0 ± 1.0	11.0	12.0	12.0	13.0
1640–1615 β-Sheet	22.0 ± 1.0	23.0 (22.6)	25.0 (22.8)	25.5 (23.0)	25.7 (25.0)

Note: The values in parenthesis are from $NaVO_3$ solution.

*The values of random obtained from D_2O solution are not included in the values from water solution. The mean deviation was 1–3.0% for the free protein and its metal ion complexes.

histidine 496 and indirectly (H-bonding) to histidine 404, positioned in the vicinity of arginine 490, arginine 360, and lysine 353 amino groups (32). Thus, the strong binding constant for VO^{2+}–HSA calculated from gel and capillary electrophoresis probably corresponds to direct cation binding to the histidine imidazole, whereas the weak binding constant probably comes from indirect binding (H-bonding) to a nonspecific site of HSA. On the other hand, it has been reported that the vanadate anion binds weakly to the lysine ε-amino group of HSA with the association constant approximately 1×10^3 M^{-1} (10). Thus, the low binding constant for the VO_3^-–HSA (6.0×10^3 M^{-1}) calculated from the capillary electrophoresis corresponds to an indirect vanadate ion interaction with ε-amino group of lysine residues in HSA.

FT-IR spectroscopy

Additional evidence regarding the complexation of oxovanadium–HSA was obtained by FT-IR spectroscopy. Figure 5 shows FT-IR spectra of the free HSA and difference spectra for the VO^{2+}–HSA and VO_3^-–HSA complexes obtained by subtraction of the free-HSA spectrum from those of the metal–protein complexes. In the free HSA, two major bands for amide I at 1657 cm^{-1} (mainly C=O stretching) and amide II band at 1542 cm^{-1} (C—N stretching coupled with N—H bending mode) (24–27) were observed (Fig. 5). In the difference spectra taken at 0.0001 mM of the oxovanadium ions, a flat line was obtained because no significant intensity changes or spectral shiftings occurred during the incubation (spectra not shown). This is indicative of no major metal–protein interaction at very low vanadium ion concentrations. As the vanadium concentration increased (0.001 mM), two negative features at 1658–1656 and 1542–1541 cm^{-1} were observed, which are attributed to the intensity decrease in the amide I and II bands in the spectra of the oxovanadium–HSA complexes. The decrease of the intensity of the amide I band is due to the reduction of the α-helix structure, whereas the decrease of the intensity of the amide II band is due to the binding of the oxovanadium ions to the nitrogen atom of the CN group. The interaction of oxovanadium ion with the nitrogen atom of the NH group is also evident from the shift of the amide A band at 3303 cm^{-1} (peptide–N-H stretching mode) (24–27), towards a lower frequency at 3290 cm^{-1} (spectrum not shown). The band at 1518 cm^{-1} of the free HSA related to the vibration of tyrosine side chain (33–37) showed no spectral changes, which is indicative of no perturbation of the tyrosine residue in the oxovanadium–HSA complexes. As the metal ion concentration increased (1 mM), the negative features in the difference spectra at 1658 –1656 and 1542–1539 cm^{-1} grew in intensity and shape due to further metal ion complexation and the reduction of the proteins' α-helix structure upon oxovanadium–HAS interaction.

A quantitative analysis of the secondary structure of the protein for HSA and its vanadium complexes in H_2O is given in Fig. 6 and Table 1. The free protein contained largely α-helix (55.0%), along with β-sheet (22.0%), turn structure (11.0%), and β-antiparallel (12.0%). The β-sheet structure is composed of three components at 1616 (inter β-strand), 1625 (intra β-strand), and 1635 cm^{-1} (hydrated) (Fig. 6), which are consistent with the recent spectroscopic studies of HSA (38, 39). In D_2O solution, due to the isotopic substitution (D/H), the presence of a new component band at 1644 cm^{-1} in the spectrum of the free HSA was assigned to the random structure (11%) (Table 1). Upon vanadium interaction, the α-helix structure was reduced from 55.0 to 50–43.5%, whereas the β-pleated increased from 22 to 23–25.7%, the turn structure from 11 to 11.5–17.8%, and the β-antiparallel from 12 to 12.5 –14% at high metal ion concentration (Fig. 6 and Table 1, 1 mM). The narrowing of the band at 1656 cm^{-1} and the broadening of the bands at 1636 and 1622 cm^{-1} in the presence of oxovanadium ions are clear evidence of the reduction of the proteins' α-helix conformation in favor of a β-sheet structure (Fig. 6). The random structure, determined from deuterated samples, showed minor changes upon cation complexation (Table 1). The observed spectral changes are consistent with the major perturbations of the HSA secondary structure upon vanadium-ion coordination. It should be noted that no major secondary structural differences were observed for complexes formed with 0.1 and 1 mM cation concentrations (Table 1). This is indicative of no further cation–protein interaction at 1 mM vanadium concentration. The reduction of the α-helix in favor of the β-sheet structure is indicative of a partial unfolding of protein, in the presence of vanadyl at high cation concentrations. Similar conformational transition from an α-helix to β-sheet structure was observed for the protein unfolding upon protonation and heat denaturation (40–42).

In conclusion, on the basis of electrophoresis and IR spectroscopic results obtained for the oxovanadium–HSA complexes in aqueous solution, the following remarks can be made: (*i*) the metal–protein interaction leads to the formation of several vanadium–protein complexes with stoichiometric ratios of 1.5–20 vanadyl cations per HSA molecule; (*ii*) vanadyl cations show strong and weak bindings with $K_1 = 7.0 \times 10^7$ M^{-1} and $K_2 = 6.5 \times 10^5$ M^{-1} (gel electrophoresis) and $K_1 = 1.2 \times 10^8$ M^{-1} and $K_2 = 8.5 \times 10^5$ M^{-1} (capil-

© 2001 NRC Canada

lary electrophoresis), respectively, whereas vanadate has only a weak binding affinity (K= 6.0 × 10^3 M^{-1}) with HSA molecule; (*iii*) the strong affinity binding for vanadyl cation is related to a direct metal ion interaction with the nitrogen atom of histidine residue, whereas the low affinity binding (6.5 × 10^5 M^{-1}) can be attributed to an indirect cation–protein complexation (H-bonding); (*iv*) the low affinity binding of vanadate anion is also due an indirect coordination of the metal ion through lysine ε-NH_3^+ group; and (*v*) metal ion complexation results in major protein secondary structural changes from that of the α-helix to β-sheet and turn structure.

Acknowledgments

We highly appreciate the financial supports received from Natural Sciences and Engineering Research Council of Canada (NSERC) and FCAR (Québec) for this work.

References

1. Y. Shechter and S.J.D. Karlish. Nature (London), **284**, 556 (1980).
2. G.R. Dubyak and A. Kleinzeller. J. Biol. Chem. **255**, 5306 (1980).
3. L.C. Cantley Jr., and P. Aisen. J. Biol. Chem. **254**, 1781 (1979).
4. J. Li, G. Elberg, D.C. Crans, and Y. Shechter. Biochemistry, **35**, 8314 (1996).
5. Y. Shechter, J. Meyerovitc., D. Gefel, R. Bruck, G. Elberg, D.S. Miller, and A. Shisheva. Mol. Cell. Biochem. **153**, 39 (1995) and refs. cited therein.
6. M.B. Anand-Srivastava, J.H. McNeill, and X.P. Yang. Mol. Cell. Biochem. **153**, 113 (1995).
7. L.M. Pierce, F. Alessandrini, J.J. Goldski, and J.D. Paulauskis. Toxicol. Appl. Pharm. **138**, 1 (1996).
8. S. Pugazhenthi and R.L. Khandelwal. Biochem. Int. **26**, 241 (1992).
9. P. Svoboda, J. Teisinger, J. Pilar, and F. Vyskocil. Biochem. Pharmacol. **33**, 2485 (1984).
10. B.R. Nechay, L.B. Nanninga, and P.S.E. Nechay. Arch. Biochem. Biophys. **251**, 128 (1996).
11. K. Fukui, H. Ohya-Nishiguchi, M. Nakai, H. Sakurai, and H. Kamada. FEBS Lett. **368**, 31 (1995).
12. L.C. Cantley Jr., M.D. Resh, and G. Guidotti. Nature (London), **272**, 552 (1978).
13. D.S. Crans, R.L. Bunch, and L.A. Theisen. J. Am. Chem. Soc. **111**, 7597 (1989).
14. X.-M. He and D.C. Carter. Nature (London) **358**, 209 (1992).
15. A. Dugiaczyk, S.W. Law, and O.E. Dennison. Proc. Natl. Acad. Sci. U.S.A. **79**, 71 (1982).
16. T. Peters. Adv. Protein Chem. **37**, 161 (1985).
17. U. Kragh-Hansen. Pharmacol. Rev. **33**, 17 (1981).
18. U.K. Laemmli. Nature (London), **227**, 680 (1970).
19. G. Scatchard. Ann. NY. Acad. Sci. **51**, 660 (1949).
20. M.I. Klotz and L.D. Hunston. Biochemistry, **10**, 3065 (1971).
21. M.I. Klotz. Science (Washington, D.C.), **217**, 1247 (1982).
22. J.F. Neault and H.A. Tajmir-Riahi. Biophys. J. **76**, 2177 (1999).
23. J.F. Neault and H.A. Tajmir-Riahi. J. Biol. Chem. **271**, 8140 (1996).
24. S. Krimm and J. Bandekar. Adv. Protein Chem. **38**, 181 (1986).
25. M. Byler and H. Susi. Biopolymers, **25**, 469 (1986).
26. E. Goormaghtigh, V. Cabiaux, and J.M. Ruysschaert. Eur. J. Biochem. **193**, 409 (1990).
27. G. Vandenbussche, A. Clercx, T. Curstedt, J. Johansson, H. Jornvall, and J.M. Ruysschaert. Eur. J. Biochem. **203**, 201 (1992).
28. A. Ahmed, H.A. Tajmir-Riahi, and R. Carpentier. FEBS Lett. **363**, 65 (1995).
29. T. Guszczynski and T. Copeland. Anal. Biochem. **260**, 212 (1998).
30. D.C. Carter and J.X. Ho. Adv. Protein Chem. **45**, 153 (1994).
31. C. Harford and B. Sarkar. Acc. Chem. Res. **30**, 123 (1997).
32. R. Rokus, H. Weiger, and R. Waver. J. Biol. Chem. **275**, 11650 (2000).
33. Y.N. Chirgadze, O.V. Federov, and N.P. Trushina. Biopolymers, **14**, 679 (1975).
34. H. Matsuura, K. Hasegawa, and T. Miyazawa. Spectrochim. Acta, **42A**, 1181 (1986).
35. J.M. Olinger, D.M. Hill, R.J. Jakobsen, and R.S. Brody. Biochim. Biophys. Acta, **869**, 89 (1986).
36. H. Fabian, C. Schultz, J. Backmann, U. Hahn, W. Saenger, H.H. Mantsch, and D. Naumann. Biochemistry, **33**, 10725 (1994).
37. T. Yamamoto and M. Tasumi. J. Mol. Struct. **242**, 235 (1991).
38. L. Boulkanz, N. Balcar, and M.H. Baron. Appl. Spectrosc. **49**, 1737 (1995).
39. E. Bramanti and E. Benedetti. Biopolymers, **38**, 639 (1996).
40. F.S. Parker. Applications of infrared, Raman, and resonance spectroscopy in biochemistry. Plenum Press, New York. 1983.
41. W.K. Surewicz, M.A. Moscarello, and H.H. Mantsch. J. Biol. Chem. **262**, 8598 (1987).
42. I.E. Holzbaur, A.M. English, and A.A. Ismail. Biochemistry, **35**, 5488 (1996).

© 2001 NRC Canada

The metal template effect on *O*-alkylation of tetrahydroxy[3.1.3.1]metacyclophane with 4-(chloromethyl)pyridine to afford tetrakis-[(4-pyridylmethyl)oxy][3.1.3.1]metacyclophanes and their conformational studies

Takehiko Yamato, Kenji Kumamaru, and Hirohisa Tsuzuki

Abstract: An attempted *O*-alkylation of the flexible macrocycle tetrahydroxy[3.1.3.1]metacyclophane (**1**) with 4-(chloromethyl)pyridine (**2a**) in the presence of NaH under THF reflux gave 1,3-di-*O*-substitution product *distal*-**3a** as a major product. In contrast, tetraol **1** was *O*-alkylated with **2a** in the presence of Cs_2CO_3 to afford a mixture of two conformers of tetra-*O*-alkylated product **4a** in a ratio of 77:23 (1,4-*alternate*-**4a**:*partial-cone*-**4a**) in 95% yield. No formation of the cone conformer in the reaction of the tetraol **1** with **2a**, in comparison with those with 2-(chloromethyl)pyridine (**2b**) or benzyl bromide (**2c**) in the presence of NaH or K_2CO_3, which predominantly afforded cone-conformer, might be attributable to the absence of contributions derived from cation–N interactions as well as cation–π interactions. The latter effect might be much smaller because of the decreased π-density of the pyridine ring compared to that of the benzene ring. The structural characterization of these products in solution as well as solid state is also discussed.

Key words: macrocycles, calixarenes, cyclophanes, [3.1.3.1]metacyclophanes, *O*-alkylation, conformation, crystal structure, cation–N interaction.

Résumé : Le produit principal obtenu lors d'un essai d'*O*-alkylation du macrocycle flexible, tétrahydroxy[3.1.3.1]métacyclophane (**1**), par la 4-(chlorométhyl)pyridine (**2a**), en présence de NaH, dans du THF au reflux, est le produit de 1,3-di-*O*-substitution *distal*-**3a**. Par opposition, la *O*-alkylation du tétraol **1** par la **2a**, en présence de Cs_2CO_3, conduit avec un rendement de 95% à un mélange 77:23 de deux conformères, 1,4-alterné:cône partiel, du produit tétra-*O*-alkylé (**4a**). Il n'y a pas de formation du conformère à cône lors de la réaction du tétraol **1** avec la **2a** et ce résultat est en opposition à ceux obtenus lors de la réaction de **1** avec la 2-(chlorométhyl)pyridine (**2b**) ou avec le bromure de benzyle (**2c**), en présence de NaH ou de K_2CO_3 qui conduisent à la formation du conformère à cône; cette différence pourrait être attribuée à l'absence d'une contribution résultant d'interactions N–cation et π–cation. L'amplitude de ce dernier effet est peut-être plus faible en raison d'une diminution de la densité π du noyau pyridine par rapport à celle d'un noyau benzénique. On discute aussi de la caractérisation structurale de ces produits en solution ainsi qu'à l'état solide.

Mots clés : macrocycles, calixarènes, cyclophanes, [3.1.3.1]métacyclophanes, *O*-alkylation, conformation, structure cristalline, interaction N–cation.

[Traduit par la Rédaction]

Introduction

Calixarene and related macrocycles have received considerable attention for their host–guest chemistry as ionophoric receptors (1–4) and as potential enzyme mimics in biology (5). Chemical modification of calixarenes represents an effective and versatile way of producing receptors with highly selective cation-binding properties (6–10). Even minor changes in the regioselective functionalization (11) or conformation (12) of the chemically modified calixarene can be associated with drastic changes in the complexation properties.

Introduction of larger alkyl groups on the phenolic oxygens of calix[4]arenes led to a situation where the OR groups within a cyclophane ring could not pass each other via the oxygen-through-the-annulus rotation (for a comprehensive review of all aspects of calixarene chemistry, see ref. 1). Although there exist four possible conformational isomers in calix[4]arenes (cone, partial cone, 1,2-alternate, and 1,3-alternate), five different conformational isomers, of which 1,4-alternate is newly counted due to the propane bridges, should be expected in tetrahydroxy[3.1.3.1]MCPs (MCP = metacyclophane) (13).

Received January 11, 2001. Published on the NRC Research Press Web site at http://canjchem.nrc.ca on October 3, 2001.

T. Yamato[1] and K. Kumamaru. Department of Applied Chemistry, Faculty of Science and Engineering, Saga University, Honjo-machi 1, Saga-shi, Saga 840-8502, Japan. **H. Tsuzuki.** Tohwa Institute for Science, Tohwa University, 1-1-1 Chikushigaoka, Minami-ku, Fukuoka-shi, Fukuoka 815-8510, Japan.

[1]Corresponding author (telephone: (0952) 28-8679; fax: (0952) 28-8591; e-mail: yamatot@cc.saga-u.ac.jp).

 DOI: 10.1139/cjc-79-10-1422 © 2001 NRC Canada

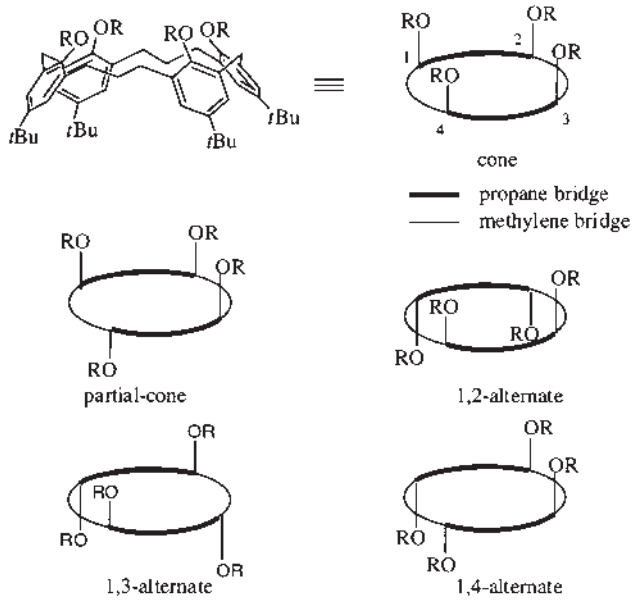
Pappalardo et al. (14) reported on the synthesis of calix[4]arenes bearing pendant pyridine groups on the lower rim as potential ligands for transition metals. Recently, we have also reported the synthesis, conformational studies, and inclusion properties of tetrakis[(2-pyridylmethyl)oxy][3.1.3.1]MCPs derived from tetrahydroxy[3.1.3.1]MCPs (15), which show strong Ag^+ and *n*-butylammonium ion affinity. ^1H NMR titration with $AgSO_3CF_3$ clearly demonstrated that a 1:1 complex is formed with retention of the original symmetry. Interestingly, the conformational changes of the pyridine moiety from the original outward orientation of the ring nitrogen to an inside orientation (toward the cyclophane cavity) was observed in the process of Ag^+ complexation. On the other hand, Reinhoudt and co-workers (16) also reported a well-defined hydrogen-bonded calix[4]arene duplex between tetrakis[(4-pyridylmethyl)oxy]calix[4]arene and calix[4]arene tetracarboxylic acid. Independently, Shinkai and co-workers (17) have extended this type of upper-rim functionalization to larger calixarenes. Thus, there is substantial interest in investigating the synthesis and structures of tetrakis[(4-pyridylmethyl)oxy][3.1.3.1]MCPs with cone and 1,4-alternate conformations, in which the former compounds are anticipated to have the property to form a hydrogen-bonded homocalix[4]arene duplex with the corresponding [3.1.3.1]MCP tetracarboxylic acid.

In this paper, we describe the metal template effect on *O*-alkylation of tetrahydroxy[3.1.3.1]MCP with 4-(chloromethyl)pyridine (**2a**) to afford tetrakis[(4-pyridylmethyl)oxy]-[3.1.3.1]MCPs with cone and 1,4-alternate conformations and their conformational studies in solution as well as in the solid state.

Results and discussion

Alkylation of the flexible macrocycles (**1**) with 10 mol equiv of 4-(chloromethyl)pyridine (**2a**) in the presence of 10 mol equiv of NaH under THF reflux gave one pure regioselective isomer, 1,3-di-*O*-substitution product *distal*-**3a**, as a major product, while other possible regioisomers were not observed. In contrast, decreasing the amount of NaH to 5 mol equiv increased the proportion of tetra-*O*-substitution product 1,4-*alternate*-**4a** dramatically (from 2 to 45%). Finally, increasing the amount of reagent to 30 mol equiv in the presence of 5 mol equiv of NaH gave complete *O*-substitution, affording the tetrakis[(4-pyridylmethyl)oxy] derivative (1,4-*alternate*-**4a**) in 95% yield. No formation of other possible conformers, as shown in Fig. 1, has been observed. Unfortunately, a significant recovery of starting compound **1** in the presence of Na_2CO_3, in spite of the condition of large excess of **2a**, was observed. When K_2CO_3 is employed for *O*-alkylation with **2a** only an intractable mixture was obtained. In contrast, tetrahydroxy[3.1.3.1]MCP (**1**) was *O*-alkylated with **2a** in the presence of Cs_2CO_3 to give a mixture of two conformers of tetra-*O*-alkylated product **4a** in a ratio of 77:23 (1,4-*alternate*-**4a**:*partial-cone*-**4a**) in 95% yield. The ratio of the number of the *O*-alkylations is governed by the nature of the base used (NaH or alkali metal carbonates). Thus, when NaH is used in this reaction, the disubstitution product *distal*-**3a** was obtained as a major product in 85% yield. On the other hand, when Cs_2CO_3 was employed, an increase in the formation of tetra-*O*-substitution product **4a** was observed. These results indicate that the

Fig. 1. Possible conformers for *O*-tetrasubstitution of tetrahydroxy[3.1.3.1]MCP (**1**).



alkali-metal cation can play an important role not only on the regioselectivity based on the template effect but also on the number of the *O*-alkylations, as previously observed in the *O*-alkylation of calixarenes (6, 7).

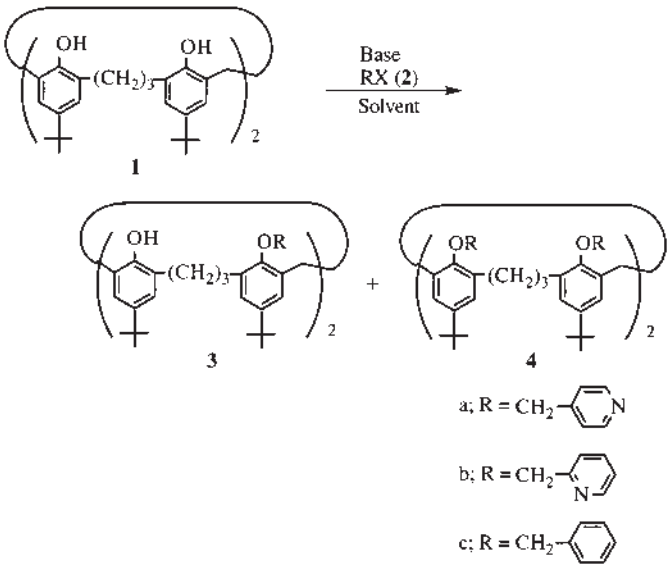
The present results are quite different from the result of *O*-benzylation of tetraol **1** with benzyl bromide **2c** in the presence of NaH, which predominantly afforded *cone*-**4c** (Scheme 1). When Cs_2CO_3 was used in this reaction, a mixture of *cone*- and 1,4-*alternate*-tetra-*O*-alkylated product **4c** in a ratio of 80:20 in quantitative yield was observed (Table 1) (13*d*).

When Cs_2CO_3 was used in this reaction, the ratio of *partial-cone*-**4a** to 1,4-*alternate*-**4a** increased. Because a much larger contribution by Cs^+ (compared to Na^+) to the template effect can be expected, as reported by Harrowfield et al. (18), the larger Cs^+ ion might enlarge the cyclophane ring, (e.g., intermediate **B**) to form sufficient space for ring inversion to afford the thermodynamically stable partial-cone conformer during the *O*-alkylation with **2a**. In contrast, the smaller Na^+ ion might increase the contribution of the metal template effect, which can hold the 4-pyridylmethyl group(s) and the oxide group(s) on the same side of the tetrahydroxy-[3.1.3.1]MCP through cation–O^- and cation–π interactions (19), similar to the *O*-benzylation. However, this effect might be smaller due to the decreased π-density of the pyridine ring as compared to that of the benzene ring (Fig. 2*a*). Therefore, no formation of cone conformer in the reaction of the tetraol **1** with **2a**, (while it was the predominant conformer when 2-(chloromethyl)pyridine (**2b**) was used) in the presence of NaH or K_2CO_3, might be attributable to the absence of contribution derived from cation–N interactions (15).

Although the reason for this finding is not clear from the available results, one might assume that the template effect of the larger alkali metal cation Cs^+ is responsible. Thus, the larger alkali metal cation Cs^+, in spite of being a weaker base when compared to NaH, obviously gives rise to the preferential formation of the cesium phenoxide intermediate

© 2001 NRC Canada

Scheme 1.



B to afford tetra-*O*-substitution product 1,4-*alternate*-**4a**. When a larger base such as Cs_2CO_3 (compared to Na^+ or K^+) is used, a much larger contribution to the template effect can be expected. Thus, the larger Cs^+ ion might enlarge the cyclophane ring of diol **3a** enough to destroy the intramolecular hydrogen bonding between the hydroxy groups on the diarylmethane units. Thus, further *O*-alkylation was observed due to the existence of the dissociated O^- groups. In contrast, the action of the much smaller Na^+ ion might lead to a decrease in the nucleophilicity of phenolic O^- anion by increasing the steric interactions in intermediate **A** during the nucleophlic attack on **2a**. Therefore, the stronger base (NaH) might suppress further *O*-alkylation, in spite of the existence of the dissociated O^- groups, and thus, only afford di-*O*-substitution product *distal*-**3a**.

Furthermore, *O*-alkylation of tetraol **1** with **2a** afforded mainly the 1,3-disubstituted product *distal*-**3a**, instead other possible isomers (1,2-disubstituted product, 1,2-*proximal*-**3a** and 1,4-disubstituted product, 1,4-*proximal*-**3a**). This finding might also be explained by the increase in steric interactions in the sodium phenoxide intermediate **C** at the 1,2-position, in comparison with that in intermediate **D** at the 1,3-position, even with a smaller alkali metal cation (Na^+) (Scheme 2). The different types of intramolecular hydrogen bonding among the hydroxyl groups between the 1,3-diarylpropane units and diarylmethane units should have an effect on the regioselectivity during the *O*-alkylation of tetrahydroxy[3.1.3.1]MCP (**1**).

To study the reaction route from tetraol **1** to tetra-*O*-alkylated product **4a** in more detail, we have attempted to carry out the *O*-alkylation of the possible intermediate **3a** with **2a** in the presence of Cs_2CO_3 (Scheme 3). Similar *O*-alkylation reaction of 1,3-di-*O*-substitution product *distal*-**3a** with **2a** was carried out in the presence of Cs_2CO_3 to yield a mixture of two conformers of tetra-*O*-alkylated product **4a** in a ratio of 86:14 (*cone*-**4a**:*partial-cone*-**4a**) in 95% yield along with the recovery of starting compound (Scheme 3). No formation of the other possible conformers was observed. However, in the presence of NaH or K_2CO_3, *O*-alkylation to afford **4a** under the same reaction conditions was not observed and only recovery of the starting compound **3a** resulted.

These results strongly indicate that, in the case of the *O*-alkylation of tetraol **1** with **2a** in the presence of Cs_2CO_3, the diol (*distal*-**3a**) with a cone conformation could not be an intermediate for the formation of 1,4-*alternate*-**4a**. Thus, the conformation to yield 1,4-*alternate*-**4a** has not been determined by the complete introduction of the second picolyl group. In other word, formation of 1,4-*alternate*-**4a** can be determined when the second picolyl group enters by the ring inversion of the O^- anion on the unmodified phenol unit in triol to form *distal*-**3a** with a 1,4-alternate conformation.

The ^{1}H NMR spectrum of *cone*-**4a** shows a singlet for the *tert*-butyl protons at δ 1.10 and two doublets (J = 2.2 Hz) of equal intensity for the aromatic protons at δ 6.78 and 6.94. Furthermore, the resonance for the Ar*CH*$_2$Ar methylene protons appear as a pair of doublets (δ 3.21 and 4.27, $J_{A,B}$ = 13.7 Hz) (relative intensity 1:1). Although these ^{1}H NMR signals correspond to either the cone or 1,4-alternate conformer, the middle methylene protons for propane bridge (ArCH$_2$*CH*$_2$CH$_2$Ar) are observed as a two multiplets for *cone*-**4a** at δ 1.58–1.68 and 1.92–2.02 (relative intensity 1:1), but only as a single multiplet for 1,4-*alternate*-**4a** at δ 1.58–1.72. The former pattern corresponds to cone conformer because the middle methylene protons for propane bridge ArCH$_2$*CH*$_2$CH$_2$Ar are in different environments, whereas the latter pattern corresponds to the 1,4-alternate conformer because the protons lie in the same environment. Therefore, *cone*-**4a** should adopt a *syn*-oriented cone conformation and not a *anti*-oriented 1,4-alternate conformation.

Although we have not yet succeeded in measuring the X-ray diffraction of cone-tetrakis[(4-pyridylmethyl)oxy][3.1.3.1]MCP (*cone*-**4a**) (15*a*) because it is a viscous oil, we have succeeded in obtaining single-crystal X-ray diffraction results for cone-tetrakis[(2-pyridylmethyl)oxy][3.1.3.1]MCP (*cone*-**4b**). The crystals were obtained by recrystallization from MeOH–$CHCl_3$, and the crystal structure and the atom numbering system of *cone*-**4b** are shown in Fig. 3.

The structure was solved by direct methods (SIR 88)[2] and refined using a full-matrix least-squares method and Fourier synthesis. Compound *cone*-**4b** crystallized in the centrosymmetric triclinic space group $P\bar{1}$ (No. 2) and is located at the general position (Z = 2). The X-ray crystallographic analysis of *cone*-**4b** clearly shows that this compound adopts a cone conformation in the solid state. The dihedral angles of the plane defined by the bridge crabons, C(1)-C(2)-C(3)-C(10)-C(17)-C(18)-C(19)-C(26) with aromatic ring C(4)-C(5)-C(6)-C(7)-C(8)-C(9), C(11)-C(12)-C(13)-C(14)-C(15)-C(16), C(20)-C(21)-C(22)-C(23)-C(24)-C(25), and C(27)-C(28)-C(29)-C(30)-C(31)-C(32) are 61.6, 62.9, 63.4, and 56.7°, respectively. The four pyridylmethyl groups located in the inner cavity point toward the outside and are not parallel with the attached phenolic aromatic planes. The dihedral angles of the pyridine rings with the phenolic rings, C(4)-C(5)-C(6)-C(7)-C(8)-C(9), C(11)-C(12)-C(13)-C(14)-C(15)-C(16), C(20)-C(21)-C(22)-C(23)-C(24)-C(25), and C(27)-C(28)-C(29)-C(30)-C(31)-C(32) are 76.3, 73.7, 69.5, and 81.7°, respec-

[2] M.C. Burla, M. Camalli, G. Cascarano, C. Giacovazzo, G. Polidori, R. Spagna, and D. Viterbo. J. Appl. Crystallogr. **22**, 389 (1989).

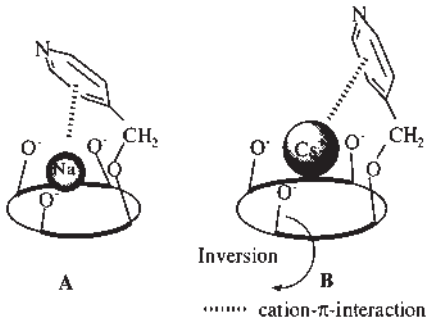
© 2001 NRC Canada

Table 1. *O*-Substitution reaction of tetraol **1** with 4-(chloromethyl)pyridine (**2a**), 2-(chloromethyl)pyridine (**2b**), and benzyl bromide (**2c**).

			Products yield (%)[a]			
Reagent	Base	**2:1** (mol ratio)	*Distal*-**3**	*Cone*-**4**	*Partial-cone*-**4**	1,4-*Alternate*-**4**
2a	NaH	10	98 (85)	0	0	2
2a	NaH[b]	10	55	0	0	45
2a	NaH[b]	30	5	0	0	95 (80)
2a	K_2CO_3[c]	30	0	0	0	0
2a	Cs_2CO_3	30	0	0	23	77 (65)
2b	Cs_2CO_3	30	0	75 (45)	20	5
2c	Cs_2CO_3	30	0	80	0	20

Note: Conditions : NaH (10 equiv) and M_2CO_3 (20 equiv) were used, unless otherwise indicated.
[a]Relative yields determined by ^{1}H NMR spectroscopy. Isolated yields are shown in parentheses.
[b]NaH (5 equiv) was used.
[c]Intractable mixture was obtained.

Fig. 2. Ring inversion of *O*-alkylation intermediate of tetraol **1**, and immobilization by metal template.



tively. In addition, the four nitrogen atoms on the pyridine rings are turned toward the *exo*-annulus direction, suggesting that this orientation might be favored to avoid electrostatic repulsion between the lone pair electrons on the nitrogen atoms.

The ^{1}H NMR spectrum of *cone*-**4b** shows a singlet for the *tert*-butyl protons at δ 1.16 and two doublets (J = 2.2 Hz) of equal intensity for the aromatic protons at δ 6.85 and 7.06. Furthermore, the resonance for the ArCH_2Ar methylene protons appears as a pair of doublets (δ 3.29 and 4.44, $J_{A,B}$ = 13.2 Hz) (relative intensity 1:1), corresponding to a symmetrical structure (C_{2v} symmetry). However, the middle methylene protons for propane bridge (Ar$CH_2CH_2CH_2$Ar) are observed as a multiplet for *cone*-**4b** at δ 1.3–1.5 and 1.8–2.0 (relative intensity 1:1), but only as a single multiplet for 1,4-*alternate*-**4b** at δ 1.59–1.64. The former pattern corresponds to cone conformer because the middle methylene protons for propane bridge Ar$CH_2CH_2CH_2$Ar are in different environments, whereas the latter pattern corresponds to the 1,4-alternate conformer because the protons are in the same environment. The similar findings were observed in the ^{1}H NMR spectrum of *cone*-**4a**. Thus, on the basis of the spectral data, a cone conformation is assigned to *cone*-**4a**.

The ^{1}H NMR spectrum of 1,4-*alternate*-**4a** shows a singlet for the *tert*-butyl protons at δ 1.10, a set of doublets ($J_{A,B}$ = 13.4 Hz) for the ArOCH_2Py methylene protons at δ 4.38 and 4.48, and two doublets of equal intensity for the aromatic protons at δ 7.00 and 8.18. Furthermore, the resonance for the ArCH_2Ar methylene protons appear as a pair of doublets (δ 3.42 and 4.43, $J_{A,B}$ = 13.2 Hz) (relative intensity 1:1). Since these ^{1}H NMR signals are observed at slightly different chemical shifts compared to those for *cone*-**4a**, a cone conformation might be also expected. However, as mentioned previously, the middle methylene protons for propane bridge (Ar$CH_2CH_2CH_2$Ar) are observed as a single multiplet at δ 1.58–1.72, which corresponds to the 1,4-alternate conformer, because the middle methylene protons for the propane bridge Ar$CH_2CH_2CH_2$Ar are same environment. Therefore, 1,4-*alternate*-**4a** should adopt an *anti*-oriented 1,4-alternate conformation and not *a syn*-oriented cone conformation. Fortunately, we have succeeded in analyzing single-crystal X-ray diffraction results of 1,4-alternate-tetrakis[(4-pyridylmethyl)oxy][3.1.3.1]MCP (1,4-*alternate*-**4a**). X-ray quality crystals were obtained via recrystallized from MeOH–$CHCl_3$, and the crystal structure and the atom numbering system of 1,4-*alternate*-**4a** are shown Fig. 4.

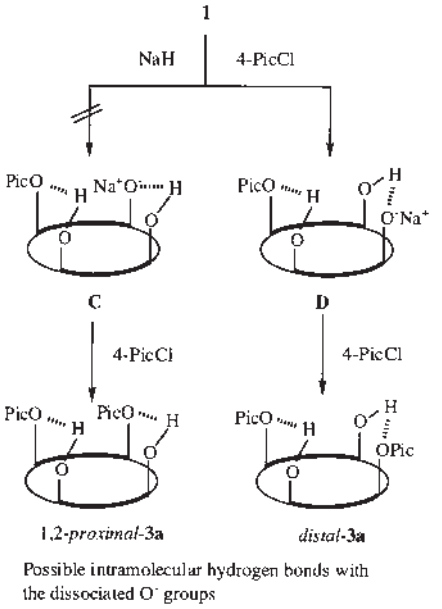
The X-ray crystal structure was solved by direct methods (MULTAN 80)[3] and refined using a full-matrix least-squares method and Fourier synthesis. Compound 1,4-*alternate*-**4a** crystallized in the centrosymmetric triclinic space group $P\bar{1}$ (No. 2) and is located at the general position (Z = 2). It is clear that this compound adopts the 1,4-alternate conformation, where the facing aromatic rings adopt an *anti*-conformation with respect to each other, and the "stepped conformation" of diphenylmethane moieties, similar to *anti*-[3.3]MCP (20), is favored. The molecular structure of the 1,4-*alternate*-**4a** possesses the following major features: (*i*) the facing phenolic aromatic rings show *anti*-conformation and are almost parallel with each other, and the *O*-appended two pyridine rings similarly adopt a parallel conformation and (*ii*) the *O*-appended two pyridine rings are located almost vertically against the phenolic aromatic rings, although the facing phenolic aromatic rings show an *anti*-conformation and are almost parallel. Thus, the four pyridine rings in 1,4-*alternate*-**4a** are almost parallel.

Ring inversion via oxygen-through-the-annulus rotation is inhibited both for *cone*-**4a** and 1,4-*alternate*-**4a** as no change in the spectrum pattern for the ArCH_2Ar methylene protons below 130°C in $CDBr_3$ is observed.

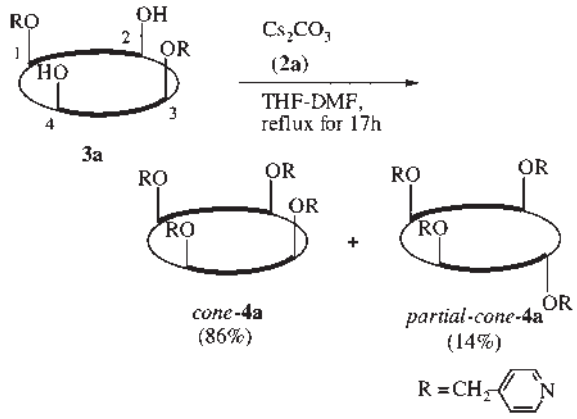
[3] P. Main, S.J. Fiske, S.E. Hull, L. Lessinger, G. Germain, J.P. DeClerq, and M.M. Woolfson. MULTAN 80, a system of computer programs for the automatic solution of crystal structures from X-ray diffraction data. University of York, England.

© 2001 NRC Canada

Scheme 2.



Scheme 3.

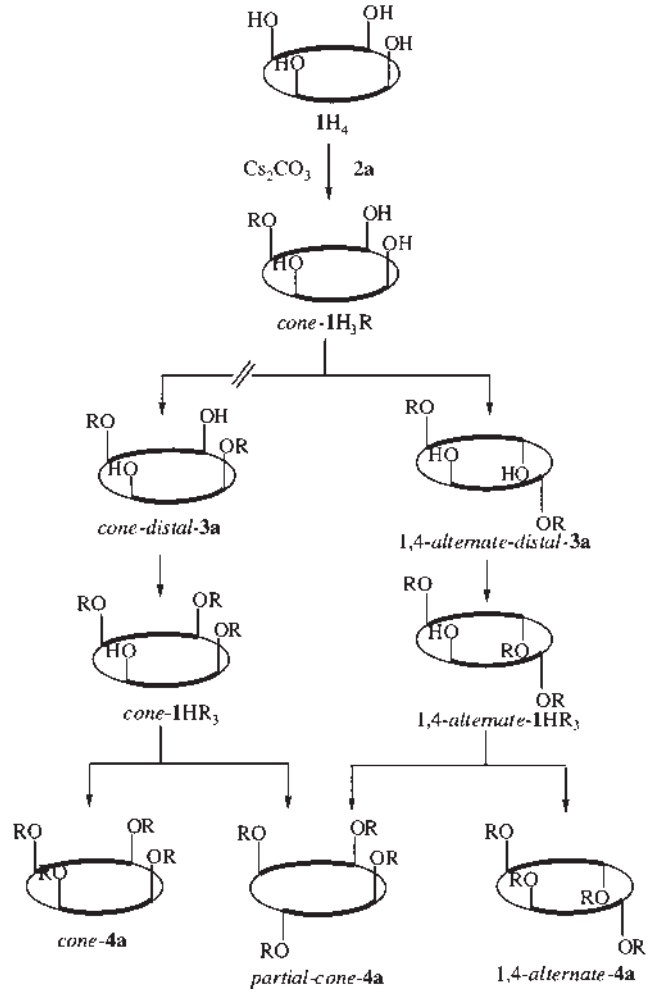


Interestingly, the heteroaromatic protons of the pyridine rings in *cone*-**4a** are exposed to ring current shielding effects (21, 22) imposed by the opposing pyridine ring among the diphenylmethane linkage and resonate at higher fields with respect to those of the reference compound **6**, which was prepared by *O*-alkylation of 4-*tert*-butyl-2,6-dimethylphenol (**5**) with **2a** in the presence of NaH in 63% yield (Scheme 5).

The magnitude of this shielding, computed as the difference between pertinent pyridine protons of *cone*-**4a** and reference compound **6**, increases significantly with protons H_2 and H_3 (see Table 2). The remarkable shielding effect experienced by the H_3 ($\delta = -0.33$ ppm) protons of the pyridine ring suggests that these protons are located much closer to the opposing pyridine ring than the H_2 ($\delta = -0.15$ ppm) protons, presumably due to the electrostatic repulsions among the nitrogens of two pyridine rings. Thus, all of the nitrogens in the pyridine rings are oriented toward the outside of the cyclophane cavity.

In contrast to *cone*-**4a**, the 1,4-alternate displays much higher upfield shifts for the H_2 (–0.62 ppm) and H_3 (–0.89 ppm) protons of the pyridine ring Since the1,4-*alternate*-**4a** adopts the "stepped conformation" for the diphenylmethane moieties, similar to *anti*-[3.3]MCP (20), face-to-face overlapping between two picolyl group is possible. Therefore, the remarkable shielding effect experienced by the H_3 (–0.89 ppm) protons suggests that these protons are located in closer to the opposing pyridine ring than the H_2 (–0.63 ppm) protons, presumably due to the repulsion among the nitrogen atoms in the pyridine rings, which are located between the diphenylmethane linkages.

Scheme 4.



In contrast, the ^{1}H NMR spectrum of *partial-cone*-**4a** shows four singlets for the *tert*-butyl protons at $\delta = 0.69$, 1.02, 1.34, and 1.45 (relative intensity 1:1:1:1) and four sets of doublets with equal intensity for the aromatic protons. Furthermore, the resonance for the aromatic protons ($H_{2,6}$ and $H_{3,5}$) appeared as four sets of doublets. These signals correspond to an unsymmetrical structure (C_S symmetric conformer). The aromatic protons in the one of the 4-pyridylmethyl groups ($H_{2'}$ and $H_{3'}$) appear at higher fields around δ 7.50 and 6.11, respectively, which strongly supports the view that **4a** adopts a partial-cone conformation. On the basis of the ^{1}H NMR studies and the consideration of CPK model of *partial-cone*-**4a**, three of the four 4-pyridylmethyl groups in the compound point upwards, while the last pyridyl group is folded into the π-cavity formed by three benzene rings and, are thus, strongly

© 2001 NRC Canada

Fig. 3. X-ray crystal structure of *cone*-**4b**. Thermal ellipsoids are drawn at 50% probability. Hydrogen atoms have been omitted for clarity.

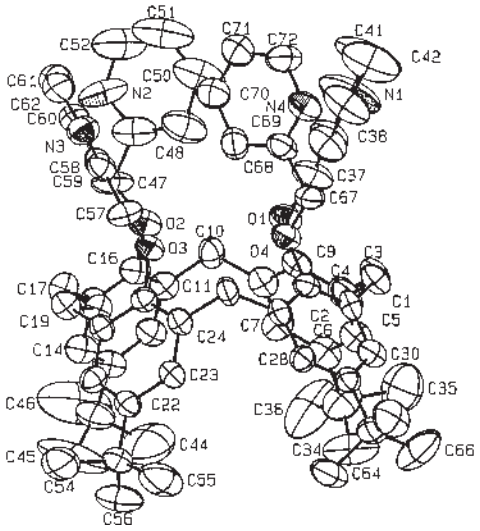
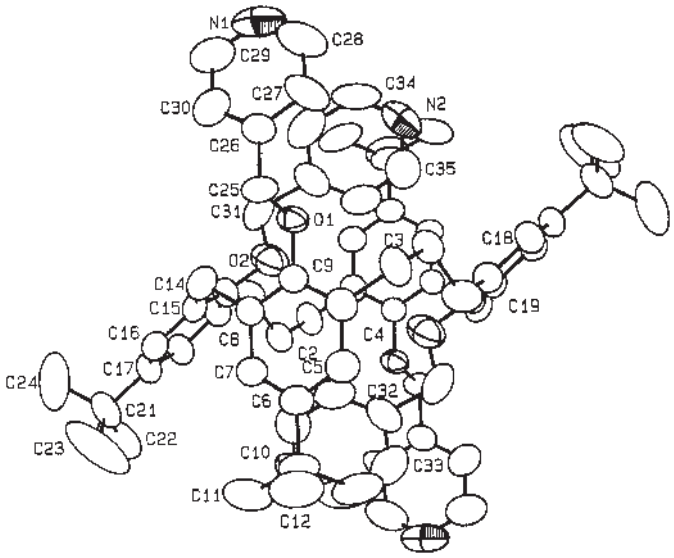


Fig. 4. X-ray crystal structure of 1,4-*alternate*-**4a**. Thermal ellipsoids are drawn at 50% probability. Hydrogen atoms have been omitted for clarity.

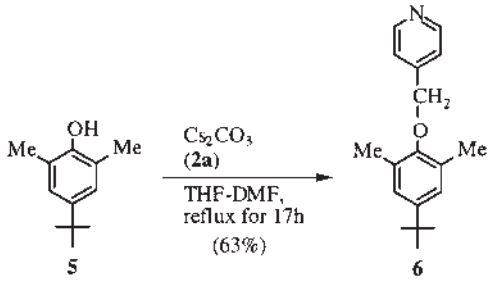


shifted upfield. Furthermore, an upfield shift at δ 0.69 for one *tert*-butyl group is observed, which is attributable to it being located on the pyridine ring of the inverted picolyl group, in spite of the sterically crowded environment. This finding might be attributed to the CH–π interaction (19) between methyl groups of the *tert*-butyl group and the pyridine ring.

In contrast, the ^{1}H NMR spectrum of **3a** shows resonances for the *tert*-butyl protons at δ 1.23 and 1.27 as singlets, for the methylene protons at δ 3.63 and 4.25 ($J_{A,B}$ = 13.2 Hz) as doublets, for the aromatic protons at δ 6.92, 7.03, 7.15, and 7.22 (J = 2.2 Hz) as doublets, and the hydroxy proton at δ 7.84 as a singlet indicating a 1,3-di-*O*-substituted structure.

Although these ^{1}H NMR signals correspond to a cone or a 1,4-alternate conformer, the IR spectrum of diol **3a** shows the absorption of the hydroxy stretching vibration at around

Scheme 5.



3379 cm^{-1}. The ^{1}H NMR spectrum in $CDCl_3$ exhibits the signal for hydroxyl groups around δ = 7.84. The υ_{OH} and δ_{OH} values in diol **3a** in which two hydroxy groups are located in distal positions, show not only a slightly lower frequency but also an upfield shift compared to those of parent compound **1** (υ_{OH} = 3254 and δ_{OH} = 9.35), which implies that a weaker hydrogen bond does exist for **3a** as compared to that in the corresponding calix[4]arene. As shown in Fig. 5, similar chemical shifts were observed as those for distal-bis-(benzyloxy)[3.1.3.1]MCP (**3c**), which adopts a cone conformation. Therefore, bis[(4-pyridylmethyl)oxy][3.1.3.1]MCP (**3a**) also might adopt a cone conformation due to the intramolecular hydrogen bonding between two hydroxy and alkoxy groups. Thus, the hydroxy and alkoxy groups can be strongly held on the same side of the [3.1.3.1]MCP *distal*-**3a**, as shown in Fig. 5.

In conclusion, an interesting result was obtained by introduction of 4-picolyl groups into the hydroxy groups of tetraol **1**. We have demonstrated for the first time that *O*-alkylation of the flexible macrocycle **1** with 4-(chloromethyl)pyridine gave tetra-*O*-alkylated products with cone or 1,4-alternate conformation, which could show promising complexation properties and interesting stereochemistry. The alkali metal cation can play an important role for the conformer distribution because of the template effect. While, to date, only three stereoisomers have been obtained, variation of the alkylation conditions and reagents could lead to different derivatives, which will serve as interesting building blocks for larger potential host molecules. Further studies of the structural and chemical properties of **3a** and **4a** are in progress.

Experimental

All melting points (Yanagimoto MP-S1) were uncorrected. Proton NMR spectra were recorded on a Nippon Denshi JEOL FT-270 spectrometer. Chemical shifts are reported as δ values (ppm) relative to internal Me_4Si. Mass spectra were obtained on a Nippon Denshi JMS-01SG-2 mass spectrometer at an ionization energy of 70 eV; *m*/*z* values reported include the parent ion peak. Infrared (IR) spectra were obtained on a Nippon Denshi JIR-AQ2OM spectrophotometer as KBr disks. Elemental analyses were performed by Yanaco MT-5. Gas–liquid chromatography (GLC) analyses were performed on a Shimadzu gas chromatograph (GC-14A; silicone OV-1, 2 m; programmed temperature rise, 12°C min^{-1}; carrier gas nitrogen, 25 mL min^{-1}).

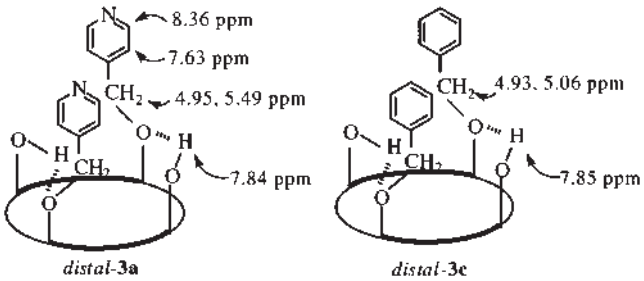
© 2001 NRC Canada

Table 2. Chemical shifts of protons in *cone*-**4a**, 1,4-*alternate*-**4a**, and reference compound **6**.

Compound	H_2	H_3	Ar protons	ArOCH_2Py	ArCH_2Ar	*t*-Bu
Cone-**4a**	8.47	7.08	6.78, 6.94	4.66	3.21, 4.27	1.10
1,4-*Alternate*-**4a**	7.99	6.52	7.00, 7.18	4.38, 4.48	3.42, 4.43	1.10
6	8.62	7.41	7.05	4.82	—	1.30

Note: In $CDCl_2$ at 27°C.

Fig. 5. Intramolecular hydrogen bonds in *distal*-**3a**.



Materials

Synthesis of 6,13,22,29-tetra-*tert*-butyl-9,16,25,32-tetrahydroxy[3.1.3.1]metacyclophane (**1**) was previously described (13*a*, *b*).

*Alkylation of **1** with 4-(chloromethyl)pyridine (**2a**) in the presence of NaH to afford distal-**3a***

A mixture of **1** (400 mg, 0.57 mmol) and NaH (230 mg, 5.70 mmol, 60%) in dry THF (10 mL) was heated at reflux for 1 h under N_2. Then a solution of 4-(chloromethyl)pyridine (**2a**) (5.56 mmol) (prepared by neutralization of 4-(chloromethyl)-pyridine hydrochloride (939 mg, 5.70 mmol) in *N*,*N*-dimethylformamide (DMF) (5.5 mL) with a solution of triethylamine (0.8 mL, 5.70 mmol) in THF (11 mL) at room temperature) was added and the mixture was heated at reflux for an additional 17 h. After cooling the reaction mixture to room temperature, it was acidified with 1 N HCl (10 mL) and extracted with CH_2Cl_2 (2 × 100 mL). The combined extracts were washed with water (2 × 50 mL), dried (Na_2SO_4), and condensed under reduced pressure to give a yellow oil. The residue was washed with either to give crude *distal*-**3a** (430 mg, 85%) as a colorless precipitate. Recrystallization from MeOH–$CHCl_3$ (3:1) afforded 6,13,22,29-tetra-*tert*-butyl-9,25-dihydroxy-16,32-bis[(4-pyridylmethyl)oxy][3.1.3.1]metacyclophane (*distal*-**3a**) as colorless prisms; mp 257–260°C. MS *m*/*z*: 886 (M^+). IR (KBr) (cm^{-1}): 3379 (OH). ^{1}H NMR ($CDCl_3$) δ: 1.23 (s, 18H), 1.26 (s, 18H), 2.17–2.45 (m, 4H,), 2.59–2.68 (m, 4H), 2.87–2.95 (m, 4H), 3.64 (d, *J* = 13.7 Hz, 2H), 4.18 (d, *J* = 13.7 Hz, 2H), 4.95 (d, *J* = 14.2 Hz, 2H), 5.49 (d, *J* = 14.2 Hz, 2H), 6.92 (d, *J* = 2.4 Hz, 2H), 7.02 (d, *J* = 2.4 Hz, 2H), 7.14 (d, *J* = 2.4 Hz, 2H), 7.22 (d, *J* = 2.4 Hz, 2H), 7.63 (d, *J* = 5.4 Hz, 2H), 7.84 (s, 2H, OH), 8.36 (d, *J* = 5.4 Hz, 2H). Anal. calcd. for $C_{60}H_{74}N_2O_4$ (887.27): C 81.22, H 8.42, N 3.16; found: C 81.49, H 8.28, N 3.27.

*Alkylation of **1** with **2a** in the presence of Cs_2CO_3*

A mixture of **1** (400 mg, 0.57 mmol) and Cs_2CO_3 (3.70 g, 11 mmol) in dry THF (10 mL) was heated at reflux for 1 h under N_2. Then a solution of **2a** (17.1 mmol) was added and the mixture heated at reflux for an additional 17 h. After cooling the reaction mixture to room temperature, it was acidified with 1 N HCl (10 mL) and extracted with CH_2Cl_2 (2 × 100 mL). The combined extracts were washed with water (2 × 50 mL), dried (Na_2SO_4), and condensed under reduced pressure to give a yellow oil. The residue was purified by column chromatography over silica gel with MeOH–CHCl, (1:1) to give a mixture of 1,4-*alternate*-**4a** and *partial-cone*-**4a** in a ratio of 77:23 as a colorless solid. Treatment with a small amount of ether gave 1,4-*alternate*-**4a** (396 mg, 55%) as a colorless solid. Attempted isolation of pure *partial-cone*-**4a** failed.

1,4-Alternate-6,13,22,29-tetra-tert-*butyl-9,16,25,32-tetrakis-[(4-pyridylmethyl)oxy][3.1.3.1]metacyclophane (1,4-*alternate-***4a**)*: Colorless prisms (MeOH–$CHCl_3$ (3:1)), mp > 300°C. MS *m*/*z*: 1068 (M^+). ^{1}H NMR ($CDC1_3$) δ: 1.10 (s, 36H), 1.58–1.72 (m, 4H), 2.13–2.24 (m, 4H), 2.51–2.64 (m, 4H), 3.42 (d, *J* = 13.2 Hz, 2H), 4.38 (d, *J* = 13.4 Hz, 4H), 4.43 (d, *J* = 13.2 Hz, 2H), 4.48 (d, *J* = 13.4 Hz, 4H), 6.52 (d, *J* = 5.9 Hz, 8H), 7.00 (d, *J* = 2.0 Hz, 4H), 7.18 (d, *J* = 2.0 Hz, 4H), 7.99 (d, *J* = 5.9 Hz, 8H). Anal. calcd. for $C_{72}H_{84}N_4O_4$ (1069.5): C 80.86, H 7.92, N 5.24; found: C 80.90, H 7.95, N 5.30.

Partial-cone-6,13,22,29-tetra-tert-*butyl-9,16,25,32-tetrakis[(4-pyridylmethyl)oxy][3.1.3.1]metacyclophane (*partial-cone-***4a**)*: Colorless oil. ^{1}H NMR ($CDCl_3$) δ: 0.69 (s, 9H), 1.02 (s, 9H), 1.34 (s, 9H), 1.45 (s, 9H), 1.6–3.0 (m, 12H), 3.40 (d, *J* = 13.2 Hz, 1H), 4.01–5.05 (m, 11H), 6.11 (d, *J* = 5.9 Hz, 2H), 6.52 (d, *J* = 5.9 Hz, 2H), 6.61 (d, *J* = 5.9 Hz, 2H), 6.63 (d, *J* = 2.4 Hz, 1H), 6.65 (d, *J* = 2.4 Hz, 2H), 6.68 (d, *J* = 2.4 Hz, 1H), 6.71 (d, *J* = 5.9 Hz, 2H), 6.82 (d, *J* = 2.4 Hz, 1H), 6.93 (d, *J* = 2.4 Hz, 1H), 7.10 (d, *J* = 2.4 Hz, 1H), 7.40 (d, *J* = 2.4 Hz, 1H), 7.50 (d, *J* = 5.9 Hz, 2H), 7.91 (d, *J* = 5.9 Hz, 2H), 8.26 (d, *J* = 5.9 Hz, 2H), 8.41 (d, *J* = 5.9 Hz, 2H).

*Alkylation of distal-**3a** with **2a** in the presence of Cs_2CO_3*

A mixture of *distal*-**3a** (200 mg, 0.225 mmol) and Cs_2CO_3 (366.5 mg, 1.13 mmol) in dry THF (5 mL) was heated at reflux for 1 h under N_2. Then a solution of **2a** (6.75 mmol) was added and the mixture heated at reflux for an additional 17 h. After cooling the reaction mixture to room temperature, it was acidified with 1 N HCl (10 mL) and extracted with CH_2Cl_2 (2 × 100 mL). The combined extracts were washed with water (2 × 50 mL), dried (Na_2SO_4), and condensed under reduced pressure to give a yellow oil. The residue was purified by column chromatography over silica gel MeOH–CHCl, (1:1) to give a mixture of *cone*-**4a** and *partial-cone*-**4a** in a ratio of 86:14 as a colorless oil. Treatment with a small amount of ether gave *cone*-**4a** (195 mg, 81%) as a colorless oil.

© 2001 NRC Canada

Table 3. Crystallographic data and data-collection details for 6,13,22,29-tetra-*tert*-butyl-9,16,25,32-tetrakis[(4-pyridylmethyl)oxy][3.1.3.1]metacyclophane (1,4-*alternate*-**4a**) and 6,13,22,29-tetra-*tert*-butyl-9,16,25,32-tetrakis[(2-pyridylmethyl)oxy][3.1.3.1]metacyclophane (*cone*-**4b**).

	1,4-*Alternate*-**4a**	*Cone*-**4b**
Formula	$C_{72}H_{84}N_4O_4$	$C_{72}H_{84}N_4O_4$
FW	1069.5	1069.5
Crystal size (mm)	0.35 × 0.35 × 0.30	0.36 × 0.23 × 0.20
Space group	Triclinic $P\bar{1}$ (No. 2)	Triclinic $P\bar{1}$ (No. 2)
a (Å)	16.443 (2)	15.093 (2)
b (Å)	16.509 (1)	19.084 (3)
c (Å)	13.119 (1)	11.423 (2)
α (°)	110.770 (8)	96.13 (1)
β (°)	106.269 (7)	102.02 (1)
γ (°)	70.363 (7)	80.66 (1)
U (Å^3)	3081.2 (5)	3166.3 (9)
Z	2	2
$\rho_{calcd.}$ (g cm^{-3})	1.153	1.121
T (K)	298	296
Radiation	Cu Kα	Cu Kα
λ (Å)	1.54184	1.54184
μ (cm^{-1})	5.16	5.02
No. of reflections	13285	12668
Unique reflections	12705	12003
R	0.113	0.116
R_w	0.165	0.143
S	5.32	2.98

Cone-6,13,22,29-tetra-tert-*butyl-9,16,25,32-tetrakis[(2-pyridylmethyl)oxy][3.1.3.1]metacyclophane (*cone-***4a***):* Colorless oil. MS *m/z*: 1068 (M^+). ^{1}H NMR ($CDC1_3$) δ: 1.10 (s, 36H) 1.58–1.68 (m, 2H), 1.92–2.02 (m, 2H), 2.27–2.38 (m, 4H), 2.48–2.64 (m, 4H), 3.21 (d, *J* = 13.7 Hz, 2H), 4.27 (d, *J* = 13.7 Hz, 2H), 4.66 (s, 8H), 6.78 (d, *J* = 2.4 Hz, 4H), 6.94 (d, *J* = 2.4 Hz, 4H), 7.08 (d, *J* = 5.9 Hz, 8H, H2), 8.47 (d, *J* = 5.9 Hz, 8H, H3). Anal. calcd. for $C_{72}H_{84}N_4O_4$ (1069.5): C 80.86, H 7.92, N 5.24; found: C 80.59, H 7.89, N 5.18.

Preparation of 4-tert-*butyl-2,6-dimethyl[(4-pyridylmethyl)oxy]-benzene (**6**)*

A mixture of 4-*tert*-butyl-2,6-dimethylphenol (**5**) (400 mg, 2.25 mmol) and NaH (580 mg, 14.5 mmol, 60%) in dry THF (20 mL) was heated at reflux for 1 h under N_2. Then a solution of **2a** (14.5 mmol) was added and the mixture heated at reflux for an additional 17 h. After cooling the reaction mixture to room temperature, it was acidified with 1 N HCl (10 mL) and extracted with CH_2Cl_2 (2 × 100 mL). The combined extracts were washed with water (2 × 50 mL), dried (Na_2SO_4), and condensed under reduced pressure to give a yellow oil. The residue was purified by column chromatography over silica gel with methanol as the eluent to give the title compound **6** (380 mg, 63%) as a colourless oil. MS *m/z*: 269 (M^+). ^{1}H NMR ($CDC1_3$) δ: 1.30 (s, 9H, *t*-Bu), 2.28 (s, 6H, Me), 4.82 (s, 2H, OCH_2Py), 7.05 (s, 2H, ArH), 7.41 (d, *J* = 5.9 Hz, 2H, H3), 8.62 (d, *J* = 5.9 Hz, 2H, H2). Anal. calcd. for $C_{18}H_{23}NO$ (269.39): C 80.26, H 8.61, N 5.2; found: C 80.55, H 8.49, N 4.9.

Crystal data and refinement details for *cone*-4b and *1,4-alternate*-4a

The unit cell constants (Table 3) were derived from least-squares analysis of the settings, on an Enraf–Nonius CAD4 FR 586 diffractometer, with 25 reflections for both cone-6,13,22,29-tetra-*tert*-butyl-9,16,25,32-tetrakis-[(2-pyridylmethyl)oxy][3.1.3.1]metacyclophane (*cone*-**4b**) and 1,4-alternate-6,13,22,29-tetra-*tert*-butyl-9,16,25,32-tetrakis[(4-pyridylmethyl)oxy][3.1.3.1]metacyclophane (1,4-*alternate*-**4a**) and in the range of 29.0° < θ < 30.7° for *cone*-**4b** and 35.0° < θ < 35.9° for 1,4-*alternate*-**4a**. The intensities of all independent reflections with 2.7° < 2θ < 144.0° for *cone*-**4b** and 5.8° < 2θ < 149.8° for 1,4-*alternate*-**4a** were measured with ω–2θ scan (ω scan width = 0.8 + 0.14 tan θ); Ni-filtered Cu Kα radiation (λ = 1.54184 Å) was used. The structure was solved uneventfully by direct method (SIR88)[2] for *cone*-**4b** and by direct method (MULTAN 80)[3] for 1,4-*alternate*-**4a**, along with difference Fourier syntheses and refined by the full-matrix least-squares method. All calculation was performed on a Micro VAX 3100 computer using a Mo1EN program package.[4]

In the case of *cone*-**4b**, full-matrix least-squares refinement on *F* with all non-hydrogen atoms anisotropic and hydrogens isotropic fixed at B_{eq} = 4.0 Å^2. The weighting scheme is $\omega = 4F_0^2/[(\sigma I_0)^2 + 0.0016F_0^4]$. Final *R* and R_w values are 0.116 and 0.143, respectively (refined on *F*). All calculation was performed on a MicroVAX3100 using Mo1EN.[4] Unfortunately, it was very difficult to improve the *R* value, even by utilizing several techniques, but the ORTEP drawing[5] depicted in Fig. 3 offers the sufficient information to discuss the conformation of

[4] Mo1EN, an interactive structure solution procedure. Enraf-Nonius, Delft, The Netherlands. 1990.
[5] C.K. Johnson Ortep-II, a fortran thermal ellipsoid plot program for crustal structure illustrations. 1976. ORNL-5138.

© 2001 NRC Canada

cone-**4b**. In the case of 1,4-*alternate*-**4a**, full-matrix least-squares refinement on F with all non-hydrogen atoms anisotropic and hydrogens isotropic fixed at B_{eq} = 5.0 Å^2. The weighting scheme is $\omega = 4F_0^2/[(\sigma I_0)^2 + 0.0016F_0^4]$. Final R and R_w values are 0.113 and 0.165, respectively (refined on F). All calculations were performed on a MicroVAX3100 using Mo1EN.[4] Unfortunately, it was very difficult to improve the R value, even by utilizing several techniques, but the ORTEP drawing[5] depicted in Fig. 4 offers the sufficient information to discuss the conformation of 1,4-*alternate*-**4a**.[6]

References

1. (*a*) C.D. Gutsche. Calixarenes. Royal Society of Chemistry, Cambridge. 1989; (*b*) J. Vicens and V. Böhmer. Calixarenes: A versatile class of macrocyclic compounds. Kluwer Academic Publishers, Cambridge. 1990; (*c*) C.D. Gutsche. Calixarenes revisited. Royal Society of Chemistry, Cambridge. 1998.
2. (*a*) S.G. Bott, A.W. Coleman, and J.L. Atwood. J. Chem. Soc. Chem. Commun. 610 (1986); (*b*) A. Arduini, A. Pochini, S. Reverber, R. Ungaro, G.D. Andreetti, and F. Ugozzoli. Tetrahedron, **42**, 2089 (1986).
3. S.-K. Chang and I. Cho. J. Chem. Soc. Perkin Trans. 1, 211 (1986).
4. (*a*) P. Zerr, M. Mussrabi, and J. Vicens. Tetrahedron Lett. **32**, 1879 (1991); (*b*) C.D. Gutsche and L.J. Bauer. J. Am. Chem. Soc. **107**, 6052 (1985).
5. (*a*) S. Shinkai. Tetrahedron, **49**, 8933 (1993); (*b*) J.-M. Lehn. Angew. Chem. **100**, 91 (1988); Angew. Chem. Int. Ed. Engl. **27**, 89 (1988); (*c*) D.J. Cram. Angew. Chem. **100**, 1041 (1988); Angew. Chem. Int. Ed. Engl. **27**, 1009 (1988).
6. V. Bocchi, D. Foina, A. Pochini, and R. Ungaro. Tetrahedron, **38**, 373 (1982).
7. G. Ferguson, B. Kaitner, M.A. McKervey, and E.M. Seward. J. Chem. Soc. Chem. Commun. 584 (1987).
8. F. Arnaud-Neu, M.-J. Schwing-Weill, K. Ziat, S. Cremin, S.J. Harris, and M.A. McKervey. New J. Chem. **15**, 33 (1991).
9. G.D. Andreetti, G. Calestani, F. Ugozzoli, A. Arduini, E. Ghidini, A. Pochini, and R. Ungaro. J. Inclusion Phenom. **5**, 123 (1987).
10. (*a*) E. Ghidini, F. Ugozzoli, R. Ungaro, S. Harkema, A. Abu El-Fadl, and D.N. Reinhoudt. J. Am. Chem. Soc. **112**, 6979 (1990); (*b*) A. Arduini, E. Ghidini, A. Pochini, R. Ungaro, G.D. Andreetti, G. Calestani, and F. Ugozzoli. J. Inclusion Phenom. **6**, 119 (1988).
11. J.A.J. Brunink, W. Verboom, J.F.J. Engbersen, S. Harkema, and D.N. Reinhoudt. Recl. Trav. Chim. Pay. B. **111**, 511 (1992).
12. R. Ungaro, A. Casnati, F. Ugozzoli, A. Pochini, J.F. Dozol, C. Hill, and H. Rouquette. Angew. Chem. Int. Ed. Engl. **33**, 1506 (1994).
13. (*a*) T. Yamato, Y. Saruwatari, S. Nagayama, K. Maeda, and M. Tashiro. J. Chem. Soc. Chem. Commun. 861 (1992); (*b*) T. Yamato, Y. Saruwatari, and M. Yasumatsu. J. Chem. Soc. Perkin Trans. 1, 1725 (1997); (*c*) T. Yamato, Y. Saruwatari, and M. Yasumatsu. J. Chem. Soc. Perkin Trans. 1, 1731 (1997); (*d*) T. Yamato, Y. Saruwatari, M. Yasumatsu, and S. Ide. Eur. J. Org. Chem. 309 (1998).
14. (*a*) S. Pappalardo, L. Giunta, M. Foti, G. Ferguson, J.F. Gallagher, and B. Kaitner. J. Org. Chem. **5**7 2611 (1992); (*b*) G. Ferguson, J.F. Gallagher, L. Giunta, P. Neri, S. Pappalardo, and M. Parisi. J. Org. Chem. **59**, 42 (1994); (*c*) S. Pappalardo, G. Ferguson, P. Neri, and C. Rocco. J. Org. Chem. **60**, 4576 (1995); (*d*) S. Pappalardo. New J. Chem. 465 (1996).
15. (*a*) T. Yamato, M. Haraguchi, T. Iwasa, and H. Tsuzuki. An. Quim.-Int. **93**, 301 (1997); (*b*) T. Yamato, M. Haraguchi, J. Nishikawa, S. Ide, and H. Tsuzuki. Can. J. Chem. **76**, 989 (1998); (*c*) T. Yamato. J. Inclusion Phenom. **32**, 195 (1988).
16. (*a*) R.H. Vreekamp, W. Verboom, and D.N. Reinhoudt. J. Org. Chem. **61**, 4282 (1996); (*b*) I. Higler, P. Timmerman, W. Verboom, and D.N. Reinhoudt. Eur. J. Org. Chem. 2689 (1998).
17. (*a*) K. Koh, K. Araki, and S. Shinkai. Tetrahedron Lett. **35**, 8255 (1994); (*b*) P. Lhoták and S. Shinkai. J. Syn. Org. Chem. Jpn. **53**, 963 (1995); (*c*) M. Takeshita and S. Shinkai. Bull. Chem. Soc. Jpn. **68**, 1088 (1995).
18. J.M. Harrowfield, M.I. Ogden, W.R. Richmond, and A.H. White. J. Chem. Soc. Chem. Commun. 1159 (1991).
19. (*a*) M. Nishio and M. Horita. Tetrahedron, **45**, 7201 (1989); (*b*) C.D. Andreetti, R. Ungaro, and A. Pochini. J. Chem. Soc. Chem. Commun. 1005 (1979); (*c*) R. Ungaro, A. Pochini, C.D. Andreetti, and O. Domiano. J. Chem. Soc. Perkin Trans. 2, 197 (1985); (*d*) M.A. McKervey, E.M. Seward, G. Ferguson, and B.L. Ruhl. J. Org. Chem. **51**, 3581 (1986); (*e*) D.J. Cram, S. Karbach, H.-E. Kim, C.B. Knobler, E.F. Marverick, J.L. Ericson, and R.C. Helgeson. J. Am. Chem. Soc. **110**, 2229 (1988); (*f*) P. Soncini, S. Bonsignore, E. Dalcanale, and F. Ugozzoli. J. Org. Chem. **57**, 4608 (1992); (*g*) J.L. Atwood, S.G. Bott, C. Jones, and C.L. Raston. J. Chem. Soc. Chem. Commun. 1349 (1992); (*h*) K. Kobayashi, Y. Asakawa, Y. Kikuvchi, H. Toi, and Y. Aoyama. J. Am. Chem. Soc. **115**, 2648 (1993); (*i*) T. Yamato, A. Miyazawa, and M. Tashiro. J. Chem. Soc. Perkin Trans. 1, 3127 (1993).
20. (*a*) K. Kobiro, M. Takashi, N. Nishikawa, K. Kikuchi, Y. Tobe, and Y. Odaira. Tetrahedron Lett. **28**, 3825 (1987); (*b*) K. Kurosawa, M. Suenaga, T. Inazu, and T. Yoshino. Tetrahedron Lett. **23**, 5335 (1982); (*c*) T. Shinmyozu, Y. Hirai, and T. Inazu. J. Org. Chem. **51**, 1551 (1986); (*d*) K. Sako, T. Hirakawa, N. Fujimoto, T. Shinmyozu, T. Inazu, and H. Horimoto. Tetrahedron Lett. **29**, 6275 (1988); (*e*) T. Meno, K. Sako, M. Suenaga, M. Mouri, T. Shinmyozu, T. Inazu, and H. Takemura. Can. J. Chem. **68**, 440 (1990); (*f*) K. Sako, T. Meno, H. Takemura, T. Shinmyozu, and T. Inazu. Chem. Ber. **123**, 630 (1990); (*g*) K. Sako, T. Shinmyozu, H. Takemura, M. Suenaga, and T. Inazu. J. Org. Chem. **57**, 6536 (1992).
21. (*a*) B.H. Smith. *In* Bridged aromatic compounds. Academic Press, New York. 1964; (*b*) F. Vögtle and P. Neumann. Angew. Chem. **84**, 75 (1972); Angew. Chem. Int. Ed. Engl. **11**, 73 (1972); (*c*) F. Vögtle and P. Newmann. Synthesis, 85 (1973); (*d*) F. Vögtle and G. Höhner. Top. Curr. Chem. **74**, 1 (1978); (*e*) P.M. Keehn and S.M. Rosenfield. Cyclophanes. Vol. 1. Academic Press, New York. 1983; (*f*) F. Vögtle. Cyclophane chemistry. John Wiley & Sons, New York. 1993.
22. (*a*) M. Tashiro and T. Yamato. J. Org. Chem. **46**, 4556 (1981); (*b*) M. Tashiro and T. Yamato. J. Org. Chem. **48**, 1461 (1983).

[6] Hydrogen coordinates, temperature factors (anisotropic for carbon atoms), scale factors, and secondary estimation coefficients have been deposited as supplementary material and may be purchased from: The Depository of Unpublished Data, Document delivery, CISTI, National Research Council Canada, Ottawa, Ontario, Canada, K1A 0S2. These data have also been deposited with the Cambridge Crystallographic Data Centre (CCDC Nos. 165 893 and 165 894) and can be obtained on request form: The Director, Cambridge Crystallographic Data Centre, University Chemical Laboratory, 12 Union Road, Cambridge, CB2 1EZ, U.K.

© 2001 NRC Canada

Binding of anti-inflammatory drug indomethacin with cyclodextrin and DNA: solubility, spectroscopic, and voltammetric studies

I.S. Shehatta and M.S. Ibrahim

Abstract: The interaction of the anti-inflammatory drug indomethacin (IMC) with α-, β-cyclodextrins (CDs) and calf thymus deoxyribonucleic acid (ct-DNA) have been investigated in the Britton–Robinson (BR) buffer (pH = 7.2) using solubility, spectroscopic, and voltammetric methods. The measurements show that the IMC molecule, acting as an intercalator, is inserted, from the *p*-chlorobenzoyl part, into the cavity of the cyclodextrins as well as into the base-stacking domain of the ct-DNA double helix. Upon addition of β-CD in a buffered IMC solution, the solubility of IMC increases and the Gibbs free energies of transfer of the drug from aqueous solution to the cavity of β-CD are negative and increase negatively with increasing β-CD concentration. The interaction of IMC with CDs and ct-DNA causes hypochromism and bathochromic shifts in the absorption spectra, along with pronounced changes in the electrochemical behaviour of the drug. The stoichiometry of complexes formed in solution is inferred to be 1:1. The binding constants were calculated from the increase of the solubility, the strong hypochromism, and the decrease in peak current of IMC upon the addition of the host molecules. IMC has a higher affinity for β-CD than for α-CD, as the IMC–β-CD interaction is the most exergonic. Binding is interpreted in terms of the intercalative (hydrophobic) interactions with the ct-DNA helix (i.e., the stacked base pairs) or within CD cavity.

Key words: cyclodextrin, ct-DNA, anti-inflammatory drug, indomethacin, binding constant, solubility, spectra, voltammetry.

Résumé : Faisant appel à des méthodes basées sur la solubilité, la spectroscopie et la voltampérométrie et opérant dans un tampon de Britton-Robinson (BR) (pH = 7,2), on a étudié l'interaction entre l'indométhacine (IMC), un antiinflammatoire, et les α- et β-cyclodextrines (CD) et l'acide désoxyribonucléique de la thyroïde du veau (ct-DNA). Les mesures montrent que la molécule d'IMC s'intercale, à partir de la portion *p*-chlorobenzoyle, dans la cavité des cyclodextrines ainsi que dans le domaine d'empilement des bases de la double hélice du ct-DNA. Par addition de β-CD dans une solution tamponnée d'IMC, la solubilité de l'IMC augmente; les énergies libres de Gibbs du transfert du médicament à partir de la solution aqueuse vers la cavité de la β-CD sont négatives et elles augmentent de façon négative avec une augmentation de la concentration de β-CD. L'interaction de l'IMC avec les CD et le ct-DNA provoque une hypochromie et une bathochromie dans les spectres d'absorption et des changements importants dans le comportement électrochimique du médicament. On fait l'hypothèse que la stoechiométrie des complexes qui se forment en solution est 1:1. Les constantes de fixation ont été calculées à partir de l'augmentation de la solubilité, la forte hypochromie et la diminution du courant de sommet de l'IMC lors de l'addition de molécules hôtes. L'affinité de l'IMC est plus grande pour la β-CD que pour la α-CD parce que l'interaction IMC–β-CD est la plus exergonique. La fixation est interprétée en termes de la facilité des interactions d'intercalation (hydrophobes) dans l'hélice de la ct-DNA (c'est-à-dire les paires de bases empilées) ou à l'intérieur de la cavité de la CD.

Mots clés : cyclodextrine, ct-DNA, médicament antiinflammatoire, indométhacine, constante de fixation, solubilité, spectres, voltampérométrie.

[Traduit par la Rédaction]

Introduction

Host–guest interactions play central roles in many biochemical processes such as the mechanism of drug action, enzyme–substrate interactions, immunological responses, and the storage and retrieval of genetic information (1, 2). There is growing interest in exploring the binding of small molecules with cyclodextrins (CDs) and DNA. Inclusion complexes of CDs have received extensive attention in the pharmaceutical field, especially in the design of drug formulation (3). Such complexation improves the aqueous solubility, dissolution, chemical stability, and bioavailability of

Received January 2, 2001. Published on the NRC Research Press Web site at http://canjchem.nrc.ca on October 9, 2001.

I.S. Shehatta.[1] Chemistry Department, Faculty of Science, Mansoura University, Mansoura, Egypt.
M.S. Ibrahim. Chemistry Department, Faculty of Science, Assiut University, Assiut 71516, Egypt.

[1]Corresponding author (fax: 009 713-767 1291; e-mail: I.shehatta@uaeu.ac.ae).

 DOI: 10.1139/cjc-79-10-1431 © 2001 NRC Canada

various drugs that are poorly soluble in water, which in turn leads to an increase in the plasma level peak resulting in a reduction in drug doses. The DNA-binding studies are important for the rational design and construction of new and more efficient drugs targeted to DNA (4, 5). These are extremely useful in understanding the DNA sequence recognition by drugs as well as by proteins. The specific interaction between a drug and DNA results in some changes in physical and chemical properties and has a potential importance for a better understanding of its therapeutic efficiency. A common feature in their structures, which characterizes both CD and DNA, are that they have a hydrophilic coat and a hydrophobic core. The hydrophilic groups (OH in CDs and PO_4^{3-} in DNA) of these macromolecules oriented to the exterior creating sites available for intercalative (hydrophobic) interactions.

Although, spectroscopic studies for CD or DNA systems are extensively reported, the voltammetric method is scarcely found in literature despite that electrochemical methods provide a useful complement to the other spectroscopic methods, e.g., for nonabsorbing species, weak absorption bands, overlap of electronic transition with those of the DNA molecule, and also when the difference of absorbance between free and complexed forms is small. Moreover, the electrochemical behaviours are valuable in elucidating some mechanisms of the drug action in vivo (6).

Indomethacin (1-(4-chlorobenzoyl)-5-methoxy-2-methyl-1-indol-3-acetic acid) is a nonsteroidal anti-inflammatory agent, widely used as an analgesic drug in the treatment of rheumatoid arthritis and other degenerative joint diseases, gout, and acute-musculoskeletal disorders. However, this compound is practically insoluble in water unless it is in alkaline media, where it undergoes hydrolysis to 5-methoxy-2-methylindol-3-yl acetate and 4-chlorobenzoate (7). Formulation of such a lipophilic drug is frequently hampered by its poor aqueous solubility, which can limit its therapeutic applications. The therapeutic activity is also impaired by the instability of the drug. To overcome these problems various methods have been used such as micellar (8) or liposomal (9) suspensions and CD derivatives (10), which affect the stability and solubility of indomethacin in aqueous solutions. Nonsteroidal, anti-inflammatory drugs generally cause ulceration as a result of slow dissolution of the drug, which provides high local drug concentraction, resulting in mucosal damage. Their ulcerogenic potencies could be reduced by CD complexation (11), which increases the dissolution and absorption rates and consequently result in a reduction of drug-induced gastric ulceration.

Therefore, and in continuation of our work (12–14)[2], the present work is devoted to study the interaction of IMC with α- and β-CDs and ct-DNA. This has been investigated by solubility, cyclic voltammetry, and differential pulse stripping voltammetry as well as UV–vis spectroscopy techniques. From the variation in the solubility, peak current, and absorption spectra, the formation constant (*K*) of these interactions were obtained.

Experimental

Instrumentation

Differential pulse stripping voltammetry (DPSV) and cyclic voltammetry (CV) were carried out using a PAR Model 264A polarographic analyzer – stripping voltammetry in conjunction with a PAR Model 303A HMDE and advanced X-Y recorder Model RE0151. An Ag/AgCl saturated KCl reference electrode and a Pt wire auxiliary electrode were used. A PAR Model 305 stirrer was also used for DPSV. The ultraviolet and visible absorption spectra were obtained using a Shimadzu UV-2101PC, UV–vis scanning spectrophotometer.

Reagents and procedure

Calf thymus deoxyribonucleic acid (ct-DNA), α-CD, β-CD, and IMC were obtained from Sigma and were used as received without further purification. Stock standard solution of ct-DNA was prepared by dissolving the ct-DNA in H_2O and stored at 4°C and discarded after no more than four days. Monitoring the absorption spectrum at 260 and 280 nm was done to check the purity of the ct-DNA. The concentration of the stock solution of ct-DNA (5.43×10^{-5} M in nucleotide phosphate, NP) was determined by UV absorbance at 260 nm using the molar extinction coefficient (ε) of 6600 M^{-1} cm^{-1} (15). It is noteworthy that the prepared ct-DNA solution in phosphate buffer gave ratio of UV absorbance at 260 and 280 nm (A_{260}:A_{280}) of approximately 1.9, indicating that the ct-DNA was sufficiently protein-free (16). Stock solutions of α-CD and β-CD were prepared by dissolving the desired weights in water. Stock solutions of IMC were prepared by dissolving an appropriate amount of the drug in methanol. The supporting electrolyte was a Britton–Robinson (BR) buffer prepared in the usual way, by adding appropriate amounts of sodium hydroxide (0.2 M) to an orthophosphoric acid, acetic acid, and boric acid mixture (0.04 M each). All chemicals were reagent grade (Merck, Darmstadt). Double-distilled water was used to prepare the solutions. The pH was measured using a pH-meter Model M64 (ORION) and is accurate to ±0.05 pH unit. In case of ct-DNA, the absorbance was recorded against a blank containing all reagents of the working sample except IMC.

For voltammetric measurements the test solution was placed in a polarographic cell of volume ≈15 mL and deoxygenated by passing nitrogen for 15 min. In the case of DPSV, the accumulation was performed on the HMDE and the solution was stirred at the accumulation potential of E_{acc}= 0.0 V for 30 s. The voltammetric response was obtained using a pulse repetition time of 0.2 s, within an amplitude of 100 mV and a scan rate of 20 mV s^{-1} (or 100 mV s^{-1} for CV, unless otherwise stated). When preconcentration of the stirred solutions was done, a quiescent period of 15 s was allowed before the potential scan was started. Typical CV peak potentials were reproducible to better than ±5 mV and DPSV peak potentials to ±2 mV.

Keeping both the concentration of the IMC and the total volume of solution constant (10 mL) the absorption and the electrochemical procedures were carried out, while varying the CD or ct-DNA concentration.

Solubility measurements were carried out according to the phase solubility method of Higuchi and Connors (17). An excess amount of the anti-inflammatory drug IMC was mixed with Britton–Robinson buffer solution (10 mL, pH = 7.2) containing various concentrations of β-CD ($0–5 \times 10^{-3}$ M).

[2] M.S. Ibrahim, I.S. Shehatta, and A. Al-Naiyle. Submitted.

© 2001 NRC Canada

Fig. 1. Phase solubility diagram of IMC in BR buffer (pH = 7.2) in the presence of different β-CD concentrations.

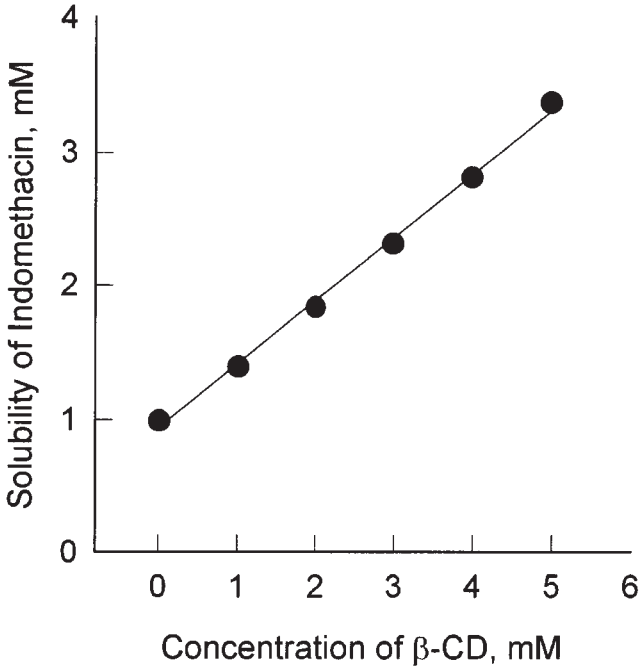


Table 1. Values of Gibbs energy of transfer of indomethacin from aqueous solution to the hydrophobic cavity of β-CD at 298.15 K.

[β-CD] (1×10^3, M)	$-\Delta_{trans}G$ (kJ mol^{-1})
1	0.87
2	1.51
3	2.09
4	2.57
5	3.02

The screw-cap glass vials containing these suspensions were shaken until equilibrium had been reached (24 h), followed by another 10 h without shaking. The contents of each vial were filtered through a Whatman filter membrane (0.2 μm pore size). The filtrate was analyzed spectrophotometrically at 266 and 319 nm for the total amount of IMC dissolved.

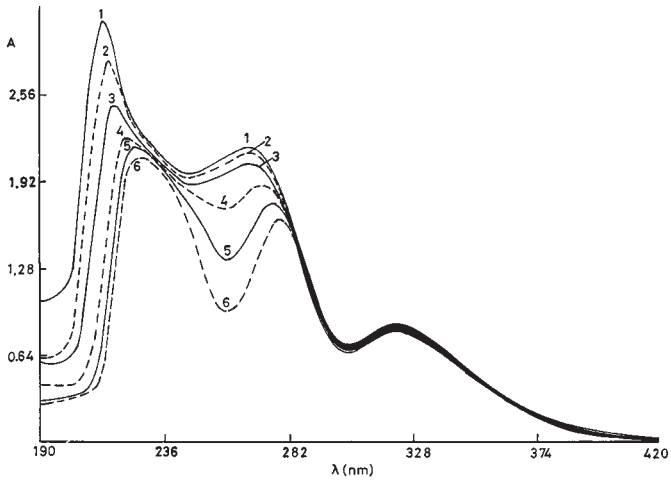
All experiments were carried out at the ambient temperature (25.0 ± 0.5°C). The solubility values are the average of the three replicates.

Methanol is the solvent of choice due to its (*i*) ability to dissolve IMC appreciably; (*ii*) structural similarity to water along with other solvents; and (*iii*) low affinity for binding with CD (18), which renders it a poor competitor with IMC for CD.

Results and discussion

Solubility, voltammetric behaviour, and absorption spectra of IMC change dramatically as a result of binding to CDs or ct-DNA. These changes have been quantified to estimate the formation constants and to evaluate the binding modes of CDs and ct-DNA. The pH value as well as the constituent of the buffer has a pronounced effect on the interaction between IMC and either CD or ct-DNA. It was found that the Britton–Robinson buffer (BR) solution (pH = 7.2) has much greater hypochromicity and cathodic peak current reduction than the other buffers investigated. This behaviour suggests that the ionized IMC species (pK_a = 4.2 (7)) are favoured for the binding with CDs or ct-DNA compared to the non-ionized ones. Moreover, such a buffer is suitable to prevent the DNA from acid or basic denaturing, as well as to avoid the DNA reduction, since it reduced in acid medium (19). Therefore, the BR buffer (pH = 7.2) was considered optimum and used throughout the present work.

Fig. 2. UV–vis spectra of IMC (1.0×10^{-4} M) in BR buffer (pH = 7.2, 20% methanol) in the (1) absence and presence of (2) 5.43; (3) 10.8; (4) 21.7; (5) 27.1; and (6) 32.5 μM ct-DNA.



Solubility studies

The IMC is known to have very poor aqueous solubility (0.004 mg mL^{-1} at 298.15 K) (20). Like all the carboxylic acids, the solubility of indomethacin is greatly influenced by pH (20). This is due to the ionization of carboxylic group being enhanced with increasing pH, hence the solubility increases. At lower pH values the solubility decreases as a result of suppression of this ionization. On the other hand, the solubilized indomethacin will decrease the pH and the depression in pH increases with increasing the solubility of IMC. Thus, in order to compare the actual relative solubilizing capacity, the measurements should be done in buffer solution with constant pH. Therefore, the solubility measurements were carried out in BR buffer solution (0.1 M, pH = 7.2). The capacity of the buffer used is sufficient and high enough to maintain a constant pH value even for the higher IMC concentrations. This is in agreement with Hammad and Müller (20). They observed that the solubility (concentration) of IMC has a constant value at ≥0.02 M phosphate buffer. They used 0.067 M phosphate buffer in measuring the solubility of IMC in different micelles. This is emphasized from the measurement of the pH of the indomethacin solutions in presence of various β-CD concentrations ($0–5 \times 10^{-3}$ M). It was found that only a very slight drop in pH occurred, e.g., the pH of the IMC solutions decreases from pH = 7.20 without β-CD to 7.17 at higher concentration of β-CD (5×10^{-3} M).

© 2001 NRC Canada

Table 2. The formation constant and Gibbs free energy of the binding of indomethacin with cyclodextrins and ct-DNA in methanol 20% (v/v) and BR buffer (pH = 7.2) at 298.15 K.

	Voltammetry[a]		Spectrophotometry	
Host	Log K	$-\Delta G$ (kJ mol^{-1})	Log K	$-\Delta G$ (kJ mol^{-1})
α-CD	2.78	15.90	—	—
β-CD	3.42	19.52	3.60	20.55
	3.25[b]	18.55[b]		
ct-DNA	4.49	25.64	4.41	25.12

[a]From differential pulse stripping voltammetry.
[b]Determined in methanol 40% (v/v) and BR buffer (pH = 7.2) at 298.15 K.

Figure 1 shows the phase solubility profile representing the effects of increasing concentrations of β-CD on the apparent solubility of IMC in aqueous solution. An increase in the solubility of the complex with respect to the free form was observed. In aqueous solutions of IMC–β-CD complexes, the free drug molecules are in equilibrium with the drug molecules entrapped within the cavity. Thus, on increasing the concentration of β-CD more IMC molecules will transfer from the aqueous solution to the hydrophobic cavity of β-CD. Therefore, one can expect that more IMC dissolved in water in the pressence of β-CD than that dissolved in absence of it and consequently, the solubility of IMC increases with increasing the concentration of β-CD. A linear plot was obtained and represented by the following equation:

$$[1] \qquad C_{IMC} = 9.38 \times 10^{-4} + 0.475 C_{\beta\text{-CD}} \qquad R = 0.998$$

Therefore, the solubility curve for IMC was classified as type A_L, according to Higuchi and Connors classification (17), indicating the formation of a 1:1 IMC–β-CD complex.

The apparent stability constant (K = 966 M^{-1}) of the formed complex was calculated from the solubility diagram according to eq. [2]

$$[2] \qquad K = \text{slope}/S_o(1 - \text{slope})$$

using the slope of the phase solubility diagram and the determined IMC solubility in water (S_o).

The Gibbs free energies of transfer of IMC from aqueous solution to the cavity of β-CD (Table 1) have been calculated from the following equation:

$$[3] \qquad \Delta_{trans}G = -RT \ln (S/S_o)$$

where S and S_o are the solubilities of IMC in presence and absence of β-CD, respectively. As can be seen from Table 1 the $\Delta_{trans}G$ values are negative and increase negatively with increasing β-CD concentration. This indicates that the transfer process is spontaneous and supports the view that β-CD is more favourable environment than water for IMC. Moreover, the interaction between IMC and β-CD increases with increasing β-CD content.

Spectrophotometric studies

Indomethacin was characterized as having ultraviolet absorbance maxima at 212, 266, and 319 nm in 20% (v/v) methanol–water BR buffer (pH = 7.2). Some important changes in the absorption spectrum of IMC were observed upon the addition of ct-DNA (Fig. 2). The absorption bands at 212 and 266 nm shifted to longer wavelength. Also, this spectrum showed strong decreases in the peak intensities (hypochromicity) on increasing the concentration of ct-DNA. A continuous decrease in the intensity of IMC absorption was followed by saturation at high concentrations of ct-DNA. Such pronounced hypochromism and bathochromism were suggested to be due to a strong intercalation of the IMC molecule into ct-DNA base pairs (21). This implies a close proximity of the IMC chromophore of the ct-DNA base pairs, i.e., a strong overlap between the electronic states of the intercalating chromophore and that of the ct-DNA bases occur. The association of the ct-DNA and guest (IMC) molecule is governed by the following thermodynamic equilibrium:

$$[4] \qquad \text{ct-DNA} + \text{IMC} \rightleftarrows \text{ct-DNA–IMC}$$

and thus the formation constant is defined as:

$$[5] \qquad K = [\text{ct-DNA–IMC}]/[\text{ct-DNA}][\text{IMC}]$$

assuming the most common host:guest ratio of 1:1.

The formation constant (K) was determined from the differences in absorbance (A) due to ct-DNA intercalation using the Hildebrand–Bensei double reciprocal plot (22)

$$[6] \qquad 1/\Delta A = (1/K[\text{IMC}]\Delta\varepsilon\, L_T) + (1/[\text{IMC}]\Delta\varepsilon)$$

in which [IMC] is the total concentration of indomethacin, L_T is the total concentration of ct-DNA, $\Delta\varepsilon$ is the difference in the molar absorpitivities for the free and the complexed IMC, and ΔA is the observed change in absorbance of the IMC at 266 nm by the addition of ct-DNA. The plot of $1/\Delta A$ vs. 1/[ct-DNA] gives good linearity with correlation coefficient ≥0.98 and was utilized to evaluate the K and $\Delta\varepsilon$ values from the intercept and slope, respectively. The formation constant is given in Table 2.

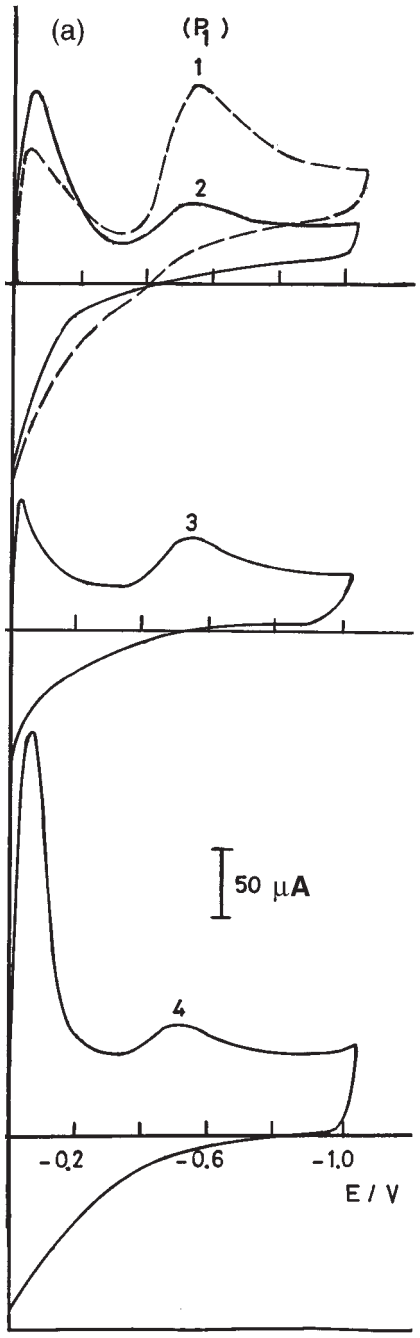
The binding constant of IMC with ct-DNA was also determined from absorption titration by using the Scatchard plot. In this method, $[\text{ct-DNA}]/(\varepsilon_A - \varepsilon_F)[\text{ct-DNA}]$ plot is constrcuted according to eq. [7] (21):

$$[7] \qquad [\text{ct-DNA}]/(\varepsilon_A - \varepsilon_F) = [\text{ct-DNA}]/(\varepsilon_B - \varepsilon_F) + 1/K(\varepsilon_B - \varepsilon_F)$$

where ε_A, ε_F, and ε_B are the apparent extinction coefficient ($\varepsilon_A = A_{observed}/[\text{IMC}]$), the extinction coefficient for free IMC ($\varepsilon_F = 2.12 \times 10^4$ M^{-1} cm^{-1} at 266 nm), and the fully bound form, respectively. From eq. [7] the K is given by the ratio of the slope to intercept. According to the experimental data of the absorption titration, the regression equation of

© 2001 NRC Canada

Fig. 3a. Cyclic voltammograms for IMC solution (1.0×10^{-4} M) obtained in BR buffer (pH = 7.2, 20% methanol) at HMDE, scan rate 200 mV s^{-1}, and potential scan from E_s = 0.0 to E_f = –1.0 V. (1) IMC only; (2) 1 + 2.39×10^{-5} M ct-DNA; (3) 1 + 5.94×10^{-3} M α-CD; and (4) 1 + 5.94×10^{-3} M β-CD.



eq. [7] is [ct-DNA]/($\varepsilon_A - \varepsilon_F$) = ($3.794 \times 10^{-4}$[ct-DNA] – 1.459×10^{-8})/K (R = 0.9797). The linear correlation revealed that the binding number was 1, i.e., one IMC molecule only interacts with one nucleotide phosphate in DNA. From the slope and the intercept of the above equation, log K = 4.41, which is exactly the value obtained using the double reciprocal method. Also, the estimated $\Delta\varepsilon = (\varepsilon_B - \varepsilon_F)$ value is 2.64×10^3 M^{-1} cm^{-1}, yielding $\varepsilon_B = 2.38 \times 10^4$ M^{-1} cm^{-1}.

On the other hand, the UV–vis absorption spectra indicate the inclusion complex formation of IMC and β-CD. The UV spectrum of IMC in BR buffer (pH = 7.2) is altered when the β-CD was added. The absorption bands at 212 and 266 nm shifted to longer wavelength as well as the absorbance peak decreased with increasing concentration of β-CD. Such observed spectral changes continue to occur until they reach a limiting value owing to the complete inclusion of the chromophore in the cavity of β-CD. The formation constant of IMC–β-CD complex (Table 2) was determined by a procedure similar to that used in the determination of K for IMC–ct-DNA complex.

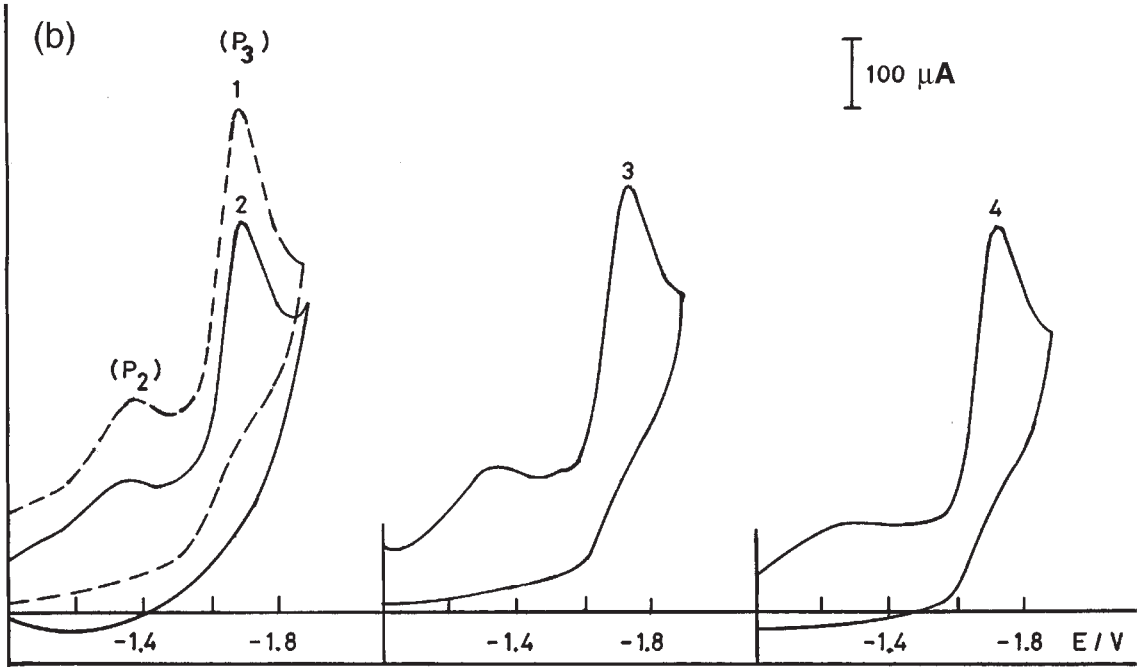
Voltammetric studies

The few previous electrochemical studies on the reduction of IMC at mercury electrode (23, 24) prompted us to use the voltammetric method to trace the interaction of IMC with asymmetric environment of the ct-DNA or with CDs. Typical cyclic voltammetric (CV) behaviours of IMC in the absence and in the presence of ct-DNA or CDs are shown in Fig. 3. Working with the HMDE, the absorbed IMC compound and its reduction products exhibit complicated voltammograms, varying with concentration, pH value, temperature, content of organic solvent, sweep rate and complex formation. Only at low concentration (9.9×10^{-5} M), 20% methanol in the BR buffer solution (pH 7.2, 25°C), and with aid of fast sweep (200 mV s^{-1}) the IMC exhibit three cathodic peaks at –0.55 (P_1), –1.40 (P_2), and –1.68 V (P_3) as shown in Fig. 3. Under these conditions the complications caused by adsorption layers and the chemical splitting reaction (25) have little effect. The first cathodic peak (P_1), which appears at less negative potential, can be assigned to the reduction of the Hg–IMC complex (26). The second peak (P_2) was attributed to the reduction of the amide carbonyl corresponding to two electrons process and the third peak (P_3) is believed to be a kinetic wave (27). Furthermore, the absence of any peaks in the reverse scan as well as the shift of the peak potential to more negative values on increasing the scan rate (v) revealed the irreversible nature of the reduction peaks.

The addition of an excess of ct-DNA in IMC solution caused the peak currents to diminish considerably (Fig. 3, curve 2). The peak current decreased to about 40, 62, and 77% for P_1, P_2, and P_3, respectively, of that in the absence of ct-DNA. In terms of this result, it seems that binding of IMC to the large, slowly diffusing ct-DNA causes the decrease in the peak current of the IMC in the presence of an excess of ct-DNA, which results in the considerable decrease in the apparent diffusion coefficient of the IMC–ct-DNA adduct. This is emphasized from the decrease in slope of the linear $i_p - v^{1/2}$ plots ($R \geq 0.9989$), where the slope values are 36.1 and 30.9 nA $mV^{-1/2}$ $s^{-1/2}$ in absence and presence of ct-DNA, respectively. From these values, the diffusion coefficient (D_f) of the free IMC was found to be 2.81×10^{-7} cm^2 s^{-1}, whereas $D_b = 2.06 \times 10^{-7}$ cm^2 s^{-1} for the bound IMC (in presence of 2.39×10^{-5} M ct-DNA, NP). These values are within the range obtained by Carter et al. (28). It is noteworthy that the cyclic voltammogram of ct-DNA solution (5.43×10^{-5} M, NP) did not exhibit any Faradaic processes at potentials between 0.0 and –1.85 V vs. Ag/AgCl electrode under our experimental condition; it showed only a small

© 2001 NRC Canada

Fig. 3b. Cyclic voltammograms for IMC solution (1.0×10^{-4} M) obtained in BR buffer (pH = 7.2, 20% methanol). Potential scan from E_s = 1.0 to E_f = –1.85 V. Other conditions as in Fig. 3*a*.



reduction (<10%) in charged current, compared to that of ct-DNA free supporting electrolyte.

In presence of α-CD or β-CD, the peak potentials as well as the peak currents of IMC are influenced (Fig. 3, curves 3 and 4). The decrease in the peak currents can be attributed to the decrease in *D* value for IMC species in presence of the host molecule (28). This is again supported by the decrease in the slope of the linear $i_p - v^{1/2}$ plots ($R \geq 0.9989$) accompanied by the addition of host molecules. It is noteworthy that the current could also be diminished if the hosts caused an increase in the solution viscosity with a corresponding decrease in the diffusion coefficients. However, no change in solution viscosity could be detected over the range 0.5–10.0 mM CDs or 5–50 μM ct-DNA.

Further evidence for the interaction of IMC with α- and β-CDs and DNA comes from the differential pulse stripping voltammetry (DPSV). In presence of different concentrations of ct-DNA (as a representative example), the cathodic peak potentials as well as the peak currents of IMC are influenced (Fig. 4). The cathodic peak potentials of the first and second peaks shifted to more positive potential, indicating that the reduction of IMC molecule is enhanced when it enters ct-DNA-stacking region, a region with lower polarity. On the other hand, the currents of the first (P_1) and second (P_2) peaks as well as the peak height of the third (P_3) are strongly decreased with increasing concentration of ct-DNA revealing that an interaction has occurred between IMC and ct-DNA.

Based on the variation in the peak current, the formation constants of the complexes formed between IMC and CDs or ct-DNA were determined. For l:1 complex the following equation could be deduced based on Feng et al. (19):

$$[8] \qquad \frac{i_o}{i_o - i} = \frac{1}{(1-C)} + \frac{1}{K(1-C)[H]}$$

where i_o and i are the peak currents of the free IMC and that in the presence of CD or ct-DNA, respectively, [*H*] is the concentration of CD or ct-DNA, and *C* is the proportional constant. According to eq. [8], from $(i_o/i_o - i)$ vs. 1/[*H*] plot, the ratio of the intercept to the slope gives the vaue of *K*. Our experimental data at pH 7.2, which are in good agreement with those obtained from spectrophotometry experiments, are listed in Table 2.

The obtained *K* value is higher than those obtained previously for IMC–β-CD (log *K* = 2.88) at 303 K using NMR spectroscopy (29) and for IMC-hydroxypropyl–β-CD (log *K* = 2.98) using the kinetic method (10). Although, the obtained *K* value for β-CD is higher than the published values, the present value is in the range of the published ones, within the experimental error of the different methods, which lends credibility to these measurements. Also, the difference in the host molecules, temperature, and other conditions, including buffer solution, its components, and its ionic strength, could contribute to the difference in *K* value.

Mode and driving forces of inclusion complex

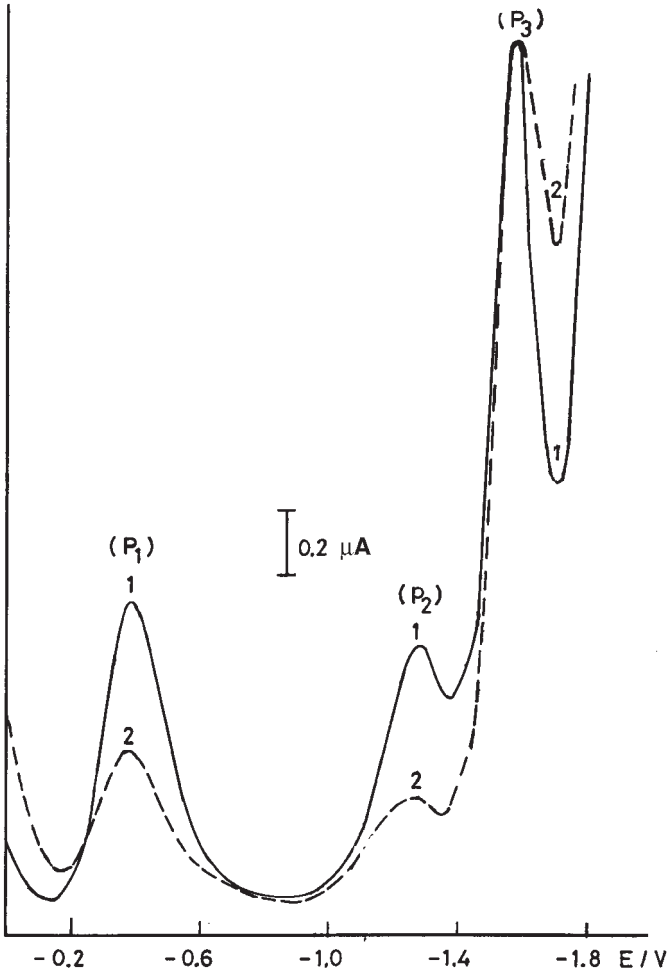
The supposed 1:1 association complex is inferred from the fitting of the experimental data from three independent techniques to the different equations. In all cases the regression coefficients ≥0.98 suggesting that IMC interacts with CD or ct-DNA in molar ratio of 1:1.

For the formation of IMC–CD complex the drug is transferred from aqueous solution to the CD cavity with the displacement of the incorporated water molecules to the bulk water, i.e.,

$$[9] \qquad \mathrm{IMC_{aq}} + [\mathrm{CD(H_2O)}_n]_{\mathrm{aq}} = [\mathrm{CD{-}IMC(H_2O)}_{n-x}] + x(\mathrm{H_2O})_{\mathrm{aq}}$$

© 2001 NRC Canada

Fig. 4. Differential pulse stripping voltammograms for IMC (1.0×10^{-4} M) in BR buffer (pH = 7.2, 20% methanol) at HMDE in the absence (1) and presence (2) of 3.8×10^{-6} M ct-DNA. Scan rate 20 mV s^{-1}, accumulation time 30 s, E_{acc} = 0.0 V, and pulse amplitude 100 mV.



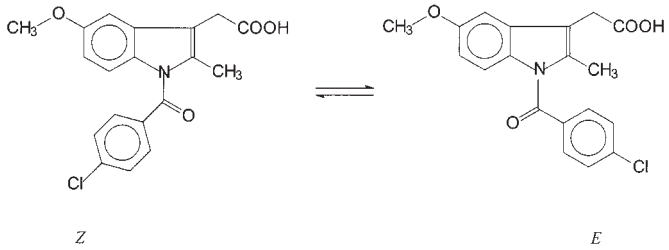
The changes in Gibbs energy values (ΔG) for the binding of IMC with the CDs or ct-DNA were calculated from the well-known relationship:

$$[10] \quad \Delta G = -RT \ln K$$

These values (Table 2) are negative indicating that the binding process is favourable and spontaneous.

The driving forces for CD inclusion complexes are still the subjects of controversy. Numerous factors have been found as contributing to the binding forces for the formation of various CD inclusion complexes (30), including hydrogen bonding between the hydroxyl groups of CD and the guest molecules, van der Waals interactions between the host and the guest molecules, hydrophobic interactions (in the present case including dehydration of the hydrophobic part of drug, i.e., the water molecules lose their lattice structure), the transfer of the high enthalpy water molecules from the cavity of CD to the bulk water, and the conformational change of the CD molecule upon the ligand binding.

Scheme 1.



Varying the percentage of methanol carried out a quantitative study of the effect of organic modifier in the binding of IMC to CD. Table 2 reports the values of *K*, determined voltammetrically for IMC–β-CD (as a representative example) at 20 and 40% (v/v) methanol. The *K* value at 40% (v/v) methanol decreased to 66% of that in 20% (v/v) methanol. This confirms that addition of methanol reduced the affinity of the IMC for the CD, and increased the affinity for the bulk buffer (31). The decrease in the *K* value and consequently the $-\Delta G$ values, with increasing methanol content suggests that water plays an important role in the association process. Thus, the hydrophobic interactions have a significant contribution to the binding reaction. The decrease in the polarity of the medium with the addition of methanol is unfavourable for hydrophobic interaction between IMC and CD.

The importance of hydrogen bonding is marginal, because the modified CD (incapable of hydrogen bonding) did not show a drastic change for the substrate binding (32). Moreover, alkanediols form less stable complexes with CD than the corresponding alkanols (12–14), in spite of the former having more hydrogen bond sites than the latter. The difference of the hydrophobicity (as indicated from the partition coefficients) between alkanols and alkanediols was suggested to be responsible for favourable binding of CD with alkanols.

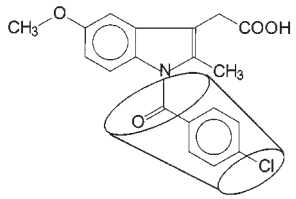
On the other hand, the release of configurational strain in the CD ring has also a minor contribution for complex formation, as indicated from the conformational energy calculation (33).

Based on the ^{1}H NMR spectroscopy (34), single crystal X-ray diffraction results (35), and theoretical calculations (36), the IMC molecule exists in solution as a mixture of *E*- and *Z*- isomers (Scheme 1) and the *Z*-isomer is the most thermodynamically stable form. But, the data obtained by both intermolecular nuclear Overhauser enhancement (NOE) and rotating overhauser enhancement (ROE) as well as the energy calculations on the IMC–β-CD complex showed that the *E*-isomer is a more favourable conformation for the entry into the CD cavity than the *Z*-isomer (34). Hence, the major complex in solution is IMC-*E*–β-CD.

Since, IMC-*E* has two different lipophilic parts (*p*-chlorobenzoyl and the indol ring) under the influences of noncovalent interactions, it can be accommodated in the host cavity by four different modes of inclusion. Two modes of entry by *p*-chlorobenzoyl part may occur either through the larger or the smaller rim of the truncated cone of the CD. The other two modes of entry involve the indol part of IMC-*E*. We believe that the IMC–β-CD complex could be formed (next page), in which the *p*-chlorobenzoyl part of IMC-*E* isomer enters the hydrophobic cavity of β-CD truncated

© 2001 NRC Canada

cone. This is in good agreement with that proposed based upon the molecular dynamics and energy calculations on the four different modes of inclusion (34).



β-CD binds IMC more strongly than α-CD as indicated from the large *K* and $-\Delta G$ values. These results indicate that the size of the cyclodextrin cavity plays an important role in the formation of the complex. On the basis of size, the cavity size of β-CD seems to be optimal for entrapment of the IMC molecule, whereas in α-CD the binding leads to the formation of a more unstable complex. In other words, the *p*-chlorobenzoyl group should fit very snugly into the β-CD cavity, and should not be able to fully penetrate into the α-CD cavity.

On the other hand, three different modes are reported for the binding of small molecules to the DNA double helix, including (*i*) electrostatic interactions with the outer negative-charged DNA phosphates; (*ii*) groove binding; and (*iii*) intercalative binding, in which the small molecule or the drug intercalates into the relatively nonpolar interior of the DNA helix, i.e., the aromatic group is stacked between base pairs. Therefore, the large hydrophobic moiety is expected to facilitate the intercalation into the helix.

The strong hypochromicity observed with IMC in the presence of increasing amounts of ct-DNA is attributable to a mode of binding that involves a strong stacking interaction between an aromatic chromophore and the base pairs of ct-DNA.Such a large hypochromic change strongly suggests that the aromatic chromophore is in close proximity to the ct-DNA bases. In addition to the strong decrease in the peak intensities, a large red shift and the appearance of an isosbestic point at 281 nm was also observed in the spectra. All of these various spectral changes show that the IMC molecule, acting as an intercalator, is inserted into the base-stacking domain of the ct-DNA double helix.

Furthermore, voltammetric data, i.e., shifts in peak potential and changes in limiting current with the addition of ct-DNA, are consistent with the interchelation of IMC into the ct-DNA base stack. Also, the large binding constant observed for IMC is indicative of the high affinity of the IMC chromophore for the DNA base pairs.

Acknowledgment

The authors would like to thank the UAE University Research Council for financial support.

References

1. J.F. Stoddart. Chem. Soc. Rev. **8**, 85 (1979).
2. I.O. Sutherland. Chem. Soc. Rev. **15**, 63 (1986).
3. J. Szejtli. *In* Cyclodextrin technology. Kluwer Academic Publishers, Dordrecht. 1988.
4. B. Lambert, J.-B. Le Peeq. *In* DNA–ligand interactions, from drugs to proteins. *Edited by* W. Guschlbauer and W. Saenger. Plenum Press, New York. 1986. pp. 141.
5. M.J. Waring. *In* Drug action at the molecular level. *Edited by* G.C.K. Roberts. Macmillan Publishers Limited, London. 1977. pp. 167–189.
6. X.-M. Wang, H.-Y. Chen, S.-Y. Li, and J.-D. Wang. Anal. Chim. Acta, **290**, 349 (1994).
7. M. O'Brien, J. MaCauley, and E. Cohen. *In* analytical profiles of drug substance. Vol. 13. *Edited by* K. Florey. Academic press, London. 1984. pp. 211–238.
8. M.S. Suleiman and N.M. Najib. Drug Dev. Ind. Pharm. **16**, 596 (1990).
9. J.B. D'Silva and R.E. Notari. J. Pharm. Sci. **71**, 1394 (1982).
10. Y.L. Loukas, V. Vraka, and G. Gregoriadis. Int. J. Pharm. **162**, 137 (1998).
11. J. Szeitli and L. Szente. Pharmazie, **36**, 694 (1985).
12. I. Shehatta. React. Funct. Polym. **28**, 183 (1996).
13. D. Hallen, A. Schon, I. Shehatta, and I. Wadsö. J. Chem. Soc. Faraday Trans. **88**, 2859 (1992).
14. M. Bastos, L.-E. Briggner, I. Shehatta, and I. Wadsö. J. Chem. Thermodyn. **22**, 1181 (1990).
15. J.K. Barton, J.M. Goldberg, C.V. Kumar, and N.J. Turro. J. Am. Chem. Soc. **108**, 2081 (1986).
16. J. Marmur. J. Mol. Bio. **3**, 208 (1961).
17. T. Higuchi and K.A. Connors. Adv. Anal. Chem. Instrum. **4**, 117 (1965).
18. A. Mounoz de la Pena, T.T. Ndou, J.B. Zung, K.L. Greene, D.H. Live, and I.M. Warner. J. Am. Chem. Soc. **113**, 1572 (1991).
19. Q. Feng, N.-Q. Li, and Y.-Y. Jiang. Anal. Chim. Acta, **344**, 97 (1997).
20. H.A. Hammad and B.W. Müller. Pharmazie, **53**, 11 (1998).
21. C.V. Kumar and E.H. Asuncion. J. Am. Chem. Soc. **115**, 8547 (1993).
22. H.A. Benesi and J.H. Hildebrand. J. Am. Chem. Soc. **71**, 2703 (1949).
23. C. Reguera, M.J. Arcos, and M.C. Ortiz. Talanta, **46**, 1493 (1998).
24. J. Arcos, J. Lopez Palacios, J.M. Leal, P. Sanchez Batanero, and F. Maata. Bull. Soc. Chim. Fr. **128**, 314 (1991).
25. G. Rao, J. Lown, and J. Plambeck. J. Electrochem. Soc. **125**, 534 (1978).
26. M.S. Ibrahim. Anal. Chim. Acta, **409**, 105 (2000).
27. G. Kazemifard and L. Holleck. Arch. Pharm. **306**, 664 (1973).
28. M.T. Carter, M. Rodriguez, and A.J. Bard. J. Am. Chem. Soc. **111**, 8901 (1989).
29. F. Djedaini, S.Z. Lin, B. Perly, and D. Wouessidjew. J. Pharm. Sci. **79**, 643 (1990).
30. M.L. Bender and M. Komiyama. *In* Cyclodextrin chemistry. Springer–Verlag, Berlin. 1978, and refs. cited therein.
31. S.A.C. Wren and R.C. Rowe. J. Chromatogr. **609**, 363 (1992).
32. F. Cramer, W. Saenger, and H. Ch. Spartz. J. Am. Chem. Soc. **89**, 14 (1967).
33. I. Tabushi, Y. Kiyosuke, T. Sugimoto, and K. Yamamura. J. Am. Chem. Soc. **100**, 916 (1978).
34. G. Fronza, A. Mele, E. Redenti, and P. Ventura. J. Org. Chem. **61**, 909 (1996).
35. T.J. Kristenmacher and R.E. Marsh. J. Am. Chem. Soc. **94**, 1340 (1972).
36. P. Gund and T.Y. Shen. J. Med. Chem. 1146 (1977).

© 2001 NRC Canada

Regioselective upper-rim functionalizations of calix[4]arene by diphenylphosphino groups

Jonathan Gagnon, Martin Vézina, Marc Drouin, and Pierre D. Harvey

Abstract: The regioselective upper-rim functionalization of calix[4]arene have been performed to prepare all the multisubstituted diphenylphosphine derivatives. In addition, the X-ray structures of 5,17-dibromo-11,23-bis(diphenylphosphino)-25,26,27,28-tetra-*n*-propoxycalix[4]arene and 5,11,17,23-tetrakis(diphenylphosphino)-25,26,27,28-tetra-*i*-propoxy-calix[4]arene have been determined. Regioselective functionalizations have been achieved using methods that involve appropriate choices of bases, alkyllithium–solvent systems, stoichiometry, and reaction times. A new and convenient method for selectively preparing derivitized calix[4]arenes at proximal positions in relative large scale quantity has been developed and involves a transesterification of the distal diester derivative into the proximal isomer.

Key words: calix[4]arenes, phosphine, upper-rim, X-ray structure, transesterification.

Résumé : On a réalisé la fonctionnalisation régiosélective de la anneau supérieure du calix[4]arène dans le but de préparer tous les dérivés multisubstitués de la diphénylphosphine. De plus, on a fait appel à la diffraction des rayons X pour déterminer les structures du 5,17-dibromo-11,23-bis(diphénylphosphino)-25,26,27,28-tétra-*n*-propoxycarix[4]arène et du 5,11,17,23-tétrakis(diphénylphosphino)-25,26,27,28-tétra-*i*-propoxycalix[4]arène. La fonctionnalisation régiosélective a été réalisée à l'aide de méthodes impliquant des choix appropriés de bases, des systèmes alkyllithium–solvant, de stoechiométrie et de temps de réaction. On a mis au point une nouvelle méthode pratique de préparer sélectivement et sur une échelle relativement grande des calix[4]arènes dérivatisés dans des positions proximales; elle implique une transestérification du diester distal en isomère proximal.

Mots clés : calix[4]arènes, phosphine, anneau supérieure, structure par diffraction des rayons X, transestérification.

[Traduit par la Rédaction]

Introduction

Calix[4]arenes are versatile molecules that are easy to synthesize (1) and are well-known for the host–guest chemical applications that they provide (1, and for an example also see ref. 2). Indeed with their ability to interact with cationic species in the ionophoric section of the cavity located at the lower rim, a great deal of important research in the area of ion transport, novel sensors, and selective receptors have been performed (3). On the other hand, the supramolecular chemistry offered with their cone conformation, also allows neutral organic guests to interact with the hydrophobic upper-rim cavity. Although multiple examples of neutral guests are already reported for molecules such as toluene (4), acetone (5), alkanes, and other substrates (6), applications have not been fully developed. The chemistry in the area of complexation of transition metals onto calix[4]arene has been mainly focused in the lower rim (7), and it is only recently that some examples of upper-rim derivatized calix[4]arene with transition metal-containing fragments, have appeared (8–10). In fact, such complexes are attractive because of potential applications in regioselective reactivity. When a metal catalyst fragment is anchored at the upper-rim, it is placed near the proximity of a cavity where a guest organic molecule may reversibly bind. Hence, the interactions between the metal fragment and the organic substrate will be molecularly localized. In addition, for multiphosphinated ligands, coordination of more than one metal is conceivable. In this way the multidentate calix[4]arene device can also act as a platform molecule for the construction of polymetallic architectures.

Recently we reported the preparation and the characterization of the monophosphinated calix[4]arene using both the diphenyl- and di-(*i*-propyl)-phosphine groups (9), along with their corresponding oxides, and some rhodium(I) and rhodium(III) complexes (9, 10). We now wish to report the preparation of the complete series of upper-rim diphenylphosphine functionalized calix[4]arenes, which are potential multidentate ligands capable of coordinating soft transition metals. During the course of this work, regioselective derivatizations were necessary. Indeed regioselective lithiation at positions 5 and 17 of a tetrabrominated calix[4]arene, and the *n*-propylation, 3,5-dinitrobenzoylation, and benzoylation at positions 25 and 27 of the tetrahydroxycalix[4]arene will be discussed. A novel and convenient method for converting the 25,27-diester- into the 25,26-diester-27,28-dihydroxycalix-[4]arene has been developed using sodium hydride.

Received April 24, 2001. Published on the NRC Research Press Web site at http://canjchem.nrc.ca on October 9, 2001.

J. Gagnon, M. Véniza, M. Drouin, and P.D. Harvey.[1]
Département de chimie, Université de Sherbrooke, Sherbrooke, QC J1K 2R1, Canada.

[1]Corresponding author (telephone: (819) 821-8000 ext 2005; fax: (819) 821-8017; e-mail: pharvey@courrier.usherb.ca).

 DOI: 10.1139/cjc-79-10-1439 © 2001 NRC Canada

Results and discussion

Tetraphosphines

To secure the cone conformation, calix[4]arene (**1**) is derivatized along the lower rim with propyl residues. It is now well-established that a three-carbon chain is the smallest group, when placed in the lower-rim, required to avoid rotations of the phenyl fragments around the bridging methylenes (11). Reinhoudt and co-workers (12) have developed an efficient propylation procedure of calix[4]arene using sodium hydride in DMF. In this work, this propylation method has been successfully applied for both *n*- and *i*-propyl leading to compounds **2a** and **2b**, respectively (Scheme 1). The cone conformation for all propylated derivatives has been confirmed by ^{1}H NMR, where the typical pattern for methylene protons is observed. Since propylation of *p*-bromocalix[4]arene is much slower than that of the parent calix[4]arene **1**, the propylation was carried out prior to bromination, which affords **3a** and **3b**, respectively.

The synthesis of 5,11,17,23-tetrakis(diphenylphosphino)-25,26,27,28-tetramethoxycalix[4]arene has been reported by Atwood and co-workers (13) with aims to design a molecular device for metal-cation extractions. Based on their procedure of using *n*-BuLi in THF at –78°C, the lithiation reaction was attempted on **3a** to synthesize the corresponding tetraphosphine derivative. However, the disubstituted 5,17-dibromo-11,23-bis(diphenylphosphino)-25,26,27,28-tetrapropoxycalix[4]arene (**5**) is selectively and reproducibly obtained, even with an excess of *n*-BuLi. Performing a subsequent lithiation and phosphination on compound **5** does not lead to the desired tetraphosphine compound **4a**. Examination of literature X-ray structures of the *n*-butyl- and *tert*-butyllithium species crystallized, in general, from ether or alkane solvents, reveals a strong tendency for aggregation (14). In ethers, tetrameric (distorted cubic) and quasi-planar dimeric structures are observed for the *n*-butyl- and *tert*-butyllithium derivatives, respectively, and one ether molecule per lithium is attached to the metal. In alkanes, octahedral and tetrahedral geometries are depicted for the *n*-butyl- and *tert*-butyllithium derivatives, respectively, with evidence for short metal–metal contacts, and no crystallization of solvent molecules. The cases where no solvent molecule is bonded to the lithium atoms offer more favorable geometries, with respect to steric interactions, for lithium–bromide exchange. Similarly, the planar dimeric structure found in [(*t*-BuLi)$_2$·(diethylether)$_2$] exhibits relatively unobscured metal atoms. In contrast, the tetrameric [(*n*-BuLi)$_4$·(1,2-dimethoxyethane)$_4$] cluster shows tetracoordinated lithium atoms that are relatively encumbered. It is anticipated that the first and second lithium–bromide exchange at the 5- and 17-positions of the tetrabromocalix[4]arene in **3a** and **3b** proceeds without any major steric restrictions. However, since the lithium atom has a strong tendency to bind ether molecules (15), the intermediate 5,17-dibromo-11,23-dilithium-25,26,27,28-tetrapropoxycalix[4]arene·2THF (speculative) appears to be severely sterically demanding for an efficient interaction with the already encumbered tetrameric [(*n*-BuLi)$_4$·(THF)$_4$]. While this speculative explanation seems reasonable, an X-ray structure of the 5,17-dibromo-11,23-dilithium derivative with THF or another ether molecule must definitely be obtained to confirm this hypothesis. As stated above, the bromide–lithium exchange followed by phosphination with chlorodiphenylphosphine affords the 5,17-diphosphine-11,23-dibromo derivative (**5**) as the sole product (discussed below).

However, we succeeded in achieving the perphosphination of **3a**. The phosphination proceeds via a bromide–lithium exchange followed by a substitution reaction with chlorodiphenylphosphine. The tetralithiated intermediate is predictably generated either with *n*-BuLi in benzene, or with *t*-BuLi in benzene or THF. Subsequently, reactions with chlorodiphenylphosphine leads to **4a** and **4b** (Scheme 1). The purification of these compounds is performed from multiple precipitations via the additions of acetone to a dichloromethane solution. This procedure leads to pure products, but the yields are modest. Among the impurities, some partially substituted calix[4]arenes, due to incomplete phosphination reactions, are found. The expected $^3J_{\mathrm{P,H\ calixarene}}$ of ~ 8 Hz is measured for **4a** and **4b**: this coupling constant is observed for all the phosphinated derivatives in this work. Both tetraphosphines **4a** and **4b** afforded single crystals of suitable quality for X-ray crystallography, but only the better quality data are reported for **4b**. The structure reveals the predicted cone conformation (Fig. 1). Three of the diphenylphosphine residues form a helical geometry, while the fourth one points in the other direction. The angles between the face-to-face phenyl groups are 88.18(0.11) and 1.19(0.20)°. The flattened bowl structure is typical in the solid state.

The success of the procedure reported by Atwood and coworkers (13) is consistent with the presence of various conformers in equilibrium (cone, partial cone, and 1,2- and 1,3-alternate) as revealed by the ^{1}H NMR data. Since the cone conformation is not retained, the bromide atoms may acquire nonsterically demanding environments in some specific geometries. This equilibrium may explain why, in this case, the tetrasubstitution can be achieved with alkyllithium in THF, which forms aggregates in this medium.

5,17-Diphosphine

Compound **5** conveniently exhibits two bromides at the remaining positions (positions 11 and 23) for further derivatizations. Single crystals of suitable quality for X-ray crystallography were obtained from slow THF–pentane vapor diffusion (Fig. 2). The structure confirms the diphenylphosphino disubstitution at positions 5 and 17 and the cone conformation. The molecule adopts a geometry belonging to the C_2 point group where the diphenylphosphine fragments are oriented in a helical fashion. In contrast with the tetraphosphine **4b**, the cone angles are very different, where the bromophenyl units are rotated inward (–16.72(0.26)°) and the diphenylphosphinophenyl groups are still rotated outward (85.2(0.12)°). Steric hindrance is likely responsible for this difference.

The 5,17-diphosphine compound (**9**) can be prepared via two alternative routes (Scheme 2). The first one is a four-step procedure from **1** and involves dipropylations, brominations, and phosphinations. Indeed, selective propylations at the distal positions (positions 25 and 27) are easily obtained using one equivalent of the weak base K_2CO_3 (16). Literature shows that these protons are the most acidic, as the resonance-stabilized dianionic species is stabilized by

© 2001 NRC Canada

Scheme 1. Syntheses of compounds **4a**, **4b**, and **5**.

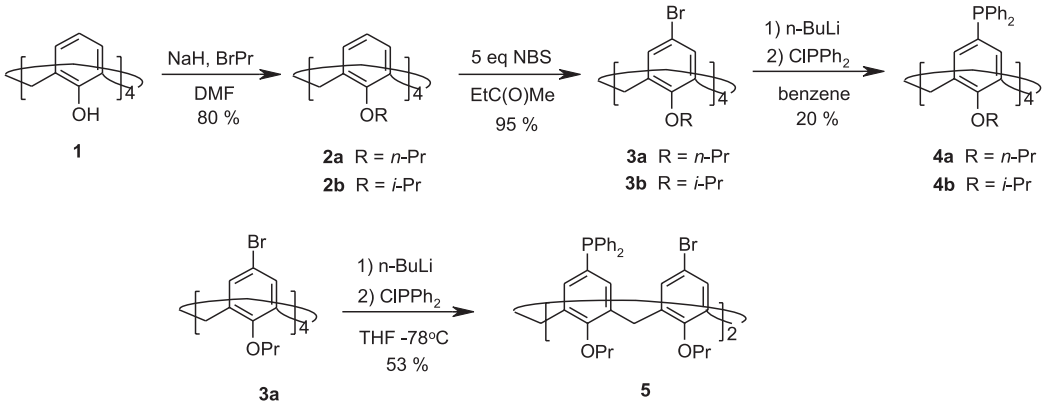


Fig. 1. ORTEP drawing for **4b**. The ellipsoids are shown with a probability of 30%. The H-atoms are not shown for clarity.

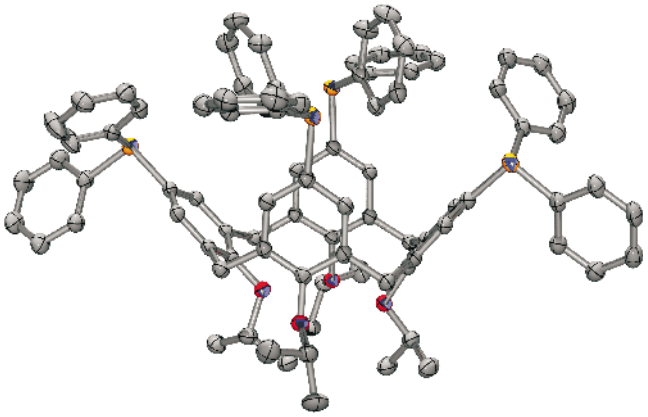
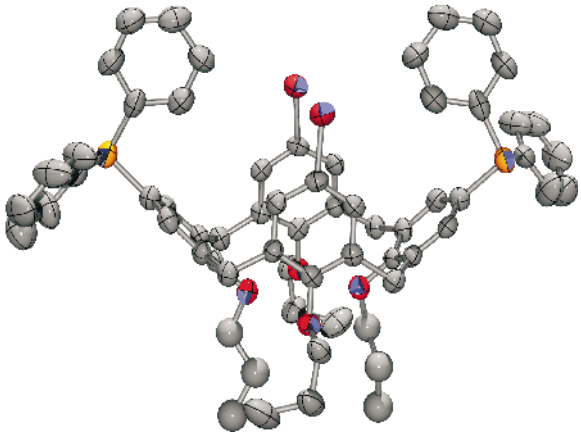


Fig. 2. ORTEP drawing for **5**. The ellipsoids are shown with a probability of 30%. The H-atoms are not shown for clarity.



intramolecular hydrogen bonds with the remaining protons. Thus, propylation of the two first hydroxy groups occurs selectively at these positions, to afford compound **6** (16) in good yields. To subsequently obtain compounds **7** and **8**, bromination followed by a second propylation is performed.

Shinkai and co-workers (17) proposed a bromination step involving the use of 2 equiv of Br_2 in $CHCl_3$ at 0°C for 1 h, to afford the desired product in 87% yield. Later Larsen and Jorgensen (18) claimed that this procedure led to a mixture of products involving several impurities, which could not be separated using recrystallization or column chromatography. Our attempts to reproduce this reaction show that in fact these impurities result from incomplete brominations. To overcome this problem, Larsen and Jorgensen (18) reported an alternative method using 8 equiv of *n*-BuLi in THF at –78°C for 30 min in the presence of **3a**, followed by quenching with water, in 88% yield. In this work, an excess of Br_2 and a shorter reaction time (5 min), allows selective and complete monobromination resulting in compound **7**, which is purified by recrystallization. This selectivity is explained by the greater reactivity of the *para*-position of the phenol group in comparison with the propoxylbenzene. This bromination procedure is a key step for the synthesis of compound **26** (triphosphine, discussed below). The propylation reaction is subsequently performed using *n*-iodopropane in DMF for 48 h to afford **8** as a sole product. The last steps consist of lithiation and phosphination reactions with *n*-BuLi and $ClPPh_2$ in THF to obtain the diphosphine **9**, which is purified by column chromatography.

Matt and co-workers (19) reported another convenient way to prepare **9** from **8** in two steps using a procedure of diphosphorylation with Ph_2POEt–$NiBr_2$ (20), which results in a bis(phosphine oxide). The next step involves the reduction of this phosphine oxide with phenylsilane to afford compound **9**. We have indeed been able to reproduce these results.

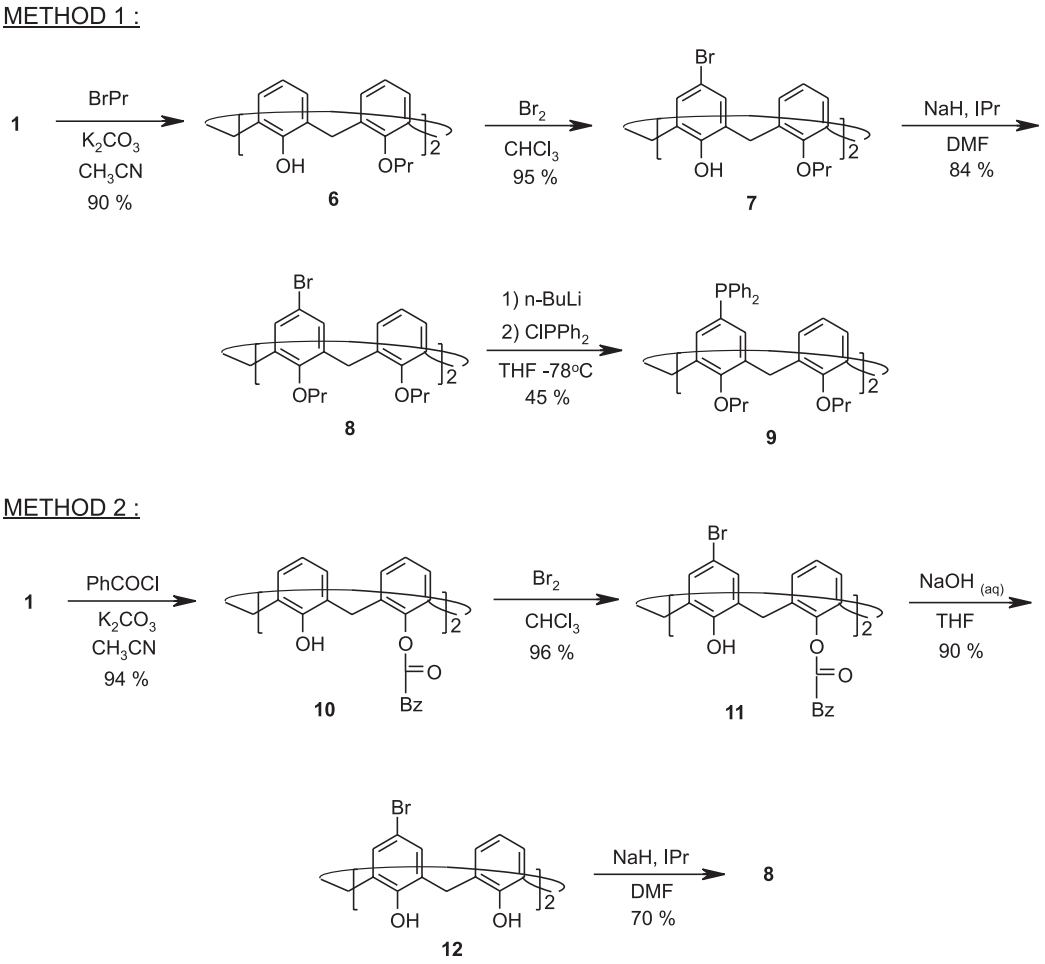
The second investigated route involves the diesterification of **1** to produce **10**, where the ester groups are anchored at the 25- and 27-positions. This reaction proceeds via a double proton abstraction of the two most acidic protons, followed by a substitution reaction with benzoyl chloride. This derivatization induces a greater difference in electron density between the phenol and phenylbenzoyl residues. In this way, the subsequent brominations can be performed selectively at the highly electron-rich phenol sites without considering reaction time. The ester groups are then easily hydrolyzed, and the cone conformation is still maintained via H-bonding as confirmed by ^1H NMR. The standard propylation of this compound provides compounds **8**, which is the precursor of the final product **9**.

5,11-Diphosphine

This desired and challenging diphosphine **17** is prepared from three alternative routes as summarized in Scheme 3.

© 2001 NRC Canada

Scheme 2. Two different synthesis pathways for compound **9**.



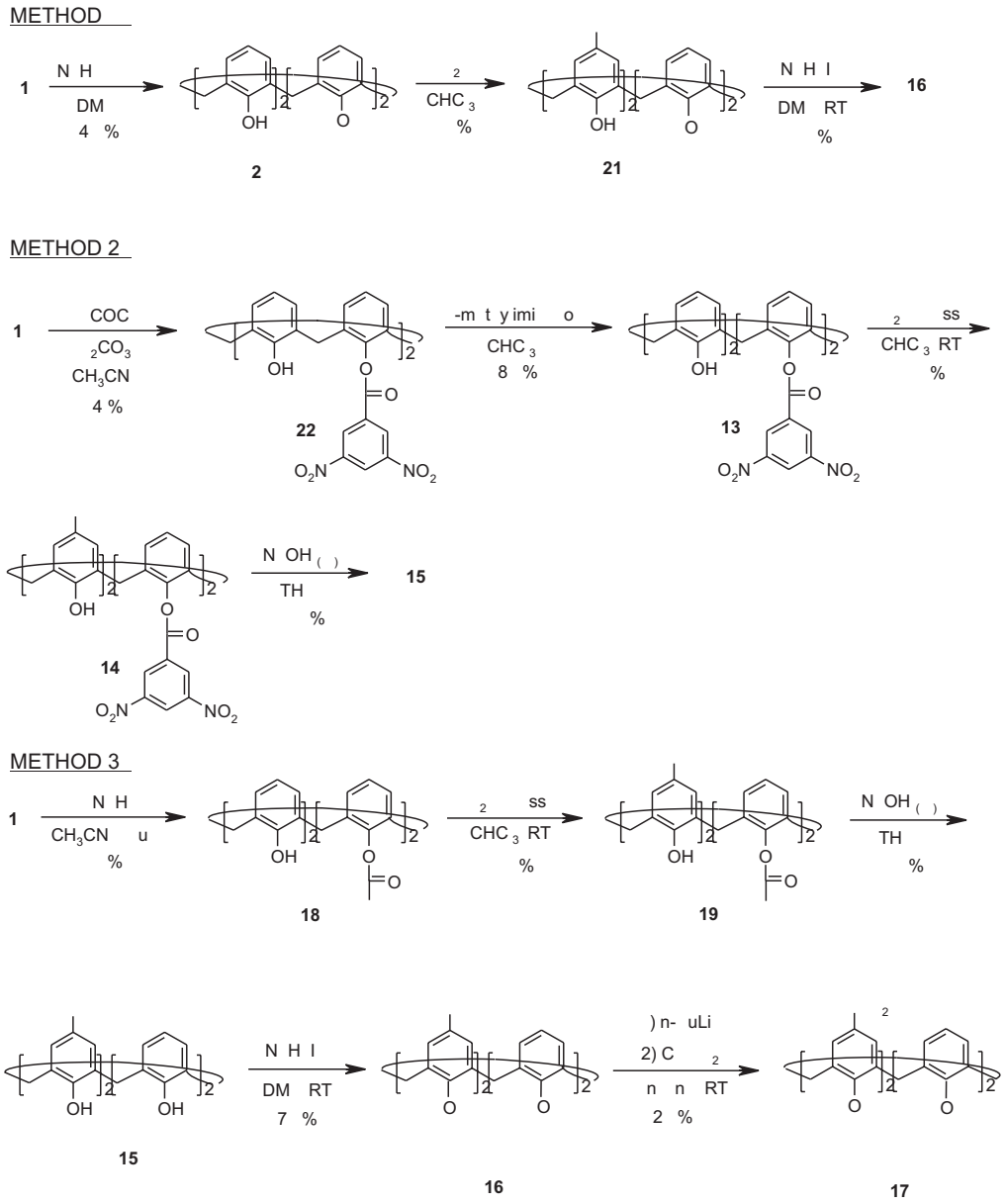
Reinhoudt et al. (21) demonstrated that propylation of **1** using NaH in DMF produce the intermediate compound 25,26-dipropoxycalix[4]arene in the cone conformation. For short reaction times, the 25,26-dipropoxycalix[4]arene compound **20** is observed as one of the intermediates. Unfortunately, the yield for this specific 1,2-disubstitution is low (45% in our work) making this route less attractive. We find that the reaction mixture also contains unreacted **1** and tetrapropylated **2a**. The relative amount of the desired product **20** is best acheived after a 2 h reaction time. Nonetheless, this compound has been prepared and used as precursor. The subsequent bromination and alkylation reactions can be performed with expected results (i.e., formation of compound **16**).

The second strategy is based on the work of Gutsche and co-workers (22), which reports the preparation of 25,26-di(3,5-dinitrobenzoyl)-27,28-dihydroxy-5,11,17,23-tetra(*tert*-butyl)calix[4]arene from 25,26,27,28-tetrahydroxy-5,11,17,23-tetra(*tert*-butyl)calix[4]arene in the presence of 3,5-dinitrobenzoyl chloride using 1-methylimidazole in acetonitrile. Indeed diester **13** can be synthesized from this methodology, but in very low yield (15–40%). Several impurities were found in the mixture, including the monoester derivative, the starting material, and the corresponding 25,27-diester. The presence of this 25,27-diester compound the is the key to understanding this mechanism and will be discussed below. Compound **13** is poorly soluble, which on one hand has the potential to allow the selective preparation of the desired product, but on the other hand, does not permit preparation on a large scale. The major drawback is that the product must be purified by column chromatography. In an attempt to avoid this important solubility problem, 3,5-dinitrobenzoyl chloride was replaced by benzoyl chloride. Surprisingly, the reaction between **1** and benzoyl chloride in presence of 1-methylimidazole in acetonitrile did not lead to the disubstituted calix[4]arene as the major product, but produced the corresponding triester as major product. Stubbornly, some of this triester compound is still formed even when only one equivalent of benzoyl chloride is used in this reaction. Nonetheless, bromination affords **14** in good yields, as anticipated. Then compound **15**, which is necessary to synthesize **17**, is convieniently obtained by ester cleavage of **14** in basic solution.

The third method involves an intramolecular transesterification of **10** to **18**. Recently, Markovsky et al. (23) reported an elegant intramolecular phosphotropic rearrangement at the lower rim of the calix[4]arene from the 25,27- to the 25,26-positions, hence providing a important clue about the mechanism. Compound **10** is prepared from **1** using K_2CO_3. Again, the two most acidic protons are readily abstracted, allowing the 25,27-diesterification of **1**. The subsequent transesterification of **10** to **18** proceeds with one equivalent of sodium hydride in good yield. This strong base in

© 2001 NRC Canada

Scheme 3. Different synthesis pathways for compound **17**.

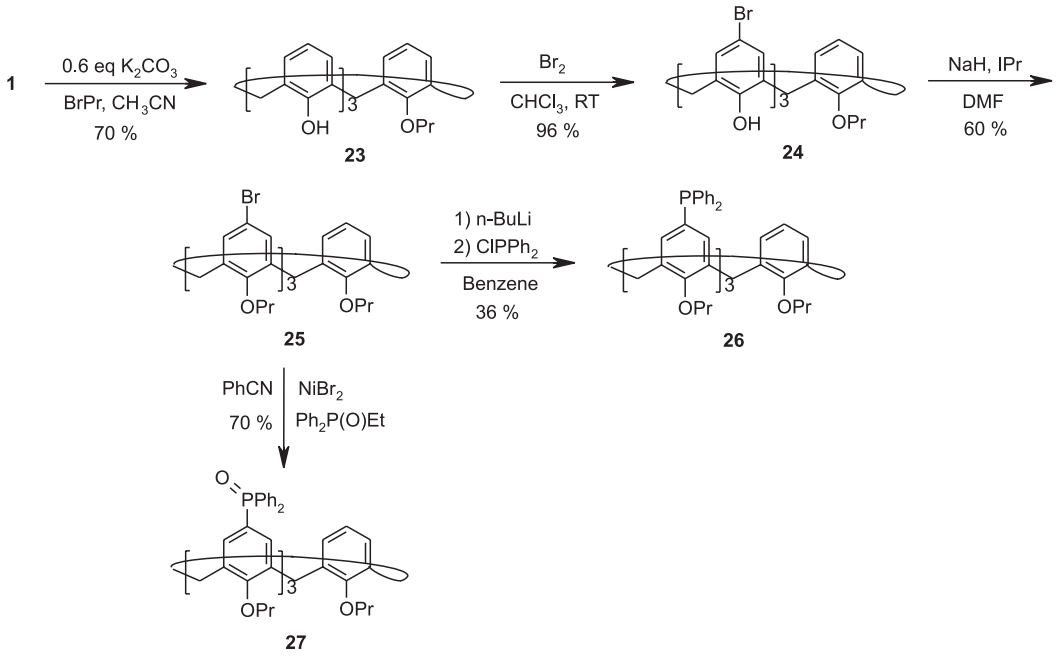


acetonitrile abstracts one of the two remaining protons, generating a phenolate intermediate over a period of 20 h, during which the transesterification occurs. This intramolecular reaction allows for equilibrium between the two disubstituted compounds. The generated 5,11-diester monoanion is stabilized by an intramolecular H-bond between the hydroxy and phenolate groups, which drives the equilibrium to the right. Acidification of the solution leads to the targeted diester **18**, which is obtained in a pure state after column chromatography to eliminate some traces of the reactant. Diester **18** exists in a partial cone conformation with both OH groups pointing in the same direction according to its ^{1}H NMR spectra. This reaction is almost complete in refluxing acetonitrile (82°C), but is not complete even after one week in refluxing THF (66°C). In addition, no transesterification is observed when two or more equivalents of sodium hydride are used. In this case, the dianionic species are generated and electrostatic repulsions between the negatively charged phenolates (doubly deprotonated calix[4]arene) may be at the origin of this selective structure. Interestingly, the 25,26-species can be converted back to the 25,27-compounds by using an excess of bases (two equivalents or more). The following steps include the well-established selective bromination, ester cleavage, propylation, and phosphination to achieve the synthesis of the desired 5,11-diphosphine compound (**17**).

Based upon these experiments, the preparation of the 25,27-di(3,5-dinitrobenzoyl)-26,28-dihydroxycalix[4]arene (**22**) in its pure state has been performed to shed some light on the mechanism for the conversion of **1** into **13**. The preparation of **22** is achieved using **1** in the presence of 3,5-dinitrobenzoyl chloride and potassium carbonate in acetonitrile. Subsequently, **22** is placed in the presence of 1-methylimidazole to produce **13**. This procedure affords better yields. In conclusion, one equivalent of potassium carbonate allows for the preparation of the corresponding

© 2001 NRC Canada

Scheme 4. Synthesis of compound **27**.



25,27-diesters. The transesterification proceeds using an additional equivalent of base to generate a monophenolated calix[4]arene anion. In this work sodium hydride and 1-methylimidazole were used for the conversion of **10** to **18** and **22** to **13**, respectively. The fact that Gutsche and co-workers (22) did not observe the 25,27-di(3,5-dinitrobenzoyl)-26,28-dihydroxy-5,11,17,23-tetra(*tert*-butyl)calix[4]arene may be related to the electron-donor inductive effect of the *tert*-butyl group rendering the corresponding monophenolate anion more basic. Hence in this case, only the monophenolated calix[4]arene is generated, which readily promotes the transesterification. When a large excess of 1-methylimidazole was used (up to 20 equivalents) to see whether the transesterification would be precluded (as seen in the reaction of **10** to **18** with an excess of sodium hydride), the transesterification was still observed.

Gutsche and co-workers (22) also reported the hydrolysis of 25,26,27-tri(3,5-dinitrobenzoyl)-28-hydroxy-5,11,17,23-tetra(*tert*-butyl)calix[4]arene to 25,26-di(3,5-dinitrobenzoyl)-27,28-dihydroxy-5,11,17,23-tetra(*tert*-butyl)calix[4]arene in the presence of 4-methylimidazole. However, the tribenzoyl ester **28** mentioned above could not be converted to **18** by this method.

From the three described methods, the last one, which utilizes benzoyl chloride and intramolecular transesterification with NaH, was found to be the most convenient. The low solubility of **13**, and also the low yield for the selective propylation of **1** into **20**, make the other described methods much less appealing.

Triphosphine

The strategy for preparing the triphosphine derivative involves the preparation of the monopropoxycalix[4]arene (**23**) (Scheme 4). This can be achieved by abstracting a proton with one equivalent of base. However, when the monophenolated calix[4]arene intermediate is generated an equilibrium sets in, to form the 25,27-diphenolate-26,28-dihydroxycalix[4]arene intermediate and **1**, as evidenced by the appearance of the dipropoxy compound **6** either with the increase or decrease in the amount of base used. By using 0.5 equivalent of K_2CO_3, the monopropoxy derivative **23** is the major product, mixed with **6** and **1**. Compound **6** is easily removed by recrystallization, and subsequently, **23** is purified by column chromatography. The yield is unavoidably low, but the preparation of the desired compound is attained. The subsequent bromination reaction is selective to the phenol residues. The following propylation reaction is preferably performed with 1-iodopropane instead of 1-bromopropane, since the propylation of the *para*-bromophenol fragments is much slower with the latter reactant. The tribromotetrapropoxy derivative **25** is then obtained. The phosphine oxide derivatization of **25** with Ph_2POEt–$NiBr_2$ was performed successfully, but the subsequent reduction of **27** using the procedure of Matt and co-workers (19), with phenylsilane to form **26**, proved very difficult either using phenylsilane-containing solutions or neat. This reaction leads to a mixture of products, which could not be separated. The desired ligand **26** is generated with *n*-BuLi in benzene, followed by a reaction with chlorodiphenylphosphine, in a modest yield. It is anticipated that the use of *n*-BuLi in THF could lead to 5,17-diphosphine-11-bromo-25,26,27,28-tetrapropoxycalix-[4]arene, similar to that describe for compound **5**. This proposed synthesis may lead to further functionalizations as suggested for **5**.

The syntheses presented can also be applied to the upper-rim multifunctionalization of calix[4]arene by dialkylphosphines. Their preparation and characterization, as well as their complexation with low-valent transition metals, will be reported in due course.

Experimental

General

All solvents were freshly distilled before use. All reac-

© 2001 NRC Canada

tions involving air- or moisture-sensitive reagents were conducted under nitrogen atmosphere. Column chromatography was performed on 230–400 mesh silica gel (60 Å). All NMR spectra were acquired (^{1}H 300 MHz, ^{13}C 75 MHz, ^{31}P 121 MHz) using the solvent as chemical shift standard, except in ^{31}P NMR, where the chemical shift are relative to D_3PO_4 (85% in D_2O). All the chemical shifts and the coupling constants are given in ppm and Hz, respectively. The lower number of signals in ^{13}C NMR spectra is due to isochronism. Mass spectra were determined at an ionizing voltage of 70 eV. Compounds **1** (23), **2a** (12), **3a** (24), **6** (16), and **23** (25) were prepared according to literature procedures. The syntheses of all new calix[4]arene compouds are reported in the Supporting Information.[2]

Crystal data for calix[4]arene 4b and 5

Crystallographic measurements were made on an Enraf-Nonius CAD-4 automatic diffractometer with graphite-monchromated Cu Kα radiation. Data were collected at 173 K for **4b** and 293 K for **5** using the θ–2θ scan technique to a maximum 2θ value of 120.0° for both compounds; no reflections above the giving angle were observed. The data collection ranges were $\pm h$, $+k$, $+l$; whereby for **4b**: $-20 \le h \le 19$, $0 \le l \le 15$, $0 \le k \le 32$; **5**: $-20 \le h \le 20$, $0 \le l \le 18$, $0 \le k \le 21$. Scans were made with a constant speed of 2.7° min^{-1} and a background time:scan time ratio of 0.25. Space group determination was based upon systematic absences, packing considerations, statistical analysis of intensity distribution, and successful solution and refinement of the structure. The NRCCAD program (26) was used for centering, indexing, and data collection. The NRCVAX programs (27) were used for crystal structure solution by application of direct methods, and the SHELX-97 program (28) was used for refinement by full-matrix least-squares on F^2.

Compound **4b** (5,11,17,23-tetrakis(diphenylphosphino)-25,26,27,28-tetra-*i*-propoxycalix[4]-arene) gives crystals belonging to the monoclinic space group $P2_1/n$ and at 173 K: a = 18.360(2), b = 13.998(2), c = 29.663(2) Å, β = 101.67(8)°, V = 7466.1(15) Å^3, Z = 4, $R(F)$ = 0.0777, and $wR(F^2)$ = 0.2218. One disordered $CHCl_3$ molecule was located on a center of symmetry, the former atoms were refined as isotropic with 0.25 occupancy factor. Compound **5** (5,17-dibromo-11,23-bis(diphenylphosphino)-25,26,27,28-tetra-*n*-propoxycalix[4]arene) gives crystals belonging to the monoclinic space group $I2/a$ and at 293(2) K: a = 17.957(2), b = 16.681(2), c = 19.336(3) Å, V = 5753.0(11) Å^3, Z = 4, $R(F)$ = 0.0694, and $wR(F^2)$ = 0.1829. The molecule is located on a glide plane, and one of the *n*-propyl ligands is disordered. The disordered atoms were refined as isotropic atoms with 0.5 occupancy factor.

Acknowledgments

This research was supported by Natural Sciences and Engineering Research Council of Canada (NSERC) and Fonds pour la Formation de Chercheurs et l'Aide à la Recherche (FCAR) for fundings. J.G. thanks NSERC for a graduate scholarship.

References

1. (*a*) C.D. Gutsche. Calixarenes. Royal Society of Chemistry, Cambridge. 1989; (*b*) Calixarenes: a versatile class of macrocyclic compounds. *Edited by* J. Vicens and V. Böhmer. Kluwer Academic Publishers, Dordrecht. 1991; (*c*) Calixarenes 50th anniversary: commemorative issue. *Edited by* J. Vicens; Z. Asfari, and J.M. Harrowfield. Kluwer Academic Publishers, Dordrecht. 1994; (*d*) C.D. Gutsche. Calixarenes revisited. Royal Society of Chemistry, Cambridge. 1998.
2. D. Diamond and M.A. McKervey. Chem. Soc. Rev. **25**, 15 (1996).
3. (*a*) V. Böhmer. Angew. Chem. Int. Ed. Engl. **34**, 713 (1995); (*b*) J. Scheerder, M. Fochi, J.F.J. Engbersen, and D.N. Reinhoudt. J. Org. Chem. **59**, 7815 (1994).
4. (*a*) T. Hascall, A.L. Rheingold, I. Guzei, and G. Parkin. Chem. Commun. 101 (1998); (*b*) L. Giannini, A. Caselli, E. Solari, C. Floriani, A. Chiesi-Villa, C. Rizzoli, N. Re, and A. Sgamellotti. J. Am. Chem. Soc. **119**, 9198 (1997); (*c*) L. Giannini, A. Caselli, E. Solari, C. Floriani, A. Chiesi-Villa, C. Rizzoli, N. Re, and A. Sgamellotti. J. Am. Chem. Soc. **119**, 9709 (1997); (*d*) M.G. Gardiner, G.A. Koutsantonis, S.M. Lawrence, P.J. Nichols, and C.L. Raston. Chem. Commun. 2035 (1996).
5. S.E. Biali, V. Bohmer, S. Cohen, G. Ferguson, C. Gruttner, F. Grynszzpan, E.F. Paulus, I. Thondorf, and W. Vogt. J. Am. Chem. Soc. **118**, 12938 (1996).
6. (*a*) E.B. Brouwer, K.A. Udachin, G.D. Enright, C.I. Ratcliffe and J.A. Ripmeester. Chem. Commun. 587 (1998); (*b*) E.B. Brouwer, G.D. Enright, and J.A. Ripmeester. J. Am. Chem. Soc. **119**, 5404 (1997); (*c*) G.D. Andreetti, O. Ori, F. Ugozzoli, C. Alfieri, A. Pochini, and R. Ungaro. J. Inclusion Phenom. **6**, 523 (1988); (*d*) M.H. Chrisholm, K. Folting, W.E. Streib, and W. De-Dong. Chem. Commun. 379 (1998); (*e*) B. Castelleno, A. Zanotti-Gerosa, E. Solari, C. Floriani, A. Chiesi-Villa, and C. Rizzoli. Organometallics, **15**, 4894 (1996); (*f*) F. Hajek, E. Graf, M.W. Hosseini, X. Delaigue, A. De Cian, and J. Fischer. Tetrahedron Lett. **37**, 1401 (1996).
7. C. Wieser, C.B. Dieleman, and D. Matt. Coord. Chem. Rev. **165**, 93 (1997).
8. (*a*) I.A. Bagatin, D. Matt, H. Thönnessen, and P.G. Jones. Inorg. Chem. **38**, 1585 (1999); (*b*) B.R. Cameron, and S.J. Loeb. Chem. Commun. 2003 (1996).
9. M. Vézina, J. Gagnon, K. Villeneuve, M. Drouin, and P.D. Harvey. Organometallics, **20**, 273 (2001).
10. M. Vézina, J. Gagnon, K. Villeneuve, M. Drouin, and P.D. Harvey. Chem. Comm. 1073 (2000).
11. (*a*) V. Bocchi, D. Foina, A. Pochini, R. Ungaro, and G.D. Andretti. Tetrahedron, **38**, 373 (1982); (*b*) C.D. Gutsche, B. Dhawan, J.A. Levine, K.H. No, and L.J. Bauer. Tetrahedron, **39**, 409 (1983).
12. E. Kelderman, L. Derhaeg, G.J.T. Heesink, W. Verboom, J.F.J. Engbersen, N.F. Van Hulst, A. Persoons, and D.N. Reinhoudt. Angew. Chem. Int. Ed. Engl. **31**, 1075 (1992).

[2] Supplementary material, including syntheses of all compounds and crystallographic data for compounds **4b** and **5**, may be purchased from the Depository of Unpublished Data, Document Delivery, CISTI, National Research Council Canada, Ottawa, ON K1A 0S2, Canada. For information on obtaining material electronically go to http://www.nrc.ca/cisti/irm/unpub_e.shtml. Crystallographic information has also been deposited with the Cambridge Crystallographic Data Centre (CCDC No. 168 292 and 169 293). Copies of the data can be obtained, free of charge, on application to the Director, CCDC, 12 Union Road, Cambridge CB2 1EZ, U.K. (fax: 44-1223-336033 or e-mail: deposit@ccdc.cam.ac.uk).

© 2001 NRC Canada

13. F. Hamada, T. Fukugaki, K. Murai, G.W. Orr, and J.L. Atwood. J. Inclusion Phenom. **10**, 57 (1991).
14. (*a*) T. Kottke, R.J. Lagow, D. Hoffmann, and R.D. Thomas. Organometallics, **16**, 789 (1997); (*b*) T. Kottke and D. Stalke. Angew. Chem. Int. Ed. Engl. **32**, 580 (1993); (*c*) M.A. Nichols and P.G. Willard. J. Am. Chem. Soc. **115**, 1568 (1993).
15. (*a*) T. Kottke, K. Sung, and R.J. Lagow. Angew. Chem. Int. Ed. Engl. **34**, 1517 (1995); (*b*) M.M. Olmstead and P.P. Power. J. Organomet. Chem. **408**, 1 (1991); (*c*) W. Zarges, M. Marsch, K. Harms, W. Koch, G. Frenking, and G. Boche. Chem. Ber. **124**, 543 (1991); (*d*) M.A. Beno, H. Hope, M.M. Olmstead, and P.P. Power. Organometallics, **4**, 2117 (1985).
16. J.D. Van Loon, A. Arduini, L. Coppi, W. Verboom, A. Pochini, R. Ungaro, S. Harkema, and D.N. Reinhoudt. J. Org. Chem. **55**, 5639 (1990).
17. P. Linnane, T.D. James, and S. Shinkai. Chem. Commun. 1997 (1995).
18. M. Larsen and M. Jørgensen. J. Org. Chem. **61**, 6651 (1996).
19. C. Wieser-Jeunesse, D. Matt, and A. De Cian. Angew. Chem. Int. Ed. Engl. **37**, 2861 (1998).
20. S. Ozegowski, B. Costisella, and J. Gloede. Phosphorus Sulfur, **1**, 209 (1996).
21. L.C. Groenen, B.H.M. Ruël, A. Casnati, P. Timmerman, W. Verboom, S. Harkema, A. Pochini, R. Ungaro, and D.N. Reinhoudt. Tetrahedron Lett. **32**, 2675 (1991).
22. K.A. See, F.R. Fronczek, W.H. Watson, R.P. Kashyap, and C.D. Gutsche. J. Org. Chem. **56**, 7256 (1991).
23. L.N. Markovsky, M.A. Visotsky, V.V. Pirozhenko, V.I. Kalchenko, J. Lipkowski, and Y.A. Simonov. Chem. Comm. 69 (1996).
24. (*a*) C.D. Gutsche and L.G. Lin. Tetrahedron, **42**, 1633 (1986); (*b*) C.D. Gutsche and M. Iqbal. Org. Synth. **68**, 234 (1989).
25. L.C. Groenen, B.H.M. Ruël, A.C. Casnati, W. Verboom, A. Pochini, R. Ungaro, S. Harkeman, and D.N. Reinhoudt. Tetrahedron, **47**, 8379 (1991).
26. Y. Le Page, P.S. White, and E.J. Gabe. Proc. Am. Crystallogr. Hamilton Meet. 1986. Abstract PA23.
27. E.J. Gabe, Y. LePage, J.-P. Charland, F.L. Lee, and P.S. White. J. Appl. Crystallogr. **22**, 384 (1989).
28. G.M. Sheldrick. SHELXL-97. University of Göttingen, Göttingen, Germany. 1997.

© 2001 NRC Canada

DISQUAC predictions on thermodynamic properties of ternary and higher multicomponent mixtures. II. Results for H^E of ternary mixtures containing nonpolar components, or one polar compound, two polar compounds, or one alcohol and hydrocarbons, or CCl_4

Juan Antonio Gonzalez, Javier Carmona, Nicolas Riesco, Isaias Garcia de la Fuente, and Jose Carlos Cobos

Abstract: The ability of the DISQUAC model for predicting excess enthalpies (H^E) of ternary systems on the basis of binary parameters only, i.e., neglecting ternary interactions is analyzed. At this end, DISQUAC results for a set of 95 ternary systems are examined. The solutions studied are formed by only hydrocarbons (or CCl_4); or by one polar compound (not alcohols) and two hydrocarbons (or CCl_4); or by two polar compounds (not alcohols) and one hydrocarbon (or CCl_4); or by one alcohol and two hydrocarbons (or CCl_4). Most of the H^Es analyzed are endothermic, and valid at 298.15 K and atmospheric pressure. The mean deviation between experimental values and DISQUAC results is 5.5% for the ternary systems and 6.5% for the constituent binaries (181 mixtures). The interaction parameters used are valid for the description of thermodynamic properties of binary systems: vapor–liquid equilibria (VLE), liquid–liquid (LLE), and solid–liquid equilibria (SLE), H^E and excess heat capacities at constant pressure (C_p^E), as well as H^E and VLE of ternary solutions. Predictions are, in most of the cases, independent of the mixture compounds, or the number of groups present in the system. Larger deviations underline typical shortcomings of the group contributions methods (e.g., Patterson's effect; branching). Note that results for the ternaries and for the constituent binaries are of the same order. This is not the case for the Dortmund version of UNIFAC. The mean deviations obtained using this model are 10.5% and 14% for the ternary and binary mixtures, respectively. Results from other models (original UNIFAC, Flory's theory, Nitta–Chao, UNIQUAC association model) for a number of systems are also compared to those obtained using DISQUAC.

Key words: predictions, H^E, ternary systems, binary parameters, geometrical methods, Flory, group contributions.

Résumé : On a analysé l'habilité du modèle « DISQUAC » à prédire les enthalpies en excès, H^E, de systèmes ternaires uniquement sur la base de paramètres binaires c'est-à-dire en négligeant les interactions ternaires. À cette fin, on a analysé les résultats « DISQUAC » obtenus pour un ensemble de 95 systèmes ternaires. Les solutions étudiées ne sont formées que d'hydrocarbures (ou de CCl_4) ou d'un composé polaire (ne comportant pas d'alcool) et de deux hydrocarbures (ou de CCl_4) ou de deux composés polaires (ne comportant pas d'alcool) et d'un hydrocarbure (ou de CCl_4) ou d'un alcool et de deux hydrocarbures (ou de CCl_4). La plupart des valeurs de H^E analysées sont endothermiques et elles sont valides à 298,15 K et à pression atmosphérique. La déviation moyenne entre les valeurs expérimentales et celles calculées à l'aide du modèle « DISQUAC » est de 5,5% pour les systèmes ternaires et de 6,5% pour les constituants binaires (181 mélanges). Les paramètres d'interaction utilisés sont valides pour la description des propriétés thermodynamiques suivantes de systèmes binaires (équilibres vapeur–liquide, VLE, liquide–liquide, LLE, et équilibre solide–liquide, SLE, H^E, capacités calorifiques en excès à pression constante, C_p^E) ainsi que pour H^E et VLE de solutions ternaires. Dans la plupart des cas, les prédictions sont indépendantes des composés présents dans les mélanges ou du nombre de groupes présents dans le système. Les déviations plus importantes observées mettent en relief les imperfections des méthodes de contributions des groupes (par exemple, l'effet de Patterson, la ramification). Il faut aussi noter que les résultats sont du même ordre pour les constituants ternaires ou binaires. Ceci n'est pas le cas pour la version Dortmund d'UNIFAC. Les déviations moyennes obtenues à l'aide de ce modèle sont de 10,5% et 14% respectivement pour les mélanges ternaires et binaires. On a aussi comparé les résultats obtenus à l'aide du modèle

Received February 15, 2001. Published on the NRC Research Press Web site at http://canjchem.nrc.ca on October 5, 2001.

J.A. González,[1] J. Carmona, N. Riesco, I.G. de la Fuente, and J.C. Cobos. Dpto. Termodinamica y Fisica Aplicada, Facultad de Ciencias, Universidad de Valladolid, 47071 Valladolid, Spain.

[1]Corresponding author (fax: +34-83-42-31-35; e-mail: jagl@termo.uva.es).

 DOI: 10.1139/cjc-79-10-1447 © 2001 NRC Canada

DISQUAC avec ceux obtenus avec d'autres modèles (UNIFAC originale, théorie de Flory, Nitta–Chao, modèle d'association UNIFAC) pour un certain nombre de systèmes.

Mots clés : prédictions, systèmes ternaires, paramètres binaires, méthodes géométriques, contributions de groupes.

[Traduit par la Rédaction]

Introduction

Although large amounts of data have been reported in the literature for binary systems, data for ternary mixtures and higher multicomponent solutions are scarce. This is due to the time and effort required to obtain a meaningful set of multicomponent data. So, one of the most important tasks of the thermodynamics is to provide predictions on thermodynamic properties of multicomponent mixtures using data obtained from more simple systems and, in the case of VLE, for pure substances.

Of course, the most essential step is to pass from binary to ternary systems and to determine the extent to which the properties in these mixtures can be predicted on the basis of binary data and to assess when data reflecting ternary interactions are absolutely needed.

In the field of correlation and prediction of multicomponent data, many efforts have been developed on the basis of statistical thermodynamics methods, several theoretical solution models, and semiempirical equations (1–20). Nevertheless, each method seems to have its own area of application limited to particular types of systems. These difficulties continue to grow with increasing the number of components. For example, in the case of alcoholic solutions, the classical association model (1), based on the so-called formation of polymeric species of alkanol molecules through hydrogen bonding, must be improved depending on the chemical nature of the remainder components (2–14). These improvements affect the physical contribution to the thermodynamic properties (5, 6, 12–14), as well as to the chemical contribution (2–14). So, in ternary mixtures with two alkanols and one active nonassociating compound, complex formation should be considered in all three combinations because of the charge transfer of the self-associating and active components.

The semiempirical equations more commonly used (Redlich–Kister, Colinet, Scatchard–Hillert, Tsao–Smith) (18–20) to predict H^E of ternary systems are geometrical methods to establish the contribution of each one of the three binaries involved to the ternary H^E. For asymmetric equations with respect to numbering of components, it is of great importance which component is designated as component 1 (19–20). An additional problem comes from that H^E of the constituent binaries must be known to apply these equations and the same occurs for association models.

Group contribution models (21–26) are powerful methods to predict ternary data (VLE and (or) H^E) neglecting ternary interactions. That is, only information from the set of binary systems which contain the groups present in the ternary system analyzed is needed. However, it must be elucidated what type of the information used is relevant to improve predictions. For example, it has been shown that the classical UNIFAC model (21) provides reliable results on H^E of ternary systems when the interaction parameters are obtained using only H^E of binary mixtures (22). However, these interaction parameters are not useful for VLE calculations.

The DORTMUND version of UNIFAC (23, 24) (hereafter, merely UNIFAC) is a modified UNIFAC model which uses a new combinatorial term and temperature-dependent interaction parameters. UNIFAC improves VLE and H^E results for binary and ternary systems in comparison to the original model (23).

We are engaged in a systematic study on the ability of the DISQUAC model (25, 26) to predict VLE and H^E of multicomponent mixtures using binary parameters only. One of the main features of DISQUAC is that the interaction parameters are assumed to be dependent on the molecular structure. Although this means to leave the classical concept of group contribution, is essential for practical purposes. As a matter of fact, it leads to improved predictions, mainly in the case of branched and cyclic molecules, and for the first members of homologous series. Results for ternary systems are also improved. For example, in the first paper of this series (27), we obtained a mean deviation of 2.2% between calculated and experimental pressures for VLE at isothermal conditions of a set of 39 mixtures. DISQUAC results are indeed reliable over a wide range of temperature and for any type of ternary system, even for those with some binary with a miscibility gap (27). Moreover, we have already shown that DISQUAC accurately describes H^E of ternary systems containing one 1-alkanol and two hydrocarbons (28), or two 1-alkanols and one alkane (29), or H^E of 1-alkanol + linear ketone + hydrocarbon mixtures (30). Here, we present DISQUAC predictions on H^E, essentially at 298.15 K, for a set of 95 ternary systems. Some of them have been studied previously, but are included to develop a more complete study. At this end, DISQUAC results are compared to those provided by UNIFAC (23) and Flory (31) models. This is interesting because of the different way of application of such models. DISQUAC uses structure-dependent interaction parameters, UNIFAC averaged parameters, and Flory parameters which are calculated from the H^E measurements of the constituent binaries of the ternary considered.

Other models, such as Nitta–Chao (20) or UNIQUAC association solution model (9, 10), are also considered briefly.

Ternary systems considered

The mixtures treated (Table 1) can be classified as follows: Group I: mixtures containing only hydrocarbons (or CCl_4); Group II: mixtures of one polar compound (not alcohols) and two hydrocarbons (or CCl_4); Group III: mixtures with two polar compounds (not alcohols) and one hydrocarbon (or CCl_4); Group IV: mixtures of one alcohol and two hydrocarbons (or CCl_4). Experimental data are valid at atmospheric pressure and most of them are at 298.15 K. On

© 2001 NRC Canada

Table 1. Comparison between DISQUAC (DQ) predictions (see *Appendix* for references of the interaction parameters used) and UNIFAC (UNIF) calculations obtained using the coefficients from literature (23, 24) with experimental (exp.), minimum (min), and maximum (max) H^E values at 298.15 K for ternary mixtures studied in this work.

			H^E_{min}			H^E_{max}			dev (H^E)		
System[a]		*N*	Exp.	DQ	UNIF	Exp.	DQ	UNIF	DQ	UNIF	Reference
Group I: mixtures containing only hydrocarbons or CCl_4											
1	C_6H_6 + *n*-C_7 + *n*-C_{14}	19	344	299	291	1156	1189	1031	0.034	0.086	56
2	C_6H_6 + *n*-C_{10} + *n*-C_{14}	21	325	298	291	1180	1206	1058	0.028	0.080	56
3	C_6H_6 + C_7H_8 + *n*-C_7[b]	7	255	264	202	695	718	604	0.039	0.095	57
4	C_6H_6 + C_7H_8 + *n*-C_{14}	20	695	732	643	1160	1153	1034	0.034	0.086	56
5	C_6H_6 + C_6H_{12} + *n*-C_6[b]	11	741	750	732	883	858	825	0.024	0.036	57
6	C_6H_6 + C_6H_{12} + *n*-C_6	50	210	238	252	920	904	848	0.039	0.059	58
7	C_6H_6 + C_6H_{12} + *n*-C_7[b]	31	489	507	439	957	914	865	0.026	0.061	59
8	C_6H_6 + C_6H_{12} + *n*-C_7	18	153	153	153	916	934	879	0.010	0.025	60
9	C_7H_8 + C_6H_{12} + *n*-C_7[b]	6	402	384	378	703	655	620	0.053	0.053	57
10	C_7H_8 + C_6H_{12} + *n*-C_7	18	107	111	118	602	641	613	0.035	0.028	60
11	C_6H_6 + CCl_4 + *n*-C_6	80	80	83	82	807	772	694	0.031	0.081	61
12	C_6H_6 + CCl_4 + *n*-C_7	140	96	99	96	847	812	738	0.026	0.068	61
13	C_6H_6 + CCl_4 + *n*-C_8	94	66	78	75	867	851	772	0.023	0.071	61
14	C_6H_6 + CCl_4 + *n*-C_9	156	87	95	89	912	893	814	0.021	0.068	61
15	C_6H_6 + C_7H_8 + C_6H_{12}[b]	6	536	528	500	741	723	710	0.050	0.059	57
16	C_6H_6 + C_6H_{12} + CCl_4	6	108	117	112	504	501	466	0.020	0.059	62
17	C_6H_6 + C_6H_{12} + CCl_4[c]	39	168	193	163	603	689	658	0.12	0.070	63
Group II: mixtures containing one polar compound (not alcohols)											
18	2CO2 + *n*-C_6 + *n*-C_9	60	121	87	91	1318	1110	1152	0.11	0.083	64
19	2CO2 + *n*-C_6 + *n*-C_{10}	58	180	164	171	1223	1151	1197	0.06	0.031	65
20	2CO2 + *n*-C_6 + *n*-C_{12}	59	156	124	129	1167	1220	1278	0.038	0.043	64
21	2CO2 + *n*-C_6 + *n*-C_{14}	59	239	194	203	1238	1090	1152	0.097	0.060	65
22	2COO2 + *n*-C_6 + *n*-C_{10}	60	122	115	99	1222	1254	1069	0.020	0.096	66
23	2COO2 + *n*-C_6 + *n*-C_{12}	60	105	84	72	1333	1324	1133	0.031	0.11	66
24	2COO2 + *n*-C_6 + *n*-C_{14}	58	154	123	106	1415	1387	1189	0.038	0.12	67
25	MTBE + *n*-C_6 + *n*-C_{10}	58	69	62	51	476	459	349	0.025	0.15	40
26	MTBE + 23DMB + *n*-C_{10}	60	72	74	62	496	458	366	0.060	0.16	68
27	MTBE + *n*-C_6 + *n*-C_{12}	59	74	79	66	521	488	369	0.036	0.16	40
28	TAME + *n*-C_6 + *n*-C_{10}	57	54	55	50	348	337	310	0.020	0.069	69
29	TAME + 23DMB + *n*-C_{10}	57	52	56	50	352	337	311	0.045	0.079	70
30	TAME + *n*-C_6 + *n*-C_{12}	57	56	58	58	402	358	330	0.070	0.12	69
31	DIPE + *n*-C_6 + *n*-C_{10}	60	55	53	18	321	274	108	0.087	0.47	71
32	DIPE + *n*-C_6 + *n*-C_{16}	59	65	56	21	513	318	125	0.25	0.51	71
33	MTBE + C_6H_{12} + *n*-C_{10}	58	89	92	78	576	579	419	0.016	0.19	68
34	TAME + C_6H_{12} + *n*-C_{10}	57	70	71	62	478	478	371	0.015	0.16	70
35	1CO4 + 12DMBZ + *n*-C_9[d]	17	217	266	239	883	944	1066	0.071	0.16	72
36	1CO1 + C_6H_{12} + CCl_4	29	419	555	584	1293	1417	1426	0.13	0.15	63
37	1CO2 + C_6H_6 + C_6H_{12}[b]	30	210	159	179	1340	1271	1251	0.072	0.13	73
38	6NH_2 + C_6H_6 + *n*-C_7	63	550	484	541	1196	1107	1202	0.074	0.013	74
39	6NH_2 + C_6H_6 + C_7H_8	37	378	322	325	668	596	644	0.096	0.055	74
Group III: mixtures containing two polar compounds (not alcohols)											
40	3O3 + MTBE + *n*-C_7	61	52	49	42	365	365	296	0.036	0.14	75
41	3O3 + MTBE + *n*-C_{10}	60	63	49	43	453	423	342	0.082	0.18	75
42	4O4 + MTBE + *n*-C_7	60	36	39	37	343	352	288	0.020	0.09	76
43	4O4 + MTBE + *n*-C_{10}	60	48	39	38	429	407	332	0.077	0.14	76

© 2001 NRC Canada

Table 1. (*continued*).

System[a]		N	H^E_{min}			H^E_{max}			dev (H^E)		
			Exp.	DQ	UNIF	Exp.	DQ	UNIF	DQ	UNIF	Reference
44	MTBE + TAME + *n*-C_7	60	58	69	55	375	387	317	0.027	0.093	77
45	MTBE + TAME + *i*-C_8	58	44	77	62	285	412	337	0.32	0.15	78
46	MTBE + TAME + *n*-C_{10}	60	70	66	59	466	446	369	0.030	0.13	77
47	MTBE + DIPE + *n*-C_7	59	52	55	30	360	376	285	0.018	0.20	79
48	MTBE + DIPE + *n*-C_{10}	60	67	56	31	457	436	327	0.080	0.26	79
49	MTBE + TAME + C_6H_{12}	59	64	74	67	447	451	389	0.016	0.085	78
50	1O2O1 + MTBE + *n*-C_7	73	121	121	104	1135	1106	929	0.033	0.13	80
51	THF + 4CN + C_6H_{12}	70	14	14	40	1214	1212	981	0.019	0.072	81
52	1CO1 + THF + C_6H_{12}	74	190	203	160	1561	1514	1530	0.024	0.031	82
53	1CO1 + $CHCl_3$ + C_6H_{12}	30	–1389	–1490	–1395	779	617	869	0.13	0.043	63
Group IV: mixtures containing one alcohol and hydrocarbons or CCl_4											
54	MeOH + C_6H_6 + *n*-C_6	36	230	196	190	1313	1297	1280	0.027	0.040	60
55	MeOH + C_6H_6 + *n*-C_7[b]	13	166	174	347	842	929	973	0.12	0.15	83
56	MeOH + C_6H_6 + *n*-C_7	38	460	501	503	1460	1157	1161	0.10	0.11	84
57	MeOH + C_6H_6 + *n*-C_7	13	149	193	366	922	1038	1048	0.087	0.13	83
58	MeOH + C_6H_6 + *n*-C_7	34	700	679	652	1321	1303	1361	0.031	0.061	85
59	MeOH + C_6H_6 + *n*-C_7[c]	13	168	213	384	986	1083	1103	0.056	0.12	83
60	MeOH + C_6H_6 + *n*-C_7[e]	13	172	234	401	1053	1133	1160	0.049	0.14	83
61	MeOH + C_7H_8 + *n*-C_7	92	364	347	344	1040	1004	1045	0.038	0.037	86
62	MeOH + C_6H_6 + C_6H_{12}	61	448	457	409	1198	1197	1288	0.057	0.083	85
63	MeOH + C_7H_8 + C_6H_{12}	55	249	249	227	1059	1058	1121	0.067	0.047	87
64	MeOH + C_6H_6 + CCl_4	45	66	72	67	671	669	696	0.030	0.034	88
65	MeOH + C_6H_{12} + CCl_4	55	114	124	92	570	737	607	0.14	0.12	89
66	EtOH + *n*-C_6 + *n*-C_{10}	62	131	109	126	684	729	776	0.048	0.11	90
67	EtOH + *n*-C_6 + *n*-C_{12}	70	141	115	134	736	792	883	0.053	0.11	90
68	EtOH + C_6H_{12} + *n*-C_6	54	142	81	98	715	738	680	0.039	0.049	91
69	EtOH + C_6H_{12} + *n*-C_7[b]	11	472	451	464	699	704	691	0.027	0.047	92
70	EtOH + C_6H_{12} + *n*-C_7	7	595	626	657	698	739	778	0.064	0.12	92
71	EtOH + C_6H_{12} + *n*-C_7	53	164	115	142	760	776	719	0.034	0.051	91
72	EtOH + C_6H_{12} + *n*-C_7[c]	7	672	665	736	796	804	863	0.012	0.095	92
73	EtOH + C_6H_{12} + *n*-C_7[f]	7	774	762	911	926	934	1064	0.016	0.16	92
74	EtOH + C_6H_{12} + *n*-C_7[g]	7	1068	1057	1322	1300	1308	1545	0.030	0.20	92
75	EtOH + C_6H_{12} + *n*-C_8	54	154	108	132	793	812	758	0.033	0.053	91
76	EtOH + C_6H_{12} + *n*-C_{10}	77	149	123	158	830	857	880	0.040	0.059	93
77	EtOH + C_6H_6 + *n*-C_6	37	343	392	531	1173	1308	1363	0.11	0.15	94
78	EtOH + C_6H_6 + *n*-C_7	26	232	198	250	1227	1385	1435	0.081	0.15	95
79	EtOH + C_6H_6 + C_6H_{12}	18	232	197	272	1274	1269	1360	0.045	0.045	60
80	EtOH + C_7H_8 + C_6H_{12}	18	223	193	202	1106	1104	1176	0.044	0.067	60
81	EtOH + C_6H_6 + CCl_4	18	264	254	347	783	679	647	0.096	0.14	96
82	1-PrOH + *n*-C_6 + *n*-C_{10}	58	93	87	88	731	754	711	0.025	0.066	97
83	1-PrOH + *n*-C_6 + *n*-C_{12}	58	106	93	94	811	823	789	0.034	0.068	97
84	1-PrOH + C_6H_{12} + *n*-C_6	54	142	79	98	715	712	680	0.032	0.049	98
85	1-PrOH + C_6H_{12} + *n*-C_7	53	165	113	142	760	755	719	0.032	0.051	98
86	1-PrOH + C_6H_{12} + *n*-C_8	54	155	107	133	794	797	758	0.030	0.053	98
87	1-PrOH + C_6H_{12} + *n*-C_{10}	59	95	100	117	856	877	823	0.022	0.039	93
88	1-PrOH + C_6H_6 + CCl_4	65	49	105	75	951	931	980	0.045	0.079	99
89	2-PrOH + C_6H_6 + m-C_6H_{12}	53	371	379	308	1496	1483	1265	0.019	0.13	100

© 2001 NRC Canada

Table 1. (*concluded*).

System[a]		*N*	H^E_{min} Exp.	H^E_{min} DQ	H^E_{min} UNIF	H^E_{max} Exp.	H^E_{max} DQ	H^E_{max} UNIF	dev (H^E) DQ	dev (H^E) UNIF	Reference
90	2-PrOH + C_6H_6 + C_6H_{12}	67	246	266	210	1537	1479	1221	0.027	0.14	101
91	2-PrOH + C_7H_8 + C_6H_{12}	56	237	258	169	1365	1295	1072	0.044	0.18	102
92	1-BuOH + C_6H_6 + C_6H_{12}	43	391	427	447	1333	1321	1335	0.026	0.033	103
93	1-PeOH + *n*-C_6 + C_6H_{12}	10	305	334	305	690	669	604	0.039	0.090	104
94	1-HxOH + *n*-C_7+ C_6H_{12}	13	571	549	488	807	702	664	0.097	0.14	105
95	1-OcOH + C_6H_6 + *n*-C_7	57	466	439	430	1567	1560	1676	0.028	0.058	74

Note: Deviations for H^E, dev (H^E), as defined by eq. [1], are also given (*N* is the number of data for each system). Detailed results for the constituent binaries are available upon request.

[a]Symbols: 3-pentanone (2CO2), ethylpropanoate (2COO2), methyl *tert*-butylether (MTBE), *tert*-amylmethylether (TAME), 2,3-dimethylbutane (23DMB), diisopropylether (DIPE), 2-hexanone (1CO4), 2-propanone (1CO1), 2-butanone (1CO2), 1,2-dimethylbenzene (12DMBZ), 1-hexylamine ($6NH_2$), di-*n*-propylether (3O3), di-*n*-butylether (4O4), 2,5-dioxahexane (1O2O1), tetrahydrofuran (THF), butanenitrile (4CN), 2-propanone (1CO1), methanol (MeOH), ethanol (EtOH), 1-propanol (1-PrOH), 1-butanol (1-BuOH), 1-pentanol (1-PeOH), 1-hexanol (1-HxOH), 1-octanol (1-OcOH), 2-propanol (2-PrOH), methyl-cyclohexane (m-C_6H_{12}).

[b]T = 293.15 K.

[c]T = 303.15 K.

[d]T = 318.15 K.

[e]T = 308.15 K.

[f]T = 313.15 K.

[g]T = 333.15 K.

the other hand, the ternary solutions studied are characterized by endothermic H^E, except the 2-propanone + $CHCl_3$ + cyclohexane system, which is strongly exothermic.

Results for the binary mixtures involved in the ternary solutions are also given. When it was possible, we considered those binaries investigated in the original works on the ternary mixtures treated.

Models

DISQUAC

Assessment of geometrical parameters

The relative molecular volumes (r_i), the surfaces (q_i), and the surface fractions (α_{si}) of all the molecular species have been calculated on the basis of the group volumes and surfaces recommended by Bondi (32), taking the volume and the surface of methane arbitrarily as unity (33). Values of r_i and q_i of the groups referred to in this work are given in the literature (see Table A1 of *Appendix* for references).

Theory

The equations used to calculate thermodynamic properties in the framework of DISQUAC are given elsewhere (34). The temperature dependence of the interaction parameters is expressed in terms of the dispersive (DIS) and quasichemical (QUAC) interchange coefficients $C^{DIS}_{st,\,l}$ and $C^{QUAC}_{st,\,l}$, where s, t are the different groups present in the mixture and l is the order of the interchange coefficient: l = 1 (Gibbs energy), l = 2 (enthalpy), l = 3 (heat capacity). For the QUAC part, the coordination number is z = 4.

Values of the interchange coefficients

Most of the interchange coefficients used in this work are available in literature (see Table A1 of the *Appendix* for references). Only a few of them have been estimated for this paper (Table A2 of *Appendix*). In mixtures containing two oxaalkanes, the interchange coefficients corresponding to the oxygen/oxygen contacts were neglected.

It should be emphasized that the DISQUAC interaction parameters are considered as dependent on the molecular structure, and so, in a given homologous series, each molecule of solute has its own set of interchange coefficients. Nevertheless, some general trends concerning their variation with the molecular structure have been pointed out. In mixtures formed by polar but not self-associated compounds, such variation is usually attributed to inductive effects on DIS coefficients and steric effects on QUAC coefficients (35, 36). On the other hand, we have found in many series containing alcohols what seems to be a general rule: the QUAC coefficients for l = 1 and l = 3 are independent of the alcohol size. This is still valid for l = 2, although some exceptions are found. So, in systems involving *sec*-alkanols one can distinguish two ensembles depending on the situation of the OH groups (e.g., 2-alkanols and 3-alkanols), each one characterized by a different second QUAC interaction parameter (37).

The regular change with the molecular structure of the interaction parameters makes it easy to estimate new parameters when experimental data are not available (38).

Modified UNIFAC (Dortmund version)

Modified UNIFAC (23) differs from the original UNIFAC (21) by the combinatorial term and the temperature dependence of the group interaction parameters. Equations used to calculate G^E and H^E are given elsewhere (23).

Assessment of geometrical and interaction parameters

In modified UNIFAC, main groups are defined to improve correlations. For example, $CHCl_3$ and methanol are considered as homogeneous molecules. The main groups may be subdivided in different subgroups, which have different geometrical parameters. The subgroups within the same main group are assumed to have identical group energy-interaction parameters.

© 2001 NRC Canada

Table 2. Comparison between DISQUAC (DQ) and Flory predictions for some of the ternary systems examined in this work.

			dev (H^E)		
System		N	DQ	Flory	Reference
Group I					
11	C_6H_6 + CCl_4 + n-C_6	80	0.031	0.036	61
12	C_6H_6 + CCl_4 + n-C_7	140	0.026	0.044	61
13	C_6H_6 + CCl_4 + n-C_8	94	0.023	0.046	61
14	C_6H_6 + CCl_4 + n-C_9	156	0.021	0.044	61
Group II					
25	MTBE + n-C_6 + n-C_{10}	58	0.025	0.020	40
26	MTBE + 23DMB + n-C_{10}	60	0.060	0.051	68
27	MTBE + n-C_6 + n-C_{12}	59	0.036	0.021	40
28	TAME + n-C_6+ n-C_{10}	57	0.020	0.034	69
29	TAME + 23DMB + n-C_{10}	57	0.045	0.024	70
30	TAME + n-C_6 + n-C_{12}	57	0.070	0.018	69
31	DIPE + n-C_6 + n-C_{10}	60	0.087	0.029	71
32	DIPE + n-C_6+ n-C_{16}	59	0.25	0.031	71
33	MTBE + C_6H_{12} + n-C_{10}	58	0.016	0.022	68
34	TAME + C_6H_{12} + n-C_{10}	57	0.015	0.041	70
Group III					
40	3O3 + MTBE + n-C_7	61	0.036	0.055	75
41	3O3 + MTBE + n-C_{10}	60	0.082	0.032	75
42	4O4 + MTBE + n-C_7	60	0.020	0.036	76
43	4O4 + MTBE + n-C_{10}	60	0.077	0.022	76
44	MTBE + TAME + n-C_7	60	0.027	0.026	77
45	MTBE + TAME + i-C_8	58	0.32	0.032	78
46	MTBE + TAME + n-C_{10}	60	0.030	0.023	77
47	MTBE + DIPE + n-C_7	59	0.018	0.034	79
48	MTBE + DIPE + n-C_{10}	60	0.080	0.024	79
49	MTBE + TAME + C_6H_{12}	59	0.016	0.051	78
50	1O2O1 + MTBE + n-C_7	73	0.033	0.031	80

Note: Deviations for H^E, dev (H^E), as defined by eq. [1], are also given (N is the number of data for each system). Detailed results for the constituent binaries are available upon request.

Table 3. Mean deviations (eq. [2]) obtained using DISQUAC and UNIFAC for the ternary and binary solutions examined in this work.

			DISQUAC		UNIFAC	
Groups/Systems	N_T[a]	N_B[b]	Ternary	Binary	Ternary	Binary
I + II + III + IV	95	181	0.053	0.063	0.103	0.141
I	17	49	0.036	0.047	0.064	0.071
II	22	40	0.066	0.070	0.142	0.192
III	14	28	0.065	0.087	0.125	0.242
IV	43	80	0.048	0.054	0.090	0.112
Only methanol	12	15	0.067	0.067	0.089	0.122

[a]Number of ternary systems.
[b]Number of binary mixtures.

The geometrical parameters, the relative van der Waals volumes, and the relative van der Waals surfaces of the different subgroups are not calculated from molecular parameters like in the original UNIFAC but fit together with the interaction parameters to the experimental values of the thermodynamic properties considered. The geometrical and interaction parameters are taken from the literature (23, 24) and used without modification.

Flory's model

The extension of Flory's theory (31) to ternary systems has been developed by Brostow and Sochanski (39). Equations are summarized elsewhere (40).

Here, a binary system is characterized by some properties of the pure compounds (molar volume, isobaric expansivity, isothermal compressibility) and by a coefficient X_{ij} which denotes the mixed-pair interchange interaction energies be-

© 2001 NRC Canada

Table 4. Mean deviations (eq. [2]) obtained using DISQUAC and Flory's model for some of the ternary and binary solutions examined in this work.

			DISQUAC		FLORY	
Groups/Systems	N_T[a]	N_B[b]	Ternary	Binary	Ternary	Binary
I + II + III + IV	95	181	0.053	0.063		
I + II + III	53	109	0.056	0.066		
I + II + III	25	33	0.058	0.071	0.033	0.022
I (nos. 13–16)	4	9	0.025	0.021	0.042	0.031
II (nos. 25–34)	10	12	0.062	0.086	0.029	0.019
III (nos 40–50)	11	19	0.067	0.113	0.033	0.015

[a]Number of ternary systems.
[b]Number of binary mixtures.

Table 5. Comparison of mean deviations (Mdev (H^E), eq. [2]) provided by different models for different set of mixtures considered in this work.

	Mdev (H^E) for systems			
Model	6–8, 17, 37, 64, 77–81, 84–86, 90, 91	6–8, 19–24, 37, 77–80, 90, 91	19–24	25, 26, 67, 68, 82, 83, 90
DISQUAC	0.052	0.049	0.047[a]	0.035
UNIFAC (A)[b]	0.072[b]			
UNIFAC (B)[c]	0.057[c]			
Kohler[d]		0.048[e]	0.024[a]	
Colinet[d]		0.042[e]	0.019[a]	
Tsao–Smith[f]		0.051[e]	0.024[a]	
Scatchard–Hillert[f]		0.033[e]		
Nitta–Chao[a]			0.072	
Local composition model[g]				0.024[g]

[a]Reference 20.
[b]Results using interaction parameters fitted to only H^E measurements (22).
[c]Results using interaction parameters fitted to H^E measurements of the constituent binaries (22). [d]Symmetric equation.
[e]Reference19.
[f]Asymmetric equation.
[g]Reference 15.

tween sites on species i and j. These coefficients were fitted to the corresponding binary H^E data assuming that the molecules are approximately spherical. H^E of the ternary solution is predicted using the three X_{ij} values calculated for the constituent binaries.

As it is known, this model provides information on H^E and excess volumes (V^E), but can only be applied to mixtures containing weakly polar compounds and inert components (e.g., methyl *tert*-butylether + *n*-hexane) (40) or compounds of identical chemical nature, such as systems containing two 1-alkanols (41) or two alkoxyethanols (42).

Results and discussion

DISQUAC and UNIFAC calculations for the ternary systems considered are listed in Table 1. Table 2 presents this comparison between DISQUAC and Flory's theory. Results are summarized in Tables 3 and 4.[2] Table 5 shows comparisons between DISQUAC and other different models. Figures 1–6 show some results in a graphical way.

In Tables 1 and 2, deviations between experimental and calculated results are included. They are defined as:

$$[1] \qquad \text{dev}(H^E) = \{[1/N\ \Sigma(H^E_{exp} - H^E_{calc}) / H^E_{max}]^2\}^{1/2}$$

where N is the number of experimental points for each system. Tables 3–5 list mean deviations for a set of N_S mixtures defined as:

$$[2] \qquad \text{Mdev}\ (H^E) = \Sigma\,\text{dev}\ (H^E)/N_S$$

From the results presented along these tables, some statements can be given: (*i*) In most of the cases, DISQUAC predictions are independent of the mixture compounds (Table 3). Certainly, the mean deviations are somewhat larger for Groups II and III. It is due to the very large discrepancies observed for some ternary mixtures. For example, for DIPE + *n*-C_6 + *n*-C_{16}, dev (H^E) = 0.25 and for MTBE + TAME + isooctane, dev (H^E) = 0.32. These results reveal some of the typical shortcomings of group contribution methods (see below): Patterson's effect (43, 44) and branching, respectively. DIPE + *n*-alkanes mixtures are characterized by interaction parameters which are independent of the *n*-alkane. Deviations for DIPE + *n*-C_6, + *n*-C_{10}, or + *n*-C_{16} are 0.022, 0.13, and 0.30, respectively, indicating that the model does not take into account the extra endothermic con-

[2]A detailed comparison between experimental data and results from DISQUAC, UNIFAC, and Flory models for the binary constituent mixtures is available upon request.

© 2001 NRC Canada

Fig. 1. H^E at 298.15 K for *n*-nonane (1) + benzene (2) + CCl_4 (3) at different x_2:x_3 ratios. Points, experimental results (61): (■) x_2:x_3 = 0.3333, (▲) x_2:x_3 = 1.000, (●) x_2:x_3 = 2.3333. Lines, DISQUAC calculations.

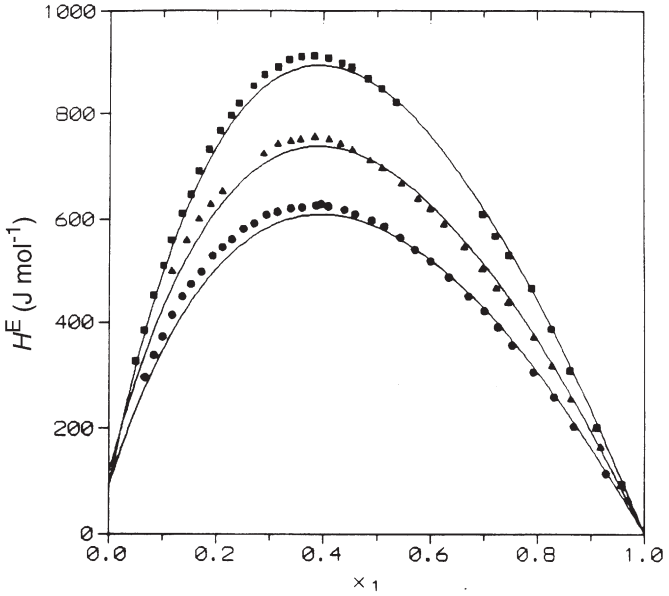
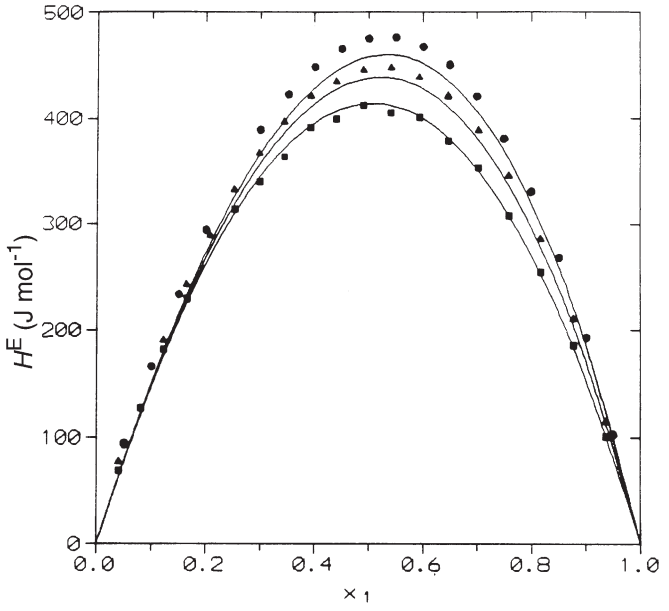


Fig. 2. H^E at 298.15 K for MTBE (1) + *n*-hexane (2) + *n*-decane (3) at different x_2:x_3 ratios. Points, experimental results (40): (●) x_2:x_3 = 0.3477, (▲) x_2:x_3 = 0.9984, (■) x_2:x_3 = 3.1408. Lines, DISQUAC calculations.



tribution to H^E due to order destruction of the longer *n*-alkanes upon mixing (43, 44). Solutions containing linear or branched alkanes (e.g., *n*-C_8 and isooctane) are characterized by the same interaction parameters. This leads to a large deviation for the MTBE + isooctane system, dev (H^E) = 0.32 (for MTBE + *n*-C_8, dev (H^E) = 0.014). Note that if in Group III, the system MTBE + TAME + isooctane is not considered, then Mdev (H^E) = 0.045.

Fig. 3. H^E at 298.15 K for ethanol (1) + *n*-hexane (2) + *n*-decane (3) at different x_2:x_3 ratios. Points, experimental results (90): (●) x_2:x_3 = 0.3339, (▲) x_2:x_3 = 2.9841. Lines, DISQUAC calculations.

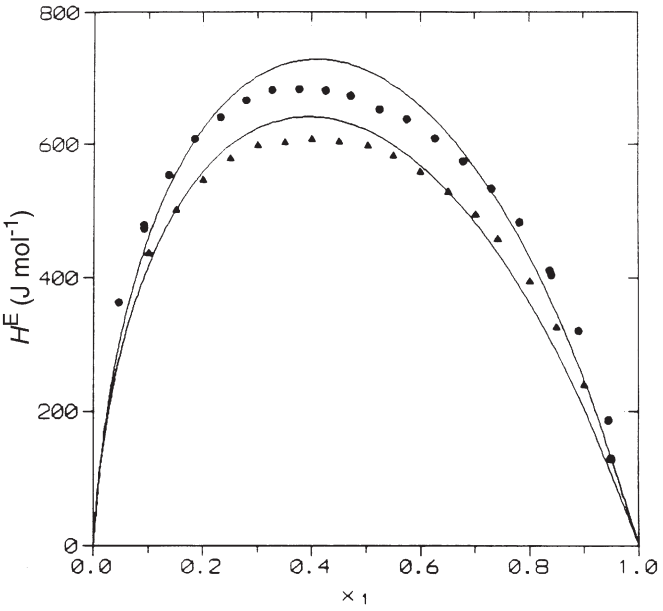
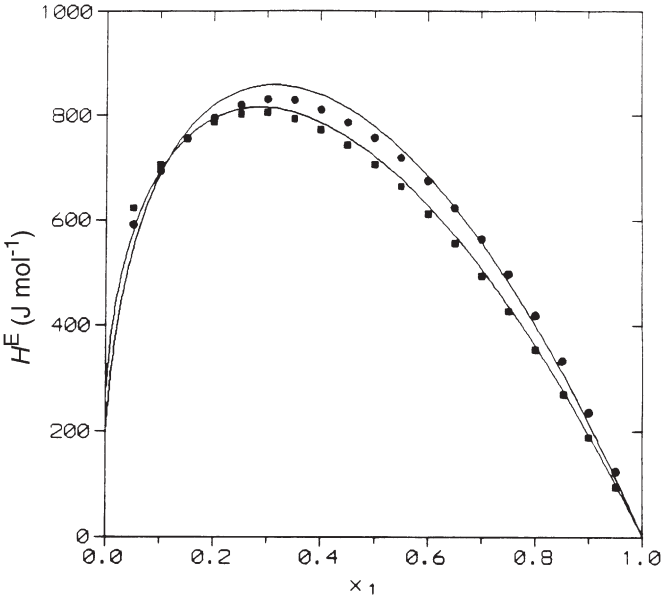


Fig. 4. H^E at 298.15 K for 1-propanol (1) + C_6H_{12} (2) + *n*-decane (3) at different x_2:x_3 ratios. Points, experimental results (93): (●) x_2:x_3 = 0.3325, (■) x_2:x_3 = 2.9995. Lines, DISQUAC calculations.



(*ii*) DISQUAC predictions are also independent of the number of contacts present in the system. For example (see Table 1), system nos. 25 (MTBE + *n*-C_6 + *n*-C_{10}) and 66 (ethanol + *n*-C_6 + *n*-C_{10}) have two different characteristic groups and one contact; system nos. 33 (MTBE + C_6H_{12} + *n*-C_{10}), 50 (2,5-dioxahexane + MTBE + *n*-C_7), or 75 (ethanol + C_6H_{12} + *n*-C_8) have three groups and three contacts, while system no. 90 (2-propanol + C_6H_6 + C_6H_{12}) has four

© 2001 NRC Canada

Fig. 5. H^E at 298.15 K for 2-propanol (1) + C_6H_6 (2) + methylcyclohexane (3) at different x_2:x_3 ratios. Points, experimental results (100): (■) x_2:x_3 = 0.3293, (▲) x_2:x_3 = 1.016, (●) x_2:x_3 = 3.014. Lines, DISQUAC calculations.

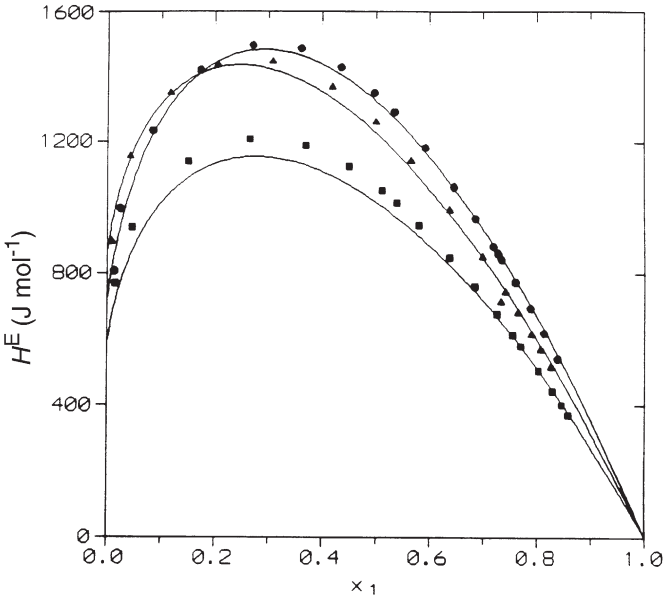
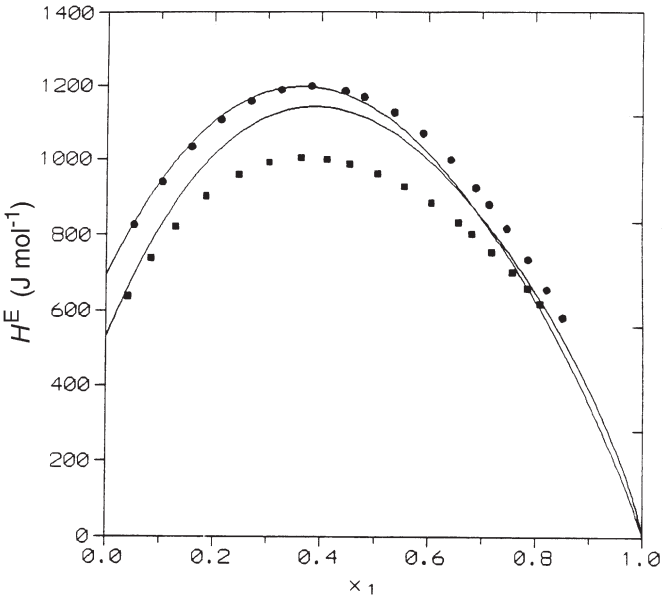


Fig. 6. H^E at 298.15 K for cyclohexane (1) + methanol (2) + C_6H_6 (3) at different x_2:x_3 ratios. Points, experimental results (85): (●) x_2:x_3 = 0.2529, (■) x_2:x_3 = 1.504. Lines, DISQUAC calculations.



groups and six contacts.[3] Deviations are similar for all of them as results depend, in some extent, on the source of the experimental measurements.

(*iii*) Deviations obtained using DISQUAC are of the same order for the ternary solutions and for the related binaries (Table 3). Therefore, the model describes consistently the data set analyzed, neglecting ternary interactions. The larger mean deviation observed for binaries included in Group III is due to the fact that those binary mixtures containing only oxaalkanes were treated, neglecting the interactions between oxygen–oxygen contacts. However, these solutions show low H^E values and this approximation is not important when calculating H^E of the related ternary mixture.

(*iv*) DISQUAC improves UNIFAC results (Tables 1, 3) due to the interaction parameters are assumed to be structure-dependent. Of course, this also means that the number of interaction parameters used in DISQUAC is higher (see below). For a similar reason, the Flory's model improves DISQUAC results for systems included in Groups II and III (Tables 2, 4) as each binary mixture is characterized by one adjustable specific interaction parameter. Note that DISQUAC and Flory's model yield similar results for solutions of Group I because they are applied in a similar way.

(*v*) However, the use of a larger number of parameters does not always imply better results. The classical UNIFAC model has been applied to predict H^E of ternary systems using interaction parameters fitted to only H^E measurements (method A in Table 5), or using interaction parameters fitted to H^E measurements of the constituent binaries (method B in Table 5) (22). The second procedure slightly improves results, which are not far from those obtained using semiempirical equations (22) (see Table 5). However, the interaction parameters were not suitable for VLE calculations. On the other hand, procedure B and semiempirical equations present the limitation of requiring the binary data related to the ternary system studied and cannot be applied when these data are not available. It is noteworthy that DISQUAC predictions are similar to those provided by semiempirical equations (Table 5) and that interaction parameters can be used to predict VLE, LLE, SLE, H^E, and C_p^E of the binary mixtures and VLE and H^E of the ternary systems.

(*vi*) UNIFAC provides quite large deviations for the binary mixtures, except for those belonging to Group I. It is remarkable that these deviations are larger than for the ternaries (Table 3). As already mentioned, the classical application of the group contribution concept leads to remove a number of very important effects in mixtures: Patterson's effect (43, 44) (in C_6H_6, C_6H_{12}, DIPE or MTBE + *n*-alkanes), cyclization (in tetrahydrofuran) (45–49), proximity effects (in 2,5-dioxahexane) (46–48), and branching (in MTBE, TAME, DIPE) (50). Such shortcomings, in some extent balanced for ternary systems, appear clearly when treating binary solutions (48–50). DISQUAC usually provides a better representation of the temperature dependence of H^E (49, 51). For example, for benzene + *n*-alkanes systems, UNIFAC predicts an increasing of H^E with temperature, while just the opposite behaviour is observed.

(*vii*) DISQUAC improves results for systems containing methanol (Tables 1, 3), assumed to be a main group in the framework of UNIFAC. That is, methanol is characterized by its own set of interaction parameters, which are different to those of the remainder alcohols. So, in this case DISQUAC and UNIFAC are applied in the same way. The same occurs for mixtures with $CHCl_3$, but now DISQUAC

[3] For example, in system no. 90, the groups are: OH, CH_2, aromatic, cyclic; and the contacts: OH–CH_2, OH–aromatic, OH–cyclic, CH_2–aromatic, CH_2–cyclic, aromatic–cyclic.

© 2001 NRC Canada

results are poorer (system no. 53). The important point is that both models yield similar mean deviations for the constituent binaries (0.044 and 0.032, for DISQUAC and UNIFAC, respectively), and that DISQUAC accurately represents systems with very strongly specific interactions, e.g., oxaalkanes + $CHCl_3$ (49). Therefore, experimental results should be taken with caution. Note that deviation is also somewhat large for system no. 17, which is taken from the same source. Nevertheless, it should be mentioned that the DISQUAC treatment of binary mixtures including $CHCl_3$ is more difficult because this molecule is considered as built by two groups. UNIFAC also improves results for the ternary systems including hexylamine (nos. 38 and 39). This is probably due to the different database used in the estimation of the interaction parameters.

Comparison with other models

Systems nos. 19–24 have been treated in terms of the Nitta–Chao model (20), which adopts the cell theory of Lee et al. (52) for the liquid state. Recently, DISQUAC provides better results (Table 5). The main advantage of this model is its ability to provide information on V^E.

Some mixtures (see Table 5) have been studied through a model based on an approximation of the radial distribution function and the quasilattice two-liquid theory (15). This model, where each binary mixture is characterized by three adjustable parameters, slightly improves results for ternary mixtures (Table 5). For 11 binary solutions related to the ternaries analyzed, the model provides Mdev (H^E) = 0.016, while DISQUAC yields 0.049.

The Mobile Order theory (13), which takes into account both contributions to the thermodynamic properties, i.e., nonspecific interactions, expressed in terms of the Nearly Ideal Binary Solvent model (53, 54), and that from the formation of the hydrogen-bonded complexes (13) has been applied to systems nos. 66, 67, 82, 83. The absolute mean deviations defined as:

$$[3] \qquad \Delta(H^E)(\text{J mol}^{-1}) = \Sigma|H^E_{calc} - H^E_{exp}|/N$$

are 12, 20, 14, and 22. DISQUAC yields (in the same order): 29, 34, 18, 28.

In the UNIQUAC association theory (9, 10), the partition function is factorized, as in any approximate model applied to complex associated systems, into two terms. The physical interactions are represented by the UNIQUAC equation (55). The chemical contribution is calculated assuming that specific interactions lead to the formation of different associated species according to a well defined set of chemical reactions, each one of them characterized by an equilibrium constant. For higher open multimers, the equilibrium constant is independent of the length of the multimer. This model has been applied widely, but no in a systematic way. For systems nos. 79, 80, 88–91, it provides (9, 10) $\Delta(H^E)$ (J mol^{-1}) = 14, 15, 16, 22, 18, 11. DISQUAC results are: 57, 44, 43, 22, 34, 44.

Therefore, the UNIQUAC association model improves DISQUAC calculations. However, it must be noted that results depend strongly on the polymeric species present in the mixture, what have to be previously elucidated to a reliable application of the model. It is typical for association models, which, on the other hand, only can be applied to mixtures where association is expected. This is their major limitation.

Conclusions

DISQUAC provides reliable predictions on H^E (and also on VLE) of the ternary systems examined using binary parameters only, i.e., neglecting interactions. These predictions are practically independent of the mixtures compounds, or of the number of groups present in the solution. Therefore, DISQUAC should be applied when interaction parameters are available. The interaction parameters used are valid for the description of thermodynamic properties of binary mixtures (VLE, LLE, SLE, H^E, C_p^E), as well as for prediction on H^Es and VLE of ternary systems.

On the other hand, deviations can be rationalized and, if necessary corrected.

The main advantage of UNIFAC is the large available matrix of interaction parameters. In the framework of this model, H^E of ternary systems are better represented than those of the constituent binaries.

Acknowledgements

This work was supported by the Programa Sectorial de Promoción General del Conocimiento de la S.E.U.I. y D. del MEC (Spain), Project no. PB97–0488 and by the Consejería de Educación y Cultura de la Junta de Castilla y León y de la Unión Europea, F.S.E under the project VA039/01. J.C. Carmona gratefully acknowledges a grant from Becas Postdoctorales del Ministerio de Educación. N.R. acknowledges the grant received from the Programa Nacional de Formación del Profesorado Universitario y Personal Investigador de la S.E.U.I. y D. del MEC.

References

1. H. Renon and J.M. Prausnitz. Chem. Eng. Sci. **22**, 299 (1967); Chem. Eng. Sci. **22**, 1891 (1967).
2. I. Nagata. Z. Phys. Chem. (Leipzig), **254**, 305 (1973).
3. T. Nitta and T. Katayama. J. Chem. Eng. Jpn. **6**, 1 (1973).
4. Sh.-A. Chen and E.B. Bagley. Chem. Eng. Sci. **33**, 161 (1978).
5. I. Nagata and Y. Kawamura. Chem. Eng. Sci. **34**, 601 (1979).
6. I. Nagata and K. Tamura. Thermochim. Acta, **57**, 331 (1982).
7. A. Nath and E. Bender. Fluid Phase Equilib. **10**, 43 (1983).
8. (*a*) I. Nagata and K. Gotoh. Thermochim. Acta, **99**, 145 (1986); (*b*) I. Nagata and K. Ohtsubo. Thermochim. Acta, **102**, 185 (1986); (*c*) I. Nagata, K. Tamura, and K. Gotoh. Thermochim. Acta, **104**, 179 (1986); (*d*) I. Nagata and K. Gotoh. Thermochim. Acta, **102**, 207 (1986); (*e*) I. Nagata and K. Gotoh. Thermochim. Acta, **258**, 77 (1995); (*f*) I. Nagata and K. Miyamoto. Thermochim. Acta, **209**, 43 (1992); (*g*) I. Nagata, K. Gotoh, and K. Miyamoto. Thermochim. Acta, **249**, 89 (1995).
9. I. Nagata and K. Inaguma. Thermochim. Acta, **97**, 51 (1986).
10. I. Nagata and K. Miyamoto. Fluid Phase Equilib. **56**, 203 (1990).
11. S.W. Campbell. Fluid Phase Equilib. **102**, 61 (1994).
12. H. Funke, M. Wetzel, and A. Heintz. Pure Appl. Chem. **61**, 1429 (1989).
13. W.E. Acree. Fluid Phase Equilib. **92**, 19 (1994).
14. S. Pandey, J.R. Powell, M.R. McHale, A.-S.M. Kauppila, and W.E. Acree. Fluid Phase Equilib. **123**, 29 (1996).

© 2001 NRC Canada

15. L. Wang, Sh. Shen, G.C. Benson, and B.C.-Y. Lu. Fluid Phase Equilib. **95**, 43 (1994).
16. T. Hofman. Fluid Phase Equilib. **107**, 61 (1995).
17. C. Figurski, J. Gregorowicz, and S. Malanowski. Fluid Phase Equilib. **56**, 235 (1990).
18. W.E. Acree. Thermodynamic properties of nonelectrolytes solutions. Academic Press, London. 1984.
19. C. Pando, J.A.R. Renuncio, J.A.G. Calzón, J.J. Christensen, and R.M. Izatt. J. Solution Chem. **16**, 503 (1987).
20. M.M. Piñeiro, B.E. Cominges, J.L. Legido, S. García-Garabal, M. López, and M.I. Paz-Andrade. J. Therm. Anal. **52**, 799 (1998).
21. A. Fredenslund, R.L. Jones, and J.M. Prausnitz. AIChE J. **21**, 1086 (1975).
22. B. Coto, J.A.G. Calzón, C. Pando, and J.A.R. Renuncio. J. Solution Chem. **20**, 71 (1991).
23. J. Gmehling, J. Li, and M. Schiller. Ind. Eng. Chem. Res. **32**, 178 (1993).
24. J. Gmehling, J. Lohmann, A. Jakob, J. Li, and R. Joh. Ind. Eng. Chem. Res. **37**, 4876 (1998).
25. H.V. Kehiaian. Fluid Phase Equilib. **13**, 243 (1983).
26. H.V. Kehiaian. Pure Appl. Chem. **57**, 15 (1985).
27. J.A. González, J.C. Carmona, I. García de la Fuente, and J.C. Cobos. Thermochim. Acta, **326**, 53 (1999).
28. J.A. González, I. García de la Fuente, J.C. Cobos, and C. Casanova. Ber. Bunsen–Ges. **98**, 106 (1994).
29. J.A. González, I. García de la Fuente, J.C. Cobos, and C. Casanova. Fluid Phase Equilib. **78**, 61 (1992).
30. J.A. González, I. García de la Fuente, and J.C. Cobos. Can. J. Chem. **75**, 1424 (1997).
31. P.J. Flory. J. Am. Chem. Soc. **87**, 1833 (1965).
32. A. Bondi. Physical properties of molecular crystals, liquids, and glasses. J. Wiley and Sons, New York. 1968.
33. H.V. Kehiaian, J.P.-E Grolier, and G.C. Benson. J. Chim. Phys. Phys.-Chim. Biol. **75**, 1031 (1978).
34. J.A. González, I. García de la Fuente, J.C. Cobos, and C. Casanova. Ber. Bunsen-Ges. **95**, 1658 (1991).
35. H.V. Kehiaian, S. Porcedda, B. Marongiu, L. Lepori, and E. Matteoli. Fluid Phase Equilib. **63**, 231 (1991).
36. H.V. Kehiaian, J.A. González, I. García, J.C. Cobos, C. Casanova, and M.J. Cocero. Fluid Phase Equilib. **69**, 81 (1991).
37. J.A. González, I. García de la Fuente, and J.C. Cobos. Fluid Phase Equilib. **123**, 39 (1996).
38. J.A. González, I. García de la Fuente, and J.C. Cobos. Fluid Phase Equilib. **168**, 31 (2000).
39. W. Brostow and J.S. Sochanski. J. Mater. Sci. **10**, 2134 (1975).
40. L. Wang, G.C. Benson, and B.C.-Y. Lu. Thermochim. Acta, **213**, 83 (1993).
41. G.C. Benson and H.D. Pflug. J. Chem. Eng. Data, **15**, 386 (1970).
42. N. Riesco, S. Villa, J.A. González, I. García de la Fuente, and J.C. Cobos. Thermochim. Acta, **362**, 89 (2000).
43. V.T. Lam, P. Picker, D. Patterson, and P. Tancrede. J. Chem. Soc. Faraday Trans. **70**, 1465 (1974).
44. M. Costas and D. Patterson. Thermochim. Acta, **120**, 161 (1987).
45. H.S. Wu and S.I. Sandler. AIChE J. **35**, 168 (1989).
46. H.V. Kehiaian, M.R. Tiné, L. Lepori, E. Matteoli, and B. Marongiu. Fluid Phase Equilib. **46**, 131 (1989).
47. H.V. Kehiaian and M.R. Tiné. Fluid Phase Equilib. **59**, 233 (1990).
48. J.A. González, I. García de la Fuente, and J.C. Cobos. Fluid Phase Equilib. **154**, 11 (1999).
49. J.A. González, I. García de la Fuente, and J.C. Cobos. Phys. Chem. Chem. Phys. **1**, 275 (1999).
50. J.A. González, F.J. Carmona, N. Riesco, I. García de la Fuente, and J.C. Cobos. Phys. Chem. Chem. Phys. **2**, 2587 (2000).
51. S. Delcros, J.R. Quint, J.P.-E. Grolier, and H.V. Kehiaian. Fluid Phase Equilib. **113**, 1 (1995).
52. T.W. Lee, R.A. Greenkorn, and K.G. Chao. Ind. Eng. Chem. Fundam **11**, 293 (1972).
53. W.E. Acree and G.L. Bertrand. J. Phys. Chem. **81**, 1170 (1977).
54. T.E. Burchfield and G.L. Bertrand. J. Solution Chem. **4**, 205 (1975).
55. D.S. Abrams and J.M. Prausnitz. AIChE J. **14**, 135 (1968).
56. P. Pfestorf, D. Kuchenbecker, and K. Quitzsch. J. Therm. Anal. **14**, 115 (1978).
57. A.R. Mathieson and J.C.J. Thynne. J. Chem. Soc. 3713 (1956).
58. K. Ridgway and P.A. Butler. J. Chem. Eng. Data, **12**, 509 (1967).
59. C.P. Brown, A.R. Mathieson, and J.C.J. Thynne. J. Chem. Soc. 4141 (1955).
60. H.W. Schnaible, H.C. Van Ness, and J.M. Smith. AIChE J. **3**, 147 (1957).
61. L. Zhou, Y. Wang, Y. Zhang, J. Shi, G.C. Benson, and B.C.-Y. Lu. J. Chem. Thermodyn. **23**, 791 (1991).
62. J.R. Goates, R.J. Sullivan, and J.B. Ott. J. Phys. Chem. **63**, 589 (1959).
63. B.S. Lark, S. Kaur, and S. Singh. Thermochim. Acta, **105**, 219 (1986).
64. M. López, E. Carballo, J.L. Legido, J. Salgado, J. Vijande, and M.I. Paz-Andrade. J. Chem. Thermodyn. **27**, 879 (1995).
65. M. López, M.I. Paz-Andrade, J. Peleteiro, J.L. Legido, L. Romaní, and E. Pérez Martell. Thermochim. Acta, **211**, 33 (1992).
66. M. López, E. Carballo, C. Franjo, J. Salgado, J. Vijande, and J.L. Legido. J. Chem. Thermodyn. **27**, 1281 (1995).
67. M. López, M.I. Paz-Andrade, J.L. Legido, L. Romaní, J. Peleteiro, and E. Jiménez. Phys. Chem. Liq. **25**, 145 (1993).
68. S. Zhu, S. Shen, G.C. Benson, and B.C.-Y. Lu. Thermochim. Acta, **235**, 161 (1994).
69. A. Knezevic-Stevanovic, Z.-L. Jin, G.C. Benson, and B.C.-Y. Lu. J. Chem. Thermodyn. **27**, 423 (1995).
70. A. Knezevic-Stevanovic, G.C. Benson, and B.C.-Y. Lu. J. Chem. Thermodyn. **27**, 531 (1995).
71. S. Zhu, S. Shen, G.C. Benson, and B.C.-Y. Lu. J. Chem. Thermodyn. **26**, 421 (1994).
72. H. Kirss, M. Kuus, E. Siimer, and L. Kudryavtseva. ELDATA: Int. Electron J. Phys.-Chem. Data, **4**, 149 (1998).
73. M.D. Donald and K. Ridgeway. J. Appl. Chem. **8**, 408 (1958).
74. A. Schumichen. Ph. D. Thesis (1978); C. Christensen, J. Gmehling, P. Rasmussen, and U. Weidlich. Heats of mixing collection. Chemistry Data Series. Vol. II. DECHEMA, Germany. 1984. Part 2.
75. D. Liao, Z. Tong, G.C. Benson, and B.C.-Y. Lu. Fluid Phase Equilib. **131**, 133 (1997).
76. Z. Tong, D. Liao, G.C. Benson, and B.C.-Y. Lu. Can. J. Chem. **75**, 308 (1997).
77. Z. Tong, G.C. Benson, L.L. Wang, and B.C.-Y. Lu. J. Chem. Eng. Data, **41**, 865 (1996).
78. D. Gravelle, Z. Tong, G.C. Benson, and B.C.-Y. Lu. J. Solution Chem. **26**, 85 (1997).
79. Z. Tong, D. Liao, G.C. Benson, and B.C.-Y. Lu. J. Chem. Thermodyn. **29**, 431 (1997).
80. G.C. Benson, L.L. Wang, and B.C.-Y. Lu. J. Chem. Thermodyn. **30**, 1533 (1998).
81. A.M. Fanni, B. Marongiu, B. Pittau, and S. Porcedda. Fluid Phase Equilib. **126**, 163 (1996).
82. B. Marongiu, C. Delitala, B. Pittau, and S. Porcedda. Fluid Phase Equilib. **109**, 67 (1995).

© 2001 NRC Canada

83. J.R. Battler and R.L. Rowley. J. Chem. Thermodyn. **17**, 719 (1985).
84. V.F. Sergeeva and I.Z. Usmanova. Zh. Obshch. Khim. **46**, 722 (1976).
85. I. Nagata. J. Chem. Thermodyn. **26**, 1293 (1994).
86. C.C. Tsao and J.M. Smith. Chem. Eng. Prog. Symp. Ser. **49**, 107 (1953).
87. I. Nagata. Thermochim. Acta, **255**, 23 (1995).
88. I. Nagata and K. Tamura. Fluid Phase Equilib. **15**, 67 (1983).
89. I. Nagata. J. Chem. Thermodyn. **27**, 207 (1995).
90. L. Wang, G.C. Benson, and B.C.-Y. Lu. J. Chem. Thermodyn. **24**, 1135 (1992).
91. S.R. Goodwin and D.M.T. Newshan. J. Chem. Thermodyn. **3**, 325 (1971).
92. H. Grosse-Wortmann, W. Jost, and H.G. Wagner. Z. Phys. Chem. (Frankfurt/Main), **49**, 74 (1966).
93. S. Zhu, S. Shen, G.C. Benson, and B.C.-Y. Lu. J. Chem. Thermodyn. **25**, 909 (1993).
94. H.K. DeQ Jones, and B.C.-Y. Lu. J. Chem. Eng. Data, **11**, 488 (1966).
95. B.C.-Y. Lu and H.K. DeQ Jones. Can. J. Chem. Eng. **44**, 251 (1966).
96. T.B. Tai, R.S. Ramalho, and S. Kaliguine. Can. J. Chem. Eng. **50**, 772 (1972).
97. L. Wang, G.C. Benson, and B.C.-Y. Lu. J. Chem. Eng. Data, **37**, 403 (1992).
98. F. Vesely, V. Dohnal, and M. Prchal. Coll. Czech. Chem. Commun. **47**, 1045 (1982).
99. I. Nagata and K. Tamura. J. Chem. Thermodyn. **18**, 827 (1986).
100. I. Nagata, H. Asano, and K. Fujiwara. Fluid Phase Equilib. **1**, 211 (1978).
101. I. Nagata, K. Fujiwara, and Y. Ogasawara. J. Chem. Thermodyn. **10**, 1201 (1978).
102. I. Nagata, Y. Kawamura, Y. Ogasawara, and S. Tokuriki. J. Chem. Thermodyn. **12**, 223 (1980).
103. K. Tamura and I. Nagata. J. Chem. Eng. Data, **32**, 45 (1987).
104. C. González Posa, L. Núñez, and E. Villar. J. Chem. Thermodyn. **4**, 275 (1972).
105. L. Núñez, E. Isorna, and M.I. Paz-Andrade. Acta Cient. Compostelana, **XIII**, 3 (1976).
106. J.A. González, I. García de la Fuente, J.C. Cobos, C. Casanova, and A. Ait-Kaci. Fluid Phase Equilib. **112**, 63 (1995).
107. A. Ait-Kaci. Ph.D. Thesis, Lyon, France, 1982.
108. H.V. Kehiaian and B. Marongiu. Fluid Phase Equilib. **40**, 23 (1988).
119. C. Delitala, B. Marongiu, S. Porcedda, Fluid Phase Equilib. **142**, 1 (1998).
110. G. Avedis, J.-P.E Grolier, J. Fernández, and H.V. Kehiaian. J. Solution Chem. **23**, 135 (1994).
111. J.A. González, I. García de la Fuente, and J.C. Cobos. J. Chem. Soc. Faraday Trans. **93**, 3773 (1997).
112. I. Velasco, J. Fernández, S. Otín, and H.V. Kehiaian. Fluid Phase Equilib. **69**, 15 (1991).
113. I. Velasco, J. Fernández, and S. Otín. Phys. Chem. Liq. **31**, 151 (1996).
114. J. Fernández, R. Garriga, I. Velasco, and S. Otín. Fluid Phase Equilib. **152**, 243 (1998).
115. B. Marongiu, B. Pittau, and S. Porcedda. Thermochim. Acta, **221**, 143 (1993).
116. J.A. González, I. García de la Fuente, J.C. Cobos, and C. Casanova. J. Solution Chem. **23**, 399 (1994).
117. J.A. González, I. García de la Fuente, J.C. Cobos, and C. Casanova. Fluid Phase Equilib. **93**, 1 (1994).
118. J.A. González, I. García de la Fuente, J.C. Cobos, and C. Casanova. Thermochim. Acta, **237**, 261 (1994).
119. J.A. González, I. García de la Fuente, and J.C. Cobos. Can. J. Chem. **78**, 1272 (2000).

© 2001 NRC Canada

Appendix

Table A1. References for DISQUAC interaction parameters for contacts listed. References are also valid for geometrical parameters of the involved groups.

	Reference
CH_2–C_6H_{12} in cyclohexane + *n*-alkanes	106
C_6H_6–CH_2 in benzene + *n*-alkanes	107
C_6H_5–CH_2 in toluene + *n*-alkanes	107
CCl_4–CH_2 in CCl_4 + *n*-alkanes	107
C_6H_{12}–C_6H_6 in cyclohexane + benzene	33
C_6H_{12}–C_6H_5 in cyclohexane + toluene	27
C_6H_{12}–CCl_4 in cyclohexane + CCl	108
C_6H_6–CCl_4 in benzene + CCl	33
O–CH_2 in linear oxaalkanes + *n*-alkanes	46
O–CH_2 in tetrahydrofuran + *n*-alkanes	46
O–C_6H_{12} in tetrahydrofuran + cyclohexane	46
O–CH_2 in tertiary alkyl ethers + *n*-alkanes	50
O–C_6H_{12} in tertiary alkyl ethers + cyclohexane	50
CO–CH_2 in linear alkanones + *n*-alkanes	35
CO–C_6H_{12} in linear alkanones + cyclohexane	35
CO–C_6H_6 in linear alkanones + benzene	109
CO–CCl_4 in linear alkanones + CCl	109
CO–O in 2-propanone + tetrahydrofuran	82
Cl–CH_2 in $CHCl_3$ + *n*-alkanes	108
Cl–C_6H_{12} in $CHCl_3$ + C_6H_{12}	108
COO–CH_2 in esters + *n*-alkanes	110
CO–Cl in linear alkanones + $CHCl_3$	111
NH_2–CH_2 in primary amines + *n*-alkanes	112
NH_2–C_6H_6 in primary amines + C_6H_6	113
NH_2–C_6H_5 in primary amines + C_7H_8	114
CN–CH_2 in n-alkanenitriles + *n*-alkanes	115
CN–C_6H_{12} in *n*-alkanenitriles + cyclohexane	115
OH–CH_2 in 1-alkanols + *n*-alkanes	116
OH–C_6H_{12} in 1-alkanols + cyclohexane	116
OH–C_6H_6 in 1-alkanols + benzene	117
OH–C_6H_5 in 1-alkanols + toluene	118
OH–CCl_4 in 1-alkanols + CCl_4	119
OH–CH_2 in *sec*-alkanols + *n*-alkanes	119
OH–C_6H_{12} in *sec*-alkanols + cyclohexane	119
OH–C_6H_6 in *sec*-alkanols + benzene	119
OH–C_6H_5 in *sec*-alkanols + toluene	119

Table A2. Interchange coefficients, dispersive (DIS) and quasichemical (QUAC), $C_{st,1}^{DIS}$ and $C_{st,1}^{QUAC}$, (l = 1, Gibbs energy; l = 2, enthalpy; l = 3, heat capacity) fitted in this work.

Contacts	$C_{st,1}^{DIS}$	$C_{st,2}^{DIS}$	$C_{st,3}^{DIS}$	$C_{st,1}^{QUAC}$	$C_{st,2}^{QUAC}$	$C_{st,3}^{QUAC}$
1,2-Dimethylbenzene + *n*-C_9						
C_6H_4–CH_2	0.3[a]	0.8	0.0	0.0	0.0	0.0
DIPE + *n*-C_n						
O–CH_2	10.6	24.0	0.0	2.8	2.9	0.0
2-Hexanone + 1,2-dimethylbenzene						
CO–C_6H_4	0.6[a]	3.6	0.0	4.45	–0.2	0.0
1-Alkanols + benzene						
1-Octanol	8.16	–0.4	–38.0	8.9	16.7	21.2
1-Decanol	12.8	1.0	–38.0	8.9	16.7	21.2
1-Tridecanol	23.4	4.0	–38.0	8.9	16.7	21.2
≥1-Hexadecanol	29.5	6.0[a]	–38.0	8.9	16.7	21.2

[a]Estimated value.

© 2001 NRC Canada

Solubility of nonpolar gases in 2,2,2-trifluoroethanol and 1,1,1,3,3,3-hexafluoropropan-2-ol at several temperatures and 101.33 kPa partial pressure of gas

Miguel Angel Sánchez, Ana María Mainar, Juan Ignacio Pardo, María Carmen López, and José Santiago Urieta

Abstract: Solubilities, expressed as mol fractions, of 14 nonpolar gases (He, Ne, Ar, Kr, Xe, H_2, N_2, O_2, CH_4, C_2H_4, C_2H_6, CO_2, CF_4, and SF_6) in 2,2,2-trifluoroethanol (TFE) at 268.15 and 283.15 K and 1,1,1,3,3,3-hexafluoropropan-2-ol (HFIP) at 273.15 and 283.15 K, with the partial pressure of gas being 101.33 kPa for all measurements, are reported. Standard changes in the thermodynamic functions (enthalpy and entropy) have been calculated from the solubilities and their variation with temperature. The Scaled Particle Theory (SPT) model has been used to determine these thermodynamic functions and also the partial molar volumes of the gases in the formed solutions.

Key words: gas solubilities, nonpolar gases, fluoroalcohols, Scaled Particle Theory.

Résumé : On rapporte les solubilités, en forme de fractions molaires, de 14 gazes apolaires (He, Ne, Ar, Kr, Xe, H_2, N_2, O_2, CH_4, C_2H_4, C_2H_6, CO_2, CF_4 et SF_6) dans 2,2,2-trifluoretanol (TFE) à 268,15 et 283,15 K et dans 1,1,1,3,3,3-hexafluorpropan-2-ol à 273,15 et 283,15 K. La pression partielle du gaz a eté 101,33 kPa en toutes les mesures. On a calculé, en utilisant les solubilités et leur variation a l'égard de la temperature, les changes standard des fonctions thermodynamiques enthalpie and entropie. On a employé le modèle SPT pour déterminer ces mêmes fonctions thermodynamiques et aussi les volumes molaires partielles des gazes dans les solutions formées.

Mots clés : solubilité du gaz, gazes apolaires, fluoralcool, Scaled Particle Theory.

Introduction

The gathering of experimental data about the thermodynamical properties of solutions and liquid mixtures is very important to the improvement of industrial equipment and processes and also to achieve a better knowledge of the molecular interactions that rule the liquid state. This is also true of the solutions of gases in liquids.

In this paper, we report the solubilities of gases in fluoroalcohols. Specifically, the solubilities of 14 nonpolar gases (He, Ne, Ar, Kr, Xe, H_2, N_2, O_2, CH_4, C_2H_4, C_2H_6, CO_2, CF_4, and SF_6) have been measured in 2,2,2-trifluoroethanol (TFE) at 268.15 and 283.15 K and 1,1,1,3,3,3-hexafluoropropan-2-ol (HFIP) at 273.15 and 283.15 K, with the partial pressure of gas being 101.33 kPa. The solubilities are expressed as mol fractions of gas dissolved in the liquid and have been determined taking the real behaviour of the gas phase into account. The aim of this work was to establish the influence of temperature on solubility for values below 298.15 K on systems that we had already studied (1, 2). Moreover, these data together with those previously reported permits us to calculate the standard changes of enthalpy ($\Delta\overline{H}^0_{m,2}$) and entropy ($\Delta\overline{S}^0_{m,2}$) for the solution process from the temperature dependence of the solubility.

The reported results are inscribed in a study of the solubilities of gases in mixtures of water and fluoroalcohol; mixtures that have gained interest because they offer the possibility of modulating the solvophobic effect, which has relevant influence on the kinetics and the selectivity of organic reactions such as Diels-Alder type reactions (3). The solubility measurement is a way of determining the solvophobic effect.

The Scaled Particle Theory (SPT), which provides expressions for the values of the changes of thermodynamic functions in the solution process, has also been applied to determine the changes in enthalpy and entropy that are then compared with those obtained from the experimental results. Another property that can be calculated with this theory is the partial molar volume of the gas in the solution. The obtained values of the partial molar volumes are compared with those provided by a model based on the regular solution (4).

Experimental

The equipment and procedure used to carry out the solubility measurements have been described in detail elsewhere

Received March 30, 2001. Published on the NRC Research Press Web site at http://canjchem.nrc.ca on October 9, 2001.

M.A. Sánchez, A.M. Mainar, J.I. Pardo, M.C. López, and J.S. Urieta.[1] Departamento de Química Orgánica-Química Física, Facultad de Ciencias, Universidad de Zaragoza, Ciudad Universitaria, Zaragoza, 50009, Spain.

[1]Corresponding author (telephone: 34 976 761 298; fax: 34 976 761 202; e-mail: urieta@posta.unizar.es).

 DOI: 10.1139/cjc-79-10-1460 © 2001 NRC Canada

(5). The apparatus is similar to that designed by Ben-Naim and Baer (6) and an scheme of it appears in Fig. 1. The experimental technique is based on the determination of the volume of wet gas (gas saturated with solvent vapour), which dissolves in a known mass of solvent at constant pressure (approximately 101.33 kPa partial pressure of gas) and temperature. The amount of wet gas is measured through the volume of mercury introduced in a system of burettes to keep the pressure balanced. The solvent is placed in a solution vessel immersed in a water bath whose temperature is maintained within 0.05 K. The whole apparatus is located in a thermostated air bath, with its temperature being controlled within 0.2 K. The temperature of the air bath is greater than that of the water bath to prevent the condensation of the solvent out of the solution vessel. The precision in the mol fraction of dissolved gas (x_2) is estimated to be 1% in the worst case, i.e., for the lowest solubility.

The gases used were: He (99.995%), Ar (99.999%), Xe (99.995%), H_2 (99.99%), N_2 (99.998%), O_2 (99.98%), CH_4 (99.95%), C_2H_4 (99.0%), C_2H_6 (99.90%), CF_4 (99.9%), SF_6 (99.5%), and CO_2 (99.998%), all from Air Liquide España, and Ne (99.9%) and Kr (99.95%) from Linde.

The liquid 2,2,2-trifluoroethanol (TFE) was a Jansen product, whereas 1,1,1,3,3,3- hexafluoropropan-2-ol (HFIP) was purchased from Fluka; both of them with a stated purity >99%. The purities of these liquids were checked by GLC.

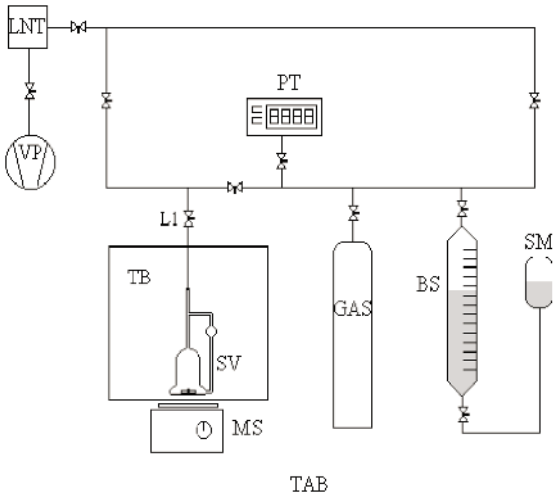
Solubilities and thermodynamic properties for the solution process

The data treatment for calculating solubility is a modification (2, 7) of the data reduction method proposed by Wilhelm and Battino (8, 9). The modification takes into account the characteristics of our apparatus, in particular that the gas phase includes solvent vapour that must be discounted and that the temperature of the gas phase in the burettes is different from the temperature in the solution vessel. The method determines the actual amount of gas dissolved in the liquid and also the actual partial pressure over the solution. Then the solubility is corrected to the partial pressure of 101.33 kPa. The calculation was carried out considering both ideal and real behaviour of the gas phase.

In the latter case the second virial coefficients (SVC) for the pure compounds and their mixtures are required. The SVC for the gases were obtained from the literature (10), while those of both pure fluoroalkanols and gas–liquid mixtures were calculated using the method of Maris and Stiel (11). The resulting SCV for HFIP and the corresponding mixtures as a function of the temperature have been reported in a previous paper (2), and those for TFE are listed in Table 1 over the temperature range of 268.15 to 309.15 K.

The differences between solubilities corresponding to the ideal and the real behaviour of the gas phase follow the pattern observed at 298.15 K (1, 2), i.e., when TFE is the solvent the deviations are above the experimental error only for the most soluble gases, whereas in the case of HFIP many of the gases show much high deviations. Table 2 shows the solubilities of gases (real behaviour) in TFE at 268.15 and 283.15 K and in HFIP at 273.15 and 283.15 K. Intervals of the same size were looked for, but were not possible in the case of HFIP whose freezing point is about 269 K. To the best of our knowledge, the solubility data for our gases either in TFE or in HFIP are not available in the literature.

Fig. 1. Scheme of the gas solubility apparatus with the following abbreviations: vacuum pump (VP), liquid nitrogen trap (LNT), pressure transducer (PT), thermostated bath (TB), solution vessel (SV), magnetic stirrer (MS), burettes system (BS), storage of mercury (SM), thermostated air bath (TAB).



The mol fractions of gas in liquid (x_2) for the temperatures considered in this paper along with those at 298.15 K (1, 2) have been adjusted as a function of the temperature using the following polynomial, which is convenient (12) for this rather narrow temperature range.

$$[1] \qquad \ln x_2 = A_0 + \frac{A_1}{T}$$

The coefficients A_0 and A_1, obtained by means of a least-squares method, are been listed in the Table 3, together with the corresponding square regression coefficients.

From the solubility values, changes in the Gibbs energy ($\Delta\bar{G}^0_{m,2}$), enthalpy ($\Delta\bar{H}^0_{m,2}$), and entropy ($\Delta\bar{S}^0_{m,2}$) can be determined for the hypothetical solution process

$$[2] \qquad \text{M (gas, hyp., 101.33 kPa)} \rightarrow \text{M (solution, hyp., } x_2 = 1)$$

using the relations reported by Clever and Battino (12) and Wilhelm et al. (13).

$$[3] \qquad \Delta\bar{G}^0_{m,2} = \mathrm{R}T \ln x_2\ (sat) = -\mathrm{R}T\left(A_0 + \frac{A_1}{T}\right)$$

$$[4] \qquad \Delta\bar{H}^0_{m,2} = \mathrm{R}T\left[\frac{\partial \ln x_2\ (sat)}{\partial \ln T}\right] = -\mathrm{R}A_1$$

$$[5] \qquad \Delta\bar{S}^0_{m,2} = \left[\frac{\partial \ln x_2\ (sat)}{\partial \ln T}\right] + \ln x_2 = RA_0$$

The values of these standard partial molar thermodynamic properties are given in Table 4 for TFE and in Table 5 for HFIP.

© 2001 NRC Canada

Table 1. Coefficients for the equation B_{ij} ($cm^3\ mol^{-1}$) = $A + BT + CT^2 + DT^3$ in the range 268.15–309.15 K, along with the corresponding square regression coefficients (r^2).

System	*A*	*B*	*C*	*D* (1×10^{-5})	r^2
TFE	–272067	9222	–28.81	—	0.9993
TFE + He	–75.387	0.8880	–0.00264	0.2702	0.9997
Ne	251.79	–3.1676	0.01220	–1.485	0.9993
Ar	–878.05	6.5591	–0.01828	1.820	0.9980
Kr	1561.8	–21.209	0.08356	–10.46	0.9967
Xe	–17830	177.97	–0.60185	68.28	0.9976
H_2	–218.76	1.7416	–0.00488	0.4973	0.9999
N_2	–148.76	–1.1459	0.00927	–1.474	0.9980
O_2	4472.8	–49.560	0.17752	–20.91	0.9980
CH_4	–1243.5	9.3597	–0.02678	2.770	0.9980
C_2H_4	683.85	–14.692	0.06526	–8.622	0.9999
C_2H_6	–3746.5	29.708	–0.08494	8.418	0.9996
CO_2	–15588	153.74	–0.51520	58.01	0.9990
CF_4	–19055	189.77	–0.63813	71.89	0.9990
SF_6	–31746	312.60	–1.0406	116.2	0.9997

Table 2. Solubility (x_2, 1×10^4) of gases in TFE and HFIP at 101.33 kPa partial pressure of gas and the indicated temperatures.

	TFE		HFIP	
Gas	268.15 K	283.15 K	273.15 K	283.15 K
He	1.13	1.41	2.24	2.38
Ne	1.73	1.99	3.66	3.79
Ar	9.21	8.87	16.26	15.51
Kr	20.88	18.81	31.61	29.91
Xe	49.48	42.59	69.16	61.28
H_2	2.13	2.43	3.50	3.84
N_2	6.02	6.23	11.61	11.68
O_2	9.36	9.29	16.60	16.37
CH_4	13.20	12.32	19.71	19.37
C_2H_4	73.61	60.42	127.0	117.2
C_2H_6	61.44	50.51	79.75	71.84
CO_2	209.7	152.2	264.8	221.9
CF_4	16.87	14.99	38.76	35.57
SF_6	89.88	68.45	230.7	186.4

Scaled Particle Theory (SPT)

General features

A model often used in the treatment of solubilities of gases in liquids is the Scaled Particle Theory (SPT) because it provides a reasonable mechanism for the solution process, leads to acceptable results for the solubility values, and allows the determination of molecular parameters for the liquid solvent, namely, the effective hard-sphere diameter and the depth of the energy well. Although the theory was developed for organic solvents with low dipole moments (14), it has yielded good results when extended to rather polar liquids (15, 16) or associated solvents like alcohols (9, 17) and even water (18–20). Therefore, its application to these systems can lead to reliable information about TFE and HFIP. According to SPT formalism (9, 13, 14, 21) the solution process takes place in two steps: (*i*) creation in the solvent of a cavity of the right size to accommodate the molecule of solute and (*ii*) insertion of the solute molecule into the cavity and then interaction between solvent and solute.

The thermodynamic functions for the first step are derived using the SPT equations for hard spheres (13, 22). The calculation of the thermodynamic properties associated to the interaction step (13) is usually carried out on the basis of an effective Lennard–Jones (6, 12) potential, corrected with terms that take the dipole–dipole and dipole-induced dipole interactions into account. The hard sphere diameter of the liquid solvent (σ_1) determined with SPT equations is identified with the distance parameter of the potential and then the energy parameter (ε_1/k) can be obtained from the values of the Gibbs energy changes.

Given that the results of the theory concerning values of solubility and change of Gibbs energies for both solvents at 298.15 K have been already considered (1, 2), in this paper we focus on the changes in enthalpy and entropy. The values of the partial molar volume of the solute in solution with

© 2001 NRC Canada

Table 3. Coefficients A_0 and A_1 for the fitting of experimental values to eq. [1] along with the corresponding square regression coefficients (r^2).

	A_0		A_1		r^2	
Gas	TFE	HFIP	TFE	HFIP	TFE	HFIP
He	–4.715	–6.595	–1174.19	–494.405	0.9994	0.9990
Ne	–5.991	–6.843	–716.191	–292.346	0.9999	0.9981
Ar	–7.686	–7.736	186.518	358.912	1.0000	0.9999
Kr	–8.175	–7.252	537.573	408.125	0.9999	0.9996
Xe	–8.100	–8.562	748.299	980.836	0.9999	0.9995
H_2	–5.872	–5.420	–696.091	–692.676	0.9996	0.9993
N_2	–6.738	–6.579	–181.527	–48.9142	0.9994	0.9986
O_2	–7.122	–6.767	39.7977	100.037	0.9990	0.9989
CH_4	–8.034	–6.454	376.993	61.5376	0.9984	0.9968
C_2H_4	–8.475	–6.557	954.837	598.097	0.9991	0.9996
C_2H_6	–8.839	–7.803	1032.24	811.785	0.9994	1.0000
CO_2	–9.797	–9.036	1590.16	1477.67	0.9998	0.9987
CF_4	–8.827	–7.754	655.867	600.523	0.9981	0.9991
SF_6	–9.521	–9.421	1287.91	1542.68	0.9980	0.9989

Table 4. Standard partial molar changes in the Gibbs energy, enthalpy, and entropy for the solution process of the gases in TFE.

	$\Delta\overline{G}^0_{m,2}$ (kJ mol^{-1})		$\Delta\overline{H}^0_{m,2}$	$\Delta\overline{S}^0_{m,2}$	$\Delta\overline{H}^{0(SPT)}_{m,2}$	$\Delta\overline{S}^{0(SPT)}_{m,2}$
Gas	268.15 K	283.15 K	(kJ mol^{-1})	(kJ K^{-1} mol^{-1})	(kJ mol^{-1})	(kJ K^{-1} mol^{-1})
He	20.26	20.87	9.762	–0.039	2.885	–0.060
Ne	19.31	20.06	5.954	–0.049	1.095	–0.061
Ar	15.58	16.54	–1.550	–0.063	–1.968	–0.062
Kr	13.76	14.77	–4.469	–0.068	–3.492	–0.062
Xe	11.84	12.85	–6.221	–0.067	–5.348	–0.063
H_2	18.85	19.59	5.754	–0.048	1.505	–0.061
N_2	16.53	17.38	1.509	–0.056	–0.465	–0.062
O_2	15.55	16.43	–0.330	–0.059	–1.650	–0.062
CH_4	14.78	15.77	–3.134	–0.066	–3.117	–0.062
C_2H_4	10.95	–7.938	–7.938	–0.070	–5.654	–0.063
C_2H_6	11.35	12.45	–8.582	–0.074	–6.192	–0.064
CO_2	8.616	9.852	–13.22	–0.081	–4.341	–0.063
CF_4	14.23	15.31	–5.452	–0.073	–1.323	–0.065
SF_6	10.50	11.73	–10.70	–0.073	–5.161	–0.067

Note: Also listed are the partial molar changes in enthalpy and entropy calculated with SPT.

each of the fluoroalcohols at 298.15 K will also be considered.

Enthalpy and entropy of solution

The change of enthalpy accompanying the solution process can be expressed (23) by

$$[6]\qquad \Delta\overline{H}^{0(SPT)}_{m,2} = \left[\frac{\partial\left(\dfrac{\Delta\overline{G}^{0(SPT)}_{m,2}}{T}\right)}{\partial\left(\dfrac{1}{T}\right)}\right]_P = \Delta\overline{H}_c + \Delta\overline{H}_i - \mathrm{R}T + \alpha_P \mathrm{R}T^2$$

where $\Delta\overline{G}^{0(SPT)}_{m,2}$ is the change in the Gibbs energy provided by the model, $\Delta\overline{H}_c$ and $\Delta\overline{H}_i$ are the changes of enthalpy in the formation of cavity and interaction steps, respectively, and α_P is the thermal expansion coefficient of the solvent.

The entropy can be directly obtained from the following relation:

$$[7]\qquad \Delta\overline{S}^{0(SPT)}_{m,2} = \frac{\Delta\overline{H}^{0(SPT)}_{m,2} - \Delta\overline{G}^{0(SPT)}_{m,2}}{T}$$

From values for σ_1 and ε_1/k, these thermodynamic functions can be obtained through SPT. Thus, the partial molar enthalpies of solution ($\Delta\overline{H}^{0(SPT)}_{m,2}$) and partial molar entropies of solution ($\Delta\overline{S}^{0(SPT)}_{m,2}$) can be found in the last columns of Tables 4 and 5. The values used for σ_1, ε_1/k, and α_P have been reported in a previous paper (2).

A point to be remarked is that the change of enthalpy for the formation of the cavity ($\Delta\overline{H}_c$) depends on the following parameter:

© 2001 NRC Canada

Table 5. Standard partial molar changes in the Gibbs energy, enthalpy, and entropy for the solution process of the gases in HFIP.

Gas	$\Delta\bar{G}^0_{m,2}$ (kJ mol^{-1}) 273.15 K	$\Delta\bar{G}^0_{m,2}$ (kJ mol^{-1}) 283.15 K	$\Delta\bar{H}^0_{m,2}$ (kJ mol^{-1})	$\Delta\bar{S}^0_{m,2}$ (kJ K^{-1} mol^{-1})	$\Delta\bar{H}^{0(SPT)}_{m,2}$ (kJ mol^{-1})	$\Delta\bar{S}^{0(SPT)}_{m,2}$ (kJ K^{-1} mol^{-1})
He	19.08	19.64	4.100	–0.054	5.040	–0.049
Ne	17.97	18.55	2.430	–0.056	3.237	–0.049
Ar	14.58	15.23	–2.983	–0.064	0.812	–0.047
Kr	13.07	13.68	–3.393	–0.060	–0.352	–0.046
Xe	11.30	11.99	–8.154	–0.071	–1.662	–0.045
H_2	18.07	18.51	5.758	–0.054	3.883	–0.049
N_2	15.35	15.90	0.406	–0.054	2.772	–0.046
O_2	14.54	15.10	–0.831	–0.056	1.190	–0.047
CH_4	14.15	14.71	–0.511	–0.053	0.138	–0.046
C_2H_4	9.915	10.47	–4.972	–0.054	–2.003	–0.045
C_2H_6	10.97	11.62	–6.749	–0.064	–1.925	–0.044
CO_2	8.246	8.965	–12.28	–0.075	–0.892	–0.045
CF_4	12.61	13.41	–4.993	–0.064	3.197	–0.042
SF_6	8.559	9.375	–12.82	–0.078	1.141	–0.038

Note: Also listed are the partial molar changes in enthalpy and entropy calculated with SPT.

$$[8] \qquad l_1 = \left(\frac{1}{\sigma_1}\right)\left(\frac{\partial\sigma_1}{\partial T}\right)_P$$

that expresses the relative variation of the hard sphere diameter as the temperature changes. The calculated enthalpies and entropies correspond to a value of $l_1 = 0$. In relation to this parameter, it is interesting to comment that the original version (14) of the model did not take into account the variation of σ_1 with the temperature. Ben-Naim and Friedman (24) pointed out that this variation should be considered and, therefore, two alternative models (18, 25) were proposed to obtain l_1. Although the temperature dependence of σ_1 has been discussed in some papers (9, 26), the values of enthalpy and entropy changes calculated with these nonzero coefficients do not lead for most gases to better values than those derived when the temperature dependence is not considered (16, 17, 27). In some cases they are actually unable to predict even the sign of the enthalpy change. This is probably because the values for σ_1 vary very slightly and the figures on which the coefficient l_1 depends on are affected by large errors.

As can be seen from the results shown in Tables 4 and 5, the predictions of the SPT formalism for the changes of enthalpy are, in general, not as good as they were for the corresponding Gibbs energy changes. On the other hand, it predicts reasonably well the changes in entropy. All this is in agreement with the acceptable performance of the model from a quantitative point of view.

Partial molar volumes of the gas solutes

The partial molar volume of a gas in the solution can be calculated (14), using the following expression:

$$[9] \qquad \bar{V}_2 = \Delta\bar{V}_c + \Delta\bar{V}_i + \kappa_T RT$$

where $\Delta\bar{V}_c$ and $\Delta\bar{V}_i$ are the volume changes upon cavity formation and charging, respectively, and κ_T is the isothermal compressibility of the solvent.

The value of $\Delta\bar{V}_i$ cannot be estimated but will be small for weakly interacting substances. Thus, for the considered gases it can be made equal to zero. The suitability of this approximation was corroborated in the original paper (14) through the comparison of the results provided by the theory for gases in several liquids. On the other hand, the partial molar volume for the cavity formation is given by

$$[10] \qquad \Delta\bar{V}_c = \left(\frac{\partial\Delta\bar{G}_c}{\partial P}\right)_{T,x} = \left(\frac{\kappa_T}{\alpha_P}\right)\Delta\bar{H}_c + \frac{\pi\sigma_2^3 N_A}{6}$$

where σ_2 is the hard sphere diameter of the gas considered.

The hard sphere diameters (σ_2) and the values of α_P can be found in ref. 2 and the isothermal compressibility (κ_T) was evaluated by means of

$$[11] \qquad \kappa_T = \frac{1}{\rho_1 u^2} + \frac{\alpha_P T V_{m,1}}{C_{P,1}}$$

with u being the speed of sound in the solvent and $C_{P,1}$ the heat capacity at constant pressure of the same solvent. The values of u were measured in our laboratory with a densimeter and sound analyzer Anton Paar DSA 48, whereas the $C_{P,1}$ values were obtained from the literature for TFE (28) and measured for HFIP.[2] The values of α_P, u, $V_{m,1}$ (2), and $C_{P,1}$ are listed in Table 6.

The calculated values of $\bar{V}_2$, for both solvents, are gathered in Table 7. It can be seen that the volumes are somewhat greater when the liquid solvent is HFIP. Given that there are no experimental data available to check the adequacy of the results, we have compared these results with those proposed by Prausnitz and Shair (4) (Table 7). These volumes are valid for nonpolar solvents.

Quite a good agreement can be observed between our results and those of Prausnitz and Shair, except in the case of nitrogen and oxygen, which exhibit rather higher deviations. This agreement is especially remarkable for noble gases in

[2] The measurement of the value of $C_{P,1}$ for HFIP was carried out by the team of Dr. L. Romaní (Universidad de Vigo) by means of a differential scanning calorimeter (Setaram Micro DSC II), which has a precision of ±0.03 J K^{-1} mol^{-1}.

© 2001 NRC Canada

Table 6. Data necessary for the calculation of the partial molar volume of the gases in solution.

Liquid	α_P (1×10^3, K^{-1})	u (ms^{-1})	$V_{m,1}$ (1×10^6, $m^3\ mol^{-1}$)	$C_{P,1}$ ($J\ mol^{-1}\ K^{-1}$)
TFE	1.255[a]	833.1	72.38[a]	177.87[b]
HFIP	1.594[a]	695.8	104.75[a]	301.6[c]

[a]Reference 2.
[b]Reference 27.
[c]Measured by the team of Dr. Romaní (Universidad de Vigo).

Table 7. Calculated partial molar volumes of the gases in the fluoroalcohols along with the values provided by Prausnitz and Shair.

	$\bar{V}_2$ (1×10^6, $m^3\ mol^{-1}$)		Prausnitz and
Gas	TFE	HFIP	Shair[a]
He	31.7	40.6	
Ne	34.7	44.0	
Ar	48.1	59.6	57.1
Kr	54.9	67.4	65.0
Xe	63.2	76.9	
H_2	36.2	45.8	31.0
N_2	55.7	68.3	32.4
O_2	49.4	61.1	33.0
CH_4	55.7	68.3	52.0
C_2H_4	66.6	80.8	65.0
C_2H_6	76.9	92.4	70.0
CO_2	62.6	76.2	55.0
CF_4	87.2	104.0	
SF_6	124.3	145.5	

[a]Reference 4.

HFIP and for the remaining ones (excluding the mentioned nitrogen and oxygen) in TFE.

The values of Prausnitz and Shair were estimated based on a model (4) that resembles that of SPT in the fact that the model divides the solution process into two steps: (*i*) isothermal condensation of the gas to a hypothetical state having a liquid-like volume and (*ii*) solution of the hypothetical liquid-like fluid into the solvent. As occurs in the SPT formalism, the change in volume accompanying the second step is zero because it is treated considering the formation of a regular solution, i.e., formation that takes place without volume variation.

From this point of view, this second step would practically coincide with the second step in SPT. Indeed, if the volume change ($\Delta\bar{V}_i$) is considered negligible, the insertion of the molecules of gas in the already created cavities and their interaction with the solvent would be a solution process almost identical to that proposed by Prausnitz and Shair. Then the volume associated with the formation of the cavities would be the volume of the hypothetical condensed liquid-like fluid to be accommodated in those cavities and it is not surprising that the two quite different models lead to similar results.

Acknowledgments

The authors gratefully acknowledge the financial support of the Dirección General de Enseñanza Superior e Investigación Científica (DGESIC) Project No. PB98–1624. They also thank Dr. Luis Romaní and his team of the Universidad de Vigo for having kindly measured the heat capacity of HFIP.

References

1. A.M. Mainar, J. Pardo, F.M. Royo, M.C. López, and J.S. Urieta. J. Solution Chem. **25**, 589 (1996).
2. A.M. Mainar, J. Pardo, J.I. García, F.M. Royo, and J.S. Urieta. J.Chem. Soc. Faraday Trans. **94**, 3595 (1998).
3. C. Cativiela, J.I. García, J. Gil, R.M. Martínez, J.A. Mayoral, L. Salvatella, J.S. Urieta, A.M. Mainar, and M.H. Abraham. J. Chem Soc. Perkin Trans. 2, 653 (1997).
4. J.M. Prausnitz and F.H. Shair. AIChE J. **7**, 682 (1961).
5. J. Carnicer, F. Gibanel, J.S. Urieta, and C. Gutiérrez Losa. Rev. Acad. Ciencias Zaragoza, **86**, 115 (1979).
6. Ben-Naim and S. Baer. J. Chem. Soc. Faraday Trans. **59**, 2735 (1963).
7. F. Gibanel, M.C. López, F. Royo, V. Rodríguez, and J.S. Urieta. J. Solution Chem. **23**, 1247 (1994).
8. E. Wilhelm and R. Battino. J. Chem. Phys. **55**, 4012 (1971).
9. E. Wilhelm. J. Chem. Phys. **58**, 3558 (1973).
10. CRC handbook of chemistry and physics. 73rd ed. *Edited by* D.R. Lide. CRC Press, Boca Raton, Florida. 1993.
11. N.P.J. Maris and L.I. Stiel. Ind. Eng. Chem. Proc. DD. **24**, 183 (1985).
12. L. Clever and R. Battino. The solubility of gases in liquids. *In* Techniques of chemistry. Vol 8. *Edited by* M.R.J. Dack. John Wiley & Sons, New York. 1975. Part 1.
13. E. Wilhelm, R. Battino, and R. Wilcock. Chem. Rev. **77**, 219 (1977).
14. R.A. Pierotti. J. Phys. Chem. **67**, 1840 (1963).
15. M.C. López, M.A. Gallardo, and J.S. Urieta. J. Chem. Eng. Data, **35**, 60 (1990).
16. M.A. Gallardo, J.M. Melendo, J.S. Urieta, and C. Gutiérrez Losa. Can. J. Chem. **65**, 2198 (1987).
17. J. Pardo, M.C. López, J. Santafé, F.M. Royo, and J.S. Urieta. Fluid Phase Equilibr. **109**, 29 (1995).
18. R.A. Pierotti. J. Phys. Chem. **69**, 281 (1965).
19. T.R. Rettich, R. Battino, and E. Wilhelm. Ber. Bunsen. Phys. Chem. **86**, 1128 (1982).
20. T.R. Rettich, R. Battino, and E. Wilhelm. J. Solution Chem. **21**, 987 (1992)
21. R.A. Pierotti. Chem. Rev. **76**, 717 (1976).
22. H. Reiss, H.L. Frisch, and J.L. Lebowitz. J. Chem. Phys. **31**, 369 (1959).
23. B.A. Cosgrove and J. Walkley. Can. J. Chem. **60**, 1896 (1982).
24. A. Ben-Naim and H.L. Friedman. J. Phys. Chem. **71**, 448 (1967).
25. R.A. Pierotti. J. Phys. Chem. **71**, 2366 (1967).
26. G. Schulze and J.M. Prausnitz. Ind. Eng. Chem. Fund. **20**, 175 (1981)
27. F. Gibanel, M.C. López, F.M. Royo, J. Pardo, and J.S. Urieta. Fluid Phase Equilibr. **87**, 285 (1993).
28. S. Miyanaga, K. Tamura, and S. Mukarami. J. Chem. Thermodyn. **24**, 291 (1992).

© 2001 NRC Canada

Solubility predictions for crystalline nonelectrolyte solutes dissolved in organic solvents based upon the Abraham general solvation model

William E. Acree, Jr. and Michael H. Abraham

Abstract: The Abraham general solvation model is used to predict the saturation solubility of crystalline nonelectrolyte solutes in organic solvents. The derived equations take the form of log $(C_S/C_W) = c + rR_2 + s\pi_2^H + a\Sigma\alpha_2^H + b\Sigma\beta_2^H + vV_x$ and log $(C_S/C_G) = c + rR_2 + s\pi_2^H + a\Sigma\alpha_2^H + b\Sigma\beta_2^H + l \log L^{(16)}$ where C_S and C_W refer to the solute solubility in the organic solvent and water, respectively, C_G is a gas-phase concentration, R_2 is the solute's excess molar refraction, V_x is McGowan volume of the solute, $\Sigma\alpha_2^H$ and $\Sigma\beta_2^H$ are measures of the solute's hydrogen-bond acidity and hydrogen-bond basicity, π_2^H denotes the solute's dipolarity and (or) polarizability descriptor, and log $L^{(16)}$ is the solute's gas-phase dimensionless Ostwald partition coefficient into hexadecane at 298 K. The remaining symbols in the above expressions are known equation coefficients, which have been determined previously for a large number of gas–solvent and water–solvent systems. Computations show that the Abraham general solvation model predicts the observed solubility behavior of anthracene, phenanthrene, and hexachlorobenzene to within an average absolute deviation of about ±35%.

Key words: solubility predictions, organic solvents, nonelectrolyte solutes, partition coefficients.

Résumé : On a utilisé le modèle général de solvatation d'Abraham pour faire des prédictions relatives à la solubilité de saturation de solutés cristallins non-électrolytes, dans des solvants organiques. Les équations dérivées sont de la forme log $(C_S/C_W) = c + rR_2 = s\pi_2^H + a\Sigma\alpha_2^H + b\Sigma\beta_2^H + vV_X$ et log $(C_S/C_G) = c + rR_2 + s\pi_2^H + a\Sigma\alpha_2^H + b\Sigma\beta_2^H + l$ log $L^{(16)}$ dans lesquelles C_S et C_W se réfèrent respectivement à la solubilité du soluté dans le solvant organique et dans l'eau, C_G est une concentration en phase gazeuse, R_2 est la réfraction molaire en excès du soluté, V_X est le volume de McGowan du soluté, $\Sigma\alpha_2^H$ et $\Sigma\beta_2^H$ sont respectivement des mesures de l'acidité et de la basicité de la liaison hydrogène du soluté, π_2^H correspond à un descripteur du caractère dipolaire et de la polarisabilité du soluté et log $L^{(16)}$ est le coefficient de partition d'Oswald, sans dimension, du soluté en phase gazeuse, dans l'hexadécane, à 298 K. Les autres symboles de ces expressions sont des coefficients d'équation connus qui ont été déterminés antérieurement pour un grand nombre de systèmes gaz–solvant et eau–solvant. Les calculs montrent que le modèle général de solvatation d'Abraham permet de prédire le comportement de solubilité observé pour l'anthracène, le phénanthrène e l'hexachlorobenzène dans les limites d'une déviation moyenne absolue d'environ ±35%.

Mots clés : prédictions de solubilité, solvants organiques, solutés non-électrolytes, coefficients de partition.

[Traduit par la Rédaction]

Introduction

Free energy of solvation is an important thermodynamic variable that quantifies the free energy difference between a molecule in the gas phase and the molecule dissolved in a solvent. Free energies of solvation provide valuable information regarding molecular interactions between dissolved solute and surrounding solvent molecules, and can be used to calculate numerical values of partition coefficients that describe the equilibrium distribution of a solute between two immiscible liquid phases. For example, the octanol–water partition coefficient is the free energy of solvation of the solute molecule in wet 1-octanol minus its free energy of solvation in water. Solvation free energies and partition coefficients are of critical importance in many pharmaceutical, environmental, and chemical engineering applications. Solute partitioning between two immiscible phases is the basis for all chromatographic separations. Correlations have been derived for predicting brain–blood partitioning of organic solutes from solutes' measured and (or) calculated free energies of solvation (1, 2), and for estimating aqueous solubilities, soil adsorptions, bioaccumulations, and toxicities of organic compounds from experimental octanol–water partition coefficient data (3–11).

Historically, many of the very early studies focussed exclusively on developing correlational equations based upon octanol–water partition coefficients. Recent studies have shown that the octanol–water partition coefficient may not necessarily be the best indicator of how likely it is for a particular solute molecule to penetrate a lipid bilayer, skin, brain, or central nervous system, or to accumulate in different tissues and body organs. Experimental studies have been expanded to include additional organic solvents, as well as

Received April 20, 2001. Published on the NRC Research Press Web site at http://canjchem.nrc.ca on October 10, 2001.

W.E. Acree, Jr.[1] Department of Chemistry, P.O. Box 305070, University of North Texas, Denton, TX 76203–5070, U.S.A.
M.H. Abraham. Department of Chemistry, University College London, 20 Gordon Street, London, WC1H 0AJ, U.K.

[1]Corresponding author (e-mail: acree@unt.edu).

 DOI: 10.1139/cjc-79-10-1466 © 2001 NRC Canada

aqueous micellar solvent media, and to use solute descriptors calculable from structural considerations and (or) easily measured thermodynamic quantities.

In this regard, Abraham and co-workers (12–19) developed expressions for describing the partition of solutes between water and a given solvent

$$[1] \quad \log P = c + rR_2 + s\pi_2^H + a\Sigma\alpha_2^H + b\Sigma\beta_2^H + vV_x$$

and between the gas phase and a given solvent

$$[2] \quad \log L = c + rR_2 + s\pi_2^H + a\Sigma\alpha_2^H + b\Sigma\beta_2^H + l \log L^{(16)}$$

The dependent variables in eqs. [1] and [2] are the log P (the partition coefficient of solute(s) between water and a given solvent) and log L (Ostwald solubility coefficient). The independent variables are the solute descriptors as follows: R_2 and V_x refer to the excess molar refraction and McGowan volume of the solute, respectively, $\Sigma\alpha_2^H$ and $\Sigma\beta_2^H$ are measures of the solute's hydrogen-bond acidity and hydrogen-bond basicity, π_2^H denotes the solute's dipolarity–polarizability descriptor, and log $L^{(16)}$ is the solute's gas-phase dimensionless Ostwald partition coefficient into hexadecane at 298 K. The numerical value of the R_2 solute descriptor can be obtained from the refractive index for solutes that are liquid at 293.15 K. For solids, the refractive index of the hyphothetical liquid at 293.15 K can be calculated, or R_2 can be obtained by the summation of fragments or substructures. The McGowan characteristic volume can be easily calculated from bond and atom contributions. It should be noted that the various c, r, s, a, b, v, and l coefficients depend on the solvent phase under consideration. The r coefficient gives the tendency of the phase to interact with solutes through polarizability-type interactions, mostly via electron pairs. The s coefficient is a measure of the solvent phase dipolarity and (or) polarity, while the a and b coefficients represent the solvent-phase hydrogen-bond basicity and hydrogen-bond acidity, respectively. The l and v coefficients are a combination of the work needed to create a solvent cavity wherein the solute will reside, and the general dispersion interaction energy between the solute and solvent phase. In the case of partition coefficients, where two solvent phases are involved, the c, r, s, a, b, v, and l coefficients represent differences in the solvent-phase properties.

Several earlier studies (20–23) developed the computational methodology for determining the various solute descriptors from measured solubility data for crystalline nonelectrolyte solutes dissolved in organic solvents for which the solvent regressional coefficients were known. In the present communication, the process is going to be reversed in that eqs. [1] and [2] will be used to predict anthracene, phenanthrene, and hexachlorobenzene solubilities in several dry organic solvents. Results of these computations will be compared to published solubility data taken from the chemical literature (24–29), and when available, to predicted values based upon Mobile Order theory, and the UNIFAC and Modified UNIFAC (Dortmund) models.

Methodology

Predictive application of eqs. [1] and [2] is relatively straightforward if: (*i*) all solute descriptors and equation coefficients are known; (*ii*) the aqueous solubility of the crystalline solute at 298 K is available; and (*iii*) the saturated vapor pressure of the solid at 298 K has been measured or can be calculated by extrapolating experimental vapor pressure data determined at slightly higher temperatures back to 298 K. These latter two quantities are needed to convert the predicted log P and log L values into saturation molar solubilities.

Let the solubility in mol dm^{-3} at 298 K be denoted C_S and C_W, respectively, in the organic solvent and in water. The partition coefficient (P) between water and the organic solvent is given by eq. [3]:

$$[3] \quad P = C_S/C_W \text{ or } \log P = \log C_S - \log C_W$$

provided that three specific conditions are met. First, the same solid phase must be in equilibrium with the saturation solutions in the organic solvent and in water (i.e., there should be no solvate or hydrate formation). Second, the secondary medium activity coefficient of the solid in the saturated solutions must be unity (or near unity). This condition generally restricts the method to those solutes that are sparingly soluble in water and nonaqueous solvents. Finally, for solutes that are ionized in aqueous solution, C_W must refer to the solubility of the neutral form.

If the three forementioned conditions are met, eqs. [1] and [3] allow one to predict the molar solubility of the solute (C_S) in all organic solvents for which equation coefficients have been determined. Readers are reminded that in selecting equation coefficients, the "dry solvent" values should be used. Equation [1] actually predicts partition coefficients, and for select solvents both "dry" and "wet" equation coefficients have been reported. For solvents that are partially miscible with water, such as 1-butanol and ethyl acetate, partition coefficients calculated using eq. [3] are not the same as those obtained from direct partition between water (saturated with the organic solvent) and organic solvent (saturated with water). Care must be taken not to confuse the two sets of partitions. In the case of solvents that are fully miscible with water, such as methanol, no confusion is possible. Only one set of equation coefficients have been reported, and the calculated log P value must refer to the hypothetical partition between the two pure solvents. And for solvents that are "almost" completely immiscible with water, such as alkanes, cyclohexane, dichloromethane, trichloromethane, tetrachloromethane, and most aromatic solvents, there should be no confusion because indirect partition through eq. [3] will be nearly identical to direct partition. Hence, if C_W is known, predicted log P values based upon eq. [1] will lead to predicted molar solubilities through eq. [3]. Currently, there are about 40 organic solvents for which dry equation coefficients have been determined.

It should be noted that other research groups (30–33) have proposed fairly similar linear solvation energy relationships for estimating partition coefficients of organic solutes between water and an organic solvent. The similar methods employ slightly different solute descriptors, and to our knowledge, all equation coefficients were determined through regressional analysis of direct experimental partition coefficient data. The equations derived from such partition coefficient data are of marginal use in estimating solute solubilities in organic solvents, except in the very special case that the organic solvent is almost completely immiscible

© 2001 NRC Canada

Table 1. Coefficients in eq. [1] and eq. [2] for various processes.[a]

Process/solvent	*c*	*r*	*s*	*a*	*b*	*v*/*l*[b]
A. Water to solvent (eq. [1])						
Hexane	0.361	0.579	–1.723	–3.599	–4.764	4.344
Heptane	0.325	0.670	–2.061	–3.317	–4.733	4.543
Octane	0.223	0.642	–1.647	–3.480	–5.067	4.526
Nonane	0.240	0.619	–1.713	–3.532	–4.921	4.482
Decane	0.160	0.585	–1.734	–3.435	–5.078	4.582
Hexadecane	0.087	0.667	–1.617	–3.587	–4.869	4.433
2,2,4-Trimethylpentane	0.288	0.382	–1.668	–3.639	–5.000	4.561
Cyclohexane	0.159	0.784	–1.678	–3.740	–4.929	4.577
Chlorobenzene	0.040	0.246	–0.462	–3.038	–4.769	4.640
Dichloromethane	0.314	0.001	0.022	–3.238	–4.137	4.259
1,2-Dichloroethane	0.227	0.278	–0.167	–2.816	–4.324	4.205
Chloroform	0.327	0.157	–0.391	–3.191	–3.437	4.191
Tetrachloromethane	0.260	0.573	–1.254	–3.558	–4.588	4.589
Acetonitrile (dry)	0.413	0.077	0.326	–1.566	–4.391	3.364
Benzene	0.142	0.464	–0.588	–3.099	–4.625	4.491
Toluene	0.143	0.527	–0.720	–3.010	–4.824	4.545
Methanol (dry)	0.329	0.299	–0.671	0.080	–3.389	3.512
Ethanol (dry)	0.208	0.409	–0.959	0.186	–3.645	3.928
1-Propanol (dry)	0.147	0.494	–1.195	0.495	–3.907	4.048
2-Propanol (dry)	0.063	0.320	–1.024	0.445	–3.824	4.067
1-Butanol (dry)	0.152	0.437	–1.175	0.098	–3.914	4.119
1-Pentanol (dry)	0.080	0.521	–1.294	0.208	–3.908	4.208
1-Hexanol (dry)	0.044	0.470	–1.153	0.083	–4.057	4.249
1-Heptanol (dry)	–0.026	0.491	–1.258	0.035	–4.155	4.415
1-Octanol (dry)	–0.034	0.490	–1.048	–0.028	–4.229	4.219
1-Decanol (dry)	–0.062	0.754	–1.461	0.063	–4.053	4.293
Ethyl acetate	0.358	0.362	–0.449	–0.668	–5.016	4.155
2-Propanone (dry)	0.335	0.349	–0.231	–0.411	–4.793	3.963
Dimethylformamide (dry)	0.105	0.317	0.462	1.154	–4.843	3.757
Carbon disulfide	0.047	0.686	–0.943	–3.603	–5.818	4.921
Ethylene glycol (dry)	–0.313	0.419	–0.409	0.906	–2.558	2.771
(Gas to water)	–0.994	0.577	2.549	3.813	4.841	–0.869
B. Gas to solvent (eq. [2])						
Hexane	0.292	–0.169	0.000	0.000	0.000	0.979
Heptane	0.275	–0.162	0.000	0.000	0.000	0.983
Octane	0.215	–0.049	0.000	0.000	0.000	0.967
Nonane	0.200	–0.145	0.000	0.000	0.000	0.980
Decane	0.156	–0.143	0.000	0.000	0.000	0.989
Hexadecane	0.000	0.000	0.000	0.000	0.000	1.000
2,2,4-Trimethylpentane	0.275	–0.244	0.000	0.000	0.000	0.972
Cyclohexane	0.163	–0.110	0.000	0.000	0.000	1.013
Chlorobenzene	0.053	–0.553	1.254	0.364	0.000	1.041
Dichloromethane	0.121	–0.450	1.677	0.404	0.786	0.940
1,2-Dichloroethane	0.011	–0.150	1.436	0.649	0.736	0.936
Chloroform	0.116	–0.467	1.203	0.138	1.432	0.994
Tetrachloromethane	0.282	–0.303	0.460	0.000	0.000	1.047
Acetonitrile	–0.007	–0.595	2.461	2.085	0.418	0.738
Benzene	0.107	–0.313	1.053	0.457	0.169	1.020
Toluene	0.121	–0.222	0.938	0.467	0.099	1.012
Methanol (dry)	–0.004	–0.215	1.173	3.701	1.432	0.769
Ethanol (dry)	0.012	–0.206	0.789	3.635	1.311	0.853
1-Propanol (dry)	–0.028	–0.185	0.648	4.022	1.043	0.869
2-Propanol (dry)	–0.060	–0.335	0.702	4.017	1.040	0.893
1-Butanol (dry)	–0.039	–0.276	0.539	3.781	0.995	0.934
1-Pentanol (dry)	–0.042	–0.277	0.526	3.779	0.983	0.932
1-Hexanol (dry)	–0.035	–0.298	0.626	3.726	0.729	0.936

© 2001 NRC Canada

Table 1. (*concluded*).

Process/solvent	*c*	*r*	*s*	*a*	*b*	*v*/*l*[b]
1-Heptanol (dry)	–0.062	–0.168	0.429	3.541	1.181	0.927
1-Octanol (dry)	–0.119	–0.203	0.560	3.576	0.702	0.940
1-Decanol (dry)	–0.136	–0.038	0.325	3.674	0.767	0.947
Ethyl acetate	0.203	–0.335	1.251	2.949	0.000	0.917
2-Propanone	0.154	–0.277	1.522	3.258	0.078	0.863
Dimethylformamide (dry)	–0.161	–0.181	2.327	4.756	0.000	0.808
Carbon disulfide	0.101	0.251	0.177	0.027	0.095	1.068
Ethylene glycol (dry)	–0.937	0.215	1.511	4.651	2.591	0.571
(Gas to water)	–1.271	0.822	2.743	3.904	4.814	–0.213

[a]The solvents denoted as dry are those for which partitions refer to transfer to the pure dry solvent. The other partitions are from water (more correctly water saturated with solvent) to the solvent saturated with water (see text).
[b]Coefficent of V_x in processes A and coefficient of log $L^{(16)}$ in processes B.

Table 2. Solute descriptors and properties for anthracene, phenanthrene, and hexachlorobenzene.

Solute	R_2	π_2^H	$\Sigma\alpha_2^H$	$\Sigma\beta_2^H$	V_x	log $L^{(16)}$	log C_W	log C_G
Anthracene	2.290	1.340	0.000	0.28	1.454	7.568	–6.43	–9.46
Phenanthrene	2.055	1.290	0.000	0.26	1.454	7.632	–5.17	–7.97
Hexachlorobenzene	1.490	0.990	0.000	0.000	1.451	7.624	–7.68	–9.18

Table 3. Comparison between experimental anthracene molar solubilities (C_S^{exp}) and predicted values based upon the Abraham general solvation model (eqs. [1] and [2]).

		Equation [1]		Equation [2]	
Solvent	C_S^{exp}	C_S^{pred}	% Dev.[a]	C_S^{pred}	% Dev.[a]
Hexane	0.00981	0.00853	–13.0	0.00715	–27.1
Heptane	0.01065	0.00887	–16.7	0.00764	–28.3
Octane	0.01132	0.01656	46.3	0.00914	–19.3
Nonane	0.01160	0.01178	0.9	0.00668	–42.4
Decane	0.01198	0.00968	–19.2	0.00713	–40.5
Hexadecane	0.01294	0.01262	–2.5	0.01282	–0.9
2,2,4-Trimethylpentane	0.00655	0.00536	–18.2	0.00410	–37.4
Cyclohexane	0.01446	0.03548	145.4	0.01311	–9.3
Chlorobenzene	0.09711	0.09223	–5.0	0.07679	–20.9
Dichloromethane	0.1437	0.08913	–38.0	0.1628	13.3
Chloroform	0.1331	0.07311	–45.1	0.1325	–0.5
Tetrachloromethane	0.04768	0.07063	48.1	0.04658	–2.3
Acetonitrile (dry)	0.0157	0.01811	15.4	0.01481	–5.7
Benzene	0.08256	0.1666	101.8	0.1282	55.3
Toluene	0.06868	0.1632	137.6	0.1248	81.7
Methanol (dry)	0.00597	0.00695	16.4	0.00686	14.9
Ethanol (dry)	0.00784	0.01319	68.2	0.00912	16.4
1-Propanol (dry)	0.00787	0.01093	38.9	0.00669	–15.0
2-Propanol (dry)	0.00534	0.00686	28.5	0.00505	–5.4
1-Butanol (dry)	0.00871	0.01100	26.3	0.00868	–0.4
1-Pentanol (dry)	0.01010	0.01359	34.6	0.00789	–21.9
1-Hexanol (dry)	0.01184	0.01539	30.0	0.00890	–24.8
1-Heptanol (dry)	0.01317	0.01733	31.6	0.01034	–21.5
1-Octanol (dry)	0.01364	0.01600	17.3	0.01040	–23.8
1-Decanol (dry)	0.01793[b]	0.02422	35.1	0.01362	–24.0
Ethyl acetate	0.04901	0.06197	26.5	0.03909	–20.2
2-Propanone (dry)	0.05812[c]	0.06528	12.3	0.04489	–22.8
Dimethylformamide (dry)	0.1011	0.1339	32.4	0.1576	55.9
Ethylene glycol (dry)	0.00128	0.00096	–25.0	0.00147	14.7
Average absolute deviation			37.1		23.0

[a]% Dev. = $100(C_S^{pred} - C_S^{exp})/C_S^{exp}$.
[b]W.E. Acree, unpublished data.
[c]Experimental value was taken from J. Mahieu (29).

© 2001 NRC Canada

Table 4. Comparison between experimental phenanthrene molar solubilities (C_S^{sat}) and predicted values based upon the Abraham general solvation model (eqs. [1] and [2]).

		Equation [1]		Equation [2]	
Solvent	C_S^{exp}	C_S^{pred}	% Dev.[a]	C_S^{pred}	% Dev.[a]
Hexane	0.2411	0.1721	–28.6	0.2795	15.9
Heptane	0.2631	0.1771	–32.7	0.2981	13.3
Octane	0.2724	0.3243	19.1	0.3345	22.8
Nonane	0.2677	0.2342	–12.5	0.2579	–3.7
Decane	0.2856	0.1983	–30.6	0.2755	–3.5
Hexadecane	0.2816	0.2407	–14.5	0.4592	63.1
2,2,4-Trimethylpentane	0.1499	0.1211	–19.2	0.1667	11.2
Cyclohexane	0.3302	0.6440	95.1	0.4991	51.2
Tetrachloromethane	1.208	1.347	11.5	1.877	55.4
Acetonitrile (dry)	0.5807	0.3727	–35.8	0.5201	–10.4
Benzene	1.814[b]	3.122	72.1	4.794	164.3
Toluene	2.005[c]	3.030	51.1	4.510	124.9
Methanol (dry)	0.1423	0.1359	–4.5	0.2181	53.3
Ethanol (dry)	0.1863	0.2541	36.4	0.3072	64.9
1-Propanol (dry)	0.1778	0.2092	17.7	0.2297	29.2
2-Propanol (dry)	0.1258	0.1409	12.0	0.1875	49.0
1-Butanol (dry)	0.1902	0.2166	13.9	0.3207	68.6
1-Pentanol (dry)	0.2268	0.2593	14.3	0.2924	28.9
1-Hexanol (dry)	0.2401	0.2990	24.5	0.3336	39.0
1-Heptanol (dry)	0.2764	0.3383	22.4	0.3615	30.8
1-Octanol (dry)	0.3426	0.3061	–10.6	0.3740	9.2
Ethyl acetate	1.400	1.230	–12.1	1.435	2.5
Ethylene glycol (dry)	0.0202	0.0164	–18.9	0.0328	62.3
Average absolute deviation			26.5		42.5

[a]% Dev = $100(C_S^{pred} - C_S^{exp})/C_S^{exp}$.
[b]Estimated by extrapolating the mol fraction solubility data of McLaughlin and Zainal (27) back to 298.15 K.
[c]Estimated by extrapolating the mol fraction solubility data of Choi and McLaughlin (28) back to 298.15 K.

with water. Our general solvation method differs from competing methods in that we have tried in recent years, to the extent possible, to build separate data bases for dry and wet solvents. This creates a problem for many of the common organic solvents. There is often very little experimental data available, and the tendency is to combine available organic solvent – water partition coefficient measurements (wet solvent) with saturation solubilities, binary liquid–vapor equilibria data, and infinite dilution activity coefficients determined from measured gas chromatographic solute retention volumes on the organic solvent stationary phase (34, 35). Lack of experimental data is the reason that we have been able to deduce *c*, *r*, *s*, *a*, *b*, *v*, and *l* coefficients for only 40 or so dry solvents.

Equation coefficients are tabulated in Table 1 for select organic solvents. The actual numerical values may differ slightly from values reported in earlier publications. Coefficients are periodically revised when additional experimental data becomes available. For example, the initial set of equation coefficients for acetonitrile were based on a data set that contained very few large polycyclic aromatic hydrocarbon solutes. Published solubility data (24, 25, 36, 37) for anthracene, pyrene, naphthalene, biphenyl, acenaphthene, acenaphthylene, fluorene, fluoranthene, and phenanthrene were later added to the database, and the equation coefficients were redetermined. Pyrene, fluoranthene, and anthracene have large excess molar refraction solute descriptors of R_2 = 2.808, R_2 = 2.377, and R_2 = 2.290, respectively. In performing the regressional analysis to determine the solvent coefficients, it is important that the data set contain solutes that span as wide of a range of solute descriptors as possible. The deficiency involving the initial parameterization for acetonitrile has now been corrected. Anthracene, phenanthrene, and other PAH solubilities were used to construct the revised acetonitrile equation. Table 1 lists the most updated set of equation coefficients that we have for each solvent.

Saturation solubilities can also be calculated from predicted log *L* values based upon eq. [2], provided that the solid saturated vapor pressure at 298 K (*VP*°) is available. *VP*° can be transformed into the gas-phase concentration (C_G), and the gas–water and gas–solvent partitions (L_W and L_S) can be obtained through eqs. [4] and [5], respectively.

$$[4] \qquad L_W = C_W/C_G \text{ or } \log L_W = \log C_W - \log C_G$$

$$[5] \qquad L_S = C_S/C_G \text{ or } \log L_S = \log C_S - \log C_G$$

As before, the predictive method will be valid if conditions (*i*)–(*iii*) above are met. In the case of the published log *L* correlations, most of the equation coefficients pertain to either dry solvents or solvents that are almost completely immiscible with water.

Katritzky et al. (38, 39) recently developed log *L* correlations for solutes dissolved in water, methanol, and ethanol

© 2001 NRC Canada

Table 5. Comparison between experimental hexachlorobenzene molar solubilities (C_S^{sat}) and predicted values based upon the Abraham general solvation model (eqs. [1] and [2]).

		Equation [1]		Equation [2]	
Solvent	C_S^{exp}	C_S^{pred}	% Dev.[a]	C_S^{pred}	% Dev.[a]
Hexane	0.01990	0.01384	–30.5	0.02109	6.0
Heptane	0.02128	0.01566	–26.4	0.02228	4.7
Octane	0.02270	0.02731	20.3	0.02160	–4.9
Nonane	0.02279	0.01949	–14.5	0.01886	–17.2
Decane	0.02348	0.01921	–18.2	0.02009	–14.4
Hexadecane	0.02316	0.01707	–26.3	0.03119	34.7
2,2,4-Trimethylpentane	0.01515	0.01393	–8.1	0.01387	–8.5
Cyclohexane	0.02712	0.04238	56.3	0.03485	28.5
1,2-Dichloroethane	0.03627	0.07895	81.3	0.1463	303.3
Methanol (dry)	0.00222	0.00336	51.3	0.00331	49.1
Ethanol (dry)	0.00401	0.00772	92.5	0.00645	60.9
1-Propanol (dry)	0.00530	0.00783	47.7	0.00607	14.5
2-Propanol (dry)	0.00387	0.00559	44.4	0.00581	50.1
1-Butanol (dry)	0.00725	0.00864	19.2	0.01057	45.8
1-Pentanol (dry)	0.00944	0.01002	6.2	0.00981	3.9
1-Hexanol (dry)	0.01149	0.01225	6.6	0.01250	8.8
1-Heptanol (dry)	0.01341	0.01536	14.5	0.01000	–25.4
1-Octanol (dry)	0.01500	0.01260	–16.0	0.01379	–8.1
1-Decanol (dry)	0.01251	0.01460	16.7	0.01476	17.8
Ethyl acetate	0.02140	0.06335	196.0	0.05670	164.9
Average absolute deviation			39.6[b]		43.6[c]

[a]% Dev. = $100(C_S^{pred} - C_S^{exp})/C_S^{exp}$.

[b]Average absolute deviation between predicted and observed values drops to 31.4% if ethyl acetate is excluded from the eq. [1] comparison.

[c]Average absolute deviation between predicted and observed values drops to 31.4% if ethyl acetate and 1,2-dichloroethane are excluded from the eq. [2] comparison.

based upon the CODESSA treatment. A major difference between our approach and that of Katritzky et al., is that we use the same exact solute descriptors in each derived correlation. Our descriptors have experimental origin. That is not the case in the Katritzky et al. treatment. There, the authors use a large pool of descriptors, whose numerical values are calculated solely from structural considerations. The authors seek the strongest correlation possible, rather than the correlations that use a common set of descriptors. The reported log *L* correlation for methanol used one set of descriptors, whereas the correlation for ethanol used different descriptors. As a consequence, the authors were unable to compare the two sets of solvent coefficients. Drawing meaningful conclusions based on the coefficients of common descriptors, when the entire descriptor set is not shared, can cause problems because of colinearity. Inert gases were omitted from the Katritzky et al. (38, 39) treatment because atomic species are not appropriate for the optimization methods used. Each approach has its advantages and disadvantages. Our approach gave the better correlations for water, methanol, and ethanol, but is limited in application to those compounds for which solute descriptors are known. Katritzky et al. treatment can be used to predict the solubility behavior of more compounds. The predictive accuracy is not as good, and at the moment, the method is limited to water, methanol, and ethanol. Though not specifically addressed, the Katritzky et al. treatment should be able to correlate organic solvent–water partition coefficients, which are related to gas–solvent and gas–water partitions through $\log P = \log L_S - \log L_W$.

Results and discussion

The chemical literature contains an enormous amount of solubility data that could be used to illustrate the computational methodology and to assess the applications and limitations of the Abraham general solvation model. Acree and co-workers experimentally determined the solubilities of several polycyclic aromatic hydrocarbons (24, 25, 37, 40–42) and pesticides (23, 26, 43) in a wide range of organic solvents of varying polarity and hydrogen-bonding characteristics. Bustamante and co-workers made similar measurements for select drug molecules (i.e., ibuprofen (44), piroxicam (45), niflumic acid (45), naproxen (46), citric acid (47), paracetamol (47), sulfamethoxypyridazine (48), diclofenac (49), and 2-hydroxybenzoic acid (49) and for the insecticide 4-methoxybenzyl 1-(4-chlorophenyl) cyclopropanecarboxylate (50). Large solubility databases also exist for thianthrene (51), *trans*-stilbene (20, 52), buckminsterfullerene (21, 53), diphenyl sulfone (54), metronidazole (55), dimetridazole (55), ipronidazole (55), benzil (56), benzoic acid (57), methyl 4-hydroxybenzoate (58), 4-hydroxybenzoic acid (58), haloperidol (59), 4-aminobenzoic acid (49), 4-nitroaniline (60), 4-nitro-*N*,*N*-dimethylaniline (60), thioxanthen-9-one (61), and ferrocene (62).

After careful consideration, we selected anthracene, phenanthrene, and hexachlorobenzene as the solutes to be studied because the solute descriptors are known, and the needed aqueous solubility and vapor pressure were readily available. The selected solutes do not contain polar func-

© 2001 NRC Canada

Table 6. Comparison between experimental anthracene mol fraction solubilities (X_S^{exp}) and predicted values based upon Mobile Order theory.

Solvent	X_S^{exp}	X_S^{pred} [a]	% Dev.[b]
Hexane	0.001290	0.001424	10.4
Heptane	0.001571	0.001519	–3.3
Octane	0.001850	0.001729	–6.5
Nonane	0.002085	0.002005	–3.8
Decane	0.002345	0.002113	–9.9
Hexadecane	0.00380	0.003015	–20.7
2,2,4-Trimethylpentane	0.001087	0.001179	8.5
Cyclohexane	0.001574	0.001746	10.9
Chlorobenzene	0.009962	0.01049	5.3
Dichloromethane	0.009387	0.01316	40.2
Chloroform	0.01084	0.01024	–5.5
Tetrachloromethane	0.00464	0.005843	25.9
Acetonitrile	0.000830	0.008202	888.1
Benzene	0.007418	0.01016	37.0
Toluene	0.00736	0.008090	9.9
Methanol	0.000243	0.000492	102.5
Ethanol	0.000460	0.000762	65.7
1-Propanol	0.000591	0.000957	61.9
2-Propanol	0.000411	0.001104	168.6
1-Butanol	0.000801	0.001212	51.3
1-Pentanol	0.001097	0.001316	20.0
1-Hexanol	0.001483	0.001266	–14.6
1-Heptanol	0.001869	0.001439	–23.0
1-Octanol	0.002160	0.001598	–26.0
1-Decanol	0.003433	0.001883	–45.2
Ethyl acetate	0.00484	0.01088	124.8
2-Propanone	0.00432[c]	0.01204	178.7
Dimethylformamide	0.007839	0.009891	26.2
Ethylene glycol	0.0000715	0.0000693	–3.1
Average absolute deviation			68.9[d]

[a]Values of a_A^{solid} = 0.01049 and V_A = 150.0 cm^3 mol^{-1} were used in the Mobile Order theory predictions.
[b]% Dev. = $100(X_S^{pred} - X_S^{exp})/X_S^{exp}$.
[c]Experimental value was taken from J. Mahieu (29).
[d]Average absolute deviation drops to 39.6% if acetonitrile is excluded from the comparison.

Table 7. Comparison between experimental phenanthrene mol fraction solubilities (X_S^{exp}) and predicted values based upon Mobile Order theory.

Solvent	X_S^{exp}	X_S^{pred} [a]	% Dev.[b]
Hexane	0.03189	0.03529	10.7
Heptane	0.03888	0.03716	–4.4
Octane	0.04443	0.04232	–4.7
Nonane	0.04785	0.04930	3.0
Decane	0.05531	0.05154	7.3
Hexadecane	0.07972	0.07194	–9.8
2,2,4-Trimethylpentane	0.02486	0.02721	9.5
Cyclohexane	0.03648	0.04724	29.5
Tetrachloromethane	0.1262	0.1807	43.2
Acetonitrile	0.03267	0.2569	686.3
Benzene	0.1809[c]	0.2561	41.6
Toluene	0.2375[d]	0.2233	–6.1
Methanol	0.00589	0.01244	111.2
Ethanol	0.01114	0.01919	72.3
1-Propanol	0.01355	0.02396	76.8
2-Propanol	0.00977	0.02811	187.7
1-Butanol	0.01771	0.03040	71.7
1-Pentanol	0.02491	0.03259	30.8
1-Hexanol	0.03028	0.03056	0.9
1-Heptanol	0.03937	0.03470	–11.9
1-Octanol	0.05418	0.03844	–29.1
Ethyl acetate	0.1499	0.2661	77.5
Ethylene glycol	0.001134	0.001457	28.5
Average absolute deviation			67.6[e]

[a]Values of a_A^{solid} = 02596 and V_A = 155.8 cm^3 mol^{-1} were used in the Mobile Order theory predictions.
[b]% Dev. = $100(X_S^{pred} - X_S^{exp})/X_S^{exp}$.
[c]Estimated by extrapolating the mol fraction solubility data of McLaughlin and Zainal (27) back to 298.15 K.
[d]Estimated by extrapolating the mol fraction solubility data of Choi and McLaughlin (28) back to 298.15 K.
[e]Average absolute deviation drops to 39.5% if acetonitrile is excluded from the comparison.

tional groups, thus decreasing the likelihood that the solutes will form solid hydrates or solvates in any of the saturated solutions. Solute properties are listed in Table 2. The numerical values for anthracene and phenanthrene were taken from our publications (12, 63, 64), as well as the solute descriptors for hexachlorobenzene. The logarithm molar solubility of hexachlorobenzene in water is log C_W = –7.68 (65). A value of log L_W = 1.66 at 294.65 K is given by Koelmans et al. (66), and we estimate that this would correspond to a value of log C_G = –9.18 at 298.15 K.

Ferrocene, *trans*-stilbene, buckminsterfullerene, diuron, and monuron were eliminated from consideration because their solute descriptors were determined from the published solubility data (20–23). For these four solutes, the calculations would not represent outright solubility predictions, but rather the ability of eqs. [1] and [2] to back-calculate the solubility data that was used as input values in the solute descriptor computations. Moreover, this information was reported at the time the solute descriptors were determined. Benzoic acid, 4-hydroxybenzoic acid, and 2-hydroxybenzoic acid were not selected due to the fact that carboxylic acid solutes are known to dimerize in hydrocarbon solvents. We did not want to complicate the analysis with concerns regarding whether the dissolved carboxylic acid solutes existed in solution in monomeric and (or) dimeric form, nor did we want to correct the measured aqueous solubilities for the extent of ionization. For solutes that ionized in aqueous solution, C_W must refer to the solubility of the neutral form. Similarly, compounds that would likely form zwitterions were excluded from consideration. Such matters will be addressed in subsequent publications. The remaining solutes were eliminated because of: (*i*) lack of aqueous solubility or vapor pressure data; (*ii*) the solute descriptors were not known; (*iii*) concerns about possible hydrate and (or) solvate formation; or (*iv*) too few of the solvents used in a given solubility study are listed in Table 1. Although not used in the present study, solubility data for these latter solutes will be added to our existing databases for possible inclusion in any additional solvent coefficient determinations.

© 2001 NRC Canada

Table 8. Comparison between experimental hexachlorobenzene mol fraction solubilities (X_S^{exp}) and predicted values based upon Mobile Order theory.

Solvent	X_S^{exp}	X_S^{pred} [a]	% Dev.[b]
Hexane	0.00262	0.00289	10.3
Heptane	0.00314	0.00307	–2.2
Octane	0.00371	0.00349	–5.9
Nonane	0.00410	0.00404	–1.5
Decane	0.00460	0.00425	–7.6
Hexadecane	0.00681	0.00601	–11.7
2,2,4-Trimethylpentane	0.00252	0.00238	–5.6
Cyclohexane	0.00295	0.00357	21.0
1,2-Dichloroethane	0.00286	0.0213	644.8
Methanol	0.0000902	0.000861	854.5
Ethanol	0.000236	0.00140	493.2
1-Propanol	0.000398	0.00179	349.7
2-Propanol	0.000298	0.00206	591.3
1-Butanol	0.000667	0.00229	243.3
1-Pentanol	0.00103	0.00251	143.7
1-Hexanol	0.00144	0.00243	68.8
1-Heptanol	0.00190	0.00277	45.8
1-Octanol	0.00238	0.00308	29.4
1-Decanol	0.00380	0.00364	–4.2
Ethyl acetate	0.00211	0.0200	847.9
Average absolute deviation			216.4

[a]Values of a_A^{solid} = 0.01943 and V_A = 155.6 cm^3 mol^{-1} were used in the Mobile Order theory predictions.
[b]% Dev. = $100(X_S^{pred} - X_S^{exp})/X_S^{exp}$.

Tables 3–5 compare observed anthracene, phenanthrene, and hexachlorobenzene molar solubilities (C_S^{exp}) to values calculated using the Abraham general solvation model. The model predicts log *P* and log *L* partitions, which were then converted to molar solubilities through eqs. [3] and [4]. For comparison purposes, we have reported the predicted values to either three or four significant figures to be as consistent as possible with the number of significant figures in the experimental values. All published mol fraction solubility data (X_S^{exp}) were converted to molarities by dividing X_S^{exp} by the ideal molar volume of the saturated solution (i.e., $C_S^{exp} \approx X_S^{exp} / [X_S^{exp} V_{solute} + (1 - X_S^{exp}) V_{solvent}]$). Solvent and solute molar volumes used in these conversions are given elsewhere (24–26). Any errors resulting from our estimations of the solutes' hypothetical supercooled liquid molar volumes (V_{solute}) or the ideal molar volume approximation should have negligible effect on the calculated C_S^{exp} values. Anthracene and hexachlorobenzene are fairly insoluble in all of the solvents considered, and the $X_S^{exp} V_{solute}$ term contributes very little to the molar volume of the saturated solution.

Examination of the numerical entries in Tables 3–5 reveals that eqs. [1] and [2] provide a very reasonable (though by no means perfect) estimation of the solubility behavior of anthracene, phenanthrene, and hexachlorobenzene in nonelectrolyte organic solvents. Overall average absolute deviations between predicted and observed values were 34.4 and 34.9% for eqs. [1] and [2], respectively. Expressed on a logarithmic molar scale basis, the Abraham general solvation model estimates the solubilities to within ±0.129 and ±0.122 log units, which is comparable in magnitude to the standard deviations associated with the *c*, *r*, *s*, *a*, *b*, *v*, and *l* coefficients for the individual solvent systems. Standard deviations for most of the individual solvent correlations fell between 0.12 and 0.20 log units. At this point in time we are unable to assign an actual uncertainty to each predicted solubility because of our limited experience in using eqs. [1] and [2] for solubility predictions. We suspect that a value of ±0.15 log units would not be too unreasonable, given the standard deviations in the individual solvent correlations and the comparisons presented in Tables 3–5 and elsewhere (20–23).

Readers will note that in the case of hexachlorobenzene, eq. [2] overpredicts the saturation solubility in several of the solvent systems studied. It might be possible to improve the overall predictive ability of eq. [2] by reestimating the numerical value of log C_G using other published vapor pressure data. It is not our intent, however, to arbitrarily select the vapor phase concentration of hexachlorobenzene that gives the best set of predicted values. Such practices would not provide an unbiased test of the applications and limitations of the Abraham general solvation model. Hexachlorobenzene does have a low vapor pressure at 298.15 K, and there is uncertainty associated both with accurately determining its vapor pressure above a saturated solution, and with extrapolating vapor pressures measured at much higher temperatures back to 298.15 K. This is one of the limitations inherent in using the log *L* correlations of the general solvation model. The computation needs accurate vapor pressure data to convert the predicted log *L* values into saturation molar solubilities. Our past experience in using different solution models has been than the better solution models will generally give predicted values that fall within ±40% or so of the observed solute solubilities. The Abraham general solvation model meets this criterion.

It should be noted that in the case of a few solvents, the measured solubility data was used in the regressional analysis to determine the equation coefficients. We do not believe that this use compromises the solubility predictions. The equation coefficients listed in Table 1 are based on data sets containing experimental solubilities and activity coefficients for more than 40 different organic and inorganic solutes. Removal of any single solute from the data set(s) should have virtually no effect on the derived coefficients.

As stated in the *Introduction*, one of the objectives of the present study is to critically examine the applicability of the Abraham solvation model in regards to solubility predictions. A better appreciation of the model's predictive ability can be gained by comparing the predictions of eqs. [1] and [2] to calculated values based upon several of the competing solution models that are currently being used in the pharmaceutical and chemical industries. Of the many solution models proposed in recent years, Mobile Order theory and the UNIFAC group contribution method are probably two of the only models that are capable of describing solute solubility behavior in such a wide range of solvent mixtures. In the case of an inert crystalline solute dissolved in a self-associating solvent, Mobile Order theory expresses the volume fraction saturation solubility (ϕ_A^{sat}) as (67–77)

© 2001 NRC Canada

Table 9. Comparison between experimental anthracene mol fraction solubilities (X_S^{exp}) and predicted values based upon the UNIFAC and Modified UNIFAC (Dortmund) models.[a]

		UNIFAC		Modified UNIFAC	
Solvent	X_S^{exp}	X_S^{pred}	% Dev.[b]	X_S^{pred}	% Dev.[b]
Hexane	0.001290	0.002380	84.5	0.001585	22.9
Heptane	0.001571	0.002407	53.2	0.001789	13.9
Octane	0.001850	0.002438	31.8	0.002385	28.9
Decane	0.002345	0.002556	9.0	0.002690	14.7
Hexadecane	0.00380	0.002920	–23.1	0.003309	12.9
2,2,4-Trimethylpentane	0.001087	0.002216	103.9	0.001902	75.0
Cyclohexane	0.001574	0.003780	140.1	0.001259	–20.0
Chlorobenzene	0.009962	0.009659	–3.0	0.001580	–84.1
Dichloromethane	0.009387	0.02225	137.0	0.006327	–32.6
Chloroform	0.01084	0.02084	92.2	0.008127	–25.0
Tetrachloromethane	0.00464	0.006433	38.6	0.002243	–51.7
Acetonitrile	0.000830	0.001447	74.3	0.002693	224.0
Benzene	0.007418	0.01234	66.3	0.005116	–31.0
Toluene	0.00736	0.01050	42.7	0.008176	11.1
Methanol	0.000243	0.000412	69.6	0.000195	–19.8
Ethanol	0.000460	0.000284	–38.3	0.000569	23.7
1-Propanol	0.000591	0.000470	–20.4	0.000508	–14.0
2-Propanol	0.000411	0.000475	15.4	0.000510	24.1
1-Butanol	0.000801	0.000664	–17.1	0.000792	–1.1
1-Pentanol	0.001097	0.000858	–21.8	0.000904	–17.6
1-Hexanol	0.001483	0.001057	–28.7	0.000918	–38.1
1-Heptanol	0.001869	0.001248	–33.2	0.000996	–46.7
1-Octanol	0.002160	0.001434	–33.6	0.001524	–29.4
Ethyl acetate	0.00484	0.005086	5.1	0.005392	11.4
Dimethylformamide	0.007839	0.003335	–57.4	0.001427	–81.8
Ethylene glycol	0.0000715	0.0000191	–73.1	0.0000528	–26.2
Average Absolute Deviation			50.5		37.8

[a]UNIFAC and Modified UNIFAC predictions were taken from Hansen et al. (81).
[b]% Dev. = $100(X_S^{pred} - X_S^{exp})/X_S^{exp}$.

$$[6]\quad \ln\phi_A^{sat} = \ln a_A^{solid} - 0.5(1 - V_A/V_{solvent})\phi_{solvent} + 0.5\ln[\phi_A^{sat} + \phi_{solvent}(V_A/V_{solvent})] - \phi_{solvent}^2 V_A(\delta_A' - \delta_{solvent}')^2(RT)^{-1} - r_{solvent}(V_A/V_{solvent})\phi_{solvent}$$

where the $r_{solvent}(V_A/V_{solvent})\phi_{solvent}$ term represents the contributions resulting from hydrogen bond formation between the solvent molecules. For most of the published applications, $r_{solvent}$ was assumed to be unity for strongly associated solvents with single hydrogen-bonded chains such as monofunctional alcohols, to be two for water or diols, and to equal zero for nonassociated solvents such as saturated hydrocarbons. Slightly more complex expressions apply in the case of solute–solvent complexation. The more complex expressions are not used in the present study as they require *a prior* knowledge of the numerical value of the solute–solvent stability equilibrium constant. While one could calculate a general numerical value for the interaction of an aromatic hydrocarbon solute with each of the different solvent classes from the observed solubility data, its subsequent use in the Mobile Order theory equations would not represent outright solubility predictions.

The symbols δ_A' and $\delta_{solvent}'$ denote the modified solubility parameters of the solute and solvent, respectively. Modified solubility parameters account for only nonspecific interactions, and in the case of the alcoholic solvents the hydrogen bonding contributions have been removed. Numerical values of $\delta_{solvent}'$ are available in several published compilations (70, 71, 73, 74), and were either deduced by regressing actual solubility data of solid *n*-alkanes in organic solvents in accordance with the configurational entropic model of Huyskens and Haulait-Pirson (78) or estimated using known values for similar organic solvents. In eq. [6], V_i is the molar volume of component *i* and a_A^{solid} is the activity of the solid solute. This latter quantity is defined as the ratio of the fugacity of the solid to the fugacity of the pure hypothetical supercooled liquid. The numerical value of a_A^{solid} can be computed from

$$[7]\quad \ln a_A^{solid} = -\Delta H_A^{fus}(T_{mp} - T)/(RTT_{mp}) + (\Delta C_{p,A}/RT)(T_{mp} - T) - (\Delta C_{p,A}/T)\ln(T_{mp}/T)$$

the solute's molar enthalpy of fusion (ΔH_A^{fus}) and heat capacity difference ($\Delta C_{p,A}$) at the normal melting point temperature (T_{mp}). Additonal term(s) must be added if the solute undergoes a phase transition prior to melting (79, 80). Ther-

© 2001 NRC Canada

modynamic models that predict solubility through activity coefficient considerations are limited to those crystalline compounds whose enthalpy of fusion is known or can be reasonably estimated. Lack of heat capacity data often necessitates that the last two terms in eq. [7] be dropped from the ln a_A^{solid} computation.

Tables 6–8 summarize the Mobile Order theory predictions for anthracene, phenanthrene, and hexachlorobenzene. Modified solubility parameters of the three solutes were obtained by forcing eq. [5] to "perfectly" describe the measured solute solubility in hexane, heptane, and octane. The resulting three preliminary δ_A' values for each solute were then averaged to give δ_A' = 20.32 $MPa^{1/2}$ (anthracene), δ_A' = 20.45 $MPa^{1/2}$ (phenanthrene), and δ_A' = 20.10 $MPa^{1/2}$ (hexachlorobenzene). The averaged values were used in all subsequent predictions. The last columns in Tables 6–8 show that Mobile Order theory predicts the observed mol fraction solubilities (X_S^{exp}) to within an average absolute deviation of ±109.5%. Mobile Order theory grossly overestimates the solubility of both anthracene and phenanthrene in acetonitrile. We suspect that the overestimation results from either failure of the Scatchard–Hildebrand solubility parameter theory to describe nonspecific interactions between acetonitrile and the two polycyclic aromatic hydrocarbons, or perhaps from an incorrect value for this solvent's modified solubility parameter. If acetonitrile is excluded from the comparison, the average absolute deviations for the anthracene and phenanthrene solubility predictions are reduced to ±39.6 and ±39.5%, respectively. The predictions for hexachlorobenzene are considerably worse. The melting point temperature of hexachlorobenzene (T_{mp} = 505.0 K) is significantly above 298.15 K, and there could be errors and (or) uncertainties associated with the a_A^{solid} calculation. The two heat capacity terms in eq. [7] were dropped from the calculation because the needed heat capacity terms were not available in the chemical literature. These terms become increasingly more important for solutes with high melting point temperature. This is an inherent problem with all thermodynamic models that predict saturation solubilities from activity coefficients based on the hypothetical supercooled liquid solute standard state. Thermodynamic models that base transfer properties upon the solute's gas-phase properties experience similar difficulties in predicting solubilities from organic solvent – gas phase partition coefficients of highly nonvolatile crystalline solutes. The needed vapor pressure data may not be known with sufficient accuracy to enable accurate solubility predictions.

Finally, the predictive ability of the Abraham general solvation model is compared to the UNIFAC and Modified UNIFAC (Dortmund) group contribution models. These latter two models estimate activity coefficients from structural considerations and molecular interactions involving the various functional groups on the dissolved solute and solvent molecules. Numerical entries in Table 9 were taken from a recent paper by Hansen et al. (81). The authors studied only three polycyclic aromatic hydrocarbons (anthracene, pyrene, and fluoranthene). For the most part, the predicted values fell with ±35% of the observed solubility data. It is expected that had the authors studied phenanthrene that the deviations would be similar. Based upon the comparisons presented above, we conclude that the Abraham general solvation model is comparable to, if not superior than, Mobile Order theory and the UNIFAC and Modified UNIFAC (Dortmund) models when it comes to predicting solute solubility in organic solvents.

Acknowledgement

Research supported in part by the University of North Texas Research Council.

References

1. F. Lombardo, J.F. Blake, and W.J. Curatolo. J. Med. Chem. **39**, 4750 (1996).
2. G.M. Keseru and L. Molnar. J. Chem. Inf. Comput. Sci. **41**, 120 (2001).
3. W.J. Lyman, W.F. Reehl, and D.H. Rosenblatt. Handbook of chemical property estimation methods. McGraw-Hill, New York. 1982. Chap. 1.
4. K. Vereschuren. Handbook of environmental data on organic chemicals. 2nd ed. Van Nostrand-Reinhold, New York. 1983.
5. A. Finizio, F. Sicbaldi, and M. Vighi. SAR QSAR Environ. Res. **3**, 71 (1995).
6. A. Finizio, M. Vighi, and D. Sandroni. Chemosphere, **34**, 131 (1997).
7. D. Domine, J. Devillers, and W. Karcher. Neural networks in QSAR and drug design. *Edited by* J. Devillers. Academic Press, New York. 1996. Chap. 2.
8. J.R. Baker, J.R. Mihelcic, D.C. Luehrs, and J.P. Hickey. Water Environ. Res. **69**, 136 (1997).
9. C. Hansch. Acc. Chem. Res. **26**, 147 (1993).
10. X. Lu, S. Tao, H. Hu, and R.W. Dawson. Chemosphere, **41**, 1675 (2000).
11. J.R. Baker, J.R. Mihelcic, and E. Shea. Chemosphere, **41**, 813 (2000).
12. M.H. Abraham. Chem. Soc. Rev. **22**, 73 (1993), and refs. therein.
13. M.H. Abraham, H.S. Chadha, G.S. Whiting, and R.C. Mitchell. J. Pharm. Sci. **83**, 1085 (1994).
14. M.H. Abraham, K. Takacs-Novak, and R.C. Mitchell. J. Pharm. Sci. **86**, 310 (1997).
15. M.H. Abraham, H.S. Chadha, G.S. Whiting, and R.C. Mitchell. J. Pharm. Sci. **83**, 1257 (1994).
16. J.A. Gratton, M.H. Abraham, M.W. Bradbury, and H.S. Chadha. J. Pharm. Pharmacol. **49**, 1211 (1997).
17. M.H. Abraham, F. Martins, and R.C. Mitchell. J. Pharm. Pharmacol. **49**, 919 (1997).
18. M.H. Abraham and P.K. Weathersby. J. Pharm. Sci. **83**, 1450 (1994).
19. M.H. Abraham, R. Kumarsingh, J.E. Cometto-Muniz, and W.S. Cain. Arch. Toxicol. **72**, 227 (1998).
20. M.H. Abraham, C.E. Green, W.E. Acree, Jr., C.E. Hernández, and L.E. Roy. J. Chem. Soc. Perkin Trans. 2, 2677 (1998).
21. M.H. Abraham, C.E. Green, and W.E. Acree, Jr. J. Chem. Soc. Perkin Trans. 2, 281 (2000).
22. M.H. Abraham, N. Benjelloun-Dekhama, J.M.R. Gola, W.E. Acree, Jr., W.S. Cain, and J.E. Commetto-Munez. New J. Chem. **24**, 825 (2000).
23. C.E. Green, M.H. Abraham, W.E. Acree, Jr., K.M. De Fina, and T.L. Sharp. Pest Manage. Sci. **56**, 1046 (2000).
24. L.E. Roy, C.E. Hernández, and W.E. Acree, Jr. Polycyclic Aromat. Compd. **13**, 105 (1999).
25. C.E. Hernández, K.M. De Fina, L.E. Roy, T.L. Sharp, and W.E. Acree, Jr. Can. J. Chem. **77**, 1465 (1999).

© 2001 NRC Canada

26. K.M. De Fina, T.T. Van, and W.E. Acree, Jr. Can. J. Chem. **78**, 459 (2000).
27. E. McLaughlin and H.A. Zainal. J. Chem. Soc. 863 (1959).
28. P.B. Chio and E. McLaughlin. AIChE J. **29**, 150 (1983).
29. J. Mahieu. Bull. Soc. Chim. Belg. **45**, 667 (1936).
30. P. Meyer and G. Maurer. I&EC Research, **32**, 2105 (1993).
31. J. Schulte, J. Dürr, S. Ritter, W.H. Hauthal, K. Quitzsch, and G. Maurer. J. Chem. Eng. Data, **43**, 69 (1998).
32. P. Meyer and G. Maurer. I&EC Research, **34**, 373 (1995).
33. J.D. Weckwerth, M.F. Vitha, and P.W. Carr. Fluid Phase Equilib. **183**–**184**, 143 (2001).
34. D.J. Giesen, G.D. Hawkins, D.A. Liotard, C.J. Cramer, and D.G. Truhlar. Theor. Chem. Acc. **98**, 85 (1997).
35. T. Zhu, J. Li, G.D. Hawkins, C.J. Cramer, and D.G. Truhlar. J. Chem. Phys. **109**, 9117 (1998).
36. I.F. Li, L.V. Semenov, A.A. Gaile, and M.N. Pul'tsin. Russ. J. Phys. Chem. **58**, 1481 (1984).
37. L.E. Roy, C.E. Hernández, and W.E. Acree, Jr. Polycyclic Aromat. Compd. **13**, 205 (1999).
38. A.R. Katritzky, L. Mu, and M. Karelson. J. Chem. Inf. Comput. Sci. **36**, 1162 (1996).
39. A.R. Katritzky, D.B. Tatham, and U. Maran. J. Chem. Inf. Comput. Sci. **41**, 358 (2001).
40. K.M. De Fina, T.L. Sharp, and W.E. Acree, Jr. Can. J. Chem. **77**, 1589 (1999).
41. K.M. De Fina, T.L. Sharp, and W.E. Acree, Jr. Can. J. Chem. **77**, 1537 (1999).
42. C.E. Hernández and W.E. Acree, Jr. Can. J. Chem. **76**, 1312 (1998).
43. K.M. De Fina, T.L. Sharp, M.A. Spurgin, I. Chuca, W.E. Acree, Jr., C.E. Green, and M.H. Abraham. Can. J. Chem. **78**, 184 (2000).
44. P. Bustamante, M.A. Pena, and J. Barra. Int. J. Pharm. **194**, 117 (2000).
45. P. Bustamante, M.A. Pena, and J. Barra. Int. J. Pharm. **174**, 141 (1998).
46. P. Bustamante, M.A. Pena, and J. Barra. J. Pharm. Pharmacol. **50**, 975 (1998).
47. J. Barra, F. Lescure, E. Doelker, and P. Bustamante. J. Pharm. Pharmacol. **49**, 644 (1997).
48. A. Martin, P. Bustamante, B. Escalera, and E. Selles. J. Pharm. Sci. **78**, 672 (1989).
49. J. Barra, M.A. Pena, and P. Bustamante. Eur. J. Pharm. Sci. **10**, 153 (2000).
50. P. Bustamante, M. Jimenez-Duran, and B. Escalera. Boll. Chim. Farma. **138**, 483 (1999).
51. K.A. Fletcher, M.E.R. McHale, J.R. Powell, K.S. Coym, and W.E. Acree, Jr. Phys. Chem. Liq. **34**, 41 (1997).
52. L.E. Roy, C.E. Hernández, K.M. De Fina, and W.E. Acree, Jr. Phys. Chem. Liq. **38**, 333 (2000).
53. M.T. Beck and G. Mandi. Fullerene Sci. Technol. **5**, 291 (1997).
54. K.M. De Fina, T.T. Van, K.A. Fletcher, and W.E. Acree, Jr. Can. J. Chem. **78**, 449 (2000).
55. D. Dumanovic, J. Jovanovic, S. Popovic, and D. Kosanovic. J. Serb. Chem. Soc. **51**, 411 (1986).
56. K.A. Fletcher, S. Pandey, M.E.R. McHale, and W.E. Acree, Jr. Phys. Chem. Liq. **33**, 181 (1996).
57. A. Beerbower, P.L. Wu, and A. Martin. J. Pharm. Sci. **73**, 179 (1984).
58. A. Martin, P.L. Wu, and A. Beerbower. J. Pharm. Sci. **73**, 188 (1984).
59. C.V.S. Subrahmanyam and S. Suresh. Eur. J. Pharm. Biopharm. **47**, 289 (1999).
60. F. Huyskens, H. Morissen, and P. Huyskens. J. Mol. Struct. **441**, 17 (1998).
61. K.A. Fletcher, K.S. Coym, L.E. Roy, C.E. Hernández, M.E.R. McHale, and W.E. Acree, Jr. Phys. Chem. Liq. **35**, 243 (1998).
62. K.M. De Fina, C. Ezell, and W.E. Acree, Jr. Phys. Chem. Liq. In press.
63. M.H. Abraham, G.S. Whiting, W.J. Shuely, and R.M. Doherty. Can. J. Chem. **76**, 703 (1998).
64. M.H. Abraham. J. Phys. Org. Chem. **6**, 660 (1993).
65. M.H. Abraham and J. Le. J. Pharm. Sci. **88**, 868 (1999).
66. A.A. Koelmans, S.F.M. Anzion, and L. Lijklema. Environ. Sci. Technol. **29**, 933 (1995).
67. P.L. Huyskens and G.G. Siegel. Bull. Soc. Chim. Belg. **97**, 821 (1988).
68. G.G. Siegel, P.L. Huyskens, and G. Vanderheyden. Ber. Bunsen–Ges. **94**, 549 (1990).
69. P.L. Huyskens. J. Mol. Struct. **274**, 223 (1992).
70. P. Ruelle, C. Rey-Mermet, M. Buchmann, H. Nam-Tran, U.W. Kesselring, and P.L. Huyskens. Pharm. Res. **8**, 840 (1991).
71. P. Ruelle, M. Buchmann, H. Nam-Tran, and U.W. Kesselring. Int. J. Pharm. **87**, 47 (1992).
72. P. Ruelle, M. Buchmann, and U.W. Kesselring. J. Pharm. Sci. **83**, 396 (1994).
73. P. Ruelle, E. Sarraf, and U.W. Kesselring. Int. J. Pharm. **104**, 125 (1994).
74. P. Ruelle, E. Sarraf, L. Van den Berge, K. Seghers, M. Buchmann, and U.W. Kesselring. Pharm. Acta Helv. **68**, 49 (1993).
75. P. Ruelle and U.W. Kesselring. J. Pharm. Sci. **87**, 998 (1998).
76. P. Ruelle. J. Phys. Org. Chem. **12**, 769 (1999).
77. P. Ruelle and U.W. Kesselring. J. Pharm. Sci. **87**, 987 (1998).
78. P.L. Huyskens and M.C. Haulait-Pirson. J. Mol. Liq. **31**, 135 (1985).
79. R.F. Weimer and J.M. Prausnitz. J. Chem. Phys. **42**, 3643 (1965).
80. H.L. Finke, J.F. Mosserly, S.H. Lee, A.G. Osborn, and D.R. Douslin. J. Chem. Thermodyn. **9**, 937 (1977).
81. H.K. Hansen, C. Riverol, and W.E. Acree, Jr. Can. J. Chem. Eng. **78**, 1168 (2000).

© 2001 NRC Canada

Synthesis of chloro(2-methylimidazole)ruthenium(III) complexes and their aqueous solution chemistry, and the crystal structure of $[2\text{-MeImH}]_2[RuCl_5\text{2-MeIm}]$

Craig Anderson

Abstract: 2-Methylimidazole (2-MeIm) reacts with $RuCl_3$ in aqueous acidic ethanolic medium to give $(2\text{-MeImH})_2[RuCl_5(2\text{-MeIm})]$ (**1**) and $(2\text{-MeImH})[RuCl_4(2\text{-MeIm})_2]$ (**2**) (2-MeImH = protonated 2-methylimidazole), the ratio depending on reaction conditions used. Molecule **1** crystallizes in the space group *Pnma*: a = 14.046(2), b = 17.294(2), and c = 8.2778(12) Å. The ^{1}H NMR spectra of these ruthenium(III) complexes have been measured and show peaks with large isotropic shifts and large line broadening characteristic of such paramagnetic complexes. The aquation of complexes **1** and **2** were followed by proton NMR spectroscopy. 1,2-Dimethylimidazole (1,2-diMeIm) reacts with $RuCl_3$ in methanolic solution to give $[RuCl_3(1,2\text{-diMeIm})(H_2O)S]$ ($S=H_2O$ (**3a**) or CH_3OH (**3b**)). The aquation reactions of complexes **3a** and **3b** were followed by ^{1}H NMR.

Key words: ruthenium, paramagnetic, antitumour, NMR.

Résumé : Le 2-méthylimidazole (2-MeIm) réagit avec le $RuCl_3$, en solution aqueuse acide, dans un milieu éthanolique, pour conduire à la formation de $(2\text{-MeImH})_2[RuCl_5(2\text{-MeIm})]$ (**1**) et de $(2\text{-MeImH})[RuCl_4(2\text{-MeIm})_2]$ (**2**) (2-MeImH = 2-méthylimidazole protoné) dans des rapports qui varient selon les conditions réactionnelles. Le composé **1** cristallise dans le groupe d'espace *Pnma*, avec a = 14,046(2), b = 17,294(2) et c = 8,2778(12) Å. On a mesuré les spectres RMN du ^{1}H de ces complexes du ruthénium(III) et ils comportent de pics présentant des larges déplacements isotropes et l'important élargissement des raies caractéristique de tels complexes paramagnétiques. On a suivi l'aquation des complexes **1** et **2** à l'aide de la RMN du proton. Le 1,2-diméthylimidazole (1,2-diMeIm) réagit avec le $RuCl_3$, en solution méthanolique, pour conduire à la formation des complexes $[RuCl_3(1,2\text{-diMeIm})(H_2O)S]$, dans lesquels $S = H_2O$ ou CH_3OH, **3a** et **3b**. Les réactions d'aquation des complexes **3a** et **3b** ont été suivies par RMN du ^{1}H.

Mots clés : ruthénium, paramagnétique, antitumoral, RMN.

[Traduit par la Rédaction]

Introduction

Interest in ruthenium imidazole complexes stems from their possible uses as anti-tumour agents (1–3), their radiosensitizability (4), more recently their potential use as immunodeciency drugs (5), and more generally, as models for transition-metal interaction with more complex biological substrates, such as the purine bases of DNA (6). Clarke and co-workers (7) have reported several papers with numerous examples of ruthenium(III) ammine complexes that also contain coordinated imidazole or purine, which are fully characterized including ^{1}H NMR spectra. The crystal structures (1), solution chemistry (8, 9), and reactivity with nitrogenous ligands (10) of $(ImH)[RuCl_4Im_2]$ (**4**) and $(ImH)_2[RuCl_5Im]$ (**5**) have been reported. Little is known, however, of analogous 2-methylimidazoles complexes, although $(2\text{-MeImH})[RuCl_4(2\text{-MeIm})_2]$ (**2**) has been reported as a red solid (1). Also, a report has been made of the reaction of ruthenium trichloride and several 2-methylimidazoles, but the products were not fully characterized (11). It is well-known that paramagnetic ruthenium(III) complexes give NMR spectra with peaks that have both large linewidths and large isotropic shifts (7, 8, 12, 13). The 2-methylimidazole complexes are no exception. However, these complexes have NMR spectra much different than for analogous 1-methylimidazole and 4-methylimidazole chloro-complexes previously reported (8). These differences can be attributed to the 2-methylimidazole ligand, which has the methyl group *ortho* to coordinated nitrogen, and therefore causes steric interactions in the bonding of the ligand to the metal centre. 2-Methylimidazole, for example, is known not to react with ruthenium(II) bipyridine species due to steric interactions, whereas other methylated analogues have (14).

The results of the formation of chloro-(2-methylimidazole)ruthenium(III) paramagnetic complexes and their aqueous solution chemistry will be reported here. An attempt has also been made to use proton NMR not only as a means of characterizing these paramagnetic compounds but also to monitor the progress of their aquatic reactions. Also to be reported here, is the first ruthenium(III) structure containing coordinated 2-methylimidazole.

Received June 1, 2001. Published on the NRC Research Press Web site at http://canjchem.nrc.ca on October 11, 2001.

C. Anderson. Department of Chemistry, Bard College, Annandale-on-Hudson, NY 12504, U.S.A. (telephone: (845) 758-7293; fax: (845) 758-7628; e-mail: canderso@bard.edu).

 DOI: 10.1139/cjc-79-10-1477 © 2001 NRC Canada

Experimental

Instruments and methods

^{1}H NMR spectra were recorded on Varian XL-300 or Bruker AMX 300 spectrometers. Sweep widths of 50 000 or 100 000 Hz were used at pulse rates of 0.04 s. The peaks were referenced to residual solvent peaks (D_2O, $\delta = 4.8$) and given with respect to Me_4Si; downfield being positive.

Infrared spectra were recorded down to 200 cm^{-1} on a PerkinElmer 1600 FT-IR apparatus as either KBr or CsI pellets. In the case of KBr pellets, noise existed below 240 cm^{-1}.

Crystal structure of (2-MeIm)$_2$[RuCl$_5$(2-MeIm)]

X-ray diffraction data were obtained with an Enraf-Nonius CAD-4 diffractometer using Mo Kα radiation. The cell parameters were calculated by least-squares refinement on 25 higher angle reflections ($20° < \theta < 23°$). Space groups *Pnma* and $Pn2_1a$ (alternate definition of $Pna2_1$) were both consistent with the systematic absences. The structure was solved in the space group *Pnma*. Crystal data are given in Table 1.

Four standards were used to monitor intensity every hour and orientation every 200 measurements. Variations remained within ±2.0% during data collection. A half sphere of data (7308 reflections) was collected by the ω–2θ scan technique. The usual corrections for the effects of Lorentz and polarization were applied.

From the Patterson map, the Ru atom was found to lie on a crystallographic mirror plane. The remaining atoms were located from structure–factor and ΔF calculations. The structure was refined on F^2 by full-matrix least-squares. All non-hydrogen atoms were refined anisotropically. The hydrogen atoms were fixed at idealized positions. All calculations were done with the SHELXTL package (15).[1]

Preparation of (2-MeIm)$_2$[RuCl$_5$(2-MeIm)] (1)

Ruthenium trichloride ($RuCl_3$) (0.413 g) was heated at reflux in a 0.5 M HCl aqueous–ethanolic solution (1:1, 40 mL) for 2 h. The solution became blue-green. The volume of the solution was then reduced to approximately 5 mL. This solution, which had subsequently turned bright red, was cooled to room temperature. To this was added 2-methylimidazole (2.4 g) in aqueous HCl (2 mL, 8 M). The resulting solution, which had remained red, was stirred and heated to 50°C for 10 min. It was cooled down to room temperature and then placed at 8°C for 24 h. Later it was placed at (–15°C) for two weeks, at which time red crystals had appeared. The solid was filtered and washed quickly with cold ethanol. The crystals were bright ruby red, but were covered with a red-brown dust or a dark red oil. The dust and (or) oil were washed away with several washings with water. A single red crystal was characterized crystallographically and shown to be (2-MeImH)$_2$[RuCl$_5$(2-MeIm)] (**1**). The brownish-red powder was assigned as (2-MeImH)[RuCl$_4$(2-MeIm)$_2$] (**2**). The NMR spectra before washing (see *Discussion*) of these materials showed a mixture of the two species (**1** and **2**) at a ratio of 4:1, respectively, but only peaks due to **1** remained after washing (Fig. 1). All the crystals in the batch had the same habit, and several crystals were taken at random from the batch and their cell parameters checked against those of the structure determination. All of these matched confirming that the crystals were the same product, namely, complex **1**. Selected IR data ν(Ru-Cl) (cm^{-1}): 270 (m), 290 (s), 305 (vs), 655 (s), 665 (s), 1080 (s), 1090 (s). Selected ^{1}H NMR data (fresh solution of **1**) (**1a**, see *Discussion*) δ: 32.2 (CH_3), –6.8 (H5); cation: 2.58 (CH_3), 7.24 (H4/H5). The pH of a fresh solution decreased from approximately 7 to 3 and then stabilized at ca. 2 after several hours. The ratio of complex **2** to complex **1** obtained was higher (1:1) when higher concentration of ligand was used. ^{1}H NMR for **2** (D_2O) δ: 38.2 (CH_3), –5.9 (H5) (see Table 2 for complete ^{1}H NMR data).

Table 1. Crystal data and conditions of data collection for (2-MeImH)$_2$[RuCl$_5$(2-MeIm)] (**1**).

Formula	$C_{15}H_{20}Cl_5N_6Ru$
Formula weight	526.66
Crystal system	Orthorhombic
Space group	*Pnma*
a (Å)	14.047(3)
b (Å)	17.294(4)
c (Å)	8.2778(17)
V (Å^3)	2010.9(7)
$D_{calcd.}$ (g cm^{-3})	1.74
Z	4
F(000)	1052
μ (mm^{-1})	14.4
No. unique reflections measured	1827
No. observed reflections	1548
T (K)	293
R [$I > 2\sigma(I)$], $wR(F^2)$	0.0453, 0.1128
R (all data), $wR(F^2)$	0.0553, 0.1202

Reaction of 2-methylimidazole and RuCl$_3$ and NMR studies of reaction products

2-MeIm reacts with commercial ruthenium chloride to give (2-MeImH)$_2$[RuCl$_5$(2-MeIm)] (**1**) (Scheme 1). The ^{1}H NMR spectrum of complex **1** measured in D_2O (Fig. 1) has one set of peaks and is assigned to the mono-aqua species [RuCl$_4$(2-MeIm)(H$_2$O)]$^-$ (**1a**) analagous to the conclusions determined for similar complexes from previous reports, i.e., that tetrachloro complexes and not pentachloro species are present immediately in aqueous solution. The peaks for **1a** appear at +32.2 ppm for the methyl group and at –6.8 ppm for the H5 proton (numbering is given in Table 3). The H5 proton is assigned due to its similar chemical shift and linewidth to those described previously (8). The H4 proton was not found in the +165 to –165 ppm region searched. The

[1] Crystallographic data (excluding structure factors) for complex **1** may be purchased from the Depository of Unpublished Data, Document Delivery, CISTI, National Research Council Canada, Ottawa, ON K1A 0S2, Canada. For information on obtaining material electronically go to http://www.nrc.ca/cisti/irm/unpub_e.shtml. Crystallographic information has also been deposited with the Cambridge Crystallographic Data Centre (CCDC No. 169 216). Copies of the data can be obtained, free of charge, on application to the Director, CCDC, 12 Union Road, Cambridge CB2 1EZ, U.K. (fax: 44-1223-336033 or e-mail: deposit@ccdc.cam.ac.uk).

© 2001 NRC Canada

Fig. 1. Proton NMR spectrum of complex **1a** in D_2O.

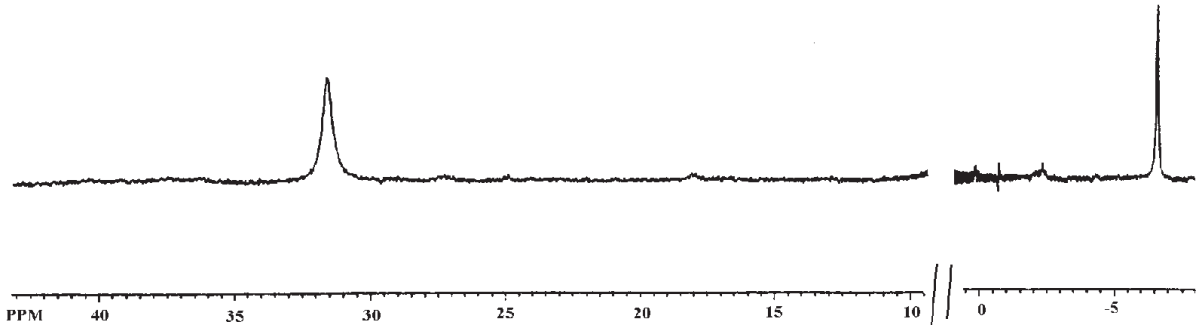
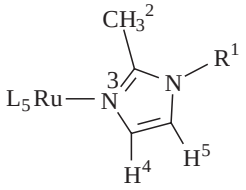


Table 2. NMR data for the ruthenium(III) complexes.

Complex	Proton	δ (ppm)	δ_{diamag} [a]	δ_{iso} [b]
$[RuCl_4(2MeIm)(H_2O)]^-$ (**1a**)	$CH_3(2)$	32.2	2.10	+30.1
	H5	–6.8	6.83	–13.6
	H4	[c]	6.83	[c]
$[RuCl_4(2MeIm)_2]^-$ (**2**)	$CH_3(2)$	38.2	2.10	36.1
	H5	–5.9	6.83	–12.7
	H4	[c]	6.83	[c]
$[RuCl_3(2MeIm)(H_2O)_2]$ (**1b**)	$CH_3(2)$	45.5	2.10	43.4
	H5	–3.8	6.83	–10.6
	H4	[c]		
$[RuCl_3(2MeIm)_2(H_2O)]$ (**2a**)	$CH_3(2)$	35.1	2.10	33.0
	H5	–4.9	6.83	11.7
	H4	[c]		
$[RuCl_3(1,2\text{-diMeIm})(H_2O)_2]$ (**3a**)	$CH_3(2)$	39.9	2.4	37.5
	H5	–6.4	6.7	–13.1
	$N1(CH_3)$	11.4	3.5	7.9
	H4	[c]	6.6	[c]
$[RuCl_3(1,2\text{-diMeIm})(H_2O)S]$ (**3b**) (S = CH_3OH)	$CH_3(2)$	33.4	2.4	31.0
	H5	–7.2	6.7	13.9
	$N1(CH_3)$	17.3	3.5	13.8
	CH_3OH	18.6	3.5	15.1
	H4	[c]		
$[RuCl_2(1,2\text{-diMeIm})(H_2O)_3]^+$ (**3c**)	$CH_3(2)$	37.2	2.4	34.8
	H5	–6.5	6.7	–13.2
	$N1(CH_3)$	11.2	3.5	7.7
	H4	[c]		

Note: The cation for complexes **1** and **2** are seen at 2.58 (CH_3) and 7.24 (H4 and H5). Numbering system is shown below, where R = H for complexes **1** and **2** and CH_3 for complexes **3**. [a]The free ligand value. [b]The difference between the observed shift and the free ligand value. [c]Peaks for these protons are not observed.



peak at low field was assigned to the methyl group because it integrated to three times the peak at higher field. The peaks for complex **2** appear at +38.2 ppm for the methyl group and –5.9 ppm for the H5 proton with the H4 proton absent. Other peaks are seen in both spectra at +2.58 and +7.24 ppm, which correspond to the methyl and H4/H5 protons, respectively, of the protonated 2-MeIm counter ion.

Species **1a** and **2** then both undergo aquation, substitution of aqua for chloride, as seen by the appearance of new peaks in the proton NMR spectra accompanied by a de-

© 2001 NRC Canada

Scheme 1.

$RuCl_3$ + HCl/EtOH → "$RuCl_3$"

"$RuCl_3$" + 2-MeIm → $(2\text{-MeImH})_2[RuCl_5(2\text{-MeIm})]$ (**1**)

"$RuCl_3$" + 2-MeIm → $(2\text{-MeImH})[RuCl_4(2\text{-MeIm})_2]$ (**2**)

1 + H_2O → $[RuCl_4(H_2O)(2\text{-MeIm})]^-$ (**1a**)

1a + H_2O → $[RuCl_3(H_2O)_2(2\text{-MeIm})]$ (**1b**)

2 + H_2O → $[RuCl_3(H_2O)(2\text{-MeIm})_2]$ (**2a**)

Table 3. Selected bond distances (Å) and angles (°) in $(2\text{-MeIm})_2[RuCl_5(2\text{-MeIm})]$ (**1**).

Bond distances (Å)			
Ru—Cl(1)	2.3676(12)	Ru—Cl(2)	2.3640(13)
Ru—Cl(3)	2.3830(19)	Ru—N(13)	2.104(5)
Bond angles (°)			
Ru-N(13)-C(12)	133.6(4)	Cl(3)-Ru-N(13)	178.29(15)
Cl(1)-Ru-Cl(2)	177.85(5)	Cl(1)-Ru-Cl(3)	89.69(6)
Cl(1)-Ru-N(13)	89.13(10)	Cl(2)-Ru-Cl(3)	88.62(6)
Cl(2)-Ru-N(13)	92.60(10)	Ru-N(13)-C(14)	119.3(4)
Cl(2)-Ru-Cl(1)*a*	88.88(5)	Cl(2)*a*-Ru-Cl(2)	89.77(7)
Cl(1)*a*-Ru-Cl(1)	92.43(6)	N(13)-C(12)-C(16)	129.2(6)

Note: Symmetry transformation used to generate equivalent atoms *a*: *x*, $-y + 3/2$, *z*.

crease in the intensity of the previously existing peaks (Table 2). The methyl peak and the H5 peak are observed at 45.5 and –3.8 ppm, respectively, for $[RuCl_3(H_2O)_2(2\text{-MeIm})]$ (**1b**) and at 35.1 and –4.9 ppm, respectively, for $[RuCl_3(H_2O)(2\text{-MeIm})_2]$ (**2a**). The peaks for methyl groups and H5 protons can be matched by comparing relative intensities (3:1). Two general points can be made: (*i*) the peaks for H5 protons shift downfield on aquation, analogous to those previously studied (8) and (*ii*) the peaks for the methyl group appear anywhere from +10 to +50 ppm and showed no general pattern of shifting upon aquation. Two differences exist in the NMR of the 2-methylimidazoleruthenium(III) complexes compared to the chlororuthenium(III) imidazole complexes already reported: (*i*) only two peaks are seen, one for the H5 proton and one for the 2-Me group, the third peak, expected for the H4 proton is either lost in the baseline or less-likely obscured by other peaks and (*ii*) the peak for the 2-Me group appears at extremely low field. No such low-field peaks for methyl resonances with other chloroimidazole complexes have been observed, however, extreme downfield peaks are observed for related ammine complexes (7).

Description of the structure

The unit cell of $(2\text{-MeImH})_2[RuCl_5(2\text{-MeIm})]$ (**1**) contains four approximately octahedral ruthenium(III) anions ($[RuCl_5(2\text{-MeIm})]^{2-}$) and eight protonated 2-methylimidazole units acting as counterions. This is analogous to $(ImH)_2[RuCl_5Im]$ already published (1). A crystallographic mirror plane including the ruthenium, the coordinated 2-MeIm, and Cl3 cuts the ruthenium moiety in half. Therefore, there are three types of chloride ligands: Cl1 and Cl2, together with their mirror images, define by the equatorial plane and Cl3, which occupies an axial site *trans* to the nitrogen. The Ru—Cl3 bond (2.383(2) Å) is significantly longer than Ru—Cl1 and Ru—Cl2 (ave. 2.366(1) Å) bonds, which are the same length within experimental error (Table 3). This same pattern was observed in the analogous $(ImH)_2[RuCl_5Im]$, for which the longer bond length is attributed to the chloride being *trans* to the strong nitrogen donor (1). The Ru—Cl *trans* to N is also much shorter than the analogous bond in $[RuCl_5Im]^{2-}$ (2.446(2) Å). The Ru—N bond length (2.104(5) Å) is normal (1). The Ru—Cl bonds *trans* to Cl are in the range found for the other ruthenium(III) compounds (16).

The 2-methylimidazole ligand lies on a crystallographic mirror plane and is therefore perfectly planar. However, coordination does not take place exactly along the N lone pair: the ligand is tilted away from the chlorides because of steric interactions between the methyl group and the chloride ligands (Fig. 2). The angle Ru-N13-C12 (133.6(4)°) is significantly larger than Ru-N13-C14 (119.3(4)°) (Table 3). No such large differences have been found for other imidazole complexes without a 2-methyl group (1, 10). This distortion is attributed to the steric effect of the methyl group as the distances between the methyl carbon and the Cl2 and Cl2a ligands is 3.44(1) Å, which is less than the sum of the Van der Waals radii (3.6–3.9 Å) (17). Therefore, the effect can be expected to be present in solution where the NMR spectra were recorded.

The $[RuCl_5(2\text{-MeIm})]^{2-}$ ions form layers in the mirror planes perpendicular to *b* at $y = 1/4$ and 3/4. Within the layer, a hydrogen bond exists between the coordinated imidazole HN11 atom and two equatorial Cl1 ligands on an adjacent anion. The N11···Cl1 distances (3.327(6) Å) (Table 3) are large, which is in agreement with this hydrogen bond being bifurcated with the hydrogen at equidistance from each chloride. The 2-methylimidazolium cations form layers between those of the anions. They show hydrogen bonding on both sides, i.e., HN21 and HN23 to the chloride ligands, thus confirming that hydrogens are present on both N21 and N23 and that the species is protonated. Two different HN23's bond to each axial Cl3, whereas one HN21 is bonded to each of the two Cl2 atoms. These interactions are strong, with the N···Cl separation being approximately 3.11 Å.

$RuCl_3$ and 1,2-dimethylimidazole: formation and NMR spectroscopy

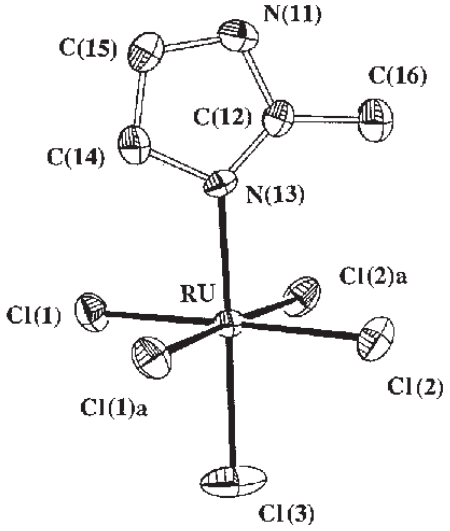
The reaction between an activated solution of ruthenium trichloride and 1,2-dimethylimidazole (1,2-diMeIm) does not form a complex with coordinated imidazole as it did in the case of 2-MeIm. Therefore, a different synthetic route was employed (Scheme 2).

The reaction was done in methanol and in the absence of acid or water. The commercial ruthenium trichloride was heated at reflux with 2 equivalents of KCl under inert atmosphere for 16 h, at which time the solution was green. The ligand was added and heated at reflux for 0.5 h and then stirred at room temperature overnight. After the solvent was removed, the residue was a blackish tar and was, therefore, characterized only by ^1H NMR spectroscopy. The products obtained from the reaction mixture decomposed within three days when left in solution.

The spectrum of the tar, measured immediately upon dissolving in D_2O, showed two major Ru(III) products assigned to $[RuCl_3(H_2O)_2(1,2\text{-}Me_2Im)]$ (**3a**) and $[RuCl_3(CH_3OH)(H_2O)(1,2\text{-}$

© 2001 NRC Canada

Fig. 2. Molecular structure of complex **1.**



MeIm)] (**3b**) on the basis of a similar study with the 9-methylhypoxanthine ligand carried out under similar conditions (18). Two sets of peaks (Table 2) were observed for the major Ru(III) products: +39.9, +11.4, and –6.4 ppm (2-Me, NMe, H5, respectively) for **3a** and +33.4, +17.3, +18.6, and –7.2 ppm (2-Me, NMe/CH_3OH, H5, respectively) for **3b**. For complex **3b** the peaks at +17.3 and +18.6 are of equal intensity and are assigned to coordinated methanol and the *N*-methyl group of the coordinated ligand, but cannot be individually assigned. Peaks present in much lesser intensity are most probably due to mixtures of *fac*- and *mer*-$[RuCl_3(MeOH)_2(1,2\text{-}Me_2Im)]$. As in the 2-MeIm system the H4 signals are not seen in the spectrum. Once the NMR solution had been aged for several hours all of **3b** had been converted to **3a** by substitution of methanol by an aqua ligand (i.e., all of the peaks associated with **3b** had disappeared and only the peaks for **3a** were present). All peaks associated with other minor species with coordinated methanol (from +12 to +30 ppm) had also disappeared and had converted to complex **3a** as well. After a period of two days, a new product, **3c** had begun to form, although the peaks associated with **3a** were still present in majority. Molecule **3c** has peaks at +37.2, +11.2, and –6.5 ppm for 2-methyl, *N*-methyl, and H5 protons, respectively, and is assigned the structure $[RuCl_2(H_2O)_3(1,2\text{-}Me_2Im)]^+$. The 3:3:1 ratio of the peaks is consistent with the assignment. However, other peaks were found in the diamagnetic portion of the spectrum indicating decomposition to ruthenium(II) complexes.

Discussion

Chlororuthenium(III) complexes with imidazole, 1-methylimidazole, and 4-methylimidazole ligands show the same general pattern in the NMR spectra, i.e., all peaks are shifted upfield compared to free ligand (8). In contrast, a downfield shift is found for the 2-methyl group of complex **1**. This is, however, in agreement with methyl protons of coordinated imidazole of ammineruthenium complexes, which have the methyl protons shifted in the opposite direction from the corresponding ring protons (i.e., downfield) (5). The H5 proton is most easily assigned to the narrowest peak and is always upfield compared to the free ligand values and virtually unchanged whether the ligand is methylated or not,

Scheme 2.

$$RuCl_3 + MeOH \rightarrow \text{“}RuCl_3\text{”}$$

$$\text{“}RuCl_3\text{”} + KCl + 1,2\text{-}Me_2Im \rightarrow [RuCl_3(1,2\text{-}Me_2Im)(H_2O)S]$$

$$S = H_2O\ (\mathbf{3a}),\ MeOH\ (\mathbf{3b})$$

$$\mathbf{3b} + H_2O \rightarrow [RuCl_3(H_2O)_2(1,2\text{-}Me_2Im)]\ (\mathbf{3a})$$

$$\mathbf{3a} + H_2O \rightarrow [RuCl_2(H_2O)_3(1,2\text{-}Me_2Im)]^+\ (\mathbf{3a})$$

similar to those previously reported (7, 8). The H4 protons of the complexes reported here are not observed and it is presumed that their linewidth are too large and therefore the peaks are lost in the baseline.

Although the metal—ligand bond lengths in complex **1** are similar to those of complexes $(ImH)[RuCl_4Im_2]$ (**4**), $(ImH)_2[RuCl_5Im]$ (**5**), and $(4\text{-}MeImH)[RuCl_4(4\text{-}MeIm)_2]$ (**6**) (1, 2), there is, however, a significant difference in the Ru-N3-C2 angle, which is much more obtuse than in all the other reported structures (1, 2, 6, 8) (133° compared to 128° for **4**, 127° for **5**, and 125° for **6**) (1). It can be concluded that this change in geometry introduces a steric factor that causes different contributions in the geometric factor for the isotropic shift term, thus the huge difference in observed shift. The 2-MeIm-complex has the methyl group closer than the accepted van derWaal radii and is, therefore, in close contact with the field of the chloride ligands. The ligand is also hindered from rotating and therefore the methyl group lies directly between the chloride ligands (7). Clarke et al. (7) have stated that ligands that have methyl groups *ortho* to the coordinated atom are unable to rotate thus changing the isotropic shift to downfield values compared to the upfield values of protons at the same position, but also admonished that it is difficult to separate isotropic shifts into their dipolar and contact components when rotation is hindered. This lack of rotation greatly effects both contact and dipolar terms (7). This effect may also account for the unobserved H4 protons. The steric bending caused by the C2 methyl group pushes the H4 proton closer to Ru and would have a pronounced effect on the contact interaction, whereas the electon donating methyl group on the ring may effect the dipolar (electronic) term (7). Recently, ruthenium pyrazine complexes have been reported where the *ortho* protons are too broad to be seen (19). Furthermore, Keppler et al. (9) have stated that the isotropic shifts for $[RuCl_4Im_2]^-$ are mainly dipolar in nature because the ratios of isotropic shifts matched well the ratio of the geometric term $(3\cos^2 s - 1)/r^3$, where s is the dihedral angle between the principal symmetry axis and the Ru–H vector, and r is the Ru–H distance (based on crystal structure). For complex **1** these ratios are 2.0:1 for isotropic shifts and 1.5:1 for geometric ratio, indicating that the shifts are perhaps not completely dipolar in nature and the contact term plays a significant role in determination.

The 2-MeIm case is clearly different from the others with respect to NMR spectroscopy. The room for quantifying these observations into chemical shifts is available, but somewhat difficult due to the controversies involved in assigning contributions to terms in the equations (5, 7). The proton NMR spectra of these complexes are sensitive to small structural and electronic perturbations, therefore, assignments and quantifying peaks must be done with caution. The NMR spectra reported here should help in determining the reactiv-

© 2001 NRC Canada

ity of these ruthenium complexes and aid in determining the reasons for their activity as anticancer drugs.

Acknowledgments

We would like to thank Michel Simard and Christian Tessier for help with the crystallographic work. We would like to thank Orgometa Laboratories for financial and moral support. Financial support from the Beretta and Keats Funds is also acknowledged.

References

1. (*a*) B.K. Keppler, W. Rupp, H. Endres, R. Niebl, and W. Balzer. Inorg. Chem. **26**, 4366 (1987); (*b*) B.K. Keppler, D. Wehe, H. Endres, and W. Rupp. Inorg. Chem. **26**, 844 (1987).
2. B.K. Keppler, M. Henn, U.M. Juhl, M.R. Berger, R. Biebl, and F.E. Wagner. Prog. Clin. Biochem. Med. **10**, 41 (1989).
3. M. Hartmann, K.G. Lipponer, and B.K. Keppler. Inorg. Chim. Acta, **267**, 137 (1998).
4. P.K.L. Chan, P.K.H. Chan, D.C. Frost, B.R. James, and K.A. Skov. Can. J. Chem. **66**, 117 (1988), and refs. therein.
5. M.J. Clarke, V.M. Bailey, P.E. Doan, C.D. Hiller, K.J. LaChance-Galang, H. Daghlian, S. Mandal, C.M. Bastos, and D. Lang. Inorg. Chem. **35**, 4896 (1996).
6. (*a*) M.J. Clarke and M. Stubbs. Met. Ions Biol. Syst. **32**, 349 (1995); (*b*) W.I. Sundquist and S.J. Lippard. Coord. Chem. Rev. 293 (1990).
7. (*a*) V.M. Bailey and M.J. Clarke. Inorg. Chem. **36**, 1611 (1997); (*b*) V.M. Bailey-Rodriguez, K.J. LaChance-Galang, P.E. Doan, and M.J. Clarke. Inorg. Chem. **36**, 1873 (1997); (*c*) K.J. LaChance-Galang, P.E. Doan, M.J. Clarke, U. Rao, A. Yamano, and B.M. Hoffman. J. Am. Chem. Soc. **117**, 3529 (1995); (*d*) K.J. LaChance-Galang, M. Zhao, and M.J. Clarke. Inorg. Chem. **35**, 6021 (1996).
8. C. Anderson and A. Beauchamp. Can. J. Chem. **73**, 471 (1995).
9. O.M. Ni Dhubhghaill, W.R. Hagen, B.K. Keppler, K.G. Lipponer, and P.J. Sadler. J. Chem. Soc. Dalton Trans. 3305 (1994).
10. (*a*) C. Anderson and A. Beauchamp. Inorg. Chim. Acta, **233**, 33 (1995); (*b*) C. Anderson and A. Beauchamp. Inorg. Chem. **34**, 4371 (1995).
11. T. Bora, M. Devi, and P.K. Gogi. Trans. Met. Chem. **11**, 467 (1986).
12. E. Alessio, G. Balucci, A. Lutman, G. Mestroni, M. Calligaris, and W.M. Attia. Inorg. Chim. Acta, **203**, 205 (1993).
13. (*a*) I. Bertinti, and C. Luchinat. NMR of paramagnetic molecules in biological systems. Benjamin-Cummings, Menlo Park, CA. 1986; (*b*) G.N. Lamar. *In* NMR of paramagnetic molecules. *Edited by* W. De Horricks, Jr. and R.H. Holm. Academic Press, New York. 1973.
14. M. Heijden, P.M. van Vliet, J.G. Haasnoot, and J. Reedijk. J. Chem. Soc. Dalton Trans. 367 (1993).
15. SHELXTL 97. Program for crystal structure refinement. Bruker Analytical X-ray Systems, Madison, WI. 1997.
16. M. Calligaris, N. Bresciani-Puhor, and R.S. Srivastava. Acta Crystallogr. C, **C49**, 448 (1993).
17. W.W. Porterfild. Inorganic chemistry: a unified approach. Addison–Wesley, Reading, MA. 1984. p.168.
18. M. Leduc. PhD thesis. Université de Montréal, Montréal. 1998.
19. E. Iengo, G. Mestroni, S. Geremia, M. Calligaris, and A. Alessio. J. Chem. Soc. Dalton Trans. 3361 (1999).

© 2001 NRC Canada

An experimental and theoretical approach to phosphonodithioato complexes: molecular orbital analysis by hybrid-DFT and EHT calculations on *trans*-bis[*O*-alkyl-phenylphosphonodithioato]Ni^{II}, and vibrational assignments

M. Carla Aragoni, Massimiliano Arca, Francesco A. Devillanova, John R. Ferraro, Francesco Isaia, Francesco Lelj, Vito Lippolis, and Gaetano Verani

Abstract: The synthesis and the full spectroscopic characterization (FT-IR, FT-Raman, ^{31}P CP MAS NMR) of *trans*-bis[*O*-ethyl-phenylphosphonodithioato]Ni^{II} (**3**) are reported. On the basis of hybrid-Density Functional Theory (DFT) calculations and Extended Hückel Theory (EHT) calculations, performed on the simpler *trans*-bis[*O*-methyl-phenylphosphonodithioato]Ni^{II} (**2**) model complex, the electronic structures of phosphonodithioato complexes in their ground states are fully described, and in particular the vibrational features are deeply analyzed, allowing an unprecedented insight into the vibrational features of *trans*-bis-*O*-methyl-phenylphosphono- and *trans*-bis(isopropylamidophosphono)-dithioato complexes of nickel(II), palladium(II), and platinum(II).

Key words: phosphonodithioato complexes, IR, Raman, DFT calculation.

Résumé : On rapporte la synthèse et la caractérisation spectroscopique complète (FT-IR, FT-Raman, ^{31}P CP MAS RMN) du *trans*-bis[*O*-éthyl-phénylphosphonodithioato]Ni^{II} (**3**). Sur la base de calculs de densité fonctionnelle hybride (DFT) et de calculs de Hückel étendus effectués (EHT) sur le complexe modèle plus simple, *trans*-bis-[*O*-méthyl-phénylphosphonodithioato]Ni^{II} (**2**), on présente une description complète des structures électroniques des complexes phosphonodithioato dans leurs états fondamentaux et, en particulier, on a analysé en détail les caractéristiques vibrationnelles ce qui permet d'obtenir une vue sans précédent des caractéristiques vibrationnelles des complexes *trans*-bis-*O*-méthyl-phénylphosphono- et *trans*-bis(isopropylamidophosphono)-dithioato du nickel(II), du palladium(II) et du platine(II).

Mots clés : complexes phosphonodithioato, IR, Raman, calculs DFT.

[Traduit par la Rédaction]

Introduction

Many reports have been published on the syntheses, characterizations, and reactivities of phosphoro- (1) and phosphinodithioates (2), since these compounds and their metal complexes have found wide application in industrial and agricultural fields (3), e.g., additives to lubricant oils (4), extraction reagents for metals (3, 5), flotation agents for mineral ores, and insecticides, rodenticides, and pesticides (3, 6). However, the chemistry of phosphono- and amido-phosphonodithioates has been only scarcely investigated, probably because of synthetic difficulties (7). Recently (8), we have reported a novel synthetic route to the preparation of square-planar metal-phosphonodithioates deriving from Lawesson's Reagent (LR, 2,4-bis(4-methoxy-phenyl)-[1,3,2,4]-dithiadiphosphetane-2,4-disulfide (**1**), see Scheme 1) (9), mainly known as thionation agent. First, these complexes were obtained as by-products in the synthesis of a new class $[M(R,R'timdt)_2]$ (M = Ni, Pd, Pt; R,R′timdt = monoreduced form of disubstituted imidazolidine-2,4,5-trithione) of neutral metal-dithiolenes (10, 11), obtained by sulphuring disubstituted imidazolidine-2-thione-4,5-diones with **1** in the presence of a suitable metal powder or salt and of an alcohol, used because of solubility reasons (8). More generally, **1** was proved to react with nucleophilic alcohols (ROH) and amines ($R'NH_2$) to induce the opening of the P_2S_2 tetra-atomic ring, yielding phosphonodithioato and amidophosphonodithioato anions. Furthermore, their reaction with Ni^{II},

Received March 7, 2001. Published on the NRC Research Press Web site at http://canjchem.nrc.ca on October 12, 2001.

M.C. Aragoni, M. Arca, F.A. Devillanova, F. Isaia, V. Lippolis, and G. Verani.[1] Dipartimento di Chimica Inorganica ed Analitica, S.S. 554 bivio per Sestu, I-09042 Monserrato – Cagliari, Italy.
J.R. Ferraro. Chemistry and Materials Science Division, Argonne National Laboratory, 9700 Soth Cass Avenue, Argonne, Illinois 60439.
F. Lelj. Dipartimento di Chimica, Via N. Sauro 85, I-85100, Potenza, Italy.

[1]Corresponding author (telephone: +39-070-675-4474; fax: +39-070-675-4456; e-mail: verani@unica.it).

 DOI: 10.1139/cjc-79-10-1483 © 2001 NRC Canada

Pd^{II}, and Pt^{II} salts (MCl_2 for M = Ni, Pd; K_2MCl_4 for M = Pd, Pt) gives the corresponding phosphono- and amido-phosphono-dithioato complexes (12). These can also be obtained in a one-pot reaction by reacting **1** and the metal salts in the presence of the nucleophilic reagent. This route proved to be particularly well-suited for the synthesis of phosphonodithioato complexes deriving from light alcohols, since these can be used directly as solvents (8). Pursuant to our interest in this field, to understand the electronic and spectroscopic features of dithiophosphonato complexes, calculations based on Density Functional Theory (DFT) (13) have been performed on *trans*-bis[*O*-methyl-phenylphosphono-dithioato]Ni^{II} (**2**, Scheme 1), chosen as a model compound. In fact, DFT calculations are assuming a primary role, since they give reliable results with inorganic compounds containing transition metals (11, 14) in their ground or excited states (15). With this in view, we have prepared *trans*-bis[*O*-ethyl-phenylphosphonodithioato]Ni^{II} (**3**), starting from 2,4-diphenyl-[1,3,2,4]-dithiadiphosphetane-2,4-disulfide (**4**). Complex **3** was previously reported, but only the cell constants and an average Ni—S distance were published (16, 17).

Results and discussion

Molecular orbital analysis

The geometry optimization of *trans*-bis[*O*-methylphenyl-phosphonodithioato]Ni^{II} (**2**, see Scheme 1) has been performed starting from the structural data determined by X-ray diffraction on *trans*-bis[*O*-ethyl-(4-methoxyphenyl)phosphono-dithioato]Ni^{II} (**5**) and has correctly led to a square-planar coordination of the central metal ion, with the phosphorus atoms slightly out of the coordination plane (Fig. 1). In Table 1, a comparison between the calculated bond distances and angles and those measured by X-ray diffraction on **5** (8) (where the phenyl is replaced by a *p*-methoxyphenyl) and *trans*-bis[isopropylamido-(4-methoxyphenyl)phosphono-dithioato]Ni^{II} (**9**) (where the ethoxy group is replaced by an isopropylamine moiety) (12) is reported. As found in the case of other hybrid-DFT calculations on Ni complexes deriving from sulphured ligands (8, 11), the metal—sulphur distances are slightly overestimated (a distance of 2.278 Å has been calculated, compared to an average value of 2.20 Å found experimentally) (17), while the remaining calculated bond distances and angles are similar to the experimental ones reported for **5** (8) and *trans*-bis[(4-methoxyphenyl)-*O*-methyl-phosphonodithioato]M^{II} (M = Pd (**7**) and Pt (**8**)) complexes (12).[2] Some differences regarding the orientation of the substituents to the phosphorus atom [S(1,2)-P(2)-O(1), S(1,2)-P(1)-C(2), P(1)-O(1)-C(1)] should be attributed to crystal packing effects. The comparison can also be extended to the reported structures of the Pd^{II} and Pt^{II} analogues of **2**, where values similar to those reported for **5** and **9** were found (17). To qualitatively understand the interactions between the atomic orbitals (AO's) of the Ni^{II} ion and the molecular orbitals (MO's) of the two ligand units, the Fragment Molecular Orbitals (FMO) approach within the Extended Hückel Theory (EHT) is employed. In Fig. 2 an interaction diagram showing the orbitals, whose eigenvalues lay in the range between –8 and –15 eV, is reported. In the idealized molecular C_{2h} point group the five 3*d* AO's span in three a_g ($d_{x^2-y^2}$, d_{z^2}, d_{xy}) and two b_g (d_{xz}, d_{yz}) representations. The $21a_g$ highest occupied molecular orbital (HOMO) of **2** is a π-MO largely made up of the $d_{x^2y^2}$ AO (25%), which is raised in energy by the antibonding interaction with the $21a_g$ FMO of the ligands, constituted by a combination of sulphur 3*p* AO's perpendicular to the coordination plane. The interaction between the $14b_g$ FMO of the ligands (in plane sulphur *p* AO's) with the d_{xz} and d_{yz} AO's (25 and 16%, respectively) origins the σ-type $14b_g$ lowest unoccupied molecular orbital (LUMO). This MO happens to lay at roughly the same energy as three other nonbonding MO's ($22a_g$, $19b_u$, $13a_u$), which are π-orbitals arising from the combinations of the 2*p* AO's of the aromatic carbon atoms. The HOMO-1 $13b_g$ also contains a contribution of Ni AO's (namely d_{yz} and d_{xz}, 25 and 15%, respectively) π-interacting with a b_g combination of 3*p* sulphur AO's. Metal *d* AO's also contribute to other MO's at lower energies, such as $20a_g$ (49% d_{z^2}, 16% d_{xy}), 18 a_g (32% $d_{x^2-y^2}$, 2% d_{z^2}, 11% d_{xy}), $15a_g$ (2% d_{z^2}, 8% d_{xy}), and $7b_g$ (28% d_{xz}).

Vibrational assignments

The calculation of harmonic frequencies from DFT energy gradients allows one to verify the optimized geometry and to obtain an unprecedented insight into the vibrational spectra of such complexes (Tables 2–4). Only two negative frequency values have been calculated (–84 and –82 cm^{-1}), which are related to rotations of methyl and phenyl groups, and therefore, are due to the presence of a constrained inversion center. A first examination of the simulated spectra (Fig. 3) shows that the use of transferable scaling factors (18), depending on the nature of the single vibrations, gives better results compared to uniform scaling factors. In this case, the slight differences found between the calculated and the experimental bond lengths and angles force the use of scaling factors that are quite different from unity, because of the unharmonic nature of the experimental vibrations. In general, scaling factors have been obtained by comparing the calculated harmonic frequency values to those measured for **3** and *trans*-bis[(4-methoxyphenyl)-*O*-methyl-phosphonodithioato]Ni^{II} (**6**), depending on the group involved in the vibrations. Because of the presence of an inversion centre, the IR spectra are expected to show only the

[2] To ascertain if the differences between the calculated and the experimental bond lengths and angles were to be attributed to the hybrid nature of the functional B3LYP, geometry optimization followed by frequency calculations have been performed with the same basis set on the simplified *trans*-bis[*O*-methyl-methylphosphonodithioato]Ni^{II} model complex, with three different functional, namely BLYP, BPW91, and B3LYP. Both the calculated geometries and frequencies are similar in the three cases. As regards the $(PS_2)_2Ni$ local moiety, the bond distances and angles calculated for the model complex are very similar to those calculated for **2** (Table 1). Although the BPW91 functional slightly reduces the overestimation of the Ni—S bond distances (2.282, 2.249, 2.278 Å for BLYP, BPW91, and B3LYP), it tends to calculate elongated P—S (2.044, 2.025, 2.020 Å for BLYP, BPW91, and B3LYP), P—O (1.656, 1.652, 1.628 Å for BLYP, BPW91, and B3LYP), and P—C (1.849, 1.836, 1.829 Å for BLYP, BPW91, and B3LYP) distances, compared to the experimental average values determined for **5** (Table 1). As regards frequency calculations, the results are also pretty similar, since the three functionals calculated the same number of bands in the same order, BLYP functional leading to smaller absolute wavenumber values.

© 2001 NRC Canada

Scheme 1.

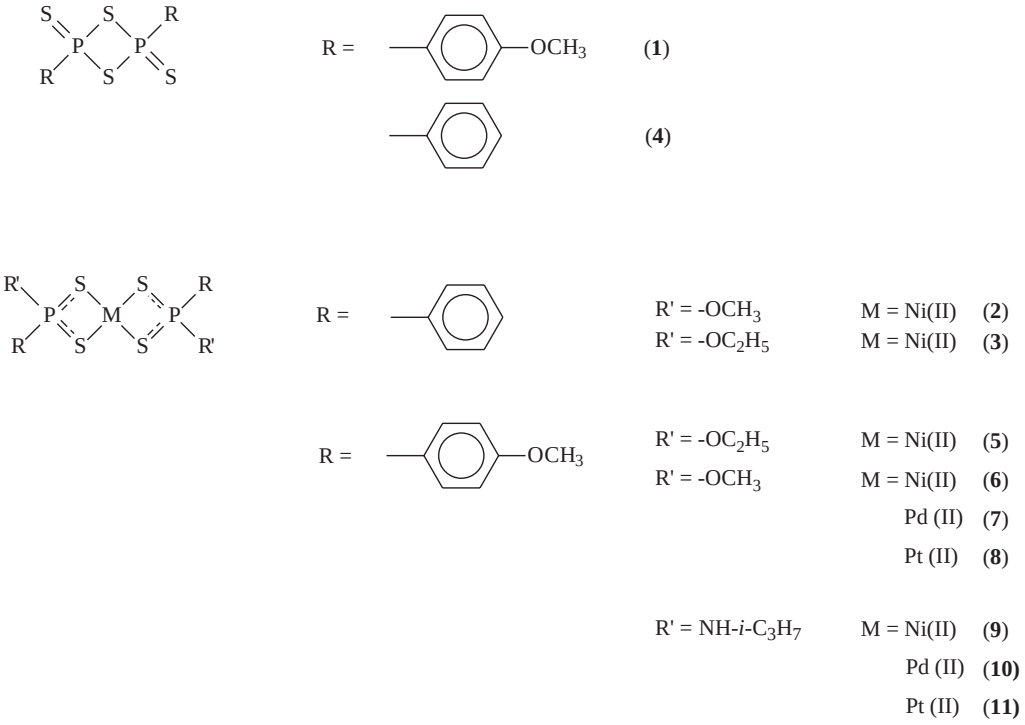


Fig. 1. Atom numbering scheme for model complex **2**.

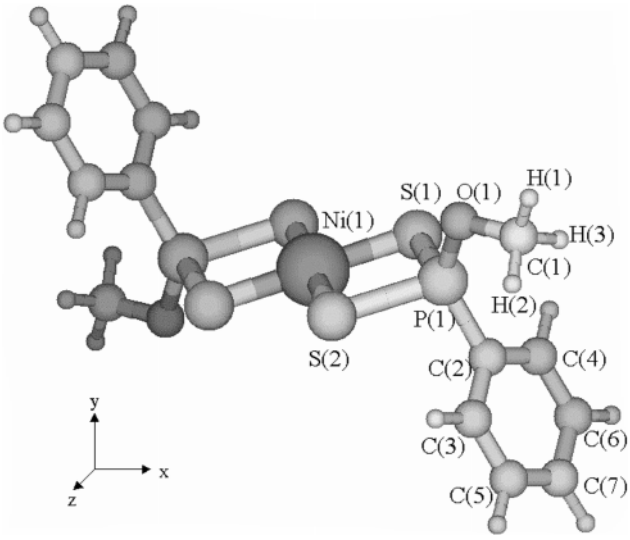


Table 1. Selected optimized bond lengths (Å), angles (°), and dihedral angles (°) for model complex *trans*-bis[*O*-methylphenylphosphonodithioato]Ni^{II} (**2**) compared with average values measured on analogue Ni complexes **5** and **9**.

	2	**5**[a]	**9**[a]
Bond lengths (Å)			
Ni(1)—S(1,2)	2.278	2.221	2.223
P(1)—S(1,2)	2.020	1.994	2.015
P(1)—O(1)	1.631	1.580	—
P(1)—C(2)	1.823	1.782	1.795
O(1)—C(1)	1.437	1.456	—
Bond angles (°)			
S(1)-Ni(1)-S(2)	88.086	88.14	87.64
S(1)-Ni(1)-S(1′)[b]	91.914	91.86	92.81
Ni(1)-S(1,2)-P(1)	80.498	83.78	84.96
S(1)-P(1)-S(2)	103.264	101.57	99.67
S(1,2)-P(1)-C(2)	112.140	113.94	112.67
S(1,2)-P(1)-O(1)	111.642	114.09	—
O(1)-P(1)-C(2)	106.160	99.85	—
P(1)-O(1)-C(1)	125.218	120.9	—

[a]Average values. Supplementary materials of refs. 8 and 12.
[b]Symmetry transformation used to generate (′): *–x*, *–y*, *–z*.

antisymmetric modes, and the Raman spectra only the symmetric ones. At any rate, as far as the ligand units are concerned, for each mode, two combinations (symmetric and antisymmetric) are possible, among which the symmetric combinations appear in the Raman spectra and the antisymmetric ones in the IR spectra. Since the two ligand groups are independent, the two combinations are almost degenerate in energy. Therefore, symmetric vibrational modes related to the two ligand units appear in the IR spectra through their antisymmetric combinations, as well as symmetric coupling of antisymmetric vibrations are Raman active.

An examination of the vibrational frequencies calculated for **2** shows that the bands having the highest energies can be found in the region 3100–2900 cm^{-1} (Table 2). In this region the symmetric and antisymmetric C—H stretching normal modes are calculated, and can be found in all the dithiophosphonato complexes, with minor differences due to the nature of the substituents.

Below 1600 cm^{-1}, the first band found in the FT-IR and Raman spectra of **6** is a strong peak at 1597 and 1590 cm^{-1}, respectively, sided by a less intense peak falling at 1567 cm^{-1} in both spectra. These peaks correspond to the two possible

© 2001 NRC Canada

Fig. 2. Qualitative EHT–FMO interaction diagram between the Ni^{II} 3*d* atomic orbitals (right side) and the ligand molecular orbitals (left side) in model complex **2**. FMO labelling refers to the C_{2h} point group. Molecular orbitals are connected to FMO's contributing for at least 20%.

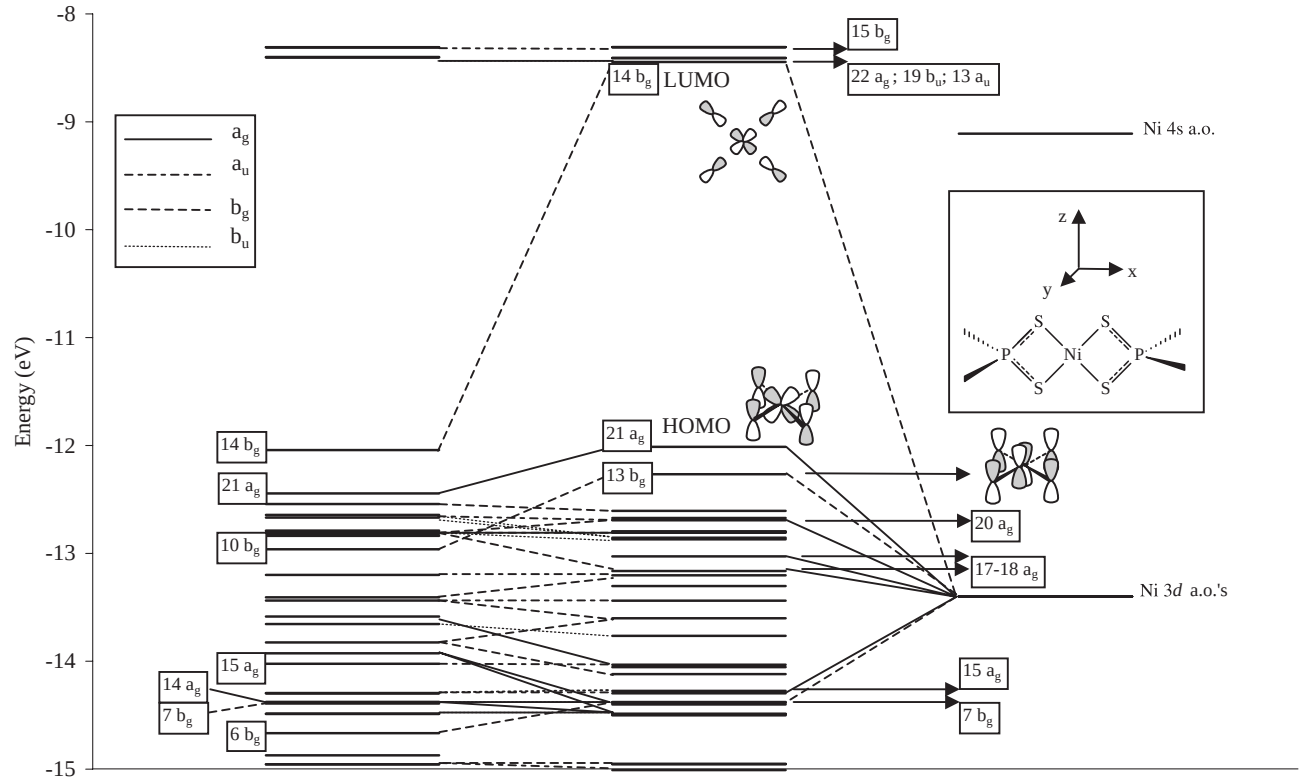


Table 2. Selected calculated scaled and unscaled harmonic frequencies (cm^{-1}), scaling factors, reduced masses (amu), calculated IR intensities (km mol^{-1}), and normal mode descriptions for model complex **2**, and corresponding FT-IR and FT-Raman (italics) experimental bands (cm^{-1}) for complexes **3** and **6**, in the region 3300–3000 cm^{-1}.

Unscaled freq. (cm^{-1})	Scaling factor	Scaled freq. (cm^{-1})	Reduc. mass (amu)	IR int. (km mol^{-1})	Exp. freq. **3** (cm^{-1})	Exp. freq. **6** (cm^{-1})	Normal mode description
3216	0.96	3088	1.098	45.7	3084 (vw)	3088 (vw)	Symmetric stretching C(3–7)—H
3211	0.96	3082	1.094	20.6			Antisymmetric stretching C(4–6)—H
3205	0.96	3076	1.091	14.3	3070 (vw)	3075 (vw), *3074*	Stretching C(3,4,7)—H
3197	0.96	3069	1.088	12.4			Antisymmetric stretching C(3–6)—H
3188	0.96	3060	1.085	0.1	*3053*		Symmetric stretching C(5–7)—H
3166	0.96	3040	1.106	40.0			Symmetric stretching C(1)—H(1,2 in phase; 3 out of phase)
3140	0.96	3015	1.108	34.5	2975 (mw)	2972 (w), *2973*	Antisymmetric stretching C(1)—H(2,3)
3064	0.96	2941	1.030	122.8	2930 (w), *2930*	2941 (mw), *2943*	Symmetric stretching C(1)—H

Note: In this region calculated symmetric and antisymmetric modes fall at the same frequencies.

combinations of ν_s and ν_{as} C—C stretching of the phenyl rings, and are very weak in the FT-IR spectrum of **3** (IR: 1585 and 1571 cm^{-1}; Raman: only 1586 cm^{-1}). In the simulated spectrum of **2** (Table 3) these two bands are also calculated to be very weak (2.2 and 0.5 km mol^{-1}, respectively). Therefore, this suggests that the presence of the methoxy substituent in the *para* position of the phenyl ring causes an enhancement in the intensity of the bands in the IR spectra, which is presumably due to the negative charges on the oxygen atoms, which enhance the variation in the dipole mo-

© 2001 NRC Canada

Table 3. Selected calculated scaled and unscaled harmonic frequencies (cm^{-1}), scaling factors, reduced masses (amu), calculated IR intensities (km mol^{-1}), and normal mode descriptions for model complex **2**, and corresponding FT-IR and FT-Raman (italics) experimental bands (cm^{-1}) for complexes **3** and **6**, in the region 1700–500 cm^{-1}.

Unscaled freq. (cm^{-1})	Scaling factor	Scaled freq. (cm^{-1})	Reduc. mass (amu)	IR int. (km mol^{-1})	Exp. freq. **3** (cm^{-1})	Exp. freq. **6** (cm^{-1})	Normal mode description
1647	0.96	1585, *1585*	5.250, *5.245*	2.2	1585 (w) *1586*	1597 (vs) *1590*	Symmetric stretching C(3,4)—C(5,6)
1632	0.96	1571, *1571*	5.138, *5.135*	0.5	1571 (w)	1567 (mw), *1566*	Antisymmetric stretching C(2,6)—C(3,7)
1530	0.95	1454, *1454*	1.927, *1.930*	8.8	1466 (mw)	1465 (mw)	Symmetric bending C(3–6)—H
1525	0.95	1449, *1449*	1.048	20.6	1449 (w), *1450*	1454 (mw), *1454*	Rocking C(1)—H(1–3)
1522	0.95	1446, *1446*	1.073, *1.072*	37.8			Scissoring C(1)—H(2,3)
1501	0.95	1426, *1426*	1.129	10.7	1436 (ms)	1426 (w), *1424*	Wagging C(1)—H(2,3)
1482	0.95	1408, *1408*	2.117	32.1	1389 (m), *1389*	1407 (mw)	Antisymmetric stretching C(3,4)—C(5,6) + symmetric bending C(5–7)—H
1365	0.95	1297, *1297*	1.914, *1.913*	10.2	1308 (mw)	1307 (ms), *1307*	Antisymmetric stretching C(2,6)—C(3,7) + bending C(3,4,7)—H
1332	0.95	1265, *1265*	2.718, *2.720*	5.6	1284 (vw), *1282*	1294 (s), *1294*	Stretching C(2)—C(3,4) + bending C(3–6)—H
1219	0.97	1182, *1182*	1.151	17.7	1182 (mw), *1184*	1186 (sh), *1175*	Symmetric bending C(3,4)-C(5,6)-H + bending C(5,6)-C(3,4)-H
1199	0.97	1165, *1165*	1.303, *1.304*	20.5	1157 (m), *1158*	1165 (m)	Out of plane wagging C(1)—H(2,3) + bending O(1)-C(1)-H(1)
1121	0.99	1113, *1113*	2.959	105.6	1113 (vs), *1113*	1118 (vs), *1118*	Stretching C(2)—P(1)
1112	0.99	1101, *1101*	1.630	2.9	1101 (sh)	1108 (sh)	Antisymmetric stretching C(3,4)—C(5,6) + bending CH aromatic
1074	0.93	1003	7.132	1018.7	1014 (vs)	1003 (vs)	Stretching O(1)—C(1)
1081		1005	7.263	—	*1027*	*1005*	
1054	1.00	1054, *1054*	2.907, *2.898*	2.7			Phenyl ring breathing
1014	1.00	1014, *1014*	5.494, *5.458*	5.4	*998*	1011 (sh)	Phenyl ring breathing C(3,4,7)
749	1.00	749	4.173	413.0	783 (s)	789 (vs)	P(1)—O(1) + deforming out of plane CH aromatic
752		752	3.094	—		*801*	
725	1.00	725	7.403	119.3			Breathing phenyl rings
726		726	7.342	—			
703	1.00	703, *703*	2.510, *2.491*	38.8			Deforming out of plane C(3,4,7)—H
657	0.96	631	21.853	103.3	627 (s)	622 (ms)	Antisymmetric stretching P(1)—S(1,2)
645		619	15.258	—	*623*	*618*	
627	1.00	627	6.893	11.9			Breathing phenyl rings
625		625	7.974	—			
582	0.96	559	11.950	224.4	565 (vs)	550 (s)	Symmetric stretching P(1)—S(1,2) + stretching P(1)—C(2)
583		560	11.804	—	*566*	*553*	

ments. Many differences can be found in the vibrational spectra of **3** and **6** in the region of 1500–1400 cm^{-1}. In particular, four normal modes are calculated to be IR-active and they fall at 1449, 1446, 1426, and 1408 cm^{-1}: the first two are due to rocking and scissoring modes of the methyl groups, the third to an umbrella wagging of the methyl

© 2001 NRC Canada

Table 4. Selected calculated scaled and unscaled harmonic frequencies (cm^{-1}), scaling factors, reduced masses (amu), calculated IR intensities (km mol^{-1}) and normal mode descriptions for model complex **2**, and corresponding FT-IR and FT-Raman (italics) experimental bands (cm^{-1}) for complexes **3** and **6**, in the region 500–50 cm^{-1}.

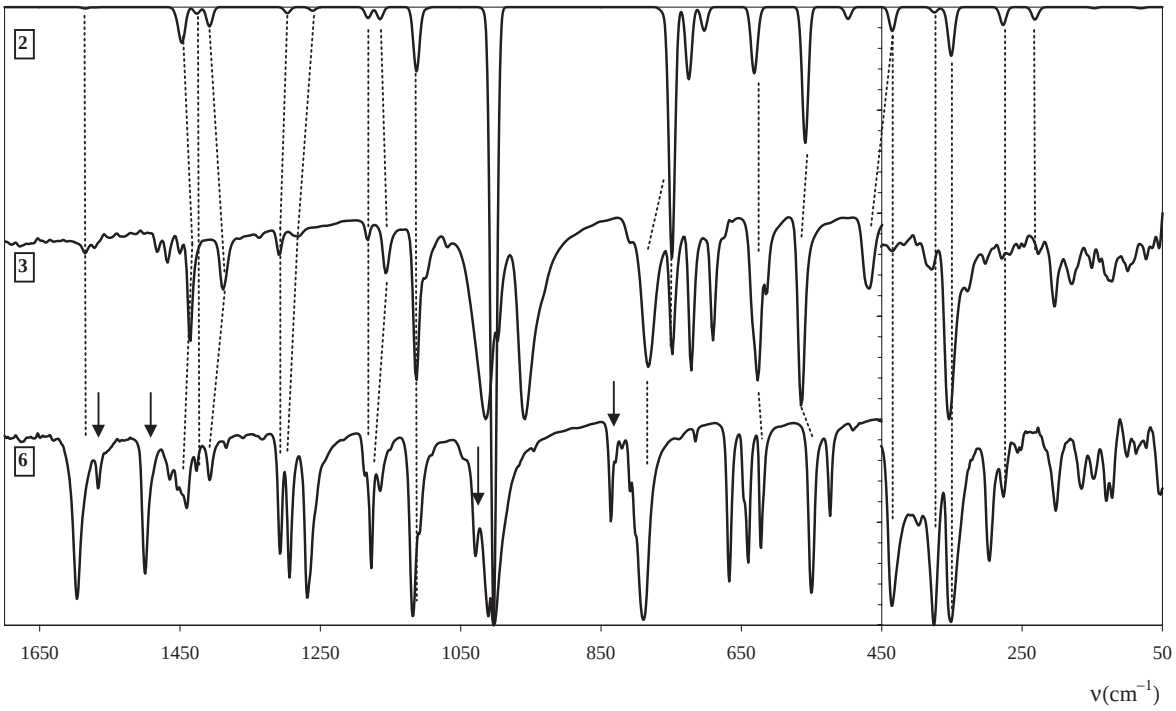
Unscaled freq. (cm^{-1})	Scaling factor	Scaled freq. (cm^{-1})	Reduc. mass (amu)	IR int. (km mol^{-1})	Exp. freq. **3** (cm^{-1})	Exp. freq. **6** (cm^{-1})	Normal mode description
498	1.00	498	4.339	19.6			Out of plane phenyl ring deforming
499		499	4.354	—		*491*	
395	1.10	435	12.401	39.4	470 (ms)	435 (m)	Bending S(1)-Ni-S(2)
401		442	12.842	—	*470*	*440*	
336	1.12	375	5.769	8.9	375 (mw)	375 (m)	Bending P(1)-O(1)-C(1) + twisting phenyl ring
337		378	5.895	—	*386*	*375*	
327	1.10	360	1.788	3.9			Bending S(1)-Ni(1)-S(1′
320	0.96	360	8.700	—			Symmetric wagging P(1)—O(1),C(2)
319	1.10	351	28.800	79.5	354 (s)	351 (m)	Antisymmetric stretching Ni—S(1,2)
313	1.10	344	27.979	1.9		*343*	Antisymmetric stretching Ni—S(1,2)
294	1.10	323	11.266	—	*308*	*314*	Symmetric stretching Ni—S(1,2) + S(1)-P(1)-S(2) bending + P(1)-O(1)-C(1) bending
259	1.07	277	5.341	29.6		277 (mw)	Bending P(1)-O(1)-C(1) + S(1)-P(1)-S(2)
248	1.10	273	15.680	—	*273*	*278*	Antisymmetric stretching Ni—S(1,2)
244	1.10	268	5.410	—			Symmetric Ni(1)—S(1,2) + bending P(1)-O(1)-C(1)
211	1.10	232	12.968	19.9	204 (mw)	202 (w)	Symmetric stretching Ni(1)—S(1,2) + bending S(1)-P(1)-S(2)
206	1.10	226	8.324	2.1			Bending S(1)-Ni(1)-S(1′ + twisting O(1)-P(1)-C(2)
136	1.10	150	9.157	—	*142*	*137*	Symmetric breathing P(1)-S(1,2)-Ni(1)
133	1.10	147	11.898	1.8			NiS_4 out of plane deforming
118	1.00	118	1.417	—		*116*	Methyl group rotation
113	1.00	113	4.150	—	*113*	*102*	Methyl group rotation + twisting NiS_4
91	1.00	91	4.859	—	*86*	*84*	NiS_4P_2 ring deformation

group, and the fourth to a combination of C—C stretching and C-C-H in plane bending of the phenyl rings. Since the first two modes are almost degenerate in frequency, these four normal modes result in three bands in the simulated spectrum. The first and the third bands are found in the FT-IR spectrum of **3** at 1436 (the shift due to the presence of an ethyl instead on a methyl group) and 1389 cm^{-1}, while the umbrella deformation is not found in **3**, since no OCH_3 group is present. With regards to **6**, the bands are more numerous due to the presence of another OCH_3 group, as a substituent, at the phenyl ring, whose C–H deformations should fall in the same region. Such deformations can be considered responsible for a very strong IR band at 1500 cm^{-1}, which is found almost identical in the corresponding complexes **7** and **8** (12), and in *trans*-bis[isopropylamido-(4-methoxyphenyl)-phosphonodithioato]M^{II} (M = Ni (**9**), Pd (**10**) and Pt (**11**)). This region of the vibrational spectrum shows only very weak bands in the Raman spectra of all compounds.

The bands between 1300 and 1100 cm^{-1} are attributed to vibrations mainly regarding bending modes of the bonds in the aromatic rings. Among them, the bands falling at 1182 and 1177 cm^{-1} in the FT-IR spectra of **3** and **6**, respectively (calculated at 1182 cm^{-1} for **2**), are also found with remarkable intensities in their symmetric combination in the Raman spectra (1184 and 1175 cm^{-1} in **3** and **6**, respectively). It is interesting to note that in this case the presence of the substitution in the phenyl ring also causes an increase in the intensities of the IR bands. Only the IR bands falling at 1113, 1113, and 1118 cm^{-1} (exactly the same values of the Raman peaks) in the simulated spectrum of **2** and in those of **3** and

© 2001 NRC Canada

Fig. 3. Simulated FT-IR spectrum based on calculated scaled harmonic frequencies for model complex **2**, experimental middle-IR (1700–450 cm^{-1}) and far-IR (450–50 cm^{-1}) spectra for complexes **3** and **6**. The bands corresponding to same normal modes are connected by dotted lines. Vertical arrows are related to bands involving the methoxy group bound to the phenyl ring in complex **6**.



6, respectively, are strong, possibly because of the P—C stretching contribution to the vibrational mode. The most intense band in the whole simulated spectrum of **2** is found at 1003 cm^{-1} and is due to a pure (calculated reduced mass 7.1 amu) C—O stretching normal mode. This band in fact is found as a very strong IR peak both in **3** (1014 cm^{-1}) and in **6** (1003 cm^{-1}). The side band found in FT-IR spectrum of **5** at 1030 cm^{-1} is absent in **3** and can, therefore, be tentatively attributed to the C—O stretching vibration of the methoxy substituent at the phenyl ring. In fact, while the peak around 1000 cm^{-1} is absent in amidophosphonodithioato complexes **9–11**, the ν_{O-CH_3} vibration is found at 1020, 1019, and 1019 cm^{-1} for **9**, **10**, and **11**, respectively. In the Raman spectra of complexes **3** and **6**, the peak around 1000 cm^{-1} is strong only for **3**, while for **6** the band is weak.

In the FT-IR spectrum of **3** the strong peak found at 959 cm^{-1} (very weak in the Raman spectrum at 961 cm^{-1}) is absent in the calculated spectrum of **2**. Therefore, this band should be due to a vibrational mode of the ethoxy substituent, since it is also absent in **6** but present in **5** at 941 and 943 cm^{-1} in the FT-IR and Raman spectra, respectively. Conversely, in the FT-IR spectrum of **6**, the band at 836 cm^{-1} (Raman 839 cm^{-1}), absent in **3** and in the simulated spectrum of **2**, appears in all the vibrational spectra of compounds derived from **1** and, consequently, it might be due to another mode of the methoxy substituent at the phenyl.

Moving to lower frequencies, a very intense IR band is found at 783 and 789 cm^{-1} (786 and 801 cm^{-1} in the Raman spectra) for compounds **3** and **6**, respectively; this band can be correlated to the vibration calculated for **2** at 749 cm^{-1}, which is due to a combination of P—O stretching and C—H out of plane deforming of the phenyl ring. These vibrations, in the region between 750 and 500 cm^{-1} (fingerprint region), are mainly due to out of plane ring deforming of the phenyl moieties and to the P—S and P—O stretching modes. In particular, the band calculated at 631 cm^{-1} is attributed to the antisymmetric stretching of the P—S bonds and appears as an intense peak in all the vibrational spectra of all the synthesized complexes (**3**: 627 (IR), 623 (Raman) cm^{-1}; **5**: 623 (IR), 616 (Raman) cm^{-1}; **6**: 622 (IR), 618 (Raman) cm^{-1}; **7**: 611 (IR), 611 (Raman) cm^{-1}; **8**: 612 (IR), 612 (Raman) cm^{-1}; **9**: 608 (IR), 600 (Raman) cm^{-1}; **10**: 599 (IR), 596 (Raman) cm^{-1}; **11**: 598 (IR), 599 (Raman) cm^{-1}).

In the far-IR region (Table 4) the antisymmetric S-Ni-S bending appears at 470 and 435 cm^{-1} for **3** and **6**, respectively. This band, calculated at 435 cm^{-1} for **2**, depends strongly on the groups bound to the phosphorus atoms, and in fact varies by about 60 cm^{-1} on passing from phosphonodithioato (435, 431, 429 cm^{-1} for **6**, **7**, and **8**, respectively) to amidophosphonodithioato complexes (496, 497, 495 cm^{-1} for **9**, **10**, and **11**, respectively), while its position is virtually independent of the metal, indicating similar force constants for this bending mode. Therefore it is not surprising that the change of the alkoxy group determines a clear variation in the position of this band. Following the same trend found for the antisymmetric stretching, the symmetric one falls in the Raman spectra at 470 cm^{-1} for **3**, 440 cm^{-1} for **6**, 432 cm^{-1} for both **7** and **8**, and 463 cm^{-1} for **9**, **10**, and **11**. The antisymmetric metal—sulphur stretching is calculated at 351 cm^{-1} to be the most intense band in this region and is found at roughly the same frequency in the FT-IR spectra of both **3** and **6**. This band falls at 356, 314, and 308 cm^{-1} for compounds **9**, **10**, and **11**, respectively, and is

© 2001 NRC Canada

found at 346, 316, and 303 cm^{-1} for **5**, **7**, and **8**, respectively. The symmetric Ni—S stretching, calculated at 323 cm^{-1}, is found in the FT-Raman spectra of all complexes: 308 (**3**), 311 (**5**), 314 (**6**), 326 (**7**), 316 (**8**), 313 (**9**), 327 (**10**), and 316 cm^{-1} (**11**), with the bands being shifted according to the ratio between the different metal–sulphur bond strength constants and the respective reduced masses. According to the previous assignments the symmetric stretching frequency is found at higher frequencies compared to the unsymmetric ones for nickel-complexes **3**, **5**, **6**, and **9**, as well as in the calculated spectrum of **2**. Surprisingly, in the case of Pd and Pt complexes **7**, **8**, **10**, and **11** this trend is inverted. Another band, calculated at 358 cm^{-1} as a symmetric combination of torsions around the P atoms, can be found in the Raman spectra at 343 (**6**), 342 (**7**), 342 (**8**), 342 (**9**), 344 (**10**), and 345 cm^{-1} (**11**). This band becomes weaker in the case of **3** and **5** (340 and 344 cm^{-1}, respectively). Finally, in the lowest frequency region of the far-IR and Raman spectra the bands are originated by deforming of the metallacycle PS_2Ni ring and by alkoxy group rotations.

Conclusions

The synthesis of *trans*-bis[*O*-ethyl-phenylphosphonodithioato]Ni^{II} (**3**) confirms the reactivity of substituted [1,3,2,4]-dithiadiphosphetane-2,4-disulfides towards nucleophilic reagents, previously explored by us on commercially available Lawesson's Reagent (**1**). The complex has been fully characterized by spectroscopic techniques. At any rate, the most interesting results come from an examination of the DFT-calculated vibrational frequencies, which allows us to deeply investigate not only the FT-IR and FT-Raman spectra of **3**, but also those of other phosphono- (**6**–**8**) and amidophosphono-dithioato (**9**–**11**) complexes previously reported by us.

Experimental

All the reagents and solvents were purchased from Aldrich or Merck and were used without further purification. Elemental analyses were performed with an EA1108 CHNS-O Fisons instrument. Fourier transform infrared spectra (FT-IR) were recorded on a Bruker IFS55 spectrometer at room temperature using a flow of dried air. Far-IR (500–50 cm^{-1}) spectra (resolution 2 cm^{-1}) were recorded as polythene pellets with a Mylar beam-splitter and polythene windows. Middle IR spectra (resolution 2 cm^{-1}) were recorded as KBr pellets, with a KBr beam-splitter and KBr windows. FT-Raman spectra were recorded with a resolution of 2 cm^{-1} on a Bruker RFS100 FT-Raman spectrometer, fitted with an In-Ga-As detector (room temperature) operating with a Nd-YAG laser (excitation wavelength 1064 nm) with a 180° scattering geometry. Solid state ^{31}P CP MAS NMR spectra were recorded on a Varian Unity Inova 400 MHz instrument operating at 161.9 MHz with samples packed into a zirconium oxide rotor. The ^{31}P NMR chemical shifts were calibrated indirectly through the H_3PO_4 85% peak (δ 0.0). Quantum-chemical calculations were performed using the commercially available suite of programs Gaussian 98 package (19). Density Functional Calculations (DFT) (13) were performed on **2** using the hybrid B3LYP functional (which uses a mixture (20) of Hartree-Fock and DFT exchange along with DFT correlation: the Lee–Yang–Parr correlation functional (21) together with the Becke's gradient correction) (22).[3] The 6–31G(*d*) basis sets (23) were employed throughout. Integration was performed numerically using a total of 7500 points for each atom (Ultrafinegrid option). Starting from geometrical parameters determined for **5** (8), and avoiding introduction of any geometrical constraints but the inversion centre, a geometry optimization was performed and the results of the calculations were examined with the Molden 3.6 program (24). The optimized structure was verified by normal-mode harmonic frequency analysis. Harmonic frequencies were obtained using the second derivatives of the DFT energy, computed by numerical differentiation of the DFT energy gradients. Calculated harmonic frequencies were extracted from the output file and converted in a simulated spectrum with the Tabfreq program after application of the scaling factors, using DFT-calculated intensities and a halfbandwidth of 10 cm^{-1}. According to a referee suggestion, the computational results[2], both the geometry optimization and the frequency calculations, have been repeated on the simpler *trans*-bis[*O*-methyl-methylphosphonodithioato]Ni^{II} model complex, using BLYP, BPW91, and B3LYP functionals and the same 6–31G(*d*) (23) basis set for all atoms. The first two functionals are pure-DFT functionals, combining the Becke's (25) 1988 exchange functional with the Lee et al.'s (including both local and nonlocal terms) (26), and Perdew and Wang's (27) 1991 gradient-corrected correlation functionals, respectively. The qualitative MO analyses have been obtained by means of Extended Hückel Theory (EHT) (28) using the CACAO (Computer Aided Composition of Atomic Orbitals) program package (29) on the hybrid-DFT optimized geometry, regularized to obtain an idealized C_{2h} symmetry. The interaction diagram was generated using the fragment molecular orbital (FMO) approach (30). Parameters used in EHT calculations were taken from the standard database of CACAO.

*Synthesis of 2,4-diphenyl-[1,3,2,4]-dithiadiphosphetane-2,4-disulfide (**4**)*

Compound **4** was synthesized according to literature methods (31), by reacting $(PhP)_3S_3$ with an excess of elemental sulphur in carbon disulfide.

*Synthesis of $C_{16}H_{20}O_2P_2S_4Ni$ (**3**)*

An excess of $NiCl_2 \cdot 6H_2O$ was reacted with **4** (2.7 g, 8 mmol) in absolute ethyl alcohol solution (100 mL). The filtered solid was recrystallized from CH_2Cl_2–EtOH (1:1 v/v) solution. Yield: 3.56 g, 7.2 mmol, 90%; mp 179°C. FT-IR (3500–450 cm^{-1} KBr; 450–50 cm^{-1} polythene) (cm^{-1}): 3050 (vvw), 3020 (vvw), 2975 (mw), 2930 (w), 2896 (w), 2857 (vvw), 1585 (w), 1571 (vw), 1481 (vw), 1468 (mw), 1449 (w), 1436 (ms), 1389 (m), 1307 (w), 1309 (w), 1282 (vw), 1182 (mw), 1157 (m), 1113 (vs), 1069 (w), 1014 (vs),

[3] Gaussian 98 *z*-matrix input and output file, optimized cartesian coordinates of atoms in complex **2**, list of unscaled calculated harmonic frequencies, IR activity, reduced mass, force constants, and atom displacements for each calculated vibration are available from author on request.

© 2001 NRC Canada

997 (ms), 959 (vs), 783 (s), 748 (s), 721 (s), 690 (ms), 627 (s), 614 (m), 565 (vs), 468 (m), 469 (m), 435 (vw), 416 (vw), 379 (w), 354 (vs), 302 (w), 279 (w), 254 (w), 227 (w), 204 (m), 179 (mw), 151 (w), 122 (mw), 99 (w), 73 (w), 55 (w). FT-Raman (solid state; in parethesis intensities scaled on the highest peak taken equal to 10.0 are reported): 3053 (3.6), 2966 (0.9), 2930 (0.9), 2919 (0.8), 2989 (0.4), 1586 (2.7), 1440 (0.5), 1158 (0.9), 1113 (2.2), 1027 (0.9), 998 (5.4), 623 (1.7), 566 (6.0), 470 (0.9), 386 (0.8), 308 (4.5), 273 (2.5), 2.42 (4.0), 142 (7.8), 114 (10.0), 86 (9.1) cm^{-1}. ^{31}P CP MAS NMR δ: 108.2, 106.9. Anal. calcd. for $C_{16}H_{20}O_2P_2S_4Ni$: C 39.0, H 4.1, S 26.0; found C 39.1, H 4.4, S 25.6.

*Synthesis of complexes **5**–**11***

The syntheses of compounds **5**–**11** were accomplished as previously reported (8, 12).

Acknowledgments

We thank the Consorzio interuniversitario per le Applicazioni di Supercalcolo per Università e Ricerca (CASPUR) and Dr. Nico Sanna for hosting the calculations on **2**, the Consorzio Interuniversitario del Nord Est Italiano per il Calcolo Automatico (CINECA) for hosting calculations on *trans*-bis[*O*-methyl-methylphosphonodithioato]Ni^{II} model complex, and the Regione Autonoma della Sardegna and MURST (Ministero dell'Università e della Ricerca Scientifica) for financial support.

References

1. J.R. Wasson, G.M. Woltermann, and H.J. Stoklosa. Forstschr. Chem. Forsch. (Topics Curr. Chem.) **35**, 65 (1973).
2. W. Kuchen and H. Hertel. Angew. Chem. Int. Ed. Engl. **8**, 89 (1969).
3. (*a*) H. So, Y.C. Lin, G.S. Huang Gibbs, and S.T. Chang. Terny. Wear, **166**, 17 (1993); (*b*) V.V. Mikhailov, Yu V. Kokhanov, K. Kazaryan, E.N. Matreeva, and A. Kozodoi. Plast. Massy, **9**, 23 (1970); (*c*). M. Fuller, M. Kasrai, J.S. Sheasby, G.M. Bancroft, K. Fyfe, and K.H. Tan. Tribol. Lett. 367 (1995).
4. (*a*) P.G. Harrison, M.J. Begley, T. Kikabhai, and F. Killer. J. Chem. Soc. Dalton Trans. 925 (1986); (*b*) Y. Lin. Lubr. Eng. **51**, 855 (1995); (*c*) A.J. Burn, I. Gosney, C.P. Warrens, and J.P. Wastle. J. Chem. Soc. Perkin Trans. 2, 265 (1995); (*d*) E.S. Yamaguchi and P.R. Ryason. Tribol. Test, **3**, 123 (1996); (*e*) S. Contarini, G. Tripaldi, G. Ponti, S. Lizzit, A. Baraldi, and G. Paolucci. Appl. Surf. Sci. **108**, 359, (1997); (*f*) B. Chen, J. Song, Y. Ye, and J. Dong. Tribologia, **29**, 207 (1998); Chem. Abst. 129:218 781.
5. R.C. Mehrotra, G. Srivastava, and B.P.S. Chauhan. Coord. Chem. Rev. **55**, 207 (1984), and refs. 2–6 therein.
6. (*a*) R.B. Fearing, E.N. Walsh, J.J. Menn, and A.H. Freiberg. J. Agr. Food Chem. **17**, 1261 (1969); (*b*) D.A. Wustner, J. Desmarchelier, and T.R. Fukuto. Life Sci. **11**, 583 (1972); (*c*) Y. Miyata, Y. Takahashi, and H. Ando. Kag. Keis. Kenkyusho Hok. Hokagaku-hen, **41**, 159 (1988); Chem. Abst. 112:92 231; (*d*) N.K. Roy. Pesticides, 1989–90, 13 (1990); Chem. Abst. 115:273 431.
7. (*a*) L. Malatesta and R. Pizzotti. Chim. e Ind. **27**, 6 (1945); (*b*) L. Malatesta and R. Pizzotti. Gazzo. Chim. Ital. **76**, 167 (1946); (*c*) P.S. Shetty, P. Jose, and Q. Fernando. J. Chem. Soc. Commun. 788 (1968); (*d*) H. Hartung. Z. Chem. **7**, 241 (1967); (*e*) J.P. Fackler, Jr. and L.D. Thompson, Jr. Inorg. Chim. Acta, **48**, 45 (1981).
8. M. Arca, A. Cornia, F.A. Devillanova, A.C. Fabretti, F. Isaia, V. Lippolis, and G. Verani. Inorg. Chim. Acta, **262**, 81 (1997).
9. M. Thorsen, T.P. Andersen, U. Pedersen, B. Yde, S.-O. Lawesson, and H.F. Hansen. Tetrahedron, **41**, 5633 (1985).
10. M. Arca, F. Demartin, F.A. Devillanova, A. Garau, F. Isaia, F. Lelj, V. Lippolis, S. Pedraglio, and G. Verani. J. Chem. Soc. Dalton Trans. 3731 (1998).
11. M.C. Aragoni, M. Arca, F. Demartin, F.A. Devillanova, A. Garau, F. Isaia, F. Lelj, V. Lippolis, and G. Verani. J. Am. Chem. Soc. **121**, 7098 (1999).
12. M.C. Aragoni, M. Arca, F. Demartin, F.A. Devillanova, C. Graiff, F. Isaia, V. Lippolis, A. Tirpicchio, and G. Verani. Eur. J. Chem. **10**, 2239 (2000).
13. J. Labanowsky and J. Andzelm. Density functional methods in chemistry. Springer–Verlag, New York. 1991.
14. C. Adamo and F. Lelj. J. Chem. Phys. **103**, 10605 (1995).
15. C. Daul. Int. J. Quantum Chem. **52**, 867 (1994).
16. J.P. Fackler, Jr. and L.D. Thompson, Jr. Inorg. Chim. Acta, **48**, 45 (1981).
17. H. Hartung. Z. Chem. **6**, 241 (1967).
18. G. Rauhut and P. Pulay. J. Phys. Chem. **99**, 3093 (1995).
19. Gaussian 98 (Revision A.7). M.J. Frisch, G.W. Trucks, H.B. Schlegel, G.E. Scuseria, M.A. Robb, J.R. Cheeseman, V.G. Zakrzewski, J.A. Montgomery, Jr. R.E. Stratmann, J.C. Burant, S. Dapprich, J.M. Millam, A.D. Daniels, K.N. Kudin, M.C. Strain, O. Farkas, J. Tomasi, V. Barone, M. Cossi, R. Cammi, B. Mennucci, C. Pomelli, C. Adamo, S. Clifford, J. Ochterski, G.A. Petersson, P.Y. Ayala, Q. Cui, K. Morokuma, D.K. Malick, A.D. Rabuck, K. Raghavachari, J.B. Foresman, J. Cioslowski, J.V. Ortiz, A.G. Baboul, B.B. Stefanov, G. Liu, A. Liashenko, P. Piskorz, I. Komaromi, R. Gomperts, R.L. Martin, D.J. Fox, T. Keith, M.A. Al-Laham, C.Y. Peng, A. Nanayakkara, C. Gonzalez, M. Challacombe, P.M.W. Gill, B. Johnson, W. Chen, M.W. Wong, J.L. Andres, C. Gonzalez, M. Head-Gordon, E.S. Replogle, and J.A. Pople. Gaussian, Inc. Pittsburgh, PA. 1998.
20. A.D. Becke. J. Chem. Phys. **98**, 1372 (1993).
21. A.D. Becke. J. Chem. Phys. **98**, 5648 (1993).
22. C. Lee, W. Yang, and R.G. Parr. Phys. Rev. B, **37**, 785 (1988).
23. (*a*) P.C. Hariharan and J.A. Pople. Theor. Chim. Acta, **28**, 213 (1973); (*b*) M.M. Francl, W.J. Petro, W.J. Hehre, J.S. Binkley, M.S. Gordon, D.J. DeFrees, and J.A. Pople. J. Chem. Phys. **77**, 3654 (1982); (*c*) V. Rassolov, J.A. Pople, M. Ratner, and T.L. Windus. J. Chem. Phys. **109**, 1223 (1998).
24. G. Schaftenaar and J.H. Noordik. Molden 3.6: a pre- and post-processing program for molecular and electronic structure. Comp.-Aided Mol. Design, **14**, 123 (2000).
25. A.D. Becke. Phys. Rev. A, **38**, 3098 (1988).
26. C. Lee, W. Yang, and R.G. Parr. Phys. Rev. B, **37**, 785 (1988).
27. J.P. Perdew and Y. Wang. Phys Rev B, **45**, 13244 (1992).
28. R. Hoffmann and W.N. Libscomb. J. Chem. Phys. **36**, 2179 (1962).
29. C. Mealli and D.M. Proserpio. J. Chem. Educ. **67**, 399 (1990).
30. H. Fujimoto and R. Hoffmann. J. Phys. Chem. **78**, 1167 (1974).
31. C. Lensch, W. Clegg, and G.M. Sheldrick. J. Chem. Soc. Dalton Trans. 723 (1984).

© 2001 NRC Canada

Tests for aromaticity applied to the pentalenoquinones — A computational study

C. Delamere, C. Jakins, and E. Lewars

Abstract: Criteria for aromaticity and antiaromaticity were applied to the four pentalenoquinones, 1,2-, 1,5-, 1,4-, and 1,6-pentalenoquinone, i.e., bicyclo[3.3.0]octa-4,6,8-triene-2,3-dione (**7a**), bicyclo[3.3.0]octa-3,5,8-triene-2,7-dione (**7b**), bicyclo[3.3.0]octa-1(5),3,7-triene-2,6-dione (**7c**), and bicyclo[3.3.0]octa-1(5),3,6-triene-2,8-dione (**7d**). Geometry optimizations and frequency calculations were done with the pBP/DN* DFT method as implemented in Spartan, and single-point HF/3-21G calculations to obtain Löwdin bond orders (Spartan), as well as HF/6-31G* NICS calculations (Gaussian 98) were also carried out. Geometries and bond orders, chemical hardness, and NICS values gave no definite indication of aromatic or antiaromatic character. However, homodesmotic ring-opening reactions to give acyclic analogues indicated that **7a** and **7b** are nonaromatic (resonance energies –11 and 5 kJ mol^{-1}) while **7c** and **7d** are antiaromatic (resonance energies –83 and –54 kJ mol^{-1}). The resonance energies were obtained with the aid of an estimate of the strain energy of the molecules **7** (86 kJ mol^{-1}) by a novel extrapolation procedure on hydropentalenes. Calculated pBP/DN* activation energies for Diels–Alder reactions with ethyne and ethene placed **7a** and **7b** in an "unreactive" class similar to 1,3-butadiene and fulvene, and **7c** and **7d** in a "reactive" class, similar to cyclopentadienone.

Key words: aromaticity, pentalenoquinones, DFT, hardness, NICS, homodesmotic, resonance energy, bicyclo[3.3.0]octatrienediones.

Résumé : On a appliqué les critères d'aromaticité et d'antiaromaticité aux quatre 1,2-, 1,5-, 1,4- et 1,6-pentalénoquinones, soit les bicyclo[3.3.0]octa-4,6,8-triène-2,3-dione (**7a**), bicyclo[3.3.0]octa-3,5,8-triène-2,7-dione (**7b**), bicyclo[3.3.0]octa-1(5),3,7-triène-2,6-dione (**7c**) et bicyclo[3.3.0]octa-1(5),3,6-triène-2,8-dione (**7d**). On a effectué les optimisations de la géométrie et les calculs de fréquences à l'aide de la méthode « pBP/DN* DFT » telle qu'implémentée dans Spartan; on a aussi effectué des calculs ponctuels HF/3-21G pour obtenir les ordres de liaison de Löwdin (Spartan) ainsi que des calculs « NICS » au niveau HF/6-31G* (Gaussian 98). Les géométries et les ordres de liaison, la dureté chimique et les valeurs « NICS » ne donnent aucune indication concernant le caractère aromatique ou antiaromatique des composés. Toutefois, des réactions d'ouverture de cycle homodesmotiques conduisant à la formation d'analogues acycliques indiquent que les composés **7a** et **7b** ne sont pas aromatiques (énergies de résonance de –11 et 5 kJ mol^{-1}) alors que les composés **7c** et **7d** sont antiaromatiques (énergies de résonance de –83 et –54 kJ mol^{-1}). Les énergies de résonance ont été obtenues à l'aide d'une évaluation de l'énergie de tension des molécules **7** (86 kJ mol^{-1}) par le biais d'une nouvelle méthode extrapolation appliquée aux hydropentalènes. Les énergies d'activation calculées par la méthode pBP/DN* pour les réactions de Diels–Alder avec l'éthyne et l'éthène suggèrent que les composés **7a** et **7b** font partie de la classe de composés non réactifs, comme le buta-1,3-diène et le fulvène alors que les composés **7c** et **7d** font partie de la classe des composés réactifs, semblables à la cyclopentadiénone.

Mots clés : aromaticité, pentalénoquinones, « DFT », dureté, « NICS », homodesmotique, énergie de résonance, bicyclo[3.3.0]octatrièndiones.

[Traduit par la Rédaction]

Introduction

In this paper we consider five probes of aromaticity (1–4), namely structure, chemical hardness, magnetic properties, energy relative to an acyclic reference molecule, and reactivity, and apply them to the pentalenoquinones.

We outline these criteria here and discuss them in detail below with reference to the title molecules. The structural criterion tends to manifest itself in the deviation of bond lengths and bond orders from those expected from the normal Kekulé structures. Chemical hardness indicates the resistance of the electronegativity of a molecule to changes in electron density. A hard molecule is like a rigid container that does not yield as electrons are forced in, so the electron density builds up, resisting the ingress of more electrons. This is associated with the relatively large HOMO–LUMO

Received February 13, 2001. Published on the NRC Research Press Web site at http://canjchem.nrc.ca on October 15, 2001.

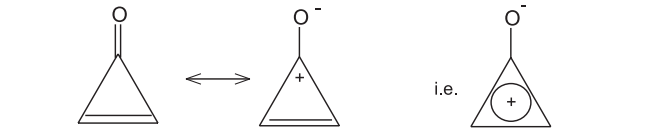
C. Delamere, C. Jakins, and E. Lewars.[1,2] Department of Chemistry, Trent University, Peterborough, ON K9J 7B8, Canada.

[1]Corresponding author (fax: (705) 748-1625; email: elewars@trentu.ca).
[2]Adjunct Professor, Department of Chemistry, Queen's University, Kingston, ON K7L 3N6, Canada.

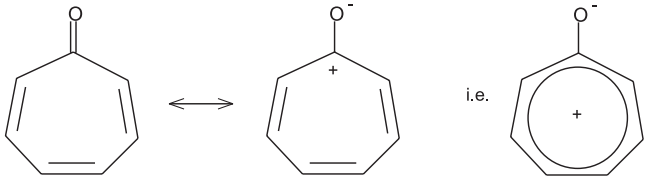
 DOI: 10.1139/cjc-79-10-1492 © 2001 NRC Canada

gaps of many aromatic molecules. The magnetic properties of aromatic molecules have been attributed to the presence of a diamagnetic ring current, the shielding effect of which on a nucleus at or above the ring center is readily calculated. Enhanced stability of a cyclic molecule relative to an acyclic reference structure is perhaps the definitive test, and the most satisfying definition, of aromaticity; we use it here as the decisive probe. Finally, chemical reactivity can provide clues to the presence of aromaticity and, more dramatically, antiaromaticity, which latter tends to be associated with extraordinarily high reactivity.

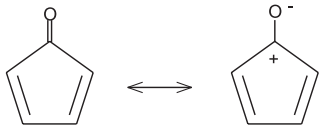
The study of aromaticity (1–4) began with hydrocarbons and moved on to consider monocations and monoanions, then ketones like cyclopropenone and cycloheptatrienone (tropone) which are potentially aromatic by virtue of possessing monocation character. Cyclopropenone (**1**) (5) and cycloheptatrienone (**2**) (6) are at least candidates for aromaticity (the status of cycloheptatrienone in this regard is debatable), because polarization of the C—O bond might confer on them some of the electronic character of, respectively, the cyclopropenyl and cycloheptatrienyl ions (Hückel 4*n* + 2 species) (1). In contrast to the three- and seven-membered ring ketones, cyclopentadienone (**3**) should, if anything, be *destabilized* by *anti*aromaticity (1, 7), since its role model, gratis carbonyl polarization, would be the cyclopentadienyl cation (8), and indeed this ketone is highly reactive (9, 10).



1

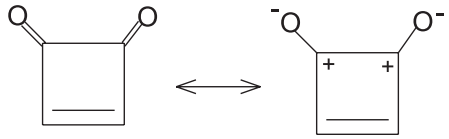


2



3

In the conceptual progression from hydrocarbons to ions to ketones, quinones are logically the next candidates for examination for possible aromatic (or antiaromatic) character. In the simplest analysis, quinones corresponding to antiaromatic hydrocarbons are candidates for aromaticity, and quinones corresponding to aromatic hydrocarbons are potentially antiaromatic. Thus, cyclobutadienoquinone (cyclobutenedione) (**4**) and the cyclooctatetraenoquinones (cyclooctatrienediones) (**5a** and **5b**) (Fig. 1), could be aromatic to the extent that the dipolar canonical form contributes to a reasonably planar structure, e.g.,



4

The dications corresponding to **4** (11) and **5a**, **5b** (12) (the cyclobutadiene dication and the cyclooctatetraene dication, respectively) are 4*n* + 2 species, and are possibly aromatic (the unsubstituted cations have apparently not been reported), while the hydrocarbons cyclobutadiene (13) and (the hypothetical) planar cyclooctatetraene are calculated (14, 15) to be antiaromatic. In comparison with the work on cyclopropenone and cycloheptatrienone, little has been reported on the question of aromaticity in quinones. Cyclobutadienoquinones are well-known, but the question of their aromaticity does not appear to have been exhaustively studied (16). The history of the cycloctatetraenoquinones has been briefly reviewed (17). The 1,2-quinone was reported in 1977 (18) and the 1,4-quinone in 1975 (19), but the question of their putative aromaticity was not specifically addressed experimentally, and apparently the only subsequent work on these compounds has been the computational study by Jakins and Lewars (17); this indicated that these quinones are nonplanar and nonaromatic. The quinones of azulene (e.g., the 1,2-quinone **6**, Fig. 1) have been relatively recently the objects of theoretical (20, 21) and experimental (22) work. As derivatives of a 10-π-electron aromatic system, they potentially have 8-π-electron perimeters and might show antiaromatic properties.

This paper addresses primarily the question of the aromaticity of the pentalenoquinones **7** (Fig. 1), using as probes geometries and bond orders (23), chemical hardness (24–26), NICS (nucleus-independent chemical shift) (27–30), a variant of isodesmic reactions (31, 32) similar to that used by Glukhovtsev et al. (15), and Diels–Alder reactivity. We classify these quinones as fulvene-like (**7a**), monocyclopentadiene-like (**7b**), and dicyclopentadiene-like (**7c** and **7d**), and designate them the 1,2-, 1,5-, 1,4-, and 1,6-quinones, respectively, using numbering based on an "aromatic" nucleus (cf. naphthalene) rather than a bicyclo[3.3.0] system. Molecules **7** are formally derivatives of the very antiaromatic pentalene **8** (33), and being almost perforce planar (in contrast to the cyclooctatetraenoquinones), they are reasonable candidates for aromatic properties. However, **7c** and **7d** may electronically resemble cyclopentadienone, rather than being peripherally delocalized, and so could be antiaromatic. In any case, the chemistry of such highly conjugated carbonyl compounds should be interesting. The pentalenoquinones are, structurally, cross-linked cyclooctatetraenoquinones (Fig. 2). Gaviña and co-workers (34–37) have trapped **7c** (34) and **7d** (35) and the 3-phenyl derivative of **7d** (36), all short-lived molecules, and reported for **7d** and its 3-phenyl derivative (and cyclopentadienone and 3-phenylcyclopentadienone) simple Hückel and MINDO/3 calculations (37).

© 2001 NRC Canada

Fig. 1. Quinones corresponding to antiaromatic and aromatic hydrocarbons. Potentially aromatic quinones are **4**, **5**, and **7**. Potentially antiaromatic: **6**. The quinones **7** of pentalene (8) are the subject of this paper.

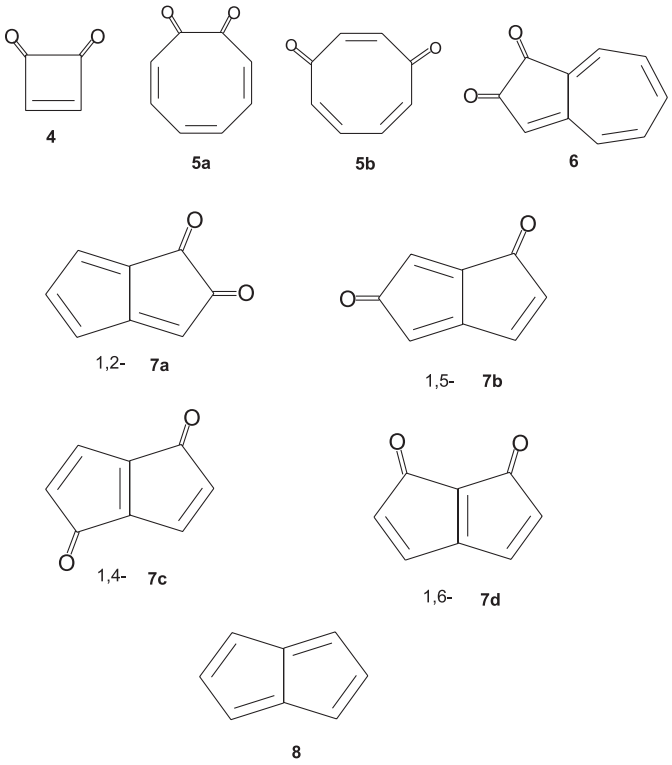
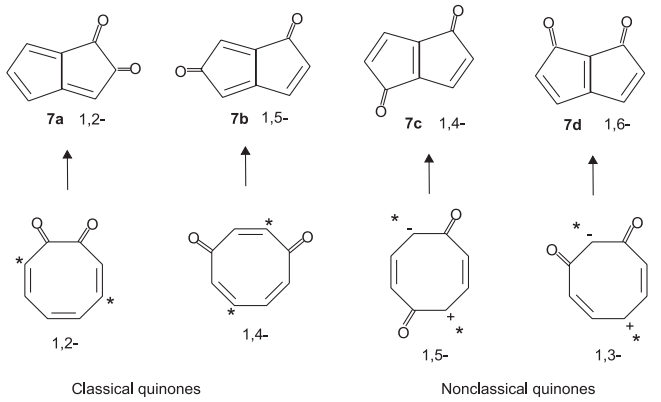


Fig. 2. The pentalenoquinones can be conceptually derived from the quinones of cyclooctatetraene by transannular cross-linking. The fulvene-like (**7a**) and monocyclopentadiene-like (**7b**) quinones are related to normal (classical) cyclooctatetraeneoquinones, while the dicyclopentadiene-like (**7c** and **7d**) quinones are related to dipolar (nonclassical) "quinones" of cyclooctatetraene.



Computational methods

Calculations were done on a 600 MHZ Pentium II computer with the Windows NT operating system. Geometries and frequencies for ab initio (38, 39) and DFT (40 (for ref. 40*a*, see refs. 25–43) calculations were obtained with the program PC Spartan Pro.[2] The DFT calculations, designated in Spartan pBP/DN*, employed the perturbational procedure (41) with the Becke–Perdew B88 and P86 functionals (42) (gradient-corrected but nonhybrid) and the numerical DN* basis set (43). The choice and accuracy of these ab initio and DFT levels are commented on below. Geometry optimizations were followed by frequency calculations (44) at the same level to verify that the structure was the desired relative minimum (no imaginary frequencies) or transition state (one imaginary frequency), and to obtain zero-point energies (ZPEs) to correct the frozen-nuclei energy. The imaginary frequency of each transition state was animated to confirm that it corresponded to the expected reaction coordinate. For pBP/DN calculations, the correction factors for ZPEs and frequencies are expected (45) to be ca. 1.01, and no correction was applied to these. Löwdin bond orders (23) were calculated with Spartan. NICS values (27–30) were calculated with the GIAO method as implemented in Gaussian 94W.[3] The NICS values are at the HF/6-31G*//pBP/DN* level, which we find gives essentially the same results as the levels (HF/6-31G* and HF/6-31+G* on B3LYP/6-31G* and MP2/6-31G* geometries) used in the original (27) work. Absolute total energies, ZPEs, and ZPE-corrected energies are available in the supplementary material tables.[4]

Results and discussion

Reliability of the computational methods

The HF/3-21G ab initio method gives good geometries[5] (46, 47) (almost as good as does the slower HF/6-31G* method), but relative energies of only modest accuracy (46, 47) (comparable to those from HF/6-31G* calculations). The pBP/DN* DFT method, implemented in Spartan in a fast and convenient manner, gives good geometries[5] and remark-

[2] PC Spartan Pro, Version 1.0.3. Wavefunction Inc., 18401 Von Karman, Suite 370, Irvine, California. January 2000.

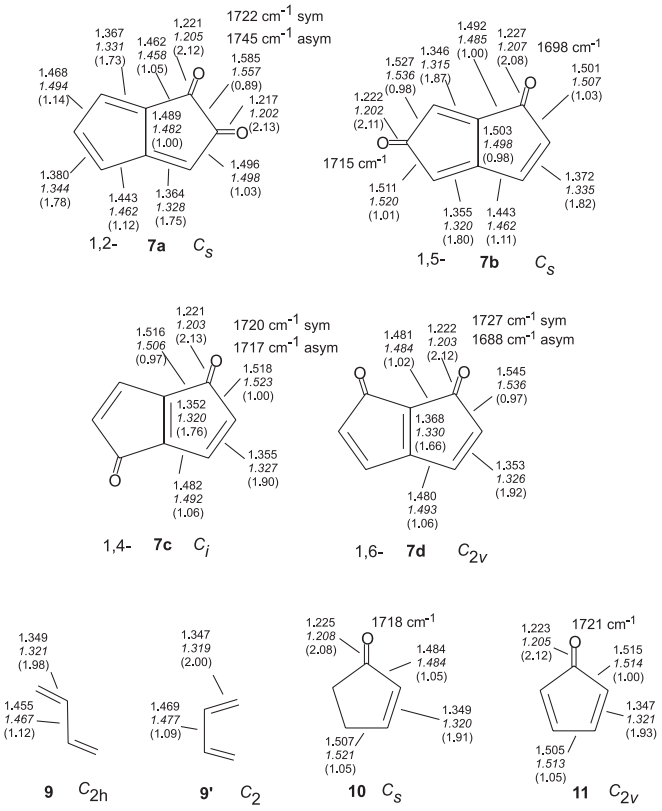
[3] M.J. Frisch, G.W. Trucks, H.B. Schlegel, P.M.W. Gill, B.G. Johnson, M.A. Robb, J.R. Cheeseman, T. Keith, G.A. Petersson, J.A. Montgomery, K. Raghavachari, M.A. Al-Laham, V.G. Zakrzewski, J.V. Ortiz, J.B. Foresman, J. Cioslowski, B.B. Stefanov, A. Nanayakkara, M. Challacombe, C.Y. Peng, P.Y. Ayala, W. Chen, M.W. Wong, J.L. Andres, E.S. Replogle, R. Gomperts, R.L. Martin, D.J. Fox, J.S. Binkley, D.J. Defrees, J. Baker, J.P. Stewart, M. Head-Gordon, C. Gonzalez, and J.A. Pople. Gaussian 94 for Windows (G94W): Gaussian 94, Revision E.1. Gaussian, Inc., Pittsburgh, Pennsylvania. 1995.

[4] Supplementary material may be purchased from the Depository of Unpublished Data, Document Delivery, CISTI, National Research Council Canada, Ottawa, ON K1A 0S2, Canada (http://www.nrc.ca/cisti/irm/unpub_e.shtml for information on ordering electronically).

[5] For a set of 20 common organic molecules, we found both HF/3-21G and HF/6-31G* calculations to give bond length errors of ca. 0.01 Å and bond angle errors of 1°; pBP/DN* also gave bond length errors of ca. 0.01 Å (slightly worse than the popular B3LYP/6-31G* method) and bond angle errors of 1°. For four isomerizations we found the pBP/DN* activation energy (a more stringent test for energy difference calculations than reaction energies) to be 5–10 kJ mol^{-1} lower than the B3LYP/6-31G* energy, which in turn was ca. 0–10 kJ mol^{-1} lower than experiment and high-accuracy (50) (CBS-Q and G2) methods.

© 2001 NRC Canada

Fig. 3. The pentalenoquinones **7**: bond lengths, bond orders, carbonyl stretching frequencies and symmetries. pBP/DN* and (italics) HF/3-21G bond lengths (Å); Löwdin bond orders (in parentheses) are from HF/3-21G single-point calculations (i.e., geometry unchanged) on the pBP/DN* geometries. The carbonyl stretching vibrations (pBP/DN, cm^{-1}) of **7a**, **7c**, and **7d** are coupled (symmetric and asymmetric), while those of **7b** are essentially independent. Information is also given for the reference molecules **9**–**11**.



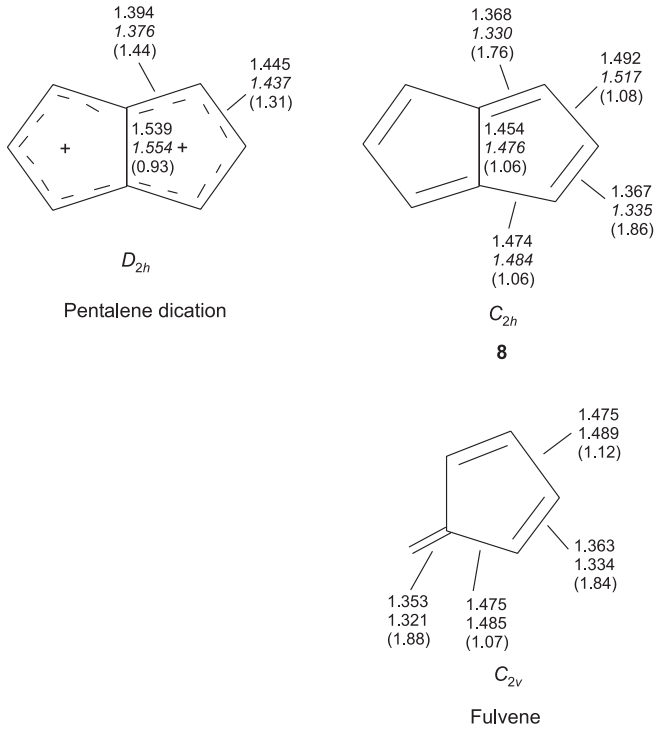
ably good energies[5] (48), which are quite similar (49) to those from the B88P86 (i.e., BP86) functional (42) with a 6-311G* basis set. Both HF/3-21G and pBP/DN* geometries should be satisfactory for the conclusions we draw. Realistic absolute energy differences are expected from the pBP calculations, which take correlation energy into account.

Probing electronic structure

Geometry and bond orders

The bond lengths, bond orders, and carbonyl stretching frequencies and symmetry designations of the quinones **7** are shown in Fig. 3, along with the corresponding parameters for the reference molecules *s-trans*-1,3-butadiene (**9**), *s-cis*-1,3-butadiene (**9′**), cyclopentenone (**10**), and cyclopentadienone (**11**). The four quinones are relative potential energy surface minima at the pBP/DN* and HF/3-21G levels (no imaginary frequencies). The bond lengths, and (more obviously) the bond orders, are about as would be expected for normal conjugated ketones. The only clear possible anomalies are the somewhat low frequency of the C-1 carbonyl of **7b**, and the low transannular bond orders (but not lengths) of the formal double bonds of **7c** and, particularly, **7d**. Small changes in bond length can be caused by subtle structural changes and the data in Fig. 3 provide no distinct evidence of unusual effects.

Fig. 4. Pentalene dication, pentalene, and fulvene: bond lengths, bond orders, and symmetries. pBP/DN* and (italics) HF/3-21G bond lengths (Å); Löwdin bond orders (in parentheses) are from HF/3-21G single-point calculations (i.e., geometry unchanged) on the pBP/DN* geometries.



Since any expectation of aromaticity in the quinones **7** is based on the postulate of an aromatic pentalene dication (cf. cycloheptatrienone and the cycloheptatrienyl cation), we give (Fig. 4) results of our calculations on this dication, as well as on pentalene **8** (both were relative potential energy surface minima at the pBP/DN* and HF/3-21G levels) and fulvene, a pentalene subunit. The bond lengths and orders, and the high symmetry of the dication, which lacks any bond length or bond order variation beyond the minimum imposed by the symmetry of a flat bicyclo[2.2.0] system, indicates it to have six-π-electron delocalization around its eight-carbon perimeter, with the transannular bond a single bond. In contrast, pentalene is, like cyclobutadiene (13), a polyene with distinct single and double bonds. The structural criteria, then, are in accord with the view that the dication is aromatic (in agreement with recent conclusions by others (51)).

Hardness

Zhou and Parr (24, 25) have shown that the chemical hardness concept as quantified by Pearson (26) can be a good measure of aromaticity. Hardness (η) is defined in terms of the resistance of chemical potential or electronegativity to a change in electron density, but practical approximate formulas for calculating it are based on HOMO–LUMO energies and on ionization energy and (or) electron affinity (26). The

© 2001 NRC Canada

simple Hückel method (52)[6], used by Zhou and Parr, is not appropriate for molecules like **7**, which are not polyenes or simple heterocyclic derivatives of polyenes, so we calculated hardness from ionization energy and electron affinity:

$$[1] \qquad \eta = \frac{I - A}{2}$$

I and *A* were obtained directly, as pBP/DN* energy differences between the neutrals and the radical ions, all at the geometry of the neutrals (vertical values), not from orbital energies, because while $-E_{HOMO}$ is a fair approximation of *I* (Koopmans' theorem), $-E_{LUMO}$ tends to be a poor approximation of *A* (53). We compare the quinones **7** with one another and with the cyclooctatetraenoquinones **4** and **5** (17). Our *I* and *A* values should be within about 0.2 eV of experimental: cf. other DFT calculations of ionization energies (54) and of electron affinities (55).

The hardness values provide no reasonable evidence for aromaticity in the pentalenoquinones **7**. This conclusion is based on the similarity of η for the bicyclic (7) and monocyclic (**5a** and **5b**) species: 3.1–3.6 eV cf. 3.6–3.9 eV. The cyclooctatetraenoquinones **5a** and **5b** in their normal, nonplanar conformations are nonaromatic, and even in the hypothetical planar conformations (hilltops with three and two imaginary frequencies, respectively) appear to possess little or no aromaticity. This is indicated (17) by the NICS (27–29) calculations, applied as plots of shielding vs. distance above the ring (30) (NICS curves see below). This conclusion from (17) is reinforced by the fact that there is no significant change in η (less than 0.1 eV) on going from nonplanar to planar **5a** and **5b**. The similarity of η for all eight species suggests that there is no special electronic effect (viz. aromaticity) at work in any of them.

NICS curves

The original (Schleyer et al. (27)) NICS test for aromaticity was based on the shielding of an idealized probe nucleus (56) placed at the center of the ring ("NICS 0"). To avoid local magnetic effects from σ bonds West et al. (28) introduced NICS 2.0, the placing of the probe nucleus 2.0 Å above the center of five-membered rings, and this has also been applied (Veszprémi et al. (29)) to three-membered rings. We use as a probe of aromaticity this very convenient test in the form of a plot of shielding vs. distance above the ring center along a line normal to the ring plane, cf. the method introduced by Morao and Cossio (30) to study aromaticity in transition states. Schleyer et al. (27) defined NICS as the negative of the isotropic shielding, i.e., as –(BQ isotropic), in Gaussian nomenclature. We chose to plot (BQ isotropic) = –NICS vs. distance (plots referred to here as NICS curves), because this gives a positive, roughly Gaussian, curve for the canonical aromatic molecule benzene. Figure 5 shows the NICS curves for **7a**–**7d** and the reference molecules benzene, cyclobutadiene, cyclobutene, cycloheptatriene, 1,2- and 1,4-benzoquinone, planar **4** and **5**, and cyclopentadienone. These curves were constructed from the HF/6-31G*//pBP/DN* NICS values at 0, 0.5, 1.0, 1.5, and 2.0 Å above the ring center. For each molecule the –NICS value at 0.0 and 2.0 Å is given.

Very different looking NICS curves are shown by the aromatic, antiaromatic, and nonaromatic molecules benzene, cyclobutadiene, and cyclobutene, respectively, (Fig. 5*a*). Were these strikingly different patterns general for these three classes of molecules there would be no problem using the shape of the NICS curve as a test for aromaticity. However, this is not the case. The cycloheptatriene curve (Fig. 5*b*) is similar in shape to that for benzene, and while appeal to the controversial notion of neutral homoaromaticity (in the triene (57), or as a general concept (58)) may be a viable option, the curves for the benzoquinones (Fig. 5*c*) also show that the shape of these curves is not really diagnostic for aromaticity; qualitatively, the 1,4-benzoquinone curve somewhat resembles that for benzene, while the 1,2-benzoquinone curve is more like that for a nonaromatic species. Evidently only –NICS 0 values more negative than about –10 can be taken as clear signs of antiaromaticity. The curves for planar (these are hilltops) 1,2- and 1,4-cyclooctatetraenoquinones **4** and **5** (Fig. 5*d*) are as expected for nonaromatic molecules, implying that the actual, nonplanar quinones are nonaromatic (17).

The molecules **7a** and **7b** (Figs. 5*e* and 5*f*) show vaguely Gaussian-shaped curves. These curves, with –NICS 0/ –NICS 2.0 values of –5.0/2.4, 1.9/2.4 (for **7a**) and –1.8/–3.9, 1.8/1.0 (for **7b**), do not provide any particular evidence for either aromatic or antiaromatic character. The molecules **7c** and **7d** (Figs. 5*g* and 5*h*) show curves very similar to that of cyclopentadienone (also shown). Interestingly, the cyclopentadienone NICS curve is itself essentially the same as that for 1,2-benzoquinone (Fig. 5*c*), another species with high Diels–Alder reactivity (59). We tentatively take this as an indication of cyclopentadienone character and a harbinger (below) of high Diels–Alder reactivity in **7c** and **7d**. The NICS curve for the pentalene dication indicates aromaticity: dication, NICS 0 = 5.9, NICS 2.0 = 5.5, cf. benzene 11.7 and 5.4.

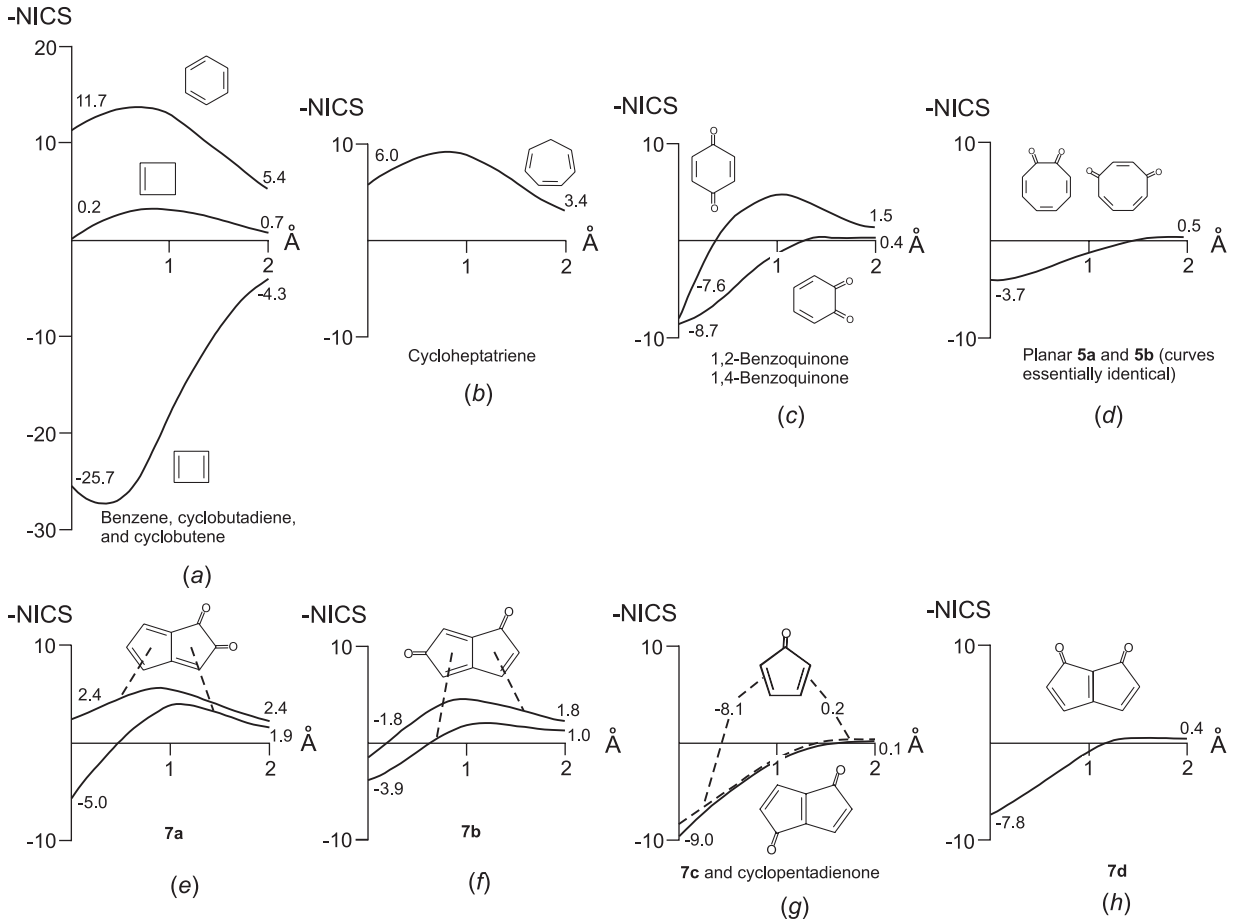
Homodesmotic aromatic stabilization energies

The most direct computational test for aromaticity is to see if the cyclic molecule enjoys distinct energetic stabilization compared to an acyclic analogue. This stabilization can be calculated as the strain-corrected (below) energy of a ring-opening reaction which, formally, preserves the numbers of each kind of bond. These *homodesmotic* reactions have been shown by Glukhovtsev et al. (15) to be a good measure of aromatic stabilization and antiaromatic destabilization. For example, to calculate the homodesmotic stabilization energy (HSE) of benzene these workers use the reaction in Scheme 1*a*. On each side of the equation there are, formally, six C—C double bonds, three sp^2-sp^2 C—C bonds, and 18 C(sp^2)—H bonds. Preserving "hybridization pairs" minimizes energy changes due just to bond energy changes (e.g., an sp^2-sp^2 C—C bond is stronger than the corresponding sp^3—sp^3 bond (60)) and should reflect π electron interaction effects. We use a similar but simpler scheme in which the cyclic molecule is opened to an all-*trans* acyclic analogue with the same number of atoms plus two hydro-

[6] An English translation of Vol. 1 is available: E. Heilbronner and H. Bock. The HMO model and its application. Basics and manipulation. Verlag Chemie, Weinheim, Germany. 1976.

© 2001 NRC Canada

Fig. 5. NICS curves (actually –NICS, see text) for benzene, cyclobutadiene, cyclobutene, cycloheptatriene, 1,2- and 1,4-benzoquinone, planar **5a** and **5b**, and the pentalenoquinones **7**, and cyclopentadienone. The –NICS values at 0.0 and 2.0 Å above the ring centers are given.



gens (Scheme 1*b*). In effect an sp^2-sp^2 C—C bond is broken using two hydrogens and an sp^2-sp^2 C—C bond is formed. At the pBP/DN* level, the HSE (the reaction energy) for (*a*) and (*b*) is 97.0 and 94.0 kJ mol^{-1}, respectively. Opening cyclobutadiene with two ethenes gives, at the same level, an HSE of –320 kJ mol^{-1}. Adding an estimated strain energy (SE) of 141 kJ mol^{-1} (15) gives –179 kJ mol^{-1} as HSE of cyclobutadiene. Compared to (*E*)-1,3,5-hexatriene, benzene is electronically stabilized by ca. 94 kJ mol^{-1} (the strain energy should be small) and compared to 1,3-butadiene cyclobutadiene is destabilized by ca. 179 kJ mol^{-1}. These numbers are very close to those calculated at the MP4SDTQ/6-31G**//MP2/6-31G** level (15). The resonance energies of benzene and of cyclobutadiene could reasonably be taken as ca. 94 and –179 kJ mol^{-1} kJ mol^{-1} (there is no single, correct definition of resonance energy (1)).

For the quinones **7**, we unzip the molecule with two pairs of hydrogens with concomitant formation of a formally identical pair of C—C bonds (Scheme 2*c*–*f*). This conserves formal conjugation involving C—C and C—O bonds and the HSE corrected for strain should reflect *cyclic* electron interaction effects, which can reasonably be considered as resonance energies; the term will be used in this sense here. Isodesmic reactions in general are not unique. They cannot be implemented unambiguously, by an algorithm, but rather sometimes require one to choose one of several possibilities; they do not represent a *model chemistry* (61). We have chosen to open **7a**–**7d** to give acyclic unbranched fully conjugated molecules, since these should be the appropriate analogs of the bicyclic species. We regard simple opening to the acyclic analogue with the same number of carbons as the most readily apprehended test of aromaticity, and concur that "The HSE (HHSE) scheme … apparently … has become the most dependable tool for obtaining numerical values of RE." (62). We applied homodesmotic reactions to estimate the resonance energies of the pentalenoquinones **7**, using the reactions of Scheme 1. Table 1 gives HSEs calculated from the ZPE-corrected pBP/DN* energies, and resonance energies calculated from the HSEs and the strain energy (below). An example of the calculation of the HSE is given in eq. [2]; using Scheme 1 and the ZPE-corrected absolute energies:

$$\begin{aligned}[2]\quad \text{HSE}\ (\mathbf{7a}) &= (E\ (\mathbf{12}) + E\ (\mathbf{13}) + E\ (\text{butadiene})) \\ &\quad -(E\ (\mathbf{7a}) + 2E\ (\text{ethanal}) + 2E\ (\text{ethene})) \\ &= -922.53187 - (-922.49488)\ \text{h} \\ &= -0.03699\ \text{h} \\ &= -0.03699 \times 2625.5\ \text{kJ mol}^{-1} \\ &= -97.1\ \text{kJ mol}^{-1}\end{aligned}$$

© 2001 NRC Canada

Scheme 1. Reactions are used to calculate homodesmic stabilization energies. The schemes *c–f* used in this paper are based on the type of ring-opening shown in *b*.

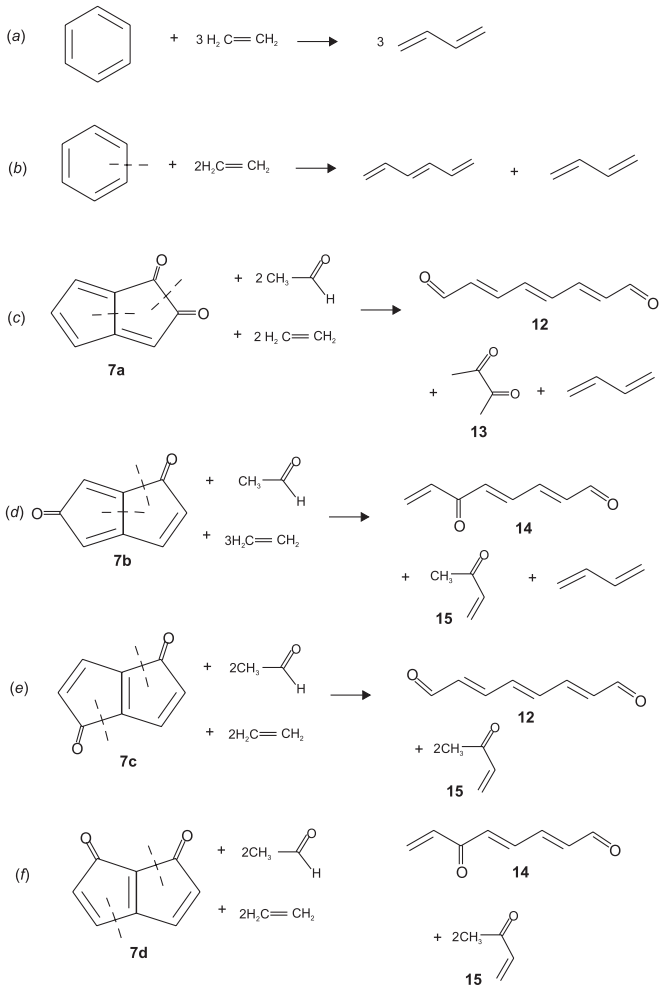


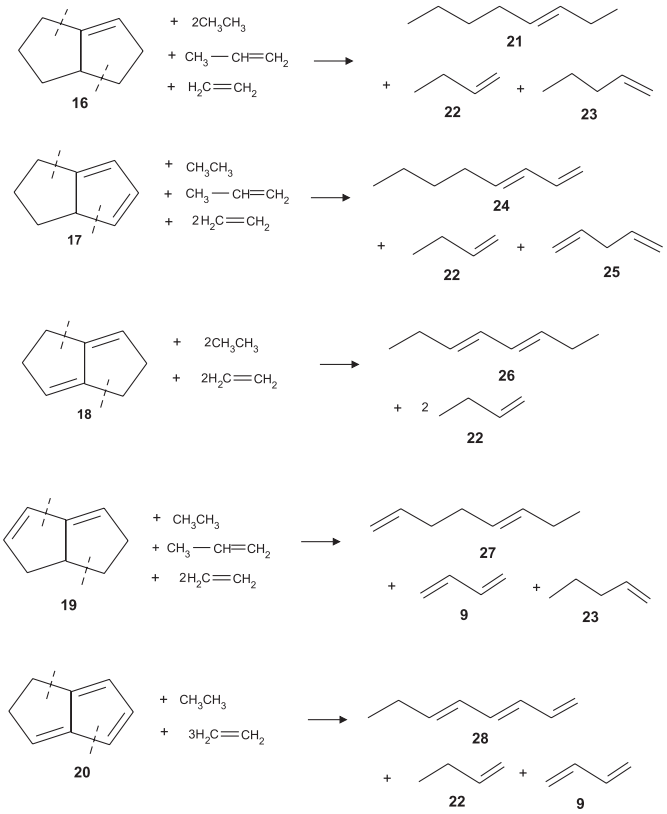
Table 1. Homodesmotic stabilization energies (HSE) and resonance energies (RE) (kJ mol^{-1}) of **7a**–**7d**.

Molecule	HSE	RE
7a	–97.1	–97.1 + 86 = –11
7b	–80.7	–80.7 + 86 = 5
7c	–169.1	–169.1 + 86 = –83
7d	–140.0	–140.0 + 86 = –54

Note: HSE was calculated using the reactions of Scheme 1 and ZPE-corrected pBP/DN* energies. RE is the sum of HSE and strain energy, which latter is estimated to be 86 kJ mol^{-1} (Fig. 6).

The resonance energy, the measure of aromaticity that we seek, is the HSE *plus* any strain energy in the cyclic species (we take the acyclic molecules to be strainless). Thus a negative HSE (a drop in energy) could be due to loss of antiaromatic destabilization, or it could be partially or wholly due to relief of strain; adding the strain energy to the HSE should leave us with the resonance energy. There is no unique definition of strain energy (63). Our purpose here is to disentangle cyclic electron interaction from strain, which appears intuitively to be associated with the σ-bond skeleton. We calculate strain energy (SE) by sneaking up on it: the

Scheme 2. The homodesmotic reactions used to calculate the strain energy (SE) of **16**–**20** (and, by extrapolation (Fig. 6), the strain energy of pentalene (**8**).

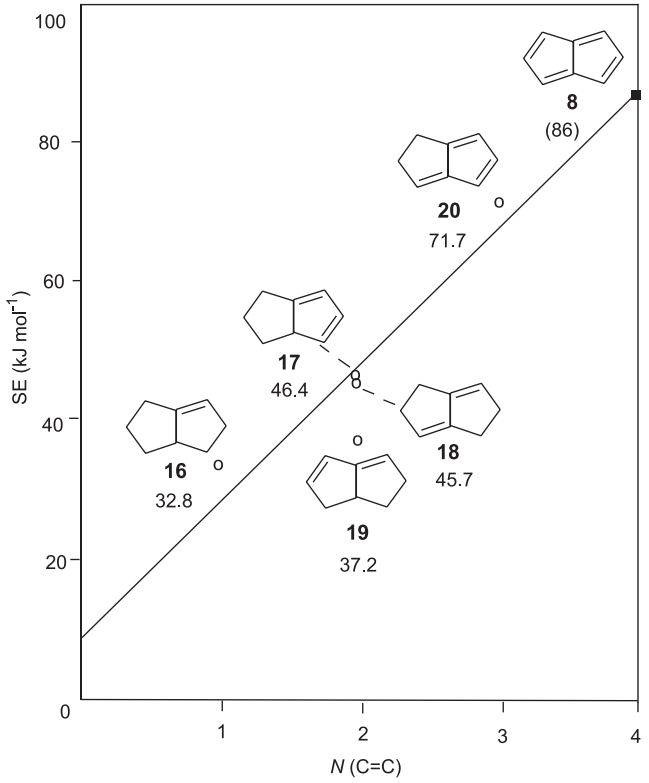


ring-opening HSE of a series of increasingly unsaturated hydropentalenes (Scheme 2) was extrapolated to the fully conjugated cyclic molecule to give an estimate (86 kJ mol^{-1}) of the SE of the putative aromatic or antiaromatic molecule: –HSE, *in the absence of any cyclic electron interaction effects*. Since the SE of a strained ring is always positive (opening a strained ring is exergonic), our SE is the extrapolated value of –HSE (*E* (reactants) – *E* (products)). We assume that the SE of the four quinones **7** is about the same as that of pentalene (**8**). The calculated SEs and the extrapolation to the SE of pentalene are shown in Fig. 6.

In estimating the SE of pentalene we avoided molecules with ring-fusion tetrahedral carbons, to sidestep the question of whether to use *cis*- or *trans*-ring fusion. Also, for consistency, double bonds were progressively added to the perimeter, maintaining conjugation. The discrepancy between the SE of the tetrahydropentalenes **17** and **18** (46.4 and 45.7 kJ mol^{-1}) and that of **19** (37.2 kJ mol^{-1}), 9 kJ mol^{-1}, is probably comparable to the error in the HSEs (the differences in 0 K enthalpies), which could well differ from experiment by about 10 kJ mol^{-1} (64). A common way of calculating strain energy is to equate it to the difference between the calculated heat of formation and the heat of formation of a hypothetical strainless structure, obtained by summing the heats of formation of appropriate molecular fragments (65). While this approach could be used for **16**–**20**, for **8** the discrepancy from the hypothetical structure would represent a mixture of strain and antiaromaticity. Our extrapolation approach avoids performing calculations on

© 2001 NRC Canada

Fig. 6. Strain energy of hydropentalenes (kJ mol^{-1}) vs. number of peripheral conjugated C—C double bonds. Extrapolation to N (C=C) = 4 for **8** gives SE = 86 kJ mol^{-1}. The correlation coefficient r^2 of this least-squares extrapolation line is 0.987.



molecules with cyclic delocalization, and consistently uses the same kind of homodesmic ring-opening reactions to calculate SEs in **16**–**20** as was used to obtain the HSEs of the quinones **7**.

Although the purpose of our extrapolation method is not to find "the" strain energy of the pentalene system, but rather what the HSE would be in the absence of antiaromaticity, we briefly supply a check on how HSE ring-opening energies compare with conventional strain energies from heats of combustion.

In Table 2, strain energies are estimated from heats of combustion per CH_2 group for cyclopropane–cyclohexane (66), and compared with HSE strain energies. The (relative to cyclohexane) SEs by the two methods are quite similar. The largest difference is 18 kJ mol^{-1}, and the biggest *change* in relative SE is only 12 kJ mol^{-1}, from cyclopentane to cyclobutane: 82 cf. 70 kJ mol^{-1}. This lends some confidence to the claim that our HSE method really calculates SE.

Adding the HSE to the SE gives the RE. These are shown for the quinones **7** in Table 1. The RE values indicate that **7a** and **7b** are essentially nonaromatic (–11 and 5 kJ mol^{-1}, respectively) and **7c**, particularly, and **7d** (–83 and –54 kJ mol^{-1}, respectively), are antiaromatic. For perspective, in considering the RE values in Table 1, recall that these ring-opening schemes with the pBP/DN* method give benzene and cyclobutadiene REs of 94 and –179 kJ mol^{-1}, respectively, (section **3a** (**4**)). It is instructive to compare the REs of **7a**–**7b** with their relative DFT energies. If all four molecules have about the same strain, the differences in "absolute" energies,

Table 2. Strain energies (SE, kJ mol^{-1}) of cyclopropane–cyclohexane estimated from heats of combustion (ΔH_c) and from pBP/DN* HSEs.

Ring size	$\Delta H_c/CH_2$	Relative $\Delta H_c/CH_2$	Relative SE From ΔH_c	From HSE
3	695.8	37.2	112	99.1
4	685.8	27.2	109	90.6
5	664.0	5.5	27	20.5
6	658.6	0.0	0.0	0.0

Note: For the HSEs, the ring C—C bond was cleaved with 2 CH_3CH_3 to give the acyclic alkane + butane. The relative ΔH_c SE is taken as the number of CH_2 groups × relative $\Delta H_c/CH_2$. The actual (not relative) HSE SE for cyclohexane was 0.95 kJ mol^{-1}.

Table 3. Relationship between the DFT (pBP/DN*) energies of the quinones **7** (ZPE-corrected) and their (Table 1) resonance energies.

Molecule	DFT energy	Relative DFT energy	RE
7a	–457.71060	1	–11
7b	–457.71098	0	5
7c	–457.68567	–66	–83
7d	–457.68825	–60	–54

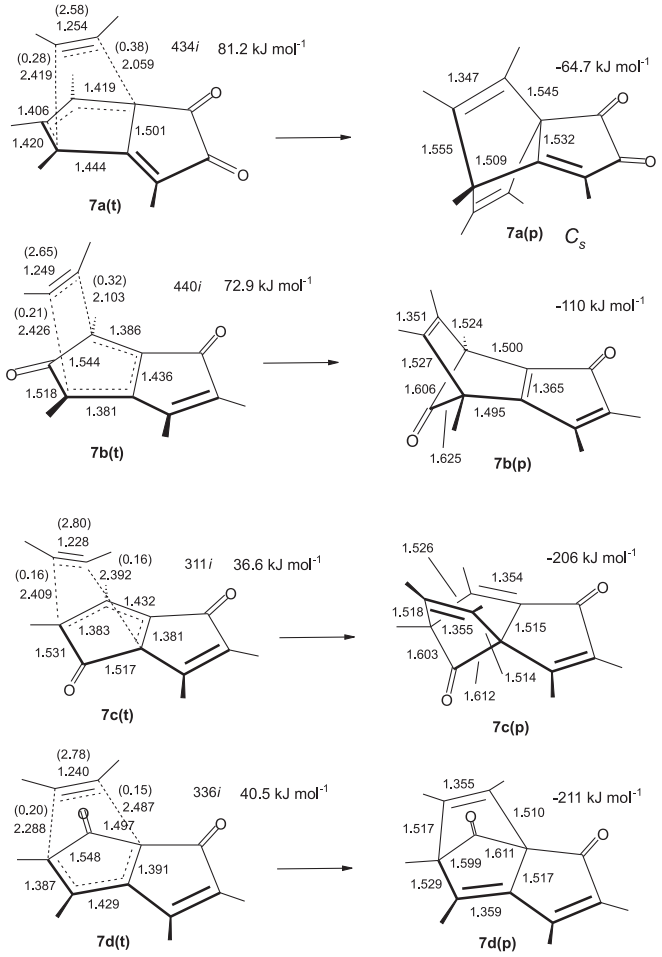
Note: The relative DFT energy of a quinone **7** is E (**7b**) – E (**7**), **7b** being the isomer of lowest energy. The DFT energies are in hartrees and the others in kJ mol^{-1}.

i.e., the relative DFT energies, should reflect the *differences* in aromaticity (or antiaromaticity). In Table 3, we compare the relative DFT energies with the REs calculated by these somewhat elaborate procedures. The maximum discrepancy is 17 kJ mol^{-1} (–66 cf. –83 kJ mol^{-1}), and the comparison is quantitatively in accord with the view that **7a** and **7b** are nonaromatic, while **7c** and **7d** are antiaromatic. The tolerable agreement between the relative energies and the REs should not be obtained if the SEs (which are incorporated in the REs) were actually very different from our estimated value. Note that in contrast to the more hard-won REs, the relative energies by themselves do not reveal the aromatic stabilization or antiaromatic destabilization of the quinones: they tell us only that **7a** and **7b** are of about the same energy, and **7c** and **7d** are about 60 kJ mol^{-1} less stable. For example, as far as the relative energies go, **7a** and **7b** might be aromatically stabilized, and **7c** and **7d** simply nonaromatic.

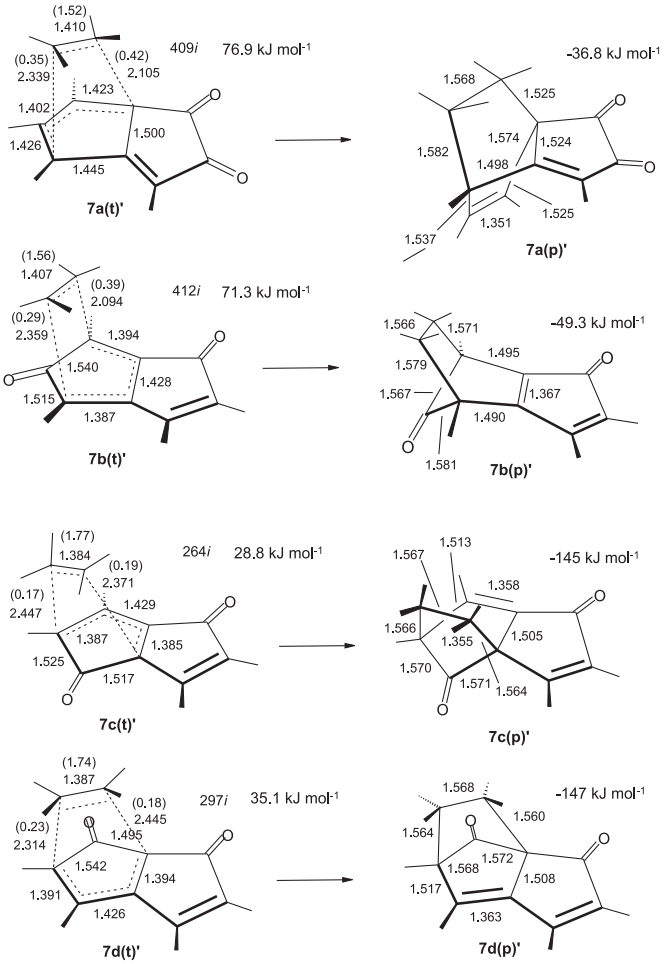
One possible complication for **7a** is that dipole–dipole repulsion of the proximal carbonyl groups raises the strain energy of this molecule above that due just to angle strain. An estimate of this dipole–dipole strain was made by comparing the energies of planar *s-cis*- and *s-trans*-ethanedial (glyoxal). The pBP/DN* energy of the *s-cis* conformer (C_{2v}, no imaginary frequencies) was found to be 18.6 kJ mol^{-1} higher than that of the *s-trans* conformation (C_{2h}, no imaginary frequencies). Raising the SE of **7a** by 19 kJ mol^{-1} gives a SE of 86 + 19 kJ mol^{-1} = 105 kJ mol^{-1}. This would give a RE of –97.1 + 105 kJ mol^{-1} = 8 kJ mol^{-1}, rather than –11 kJ mol^{-1}, which makes no difference to the above arguments (in fact, it makes **7a** and **7b** even more similar).

© 2001 NRC Canada

Scheme 3. Selected C—C bond lengths (Å) and (parentheses) Löwdin bond orders of transition states and products from Diels–Alder reactions of **7a**–**7b**, with the quinones acting as dienes toward the dienophile ethyne. The hydrogens at the ends of the C—H bonds have been omitted for clarity. All species are of C_1 symmetry except **7a(p)** (C_s). The imaginary frequency of each transition state is given, as well as, beside each transition state and product respectively, the activation energy and the reaction energy. pBP/DN* calculations.



Scheme 4. Selected C—C bond lengths (Å) and (parentheses) Löwdin bond orders of transition states and products from Diels–Alder reactions of **7a** and **7b**, with the quinones acting as dienes toward the dienophile ethene. The hydrogens at the ends of the C—H bonds have been omitted for clarity. All species are of C_1 symmetry. The imaginary frequency of each transition state is given, as well as, beside each transition state and product, respectively, the activation energy and the reaction energy. pBP/DN* calculations.



Diels–Alder reactivity

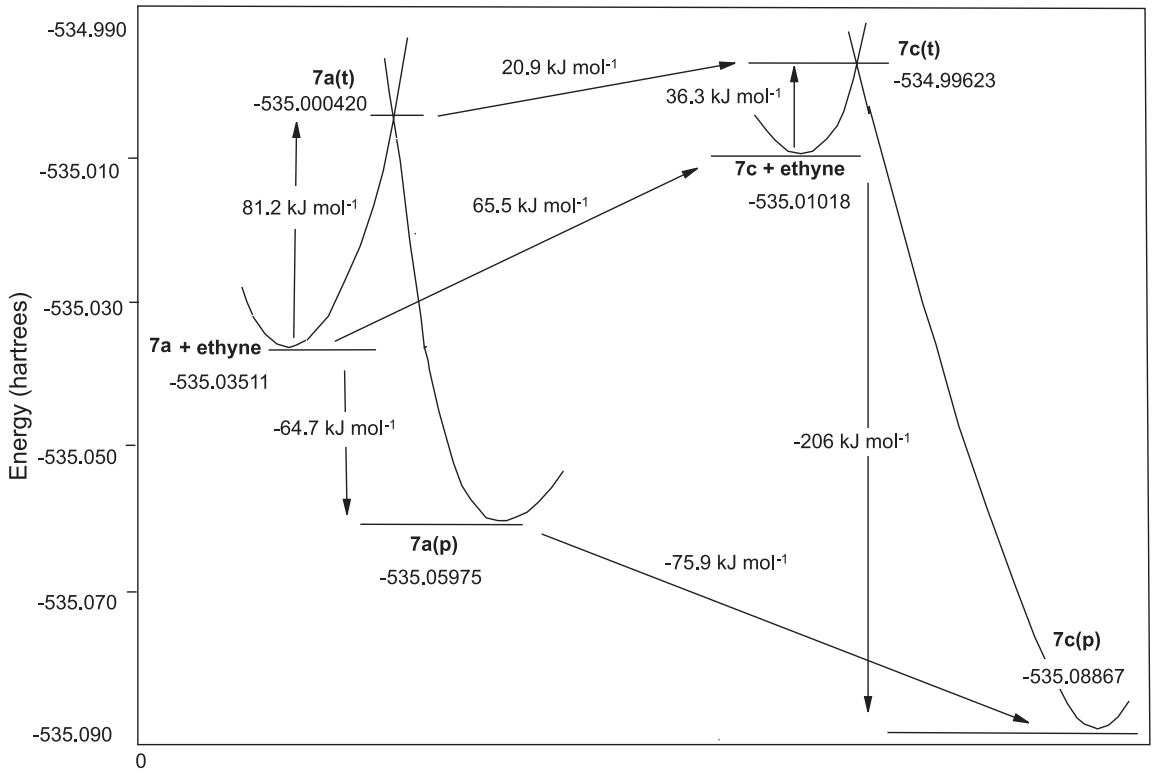
The four quinones can in principle undergo the Diels–Alder reaction. Indeed, **7c** and **7d** (34, 35) and the 3-phenyl derivative of **7d** (36) have been trapped as both dienes and dienophiles. Considering **7a**–**7d** as potential dienophiles, if we limit ourselves to those C—C double bonds in immediate conjugation with a carbonyl group then the number of different possible ways the quinones can act as dienophiles is: **7a** 2, **7b** 3, **7c** 2, **7d** 2.

Limiting ourselves to the stereochemically feasible cycloaddition to an *s-cis* moiety, the number of different ways each quinone can act as a *diene* is only one. To facilitate a simple comparison of the Diels–Alder reactivity of the four quinones, we therefore examined computationally the reactivity of **7a**–**7d** and related molecules as dienes, using ethyne and ethene as the dienophiles. The results of these calculations are given in Schemes 3 and 4.

From Scheme 3, the Diels–Alder **7**–ethyne transition states fall into two groups: **7a(t)** and **7b(t)** are (the terms are used here semiquantitatively for descriptive purposes and should not be taken too literally) high-frequency, high-activation energy, and lead to mildly exothermic reactions, while **7c(t)** and **7d(t)** are low-frequency, low-activation energy, and lead to strongly exothermic reactions. In the first group, the imaginary frequency (in all cases animation confirmed that this corresponded to the formation of the two new bonds in a Diels–Alder cycloaddition) is ca. 437*i*, the activation energy is ca. 75 kJ mol^{-1}, and the reaction is 65–110 kJ mol^{-1} exothermic. In the second group, the imaginary frequency is ca. 324*i*, the activation energy is ca. 40 kJ mol^{-1}, and the reaction is ca. 210 kJ mol^{-1} exothermic. Evidently **7a** and **7b** are kinetically and thermodynamically significantly less reactive dienes than **7c** and **7d**. The frequency of a vibrational mode is an indication of the curvature of the potential energy hypersurface along that direction, since fre-

© 2001 NRC Canada

Fig. 7. Change in reaction profile on going from the **7a**–ethyne reaction to the **7c**–ethyne reaction. The transition states are approximated as the crossing points of the reactant and product reaction coordinate curves. Transition state **7c(t)** is "dragged down" by the low-energy product **7c(p)**.



quencies are proportional to (mass-weighted) second derivatives of energy with respect to geometry (67). Relatively "large" imaginary frequencies tend to correspond to relatively high curvature of the potential energy surface along the reaction coordinate in the region of a somewhat late transition state; this also corresponds to a relatively high activation energy and tends to correspond to a relatively weakly exothermic reaction (68). The electronic structures of the transition states agree with this interpretation. Bond orders provide a measure of the lateness of the transition state (69). One can consider the sum of the bond orders of the two forming single bonds, or the bond order of the ethyne central bond. For **7a(t)** and **7b(t)**, the sum of the bond orders for the forming single bonds is 0.28 + 0.38 = 0.66, and 0.21 + 0.32 = 0.53, respectively. For **7c(t)** and **7d(t)**, it is 0.16 + 0.16 = 0.32, and 0.20 + 0.15 = 0.35, respectively. The ethyne C—C bond order is ca. 2.6 for the former two, and ca. 2.8 for the latter two. Bond lengths also are (albeit less obviously) in accord in accord with **7c(t)** and **7d(t)** being earlier than **7a(t)** and **7b(t)**. For example, the ethyne moiety in **7c(t)** and **7d(t)** has a shorter C—C bond than in the other two. For **7c(t)** and **7d(t)** too, the forming C—C bonds are seen to have to "travel" a greater distance toward the bond lengths in the products, if one compares the sum of the bond lengths in the transition state with that in the corresponding product: Σ (lengths in ts) – Σ (lengths in product) (Å): **7a(t)** 1.37, **7b(t)** 1.48, **7c(t)** 1.77, **7d(t)** 1.75.

The long single bond lengths to one of the carbonyl groups in **7b(p)**, **7c(p)**, and **7d(p)**, ca. 1.6 Å, can be ascribed to these bonds being those that tether the carbonyl group in a norbornadienone, a system where these bonds break exceedingly readily with extrusion of carbon monoxide and formation of a benzene ring (70). The corresponding pBP/DN* lengths in norbornadienone itself and in norbornenone are 1.594 and 1.557 Å, respectively.

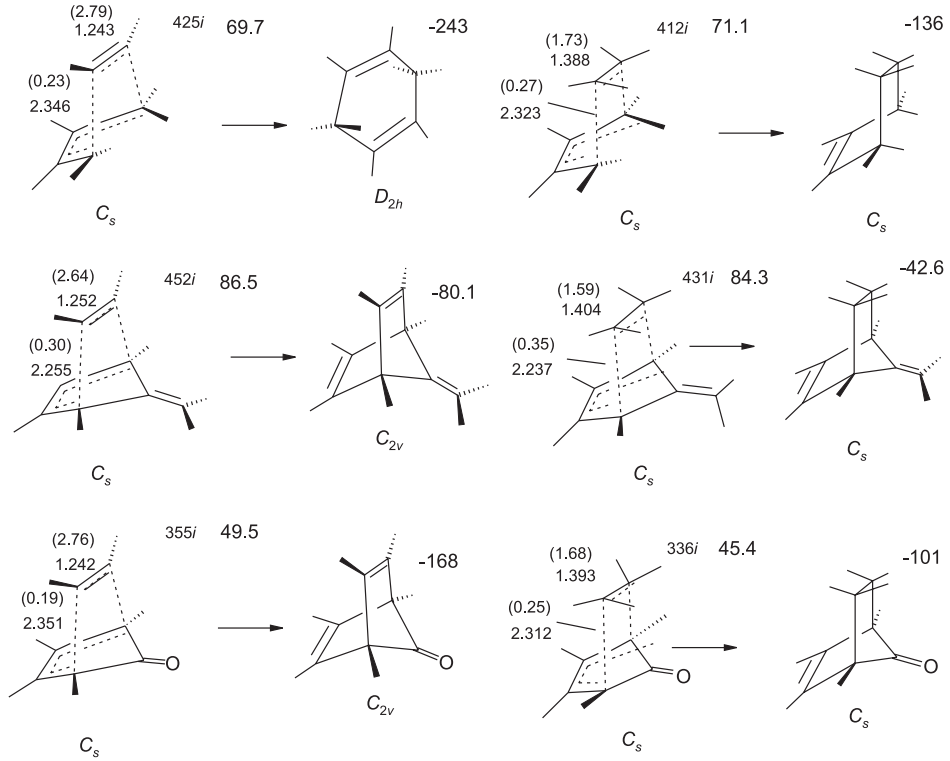
We also performed calculations on the Diels–Alder reactivity of the quinones **7** with ethene (rather than ethyne). The results are summarized in Scheme 4, which shows the transition states **7(t)′** and products **7(p)′**. The geometric and energetic similarities between the ethyne and ethene reactions are clear. For these Diels–Alder reactions, then, activation and reaction energies, transition state imaginary frequencies, and bond lengths and orders all support the conclusion that **7a(t)** and **7b(t)** are significantly less reactive dienes than **7c(t)** and **7d(t)**.

A referee invoked the Bell–Evans–Polanyi principle (71) and suggested[7] that the lower activation barriers for **7c** and **7d** compared to **7a** and **7b** may be due to the greater product stability for the **7c** and **7d** reactions, and so may not really reflect electronic destabilization in going from **7a** or **7b** to **7c** or **7d**. This may well be the case, as shown by Fig. 7, which depicts changes in absolute DFT energies on going from the **7a** reaction to the **7c** reaction, with the dienophile ethyne (the situation is similar for the other high-barrier and

[7] We thank the referee for this suggestion.

© 2001 NRC Canada

Scheme 5. Selected C—C bond lengths (Å) and (parentheses) Löwdin bond orders of transition states and products from Diels–Alder reactions of 1,3-butadiene, fulvene, and cyclopentadienone with ethyne and with ethene. The hydrogens at the ends of the C—H bonds have been omitted for clarity. The imaginary frequency of each transition state is given, as well as, beside each transition state and product, respectively, the activation energy and the reaction energy. pBP/DN* calculations.



low-barrier pairs, and for the ethene reactions); the transition state is approximated by the crossing of reactant and product reaction coordinate curves. Going from the **7a** to the **7c** reaction, both the reactant energy (taken as the pentalenequinone energy plus the ethyne energy) and the transition state energy increase, but the transition state energy increases less, apparently because it is "dragged down" by the product.

To put these results for the Diels–Alder reactions of ethyne and ethene with the quinones **7** in perspective, we compared them with pBP/DN* calculations on the more familiar Diels–Alder reactions of ethyne and ethene with 1,3-butadiene (the prototypical reactions), with fulvene (cf. the fulvenoid diene system of **7a**), and with cyclopentadienone (cf. the cyclopentadienone systems of **7b**–**7d**). The results of these model calculations are given in Scheme 5. The magnitude of the imaginary frequencies and the bond lengths and orders, and particularly the activation energies, indicate that the cyclopentadienone–ethyne transition state is earlier and of lower activation energy than those for butadiene and fulvene, and of course cyclopentadienone is known to be extraordinarily reactive as a diene (10). The activation and reaction energies place **7c** and **7d** in the same class as cyclopentadienone, with the quinones being a bit more reactive. The butadiene–ethene reaction seems to be anomalous in that its activation energy is between that for fulvene and cyclopentadienone, yet it is more exothermic than the fulvene reaction. That **7a** and **7b** are of the same energy (to within 1 millihartree, 3 kJ mol^{-1}), and that **7b** is calculated to be only slightly more reactive as a Diels–Alder diene than **7a** (activation energy 72.9 cf. 81.2 kJ mol^{-1}), is surprising considering that, formally, **7b** is a cyclopentadienone and **7a** is a fulvene.

The pBP/DN* method may give somewhat low values for Diels–Alder activation energies; for the butadiene–*ethene* reaction, the experimental activation and reaction energies are (72) 105 and –167 kJ mol^{-1}, cf. the pBP/DN* values of 71.1 and –136 kJ mol^{-1}, respectively. However, for a series of molecules, all using this method, comparisons should be reliable. These pBP/DN* parameters are better than those from high-level ab initio (CASSCF) calculations, which gave activation and reaction energies of 156 and –109 kJ mol^{-1}, respectively (72).

There is a relationship between the dienophile LUMO – diene HOMO energy gap and the rates of Diels–Alder reactions (the smaller the gap, the faster the reaction) (73). For the pentalenoquinones reacting with ethyne and with ethene, the activation energy does indeed decrease as the dienophile LUMO – diene HOMO gap decreases. For the reaction with ethyne we have (in the order **7a**, **7b**, **7d**, **7c**) LUMO-(dienophile)–HOMO(diene), eV/activation energy, kJ mol^{-1}: **7a** 15.35/81.2, **7b** 15.28/72.9, **7d** 15.03/40.5, **7c** 14.79/36.6. For the reaction with ethene: 14.32/76.9, 14.25/71.3, 14.00/35.1, 13.76/28.8.

Conclusions

Criteria for aromaticity were applied to the pentalenoquinones **7a**–**7d** using primarily pBP/DN* DFT calculations. Five molecular characteristics were examined: structure

© 2001 NRC Canada

(bond lengths and bond orders), chemical hardness, nucleus-independent chemical shift (NICS) curves, resonance energies (REs), and Diels–Alder reactivity toward dienophiles (ethyne and ethene). The bond lengths and orders and the hardness values gave no obvious indication of unusual electronic characteristics. The NICS curves are intriguing but do not provide any definite evidence for aromaticity or antiaromaticity in the quinones, beyond suggesting that **7c** and **7d** are electronically cyclopentadiene-like, in contrast to **7a** and **7b**.

The clearest evidence for the electronic nature of the pentalenoquinones comes from their calculated REs. These were obtained by adding the strain energy (SE) to the homodesmotic energy change for ring-opening to an acyclic analogue. The SE was taken as that of pentalene, which was estimated by calculating SE as the homodesmotic energy decrease on ring-opening of a series of hydropentalenes and extrapolating to a hypothetical nonantiaromatic pentalene. The REs of **7a** and **7b** are not significantly different from zero, indicating they are simply nonaromatic, but those of **7c** and **7d** are –83 and –54 kJ mol^{-1}, respectively, indicating antiaromaticity. The REs are comparable to the simple relative energies of the quinones, indicating that the values calculated by this somewhat elaborate procedure are meaningful.

The calculated Diels–Alder activation energies (with the quinones acting as dienes), too, divide **7a** and **7b** from **7c** and **7d**. The former pair have activation energies with ethyne (the values with ethene are similar) of ca. 75 kJ mol^{-1}, the latter ca. 40 kJ mol^{-1}. The "unreactive" former pair are similar in activation energies to 1,3-butadiene and fulvene, the "reactive" latter pair to cyclopentadienone. The possibility that the lower activation energies of **7c** and **7d** is due to the greater product stability makes it uncertain to what extent these energies reflect electronic destabilization.

Acknowledgements

We thank the Natural Sciences and Engineering Research Council of Canada (NSERC) for financial support.

References

1. V.I. Minkin, M.N. Glukhovtsev, and B.Ya. Simkin. Aromaticity and antiaromaticity. Wiley, New York. 1994.
2. M. Glukhovtsev. Chem. Educ. **74**, 132 (1997).
3. P. Von R. Schleyer and H. Jiao. Pure Appl. Chem. **68**, 209 (1996).
4. D. Lloyd. J. Chem. Inf. Comput. Sci. **36**, 442 (1996).
5. T. Eicher and J.L. Weber. Top. Curr. Chem. **57**, 1 (1975).
6. D.W. Rogers, A. Podosenin, and J.F. Liebman. J. Org. Chem. **58**, 2589 (1993).
7. N.L. Bauld, T.L. Welsher, J. Cassac, and R.L. Holloway. J. Am. Chem. Soc. **100**, 6920 (1978).
8. M.N. Glukhovtsev, B. Reindl, and P. Von R. Schleyer. Mendeleev Commun. 100 (1993).
9. F. Gaviña, A.M. Costero, P. Gil, and S.V. Luis. J. Am. Chem. Soc. **106**, 2077 (1984).
10. C.H. DePuy, M. Isaks, K.L. Eilers, and G.F. Morris. J. Org. Chem. **29**, 3503 (1964).
11. (*a*) M. Bremer and P.v.R. Schleyer. J. Am. Chem. Soc. **111**, 1147 (1989); (*b*) K. Krogh-Jespersen, P.v.R. Schleyer, J.A. Pople, and D. Cremer. J. Am. Chem. Soc. **100**, 4301 (1784).
12. (*a*) G.A. Olah, I.S. Staral, G. Liang, L.A. Paquette, W.P. Melega, and M.I. Carmody. J. Am. Chem. Soc. **99**, 3349 (1977); (*b*) L. Radom and H.F. Schaefer. J. Am. Chem. Soc. **99**, 7522 (1977); (*c*) I. Willner and M. Rabinowitz. Nouv. J. Chim. **6**, 129 (1982).
13. (*a*) A.A. Deniz, K.S. Peters, and G.J. Snyder. Science (Washington, D.C.), **286**, 1119 (1999); B.K. Carpenter. *In* Advances in molecular modelling. *Edited by* D. Liotta. JAI Press, Greenwich, Connecticut. 1988. pp. 41–100.
14. V.I. Minkin, M.N. Glukhovtsev, and B.Ya. Simkin. Aromaticity and antiaromaticity. Wiley, New York. 1994. pp. 165–169.
15. M.N. Glukhovtsev, R.D. Bach, and S. Laiter. J. Mol. Struct: THEOCHEM, **417**, 123 (1997).
16. M.P. Cava and M.J. Mitchell. Cyclobutadiene and related compounds. Academic Press, New York. 1967. Chap. 4.
17. C. Jakins and E. Lewars. J. Mol. Struct: THEOCHEM, **531**, 181 (2000).
18. M. Oda, M. Oda, S. Miyakoshi, and Y. Kitahara. Chem. Lett. 293 (1977).
19. M. Oda, Y. Kayama, H. Miyazaki, and Y. Kitahara. Angew. Chem. **87**, 414 (1975).
20. L.T. Scott, M.D. Rozenboom, K.N. Houk, T. Fukunaga, H.J. Lindner, and K. Hafner. J. Am. Chem. Soc. **102**, 5169 (1980).
21. B.-C. Wang, Y.-S. Lin, J.-C. Chang, and P.-Y. Wang. Can. J. Chem. **78**, 224 (2000).
22. (*a*) L.T. Scott. *In* The chemistry of the quinonoid compounds. Vol. 2, Part 2. *Edited by* S. Patai and Z. Rapaport. Wiley, Chichester, U.K. 1998; (*b*) T. Marita, F. Ice, and K. Takahe. Chem. Lett. **8**, 1303 (1982); (*c*) L.T. Scott and C.M. Adams. J. Am. Chem. Soc. **106**, 4857 (1984); (*d*) T. Nozoe and H. Takesita. Bull. Chem. Soc. Jpn. **69**, 1149 (1996); (*e*) T. Nozoe, H. Wakabayashi, K. Shindo, and S. Iskikawa. Chem. Lett. **1**, 27 (1995).
23. M.A. Natiello and J.A. Medrano. Chem Phys. Lett. **105**, 180 (1984); Chem Phys. Lett. **110**, 445 (1984).
24. Z. Zhou and R.G. Parr. J. Am. Chem. Soc. **111**, 7371 (1989).
25. Z. Zhou and R.G. Parr. Tetrahedron Lett. 4842 (1988).
26. R.G. Pearson. J. Chem. Educ. **76**, 267 (1999), and refs. therein.
27. P.v.R. Schleyer, C. Maerker, A. Dransfeld, H. Jiao, and N.J.R. Van Eikema Hommes. J. Am. Chem. Soc. **118**, 6317 (1996).
28. R. West, J. Buffy, M. Haaf, T. Müller, B. Gehrhus, M.F. Lappert, and Y. Apeloig. J. Am. Chem. Soc. **120**, 1639 (1998).
29. T. Veszprémi, M. Takahashi, B. Hajgató, J. Ogasarawa, K. Sakamoto, and M. Kira. J. Phys. Chem. A. **102**, 10 530 (1998).
30. I. Morao and F.P. Cossio. J. Org. Chem. **64**, 1868 (1999).
31. D.A. Ponomarev and V.V. Takhistov. J. Chem. Educ. **74**, 201 (1997).
32. V.I. Minkin, M.N. Glukhovtsev, and B.Ya. Simkin. Aromaticity and antiaromaticity. Wiley, New York. 1994. pp. 29–37.
33. V.I. Minkin, M.N. Glukhovtsev, and B.Ya. Simkin. Aromaticity and antiaromaticity. Wiley, New York. 1994. pp. 196–198.
34. F. Gaviña, A.M. Costero, A.M. González, and S.V. Luis. J. Org. Chem. **52**, 2997 (1987).
35. F. Gaviña, A.M. Costero, and A.M. González. J. Org. Chem. **55**, 2060 (1990).
36. F. Gaviña, A.M. Costero, and S.V. Luis. J. Org. Chem. **49**, 4616 (1984).
37. F. Gaviña, A.M. Costero, A.M. González, and J.B. Lluch. An. Quim. **87**, 283 (1991).
38. W.J. Hehre, L. Radom, P.V.R. Schleyer and J.A. Pople. Ab initio molecular orbital theory. Wiley–Interscience, New York. 1986.
39. J.B. Foresman and A. Frisch. Exploring chemistry with electronic structure methods. 2nd ed. Gaussian Inc., Pittsburgh. 1996.
40. (*a*) F. Eckert and G. Rauhut. J. Am. Chem. Soc. **120**. 13478 (1998); (*b*) E.R. Davidson. Int. J. Quantum Chem. **69**. 241 (1998); (*c*) W. Kohn, A.D. Becke, and R.G. Parr. J. Phys.

© 2001 NRC Canada

Chem. **100**, 12 974 (1996); (*e*) R.D. Parr and W. Yang. Ann. Rev. Phys. Chem. **46**, 701 (1995); (*f*) C.W. Bauschlicher. Chem. Phys. Lett. **246**, 40 (1995).

41. I.N. Levine. Quantum chemistry. 5th ed. Prentice Hall, Upper Saddle River, New Jersey. 2000. p. 589.
42. (*a*) A.D. Becke. Phys. Rev. A. **38**, 3089 (1988); (*b*) A.D. Becke. Phys. Rev. A. **33**, 2786 (1986); (*c*) J.P. Perdew. Phys. Rev. B. **33**, 8822 (1988).
43. B. Delley and D.E. Ellis. J. Chem. Phys. **76**, 1949 (1982).
44. W.J. Hehre, L. Radom, P.V.R. Schleyer and J.A. Pople. Ab initio molecular orbital theory. Wiley–Interscience, New York. 1986. Section 6.3; J.B. Foresman and A. Frisch. Exploring chemistry with electronic structure methods. 2nd ed. Gaussian Inc., Pittsburgh. 1996. Chap. 4.
45. A.P. Scott and L. Radom. J. Phys. Chem. **100**, 16 502 (1996).
46. W.J. Hehre, L. Radom, P.V.R. Schleyer and J.A. Pople. Ab initio molecular orbital theory. Wiley–Interscience, New York. 1986. Chap.6.
47. W.J. Hehre. Practical strategies for electronic structure calculations. Wavefunction Inc., Irvine, California. 1995.
48. E. Lewars. Can. J. Chem. **78**, 297 (2000).
49. W.J. Hehre and L. Lou. A guide to density functional calculations in Spartan. Wavefunction Inc., Irvine, California. 1997.
50. J.B. Foresman and A. Frisch. Exploring chemistry with electronic structure methods. 2nd ed. Gaussian Inc., Pittsburgh. 1996. Chap. 7.
51. T.K. Zywietz, H. Jiao, P.v.R. Schleyer, and A. de Meijere. J. Org. Chem. **63**, 3417 (1998).
52. (*a*) I.N. Levine. Quantum chemistry. 5th ed. Prentice Hall, Upper Saddle River, New Jersey. 2000. pp. 629–649; (*b*) J.D. Roberts. Notes on molecular orbital calculations. Benjamin, New York. 1962; (*c*) A. Streitweiser. Molecular orbital theory for organic chemists. Wiley, New York. 1961; (*d*) H.E. Zimmerman. Quantum mechanics for organic chemists. Academic Press, New York. 1975; (*e*) E. Heilbronner and H. Bock. Das HMO Modell und seine Anwendung. Vol. 1 (basics and implementation). Verlag Chemie, Weinheim, Germany. 1968; E. Heilbronner and H. Bock. Das HMO Modell und seine Anwendung. Vol. 2 (examples and solutions). 1970; E. Heilbronner and H. Bock. Das HMO Modell und seine Anwendung. Vol. 3 (tables of experimental and calculated quantities). 1970.
53. F. Jensen. Introduction to computational chemistry. Wiley, New York. 1999. pp. 64–65; A.R. Leach. Molecular modelling. Longman, Harlow. pp. 110.
54. H.M. Muchall, N.H. Werstiuk, and B. Choudhury. Can. J. Chem. **76**, 221 (1998).
55. (*a*) S.T. Brown, J.C. Rienstra-Kiracofe, and H.F. Schaefer. J. Phys. Chem. A. **103**, 4065 (1999); (*b*) S.E. Boesch, A.K. Grafton, and R.A. Wheeler. J. Phys. Chem. **100**, 10 083 (1996).
56. A. Frisch and M.J. Frisch. Gaussian 94 user's reference. Gaussian Inc., Pittsburgh. 1994. p. 253.
57. D.W. Rogers, A. Podosenin, and J.F. Liebman. J. Org. Chem. **58**, 2589 (1993).
58. S.P. Verevkin, H.-D. Beckhaus, C. Rüchardt, R. Haag, S.I. Kozhushkov, T. Zywietz, A. de Meijere, H. Jiao, and P.v.R. Schleyer. J. Am. Chem. Soc. **120**, 11 130 (1998).
59. K.T. Finley. *In* The chemistry of the quinonoid compounds. Vol. 2, Part 1. *Edited by* S. Patai and Z. Rapaport. Wiley, Chichester, U.K. 1988.
60. T.H. Lowry and K.S. Richardson. Mechanism and theory in organic chemistry. Harper and Row, New York. 1981. p. 146.
61. J.B. Foresman and A. Frisch. Exploring chemistry with electronic structure methods. 2nd ed. Gaussian Inc., Pittsburgh. 1996. p. 183.
62. V.I. Minkin, M.N. Glukhovtsev, and B. Ya. Simkin. Aromaticity and antiaromaticity. Wiley, New York. 1994. p. 37.
63. K. Wiberg. Angew. Chem. Int. Ed. Engl. **25**, 312 (1986).
64. D.B. Chestnut. J. Comput. Chem. **16**, 1227 (1995).
65. E. Lewars. J. Mol. Struct: THEOCHEM, **507**, 165 (2000), and refs. therein.
66. M.B. Smith and J. March. March's advanced organic chemistry. Wiley, New York. 2001. p. 186.
67. W.J. Hehre, L. Radom, P.V.R. Schleyer and J.A. Pople. Ab initio molecular orbital theory. Wiley–Interscience, New York. 1986. p. 228.
68. (*a*) G.S. Hammond. J. Am. Chem. Soc. **77**, 334 (1955); D. Fárcasiu. J. Chem. Educ. **52**, 76 (1975). (*b*) S. S. Shaik, H. B. Schlegel, and S. Wolfe. Theoretical aspects of physical organic chemistry. Wiley, New York. 1992. Chaps. 1 and 2.
69. G. Lendvay. J. Phys. Chem. **98**, 6098 (1994).
70. (*a*) D.M. Birney, K.B. Wiberg, and J.A. Berson. J. Am. Chem. Soc. **110**, 6631 (1988); (*b*) B.F. LeBlanc and R.S. Sheridan. J. Am. Chem. Soc. **107**, 4554 (1985).
71. S.S. Shaik, H.B. Schlegel, and S. Wolfe. Theoretical aspects of physical organic chemistry. Wiley, New York. 1992. pp. 16, 17.
72. Y. Li and K.N. Houk. J. Am. Chem. Soc. **115**, 7478 (1993), and refs. therein.
73. (*a*) R. Sustmann and R. Schubert. Angew. Chem. Int. Ed. Engl. **11**, 840 (1972); (*b*) I. Fleming. Frontier orbitals and organic chemical reactions. Wiley, New York. 1976.

© 2001 NRC Canada

Oxidative coupling of naphtho-9-crown-3 ether: X-ray crystal structure and solution and solid-state NMR analysis of the dimer

G.W. Buchanan, M.F. Rastegar, G.P.A. Yap, A. Moghimi, and M. Ghandi

Abstract: Treatment of naphtho-9-crown-3 ether with $FeCl_3$ and aqueous H_2SO_4 generates bis-naphtho-9-crown-3 ether in ca. 30% yield. This compound crystallizes in the monoclinic $P2_1/n$ space group; a = 9.2004(9), b = 18.0868(17), and c = 13.2078(13) Å, β = 97.799(2)° and Z = 4. ^1H and ^{13}C NMR data have been obtained in solution, and the solid-state ^{13}C NMR spectrum is included for comparison. A chemical shift range of ca. 12 ppm has been found for the oxygenated aliphatic carbons in the solid state, in contrast to the 3 ppm range in the solution ^{13}C NMR spectrum. These results are discussed in terms of the torsional environments of the carbon sites in the crystal structure.

Key words: crown ether, stereochemistry, oxidative dimerization.

Résumé : Le traitement de l'éther naphto-9-couronne-3 par du $FeCl_3$ et du H_2SO_4 aqueux conduit à la formation de l'éther bis-naphto-9-couronne-3 avec un rendement d'environ 30%. Ce composé cristallise dans le groupe d'espace $P2_1/n$ avec a = 9,2004(9), b = 18,0868(17) et c = 13,2078(13) Å, β = 97,799(2)° et Z = 4. On a mesuré les spectres RMN du ^1H et du ^{13}C en solution et on a aussi déterminé le spectre RMN du ^{13}C à l'état solide. Dans les spectres RMN du ^{13}C à l'état solide, les déplacements chimiques des carbones aliphatiques oxygénés sont de l'ordre de 12 ppm alors qu'en solution on les retrouve vers 3 ppm. On discute de ces résultats en termes de l'environnement torsionnel des sites carbonés dans la structure cristalline.

Mots clés : éther couronne, stéréochimie, dimérisation oxydante.

[Traduit par la Rédaction]

Introduction

Recent work from these laboratories (1) described the results of oxidative trimerization of benzo-9-crown-3 ether leading to a novel tris(9-crown-3)triphenylene system. We are interested in comparing the behaviour of the corresponding naphtho-9-crown-3 system, to determine if extended conjugation would lead to a similar type of trimerization, in which case enhanced liquid crystalline properties could result due to the increased propensity for π stacking between layers of the aromatic rings.

Results and discussion

The synthesis, NMR spectra, and X-ray crystal structure of naphtho-9-crown-3 ether (**1**), have been reported previously (2, 3). In the current study, we have found that **1**, in the presence of $FeCl_3$ and aqueous H_2SO_4 at 313 K, dimerizes in 30% yield to afford the bis-naphtho-9-crown-3 system (**2**). This is in contrast to the benzo-9-crown-3 analog, which trimerizes in 25% yield under identical conditions to give a tris(9-crown-3)triphenylene system (1).

Figure 1 shows the ORTEP diagram for **2** and the solid-state ^{13}C NMR spectrum is shown in Fig. 2. Table 1 contains selected atomic bond lengths and angles. Selected torsion angles are collected in Table 2, while crystallographic data are presented in Table 3. Atomic coordinates and anisotropic temperature factors are available as Supplementary Data. Solution ^1H NMR data are in Table 4, and the ^{13}C NMR data collected in Table 5.

X-ray crystal structure

The crystal structure of **2** is found to show some disorder at the O1 and C9 positions, with the refined distribution being 70/30. Details of the structural differences between the disordered forms are described below.

For example, in the major form the C9-O1-C8-C7 torsion angle is 89.8(5)°, while the angle for the C9′-O1′-C8-C7 unit in the minor form is –174.2(8)°. In the case of C9-O1-C8-C13, the torsion angle is –101.2(4)°, whereas that for the C9′-O1′-C8-C13 counterpart is 14.9(13)°. For C11-O(3)-C10-C9, the angle is 123.9(4)°, while that for the same network with the C9′ terminus is 69.0(7)°. Finally, for the O1-C9-C10-O2 unit, a smaller difference is found between the two forms. The torsion angle in this case is –80.8(5)°, while that for the O1′-C9′-C10-O2 counterpart is 68.7(9)°.

Regarding the interplanar angle between the two naphthalene rings, the C13-C14-C15-C16 angle has been found to

Received May 21, 2001. Published on the NRC Research Press Web site at http://canjchem.nrc.ca on October 15, 2001.

G.W. Buchanan,[1] M.F. Rastegar, and G.P.A. Yap. Ottawa-Carleton Chemistry Institute, Department of Chemistry, Carleton University, Ottawa, ON K1S 5B6, Canada.
A. Moghimi and M. Ghandi. Department of Chemistry, Imam Hossein University, Tehran, Iran.

[1]Corresponding author (telephone: (613) 520-3841; fax: (613) 520-3749; e-mail: gwbuchan@ccs.carleton.ca).

 DOI: 10.1139/cjc-79-10-1505 © 2001 NRC Canada

Table 1a. Selected bond lengths (Å) for **2**.

O(1)—C(9′)	1.422(16)	O(1)—C(9)	1.458(7)	O(1)—C(8)	1.418(5)
O(1′)—C(8)	1.348(10)	O(2)—C(11)	1.393(4)	O(2)—C(10)	1.399(5)
O(3)—C(13)	1.369(3)	O(3)—C(12)	1.413(4)	O(4)—C(16)	1.359(4)
O(4)—C(17)	1.455(4)	O(5)—C(19)	1.414(4)	O(5)—C(18)	1.417(4)
O(6)—C(21)	1.378(4)	O(6)—C(20)	1.445(4)	C(7)—C(8)	1.356(5)
C(8)—C(13)	1.415(4)	C(9)—C(10)	1.505(7)	C(9′)—C(10)	1.479(12)
C(11)—C(12)	1.507(5)	C(13)—C(14)	1.366(4)	C(14)—C(15)	1.493(4)
C(15)—C(16)	1.378(4)	C(15)—C(28)	1.430(4)	C(16)—C(21)	1.436(4)
C(17)—C(18)	1.499(5)	C(19)—C(20)	1.488(5)	C(21)—C(22)	1.348(5)

Fig. 1. ORTEP plot for **2**.

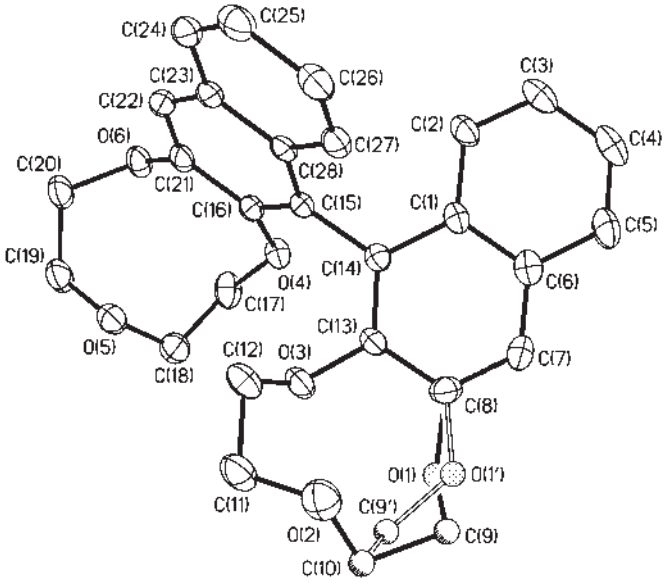
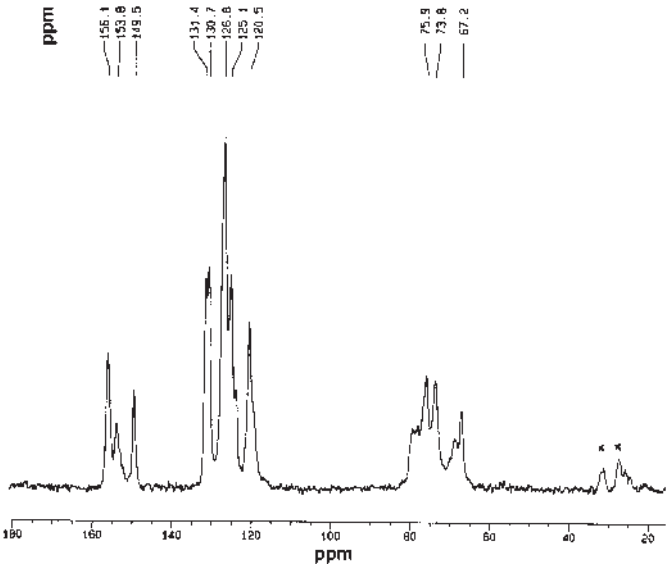


Fig. 2. 50.3 MHz ^{13}C solid-state NMR spectrum of **2**.



be –67.5(4)°, indicating a gauche type relationship between these two essentially planar aromatic units.

It is also of interest to compare the 9-membered ring geometries present in **2** with that which has been determined in naphtho-9-crown-3 itself (3). Table 6 contains a tabulation of the pertinent torsional angle data. It is evident that the major conformation of the C8–C13 ring of **2** bears a remarkable similarity in geometry with that present in the monomer, with the largest difference in torsional angles being only ca. 15°. In contrast, there are very large differences (up to ca. 80°) present in the C16–C21 ring of **2** for three of the nine torsional networks of the 9-membered ring. Since this is a solid-state structure, the conformational differences are most likely due to crystal packing effects.

Table 1b. Selected bond angles (°) for **2**.

C(9′)-O(1′)-C(8)	125.8(8)	C(9)-O(1)-C(8)	111.1(4)
C(11)-O(2)-C(10)	116.1(3)	C(13)-O(3)-C(12)	116.9(3)
C(16)-O(4)-C(17)	123.7(2)	C(19)-O(5)-C(18)	113.7(3)
C(21)-O(6)-C(20)	114.3(3)	O(1′)-C(8)-C(7)	111.6(5)
O(1′)-C(8)-C(13)	127.4(5)	C(7)-C(8)-O(1)	121.5(3)
C(7)-C(8)-C(13)	120.4(3)	O(1)-C(8)-C(13)	117.2(3)
O(1)-C(9)-C(10)	112.1(4)	O(1′)-C(9′)-C(10)	109.2(9)
O(2)-C(10)-C(9′)	115.6(6)	O(2)-C(10)-C(9)	111.0(4)
O(2)-C(11)-C(12)	110.5(3)	O(3)-C(12)-C(11)	109.1(3)
O(3)-C(13)-C(8)	117.1(3)	C(13)-C(14)-C(15)	121.7(3)
C(1)-C(14)-C(15)	119.1(3)	C(16)-C(15)-C(28)	120.4(2)
C(16)-C(15)-C(14)	119.5(3)	O(4)-C(16)-C(21)	124.7(3)
O(4)-C(17)-C(18)	113.5(3)	O(5)-C(18)-C(17)	115.5(3)
O(5)-C(19)-C(20)	110.5(3)	O(6)-C(20)-C(19)	111.0(3)
C(22)-C(21)-O(6)	120.7(3)	C(22)-C(21)-C(16)	120.1(3)
O(6)-C(21)-C(16)	119.1(3)		

NMR spectral result

Because of rapid conformational interconversion on the NMR timescale, **2** can be regarded, for solution NMR purposes, as having a twofold axis of symmetry bisecting the C14—C15 bond. Hence, we will discuss assignments for C1–C14 only. Spectra were temperature independent to 173 K.

The starting point for the ^{1}H NMR assignments is the singlet observed for H7 at 7.594 ppm. From results of a NOESY experiment, the correlation to the peri-H5 proton was established. Subsequent ^{1}H–^{1}H COSY results permitted facile assignments of the H4, H3, and H2 resonances.

The coupling constants between the aromatic protons listed in Table 4 were obtained by first-order analysis.

For the aliphatic protons, the ^{1}H–^{1}H COSY experiment permitted establishment of the H9–H10 connectivity. These four protons, which give rise to a complex AA′BB′ spectrum, have chemical shifts that are nearly identical to those found in naphtho-9-crown-3 (2). The internal protons on C11 and

© 2001 NRC Canada

Table 2. Selected torsion angles (°) for **2**.

C(6)-C(7)-C(8)-O(1)	166.9(3)	C(6)-C(7)-C(8)-O(1′)	–173.4(5)
C(6)-C(7)-C(8)-C(13)	–1.7(5)	C(9′)-O(1′)-C(8)-C(7)	–174.2(8)
C(9)-O(1)-C(8)-C(7)	89.8(5)	C(9)-O(1)-C(8)-C(13)	–101.2(4)
C(9′)-O(1′)-C(8)-C(13)	14.9(13)	C(8)-O(1)-C(9)-C(10)	101.8(4)
C(8)-O(1′)-C(9′)-C(10)	–98.3(11)	C(11)-O(2)-C(10)-C(9′)	69.0(7)
C(11)-O(2)-C(10)-C(9)	123.9(4)	O(1′)-C(9′)-C(10)-O(2)	68.7(9)
O(1)-C(9)-C(10)-O(2)	–80.8(5)	C(10)-O(2)-C(11)-C(12)	–109.5(4)
C(13)-O(3)-C(12)-C(11)	–110.2(3)	O(2)-C(11)-C(12)-O(3)	62.0(4)
C(12)-O(3)-C(13)-C(14)	–70.1(4)	C(12)-O(3)-C(13)-C(8)	116.1(3)
O(1)-C(8)-C(13)-C(14)	–168.5(3)	O(1′)-C(8)-C(13)-C(14)	170.9(6)
C(7)-C(8)-C(13)-O(3)	174.6(3)	O(1)-C(8)-C(13)-O(3)	5.5(5)
O(1′)-C(8)-C(13)-O(3)	–15.2(7)	O(3)-C(13)-C(14)-C(1)	–171.4(3)
C(8)-C(13)-C(14)-C(1)	2.3(5)	O(3)-C(13)-C(14)-C(15)	6.5(5)
C(8)-C(13)-C(14)-C(15)	–179.8(3)	C(6)-C(1)-C(14)-C(15)	178.0(3)
C(2)-C(1)-C(14)-C(15)	–2.9(4)	C(13)-C(14)-C(15)-C(16)	–67.7(4)
C(1)-C(14)-C(15)-C(16)	110.2(3)	C(13)-C(14)-C(15)-C(28)	113.0(3)
C(1)-C(14)-C(15)-C(28)	–69.1(4)	C(17)-O(4)-C(16)-C(15)	150.9(3)
C(17)-O(4)-C(16)-C(21)	–35.3(4)	C(28)-C(15)-C(16)-O(4)	174.9(2)
C(14)-C(15)-C(16)-O(4)	–4.3(3)	C(28)-C(15)-C(16)-C(21)	0.8(4)
C(14)-C(15)-C(16)-C(21)	–178.4(3)	C(16)-O(4)-C(17)-C(18)	–60.5(4)
C(19)-O(5)-C(18)-C(17)	67.6(4)	O(4)-C(17)-C(18)-O(5)	70.5(4)
C(18)-O(5)-C(19)-C(20)	–112.9(3)	C(21)-O(6)-C(20)-C(19)	–95.0(4)
O(5)-C(19)-C(20)-O(6)	56.1(4)	C(20)-O(6)-C(21)-C(22)	–69.0(4)
C(20)-O(6)-C(21)-C(16)	114.5(3)	O(4)-C(16)-C(21)-C(22)	–171.8(3)
O(4)-C(16)-C(21)-O(6)	4.7(4)	C(15)-C(16)-C(21)-O(6)	178.2(2)
O(6)-C(21)-C(22)-C(23)	–179.3(3)	C(16)-C(21)-C(22)-C(23)	–2.8(4)
C(21)-C(22)-C(23)-C(28)	1.3(4)	C(22)-C(23)-C(28)-C(15)	1.2(4)
C(14)-C(15)-C(28)-C(27)	–3.5(4)	C(14)-C(15)-C(28)-C(23)	177.0(2)

Table 3. Crystallographic data for **2**.

Formula	$C_{28}H_{26}O_6$
Formula mass (g mol^{-1})	458.49
Temperature (K)	203(2)
Crystal system	Monoclinic
Space group	$P2_1/n$
a (Å)	9.2004(9)
b (Å)	18.0868(17)
c (Å)	13.2078(13)
β (°)	97.799(2)
Volume (Å^3)	2177.5(4)
Z (molecules per unit cell)	4
D_c (gm cm^{-3})	1.399
Crystal Dimensions (mm)	0.1 × 0.1 × 0.1
Radiation (λ, Å)	Mo Kα, 0.71073
Octants measured	h (–11–11), k (0–22), l (0–16)
Theta range (°)	1.92–26.37
No. of unique reflections	4429
No. of reflections measured	17 087
No. of reflections with $I > 2\sigma(I)$	4397
R_1 ($I > 2\sigma(I)$)	0.0691
R_1 (all data)	0.1199
wR_2 (all data)	0.2155
wR_2 ($I > 2\sigma(I)$)	0.1913
GoF	1.100
Largest diff. peak and hole (e Å^{-3})	0.619 and –0.495

Table 4. ^{1}H NMR chemical shifts (δ, ppm from TMS) and coupling constants (J, Hz) for a 0.05 M solution of **1** in $CDCl_3$.

Site	δ	^3J	^4J	^5J
H(2), H(27)	7.095	8.3	1.3	0.6
H(3), H(26)	7.157	8.3, 8.4	1.2	
H(4), H(25)	7.345	8.4, 8.4	1.3	
H(5), H(24)	7.771	8.4	1.2	0.6
H(7), H(22)	7.594			
H(9), H(20)	4.454[a]			
H(10), H(19)	3.936[a]			
H(11), H(18)	3.772[a]			
H(12), H(17)	3.924[a]			

[a]Part of a complex AA′BB′ spin system.

C12 are shielded relative to those on C10 and C9, respectively. This shielding is likely due to the intramolecular aromatic ring current of the nonbonded naphthalene ring. The X-ray geometry indicates a gauche relationship between the two naphthyl moieties; however, oscillatory freedom in solution would bring the C12 and C11 protons into the shielding cone of the nonbonded naphthyl unit at least some of the time.

With respect to the assignment of the solution ^{13}C NMR resonances, results of a heteronuclear multiple quantum correlation (HMQC) experiment gave assignments for all the carbons bearing hydrogen atoms, since all ^{1}H assignments are in hand. Regarding the quaternary carbons, the chemical shift of C8 was established via a heteronuclear multiple bond correlation (HMBC) experiment and is identical to that found in naphtho-9-crown-3 (2), whereas the C13 site is shielded by ca. 3 ppm. Intramolecular ring-current effects may again be the origin of this shielding phenomenon. Dis-

© 2001 NRC Canada

Table 5. ^{13}C NMR chemical shifts (δ_c from TMS ± 0.1) for **2**.

Site	Solution (0.1 M in $CDCl_3$)	Solid-state
C(1)	130.4	130.8[a]
C(2)	125.9	126.8
C(3)	125.6	125.1
C(4)	125.0	125.1
C(5)	126.9	126.8
C(6)	131.0	131.4[a]
C(7)	118.9	120.5
C(8)	152.5	156.1
C(9)	74.9	79.0
C(10)	71.9	78.1
C(11)	72.9	73.8[b]
C(12)	74.5	75.9
C(13)	149.8	149.5
C(14)	126.2	127.1
C(15)	126.2	127.1
C(16)	149.8	153.8
C(17)	74.5	67.2
C(18)	72.9	69.5[b]
C(19)	71.9	73.8[b]
C(20)	74.9	75.9
C(21)	152.5	156.1
C(22)	118.9	120.5
C(23)	131.0	131.4[a]
C(24)	126.9	126.8
C(25)	125.0	125.1
C(26)	125.6	125.1
C(27)	125.9	126.8
C(28)	130.4	130.7[a]

[a, b]Denotes possible assignment interchange.

tinction between C1 and C6 was also accomplished via HMBC, with the C6 shift of 131.0 ppm being identical to that in naphtho-9-crown-3 (2). Here the internal carbon C1 is again shielded, in this case by 0.6 ppm relative to the external C6 site. Finally, the remaining quaternary resonance at 126.2 ppm is attributed to C14.

The 50.3 MHz solid-state ^{13}C NMR spectrum of **2** is shown in Fig. 2. Due to the nonaveraged conformational situation in the solid, the spectrum is a good deal more complex than that observed in solution and some very interesting chemical shifts are observed. For example, in the aliphatic region, only four resonances are observed in solution, with chemical shifts ranging from 71.9 to 74.9 ppm. In contrast, the solid-phase spectrum shows six resolved peaks in the range of 67.2 to 79.0 ppm with relative intensities of approximately 1:1:2:2:1:1. The fact that there is disorder present at the C9/C9′ position in the crystal with a population ratio of ca. 3:1 (vide supra) will introduce some additional complexity into the spectrum. However, it is useful to attempt to assign the resonances based on their torsional environments, since previous work in this field has been remarkably successful with respect to crown ethers, particularly for benzo-9-crown-3 ether (4).

An important part of this discussion is based on the previous results (4) of ab initio calculations of the total shielding of the methyl group of anisole as a function of dihedral angle using a localized orbital local origin (LORG) approach. These results are depicted in Fig. 3.

From the X-ray crystal data, one can compare the two C*-O-C-C torsional environments of the C9, C12, C17, and C20 positions, since these are the sites in **2** that are similar to the methyl group of anisole. Then an estimate of the total relative shielding at each of these carbons can be obtained using Fig. 3. For example, the C12-O3-C13-C8 angle is 116.1°, which would give a total shielding of ca. 138 ppm. Similarly, the C12-O3-C13-C14 angle of 70.1° leads to a total shielding of ca. 137.5 ppm. Thus, the total relative shielding for C12 using this approach is expected to be (138.0 + 137.5 ppm) 275.5 ppm. In contrast, the C17-O4-C16-C21 torsion angle is 35.3°, leading to a total shielding of 142 ppm (Fig. 3). For the C17-O4-C16-C15 unit, the torsion angle is 150.9, also leading to a total shielding of ca. 142 ppm. Hence for C17, the contribution would be 142 + 142 = 284 ppm. A similar approach for C9 and C20 leads to values of ca. 272 and 276 ppm, respectively. Thus, a range of chemical shifts of ca. (284–272 ppm) 12 ppm is expected based on this approach, in excellent accord with our experiment. Accordingly, we assign the most shielded aliphatic carbon at 67.2 ppm to C17, and the most deshielded (at 79.0 ppm) to C9. The resonance at 75.9 ppm of relative intensity 2 is assigned to C12 and C20.

With regard to the remaining C10, C11, C18, and C19 sites, some ambiguity in the assignments exists. For C10, the resonance at 78.1 ppm has been assigned. This is because in naphtho-9-crown-3 (**1**), the corresponding carbon has an identical chemical shift in the solid state and the major form of the C8–C13 ring of **2** has essentially the same conformation as that present in **1**. For C11, C18, and C19, we have no clear method to distinguish their chemical shifts, hence the assignments for these carbons at 73.8 (intensity 2) and 69.5 ppm may be interchangeable as noted in Table 5.

Finally, for the quaternary carbons, three distinct resonances are observed in the solid-state spectrum at 156.1 (relative intensity 2), 153.8, and 149.5 ppm. In solution, C8 and C21 appear at 152.5 ppm, while C13 and C16 are at 149.8 ppm. Our assignments in these instances are C8 and C21 at 156.1 ppm, with a distinction between C13 and C16 being made on the basis of the C—O bond lengths in the X-ray crystal structure. The C16—O4 bond length is 1.359(4) Å, while the C13—O3 bond length is 1.369(3) Å. A shorter C—O bond accompanies more double-bond character and thus the carbon would be expected to be deshielded, based on the well-established chemical shift patterns in ^{13}C NMR spectra (5). Accordingly we assign the peak at 153.8 ppm to C16 and the resonance at 149.5 to C13.

Experimental

Materials

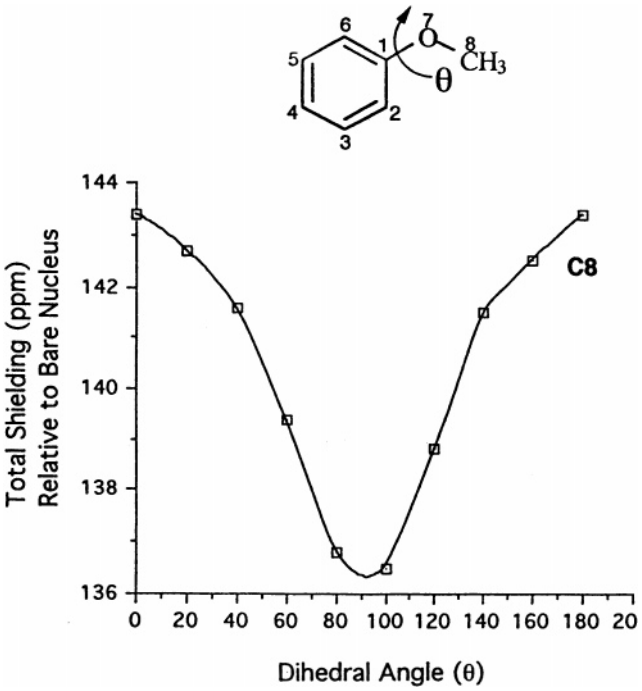
The following method was employed for the synthesis of **2**: $FeCl_3$ (9.01 g, 0.0561 mol), concentrated H_2SO_4 (0.5 mL), and dichloromethane (250 mL) were placed in a 500 mL round-bottom flask. To this was added, dropwise with stirring, naphtho-9-crown-3 ether (**1**) (4.30 g, 0.0187 mol) dissolved in dichloromethane (50 mL). The reaction mixture was heated at reflux for 24 h followed by slow addition of

© 2001 NRC Canada

Table 6. 9-Membered ring torsion angles (°) in **2** compared to naphtho-9-crown-3 (**1**).

C(16)–C(21) ring		C(8)–C(13) ring		Naphtho-9-crown-3
O(6)-C(20)-C(19)-O(5)	56.1	O(1)-C(9)-C(10)-O(2)	–80.8	–65.5
C(20)-C(19)-O(5)-C(18)	–112.9	C(9)-C(10)-O(2)-C(11)	123.9	116.0
C(19)-O(5)-C(18)-C(17)	67.6	C(10)-O(2)-C(11)-C(12)	–109.5	–119.5
O(5)-C(18)-C(17)-O(4)	70.5	O(2)-C(11)-C(12)-O(3)	62.0	70.7
C(18)-C(17)-O(4)-C(16)	–60.5	C(11)-C(12)-O(3)-C(13)	–110.2	–105.1
C(17)-O(4)-C(16)-C(21)	–35.3	C(12)-O(3)-C(13)-C(8)	116.1	104.8
O(4)-C(16)-C(21)-O(6)	4.7	O(3)-C(13)-C(8)-O(1)	5.5	1.6
C(16)-C(21)-O(6)-C(20)	114.5	C(13)-C(8)-O(1)-C(9)	–101.2	–112.4
C(21)-O(6)-C(20)-C(19)	–95.0	C(8)-O(1)-C(9)-C(10)	101.8	103.5

Fig. 3. LORG calculation of the angular dependence of total ^{13}C shielding for the methyl group of anisole.



methanol (100 mL) and heated at reflux for another 3 h. After cooling to room temperature, an additional 300 mL of dichloromethane was added and the solution was washed with distilled water (3 × 300 mL). The organic layer was dried over anhydrous sodium sulfate and after filtration the solvent was removed in vacuo to yield 4.2 g of a brown solid. This solid was boiled with hexane (3 × 200 mL), filtered, and dried in vacuo. Column chromatography over silica gel with dichloromethane–diethyl ether (1:9) afforded a light yellow oil, which changed to a solid upon trituration with diethyl ether. Recrystallization from dichloromethane–diethyl ether yielded 1.51 g (35.2%) of pure **2**, mp 209 to 210°C.

NMR spectra

Solution NMR spectra were recorded in $CDCl_3$ solution at 300 K using a Bruker AMX-400 instrument. An Aspect 3000 processing controller was used and all standard microprograms employed are in the Bruker software library.

For the heteronuclear multiple quantum correlation (HMQC) experiment, delays were set for couplings of 135 Hz, whereas for the heteronuclear multiple bond correlation (HMBC) experiment, delays were set for couplings of 7.5 Hz.

The solid-phase ^{13}C NMR spectra were recorded at 50.3 MHz at 300 K using a Bruker ASX-200 solid-state NMR spectrometer equipped with a Bruker 7 mm triple-resonance probe. The magic angle was set accurately using the ^{79}Br resonance of KBr and maximizing the number of rotational echoes in the FID. Magic-angle spinning rates were approximately 5 kHz. ^1H 90° pulses were 3.5–3.8 μs with contact times of 1 ms. Chemical shifts were referenced to the ^{13}C resonance of $Si(Si(CH_3)_3)_4$, which has a chemical shift of 3.7 ppm relative to TMS.

X-ray crystallographic studies and structure refinement[2]

Suitable crystals were selected and mounted on thin glass fibers using viscous oil. Data were collected on a Bruker AX SMART 1k CCD diffractometer using 0.3° scans at 0, 90, and 180°.

Unit-cell parameters were determined from 60 data frames collected at different sections of the Ewald sphere. Semi-empirical absorption corrections based on equivalent reflections were applied (6). The unit-cell parameters and systematic absences in the diffraction data are consistent with the space group $P2_1/n$. The structure was solved by direct methods, completed with difference Fourier syntheses and refined with full-matrix least-squares procedures based on F^2. Atoms O1 and C9 were found disordered with a refined site occupancy of 70/30. The presumed disorder at C10 could not be resolved. Disordered atoms were refined with major and minor contributions at common isotropic parameters. All other nonhydrogen atom positions were refined with anisotropic displacement parameters, and hydrogen atoms

[2] Supplementary material may be purchased from the Depository of Unpublished Data, Document Delivery, CISTI, National Research Council Canada, Ottawa, ON K1A 0S2, Canada. For information on obtaining material electronically go to http://www.nrc.ca/cisti/irm/unpub_e.shtml. Crystallographic information has also been deposited with the Cambridge Crystallographic Data Centre. Copies of the data can be obtained, free of charge, on application to the Director, CCDC, 12 Union Road, Cambridge CB2 1EZ, U.K. (fax: 44-1223-336033 or e-mail: deposit@ccdc.cam.ac.uk).

© 2001 NRC Canada

were treated as idealized contributions. All scattering factors are contained in the SHEXTL 5.1 program library.

Acknowledgments

GWB thanks the Natural Sciences and Engineering Research Council of Canada (NSERC) for continuing financial support. MFR thanks the Iranian Ministry of Education for a Fellowship.

References

1. G.W. Buchanan, M.F. Rastegar, and G.P.A. Yap. Can. J. Chem. **79**, 195 (2001).
2. A. Moghimi, M.F. Rastegar, M. Ghandi, G.W. Buchanan, and H. Rahbarnoohi. J. Mol. Struct. **526**, 185 (2000).
3. G.W. Buchanan, M.F. Rastegar, and G.P.A. Yap. J. Mol. Struct. **561**, 43 (2001).
4. G.W. Buchanan, A.B. Driega, A. Moghimi, C. Bensimon, R.A. Kirby, and T.D. Bouman. Can. J. Chem. **71**, 1983 (1993).
5. J.B. Stothers. Carbon-13 NMR spectroscopy. Academic Press, New York, N.Y. 1972.
6. R. Blessing. Acta Crystallogr. A, **A51**, 33 (1995).

© 2001 NRC Canada

Canadian Journal of Chemistry

Author Index
Volume 79, 2001

Revue canadienne de chimie

Index des auteurs
Volume 79, 2001

Abdur-Rashid, K., 964
Abraham, M.H., 1466
Acree, Jr., W.E., 1466
Adams, H., 731, 760
Agustinho, S.C.M., 760
Akim, L.G., 201
Albinati, A., 693
Albrecht, M., 709
Alexiou, C., 992
Alguindigue, S.S., 809
Alper, H., 587
Amoroso, D., 958
Anderson, C., 1477
Angelici, R.J., 578
Aragoni, M.C., 1483
Arakawa, H., 1415
Arca, M., 1483
Aresta, M., 570
Argyropoulos, D.S., 201, 1394
Armstrong, D.A., 405
Asadi, M., 70, 1360
Ashby, M.T., 809
Askalany, A.H., 42
Atwood, J.D., 1036
Aylward, W.M., 1
Baboulène, M., 1153
Bachmann, P., 519
Baerlocher, M.O., 1115
Baerlocher, F.J., 1115
Bailey, A.J., 792
Baines, K.M., 461
Baird, M.C., 1012
Baker, P.K., 263
Bakhmutov, V.I., 479
Bakhmutova, E.V., 479
Bakos, J., 725, 1040
Balakrishnan, V.K., 157
Balch, A.L., 922
Balci, M., 35
Ball, J.M., 304
Barba, V., 1229
Barthazy, P., 904
Bartosh, K., 1026
Bartosz-Bechowski, H., 752
Basickes, L., 854
Batchelor, R.J., 938, 1272
Batista, A.A., 1030
Battaglia, L., 621
Beagley, P., 731
Belchior, J.C., 211
Belkova, N.V., 479
Bennett, M.A., 655
Benson, G.C., 388
Bényei, A.C., 635
Bergens, S.H., 1019
Berges, J., 405
Bergman, R.G., 525
Berners-Price, S.J., 1030
Bertotti, M., 679
Besenyei, G., 649, 688
Bhattacharyya, S., 938
Bianchini, C., 479
Blanco, C.A., 448
Blaser, H.-U., 566
Boch, R., 1068
Bond, A.M., 613
Bonilla, R.J., 719
Bottomley, F., 1321
Boule, P., 1179
Bourgeois, M.-J., 257
Bowden, A.A., 1036
Boyd, S.E., 1030
Braga, J.P., 211
Brechbiel, M.W., 1105
Breed, P.G., 1049
Broggini, D., 904
Brouillard, R., 1173
Brown, J.M., 1049
Brown, M.A., 463
Bruce, D.W., 472
Buchanan, G.W., 195, 1505
Buckley, A.V., 1284
Buckley, R.W., 1030
Buncel, E., 157
Bunn, A.G., 854
Burford, N., 342
Butler, D.C.D., 472
Cadoret, J., 626
Cai, Z.-S., 29
Calderazzo, F., 495
Cameron, T.S., 342
Campagnole, M., 257
Cantin, A.M., 377
Cao, D., 455
Cao, S., 272
Carpenter, B.E., 291, 857
Carmona, J., 1447
Casagrande, B., 566
Casey, C.P., 1002
Castellano, E.E., 1030
Catellani, M., 742
Centoducatte, R., 121
Chapados, C., 13
Chen, L., 29
Chen, Y.-T., 221, 455
Chim, J.L.C., 607
Choi, H.Y., 337
Chomka, K., 760
Chow, A., 437
Chung, M.-K., 949
Ciunik, Z., 752, 868
Claver, C., 560
Cobos, J.C., 1447
Cole-Hamilton, D.J., 472
Colodette, J.L., 201
Cooper, L., 490
Cordes, A.W., 1352
Coulter, K.R., 930
Cowan, J.J., 792
Cromer, M., 370
Crowe, D.A.J., 1145
Cserépi-Szűcs, S., 725
Cuahutle, D., 1229
Cugini, F., 742
Das, P.K., 809
Dave, V., 461
Davies, P., 731
Davies, S.C., 490
Dawid, M., 110, 1294
de Almeida Santos, R.H., 679
de Blois, S., 13
de Castro, E.V.R., 121
de Vries, J.G., 1086
Dean, P.A.W., 1293, 1330
Decken, A., 1115, 1321
Delamere, C., 1492
Delaude, L., 529
Delmarre, D., 1068
del Rio, I., 560
Demchenko, A.P., 358
Demonceau, A., 529

© 2001 NRC Canada

den Reijer, C.J., 693
Devillanova, F.A., 1483
Dibenedetto, A., 570
Dileo, C., 570
Dilworth, J.R., 490
Dobó, A., 1040
Dolphin, D., 1068
dos Santos Silva, H.A., 679
Dotta, P., 693
Drake, J.E., 983
Drew, M.G.B., 263
Drouin, M., 1439
Durran, S.E., 780
Duś, D., 868
Dust, J.M., 157
Duval, P.B., 536
Dworschak, R.G., 437
Dyson, P.J., 705
Ebadi, M., 992
Einstein, F.W.B., 938, 1272
Ellena, J., 1030
Ellis, D.J., 705
Elzner, S., 593
Emmett, M.R., 546
Englert, U., 495
Ens, W., 437
Epstein, L.M., 479
Escher, E., 377
Evans, D.S., 263
Fabbri, D., 670
Fackler, J.P., Jr., 896
Fang, Q., 174
Farcas, S.I., 983
Farfán, N., 1229
Faria, R.B., 1135
Feng, J.-K., 1366
Ferguson, G., 949
Ferraro, J.R., 1483
Fish, R.H., 888
Fitzpatrick, S.J., 1101
Fleischer, M.A., 75
Fogg, D.E., 958
Fornika, R., 642
Fougerousse, A., 1173
Franco, D.W., 679
Fryzuk, M.D., 536, 1194
Fu, W., 1366
Funahashi, S., 1344
Gagnon, J., 1439
Gaisberger, B., 394
Gałęzowski, W., 1128
Gao, H., 578
Gao, Y., 915
Garcia de la Fuente, I., 1447
Gay, I.D., 1272
Gelbrich, T., 780
Geletti, Y.V., 792
Gill, M.A., 1101
Gillis, H.A., 80
Ghandi, M., 1505
Gladiali, S., 670
Gömöry, Á., 725
Gonzalez, E., 1173
Gonzalez, J.A., 1447
Görls, H., 642
Graziano, G., 105, 1310
Greaney, M., 546
Griffith, W.P., 598
Grundwald-Wyspiańska, M., 775
Grześkowiak, I., 1128
Guliński, J., 775
Gulyás, H., 1040
Gupta, R.N., 418
Haines, R.I., 54
Harrod, J.F., 1075
Hartman, J.S., 426
Harvey, P.D., 552, 1439
Hassan, A.A., 42
He, D., 1213
He, S., 510
He, W., 127
Healy, P.C., 1030
Hegedüs, C., 725
Hemscheidt, T., 418
Hendrickson, C.L., 546
Henry, B.R., 279
Herraiz-Sierra, I., 448
Hidai, M., 632
Hill, C.L., 792
Hill, J.M., 817
Hioka, N., 1068
Hiyama, T., 593
Hnatiw, J.B., 304
Holly, S., 649
Hook, J.M., 1330
Horikawa, Y., 388
Hou, Z., 29
Hsieh, Y.-H., 1272
Hu, T.Q., 1201
Huang, Y., 719
Hughes, D.L., 490
Hursthouse, M.B., 780, 983
Hutchings, D.R., 54
Ibrahim, M.S., 1431
Isaia, F., 1483
Iwatsuki, S., 1344
Jablonski, C., 463
Jafarpour, L., 626
Jakins, C., 1492
James, B.R., 1201
James, S.L., 709
Jamshid, K.A., 70
Jan, D., 529
Jarczewski, A., 1128
Jenkins, H.A., 1293, 1330
Jennings, M., 1330
Jennings, M.C., 915
Jensen, C.M., 823
Jessop, P.G., 719
Jezierski, A., 570
Jiang, M.H., 174
Jiang, X., 127
Joó, F., 635
Jorge, F.E., 121
Jurasek, L., 1394
Kashiwabara, K., 1344
Kenawy, I., 42
Kessler, M., 642
Khan, M.A., 830
Khomutov, O.G., 183
Kim, C.-K., 1238
Kinal, A., 35
King, J.F., 461
Kirby, C.W., 296
Kleinke, H., 1338
Kliegel, W., 226
Klymchenko, A.S., 358
Knoblauch, S., 977
Koch, H.F., 977
Kodess, M.I., 183
Konkol, M., 490
Koshino, N., 1344
Koteva, K.P., 377
Kovács, J., 635
Krisdhasima, V., 848
Krištofová, L., 1394
Krüger, C., 642
Kumamaru, K., 1422
Kurokawa, G.S., 1058
Lam, K.C., 342
Langner, R., 1376
Lau, M.-K., 607
Laurenczy, G., 635
Le, N., 238
LeBlanc, D.J., 342
Lee, D.W., 823
Lee, J., 830
Lee-Ruff, E., 114
Legzdins, P., 502
Leitner, W., 642
Lelj, F., 1483
Lemes, N.H.T., 211
Lemieux, R.U., 238
Leung, W.-H., 607
Lever, A.B.P., 992
Lewandowski, M., 775
Lewars, E., 1492
Leznoff, C.C., 878

© 2001 NRC Canada

Li, H.L., 328
Li, W., 1366
Li, Y.-N., 29
Light, M.E., 780, 983
Lightfoot, P., 472
Lin, H.-K., 221, 455
Ling, C.-C., 238
Lippolis, V., 1483
Liu, S., 1058
Long, G.S., 1026
Loop, I., 183
López, M.C., 1460
López-de-Luzuriaga, J.M., 896
Lord, G., 337
Lork, E., 183
Lough, A.J., 964
Lu, A.Z., 1201
Lu, B.C.-Y., 388
Lu, J., 127
Lu, X., 319, 364
Lubell, W.D., 94
Lubkowitz, G., 226
Lucas, R.J., 54
Luo, H., 1105
Ma, M., 1213
Macdonald, C.L.B., 342
Machado, S.P., 1135
Machuca-Herrera, J.O., 1135
MacRae, A.I., 1101
Magnuson, K., 823
Mahajan, D., 848
Mahiuddin, S., 1207
Mainar, A.M., 1460
Małecka, E., 775
Małgorzata, D., 1294
Malonga, H., 1415
Mamer, O., 1381
Mann, B.E., 760
March, R.E., 124
Marciniec, B., 775
Markó, L., 725
Marshall, A.G., 546
Martin, M., 519
Martinez, H.E., 50
Martinsson, A., 938
Masi, D., 479
Max, J.-J., 13
McAuley, A., 930
McComb, M.E., 437
McDonald, R., 291
McGarvey, B.R., 679
McGlinchey, M.J., 1295
Medici, S., 670
Meilleur, D., 552
Mele, G., 587
Menzek, A., 35
Merkley, N., 312
Meunier, L., 1179
Mezzetti, A., 904
Miller, D., 54
Miller, J.M., 1220, 1224
Mingie, J.R., 1352
Mitchell, T.R.B., 655
Mizobe, Y., 632
Moghimi, A., 1505
Moineau, C., 587
Montaudon, E., 257
Morales-Morales, D., 823
Mori, V., 679
Morlay, C., 370
Morris, R.H., 964
Mouginot, Y., 370
Moulik, S.P., 1
Murray, M.C., 1012
Nâdasdi, L., 635
Narracci, M., 570
Natansohn, A., 1093
Neault, J.F., 1415
Neil, M.A., 1321
Neszmélyi, A., 649
Netherton, M.R., 461
Neugebauer, W.A., 377
Ng, F.T.T., 817
Niesyty, K., 752
Nikolcheva, L.G., 1115
Noels, A.F., 529
Nolan, S.P., 626
Noll, B.C., 922
Norman, D.W., 1115
North, M.R., 75
Nozaki, K., 593
Oakley, R.T., 1352
Obeyama, K., 1344
Okajima, T., 22
Oleschuk, R.D., 437
Olmstead, M.M., 922
Opolski, A., 868
Orvig, C., 1058
Osmond, D.A., 1201
Ozturk, T., 358
Palepu, R., 1
Pampaloni, G., 495
Pan, P., 131
Panosyan, F.B., 1110
Papp, G., 635
Pardo, J.I., 1460
Park, D.K., 337
Park, Y.S., 337
Párkányi, L., 649
Parvez, M., 857
Pashkevich, K.I., 183
Passarelli, V., 495
Patrick, B.O., 1194, 1201
Pawliszyn, J., 1403
Perez-Encabo, A., 448
Perreault, H., 437
Peruzzini, M., 479
Petryk, M.W.P., 279
Phillips, A.D., 342
Phillips, S., 922
Piers, W.E., 291, 857
Pilichowski, J.-F., 1179
Pincock, J.A., 63
Pinna, F., 621
Pirri, G., 670
Pivovarenko, V.G., 358
Pokriefke, J.O., 226
Polydore, C., 977
Pope, M.T., 802
Povar, I., 1166
Powell, D.R., 830, 1002
Power, W.P., 296
Pregosin, P.S., 693
Preston, K.R., 437
Pruchnik, F.P., 868
Puddephatt, R.J., 915
Pulacchini, S., 670
Purcell, M., 1415
Qian, K., 546
Qian, X., 272
Qian, Y., 127
Queiroz, S.L., 1030
Quickenden, T.I., 80
Rabion, A., 888
Rajalingam, U., 1293, 1330
Ramnauth, J., 114
Ramos, J.F., 50
Ramsden, J.A., 1049
Rastegar, M.F., 195, 1505
Rauk, A., 405
Redón, R., 823
Reed, R.W., 1352
Reid, D.L., 319
Rettig, S.J., 226, 502, 536, 857, 930
Rheingold, A.L., 342
Richards, R.L., 490
Richardt, P.J.S., 613
Richter-Addo, G.B., 830
Riesco, N., 1447
Rifai, S., 63
Riggio, R., 50
Ro, S., 1238, 1259
Robertson, V., 949
Rocha, R.C., 145
Rochon, P., 1093
Rodgers, R.P., 546
Roehri-Stoeckel, C., 1173
Rogers, R.D., 1105

© 2001 NRC Canada

Rojas, A., 448
Röschenthaler, G.-V., 183
Rösler, R., 983
Rotar, A., 983
Roundhill, D.M., 977
Samonte, J.L., 802
Samuel, E., 1075
Sánchez, M.A., 1460
Sanders, J.R., 490
Santillan, R., 1229
Santos, C.M.P., 1135
Saraçoglu, N., 35
Sarvestani, A.H., 1360
Sauriol, F., 1381
Sayer, B.G., 418
Scheffer, J.R., 349
Schlaf, M., 949
Seino, H., 632
Sen, A., 1026
Serni, G., 495
Sevenard, D.V., 183
Seward, C., 1187
Shehetta, I., 42
Shehatta, I.S., 1431
Sheldon, R.A., 688
Shi, Y.-L., 328
Shi, Z., 1238, 1259, 1278
Shibahara, F., 593
Shoemaker, J.A.W., 426
Shu, R., 1075
Shubina, E.S., 479
Siebenhaar, B., 566
Silvestru, A., 983
Silvestru, C., 983
Simal, F., 529
Simándi, L.I., 649
Singer, S.W., 1002
Six, C., 642
Slawin, A.M.Z., 780
Smith, D.C., Jr., 626
Smith, K.M., 502
Smith, M.B., 780
Smith, P.J., 1145
Smith, S., 760
Snedeker, B., 1026
Sobota, P., 490
Solar, S., 394
Somogyi, L., 1159
Song, B., 1058
Song, G., 272
Song, H., 29
Song, J.H., 337
Souirti, S., 1153
Spek, A.L., 709
Spenser, I.D., 418
Spey, S., 760
Spinney, H.A., 1115
Spirlet, M.R., 529
Spohr, U., 238
Sproull, R.D., 848
Squires, C., 760
Standing, K.G., 437
Staples, R.J., 896
Stark, L., 342
Starosta, R., 868
Stefanova, R., 63
Sternberg, E., 1068
Stevens, E.D., 626
Stevens, M.R., 655
Still, I.W.J., 1110
Stojanovic, N., 1101
Strukul, G., 621
Studer, M., 566
Stynes, D.V., 795
Su, X.-C., 221, 455
Suchozak, B., 878
Sun, D.-A., 1381
Sun, H.-W., 221
Sun, Y., 1394
Suriaatmaja, M., 598
Suzuki, T., 1344
Swaddle, T.W., 75, 841
Symons, M.C.R., 124
Szöllősy, Á., 725
Tajmir-Riahi, H.A., 1415
Takagi, F., 632
Takagi, H.D., 1344
Tellers, D.M., 525
Thomas, C.A., 719
Tiefenthaler, D., 742
Toma, H.E., 145
Tommasi, I., 570
Tracey, A.S., 938
Tregloan, P.A., 613
Trotter, J., 226
Trzeciak, A.M., 752
Tsuzuki, H., 1422
Urieta, J.S., 1460
van Koten, G., 709
van Leeuwen, P.W.N.M., 560
vanLoon, G.W., 157
van Zyl, W.E., 896
Veilleux, A., 13
Veldman, N., 709
Venneri, P.C., 110, 312, 1294
Verani, G., 1483
Verspui, G., 688
Vézina, M., 1439
Vialemaringe, M., 257
Vincent, J.-M., 888
Vittori, O., 370
Vogels, C.M., 1115
Vorontsov, E.V., 479
Wagner, B.D., 1101
Wahab, A., 1207
Walsh, D., 342
Wang, C., 174
Wang, H., 1213
Wang, R., 495
Wang, S., 1187
Wang, Z., 328, 388, 823
Wang, X.M., 174
Warkentin, J., 110, 312, 319, 364, 1294
Wayland, B.B., 854
Wedd, A.G., 613
Wei, L., 94
Wei, Q.-L., 29
Weinberg, N., 1284
Weinstock, I.A., 792
Welton, T., 705
Werner, H., 519
Werner, M.L., 1026
Westaway, K.C., 1145
Westcott, S.A., 1115
White, C., 731
White, J.M., 613
Wietrzyk, J., 868
Wiles, J.A., 1019
Williams, I.D., 607
Willis, A.C., 655
Withers, S.G., 510
Wojdat, E., 868
Wolfe, S., 1238, 1259, 1272, 1278, 1284
Wong, A.W., 510
Wong, W.-T., 607
Woo, H.-G., 1075
Wu, B.-X., 29
Xie, Y., 127
Yachandra, V.K., 888
Yamato, T., 1422
Yan, P., 127
Yap, G.P.A., 195, 857, 958, 1505
Yi, G.-B., 830
Young, V.G., Jr., 1019
Yu, P., 1194
Yu, W.T., 174
Yung, C., 823
Zahir, K.O., 1124
Zamir, L.O., 1381
Zanobini, F., 479
Zhang, H., 1352
Zhang, H.-X., 1366
Zhao, G.-H., 221
Zhao, R., 131
Zhao, X., 174
Zhao, X.-Z., 29
Zhou, J., 841
Zhou, P., 1213

© 2001 NRC Canada

Zhou, Y.F., 174
Zhou, Z.-F., 221, 455
Zhu, S.-R., 221, 455
Zhuang, Q., 1220, 1224
Ziolkowski, J., 570
Ziólkowski, J.J., 752
Znamirowski, M., 437
Zobi, F., 795
Zundel, G., 1376

© 2001 NRC Canada

PREVIEW / APERÇU

Forthcoming special issues / Numéros spécials à paraître

November 2001	In honour of Professor Victor Snieckus
June 2002	In honour of Professor J. Bryan Jones
August 2002	In honour of Professor Ray Lemieux
November 2002	In honour of Professor Tris Chivers
June 2003	In honour of Professor Don Arnold

Forthcoming articles / Articles à paraître

Efficient and regioselective synthesis of bridged ring systems by domino Knoevenagel – hetero-Diels–Alder reaction	L.F. Tietze, C. Ott, and F. Haunert
Total synthesis of polyoximic acid	S. Hanessian and J. Fu
A highly efficient strategy for the synthesis of 3-substituted salicylic acids by either directed ortho-lithiation or halogen–metal exchange of substituted MOM-protected phenols followed by carboxylation	S.Y.W. Lau and B.A. Keay
Organometallic reactions in aqueous media — Antimony-mediated allylation of carbonyl compounds and the nature of allylstibine intermediates	L.-H. Li and T.K. Chan
The versatile reactivity of 2-aryl-4,6-dinitrobenzotriazole 1-oxides in Diels–Alder type condensations and in σ-complexation — A relationship between superelectrophilicity and pericyclic reactivity	D. Vichard, T. Boubaker, F. Terrier, M.-J. Pouet, J.M. Dust, and E. Buncel
Stereoscopic studies of the electrophilic activation of amides with triflic anhydride and pyridine	A.B. Charette and M. Grenon
Absolute stereochemistry of the spiroxins	T. Wang, O. Shirota, K. Nakanishi, N. Berova, L.A. McDonald, L.R. Barbieri, and G.T. Carter
Studies on enolate chemistry of 8-thiabicyclo[3.2.1]octan-3-one — Enantioselective deprotonation and synthesis of sulfur analogs of tropane alkaloids	M. Majewski, M. DeCaire, P. Nowak, and R. Wang
Attempted enantiotopic group seletive cyanohydrin formation from α-alkoxy aldehydes by double stereodifferentiation	D.E. Ward, M. Sales, and M.J. Hrapchak
Synthesis of substituted phenols by directed *ortho*-lithiation of in situ *N*-silyl-protected *O*-aryl *N*-monoalkylcarbamates	M. Kauch and D. Hoppe
Synthesis of trichiliasterones A and B — 16-Ketosteroids isolated from *Trichilia hirta* and *Trichilia americana*	S.M. Hantos, S. Tripathy, N. Alibhai, and T. Durst
Applications of crotyldiisopinocampheylboranes in synthesis — A formal total synthesis of (+)-calyculin A	O.P. Anderson, A.G.M. Barrett, J.J. Edmunds, S.-I. Hachiya, J.A. Hendrix, K. Horita, J.W. Malecha, C.J. Parkinson, and A. VanSickle
The total synthesis of (+)-aspicilin using 2,3-butane diacetal protected butane tetrols via a chiral memory protocol	D.J. Dixon, A.C. Foster, and S.V. Ley
Traceless solid-phase synthesis of 5-benzoylbenzimidazoles	K.J. Lee and K.D. Janda

© 2001 NRC Canada

National Research Council Canada
Ottawa, Canada K1A 0R6

Conseil national de recherches Canada
Ottawa, Canada K1A 0R6

Postage paid at Ottawa
Publications mail
Registration No. 1240447

Port payé à Ottawa
Poste-publication
Enregistrement n° 1240447

Canadian Journal of Chemistry

Volume 79, Number 11, November 2001

Revue canadienne de chimie

Volume 79, numéro 11, novembre 2001

This issue is dedicated to Professor Victor Snieckus
Ce tirage est dédié au Professeur Victor Snieckus

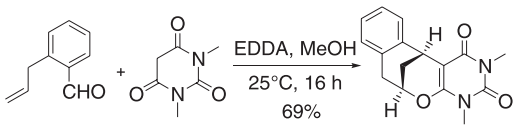
Dedication iii
Bibliography v

Dédicace iii
Bibliographie v

Efficient and regioselective synthesis of bridged ring systems by domino Knoevenagel – hetero-Diels–Alder reaction

Lutz F. Tietze, Christian Ott, and Frank Haunert

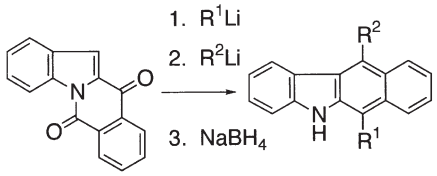
1511–1514



A synthesis of 6,11-disubstituted benzo[*b*]carbazoles

Heidi L. Fraser and Gordon W. Gribble

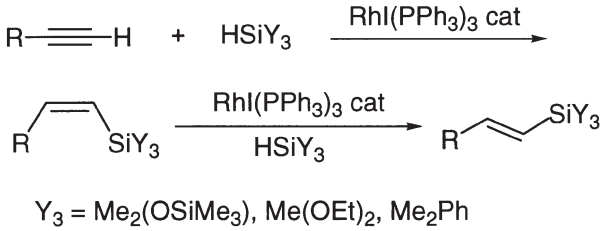
1515–1521



Isomerization of (*Z*)-alkenylsilanes to (*E*)-isomers with hydrosilane and $RhI(PPh_3)_3$

Atsunori Mori, Eisuke Takahisa, Yasushi Nishihara, and Tamejiro Hiyama

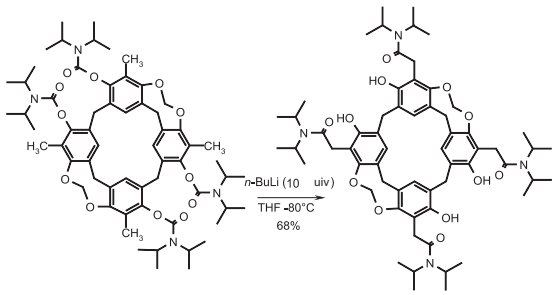
1522–1524



Fourfold homologous anionic *ortho*-Fries rearrangement on a partially bridged resorc[4]arene

Oskar Middel, Willem Verboom, and David N. Reinhoudt

1525–1527



Continued on inside back cover / Suite au verso

Canada

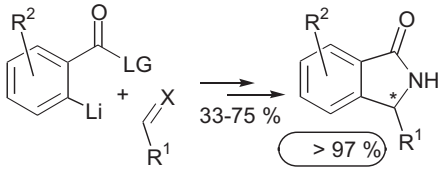
Printed in Canada by / Imprimé au Canada par
University of Toronto Press Inc.
Typesetting by / Typographie par
NRC Research Press / Presses scientifiques du CNRC

000 -4042 200111 79 11 1-

Asymmetric synthesis of 3-aryl-substituted 2,3-dihydro-1*H*-isoindol-1-ones

Dieter Enders, Volker Braig, and Gerhard Raabe

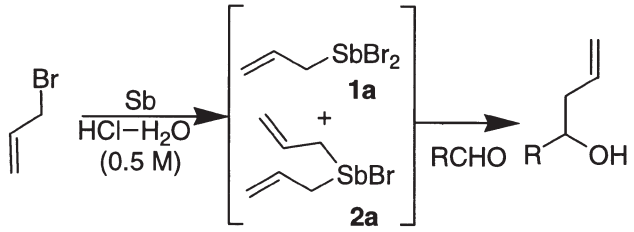
1528–1535



Organometallic reactions in aqueous media — Antimony-mediated allylation of carbonyl compounds and the nature of allylstibine intermediates

Lian-Hai Li and Tak Hang Chan

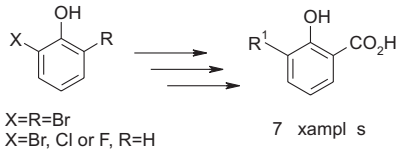
1536–1540



A highly efficient strategy for the synthesis of 3-substituted salicylic acids by either directed *ortho*-lithiation or halogen–metal exchange of substituted MOM protected phenols followed by carboxylation.

Stephen Y.W. Lau and Brian A. Keay

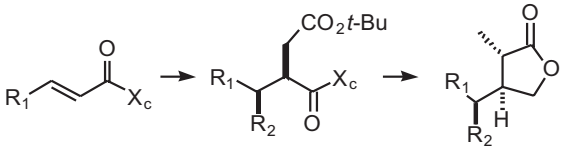
1541–1545



Enantioselective synthesis of peperomins A, C, D, and analogs — Examination of diastereoselective cuprate conjugate additions to *N*-enoyl-4-diphenylmethyl-2-oxazolidinones

Mukund P. Sibi, Michael D. Johnson, and T. Punniyamurthy

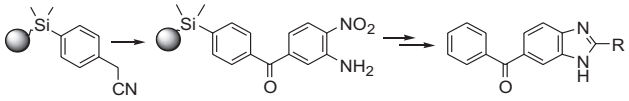
1546–1555



Traceless solid-phase synthesis of 5-benzoylbenzimidazoles

Kyung Joo Lee and Kim D. Janda

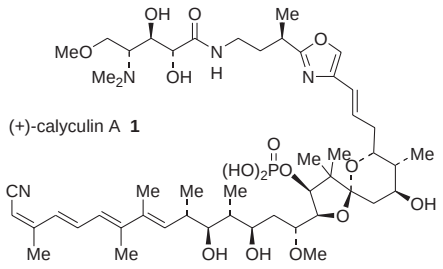
1556–1561



Applications of crotyldiisopinocampheylboranes in synthesis: a formal total synthesis of (+)-calyculin A

Oren P. Anderson, Anthony G.M. Barrett, Jeremy J. Edmunds, Shun-Ichiro Hachiya, James A. Hendrix, Kiyoshi Horita, James W. Malecha, Christopher J. Parkinson, and Andrew VanSickle

1562–1592

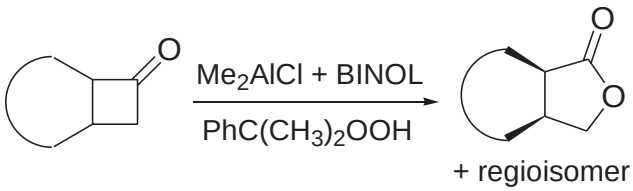


Continued on facing page / Suite à la page précédente

Chiral aluminum complexes as catalysts in asymmetric Baeyer-Villiger reactions of cyclobutanones

Carsten Bolm, Oliver Beckmann, and Chiara Palazzi

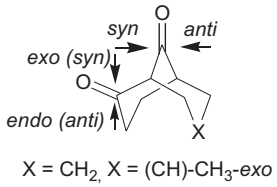
1593–1597



Stereoelectronic and conformational effects on the stereochemical course of reduction of bicyclo[3.3.1]nonane 1,3-diketones

Eugenius Butkus, Arvydas Stončius, Julė Malinauskienė, Shuji Tomoda, and Daisuke Kaneno

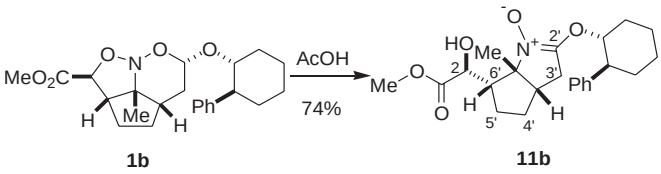
1598–1605



Studies on the reduction and hydrolysis of nitroso acetals

Scott E. Denmark, Vito Guagnano, and Jean Vaugeois

1606–1616



The versatile reactivity of 2-aryl-4,6-dinitrobenzotriazole 1-oxides in Diels–Alder type condensations and in σ-complexation — A relationship between superelectrophilicity and pericyclic reactivity

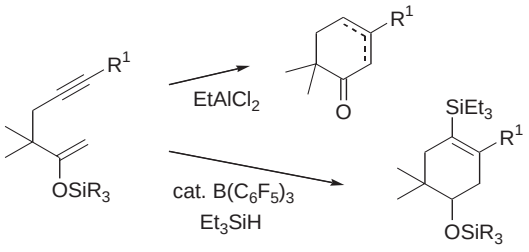
Dominique Vichard, Taoufik Boubaker, François Terrier, Marie-José Pouet, Julian M. Dust, and Erwin Buncel

1617–1623

Lewis acid-mediated intramolecular addition of silyl enol ethers to internal unactivated alkynes

Ken-ichiro Imamura, Eiji Yoshikawa, Vladimir Gevorgyan, Tomoko Sudo, Naoki Asao, and Yoshinori Yamamoto

1624–1631

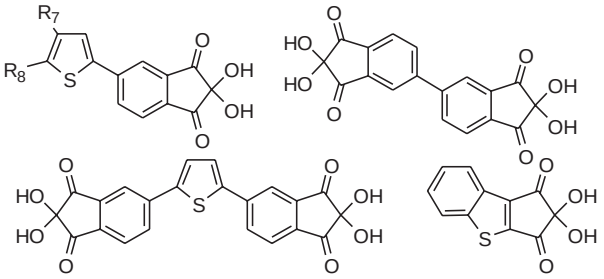


Continued on previous page / Suite à la page précédente

Synthetic studies of novel ninhydrin analogs

Richard R. Hark, Diane B. Hauze, Olga Petrovskaia, and Madeleine M. Joullié

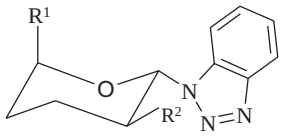
1632–1654



An ^{1}H and ^{13}C NMR conformational study of 2-(benzotriazol-1-yl)-substituted tetrahydropyrans

Alan R. Katritzky, Novruz G. Akhmedov, Sergey N. Denisenko, and Subbu Perumal

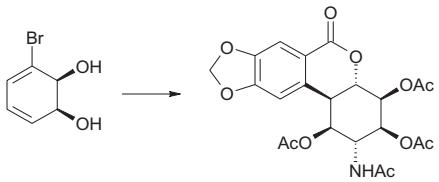
1655–1658



Structure assignment of aminoconduritols by ^{15}N NMR correlation spectroscopy; synthesis of a positional isomer of 7-deoxypancratistatin

Stefan Schilling, Uwe Rinner, Collin Chan, Ion Ghiviriga, and Tomas Hudlicky

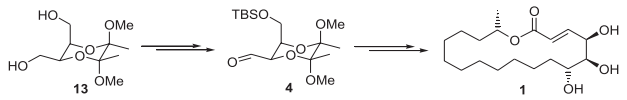
1659–1667



The total synthesis of (+)-aspicilin using 2,3-butane diacetal protected butane tetrols via a chiral memory protocol

Darren J. Dixon, Alison C. Foster, and Steven V. Ley

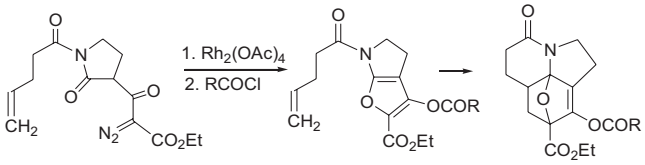
1668–1680



Cyclization–cycloaddition cascades for the construction of azapolycyclic ring systems

Albert Padwa, William S. Kissell, and Cheryl K. Eidell

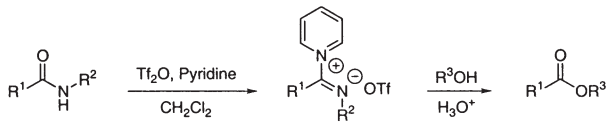
1681–1693



Spectroscopic studies of the electrophilic activation of amides with triflic anhydride and pyridine

André B. Charette and Michel Grenon

1694–1703

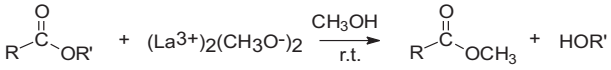


Continued on facing page / Suite à la page précédente

Catalysis of transesterification reactions by lanthanides — Unprecedented acceleration of methanolysis of aryl and alkyl esters promoted by $La(OTf)_3$ at neutral $^{s}_{s}$pH and ambient temperatures

Alexei. A. Neverov, Todd McDonald, Graham Gibson, and R.S. Brown

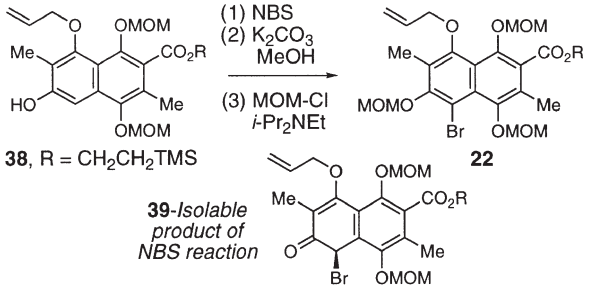
1704–1710



Synthesis of highly functionalized naphthoate precursors to damavaricin D — Observation of kinetically stable benzocyclohexadienones in the bromination reactions of highly functionalized β-naphthol derivatives

William R. Roush, David J. Madar, and D. Scott Coffey

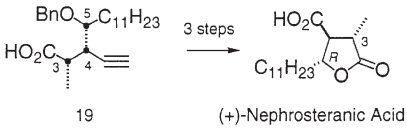
1711–1726



Enantioselective syntheses of (+)- and (–)-nephrosteranic acid employing the Nicholas–Schreiber reaction

Peter A. Jacobi and Prudencio Herradura

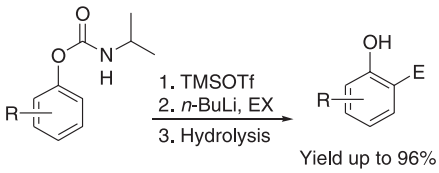
1727–1735



Synthesis of substituted phenols by directed *ortho*-lithiation of in situ *N*-silyl-protected *O*-aryl *N*-monoalkylcarbamates

Matthias Kauch and Dieter Hoppe

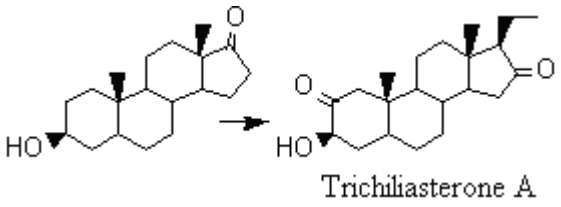
1736–1746



Synthesis of trichiliasterones A and B — 16-Ketosteroids isolated from *Trichilia hirta* and *Trichilia americana*

Susanne M. Hantos, Sasmita Tripathy, Najma Alibhai, and Tony Durst

1747–1753

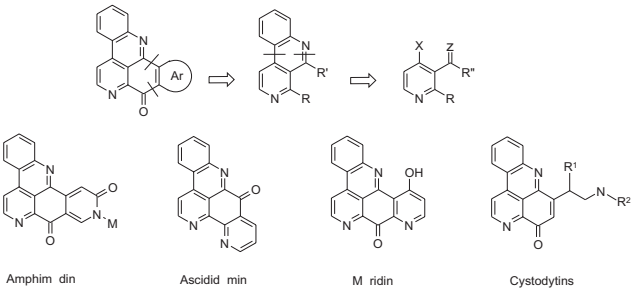


Continued on previous page / Suite à la page précédente

Ortho-directed metallation of π-deficient heterocycles in connection with palladium-catalyzed biaryl cross-coupling — Synthesis of marine alkaloids of the pyridoacridine series

A. Godard, P. Rocca, F. Guillier, G. Duvey, F. Nivoliers, F. Marsais, and G. Quéguiner.

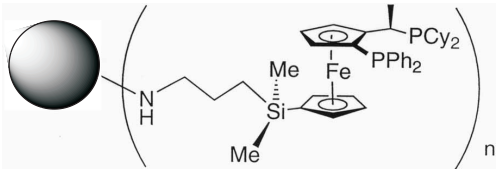
1754–1761



Synthesis, characterization, and application in asymmetric catalysis of dendrimers containing chiral ferrocenyl diphosphines

Christoph Köllner and Antonio Togni

1762–1774



Attempted enantiotopic group selective cyanohydrin formation from α-alkoxy aldehydes by double stereodifferentiation

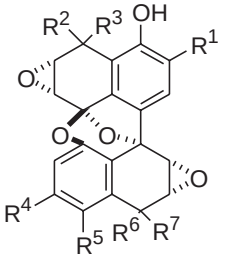
Dale E. Ward, Marcelo Sales, and Matthew J. Hrapchak

1775–1785

Absolute stereochemistry of the spiroxins

Tao Wang, Osamu Shirota, Koji Nakanishi, Nina Berova, Leonard A. McDonald, Laurel R. Barbieri, and Guy T. Carter

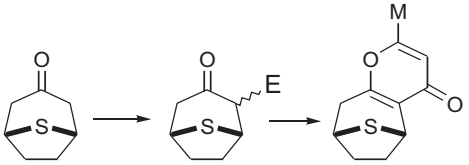
1786–1791



Studies on enolate chemistry of 8-thiabicyclo[3.2.1]-octan-3-one: enantioselective deprotonation and synthesis of sulfur analogs of tropane alkaloids

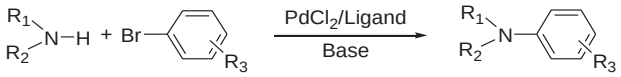
Marek Majewski, Marc DeCaire, Pawel Nowak, and Fan Wang

1792–1798



Concluded on facing page / Suite et fin à la page précédente

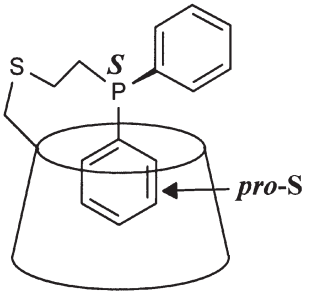
The use of palladium chloride as a precatalyst for the amination of aryl bromides



Xiao-Xiang Zhang, Michele C. Harris, Joseph P. Sadighi, and Stephen L. Buchwald

1799–1805

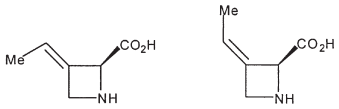
Diastereotopic group recognition in the solid state — A unique intramolecular β-cyclodextrin inclusion complex



Manfred T. Reetz, Joachim Rudolph, and Richard Goddard

1806–1811

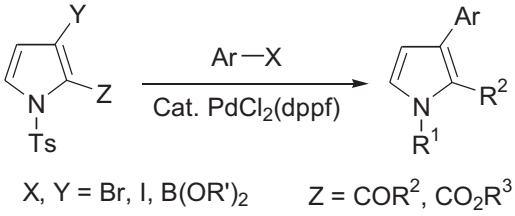
Total synthesis of polyoximic acid



Stephen Hanessian and Jian-min Fu

1812–1826

Studies of palladium-catalyzed coupling reactions for preparation of hindered 3-arylpyrroles relevant to (–)-rhazinilam and its analogues



Léon Ghosez, Cécile Franc, Frédéric Denonne, Claire Cuisinier, and Roland Touillaux

1827–1839

The Canadian Journal of Chemistry is affiliated with the Canadian Society for Chemistry and publishes papers in all areas of chemistry.

La Revue canadienne de chimie est affiliée à la Société canadienne de chimie et publie des articles dans tous les domaines de la chemie.

Efficient and regioselective synthesis of bridged ring systems by domino Knoevenagel – hetero-Diels–Alder reaction

Lutz F. Tietze, Christian Ott, and Frank Haunert

Abstract: The bridged heterocycles **10**–**12** were efficiently prepared by a domino Knoevenagel – hetero-Diels–Alder reaction of *N*,*N*′-dimethylbarbituric acid **2** and the aldehydes **6**–**8** which contain an allyl moiety as dienophile. In contrast, reaction of **2** and aldehyde **5** with a dimethylallyl moiety leads to the annulated product **9.** For the formation of **10**–**12,** an *exo-Z-syn* and for that of **9** an *endo-E-syn* transition structure is proposed.

Key words: bridged compounds, domino reaction, Diels–Alder reaction, heterocycles, Knoevenagel reaction.

Résumé : On a préparé de façon efficace les hétérocycles pontés **10**–**12** par le biais d'une réaction de Knoevenagel – hétéro-Diels–Alder en domino de l'acide *N*,*N*′-diméthylbarbiturique (**2**) avec les aldéhydes **6**–**8** qui contiennent une partie allylique agissant comme diénophile. Par ailleurs, la réaction du composé **2** avec l'aldéhyde **5** qui contient une partie diméthylallylique conduit à la formation du produit **9** résultant d'une annellation. Pour la formation des composés **10**–**12**, on suggère l'implication d'une structure de transition *exo-Z-syn* alors que celle impliquée dans la formation du produit **9** serait *endo-E-syn*.

Mots clés : composés pontés, réaction en domino, réaction de Diels–Alder, hétérocycles, réaction de Knoevenagel.

[Traduit par la Rédaction]

Introduction

The domino Knoevenagel – hetero-Diels–Alder reaction (reviews, see ref. 1), which was introduced by us as a powerful sequential transformation, has been proven to be a valuable method for the construction of heterocyclic ring systems (2). The reaction can be performed as a two-, three- or four-component transformation using an aldehyde, a 1,3-dicarbonyl, or a hetero-analogous compound and an enol ether or alkene as a dienophile. For the two-component transformation, any type of aromatic aldehyde such as substituted benzaldehydes, heteroaromatic aldehydes, or aliphatic aldehydes containing a double bond in the side chain can be employed to give annulated compounds. The transformations are highly stereoselective leading either to the *cis*-annulated heterocycles with aromatic and α,β-unsaturated aliphatic aldehydes or to the *trans*-annulated compounds with aliphatic aldehydes (2). Thus, reaction of the aromatic aldehyde **1** with *N*,*N*′-dimethylbarbituric acid **2** at room temperature gives exclusively the *cis*-fused tetracycle **4** via **3** in 91% yield (Scheme 1) (3).

So far this domino reaction has been used mostly for the generation of annulated five- to seven-membered ring systems; however; it is also very suitable for the synthesis of bridged heterocycles as described in this paper (4).

Results and discussion

In the domino Knoevenagel – hetero-Diels–Alder reaction of **1** and **2**, a 1-oxa-1,3-butadiene **3** is formed first which undergoes a hetero-Diels–Alder reaction (5) with inverse electron demand. Since the regioselectivity of the cycloaddition is controlled by the coefficients at the dienophile according to the Klopman–Salem eq. [6], a change of the substituents at the dienophile should allow a switch from annulated to bridged products.

For the synthesis of the desired bridged heterocycles we prepared the aromatic and aliphatic aldehydes **6**–**8** with an allyl moiety as dienophile; in addition we have also synthesized aldehyde **5** with a dimethylallyl group as a side chain (Fig. 1). 2-(3-Methyl-3-butenyl)-benzaldehyde **5** and 2-allylbenzaldehyde **6** were easily accessible from 2-bromo-benzaldehyde by formation of an acetal, successive Stille-coupling with the corresponding stannane reagents, and cleavage of the acetal (7). The aliphatic 2-allyl-carbaldehydes **7** and **8** were prepared by allylation and successive oxy-Cope-rearrangement of the corresponding 1-cycloalkene-1-carbaldehydes (8).

First, aldehyde **5** was treated with *N*,*N*′-dimethylbarbituric acid **2** in methanol in the presence of catalytic amounts of ethylenediammonium diacetate (EDDA) for 16 h at room temperature. As expected, the annulated five-membered

Received October 10, 2000. Published on the NRC Research Press Web site at http://canjchem.nrc.ca on October 18, 2001.

Dedicated to Professor Vic Snieckus, a good friend and an excellent scientist who has contributed so much to chemistry.

L.F. Tietze,[1] C. Ott, and F. Haunert. Institut für Organische Chemie der Georg-August Universitat Göttingen, Tammannstrasse 2, D-37077 Göttingen, Germany.

[1]Corresponding author (telephone: (49) 551393271/72; fax: 49 551 3994 76; e-mail: ltietze@gwdg.de).

 DOI: 10.1139/cjc-79-11-1511 © 2001 NRC Canada

Scheme 1. Synthesis of the *cis*-annulated tetracyclic dihydropyran **4**.

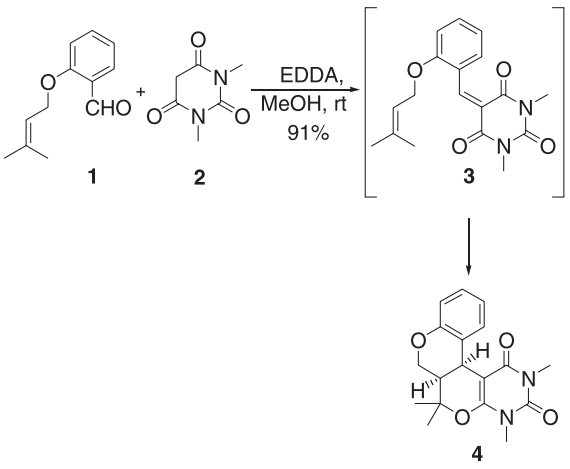
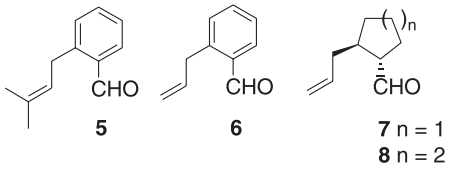


Fig. 1. Substrates for the domino Knoevenagel – hetero-Diels–Alder reaction.



heterocycle **9** was obtained exclusively in 51% yield (Scheme 2). This result is consistent with the large HOMO-coefficient at the terminal carbon of the dienophile moiety in **5**. However, for the regioselectivity of the hetero-Diels–Alder reaction steric effects may also play a role. We assume that the cycloaddition proceeds in a concerted way via an *endo-E-syn* transition structure (Fig. 2) (3).

In contrast, the domino Knoevenagel – hetero-Diels–Alder reaction of **6**, **7**, and **8** with *N*,*N*′-dimethylbarbituric acid **2** in methanol at room temperature with ethylenediammonium acetate as catalyst efficiently provided the novel bridged heterocycles **10**–**12** in 43–69% yield (Scheme 3).

The domino process is highly regioselective, thus, formation of the bridged cycloadducts was observed exclusively. This result is again in agreement with the expectation since the HOMO-coefficient at the terminal carbon of the dienophile should now be much smaller. Here we propose an *exo-Z-syn* transition structure for the hetero-Diels–Alder reaction of the 1-oxa-1,3-butadiene to give a *meta*-addition (Fig. 2) (9). Thus, the intermediate formed benzylidene- and alkylidene-1,3-dicarbonyl compounds have the unique feature that they are not only highly activated 1-oxa-1,3-butadienes due to the second carbonyl group, but they also contain a (*Z*)- and an (*E*)-1-oxa-1,3-butadiene moiety in the same molecule which both can undergo a reaction.

Structure elucidation

The structures of the newly formed compounds were mainly determined by NMR spectroscopy. Exemplary, the ^{1}H and ^{13}C NMR spectra of the bridged heterocycles **10** and **11** are discussed. In the ^{1}H NMR spectrum of **10** the signals

Scheme 2. Synthesis of the *cis*-annulated cycloadduct **9**.

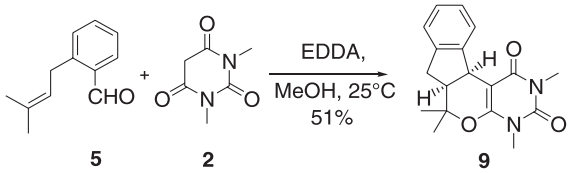
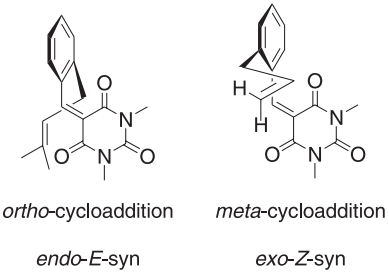
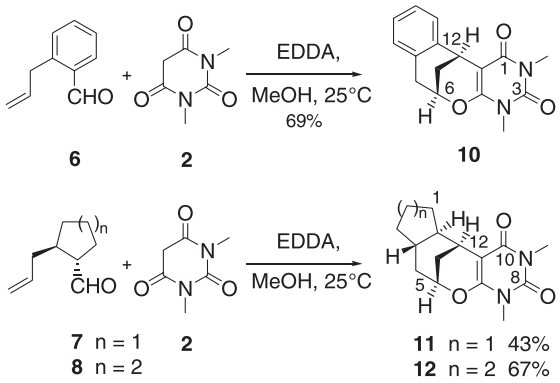


Fig. 2. Proposed transition structures for the *ortho*- and *meta*-cycloaddition.



Scheme 3. Synthesis of the bridged heterocycles **10**–**12**.



for the diasterotopic protons at C-13 are found at δ = 1.34 and δ = 1.43 with a large geminal coupling of J = 14.3 Hz. 12-H resonates as dd at δ = 4.15 with J = 3.1 and 2.0 Hz. In the ^{13}C NMR spectrum, the resonance for the tertiary carbon C-6 is found at δ = 74.8. In the ^{1}H NMR spectrum of **11**, the signals for 11-H and 5-H are observed as a multiplet at δ = 2.94 and as a ddd at δ = 5.03 with J = 9.2, 3.4, 1.9 Hz, respectively. 4-H_{eq} resonates at δ = 2.48 with J = 13.0, 9.2, and 3.4 Hz and one of the diasterotopic protons of the methano-bridge (C-12) at δ = 1.46 as dt with a large geminal (J = 13.9 Hz) and two smaller vicinal couplings (J = 3.4 Hz). The signal of the second 12-H is shielded in a multiplet at δ = 1.93–2.05 but definitely identified by a ^{1}H–^{1}H-COSY experiment. In the ^{13}C NMR spectrum, the tertiary carbon C-5 resonates at δ = 76.1 and thus confirms the bridged structure of **11**.

Experimental

All reactions were performed under nitrogen or argon atmosphere in flame-dried flasks, and the reactants were introduced by syringe. All solvents were dried by standard methods. All reagents obtained from commercial sources were used without further purification. Thin-layer chroma-

© 2001 NRC Canada

tography (TLC) was performed on precoated silica gel SIL G/UV_{254} plates (Macherey-Nagel GmbH & Co. KG), and silica gel 32–63 (0.032–0.064 mm) (Macherey-Nagel GmbH & Co. KG) was used for column chromatography. UV–vis spectra were taken in CH_3CN with a PerkinElmer Lambda 2 spectrometer. IR spectra were recorded as KBr pellets or as films with a Bruker IFS 25 spectrometer. ^1H and ^{13}C NMR spectra were recorded with a Varian XL 200, VXR 200, and VXR 500 or a Bruker AMX-300 with tetramethylsilane (TMS) as internal standard in chloroform-d_1 or benzene-d_6. Multiplicities of ^{13}C NMR peaks were determined with the APT pulse sequence. Mass spectra were measured at 70 eV with a Varian MAT 311A, high-resolution mass spectra with a Varian MAT 731 instrument. Melting points are uncorrected and were measured with a Mettler FP 61. The following abbreviations are used in the text: DE = diethyl ether, EE = ethyl acetate, PE = petroleum ether, EDDA = ethylenediammonium diacetate.

(6*aS*,11*bR*)-(±)-2,4,6,6-Tetramethyl-6,6*a*,7,11*b*-tetrahydro-4*H*-5-oxa-2,4-diaza-benzo[*c*]fluorene-1,3-dione (9)

A solution of aldehyde **5** (331 mg, 1.90 mmol) in CH_2Cl_2 (1 mL) was slowly added to a suspension of *N*,*N*′-dimethylbarbituric acid (312 mg, 2.00 mmol) and 20 mg EDDA in dry methanol (10 mL) and the reaction mixture was stirred 16 h at room temperature. The solvent was evaporated in vacuo and the crude product purified by column chromatography (EE:PE = 1:1) to give 302 mg of **9** (0.97 mmol, 51% yield). R_f = 0.26 (EE:PE = 1:2). MS (70 eV, EI) *m*/*z* (%): = 312 (100) [M^+], 297 (80) [M^+ – CH_3], 156 (63) [$C_6H_8N_2O_3^+$], 41 (43) [$C_3H_5^+$]. UV (CH_3CN) λ_{max} (log ε) (nm): 265 (3.98). IR (film) (cm^{-1}) = 3020, 2998, 2930 (C-H), 1706 (C=O), 1648, 1626 (C=C), 1478, 1460 (CH_2, CH_3). ^1H NMR (300 MHz, $CDCl_3$) δ: 1.42 (s, 3 H, 6-CH_3), 1.46 (s, 3 H, 6-CH_3), 2.77 (q, *J* = 8.2 Hz, 1 H, 6*a*-H), 2.98 (m, 2 H, 7-H_2), 3.30 (s, 3 H, N-CH_3), 3.32 (s, 3 H, N-CH_3), 4.28 (d, *J* = 8.2 Hz, 1 H, 11*b*-H), 7.11–7.22 (m, 3 H, 8-H, 9-H, 10-H), 7.36–7.43 (m, 1 H, 11-H). ^{13}C NMR (125.7 MHz, $CDCl_3$) δ: 25.3 (6-CH_3), 25.7 (6-CH_3), 27.9 (N-CH_3), 28.6 (N-CH_3), 33.1 (C-7), 38.7 (C-11*b*), 48.1 (C-6*a*), 82.28 (C-6), 88.8 (C-11*c*), 123.9 (C-8), 126.5 (C-9), 127.2, 127.8 (C-10, C-11), 141.2 (C-11*a*), 143.6 (C-7*a*), 151.1 (C-3), 154.7 (C-4*a*), 162.9 (C-1). Anal. calcd. $C_{18}H_{20}N_2O_3$ (312.4): 312.1474; found: 312.1473.

(6*S*,12*R*)-(±)-6,12-Methano-2,4-dimethyl-4,6,7,12-tetrahydro-5-oxa-2,4-diaza-dibenzo[*a*,*d*]cyclooctene-1,3-dione (10)

A solution of aldehyde **6** (190 mg, 1.30 mmol) in CH_2Cl_2 (1 mL) was slowly added to a suspension of *N*,*N*′-dimethylbarbituric acid (234 mg, 1.50 mmol) and 20 mg EDDA in dry methanol (10 mL) and the reaction mixture was stirred 16 h at room temperature. The solvent was evaporated in vacuo and the residue purified by column chromatography (EE:PE = 1:1) to give 256 mg of **10** (0.90 mmol, 69% yield); mp 176°C. R_f = 0.29 (EE:PE = 1:1). MS (70 eV, EI) *m*/*z* (%): 283 (100) [M^+ – H], 43 (37) [$C_3H_7^+$]. UV (CH_3CN) λ_{max} (log ε) (nm): 264 (3.92). IR (film) (cm^{-1}): 3010, 2942, 2928 (C-H), 1700 (C=O), 1632 (C=C), 1464 (CH_2, CH_3). ^1H NMR (300 MHz, C_6D_6) δ: 1.34 (ddd, *J* = 14.3, 3.1, 2.0 Hz, 1 H, 13-H), 1.43 (dtd, *J* = 14.3, 4.2, 1.0 Hz, 1 H, 13-H), 2.60–2.66 (m, 2 H, 7-H_2), 2.80 (s, 3 H, N-CH_3), 3.25 (s, 3 H, N-CH_3), 4.15 (dd, *J* = 4.2, 3.1 Hz, 1 H, 12-H), 4.32 (m, 1 H, 6-H), 6.82 (d, *J* = 7.5 Hz, 1 H, 8-H), 6.93–7.07 (m, 2 H, 9-H, 10-H), 7.88 (dd, *J* = 7.5, 1.0 Hz, 1 H, 11-H). ^{13}C NMR (50.3 MHz, $CDCl_3$) δ: 26.9 (C-13), 27.3 (C-12), 27.9 (N-CH_3), 28.5 (N-CH_3), 36.9 (C-7), 74.8 (C-6), 92.1 (C-12*a*), 126.4, 126.5 (C-9, C-10), 128.1, 128.8 (C-8, C-11), 130.4 (C-11*a*), 140.6 (C-7*a*), 150.8 (C-3), 155.1 (C-4*a*), 161.6 (C-1). Anal. calcd. $C_{16}H_{16}N_2O_3$ (284.3): C 67.59, H 5.57; found: C 67.59, H 5.67.

(3*aS*,5*R*,11*R*,11*aR*)-(±)-5,11-Methano-7,9-dimethyl-2,3,3*a*,4,5,7,11,11*a*-octahydro-1*H*-6-oxa-7,9-diaza-benzo[*a*]cyclopenta[*d*]cyclooctene-8,10-dione (11)

A solution of aldehyde **7** (333 mg, 2.41 mmol) in CH_3CN (1 mL) was slowly added to a suspension of *N*,*N*′-dimethylbarbituric acid (390 mg, 2.50 mmol) and 12 mg EDDA in dry acetonitrile (20 mL) and the reaction mixture was stirred 2 h at room temperature (formation of the Knoevenagel product) and then heated for 30 h at reflux. The solvent was evaporated in vacuo and the crude product purified by column chromatography (EE:PE = 1:2) to give 286 mg of **11** (1.04 mmol, 43% yield) as colorless crystals; mp 128°C. R_f = 0.18 (EE:PE = 1:2). MS (70 eV, EI) *m*/*z* (%): 276 (94) [M^+], 193 (100) [M^+ – C_6H_{11}]. UV (CH_3CN) λ_{max} (log ε) (nm): 263 (3.96). IR (film) (cm^{-1}): 2954, 2930 (C-H), 1702 (C=O), 1632 (C=C), 1458 (CH_2, CH_3). ^1H NMR (300 MHz, $CDCl_3$) δ: 0.82–1.37 (m, 5 H, 1-H_{ax}, 3-H_{ax}, 3*a*-H, 4-H_{ax}, 11*a*-H), 1.46 (dt, *J* = 13.9, 3.4 Hz 1 H, 12-H), 1.59–1.72 (m, 3 H, 2-H_2, 3-H_{eq}),1.93–2.05 (m, 2H, 12-H, 1-H_{eq}), 2.48 (ddd, *J* = 13.0, 9.2, 3.4 Hz, 1 H, 4-H_{eq}), 2.94 (m, 1 H, 11-H), 3.27 (s, 3 H, N-CH_3), 3.29 (s, 3 H, N-CH_3), 5.03 (ddd, *J* = 9.2, 3.4, 1.9 Hz, 1 H, 5-H). ^{13}C NMR (20 MHz, $CDCl_3$) δ: 22.4 (C-2), 23.4 (C-11), 23.9 (C-12), 27.8 (N-CH_3), 28.1. (C-3), 28.4 (N-CH_3), 29.9 (C-1), 35.4 (C-4), 35.7 (C-3*a*), 53.3 (C-11*a*), 76.1 (C-5), 97.0 (C-10*a*), 151.2 (C-8), 153.3 (C-6*a*), 162.0 (C-10). Anal. calcd. $C_{15}H_{20}N_2O_3$ (276.3): C 65.20, H 7.29; found: C 65.14, H 7.27.

(4*aS*,6*R*,12*R*,12*aR*)-(±)-6,12-Methano-8,10-dimethyl-1,2,3,4,4*a*,5,6,8,12,12*a*-decahydro-7-oxa-8,10-diaza-dibenzo[*a*,*d*]cyclooctene-9,11-dione (12)

A solution of aldehyde **8** (107 mg, 0.70 mmol) in CH_2Cl_2 (1 mL) was slowly added to a suspension of *N*,*N*′-dimethylbarbituric acid (104 mg, 0.67 mmol) and 20 mg EDDA in dry methanol (10 mL) and the reaction mixture was stirred 16 h at room temperature. The solvent was evaporated in vacuo and the crude product purified by column chromatography (DE:PE = 1:5) to give 132 mg of **12** (0.45 mmol, 67% yield) as colorless crystals; mp 142°C. R_f = 0.10 (DE:PE = 1:5). MS (70 eV, EI) *m*/*z* (%): 290 (20) [M^+], 81 (84) [$C_6H_9^+$], 41 (100) [$C_3H_5^+$]. UV (CH_3CN) λ_{max} (log ε) (nm): 262 (3.80). IR (film) (cm^{-1}) 2926, 2854 (C-H), 1700 (C=O), 1640 (C=C), 1450 (CH_2, CH_3). ^1H NMR (200 MHz, $CDCl_3$) δ: 1.76–2.39 (m, 14 H, 1-H_2, 2-H_2, 4-H_2, 5-H_2, 13-H_2, 4*a*-H, 12*a*-H), 2.63 (m, 1 H, 12-H), 3.31 (s, 3 H, N-CH_3), 3.35 (s, 3 H, N-CH_3), 5.03 (ddt, *J* = 10.0, 5.0, 2.5 Hz 1 H, 6-H). ^{13}C NMR (20 MHz, $CDCl_3$) δ: 22.9 (C-2)*, 26.9 (C-4)*, 26.9 (C-3)*, 27.1 (C-12), 27.8 (N-CH_3), 28.4 (N-CH_3), 32.7 (C-1), 33.9 (C-4*a*), 34.1 (C-13), 36.9

© 2001 NRC Canada

(C-5), 49.1 (C-12*a*), 75.5 (C-6), 95.8 (C-11*a*), 151.3 (C-9), 152.6 (C-7*a*), 162.4 (C-11). Anal. calcd. $C_{16}H_{22}N_2O_3$ (290.2): C 290.1630; found: 290.1630.

Conclusion

In addition to the synthesis of annulated heterocycles the domino Knoevenagel – hetero-Diels–Alder reaction is also a very efficient method for the preparation of bridged heterocyclic compounds.

Acknowledgment

This work was supported by the Deutsche Forschungsgemeinschaft and the Fonds der Chemischen Industrie. F. H. thanks the Fonds der Chemischen Industrie for a Ph.D fellowship.

References

1. (*a*) L.F. Tietze and U. Beifuss. Angew. Chem. **105**, 137 (1993); Angew. Chem. Int. Ed. Engl. **32**, 131 (1993); (*b*) L.F. Tietze. Chem. Rev. **96**, 115 (1996); (*c*) L.F. Tietze and M. Lieb. Curr. Opin. Chem. Biol. **2**, 363 (1998); (*d*) L.F. Tietze and A. Modi. Med. Res. Rev. **20**, 304 (2000); (*e*) L.F. Tietze and F. Haunert. *In* Stimulating concepts in chemistry. *Edited by* F. Vögtle, J.F. Stoddart, and M. Shibasaki. Wiley–VCH, Weinheim. 2000. p. 39.
2. (*a*) L.F. Tietze, G.V. Kiedrowski, K. Harms, W. Clegg, and G.M. Sheldrick. Angew. Chem. **92**, 130 (1980); Angew. Chem. Int. Ed. Engl. **19**, 134 (1980); (*b*) L.F. Tietze, T. Brumby, and M. Pretor. Synthesis, 700 (1987); (*c*) L.F. Tietze, S. Brand, T. Pfeiffer, J. Antel, K. Harms, and G.M. Sheldrick. J. Am. Chem. Soc. **109**, 921 (1987); (*d*) L.F. Tietze, T. Brumby, and T. Pfeiffer. Liebigs Ann. Chem. 9 (1988); (*e*) L.F. Tietze, H. Geissler, J. Fennen, T. Brumby, S. Brand, and G. Schulz. J. Org. Chem. **59**, 182 (1994); (*f*) L.F. Tietze and Y. Zhou. Angew. Chem. **111**, 2076 (1999); Angew. Chem. Int. Ed. Engl. **38**, 2045 (1999).
3. L.F. Tietze, H. Stegelmeier, K. Harms, and T. Brumby. Angew. Chem. **94**, 868 (1982); Angew. Chem. Int. Ed. Engl**. 21**, 863 (1982).
4. L.F. Tietze and P. Saling. Chirality, **5**, 329 (1993).
5. (*a*) L.F. Tietze and G. Kettschau. Top. Curr. Chem. **189**, 1 (1997); (*b*) L.F. Tietze, G. Kettschau, J.A. Gewert, and A. Schuffenhauer. Curr. Org. Chem. **2**, 19 (1998).
6. (*a*) G. Klopman. J. Am. Chem. Soc. **90**, 223 (1968); (*b*) L. Salem. J. Am. Chem. Soc. **90**, 543 (1968); (*c*) L. Salem. J. Am. Chem. Soc. **90**, 553 (1968).
7. R. McKean, G. Parinello, A.F. Renaldo, and J.K. Stille. J. Org. Chem. **52**, 422 (1987).
8. (*a*) Y. Okude, S. Hirano, T. Hiyamo, and H. Nozaki. J. Am. Chem. Soc. **99**, 3179 (1977); (*b*) D.A. Evans and J.V. Nelson. J. Am. Chem. Soc. **102**, 774 (1980); (*c*) T. Hiyama, K. Kimura, and H. Nozaki. Tetrahedron Lett. **22**, 1037 (1981).
9. G. Brieger and J.N. Bennett. Chem. Rev. **80**, 63 (1980).

© 2001 NRC Canada

A synthesis of 6,11-disubstituted benzo[*b*]carbazoles

Heidi L. Fraser and Gordon W. Gribble

Abstract: Sequential regioselective addition of organolithium reagents to indolo[1,2-*b*]isoquinoline-6,11-quinone (**7**) followed by sodium borohydride reduction of the intermediate diol **10**, which is not isolated, affords 6,11-disubstituted 5*H*-benzo[*b*]carbazoles **11**. The tandem combination of methyllithium and lithium triethylborohydride (Super Hydride) gives 6-methylbenzo[*b*]carbazole (**24**).

Key words: benzo[*b*]carbazole, organolithiums, indolo[1,2-*b*]isoquinoline-6,11-quinone, ellipticine, indole.

Résumé : L'addition régiosélective séquentielle de réactifs organolithiens à l'indolo[1,2-*b*]isoquinoléine-6,11-quinone (**7**), suivie d'une réduction par le borohydrure de sodium du diol intermédiaire **10** qui n'a pas été isolé, conduit à la formation de 5*H*-benzo[*b*]carbazoles 6,11-disubstitués (**11**). La combinaison en tandem du méthyllithium et du triéthylborohydrure de lithium (« Super Hydrure ») conduit au 6-méthylbenzo[*b*]carbazole (**24**).

Mots clés : benzo[*b*]carbazole, organolithiens, indolo[1,2-*b*]isoquinoléine-6,11-quinone, ellipticine, indole.

[Traduit par la Rédaction]

The ellipticine family of alkaloids and related pyridocarbazoles and benzocarbazoles (**1**–**6**, Fig. 1) continue to be intensively studied as novel DNA active compounds and potential anticancer agents (for reviews see ref. 1; for recent work, see ref. 2). For example, S16020–2 (**4**) is one of the most potent such analogues yet discovered, and 9-chloro-4-hydroxy-2,3,5,11-tetramethyl-6*H*-pyrido[3,2-*b*]carbazole (**6**) has high in vivo antitumor activity against L1210 and P388 leukemia, B16 melanoma, and M5076 sarcoma (2).

As an extension of our previous work on the synthesis of ellipticine and other pyridocarbazoles (for reviews of our early work see ref. 3; 4, 5), we describe herein the synthesis of 6,11-disubstituted benzo[*b*]carbazoles **11**. Thus, sequential regioselective addition of organolithiums to indolo[1,2-*b*]isoquinoline-6,11-quinone (**7**) followed by reduction of the intermediate diol **10** gives **11** (Scheme 1). Our earlier experience showed that low temperatures are necessary during the organolithium addition to preclude the ring-opening **8** → **9** prior to consumption of all of the organolithium reagents. If this does occur, then ketone **9** can react with the organolithium to give tertiary alcohol **12**, useless for this approach.

Results and discussion

As we have shown earlier (5), indole (**13**) is readily converted to quinone **7** in 67% overall yield (Scheme 2). Thus, a standard C-2 lithiation of 1-(phenylsulfonyl)indole (**14**) with LDA (6) followed by reaction with phthalic anhydride (**15**) affords keto acid **16** in 86% overall yield from indole. Cleavage of the phenylsulfonyl group and cyclization with hot acetic anhydride furnishes the desired quinone **7**. Treatment of **7** with methyllithium (2 equiv) followed by reduction of the crude diol mixture with sodium borohydride gives 6,11-dimethyl-5*H*-benzo[*b*]carbazole (**18**) in 87% yield (5). With this result it became of interest to examine the sequential addition of different organolithium reagents to quinone **7**.

Based on our previous studies (5–7), we anticipated that the ketone carbonyl in **7** would be more reactive than the lactam carbonyl towards organolithium addition. Indeed, treatment of **7** with 1 equiv of methyllithium at –100°C followed by the addition of 1 equiv of *n*-butyllithium affords, after reductive work-up, 11-*n*-butyl-6-methylbenzo[*b*]carbazole (**19**) as the major product (61% yield). The regioisomeric 6-*n*-butyl-11-methylbenzo[*b*]carbazole (**20**) is obtained in 12% yield (Scheme 3). Reversing the order of addition yields **20** exclusively in 72% yield.

The isomer assignments of **19** and **20** are based on the respective methyl proton chemical shifts, which in turn were established from NOESY data obtained with 6,11-dimethylbenzo[*b*]carbazole (**18**). Thus, the C-6 methyl protons (2.85 ppm) show a NOESY cross peak with the indole NH (7.91 ppm) and one adjacent aromatic proton (H-7, 8.10 ppm). In contrast, the C-11 methyl protons (3.25 ppm) interact with *two* aromatic protons (H-1, 8.37 ppm and H-10, 8.31 ppm). Moreover, as we have observed previously with

Received December 4, 2000. Published on the NRC Research Press Web site at http://canjchem.nrc.ca on October 18, 2001.

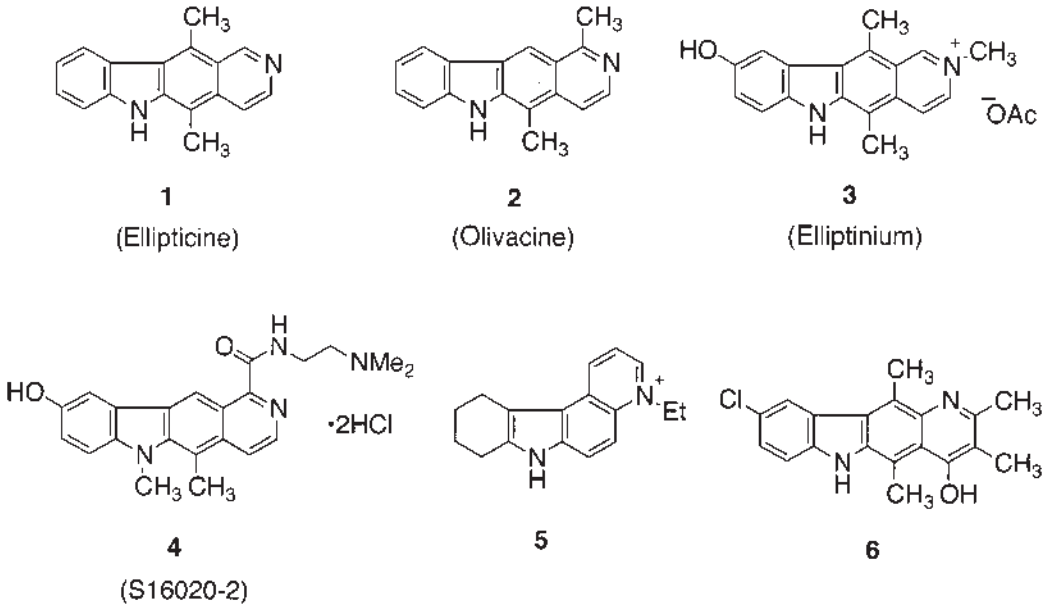
Dedicated to Victor Snieckus, a friend and colleague for nearly 40 years, in celebration of his many contributions to organic chemistry and his outstanding service to our community.

H.L. Fraser and G.W. Gribble.[1] Department of Chemistry, 6128 Burke Laboratory, Dartmouth College, Hanover, NH 03755 U.S.A.

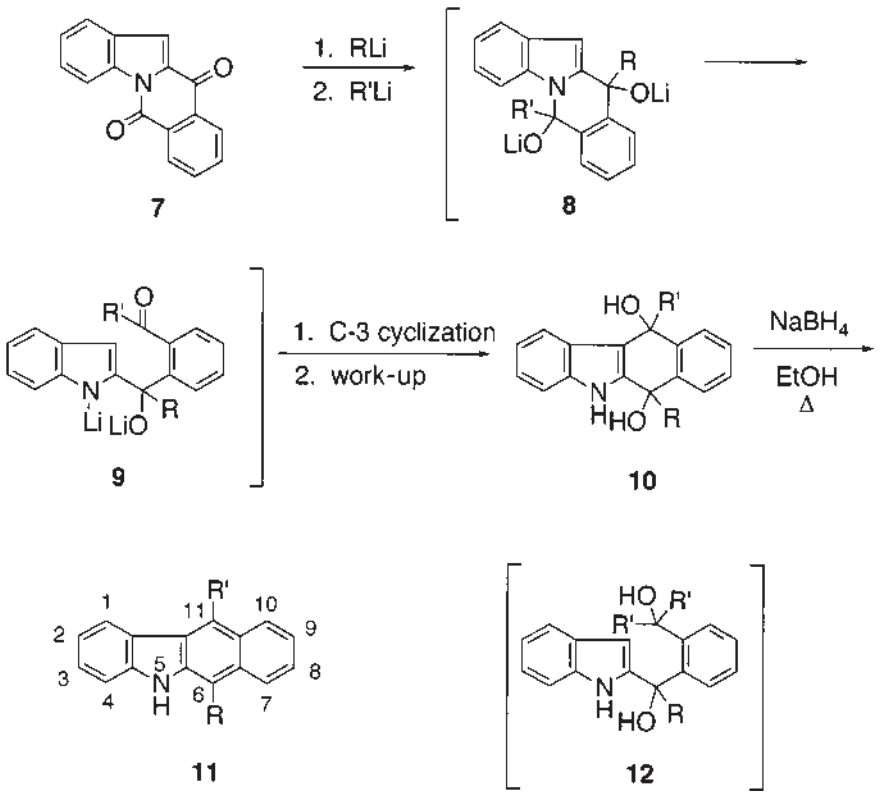
[1]Corresponding author (telephone: (603) 646-3118; fax: (603) 646-3946; e-mail: grib@dartmouth.edu).

 DOI: 10.1139/cjc-79-11-1515 © 2001 NRC Canada

Fig. 1. Ellipticine alkaloids and related antitumor pyridocarbazoles.



Scheme 1.



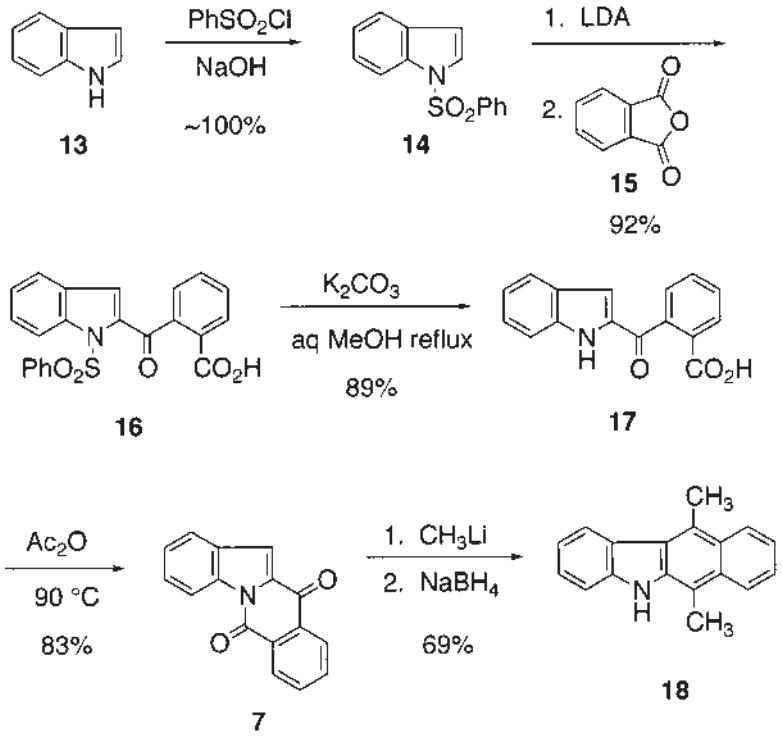
pyridocarbazoles (5, 7), a methyl group in the C-11 position is significantly deshielded by the indole benzene ring. The methyl group chemical shifts observed for **19** (2.81 ppm) and **20** (3.67 ppm) are consistent with this deshielding effect.

Similar results were obtained with reactions of phenyllithium with quinone **7**. Thus, treatment of **7** with 2 equiv of phenyllithium affords 6,11-diphenylbenzo[*b*]carbazole (**21**), in 70% yield after reductive work-up. Sequential treatment of **7** with 1 equiv each of phenyllithium then methyllithium affords **22** (37%) and **23** (22%). The reverse order of organolithium addition is somewhat more regioselective giving **23** (47%) and **22** (18%). These two isomers were distinguished by their characteristic methyl group chemical shifts (3.28 ppm for **22**; 2.91 ppm for **23**).

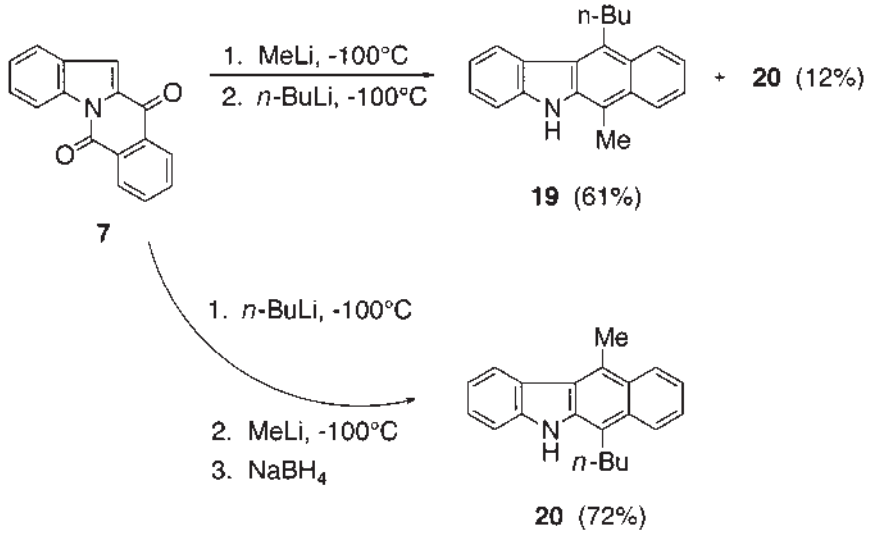
The use of hydride nucleophiles has been more problematic and only one combination of reagents has been fruitful.

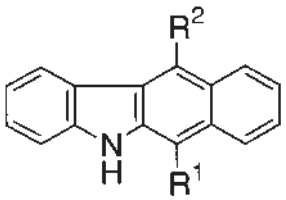
© 2001 NRC Canada

Scheme 2.



Scheme 3.



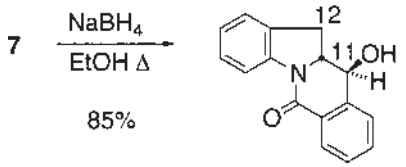


21, $R^1 = R^2 = Ph$
22, $R^1 = Ph$, $R^2 = Me$
23, $R^1 = Me$, $R^2 = Ph$
24, $R^1 = Me$, $R^2 = H$

Treatment of quinone **7** with methyllithium followed by Super Hydride ($LiBHEt_3$) affords 6-methylbenzo[*b*]carbazole (**24**) in 56% yield, after reduction of the intermediate diol with sodium borohydride. The reverse sequence of reagents as well as several attempts (Super Hydride, DIBAL, $LiAlH_4$) to effect hydride addition to both carbonyl groups, which would give the parent 5*H*-benzo[*b*]carbazole, were unsuccessful and led only either to complex mixtures or partial reduction. For example, reduction of **7** with sodium borohydride alone affords the hydroxy lactam **25** (86% yield) resulting from conjugate reduction of the indole double bond and ketone reduction (Scheme 4). The stereochemistry of **25** was established by 2D NMR experiments (COSY, NOESY) and coupling constants. The methine proton at C-11 is trans to the

© 2001 NRC Canada

Scheme 4.



25

proton at C-11a (J = 11.5 Hz), and the coupling constants between C-11a-H and the protons at C-12 (J = 8.7 and 9.4 Hz) are consistent with this stereochemistry.

In summary, we have shown that 6,11-disubstituted benzo[*b*]carbazoles are accessible via the sequential addition several organolithium reagents to indolo[1,2-*b*]isoquinoline-6,11-quinone (**7**). The use of Super Hydride in this strategy allows for the synthesis of 6-methylbenzo[*b*]carbazole (**24**).

Experimental section

General experimental

Melting points were determined in open capillaries and are uncorrected. Elemental analyses were done by Atlantic Microlab Inc., Atlanta, Georgia. High resolution mass spectra (HRMS) were carried out at the University of Illinois at Urbana-Champaign, School of Chemical Sciences, Mass Spectrometry Laboratory, Urbana, Illinois. All ^{1}H NMR, ^{13}C NMR, HMQC, COSY, and NOESY spectra were generated with a Varian Unity Plus NMR spectrometer (300 Hz) unless specified otherwise. Tetramethylsilane (TMS) and deuterated solvents were used as internal reference ($CDCl_3$, acetone-d_6, DMSO-d_6, or CD_3OD). Chemical shifts are reported in parts per million (δ) downfield from TMS. The apparent multiplicity (s = singlet, d = doublet, t = triplet, q = quartet, m = multiplet, b = broad), number of protons, and coupling constants (J = xHz) are reported where appropriate. Low resolution mass spectral data were generated on a Hewlett-Packard 5890 (70 eV). Infrared spectra were taken with a PerkinElmer 1600 series FT IR spectrophotometer and are referenced to the 1601 cm^{-1} band of polystyrene. Ultraviolet spectra were taken with a Hewlett-Packard 8451A diode array spectrophotometer in 95% ethanol. Thin layer chromatography was done on Whatman brand 20 × 20 cm polyester backed silica plates with fluorescent indicator. Plates were visualized by 254 nm UV light. Alternative visualization was accomplished by treatment with a solution of ceric ammonium sulfate in 10% H_2SO_4. Preparative TLC was done on silica gel 60 F254 1 mm 20 × 20 plates from VWR. Flash chromatography was carried using Fisher or SELECTO brand silica gel 60 PF254 (230–400 mesh). Alkyllithiums were standardized prior to use by titration against dried diphenylacetic acid under an atmosphere of N_2 at 0°C. Tetrahydrofuran was freshly distilled from sodium–benzophenone under N_2. Anhydrous reactions were done with glassware dried for 24 h at a temperature of 120°C or greater. Apparatus was assembled hot and cooled under an atmosphere of N_2. Alternatively, glassware was assembled and dried by treatment with flame of a propane torch and cooled under an atmosphere of N_2.

*1-(Phenylsulfonyl)indole (**14**) (8)*

To a stirred suspension of powdered sodium hydroxide (67.45 g, 1.69 mol) and tetra-*n*-butylammonium hydrogen sulfate (4.70 g, 0.014 mol) in methylene chloride (660 mL) at 0°C, indole (**13**) (60.58 g, 0.517 mol) was added neat via a powder funnel under N_2. A solution of benzenesulfonyl chloride (63.8 mL, 0.50 mol) in methylene chloride (40 mL) was added to the ice-cold suspension over 20 min, not allowing the temperature to surpass 20°C. The reaction mixture was stirred vigorously for 3 h via mechanical stirring. The resulting solid was filtered and the filtrate was concentrated in vacuo to give a light pink solid (144.7 g), which was triturated with hexanes to yield 133.1 g (100%) of **14** as white crystals: mp 77–79°C (lit. (8) mp 78 to 79°C).

*1-(Phenylsulfonyl)indol-2-yl 2-carboxyphenyl ketone (**16**) (5)*

To a stirred solution of LDA in THF (10 mL) (generated from diisopropylamine (0.60 mL, 4.25 mmol) and *n*-BuLi (1.7 mL, 4.27 mmol, 2.5 M in hexane) at –78°C), was added 1-(phenylsulfonyl)indole (**14**) (1.11 g, 4.27 mmol) in THF (10 mL) at –78°C under N_2 over 5 min. The reaction mixture was stirred at –78°C for 2 h and was then warmed to 14°C over 30 min. The reaction mixture was recooled to –78°C, followed by rapid addition of a solution of phthalic anhydride (**15**) (0.64 g, 4.27 mmol) in THF (5 mL). The reaction mixture was allowed to warm to room temperature overnight. The reaction mixture was concentrated in vacuo, and the residue was dissolved in water (20 mL). The solution was cooled to 0°C and acidified with 20% HCl. The tan solid which formed upon acidification was collected by vacuum filtration and dried in vacuo to afford 1.60 g (92%) **16** as a tan solid. The solid was recrystallized from acetone to yield 9.12 g of **16** as a tan solid (89%): mp 212 to 213°C (lit. (5) mp 212 to 213°C). ^{13}C NMR (acetone-d_6) δ (ppm): 186.0, 167.5, 134.3, 131.7, 131.3, 130.1, 129.6, 129.4, 128.1, 128.0, 124.3, 123.6, 120.7, 115.6.

*2-Carboxyphenyl 2-indolyl ketone (**17**) (5)*

A solution of keto acid **16** (6.94 g, 17.14 mmol) and K_2CO_3 (9.6 g, 0.068 mol) in MeOH (175 mL) and H_2O (60 mL) was refluxed for 5 h under N_2. The reaction mixture was cooled, and the MeOH was removed in vacuo. Water (100 mL) was added, and the acidity was adjusted to pH 2 with 20% HCl. The aqueous layer was extracted with EtOAc (3 × 200 mL), the organic layers were combined and washed with brine (2 × 50 mL), dried (Na_2SO_4), and concentrated in vacuo. The crude solid was recrystallized from acetone to yield 4.03 g (89%) of **17** as a tan solid: mp 234–236°C (lit. (5) mp 234 to 235°C).

*Indolo[1,2-*b*]isoquinoline-6,11-quinone (**7**) (5)*

Keto acid **17** (3.01 g, 11.4 mmol) was suspended in acetic anhydride (560 mL) and heated to 90–109°C for 24 h under N_2. The reaction mixture was cooled to room temperature and kept at 0°C for 12 h. The gold needles that formed were collected by vacuum filtration (1.84 g, 65%). The Ac_2O present in the filtrate was removed by vacuum distillation (10–20 torr (1 torr = 133.322 Pa)) and the residue was recrystallized from acetone to yield 0.49 g of **7** as gold needles (overall yield 83%): mp 217 to 218°C (lit. (5) mp 217 to 218°C). ^{1}H NMR (acetone-d_6) δ (ppm): 8.41 (d, 1H), 8.24 (dd, 1H), 8.15

© 2001 NRC Canada

(dd, 1H), 7.93–7.79 (m, 3H), 7.65 (s, 1H), 7.57 (t, 1H), 7.36 (t, 1H).

*6,11-Dimethyl-5*H*-benzo[*b*]carbazole (**18**) (5)*

To a stirred solution of quinone **7** (130 mg, 0.530 mmol) in THF (25 mL) at –100°C under N_2 was added MeLi (0.8 mL, 1.13 mmol, 1.4 M in ether) dropwise via syringe. The resulting dark green solution was stirred at –90°C for 2 h and was warmed to room temperature overnight. The solvent was removed in vacuo and the residue was dissolved in absolute EtOH (50 mL). The solution was then heated to reflux and $NaBH_4$ (1 pellet, 1.0 g, 27.0 mmol) was added; another pellet of $NaBH_4$ was then added after every 24 h of reflux. The reaction was refluxed for a total of 78 h. The reaction was cooled to room temperature, the EtOH was removed in vacuo, and the residue was partitioned between H_2O (300 mL) and CH_2Cl_2 (200 mL) with stirring for 48 h. The layers were separated, the aqueous layer was acidified with concd HCl to pH 2 and extracted with CH_2Cl_2 (1 × 100 mL); the aqueous layer was basified with KOH pellets to pH 12 and extracted with CH_2Cl_2 (1 × 100 mL); the aqueous layer was then neutralized with concentrated HCl and extracted with CH_2Cl_2 (1 × 100). This process was repeated twice. The organic layers were combined, dried over (Na_2SO_4), and concentrated in vacuo to yield 0.24 g of a yellow residue, which was chromatographed (2:1, hexanes:CH_2Cl_2) to yield 90.3 mg (69%) of **18** as a light yellow solid: mp 211 to 212°C (lit. (5) mp 211–213°C). ^{1}H NMR (DMSO-d_6) δ (ppm): 8.39 (t, 2H), 8.16 (d, 1H), 7.91 (br s, 1H), 7.62–7.45, (m, 4H), 3.25 (s, 3H), 2.85 (s, 3H). ^{13}C NMR (acetone-d_6) δ (ppm): 126.7, 124.7, 124.5, 123.9, 123.4, 121.9, 118.9, 110.5, 15.6, 12.9.

*11-*n*-Butyl-6-methyl-5*H*-benzo[*b*]carbazole (**19**)*

To a stirred yellow solution of quinone **7** (119.6 mg, 0.450 mmol) in THF (20 mL) at –100°C under N_2 was added 1 equiv of MeLi (0.3 mL, 0.450 mmol, 1.4 M in ether). The solution was stirred for 15 min at –100°C, then 1 equiv of *n*-BuLi (0.2 mL, 0.450 mmol, 2.0 M in hexanes) was added, increasing the temperature to –95°C which was recooled to –100°C immediately. The reaction mixture was warmed to room temperature gradually overnight. The solvent was removed by vacuum, the residue was dissolved in 95% EtOH (50 mL) to which a $NaBH_4$ pellet (1 pellet = 1.0 g, 27 mmol, crushed) was added, and the solution was heated to reflux. Another $NaBH_4$ pellet was added after 24 h of refluxing. The reaction mixture was refluxed for a total of 67 h, cooled to room temperature, and concentrated in vacuo. The residue was partitioned between CH_2Cl_2 (200 mL) and H_2O (100 mL) and the two layers were stirred for 12 h. The layers were separated. The originally basic aqueous layer was acidified to pH 2 with concd HCl and extracted with CH_2Cl_2 (1 × 50 mL). The aqueous acid layer was neutralized with NaOH pellets and extracted with CH_2Cl_2 (1 × 50 mL). The aqueous layer was rebasified with NaOH pellets to pH 12 and extracted with CH_2Cl_2 (1 × 50 mL). The entire extraction process was repeated. The organic layers were combined, washed with brine (2 × 25 mL), dried (Na_2SO_4) and concentrated in vacuo to give 156.7 mg of a brown oil. The oil was then chromatographed (1:1, hexanes:CH_2Cl_2) to obtain 61% (78.5 mg) of the major isomer as a film and 12% (15.5 mg) of the minor isomer also as a film. Attempts to purify these compounds for elemental analysis were unsuccessful. Major isomer **19**: MS *m*/*z*: 287 (M^+), 273, 244 (100%), 230, 202, 143, 120. HRMS calcd. *m*/*z*: 287.1674; found *m*/*z*: 287.1666. UV (95% EtOH) λ_{max} (nm): 296 (5.70), 320 (5.17), 334 (4.23), 380 (5.05), 398 (5.09). IR (film) (cm^{-1}): 3733, 2922, 2355, 1211, 1151, 638, 502. ^{1}H NMR ($CDCl_3$) δ (ppm): 8.41 (d, *J* = 8.7 Hz, 1H), 8.33 (d, *J* = 8.1 Hz, 1H), 8.19 (d, *J* = 8.1 Hz), 7.94 (bs, 1H), 7.67 (m, 4H), 7.36 (t, *J* = 7.2, 1H), 3.75 (t, 2H), 2.81 (s, 3H), 1.95 (m, 2H), 1.78 (m, 2H), 1.52 (t, *J* = 7.2 Hz, 3H). ^{13}C NMR ($CDCl_3$) δ (ppm): 127.3, 126.8, 124.8, 123.9, 123.6, 122.4, 119.7, 111.6, 110.5, 32.5, 31.2, 29.2, 23.8, 14.5.

*6-*n*-Butyl-11-methyl-5*H*-benzo[*b*]carbazole (**20**)*

To a stirred solution of quinone **7** (145.2 mg, 0.550 mmol) at –60°C under N_2 was added 1 equiv of *n*-BuLi (0.3 mL, 0.55 mmol, 2.1 M in hexanes). This was stirred for 15 min while cooling the reaction to –100°C, at which time 1 equiv of MeLi (0.4 mL, 0.55 mmol, 1.4 M in diethyl ether) was added. The solution was then warmed to room temperature overnight. The solvent was removed in vacuo, the residue was dissolved in EtOH (60 mL) and treated with a $NaBH_4$ pellet (1 pellet = 1.0 g, 27 mmol, crushed), and the solution was refluxed. After refluxing for 15 h, another $NaBH_4$ pellet (1 pellet = 1.0 g, 27 mmol, crushed) was added to the refluxing solution. The reaction mixture was refluxed for a total of 80 h. The reaction was cooled and the solvent was removed by vacuum. The residue was partitioned between CH_2Cl_2 (200 mL) and H_2O (100 mL) and the two phases were stirred over 12 h. The layers were separated. The basic aqueous layer was acidified to pH 2 with concd HCl and extracted with CH_2Cl_2 (1 × 50 mL). The aqueous layer was neutralized with NaOH pellets and extracted with CH_2Cl_2 (1 × 50 mL). The aqueous layer was rebasified with NaOH pellets to pH 12 and extracted with CH_2Cl_2 (1 × 50 mL). The extraction process was repeated. The organic layers were combined, washed with brine (2 × 25 mL), dried (Na_2SO_4), and concentrated in vacuo to yield an orange oil. The oil was chromatographed (3:1, hexanes:CH_2Cl_2) to give 113.7 mg (72%) of **20** as a light yellow film. This compound could not be crystallized. MS *m*/*z*: 287 (M^+), 244 (100%), 229, 202, 120. HRMS calcd. *m*/*z*: 287.1674; found: *m*/*z* 287.1666. UV (95% EtOH) λ_{max} (nm): 298 (5.80), 322 (5.31), 336 (5.21), 386 (5.12), 404 (5.17). IR (film) (cm^{-1}): 3411, 2922, 2856, 1617, 1467, 1400, 1372, 1322, 1228, 1078, 878, 778, 739. ^{1}H NMR δ (ppm): 8.39 (s, 1H), 8.14 (d, 1H, *J* = 7.7 Hz), 8.08 (d, 1H, *J* = 8.4 Hz), 8.01 (d, 1H, *J* = 8.7 Hz), 7.80 (s, 1H), 7.51–7.32 (m, 3H), 7.20 (t, 1H), 3.67 (s, 3H), 3.25 (t, 2H, *J* = 7.8 Hz), 1.83–1.70 (m, 2H), 1.58–1.44 (m, 2H), 0.95 (t, 3H, *J* = 7.3 Hz). ^{13}C NMR ($CDCl_3$) δ (ppm): 146.9, 142.2, 129.6, 127.5, 125.2, 123.0, 122.6, 121.4, 119.7, 117.2, 111.4, 110.6, 54.2, 32.4, 27.7, 23.6, 14.4.

*6,11-Diphenyl-5*H*-benzo[*b*]carbazole (**21**)*

To a stirred solution of quinone **7** (136.9 mg, 0.52 mmol) in THF (25 mL) at –100°C was added 2 equiv of PhLi (1.8 mL, 1.0 mmol, 1.8 M in hexanes). The reaction mixture immediately turned dark and it was warmed to room temperature overnight. In the morning the solution was golden yellow, the solvent was removed by rotary evaporation, and the

© 2001 NRC Canada

residue was dissolved in EtOH (30 mL) and a $NaBH_4$ pellet was added (1 pellet = 1 g, 27 mmol, crushed). The reaction was refluxed for a total of 80.5 h. The EtOH was then removed by vacuum, the residue was partitioned between CH_2Cl_2 (200 mL) and H_2O (100 mL), and the two phases were stirred for 12 h. The layers were separated and the basic aqueous layer was acidified to pH 2 with concd HCl and extracted with CH_2Cl_2 (1 × 50 mL). The aqueous layer was neutralized with NaOH pellets and extraction with CH_2Cl_2 (1 × 50 mL). The aqueous layer was rebasified with NaOH pellets to pH 12 and extracted with CH_2Cl_2 (1 × 50 mL). The extraction process was repeated. The organic layers were combined, washed with brine (2 × 25 mL), dried (Na_2SO_4), and concentrated in vacuo to give a brown oil which was chromatographed (1:1, hexanes:CH_2Cl_2) to give 255 mg of a yellow oil. The oil was then triturated with hexanes to give 132.7 mg (70%) of **21** as a tan film. MS *m*/*z*: 369 (100%, M+), 316, 291, 183, 146, 105. HRMS calcd. *m*/*z*: 369.1518; found *m*/*z*: 369.1516. UV (95% EtOH) λ_{max} (nm): 298 (3.80), 324 (3.26), 338 (3.25), 360 (2.94), 366 (3.02), 404 (3.27). IR (film) (cm^{-1}): 3756, 2992, 2356, 1206, 1150, 639, 500. ^1H NMR ($CDCl_3$) δ (ppm): 8.22 (d, 1H, *J* = 6.8 Hz), 7.95 (s, 1H), 7.93 (d, 1H, *J* = 8.4 Hz), 7.80–7.62 (m, 6H), 7.58–7.26 (m, 6H), 7.02 (dd, 3H, *J*′ = 1.2 Hz, *J*′′ = 6.3 Hz). ^{13}C NMR ($CDCl_3$) δ (ppm): 139.4, 131.2, 130.5, 129.6, 129.2, 128.4, 126.9, 126.1, 124.7, 122.8, 119.4.

*11-Methyl-6-phenyl-5*H*-benzo[*b*]carbazole (**22**)*

To a stirred solution of quinone **7** (120.7 mg, 0.460 mmol) at –78°C under N_2 in THF (15 mL) was added 1 equiv of PhLi (0.3 mL, 0.460 mmol, 1.8 M hexane). This was stirred for 20 min while the solution was cooled to –100°C. At this time 1 equiv of MeLi (0.3 mL, 0.460 mmol, 1.4 M in ether) was added, and the solution was warmed gradually to room temperature overnight. The solvent was then removed by rotary evaporation and the residue was dissolved in EtOH (30 mL). The ethanolic solution was treated with $NaBH_4$, 1 pellet was added (1 pellet = 1 g, 27 mmol, crushed) and refluxed, another $NaBH_4$ pellet was added after 24 h of reflux. The reaction was refluxed for a total of 82 h and was cooled to room temperature and the solvent was removed in vacuo. The residue was partitioned between CH_2Cl_2 (200 mL) and H_2O (100 mL) and stirred over 12 h. The layers were separated. The basic aqueous layer was acidified to pH 2 with concd HCl and extracted with CH_2Cl_2 (1 × 50 mL). The aqueous layer was neutralized with NaOH pellets and extracted with CH_2Cl_2 (1 × 50 mL). The aqueous layer was rebasified with NaOH pellets to pH 12 and extracted with CH_2Cl_2 (1 × 50 mL). The extraction process was repeated. The organic layers were combined, washed with brine (2 × 25 mL), dried (Na_2SO_4) and concentrated in vacuo to give a brown oil (>100%). The oil was chromatographed to give 51.8 mg (37%) of **22** and 31.2 mg (22%) of **23**, both as films for an overall yield of 59%. The major isomer was crystallized from pentane–$CHCl_3$; (major **22**) mp 231–233°C. MS *m*/*z*: 307 (100%, M^+), 293, 230, 146. HRMS calcd. *m*/*z*: 307.1361; found *m*/*z*: 307.1358. UV (95% EtOH) λ_{max} (nm): 298 (4.24), 324 (3.72), 338 (3.72), 404 (3.78). IR (film) (cm^{-1}): 3451, 3057, 2360, 1609, 1484, 1488, 1391, 1344, 1315, 1251, 1258, 1144, 1028, 907, 746, 700, 667. ^1H NMR ($CDCl_3$) δ (ppm): 7.81 (m, 1H), 7.74 (d, 1H, *J* = 8.4 Hz), 7.63–7.50 (m, 7H), 7.37 (td, 1H, *J* = 7.6 Hz, *J* = 1.6 Hz), 7.31–7.20 (m, 2H), 6.85 (s, 1H), 3.28 (s, 3H). ^{13}C NMR ($CDCl_3$) δ (ppm): 153.3, 140.2, 131.9, 131.6, 131.3, 130.4, 130.1, 128.9, 128.1, 127.7, 126.1, 125.5, 124.2, 123.0, 122.3, 118.4, 111.0, 109.5, 14.5.

*6-Methyl-11-phenyl-5*H*-benzo[*b*]carbazole (**23**)*

To a stirred solution of quinone **7** (141.8 mg, 0.540 mmol) at –78°C under N_2 was added 1 equiv of MeLi (0.4 mL, 0.540 mmol, 1.4 M in ether). This was stirred for 20 min while the solution was cooled to –100°C. Then 1 equiv of PhLi (0.3 mL, 0.540 mmol, 1.8 M hexane) was added, and the solution was warmed gradually to room temperature overnight. The solvent was removed by rotary evaporation, and the residue was dissolved in EtOH (50 mL). The ethanolic solution was treated with one $NaBH_4$ pellet (1 pellet = 1 g, 27 mmol, crushed) and refluxed, another $NaBH_4$ pellet was added after 48 h of reflux. The reaction was refluxed for a total of 72 h. The reaction was cooled to room temperature, and the solvent was removed in vacuo. The residue was partitioned between CH_2Cl_2 (200 mL) and H_2O (100 mL) and the two phases were stirred for 12 h. The layers were separated. The basic aqueous layer was acidified to pH 2 with concd HCl and extracted with CH_2Cl_2 (1 × 50 mL). The aqueous layer was neutralized with NaOH pellets and extracted with CH_2Cl_2 (1 × 50 mL). The aqueous layer was rebasified with NaOH pellets to pH 12 and extracted with CH_2Cl_2 (1 × 50 mL). The extraction process was repeated. The organic layers were combined, washed with brine (2 × 25 mL), dried (Na_2SO_4), and concentrated in vacuo to give a brown oil (>100%). The oil was chromatographed to give 78.4 mg (47%) of **23** and 30.5 mg (18%) of **22** both as films for an overall yield of 65%. **23**: MS *m*/*z*: 307 (M^+), 231 (100%), 202, 146, 116. HRMS calcd. *m*/*z*: 307.1361; found *m*/*z*: 307.1357. UV (95% EtOH) λ_{max} (nm): 298 (5.87), 320 (5.51), 334 (5.51), 380 (5.32), 400 (5.38). IR (film) (cm^{-1}): 3733, 2356, 1215, 1152, 638, 503. ^1H NMR δ (ppm): 8.40 (s, 1H), 8.14, (d, 1H, *J* = 7.7 Hz), 8.04 (d, 1H, *J* = 8.7 Hz), 8.01 (d, 1H, *J* = 8.4 Hz), 7.70 (d, 1H, *J* = 8.7 Hz), 7.62–7.22 (m, 8H), 7.20 (td, 1H, *J* = 1.7 Hz, *J* = 6.3 Hz), 2.91 (s, 3H). ^{13}C NMR ($CDCl_3$) δ (ppm): 147.8, 131.1, 129.9, 129.6, 128.4, 127.9, 127.6, 125.6, 125.5, 124.7, 123.5, 123.1, 121.8, 120.2, 119.9, 111.0, 13.5.

*6-Methyl-5*H*-benzo[*b*]carbazole (**24**)*

To a stirred solution of quinone **7** (538.8 mg, 2.18 mmol) in THF (150 mL) under N_2 at –100°C was added MeLi (2.2 mL, 2.18 mmol, 1.0 M in ether). The solution immediately turned deep purple. After stirring at –100°C for 15 min, 1 equiv of Super Hydride ($LiBHEt_3$) (2.2 mL, 2.18 mmol, 1.0 M in THF) was added and the solution was warmed to room temperature overnight. The solvent was removed by vacuum; the residue was dissolved in EtOH (275 mL) to which was added a $NaBH_4$ pellet (1 pellet = 1.0 g, 27 mmol), and the solution was heated to reflux. After refluxing for 6 h another $NaBH_4$ pellet was added; additional $NaBH_4$ pellets were added every 24 h. The reaction mixture was refluxed for a total of 72 h, at which time the solvent was removed by vacuum to give an orange oil. The orange oil was treated with $CHCl_3$ and the fine insoluble solid was removed by filtration to give 0.56 g of an orange oil, which was chromatographed (1:1, hexanes:CH_2Cl_2) to yield 285 mg (56%) of **24**

© 2001 NRC Canada

as a light yellow solid: mp 209–212°C (lit. (9) mp 210 to 211°C). GC–MS *m*/*z*: 231 (M^+, 100%), 216, 202, 115, 88, 44. UV (95% EtOH) λ_{max} (nm) 331, 320, 298, 285, 272, 234, 203. ^{1}H NMR ($CDCl_3$) δ (ppm): 8.46 (1H, s), 8.21 (1H, d, *J* = 7.5 Hz), 8.14 (1H, d, *J* = 8.7 Hz), 8.08 (1H, d, *J* = 8.1 Hz), 7.85 (1H, s), 7.69–7.41 (4H, m), 7.28 (1H, td, *J* = 7.6 Hz, *J* = 1.6 Hz), 2.85 (3H, s). ^{13}C NMR ($CDCl_3$) δ (ppm): 142.3, 138.6, 131.3, 129.5, 129.0, 127.5, 125.3, 125.2, 124.0, 123.1, 122.7, 121.4, 119.8, 117.0, 111.6, 110.6, 13.0.

*11,11a-Dihydroindolo[1,2-*b*]isoquinoline-6,11-hydroquinone (**25**)*

An ethanol solution of quinone **7** under N_2 (108.6 mg, 0.410 mmol) was treated with $NaBH_4$ (1 pellet = 1 g, 27 mmol, crushed) and refluxed for 24 h, then stirred at room temperature for 24 h. The EtOH was removed by vacuum and the residue was partitioned between CH_2Cl_2 (200 mL) and H_2O (100 mL) and the two phases were stirred for 12 h. The layers were separated. The basic aqueous layer was acidified to pH 2 with concd HCl and extracted with CH_2Cl_2 (1 × 50 mL). The aqueous layer was neutralized with NaOH pellets and extracted with CH_2Cl_2 (1 × 50 mL). The aqueous layer was rebasified with NaOH pellets to pH 12 and extracted with CH_2Cl_2 (1 × 50 mL). The extraction process was repeated. The organic layers were combined, washed with brine (2 × 25 mL), dried (Na_2SO_4), and concentrated in vacuo. The resulting residue was chromatographed to give 94.9 mg (86%) of the indoline alcohol **25** (89% yield with recovered starting material): mp 244–247°C. MS *m*/*z*: 251 (M^+), 234, 204, 134, 118 (100%), 105, 91, 77. HRMS calcd. *m*/*z*: 251.0946; found *m*/*z*: 251.0953. UV (95% EtOH) λ_{max} (nm): 258, 274, 284, 304, 364. UV (95% EtOH + HCl) λ_{max} (nm): 254, 304, 364. IR (film) (cm^{-1}): 2918, 2357, 1480, 1211, 1150, 633, 501. ^{1}H NMR (acetone-d_6) δ (ppm): 8.31 (1H, d, *J* = 8.0 Hz), 8.08 (1H, d, *J* = 7.5 Hz), 7.79 (1H, d, *J* = 7.8 Hz), 7.66 (1H, t, *J* = 7.6 Hz), 7.50 (1H, t, *J* = 7.6 Hz), 7.34 (1H, d, *J* = 6.8 Hz), 7.26 (1H, t, *J* = 7.8 Hz), 7.08 (1H, t, *J* = 7.5 Hz), 5.05 (1H, d, *J* = 11.5 Hz), 4.34 (1H, ddd, *J* = 11.5 Hz, *J* = 9.6 Hz, *J* = 8.7 Hz), 3.51 (1H, dd, *J* = 8.7 Hz, *J* = 16.1 Hz), 3.29 (1H, dd, *J* = 9.9 Hz, *J* = 16.2 Hz), 2.85 (1H, s). ^{13}C NMR ($CDCl_3$) δ (ppm): 171.8, 132.9, 130.2, 128.7, 128.6, 128.2, 125.1, 124.5, 123.6, 117.0, 30.0, 29.9, 23.0.

Acknowledgements

This work was supported in part by the Donors of the Petroleum Research Fund (PRF), administered by the American Chemical Society. We also thank Wyeth–Ayerst for their support. H.L.F. acknowledges receipt of an Arthur Dunhan Holmes 1906 Graduate Fellowship in Nutritional Chemistry.

References

1. G.W. Gribble. *In* The alkaloids. Vol. 39. *Edited by* A. Brossi. Academic Press, San Diego. 1990. pp. 239–352.
2. (*a*) S. Léonce, V. Perez, M.-R. Casabianca-Pignede, M. Anstett, E. Bisagni, A. Pierré, and G. Atassi. Invest. New Drugs, **14**, 169 (1996); (*b*) M.G. Ferlin, G. Chiarelotto, C. Marzano, E. Severin, F. Baccichetti, F. Carlassare, M. Simonato, and F. Bordin. Farmaco, **53**, 431 (1998); (*c*) V. Moinet-Hedin, T. Tabka, L. Poulain, T. Godard, M. Lechevrel, D. Saturnino, J.-C. Lancelot, J.-Y. LeTalaër, and P. Gaudchon. Anti-Cancer Drug Des. **15**, 109 (2000).
3. G.W. Gribble. *In* Advances in heterocyclic natural product synthesis. Vol. 1. *Edited by* W.H. Pearson. JAI Press, Greenwich, Connecticut. 1990. pp. 43–94; G.W. Gribble. Synlett, 289 (1991).
4. M.G. Saulnier and G.W. Gribble. J. Org. Chem. **47**, 2810 (1982).
5. G.W. Gribble, M.G. Saulnier, J.A. Obaza-Nutaitis, and D.M. Ketcha. J. Org. Chem. **57**, 5891 (1992).
6. M.G. Saulnier and G.W. Gribble. J. Org. Chem. **47**, 757 (1982).
7. M.G. Saulnier and G.W. Gribble. Tetrahedron Lett. **24**, 3831 (1983).
8. S.C. Conway and G.W. Gribble. Heterocycles, **30**, 6278 (1990).
9. S. Kano, E. Sugino, S. Shibuya, and S. Hibino. J. Org. Chem. **46**, 2979 (1981).

© 2001 NRC Canada

Isomerization of (*Z*)-alkenylsilanes to (*E*)-isomers with hydrosilane and $RhI(PPh_3)_3$

Atsunori Mori, Eisuke Takahisa, Yasushi Nishihara, and Tamejiro Hiyama

Abstract: Isomerization of (*E*)-2-phenylethenylsilanes to the (*Z*)-isomers is found to easily take place at 60°C within 1 h using 20–100 mol% of a hydrosilane and 0.1 mol% of $RhI(PPh_3)_3$ and is understood in terms of insertion of alkenylsilanes to hydridorhodium followed by β-hydride elimination.

Key words: hydrosilylation, isomerization, $RhI(PPh_3)_3$, alkenylsilane, hydrosilane.

Résumé : On a observé que l'isomérisation des (*E*)-2-phényléthénylsilanes en isomère (*Z*) se produit facilement à 60°C, pendant une heure, en présence de 20 à 100% d'un hydrosilane et de 0,1 mol % de $RhI(PPh_3)_2$. On peut l'expliquer en termes d'une insertion d'alcénylsilanes sur l'hydridorhodium, suivie d'une élimination β d'hydrure.

Mots clés : hydrosilylation, isomérisation, $RhI(PPh_3)_2$, alcénylsilane, hydrosilane.

[Traduit par la Rédaction]

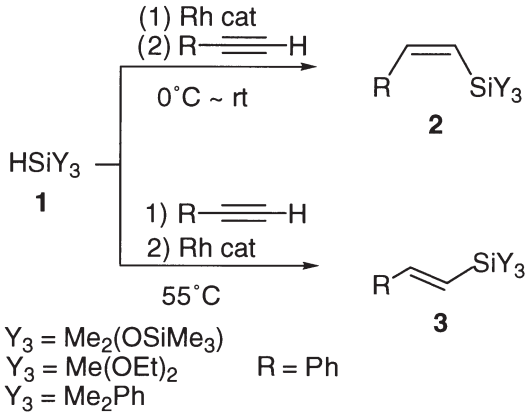
Introduction

Regio- and stereoselective hydrosilylaton of terminal alkynes leading to alkenylsilanes is a significant reaction in organic synthesis as well as organometallic chemistry (1). Among a number of transition-metal catalysts endowed with a variety of features, rhodium complexes show high activity as well as characteristic selectivities. We recently disclosed that rhodium-catalyzed hydrosilylation of terminal alkynes using a hetereoatom-substituted hydrosilane (e.g., **1a** and **1b**) produced (*Z*)-alkenylsilanes (**2**) or (*E*)-alkenylsilanes (**3**) depending on the reaction procedure as shown in Scheme 1 (2).

Meanwhile, we observed that (*E*)-alkenylsilanes **3** were obtained through isomerization of initially produced (*Z*)-isomers **2**. This observation suggests that the hydrosilylation might have occurred through *trans*-addition of a hydrosilane to give **2** followed by isomerization to *cis*-adduct **3**. This isomerization is unusual in view of stereochemistry of hydrosilylation (3, 4)[3,4]. We report here that the isomerization of **2** to **3** is promoted by the presence of a hydrosilane and $RhI(PPh_3)_3$. We also discuss the mechanistic aspect of the isomerization.

When a mixture of phenylacetylene and pentamethyldisiloxane (**1a**) was heated at 60°C in the presence of 0.1 mol% of $RhI(PPh_3)_3$, the reaction leading to (*E*)-2-phenylethenylsilane **3a** proceeded highly selectively (1). At 26% conversion, the ratio of resulting (*Z*)-2-phenylethenylsilane (**2a**) and (*E*)-isomer (**3a**) was 92:8. The isomer ratio gradually changed in favor of **3a** as the reaction proceeded. At 89% conversion, the ratio was 37:62; at >99% conversion, 0:100 (Scheme 2).

Scheme 1.



In the presence of 0.1 mol% of $RhI(PPh_3)_3$ only, **2a** did not isomerize at 60°C in 24 h (see Table 1, entry 1), whereas the isomerization started to take place rapidly when 10 mol% of pentamethyldisiloxane (**1a**) was added to the mixture, and after 1 h a 65:35 mixture of (*Z*)-isomer **2a** and

Received December 22, 2000. Published on the NRC Research Press Web site at http://canjchem.nrc.ca on October 18, 2001.

Dedicated to Professor Victor Snieckus for his contributions to Canadian chemistry.

A. Mori, E. Takahisa, Y. Nishihara, and T. Hiyama.[1,2] Chemical Resources Laboratory, Tokyo Institute of Technology, Nagatsuta, Yokohama 226–8503, Japan.

[1]Present address: Department of Material Chemistry, Graduate School of Engineering, Kyoto University, Sakyo-ku, Kyoto 606–8501, Japan.
[2]Corresponding author (fax: +81-75-753-5555; e-mail: thiyama@NPC05.kuic.kyoto-u.ac.jp).

[3]Wilkinson complex $RhCl(PPh_3)_3$ is reported to catalyze the reaction of 1-alkynes with trialkylsilane leading to (*Z*)-alkenylsilanes. The stereochemical outcome is understood in terms of initial *cis*-addition to give (*E*)-products followed by isomerization to (*Z*)-isomers.
[4]Isomerization of (*Z*)-alkenyltriethylsilanes to (*E*)-isomers catalyzed by iridium complexes.

 DOI: 10.1139/cjc-79-11-1522 © 2001 NRC Canada

Scheme 2.

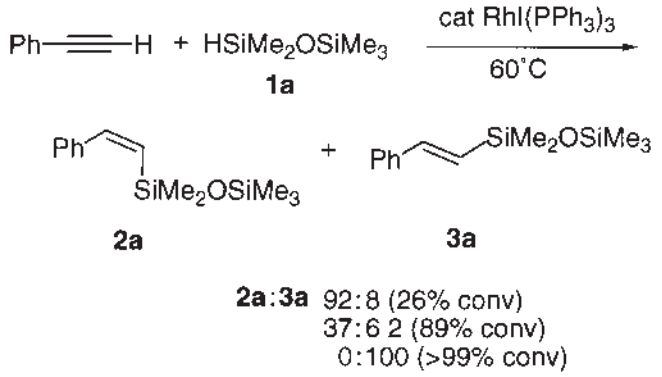
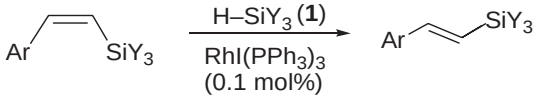


Table 1. Isomerization of (*Z*)-alkenylsilanes.[a]

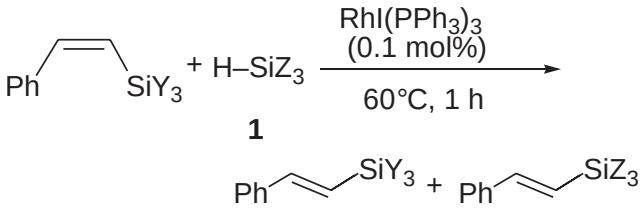


Entry	(Z)-Alkenyl-silane (% Z)	1	Mol	Time (h)	(*Z*):(*E*)[b]
1	**2a** (99)		None	24	97:3
2		**1a**	0.1	1	65:35
3				2	61:39
4			+0.6[c]	1	0:100
5			0.2	1	24:76
6			0.3	1	0:100
7	**2a′**[d] (95)		0.1	1	27:73
8			0.2	1	0:100
9	**2b** (93)	**1b**	0.1	1	2:98

[a]All reactions were carried out using 0.1 mol% of $RhI(PPh_3)_3$ at 60°C.
[b]The ratio was determined by ^1H NMR.
[c]An additional 0.6 mol of hydrosilane was added to the product mixture resulting from the experiment in entry 3.
[d]Ar = 4-Me-C_6H_4, $Y_3 = Me_2OSiMe_3$.

(*E*)-isomer **3a** resulted. The ratio did not change 1 h thereafter, while most of **1a** was confirmed (5).[5] Addition of **1a** (0.6 mol) to the reaction mixture reinitiated the isomerization to complete the transformation to (*E*)-isomer **3a** within 1 h. Use of a larger amount of **1a** accelerated the isomerization more (entries 4–6). Thus, the isomerization appears to be competitive with consumption of hydrosilane **1a**, a pathway independent of the isomerization, both presumably being catalyzed by the rhodium complex. (*Z*)-Isomer **2a′** with a *p*-tolyl group in place of the phenyl group isomerized faster than **2a** to give (*E*)-isomer **3a′** exclusively using 20 mol% of **1a** in 1 h at 60°C (entry 8). Isomerization of (*Z*)-isomer **2b** to (*E*)-isomer **3b** also occurred similarly in the presence of diethoxy(methyl) silane (**1b**) (6).[6]

Table 2. Isomerization of *Z*-alkenylsilanes using hydrosilane with different substituents.



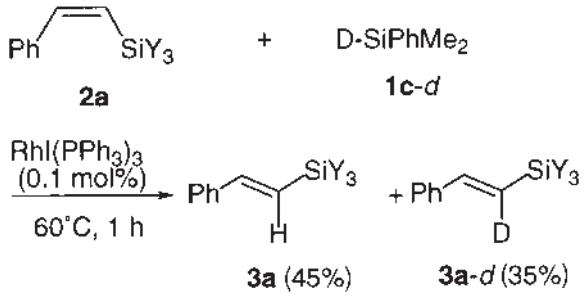
Entry	(*Z*)-Silane	1	Products[a] (%) –SiY3	Products[a] (%) –SiZ3
1	**2b**	**1a**	86	0
2	**2a**	**1b**	87	6
3	**2a**	**1c**	80	0

[a]Yields determined by ^1H NMR.

Table 2 shows scrambling experiments using an equimolar mixture of (*Z*)-2-phenylethenylsilane **2** and hydrosilane **1** with a different silyl group (SiY_3 or SiZ_3). Scrambling of a silyl group was at best 6% after isomerization at 60°C for 1 h. These results show that the silyl exchange does not occur extensively during the isomerization to the corresponding (*E*)-silane **3**.

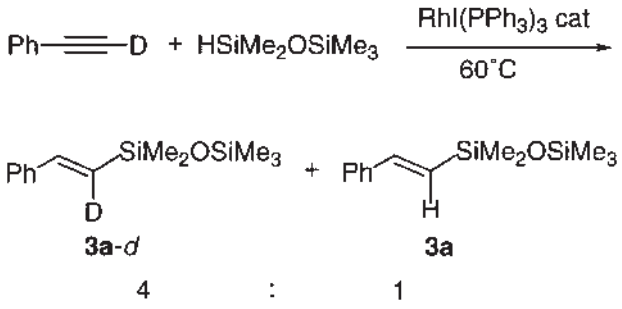
On the other hand, the scrambling experiments using $DSiMe_2Ph$ (**1c**-*d*) revealed that a fair amount of deuterium was incorporated into the product. For example, as illustrated in Scheme 3, when the isomerization was carried out starting with an equimolar mixture of **1c**-*d* and (*Z*)-2-phenylethenylsilane **2a**, a 1.3:1 mixture of (*E*)-isomer **3a** and 1-deuterio-2-phenylethenylsilane **3a**-*d* resulted.[7,8]

Scheme 3.



[5]Reaction of **3a** in the presence of 0.1 mol% of $RhI(PPh_3)_3$ afforded the corresponding disilane as confirmed by ^1H NMR.
[6]We also observed the similar isomerization in the use of 0.1 mol% of $RhCl(PPh_3)_3$.
[7]Typical experimental procedure: To a screw-capped glass tube were added (*Z*)-2-phenylethenylsilane **2** (1.0 mmol), a hydrosilane (0.1–0.3 mmol), and $RhI(PPh_3)_3$ (0.1 mol%, 1 mg). The resulting mixture was heated at 60ºC for 1 h. The isomerization was monitored by taking an aliquot of the solution and measuring ^1H NMR spectra in a $CDCl_3$ solution. After the isomerization was completed, the corresponding (*E*)-silane **3** was isolated by bulb-to-bulb distillation.
[8]The major product of the following equation showed ^1H NMR spectrum identical to the deuterated product in Scheme 3. ^1H NMR ($CDCl_3$, 300 MHz) δ: 6.92 (t, *J* = 2.7 Hz, 1 H, Ph*CH*=CDSi) for **3a**-d; 6.95 (d, *J* = 19.2 Hz, 1 H, Ph*CH*=CHSi) for **3a**.

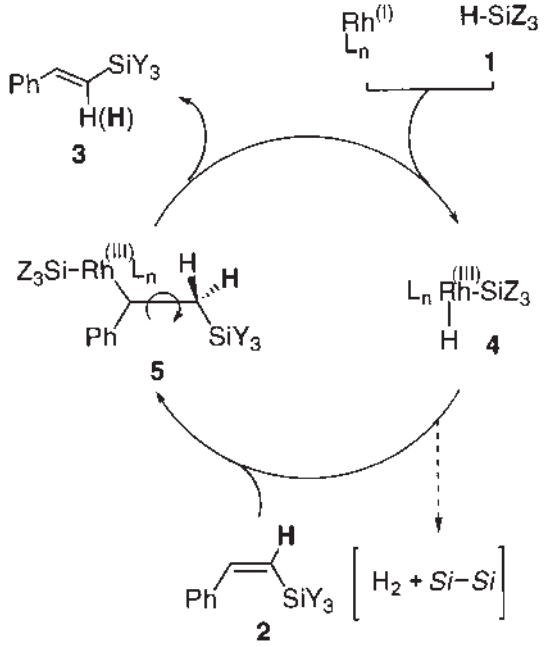
© 2001 NRC Canada



Above observations lead to a mechanism shown in Scheme 4: oxidative addition of $HSiZ_3$ to $Rh(I)L_n$ followed by insertion of (*Z*)-alkenylsilane **2** to the resulting of Rh(III) species **4** would furnish intermediate **5**. The scrambling experiments shown in Table 2 and Scheme 3 suggest that the insertion occurs at a Rh(III)—H bond in **4** rather than a Rh(III)—Si bond. The results contrast sharply to the fact that insertion of a carbon—carbon triple bond towards a H-Rh(III)-SiZ_3 species is considered to occur at a rhodium—silicon bond (3)[3]. Thus, the isomerization proceeds via an insertion–β-elimination mechanism, which is rarely considered for alkenylsilane isomerization though often discussed in olefin isomerization (7).[6] The regiochemistry is controlled to give **5** so that the rhodium atom is located at the β-position of SiY_3. Successive β-elimination leading to (*E*)-alkenylsilanes **3** would occur after C—C bond rotation to induce *syn*-periplanar conformation of a Rh-C-C-H moiety.

We have found that the rhodium-catalyzed isomerization of (*Z*)-2-phenylethenylsilane **2** to (*E*)-isomers **3** takes place in the presence of a catalytic amount of hydrosilane and a rhodium catalyst. Since hydrosilylation of 1-alkynes also proceeds in a similar stereochemical manner, it would be reasonable to assume that a similar isomerization pathway is involved in these cases also. In addition, the isomerization was demonstrated to proceed through insertion–β-elimination of a hydridorhodium (H-Rh(III)-Si) to alkenylsilane in contrast to the reaction of the species with a triple bond which has been considered for insertion at the rhodium—silicon bond.

Scheme 4.



Acknowledgement

This work was supported by Yamada Science Foundation and by a Grant-in-Aid for Scientific Research on Priority Areas "The Chemistry of Inter-element Linkage" (No. 09239102) from the Ministry of Education, Science, Sports and Culture, Japan. We thank Shin-Etsu Chemical Co. Ltd. for kind donation of organosilicon reagents.

References

1. T. Hiyama and T. Kusumoto. Hydrosilylation of C=C and C≡C in comprehensive organic synthesis. Vol. 8. Pergamon Press, Oxford. 1991.
2. (*a*) A. Mori, E. Takahisa, H. Kajiro, K. Hirabayashi, Y. Nishihara, and T. Hiyama. Chem. Lett. 443 (1998); (*b*) A. Mori, E. Takahisa, K. Kajiro, Y. Nishihara, and T. Hiyama. Polyhedron, **19**, 567 (2000).
3. I. Ojima, N. Clos, R.J. Donovan, and P. Ingallina. Organometallics, **9**, 3127 (1990); R. Takeuchi, S. Nitta, and D. Watanabe. J. Org. Chem. **60**, 3045 (1995), and refs. cited therein.
4. M.A. Esteruelas, O. Nürnberg, M. Oliván, L.A. Oro, and H. Werner. Organometallics, **12**, 3264 (1993).
5. K. Shintani, O. Ooi, A. Mori, and Y. Kawakami. Polym. Bull. **38**, 1 (1997).
6. H.M. Dickers, R.N. Haszeldine, A.P. Mather, and R.V. Parish. J. Organomet. Chem. **161**, 91 (1978).
7. J.P. Collman, L.S. Hegedus, J.R. Norton, and R.G. Finke. *In* Principles and application of organotransition metal chemistry. University Science Books, Mill Valley, California. 1987. Chap. 10. p. 523.

© 2001 NRC Canada

Fourfold homologous anionic *ortho*-Fries rearrangement on a partially bridged resorc[4]arene

Oskar Middel, Willem Verboom, and David N. Reinhoudt

Abstract: Fourfold homologous anionic *ortho*-Fries rearrangement in the twofold bridged tetra-*O*-carbamate **3** gave the tetrakis(carboxamidomethyl)resorc[4]arene **4** in 68% yield. Compound **3** was prepared by selective carbamoylation of methylresorc[4]arene **1**, followed by the bridging of the remaining OH groups in tetra-*O*-carbamate **2**.

Key words: resorc[4]arenes, selective functionalizations, homologous anionic *ortho*-Fries rearrangement.

Résumé : Le réarrangement *ortho*-Fries anionique homologue quaternaire du tétra-*O*-carbamate **3** à pont binaire conduit à la formation du tétrakis(carboxamidométhyl)résorc[4]arène, **4**, avec un rendement de 68%. Le composé **3** a été préparé par carbamoylation sélective du méthylrésorc[4]arène, **1**, suivie de la formation d'un pont des groupes OH résiduels du tétra-*O*-carbamate **2**.

Mots clés : résorc[4]arènes, fonctionnalisation sélective, réarrangement *ortho*-Fries anionique homologue.

[Traduit par la Rédaction]

Over a time period of about 20 years the directed *ortho*-metalation strategy (D*o*M) (for recent examples see ref. 1*a*, 1*b*; for a review see ref. 1*c*) has developed as a common synthetic concept in aromatic chemistry. The Snieckus group is one of the leaders in this emerging field in synthetic organic chemistry and by their contemporary developments and collaborations, this synthetic concept has been applied in pharmaceutical chemistry, industrial processes, and the total syntheses of complex natural products. Recently, we (2) introduced the D*o*M concept in supramolecular chemistry as the first synthetic tool for the direct, selective introduction of functional groups at the lateral positions of the calix[4]arene skeleton.

Resorc[4]arenes (for a review see ref. 3) (octols), are the cyclic condensation products of aldehydes and resorcinol and the insertion of methylene bridges between adjacent phenolic moieties results in the formation of cavitands (3, 4). Only a few (selective) resorc[4]arene functionalizations, other than methylene bridge formation (4), are known, e.g., the Mannich reaction (5), radical aromatic bromination (6), and the alkylation (7) and (sulfonate) esterification (8, 9) of the phenolic groups. In this communication, we report our first results on the application of the D*o*M concept for the introduction of upper rim functional groups via a unique fourfold anionic *ortho*-Fries rearrangement (10) at the partially bridged resorc[4]arene **3**.

Results and Discussion

Synthesis[2]

Reaction of resorc[4]arene **1** (11) with diisopropylcarbamoyl chloride (20 equiv) in the presence of a large excess of NaH as a base in DMF at 65°C for 72 h afforded a mixture of tetra-*O*-carbamate regioisomers. Fractional crystallization of this mixture from MeOH–H_2O gave regioisomer **2**, having two diametrical pairs of substituted adjacent phenol groups, in 32% isolated yield.[3] The predominant formation of **2** is probably due to a stabilizing effect of the hydrogen bond between adjacent phenol groups. The selective formation of (tetrasulfonate) esters of resorc[4]arenes described by Shivanyuk and co-workers (8*a*), in which on two diametrical aryl rings two sulfonate esters were introduced, was explained by the formation of a strong hydrogen bond between a sulfonate ester and an adjacent phenol moiety.[4]

Received March 1, 2001. Published on the NRC Research Press Web site at http://canjchem.nrc.ca on October 19, 2001.

Dedicated to Professor Victor Snieckus for his contributions to Canadian chemistry.

O. Middel, W. Verboom, and D.N. Reinhoudt.[1] Laboratory of Supramolecular Chemistry and Technology, MESA$^+$ Research Institute, University of Twente, P.O. Box 217, NL-7500 AE Enschede, The Netherlands.

[1]Corresponding author (fax: +31 534894645; e-mail: smct@ct.utwente.nl).

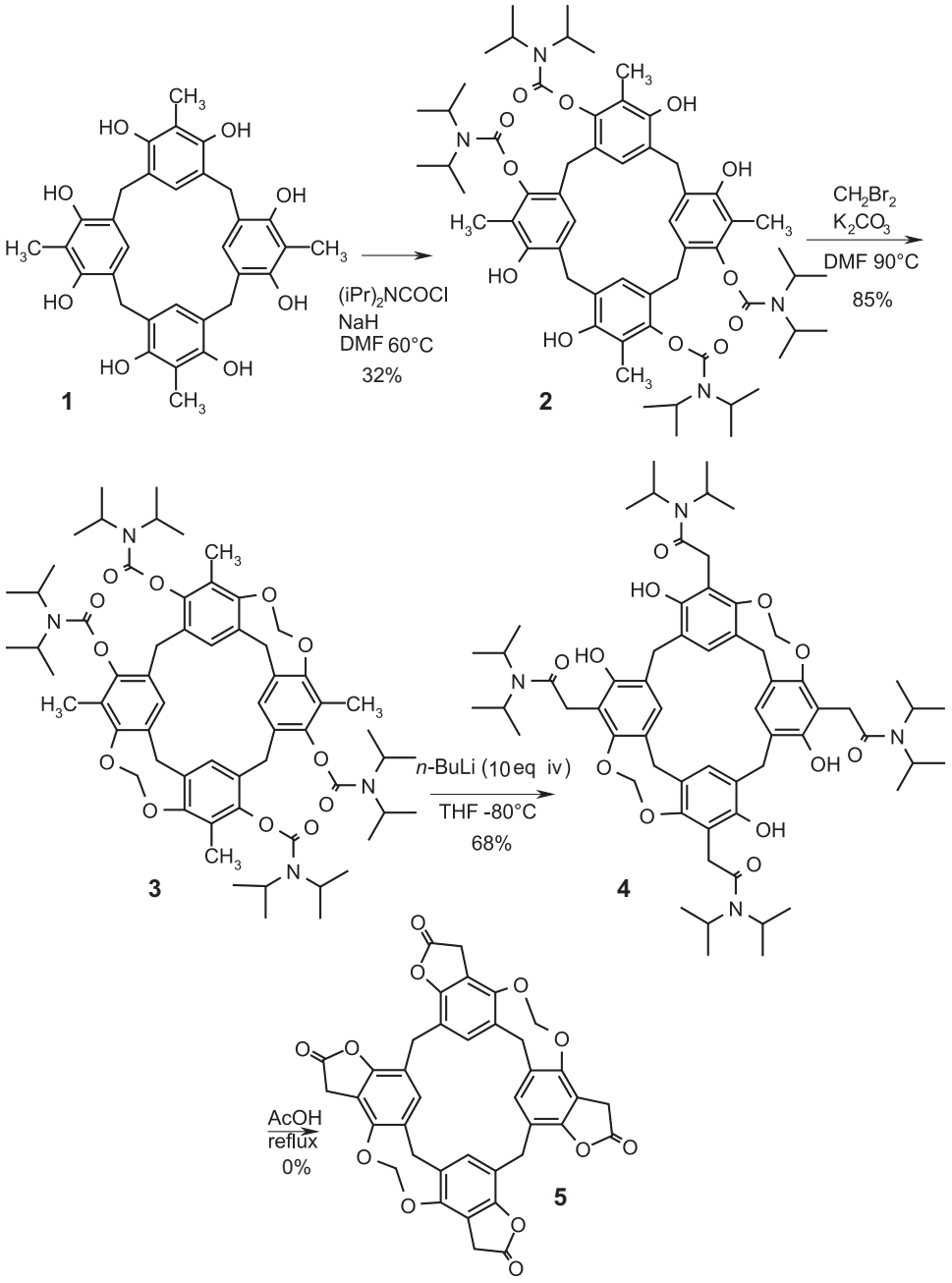
[2]Experimental and spectroscopic data of resorc[4]arenes **2**–**5** have been deposited as supplementary material. Supplementary material may be purchased from the Depository of Unpublished Data, Document Delivery, CISTI, National Research Council Canada, Ottawa, ON K1A 0S2, Canada (http://www.nrc.ca/cisti/irm/unpub_e.shtml for information on ordering electronically).

[3]Octols having lower rim substituents gave complicated reaction mixtures of multiple substitutions. Other examples giving other regioisomers: see ref. 8.

[4]In the case of esters, a dependence on solvent, base, and acylating agents was observed: see ref. 8*b*.

 DOI: 10.1139/cjc-79-11-1525 © 2001 NRC Canada

Scheme 1.



In our case, a corresponding hydrogen bond between an *O*-carbamate and a phenol moiety is probably disfavored by the steric hindrance caused by the diisopropylamine groups.

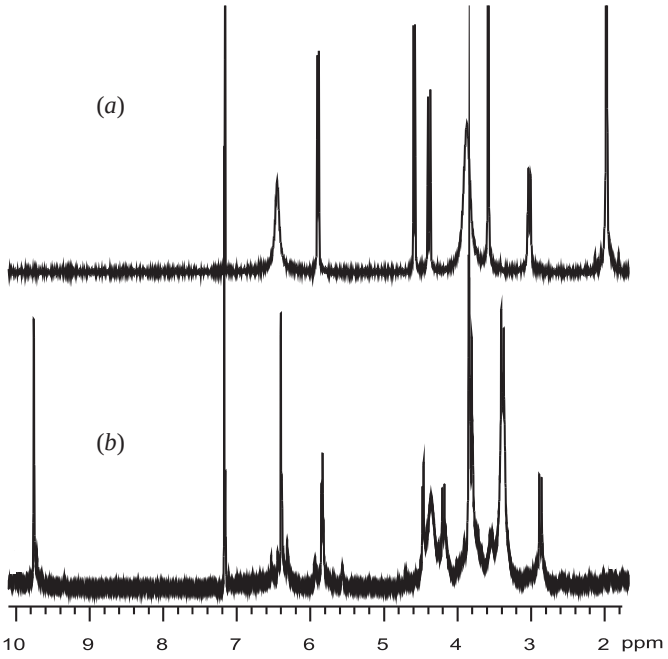
At temperatures between 297 and 333 K, compound **2** shows a broad ^{1}H NMR spectrum in $CDCl_3$, indicating the presence of rotational barriers in parts of the molecule caused by the *O*-carbamate moieties. The molecule equilibrates with rather high-energy barriers, via a *crown*[5] conformer (4), between all possible conformations almost equal in energy. Only the OH-, ArH-, and ArMe signals reside as slightly broadened singlets which suggests the presence of C_{2v}-planes of symmetry in the molecule. This symmetry element leaves two regioisomeric possibilities of which only one was isolated. Elemental analysis and FAB-MS prove that a tetra-*O*-carbamate regioisomer was obtained. However, in combination with ^{1}H NMR we have no conclusive evidence which of the two regioisomers was formed.

Definite proof for the formation of **2** was obtained by its reaction with CH_2Br_2 in the presence of K_2CO_3 as a base in DMF at 90°C for 60 h to give twofold-bridged resorc[4]arene **3** in 85% yield. The introduction of methylene bridges is only possible when adjacent phenol groups are present. The

[5] Two octol conformations are the most common: the *chair* and *crown* conformations which both can be bridged to a cavitand giving pairs of axial and equatorial lower rim substituents or exclusively axial substituents, respectively.

© 2001 NRC Canada

Fig. 1. ^{1}H NMR spectra of: (*a*) tetra-*O*-carbamate **3**; and (*b*) tetraamide **4**.



bridging reaction requires a higher reaction temperature and consequently, the use of CH_2Br_2 instead of CH_2BrCl[6], compared to the standard procedure for the fourfold bridging of both crown (3) and chair resorc[4]arenes (4). This is probably caused by the rather high rotational barriers in **2** (vide supra). Since there are no lateral substituents in **2**, the different conformers all give the same reaction product. The ^{1}H NMR spectrum of **3** (Fig. 1*a*) clearly proves the introduction of two bridges and shows a symmetry in which all ArH and $ArCH_3$ positions are equivalent in agreement with the proposed structure. This is an additional proof of the structure of the tetra-*O*-carbamate **2**.

Ortho-lithiation was accomplished by treating **3** with 10 equiv of *n*-BuLi in THF at –80°C. Upon warming, the reaction mixture slowly to room temperature and stirring at that temperature for 36 h, followed by quenching with aq NH_4Cl, the tetracarboxamide migrated compound **4** was obtained in 68%. The homologous anionic *ortho*-Fries rearrangement resulted in the migration of the carboxamide moieties to the methyl groups since they have the most acidic hydrogen atom upon *ortho*-lithiation in the presence of the *ortho*-directing diisopropyl-*O*-carbamates. The lateral bridge positions are less acidic and are sterically, as well as energetically disfavored for deprotonation since the formation of a five-membered intermediate structure (4) is not easily accomplished. Figure 1 shows the ^{1}H NMR spectra of the starting material (**3**) (*a*) and the rearranged product (**4**) (*b*), clearly visualizing the disappearance of the methyl groups upon migration. Furthermore, the signals for the phenolic groups and the resulting carboxamidomethyl moieties (Fig. 1*b*) reside as a singlet at δ 9.90 and as a double doublet at δ 3.52 and 3.93 (J_{AB} = 13.8 Hz), respectively. Consecutive functional group transformations using the phenol moieties, is demonstrated by the synthesis of tetra-γ-lactone **5,** which is obtained in 70% yield upon refluxing tetraamide **4** in AcOH for 24 h. The lack of isopropyl and ArOH signals in the ^{1}H NMR spectrum, the typical γ-lactone signal at 1812 cm^{-1} in the IR spectrum, and the molecular mass peak (EI–MS) prove the formation of tetra-γ-lactone **5**.

In conclusion, to the best of our knowledge, in this communication we have described the first example of a fourfold homologous anionic *ortho*-Fries rearrangement. By making use of the D*o*M concept, the twofold-bridged tetrakis-(carboxamidomethyl)resorc[4]arene **4** was obtained, which is, upon further transformations, of interest as a building block in supramolecular chemistry.

Acknowledgements

We are grateful to NATO (grant 930740-Supramolecular Chemistry Program) and the Council for Chemical Sciences of the Netherlands Organization for Scientific Research (CW-NWO) for financial support. O.M. warmly thanks the Snieckus lab for the personal guidance in the field of D*o*M and the hospitality during his stay at Queen's University.

References

1. (*a*) J.M. Fu and V. Snieckus. Can. J. Chem. **78**, 905 (2000); (*b*) C. Lane and V. Snieckus. Synlett, 1294 (2000); (*c*) V. Snieckus, Chem. Rev. **90**, 879 (1990).
2. O. Middel, Z. Greff, N.J. Taylor, W. Verboom, D.N. Reinhoudt, and V. Snieckus. J. Org. Chem. **65**, 667 (2000).
3. P. Timmerman, W. Verboom, and D.N. Reinhoudt. Tetrahedron, **52**, 2663 (1996).
4. (*a*) O. Middel, W. Verboom, R. Hulst, H. Kooijman, A.L. Spek, and D.N. Reinhoudt. J. Org. Chem. **63**, 8259 (1998), and refs. therein. (*b*) W. Verboom. Cavitands. *In* Calixarenes 2001. *Edited by* Z. Asfari, V. Böhmer, J. Harrowfield, and J. Vicens. Kluwer Academic Publishers, Dordrecht. 2001.
5. A. Shivanyuk, C. Schmidt, V. Böhmer, E.F. Paulus, O.V. Lukin, and W.J. Vogt. J. Am. Chem. Soc. **120**, 4319 (1998).
6. J.C. Sherman, C.B. Knobler, and D.J. Cram. J. Am. Chem. Soc. **113**, 2194 (1991).
7. (*a*) O. Haba, K. Haga, and M. Ueda. Chem. Mater. **11**, 427 (1999); (*b*) H. Konishi, T. Tamura, H. Ohkubo, K. Kobayashi, and O. Morikawa. Chem. Lett. 685 (1996).
8. (*a*) O. Lukin, A. Shivanyuk, V.V. Pirozhenko, I.F. Tsymbal, and V.I. Kalchenko. J. Org. Chem. **63**, 9510 (1998); (*b*) A. Shivanyuk, E. Paulus, V. Böhmer, and W.J. Vogt. J. Org. Chem. **63**, 6448 (1998).
9. J.R. Fransen and P.J. Dutton. Can. J. Chem. **73**, 2217 (1995).
10. A.V. Kalinin, M.A.J. Miah, S. Chattopadhyay, M. Tsukazaki, M. Wicki, T. Nguen, A.L. Coelho, M. Kerr, and V. Snieckus. Synlett, 839 (1997).
11. H. Konishi, Y. Iwasaki, O. Morikawa, T. Okano, and J. Kiji. Chem. Express, **5**, 869 (1990).

[6] Using bromochloromethane at 60°C, a complex reaction product mixture was obtained.

© 2001 NRC Canada

Asymmetric synthesis of 3-aryl-substituted 2,3-dihydro-1*H*-isoindol-1-ones

Dieter Enders, Volker Braig, and Gerhard Raabe

Abstract: The first asymmetric synthesis of 3-aryl substituted 2,3-dihydro-1*H*-isoindol-1-ones via a tandem nucleophilic 1,2-addition ring closure procedure from SAMP and (or) RAMP hydrazones and subsequent oxidative cleavage of the auxiliary is reported.

Key words: isoindolinones, asymmetric synthesis, hydrazones, 1,2-addition, N—N bond cleavage.

Résumé : On a réalisé la première synthèse asymétrique de 2,3-dihydro-1*H*-isoindol-1-ones substituées en position 3 par un groupe aryle; la synthèse est réalisée par le biais d'une réaction de fermeture de cycle par addition nucléophile 1,2 en tandem à partir des hydrazones SAMP et (ou) RAMP, suivie d'une fermeture oxydante de l'auxiliaire.

Mots clés : isoindolinones, synthèse asymétrique, hydrazones, addition-1,2, clivage de liaisons N—N.

[Traduit par la Rédaction]

Introduction

2,3-Dihydro-1*H*-isoindol-1-ones **1** are known under different names in the literature such as isoindolinones or phthalimidines and are found as a core unit in various natural products. Shamma and co-workers (1) isolated the compounds neuvamine **2**, chilenine **3**, lennoxamine **4**, magallanesine **5**, and pictonamine **6** (Fig. 1). Isoindolinone moieties can also be found in pharmacologically active synthetic substances. For example, compound **7** inhibits the activity of thromboxane A_2 analogue (U-46619)-induced vasoconstriction (2). 3-Substituted 2,3-dihydro-1*H*-isoindol-1-ones can also modulate the common allosteric binding site of the muscarine M_2 receptors, for example the dimer **8** (3). Finally, compounds such as **9** are inhibitors of the HIV-1 reverse transcriptase (4; for further examples see ref. 5).

There are many methods for the synthesis of 3-carbon-substituted isoindolinones described in the literature. The most common strategies are shown retrosynthetically in Fig. 2.

Method **I** may be achieved via substitution of a 3-chloroisoindolinone (6), a nucleophilic addition to either an *N*-acyliminium ion (7) or to a carbonyl group and subsequent reduction of the *N*,*O*-acetal (8, 6*b*). Another possibility for the cut **I** is the addition of an electrophile to a deprotonated isoindolinone (9, 10). Ring closure reactions are involved in methods **II**–**IV.** Method **II** is either possible via radical cyclisations (11) or as palladium-catalyzed ring closure reactions (12). 2-Vinyl-benzamides (13), 2-vinyl-benzonitriles (13*b*), or 2-acyl-benzamides (14) can be cyclised according to method **III**. The important reaction of method **IV** is the formation of the lactam ring (15). The common feature of methods **V**–**VII** is that the isoindolinone is built with two reactants, one is a substituted benzene and the other reactant contributes to the isoindolinone ring a one-atom unit. In method **V**, the 3-position carbon atom is brought into the ring (16). Method **VI** involves the reaction of an amine with either 2-acyl or 2-aroyl benzoic acids or esters (17), 2-(bromo-ethoxycarbonyl-methyl)-benzoic acid ethyl ester (18), or 2-(2-nitro-ethylen)-benzoic acid methyl ester (19). A newer version of method **VI** is based on *N*,*O*-acetals as intermediates, which can be opened, leading to enantiomerically enriched 3-subsituted isoindolinones (20). Method **VII** offers the possibility to obtain chiral 3-substituted isoindolinones, because the 3-position is not involved in the reaction (21). Method **VIII** is based on a nucleophilic addition to a C—N double bond to build the isoindolinone unit (22). It is also possible to synthesize isoindolinones via rearrangements (6*a*, 3*b*, 23) or the reduction of 3-alkylidene-isoindolinones to 3-alkyl-isoindilinones (24, 19).

In this paper, we report on the first asymmetric synthesis of 3-aryl-substituted isoindolinones via nucleophilic 1,2 addition to RAMP-hydrazones according to method **VIII**.

Results and Discussion

As shown in Scheme 1 the RAMP or SAMP hydrazones were prepared in good yields in a facile procedure. The freshly distilled aldehydes were condensed with neat RAMP or SAMP, to obtain the corresponding hydrazones **11a**–**c** in almost quantitative yields (Table 1).

The nucleophilic 1,2-addition to SAMP or RAMP hydrazones is a well-established method to obtain enantiopure

Received February 27, 2001. Published on the NRC Research Press Web site at http://canjchem.nrc.ca on October 19, 2001.

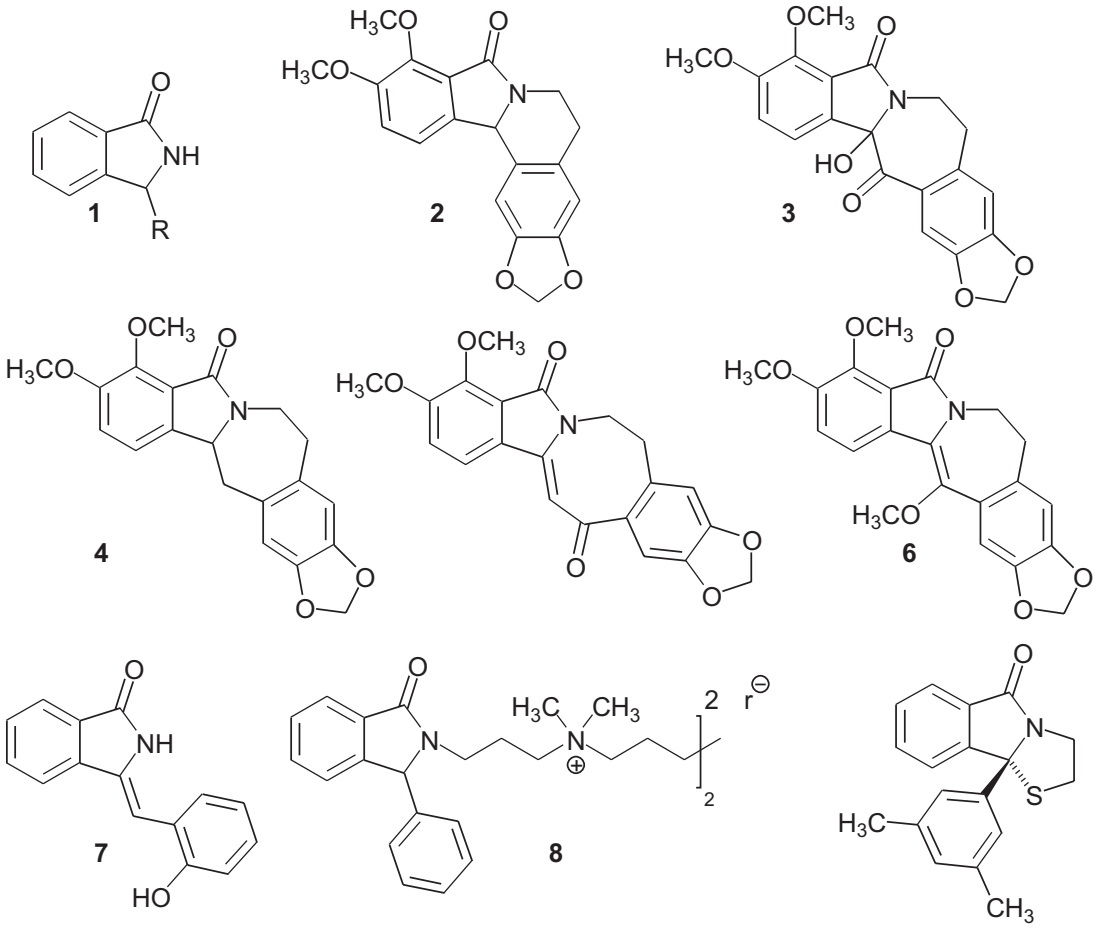
Dedicated to Professor Victor Snieckus for his contributions to Canadian chemistry.

Dieter Enders,[1] Volker Braig, and Gerhard Raabe. Institut für Organische Chemie, Rheinisch-Westfälische Technische Hochschule, Professor-Pirlet-Straβe 1, 52074 Aachen, Germany.

[1]Corresponding author (fax: +49 (0)241/8092-127; e-mail: Enders@RWTH-Aachen.de).

 DOI: 10.1139/cjc-79-11-1528 © 2001 NRC Canada

Fig. 1.



amines (25). For example, a recent application led to syntheses of the pheromone harmonine (26) and the defence alkaloid of the mexican bean beetle, *Epilachana varivestis* (Coccinellidae) (27). In our synthesis we applied lithiated diethylbenzamides as nucleophiles, generated by directed *ortho*-metalation (DoM) (28), which underwent smooth nucleophilic 1,2-addition to the C—N double bond of aldehydehydrazones **11a**–**c** followed by in situ ring closure to afford the corresponding isoindolinones **13a**–**e.** This tandem reaction was performed in satisfactory to good yields (Table 2) and high diastereomeric excesses.[2] To drive the reaction to completion, we had to use 11 equiv of diethylbenzamides **12a**–**b** and 10 equiv of *sec*-butyllithium. Reaction of only 4.5 equiv of both substrates gave a poor yield (17% of compound (*S*,*S*)-**13e**). We also investigated halogen metal exchange of 2-iodobenzoic acid esters and DoM of methylbenzamide instead of the diethylbenzamides **12a**–**b**, but no product was observed. Recrystallization of the SAMP-derivative (*S*,*S*)-**13e** allowed the assignment of the configuration of the new generated stereocenter by X-ray analysis (Fig. 3). It was found to be *S*-configured, as expected (29).

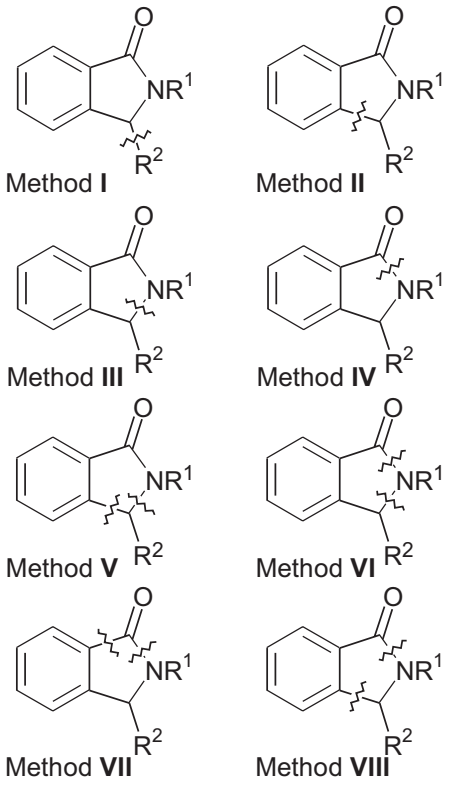
To obtain a good diastereomeric excess, careful control of the reaction temperature is important: if the warm-up of the reaction mixture was too fast the diastereomeric excesses were observed to decrease. To see if the reaction tolerated substitution at the aromatic ring, we used the benzamide **12b** with success. To further extend the scope of this reaction aliphatic hydrazones (R^1 = *tert*-butyl, isopropyl) were screened but no acceptable results could be obtained.

We next examined the N—N bond cleavage of the auxiliary to release the enantio-enriched amines (30). A variety of methods were applied to the hydrazines **13a**–**e**, but we obtained either a complex mixture (BH_3·THF, O_3, Raney Ni–H_2), no reaction at all ($Na_2S_2O_4$), or cleavage but racemisation (Li–NH_3(l), Ca–NH_3(l), Zn–AcOH). The only method we could apply with success was the oxidative cleavage with magnesium monoperoxyphthalate hexahydrate (MMPP) developed by Lassaletta and co-workers (31). They used MMPP to cleave N—N bonds of SAMP-derivatives. The *N*-unsubstituted isoindolinones **14a**–**e** were obtained in very good yields and high enantiopurity. Three compounds were purified via crystallization (**14a**, **14b**, **14e**) resulting an enantiomeric excess higher than 99%. Compounds **14c** and **14d** were purified via flash chromatography, leading to an enantiomeric excess of 97% and 99%. This indicates that we could remove the auxiliary without racemization. Enantiomeric excesses were determined by HPLC on a chiral stationary phase. The racemates were prepared by racemization

[2] Determination of the diastereomeric excess of the isoindolinones **13a**–**e** was achieved by ^{1}H NMR analysis of the crude products. The singlet due to the hydrogen at the 3-position of the isoindolinone ring was used (e.g., (*S*,*S*)-**13e** δ: 5.60 ppm; (*R*,*S*)-**13e** δ: 5.07 ppm).

© 2001 NRC Canada

Fig. 2. Retrosynthetic cuts for the synthesis of isoindolinones.



of the enantiopure compounds with lithium diisopropylamide (LDA) in THF at 0°C.

In conclusion, we have developed the first asymmetric synthesis of 3-aryl-substituted 2,3-dihydro-1*H*-isoindol-1-ones via a tandem nucleophilic 1,2-addition ring closure procedure to SAMP- and (or) RAMP-hydrazones and subsequent oxidative removal of the auxiliary.

Experimental

All melting points (Büchi 510, system Dr. Tottoli) are uncorrected. Proton and carbon nuclear magnetic resonance (^{1}H NMR and ^{13}C NMR) were recorded on Varian Inova 400 (^{1}H NMR: 400 MHz; ^{13}C NMR: 100 MHz) or Varian Unity 500 (^{1}H NMR: 500 MHz; ^{13}C NMR: 125 MHz) spectrometers. Chemical shifts are reported as δ values (ppm) relative to internal Me_4Si. Coupling constants are given in Hertz (Hz). The following abbreviations report the multiplicity and shape of the signals: s (singlet), d (doublet), t (triplet), q (quartet), m (multiplet), and combinations e.g., dd (doublet of doublets). Mass spectra (MS) were obtained on Varian MAT 212 (EI: 70 eV; CI: 100 eV, Isobutan) or Finnigan MAT 95 (high resolution MS (HRMS): 70 eV). Intensities are given relative to the base peak. Infrared (IR) spectra were obtained on a PerkinElmer FT IR 1750. Elemental analyses were performed on a Heraeus CHN-O-Rapid. Optical rotations were measured with a PerkinElmer P 241 polarimeter. Reactions and the progress of chromatographic separations were monitored by TLC on silica gel (Merck Kieselgel 60 F_{254}). Flash chromatography was performed on silica gel (Merck Kieselgel 60). Reactions with moisture- or air-sensitive reagents were performed with Schlenk technique under an argon atmosphere. Tetrahydrofuran (THF) was freshly distilled from sodium lead alloy (5% Na) – benzophenone ketyl.

Synthesis of the RAMP or SAMP hydrazones 11a–c

After cooling of the aldehydes **10a–c** (1.2–2.4 equiv) to 0°C RAMP or SAMP (1 equiv) was added. This mixture was stirred for 30 min at 0°C. First, diethyl ether (4.2 mL per mmol SAMP and (or) RAMP) and then $MgSO_4$ were added. The reaction mixture was stirred overnight at room temperature. The removal of $MgSO_4$ and of the solvent afforded the oily crude hydrazones in virtually quantitative yield, which were purified by Kugelrohr distillation under reduced pressure. This reaction was typically run on a scale of 30 mmol.

*[(*E*)-Benzylidene]-[(2*R*)-2-methoxymethyl-pyrrolidine-1-yl]-amine ((*R*)-**11a**)*

Compound (*R*)-**11a** was prepared earlier in our group (29).

*[(*E*)-Benzylidene]-[(2*S*)-2-methoxymethyl-pyrrolidine-1-yl]-amine ((*S*)-**11a**)*

Compound (*S*)-**11a** was prepared earlier in our group (29).

*[(*E*)-4-Methoxy-benzylidene]-[(2*R*)-2-methoxymethyl-pyrrolidine-1-yl]-amine ((*R*)-**11b**)*

Pale yellow solid, mp 24°C. $[\alpha]_D^{23}$ = +164.6 (c = 1.02, $CHCl_3$). *m/z* (EI): 248 (3%)$(M)^+$, 203 (100)$(M\text{-}CH_3OCH_2)^+$. ν_{max} (film) (cm^{-1}): 1510, 1249, 1125, 1034, 831. ^{1}H NMR (C_6D_6, 400 MHz) δ: 1.48–1.52 (m, 1H, $NCH_2CH\mathit{H}$), 1.67–1.82 (m, 3H, $NCH_2CH\mathit{H}C\mathit{H}_2$), 2.66–2.72 (m, 1H, $NCH\mathit{H}$), 3.10–3.19 (m, 4H, $NC\mathit{H}H$, $OC\mathit{H}_3$), 3.34 (s, 3H, $OC\mathit{H}_3$), 3.42–3.48 (m, 1H, $C\mathit{H}HOCH_3$), 3.71–3.77 (m, 2H, $NC\mathit{H}C\mathit{H}HOCH_3$), 6.83–6.88 (m, 2H, N=CHCCH=C*H*), 7.15 (s, 1H, N=C*H*), 7.63–7.67 (m, 2H, N=CHCC*H*=CH). ^{13}C NMR (C_6D_6, 100 MHz) δ: 22.4, 27.3, 48.8, 54.7, 58.8, 63.4, 75.3, 114.1, 126.8, 103.9, 131.9, 159.2. Anal. calcd. for $C_{14}H_{20}N_2O_2$: C 67.71, N 11.28, H 8.12; found: C 67.66, N 10.87, H 8.11.

*[(*E*)-4-tert-Butyl-benzylidene]-[(2*R*)-2-methoxymethyl-pyrrolidine-1-yl]-amine ((*R*)-**11c**)*

Pale yellow solid, mp 38°C. $[\alpha]_D^{23}$ = +131.9 (c = 1.02, $CHCl_3$). *m/z* (EI): 274 (14%) $(M)^+$, 229 (100)$(M\text{-}CH_3OCH_2)^+$. ν_{max} (film) (cm^{-1}): 2962, 1114. ^{1}H NMR (C_6D_6, 400 MHz) δ: 1.24 (s, 9H, $C(C\mathit{H}_3)_3$), 1.45–1.55 (m, 1H, $NCH_2CH\mathit{H}$), 1.65–1.81 (m, 3H, $NCH_2CH\mathit{H}C\mathit{H}_2$), 2.65–2.74 (m, 1H, $NCH\mathit{H}$), 3.06–3.13 (m, 1H, $NC\mathit{H}H$), 3.16 (s, 3H, $OC\mathit{H}_3$), 3.42–3.48 (m, 1H, $C\mathit{H}HOCH_3$), 3.70–3.77 (m, 2H, $NC\mathit{H}C\mathit{H}HOCH_3$),7.17 (s, 1H, N=C*H*), 7.33–7.37 (m, 2H, N=CCC*H*=CH), 7.71–7.74 (m, 2H, N=CCCH=C*H*). ^{13}C NMR (C_6D_6, 100 MHz) δ: 22.4, 27.2, 31.4, 34.5, 48.6, 58.8, 63.2, 75.2, 125.4, 131.6, 135.4, 149.6. Anal. calcd. for $C_{17}H_{26}N_2O$: C 74.41, N 10.21, H 9.55; found: C 74.67, N 9.96, H 9.53.

1,2-Addition to aldehyde–SAMP-hydrazones 11 to afford the isoindolinones 13a–e

sec-Butyllithium (10.0 equiv, ca. 1.3 M in cyclohexane) was added dropwise to a solution of *N*,*N*-diethylbenzamide **12a–b** (11.0 equiv) in dry THF (7.0 mL per mmol diethylamide) at –78°C. After 2 h 30 min of stirring at –78°C, a solution of the hydrazone **11a–c** (1.0 equiv) in abs THF

© 2001 NRC Canada

Scheme 1. Asymmetric synthesis of 3-aryl-substituted isoindolinones via nucleophilic 1,2-addition to RAMP-hydrazones and subsequent intramolecular lactamization (**13e** and **14e** enantiomers prepared with SAMP instead of RAMP).

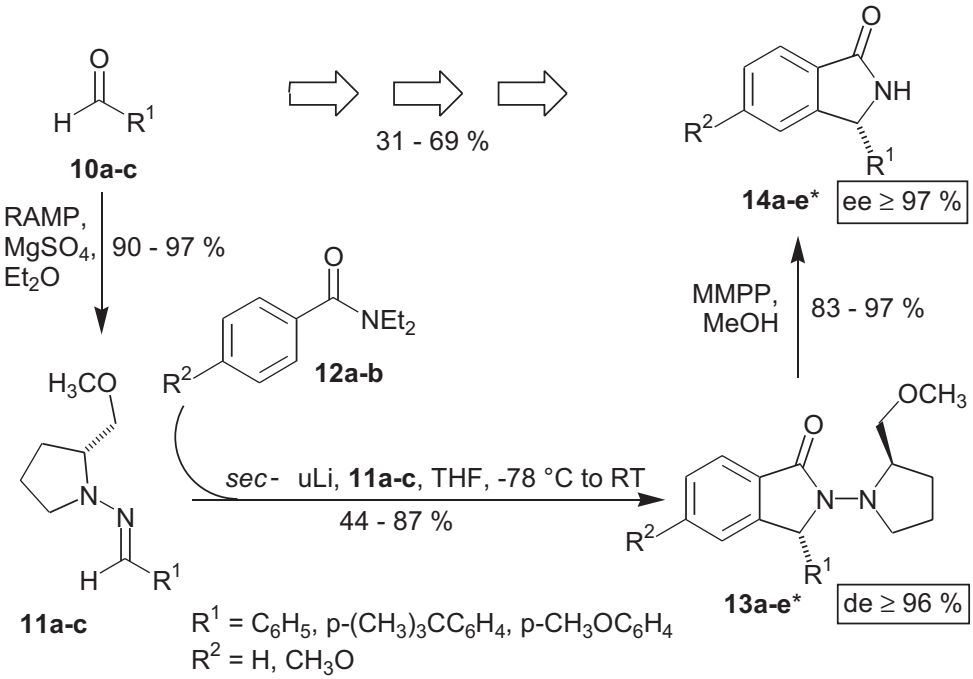


Table 1. Synthesis of the RAMP and (or) SAMP hydrazones **11a–c**.

Entry	R_1	Compound	Yield (%)
1	Phenyl	(*R*)-**11a**	95
2	Phenyl	(*S*)-**11a**	95
3	*p*-Methoxyphenyl	(*R*)-**11b**	97
4	*p-tert*-Butylphenyl	(*R*)-**11c**	90

(6.0 mL per mmol hydrazone) was added slowly. The reaction mixture was warmed slowly overnight to a temperature between –40°C and –20°C, then the reaction mixture was warmed quickly to 0°C and quenched with sat. aq NH_4Cl (5.0 mL/mmol hydrazone). After phase separation and extraction of the aqueous layer with ether, the combined organic extracts were dried over $MgSO_4$. The removal of $MgSO_4$ and solvent in vacuo at 45°C afforded an oily residue, which was purified by column chromatography.

*(3*R*)-5-Methoxy-2-[(2*R*)-2-methoxymethyl-pyrrolidine-1-yl]-3-phenyl-2,3-dihydro-1*H*-isoindol-1-one ((*R,R*)-**13a**)*

Pale yellow oil. $[\alpha]_D^{23}$ = –11.1 (c = 1.03, $CHCl_3$). *m/z* (EI): 352 (2%) $(M)^+$, 307 (100)$(M\text{-}CH_3OCH_2)^+$. *m/z* (HRMS): 307.1444 $(M–CH_3OCH_2)^+$, (calcd. for $C_{19}H_{19}N_2O_2$: 307.1447). ν_{max} (film) (cm^{-1}): 1693. ^{1}H NMR (C_6D_6, 400 MHz) δ: 1.19–1.42 (m, 2H, $NCH_2CH\mathit{H}CH\mathit{H}$), 1.65–1.75 (m, 1H, $NCH_2CH\mathit{H}$), 1.95–2.05 (m, 1H, $NCH_2CH_2CH\mathit{H}$), 2.72 (dt, *J* = 7.8, 3.5, 1H, NCH*H*), 3.06–3.15 (m, 7H, $OC\mathit{H}_3$, $OC\mathit{H}_3$, $CH\mathit{H}OCH_3$), 3.29 (dd, *J* = 7.7, 9.3, 1H, $CH\mathit{H}OCH_3$), 3.85 (dd, *J* = 8.1, 16.3, 1H, NCH*H*), 4.37–4.44 (m, 1H, $C\mathit{H}CH_2OCH_3$), 5.62 (s, 1H, NC*H*Ar), 6.53 (d, *J* = 2.2, 1H, O=CCC=C*H*), 6.71 (dd, *J* = 2.5, 8.5, 1H, O=CC=CHC*H*), 7.06–7.19 (m, 5H $C\mathit{H}_{Phenyl}$), 7.91 (d, ^3J = 8.5 Hz, 1H, O=CC=C*H*CH). ^{13}C NMR (C_6D_6, 100 MHz) δ: 23.1, 27.4, 53.5, 54.8, 58.4, 60.2, 67.5, 77.3, 108.1, 115.0, 124.8, 125.2, 128.6, 139.1, 147.3, 163.0, 166.1.

*(3*R*)-5-Methoxy-2-[(2*R*)-2-methoxymethyl-pyrrolidine-1-yl]-3-(4-methoxy-phenyl)-2,3-dihydro-1*H*-isoindol-1-one ((*R,R*)-**13b**)*

Colorless oil. $[\alpha]_D^{26}$ = +20.4 (c = 1.17, $CHCl_3$). *m/z* (EI): 382 (2%) $(M)^+$, 337 (100)$(M\text{-}CH_3OCH_2)^+$. *m/z* (HRMS): 382.1892 $(M)^+$, (calcd. for $C_{22}H_{26}N_2O_4$: 382.1893). ν_{max} (film) (cm^{-1}): 1691, 1242. ^{1}H NMR (C_6D_6, 400 MHz) δ: 1.22–1.45 (m, 2H, $NCH_2CH\mathit{H}CH\mathit{H}$), 1.67–1.76 (m, 1H, $NCH_2CH\mathit{H}$), 1.97–2.07 (m, 1H, $NCH_2CH_2CH\mathit{H}$), 2.75 (dt, *J* = 7.7, 4.9, 1H, NCH*H*), 3.12–3.18 (m, 7H, $OC\mathit{H}_3$, $CH\mathit{H}OC\mathit{H}_3$), 3.30–3.36 (m, 4H, $OC\mathit{H}_3$, $CH\mathit{H}OCH_3$), 3.85 (dd, *J* = 8.2, 16.4, 1H, NCH*H*), 4.38–4.46 (m, 1H, $C\mathit{H}CH_2OCH_3$), 5.59 (s, 1H, NC*H*Ar), 6.60 (d, *J* = 2.2, 1H, O=CCC=C*H*), 6.71–6.77 (m, 3H, O=CC=CHC*H*, NCHC=C*HCH*), 7.08–7.12 (m, 2H, NCHC=C*HCH*), 7.92 (m, *J* = 8.5, 1H, O=CC=C*H*). ^{13}C NMR (C_6D_6, 100 MHz) δ: 23.1, 27.4, 53.4, 54.7, 54.9, 58.4, 60.2, 66.9, 77.3, 108.1, 114.1, 115.0, 124.7, 125.3, 129.8, 130.8, 147.6, 159.8, 163.0, 165.9.

*(3*R*)-3-(4-*tert*-Butyl-phenyl)-2-[(2*R*)-2-methoxymethyl-pyrrolidine-1-yl]-2,3-dihydro-1*H*-isoindol-1-one ((*R,R*)-**13c**)*

Colorless solid, mp = 123°C. $[\alpha]_D^{26}$ = +71.7 (c = 1.15, $CHCl_3$). *m/z* (EI): 378 (2%) $(M)^+$, 333 (100)$(M\text{-}CH_3OCH_2)^+$. ν_{max} (KBr) (cm^{-1}): 1687. ^{1}H NMR (C_6D_6, 400 MHz) δ: 1.15–1.36 (m, 11H, $NCH_2CH\mathit{H}CH\mathit{H}$, $C(C\mathit{H}_3)_3$), 1.64–1.74 (m, 1H, $NCH_2CH\mathit{H}$), 1.94–2.04 (m, 1H, $NCH_2CH_2CH\mathit{H}$), 2.79–2.84 (m, 1H, NCH*H*), 3.08 (s, 3H, $OC\mathit{H}_3$), 3.11 (dd, *J* = 4.5, 9.5, 1H, $CH\mathit{H}OCH_3$), 3.29 (dd, *J* = 7.7, 9.6, 1H, $CH\mathit{H}OCH_3$), 3.90 (dd, *J* = 8.1, 16.1, 1H, NCH*H*), 4.36–4.45 (m, 1H, $C\mathit{H}CH_2OCH_3$), 5.66 (s, 1H, NC*H*Ar), 6.84–6.88 (m, 1H, O=CCC=C*H*), 6.99–7.07 (m, 2H, O=CC=CHC*H*=C*H*),

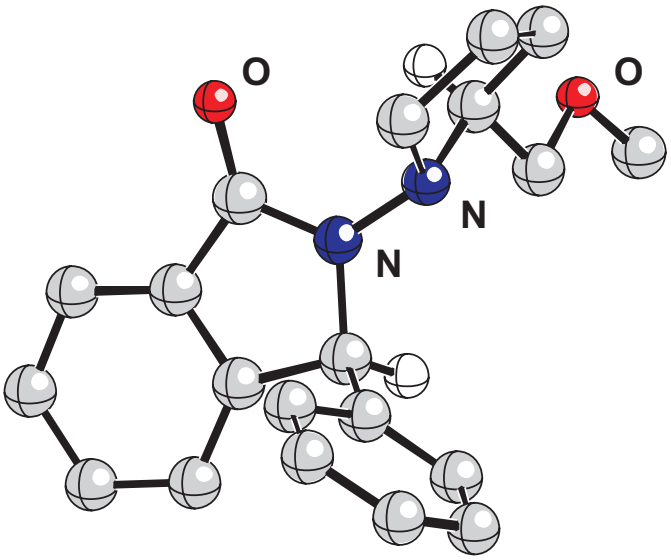
© 2001 NRC Canada

Table 2. Synthesis of compounds **13a**–**e**.

Entry	R_1	R_2	Compound	Yield (%)	de (%)[a]
1	Phenyl	CH_3O	(*R*,*R*)-**13a**	44	≥96
2	*p*-Methoxyphenyl	CH_3O	(*R*,*R*)-**13b**	55	94, ≥96[b]
3	*p*-*tert*-Butylphenyl	H	(*R*,*R*)-**13c**	77	≥96
4	*p*-*tert*-Butylphenyl	CH_3O	(*R*,*R*)-**13d**	76	≥96
5	Phenyl	H	(*S*,*S*)-**13e**[c]	87	≥96

[a]Determined by NMR of the crude product.
[b]After chromatography.
[c]Prepared with SAMP instead of RAMP.

Fig. 3. X-ray structure of (3*S*)-2-[(2*S*)-2-methoxymethyl-pyrrolidin-1-yl)-3-phenyl-2,3-dihydro-1*H*-isoindol-1-one ((*S*,*S*)-**13e**).



7.12–7.17 (m, 2H, NCHC=C*H*C*H*=CC$(CH_3)_3$), 7.20–7.24 (m, 2H, NCHC=C*H*C*H*=CC$(CH_3)_3$), 7.97–8.01 (m, 1H, O=CC=C*H*). ^{13}C NMR (C_6D_6, 100 MHz) δ: 23.1, 27.4, 31.3, 34.4, 53.4, 58.4, 60.4, 67.4, 77.2, 123.2, 123.3, 125.5, 128.0, 128.3, 131.4,132.6, 135.8, 145.5, 150.8, 166.1. Anal. calcd. for $C_{24}H_{30}N_2O_2$: C 76.16, N 7.40, H 7.99; found: C 76.10, N 7.34, H 7.71.

*(3*R*)-3-(4*-tert-*Butyl-phenyl)-5-methoxy-2-[(2*R*)-2-methoxymethyl-pyrrolidine-1-yl]-2,3-dihydro-1*H*-isoindol-1-one ((*R,R*)-**13d**)*

Colorless solid, mp 138°C. $[\alpha]_D^{28}$ = –6.6 (c = 1.09, $CHCl_3$). *m*/*z* (EI): 408 (2%) $(M)^+$, 363 (100)$(M\text{-}CH_3OCH_2)^+$. ν_{max} (KBr) (cm^{-1}): 1684, 1608, 1286. ^{1}H NMR (C_6D_6, 400 MHz) δ: 1.15–1.37 (m, 11H, $NCH_2CHHCHH$, $C(CH_3)_3$), 1.66–1.76 (m, 1H, NCH_2CHH), 1.97–2.06 (m, 1H, NCH_2CH_2CHH), 2.80–2.86 (m, 1H, NCH*H*), 3.03 (s, 3H, OCH_3), 3.12 (s, 3H, OCH_3), 3.15 (dd, *J* = 4.5, 9.5, 1H, $CHHOCH_3$), 3.33 (dd, *J* = 7.7, 9.4, 1H, $CHHOCH_3$), 3.92 (dd, *J* = 8.2, 16.2, 1H, NCH*H*), 4.39–4.46 (m, 1H, $CHCH_2OCH_3$), 5.67 (s, 1H, NC*H*Ar), 6.55 (d, *J* = 2.5, 1H, O=CCC=C*H*), 6.71 (dd, *J* = 2.2, 8.2, 1H, O=CC=CHC*H*), 7.19–7.27 (m, 4H, $(CH_3)_3CCCH$=C*H*), 7.92 (d, *J* = 8.2, 1H, O=CC=C*H*). ^{13}C NMR (C_6D_6, 100 MHz) δ: 23.1, 27.4, 31.3, 34.5, 53.5, 54.7, 58.4, 60.4, 67.3, 77.3, 108.0, 115.1, 124.8, 125.1, 125.6, 128.3, 136.2, 147.6, 150.8, 163.0, 166.1. Anal. calcd. for $C_{25}H_{32}N_2O_3$: C 73.50, N 6.86, H 7.90; found: C 73.41, N 6.69, H 7.95.

*(3S)-2-[(2S)-2-Methoxymethyl-pyrrolidine-1-yl]-3-phenyl-2,3-dihydro-1*H*-isoindol-1-one ((*S,S*)-**13e**)*

Colorless solid, mp = 96°C. $[\alpha]_D^{28}$ = +69.6 (c = 0.65, $CHCl_3$). *m*/*z* (CI): 323 (100%) $(MH)^+$. ν_{max} (KBr) (cm^{-1}): 1685. ^{1}H NMR (C_6D_6, 500 MHz) δ: 1.19–1.36 (m, 2H, $NCH_2CHHCHH$), 1.64–1.72 (m, 1H, NCH_2CHH), 1.93–2.02 (m, 1, NCH_2CH_2CHH), 2.70 (dt, *J* = 7.8, 3.7, 1H, NCH*H*), 3.03 (s, 3H, OCH_3), 3.09 (dd, *J* = 4.3, 9.5, 1H, $CHHOCH_3$), 3.25 (dd, *J* = 7.6, 9.5, 1H, $CHHOCH_3$), 3.82 (dd, *J* = 8.2, 16.5, 1H, NCH*H*), 4.35–4.41 (m, 1H, $CHCH_2OCH_3$), 5.60 (s, 1H, NC*H*Ar), 6.81–6.85 (m, 1H, O=CCC=C*H*), 7.02–7.18 (m, 7H, O=CC=CHC*H*=C*H*, CH_{Phenyl}), 7.94–7.98 (m, 1H, O=CC=C*H*). ^{13}C NMR (C_6D_6, 125 MHz) δ: 23.1, 27.4, 53.4, 58.4, 60.4, 67.7, 77.3, 123.3, 123.4, 128.2, 128.2, 128.7, 131.6,132.8, 139.0, 145.3, 166.2. Anal. calcd. for $C_{20}H_{22}N_2O_2$: C 74.51, N 8.69, H 6.88; found: C 74.63, N 8.66, H 6.96.

*Crystal data and refinement details for (S,S)-**13e**:* $C_{20}H_{22}N_2O_2$; fw = 322.41; orthorhombic; space group $P2_12_12_1$ (no. 19); *a* = 6.1386(8), *b* = 12.392(1), *c* = 22.328(6) Å; *V* = 1698.5(5) $Å^3$; *Z* = 4; ρ_c = 1.261 g cm^{-3}; μ = 6.51 cm^{-1}, no absorption correction; *T* = 150 K; CuKα (1.54179 Å). An irregularly shaped crystal (~0.3 × 0.3 × 0.3 mm^3) was mounted on top of a capillary in a stream of cooled nitrogen. 3472 unique reflections were collected in the range: *h*: ±7, *k*: ±15, and *l*: ±27 (r_{av} = 0.01(5)) on an Enraf–Nonius CAD4 diffractometer in the ω/2Θ mode. The structure has been solved by direct methods (GENSIN/GENTAN) as implemented in the Xtal3.4 suite of crystallographic routines (32). 3130 observed reflections ($I > 2\sigma(I)$) in the final full-matrix least-squares refinement of 217 variables terminating at *r* = 0.061 (r_w = 0.066, $w = \sigma^{-2}$), a residual electron density of –0.33/+0.40 e $Å^{-3}$, a max shift/error of 0.13 × 10^{-3}, and a goodness-of-fit of 1.744. The atomic scattering factors are those from ref. 33. No extinction correction. Hydrogen atoms were calculated in idealized positions and their *U*s were fixed at 1.5 times *U* of the relevant heavy atom prior to final refinement. No refinement of hydrogen positions. The chirality of the new generated stereocenter was fixed using the known configuration of the auxiliary (Fig. 3).

The refined non-hydrogen atomic coordinates for (*S*,*S*)-**13e** are listed in Table 4 while the hydrogen coordinates, temperature factors (anisotropic for carbon atoms), scale factor, and

© 2001 NRC Canada

Table 3. Synthesis of compounds **14a–e**.

Entry	R_1	R_2	Compound	Yield (%)	ee (%)[a]
1	Phenyl	CH_3O	(*R*)-**14a**	74	≥99
2	*p*-Methoxyphenyl	CH_3O	(*R*)-**14b**	85	≥99
3	*p*-*tert*-Butylphenyl	H	(*R*)-**14c**	97	97[b]
4	*p*-*tert*-Butylphenyl	CH_3O	(*R*)-**14d**	85	99[b]
5	Phenyl	H	(*S*)-**14e**[c]	83	≥99

[a]Determined by HPLC on chiral phase.
[b]Purified by column chromatography.
[c]Prepared with SAMP instead of RAMP.

secondary estimation coefficient for (*S*,*S*)-**13e** are available on request.[3]

N—N bond cleavage for the synthesis of title compounds 14a–e

MMPP·6 H_2O (2.0 to 2.5 equiv) was added to a solution of hydrazine **13a–e** (1.0 equiv) in methanol (13.0 mL per mmol hydrazine). Stirring at room temperature (24–96 h) was continued until no hydrazine remained (TLC monitoring). If the reaction stops before all hydrazine has reacted, it is possible to add a further amount of MMPP·6 H_2O (0.5 equiv). After dilution of the reaction mixture with ether (60.0 mL per mmol hydrazine), a sat. aq $NaHCO_3$ solution (43.0 mL per mmol hydrazine) was added. The aqueous layer was extracted with chloroform after phase separation. The combined organic extracts were dried ($MgSO_4$) and the solvent was removed in vacuo. The residue was either purified by flash chromatography or crystallization from ethyl acetate.

*(3*R*)-5-Methoxy-3-phenyl-2,3-dihydro-1*H*-isoindol-1-one ((*R*)-**14a**)*

Colorless solid, mp = 219°C. $[\alpha]_D^{26}$ = –52.2 (c = 0.81, $CHCl_3$). *m*/*z* (EI): 239 (100%)$(M)^+$, 208 (43)$(M\text{-}CH_3O)^+$, 162 (34)$(M\text{-}Ph)^+$. ν_{max} (KBr) (cm^{-1}): 1690, 1664, 1610. ^1H NMR (d_6-DMSO, 400 MHz) δ: 3.69 (s, 3H, OC*H*$_3$), 5.60 (s, 1H, NHC*H*), 6.73 (d, *J* = 1.5, 1H, O=CCCC*H*), 6.98 (dd, *J* = 8.5, 1.9, 1H, O=CCCH=C*H*), 7.21–7.35 (m, 5H, C*H*$_{Phenyl}$), 7.59 (d, *J* = 8.5, 1H, O=CCC*H*=CH), 8.81 (s, 1H, N*H*). ^{13}C NMR (d_6-DMSO, 100 MHz) δ: 56.4, 60.1, 108.7, 115.5, 124.4, 125.0, 127.2, 128.6, 129.4, 140.3, 151.1, 163.1, 170.3. Anal. calcd. for $C_{15}H_{13}NO_2$: C 75.30, N 5.85, H 5.48; found: C 74.96, N 5.84, H 5.76.

*(3*R*)-5-Methoxy-3-(4-methoxy-phenyl)-2,3-dihydro-1*H*-isoindol-1-one ((*R*)-**14b**)*

Colorless solid, mp = 168°C. $[\alpha]_D^{27}$ = +3.6 (c = 0.73, $CHCl_3$). *m*/*z* (EI): 269 (100%)$(M)^+$, 238 (38)$(M\text{-}CH_3O)^+$. *m*/*z* (HRMS): 269.10513 $(M)^+$, (calcd. for $C_{16}H_{15}NO_3$: 269.10519). ν_{max} (KBr) (cm^{-1}): 1706, 1620, 1278, 1241. ^1H NMR($CDCl_3$, 400 MHz) δ: 3.78 (s, 3H, OC*H*$_3$), 3.79 (s, 3H, OC*H*$_3$), 5.51 (s, 1H, NHC*H*), 6.66 (d, *J* = 2.2, 1H, O=CCCC*H*), 6.83 (s, 1H, N*H*), 6.85–6.89 (m, 2H, NHCHCCH=C*H*) 6.97 (dd, *J* = 8.2, 2.2, 1H, O=CCCH=C*H*), 7.15–7.19 (m, 2H, NHCHCC*H*=CH), 7.77 (d, *J* = 8.5, 1H, O=CCC*H*=CH). ^{13}C NMR ($CDCl_3$, 100 MHz) δ: 55.6, 55.9, 60.4, 108.1, 114.6, 115.3, 124.7, 125.3, 128.3, 130.7, 150.9, 159.9, 163.5, 171.0.

Table 4. Fractional atomic coordinates for non-hydrogen atoms, with estimated standard deviations in parentheses, for (3*S*)-2-[(2*S*)-2-methoxymethyl-pyrrolidin-1-yl)-3-phenyl-2,3-dihydro-1*H*-isoindol-1-one ((*S*,*S*)-**13e**) and the isotropic equivalent displacement parameters.

Atom	*x*	*y*	*z*	U_{eq} (Å^2)
N1	0.9131(5)	0.4598(2)	0.6268(1)	0.0264(9)
N2	0.8949(5)	0.4844(2)	0.6877(1)	0.0268(9)
O1	1.2427(5)	0.3690(2)	0.6257(1)	0.0371(8)
O2	0.6337(4)	0.2484(2)	0.7545(1)	0.0369(9)
C1	1.0743(7)	0.5517(3)	0.7110(2)	0.036(1)
C2	1.0645(7)	0.5341(4)	0.7781(2)	0.046(2)
C3	0.9234(9)	0.4338(4)	0.7883(2)	0.053(2)
C4	0.8745(7)	0.3892(3)	0.7264(2)	0.029(1)
C5	0.7408(7)	0.4930(3)	0.5854(2)	0.027(1)
C6	0.8195(6)	0.4436(3)	0.5276(2)	0.027(1)
C7	0.7257(7)	0.4432(3)	0.4706(2)	0.034(1)
C8	0.8349(8)	0.3933(3)	0.4242(2)	0.039(1)
C9	1.0373(8)	0.3453(3)	0.4337(2)	0.039(1)
C10	1.1332(7)	0.3463(3)	0.4904(2)	0.034(1)
C11	1.0223(6)	0.3952(3)	0.5369(2)	0.027(1)
C12	1.0796(6)	0.4043(3)	0.5997(2)	0.027(1)
C13	0.6479(7)	0.3438(3)	0.7207(2)	0.032(1)
C14	0.4219(8)	0.2016(3)	0.7506(2)	0.049(1)
C15	0.7126(6)	0.6140(3)	0.5829(2)	0.025(1)
C16	0.5187(7)	0.6629(3)	0.5983(2)	0.038(1)
C17	0.4961(8)	0.7724(4)	0.5961(2)	0.052(2)
C18	0.6681(9)	0.8370(3)	0.5786(2)	0.049(2)
C19	0.8625(8)	0.7891(3)	0.5625(2)	0.044(1)
C20	0.8850(7)	0.6791(3)	0.5647(2)	0.036(1)

*(3*R*)-3-(4-*tert*-Butyl-phenyl)-2,3-dihydro-1*H*-isoindol-1-one ((*R*)-**14c**)*

Colorless solid, mp = 226°C. $[\alpha]_D^{27}$ = –117.4 (c = 1.00, $CHCl_3$). *m*/*z* (EI): 265 (100%)$(M)^+$, 250 (67)$(M\text{-}CH_3)^+$, 208 (34)$(M\text{-}C(CH_3)_3)^+$. ν_{max} (KBr) (cm^{-1}): 1698, 1657. ^1H NMR ($CDCl_3$, 400 MHz) δ: 1.29 (s, 9H, C(C*H*$_3$)$_3$), 5.61 (s, 1H, NHC*H*), 7.18–7.22 (m, 2H, NHCHCC*H*=CH), 7.23–7.27 (m, 1H, O=CC=CC*H*), 7.30 (s, 1H, N*H*), 7.34–7.38 (m, 2H,

[3]Supplementary material may be purchased from the Depository of Unpublished Data, Document Delivery, CISTI, National Research Council Canada, Ottawa, ON K1A 0S2, Canada (http://www.nrc.ca/cisti/irm/unpub_e.shtml for information on ordering electronically). Crystallographic data for the structure reported in this paper have been deposited with the Cambridge Crystallographic Data Centre (CCDC 158 453). Copies of the data can be obtained, free of charge, on application to the Director, CCDC, 12 Union Road, Cambridge CB2 1EZ, U.K. (Fax: +44-1223-336033 or e-mail: deposit@ccdc.cam.ac.uk).

© 2001 NRC Canada

NHCHCCH=C*H*), 7.42–7.51 (m, 2H, O=CCCH=C*HCH*), 7.85–7.88 (m, 1H, O=CCC*H*). ^{13}C NMR ($CDCl_3$, 100 MHz) δ: 31.6, 34.9, 60.9, 123.6, 123.9, 126.2, 126.7, 128.4, 131.1, 132.4, 135.5, 148.3, 151.7, 171.4. Anal. calcd. for $C_{18}H_{19}NO$: C 81.48, N 5.28, H 7.22; found: C 81.18, N 5.14, H 7.31.

*(3*R*)-3-(4*-tert-*Butyl-phenyl)-5-methoxy-2,3-dihydro-1*H*-isoindol-1-one ((*R*)-**14d**)*

Colorless solid, mp = 211°C. $[\alpha]_D^{26}$ = −4.2 (c = 0.78, $CHCl_3$). ν_{max} (KBr) (cm^{-1}): 1690, 1652, 1621. *m/z* (EI): 295 (100%)$(M)^+$, 294 (43)$(M\text{-}CH_3)^+$, 264 (42)$(M\text{-}OCH_3)^+$, 238 (49)$(M\text{-}C(CH_3)_3)^+$. ^{1}H NMR (d_6-DMSO, 400 MHz) δ: 1.26 (s, 9H, $C(CH_3)_3$), 3.75 (s, 3H, OCH_3), 5.61 (s, 1H, NHC*H*), 6.78 (d, *J* = 1.9, 1H, O=CCCC*H*), 7.03 (dd, *J* = 8.5, 2.2, 1H, O=CCCH=C*H*), 7.18–7.23 (m, 2H, NHCHCC*H*=CH), 7.37–7.41 (m, 2H, NHCHCCH=C*H*), 7.63 (d, *J* = 8.3, 1H, O=CCC*H*=CH), 8.79 (s, 1H, N*H*). ^{13}C NMR (d_6-DMSO, 100 MHz) δ: 30.9, 34.1, 55.4, 58.9, 107.9, 114.4, 123.6, 124.1, 125.2, 126.0, 136.3, 150.0, 150.2, 162.1, 169.2. Anal. calcd. for $C_{19}H_{21}NO_2$: C 77.26, N 4.74 H, 7.17; found: C 77.13, N 4.62, H 6.96.

*(3*S*)-3-(Phenyl)-5-methoxy-2,3-dihydro-1*H*-isoindol-1-one ((*S*)-**14e**)*

The analytical and spectroscopic data were in agreement with recent literature (20*c*).

Acknowledgments

We thank Bayer AG, BASF AG, and Degussa AG for the donation of chemicals, the DFG (SFB 380) for financial support, and Mr. Thomas Klumpen who carried out parts of the work during an undergraduate research program.

References

1. (*a*) V. Fajardo, V. Elango, B.K. Cassels, and M. Shamma. Tetrahedron Lett. **23**, 39 (1982); (*b*) E. Valencia, J. Freyer, and M. Shamma. Tetrahedron Lett. **25**, 599 (1984); (*c*) E. Valencia, I. Weiss, S. Firdous, A.J. Freyer, and M. Shamma. Tetrahedron, **40**, 3957 (1984); (*d*) E. Valencia, V. Fajardo, A.J. Freyer, and M. Shamma. Tetrahedron Lett. **26**, 993 (1985).
2. Y. Kato, M. Takemoto, and K. Achiwa. Chem. Pharm. Bull. **41**, 2003 (1993).
3. (*a*) U. Holzgrabe, W. Bender, H.M Botero Cid, M. Staudt, R. Pick, C. Pfletschinger, E. Balatková, C. Tränkle, and K. Mohr. Pharm. Helv. Acta, **74**, 149 (2000); (*b*) H.M Botero Cid, C. Tränkle, K. Baumann, R. Pick, E. Mies-Klomfass, E. Kostenis, K. Mohr, and U. Holzgrabe. J. Med. Chem. **43**, 2155 (2000).
4. (*a*) A. Mertens, H. Zilch, B. König, W. Schäfer, T. Poll, W. Kampe, H. Seidel, U. Leser, and H. Leinert. J. Med. Chem. **36**, 2526 (1993); (*b*) P.P. Mager. Drug Des. Discovery, **14**, 241 (1996).
5. N.G. Kundu and M.W. Khan. Tetrahedron, **56**, 4777 (2000).
6. (*a*) R.P. Kreher, H. Hennige, M. Konrad, J. Uhrig, and A. Clemens. Z. Naturforsch. **B 46**, 809 (1991); (*b*) M. Othman, P. Pigeon, and B. Decroix. Tetrahedron, **53**, 2495 (1997).
7. (*a*) S.M. Allin, C.J. Northfield, M.I. Page, and A.M.Z. Slawin. Tetrahedron Lett. **39**, 4905 (1998); (*b*) P. Pigeon and B. Decroix. Tetrahedron Lett. **38**, 1041 (1997); (*c*) R. Alonso, L. Castedo, and D. Domínguez. Tetrahedron Lett. **26**, 2925 (1985).
8. E. Deniau and D. Enders. Tetrahedron Lett. **41**, 2347 (2000).
9. (*a*) A. Couture, E. Deniau, D. Ionescu, and P. Grandclaudon. Tetrahedron Lett. **39**, 2319 (1998); (*b*) E. Deniau and D. Enders. Tetrahedron. In press (2001).
10. V.A. Kovtunenko, T.T. Dobrenko, A.K. Tiltin, and F.S. Babichev. Chem. Heterocycl. Compd. (N.Y.), **21**, 830, (1985); Khim. Geterotsikl. Soedin. 996, (1985).
11. (*a*) H. Ishibashi, H. Kawanami, H. Iriyama, and M. Ikeda. Tetrahedron Lett. **36**, 6733 (1995); (*b*) W. Zhang and G. Pugh. Tetrahedron Lett. **40**, 7591 (1999); (*c*) H. Ishibashi, H. Kawanami, and M. Ikeda. J. Chem. Soc. Perkin Trans. 1, 817 (1997); (*d*) M. Black, J.I.G. Cadogan, and H. McNab. J. Chem. Soc. Perkin Trans. 1, 155 (1994); (*e*) D.P. Curran and H. Liu. J. Chem. Soc. Perkin Trans. 1, 1377 (1994); (*f*) V. Snieckus, J.-C. Cuevas, C.P. Sloan, H. Liu, and D.P. Curran. J. Am. Chem. Soc. **112**, 896 (1990).
12. B. Burns, R. Grigg, V. Santhakumar, V. Sridharan, P. Stevenson, and T. Worakun. Tetrahedron, **48**, 7297 (1992).
13. (*a*) R.S. Mali and S. Yeola. Synthesis, 755 (1986); (*b*) T.R. Belliotti, W.A. Brink, S.R. Kesten, J.R. Rubin, D.J. Wustrow, K.T. Zoski, S.Z. Whetzel, A.E. Corbin, T.A. Pugsley, T.G. Heffner, and L.D. Wise. Bioorg. Med. Chem. Lett. **8**, 1499 (1998); (*c*) E. Napolitano, R. Fiaschi, and A. Marsili. Tetrahedron Lett. **24**, 1319 (1983).
14. (*a*) S. Gabriel and R. Stelzner. Chem. Ber. **29**, 2743 (1896); (*b*) S. Gabriel and G. Giebe. Chem. Ber. **29**, 2518 (1896); (*c*) F.A. Mason and W.H. Perkin, Jr. J. Chem. Soc. **105**, 2013 (1914).
15. G. Cauquis and A. Deronzier. J. Chem. Soc. Chem. Commun. 807 (1978).
16. N. Barr, J.P. Bartley, P.W. Clark, P. Dunstan, and S.F. Dyke. J. Organomet. Chem. **302**, 117 (1986).
18. (*a*) M. Othman and B. Decroix. Synth. Commun. **26**, 2803 (1996); (*b*) M. Othman, P. Pigeon, and B. Decroix. Tetrahedron, **54**, 8737 (1998); (*c*) M. Othman, P. Pigeon, and B. Decroix. J. Heterocycl. Chem. **36**, 735 (1999).
19. J.-M. Ferland, C.A. Demerson, and L.G. Humber. Can. J. Chem. **63**, 361 (1985).
20. (*a*) S.M. Allin, C.J. Northfield, M.I. Page, and A.M.Z. Slawin. Tetrahedron Lett. **40**, 141 (1999); (*b*) S.M. Allin, C.J. Northfield, M.I. Page, and A.M.Z. Slawin. Tetrahedron Lett. **40**, 143 (1999); (*c*) S.M. Allin, C.J. Northfield, M.I. Page, and A.M.Z. Slawin. J. Chem. Soc. Perkin Trans. 1, 1715 (2000).
21. (*a*) W. Oppolzer, M. Wills, M.J. Kelly, M. Signer, and J. Blagg. Tetrahedron Lett. **31**, 5015 (1990); (*b*) A. Böhm, K. Polborn, K. Sünkel, and W. Beck. Z. Naturforsch. **B 53**, 448 (1998).
22. J. Campbell, R.F. Dedinas, and S.A. Trumbower-Walsh. J. Org. Chem. **61**, 6205 (1996).
23. J.L. Moniot, D.M. Hindenlang, and M. Shamma. J. Org. Chem. **44**, 4343 (1979).
24. (*a*) P. Pigeon, and B. Decroix. Tetrahedron Lett. **37**, 7707 (1996); (*b*) N.G. Kundu, M.W. Kahn, and R. Mukhopadhyay. Tetrahedron, **55**, 12 361 (1999); (*c*) A. Couture, E. Deniau, P. Grandclaudon, and C. Hoarau. Tetrahedron, **56**, 1491 (2000); (*d*) J. Honzl. Coll. Czech. Chem. Commun. **21**, 725 (1956); (*e*) S. Sugasawa and Y. Kanaoka. Pharm. Bull. **3**, 266 (1955); (*f*) J.H. Helberger, and D.B. Hevér. Ann. Chem. **536**, 173 (1938); (*g*) S. Natelson and S.P. Gottfried. J. Am. Chem. Soc. **63**, 487 (1941); (*h*) P.L. Barili, R. Fiaschi, E. Napolitano, L. Pistelli, V. Scartoni, and A. Marsili. J. Chem. Soc. Perkin Trans. 1, 1654 (1981); (*i*) H.P. Soetens and U.K. Pandit. Recl. J. Royal Neth. Chem. Soc. **99**, 271 (1980); (*j*) R.P. Linstead and G.A. Rowe. J. Chem. Soc. 1070 (1940).
25. D. Enders, H. Schubert, and C. Nübling. Angew. Chem. **98**, 1118 (1986); Angew. Chem. Int. Ed. Engl. **25**, 1109 (1986).
26. D. Enders and D. Bartzen. Liebigs Ann. Chem. 569 (1991).

© 2001 NRC Canada

27. D. Enders and C. Thiebes. Synthesis, 510 (2000).
28. V. Snieckus. Chem. Rev. **90**, 879 (1990).
29. D. Enders, C. Nübling, and H. Schubert. Liebigs Ann. 1089 (1997).
30. D. Enders, R. Lochtman, M. Meiers, S. Müller, and R. Lazny. Synlett, 1182 (1998).
31. R. Fernández, A. Ferrete, J.M. Lassaletta, J.M. Llera, and A. Monge. Angew. Chem. **112**, 3015 (2000); Angew. Chem. Int. Ed. **39**, 2893 (2000).
32. S.R. Hall, G.S.D. King, and J.M. Stewart (*Editors*). Xtal3.4 User's Manual. Universities of Western Australia, Leuven, and Maryland. Lamb, Perth. 1995.
33. D.T. Cromer, and J.T. Weber. *In* International tables for X-ray crystallography. *Edited by* J.A. Ibers and W.C. Hamicton. Vol. IV. Kluwer Academic Publishers, Dordrecht. 1989. Tables 2.2B and 2.3.1.

© 2001 NRC Canada

Organometallic reactions in aqueous media — Antimony-mediated allylation of carbonyl compounds and the nature of allylstibine intermediates

Lian-Hai Li and Tak Hang Chan

Abstract: Commercial antimony metal, in aqueous 1 M H(D)Cl solution, reacts with allyl bromide and aldehydes to give the corresponding homoallylic alcohols in good yield. The reaction proceeds through the formation of allylstibine intermediates. The structures of the allylstibine intermediates are likely to be allylstibine dibromide and diallylstibine bromide.

Key words: allylation reaction, aqueous organometallic reactions, homoallylic alcohols, allylstibine dibromide, diallylstibine bromide.

Résumé : En solution aqueuse de H(D)Cl 1 M, l'antimoine métallique commercial réagit avec le bromure d'allyle et les aldéhydes pour donner lieu à la formation, avec de bons rendements, des alcools homoallyliques correspondants. La réaction se produit par le biais de la formation d'intermédiaires allylstibines. Les structures des allylstibines intermédiaires sont vraisemblablement celles du dibromure d'allylstibine et du bromure de diallylstibine.

Mots clés : réaction d'allylation, réactions d'organométalliques en milieu aqueux, alcools homoallyliques, dibromure d'allylstibine, bromure de diallylstibine.

[Traduit par la Rédaction]

Introduction

The allylation of carbonyl compounds has proved to be a very important reaction in organic synthesis. Numerous reagents and methods have been developed to accomplish this transformation (for general reviews, see ref. 1). The discovery (for reviews see ref. 2) in the past decade that this transformation could be achieved in aqueous media through a Barbier type reaction (for a recent monograph see ref. 3*b*), has drawn even more attention to this area of chemistry. Metals such as Zn (4), In (5), Bi (6), Sn (7), Pb (8), Mn (9), Mg (10), or Sb (11) have been reported to be effective in mediating the coupling between allyl halides and carbonyl compounds to give the corresponding homoallylic alcohols (Scheme 1). Among these reported metals, all of them except Sb were found to effect the transformation with commercially available metal powder, even though in cases such as Sn or Zn, activation was needed. In the case of antimony, however, commercial antimony metal was apparently not successful in mediating the allylation reaction in aqueous media (Barbier–Grignard type allylation of aldehydes with metallic antimony can be accomplished in nonaqueous media by refluxing in THF–HMPA (1:1) (see ref. 12*a*); recently, activation of antimony with fluoride salts in aqueous media has been reported (see ref. 12*b*)). Several publications have appeared in the literature to indicate that the antimony metal must be formed in situ through the reduction of antimony trichloride with a reducing reagent such as Al or Fe (11*a*) or $NaBH_4$ (11*b*). The "active" antimony, thus generated, could then mediate the allylation reaction in an aqueous and (or) organic solvent system. As part of our general program to study organometallic reactions in aqueous media, we are interested in finding conditions that can allow the use of commercial antimony directly without the need for the reductive generation step (12). Another objective is to have a better understanding of the mechanism of these reactions. Recently, we have investigated the nature of the organometallic intermediates that may be implicated in these reactions. We were able to conclude that in the indium mediated allylation reaction, an allylindium(I) intermediate rather than an allylindium(III) species was formed (13). In the tin-mediated allylation reaction, both diallyltin(IV) dibromide and allyltin(II) bromide were formed (14). On the other hand, in the zinc- or magnesium-mediated allylation reactions, there had been suggestion that the reaction may have occurred on the metal surface (10). We are interested therefore in the antimony-mediated reaction to see if any organostibine intermediate(s) were formed in the aqueous allylation reaction and to explore the nature of these intermediates.

Results and discussion

Investigations on the use of commercial antimony powder

Our investigation started with performing the reaction with commercial antimony powder in aqueous media. In agree-

Received December 12, 2000. Published on the NRC Research Press Web site at http://canjchem.nrc.ca on October 22, 2001.

Dedicated to Professor Victor Snieckus for his contributions to Canadian chemistry.

L.-H. Li and T.H. Chan.[1] Department of Chemistry, McGill University, Montreal, QC H3A 2K6, Canada.

[1]Corresponding author (telephone: (514)-398-6932; fax: (514)-398-3797; e-mail: thchan@chemistry.mcgill.ca).

 DOI: 10.1139/cjc-79-11-1536 © 2001 NRC Canada

Scheme 1.

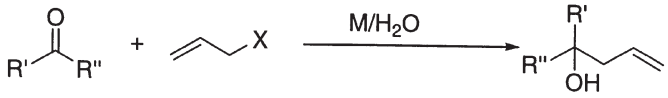


Table 1. The allylation of carbonyl compounds with allyl bromide mediated by Sb powder.

Entry	R′, R′′	Reaction conditions[a] (promoters in H_2O)	Time (h)	Isolated yields[b]
1	Ph, H	A (neat H_2O)	1 week	0
2	Ph, H	A (17% NH_4Cl)	3 days	30[c]
3	Ph, H	A (29% NH_4Cl)	3 days	100
4	Ph, H	B (29% NH_4Cl)	3 days	18[c]
5	Ph, H	A (0.1 M HCl)	16	100
6	Ph, H	B (0.1 M HCl)	4 days	52
7	Ph, H	C (0.1 M HCl)	4 days	93
8	Ph, H	D (0.1 M HCl)	4 days	95
9	Ph, H	C (0.5 M HCl)	16	100
10	*n*-C_6H_{13}, H	C (0.5 M HCl)	24	94
11	*p*-ClC_6H_4, H	C (0.5 M HCl)	16	92
12	*p*-$MeOC_6H_4$, H	C (0.5 M HCl)	16	96
13	*p*-$NO_2C_6H_4$, H	C (0.5 M HCl)	16	89
14	*p*-MeC_6H_4, H	C (0.5 M HCl)	16	100
15	*p*-$CF_3C_6H_4$, H	C (0.5 M HCl)	16	100
16	1-Naphthyl, H	C (0.5 M HCl)	16	100
17	Cyclohexyl, H	C (0.5 M HCl)	24	96
18	Cinnamaldehyde	C (0.5 M HCl)	16	97
19	Ph, Me	C (0.5 M HCl)	3 days	0
20	$(CH_2)_5$	C (0.5 M HCl)	3 days	0

[a]The molar ratio of carbonyl compound:allyl bromide:Sb is shown as: A 1:2.5:5, B 1:2.5:1.2, C 1:2.5:2, D 1:2.5:3.
[b]While the yield was low, the starting carbonyl compound was recovered unchanged in good mass balance.
[c]Yield based on ^1H NMR spectrum analysis of the crude products mixture.

ment with previous reports, the reaction performed in distilled water with the molar ratio of Sb:benzaldehyde:allyl bromide at 5:1:2.5 gave no trace of the corresponding homoallylic alcohol even after a week of vigorous stirring of the reaction mixture (entry 1, Table 1). It was obvious that activation of the metal was needed for this reaction to proceed. Previous investigations of other metals showed that catalytic amount of acid such as hydrobromic acid (7), ammonium chloride (4), higher reaction temperature (7), or ultrasonic radiation (4) might be helpful in promoting such reactions. We tried, therefore, saturated ammonium chloride solution with the same ratio of the reactants and found the reaction did work but slowly (entry 2, Table 1). Increasing the concentration of the ammonium chloride helped improve the yield of the reaction but it was still too slow to be practical (entry 3, Table 1). The role of ammonium chloride might be due to increasing acidity or the effect of the chloride ion. When the ammonium chloride solution was substituted with a 0.1 M of hydrochloric acid solution, the reaction was found to proceed smoothly and be completed in 16 h (entry 5, Table 1). These results suggested that acidity played a role in promoting the reaction. Attempts to reduce the amount of the Sb used for the reaction caused the prolonging of the reaction time (entries 6–8, Table 1). The use of 2 equiv of Sb was found to be optimal. On the other hand, the use of 0.5 M instead of 0.1 M hydrochloric acid as solvent was found to accelerate the reaction (entry 9, Table 1). With these conditions, other aldehydes could be allylated to give excellent yields of the products (entries 10–18, Table 1). The results in Table 1 showed some interesting features of the antimony mediated allylation reaction. First, the reaction was not sensitive to the nature of the aldehydes used. The reaction proceeded well with either aromatic or aliphatic aldehydes. The allylation of α,β-unsaturated aldehyde as represented by *trans*-cinnamaldehyde (entry 18, Table 1) occurred in a regiospecific manner and gave solely the 1,2-addition product. Furthermore, electron donating or withdrawing groups on the aromatic ring did not seem to affect the reaction significantly either in the yield of the product or the rate of the reaction. Thirdly, the reaction conditions appeared not to be reductive in nature. Thus, we did not detect alcohols or pinacols as side products of the reactions as often found with Zn or Mg. In the same vein, nitro function was not reduced under the reaction conditions. Thus, *p*-nitrobenzaldehyde was successfully allylated. Usually, the nitro group was sensitive to reduction by metals and *p*-nitrobenzaldehyde could not be allylated under Barbier conditions by Zn, Sn, or In (15). Finally, the reaction was chemoselective. Efforts to allylate ketones failed (entries 19 to 20, Table 1) in agreement with previous literature reports using active antimony (11). In this respect, antimony seems to be different from indium, the commonly employed metal, in that indium mediates the allylation of both aldehydes and ketones effectively.

Table 2. The effect of acid sensors on antimony-mediated allylation of benzaldehyde.[a]

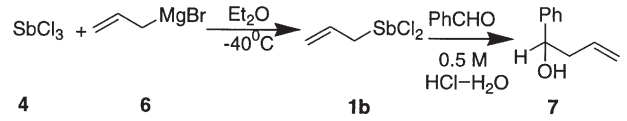
Entry	Solvents (in H_2O)	Time (h)	Isolated yields[b]
1	0.1 M HCl	4 days	93
2	0.5 M HCl	16	100
3	1 M HCl	8	89
4	0.5 M HBr	16	43
5	0.25 M H_2SO_4	16	81
6	0.5 M D-Tartaric acid	16	100[c]
7	0.5 M Oxalic acid	1	26
8	0.1 M Oxalic acid	1.5	70
9	0.025 M Oxalic acid	6	19

[a]The molar ratio of benzaldehyde:allyl bromide:Sb was 1:2.5:2 and the solvent used was 5 mL of benzaldehyde (1 mmol).
[b]While the yield was low benzaldehyde was recovered unchanged in good mass balance.
[c]No optical rotation could be observed.

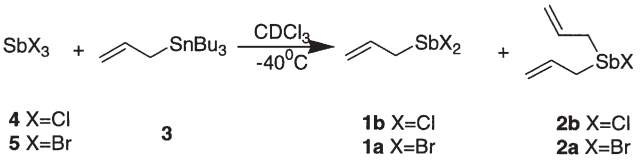
We have also briefly examined other acids as promoters of the reaction. When hydrochloric acid was replaced by a 0.25 M aq H_2SO_4 solution, the reaction gave lower yield (Table 2, entry 5) in comparison with the same reaction in hydrochloric acid solution (Table 2, entry 2). These results showed that in addition to acidity, the counter anion might play a role in the reaction. In support of this observation, we found that the reaction can be promoted by oxalic acid or tartaric acid (entry 6, Table 2), even though the yield with oxalic acid (entries 7–9, Table 2) was lower. In the case of D-tartaric acid, it was a very effective promoter of the reaction; however, the product homoallylic alcohol derived from benzal-

© 2001 NRC Canada

Scheme 2.



Scheme 3.



dehyde unfortunately did not show any optical activity. No asymmetric induction was observed (16).

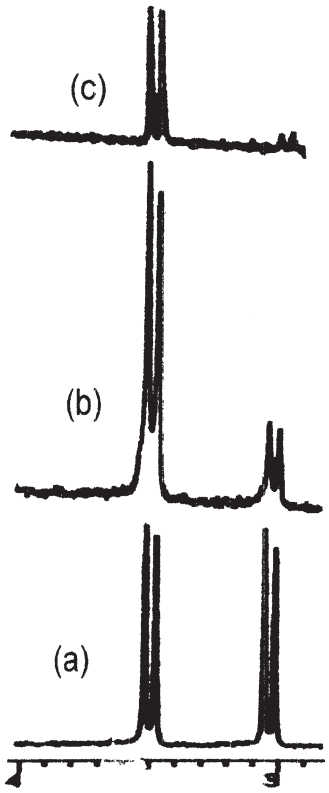
Investigations of the allylstibine intermediate

First, we tried to determine if an allylantimony intermediate can survive the aqueous conditions and allylate aldehydes. The reaction between a Grignard reagent and antimony(III) halide has been known to give the alkylantimony(III) dihalide (17). We therefore carried out the reaction of antimony trichloride with allylmagnesium bromide in ether (Scheme 2). When the supposed allylstibine dichloride (from 5 mmol of the Grignard reagent) prepared in this way was treated with benzaldehyde (1 mmol) in 0.5 M hydrochloric acid aqueous solution, the desired homoallylic alcohol was obtained in 81% yield. These results showed that the allylantimony species, whatever its structure, was able to exist in the aqueous media to some extent and perform the addition reaction to carbonyl compound in acidic conditions. We were, however, not able to isolate and characterize the presumed allylstibine intermediate by the usual method of isolation or purification.

Since in the indium and tin cases, we had some success in the direct observation of the reaction of metal with allyl bromide in aqueous media (as D_2O) using ^1H NMR analysis (13, 14), we followed the reaction of allyl bromide with antimony powder in 0.5 M DCl–D_2O (prepared by the hydrolysis of TMSCl in D_2O) by ^1H NMR but detected no new signals. However, when a 1 M DCl–D_2O solution was used as the solvent instead, two new doublets, one at about 3.8 ppm and the other at about 3.3 ppm were observed in about 12 min. These signals grew in intensity for about 45 min and then disappeared after 90 min. At the same time, the doublet at 3.7 ppm, due to the methylenic protons of allyl bromide, declined in intensity correspondingly. These results suggested that some allylstibine intermediates were formed in the reaction mixture.

What are the structures of these intermediates? The likely candidates are: allylstibine(III) dibromide (**1a**) and diallylstibine(III) bromide (**2a**) as well as their chloride counterparts **1b** and **2b** due to possible halide exchange in the presence of DCl. In the literature, allylstibine(III) dichloride (**1b**) had been prepared in situ by the reaction of antimony trichloride with allyltributyltin (**3**) in $CDCl_3$. Its NMR in $CDCl_3$ had been observed and the chemical shift of the allylic protons was reported to be at 3.51 ppm at –40°C (18). We, therefore, examined in some details the reaction between allyltributyltin

Fig. 1. Partial ^1H NMR spectra of the in situ-formed allylstibine intermediates by the reaction of antimony(III) chloride with allyltributyltin in $CDCl_3$ at –40°C. (*a*) Mol ratio $SbCl_3$:allyltributyltin = 1:1; (*b*) mol ratio $SbCl_3$:allyltributyltin = 1:0.66; (*c*) mol ratio $SbCl_3$:allyltributyltin = 1:0.33.



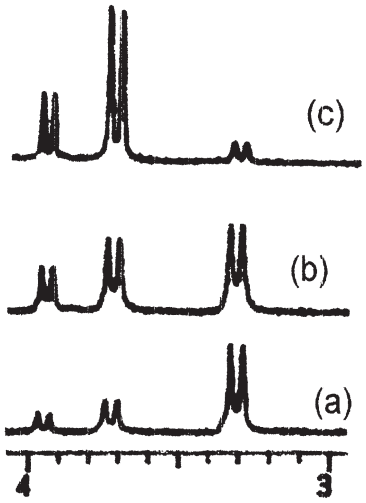
with antimony halides in $CDCl_3$ to generate the allylstibine halide intermediates (Scheme 3). When compound **3** and antimony trichloride (**4**) in equal molar amounts were mixed in $CDCl_3$ at –40°C, a doublet at 3.5 ppm, in agreement with literature report for **1b** (18), was observed in the ^1H NMR. However, another doublet at 3.0 ppm was observed as well. We attributed the presence of the second doublet at 3.0 ppm to diallylstibine chloride **2b.** In accordance with this explanation, it was found that when the amount of **3** added was reduced, the intensity of the doublet at 3.0 ppm declined relative to that of 3.5 ppm, as one would expect (Fig. 1*a*–*c*). Allylstibine chlorides **1b** and **2b,** thus prepared from a one-third molar amount of compound **3** to **4** in $CDCl_3$, were extracted into a solution of DCl–D_2O at 0°C and the ^1H NMR was observed. Signals at 3.6 and 3.0 ppm were observed, suggesting that the same allylstibine chlorides **1b** and **2b** existed in the aqueous media.[2]

Similar patterns were observed in the reaction of allyltributyltin (**3**) with antimony tribromide (**5**). When compounds **3** and **5** were mixed in equal molar amounts in $CDCl_3$ at –40°C, the ^1H NMR showed two doublets at 3.7 and 3.3 ppm. These two doublets are assigned to allylstibine dibromide **1a** and diallylstibine bromide **2a**, respectively. Again, as the amount of compound **3** was reduced successively from equal amount to one-half and then to one-third of **5**, the relative intensity of the 3.3 ppm doublet decreased

[2] Additional doublet at 2.3 ppm could be observed in DCl–D_2O which may be due to hydrolysis product under these conditions.

© 2001 NRC Canada

Fig. 2. Partial ^{1}H NMR spectra of the in situ-formed allylstibine intermediates by the reaction of antimony(III) bromide with allyltributyltin in $CDCl_3$ at –40°C. (*a*) Mol ratio $SbBr_3$:allyltributyltin = 1:1; (*b*) mol ratio $SbBr_3$:allyltributyltin = 1:0.66; (*c*) mol ratio $SbBr_3$:allyltributyltin = 1:0.33. The doublet at 3.95 ppm was due to the methylenic proton of allyl bromide which was found as a side product.



eventually to about one-tenth of the intensity of the 3.7 ppm doublet (Fig. 2*a*–*c*). Similar extraction of **1a** and **2a** from $CDCl_3$ solution into DBr–D_2O solution showed doublets at 3.8 and 3.4 ppm,[3] at nearly the same positions as those observed from the direct reaction between allyl bromide and antimony in DCl–D_2O.[4]

Experimental section

General procedure

All the reactions were carried out in distilled water. Purification of products with flash chromatography was performed over silica gel. The ^{1}H NMR spectra of the products were performed on a Gemini-200 spectrometer in chloroform-*d* with the solvent signal used as the internal standard. The DCl–D_2O solution was prepared by hydrolysis of trimethylchlorosilane (TMSCl) in D_2O. The antimony powder (325 mesh) was purchased from Alfa Aesar. The hydrochloric solution was prepared by dilution of reagent grade concentrated hydrochloric acid (36.5–38%) and was not titrated again. The aldehydes and ketones were used as purchased as long as their ^{1}H NMR spectra were satisfactory.

Standard procedures for the allylation of aldehydes

To a mixture of aldehyde (1 mmol) and allyl bromide (2.5 mmol) in 0.5 M hydrochloric acid solution (4 mL), antimony powder (2 mmol) was added in one portion and the mixture was vigorously stirred until the antimony powder was reacted (usually overnight). Ethyl ether was added to the reaction mixture and the organic layer was separated. The aqueous phase was extracted with ethyl ether. The organic extracts were combined and dried over Na_2SO_4, and were filtered and evaporated. The residue, for most of the aldehydes, afforded the corresponding homoallylic alcohols of sufficient purity according to ^{1}H NMR without the need for further purification. If necessary, purification was performed by flash chromatography over silica gel using hexane – ethyl acetate as eluent. All the homoallylic alcohols reported in Table 1 are known compounds: 1-phenylbut-3-en-1-ol (19), 1-decen–4-ol (20), 1-(4-chlorophenyl)but-3-en-1-ol (21), α-propenyl-cyclohexanemethanol (22), 1-phenyl-1,5-hexadien-3-ol (23), 1-(4-nitrophenyl)but-3-en-1-ol (24), 1-(4-methoxyphenyl)but-3-en-1-ol (25), 1-naphthylbut-3-en-1-ol (24), 1-(4-trifluoromethylphenyl)but-3-en-1-ol (26), 1-(4-methylphenyl)but-3-en-1-ol (26).

Procedures for the monitoring of the reaction intermediates by ^{1}H NMR in 1 M DCl–D_2O

To a stirring mixture of allyl bromide (2.5 mmol) in D_2O (5 mL) at room temperature, TMSCl (5 mmol) was added dropwise. The resulting mixture was stirred at room temperature for 10 min and then antimony powder (2 mmol) was added in one portion. The resulting reaction mixture was stirred vigorously. After the reaction mixture was stirred for 12 min, 30 min, 60 min, or 90 min, a sample was taken while stirring and the ^{1}H NMR spectrum was observed immediately (132 scans). The resulting spectrua showed that two new doublets at 3.8 and 3.3 ppm could be observed until the sample taken after 75 min.

Procedures for the allylation of benzaldehyde with allylstibine dichloride in water

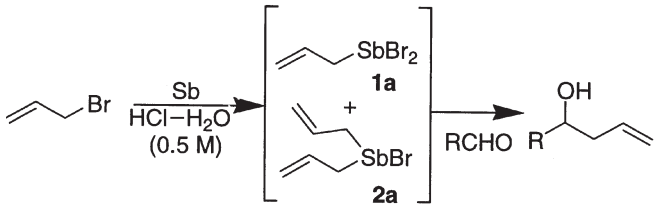
At –78°C, under Ar atmosphere, allylmagnesium bromide (5 mL, 1 M in Et_2O) was added dropwise to a solution of antimony trichloride (5 mmol) in ether (40 mL). The resulting mixture was stirred at –40°C for 3 h. The solvent was then removed by high vacuum at –40°C and the solid residue was subjected to high vacuum at this temperature for 4 h. The solid residue was broken up with a spatula at –40°C under an Ar atmosphere in the flask. Then the cooling bath was removed and, at room temperature, a solution of 0.5 M aqueous hydrochloric acid solution (10 mL) or distilled water with benzaldehyde (106 mg, 1 mmol) was added to the flask containing the solid. The resulting mixture was stirred at room temperature for 2 h. Ethyl ether was used to extract the reaction mixture. The organic extracts were combined and dried over Na_2SO_4. The residue after evaporation was purified through flash chromatography (10% EtOAc–hexane) to afford the corresponding homoallylic alcohol as a colorless oil (120 mg, 81% yield).

[3] Additional doublets of weaker intensities at 3.6, 3.0, 2.7, and 2.5 ppm could be observed in DBr–D_2O which may be due to hydrolysis products under these conditions.

[4] The possibility of halide exchanges cannot be resolved completely. We were able to extract **1b** and **2b** from $CDCl_3$ into DBr–D_2O and found that the allylic signals were observed at 3.8 and 3.4 ppm. This observation suggested that **1b** and **2b** may have been converted to **1a** and **2a** through halide exchange. We were however not able to obtain good spectra by extracting **1a** and **2a** from $CDCl_3$ into DCl–D_2O to confirm that the reverse exchange did not take place.

© 2001 NRC Canada

Scheme 4.



Conclusions

The above studies demonstrate that antimony, in aq 1 M H(D)Cl solution, is able to react with allyl bromide and aldehydes to give the corresponding homoallylic alcohols in good yield. The reaction proceeds through the formation of allylstibine intermediates. The structures of the allylstibine intermediates are likely to be allylstibine dibromide **1a** and diallylstibine bromide **2a** (Scheme 4). Compounds **1a** and **2a** have been independently generated by transmetalation reaction between allyltributyltin and antimony tribromide. Together with the results in the cases of indium (13) and tin (14) where formation of allylindium and allyltin intermediates were observed, a general picture on the Barbier reaction in aqueous media begins to emerge. For these three metals (In, Sn, and Sb), discreet organometallic intermediates can be formed directly from allyl bromide and the metal in aqueous media. These allylic organometallic intermediates have finite stability in water, and sufficient reactivity with carbonyl compounds to make them useful synthetic reagents in aqueous media. It remains to be seen whether for other metals such as Bi, Pb, or Mn, discreet organometallic intermediates can equally exist in water with finite lifetimes.

Acknowledgement

We thank the Natural Sciences and Engineering Research Council of Canada (NSERC) for financial support of this research.

References

1. Y. Yamamoto and N. Asao. Chem. Rev. **93**, 2207 (1993).
2. (*a*) C.J. Li and T.H. Chan. Organic reactions in aqueous media. John Wiley and Sons Inc., New York. 1993; (*b*) C.J. Li. Chem. Rev. **93**, 2023 (1993); (*c*) T.H. Chan, C.J. Li, M.C. Lee, and Z.Y. Wei. Can. J. Chem. **72**, 1181 (1994); (*d*) A. Lubineau, J. Auge, and Y. Queneau. Synthesis, 741 (1994); (*e*) C.J. Li. Tetrahedron, **52**, 5643 (1996).
3. (*a*) P. Barbier. Comp. Rend. **128**, 110 (1899); (*b*) C. Blomberg. The Barbier reaction and related one-step processes. *In* Reactivity and structure: concepts in organic chemistry. *Edited by* K. Hafner, J.M. Lehn, C.W. Rees, P. von Rague Schleyer, B.M. Trost, and R. Zahradnik. Springer–Verlag, New York. 1993.
4. (*a*) J. Nokami, J. Otera, T. Sudo, and R. Okawara. Organometallics, **2**, 191 (1983); (*b*) C. Petrier and J.L. Luche. J. Org. Chem. **50**, 910 (1983).
5. (*a*) C.J. Li and T.H. Chan. Tetrahedron Lett. **32**, 7017 (1991); (*b*) L.A. Paquette, G.D. Bennett, M.B. Isaac, and A. Chhatriwalla. J. Org. Chem. **63**, 1836 (1998).
6. M. Wada, H. Ohki, and K.Y. Akiba. Bull. Chem. Soc. Jpn. **63**, 2751 (1990).
7. (*a*) J. Nokami, J. Otera, T. Sudo, and R. Okawara. Organometallics, **2**, 191 (1983); (*b*) J. Nokami, S. Wakabayashi, and R. Okawara. Chem. Lett. 869 (1984); (*c*) K. Uneyama, N. Kamaki, A. Moriya, and S. Torii. J. Org. Chem. **50**, 5396 (1985); (*d*) S.H. Wu, B.Z. Huang, T.M. Zhu, D.Z. Yiao, and Y.L. Chu. Acta Chim. Sinica, **48**, 372 (1990); (*e*) C. Einhorn, and J.L. Luche. J. Organomet. Chem. **322**, 177 (1987).
8. J.Y. Zhou, Y. Jia, G.F. Sun, and S.H. Wu. Synth. Commun. **27**, 1899 (1997).
9. C.J. Li, Y. Meng, X.H. Yi, J.H. Ma, and T.H. Chan. J. Org. Chem. **63**, 7498 (1998).
10. W.C. Zhang and C.J. Li. J. Org. Chem. **64**, 3230 (1999).
11. (*a*) W. Wang, L. Shi, and Y. Huang. Tetrahedron, **46**, 3315 (1990); (*b*) P.D. Ren, Q.H. Jin, and Z.P. Yao. Synth. Commun. **27**, 2761 (1997).
12. (*a*) Y. Butsugan, H. Ito, and S. Araki. Tetrahedron Lett. **28**, 3707 (1987); (*b*) L.-H. Li, and T.H. Chan. Tetrahedron Lett. **41**, 5009 (2000).
13. (*a*) T.H. Chan and Y. Yang. J. Am. Chem. Soc. **121**, 3228 (1999); (*b*) Y. Yang and T.H. Chan. J. Am. Chem. Soc. **122**, 402 (2000).
14. T.H. Chan, Y. Yang, and C.J. Li. J. Org. Chem. **64**, 4452 (1999).
15. T.H. Chan and B.M. Issac. Pure Appl. Chem. **68**, 919 (1996).
18. S.L. Serre and J.-C. Guillemin. J. Org. Chem. **63**, 59 (1998).
19. S. Araki, H. Ito, and Y. Butsugan. J. Organometal. Chem. **347**, 5 (1988).
20. C.J. Kowalski and J.S. Dung. J. Am. Chem. Soc. **102**, 7950 (1980).
21. W. Makoto, O. Hidenori, and A. Kinya. Bull Chem. Soc. Jpn. **63**, 1738 (1990).
22. W.R. Roush, A.E. Walts, and L.K. Hoong. J. Am. Chem. Soc. **107**, 8186 (1985).
23. N. Minowa and T. Mukaiyama. Bull. Chem. Soc. Jpn. **60**, 3697 (1987).
24. Y. Yamamoto Y. Saito, K. Marayama, J. Org. Chem. **48**, 5408 (1983).
25. X.H. Yi, J.X. Haberman, and C.J. Li. Synth. Commun. **28**, 2999 (1998).
26. H. Yamataka and K. Nishikawa. Bull. Chem. Soc. Jpn. **65**, 2145 (1992).

© 2001 NRC Canada

A highly efficient strategy for the synthesis of 3-substituted salicylic acids by either directed *ortho*-lithiation or halogen–metal exchange of substituted MOM protected phenols followed by carboxylation.

Stephen Y.W. Lau and Brian A. Keay

Abstract: A highly efficient synthesis of various 3-substituted salicylic acids is described starting from inexpensive starting materials and requiring no special apparatus.

Key words: salicylic acids, *ortho*-metalation, halogen–metal exchange, methoxymethyl group.

Résumé : On décrit une synthèse très efficace d'acides salicyliques substitués en position 3, à partir de produits peu dispendieux et ne requérant pas d'appareils spéciaux.

Mots clés : acides salicyliques, *ortho*-métallation, échange halogène–métal, groupe méthoxyméthyle.

[Traduit par la Rédaction]

Introduction

During the course of our study on the effect of remote substituents on the enantioselectivity of a palladium-catalyzed polyene cyclization (**3** → **4**) (1), which has been used in the synthesis of (+)-xestoquinone (2), we required various 3-substituted salicylic acid derivatives **1** (Scheme 1). As only 3-chlorosalicylic acid was commercially available, other methods for the preparation of 3-substituted salicylic acids were found in the literature. Currently, there exist relatively few direct methods for the synthesis of 3-substituted salicylic acids (3, and for recent reports involving the use of 3-halogen substituted salicylic acids, see ref. 4). Some salicylic acid derivatives can be synthesized directly from their corresponding phenols via a Kolbe–Schmidt carboxylation (5), however, we did not possess the proper apparatus to work with carbon dioxide at high pressures and temperatures. Another common route is through Reimer–Tiemann (6) or Duff formylations (7) of the 2-substituted phenols to give the 3-substituted salicylaldehydes followed by oxidation to the acid (8). The main drawback of this reaction is that the formylation is rarely selective and the aldehyde can be introduced *ortho* and (or) *para* to the phenol (9). In our hands, formylation of 2-substituted phenols provided a mixture in which the *para* isomer was the major product. Other strategies, such as the direct bromination of salicylic acid, which is reported to give only the 3-brominated isomer (10), gave us mixtures of the 5-bromo- and 3,5-dibromo- products and never the desired isomer. An alternative synthesis of 3-bromosalicyclic acid was reported in 1923 (11) in which the 5-position of salicyclic acid could be blocked as a sulfonic acid, brominated in the 3-position, and then the sulfonic acid removed. However, bromination of 5-protected salicyclic acid gave only 2,4,6-tribromophenol. As we had no luck with existing procedures we designed a new synthetic strategy for preparing various 3-substituted salicyclic acids and report herein simple and inexpensive procedures for their preparation.

Our initial attempts at synthesizing 3-chlorosalicylic acid from 2-chlorophenol, using either 2 equiv. of *n*-BuLi or 1 equiv. of NaH and 1 equiv. of *n*-BuLi followed by treatment with CO_2 gas at ambient pressure, met with little success due to the weakness of the phenolic OLi group as an *ortho*-lithiation director (12). The methoxymethyl (MOM) ether of phenols is known to be a more efficient *ortho*-lithiation director than phenolic hydroxyl groups (13). Thus, treatment of either the *ortho*-fluoro- (**5**) or *ortho*-chlorophenol MOM ether (**6**) (14) with 1 equiv. of *n*-BuLi generated the *ortho*-anion, which was trapped with gaseous CO_2 at low temperature (15). An acidic workup with 6 M HCl protonated the carboxylic acid and cleaved the MOM ether in situ to afford the 3-fluoro- (**7**) or 3-chlorosalicylic acid (**8**) in 86 and 91% yields, respectively (Scheme 2). As expected, there was no evidence of halogen–lithium exchange with either sample. This method for the preparation of 3-fluorosalicyclic acid (**7**) is more efficient than a recently reported synthesis (3).

The 3-bromo derivative could not be synthesized in the same manner from *ortho*-bromophenol because, in this case,

Received February 5, 2001. Published on the NRC Research Press Web site at http://canjchem.nrc.ca on October 23, 2001.

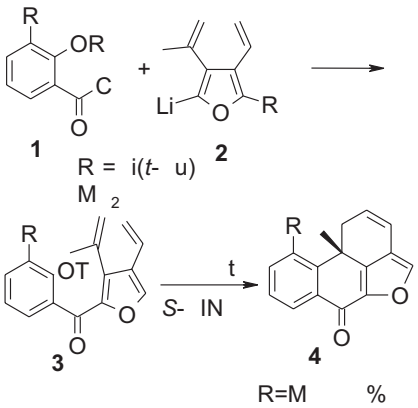
In recognition of Victor Snieckus' contributions to organic chemistry.

S.Y.W. Lau and B.A. Keay.[1] Department of Chemistry, University of Calgary, Calgary, AB T2N 1N4. Canada.

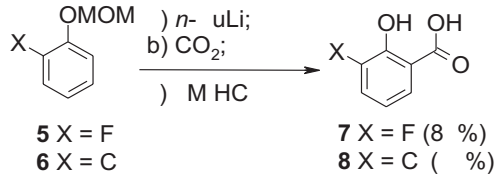
[1]Corresponding author (fax: (403) 289-9488; e-mail: keay@ucalgary.ca).

 DOI: 10.1139/cjc-79-11-1541 © 2001 NRC Canada

Scheme 1.



Scheme 2.

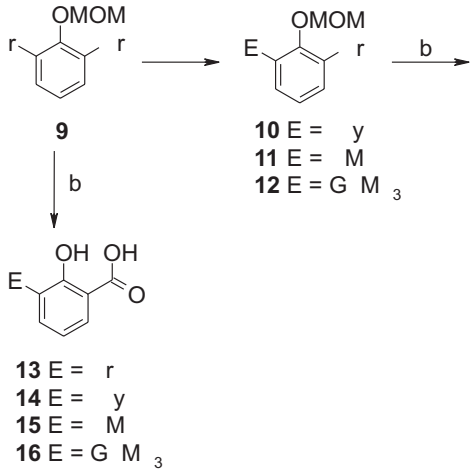


halogen–lithium exchange would occur more rapidly than deprotonation. We, thus, developed an alternative strategy starting from 2,6-dibromophenol that was easily prepared by treatment of a mixture of phenol and *tert*-butylamine with 2 equiv. of bromine at low temperature (16). The MOM protected 2,6-dibromophenol **9** (Scheme 3) was subjected to a monohalogen–lithium exchange with 2.1 equiv. of *t*-BuLi followed by quenching the anion with carbon dioxide. An acidic workup afforded the desired 3-bromosalicylic acid **13** in 97% yield.

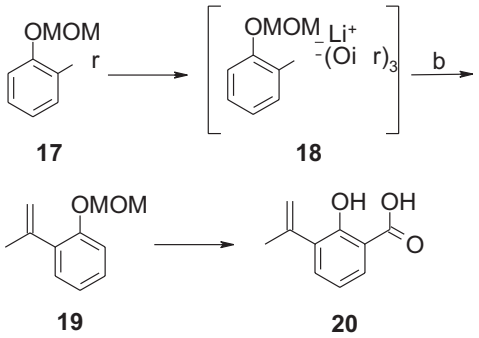
We decided to extend the above strategy towards other 3-substituted salicylic acids by using **9** as the starting material. By trapping the initial anion formed by a monohalogen–metal exchange with suitable electrophiles, the remaining bromide could subsequently be exchanged and trapped with carbon dioxide to give 3-substituted salicylic acids. Allyl bromide, dimethyl disulfide, and trimethygermanium bromide were used as electrophiles to quench the initial anion to give the corresponding products (Scheme 3). 3-Substituted salicylic acids were prepared in high yield by subsequent treatment of **10**–**12** with *t*-BuLi followed by the addition of carbon dioxide and acidic workup. We realized that **14**–**16** could have been obtained from the MOM-ether of phenol via successive deprotonations *ortho* to the MOM group followed by quenching with suitable electrophiles; however, problems could arise in the second lithiation if the first electrophile introduced is itself an *ortho*-lithiation director. For example, it is well-documented that an SMe group will direct an *ortho*-lithiation (17). Thus, the second lithiation of 2-methylthio-*O*-methoxymethylphenol might have led to some lithiation *ortho* to the thiomethyl group. Having the bromide in compound **11** ensured that the subsequent anion would be formed *ortho* to the MOM group.

Finally, we decided to extend this strategy towards our in situ Suzuki coupling methodology (1*c*, 18) to synthesize various 3-substituted salicylic acids in which the substituent could

Scheme 3. Reagents: (*a*) 2.1 equiv. *t*-BuLi, Et_2O, then allyl bromide, MeSSMe or Me_3GeBr; (*b*) 2.1 equiv. *t*-BuLi, THF, then CO_2, then 6 M HCl.



Scheme 4. Reagents: (*a*) 2.1 equiv. *t*-BuLi, THF, $B(O\text{-}i\text{-}Pr)_3$; (*b*) 2 M Na_2CO_3, $Pd(PPh_3)_4$, 2-bromopropene; (*c*) 1.1 equiv. *n*-BuLi, THF, CO_2 then 6 M HCl.



not be obtained via conventional nucleophilic displacement of a halide. This method, however, precluded the use of **9** as a starting material to prevent homo-coupling of **9** and possible polymerization. Thus the MOM ether of *ortho*-bromophenol **17** underwent a halogen–lithium exchange with *t*-BuLi and the resulting anion was treated with triisopropylborate to form **18** in situ (Scheme 4). After stirring the mixture for 4 h, 2-bromopropene, $Pd(PPh_3)_4$, and Na_2CO_3 (2 M) were added and the mixture was heated at reflux to afford **19**. Subsequent *ortho*-lithiation of **19** followed by trapping the anion with carbon dioxide afforded 3-isopropenylsalicylic acid (**20**) in 87% yield after an acidic workup.

In conclusion, we have developed an efficient, high yielding strategy for the synthesis of 3-substituted salicylic acids beginning with inexpensive starting materials that requires no special equipment. Although salicylic acid derivatives were our target, this strategy certainly permits further elaboration, allowing one to synthesize various 2,6-disubstituted phenols with ease.

Experimental

General

Nuclear magnetic resonance (NMR) spectra were recorded on a Bruker ACE-200 (^{1}H 200 MHz, ^{13}C 50 MHz)

© 2001 NRC Canada

spectrometer. All spectra were obtained in $CDCl_3$ and the chemical shifts (ppm) are relative to the $CHCl_3$ peak as an internal reference (^{1}H 7.27 ppm, ^{13}C 77.00 ppm). Infrared (IR) spectra were recorded using a Mattson Galaxy Series 4030 FT-IR or a Nicolet Nexus 470 FT-IR ESP spectrophotometer. Mass spectra (MS) were run on either a Hewlett-Packard 5890 Series II gas chromatograph interfaced to a Hewlett-Packard 5971A mass selective detector or acquired by Mrs. Q. Wu, Department of Chemistry, University of Calgary, using a VG 7070 instrument. High resolution mass spectra (HRMS) were obtained by Mrs. D. Fox, Department of Chemistry, University of Calgary, on a Kratos MS-80 spectrometer. Elemental analyses were also performed by Mrs. D. Fox using a Control Equipment Corporation 440 Elemental Analyzer. All melting and boiling points are uncorrected. Anhydrous THF was distilled from sodium benzophenone ketyl. Anhydrous diethyl ether was distilled from CaH_2.

General procedure for the MOM protection of phenols (19)

Dry sodium hydride (432 mg, 18 mmol) was suspended in THF (10 mL) and was cooled to 0°C under N_2. A suitable phenol (12 mmol) was dissolved in THF (10 mL) and was added slowly dropwise to the NaH suspension over 10 min. The reaction mixture was allowed to stir at room temperature for 2 h. MOMCl (20) (6 mL, 6 M in methyl acetate, 36 mmol) was then added to the reaction mixture over 10 min and the reaction was stirred 2 h. The reaction mixture was concentrated in vacuo and the residue partitioned between diethyl ether and NaOH (0.1 M). The aqueous layer was extracted with diethyl ether and the organic layers were combined, washed once with NaOH (0.1 M), then with brine, dried over $MgSO_4$, and concentrated in vacuo. The resulting oil was purified via air bath distillation at reduced pressure to give a colorless oil.

*1-Fluoro-2-methoxymethoxybenzene (**5**)*

Yield 1.70 g (94%, 10.9 mmol); bp 90°C at 13 torr (lit. (21) 100°C at 20 torr) (1 torr = 133.322 Pa). ^{1}H NMR δ: 3.52 (s, 3H), 5.22 (s, 2H), 6.9–7.3 (m, 4H).

*1-Chloro-2-methoxymethoxybenzene (**6**)*

Yield 1.92 g (96%, 11.1 mmol); bp 100–110°C at 13 torr (lit. (21) 100–102°C at 11 torr). ^{1}H NMR δ: 3.53 (s, 3H), 5.27 (s, 2H), 6.9–7.01 (m, 1H), 7.18–7.23 (m, 2H), 7.34–7.41 (m, 1H).

*1-Bromo-2-methoxymethoxybenzene (**17**)*

Yield 2.18 g (91%, 10.1 mmol); bp 105–110°C at 13 torr (lit. (22) 98–99°C at 6 torr). ^{1}H NMR δ: 3.54 (s, 3H), 5.27 (s, 2H), 6.90 (ddd, J = 1.71, 7.13, 7.86 Hz, 1H), 7.16 (dd, J = 1.71, 8.29 Hz, 1H), 7.20–7.32 (m, 1H), 7.56 (dd, J = 1.54, 7.86 Hz, 1H).

*1,3-Dibromo-2-methoxymethoxybenzene (**9**)*

Yield 3.38 g (99%, 11.5 mmol); bp 60°C at 0.08 torr (lit. (23) 118–121°C at 5 torr). ^{1}H NMR δ: 3.73 (s, 3H), 5.20 (s, 2H), 6.90 (t, J = 8.0 Hz, 1H), 7.52 (d, J = 8.0 Hz, 2H).

*1-Isopropenyl-2-methoxymethoxybenzene (**19**)*

1-Bromo-2-methoxymethoxybenzene (11 mmol) was dissolved in THF (10 mL) and cooled to –78°C under N_2. *t*-BuLi (13.6 mL, 1.7 M in pentane, 23.1 mmol) was added dropwise over 10 min and then allowed to stir at –78°C for 1 h. Triisopropylborate (13.2 mmol) was added dropwise over 5 min and reaction mixture was stirred at room temperature for 4 h. Na_2CO_3 (6.6 mL, 2 M in H_2O, 13.2 mmol) was added and the mixture was allowed to stir for 10 min. $Pd(PPh_3)_4$ (0.55 mmol, 5 mol%) and 2-bromopropene (24.2 mmol) were added and the reaction mixture was heated to 50°C with vigorous stirring overnight. The reaction was diluted with diethyl ether and quenched with saturated sodium bicarbonate solution. The aqueous layer was extracted with diethyl ether and the organic layers were combined, washed with brine, dried over $MgSO_4$, and concentrated in vacuo. The resulting oil was purified via air bath distillation at reduced pressure to give a colourless oil. Yield 1.63 g (83%, 9.1 mmol); bp 100°C at 13 torr. MS *m*/*z* (%): 178 (25, M^+), 163 (13, $[M - 15]^+$). HRMS calcd. for $C_{11}H_{14}O_2$: 178.0994; found: 178.1005. IR (thin film) (cm^{-1}): 1598 (C=C), 1229 (C–O). ^{1}H NMR δ: 2.10–2.20 (m, 3H), 3.50 (s, 3H), 5.00–5.10 (m, 1H), 5.10–5.20 (m, 1H), 5.22 (s, 2H), 6.90–7.05 (m, 1H), 7.05–7.18 (m, 1H), 7.18–7.25 (m, 2H). ^{13}C NMR δ: 23.3, 56.1, 94.6, 114.9, 115.1, 121.8, 128.2, 129.5, 133.7, 144.1, 154.1.

General procedure for the formation of 2-bromo-6-substituted MOM protected phenols

1,3-Dibromo-2-methoxymethoxybenzene (12 mmol) was dissolved in diethyl ether (10 mL) and was cooled to –78°C under N_2. *t*-BuLi (15.5 mL, 1.7 M in pentane, 26.4 mmol) was added dropwise over 10 min and was allowed to stir at –78°C for 1 h. A suitable electrophile (14.4 mmol) was added dropwise over 5 min and the reaction mixture was stirred at room temperature for 1 h. The reaction mixture was diluted with diethyl ether and quenched with saturated sodium bicarbonate solution (10 mL). The aqueous layer was extracted with diethyl ether and the organic layers were combined, washed with brine, dried over $MgSO_4$, and concentrated in vacuo. The product was purified via air bath distillation at reduced pressure to give a colorless oil.

*1-Allyl-3-bromo-2-methoxymethoxybenzene (**10**)*

Yield 2.70 g (88%, 10.6 mmol); bp 70°C at 0.08 torr. MS *m*/*z* (%): 256 (3, M^+), 258 (3, $[M + 2]^+$). HRMS calcd. for $C_{11}H_{13}O_2{}^{79}Br$: 256.0099; found: 256.0092. IR: (thin film) (cm^{-1}): 1159 (C–O). ^{1}H NMR δ: 3.48–3.55 (m, 2H), 3.67 (s, 3H), 5.0–5.15 (m, 2H), 5.10 (s, 2H), 5.88–6.10 (m, 1H), 6.97 (t, J = 7.78 Hz, 1H), 7.15 (dd, J = 1.71, 7.78 Hz, 1H), 7.42 (dd, J = 1.71, 7.78 Hz, 1H). ^{13}C NMR δ: 34.7, 57.7, 99.8, 116.2, 117.5, 125.6, 129.5, 131.5, 135.8, 136.5, 152.7. Anal. calcd. for $C_{11}H_{13}BrO_2$: C 51.38, H 5.10; found: C 50.07, H 5.10.

*1-Bromo-2-methoxymethoxy-3-methylsulfanylbenzene (**11**)*

Yield 2.45 g (78%, 9.4 mmol); bp 80–85°C at 0.08 torr. MS *m*/*z* (%): 262 (56, M^+), 264 (56, $[M + 2]^+$), 232 (42, $[M - 30]^+$), 234 (42, $[(M + 2) - 30]^+$. HRMS calcd. for $C_9H_{11}O_2S^{79}Br$: 261.9663; found: 261.9646. IR (thin film) (cm^{-1}): 1562 (C=C), 1158 (C–O). ^{1}H NMR δ: 2.43 (s, 3H), 3.73 (s, 3H), 5.15 (s, 2H), 6.95 (t, J = 7.8 Hz, 1H), 7.10

© 2001 NRC Canada

(dd, *J* = 1.7, 7.8 Hz, 1H), 7.35 (dd, *J* = 1.7, 7.8 Hz, 1H) (23). ^{13}C NMR δ: 15.1, 58.3, 99.0, 117.5, 125.3, 125.8, 128.1, 129.8, 135.4, 150.7. Anal. calcd. for $C_9H_{11}BrO_2S$: C 41.08, H 4.21; found: C 42.18, H 4.23.

*3-Bromo-2-methoxymethoxy-1-(trimethylgermanyl)benzene (**12**)*

Yield 3.33 g (83%, 10.0 mmol); bp 90–95°C at 0.08 torr. MS *m*/*z* (%): 334 (1, M^+), 319 (100, $[M - 15]^+$), 289 (62, $[M - 45]^+$). HRMS calcd. for $C_{10}H_{14}O_2{}^{79}Br^{74}Ge$: 318.9389 ($[M + CH_3]$); found 318.9390. IR: (thin film) (cm^{-1}): 1164 (C–O). ^{1}H NMR δ: 0.47 (s, 9H), 3.64 (s, 3H), 5.12 (s, 2H), 6.99 (t, *J* = 7.5 Hz, 1H), 7.35 (dd, *J* = 1.6, 7.5 Hz, 1H), 7.55 (dd, *J* = 1.6, 7.5 Hz, 1H). ^{13}C NMR δ: –0.4, 58.0, 99.6, 116.9, 125.5, 128.3, 133.9, 134.3, 135.8, 138.1, 157.5. Anal. calcd. for $C_{11}H_{17}BrO_2Ge$: C 39.58, H 5.19; found: C 39.40, H 5.13.

General procedure for (*i*) *ortho*-lithation; (*ii*) direct carboxylation; (*iii*) deprotection

The 1-substituted-2-methoxymethoxybenzene (11 mmol) was dissolved in THF (10 mL) and cooled to 0°C under N_2. *n*-BuLi (8.6 mL, 1.4 M in hexanes, 12.1 mmol) was added dropwise over 5 min and the reaction mixture was stirred at 0°C for 1.5 h. The mixture was then cooled to –78°C and CO_2(g) was passed through a column of Drierite and bubbled into the reaction for 1.5 h. The mixture was allowed to warm to room temperature, HCl (6 M, 10 mL) was added, and the reaction mixture was stirred vigorously overnight. The reaction mixture was extracted with diethyl ether and the combined organic layers was washed with brine, dried over $MgSO_4$, and concentrated in vacuo to give a solid, which was purified by flash chromatography.

*3-Fluorosalicylic acid (**7**)*

Yield 1.48 g (86%, 9.5 mmol); mp 144–147°C (lit. (3) 146–148°C). ^{1}H NMR δ: 6.84 (dt, *J* = 1.54, 8.04 Hz, 1H), 7.22–7.36 (m, 1H), 7.68 (dt, *J* = 4.62, 8.04 Hz, 1H).

*3-Chlorosalicylic acid (**8**)*

Yield 1.72 g (91%, 10.0 mmol); mp 183–185°C (lit. (24) 184–185°C). ^{1}H NMR δ: 6.90 (t, *J* = 8.0 Hz, 1H), 7.60 (dd, *J* = 1.7, 8.0 Hz, 1H), 7.87 (dd, *J* = 1.7, 8.0 Hz, 1H).

*3-Isopropenylsalicylic acid (**20**)*

Yield 1.71 g (87%, 9.6 mmol); mp 98–100°C (lit. (25) 110–110.5°C). MS *m*/*z* (%): 178 (1, M^+), 160 (54, $[M - 18]^+$). HRMS calcd. for $C_{10}H_{10}O_3$: 178.0630; found 178.0613. IR ($CHCl_3$) (cm^{-1}): 3063 (br, OH), 1655 (C=O). ^{1}H NMR δ: 6.90 (dd, *J* = 7.52, 8.04 Hz, 1H), 7.46 (dd, *J* = 1.71, 7.52 Hz, 1H), 7.88 (dd, *J* = 1.71, 8.04 Hz, 1H), 10.75 (br s, 1H). ^{13}C NMR δ: 22.8, 111.1, 116.1, 119.1, 129.9, 132.7, 136.4, 142.6, 159.6, 174.7. Anal. calcd. for $C_{11}H_{14}O_2$: C 67.41, H 5.66; found: C 67.51, H 5.80.

General procedure for (*i*) *ortho*-lithiation via lithium–bromide exchange; (*ii*) direct carboxylation; (*iii*) deprotection

The 1-bromo-3-substituted-2-methoxymethoxybenzene (11 mmol) was dissolved in THF (10 mL) and cooled to –78°C under N_2. *t*-BuLi (13.6 mL, 1.7 M in pentane, 23.1 mmol) was added dropwise over 10 min and the reaction mixture was stirred at –78°C for 1.5 h. CO_2(g) was passed through a column of Drierite and bubbled into the reaction for 1.5 h. The mixture was allowed to warm to room temperature, HCl (6 M, 10 mL) was added, and the reaction mixture was stirred vigorously overnight. The reaction mixture was extracted with diethyl ether and the organic layers were combined, washed with brine, dried over $MgSO_4$, and concentrated in vacuo to give a beige solid, which was purified by flash chromatography.

*3-Bromosalicylic acid (**13**)*

Yield 2.30 g (97%, 10.7 mmol); mp 177–180°C (lit. (10) 181–181.5°C). ^{1}H NMR δ: 6.84 (t, *J* = 7.95 Hz, 1H), 7.78 (dd, *J* = 1.71, 7.95 Hz, 1H), 7.90 (dd, *J* = 1.71, 7.95 Hz, 1H).

*3-Allylsalicylic acid (**14**)*

Yield 1.78 g (91%, 10.0 mmol); mp 90–92°C (lit. (26) 90–91°C). ^{1}H NMR δ: 6.88 (dd, *J* = 7.52, 7.86 Hz, 1H), 7.41 (dd, *J* = 1.71, 7.52 Hz, 1H), 7.82 (dd, *J* = 1.71, 7.86 Hz, 1H).

*3-Methylsulfanylsalicylic acid (**15**)*

Yield 1.36 g (67%, 7.4 mmol); mp 165–169°C (lit. (27) 168–170°C). ^{1}H NMR (lit. (27)) δ: 2.49 (s, 3H), 6.95 (t, *J* = 7.95 Hz, 1H), 7.44 (dd, *J* = 1.54, 7.95 Hz, 1H), 7.78 (dd, *J* = 1.54, 7.95 Hz, 1H).

*3-Trimethylgermanylsalicylic acid (**16**)*

Yield 2.51 g (89%, 9.8 mmol); mp 138–141°C. MS *m*/*z* (%): 256 (2, M^+), 241 (72, $[M - 15]^+$), 223 (100, $[(M - 15) - 18]^+$). HRMS calcd. for $C_{10}H_{14}O_3{}^{74}Ge$: 256.0155; found 256.0131. IR ($CHCl_3$) (cm^{-1}): 3073 (br, OH), 1660 (C=O). ^{1}H NMR δ: 0.46 (s, 9H), 6.93 (dd, *J* = 7.10, 7.95 Hz, 1H), 7.60 (dd, *J* = 1.71, 7.10 Hz, 1H), 7.91 (dd, *J* = 1.71, 7.95 Hz, 1H), 10.61 (s, 1H). ^{13}C NMR δ: –1.6, 110.0, 119.3, 131.3, 141.7, 163.2, 165.8, 174.6. Anal. calcd. for $C_{10}H_{14}O_3Ge$: C 47.14, H 5.54; found: C 47.99, H 5.70.

Acknowledgments

We thank Natural Sciences and Engineering Research Council of Canada (NSERC) and the University of Calgary for financial support. S.Y.W.L. also thanks NSERC for postgraduate scholarships.

References

1. (*a*) S.Y.W. Lau and B.A. Keay. Synlett, 605 (1999); (*b*) S.Y.W. Lau, N.G. Andersen, and B.A. Keay. Org. Lett. **3**, 181 (2001). (*c*) W.A. Cristofoli and B.A. Keay. Synlett, 625 (1994).
2. (*a*) S.P. Maddaford, N.G. Andersen, W.A. Cristofoli, and B.A. Keay. J. Am. Chem. Soc. **118**, 10766 (1996); (*b*) B.A. Keay, S.P. Maddaford, W.A. Cristofoli, N.G. Andersen, M.S. Passafaro, N.S. Wilson, and J.A. Nieman. Can. J. Chem. **75**, 1163 (1997).
3. M.L. Micklatcher and M. Cushman. Synthesis, 1878 (1999).
4. (*a*) R. Kluger and V. DeStafano. J. Org. Chem. **65**, 214 (2000); (*b*) T. Kline, J. Bowman, B.H. Iglewski, T. DeKievit, Y. Kakai, and L. Passador. Bioorg. Med. Chem. Lett. **9**, 3447 (1999); (*c*) J. Chen, B.R. Dixon, J. Dumas, and D. Brittelli. Tetrahedron Lett. **40**, 9195 (1999); (*d*) J.A. Ruell, E. DeClerq, C. Pannecouque, M. Witvrow, T.L. Stup, J.A. Turpin, R.W. Buckheit, and M. Cushman. J. Org. Chem. **64**, 5858 (1999); (*e*) T. Hattori,

© 2001 NRC Canada

A. Takeda, K. Suzuki, N. Koike, E. Koshiishi, and S. Mizano. J. Chem. Soc. Perkin Trans. 1, 3661 (1998).
5. A.S. Lindsey. Chem. Rev. **57**, 583 (1957).
6. H. Wynberg. Chem. Rev. **60**, 169 (1960).
7. L.N. Ferguson. Chem. Rev. **46**, 230 (1946).
8. (*a*) L.N. Ferguson. J. Am. Chem. Soc. **68**, 2502 (1946); (*b*) S.H. Dandegaonker and G.R. Revankar. Monatsh. Chem. **96**, 450 (1965).
9. (*a*) M. Komiyama and H. Hirai. J. Am. Chem. Soc. **105**, 2018 (1983); (*b*) A. Theor, G. Denis, M. Delmas, and A. Gaset. Synth. Commun. **18**, 2095 (1988); (*c*) R. Neumann and Y. Sasson. Synthesis, 569 (1986).
10. J.M. Shackelford. J. Org. Chem. **26**, 4908 (1961).
11. A.N. Meldrum and M.S. Shah. J. Chem. Soc. 1986 (1923).
12. (*a*) G.H. Posner and K.A. Canella. J. Am. Chem. Soc. **107**, 2571 (1985); (*b*) N.S. Narasimhan and R.S. Mali. Synthesis, 965 (1983); (*c*) M. Gilman, C.E. Arntzen, and F.J. Webb. J. Org. Chem. **10**, 374 (1945). For reviews on *ortho*-lithiation, see: (*d*) H.W. Gschwend and H.R. Rodriguez. Org. React. **26**, 1 (1979); (*e*) V. Snieckus. Chem. Rev. **90**, 879 (1990).
13. (*a*) M.R. Winkle and R.C. Ronald. J. Org. Chem. **47**, 2101 (1982); (*b*) R.C. Ronald and M.R. Winkle. Tetrahedron, **39**, 2031 (1983); (*c*) D.L. Comins and J.K. Saha. Tetrahedron Lett. **36**, 7995 (1995).
14. H. Christensen. Synth. Commun. **5**, 65 (1975).
15. A.R. Katritzky, H. Lang, and X. Lan. Synth. Commun. **23**, 1175 (1993).
16. D.E. Pearson, R.D. Wysong, and C.V. Breder. J. Org. Chem. **32**, 2358 (1967).
17. (*a*) L. Horner, A.J. Lawson, and G. Simons. Phosphorus Sulfur, **12**, 353 (1981); (*b*) S. Cabiddu, C. Fattuoni, C. Floris, G. Gelli, S. Melis, and F. Sotgiu. Tetrahedron, **46**, 861 (1990); (*c*) C.A. Coburn, M.B. Young, R.W. Hungate, R.C.A. Isaacs, J.P. Vacca, and J.R. Huff. Bioorg. Med. Chem. Lett. **6**, 1937 (1996).
20. A. Amato, S. Karady, M. Sletzinger, and L.M. Weinstock. Synthesis, 970 (1979).
21. S. Labidalle, Z.Y. Min, A. Reynet, H. Moskowitz, J.-M. Vierford, and M. Miocque. Tetrahedron, **44**, 1159 (1988).
23. Y. Morita, A. Kashiwagi, and N. Kazuhiro. J. Org. Chem. **62**, 7464, 1997.
24. A.E. Bird and A.C. Marshall. J. Chem. Soc. C, 2418 (1969).
25. S. Seki. Nippon Kagaku Zasshi, **80**, 667 (1959); Chem. Abs. 4410 (1961).
26. P. Stanetty, H. Koller, and G. Pürstinger. Monatsh. Chem. **121**, 883 (1990).
27. (*a*) May and Baker Ltd. Ger. Offen. No. 2 749 518 (Cl. C07D257/06) (1978); Chem. Abs. **89**. 109 509m (1978); (*b*) A. Kalgutkar, K.R. Kozak, B.C. Crews, G.P. Hochgesang, Jr., and L.J. Marnett. J. Med. Chem. **41**, 4800 (1998).

© 2001 NRC Canada

Enantioselective synthesis of peperomins A, C, D, and analogs — Examination of diastereoselective cuprate conjugate additions to *N*-enoyl-4-diphenylmethyl-2-oxazolidinones

Mukund P. Sibi, Michael D. Johnson, and T. Punniyamurthy

Abstract: A concise and general route to secolignans has been developed. The first total synthesis of secolignans peperomin A (**1a**), peperomin C (**1b**), and peperomin D (**1c**) was accomplished in ~28% overall yield over five synthetic steps. Peperomin analogs (**1d**) and (**1e**), possessing two differentially substituted aryl groups, were synthesized by a highly selective conjugate addition. The overall yield for the analogs **1d** and **1e** were 27 and 26%, respectively.

Key words: peperomins, secoliganans, conjugate additions, 4-diphenylmethyl-oxazolidin-2-one.

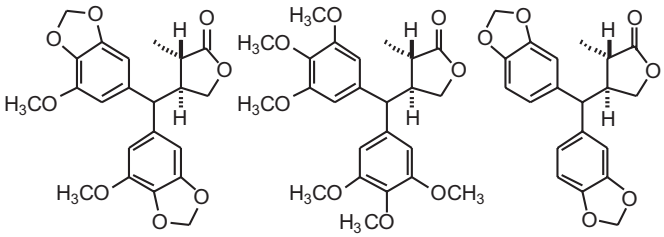
Résumé : On a mis au point une voie d'accès concise et générale conduisant aux sécolignanes. On a réalisé la première synthèse totale des sécolignanes pépéromine A (**1a**), pépéromine C (**1b**) et pépéromine D (**1c**), avec un rendement global d'environ 28% sur cinq étapes. Les analogues **1d** et **1e** de la pépéromine qui possèdent deux groupes aryles substitués de façon différente ont aussi été synthétisés par le biais d'une addition conjuguée hautement sélective. Les rendements globaux des synthèses des analogues **1d** et **1e** sont respectivement de 27 et 26%.

Mots clés : pépéromines, sécolignanes, additions conjuguées, 4-diphénylméthyloxazolidin-2-one.

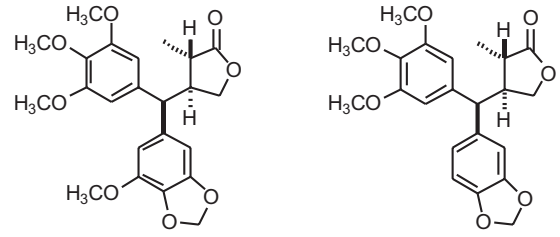
[Traduit par la Rédaction]

Introduction

Recently, a novel and unusual class of lignans were isolated from *Peperomia japonica* Makino by Chen et al. (1). Three lignans, peperomins A, B, and C, with a novel seco structure, were isolated from this perennial herb. Peperomin D was also recently isolated from *Peperomia glabella* (2). The use of aqueous and alcoholic decoctions of the herb as folk medicine for the treatment of malignant tumors has been noted (1). Two other secolignans with insect antifeedant activity have also been isolated from *Peperomia dindigulensis* (3). These secolignans have structural features that are present in the combretastatins (4) and podophyllotoxin (5). In view of the high tubulin inhibitory activity of the combretastatins and podophyllotoxin, the evaluation of the biological activity of peperomins and their analogs could be important. The structure-activity relationship in this novel secolignan series could shed more light on the conformational requirements for tubulin binding at the colchicine–podophyllotoxin site. Towards this end we have started a program on the preparation and biological evaluation of peperomins and analogs. Only a single racemic synthesis of peperomin C has been reported in the literature so far (6). This paper describes the first total synthesis of peperomins A, C, D, and two analogs.



1a eperomin **1b** eperomin C **1c** eperomin D



1d eperomin analog **1e** eperomin analog

We have been investigating methodologies for the preparation of succinates with various substituents on the carbon backbone and their application to the synthesis of butyrolactone

Received January 10, 2001. Published on the NRC Research Press Web site at http://canjchem.nrc.ca on October 22, 2001.

Dedicated with heartfelt appreciation to Victor Snieckus — mentor, teacher, and a friend.

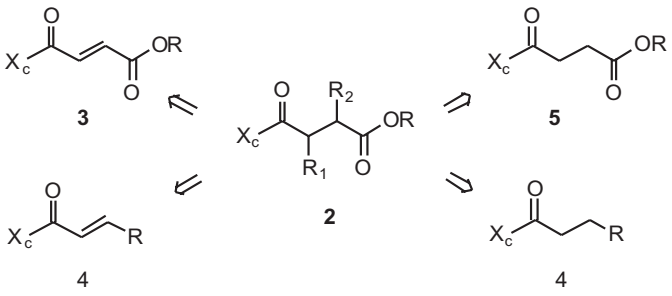
M.P. Sibi,[1] M.D. Johnson,[2] and T. Punniyamurthy. Department of Chemistry, North Dakota State University, Fargo, ND 58105–5516, U.S.A.

[1]Corresponding author (telephone: (701) 231-8251; fax: (701) 231-8831; e-mail: Mukund_Sibi@ndsu.nodak.edu).

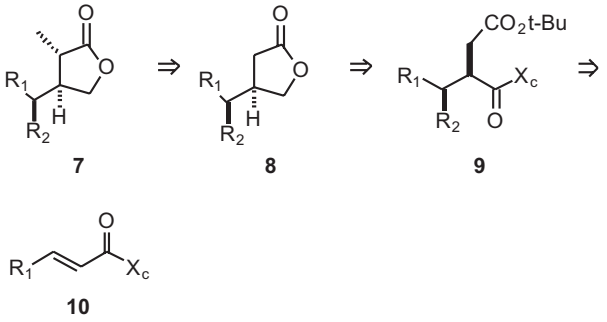
[2]Taken in part from the M.S. thesis of M.D. Johnson, North Dakota State University, Fargo, North Dakota, October 1998.

 DOI: 10.1139/cjc-79-11-1546 © 2001 NRC Canada

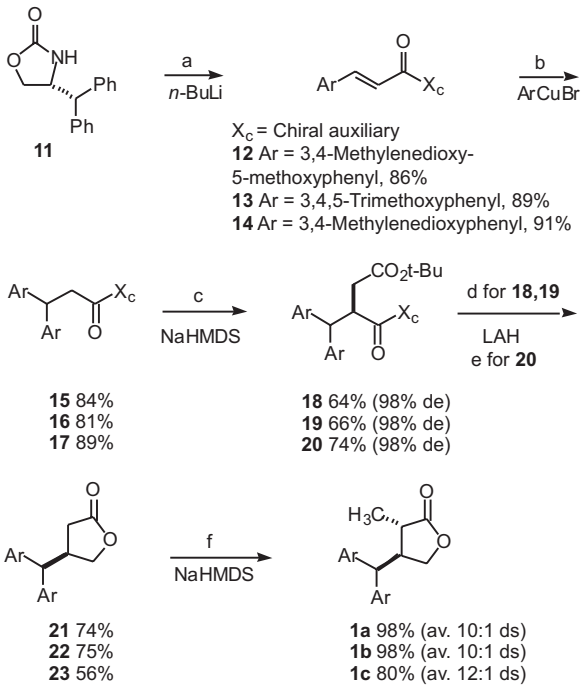
Scheme 1.



Scheme 2.



Scheme 3.



Key: (a) 1.0 equiv. n-BuLi, 1.1 equiv. ClCOAr, -78°C, 3h, THF; (b) (i) 3.1 equiv. Mg, (ii) 3.0 equiv. ArBr, (iii) 1.5 equiv. CuBr-$(CH_3)_2S$, -48 to 0°C, 3 h, 3:1 THF-$(CH_3)_2S$; (c) (i)1.1 equiv. NaHMDS, (ii)1.5 equiv. *t*-BuO_2CCH_2I,-78 to -48°C, 6 h, THF; (d) (i) 5.0 equiv. LAH (1 M), 20 h, THF, (ii) Silica gel; (e) (i) $LiOH/H_2O_2$; (ii) BH_3, (iii) PTSA; (f) (i)1.1 equiv. NaHMDS, (ii)1.5 equiv. CH_3I, 3 h, -78°C.

natural products (Scheme 1) (for other selected approaches to substituted succinates see refs. 7*a–c*; for an example of enolate alkylation leading to similar structures see ref. 7*d*). Recently, we described a novel route to paraconic and lignan natural products by the conjugate addition of radical intermediates starting from fumarates (**3** → **2**) (8). We have also reported on alternate routes to paraconic acids using succinates as starting materials (**5** → **2**) (9). The chiral auxiliary appended β-aryl propionates have also served as starting materials in the synthesis of lignan natural products (**6** → **2**) (10). These three disconnections, however, were not suited for the preparation of the secolignans and an alternate approach (**4** → **2**) was required.

The synthetic strategy for the preparation of peperomins is shown in Scheme 2. The design is based on the conjugate addition of an aryl group to the enoyloxazolidinone **10** (X_c = chiral auxiliary). The conjugate addition is followed by electrophile incorporation in a step-wise manner to furnish **9**. The strategy provides the flexibility for the introduction of different aryl groups by either varying the nucleophile or the enoyloxazolidinone leading to a variety of β,β-diaryl propionic acids (for procedures describing methodologies for the synthesis of enantiomerically enriched 3,3-diaryl propanoic acids and derivatives see refs. 11*a–f*; for a recent effort see ref. 11*g*). The next step in the sequence involves chemoselective reduction of the carbonyl bearing the chiral auxiliary and cyclization to provide **8**. Enolate alkylation of **8** from the less-hindered face establishes the required *trans* stereochemistry in the natural products. The key bond construction in our synthesis is a conjugate addition of an aryl copper reagent to a chiral enoate. Of the variety of chiral auxiliaries examined for conjugate additions, the oxazolidinones have generally been inferior in terms of selectivity. Recently, several groups have undertaken a study of various auxiliaries in the addition of copper reagents to enoates (for a comparative study of chiral auxiliaries see ref. 12). Hruby and co-workers (13; for NMR studies see ref. 13*b*) have shown that the oxazolidinone derived from phenylglycinol provides high selectivity in the addition of aryl coppers to cinnamates. We describe the use of an oxazolidinone derived from diphenylalanine in conjugate additions to acyclic systems using copper nucleophiles and determine its effectiveness in controlling stereochemistry at the β-carbon with the traditional oxazolidinones.

Results and discussion

Initial targets for examining the feasibility of our methodology were the simpler peperomins A, C, and D, since these compounds do not possess a chiral center at the benzylic carbon. This would allow us to establish reaction conditions for the conjugate additions (protocols for conjugate additions to enoyloxazolidinones has been established, see ref. 14*a*; for other contributions from the Hruby group see ref. 14*b*; 14*c–h*; for work on superquat oxazolidinone auxiliaries see ref. 14*i*). The synthesis of peperomin A, C, and D started with the acylation of the 4-diphenylmethyl-2-oxazolidinone auxiliary developed in our laboratory (Scheme 3) (15).[3] Treatment of **11** with *n*-BuLi provided the anion which was acylated with 3-[3′,4′-methylenedioxy-5′-methoxy-phenyl]-2-propenoyl

[3] For the synthesis of chiral auxiliary **11** see ref. 15*a*. This chiral auxiliary is available commercially from Aldrich Chemical Company; see ref. 15*b*. For the application of this auxiliary in synthesis see ref. 15*c*.

© 2001 NRC Canada

chloride (16).[4] 3,4-(Methylenedioxy)-5-methoxybenzaldehyde was transformed into the corresponding acid chloride: (*a*) $Ph_3P{=}CHCO_2Et$ (1.1 equiv), 70°C, 16 h, C_6H_6, 92% (96% *E*-isomer); (*b*) (*i*) 2.2 equiv NaOH, reflux, 20 min, 99%; (*ii*) 3.2 equiv oxalyl chloride, 25°C, 3 h, 93%. to furnish **12** in high yield. The required cinnamic acid (17) was prepared by HWE reaction between 3,4-methylenedioxy-5-methoxybenzaldehyde (18) and phosphanoacetic acid. Cinnamates **13** and **14** were prepared in high yields using 3-[3′,4′,5′-trimethoxyphenyl]-2-propenoyl chloride and 3-[3′,4′-methylenedioxyphenyl]-2-propenoyl chloride and lithiated **11**, respectively. The two-step protocol for the introduction of the substituents was then undertaken (19).[5] Reaction of **12** with the copper reagent prepared from 3,4-methylenedioxy-5-methoxy bromobenzene (20) gave **15** in 84% yield. Similarly, treatment of **13** and **14** with the copper reagent derived from 3,4,5-trimethoxy bromobenzene and 3,4-methylenedioxy bromobenzene (21) gave **16** and **17**, respectively. The next step involved the introduction of the acetic acid chain. This was accomplished in respectable chemical yield and excellent diastereoselectivity (>98%) by treatment of **15** and **16** with sodium hexamethyldisilazide followed by quenching of the sodium enolate with *tert*-butylbromoacetate. The diastereoselectivity in the alkylation step was established by ^1H NMR analysis (400 MHz) of the crude product. The alkylation of **17** using bromo-*tert*-butylacetate gave moderate yields (60%). A change of the leaving group to an iodo group gave **20** in higher yields (74%). Similar small increments in chemical efficiency were also noted for simple substrates as well as the alkylation precursor for peperomin analogs (vide infra). Thus, the iodoacetates were used in all the alkylation reactions (for a recent example of variation in chemical efficiency and selectivity in enolate alkylations with haloacetates see ref. 22).

With the desired succinates at hand, chemoselective reduction of the carbonyl attached to the chiral auxiliary was achieved by using LAH at low temperatures (23). Work-up of the reduction product followed by silica gel column chromatography furnished the butyrolactones **21** and **22** directly in good yields over two steps.[6] Reduction of **20** using LAH was not clean, providing the desired alcohol as well as an over-reduced diol (reduction of imide as well as the ester). Thus, an alternate sequence was devised. The chiral auxiliary in **20** was selectively hydrolyzed using $LiOH–H_2O_2$ (24). The resulting acid ester was reduced chemoselectively using borane (25). Lactonization using catalytic amounts of *p*-toluenesulfonic acid gave **23**. The three-step sequence could be carried out with good efficiency without isolation of the intermediates.

Introduction of the 3-substituent in butyrolactones by enolate alkylation has been well established in the literature (for some examples of diastereoselective alkylation at the 3-position see ref. 26). Generation of the sodium enolate of **21** and quenching with methyl iodide gave a 10:1 to 12:1 mixture of the methylated product. The use of LDA as the base in the alkylation gave a 8:1 mixture of the alkylated products (stereoselectivity of alkylations in substituted butyrolactones has been examined, see ref. 27). Attempts to improve diastereoselectivity by variation of reaction conditions were unrewarding. The two diastereomers were inseparable by chromatographic methods. However, the major diastereomer (**1a**) could be separated and purified by careful recrystallization. The major diastereomer was established to posses the 3,4-*trans* stereochemistry by comparison of its spectral data with those reported for peperomin A (1). The synthesis of **1b** followed a similar reaction sequence but starting with **22** and spectral data of the major diastereomer (~10:1 ds) was consistent with those reported for peperomin C (1). The overall yields for peperomin A (**1a**) and peperomin C (**1b**) were 28% (five steps) and 28% (five steps), respectively. The alkylation of **23** using NaHMDS as the base gave peperomin D (**1c**) with moderate to good diastereoselectivity and chemical yield. The spectral characteristics of the synthetic material were consistent with those reported in the literature for the natural product (2). The overall yield for peperomin D (**1c**) is ~27% over seven steps.

The synthesis of peperomin analogs (**1d** and **1e**) required the development of a diastereoselective conjugate addition protocol using copper reagents. Several groups have recently compared the effectiveness of different auxiliaries in conjugate additions and noted that the camphor sultams are quite good (28).[7] Hruby and co-workers (see ref. 13. For selected examples from a large body of work see ref. 29)[8] have also demonstrated that an oxazolidinone derived from phenylglycinol is an excellent chiral auxiliary in conjugate addition to enoates using organocuprates as nucleophiles. We have recently shown that a chiral auxiliary derived from diphenylalanine is superior to Evans-type oxazolidinones in conjugate radical additions (30). Thus, we wished to briefly evaluate the utility of this auxiliary in conjugate addition using cuprates as nucleophiles. The protocol developed by Hruby and co-workers was adapted as the standard reaction conditions (the addition of Grignard reagent with the use of copper bromide – dimethyl sulfide complex as the copper source). Reactions with a variety of substrates with simple as well as more functionalized aromatic nucleophiles were investigated. Results from these experiments are shown in Table 1. The diastereoselectivity in the conjugate additions was determined by NMR and HPLC analyses. The data in the table indicates that the diastereoselectivity was very high. The addition of Grignard reagent derived from 3,4-methylenedioxy-5-methoxy-

[4] 3,4-(Methylenedioxy)-5-methoxybenzaldehyde was transformed into the corresponding acid chloride: (*a*) $Ph_3P{=}CHCO_2Et$ (1.1 equiv), 70°C, 16 h, C_6H_6, 92% (96% *E*-isomer); (*b*) (*i*) 2.2 equiv NaOH, reflux, 20 min, 99%; (*ii*) 3.2 equiv oxalyl chloride, 25°C, 3 h, 93%.

[5] For a review on enantioselective conjugate addition see ref. 19*b*. For other recent reviews see ref. 19*c*.

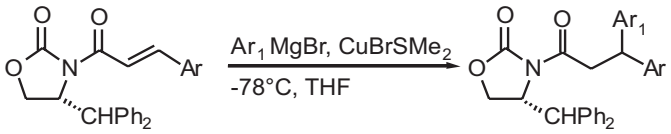
[6] The chiral auxiliary was recovered in >95% yield.

[7] (*S*)-4,4-Dimethylpyroglutamate as a chiral auxiliary, see ref. 28*a*. Addition of Yamamoto's reagent with high selectivity to *N*-enoyloxazolidinones; see ref. 28*b*. Comparison of auxiliaries see ref. 28*c*. Others: Oppolzer and Helmchen auxiliary; see ref. 28*d–f*. Addition of aryl Grignards and (or) coppers to oxazolidinone enoates see ref. 28*g*. Addition to 4-phenyl-oxazolidinone derived enoates see ref. 28*h*. For other efforts in the area see ref. 28*i*.

[8] Williams has recently shown that 4-benzyloxazolidinone is a useful chiral auxiliary in conjugate additions using Yamamoto's reagent. See ref. 12*b*.

© 2001 NRC Canada

Table 1. Diastereoselective conjugate additions to enoyloxazolidinones.



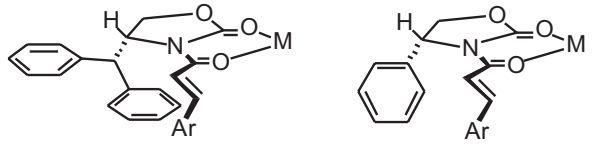
12, 13,14, 24 **25-30**

Entry	Ar	Ar_1	Product	Yield (%)	de (%)
1	3,4-(OCH_2O)-5-MeOPh (**12**)	Ph	**25**	90	94
2	3,4,5-$(MeO)_3$Ph (**13**)	3,4-(OCH_2O)-5-MeOPh	**26**	89	97
3	3,4,5-$(MeO)_3$Ph (**13**)	3,4-(OCH_2O)Ph	**27**	88	95
4	3,4,5-$(MEO)_3$Ph (**13**)	Ph	**28**	90	96
5	3,4-(OCH_2O)Ph (**14**)	Ph	**29**	97	97
6	Ph (**24**)	3,4-(OCH_2O)Ph	**30**	95	92

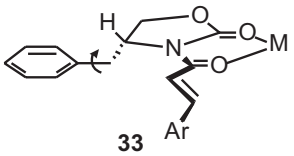
[a]Yields are for purified materials.
[b]des were determined by NMR analysis.

bromobenzene (31) to **13** gave **26**, the intermediate in peperomin analog (**1d**) synthesis, in excellent yield and diastereoselectivity (entry 2). Similarly, intermediate for analog **1e**, was also obtained with high efficiency (entry 3). Conjugate additions to other substrates either varying the nucleophile or the acceptor did not diminish the selectivity (entries 1, 4, 5, and 6). Thus, the 4-diphenylmethyl substituted enoyl oxazolidinones undergo conjugate additions with high selectivity.

The efficient shielding of the β-carbon in conjugate additions by 4-phenyl- and 4-diphenylmethyl-oxazolidinones may suggest that these likely have similar structural organization in the transition states (structures **31** and **32**). In conjugate additions with 4-benzyloxazolidinones (13), the C-4-benzyl bond rotation (**33**) may play a role in the observed low selectivity. The high selectivity observed for organocuprate addition to 4-phenyl and 4-diphenylmethyl derived enoates is in stark contrast to conjugate radical additions where only auxiliary **11** showed high selectivity. Thus, the results depicted in the table and previous work from our laboratory (30) clearly show that the diphenylalanine-derived oxazolidinone can shield the β-carbon effectively in both organocuprate and radical conjugate additions.



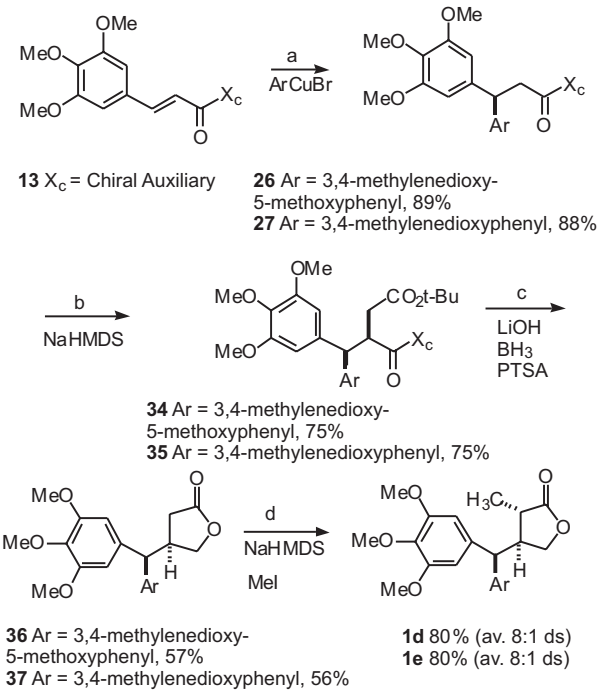
31 M = Lewis acid **32**



33

The basic methodology used in the synthesis of peperomins A, C, and D was adapted for the synthesis of the more complex analogs **1d** and **1e** (Scheme 4). Installation of the two-carbon chain on the conjugate addition products **26** and **27** furnished **34** and **35**. The diastereoselectivity in these alkylations was high with the chiral auxiliary controlling the face selectivity. The succinates were converted to the lactones **36** and **37**, respectively by a hydrolysis–reduction–lactonization sequence. The overall yield for the three steps without purification of the intermediates was excellent. With the lactones at hand, the final installation of the C-3 methyl group was uneventful. As observed in the previous alkylations (vide supra), the diastereoselectivities in these reactions were only moderate (highest ds of 8:1). All attempts at purification of the diastereomeric mixture were not successful. The structural characteristics (^1H and ^{13}C NMR chemical shifts) of analog **1d** are similar to those reported for the natural product peperomin B (1). The structure for the major

Scheme 4.



13 X_c = Chiral Auxiliary

26 Ar = 3,4-methylenedioxy-5-methoxyphenyl, 89%
27 Ar = 3,4-methylenedioxyphenyl, 88%

34 Ar = 3,4-methylenedioxy-5-methoxyphenyl, 75%
35 Ar = 3,4-methylenedioxyphenyl, 75%

36 Ar = 3,4-methylenedioxy-5-methoxyphenyl, 57%
37 Ar = 3,4-methylenedioxyphenyl, 56%

1d 80% (av. 8:1 ds)
1e 80% (av. 8:1 ds)

Key: (a) (i) 3.1 equiv. Mg, (ii) 3.0 equiv. ArBr, (iii) 1.5 equiv. CuBr-$(CH_3)_2S$, -48 to 0°C, 3 h, 3:1 THF-$(CH_3)_2S$; (b) (i)1.1 equiv. NaHMDS, (ii)1.5 equiv. t-BuO_2CCH_2I,-78 to -48°C, 6h , THF; (c) (i) $LiOH/H_2O_2$, (ii) BH_3, (iii) PTSA; (d) (i)1.1 equiv. NaHMDS, (ii)1.5 equiv. CH_3I, 3h, -78°C.

© 2001 NRC Canada

diastereomer (*trans* stereochemistry) of **1d** and **1e** are consistent with the observed ^{1}H NMR coupling constants and spectral similarities to the natural peperomins. The overall yield for **1d** and **1e** were 27 and 26%, respectively.

In conclusion, we have developed a simple and efficient strategy for the synthesis of secolignans peperomin A, C, D, and two analogs. Additionally, we have also shown that 4-diphenylmethyl oxazolidin-2-one (**11**) is an excellent auxiliary in diastereoselective conjugate addition of organocuprates to enoates. The extension of the present methodology for the synthesis of analogs and biological evaluation of the secolignans is currently underway in our laboratory.

Experimental

General experimental details

Methylene chloride (CH_2Cl_2) was distilled from calcium hydride. Tetrahydrofuran (THF), diethyl ether (Et_2O), and benzene were distilled from benzophenone–ketyl prior to use. Methanol (MeOH) was distilled from magnesium turnings and I_2. Acetone was dried from $KMnO_4$ and K_2CO_3. Most of the organic compounds utilized in this study were purchased from Aldrich Chemical Company. All glassware were oven dried, assembled hot, and cooled under a stream of dry nitrogen before use. Reactions with air-sensitive materials were carried out by standard syringe techniques. All reactions were run under an atmosphere of nitrogen unless otherwise noted.

Chromatography and instrumentation

Thin layer chromatographic analyses (TLC) were performed on silica gel Whatmann-60F glass plates and components were visualized by illumination with UV light or by staining with phosphomolybdic acid. Flash column chromatography was performed using E. Merck silica gel 60 (230–400 mesh). ^{1}H NMR was recorded on a 500, 400, or 300 MHz spectrometer. ^{13}C NMR was recorded on 500 (125) MHz, 400 (100) MHz, and 300 (75) MHz spectrometers using broad band proton decoupling. Rotations were recorded on a JASCO-DIP-370 instrument. Elemental analyses were performed on a PerkinElmer Series II CHNS/O analyzer 2400. Melting points was determined using a Fisher–Johns melting point apparatus without correction.

Representative procedure for the acylation of (*R*)-4-diphenylmethyl-2-oxazolidinone (compound 13)

To an oven-dried 100 mL three- neck round- bottomed flask purged with N_2 was added 3.50 g (14.69 mmol) of 3,4,5-trimethoxycinnamic acid. To the solid was added 5 mL (57.23 mmol) of oxalyl chloride dropwise over 2 min and the mixture was allowed to stir at room temperature (rt) for 1 h. Removal of the excess oxalyl chloride under reduced vacuum gave 3.65 g of pure acid chloride (97% yield). To an oven-dried 250 mL three-neck round-bottomed flask purged with N_2 was added 3.0 g (11.86 mmol) of 4-diphenylmethyl-2-oxazolidinone **11** and 40 mL of dry THF. The reaction mixture was cooled to –78°C in an acetone – dry ice bath. To the mixture was added 5.19 mL (12.45 mmol) of *n*-BuLi dropwise over 10 min and the mixture was allowed to stir for 30 min. A solution of 3.35 g (13.05 mmol) of the 3,4,5-trimethoxy cinnamoyl chloride dissolved in 15 mL of dry THF was added dropwise to the solution over 8 min. The solution was stirred at –78°C for 3 h. The reaction was quenched with 10 mL NH_4Cl. The reaction mixture was extracted with ethyl acetate. The combined organics were washed with water followed by brine and dried over $MgSO_4$. Removal of solvent under reduced pressure followed by flash column purification of the crude mixture gave 5.0 g of the acylated product (89% yield).

*(4*R*)-4-(Diphenylmethyl)-3-[3-(3′,4′-methylenedioxy-5′-methoxyphenyl)-2(*E*)-propenoyl]-2-oxazolidinone (**12**)*

Yield: 86%; mp 88–90°C. $[\alpha]_D^{25}$ –192.8 (*c* 0.98, $CHCl_3$). R_f 0.7 (50:50, EtOAc:hexanes). ^{1}H NMR (400 MHz, $CDCl_3$) δ: 3.94 (s, 3H), 4.48 (dd, *J* = 2.7, 8.0 Hz, 2H), 4.81 (d, *J* = 5.4 Hz, 1H), 5.44 (m, 1H), 6.04 (s, 2H), 6.78 (d, *J* = 1.1 Hz, 1H), 6.85 (d, *J* = 1.1 Hz, 1H), 7.22 (m, 10H), 7.70 (s, 2H). ^{13}C NMR (100 MHz, $CDCl_3$) δ: 50.6, 56.4, 56.5, 64.7, 102.0, 109.6, 115.1, 127.0, 127.7, 128.3, 128.6, 128.7, 128.8, 129.3, 138.0, 139.6, 143.6, 146.2, 149.2, 153.4, 164.9. Anal. calcd. for $C_{27}H_{23}NO_6$: C 70.89, H 5.07, N 3.06; found: C 70.81, H 5.12, N 2.91.

*(4*R*)-4-(Diphenylmethyl)-3-[3-(3′,4′,5′-trimethoxyphenyl)-2(*E*)-propenoyl]-2-oxazolidinone (**13**)*

Yield: 89%; mp 70 to 71°C. $[\alpha]_D^{25}$ –182.4 (*c* 0.95, $CHCl_3$). R_f 0.5 (50:50, EtOAc:hexanes). ^{1}H NMR (400 MHz, $CDCl_3$) δ: 3.89 (overlapping s, 9H), 4.45 (m, 2H), 4.82 (d, *J* = 5.4 Hz, 1H), 5.44 (m, 1H), 6.82 (s, 2H), 7.22 (m, 10H), 7.75 (d, *J* = 2.2 Hz, 2H). ^{13}C NMR (100 MHz, $CDCl_3$) δ: 50.5, 56.1, 56.4, 60.9, 64.8, 105.6, 115.8, 126.9, 127.7, 128.3, 128.6, 128.8, 129.3, 129.9, 138.0, 139.6, 140.4, 146.5, 153.3, 153.5, 164.9. Anal. calcd. for $C_{28}H_{27}NO_6$: C 71.02, H 5.75, N 2.96; found: C 70.94, H 5.76, N 2.84.

*(4*R*)-4-(Diphenylmethyl)-3-[3-(3′,4′-methylenedioxyphenyl)-2(*E*)-propenoyl]-2-oxazolidinone (**14**)*

Yield: 91%; mp 188 to 189°C. $[\alpha]_D^{25}$ –163.3 (*c* 1.0, CH_2Cl_2). R_f 0.56 (50:50, EtOAc:hexanes). ^{1}H NMR (400 MHz, $CDCl_3$) δ: 4.45 (m, 2H), 4.80 (d, *J* = 5.1 Hz, 1H), 5.42 (m, 1H), 6.01 (s, 2H), 6.81 (d, *J* = 8.1 Hz, 1H), 7.22 (m, 12H), 7.70 (s, 2H). ^{13}C NMR (100 MHz, $CDCl_3$) δ: 50.7, 56.6, 64.9, 101.8, 107.1, 108.6, 114.8, 125.4, 127.1, 127.9, 128.5, 128.8, 128.9, 129.1, 129.5, 138.3, 139.8, 146.4, 148.4, 150.1, 153.6, 165.2. Anal. calcd. for $C_{26}H_{21}NO_5$: C 73.06, H 4.95, N 3.28; found: C 72.57, H 5.10, N 3.29.

Representative procedure for the conjugate addition — Preparation of 26

To an oven-dried 100 mL round-bottomed flask purged with N_2 was added 1.43 g (58.9 mmol) of magnesium turnings and 10 mL of dry THF. The flask was placed in a ultrasonic bath for 3 min before dropwise addition of 13.18 g (57 mmol) 5-bromo-3-methoxy-1,2-methylenedioxybenzene (dissolved in 24 mL of dry THF) over 20 min. To an oven-dried three-neck 500 mL round-bottomed flask purged with N_2 was added 5.86 g (28.5 mmol) of copper(I) bromide – dimethyl sulfide complex and 40 mL of dimethyl sulfide and 80 mL of dry THF. The reaction mixture was cooled to –48°C in an acetonitrile – dry ice bath. To the mixture was added the Grignard reagent dropwise over 30 min and the mixture was allowed to stir for 30 min. A solution of 9.0 g

© 2001 NRC Canada

(19.0 mmol) of the cinnamate **13** dissolved in 36 mL of dry THF was added dropwise to the solution over 30 min. The solution was stirred at −48°C for 4.5 h. The reaction was quenched with 30 mL NH_4Cl. Excess dimethyl sulfide was removed using a water aspirator. The residue was extracted with ethyl acetate. The combined organics was washed with 10% NH_4OH, water, followed by brine, and dried over $MgSO_4$. Removal of solvent under reduced pressure followed by flash column purification of the crude mixture gave 10.58 g of the addition product **26** (89% yield).

*(4*R*)-4-(Diphenylmethyl)-3-[3-(3,3-bis-3′,4′-methylenedioxy-5′-methoxyphenyl)-propanoyl]-2-oxazolidinone (**15**)*

Yield: 84%; mp 90 to 91°C. $[\alpha]_D^{25}$ –130.8 (*c* 1.0, $CHCl_3$). R_f 0.53 (50:50, EtOAc:hexanes). ^{1}H NMR (400 MHz, $CDCl_3$) δ: 3.55 (m, 2H), 3.87 (two s, 6H), 4.40 (d, *J* = 5.4 Hz, 2H), 4.45 (t, *J* = 7.5, 1H), 4.62 (d, *J* = 4.8 Hz, 1H), 5.24 (m, 1H), 5.93 (m, 4H), 6.46 (m, 4H), 6.90 (s, 2H), 7.03 (d, *J* = 7.0 Hz, 2H), 7.27 (m, 6H). ^{13}C NMR (100 MHz, $CDCl_3$) δ: 40.9, 46.1, 50.3, 56.4, 56.6, 64.8, 101.3, 101.7, 101.8, 107.1, 107.4, 127.0, 127.8, 128.2, 128.6, 128.8, 129.3, 133.7, 133.8, 137.7, 138.1, 138.2, 139.4, 143.4, 143.5, 148.8, 148.9, 153.4, 170.8. Anal. calcd. for $C_{35}H_{31}NO_9$: C 68.96, H 5.03, N 2.30; found: C 68.70, H 4.66, N 2.68.

*(4*R*)-4-(Diphenylmethyl)-3-[3-(3,3-bis-3′,4′,5′-trimethoxyphenyl)-propanoyl]-2-oxazolidinone (**16**)*

Yield: 81%; mp 75 to 76°C. $[\alpha]_D^{25}$ –121.2 (*c* 0.98, $CHCl_3$). R_f 0.43 (50:50, EtOAc:hexanes). ^{1}H NMR (400 MHz, $CDCl_3$) δ: 3.60 (dd, *J* = 7.5, 16.7 Hz, 1H), 3.67 (dd, *J* = 7.5, 16.7 Hz, 1H), 3.82 (three s, 18H), 4.37 (m, 2H), 4.53 (t, *J* = 7.5 Hz, 1H), 4.60 (d, *J* = 4.8 Hz, 1H), 5.22 (m, 1H), 6.51 (s, 2H), 6.56 (s, 2H), 6.85 (m, 2H), 7.02 (d, *J* = 7.5 Hz, 2H), 7.26 (m, 6H). ^{13}C NMR (100 MHz, $CDCl_3$) δ: 40.6, 47.1, 50.3, 56.1, 56.4, 60.8, 64.7, 104.7, 104.9, 127.0, 127.8, 128.1, 128.6, 128.8, 129.2, 136.6, 136.7, 137.7, 138.8, 138.9, 139.4, 153.1, 153.4, 171.0. Anal. calcd. for $C_{37}H_{39}NO_9$: C 69.25, H 6.13, N 2.18; found: C 69.15, H 6.19, N 2.01.

*(4*R*)-4-(Diphenylmethyl)-3-[3-(3,3-bis-3′,4′-methylenedioxyphenyl)-propanoyl]-2-oxazolidinone (**17**)*

Yield: 89%; mp 86 to 87°C. $[\alpha]_D^{25}$ –112.7 (*c* 1.03, CH_2Cl_2). R_f 0.50 (50:50, EtOAc:hexanes). ^{1}H NMR (400 MHz, $CDCl_3$) δ: 3.51 (dd, *J* = 7.5, 17.4 Hz, 1H), 3.58 (dd, *J* = 7.5, 17.4 Hz, 1H), 4.38 (d, *J* = 4.8 Hz, 2H), 4.46 (t, *J* = 7.8 Hz, 1H), 4.61 (d, *J* = 5.1 Hz, 1H), 5.23 (m, 1H), 5.89 (s, 2H), 5.92 (s, 2H), 6.73 (m, 6H), 6.92 (d, *J* = 3.2 Hz, 2H), 7.03 (d, *J* = 6.7 Hz, 2H), 7.27 (m, 6H). ^{13}C NMR (100 MHz, $CDCl_3$) δ: 41.2, 45.5, 50.4, 56.4, 64.9, 101.1, 108.3, 108.4, 120.5, 120.8, 127.1, 127.9, 128.3, 128.7, 128.9, 129.4, 137.7, 137.9, 139.5, 146.2, 146.3, 147.8, 147.9, 153.5, 170.9. Anal. calcd. for $C_{33}H_{27}NO_7$: C 72.12, H 4.95, N 2.55; found: C 71.64, H 5.00, N 2.54.

*(3(3*S*),4*R*)-4-(Diphenylmethyl)-3-[3-(3,3-(phenyl)-(3″,4″-methylenedioxy-5″-methoxyphenyl)-propanoyl]-2-oxazolidinone (**25**)*

Yield: 90%; mp 146–148°C. $[\alpha]_D^{25}$ –140.0 (*c* 0.69, CH_2Cl_2). ^{1}H NMR (500 MHz, $CDCl_3$) δ: 3.59 (dd, *J* = 17.3, 7.1 Hz, 1H), 3.70 (dd, *J* = 17.3, 8.1 Hz, 1H), 3.89 (s, 3H), 4.38 (m, 2H), 4.57 (t, *J* = 7.5 Hz, 1H), 4.63 (d, *J* = 5.0 Hz, 1H), 5.24 (m, 1H), 5.93 (m, 2H), 6.53 (s, 2H), 6.91 (m, 2H), 7.05 (m, 2H), 7.25 (m, 11H). ^{13}C NMR (125 MHz, $CDCl_3$) δ: 41.1, 46.5, 50.5, 56.6, 56.9, 65.0, 101.6, 102.3, 107.8, 126.9, 127.3, 127.8, 128.1, 128.5, 128.9, 134.1, 138.0, 138.6, 139.7, 143.8, 149.2, 153.7, 171.3. Anal. calcd. for $C_{33}H_{29}NO_6$: C 74.00, H 5.46, N 2.62; found: C 73.74, H 5.33, N 2.73.

*(3(3*S*),4*R*)-4-(Diphenylmethyl)-3-[3-(3,3-(3′,4′,5′-trimethoxyphenyl)-(3″,4″-methylenedioxy-5″-methoxyphenyl)-propanoyl]-2-oxazolidinone (**26**)*

Yield: 89%; mp 88 to 89°C. $[\alpha]_D^{25}$ –95.1 (c 1.0, CH_2Cl_2). R_f 0.42 (50:50, EtOAc:hexanes). ^{1}H NMR (400 MHz, $CDCl_3$) δ: 3.53 (dd, *J* = 7.5, 17.2 Hz, 1H), 3.66 (dd, *J* = 7.5, 16.9 Hz, 1H), 3.81 (s, 3H), 3.84 (s, 6H), 3.87 (s, 3H), 4.39 (d, *J* = 5.1 Hz, 2H), 4.49 (t, *J* = 7.2 Hz, 1H), 4.60 (d, *J* = 5.4 Hz, 1H), 5.23 (m, 1H), 5.92 (s, 2H), 6.46 (s, 2H), 6.52 (s, 2H), 6.82 (d, *J* = 5.6 Hz, 2H), 7.01 (d, *J* = 6.7 Hz, 2H), 7.26 (m, 6H). ^{13}C NMR (100 MHz, $CDCl_3$) δ: 40.9, 46.7, 50.4, 56.3, 56.6, 56.8, 60.9, 64.8, 101.4, 101.8, 104.9, 107.4, 127.1, 128.0, 128.3, 128.7, 128.9, 129.3, 133.9, 136.7, 137.8, 138.2, 139.2, 139.6, 143.5, 149.0, 153.3, 153.6, 171.1. Anal. calcd. for $C_{36}H_{35}NO_9$: C 69.11, H 5.64, N 2.24; found: C 69.49, H 5.79, N 2.04.

*(3(3*S*),4*R*)-4-(Diphenylmethyl)-3-[3-(3,3-(3′,4′,5′-trimethoxyphenyl)-(3″,4″-methylenedioxyphenyl)-propanoyl]-2-oxazolidinone (**27**)*

Yield: 88%; mp 84 to 85°C. $[\alpha]_D^{25}$ –105.2 (*c* 1.0, CH_2Cl_2). R_f 0.42 (50:50, EtOAc:hexanes). ^{1}H NMR (400 MHz, $CDCl_3$) δ: 3.50 (dd, *J* = 7.5, 17.2 Hz, 1H), 3.70 (dd, *J* = 7.8, 17.2 Hz, 1H), 3.81 (s, 3H), 3.84 (s, 6H), 4.39 (d, *J* = 4.8 Hz, 2H), 4.51 (t, *J* = 7.2 Hz, 1H), 4.60 (d, *J* = 5.1 Hz, 1H), 5.23 (m, 1H), 5.91 (s, 2H), 6.52 (s, 2H), 6.74 (m, 3H), 6.82 (d, *J* = 5.9 Hz, 2H), 7.01 (d, *J* = 7.2 Hz, 2H), 7.24 (m, 6H). ^{13}C NMR (100 MHz, $CDCl_3$) δ: 40.9, 46.4, 50.3, 56.2, 56.6, 60.9, 64.8, 101.1, 104.9, 108.3, 120.4, 127.1, 127.9, 128.3, 128.4, 128.7, 128.9, 129.3, 136.6, 137.5, 137.8, 139.4, 139.6, 146.3, 147.9, 153.3, 153.5, 171.1. Anal. calcd. for $C_{35}H_{33}NO_8$: C 70.58, H 5.58, N 2.35; found: C 70.57, H 5.86, N 1.92.

*(3(3*S*),4*R*)-4-(Diphenylmethyl)-3-[3-(3,3-(phenyl)-(3′,4′,5′-trimethoxyphenyl)-propanoyl]-2-oxazolidinone (**28**)*

Yield: 90%; mp 125–127°C. $[\alpha]_D^{25}$ –131.2 (*c* 0.42, CH_2Cl_2). ^{1}H NMR (500 MHz, $CDCl_3$) δ: 3.61 (dd, *J* = 17.0, 7.1 Hz, 1H), 3.82 (dd, *J* = 17.0, 8.2 Hz, 1H), 3.85 (s, 3H), 3.88 (s, 6H), 4.41 (m, 2H), 4.65 (m, 2H), 5.25 (m, 1H), 6.59 (s, 2H), 6.85 (m, 2H), 7.27 (m, 13H). ^{13}C NMR (125 MHz, $CDCl_3$) δ: 40.9, 47.0, 50.5, 56.4, 56.7, 61.1, 65.0, 105.3, 126.9, 127.3, 127.9, 128.1, 128.4, 128.9, 129.1, 129.5, 136.8, 138.0, 139.5, 140.0, 143.7, 153.5, 171.4. Anal. calcd. for $C_{34}H_{33}NO_6$: C 74.03, H 6.03, N 2.54; found: C 74.01, H 5.95, N 2.53.

*(3(3*S*),4*R*)-4-(Diphenylmethyl)-3-[3-(3,3-(3′,4′-methylenedioxyphenyl)-(phenyl)-propanoyl]-2-oxazolidinone (**29**)*

Yield: 97%; mp 164–166°C. $[\alpha]_D^{25}$ –142.5 (*c* 0.56, CH_2Cl_2). ^{1}H NMR (500 MHz, $CDCl_3$) δ: 3.60 (dd, *J* = 17.5, 7.5 Hz, 1H), 3.67 (dd, *J* = 17.5, 7.4 Hz, 1H), 4.37 (m, 2H), 4.57 (t, *J* = 7.6 Hz, 1H), 4.63 (d, *J* = 5.2 Hz, 1H), 5.23 (m,

© 2001 NRC Canada

1H), 5.92 (m, 2H), 6.77 (m, 3H), 6.93 (m, 2H), 7.05 (m, 2H), 7.26 (m, 11H). ^{13}C NMR (125 MHz, $CDCl_3$) δ: 41.2, 46.0, 50.5, 56.6, 65.0, 101.2, 108.5, 108.8, 121.2, 126.8, 127.3, 127.9, 128.1, 128.5, 128.9, 129.1, 129.6, 137.9, 138.0, 139.7, 143.9, 146.4, 148.0, 153.7, 171.2. Anal. calcd. for $C_{32}H_{27}NO_5$: C 76.02, H 5.38, N 2.77; found: C 76.14, H 5.41, N 2.66.

*(3(3*R*),4*R*)-4-(Diphenylmethyl)-3-[3-(3,3-(3′,4′-methylenedioxyphenyl)-(phenyl)-propanoyl]-2-oxazolidinone (**30**)*

Yield: 95%; mp 78–81°C. $[\alpha]_D^{25}$ –142.2 (*c* 0.49, CH_2Cl_2). ^{1}H NMR (500 MHz, $CDCl_3$) δ: 3.57 (dd, *J* = 17.6, 7.3 Hz, 1H), 3.69 (dd, *J* = 17.8, 7.8 Hz, 1H), 4.38 (m, 2H), 4.57 (t, *J* = 7.5 Hz, 1H), 4.63 (d, *J* = 5.2 Hz, 1H), 5.25 (m, 1H), 5.90 (s, 2H), 6.76 (m, 3H), 6.92 (m, 2H), 7.05 (m, 2H), 7.27 (m, 11H). ^{13}C NMR (125 MHz, $CDCl_3$) δ: 41.3, 46.0, 50.5, 56.6, 65.1, 101.2, 108.5, 108.7, 120.9, 126.9, 127.3, 127.9, 128.1, 128.5, 128.9, 129.1, 129.6, 137.9, 138.0, 139.7, 144.1, 146.3, 148.0, 153.7, 171.3. Anal. calcd. for $C_{32}H_{27}NO_5$: C 76.02, H 5.38, N 2.77; found: C 76.20, H 5.32, N 2.87.

Representative procedure for alkylation (compound 34)

To an oven-dried 250 mL three- neck round-bottomed flask purged with N_2 was added 10.5 g (16.78 mmol) of **26** and 120 mL of dry THF. The reaction mixture was cooled to –78°C in an acetone –dry ice bath. To the mixture was added 18.46 mL (18.46 mmol) of a 1 M NaHMDS–THF solution dropwise over 20 min and the mixture was allowed to stir for 1 h. To the solution was added 2.92 mL (20.14 mmol) of *tert*-butyl iodoacetate dropwise over 6 min. The solution was stirred at –78°C for 6 h. The reaction was quenched with 20 mL NH_4Cl. The reaction mixture was extracted with ethyl acetate. The combined organics were washed with water, followed by brine, and dried over $MgSO_4$. Removal of solvent under reduced pressure followed by flash column purification of the crude mixture led to 9.3 g of the alkylated product **34** (75% yield).

*(3(2*S*),4*R*)-4-(Diphenylmethyl)-3-[bis-(3′,4′-methylenedioxy-5′-methoxyphenyl)-methyl]-(4-oxo-butyric acid* tert*-butyl ester)-2-oxazolidinone (**18**)*

Yield: 64%; mp 189 to 190°C. $[\alpha]_D^{25}$ –289.9 (*c* 1.09, $CHCl_3$). R_f 0.63 (50:50, EtOAc:hexanes). ^{1}H NMR (400 MHz, $CDCl_3$) δ: 1.48 (s, 9H), 2.48 (dd, *J* = 3.2, 17.2 Hz, 1H), 2.82 (dd, *J* = 10.8, 17.2 Hz, 1H), 3.77 (m, 2H), 3.83 (s, 3H), 3.90 (s, 3H), 4.22 (d, *J* = 8.6 Hz, 1H), 4.70 (m, 2H), 5.17 (ddd, *J* = 3.2, 3.8, 10.8 Hz, 1H), 5.93 (m, 4H), 6.42 (d, *J* = 5.9 Hz, 2H), 6.51 (s, 1H), 6.62 (s, 1H), 6.99 (d, *J* = 7.5 Hz, 2H), 7.28 (m, 8H). ^{13}C NMR (100 MHz, $CDCl_3$) δ: 28.1, 37.3, 42.9, 50.1, 55.6, 56.3, 56.6, 56.9, 63.9, 80.9, 101.3, 101.4, 101.8, 102.4, 106.9, 107.7, 126.8, 127.5, 128.0, 128.4, 128.6, 129.6, 133.8, 134.2, 135.1, 135.8, 137.9, 140.0, 143.1, 143.6, 148.3, 149.2, 170.9, 174.8. Anal. calcd. for $C_{41}H_{41}NO_{11}$: C 68.04, H 5.71, N 1.94; found: C 68.03, H 5.73, N 1.73.

*(3(2*S*),4*R*)-4-(Diphenylmethyl)-3-[bis-(3′,4′,5′-trimethoxyphenyl)-methyl]-(4-oxo-butyric acid* tert*-butyl ester)-2-oxazolidinone (**19**)*

Yield: 66%; mp 90 to 91°C. $[\alpha]_D^{25}$ –265.4 (*c* 0.95, CH_2Cl_2). R_f 0.33 (50:50, EtOAc:hexanes). ^{1}H NMR (400 MHz, $CDCl_3$) δ: 1.46 (s, 9H), 2.46 (dd, *J* = 3.5, 16.9 Hz, 1H), 2.87 (dd, *J* = 10.9, 16.9 Hz, 1H), 3.61 (t, *J* = 8.5 Hz, 1H), 3.76 (s, 3H), 3.79 (s, 6H), 3.80 (d, *J* = 11 Hz, 1H), 3.82 (s, 3H), 3.87 (s, 6H), 4.12 (dd, *J* = 1.8, 7.3 Hz, 1H), 4.52 (dd, *J* = 2.4, 8.2 Hz, 1H), 4.65 (d, *J* = 2.5 Hz, 1H), 5.26 (ddd, *J* = 3.2, 3.5, 11.0 Hz, 1H), 6.48 (s, 2H), 6.64 (s, 2H), 6.93 (d, *J* = 6.9 Hz, 2H), 7.25 (m, 8H). ^{13}C NMR (100 MHz, $CDCl_3$) δ: 28.3, 37.7, 43.3, 50.1, 56.1, 56.3, 56.9, 57.2, 60.8, 60.9, 63.9, 81.1, 105.0, 126.9, 127.7, 128.1, 128.5, 128.8, 129.8, 136.3, 136.6, 137.2, 137.9, 140.2, 152.8, 153.3, 153.6, 171.3, 175.2. Anal. calcd. for $C_{43}H_{49}NO_{11}$: C 68.33, H 6.53, N 1.85; found: C 67.97, H 6.45, N 1.76.

*(3(2*S*),4*R*)-4-(Diphenylmethyl)-3-[bis-(3′,4′-methylenedioxyphenyl)-methyl]-(4-oxo-butyric acid* tert*-butyl ester)-2-oxazolidinone (**20**)*

Yield: 74%; mp 104 to 105°C. $[\alpha]_D^{25}$ –252.3 (*c* 0.55, $CHCl_3$). R_f 0.62 (50:50, EtOAc:hexanes). ^{1}H NMR (400 MHz, $CDCl_3$) δ: 1.47 (s, 9H), 2.50 (dd, *J* = 3.2, 17.2 Hz, 1H), 2.82 (dd, *J* = 10.8, 17.2 Hz, 1H), 3.69 (t, *J* = 8.9 Hz, 1H), 3.85 (d, *J* = 11.3 Hz, 1H), 4.19 (d, *J* = 8.8 Hz, 1H), 4.69 (s, 2H), 5.18 (ddd, *J* = 3.2, 3.2, 11.0 Hz, 1H), 5.85 (m, 2H), 5.93 (s, 2H), 6.77 (m, 6H), 7.00 (d, *J* = 8.3 Hz, 2H), 7.28 (m, 8H). ^{13}C NMR (100 MHz, $CDCl_3$) δ: 28.3, 37.4, 43.1, 50.2, 55.0, 57.0, 64.0, 81.0, 101.1, 107.8, 108.5, 108.7, 108.8, 121.3, 127.0, 127.6, 128.2, 128.4, 128.6, 128.8, 130.0, 134.6, 135.5, 138.1, 140.3, 146.4, 146.6, 147.5, 148.2, 152.9, 171.2, 175.1. Anal. calcd. for $C_{39}H_{37}NO_9$: C 70.58, H 5.62, N 2.11; found: C 70.29, H 5.60, N 1.96.

*(3(2*S*),3(3*S*),4*R*)-4-(Diphenylmethyl)-3-[(3′,4′,5′-trimethoxyphenyl)-(3″,4″-methylenedioxy-5″-methoxyphenyl)-methyl]-(4-oxo-butyric acid* tert*-butyl ester)-2-oxazolidinone (**34**)*

Yield: 75%; mp 231 to 232°C. $[\alpha]_D^{25}$ –251.4 (*c* 1.0, CH_2Cl_2). R_f 0.46 (50:50, EtOAc:hexanes). ^{1}H NMR (400 MHz, $CDCl_3$) δ: 1.46 (s, 9H), 2.46 (dd, *J* = 3.2, 16.7 Hz, 1H), 2.82 (dd, *J* = 10.8, 16.9 Hz, 1H), 3.72 (t, *J* = 9.1 Hz, 1H), 3.81 (s, 3H), 3.82 (s, 3H), 3.83 (d, *J* = 11.3 Hz, 1H) 3.86 (s, 6H), 4.20 (d, *J* = 7.6 Hz, 1H), 4.68 (d, *J* = 3.5 Hz, 2H), 5.23 (m, 1H), 5.88 (m, 2H), 6.44 (d, *J* = 10.2 Hz, 2H), 6.57 (s, 2H), 6.98 (d, *J* = 7.3 Hz, 2H), 7.26 (m, 8H). ^{13}C NMR (100 MHz, $CDCl_3$) δ: 28.3, 37.6, 43.1, 50.2, 56.2, 56.4, 57.1, 60.9, 64.1, 81.1, 101.6, 102.6, 104.9, 107.2, 127.0, 127.7, 128.2, 128.6, 128.8, 129.8, 134.0, 135.8, 136.4, 137.1, 138.0, 140.2, 143.2, 148.5, 153.1, 153.6, 171.2, 175.0. Anal. calcd. for $C_{42}H_{45}NO_{11}$: C 68.19, H 6.13, N 1.89; found: C 67.94, H 6.09, N 1.92.

*(3(2*S*),3(3*S*),4*R*)-4-(Diphenylmethyl)-3-[(3′,4′,5′-trimethoxyphenyl)-(3″,4″-methylenedioxyphenyl)-methyl]-(4-oxo-butyric acid* tert*-butyl ester)-2-oxazolidinone (**35**)*

Yield: 75%; mp 214 to 215°C. $[\alpha]_D^{25}$ –261.8 (*c* 1.0, CH_2Cl_2). R_f 0.55 (50:50, EtOAc:hexanes). ^{1}H NMR (400 MHz, $CDCl_3$) δ: 1.47 (s, 9H), 2.46 (dd, *J* = 3.2, 16.9 Hz, 1H), 2.83 (dd, *J* = 11.0, 17.0 Hz, 1H), 3.62 (t, *J* = 8.3 Hz, 1H), 3.76 (s, 3H), 3.79 (s, 6H), 3.79 (d, *J* = 11.3 Hz, 1H), 4.12 (dd, *J* = 1.9, 8.9 Hz, 1H), 4.53 (dd, *J* = 2.7, 5.9 Hz, 1H), 4.66 (d, *J* = 2.7 Hz, 1H), 5.23 (ddd, *J* = 3.0, 3.5, 11.6 Hz, 1H), 5.94 (s, 2H), 6.42 (s, 2H), 6.78 (d, *J* = 8.0 Hz, 1H), 6.92 (m, 4H), 7.25 (m, 8H). ^{13}C NMR (100 MHz, $CDCl_3$) δ: 28.3, 37.6, 43.0, 50.1, 56.1, 57.2, 60.8,

© 2001 NRC Canada

63.9, 81.0, 101.3, 104.9, 108.4, 108.7, 121.1, 126.9, 127.6, 128.1, 128.5, 128.8, 129.8, 134.5, 136.4, 137.1, 138.0, 140.2, 146.8, 148.2, 152.9, 153.2, 171.2, 175.2. Anal. calcd. for $C_{41}H_{43}NO_{10}$: C 69.38, H 6.11, N 1.97; found: C 69.17, H 6.17, N 1.99.

General procedure for the LAH reduction–cyclization (compounds 21 and 22)

To an oven-dried 25 mL two-neck round-bottomed flask purged with N_2 was added 1.00 g of **18** (1.38 mmol) of alkylated product and 2 mL of dry THF. The reaction mixture was cooled to –78°C in an acetone – dry ice bath. To the solution was added 265 mg (6.99 mmol) of LAH in 7 mL of dry THF dropwise over 15 min. The reaction was stirred at –78°C for 20 h before quenching with ethyl acetate. The mixture was filtered through Celite and dried over $MgSO_4$. Removal of solvent under reduced pressure led to the crude alcohol. The crude alcohol cyclized on standing and (or) during column chromatography over silica gel. Lactone (410 mg) was obtained after column chromatography (74% yield for **21**).

General procedure for hydrolysis–reduction–cyclization (for compounds 23, 36, 37)

To an oven-dried 250 mL three-neck round-bottomed flask purged with N_2 was added 3.00 g (4.05 mmol) of alkylated product **34**, 60 mL of THF, and 15 mL of H_2O. The reaction mixture was cooled to 0°C before the dropwise addition of 3.31 mL (32.4 mmol) of 30% H_2O_2 over 10 min. To the solution was added 747 mg (17.82 mmol) of LiOH–H_2O in 15 mL of H_2O dropwise over 20 min. The reaction was stirred at 0°C for 5 h before being allowed to warm to room temperature and stirred for 14 h. The reaction was cooled to 0°C before quenching with 4.20 g of Na_2SO_3 in 20 mL of H_2O. The mixture was washed with H_2O and extracted with CH_2Cl_2. The aqueous layer was acidified to pH = 2 with 5 M HCl before extraction with ethyl acetate. The organic extracts were not combined and both were dried over $MgSO_4$. Removal of solvent from the acid wash under reduced pressure led to 1.75 g of crude acid (86% yield). Evaporation of the neutral fraction provided crude chiral auxiliary.

General procedure for the borane reduction

To an oven-dried 100 mL three-neck round-bottomed flask purged with N_2 was added 1.90 g (3.77 mmol) of crude acid and 50 mL of dry THF. The reaction mixture was cooled to –10°C in an acetone – ice bath. To the solution was added 7.54 mL (7.54 mmol) of a 1 M BH_3–THF solution dropwise over 15 min. The reaction was stirred at –10°C for 6 h before warming to room temperature and stirred for 14 h. The reaction was quenched with 4 mL of a 1:1 solution of acetic acid and water. The aqueous layer was washed with a cold saturated solution of $NaHCO_3$ and extracted with ethyl acetate while being dried over $MgSO_4$. Removal of solvent under reduced pressure led to 1.43 g of crude alcohol (75% yield).

Lactonization

To an oven-dried 50 mL two-neck round- bottomed flask set up with a condenser purged with N_2 was added 1.60 g (3.26 mmol) of crude alcohol, 15 mg of PTSA, and 30 mL of benzene. The solution was heated to reflux for 2.0 h before being allowed to cool to room temperature. The mixture was washed with $NaHCO_3$ and water before extracting with ethyl acetate and drying over $MgSO_4$. Removal of solvent under reduced pressure followed by flash column purification of the crude mixture led to 1.2 g of the lactone **36** (89% yield).

*(4S)-4-[1-Bis(3′,4′-methylenedioxy-5′-methoxyphenyl)methyl]-butyrolactone (**21**)*

Overall yield over two steps: 74% (average of three runs); mp 147 to 148°C. $[\alpha]_D^{25}$ –9.2 (*c* 0.59, CH_2Cl_2). R_f 0.4 (50:50, EtOAc:hexanes). ^{1}H NMR (400 MHz, $CDCl_3$) δ: 2.26 (dd, *J* = 7.5, 10.2 Hz, 1H), 2.59 (dd, *J* = 8.3, 9.4 Hz, 1H), 3.24 (m, 1H), 3.57 (d, *J* = 11.8 Hz, 1H), 3.89 (s, 6H), 3.96 (dd, *J* = 6.4, 9.4 Hz, 1H), 4.28 (dd, *J* = 7.2, 9.4 Hz, 1H), 5.92 (two s, 4H), 6.39 (two s, 4H). ^{13}C NMR (100 MHz, $CDCl_3$) δ: 34.1, 40.1, 55.3, 57.0, 72.0, 101.1, 101.6, 107.7, 134.3, 136.4, 136.8, 143.7, 149.5, 176.5. Anal. calcd. for $C_{21}H_{20}O_8$: C 63.00, H 5.03; found: C 63.34, H 5.05.

*(4S)-4-[1-Bis(3′,4′,5′-trimethoxyphenyl)methyl]-butyrolactone (**22**)*

Overall yield over two steps: 75% (average of three runs); mp 168 to 169°C. $[\alpha]_D^{25}$ –13.0 (*c* 1.0, $CHCl_3$). R_f 0.16 (50:50, EtOAc:hexanes). ^{1}H NMR (400 MHz, $CDCl_3$) δ: 2.26 (dd, *J* = 7.5, 17.8 Hz, 1H), 2.59 (dd, *J* = 8.0, 18.0 Hz, 1H), 3.32 (m, 1H), 3.64 (d, *J* = 11.8 Hz, 1H), 3.80 (s, 6H), 3.84 (s, 12H), 3.98 (dd, *J* = 6.7, 9.4 Hz, 1H), 4.27 (dd, *J* = 7.2, 9.4 Hz, 1H), 6.45 (s, 4H). ^{13}C NMR (100 MHz, $CDCl_3$) δ: 31.9, 38.1, 53.7, 54.2, 58.8, 70.0, 102.7, 135.5, 135.9, 151.8, 174.9. Anal. calcd. for $C_{23}H_{28}O_8$: C 63.88, H 6.53; found: C 63.56, H 6.30.

*(4S)-4-[1-Bis(3′,4′-methylenedioxyphenyl)methyl]-butyrolactone (**23**)*

Overall yield over three steps: 56% (average of three runs); mp 66 to 67°C. $[\alpha]_D^{25}$ –4.3 (*c* 1.0, CH_2Cl_2). R_f 0.44 (50:50, EtOAc:hexanes). ^{1}H NMR (400 MHz, $CDCl_3$) δ: 2.24 (dd, *J* = 8.1, 18.0 Hz, 1H), 2.56 (dd, *J* = 8.6, 18.0 Hz, 1H), 3.27 (m, 1H), 3.64 (d, *J* = 11.6 Hz, 1H), 3.94 (dd, *J* = 7.0, 9.4, 1H), 4.25 (dd, *J* = 7.5, 9.4 Hz, 1H), 5.90 (two s, 4H), 6.70 (m, 6H). ^{13}C NMR (100 MHz, $CDCl_3$) δ: 31.1, 34.1, 40.0, 54.8, 72.2, 101.2, 107.7, 108.6, 120.5, 120.6, 128.4, 135.9, 136.4, 146.6, 146.7, 148.2,176.7. Anal. calcd. for $C_{19}H_{16}O_6$: C 67.06, H 4.74; found: C 67.25, H 4.96.

*(4(1S),4S)-4-[1,1-(3′,4′,5′-Methoxyphenyl)-(3″,4″-methylenedioxy-5″-methoxyphenyl)methyl]-butyrolactone (**36**)*

Overall yield over three steps: 57% (average of three runs); mp 77 to 78°C. $[\alpha]_D^{25}$ –12.8 (*c* 0.9, CH_2Cl_2). R_f 0.20 (50:50, EtOAc:hexanes). ^{1}H NMR (400 MHz, $CDCl_3$) δ: 2.26 (dd, *J* = 7.5, 17.7 Hz, 1H), 2.59 (dd, *J* = 8.0, 17.7 Hz, 1H), 3.29 (m, 1H), 3.61 (d, *J* = 11.8 Hz, 1H), 3.80 (s, 3H), 3.84 (s, 6H), 3.90 (s, 3H), 3.98 (dd, *J* = 6.4, 9.4 Hz, 1H), 4.28 (dd, *J* = 7.0, 9.4 Hz, 1H), 5.93 (d, *J* = 2.7 Hz, 2H), 6.41 (m, 4H). ^{13}C NMR (100 MHz, $CDCl_3$) δ: 27.4, 34.1, 40.1, 55.5, 56.3, 57.0, 60.9, 72.1, 101.1, 101.6, 104.5, 107.8, 134.3, 136.4, 137.1, 137.9, 143.7, 149.5, 153.5, 176.6. Anal. calcd. for $C_{22}H_{24}O_8$: C 63.45, H 5.81; found: C 63.39, H 6.04.

© 2001 NRC Canada

*(4(1S),4S)-4-[1,1-(3′,4′,5′-Methoxyphenyl)-5-(3″,4″-methylenedioxyphenyl)methyl]-butyrolactone (**37**)*

Overall yield over three steps: 56% (average of three runs); mp 69 to 70°C. $[\alpha]_D^{25}$ –4.6 (*c* 1.0, CH_2Cl_2). R_f 0.26 (50:50, EtOAc:hexanes). ^{1}H NMR (400 MHz, $CDCl_3$) δ: 2.25 (dd, *J* = 8.6, 17.7 Hz, 1H), 2.56 (dd, *J* = 9.1, 17.7 Hz, 1H), 3.30 (m, 1H), 3.64 (d, *J* = 11.6 Hz, 1H), 3.78 (s, 3H), 3.82 (s, 6H), 3.94 (dd, *J* = 7.0, 16.4 Hz, 1H), 4.25 (dd, *J* = 9.4, 19.1 Hz, 1H), 5.90 (m, 2H), 6.41 (s, 2H), 6.71 (m, 3H). ^{13}C NMR (100 MHz, $CDCl_3$) δ: 34.1, 40.0, 55.3, 56.3, 60.9, 72.1, 101.3, 104.4, 107.7, 108.6, 120.5, 128.4, 135.6, 136.1, 137.0, 137.7, 138.1, 146.8, 148.2, 153.5, 176.6. Anal. calcd. for $C_{21}H_{22}O_7$: C 65.28, H 5.74; found: C 64.81, H 5.46.

Representative methylation procedure (compound 1d)

To an oven-dried 25 mL two-neck round-bottomed flask purged with N_2 was added 400 mg (0.961 mmol) of the lactone **36** and 7 mL of dry THF. The reaction mixture was cooled to –78°C in an acetone – dry ice bath. To the mixture was added 1.15 mL (1.15 mmol) of a 1 M NaHMDS–THF solution dropwise over 3 min and the mixture was allowed to stir for 50 min. To the solution was added 0.12 mL (1.92 mmol) of methyl iodide over 1 min. The solution was stirred at –78°C for 5 h. The reaction was quenched with 1 mL NH_4Cl. The reaction mixture was extracted with ethyl acetate. The combined organics were washed with water, followed by brine, and dried over $MgSO_4$. Removal of solvent under reduced pressure followed by flash column purification of the crude mixture led to 331 mg of the natural product peperomin B (**1d**) along with the diastereomer (80% yield).

*(3S,4S)-3-Methyl-4-[1-bis(3′,4′-methylenedioxy-5′-methoxyphenyl)methyl]-butyrolactone (peperomin A (**1a**))*

Yield: 98%; mp 143 to 144°C (abs. EtOH) (lit. (1) 143–145°C). $[\alpha]_D^{25}$ 22.7 (*c* 0.13, $CHCl_3$) (lit. (1) $[\alpha]_D^{27}$ 20.6 (*c* 0.14, $CHCl_3$)). R_f 0.5 (50:50, EtOAc:hexanes). ^{1}H NMR (400 MHz, $CDCl_3$) δ: 0.94 (d, *J* = 7.2 Hz, 3H), 2.34 (m, 1H), 2.84 (m, 1H), 3.57 (d, *J* = 11.3 Hz, 1H), 3.80 (dd, *J* = 7.8, 9.7 Hz, 1H), 3.89 (s, 6H), 4.30 (dd, *J* = 7.5, 9.6 Hz, 1H), 5.93 (s, 4H), 6.38–6.44 (m, 4H). ^{13}C NMR (100 MHz, $CDCl_3$) δ: 15.9, 40.3, 47.3, 56.2, 57.0, 70.4, 101.2, 101.4, 101.6, 107.7, 134.3, 136.2, 136.8, 143.6, 149.4, 179.7. Anal. calcd. for $C_{22}H_{22}O_8$: C 63.76, H 5.35; found: C 63.84, H 5.22.

*(3S,4S)-3-Methyl-4-[1-bis(3′,4′,5′-trimethoxyphenyl)methyl]-butyrolactone (peperomin C (**1b**))*

Yield: 98%; mp 156 to 157°C (EtOAC–hexane), (lit. (1) 158–160°C). $[\alpha]_D^{25}$ 43.3 (*c* 0.06, $CHCl_3$) (lit. (1) $[\alpha]_D^{27}$ 42.7 (*c* 0.06, $CHCl_3$)). R_f 0.22 (50:50, EtOAc:hexanes). ^{1}H NMR (400 MHz, $CDCl_3$) δ: 0.94 (d, *J* = 7.2 Hz, 3H), 2.37 (m, 1H), 2.92 (m, 1H), 3.64 (d, *J* = 11.3 Hz, 1H), 3.81 (s, 6H), 3.83 (m, 1H), 3.84 (s, 6H), 3.86 (s, 6H), 4.30 (dd, *J* = 7.8, 9.7 Hz, 1H), 6.48 (s, 4H). ^{13}C NMR (100 MHz, $CDCl_3$) δ: 15.9, 40.4, 47.5, 56.3, 56.7, 61.0, 70.5, 104.7, 104.9, 137.2, 137.4, 137.6, 153.6, 179.7. Anal. calcd. for $C_{24}H_{30}O_8$: C 64.56, H 6.77; found: C 64.29, H 6.40.

*(3S,4S)-3-Methyl-4-[1-bis(3′,4′-methylenedioxyphenyl)methyl]-butyrolactone (peperomin D (**1c**))*

Yield: 80%; mp 120–122°C (lit. (2) 122–124°C). $[\alpha]_D^{25}$ 18.4 (*c* 0.13, $CHCl_3$) (lit. (2) $[\alpha]_D^{27}$ 23.0 (*c* 0.1, $CHCl_3$)). R_f 0.50 (50:50, EtOAc:hexanes). ^{1}H NMR (400 MHz, $CDCl_3$) δ: 0.89 (d, *J* = 7.3 Hz, 3H), 2.33 (m, 1H), 2.87 (m, 1H), 3.63 (d, *J* = 11.2 Hz, 1H), 3.76 (dd, *J* = 8.2, 9.4 Hz, 1H), 4.28 (dd, *J* = 7.6, 9.4 Hz, 1H), 5.90 (s, 4H), 6.70 (m, 6H). ^{13}C NMR (100 MHz, $CDCl_3$) δ: 15.8, 40.4, 47.3, 55.7, 70.5, 101.2, 107.7, 107.8, 108.6, 108.7, 120.4, 120.8, 135.7, 136.3, 146.7, 148.2, 148.3, 179.8. Anal. calcd. for $C_{20}H_{18}O_6$: C 67.68, H 5.12; found: C 67.21, H 5.08.

*(3S,4S,5R)-3-Methyl-4-[1,1-(3′,4′,5′-methoxyphenyl)-5-(3″,4″-methylenedioxy-5″-methoxyphenyl)methyl]-butyrolactone (peperomin analog (**1d**))*

The minor diastereomer could not be separated. Chemical shifts for the major compound are reported. Yield: 80%; mp 84 to 85°C. $[\alpha]_D^{25}$ 13.9 (*c* 0.49, $CHCl_3$). R_f 0.26 (50:50, EtOAc:hexanes). ^{1}H NMR (400 MHz, $CDCl_3$) δ: 0.93 (d, *J* = 7.3 Hz, 3H), 2.35 (m, 1H), 2.90 (m, 1H), 3.61 (d, *J* = 11.3 Hz, 1H), 3.80 (s, 3H), 3.80 (overlapping with OMe peaks, dd, 1H) 3.84 (s, 6H), 3.90 (s, 3H), 4.30 (dd, *J* = 7.6, 9.7 Hz, 1H), 5.94 (s, 2H), 6.41 (d, *J* = 1.6 Hz, 1H), 6.44 (s, 2H), 6.48 (d, *J* = 1.6 Hz, 1H). ^{13}C NMR (100 MHz, $CDCl_3$) δ: 16.0, 40.3, 47.3, 56.3, 56.4, 57.1, 61.0, 70.4, 101.2, 101.6, 104.7, 107.9, 128.4, 134.4, 136.2, 137.3, 137.7, 143.7, 149.5, 153.6, 179.7. Anal. calcd. for $C_{23}H_{26}O_8$: C 64.18, H 6.01; found: C 64.14, H 5.55.

*(3S,4S,5R)-3-Methyl-4-[1,1-(3′,4′,5′-methoxyphenyl)-5-(3″,4″-methylenedioxyphenyl)methyl]-butyrolactone (peperomin analog (**1e**))*

The minor diastereomer could not be separated. Chemical shifts for the major compound are reported. Yield: 80%; mp 181 to 182°C. $[\alpha]_D^{25}$ 35.3 (*c* 0.17, $CHCl_3$). R_f 0.34 (50:50, EtOAc:hexanes). ^{1}H NMR (400 MHz, $CDCl_3$) δ: 0.93 (d, *J* = 7.2 Hz, 3H), 2.35 (m, 1H), 2.90 (m, 1H), 3.63 (d, *J* = 11.3 Hz, 1H), 3.79 (s, 3H), 3.80 (overlapping with OMe peaks, dd, 1H), 3.83 (s, 6H), 4.28 (dd, *J* = 7.6, 9.6 Hz, 1H), 5.92 (s, 2H), 6.43 (s, 2H), 6.74 (s, 3H). ^{13}C NMR (100 MHz, $CDCl_3$) δ: 15.9, 40.4, 47.2, 56.2, 56.3, 60.9, 70.4, 101.3, 104.7, 107.8, 108.7, 120.5, 135.5, 137.2, 137.9, 146.8, 148.3, 153.5, 179.8. Anal. calcd. for $C_{22}H_{24}O_7$: C 65.99, H 6.04; found: C 65.92, H 5.86.

Acknowledgement

We thank the National Institutes of Health (CA-60030) for financial support. We would also like to thank Dr. Jianxie Chen and Shankar Manyem for experimental assistance.

References

1. C.-M. Chen, F.-Y. Jan, M.-T. Chen, and T.-J. Lee. Heterocycles, **29**, 411 (1989).
2. F. Delle Monache and R.S. Compagnone. Phytochemistry, **43**, 1097 (1996).
3. T.R. Govindachari, G.N. Krishna Kumari, and P.D. Partho. Phytochemistry, **49**, 2129 (1998).
4. C.M. Lin, S.B. Singh, P.S. Chu, R.O. Dempey, J.M. Schmidt, G.R. Petit, and E. Hamel. Mol. Pharmacol. **34**, 200 (1984).
5. J.D. Loike, C.F. Brewer, H. Sternlicht, W.J. Gensler, and S.B. Horwitz. Cancer. Res. **38**, 2688 (1978**)**.
6. R. Cruz-Almanza and F.P. Higareda. Heterocycles, **34**, 2323 (1992).

© 2001 NRC Canada

7. (*a*) C.-B. Xue and C.P. Dicicco. J. Med. Chem. **41**, 1745 (1998); (*b*) R.P. Becket, M.J. Crimmins, M.H. Davis, and Z.A. Spavold. Synlett, 137 (1993); (*c*) J.L. Charlton and G. Chee. Can. J. Chem. **75**, 1076 (1997). (*d*) T. Nishi, M. Sakurai, S. Sato, M. Kataoka, and Y. Morisawa. Chem. Pharm. Bull. **37**, 2200 (1989).
8. M.P. Sibi, P. Liu, J. Ji, S. Hajra, and J. Chen. J. Org. Chem. In press (2001).
9. M.P. Sibi, P.K. Deshpande, and A.J. La Loggia. Synlett, 343 (1996).
10. M.P. Sibi, P. Liu, and M.D. Johnson. Can. J. Chem. **78**, 133 (2000).
11. (*a*) L.F. Frey, R.D. Tillyer, A.-S. Caille, E.J.J. Grabowski, and P.J. Reider. J. Org. Chem. **63**, 3120 (1998); (*b*) A. Alexakis, R. Sedrani, P. Mangeney, and J.F. Normant. Tetrahedron Lett. **29**, 4411 (1988); (*c*) F. Xu, R.D. Tillyer, D.M. Tschaen, E.J.J. Grabowski, and P.J. Reider. Tetrahedron: Asymmetry, **9**, 1651 (1998); (*d*) Z.J. Song, M. Zhao, R. Desmond, P. Devine, D.M. Tschaen, R. Tillyer, L. Frey, R. Heid, F. Xu, B. Foster, J. Li, R. Reamer, P. Volante, E.J.J. Grabowski, U.H. Dolling, P.J. Reider, S. Okada, Y. Kato, and E. Mano. J. Org. Chem. **64**, 9658 (1999); (*e*) E.J. Corey and T.G. Gant. Tetrahedron Lett. **35**, 5373 (1994); (*f*) K. Tanaka, M. Nuruzzaman, M. Yoshida, N. Asakawa, X.S. Yang, K. Tsubaki, and K. Fuji. Chem. Pharm. Bull. **47**, 1053 (1999); (*g*) D.B. Berkowitz, S. Choi, and J.-H. Maeng. J. Org. Chem. **65**, 847 (2000).
12. (*a*) P.G. Andersson, H.E. Schink, and K. Österlund. J. Org. Chem. **63**, 8067 (1998); (*b*) D.R. Williams, W.S. Kissel, and J.J. Li. Tetrahedron Lett. **39**, 8593 (1998).
13. (*a*) E. Nicholas, K.C. Russell, and V.J. Hruby. J. Org. Chem. **58**, 766 (1993); (*b*) B.-S. Lou, G. Li, F.-D. Lung, and V.J. Hruby. J. Org. Chem. **60**, 5509 (1995).
14. (*a*) E. Nicholas, K.C. Russell, and V.J. Hruby. J. Org. Chem. **58**, 766 (1993); B.-S. Lou, G. Li, F.-D. Lung, and V.J. Hruby. J. Org. Chem. **60**, 5509 (1995); (*b*) Y. Han and V.J. Hruby. Tetrahedron Lett. **38**, 7317 (1997); (*c*) B.-S. Lou, G. Li, F.-D. Lung, and V.J. Hruby. J. Org. Chem. **60**, 5509 (1995); (*d*) A. Snider, T. Hintermann, and D. Seebach. Helv. Chim. Acta, **78**, 1185 (1995); (*e*) C. Schneider and O. Reese. Synthesis, 1689 (2000); (*f*) P.S. van Hereden, B.C.B. Bezuidenhoudt, and D. Ferreira. Tetrahedron Lett. **38**, 1821 (1997); (*g*) A. Bongini, G. Cardillo, A. Mingardi, and C. Tomasini. Tetrahedron: Asymmetry, **7**, 1457 (1996); (*h*) R. Amoroso, G. Cardillo, P. Sabatino, C. Tomasini, and A. Trere. J. Org. Chem. **58**, 5615 (1993); (*i*) S.G. Davies and H.J. Snaganee. Tetrahedron: Asymmetry, **6**, 671 (1995).
15. (*a*) M.P. Sibi, P.K. Deshpande, A.J. La Loggia, and J.W. Christensen. Tetrahedron Lett. **36**, 8961 (1995); (*b*) M.P. Sibi. Aldrichimica Acta, **32**, 93 (1999); (*c*) M.P. Sibi, P.K. Deshpande, and J. Ji. Tetrahedron Lett. **36**, 8965 (1995); M.P. Sibi, C.P. Jasperse, and J. Ji. J. Am. Chem. Soc. **117**, 10 779 (1995); M.P. Sibi and J. Ji. Angew. Chem. Int. Ed. Engl. **35**, 190 (1996).
16. G.E. Schneiders and R. Stevenson. J. Org. Chem. **46**, 2969 (1981).
17. J. Surrey. J. Am. Chem. Soc. **70**, 2887 (1948).
18. C. Chung, M. Ho, K. Lun, and M.O. Wong. Synth. Commun. **18**, 507 (1988).
19. (*a*) P. Perlmutter. Conjugate addition reactions in organic synthesis. Pergamon, Oxford. 1992; (*b*) M.P. Sibi and S. Manyem. Tetrahedron, **51**, 8033 (2000); (*c*) J. Leonard, E. Diez-Barra, and S. Merino. Eur. J. Org. Chem. 2051 (1998).
20. T. Shirasaka, Y. Takuma, and N. Imaki. Synth. Commun. **20**, 1223 (1990).
21. M. Jung, P. Lam, M. Mansuri, and L. Speltz. J. Org. Chem. **50**, 1087 (1985).
22. I.B. Parr, A.B. Dribben, S.R Norris, M.G. Hinds, and N.G.J. Richards. J. Chem. Soc. Perkin Trans. 1, 1029 (1999).
23. L.F. Tietze and C. Schunke. Angew. Chem. Int. Ed. Engl. **34**, 1731 (1995).
24. (*a*) D.A. Evans, T.C. Britton, and J.A.Ellman. Tetrahedron Lett. **28**, 6141 (1987); (*b*) D.A. Evans, T.C. Britton, R.L. Dorow, and J.F. Dellaria, Jr. Tetrahedron, **44**, 5525 (1988).
25. Y. Matsumoto, K. Mikani, and A. Yoshida. Tetrahedron Lett. **37**, 8515 (1996).
26. K. Tomioka, H. Mizuguchi, and K. Koga. Tetrahedron Lett. **20**, 3315 (1979); S. Kuwahara, Y. Shibata, and A. Hiramatsu. Liebigs Ann. Chem. 993 (1992); M.P. Collis, D.C.R. Hockless, and P. Perlmutter. Tetrahedron Lett. **36**, 7133 (1995); H. Yoda, H. Kitayama, T. Katagiri, and K. Takabe. Tetrahedron, **48**, 3313 (1992).
27. T.J. Sprules, and J.-F. Lavallée. J. Org. Chem. **60**, 5041 (1995).
28. (*a*) J. Ezquerra, L. Prieto, C. Avendaño, J.L. Martos, and E. de la Cuesta. Tetrahedron Lett. **40**, 1575 (1999); (*b*) D.R. Williams, W.S. Kissel, and J.J. Li. Tetrahedron Lett. **39**, 8593 (1998); (*c*) P.G. Andersson, H.E. Schink, and K. Österlund. J. Org. Chem. **63**, 8067 (1998); (*d*) W. Oppolzer, P. Dudfield, T. Stevenson, and T. Godel. Helv. Chim. Acta, **68**, 212 (1985); (*e*) W. Opplozer, R.J. Mills, W. Pachinger, and T. Stevenson. Helv. Chim. Acta, **68**, 1542 (1986); (*f*) M.D. Fletcher, J.R. Harding, R.A. Hughes, N.M. Kelly, H. Schmalz, A. Sutherland, and C.L. Willis. J. Chem. Soc. Perkin Trans. 1, 43 (2000). (*g*) D.B. Berkowitz, S. Choi, and J.-H. Maeng. J. Org. Chem. **65**, 847 (2000); (*h*) T.M. Judge, G. Philipps, J.K. Morris, K.D. Lovasz, K.R. Romines, G.P. Luke, J. Tulinsky, J.M. Tustin, R.A. Chrusciel, L.A. Dolak, S.A. Mizsak, W. Watt, J. Morris, S.L. Vander Velde, J.W. Strohbach, and R. B. Gammill. J. Am. Chem. Soc. **119**, 3627 (1997); D.R. Willimas, P.D. Lowder, and Y.-G. Gu. Tetrahedron Lett. **41**, 9397 (2000); (*i*) C. Einhorn, J. Einhorn, P. Delair, and J. Luche. J. Org. Chem. **59**, 4680 (1994); K. Koga, K. Tomioka, and T. Suenaga. Tetrahedron Lett. **27**, 369 (1986); M. Nilsson, M. Bergdahl, T. Iliefski, and T. Olsson. Tetrahedron Lett. **36**, 3227 (1995).
29. (*a*) J. Lin, S. Liao, V.J. Hruby. Tetrahedron Lett. **39**, 3117 (1998); (*b*) S. Liao, Y. Han, W. Qiu, M. Bruck, and V.J. Hruby. Tetrahedron Lett. **37**, 7917 (1996).
30. M.P. Sibi, J. Ji, J.B. Sausker, and C.P. Jasperse. J. Am. Chem. Soc. **121**, 7517 (1999).
31. S. Larsson and G.E. Miksche. Acta Chem. Scand. **26**, 2031 (1972).

© 2001 NRC Canada

Traceless solid-phase synthesis of 5-benzoylbenzimidazoles

Kyung Joo Lee and Kim D. Janda

Abstract: A traceless linker strategy for the solid-supported synthesis of 5-benzoylbenzimidazoles has been developed. A benzyl cyanide functional group was linked to 2% divinylbenzene cross-linked polystyrene through a dimethylsilyl linker. Coupling with 5-chloro-2-nitroaniline followed by oxidative decyanation gave benzophenone **11** as a key intermediate in an efficient one-pot reaction procedure. After reduction of the nitro group and oxidative cyclization with a variety of aldehydes in the presence of DDQ, a series of polymer-supported benzimidazoles was produced. Final traceless cleavage of the arylsilane linker with TBAF provided a small library of 5-benzoylbenzimidazoles.

Key words: solid-support, traceless linker, arylsilane, 5-benzoylbenzimidazole.

Résumé : On a développé une stratégie d'ancrage sans trace pour la synthèse sur support solide de 5-benzoylbenzimidazoles. Utilisant un diméthylsilyle comme ancre, on a relié un cyanure de benzyle fonctionnalisé à du polystyrène réticulé à 2% de divinylbenzène. Son couplage avec de la 5-chloro-2-nitroaniline, suivi d'une décyanation oxydante, conduit à la benzophénone **11**, un intermédiaire clé dans une réaction monotope efficace. Après réduction du groupe nitro et cyclisation oxydante avec une variété d'aldéhydes, en présence de DDQ, on obtient une série de benzimidazoles supportés par un polymère. Un clivage final sans laisser de trace de l'ancre arylsilane, par du TBAF, conduit à une série de 5-benzoylbenzimidazoles.

Mots clés : support solide, ancre sans trace, arylsilane, 5-benzoylbenzimidazole.

[Traduit par la Rédaction]

Introduction

Benzimidazoles and in particular 2-substituted benzimidazoles show a broad range of medicinal activity including fungicidal, antitumor, and antiviral, with the antiulcerative Omeprazole (1) and antihistamine Astemizole (2) being clinical examples. In addition, benzimidazole-based compounds have been found to be inhibitors of phosphodiesterase IV (3) and antagonists of angiotensin I (4). Because of their medicinal importance, the solid-phase synthesis of heterocycles such as benzimidazoles, diketopiperazines, diazines, and hydantoins that contain one or more nitrogen atoms has received considerable attention. Consequently, a general method for the rapid synthesis of a library of benzimidazoles might provide new lead compounds in drug discovery based efforts.

Our efforts in the library preparation of benzimidazoles were centered upon structures such as **1**, 2-substituted-5-benzoylbenzimidazole. We envisioned that this benzimidazole and the related supported intermediate **12** could be utilized as precursors to a range of medicinally important molecules such as Enviroxime, Enviradene, and Itemazole (5). In accessing such structures via a solid-supported methodology, linking group strategies must be considered a key element in the synthetic design. Indeed, major drawbacks inherent to solid-phase synthesis are related to the linking of the molecule to the support, the linker's chemical inertness, and ease of detachment of the final molecule. A further consideration is the potential remains of the linking functionality. Thus, carboxyl, carboxamide, amine, or hydroxyl functionalities are often left embedded within the target molecule as a result of the linking strategies engaged. Clearly, these moieties can affect the physico-chemical and biological properties of the target molecule. Therefore, the development of traceless linker strategies is an important challenge in solid-phase combinatorial synthesis.

Recently, several novel tactics that utilize a resin-bound arylsilane as a traceless linker have been successfully applied to the solid-phase synthesis of aromatic and heteroaromatic compounds including 1,4-benzodiazepines (6), benzofurans (7), tricyclics (8), and biaryl (9) structures. Furthermore, a number of papers describing the solid or soluble-polymer supported synthesis of benzimidazole derivatives (10, 11) have also appeared. However, in these reports of benzimidazoles, all the structures described show retained linker functionality within the final compound. Herein, we report the traceless solid-phase synthesis of 5-benzoylbenzimidazoles employing an arylsilane linkage.

Received February 13, 2001. Published on the NRC Research Press Web site at http://canjchem.nrc.ca on October 24, 2001.

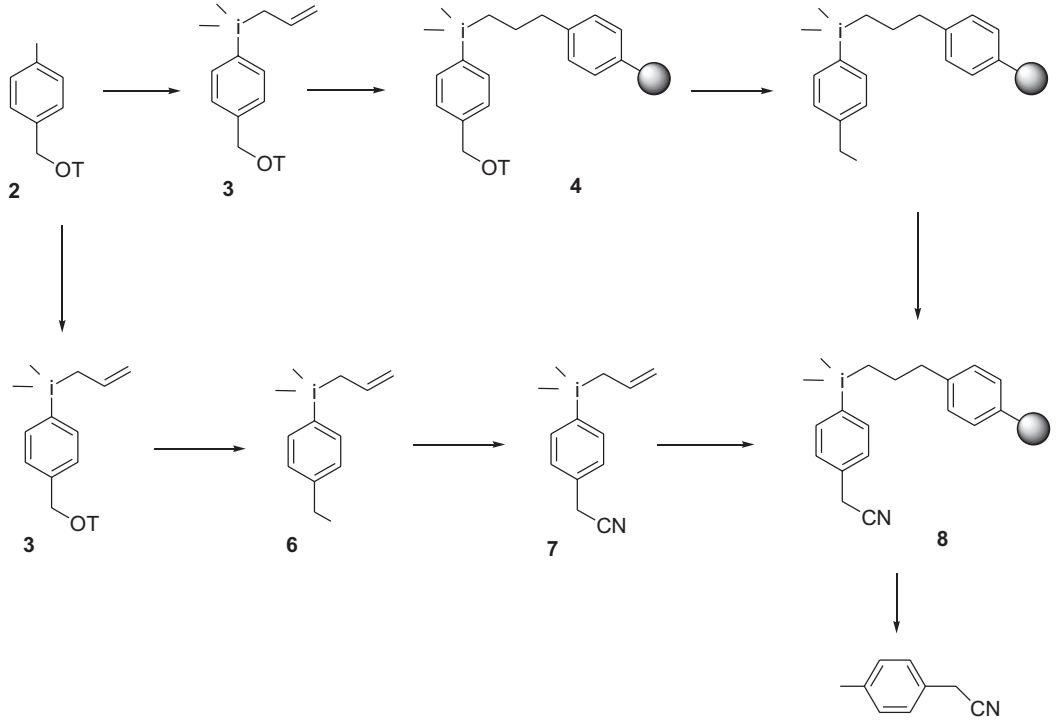
We dedicated this paper to our good friend Professor Victor Snieckus.

K.J. Lee and K.D. Janda.[1] Department of Chemistry and The Skaggs Institute for Chemical Biology, The Scripps Research Institute, 10550 North Torrey Pines Road, La Jolla, California 92037, U.S.A.

[1]Corresponding author (telephone: +1 858-784-2516; fax: +1 858-784-2595; e-mail: kdjanda@scripps.edu).

 DOI: 10.1139/cjc-79-11-1556 © 2001 NRC Canada

Scheme 1. Reagents and conditions: (*a*) *n*-BuLi, THF, –78°C, then allylchloro-dimethylsilane; (*b*) 9-BBN, THF, rt, 3.5 h, then 4-bromopolystyrene, THF, $Pd(PPh_3)_4$, 2 M Na_2CO_3, 60°C, 72 h; (*c*) *p*-TsOH·H_2O (0.1 equiv.), THF, H_2O, rt; (*d*) Ph_3P, CBr_4, CH_2Cl_2, rt; (*e*) NaCN, DMF–H_2O, reflux, 1 h; (*f*) Br_2, CH_2Cl_2, rt, 1 h.



Results and discussion

We envisioned diamine **12** as the key intermediate in our approach to 5-benzoylbenzimidazoles (see below). In solution phase synthesis, this type of benzophenone can be prepared readily from a Friedel-Crafts acylation reaction; however, this strategy cannot be implemented in a polystyrene-based system due to the presence of the aromatic backbone on the resin. Alternatively, **12** could be prepared from an aldehyde and organolithium or organomagnesium reagent followed by oxidation of the resultant secondary alcohol; however, this reaction sequence requires rigorous anhydrous conditions not readily adaptable to a solid support and ultimately automation of the process.

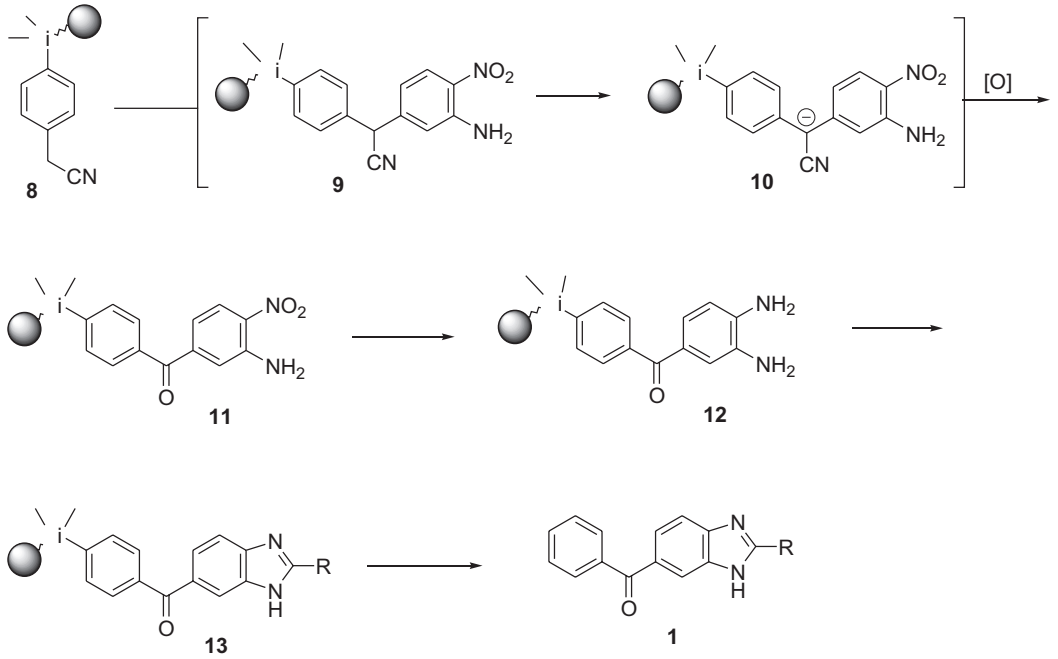
We thus envisioned that **11** could be prepared by oxidative decyanation (12) of diaryl cyanide **9**. It was our contention that **9** could be obtained from the nucleophilic substitution reaction of 5-chloro-2-nitroaniline with the anion of solid-supported benzyl cyanide **8**. This kind of oxidative decyanation has been exemplified in the solution phase synthesis of various benzophenone derivatives (5*a*).

Our route to solid-supported benzyl cyanide **8** is illustrated in Scheme 1. Thus, **2** was lithiated and quenched with chlorodimethylallylsilane to give the arylsilane derivative **3** that was attached subsequently to the polymer in a two step procedure. Hydroboration of the allylsilane followed by in situ Suzuki coupling (13) with bromophenylsubstituted resin (1.97 mmol g^{-1}) provided the silyl-derivatized resin **4**. Deprotection of the TBS group with acid followed by bromination of the resultant alcohol gave the benzyl bromide derivative **5**. The key intermediate, polymer-supported benzyl cyanide **8** was then obtained from the reaction of **5** with sodium cyanide in a DMF–water solvent system. The loading level of **8** was determined to be 1.2 mmol g^{-1} by mass balance of 4-bromobenzyl cyanide, which was obtained from the electrophilic cleavage reaction of a small aliquot of the resin with Br_2. Alternatively, **8** could be accessed if the hydroboration–Suzuki coupling protocol was conducted at a later stage with preformed benzyl cyanide **7**. With intermediate **8** in hand, our 5-benzoylbenzimidazole library synthesis was accomplished as shown in Scheme 2.

Solid-supported benzyl cyanide **8** was treated with 5-chloro-2-nitroaniline in the presence of an excess of potassium *tert*-butoxide at room temperature. The requirement for excess base (>2 equiv.) is essential to drive the first step (nucleophilic aromatic substitution) of the reaction sequence to completion due to the increased acidity of the α-hydrogen found on the disubstituted nitrile product **9**. Oxidation of **9** was performed in situ with 30% aqueous hydrogen peroxide to afford the desired benzophenone derivative **11** after acidification, so that the overall reaction sequence to give ketone **11** can be accomplished conveniently in a one-pot procedure. To confirm the structure and to determine the loading value, an aliquot of **11** was subjected to cleavage. Usually, the aryl—silicon bond is cleaved by trifluoroacetic acid (i.e., protodesilylation). However, an aryl—silicon bond can be quite stable if the aromatic ring possesses a strong electron-withdrawing group within its nucleus. In this scenario the ipso-substituted intermediate, needed to generate a carbonium ion β to the silicon moiety is prevented. In such cases, fluoride ion has proven to be an effective alternative (9–11, 14). Thus, the benzophenone resin **11** was cleaved effectively with tetrabutylammonium fluoride (TBAF) to give 5-benzoyl-2-nitroaniline. This was confirmed by ^1H NMR as

© 2001 NRC Canada

Scheme 2. Reagents and conditions: (*a*) (*i*) 5-chloro-2-nitroaniline, *t*-BuOK, rt, 21 h, (*ii*) 30% H_2O_2, 0°C to rt, 22 h, (*iii*) 1 N HCl, rt, 15 min; (*b*) $SnCl_2 \cdot 2H_2O$, DMF, 65°C, 27 h; (*c*) RCHO (5 equiv.), DDQ (2 equiv.), DMF, rt, 7 h; (*d*) 1 M TBAF, THF, 60°C, 24 h.



well as high resolution mass spectrometry (HRMS) and a loading value between 0.34~0.5 mmol g^{-1} was calculated for **11**. Reduction of the polymer-supported nitroaniline **11** was achieved by treatment with $SnCl_2$ in DMF at 60°C (incomplete reduction was observed at room temperature even with a prolonged reaction time), and was confirmed by ^{1}H NMR after cleavage of a small amount of the resin with TBAF.

Among the many procedures for the preparation of benzimidazoles from diamines, 2,3-dichloro-5,6-dicyano-1,4-benzoquinone (DDQ) mediated oxidative cyclocondensation with an aldehyde is attractive because of its mild reaction conditions (6*c*, 6*f*, 15). Thus, treatment of resin **12** with an aldehyde (5 equiv.) and DDQ (2 equiv.) in DMF at room temperature gave the resin bound benzimidazole **13**. Cleavage from the support was accomplished by treatment with TBAF in warm THF (60°C) to provide the desired 5-benzoylbenzimidazoles **1a**–**k** (Table 1).

In general, the purities of the crude products as determined by ^{1}H NMR were greater than 85%. The isolated yields (following purification over silica gel), calculated based on the substitution level of the benzophenone resin **11**, were between 48 and 70%. The cyclocondensation–oxidation reaction was efficient with electron-rich aromatic (**1c**, **1g**), electron-deficient aromatic (**1b**, **1d**), heteroaromatic (**1e**, **1f**), and aliphatic (**1h**–**k**) aldehydes. All final compounds were characterized by ^{1}H NMR, ^{13}C NMR, and HRMS.

In summary, we have developed a traceless linker strategy for the solid-supported synthesis of 2-substituted-5-benzoylbenzimidazoles **1**. The key feature of our synthetic strategy was the oxidative decyanation of **9** to give ketone **11** in an efficient one-pot procedure. It is anticipated that resin-bound intermediates **12** and **13** could serve as scaffolds for more diversified compound libraries. For example, regiospecific acylation or sulfonylation of **12** and subsequent cyclization would give 1,2-disubstituted-5-benzoylbenzimidazoles. Furthermore, reduction of the carbonyl group found in **13** and subsequent derivatization of the resultant alcohol would give 2,5-disubstitutedbenzimidazoles. Efforts along these lines to construct more diversified libraries in the pursuit of interesting biological active compounds are currently in progress.

Experimental

General

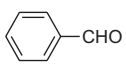
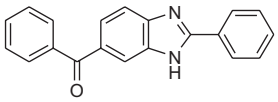
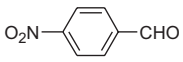
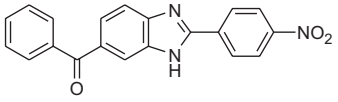
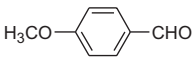
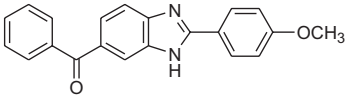
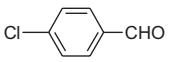
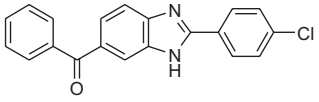
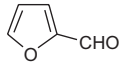
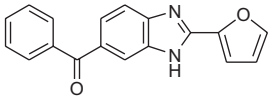
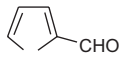
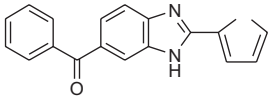
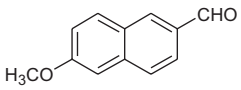
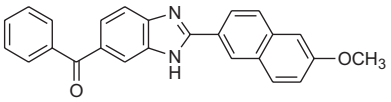
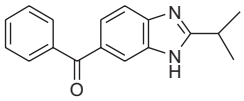
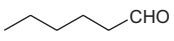
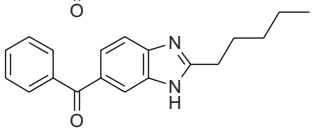
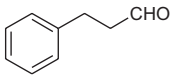
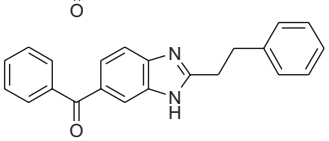
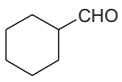
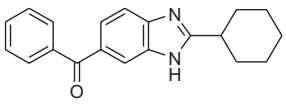
Unless otherwise noted, materials were obtained from commercial suppliers and used without further purification. Tetrahydrofuran (THF) was distilled immediately before use from sodium–benzophenone under N_2. Anhydrous dimethylformamide (DMF) was obtained from Aldrich in a SureSeal bottle. All reactions were run under an inert atmosphere with dry reagents and solvents and flame-dried glassware. Flash column chromatography was carried out using Merck 60 230–400 mesh silica gel. Thin layer chromatography was performed using 0.25 mm silica gel coated Kieselgel 60 F_{254} plates and visualized using aqueous cerium molybdate with heating. ^{1}H NMR and ^{13}C NMR spectra were recorded on a Bruker AMX-400 spectrometer at 400 and 100 MHz, respectively, in $CDCl_3$ or CD_3OD at 25°C. Chemical shifts are reported in ppm on the δ scale from an internal TMS standard. 4-Bromopolystyrene resin was purchased from Novabiochem (San Diego, CA). Large scale solid-phase reactions were performed in peptide-flasks with glass tubes equipped for vacuum filtration (ChemGlass Inc., Vineland, NJ) and were agitated with a Ika-Vibrax-Vxr shaker (Germany).

O-tert-Butyldimethylsilyl-4-allyldimethylsilylbenzyl ether (3)

To a solution of *tert*-butyldimethylsilyl-4-bromobenzyl ether (**1**, 14.4 g, 47.8 mmol) in dry THF (150 mL) at –78°C was slowly added *n*-BuLi (29.9 mL, 1.6 M solution in hexane,

© 2001 NRC Canada

Table 1.

Entry	Aldehydes	Benzimidazoles	Yield %[a]
1a			70
1b			64
1c			52
1d			60
1e			56
1f			66
1g			48
1h			56
1i			68
1j			61
1k			66

[a] Isolated yields after purification by silica gel chromatography.

47.8 mmol). After 20 min of further stirring at –78°C, allylchlorodimethylsilane (6.98 mL, 47.8 mmol) was added slowly and the reaction mixture was warmed to room temperature. After 30 min, saturated NH_4Cl (1 mL) was added followed by sodium sulfate and the reaction mixture was then filtered, concentrated, and purified by column chromatography (ethyl acetate–hexane, 1:20) to give a colorless liquid (14.2 g, 93%). ^{1}H NMR ($CDCl_3$) δ: 7.50 (d, J = 7.9 Hz, 2H), 7.36 (d, J = 7.9 Hz, 2H), 5.79 (m, 1H), 4.86 (m, 2H), 4.77 (s, 2H), 0.98 (s, 9H), 0.29 (s, 6H), 0.13 (s, 6H). ^{13}C NMR ($CDCl_3$) δ: 142.3, 136.9, 134.7, 133.6, 125.4, 113.3, 64.9, 26.0, 23.8, 18.5, –3.4, –5.2.

© 2001 NRC Canada

Preparation of 4

To a solution of **3** (3.0 g, 9.4 mmol) in dry THF (30 mL) was added 9-BBN (18.7 mL, 0.5 M solution in THF) at room temperature. After stirring for 3 h, $Pd(PPh_3)_4$ (324 mg, 3 mol%), a 2 M Na_2CO_3 solution (4.8 mL, 9.6 mmol), and 4-bromopolystyrene (3 g, 1.97 mmol g^{-1}, 5.9 mmol) were added and the reaction mixture was stirred gently at 65°C in the dark. After 48 h, additional $Pd(PPh_3)_4$ (160 mg) was added and the heating and stirring was continued for 24 h. After a total of 72 h of heating, the mixture was allowed to cool to room temperature. The resin was filtered and washed with THF, THF–H_2O (1:1), H_2O, MeOH, DMF, MeOH, and [CH_2Cl_2, MeOH]$_3$ and then dried under vacuum to give 3.6 g of polymer.

Preparation of 8

To a mixture of resin **4** (3.6 g) in THF–water (20:1 mL) was added a catalytic amount of *p*-TsOH·H_2O (50 mg). After shaking overnight at room temperature, the resin was washed with THF, THF–H_2O (1:1), H_2O, MeOH, and [CH_2Cl_2, MeOH]$_3$ and then dried under vacuum. To a mixture of this resin and Ph_3P (1.4 g) in CH_2Cl_2 (40 mL) was slowly added CBr_4 (1.7 g). After shaking overnight at room temperature, the resin was filtered and washed with THF, CH_2Cl_2, MeOH, and [CH_2Cl_2, MeOH]$_3$ and then dried under vacuum to give polymer **5**.

To the above resin **5** (3.5 g) swelled in DMF–H_2O (20:10 mL) was added an excess of sodium cyanide (2.0 g) and the suspension was stirred gently at 80°C for 3 h. The resin was filtered and washed with THF–H_2O (1:1), H_2O, MeOH, THF, and [MeOH, CH_2Cl_2]$_3$ and then dried under vacuum to give polymer **8**. To determine the loading level of resin **8**, 100 mg of the resin was swelled in 5 mL of CH_2Cl_2 and Br_2 (30 μL) was added. After stirring for 1 h at room temperature, the resin was filtered and washed with CH_2Cl_2. The combined filtrate was concentrated to give 4-bromobenzylcyanide (23.4 mg, 1.2 mmol g^{-1}), whose identity was confirmed by ^{1}H NMR and mass spectrometry.

Preparation of 11

To a mixture of resin **8** (3.0 g, 3.6 mmol) and 5-chloro-2-nitroaniline (2.4 g, 14.4 mmol) in anhydrous DMF (40 mL) was added potassium *tert*-butoxide (2.4 g, 21.6 mmol) in one portion at 0°C. The reaction mixture immediately turned to an intense dark red color. The mixture was stirred gently for 21 h at room temperature and then cooled to 0°C with an ice bath. Hydrogen peroxide (7.5 mL, 30% solution) was added and the mixture was stirred for 22 h at room temperature. At this time, the color changed to dark green. After the addition of 1 N HCl (45 mL) and stirring for 15 min, the color of the mixture turned bright yellow. The resin was washed thoroughly with THF, H_2O (5 times), DMF, H_2O, [THF, MeOH]$_3$, and [CH_2Cl_2, MeOH]$_3$ to give yellow beads (3.7 g). A portion of the above resin (100 mg) was treated with a 1 M solution of TBAF (50 μL) in THF at room temperature overnight. The resin was filtered, rinsed with THF and MeOH, and the combined filtrate was concentrated to afford a residue that was subjected to extractive work up with CH_2Cl_2–H_2O. The residue obtained from concentration of the CH_2Cl_2 layer was taken up in CH_2Cl_2 and further extracted with water to remove a small amount of residual TBAF. Removal of CH_2Cl_2 under reduced pressure provided 5-benzoyl-2-nitroaniline (10 mg, 0.41 mmol) as a bright yellow solid whose structure was confirmed by ^{1}H NMR and mass spectrometry.

Preparation 12

To resin **11** (3.0 g, 1.23 mmol) in DMF (30 mL) was added an excess of $SnCl_2 \cdot 2H_2O$ (4 g, 12.3 mmol) and the mixture was stirred gently at 65°C. After 10 h, additional $SnCl_2 \cdot 2H_2O$ (4 g) was added and the mixture was stirred for a further 10 h. The reaction mixture was cooled to room temperature and the resin was filtered, washed with DMF several times, and dried under vacuum to provide a dark red resin (2.9 g).

General procedure for the preparation of 5-benzoyl-benzimidazoles (1)

To resin **12** (0.2 g, 0.08 mmol) in DMF (5 mL) was added an aldehyde (5 equiv.) and DDQ (2 equiv.) and the mixture was stirred gently for 7 h at room temperature. The resulting resin was washed with CH_2Cl_2, DMF, and [CH_2Cl_2, MeOH]$_3$ and dried under vacuum to provide the resin bound benzimidazoles **13**. The resin was cleaved with 1 M solution of TBAF (2 mL) in THF at 65°C overnight and worked-up as in the cleavage of resin **11** vide supra. The crude residue was redissolved and purified by column chromatography ($CHCl_3$–MeOH, 20:1) to give **1a**–**k**.

***1a**:* Prepared from benzaldehyde, 70%. HRMS calcd. for $C_{20}H_{15}N_2O$: 299.1179; found: 299.1167. ^{1}H NMR ($CDCl_3$) δ: 8.17, (s, 1H), 8.10 (m, 2H), 7.84 (m, 3H), 7.58 (t, 1H).

***1b**:* Prepared from 4-nitrobenzaldehyde, 64%. HRMS calcd. for $C_{20}H_{12}N_3O_3$: 342.0884; found: 342.0888. ^{1}H NMR (DMSO-d_6) δ: 7.60 (s, 1H), 7.40 (m, 1H), 7.30 (m, 4H), 7.22 (m, 3H), 7.11 (m, 4H).

***1c**:* Prepared from *p*-anisaldehyde, 52%. HRMS calcd. for $C_{21}H_{17}N_2O_2$: 329.1285; found: 329.1282. ^{1}H NMR ($CDCl_3$) δ: 8.08 (m, 3H), 7.78 (m, 3H), 7.55 (m, 2H), 7.46 (m, 2H), 6.93 (d, J = 9.1 Hz, 2H), 3.82 (s, 3H). ^{13}C NMR ($CDCl_3$) δ: 197.2, 161.6, 138.2, 132.1, 131.9, 130.0, 128.5, 128.2, 125.4, 121.7, 114.5, 55.4.

***1d**:* Prepared from 4-chlorobenzaldehyde, 60%. HRMS calcd. for $C_{20}H_{13}ClN_2O$: 333.0789; found: 333.0776. ^{1}H NMR (MeOH-d_4) δ: 7.98 (s, 1H), 7.96 (s, 1H), 7.95 (m, 1H), 7.73 (m, 1H), 7.66 (m, 3H), 7.52 (m, 3H), 7.43 (m, 3H). ^{13}C NMR (MeOH-d_4) δ: 198.2, 154.4, 141.6, 139.4, 139.1, 138.5, 134.7, 133.8, 131.1, 130.9, 130.0, 129.7, 127.7, 127.3, 119.1, 115.7.

***1e**:* Prepared from 2-furylaldehyde, 56%. HRMS calcd. for $C_{18}H_{13}N_2O_2$: 289.0972; found: 289.0969. ^{1}H NMR (MeOH-d_4) δ: 7.91 (s, 1H), 7.67 (m, 4H), 7.54 (m, 2H), 7.43 (m, 2H), 7.18 (d, J = 2.96 Hz, 1H), 6.61 (m, 1H). ^{13}C NMR (MeOH-d_4) δ: 198.6, 146.7, 146.1, 139.8, 133.7, 133.6, 131.1, 129.6, 126.6, 113.6, 113.3.

***1f**:* Prepared form 2-thiophenecarboxaldehyde, 66%. HRMS calcd. for $C_{18}H_{13}N_2OS$: 305.0743; found: 305.0747. ^{1}H NMR (MeOH-d_4) δ: 7.89 (m, 1H), 7.77 (m, 2H), 7.66 (m, 2H), 7.59 (m, 1H), 7.54 (m, 2H), 7.43 (m, 2H), 7.12 (dd, J =

© 2001 NRC Canada

5.0, 3.5 Hz, 1H). ^{13}C NMR (MeOH-d_4) δ: 197.5, 138.6, 132.4, 132.3, 129.9, 129.7, 128.5, 128.4, 128.3, 128.1.

1g: Prepared from 5-methoxynaphthaldehyde, 48%. HRMS calcd. for $C_{25}H_{19}N_2O_2$: 379.1441; found: 379.1449. ^{1}H NMR (MeOH-d_4) δ: 8.34 (s, 1H), 7.99 (dd, *J* = 7.0, 1.5 Hz, 1H), 7.92 (s, 1H), 7.75 (m, 2H), 7.65 (m, 3H), 7.55 (m, 2H), 7.43 (t, *J* = 6.2 Hz, 2H), 7.15 (d, *J* = 2.1 Hz, 1H), 7.07 (dd, *J* = 7.2, 2.0 Hz, 1H). ^{13}C NMR (MeOH-d_4) δ: 197.5, 138.7, 136.4, 132.4, 132.2, 130.2, 129.9, 128.9, 128.4, 127.9, 126.8, 125.2, 124.2, 124.1, 119.9, 54.9.

1h: Prepared from 2-butyraldehyde, 56%. HRMS calcd. for $C_{17}H_{17}N_2O$: 265.1335; found: 265.1343. ^{1}H NMR ($CDCl_3$) δ: 8.05 (s, 1H), 7.80 (m, 3H), 7.55 (m, 2H), 7.46 (t, *J* = 7.9 Hz, 2H), 3.38 (quintet, *J* = 7.0 Hz, 1H), 1.47 (d, *J* = 6.8 Hz, 6H). ^{13}C NMR ($CDCl_3$) δ: 197.1, 138.3, 132.0, 131.8, 130.0, 128.2, 124.9, 29.1, 21.3.

1i: Prepared from 1-hexanal, 68%. HRMS calcd. for $C_{19}H_{21}N_2O$: 293.1648; found: 293.1635. ^{1}H NMR ($CDCl_3$) δ: 8.25 (s, 1H), 7.85 (m, 2H), 7.77 (m, 2H), 7.51 (m, 4H), 3.36 (t, *J* = 7.6 Hz, 1H), 3.21 (m, 1H), 2.04 (m, 2H), 1.29 (m, 4H), 0.77 (t, *J* = 7.1 Hz, 3H). ^{13}C NMR ($CDCl_3$) δ: 195.1, 156.3, 136.9, 135.5, 133.2, 132.9, 130.4, 129.9, 128.5, 127.7, 116.2, 113.9, 31.0, 27.3, 26.7, 22.0, 13.8.

1j: Prepared from 3-phenylpropanal, 61%. HRMS calcd. for $C_{22}H_{19}N_2O$: 327.1492; found: 327.1495. ^{1}H NMR (MeOH-d_4) δ: 7.99 (s, 1H), 7.88 (m, 1H), 7.75 (m, 1H), 7.70 (m, 2H), 7.56 (m, 1H), 7.45 (m, 2H), 7.21 (m, 3H), 7.13 (m, 2H), 3.43 (t, *J* = 5.9 Hz, 2H), 3.17 (t, *J* = 6.0 Hz, 2H). ^{13}C NMR (MeOH-d_4) δ: 196.9, 157.6, 139.9, 138.6, 137.1, 135.1, 134.3, 132.3, 131.2, 130.1, 129.9, 129.4, 129.1, 128.4, 117.1, 114.9, 34.1, 30.2.

1k: Prepared from cyclohexylcarboxaldehyde, 66%. HRMS calcd. for $C_{20}H_{21}N_2O$: 305.1648; found: 305.1659. ^{1}H NMR (MeOH-d_4) δ: 7.85 (s, 1H), 7.66 (s, 1H), 7.64 (m, 1H), 7.61 (dd, *J* = 6.8, 1.2 Hz, 1H), 7.52 (m, 2H), 7.42 (m, 2H), 2.84 (m, 1H), 2.01 (d, *J* = 11.2 Hz, 2H), 1.80 (m, 2H), 1.70 (m, 1H), 1.56 (m, 2H), 1.39 (m, 2H), 1.27 (m, 1H). ^{13}C NMR (MeOH-d_4) δ: 197.8, 138.8, 132.3, 131.8, 129.9, 128.4, 124.7, 38.9, 31.7, 26.1, 25.9.

Acknowledgments

Funding for this project was provided to K.D.J. by The Skaggs Institute for Chemical Biology, The Scripps Research Institute, and the National Institute of Health (GM 56154). We thank Thomas S. Reger for proofreading of the manuscript.

References

1. J.E. Richter. Am. J. Gastroenterol. **92**, 34 (1997).
2. H.J. Al-Muhaimeed. Int. Med. Res. **25**, 175 (1997).
3. J.B. Cheng, K. Cooper, A.J. Duplantier, J.F. Eggler, K.G. Kraus, S.C. Marshall, A. Marfat, H. Masamune, J.T. Shirley, J.E. Tickner, and J.P. Umland. Bioorg. Med. Chem. Lett. **5**, 1969 (1995).
4. K. Kubo, Y. Inada, Y. Kohara, Y. Sugiura, M. Ojima, K. Itoh, Y. Furukawa, K. Nishikawa, and T.J. Naka. J. Med. Chem. **36**, 1772 (1993).
5. (*a*) M.J. Tebbe, W.A. Spitzer, F. Victor, S.C. Miller, C.C. Lee, T.R. Sattelberg, E. McKinney, and J.C. Tang. J. Med. Chem. **40**, 3937 (1997); (*b*) F. Victor, R. Loncharich, J. Tang, and W.A. Spitzer. J. Med. Chem. **40**, 3478 (1997); (*c*) F. Victor, T.J. Brown, K. Campanale, B.A. Heinz, L.A. Shipley, K.S. Su, J. Tang, L.M. Vance, and W.A. Spitzer. J. Med. Chem. **40**, 1511 (1997).
6. (*a*) M.J. Plunkett and J.A. Ellman. J. Org. Chem. **62**, 2885 (1997); (*b*) M.J. Plunkett and J.A. Ellman. J. Org. Chem. **60**, 6006 (1995).
7. T.L. Boehm, H.D.H. Showalter, M.J. Plunkett, and J.A. Ellman. J. Org. Chem. **61**, 6498 (1996).
8. F.X. Woolard, J. Paetsch, J.A. Ellman, and M.J. Plunkett. J. Org. Chem. **62**, 6102 (1997).
9. B. Chenera, J.A. Finkelstein, and D.F. Veber. J. Am. Chem. Soc. **117**, 11999 (1995).
10. (*a*) J.P. Kilburn, J. Lau, and R.C.F. Jones. Tetrahedron Lett. **41**, 5419 (2000); (*b*) A. Mazurov. Bioorg. Med. Chem. Lett. **10**, 67 (2000); (*c*) T.S. Yokum, J. Alsina, and G. Barany. J. Comb. Chem. **2**, 282 (2000); (*d*) D. Tumelty, M.K. Schwarz, K. Cao, and M.C. Needles. Tetrahedron Lett. **40**, 6185 (1999); (*e*) D. Tumelty, M.K. Schwarz, K. Cao, and M.C. Needles. Tetrahedron Lett. **39**, 7467 (1998); (*f*) J.P. Mayer, G.S. Lewis, C. McGee, and D. Bankaitis-Davis. Tetrahedron Lett. **39**, 6655 (1998).
11. (*a*) Y.-C. Chi and C.-M. Sun. Synlett, 591 (2000); (*b*) C.-M. Yeh, C.-L. Tung, and C.-M. Sun. J. Comb. Chem. **2**, 341 (2000); (*c*) C.G. Blettner, W.A. Koenig, G. Ruehter, W. Stenzel, and T. Schotten. Synlett, 307 (1999).
12. (*a*) S.S. Kulp and M.J. McGee. J. Org. Chem. **48**, 4097 (1983); (*b*) A. Donetti, O. Boniardi, and A. Ezhaya. Synthesis. 1009 (1980).
13. N. Miyarura and A. Suzuki. Chem. Rev. **95**, 2457 (1995).
14. Y. Hu, J.A. Porco, Jr., J.W. Labadie, O.W. Gooding, and B.M. Trost. J. Org. Chem. **63**, 4518 (1998).
15. J.J.V. Eynde, F. Delfosse, and Y.V. Haverbeke. Tetrahedron, **51**, 5813 (1995).

© 2001 NRC Canada

Applications of crotyldiisopinocampheylboranes in synthesis: a formal total synthesis of (+)-calyculin A

Oren P. Anderson, Anthony G.M. Barrett, Jeremy J. Edmunds, Shun-Ichiro Hachiya, James A. Hendrix, Kiyoshi Horita, James W. Malecha, Christopher J. Parkinson, and Andrew VanSickle

Abstract: The formal total synthesis of the marine metabolite (+)-calyculin A is reported. The key steps involve (*i*) the use of Brown allylboration chemistry to control the relative and absolute stereochemistry of homoallylic alcohol arrays, thus setting eight of the desired stereocenters; (*ii*) Stille coupling methodology in the construction of the cyano tetraene unit of the natural product; and (*iii*) a modified Cornforth–Meyers approach to the synthesis of the oxazole fragment.

Key words: calyculin, marine natural product, phosphatase inhibitor, total synthesis, palladium catalyzed coupling reactions, allylboration reactions, aldol reactions, spiroketal, Cornforth–Meyers oxazole reaction.

Résumé : Une synthèse total d'un métabolite d'origine marine, la (+)-calyculine A, été descrite. Les étapes clés de la synthèse reposent sur l'utilisation: de la chimie d'allylboration de Brown afin de contrôler la stéréochemie relative et absolue d'une série d'alcools homoallyliques ayant ainsi permis la création de 8 centres asymétriques; de la réaction de couplage de Stille dans la construction du motif cyanotétraène du produit naturel; d'une approache modifiée de Cornforth–Meyers pour la préparation de la partie oxazole.

Mots clés : calyculine, produit naturel d'origine marine, inhibiteur de la phosphatase, synthèse totale, réactions de couplage catalysées par la palladium, réactions d'allylborations, réactions d'aldolisations, spirocétal, réaction d'oxazole selon Cornforth–Meyers.

[Traduit par la Rédaction]

Introduction

The calyculins represent a group of marine natural products isolated from the sponge *Discodermia calyx* (1). These structurally remarkable compounds have shown potent inhibitory activity toward phosphatase enzymes, notably the serine–threonine PP-1 and PP-2A protein phosphatases. For example, (–)-calyculin A, the antipode of **1**, is active against rabbit skeletal muscle type PP-2A phosphatases at 0.5–1.0 nmol dm^{-3} concentrations and is also 20–300 times more potent than okadaic acid against various PP-1 enzymes. (–)-Calyculin A is a representative member of a series of eight similar structures (calyculins B–H) (2), the other calyculins differing by the presence of an additional methyl unit at C-32 and (or) geometric differences at Δ^2 and (or) Δ^6. A further five related structures, calyculin J, the caliculinamides A, B, and F, and des-*N*-methylcalyculin A have recently been isolated (3). The dephosphono derivative of calyculin A has been obtained from the same marine organism (4). This compound also inhibits protein phosphatases, an unexpected phenomenon, as the presence of the phosphate group was believed to be key to the calyculins' biological activity (5). The relative stereochemistry of **1** was determined by X-ray analysis (1) and the absolute configuration later elucidated by Matsunaga and Fusetani (6), through analysis of the C(37)–C(33) and C(32)–C(29) degradation fragments and Shioiri and co-workers (7) through asymmetric synthesis of the C(37)–C(33) fragment. Total synthesis of (+)-calyculin **1**, the antipode of the natural product, by Evans et al. (8) later corroborated this absolute stereochemical assignment.

Due to the structural complexity of these marine metabolites and their associated biological profile, they have attracted a great deal of synthetic attention (for other synthetic efforts toward the synthesis of the calyculins, see ref. 9). This has culminated in several total syntheses of the calyculin family, the first reported by Evans et al. (8). Their approach centered on the union of a "southern" C(1)–C(25) spiroketal unit and "northern" C(26)–C(37) amide oxazole fragment through Wittig chemistry, the former subunit also

Received January 30, 2001. Published on the NRC Research Press Web site at http://canjchem.nrc.ca on October 29, 2001.

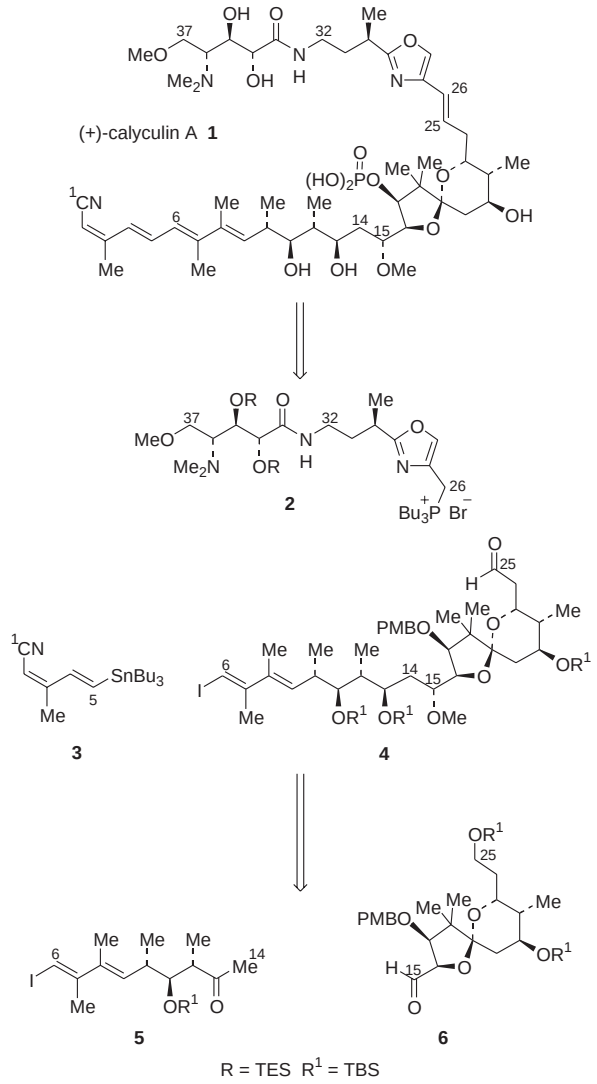
Dedicated to Professor Victor Snieckus on the occasion of his 64th birthday. Happy Birthday Vic.

O.P. Anderson, J.A. Hendrix, K. Horita, and J.W. Malecha. Department of Chemistry, Colorado State University, Fort Collins, CO 80523, U.S.A.
A.G.M. Barrett,[1] S.-I. Hachiya, C.J. Parkinson, and A. VanSickle. Department of Chemistry, Imperial College of Science, Technology and Medicine, South Kensington, London, SW7 2AZ, U.K.
J.J. Edmunds. Department of Chemistry, Northwestern University, Evanston, IL 60208, U.S.A.

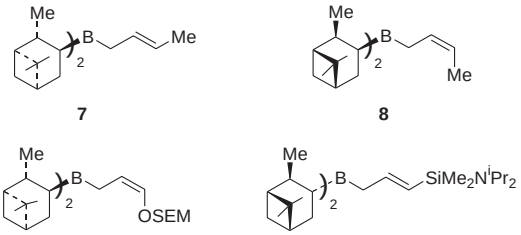
[1]Corresponding author (telephone: (44)-207-594-5767; fax: (44)-207-594-5766; e-mail: agmb@ic.ac.uk).

 DOI: 10.1139/cjc-79-11-1562 © 2001 NRC Canada

Scheme 1.



being constructed using this methodology at C(8)–C(9). Enantioselective synthesis of these fragments was achieved using auxiliary-based asymmetric aldol methodology, establishing ten of the fifteen stereocenters present in **1**. The approach to calyculin A **1** adopted by Masamune and co-workers (10) employed Wadsworth–Emmons type coupling to elaborate the C(8)–C(9) olefin with Stille coupling, was also used in the synthesis of the C(5)–C(6) bond, paralleling other synthetic endeavors in this area. Interestingly, they constructed the C(25)–C(26) alkene by utilizing a Julia-olefination approach to link up the "northern" and "southern" hemispheres. Smith et al. (11) have also recently published total syntheses of both ent-**1** and (–)-calyculin B utilizing an advanced intermediate to synthesize either compound through Peterson olefination at C(2). Their approach also elected to construct the C(25)–C(26) alkene through phosphonium ylide chemistry, as does the formal synthesis of calyculin A (**1**) by Shioiri and co-workers (12). Calyculin C has also succumbed to total synthesis through the efforts of Ogawa and Armstrong (13) using allylborane reagents in the elaboration of the spiroketal unit, notably the novel use of a tetrasubstituted allylborane in the synthesis of the *gem*-dimethyl moiety present in this subunit. Retrosynthetically, we considered that (+)-calyculin A **1** should be accessible from the oxazole amide **2**, the cyanostannane **3**, and the spiroketal fragment **4**, the later being constructed using aldol methodology between the methyl ketone **5** and aldehyde **6** to establish the C(14)–C(15) bond (Scheme 1). Key to our overall strategy, is the employment of the elegant masked aldol chemistry developed by Brown and co-workers (14*b*–*d*, *g*, *h*), employing the derivatives of diisopinocampheylborane **7**–**10** as versatile reagents for the construction of homoallylic alcohols. Our synthetic plan also parallels other endeavors (8, 11–13) in the synthesis of calyculin A **1**, whereby the coupling of oxazole **2** and spiroketal **4** fragments was based upon Wittig chemistry (for our previous publications towards the total synthesis of (+)-calyculin A, see ref. 15).



Results and discussion

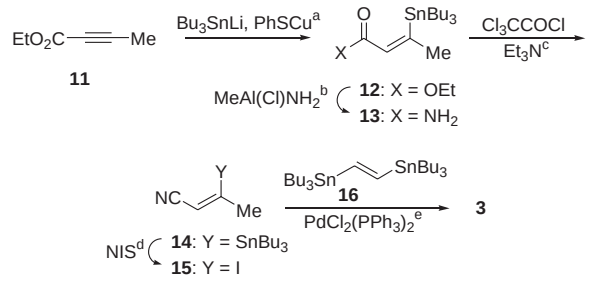
Synthesis of the C(1)–C(5) cyanodiene fragment 3

Construction of the (*Z*,*E*)-cyano diene **3** was based upon the use of Stille chemistry for the elaboration of the C(3)–C(4) bond. This approach would also facilitate the elaboration of the (*E*,*E*)-isomer, an appropriate building block for the synthesis of other calyculins with this geometry at Δ^2. Therefore, conjugate addition of tributylstannyl cuprate (16) to ethyl but-2-ynoate **11** and quenching with methanol gave the (*Z*)-β-stannylcrotonate **12** (52%) and the corresponding (*E*)-isomer **17** (7%). The *trans*-geometry of the major product was established by measurement of the ^{117,119}Sn–H coupling constant (J = 97 Hz) in the ^{1}H NMR spectrum (17). Conversion of ester **12** to the corresponding amide **13** was achieved using the methodology of Weinreb and co-workers (18), and subsequent dehydration using trichloroacetyl chloride and triethylamine gave the nitrile **14**. Iododestannylation afforded solely the desired (*Z*)-iodide **15** and this was smoothly coupled with the distannane **16** (19) using Stille methodology to give the requisite C(1)–C(5) diene coupling fragment **3** with complete geometric retention (Scheme 2). For ease of synthesis upon scale up, in situ generation of the vinyl iodide **15**, using iodine in DMF and subsequent addition of bis(triphenylphosphino)palladium dichloride and distannane **16** gave the cyanodiene **3** in moderate yield (50%) in a one-pot procedure. This protocol also circumvented the need for the isolation of the volatile iodide intermediate **15**.

In parallel to the synthesis of stannane **3**, the minor *trans*-isomer **17** was converted by sequential reaction with trimethylaluminum and ammonium chloride (72%), trichloroacetyl chloride and triethylamine (95%), and iodine followed by stannane **16** and palladium(0) catalysis (39%) into the (*E*,*E*)-isomer **22**. Comparisons of spectral data for each in-

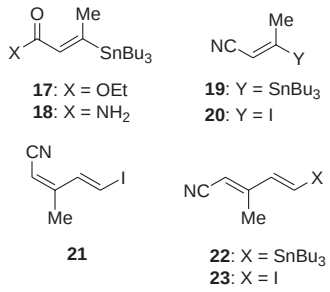
© 2001 NRC Canada

Scheme 2.



Reagents and Conditions: (a) $Bu_3SnSnBu_3$, *n*-BuLi, PhSCu, THF, -35°C then MeOH, Et_2O (52%); (b) $AlMe_3$, NH_4Cl, PhH, 50°C (76%); (c) Cl_3CCOCl, Et_3N, CH_2Cl_2, 0°C (95%); (d) NIS, THF, Et_2O (65%); (e) **16**, $PdCl_2(PPh_3)_2$ (cat) THF 60°C (55%)

termediate **12**, **13**, **14**, **15**, and **3** with the data for the corresponding (*E*)- and (*E*,*E*)-isomers **17**, **18**, **19**, **20**, and **22**, respectively, were fully consistent with assignment of stereochemistry in each case. Finally, separate iododestannylation of both **3** and **22** gave the corresponding (*Z*,*E*)- and (*E*,*E*)-dienyl iodides **21** and **23** with retention of geometry. These results unequivocally established the geometric integrity and purity of the key intermediate **3**.

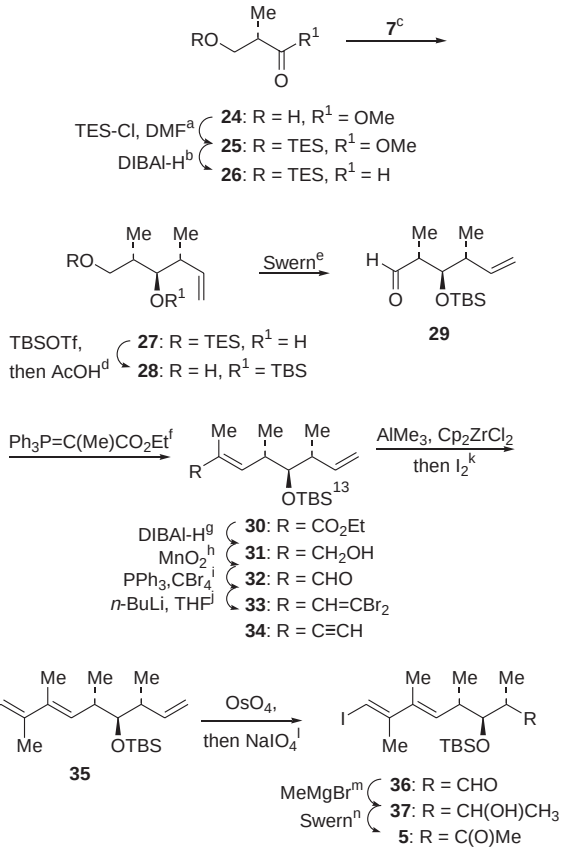


Synthesis of the C(6)–C(14) vinyl iodide subunit 5

We envisaged that construction of the vinyl iodide **5** would arise from the methylzirconation–iodinolysis of alkyne **34** according to the procedure of Negishi et al. (20). Alkyne **34** would in turn come from the suitably elaborated aldehyde **29**, the synthesis of which involves a key Brown homologation to unambiguously set the C(11) and C(12) stereochemistry (Scheme 3). Thus, synthesis of vinyl iodide **5** commenced from aldehyde **26**, prepared from commercially available methyl (*S*)-(+)-3-hydroxy-2-methylpropanoate **24** via triethylsilyl protection of the alcohol and DIBAl-H reduction. Brown homologation (14) of aldehyde **26** using the borane reagent **7** derived from (–)-pinene gave the homoallylic alcohol **27**, which was formed in excellent diastereomeric excess (>96%) as judged by ^1H NMR analysis.

In parallel to the conversion of ester **24** into ether **27** in Scheme 3, the early transformations were repeated in the antipode series starting from methyl (2*R*)-2-methyl-3-triethylsilyloxypropanoate. Whilst the intermediate **38** was not transformed further towards calyculin, it was used to confirm the stereochemistry of the key intermediate **28**. Conversion of the silyl ether **38** into the *meso*-triacetate **42** is outlined in Scheme 4. This was accomplished through catalytic osmium tetraoxide mediated dihydroxylation and periodate cleavage of the olefin giving aldehyde **39**. Subsequent re-

Scheme 3.

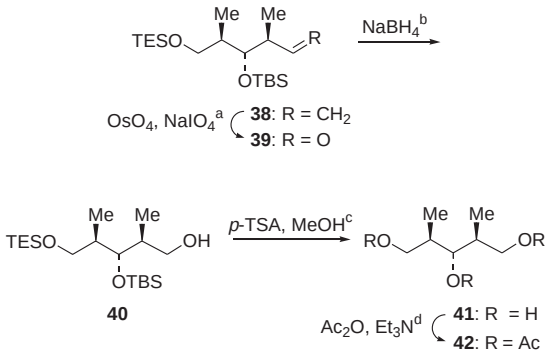


Reagents and Conditions: (a) TES-Cl, CH_2Cl_2, imidazole, DMAP (cat.) (90%); (b) DIBAl-H, hexanes, -70°C (89%); (c) **7**, THF, -78°C then $NaBO_3{\cdot}4H_2O$, H_2O (76%); (d) THF, TBSOTf, 2,6-lutidine, -78°C then AcOH, 25°C (84%); (e) $(COCl)_2$, DMSO, Et_3N, CH_2Cl_2 (78%); (f) $Ph_3P{=}C(Me)CO_2Et$, THF, reflux (96%); (g) DIBAl-H, THF, 25°C (86%); (h) MnO_2, CH_2Cl_2 (81%); (i) PPh_3, CBr_4, CH_2Cl_2 (89%); (j) *n*-BuLi, THF, -78°C (80%); (k) $AlMe_3$, Cp_2ZrCl_2, CH_2Cl_2 then I_2 (69-86%); (l) OsO_4 (cat.), NMO, acetone, H_2O (<61%) then $NaIO_4$, THF, MeOH, H_2O; (m) MeMgBr, THF, -78°C (80%, 2 steps); (n) $(COCl)_2$, DMSO, Et_3N, CH_2Cl_2 (79%).

duction with sodium borohydride gave alcohol **40** that was desilylated and per-acetylated to furnish the triacetate **42.** Both the lack of optical rotation and the ^1H and ^{13}C NMR spectra of **40** were fully consistent with the expected *meso*-stereochemistry. Since the synthesis of alcohol **27** started from methyl (2*S*)-2-methyl-3-triethylsilyloxypropanoate (**24**), this correlation established both the relative and absolute stereochemistry of the two CHMe stereocenters. The C(2)–C(3) *anti*-stereochemistry followed from the known stereochemical bias of the Brown crotylboration reaction (14) using reagent **7**. With the knowledge that the desired stereochemical configuration was in place, the synthesis of ketone **5** proceeded with the selective *tert*-butyldimethylsilylation and detriethylsilylation (21) of alcohol **27** to give ether **28**. Oxidation under Swern (22) conditions and homologation of the resulting aldehyde **29** gave the α,β-unsaturated ester **30** with excellent (*E*)-selectivity (>95%). Ester **30** was transformed via aldehyde **32** and homologated under the protocol of Corey and Fuchs (23) into the acetylene **34**. Elimination of

© 2001 NRC Canada

Scheme 4.



Reagents and Conditions: (a) OsO_4 , *N*-methylmorpholine -*N*-oxide, Me_2CO, H_2O; $NaIO_4$, THF, MeOH; (b) $NaBH_4$, MeOH, 0°C (93%); (c) *p*-$MeC_6H_4SO_3H$, MeOH (100%); (d) Ac_2O, Et_3N, DMAP, CH_2Cl_2 (97%).

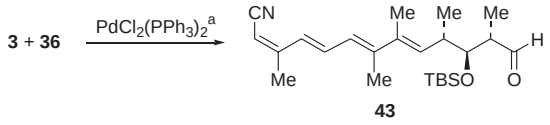
the intermediate dibromide **33** was carried out using either lithium diisopropylamide (15) or *n*-butyllithium. However, in either case, rapid purification of **33** was required to obtain the acetylene **34** in acceptable yields. *Syn*-methylzirconation (20) of acetylene **34** followed by in-situ iodinolysis of the vinyl alane intermediate gave triene **35** exclusively as the (*E*)-isomer. This reaction, however, proved highly dependent upon the nature of the C(13) substituent. Attempted methylzirconation of protected derivatives of the analogous C(13) primary alcohol, C(13), C(14) diol, or the C(13) aldehyde gave intractable product mixtures. Quite remarkably, osmylation of triene **35** resulted in selective oxidation of the terminal olefin (Δ^{13}) thereby providing a route to the key ketone **5**. Subsequent periodate cleavage of the vicinal diol (24) gave aldehyde **36**, which was transformed through methylmagnesium bromide addition and subsequent Swern oxidation to the desired C(6)–C(14) calyculin A methyl ketone **5** (Scheme 3). Whilst this sequence of transformations from triene **35** into the C(13) ketone **5** did indeed work acceptably, it unfortunately proceeded in variable yields especially on scale up. However sufficient material was accumulated to further progress the synthesis.

Our projected route toward calyculin A **1** is flexible in the timing of the construction of the C(5)–C(6) bond. However, we wished at this stage to explore this chemistry and hence attempted the palladium(0) catalyzed reaction of the vinyl iodide **36** with the vinyl stannane **3** (Scheme 5). Much to our delight, this Stille coupling (25) afforded the tetraene nitrile **43** as a single geometric isomer in good yield (75%) and thus indicated the viability of our disconnection strategy.

Synthesis of the C(15)–C(25) spiroketal subunit

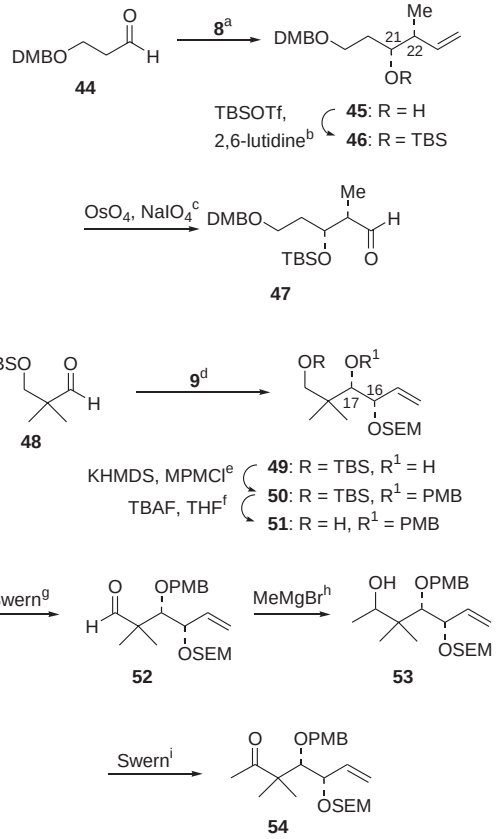
Our first synthetic approach toward the spiroketal core of the calyculins employed a convergent strategy, again using Brown allylborane chemistry to control the relative and absolute stereochemistry of the two fragments **47** and **54** prior to aldol reaction. Thus, reaction of aldehyde **44** with (–)-(*Z*)-crotonyldiisopinocampheylborane **8**, derived from (+)-pinene, furnished the corresponding homoallylic alcohol **45**. This established the desired *syn*-relative stereochemistry at C(21) and C(22) (>95% as determined by ^{1}H NMR analysis) with

Scheme 5.



Reagents and Conditions: (a) $PdCl_2(PPh_3)_2$ (cat.), THF, 60°C (75%).

Scheme 6.

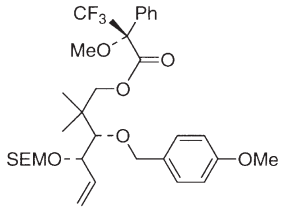


Reagents and Conditions: (a) **8**, THF, Et_2O, -78°C then $NaBO_3{\cdot}4H_2O$, H_2O (72%); (b) TBSOTf, 2,6-lutidine, CH_2Cl_2, (94%); (c) OsO_4 (cat.), NMO, acetone, H_2O then $NaIO_4$, THF, H_2O (88%); (d) **9**, THF, Et_2O, -78°C then $HOCH_2CH_2NH_2$, NaH (cat.) (60%); (e) KHMDS, THF, DMF, *p*-$MeOC_6H_4CH_2Cl$; (f) TBAF, THF (98% over both steps); (g) $(COCl)_2$, DMSO, Et_3N, CH_2Cl_2, -78 to 20°C, (89%); (h) MeMgBr, THF (95%); (i) $(COCl)_2$, DMSO, Et_3N, CH_2Cl_2, -78 to 20°C, (85%).

excellent enantiomeric excess, vide infra. Protection of the resultant alcohol as the *tert*-butyldimethylsilyl ether **46** and conversion of the terminal olefin into the corresponding aldehyde **47** was carried out via osmylation and periodate cleavage (Scheme 6). Addition of the (*Z*)-borane **9** to aldehyde **48** proceeded smoothly to yield the *syn*-diol derivative **49**, again with excellent control of relative (>95%) and absolute (>95%) stereochemistry, as estimated through ^{1}H NMR and Mosher ester **55** analysis (26). With the desired C(16) and C(17) stereochemistry established, transformation of alkene **49** into the methyl ketone **54** was accomplished using

© 2001 NRC Canada

standard methodology. Thus, protection of the newly formed C(17) alcohol gave the *p*-methoxybenzyl ether **50**. Deprotection of the *tert*-butyldimethylsilyl ether using tetrabutylammonium fluoride, oxidation under Swern conditions, methyl Grignard addition, and reoxidation afforded the methyl ketone **54** in excellent overall yield (52% over 6 steps).



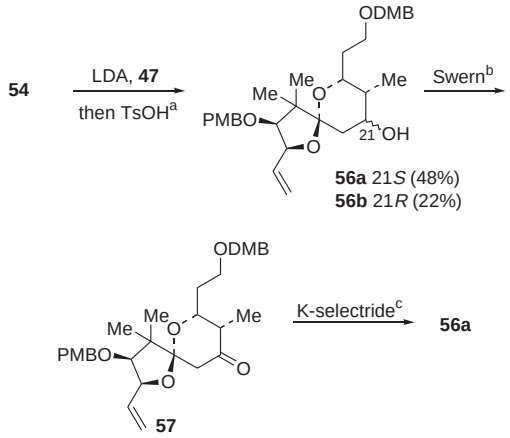
55

Lithium diisopropylamide mediated aldol coupling between ketone **54** and aldehyde **47** and subsequent acidification gave the spiroketal core as a mixture of C(21)-epimeric alcohols **56a** and **56b**. Much to our delight, the initial aldol adduct underwent clean cleavage of the robust SEM protecting group (21), removal of the *tert*-butyldimethylsilyl ether, and spiroketalization in a single operation under mild acidic conditions. The epimeric alcohols **56** could be easily separated and individually authenticated but on a larger scale the mixture was oxidized under Swern conditions to produce the ketone **57**, which was stereoselectively reduced using K-Selectride (27) yielding the desired axial diastereoisomer **56a** (Scheme 7). The final spiroketal **56a** was obtained free from other diastereoisomers (TLC, NMR; after the correction at C(21)). Since the high enantiomeric purity of alcohol **51** was established by ^{1}H NMR spectral analysis of ester **55**, the initial allylboration reaction and chromatographic purification must have given alcohol **45** with high absolute as well as relative stereocontrol.

A second approach towards the spiroketal unit was developed to provide additional material for the total synthesis. Thus, the commercial ester **58**, as employed in the construction of **38** (vide supra), was protected as the benzyloxymethyl ether **59** (21), reduced to the alcohol **60** using lithium aluminum hydride, and oxidized under Swern conditions to give aldehyde **61** (Scheme 8). Wittig homologation and reduction of the resultant α,β-unsaturated ester **62** with DIBAL-H furnished the allylic alcohol **63**. Sharpless asymmetric epoxidation (28) was used to elaborate the epoxy alcohol **64**, thereby controlling the absolute stereochemistry of C(23). Epoxide ring opening, through intramolecular hydride delivery upon treatment with Red-Al, gave diol **65**, which was smoothly converted to the corresponding acetonide **66** under standard conditions. Deprotection of the benzyloxymethyl ether using sodium in ammonia and Swern oxidation of the resultant primary alcohol gave the aldol partner **68** in excellent overall yield (77% over 10 steps, Scheme 8).

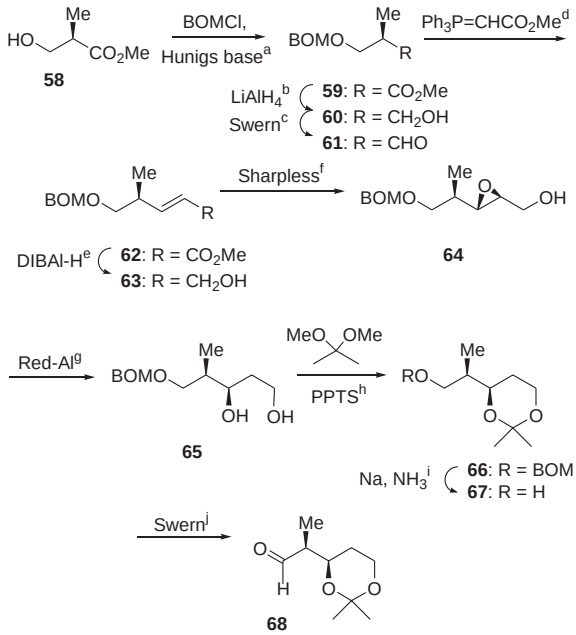
Aldol reaction of ketone **54** and aldehyde **68** gave, after acidification, the spiroketal system **69**, again as an epimeric mixture (Scheme 9). Oxidation gave the keto-aldehyde **70**, which upon reduction using K-Selectride gave diol **71** as a single diastereoisomer. The constitution and relative stereochemistry of spiroketal **71** was established by a single crystal X-ray structure determination (Fig. 1). The structure of

Scheme 7.



Reagents and Conditions: (a) LDA, THF, -78°C; **47**; TsOH, MeOH, 25°C (70%); (b) $(COCl)_2$, DMSO, Et_3N, CH_2Cl_2 (95% from **56a**, 100% from **56b**); (c) KBH^sBu_3, THF, -78°C to -10°C then NaOH, H_2O_2 (93%).

Scheme 8.



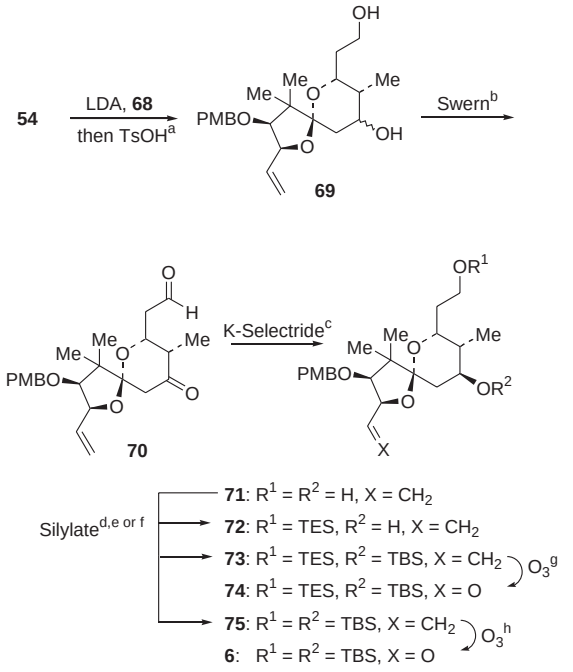
Reagents and Conditions: (a) $PhCH_2OCH_2Cl$, $^iPr_2NEt$, CH_2Cl_2, -78 to -10°C; (b) $LiAlH_4$, Et_2O; (c) $(COCl)_2$, DMSO, Et_3N, CH_2Cl_2; (d) $Ph_3P{=}CHCO_2Me$, $ClCH_2CH_2Cl$ (95% over four steps); (e) DIBAl-H, CH_2Cl_2 (99%); (f) $Ti(O^iPr)_4$, L-(+)-diethyl tartrate, 3Å molecular sieves, ^tBuOOH, CH_2Cl_2, -20°C (90%); (g) $NaAlH_2(OCH_2CH_2OMe)_2$, THF; (h) PPTS, $Me_2C(OMe)_2$, PhH (100% over 2 steps); (i) Na, NH_3, THF (100%); (j) $(COCl)_2$, DMSO, Et_3N, CH_2Cl_2, -78 to -20°C, (93%).

BOM = $PhCH_2OCH_2$

the spiroketal core of **71** is similar to that found for calyculin A (1), but some interesting differences exist. For example, the intra-ring angles at C(19) in **71** are as follows: O(8)-

© 2001 NRC Canada

Scheme 9.



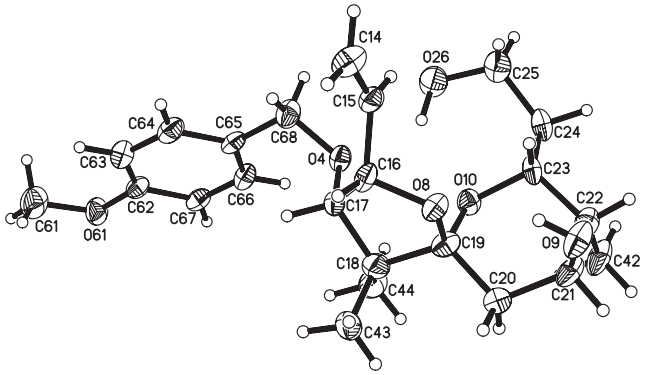
Reagents and Conditions: (a) LDA, THF, -78°C, **68** (96%) then TsOH, MeOH, 25°C (85%); (b) $(COCl)_2$, DMSO, Et_3N, CH_2Cl_2, -78 to -20°C; (c) $KBH^{s}Bu_3$, THF, -78°C to -10°C then NaOH, H_2O_2 (76% over both steps); (d) TESCl, Et_3N, imidazole, CH_2Cl_2, -40°C (78%); (e) TBSOTf, $^{iso}Pr_2NEt$, CH_2Cl_2, -50 to -20 °C (100%); (f) TBSOTf, 2,6-lutidine, CH_2Cl_2, -5°C (90%); (g) O_3, CH_2Cl_2, -78 °C; Me_2S, -78°C to 25 °C (76%); (h) O_3, CH_2Cl_2, -78 °C; Me_2S, -78°C to 25 °C (89%).

C(19)-C(18) = 104.0(5)° (**71**), 108.2° (calyculin A); O(10)-C(19)-C(20) = 110.2(5)° (**71**), 105.6° (calyculin A). The inter-ring angles about C(19) differ less dramatically, if at all: O(8)-C(19)-O(10) = 110.8(5)° (**71**), 109.5° (calyculin A); C(18)-C(19)-C(20) = 116.6(5)° (**71**), 116.4° (calyculin A). Since one would expect that different crystal packing forces might exert maximum effect on the inter-ring angles, the observed differences in the intra-ring angles presumably result from the changes in the substituent pattern in the fused five- and six-membered rings in **71**. Since the spiroketal **71** was derived ultimately from methyl (*R*)-2-methyl-3-hydroxypropanoate, the ORTEP clearly identifies all the stereocenters are of correct absolute stereochemistry. The diol **71** was converted into the three silyl ethers **72**, **73**, and **75** by double triethylsilylation, selective C(25)-OH triethylsilylation followed by C(21)-OH *tert*-butyldimethylsilylation and double *tert*-butyldimethylsilylation respectively. Finally ozonolysis of alkenes **73** and **75** gave the corresponding aldehydes **74** and **6**, respectively, thereby completing the second calyculin building block, the C(15)–C(25) spiroketal unit.

Synthesis of the C(1)–C(25) spiroketal tetraene nitrile

We sought to construct the C(15)–C(25) tetraene nitrile entity of calyculin by aldol addition of the enolate derived from ketone **5** with the spiroketal **6** followed by alteration of

Fig. 1. Thermal ellipsoid plot for spiroketal **71**. Most hydrogen atoms have been omitted for clarify.

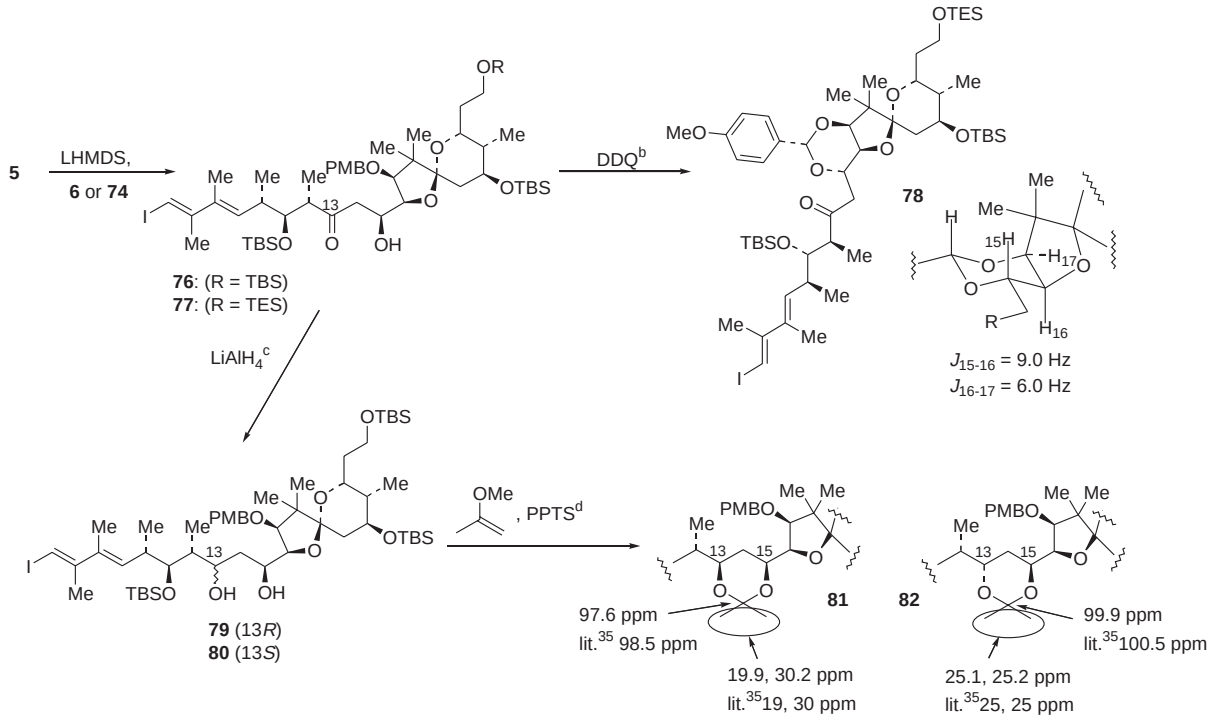


the C(13), C(15)-oxygen substituents and late palladium(0) catalyzed coupling with the dienylstannane **3**. Enolization of the ketone **5** using lithium hexamethyldisilazide and subsequent reaction with the C(1)–C(25) aldehydes **6** and **74** gave the β-hydroxy ketones **76** (76%) and **77** (43%), respectively. In the second unoptimized aldol reaction quantities of the starting ketone **5** (54%) and the aldehyde **74** (35%) were recovered unchanged. Both reactions proceeded with complete diastereoselectivity as judged by ^{1}H NMR spectroscopy of the crude reaction mixture. In the case of β-hydroxy ketone **77** the stereochemistry at C(15) was established by partial DDQ oxidation to produce the corresponding acetal **78** and analysis of the ^{1}H NMR spectrum. Thus, reaction of aldol **77** with DDQ in dichloromethane in the presence of molecular sieves (3 Å) gave the *p*-methoxybenzylidene acetal **78** (29). Analysis of its ^{1}H NMR spectrum (inter alia δ: 5.52 (s, 1H, ArC*H*), 4.04 (dd, 1H, *J* = 9.0, 6.0 Hz, 16-CH), 3.74 (d, 1H, *J* = 6.0 Hz, 17-CH), 2.83 (dd, 1H, *J* = 15.5, 3.0 Hz, 14-CH), 2.60 (dd, 1H, *J* = 15.5, 8.0 Hz, 14-CH)) was consistent with a *trans* disposition of H(15) and H(16) (*J* = 9 Hz) and a *cis* configuration of H(16) and H(17) (*J* = 6 Hz) corresponding to the (15*S*)-stereochemistry, the opposite to that found in (+)-calyculin A. It is not clear, without additional experimentation, as to the exact origin of this high stereochemical bias. Possibly it is the result of the aldol reaction proceeding by a chelation controlled addition pathway (tetrahydrofuran ether as the Lewis basic site) or via a Felkin-type addition pathway. Significant efforts to alter the stereochemical outcome of this key aldol reaction were unsuccessful.

Reduction of the β-hydroxy ketone **76** with lithium aluminum hydride, which presumably took place via ligand exchange at aluminum by the C(15) alcohol and intramolecular hydride delivery, gave a 5:1 mixture of the diols **79** and **80**. The stereochemistries of the two isomers **79** and **80** were determined by formation of the derived acetonides **81** and **82**, respectively, and Rychnovsky (30) analysis of the ^{13}C NMR spectra. The acetonide **81** derived from the major diol **79** showed inter alia ^{13}C NMR δ: 97.6, 30.2, and 19.9 (CMe_2), whereas the isomer **82** showed inter alia ^{13}C NMR δ: 99.9, 25.2, and 25.1 (CMe_2) consistent with the *syn*-acetonide and the *anti*-acetonide structures, respectively. Rychnovsky and co-workers have reported that *syn*-acetonides show the three isopropylidene resonances typically at δ 98.5, 30, and 19,

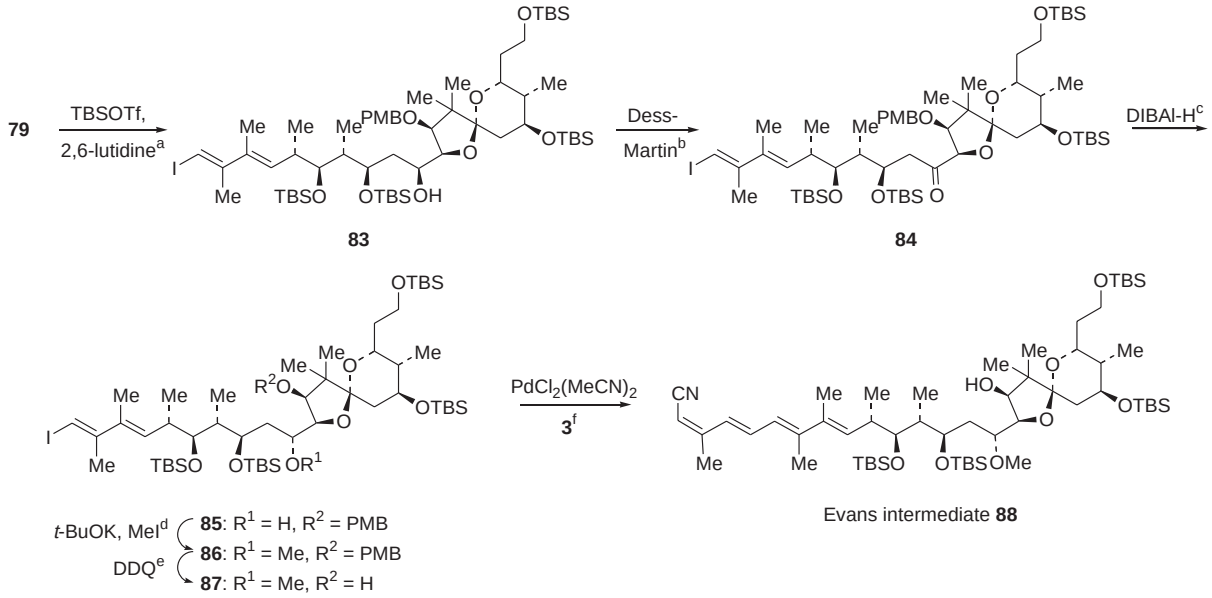
© 2001 NRC Canada

Scheme 10.



Reagents and Conditions: (a) LiHMDS, THF, -78°C then **6** (**76** 76%; **77** 34%); (b) (R = TES) DDQ, 3Å mol. sieves, CH_2Cl_2, -20°C to 0°C (49%); (c) $LiAlH_4$, THF, -78°C (**79** 73%; **80** 15%); (d) $CH_3C(OMe)=CH_2$, PPTS, CH_2Cl_2, 0°C to 25°C (**81** (13*R*) 65%; **82** (13*S*) 77%).

Scheme 11.



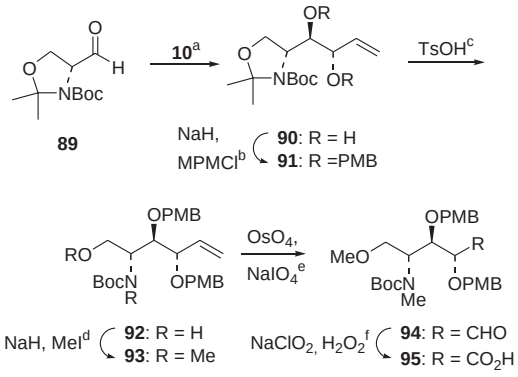
Reagents and Conditions: (a) TBSOTf, 2,6-lutidine, MeCN-CH_2Cl_2 (1:1), -78°C (74%); (b) Dess-Martin periodinane, CH_2Cl_2 (80%); (c) DIBAl-H, CH_2Cl_2, -78°C (97%); (d) *t*-BuOK, MeI, THF, -78°C (87%); (e) DDQ, CH_2Cl_2-pH 7 buffer-*i*-PrOH (5:2:2) (100%); (f) $PdCl_2(MeCN)_2$, NMP, **3**, -5°C to 5°C (91%).

whereas the corresponding signals for *anti*-acetonides are at δ 100.5, 25, and 25 (Scheme 10).

Selective monosilylation of the C(13) alcohol in diol **79** was carried out using *tert*-butyldimethylsilyl triflate in acetonitrile and dichloromethane at –78°C to produce an alcohol most probably the C(15) alcohol **83** (Scheme 11). Subsequent oxidation using the Dess-Martin periodinane (31) gave a product that was assigned as the C(15) ketone

© 2001 NRC Canada

Scheme 12.



Reagents and Conditions: (a) **10**, THF, Et_2O, -78°C then H_2O_2, KF, $KHCO_3$ (reference 30); (b) NaH, DMF, *p*-$MeOC_6H_4CH_2Cl$, (65%); (c) TsOH, MeOH (90%); (d) NaH, MeI, DMF (72%); (e) OsO_4 (cat.), NMO, *t*-BuOH, Me_2CO then $NaIO_4$, MeOH, H_2O; (f) $NaClO_2$, H_2O_2, MeCN, NaH_2PO_4 (65% from **93**).

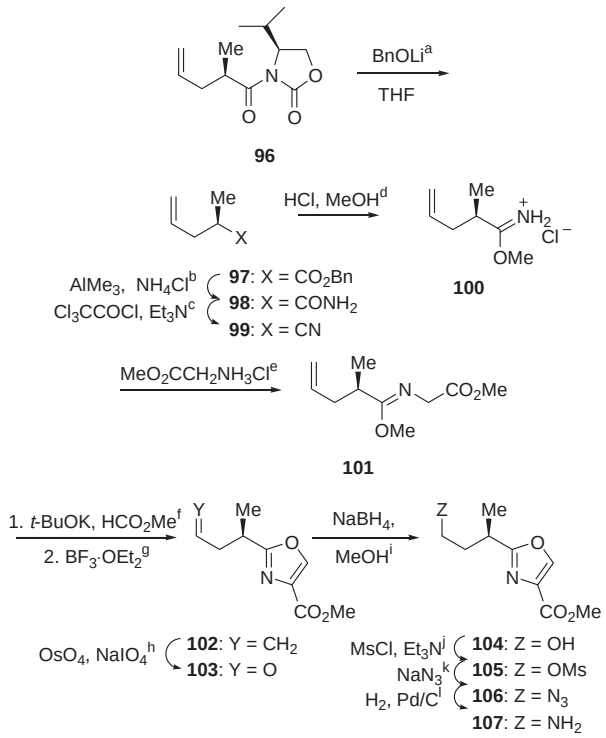
84. Since the NMR spectra of this compound and that of ketone **76** showed myriad resonance differences notwithstanding only the presence of an additional TBS group, the compound was most likely the C(15) ketone **84**. This assignment was consistent with changes in the positions of key peaks in the ^{1}H NMR spectra including the C(9) and (11) methyl peaks, the C(14) methylene and the C(16) and (17) methine peaks [(**76**: 3.64 (d, 1H, *J* = 5.7 Hz, 17-H), 3.20 (d, 1H, *J* = 18 Hz, 14-H), 2.45 (dd, 1H, *J* = 18, 10.3 Hz, 14-H), 1.00 and 0.81 (2d, each 3H, *J* = 7 Hz, 10-Me, 12-Me); **84**: 4.67 (d, 1H, *J* = 5.6 Hz, 16-H), 3.60 (d, 1H, *J* = 5.7 Hz, 17-H), 3.56 (dd, 1H, *J* = 18.5, 8.7 Hz, 14-H), 2.57 (dd, 1H, *J* = 18.5, 2.0 Hz, 14-H), 1.16 and 0.97 (2d, each 3H, *J* = 7 Hz, 10-Me, 12-Me)). As expected on the basis of the stereochemistry of the key aldol reaction to produce **76** and **77**, DIBAL-H reduction of ketone **84** proceeded to produce the (15*R*)-alcohol **85** (Scheme 11). The inversion of C(15) stereochemistry in the oxidation reduction sequence, which may have been the result of a chelation controlled addition pathway (tetrahydrofuran ether as the Lewis basic site) or via a Felkin-type addition pathway, was clearly apparent from comparisons of the ^{1}H NMR and ^{13}C NMR spectra.

Methylation of alcohol **85**, using excess potassium *tert*-butoxide and methyl iodide proceeded smoothly and gave methyl ether **86** in good yield (76%). Subsequent deprotection of the *p*-methoxybenzyl residue at C(17) using DDQ oxidation proceeded in quantitative yield to give the alcohol **87**. Finally, Stille coupling (25) of the dienyl stannane **3** with the dienyl iodide **87** using $PdCl_2(MeCN)_2$ as the catalyst at –5 to 5°C gave the (*Z*,*E*,*E*,*E*)-tetraene nitrile **88** (91%). Stille coupling at higher temperatures resulted in partial isomerization of the delicate tetraene entity. The product C(1)–C(25) (+)-calyculin A intermediate **88** showed data in agreement with that reported by the Evans group in their total synthesis of (+)-calyculin A (**1**) (8).

Synthesis of C(26)–C(37) amide-oxazole unit

We sought to prepare the amide oxazole entity **2** using a convergent strategy with late elaboration of the amide bond linking the C(37)–C(33) γ-amino acid with the C(32)–C(26) aminoalkyl oxazole. Again an allylboration strategy was used to elaborate the C(37)–C(33) γ-amino acid unit **95**. The diol **90** was prepared from the Garner aldehyde **89** (32) and the allylborane derivative **10** (33) with oxidative cleavage of the intermediate C–Si bond (for a review on the oxidation of the carbon–silicon bond, see ref. 34). Dialkylation with 4-methoxybenzyl bromide gave the diether **91** (Scheme 12). Selective hydrolysis of the isopropylidene ketal using 4-toluenesulfonic acid gave alcohol **92**, which was doubly methylated by reaction with methyl iodide and sodium hydride to produce the *O*,*N*-dimethylated ether **93**. Sequential catalytic osmium tetraoxide mediated dihydroxylation and periodate cleavage gave the corresponding aldehyde **94**, which was further oxidized using sodium chlorite and hydrogen peroxide (35) to produce the key carboxylic acid **95**.

Scheme 13.

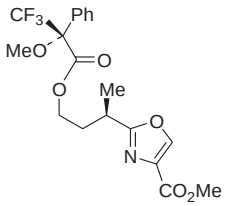


Reagents and Conditions: (a) n-BuLi, $PhCH_2OH$, THF, -20°C (97%); (b) NH_4Cl, $AlMe_3$, PhMe, 60°C (81%); (c) Cl_3CCOCl, Et_3N, CH_2Cl_2, 0°C (78%); (d) HCl, MeOH, -5°C (96%); (e) $MeO_2CCH_2NH_3Cl$, Et_3N, CH_2Cl_2, -10°C to 25°C (69%); (f) *t*-BuOK, HCO_2Me, THF, -10°C to 25°C; (g) $BF_3{\cdot}OEt_2$, THF, -78°C to 25°C (77% over both steps); (h) OsO_4, $NaIO_4$, H_2O, Me_2CO (79%); (i) $NaBH_4$, MeOH, -12°C (93%); (j) Et_3N, $MeSO_2Cl$, Et_2O, -10°C (84%); (k) Me_2SO, NaN_3, 70°C (87%); (l) H_2, Pd/C (cat.), MeOH (98%).

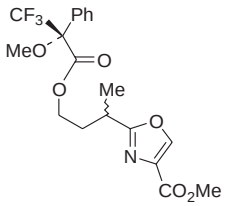
The synthesis of the oxazole unit was accomplished using a modified Cornforth–Meyers approach (Scheme 13) (36). Benzyl ester **97** was readily prepared using Evans alkylation (37) and cleavage of the resultant oxazolidinone **96** using lithium benzyloxide. Ester **97** was converted to the nitrile **99** via Weinreb amide (18) synthesis using trimethylaluminum and ammonium chloride and subsequent dehydration using

© 2001 NRC Canada

trichloroacetyl chloride and triethylamine (Scheme 13). The addition of methanol and hydrogen chloride (36) to nitrile **99** gave the imidate **100** that was allowed to react with glycine methyl ester to produce the *trans*-imidation product **101**. *C*-Formylation, using the Cornforth–Meyers protocol with methyl formate in the presence of potassium *tert*-butoxide, and boron trifluoride diethyl etherate mediated cyclization gave the oxazole **102**. Lewis acid catalysis in this step was found to be superior to the use of acetic acid (15). The alkene **102** was converted into the corresponding aldehyde **103** by osmium tetraoxide mediated dihydroxylation and periodate cleavage. Subsequent reduction with sodium borohydride in methanol proceeded smoothly to produce the alcohol **104**. Gratifyingly, this whole sequence of transformations from oxazolidinone **96** to alcohol **104** proceeded without any significant racemization. Thus, esterification of alcohol **104** with (*R*)-α-methoxy-α-(trifluoromethyl)phenylacetic acid, 4-(*N*,*N*-dimethylamino)pyridine, and 1,3-dicyclohexyl carbodiimide gave the Mosher ester **108**. In parallel, racemic benzyl 2-methyl-4-pentenoate was converted into the racemic modification of the alcohol **104** using exactly the same methods as in Scheme 13 and converted into the ester mixture **109**. Comparison of the ^{1}H NMR spectra for esters **108** and **109** were fully consistent with the diastereoisomic purity of **108** and the enantiomeric purity of alcohol **104**, respectively.



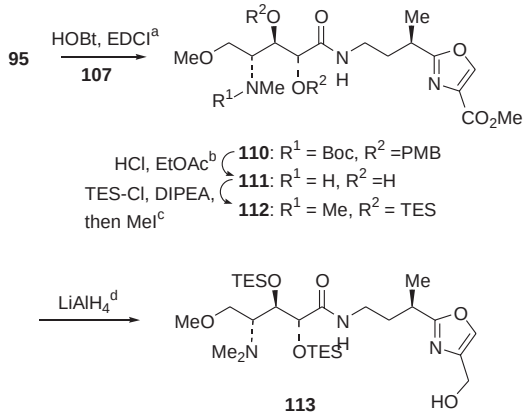
108



109

The alcohol **104** was converted into the corresponding amine **107** via methanesulfonylation, azide displacement, and hydrogenation over palladium on carbon. Initial attempts at coupling the C(26)–C(32)amine **107** with the C(33)–C(37) carboxylic acid **95** employed DCC and 1-hydroxybenzotriazole (HOBT) hydrate as coupling agents, but yields of amide **110** (Scheme 14) were disappointingly low and removal of the side product dicyclohexylurea proved troublesome. However, coupling of **95** with **107** using 1-ethyl-3-(3-dimethylaminopropyl)carbodiimide hydrochloride (EDCI) and dehydrated HOBT in the presence of powdered molecular sieves (4 Å) in DMF proceeded in superior yields and gave the amide **110** (72%). Conversion of ester **110** to the Evans intermediate **112** (8) was achieved via cleavage of the Boc and 4-methoxybenzyl protecting groups upon treatment with a saturated solution of hydrogen chloride in ethyl acetate and direct triethylsilylation and *N*-methylation. These three transformations were most conveniently accomplished in a one-pot procedure. The product C(26)–C(37) amide-oxazole **112** showed data in agreement with that reported by the Evans group in their total synthesis of (+)-calyculin A (1) (8). Finally, lithium aluminum hydride reduction of the ester **112** gave the corresponding alcohol **113**. The product alcohol **113** also showed data in agreement with that reported by the Evans group in their total synthesis of (+)-calyculin A (**1**) (8).

Scheme 14.



Reagents and Conditions: (a)EDCI,1-HOBt, 4Å mol. sieves; **107**, DMF (72%); (b) HCl, EtOAc; (c) MeCN, ^{i}Pr$_2$NEt, TES-Cl; MeI (59% over both steps); (d) Et_2O, $LiAlH_4$, -78°C (62%).

Conclusions

We have demonstrated the synthetic utility of the powerful Brown allylboration methodology for the diastereoselective construction of heavily functionalized homoallylic alcohols and the use of this masked aldol methodology in the succinct preparation of complex natural product arrays. Utilizing this methodology, we have completed the synthesis of the C(1)–C(25) tetraene nitrile **88** and C(26)–C(37) oxazole amide **113** intermediates reported by Evans in his total synthesis of synthesis of (+)-calyculin (**1**). This work therefore constitutes a formal total synthesis of the (+)-antipode of this remarkable natural product.

Experimental

General procedures

All reactions were carried out under a dry argon or nitrogen atmosphere at ambient temperature unless otherwise stated. Low reaction temperatures were recorded as bath temperatures. Chromatography refers to column chromatography using E. Merck or BDH silica gel 60, 230–400 mesh (eluants are given in parenthesis). Analytical thin layer chromatography (TLC) was performed on E. Merck precoated silica gel 60 F_{254} plates. Solvents were purified by distillation. Anhydrous THF, Et_2O, PhH, and PhMe were distilled from sodium benzophenone ketyl. DMF was distilled at reduced pressure from BaO or Al_2O_3 and stored over molecular sieves (4 Å). CH_2Cl_2 was distilled from CaH_2. Et_3N and *i*-Pr_2EtN were distilled from CaH_2 and stored over KOH. All other chemicals were used without further purification unless otherwise stated. Optical rotations were measured in $CHCl_3$ solution.

Ethyl 3-(tributylstannyl)-(2*Z*)-propenoate (12)

$Bu_3SnSnBu_3$ (9.84 g, 17.0 mmol) was dissolved in THF (125 mL), cooled to 0°C and *n*-BuLi in hexanes (1.6 M, 10.6 mL, 0.017 mol) was added to generate a faint yellow solution. After stirring at 0°C for 5 min, the mixture was

© 2001 NRC Canada

cooled to –20°C and PhSCu (2.99 g, 17.3 mmol) added to generate a red-black mixture after stirring at –20°C for 15 min. The mixture was cooled to –78°C and treated with ester **11** (1.46 g, 13.0 mmol) in THF (25 mL). The mixture was stirred at –78°C for 10 min, then allowed to warm to –35°C and stirred between –35°C and –50°C for a further 3.5 h. MeOH (10 mL) and Et_2O (100 mL) were added sequentially and the mixture was allowed to warm to room temperature. The resulting solution was filtered through silica eluting with Et_2O. Chromatography (hexanes) afforded stannane **12** (2.72 g, 52%) and the corresponding *trans* stannyl ester **17** (0.409 g, 7%). The *cis*-isomer **12** was obtained as a colorless oil. TLC R_f = 0.2 (hexanes). EI-MS *m*/*z*: 401, 375, 347 ([M – Bu]$^+$), 319, 233, 205, 137, 57. EI-HRMS calcd. for $C_{14}H_{27}O_2Sn$: 347.1033 ([M – Bu]$^+$); found: 347.1042 ([M – Bu]$^+$). IR (film) (cm^{-1}): 1702, 1601, 1458, 1368, 1316, 1197, 1044, 863. ^{1}H NMR (400 MHz, $CDCl_3$) δ: 6.41 (br s, 1H, $J_{Sn,H}$ = 106 Hz), 4.17 (q, 2H, J = 7.1 Hz), 2.13 (br d, 3H, J = 2 Hz, $J_{Sn,H}$ = 41 Hz), 1.47–0.88 (m, 30H). ^{13}C NMR (68 MHz, $CDCl_3$) δ: 171.4, 167.8, 129.3, 60.0, 29.2 (d, $J_{Sn,C}$ = 18.6 Hz), 27.4 (d, $J_{Sn,C}$ = 29 Hz), 27.3, 14.3, 13.7, 10.9. Anal. calcd. for $C_{18}H_{36}O_2Sn$: C 53.62, H 9.00; found: C 53.54, H 9.22. Stannyl ester **17** was obtained as a colorless oil. TLC R_f = 0.2 (hexanes). EI-MS *m*/*z*: 347 ([M – Bu]$^+$), 291, 235, 179, 113. IR (neat) (cm^{-1}): 1715, 1176. ^{1}H NMR (400 MHz, $CDCl_3$) δ: 5.96 (m, 1H, $J_{Sn,H}$ = 64.4 Hz), 4.16 (q, 2H, J = 7.1 Hz), 2.40 (d, 3H, J = 1.5 Hz), 1.50, 1.30, 0.90 (3m, 30H). ^{13}C NMR (68 MHz, $CDCl_3$) δ: 168.8, 164.3, 128.2, 59.4, 28.9, 27.3, 22.3, 14.3, 13.5, 9.4. Anal. calcd. for $C_{18}H_{36}O_2Sn$: C 53.62, H 9.00; found: C 53.38, H 9.19.

3-(Tributylstannyl)-(2*Z*)-butenamide (13)

$AlMe_3$ in PhMe (2 M, 1.87 mL, 3.74 mmol) was added dropwise with stirring to a suspension of NH_4Cl (200 mg, 3.74 mmol) in PhH (20 mL) at 0°C. The colorless solution was stirred at 0°C for 30 min and at room temperature for 1 h. This mixture was transferred to ester **12** (500 mg, 1.24 mmol) in dry PhH (5 mL) and heated at 50°C for 24 h. The mixture was cooled, carefully quenched with H_2O, diluted with Et_2O, and stirred for 30 min. Buffer (pH 7) and saturated aqueous Na_2SO_4 were added and the mixture was filtered through Celite eluting with EtOAc (125 mL). The filtrate was washed with brine, dried ($MgSO_4$), and chromatographed (hexanes–Et_2O, 1 :1) to give stannane **13** (354 mg, 76%) as a crystalline solid: mp 35°C. TLC R_f = 0.25 (hexanes–Et_2O, 1:1). EI-MS *m*/*z*: 318 ([M – Bu]$^+$), 204, 184, 136, 57. EI-HRMS calcd. for $C_{12}H_{24}NOSn$: 318.0880 ([M – Bu]$^+$); found: 318.0848 ([M – Bu]$^+$). IR (CCl_4) (cm^{-1}): 3495, 3334, 1670, 1593, 1275, 788, 669. ^{1}H NMR (400 MHz, $CDCl_3$) δ: 6.41 (m, 1H, $J_{Sn,H}$ = 107 Hz), 5.50, 5.30 (2 br s, 2H, NH_2), 2.14 (m, 3H, $J_{Sn,H}$ = 40 Hz), 1.45, 1.30, 0.90 (m, 27H). ^{13}C NMR (68 MHz, $CDCl_3$) δ: 169.4, 168.7, 129.3, 29.3 (d, $J_{Sn,C}$ = 10 Hz), 27.4, 26.7, 13.7, 11.5. Anal. calcd. for $C_{16}H_{33}NOSn$: C 51.36, H 8.89, N 3.74; found: C 51.42, H 9.07, N 3.77. A similar reaction of ester **17** with $AlMe_3$ and NH_4Cl gave amide **18** (72%) as low melting solid: mp 38–40°C. TLC R_f = 0.23 (hexanes–Et_2O, 1:1). EI-MS *m*/*z*: 318 ([M – Bu]$^+$), 298, 262, 242, 204, 179, 121. EI-HRMS calcd. for $C_{12}H_{24}NOSn$: 318.0880 ([M – Bu]$^+$); found: 318.0861 ([M – Bu]$^+$). IR (KBr disc) (cm^{-1}): 3403, 3209, 1656, 1596, 1458, 1399, 1315, 876. ^{1}H NMR (400 MHz, $CDCl_3$) δ: 5.93 (m, 1H, $J_{Sn,H}$ = 64.8 Hz), 5.30 (br s, 2H, NH_2), 2.36 (m, 3H, $J_{Sn,H}$ = 44.0 Hz), 1.50, 1.30, 0.90 (3m, 27H). ^{13}C NMR (68 MHz, $CDCl_3$) δ: 167.9, 161.9, 130.7, 28.8, 27.2, 21.9, 13.5, 9.2. Anal. calcd. for $C_{16}H_{33}NOSn$: C 51.36, H 8.89, N 3.74; found: C 51.28, H 8.86, N 3.59.

3-(Tributylstannyl)-(2*Z*)-butenonitrile (14)

Freshly distilled Cl_3CCOCl (2.72 mL, 0.024 mol) in CH_2Cl_2 (10 mL) was added dropwise over 5 min to **13** (7.00 g, 0.019 mol) and Et_3N (5.2 mL, 0.037 mol) in ice cold dry CH_2Cl_2 (60 mL). The resulting yellow suspension was stirred at 0°C for 90 min, added to pH 7 buffer (50 mL), extracted with CH_2Cl_2 (125 mL) and then the extract was dried (Na_2SO_4) and chromatographed (hexanes–Et_2O, 9:1) to give nitrile **14** (6.7 g, 95%) as a faint green oil. TLC R_f = 0.75 (hexanes–Et_2O, 9:1). EI-MS *m*/*z*: 356 (M$^{\cdot+}$), 300 ([M – Bu]$^+$), 244, 186, 159, 121. EI-HRMS calcd. for $C_{12}H_{22}NSn$: 300.0774 ([M – Bu]$^+$); found: 300.0773 ([M – Bu]$^+$). IR (film) (cm^{-1}): 2214, 1458, 1377, 1074, 813. ^{1}H NMR (400 MHz, $CDCl_3$) δ: 5.90 (m, 1H, $J_{Sn,H}$ = 94.4 Hz), 2.12 (br d, 3H, J = 1.8 Hz, $J_{Sn,H}$ = 34.5 Hz), 1.52 (m, 6H), 1.32 (m, 6H), 1.12 (m, 6H), 0.9 (m, 9H). ^{13}C NMR (68 MHz, $CDCl_3$) δ: 176.3, 118.8, 109.2, 28.9, 28.4, 27.3, 13.7, 10.0. Anal. calcd. for $C_{16}H_{31}NSn$: C 53.96, H 8.78, N 3.93; found: C 53.57, H 8.75, N 3.69. A similar dehydration of amide **18** using Cl_3CCOCl and Et_3N gave nitrile **19** (95%) as a colorless oil. TLC R_f = 0.9 (hexanes–Et_2O, 9: 1). EI-MS *m*/*z*: 357 (M$^{\cdot+}$), 300 ([M – Bu]$^+$), 244, 188, 159, 121. EI-HRMS calcd. for $C_{12}H_{22}NSn$: 300.0774 ([M – Bu]$^+$); found: 300.0783 ([M – Bu]$^+$). IR (film) (cm^{-1}): 2209, 1459, 1376, 1074, 995, 875, 810, 669. ^{1}H NMR (270 MHz, $CDCl_3$) δ: 5.43 (m, 1H, $J_{Sn,H}$ = 47.7 Hz), 2.27 (m, 3H, $J_{Sn,H}$ = 35.8 Hz), 1.50, 1.30, 0.94 (3m, 27H). ^{13}C NMR (68 MHz, $CDCl_3$) δ: 175.4, 115.0, 106.9, 28.8, 27.2, 24.8, 13.5, 9.6. Anal. calcd. for $C_{16}H_{31}NSn$: C 53.96, H 8.78, N 3.93; found: C 53.79, H 8.77, N 3.77.

3-Iodo-(2*Z*)-butenonitrile (15)

N-Iodosuccinimide (683 mg, 3.04 mmol) was added to nitrile **14** (1.0 g, 2.81 mmol) in THF (10 mL). After 12 h, more *N*-iodosuccinimide (340 mg, 1.51 mmol) (total 1.6 equiv.) was added and the stirring maintained a further 8 h. Silica was added, the mixture was rotary evaporated, and chromatographed (hexanes–Et_2O, 4:1) to give nitrile **15** (353 mg, 65%) as low melting colorless hexagonal crystals. TLC R_f = 0.20 (hexanes–Et_2O, 9:1). EI-MS *m*/*z*: 193 (M$^{\cdot+}$), 165, 149, 129, 109, 95. EI-HRMS calcd. for C_4H_4IN: 192.9389 (M$^{\cdot+}$); found: 192.9395 (M$^{\cdot+}$). IR (film) (cm^{-1}): 2224, 1613, 1376, 1272, 1101, 796 cm^{-1}. ^{1}H NMR (400 MHz, $CDCl_3$) δ: 6.13 (m, 1H), 2.69 (d, 3H, J = 1.6 Hz). ^{13}C NMR (101 MHz, $CDCl_3$) δ: 122.6, 118.1, 110.2, 34.6.

3-Methyl-5-(tributylstannyl)-(2*Z*,4*E*)-pentadienenitrile (3)

$PdCl_2(PPh_3)_2$ (143 mg, 0.2 mmol) and stannane **16** (2.0 g, 3.3 mmol, 1.8 equiv.) in THF (4 mL) were added sequentially to nitrile **15** (353 mg, 1.82 mmol) in THF (9 mL). The resulting yellow mixture was stirred for 14 h producing a dull red solution. After a further 2 h at reflux, silica was added, the mixture rotary evaporated, and chromatographed to give nitrile **3** (382 mg, 55%) as a colorless oil. TLC R_f =

© 2001 NRC Canada

0.8 (hexanes–Et_2O, 9:1). EI-MS *m/z*: 361, 326 ([M – Bu]$^+$), 300, 270, 212, 177, 121, 94. EI-HRMS calcd. for $C_{14}H_{24}NSn$: 326.0931 ([M – Bu]$^+$); found: 326.0933 ([M – Bu]$^+$). IR (film) (cm^{-1}): 2213, 1459, 1377, 1342, 1073, 984, 874, 809. ^{1}H NMR (270 MHz, $CDCl_3$) δ: 7.14 (d, 1H, *J* = 19 Hz), 6.87 (d, 1H, *J* = 19 Hz), 5.18 (q, 1H, *J* = 0.7 Hz), 1.99 (d, 3H, *J* = 1.5 Hz), 1.50, 1.32, 0.90 (3m, 27H). ^{13}C NMR (68 MHz, $CDCl_3$) δ: 156.0, 142.8, 142.3, 109.1, 95.5, 29.0, 27.2, 13.6, 9.7. Stannane **3** was further authenticated by conversion into the corresponding dienyl iodide **21**. I_2 (50 mg, 0.2 mmol) was added to stannane **3** (68 mg, 0.18 mmol) in Et_2O (3 mL) at 0°C. After 17 h, KF (70 mg), sodium thiosulfate (100 mg), MeOH (2 drops), H_2O (2 drops), and Et_2O (5 mL) were added and the mixture stirred vigorously until colorless. The mixture was filtered through Celite–$MgSO_4$–sand, rotary evaporated, and chromatographed (hexanes–Et_2O, 4:1) to give iodide **21** (27mg, 70%) as a colorless low melting crystalline solid. TLC R_f = 0.3 (hexanes–Et_2O, 9:1). EI-MS *m/z*: 219 (M$^{\cdot+}$), 127, 92. EI-HRMS calcd. for C_6H_6IN: 218.9545 (M$^{\cdot+}$); found: 218.9547 (M$^{\cdot+}$). IR (KBr disc) (cm^{-1}): 2215, 1599, 1557, 946, 809, 724. ^{1}H NMR (300 MHz, $CDCl_3$) δ: 7.67 (d, 1H, *J* = 14.7 Hz), 7.07 (d, 1H, *J* = 14.7 Hz), 5.15 (br s, 1H), 2.01 (br s, 3H). ^{13}C NMR (101 MHz, $CDCl_3$) δ: 155.2, 142.3, 116.2, 97.2, 88.7, 18.9. Anal. calcd. for C_6H_6IN: C 32.90, H 2.76, N 6.40; found: C 32.85, H 2.83, N 6.01. A similar iododestannylation of nitrile **19** (286 mg) and $PdCl_2(PPh_3)_2$ catalyzed coupling of the resultant iodide **20** with stannane **16** gave nitrile **22** (39% overall) as a colorless oil. TLC R_f = 0.8 (hexanes–Et_2O, 9:1). EI-MS *m/z*: 352, 326 ([M – Bu]$^+$), 300, 270, 244, 214. EI-HRMS calcd. for $C_{14}H_{24}NSn$: 326.0931 ([M – Bu]$^+$); found: 326.0931 ([M – Bu]$^+$). IR (film) (cm^{-1}): 2211, 1458, 985, 600. ^{1}H NMR (400 MHz, $CDCl_3$) δ: 6.80 (d, 1H, *J* = 19.4 Hz), 6.58 (d, 1H, *J* = 19.4 Hz), 5.17 (br s, 1H), 2.13 (br s, 3H), 1.5, 1.3, 0.8 (3m, 27H). ^{13}C NMR (101 MHz, $CDCl_3$) δ: 157.3, 145.5, 141.4, 117.9, 97.3, 29.0, 27.2, 16.0, 13.7, 9.6. Stannane **22** was further authenticated by iododestannylation giving nitrile **23** (65%) as a colorless oil. TLC R_f = 0.3 (hexanes–Et_2O, 9:1). EI-MS *m/z*: 219 (M$^{\cdot+}$), 127. EI-HRMS calcd. for C_6H_6IN: 218.9545 (M$^{\cdot+}$); found: 218.9553 (M$^{\cdot+}$). IR (KBr disc) (cm^{-1}): 2213, 1594, 1559, 1439, 947, 831, 763, 726. ^{1}H NMR (400 MHz, $CDCl_3$) δ: 7.15 (d, 1H, *J* = 14.8 Hz), 6.99 (d, 1H, *J* = 14.8 Hz), 5.23 (br s, 1H), 2.14 (br s, 3H). ^{13}C NMR (101 MHz, $CDCl_3$) δ: 155.7, 145.0, 116.7, 98.9, 86.9, 16.2. Anal. calcd. for C_6H_6IN: C 32.90, H. 2.76, N 6.40; found: C 32.65, H 2.75, N 6.34.

Methyl (2*S*)-2-methyl-3-(triethylsilyl)oxypropanoate (25)

Et_3SiCl (40 mL, 0.238 mol) followed by **24** (24.0 g, 0.203 mol) and DMAP (10 mg) were added to ice cooled imidazole (33.3 g, 0.489 mol) in CH_2Cl_2 (100 mL). After 3 h at 0°C and 1 h at room temperature, the mixture was poured into pH 7 buffer and extracted with CH_2Cl_2, washed with pH 7 buffer, and the aqueous phase re-extracted with Et_2O. The combined organic phases were dried ($MgSO_4$) and filtered through alumina. The filtrate was rotary evaporated and the residue distilled (135°C) to afford ester **25** (49.5 g, 90%) as a colorless oil: bp 90°C (15–16 mm Hg). TLC R_f = 0.9 (hexanes–Et_2O, 9:1). $[\alpha]_D^{23}$ = +17.5° (*c* = 13.65). EI-MS *m/z*: 203 ([M – Et]$^+$), 119, 117. IR (film) (cm^{-1}): 1744, 1241, 1199, 1177, 1094. ^{1}H NMR (270 MHz, $CDCl_3$) δ: 3.77 (dd, 1H, *J* = 9.4, 6.9 Hz), 3.66 (s, 3H), 3.62 (dd, 1H, *J* = 9.9, 6.2 Hz), 2.63 (m, 1H), 1.12 (d, 3H, *J* = 7.0 Hz), 0.92 (m, 9H), 0.55 (m, 6H). ^{13}C NMR (101 MHz, $CDCl_3$) δ: 175.5, 64.9, 51.5, 42.5, 13.5, 6.6, 4.3. Anal. calcd. for $C_{11}H_{24}O_3Si$: C 56.85, H 10.41; found: C 56.97, H 10.57.

(2*S*)-2-Methyl-3-(triethylsilyl)oxypropanal (26)

DIBAl-H in hexanes (1.24 M, 50 mL, 0.062 mol) was added to ester **25** (14.4 g, 0.062 mol) in hexane (100 mL) at –70°C so as to maintain an internal temperature of –70°C. After 2 h at –70°C, MeOH (6 mL) was added and the cold mixture added to Na_2SO_4 (60 g) in H_2O (300 mL) and Et_2O (500 mL). After 1 h standing, the mixture was filtered through Celite and the organic phase was separated, washed with brine, dried ($MgSO_4$), and rotary evaporated. The resulting oil was dried under vacuum (65°C at 4 mm Hg) to afford aldehyde **26** (11.16 g, 89%) as a colorless oil: bp 145°C (20 mm Hg). TLC R_f = 0.43 (hexanes–Et_2O, 9:1). $[\alpha]_D^{23}$ = +31.4° (*c* = 9.65). IR (film) (cm^{-1}): 2726. ^{1}H NMR (400 MHz, $CDCl_3$) δ: 9.74 (s, 1H), 3.83, (m, 2H), 2.55 (m, 1H), 1.09 (d, 3H, *J* = 7.0 Hz), 0.95 (m, 9H), 0.56 (m, 6H). ^{13}C NMR (101 MHz, $CDCl_3$) δ: 204.6, 63.2, 48.8, 10.2, 6.6, 4.2. This crude product was used directly without further purification.

(2*S*,3*R*,4*R*)-2,4-Dimethyl-1-(triethylsilyl)oxy-5-hexen-3-ol (27)

trans-2-Butene (5 mL) was added to *t*-BuOK in THF (1 M, 7.3 mL, 7.3 mmol) at –78°C. *n*-BuLi in hexanes (1.58 M, 4.62 mL, 7.3 mmol) was added dropwise at –78°C and the deep yellow solution stirred at –50°C for 10 min. The solution was recooled to –78°C and (+)-*B*-methoxydiisopinocampheylborane (2.77 g, 8.77 mmol) in Et_2O (8 mL) was added dropwise. After 30 min, $BF_3{\cdot}OEt_2$ (1.2 mL, 9.76 mmol) followed by aldehyde **26** (1.1 g, 5.44 mmol) in Et_2O (8 mL) were added dropwise. The mixture was stirred for 3 h at –78°C, then saturated aqueous sodium perborate (10 mL) was added and the mixture allowed to warm up to room temperature. Additional saturated aqueous sodium perborate (20 mL) was added, the mixture stirred for 12 h, and subsequently extracted with Et_2O (3 × 70 mL). The organic phase was washed with brine, dried (Na_2SO_4), and rotary evaporated to give alcohol **27** (1.064 g, 76%) as a colorless oil: bp 105°C (1 mm Hg). TLC R_f = 0.3 (hexanes–Et_2O, 9:1). $[\alpha]_D^{23}$ = +20.7° (*c* = 5.2). EI-MS *m/z*: 259 (M$^{\cdot+}$), 229 ([M – Et]$^+$), 203, 187, 173. EI-HRMS calcd. for $C_{12}H_{25}O_2Si$: 229.1624 ([M – Et]$^+$); found: 229.1622 ([M – Et]$^+$). IR (film) (cm^{-1}): 3495, 1077, 1006, 788, 744, 730. ^{1}H NMR (270 MHz, $CDCl_3$) δ: 5.90 (m, 1H), 5.05 (m, 2H), 3.98 (dd, 1H, *J* = 2.6, 0.7 Hz), 3.72 (m, 1H), 3.60 (m, 1H), 3.40 (m, 1H), 2.35 (m, 1H), 1.80 (m, 1H), 1.10 (d, 3H, *J* = 6.9 Hz), 0.96 (t, 9H, *J* = 7.6 Hz), 0.81 (d, 3H, *J* = 7.0 Hz), 0.61 (q, 6H, *J* = 7.6 Hz). ^{13}C NMR (101 MHz, $CDCl_3$) δ: 139.6, 114.6, 80.3, 68.5, 41.5, 38.0, 17.9, 13.0, 6.9, 4.3. Anal. calcd. for $C_{14}H_{30}O_2Si$: C 65.05, H 11.70; found: C 64.70, H 11.75.

(2*S*,3*R*,4*R*)-2,4-Dimethyl-3-((*tert*-butyldimethylsilyl)oxy)-5-hexen-1-ol (28)

2,6-Lutidine (200 μL, 1.74 mmol) followed by *t*-

© 2001 NRC Canada

$BuMe_2SiOTf$ (295 μL, 1.28 mmol) were added dropwise to alcohol **27** (0.30 g, 1.16 mmol) in THF (5 mL) at –78°C. After stirring for 10 min at –78°C, AcOH (5 mL) and H_2O (1 mL) were added and the mixture allowed to warm to room temperature. After a further 3 h stirring, Et_2O (40 mL) and saturated aqueous $NaHCO_3$ were added in sequence to neutrality and the mixture was extracted with Et_2O. The organic phase was dried ($MgSO_4$), rotary evaporated, and chromatographed (hexanes–Et_2O, 9:1 to 4:1) to give ether **28** (252 mg, 84%) as a colorless oil. TLC R_f = 0.2 (hexanes–Et_2O, 4:1). $[\alpha]_D^{23}$ –5.30° (*c* = 6.3). EI-MS *m*/*z*: 204, 202, 201, 200, 199, 159. EI-HRMS calcd. for $C_{10}H_{21}O_2Si$: 201.1337 ($[M - Bu]^+$); found: 201.1322 ($[M - Bu]^+$). IR (film) (cm^{-1}): 3338, 1473, 1256, 1036, 836, 774, 669. ^1H NMR (400 MHz, $CDCl_3$) δ: 5.80 (m, 1H), 5.02 (m, 2H), 3.60 (m, 2H), 2.48 (m, 1H), 2.42 (m, 1H), 1.82 (m, 1H), 1.06 (d, 3H, *J* = 7.0 Hz), 0.94 (d, 3H, *J* = 7.0 Hz), 0.91 (s, 9H), 0.10 (s, 3H), 0.00 (s, 3H). ^{13}C NMR (101 MHz, $CDCl_3$) δ: 140.9, 114.6, 80.7, 66.0, 43.2, 37.5, 26.0, 25.7, 18.2, 18.0, 16.02, 15.96, –3.6, –4.0. Anal. calcd. for $C_{14}H_{30}O_2Si$: C 65.05, H 11.70; found: C 64.04, H 11.76.

(2*R*,3*R*,4*R*)-2,4-Dimethyl-3-(*tert*-butyldimethylsilyl)oxy-5-hexenal (29)

DMSO (0.413 mL, 5.8 mmol) in CH_2Cl_2 (2 mL) was added dropwise with stirring over 10 min to $(COCl)_2$ (0.413 mL, 4.34 mol) in CH_2Cl_2 (6 mL) at –78°C. After 25 min, alcohol **28** (0.9 g, 3.49 mmol) in CH_2Cl_2 (2 mL) was added dropwise. The mixture was stirred at –78°C for 45 min, then Et_3N (2.74 mL, 19.95 mmol) was added dropwise and stirring continued at –78°C for 45 min. The solution was allowed to warm to room temperature and pH 7 buffer (6 mL) and Et_2O (25 mL) were added. The ethereal layer was washed with brine and dried ($MgSO_4$). Chromatography (hexanes–Et_2O, 4:1) afforded aldehyde **29** (695 mg, 78%) as a colorless oil. TLC R_f = 0.3 (hexanes–Et_2O, 9:1). $[\alpha]_D^{23}$ = – 49.8° (*c* = 7.6). EI-MS *m*/*z*: 257 ($[M + H]^+$), 199 ($[M - Bu]^+$), 173, 143, 129. EI-HRMS calcd. for $C_{10}H_{19}O_2Si$: 199.1154 ($[M - Bu]^+$); found: 199.1158 ($[M - Bu]^+$). IR (film) (cm^{-1}): 1725, 1256, 1040, 1006, 915, 837, 775, 670. ^1H NMR (400 MHz, $CDCl_3$) δ: 9.78 (d, 1H, *J* = 2.7 Hz), 5.80 (m, 1H), 5.02, (m, 2H), 3.80 (t, 1H, *J* = 4.4 Hz), 2.56 (m, 1H), 2.42 (m, 1H), 1.07 (d, 3H, *J* = 7.1 Hz), 1.05 (d, 3H, *J* = 7.0 Hz), 0.90 (s, 9H), 0.08 (s, 3H), 0.05 (s, 3H). ^{13}C NMR (68 MHz, $CDCl_3$) δ: 204.7, 139.9, 115.3, 78.0, 49.9, 43.2, 25.9, 16.2, 16.1, 12.1, –4.1, – 4.4. Anal. calcd. for $C_{14}H_{28}O_2Si$: C 65.57, H 11.00; found: C 65.31, H 10.99.

Ethyl (4*S*,5*R*,6*R*)-2,4,6-trimethyl-5-(*tert*-butyldimethylsilyl)oxy-(2*E*,7)-octadienoate (30)

$Ph_3P{=}C(Me)CO_2Et$ (3.77 g, 10.40 mmol) in THF (10 mL) was added to aldehyde **29** (1.325 g, 5.176 mmol) in THF (10 mL). The resulting yellow mixture was heated 75°C for 3 days and cooled to room temperature, whereupon unreacted ylide precipitated. This was dissolved in $CHCl_3$ and then silica gel was added. Rotary evaporation and chromatography (hexanes–Et_2O, 9:1) gave ester **30** (1.772 g, 96%) as a colorless oil. TLC R_f 0.3 (hexanes–Et_2O, 9:1). $[\alpha]_D^{23}$ = –35.4° (*c* = 2.75). EI-MS *m*/*z*: 325 ($[M - Me]^+$), 285, 283 ($[M - Bu]^+$), 199, 171, 143, 125. EI-HRMS calcd. for $C_{18}H_{31}O_3Si$: 325.2110 ($[M - Me]^+$); found: 325.2222 ($[M - Me]^+$). IR (neat) (cm^{-1}): 1712, 1648, 1463, 1366, 1256, 1097, 1038, 862, 837, 774, 772. ^1H NMR (300 MHz, $CDCl_3$) δ: 6.82 (br d, 1H, *J* = 10.2 Hz), 5.85 (m, 1H), 5.00 (m, 2H), 4.17 (m, 2H), 3.51 (t, 1H, *J* = 4.9 Hz), 2.65 (m, 1H), 2.35 (m, 1H), 1.81 (d, 3H, *J* = 1.5 Hz), 1.28 (t, 3H, *J* = 7.1 Hz), 0.98 (d, 3H, *J* = 6.9 Hz), 0.96 (d, 3H, *J* = 6.4 Hz), 0.89 (s, 9H), 0.05 (s, 3H), 0.03 (s, 3H). ^{13}C NMR (75 Hz, $CDCl_3$) δ: 168.4, 145.4, 140.9, 126.4, 114.4, 79.6, 60.3, 43.0, 37.2, 26.1, 18.3, 17.7, 16.5, 14.3, 12.5, –3.7, – 4.0. Anal. calcd. for $C_{19}H_{36}O_3Si$: C 67.00, H 10.66; found: C 66.81, H 10.78.

(4*S*,5*R*,6*R*)-2,4,6-Trimethyl-5-(*tert*-butyldimethylsilyl)oxy-(2*E*,7)-octadien-1-ol (31)

DIBAl-H in hexanes (1 M, 13.0 mL, 0.013 mol) was added over 5 min to the ester **30** (2.0 g, 5.88 mmol) in CH_2Cl_2 (100 mL) at –78°C. After 1 h, the mixture was allowed to warm to –20°C over 1 h, recooled to –78°C and MeOH (1 mL) and saturated aqueous Na_2SO_4 (30 mL) were added sequentially. After allowing to warm to room temperature, the CH_2Cl_2 layer was removed by decantation. The remaining crystalline residue was washed with CH_2Cl_2 (100 mL) and the combined CH_2Cl_2 extracts washed with brine, dried ($MgSO_4$), and rotary evaporated. Chromatography (hexanes–Et_2O, 4:1 to 1:1) gave alcohol **31** (1.553 g, 86%) as a colorless oil. TLC R_f = 0.25 (hexanes–Et_2O, 4:1). $[\alpha]_D^{23}$ = –7.57° (*c* = 2.8). EI-MS *m*/*z*: 243 ($[M - C_4H_7]^+$), 225, 199, 159, 115. EI-HRMS calcd. for $C_{13}H_{27}O_2Si$: 243.1780 ($[M - C_4H_7]^+$), 225.1675 ($[M - C_4H_9O]^+$); found: 243.1786 ($[M - C_4H_7]^+$), 225.1671 ($[M - C_4H_9O]^+$). IR (film) (cm^{-1}): 3309, 1254, 1039, 836, 773. ^1H NMR (400 MHz, $CDCl_3$) δ: 5.85 (m, 1H), 5.43 (d, 1H, *J* = 9.8 Hz), 4.99 (dd, 1H, *J* = 6.9, 1.0 Hz), 4.96 (s, 1H), 4.00 (br s, 2H), 3.43 (t, 1H, *J* = 4.4 Hz), 2.55 (m, 1H), 2.34 (m, 1H), 1.64 (s, 3H), 0.97 (d, 3H, *J* = 6.9 Hz), 0.91 (d, 3H, *J* = 7.0 Hz), 0.89 (s, 9H), 0.04 (s, 3H), 0.03 (s, 3H). ^{13}C NMR (101 MHz, $CDCl_3$) δ: 141.6, 133.2, 129.7, 113.9, 79.7, 69.3, 42.7, 36.2, 26.1, 18.5, 18.4, 17.2, 13.9, –3.76, –3.82. Anal. calcd. for $C_{17}H_{34}O_2Si$: C 68.39, H 11.48; found: C 68.48, H 11.61.

(4*S*,5*R*,6*R*)-2,4,6-Trimethyl-5-(*tert*-butyldimethylsilyl)oxy-(2*E*,7)-octadienal (32)

Activated MnO_2 (8.5 g, 97.8 mmol) was added to allylic alcohol **31** (1.50 g, 5.03 mmol) in CH_2Cl_2 (50 mL), the black mixture was stirred for 16 h and filtered through Celite eluting with CH_2Cl_2. Rotary evaporation and chromatography (hexanes–Et_2O, 9:1) gave aldehyde **32** (1.255 g, 81%) as a colorless oil. TLC R_f = 0.9 (hexanes–Et_2O, 9:1). $[\alpha]_D^{22}$ = –9.7° (*c* = 5.35). EI-MS *m*/*z*: 281 ($[M - Me]^+$), 241, 199, 155, 115. EI-HRMS calcd. for $C_{16}H_{29}O_2Si$: 281.1937 ($[M - Me]^+$); found: 281.1932 ($[M - Me]^+$). IR (film) (cm^{-1}): 1690, 1641, 1462, 1377, 1255, 1099, 1034, 837, 774, 679. ^1H NMR (400 MHz, $CDCl_3$) δ: 9.40 (s, 1H), 6.63 (dd, 1H, *J* = 10.0, 1.3 Hz), 5.81 (m, 1H), 5.03 (br s, 1H), 5.00 (br d, 1H, *J* = 8.8 Hz), 3.60 (t, 1H, *J* = 4.1 Hz), 2.85 (m, 1H), 2.32 (m, 1H), 1.72 (d, 3H, *J* = 1.3 Hz), 1.03 (d, 3H, *J* = 7.0 Hz), 0.95 (d, 3H, *J* = 7.0 Hz), 0.91 (s, 9H), 0.08 (s, 3H), 0.05 (s, 3H). ^{13}C NMR (101 MHz, $CDCl_3$) δ: 195.8, 157.8, 140.6, 137.6, 114.8, 79.2, 43.5, 36.9, 26.0, 18.3, 18.1, 15.7, 9.3, –3.7, –3.9.

© 2001 NRC Canada

(5*S*,6*R*,7*R*)-1,1-Dibromo-3,5,7-trimethyl-6-(*tert*-butyldimethylsilyl)oxy-(1,3*E*,8)-nonatriene (33)

CBr_4 (3.36 g, 0.01 mol) was added in one portion to PPh_3 (5.30 g, 0.020 mol) in CH_2Cl_2 (20 mL) at 0°C. The mixture was stirred 5 min, then aldehyde **32** (1.20 g, 4.05 mmol) in CH_2Cl_2 (10 mL) was added. After stirring for 5 min, the mixture was filtered through silica eluting with hexanes and rotary evaporated at low temperature. Chromatography (hexanes) gave dibromide **33** (1.648 g, 89%) as an unstable colorless oil. TLC R_f = 0.9 (hexanes). $[\alpha]_D^{22}$ = –7.1° (*c* = 2.85). EI-MS *m*/*z*: 452 ($M^{\cdot+}$), 395, 253, 199, 172, 143, 115. EI-HRMS calcd. for $C_{18}H_{32}Br_2OSi$: 452.0569 ($M^{\cdot+}$), 394.9864 ($[M - Bu]^+$); found: 452.0548 ($M^{\cdot+}$), 394.9929 ($[M - Bu]^+$). IR (CCl_4) (cm^{-1}): 1640, 1255, 1037, 837, 788. ^1H NMR (400 MHz, $CDCl_3$) δ: 6.93 (s, 1H), 5.82 (m, 1H), 5.72 (d, 1H, *J* = 9.9 Hz), 5.00 (d, 1H, *J* = 3.2 Hz), 4.97 (s, 1H), 3.46 (t, 1H, *J* = 4.1 Hz), 2.60 (m, 1H), 2.32 (m, 1H), 1.85 (s, 3H), 0.95 (d, 3H, *J* = 7.0 Hz), 0.94 (d, 3H, *J* = 7.0 Hz), 0.91 (s, 9H), 0.05 (s, 3H), 0.03 (s, 3H). ^{13}C NMR (101 MHz, $CDCl_3$) δ: 141.4, 141.2, 139.0, 130.0, 114.2, 85.3, 79.5, 43.1, 36.4, 26.1, 18.3, 18.2, 16.6, 15.4, –3.7, –3.8.

(5*S*,6*R*,7*R*)-3,5,7-trimethyl-6-(*tert*-butyldimethylsilyl)oxy-(3*E*,8)-nonadien-1-yne (34)

n-BuLi in hexanes (2.28 M, 5.0 mL, 11.4 mmol) was added dropwise to dibromide **33** (2.36 g, 5.22 mmol) in THF (25 mL) at –78°C generating a yellow solution. After 1 h, the mixture was allowed to warm to room temperature and stirred for 1 h. Water (1 mL) was added, the mixture rotary evaporated, and Et_2O was added. The organic phase was washed with brine, dried ($MgSO_4$), and chromatographed (hexanes–Et_2O, 49:1) to give alkyne **34** (1.23 mg, 80%) as a colorless oil. TLC R_f = 0.8 (hexanes). $[\alpha]_D^{22}$ = –48.4° (*c* = 3.7). EI-MS *m*/*z*: 292 ($M^{\cdot+}$), 277, 237, 199, 179, 161, 115. EI-HRMS calcd. for $C_{18}H_{32}OSi$: 292.2222 ($M^{\cdot+}$); found: 292.2238 ($M^{\cdot+}$). IR (film) (cm^{-1}): 3315, 2097, 1463, 1256, 1102, 1037, 1032, 880, 836, 774, 636, 609, 606. ^1H NMR (400 MHz, $CDCl_3$) δ: 5.95 (dd, 1H, *J* = 9.1, 1.2 Hz), 5.84 (m, 1H), 5.00 (m, 2H), 3.43 (t, 1H, *J* = 4.5 Hz), 2.76 (s, 1H), 2.61 (m, 1H), 2.35 (m, 1H), 1.78 (d, 3H, *J* = 1.4 Hz), 0.98 (d, 3H, *J* = 6.9 Hz), 0.92 (d, 3H, *J* = 6.9 Hz), 0.91 (s, 9H), 0.06 (s, 3H), 0.05 (s, 3H). ^{13}C NMR (101 MHz, $CDCl_3$) δ: 143.1, 141.1, 115.5, 114.3, 87.2, 79.4, 73.5, 42.8, 37.0, 26.1, 18.3, 17.9, 17.2, 16.8, –3.78, –3.82.

(5*S*,6*R*,7*R*)-1-Iodo-2,3,5,7-tetramethyl-6-(*tert*-butyldimethylsilyl)oxy-(1*E*,3*E*,8)-nonatriene (35)

$AlMe_3$ in PhMe (2 M, 1.92 mL, 3.84 mmol) was added dropwise to Cp_2ZrCl_2 (560 mg, 1.916 mmol) in CH_2Cl_2 (8 mL) and, after 10 min, alkyne **34** (510 mg, 1.75 mmol) in CH_2Cl_2 (6 mL) was added. After 16 h, I_2 (530 mg, 2.088 mmol) in THF (10 mL) was added and, after a further 30 min stirring, the solution was cooled to 0°C and carefully treated with H_2O (3 mL). The solution was filtered through Celite eluting with Et_2O and the organic phase was washed with pH 7 buffer and brine and dried ($MgSO_4$). Rotary evaporation and chromatography (hexanes) gave iodide **35** (520 mg, 69%) as an unstable oil that turned purple upon prolonged standing. TLC R_f = 0.9 (hexanes). EI-MS *m*/*z*: 379, 377 ($[M - Bu]^+$), 251, 199. EI-HRMS calcd. for $C_{15}H_{26}IOSi$: 377.0798 ($[M - Bu]^+$); found: 377.0795 ($[M - Bu]^+$). IR (film) (cm^{-1}): 1253, 1111, 1048, 1034, 836, 772. ^1H NMR (270 MHz, $CDCl_3$) δ: 6.26 (s, 1H), 5.80 (m, 2H), 5.00 (m, 2H), 3.49 (t, 1H, *J* = 4.4 Hz), 2.60 (m, 1H), 2.30 (m, 1H), 2.04 (d, 3H, *J* = 0.6 Hz), 1.77 (d, 3H, *J* = 1.0 Hz), 0.95 (d, 3H, *J* = 7.0 Hz), 0.91 (d, 3H, *J* = 7.0 Hz), 0.91 (s, 9H), 0.05 (s, 3H), 0.03 (s, 3H). ^{13}C NMR (101 MHz, $CDCl_3$) δ: 148.5, 141.5, 132.8, 132.4, 114.1, 79.6, 78.1, 43.3, 36.6, 26.1, 22.6, 18.9, 18.3, 16.3, 14.5, –3.7, –4.0. Reaction on a smaller scale proceeded in superior yield to give iodide **35** (191 mg, 86%).

(5*S*,6*R*,7*S*)-6-(*tert*-Butyldimethylsilyl)oxy-1-iodo-8-oxo-2,3,5,7-tetramethylnonan-1*E*,3*E*-diene (5)

OsO_4 in THF (0.065 M, 3.5 mL, 0.244 mmol) and pyridine (77 μL) were added to diene **35** (88 mg, 0.203 mmol) in dry THF (4 mL) at room temperature. The mixture was stirred for 1.7 h when Celite (500 mg) and saturated aqueous sodium bisulfite (3 mL) were added. After further stirring for 2.5 h, the mixture was filtered and diluted with Et_2O (20 mL). The organic phase was washed with H_2O, 1 M HCl, aqueous $NaHCO_3$ (10%), and brine and dried (Na_2SO_4). Rotary evaporation and chromatography (hexanes–Et_2O, 1:2.5) gave the crude diol (51 mg, 54%) as a colorless oil. TLC R_f = 0.5 (Et_2O). EI-HRMS calcd. for $C_{18}H_{34}IO_2Si$: 437.1373 ($[M - CH_2OH]^+$); found: 437.1388 ($[M - CH_2OH]^+$). IR (CCl_4) (cm^{-1}): 3399, 1253, 1075, 1032, 837, 773, 600. ^1H NMR (400 MHz, $CDCl_3$) major diastereoisomer δ: 6.28 (s, 1H), 5.69 (d, 1H, *J* = 9.9 Hz), 3.72–3.35 (m, 5H), 2.72 (m, 1H), 2.02 (s, 3H), 1.80 (s, 3H), 1.79 (m, 1H), 1.00 (d, 3H, *J* = 6.9 Hz), 0.92 (s, 9H), 0.79 (d, 3H, *J* = 7.1 Hz), 0.11 (s, 3H), 0.10 (s, 3H). ^{13}C NMR (101 MHz, $CDCl_3$) major diastereoisomer δ: 148.2, 133.7, 131.3, 79.6, 78.6, 74.0, 64.7, 39.4, 37.4, 26.0, 22.6, 18.1, 17.9, 14.7, 14.3, –4.0, –4.4. *N*-Methylmorpholine-*N*-oxide (10 mg, 87 μmol) and OsO_4 in H_2O (0.3 M, ca 10 μL) were added to diene **35** (29 mg, 67 μmol) in Me_2CO and H_2O (1:1, 1 mL) at room temperature. The mixture was stirred for 7 h when sodium bisulfite was added and, after 20 min, the mixture was filtered through Celite. Rotary evaporation and chromatography (Et_2O) gave the crude diol (19 mg, 61%) and recovered triene **35** (6 mg, 21%). Both of these osmylation processes proved to be capricious and proceeded in variable yield on scale up. The crude diol from either preparation was used directly in the next step. The crude 1,2-diol (147 mg, 0.314 mmol) was allowed to react with $NaIO_4$ (174 mg, 0.91 mmol) in THF (5 mL), MeOH (0.8 mL), and H_2O (2 mL) for 30 min at room temperature. The resulting mixture was diluted with CH_2Cl_2 (50 mL) and washed with H_2O and brine. The organic layer was dried (Na_2SO_4) and rotary evaporated to leave the crude aldehyde **36** as a pale yellow oil. TLC R_f = 0.4 (hexanes–Et_2O, 9:1). $[\alpha]_D^{22}$ = +0.41° (*c* = 3.15). EI-MS *m*/*z*: 379 ($[M - Bu]^+$), 252, 201, 173, 145. IR (film) (cm^{-1}): 1723, 1463, 1378, 1254, 1075, 1034, 1006, 939, 838, 773, 673. ^1H NMR (400 MHz, $CDCl_3$) δ: 9.76 (d, 1H, *J* = 2.6 Hz), 6.31 (s, 1H), 5.68 (d, 1H, *J* = 9.5 Hz), 3.84 (t, 1H, *J* = 3.8 Hz), 2.65 (m, 1H), 2.48 (m, 1H), 2.03 (s, 3H), 1.79 (s, 3H), 1.06 (d, 3H, *J* = 7.0 Hz), 1.00 (d, 3H, *J* = 6.9 Hz), 0.90 (s, 9H), 0.08 (s, 3H), 0.06 (s, 3H). ^{13}C NMR (101 MHz, $CDCl_3$) δ: 204.7, 148.1, 134.9, 130.2, 79.1, 77.7, 51.1, 37.9, 25.9, 22.6, 18.2, 17.8, 14.7, 11.8, –4.0, –4.1. The crude aldehyde **36** was used in the

© 2001 NRC Canada

next reaction without further purification. Aldehyde **36** (134 mg, crude) in dry THF (3.0 mL) was added dropwise to MeMgBr in PhMe and THF (3:1) (1.4 M, 722 μL, 1.0 mmol) in dry THF (4 mL) at –78°C. After 30 min, the mixture was poured into saturated aqueous NH_4Cl and ice and extracted with Et_2O. The extracts were combined, washed with brine, and dried ($MgSO_4$). Rotary evaporation and chromatography (Et_2O–hexanes, 1:3) gave alcohol **37** (114 mg, 80% from the diol). Since the alcohol **37** was unstable, it was used directly in the next reaction. DMSO (86 μL, 1.21 mmol) in dry CH_2Cl_2 (3 mL) was added dropwise to oxalyl chloride (88 μL, 1.01 mmol) in dry CH_2Cl_2 (4 mL) at –78°C. After 8 min, alcohol **37** (114 mg, 0.252 mmol) in dry CH_2Cl_2 (3 mL) was added and stirring was continued for 10 min at –78°C, when Et_3N (296 μL, 2.12 mmol) was added dropwise. The mixture was allowed to warm up to –30°C over 15 min and then diluted with Et_2O (50 mL). The organic phase was washed with H_2O, 0.5 M HCl, H_2O, saturated aqueous $NaHCO_3$, and brine and then dried ($MgSO_4$). Rotary evaporation and chromatography (hexanes–Et_2O, 6:1) gave ketone **5** (90 mg, 79%) as a colorless oil. TLC R_f = 0.43 (hexanes–Et_2O, 5:1). $[\alpha]_D^{20}$ = +23° (*c* = 0.70). EI-MS *m*/*z*: 435 ($[M - Me]^+$), 393, 301, 251, 215. EI-HRMS calcd. for $C_{18}H_{32}IO_2Si$: 435.1216 ($[M - Me]^+$); found: 435.1208 ($[M - Me]^+$). IR (film) (cm^{-1}): 1718, 1462, 1377, 1253. ^1H NMR (300 MHz, $CDCl_3$) δ: 6.28 (s, 1H), 5.80 (dq, 1H, *J* = 9.5, 1.0 Hz), 3.88 (dd, 1H, *J* = 7.5, 2.5 Hz), 2.64 (q, 1H, *J* = 7.5 Hz), 2.57 (ddt, 1H, *J* = 9.5, 7.5, 2.5 Hz), 2.14 (s, 3H), 2.03 (d, 3H, *J* = 1.0 Hz), 1.78 (d, 3H, *J* = 1.0 Hz), 0.97 (d, 3H, *J* = 7.5 Hz), 0.93 (d, 3H, *J* = 7.5 Hz), 0.87 (s, 9H), 0.06 (s, 3H), 0.02 (s, 3H). ^{13}C NMR (85 MHz, $CDCl_3$) δ: 211.9, 148.3, 134.3, 130.3, 78.8, 77.6, 52.0, 36.6, 31.1, 26.2, 22.7, 18.5, 18.3, 14.7, 13.4, –3.9, –4.3.

(2*R*,4*S*)-2,4-Dimethyl-1,3,5-pentanetriyl triacetate (42)

The silyl ether **38** was prepared from methyl (2*R*)-2-methyl-3-triethylsilyloxypropanoate (ent-**24**) (17.5 g) and (–)-*B*-methoxydiisopinocampheylborane following the methods as for the (*S*)-antipode **27**. Ether **38** was dissolved in Me_2CO (50 mL) and H_2O (5 mL), then OsO_4 in H_2O (5%, 1 mL) and *N*-methylmorpholine-*N*-oxide (9.5 g, 0.0698 mol) were added. After stirring for 6 h at room temperature, saturated aqueous sodium metabisulfite (20 mL) and Celite (20 g) were added and, after 3 h, the mixture was filtered. The filtrate was rotary evaporated, the resultant solid extracted with Et_2O (300 mL), and the filtrate washed with H_2O (2 × 50 mL), 1 M HCl (50 mL), H_2O (50 mL), 10% aqueous $NaHCO_3$ (50 mL), and brine and dried (Na_2SO_4). Rotary evaporation and chromatography (hexanes–EtOAc, 8:1 to 3:2) gave the crude vicinal diol (14.2 g, 40% overall from ester ent-**24**). $NaIO_4$ (1.11 g, 6.21 mmol), MeOH (5 mL), and H_2O (2 mL) were added to an aliquot of the diol (2.1 g, 5.17 mmol) in THF (15 mL) and the mixture stirred for 20 min at room temperature. An insoluble solid was removed by filtration and the filtrate was extracted with CH_2Cl_2 (3 × 50 mL). The extracts were washed with H_2O and brine and dried (Na_2SO_4). Rotary evaporation and chromatography (hexanes–Et_2O, 22:1) gave the crude aldehyde **39** (1.93 g, 100%). $NaBH_4$ (6.6 mg, 0.175 mmol) was added to an aliquot of the aldehyde **39** (80 mg, 0.175 mmol) in MeOH (1 mL) with ice cooling. After 20 min, rotary evaporation and chromatography (hexanes–EtOAc, 5:1) gave the crude alcohol **40** (75 mg, 93%). $TsOH \cdot H_2O$ (3 mg, 0.017 mmol) was added to alcohol **40** (75 mg, 0.163 mmol) in MeOH (1.6 mL) at room temperature. After 3 h, Et_3N (50 μL) was added and the mixture rotary evaporated and chromatographed (hexanes–EtOAc, 1:1 then MeOH:CH_2Cl_2, 1:9) to give the crude triol **41** (24 mg, 100%). Ac_2O (60 μL), Et_3N (80 μL), and DMAP (5 mg) were added to triol **41** (24 mg, 0.16 mmol) in CH_2Cl_2 (1 mL). After 30 min, excess Ac_2O was quenched with MeOH (0.1 mL). Rotary evaporation and chromatography (hexanes–EtOAc, 2:1) gave triester **42** (45 mg, 97%) as a colorless oil. $[\alpha]_D^{20}$ = 0° (*c* = 2.25). IR (film) (cm^{-1}): 2973, 1739, 1460, 1376, 1228, 1128. ^1H NMR (300 MHz, $CDCl_3$) δ: 4.90 (t, 1H, *J* = 6.5 Hz), 4.06 (dd, 2H, *J* = 4.5, 11.0 Hz), 3.92 (dd, 2H, *J* = 11.0, 6.5 Hz), 2.22–2.13 (m, 2H), 2.05 (s, 3H), 2.04 (s, 6H), 1.00 (d, 6H, *J* = 7.0 Hz). ^{13}C NMR (75 MHz, $CDCl_3$) δ: 171.1, 170.6, 76.5, 65.5, 34.3, 21.0, 20.8, 14.9.

(10*S*,11*S*,12*S*)-3,7,8,10,12-Pentamethyl-13-oxo-11-(*tert*-butyldimethylsilyl)oxy-(2*Z*,4*E*,6*E*,8*E*)-tridecatetraenenitrile (43)

$PdCl_2(PPh_3)_2$ (3 mg) in THF (0.5 mL) was added to the aldehyde **36** (75 mg, 0.172 mmol) and stannyl nitrile **3** (80 mg, 0.21 mmol) in THF (0.5 mL) and the yellow mixture was heated with stirring at 60°C for 2 h. The resultant black mixture was cooled and directly chromatographed (hexanes–Et_2O, 4:1) to afford the tetra-ene nitrile **43** (52 mg, 75%) as a yellow oil. TLC R_f = 0.25 (hexanes–Et_2O, 9:1). $[\alpha]_D^{22}$ = +70.6° (*c* = 2.3). EI-MS *m*/*z*: 401 ($M^{\cdot+}$), 344, 315, 286, 252, 201, 173, 145, 115. EI-HRMS calcd. for $C_{24}H_{39}NO_2Si$: 401.2750 ($M^{\cdot+}$); found: 401.2751 ($M^{\cdot+}$). IR (film) (cm^{-1}): 2208, 1723, 1592, 1583, 1462, 1379, 1254, 1040, 1034, 962, 838, 775. ^1H NMR (400 MHz, $CDCl_3$) δ: 9.76 (d, 1H, *J* = 2.7 Hz), 6.99 (dd, 1H, *J* = 14.2, 11.2 Hz), 6.85 (d, 1H, *J* = 14.8 Hz), 6.36 (d, 1H, *J* = 10.8 Hz), 5.82 (d, 1H, *J* = 9.5 Hz), 5.09 (br s, 1H), 3.86 (t, 1H, *J* = 4.7 Hz), 2.77 (m, 1H), 2.50 (m, 1H), 2.07 (d, 3H, *J* = 1.3 Hz), 2.00 (s, 3H), 1.86 (s, 3H), 1.07 (d, 3H, *J* = 7.0 Hz), 1.03 (d, 3H, *J* = 6.9 Hz), 0.90 (s, 9H), 0.09 (s, 3H), 0.06 (s, 3H). ^{13}C NMR (101 MHz, $CDCl_3$) δ: 204.6, 156.5, 143.4, 136.1, 133.5, 131.7, 129.1, 125.0, 117.4, 95.1, 77.8, 51.2, 38.3, 34.1, 25.9, 22.3, 19.4, 18.2, 17.8, 14.6, 14.3, 14.1, 11.8, –4.0, –4.2.

3-(3,4-Dimethoxybenzyl)oxypropan-1-ol

Camphorsulfonic acid (50 mg) and 3,4-dimethoxybenzaldehyde (20 g, 0.120 mol) were added to 1,3-propanediol (22 g, 0.289 mol) in PhH (100 mL). The mixture was heated to reflux (Dean-Stark) for 12 h, cooled to room temperature, and treated with pH 7 buffer (50 mL). The organic phase was separated,washed with brine (2 × 100 mL), and dried ($MgSO_4$). The mixture was heated to reflux (Dean-Stark) for a further 2 h and cooled to 0°C. DIBAl-H in PhMe (1.46 M, 25 mL, 0.365 mmol) was added dropwise at 0°C, stirred for 5 min at 0°C and then 1 h at room temperature. A further aliquot of DIBAl-H in PhMe (1.46 M, 8 mL) was added and the mixture stirred at room temperature for 30 min. The solution was cooled to 0°C and quenched with EtOAc (10 mL) and aqueous NaOH (3 M, 7 mL). The resulting solution was filtered through Celite eluting with EtOAc and the organic fraction washed with

© 2001 NRC Canada

H_2O and brine and dried ($MgSO_4$). Rotary evaporation and chromatography (hexanes–EtOAc, 1:1, then EtOAc) gave 3-(3,4-dimethoxybenzyl)oxy-1-propanol (10 g, 37%) as a viscous oil: TLC R_f = 0.25 (Et_2O). EI-MS *m/z*: 226 ($M^{\cdot+}$), 211, 195, 167, 151. EI-HRMS calcd. for $C_{12}H_{18}O_4$: 226.1205 ($M^{\cdot+}$); found: 226.1197 ($M^{\cdot+}$). IR (film) (cm^{-1}): 3466, 1593, 1515, 1465, 1420, 1365, 1360, 1265, 1238, 1157, 1090, 1028, 820, 811, 765. ^1H NMR (400 MHz, $CDCl_3$) δ: 6.87–6.83 (m, 3H), 4.45 (s, 2H), 3.88 (s, 3H), 3.87 (s, 3H), 3.79–3.75 (m, 2H), 3.65–3.62 (m, 2H), 2.34 (m, 1H), 1.87–1.84 (m, 2H). ^{13}C NMR (101 MHz, $CDCl_3$) δ: 149.0, 148.6, 130.6, 120.2, 110.9, 110.9, 73.2, 69.1, 61.9, 55.91, 55.88, 55.84, 55.80, 32.1. Anal. calcd. for $C_{12}H_{18}O_4$: C 63.70, H 8.02; found: C 63.48, H 8.17.

3-(3,4-Dimethoxybenzyl)oxypropanal (44)

DMSO (3 mL, 0.042 mmol) in CH_2Cl_2 (4 mL) was added dropwise over 10 min to $(COCl)_2$ (3 mL, 0.034 mol) in CH_2Cl_2 (50 mL) at –78°C. After stirring at –78°C for 25 min, 3-(3,4-dimethoxybenzyl)oxypropan-1-ol (6.0 g, 0.0265 mol) in CH_2Cl_2 (4 mL) was added dropwise. After 45 min, Et_3N (20 mL, 0.143 mol) was added dropwise at –78°C and stirring was continued for a further 45 min; the solution was then allowed to warm to room temperature. Buffer (pH 7, 50 mL) and Et_2O (200 mL) were added and the ethereal layer was washed with brine and dried ($MgSO_4$). Chromatography (hexanes–EtOAc, 1:1) gave aldehyde **44** (4.59 g, 77%) as a colorless oil. TLC R_f = 0.4 (hexanes–Et_2O, 3:7). EI-MS *m/z*: 224 ($M^{\cdot+}$), 209, 193, 167, 151, 139. EI-HRMS calcd. for $C_{12}H_{16}O_4$: 224.1049 ($M^{\cdot+}$); found: 224.1046 ($M^{\cdot+}$). IR (film) (cm^{-1}): 1723, 1712, 1593, 1515, 1465, 1420, 1363, 1265, 1258, 1157, 1092, 1028, 856, 812, 766. ^1H NMR (300 MHz, $CDCl_3$) δ: 9.80, (t, 1H, *J* = 1.8 Hz), 7.2–6.8 (m, 3H), 4.45 (s, 2H), 3.89 (s, 3H), 3.88 (s, 3H), 3.82 (t, 2H, *J* = 6.1 Hz), 2.70 (dt, 2H, *J* = 6.1, 1.8 Hz). ^{13}C NMR (75 MHz, $CDCl_3$) δ: 200.7, 149.1, 148.8, 130.4, 120.2, 111.2, 73.0, 63.5, 55.9, 43.8.

(3*R*,4*R*)-1-(3,4-Dimethoxybenzyl)oxy-4-methyl-5-hexen-3-ol (45)

Freshly condensed *cis*-2-butene (5 mL) was added to *t*-BuOK (2.675 g, 0.0238 mol) in THF (50 mL) at –78°C. *n*-BuLi in hexanes (1.6 M, 15 mL, 0.024 mol) was added dropwise resulting in the formation of a yellow precipitate, which was allowed to warm to –55°C and stirred for an additional 20 min. Upon recooling to –78°C, (–)-*B*-methoxydiisopinocampheylborane (8.27 g, 0.0262 mol) in Et_2O (30 mL) was added dropwise over 10 min. The colorless mixture was stirred at –78°C for 30 min, then $BF_3.OEt_2$ (4.19 mL, 0.034 mol) was added in one portion followed by aldehyde **44** (4.45 g, 0.020 mol) in Et_2O (25 mL) dropwise. The mixture was stirred at –78°C for 4 h and H_2O (20 mL) was added when the mixture was allowed to warm to room temperature. Sodium perborate (20 g) was added and the mixture was stirred vigorously overnight. The mixture was extracted with Et_2O (200 mL) and the extracts were washed with H_2O and brine, dried ($MgSO_4$), and rotary evaporated. Chromatography (hexanes–Et_2O, 1:1) gave alcohol **45** (4.00 g, 72%) as a colorless oil. TLC R_f = 0.4 (hexanes–Et_2O, 3:7). $[\alpha]_D^{23}$ = +9.5° (*c* = 9.95). EI-MS *m/z*: 280 ($M^{\cdot+}$), 224, 167, 151, 137, 107. EI-HRMS calcd. for $C_{16}H_{24}O_4$: 280.1675 ($M^{\cdot+}$); found: 280.1678 ($M^{\cdot+}$). IR (CCl_4) (cm^{-1}): 3469, 1612, 1593, 1465, 1420, 1364, 1265, 1239, 1168, 1139, 1088, 1030, 916, 767, 765. ^1H NMR (400 MHz, $CDCl_3$) δ: 6.87–6.82 (m, 3H), 5.78 (m, 1H), 5.05 (m, 2H), 4.46 (s, 2H), 3.89 (s, 3H), 3.88 (s, 3H), 3.65 (m, 3H), 2.85 (d, 1H, *J* = 3.4 Hz), 2.26 (m, 1H), 1.75 (m, 2H), 1.05 (d, 3H, *J* = 6.8 Hz). ^{13}C NMR (75 MHz, $CDCl_3$) δ: 149.0, 148.5, 140.8, 130.5, 120.0, 114.4, 111.1, 73.8, 72.8, 68.6, 55.7, 55.6, 43.6, 33.4, 14.8. Anal. calcd. for $C_{16}H_{24}O_4$: C 68.54, H 8.63; found: C 68.45, H 8.84.

(3*R*,4*R*)-1-(3,4-Dimethoxybenzyl)oxy-4-methyl-3-(*tert*-butyldimethyl)oxy-5-hexene (46)

2,6-Lutidine (1 mL, 8.59 mmol) followed by *t*-$BuMe_2SiOTf$ (1.3 mL, 5.62 mmol) were added to alcohol **45** (1.43 g, 5.11 mmol) in CH_2Cl_2 (15 mL) at –78°C. The mixture was allowed to warm to room temperature over 90 min and quenched with pH 7 buffer (5 mL). The solution was diluted with Et_2O (100 mL), washed with brine, dried ($MgSO_4$), and evaporated to dryness. Chromatography (hexanes–Et_2O, 9:1) afforded the silyl alcohol **46** (1.89 g, 94%) as a colorless oil. TLC R_f = 0.5 (hexanes–Et_2O, 1:1). $[\alpha]_D^{22}$ = +28.1° (*c* = 7.2). EI-MS *m/z*: 394 ($M^{\cdot+}$), 339, 281, 251, 224, 199, 173, 167, 151. EI-HRMS calcd. for $C_{22}H_{38}O_4Si$: 394.2539 ($M^{\cdot+}$); found: 394.2524 ($M^{\cdot+}$). IR (film) (cm^{-1}): 1594, 1517, 1465, 1420, 1362, 1259, 1106, 1092, 1032, 912, 837, 774. ^1H NMR (400 MHz, $CDCl_3$) δ: 6.85 (m, 3H), 5.88 (m, 1H), 5.00 (m, 2H), 4.44 (d, 1H, *J* = 11.3 Hz), 4.39 (d, 1H, *J* = 11.3 Hz), 3.88 (s, 3H), 3.87 (s, 3H), 3.71 (m, 1H), 3.50 (m, 2H), 2.30 (m, 1H), 1.8–1.6 (m, 2H), 0.96 (d, 3H, *J* = 6.9 Hz), 0.88 (s, 9H), 0.04 (s, 6H). ^{13}C NMR (101 MHz, $CDCl_3$) δ: 148.9, 148.4, 140.8, 131.1, 120.2, 114.2, 110.9, 110.8, 72.9, 72.8, 66.8, 55.9, 55.7, 43.0, 33.4, 25.9, 18.1, 14.8, –4.4, –4.6. Anal. calcd. for $C_{22}H_{38}O_4Si$: C 66.96, H 9.71; found: C 67.10, H 9.96.

(2*S*,3*R*)-5-(3,4-Dimethoxybenzyl)oxy-2-methyl-3-(*tert*-butyldimethylsilyl)oxypentanal (47)

Aqueous OsO_4 (0.3 M, 10 drops) was added to alkene **46** (520 mg, 1.320 mmol) in THF and H_2O (1:1, 5 mL) and *N*-methylmorpholine-*N*-oxide (235 mg, 1.74 mmol) and the brown solution was stirred at room temperature for 7 h. $NaIO_4$ (370 mg, 1.73 mmol) was added and the resulting mixture was stirred for a further 2 h, filtered through Celite, eluting with Et_2O (100 mL), and the ethereal layer was washed with pH 7 buffer and brine and dried (Na_2SO_4). Chromatography (hexanes–Et_2O, 9:1 to 1:1) gave aldehyde **47** (432 mg, 88%) as a tan oil. TLC R_f = 0.4 (hexanes–Et_2O, 1:1). $[\alpha]_D^{21}$ = +44.1° (*c* = 3.2). EI-MS *m/z*: 396 ($M^{\cdot+}$), 339, 282, 264, 236, 224, 189. EI-HRMS calcd. for $C_{21}H_{36}O_5Si$: 396.2332 ($M^{\cdot+}$); found: 396.2286 ($M^{\cdot+}$). IR (film) (cm^{-1}): 1726, 1593, 1515, 1463, 1419, 1362, 1259, 1157, 1103, 1033, 939, 888, 777, 669. ^1H NMR (400 MHz, $CDCl_3$) δ: 9.78 (s, 1H), 6.87–6.82 (m, 3H), 4.44 (d, 1H, *J* = 11.6 Hz), 4.38 (d, 1H, *J* = 11.5 Hz), 4.32 (m, 1H), 3.89 (s, 3H), 3.88 (s, 3H), 3.49 (m, 2H), 2.48 (m, 1H), 1.80 (m, 2H), 1.05 (d, 3H, *J* = 7.0 Hz), 0.86 (s, 9H), 0.07 (s, 3H), 0.04 (s, 3H). ^{13}C NMR (101 MHz, $CDCl_3$) δ: 205.1, 148.9, 148.5, 130.7, 120.2, 110.9, 110.8. 72.9, 69.3, 66.3, 55.9, 55.8, 55.7, 51.6, 34.5, 25.7, 18.0, 7.9, –4.5, –4.6.

© 2001 NRC Canada

2,2-Dimethyl-3-(*tert*-butyldimethylsilyl)oxypropanal (48)

Imidazole (15 g, 0.220 mol) followed by *t*-$BuMe_2SiCl$ (15 g, 0.1 mol) were added to 2,2-dimethyl-1,3-propanediol (20 g, 0.192 mol) in DMF (10 mL). The resulting viscous mixture was stirred at room temperature for 16 h, then Et_2O (200 mL) and H_2O (200 mL) were added. The ethereal layer was washed with pH 7 buffer (2 × 100 mL) and brine and dried ($MgSO_4$). After rotary evaporation, the residue was distilled to leave 2,2-dimethyl-3-(*tert*-butyldimethylsilyl)oxy-1-propanol (15.8 g, 63%) as a colorless oil. DMSO (1 mL, 0.014 mol) in CH_2Cl_2 (2 mL) was added to $(COCl)_2$ (1 mL, 0.011 mol) in CH_2Cl_2 (25 mL) at –78°C such that the internal reaction temperature did not increase by more than 5°C. This mixture was stirred at –78°C for 30 min and then the alcohol (2 g, 7.87 mmol) in CH_2Cl_2 (5 mL) was added dropwise. The mixture was stirred at –78°C for 35 min, then Et_3N (6 mL, 0.043 mmol) was added slowly and the mixture allowed to warm to –10°C. Buffer (pH 7, 20 mL) and Et_2O (100 mL) were added and the ethereal fraction washed with pH 7 buffer and brine and dried (Na_2SO_4). Chromatography (hexanes–Et_2O, 9:1) afforded aldehyde **48** (1.72 g, 86%) as a colorless oil. TLC R_f = 0.75 (hexanes–Et_2O, 9:1). IR (film) (cm^{-1}): 1730, 1472, 1362, 1401, 1256, 1103, 1006, 897, 864, 842, 775, 669. ^1H NMR (400 MHz, $CDCl_3$) δ: 9.57 (s, 1H), 3.59 (s, 2H), 1.04 (s, 6H), 0.86 (s, 9H), 0.03 (s, 6H). ^{13}C NMR (101 MHz, $CDCl_3$) δ: 206.2, 68.4, 48.1, 25.8, 18.6, 18.2, –5.6. The crude aldehyde **48** was used directly in the next step without any further purification.

(3*S*,4*S*)-2,2-Dimethyl-1-(*tert*-butyldimethylsilyl)oxy-4-(2-(trimethylsilyl)ethoxy)methoxy-5-hexen-3-ol (49)

sec-BuLi in hexanes (1.4 M, 20 mL, 0.028 mol) was added over 10 min to $Me_3SiCH_2CH_2OCHsOCH_2CH{=}CH_2$ (5.30 g, 0.028 mol) in THF (75 mL) at –78°C. The resulting yellow mixture was stirred at –78°C for a further 30 min, then (+)-*B*-methoxydiisopinocampheylborane (9.74 g, 0.031 mol) in Et_2O (30 mL) was added dropwise over 20 min to yield a colorless solution. After a further 20 min at –78°C, $BF_3{\cdot}OEt_2$ (4.9 mL, 0.0389 mol) was added immediately followed by the dropwise addition of aldehyde **48** (6.50 g, 0.026 mol) in Et_2O (30 mL). This viscous mixture was stirred for 4 h at –78°C and allowed to slowly warm to –40°C. Ethanolamine (10 mL, 0.166 mol) was added and the mixture allowed to warm up to room temperature and stirred for 1 h. Additional ethanolamine (10 mL) was added followed by NaH dispersion in oil (50%, 50 mg). After stirring for 12 h, the mixture was extracted with EtOAc–Et_2O (1:1, 500 mL), the extracts were washed with pH 7 buffer and brine, and dried ($MgSO_4$). Chromatography (hexanes–Et_2O, 9:1) afforded alcohol **49** (6.28 g, 60%) as a colorless oil. TLC R_f = 0.45 (hexanes–Et_2O, 9:1). $[\alpha]_D^{22}$ = +74.1° (*c* = 2.35). EI-MS *m*/*z*: 405 ($[M + H]^+$), 331, 289, 257, 217. EI-HRMS calcd. for $C_{17}H_{35}O_4Si$: 331.2305 ($[M - SiMe_3]^+$); found: 331.2148 ($[M - SiMe_3]^+$). IR (film) (cm^{-1}): 3500, 1473, 1389, 1251, 1099, 1025, 933, 837, 786. ^1H NMR (400 MHz, $CDCl_3$) δ: 5.94 (m, 1H), 5.25 (m, 2H), 4.73 (d, 1H, *J* = 7.0 Hz), 4.63 (d, 1H, *J* = 7.0 Hz), 4.22 (dd, 1H, *J* = 8.2, 2.4 Hz), 3.75 (m, 1H), 3.54 (d, 1H, *J* = 9.3 Hz), 3.52 (m, 1H), 3.48 (d, 1H, *J* = 2.7 Hz), 3.40 (d, 1H, *J* = 9.4 Hz), 1.02 (s, 3H), 0.93 (s, 3H), 0.89 (s, 9H), 0.88 (m, 2H), 0.05 (s, 6H), 0.01 (s, 9H). ^{13}C NMR (101 MHz, $CDCl_3$) δ: 136.9, 118.2, 91.7, 79.1, 77.3, 72.5, 65.8, 39.0, 25.8, 21.9, 20.4, 18.2, 18.1, –1.5, –5.6. Anal. calcd. for $C_{20}H_{44}O_4Si_2$: C 59.35, H 10.96; found: C 59.15, H 11.11.

(3*S*,4*S*)-3-(4-Methoxybenzyl)oxy-2,2-dimethyl-4-(2-trimethylsilylethoxy)-methoxy-5-hexen-1-ol (51)

$KN(SiMe_3)_2$ (3.14 g, 0.0157 mol) in THF (20 mL) was added to alcohol **49** (5.60 g, 0.0138 mol) in THF (30 mL) at –78°C. After stirring for 10 min at –78°C, the mixture was stirred at 0°C for 10 min and treated with 4-$MeOC_6H_4CH_2Cl$ (2.2 mL, 0.0162 mol). After 1 h, the mixture was allowed to warm up to room temperature and DMF (10 mL) added. After 30 min, saturated aqueous NH_4Cl (10 mL) was added and the mixture was diluted with Et_2O (400 mL), washed with brine, and dried ($MgSO_4$). Rotary evaporation gave silyl ether **50** as a colorless oil. TLC R_f = 0.45 (hexanes–Et_2O, 1:1). EI-MS *m*/*z*: 524 ($M^{\cdot+}$), 409, 393, 289, 257. EI-HRMS calcd. for $C_{28}H_{52}O_5Si_2$: 524.3353 ($M^{\cdot+}$); found: 524.3357 ($M^{\cdot+}$). IR (CCl_4) (cm^{-1}): 1613, 1514, 1472, 1389, 1361, 1259, 1250, 1173, 1094, 1036, 924, 837, 775, 668. ^1H NMR (400 MHz, $CDCl_3$) δ: 7.29 (d, 2H, *J* = 8.5 Hz), 6.85 (d, 2H, *J* = 8.5 Hz), 5.92 (m, 1H), 5.28 (m, 1H), 5.24 (m, 1H), 4.72 (d, 1H, *J* = 7.1 Hz), 4.68 (d, 1H, *J* = 6.9 Hz), 4.66 (d, 1H, *J* = 6.9 Hz), 4.51 (d, 1H, *J* = 10.8 Hz), 4.32 (dd, 1H, *J* = 7.9, 3.1 Hz), 3.80 (s, 3H), 3.79 (m, 1H), 3.54 (m, 3H), 3.27 (d, 1H, *J* = 9.6 Hz), 0.99 (s, 3H), 0.98 (s, 3H), 0.91 (s, 9H), 0.90 (m, 2H), 0.05 (s, 3H), 0.04 (s, 3H), 0.00 (s, 9H). ^{13}C NMR (101 MHz, $CDCl_3$) δ: 158.9, 137.7, 131.4, 129.4, 117.4, 113.6, 92.2, 84.4, 78.2, 75.6, 70.2, 65.7, 55.2, 40.8, 25.9, 21.8, 21.2, 18.3, 18.1, –1.5, –5.4, –5.5. Anal. calcd. for $C_{28}H_{52}O_5Si_2$: C 64.07, H 9.99; found: C 63.89, H 10.19. The silyl ether **50** was dissolved in Bu_4NF in THF (1 M, 0.040 mL) and maintained at room temperature for 16 h. Et_2O (400 mL) and H_2O (100 mL) were added, and the ethereal layer was washed with brine and dried ($MgSO_4$). Chromatography (hexanes–Et_2O, 3:2) gave alcohol **51** (5.65 g, 98%) as a colorless oil. TLC R_f = 0.45 (hexanes–Et_2O, 1:1). $[\alpha]_D^{21}$ = +39.6° (*c* = 5.8). EI-MS *m*/*z*: 410 ($M^{\cdot+}$), 308, 279, 252, 179. EI-HRMS calcd. for $C_{22}H_{38}O_5Si$: 410.2489 ($M^{\cdot+}$); found: 410.2477 ($M^{\cdot+}$). IR (film) (cm^{-1}): 3465, 1613, 1586, 1514, 1465, 1302, 1249, 1174, 1100, 1036, 931, 859, 836, 759, 694. ^1H NMR (400 MHz, $CDCl_3$) δ: 7.27 (d, 2H, *J* = 9.3 Hz), 6.86 (d, 2H, *J* = 8.6 Hz), 5.95 (m, 1H), 5.30 (dm, 1H, *J* = 16.0 Hz), 5.26 (dm, 1H, *J* = 9.4 Hz), 4.73 (d, 1H, *J* = 7.0 Hz), 4.69 (d, 1H, *J* = 11.0 Hz), 4.68 (d, 1H, *J* = 7.0 Hz), 4.50 (d, 1H, *J* = 11.0 Hz), 4.36 (dd, 1H, *J* = 7.4, 3.3 Hz), 3.79 (s, 3H), 3.78 (m, 1H), 3.50 (m, 3H), 3.35 (m, 3H), 2.82 (br t, 1H, *J* = 5 Hz), 1.02 (s, 3H), 0.97 (s, 3H), 0.9 (m, 2H), 0.00 (s, 9H). ^{13}C NMR (101 MHz, $CDCl_3$) δ: 159.3, 137.0, 130.6, 129.3, 117.4, 113.8, 92.6, 87.4, 77.7, 75.3, 70.1, 65.9, 55.2, 40.4, 23.4, 22.4, 22.2, 18.1, –1.5. Anal. calcd. for $C_{22}H_{38}O_5Si$: C 64.35, H 9.33; found: C 64.06, H 9.42. DCC (26 mg, 0.127 mmol) was added to alcohol **51** (40 mg, 0.0976 mmol), (*R*)-(+)-α-methoxy-α-(trifluoromethyl)phenylacetic acid (30 mg, 0.127 mmol), and DMAP (3 mg) in dry CH_2Cl_2 (0.6 mL) at 0°C under Ar. After stirring for 30 min at 0°C and 1.5 h at room temperature, excess DCC was quenched with AcOH (0.1 mL). The mixture was diluted with Et_2O (30 mL), and the resulting insolu-

© 2001 NRC Canada

ble solid was removed by filtration. The filtrate was washed with 10% aqueous $NaHCO_3$ and brine, and the organic layer was dried ($MgSO_4$). Rotary evaporation and chromatography (Et_2O–hexanes, 1:2) gave (3*S*,4*S*)-3-(4-methoxybenzyl)oxy-2,2-dimethyl-4-(2-trimethylsilylethoxy)-methoxy-5-hexen-1-yl-(*R*)-(+)-α-methoxy-α-(trifluoromethyl)phenylacetate (**55**) (50 mg, 82%) as a colorless oil. ^{1}H NMR (300 MHz, $CDCl_3$) δ: 7.50–7.46 (m, 2H), 7.39–7.34 (m, 3H), 7.20 (d, 2H, *J* = 8.5 Hz), 6.83 (d, 2H, *J* = 8.5 Hz), 5.82 (ddd, 1H, *J* = 17.5, 10.0, 7.5 Hz), 5.19–5.18 (m, 2H), 4.65 (d, 1H, *J* = 7.0 Hz), 4.64 (d, 1H, *J* = 10.5 Hz), 4.61 (d, 1H, *J* = 7.0 Hz), 4.32 (d, 1H, *J* = 10.5 Hz), 4.30 (d, 1H, *J* = 10.5 Hz), 4.24 (dd, 1H, *J* = 7.5, 3.5 Hz), 3.77 (s, 3H), 3.70 (dt, 1H, *J* = 9.5, 7.5 Hz), 3.50 (q, 3H, *J* = 1.0 Hz), 3.55–3.46 (m, 1H), 3.26 (d, 1H, *J* = 3.5 Hz), 1.02 (s, 3H), 1.00 (s, 3H), 0.97–0.83 (m, 2H), –0.04 (s, 3H). ^{13}C NMR (101 MHz, $CDCl_3$) δ: 166.5, 159.3, 137.1, 132.5, 130.9, 129.8, 129.4, 128.6, 127.7, 118.1, 113.9, 92.4, 85.1, 77.8, 75.8, 73.0, 66.1, 55.5, 39.7, 22.1, 21.7, 18.3, –1.3.

(2*R*/*S*,4*S*,5*S*)-4-(4-Methoxybenzyl)oxy-3,3-dimethyl-5-((2-trimethylsilyl)ethoxy)methoxy-6-hepten-2-ol (53)

DMSO (1.6 mL, 0.023 mol) in CH_2Cl_2 (3 mL) was added dropwise to $(COCl)_2$ (1.6 mL, 0.0183 mol) in CH_2Cl_2 (65 mL) at –78°C. After 30 min, alcohol **51** (5.65 g, 0.0138 mol) in CH_2Cl_2 (20 mL) was added over 10 min. Following an additional 40 min at –78°C, Et_3N (10 mL, 0.072 mol) was added and the mixture allowed to warm to room temperature. The solution was diluted with Et_2O (300 mL) and washed with pH 7 buffer (100 mL) and brine and dried ($MgSO_4$). Rotary evaporation gave aldehyde **52** (5.04 g, 89%) as a yellow oil, which was used directly in the next step without any further purification. MeMgBr in Et_2O (3.0 M, 7.2 mL, 0.0216 mol) was added to aldehyde **52** (5.04 g, 0.0123 mol) in THF (20 mL) at –78°C. The mixture was allowed to slowly warm to 0°C, then saturated aqueous NH_4Cl (10 mL) was cautiously added. The mixture was diluted with Et_2O (200 mL), washed with H_2O and brine, and dried ($MgSO_4$). Chromatography (hexanes–Et_2O, 1:1) afforded alcohol **53** (4.96 g, 95%) as a colorless oil. TLC R_f = 0.5 (hexanes–Et_2O, 1:1). FAB-MS *m*/*z*: 447 ($[M + Na]^+$), 425 ($[M + H]^+$), 293, 226, 199, 179. FAB-HRMS calcd. for $C_{23}H_{40}O_5SiNa$: 447.2543 ($[M + Na]^+$); found: 447.2579 ($[M + Na]^+$). IR (film) (cm^{-1}): 3467, 1613, 1609, 1515, 1466, 1390, 1255, 1249, 1173, 1101, 925, 836, 758, 702. ^{1}H NMR (400 MHz, $CDCl_3$) δ: 7.28 (d, 2H, *J* = 8.7 Hz), 6.87 (d, 2H, *J* = 8.8 Hz), 5.98 (m, 1H), 5.29 (dm, 1H, *J* = 17.3 Hz), 5.24 (dm, 1H, *J* = 10.5 Hz), 4.74 (d, 1H, *J* = 6.9 Hz), 4.70 (d, 1H, *J* = 7.0 Hz), 4.48 (d, 1H, *J* = 10.8 Hz), 4.44 (m, 1H), 3.90 (m, 1H), 3.80 (s, 3H), 3.76 (m, 1H), 3.56 (m, 1H), 3.43 (d, 1H, *J* = 3.4 Hz), 3.41 (d, 1H, *J* = 3.5 Hz), 1.08 (d, 3H, *J* = 6.4 Hz), 0.96 (s, 3H), 0.92 (m, 2H), 0.89 (s, 3H), 0.01 (s, 9H). ^{13}C NMR (75 MHz, $CDCl_3$) δ: 159.33, 159.25, 137.7, 137.0, 130.7, 130.4, 129.3, 117.6, 117.0, 113.9, 113.8, 92.9, 92.4, 90.3, 87.7, 77.5, 77.3, 75.9, 74.7, 71.6, 71.4, 66.0, 55.2, 43.5, 42.2, 23.0, 21.9, 19.8, 18.3, 18.2, 17.4, 17.3, –1.4.

(4*S*,5*S*)-4-(4-Methoxybenzyl)oxy-3,3-dimethyl-5-((2-trimethylsilyl)ethoxy)methoxy-6-hepten-2-one (54)

DMSO (1.3 mL, 0.0183 mol) in CH_2Cl_2 (3 mL) was added dropwise to $(COCl)_2$ (1.3 mL, 0.0149 mol) in CH_2Cl_2 (50 mL) at –78°C. After 20 min, alcohol **53** (4.90 g, 0.0116 mol) in CH_2Cl_2 (15 mL) was added dropwise over 10 min. The mixture was stirred at –78°C for 40 min, then Et_3N (10 mL, 0.0717 mol) was added and the mixture allowed to slowly warm up to room temperature. The solution was diluted with Et_2O (200 mL), washed with pH 7 buffer and brine, and dried ($MgSO_4$). Chromatography (hexanes–Et_2O, 4:1) gave ketone **54** (4.18 g, 85%) as a yellow oil. TLC R_f = 0.7 (hexanes–Et_2O, 1:1). $[\alpha]_D^{23}$ = +23.9° (*c* = 5.5). FAB-MS *m*/*z*: 445 ($[M + Na]^+$), 437, 363, 303, 275, 252. EI-HRMS calcd. for $C_{23}H_{38}O_5SiNa$: 445.2386 ($[M + Na]^+$); found: 445.2345 ($[M + Na]^+$). IR (film) (cm^{-1}): 1702, 1514, 1354, 1257, 1248, 1173, 1101, 1036, 934, 836. ^{1}H NMR (400 MHz, $CDCl_3$) δ: 7.25 (d, 2H, *J* = 8.7 Hz), 6.85 (d, 2H, *J* = 8.7 Hz), 5.72 (m, 1H), 5.27 (m, 1H), 5.24 (m, 1H), 4.77 (d, 1H, *J* = 10.7 Hz), 4.64 (d, 1H, *J* = 6.9 Hz), 4.58 (d, 1H, *J* = 6.9 Hz), 4.51 (d, 1H, *J* = 10.7 Hz), 4.17 (dd, 1H, *J* = 8.2, 5.5 Hz), 3.80 (s, 3H), 3.75 (d, 1H, *J* = 5.6 Hz), 3.68 (m, 1H), 3.50 (m, 1H), 2.14 (s, 3H), 1.18 (s, 3H), 1.16 (s, 3H), 0.88 (apparent t, 2H), –0.02 (s, 9H). ^{13}C NMR (101 MHz, $CDCl_3$) δ: 212.7, 159.0, 136.1, 130.8, 129.2, 118.8, 113.6, 92.3, 85.9, 78.7, 75.6, 65.5, 55.2, 51.6, 27.1, 23.2, 21.1, 18.0, –1.5. Anal. calcd. for $C_{23}H_{38}O_5Si$: C 65.36, H 9.06; found: C 65.15, H 9.28.

(2*R*,3*R*,4*S*,6*R*,8*S*,9*S*)-2-(2-(3,4-Dimethoxybenzyloxy)ethyl)-8-ethenyl-9-(4-methoxybenzyl)oxy-3,10,10-trimethyl-1,7-dioxaspiro[4.5]decan-4-ol (56a) and (2*R*,3*R*,4*R*,6*R*,8*S*,9*S*)-2-(2-(3,4-dimethoxybenzyloxy)ethyl)-8-ethenyl-9-(4-methoxybenzyl)oxy-3,10,10-trimethyl-1,7-dioxaspiro[4.5]decan-4-ol (56b)

n-BuLi in hexanes (1.6 M, 4.0 mL, 6.39 mmol) was added dropwise to *i*-Pr_2NH (913 μL, 6.51 mmol) in THF (8 mL) at 0°C. After 10 min, the mixture was cooled to –78°C and ketone **54** (2.29 g, 5.43 mmol) in THF (11 mL) was added dropwise. The mixture was stirred at –55 to –45°C for 15 min, cooled to –78°C, and then aldehyde **47** (1.66 g, 4.19 mmol) in THF (13 mL) was added. Following an additional 20 min at –78°C, the solution was allowed to warm slowly to –25°C over 1 h. Saturated aqueous NH_4Cl was added and the mixture was allowed to warm to room temperature. After dilution with Et_2O (50 mL), the mixture was extracted with Et_2O (2 × 100 mL), and the extracts were washed with brine and dried (Na_2SO_4). Rotary evaporation and chromatography (hexanes–EtOAc, 5:2) gave recovered **54** (440 mg) and the aldol product (3.39 g, 99%) as a colorless oil. The aldol product was treated with $TsOH \cdot H_2O$ (960 mg) in MeOH (60 mL) for 1.5 h at 0°C and 4 h at room temperature. After neutralization with Et_3N (0.5 mL), rotary evaporation and chromatography (hexanes–EtOAc, 1:1) gave spiroketal **56a** (1.10 g, 48%) and **56b** (515 mg, 22%). Spiroketal **56a** was obtained as a colorless oil. TLC R_f = 0.40 (Et_2O). $[\alpha]_D^{25}$ = +67.3° (*c* = 4.5). EI-MS *m*/*z*: 556 ($M^{\cdot+}$), 538, 435, 417, 405. EI-HRMS calcd. for $C_{32}H_{44}O_8$: 556.3036 ($M^{\cdot+}$); found: 556.3033 ($M^{\cdot+}$). IR (film) (cm^{-1}): 3519, 1611, 1515, 1465, 1420, 1414, 1302, 1248, 1119, 1111, 1071, 1031, 887, 881, 788, 765. ^{1}H NMR (300 MHz, $CDCl_3$) δ: 7.27 (d, 2H, *J* = 8.6 Hz), 6.84 (d, 2H, *J* = 8.7 Hz), 6.80 (m, 3H), 6.02 (m, 1H), 5.23 (dm, 1H, *J* = 17.4 Hz), 5.10 (dm, 1H, *J* = 10 Hz), 4.63 (dd, 1H, *J* = 8.6, 6.4 Hz), 4.43 (d, 1H, *J* = 11.0 Hz), 4.33 (d, 1H, *J* = 11.0 Hz), 4.30 (m, 1H), 4.14

© 2001 NRC Canada

(d, 1H, *J* = 11.5 Hz), 4.02 (d, 1H, *J* = 11.4 Hz), 3.87 (s, 3H), 3.86 (s, 3H), 3.79 (br d, 1H), 3.72 (s, 3H), 3.50 (m, 3H), 1.8–1.5 (m, 4H), 1.13 (s, 3H), 0.94 (s, 3H), 0.82 (d, 3H, *J* = 7.1 Hz). ^{13}C NMR (75 MHz, $CDCl_3$) δ: 159.0, 149.0, 148.4, 136.7, 131.6, 130.8, 129.2, 119.9, 117.4, 113.5, 111.13, 111.07, 108.3, 88.1, 83.6, 73.9, 72.3, 71.1, 67.4, 63.2, 55.9, 55.8, 55.1, 50.6, 37.8, 33.0, 29.2, 23.7, 17.0, 10.8. Spiroketal **56b** was obtained as a colorless oil. TLC R_f = 0.25 (Et_2O). $[\alpha]_D^{25}$ = +74.0° (*c* = 2.25). EI-MS *m*/*z*: 556 ($M^{\cdot+}$), 538, 435, 417, 405. EI-HRMS calcd. for $C_{23}H_{44}O_8$: 556.3036 ($M^{\cdot+}$); found: 556.3066 ($M^{\cdot+}$). IR (film) (cm^{-1}): 3438, 1611, 1515, 1466, 1450, 1363, 1248, 1139, 1104, 1032, 992, 908, 788, 785. ^{1}H NMR (300 MHz, $CDCl_3$) δ: 7.26, (d, 2H, *J* = 8.5 Hz), 6.84 (d, 2H, *J* = 8.5 Hz), 6.80 (m, 3H), 6.02 (m, 1H), 5.23 (dm, 1H, *J* = 17.2 Hz), 5.12 (dm, 1H, *J* = 10.0 Hz), 4.60 (dd, 1H, *J* = 8.6, 5.6 Hz), 4.43 (d, 1H, 10.9 Hz), 4.34 (d, 1H, *J* = 10.9 Hz), 4.19 (m, 1H), 4.17 (d, 1H, *J* = 11.5 Hz), 4.04 (d, 1H, *J* = 11.5 Hz), 4.00 (dm, 1H, *J* = 10.5 Hz), 3.87 (s, 3H), 3.85 (s, 3H), 3.73 (s, 3H), 3.55 (d, 1H, *J* = 5.6 Hz), 3.47 (m, 2H), 1.9–1.4 (m, 4H), 1.14 (s, 3H), 0.96 (s, 3H), 0.81 (d, 3H, *J* = 6.9 Hz). ^{13}C NMR (75 MHz, $CDCl_3$) δ: 159.1, 149.1, 148.5, 137.2, 131.6, 131.1, 129.2, 120.1, 117.1, 113.6, 111.3, 111.1, 108.3, 88.7, 83.1, 73.8, 72.5, 68.6, 67.6, 67.5, 56.0, 55.9, 55.2, 50.3, 38.4, 33.1, 32.2, 23.9, 17.0, 4.0.

(2*R*,3*S*,6*R*,8*S*,9*S*)-2-(2-(3,4-Dimethoxybenzyl)oxyethyl)-8-ethenyl-9-(4-methoxybenzyl)oxy-3,10,10-trimethyl-1,7-dioxaspiro[4.5]-decan-4-one (57)

From **56a**: DMSO (243 μL, 3.42 mmol) in CH_2Cl_2 (5 mL) was added dropwise to $(COCl)_2$ (230 μL, 2.63 mmol) in CH_2Cl_2 (5 mL) at –78°C. After 5 min, spiroketal **56a** (1.05 g, 1.88 mmol) in CH_2Cl_2 (12 mL) and, after 10 min, Et_3N (767 μL, 5.5 mmol) were both slowly added. The mixture was allowed to warm up to 0°C over 15 min and diluted with Et_2O (80 mL). The ethereal layer was washed with H_2O (2 × 30 mL) and brine and dried (Na_2SO_4). Rotary evaporation and chromatography (hexanes–EtOAc, 3:2) gave ketone **57** (992 mg, 95%) as a colorless oil. TLC R_f = 0.6 (Et_2O). ^{1}H NMR (400 MHz, $CDCl_3$) δ: 7.27 (d, 2H, *J* = 9.5 Hz), 6.86 (d, 2H, *J* = 8.7 Hz), 6.79 (d, 2H, *J* = 8.0 Hz), 6.74 (m, 2H), 6.00 (m, 1H), 5.24 (dm, 1H, *J* = 16.2 Hz), 5.11 (dm, 1H, *J* = 10.0 Hz), 4.63 (dd, 1H, *J* = 8.6, 5.3 Hz), 4.44 (d, 1H, *J* = 10.9 Hz), 4.37 (d, 1H, *J* = 10.9 Hz), 4.32 (dm, 1H, *J* = 10.6 Hz), 4.15 (d, 1H, *J* = 11.6 Hz), 4.02 (d, 1H, *J* = 11.3 Hz), 3.87 (s, 3H), 3.86 (s, 3H), 3.74 (s, 3H), 3.58 (d, 1H, *J* = 5.4 Hz), 3.50 (m, 2H), 2.57 (d, 1H, *J* = 14.2 Hz), 2.30 (m, 1H), 2.21 (d, 1H, *J* = 15.0 Hz), 1.85 (m, 1H), 1.24 (s, 3H), 1.08 (m, 1H), 1.07 (d, 3H, *J* = 7.2 Hz), 0.96 (s, 3H). Alcohol **56b** (515 mg, 0.926 mmol) was converted into **57** (510 mg, 100%) under identical Swern oxidation conditions. The crude ketone from both experiments **57** was reduced directly without any further purification.

(2*R*,3*R*,4*S*,6*R*,8*S*,9*S*)-2-[2-(3,4-Dimethoxybenzyloxy)ethyl]-8-ethenyl-9-(4-methoxybenzyl)oxy-3,10,10-trimethyl-1,7-dioxaspiro[4.5]decan-4-ol (56a)

Ketone **57** (1.25 g, 2.17 mmol) in THF (20 mL) was added dropwise to K-Selectride in THF (0.5 M, 8.7 mL, 4.34 mmol) in THF (10 mL) at –78°C. After 2 h, the mixture was allowed to warm up to –20°C over 20 min. Excess K-Selectride was quenched with MeOH (2 mL), and then NaOH (3 M, 5 mL) and H_2O_2 (30%, 5 mL) were added. The resulting aqueous mixture was stirred for 1.5 h at 0°C and diluted with Et_2O (100 mL). The ethereal layer was washed with H_2O (2 × 30 mL) and brine (50 mL) and dried (Na_2SO_4). Rotary evaporation and chromatography (hexanes–EtOAc, 3:2) gave spiroketal **56a** (1.12 g, 93%).

(2*S*)-3-(Benzyloxy)methoxy-2-methyl-1-propanol (60) (38)

$PhCH_2OCH_2Cl$ (13.8 g, 0.088 mmol) was added to alcohol **58** (8.0 g, 0.067 mmol) and *i*-Pr_2NEt (18.5 mL, 0.106 mmol) in CH_2Cl_2 (30 mL) at 0°C. The mixture was subsequently stirred at room temperature for 12 h when MeOH (15 mL) was added. The solution was diluted with Et_2O (200 mL), washed sequentially with 1 M HCl, H_2O, 10% aqueous $NaHCO_3$, and brine. The organic layer was dried ($MgSO_4$) and rotary evaporated to leave a colorless oil, which was dissolved in Et_2O (100 mL) and added to $LiAlH_4$ (3.8 g, 1.0 mmol) in Et_2O (150 mL) at 0°C. After stirring for 15 min at 0°C and 1 h at room temperature, excess $LiAlH_4$ was quenched by the careful addition of MeOH. Following further stirring for 30 min, H_2O (15.2 mL) and aqueous NaOH (15%, 4 mL) were added and, after 1 h, the insoluble solid was removed by filtration. Rotary evaporation of the filtrate and chromatography (hexanes–Et_2O, 1:3) gave alcohol **60** (14.8 g, 100%).

Methyl (4*S*)-5-(benzyloxy)methoxy-4-methyl-2-pentenoate (62)

DMSO (9.5 g, 0.122 mol) in CH_2Cl_2 (80 mL) was added dropwise to $(COCl)_2$ (8.1 mL, 92.9 mmol) in CH_2Cl_2 (80 mL) at –78°C. After 10 min, alcohol **60** (14.0 g, 66.7 mmol) in CH_2Cl_2 (100 mL) was added, stirring was continued for 15 min at –78°C and Et_3N (33.7 mL, 0.241 mol) was slowly added. After stirring for 10 min, the resulting mixture was allowed to warm up to –10°C for 15 min, diluted with CH_2Cl_2 (100 mL), and washed with H_2O (3 × 15 mL) and brine. The organic layer was dried (Na_2SO_4) and rotary evaporated to leave the crude aldehyde **61**, which was used without further purification. $Ph_3P{=}CHCO_2Me$ (29.0 g, 0.867 mmol) was added to the aldehyde in $ClCH_2CH_2Cl$ (200 mL) and the mixture was heated at 70°C for 16 h. After rotary evaporation, the residue was diluted with Et_2O (200 mL). Filtration, rotary evaporation, and chromatography (hexanes–EtOAc, 7:1) gave ester **62** (for the (*R*)-antipode of **62**, see ref. 39) (16.7 g, 95%) as a colorless oil. $[\alpha]_D^{25}$ = –16° (*c* = 1.6). ^{1}H NMR (300 MHz, $CDCl_3$) δ: 7.26–7.25 (m, 5H), 6.95 (dd, 1H, *J* = 16.0, 7.0 Hz), 5.87 (dd, 1H, *J* = 16.0, 1.5 Hz), 4.73 (s, 2H), 4.57 (s, 2H), 3.71 (s, 3H), 3.51 (d, 2H, *J* = 6.5 Hz), 2.66–2.57 (m, 1H), 1.08 (d, 3H, *J* = 7.0 Hz). ^{13}C NMR (75 MHz, $CDCl_3$) δ: 167.0, 151.3, 137.9, 128.5, 127.9, 127.8, 120.8, 94.8, 71.7, 69.5, 51.5, 36.8, 16.1.

(4*S*)-5-(Benzyloxy)methoxy-4-methyl-2-penten-1-ol (63)

Ester **62** (16.2 g, 61.4 mmol) in CH_2Cl_2 (100 mL) was added dropwise to DIBAl-H in PhMe (1.5 M, 90 mL, 135 mmol) in CH_2Cl_2 (100 mL) at –78°C and, after 1 h, excess DIBAl-H was quenched with MeOH (30 mL). Stirring was continued until H_2 evolution ceased, then H_2O (40 mL) in THF (40 mL) was carefully added to the clear solution.

© 2001 NRC Canada

This was allowed to warm up to 0°C over 15 min and the resulting suspension stirred vigorously for 1.5 h. Filtration, rotary evaporation, and chromatography (hexanes–EtOAc, 1:1) gave alcohol **63** (for the (*R*)-antipode of **63**, see ref. 40) (14.3 g, 99%) as a colorless oil. ^{1}H NMR (300 MHz, $CDCl_3$) δ: 7.36–7.26 (m, 5H), 5.77–5.63 (m, 2H), 4.76 (s, 2H), 4.60 (s, 2H), 4.13–4.10 (m, 2H), 3.51 (dd, 1H, *J* = 9.5, 6.5 Hz), 3.46 (dd, 1H, *J* = 9.5, 6.5 Hz), 2.54–2.46 (m, 1H), 1.28 (t, 1H, *J* = 6.0 Hz), 1.06 (d, 3H, *J* = 7.0 Hz). The product was used directly without further purification.

(2*S*,3*S*)-2-[1-(Benzyloxy)methoxy-(2*R*)-propyl]-3-(hydroxymethyl)oxirane (64)

L-(+)-Diethyl tartrate (1.9 g, 9.21 mmol) and alkene **63** (14.3 g, 60.6 mmol) in CH_2Cl_2 (50 mL) were added sequentially to a suspension of powdered molecular sieves (3 Å, 8 g) in CH_2Cl_2 (50 mL). The mixture was cooled to –20°C and Ti(O-*i*-Pr)$_4$ (2.4 mL, 8.13 mmol) was added with stirring. After 20 min at –20°C, *t*-BuOOH in 2,2,4-trimethylpentane (3 M, 24 mL, 72.0 mmol) was added slowly and the mixture stirred for 1.5 h at room temperature. The solution was filtered through Celite, washing with CH_2Cl_2, and the combined washings dried (Na_2SO_4). Rotary evaporation and chromatography (hexanes–Et_2O, 1:2) gave epoxide **64** (13.7 g, 90%) as a colorless oil. TLC R_f = 0.40 (hexanes–EtOAc, 1:1). $[\alpha]_D^{25}$ = –26° (*c* = 4.35). EI-MS *m*/*z*: 221 ([M – CH_2OH]$^+$), 191, 174, 91. EI-HRMS calcd. for $C_{13}H_{17}O_3$: 221.1178 ([M – CH_2OH]$^+$); found: 221.1182 ([M – CH_2OH]$^+$). IR (film) (cm^{-1}): 3448, 1497, 1455. ^{1}H NMR (300 MHz, $CDCl_3$) δ: 7.37–7.29 (m, 5H), 4.75 (s, 2H), 4.60 (s, 2H), 3.89 (ddd, 1H, *J* = 12.5, 4.5, 2.5 Hz), 3.64 (ddd, 1H, *J* = 12.5, 4.5, 2.5 Hz), 3.55–3.53 (m, 2H), 3.05 (dt, 1H, *J* = 4.5, 2.5 Hz), 2.90 (dd, 1H, *J* = 7.0, 2.5 Hz), 1.77 (sept, 1H, *J* = 7.0 Hz), 1.67–1.64 (br m, 1H), 1.04 (d, 3H, *J* = 7.0 Hz). ^{13}C NMR (75 MHz, $CDCl_3$) δ: 137.9, 128.6, 127.9, 127.8, 94.9, 70.4, 69.5, 62.0, 58.5, 58.0, 35.9, 13.6. Anal. calcd. for $C_{14}H_{20}O_4$: C 66.64, H 7.99; found: C 66.90, H 8.03.

(4*R*)-4-(1-(Benzyloxy)methoxy)-(2*R*)-propyl)-2,2-dimethyl-1,3-dioxane (66)

Epoxide **64** (13.7 g, 0.0544 mmol) in THF (80 mL) was added dropwise to Red-Al in PhMe (3.4 M, 22.6 mL, 76.8 mmol) in THF (80 mL) at –20°C. The solution was allowed to warm to room temperature over 15 min and left at this temperature for 3 h, after which excess Red-Al was quenched with MeOH at 0°C. H_2O (24 mL) and aqueous NaOH (15%, 24 mL) were added, the mixture was stirred for 1 h at room temperature, and the resulting insoluble solid removed by filtration. The filtrate was evaporated under reduced pressure and the residue chromatographed (hexanes–EtOAc, 1:5) to give the diol **65** (15.0 g) as a colorless oil. TLC R_f = 0.38 (hexanes–EtOAc, 1:2). $[\alpha]_D^{25}$ = +3.3° (*c* = 6.85). EI-MS *m*/*z*: 255 ([M + H]$^+$), 223 ([M – CH_2OH]$^+$), 205, 148. EI-HRMS calcd. for $C_{13}H_{19}O_3$: 223.1334 ([M – CH_2OH]$^+$); found: 223.1340 ([M – CH_2OH]$^+$). IR (film) (cm^{-1}): 3390, 1497, 1454. ^{1}H NMR (300 MHz, $CDCl_3$) δ: 7.32–7.23 (m, 5H), 4.71 (s, 2H), 4.56 (s, 2H), 3.98–3.92 (m, 1H), 3.83–3.77 (m, 2H), 3.61–3.54 (m, 2H), 2.92 (d, 1H, *J* = 4.0 Hz), 2.58 (br t, 1H, *J* = 4.5 Hz), 1.87–1.70 (m, 2H), 1.58–1.48 (m, 1H), 0.90 (d, 3H, *J* = 7.0 Hz). ^{13}C NMR (75 MHz, $CDCl_3$) δ: 138.5, 129.0, 128.4, 128.3, 95.4, 73.8, 72.2, 70.2, 62.2, 39.0, 36.0, 11.7. The diol **65** was used directly in the next step. Diol **65** (15 g) was allowed to react with $(MeO)_2CMe_2$ (20 mL) and pyridinium 4-toluenesulfonate (500 mg, 1.98 mmol) in PhH (100 mL) at room temperature for 3 h. Et_3N (ca. 1.0 mL) was added, and rotary evaporation and chromatography (hexanes–Et_2O, 1:1) gave ether **66** (15.9 g, 100% from epoxide **64**) as a colorless oil. $[\alpha]_D^{25}$ = –11.7° (*c* = 13.8). EI-MS *m*/*z*: 294 (M$^{\cdot+}$), 279, 115, 91. EI-HRMS calcd. for $C_{17}H_{26}O_4$: 294.1831 (M$^{\cdot+}$); found: 294.1817 (M$^{\cdot+}$). IR (film) (cm^{-1}): 3031, 1497, 1455. ^{1}H NMR (300 MHz, $CDCl_3$) δ: 7.34–7.25 (m, 5H), 4.73 (s, 2H), 4.58 (s, 2H), 3.93 (dt, 1H, *J* = 11.5, 3.0 Hz), 3.89 (ddd, 1H, *J* = 8.5, 6.0, 2.5 Hz), 3.82 (ddd, 1H, *J* = 11.5, 5.5, 1.5 Hz), 3.58 (dd, 1H, *J* = 9.5, 6.0 Hz), 3.44 (dd, 1H, *J* = 9.5, 6.0 Hz), 1.79–1.63 (m, 2H), 1.41 (s, 3H), 1.34 (s, 3H), 1.37–1.30 (m, 1H), 0.96 (d, 3H, *J* = 7.0 Hz). ^{13}C NMR (75 MHz, $CDCl_3$) δ: 138.0, 128.5, 127.9, 127.7, 98.2, 94.9, 69.9, 69.5, 69.3, 60.1, 38.6, 30.0, 28.5, 19.3, 12.2. Anal. calcd. for $C_{17}H_{26}O_4$: C 69.36, H 8.90; found: C 69.24, H 9.00.

(2*R*,3*R*)-3,5-Isopropylidenedioxy-2-methyl-propane-1-ol (67)

Ether **66** (3.4 g, 11.5 mmol) in THF (10 mL) was added dropwise to Na (630 mg, 27.3 mmol) in liquid NH_3 (10 mL) at –78°C. After 1 h, the mixture was allowed to warm to room temperature, for the NH_3 to vent, and then rotary evaporated. The residue was extracted with CH_2Cl_2, filtered, rotary evaporated, and chromatographed (hexanes–Et_2O, 1:1) to give alcohol **67** (2.09 g, 100%) as a colorless oil. $[\alpha]_D^{25}$ = –11° (*c* = 5.05). EI-MS *m*/*z*: 159 ([M – Me]$^+$), 115. EI-HRMS calcd. for $C_8H_{15}O_3$: 159.1021 ([M – Me]$^+$); found: 159.1025 ([M – Me]$^+$). IR (film) (cm^{-1}): 3425, 1461, 1382, 1271. ^{1}H NMR (300 MHz, $CDCl_3$) δ: 4.05 (ddd, 1H, *J* = 12.0, 4.0, 2.5 Hz), 3.96 (dt, 1H, *J* = 11.5, 2.5 Hz), 3.86 (ddd, 1H, *J* = 11.5, 5.5, 2.5 Hz), 3.68 (ddd, 1H, *J* = 11.0, 7.5, 4.5 Hz), 3.55 (ddd, 1H, *J* = 11.0, 6.5, 4.0 Hz), 2.63 (dd, 1H, *J* = 6.5, 4.5 Hz), 1.90–1.77 (m, 2H), 1.43 (s, 3H), 1.36 (s, 3H), 1.34–1.27 (m, 1H), 0.88 (d, 3H, *J* = 7.0 Hz). ^{13}C NMR (75 MHz, $CDCl_3$) δ: 98.4, 71.9, 65.2, 60.0, 39.3, 29.9, 26.9, 19.1, 11.6. Anal. calcd. for $C_9H_{18}O_3$: C 62.04, H 10.41; found: C 61.71, H 10.64.

(2*S*)-(2,2-Dimethyl-1,3-dioxolan-(4*R*)-yl)propanal (68)

DMSO (1.8 mL, 25.4 mmol) in CH_2Cl_2 (15 mL) was added to $(COCl)_2$ (1.8 mL, 20.9 mmol) in CH_2Cl_2 (20 mL) at –78°C. After 5 min, alcohol **67** (2.8 g, 16.1 mmol) in CH_2Cl_2 (15 mL) was added and stirring was continued for 10 min at –78°C, then Et_3N (7.0 mL, 50.0 mmol) was added slowly. The solution was allowed to warm to –20°C over 15 min and poured into H_2O. The aqueous mixture was extracted with CH_2Cl_2 (2 × 100 mL) and the extracts washed with H_2O and brine. The organic layer was dried (Na_2SO_4), rotary evaporated, and chromatographed (hexanes–Et_2O, 3:2) to give aldehyde **68** (2.65 g, 95%) as a colorless oil. IR (film) (cm^{-1}): 2993, 1725, 1458, 1382. ^{1}H NMR (300 MHz, $CDCl_3$) δ: 9.74 (d, 1H, *J* = 1.0 Hz), 4.24 (ddd, 1H, *J* = 12.0, 5.0, 2.5 Hz), 3.97 (dt, 1H, *J* = 12.0, 3.0 Hz), 3.84 (ddd, 1H, *J* = 12.0, 5.0, 1.5 Hz), 2.48–2.39 (m, 1H), 1.76–1.58 (m, 2H), 1.09 (d, 3H, *J* = 7.0 Hz). ^{13}C NMR (75 MHz, $CDCl_3$) δ: 204.1, 98.5, 68.8, 59.6, 50.7, 29.7, 28.0,

© 2001 NRC Canada

19.0, 8.3. The unstable aldehyde **68** was used directly without further purification.

(2*R*,3*R*,4*RS*,6*R*,8*S*,9*S*)-8-Ethenyl-2-(2-hydroxyethyl)-9-(4-methoxybenzyl)oxy-3,10,10-trimethyl-1,7-dioxaspiro[4.5]-decan-4-ol (69)

n-BuLi in hexanes (1.6 M, 9.4 mL, 15.0 mmol) was added dropwise to *i*-Pr_2NH (2.1 mL, 15.0 mmol) in THF (15 mL) at 0°C. The clear solution was stirred for 10 min at 0°C and the cooled to –78°C, at which point ketone **54** (6.4 g, 15.2 mmol) in THF (30 mL) was slowly added over 10 min. The mixture was stirred at –60 to –45°C for 20 min and recooled to –78°C. Aldehyde **68** (2.6 g, 14.9 mmol) in THF (15 mL) was added dropwise and the mixture stirred for 30 min at –78°C and then allowed to warm to –20°C. The solution was poured into a mixture of saturated aqueous NH_4Cl and ice. The mixture was extracted with Et_2O (3 × 100 mL) and the organic phase washed with H_2O and brine and dried (Na_2SO_4). Rotary evaporation and chromatography (hexanes–Et_2O, 3:2) gave recovered ketone **54** (2.4 g, 38%) and the aldol adduct (5.4 g, 61%; 96% allowing for recovered **54**). $TsOH·H_2O$ (100 mg, 0.526 mmol) was added to this adduct (4.9 g, 8.25 mmol) in MeOH (100 mL) and the mixture stirred for 3.5 h at room temperature. Et_3N (3 mL) was added, at which point rotary evaporation and chromatography (hexanes–EtOAc, 1:2) gave spiroketal **69** (2.86 g, 85%) as a mixture of diastereomeric alcohols, which were directly oxidized to produce the corresponding ketone **70**.

(2*R*,3*R*,4*S*,6*R*,8*S*,9S)-8-Ethenyl-2-(2-hydroxyethyl)-9-(4-methoxybenzyl)oxy-3,10,10-trimethyl-1,7-dioxaspiro[4.5]-decan-4-ol (71)

DMSO (716 μL, 10.1 mmol) in CH_2Cl_2 (7.5 mL) was added to $(COCl)_2$ (732 μL, 8.39 mmol) in CH_2Cl_2 (10 mL) at –78°C. After stirring for 5 min, the diastereomeric alcohols **69** (1.31 g, 3.23 mmol) in CH_2Cl_2 (10 mL) were added and stirring was continued for 10 min at –78°C. Et_3N (2.8 mL, 20.1 mmol) was added slowly, the solution was allowed to warm up to –20°C over 15 min and then poured into H_2O. The aqueous mixture was extracted with CH_2Cl_2 (2 × 100 mL) and the extracts washed with H_2O and brine. The organic layer was dried (Na_2SO_4) and rotary evaporated to give the crude keto-aldehyde **70** (1.25 g). This compound in THF (25 mL) was added dropwise to K-Selectride in THF (0.5 M, 17 mL, 8.5 mmol) in THF (10 mL) at –78°C. The mixture was stirred for 2 h at –78°C and excess K-Selectride quenched with MeOH (10 mL). The solution was allowed to warm up to –10°C and aqueous NaOH (15%, 8 mL) and aqueous H_2O_2 (30%, 10 mL) were added sequentially at –5°C. The resulting alkaline mixture was vigorously stirred for 2 h at 0°C when it was extracted with CH_2Cl_2 (10 mL) and the extract washed with H_2O and brine and dried (Na_2SO_4.). Rotary evaporation and chromatography (hexanes–EtOAc, 1:2) gave diol **71** (0.997 g, 76% from **69**) as colorless crystals: mp 96.5–98°C (from EtOAc–hexanes). TLC R_f = 0.41 (hexanes–EtOAc, 3:1). $[\alpha]_D^{20}$ = +10° (*c* = 1.1). EI-MS *m*/*z*: 406 ($M^{\cdot+}$), 388, 270, 234, 229, 211, 163. EI-HRMS calcd. for $C_{23}H_{34}O_6$: 406.2350 ($M^{\cdot+}$); found: 406.2346 ($M^{\cdot+}$). IR (film) (cm^{-1}): 3536, 3449, 1611, 1586, 1510, 1452. ^1H NMR (300 MHz, $CDCl_3$) δ: 7.19 (d, 2H, *J* = 8.0 Hz), 6.82 (d, 2H, *J* = 8.0 Hz), 6.05 (ddd, 1H, *J* = 17.5, 9.5, 8.0 Hz), 5.30 (dd, 1H, *J* = 17.5, 1.0 Hz), 5.26 (dd, 1H, *J* = 9.5, 1.0 Hz), 4.59 (dd, 1H, *J* = 8.0, 5.0 Hz), 4.55 (d, 1H, *J* = 12.5 Hz), 4.43 (br d, 1H, *J* = 11.0 Hz), 4.29 (dd, 1H, *J* = 11.0, 2.0 Hz), 4.25 (d, 1H, *J* = 12.5 Hz), 3.82–3.73 (m, 4H), 3.78 (s, 3H), 3.48 (d, 1H, *J* = 5.0 Hz), 1.96–1.90 (m, 1H), 1.76 (br d, 1H, *J* = 14.0 Hz), 1.64–1.57 (m, 1H), 1.53 (br d, 1H, *J* = 14.0 Hz), 1.35–1.34 (m, 1H), 0.93 (s, 3H), 0.84 (d, 3H, *J* = 7.0 Hz), 0.81 (s, 3H). ^{13}C NMR (75 MHz, $CDCl_3$) δ: 159.5, 135.7, 130.6, 129.6, 118.4, 113.7, 108.6, 86.1, 83.9, 73.3, 70.8, 69.6, 63.3, 55.3, 50.5, 38.4, 35.2, 29.0, 23.4, 17.4, 11.1. Anal. calcd. for $C_{23}H_{34}O_6$: C 67.95, H 8.43; found: C 67.60, H 8.03. Diffraction data from a single crystal of **71** was obtained on a Bruker P4 four-circle diffractometer operating in the θ–2θ scan mode at –100°C. The unit cell constants were obtained by refinement against the setting angles for 25 reflections widely distributed in reciprocal space. The diffraction pattern exhibited symmetry consistent with the space group $P2_12_12_1$ in the orthorhombic crystal system. The structure was solved by direct methods and refined by full-matrix least-squares.[2] All non-hydrogen atoms were refined with anisotropic thermal displacement parameters. Hydrogen atoms were placed in idealized positions, with the exception of H26 and H9, which were located in the difference Fourier map and were refined independently with isotropic thermal displacement parameters.

(2*R*,3*R*,4*S*,6*R*,8*S*,9*S*)-8-Ethenyl-9-(4-methoxybenzyl)oxy-2-(triethylsilyl)oxyethyl-3,10,10-trimethyl-1,7-dioxaspiro-[4.5]decan-4-ol (72)

Et_3SiCl (509 μL, 3.03 mmol) was slowly added over 1.5 h to diol **71** (1.1 g, 2.71 mmol), Et_3N (0.7 mL), and imidazole (454 mg, 6.67 mmol) in dry CH_2Cl_2 (30 mL) at –40°C (Ar). After the mixture was stirred for 2 h at –20°C, excess reagent was quenched with MeOH (1.0 mL) and the resultant mixture diluted with CH_2Cl_2 (50 mL). The solution was washed with H_2O and brine and dried (Na_2SO_4). Rotary evaporation and chromatography (hexanes–EtOAc, 5:1) gave **72** (1.1 g, 78%) as a colorless oil. TLC R_f = 0.39 (hexanes–Et_2O, 1:1). $[\alpha]_D^{20}$ = +49.0° (*c* = 2.35). EI-MS *m*/*z*: 520 ($M^{\cdot+}$), 484, 429, 401, 317, 289, 241. EI-HRMS calcd. for $C_{29}H_{48}O_6Si$: 520.3220 ($M^{\cdot+}$); found: 520.3213 ($M^{\cdot+}$). IR (film) (cm^{-1}): 3535, 2953, 1613, 1587, 1514, 1466. ^1H NMR (300 MHz, $CDCl_3$) δ: 7.20 (d, 2H, *J* = 8.5 Hz), 6.82 (d, 2H, *J* = 8.5 Hz), 6.11 (ddd, 1H, *J* = 17.5, 10.0, 9.0 Hz), 5.20 (dd, 1H, *J* = 17.5, 1.0 Hz), 5.17 (dd, 1H, *J* = 10.0, 1.0 Hz), 4.58 (dd, 1H, *J* = 9.0, 6.0 Hz), 4.45 (d, 1H, *J* = 12.0 Hz), 4.28 (d, 1H, *J* = 12.0 Hz), 4.29–4.24 (m, 1H), 3.80 (d, 1H, *J* = 10.0 Hz), 3.80–3.64 (m, 3H), 3.78 (s, 3H), 3.47 (d, 1H, *J* = 6.0 Hz), 1.78–1.41 (m, 5H), 1.03 (s, 3H), 0.91 (t, 9H,

[2] Supplementary material may be purchased from the Depository of Unpublished Data, Document Delivery, CISTI, National Research Council Canada, Ottawa, ON K1A 0S2, Canada. For information on obtaining material electronically go to http://www.nrc.ca/cisti/irm/unpub_e.shtml. Crystallographic information has also been deposited with the Cambridge Crystallographic Data Centre. Copies of the data can be obtained, free of charge, on application to the Director, CCDC, 12 Union Road, Cambridge CB2 1EZ, U.K. (fax: 44-1223-336033 or e-mail: deposit@ccdc.cam.ac.uk).

© 2001 NRC Canada

J = 8.0 Hz), 0.87 (s, 3H), 0.81 (d, 3H, *J* = 7.0 Hz), 0.53 (q, 6H, *J* = 8.0 Hz). ^{13}C NMR (75 MHz, $CDCl_3$) δ: 159.2, 137.1, 131.0, 129.3, 117.6, 113.7, 108.5, 87.6, 83.9, 73.7, 71.3, 63.3, 60.4, 55.4, 50.6, 38.1, 36.5, 29.4, 24.1, 17.3, 11.1, 7.0, 4.7. Anal. calcd. for $C_{29}H_{48}O_6Si$: C 66.88, H 9.29; found: C 67.13, H 9.29.

(2*R*,3*R*,4*S*,6*R*,8*S*,9*S*)-4-(*tert*-Butyldimethylsilyl)oxy-8-ethenyl-9-(4-methoxybenzyl)oxy-2-(triethylsilyl)oxyethyl-3,10,10-trimethyl-1,7-dioxaspiro[4.5]decane (73)

t-$BuMe_2SiOSO_2CF_3$ (477 μL, 2.08 mmol) was added to **72** (900 mg, 1.73 mmol) and *i*-Pr_2NEt (906 μL, 5.2 mmol) in dry CH_2Cl_2 (10 mL) at –50°C (Ar). The reaction mixture was allowed to warm to –20°C during 1.5 h. After excess reagent was quenched with MeOH (2.0 mL), the mixture was rotary evaporated and then chromatographed (hexanes–EtOAc, 11:1) to give **73** (1.11 g, 100%) as a colorless oil. TLC R_f = 0.43 (hexanes–Et_2O, 11:1). $[\alpha]_D^{20}$ = +55° (*c* = 1.35). EI-MS *m*/*z*: 634 ($M^{\cdot+}$), 577, 502, 484, 457, 441, 385. EI-HRMS calcd. for $C_{35}H_{62}O_6Si_2$: 634.4085 ($M^{\cdot+}$); found: 634.4075 ($M^{\cdot+}$). IR (film) (cm^{-1}): 2953, 1614, 1587, 1515, 1464, 1422. ^{1}H NMR (300 MHz, $CDCl_3$) δ: 7.21 (d, 2H, *J* = 8.5 Hz), 6.82 (d, 2H, *J* = 8.5 Hz), 6.06 (ddd, 1H, *J* = 17.5, 10.0, 8.0 Hz), 5.16 (dd, 1H, *J* = 17.5, 1.0 Hz), 5.06 (dd, 1H, *J* = 10.0, 1.0 Hz), 4.49 (dd, 1H, *J* = 8.0, 6.0 Hz), 4.46 (d, 1H, *J* = 12.0 Hz), 4.37 (dt, 1H, *J* = 9.0, 3.0 Hz), 4.29 (d, 1H, *J* = 12.0 Hz), 3.78 (s, 3H), 3.81–3.73 (m, 2H), 3.65–3.57 (m, 1H), 3.44 (d, 1H, *J* = 6.0 Hz), 1.71–1.55 (m, 2H), 1.44–1.32 (m, 3H), 1.01 (s, 3H), 0.91 (t, 9H, *J* = 8.0 Hz), 0.85 (s, 9H), 0.79 (d, 3H, *J* = 7.0 Hz), 0.53 (q, 6H, *J* = 8.0 Hz), –0.01 (s, 3H), –0.02 (s, 3H). ^{13}C NMR (75 MHz, $CDCl_3$) δ: 159.0, 138.2, 131.5, 129.1, 115.7, 113.6, 106.9, 88.2, 82.6, 73.5, 71.2, 63.4, 61.0, 55.3, 50.9, 38.8, 36.6, 30.7, 25.9, 24.2, 18.2, 17.4, 10.7, 7.0, 4.7, –4.4, –4.7. Anal. calcd. for $C_{35}H_{62}O_6Si_2$: C 66.20, H 9.84; found: C 66.48, H 9.95.

(2*R*,3*R*,4*S*,6*R*,8*R*,9*S*)-4-(*tert*-Butyldimethylsilyl)oxy-9-(4-methoxybenzyl)oxy-2-(triethylsilyl)oxyethyl-3,10,10-trimethyl-1,7-dioxaspiro[4.5]decane-8-carboxaldehyde (74)

O_3–O_2 was bubbled through alkene **73** (43 mg, 0.0726 mmol) in CH_2Cl_2 (3 mL) at –78°C. The solution, saturated with O_3, was stirred for 10 min and purged with Ar when Me_2S (1 mL) was added and the mixture was allowed to warm up to room temperature over 1 h. Rotary evaporation and chromatography (hexanes–Et_2O, 7:1) gave **74** (35 mg, 76%) as a colorless oil. TLC R_f = 0.50 (hexanes–Et_2O, 4:1). $[\alpha]_D^{20}$ = +97° (*c* = 1.64). EI-MS *m*/*z*: 636 ($M^{\cdot+}$), 608, 579, 441, 339, 163. EI-HRMS calcd. for $C_{34}H_{60}O_7Si_2$: 636.3878 ($M^{\cdot+}$); found: 636.3888 ($M^{\cdot+}$). IR (film) (cm^{-1}): 2953, 1723, 1613, 1514, 1464, 1385. ^{1}H NMR (300 MHz, $CDCl_3$) δ: 9.63 (d, 1H, *J* = 3.0 Hz), 7.16 (d, 2H, *J* = 8.5 Hz), 6.81 (d, 2H, *J* = 8.5 Hz), 4.63 (dt, 1H, *J* = 9.5, 2.5 Hz), 4.39 (d, 1H, *J* = 11.0 Hz), 4.35 (dd, 1H, *J* = 6.5, 3.0 Hz), 4.28 (d, 1H, *J* = 11.0 Hz), 3.83 (q, 1H, *J* = 3.0 Hz), 3.77 (s, 3H), 3.75 (d, 1H, *J* = 6.5 Hz), 3.59–3.54 (m, 2H), 1.69–1.54 (m, 1H), 1.47–1.41 (m, 2H), 1.03 (s, 3H), 0.89 (t, 9H, *J* = 8.0 Hz), 0.87 (s, 9H), 0.81 (d, 3H, *J* = 7.0 Hz), 0.79 (s, 3H), 0.50 (q, 6H, *J* = 8.0 Hz), 0.00 (s, 3H), –0.01 (s, 3H). ^{13}C NMR (75 MHz, $CDCl_3$) δ: 206.1, 159.2, 130.4, 129.6, 113.6, 109.2, 88.8, 85.0, 74.1, 70.7, 63.2, 59.5, 55.3, 50.9, 38.6, 36.4, 30.4, 25.8, 23.6, 18.1, 17.0, 10.6, 6.9, 4.6, –4.4, –4.8.

(2*R*,3*R*,4*S*,6*R*,8*S*,9*S*)-4-(*tert*-Butyldimethylsilyl)oxy-2-(*tert*-butyldimethylsilyl)oxyethyl-8-ethenyl-9-(4-methoxybenzyl)oxy-3,10,10-trimethyl-1,7-dioxaspiro[4.5]decane (75)

2,6-Lutidine (1.35 mL, 11.6 mmol) and *t*-$BuMe_2SiOTf$ (739 μL, 3.22 mmol) were added to diol **71** (328 mg, 0.808 mmol) in CH_2Cl_2 (5.0 mL) at –10°C. After 1 h at –5°C, the mixture was quenched with MeOH (2 mL), diluted with Et_2O (10 mL), washed with H_2O and brine, and dried (Na_2SO_4). Rotary evaporation and chromatography (hexanes–PhMe, 1:2) gave spiroketal **75** (475 mg, 90%) as a colorless oil. $[\alpha]_D^{25}$ = +58.3° (*c* = 0.23). IR (film) (cm^{-1}): 1614, 1513, 1471, 1252, 1115, 1086, 917, 899, 773. ^{1}H NMR (300 MHz, $CDCl_3$) δ: 7.24 (d, 2H, *J* = 8.5 Hz), 6.84 (d, 2H, *J* = 8.5 Hz), 6.08 (m, 1H), 5.19 (dd, 1H, *J* = 17.3, 1.4 Hz), 5.09 (dd, 1H, *J* = 10.0, 1.9 Hz), 4.54 (m, 1H), 4.48 (d, 1H, *J* = 11.5 Hz), 4.42 (m, 1H), 4.31 (d, 1H, *J* = 11.5 Hz), 3.81 (m, 1H), 3.79 (s, 3H), 3.81–3.64 (m, 2H), 3.46 (d, 1H, *J* = 5.9 Hz), 1.67 (m, 1H), 1.61 (dd, 1H, *J* = 14.0, 3.6 Hz), 1.48–1.38 (m, 2H), 1.37 (dd, 1H, *J* = 14.0, 2.0 Hz), 1.04 (s, 3H), 0.88 (s, 18H), 0.85 (s, 3H), 0.81 (d, 3H, *J* = 7.1 Hz), 0.02 (s, 3H), 0.00 (s, 9H). ^{13}C NMR (75 MHz, $CDCl_3$) δ: 158.8, 138.1, 131.4, 129.0, 115.7, 113.5, 106.8, 88.1, 82.5, 73.3, 71.0, 63.1, 61.0, 55.2, 50.8, 38.7, 36.4, 30.6, 26.0, 25.8, 24.1, 18.3, 18.1, 17.3, 10.6, –4.5, –4.8, –5.2, –5.3.

(2*R*,3*R*,4*S*,6*R*,8*R*,9*S*)-4-(*tert*-Butyldimethylsilyl)oxy-2-(*tert*-butyldimethylsilyl)oxyethyl-9-(4-methoxybenzyl)oxy-3,10,10-trimethyl-1,7-dioxaspiro[4.5]decane-8-carboxaldehyde (6)

Ozone was bubbled through spiroketal **75** (83.5 mg, 0.128 mmol) in CH_2Cl_2 (4 mL) at –78°C for 1 min, then Me_2S (1 mL) was immediately added. The solution was purged with N_2 and allowed to warm to room temperature. After 1 h, the mixture was filtered through Na_2SO_4, rotary evaporated, and chromatographed (hexanes–Et_2O, 9:1) to give spiroketal **6** (72.5 mg, 89%) as a pale yellow oil. $[\alpha]_D^{25}$ = +72.9° (*c* = 0.17). IR (film) (cm^{-1}): 1726, 1614, 1516, 1466, 1386, 1252, 1128, 1113, 1083, 835, 775. ^{1}H NMR (300 MHz, $CDCl_3$) δ: 9.65 (d, 1H, *J* = 3.0 Hz), 7.15 (d, 2H, *J* = 8.5 Hz), 6.80 (d, 2H, *J* = 8.5 Hz), 4.66 (m, 1H), 4.38 (d, 1H, *J* = 11.0 Hz), 4.36 (dd, 1H, *J* = 6.5, 3.0 Hz), 4.28 (d, 1H, *J* = 11.0 Hz), 3.84 (m, 1H), 3.76 (s, 3H), 3.75 (d, 1H, *J* = 6.5 Hz), 3.59 (m, 1H), 3.49 (m, 1H), 1.66 (dd, 1H, *J* = 14.0, 3.5 Hz), 1.57 (m, 1H), 1.45 (dd, 1H, *J* = 14.0, 2.5 Hz), 1.48–1.34 (m, 2H), 1.04 (s, 3H), 0.85 (s, 9H), 0.83 (s, 9H), 0.80 (d, 3H, *J* = 7.1 Hz), 0.80 (s, 3H), 0.00 (s, 3H), –0.01 (s, 3H), –0.03 (s, 3H), –0.05 (s, 3H). ^{13}C NMR (75 MHz, $CDCl_3$) δ: 206.0, 159.0, 130.4, 129.5, 113.5, 109.1, 88.8, 84.9, 74.0, 70.6, 62.9, 59.4, 55.2, 50.7, 38.5, 36.3, 30.3, 25.9, 25.7, 23.5, 18.2, 18.0, 16.8, 10.5, –4.6, –4.9, –5.4.

(2*R*,3*R*,4*S*,6*R*,8*S*,9*S*)-4-(*tert*-Butyldimethylsilyl)oxy-2-(*tert*-butyldimethylsilyl)oxyethyl-((1*S*,4*S*,5*S*,6*S*)-5-(*tert*-butyldimethylsilyl)oxy-1-hydroxy-10-iodo-3-oxo-4,6,8,9-tetramethyldeca–7,9-dien-1-yl)-9-(4-methoxybenzyl)oxy-3,10,10-trimethyl-1,7-dioxaspiro[4.5]decane (76)

n-BuLi in hexanes (2.5 M, 94.3 μL, 0.236 mmol) was added dropwise to $(Me_3Si)_2NH$ (54.9 μL, 0.260 mmol) in THF (0.5 mL) at –30°C and the mixture stirred at –20°C for 20 min and then cooled to –78°C. Ketone **5** (106 mg,

© 2001 NRC Canada

0.236 mmol) in THF (1.5 mL) was added over 7 min and the mixture stirred for an additional 7 min at –78°C. Aldehyde **6** (140 mg, 0.219 mmol) in THF (1.25 mL) was added over 7 min and the mixture left for 7 min at –78°C. The mixture was quenched with saturated aqueous NH_4Cl (1.0 mL) and allowed to warm up to room temperature over 2 h. The solution was diluted with Et_2O (10 mL), washed with H_2O (1 mL) and brine (1 mL), and dried (Na_2SO_4). Rotary evaporation and chromatography (hexanes–Et_2O, 9:1) gave ketone **76** (181 mg, 76% from **6**) as a pale yellow oil. $[\alpha]_D^{20}$ = +22.4° (*c* = 0.17). FAB-HRMS (NaI added) calcd. for $C_{53}H_{95}IO_9Si_3Na$: 1109.5226 ($[M + Na]^+$); found: 1109.5277 ($[M + Na]^+$). IR (film) (cm^{-1}): 3560, 1707, 1613, 1514, 1464, 1384, 1361, 1251, 1110, 1083, 1023, 836, 776. ^1H NMR (300 MHz, $CDCl_3$) δ: 7.29 (d, 2H, *J* = 8.6 Hz), 6.87 (d, 2H, *J* = 8.6 Hz), 6.32 (s, 1H), 5.92 (d, 1H, *J* = 9.5 Hz), 4.61 (d, 1H, *J* = 11.5 Hz), 4.54 (d, 1H, *J* = 11.5 Hz), 4.33 (m, 1H), 4.04 (m, 2H), 3.90 (dd, 1H, *J* = 9.6, 5.7 Hz), 3.84 (m, 1H), 3.80 (s, 3H), 3.77 (m, 1H), 3.64 (d, 1H, *J* = 5.7 Hz), 3.38 (m, 1H), 3.20 (d, 1H, *J* = 18.0 Hz), 3.17 (m, 1H), 2.65 (m, 1H), 2.62 (m, 1H), 2.45 (dd, 1H, *J* = 18.5, 10.3 Hz), 2.07 (s, 3H), 1.82 (s, 3H), 1.76 (m, 1H), 1.61 (dd, 1H, *J* = 14.0, 3.5 Hz), 1.46–1.36 (m, 2H), 1.28 (m, 1H), 1.02 (s, 3H), 1.00 (d, 3H, *J* = 6.9 Hz), 0.91 (s, 9H), 0.88 (s, 3H), 0.87 (s, 9H), 0.86 (s, 9H), 0.84 (s, 3H), 0.81 (d, 3H, *J* = 7.1 Hz), 0.10 (s, 3H), 0.03 (s, 3H), 0.01 (s, 3H), 0.00 (s, 3H), –0.03 (s, 6H). ^{13}C NMR (75 MHz, $CDCl_3$) δ: 214.7, 159.0, 148.0, 133.6, 131.4, 130.3, 129.2, 113.7, 106.9, 86.8, 82.0, 78.7, 76.0, 74.7, 70.9, 66.8, 64.2, 62.0, 55.2, 52.5, 51.0, 47.6, 38.6, 36.3, 35.8, 30.2, 26.2, 26.0, 25.8, 23.6, 22.7, 18.7, 18.3, 17.9, 17.3, 14.4, 12.9, 10.6, –3.8, –4.3, –4.7, –5.2, –5.3, –5.5.

(2*R*,3*R*,4*S*,6*R*,8*S*,9*S*)-4-(*tert*-Butyldimethylsilyl)oxy-2-(triethylsilyl)oxyethyl-((1*S*,4*S*,5*S*,6*S*)-5-(*tert*-butyldimethylsilyl)oxy-1-hydroxy-10-iodo-3-oxo-4,6,8,9-tetramethyldeca-7,9-dien-1-yl)-9-(4-methoxybenzyl)oxy-3,10,10-trimethyl-1,7-dioxaspiro[4.5]decane (77)

Ketone **5** (78 mg, 0.173 mmol) in dry THF (1 mL) was slowly added to $LiN(SiMe_3)_2$ in THF (0.26 M, 665 μL, 0.173 mmol), freshly prepared from $HN(SiMe_3)_2$ and *n*-BuLi at –78°C (Ar). After 7 min, aldehyde **74** (99 mg, 0.156 mmol) in dry THF (1 mL) was added at –78°C. After stirring for 30 min at –78°C, the mixture was allowed to warm to –50°C over 15 min, then solid NH_4Cl (100 mg) was added and the mixture was diluted with Et_2O (50 mL). The mixture was washed with H_2O and brine and dried (Na_2SO_4). Rotary evaporation and chromatography (hexanes–Et_2O, 9:1) gave **77** (73.5 mg, 43%) along with recovered starting ketone **5** (43 mg, 54%) and aldehyde **74** (35 mg, 35%). The aldol adduct **77** was obtained as a colorless oil. TLC R_f = 0.23 (hexanes–Et_2O, 6:1). $[\alpha]_D^{20}$ = +22° (*c* = 0.60). IR (film) (cm^{-1}): 3571, 1706, 1614, 1514, 1463, 1382, 1302. ^1H NMR (300 MHz, $CDCl_3$) δ: 7.26 (d, 2H, *J* = 8.5 Hz), 6.84 (d, 2H, *J* = 8.5 Hz), 6.28 (s, 1H), 5.88 (d, 1H, *J* = 9.5 Hz), 4.57 (d, 1H, *J* = 11.5 Hz), 4.52 (d, 1H, *J* = 11.5 Hz), 4.31–4.25 (m, 1H), 4.01 (dd, 1H, *J* = 7.5, 2.0 Hz), 3.99 (dt, 1H, *J* = 9.0, 2.5 Hz), 3.88–3.73 (m, 3H), 3.77 (s, 3H), 3.60 (d, 1H, *J* = 5.5 Hz), 3.36 (dt, 1H, *J* = 10.0, 5.5 Hz), 3.15 (d, 1H, *J* = 2.5 Hz), 3.11 (dd, 1H, *J* = 18.5, 1.5 Hz), 2.64–2.54 (m, 2H), 2.41 (dd, 1H, *J* = 18.5, 10.5 Hz), 2.03 (s, 3H), 1.78 (s, 3H), 1.77–1.67 (m, 1H), 1.41–1.21 (m, 4H), 0.97 (d, 3H, *J* = 7.0 Hz), 0.97 (s, 3H), 0.91–0.77 (m, 18H), 0.88 (s, 9H), 0.84 (s, 9H), 0.50 (q, 6H, *J* = 8.0 Hz), 0.07 (s, 3H), 0.00 (s, 3H),–0.01 (s, 3H), –0.03 (s, 3H). ^{13}C NMR (75 MHz, $CDCl_3$) δ: 214.9, 159.1, 148.2, 133.7, 131.5, 130.5, 129.5, 113.8, 107.0, 86.8, 82.2, 78.8, 76.1, 74.8, 71.0, 67.0, 64.2, 61.7, 55.4, 52.7, 51.1, 47.7, 38.8, 36.6, 36.0, 30.4, 26.4, 26.0, 23.8, 22.8, 18.8, 18.6, 18.1, 17.5, 14.6, 13.0, 10.7, 7.0, 4.5, -3.6, –4.1, –4.5, –5.0. DDQ (3.4 mg, 16.6 μmol) was added to spiroketal **77** (15.0 mg, 13.8 μmol) and molecular sieves (3 Å, 10 mg) in CH_2Cl_2 (1 mL) at –20°C. The mixture was allowed to warm to 0°C and stirred for 10 min when it was diluted with Et_2O and quenched with saturated aqueous $NaHCO_3$. The organic phase was washed with H_2O (1 mL) and brine (1 mL) and dried (Na_2SO_4). Rotary evaporation and chromatography (hexanes–Et_2O, 6:1) gave acetal **78** (7.0 mg, 49%) as a colorless oil. TLC R_f = 0.44 (2 developments, hexanes–Et_2O, 7:1). ^1H NMR (300 MHz, $CDCl_3$) δ: 7.40 (d, 2H, *J* = 8.5 Hz), 6.83 (d, 2H, *J* = 8.5 Hz), 6.23 (s, 1H), 5.77 (d, 1H, *J* = 9.0 Hz), 5.52 (s, 1H), 4.21–4.14 (m, 2H), 4.04 (dd, 1H, *J* = 9.0, 6.0 Hz) 3.93 (dd, 1H, *J* = 6.5, 2.5 Hz), 3.77 (s, 3H), 3.74 (d, 1H, *J* = 6.0 Hz), 3.77–3.73 (m, 1H), 3.60–3.52 (m, 1H), 3.49–3.41 (m, 1H), 2.83 (dd, 1H, *J* = 15.5, 3.0 Hz), 2.68 (dq, 1H, *J* = 7.0, 6.5 Hz), 2.60 (dd, 1H, *J* = 15.5, 8.0 Hz), 2.47 (dq, 1H, *J* = 7.0, 2.5 Hz), 2.00 (s, 3H), 1.70 (s, 3H), 1.66–1.37 (m, 5H), 1.09 (s, 3H), 0.90–0.79 (m, 39H), 0.49 (q, 6H, *J* = 8.0 Hz), 0.03 (s, 3H), 0.01 (s, 3H), –0.02 (s, 3H), –0.05 (s, 3H).

(2*R*,3*R*,4*S*,6*R*,8*S*,9*S*)-4-(*tert*-Butyldimethylsilyl)oxy-2-(*tert*-butyldimethylsilyl)oxyethyl-((1*S*,3*R*,4*S*,5*S*,6*S*)-5-(*tert*-butyldimethylsilyl)oxy-1,3-dihydroxy-10-iodo-4,6,8,9-tetramethyldeca-7,9-dien-1-yl)-9-(4-methoxybenzyl)oxy-3,10,10-trimethyl-1,7-dioxaspiro[4.5]decane (79) and (2*R*,3*R*,4*S*,6*R*,8*S*,9*S*)-4-(*tert*-butyldimethylsilyl)oxy-2-(*tert*-butyldimethylsilyl)oxyethyl-((1*S*,3*S*,4*S*,5*S*,6*S*)-5-(*tert*-butyldimethylsilyl)oxy-1,3-dihydroxy-10-iodo-4,6,8,9-tetramethyldeca-7,9-dien-1-yl)-9-(4-methoxybenzyl)oxy-3,10,10-trimethyl-1,7-dioxaspiro[4.5]decane (80)

$LiAlH_4$ in THF (1 M, 76 μL, 79 μmol) was added dropwise to ketone **76** (20.9 mg, 19.0 μmol) in THF (1 mL) at –78°C. After 1 h, the mixture was quenched with H_2O (100 μL) and allowed to warm to room temperature. The solution was diluted with CH_2Cl_2 and Celite and anhydrous Na_2SO_4 were added with vigorous stirring. After 30 min, the mixture was filtered through Celite with CH_2Cl_2. Rotary evaporation and chromatography (hexanes–Et_2O, 5:1) gave diol **80** (3.1 mg, 15%) and diol **79** (15.0 mg, 73%) both as pale yellow oils. Data for diol **80**: TLC R_f = 0.46 (hexanes–Et_2O, 5:1). $[\alpha]_D^{24}$ = +29.7° (*c* = 0.28). FAB-HRMS (NaI added) calcd. for $C_{53}H_{97}IO_9Si_3Na$: 1111.5383 ($[M + Na]^+$); found: 1111.5403 ($[M + Na]^+$). IR (film) (cm^{-1}): 3508, 1514, 1471, 1252, 1111, 1080, 835, 773. ^1H NMR (300 MHz, $CDCl_3$) δ: 7.27 (d, 2H, *J* = 8.5 Hz), 6.87 (d, 2H, *J* = 8.5 Hz), 6.27 (s, 1H), 5.81 (d, 1H, *J* = 10.0 Hz), 4.71 (d, 1H, *J* = 11.3 Hz), 4.35 (d, 1H, *J* = 11.3 Hz), 4.35–4.17 (m, 2H), 4.03–4.00 (m, 2H), 3.80 (s, 3H), 3.82–3.58 (m, 5H), 2.89–2.84 (m, 2H), 2.76 (m, 1H), 2.03 (s, 3H), 1.96 (m, 1H), 1.81 (s, 3H), 1.69 (m, 1H), 1.60–1.22 (m, 6H), 0.97 (d, 3H, *J* = 7.0 Hz), 0.93 (s, 3H), 0.90 (s, 9H), 0.89 (s, 3H), 0.87 (s,

© 2001 NRC Canada

9H), 0.86 (s, 9H), 0.86 (m, 3H), 0.82 (d, 3H, *J* = 7.1 Hz), 0.12 (s, 3H), 0.06 (s, 6H), 0.00 (s, 9H). Data for diol **79**: TLC R_f = 0.54 (hexanes–Et_2O, 5:1). $[\alpha]_D^{24}$ = +25.2° (*c* = 0.27). IR (film) (cm^{-1}): 3489, 1514, 1471, 1252, 1109, 1080, 970, 939, 899, 835, 739. ^1H NMR (300 MHz, $CDCl_3$) δ: 7.25 (d, 2H, *J* = 8.6 Hz), 6.87 (d, 2H, *J* = 8.6 Hz), 6.20 (s, 1H), 5.97 (d, 1H, *J* = 9.7 Hz), 4.71 (d, 1H, *J* = 11.3 Hz), 4.33 (d, 1H, *J* = 11.3 Hz), 4.23 (m, 1H), 4.08 (m, 1H), 4.02 (dd, 1H, *J* = 4.5, 2.1 Hz), 3.88 (dd, 1H, *J* = 8.8, 6.2 Hz), 3.80 (s, 3H), 3.77 (m, 2H), 3.72 (d, 1H, *J* = 6.2 Hz), 3.60 (m, 1H), 3.47 (m, 1H), 3.18 (m, 1H), 2.74 (m, 1H), 2.11 (br d, 1H, *J* = 14.5 Hz), 2.02 (s, 3H), 1.79 (s, 3H), 1.72–1.23 (m, 8H), 1.14 (s, 3H), 0.99 (d, 3H, *J* = 6.9 Hz), 0.91 (s, 9H), 0.87 (s, 9H), 0.85 (s, 3H), 0.84 (s, 9H), 0.82 (d, 3H, *J* = 7.1 Hz), 0.74 (d, 3H, *J* = 7.0 Hz), 0.08 (s, 6H), 0.00 (s, 6H), –0.01 (s, 6H). ^{13}C NMR (75 MHz, $CDCl_3$) δ: 159.4, 148.3, 133.2, 130.0, 129.6, 114.2, 107.1, 87.6, 82.4, 77.7, 76.2, 75.0, 74.5, 72.3, 70.8, 64.2, 61.8, 55.2, 51.1, 46.0, 39.3, 38.4, 36.3, 34.8, 30.2, 26.0, 25.9, 24.0, 22.6, 19.8, 18.30, 18.29, 17.5, 14.5, 12.0, 10.7, –4.0, –4.6, –4.7, –5.0, –5.2, –5.3.

(2*R*,3*R*,4*S*,6*R*,8*S*,9*S*)-4-(*tert*-Butyldimethylsilyl)oxy-2-(*tert*-butyldimethylsilyl)oxyethyl-8-((4*R*,6*S*)-((2*S*,3*S*,4*S*)-3-(*tert*-butyldimethylsilyl)oxy-8-iodo-4,6,7-trimethylocta-5,7-dien-2-yl)-2,2-dimethyl-1,3-dioxan-6-yl)-9-(4-methoxybenzyl)oxy-3,10,10-trimethyl-1,7-dioxaspiro[4.5]decane (81)

Pyridinium toluene-4-sulfonate (6.5 mg, 26 μL) was added to diol **79** (28.4 mg, 26 μmol) and 2-methoxypropene (50 μL, 521 μmol) in CH_2Cl_2 (1.0 mL) at 0°C and the mixture stirred for 1 h at room temperature. Et_3N (0.1 mL) was added at 0°C, and the mixture was rotary evaporated to 30% by volume, diluted with Et_2O (10 mL), washed with H_2O (1 mL) and brine (1 mL), and dried (Na_2SO_4). Rotary evaporation and chromatography (hexanes–PhMe, 1:2 to 1:3) gave ketal **81** (19.2 mg, 65%) as a pale yellow oil. TLC R_f = 0.66 (hexanes–Et_2O, 6:1). $[\alpha]_D^{26}$ = –6.5° (*c* = 0.18). FAB-HRMS (NaI added) calcd. for $C_{56}H_{101}IO_9Si_3Na$: 1151.5696 ($[M + Na]^+$); found: 1151.5779 ($[M + Na]^+$). IR (film) (cm^{-1}): 1614, 1514, 1463, 1379, 1252, 969, 774, 732, 669. ^1H NMR (400 MHz, $CDCl_3$) δ: 7.26 (d, 2H, *J* = 8.6 Hz), 6.85 (d, 2H, *J* = 8.6 Hz), 6.22 (s, 1H), 6.00 (d, 1H, *J* = 9.4 Hz), 4.57 (d, 1H, *J* = 11.5 Hz), 4.39 (d, 1H, *J* = 11.5 Hz), 4.15 (m, 2H), 3.93 (dd, 1H, *J* = 5.0, 2.5 Hz), 3.91 (dd, 1H, *J* = 9.5, 5.5 Hz), 3.89 (dt, 1H, *J* = 10.0, 5.3 Hz), 3.80 (s, 3H), 3.76 (m, 1H), 3.68 (ddd, 1H, *J* = 11.5, 9.0, 2.5 Hz), 3.53 (d, 1H, *J* = 5.5 Hz), 3.51 (dt, 1H, *J* = 10.0, 6.0 Hz), 2.61 (ddt, 1H, *J* = 9.4, 7.0, 2.0 Hz), 2.03 (s, 3H), 1.89 (dt, 1H, *J* = 12.5, 2.5 Hz), 1.78 (br s, 3H), 1.73 (m, 1H), 1.71 (m, 1H), 1.58 (dd, 1H, *J* = 14.2, 3.6 Hz), 1.46 (m, 1H), 1.39 (m, 1H), 1.35 (s, 3H), 1.32 (m, 1H), 1.30 (s, 3H), 1.20 (q, 1H, *J* = 12.5 Hz), 0.94 (d, 3H, *J* = 7.0 Hz), 0.93 (s, 3H), 0.92 (s, 9H), 0.87 (s, 9H), 0.86 (s, 9H), 0.81 (d, 3H, *J* = 6.9 Hz), 0.80 (s, 3H), 0.77 (d, 3H, *J* = 7.1 Hz), 0.08 (s, 3H), 0.05 (s, 3H), 0.01 (s, 3H), –0.01 (s, 6H), –0.04 (s, 3H). ^{13}C NMR (100 MHz, $CDCl_3$) δ: 158.7, 148.5, 132.9, 131.7, 131.4, 129.0, 113.4, 106.8, 97.6, 86.2, 83.7, 77.7, 75.0, 74.5, 70.9, 70.8, 67.6, 63.8, 61.8, 55.2, 50.4, 45.5, 38.5, 36.5, 34.5, 33.7, 30.5, 30.2, 26.0, 25.93, 25.86, 23.6, 22.5, 19.9, 18.3, 18.2, 18.0, 17.3, 14.5, 10.6, 10.2, 4.0, –4.5, –4.8, –5.0, –5.2.

(2*R*,3*R*,4*S*,6*R*,8*S*,9*S*)-4-(*tert*-Butyldimethylsilyl)oxy-2-(*tert*-butyldimethylsilyl)oxyethyl-8-((4*S*,6*S*)-((2*S*,3*S*,4*S*)-3-(*tert*-butyldimethylsilyl)oxy-8-iodo-4,6,7-trimethylocta-5,7-dien-2-yl)-2,2-dimethyl-1,3-dioxan-6-yl)-9-(4-methoxybenzyl)oxy-3,10,10-trimethyl-1,7-dioxaspiro[4.5]decane (82)

Ketal **82** (18 mg, 77%), which was prepared in an identical manner to that reported for ketal **81**, was obtained as a colorless oil. TLC R_f = 0.46 (hexanes–PhMe, 1:3). $[\alpha]_D^{26}$ = –2.8° (*c* = 0.56). FAB-HRMS (NaI added) calcd. for $C_{56}H_{101}IO_9Si_3Na$: 1151.5696 ($[M + Na]^+$); found: 1151.5679 ($[M + Na]^+$). IR (film) (cm^{-1}): 1614, 1514, 1463, 1380, 1250, 1083, 1029, 836, 774. ^1H NMR (400 MHz, $CDCl_3$) δ: 7.26 (d, 2H, *J* = 8.6 Hz), 6.84 (d, 2H, *J* = 8.6 Hz), 6.20 (s, 1H), 6.03 (d, 1H, *J* = 9.4 Hz), 4.56 (d, 1H, *J* = 11.5 Hz), 4.43 (d, 1H, *J* = 11.5 Hz), 4.16 (m, 1H), 4.12 (m, 1H), 4.04 (dd, 1H, *J* = 9.6, 5.6 Hz), 3.92 (dt, 1H, *J* = 15.0, 5.0 Hz), 3.78 (s, 3H), 3.82–3.75 (m, 2H), 3.67 (dd, 1H, *J* = 5.0, 1.0 Hz), 3.56 (m, 1H), 3.55 (d, 1H, *J* = 5.7 Hz), 2.77 (m, 1H), 2.03 (br s, 3H), 1.90 (m, 1H), 1.83 (m, 1H), 1.81 (m, 1H), 1.77 (d, 3H, *J* = 0.8 Hz), 1.60 (dd, 1H, *J* = 14.0, 3.5 Hz), 1.58 (m, 1H), 1.46 (m, 1H), 1.41 (m, 1H), 1.34 (dd, 1H, *J* = 14.0, 2.0 Hz), 1.31 (s, 3H), 1.13 (s, 3H), 0.96 (d, 3H, *J* = 7.0 Hz), 0.96 (s, 3H), 0.93 (s, 9H), 0.87 (s, 9H), 0.86 (s, 9H), 0.84 (d, 3H, *J* = 7.1 Hz), 0.83 (s, 3H), 0.82 (d, 3H, *J* = 7.0 Hz), 0.08 (s, 6H), 0.02 (s, 3H), 0.00 (s, 3H), –0.04 (s, 3H), –0.05 (s, 3H). ^{13}C NMR (100 MHz, $CDCl_3$) δ: 158.5, 148.6, 132.7, 131.6, 131.2, 128.3, 113.4, 106.6, 99.9, 86.1, 82.9, 78.6, 77.5, 74.4, 70.8, 67.4, 65.1, 63.7, 61.8, 55.2, 50.9, 44.9, 36.7, 35.3, 35.2, 30.2, 26.0, 25.8, 25.2, 25.1, 23.6, 22.5, 20.2, 18.3, 18.2, 18.0, 17.1, 14.3, 10.5, 8.6, –4.1, –4.3, –4.6, –5.0, –5.2, –5.3.

(2*R*,3*R*,4*S*,6*R*,8*S*,9*S*)-4-(*tert*-Butyldimethylsilyl)oxy-2-(*tert*-butyldimethylsilyl)oxyethyl-((1*S*,3*R*,4*S*,5*S*,6*S*)-3,5-di(*tert*-butyldimethylsilyl)oxy-1-hydroxy-10-iodo-4,6,8,9-tetramethyldeca-7,9-dien-1-yl)-9-(4-methoxybenzyl)oxy-3,10,10-trimethyl-1,7-dioxaspiro[4.5]decane (83)

t-$BuMe_2SiOTf$ (2.37 μL, 6.61 μmol) in dry CH_3CN (23.7 μL) was added to diol **79** (6 mg, 5.3 μmol) and 2,6-lutidine (20.0 μL, 0.17 mmol) in CH_2Cl_2–CH_3CN (1:1, 0.8 mL) at –50°C. After 10 min, the solution was cooled to –78°C when additional *t*-$BuMe_2SiOTf$ (2.37 μL, 6.61 μmol) in dry CH_3CN (23.7 μL) was added. After 10 min, further *t*-$BuMe_2SiOTf$ (2.37 μL, 6.61 μmol) in dry CH_3CN (23.7 μL) was added and, after a further 15 min, the reaction mixture was quenched with precooled MeOH at –78°C. The mixture was diluted with Et_2O (10 mL), washed with H_2O (1 mL) and brine (1 mL), and dried (Na_2SO_4). Rotary evaporation and chromatography (hexanes–Et_2O, 24:1 to 15:1) gave alcohol **83** (4.7 mg, 74%) as a colorless oil. $[\alpha]_D^{26}$ = +30.6° (*c* = 0.29). FAB-HRMS (NaI added) calcd. for $C_{59}H_{111}IO_9Si_4Na$: 1225.6248 ($[M + Na]^+$); found: 1225.6307 ($[M + Na]^+$). IR (film) (cm^{-1}): 3480, 1514, 1471, 1252, 1078, 1030, 836, 775. ^1H NMR (300 MHz, $CDCl_3$) δ: 7.25 (d, 2H, *J* = 8.6 Hz), 6.81 (d, 2H, *J* = 8.6 Hz), 6.23 (s, 1H), 5.96 (d, 1H, *J* = 9.3 Hz), 4.57 (d, 1H, *J* = 11.4 Hz), 4.51 (d, 1H, *J* = 11.4 Hz), 4.19 (m, 2H), 3.99 (m, 1H), 3.81 (m, 1H), 3.77 (s, 3H), 3.76 (m,

© 2001 NRC Canada

1H), 3.69 (m, 2H), 3.60 (m, 1H), 3.58 (m, 1H), 3.47 (m, 1H), 2.57 (m, 1H), 2.01 (s, 3H), 1.75 (s, 3H), 1.87–1.08 (m, 8H), 1.01 (s, 3H), 0.95 (d, 3H, *J* = 7.0 Hz), 0.91 (s, 9H), 0.87 (s, 3H), 0.86 (s, 9H), 0.84 (s, 9H), 0.83 (s, 9H), 0.79 (d, 3H, *J* = 7.1 Hz), 0.71 (d, 3H, *J* = 7.1 Hz), 0.09 (s, 3H), 0.06 (s, 3H), 0.05 (s, 3H), 0.04 (s, 3H), 0.00 (s, 3H), –0.01 (s, 3H), –0.06 (s, 3H), –0.07 (s, 3H). ^{13}C NMR (75 MHz, $CDCl_3$) δ: 158.9, 148.3, 132.7, 131.5, 131.1, 129.0, 113.6, 107.0, 87.4, 84.1, 78.1, 76.6, 74.1, 73.0, 71.2, 69.5, 64.4, 61.2, 55.2, 50.5, 46.3, 38.0, 35.9, 35.4, 31.0, 26.4, 26.0, 23.7, 22.6, 19.1, 18.5, 18.2, 17.9, 17.6, 14.4, 10.9, 10.2, –4.0, –4.1, –4.5, –4.8, –5.2.

(2*R*,3*R*,4*S*,6*R*,8*S*,9*S*)-4-(*tert*-Butyldimethylsilyl)oxy-2-(*tert*-butyldimethylsilyl)oxyethyl-((3*R*,4*S*,5*S*,6*S*)-3,5-di(*tert*-butyldimethylsilyl)oxy-10-iodo-1-oxo-4,6,8,9-tetramethyldeca-7,9-dien-1-yl)-9-(4-methoxybenzyl)oxy-3,10,10-trimethyl-1,7-dioxaspiro[4.5]decane (84)

Dess-Martin periodinane (31) (28.4 mg, 6.7 μmol) was added to alcohol **83** (16.1 mg, 13.3 μmol) in CH_2Cl_2 (1 mL). After 40 min, the mixture was diluted with Et_2O and quenched with saturated aqueous $NaHCO_3$ and saturated aqueous Na_2SO_3 at 0°C. After vigorous stirring for 30 min, the organic phase was washed with H_2O (1 mL) and brine (1 mL) and dried (Na_2SO_4). Rotary evaporation and chromatography (hexanes–PhMe, 2:5) gave ketone **84** (12.8 mg, 80%) as a pale yellow oil. $[\alpha]_D^{26}$ = +50.7° (*c* = 0.15). FAB-HRMS (NaI added) calcd. for $C_{59}H_{109}IO_9Si_4Na$: 1223.6091 ($[M + Na]^+$); found: 1223.6146 ($[M + Na]^+$). IR (film) (cm^{-1}): 1718, 1514, 1471, 1252, 1106, 1079, 1035, 836, 775. ^{1}H NMR (300 MHz, C_6D_6) δ: 7.24 (d, 2H, *J* = 8.7 Hz), 6.84 (d, 2H, *J* = 8.7 Hz), 6.28 (s, 1H), 6.23 (d, 1H, *J* = 9.1 Hz), 4.78 (m, 2H), 4.67 (d, 1H, *J* = 5.6 Hz), 4.53 (d, 1H, *J* = 11.5 Hz), 4.25 (d, 1H, *J* = 11.5 Hz), 3.95 (m, 1H), 3.84 (m, 1H), 3.79 (m, 2H), 3.60 (d, 1H, *J* = 5.7 Hz), 3.56 (dd, 1H, *J* = 18.5, 8.7 Hz), 3.37 (s, 3H), 2.81 (m, 1H), 2.57 (dd, 1H, *J* = 18.5, 2.0 Hz), 2.15 (s, 3H), 2.00 (m, 1H), 1.83 (m, 1H), 1.69 (s, 3H), 1.45 (dd, 1H, *J* = 14.5, 3.5 Hz), 1.38 (dd, 1H, *J* = 14.5, 2.5 Hz), 1.33 (m, 2H), 1.16 (d, 3H, *J* = 7.0 Hz), 1.11 (s, 9H), 1.07 (s, 3H), 1.06 (s, 9H), 1.05 (s, 9H), 1.02 (2s, 12H), 0.97 (d, 3H, *J* = 7.0 Hz), 0.91 (d, 3H, *J* = 7.1 Hz), 0.35 (s, 3H), 0.33 (s, 3H), 0.23 (s, 3H), 0.14 (s, 3H), 0.13 (2s, 6H), 0.12 (s, 3H), 0.09 (s, 3H). ^{13}C NMR (75 MHz, $CDCl_3$) δ: 211.1, 158.8, 148.4, 132.5, 131.2, 130.9, 128.5, 113.5, 109.1, 88.4, 87.2, 78.0, 76.5, 74.1, 70.5, 67.7, 66.1, 60.9, 55.3, 50.7, 45.9, 43.5, 37.6, 35.6, 35.1, 31.0, 26.2, 26.0, 25.94, 25.89, 23.2, 22.5, 19.5, 18.4, 18.2, 18.1, 17.1, 14.3, 10.5, 10.2, –3.4, –4.1, –4.3, –4.60, –4.64, –5.0, –5.3.

(2*R*,3*R*,4*S*,6*R*,8*S*,9*S*)-4-(*tert*-Butyldimethylsilyl)oxy-2-(*tert*-butyldimethylsilyl)oxyethyl-((1*R*,3*R*,4*S*,5*S*,6*S*)-3,5-di(*tert*-butyldimethylsilyl)oxy-1-hydroxy-10-iodo-4,6,8,9-tetramethyldeca-7,9-dien-1-yl)-9-(4-methoxybenzyl)oxy-3,10,10-trimethyl-1,7-dioxaspiro[4.5]decane (85)

Ketone **84** (31.5 mg, 26.2 μmol) in CH_2Cl_2 (2 mL) was added to DIBAl-H in hexanes (1 M, 300 μL, 300 μmol) in CH_2Cl_2 (1 mL) at –78°C. After 30 min, the mixture was quenched with precooled MeOH at –78°C, diluted with Et_2O (10 mL), and saturated aqueous potassium sodium tartrate was added with vigorous stirring. After 2 h, the mixture was washed with H_2O (1 mL) and brine (1 mL) and dried (Na_2SO_4). Rotary evaporation and chromatography (hexanes–Et_2O, 16:1) gave alcohol **85** (30.6 mg, 97%) as a pale yellow oil. $[\alpha]_D^{25}$ = +45.0° (*c* = 0.24). FAB-HRMS (NaI added) calcd. for $C_{59}H_{111}IO_9Si_4Na$: 1225.624 8 ($[M + Na]^+$); found: 1225.6286 ($[M + Na]^+$). IR (film) (cm^{-1}): 3526, 1614, 1515, 1471, 1252, 1106, 1071, 836, 775. ^{1}H NMR (300 MHz, $CDCl_3$) δ: 7.21 (d, 2H, *J* = 8.6 Hz), 6.81 (d, 2H, *J* = 8.6 Hz), 6.23 (s, 1H), 5.96 (d, 1H, *J* = 9.3 Hz), 4.49 (d, 1H, *J* = 11.3 Hz), 4.42 (d, 1H, *J* = 11.3 Hz), 4.34 (m, 1H), 4.17 (m, 1H), 3.98 (m, 1H), 3.92 (m, 1H), 3.75 (m, 1H), 3.75 (s, 3H), 3.52 (d, 1H, *J* = 5.5 Hz), 3.63–3.47 (m, 2H), 3.43 (m, 1H), 3.28 (s, 1H), 2.56 (m, 1H), 2.00 (s, 3H), 1.78 (s, 3H), 1.69–1.12 (m, 8H), 0.99 (s, 3H), 0.96 (d, 3H, *J* = 7.1 Hz), 0.89 (s, 9H), 0.86 (s, 3H), 0.85 (s, 9H), 0.81 (s, 9H), 0.80 (s, 9H), 0.78 (d, 3H, *J* = 7.1 Hz), 0.69 (d, 3H, *J* = 6.8 Hz), 0.21 (s, 3H), 0.04 (s, 3H), 0.00 (s, 6H), –0.01 (s, 3H), –0.03 (s, 3H), –0.09 (s, 6H). ^{13}C NMR (75 MHz, $CDCl_3$) δ: 159.2, 148.4, 133.3, 131.0, 130.1, 129.4, 113.8, 106.6, 89.3, 83.6, 78.0, 76.9, 74.8, 71.0, 68.7, 67.2, 64.5, 61.2, 55.2, 50.8, 45.4, 37.9, 36.6, 36.3, 35.8, 30.7, 26.6, 26.0, 23.8, 22.6, 18.7, 18.4, 18.1, 17.3, 14.4, 10.9, 9.9, –2.9, –3.7, –4.2, –4.4, –4.6, –4.8, –5.3.

(2*R*,3*R*,4*S*,6*R*,8*S*,9*S*)-4-(*tert*-Butyldimethylsilyl)oxy-2-(*tert*-butyldimethylsilyl)oxyethyl-((1*R*,3*R*,4*S*,5*S*,6*S*)-3,5-di(*tert*-butyldimethylsilyl)oxy-10-iodo-1-methoxy-4,6,8,9-tetramethyldeca-7,9-dien-1-yl)-9-(4-methoxybenzyl)oxy-3,10,10-trimethyl-1,7-dioxaspiro[4.5]decane (86)

t-BuOK in THF (1 M, 200 μL, 200 μmol) and MeI (36 μL, 589 μmol) were added dropwise in sequence to alcohol **85** (28.4 mg, 23.6 μmol) in THF (3.0 mL) at –78°C. Three further additions of MeI (20 μL, 330 μmol) were made at 10 min intervals. The mixture was poured onto ice cooled saturated aqueous $NaHCO_3$, extracted with Et_2O, and the organic phase washed with H_2O (1 mL) and brine (1 mL) and dried (Na_2SO_4). Rotary evaporation and chromatography (hexanes–Et_2O, 40:1 to 24:1) gave ether **86** (25.1 mg, 87%) as a pale yellow oil. $[\alpha]_D^{26}$ = +47.7° (*c* = 0.14). FAB-MS (NaI added) *m*/*z*: 1239 ($[M + Na]^+$), 782, 629. IR (film) (cm^{-1}): 1615, 1515, 1471, 1250, 1106, 1080, 835, 774. ^{1}H NMR (300 MHz, $CDCl_3$) δ: 7.29 (d, 2H, *J* = 8.7 Hz), 6.81 (d, 2H, *J* = 8.7 Hz), 6.28 (s, 1H), 5.90 (d, 1H, *J* = 8.9 Hz), 4.47 (d, 1H, *J* = 11.3 Hz), 4.46 (m, 1H), 4.42 (d, 1H, *J* = 11.3 Hz), 4.27 (m, 1H), 4.02 (dd, 1H, *J* = 8.8, 5.0 Hz), 3.82 (m, 1H), 3.79 (s, 3H), 3.64 (s, 3H), 3.70–3.58 (m, 3H), 3.45 (dd, 1H, *J* = 5.0, 2.5 Hz), 3.38 (d, 1H, *J* = 5.0 Hz), 2.63 (m, 1H), 2.05 (s, 3H), 1.81 (s, 3H), 1.80 (m, 1H), 1.69 (dd, 1H, *J* = 14.1, 3.8 Hz), 1.60–1.51 (m, 4H), 1.44 (m, 1H), 1.26 (m, 1H), 1.09 (s, 3H), 1.00 (d, 3H, *J* = 7.0 Hz), 0.94 (s, 9H), 0.92 (s, 3H), 0.89 (s, 9H), 0.87 (s, 9H), 0.84 (d, 3H, *J* = 7.1 Hz), 0.71 (m, 3H), 0.70 (s, 9H), 0.18 (s, 3H), 0.06 (s, 3H), 0.02 (s, 3H), 0.00 (s, 9H), –0.01 (s, 6H). ^{13}C NMR (75 MHz, $CDCl_3$) δ: 158.6, 148.4, 133.3, 131.6, 131.3, 128.1, 113.4, 107.1, 87.5, 86.9, 78.03, 77.95, 77.6, 73.9, 71.5, 67.9, 64.3, 60.9, 60.2, 55.2, 50.7, 44.8, 37.8, 37.2, 35.9, 33.9, 31.0, 26.4, 26.1, 26.0, 23.4, 22.5, 18.6, 18.3, 18.1, 18.0, 17.3, 14.5, 10.5, 10.4, –3.5, –3.7, –4.0, –4.6, –5.0, –5.1, –5.2.

© 2001 NRC Canada

(2*R*,3*R*,4*S*,6*R*,8*S*,9*S*)-4-(*tert*-Butyldimethylsilyl)oxy-2-(*tert*-butyldimethylsilyl)oxyethyl-((1*R*,3*R*,4*S*,5*S*,6*S*)-3,5-di(*tert*-butyldimethylsilyl)oxy-10-iodo-1-methoxy-4,6,8,9-tetramethyldeca-7,9-dien-1-yl)-9-hydroxy-3,10,10-trimethyl-1,7-dioxaspiro[4.5]decane (87)

DDQ (7.5 mg, 33.4 μmol) was added to ether **86** (7.4 mg, 6.07 μmol) in CH_2Cl_2 (0.5 mL), pH 7 buffer (0.2 mL), and isopropanol (0.2 mL). After 1 h, further DDQ (7.5 mg, 33.4 μmol) was added. After 1.5 h stirring, the mixture was diluted with Et_2O and the reaction mixture quenched with saturated aqueous $NaHCO_3$. The organic phase was washed with H_2O (1 mL) and brine (1 mL) and dried (Na_2SO_4). Rotary evaporation and chromatography (hexanes–Et_2O, 24:1) gave alcohol **87** (6.7 mg, 100%) as a pale yellow oil. $[\alpha]_D^{25}$ = +43.2° (*c* = 0.13). FAB-HRMS (NaI added) calcd. for $C_{52}H_{105}IO_8Si_4Na$: 1119.5829 ([M + Na]$^+$); found: 1119.5850 ([M + Na]$^+$). IR (film) (cm^{-1}): 3496, 1471, 1388, 1254, 1101, 1073, 836, 774. ^{1}H NMR (300 MHz, $CDCl_3$) δ: 6.24 (s, 1H), 5.89 (d, 1H, *J* = 9.1 Hz), 4.55 (m, 1H), 4.20 (m, 1H), 3.93 (dd, 1H, *J* = 8.8, 4.0 Hz), 3.91 (m, 1H), 3.60 (s, 3H), 3.60–3.56 (m, 2H), 3.51–3.41 (m, 3H), 3.37 (d, 1H, *J* = 12.0 Hz), 2.61 (m, 1H), 2.01 (s, 3H), 1.78 (s, 3H), 1.81–1.51 (m, 6H), 1.46 (m, 1H), 1.24 (m, 1H), 1.07 (s, 3H), 0.96 (d, 3H, *J* = 7.0 Hz), 0.90 (s, 9H), 0.85 (s, 18H), 0.84 (s, 12H), 0.80 (d, 3H, *J* = 7.1 Hz), 0.72 (d, 3H, *J* = 7.1 Hz), 0.14 (s, 3H), 0.06 (s, 3H), 0.04 (s, 3H), 0.03 (s, 3H), 0.02 (s, 3H), 0.00 (s, 6H), –0.01 (s, 3H). ^{13}C NMR (75 MHz, $CDCl_3$) δ: 133.2, 131.7, 108.6, 88.0, 80.3, 79.0, 78.0, 77.4, 70.6, 68.4, 65.4, 60.1, 60.0, 49.3, 45.0, 37.4, 37.0, 35.6, 34.2, 30.4, 26.4, 26.0, 25.9, 22.6, 22.1, 18.6, 18.4, 18.1, 16.6, 14.5, 10.4, 10.2, –3.5, –3.7, –4.1, –4.7, –5.0, –5.3.

(10*S*,11*S*,12*R*,13*R*)-11,13-Di(*tert*-butyldimethylsilyl)oxy-((2*R*,3*R*,4*S*,6*R*,8*S*,9*S*)-4-(*tert*-butyldimethylsilyl)oxy-2-(*tert*-butyldimethylsilyl)oxyethyl-9-hydroxy-3,10,10-trimethyl-1,7-dioxaspiro[4.5]decane-8-yl)-15-methoxy-3,7,8,10,12-pentamethyl-pentadeca-2,4,6,8-tetraenenitrile (88) (8)

Stannyl diene **3** (41.2 mg, 107 μmol) in *N*-methylpyrrolidinone (2.0 mL) was added dropwise to iodide **87** (14.8 mg, 13.5 μmol) and $Pd(MeCN)_2Cl_2$ (2.0 mg, 7.71 μmol) in *N*-methylpyrrolidinone (2.0 mL) at –5°C. After 30 min, further $Pd(MeCN)_2Cl_2$ (2.0 mg, 7.71 μmol) was added and the solution was allowed to warm up to 5°C over 20 min. After 1 h, the mixture was poured into ice cooled saturated aqueous $NaHCO_3$, extracted with Et_2O (3 × 5 mL), and the combined extracts washed with H_2O (1 mL) and brine (1 mL) and dried (Na_2SO_4). Rotary evaporation and chromatography (hexanes–Et_2O, 7:1) gave **88** (8) (13.0 mg, 91%) as a white foam. $[\alpha]_D^{22}$ = +73.9° (*c* = 0.18). FAB-HRMS (NaI added) calcd. for $C_{58}H_{111}NO_8Si_4Na$: 1084.7285 ([M + Na]$^+$); found: 1084.7249 ([M + Na]$^+$). IR (film) (cm^{-1}): 3492, 2210, 1592, 1471, 1380, 1361, 1254, 1102, 1073, 1031, 1006, 961, 877, 836, 775. ^{1}H NMR (400 MHz, $CDCl_3$) δ: 7.01 (dd, 1H, *J* = 15.0, 11.1 Hz), 6.83 (d, 1H, *J* = 15.0 Hz), 6.35 (d, 1H, *J* = 11.1 Hz), 6.07 (d, 1H, *J* = 9.1 Hz), 5.06 (s, 1H), 4.58 (m, 1H), 4.24 (m, 1H), 3.96 (dd, 1H, *J* = 8.8, 4.0 Hz), 3.82 (m, 1H), 3.62 (s, 3H), 3.61 (m, 2H), 3.53–3.46 (m, 3H), 3.39 (d, 1H, *J* = 12.0 Hz), 2.75 (m, 1H), 2.07 (s, 3H), 2.00 (s, 3H), 1.87 (s, 3H), 1.83 (m, 1H), 1.75 (dd, 1H, *J* = 14.3, 3.9 Hz), 1.69–1.58 (m, 4H), 1.49 (m, 1H), 1.29 (m, 1H), 1.09 (s, 3H), 1.02 (d, 3H, *J* = 7.0 Hz), 0.94 (s, 9H), 0.88 (s, 18H), 0.87 (s, 12H), 0.83 (d, 3H, *J* = 7.1 Hz), 0.77 (d, 3H, *J* = 7.1 Hz), 0.17 (s, 3H), 0.09 (s, 3H), 0.08 (s, 3H), 0.05 (2s, 6H), 0.03 (s, 6H), 0.02 (s, 3H). ^{13}C NMR (100 MHz, $CDCl_3$) δ: 156.7, 144.3, 134.4, 133.9, 133.4, 128.5, 124.0, 117.5, 108.5, 94.6, 87.9, 80.2, 78.9, 77.6, 70.6, 68.4, 65.3, 60.1, 60.0, 49.3, 45.1, 37.3, 35.5, 34.1, 30.3, 26.4, 26.00, 25.96, 25.9, 22.1, 19.4, 18.6, 16.6, 14.5, 14.0, 10.3, 10.1, –3.5, –3.76, –3.83, –4.2, –4.7, –5.0, –5.4. The ^{1}H and ^{13}C NMR spectra of **88** were in agreement with spectra of authentic material kindly provided by Professor David A. Evans. The corresponding data reported by Evans et al. (8) were as follows: $[\alpha]_{577}^{25}$ = +76.6° (CH_2Cl_2, *c* = 0.59). FAB-HRMS (NaI added) calcd. for $C_{58}H_{111}NO_8Si_4Na$: 1084.7284 ([M + Na]$^+$); found: 1084.7275 ([M + Na]$^+$). IR (film) (cm^{-1}): 3498, 2953, 2927, 2856, 2210, 1591, 1471, 1380, 1360, 1253, 1101, 1072, 1030, 1006, 960, 876, 835, 774. ^{1}H NMR (500 MHz, $CDCl_3$) δ: 7.02 (dd, 1H, *J* = 14.9, 11.2 Hz), 6.83 (d, 1H, *J* = 15.0 Hz), 6.35 (d, 1H, *J* = 11.1 Hz), 6.08 (d, 1H, *J* = 9.1 Hz), 5.06 (s, 1H), 4.58 (m, 1H), 4.25 (m, 1H), 3.96 (dd, 1H, *J* = 8.8, 4.1 Hz), 3.82 (m, 1H), 3.63 (s, 3H), 3.61 (m, 2H), 3.53–3.46 (m, 3H), 3.38 (d, 1H, *J* = 12.0 Hz), 2.75 (m, 1H), 2.07 (s, 3H), 2.01 (s, 3H), 1.87 (s, 3H), 1.83 (m, 1H), 1.75 (dd, 1H, *J* = 14.3, 3.8 Hz), 1.69–1.58 (m, 4H), 1.49 (m, 1H), 1.29 (m, 1H), 1.10 (s, 3H), 1.02 (d, 3H, *J* = 7.0 Hz), 0.94 (s, 9H), 0.88 (s, 18H), 0.87 (s, 12H), 0.83 (d, 3H, *J* = 7.1 Hz), 0.77 (d, 3H, *J* = 7.1 Hz), 0.18 (s, 3H), 0.09 (s, 3H), 0.08 (s, 3H), 0.06 (s, 3H), 0.05 (s, 3H), 0.03 (s, 6H), 0.02 (s, 3H). ^{13}C NMR (100 MHz, $CDCl_3$) δ: 156.7, 144.2, 134.4, 133.9, 133.4, 128.5, 124.0, 117.5, 108.5, 94.6, 87.9, 80.2, 78.9, 77.6, 70.5, 68.4, 65.3, 60.1, 60.0, 49.3, 45.1, 37.3, 37.3, 35.5, 34.1, 30.3, 26.4, 26.0, 26.0, 25.9, 22.1, 19.4, 18.6, 16.6, 14.5, 14.0, 10.3, 10.1, –3.5, –3.8, –3.8, –4.2, –4.7, –5.0, –5.4.

***tert*-Butyl-(4*R*)-4-((1*R*,2*S*)-1,2-di(4-methoxybenzyl)oxy-3-buten-1-yl)-2,2-dimethyl-3-oxazolidinecarboxylate (91)**

NaH (60% dispersion in oil, 0.57 g, 14.00 mmol) was added in 2 portions with stirring over 15 min to diol **90** (33) (1.31 g, 4.56 mmol) and 4-$MeOC_6H_4CH_2Cl$ (2.17 g, 13.9 mmol) in DMF (9 mL) at 0°C. The mixture was allowed to warm to room temperature and stirred for 16 h. Excess NaH was quenched with pH 7 buffer and the mixture partitioned between H_2O and Et_2O. The ethereal layer was washed with brine and dried (Na_2SO_4). Rotary evaporation and chromatography (PhMe–EtOAc, 1:49 to 1:19) gave carbamate **91** (1.57 g, 65%) as an oil. $[\alpha]_D^{25}$ = 77.5° (*c* = 1.02). CI-MS *m/z*: 528 ([M + H]$^+$). IR (film) (cm^{-1}): 1695, 1514, 1391, 1366, 1249, 1173, 1068, 1036. ^{1}H NMR (250 MHz, DMSO-d_6, 350 K) δ: 7.20 (m, 4H), 6.88 (m, 4H), 5.85 (m, 1H), 5.30 (m, 2H), 4.54 (d, 1H, *J* = 11.1 Hz), 4.48 (d, 1H, *J* = 11.8 Hz), 4.43 (d, 1H, *J* = 11.2 Hz), 4.28 (d, 1H, *J* = 11.7 Hz), 4.01 (m, 4H), 3.77 (m, 1H), 3.75 (s, 3H), 3.74 (s, 3H), 1.41 (br s, 15H). ^{13}C NMR (62.5 MHz, DMSO-d_6, 350 K) δ: 158.5, 151.2, 135.5, 130.1, 130.0, 128.6, 128.5, 117.4, 113.4, 113.3, 92.6, 79.8, 78.9, 78.7, 72.2, 69.5, 62.7, 56.9, 54.7, 27.7, 25.5, 24.2. Anal. calcd. for $C_{30}H_{41}NO_7$: C 68.29, H 7.83, N 2.65; found: C 68.10, H 7.88, N 2.75.

© 2001 NRC Canada

(2*R*,3*R*,4*S*)-2-(*tert*-Butyloxycarbonyl)amino-3,4-di(4-methoxybenzyl)oxy-5-hexen-1-ol (92)

$TsOH \cdot H_2O$ (97 mg, 0.51 mmol) was added to acetonide **91** (1.34 g, 2.54 mmol) in MeOH (40 mL) and, after 9 h at room temperature, Et_3N (0.11 mL, 0.77 mmol) was added. Rotary evaporation and chromatography (hexanes–EtOAc, 2:1) gave alcohol **92** (1.11 g, 90%) as an oil. $[\alpha]_D^{25}$ = 78.4° (*c* = 1.14). CI-MS *m*/*z*: 488 ($[M + H]^+$), 432, 241, 154, 137, 121. IR (film) (cm^{-1}): 3426, 1713, 1694, 1514, 1249, 1173, 1037. ^1H NMR (270 MHz, $CDCl_3$) δ: 7.22 (m, 4H), 6.85 (m, 4H), 5.88 (m, 1H), 5.39 (m, 2H), 5.09 (br d, 1H), 4.61 (d, 1H, *J* = 7.3 Hz), 4.57 (d, 1H, *J* = 7.8 Hz), 4.41 (d, 1H, *J* = 11.0 Hz), 4.28 (d, 1H, *J* = 11.5 Hz), 3.94 (m, 1H), 3.82 (m, 2H), 3.78 (s, 6H), 3.69 (m, 1H), 3.51 (m, 1H), 2.6 (br s, 1H), 1.40 (s, 9H). ^{13}C NMR (62.5 MHz, $CDCl_3$) δ: 159.2, 159.0, 155.3, 134.9, 129.8, 129.54, 129.51, 129.2, 119.8, 113.7, 113.6, 81.9, 79.7, 79.0, 73.3, 69.8, 62.3, 55.0, 54.9, 51.6, 28.1. Anal. calcd. for $C_{27}H_{37}NO_7$: C 66.51, H 7.65, N 2.87; found: C 66.87, H 7.82, N 2.98.

(3*S*,4*R*,5*R*)-5-(*N*-*tert*-Butyloxycarbonyl)-*N*-methylamino-6-methoxy-3,4-di(4-methoxybenzyl)oxy-1-hexene (93)

NaH (60% dispersion in oil, 0.71 g, 18 mmol) was added portionwise over 1.5 h to amine **92** (2.90 g, 5.95 mmol) and MeI (6.77 g, 47.7 mmol) in DMF (24 mL) and stirred for 28 h at room temperature. The mixture was poured into H_2O (100 mL), extracted into Et_2O (3 × 50 mL), and the combined organics washed with brine and dried (Na_2SO_4). Rotary evaporation and chromatography (gradient Et_2O–CH_2Cl_2, 1:9 to 1:4) gave carbamate **93** (2.20 g, 72%) as a colorless oil. $[\alpha]_D^{25}$ = +69.7° (*c* = 0.98). CI-MS *m*/*z*: 516 ($[M + H]^+$), 460. 416, 241, 137, 121. IR (film) (cm^{-1}): 1693, 1682, 1614, 1514, 1249, 1156, 1036, 826. ^1H NMR (250 MHz, DMSO-d_6, 350 K) δ: 7.23 (m, 4H), 6.89 (m, 4H), 5.89 (m, 1H), 5.30 (m, 2H), 4.67 (d, 1H, *J* = 11.0 Hz), 4.51 (d, 1H, *J* = 11.8 Hz), 4.42 (d, 1H, *J* = 11.0 Hz), 4.33 (d, 1H, *J* = 11.8 Hz), 4.03 (m, 1H), 3.87 (m, 1H), 3.78 (m, 1H), 3.75 (s, 6H), 3.57 (m, 1H), 3.46 (m, 1H), 3.19 (s, 3H), 2.65 (s, 3H), 1.36 (s, 9H). ^{13}C NMR (62.5 MHz, DMSO-d_6, 350 K) δ: 158.5, 154.5, 134.3, 130.2, 130.1, 128.8, 128.5, 118.1, 113.4, 113.3, 80.2, 79.8, 78.2, 72.2, 69.4, 69.3, 57.5, 55.0, 54.7, 30.3, 27.6. Anal. calcd. for $C_{29}H_{41}NO_7$: C 67.55, H 8.01, N 2.72; found: C 67.77, H 8.32, N 2.71.

(3*R*,4*R*,5*R*)-4-(*N*-*tert*-Butyloxycarbonyl)-*N*-methylamino-5-methoxy-2,3-di(4-methoxybenzyl)oxyhexanoic acid (95)

OsO_4 (57 mg, 0.22 mmol) and *N*-methylmorpholine-*N*-oxide (1.72 g, 14.7 mmol) followed by H_2O (6 mL) were added to alkene **93** (6.31 g, 12.2 mmol) in *t*-BuOH (24 mL) and Me_2CO (12 mL). After stirring for 16 h, the solution was diluted with Et_2O (75 mL) and washed successively with 10% aqueous $Na_2S_2O_3$ (20 mL) and brine (20 mL). The organic phase was dried (Na_2SO_4) and rotary evaporated. The resulting oil was dissolved in MeOH (102 mL) and treated with $NaIO_4$ (3.12 g, 14.6 mmol) in H_2O (25 mL). After 20 min, solid material was removed via filtration through Celite and the filtrate rotary evaporated. The residue was partitioned between brine (20 mL) and Et_2O (60 mL) and the organic phase washed with 10% aqueous $Na_2S_2O_3$ (20 mL) and brine (20 mL) and then dried (Na_2SO_4). Rotary evaporation gave an oil, presumably containing the crude aldehyde **94**, which was dissolved in CH_3CN (25 mL) and mixed with $NaH_2PO_4 \cdot H_2O$ (0.69 g, 5.0 mmol) in 27% aqueous H_2O_2 (6.1 mL, 50 mmol). $NaClO_2$ (1.09 g, 12.0 mmol) was added in small portions over 1 h to this vigorously stirred mixture and stirring was maintained for 12 h. The mixture was diluted with PhMe (50 mL) and washed successively with brine (2 × 50 mL) and 20% aqueous $Na_2S_2O_3$ (50 mL). The product was extracted with aqueous KOH (0.21 M, 100 mL) and the aqueous layer back extracted with hexanes. The aqueous fraction was acidified with aqueous H_3PO_4 (0.49 M, 10 mL) and extracted with CH_2Cl_2 (2 × 50 mL). The extracts were dried (Na_2SO_4) and rotary evaporated to give acid **95** (4.26 g, 65%) as a foam. R_f = 0.40 (MeOH–$CHCl_3$, 1:9). $[\alpha]_D^{25}$ = +63.6° (*c* = 0.98). IR (film) (cm^{-1}): 3400, 1749, 1691, 1613, 1513, 1250, 1172. ^1H NMR (250 MHz, DMSO-d_6, 350 K) δ: 7.28 (m, 2H), 7.21 (m, 2H), 6.89 (m, 2H), 6.86 (m, 2H), 4.67 (d, 1H, *J* = 5.6 Hz), 4.62 (d, 1H, *J* = 5.0 Hz), 4.38 (d, 1H, *J* = 5.3 Hz), 4.34 (d, 1H, *J* = 5.8 Hz), 4.39 (br m, 1H), 4.06 (br m, 1H), 3.98 (m, 1H), 3.75 (s, 3H), 3.74 (s, 3H), 3.55 (m, 2H), 3.19 (s, 3H), 2.70 (s, 3H), 1.36 (s, 9H). ^{13}C NMR (62.5 MHz, DMSO-d_6, 350 K) δ: 171.1, 158.6, 154.6, 130.0, 129.8, 129.0, 128.7, 113.4, 79.6, 78.5, 78.2, 71.7, 71.0, 69.5, 57.5, 56.0, 54.8, 31.6, 27.7. Anal. calcd. for $C_{28}H_{39}NO_9$: C 63.02, H 7.37, N 2.63; found: C 62.78, H 7.08, N 2.45.

(2*R*)-Benzyl-2-methyl-4-pentenoate (97)

n-BuLi in hexanes (1.6 M, 125 mL, 200 mmol) was added to $PhCH_2OH$ (27.6 mL, 266 mmol) in THF (150 mL) at –23°C. After 1 h, the 1,3-oxazolidinone **96** (37) (30.0 g, 133 mmol) in THF (125 mL) was added and the solution was kept at –20°C for 2.5 h. Half-saturated NH_4Cl (250 mL) was added, the mixture rotary evaporated and the aqueous residue extracted with CH_2Cl_2 (3 × 350 mL). The combined extracts were washed with pH 7 buffer (300 mL) and brine (200 mL), dried, rotary evaporated, and chromatographed (hexanes–EtOAc, 9:1) to give ester **96** (26.5 g, 97%) as a colorless oil. R_f = 0.52 (hexanes–EtOAc, 9:1).$[\alpha]_D^{25}$ = –2.7° (*c* = 2.5). EI-MS *m*/*z*: 204 ($M^{\cdot+}$), 130, 91, 69, 41. EI-HRMS calcd for $C_{13}H_{16}O_2$: 204.1150 ($M^{\cdot+}$); found: 204.1156 ($M^{\cdot+}$). IR (film) (cm^{-1}): 2977, 1736, 1642, 1456, 1382, 1275, 1173, 917. ^1H NMR (400 MHz, $CDCl_3$) δ: 7.34 (m, 5H), 5.72 (m, 1H), 5.11 (s, 2H), 5.06 (m, 2H), 2.58 (m, 1H), 2.43 (m, 1H), 2.19 (m, 1H), 1.17 (d, 3H, *J* = 6.8 Hz). ^{13}C NMR (101 MHz, $CDCl_3$) δ: 175.8, 136.1, 135.3, 128.5, 128.1, 116.9, 66.1, 39.2, 37.7, 16.5.

(2*R*)-2-Methyl-4-pentenamide (98)

$AlMe_3$ in PhMe (2 M, 55 mL, 110 mmol) was added slowly to a suspension of NH_4Cl (5.9 g, 110 mmol) in PhMe (200 mL) at 0°C. After 1 h at 0°C and 1.5 h at room temperature, gas evolution had ceased and the solution was transferred to ester **97** (7.5 g, 36.7 mmol) in PhMe (50 mL). The mixture was heated at 60°C for 36 h and allowed to cool to room temperature. HCl (5%) was added as a quench and the resulting precipitate removed by filtration, washing with EtOAc. The combined organic extracts were dried (Na_2SO_4), rotary evaporated, and chromatographed (hexanes–EtOAc, 1:1) to give amide **98** (3.40 g, 81%) as a colorless solid. R_f = 0.39 (EtOAc); mp 79 to 80°C. $[\alpha]_D^{25}$ = –22.9° (*c* = 1.3). EI-MS *m*/*z*: 113 ($M^{\cdot+}$). EI-HRMS calcd. for $C_6H_{11}NO$:

© 2001 NRC Canada

113.0840 ($M^{\cdot+}$); found: 113.0844 ($M^{\cdot+}$). IR ($CHCl_3$) 3354, 3186, 2974, 1659. ^{1}H NMR (400 MHz, $CDCl_3$) δ: 6.44 (br s, 1H), 5.91 (br s, 1H), 5.87 (m, 1H), 5.77 (m, 2H), 2.38 (m, 2H), 2.16 (m, 1H), 1.16 (d, 3H, J = 6.8 Hz). ^{13}C NMR (100 MHz, $CDCl_3$) δ: 178.9, 135.6, 116.8, 40.3, 38.1, 17.1. Anal. calcd. for $C_6H_{11}NO$: C 63.69, H 9.80; N. 12.37; found: C 63.49, H 9.73; N. 12.39.

(2*R*)-2-Methyl-4-pentenenitrile (99)

Et_3N (12.3 mL, 88.4 mmol) and Cl_3CCOCl (9.9 mL, 88.4 mmol) in CH_2Cl_2 (20 mL) were added to amide **98** (5.0 g, 44.2 mmol) in CH_2Cl_2 (140 mL) at 0°C. The mixture was stirred at 0°C for 3 h, diluted with pH 7 buffer (75 mL), and extracted with CH_2Cl_2 (3 × 100 mL). The combined extracts were dried ($MgSO_4$) and rotary evaporated. The residue was distilled under reduced pressure to give nitrile **99** (3.3 g, 78%) as a colorless oil; bp 68°C (151 mm Hg). $[\alpha]_D^{25}$ = –17.4° (c = 1.1). EI-MS m/z: 95 ($M^{\cdot+}$). EI-HRMS calcd. for C_6H_9N: 95.0891 ($M^{\cdot+}$); found: 95.0753 ($M^{\cdot+}$). IR (film) (cm^{-1}): 2985, 2241, 1644. ^{1}H NMR (300 MHz, $CDCl_3$) δ: 5.80 (m, 1H), 5.21 (m, 2H), 2.66 (m, 1H), 2.33 (m, 2H), 1.31 (d, 3H, J = 6.9 Hz). ^{13}C NMR (75 MHz, $CDCl_3$) δ: 132.8, 122.2, 118.5, 37.6, 25.0, 17.1.

(2*R*)-Methyl 2-methyl-4-pentenimidate hydrochloride (100)

Anhydrous HCl was bubbled through nitrile **99** (2.64 g, 29.9 mmol) in MeOH (1.3 mL, 32.0 mmol) at –10°C until the solution was saturated. On standing at –5°C for 24 h, the mixture solidified and the solid was dried in vacuo, triturated with Et_2O, and the solid isolated by filtration to give hydrochloride **100** (4.66 g, 96%) as a colorless powder; mp 106 to 107°C. $[\alpha]_D^{25}$ = +35.8° (c = 1.0). EI-MS m/z: 126 ([M – H_2Cl]$^+$). EI-HRMS calcd. for $C_7H_{12}NO$: 126.0918 ([M – H_2Cl]$^+$); found: 126.0913 ([M – H_2Cl]$^+$). IR ($CHCl_3$) (cm^{-1}): 2886, 1654. ^{1}H NMR (400 MHz, $CDCl_3$) δ: 5.76 (m, 1H), 5.12 (m, 2H), 4.29 (s, 3H), 3.27 (m, 1H), 2.48–2.32 (m, 2H), 1.30 (d, 3H, J = 6.8 Hz). ^{13}C NMR (100 MHz, $CDCl_3$) δ: 182.5, 133.3, 118.5, 60.6, 38.2, 37.7, 16.7.

(5*R*)-Methyl 3-aza-4-methoxy-5-methyl-3,7-octadienoate (101)

Glycine methyl ester hydrochloride (3.86 g, 30.7 mmol) was added to hydrochloride **100** (4.79 g, 29.3 mmol) and glass chips in CH_2Cl_2 cooled to –10°C. This was followed by dropwise addition of Et_3N (4.16 mL, 29.9 mmol) over 2 h (syringe pump). After stirring for 1 h, the mixture was allowed to warm to room temperature and stirred for an additional 43 h. The solution was cooled to 0°C and quenched with cold pH 7 buffer (1.5 M, 100 mL), extracted with Et_2O (2 × 50 mL), and the combined ethereal extracts dried (Na_2SO_4). Rotary evaporation and distillation (Kugelrohr) gave imidate **101** (4.03 g, 69%) as a colorless liquid; bp 70°C (0.35 mm Hg). $[\alpha]_D^{25}$ = +22.6° (c = 1.7). EI-MS m/z: 199 ($M^{\cdot+}$). EI-HRMS calcd. for $C_{10}H_{17}NO_3$: 199.1208 ($M^{\cdot+}$); found: 199.1208 ($M^{\cdot+}$). IR (film) (cm^{-1}): 2947, 1752, 1674. ^{1}H NMR (300 MHz, $CDCl_3$) δ: 5.66 (m, 1H), 5.00 (m, 2H), 4.09 (s, 2H), 3.72 (s, 3H), 3.66 (s, 3H), 2.66 (m, 1H), 2.30 (m, 1H), 2.12 (m, 1H), 1.10 (d, 3H, J = 6.8 Hz). ^{13}C NMR (100 MHz, $CDCl_3$) δ: 171.1, 169.1, 135.7, 116.7, 52.6, 51.9, 49.9, 38.1, 33.2, 17.1. Anal. calcd. for $C_{10}H_{17}NO_3$: C 60.28, H 8.59, N 7.02; found: C 60.42, H 8.75, N 6.83.

Methyl 2-(4-penten-(2*R*)-yl)-4-oxazolecarboxylate (102)

Imidate **101** (1.64 g, 8.24 mmol) and HCO_2Me (0.6 mL, 9.9 mmol) in THF (12 mL) were added dropwise over 0.5 h to *t*-BuOK in THF (1 M, 8.2 mL, 8.2 mmol) at –10°C. The mixture was stirred for 3 h at –10°C and for 14 h at room temperature and then rotary evaporated. The residue was suspended in THF (40 mL), cooled to –78°C whereupon $BF_3{\cdot}OEt_2$ (2.2 mL, 18.0 mmol) was added over 5 min. The mixture was allowed to warm to room temperature over 1 h and stirred for a further 45 h. The resulting orange solution was poured into 10% aqueous $NaHCO_3$ (200 mL), extracted with Et_2O (2 × 100 mL), and the combined organic phases were washed with brine and dried (Na_2SO_4). Rotary evaporation and chromatography (hexanes–EtOAc, 4:1) gave oxazole **102** (1.23 g, 77%) as a colorless oil. R_f = 0.63 (hexanes–EtOAc, 3:1). $[\alpha]_D^{25}$ = –4.5° (c = 1.0). EI-MS m/z: 195 ($M^{\cdot+}$). EI-HRMS calcd. for $C_{10}H_{13}NO$: 195.0895 ($M^{\cdot+}$); found: 195.0901 ($M^{\cdot+}$). IR (film) (cm^{-1}): 2979, 1748, 1584. ^{1}H NMR (300 MHz, $CDCl_3$) δ: 8.21 (s, 1H), 5.77 (m, 1H), 5.03 (m, 2H), 3.91 (s, 3H), 3.13 (m, 1H), 2.58 (m, 1H), 2.41 (m, 1H), 1.37 (d, 3H, J = 7.0 Hz). ^{13}C NMR (75 MHz, $CDCl_3$) δ: 168.3, 161.3, 143.3, 134.5, 132.6, 116.9, 51.5, 38.6, 33.3, 17.2. Anal. calcd. for $C_{10}H_{13}NO$: C 61.52, H 6.71, N 7.17; found: C 61.15, H 6.69, N 7.08.

Methyl 2-(4-oxo-(2*R*)-butyl)-4-oxazolecarboxylate (103)

$NaIO_4$ (5.90 g, 27.6 mmol) in H_2O (50 mL) was added dropwise to oxazole **102** (2.57 g, 13.14 mmol) and OsO_4 in H_2O (2.5%, 16 drops) in Me_2CO (25 mL) and H_2O (25 mL). The mixture was stirred for 5 h, poured into H_2O (200 mL), and extracted with $CHCl_3$ (5 × 50 mL). After drying (Na_2SO_4) of the extracts, rotary evaporation, and chromatography (hexanes–EtOAc, 2:1 to 1:1) gave aldehyde **103** (2.05 g, 79%) as a colorless liquid. R_f = 0.34 (hexanes–EtOAc, 1:1). EI-MS m/z: 197 ($M^{\cdot+}$). EI-HRMS calcd. for $C_9H_{11}NO_4$: 197.0688 ($M^{\cdot+}$); found: 197.0681 ($M^{\cdot+}$). IR (film) (cm^{-1}): 3161, 2955, 1732, 1584. ^{1}H NMR (300 MHz, $CDCl_3$) δ: 9.76 (s, 1H), 8.12 (s, 1H), 3.86 (s, 3H), 3.55 (m, 1H), 3.14 (dd, 1H, J = 18.2, 7.0 Hz), 2.76 (dd, 1H, J = 18.2, 6.7 Hz), 1.36 (d, 3H, J = 7.1 Hz). ^{13}C NMR (100 MHz, $CDCl_3$) δ: 199.1, 167.5, 161.3, 143.6, 132.9, 51.7, 47.6, 27.7, 18.2.

Methyl 2-(4-hydroxy-(2*R*)-butyl)-4-oxazolecarboxylate (104)

$NaBH_4$ (0.39 g, 10.3 mmol) was added in small portions over 5 min to aldehyde **103** (2.03 g, 10.28 mmol) in MeOH (100 mL) at –12°C. After 1 h, chilled (5°C) aqueous $KHSO_4$ (1 M, 50 mL) was added, the mixture was extracted with $CHCl_3$ (5 × 50 mL), and the extracts dried (Na_2SO_4). Rotary evaporation and chromatography (hexanes–EtOAc, 1:1, then EtOAc) gave alcohol **104** (1.90 g, 93%) as a colorless oil. R_f = 0.42 (EtOAc). $[\alpha]_D^{25}$ = –25.0° (c = 1.0). CI-MS m/z: 200 ([M + H]$^+$). CI-HRMS calcd. for $C_9H_{13}NO_4$: 199.0844 ($M^{\cdot+}$); found: 199.0829 ($M^{\cdot+}$). IR (film) (cm^{-1}): 3413, 2953, 1736, 1585. ^{1}H NMR (300 MHz, $CDCl_3$) δ: 8.03 (s, 1H), 3.72 (s, 3H), 3.49 (m, 3H), 3.08 (m, 1H), 1.89 (m, 1H), 1.72 (m, 1H), 1.20 (d, 3H, J = 6.9 Hz). ^{13}C NMR (75 MHz, $CDCl_3$) δ: 168.9, 161.4, 143.4, 132.3, 59.2, 51.6, 37.0, 30.1, 17.9. (*R*)-α-methoxy-α-(trifluoromethyl)phenylacetic acid

© 2001 NRC Canada

(26 mg, 0.11 mmol) in CH_2Cl_2 (0.25 mL), 1,3-dicyclohexyl carbodiimide (22 mg, 0.11 mmol), and DMAP (2 mg) were added sequentially with stirring to alcohol **104** (20 mg, 0.10 mmol). After 2 h, the mixture was diluted with Et_2O (10 mL) and filtered. The organic solution was evaporated and the residue chromatographed (hexanes–EtOAc, 1:1) to furnish ester **108** (38 mg, 91%) as a colorless oil. R_f = 0.50 (hexanes–EtOAc, 1:1). EI-MS *m*/*z*: 415 ($M^{\cdot+}$), 189, 150, 105. EI-HRMS calcd for $C_{19}H_{20}F_3NO_6$: 415.1217 ($M^{\cdot+}$); found: 415.1222 ($M^{\cdot+}$). IR (film) (cm^{-1}): 1756, 1274, 1166, 1114. ^1H NMR (300 MHz, $CDCl_3$) δ: 8.09 (s, 1H), 7.46–7.34 (m, 5H), 4.35 (m, 2H), 3.90 (s, 3H), 3.52 (s, 3H), 3.08 (m, 1H), 2.26 (m, 1H), 2.02 (m, 1H), 1.33 (d, 3H, *J* = 7.0 Hz). The mixture of diastereoisomeric Mosher esters **109** prepared in the same way from the corresponding racemic alcohol (±)-**104** showed: ^1H NMR (400 MHz, $CDCl_3$) δ: 8.11 (s, 1H), 7.48–7.36 (m, 5H), 4.35 (m, 2H), 3.91 (s, 3H), 3.53 (s, 3H), 3.09 (m, 1H), 2.26 (m, 1H), 2.02 (m, 1H), 1.36 (d, 1.5H, *J* = 7.0 Hz), 1.35 (d, 1.5H, *J* = 7.0 Hz).

Methyl 2-(4-(methanesulfonyl)oxy-(2*R*)-butyl)-4-oxazolecarboxylate (105)

Et_3N (2.3 mL, 16.0 mmol) and $MeSO_2Cl$ (0.9 mL, 10 mmol) were added to alcohol **104** (1.61 g, 8.09 mmol) in Et_2O (40 mL) at –10°C. The mixture was stirred at –10°C for 45 min, diluted with H_2O (25 mL), and extracted with $CHCl_3$ (3 × 25 mL). The combined extracts were dried (Na_2SO_4), rotary evaporated, and chromatographed (EtOAc–CH_2Cl_2, 1:9) to give mesylate **105** (1.89 g, 84%) as a colorless solid; mp 61–63°C. R_f = 0.69 (EtOAc). $[\alpha]_D^{25}$ = –34.0° (*c* = 1.0). EI-MS *m*/*z*: 277 ($M^{\cdot+}$). EI-HRMS calcd. for $C_{10}H_{15}NO_4S$: 277.0620 ($M^{\cdot+}$); found: 277.0619 ($M^{\cdot+}$). IR ($CHCl_3$) (cm^{-1}): 3098, 1726. ^1H NMR (300 MHz, $CDCl_3$) δ: 8.07 (s, 1H), 4.15 (m, 2H), 3.76 (s, 3H), 3.13 (m, 1H), 2.88 (s, 3H), 2.17 (m, 1H), 1.97 (m, 1H), 1.27 (d, 3H, *J* = 7.1 Hz). ^{13}C NMR (75 MHz, $CDCl_3$) δ: 167.4, 161.2, 143.6, 132.6, 67.1, 51.7, 36.9, 33.5, 29.8, 17.9. Anal. calcd. for $C_{10}H_{15}NO_6S$: C 43.31, H 5.45, N 5.05; found: C 43.29, H 5.48, N 4.91.

Methyl 2-(4-azido-(2*R*)-butyl)-4-oxazolecarboxylate (106)

NaN_3 (1.11 g, 17.1 mmol) was added to mesylate **105** (1.89 g, 6.82 mmol) in DMSO (45 mL), the mixture was heated to 70°C for 7 h, cooled to room temperature, and diluted with cold H_2O (200 mL). The mixture was extracted with EtOAc (3 × 50 mL) and the combined extracts dried (Na_2SO_4). Rotary evaporation and chromatography (hexanes–EtOAc, 1:1 to 1:2) gave azide **106** (1.33 g, 87%) as a colorless liquid. R_f = 0.56 (hexanes–EtOAc, 1:1). $[\alpha]_D^{25}$ = –39.0° (*c* = 2.3). EI-MS *m*/*z*: 225 ($[M + H]^+$). CI-HRMS calcd. for $C_9H_{12}N_4O_3$: 224.0909 ($M^{\cdot+}$); found: 224.0922 ($M^{\cdot+}$). IR (film) (cm^{-1}): 2953, 2099, 1747, 1584. ^1H NMR (300 MHz, $CDCl_3$) δ: 8.10 (s, 1H), 3.81 (s, 3H), 3.26 (t, 2H, *J* = 6.8 Hz), 3.09 (m, 1H), 2.05 (m, 1H), 1.81 (m, 1H), 1.29 (d, 3H, *J* = 7.1 Hz). ^{13}C NMR (75 MHz, $CDCl_3$) δ: 167.8, 161.4, 143.6, 132.8, 51.8, 48.7, 33.5, 30.9, 18.1. Anal. calcd. for $C_9H_{12}N_4O_3$: C 48.21, H 5.39, N 24.98; found: C 47.90, H 5.28, N 24.76.

Methyl 2-(4-amino-(2*R*)-butyl)-4-oxazolecarboxylate (107)

A suspension of 10% Pd(C) (8 mg) and azide **106** (96 mg, 0.43 mmol) in MeOH (1.5 mL) was purged with Ar and then maintained under a H_2 atmosphere for 2 h. The catalyst was removed by filtration and the filtrate rotary evaporated to leave amine **107** (83 mg, 98%) as a colorless oil. $[\alpha]_D^{25}$ = –29.6° (*c* = 1.1). EI-MS *m*/*z*: 198 ($M^{\cdot+}$). EI-HRMS calcd. for $C_9H_{14}N_2O_3$: 198.1004 ($M^{\cdot+}$); found: 198.0997 ($M^{\cdot+}$). IR (film) (cm^{-1}): 2927, 2877, 1742, 1671, 1622. ^1H NMR (300 MHz, $CDCl_3$) δ: 8.06 (s, 1H), 3.78 (s, 3H), 3.05 (m, 1H), 2.57 (t, 2H, *J* = 7.1 Hz), 1.85 (m, 1H), 1.66 (m, 1H), 1.24 (d, 3H, *J* = 7.9 Hz), 1.19 (br s, 2H). ^{13}C NMR (75 MHz, $CDCl_3$) δ: 168.9, 161.2, 143.4, 132.7, 51.8, 39.5, 38.5, 31.2, 18.2.

(2*R*,3*R*,4*R*)-4-(*N*-(*tert*-Butyloxy)carbonyl-*N*-methyl)amino-2,3-di(4-methoxybenzyl)oxy-5-methoxy-*N*-(3*R*-((4-methoxycarbonyl)-2-oxazolyl)-1-butyl)pentamide (110)

1-Hydroxybenzotriazole (1.21 g, 8.96 mmol), powdered molecular sieves (4 Å, 3.0 g), and 1-ethyl-3-(3-dimethylaminopropyl)carbodiimide hydrochloride (0.855 g, 4.46 mmol) were added sequentially to acid **95** (2.49 g, 4.67 mmol) in DMF (10 mL) at 0°C. After 1 h, amine **107** (0.88 g, 4.5 mmol) in DMF (10 mL) was added and the mixture allowed to warm to room temperature and stirred for 10 h. The mixture was filtered and the filtrate rotary evaporated. The residue was partitioned between Et_2O (75 mL) and 10% aqueous $NaHCO_3$ (25 mL), the organic phase washed with aqueous citric acid (0.1 M, 25 mL) and brine (2 × 25 mL) and dried (Na_2SO_4). Chromatography (EtOAc–PhMe, 2:1) gave amide **110** (2.28 g, 72%) as a yellow oil. R_f = 0.55 (MeOH–$CHCl_3$, 1:9). $[\alpha]_D^{25}$ = +21.4° (*c* = 1.02). FAB-MS *m*/*z*: 714 ($M^{\cdot+}$). IR (neat) (cm^{-1}): 3420, 1745, 1688, 1612, 1584, 1513, 1455, 1246, 821, 775. ^1H NMR (250 MHz, DMSO-d_6, 350 K) δ: 8.61 (s, 1H), 7.60 (br s, 1H), 7.29 (m, 2H), 7.20 (m, 2H), 6.88 (m, 4H), 4.56 (m, 2H), 4.45 (d, 1H, *J* = 11.7 Hz), 4.36 (d, 1H, *J* = 10.9 Hz), 4.20 (br m, 1H), 3.96 (m, 2H), 3.80 (s, 3H), 3.75 (s, 3H), 3.74 (s, 3H), 3.61 (br m, 1H), 3.50 (m, 1H), 3.19 (s, 3H), 3.13 (m, 2H), 3.03 (m, 1H), 2.67 (s, 3H), 1.95 (m, 1H), 1.72 (m, 1H), 1.35 (s, 9H), 1.27 (d, 3H, *J* = 7.0 Hz). Anal. calcd. for $C_{37}H_{51}N_3O_{11}$: C 62.26, H 7.20, N 5.89; found: C 61.93, H 7.27, N 5.81.

(2*R*,3*R*,4*R*)-4-Dimethylamino-5-methoxy-*N*-(3*R*-((4-methoxycarbonyl)-2-oxazolyl)-1-butyl)-2,3-di((triethylsilyl)oxy)pentamide (112)

Oxazole-amide **110** (586 mg, 0.821 mmol) was dissolved in EtOAc saturated with aqueous HCl (2.8M, 12 mL) and stirred at room temperature for 4 h. After rotary evaporation, the residue was washed with Et_2O and dissolved in CH_3CN (8.0 mL). Et_3SiCl (0.34 mL, 2.05 mmol) and *i*-Pr_2NEt (1.4 mL, 8.20 mmol) were added. After stirring for 2 h, MeI (0.26 mL, 4.10 mmol) was added. Following 10 h stirring at room temperature, the mixture was diluted with Et_2O and quenched with saturated aqueous $NaHCO_3$. The organic phase was washed with H_2O (1.0 mL) and brine (1.0 mL) and then dried (Na_2SO_4). Rotary evaporation and chromatography (hexanes–EtOAc, 1:2 to 1:4) gave oxazole **112** (8) (300 mg, 59%) as a yellow oil. $[\alpha]_D^{25}$ = +4.4° (*c* = 0.89). FAB-HRMS calcd. for $C_{29}H_{58}N_3O_7Si_2$: 616.3813 ($[M + H]^+$); found: 616.3734 ($[M + H]^+$). IR (film) (cm^{-1}): 3438, 2958, 2877, 1750, 1676, 1584, 1519, 1459, 1323, 1237, 1197, 1142, 1110, 1076, 1007, 857, 839, 740. ^1H NMR (400 MHz, $CDCl_3$) δ: 8.14 (s, 1H), 6.54 (m, 1H), 4.26 (s,

© 2001 NRC Canada

1H), 4.03 (d, 1H, *J* = 9.8 Hz), 3.89 (s, 3H), 3.51 (d, 2H, *J* = 5.6 Hz), 3.27 (s, 3H), 3.23 (m, 1H), 3.14 (m, 1H), 3.10–3.04 (m, 2H), 2.23 (s, 6H), 2.03 (m, 1H), 1.80 (m, 1H), 1.37 (d, 3H, *J* = 7.0 Hz), 0.95 (m, 18H), 0.64 (m, 12H). ^{13}C NMR (100 MHz, $CDCl_3$) δ: 171.9, 168.5, 161.8, 143.7, 133.0, 77.3, 73.7, 70.5, 61.5, 58.4, 52.1, 41.7, 36.8, 34.7, 31.6, 18.3, 6.9, 6.8, 4.9, 4.7. The corresponding data reported by Evans (8) were as follows: $[\alpha]_D^{25}$ = +4.3° (CH_2Cl_2, *c* = 0.70). FAB-HRMS$^+$ calcd. for $C_{29}H_{57}N_3O_7Si_2Na$: 638.3633 ([M + Na]$^+$); found: 638.3651 ([M + Na]$^+$). IR (film) (cm^{-1}): 3435, 2960, 2882, 1756, 1680, 1587, 1518, 1460, 1321, 1236, 1196, 1141, 1110, 1073, 1005, 857, 838, 740. ^{1}H NMR (500 MHz, $CDCl_3$) δ: 8.16 (s, 1H), 6.56 (t, 1H, *J* = 5.8 Hz), 4.28 (s, 1H), 4.05 (d, 1H, *J* = 10.1 Hz), 3.91 (s, 3H), 3.53 (d, 2H, *J* = 6.2 Hz), 3.29 (s, 3H), 3.27 (m, 1H), 3.15 (m, 1H), 3.11–3.05 (m, 2H), 2.24 (s, 6H), 2.04 (m, 1H), 1.82 (m, 1H), 1.39 (d, 3H, *J* = 7.1 Hz), 0.97 (m, 18H), 0.67 (m, 12H). ^{13}C NMR (100 MHz, $CDCl_3$) δ: 171.9, 168.5, 161.7, 143.7, 133.0, 77.3, 73.8, 70.5, 61.5, 58.3, 52.1, 41.7, 36.8, 34.7, 31.6, 18.3, 6.9, 6.8, 4.9, 4.7.

(2*R*,3*R*,4*R*)-4-Dimethylamino-5-methoxy-*N*-(3*R*-((4-hydroxymethyl)-2-oxazolyl)-1-butyl)-2,3-di((triethylsilyl)-oxy)pentamide (113)

$LiAlH_4$ in Et_2O (1.0 M, 1.5 mL, 1.50 mmol) was added dropwise to ester **112** (300 mg, 0.487 mmol) in Et_2O (5 mL) at –78°C and the mixture stirred for 1.5 h. EtOAc was added to quench excess $LiAlH_4$ and the solution allowed to warm to room temperature. H_2O (3.0 mL) and, after 10 min, anhydrous Na_2SO_4 were added and the mixture stirred vigorously for 30 min. Filtration, rotary evaporation, and chromatography (hexanes–EtOAc, 1:2 to 1:9) gave oxazole **113** (8) (177 mg, 62%) as a pale yellow oil. $[\alpha]_D^{25}$ = +5.8° (*c* = 1.2). FAB-HRMS calcd. for $C_{28}H_{58}N_3O_6Si_2$: 588.3864 ([M + H]$^+$); found: 588.3810 ([M + H]$^+$). IR (film) (cm^{-1}): 3430, 2955, 2878, 1665, 1525, 1459, 1239, 1129, 1070, 1008, 741. ^{1}H NMR (300 MHz, $CDCl_3$) δ: 7.48 (s, 1H), 6.58 (m, 1H), 4.55 (s, 2H), 4.26 (s, 1H), 4.05 (d, 1H, *J* = 9.8 Hz), 3.52 (d, 2H, *J* = 5.8 Hz), 3.27 (s, 3H), 3.27–3.14 (m, 2H), 3.10–2.98 (m, 2H), 2.38 (m, 1H), 2.23 (s, 6H), 1.96 (s, 1H), 1.78 (m, 1H), 1.37 (d, 3H, *J* = 7.0 Hz), 0.96 (m, 18H), 0.64 (m, 12H). ^{13}C NMR (75 MHz, $CDCl_3$) δ: 171.9, 168.0, 140.0, 134.6, 77.4, 73.7, 70.5, 61.6, 58.4, 56.7, 41.7, 36.8, 34.9, 31.6, 18.4, 7.0, 6.8, 4.9, 4.7. The ^{1}H and ^{13}C NMR spectra of **113** were in agreement with spectra of authentic material kindly provided by Professor David A. Evans. The corresponding data reported by Evans (8) were as follows: $[\alpha]_D^{25}$ = +4.8° (CH_2Cl_2, *c* = 1.12). FAB-HRMS calcd. for $C_{28}H_{57}N_3O_6Si_2$: 588.3864 ([M + H]$^+$); found: 588.3846 ([M + H]$^+$). IR (film) (cm^{-1}): 3400, 2960, 2870, 1660, 1530, 1455, 1070, 1010. ^{1}H NMR (400 MHz, $CDCl_3$) δ: 7.48 (s, 1H), 6.58 (br s, 1H), 4.55 (s, 2H), 4.26 (s, 1H), 4.04 (d, 1H, *J* = 9.7 Hz), 3.52 (d, 2H, *J* = 5.8 Hz), 3.28 (s, 3H), 3.20 (m, 2H), 3.02 (m, 2H), 2.23 (s, 6H), 1.96 (m, 1H), 1.78 (m, 1H), 1.34 (d, 3H, *J* = 7.0 Hz), 0.96 (m, 18H), 0.63 (m, 12H). ^{13}C NMR (100 MHz, $CDCl_3$) δ: 171.9, 168.0, 139.9, 134.6, 77.4, 73.7, 70.5, 61.5, 58.4, 56.8, 41.7, 36.8, 34.9, 31.5, 18.4, 6.9, 6.8, 4.9, 4.7.

Acknowledgments

We thank the National Institutes of Health for support of this program (AI-20644), G. D. Searle & Company (now Pharmacia) for unrestricted support and microanalyses, Glaxo Wellcome for the endowment (to A.G.M.B.), the Uehara Memorial Life Science Fund for a fellowship (to K. H.), and the Wolfson Foundation for establishing the Wolfson Centre for Organic Chemistry in Medical Science at Imperial College. We additionally thank Professor David A. Evans for sending us copies of the ^{1}H and ^{13}C NMR spectra of **88** and **113** and Dr. Nick S. Stock for assistance with drafting the manuscript.

References

1. Y. Kato, N. Fusetani, S. Matsunaga, and K. Hashimoto. J. Am. Chem. Soc. **108**, 2780 (1986).
2. (*a*) Y. Kato, N. Fusetani, S. Matsunaga, K. Hashimoto, and K. Koseki. J. Org. Chem. **53**, 3930 (1988); (*b*) S. Matsunaga, H. Fujiki, D. Sakata, and N. Fusetani. Tetrahedron, **47**, 2999 (1991).
3. (*a*) S. Matsunaga, T. Wakimoto, and N. Fusetani. J. Org. Chem. **62**, 2640 (1997); (*b*) E.J. Dumdei, J.W. Blunt, M.H.G. Munro, and L.K. Pannell. J. Org. Chem. **62**, 2636 (1997); (*c*) S. Matsunaga, T. Wakimoto, and N. Fusetani. Tennen Yuki Kagobutsu Toronkai Koen Yoshishu, **39**, 181 (1997**)**; (*d*) K.G. Steube, C. Meyer, P. Proksch, A Supriyono, W. Sumaryono, and H.G. Drexler. Anticancer Res. **18**, 129 (1998); (*e*) S. Matsunaga, T. Wakimoto, and N. Fusetani. J. Org. Chem. **62**, 9388 (1997).
4. S. Matsunaga, T. Wakimoto, N. Fusetani, and M. Suganuma. Tetrahedron Lett. **38**, 3763 (1997).
5. J.R. Bagu, B.D. Sykes, M.M Craig, and C.F. Holmes. J. Biol. Chem. **272**, 5087 (1997), and refs. cited therein.
6. S. Matsunaga and N. Fusetani. Tetrahedron Lett. **32**, 5605 (1991).
7. (*a*) Y. Hamada, Y. Tanada, F. Yokokawa. and T. Shioiri. Tetrahedron Lett. **32**, 5983 (1991); (*b*) D.A. Evans, J.L. Leighton, and J.R. Gage. Recent advances in the chemistry of anti-infective agents. Special publication. No. 119. *Edited by* P.H. Bentley and R. Ponsford. Royal Society of Chemistry, Cambridge. 1993. p. 117.
8. D.A. Evans, J.R. Gage, and J.L. Leighton. J. Am. Chem. Soc. **114**, 9434 (1992).
9. (*a*) D.A. Evans and J.R. Gage. Tetrahedron Lett. **31**, 6129 (1990); (*b*) O. Hara, K. Nakao, Y. Tanada, A. Nishio, J. Matsubara, F. Yokokawa, Y. Hamada, and T. Shioiri. Tennen Yuki Kagobutsu Toronkai Koen Yoshishu, **32**, 617 (1990); (*c*) O.Hara, Y. Hamada, and T. Shioiri. Synlett, 283 (1991); (*d*) O. Hara, Y. Hamada, and T. Shioiri. Synlett, 285 (1991); (*e*) A.B. Smith III, J.J.-W. Duan, K.G. Hull, and B.A. Salvatore. Tetrahedron Lett. **32**, 4855 (1991); (*f*) A.B. Smith III, B.A. Salvatore, K.G. Hull, and J.J.-W. Duan. Tetrahedron Lett. **32**, 4859 (1991); (*g*) R.W. Armstrong and J.A. DeMattei. Tetrahedron Lett. **32**, 5749 (1991); (*h*) Y. Hamada, Y. Tanada, F. Yokokawa, and T. Shioiri. Tetrahedron Lett. **32**, 5983 (1991); (*i*) A.M.P. Koskinen and J. Chen. Tetrahedron Lett. **32**, 6977 (1991); (*j*) D.A. Evans, J.R. Gage, J.L. Leighton, and A.S. Kim. J. Org. Chem. **57**, 1961 (1992); (*k*) D.A. Evans, J.R. Gage, and J.L. Leighton. J. Org. Chem. **57**, 1964 (1992); (*l*) D.A. Evans and J.R. Gage. J. Org. Chem. **57**, 1958 (1992); (*m*) F. Yokokawa, Y. Hamada, and T. Shioiri. Synlett, 149 (1992); (*n*) F. Yokokawa, Y. Hamada, and T. Shioiri. Synlett, 151 (1992); (*o*) H.A. Vaccaro, D.E. Levy, A. Sawabe, T. Jaetsch, and S. Masamune. Tetrahedron Lett. **33**, 1937 (1992);

© 2001 NRC Canada

(*p*) J. Matsubara, K. Nakao, Y. Hamada, and T. Shioiri. Tetrahedron Lett. **33**, 4187 (1992); (*q*) F. Yokokawa, Y. Hamada, and T. Shioiri. Synlett, 703 (1992); (*r*) A. Sawabe, S.A. Filla, and S. Masamune. Tetrahedron Lett. **33**, 7685 (1992); (*s*) F. Yokokawa, Y. Hamada, and T. Shioiri. Tetrahedron Lett. **34**, 6559 (1993); (*t*) J.J.-W. Duan and A.B. Smith III. J. Org. Chem. **58**, 3703 (1993); (*u*) F. Yokokawa, Y. Hamada, and T. Shioiri. Tennen Yuki Kagobutsu Toronkai Koen Yoshishu, **35**, 127 (1993); (*v*) B.A. Salvatore and A.B. Smith III. Tetrahedron Lett. **35**, 1329 (1994); (*w*) K. Takebuchi, Y. Hamada and T. Shioiri. Tetrahedron Lett. **35**, 5239 (1994); (*x*) B.M. Trost and J.A. Flygare. Tetrahedron Lett. **35**, 4059 (1994); (*y*) A.M.P Koskinen and P.M. Pihko. Tetrahedron Lett. **35**, 7417 (1994); (*z*) A.B. Smith III and M. Iwashima. Tetrahedron Lett. **35**, 6051 (1994); (*aa*) M. Iwashima, T. Kinsho, and A.B. Smith III. Tetrahedron Lett. **36**, 2199 (1995); (*bb*) K. Shinozaki, K. Mizuno, H. Wakamatsu, and Y. Masaki. Chem. Pharm. Bull. **44**, 1823 (1996); (*cc*) A.K. Ogawa, J.A. DeMattei, G.R. Scarlato, J.E. Tellew, L.S. Chong, and R.W. Armstrong. J. Org. Chem. **61**, 6153 (1996); (*dd*) G.R. Scarlato, J.A. DeMattei, L.S. Chong, A.K. Ogawa, M.R. Lin, and R.W. Armstrong. J. Org. Chem. **61**, 6139 (1996); (*ee*) K. Shinozaki, K. Mizuno, and Y. Masaki. Heterocycles, **43**, 11 (1996); (*ff*) Y. Hamada, F. Yokokawa, M. Kabeya, K. Hatano, Y. Kurono, and T. Shioiri. Tetrahedron, **52**, 8297 (1996); (*gg*) Y. Hamada. Ikagaku Oyo Kenkyu Zaidan Kenkyu Hokoku, **15**, 293 (1997); (*hh*) M. Kabeya, Y. Hamada, and T. Shioiri. Tetrahedron, **53**, 13969 (1997); (*ii*) M. Kabeya, Y. Hamada, and T. Shioiri. Tetrahedron, **53**, 9769 (1997); (*jj*) M. Kabeya, Y. Hamada, and T. Shioiri. Tetrahedron, **53**, 9777 (1997); (*kk*) P.M. Pihko and A.M.P. Koskinen. J. Org. Chem. **63**, 92 (1998); (*ll*) M.F. Jacobs and W. Kitching. Curr. Org. Chem. **2**, 395 (1998); (*mm*) P.M. Pihko and A.M.P. Koskinen. Synlett, 1966 (1999); (*nn*) P.M. Pihko, A.M.P. Koskinen, M.J. Nissinen, and K. Rissanen. J. Org. Chem. **64**, 652 (1999).

10. N. Tanimoto, S.W. Gerritz, A. Sawabe, T. Noda, S.A. Filla, and S. Masamune. Angew. Chem. Int. Ed. Engl. **33**, 673 (1994).
11. (*a*) A.B. Smith III, G.K. Friestad, J.J.-W. Duan, J. Barbosa, K.G. Hull, M. Iwashima, Y. Qiu, P.G. Spoors, E. Bertounesque, and B.A. Salvatore. J. Org. Chem. **63**, 7596 (1998); (*b*) A.B. Smith III, G.K. Friestad, J. Barbosa, E. Bertounesque, K.G. Hull, M. Iwashima, Y. Qiu, B.A. Salvatore, P.G. Spoors, and J.J.-W. Duan. J. Am. Chem. Soc. **121**, 10468 (1999); (*c*) A.B. Smith III, G.K. Friestad, J. Barbosa, E. Bertounesque, J.J.-W. Duan, K.G. Hull, M. Iwashima, Y. Qiu, P.G. Spoors, and B.A. Salvatore. J. Am. Chem. Soc. **121**, 10478 (1999).
12. F. Yokokawa, Y. Hamada and T. Shioiri. Chem. Commun. 871 (1996).
13. A.K. Ogawa and R.W. Armstrong. J. Am. Chem. Soc. **120**, 12435 (1998), and refs. cited therein.
14. (*a*) W.R. Roush. Allyl organometallics. *In* Comprehensive organic synthesis. Vol. 2. *Edited by* B.M. Trost, I. Fleming, and C.H. Heathcock. Pergamon Press, New York. 1991. pp. 1–53, and refs. therein; (*b*) H.C. Brown and P.K. Jadhav. J. Am. Chem. Soc. **105**, 2092 (1983); (*c*) H.C. Brown, P.K. Jadhav, and P.T. Perumal. Tetrahedron Lett. **25**, 5111 (1984); (*d*) H.C. Brown and K.S. Bhat. J. Am. Chem. Soc. **108**, 5919 (1986); (*e*) P.K. Jadhav, K.S. Bhat, P.T. Perumal, and H.C. Brown. J. Org. Chem. **51**, 432 (1986); (*f*) M. Srebmik and P.V. Ramachandran. Aldrichim. Acta, **20**, 9 (1987); (*g*) H.C. Brown, P.K. Jadhav, and K.S. Bhat. J. Am. Chem. Soc. **110**, 1535 (1988); (*h*) U.S. Racherla and H.C. Brown. J. Org. Chem. **56**, 401 (1991).
15. *(A)* A.G.M. Barrett, J.J. Edmunds, K. Horita, and C.J. Parkinson. J. Chem. Soc. Chem. Commun. 1236 (1992); (*b*) A.G.M. Barrett, J.J. Edmunds, J.A. Hendrix, K. Horita, and C.J. Parkinson. J. Chem. Soc. Chem. Commun. 1238 (1992); (*c*) A.G.M. Barrett, J.J. Edmunds, J.W. Malecha, and C.J. Parkinson. J. Chem. Soc. Chem. Commun. 1240 (1992).
16. E. Piers, J.M. Chong, and H.E. Morton. Tetrahedron, **45**, 363 (1989).
17. A.J. Leusink, H.A. Budding, and J.W. Marsman. J. Organomet. Chem. **9**, 285 (1967).
18. A. Basha, M. Lipton, and S.M. Weinreb. Tetrahedron Lett. **18**, 4171 (1977).
19. E.J. Corey and R.H. Wollenberg. J. Org. Chem. **40**, 3788 (1975).
20. E.-I. Negishi, D.E. Van Horn, and T. Yoshida. J. Am. Chem. Soc. **107**, 6639 (1985).
21. (*a*) T.W. Green. Protective groups in organic synthesis. Wiley, New York. 1981; (*b*) T.W. Green and P.G. Wuts. Protective groups in organic synthesis. 2nd ed. Wiley, New York. 1991; (*c*) H. Kunz and H. Waldmann. Protecting groups. *In* Comprehensive organic synthesis. Vol. 6. *Edited by* B.M. Trost, I. Fleming, and E. Winterfeldt. Pergammon Press, Oxford. 1991. p. 631.
22. A.J. Mancuso, D.S. Brownfain, and D. Swern. J. Org. Chem. **44**, 4148 (1979).
23. E.J. Corey and P.J. Fuchs. Tetrahedron Lett. 3769 (1972).
24. R. Pappo, D.S. Allen Jr., R.U. Lemieux, and W.S. Johnson. J. Org. Chem. **21**, 478 (1956).
25. J.K. Stille and B.L. Groh. J. Am. Chem. Soc. **109**, 813 (1987).
26. J.A. Dale, D.L. Dull, and H.S. Mosher. J. Org. Chem. **34**, 2543 (1969).
27. C.A. Brown. J. Am. Chem. Soc. **95**, 4100 (1973).
28. P. Ma, V.S. Martin, S. Masamune, K.B. Sharpless, and S.M. Viti. J. Org. Chem. **47**, 1378 (1982).
29. (*a*) Y. Oikawa, Y. Yoshioka, and O. Yonemitsu. Tetrahedron Lett. 23, 889 (1982); (*b*) K. Horita, T. Yoshioka, T. Tanaka, Y. Oikawa, and O. Yonemitsu. Tetrahedron, **42**, 3021 (1986).
30. (*a*) S.D. Rychnovsky, B. Rogers, and G. Yang. J. Org. Chem. **58**, 3511 (1993); (*b*) P. Cieplak, A.E. Howard, J.P. Powers, S.D. Rychnovsky, and P.A. Kollman. J. Org. Chem. **61**, 3662 (1996); (*c*) for an example of the use of this analytical NMR technique in more complicated 1,3-polyol systems see: D.A. Evans, D.L. Rieger, and J.R. Gage. Tetrahedron Lett. **31**, 7099 (1990).
31. D.B. Dess and J.C. Martin. J. Am. Chem. Soc. **113**, 7277 (1991).
32. P. Garner and J.M. Park. J. Org. Chem. **52**, 2361 (1987).
33. A.G.M. Barrett and J.W. Malecha. J. Org. Chem. **56**, 5243 (1991).
34. (*a*) G.R. Jones and Y. Landais. Tetrahedron, **52**, 7599 (1996); (*b*) I. Fleming, Chemtracts: Org. Chem. 1 (1996).
35. B.O. Lindgren and T. Nilsson. Acta Chem. Scand. **27**, 888 (1973).
36. (*a*) A.I. Meyers, J.P. Lawson, D.G. Walker, and R.J. Linderman. J. Org. Chem. **51**, 5111 (1986), and refs. cited therein. For other pertinent examples of 2,4-disubstituted oxazole syntheses see: (*b*) Z. Zhao, G.R. Scarlato, and R.W. Armstrong. Tetrahedron Lett. **32**, 1609 (1991); (*c*) F. Yokokawa, Y. Hamada, and T. Shioiri. Synlett, 153 (1992); (*d*) R. Shapiro. J. Org. Chem. **58**, 5759 (1993).
37. D.A. Evans, M.D. Ennis, and D.J. Mathre. J. Am. Chem. Soc. **104**, 1737 (1982).
38. (*a*) M. Tsuda, A. Hatakeyama, and J. Kobayashi. J. Chem. Soc. Perkin Trans. 1, 149 (1998); (*b*) Y. Oikawa, T. Yoshioka, and O. Yonemitsu. Tetrahedron Lett. **23**, 889 (1982).

© 2001 NRC Canada

39. (*a*) R.K. Boeckmann Jr., A.B. Charette, T. Asberom, and B.H. Johnston. J. Am. Chem. Soc. **113**, 5337 (1991); (*b*) for the racemic compound see: S. Thaisrivongs and D. Seebach. J. Am. Chem. Soc. **105**, 7407 (1983).

40. J. Kobayashi, A. Hatakeyama and M. Tsuda. Tetrahedron, **54**, 697 (1998).

© 2001 NRC Canada

Chiral aluminum complexes as catalysts in asymmetric Baeyer-Villiger reactions of cyclobutanones

Carsten Bolm, Oliver Beckmann, and Chiara Palazzi

Abstract: BINOL-aluminum complexes were successfully employed as mediators and catalysts in asymmetric Baeyer-Villiger rearrangements of cyclobutanones. Good enantioselectivies were achieved with only 15 mol% of the chosen chiral Lewis acid. The enantiomeric excesses obtained have never been reached before in such metal-catalyzed Baeyer-Villiger reactions.

Key words: aluminum, asymmetric catalysis, lactones, oxidations, rearrangement.

Resumé : Des complexes d'aluminium-BINOL ont été employés avec succès en tant que médiateurs et catalyseurs dans des réactions de Baeyer-Villiger asymétriques de cyclobutanones. Avec des taux catalytiques pouvant aller jusqu'à seulement 15 mol% en acide de Lewis chiral, il a été possible d'obtenir des excès énantiomériques jamais atteints auparavant dans de tels oxydations de Baeyer-Villiger catalysées par des métaux.

Mots clés : aluminium, catalyse asymétrique, lactones, oxydation, réarrangement.

Introduction

More than 100 years after its discovery, the Baeyer-Villiger oxidation has become a valuable tool in organic synthesis, owing to its tolerance of functional groups, its regioselectivity, and retention of configuration during the migration step (1). However, the search for an asymmetric metal catalysis for this rearrangement is still a challenging task in modern chemistry. The metal systems that have been devised to render the reaction asymmetric either lack a broader scope of substrates and enantioselectivity or exhibit the drawback of relying on stoichiometric amounts of the metal (2).[3] Existing catalytic procedures employ platinum (3) or copper complexes (4), while (over)stoichiometric variants make use of titanium, tin, zinc, or zirconium (5). These approaches have in part provided appreciable results with respect to enantiomeric excesses, but none represent a practical, synthetically useful method. Thus, further development in this field of asymmetric oxygen insertion is still necessary.

In the present report we introduce a novel catalyst involving a BINOL-aluminum promoter, which has already been successfully applied to other reactions (6): the combination of Me_2AlCl with enantiopure BINOL under a dry, inert gas atmosphere furnishes a catalyst, which is able to oxidize cyclobutanones in an enantioselective manner upon addition of a hydroperoxide (Scheme 1).

To the best of our knowledge this is the first example of a main group metal complex that can mediate in substoichiometric amounts asymmetric Baeyer-Villiger oxidations.[4] The γ-butyrolactones formed are valuable intermediates in the synthesis of pharmaceuticals or natural products, particularly when they are obtained in an enantiomerically pure form, and hence there is a notable effort to gain synthetic access to these important building blocks (7).

Results and discussion

In principle, if a bicyclic cyclobutanone derivative such as **1** is oxidized, two regioisomeric lactones may be formed, since the insertion of oxygen can occur on either side of the carbonyl group. Thus, when the racemic bicyclooctanone **1** was used as the substrate, the novel Al-mediated oxidation afforded not only 7-oxabicyclo[4.3.0]nonan-8-one (**2a**), which is the normal predominately formed lactone in common Baeyer-Villiger reactions (1), but also its regioisomer, 8-oxabicyclo[4.3.0]nonan-7-one (**2b**), in fairly large quantity. With (*S*)-BINOL in combination with Me_2AlCl (metal-to-ligand ratio = 1:1, 50 mol%), the products were (+)-(1*R*,6*R*)-**2a** with 34% ee and (+)-(1*R*,6*S*)-**2b** with 96% ee, exhibiting a remarkably low ratio **2a**:**2b** of 2.7 (Table 1, entry 1). Apparently, this transformation represents an example of an enantiodivergent reaction. Hence, the regioisomeric, enantio-

Received February 7, 2001. Published on the NRC Research Press Web site at http://canjchem.nrc.ca on October 26, 2001.

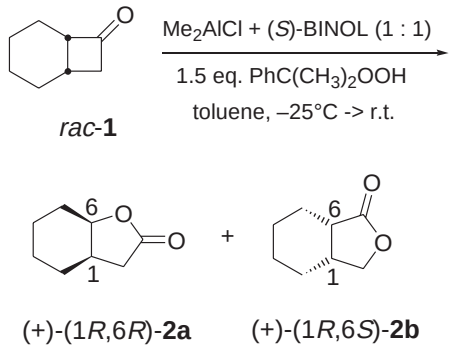
This article is dedicated to Professor Victor Snieckus for his outstanding contributions to the art of organic synthesis.

C. Bolm,[1] O. Beckmann,[2] and C. Palazzi. Institut für Organische Chemie der RWTH Aachen, Prof.-Pirlet-Str. 1, D-52056 Aachen, Germany.

[1]Corresponding author (telephone: +49 241 80 946 75; fax: +49 241 80 92 391; e-mail: carsten.bolm@oc.rwth-aachen.de).
[2]Present address: UMR 6509 CNRS, Université de Rennes 1, Organométalliques et Catalyse, Campus de Beaulieu, F-35042 Rennes CEDEX, France.
[3]For reviews on asymmetric metal-mediated Baeyer-Villiger reactions see ref. 2.
[4]The aforementioned nonstoichiometric variants known to date are based on transition metals platinum or copper (3, 4).

 DOI: 10.1139/cjc-79-11-1593 © 2001 NRC Canada

Scheme 1.



merically enriched lactone **2a** is produced chiefly from one enantiomer of the racemic starting material *rac*-**1**, while the substrate antipode gives rise to the other nonracemic regioisomeric product **2b**. Such a behavior has previously been found in biocatalytic Baeyer-Villiger reactions (8) and in the copper-catalyzed Baeyer-Villiger oxidation of the same substrate, *rac*-**1** (4b). Mathematically it was described by Kagan (9).

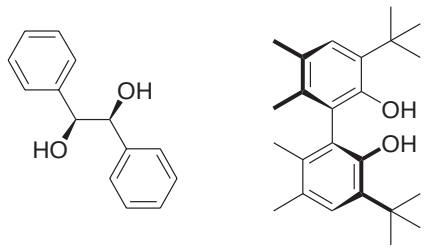
Furthermore, the bicyclic, commercially available ketone *rac*-**3** and the indene-derived cyclobutanone *rac*-**5** each led to two regioisomeric lactones (Table 1, entries 2 and 3). Here, the ratio **a**:**b** of regioisomers had shifted even more in favor of the unusual Baeyer-Villiger product (i.e., toward **4b** and **6b**, respectively). In parallel, the enantiomeric excesses of either lactone are leveling to nearly the same value. In addition, under the applied conditions, the olefinic ketone *rac*-**3** did not seem susceptible to epoxidation according to GC analysis.

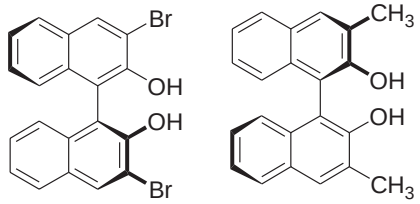
Besides the racemic disubstituted ketones **1**, **3**, and **5**, prochiral 3-monosubstituted cyclobutanones **7**, **9**, **11**, **13**, and **15** were also tested. These are accessible by means of [2+2]-cycloaddition of dichloroketene to an olefin with subsequent dehalogenation (11). The oxidation of 3-phenylcyclobutanone (**7**) yielded the corresponding lactone with 71% ee when 50 mol% of the Al-BINOL mixture was used (Table 1, entry 4). On reducing the catalyst loading to 15 mol%, the ee dropped only slightly to 68%,[5] which is the highest value reached to date in metal-catalyzed Baeyer-Villiger reactions of this substrate (2, 4*d*).

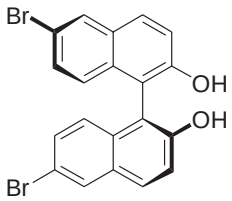
Neither the introduction of a chloro substituent on the arene nor the replacement of the aromatic substituent by an alkyl group at positon C3 had a detrimental effect with respect to the conversion and enantiomeric excess (Table 1, entries 5 and 6). In addition, 3-benzylcyclobutanones, whose lactones are intermediates in syntheses of pharmaceuticals and lignanes (7*e*, 12), proved to be suitable substrates for this (catalytic) asymmetric transformation. Albeit, piperonyl lactone **16** showed a modest ee of 58% in comparison to lactone **14** with 73% ee (Table 1, entries 7 and 8). All oxidations were complete within 12 h. No ketone could be detected by GC analysis and lactones **10** and **14** were isolated after column chromatography in 82 and 87% yield, respectively.

During the evaluation of the new Al-based Baeyer-Villiger system, different metal sources were employed. Aluminum reagents such as $EtAlCl_2$, $AlCl_3$, and $Al(O\text{-}t\text{-}Bu)_3$ in combination with BINOL did not lead to complete oxidation and afforded products with low ee's. Me_3Al with BINOL allowed full conversion but gave a racemate. Solely when dialkyl aluminum chlorides (R_2AlCl with R = Me, Et) were used was the reaction successful. Of the compounds tested, the dimethyl derivative gave somewhat higher enantiomeric excesses than the diethyl metalhalide (e.g., 71 vs. 63% ee for lactone **8** and 68 vs. 54% ee for lactone **10**). The different performances of dialkyl precursors with BINOL as ligand may be indicative of an intricate, oligomeric active species. Since Me_3Al is not an appropriate metal source, even though it readily reacts with diols, a simple mononuclear (BINOL)AlMe structure formed by reaction of BINOL with Me_2AlCl may be excluded as the catalyzing complex, since it should also be expected to be formed from Me_3Al. On the other hand a (BINOL)AlCl species cannot play a decisive role in the enantioselection because of the aforementioned influence of the alkyl rest, i.e., alkyl groups are likely to be still bound to an active aluminum complex. Thus, aluminum catalyst(s) incorporating two or more metal centers and bridging ligands are probable.[6]

A survey of various chiral diols as ligands revealed the binaphthyl scaffold to be the most effective one for achieving





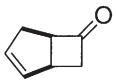
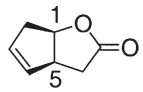
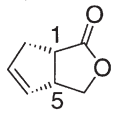
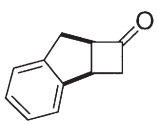
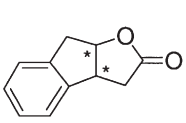
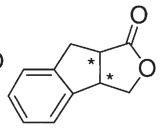
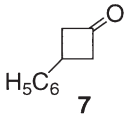
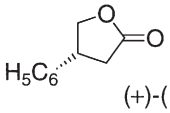
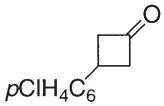
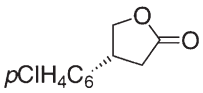
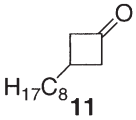
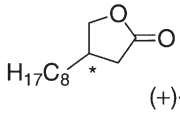
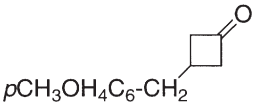
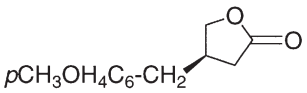
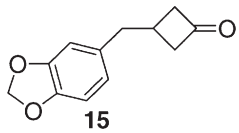
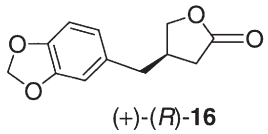


[5] A reduction of catalyst loading to 15 mol% was possible with 4-chlorophenyl cyclobutanone **9** as well (ee dropped from 68 to 57% at full conversion), but not with bicyclooctanone *rac*-**1**. In the latter case full conversion with 25 mol% of BINOL-Al (1:1) could no longer be achieved. However, when 25 mol% of BINOL and 50 mol% of Me_2AlCl were used, the oxidation of *rac*-**1** was still complete, albeit the enantioselectivity deteriorated (**2a**: 5% ee; **2b**: 80% ee).

[6] A similar interpretation was supported by ^{27}Al NMR studies and molecular weight determinations as described in ref. 13.

© 2001 NRC Canada

Table 1. Asymmetric Baeyer-Villiger reaction of various cyclobutanone derivatives mediated by the (*S*)-BINOL-Al system (50 mol%).

Entry	Ketone	Product(s)	ee (%) of product(s)	Ratio of lactones **a**:**b**[a]
1	*rac*-**1**	(+)-(1*R*,6*R*)-**2a** (+)-(1*R*,6*S*)-**2b**	34 (**2a**) 96 (**2b**)	2.7
2	 *rac*-**3**	 (+)-(1*R*,5*S*)-**4a**	 (+)-(1*S*,5*R*)-**4b**	79 (**4a**)[b] 74 (**4b**)	0.8
3	 *rac*-**5**	 **6a**	 **6b**	78 (**6a**) 68 (**6b**)	0.9
4	 **7**	 (+)-(*S*)-**8**	71	–
5	 **9**	 (+)-(*S*)-**10**	68	–
6	 **11**	 (+)-**12**	67	–
7	 **13**	 (+)-(*R*)-**14**	73	–
8	 **15**	 (+)-(*R*)-**16**	58	–

Note: For details see *Experimental*. (*R*)-BINOL as ligand gave the same results yet with inverted absolute configuration of the product.

[a]Calculated from area percentages in the GC.

[b]The ee analysis by chiral GC did not give baseline-separated signals.

enantioselectivity. Me_2AlCl in combination with L-diethyl tartrate, (*R*,*R*)-TADDOL, dianhydro D-mannitol, or D-erythrono lactone was not able to promote an asymmetric oxidation of ketone *rac*-**1** and **7**, and in some cases even failed to afford full conversion to the corresponding lactones. Furthermore, nitrogen-containing diols (salen-type ligands) prevented the ketones from being oxidized, which is consistent with the observed inhibitory effect of additives such as triethylamine, triphenylphosphine oxide, or tetrahydrofuran bearing coordinating sites. Eventually, it was (*S*,*S*)-hydrobenzoin **17**, (*S*)-$BIPHENH_2$ **18** (14*a*), and BINOL and derivatives thereof, in particular **21** (14b), that brought about noticeable enantiomeric excesses with a full conversion.

The test reaction involving 3-phenyl cyclobutanone (**7**) as the substrate and 3,3′-disubstituted BINOLs such as **19**, with two bromo substitutents, or BINOL with two biphenyl or naphthyl moieties, at C3 and C3′ (15), respectively, merely led to racemic lactones if they showed full conversion at all.[7] Only when 3,3′-dimethyl-BINOL ((*R*)-**20**) was used as the ligand, did the oxidation go to completion. Lactone **8** having

[7]We are grateful to Prof. K.A. Jørgensen (Aarhus University) for a kind donation of (*R*)-3,3′-bis(2,5-dimethoxyphenyl)-2,2′-dihydroxy-1,1′-dinaphthyl, which when employed as ligand unfortunately inhibited the Baeyer-Villiger oxidation.

© 2001 NRC Canada

an (*R*)-configuration was achieved with an enantiomeric excess of 40%.[8] However, 6,6′-disubstituted BINOL (*S*)-**21** proved to be the most effective ligand, leading to (*S*)-**8** with 77% ee, which is an even higher enantioselectivity than the one the unsubstituted BINOL ligand induced in the oxidation of **7**.[9] Hence, modifications at this end of the BINOL scaffold with different groups seem to be promising in regards to further improvement of the enantioselectivity. We are currently investigating these BINOL derivatives along with other oxidants and substrates in the aluminum-mediated Baeyer-Villiger oxidation.

Experimental

In a typical procedure, a solution of Me_2AlCl in hexanes (0.10 mL, 1.0 M, 0.10 mmol) was injected to enantiopure BINOL (29 mg, 0.10 mmol; obtained by resolution according to ref. 18) in absolute toluene under argon atmosphere. After stirring for 0.5–1 h at ambient temperature, the ketone (0.20 mmol) was added to the suspension, which within 15 min at room temperature became less turbid. The mixture was cooled down to –25°C before the addition of cumene hydroperoxide (technical grade 80%, 57 mg, 0.30 mmol) and then slowly let warm to room temperature again. After 12 h of stirring the mixture was treated with aq. HCl (0.5 M), then diluted with ether, washed with saturated. aq. $NaHCO_3$ and brine, and finally dried over $MgSO_4$. The obtained solution was directly subjected to GC analysis for the determination of the conversion (calculated from area percentages in the GC) and the ee (using chiral columns). The peak assignments were assured by comparison with chromatograms of ketones and racemic lactones.

For the correlations of optical rotations and absolute configurations, see ref. 10*a* for **2a**, ref. 10*b* for **2b**, ref. 10*c* for **8**, ref. 10*d* for **10**, ref. 7*e* for **14**, and ref. 10*e* for **16**. In ref. 7*a*, (*R*)-configurated 3-pentyl- and 3-hexyl-butyrolactones were shown to have a positive sign of optical rotation. Thus, the absolute configuration of octyl-bearing lactone (+)-**12** is supposed to be (*R*) too.

When isolated yields were to be determined, 1 to 2 mmol of ketone were employed and the product purified by column chromatography on silica gel.

Acknowledgments

We are grateful to the Deutsche Forschungsgemeinschaft (Schwerpunktprogramm Sauerstofftransfer/Peroxidchemie, Graduiertenkolleg 440) and the Fonds der Chemischen Industrie for support of our research program.

References

1. (*a*) A. Baeyer and V. Villiger. Ber. Deut. Chem. Ges. **32**, 3625 (1899); (*b*) G. Krow. Org. Reactions, **43**, 251 (1993); (*c*) M. Renz and B. Meunier. Eur. J. Org. Chem. 737 (1999).
2. (*a*) C. Bolm. *In* Advances in catalytic processes. Vol. 2. *Edited by* M.P. Doyle. JAI Press, Greenwich. 1997. p. 43; (*b*) C. Bolm, O. Beckmann, and T.K.K. Luong. *In* Transition metals for organic synthesis. Vol. 2. *Edited by* M. Beller and C. Bolm. Wiley–VCH, Weinheim. 1998. p. 213; (*c*) G. Strukul, Angew. Chem. **110**, 1256 (1998); Angew. Chem. Int. Ed. Engl. **37**, 1198 (1998); (*d*) C. Bolm and O. Beckmann. *In* Comprehensive asymmetric catalysis. *Edited by* E.N. Jacobsen, A. Pfaltz, and H. Yamamoto. Springer, Berlin. 1999. p. 803.
3. (*a*) A. Gusso, C. Baccin, F. Pinna, and G. Strukul. Organometallics, **13**, 3442 (1994); (*b*) G. Strukul, A. Varagnolo, and F. Pinna. J. Mol. Catal. **117**, 413 (1997); (*c*) C. Paneghetti, R. Gavagnin, F. Pinna, and G. Strukul. Organometallics, **18**, 5057 (1999).
4. (*a*) C. Bolm, G. Schlingloff, and K. Weickhardt. Angew. Chem. **106**, 1944 (1994); Angew. Chem. Int. Ed. Engl. **33**, 1848 (1994); (*b*) C. Bolm and G. Schlingloff. J. Chem Soc. Chem. Commun. 1247 (1995); (*c*) C. Bolm, G. Schlingloff, and F. Bienewald. J. Mol. Cat. **117**, 347 (1997); (*d*) C. Bolm, T.K.K. Luong, and G. Schlingloff. Synlett, 1151 (1997); (*e*) C. Bolm, O. Beckmann, and T.K.K. Luong. *In* Asymmetric oxidation reactions: a practical approach. *Edited by* T. Katsuki. Oxford University Press, Oxford. 2001. p. 1476.
5. (*a*) M. Lopp, A. Paju, T. Kanger, and T. Pehk. Tetrahedron Lett. **37**, 7583 (1996); (*b*) T. Kanger, K. Kriis, A. Paju, T. Pehk, and M. Lopp. Tetrahedron: Asymmetry, **9**, 4475 (1998); (*c*) T. Sugimura, Y. Fujiwara, and A. Tai. Tetrahedron Lett. **38**, 6019 (1997); (*d*) T. Shinohara, S. Fujiora, and H. Kotsuki. Heterocycles, **55**, 237 (2001); (*e*) C. Bolm and O. Beckmann. Chirality, **12**, 523 (2000).
6. (*a*) K. Maruoka and H. Yamamoto. *In* Catalytic asymmetric synthesis *Edited by* I. Ojima. VCH, New York. 1993. p. 413; (*b*) T. Ooi and K. Maruoka. *In* Comprehensive asymmetric catalysis. Vol. 3. *Edited by* E.N. Jacobsen, A. Pfaltz, and H. Yamamoto. Springer, Berlin. 1999. p. 1237; (*c*) C. Chapuis and J. Jurczak. Helv. Chim. Acta, **70**, 436 (1987); (*d*) J. Bao, W.D. Wulff, and A.L. Rheingold. J. Am. Chem. Soc. **115**, 3814 (1993); (*e*) H. Urabe, K. Yamashita, K. Suzuki, K. Kobayashi, and F. Sato. J. Org. Chem. **60**, 3576 (1995); (*f*) M.S. Sigman and E.N. Jacobsen. J. Am. Chem. Soc. **120**, 5315 (1998); (*g*) Y. Hamashima, D. Sawada, M. Kanai, and M. Shibasaki. J. Am. Chem. Soc. **121**, 2641 (1999); (*h*) K. Maruoka, T. Itoh, T. Shirasaka, and H. Yamamoto. J. Am. Chem. Soc. **110**, 310 (1988); (*i*) K.B. Simonsen, N. Svenstrup, M. Roberson, and K.A. Jørgensen. Chem. Eur. J. **6**, 123 (2000); (*j*) M. Takamura, Y. Hamashima, H. Usuda, M. Kanai, and M. Shibasaki. Angew. Chem. **112**, 1716 (2000); Angew. Chem. Int. Ed. **39**, 1650 (2000).
7. (*a*) H. Kosugi, K. Tagami, A. Takashi, H. Kanna, and H. Uda. J. Chem. Soc. Perkin Trans. 1, 935 (1989); (*b*) A. Pelter, R.S. Ward, D.M. Jones, and P. Maddocks. J. Chem. Soc. Perkin Trans. 1, 2621 (1993); (*c*) S.S. Canan Koch and A.R. Chamberlin. J. Org. Chem. **58**, 2725 (1993); (*d*) M.P. Doyle, M.N. Protopopova, Q.–L. Zhou, J.W. Bode, S.H. Simonsen, and V. Lynch. J. Org. Chem. **60**, 6654 (1995); (*e*) Shiotani, H. Okada, T. Yamamoto, K. Nakamata, J. Adachi, and H. Nakamoto. Heterocycles, **43**, 113 (1996); (*f*) C. Mazzini, J. Lebreton, V. Alphand, and R. Furstoss. Tetrahedron Lett. **38**, 1195 (1997); (*g*) A. Krief, A. Ronvaux, and A. Tuch. Bull. Soc. Chim. Belg. **106**, 699 (1997); (*h*) K. Hirayama and K. Mori. Eur. J. Org. Chem. 2211 (1999); (*i*) B.M. Trost and Y.H. Rhee. J. Am. Chem. Soc. **121**, 11680 (1999); (*j*) Y. Takaya, T. Senda, H. Kurushima, M. Ogasawara, and T. Hayashi. Tetrahedron: Asymmetry, **10**, 4047 (1999); (*k*) G. Fardella, P. Barbetti, G. Grandolini, I. Chiappini, V. Ambrogi, V. Scarcia, and A.

[8] This is not the first example of sheer BINOL being a superior ligand in comparison to its 3,3′-substituted derivatives, cf.: ref. 16.
[9] For other catalyses exhibiting a marked improvement when, instead of BINOL, 6,6′-dibromo-BINOL was used, see ref. 17.

© 2001 NRC Canada

Furlani Candiani. Eur. J. Med. Chem. **34**, 515 (1999); (*l*) D. Takano, M. Doe, Y. Morimoto, K. Yoshihara, and T. Kinoshita. J. Heterocyclic Chem. **36**, 221 (1999); (*m*) N. Gathergood and K.A. Jørgensen. Chem. Commun. 1869 (1999); (*n*) E.J. Bergner and G. Helmchen. Eur. J. Org. Chem. 419 (2000).

8. V. Alphand, A. Archelas, and R. Furstoss. Tetrahedron Lett. **30**, 3663 (1989).
9. H.B. Kagan. Croatica Chem. Acta, **69**, 669 (1996).
10. (*a*) W.H. Pirkle and P.E. Adams. J. Org. Chem. **45**, 4111 (1980); (*b*) I.J. Jakovac, H.B. Goodbrand, K.P. Lok, and J.B. Jones. J. Am. Chem. Soc. **104**, 4659 (1982); (*c*) G. Helmchen and G. Nill. Angew. Chem. **91**, 66 (1979); Angew. Chem. Int. Ed. Engl. **18**, 65 (1979); (*d*) J.W. Lawston and T.D. Inch. J. Chem. Soc. Perkin Trans. 1, 2629 (1983); (*e*) M. Kuhn and A. von Wartburg. Helv. Chim. Acta, **50**, 1546 (1967).
11. (*a*) L. Ghosez, R. Montaigne, A. Roussel, A. Vanlierde, and P. Mollet. Tetrahedron, **27**, 615 (1971); (*b*) L.R. Krepski and A. Hassner. J. Org. Chem. **43**, 2879 (1978); (*c*) V. Kaiwar, C.B. Reese, E.J. Gray, and S. Neidle. J. Chem. Soc. Perkin Trans. 1, 2281 (1995).
12. R.S. Ward. Tetrahedron, **46**, 5029 (1990).
13. M. Brunner. PhD thesis. RWTH Aachen, Germany. 1995.
14. (*a*) J.B. Alexander, D.S. La, D.R. Cefalo, A.H. Hoveyda, and R.R. Schrock. J. Am. Chem. Soc. **120**, 4041 (1999); (*b*) G.D.Y. Sogah and D.J. Cram. J. Am. Chem. Soc. **101**, 3035 (1979).
15. (*a*) S.S. Zhu, D.R. Cefalo, D.S. La, J.Y. Jamieson, W.M. Davies, A.H. Hoveyda, and R.R. Schrock. J. Am. Chem. Soc. **121**, 8251 (1999); (*b*) K.B. Simonsen, K.V. Gothelf, and K.A. Jørgensen. J. Org. Chem. **63**, 7536 (1998); (*c*) P. Kratky, U. Haslinger, and M. Widhalm. Monatsh. Chem. **129**, 1319 (1998).
16. A. Graven, M. Johannsen, and K.A. Jørgensen. Chem. Commun. 2372 (1996).
17. (*a*) M. Terada, Y. Motoyama, and K. Mikami. Tetrahedron Lett. **35**, 6693 (1994); (*b*) H. Ishitani, M. Keno, and S. Kobayashi. J. Am. Chem. Soc. **119**, 7153 (1997).
18. D. Cai, D.L. Hughes, T.R. Verhoeven, and P.J. Reider. Tetrahedron Lett. **36**, 7991 (1995).

© 2001 NRC Canada

Stereoelectronic and conformational effects on the stereochemical course of reduction of bicyclo[3.3.1]nonane 1,3-diketones

Eugenius Butkus, Arvydas Stončius, Julė Malinauskienė, Shuji Tomoda, and Daisuke Kaneno

Abstract: The stereoselectivity of the reduction of bicyclo[3.3.1]nonane 1,3-diketones was studied. The experimental data of π-facial stereoselection of the reduction of the carbonyl group were successfully rationalized by the application of the exterior frontier orbital extension (EFOE) model. The observed facial diastereoselectivity of the carbonyl reduction of bicyclo[3.3.1]nonane diketones could be reasonably explained by the ground-state facial anisotropy of the frontier orbital extension, steric effects, and the intrinsic reactivity of carbonyl groups. Although the EFOE density and PDAS values predicted the enhanced reactivity at the C-2 carbonyl compared to C-9 carbonyl, transition-state calculations at the B3LYP/6-31+G(d,p) level showed that the reactivity of C-9 and C-2 in a hydride addition to both carbonyl groups should be nearly the same. The EFOE analysis also strongly indicated that in the second hydride reduction step the corresponding oxobicyclononanolates are most likely to be involved in the reduction as the major species rather than the free hydroxyketones. The antiperiplanar effects in the transition states of the $LiAlH_4$ reduction as measured by both the elongation and the natural bond population of the antiperiplanar bonds clearly indicated they should not be an essential factor of the facial diastereoselection of studied diketones.

Key words: bicyclo[3.3.1]nonanedione, EFOE model, reduction, stereoselectivity, transition state.

Résumé : On a étudié la stéréosélectivité de la réduction de bicyclo[3.3.1]nonane-1,3-diones. On a pu rationaliser facilement les données expérimentales de la stéréosélectivité π-faciale de la réduction du groupe carbonyle par l'application du modèle de l'extension des orbitales frontières extérieures (« EFOE »). La diastéréosélectivité faciale observée de la réduction du carbonyle des bicyclo[3.3.1]nonanediones peut s'expliquer raisonnablement par l'anisotropie faciale de l'état fondamental de l'extension de l'orbitale frontière, par des effets stériques et par la réactivité intrinsèque des groupes carbonyles. Même si la densité EFOE et les valeurs de « PDAS » ont permis de prédire la plus grande réactivité du carbonyle en C-2 par rapport à celle du carbonyle en C-9, les calculs d'état de transition au niveau B3LYP/6-31+G(d,p) montrent que les réactivités des deux groupes carbonyles en C-2 et en C-9 vis-à-vis de l'hydrure devraient être assez semblables. L'analyse EFO" indique aussi fortement que, dans la deuxième étape de réduction par l'hydrure, il est probable que les oxobicyclononanolates correspondants sont impliqués dans la réduction sous la forme d'espèces majeures plutôt que sous la forme d'hydroxycétones libres. Les effets antipériplanaires dans les états de transition des réductions par $LiAlH_4$, tels que mesurés par l'élongation ainsi que la population naturelle de liaison des liaisons antipériplanaires, indiquent clairement qu'ils ne sont pas des facteurs essentiels de la diastéréosélectivité faciale des dicétones étudiées.

Mots clés: bicyclo[3.3.1]nonanedione, modèle EFOE, réduction, stéréosélectivité, état de transition.

[Traduit par la Rédaction]

Introduction

The most important aspect of the conversion of organic molecules containing one or more stereogenic centers is usually that of stereochemical control. The problem of π-facial stereoselection is one of the fundamental topics in theoretical and experimental organic chemistry. The state of art of this problem was recently reviewed in a special issue of *Chem. Rev.* (1). The origin of π-facial stereoselectivity is accounted for by two different transition-state (TS) models,

Received January 18, 2001. Published on the NRC Research Press Web site at http://canjchem.nrc.ca on October 26, 2001.

Dedicated to Professor Victor Algirdas Sniečkus in recognition of his significant contribution to the development of organic synthesis.

E. Butkus,[1] A. Stončius, and J. Malinauskienė. Department of Organic Chemistry, Vilnius University, 2734 Vilnius, Lithuania.
S. Tomoda[1] and D. Kaneno. Department of Life Sciences, Graduate School of Arts and Sciences, The University of Tokyo, Komaba, Meguro, Tokyo 153–8902, Japan.

[1]Corresponding authors ((EB): telephone: +370-2-336517; fax: +370-2-330987; e-mail: eugenijus.butkus@chf.vu.lt; (ST) e-mail: tomoda@selen.c.u-tokyo.ac.jp).

 DOI: 10.1139/cjc-79-11-1598 © 2001 NRC Canada

known as the Felkin–Ahn model (2) and Cieplak model (3). The former assumes that torsional and steric effects arise by interaction between the bonding orbital being formed and the antibonding orbitals of adjacent bonds can account for the experimental results (4). The Cieplak model places more importance in the interaction between the antibonding orbital of the incipient bond and the bonding orbitals of the adjacent bonds, and some interesting results in sterically unbiased systems were reviewed (5). An attempt to evaluate contributions of the above-mentioned approaches to explain the reaction selectivities by combining the stabilizing interactions was made by Li and le Noble (6) and Gung (7). Klein (8) introduced the frontier molecular orbital (FMO) distortion approach to π-facial selectivity. He pointed out that the anisotropic distribution of LUMO with respect to the carbonyl plane of the substrate in the ground state is governing the approach of nucleophile. The FMO approach was supported by ab initio calculations performed by Frenking et al. (9). The polarized π-frontier molecular orbital theory was shown to have some advantage over both the Anh and Cieplak models in the understanding of selectivity in some π-systems (10). However, these assumptions have been strongly criticized, and Felkin's torsional strain in the transition state maintained as the main factor governing the stereochemical outcome of π-facial additions (11). In spite of this, the electronic effects in terms of remote electrostatic effect or even the through-space orbital interaction in transition state were recognized as playing the significant role in nucleophile addition to carbonyl in sterically unhindered systems (12).

Recently the "exterior frontier orbital extension" (EFOE) model based on the Salem–Klopman kinetic equation has been suggested (13). The π-facial stereoselection in carbonyl group reduction and other nucleophilic addition reactions assumes the importance of the ground-state conformational and electronic properties of substrates generated over the exterior area of substrate ketones in the early stages of reaction, whereas the transition-state effects are most likely to have minor effects on facial selection (14). The calculation of the EFOE density and π-plane-divided accessible space (PDAS) provides a strong theoretical model for prediction of facial stereoselectivity of a hydride reduction and nucleophilic additions of a variety of ketones (15).

Further, an interesting study on diastereoselectivity observed in gas-phase reduction of a series of bicyclic ketones by silicon hydride has been published (16). The diastereoselectivity was remarkably consistent with results obtained in solution and in accord with the predictions by molecular orbital calculations. The results are rationalized in terms of competition among steric, torsional, and electrostatic effects, and also suggest that reduction stereoselectivity might be attributed to the intrinsic nature of the reactants.

However, it should be recognized that despite the power of prediction in many cases, the available models and procedures could not rationalize a number of stereochemical outcomes of π-facial additions. Consideration and comparison of the methods that are based entirely on second-order perturbation to predict diastereofacial selectivity led to a conclusion that there is no general explanation for the selectivities observed (17).

Earlier we studied the stereoselectivity of reduction of bicyclo[3.3.1]nonane ketones which seem to be suitable models to understand the stereochemical control of the reaction (18). However, an analysis of the TS structures at the 3-21G level and by the MNDO method did not give any definite explanation of stereoselectivites observed for bicyclo[3.3.1]nonane-2,9-dione. EFOE analysis is based upon a hybrid of ground-state (GS) and transition-state arguments. Therefore, a study of the applicability of the EFOE method to explain the stereoselectivity of the reduction of two diketones of this bicyclic structure was undertaken to interpret the stereoselectivity of the reaction.

Results and discussion

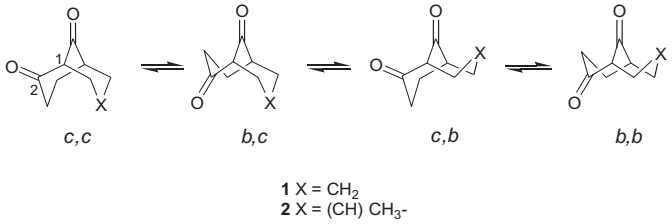
Reduction of bicyclo[3.3.1]nonanediones

The reduction of bicyclo[3.3.1]nonane-2,9-dione **1** and *exo*-7-methylbicyclo[3.3.1]nonane-2,9-dione **2** (Scheme 1) was performed using $NaBH_4$, $NaBH_3CN$, and $LiAlH_4$ in an appropriate solvent. The examination of a reaction course of bicyclo[3.3.1]nonane-2,9-dione **1** and $NaBH_4$ in methanol by GC and ^1H NMR showed that reduction of the first carbonyl group was not regioselective but was totally diastereoselective (18*a*). Though solvent effect on the reduction stereoselectivity could not be excluded in $NaBH_4$ reduction (19), there was no significant influence of it in this work. Only two of four possible hydroxyketones, i.e., the *anti*-9-hydroxybicyclo[3.3.1]nonan-2-one **1A** and the *endo*-2-hydroxybicyclo[3.3.1]nonan-9-one **1B** (Scheme 2) were formed in almost equal amounts. This ratio of hydroxyketones was found to be nearly constant during the reaction course. The stereochemical course of reduction of individual hydroxyketones was determined from the final ratio and configuration of diols, which in turn is dependent on the ratio of hydroxyketones formed in a reaction.

The examination of mixtures of diastereomeric diols obtained after a complete reduction of diketones by ^1H NMR, GC–MS, and circular dichroism spectroscopy of resolved enantiomeric derivatives provided us with the ratio of formed diols (Table 1). The reduction of bicyclo[3.3.1]nonane-2,9-dione **1** led to two main diols **1a** and **1b**, and an insignificant amount of the minor diol **1c** (4 ~ 8%). Essentially the same stereochemical course was observed in the reduction of *exo*-7-methylbicyclo[3.3.1]nonane-2,9-dione **2**. The distribution of the corresponding diastereomeric diols slightly varied in the reduction of **1** and **2** depending upon the hydride used and temperature of a reaction mixture. The most striking features of the investigated reduction of diones **1** and **2** was the low regioselectivity as contrasted with the high diastereoselectivity upon reduction of the first carbonyl group. At the first reduction step, hydride ion attacks the C-2 carbonyl group at the ring position from *exo*-face or the bridge C-9 carbonyl from *syn*-face, consequently *syn* attack with respect to both carbonyl groups occurs exclusively. Taking into account the fact that two hydroxyketones were forming in a substantial amount and the ratio of these hydroxyketones was found to be nearly constant during the reduction course, let us consider the reduction reaction as a two-step process. First, the reduction of one of the carbonyl groups of diketone leading to a formation of hydroxyketones, and second, a subsequent reduction of hydroxyketones. An attempt to interpret the product distribution was made by

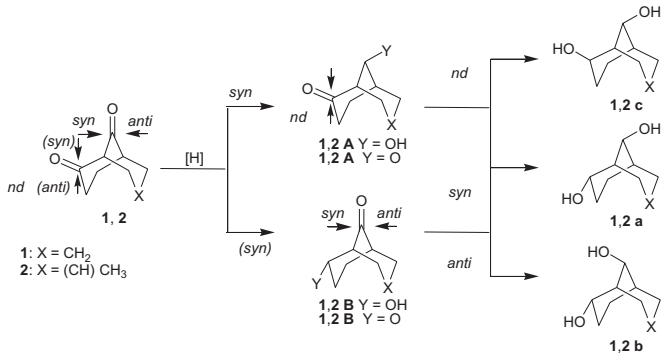
© 2001 NRC Canada

Scheme 1. Conformers of investigated bicyclo[3.3.1]nonan-2,9-dione **1** and *exo*-7-methylbicyclo[3.3.1]nonan-2,9-dione **2**: *c*,*c* chair–chair, *b*,*c* boat–chair, *c*,*b* chair–boat, and *b*,*b* boat–boat.



theoretical evaluation of the TS although a good explanation could not be given (18*a*).

Scheme 2. Reduction scheme of bicyclo[3.3.1]nonan-2,9-diones **1** and **2**.



Ground state conformational and EFOE analyses

An approach of the use of the EFOE model to account for the stereochemistry of the reduction of bicyclo[3.3.1]nonane-2,9-dione **1** and *exo*-7-methylbicyclo[3.3.1]nonane-2,9-dione **2** by complex metal hydrides is presented in this work. To explain the stereo- and regioselectivity of reduction, the theoretical calculation of properties of starting diketones and intermediate reduction products forming during the reaction was performed. The theoretical explanation of the stereochemical course of the reduction seems to be complicated due to the complexity of conformational and electronic properties of bicyclic diketones. A conformational mobility of investigated bicyclo[3.3.1]nonan-2,9-diones should be taken into account. Two six-membered rings of bicyclo[3.3.1]nonan-2,9-dione may adopt four possible conformations, namely *c*,*c*, *b*,*c*, *c*,*b*, and *b*,*b* (Scheme 1). Numerous calculations performed earlier (18*a*, 23*b*) and in this work (20) showed that only *c*,*c* and *b*,*c* conformations are significantly populated and the latter appeared to be more stable. In addition, a transannular interaction between the carbonyl groups should not be neglected in bicyclic diketones as demonstrated by ^{13}C NMR (21), photoelectron spectroscopy and calculations (22), or CD spectroscopy (23) experiments.

EFOE theory is based on a hypothesis that facial diastereoselection should not be dependent on thermodynamic stabilization effects towards the TS and one doesn't need to focus on the latter. Namely, the information on the facial diastereoselection is contained in the initial properties (interactions) of the reactants. Since the same reagent attacks two π-faces, one can predict diastereoselectivity by looking at the properties of the substrate (ketone). Thus the GS interactions might be decisive, and EFOE analysis, which implies evaluation of these interactions, provides a method for analyzing the polarization of π-wave functions. It is commonly accepted that properties of virtual orbitals are not as precise as the occupied orbitals. However, those of LUMO are pretty accurately predicted, because LUMO most significantly reflects the properties of occupied MOs through iterative variation procedure during MO calculation. Within the framework of the same method and basis sets (in this case, HF/6-31G(d)), one can reasonably compare the energies and spatial extension of LUMOs.

Two of the calculated MOs of the investigated bicyclic 1,3-diketones (**1**,**2**) could be recognized as π* MO, i.e., LUMO (lower energy) and LUMO + 1 (higher energy). These two MOs are located on both carbonyl groups and could be involved in π-facial stereoselection in investigated diketones. The difference in energy of LUMO and LUMO + 1, namely 0.42 ~ 1.2 eV at HF/6-31G(*d*) level (24), enabled us to consider that only the lower energy LUMO could be responsible for the new bond formation upon the hydride addition to the carbonyl group.

The EFOE analysis (13, 14) of a complete set of conformers of **1** showed that conformers should demonstrate significantly different reactivity in nucleophilic addition reactions. LUMO of **1***c*,*c* is the lowest one (3.56 eV) and gives significantly larger values of both EFOE density and PDAS over the *syn*-face of both carbonyls (Table 2). The LUMO of the main conformer **1***b*,*c* and of scantily populated conformers *c*,*b* and *b*,*b* showed much reduced values of both the EFOE density and PDAS. Therefore, the most reactive conformation that mainly contributes to the reaction should be **1***c*,*c* despite the slightly higher population of **1***b*,*c*. Similar values of the EFOE density and PDAS were obtained for LUMO of the most populated conformers of the diketone **2** (Table 2).

Overall, the EFOE model correctly predicted the preferred hydride approach from the *syn*-face to both carbonyls in agreement with experimental results, although the absence of regioselectivity at the first reduction step could not be understood by this approach. According to the EFOE analysis, the carbonyl group at C-2 is predicted to be more reactive compared to carbonyl at C-9 since both EFOE quantities of the LUMO for the *syn*-face are larger in the former group.

However, the thermodynamic stability of the products should affect the reaction rate according to the Marcus theory (25). The regioselectivity of some reactions of investigated diketones (26) and molecular mechanics, semiempirical or ab initio estimation of the relative stability of hydroxyketones **A** and **B** gave the following results: **1A***c*,*c* is more stable by 1.65 kcal mol^{-1} than **1B***c*,*c*, and **2A***c*,*c* is more stable by 2.90 kcal mol^{-1} than **2B***c*,*c*. It should be noted that exactly the same trend for the corresponding alkoxy anions (**1A**$^-$ < **1B**$^-$ (2.84 kcal mol^{-1}) and **2A**$^-$ < **2B**$^-$ (3.00 kcal mol^{-1})) was observed (Table 3).

Analysis of the transition states on addition of $LiAlH_4$

Transition states possibly forming in the reduction of the first carbonyl group were calculated. Lithium bicoordinate transition complexes of $LiAlH_4$ (Table 4) and substrate diketones were found to be uniformly more stable by about 1.5 kcal mol^{-1} over the Li-tricoordinate transition states. Ac-

© 2001 NRC Canada

Table 1. Results of hydride reduction of bicyclo[3.3.1]nonan-2,9-diones **1** and **2**.

Hydride/solvent	Diketone	**a** (*anti-endo*) (%)	**b** (*syn-endo*) (%)	**c + d** (*anti-exo*) + (*syn-exo*) (%)
$NaBH_4$/MeOH	**1**	59	36	4
	2	68	27	<5
$LiAlH_4$/THF	**1**	58	32	8
	2	63	36	<1
$NaBH_3CN$/MeOH	**1**	62	38	—
	2	73	24	<3

Table 2. EFOE analysis of bicyclo[3.3.1]nonan-2,9-diones **1** and **2**.[a]

Compound and conformer	ΔE (kcal mol^{-1})[b]	MO *E* (eV)	Carbonyl	EFOE density (%)		PDAS (au^3)		Observed (%)
				syn	*anti*	*syn*	*anti*	*syn*:*anti*[c]
1*c*,*c*	0.49	LUMO	C-9	0.7807	0.2339	15.87	8.84	99:1
		3.56	C-2	1.2559	0.2766	51.07	9.32	
		LUMO+1	C-9	0.1512	0.6373			
		4.67	C-2	0.3152	0.0106			
1*b*,*c*	0.0	LUMO	C-9	0.0162	0.0631	8.89	8.00	
		3.87	C-2	0.3500	0.7028	44.64	4.71	
		LUMO + 1	C-9	0.8443	0.6739			
		4.29	C-2	0.0936	0.0755			
1*c*,*b*	3.62	LUMO	C-9	0.8336	0.1914	11.48	6.38	
		3.59	C-2	1.1915	0.1982	31.82	11.05	
		LUMO + 1	C-9	0.0165	0.7346			
		4.80	C-2	0.4725	0.0033			
1*b*,*b*	6.66	LUMO	C-9	0.3015	0.3253	7.41	5.56	
		3.82	C-2	0.3726	0.4951	42.31	9.42	
		LUMO + 1	C-9	0.2799	0.2770			
		4.62	C-2	0.1241	0.5971			
2*c*,*c*	0.58	LUMO	C-9	0.7925	0.2491	15.62	9.0	
		3.56	C-2	1.2050	0.2645	51.64	8.95	
2*b*,*c*	0.0	LUMO	C-9	0.0432	0.1075	8.75	8.27	
		3.89	C-2	0.3350	0.6127	44.28	4.51	

[a]RHF/6-31G(d)//RHF/6-31G(d), lattice unit = 0.1 au^3.
[b]Relative stabilities of conformers obtained at the same level.
[c]Ratio of diastereomeric hydroxyketones formed in reaction with $NaBH_4$ in respect to the direction of the hydride attack.

cording to results at the HF/3-21* level, the first reduction step should proceed mainly via *c*,*c*-TS, which is lowest in energy (Table 4). Overwhelming *exo* preference was manifested by the large facial difference in the energy between the *exo*- and *endo*-*c*,*c*-C-2 TS (3.29 kcal mol^{-1}). The *c*,*c*-*syn*-C-9 transition state was found to be slightly more stable (0.46 kcal mol^{-1}) (Table 4). This is consistent with the prediction by the EFOE analysis. The energy of *b*,*c*-C-9 TS was found to be just slightly higher compared to that of the *c*,*c*-*exo*-C-2 or *c*,*c*-*syn*-C-9 TS. However, considering that the *b*,*c* conformation is more stable than *c*,*c*, the activation energy of the former is much higher compared to the latter.

Li-bicoordinate transition states of $LiAlH_4$ attack, calculated at the B3LYP/6-31+G(d,p) level taking into account the electron correlation effect, indicated that the energies of transition states of the C-2 and C-9 carbonyls are nearly the same and even more — *syn*-TS at C-9 is a bit more stable than the *exo*-TS at C-2 (Table 5 and Fig. 1).

Thus, in facial diastereoselection processes of hydride reductions, the kinetic activation energy (intrinsic barrier) has to prevail with a small effect of the thermodynamic activation energy. Consequently, in terms of the EFOE model, which reflects the kinetic part of the activation energy, it is predicted that C-2 may be kinetically more reactive compared to C-9. Owing to the strain relief at C-9 along the reaction pathway, thermodynamic activation energy at C-9 process lowers the TS more significantly than that at C-2, because the former is possibly much larger than the latter. As a result, the C-9 carbonyl may become slightly more reactive compared to C-2. This could be understood in terms of strain release and possible higher intrinsic reactivity of bridge carbonyl at C-9. However, this tendency was not observed at the MP2/6-311+G(2d,p) level. Finally, assuming that the initial complexes have nearly the same energy, the reactivity of the C-2 and C-9 carbonyls should be almost the same.

It is interesting to note that the antiperiplanar (AP) effect in transition states can not be used for the prediction of stereoselectivity in the studied molecules. We performed the natural bond population (NBO) analysis of all calculated transition states. The obtained values of population of antiperiplanar (AP) bonds along with the elongation of these bonds in comparison to the corresponding ground state values surprisingly predicted the opposite stereoselectivity to

© 2001 NRC Canada

Table 3. The EFOE analysis of hydroxyketones **1A**, **2B** and **2A**, **2B** and the corresponding oxobicyclo[3.3.1]nonanolates.[a]

				EFOE density (%)		PDAS (au^3)		Observed (%)[c]
Compound and conformer	Rotamer	ΔE (kcal mol^{-1})[b]	LUMO E (eV)	*syn*	*anti*	*syn*	*anti*	*syn*:*anti*
1A*c*,*c*	1	0.17	4.31	1.7112	0.3073	29.87	10.93	93:7
1A*c*,*c*	2	0.0	4.25	1.7007	0.3604	27.93	11.86	
1A*b*,*c*	1	2.38	4.15	0.3249	0.8695	41.06	4.53	
1A$^-$*c*,*c*	—	0.0	8.35	1.7216	0.4116	20.68	15.95	
1A$^-$*b*,*c*	—	1.63	8.18	0.2866	1.2172	37.72	5.63	
1B*c*,*c*	1	1.65	4.45	1.0899	1.0773	9.07	10.45	20:80
1B*c*,*c*	2	2.04	4.49	1.0377	1.0235	9.53	9.79	
1B*c*,*c*	3	2.89	4.36	1.0218	1.0844	9.25	9.98	
1B$^-$*c*,*c*	—	2.84	8.53	0.8636	1.5489	7.11	14.14	
2A*c*,*c*	1	0.0	4.31	1.7156	0.2915	30.46	10.57	
2A$^-$*c*,*c*	—	0.0	8.31	1.7067	0.4077	21.21	15.68	
2B*c*,*c*	1	2.90	4.32	0.9448	1.0806	9.10	10.05	
2B*c*,*c*	2	2.06	4.46	0.9675	1.0403	9.34	9.90	
2B$^-$*c*,*c*	—	3.00	8.41	0.7060	1.4075	6.92	14.46	

[a]RHF/6-31G(d)//RHF/6-31G(d), lattice unit = 0.1 au^3.
[b]Relative stability of conformers obtained at the same level in comparison to the most stable derivative in series **1** and **2,** and oxobicyclononanolates are compared separately.
[c]Ratio of diastereomeric diols formed in reaction with $NaBH_4$ in respect to hydride attack direction.

Table 4. Energetic parameters for the Li-bicoordinate transition states (TS) of bicyclo[3.3.1]nonan-2,9-dione **1** with $LiAlH_4$ at the HF/3-21G* level.

Conformer	Carbonyl	TS	ν_i (cm^{-1})[a]	ZPVE (kcal mol^{-1})[b]	E (au)[c]
c,*c*	C-2	*exo*	–490.0590	153.36555	–745.146725
		endo	–455.4593	153.28924	–745.141486
Difference (kcal mol^{-1})				–0.00097	3.29
c,*c*	C-9	*syn*	–449.012	153.25186	–745.145190
		anti	–368.981	153.25496	–745.144462
Difference (kcal mol^{-1})				–0.0031	0.46
b,*c*	C-2	*exo*	–573.7541	153.30492	–745.141261
		endo	–504.4308	153.30589	–745.137637
Difference (kcal mol^{-1})				–0.00097	2.27
b,*c*	C-9	*syn*	–448.9124	153.10611	–745.143812
		anti	–385.3477	153.17342	–745.143962
Difference (kcal mol^{-1})				–0.06731	–0.09
c,*b*	C-2	*exo*	–448.2290	153.16733	–745.142831
		endo	–431.5670	153.18556	–745.140177
Difference (kcal mol^{-1})				–0.01823	1.67
c,*b*	C-9	*syn*	–448.7359	153.24029	–745.138380
		anti	–377.7363	153.09607	–745.134713
Difference (kcal mol^{-1})				0.14422	2.30

[a]Imaginary vibrational frequency.
[b]Zero point vibration energy.
[c]Total electron energy.

that observed in the experiment. The greater loss of electrons and, respectively, the greater elongation of AP bonds was obtained for less energetically favored TSs in all cases (Table 6).

The EFOE analysis correctly predicted the observed stereoselectivity in the reduction of the first carbonyl group and the absence of regioselectivity at this reduction step could be understood in terms of combination of kinetic and thermodynamic components of the activation energy.

EFOE consideration of hydroxyketones

Hydroxyketones formed in the first reduction step undergo subsequent reduction. The reduction of *anti*-9-hydroxyketones **A** is stereoselective where *exo*-hydride approach prevails and the main *anti*-9-*endo*-2-diol **a** and only a small amount of *anti*-9-*exo*-2-diol **c** were formed (**1a**:**1c** = 93:7). The reduction of *endo*-2-hydroxyketones **1B** and **2B** yielded *syn*-9-*endo*-2-diols **1b**, **2b** and *anti*-9-*endo*-2-diols **1a**, **2a**, respectively. Approach of hydride from the *anti*-face of the bridge carbonyl group is prevailing and corresponding **b** was formed preferably over **a** (**1b**:**1a** = 80:20).

The EFOE analysis performed for hydroxyketones **A** and **B** in general correctly predicts the stereoselectivity observed experimentally (Table 3). The stereoselectivity is predicted to be large in reduction of hydroxyketone **A** by superiority of both the EFOE and PDAS values over the *exo*-face of the

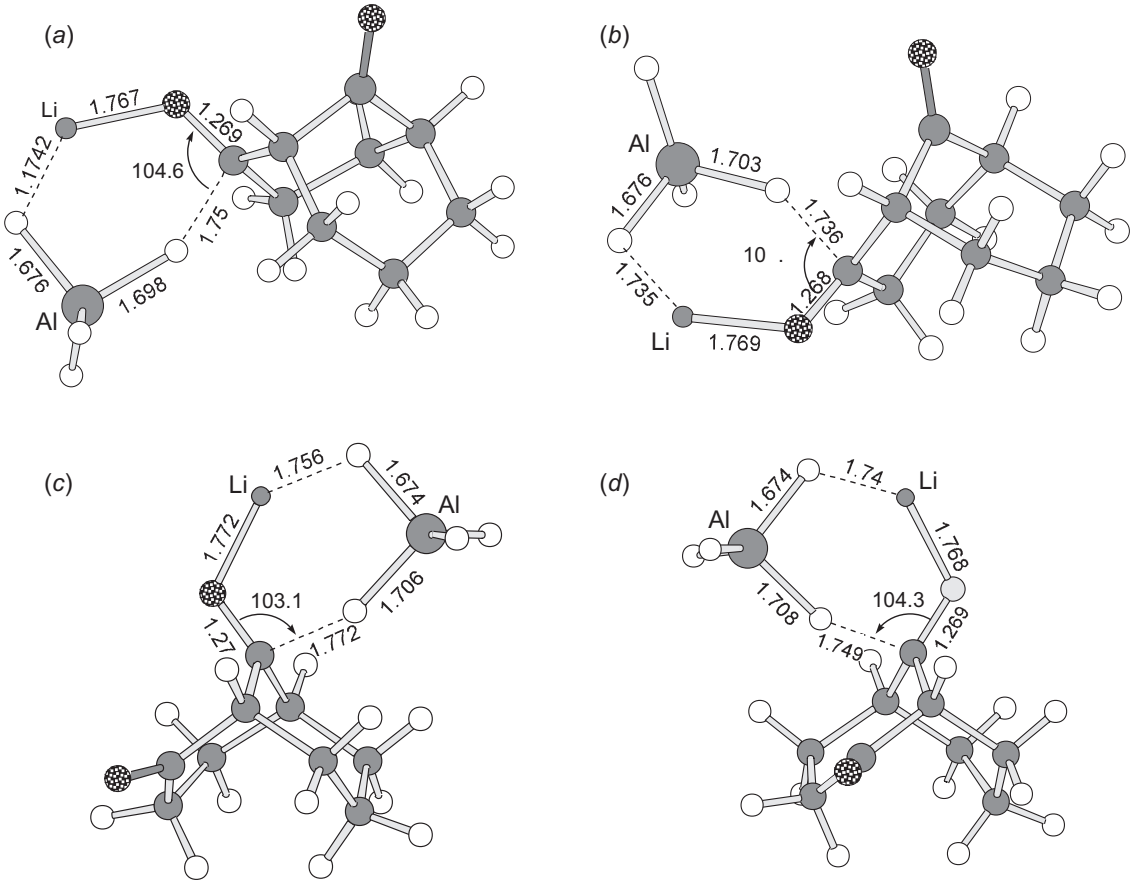
© 2001 NRC Canada

Table 5. Energy parameters for the Li-bicoordinate transition states (TS) of bicyclo[3.3.1]nonan-2,9-dione **1** with $LiAlH_4$ at the RB3LYP/6-31+G(d,p) level.

Conformer	Carbonyl	TS	ν_i (cm^{-1})[a]	*ZPE* (kcal mol^{-1})[b]	*E* (au)[c]	*H* (au)	*G* (au)	MP2/6-311+G(2d,p) (kcal mol^{-1})
c,c	C-2	*exo*	–272.5833	142.25962	–753.0560853	–752.814563	–752.870139	–751.2774406
		endo	–238.4634	142.26402	–753.0535101	–752.811978	–752.867660	–751.2735302
Difference (kcal mol^{-1})				–0.0044	1.616	1.622	1.556	2.45381
c,c	C-9	*syn*	–211.6242	142.25621	–753.0560934	–752.814666	–752.870040	–751.2767285
		anti	–251.4827	142.18321	–753.0559506	–752.814585	–752.869877	–751.2765169
Difference (kcal mol^{-1})				0.0730	0.090	0.051	0.102	0.13278

[a]Imaginary vibrational frequency.
[b]Zero point vibration energy.
[c]Total electron energy.

Fig. 1. Geometries of Li-bicoordinate transition states at the B3LYP/6-31+G(d,p) level: (*a*) *endo*-C-2 TS; (*b*) *exo*-C-2 TS; (*c*) *anti*-C-9 TS; and (*d*) *syn*-C-9 TS. Distances are presented in Å, angles in degrees.



C-2-carbonyl leading to the *endo*-isomer **a**. However, the stereoselection in the hydroxyketone **B** should be weak due to almost equal EFOE values over two C-9-carbonyl faces (the *syn*-stereoselectivity is very slightly preferred) and a slightly different PDAS value (the opposite weak *anti*-stereoselectivity is predicted).

Both neutral hydroxyketone (**A** or **B**) and lithium or sodium oxobicyclononanolate ($\mathbf{A}^-$or $\mathbf{B}^-$) species could be formed in a reduction process. In particular, in the reduction of **B** the EFOE data strongly indicated that $\mathbf{B}^-$ should be the diastereoselectivity-determining species. The *anti*-face of $\mathbf{B}^-$ is far more reactive (EFOE density = 1.5489% and PDAS = 14.14 au^3) than any rotamer of **1B** *c,c* (rotation around the C—OH bond does not cause any significant changes in EFOE and PDAS data in all cases). Consequently, $\mathbf{B}^-$ should most significantly contribute to the production of the *syn*-isomer **b**.

The reason for the significant effects of the hydroxyanion group is that it is a strong electron-donating substituent. Substitution at C-3 of cyclohexanone by an electron-donating group causes a decrease in the PDAS value over the axial area owing to the ground-state Cieplak mode hyperconjugation between π^*(C=O) and C-2—C-3 (C-2—C-6) bonds (27) as it appears in $\mathbf{B}^-$. However, no significant

© 2001 NRC Canada

Table 6. Antiperiplanar effects in transition states.

		AP bond length (Å)[a]				Bond population (e)[c]		
Carbonyl	TS	TS	GS	Δ*BL*	Δ*BE* (%)[b]	TS	GS	Δ*BP*
$LiAlH_4$ bicoordinate HF/3-21*								
C-2	*exo*	1.5576	1.5601	–0.0025	–0.16	1.95755	1.95691	+0.00064
		1.0823	1.0829	–0.0006	–0.06	1.96748	1.97132	–0.00384
	endo	1.5272	1.5083	+0.0189	+1.25	1.96337	1.97869	–0.01532
		1.5581	1.5432	+0.0149	+0.97	1.97119	1.98563	–0.01444
C-9	*syn*	1.5639	1.5601	+0.0038	+0.24	1.95244	1.95691	–0.00447
		1.5589	1.5499	+0.009	+0.58	1.96155	1.97431	–0.01258
	anti	1.5343	1.5201	+0.0142	+0.93	1.96413	1.97750	–0.01337
		1.5614	1.5469	+0.0145	+0.94	1.95910	1.97381	–0.01471
$LiAlH_4$ bicoordinate B3LYP/6-31+G(d,p)								
C-2	*exo*	1.5643	1.5647	–0.0004	–0.03	1.94158	1.94287	–0.00129
		1.0973	1.0974	–0.0001	0.0	1.95312	1.95774	–0.00462
	endo	1.5394	1.5215	+0.0179	+1.18	1.96337	1.96826	–0.00489
		1.5519	1.5451	+0.0068	+0.44	1.97119	1.98235	–0.01116
C-9	*syn*	1.5639	1.5647	–0.0008	–0.05	1.93622	1.94287	–0.00625
		1.5589	1.5534	+0.0055	+0.35	1.94998	1.96627	–0.01629
	anti	1.5492	1.5347	+0.0145	+0.94	1.94750	1.96566	–0.01816
		1.5617	1.5522	+0.0095	+0.61	1.94816	1.96560	–0.01744

[a]AP bond: antiperiplanar bonds with respect to the incipient bond; TS: transition state; GS: ground state; Δ*BL* = bond length (TS) – bond length (GS).
[b]*BE* (%): bond elongation (%) = Δ*BL*/bond length (GS) × 100 (%).
[c]Δ*BP* = bond population (TS) – bond population (GS) (electrons).

differences in both EFOE and PDAS values were found for **A** and $\mathbf{A}^-$ (Table 3).

The energies of LUMO for the hydroxyanions were uniformly significantly high (ca. 8 eV) compared to the neutral species (ca. 4 eV). This implies that the intermediate oxobicyclononanolate may be less reactive than any neutral ketones present in the reaction mixture. Namely, the second reduction may be slower than the first reduction step.

The EFOE data also strongly suggested that **A** should be more reactive than **B** due to the significantly larger EFOE densities and PDAS values in the *syn*-face of **A** and $\mathbf{A}^-$ than those in the *anti*-face of **B** and $\mathbf{B}^-$. However, the angle strain at C-9 should make hydroxyketones **B** more reactive. As a consequence of these competing factors their reactivities may become comparable.

Again, *b,c* conformers of hydroxyketones should make much less contribution to the diastereoselection compared to *c,c* conformers, which were found to be most stable and populated for all hydroxyketones (Table 3). The minor species $\mathbf{1A}^-$*b,c* are predicted to be very unreactive over both π-faces. The *anti*-face of the minor species $\mathbf{1A}^-$*b,c* is extremely sterically crowded, i.e., PDAS = 5.63 au^3 and the PDAS values for about 5 au^3 usually can be interpreted in this way. Thus, hydride approach from this face is essentially prohibited even though this face is electronically quite activated (EFOE density = 1.2172%). The *syn*-face of $\mathbf{1A}^-$*b,c* is sterically the most relaxed (PDAS = 37.72 au^3) but this face is electronically very unactivated (EFOE density = 0.2866%) and therefore these species may not contribute to the *syn*-stereochemical preference of this ketone. Consequently, the most reactive species should be **1A***c,c* and $\mathbf{1A}^-$*c,c*. Thus, taking into account the formation of oxobicyclo[3.3.1]nonanolates during the reaction course and conformational distribution along with the relative reactivity of conformers of hydroxyketones and corresponding oxobicyclononanolates, the EFOE model demonstrated the superior stereochemistry predicting abilities in the studied molecules.

Conclusions

The EFOE model correctly predicted the experimentally observed π-facial diastereoselectivity in the reduction of bicyclo[3.3.1]nonan-2,9-diones. The obtained results strongly indicate that among the four possible conformers of diketones, the double chair *c,c* conformer, which is slightly less stable than the most populated *b,c* conformer, might be the most reactive one. This is clearly demonstrated by the EFOE and PDAS values of the corresponding conformers. Although the EFOE density and PDAS values predicted enhanced reactivity at C-2 compared to C-9, transition-state calculations at the B3LYP/6-31+G(d,p) level showed that C-9 should be imperceptibly more reactive than C-2, which is in agreement with the experimental observations. EFOE analysis also strongly suggested that in the second hydride reduction step, the corresponding oxobicyclononanolates are most likely to be involved in the reduction as the major species rather than the free hydroxyketones. The antiperiplanar effects in the transition states of the $LiAlH_4$ reduction as measured by both the elongation and the bond population of the antiperiplanar bonds clearly indicated that they should not be an essential factor of the facial diastereoselection of studied diketones.

Acknowledgements

Collaboration between the Vilnius and Tokyo groups originated from the BOS 2000 meeting initiated by Professor V.A. Snieckus in Vilnius, June 26–29, 2000. The Vilnius group wishes to thank him for his encouragement and long

© 2001 NRC Canada

lasting friendship, and ST expresses his special gratitude to Professor V. Snieckus for his hospitality at the BOS conference. This work was supported by Grant-in-Aids for Scientific Research No. 09440215 (Japanese Government) and (in part) by the Lithuanian Science and Studies Foundation.

References

1. B.W. Gung and B. le Noble. Chem. Rev. **99**, 1067 (1999).
2. (*a*) M. Cherest and H. Felkin. Tetrahedron Lett. 2205 (1968); (*b*) N.T. Anh, O. Eisenstein, J.-M. Lefour, and M.E. Tran Huu Dau. J. Am. Chem. Soc. **95**, 6146 (1976); (*c*) D. Mukherjee, Y.-D. Wu, F.R. Fronczek, and K.N. Houk. J. Am. Chem. Soc. **110**, 3328 (1988); (*d*) S.S. Wong and M.N. Paddon-Row. J. Chem. Soc. Chem. Commun. 456 (1990).
3. (*a*) A.S. Cieplak. J. Am. Chem. Soc. **103**, 4540 (1981); (*b*) A.S. Cieplak. Chem. Rev. **99**, 1265 (1999).
4. Y.-D. Wu, J.A. Tucker, and K.N. Houk. J. Am. Chem. Soc. **113**, 5018 (1991).
5. M. Kaselj, W.-S. Chung, and W. le Noble. Chem. Rev. **99**, 1387 (1999).
6. H. Li and W. le Noble. Recl. Trav. Chim. Pays–Bas, **111**, 199 (1992).
7. B.W. Gung. Tetrahedron, **52**, 5263 (1996).
8. J. Klein. Tetrahedron Lett. **14**, 4307 (1973).
9. G. Frenking, K.F. Köhler, and M.T. Reetz. Angew. Chem. Int. Ed. Engl. **30**, 1146 (1991).
10. (*a*) X.L. Huang, J.J. Dannenberg, M. Duran, and J. Bertran. J. Am. Chem. Soc. **115**, 4024 (1993); (*b*) X.L. Huang and J.J. Dannenberg. J. Am. Chem. Soc. **115**, 6017 (1993).
11. Y.-D. Wu, K.N. Houk, and M.N. Paddon-Row. Angew. Chem. Int. Ed. Engl. **31**, 1019 (1992).
12. (*a*) J.M. Coxon, K.N. Houk, and R.T. Luibrand. J. Org. Chem. **60**, 418 (1995); (*b*) R.R. Fraser, N.C. Faibish, F.Z. Kong, and K. Bednarski. J. Org. Chem. **62**, 6164 (1997); (*c*) G. Mehta, F.A. Khan, B. Ganguly, and J. Chandrasekhar. J. Chem. Soc. Perkin Trans. 2, 2275 (1994).
13. (*a*) S. Tomoda and T. Senju. Tetrahedron, **53**, 9057 (1997); (*b*) S. Tomoda. Chem. Rev. **99**, 1243 (1999).
14. S. Tomoda and T. Senju. Chem. Commun. 423 (1999).
15. (*a*) S. Tomoda and T. Senju. Tetrahedron, **55**, 5303 (1999); (*b*) S. Tomoda and T. Senju. Chem. Lett. 625 (1999).
16. A. Artou, Y. Ho, H. Kenttama, and R.R. Squires. J. Am. Chem. Soc. **121**, 7130 (1999).
17. J.J. Dannenberg. Chem. Rev. **99**, 1225 (1999).
18. (*a*) U. Berg, E. Butkus, and A. Stončius. J. Chem. Soc., Perkin Trans. 2, 97 (1995); (*b*) E. Butkus, J. Malinauskienė, and P. Kadziauskas. Z. Chem. 103 (1980).
19. T.E. Goodwin, J.M. Meacham, and M.E. Smith. Can. J. Chem. **76**, 1308 (1998).
20. PC Spartan Pro, Version 1.0.5. Wavefunction, Inc., 18401 Von Karman Avenue, Suite 370, Irvine, California.
21. (*a*) J.E. Gurst, E.M. Schubert, S.E. Boiadjiev, and D.A. Lightner. Tetrahedron, **49**, 9191 (1993); (*b*) M.N. Paddon-Row. Tetrahedron, **50**, 10813 (1994).
22. T. Doerner, R. Gleiter, T.A. Robbins, P. Chayangkoon, and D.A. Lightner. J. Am. Chem. Soc. **114**, 3235 (1992).
23. (*a*) J. Perard-Viret and A. Rassat. Tetrahedron: Asymmetry, **5**, 1 (1994); (*b*) U. Berg and E. Butkus. J. Chem. Res. Synop. 116 (1993).
24. Gaussian 94, Version SGI-G94, Revision D.1. M.J. Frisch, G.W. Trucks, H.B. Schlegel, P.M.W. Gill, B.G. Johnson, M.A. Robb, J.R. Cheeseman, T. Keith, G.A. Petersson, J.A. Montgomery, K. Raghavachari, M.A. Al-Laham, V.G. Zakrzewski, J.V. Ortiz, J.B. Foresman, J. Cioslowski, B.B. Stefanov, A. Nanayakkara, M. Challacombe, C.Y. Peng, P.Y. Ayala, W. Chen, M.W. Wong, J.L. Andres, E.S. Replogle, R. Gomperts, R.L. Martin, D.J. Fox, J.S. Binkley, D.J. Defrees, J. Baker, J.P. Stewart, M. Head-Gordon, C. Gonzalez, and J.A. Pople. Gaussian, Inc., Pittsburgh Pennsylvania. 1995.
25. (*a*) R.A. Marcus. Angew. Chem. Int. Ed. Engl. **32**, 1111 (1993); (*b*) R.A. Marcus. Annu. Rev. Phys. Chem. **15**, 155 (1964).
26. E. Butkus, U. Berg, A. Stončius, and A. Rimkus. J. Chem. Soc. Perkin Trans. 2, 2547 (1998).
27. S. Tomoda and T. Senju. Tetrahedron, **55**, 3871 (1999).

© 2001 NRC Canada

Studies on the reduction and hydrolysis of nitroso acetals

Scott E. Denmark, Vito Guagnano, and Jean Vaugeois

Abstract: Chemical transformation of nitroso acetals derived from tandem [4 + 2]/[3 + 2] cycloadditions of nitroalkenes have been investigated. New reduction methods were surveyed in an attempt to supplant the use of hydrogen and Raney nickel. Homogeneous catalytic hydrogenation was not successful, but samarium diiodide did effectively and selectively cleave one of the N—O bonds in a number of nitroso acetals. Acid-promoted hydrolysis of the nitroso acetals produced both α-alkoxy nitrones and hydroxamic acids selectively via expected pathways.

Key words: nitroso acetals, hydroxamic acids, α-alkoxy nitrones, reduction, hydrolysis.

Résumé : On a étudié les réactions de transformation chimique des acétals nitrosés obtenus par les cycloadditions en tandem [4 + 2]/[3 + 2] de nitroalcènes. On a évalué de nouvelles méthodes de réduction qui pourraient éventuellement supplanter l'utilisation de l'hydrogène et du nickel de Raney. L'hydrogénation catalytique homogène a été essayée sans succès; toutefois, le diiodure de samarium permet de cliver de façon efficace et sélective l'une des liaisons N—O dans un grand nombre d'acétals nitrosés. L'hydrolyse acidocatalysée des acétals nitrosés conduit à la formation sélective d'α-alkoxynitrones ainsi que d'acides hydroxamiques par le biais des voies prévues.

Mots clés : acétals nitrosés, acides hydroxamiques, α-alkoxynitrones, réduction, hydrolyse.

[Traduit par la Rédaction]

Introduction

The tandem [4 + 2]/[3 + 2] cycloadditions of nitroalkenes have evolved as a powerful strategy for the construction of highly functionalized polycyclic compounds adorned with multiple stereogenic centers (1). Over the past decade, we have extensively explored the development of this process in all of its manifold incarnations, i.e., with regard to the inter- or intramolecular nature of the two component cycloadditions. By far the most heavily investigated variant to date is the tandem intermolecular [4 + 2]/intramolecular [3 + 2] process. The unique feature of this mode that makes it attractive for synthesis is the diversity of product structures that are accessible by simply changing the point of attachment of the dipolarophilic tether as illustrated in Fig. 1. The critical transformation that makes all of these pathways useful is the hydrogenolysis of the nitroso acetals to reveal the final product. In general, the hydrogenolyses are mild, high yielding reactions that not only allow for the production of the target skeletons, but also provide for the release (and recovery) of the chiral auxiliary (G*OH) which controls the absolute stereochemical course of the cycloadditions.

The successful total syntheses of a variety of alkaloids disclosed from these laboratories (inter alia, rosmarinecine (1*a*), crotanecine (2*b*), detoxine (2*c*), castanospermine (2*d*), casuarine (2*e*), and mesembrine (2*f*)) made good use of the hydrogenolytic process to construct a pyrrolidine unit from the fused-mode cycloadduct. Similarly, spiro- (3) and bridge-mode (4) nitroso acetal cycloadducts have been cleanly transformed to cyclopentanes and cyclohexanes by this procedure.

To expand the scope of synthetic manipulations of the tandem cycloadducts, we have embarked on a broadly based examination of the chemistry of the nitroso acetals, a relatively unexplored class of compounds (for reviews see ref. 5). Our recognition that the tandem process represents a multicomponent reaction that may lend itself to solid-phase synthesis for combinatorial chemistry was another reason for finding new unmasking procedures. One such strategy for solid-phase applications would involve the attachment of the solid support linker at the vinyl ether moiety. Thus, unmasking would be coupled with cleavage from the resin. Clearly, catalytic heterogeneous hydrogenation is incompatible with the solid supported compounds, thus emphasizing the need for developing homogeneous methods for transforming these cycloadducts.

Background

Traditionally, Raney nickel has proven to be the promoter of choice in the hydrogenolysis of nitroso acetals. Other heterogeneous catalysts such as Pd/C, $Pd(OH)_2$, and PtO_2, have provided less satisfactory results (6). To our knowledge, no

Received January 30, 2001. Published on the NRC Research Press Web site at http://canjchem.nrc.ca on October 29, 2001.

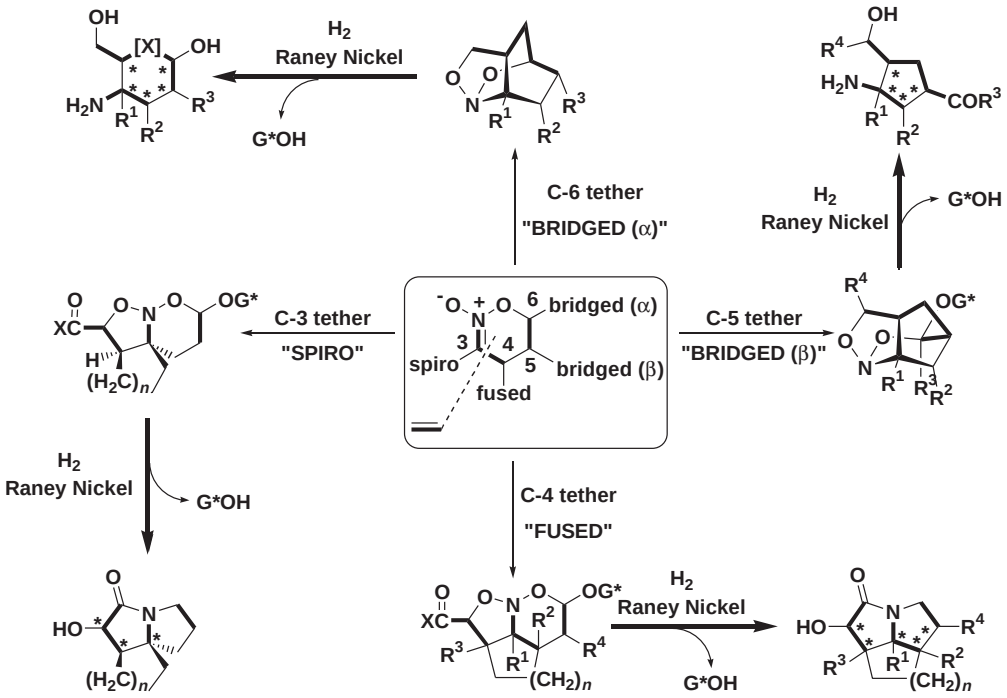
Dedicated to Professor Victor Snieckus for his contributions to chemistry worldwide, his inspiring enthusiasm, and his friendship.

S.E. Denmark,[1] V. Guagnano, and J. Vaugeois. 245 Roger Adams Laboratory, Box 18, Department of Chemistry, University of Illinois, 600 South Mathews Avenue, Urbana, IL 61801, U.S.A.

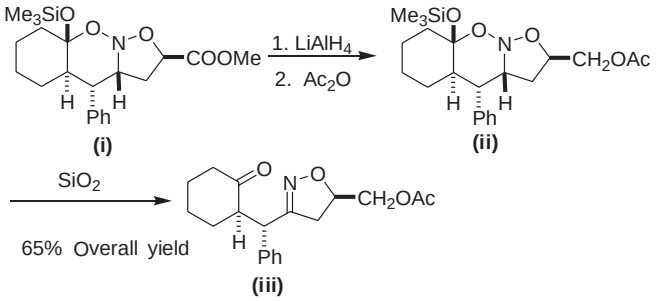
[1]Corresponding author (telephone: (217) 333-0066; fax: (217) 333-3984; e-mail: denmark@scs.uiuc.edu).

 DOI: 10.1139/cjc-79-11-1606 © 2001 NRC Canada

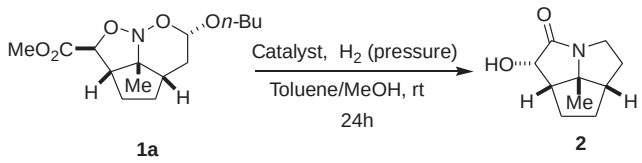
Fig. 1. Family of tandem inter-[4 + 2]/intra-[3 + 2] cycloadditions.



Scheme 1.



Scheme 2.



examples of homogeneous catalytic hydrogenation of nitroso acetals has been reported. Furthermore, the reductive cleavage of nitroso acetals by means of hydride sources has been attempted without much success. For example, Brook and Seebach (7) have shown that the reduction of nitroso acetal **i** with $LiAlH_4$ results in the selective reduction of the ester functionality, whereas the two N—O bonds remained untouched (Scheme 1). The resulting nitroso acetal **ii** underwent silica gel-catalyzed ring opening during column chromatography to afford isoxazoline **iii**. This interesting acid-catalyzed conversion of nitroso acetals to isoxazolines has been previously reported (8).

The paucity of attempts to explore the synthetic utility of nitroso acetals demonstrate that the chemistry of these compounds is still underinvestigated. Whereas there are no reported studies on the reductive cleavage of nitroso acetals, there are several methods for the homogenous reduction of other N—O containing compounds such as nitro groups, oximes, hydroxamic acids, and hydroxylamines (9). Among these the most appealing for our application are: (*i*) $TiCl_3$ in aqueous methanol (10); (*ii*) Zn in aq HCl or acetic acid (11); (*iii*) $Mo(CO)_6$ (12); (*iv*) $Fe_2(CO)_9$ (13); and (*v*) samarium diiodide (14). We report herein our efforts to develop mild, homogeneous methods for the reductive unmasking of nitroso acetals. In the course of these studies, we have discovered a series of novel acid-catalyzed transformations that would be suitable for application to solid-phase synthesis.

Results and discussion

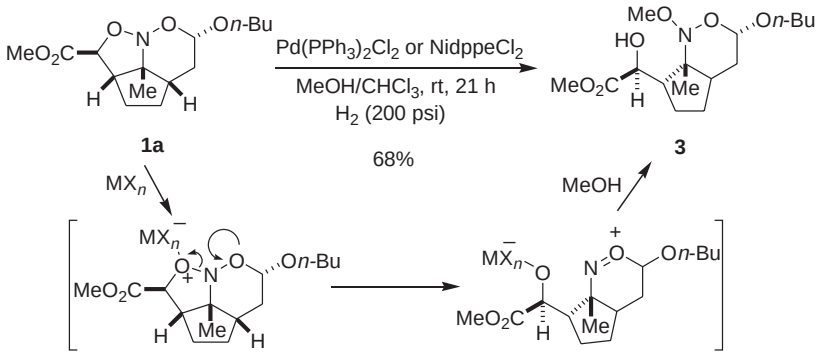
Catalytic homogenous hydrogenation of nitroso acetals

The absence of literature reports documenting the homogenous catalytic reduction of nitroso acetals led us to investigate the use of homogenous catalysts that are commonly employed in the hydrogenation of related compounds. For example, ruthenium(II)-based catalysts have found application in the homogenous reduction of nitroalkanes to amines (15). These reactions are usually carried out at high temperatures and high hydrogen pressure and require the presence of a base. Furthermore, it is known that copper(I) salts are efficient homogenous catalysts for the hydrogenation of nitroalkanes to oximes in alkylpolyamines solvent (16).

Nitroso acetal **1a** (Scheme 2) was selected as the model substrate because of its thermal stability and its well-documented ability to undergo clean and high yielding hydrogenation in the presence of Raney nickel (82–85% yield) (17). In orienting experiments, the hydrogenation of **1a** was conducted in the presence of the Wilkinson's catalyst

© 2001 NRC Canada

Scheme 3.



$(Rh(PPh_3)_3Cl)$ and of its congener $Ru(PPh_3)_3Cl_2$. No α-hydroxy lactam was ever detected and no other product could be isolated, while the starting material was recovered in good yield. An increase of the hydrogen pressure effected no improvement. Also, the ionic complex (1,5-cyclooctadiene)(pyridine)(tricyclohexylphosphine)iridium(I) hexafluorophosphate proved to be an unsuitable catalyst for the hydrogenation of nitroso acetal **1a**, since a low conversion of the starting material to a mixture of products was obtained.

The use of several palladium-based catalysts was also examined. Only three of the catalysts employed ($Pd(dba)_2$, $Pd_2(dba)_3$, $Pd(OAc)_2$) were able to partially convert **1a** into the lactam **2**, (17*e*) in methanol at 200 psi of H_2 pressure and at room temperature. In all the other instances, the reaction provided mixtures of products in which **2** could not be detected.[2] All the palladium catalysts were only sparingly soluble in methanol but quite soluble in the mixture MeOH–$CHCl_3$. Nonetheless, the hydrogenations carried out in this solvent mixture also provided unsatisfactory results. It is also noteworthy that, in all the cases examined, the reaction mixture after hydrogenation showed the presence of a black precipitate, which is presumed to be metallic Pd(0). Furthermore, whereas a 50% conversion of nitroso acetal **1a** into lactam **2** required 24 h, the formation of black Pd(0) was achieved in less than an hour. This observation leads to the conclusion that the formation of **2** was catalyzed by the metallic Pd(0) rather than by the starting complexes.

When the hydrogenation of nitroso acetal **1a** was carried out in the presence of either $Pd(PPh_3)_2Cl_2$ or $Ni(dppe)Cl_2$, a new compound was obtained as a mixture of stereoisomers (Scheme 3). On the basis of ^1H NMR and mass spectroscopic data, this compound is believed to be the bicyclic nitroso acetal **3** arising from methanolysis of the isoxazolidine ring of **1a**. The existence of two stereoisomers is explained by the presence of a noninverting nitrogen (18). The formation of **3** is proposed to involve initial coordination of the Lewis acidic metal to the oxygen in the five-membered ring, followed by assisted opening of the isoxazolidine and nucleophilic attack of MeOH to the nitrogen center. In support of this hypothesis, **3** was also obtained from **1a** in methanolic acetic acid (vide infra).

Samarium diiodide cleavage of N—O bonds in nitroso acetals

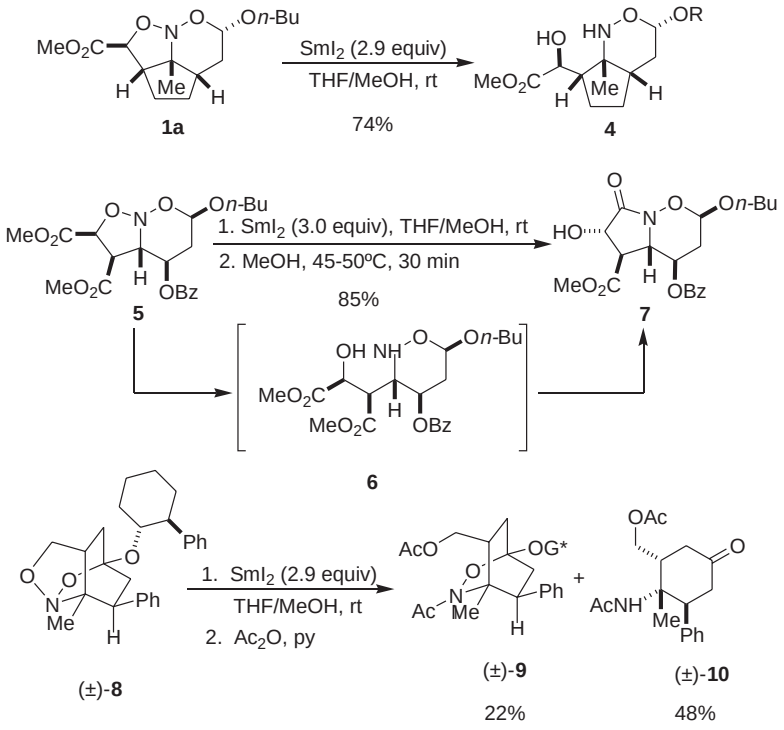
Our search for a general method for the cleavage of nitroso acetals under homogeneous conditions next turned to the use of $Mo(CO)_6$ and SmI_2 which have been shown to reduce N—O bonds in hydroxylamines, isoxazolidines, and oxazines (12, 14). Unfortunately, $Mo(CO)_6$ proved to be unsuitable for this purpose. Treatment of nitroso acetal **1a** with $Mo(CO)_6$ in aqueous acetonitrile at reflux for 1 h resulted in the complete conversion of the starting material into an intractable mixture of products. Much better results were obtained from the reaction of nitroso acetal **1a** with SmI_2. Although optimization was required to make the initially low yielding process synthetically attractive, we were eventually able to develop a protocol for the selective reduction of the N—O bond of the isoxazolidine ring in nitroso acetal **1a**. Thus, treatment of **1a** with 2.9 equiv of SmI_2 in THF–MeOH afforded the bicyclic oxazine **4** in 74% yield (Scheme 4). To assess the scope of this reaction, nitroso acetal **5** (derived from a tandem double intermolecular cycloaddition (19)) was subjected to the same reaction conditions. We were pleased to find that SmI_2 promoted the analogous reduction to afford the oxazine **6**. This compound underwent partial intramolecular cyclization at room temperature to afford the corresponding lactam **7**. The bicyclic product **7** could be obtained reproducibly and in high yield (85%) by heating a methanolic suspension of the crude oxazine **6** at 45–50°C for 30 min. Attempts to cleave the remaining N—O bond in lactam **7** were unsuccessful. Finally, the bridged nitroso acetal **8** underwent both single and double N—O bond cleavage under similar conditions to provide, after acetylation, a mixture of the bicyclic oxazine **9** and the aminocyclohexanone **10** in 22% and 48% yield, respectively, (Scheme 4).

The preferential cleavage of the isoxazolidine rings in **1a**, **5**, and **8** with SmI_2 implies that the LUMO has a large coefficient at that N—O bond and that there may be a significant strain release upon opening the five-membered ring. A similar observation was made in the partial hydrogenolysis of tricyclic nitroso acetals related to **1a** (six-membered carbocyclic ring) and **8**. Although this is fundamentally interesting, this cleavage mode does not lead to unraveling of the oxazine wherein the auxiliary or the linker to the solid phase would

[2] Although lactam **2** (when produced) was never isolated, its presence in the crude reaction mixture was confirmed by the appearance in the ^1H NMR spectrum of two diagnostic signals (a doublet at 4.70 ppm and a multiplet in the region 4.00–3.80 ppm).

© 2001 NRC Canada

Scheme 4.



Scheme 5.

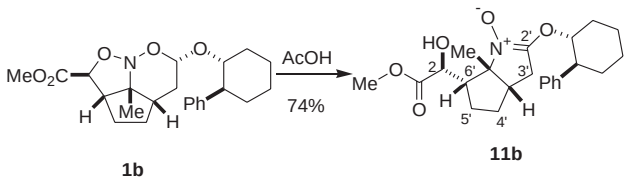


Table 1. Selected spectral data for compounds **11a** and **11b.**

^{1}H NMR (δ, ppm)		^{13}C NMR (δ, ppm)		IR (cm^{-1})	
11a	**11b**	**11a**	**11b**	**11a**	**11b**
4.38 t, 1H	4.81 d, 1H	173.33	173.41	1742	1756
4.29 dd, 1H	4.06 d, 1H	153.67	153.48	1648	1644
3.75 s, 3H	3.76 s, 3H	80.59	81.04		
3.01 dd, 1H	2.39 dd, 1H				

be attached. We thus began an investigation of dissolving metal type reductions in the hope that the acetal type function in the oxazine would exhibit enhanced reactivity.

Acetic acid cleavage of nitroso acetals

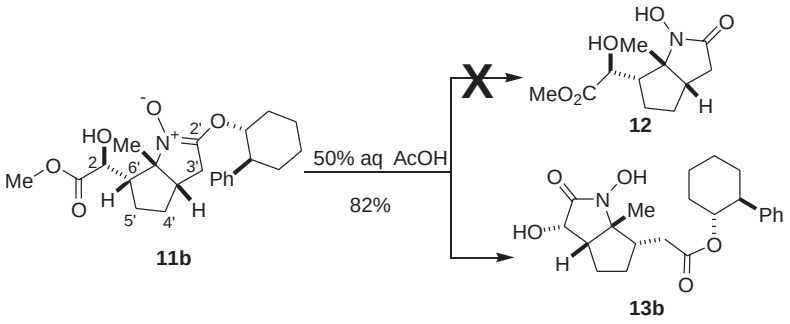
For this series of experiments we employed the same nitroso acetal subunit as in **1a** but this time derived from the 2-phenylcyclohexanol vinyl ether dienophile (**1b**) (17). Upon treating **1b** with Zn in acetic acid overnight, a new compound **11b** was obtained that differed from the Raney nickel reduction product **2**. That this new compound did not arise from a reductive process was revealed by a control experiment in acetic acid (without zinc) which afforded the same product. The diagnostic spectroscopic data for **11b** are collected in Table 1. Of primary importance was the mass spectral data which revealed that **11b** is an isomer of **1b**! ^{1}H NMR, ^{13}C NMR, and IR data supported the persistence of a methyl ester (δ 3.78 ppm, δ 173.3 ppm, and 1756 cm^{-1}) most likely flanked by a hydroxyl bearing methine group (δ 4.06 ppm, 3437 cm^{-1}). However, identifying a chemical function that fit the second combination of signals at δ 4.81 ppm, δ 153.5 ppm, and 1644 cm^{-1} proved more challenging. The signal at 153 ppm in the ^{13}C NMR is suggestive of carbonates or carbamates but their carbonyl stretching frequencies are usually 1800 and 1720 cm^{-1}. Unknown compound **11b** clearly does not contain any of these functions.

The structure of **11b** was ultimately secured by single crystal X-ray analysis.[3] Crystals suitable for X-ray crystallography were deposited from hexane – ethyl acetate in 73% yield. As we surmised, the α-hydroxy methyl ester moiety is indeed present (Scheme 5). The core of the structure is an azabicyclic[3.3.0] system containing two C—N bonds whose lengths are 1.293(2) and 1.501(2) Å, respectively. This indicates the presence of both C—N double and single bonds. The presence of one N—O bond of 1.3334(12) Å, typical

[3] Supplemenatry material has been deposited with the Depository of Unpublished Data, CISTI, National Research Council Canada, Ottawa, ON K1A 0S2, Canada ((http://www.nrc.ca/cisti/irm/unpubl_e.shtml for information on ordering electronically). The crystallographic coordinates of **11b** and **13b** have been deposited with the Cambridge Crystallographic Data Centre (CCDC nos. 158 466 and 158 467). Copies of the data are available, free of charge, from the Director, CCDC, 12 Union Road, Cambridge CB2 1EZ, U.K. (Fax: 44-1223-336033 or e-mail: deposit@ccdc.cam.ac.uk).

© 2001 NRC Canada

Scheme 6.



of *N*-oxides, is also noted. Hence the unexplained ^{13}C NMR (δ 153.5 ppm) and IR (1644 cm^{-1}) resonances arise from the rather uncommon α-alkoxy nitrone function (20).

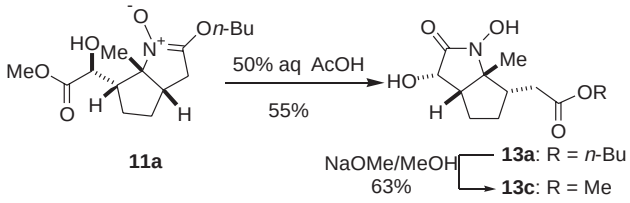
To establish the generality of this new transformation, compound **1a** was treated with glacial acetic acid for 2 h. After evaporation of the solvent, purification by column chromatography and recrystallization from dry dichloromethane–hexane under N_2, compound **11a** was obtained as a white crystalline solid in 56% yield. The identity of this structure was easily made by comparison of the spectroscopic data to those from **11b** (see Table 1). Although there are some differences in the ^{1}H NMR data primarily due to the anisotropic effect of the 2-phenylcyclohexyl moiety, one can confidently assign the structure by analogy on the basis of the ^{13}C NMR and IR spectra.

Although the transformation of **1** to **11** is interesting, it failed to accomplish our objective of separating the dienophile alkoxy group from the nitroso acetal. Therefore, we attempted to hydrolyze the α-alkoxy nitrone in hope of obtaining hydroxamic acid **12** (Scheme 6). Treatment of **11b** with 50% aqueous acetic acid at room temperature for 16 h afforded a new crystalline compound after recrystallization from acetonitrile–water. Much to our surprise, the ^{1}H NMR spectrum of the product indicated that the 2-phenylcyclohexyloxy group remained whereas the methyl ester did not. Moreover, the 2-phenylcyclohexyloxy carbinol proton was shifted downfield to δ 5.02 ppm and remained a doublet of triplets. The ^{13}C NMR spectrum of this compound displayed signals at δ 173.0 and 169.5 ppm and the IR spectrum showed strong absorbencies at 1740 and 1677 cm^{-1}. These data suggested that both ester and amide functionalities were present. The FAB mass spectrum shows an M + 1 signal at *m*/*z* 388.2 indicating loss of a methylene group from **11b**. Taken together, this information led to the formulation of hydroxamic acid **13b** as the structure of the new compound (Scheme 6). Our hypothesis was again validated by a single crystal X-ray analysis.[3]

The unexpected formation of **13b** could be attributed to the steric congestion in the vicinity of the hindered phenylcyclohexyl ester. Accordingly, compound **11a** was submitted to aqueous acetic acid with the expectation that an *n*-butyl group might allow formation of **12**. However, treatment of **11a** under similar conditions followed by purification by recrystallization from acetonitrile afforded a new material (**13a**) in 55% yield whose structure was easily assigned by analogy to compound **13b** (Scheme 7).

To streamline the hydrolytic transformation, we reasoned that compounds **13a** and **13b** should be accessible directly

Scheme 7.

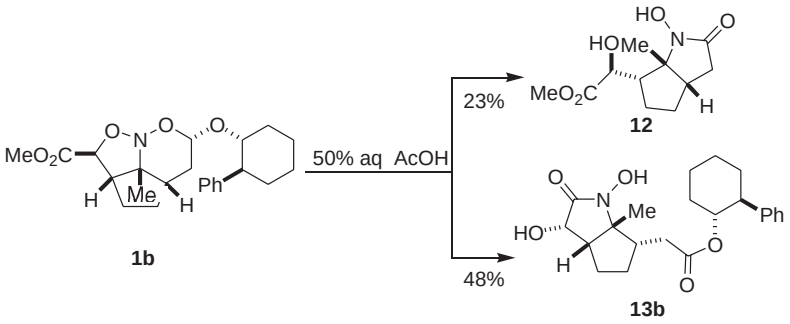


from nitroso acetals **1a** and **1b** using a one-step treatment with aqueous acetic acid. Thus, compound **1b** was stirred with 50% aqueous acetic acid for 16 h at room temperature. The ^{1}H NMR spectrum of the white solid obtained clearly indicated the presence of **13b** along with 2-phenylcyclohexanol and another unknown compound. Because this new product retained the methyl ester signal we suspected that **12** had indeed been produced. The ratio of **13b** to **12** as determined by ^{1}H NMR integration was 2:1; however, isolation of **12** proved difficult. Purification of the mixture by column chromatography on silica gel with toluene – acetone – acetic acid (60:38:2), afforded a reddish solid! Elemental analysis of the reddish compound showed that it contained copper. We surmised that the powerful, metal-chelating hydroxamic acid moieties in both **13b** and **12** were leaching this trace metal from the adsorbent (21). Thus, the silica gel was extensively washed, dried, and then used for separation. In this fashion, we successfully obtained hydroxamic acids **13b** and **12** in 48 and 23% yield, respectively. The spectroscopic data from **12** (^{1}H NMR, ^{13}C NMR, IR, and MS) were fully consistent with the structure assigned (Scheme 8).

Although compound **12** is structurally distinct from the kinds of products usually produced from unmasking nitroso acetals, our goal for implementing tandem cycloadditions on the solid phase did not have a specific structural objective. Therefore, we were pleased to have identified a cleavage procedure that could function under mild, homogeneous conditions and next assayed the optimization of this hydrolytic process for the production of **12**. Unfortunately, all attempts to do so by varying acid concentration, temperature, or solvent proved fruitless. The only variable that influenced the ratio of **12**:**13b** was the reaction temperature. However lowering the temperature required that the reaction be left for much longer periods of time in order for **1b** to dissolve fully. Regrettably, the ratio of **12**:**13b** slightly decreased to 1:1 after 7 days at –10°C. As we could not favor the formation of only one compound in this fashion, the one-step avenue was abandoned.

© 2001 NRC Canada

Scheme 8.



Having failed to achieve a direct hydrolysis of **1b** to **12**, we next sought a procedure that might deliver **13b** directly from **1b** and thence to devise a protocol to cleave the pendant alkoxy moiety by ester saponification. Thus, compound **1b** was first treated with glacial acetic acid for 2 h and then an equal volume of distilled, deionized water was added and the solution was stirred for 16 h. By this protocol, **13b** was obtained in 87% yield after recrystallization. This represents a significant improvement compared to the two-pot procedure (59% yield). In a similar fashion, **1a** afforded **13a** in only a marginally higher yield (33% vs. 30% for the two-pot procedure).

With a high yielding procedure for the production of **13b** in hand, we turned our attention to the base promoted cleavage of the ester group. Remarkably, **13b** proved resistant to trans-esterification with sodium methoxide in methanol. Even attempts to engage the *N*-hydroxyl group of the hydroxamic acid with DMAP or K_2CO_3 in toluene at room temperature or at reflux resulted in recovery of the starting material. This surprising resistance to reaction at the ester carbonyl group in **13b** may be due to the shielding from the phenylcyclohexyl moiety. Support for this hypothesis was forthcoming in the successful trans-esterification of **13a** with sodium methoxide in methanol. After neutralization with acidic Dowex resin and recrystallization from acetonitrile, methyl ester acid **13c** was obtained in 63% yield (Scheme 7). We were thus, finally in possession of non-hydrogenolytic means to cleave the alkoxy moiety from a nitroso acetal created by a tandem [4 + 2]/[3 + 2] nitroalkene cycloaddition

Mechanistic analysis

The divergent hydrolytic behavior of nitroso acetals **1a** and **1b** is intriguing. In glacial acetic acid, only alkoxy nitrones **11a**:**11b** are produced. Further, hydrolysis of **11a**:**11b** in 50% aqueous acetic acid leads exclusively to hydroxamic acid **13a**:**13b**. The alternate hydroxamic acid **12** is only formed by direct hydrolysis of **1b** with 50% aqueous acetic acid. A mechanistic scenario that can accommodate these unusual selectivities under various conditions is presented in Scheme 9.

The initial event in glacial acetic acid is proposed to be the fragmentation of the protonated nitroso acetal to produce the nitroso oxocarbenium ion **iv** (Glacial acetic acid pathway). In the absence of any nucleophile other than acetate, this species collapses by attack of the nitrogen atom on the oxocarbenium ion to produce a nitrosonium cation **v** which leads directly to the alkoxy nitrone **11** by simple deprotonation. Recall that if methanol is present, the cation **iv** can be intercepted to afford the opened nitroso acetal **3**.

One of the most unexpected results was the exclusive formation of **13b** from hydrolysis of **11b** in aqueous acetic acid and the observation of *both* **13b** and **12** from hydrolysis of **1b** under the same conditions. This clearly implies that the hydrolysis of **11b** and **1b** proceed through different intermediates. To accommodate these facts, two mechanistic scenarios are proposed in Scheme 9. Aqueous hydrolysis of **11b** is suggested to proceed by hydration the alkoxy nitrone to give **ix** which collapses to hydroxylamine ester **x**. For reasons that are not completely understood, the hydroxylamine moiety reacts exclusively with the α-hydroxy ester (most likely due to the activated nature of the carbonyl group) to afford **13b**.

To explain the formation of both **12** and **13b** from **1b** under these conditions requires that **12** arise from an independent pathway not involving hydroxylamine **x**. Accordingly, we propose that in aqueous acetic acid, two pathways are operative; the first is the Glacial acetic acid pathway and the second, Aqueous acetic acid pathway (Scheme 9). In this latter pathway, the alkoxy group OG in **1** is hydrolyzed to a hydroxyl group (by any of a number of mechanisms). As was proposed above, nitroso acetal fragmentation leads to nitroso oxocarbenium ion **vi** which again collapses to a nitronium ion **vii**. Now, however, the deprotonation of **vii** leads to a hydroxy nitrone which simply tautomerizes to the hydroxamic acid **12**. Most certainly, alternative mechanisms are conceivable, but all must provide a pathway for the formation of **12** which does not proceed via **x**.

Experimental

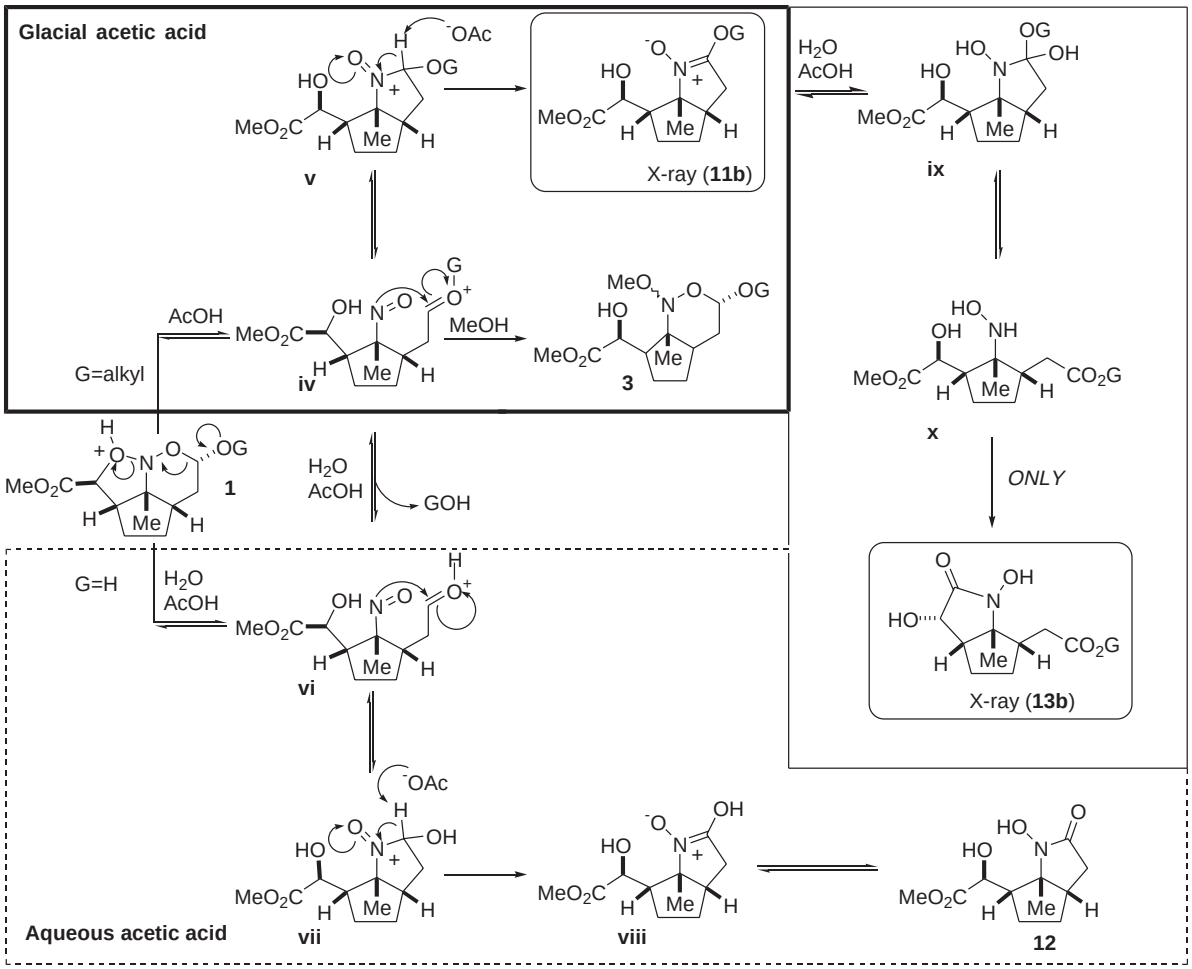
General experimental

All reactions were performed under an atmosphere of dry nitrogen in flame- or oven-dried (140°C) glassware. Solvents for chromatography and recrystallization were reagent grade or better. Reaction solvents were distilled from the indicated drying agents: dichloromethane (P_2O_5), methanol ($Mg(OMe)_2$). TLC was performed on Merck silica gel plates with QF-254 indicator. Plates were visualized using UV radiation (254 nm) in conjunction with the following reagents: $KMnO_4$ (alkenes, nitro compounds, alcohols), anisaldehyde (nitroso acetals), $FeCl_3$ (hydroxamic acids), or I_2 (alkenes, aromatics). Column (flash) chromatography was performed using 230–400 mesh silica gel purchased from EM Science or alumina purchased from Aldrich.

Melting points (mp) were determined on a Thomas–Hoover capillary melting point apparatus in vacuum sealed tubes and are uncorrected. ^1H and ^{13}C NMR spectra were recorded at

© 2001 NRC Canada

Scheme 9.



400 MHz, ^{1}H (100 MHz ^{13}C) or 500 MHz ^{1}H (125 MHz ^{13}C) in deuteriochloroform ($CDCl_3$) with chloroform (7.27 ppm ^{1}H, 77.0 ppm ^{13}C) as an internal reference. Chemical shifts are given in ppm (δ); multiplicities are indicated by s (singlet), d (doublet), t (triplet), q (quartet), m (multiplet), or b (broadened). Coupling constants (*J*) are reported in Hz. Infrared spectra (IR) were obtained on a Mattson Galaxy 5020 spectrophotometer. Peaks are reported in cm^{-1} with the following relative intensities: s (strong, 67–100%), m (medium, 34–66%), w (weak, 0–33%). Mass spectra were obtained through the Mass Spectrometry Laboratory, School of Chemical Sciences, University of Illinois. Low-resolution fast atom bombardment (FAB) spectra were obtained on a VG ZAB-SE spectrometer in magic bullet (3:1, dithiothreitol–dithioerythitol) or 3-nitrobenzyl alcohol. Data are reported in the form *m*/*z* (intensity relative to base = 100). Elemental analyses were performed by the University of Illinois Microanalytical Service Laboratory and are the average of two combustions.

2-Aza-4-butoxy-9-[(carbomethoxyhydroxy)methyl]-N-*methoxy-3-oxabicyclo[4.3.0]nonane (**3**)*

Acetic acid (0.057 mL, 1.0 mmol, 2 equiv) was added to a solution of nitroso acetal **1a** (150 mg, 0.5 mmol, 1 equiv) in MeOH (10 mL). The reaction mixture was stirred for 2 h and 30 min at room temperature (rt). After removal of MeOH and AcOH under vacuo, the resulting blue residue was dissolved in EtOAc (50 mL) and treated with SiO_2 (20 g). The suspension was stirred for 18 h at rt, then filtered and concentrated. The residue was dissolved in benzene and purified by silica gel column chromatography (hexane–EtOAc, 6:1) to afford 59.2 mg of a mixture of **3**:**3′** (1.44:1) and 53.3 mg of **3** for a combined yield of 112.5 mg (68%). Data for **3**:**3′** (1.44:1): MS (CI, CH_4) *m*/*z*: 300 (M^+-31, 25), 270 (13), 269 (67), 258 (20), 242 (44), 227 (57), 226 (24), 213 (28), 209 (26), 196 (17), 195 (100), 177 (43), 169 (14), 152 (20), 139 (12), 116 (58), 106 (15). ^{1}H NMR (400 MHz, $CDCl_3$) δ: 4.42 (dd, *J* = 3.6, 7.6, 0.41H, HC(4)), 4.32 (dd, *J* = 4.0, 7.2, 0.59H, HC(4)), 4.20 (d, *J* = 9.6, 0.41H, HC(1′″)), 4.09 (d, *J* = 7.6, 0.59H, HC(1′″)), 3.79 (s, 1.23H, H_3CO_2C), 3.74 (s, 1.77H, H_3CO_2C), 3.60–3.30 (m, 2H, $H_2C(1')$), 3.29 (s, 1.23H, H_3CO), 3.20 (s, 1.77H, H_3CO), 3.12–2.98 (m, 0.59H), 2.80–2.70 (m, 0.59H), 2.62–2.34 (m, 2.77H), 2.22–1.78 (m, 3.46H), 1.76 (s, 1.23H, $H_3C(1')$), 1.62–1.29 (m, 4H), 1.18 (ddd, *J* = 3.6, 10.4, 13.6, 0.41H), 1.00–0.80 (m, 3.59H), 0.70 (m, 1.77H, $H_3C(1')$), 0.62–0.52 (m, 0.59H). Data for **3**: ^{1}H NMR (400 MHz, $CDCl_3$) δ: 4.42 (dd, *J* = 3.6, 7.6, 1H, HC(4)), 4.20 (d, *J* = 9.6, 1H, HC(1′″)), 3.79 (s, 3H, H_3CO_2C), 3.56 (dt, J_d = 9.5, J_t = 6.5, 1H, HC(1′)), 3.38 (dt, J_d = 9.5, J_t = 6.5, 1H, HC(1′)), 3.29 (s, 3H, H_3CO), 2.90–2.75 (bs, 1H, OH), 2,42 (dd, *J* = 8.8, 10.0, 1H, HC(9)), 2.18–1.77 (m, 6H), 1.76

© 2001 NRC Canada

(s, 3H, $H_3C(1')$), 1.60–1.50 (m, 2H, $H_2C(2'')$), 1.42–1.31 (m, 2H, $H_2C(3'')$), 1.18 (ddd, J = 3.6, 10.4, 13.6, 1H), 0.92 (t, J = 7.2, 3H, $H_3C(4'')$).

rel-*(1*R,*4*S,*6*S,*9*S)-*2-Aza-4-butoxy-9-[(carbomethoxyhydroxy)-methyl]-3-oxabicyclo[4.3.0]nonane **(4)***

A solution of nitroso acetal **1a** (149.6 mg, 0.50 mmol) in MeOH (5 mL) was added quickly to a solution of SmI_2 in THF (0.036 N, 40 mL, 1.45 mmol, 2.9 equiv) at rt. The flask containing **1a** was rinsed with MeOH (2 mL). In a few seconds, the color of the reaction mixture turned from blue to yellow. The solvents were removed under vacuo. The residue was dissolved in CH_2Cl_2 (300 mL) and washed with H_2O (100 mL). The aqueous layer was back-extracted with CH_2Cl_2 (2 × 300 mL). The combined organic phase was dried (Na_2SO_4), filtered, and concentrated. The residue was dissolved in benzene and purified by silica gel column chromatography to afford 112.1 mg (74%) of **4** in analytically pure form. Data for **4**: TLC: R_f 0.25 (hexane–EtOAc, 2:1). MS (CI, CH_4) *m*/*z*: 302 (M^++1, 18), 300 (3), 284 (7), 256 (10), 242 (3), 229 (16), 228 (100), 227 (5), 210 (4), 168 (6), 139 (12). IR ($CHCl_3$) υ (cm^{-1}): 3302 (w), 3026 (m), 3011 (s), 2959 (s), 2935 (s), 2875 (s), 1737 (s), 1458 (s), 1371 (m), 1264 (s), 1233 (s), 1216 (s), 1128 (s), 1113 (s), 1074 (s), 1014 (s), 996 (s), 972 (m), 772 (m). ^{1}H NMR (400 MHz, $CDCl_3$) δ: 5.76–5.46 (bs, 1H, HN), 4.69 (t, J = 4.6, 1H, HC(4)), 4.26 (d, J = 4.6, 1H, HC(1′′)), 4.24–4.14 (bs, 1H, OH), 3.77 (s, 3H, H_3CO_2C), 3.72 (dt, J_d = 9.6, J_t = 6.8, 1H, HC(1′)), 3.38 (dt, J_d = 9.6, J_t = 6.8, 1H, HC(1′)), 2.24–2.16 (m, 1H, HC(9)), 2.02–1.66 (m, 7H, $H_2C(5)$, HC(6), $H_2C(7)$, $H_2C(8)$), 1.64–1.52 (m, 2H, $H_2C(2')$), 1.44–1.34 (m, 2H, $H_2C(3')$), 1.33 (s, 3H, $H_3C(1'')$), 0.93 (t, J = 7.4, 3H, $H_3C(4')$). ^{13}C NMR (100 MHz, $CDCl_3$) δ: 174.85 (H_3CO_2C), 98.59 (C(4)), 71.82 (C(1′′)), 67.78 (C(1′)), 64.98 (C(1)), 52.18 (C(9)), 52.01 (H_3CO_2C), 40.84 (C(6)), 31.61 (C(2′)), 28.50 (CH_2), 28.22 (CH_2), 27.01 (CH_2), 24.75 (C(1′′)), 19.28 (C(3′)), 13.78 (C(4′)). Anal. calcd. for $C_{15}H_{27}NO_5$: C 59.78, H 9.03, N 4.65; found: C 59.54, H 8.81, N 4.88.

rel-*(3*R,*5*R,*6a*S,*7*R,*8*S)-*5-Benzoyloxy-3-butoxy-7-carbomethoxy-8-hydroxy-2-oxa-9-oxobicyclo[4.3.0]nonane **(7)***

A solution of nitroso acetal **5** (149.6 mg, 0.50 mmol) in MeOH (5 mL) was added quickly to a solution of SmI_2 in THF (0.036 N, 42 mL, 1.5 mmol, 3.0 equiv) at rt. The flask containing **5** was rinsed with MeOH (5 mL). The solvents were removed under vacuo. The residue was dissolved in CH_2Cl_2 (350 mL) and washed with NH_4Cl (100 mL). The aqueous layer was back-extracted with CH_2Cl_2 (3 × 100 mL). The combined organic phase was dried (Na_2SO_4), filtered, and concentrated. The residue was suspended in MeOH (25 mL) and stirred at 45–50°C for 30 min. The solvent was removed in vacuo; the residue was dissolved in benzene and purified by silica gel column chromatography (hexane–EtOAc, 2:1, 1:1, 1:2) to afford 173.0 mg (85%) of **7** in analytically pure form. Data for **7**: mp 135 to 136°C (hexane–EtOAc). TLC: R_f 0.13 (hexane–EtOAc, 1:1). MS (CI, CH_4) *m*/*z*: 408 (M^++1, 45), 334 (11), 314 (15), 287 (20), 286 (100), 285 (26), 268 (21), 212 (28), 184 (16), 123 (16), 105 (10). IR ($CHCl_3$) υ (cm^{-1}): 3300 (w), 3031 (w), 2959 (w), 2875 (w), 1737 (s), 1439 (w), 1268 (s), 1232 (m), 1171 (m), 1114 (m), 1094 (m), 1027 (m), 934 (w). ^{1}H NMR (400 MHz, $CDCl_3$) δ: 8.04–7.98 (m, 2H, Ph), 7.64–7.58 (m, 1H, Ph), 7.51–7.43 (m, 2H, Ph), 5.26 (ddd, J = 5.0, 9.4, 11.4, 1H, HC(5)), 5.02–4.93 (m, 2H, HC(3), OH), 4.64 (dd, J = 5.2, 7.6, 1H, HC(8)), 4.10 (dt, J_d = 9.6, J_t = 6.7, 1H, HC(1′)), 3.88 (dd, J = 6.8, 9.2, 1H, HC(6)), 3.73 (dt, J_d = 9.6, J_t = 6.7, 1H, HC(1′)), 3.51 (s, 3H, H_3CO_2C), 3.10 (t, J = 7.2, 1H, HC(7)), 2.54 (ddd, J = 1.2, 4.8, 8.0, 1H, HC(4)), 2.00–1.86 (m, 1H, HC(4)), 1.68–1.54 (m, 2H, $H_2C(2')$), 1.46–1.31 (m, 2H, $H_2C(3')$), 0.92 (t, J = 7.2, 3H, $H_3C(4')$). ^{13}C NMR (100 MHz, $CDCl_3$) δ: 170.94, 165.74, 165.33, 133.59 (C(4′′)), 129.65 (C(2′′)), 128.92 (C(1′′)), 128.48 (C(3′′)), 103.39 (C(3)), 71.22 (C(5)), 71.15 (C(1′)), 70.22 (C(8)), 57.03 (C(6)), 52.65 (H_3CO_2C), 49.12 (C(7)), 35.79 (C(4)), 31.51 (C(2′)), 18.94 (C(3′)), 13.75 (C(4′)). Anal. calcd. for $C_{20}H_{25}NO_8$: C 58.96, H 6.19, N 3.44; found: C 58.88, H 6.04, N 3.34.

rel-*(1*R,*4*S,*5*S,*8*R*)–8-Acetoxymethyl*-N-*acetyl-3-aza-2-oxa-5-phenyl–1-[(1*R**,*2*S**)-(2-phenyl-cyclohexyl)oxy]bicyclo-[2.2.2]octane ((±)9) and* rel-*(1*R,*2*S,*3*S)-*2-acetylamino-2-methyl-5-oxo-3-phenylcyclohexanemethyl acetate ((±)**10)***

A solution of nitroso acetal (±)**8** (20.3 g, 0.05 mmol) in MeOH (0.5 mL) was added quickly to a solution of SmI_2 in THF (0.036 N, 4.0 mL, 1.45 mmol, 2.9 equiv) at rt. The flask containing (±)**8** was rinsed with MeOH (0.5 mL). The solvents were removed under vacuo. The residue was suspended in pyridine (1.0 mL) and treated with acetic anhydride (1.0 mL). The reaction mixture was stirred for 16 h at rt. Pyridine and acetic anhydride were removed by bulb-to-bulb distillation (40°C, 0.1 mmHg (1 mmHg = 133.322 Pa)). The residue was dissolved in THF, filtered through a plug of silica gel, concentrated, dissolved in benzene, and purified by silica gel column chromatography (hexane–EtOAc, 3:1, 1:2) to afford 54 mg (22%) of (±)**10** and 76 mg (48%) of (±)**9**. The ^{1}H NMR spectra of (±)**10** and (±)**9** were consistent with those of the compounds obtained from the Raney-nickel-promoted hydrogenations of nitroso acetal (±)**8** (4*b*).

rel-*{[(3a*S,*6*S,*6a*R*)-6a-Methyl-(1*R,*2*S)-2-(2-phenylcyclo-hexyl)oxy]-3,3a,4,5,6-pentahydrocyclopenta[*d*]pyrrol-6-yl-*N-*oxide}-(2*S)-hydroxy acetic acid methyl ester **(11b)***

In a round bottom flask equipped with a magnetic stirring bar and a stopper was dissolved 1.08 g (2.7 mmol) of **1b** in 10 mL of CH_3CO_2H. The solution was stirred for 2 h (solution turns light blue after ca. 20 min). The solvent was removed in vacuo and the light blue viscous oil was kept at 0.2 mmHg (1 mmHg = 133.322 Pa) and rt for 18 h. The residue was separated by chromatography on SiO_2 column (40 × 150 mm) with 5% (v/v) CH_3OH in CH_2Cl_2. The white solid obtained was recrystallized from hexane and ethyl acetate to afford 780 mg (73%) of **11b** as white crystals. Data for **11b**: mp 162°C. TLC: R_f 0.45 (CH_2Cl_2–CH_3OH, 9:1). MS (FAB) *m*/*e*: 402.3 (75), 244.1 (100), 118.95 (21). IR (KBr) υ (cm^{-1}): 3437 (s), 3119 (s), 2935 (s), 1756 (s), 1644 (s), 1401 (s), 1193 (s), 701 (s). ^{1}H NMR (500 MHz, $CDCl_3$) δ: 7.37–7.23 (m, 5H), 4.81 (dt, J = 4.7, 10.6, 1H, HC(1′′)), 4.06 (d, J = 8.6, 1H, HC(2)), 3.76 (s, 3H, CH_3O), 2.80 (dt, J = 3.6, 11.4, 1H, H(C2′′)), 2.39 (dd, J = 10.4, 17.8, 1H, HC(3′)), 2.29–2.26 (m, 1H, HC(6′′)), 2.20–2.15 (m, 1H, HC(3a′)), 2.09–2.03 (m, 1H, HC(6′)), 1.98–1.91 (m, 2H), 1.82–1.32 (m, 8H), 1.49 (s, 3H, H3(C7′)), 1.14 (dd, J = 6.0,

© 2001 NRC Canada

13.0, 1H, HC(4′)), 1.04–0.94 (m, 1H, HC(5′)). ^{13}C NMR (126 MHz, $CDCl_3$) δ: 173.33 (C(1)), 153.48 (C(2′)), 142.39, 128.85, 128.07, 127.32, 85.45 (C(1′′)), 80.60 (C(6a′)), 72.58 (C(2)), 53.95 (C(6′)), 51.92 (CH_3O), 50.82 (C(2′′)), 41.82 (C(3a′)), 33.25, 32.41, 32.27, 30.94, 27.62, 25.78, 25.33, 24.77. Anal. calcd. for $C_{23}H_{31}NO_5$: C 68.80, H 7.78, N 3.49; found: C 68.72, H 7.63, N 3.51.

rel-*(3*S*,3a*S*,6*S*,6a*S*)*-N-*Hydroxy-3-hydroxy-6a-methylpenta-hydrocyclopenta[*b*]pyrrol-2-on-6-yl acetic acid (1*R*,2*S*)-2-phenylcyclohexyl ester (**13b**)*

In a round bottom flask equipped with a magnetic stirring bar and a stopper was dissolved 433 mg (1.07mmol) of **11b** in 20 mL of CH_3CO_2H–H_2O (1:1) (distilled and deionized) and was stirred for 16 h. The solution was diluted with 30 mL of H_2O and washed twice with 50 mL of CH_2Cl_2. The combined organic phase was concentrated in vacuo and kept at 0.2 mmHg (1 mmHg = 133.322 Pa) and rt for 24 h. The residue was recrystallized in CH_3CN and H_2O to afford 345 mg (82%) of **13b** as white crystals. Data for **13b**: mp 131 to 132°C. TLC: R_f 0.45 (CH_2Cl_2–CH_3OH, 9:1). MS (FAB) *m*/*z*: 388.2 (M^++1, 100), 230.1 (37), 159.1 (30), 118.9 (23). IR (KBr) υ (cm^{-1}): 3403 (br), 2935 (s) 2860 (s), 1740 (s), 1677 (s), 1446, 1385, 1180 (s), 1011, 703. ^{1}H NMR (500 MHz, $CDCl_3$) δ: 9.6 (broad s, 1 H, OH), 7.26–7.14 (m, 5 H), 5.02 (dt, *J* = 4.3, 10.6, 1 H, H(C(1′′)), 4.31 (d, *J* = 9.3, 1 H, HC(3′)), 2.67–2.62 (m, 1 H, HC(2′′)), 2.55–2.49 (m, 2 H, HC(2), HC(3a)), 2.19 (dd, *J* = 10.6, 15, 1 H, HC(2)), 2.10–2.07 (m, 1 H, HC(6′)), 1.97–1.76 (m, 5 H), 1.59–1.30 (m, 5 H), 1.30 (s, 3 H, H_3C(7′)), 1.17–1.12 (m, 1 H, HC(5′)), 0.87–0.80 (m, 1 H, HC(5′)). ^{13}C NMR (126 MHz, $CDCl_3$) δ: 173.00 (C(1), 169.46 (C(2′)), 143.16, 128.30, 127.63, 126.42, 76.11 (C(1′′)), 71.54 (C(6a′)), 66.62 (C(3′)), 49.8 (C(2′′)), 47.24 (C(6′)), 46.14 (C(3a′)), 34.00 (C(2)), 33.94 (C(3′′)), 32.30 (C(6′′)), 29.78 (C(5′)), 25.76 (C(4′′)), 24.75 (C(5′′)), 21.31 (C(4′)), 20.93 (C(5′). Anal. calcd. for $C_{22}H_{29}NO_5$: C 68.20, H 7.54, N 3.61; found: C 68.07, H 7.49, N 3.67.

rel-*{[(3a*S*,6*S*,6a*R*)-2-Butyloxy-6a-methyl]-3,3a,4,5,6-penta-hydrocyclopenta[*d*]pyrrol-6-yl*-N-*oxide}-(2*S*)-hydroxyacetic acid methyl ester (**11a**)*

In a round bottom flask equipped with a magnetic stirring bar and a stopper was dissolved 325 mg (1.08 mmol) of **1a** in 7.5 mL of CH_3CO_2H. The solution was stirred for 2 h (solution turns light blue after ca. 20 min). The solvent was removed in vacuo and the light blue viscous oil was kept at 0.2 mmHg (1 mmHg = 133.322 Pa) and rt for 18 h. The residue was separated by chromatography on SiO_2 column (20 × 150 mm) with 5% (v/v) CH_3OH in CH_2Cl_2. The white solid obtained was recrystallized from dry CH_2Cl_2 and hexane under N_2 to afford 182 mg (56%) of **11a** as white crystals. Data for **11a**: mp 100 to 100.5°C. TLC R_f 0.40 (CH_2Cl_2–CH_3OH, 9:1). MS (FAB) *m*/*z*: 300.2 (M^++1, 100). IR (KBr) υ (cm^{-1}): 3600–3100 (br), 2960 (s), 1742(s), 1648 (s), 1412 (s), 1195 (s). ^{1}H NMR (500 MHz, $CDCl_3$) δ: 7.48 (d, *J* = 5.8, 1H, OH), 4.38 (t, *J* = 6.7, 1H, HC(1′′), 4.29 (dd, *J* = 5.8, 8.3, 1H, HC(2), 3.75 (s, 3H, CH_3O), 3.01 (dd, *J* = 10.4, 18.0, HC(3′)), 2.56–2.50 (m, 1H, HC(3a)), 2.35 (dd, *J* = 4.2, 18.0, HC(3′)), 2.30–2.24 (m, 1H, HC(6′)), 1.90–1.84 (m, 1H, HC(4′)), 1.80–1.71 (m, 3H), 1.65 (s, 3H, HC(7′)), 1.65–1.52 (m, 2H), 1.48–1.40 (m, 2H, HC(3′′)), 0.94 (t, *J* = 7.5, 3H, HC(4′′)). ^{13}C NMR (126 MHz, $CDCl_3$) δ: 173.41 (C(1)), 153.67 (C(2′)), 81.04 (C(6a)), 72.65 (C(2)), 71.90 (C(1′′)), 53.90 (C(6′)), 52.02 (CH_3O), 41.84 (C(3a′)), 32.44 (C(3′)), 31.63 (C(2′′)), 31.55 (C(4′)), 28.16 (C(5′)), 25.75 (C(7′)), 18.71 (C(3′′)), 13.64 (C(4′′). Anal. calcd. for $C_{15}H_{25}NO_5$: C 60.18, H 8.42, N 4.68; found: C 59.94, H 8.49, N 4.78.

rel-*(3*S*,3a*S*,6*S*,6a*S*)*-N-*Hydroxy-3-hydroxy-6a-methylpenta-cyclopenta[*b*]pyrrol-2-on-6-yl acetic acid butyl ester (**13a**)*

In a round bottom flask equipped with a magnetic stirring bar and a stopper was dissolved 695 mg (2.32 mmol) of **11a** in 20 mL of CH_3CO_2H–H_2O (1:1) (distilled and deionized) and was stirred for 18 h. The solution was diluted with 50 mL of H_2O and washed twice with 50 mL of CH_2Cl_2. The combined organic phase was concentrated in vacuo and kept at 0.2 mmHg (1 mmHg = 133.322 Pa) and rt for 48 h. The residue was recrystallized in CH_3CN to afford 360 mg (55%) of **7a** as white crystals. Data for **13a**: mp 145 to 146°C. TLC: R_f 0.28 (CH_2Cl_2–CH_3OH, 9:1). MS (FAB) *m*/*z*: 286.2 (M^++1, 69), 154.1 (100), 136.1 (71.45). IR (KBr) υ (cm^{-1}): 3428 (s, br), 3066 (s, br), 2935 (s) 2872 (s), 1735 (s), 1686 (s), 1636 (s), 1446, 1385, 1180 (s), 1027. ^{1}H NMR (500 MHz, $CDCl_3$) δ: 9.40 (br s, 1H), 4.41 (d, *J* = 9.5, 1H, HC(3′)), 4.08 (t, *J* = 6.7, 2H, HC(1′′)), 2.79 (dd, *J* = 4.1, 15.6, HC(2)), 2.65 (dt, *J* = 2.9, 10.2, 1H, HC(3a′)), 2.55 (dd, *J* = 10.2, 15.6, 1H, HC(2)), 2.20–2.00 (m, 2H, HC(4′), HC(6′)), 1.90–1.82 (m, 1H, HC(5′)), 1.65–1.51 (m, 3H, HC(4′), HC(2′′)), 1.45 (s, 3H, HC(7)), 1.42–1.25 (m, 3H, HC(3′′), HC(5′)), 0.92 (t, *J* = 7.3, 3H, HC(4′′)). ^{13}C NMR (126 MHz, $CDCl_3$) δ: 173.83 (C(1)), 169.62 (C(2′)), 71.62 (C(6a′)), 66.67 (C(3′)), 64.52 (C(1′′)), 47.22 (C(6′)), 46.25 (C(3a′)), 33.88 (C(2)), 30.58, 30.46, 21.48 (C(2′′)), 21.10 (C(7)), 19.09 (C(3′′)), 13.67 (C(4′′)). Anal. calcd. for $C_{14}H_{23}NO_5$: C 58.93, H 8.02, N 4.91; found: C 58.99, H 8.05, N 4.88.

rel-*(3*S*,3a*S*,6*S*,6a*S*)-[*N*-Hydroxy-3-hydroxy-6a-methylpenta-hydrocyclopenta[*b*]pyrrol-2-on-6-yl] acetic acid methyl ester (**13c**)*

In a round bottom flask equipped with a magnetic stirring bar and a rubber septum was placed 302 mg (105 mmol) of **13a**. The flask was evacuated and a freshly prepared solution of $NaOCH_3$ in 25 mL of CH_3OH (Na 497 mg, 22 mmol, 20 equiv) under N_2 was transferred by cannula. The solution was stirred for 16 h under N_2 and was transferred by cannula to a flask containing 6.0 g of dry acidic ion exchange (Bio-Rad, AG-50WX8). The resin was filtered and rinsed four times with 50 mL of CH_3OH. The combined organic phase was concentrated in vacuo and kept at 0.2 mmHg (1mmHg = 133.322 Pa) and room temperature overnight. The residue was recrystallized in CH_3CN to afford 160 mg (63%) of **7c** as white crystals. Data for **7c**: mp 190–192°C. TLC: R_f 0.32 (CH_2Cl_2–CH_3OH, 9:1). MS (FAB) *m*/*z*: 244.1 (M^++1), 155.1 (22) 135.0 (23), 119.0 (55). ^{1}H NMR (500 MHz, DMSO-d_6) δ: 9.50 (s, 1H), 5.63 (d, *J* = 5.6, 1H), 4.14 (dd, *J* = 5.6, 9.2, 1H, HC(3′)), 3.56 (s, 3H, CH_3O), 2.64 (dd, *J* = 3.7, 16.1, 1H, HC(2)), 2.48–2.40 (m, 1H, HC(3a′)), 2.31 (dd, *J* = 11.0, 16.1, 1H, HC(2)), 1.98–1.88 (m, 2H, HC(6′), HC(4′)), 1.69–1.65 (m, 1H, HC(5′)), 1.45–1.38 (m, 1H, HC(4′)), 1.24 (s, 3H, HC(7′)), 1.17–1.12 (m, 1H, HC(5′)). ^{13}C NMR

© 2001 NRC Canada

(126 MHz, DMSO-d_6) δ: 173.72 (C(1)), 169.76 (C(2′′)), 69.7 (C(6a′)), 66.16 (C(3′)), 51.76 (CH_3O), 47.14 (C(6′)), 46.17 (C(3a′)), 33.78 (C(2)), 30.33 (C(5′)), 21.59 (C(4′)), 20.98 (C(7′). IR (KBr) υ (cm^{-1}): 3433 (s, br), 3069 (s, br), 2935 (s) 2872 (s), 1742 (s), 1685 (s), 1632 (s), 1439, 1385, 1177 (s), 1025. Anal. calcd. for $C_{11}H_{17}NO_5$: C 54.31, H 7.04, N 5.76; found: C 54.43, H 7.01, N 5.75.

rel*[(3a*S*,6*S*,6a*S*)*-N*-Hydroxy-6a-methylpentacyclopenta[*b*]-pyrrol-2-on-6-yl](2*R*)-2-hydroxy acetic acid methyl ester (**12**)*

In a round bottom flask equipped with a magnetic stirring bar and a stopper was dissolved 320 mg (0.8 mmol) of **1b** in 40 mL of CH_3CO_2H–H_2O (1:1) (distilled and deionized) and was stirred for 48 h. The solvents are removed in vacuo and the residue kept at 0.2 mmHg (1 mmHg = 133.322 Pa) and rt for 48 h. The residue was separated by chromatography on a SiO_2 (previously washed with HCl, HNO_3, and NH_4OH) column (20 × 150 mm) with toluene–acetone–CH_3CO_2H (60:38.5:1.5) to afford 186 mg (48%) of **13b** and 58 mg (23%) of **12**. Data for **12**: TLC: R_f 0.44 (CH_2Cl_2–CH_3OH, 9:1). MS (FAB) *m*/*z*: 244.1 (M^++1), 155.1 (34) 135.0 (29), 119.0 (65). HRMS calcd. for $C_{22}H_{30}NO_5$: 244.11849; found: 244.118860. ^{1}H NMR (500 MHz, $CDCl_3$) δ: 4.41 (d, *J* = 7.3, 1H, HC(2)), 3.77 (s, 3H, CH_3O), 2.65 (dd, *J* = 10.7, 17.2, 1H), 2.50–2.45 (m, 1H), 2.17–2.04 (m, 2H), 1.88–1.64 (m, 4H), 1.55–1.48 (m, 1H), 1.48 (s, 3H, HC(7′)). ^{13}C NMR (126 MHz, $CDCl_3$) δ: 173.13 (C(1)), 169.35 (C(2′)), 72.02 (C(6a)), 71.18 (C(2)), 52.58, 52.00, 42.18, 34.16, 31.00, 27.87, 24.66. IR (KBr) υ (cm^{-1}): 3173 (s, br), 2952 (s) 2874 (s), 1742 (s), 1685 (s), 1199.

Conclusion

A number of new transformations of nitroso acetals have been developed. For the reduction of nitroso acetals derived from tandem cycloadditions of nitroalkenes, catalytic hydrogenation over Raney nickel remains the method of choice. Hydrogenation under homogeneous conditions was shown to be unsuitable for this transformation. Samarium iodide was able to effect a selective cleavage of the N—O bond of the isoxazolidine ring in a number of structurally diverse cycloadducts.

The acid-promoted ring opening of nitroso acetal **1** has revealed new and interesting aspects of the chemistry of these compounds. α-Alkoxy nitrones and hydroxamic acids could be selectively produced under different reaction conditions. A two-step protocol was developed for the cleavage of the alkoxy group of which may find use in the application of tandem cycloaddition technology in combinatorial chemistry. Further studies on the chemistry of nitroso acetals and the implementation of tandem cycloadditions on the solid phase are planned.

Acknowledgment

We wish to thank the National Institutes of Health (R01 GM-30938) for financial support. We thank Dr. Scott R. Wilson for assistance with the X-ray crystallographic analyses.

References

1. (*a*) S.E. Denmark and A. Thorarensen. Chem. Rev. **96**, 137 (1996); (*b*) S.E. Denmark, C.B. Senanayake, M.E. Schnute, Y.-C. Moon, G.-D. Ho, and D.S. Middleton. Proc. Int. Kyoto Conf. New Aspects Org. Chem. VCH Verlagsgesellschaft and Kodansha Ltd, Weinheim/Tokyo. 1992.
2. (*a*) S.E. Denmark, A. Thorarensen, and D.S. Middleton. J. Am. Chem. Soc. **118**, 8266 (1996); (*b*) S.E. Denmark and A. Thorarensen. J. Am. Chem. Soc. **119**, 125 (1997); (*c*) S.E. Denmark, A.R. Hurd, and H.J. Sacha. J. Org. Chem. **62**, 1668 (1997); (*d*) S.E. Denmark and E.A. Martinborough. J. Am. Chem. Soc. **121**, 3046 (1999); (*e*) S.E. Denmark and A.R. Hurd. J. Org. Chem. **65**, 2875 (2000); (*f*) S.E. Denmark and L.R. Marcin. J. Org. Chem. **62**, 1675 (1997).
3. S.E. Denmark and D.S. Middleton. J. Org. Chem. **63**, 1604 (1998).
4. (*a*) S.E. Denmark, A. Stolle, J.A. Dixon, and V. Guagnano. J. Am. Chem. Soc. **117**, 2100 (1995); (*b*) S.E. Denmark, V. Guagnano, J.A. Dixon, and A. Stolle. J. Org. Chem. **62**, 4610 (1997); (*c*) S.E. Denmark and J.A. Dixon. J. Org. Chem. **63**, 6167 (1998); (*d*) S.E. Denmark and J.A. Dixon. J. Org. Chem. **63**, 6178 (1998).
5. (*a*) V.F. Rudchenko. Chem. Rev. **93**, 725 (1993); (*b*) K.B.G. Torssell. *In* Nitrile oxides, nitrones and nitronates in organic synthesis. VCH, Weinheim. 1988. Chap. 4.
6. S.E. Denmark and A. Thorarensen. J. Org. Chem. **59**, 5672 (1994).
7. M.A. Brook and D. Seebach. Can. J. Chem. **65**, 836 (1987).
8. P.A. Wade, N.V. Amin, H.-K. Yen, D.T. Price, and G.F. Huhn. J. Org. Chem. **49**, 4595 (1984).
9. G.W. Kabalka and T.L. Gilchrist. *In* Comprehensive organic synthesis, combining C-C π-bonds. Vol. 5. *Edited by* L.A. Paquette. Pergamon Press, Oxford. 1991. pp. 363–402.
10. S.-I. Murahashi and Y. Kodera. Tetrahedron Lett. **26**, 4633 (1985).
11. S.-I. Murahashi, Y. Imada, Y. Taniguchi, and Y. Kodera. Tetrahedron Lett. **26**, 2973 (1988).
12. (*a*) S. Cicchi, A. Goti, A. Brandi, A. Guarna, and F. De Sarlo. Tetrahedron Lett. **31**, 3351 (1990); (*b*) M. Nitta and T. Kobayashi. J. Chem. Soc. Chem. Commun. 877 (1982); (*c*) P.G. Baraldi, A. Barco, S. Benetti, S. Manfredini, and D. Simoni. Synthesis, 276 (1987); (*d*) D. Zhang, A. Ghosh, C. Sülig, and M.J. Miller. Tetrahedron Lett. **37**, 3799 (1996).
13. Y. Becker, A. Eisenstadt, and Y. Shvo. Tetrahedron, **34**, 799 (1978).
14. (*a*) N.R. Natale. Tetrahedron Lett. **23**, 5009 (1982); (*b*) J.L. Chiara, C. Destabel, P. Gallego, and J. Marco-Contelles. J. Org. Chem. **61**, 359 (1996).
15. J. Knifton. J. Org. Chem. **40**, 519 (1975).
16. (*a*) J. Knifton. J. Org. Chem. **38**, 3296 (1973); (*b*) J. Knifton. J. Catal. **33**, 289 (1974).
17. (*a*) S.E. Denmark, Y.C. Moon, and C.B.W. Senanayake. J. Am. Chem. Soc. **112**, 311 (1990), and refs. cited therein; (*b*) S.E. Denmark, C.B.W. Senanayake, and G.D. Ho. Tetrahedron, **46**, 4857 (1990); (*c*) S.E. Denmark and M.E. Schnute. J. Org. Chem. **56**, 6738 (1991); (*d*) S.E. Denmark and C.B.W. Senanayake. J. Org. Chem. **58**, 1853 (1993); (*e*) S.E. Denmark, M.E. Schnute, and C.B.W. Senanayake. J. Org. Chem. **58**, 1859 (1993).
18. (*a*) J.B. Lambert. Top. Stereochem. **6**, 19 (1971); (*b*) M. Raban and D. Kost. *In* Acyclic organonitrogen stereodynamics. *Edited by* J.B. Lambert and Y. Takekuchi. VCH, Weinheim. 1992. Chap. 2.

© 2001 NRC Canada

19. S.E. Denmark and A.R. Hurd. J. Org. Chem. **63**, 3045 (1998).
20. J.A. Warshaw, D.E. Gallis, B.J. Acken, O.J. Gonzalez, and D.R. Crist. J. Org. Chem. **54**, 1736 (1989); (*b*) B.J. Acken, J.A. Warshaw, D.E. Gallis, and D.R. Crist. J. Org. Chem. **54**, 1743 (1989).
21. (*a*) V.C. Bass and J.H. Yoe. Talanta, **13**, 735 (1966); (*b*) T.J. King and P.G. Harrison. J. Chem. Soc. Chem. Commun. 815 (1972).

© 2001 NRC Canada

The versatile reactivity of 2-aryl-4,6-dinitrobenzotriazole 1-oxides in Diels–Alder type condensations and in σ-complexation — A relationship between superelectrophilicity and pericyclic reactivity

Dominique Vichard, Taoufik Boubaker, François Terrier, Marie-José Pouet, Julian M. Dust, and Erwin Buncel

Abstract: A two-pronged study of a series of 2-aryl-4,6-dinitrobenzotriazole 1-oxide substrates (**2a**–**c**) is reported: Diels–Alder type pericyclic reactivity and covalent hydration to yield Meisenheimer type hydroxy anionic σ-adducts. The most activated benzotriazole 1-oxide **2a** is found to exhibit both dienophilic and heterodienic behaviour on treatment with cyclopentadiene, providing a highly functionalized stereoselective diadduct (**7**). This diadduct is shown to be the result of two consecutive inverse demand Diels–Alder condensations proceeding through the *endo* mode with a *trans* addition of two cyclopentadiene molecules. Kinetic and thermodynamic measurements of the ease of covalent hydration of **2a**–**c** to give σ-adducts **4a**–**c** in aqueous solution indicate that the electrophilic reactivity of the 4,6-dinitrobenzotriazole 1-oxide structure is much closer to that of the superelectrophilic 4,6-dinitrobenzofuroxan (DNBF, **1a**) than that of the standard Meisenheimer electrophile 1,3,5-trinitrobenzene (TNB). The pK_a values range from 6.70 for the 2-(2′,4′,6′-trinitrophenyl)-4,6-dinitrobenzotriazole 1-oxide (Pi-DNBT, **2a**) to 10.73 for the 2-phenyl-4,6-dinitrobenzotriazole 1-oxide (Ph-DNBT, **2c**). The observation that the most activated benzotriazole 1-oxide structure **2a** which resembles 4,6-dinitrobenzofuroxan (DNBF) in superelectrophilic behaviour, is the only one that undergoes Diels–Alder reactions, points to a direct relationship between superelectrophilic and pericyclic reactivity.

Key words: σ-complexes, arylnitrobenzotriazole 1-oxides, super-electrophiles, Diels–Alder condensations, pericyclic reactions.

Résumé : On a réalisé une étude d'une série de substrats 1-oxyde de 2-aryl-4,6-dinitrobenzotriazole (**2a**–**c**) et elle a été menée sur deux fronts: la réactivité péricyclique de type Diels–Alder et l'hydratation covalente conduisant à des adduits σ, des hydroxy anioniques de type Meisenheimer. On a observé que le traitement de l'oxyde de benzotriazole le plus activé (**2a**) avec du cyclopentadiène donne lieu à des comportements à la fois diénophile et hétérodiénique et qu'il permet d'obtenir un diadduit stéréosélectif hautement fonctionnalisé (**7**). On a démontré que ce diadduit résulte de deux condensations consécutives de Diels–Alder ayant des demandes inverses et qu'elles se produisent par le mode *endo* avec une addition *trans* de deux molécules de cyclopentadiène. Des mesures cinétiques et thermodynamiques de la facilité d'hydratation covalente des composés **2a**–**c** qui conduit à la formation des adduits σ correspondants (**4a**–**c**) indiquent que, en solution aqueuse, la réactivité électrophile de la structure 1-oxyde de 4,6-dinitrobenzotriazole est beaucoup plus proche de celle du 4,6-dinitrobenzofuroxane (DNBF, **1a**) superélectrophile que de celle du 1,3,5-trinitrobenzène (TNB), l'électrophile de Meisenheimer de référence. Les valeurs de pK_a vont de 6,70 pour le 1-oxyde de 2-(2′4′6′-trinitrophényl)-4,6-dinitribenzotriazole (Pi-DNBT, **2a**) à 10,73 pour le 1-oxyde de 2-phényl-4,6-dinitrobenzotriazole (P-DNBT, **2c**). On a observé que la seule structure à subir des réactions de Diels–Alder est la structure la structure la plus activée du 1-oxyde de benzotriazole (**2a**), qui ressemble au 4,6-dinitrobenzofuroxnae

Received August 29, 2000. Published on the NRC Research Press Web site at http://canjchem.nrc.ca on October 31, 2001.

Dedicated to Professor Victor Snieckus in recognition of his contributions to Canadian chemistry.

D. Vichard, F. Terrier, and M.-J. Pouet. Institute Lavoiser-Franklin, UPRESA 8086, Université de Versailles, 45 Avenue des Etats-Unis, 78035 Versailles CEDEX, France.
T. Boubaker. Unité de Recherche de Physico-Chimie Moléculaire, Faculté des Sciences de Monastir, Avenue de l'Environnement 5000, Monatir, Tunisie.
J.M. Dust. Departments of Chemistry and Environmental Science, Sir Wilfred Grenfell College, Corner Brook, NF, A2H 6P9, Canada.
E. Buncel.[1] Department of Chemistry, Queen's University, Kingston, ON K7L 3N6, Canada.

[1]Corresponding authors (EB) (telephone: (613) 533-2653; fax: (613) 533-6669; e-mail: buncele@chem.queensu.ca); (JD) (telephone: (709) 637-6330; fax: (709) 639-8125; e-mail: jdust@swgc.mum.ca; (FT) (telephone: 33-1-39-25-44-50; fax: 33-1-39-25-44-52; e-mail: terrier@chimie.uvsq.fr.).

 DOI: 10.1139/cjc-79-11-1617 © 2001 NRC Canada

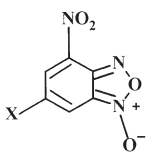
(DNBF) en comportement supe-électrophile; cette observation suggère qu'il existe une relation directe entre un comportement superélectrophile et la réactivité péricyclique.

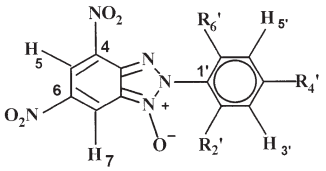
Mots clés : complexes-σ, 1-oxydes d'arylnitrobenzotriazole, superélectrophiles, condensations de Diels–Alder, réactions péricycliques.

[Traduit par la Rédaction]

Introduction

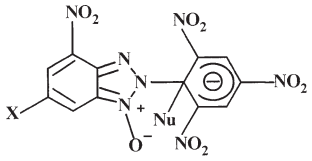
Following the discovery of the extremely strong electrophilic character of the carbocyclic ring of 4,6-dinitrobenzofuroxan (DNBF, **1a**) (1–9), we have been engaged in an effort to design analogues of **1a** in which the oxygen atom in the furoxan ring is replaced by other electron-withdrawing moieties (10, 11). We thus found that 2-(2′,4′,6′-trinitrophenyl)-4,6-dinitrobenzotriazole 1-oxide (Pi-DNBT, **2a**) is also a powerful electrophilic heterocycle that undergoes facile σ-complexation at C-7 of the carbocyclic ring with a number of nucleophiles, including weak neutral nucleophiles like water, methanol, or ethanethiol (10*a*). A contrasting feature of **2a** is that the C-1′ carbon of the picryl ring is also susceptible to reaction with nucleophiles, giving rise to an S_NAr displacement reaction via the metastable σ-adduct **3a** (10, 11). The ambident (C-7 vs. C-1′) electrophilicity of **2a** (and other members of benzotriazole 1-oxides series, e.g., **2b**) has given new impetus to the study of reactivity–selectivity relationships in reactions of this and related ambident electrophiles with ambident nucleophiles (9*b*, 11).





1a X = NO_2 (DNBF)
1b X = H (NBF)

2a R_2' = R_4' = R_6' = NO_2 (Pi-DNBT)
2b R_2' = R_6' = H ; R_4' = NO_2 (NP-DNBT)
2c R_2' = R_4' = R_6' = H (Ph-DNBT)

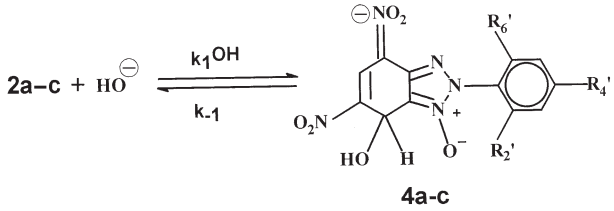


3a

In probing the manifold reactivity of electron-deficient heteroaromatics like **1a**, we have discovered that nitrobenzofuroxans are also remarkably versatile reagents in pericyclic reactions such as the Diels–Alder, being capable of acting as dienophiles, carbodienes, or heterodienes depending upon the experimental conditions and reaction partners employed (12). To test whether this diverse pericyclic reactivity is a reflection of the low aromaticity of the carbocyclic ring of such compounds, studies have been undertaken of the 2-aryl-4,6-dinitrobenzotriazole 1-oxides (**2a**–**c**) in which the electron-withdrawing power of the 2-aryl moiety is systematically decreased through the sequential removal of nitro groups. In this paper, we report that **2a** exhibits ambident Diels–Alder reactivity towards cyclopentadiene (Cp). This discovery opens the way to the synthesis of highly functionalized benzotriazole derivatives with defined stereochemistry. Importantly, the results point to a direct relationship between superelectrophilic and pericyclic behaviour.

So far no firm assessment of the electrophilic reactivity of **2a** or related benziotriazole systems, in terms of meaningful thermodynamic and kinetic data, has been reported. Therefore, we have carried out a kinetic and thermodynamic study of the reactions of hydroxide ion in water with the various substrates **2a**–**c** yielding the hydroxide adducts **4a**–**c** according to eq. [1]. Our results reveal that the reactivity of compounds **2a**–**c** is greater than that of the conventional Meisenheimer electrophile 1,3,5-trinitrobenzene (TNB) (9), but only that of **2a** is found to approach that of **1a**, providing further evidence of the superelectrophilic behaviour of structure **2**.

[1]

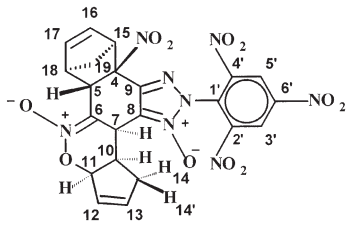


4a-c

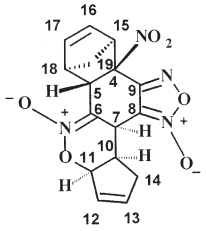
Results

Reaction of Pi-DNBT (2a) with cyclopentadiene

Treatment of **2a** with excess cyclopentadiene in a CH_2Cl_2–THF mixture at room temperature results in nearly quantitative formation of a product (5 h), which was readily isolated as a pale yellow solid after addition of pentane. ^1H and ^{13}C NMR spectra of this solid (CD_3CN solvent) consisted of only one set of signals, indicating that the reaction has proceeded with a high stereoselectivity, affording only the diastereomer **7** (only one enantiomer is shown).



7



8

The proposed stereochemistry for **7** has been derived from a detailed NMR analysis which has included COSY, HETCOR, as well as *J*-modulation and NOE experiments. In particular, 2D-NOE experiments have revealed that the H-7, H-10, H-11, and

© 2001 NRC Canada

H-14 protons (but not the H-14′ proton) are located on the same side of the dihydrooxazine *N*-oxide and cyclopentene rings of **7**. The values of the related ^3J coupling constants ($^3J_{H7\text{-}H10}$ = 5.6, $^3J_{H10\text{-}H11}$ = 8.9 Hz) agree with the *cis* arrangement of the H-7, H-10, and H-11 protons (12*a*). On the other hand, the observation of a W-type ^4J coupling constant between the H-5 and H-7 protons ($^4J_{H5\text{-}H7}$ = 2.8 Hz) implies a *trans* addition of the two Cp molecules (13, 14). In accord with the strong electron-withdrawing effect of the O-N^+-O^- fragment of the dihydrooxazine ring, both the sp^3 carbon C-11 and the related H-11 proton of **7** are strongly deshielded (δC_{11} = 93.02, δH_{11} = 5.77 ppm in CD_3CN) with the C-11 resonance comparing well with that of the nitro-substituted quaternary carbon C-4 (δC_4 = 93.17 ppm) (15). The close analogy between the resonances of the protons and carbons of the three carbocyclic rings of **7** with those of the related DNBF adduct **8** further supports our stereochemical assignment (Tables 1 and 2) (12*c*). Note that the stereochemistry illustrated in structure **8** was determined independently by X-ray diffraction studies. That the benzotriazole **2a** undergoes addition of 2 mol of cyclopentadiene to give the diadduct **7** was also confirmed by mass spectrometry (HRMS). Attempts to get precise information on the reaction sequence leading to **7** by carrying out similar experiments at 0°C have been unsuccessful because of solubility problems.

Reactions of the 2-aryl-4,6-dinitrobenzotriazole 1-oxide series (2a–c) with OH^-

All rate and equilibrium measurements pertaining to eq. [1] were made at 25°C and constant ionic strength of 0.2 mol dm^{-3} maintained with KCl. Measurements of absorbance at λ max of the σ-adducts **4a–c** (λ max ca. 470 nm) were first made at equilibrium as a function of pH. These describe clear-cut acid–base behaviour, as evidenced by the observation of excellent straight lines with unit slopes fitting eq. [2]. Here, pK_a refers to the reaction of **2a–c** with water to produce **4a–c** and a proton.

$$[2] \qquad \log [\mathbf{4a\text{–}c}]/[\mathbf{2a\text{–}c}] = pH - pK_a$$

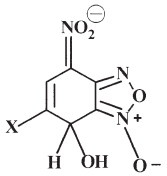
Plots are shown in Fig. 1 and yield the following pK_a values: **2a** 6.70 ± 0.05, **2b** 9.0 ± 0.05, **2c** 10.73 ± 0.05. The pH ranges required for these pK_a determinations were conveniently covered by using amine buffers made up from *N*-substituted aminoethane or propane sulfonic acids, namely TES, HEPES, TAPS, and CAPS which are known to be rather unreactive in nucleophilic processes (16).

Using a stopped-flow apparatus, the interconversions of **2a–c** and **4a–c** were then kinetically investigated under pseudo-first-order conditions. Solutions of the substrates (ca. 3×10^{-5} mol dm^{-3}) in water containing HCl (1×10^{-3} mol dm^{-3}) were mixed with the appropriate KOH solutions (2×10^{-3} – 6.1×10^{-2} mol dm^{-3}). In agreement with the direct equilibrium approach described by eq. [1], only one relaxation time corresponding to the complete formation of the adducts **4a–c** was observed in all cases. For each of the reactions studied, plots of k_{obsd} vs. the KOH concentration afforded excellent straight lines with zero intercepts. This shows that the k_{-1} pathway makes a negligible contribution so that the k_{obsd} values are given by the simple eq. [3] (Fig. 2). From the slopes of these lines, values of k_1^{OH} were readily determined. Then the k_{-1} values could be calculated by means of eq. [4].

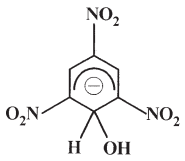
$$[3] \qquad k_{obsd} = k_1^{OH}[OH^-]$$

$$[4] \qquad k_{-1} = k_1^{OH} K_e [K_a]^{-1}$$

Values of the various rate and equilibrium parameters for the formation and decomposition of **4a–c** together with the related parameters for the DNBF adduct **5a**, the 4-nitrobenzofuroxan (NBF, **1b**) adduct **5b**, and the TNB adduct **6** are given in Table 3 for purposes of comparison.



5a X = NO_2
5b X = H



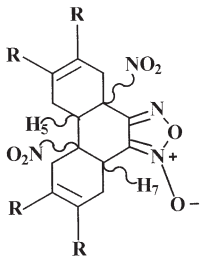
6

Discussion

The Diels–Alder reactivity of Pi-DNBT (2a)

Two main factors have long been suggested as contributing to the exceptional ease of formation and stability of adducts such as **5a** formed by reaction with the superelectrophile **1a**. The first is the combination of the strong electron-withdrawing effects of the nitro groups and the annelated furoxan ring (1–5). The result is not only a high electron deficiency at C-7 of the carbocyclic ring, and hence a high susceptibility of this ring position to nucleophilic attack, but also a high stability for the resultant σ-adducts, as a function of the high electron-delocalizing capability of the ring structure. The second factor is the relatively low aromaticity of the benzofuroxan system which is expected to favour covalent addition compared to most common aromatic and heteroaromatic systems, e.g., TNB or 3,5-dinitropyridine (9*a*, 17).

Evidence that the aromaticity factor is actually very important in determining the electrophilic reactivity of the nitrobenzofuroxan system has recently come from the discovery that DNBF is a remarkably versatile reagent in Diels–Alder reactions. We have shown that it may act as dienophile or heterodiene, depending upon the reaction partners employed and the experimental conditions (12, 18). In this regard, an early report by Kresze and Bathelt (19) that DNBF reacts to some extent with 2,3-dimethylbutadiene and 1,3-butadiene to afford the adducts **9** has remained essentially unnoticed in the literature.



9 R = H, CH_3

© 2001 NRC Canada

Table 1. ^{13}C NMR data for the benzotriazole 1-oxide **2a** and the diadducts **7** and **8**.[a]

Compound	C_4	C_5	C_6	C_7	C_8	C_9	C_{10}	C_{11}	C_{12}	C_{13}
2a	137.5	124.2	144.5	119.9	125.6[b]	136.3[b]				
7[c]	93.17	49.04	123.11	33.53	124.45	145.71	38.45	93.02	128.31	140.43
8[d]	91.27	47.54	121.82	32.17	111.35	152.69	36.61	91.67	127.52	139.36
Compound	C_{14}	C_{15}	C_{16}	C_{17}	C_{18}	C_{19}	$C_{1'}$	$C_{2',6'}$	$C_{3',5'}$	$C_{4'}$
2a							122.2[b]	145.5	126.4	150.0
7[c]	35.34	55.17	135.40	142.33	47.45	47.08	128.3	147.2 (broad)		150.4
8[d]	34.60	54.56	134.27	141.90	46.11	46.24			124.44	

[a]δ in ppm relative to TMS in Me_2SO-d_6, unless otherwise specified; numbering is given in the structures **2a**, **7**, and **8** in the text.
[b]These values are based on the analysis of lone distance C—H coupling constants, allowing a complete and more reliable assignment of previously reported data (11*c*).
[c]In acetonitrile-d_3.
[d]Data taken from ref. 12*c*.

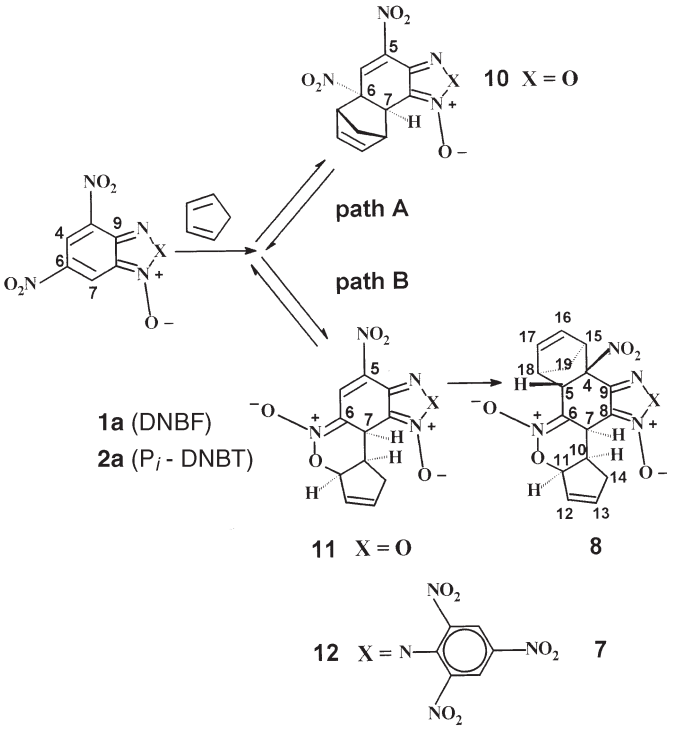
Most importantly, strong pericyclic reactivity could be observed with other highly activated nitrobenzofuroxans, e.g., the 4-nitro-6-trifluoromethylsulfonyl and 4-aza-6-nitrobenzo-furoxans for which pK_a values of 2.95 and 3.8 have been measured, respectively, for water addition in aqueous solution, but not with less activated compounds such as 4-nitrobenzofuroxan itself (pK_a = 10.32) (18, 20, 21)[2]. It thus appears that there is a clear correlation between the superelectrophilic and pericyclic behaviours in this series of 10 π electron heteroaromatic substrates.

Since pericyclic reactions are governed by HOMO–LUMO interactions (22) and similarly electrophile–nucleophile reactions are governed by the LUMO energy of the electrophilic partner and the HOMO energy of the nucleophilic partner (23), this observed correspondence between pericyclic and superelectrophilic reactivity follows the parallelism in the fundamental nature of both types of processes. We emphasize the salient point that *it is only the most superelectrophilic member of the series of benzotriazole 1-oxides,* ***2a****, that also displays Diels–Alder reactivity.*

In this context, our finding that **2a** reacts with cyclopentadiene (Cp) at room temperature to afford the highly functionalized stereoselective diadduct **7** supports the idea that the 4,6-dinitro-substituted carbocyclic ring of the most activated benzotriazole has a relatively low aromaticity. Interestingly, neither the *N-para*-nitrophenyl nor the *N*-phenyl analogues **2b** and **2c** which have pK_a values comparable to that of NBF (**1b**) show similar pericyclic reactivity upon treatment with cyclopentadiene, thus adding to the evidence of a close relationship between the degree of electron deficiency of the carbocyclic ring and the Diels–Alder reactivity of this ring.

In the case of the reaction of **1a** with Cp, it has been clearly demonstrated that the formation of the diadduct **8** proceeds according to Scheme 1 (12*c*). Following a diastereoselective and regioselective normal electron-demand condensation leading to the formation of the monoadduct **10** under kinetic control (path A), the diadduct **8** is formed as the result of two consecutive inverse and normal electron demand processes which take place with a high stereoselectivity at the C-6—C-7 and C-4—C-5 double bonds of the carbocyclic ring. This reaction sequence is consistent with theoretical calculations which point to the activated 6,7-double bond of DNBF as being the preferred site for

Scheme 1.



normal as well as inverse Diels–Alder reactivity (24). Then, a second cycloaddition can take place at the remaining activated C-4—C-5 double bond of the resulting monoadduct **11**, akin to the reactivity of nitroolefins (25, 26). Although we were not able to carry out a similarly detailed study of the behaviour of **2a** at low temperatures (vide supra), it is reasonable to assume by analogy that the formation of the diadduct **7** is the result of the two-step sequence of path B in Scheme 1. That the two condensations leading to **12** and then to **7** proceed through *endo* processes with a *trans* addition of the two cyclopentadiene molecules is reminiscent of the situation which prevails in the formation of all DNBF diadducts (6*b*, 6*c*, 18, 20).

The electrophilic character of the 2a–c series

So far, the pK_a values of DNBF (3.73) (1*a*) and TNB (13.43) (26) represent the extremes in the scale of measuring

[2] F. Terrier, G. Moutiers, M. Mokhtari, and J.C. Hallé. Unpublished results.

© 2001 NRC Canada

Table 2. ^{1}H NMR data for the diadducts **7** and **8**.[a]

Diadduct	Solvent	H-5	H-7	H-10	H-11	H-12	H-13	H-14	H-15	H-16	H-17	H-18	H-19	Hmm′	Coupling constants
7	$CDCl_3$	3.49	4.06	3.98	5.77	5.95	6.21	2.41	4.06	6.38	6.69	3.49	1.80		$^2J_{14a/14b}$ = 18.0, $^2J_{19a/19b}$ = 10.2
								2.16					1.18		$^3J_{11/10}$ = 8.9, $^3J_{12/13}$ = 5.8
															$^3J_{14a/10}$ = 8.8, $^3J_{14b/10}$ = $^3J_{16/15}$ = 2.8
															$^3J_{17/16}$ = 5.7
8[b]	CD_3CN	3.41	4.32	4.07	5.78	5.87	6.21	2.36	3.84	6.32	6.68	3.37	1.73	9.23	$^2J_{14a/14v}$ = 18.2, $^2J_{19a/19b}$ = 10.3
								2.12					1.42		$^3J_{11/10}$ = 8.9, $^3J_{7/10}$ = 5.4
															$^3J_{12/13}$ = 5.7, $^3J_{14a/10}$ = 8.9
															$^3J_{17/16}$ = 5.7, $^3J_{14b/10}$ = 3.2
															$^3J_{5/7}$ = $^3J_{5/19}$ = $^3J_{16/15}$ = 2.8

[a]δ in ppm relative to TMS, *J* in Hertz (Hz); numbering is given in structures **7** and **8** in the text.
[b]Data taken from ref. 12*c*.

the electron deficiency of aromatic and heteroaromatic substrates as derived from the susceptibility of these compounds to undergo covalent hydration in aqueous solution (9). In this regard, Table 3 shows that the pK_a values for the three benzotriazole 1-oxides **2a–c** fall in the midrange between those of DNBF and TNB with the *N*-phenyl-substituted derivative **2c** being the weakest electrophile of the family, as expected, with a pK_a value (10.73) close to that of 4-nitrobenzofuroxan (10.32). Introduction of nitro groups in the phenyl ring of **2c** has a major effect on the ease of σ-complexation of the 4,6-dinitro-substituted carbocyclic ring, as evidenced by the measurement of pK_a values of 9.0 and 6.70 for formation of the hydroxy adducts **4b** and **4a** derived from the *N*-(4′-nitrophenyl) and *N*-(2′,4′,6′-trinitrophenyl) compounds **2b** and **2a**, respectively. This corresponds to a major shift in electrophilic character from that of the reference electrophile TNB, approaching in the case of **2a** the recognized superelectrophilic character of DNBF (1, 5–9). Interestingly, an X-ray analysis of **2a** has revealed that the picryl ring and the benzotriazole ring system are in an almost orthogonal orientation, due to a strong steric compression of the adjacent ortho–nitro and *N*-oxide functions (10*a*). This type of steric compression may be reasonably expected to also prevail in the corresponding adduct **4a**. Based on this, the strong activating effect exerted by the picryl ring on the susceptibility of the 4,6-dinitro-substituted carbocyclic ring of **2a** to covalent hydration must be the result of inductive and (or) field effects rather than conjugation effects.

Using again the data for the DNBF and TNB as the references, Table 3 also reveals that the k_1^{OH} rate constants for the hydroxide ion attack on our three benzotriazole 1-oxides (**2a–c**) to generate the adducts **4a–c** (eq. [1]), are intermediate between the two extremes, with relatively minor variations on going from **2c** to **2a**. In fact, a most noteworthy finding is that the k_{-1} values that measure the tendency of the three adducts **4a–c** to undergo spontaneous decomposition are all much lower than the value measured for the TNB adduct **6**. On the other hand, it is also of much interest that the changes in k_{-1} are essentially responsible for changes in the pK_a values for **2a–c**. This is clearly consistent with the idea that the Marcus intrinsic barrier for the σ-complexation process increases on going from **2c** to **2a**. This effect of nitro substitution on the intrinsic barrier may be understood as the result of charge delocalization being extensive in the resulting adducts **4a–c**, but only slightly developed at the transition state (27). In the case of **4c**, the k_{-1} value is about 30-fold greater than for the mononitrobenzofuroxan adduct **5b**, suggesting that some electron donation from the monosubstituted phenyl ring to the heterocyclic framework of the benzotriazole may occur in this instance.

Conclusions

The present work has shown definitively that the 4,6-dinitrobenzotriazole 1-oxide structure **2**, when appropriately substituted as in **2a**, can exhibit overall ambident pericyclic reactivity, i.e., normal and inverse electron demand cycloadditions take place with high stereoselectivity. This behaviour, which was found previously for **1a**, may extend to a wide range of low aromaticity heteroaromatics and investigation of the generality of such reaction is a thrust of inves-

© 2001 NRC Canada

Fig. 1. Variation of the ratio of ionized to non-ionized benzotriazole 1-oxides **2a**–**c** as a function of pH in aqueous solution. T = 25°C, I = 0.2 mol dm^{-3} KCl.

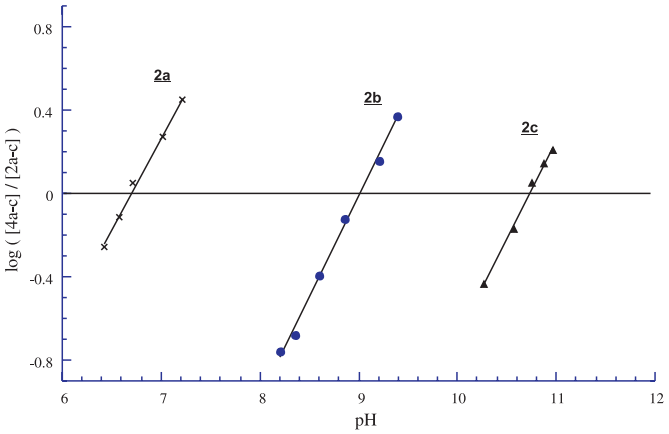


Fig. 2. Effect of the hydroxide ion concentration on the σ-complexation of **2a**–**c** in aqueous solution. T = 25°C, I = 0.2 mol dm^{-3} KCl.

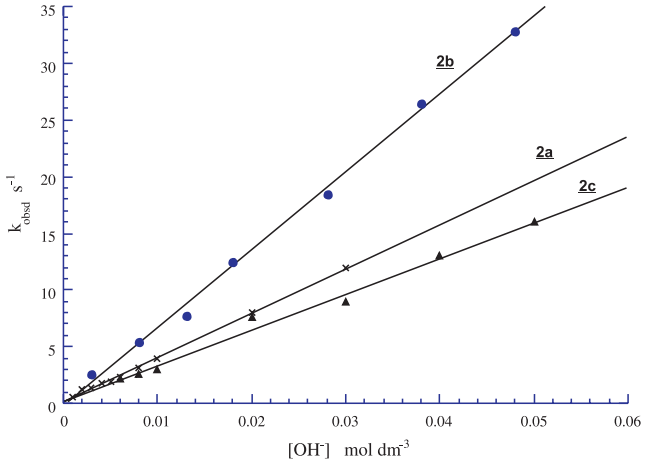


Table 3. Kinetic and thermodynamic parameters for the formation and decomposition of hydroxy σ-adducts ion aqueous solution.[a]

Adduct	pK_a	k_1^{OH} (dm^3 mol^{-1} s^{-1})	k_{-1} (s^{-1})
5a[b]	3.75	3.35 × 10^4	2.6 × 10^{-6}
4a	6.70	392	1.96 × 10^{-5}
4b	9.00	680	3.54 × 10^{-3}
4c	10.73	317	0.19
5b[c]	10.32	25	6 × 10^{-3}
6[d]	13.43	37.5	9.8

[a] T = 298 K; I = 0.2 mol dm^{-3} KCl.
[b] Reference 1*a*.
[c] Reference 1*b*.
[d] Reference 25, I = 0.1 mol dm^{-3} NaCl.

tigations in our laboratories. It is also important to note that the relative ease of displacement of the picryl moiety from adducts such as **7** by nucleophiles would afford a facile route to the synthesis of functionalized triazole deriviatives of defined stereochemistry with potential pharmacological activity.

The kinetic and equilibrium data reported here show that the electrophilic character of the 4,6-dinitrobenzotriazole 1-oxide strudcture is closer to that of the nitrobenzofuroxans (i.e., **1a**, **1b**) than that of the standard aromatic electrophile TNB. This result is believed to be largely the reflection of a rleatively low aromaticity of the carbocyclic ring. Overall, the finding of a dual electrophilic and pericyclic behaviour for **2a** adds a new facet to the extremely rich chemistry of the benzotriazole 1-oxide structure (32, 33).

Experimental

Materials

The 4,6-dinitrobenzotriazole 1-oxides **2a** and **2b** were available from previous studies (11); the preparation of **2c** is described below. Reagent grade TES (2-*N*-[tris(hydromethyl) methyl]aminoethane sulfonic acid), HEPES (*N*-2-hydroxylethylpiperazine-*N*′-2-ethanesulfonic acid, (3-*N*-[tris(hydroxylmethyl)methyl]aminopropanesulfonic acid), and CAPS (3-[cyclohexylamino]propanesulfonic acid) were of the highest purity obtainable from commerical sources and used without further purification to prepare buffer solutions if the pH range required for the pK_a determinations of **2a**–**2c**. KOH solutions were prepared from Titrisol.

Synthesis of 2c

1-Chloro-2,4,6-trinitrobenzene (picryl chloride, 3.0 g, 0.012 mol) was dissolved in 95% ethanol (ca. 25 mL) in a 50 mL round-bottomed flask. Phenylhydrazine (2.8 g, 2.4 mL, 0.025 mol) was dripped into the stirring solution. The brick red picrylhydrazobenzene solidified in the flask, more ethanol was added (15 mL), and the suspension was stirred and warmed for 3 h. The final suspension was cooled to room temperature and the crude product collected by suction filtration, washed with dilute HCl (0.3 M), and then distilled water. The product was dried in a vacuum dry-box and recrystallized from 95% ethanol to give picrylhydrazobenzene (2.65 g, 69%), mp 179 to 180°C (lit. (29) 181°C). R_f (TLC, CH_2Cl_2) 0.26. Picrylhydrazobenzene (0.50 g, 1.6 mmol) was cyclized in glacial acetic acid to 2-phenyl-4,6-dinitrobenzotriazole 1-oxide (**2c**) according to the method of Joshi and Deorha (30). Yield (after recrystallization from CH_3CN): 0.25 g, 51% (metallic, golden plates), mp 248–254°C (lit. (31) 249 to 250°C). R_f (CH_2Cl_2) 0.36.

Synthesis of 7

2-(2′,4′,6′-Trinitrophenyl)-4,6-dinitrobenzotriazole 1-oxide (**2a**) (86 mg, 0.197 mmol) was dissolved in a CH_2Cl_2–THF mixture and an excess of freshly distilled cyclopentadiene (1 mL) was added. The solution was maintained under stirring at room temperature for 5 h, then concentrated under reduced pressure. After addition of an excess of pentane, a pale yellow solid was isolated and dried under pump vacuum. Compound **7** was obtained in 92% yield (103 mg) and gave satisfactory analytical data. ^{1}H NMR: 300 MHz, acetonitrile-d_3, see Table 2. ^{13}C NMR: (see Table 1). FAB$^+$-MS mass spectrum (obsd). *m*/*z*: 569.1017 (reference *m*-nitrobenzyl alcohol), $C_{22}H_{14}N_8O_{11}$ requires 569.0984.

© 2001 NRC Canada

Rate and pK_a measurements

Stopped-flow determinations were performed on an Applied Photophysics spectrophotometer, the cell compartment of which was maintained at 25° ± 0.2°C. Other kinetic and pK_a measurements were made using a Varian Cary 1E spectrophotometer. All kinetic runs were carried out in triplicate under pseudo-first-order conditions with a substrate concentration of 2 to 3 × 10^{-5} mol dm^{-3}. In the case of **2c**, the measurements have been made in 90% H_2O – 10% Me_2SO (v/v) to overcome solubility problems but this low Me_2SO content does not have any major influence on the discussion of the results (1*b*). All rate constants are accurate to ±3%.

Acknowledgements

We are grateful for the financial support of this research by CNRS (F.T.), the Natural Sciences and Engineering Research Council of Canada (NSERC) (E.B.), and the Principal's Research Fund of Sir Wilfred Grenfell College (J.M.D.).

References

1. (*a*) F. Terrier, F. Millot, and W.P. Norris. J. Am. Chem. Soc. **98**, 5883 (1976); (*b*) F. Terrier. Chem. Rev. **82**, 77 (1982); (*c*) F. Terrier, A.P. Chatrousse, Y. Soudais, and M. Hlaibi. J. Org. Chem. **49**, 4176 (1984).
2. (*a*) M.J. Strauss, R.A. Renfrow, and E. Buncel. J. Am. Chem. Soc. **105**, 1555 (1983); (*b*) E. Buncel, R.A. Renfrow, and M.J. Strauss. J. Org. Chem. **52**, 488 (1987).
3. (*a*) R.J. Spear, W.P. Norris, and R.W. Read. Tetrahedron. Lett. **24**, 1555 (1983); (*b*) W.P. Norris, R.J. Spear, and R.W. Read. Aust. J. Chem. **36**, 297 (1983).
4. (*a*) F. Terrier, E. Kizilian, J.C. Hallé, and E. Buncel. J. Am. Chem. Soc. **114**, 1740 (1992); (*b*) F. Terrier, M.J. Pouet, J.C. Hallé, S. Hunt, J.R. Jones, and E. Buncel. J. Chem. Soc. Perkin Trans. 2, 1665 (1993); (*c*) F. Terrier, R. Goumont, M.J. Pouet, and J.C. Hallé. J. Chem. Soc. Perkin Trans. 2, 1629 (1995); (*d*) F. Terrier, M.J. Pouet, J.C. Hallé, E. Kizilian, and E. Buncel. J. Phys. Org. Chem. **11**, 707 (1998).
5. (*a*) M.R. Crampton, L.C. Rabbitt, and F. Terrier. Can. J. Chem. **77**, 639 (1999); (*b*) M.R. Crampton and L.C. Rabbitt. J. Chem. Soc. Perkin Trans. 2, 1669 (1999).
6. J. Kind and H. Niclas. Synth. Commun. **23**, 1569 (1993).
7. M.J. Evgen'yev, S.Y. Garmonov, I.I. Evgen'yeva, and L.S. Gazizullina. J. Anal. Chem. **53**, 571 (1998).
8. (*a*) E. Buncel, R.A. Manderville, and J.M. Dust. J. Chem. Soc. Perkin Trans. 2, 1019 (1997); (*b*) R.A. Manderville and E. Buncel. J. Chem. Soc. Perkin Trans. 2, 1887 (1993).
9. (*a*) F. Terrier. Nucleophilic aromatic displacement. The influence of the nitro group. VCH, New York. 1991; (*b*) E. Buncel, J.M. Dust, and F. Terrier. Chem. Rev. **95**, 2261 (1995).
10. (*a*) R.A. Renfrow, M.J. Strauss, S. Cohen, and E. Buncel. Aust. J. Chem. **36**, 1843 (1983); (*b*) J.M. Dust and E. Buncel. Can. J. Chem. **69**, 978 (1991).
11. (*a*) E. Buncel and J.M. Dust. Can. J. Chem. **66**, 1712 (1988); (*b*) J.M. Dust and E. Buncel. Can. J. Chem. **72**, 218 (1994); (*c*) J.M. Dust and R. Manderville. Can. J. Chem. **76**, 662 (1998).
12. (*a*) J.C. Hallé, D. Vichard, M.J. Pouet, and F. Terrier. J. Org. Chem. **62**, 7178 (1997); (*b*) D. Vichard, J.C. Hallé, B. Huguet, M.J. Pouet, D. Riou, and F. Terrier. Chem. Commun. 791 (1998); (*c*) P. Sépulcri, J.C. Hallé, R. Goumont, D. Riou, and F. Terrier. J. Org. Chem. **64**, 9254 (1999).
13. H. Günther. NMR spectroscopie 3/E. George Thieme Verlag, Dusseldorf. 1992. Chap. 4.
14. (*a*) W. Danchura, T. Schaefer, J.B. Rowbothaus, and D.J. Wood. Can. J. Chem. **52**, 3986 (1994); (*b*) M.P. Simonnin, H.Q. Xie, F. Terrier, J. Lelièvre, and P.G. Farrell. J. Chem. Soc. Perkin Trans. 2, 1553 (1989).
15. A. Ejchardt. Org. Magn. Reson. **10**, 263 (1977).
16. (*a*) N.E. Good, G.D. Winget, W. Winter, T.N. Connolly, S. Izawa, and R.M.M. Singh. Biochemistry, **5**, 467 (1966); (*b*) C.A. Vega and J.C. Hallé. Bull. Soc. Chim. Fr. **I**, 124 (1979).
17. E. Buncel, M.R. Crampton, M.J. Strauss, and F. Terrier. Electron-deficient aromatic and heteroaromatic-base interactions. The chemistry of anionic σ-complexes. Elsevier, Amsterdam. 1984.
18. P. Sépulcri, R. Goumont, J.C. Hallé, J. Marrot, and F. Terrier. J. Chem. Soc. Perkin Trans. 2, 51 (2000).
19. G. Kresze and H. Bathelt. Tetrahedron, **29**, 1043 (1973).
20. F. Terrier, M. Sebban, R. Goumont, J.C. Hallé, G. Moutiers, I. Cangelosi, and E. Buncel. J. Org. Chem. **65**, 7391 (2000).
21. L.M. Yagupolskii, I.V. Gogoman, G.M. Shchupak, and V.N. Boiko. J. Org. Chem. USSR **22**, 664 (1986).
22. I. Fleming. Frontier orbitals and organic chemical reactions. Wiley, New York. 1976.
23. E. Buncel, R.M. Tarkka, and J.M. Dust. Can. J. Chem. **72**, 1709 (1994), and refs. therein.
24. S. Pugnaud, D. Masure, J.C. Hallé, and S. Chaquin. J. Org. Chem. **62**, 8687 (1997).
25. (*a*) S.E. Denmark, B.S. Kessler, and Y.C. Moon. J. Org. Chem. **57**, 4912 (1992); (*b*) S.E. Denmark and A. Thorarensen. Chem. Rev. **96**, 137 (1996), and refs. therein; (*c*) S.E. Denmark and A. Thorarensen. J. Am. Chem. Soc. **119**, 127 (1997); (*d*) S.E. Denmark, R.A. Hund, and H.J. Sacha. J. Org. Chem. **62**, 1668 (1997); (*e*) S.E. Denmark and L.R. Marciu. J. Org. Chem. **62**, 1675 (1997); (*f*) S.E. Denmark and M. Seierstad. J. Org. Chem. **64**, 1610 (1999).
26. C.F. Bernasconi. J. Am. Chem. Soc. **92**, 4682 (1970).
27. C.F. Bernasconi. Adv. Phys. Org. Chem. **27**, 119 (1992).
28. E. Fischer. Liebigs Ann. **190**, 67 (1878).
29. (*a*) S.S. Joshi and D.S. Deorha. J. Indian Chem. Soc. **34**, 77 (1957), and refs. therein; (*b*) D.S. Deorha and S.S. Joshi. J. Indian Chem. Soc. **38**, 690 (1961).
30. R. Andrisano and D. Dalmonte-Casoni. Boll. Sci. Fac. Chim. Ind. Bologna, **1**, 1 (1943); Chem. Abstr. **41**, 723d.
31. L.R. Domingo and A. Ascensio. J. Org. Chem. **65**, 1076 (2000).
32. (*a*) A.R. Katritzky, X. Lan, I.Z. Yang, and O. Denissko. Chem. Rev. **98**, 409 (1998); (*b*) A.R. Katritzky, L. Xie, and D. Cundy. Synth. Commun. **25**, 539 (1995); (*c*) A.R. Katritzky, G. Zhang, L. Xie, and I. Ghiviriga. J. Org. Chem. **61**, 7558 (1996); (*d*) A.R. Katritzky and X. Lan. Chem. Soc. Rev. 363 (1994).
33. (*a*) A.R. Katritzky, H. Lang, and X. Lan. Tetrahedron, **49**, 7445 (1993); (*b*) A.R. Katritzky, Z. Zhang, X. Lan, and H. Lang. J. Org. Chem. **59**, 1900 (1994); (*c*) A.R. Katritzky, Z. Zhang, H. Lang, and X. Lan. J. Org. Chem. **59**, 7209 (1994); (*d*) A.R. Katritzky, H. Lang, Z. Wang, Z. Zhang, and H. Song. J. Org. Chem. **59**, 7619 (1995); (*e*) A.R. Katritzky, P. Czerney, and J.R. Levell. J. Org. Chem. **62**, 8198 (1997).

© 2001 NRC Canada

Lewis acid-mediated intramolecular addition of silyl enol ethers to internal unactivated alkynes

Ken-ichiro Imamura, Eiji Yoshikawa, Vladimir Gevorgyan, Tomoko Sudo, Naoki Asao, and Yoshinori Yamamoto

Abstract: The $EtAlCl_2$-mediated intramolecular addition of silyl enol ethers to both terminal and internal unactivated alkynes, bearing alkyl and phenyl susbstituents at the alkyne moiety, gave mono- and bicyclic β,γ-unsaturated ketones in good to excellent yields. On the other hand, the silyloxy-substituted cyclic vinylsilanes were obtained in moderate to high yields when the reactions were catalyzed by $B(C_6F_5)_3$ in the presence of triethylsilane. All the reactions proceeded via *endo*-fashion exclusively. The mechanisms of these regiospecific Lewis acid-assisted carbocyclizations are proposed.

Key words: Lewis acid, silyl enol ethers, carbocyclization, alkynes.

Résumé : La réaction, catalysée par le $EtAlCl_2$, d'addition intramoléculaire d'éthers énoliques silylés sur des alcynes internes ou en position terminale portant des substituants alkyles et phényles au niveau de l'alcyne conduit à la formation de cétones β,γ-insaturées mono- et bicycliques, avec des rendements allant de bons à excellents. Par ailleurs, les réactions catalysées par du $B(C_6F_5)_3$ en présence de triéthylsilane conduisent à la formation de vinylsilanes cycliques, substitués par des groupes silyloxy, avec des rendements allant de modérés à élevés. Toutes les réactions se produisent exclusivement de façon *endo*. On propose des mécanismes pour ces carbocyclisations régiospécifiques assistées par des acides de Lewis.

Mots clés : acide de Lewis, éthers énoliques, carbocyclisation, alcynes.

[Traduit par la Rédaction]

Introduction

The development of new selective carbocyclization methodologies is an important task for synthetic organic chemists (for reviews see ref. 1). Carbocyclization of alkynes is of particular interest since it provides an access to unsaturated carbo- and heterocycles (for a review, see for example ref. 2). Among several known methods of carbocyclization of alkynes (1, 2), the intramolecular addition of silyl enol ethers to acetylenes has proven to become one of the effective complementary tools towards medium-sized carbocycles. Two approaches are known to date to encourage a weak nucleophile, such as a silyl enol ether, to add intramolecularly across a carbon—carbon triple bond (3).[2] First is a well explored $HgCl_2$-mediated *exo*-carbocyclization (eq. [1]) (4, 5),[3] in which mercury activates an enolate moiety of **1** by forming a transient α-keto mercurial species **2**. Either the product **4** or the isomeric *trans*-addition product **6** is obtained through *syn*-addition of enolate to the η^2 neutral **3** (pathway **A**) or *anti*-addition to the η^2 cationic **5** (pathway **B**) species, respectively.

The second is a very recent approach where a W complex catalytically activates an alkyne moiety (toward nucleophilic addition of enolate) via formation of the alkyne–vinilydene intermediate **7**, which, after concomitant *anti*-addition of silyl enol ether to its electrophilic central carbon, forms an *endo*-carbocyclization product **8** (eq. [2]) (6).[4]

Despite the obvious synthetic importance of the mentioned methodologies (7),[5] the scope of their application is limited to use of terminal (4–6)[3,4] and masked terminal (silyl-protected) (4*c*-4*d*, 7)[5] alkynes. Recently, we reported the first examples of the third alternative approach: Lewis acid-mediated intramolecular addition of silyl enol ethers to both terminal and internal unactivated alkynes (8). Now we report the $B(C_6F_5)_3$-catalyzed cyclization reactions of the carbon-tethered alkynyl silyl enol ether in the presence of

Received January 31, 2001. Published on the NRC Research Press Web site at http://canjchem.nrc.ca on October 30, 2001.

This paper is dedicated to Professor Victor Snieckus in recognition of his contributions to organic chemistry.

K. Imamura, E. Yoshikawa, V. Gevorgyan, T. Sudo, N. Asao, and Y. Yamamoto.[1] Department of Chemistry, Graduate School of Science, Tohoku University, Sendai 980–8578, Japan.

[1]Corresponding author (telephone: +81-22-217-6581; fax: +81-22-217-6784; e-mail: yoshi@yamamoto1.chem.tohoku.ac.jp).

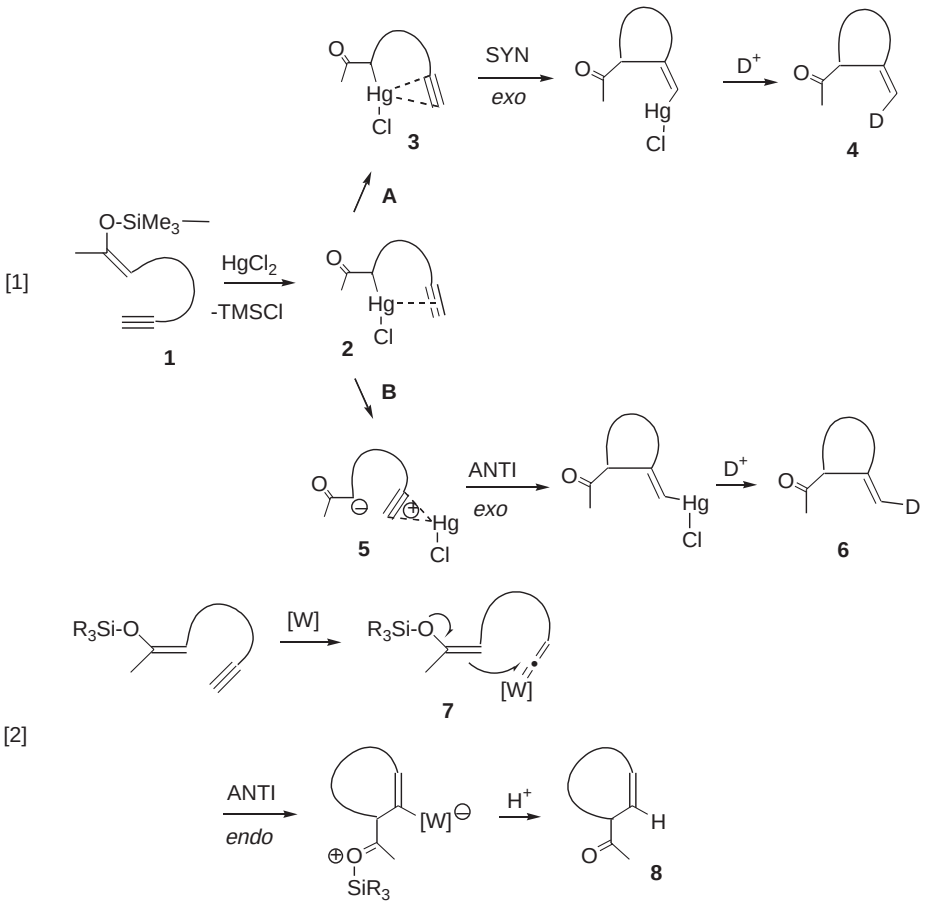
[2]There are reports on the intermolecular addition of silyl enol ethers to terminal alkynes mediated by the $SnCl_4$–Bu_3N system and by $GaCl_3$, proceeding via *syn*-addition of metal enolates to metalacetylides. See ref. 3.

[3]There are reports in which the authors state an exclusive *anti*-selective addition of α-keto carbons to the terminal alkynes mediated by mercuric chloride. See ref. 5.

[4]When this project was undergoing in our labs, a paper describing a W-catalyzed *endo*-selective carbocyclization of silyl enol ethers with terminal alkynes had appeared. See ref. 6.

[5]Mercury-mediated carbocylization approach was recently successfully used for the natural products syntheses. See ref. 7.

 DOI: 10.1139/cjc-79-11-1624 © 2001 NRC Canada

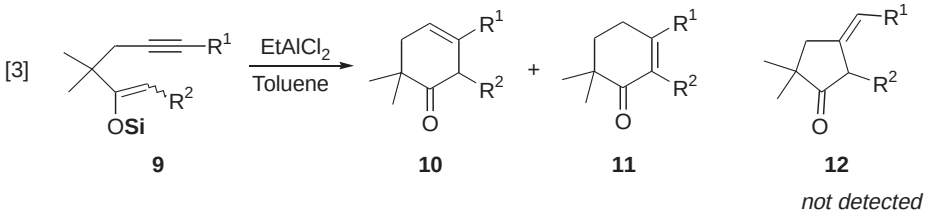


triethylsilane along with a detailed study on the $EtAlCl_2$-mediated reactions (Lewis acid-catalyzed intramolecular carbosilylation of alkynes are reported; see ref. 9).

Results and discussion

$EtAlCl_2$-mediated intramolecular addition of silyl enol ether to alkynes

As we have previously shown, the intramolecular addition of silyl enol ethers of **9** to internal alkynes is mediated by $EtAlCl_2$ to give cyclic products **10** in good to high yields (eq. [3], Table 1). The reaction of **9a** in the presence of stoichiometric amounts of $EtAlCl_2$[6] afforded the cyclization product **10a** in 70% isolated yield (entry 1). The reaction of **9b** bearing *t*-Bu-Me_2Si group instead of Me_3Si group also proceeded smoothly to give **10a** in 63% (entry 2). Optimization experiments revealed that the reaction under 0.1 mol L^{-1} concentration gave the best result (entries 1, 3–5). The carbocyclizations of methyl- (**9c**) and butyl-substituted (**9d**) alkynyl silyl enol ethers gave β,γ-unsaturated ketones **10b–c** in 57 and 80%, respectively. The reaction of the silyl enol ether containing trisubstituted alkene **9e** also proceeded smoothly to give **10d** in 76% yield. In all above cases, the β,γ-unsaturated ketones **10a–d** were accompanied with detectable amounts of isomeric α,β-unsaturated cyclohexenones **11a–d**, which are obviously the thermodynamic products.[7] It should be pointed out that in all cases the carbocyclizations proceeded in exclusive *endo*-fashion and no traces of *exo*-cyclization product **12** were detected by GC–MS and NMR analyses of the crude reaction mixtures.



9 **10** **11** **12**

not detected

[6] Other Lewis acids such as $HfCl_4$, $ZrCl_4$, and $InCl_3$ did not mediate this carbocyclization, whereas the use of $AlBr_3$, $MeAlCl_2$, Et_2AlCl, and $GaCl_3$ in some cases gave the carbocyclization products although the chemical yields with these Lewis acids were low (≤40%).

[7] The control experiments have confirmed that β,γ-enone **10** is the kinetic product, which isomerized into the thermodynamic product (α,β-enone **11**) under the reaction conditions. Thus, normally the carbocyclization of **9c** gives about a 95:5 ratio of **10c**:**11c** (eq. [3]); after being stirred for an additional 3 h at room temperature, the mentioned ratio changed to 44:56, whereas after 12 h, the isomeric **11c** became the major reaction product accompanied by traces of **10c**.

© 2001 NRC Canada

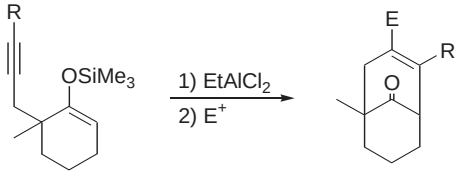
Table 1. $EtAlCl_2$-mediated cyclization reaction of **9**.[a]

Entry	Si	R^1	R^2	9	Lewis acid (equiv)		(mol L^{-1})	Yield (%) 10		11	
1	Me_3Si	Ph	H	**9a**	$EtAlCl_2$	(1.2)	0.4	**10a**	70	**11a**	6
2	*t*-Bu-Me_2Si	Ph	H	**9b**	$EtAlCl_2$	(1.2)	0.4	**10a**	63	**11a**	11
3	Me_3Si	Ph	H	**9a**	$EtAlCl_2$	(1.2)	0.1	**10a**	75	**11a**	4
4	Me_3Si	Ph	H	**9a**	$EtAlCl_2$	(1.5)	0.08	**10a**	77	**11a**	5
5	Me_3Si	Ph	H	**9a**	$EtAlCl_2$	(1.2)	0.01	**10a**	60	**11a**	4
6	Me_3Si	Me	H	**9c**	$EtAlCl_2$	(1.2)	0.1	**10b**	57	**11b**	11
7	Me_3Si	Bu	H	**9d**	$EtAlCl_2$	(1.2)	0.1	**10c**	80	**11c**	6
8	Me_3Si	Ph	Me	**9e**	$EtAlCl_2$	(1.2)	0.1	**10d**	76	**11d**	8

[a]Reactions were conducted in toluene at 0°C for 3 h.

$EtAlCl_2$-mediated carbocyclization of cyclic substrates **13**, as well as that of their acyclic analogues **9**, proceeded in exclusive *endo*-fashion to give bicylic β,γ-cyclohexenones **14** in good yields (eq. [4]). Substrates possessing both terminal (**13a**) and internal (**13b**) alkynyl moieties effectively cyclized to give the bicylic **14a** and **14c** in 78 and 84% isolated yields, respectively. Furthermore, quenching the reaction mixtures with electrophiles, such as D_2O and I_2, afforded the corresponding D- (**14b**) and I-containing (**14d**) products in good yields.

[4]

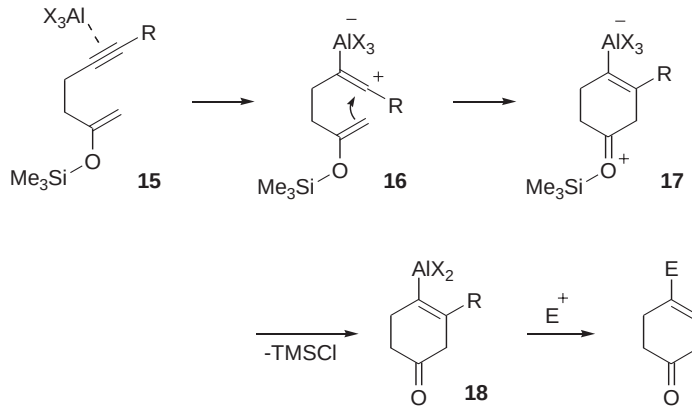


13 a: R=H
b: R=Me

14 a: R=E=H, 78%
b: R=H, E=D, 71%
c: R=Me, E=H, 84%
d: R=Me, E=I, 75%

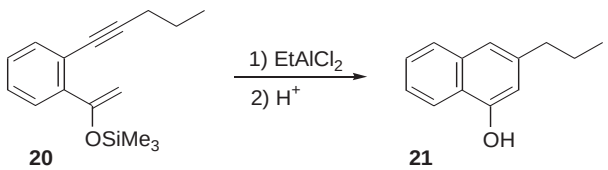
We propose the following plausible mechanism for the observed Lewis acid-mediated exclusive *endo*-carbocyclization of carbon-tethered alkynyl silyl enol ethers. As we previously proposed for the Lewis acid-catalyzed hydro- and allylmetalation of alkynes (9), the coordination of the triple bond of **15** to Lewis acid would form zwitterionic intermediate **16** (eq. [5]). The double bond of silyl enol ether moiety would attack the vinyl cation of **16** at the most nucleophilic terminal position in an *anti*-fashion affording the *endo*-mode cyclization intermediate **17**. The elimination of the TMSCl from **17** would form the vinyl metal **18**, which after trapping with an electrophile would produce **19**.

[5]



An application of the above methodology is shown in eq. [6]. Naphthol **21** could be synthesized from the unsaturated analogue **20**, although in modest unoptimized yield (40% by ^1H NMR, eq. [6]).

[6]

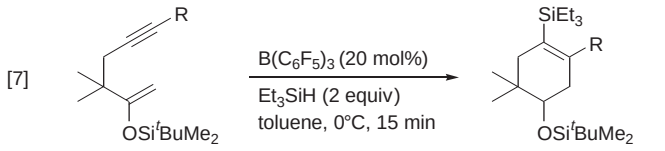


20 **21**

© 2001 NRC Canada

$B(C_6F_5)_3$-catalyzed intramolecular addition of silyl enol ether to alkynes

Although the above mentioned carbocyclization reaction demonstrated the first example of the Lewis acid-mediated addition of silyl enol ethers to internal unactivated alkynes, the synthetic utility of this methodology is limited by the fact that a stoichiometric amount of $EtAlCl_2$ is needed. This prompted us to search for a more synthetically useful catalyst for this reaction. Attempted reaction of **9b** in the presence of a catalytic amount of $B(C_6F_5)_3$ did not proceed at all. However, the $B(C_6F_5)_3$-catalyzed reaction proceeded dramatically by addition of triethylsilane and the silyloxy-substituted cyclic vinylsilane **22a** was obtained in 49% yield (eq. [7]) (10).[8] The compound **10a**, which was produced in the $EtAlCl_2$-mediated reaction, was not formed at all. The $B(C_6F_5)_3$-catalyzed cyclization reaction using other substituted substrates **9f** and **9g** also proceeded smoothly under the same conditions as those in the case of **9b** to afford **22b** and **22c** in 61 and 63% yield, respectively.



9b: R=Ph
9f : R=Me
9g: R=Bu

22a: R=Ph 49%
22b: R=Me 61%
22c: R=Bu 63%

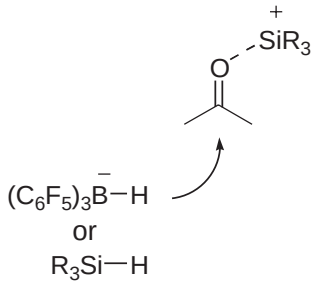
Piers and co-workers (10)[8] proposed the interesting silane activation mechanism in the $B(C_6F_5)_3$-catalyzed hydrosilylation of aldehydes and ketones; the ordinary mechanism, in which the carbonyl oxygen of the electrophiles coordinates to $B(C_6F_5)_3$ and thus carbonyl substrates are activated, is not operative in the $B(C_6F_5)_3$-catalyzed reduction. Their extensive mechanistic studies clarify that $B(C_6F_5)_3$ activates the silane via hydride abstraction to form the incipient silylium species which enhances the electrophilicity of carbonyl group, facilitating the reduction by $[HB(C_6F_5)_3]^-$ or R_3SiH (Fig. 1).

Most probably, silylium species **23** is generated here also and a plausible mechanism for the $B(C_6F_5)_3$-catalyzed cyclization reaction of **9** is shown in Scheme 1. The π-coordination of acetylenic bond of **9** to the silylium species would form the cationic intermediate **24**. The silyl enol ether moiety would attack the electron deficient triple bond from the side opposite to the silylium species to produce an oxonium cation **25**. The reduction of an intermediate **25** by $[HB(C_6F_5)_3]^-$ would form cyclization products **22** and regenerate $B(C_6F_5)_3$.

Experimental

^1H and ^{13}C NMR spectra were recorded on a JEOL LA-300 (300 MHz) and JEOL α–500 (500 MHz) spectrometers. IR spectra were recorded on a Shimadzu FT IR-8200A spectrometer. High-resolution mass spectra were recorded on a JEOL HX-110 spectrometer. Elemental analyses were carried out at the Analytical Center of Tohoku University. GC–MS analysis was performed on a Hewlett-Packard Model 6890 GC interfaced to a Hewlett-Packard Model 5973 mass selective detector (30 m × 0.25 mm capillary column). Column chromatography was carried out employing Merck silica gel (Kieselgel 230–400 mesh), and analytical thin layer chromatography (TLC) was performed on 0.2-mm precoated silica gel plates (Kieselgel 60 F_{254}). All manipulations were conducted under an argon atmosphere using standard Schlenk techniques. Anhydrous solvents were purchased from Kanto Chemicals. Alkyl-tethered alkynyl silyl enol ethers **9** were obtained by consecutive ester propargylation (for a review see ref. 13), conversion to ketone, and silyl enolization (for a review see ref. 14). All other compounds used were commercially available and purchased from Aldrich.

Fig. 1. Mechanism of the $B(C_6F_5)_3$-catalyzed hydrosilylation of the carbonyl group.



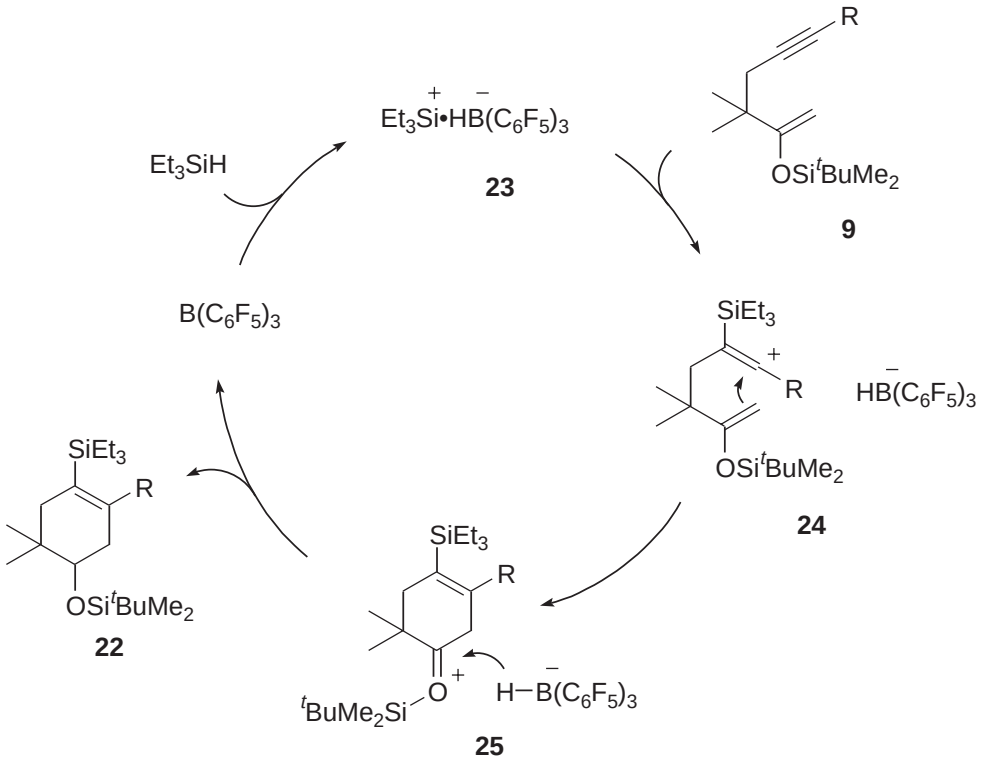
Preparation of alkynyl silyl enol ethers 9

The preparation of **9e** is representative. (*i*) To a solution of diisopropylamine (6.73 mL, 48 mmol) in THF (40 mL) was added *n*-BuLi (1.61 M in hexane, 28.6 mL) at 0°C. After being stirred for 30 min, the mixture was cooled to –78°C. To the solution was added methyl isobutyrate (4.58 mL, 40 mmol), and the reaction mixture was stirred for 1 h. To the resulting mixture, phenylpropargyl *p*-toluenesulfonate (11.4 g, 40 mmol) in THF (20 mL) – 1,3-dimethyl-3,4,5,6-tetrahydro-2(1*H*)-pyrimidinone (5.0 mL) was added. The mixture was stirred for 15 min, and then allowed to warm to 0°C. After being stirred for additional 10 min at this temperature, the mixture was quenched with ice-cold saturated, aq NH_4Cl solution and three times extracted with ether. The combined organic phase was washed with H_2O, brine, dried over $MgSO_4$, filtered, and concentrated. The crude product was purified by column chromatography (silica gel, eluent: hexane – ethyl acetate, 15:1) to give methyl 2,2-dimethyl-5-phenyl-4-pentylate (6.96 g, 80% yield). ^1H NMR (300 MHz, $CDCl_3$) δ: 7.41–7.35 (m, 2H), 7.30–7.24 (m, 3H), 3.71 (s, 3H), 2.66 (s, 2H), 1.34 (s, 6H). (*ii*) To a solution of methyl 2,2-dimethyl-5-phenyl-4-pentylate (1.92 g, 8.9 mmol) in THF (18 mL) were added sequentially $TMSCH_2Li$ (1.0 M in pentane, 19.5 mL) and 1,3-dimethyl-3,4,5,6-tetrahydro-2(1*H*)-pyrimidinone (2.15 mL, 18 mmol) at –78°C. After being stirred for 30 min, the mixture was quenched with ice-cold saturated, aq NH_4Cl solution and three times extracted with ether. The combined organic phase was washed with H_2O, brine, dried over $MgSO_4$, filtered, and concentrated. The crude product was purified by column chromatography (silica gel, eluent: hexane – ethyl acetate, 30:1) to give 1-(trimethylsilyl)-3,3-dimethyl-6-phenyl-5-hexyn-2-one (1.85 g, 76% yield). ^1H NMR (300 MHz, $CDCl_3$) δ: 7.40–7.34 (m, 2H), 7.30–7.24 (m, 3H), 2.59 (s,

[8] Piers and his co-workers found that $B(C_6F_5)_3$-catalyzed hydrosilylation of carbonyl functions, such as aldehydes, ketones, and esters, proceeded very smoothly to give the corresponding reduced compounds in high yields.

© 2001 NRC Canada

Scheme 1.



2H), 2.27 (s, 2H), 1.27 (s, 6H), 0.13 (s, 9H). (*iii*) To a mixture of 1-(trimethylsilyl)-3,3-dimethyl-6-phenyl-5-hexyn-2-one (1.85 g, 6.8 mmol) and NaI (1.22 g, 8.1 mmol) in CH_3CN (14 mL) were added sequentially Et_3N (4.54 mL, 33 mmol) and TMSCl (2.58 mL, 20 mmol) at room temperature. After being stirred for 30 min, the mixture was quenched with saturated, aq $NaHCO_3$ solution and three times extracted with pentane. The combined organic phase was washed with brine, dried over $MgSO_4$, filtered, and concentrated. The crude product was purified by column chromatography (silica gel, eluent: hexane – ethyl acetate – pyridine, 20:1:0.1) to give **9a** (1.81 g, 98% yield). (*iv*) To a solution of **9a** (1.33 g, 4.9 mmol) in THF (9.8 mL) was added *n*-BuLi (1.54 M in hexane, 3.32 mL) at 0°C, and the mixture was stirred for 20 min. To the resulting mixture was added MeI (455 μL, 7.3 mmol), and the mixture was allowed to warm to room temperature. After being stirred for 25 min, the reaction mixture was quenched with ice-cold saturated, aq NH_4Cl solution and three times extracted with ether. The combined organic phase was washed with brine, dried over $MgSO_4$, filtered, and concentrated. The crude product was purified by column chromatography (silica gel, eluent: hexane – ethyl acetate, 30:1) to give 4,4-dimethyl-7-phenyl-6-heptyn-3-one (327 mg, 31% yield). ^{1}H NMR (300 MHz, $CDCl_3$) δ: 7.40–7.33 (m, 2H), 7.30–7.24 (m, 3H), 2.61 (s, 2H), 2.59 (q, *J* = 7.2 Hz, 2H), 1.28 (s, 6H), 1.06 (t, *J* = 7.2 Hz, 3H). (*v*) To a solution of 4,4-dimethyl-7-phenyl-6-heptyn-3-one (281 mg, 1.3 mmol) in CH_2Cl_2 (2.8 mL) were added sequentially Et_3N (274 μL, 2.0 mmol) and TMSOTf (304 μL, 1.6 mmol) at 0°C. The mixture was stirred for 30 min, and then allowed to warm to room temperature. After being stirred for an additional 1 h at this temperature, the mixture was quenched with saturated, aq $NaHCO_3$ solution and three times extracted with pentane. The combined organic phase was washed with brine, dried over $MgSO_4$, filtered, and concentrated. The crude product was purified by column chromatography (silica gel, eluent: hexane – ethyl acetate – pyridine, 20:1:0.1) to give **9e** (302 mg, 81% yield).

*2-(Trimethylsilyloxy)-3,3-dimethyl-6-phenyl-1-hexen-5-yne (**9a**):* colorless oil. HRMS calcd. for $C_{17}H_{24}OSi$ 272.1597; found 272.1600. IR (neat) (cm^{-1}): 3125, 1654, 1624, 1599, 1254, 1021, 847, 755, 691. ^{1}H NMR (300 MHz, $CDCl_3$) δ: 7.41–7.36 (m, 2H), 7.30–7.24 (m, 3H), 4.18 (d, *J* = 1.7 Hz, 1H), 4.04 (d, *J* = 1.7 Hz, 1H), 2.48 (s, 2H), 1.19 (s, 6H), 0.23 (s, 9H). ^{13}C NMR (75.5 MHz, $CDCl_3$) δ: 164.4, 131.5, 128.1, 127.4, 124.2, 88.4, 87.4, 82.2, 40.0, 30.8, 25.4, 0.2. Anal. calcd. for $C_{17}H_{24}OSi$: C 74.94, H 8.88; found: C 74.72, H 8.68.

*2-(*tert*-Butyldimethylsilyloxy)-3,3-dimethyl-6-phenyl-1-hexen-5-yne (**9b**):* colorless oil. HRMS calcd. for $C_{20}H_{30}OSi$: 314.2066; found: 314.2067. ^{1}H NMR (300 MHz, $CDCl_3$) δ: 7.41–7.37 (m, 2H), 7.28–7.26 (m, 2H), 4.15 (d, *J* = 1.8 Hz, 1H), 4.03 (d, *J* = 1.8 Hz, 1H), 2.50 (s, 2H), 1.20 (s, 6H), 0.96 (s, 9H), 0.21 (s, 6H). ^{13}C NMR (75.5 MHz, $CDCl_3$) δ: 164.4, 134.5, 128.1, 127.4, 124.2, 88.4, 86.2, 82.2, 40.4, 30.9, 25.8, 25.5, 18.2, –4.8. Anal. calcd. for $C_{20}H_{30}OSi$: C 76.37, H 9.61; found: C 76.22, H 9.56.

*2-(Trimethylsilyloxy)-3,3-dimethyl-1-hepten-5-yne (**9c**):* colorless oil. HRMS calcd. for $C_{12}H_{22}OSi$: 210.1440; found: 210.1422. IR (neat) (cm^{-1}): 3125, 1655, 1622, 1254, 1021, 848. ^{1}H NMR (300 MHz, $CDCl_3$) δ: 4.12 (d, *J* = 1.6 Hz, 1H), 3.99 (d, *J* = 1.6 Hz, 1H), 2.20 (q, *J* = 2.6 Hz, 2H), 1.78

© 2001 NRC Canada

(t, J = 2.6 Hz, 3H), 1.10 (s, 6H), 0.21 (s, 9H). ^{13}C NMR (75.5 MHz, $CDCl_3$) δ: 164.9, 87.2, 39.7, 30.2, 25.2, 3.5, 0.1. Anal. calcd. for $C_{12}H_{22}OSi$: C 68.51, H 10.54; found: C 68.50, H 10.21.

*2-(Trimethylsilyloxy)-3,3-dimethyl-1-decen-5-yne (**9d**):* colorless oil. HRMS calcd. for $C_{15}H_{28}OSi$: 252.1909; found: 252.1911. IR (neat) (cm^{-1}): 3125, 1658, 1622, 1254, 1021, 846. ^{1}H NMR (300 MHz, $CDCl_3$) δ: 4.11 (d, J = 1.7 Hz, 1H), 3.99 (d, J = 1.7 Hz, 1H), 2.22 (t, J = 2.3 Hz, 2H), 2.15 (tt, J = 6.8, 2.3 Hz, 2H), 1.51–1.34 (m, 4H), 1.10 (s, 6H), 0.90 (t, J = 7.2 Hz, 3H), 0.21 (s, 9H). ^{13}C NMR (75.5 MHz, $CDCl_3$) δ: 164.8, 87.2, 81.9, 77.9, 39.8, 31.3, 30.2, 25.2, 21.9, 18.4, 13.6, 0.1. Anal. calcd. for $C_{15}H_{28}OSi$: C 71.36, H 11.18; found: C 71.22, H 10.92.

*3-(Trimethylsilyloxy)-4,4-dimethyl-7-phenyl-2-hepten-6-yne (**9e**):* colorless oil. HRMS calcd. for $C_{18}H_{26}OSi$: 286.1752; found: 286.1758. IR (neat) (cm^{-1}): 1664, 1598, 1253, 1074, 842, 755, 691. ^{1}H NMR (300 MHz, $CDCl_3$, a major isomer) δ: 7.41–7.36 (m, 2H), 7.30–7.24 (m, 3H), 4.70 (q, J = 6.8 Hz, 1H), 2.47 (s, 2H), 1.55 (d, J = 6.8 Hz, 3H), 1.18 (s, 6H), 0.26 (s, 9H). ^{13}C NMR (75.5 MHz, $CDCl_3$) δ: 156.8, 131.5, 128.1, 127.4, 124.2, 99.3, 88.6, 82.4, 39.9, 31.1, 25.8, 11.8, 1.2.

*2-(*tert*-Butyldimethylsilyloxy)-3,3-dimethyl-1-hepten-5-yne (**9f**):* colorless oil. HRMS calcd. for $C_{15}H_{28}OSi$: 252.1910; found: 252.1908. ^{1}H NMR (300 MHz, $CDCl_3$) δ: 4.08 (d, J = 1.7 Hz, 1H), 3.97 (d, J = 1.7 Hz, 1H), 2.22 (q, J = 2.6 Hz, 2H), 1.78 (t, J = 2.6 Hz, 3H), 1.11 (s, 6H), 0.93 (s, 9H), 0.18 (s, 6H). ^{13}C NMR (75.5 MHz, $CDCl_3$) δ: 164.9, 86.5, 77.2, 76.9, 40.0, 30.3, 25.8, 25.3, 18.2, 3.5, –4.8. Anal. calcd. for $C_{15}H_{28}OSi$: C 71.36, H 11.18; found: C 71.34, H 10.92.

*2-(*tert*-Butyldimethylsilyloxy)-3,3-dimethyl-1-decen-5-yne (**9g**):* colorless oil. ^{1}H NMR (300 MHz, $CDCl_3$) δ: 4.08 (d, J = 1.7 Hz, 1H), 3.97 (d, J = 1.7 Hz, 1H), 2.24 (t, J = 2.4 Hz, 2H), 2.15 (tt, J = 6.8 and 2.4 Hz, 2H), 1.51–1.34 (m, 4H), 1.11 (s, 6H), 0.94 (s, 9H), 0.90 (t, J = 7.2 Hz, 3H), 0.38 (s, 6H). ^{13}C NMR (75.5 MHz, $CDCl_3$) δ: 164.8, 86.5, 81.8, 77.9, 40.1, 31.3, 30.3, 25.8, 25.3, 21.9, 18.4, 18.2, 13.6, –4.8. Anal. calcd. for $C_{18}H_{34}OSi$: C 73.40, H 11.63; found: C 73.32, H 11.57.

*2-(Trimethylsilyloxy)-3-methyl-3-(2-propynyl)-1-cyclohexene (**13a**):* colorless oil. HRMS calcd. for $C_{13}H_{22}OSi$: 222.1439; found: 222.1446. IR (neat) (cm^{-1}): 2962, 2933, 2118, 1713, 1659, 1458, 1252, 1178. ^{1}H NMR (300 MHz, $CDCl_3$) δ: 4.72 (t, J = 4.0 Hz, 1H), 2.35 (dd, J = 16.2, 2.7 Hz, 1H), 2.27 (dd, J = 16.2, 2.7 Hz, 1H), 2.03–1.95 (m, 2H), 1.95 (t, J = 2.7 Hz, 1H), 1.87–1.74 (m, 1H), 1.60–1.48 (m, 3H), 1.10 (s, 3H), 0.17 (s, 9H). ^{13}C NMR (75.5 MHz, $CDCl_3$) δ: 154.7, 102.6, 82.6, 69.8, 37.9, 35.0, 28.8, 24.5, 24.2, 19.2, 0.4.

*2-(Trimethylsilyloxy)-3-(2-butynyl)-3-methyl-1-cyclohexene (**13b**):* colorless oil. HRMS calcd. for $C_{14}H_{24}OSi$: 236.1596; found: 236.1600. IR (neat) (cm^{-1}): 2962, 2932, 2126, 1656, 1252, 1178, 842. ^{1}H NMR (300 MHz, $CDCl_3$) δ: 4.70 (t, J = 4.0 Hz, 1H), 2.28 (dq, J = 16.5, 2.5 Hz, 1H), 2.19 (dq, J = 16.5, 2.5 Hz, 1H), 1.98 (dt, J = 6.0, 4.0 Hz, 2H), 1.85–1.76 (m, 1H), 1.78 (t, J = 2.5 Hz, 3H), 1.58–1.46 (m, 2H), 1.50–1.42 (m, 1H), 1.06 (s, 3H), 0.17 (s, 9H). ^{13}C NMR (75.5 MHz, $CDCl_3$) δ: 155.3, 102.4, 77.04, 76.95, 38.1, 35.1, 29.1, 24.6, 24.2, 19.3, 0.4. Anal. calcd. for $C_{14}H_{24}OSi$: C 71.12, H 10.23; found: C 70.93, H 10.06.

α*-(Trimethylsilyloxy)-*o*-(1-pentynyl)styrene (**20**):* colorless oil. HRMS calcd. for $C_{16}H_{22}OSi$: 258.1439; found: 258.1465. IR (neat) (cm^{-1}): 2963, 2933, 2235, 1621, 1480, 1307, 1253, 1014, 848. ^{1}H NMR (300 MHz, $CDCl_3$) δ: 7.54–7.45 (m, 2H), 7.28–7.23 (m, 2H), 5.13 (d, J = 1.2 Hz, 1H), 4.07 (d, J = 1.2 Hz, 1H), 2.46 (t, J = 7.0 Hz, 2H), 1.68 (tq, J = 7.0, 7.0 Hz, 2H), 1.10 (t, J = 7.0 Hz, 3H), 0.27 (s, 9H). ^{13}C NMR (75.5 MHz, $CDCl_3$) δ: 154.8, 139.9, 133.5, 127.7, 127.4, 127.2, 121.4, 95.9, 94.3, 80.4, 22.1, 21.7, 13.6, 0.0.

$EtAlCl_2$-mediated carbocyclization of 9 (general procedure)

$EtAlCl_2$ (1.2 equiv) was added to a stirred solution of **9** (0.5 mmol) in toluene (5.0 mL) at 0°C. After being stirred for 3 h, the reaction mixture was quenched with Et_2NH, diluted with saturated, aq $NaHCO_3$ solution, and extracted with ether three times. The combined organic phase was washed with brine, dried over $MgSO_4$, filtered, and concentrated. The products (**10** and **11**) were purified by column chromatography (silica gel, eluent: hexane – ethyl acetate).

*6,6-Dimethyl-3-phenyl-3-cyclohexenone (**10a**):* colorless oil. HRMS calcd. for $C_{14}H_{16}O$: 200.1201; found: 200.1211. IR (neat) (cm^{-1}): 1714, 1672, 1599, 751, 694. ^{1}H NMR (300 MHz, $CDCl_3$) δ: 7.41–7.25 (m, 5H), 6.22 (tt, J = 4.2, 1.8 Hz, 1H), 3.31 (dt, J = 1.8, 1.8 Hz, 2H), 2.46 (dt, J = 4.2, 1.8 Hz, 2H), 1.20 (s, 6H). ^{13}C NMR (75.5 MHz, CDCl3) δ: 213.4, 139.4, 134.2, 128.5, 127.5, 124.9, 122.1, 43.3, 40.8, 40.1, 24.3. Anal. calcd. for $C_{14}H_{16}O$: C 83.96, H 8.05; found: C 83.91, H 8.01.

*6,6-Dimethyl-3-phenyl-2-cyclohexenone (**11a**):* colorless oil. HRMS calcd. for $C_{14}H_{16}O$: 200.1201; found: 200.1201. IR (CCl_4) (cm^{-1}): 1667, 1611, 1573, 725, 693. ^{1}H NMR (300 MHz, $CDCl_3$) δ: 7.58–7.52 (m, 2H), 7.44–7.38 (m, 3H), 6.35 (t, J = 1.5 Hz, 1H), 2.79 (td, J = 6.1, 1.5 Hz, 2H), 1.98 (t, J = 6.1 Hz, 2H), 1.18 (s, 6H). ^{13}C NMR (75.5 MHz, $CDCl_3$) δ: 204.7, 157.3, 138.5, 129.8, 128.7, 126.0, 123.8, 40.4, 36.4, 25.2, 24.1.

*3,6,6-Trimethyl-3-cyclohexenone (**10b**):* colorless oil. HRMS calcd. for $C_9H_{14}O$: 138.1045; found: 138.1067. IR (neat) (cm^{-1}): 3041, 1715. ^{1}H NMR (300 MHz, $CDCl_3$) δ: 5.44 (ttq, J = 3.9, 1.8, 1.4 Hz, 1H), 2.80 (dtq, J = 1.8, 1.8, 0.9 Hz, 2H), 2.21 (dtq, J = 3.9, 1.8, 1.8 Hz, 2H), 1.70 (tdt, J = 1.8, 1.4, 0.9 Hz, 3H), 1.11 (s, 6H). ^{13}C NMR (75.5 MHz, $CDCl_3$) δ: 214.1, 131.5, 119.7, 43.3, 42.7, 40.6, 24.3, 22.4. Anal. calcd. for $C_9H_{14}O$: C 78.21, H 10.21; found: C 77.92, H 10.67.

*3,6,6-Trimethyl-2-cyclohexenone (**11b**):* colorless oil. HRMS calcd. for $C_9H_{14}O$: 138.1045; found: 138.1045. IR (neat) (cm^{-1}): 3031, 1670, 1638. ^{1}H NMR (300 MHz, $CDCl_3$) δ: 5.77 (tq, J = 1.5, 1.3 Hz, 1H), 2.29 (tdq, J = 6.1, 1.5, 0.7 Hz, 2H), 1.92 (dt, J = 1.3, 0.7 Hz, 3H), 1.80 (t, J = 6.1 Hz, 2H), 1.08 (s, 6H). ^{13}C NMR (75.5 MHz, $CDCl_3$) δ: 204.5, 160.3, 125.1, 40.1, 36.3, 28.4, 24.2, 24.0.

© 2001 NRC Canada

*3-Butyl-6,6-dimethyl-3-cyclohexenone (**10c**):* colorless oil. HRMS calcd. for $C_{12}H_{20}O$: 180.1514; found: 180.1510. IR (neat) (cm^{-1}): 3043, 1717, 1676. ^1H NMR (300 MHz, $CDCl_3$) δ: 5.45 (ttt, *J* = 3.9, 1.8, 1.3 Hz, 1H), 2.81 (dtt, *J* = 1.8, 1.7, 0.7 Hz, 2H), 2.23 (dtt, *J* = 3.9, 1.7, 1.6 Hz, 2H), 2.00 (ttdt, *J* = 6.8, 1.6, 1.3, 0.7 Hz, 2H), 1.44–1.24 (m, 4H), 1.12 (s, 6H), 0.90 (t, *J* = 7.2 Hz, 3H). ^{13}C NMR (75.5 MHz, $CDCl_3$) δ: 214.5, 135.6, 119.1, 43.5, 41.1, 40.6, 36.1, 29.5, 24.4, 22.3, 13.9. Anal. calcd. for $C_{12}H_{20}O$: C 79.94, H 11.18; found: C 79.77, H 10.96.

*3-Butyl-6,6-dimethyl-2-cyclohexenone (**11c**):* colorless oil. HRMS calcd. for $C_{12}H_{20}O$: 180.1514; found: 180.1515. IR (neat) (cm^{-1}): 3028, 1668, 1632. ^1H NMR (300 MHz, $CDCl_3$) δ: 5.76 (tt, *J* = 1.3, 0.9 Hz, 1H), 2.29 (tdt, *J* = 6.1, 1.3, 0.7 Hz, 2H), 2.18 (tdt, *J* = 7.4, 0.9, 0.7 Hz, 2H), 1.80 (t, *J* = 6.1 Hz, 2H), 1.53–1.43 (m, 2H), 1.38–1.25 (m, 2H), 1.09 (s, 6H), 0.91 (t, *J* = 7.2 Hz, 3H). ^{13}C NMR (75.5 MHz, $CDCl_3$) δ: 204.8, 164.3, 124.1, 40.4, 37.4, 36.4, 29.2, 27.0, 24.2, 22.3, 13.8.

*2,6,6-Trimethyl-3-phenyl-3-cyclohexenone (**10d**):* colorless oil. HRMS calcd. for $C_{15}H_{18}O$: 214.1357; found: 214.1322. IR (neat) (cm^{-1}): 1710, 1599, 756, 698. ^1H NMR (300 MHz, $CDCl_3$) δ: 7.38–7.24 (m, 5H), 5.98 (ddd, *J* = 5.4, 3.3, 1.5 Hz, 1H), 3.48 (qddd, *J* = 7.3, 1.8, 1.5, 0.9 Hz, 1H), 2.43 (ddd, *J* = 17.6, 3.3, 1.8 Hz, 1H), 2.37 (ddd, *J* = 17.6, 5.4, 0.9 Hz, 1H), 1.24 (s, 3H), 1.19 (s, 3H), 1.15 (d, *J* = 7.3 Hz, 3H). ^{13}C NMR (75.5 MHz, $CDCl_3$) δ: 216.0, 141.2, 140.3, 128.4, 127.2, 126.1, 122.7, 43.0, 39.8, 25.2, 24.6, 15.4.

*2,6,6-Trimethyl-3-phenyl-2-cyclohexenone (**11d**):* colorless oil. HRMS calcd. for $C_{15}H_{18}O$: 214.1357; found: 214.1361. IR (neat) (cm^{-1}): 1665, 1625, 1599, 751, 701. ^1H NMR (300 MHz, $CDCl_3$) δ: 7.42–7.28 (m, 3H), 7.21–7.17 (m, 2H), 2.62 (tq, *J* = 6.0, 2.0 Hz, 2H), 1.93 (t, *J* = 6.0 Hz, 2H), 1.70 (t, *J* = 2.0 Hz, 3H), 1.18 (s, 6H). ^{13}C NMR (75.5 MHz, $CDCl_3$) δ: 204.7, 154.4, 141.4, 129.9, 128.3, 127.7, 127.1, 40.3, 36.1, 29.6, 24.6, 13.4.

*5-Methyl-9-oxobicyclo[3,3,1]non-2-ene (**14a**):* colorless oil. HRMS calcd. for $C_{10}H_{14}O$: 150.1044; found: 150.1044. IR (neat) (cm^{-1}): 2929, 1718, 1445. ^1H NMR (300 MHz, $CDCl_3$) δ: 5.86 (dt, *J* = 9.5, 3.5 Hz, 1H), 5.55 (dddd, *J* = 9.5, 5.5, 2.0, 1.5 Hz, 1H), 2.91 (dt, *J* = 5.5, 3.0 Hz, 1H), 2.54 (ddd, *J* = 18.5, 3.5, 1.5 Hz, 1H), 2.37 (d, *J* = 18.5 Hz, 1H), 2.15–1.98 (m, 1H), 1.88–1.80 (m, 3H), 1.63–1.47 (m, 2H), 1.03 (s, 3H). ^{13}C NMR (75.5 MHz, $CDCl_3$) δ: 217.1, 129.4, 127.1, 48.2, 46.3, 44.8, 44.5, 33.2, 23.7, 18.1.

*3-Deuterio-5-methyl-9-oxobicyclo[3,3,1]non-2-ene (**14b**):* colorless oil. HRMS calcd. for $C_{10}H_{13}DO$: 151.1106; found: 151.1096. IR (neat) (cm^{-1}): 2929, 1720, 1445. ^1H NMR (300 MHz, $CDCl_3$) δ: 5.58–5.53 (m, 1H), 2.91 (dt, *J* = 5.5, 3.0 Hz, 1H), 2.54 (dd, *J* = 18.5, 1.5 Hz, 1H), 2.37 (d, *J* = 18.5 Hz, 1H), 2.15–1.98 (m, 1H), 1.88–1.80 (m, 3H), 1.63–1.47 (m, 2H), 1.03 (s, 3H). ^{13}C NMR (75.5 MHz, $CDCl_3$) δ: 217.1, 129.4 (*C*—D), 129.1 (*C*—D), 128.8 (*C*—D), 126.9, 48.1, 46.3, 44.8, 44.4, 33.2, 23.7, 18.0.

*2,5-Dimethyl-9-oxobicyclo[3,3,1]non-2-ene (**14c**):* colorless oil. HRMS calcd. for $C_{11}H_{16}O$: 164.1200; found: 164.1205. IR (neat) (cm^{-1}): 2966, 2927, 1716, 1446, 1379. ^1H NMR (300 MHz, $CDCl_3$) δ: 5.54 (tq, *J* = 4.0, 1.5 Hz, 1H), 2.70 (t, *J* = 3.0 Hz, 1H), 2.43 (ddq, *J* = 18.0, 4.0, 2.0 Hz, 1H), 2.27 (d, *J* = 18.0 Hz, 1H), 2.00–1.87 (m, 2H), 1.84–1.75 (m, 2H), 1.66 (dt, *J* = 2.0, 1.5 Hz, 3H), 1.62–1.46 (m, 2H), 1.01 (s, 3H). ^{13}C NMR (75.5 MHz, $CDCl_3$) δ: 217.2, 133.8, 122.8, 52.8, 45.1, 44.7, 43.3, 31.5, 23.5, 21.3, 18.5. Anal. calcd. for $C_{11}H_{16}O$: C 80.44, H 9.82; found: C 80.42, H 9.93.

*2,5-Dimethyl-3-iodo-9-oxobicyclo[3,3,1]non-2-ene (**14d**):* colorless oil. HRMS calcd. for $C_{11}H_{15}IO$: 290.0167; found: 290.0177. IR (neat) (cm^{-1}): 2932, 2864, 1720, 1446. ^1H NMR (300 MHz, $CDCl_3$) δ: 2.95 (t, *J* = 3.0 Hz, 1H), 2.95 (dd, *J* = 18.0, 2.0 Hz, 1H), 2.76 (d, *J* = 18.0 Hz, 1H), 2.05–1.70 (m, 7H), 1.63–1.53 (m, 2H), 1.00 (s, 3H). ^{13}C NMR (75.5 MHz, $CDCl_3$) δ: 213.5, 138.3, 95.3, 57.0, 54.8, 49.0, 44.4, 31.9, 27.5, 22.6, 18.8. Anal. calcd. for $C_{11}H_{15}IO$: C 45.54, H, 5.21, I 43.74; found: C 45.63, H 5.24, I 43.84.

*3-Propyl-1-naphthol (**21**):* colorless oil. HRMS calcd. for $C_{13}H_{14}O$: 186.1044; found: 186.1045. IR (neat) (cm^{-1}): 3393, 2958, 2929, 1638, 1599, 1578. ^1H NMR (300 MHz, $CDCl_3$) δ: 8.13–8.08 (m, 1H), 7.75–7.71 (m, 1H), 7.48–7.38 (m, 2H), 7.22 (s, 1H), 6.67 (s, 1H), 5.39 (s, 1H), 2.67 (t, *J* = 7.5 Hz, 2H), 1.70 (tq, *J* = 7.5, 7.5 Hz, 2H), 0.96 (t, *J* = 7.5 Hz, 3H). ^{13}C NMR (75.5 MHz, $CDCl_3$) δ: 151.2, 140.6, 134.8, 127.2, 126.4, 124.4, 122.8, 121.3, 119.2, 110.1, 38.2, 24.2, 13.8.

$B(C_6F_5)_3$-mediated carbocyclization of 9 (general procedure)

To a solution of $B(C_6F_5)_3$ (0.1 mmol, 20 mol%) in toluene (1.0 mL) were added triethylsilane (0.16 mL, 1.0 mmol) and substrate **9** (0.5 mmol) at 0°C, successively. After being stirred for 15 min, the reaction mixture was diluted with pentane, quenched with Et_2NH, filtered through Al_2O_3, and concentrated. The product was purified by column chromatography (silica gel, eluent: hexane).

*[5-(*tert*-Butyldimethylsilyloxy)-4,4-dimethyl-2-(triethylsilyl)-cyclohex-1-enyl]-benzene (**22a**):* colorless oil. HRMS calcd. for $C_{26}H_{46}OSi$: 430.3087; found: 430.3081. ^1H NMR (300 MHz, $CDCl_3$) δ: 7.27–7.23 (m, 3H), 7.10–7.07 (m, 2H), 3.57 (dd, *J* = 6.8 and 4.9 Hz, 1H), 2.45 (ddt, *J* = 18.3, 5.1, and 2.0 Hz, 1H), 2.18 (ddt, *J* = 18.3, 5.1, and 2.0 Hz, 1H), 2.12 (dt, *J* = 17.4 and 1.7 Hz, 1H), 1.89 (dt, *J* = 17.4 and 1.7 Hz, 1H), 0.96 (s, 3H), 0.92 (s, 3H), 0.89 (s, 9H), 0.79 (t, *J* = 6.4 Hz, 9H), 0.21 (q, *J* = 6.4 Hz, 6H), 0.04 (d, *J* = 5.3 Hz, 6H). ^{13}C NMR (75.5 MHz, $CDCl_3$) δ: 147.0, 145.8, 130.0, 128.3, 127.7, 126.5, 74.1, 42.3, 35.9, 33.9, 26.7, 25.8, 21.6, 18.0, 15.3, 7.5, 3.4, –4.1, –4.9. Anal. calcd. for $C_{26}H_{46}OSi$: C 72.49, H 10.76; found: C 72.36, H 10.77.

*5-(*tert*-Butyldimethylsilyloxy)-1,4,4-trimethyl-2-(triethylsilyl)-cyclohexene (**22b**):* colorless oil. HRMS calcd. for $C_{21}H_{44}OSi_2$: 368.2931; found: 368.2938. ^1H NMR (300 MHz, $CDCl_3$) δ: 3.46 (dd, *J* = 7.7 and 5.6 Hz, 1H), 2.17–1.76 (m, 4H), 1.70 (s, 3H), 0.91 (t, *J* = 7.9 Hz, 9H), 0.89 (s, 9H), 0.85 (s, 3H), 0.77 (s, 3H), 0.64 (q, *J* = 7.9 Hz, 6H), 0.03 (d, *J* = 2.8 Hz, 6H). ^{13}C NMR (75.5 MHz, $CDCl_3$) δ: 141.2, 125.2, 74.3, 43.2, 40.8, 34.0, 27.2, 25.8, 23.1, 20.5, 18.3, 7.6, 4.2, –4.1, –4.9. Anal. calcd. for $C_{21}H_{44}OSi_2$: C 68.40, H 12.03; found: C 68.27, H 12.17.

© 2001 NRC Canada

*1-Butyl-5-(*tert*-butyldimethylsilyloxy)-4,4-dimethyl-2-(triethylsilyl)-cyclohexene (**22c**):* colorless oil. HRMS calcd. for $C_{24}H_{50}OSi_2$: 410.3401; found: 410.3400. ^{1}H NMR (300 MHz, $CDCl_3$) δ: 3.46 (dd, *J* = 7.5 and 5.5 Hz, 1H), 2.12–1.73 (m, 6H), 1.39–1.26 (m, 4H), 0.91 (t, *J* = 8.0 Hz, 9H), 0.88 (s, 3H), 0.77 (s, 3H), 0.62 (q, *J* = 8.0 Hz, 6H), 0.03 (d, *J* = 3.7 Hz, 6H). ^{13}C NMR (75.5 MHz, $CDCl_3$) δ: 145.9, 125.1, 74.4, 43.1, 37.7, 37.4, 34.1, 31.6, 31.3, 27.1, 25.9, 23.1, 22.7, 20.7, 18.0, 14.2, 7.6, 4.3, −4.0, − 4.9.

Conclusion

We demonstrated for the first time an intramolecular addition of silyl enol ethers to both terminal and internal unactivated alkynes by using Lewis acid. While the $EtAlCl_2$-mediated reaction gave cyclohexenone derivatives, the silyloxy-substituted cyclic vinylsilanes were produced in the $B(C_6F_5)_3$-catalyzed reaction in the presence of Et_3SiH. The presented *endo*-selective method could be used for the construction of mono- and bicyclic compounds possessing a cyclohexenone framework.

References

1. (*a*) I. Ojima, M. Tzamarioudaki, Z. Li, and R.J. Donovan. Chem. Rev. **96**, 635 (1996); (*b*) R. Grigg and V. Sridharan. *In* Comprehensive organometallic chemistry II. Vol. 12. *Edited by* E.W. Abel, F.G.A. Stone, and G. Wilinson. Pergamon, Oxford. 1995. pp. 299.
2. (*a*) M. Lautens, W. Klute, and W. Tam. Chem. Rev. **96**, 49 (1996); (*b*) T. Harada, T. Otani, and A. Oku. Tetrahedron Lett. **38**, 2855 (1997); (*c*) H. Huang and C.J. Forsyth. J. Org. Chem. **62**, 8595 (1997).
3. (*a*) M. Yamamguchi, A. Hayashi, and M. Hirama. J. Am. Chem. Soc. **115**, 3362 (1993); (*b*) T. Tsukagoshi, Y. Kido, M. Arisawa, T. Sugihara, and M. Yamaguchi. *In* Int. Symp. Carbanion Chem. (ISCC-5), 5th, 1998. Sendai. pp. 144.
4. (*a*) J. Drouin, M.A. Boaventura, and J.M. Conia. J. Am. Chem. Soc. **107**, 1726 (1985); (*b*) J. Drouin and M.A. Boaventura. Tetrahedron Lett. **28**, 3923 (1987); (*c*) M.A. Boaventura, J. Drouin, F. Theobald, and N. Rodier. Bull. Soc. Chim. Fr. 1006 (1987); (*d*) M.A. Boaventura and J. Drouin. J. Bull. Soc. Chim. Fr. 1015 (1987).
5. (*a*) C.J. Forsyth and J. Clardy. J. Am. Chem. Soc. **112**, 3497 (1990); (*b*) H. Huang and C.J. Forsyth. J. Org. Chem. **60**, 2773 (1995); (*c*) H. Huang and C.J. Forsyth. J. Org. Chem. **60**, 5746 (1995).
6. K. Maeyama and N. Iwasawa. J. Am. Chem. Soc. **120**, 1928 (1998).
7. (*a*) A.J. Frontier, S. Raghavan, and S.J. Danishefsky. J. Am. Chem. Soc. **119**, 6686 (1997); (*b*) H. Huang and C.J. Forsyth. J. Org. Chem. **60**, 5746 (1995).
8. K.-i. Imamura, E. Yoshikawa, V. Gevorgyan, and Y. Yamamoto. Tetrahedron Lett. **40**, 4081 (1999).
9. (*a*) N. Asao and Y. Yamamoto. Bull. Chem. Soc. Jpn. **73**, 1071 (2000); (*b*) N. Asao, T. Shimada, and Y. Yamamoto. J. Am. Chem. Soc. **121**, 3797 (1999); (*c*) K. Imamura, E. Yoshikawa, V. Gevorgyan, and Y. Yamamoto. J. Am. Chem. Soc. **120**, 5339 (1998).
10. (*a*) D.J. Parks and W.E. Piers. J. Am. Chem. Soc. **118**, 9440 (1996); (*b*) D.J. Parks, J.M. Blackwell, and W.E. Piers. J. Org. Chem. **65**, 3090 (2000).
11. N. Petragnani and M. Yonashiro. Synthesis, 521 (1982).
12. P. Brownbridge. Synthesis, 1 (1983).

© 2001 NRC Canada

Synthetic studies of novel ninhydrin analogs

Richard R. Hark, Diane B. Hauze, Olga Petrovskaia, and Madeleine M. Joullié

Abstract: Ninhydrin is an essential tool in the analysis of amino acids, peptides, and proteins, and the preferred reagent for the detection of latent fingerprints on porous surfaces. The goal of this investigation was to prepare ninhydrin analogs with enhanced chromogenic and fluorogenic properties. Target compounds included structures with extended conjugation and (or) with the presence of sulfur-containing moieties. We have devised general convergent routes for novel heterocyclic and aryl-substituted ninhydrin analogs for use as reagents for amino acid detection.

Key words: ninhydrin analogs, synthesis, ketals, Suzuki cross-coupling reactions, Stille cross-coupling reactions.

Résumé : La ninhydrine est un outil essentiel pour l'analyse des acides aminés, des peptides et des protéines ainsi que le réactif privilégié pour la détection d'empreintes digitales latentes sur des surfaces poreuses. Le but de ce travail était de préparer des analogues de la ninhydrine ayant des propriétés chromogènes et fluorogènes accrues. Les composés cibles incluaient des structures avec conjugaison accrue et/ou comportant la présence de portions contenant du soufre. On a mis au point des voies générales convergentes permettant de préparer de nouveaux analogues hétérocycliques de la ninhydrine ainsi que d'autres portant des substituants aryles pour utiliser comme réactifs de détection des acides aminés.

Mots clés : analogues de la ninhydrine, synthèses, cétals, réaction de couplage croisé de Suzuki, réactions de couplage croisé de Stille.

[Traduit par la Rédaction]

Introduction

Ninhydrin or 2,2-dihydroxy-1,3-indanedione (**1**, Fig. 1) has earned a prominent place in chemistry, biochemistry, and forensic science due to its color-forming reaction with amino acids and amines found in fingerprint residues (1). The chemistry of this interesting compound has been the subject of several reviews (2–6).

Since its serendipitous discovery by Ruhemann (7), ninhydrin (**1**) has been a widely used reagent in several areas of chemistry. Although **1** reacts with a plethora of reagents to give a wide variety of structures (5), it is best known for its reactions with amines and amino acids to give the colored compound known as Ruhemann's purple (8, 9). These complex reactions have been a subject of prolonged investigations (5) and are still of current interest (10). Of particular relevance is the work of Grigg and co-workers (11–13), who established the intermediacy of 1,3-dipoles in the formation of Ruhemann's purple and the studies of the transition-metal complexes of Ruhemann's purple by Davies et al. (14, 15).

Our interest in the synthesis of novel ninhydrin analogs to be used in the detection of latent fingerprints has led us to investigate previously reported approaches to ninhydrin to prepare new reagents with enhanced optical properties. During the course of these investigations, we have examined several chemical and physical properties of substituted ninhydrin analogs and have devised new synthetic approaches to some of these compounds.

Ninhydrin (**1**) is the forensic specialist's top choice for latent print detection on porous surfaces (1). It is affordable and easy to apply. The developed dark purple fingerprints are easy to detect by the naked eye and do not require special viewing conditions. The ninhydrin reaction has the advantage of forming a product with a high molar extinction coefficient under very mild reaction conditions.

However, despite its obvious advantages for forensic applications, the fluorogenic and chromogenic properties of ninhydrin can be improved. For example, Herod and Menzel (16) reported that fingerprints which were developed with ninhydrin could be made to fluoresce after treatment with zinc chloride. Formation of fluorescent complexes resulted in enhanced sensitivity and improved contrast between the fingerprint and the background but at the expense of introducing an extra step in processing the prints. An ideal reagent should display high sensitivity as both a chromogen and a fluorogen without secondary treatment.

The high polarity of ninhydrin does not allow much versatility in choosing solvent formulations. The choice of sol-

Received March 14, 2001. Published on the NRC Research Press Web site at http://canjchem.nrc.ca on October 31, 2001.

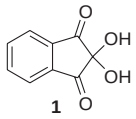
Dedicated to Professor Victor Snieckus with appreciation for his many contributions to organic synthesis.

R.R. Hark,[1] D.B. Hauze,[2] O. Petrovskaia,[3] and M.M. Joullié.[4] Department of Chemistry, University of Pennsylvania, Philadelphia, PA 19104–6323, U.S.A.

[1]Department of Chemistry, Marietta College, Marietta, OH 45750. Current address: Juniata College, Huntingdon, PA 16652, U.S.A.
[2]Chemical Sciences, Wyeth-Ayerst Research, 145 King of Prussia Road, Radnor, PA 19087, U.S.A.
[3]PPG Industries, 400 College Park Drive, Monroeville, PA 15146, U.S.A.
[4]Corresponding author (telephone: (215) 898-3158; fax: (215) 898-5129; e-mail: mjoullie@sas.upenn.edu).

 DOI: 10.1139/cjc-79-11-1632 © 2001 NRC Canada

Fig. 1. Ninhydrin.



1

vents presents a serious challenge (17) since the solvent has to be volatile, nontoxic, nonflammable, environmentally safe (ozone friendly), and affordable. Polar solvents, such as methanol, diffuse the ink frequently found in pieces of evidence and therefore are unsuitable for forensic applications. Previously used freon-based ninhydrin formulations that were once considered ideal are no longer acceptable because of the environmental impact of freons. The constraints imposed by solubility are a factor that must be considered in the design of new analogs.

Modifications in the structure of ninhydrin are an attractive approach for obtaining a highly effective amino acid reagent for forensic and analytical applications. Expansion of the conjugated system and introduction of appropriate substituents, such as amino, alkoxy, or thioalkoxy groups, can in principle, cause an increase in molar extinction coefficients, as well as blue or red shifts in absorption maxima of Ruhemann's purple analogs. An array of ninhydrin-type reagents with a wide range of absorption maxima allows for the optimal selection of visualizing reagents for specific backgrounds. Modifications of the chromophore can also induce fluorescence. Appended nonpolar moieties can improve the solubility of the reagent. The structural changes that affect the spectral properties of the products in the amino acid reactions should not, however, adversely affect the reactivity of the vicinal triketone fragment.

In view of these considerations, a large number of ninhydrin analogs has been synthesized and evaluated. By 1992, the data on approximately 30 ninhydrin analogs had been reported in the literature (18). At the present time, due to our efforts and those of other groups, this number has tripled. The term "ninhydrin analogs" is typically used to describe compounds with a vicinal cyclopentatrione moiety fused to an aromatic ring. They are usually represented in their most stable hydrate form (19).

Figure 2 gives an extensive overview of all known ninhydrin analogs, some of which will be subsequently described.

The first ninhydrin analog, **38**, was synthesized by Ruhemann in an attempt to prepare a compound with greater solubility in organic solvents (20, 21). Since that time numerous analogs (e.g., **5**, **7**, **13** (22), **8** (23), **40** (24), **73** (25), **80** (26, 27), **81**, **83** (28), **74**, **75** (29, 30), **73** (31), **34** (20), **44** (32), **72** (33), **76** (34), **78** (35), and **9**[5]) have been prepared for a variety of uses, including natural product synthesis and studies of reaction kinetics and charge transfer complexes. The majority of ninhydrin analogs have been prepared for forensic evaluation. Compounds **2**, **6**, **15**, **36**, **37**, **43**, **45**, **46**, and **69** were studied by Lennard et al. (36, 37). Joullié and co-workers have synthesized compounds **68** (38), **70**, **84** (38, 39), **23** (40), **10**, **47**–**49**, **52**–**62**, **67**, **86**, **87** (41, 18), **22**, and **85** (42). To identify potential fingerprint reagents, Almog et al. (43–47) have conducted extensive evaluations of ninhydrin analogs, many of which they have synthesized (**3**, **4**, **11**, **12**, **14**, **16**, **21**, **24**, **28**, **41**, **71**, and **77**). Recently, Della and co-workers (48–50) synthesized compounds **17**–**20**, **25**–**27**, **29**–**32**, **39**, **50**, **64**, and **79**.

At the time the present work was initiated, Cantu et al. (51) reported the forensic evaluation of eight ninhydrin analogs as well as **1**. Subsequently, other analogs were developed and evaluated by different groups (43, 52, 1, 53–55). Compounds **23** and **84** were considered to be the most promising reagents. These compounds displayed a combination of good chromogenic properties with good fluorogenic properties after zinc chloride treatment. These analogs were not commercially available, although **23** can now be obtained from BVDA International, Haarlem, Netherlands. It was therefore necessary to design a high-yielding and cost-effective synthesis that would allow a variety of fragments to be appended to the ninhydrin moiety for the purpose of generating an array of new reagents which could be screened for improved properties.

The syntheses of ninhydrin and its analogs usually involve oxidation of 1-indanones (**88**) or 1,3-indanediones (**89**). A retrosynthetic analysis of ninhydrins from these precursors is shown in Scheme 1.

1-Indanones are routinely obtained via Friedel–Crafts cyclization of the corresponding 3-phenylpropionic acids (**90**), which in turn can be obtained from aromatic aldehydes (**94**). An alternative approach to the synthesis of 1-indanones was devised by reacting substituted benzenes with 3-chloropropanoic acid chloride (56, 49). Sartori et al. (57) suggested a method of indanone ring closure that was somewhat similar to this approach. Attempts to reproduce this synthesis, as well as the 1,3-indanedione synthesis reported by the same group, were unsuccessful (58). A complex formed from dimethylacrylamide and triflic anhydride was found to react with some 1,2-dialkoxybenzenes and 1,2,3-trialkoxybenzenes to give the corresponding 1-indanones in good yields (59).

1,3-Indanediones (**89**) are usually obtained from the corresponding diesters (**91**) or phthalic anhydrides (**92**). 2-Indanone is a less suitable precursor for ninhydrin synthesis due to its low stability, and no syntheses of ninhydrin analogs from 2-indanones have been reported.

Since our review of synthetic methods, a few potential approaches to the carbon framework have appeared such as the ring contraction of pyranones (60, 61), the Pauson–Khand reaction (62), and other metal-catalyzed cyclizations. The disadvantage of such methods is the reaction complexity and the cost of the required starting materials. Our efforts were focused on the synthesis of a broad variety of ninhydrin analogs which could be assayed for utility as affordable, efficient reagents for the detection of amino acids.

Ninhydrin analogs

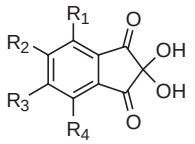
Our approach was to synthesize a broad variety of affordable, efficient analogs classified in three main categories.

Bisninhydrins in which a single molecule would contain two cyclopenta-1,2,3-trione moieties. The reaction of these compounds with amino acids in principle could afford polymeric Ruhemann's purple species.

[5] A. Pounds. Unpublished results. 1990.

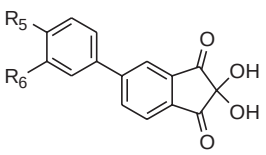
© 2001 NRC Canada

Fig. 2. Overview of ninhydrin analogs.

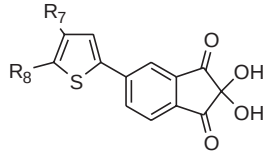


$R_{1,2,3,4}$ = H, unless shown otherwise

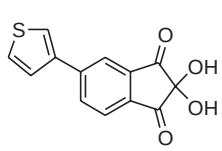
2 R_1 = Me
3 R_1 = NH_2
4 R_1 = NMe_2
5 R_1 = NO_2
6 R_1 = OMe
7 R_1 = Cl
8 R_2 = Me
9 R_2 = $(CH_2)_{15}CH_3$
10 R_2 = $(CH_2)_2COOH$
11 R_2 = NH_2
12 R_2 = NMe_2
13 R_2 = NO_2
14 R_2 = OH
15 R_2 = OMe
16 R_2 = OEt
17 R_2 = OPh
18 R_2 = OC_6H_4-*p*-NMe_2
19 R_2 = OC_6H_4-*p*-OMe
20 R_2 = OC_6H_4-*p*-NO_2
21 R_2 = OAc
22 R_2 = F
23 R_2 = SMe
24 R_2 = S-*i*-Pr
25 R_2 = SBu
26 R_2 = SC_7H_{15}
27 R_2 = SPh
28 R_2 = SCN
29 R_2 = Cl
30 R_2 = SeMe
31 R_2 = SeC_5H_{11}
32 R_2 = SePh
33 R_2 = Br
34 R_1 = R_2 = OMe
35 R_1, R_2 = OCH_2O
36 R_2 = R_3 = Me
37 R_2 = R_3 = OMe
38 R_2, R_3 = OCH_2O
39 R_1 = R_4 = OMe
40 R_2 = R_3 = Cl
41 R_2 = OMe; R_3 = Cl
42 R_1 = Br; R_3, R_4 = OCH_2O
43 R_1 = R_4 = Me; R_2 = R_3 = Ph
44 R_1 = R_2 = R_3 = R_4 = F
45 R_1 = R_2 = R_3 = R_4 = Cl
46 R_1 = R_2 = R_3 = R_4 = Br



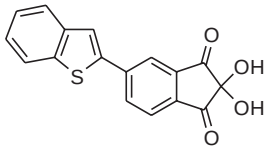
47 R_5 = R_6= H
48 R_5 = Ph; R_6 = H
49 R_5 = NMe_2; R_6 = H
50 R_5 = NO_2; R_6 = H
51 R_5 = OH; R_6 = H
52 R_5 = OMe; R_6 = H
53 R_5, R_6 = OCH_2O
54 R_5 = SMe; R_6 = H



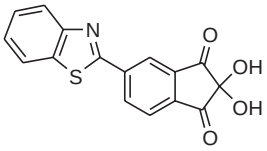
55 R_7 = R_8 = H
56 R_7 = Me; R_8 = H
57 R_7 = H; R_8 = Me
58 R_7 = H; R_8 = Et



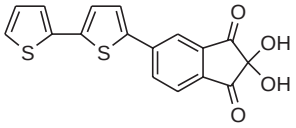
59



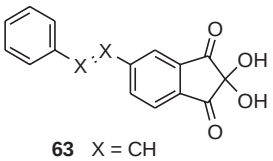
60



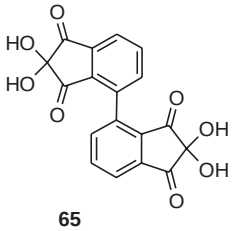
61



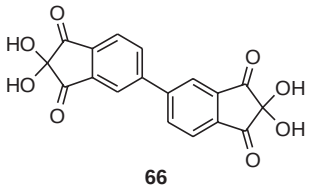
62



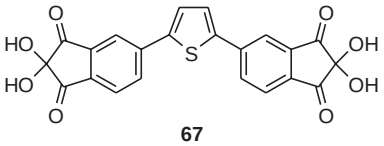
63 X = CH
64 X = N



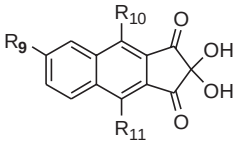
65



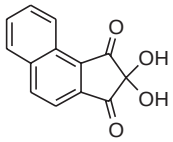
66



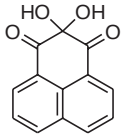
67



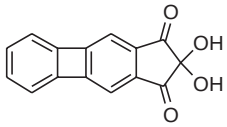
68 R_9 = R_{10} = R_{11} = H
69 R_9 = H; R_{10} = R_{11} = Ph
70 R_9 = OMe; R_{10} = R_{11} = H



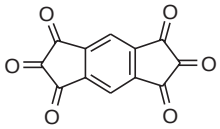
71



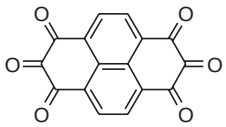
72



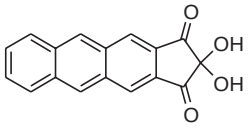
73



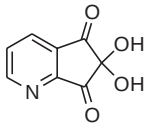
74



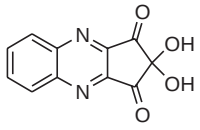
75



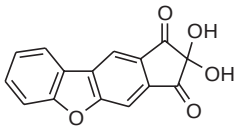
76



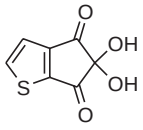
77



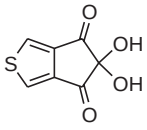
78



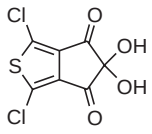
79



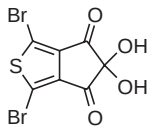
80



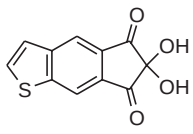
81



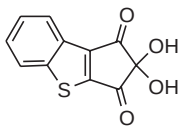
82



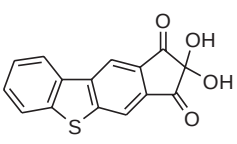
83



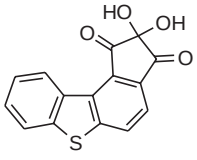
84



85



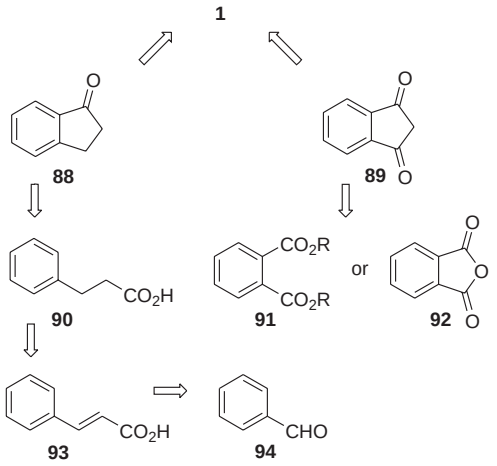
86



87

© 2001 NRC Canada

Scheme 1.



Sulfur-containing ninhydrin analogs based on the similarity of the physical properties of thiophene and benzene derivatives. The incorporation of sulfur into the aromatic ring fused to the tricarbonyl system was previously shown to produce analogs exhibiting superior color and fluorescence.

Aryl and heteroaryl analogs that extend the conjugation of the ninhydrin system. The parent compound of this series is 5-phenylninhydrin. Compounds with *para*-substituted phenyl groups were expected to produce interesting analogs, which are biphenyl derivatives.

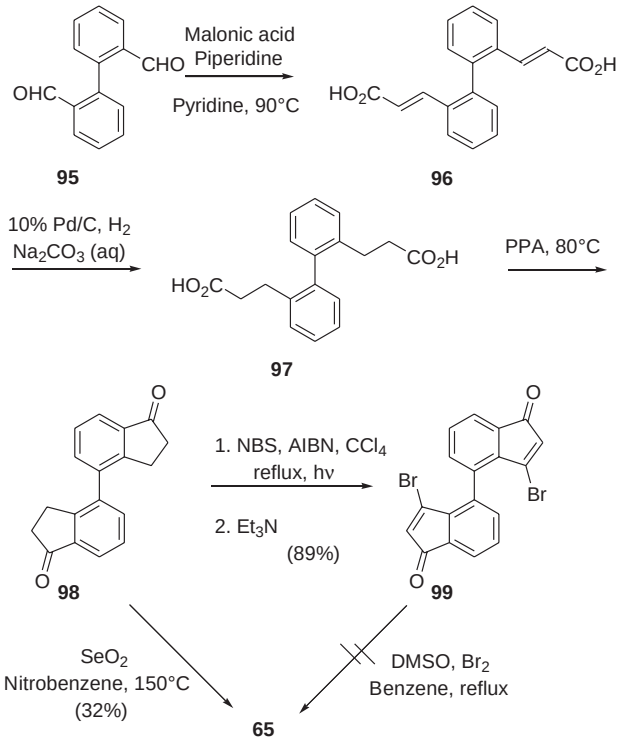
Bisninhydrin analogs

We first envisaged a 4,4′-bisninhydrin (**65**) which could be prepared by the same sequence of reactions used to prepare 5-methoxyninhydrin from anisaldehyde (39). Application of this protocol to synthesize 4,4′-bisninhydrin from 2,2′-biphenylcarboxaldehyde appeared to be a suitable route (Scheme 2).

The requisite 2,2′-biphenyldicarboxaldehyde (**95**) was prepared in good yield by ozonolysis of phenanthrene, followed by in situ reduction with sodium iodide in glacial acetic acid according to a known procedure (63). Knoevenagel condensation of dialdehyde **95** gave diacid **96** in only modest yield since the aldehyde groups are somewhat hindered due to the conformation of the biphenyl system. Catalytic hydrogenation of the unsaturated diacid **96** afforded diacid **97**, which was cyclized using polyphosphoric acid (PPA) to give bisindanone **98** (64).

The bisindanone **98** was oxidized with *N*-bromosuccinimide to form a tetrabromide, which subsequently eliminated hydrogen bromide and formed the bis-β-bromoindenone **99** in high yield. Attempts to transform this penultimate precursor into the desired bisninhydrin **65** using a modification of the Kornblum oxidation (40) led to a complex reaction mixture with substantial decomposition. Again, it is believed that steric congestion in the biphenyl system hindered the approach of the oxidizing agent. Originally, we had considered selenium dioxide to be an inferior choice for oxidizing indanones because of the relatively poor yields reported in the syntheses of other ninhydrin analogs. Selenium dioxide was also known to be toxic and had to be used in stoichiometric quantities while the two-step oxidation

Scheme 2.



method developed by Heffner and Joullié (39) was efficient and convenient. Selenium dioxide did have the advantage, however, of oxidizing indanones to ninhydrins in a single step.

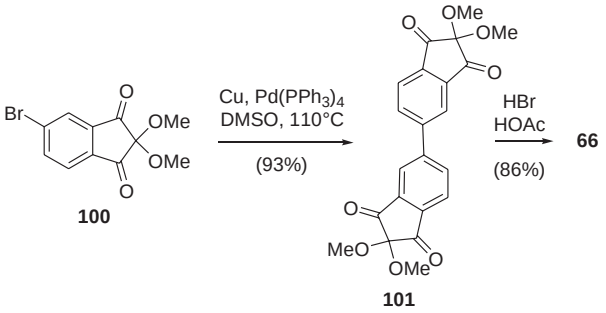
Selenium dioxide oxidation of the bisindanone **98** gave a 15% yield of the desired bisninhydrin **65**, which was contaminated with a small amount of selenium by-products. Selenous acid and other selenium-containing compounds must be removed from the final product since these contaminants may act as a bleaching agent and would prevent the formation of the characteristic purple color (65). When the reaction was run in nitrobenzene at 150°C, selenium-containing by-products were easily removed from the reaction mixture and **65** was obtained in 32% yield (Scheme 2). Though ninhydrin itself is relatively easy to purify, substituted ninhydrins are generally more difficult to obtain in pure form, as methods which were successful in the case of ninhydrin were frequently not applicable.

Preliminary testing showed that the new bisninhydrin (**65**) reacted with amino acids to give the characteristic Ruhemann's purple color but no special optical properties were observed. This result suggested that the steric hindrance of the keto groups at the 3- and 3′-positions of the biphenyl ring prevented the two ninhydrin systems from being significantly conjugated. Each half of the compound behaved essentially as an isolated ninhydrin molecule.

The 5,5′-bisninhydrin (**66**, Fig. 2) was expected to show altered properties since no similar hindrance to conjugation existed other than that which is usual for an unsubstituted biphenyl system. However, this conjugative overlap made its preparation somewhat problematic. The synthesis of **66** following a route similar to that used to prepare **65** contained

© 2001 NRC Canada

Scheme 3.



several low yielding steps, therefore we opted for a different route.

The new approach is shown in Scheme 3.

Palladium chemistry provided an entry to not only aryl- and heteroaryl-substituted ninhydrins, whose syntheses will be described later, but also to this class of bisninhydrins (66). A key intermediate (2,2-dimethoxy-5-bromoindan-1,3-dione (**100**)), described later, was used in an Ullmann-type reaction to afford the desired bisninhydrin (**66**) in good yield after hydrolysis of the diketal precursor **101**. It is noteworthy that neither copper nor palladium(0) alone were sufficient to induce the coupling reaction. 5,5′-Bisninhydrin (**66**) exhibited low solubility in various solvents, and did not display any enhanced chromogenic or fluorogenic properties.

Sulfur-containing ninhydrin analogs

The sulfur-containing analogs are based on inclusion of a thiophene ring in the molecule. Thieno[*e*]ninhydrin (**85**), is an isomer of the superior reagent thieno[*f*]ninhydrin (51) (**84**) in which the five-membered tricarbonyl fragment is fused to a thiophene ring instead of a benzene ring (39). We were interested in examining the fluorescence of the Ruhemann's purple of **85**, and also in developing a reagent which would be easier to synthesize than the challenging thieno[*f*]ninhydrin (**84**).

A Heck coupling reaction was chosen to attach the propenoic acid side chain to the aryl core. The tricyclic indanone **102** was obtained in three steps from benzo[*b*]thiophene using published procedures (42).

It was believed that indanone **102** (Scheme 4) would withstand the high temperature (145°C) used in selenium dioxide oxidations in nitrobenzene. However, the conversion proceeded in only 11% yield. The modification of the Kornblum reaction (39) also failed. As enamine formation and subsequent oxidation were successful in the synthesis of thianinhydrin (42); the same methodology was investigated in this case. We were interested in improving the synthesis of thieno[*e*]ninhydrin, and exploring the general applicability of this new approach.

Dibromination of indanone **102** proceeded in quantitative yield (Scheme 4).

The crude dibromide (**103**) was immediately hydrolyzed to avoid the problems experienced earlier in the bromination–elimination method. 1,3-Dione **104** was obtained in 78% yield after column chromatography. Reaction of the dione with DMF-dimethyl acetal proceeded in nearly quantitative

Scheme 4.

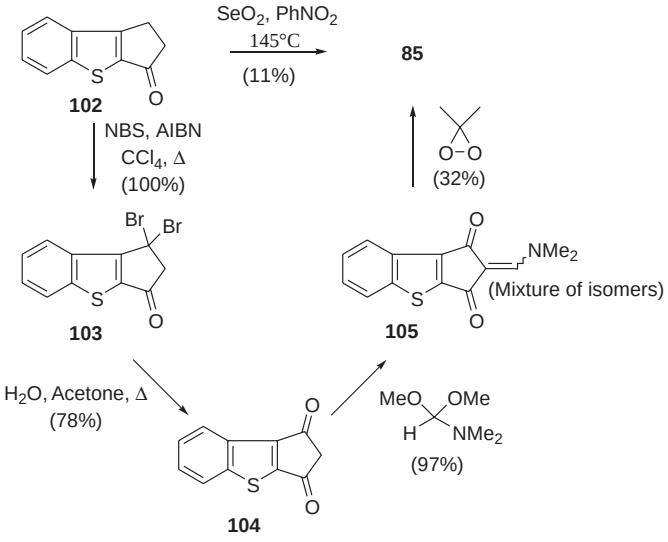
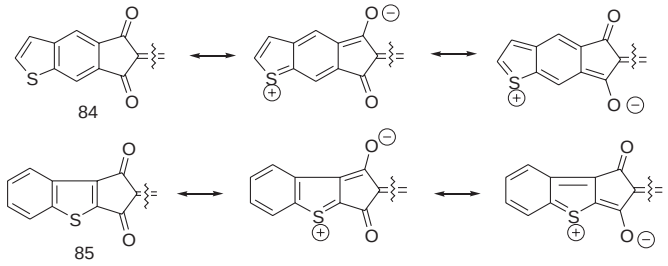


Fig. 3. Relationship between *p*-quinoid resonance structures and fluorescence for compounds **84** and **85.**



yield, and the enamine **105** was oxidized cleanly to thieno[*e*]ninhydrin (**85**) in 32% yield using dimethyl dioxirane.

Evaluation of thieno[*e*]ninhydrin (**85**) as a reagent for the development of latent fingerprints showed that the strong fluorescence of the Ruhemann's purple analog derived from **84** was not exhibited by **85**.

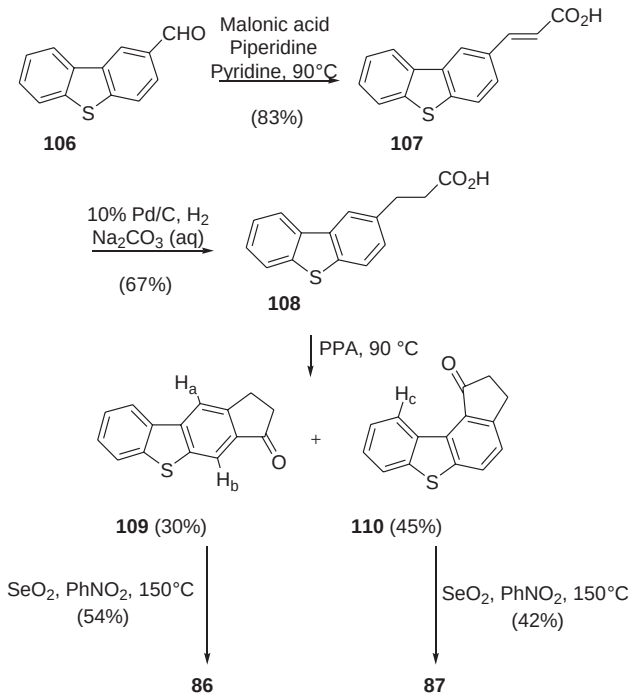
The disappointing results obtained for the sulfur analogs thianinhydrin (**80**) and for thieno[*e*]ninhydrin (**85**) might be rationalized as resulting from the lack of *p*-quinoid resonance structures of their Ruhemann's purple species. The Ruhemann's purple species of the superior reagents 5-(methylthio)ninhydrin (**23**) and thieno[*f*]ninhydrin (**84**) have resonance structures that exhibit an extended *p*-quinoid character from release of electron density of sulfur into the aromatic system. Analogs **80** and **85** cannot adopt such structures and, therefore, do not exhibit the strong fluorescence on reaction with amino acids.

The relationship between the *p*-quinoid resonance structure and fluorescence may explain the differences in fluorescence intensity of the Ruhemann's purple analogs of thieno[*f*]ninhydrin and thieno[*e*]ninhydrin (Fig. 3). Benzo[*f*]ninhydrin (**68**), which reacts with amino acids to afford a highly fluorescent species, also has a Ruhemann's purple which can adopt a *p*-quinoid resonance structure. The weakly fluorescent Ruhemann's purple analog of benzo[*e*]ninhydrin adopts an *o*-quinoid structure.

What cannot be explained by this theory is the fluorescence of the Ruhemann's purple species derived from

© 2001 NRC Canada

Scheme 5.



dichlorothia[*c*]ninhydrin (**82**) (42) which cannot adopt the *p*-quinoid structure, yet is fluorescent without secondary treatment. However, the presence of the two chlorine substituents adds complexity to any interpretation of this result.

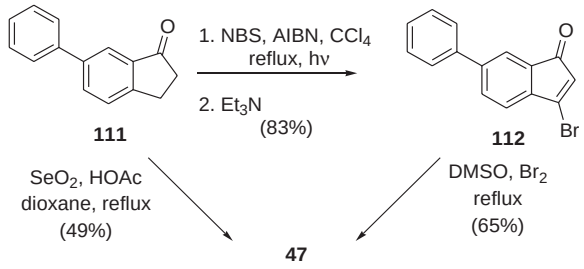
In an attempt to improve the properties of thieno[*f*]ninhydrin (**84**) (67), we initiated the synthesis of thianaphtheno[*f*]ninhydrin (**86**, Scheme 5) (18).

Knoevenagel condensation of aldehyde **106** (69) gave a 83% yield of the unsaturated acid (**107**). Catalytic hydrogenation afforded a 67% yield of **108** after recrystallization.

Cyclization of the saturated acid could lead to two potential regioisomers, with the linear isomer (**109**) predicted to predominate based on steric considerations. When the carboxylic acid was cyclized with PPA, two isomers were produced in an overall yield of 75%, with the nonlinear ketone (**110**) as the major product in a 3:2 ratio (Scheme 5) (18). These isomeric ketones could be readily distinguished by ^{1}H NMR. The proton in the 8-position of the nonlinear isomer (**110**) displayed a large down-field shift due to its proximity to the deshielding region of the neighboring carbonyl group. With sufficient quantities of **109** and **110** in hand, we elected to oxidize both ketones. The ninhydrin analog (**87**) derived from **110**, although not one of our original target molecules, was also prepared.

Purification problems associated with selenium dioxide oxidations were avoided by carrying out the reaction in nitrobenzene. The elevated reaction temperature caused the red allotropic form of selenium to undergo a phase transition (which occurs at 140°C) so that nearly all of the selenium metal by-product could easily be removed by filtration in its black form. The solvent can then be removed by steam distillation of the crude mixture. The selenium dioxide oxidation of the isomeric ketones afforded a 54% and 42% yield of **86** and **87**, respectively, (Scheme 5). These analogs did not display superior fluorogenic properties.

Scheme 6.



Aryl and heteroaryl ninhydrin analogs

We expected that extending the conjugation of the substituents on a ninhydrin ring would increase the fluorescence of the corresponding Ruhemann's purple species. Addition of an aryl substituent at the 5-position of ninhydrin should accomplish this goal. Substituents at the 4-position were not considered because some reported 4-substituted analogs did not show the desired properties (46).

We first synthesized phenylninhydrin (**47**) starting from biphenyl carboxaldehyde using the protocol previously described for the preparation of **109** and **110** (Scheme 5). Radical bromination of ketone **111** with NBS provided **112** in 83% yield (Scheme 6) (39).

The bromide was oxidized to phenylninhydrin with DMSO and heat in 65% yield. One-step oxidation with selenium dioxide gave a 49% yield of **47**. Although analog **47** was similar to ninhydrin in most of its properties, on reaction with amino acids, a short-lived phosphorescence was observed. A similar method was also used to prepare 5-fluoroninhydrin (**22**) from commercially available 6-fluoro-1-indanone (Aldrich). The chromogenic and fluorogenic properties of analog **22** were also similar to those of **1**.

The synthetic protocol illustrated in Scheme 6 was a good method for the preparation of an aryl ninhydrin analog. However, a more convergent route was needed to synthesize a large number of analogs. Scheme 7 shows the retrosynthetic analysis of our approach.

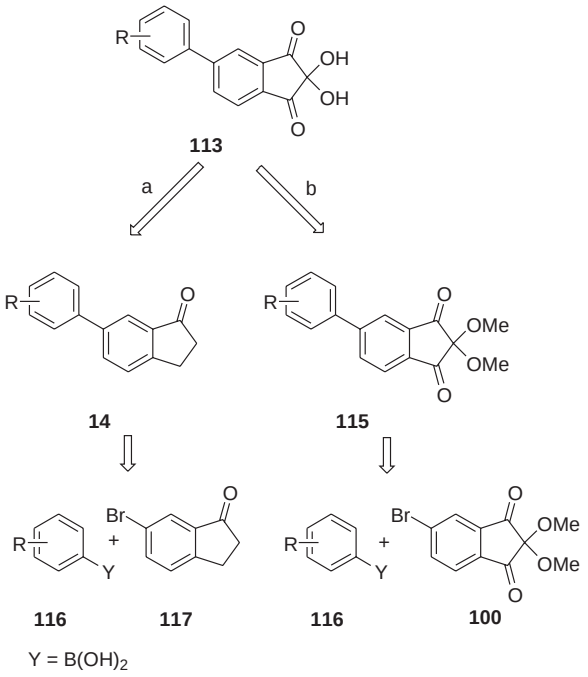
We envisioned employing metal-catalyzed coupling reactions to append a large number of aryl substituents to the ninhydrin nucleus. Our initial efforts utilized the Suzuki cross-coupling (69–71) reaction in which a suitably substituted boronic acid (**116**, Scheme 7) would be coupled to a bromo-substituted ninhydrin precursor (**100** or **117**). The introduction of a dimethyl ketal in the 2-position is necessary since ninhydrin is unstable under the basic conditions (72) required for Suzuki couplings. Of the two routes pictured in Scheme 7, route b was considered to be more attractive since it required only deprotection of a ketal as the final step.

The choice of the protecting groups for the overall synthetic sequence is somewhat limited by the logic of the synthesis and the nature of the substrates. Protecting groups that are highly base-sensitive cannot be employed, since the tricarbonyl will undergo ring opening upon generation under basic conditions (73).

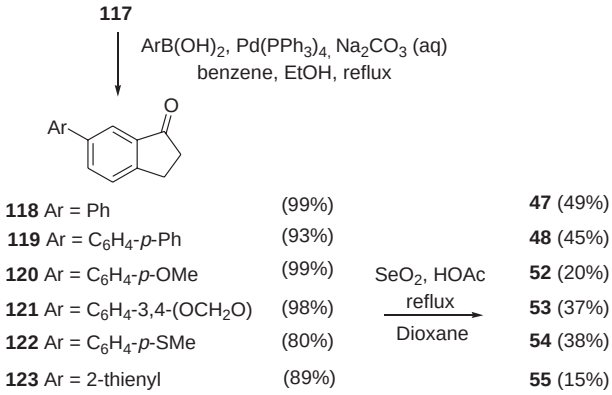
Since 5-bromo-2,2-dibromo-1,3-indanedione was available (18), we decided to use this compound directly in a Suzuki coupling (69, 70). The reaction of this compound with a boronic acid gave none of the desired product but led

© 2001 NRC Canada

Scheme 7.



Scheme 8.

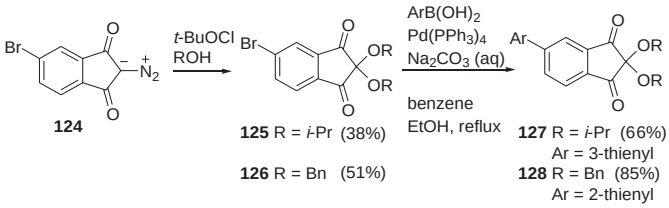


only to decomposition of the starting material. A possible explanation for this behavior was that the aqueous base had hydrolyzed the geminal dibromide to give 5-bromoninhydrin (**33**), which was not stable in basic solution. This result ruled out the possibility that the dibromo derivative could be used in a Suzuki coupling reaction.

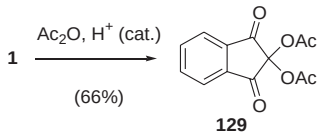
5-Bromo-1,3-indanedione was likewise unsuitable for the Suzuki conditions presumably due to enolization of the 1,3-dione and subsequent reactions of the resulting enol with palladium species. Therefore, a 2,2-dimethyl ketal seemed to be the most practical intermediate for any coupling procedure involving basic conditions.

The stability of 2,2-dimethoxy-1,3-indandione in the presence of acids resembles that of an ether. The conditions for its deprotection are quite harsh (HBr – acetic acid – water, 80°C). Since some of the heterocycles that could be appended to the ninhydrin moiety decompose under these conditions, it was necessary to investigate alternative protocols. A number of protic acids (chloroacetic acid, formic acid, trifluoroacetic acid, hydrochloric acid, toluenesulfonic acid) in solvents ranging from benzene to water failed to achieve the deprotection. Trimethylsilyl iodide also failed to yield a product. Hydroiodic acid, and addition of potassium iodide, a logical choice as a source of a nucleophile in ketal deprotection, did not offer any significant improvement.

Scheme 9.



Scheme 10.



To test the viability of route a in Scheme 7, we used the Suzuki coupling to prepare a series of 6-aryl-1-indanones. The boronic acids used in this project were prepared from commercially available aryl halides according to published procedures (18, 66). All of the boronic acids used were known compounds. The reactions of **117** with several boronic acids proceeded in high yield to give the corresponding 1-indanones (**118**–**123**). Conversion of these ketones to the corresponding ninhydrins (**47**, **48**, **52**–**55**) using the one-step selenium dioxide oxidation was accomplished in poor to moderate yields (Scheme 8).

Other alternatives to the dimethoxy ketal were explored (Scheme 9).

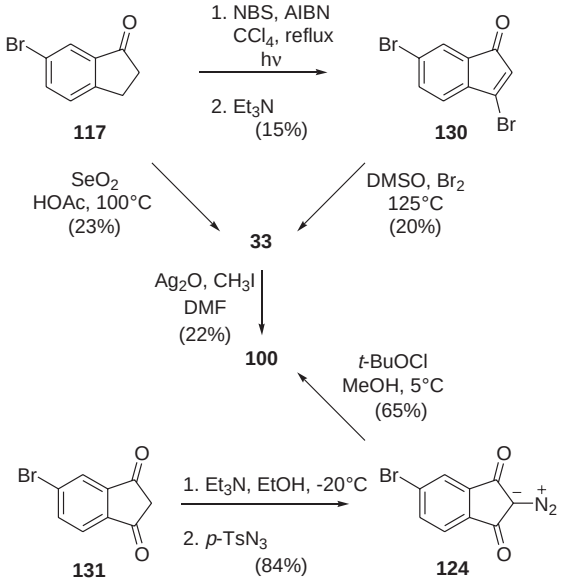
The diisopropyl (**125**) and dibenzyl ketals (**126**) were synthesized from diazodione **124**. Suzuki cross-coupling of these compounds with thienylboronic acids gave compounds **127** and **128** in good yields. Deprotection of the diisopropyl ketal **127** in trifluoroacetic acid at room temperature caused decomposition of the product due to the presence of the thiophene ring. Ketal **125** could be deprotected with trifluoroacetic acid to give 5-bromoninhydrin (**33**). The benzyl group in **128** could not be removed using mild acidic conditions, hydrogenolysis, DDQ, or dimethyldioxirane oxidation (74). An alternative approach, which merits further investigation, is the use of a 2,2-diacetoxy-protecting group. 2,2-Diacetoxy-1,3-indandione was synthesized from **1** (**129**, Scheme 10) and was stable under mildly basic conditions.

Use of the diacetoxy-protecting group may be more compatible with acid-sensitive heteroaromatic moieties, since acidic hydrolysis of the ester group in the presence of water could be carried out under conditions that are milder than the ones required for hydrolysis of dimethyl ketals.

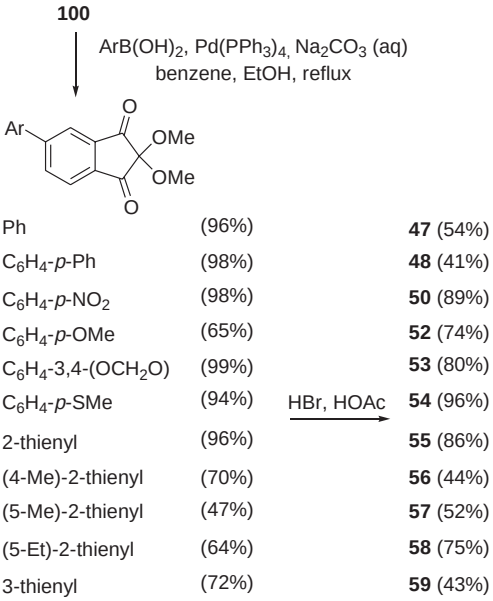
The most straightforward approach to 2,2-dimethoxy-5-bromoindan-1,3-dione (**100**) was the direct bromination of ninhydrin using dibromoisocyanuric acid (DBI) (75), followed by formation of its ketal using methyl iodide and silver oxide. The reaction of DBI with ninhydrin in concentrated

© 2001 NRC Canada

Scheme 11.

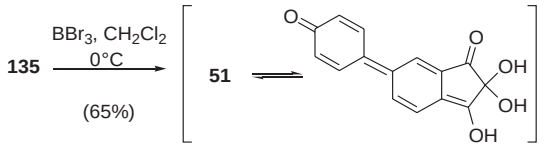


Scheme 12.



132 Ar = Ph	(96%)	**47** (54%)
133 Ar = C_6H_4-*p*-Ph	(98%)	**48** (41%)
134 Ar = C_6H_4-*p*-NO_2	(98%)	**50** (89%)
135 Ar = C_6H_4-*p*-OMe	(65%)	**52** (74%)
136 Ar = C_6H_4-3,4-(OCH_2O)	(99%)	**53** (80%)
137 Ar = C_6H_4-*p*-SMe	(94%)	**54** (96%)
138 Ar = 2-thienyl	(96%)	**55** (86%)
139 Ar = (4-Me)-2-thienyl	(70%)	**56** (44%)
140 Ar = (5-Me)-2-thienyl	(47%)	**57** (52%)
141 Ar = (5-Et)-2-thienyl	(64%)	**58** (75%)
142 Ar = 3-thienyl	(72%)	**59** (43%)

Scheme 13.



sulfuric acid gave an intractable mixture of polyhalogenated products. 5-Bromoninhydrin (**33**) was prepared in modest yield by selenium dioxide oxidation of 6-bromo-1-indanone (**117**) or using the two-step oxidation (Scheme 11).

Conversion of **33** to ketal **100** could only be accomplished in low yield. To obtain sufficient amounts of **100**, a new synthesis was devised starting from 5-bromo-1,3-indanedione (**131**) (76, 77). The investigations of Regitz and co-workers (78–81) with diazo group transfer reactions afforded a reliable method for the preparation of **100** (Scheme 11). Deprotonation of dione **131** with triethylamine at –20°C, followed by addition of *p*-toluenesulfonyl azide gave an 84% yield of **124**. The diazodione is unstable when heated and decomposed explosively at its melting point. *p*-Toluenesulfonyl azide is toxic, shock sensitive, and potentially explosive at elevated temperatures so due care should be exercised in its use. The diazo transfer reagent 4-dodecylbenzenesulfonyl azide or *p*-acetamidobenzenesulfonyl azide are safer alternatives (82, 83). Slow addition of *tert*-butylhypochlorite to a cooled slurry of **124** in methanol gave ketal **100** in 65% yield. The temperature of this reaction must be carefully monitored since *tert*-butylhypochlorite has been known to explode as a result of improper temperature control (84).

With multi-gram quantities of common intermediate **100** and suitable boronic acid partners in hand, we turned our attention to the coupling and (or) deprotection reactions. In moderate scale reactions, the Suzuki coupling typically gave high yields of ketals **132**–**142** (Scheme 12).

Deprotection using a 1:1:1 mixture of 48% hydrogen bromide, glacial acetic acid, and water was found effective for most ketals. This protocol was used to prepare the compounds shown in Scheme 12.

Deprotection of ketal **135** presented an interesting question since it was known that 48% hydrobromic acid could convert aryl methyl ethers into phenols (85). After refluxing **135** using a less concentrated HBr solution, a 74% yield of product (**52**) was obtained with no evidence of ether cleavage. Boron tribromide was used to simultaneously cleave the ether and deprotect the ketal to give 65% yield of **51** as a dark green solid (Scheme 13) (86).

^{1}H and ^{13}C NMR indicated that the compound existed as a mixture of tautomeric forms. The presence of a small amount of the quinoid tautomer could be responsible for the green coloration of the solid as evidenced by weak electronic transitions in the visible region at 594 and 492 nm. Another possibility would be the presence of a small amount of trione.

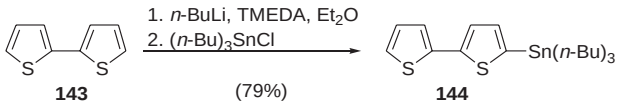
The Suzuki cross-coupling protocol served very well to synthesize a number of ninhydrin analogs. However, there were still several compounds which could not be made by this method due to the difficulty of preparing the required boronic acids. The Stille reaction provided an alternative coupling technique that could be used to make additional novel ninhydrin analogs (88, 89). The synthesis of many other stannanes have been reported in the literature and could potentially be used to produce new ninhydrin analogs (89–94). In another report, Lee and Dai (95) described the synthesis of a variety of arylstannanes in high yield via a sonochemical Barbier reaction.

The synthesis of 5-(tributylstannyl)-2,2′-bithiophene (**144**) began with treatment of **143** with *n*-butyllithium and TMEDA at –78°C to generate a 5-lithio species in situ. This species was quenched with tributyltin chloride (Scheme 14). The product was purified by distillation under reduced pressure to afford a 79% yield of **144**.

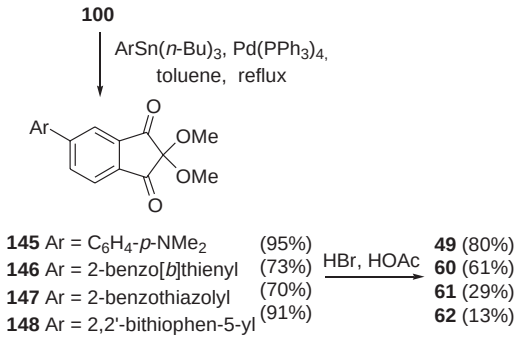
The other stannanes were prepared directly from *p*-dimethylaminobenzene, benzo[*b*]thiophene, and benzothiazole in good yields by a similar method. The common intermediate

© 2001 NRC Canada

Scheme 14.



Scheme 15.



100 was heated with an equimolar amount of arylstannane in toluene with a catalytic amount of $Pd(PPh_3)_4$ to give good yields of coupled products (**145**–**148**, Scheme 15).

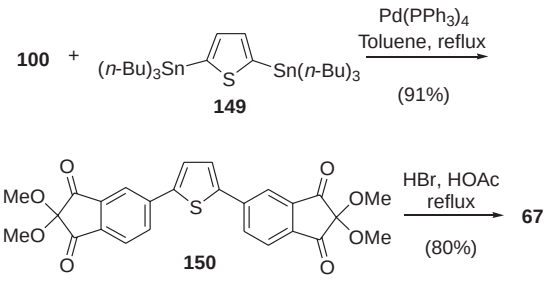
Deprotection under acidic conditions gave poor to good yields of the corresponding ninhydrin analogs (**49**, **60**–**62**) possibly due to decomposition of the heterocyclic rings of **147** and **148**. As compound **49** was not accessible using the Suzuki procedure, its synthesis demonstrates the complementary nature of the Stille methodology.

We next turned our attention to the synthesis of a bisninhydrin analog using the Stille methodology. A previous attempt to accomplish a double coupling of a diboronic acid using Suzuki conditions had been unsuccessful. Literature precedent showed that such a tandem coupling was possible using the Stille reaction (96). Based on the apparent utility of 5-(2-thienyl)ninhydrin (**55**) (41, 67), we were particularly interested in preparing the analog which consisted of two ninhydrin molecules tethered together by a thiophene moiety (**67**). This type of compound incorporates all the ideas for improving the properties of ninhydrin analogs.

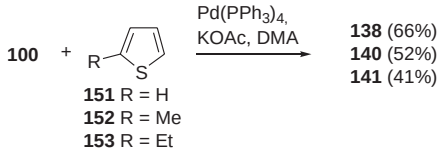
Synthesis of 2,5-bis(tributylstannyl)thiophene (**149**, Scheme 16) proceeded smoothly in good yield (97). The direct syntheses of several dilithio heteroarene species, such as **149**, have been reported (97, 98). Stille coupling of **100** and **149** afforded a high yield of ketal **150**, which was deprotected in acid to give **67**.

Compound **55** (Fig. 2) showed good initial development and good fluorescent properties (51, 18). This finding led us to the investigation of other thienyl-substituted analogs. Thienyl ninhydrins with alkyl chains on the thiophene ring were of interest since these side chains could potentially improve the solubility of target analogs in solvents of lower polarity. Initially, Suzuki coupling of **100** with substituted thienyl boronic acids was chosen as the method to append heterocyclic moieties to the ninhydrin framework. Unfortunately, these boronic acids (99, 100) could only be obtained in low yields due to side-chain deprotonation in the lithiation step. Alkyl-substituted thienyl boronic acids were difficult to purify and as a consequence were used crude and in excess

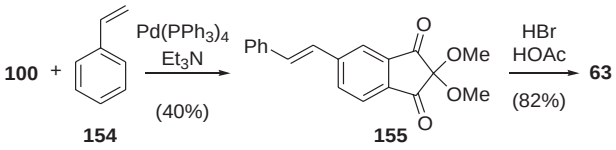
Scheme 16.



Scheme 17.



Scheme 18.



in Suzuki couplings to give modest yields of coupled products (**138**–**142**, Scheme 12).

An alternative procedure was tested to circumvent the difficulties encountered in the synthesis of several boronic acids. Electron-rich heterocycles such as furans, benzofurans, thiophenes, and benzothiophenes are known to undergo palladium-catalyzed cross-coupling reactions with electron-poor aryl halides (101, 102). Although the mechanistic details of this uncommon cross-coupling reaction were not discussed by the authors, it is reasonable to assume that the mechanism is similar to the Heck coupling. Thiophene (**151**), 2-methyl thiophene (**152**), and 2-ethyl thiophene (**153**) were reacted with compound **100** to yield coupled products (**138**, **140**, **141**, Scheme 17) in moderate yields.

The low yields encountered in deprotection of thienyl-substituted analogs (**139**, **140**, **142**, Scheme 12) are due to the formation of high molecular weight side products as observed in the thiophene–isatin condensation (known also as the indophenine reaction) in the presence of sulfuric acid. The term refers to formation of a colored product obtained by condensation of thiophene compounds that have no substitution in 2,5- or 2,3-positions with vicinal polycarbonyls, such as benzil or ninhydrin (103).

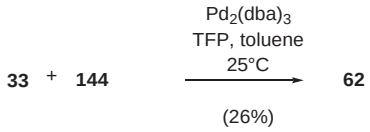
The Heck coupling reaction conditions were used to obtain yet another compound in the series of substituted ninhydrins, a styryl ninhydrin (**63**, Scheme 18), which is an ethylenic homolog of 5-phenylninhydrin (**47**).

Ketal **100** was coupled with styrene (**154**) to afford **155**, which was deprotected in excellent yield. Other interesting compounds could be made using this methodology.

An effective palladium catalyst, using tri-2-furylphosphine (TFP) as a ligand, had been reported (104). The dramatic increase in reactivity of this catalyst provided a solution for

© 2001 NRC Canada

Scheme 19.



Stille reactions that required excessive temperatures (105). This catalyst was easily prepared in situ by ligand exchange with tris-(dibenzylideneacetone)dipalladium(0) (106). Both compounds are commercially available (107). To test the efficacy of this milder coupling procedure, we chose the analog (**62**) that had given us the poorest yield in the deprotection step. The reaction is shown in Scheme 19.

After formation of the catalyst, 5-bromoninhydrin (**33**) and stannane **144** were added to the solution at room temperature. The product was obtained in 26% yield. This yield represents an overall yield of 20% for three steps from 5-bromo-1,3-indanedione (**131**) as compared to 6.4% for the corresponding coupling and (or) deprotection route. This attractive approach deserves to be explored and optimized.

The goal of the described structural modifications was the optimization of the chromophoric and luminescent properties of the Ruhemann's purple product arising from the reaction of ninhydrin analogs with amino acids. It is difficult to predict a priori which modifications will result in enhanced optical properties. Therefore, in spite of the large number of analogs synthesized, only a few were found to afford significant improvement over ninhydrin.

In conclusion, new chromogenic and fluorogenic reagents for amino acid detection were synthesized and evaluated. Evaluation of the analogs showed that thienyl-substituted compounds, especially **55** and **59**, were promising reagents, exhibiting fluorogenic properties without secondary treatment. Some correlations between the structure of ninhydrin analogs and the spectral properties of the resulting Ruhemann's purple analog have been demonstrated but no general method of predicting the spectral properties has evolved, thereby making evaluation of modified structures the only available route to better reagents.

Although a wide variety of reagents is currently known and employed for the detection of amines and amino acids in analytical chemistry, only a few of these reagents have found their way into forensic practice because of the different requirements of reactions occurring in solution and on porous surfaces.

Experimental section

General procedures

All solvents were reagent grade and were distilled from appropriate drying agents. *N*-Bromosuccinimide (NBS) was recrystallized from water. Tri-*n*-butylstannyl chloride was distilled under reduced pressure. Organic acids were reagent grade. *n*-Butyllithium was purchased as a solution in hexanes (1.6 M). Tetrakis(triphenylphosphine)palladium(0) ($Pd(PPh_3)_4$) was purchased commercially and stored in a refrigerator (5°C) under a N_2 atmosphere. Tosyl azide (81, 80) and dimethyl dioxirane (108, 109) were prepared as described in the literature. Melting points (mp) were determined with a Thomas–Hoover capillary melting point apparatus and are uncorrected. Analytical thin layer chromatography (TLC) was performed on Merck silica gel (60F-254) plates (0.25 mm), precoated with a fluorescent indicator. Visualization was effected with ultraviolet light or a suitable chemical reagent. Flash column chromatography was carried out on E. Merck silica gel 60 (240–400 mesh) using the solvent systems listed under the individual experiments. Proton magnetic resonance spectra (^{1}H NMR) and carbon magnetic resonance spectra (^{13}C NMR) were recorded on a Bruker/IBM AC-250 (250 MHz) (or a Bruker AMX-500 (500 MHz) where noted) Fourier transform (FT) spectrometer using $CDCl_3$, DMSO-d_6, D_2O, or acetone-d_6, as solvents. Chemical shifts are measured in parts per million (δ) relative to tetramethylsilane (TMS) or chloroform as the internal standard. Coupling constants (*J* values) are in Hertz (Hz). Infrared spectra (IR) were obtained on a PerkinElmer Model 281-B or a PerkinElmer Model 781 spectrometer. Solid samples were analyzed as potassium bromide (KBr) disks. Liquids or oils were analyzed as neat films between sodium chloride plates. Absorptions are reported in wave numbers (cm^{-1}), and intensities are designated as broad (br), strong (s), medium (m), or weak (w). The spectra taken were referenced to the 1601 cm^{-1} band of polystyrene, and only the most prominent or characteristic absorptions are noted. High resolution mass spectra (HRMS) were obtained on VG 7070H or VG ZAB-E high resolution, double focusing, mass spectrometers, employing either chemical ionization (CI) or fast atom bombardment (FAB) using a Cesium (Cs) ion gun. The mass spectrometers were interfaced with a VG/DEC 11–73 data system. Ultraviolet spectra (UV) were recorded on an IBM 9420 UV–vis spectrophotometer. Elemental analyses were performed by National Chemical Consulting, Inc., Tenafly, New Jersey or at the elemental analysis facility of the University of Pennsylvania.

*3,3′-Dibromo[4,4′]biindenyl-1,1′-dione (**99**)*

To a solution of dione **98** (620 mg, 2.37 mmol) in CCl_4 (115 mL) at 25°C was added NBS (1.77 g, 9.94 mmol) and a catalytic amount of AIBN. The mixture was heated at reflux, while being irradiated with a 150 W light. After 3.5 h, the reaction was cooled to 5°C in an ice bath, triethylamine (2.40 mL, 16.5 mmol) was added, and the reaction was then allowed to stir for 1 h at 25°C. A precipitate was removed by filtration and the solid was washed with CCl_4 (25 mL). The filtrate was evaporated in vacuo to give a dark residue which was dissolved in Et_2O (100 mL), washed first with 0.1 M HCl (100 mL), and then water (1 × 50 mL). The solution was dried over Na_2SO_4 and filtered. The solvent was evaporated in vacuo to afford 970 mg of an orange-red solid. The crude product was purified by column chromatography (EtOAc – petroleum ether, 1:9 and 1:4) to provide 876 mg (89% yield) of **99** as an orange solid; mp 183–186°C dec. R_f 0.30 (Et_2O – petroleum ether, 1:1). HRMS–CI (NH_3) calcd. for $C_{18}H_8Br_2O_2$ $(M)^+$: 413.8891; found: 413.8938. IR (KBr) (cm^{-1}): 1700 (s). ^{1}H NMR ($CDCl_3$) δ: 7.46 (dd, J = 7.1 Hz, J = 1.1 Hz, 2H), 7.34 (dd, J = 9.0 Hz, J = 7.1 Hz, 2H), 7.23 (dd, J = 9.0 Hz, J = 1.1 Hz, 2H), 6.24 (s, 2H). ^{13}C NMR ($CDCl_3$) δ: 193.4, 147.8, 136.4, 132.1, 130.1, 130.6, 129.7, 129.4, 127.5, 122.0.

© 2001 NRC Canada

*2,2,2′,2′-Tetrahydroxy[4,4′]biindenyl-1,3,1′,3′-tetrone (**65**)*

Method A: A mixture of dione **98** (510 mg, 1.94 mmol) and SeO_2 (1.08 g, 9.72 mmol) in glacial acetic acid (25 mL) was heated at 100°C for 2 h. The reaction mixture was filtered through Celite while still hot to remove a red precipitate. The precipitate was washed with water (25 mL) and the filtrates were combined. Upon cooling in an ice bath, a precipitate formed which was collected and dried to give a yellow-orange solid (120 mg). The volume of the solution was reduced several times by heating to obtain additional crops of material (198 mg) for a total yield of 15%.

Method B: A mixture of dione **98** (0.87 g, 3.3 mmol) and selenium dioxide (1.49 g, 13.4 mmol) in nitrobenzene (5 mL) was heated at 145–150°C. After 50 min, the reaction was filtered through Celite while still hot to remove a dark precipitate. The precipitate was washed with EtOAc (15 mL) and the filtrates were combined. Water (300 mL) was added and the organic solvents were removed by steam distillation. The solution was filtered again while still hot to remove a dark, sticky precipitate. Additional precipitate, which formed after standing at room temperature overnight, was also removed by filtration. The filtrate was extracted with EtOAc (3 × 50 mL) and the combined extracts were dried over Na_2SO_4, filtered, and the solvent evaporated under reduced pressure. The residue was dried in vacuo to provide 390 mg (32% yield) of **65** as a pink solid, mp 200–202°C dec. R_f 0.40 (CH_2Cl_2 – MeOH – acetic acid, 90:10:1). UV (CH_3CN) (nm): 242 (ε 33 000). IR (KBr) (cm^{-1}): 3650–2100 (br, s), 1705 (s), 1180 (s), 1160 (s). ^1H NMR (DMSO-d_6) δ: 8.06–8.13 (m, 4H), 7.90 (m, 2H), 7.49 (br s, 4H, exchangeable with D_2O). ^{13}C NMR (DMSO-d_6) δ: 196.7, 196.1, 138.7, 138.4, 136.5, 135.9, 135.6, 123.9, 87.3. Anal. calcd. for $C_{18}H_{10}O_8$: C 61.02, H 2.85; found: C 60.83, H 3.17.

*2,2,2′,2′-Tetramethoxy[5,5′]biindenyl-1,3,1′,3′-tetrone (**101**)*

Powdered Cu (495 mg, 7.80 mmol) was added to a solution of **100** (556 mg, 1.95 mmol) in DMSO (3 mL). The reaction mixture was flushed with N_2 and then stirred in a N_2 atmosphere for 2 h. $Pd(PPh_3)_4$ (115 mg, 5% mol) was added, and the reaction mixture was allowed to stir at 110–120°C under N_2 for 17 h in a dark hood. At that time, the reaction mixture was diluted with EtOAc, and inorganic solids were removed by filtration. The solvents were evaporated under reduced pressure to yield an oil that was purified by column chromatography (acetone – petroleum ether (1:4), and CH_2Cl_2) to afford 90 mg (16% recovery) of **100** and 310 mg (78% yield, 93% yield based on recovered starting material) of **101** as a yellow solid, mp 210°C. R_f 0.46 (EtOAc – petroleum ether, 2:3). HRMS–CI(NH_3) calcd. for $C_{22}H_{22}NO_8$ $(M+NH_4)^+$: 428.1346; found: 428.1340. IR (KBr) (cm^{-1}): 1747 (s), 1718 (s), 1179 (s), 1037 (s). ^1H NMR ($CDCl_3$) δ: 8.07 (d, J = 8.4 Hz, 2H), 7.58 (dd, J = 8.4 Hz, J = 2.2 Hz, 2H), 7.47 (d, J = 2.3 Hz, 2H), 3.65 (s, 12 H). ^{13}C NMR ($CDCl_3$) δ: 193.0, 192.7, 146.9, 140.2, 39.2, 135.7, 125.3, 122.9, 91.2, 51.8. Anal. calcd. for $C_{22}H_{18}O_8$: C 64.39, H 4.42; found: C 64.03, H 4.61.

*2,2,2′,2′-Tetrahydroxy[5,5′]biindenyl-1,3,1′,3′-tetrone (**66**)*

Tetrone **101** (140 mg, 0.341 mmol) was dissolved in glacial acetic acid (2 mL) and an equal amount of water and concd aq HBr (48%) were added to form a fine suspension. The reaction mixture was heated at reflux for 2 h and filtered while hot. The filtrate was diluted with water and the precipitate which formed after cooling in an ice bath was collected by filtration, washed with water, and air dried to give 103 mg (86% yield) of **66** as a beige solid. IR (KBr) (cm^{-1}): 3270 (s), 1754 (s), 1719 (s), 1182 (s). ^1H NMR (DMSO-d_6) δ: 8.53 (dd, J = 8.1 Hz, J = 1.4 Hz, 2H), 8.46 (s, 2H), 8.15 (d, J = 8.0 Hz, 2H), 7.61 (br s, 1.2 H). ^{13}C NMR (DMSO-d_6) δ: 196.6, 196.5, 146.2, 139.2, 138.2, 136.5, 124.6, 122.9, 87.9. Anal. calcd. for $C_{18}H_{10}O_8 \cdot H_2O$: C 58.07, H 3.25; found: C 58.08, H 2.99.

*1,1-Dibromo-1,2-dihydrobenzo[*b*]cyclopenta[*d*]thiophen-3-one (**103**)*

To a solution of **102** (0.203 g, 1.08 mmol) in CCl_4 (12 mL) was added NBS (0.422 g, 2.37 mmol) and a catalytic amount of AIBN. The mixture was heated at reflux for 5 h while following the reaction by TLC. The mixture was cooled and filtered. The collected solid was washed with additional CCl_4 (8 mL) and the filtrate was concentrated under reduced pressure to afford **103** (0.372 g) in quantitative yield. The crude solid was used in the next step without further purification. R_f 0.71 (CH_2Cl_2 – petroleum ether, 1:1). HRMS–CI (NH_3) calcd. for $C_{11}H_{10}NOSBr_2$ $(M+NH_4)^+$: 361.8850; found: 361.8857. ^1H NMR (500 MHz, $CDCl_3$) δ: 8.35 (m, 1H), 7.90 (m, 1H), 7.59 (m, 2H), 4.24 (s, 2H). ^{13}C NMR (125 MHz, $CDCl_3$) δ: 188.5, 162.8, 148.4, 139.3, 131.3, 129.1, 125.7, 125.1, 124.4, 66.7, 42.1.

*Benzo[*b*]cyclopenta[*d*]thiophene-1,3-dione (**104**)*

To a solution of **103** (0.372 g, 1.08 mmol) in acetone (15 mL) was added H_2O (25 mL) and the mixture was heated at reflux for 3 h. The mixture was cooled and the acetone was removed under reduced pressure. The aqueous layer was extracted with $CHCl_3$ (3 × 15 mL). The combined organic layers were dried (Na_2SO_4), filtered, and concentrated under reduced pressure. The orange solid was purified using column chromatography (CH_2Cl_2 and 2% MeOH–CH_2Cl_2) to afford 0.169 g (78% yield) of **104** as a bright yellow solid, mp > 280°C. R_f 0.57 (2% MeOH–CH_2Cl_2). HRMS–CI (NH_3) calcd. for $C_{11}H_{10}NO_2S$ $(M+NH_4)^+$: 220.0166; found: 220.0166. IR (KBr) (cm^{-1}): 3500–2500 (br, w), 1735 (m), 1701 (s), 1671 (s). ^1H NMR (500 MHz, $CDCl_3$) δ: 8.37 (m, 1H) 7.95 (m, 1H), 7.58 (m, 2H), 3.51 (s, 2H). ^{13}C NMR (125 MHz, $CDCl_3$) δ: 190.2, 189.9, 157.9, 152.7, 148.1, 130.4, 129.2, 127.1, 126.0, 124.0, 49.1.

*2-Dimethylaminomethylenebenzo[*b*]cyclopenta[*d*]thiophene-1,3-dione (**105**)*

To a solution of **104** (0.169 g, 0.837 mmol) in CH_2Cl_2 (4 mL) was added dimethylformamide dimethyl acetal (0.22 mL, 1.67 mmol) and the solution was stirred at ambient temperature for 24 h. The crude material was purified directly using column chromatography (1% MeOH–CH_2Cl_2 and 2% MeOH–CH_2Cl_2) to afford 0.211 g (97% yield) of **105** (mixture of isomers) as an orange solid, mp 182–184°C. R_f 0.48 (2% MeOH–CH_2Cl_2). HRMS–CI(NH_3) calcd. for $C_{14}H_{12}NO_2S$ $(M+H)^+$: 258.0589; found: 258.0594. IR (neat) (cm^{-1}): 1698 (m), 1652 (s), 1610 (s). ^1H NMR (500 MHz, $CDCl_3$) δ: 8.29 (d, J = 7.9 Hz, 1H), 7.88 (m, 1H), 7.45 (m,

© 2001 NRC Canada

2H), 7.25 (m, 1H), 3.67 (s, 3H), 3.29 (s, 3H). ^{13}C NMR (125 MHz, $CDCl_3$) δ: 187.5, 184.2, 154.6, 151.1, 149.5, 146.7, 131.8, 126.9, 126.1, 124.8, 123.8, 104.2, 47.5, 43.2.

*2,2-Dihydroxybenzo[*b*]cyclopenta[*d*]thiophene-1,3-dione (**85**)*

Method A: Ketone **102** (0.373 g, 1.98 mmol) was oxidized with SeO_2 (0.839 g, 4.46 mmol) in nitrobenzene using a procedure similar to that described for the preparation of compound **65** to give an orange oil. The oil was purified by recrystallization from H_2O and decolorizing carbon to give 50 mg (11% yield) of **85** as a yellow solid.

Method B: To a solution of enamine **105** (0.211 g, 0.823 mmol) in acetone (10 mL) was added dimethyldioxirane in acetone (excess, 5 mL) and the golden solution turned pale yellow within 2 min. After stirring for 15 min, the solution was concentrated under reduced pressure. The crude solid was dissolved in hot H_2O (50 mL), Norit was added, and the suspension was filtered hot. The filtrate was concentrated to 10 mL and refrigerated overnight to give 62 mg (32% yield) of **85** as peach colored needles. HRMS–CI calcd. for $C_{11}H_5O_3S$ $(M)^+$: 216.9959; found: 216.9963. IR (KBr) (cm^{-1}): 3400 (s, br), 1740 (s), 1705 (s, br), 1070 (s). ^{1}H NMR (500 MHz, acetone-d_6) δ: 8.85 (m, 1H), 8.76 (m, 1H), 8.27–8.28 and 8.34 (m, 2H, exchangeable with D_2O), 8.21 (m, 2H). ^{13}C NMR (125 MHz, acetone-d_6) δ: 200.8, 200.5, 165.2, 158.5, 158.0, 141.2, 140.5, 138.0, 136.2, 135.2.

*3-Dibenzothiophen-2-yl-acrylic acid (**107**)*

A solution of aldehyde **106** (3.41 g, 16.0 mmol), malonic acid (2.50 g, 24.0 mmol), pyridine (16 mL), and piperidine (10 drops) was heated to 95°C for 2 h and then at reflux for 15 min. After brief cooling, the mixture solidified. The solid was mixed with 2 M HCl (250 mL) and the precipitate was collected. The solid was washed with 2 M HCl (250 mL) and water (50 mL) and then dried overnight in an oven (70°C) to afford 3.03 g (83% yield) of 107 as small off-white crystals after recrystallization from 2-propanol–water, mp 275–277°C dec. R_f 0.41 (Et_2O). HRMS–CI (NH_3) calcd. for $C_{15}H_{14}NO_2S$ $(M+NH_4)^+$: 272.0745; found: 272.0740. IR (KBr) (cm^{-1}): 3300–2200 (br, s), 1690 (s), 1630 (s), 1350 (s). ^{1}H NMR (DMSO-d_6) δ: 12.45 (br s, 1H, exchangeable with D_2O), 8.74 (d, J = 1.3 Hz, 1H), 8.45 (m, 1H), 8.04 (d, J = 8.4 Hz, 1H), 8.02 (m, 1H), 7.82 (dd, J = 8.4 Hz, J = 1.3 Hz, 1H), 7.77 (d, J = 16.0 Hz, 1H), 7.49–7.56 (m, 2H), 6.74 (d, J = 16.0 Hz, 1H). ^{13}C NMR (DMSO-d_6) δ: 167.8, 144.0, 140.5, 139.0, 135.7, 134.8, 131.2, 127.5, 126.8, 125.0, 123.4, 123.2, 122.4, 122.0, 119.1.

*3-Dibenzothiophen-2-yl-propionic acid (**108**)*

Unsaturated acid **107** (5.67 g, 22.3 mmol) was hydrogenated in 0.5 M Na_2CO_3 (90 mL) with 10% Pd on activated carbon (402 mg) in a Parr apparatus. When TLC indicated that the reaction was complete, the mixture was filtered through Celite and the solids were washed with water (50 mL). The filtrate was then acidified with 1 M HCl and the precipitate was collected and recrystallized from 2-propanol–water to afford 3.82 g (67% yield) of **108** as white crystals, mp 123–125°C dec. R_f 0.48 (Et_2O). HRMS–CI (NH_3) calcd. for $C_{15}H_{16}NO_2S$ $(M+NH_4)^+$: 274.0901; found: 274.0913. IR (KBr) (cm^{-1}): 3400–2350 (br, s), 1690 (s). ^{1}H NMR (DMSO-d_6) δ: 12.24 (br s, 1H, exchangeable with D_2O), 8.29 (m, 1H), 8.21 (s, 1H), 7.97 (m, 1H), 7.87 (d, J = 8.1 Hz, 1H), 7.47 (m, 2H), 7.38 (d, J = 8.1 Hz, 1H), 3.01 (m, 2H), 2.67 (m, 2H). ^{13}C NMR (DMSO-d_6) δ: 173.9, 139.0, 137.8, 136.3, 135.3, 135.0, 127.8, 127.0, 124.7, 123.1, 122.8, 122.0, 121.5, 35.6, 30.5.

*2,3-Dihydro-9-thiacyclopenta[*b*]fluoren-1-one (**109**) and 2,3-dihydro-6-thiacyclopenta[*c*]fluoren-1-one (**110**)*

To a mechanically stirred solution of polyphosphoric acid (165 g) in a 400 mL beaker heated at 80°C in an oil bath, was carefully added a solution of acid **108** (4.43 g, 17.3 mmol) in CH_2Cl_2 (20 mL). The color of the mixture changed from light yellow to deep red. After 30 min, the reaction was poured over ice (500 g) and water (250 mL) was used to wash the residue from the beaker. The resulting mixture was extracted with CH_2Cl_2 (3 × 150 mL). The organic extracts were combined, washed first with saturated $NaHCO_3$ (2 × 100 mL) and then water (2 × 100 mL), dried over Na_2SO_4, and filtered. The solvent was evaporated under reduced pressure to give 4.03 g of a yellow solid which contained two products as indicated by TLC. The crude product was purified by column chromatography (Et_2O – petroleum ether, 3:7) to afford 919 mg (22% yield) of pure ketone **110** as a white solid and 654 mg (16% yield) of pure ketone **109** as a yellow solid. Analytical samples of each compound were obtained by collecting the crystals that formed in several chromatography fractions. The mixed fractions were combined and evaporated under reduced pressure to give a light yellow solid (1.50 g). ^{1}H NMR analysis indicated this solid contained a mixture of only the two isomeric ketones in the ratio of 62:38 (**110**:**109**). Therefore, the total yield of ketone **109** was 30% and the total yield of ketone **110** was 45%. The physical and spectroscopic data for each compound are given below.

*2,3-Dihydro-9-thiacyclopenta[*b*]fluoren-1-one (**109**):* Yellow crystals, mp 217 to 218°C. R_f 0.48 (Et_2O – petroleum ether, 1:1). HRMS–CI (NH_3) calcd. for $C_{15}H_{10}OS$ $(M)^+$: 238.0453; found: 238.0438. IR (KBr) (cm^{-1}): 1690 (s). ^{1}H NMR ($CDCl_3$) δ: 8.13 (m, 1H), 7.41–7.53 (m, 2H), 7.81 (m, 1H), 8.15 (m, 1H), 8.11 (m, 1H), 3.23 (m, 2H), 2.76 (m, 2H). ^{13}C NMR ($CDCl_3$) δ: 206.0, 150.4, 141.6, 138.8, 135.7, 134.1, 133.0, 128.2, 124.6, 123.0, 122.5, 118.8, 118.2, 37.0, 25.5. Anal. calcd. for $C_{15}H_{10}OS$: C 75.60, H 4.23; found: C 75.46, H 4.00.

*2,3-Dihydro-6-thiacyclopenta[*c*]fluoren-1-one (**110**):* White needles, mp 167 to 168°C. R_f 0.60 (Et_2O – petroleum ether, 1:1). HRMS–CI (NH_3) calcd. for $C_{15}H_{10}OS$ $(M)^+$: 238.0453; found: 238.0434. UV (CH_3CN) (nm): 356 (ε 5 700), 345 (ε 4300), 314 (ε 10 600), 276 (ε 5200). IR (KBr) (cm^{-1}): 1700 (s). ^{1}H NMR (DMSO-d_6) δ: 9.77 (m, 1H), 7.87 (d, J = 8.1 Hz, 1H), 7.82 (m, 1H), 7.46–7.50 (m, 2H), 7.31 (d, J = 8.1 Hz, 1H), 3.12 (m, 2H), 2.73 (m, 2H). ^{13}C NMR ($CDCl_3$) δ: 206.5, 155.0, 140.0, 139.0, 135.3, 133.2, 133.1, 128.7, 128.5, 127.3, 124.4, 124.0, 121.9, 36.8, 26.3. Anal. calcd. for $C_{15}H_{10}OS$: C 75.60, H 4.23; found: C 75.26, H 4.08.

*2,2-Dihydroxy-9-thiacyclopenta[*b*]fluoren-1,3-dione (**86**)*

Ketone **109** (740 mg, 3.10 mmol) was oxidized with SeO_2 (689 mg, 6.20 mmol) in nitrobenzene using a procedure sim-

© 2001 NRC Canada

ilar to that described for the preparation of compound **65** to give 480 mg (54% yield) of **86** as an off-white solid after recrystallization from water, mp 296–298°C dec. R_f 0.18 (benzene – EtOAc – formic acid, 85:15:5). HRMS–CI (NH_3) calcd. for $C_{15}H_8O_4S$ $(M)^+$: 284.0143; found: 284.0159. UV (CH_3CN) (nm): 295 (ε 43 300), 267 (ε 13 800). IR (KBr) (cm^{-1}): 3650–2600 (br, s), 1755 (s), 1715 (s), 1175 (s), 1075 (s). ^1H NMR (DMSO-d_6) δ: 9.02 (s, 1H), 8.75 (s, 1H), 8.70 (d, J = 7.7 Hz, 1H), 8.13 (d, J = 7.7 Hz, 1H), 7.56–7.69 (m, 2H), 7.59 (s, 2H, exchangeable with D_2O). ^{13}C NMR (DMSO-d_6) δ: 196.7, 196.6, 147.5, 142.0, 140.8, 135.7, 134.9, 133.7, 129.6, 125.7, 124.2, 123.5, 119.3, 117.4, 88.6.

*2,2-Dihydroxy-6-thiacyclopenta[c]fluoren-1,3-dione (**87**)*

Ketone **110** (920 mg, 3.80 mmol) was oxidized with SeO_2 (860 mg, 7.70 mmol) in nitrobenzene using a procedure similar to that described for the preparation of compound **65** to give 234 mg (21% yield) of **87** as a light orange solid after column chromatography (Et_2O and EtOAc), mp 286–288°C dec. R_f 0.29 (benzene – EtOAc – formic acid, 85:15:5). HRMS–CI (NH_3) calcd. for $C_{15}H_8O_4S$ $(M)^+$: 284.0143; found: 284.0154. UV (CH_3CN) (nm): 304 (ε 22 900), 268 (ε 15 700). IR (KBr) (cm^{-1}): 3600–2900 (br, s), 1740 (s), 1710 (s). ^1H NMR (DMSO-d_6) δ: 9.66 (m, 1H), 8.70 (d, J = 8.2 Hz, 1H), 8.15 (m, 1H), 8.06 (d, J = 8.2 Hz, 1H), 7.67 (s, 2H, exchangeable with D_2O) 7.59–7.71 (m, 2H). ^{13}C NMR (DMSO-d_6) δ: 197.5, 196.4, 148.3, 140.1, 137.7, 134.1, 133.5, 132.0, 132.0, 128.9, 127.1, 125.4, 123.2, 120.5, 87.7. Anal. calcd. for $C_{15}H_8O_4S$: C 63.37, H 2.84; found: C 63.15, H 2.76.

*3-Bromo-6-phenylinden-1-one (**112**)*

To a solution of ketone **111** (1.50 g, 7.17 mmol) in CCl_4 (60 mL) at 25°C was added NBS (4.20 g, 23.6 mmol) and a catalytic amount of AIBN. The mixture was heated at reflux, while being irradiated with a 150 W light. After 4 h, the reaction was cooled to 5°C in an ice bath, triethylamine (4.00 mL, 28.7 mmol) was added, and the reaction was then allowed to stir for 90 min at 25°C. A precipitate was removed by filtration and the solid was washed with CCl_4 (25 mL). The filtrate was washed first with 2 M HCl (2 × 100 mL) and then water (3 × 75 mL), dried over Na_2SO_4, and filtered. The solvent was evaporated in vacuo and the residue was purified by column chromatography (petroleum ether and EtOAc – petroleum ether, 1:9) to provide 1.70 g (83% yield) of **112** as an orange solid, mp 213–215°C. R_f 0.55 (Et_2O – petroleum ether, 1:1). HRMS–CI (CH_4) calcd. for $C_{15}H_9BrO$ $(M)^+$: 283.9837; found: 283.9810. IR (KBr) (cm^{-1}): 1705 (s), 1595 (m). ^1H NMR ($CDCl_3$) δ: 7.57–7.69 (m, 3H), 7.24–7.56 (m, 5H), 6.24 (s, 1H). ^{13}C NMR ($CDCl_3$) δ: 148.7, 139.5, 131.7, 129.0, 128.2, 127.5, 126.9, 121.6, 120.9 (note: only 9 out of a potential 13 signals were observed.). Anal. calcd. for $C_{15}H_{12}O$: C 86.51. H 5.81; found: C 86.14, H 5.92.

*2,2-Dihydroxy-5-phenylindan-1,3-dione (**47**)*

Method A: To a solution of **112** (960 mg, 3.30 mmol) in DMSO (50 mL) was added Br_2 (1 drop). The solution was heated at reflux for 8 h, cooled to 25°C, and then poured into water (200 mL) to form a viscous orange mixture. The mixture was extracted with EtOAc (4 × 100 mL). The combined organic extracts were washed with brine (3 × 25 mL), dried over Na_2SO_4, and filtered. The solvent was removed under reduced pressure to give a red oil which was dried in vacuo to afford 550 mg (65% yield, mp 64 to 65°C dec) of **47** as an orange-red foam.

Method B: A mixture of **111** (1.04 g, 5.00 mmol) and SeO_2 (1.22 g, 11.0 mmol) in dioxane (12 mL) and glacial acetic acid (2 mL) was heated at reflux for 2 h. The reaction mixture was filtered through Celite while still hot and the solids were washed with EtOAc. The filtrate was poured into water and the mixture was extracted with EtOAc. The organic extracts were combined, washed with brine, dried over Na_2SO_4, and filtered. The solvent was evaporated under reduced pressure and the residue heated at reflux with water and a small amount of decolorizing carbon. The mixture was filtered while hot and allowed to cool. No solid formed even after reducing the volume of the mixture so the solution was extracted with EtOAc (2 × 100 mL) and the combined organic extracts were washed with brine (1 × 50 mL), dried over $MgSO_4$, and filtered. The solvent was removed under reduced pressure and the residue dried in vacuo to afford 0.59 g of **47** as a yellow solid (49% yield), mp 86–88°C dec. R_f 0.51 (CH_2Cl_2 – MeOH – acetic acid, 90:10:1). HRMS–CI (NH_3) calcd. for $C_{15}H_{10}O_4$ $(M)^+$: 254.0579; found: 254.0539. UV (CH_3CN) (nm): 294 (ε 17 400). IR (KBr) (cm^{-1}): 3700–2600 (br, s), 1755 (s), 1730 (s), 1715 (s), 1600 (s). ^1H NMR (DMSO-d_6) δ: 8.31 (d, J = 8.0 Hz, 1H), 8.19 (s, 1H), 8.07 (d, J = 8.0 Hz, 1H), 7.82 (m, 2H), 7.62 (s, 2H, exchangeable with D_2O), 7.43–7.54 (m, 3H). ^{13}C NMR (DMSO-d_6) δ: 197.2, 196.7, 148.7, 139.4, 137.9, 137.3, 135.8, 129.4, 127.6, 124.8, 121.4, 88.1. Anal. calcd. for $C_{15}H_{10}O_4$: C 70.86, H 3.96; found: C 71.13, H 4.01.

Suzuki coupling reactions of 117

To a solution of **117** (1.0 equiv) in benzene (0.20–0.50 M) was added aq 2 M Na_2CO_3 (2.0 equiv) and a solution of a boronic acid (1.1–1.3 equiv) dissolved in ethanol (1.0–1.5 M). Dissolved oxygen was removed by placing the reaction flask in a dry ice – acetone bath followed by evacuation under reduced pressure. The evacuated flask was then filled with N_2 and allowed to warm to room temperature. When the contents of the flask were completely fluid, the freeze–pump–thaw process was repeated two more times. A catalytic amount of $Pd(PPh_3)_4$ (1–3 mol%) was added and the mixture was heated at reflux under a N_2 atmosphere and protected from light. When the reaction was completed (1–6 h as determined by TLC), 30% hydrogen peroxide (0.5 mL) was added and the reaction mixture was stirred. After 45 min, the contents of the flask were poured into water and the mixture was extracted with Et_2O or CH_2Cl_2. The organic extract was washed with brine, dried over Na_2SO_4, filtered, and the solvent was evaporated under reduced pressure. The crude product was purified by column chromatography.

*6-Phenylindan-1-one (**118**)*

Compound **117** (528 mg, 2.50 mmol) was coupled with phenylboronic acid (335 mg, 2.75 mmol) to afford 546 mg of a yellow solid after purification by column chromatography (Et_2O – petroleum ether, 1:1). The solid was dissolved in CH_2Cl_2 (50 mL) and the solution was stirred with decolorizing carbon for several hours at 25°C. The mixture

© 2001 NRC Canada

was filtered through a pad of Celite and the solvent evaporated in vacuo to provide 515 mg (99% yield) of **118** as an off-white solid, mp 108–110°C (18). R_f 0.33 (Et_2O – petroleum ether, 1:1). HRMS–CI (NH_3) calcd. for $C_{15}H_{12}O$ $(M)^+$: 208.0888; found: 208.0885. UV (CH_3CN) (nm): 306 (ε 2100), 239 (ε 32 300). IR (KBr) (cm^{-1}): 1710 (s). ^1H NMR ($CDCl_3$) δ: 7.94 (s, 1H), 7.78 (d, J = 8.0 Hz, 1H), 7.57 (d, J = 8.0 Hz, 1H), 7.30–7.55 (m, 5H), 3.11 (m, 2H), 2.69 (m, 2H). ^{13}C NMR ($CDCl_3$) δ: 206.8, 153.9, 140.4, 139.7, 137.5, 133.5, 128.8, 127.5, 126.9, 126.8, 121.5, 35.4, 25.4.

*6-Biphenyl-4-yl-indan-1-one (**119**)*

Compound **117** (2.12 g, 10.0 mmol) was coupled with 4-biphenylboronic acid (2.98 g, 15.0 mmol) to afford 2.66 g (93% yield) of **119** as a yellow solid after purification by column chromatography (Et_2O – petroleum ether, 1:4, 1:1; and CH_2Cl_2–Et_2O, 1:1). An analytical sample was prepared by recrystallization from $CHCl_3$–MeOH (1:1) using decolorizing carbon to give small, white crystals which were dried in vacuo for 48 h, mp 213.5 to 215°C. R_f 0.36 (Et_2O – petroleum ether, 1:1). UV (CH_3CN) (nm): 280 (ε 29 000), 250 (ε 16 900). IR (KBr) (cm^{-1}): 1700 (s). HRMS–CI (NH_3) calcd. for $C_{21}H_{17}O$ $(M+H)^+$: 285.1279; found: 285.1271. ^1H NMR ($CDCl_3$) δ: 8.02 (d, J = 1.6 Hz, 1H); 7.87 (dd, J = 8.0 Hz, J = 1.6 Hz, 1H), 7.67 (m, 4H), 7.63 (d, J = 8.0 Hz, 3H), 7.32–7.56 (m, 5H), 3.18 (m, 2H), 2.75 (m, 2H). ^{13}C NMR ($CDCl_3$) δ: 207.1, 154.2, 140.6, 140.4, 140.1, 138.8, 137.7, 133.6, 128.8, 127.6, 127.5, 127.1, 127.0, 121.7, 36.6, 25.6 (note: only 16 of a possible 17 signals were observed).

*6-(4-Methoxyphenyl)indan-1-one (**120**)*

Compound **117** (2.12 g, 10.0 mmol) was coupled with 4-methoxyphenylboronic acid (2.28 g, 15.0 mmol) to afford 1.63 g (68% yield, mp 145–147°C) of **120** as orange crystals after recrystallization (THF–hexane, 1:4). A small analytical sample was purified by column chromatography (Et_2O – petroleum ether, 1:4) to give 153 mg (6% yield) of light yellow crystals (74% overall yield), mp 149 to 150°C (lit. (110) mp 148 to 149°C), purified by column chromatography eluting with EtOAc–cyclohexane, 1:1). R_f 0.31 (Et_2O – petroleum ether, 1:1). HRMS–CI (NH_3) calcd. for $C_{16}H_{14}O_2$ $(M+H)^+$: 239.1072; found: 239.1059. UV (CH_3CN) (nm): 312 (ε 1300), 263 (ε 18 600). IR (KBr) (cm^{-1}): 1690 (s), 1245 (s), 1175 (s). ^1H NMR ($CDCl_3$) δ: 7.87 (s, 1H), 7.74 (d, J = 8.0 Hz, 1H), 7.44–7.51 (m, 3H), 6.94 (m, 2H), 3.80 (s, 3H), 3.09 (m, 2H), 2.68 (m, 2H). ^{13}C NMR ($CDCl_3$) δ: 207.0, 159.3, 153.4, 140.0, 137.5, 133.1, 132.2, 128.0, 126.8, 121.0, 114.2, 55.2, 36.5, 25.4. Anal. calcd. for $C_{16}H_{14}O_2$: C 80.65, H 5.92; found: C 80.49, H 5.93.

*6-Benzo[1,3]dioxo-5-yl-indan-1-one (**121**)*

Compound **117** (730 mg, 3.45 mmol) was coupled with benzo[1,3]dioxole-5-boronic acid (630 mg, 3.80 mmol) to afford 820 mg (94% yield) of **121** after purification by column chromatography (Et_2O – petroleum ether, 1:4 and 1:1). It was necessary to use CH_2Cl_2 to extract the product from the crude reaction mixture. An analytical sample was prepared by recrystallization from Et_2O–CH_2Cl_2 to give light yellow crystals, mp 160–162°C. R_f 0.33 (Et_2O – petroleum ether, 1:1). HRMS–CI (NH_3) calcd. for $C_{16}H_{12}O_3$ $(M)^+$: 252.0786; found: 252.0786. UV (CH_3CN) (nm): 298 (ε 7900), 268 (ε 8900). IR (KBr) (cm^{-1}): 1700 (s), 1480 (s), 1220 (s), 1035 (s). ^1H NMR ($CDCl_3$) δ: 7.82 (d, J = 2.0 Hz, 1H), 7.69 (dd, J = 8.0 Hz, J = 2.0 Hz, 1H), 7.44 (d, J = 8.0 Hz, 1H), 7.00–7.03 (m, 2H), 6.82 (m, 1H), 5.95 (s, 2H), 3.08 (m, 2H), 2.67 (m, 2H). ^{13}C NMR ($CDCl_3$) δ: 206.8, 153.6, 148.2, 147.3, 140.2, 137.5, 134.1, 133.3, 126.8, 121.3, 120.6, 108.6, 107.4, 101.2, 36.5, 25.4. Anal. calcd. for $C_{16}H_{12}O_3$: C 76.18, H 4.80; found: C 76.03, H 4.70.

*6-(4-Methysulfanylphenyl)indan-1-one (**122**)*

Compound **117** (211 mg, 1.00 mmol) was coupled with 4-methylsulfanylphenylboronic acid (252 mg, 1.50 mmol) to afford 202 mg (80% yield, mp 120–124°C) of **122** after purification by column chromatography (Et_2O – petroleum ether, 1:4 and 1:1). An analytical sample was prepared by recrystallization from MeOH to afford yellow crystals, mp 126 to 127°C. R_f 0.35 (Et_2O – petroleum ether, 1:1). HRMS-CI (NH_3) calcd. for $C_{16}H_{18}NOS$ $(M+NH_4)^+$: 272.1108; found: 272.1120.UV (CH_3CN) (nm): 284 (ε 24 400). IR (KBr) (cm^{-1}): 1700 (s). ^1H NMR ($CDCl_3$) δ: 7.91 (s, 1H), 7.77 (d, J = 8.0 Hz, 1H), 7.48–7.51 (m, 3H), 7.29 (d, J = 8.1 Hz, 2H), 2.50 (s, 3H), 3.13 (m, 2H), 2.70 (m, 2H). ^{13}C NMR ($CDCl_3$) δ: 206.9, 153.9, 139.7, 138.2, 137.5, 136.4, 133.2, 127.2, 126.9, 126.7, 121.2, 36.5, 25.4, 15.5. Anal. calcd. for $C_{16}H_{14}OS$: C 75.17, H 5.71; found: C 75.57, H 5.55.

*6-Thiophen-2-yl-indan-1-one (**123**)*

Compound **117** (1.10 g, 5.21 mmol) was coupled with thiophen-2-ylboronic acid (1.00 g, 7.82 mmol) to afford 993 mg (89% yield) of **123** as a white solid after purification by column chromatography (Et_2O – petroleum ether, 1:1), mp 115 to 116°C. R_f 0.40 (Et_2O – petroleum ether, 1:1). HRMS–CI (NH_3) calcd. for $C_{13}H_{10}OS$ $(M)^+$: 214.0452; found: 214.0445. UV (CH_3CN) (nm): 285 (ε 15 300). IR (KBr) (cm^{-1}): 1705 (s). ^1H NMR ($CDCl_3$) δ: 7.94 (dd, J = 1.8 Hz, J = 0.6 Hz, 1H), 7.80 (dd, J = 8.0 Hz, J = 1.8 Hz, 1H), 7.45 (dd, J = 8.0 Hz, J = 0.6 Hz, 1H), 7.33 (dd, J = 3.6 Hz, J = 1.1 Hz, 1H), 7.27 (dd, J = 5.1 Hz, J = 1.1 Hz, 1H), 7.06 (dd, J = 5.1 Hz, J = 3.6 Hz, 1H), 3.11 (m, 2H), 2.70 (m, 2H). ^{13}C NMR ($CDCl_3$) δ: 206.2, 160.6, 153.4, 137.1, 133.2, 131.7, 127.6, 126.6, 126.5, 124.7, 123.1, 119.7, 35.9, 25.0. Anal. calcd. for $C_{13}H_{10}OS$: C 72.86, H 4.70; found: C 73.02, H 4.55.

Selenium dioxide oxidation of 6-aryl-substituted indanones

These compounds were prepared according to the general procedure described for **47**. The solid which formed after recrystallization from water and decolorizing carbon was collected, washed with water, and dried in vacuo. The yields were not optimized.

*5-Biphenyl-4-yl-2,2-dihydroxyindan-1,3-dione (**48**)*

Dark yellow solid (45% yield), mp 270–272°C dec. R_f 0.56 (MeOH – CH_2Cl_2 – acetic acid, 90:10:1). HRMS–CI (NH_3) calcd. for $C_{21}H_{14}O_4$ $(M)^+$: 330.0892; found: 330.0878. UV (CH_3CN) (nm): 312 (ε 25 400), 254 (ε 21 100). IR (KBr) (cm^{-1}): 3600–2600 (br, s), 1720 (s), 1175 (s). ^1H NMR (DMSO-d_6) δ: 8.38 (dd, J = 8.1 Hz, J = 1.6 Hz, 1H), 8.28 (d, J = 1.6 Hz, 1H), 8.08 (d, J = 8.1 Hz, 1H), 7.95 (d, J = 8.4 Hz, 2H), 7.81 (d, J = 8.4 Hz, 2H), 7.73 (m, 2H), 7.61 (s,

© 2001 NRC Canada

2H, exchangeable with D_2O), 7.48 (m, 2H), 7.38 (m, 1H). ^{13}C NMR (DMSO-d_6) δ: 197.1, 196.6, 148.0, 141.0, 139.4, 139.1, 137.3, 136.8, 135.5, 129.1, 128.1, 128.0, 127.5, 126.8, 124.7, 121.1, 88.1. Anal. calcd. for $C_{21}H_{14}O_4$: C 76.35, H 4.27; found: C 76.45, H 4.44.

*2,2-Dihydroxy-5-(4-methoxyphenyl)-indan-1,3-dione (**52**)*

Dark yellow solid (20% yield), mp 52–55°C dec. R_f 0.20 (benzene – EtOAc – formic acid, 85:10:5). HRMS–CI (NH_3) calcd. for $C_{16}H_{12}O_5$ $(M)^+$: 284.0685; found: 284.0682. UV (CH_3CN) (nm): 321 (ε 13 600). IR (KBr) (cm^{-1}): 3700–2600 (br, s), 1750 (s), 1715 (s), 1595 (s), 1250 (s), 1180 (s). ^1H NMR (DMSO-d_6) δ: 8.25 (d, J = 8.1 Hz, 1H), 8.14 (s, 1H), 8.02 (d, J = 8.1 Hz, 1H), 7.78 (d, J = 8.7 Hz, 2H), 7.61 (s, 2H, exchangeable with D_2O), 7.03 (d, J = 8.7 Hz, 2H), 3.78 (s, 3H). ^{13}C NMR (DMSO-d_6) δ: 197.2, 196.5, 160.4, 148.3, 139.4, 136.6, 134.9, 130.0, 128.9, 124.6, 120.3, 114.8, 88.1, 55.4.

*5-Benzo[1,3]dioxo-5-yl-2,2-dihydroxyindan-1,3-dione (**53**)*

Yellow solid (37% yield), mp 231–233°C dec. R_f 0.22 (benzene – EtOAc – formic acid, 85:10:5). HRMS–CI (NH_3) calcd. for $C_{16}H_{11}O_6$ $(M+H)^+$: 299.0555; found: 299.0561. UV (CH_3CN) (nm): 332 (ε 8300). IR (KBr) (cm^{-1}): 3650–2500 (br, s), 1755 (s), 1720 (s), 1705 (s). ^1H NMR (DMSO-d_6) δ: 8.26 (d, J = 8.1 Hz, 1H), 8.14 (s, 1H), 8.01 (d, J = 8.1 Hz, 1H), 7.56 (s, 2H, exchangeable with D_2O), 7.47 (d, J = 1.6 Hz, 1H), 7.36 (dd, J = 8.2 Hz, J = 1.6 Hz, 1H), 7.04 (d, J = 8.2 Hz, 1H), 6.09 (s, 2H). ^{13}C NMR (DMSO-d_6) δ: 197.1, 196.5, 148.5, 148.4, 148.3, 139.4, 136.8, 135.3, 132.0, 124.6, 122.0, 120.8, 109.0, 107.8, 101.7, 88.1. Anal. calcd. for $C_{16}H_{10}O_6$: C 64.43, H 3.38; found: C 64.74, H 3.65.

*2,2-Dihydroxy-5-(4-methylsulfanylphenyl)indan-1,3-dione (**54**)*

Orange crystals (37% yield), mp 228–230°C dec, which were dried in vacuo for 24 h to provide an analytical sample. R_f 0.25 (benzene – EtOAc –mformic acid, 85:10:5). HRMS–CI (NH_3) calcd. for $C_{16}H_{12}O_4S$ $(M)^+$: 300.0456; found: 300.0450. UV (CH_3CN) (nm): 331 (ε 14 500). IR (KBr) (cm^{-1}): 3600–2400 (br, s), 1750 (s), 1725 (s), 1715 (s), 1160 (s). ^1H NMR (DMSO-d_6) δ: 8.33 (d, J = 8.1 Hz, 1H), 8.20 (s, 1H), 8.05 (d, J = 8.1 Hz, 1H), 7.83 (d, J = 8.4 Hz, 2H), 7.55 (s, 2H, exchangeable with D_2O), 7.39 (d, J = 8.4 Hz, 2H), 2.53 (m, 1H). ^{13}C NMR (DMSO-d_6) δ: 197.1, 196.5, 148.0, 140.4, 139.4, 137.0, 135.2, 133.9, 127.9, 126.2, 124.6, 120.7, 88.0, 14.3. Anal. calcd. for $C_{16}H_{12}O_4S$: C 63.98, H 4.03; found: C 63.50, H 3.94.

*2,2-Dihydroxy-5-thiophen-2-yl-indan-1,3-dione (**55**)*

Yellow solid (25% yield), mp 90–92°C dec. R_f 0.23 (benzene – EtOAc – formic acid, 85:10:5). HRMS–CI (NH_3) calcd. for $C_{13}H_8O_4S$ $(M)^+$: 260.0143; found: 260.0130. UV (CH_3CN) (nm): 331 (ε 17 900). IR (KBr) (cm^{-1}): 3600–2300 (br, s), 1740 (m), 1705 (s), 1145 (s), 1105 (s). ^1H NMR (DMSO-d_6) δ: 8.30 (dd, J = 8.1 Hz, J = 1.6 Hz, 1H), 8.18 (d, J = 1.6 Hz, 1H), 8.02 (d, J = 8.1 Hz, 1H), 7.79 (d, J = 5.0 Hz, 1H), 7.56 (s, 2H, exchangeable with D_2O), 7.24 (dd, J = 5.0 Hz, J = 3.8 Hz, 1H), 7.11 (d, J = 3.8 Hz, 1H). ^{13}C NMR (DMSO-d_6) δ: 197.0, 196.1, 141.9, 139.5, 136.8, 133.7, 131.4, 129.3, 128.7, 127.6, 125.0, 119.0, 87.9. Anal. calcd. for $C_{13}H_8O_4S \cdot H_2O$: C 56.11, H 3.62; found: C 55.78, H 3.30.

Suzuki coupling reactions of ketal intermediates

Compounds **100**, **125**, or **126** were coupled to a variety of boronic acids using the procedure described for the coupling reactions of **117**.

*2,2-Dimethoxy-5-phenyl-indan-1,3-dione (**132**)*

Compound **100** (1.43 g, 5.00 mmol) was coupled with phenylboronic acid (920 mg, 7.50 mmol) to afford 1.36 g (96% yield) of **132** after purification by column chromatography (Et_2O – petroleum ether, 1:1). A yellow, crystalline precipitate, which formed in several of the chromatography fractions, was collected and dried in vacuo to afford an analytical sample, mp 145 to 146°C. R_f 0.31 (Et_2O – petroleum ether, 1:4). HRMS–CI (CH_4) calcd. for $C_{17}H_{14}O_4$ $(M)^+$: 282.0892; found: 282.0880.UV (CH_3CN) (nm): 297 (ε 13 700), 249 (ε 16 800). IR (KBr) (cm^{-1}): 1750 (s), 1720 (s), 1160 (s), 1050 (s). ^1H NMR ($CDCl_3$) δ: 8.13 (dd, J = 1.7 Hz, J = 0.6 Hz, 1H), 8.08 (dd, J = 8.0 Hz, J = 1.7 Hz, 1H), 8.01 (dd, J = 8.0 Hz, J = 0.6 Hz, 1H), 7.62 (s, 2H), 7.42–7.51 (m, 3H), 3.65 (s, 6H). ^{13}C NMR ($CDCl_3$) δ: 193.6, 193.0, 149.8, 140.0, 138.4, 137.9, 135.5, 129.3, 129.22, 127.4, 124.7, 122.0, 91.1, 51.7. Anal. calcd. for $C_{17}H_{14}O_4$: C 72.34, H 5.00; found: C 72.25, H 4.96.

*5-Biphenyl-4-yl-2,2-dimethoxyindan-1,3-dione (**133**)*

Compound **100** (1.43 g, 5.00 mmol) was coupled with 4-biphenylboronic acid (1.49 g, 7.50 mmol) to afford 1.75 g (98% yield) of **133** after purification by column chromatography (Et_2O – petroleum ether, 1:1). A white-yellow, crystalline precipitate, which formed in several of the chromatography fractions, was collected and dried in vacuo to afford an analytical sample, mp 156 to 157°C. R_f 0.30 (Et_2O – petroleum ether, 1:4). HRMS–CI (NH_3) calcd. for $C_{23}H_{22}NO_4$ $(M+NH_4)^+$: 376.1548; found: 376.1553. UV (CH_3CN) (nm): 320 (ε 23 400), 254 (ε 17 900). IR (KBr) (cm^{-1}): 1750 (s), 1720 (s), 1190 (s), 1165 (s), 1035 (s). ^1H NMR ($CDCl_3$) δ: 8.20 (d, J = 1.6 Hz, 1H), 8.13 (dd, J = 8.0 Hz, J = 1.6 Hz, 1H), 8.04 (d, J = 8.0 Hz, 1H), 7.72 (s, 4H), 7.63 (m, 2H), 7.33–7.49 (m, 3H), 3.68 (s, 6H). ^{13}C NMR ($CDCl_3$) δ: 193.6, 149.3, 142.2, 140.1, 139.9, 138.0, 137.1, 135.3, 128.9, 127.9, 127.9, 127.8, 127.0, 124.8, 121.8, 91.2, 51.7 (note: only 22 of a potential 23 signals were observed observed). Anal. calcd. for $C_{23}H_{18}O_4$: C 77.08, H 5.06; found: C 77.19, H 4.89.

*2,2-Dimethoxy-5-(4-nitrophenyl)indan-1,3-dione (**134**)*

Compound **100** (428 mg, 1.5 mmol) was coupled with 4-nitrophenylboronic acid (250 mg, 1.5 mmol) to afford 321 mg (66% yield) of **134** as a yellow solid after purification by column chromatography (EtOAc – petroleum ether, 1:3), mp 155 to 156.5°C. R_f 0.50 (EtOAc – petroleum ether, 1:3). HRMS calcd. for $C_{17}H_{14}NO_6$ $(M+H)^+$: for 328.0821; found: 328.0813. IR (KBr) (cm^{-1}): 1751 (s), 1719 (s), 1163 (s), 1038 (s), 973 (m), 883 (m). ^1H NMR (500 MHz, $CDCl_3$) δ: 8.36–8.38 (m, 2H), 8.20 (d, J = 1.3 Hz, 1H), 8.11 (d, J = 1.0 Hz, 2H), 7.81 (dd, ^1J = 6.9 Hz, ^2J = 2.0 Hz, 2H), 3.67 (s, 6H). ^{13}C NMR (125 MHz, $CDCl_3$) δ: 193.2, 192.8, 148.3, 147.2, 144.7, 140.1, 139.0, 135.6, 128.5, 125.1, 124.5, 122.7, 91.2, 51.8. Anal. calcd. for $C_{17}H_{13}NO_6$: C 62.39, H 4.00, N 4.28; found: C 62.65, H 3.80, N 4.68.

© 2001 NRC Canada

*2,2-Dimethoxy-5-(4-methoxyphenyl)indan-1,3-dione (**135**)*

Compound **100** (1.26 g, 4.42 mmol) was coupled with 4-methoxyphenylboronic acid (1.01 g, 6.63 mmol) to afford 1.37 g (99% yield), mp 105–108°C of **135** after purification by column chromatography (Et_2O – petroleum ether, 1:1). Slow evaporation of a CH_2Cl_2 solution of the product gave yellow crystals which were washed with cold Et_2O (1.0 mL) and dried in vacuo to afford an analytical sample, mp 112–114°C. R_f 0.28 (Et_2O – petroleum ether, 1:4). HRMS–CI (NH_3) calcd. for $C_{18}H_{20}NO_5$ $(M+NH_4)^+$: 330.1341; found: 330.1334. UV (CH_3CN) (nm): 326 (ε 19 700). IR (KBr) (cm^{-1}): 1710 (s), 1590 (s), 1245 (s), 1170 (s), 1160 (s), 1030 (s). ^1H NMR ($CDCl_3$) δ: 8.01 (d, *J* = 1.5 Hz, 1H), 7.98 (dd, *J* = 8.1 Hz, *J* = 1.5 Hz, 1H), 7.91 (d, *J* = 8.1 Hz, 1H), 7.52 (d, *J* = 8.8 Hz, 2H), 6.93 (d, *J* = 8.8 Hz, 2H), 3.79 (s, 3H), 3.62 (s, 6H). ^{13}C NMR ($CDCl_3$) δ: 193.6, 192.8, 160.6, 149.2, 139.9, 137.2, 134.7, 130.4, 128.5, 124.5, 120.9, 114.6, 91.1, 55.2, 51.5.

*5-Benzo[1,3]dioxo-5-yl-2,2-dimethoxyindan-1,3-dione (**136**)*

Compound **100** (1.43 g, 5.00 mmol) was coupled with benzo[1,3]dioxole-5-boronic acid (1.24 g, 7.50 mmol) to afford 1.62 g (99% yield) of **136** after purification by column chromatography (Et_2O – petroleum ether, 1:1). A yellow, crystalline precipitate, which formed in one of the chromatography fractions, was collected and dried in vacuo to afford an analytical sample, mp 158–160°C. R_f 0.24 (Et_2O – petroleum ether, 1:4). HRMS–CI (CH_4) calcd. for $C_{18}H_{14}O_6$ $(M)^+$: 326.0790; found: 326.0796. UV (CH_3CN) (nm): 341 (ε 12 600). IR (KBr) (cm^{-1}): 1740 (m), 1710 (s), 1235 (s), 1030 (s). ^1H NMR ($CDCl_3$) δ: 7.97–8.02 (m, 3H), 7.06 (s, 1H), 7.10 (d, *J* = 8.1 Hz, 1H), 6.87 (d, *J* = 8.1 Hz, 1H), 6.01 (s, 2H), 3.64 (s, 6H). ^{13}C NMR ($CDCl_3$) δ: 193.6, 192.9, 149.4, 148.8, 148.6, 140.0, 137.5, 135.0, 132.4, 124.6, 121.6, 121.4, 108.9, 107.5, 101.6, 91.1, 51.7. Anal. calcd. for $C_{18}H_{14}O_6$: C 66.25, H 4.32; found: C 66.14, H 4.36.

*2,2-Dimethoxy-5-(4-methylsulfanylphenyl)indan-1,3-dione (**137**)*

Compound **100** (2.85 g, 10.0 mmol) was coupled with 4-methylsulfanylphenylboronic acid (2.52 g, 15.0 mmol) to afford 3.08 g (95% yield) of **137** after purification by column chromatography (Et_2O – petroleum ether, 1:1). A yellow, crystalline precipitate, which formed in the chromatography fractions, was collected and dried in vacuo to give an analytical sample, mp 112 to 113°C. R_f 0.25 (Et_2O – petroleum ether, 1:4). HRMS–CI(CH_4) calcd. for $C_{18}H_{16}O_4S$ $(M)^+$: 328.0769; found: 328.0765. UV (CH_3CN) (nm): 339 (ε 19 900). IR (KBr) (cm^{-1}): 1715 (s), 1585 (s), 1190 (s), 1160 (s), 1030 (s). ^1H NMR ($CDCl_3$) δ: 8.02 (dd, *J* = 1.6 Hz, *J* = 0.5 Hz, 1H), 7.99 (dd, *J* = 8.1 Hz, *J* = 1.6 Hz, 1H), 7.93 (dd, *J* = 8.1 Hz, *J* = 0.5 Hz, 1H), 7.49 (d, *J* = 8.5 Hz, 2H), 7.24 (d, *J* = 8.5 Hz, 2H), 2.45 (s, 3H), 3.61 (s, 6H). ^{13}C NMR ($CDCl_3$) δ: 193.4, 192.7, 148.8, 140.9, 139.8, 137.5, 134.8, 134.3, 127.4, 126.2, 124.6, 121.1, 91.0, 51.5, 15.0. Anal. calcd. for $C_{18}H_{16}O_4S$: C 65.83, H 4.91; found: C 65.69, H 4.86.

*2,2-Dimethoxy-5-thiophen-2-yl-indan-1,3-dione (**138**)*

Compound **100** (4.28 g, 15.0 mmol) was coupled with 2-thienylboronic acid (2.88 g, 22.5 mmol) to afford 4.18 g (96% yield) of **138** after purification by column chromatography (Et_2O – petroleum ether, 1:1 and CH_2Cl_2). A yellow, crystalline precipitate, which formed in the chromatography fractions, was collected and dried in vacuo to afford an analytical sample, mp 133 to 134°C. R_f 0.28 (Et_2O – petroleum ether, 1:4). HRMS–CI (CH_4) calcd. for $C_{15}H_{12}O_4S$ $(M)^+$: 288.0456; found: 288.0475. UV (CH_3CN) (nm): 335 (ε 16 600), 250 (ε 12 000), 224 (ε 18 500). IR (KBr) (cm^{-1}): 1740 (s), 1710 (s), 1585 (s), 1185 (s), 1155 (s), 1040 (s), 1020 (s), 720 (s). ^1H NMR ($CDCl_3$) δ: 8.05 (dd, *J* = 1.7 Hz, *J* = 0.6 Hz, 1H), 8.30 (dd, *J* = 8.1 Hz, *J* = 1.7 Hz, 1H), 8.02 (dd, *J* = 8.1 Hz, *J* = 0.6 Hz, 1H), 7.47 (dd, *J* = 5.1 Hz, *J* = 1.1 Hz, 1H), 7.41 (dd, *J* = 3.8 Hz, *J* = 1.1 Hz, 1H), 7.09 (dd, *J* = 5.1 Hz, *J* = 3.8 Hz, 1H), 3.66 (s, 6H). ^{13}C NMR ($CDCl_3$) δ: 193.4, 192.4, 142.5, 141.2, 140.1, 137.4, 133.4, 128.7, 128.3, 126.3, 124.8, 119.7, 91.0, 51.6. Anal. calcd. for $C_{15}H_{12}O_4S$: C 62.15, H 4.20; found: C 62.48, H 4.06.

*2,2-Dimethoxy-5-(4-methylthiophen-2-yl)indan-1,3-dione (**139**)*

Compound **100** (4.28 g, 15 mmol) was coupled with 2-(4-methylthienyl)boronic acid (3.42 g, 22.5 mmol) to afford 3.18 g (70% yield) of **139** as a yellow solid after purification by column chromatography (Et_2O – petroleum ether, 1:4), mp 108 to 109°C. R_f 0.27 (Et_2O – petroleum ether, 1:4). HRMS–CI calcd. for $C_{16}H_{18}O_4S$ $(M+NH_4)^+$: 320.0957; found: 320.0963. IR ($CHCl_3$) (cm^{-1}): 1750 (s), 1725 (s), 1165 (s), 1065 (s). ^1H NMR (500 MHz, $CDCl_3$) δ: 8.08 (d, *J* = 1.2 Hz, 1H), 8.02 (dd, *J* = 8.1 Hz, *J* = 1.7 Hz, 1H), 7.93 (dd, *J*= 8.4 Hz, *J* = 0.6 Hz, 1H), 7.34 (d, *J* = 1.2 Hz, 1H), 7.02 (d, *J* = 1.1 Hz, 1H), 3.64 (s, 6H), 2.28 (s, 3H). ^{13}C NMR ($CDCl_3$) δ: 193.3, 192.3, 141.0, 133.4, 128.6, 125.1, 124.9, 124.0, 119.6, 91.2, 51.8, 15.8. Anal. calcd. for $C_{16}H_{14}O_4S$: C 63.56, H 4.67; found: C 63.86, H 4.70.

*2,2-Dimethoxy-5-(5-methylthiophen-2-yl)indan-1,3-dione (**140**)*

Compound **100** (3.5 g, 12.3 mmol) was coupled with 2-(5-methylthienyl)boronic acid (2.6 g, 18.4 mmol) to afford 1.75 g (47% yield) of **140** as a yellow solid after purification by column chromatography (Et_2O – petroleum ether, 1:4), mp 113 to 114°C. R_f 0.27 (Et_2O – petroleum ether, 1:4). HRMS–CI calcd. for $C_{16}H_{14}O_4S$ $(M+NH_4)^+$: 320.0957; found: 320.0950. IR ($CDCl_3$) (cm^{-1}): 1750 (s), 1720 (s), 1155 (s), 1055 (s). ^1H NMR (500 MHz, $CDCl_3$) δ: 8.02 (d, *J* = 1.9 Hz, 1H), 7.97 (dd, *J*= 8.1 Hz, *J*= 1.6 Hz, 1H), 7.90 (dd, *J* = 7.4, *J* = 3.5 Hz, 1H), 7.32 (d, *J* = 3.6 Hz, 1H), 6.77 (d, *J* = 3.7 Hz, 1H), 3.67 (s, 6H), 2.51 (s, 3H). ^{13}C NMR (125 MHz, $CDCl_3$) δ: 193.6, 192.5, 143.0, 140.2, 138.9, 137.2, 133.0, 127.2, 126.5, 124.8, 119.1, 91.2, 51.7, 15.6. Anal. calcd. for $C_{16}H_{14}O_4S$: C 63.56, H 4.67; found: C 63.83, H 4.64.

*2,2-Dimethoxy-5-(5-ethylthiophen-2-yl)indan-1,3-dione (**141**)*

Compound **100** (4.9 g, 17.2 mmol) was coupled with 2-(5-ethylthienyl)boronic acid (4.0 g, 25.6 mmol) to afford 3.27 g (64% yield, based on recovery of 0.31 g of 100) of **141** as a yellow solid after purification by column chromatography (Et_2O – petroleum ether, 1:4), mp 61 to 62°C. R_f 0.28 (Et_2O – petroleum ether, 1:4). HRMS–CI calcd. for $C_{17}H_{20}NO_4S$ $(M+NH_4)^+$: 334.1113; found: 334.1106. IR ($CDCl_3$) (cm^{-1}): 1750 (s), 1720 (s), 1160 (s), 1035 (s). ^1H NMR (500 MHz, $CDCl_3$) δ: 8.00 (d, *J* = 1.8 Hz, 1H), 7.98 (dd, *J* = 8.1 Hz, *J* =

© 2001 NRC Canada

1.6 Hz, 1H), 7.91 (d, *J* = 8.1 Hz, 1H), 7.35 (d, *J* = 3.7 Hz, 1H), 6.81 (d, *J* = 3.7 Hz, 1H), 3.63 (s, 6H), 2.86 (q, *J* = 7.5 Hz, 2H), 1.32 (t, *J* = 7.5 Hz, 3H). ^{13}C NMR (125 MHz, $CDCl_3$) δ: 193.5, 192.5, 151.5, 143.1, 140.2, 138.5, 137.2, 133.0, 126.3, 125.4, 124.8, 119.1, 91.2, 51.7, 23.7, 15.7. Anal. calcd. for $C_{17}H_{16}O_4S$: C 64.54, H 5.10; found: C 64.91, H 4.98.

*2,2-Dimethoxy-5-(thiophen-3-yl)indan-1,3-dione (**142**)*

Compound **100** (7.00 g, 24.6 mmol) was coupled with 3-thienylboronic acid (4.70 g, 36.7 mmol) to give 5.07 g (72% yield) of **142** as a yellow solid after purification by column chromatography (Et_2O – petroleum ether, 1:4), mp 163°C. R_f 0.23 (Et_2O – petroleum ether, 1:4). HRMS–CI calcd. for $C_{15}H_{16}NO_4S$ $(M+NH_4)^+$: 306.0800; found: 306.0812. IR ($CDCl_3$) (cm^{-1}): 1750 (s), 1720 (s), 1155 (s), 1030 (s). ^{1}H NMR (500 MHz, $CDCl_3$) δ: 8.10 (d, *J* = 1.3 Hz, 1H), 8.06 (dd, *J* = 8.5 Hz, *J* = 1.5 Hz, 1H), 7.96 (d, *J* = 8.1 Hz, 1H), 7.67 (dd, *J*= 2.9, *J* = 0.9 Hz, 1H), 7.43 (m, 2H), 3.64 (s, 6H). ^{13}C NMR (125 MHz, $CDCl_3$) δ: 193.7, 192.7, 144.0, 140.2, 139.6, 137.6, 134.5, 127.6, 125.9, 124.8, 124.0, 120.8, 91.1, 51.7. Anal. calcd. for$C_{15}H_{16}NO_4S$: C 62.15, H 4.20; found: C 61.96, H 4.16.

*2,2-Diisopropoxy-5-(thiophen-3-yl)indan-1,3-dione (**127**)*

Compound **125** (1.2 g, 3.5 mmol) was coupled with 3-thienylboronic acid (0.96 g, 7.5 mmol) to give 790 mg (66% yield) of **127** as a yellow solid after purification by column chromatography (Et_2O – petroleum ether, 1:9), mp 127 to 127.5°C. R_f 0.28 (Et_2O – petroleum ether, 1:9). HRMS–CI calcd. for $C_{19}H_{21}O_4S$ $(M+H)^+$: 345.1161; found: 345.1163. IR (KBr) (cm^{-1}): 1748 (s), 1718 (s), 1161 (s), 1042 (s). ^{1}H NMR ($CDCl_3$) δ: 8.14 (d, *J* = 1.6 Hz, 1H), 8.10 (dd, *J* = 8.1 Hz, *J* = 1.6 Hz, 1H), 8.00 (d, *J* = 8.1 Hz, 1H), 7.69 (m, 1H), 7.47 (m, 2H), 4.68 (m, 2H), 1.16 (d, *J* = 6.1 Hz, 12 H). ^{13}C NMR (125 MHz, $CDCl_3$) δ: 195.2, 194.3, 143.9, 140.0, 139.8, 137.5, 134.4, 127.6, 126.0, 124.8, 123.9, 120.8, 91.4, 67.2, 23.8. Anal. calcd. for $C_{19}H_{20}O_4S$: C 66.26, H 5.85; found: C 66.46, H 5.87.

*2,2-Dibenzyloxy-5-(thiophen-2-yl)indan-1,3-dione (**128**)*

Compound **126** (1.31 g, 3.0 mmol) was coupled with 2-thienylboronic acid (576 mg, 4.5 mmol) to give 1.13 g (85% yield) of **128** as a yellow solid after purification by column chromatography (EtOAc – petroleum ether, 1:3). R_f 0.50 (EtOAc – petroleum ether, 1:3). HRMS–CI calcd. for $C_{27}H_{21}O_4S$ $(M+H)^+$: 441.1161; found: 441.1156. IR (KBr) (cm^{-1}): 1742 (s), 1715 (s), 1155 (s), 1059 (s), 1015 (s). ^{1}H NMR ($CDCl_3$) δ: 8.16 (d, *J* = 1.5 Hz, 1H), 8.10 (dd, *J* = 8.2 Hz, *J* = 1.6 Hz, 1H), 7.99 (d, *J* = 8.0 Hz, 1H), 7.55 (dd, *J* = 3.7 Hz, *J* = 1.1 Hz, 1H), 7.47 (dd, *J* = 5.1 Hz, *J* = 1.2 Hz, 1H), 7.26–7.33 (m, 10H), 7.16 (dd, *J* = 4.5 Hz, *J* = 1.3 Hz, 1H), 5.09 (s, 4H). ^{13}C NMR ($CDCl_3$) δ: 193.3, 192.3, 142.8, 141.4, 140.3, 137.7, 137.1, 133.7, 128.9, 128.4, 127.8, 126.4, 125.1, 120.0, 91.7, 66.2. Anal. calcd. for $C_{27}H_{20}O_4S$: C 73.45, H 4.79; found: C 73.26, H 4.46.

*3,6-Dibromoinden-1-one (**130**)*

Ketone **117** (2.11 g, 10.0 mmol) was reacted with NBS (5.78 g, 32.5 mmol) and a catalytic amount of AIBN in CCl_4 (50 mL) according to the procedure previously described for the preparation of **99** to provide 420 mg (15% yield) of **130** as an orange solid after column chromatography (petroleum ether and Et_2O – petroleum ether, 15:85), mp 266–268°C. R_f 0.46 (Et_2O – petroleum ether, 1:4). HRMS–CI (NH_3) calcd. for $C_9H_4Br_2O$ $(M)^+$: 285.8629; found: 285.8596. IR (KBr) (cm^{-1}): 1715 (s). ^{1}H NMR ($CDCl_3$) δ: 7.58 (dd, *J* = 7.8 Hz, *J* = 1.8 Hz, 1H), 7.49 (d, *J* = 1.8 Hz, 1H), 7.05 (d, *J* = 7.8 Hz, 1H), 6.20 (s, 1H). ^{13}C NMR ($CDCl_3$) δ: 192.2, 148.2, 141.3, 135.8, 131.6, 127.3, 125.1, 124.6, 122.5.

*5-Bromo-2,2-dihydroxyindan-1,3-dione (**33**)*

Method A: Enone **130** (200 mg, 0.69 mmol) was heated with Br_2 (1 drop) in DMSO (10 mL) for 3.5 h according to the procedure previously described for the preparation of **112** to provide 35 mg (20% yield) of **33** as a light green solid after column chromatography (petroleum ether and Et_2O – petroleum ether, 1:1 and CH_2Cl_2).

Method B: Ketone **117** (500 mg, 2.37 mmol) was heated with SeO_2 (1.30 g, 11.8 mmol) in dioxane (50 mL) for 2 h according to the procedure previously described for the preparation of **65** to afford 140 mg (23% yield) of **33** as a yellow-green foam, mp 68–72°C. R_f 0.24 (Et_2O – petroleum ether, 1:1). HRMS–CI (NH_3) calcd. for $C_9H_5BrO_4$ $(M)^+$: 255.9371; found: 255.9358. UV (CH_3CN) (nm): 338 (ε 890), 265 (ε 13 200). IR (KBr) (cm^{-1}): 3700–2200 (br, s), 1720 (s), 1175 (s). ^{1}H NMR (D_2O) δ: 7.89–7.93 (m, 2H), 7.68 (d, *J* = 8.1, 1H) (note: the hydroxyl protons do not appear in the spectrum due to exchange with D_2O). ^{13}C NMR (D_2O) δ: 195.7, 195.3, 139.2, 136.6, 132.5, 131.6, 129.6, 124.1, 86.6.

*5-Bromo-2-diazoindan-1,3-dione (**124**)*

A suspension of finely divided **131** (48.0 g, 213 mmol, passed through a 40 mesh screen) in absolute EtOH (100 mL) was cooled to –30°C in a dry ice – acetone bath. Triethylamine (38.6 mL, 278 mmol) was added all at once to the slurry. The mixture immediately turned dark red, the solid dissolved, and the temperature rose to approximately –10°C. After stirring for 10 min, tosyl azide (53.4 g, 271 mmol) (CAUTION: toxic, potentially explosive at elevated temperatures) was slowly added over 10 min and the flask was transferred to an ice bath. The mixture gradually turned purple and a precipitate formed. After stirring for 1 h, the precipitate was collected, dried in air (1 h), and then in vacuo (2 h) to afford 45.0 g (84% yield) of **120** as a purple solid, mp 131 to 132°C dec. R_f 0.37 (Et_2O – petroleum ether, 1:4). HRMS–CI (CH_4) calcd. for $C_9H_3BrN_2O_2$ $(M)^+$: 249.9378; found: 249.9365. IR (KBr) (cm^{-1}): 2320 (w), 2125 (s), 1680 (s). ^{1}H NMR ($CDCl_3$) δ: 7.91 (d, *J* = 1.7 Hz, 1H), 7.83 (dd, *J* = 8.0 Hz, *J* = 1.7 Hz, 1H), 7.65 (d, *J* = 8.0 Hz, 1H). ^{13}C NMR ($CDCl_3$) δ: 180.8, 180.4, 138.3, 137.5, 135.3, 130.0, 125.8, 123.9 (note: a signal for C-2 was not observed).

*5-Bromo-2,2-dimethoxyindan-1,3-dione (**100**)*

Method A: Compound **33** (200 mg, 0.78 mmol) was dissolved in DMF (10 mL). Methyl iodide (870 mg, 14.0 mmol), silver(I) oxide (415 mg, 1.79 mmol), and water (5 drops) were added and the mixture was stirred at 25°C overnight. $CHCl_3$ (50 mL) was added and a precipitate was collected. The

© 2001 NRC Canada

solid was washed with $CHCl_3$ (25 mL) and the filtrates were combined. The $CHCl_3$ solution was treated with 5% aq KCN (50 mL), washed with water (2 × 50 mL), dried over Na_2SO_4, and filtered. The solvent was evaporated under reduced pressure and the residue was purified by column chromatography (petroleum ether and Et_2O – petroleum ether, 1:1) to give 48 mg (22% yield, mp 103–105°C) of **100** as a yellow solid.

Method B: A mixture of diazodione **124** (45.0 g, 179 mmol) and MeOH (100 mL) was cooled to 5°C in an ice bath. To the purple slurry was added *tert*-butyl hypochlorite (23.4 mL, 195 mmol) over 10 min. Gentle bubbling (loss of N_2) was observed and a yellow precipitate formed. The solid was collected after 1 h, washed with ice cold MeOH (20 mL), dried in air and then in vacuo to give 33.0 g (65% yield, mp 103.5 to 104.5°C) of **100** as a yellow solid. An analytical sample of the product was obtained by recrystallization from MeOH to afford yellow crystals, mp 106 to 107°C. R_f 0.38 (Et_2O – petroleum ether, 1:4). ^{1}H NMR ($CDCl_3$) δ: 8.05 (d, J = 1.1 Hz, 1H), 7.94 (dd, J = 8.1 Hz, J = 1.1 Hz, 1H), 7.79 (d, J = 8.1 Hz, 1H), 3.58 (s, 6H). ^{13}C NMR ($CDCl_3$) δ: 192.3, 192.1, 140.4, 139.8, 137.8, 132.4, 127.3, 125.6, 90.8, 51.7. IR (KBr) (cm^{-1}): 1720 (s). HRMS–CI (NH_3) calcd. for $C_{11}H_{13}BrNO_4$ $(M+NH_4)^+$: 302.0027; found: 302.0049. Anal. calcd. for $C_{11}H_9BrO_4$: C 46.34, H 3.18; found: C 46.35, H 3.05.

*5-Bromo-2,2-diisopropoxyindan-1,3-dione (**125**)*

A mixture of diazodione **124** (2.27 g, 9.00 mmol) and 2-propanol (10 mL) was treated with *tert*-butyl hypochlorite (1.11 g, 10 mmol) according to the procedure described for compound **100** to give 1.15 g (38% yield) of **125**, mp 97 to 97.5°C. R_f 0.52 (Et_2O – petroleum ether, 1:9). HRMS calcd. for $C_{15}H_{18}BrO_4$ $(M+H)^+$: 341.0389; found: 341.0392. IR (KBr) (cm^{-1}): 1755 (s), 1728 (s), 1171 (s), 1042 (s). ^{1}H NMR ($CDCl_3$) δ: 8.11 (d, J = 1.3 Hz, 1H), 7.98 (dd, J = 8.2 Hz, J = 1.7 Hz, 1H), 7.85 (d, J = 8.0 Hz, 1H), 4.55–4.70 (m, 2H), 1.14 (d, J = 6.2 Hz, 12 H). ^{13}C NMR (125 MHz, $CDCl_3$) δ: 193.9, 193.6, 140.2, 139.7, 137.5, 132.2, 127.2, 125.5, 91.4, 67.3, 23.7. Anal. calcd. for $C_{15}H_{17}BrO_4$: C 52.80, H 5.02; found: C 52.25, H 5.12.

*5-Bromo-2,2-dibenzyloxyindan-1,3-dione (**126**)*

A mixture of diazodione **124** (2.0 g, 8.0 mmol) and benzyl alcohol (4 mL) was treated with *tert*-butyl hypochlorite (2.6 g, 24 mmol) according to the procedure described for compound **100** to give 1.77 g (51% yield) of **126**. R_f 0.63 (EtOAc – petroleum ether, 1:3). HRMS–CI calcd. for $C_{23}H_{18}BrO_4$ $(M+H)^+$: 437.0389; found: 437.0386. IR (KBr) (cm^{-1}): 1754 (m), 1717 (s), 1174 (s), 1055 (s). ^{1}H NMR ($CDCl_3$) δ: 8.13 (d, J = 1.2 Hz, 1H), 7.99 (dd, J = 8.1 Hz, J = 1.6 Hz, 1H), 7.85 (d, J = 8.1 Hz, 1H), 7.27–7.29 (m, 10 H), 5.05 (s, 4H). ^{13}C NMR (125 MHz, $CDCl_3$) δ: 192.2, 191.9, 140.5, 139.9, 137.8, 136.9, 132.5, 128.4, 127.9, 127.8, 127.4, 125.7, 91.3, 66.2. Anal. calcd. for $C_{23}H_{17}BrO_4$: C 63.17, H 3.92; found: C 63.09, H 4.03.

*2,2-Diacetoxy-1,3-indandione (**129**)*

Ninhydrin (**1**) (2.0 g, 11.2 mmol) was added to 5 mL (53 mmol) of acetic anhydride. One drop of concentrated (98%) sulfuric acid was added, and the temperature of the reaction mixture increased to ~40°C. The reaction mixture was stirred for 15 min at room temperature and then heated in an oil bath at 100°C for 48 h. Upon cooling the reaction mixture solidified. The solid was washed with Et_2O and recrystallized from EtOAc to yield 1.94 g (66% yield) of **129** as transparent crystals, mp 174.5 to 175.5°C. R_f 0.63 (EtOAc – petroleum ether, 2:3). HRMS calcd. for $C_{13}H_{11}O_6$ $(M+H)^+$: 263.0556; found: 263.0556. IR (KBr) (cm^{-1}): 1749 (s), 1728 (s), 1222 (s), 1066 (s). ^{1}H NMR ($CDCl_3$) δ: 7.93–7.98 (m, 2H), 7.85–7.90 (m, 2H), 2.11 (s, 6H). ^{13}C NMR (125 MHz, $CDCl_3$) δ: 190.5, 168.0, 139.1, 136.2, 123.4, 19.9 (note: one quaternary carbon signal was not observed). Anal. calcd. for $C_{13}H_{10}O_6$: C 59.55, H 3.84; found: C 59.20, H 3.81.

Deprotection of ketals

The ketal was dissolved in glacial acetic acid (0.2 M) and an equal amount of water and concentrated aqueous hydrobromic acid (48%) were added to form a fine suspension. The reaction mixture was heated at reflux for 2 h and filtered while hot. The filtrate was diluted with water and the precipitate which formed after cooling in an ice bath was collected by filtration, washed with water, and air-dried to give the ninhydrin analog without further purification, in most cases.

*2,2-Dihydroxy-5-phenylindan-1,3-dione (**47**)*

Ketal **132** (930 mg, 3.29 mmol) was deprotected to give 450 mg (54% yield) of **47** as an orange-brown solid, mp 70–73°C dec.

*5-Biphenyl-4-yl-2,2-dihydroxyindan-1,3-dione (**48**)*

Ketal **133** (870 mg, 2.42 mmol) was deprotected to give 330 mg (41% yield) of **48** as an orange-brown solid, mp 228–231°C dec.

*2,2-Dihydroxy-5-(4-nitrophenyl)indan-1,3-dione (**50**)*

Ketal **134** (90 mg, 0.275 mmol) was deprotected to give 65 mg (89% yield) of **50** as a beige solid, mp 229–230°C dec. R_f 0.35 (EtOAc – petroleum ether, 2:3). IR (KBr) (cm^{-1}): 3412 (br), 1757 (s), 1715 (s), 1706 (s). ^{1}H NMR (DMSO-d_6) δ: 8.44 (dd, J = 8 Hz, J = 1.5 Hz, 1H), 8.35–8.38 (m, 3H), 8.13–8.19 (m, 3H), 7.62 (s, 2H). ^{13}C NMR (125 MHz, DMSO-d_6) δ: 196.2, 196.1, 147.8, 146.1, 144.2, 139.2, 138.1, 136.1, 129.1, 124.7, 124.2, 122.4, 106.1, 87.9. Anal. calcd. for $C_{15}H_9NO_6$: C 60.21, H 3.03; found: C 60.07, H 2.99.

*2,2-Dihydroxy-5-(4-methoxyphenyl)indan-1,3-dione (**52**)*

Ketal **135** (312 mg, 1.00 mmol) was deprotected to give 211 mg (74% yield) of **52** as an orange foam after column chromatography (Et_2O – petroleum ether, 1:4, and Et_2O), mp 62–65°C dec.

*5-Benzo[1,3]dioxo-5-yl-2,2-dihydroxyindan-1,3-dione (**53**)*

Ketal **136** (1.21 g, 3.71 mmol) was deprotected to give 890 mg (80% yield) of **53** as a dark yellow solid, mp 112–115°C dec (hydrated form); an orange-red foam was obtained after drying an analytical sample sample in vacuo for 48 h, mp 236–239°C dec.

© 2001 NRC Canada

*2,2-Dihydroxy-5-(4-methylsulfanylphenyl)indan-1,3-dione (**54**)*

Ketal **137** (750 mg, 2.28 mmol) was deprotected to give 660 mg (96% yield) of **54** as a yellow solid, mp 77 to 78°C dec.

*2,2-Dihydroxy-5-thiophen-2-yl-indan-1,3-dione (**55**)*

Ketal **138** (1.00 g, 3.47 mmol) was deprotected to give 770 mg (86% yield) of **55** as a yellow-tan solid, mp 260–262°C dec.

*2,2-Dihydroxy-5-(4-methylthiophen-2-yl)indan-1,3-dione (**56**)*

Ketal **139** (2.65 g, 8.75 mmol) was deprotected to give 1.05 g (44% yield) of **56** as cream-colored flakes. HRMS–CI calcd. for $C_{14}H_8O_3S$ $(M\text{-}H_2O)^+$: 256.0194; found: 256.0199. IR (KBr) (cm^{-1}): 3280 (m), 1750 (s), 1715 (s), 1165 (s). ^1H NMR (DMSO-d_6) δ: 8.14 (dd, J = 8.2 Hz, J = 1.6 Hz, 1H), 8.12 (s, 1H), 7.99 (d, J = 8.1 Hz, 1H), 7.78 (s, 1H), 7.50 (s, 2H, exchangeable with D_2O), 7.37 (s, 1H), 2.26 (s, 3H). ^{13}C NMR (125 MHz, DMSO-d_6) δ: 196.9, 196.0, 142.0, 140.2, 139.5, 139.3, 136.7, 133.4, 129.7, 124.9, 124.5, 118.6, 87.9, 15.4. Anal. calcd. for $C_{14}H_{10}O_4S$: C 61.31, H 3.67; found: C 60.94, H 3.55.

*2,2-Dihydroxy-5-(5-methylthiophen-2-yl)indan-1,3-dione (**57**)*

Ketal **140** (410 mg, 1.36 mmol) was deprotected to give 195 mg (52% yield) of **57** as cream-colored flakes. HRMS calcd. for $C_{14}H_{10}O_4S$ $(M)^+$: 274.0300; found: 274.0306. IR (KBr) (cm^{-1}): 3250 (s), 1745 (s), 1710 (s), 1160 (s). ^1H NMR (500 MHz, acetone-d_6) δ: 8.40 (dd, J = 8.1 Hz, J = 1.7 Hz, 1H), 8.26 (d, J = 1.3 Hz, 1H), 8.17 (d, J = 8.2 Hz, 1H), 7.83 (d, J = 3.6 Hz, 1H), 7.09 (d, J = 3.6 Hz, 1H), 6.65 (s, 2H, exchangeable with D_2O), 3.01 (s, 3H). ^{13}C NMR (125 MHz, DMSO-d_6) δ: 197.0, 195.9, 143.2, 142.0, 139.5, 138.3, 136.4, 133.1, 127.8, 127.7, 124.9, 118.2, 87.9, 15.2. Anal. calcd. for $C_{14}H_{10}O_4S$: C 61.31, H 3.67; found: C 61.20, H 3.47.

*2,2-Dihydroxy-5-(5-ethylthiophen-2-yl)indan-1,3-dione (**58**)*

Ketal **141** (3.27 g, 10.35 mmol) was deprotected to give 2.23 g (75% yield) of **58** as cream-colored flakes, mp 108 to 109.5°C dec. R_f 0.40 (benzene – EtOAc – formic acid, 85:10:5). IR (KBr) (cm^{-1}): 3285 (m), 1745 (s), 1710 (s), 1160 (s). HRMS calcd. for $C_{15}H_{12}O_4S$ $(M)^+$: 288.0456; found: 288.0449. ^1H NMR (500 MHz, acetone-d_6) δ: 8.38 (dd, J = 8.1 Hz, J = 1.8 Hz, 1H), 8.25 (dd, J = 1.5 Hz, J = 0.5 Hz, 1H), 8.15 (dd, J = 8.2 Hz, J = 0.7 Hz, 1H), 7.81 (d, J = 3.7 Hz, 1H), 7.10 (d, J = 3.8 Hz, 1H), 3.07 (q, J = 7.5 Hz, 2H), 1.48 (t, J = 7.5 Hz, 3H). ^{13}C NMR (125 MHz, DMSO-d_6) δ: 197.0, 195.9, 150.6, 142.1, 139.5, 137.9, 136.4, 133.1, 127.6, 126.1, 124.9, 118.2, 87.9, 23.0, 15.6. Anal. calcd. for $C_{15}H_{12}O_4S$: C 62.49, H 4.20; found: C 62.25, H 4.19.

*2,2-Dihydroxy-5-(thiophen-3-yl)indan-1,3-dione (**59**)*

Ketal **142** (2.01 g, 7.0 mmol) was deprotected to give 0.78 g (43% yield) of **59** as cream-colored flakes, mp 124–126°C dec. IR (KBr) (cm^{-1}): 3370 (m), 1745 (s), 1710 (s). HRMS–CI calcd. for $C_{13}H_8O_4S$ $(M)^+$: 260.0143; found: 260.0150. ^1H NMR (500 MHz, acetone-d_6) δ: 8.57 (dd, J = 8.6 Hz, J = 1.8 Hz, 1H), 8.44 (d, J = 1.2 Hz, 1H), 8.36 (dd, J = 2.9 Hz, J = 1.4 Hz, 1H), 8.22 (dd, J = 7.9 Hz, J = 0.5 Hz, 1H), 7.94 (dd, J = 5.1 Hz, J = 1.4 Hz, 1H), 7.85 (dd, J = 4.0 Hz, J = 2.0 Hz, 1H), 6.66 (s, 2H, exchangeable with D_2O). ^{13}C NMR (125 MHz, acetone-d_6) δ: 210.6, 210.4, 149.0, 145.2, 144.9, 142.6, 139.8, 132.8, 131.4, 129.8, 129.7, 125.6, 93.0. Anal. calcd. for $C_{13}H_8O_4S\cdot H_2O$: C 56.11, H 3.62; found: C 55.93, H 3.43.

*5-(4-Dimethylaminophenyl)-2,2-dihydroxyindan-1,3-dione (**49**)*

Ketal **145** (1.00 g, 3.07 mmol) was deprotected to give 730 mg (80% yield) of **49** as a brown solid. An analytical sample was purified by column chromatography (EtOAc – petroleum ether, 1:4 and 1:1) to give a khaki-colored solid, mp 90–94°C. R_f 0.33 (MeOH–CH_2Cl_2, 4:96). HRMS–CI (NH_3) calcd. for $C_{17}H_{14}NO_3$ $(M\text{-}OH)^+$: 280.0974; found: 280.0963. UV (CH_3CN) (nm): 625 (ε 300), 396 (ε 13 900), 258 (ε 14 400). IR (KBr) (cm^{-1}): 3600–2800 (br, m), 1740(m), 1720(s). ^1H NMR (DMSO-d_6) δ: 8.28 (m, 1H), 8.10 (m, 1H), 7.96 (m, 1H), 7.79 (m, 2H), 7.62 (br s, 2H, exchangeable with D_2O), 6.82 (m, 2H), 3.33 (s, 6H). ^{13}C NMR (DMSO-d_6) δ: 197.7, 196.5, 151.4, 149.1, 139.8, 135.9, 134.1, 128.5, 125.1, 124.4, 119.2, 112.8, 88.3 (note: the absorption for the dimethylamino-group carbons occurs in a region where it is obscured by the multiplet associated with DMSO-d_6).

*5-(2-Benzo[*b*]thienyl)-2,2-dihydroxy-1*H*-indene-1,3(2*H*)-dione (**60**)*

Ketal **146** (2.17 g, 6.41 mmol) was deprotected to give 1.22 g (61% yield) of **60** as a yellow-tan solid, mp 309–311°C dec. R_f 0.25 (benzene – EtOAc – formic acid, 85:10:5). HRMS–CI (NH_3) calcd. for $C_{17}H_{10}O_4S$ $(M)^+$: 310.0300; found: 310.0316. UV (CH_3CN) (nm): 340 (ε 17 700), 258 (ε 13 000). IR (KBr) (cm^{-1}): 3600–2300 (br, s), 1740 (s), 1730 (s), 1710 (s), 1250 (s), 1180 (s), 1145 (s), 1080 (s). ^1H NMR (DMSO-d_6) δ: 8.35 (d, J = 8.1 Hz, 1H), 8.26 (s, 2H), 8.04 (d, J = 8.1 Hz, 1H), 7.87–8.03 (m, 2H), 7.62 (br s, 2H, exchangeable with D_2O), 7.41 (m, 2H). ^{13}C NMR (DMSO-d_6) δ: 196.9, 196.2, 141.6, 140.4, 140.1, 139.5, 139.4, 137.4, 134.3, 126.0, 125.3, 125.0, 124.7, 124.3, 122.7, 120.0, 88.0. Anal. calcd. for $C_{17}H_{10}O_4S$: C 65.79, H 3.25; found: C 65.65, H 3.02.

*5-Benzothiazol-2-yl-2,2-dihydroxyindan-1,3-dione (**61**)*

Ketal **147** (890 mg, 2.62 mmol) was deprotected to give 238 mg (29% yield) of **61** as a light tan solid, mp 272–274°C dec. R_f 0.21 (benzene – EtOAc – formic acid, 85:10:5). HRMS–CI (NH_3) calcd. for $C_{16}H_8NO_4S$ $(M\text{-}OH)^+$: 294.0225; found: 294.0211. UV (CH_3CN) (nm): 334 (ε 12 200). IR (KBr) (cm^{-1}): 3600–2300 (br,s), 1760 (s), 1720 (s), 1140 (s), 1110 (s). ^1H NMR (DMSO-d_6) δ: 8.63 (d, J = 8.0 Hz, 1H), 8.48 (s, 1H), 8.09–8.19 (m, 3H), 7.68 (s, 2H, exchangeable with D_2O), 7.48–7.60 (m, 2H). ^{13}C NMR (DMSO-d_6) δ: 196.5, 196.4, 164.8, 153.4, 140.1, 139.5, 139.2, 135.3, 135.1, 127.2, 126.6, 125.2, 123.6, 122.7, 121.6, 88.0. Anal. calcd. for $C_{16}H_9NO_4S\cdot(H_2O)_{0.5}$: C 59.99, H 3.15; found: C 60.14, H 2.77.

*5-[2,2′-Bithiophen-5-yl]-2,2-dihydroxyindan-1,3-dione (**62**)*

Ketal **148** (2.15 g, 5.81 mmol) was deprotected to give 267 mg (13% yield) of **62** as an orange brown solid, mp 90–93°C dec. The solid was dried in vacuo for 48 h to provide a dark green-brown solid which was used as an analytical

© 2001 NRC Canada

sample (mp > 360°C). R_f 0.33 (benzene – EtOAc – formic acid, 85:10:5). HRMS–CI (NH_3) calcd. for $C_{17}H_9O_3S_2$ $(M-OH)^+$: 324.9993; found: 324.9989. UV (CH_3CN) (nm): 383 (ε 18 100). IR (KBr) (cm^{-1}): 3600–2700(br, s), 1765(m), 1725(s), 1160(s), 1070(s). ^1H NMR (DMSO-d_6) δ: 8.26 (d, J = 8.2 Hz, 1H), 8.17 (s, 1H), 8.00 (d, J = 8.2 Hz, 1H), 7.90 (d, J = 3.9 Hz, 1H), 7.58 (s, 2H, exchangeable with D_2O), 7.57 (m, 1H), 7.40–7.43 (m, 2H), 7.11 (m, 1H). ^{13}C NMR (DMSO-d_6) δ: 197.0, 196.0, 141.4, 139.5, 139.3, 139.1, 136.8, 135.7, 133.4, 128.8, 128.6, 126.7, 125.7, 125.2, 125.0, 118.8, 88.0. Anal. calcd. for $C_{17}H_{10}O_4S_2$: C 59.63, H 2.94; found: C 59.52, H 2.75.

*5-[5′-(2,2-Dihydroxy-1,3-dioxoindan-5-yl)-thiophen-2-yl]-2,2-dihydroxyindan-1,3-dione (**67**)*

Ketal **150** (1.23 g, 2.50 mmol) was deprotected to give 880 mg (80% yield) of **67** as a bright yellow solid, mp 298–300°C dec. R_f 0.27 (MeOH–CH_2Cl_2, 4:96). UV (CH_3CN) (nm): 380 (ε 30 900). IR (KBr) (cm^{-1}): 3600–2500 (br, s), 1700 (s), 1150 (s). ^1H NMR (DMSO-d_6) δ: 8.38 (d, J = 8.2 Hz, 2H), 8.30 (s, 2H), 8.09 (s, 2H), 8.07 (d, J = 8.2 Hz, 2H), 7.58 (s, 4H, exchangeable with D_2O). ^{13}C NMR (DMSO-d_6) δ: 196.9, 196.1, 143.0, 141.0, 139.5, 137.3, 133.8, 129.4, 125.1, 119.4, 87.9. Anal. calcd. for $C_{22}H_{12}O_8S\cdot(H_2O)_{1.5}$: C 57.02, H 3.26; found: C 57.22, H 3.60.

*2,2-Dihydroxy-5-styrylindan-1,3-dione (**63**)*

Ketal **155** (154 mg, 0.5 mmol) was deprotected to give 120 mg (82% yield) of **63** as a beige solid. IR (KBr) (cm^{-1}): 1747 (s), 1711 (s). ^1H NMR (DMSO-d_6) δ: 8.26 (d, J = 8.1 Hz, 1H), 8.20 (s, 1H), 8.00 (d, J = 8.0 Hz, 1H), 7.67–7.37 (m, 3H), 7.53 (d, J = 13.3 Hz, 1H), 7.50 (s, 2H), 7.35–7.49 (m, 3H). ^{13}C NMR (125 MHz, DMSO-d_6) δ: 197.2, 196.2, 146.0, 139.3, 137.0, 136.2, 134.9, 134.0, 128.8, 127.2, 126.5, 124.4, 120.7, 87.9 (note: the signal for one aromatic carbon was not detected). Anal. calcd. for $C_{17}H_{12}O_4$: C 72.85, H 4.32; found: C 72.99, H 4.26.

*2,2-Dihydroxy-5-(4-hydroxyphenyl)indan-1,3-dione (**51**)*

A solution of ketal **135** (376 mg, 1.20 mmol) in CH_2Cl_2 (50 mL) was placed under an N_2 atmosphere and cooled to 5°C in an ice bath. Boron tribromide in CH_2Cl_2 (6.00 mL, 6.00 mmol) was added via a syringe over 10 min and the color of the solution changed from yellow to red. The reaction mixture was stirred for 3 h at 25°C and then poured into 1 M HCl (50 mL). Water (50 mL) was added and the mixture was extracted with EtOAc (2 × 150 mL), washed with brine (50 mL), dried over Na_2SO_4, and filtered. The solvent was evaporated under reduced pressure and the residue heated at reflux with water and a small amount of decolorizing carbon. The mixture was filtered while hot and allowed to cool. No solid formed even after reducing the volume of the mixture so the solution was extracted with EtOAc (6 × 100 mL) and the combined organic extracts were washed with brine (50 mL), dried over $MgSO_4$, and filtered. The solvent was removed under reduced pressure and the residue dried in vacuo to afford 211 mg (65% yield) of **51** as a dark green solid, mp 112–114°C dec. R_f 0.27 (benzene – EtOAc – formic acid, 85:10:5). FAB–HRMS (NBA) calcd. for $C_{15}H_{10}O_5$ $(M)^+$: 270.0528; found: 270.0533. UV (CH_3CN) (nm): 594 (ε 280), 492 (ε 740), 323 (ε 12 200). IR (KBr) (cm^{-1}): 3700–2200 (br, s), 1710 (s), 1260 (s), 1170 (s). ^1H NMR (DMSO-d_6) δ: 9.96 (s, 1H, exchangeable with D_2O), 8.27 (d, J = 8.2 Hz, 1H), 8.12 (s, 1H), 8.01 (d, J = 8.2 Hz, 1H), 7.73 (d, J = 8.3 Hz, 2H), 7.70 (s, 2H, exchangeable with D_2O), 6.90 (d, J = 8.3 Hz, 2H). ^{13}C NMR (DMSO-d_6) δ: 197.2, 196.4, 159.0, 148.7, 139.4, 136.3, 134.7, 129.0, 128.3, 124.5, 119.9, 116.2, 88.0 (note: only the signals associated with the major tautomer are given for ^1H and ^{13}C NMR).

*5-Tributylstannyl[2,2′]bithiophene (**144**)*

A flame-dried 500 mL two-necked, round-bottomed flask under a dry N_2 atmosphere, was charged with anhyd Et_2O (100 mL) and *n*-BuLi in hexanes (12.0 mL, 30.0 mmol). TMEDA (4.50 mL, 30.0 mmol) was added via a syringe. The solution was stirred for 10 min, cooled to 5°C in an ice bath and 2,2′-bithienyl (**143**, 5.00 g, 30.0 mmol) was added. After 30 min, tributyltin chloride (8.10 mL, 30.0 mmol) was added via a syringe. The mixture was warmed to 25°C and stirred overnight. To remove unreacted tributyltin chloride in the form of polymeric tributyltin fluoride, potassium fluoride (1.4 g, 28 mmol) was then added and the mixture was stirred for 1 h. Solids were collected by filtration and rinsed with CH_2Cl_2 (50 mL). The filtrate was evaporated under reduced pressure and the residue was dried in vacuo to give a yellow-orange oil (14.3 g). The oil was purified by distillation under reduced pressure to afford 10.8 g (79% yield, bp 190–205°C at 1 torr (1 torr = 133.322 Pa)) of **144** as a yellow oil. R_f 0.51, (petroleum ether). HRMS–CI (NH_3) calcd. for $C_{20}H_{32}S_2Sn$ $(M)^+$: 456.0967; found: 456.0988. IR (neat) (cm^{-1}): 2970 (s), 2940 (s), 2880 (s), 2860 (s). ^1H NMR ($CDCl_3$) δ: 7.96 (d, J = 4.8 Hz, 1H), 7.33 (d, J = 3.3 Hz, 1H), 7.21 (d, J = 3.3 Hz, 1H), 7.11 (d, J = 3.3 Hz, 1H), 7.02 (dd, J = 4.8 Hz, J = 3.3 Hz, 1H), 0.96–1.64 (m, 27H). ^{13}C NMR ($CDCl_3$) δ: 142.7, 137.6, 136.5, 136.0, 127.6, 124.9, 123.9, 123.4, 28.9, 27.2, 13.6, 10.8.

Stille coupling reactions

To a solution of compound **100** (1.0 equiv) in toluene (0.10 M) was added a stannane (1.0 to 1.1 equiv). A catalytic amount of $Pd(PPh_3)_4$ (2 mol%) was added and the mixture was heated at reflux under an N_2 atmosphere and protected from light. After 6 h, the reaction mixture was evaporated under reduced pressure and the residue was purified by column chromatography using petroleum ether and Et_2O – petroleum ether (1:1) and (or) recrystallization. In some instances, the crude residue was washed with hexanes and (or) taken up in Et_2O and stirred with an excess of potassium fluoride for 36 h to remove tributylstannyl chloride as polymeric tributyltin fluoride before further purification.

*5-(4-Dimethylaminophenyl)-2,2-dimethoxyindan-1,3-dione (**145**)*

Compound **100** (2.85 g, 10.0 mmol) was coupled with 4-tributylstannyldimethylaniline (4.11 g, 10.0 mmol) to afford 3.08 g (95% yield) of **145** as a yellow solid, mp 101–103°C. R_f 0.15 (Et_2O – petroleum ether, 1:4). HRMS–CI (NH_3) calcd. for $C_{19}H_{20}NO_4$ $(M+H)^+$: 326.1392; found: 326.1394. UV (CH_3CN) (nm): 626 (ε 100), 396 (ε 28 100), 258 (ε 26 100). IR (KBr) (cm^{-1}): 1740 (m), 1710 (s), 1185 (s), 1160 (s), 1030 (s). ^1H NMR ($CDCl_3$) δ: 8.06 (d, J = 1.6 Hz,

© 2001 NRC Canada

1H), 8.02 (dd, *J* = 8.1 Hz, *J* = 1.6 Hz, 1H), 7.93 (dd, *J* = 8.1 Hz, 1H), 7.55 (d, *J* = 8.9 Hz, 2H), 6.73 (d, *J* = 8.9 Hz, 2H), 3.66 (s, 6H), 3.00 (s, 6H). ^{13}C NMR ($CDCl_3$) δ: 194.1, 192.8, 151.1, 149.7, 140.1, 136.5, 133.9, 128.2, 125.0, 124.5, 119.8, 112.3, 91.3, 51.7, 40.1. Anal. calcd. for $C_{19}H_{19}NO_4$: C 70.14, H 5.89, N 4.31; found: C 69.95, H 5.97, N 4.37.

*5-Benzo[*b*]thiophen-2-yl-2,2-dimethoxyindan-1,3-dione (**146**)*

Compound **100** (4.30 g, 15.0 mmol) was coupled with 2-tributylstannylbenzo[*b*]thiophene (6.35 g, 15.0 mmol) to afford 3.73 g (73% yield) of **146** as light yellow crystals, mp 182 to 183°C (MeOH). R_f 0.35 (Et_2O – petroleum ether, 1:1). HRMS–CI (NH_3) calcd. for $C_{19}H_{14}O_4S$ $(M)^+$: 338.0613; found: 338.0625. UV (CH_3CN) (nm): 344 (ε 25 800), 258 (ε 17 900). IR (KBr) (cm^{-1}): 1735 (s), 1710 (s), 1180 (s), 1145 (s), 1030 (s). ^{1}H NMR ($CDCl_3$) δ: 8.80 (dd, *J* = 8.1 Hz, *J* = 1.6 Hz, 1H), 8.16 (d, *J* = 1.6 Hz, 1H), 7.92 (d, *J* = 8.1 Hz, 1H), 7.73–7.80 (m, 2H), 7.69 (s, 1H), 7.32–7.36 (m, 2H), 3.66 (s, 6H). ^{13}C NMR ($CDCl_3$) δ: 193.3, 192.5, 142.5, 140.8, 140.2, 140.0, 140.0, 138.0, 134.0, 125.8, 125.1, 124.8, 124.4, 123.1, 122.4, 120.6, 91.1, 51.7. Anal. calcd. for $C_{19}H_{14}O_4S$: C 67.44,H 4.17; found: C 67.81, H 4.18.

*5-Benzothiazol-2-yl-2,2-dimethoxyindan-1,3-dione (**147**)*

Compound **100** (4.30 g, 15.0 mmol) was coupled with 2-tributylstannylbenzothiazole (7.00 g, 16.5 mmol) to afford 3.50 g (70%) of **147** as yellow crystals, mp 176 to 177°C (MeOH). R_f 0.42 (Et_2O – petroleum ether, 1:1). HRMS–CI (NH_3) calcd. for $C_{18}H_{13}NO_4S$ $(M)^+$: 339.0565; found: 339.0553. UV (CH_3CN) (nm): 334 (ε 25 500). IR (KBr) (cm^{-1}): 1750 (m), 1720 (s), 1185 (s), 1150 (s), 1055 (s). ^{1}H NMR ($CDCl_3$) δ: 8.59 (dd, *J* = 8.1 Hz, *J* = 1.5 Hz, 1H), 8.52 (dd, *J* = 1.5 Hz, *J* = 0.6 Hz, 1H), 8.06 (m, 1H), 8.02 (dd, *J* = 8.0 Hz, *J* = 0.5 Hz, 1H), 7.89 (dd, *J* = 8.0 Hz, *J* = 0.8 Hz, 1H), 7.38–7.54 (m, 2H), 3.66 (s, 6H). ^{13}C NMR ($CDCl_3$) δ: 192.8, 192.6, 164.4, 153.8, 141.1, 140.0, 139.9, 135.4, 135.0, 126.9, 126.4, 124.8, 124.0, 122.6, 121.8, 91.0, 51.7.

*5-[2,2′-Bithiophen-5-yl]-2,2-dimethoxyindan-1,3-dione (**148**)*

Compound **100** (4.30 g, 15.0 mmol) was coupled with 5-tributylstannyl-[2,2′]bithiophene (6.82 g, 15.0 mmol) to afford 5.07 g (91% yield) of **148** as bright yellow crystals, mp 126–128°C (Et_2O – petroleum ether). R_f 0.17 (Et_2O – petroleum ether, 1:4). HRMS–CI (NH_3) calcd. for $C_{19}H_{14}O_4S_2$ $(M)^+$: 370.0334; found: 370.0330. UV (CH_3CN) (nm): 387 (ε 23 500). IR (KBr) (cm^{-1}): 1745 (s), 1715 (s), 1155 (s), 1030 (s). ^{1}H NMR ($CDCl_3$) δ: 8.09 (d, *J* = 1.5 Hz, 1H), 8.04 (dd, *J* = 8.1 Hz, *J* = 1.5 Hz, 1H), 7.96 (d, *J* = 8.1 Hz, 1H), 7.46 (d, *J* = 3.9 Hz, 1H), 7.30 (dd, *J* = 4.8 Hz, *J* = 0.7 Hz, 1H), 7.24 (dd, *J* = 3.6 Hz, *J* = 0.7 Hz, 1H), 7.19 (d, *J* = 3.9 Hz, 1H), 7.06 (dd, ^1J = 4.8 Hz, ^2J = 3.6 Hz, 1H), 3.70 (s, 6H). ^{13}C NMR ($CDCl_3$) δ: 193.5, 192.4, 142.2, 140.5, 140.1, 139.4, 137.3, 136.3, 133.0, 128.1, 127.1, 125.6, 125.0, 124.9, 124.6, 119.2, 91.1, 51.7.

*5-[5′-(2,2-Dimethoxy-1,3-dioxoindan-5-yl)thiophen-2-yl]-2,2-dimethoxyindan-1,3-dione (**150**)*

Compound **100** (5.70 g, 20.0 mmol) was coupled with 2,5-bis(tributylstannyl)thiophene (6.60 g, 10.0 mmol) and toluene (100 mL) was added $Pd(PPh_3)_4$ (347 mg, 1.5 mol%). The mixture was heated at reflux under a nitrogen atmosphere for 6 h. The mixture was concentrated and the residue purified by chromatography (petroleum ether, Et_2O – petroleum ether) to afford a solid (5.10 g) contaminated with organotin products. The crude solid was recrystallized from CH_2Cl_2–hexanes to afford 4.45 g (91% yield) of **150** as an orange powder, mp 232–235°C (CH_2Cl_2–hexanes). R_f 0.26 (Et_2O – petroleum ether, 1:1). FAB–HRMS (NBA) calcd. for $C_{26}H_{20}O_8S$ $(M)^+$: 492.0879; found: 492.0883. UV (CH_3CN) (nm): 383 (ε 46 700). IR (KBr) (cm^{-1}): 1750 (s), 1720 (s), 1155 (s), 1030 (s). ^{1}H NMR ($CDCl_3$) δ: 8.13 (s, 2H), 8.08 (d, *J* = 8.1 Hz, 2H), 7.98 (d, *J* = 8.1 Hz, 2H), 7.57 (s, 2H), 3.64 (s, 12H). ^{13}C NMR ($CDCl_3$) δ: 193.2, 192.3, 143.6, 141.5, 140.2, 138.1, 133.4, 127.7, 125.1, 119.9, 91.0, 51.7. Anal. calcd. for $C_{26}H_{20}O_8S$: C 63.41, H 4.09; found: C 63.46, H 3.94.

*5-[2,2′-Bithiophen-5-yl]-2,2-dihydroxyindan-1,3-dione (**62**)*

A solution of 174 mg of tris(dibenzylideneacetone)dipalladium ($Pd_2(dba)_3$) and 90 mg of tri-2-furylphosphine (TFP) and toluene under an N_2 atmosphere was stirred at 25°C for 10 min. The initial purple color of the solution slowly turned to yellow. After in situ preparation of the catalyst, **33** (975 mg, 3.08 mmol) and **144** (1.72 g, 3.77 mmol) were added and the solution was stirred at 25°C. A precipitate began to form after 30 min. After 21 h, the precipitate was collected, washed with hot hexanes (bp 68 to 69°C), and dried in vacuo to give 274 mg (26% yield) of **62** as a yellow-orange solid.

*2,2-Dimethoxy-5-styrylindan-1,3-dione (**155**)*

Ketal **100** (1.43 g, 5 mmol), styrene (1 mL, 8.74 mmol), and freshly distilled triethylamine (2 mL) were placed in a sealed tube. The reaction mixture was flushed with N_2 and then stirred in an atmosphere of N_2 for 2 h. $Pd(PPh_3)_4$ (58 mg, 1 mol%) was added, and the reaction mixture was stirred at 100°C under N_2 for 8 h in a dark hood. Triethylamine and unreacted styrene were removed under reduced pressure. The resulting solid was dissolved in CH_2Cl_2 and washed with water. The CH_2Cl_2 solution was dried over anhyd Na_2SO_4, and filtered. The solvent was then removed under reduced pressure. Upon purification of the residue by column chromatography (Et_2O – petroleum ether, 1:4) 0.61 g (40% yield) of **155** was obtained as a yellow solid, mp 134°. R_f 0.23 (Et_2O – petroleum ether, 1:4). HRMS calcd. for $C_{19}H_{16}O_4$ $(M)^+$: 308.1049; found: 308.1043. IR (KBr) (cm^{-1}): 1744 (s), 1713 (s), 1203 (s), 1191 (s), 1152 (s), 1033 (s). ^{1}H NMR (DMSO-d_6) δ: 8.28 (d, *J* = 8.1 Hz, 1H), 8.22 (s, 1H), 7.98 (d, *J* = 8.1 Hz, 1H), 7.68–7.76 (m, 3H), 7.52 (d, *J* = 16.5 Hz, 1H), 7.32–7.46 (m, 3H), 3.51 (s, 6H). ^{13}C NMR (125 MHz, $CDCl_3$) δ: 193.7, 192.7, 146.2, 140.1, 138.0, 135.9, 134.7, 134.5, 129.2, 128.9, 127.2, 126.1, 124.6, 120.8, 91.2, 51.7. Anal. calcd. for $C_{19}H_{16}O_4$: C 74.07, H 5.23; found: C 74.42, H 5.12.

Coupling procedure

Ketal **100** (1 equiv), an electron-rich heterocycle (**151**–**153**, 3 to 4 equiv) and potassium acetate (1.5 equiv) were stirred in DMA under N_2 for 2 h. $Pd(PPh_3)_4$ (1–3 mol%) was added, and the reaction mixture was stirred at 90°C in a

© 2001 NRC Canada

sealed tube under N_2 for 24 h. The solvent was removed under reduced pressure and the residue was dissolved in CH_2Cl_2 and washed with water. The organic phase was separated, dried over Na_2SO_4, and the solvent was removed under reduced pressure. The crude product was purified by column chromatography.

*2,2-Dimethoxy-5-(thiophen-2-yl)indan-1,3-dione (**138**)*

Ketal **100** (1.95 g, 6.84 mmol) was reacted with an excess of thiophene (**151**) to give 1.3 g (66% yield) of **138** as a yellow solid.

*2,2-Dimethoxy-5-(5-methylthiophen-2-yl)indan-1,3-dione (**140**)*

Ketal **100** (2.85 g, 10.0 mmol) was reacted with an excess of 2-methylthiophene (**152**) to give 1.57 g (52% yield) of **140** as a yellow solid.

*2,2-Dimethoxy-5-(5-ethylthiophen-2-yl)indan-1,3-dione (**141**)*

Ketal **100** (1.43 g, 5.00 mmol) was reacted with an excess of 2-ethylthiophene (**153**) to give 0.65 g (41% yield) of **141** as a yellow solid.

Acknowledgments

We are grateful for the financial support provided by the National Institutes of Justice (92-IJ-CX-K015), Unites States Secret Service, National Institutes of Health (CA-40081), and National Science Foundation (CHE-01449). We thank Dr. Antonio Cantu and Mr. Robert Ramotowski of the United States Secret Service, Dr. Josef Almog of the Israel National Police and Professor Chris Lennard of the Canberra Forensic Science Division for testing of compounds and for helpful discussions.

References

1. J. Almog. Fingerprint development by ninhydrin and its analogues. *In* Advances in fingerprint technology. *Edited by* H.C. Lee and R.E. Gaensslen. Elsevier Science Publishing Co., Inc., New York. 1991.
2. D.J. McCaldin. Chem. Rev. **60**, 39 (1960).
3. M.B. Rubin. Chem. Rev. **75**, 177 (1975).
4. A. Schönberg and E. Singer. Tetrahedron, **34**, 1285 (1978).
5. M.M. Joullié, T.R. Thompson, and N.H. Nemeroff. Tetrahedron, **47**, 8791 (1991).
6. M.B. Rubin and R. Gleiter. Chem. Rev. **100**, 1121 (2000).
7. S. Ruhemann. Trans. Chem. Soc. **97**, 1438 (1910).
8. Z. Khan, Z.A. Rafiquee, and A.A. Khan. J. Indian Chem. Soc. **73**, 305 (1996).
9. F. Dietz, K. Rommel-Möhle, A. Schleitzer, and N. Tyutyulkov. Z. Naturforsch. B: Chem. Sci. **48b**, 1133 (1993).
10. B. Breur and H. Breur. Prax. Naturwiss. Chem. **45**, 18 (1996).
11. R. Grigg and S. Thianpatanagul. J. Chem. Soc. Chem. Comm. 180 (1984).
12. R. Grigg. Chem. Soc. Rev. **16**, 89 (1987).
13. R. Grigg and V. Sridharan. Azomethine ylide cycloadditions via 1,2-prototropy and metallo-dipole formation from imines. *In* Advances in cycloaddition. Vol. 3. *Edited by* D.P. Curran. JAI Press, Greenwich, Connecticut. 1993. pp. 161.
14. P.J. Davies, H.J. Kobus, M.R. Taylor, and K.P. Wainwright. J. Forensic Sci. **40**, 565 (1995).
15. P.J. Davies, M.R. Taylor, and K.P. Wainwright. Acta Crystallogr. Sect. C: Cryst. Struct. Commun. **C51**, 1802 (1995).
16. D.W. Herod and E.R. Menzel. J. Forensic Sci. **27**, 513 (1982).
17. D.F. Hewlett and V.G. Sears. Proc. Int. Symp. Fingerprint Detection and Identification. Ne'urim, Israel. 1995.
18. R.R. Hark. Ph.D. Dissertation, University of Pennsylvania, 1996.
19. K. Bowden and S. Rumpal. J. Chem. Res. Synop. 35 (1997).
20. S. Ruhemann. Trans. Chem. Soc. **101**, 780 (1912).
21. T. Kametani, S. Hibino, and S. Takano. J. Chem. Soc. Perkin Trans. 1, 391 (1972).
22. D.E. Prikule and O.Y. Neiland. Zh. Org. Khim. **17**, 2119 (1981).
23. L.W. Deady, J. Desneves, and A.C. Ross. Tetrahedron, **49**, 9823 (1993).
24. K. Bowden and M. Chele-Amiran. J. Chem. Soc. Perkin Trans. 2, 2035 (1986).
25. P.R. Buckland and J.F.W. McOmie. Tetrahedron, **33**, 1797 (1977).
26. P. Dallemagne, S. Rault, and M. Robba. Bull. Soc. Chim. Fr. **128**, 260 (1991).
27. D.B. Hauze, M.M. Joullié, R. Ramotowski, and A. Cantu. Tetrahedron, **53**, 4239 (1997).
28. L.P. Khanh, P. Dallemagne, and S. Rault. Synlett. 1450 (1999).
29. R. Gleiter, R. Kraemer, H. Irngartinger, and C. Bissinger. J. Org. Chem. **57**, 252 (1992).
30. R. Gleiter and P. Schang. Angew. Chem. Int. Ed. Engl. **19**, 715 (1980).
31. B. Nalliah, Q.A. Ahmed, and R.H.F. Manske. Can. J. Chem. **50**, 1819 (1972).
32. S.A. Osadchii and V.A. Barkhash. Zh. Org. Khim. **6**, 1815 (1970); Chem. Abstr. **73**, 120381 (1970).
33. G. Errera. Gazz. Chim. Ital. **43I**, 583 (1913).
34. J.L. Hallman and R.A. Bartsch. J. Org. Chem. **56**, 6243 (1991).
35. F.J. Frank, B. Borup, J.A. Brookman, A.J. Carr, K.L. Hurd, M. Renner, and J.K. Stowell. Poster presented at SPECTRUM 91. Int. Symp. Forensic Techniques. Detroit, Michigan. 1991.
36. C.J. Lennard, P.A. Margot, M. Stoilovic, and R.N. Warrener. Forensic Science Soc. J. **26**, 323 (1986).
37. C.J. Lennard, P.A. Margot, M. Stoilovic, and R.N. Warrener. J. Forensic Sci. Soc. **28**, 3 (1988).
38. R. Heffner, J.E. Safaryn, and M.M. Joullié. Tetrahedron Lett. **28**, 6539 (1987).
39. R.J. Heffner and M.M. Joullié. Synth. Commun. **21**, 1055 (1991).
40. R.J. Heffner and M.M. Joullié. Synth. Commun. **21**, 2231 (1991).
41. R.R. Hark, D.B. Hauze, O. Petrovskaia, M.M. Joullié, R. Jaouhari, and P. McComiskey. Tetrahedron Lett. **35**, 7719 (1994).
42. D.B. Hauze. Ph.D. Dissertation, University of Pennsylvania, 1996.
43. J. Almog, A. Hirshfeld, and J.T. Klug. J. Forensic Sci. **27**, 912 (1982).
44. J. Almog and A. Hirshfeld. J. Forensic Sci. **33**, 1027 (1988).
45. J. Almog, A. Hirshfeld, A. Frank, H. Grant, Z. Harel, and Y. Ittah. J. Forensic Sci. **37**, 688 (1992).
46. J. Almog, A. Hirshfeld, A. Frank, J. Sterling, and E.D. Leonov. J. Forensic Sci. **36**, 104 (1991).
47. J. Almog, V.G. Sears, E. Springer, D.F. Hewlett, S. Walker, S. Wiesner, R. Lidor, and E. Bahar. J. Forensic Sci. **44**, 538 (1999).
48. H.J. Kobus, P.E. Pigou, E.W. Della, B. Taylor, K.P. Wainwright, and P.J. Davies. Proc. Int. Symp. Fingerprint Detection and Identification. Ne'urim, Israel. 1995.
49. B.M. Taylor. Ph.D. Dissertation, Flinders University, Australia. 1997.
50. E.W. Della, W.K. Janowski, P.E. Pigou, and B.M. Taylor. Synthesis, 2119 (1999).
51. A.A. Cantu, D.A. Leben, M.M. Joullié, R.J. Heffner, and R.R. Hark. J. Forensic Identi. **43**, 44 (1993).

© 2001 NRC Canada

52. E.R. Menzel and J. Almog. J. Forensic Sci. **30**, 371 (1985).
53. J. Almog, V.G. Sears, E. Springer, D.F. Hewlett, S. Walker, S. Wiesner, R. Lidor, and E. Bahar. J. Forensic Sci. **44**, 538 (1999).
54. R. Ramotowski. Proc. Int. Symp. Fingerprint Detection and Identification. Ne'urim, Israel. 1995.
55. C.J. Lennard. Ph.D. Dissertation, Australian National University, Canberra, Australia. 1986.
56. R.T. Hart and R.F. Tebbe. J. Am. Chem. Soc. **72**, 3286 (1950).
57. G. Sartori, R. Maggi, F. Bigi, C. Porta, X. Tao, G.L. Bernardi, S. Ianelli, and M. Nardelli. Tetrahedron, **51**, 12179 (1995).
58. G. Sartori, F. Bigi, R. Maggi, D. Baraldi, and G. Casnati. J. Chem. Soc. Perkin Trans. 1, 2985 (1992).
59. V. Nenajdenko, I.L. Baraznenok, and E.S. Balenkova. Tetrahedron Lett. **37**, 4199 (1996).
60. H.C. Kolb and M.R. Hoffman. Tetrahedron, **46**, 5127 (1990).
61. S. Caddick and S. Khen. J. Chem. Soc. Chem. Commun. 1971 (1995).
62. N.E. Schore. Org. React. (N.Y.), **40**, 1 (1991).
63. P.S. Bailey and R.E. Erickson. Diphenaldehyde (biphenyl, 2,2′-diformyl-). *In* Organic syntheses. Coll. Vol. V. *Edited by* H.E. Baumgarten. John Wiley, New York. 1973. pp. 493.
64. L. Horner, P.V. Subramaniam, and K. Eiben. Liebigs Ann. Chem. **714**, 91 (1968).
65. F. Feigl. Anal. Chim. Acta, **24**, 501 (1961).
66. O.G. Petrovskaia. Ph.D. Thesis, University of Pennsylvania. 1999.
67. R. Ramotowski, A. Cantu, M.M. Joullié, and O. Petrovskaia. Fingerprint Whorld, **23**, 131 (1997).
68. L.F. Fieser and R.G. Kennelly. J. Am. Chem. Soc. **57**, 1611 (1935).
69. A. Suzuki. Acc. Chem. Res. **15**, 178 (1982).
70. A. Suzuki. Pure Appl. Chem. **57**, 1749 (1985).
71. A. Suzuki. Pure Appl. Chem. **58**, 629 (1986).
72. K. Bowden and S. Rumpal. J. Chem. Soc. Perkin Trans. 2, 983 (1997).
73. S. Ruhemann. J. Chem. Soc. **97**, 2025 (1910).
74. R. Csuk and P. Dörr. Tetrahedron, **50**, 9983 (1994).
75. W. Gottardi. Monatsh. Chem. **99**, 815 (1968).
76. D.R. Buckle, N.J. Morgan, J.W. Ross, H. Smith, and B.A. Spicer. J. Med. Chem. **16**, 1334 (1973).
77. H.N. Stephens. J. Am. Chem. Soc. **43**, 1950 (1921).
78. M. Regitz, H. Schwall, G. Heck, B. Eistert, and G. Bock. Liebigs Ann. Chem. **690**, 125 (1965).
79. M. Regitz and H.-G. Adolph. Chem. Ber. **101**, 3604 (1968).
80. M. Regitz and H.-G. Adolph. Liebigs Ann. Chem. **723**, 47 (1969).
81. M. Regitz. Ang. Chem. Int. Ed. Engl. **6**, 733 (1967).
82. G.G. Hazen, F.W. Bollinger, F.E. Roberts, W.K. Russ, J.J. Seman, and S. Staskiewicz. Org. Synth. **73**, 144 (1995).
83. J.S. Baum, D.A. Shook, H.M.L. Davies, and H.D. Smith. Synth. Commun. **17**, 1709 (1987).
84. M.J. Mintz and C. Walling. *tert*-Butyl hypochlorite. *In* Organic syntheses. Coll. Vol. V. *Edited by* H.E. Baumgarten. John Wiley, New York. 1973. pp. 183.
85. I. Kawasaki, K. Matsuda, and T. Kaneko. Bull. Chem. Soc. Jpn. **44**, 1986 (1971).
86. J.F.W. McOmbie and D.E. West. 3,3′-Dihydroxybiphenyl. *In* Organic syntheses. Coll. Vol. V. *Edited by* H.E. Baumgarten. John Wiley, New York. 1973. pp. 412.
87. J.K. Stille and D. Milstein. J. Am. Chem. Soc. **100**, 3636 (1978).
88. J.K. Stille. Angew. Chem. Int. Ed. Engl. **25**, 508 (1986).
89. L. Balas, B. Jousseaume, H. Shin, J.-B. Verlhac, and F. Wallian. Organometallics, **10**, 366 (1991).
90. L.S. Liebeskind and J. Wang. J. Org. Chem. **58**, 3550 (1993).
91. F.H. Pinkerton and S.F. Thames. J. Heterocycl. Chem. 257 (1971).
92. K.C. Molloy, P.C. Waterfield, and M.F. Mahon. J. Organomet. Chem. **365**, 61 (1989).
93. J. Malm, P. Björk, S. Gronowitz, and A.-B. Hörnfeldt. Tetrahedron Lett. **33**, 2199 (1992).
94. P.J. Stang, R. Tykwinski, and V.V. Zhdankin. J. Heterocycl. Chem. **29**, 815 (1992).
95. A.S.-Y. Lee and W.-C. Dai. Tetrahedron Lett. **37**, 495 (1996).
96. J.M. Tour and R. Wu. Macromolecules, **25**, 1901 (1992).
97. Z. Bao, W. Chan, and L. Yu. Chem. Mater. **5**, 2 (1993).
98. D.J. Chadwick and C. Willbe. J. Chem. Soc. Perkin Trans. 1, 887 (1977).
99. S. Gronowitz and A. Bugge. Acta Chem. Scand. **19**, 1271 (1965).
100. S. Gronowitz, A.B. Hörnfeldt, and Y. Yang. IUPAC Symp., 6th. 1965.
101. A. Ohta, Y. Akita, T. Ohkuwa, M. Chiba, R. Fukunaga, A. Miyafuji, T. Nakata, N. Tani, and Y. Aoyagi. Heterocycles, **31**, 1951 (1990).
102. Y. Aoyagi, A. Inoue, I. Koizumi, R. Hashimoto, K. Tokunaga, K. Gohma, J. Komatsu, K. Sekine, A. Miyafuji, J. Kunoh, R. Honma, Y. Akita, and A. Ohta. Heterocycles, **33**, 257 (1992).
103. F. Feigl, V. Anger, and R.E. Oesper. Spot tests in organic analysis. VII ed. Elsevier Publishing Company, Amsterdam. 1966.
104. V. Farina and B. Krishnan. J. Am. Chem. Soc. **113**, 9585 (1991).
105. V. Farina, S.R. Baker, D.A. Benigni, S.I. Hauck, and C. Sapino. J. Org. Chem. **55**, 5833 (1990).
106. M.F. Rettig and P.M. Maillis. Tetrakis(*t*-butyl-isocyanide)di-μ-chlorodipalladium(I). *In* Inorg. Synth. Vol. 17. *Edited by* A.G. MacDiarmid. McGraw Hill, New York. 1976. pp. 134.
107. D.W. Allen and B.F. Taylor. J. Chem. Soc. Dalton Trans. 51 (1982).
108. R.W. Murray and R. Jeyaraman. J. Org. Chem. **50**, 2847 (1985).
109. A. Saba. Synth. Commun. **24**, 695 (1994).
110. M. Minssen-Guetté, M. Dvolaitzky, and J. Jacques. Bull. Soc. Chim. Fr. **5**, 2111 (1968).

© 2001 NRC Canada

An ^{1}H and ^{13}C NMR conformational study of 2-(benzotriazol-1-yl)-substituted tetrahydropyrans

Alan R. Katritzky, Novruz G. Akhmedov, Sergey N. Denisenko, and Subbu Perumal

Abstract: Proton and carbon NMR signals for 2-(benzotriazol-1-yl)tetrahydropyrans are assigned on the basis of spin decoupling, *H*,*H*-COSY, HETCOR, and nuclear Overhauser enhancement experiments. Conformational preferences are deduced. It was found that 2-(benzotriazol-1-yl) substituents: (*i*) prefer the equatorial orientation; and (*ii*) display a rotameric preference to minimize the electronic repulsion and (or) steric interaction.

Key words: anomeric, NMR, tetrahydropyrans.

Résumé : On a attribué les signaux RMN du proton et du carbone de 2-(benzotriazol-1-yl)tétrahydropyranes grâce à des expériences de: découplage de spin, « *H*,*H*-COSY », « HETCOR » ainsi que de rehaussement Overhauser nucléaire. On en a déduit les préférences conformationnelles. On a trouvé que les substituants 2-(benzotriazol-1-yles) : (*i*) préfèrent occuper une orientation équatoriale et (*ii*) montrent une préférence rotamérique pour minimiser la répulsion électronique et/ou l'interaction stérique.

Mots clés : anomère, RMN, tétrahydropyranes.

[Traduit par la Rédaction]

Introduction

The normal (or *endo*-) anomeric effect in tetrahydropyrans causes a significant preference for the conformer with the anomeric substituent in the axial orientation (α-anomer) compared to that with the anomeric substituent equatorial (β-anomer). This effect is believed to originate from an overlap between the unshared electrons of the ring oxygen atom and the antibonding σ* orbital of the anticoplanar anomeric carbon—heteroatom bond (1–3) (Scheme 1). Nitrogen-containing substituents in an anomeric position behave differently from their oxygen and halogen analogs. Neutral 2-aminotetrahydropyrans and their heterocyclic derivatives exist with the *N*-linked substituent equatorial (3, 4) due to the *exo*-anomeric effect. This conformational preference is rationalized (3, 5) by delocalization of electron density from the *exo*-cyclic substituent X to the antibonding orbital of the carbon—oxygen bond. Thus, the overall anomeric effect is a balance between the sum of the *endo*- and *exo*-anomeric effects (3) in both the equatorial and axial conformers (Scheme 1). However, this "double bond – no-bond resonance" model fails to explain the so-called reverse anomeric effect postulated for the glycosyl imidazolinium ions and glycosyl pyridinium ions (6).

In the present study, the NMR spectra of 2-(benzotriazol-1-yl)-substituted tetrahydropyrans **1**–**3** (Scheme 2) have been recorded and their chemical shifts and coupling constants used to investigate the conformational preferences of these molecules.

Investigation of the stereochemical preference of a benzotriazol-1-yl group attached to an anomeric carbon in the tetrahydropyran system is relevant particularly in view of the: (*i*) known dual nature of the benzotriazolyl group which can act either as an electron-withdrawing (nucleofuge) or as an-electron donating (nucleophile) moiety in many important synthetic transformations (7*a*); and (*ii*) evidence for the vinylogues anomeric effect in 4-(benzotriazol-1-yl)pyrans (7*b*).

Recent photoelectron spectra and electronic structure studies of 1-fluoromethyl- and 1-chloromethyl-1*H*-benzotriazoles (8) shown significant interactions of the benzotriazole HOMO orbital with an α-C—heteroatom bond. By contrast, the ionization potential for the unshared oxygen electron pair was higher in 1-methoxymethyl-1*H*-benzotriazole as compared to dimethyl ether. This was ascribed to the electron acceptor character of the benzotriazole system. Thus, both *exo*- and *endo*-anomeric effect could be important factors for the stereochemical behavior of 2-(benzotriazol-1-yl)-substituted tetrahydropyrans **1**–**3**.

Results and discussion

Studies on 2-(benzotriazol-1-yl)tetrahydropyrans 1–3

The proton chemical shifts for unsubstituted 2-(benzotriazol-1-yl)tetrahydropyran (1) were assigned as follows: (*i*) the protons of the benzotriazolyl ring in **1** gave four signals in the far down-field region (see Table 1). These signals are

Received March 6, 2001. Published on the NRC Research Press Web site at http://canjchem.nrc.ca on November 2, 2001.

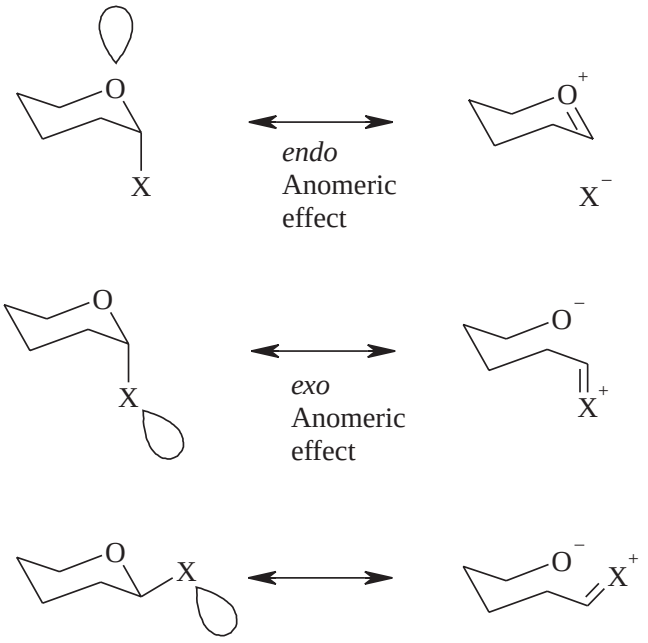
Dedicated to Professor Victor Snieckus for his contributions to Canadian chemistry.

A.R. Katritzky,[1] N.G. Akhmedov, S.N. Denisenko, and S. Perumal. Center for Heterocyclic Compounds, Department of Chemistry, University of Florida, P.O. Box 117200, Gainesville, FL 32611–7200, U.S.A.

[1]Corresponding author (telephone: (352) 392-0554; fax: (352) 392-9199; e-mail: KATRITZKY@chem.ufl.edu).

 DOI: 10.1139/cjc-79-11-1655 © 2001 NRC Canada

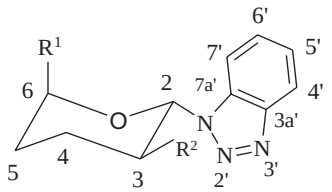
Scheme 1.



readily assignable to the aromatic protons of the benzotriazol-1-yl ring as shown in Table 1 on the basis of the *H*,*H*-COSY and HETCOR spectra; (*ii*) the doublet of doublets of **1** appearing far down-field at 6.02 ppm, with $^3J_{H-2,H-3}$ values of 8.3 and 3.0 Hz, is assigned to H-2 of the tetrahydropyran ring on the basis that only H-2 has just two vicinal protons. The other tetrahydropyran ring protons have either a geminal or more than two vicinal protons and furnish more complex multiplets. That the chemical shift of H-2 appears far downfield is probably due to the interplay of several factors including the ring current effect of the aromatic benzotriazole system and the rotamer preference; (*iii*) the unresolved multiplets centered at ~2.18 and ~1.80 ppm are assigned to the overlapping resonances of (H-3*ax* + H-4*eq*) and (H-4*ax* + H-5*ax* + H-5 *eq*), on the basis of COSY and spin-decoupling experiments, respectively. Individual coupling constants were not resolved. Cross-peaks were observed in the COSY spectrum between the doublet of doublets at 6.02 ppm for H-2*ax* and each of the resonance signals at 2.18 and 2.60 ppm; these latter are therefore assigned to H-3*ax* and H-3*eq*, respectively. Irradiation of the overlapping signals centered at 1.80 ppm (H-4*ax* + H-5*ax* + H-5 *eq*) simplifies the multiplets centered at 3.78 ppm (H-6*ax*) and 3.94 ppm (H-6 *eq*), which appeared in the selectively decoupled ^{1}H NMR spectrum as doublets of doublets with $^2J_{AB}$ of 12.6 Hz; (*iv*) the chemical shifts of the remaining protons of **1** were assigned in a similar manner as listed in Table 1. The H-3*ax* and H-5*ax* gave signals, which are shifted slightly downfield compared to those of the corresponding equatorial protons; this is ascribable to the van der Waals interactions between each of the axial protons and the axial unshared pair of electrons of oxygen.

Compound **1** could adopt several rotameric forms depending on the H-C(2)-N(1′)-C(7a′) dihedral angle (Φ) (Scheme 3). In

Scheme 2.



1: $R^1 = R^2 = H$; **2**: $R^1 = OCH_3$; $R^2 = H$; **3**: $R^1 = H$; $R^2 = CH_2N(Me)Ph$

the two rotamers **1a** (Φ = 20°) and **1b** (Φ = 160°) shown in Scheme 3, *exo*-anomeric interaction between the N-1′ π electron orbital and the σ^*_{C-O} orbital should be developed most strongly. Rotamer **1b** should have strong van der Waals interaction between H-3*ax* and H-7′. Rotamer **1a** is likely to suffer from repulsion between anomeric H-2*ax* and H-7′. Indeed, we observed a NOE effect of 5% for H-7′ while irradiating H-2*ax*, however no NOE effect was found between H-7′ and H-3*ax*. Two other possible rotamers with the N-1′ π orbital orthogonal to the C—O bond are less likely to be preferred due to dipole–dipole repulsions between lone pairs of the O and N-2′ atoms and (or) repulsion between the lone pairs of the O and H-7′. Nevertheless, a small NOE effect was observed for H-3*eq* while irradiating H-7′, suggesting at least partial population of the rotamer **1c** (Scheme 3).

Detailed ^{1}H, ^{13}C, and two-dimensional NMR spectroscopic measurements have been made for two bis-substituted tetrahydropyrans **2** and **3** (Scheme 4). In **2** and **3,** the presence of an additional substituent could bias the conformational equilibrium in favor of a single conformer. We expected that the OCH_3 group in position 6[2] of **2** should favor the axial orientation as a result of classical anomeric effect, while the large *N*-methyl-*N*-phenylaminomethyl group of **3** would be in the equatorial orientation (9). Indeed, only the *trans* diastereomer of 2-methoxy-6-(benzotriazol-1-yl)tetrahydropyran **2** was obtained from the reaction of benzotriazole and 2-methoxy-3,4-dihydropyran (10), in consonance with the known axial preference of the anomeric methoxy group.

The chemical shifts of **2** are listed in Table 1. The H-2 signal at 6.41 ppm is shifted downfield 0.39 ppm compared to that of H-2 in **1**, which is ascribable to the van der Waals interaction with the axial methoxy group. The H-2 appears as a doublet of doublet with $^3J_{H-2,H-3}$ couplings of 10.7 and 2.7 Hz. The broadened triplet (overlapping doublet of doublets) at 4.92 ppm was assigned to the H-6*eq* proton. The axial orientation of the OCH_3 group, and the corresponding equatorial orientation of H-6, is supported by the $^3J_{H-6,H-5}$ value of 2.3 Hz, as well as by the NOE effect between OCH_3 and both H-2*ax* and H-6*eq*.

The chemical shifts and coupling constants for *trans*-2-(benzotriazol-1-yl)-3-(*N*-methyl-*N*-phenylaminomethyl)tetrahydropyran **3** are listed in Table 1. The doublet for the H-2 of **3** at 5.87 ppm (with $^3J_{H-2,H-3}$ = 7.5 Hz) is in accord with the diequatorial arrangement of the two substituents. Interestingly, strong steric repulsion between these groups could be detected by a 4.5% Overhauser effect for the H-7′ proton while irradiating C-3-CH_2-N protons. Similarly to the com-

[2] Here, we use an unconventional numbering of the carbon atoms of the tetrahydropyran ring, assigning the number 2 for the carbon atom connected to the benzotriazole substituent (Scheme 4).

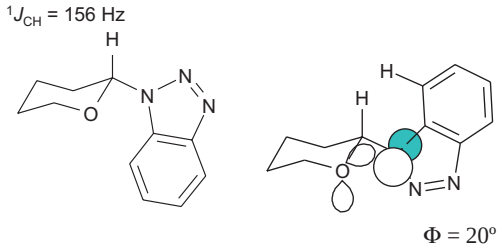
© 2001 NRC Canada

Table 1. The ^{1}H NMR chemical shifts (ppm), multiplicity, and coupling constants (Hz) for compounds **1**–**3** in $CDCl_3$ at ambient temperature.

Compound					
Tetrahydropyran protons					
	H-2*ax*	H-3*eq*	H-6*ax*	H-6*eq*	Others
1	6.02 dd			3.94 dt	H-4*ax* + H-5*ax* + H-5*eq*
	(8.3, 3.0)	2.55–2.67 m	3.73–3.82 m	(12.6, 4.5)	1.70 – 1.89 m
2[a]	6.41 dd	2.50–2.64 m	—	4.92 br t	H-4*eq* + H-5*ax* + H-5*eq*
	(10.7, 2.7)			(2.3)	1.84 – 1.99 m
3[b]	5.87 d	3.07 m	3.76 ddd	3.96 dtd	H-4*ax* + H-5*ax* + H-5*eq*
	(7.5)		(12.6, 8.8, 3.6)	(12.6, 4.3, 3.6)	1.54–1.87 m
Benzotriazolyl protons					
	H-4′	H-5′	H-6′	H-7′	
1	8.05 dt	7.37 ddd	7.48 ddd	7.74 dt	
	(8.2, 0.9)	(8.2, 6.9, 0.9)	(8.4, 6.9, 0.9)	(8.4, 0.9)	
2	8.07 dt	7.38 ddd	7.50 ddd	7.73 dt	
	(8.2, 0.9)	(8.2, 6.9, 0.9)	(8.2, 6.9, 0.9)	(8.2, 0.9)	
3	8.08 dt	7.39 ddd	7.48 ddd	7.67 dt	
	(8.3, 0.9)	(8.2, 7.0, 0.9)	(8.2, 7.0, 0.9)	(8.3, 0.9)	

[a]Additional signals: compound **2**: δ 3.5 (s, OCH_3).
[b]Compound **3**: δ 2.81 (s, NCH_3); 3.21 (AB spin system, A part: dd, 14.4 Hz; 6.0 Hz; B part: d, 14.4 Hz; CH_2N); 6.46 (d, 7.9 Hz, 2H, *ortho*-Ph); 7.09 (t, 7.2 Hz, 2H, *meta*-Ph); 6.64 (dd, 7.3 Hz; 7.9 Hz, 1H, *para*-Ph).

Scheme 3.

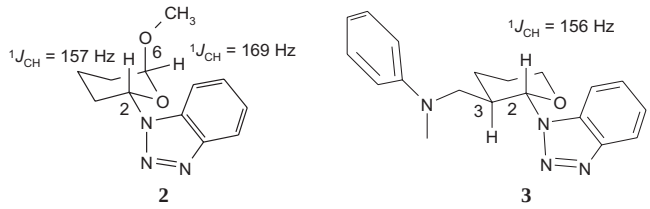


1 **1a** **1b** **1c**

pound **1**, a rotamer with strong interaction of the H-2 and H-7′ was indicated by NOE between these protons. The 0.15 ppm upfield shift of H-2 in **3** as compared to **1** may be due to shielding H-2 in **3** by the aniline ring in some of the populated conformations.

The $^3J_{H\text{-}2,H\text{-}3}$ values of the coupling constants for H-2 in compounds **1**–**3** each indicate the predominance of the equatorial orientation for the benzotriazol-1-yl group. However, the $^3J_{H\text{-}2,H\text{-}3ax}$ values in **1** and **3** (8.3 and 7.5 Hz, respectively) are significantly less than that in **2** (10.7 Hz). This could suggest significant contributions to the conformational equilibrium of **1** and **3** from conformers with the axial benzotriazolyl group. However, a low-temperature ^{1}H NMR study of **1** in CD_2Cl_2 at about –92°C did not reveal the existence of any other conformer. Thus, the ^{1}H NMR spectrum of **1** shows at –92°C neither new signals nor any significant change in the chemical shifts. The only variation found is the lack of fine splitting for the aliphatic protons of the tetrahydropyran ring, probably ascribable to the rapid spin-lattice relaxation or increasing viscosity at a low temperature. We believe that variations in the rotameric conformational populations of the benzotriazolyl ring system in these molecules are probably responsible for the variation in the $^3J_{H\text{-}2,H\text{-}3}$ values in **1**–**3**, with the equatorial conformer uniformly preferred throughout.

Scheme 4.



2 **3**

The equatorial orientation of the benzotriazole group in **1**–**3** is also supported by the values of the direct CH coupling constant $^1J_{CH}$, which are different for protons in the α- or β-anomeric position (11). Whereas the equatorial proton at C-6 in **2** causes splitting of carbon signal with a constant of 169 Hz, the axial proton at C-2 couples with its carbon with $^1J_{CH}$ = 156 to 157 Hz in **1**–**3** (Schemes 3 and 4). The ^{13}C NMR chemical shifts of mono- and di-substituted tetrahydropyrans **1**–**3** are shown in Table 2.

Consequently, the preference of the equatorial orientation by the benzotriazolyl group in these compounds appears to be due to the influence of both steric and electronic factors. The preference of the benzotriazolyl group equatorially orientated conformers for **1**–**3** may be ascribed to: (*i*) hyperconjugative interaction of the π orbital on the N-1′ with the C-O antibonding orbital in the so-called *exo*-anomeric effect; and (*ii*) steric interactions that may be encountered when the

© 2001 NRC Canada

Table 2. ^{13}C NMR chemical shifts (in ppm) of 2-(benzotriazol-1-yl)tetrahydropyrans **1**–**3**.

	Tetrahydropyran carbons					Benzotriazole carbons					
Compound	C-2	C-3	C-4	C-5	C-6	C-4′	C-5′	C-6′	C-7′	C-7a′	C-3a′
1	85.5	29.0	21.4	24.6	66.7	119.6	124.0	127.1	110.9	132.1	146.3
2[a]	80.2	29.4	17.7	28.9	100.3	120.0	124.1	127.5	110.6	132.2	146.4
3[b]	87.9	37.9	23.9	26.4	66.9	120.2	124.3	127.9	110.1	132.2	146.5

[a]Numbering is not conventional; δ (OCH_3) = 55.5 ppm.
[b]Phenyl group: 2/C_{ortho} = 112.3; 2/C_{meta} = 129.1; C_{para} = 116.9; δ (NCH_2) = 53.9 ppm; δ (NCH_3) = 39.5 ppm.

benzotriazole ring takes up an axial orientation with the 1,3-*syn*-axial hydrogen atoms. Similar behavior was reported (12) for 2-methylaminotetrahydropyran, where the basic nitrogen (good donor, poor acceptor) gives rise to a strong *exo*-anomeric effect.

Experimental

The ^1H, ^{13}C, and two-dimensional NMR spectra (*H*,*H*-COSY, *C*,*H*-COSY) and difference NOE experiments were recorded using Varian instruments (VXR-S-300 MHz and Mercury-300 MHz) in 5 mm NMR tubes in $CDCl_3$ solution (Cambridge Isotope Laboratories) at 25°C. Chemical shifts are expressed in parts per million (ppm) from tetramethylsilane as an internal standard.

The two-dimensional homonuclear correlation (*H*,*H*-COSY) spectra were recorded with a 1024 × 1024 data matrix and 256 time increments each of 16 scans, in magnitude mode, and processed with zero-filling in F1 and unshifted sine-bell apodization function. For the proton composite pulse decoupled (WALTZ-16) ^{13}C NMR experiments, the conditions were as follows: spectral width 14 000 Hz (220 ppm), number of data points 65 K, acquisition time 0.8 s, recycle delay 2 s, flip angle 30°. The FIDs in ^1H and ^{13}C NMR experiments were apodized by an exponential windowing prior to Fourier transformation (WFT) to improve the signal-to-noise ratio in the NMR spectra.

2-(Benzotriazol-1-yl)tetrahydropyrans **1**–**3** were prepared according to literature procedures (10, 13).

Conclusions

The conformational behavior of the 2-(benzotriazol-1-yl)-substituted tetrahydropyrans **1**–**3** is determined by a balance of electronic and steric effects. The *exo*-anomeric effect is pronounced, resulting in equatorial orientations for the benzotriazolyl moieties. This study further reveals that, with respect to the conformational preferences of tetrahydropyrans, the 2-(benzotriazol-1-yl) group stands closer to the other nitrogen heterocyclic groups than to a halogen or an alkoxy group.

References

1. G.R.J. Thatcher. Anomeric and associated stereoelectronic effects: Scope and controversy. *In* The anomeric effect and associated stereoelectronic effects. ACS Symp. Ser. 539. *Edited by* G.R.J. Thatcher. American Chemical Society, Washington, D.C. 1993. pp. 6–25.
2. V.G.S. Box. Heterocycles, **48**, 2389 (1998).
3. B.M. Pinto and R.Y.N. Leung. X-C-Z anomeric effect and Y-C-C-Z gauche effect (X,Y = O, S; Z = O, N). *In* The anomeric effect and associated stereoelectronic effects. ACS Symp. Ser. 539. *Edited by* G.R.J. Thatcher. American Chemical Society, Washington, D.C. 1993. pp. 126–155.
4. E. Juaristi and G. Cuevas. Tetrahedron, **48**, 5019 (1992).
5. J.-P. Praly and R.U. Lemieux. Can. J. Chem. **65**, 213 (1987).
6. V.G.S. Box. J. Mol. Struct. **522**, 145 (2000).
7. (*a*) A.R. Katritzky, X. Lan, J.Z. Yang, and O.V. Denisko. Chem. Rev. **98**, 409 (1998); (*b*) A.R. Katritzky, P. Steel, and S.N. Denisenko. Tetrahedron, **57**, 3309 (2001).
8. P. Rademacher, K. Kowski, A.R. Katritzky, and S.N. Denisenko. J. Mol. Struct. **513**, 47 (1999).
9. H. Booth, K.A. Khedhair, and S.A. Readshaw. Tetrahedron, **43**, 4699 (1987).
10. A.R. Katritzky, S. Rachwal, and B. Rachwal. J. Chem. Soc. Perkin Trans. 1, 1717 (1990).
11. G.V. Shustov, S.N. Denisenko, I.I. Chervin, N.L. Asfandiarov, and R.G. Kostyanovsky. Tetrahedron, **41**, 5719 (1985).
12. H. Booth, J.M. Dixon, K.A. Khedhair, and S.A. Readshaw. Tetrahedron, **46**, 1625 (1990).
13. A.R. Katritzky, B. Rachwal, and S. Rachwal. J. Org. Chem. **60**, 2588 (1995).

© 2001 NRC Canada

Structure assignment of aminoconduritols by ^{15}N NMR correlation spectroscopy; synthesis of a positional isomer of 7-deoxypancratistatin

Stefan Schilling, Uwe Rinner, Collin Chan, Ion Ghiviriga, and Tomas Hudlicky

Abstract: A positional isomer of 7-deoxypancratistatin was synthesized in 12 steps from epoxyaziridines **4** and **5**. An intermolecular opening of the aziridine rather than the epoxide in the early stages of the synthesis led to **13**, which did not match the properties of tetraacetate **10** derived from 7-deoxypancratistatin. At no stage of the synthesis did standard NMR techniques, involving ^{1}H–^{1}H or ^{1}H–^{13}C coupling, prove adequate for the structure assignment. Unambiguous structure was assigned by ^{1}H–^{15}N correlation NMR spectroscopy as well as by the conversion of epoxide **11** to diol **29** synthesized independently by another route. Experimental and spectral details are reported for all new compounds.

Key words: ^{15}N NMR spectroscopy, iso-7-deoxypancratistatin, Lewis acid catalyzed intramolecuar opening of epoxides, aminoconduritols.

Résumé : On a synthétisé un isomère de position de la 7-désoxypancrastistatine en douze étapes à partir des époxyaziridines **4** et **5**. Au cours des premières étapes de la synthèse, une ouverture intermoléculaire de l'aziridine à la place d'une ouverture de l'époxyde a conduit au produit **13** dont les propriétés ne correspondent pas à celles du tétraacétate **10** qui dérive de la 7-désoxypancratistatine. Les techniques normales de RMN impliquant les couplages ^{1}H–^{1}H ou ^{1}H–^{13}C ne se sont avérés adéquates pour faire des attributions de structures. La structure a été attribuée sans ambiguïté par spectroscopie RMN de corrélation ^{1}H–^{15}N ainsi que par conversion de l'époxyde **11** en diol **29** qui a été synthétisé de façon indépendante par une autre voie. On rapporte les détails expérimentaux et les spectres de tous les nouveaux composés.

Mots clés : spectroscopie ^{15}N RMN, iso-7-désoxypancratistatine, ouverture intramoléculaire d'époxydes catalysée par un acide de Lewis, aminoconduritols.

[Traduit par la Rédaction]

Introduction

Several total syntheses of the Amaryllidaceae alkaloids have been recently completed by our research group and by others (1–4). We have reported the first asymmetric synthesis of pancratistatin (1*b*, *c*), as well as brief routes to lycoricidine (4*j*), 7-deoxypancratistatin (2*c*), *ent*-7-deoxypancratistatin (5), and narciclasine (3*b*). Attempting to improve on the 14-step preparation of pancratistatin, which featured an intermolecular aziridine opening by an aryl cuprate (2*c*), we chose to pursue what appeared to be a more efficient strategy based on a novel intramolecular opening of the aziridine in **3**, Fig. 1.

Our strategy, shown in Fig. 1, relies on the availability of epoxyaziridines **4** and **5**, which can be rapidly synthesized from the commercially available diene **8** by established methods (6). Stereoelectronic considerations indicate that the nucleophilic opening of either isomer of epoxide with piperonol **6** followed by alkylation of the resulting alcohol with piperonyl bromide **7** will provide an intermediate in which both oxygens bear identical functionality. Such redundant operations (7) greatly improve the practicality of a synthesis because no attention need be paid either to the control of stereochemistry at the intermediate stage or to the separation of the isomers of epoxides **4** and **5**. Lewis acid catalyzed aziridine opening, oxidation, and recyclization would lead to the phenanthridine core of the alkaloid. We are aware of only three previous examples of intramolecular opening of aziridines (8) before we applied the technique to our synthesis, which is conceptually similar to the opening of the epoxide derived from *myo*-inositol as reported by Bender (9).

In this paper we report the synthesis of tetracetate **13,** a positional isomer of **10**, shown in Fig. 2. The latent func-

Received February 22, 2001. Published on the NRC Research Press Web site at http://canjchem.nrc.ca on November 12, 2001.

Dedicated to Professor Victor A. Snieckus in recognition of his contributions to synthetic organic chemistry.

S. Schilling, U. Rinner, C. Chan,[1] I. Ghiviriga,[2] and T. Hudlicky.[3] Department of Chemistry, University of Florida, Gainesville, Fl 32611, U.S.A.

[1]NSF REU participant, Summer 2000.
[2]Author to whom correspondence regarding NMR work may be addressed (telephone: (352) 846- 3001; fax: (352) 846-3001; e-mail: ion@chem.ufl.edu).
[3]Corresponding author (telephone: (352) 392-9844; fax: (352) 846-1203; e-mail: hudlicky@chem.ufl.edu).

 DOI: 10.1139/cjc-79-11-1659 © 2001 NRC Canada

Fig. 1. Design of synthesis.

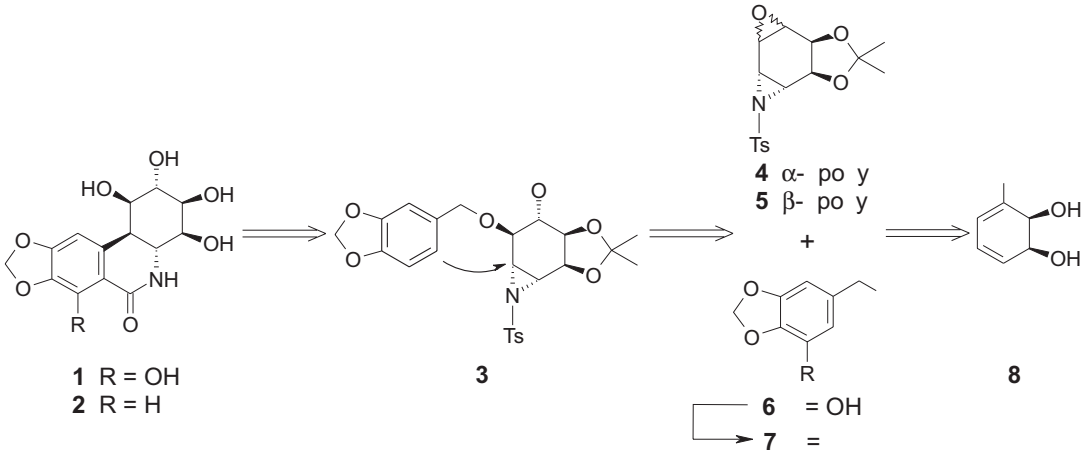
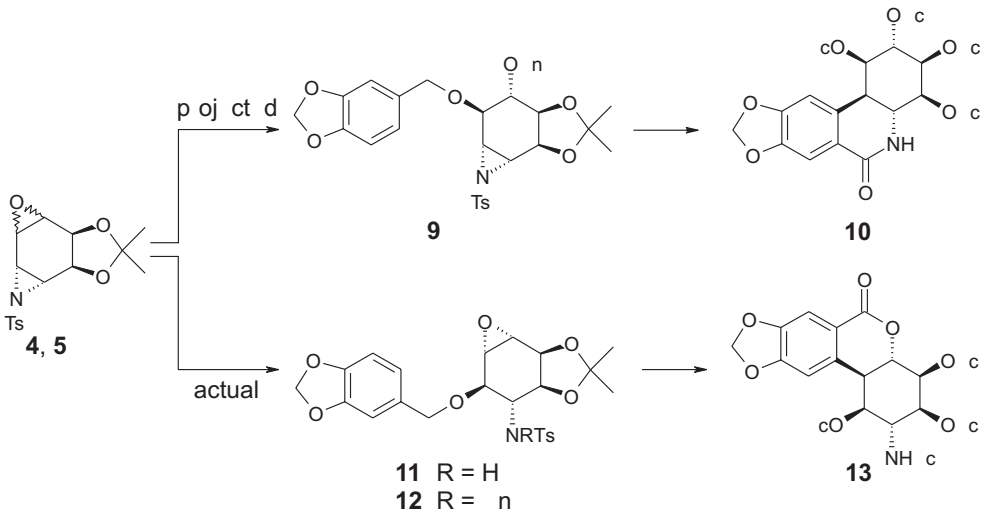


Fig. 2. Pathway to positional isomer of 7-deoxypancratistatin.



tional symmetry of epoxyaziridines **4** and **5** and their tendency to react with nucleophiles made structural assignment difficult throughout the synthesis. The inherent difficulties in precise stereochemical and regiochemical assignments in all intermediates propagated the errors resulting from the initial incorrect assignment of regiochemistry in the opening of aziridines **4** and **5** under basic conditions. A full structural correlation is reported along with experimental details for the preparation of tetraacetyl aminolactone **13**.

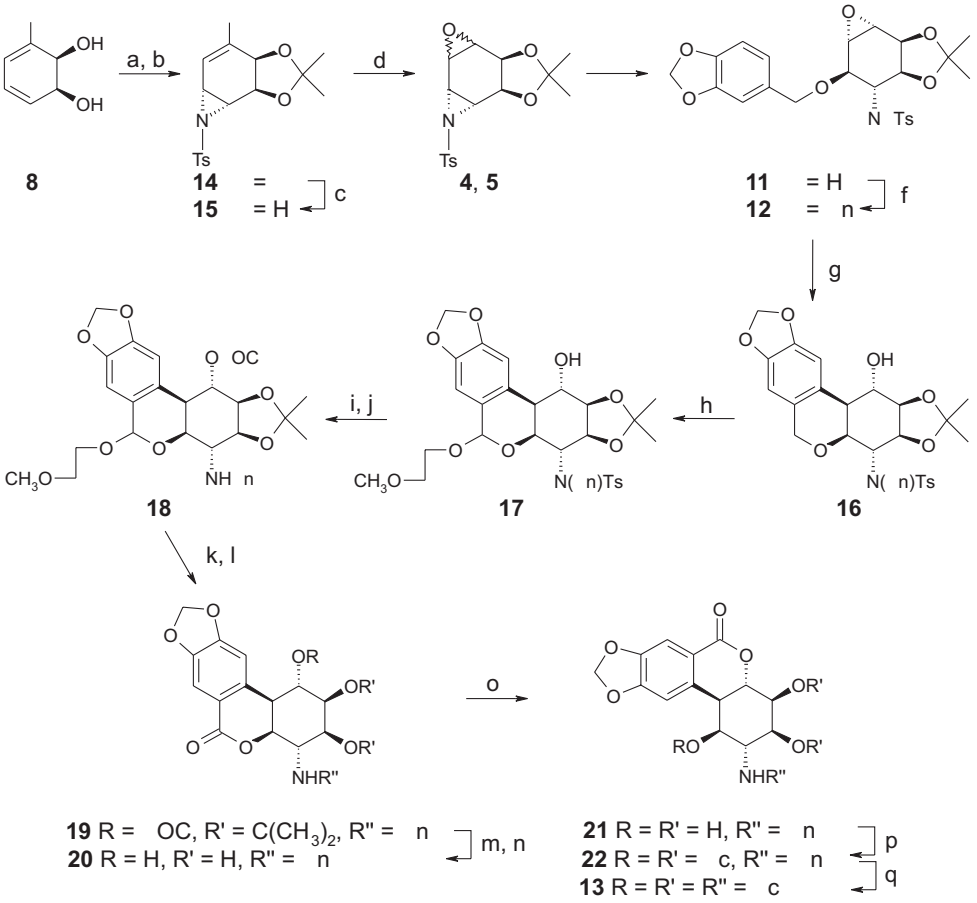
Results and discussion

Enantiomerically pure diol **8** was obtained by whole-cell biooxidation with recombinant *E. coli* JM109 (pDTG601) according to the established procedure (10). Diol **8** was protected as its acetonide and then reacted with (*N*-tosylimino)phenyliodinane according to the protocol established by Evans et al. (11*a*) and Jacobsen and co-workers (11*b*) to produce aziridine **14** in 45% overall yield (1*c*), as shown in Scheme 1. Dehalogenation of **14** with *n*-Bu_3SnH–THF generated vinylaziridine **15** (1*c*), which was subsequently oxidized (*m*CPBA, 1,2-dichloroethane, 85°C) to furnish an inseparable mixture (2.6:1) of α- and β-epoxyaziridines **4** and **5**, respectively. In our group, earlier work on nucleophilic opening of this material indicated that carboxylate salts (12) opened the epoxide under slightly basic conditions and that alcohols (13) under $BF_3 \cdot Et_2O$ catalysis also opened the epoxide with the aziridine ring intact. Following this precedent, the potassium salt of piperonol was reacted with the epoxyaziridines **4** and **5** and the product subjected to benzylation. Spectroscopic evidence, as presented below, suggested that compound **9** had been obtained, and therefore the rest of the synthesis was carried out. However, the compound, isolated in 71% yield as a single isomer, turned out to be epoxide **12**, ascertained only at the end of the synthesis when tetracetate **13** was identified.

The analysis of ^1H NMR spectra of conduramine and conduritol derivatives is not trivial, viz. the patterns of epoxy vs. aziridinyl methines and the chemical shift differences between *O*-benzyl vs. *N*-benzyl groups in structures where various shielding parameters could lead to pronounced shifts of the benzylic protons. This error in structure assignment was propagated through 12 steps without detection or ambiguity. The functional symmetry of epoxy aziridines **4** and **5** and the difficulty in deciphering the outcome of the first step contributed to the error.

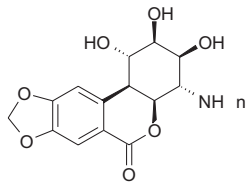
© 2001 NRC Canada

Scheme 1. Reagents and conditions: (*a*) DMP, *p*-TSA (cat.), acetone, rt; (*b*) PhI=NTs, $Cu(acac)_2$, CH_3CN, rt, 63% (over 2 steps); (*c*) Bu_3SnH, AIBN, THF, reflux, 78%; (*d*) *m*CPBA, $C_2H_4Cl_2$, reflux, 80%; (*e*) potassium piperonoxide, 18-C-6, DME, rt; (*f*) (*i*) NaH, THF, (*ii*) BnBr, Bu_4NI, rt, 71% (over 2 steps); (*g*) Me_2AlCl, CH_2Cl_2, –25°C, 77%; (*h*) DDQ, 2-methoxyethanol, CH_2Cl_2, rt, 78%; (*i*) NaH, $(BOC)_2O$, THF, reflux; (*j*) Na–naphthalene, DME, –50°C, 85% (over 2 steps); (*k*) CSA, THF, H_2O, rt; (*l*) PCC, CH_2Cl_2, rt, 72% (over 2 steps); (*m*) $C_6H_5CO_2Na$, MeOH–H_2O, reflux; (*n*) *p*-TsOH, MeOH, 84% (over 2 steps); (*o*) K_2CO_3, MeOH, 44%; (*p*) Ac_2O, DMAP, pyridine, 61%; (*q*) (*i*) H_2, $Pd(OH)_2$, MeOH, (*ii*) Ac_2O, DMAP, pyridine, 55% (over 2 steps).

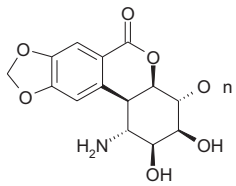


The actual sequence of steps was as follows: treatment of piperonyl ether **12** with Me_2AlCl resulted in cyclization to pentacycle **16** in 77% yield. Benzylic oxidation of ether **16** by means of 2,3-dichloro-5,6-dicyano-1,4-benzoquinone (DDQ) in the presence of 2-methoxyethanol gave acetal **17** in 78% yield. Acylation of acetal **17** followed by reductive detosylation (sodium–naphthalene–DME) generated acetal **18** in 85% overall yield. Deprotection of the acetal followed by oxidation of the resulting lactol provided lactone **19** in 72% yield. Removal of the carbamate by thermolysis followed by deketalization gave amino diol **20**, which upon hydrolysis (K_2CO_3–methanol) furnished lactone **21** in 44% yield.

The last stages of the synthesis were reached with what we thought to be lactone **23**, to which the conditions of Paulsen (2*b*) were applied for the final lactone–lactam interconversion, a sequence driven by the greater stability of the *trans*-fused lactam. Following this rearrangement, a protocol for debenzylation was carried out, ultimately leading to the isolation of a compound whose tetraacetate provided ^1H NMR remarkably similar to the ^1H NMR of the known tetraacetate of 7-deoxypancratistatin (2*c*), but whose R_f value in thin layer chromatography was lower by 0.6. The interesting point here is that lactone **20** did isomerize to the more stable lactone **21**, with distinctly different chromatographic and spectral properties; at the time we assumed that we were observing the expected equilibrium-driven transformation to the lactam.



20 actual



23 p oj ct d

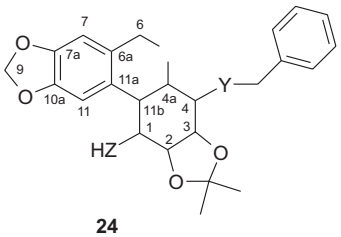
^1H NMR, ^{13}C NMR, and other analytical methods failed to confirm the structure of this material, which had evidently undergone a lactone rearrangement of some kind. An unambiguous assignment was finally made by means of ^{15}N HMQC spectroscopy, described in the next section.

Assignment of regio- and stereochemistry of tosylamide 16

Throughout the synthesis, 2D NMR was employed to confirm the structural integrity of key compounds, namely **16**,

© 2001 NRC Canada

19, and **21**. However, the $^1H–^1H$ couplings and NOE's, and the one-bond and long-range $^1H–^{13}C$ couplings fail to discriminate between compounds from the projected and actual series. In the case of compound **16** for instance, the $^1H–^1H$ and $^1H–^{13}C$ correlations indicate functionalized benzophyranyl system **24**, where X, Y, and Z are two O atoms and one NTs group. Uncertainty arises because there can be no $^1H–^{13}C$ long range coupling between atoms in the tosyl group and atoms at its point of attachment.



24

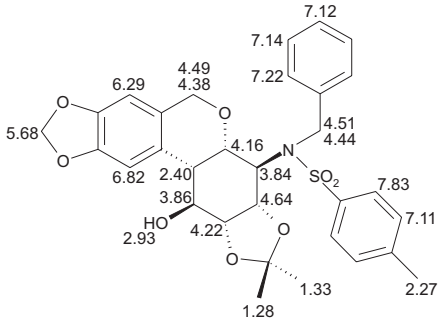
Formula **24** describes a compound in the projected series for X, Y = O and Z = NTs, as well as the actual **16**, for X, Z = O and Y = NTs. The same ambiguity is seen in compound **17**; however, compounds produced after the reductive detosylation step possess a proton attached to nitrogen, which in theory can be used to reveal the location of the trivalent nitrogen. In reality though, fast exchange with residual water in the sample precluded the observation of any coupling of this proton and even of its chemical shift for both **18** and **19**. The peracetylated derivative of **20** (R = R′ = R″ = Ac) displayed coupling of the NH proton with the proton in position 4 and not with the proton in position 1 as expected, thus revealing that the compounds synthesized were different from the projected ones.

Direct evidence for the structure of compound **16** came from the long-range $^1H–^{15}N$ couplings, revealed by the gHMBC spectrum at natural abundance (Fig. 3). Enough sample for the experiment was obtained by repeating the synthesis to provide 100 mg of tosylamide **16**. The nitrogen signal at 277.9 ppm on the nitromethane scale displayed cross-peaks with the benzylic protons (4.44 and 4.51 ppm) and the proton at 4.16 ppm of the cyclohexyl unit.

Chemical proof via structure correlation

In addition to the evidence for the structure of tosylamide **16** based on spectroscopy, including $^1H–^{13}C$ as well as $^1H–^{15}N$ correlation experiments, its structural integrity was confirmed through an independent synthesis. As illustrated in Scheme 2, opening of vinylaziridine **15** with the potassium salt of piperonol generated tosylamide **25**, which was converted to olefin **26** following benzylation. Stereoselective dihydroxylation of the olefin furnished *cis*-diol **27**; moreover, opening of epoxide **12**, derived from opening of the mixture of epoxyaziridines **4** and **5**, with hydroxide provided the *trans*–diol **28**. Cleavage of the diol functionalities in both tosylamides **27** and **28** gave rise to the corresponding dialdehydes, which upon reduction afforded *N*-benzyl tosylamide **29**, whose spectral and physical properties (^1H NMR, R_f, mass spectrum fragmentation pattern) were identical for the materials obtained by two independent synthetic routes.

Fig. 3. Proton assignment of tosylamide **16**.



16

Conclusion

The latent functional symmetry of epoxyaziridines **4** and **5** made it difficult to differentiate clearly the outcome of the initial nucleophilic opening of either of the three-membered rings. Standard structural assignment could not distinguish between the two regioisomers during a 12 step synthesis until a physical match was made. Philosophically, this case should raise interesting questions about the global probability of similar errors, undetected because of limited or nonexisting comparisons of physical properties, in today's literature.

Experimental

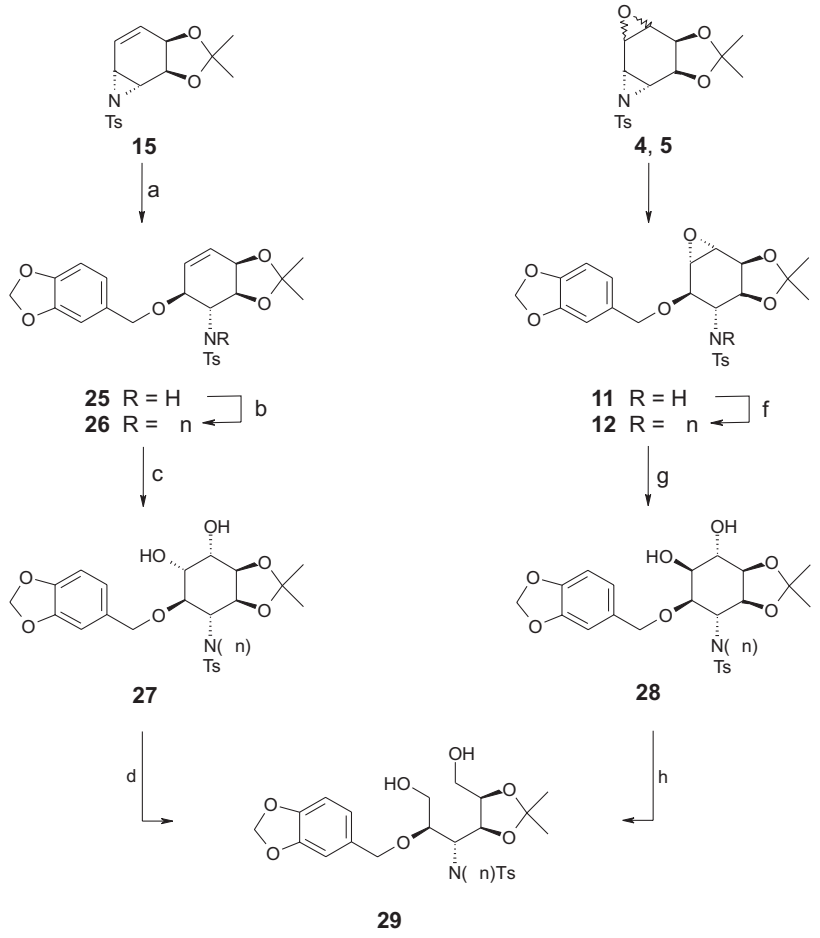
All reactions were carried out in an argon atmosphere with standard techniques for the exclusion of air and moisture. Glassware used for moisture-sensitive reactions was flame-dried under vacuum. Tetrahydrofuran (THF) and 1,2-dimethoxyethane (DME) were distilled from sodium benzophenone ketyl. Dichloromethane and 1,2-dichloroethane were distilled from calcium hydride. Reactions were monitored by thin layer chromatography on K6F silica gel (Whatman) plates. Flash column chromatography was performed on Merck silica gel (grade 60, 230–400 mesh). Melting points were determined on a Thomas-Hoover Unimelt apparatus and are uncorrected. Infrared spectra were obtained on a PerkinElmer 1600 Series FT-IR spectrometer. High resolution mass spectra (HRMS) were measured on a Finnigan Mat 95Q mass spectrometer. Nuclear magnetic resonance spectra were recorded on either a Varian VXR-300, Gemini 300, or Inova 500 FT NMR spectrometer in $CDCl_3$ unless otherwise noted. Coupling constants are measured in Hertz and chemical shifts are reported in ppm downfield from tetramethylsilane. Optical rotations were measured on a PerkinElmer model 341 polarimeter.

(1*S*,2*S*,4*R*,5*S*,6*S*,7*S*)-5,6-(Isopropylidenedioxy)-3-(4′-methylphenylsulfonyl)-8-oxa-3-aza-tricyclo[5.1.0.0]octane (4) and (1*R*,2*S*,4*R*,5*S*,6*S*,7*R*)-5,6-(isopropylidenedioxy)-3-(4′-methylphenylsulfonyl)-8-oxa-3-aza-tricyclo[5.1.0.0]-octane (5)

To a degassed solution of aziridine **15** (2.18 g, 6.79 mmol) in 1,2-dichloroethane (70 mL) was added *m*CPBA (8.37 g, 70%, 34.0 mmol) along with 3-*tert*-butyl-4-hydroxy-5-

© 2001 NRC Canada

Scheme 2. Reagents and conditions: (*a*) potassium piperonoxide, 18-C-6, DME, rt, 56%; (*b*) (*i*) NaH, THF, (*ii*) BnBr, Bu_4NI, rt, 84%; (*c*) $RuCl_3 \cdot 3H_2O$, $NaIO_4$, CH_3CN, EtOAc, 0°C, 66%; (*d*) (*i*) $NaIO_4$, CH_3COCH_3, H_2O, (*ii*) $NaBH_4$, MeOH, rt, 52% (over 2 steps); (*e*) potassium piperonoxide, 18-C-6, DME, rt; (*f*) (*i*) NaH, THF, (*ii*) BnBr, Bu_4NI, rt 71%; (*g*) KOH, H_2O, 1,4-dioxane, reflux, 56%; (*h*) (*i*) $NaIO_4$, CH_3COCH_3, H_2O, (*ii*) $NaBH_4$, MeOH, rt, 49% (over 2 steps).



methylphenyl sulfide (1.21 g, 3.40 mmol) as a radical inhibitor. The resulting solution was heated at reflux for 12 h. After allowing the solution to cool to room temperature, the reaction mixture was diluted with CH_2Cl_2 and washed sequentially with saturated $NaHSO_3$ and saturated $NaHCO_3$ solution. The organic phase was dried over Na_2SO_4 and the solvent was removed under reduced pressure. The residue was purified by chromatography (10% deactivated silica gel, hexanes – ethyl acetate, 4:1) to give a mixture of epoxyaziridines **4** and **5** (1.83 g, 80%) as a white solid; mp 107–108°C. $[\alpha]_D^{28}$ –56.5 (*c* 0.8, $CHCl_3$). R_f = 0.43 (hexanes – ethyl acetate, 2:1) FAB-HRMS calcd. for $C_{16}H_{20}NO_5S$: 338.1062; found: 338.1061. IR (neat) (cm^{-1}): 3000, 1595, 1330, 1255, 1158, 1082. ^1H NMR (300 MHz, $CDCl_3$) δ: 7.84 (d, *J* = 8.4 Hz, 2H), 7.35 (d, *J* = 8.1 Hz, 2H), 4.36 (d, *J* = 5.7 Hz, 1H), 4.24 (d, *J* = 6.3 Hz, 1H), 3.53 (t, *J* = 3.6 Hz, 1H), 3.37 (dd, *J* = 6.8, 3.8 Hz, 1H), 3.12 (dd, *J* = 3.3, 1.2 Hz, 1H), 3.03 (dd, *J* = 6.9, 1.2 Hz, 1H), 2.45 (s, 3H), 1.44 (s, 3H), 1.35 (s, 3H). ^{13}C NMR (75 MHz, $CDCl_3$) δ: 144.8, 134.1, 129.6, 127.7, 109.9, 70.6, 69.5, 49.9, 46.5, 37.1, 35.4, 27.2, 25.0, 21.5. Anal. calcd. for $C_{16}H_{19}NO_5S$: C 56.97, H 5.68, N 4.56; found: C 57.37, H 5.96, N 3.72.

N-Benzyl-*N*-[(1*R*,2*R*,3*S*,4*S*,5*S*,6*S*)-2-(benzo[1,3]dioxolo-5-ylmethoxy)-4,5-(isopropylidenedioxy)-7-oxa-bicyclo-[4.1.0]hept-3-yl]-4′-methylbenzenesulfonamide (12)

To a suspension of KH (757 mg, 18.9 mmol) in DME (12 mL) was added a solution of piperonol (2.51 g, 16.5 mmol) in DME (7 mL), and the mixture was stirred for 20 min. A solution of epoxyaziridine **4**, **5** (1.59 g, 4.72 mmol) in DME (8 mL) was added dropwise followed by the addition of 18-crown-6 (436 mg, 1.65 mmol). The resulting solution was stirred for 20 h. The reaction was quenched with saturated NH_4Cl solution and the reaction mixture was extracted with CH_2Cl_2 (4 × 75 mL). The combined organic extracts were dried over $MgSO_4$ and concentrated in vacuo to provide **11**, which was used without further purification. A solution of the remaining residue in THF (35 mL) was added dropwise to a suspension of NaH (841 mg, 35.0 mmol) in THF (35 mL). The solution was stirred for 20 min, then benzyl bromide (4.30 mL,

© 2001 NRC Canada

36.2 mmol) was added followed by a catalytic amount of tetrabutylammonium iodide. The solution was allowed to stir for 44 h and then quenched with water. The reaction mixture was extracted with ethyl acetate (4 × 60 mL), and the combined organic extracts were dried over $MgSO_4$. The solvent was removed under reduced pressure and the residue purified by chromatography (silica gel, hexanes – ethyl acetate, 5:1) to provide epoxide **12** (1.40 g, 71%) as a white solid; mp 63–65°C. $[\alpha]_D^{26}$ –6.9 (*c* 1.0, $CHCl_3$). R_f = 0.27 (hexanes – ethyl acetate, 3:1) FAB-HRMS calcd. for $C_{31}H_{34}NO_8S$: 580.2005; found: 580.2050. IR (KBr) (cm^{-1}): 2987, 1492, 1445, 1251, 1036. ^1H NMR (300 MHz, $CDCl_3$) δ: 7.82 (d, *J* = 8.0 Hz, 2H), 7.18–7.10 (m, 7H), 6.81–6.79 (m, 3H), 5.99 (s, 2H), 4.54–4.48 (m, 2H), 4.31–4.26 (m, 2H), 4.16–4.04 (m, 3H), 3.38 (d, *J* = 3.3 Hz, 1H), 3.30 (d, *J* = 3.0 Hz, 1H), 2.40 (s, 3H), 1.46–1.33 (m, 6H). ^{13}C NMR (75 MHz, $CDCl_3$) δ: 147.7, 147.4, 142.8, 138.0, 136.4, 130.9, 129.0, 128.7, 128.3, 128.2, 127.6, 122.1, 110.1, 109.2, 108.0, 101.0, 72.7, 71.3, 57.2, 52.1, 27.3, 25.6, 21.5. Anal. calcd. for $C_{31}H_{33}NO_8S$: C 64.23, H 5.74, N 2.42; found: C 64.51, H 5.93, N 2.28.

(1*S*,2*R*,3*S*,4*R*,5*S*,6*R*)-1-Hydroxy-2,3-(isopropylidenedioxy)-4-[*N*-benzyl-(4′-methylphenylsulfonyl)amino]-2,3,4,4a,6,11b-hexahydro-1*H*-5,8,10-trioxa-cyclopenta-[*b*]phenanthrene (16)

A solution of epoxide **12** (210 mg, 0.36 mmol) in CH_2Cl_2 (25 mL) at –25°C was treated with a 1.0 M solution of Me_2AlCl in hexanes (400 μL, 0.4 mmol) and stirred at –25°C for 2 h; it was slowly warmed to room temperature. The reaction was quenched with saturated NH_4Cl solution, and the reaction mixture was extracted with CH_2Cl_2 (4 × 20 mL). The combined organic extracts were dried over $MgSO_4$ and the solvent removed under reduced pressure. The remaining residue was purified by chromatography (silica gel, hexanes – ethyl acetate, 4:1) to furnish tosylamide **16** (161 mg, 77%) as a white solid; mp 114–116°C. $[\alpha]_D^{27}$ –49.0 (*c* 1.0, $CHCl_3$). R_f = 0.44 (hexanes – ethyl acetate, 1:1) CI-HRMS calcd. for $C_{31}H_{34}NO_8S$: 580.2005; found: 580.2001. IR (KBr) (cm^{-1}): 3504, 1484, 1329, 1238, 1156, 1038. ^1H NMR (500 MHz, $CDCl_3$) δ: 7.83 (d, *J* = 7.8 Hz, 2H), 7.26 (d, *J* = 9.0 Hz, 2H), 7.19 (m, 5H), 6.75 (s, 1H), 6.43 (s, 1H), 5.89 (s, 2H), 4.75 (dd, *J* = 9.7, 7.4 Hz, 1H), 4.58 (d, *J* = 15.1 Hz, 1H), 4.55–4.43 (m, 3H), 4.28 (t, *J* = 7.4 Hz, 1H), 4.21 (dd, *J* = 5.9, 4.5 Hz, 1H), 3.89 (dd, *J* = 11.2, 7.1 Hz, 1H), 3.69 (dd, *J* = 9.4, 6.6 Hz, 1H), 2.47 (dd, *J* = 11.6, 4.2 Hz, 1H), 2.42 (s, 3H), 1.92 (s, 1H), 1.30 (m, 6H). ^{13}C NMR (75 MHz, $CDCl_3$) δ: 146.8, 145.9, 143.2, 137.9, 136.1, 129.3, 128.7, 128.2, 128.1, 127.8, 127.6, 123.4, 111.1, 109.8, 104.1, 100.9, 81.0, 75.9, 73.3, 70.9, 67.4, 64.3, 52.4, 39.8, 27.1, 25.0, 21.5. Anal. calcd. for $C_{31}H_{33}NO_8S$: C 64.23, H 5.74, N 2.42; found: C 63.97, H 5.87, N 2.36.

(1*S*,2*R*,3*S*,4*R*,5*S*,6*R*)-1-Hydroxy-2,3-(isopropylidenedioxy)-6-(2′-methoxyethoxy)-4-[*N*-benzyl-(4′-methylphenyl-sulfonyl)-amino]-2,3,4,4a,6,11b-hexahydro-1*H*-5,8,10-trioxa-cyclopenta[*b*]phenanthrene (17)

A degassed solution of tosylamide **16** (320 mg, 0.55 mmol) in CH_2Cl_2 (25 mL) and 2-methoxyethanol (0.33 mL, 4.2 mmol) was treated with DDQ (188 mg, 0.828 mmol). The resulting solution was stirred at room temperature for 23 h. The solvent was removed under reduced pressure and the remaining residue was purified by chromatography (silica gel, hexanes – ethyl acetate – triethylamine, 2.5:2:1) to afford acetal **17** (282 mg, 78%) as a white solid ; mp 87–90°C. $[\alpha]_D^{27}$ +2.7 (*c* 1.0, $CHCl_3$). R_f = 0.31 (hexanes – ethyl acetate, 1:1) FAB-HRMS calcd. for $C_{34}H_{40}NO_{10}S$: 654.2373; found: 654.2409. IR (KBr) (cm^{-1}): 3448, 1485, 1328, 1242, 1039. ^1H NMR (500 MHz, $CDCl_3$) δ: 7.83 (d, *J* = 8.0 Hz, 2H), 7.25 (d, *J* = 8.5 Hz, 2H), 7.19–7.13 (m, 5H), 6.72 (s, 1H), 6.69 (s, 1H), 5.91 (m, 2H), 5.46 (s, 1H), 4.73–4.62 (m, 2H), 4.44 (ABq, *J* = 15.3 Hz, 2H), 4.30 (t, *J* = 7.3 Hz, 1H), 3.93–3.86 (m, 3H), 3.71–3.59 (m, 3H), 3.43 (s, 3H), 2.42 (s, 3H), 2.38 (d, *J* = 12.0 Hz, 1H), 2.07 (s, 1H), 1.35–1.33 (m, 6H). ^{13}C NMR (75 MHz, $CDCl_3$) δ: 147.2, 146.9, 143.1, 137.8, 135.7, 129.2, 129.0, 128.2, 128.0, 127.7, 127.3, 124.5, 110.5, 109.8, 107.1, 101.0, 96.8, 81.1, 73.7, 72.0, 69.7, 68.3, 67.2, 63.6, 59.0, 52.5, 39.6, 27.1, 24.9, 21.5.

(1*S*,2*R*,3*S*,4*R*,5*S*,6*R*)-4-Benzylamino-1-(*tert*-butoxy-carbonyloxy)-2,3-(isopropylidenedioxy)-6-(2′-methoxy-ethoxy)-2,3,4,4a,6,11b-hexahydro-1*H*-5,8,10-trioxa-cyclopenta[*b*]phenanthrene (18)

To a suspension of NaH (12 mg, 0.50 mmol) in THF (5 mL) was added a solution of acetal **17** (208 mg, 0.319 mmol) in THF (8 mL). The resulting solution was stirred at room temperature for 20 min after which a solution of di-*tert*-butyl dicarbonate (105 mg, 0.481 mmol) in THF (2 mL) was added dropwise. The solution was heated at reflux for 5 h. After the solution cooled to room temperature, the reaction was quenched with water, and the mixture extracted with ethyl acetate (3 × 30 mL). The combined organic extracts were dried over $MgSO_4$ and concentrated in vacuo. A solution of the remaining residue in DME (5 mL) cooled to –50°C was treated with a 0.6 M solution of Na–naphthalene in DME until a dark color persisted. The resulting solution was stirred at –50°C for 30 min, and then the reaction was quenched with water. After it had warmed to room temperature, the reaction mixture was extracted with ethyl acetate (3 × 25 mL), and the combined organic extracts were dried over $MgSO_4$. Removal of the solvent under reduced pressure and purification of the residue by chromatography (hexanes – ethyl acetate – triethylamine, 3:1:1) gave carbonate **18** (163 mg, 85%) as a white foam; $[\alpha]_D^{25}$ +21.5 (*c* 1.0, $CHCl_3$). R_f = 0.24 (hexanes – ethyl acetate, 1:1). FAB-HRMS calcd. for $C_{32}H_{42}NO_{10}$: 600.2809; found: 600.2813. IR (KBr) (cm^{-1}): 3448, 1751, 1508, 1490, 1243, 1039. ^1H NMR (300 MHz, $CDCl_3$) δ: 7.34–7.32 (m, 5H), 6.74 (s, 1H), 6.63 (s, 1H), 5.86 (d, *J* = 18.0 Hz, 2H), 5.64 (s, 1H), 5.09 (dd, *J* = 11.7, 7.8 Hz, 1H), 4.43–4.38 (m, 2H), 4.20 (t, *J* = 5.9 Hz, 1H), 4.01–3.82 (m, 4H), 3.58 (m, 2H), 3.34 (s, 3H), 3.23 (dd, *J* = 6.7, 3.3 Hz, 1H), 2.64 (dd, *J* = 11.6, 2.9 Hz, 1H), 1.69 (br s, 1H), 1.45 (s, 3H), 1.35 (s, 3H), 1.32 (s, 9H). ^{13}C NMR (75 MHz, $CDCl_3$) δ: 152.8, 147.7, 147.3, 140.3, 128.9, 128.7, 127.6, 126.6, 112.6, 110.2, 109.9, 108.1, 101.3, 98.0, 82.6, 78.0, 77.9, 76.4, 72.4, 69.9, 68.0, 59.4, 59.2, 52.7, 38.8, 28.3, 27.9, 26.4.

© 2001 NRC Canada

(1*S*,2*R*,3*S*,4*R*,5*S*,6*R*)-4-Benzylamino-1-(*tert*-butoxycarbonyloxy)-2,3-(isopropylidenedioxy)-2,3,4,4a,6,11b-hexahydro-1*H*-5,8,10-trioxa-cyclopenta[*b*]phenanthrene-6-one (19)

A solution of acetal **18** (204 mg, 0.340 mmol) in 30% aqeous THF (13 mL) was treated with CSA (395 mg, 1.70 mmol) and stirred at room temperature for 21 h. The solution was then diluted with ethyl acetate and washed successively with saturated $NaHCO_3$ solution, water, and brine. The organic layer was dried over Na_2SO_4 and then concentrated in vacuo. To a solution of the remaining residue in CH_2Cl_2 (9 mL) and molecular sieves (3 Å) was added PCC (112 mg, 0.520 mmol). The resulting solution was stirred at room temperature for 3 h. The reaction mixture was then filtered over silica and was subsequently washed with several portions of CH_3OH. Removal of the solvent under reduced pressure and purification of the residue by chromatography (silica gel, hexanes – ethyl acetate, 1:1) provided lactone **19** (131 mg, 72%) as a white solid; mp 201–203°C. $[\alpha]_D^{27}$ –28.1 (*c* 1.0, $CHCl_3$). R_f = 0.23 (hexanes – ethyl acetate, 1:1) FAB-HRMS calcd. for $C_{29}H_{34}NO_9$: 540.2234; found: 540.2238. IR (KBr) (cm^{-1}): 3318, 1733, 1702, 1501, 1485, 1260, 1038. ^1H NMR (500 MHz, $CDCl_3$) δ: 7.55 (s, 1H), 7.33–7.26 (m, 5H), 6.72 (s, 1H), 6.05 (m, 1H), 5.96 (m, 1H), 5.07 (dd, *J* = 11.5, 7.5 Hz, 1H), 4.72 (t, *J* = 3.5 Hz, 1H), 4.40 (dd, *J* = 7.5, 5.8 Hz, 1H), 4.22 (t, *J* = 5.4 Hz, 1H), 3.94 (ABq, *J* = 12.9 Hz, 2H), 3.48 (dd, *J* = 5.0, 3.4 Hz, 1H), 2.99 (dd, *J* = 11.5, 3.4 Hz, 1H), 1.63 (br s, 1H), 1.43 (s, 3H), 1.36 (s, 3H), 1.30 (s, 9H). ^{13}C NMR (75 MHz, $CDCl_3$) δ: 163.5, 152.2, 152.1, 148.1, 139.6, 134.6, 128.8, 128.4, 127.6, 118.9, 110.3, 110.2, 108.7, 102.2, 82.9, 79.3, 77.4, 76.9, 75.2, 58.3, 52.7, 38.8, 28.1, 27.6, 26.2.

(1*S*,2*R*,3*S*,4*R*,5*S*,6*R*)-4-Benzylamino-1,2,3-trihydroxy-2,3,4,4a,6,11b-hexahydro-1*H*-5,8,10-trioxa-cyclopenta-[*b*]phenanthrene-6-one (20)

A solution of carbonate **19** (17.5 mg, 0.0295 mmol) in MeOH–H_2O (3:2, 3.5 mL) was treated with a catalytic amount of sodium benzoate and then heated at reflux for 17 h. After the solution cooled to ambient temperature, the reaction mixture was extracted with ethyl acetate (4 × 15 mL). The combined organic extracts were dried over Na_2SO_4 and the solvent removed under reduced pressure. The residue was dissolved in MeOH (1.2 mL) to which *p*-toluenesulfonic acid (95 mg, 0.50 mmol) was added. The resulting solution was stirred at room temperature for 38 h. The reaction mixture was diluted with ethyl acetate, and the organic phase was washed with saturated $NaHCO_3$ solution. Following separation of the aqueous and organic phases, the aqueous phase was extracted with ethyl acetate (4 × 25 mL). The combined organic extracts were dried over Na_2SO_4 and the solvent removed under reduced pressure. The residue was purified by chromatography (silica gel, $CHCl_3$–MeOH, 9:1) to give diol **20** (9.9 mg, 84% over two steps) as a white solid; mp 173–176°C (dec.). $[\alpha]_D^{26}$ –81.0 (*c* 1.0, $CHCl_3$). R_f = 0.28 ($CHCl_3$–MeOH, 9:1) FAB-HRMS calcd. for $C_{21}H_{22}NO_7$: 400.1396; found: 400.1312. IR (KBr) (cm^{-1}): 3417, 1703, 1503, 1482, 1260, 1034. ^1H NMR (500 MHz, acetone) δ: 7.38 (d, *J* = 7.4 Hz, 2H), 7.32 (s, 1H), 7.29 (t, *J* = 7.4 Hz, 2H), 7.21 (t, *J* = 7.4 Hz, 1H), 6.89 (s, 1H), 6.10 (m, 2H), 4.75 (td, *J* = 2.9, 1.3 Hz, 1H), 4.14 (m, 1H), 3.91 (ABq, *J* = 14.0 Hz, 2H), 3.85 (m, 2H), 3.68–3.38 (m, 4H); 3.32 (t, *J* = 2.6 Hz, 1H), 3.11 (m, 1H). ^{13}C NMR (75 MHz, $CDCl_3$) δ: 164.8, 152.0, 147.5, 137.8, 129.8, 128.5, 128.3, 128.1, 117.2, 109.7, 108.9, 101.9, 78.7, 72.8, 69.8, 59.4, 52.3, 41.1.

(1*S*,2*R*,3*S*,4*R*,4a*S*,11b*R*)-2-Benzylamino-1,3,4-trihydroxy-1,2,3,4,4a,11b-hexahydro-1*H*-5,8,10-trioxa-cyclopenta[*b*]-phenanthrene-6-one (21)

A solution of triol **20** (43 mg, 0.11 mmol) in MeOH (4 mL) was treated with K_2CO_3 (31 mg, 0.22 mmol) and subsequently heated at reflux for 13 h. The reaction was diluted with ethyl acetate and quenched with saturated NH_4Cl solution. The organic and aqueous phases were separated and the aqueous phase was extracted with ethyl acetate (4 × 30 mL). The combined organic extracts were dried over Na_2SO_4 and the solvent removed under reduced pressure. The remaining residue was purified by chromatography (silica gel, $CHCl_3$–MeOH, 9:1) to give triol **21** (19 mg, 44%) as a thin film: $[\alpha]_D^{25}$ –60.4 (*c* 1.0, $CHCl_3$). R_f = 0.42 ($CHCl_3$–MeOH, 9:1). FAB-HRMS calcd. for $C_{21}H_{22}NO_7$: 400.1396; found: 400.1379. IR (neat) (cm^{-1}): 3410, 1690, 1484, 1261, 1026. ^1H NMR (500 MHz, acetone) δ: 7.40 (d, *J* = 7.2 Hz, 2H), 7.36 (s, 1H), 7.30 (t, *J* = 7.7 Hz, 2H), 7.22 (t, *J* = 7.2 Hz, 1H), 6.94 (d, *J* = 0.8 Hz, 1H), 6.10 (m, 2H), 4.68 (s, 1H), 4.58 (dd, *J* = 12.2, 9.4 Hz, 1H), 4.37 (s, 1H), 4.27 (td, *J* = 3.2, 1.3 Hz, 1H), 4.22 (dd, *J* = 9.4, 3.2 Hz, 1H), 3.91 (s, 2H), 3.45 (ddd, *J* = 12.3, 2.6, 0.7 Hz, 1H), 3.38 (t, *J* = 2.8 Hz, 1H), 3.0–2.62 (m, 3H). ^{13}C NMR (126 MHz, acetone) δ: 163.8, 152.5, 147.0, 140.8, 138.0, 128.3, 126.9, 120.1, 108.7, 105.6, 102.3, 78.5, 74.2, 70.3, 69.1, 60.3, 52.0, 39.7.

(1*S*,2*R*,3*S*,4*R*,4a*S*,11b*R*)-2-Benzylamino-1,3,4-triacetoxy-1,2,3,4,4a,11b-hexahydro-1*H*-5,8,10-trioxa-cyclopenta-[*b*]phenanthrene-6-one (22)

A solution of triol **21** (8.2 mg, 0.016 mmol) in pyridine (0.25 mL) was treated with neat acetic anhydride (58 μL, 0.61 mmol) and a catalytic amount of DMAP. The reaction was allowed to stir for 32 h. The solvent was removed and the remainder purified by chromatography (silica gel, hexanes – ethyl acetate, 1:1) to give triacetate **22** (6.6 mg, 61%) as an oil: $[\alpha]_D^{26}$ –16.2 (*c* 1.0, $CHCl_3$). R_f = 0.44 (hexanes – ethyl acetate, 1:1). FAB-HRMS calcd. for $C_{27}H_{28}NO_{10}$: 526.1713; found: 526.1718. IR (neat) (cm^{-1}): 3441, 1742, 1505, 1485, 1372, 1230, 1040. ^1H NMR (300 MHz, $CDCl_3$) δ: 7.54 (s, 1H), 7.38–7.28 (m, 5H), 6.40 (s, 1H), 6.06 (m, 2H), 5.61–5.56 (m, 2H), 5.52 (m, 1H), 4.91 (dd, *J* = 20.7, 12.2 Hz, 1H), 3.96 (ABq, *J* = 13.2 Hz, 2H), 3.77 (dd, *J* = 12.3, 3.0 Hz, 1H), 3.30 (t, *J* = 2.6 Hz, 1H), 2.10 (s, 3H), 2.05 (s, 3H), 1.98 (s, 3H), 1.7 (br s, 1H).

(1*S*,2*R*,3*S*,4*R*,4a*S*,11b*R*)-2-Acetylamino-1,3,4-triacetoxy-1,2,3,4,4a,11b-hexahydro-1*H*-5,8,10-trioxa-cyclopenta-[*b*]phenanthrene-6-one (13)

A solution of triacetate **22** (5.7 mg, 0.011 mmol) and $Pd(OH)_2$ (25 mg) in MeOH (1.5 mL) was subjected to an atmosphere of hydrogen for 40 min. The reaction mixture was

© 2001 NRC Canada

filtered over Celite, and the filtrate concentrated in vacuo. The remaining residue was dissolved in pyridine to which acetic anhydride (15 μL, 0.16 mmol) was added followed by a catalytic amount of DMAP. The reaction was stirred for 19 h. The solvent was removed and the residue purified by chromatography (hexanes – ethyl acetate, 1:1) to provide tetraacetate **13** (2.8 mg, 55%) as a film. ^{1}H NMR (300 MHz, $CDCl_3$) δ: 7.44 (s, 1H), 6.99 (d, J = 8.1 Hz, 1H), 6.62 (s, 1H), 6.06 (m, 2H), 5.71 (s, 1H), 5.53–5.46 (m, 2H), 4.89 (dd, J = 12.2, 10.1 Hz, 1H), 4.54 (m, 1H), 3.53 (dd, J = 10.5, 1.8 Hz, 1H), 2.08 (m, 9H), 1.98 (s, 3H).

N-[(1*R*,2*S*,5*R*,6*S*)-2-(Benzo[1,3]dioxol-5-ylmethoxy)-5,6-(isopropylidenedioxy)cyclohex-3-enyl]-4′-methylbenzenesulfonamide (25)

To a suspension of KH (108 mg, 2.69 mmol) in DME (3 mL) was added a solution of piperonol (378 mg, 2.49 mmol) in DME (5 mL). The resulting solution was stirred for 20 min, then a solution of vinylaziridine **15** (228 mg, 0.710 mmol) in DME (3 mL) was added dropwise followed by 18-crown-6 (66 mg, 0.25 mmol). The reaction mixture was stirred for 24 h and then the reaction quenched with saturated NH_4Cl solution. The reaction mixture was extracted with CH_2Cl_2 (4 × 50 mL) and the combined organic extracts dried over Na_2SO_4. The solvent was removed under reduced pressure and the remainder purified by chromatography (silica gel, hexanes – ethyl acetate, 2:1) to furnish tosylamide **25** (223 mg, 56%) as a white foam; $[\alpha]_D^{29}$ –10.5 (*c* 1.0, $CHCl_3$). R_f = 0.38 (hexanes – ethyl acetate, 1:1). FAB-HRMS calcd. for $C_{24}H_{28}NO_7S$: 474.1586; found: 474.1587. IR (neat) (cm^{-1}): 3269, 1503, 1599, 1492, 1445, 1326, 1251, 1156, 1094, 1039. ^{1}H NMR (500 MHz, $CDCl_3$) δ: 7.80 (d, J = 8.3 Hz, 2H), 7.19 (d, J = 8.3 Hz, 2H), 6.73 (d, J = 8.0 Hz, 1H), 6.72 (d, J = 1.6 Hz, 1H), 6.68 (dd, J = 7.9, 1.8 Hz, 1H), 5.94 (s, 2H), 5.88 (dd, J = 10.3, 1.0 Hz, 1H), 5.84 (ddd, J = 10.1, 3.2, 1.8 Hz, 1H), 5.10 (d, J = 7.4 Hz, 1H), 4.53 (dd, J = 6.3, 3.4 Hz, 1H), 4.36 (d, J = 11.6 Hz, 1H), 4.27 (d, J = 11.5 Hz, 1H), 4.05 (dd, J = 9.4, 6.1 Hz, 1H), 3.80 (dq, J = 9.2, 1.6 Hz, 1H), 3.55 (td, J = 9.2, 7.4 Hz, 1H), 2.37 (s, 3H), 1.36 (s, 3H), 1.29 (s, 3H). ^{13}C NMR (126 MHz, $CDCl_3$) δ: 147.9, 147.2, 142.9, 139.0, 132.6, 131.9, 129.3, 127.6, 124.5, 121.6, 110.8, 109.0, 108.2, 101.0, 76.4, 75.7, 72.2, 70.8, 57.3, 27.8, 26.0, 21.7.

N-Benzyl-*N*-[(1*R*,2*S*,5*R*,6*S*)-2-(benzo[1,3]dioxol-5-ylmethoxy)-5,6-(isopropylidenedioxy)cyclohex-3-enyl]-4′-methylbenzenesulfonamide (26)

To a suspension of NaH (10.8 mg of 60% reagent, 0.270 mmol) in THF (2 mL) was added a solution of tosylamide **25** (117 mg, 0.208 mmol) in THF (5 mL). The resulting solution was stirred for 20 min then benzyl bromide (36 μL, 0.28 mmol) was added, followed by a catalytic amount of tetrabutylammonium iodide. The solution was stirred for 18 h and then quenched with water. The reaction was diluted with ethyl acetate and the aqueous and organic layers separated. The aqueous phase was extracted with ethyl acetate (4 × 40 mL) and the combined organic extracts dried over Na_2SO_4. Removal of the solvent in vacuo provided a residue which was purified by chromatography (silica gel, hexanes – ethyl acetate, 3:1) generating tosylamide **26** (114 mg, 84%) as a solid; mp 157–160°C. $[\alpha]_D^{25}$ +3.2 (*c* 1.0, $CHCl_3$). R_f = 0.21 (hexanes – ethyl acetate, 5:1). FAB-HRMS calcd. for $C_{31}H_{34}NO_7S$: 564.2056; found: 564.2099. IR (neat) (cm^{-1}): 1599, 1503, 1492, 1445, 1330, 1251, 1156, 1040. ^{1}H NMR (300 MHz, $CDCl_3$) δ: 7.86 (d, J = 8.1 Hz, 2H), 7.22–7.15 (m, 7H), 6.81–6.78 (m, 3H), 5.97–5.94 (m, 3H), 5.80 (d, J = 9.9 Hz, 1H), 4.57–4.31 (m, 6H), 2.40 (s, 3H), 1.32–1.25 (m, 6H). ^{13}C NMR (75 MHz, $CDCl_3$) δ: 147.6, 142.9, 138.1, 136.4, 133.0, 131.7, 129.1, 128.9, 128.2, 127.5, 123.0, 121.6, 112.0, 110.3, 108.9, 107.9, 100.9, 73.6, 72.7, 70.6, 27.5, 25.7, 21.5.

(1*R*,2*R*,3*S*,4*S*,5*S*,6*S*)-3,4-Dihydroxy-5,6-(isopropylidenedioxy)-2-(3′,4′-methylenedioxyphenylmethyl)-1-cyclohexylbenzenesulfonamide (27)

A solution of tosylamide **26** (16.2 mg, 0.0288 mmol) in CH_3CN–EtOAc (1:1, 0.80 mL) at 0°C was treated with a solution of $NaIO_4$ (10.1 mg, 0.0432 mmol) and a catalytic amount of $RuCl_3 \cdot 3H_2O$ in water (0.5 mL). The resulting solution was stirred at 0°C for 3 min and then quenched with saturated $Na_2S_2O_3$ solution. The reaction mixture was extracted with CH_2Cl_2 (4 × 10 mL) and the combined organic extracts dried over Na_2SO_4. The solvent was removed under reduced pressure and the residue purified by chromatography (silica gel, hexanes – ethyl acetate, 1:2) to provide diol **27** (11.3 mg, 66%) as a film; $[\alpha]_D^{26}$ –27.9 (*c* 1.0, $CHCl_3$). R_f = 0.34 (hexanes – ethyl acetate, 1:2). FAB-HRMS calcd. for $C_{31}H_{36}NO_9S$: 598.2111; found: 598.2108. IR (neat) (cm^{-1}): 3460, 1504, 1492, 1445, 1328, 1251, 1156, 1040. ^{1}H NMR (300 MHz, acetone) δ: 7.75 (d, J = 7.8 Hz, 2H), 7.24–7.15 (m, 7H), 6.88 (s, 1H), 6.80–6.78 (m, 2H), 6.00 (s, 2H), 4.60 (d, J = 11.1 Hz, 1H), 4.45–4.38 (m, 3H), 4.28–4.14 (m, 4H), 4.03–3.79 (m, 3H), 3.93 (br s, 1H), 2.38 (s, 3H), 1.28–1.24 (m, 6H). ^{13}C NMR (75 MHz, $CDCl_3$) δ: 147.7, 147.3, 142.8, 138.3, 136.2, 131.8, 129.1, 128.8, 128.2, 128.0, 127.5, 122.1, 109.3, 109.2, 108.1, 101.0, 76.5, 73.0, 69.7, 27.4, 25.4, 21.4.

(1*R*,2*R*,3*R*,4*S*,5*S*,6*S*)-3,4-Dihydroxy-5,6-(isopropylidenedioxy)-2-(3′,4′-methylenedioxyphenylmethyl)-1-cyclohexylbenzenesulfonamide (28)

A solution of epoxide **12** (17.2 mg, 0.0297 mmol) in a mixture of 1,4-dioxane–H_2O (1:1, 1 mL) was treated with KOH (16.7 mg, 0.297 mmol) and then heated at reflux for 48 h. The reaction mixture was diluted with ethyl acetate and the organic and aqueous layers were separated. The aqueous layer was extracted with ethyl acetate (4 × 20 mL) and the combined organic extracts dried over Na_2SO_4. Removal of the solvent under reduced pressure afforded a residue that was purified by chromatography (silica gel, hexanes – ethyl acetate, 1:4) to give diol **28** (9.9 mg, 56%) as a film; $[\alpha]_D^{27}$ –35.4 (*c* 1.0, $CHCl_3$). R_f = 0.36 (hexanes – ethyl acetate, 1:24). FAB-HRMS calcd. for $C_{31}H_{35}NO_9S$ + Na: 620.1930; found: 620.1910. IR (neat) (cm^{-1}): 3478, 1493, 1445, 1326, 1246, 1156, 1038. ^{1}H NMR (300 MHz, $CDCl_3$) δ: 7.82 (d, J = 8.1 Hz, 2H), 7.24–7.20 (m, 7H), 6.76–6.75 (m, 3H), 5.97 (s, 2H), 4.48 (m, 2H), 4.38–4.24 (m, 3H), 4.10–4.06 (m, 2H), 3.98–3.90 (m, 2H), 3.73 (t, J = 6.0 Hz, 1H), 2.42 (s, 3H), 1.35 (s, 3H), 1.25 (s, 3H). ^{13}C NMR (75 MHz, $CDCl_3$) δ: 147.7, 147.4, 143.1, 137.8, 136.3, 131.2, 129.2, 128.8, 128.4, 128.0, 127.7, 122.0,

© 2001 NRC Canada

109.5, 109.1, 108.1, 101.0, 77.8, 75.3, 74.1, 72.5, 70.5, 69.4, 61.0, 50.9, 27.4, 25.2, 21.5.

(2*R*,3*R*,4*S*,5*R*)-[2-(Benzo[1,3]-dioxol-5-ylmethoxy)-3-(*N*-benzyl-(4′-methylphenylsulfonyl)amino)-1,6-dihydroxy-4,5-(isopropylidenedioxy)]hexane (29)

A solution of diol **27** (21.1 mg, 0.0353 mmol) in a 40% aqueous acetone solution (2 mL) was treated with a solution of $NaIO_4$ (10.2 mg, 0.0477 mmol) in water (0.2 mL) and stirred at room temperature for 3 h. The reaction mixture was concentrated in vacuo and the resulting solution was extracted with ethyl acetate (4 × 25 mL). The combined organic extracts were dried over Na_2SO_4 and the solvent removed under reduced pressure. The remaining residue was dissolved in MeOH (1 mL), cooled to 0°C, and treated with neat $NaBH_4$. The solution was slowly warmed to room temperature and stirred for 18 h. The reaction mixture was treated with water and then concentrated in vacuo. The remaining solution was extracted with ethyl acetate (4 × 20 mL) and the combined organic extracts dried over Na_2SO_4. Removal of the solvent under reduced pressure gave a residue, which was purified by chromatography (silica gel, hexanes – ethyl acetate, 1:2) furnishing diol **29** (11.1 mg, 52%) as a film; $[\alpha]_D^{25}$ +66.8 (*c* 1.0, $CHCl_3$). R_f = 0.30 (hexanes – ethyl acetate, 1:2). FAB-HRMS calcd. for $C_{31}H_{38}NO_9S$: 600.2267; found: 600.2264. IR (neat) (cm^{-1}): 3501, 1503, 1491, 1445, 1332, 1251, 1157, 1039. ^1H NMR (300 MHz, $CDCl_3$) δ: 7.56 (d, *J* = 8.1 Hz, 2H), 7.36–7.34 (m, 2H), 7.21–1.15 (m, 5H), 6.73 (d, *J* = 8.7 Hz, 1H), 6.62–6.60 (m, 2H), 5.93 (m, 2H), 4.60 (d, *J* = 15.9 Hz, 1H), 4.39–4.27 (m, 4H), 4.13 (d, *J* = 11.7 Hz, 1H), 3.93 (m, 1H), 3.69–3.58 (m, 2H), 3.44–3.40 (m, 4H), 2.37 (s, 3H), 2.03 (br s, 1H), 1.13 (s, 3H), 1.0 (s, 3H). ^{13}C NMR (75 MHz, $CDCl_3$) δ: 147.8, 147.5, 143.0, 138.1, 137.0, 131.2, 128.8, 128.0, 127.7, 126.8, 121.9, 108.8, 108.0, 107.9, 101.1, 78.5, 73.2, 72.3, 61.2, 58.9, 55.2, 49.6, 27.7, 25.0, 21.4. (Note: an analagous procedure can be applied to diol **28** which also affords diol **29**).

Acknowledgments

The authors thank the National Science Foundation (CHE-9 615 112), TDC Research, Inc., and the University of Florida for financial support.

References

1. Pancratistatin: (*a*) S. Danishefsky and J.Y. Lee. J. Am. Chem. Soc. **111**, 4829 (1989); (*b*) X. Tian, T. Hudlicky, and K. Königsberger. J. Am. Chem. Soc. **117**, 3643 (1995); (*c*) T. Hudlicky, X. Tian, K. Königsberger, R. Maurya, J. Rouden, and B. Fan. J. Am. Chem. Soc. **118**, 10752 (1996); (*d*) B.M. Trost and S.R. Pulley. J. Am. Chem. Soc. **117**, 10143 (1995).(*e*) T.J. Doyle, M. Hendrix, D. VanDerveer, S. Javanmard, and J. Haseltine. Tetrahedron, **53**, 11153 (1997); (*f*) P. Magnus and I.K. Sebhat. J. Am. Chem. Soc. **120**, 5341 (1998); (*g*) J.H. Rigby, U.S.M. Maharoof, and M.E. Mateo. J. Am. Chem. Soc. **122**, 6624 (2000).
2. 7-Deoxypancratistatin: (*a*) S. Ohta and and S. Kimoto. Chem. Pharm. Bull. **24**, 2977 (1976); (*b*) G.E. Keck, S.F. McHardy, and J.A. Murry. J. Am. Chem. Soc. **117**, 7289 (1995); (*c*) X. Tian, R. Maurya, K. Königsberger, and T. Hudlicky. Synlett, 1125 (1995); (*d*) N. Chida, M. Jitsuoka, and Y. Yamamoto. Heterocycles, **43**, 1385 (1996); (*e*) G.E. Keck, T.T. Wager, and S.F. McHardy. J. Org. Chem. **63**, 9164 (1998); (*f*) G.E. Keck, S.F. McHardy, and J.A. Murry. J. Org. Chem. **64**, 4465 (1999); (*g*) J.L. Acena, O. Arjona, M.L. Leon, and J. Plumet. Org. Lett. **2**, 3683 (2000).
3. Narciclasine: (*a*) J.H. Rigby and M.E. Mateo. J. Am. Chem. Soc. **119**, 12655 (1997); (*b*) D. Gonzalez, T Martinot, and T. Hudlicky. Tetrahedron Lett. **40**, 3077 (1999); (*c*) G.E. Keck, T.T. Wager, and J.F.D. Rodriguez. J. Am. Chem. Soc. **121**, 5176 (1999).
4. Lycoricidine: (*a*) S. Ohta and S. Kimoto. Tetrahedron Lett. **23**, 2279 (1975); (*b*) S. Ohta and S. Kimoto. Chem. Pharm. Bull. **24**, 2969, (1976); (*c*) S. Ohta and S. Kimoto. Chem. Pharm. Bull. **24**, 2977 (1976); (*d*) H. Paulsen and M. Stubbe. Tetrahedron Lett. **23**, 3171 (1982); (*e*) H. Paulsen and M. Stubbe. Liebigs Ann. Chem. 535 (1983); (*f*) S. Ogawa, M. Ohtsuka, and N. Chida. Tetrahedron Lett. **32**, 4525 (1991); (*g*) T. Hudlicky and H.F. Olivo. J. Am. Chem. Soc. **114**, 9694 (1992); (*h*) S.F. Martin and H.H. Tso. Heterocycles, **35**, 85 (1993); (*i*) S. Ogawa, M. Ohtsuka, and N. Chida. J. Org. Chem. **58**, 4441 (1993); (*j*) T. Hudlicky, H.F. Olivo, and B. McKibben. J. Am. Chem. Soc. **116**, 5108 (1994).
5. H. Akgun amd T. Hudlicky. Tetrahedron Lett. **40**, 3081 (1999).
6. (*a*) H.G. Viehe amd J.L. Vaerman. Tetrahedron, **45**, 3183 (1989); (*b*) H.G. Viehe, J.L. Vaerman, F.P. Schmidtchen, G. Kresze, W. Burger, and H. Braun. Tetrahedron: Asymmetry, **1**, 403 (1990).
7. For definitions of redundant operations, see T. Hudlicky. Chem. Rev. **96**, 3 (1996).
8. (*a*) S.C. Bergmeier, W.K. Lee, and H. Rapoport. J. Org. Chem. **58**, 5019 (1993); (*b*) S.C. Bergmeier, and P.P. Seth. Tetrahedron Lett. **36**, 3793 (1995); (*c*) S.C. Bergmeier and P.P. Seth. J. Org. Chem. **64**, 3237 (1999); (*d*) S.C. Bergmeier, S.L. Fundy, and P.P. Seth. Tetrahedron, **55**, 8025 (1999).
9. D.R. Gauthier and S.L. Bender. Tetrahedron Lett. **37**, 13 (1996).
10. (*a*) T. Hudlicky, E.E. Boros, and C.H. Boros. Tetrahedron: Asymmetry, **4**, 1365, (1993); (*b*) T. Hudlicky, E.E. Boros, and C.H. Boros. Synthesis, 174 (1992); (*c*) T. Hudlicky, M.R. Stabile, D.T. Gibson, and G.M. Whited. Org. Syn. **76**, 77 (1999).
11. (*a*) D.A. Evans, M.M. Faul, and M.T. Bilodeau. J. Org. Chem. **56**, 6744 (1991); (*b*) Z. Li, K.R. Conser, and E.N. Jacobsen. J. Am. Chem. Soc. **115**, 5326 (1993); (*c*) J.G. Knight and M.P. Muldowney. Synlett, 949 (1995).
12. (*a*) S. Miah. Unpublished results. 1995; (*b*) R.D. Guthrie, I.D. Jenkins, S. Thang, J. Watters, and R. Yamasaki. Carbohydr. Res. **103**, 1 (1982).
13. S. McLamore. Studies directed towards the total synthesis of *ent*-7-deoxypancratistatin. PhD thesis. University of Florida. 1997.

© 2001 NRC Canada

The total synthesis of (+)-aspicilin using 2,3-butane diacetal protected butane tetrols via a chiral memory protocol

Darren J. Dixon, Alison C. Foster, and Steven V. Ley

Abstract: The total syntheses of the polyhydroxylated macrolactone (+)-aspicilin and a diastereoisomer have been achieved via a concise route, starting from the spatially desymmetrized (*R′*,*R′*,*R*,*S*)-2,3-butanediacetal-protected butane tetrol **13**. The key steps include a regioselective silyl protection of **13** and a stereoselective Lewis acid mediated addition of allyltributylstannane to the equatorially disposed aldehyde of **4**. Macrocyclization is achieved using ring closing metathesis, after which selective hydrogenation and protecting group removal yields the natural product.

Key words: aspicilin, butanediacetal, desymmetrization, macrolactone, metathesis.

Résumé : Les synthèses totales de la macrolactone polyhydroxylée (+)-aspiciline et d'une de ses diastéréoisomères ont été effectvé par le biais d'une route concise partant d'un butanetétrol désymétrisé d'un point de vue spacial sous la forme de (*R′*,*R′*,*R*,*S*)-butanediacétal protégé, **13**. Les étapes clés impliquent une protection régiosélective du composé **13** par un silyle et une addition stéréosélective, catalysée par un acide de Lewis, de l'allyltributylstannane sur un aldéhyde en position équatoriale du composé **4**. On réalise la macrocyclisation en exploitant à une réaction de fermeture de cycle par métathèse, suivie d'une hydrogénation sélective et d'une élimination du groupe protecteur pour conduire au produit naturel.

Mots clés : aspiciline, butanediacétal, désymétrisation, macrolactone, métathèse.

[Traduit par la Rédaction]

Introduction

The desymmetrization of *meso* compounds as a method for obtaining enantiomerically enriched products has become a powerful tool for synthetic organic chemists. Enzymes are frequently used to effect this kind of transformation (1); however, considerable work has also been carried out using chiral reagents or catalysts (2).

Tartaric acid is a readily available four-carbon building block in either the (+)-, (–)-, or *meso* forms. Terminal group manipulation of the two homochiral tartrates affords the *syn*-1,2-diol motif, whereas elaboration of the *meso* form provides *anti*-1,2-diols but as a racemate. Polyhydroxylated natural products are important synthetic targets, consequently several methods have been devised for the introduction of a 1,2-diol. However, the number of ways to prepare *anti*-1,2-diols is much less than for the corresponding *syn*-1,2 unit. Even the powerful Sharpless asymmetric dihydroxylation procedure favors *syn*-1,2-diol formation from *trans* alkenes in a higher enantiomeric excess (ee) than when *cis* alkenes are used as precursors for the *anti*-1,2-diol motif (3). Alternative methods for the introduction of enantiomerically pure *anti*-1,2-diols are therefore crucial to expand the repertoire of the synthetic organic chemist.

Previous work developed in our group using the homochiral C_2 symmetric bis(dihydropyran) (BDP) unit to protect 1,2-diols was one solution to the problem, allowing for the desymmetrization of *meso* compounds such as glycerol and *myo*-inositol (4–7). This protecting group makes use of the anomeric stabilization effect and the preference for all other substituents to be placed in equatorial environments. Here we report in full a cheaper alternative process that relies on the use of 1,2-butane diacetals operating through a chiral memory protocol to obtain the desired desymmetrized *meso* tartaric acid derivatives and then use of this in the synthesis of the *anti*-1,2-diol containing macrolactone natural product (+)-aspicilin **1**.

This 18-membered macrolactone metabolite, was first isolated from *Lecanoraceae* lichen in 1900 by Hesse (9, 10), but despite the elucidation of the connective structure in 1973 (8), the relative and absolute stereochemistry remained unknown until 1985 (11). Although no biological function for **1** has been reported, its structure, which contains four stereogenic centres, three of which occur as an *anti*, *syn*-triol unit, consequently makes it an ideal target to explore the use of our new chiral building blocks in a stereoselective synthesis of **1** (12). Other syntheses of (+)-aspicilin have also been reported (13–27).

Received March 15, 2001. Published on the NRC Research Press Web site at http://canjchem.nrc.ca on November 20, 2001.

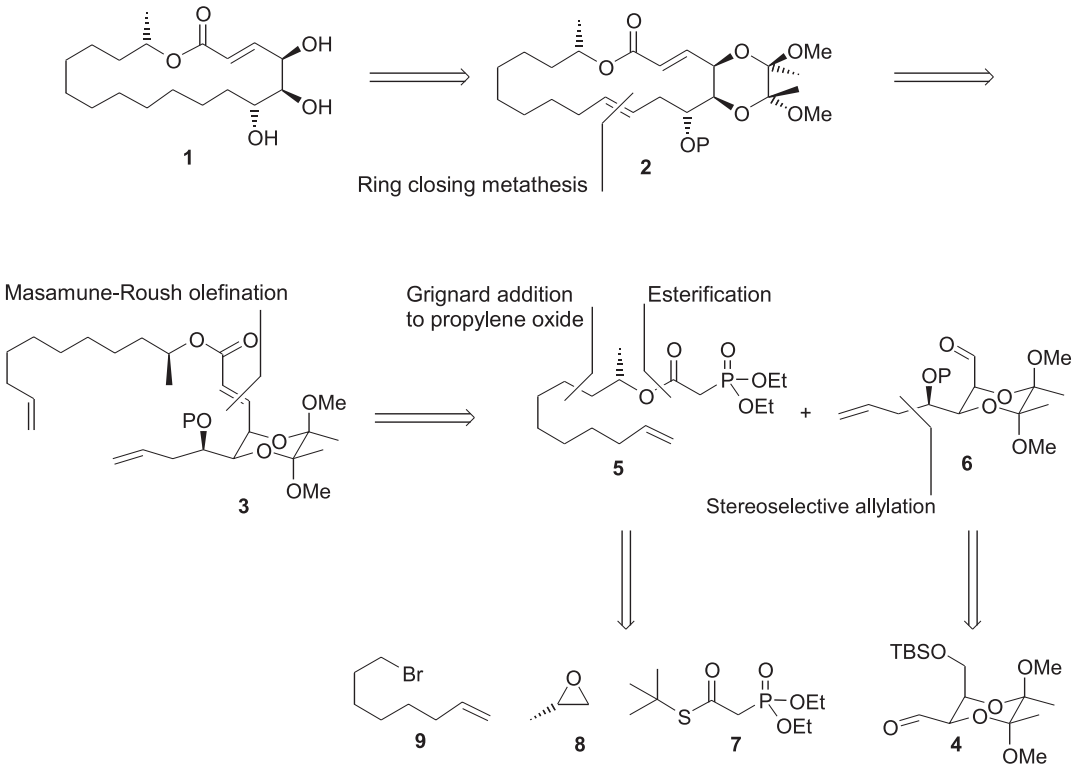
Dedicated to Professor Victor Snieckus for his contributions to chemistry and the training of students worldwide.

D.J. Dixon, A.C. Foster, and S.V. Ley.[1] Department of Chemistry, University of Cambridge, Lensfield Road, Cambridge, CB2 1EW, U.K.

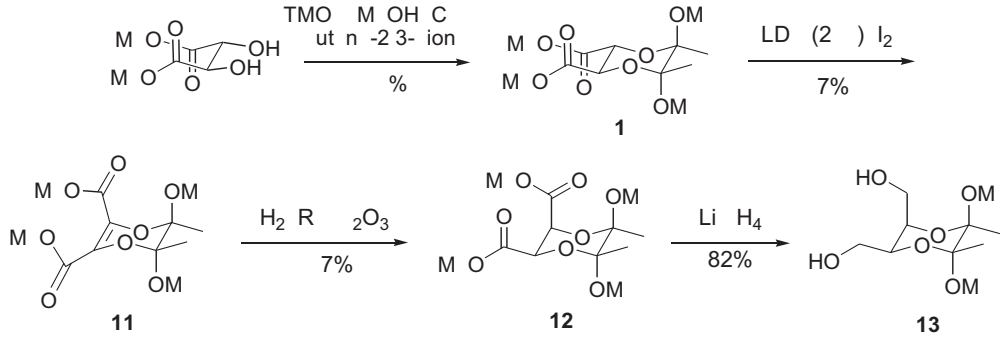
[1]Corresponding author (telephone: 44 1233 336 398; fax: 44 1233 336 442; e-mail: svl1000@cam.ac.uk).

 DOI: 10.1139/cjc-79-11-1668 © 2001 NRC Canada

Scheme 1.



Scheme 2.



Our general route to aspicilin is shown in Scheme 1. Ring closing metathesis of **3** to give the large ring olefin **2** suggests that **3** could be constructed by a stereoselective Masamune–Roush coupling of the phosphonoacetate **5** and aldehyde **6**. In turn compound **5** should be available from ring opening of propylene oxide **8** with the Grignard derived from **9**, and finally esterification with **7** (28). The preparation of **6** follows from an anticipated stereoselective addition of an allyl side chain to the *R,R,R′,R′*-butane diacetal protected aldehyde derivative **4**. Compound **4** would be obtained by chemistry already established in our group.

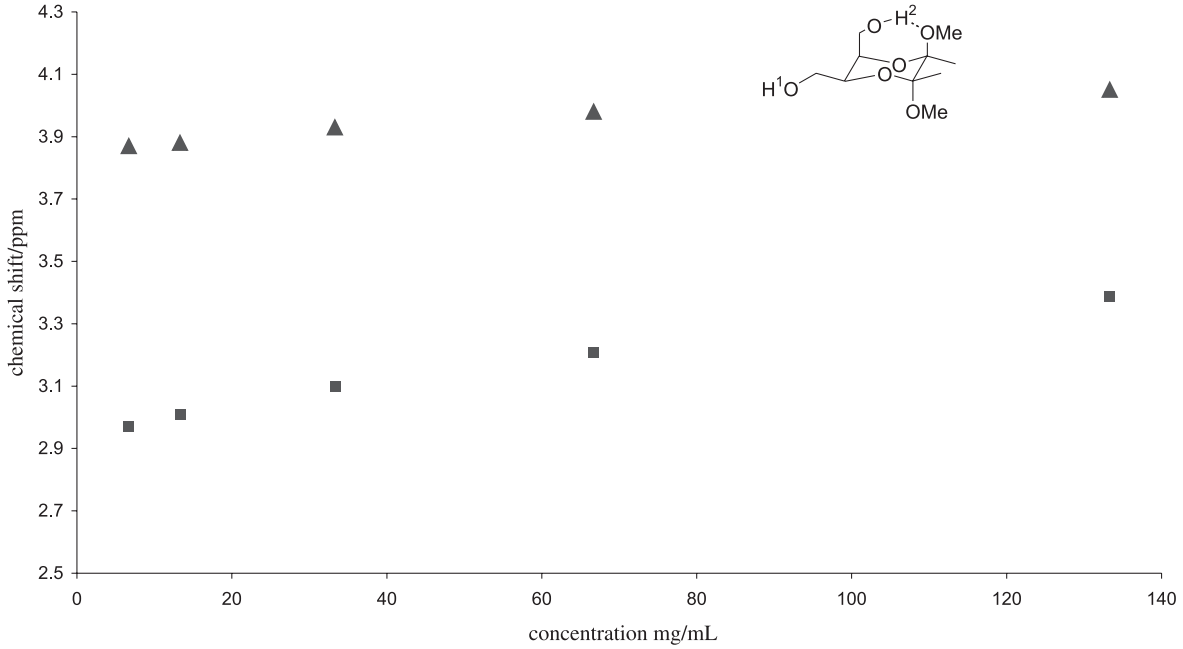
The synthesis begins from commercially available dimethyl L-tartrate, which was transformed to the desymmetrized diol **13** using our recently developed chiral memory protocol (29, 30). Firstly, the enantiopure diester was protected as the butane diacetal **10** using butane-2,3-dione and catalytic acid. The resulting diacetal was then oxidized, via double deprotonation and treatment with iodine, to give the unsaturated diester **11**. Upon hydrogenation using rhodium on alumina as the catalyst, the spatially desymmetrized diester **12** was produced. All the compounds in Scheme 2 are highly crystalline therefore avoiding the need for tedious chromatographic purification. Diester **12** was then reduced to give the diol **13** where the two hydroxyl groups are in spatially differentiated environments, one being axially and the other equatorially disposed. This efficient four-step protocol was carried out in multigram quantities.

The two hydroxyl protons of the diol **13** were clearly identified in the ^{1}H NMR spectrum. The relative chemical shifts indicate the axial hydroxyl proton to be in a more electronegative environment and this together with ^{1}H NMR studies at varying concentrations revealed the axial hydroxyl group to be involved in an intramolecular hydrogen bond to the backbone methoxy group (Fig. 1).

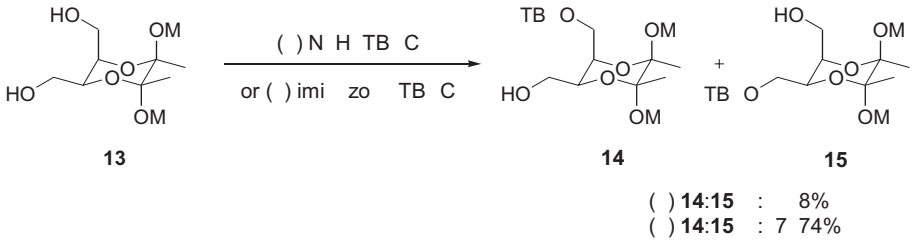
Either hydroxyl group of **13** could be selectively protected as a *tert*-butyl dimethyl silyl ether. The two diastereomeric

© 2001 NRC Canada

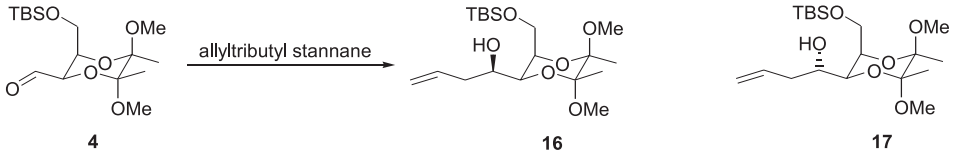
Fig. 1. Effect of concentration on hydroxyl proton chemical shift (■ H^1, ▲ H^2).



Scheme 3.



Scheme 4.



ethers **14** and **15** are readily separable by column chromatography to afford pure materials. Upon treatment of the diol with one equivalent of sodium hydride a mono-alkoxide precipitates, which then reacts with the silylating reagent to give predominantly the axial ether **14** (7:1), whereas treatment of the diol **13** with imidazole and the silyl chloride gave the equatorial ether **15** as the major product (17:1) (Scheme 3).

Thus we can infer that the alkoxide that precipitates upon treatment with sodium hydride is consistent with deprotonation of the hydroxyl group on the axial ring substituent, with this being thermodynamically more stable due to the interactions with the lone pair electrons on the oxygen atom as shown in Fig. 1. The equatorial alcohol is preferentially silylated in the presence of imidazole due to the less sterically hindered nature of this hydroxyl group.

Once the two alcohols had been differentiated, oxidation of the free hydroxyl occurred smoothly using the method of Swern to give the aldehyde **4** (31). The key stereoselective addition of an allyl group to this aldehyde using allyltributylstannane as the nucleophile was then investigated. Following similar conditions for the analogous addition to aldehydes derived from (*R*′,*R*′,*S*,*S*)- and (*S*′,*S*′,*R*,*R*)-2,3-butanediacetal protected butane tetrols (32), aldehyde **4** was dissolved in diethyl ether and lithium perchlorate was added until the solution was saturated (~5 M). Allyltributyl stannane (3 equiv.) was added and the reaction left to stir overnight at room temperature. On work up, two diastereomeric products **16** and **17** were detected in the ratio of 9:1, respectively. Chromatographic purification afforded the diastereomerically pure homoallylic alcohol **16** in 70% yield. However, even after extended reaction times a small amount of aldehyde starting material could still be detected in this reaction.

During the course of investigations to increase the yield as well as the observed selectivity of this addition reaction we observed an interesting result. When zinc chloride was used

© 2001 NRC Canada

Table 1.

Lewis acid	Ratio of **16**:**17**	Reaction yield (%)
$ZnCl_2$	1:9	89
$LiClO_4$	9:1	70[a]
$Yb(OTf)_3$	1.4:1	87
$MgBr_2$	13:5	92

[a]Isolated yield of **16** only.

as the Lewis acid, the reaction proceeded to completion in a shorter time and in improved yield. However, the opposite sense of stereochemical induction was observed giving products **17** and **16** in a ratio of 9:1 (Scheme 4). In an attempt to explain this result the reaction was repeated using other Lewis acids. The use of ytterbium(III) triflate gave essentially a 1:1 ratio of alcohols, whilst magnesium bromide gave a lower ratio than (but with the same major product) the reaction with lithium perchlorate. A straightforward addition of allylmagnesium bromide gave a ratio of 2:1 in favor of the alcohol **16** (Table 1).

Attempts to determine the stereochemistry of the newly formed secondary alcohols by formation of the Mosher esters were not successful due to the hindered nature of these alcohols. However, a single crystal X-ray structure of the diol derived from the major product **16** confirmed that the sense of the asymmetric induction in the lithium perchlorate mediated reaction was consistent with addition occurring through chelation control.[2]

With these compounds available the synthesis of both natural and 6-*epi* aspicilin was investigated (Scheme 5). The preparation of both these diastereoisomers began with protection of the corresponding homoallylic alcohol as the methoxymethyl (MOM) ether. This was possible but required forcing conditions analogous to those used for the protection of tertiary alcohols (33). Thus alcohol **16** was treated with in situ generated methoxymethyliodide and Hünig's base in DME at reflux for 13 h affording the desired MOM protected compound **18** in 72% yield after chromatographic purification. Standard TBS removal and Swern oxidation gave the axially disposed aldehyde **19** in quantitative yield over 2 steps.

The phosphonate **5** required for the olefination reaction was obtained in a two step process (Scheme 6). Firstly, the Grignard reagent was generated in situ from the commercially available 8-bromooct-1-ene (**9**) and reacted with (*S*)-propylene oxide (**8**) in the presence of $CuLi_2Cl_4$ to give the long chain alcohol **20** in good yield. A transesterification of the thioester **7** with long chain alcohol **20** was mediated by silver trifluoroacetate and gave the required phosphonate **5** in 84% yield. To minimize the possibility of epimerization of the axially disposed aldehyde, the Masamune–Roush conditions were chosen for the subsequent olefination reaction (34). Accordingly, aldehyde **19** was treated with phosphonate ester **5**, lithium chloride, and Hünig's base at room temperature for 14 h to give the corresponding olefin as a 10:1 mixture of *E*:*Z* isomers. Chromatographic purification afforded the isomerically pure *E*-isomer **21** in 58% yield as well as the *Z*-isomer in 8% yield (Scheme 5). The axial nature of the side chain could clearly be seen from the size of the coupling constant between H-2 and H-3 (J = 4 Hz).

Macrocyclization of triene **21** was possible using standard ring-closing metathesis (RCM) conditions (35). Thus, a dilute solution of **21** in dichloromethane at room temperature was treated with a catalytic quantity of Grubb's catalyst (10%) for 14 h and afforded the desired material **22** in 73% yield and as a 1.5:1 mixture of *Z*:*E* isomers. The product of RCM across the double bond of the α,β-unsaturated ester, cyclohexene **23**, was also detected in 26% yield (Scheme 5).

Co-elution of the starting material and product meant that early attempts to reduce only the isolated double bond resulted in formation of the fully saturated system due to over-reduction. Partial hydrogenation of the isomeric mixture of alkenes **22**, however, occurred smoothly using palladium on barium sulfate in ethyl acetate under an atmosphere of hydrogen, when the reaction time was limited to 40 min, to give fully protected aspicilin in 100% yield.

The synthesis of protected 6-*epi*-aspicilin was carried out in an analogous manner, the yields at all stages up to this point being comparable to those of the natural system. Global deprotection using the standard conditions for BDA removal, namely treatment with a 90% aqueous solution of trifluoroacetic acid followed by removal of volatiles in vacuo was first attempted on the unnatural diastereoisomer. The reaction proceeded smoothly in this case to give the triol product **24** in 44% yield (Scheme 7).

When these deprotection conditions were applied to the natural diastereoisomer the reaction gave no desired product. However, treatment with ethanedithiol and boron trifluoride etherate afforded (+)-aspicilin **1** in 73% yield. The ^1H and ^{13}C NMR, IR, melting point, MS, and specific rotation ($[\alpha]_D^{26}$ +35.0 (*c* 0.20, $CHCl_3$) (lit. $[\alpha]_D^{26}$ +37.5 (*c* 0.55, $CHCl_3$)) of the synthesized material were in excellent agreement with the reported data and that of an authentic sample.[3]

In summary, a short and efficient stereoselective synthesis of the polyhydroxylated natural product (+)-aspicilin **1** and that of its C-6 epimer **24**, has been achieved using (*R*′,*R*′,*R*,*S*)-2,3-butanediacetal protected butane tetrol **13** as the starting material. The key step relied on the stereoselective allylation of the equatorially disposed aldehyde in **4**. Terminal group manipulation and olefination using phosphonate ester **5** followed by macrocyclization via ring closing metathesis afforded, after partial hydrogenation and global deprotection, the target compounds. Both diastereoisomers of aspicilin have been submitted for full biological evaluation.

Experimental

(–)-(2*R*,3*R*,5*R*,6*R*)-5,6-Dimethoxy-5,6-dimethyl-1,4-dioxane-2,3-dimethyl dicarboxylate (10)

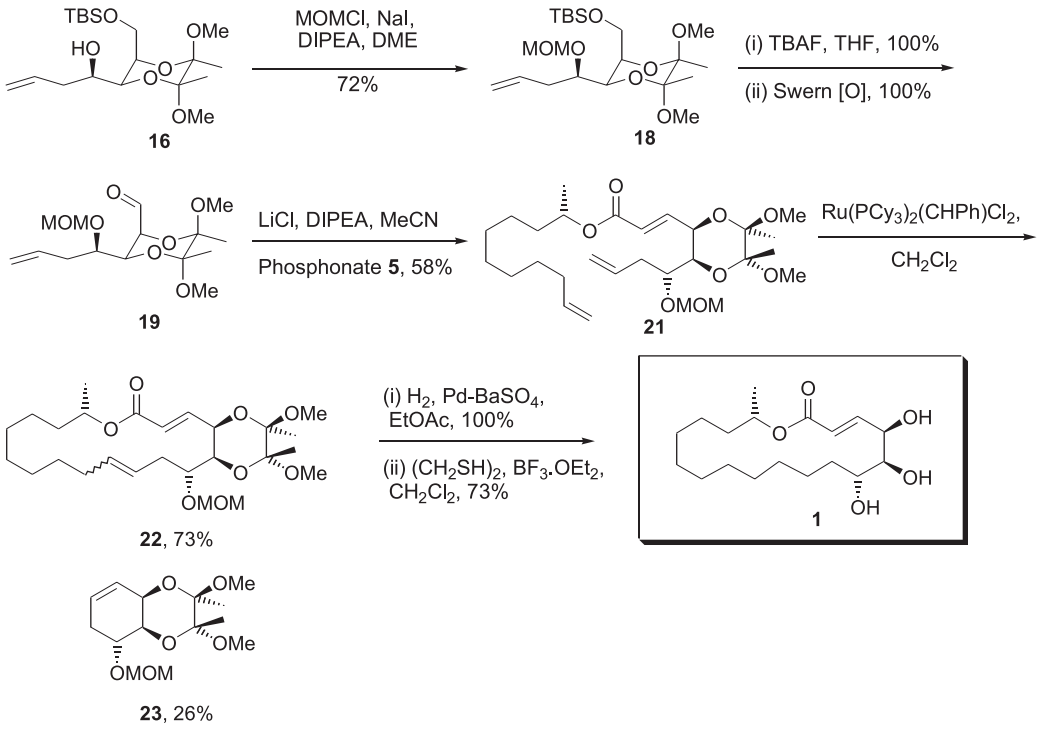
TMOF (123 mL, 1123 mmol), butane-2,3-dione (54 mL, 617 mmol), and CSA (6.52 g, 28 mmol) were added to a solu-

[2] Supplementary material may be purchased from the Depository of Unpublished Data, Document Delivery, CISTI, National Research Council Canada, Ottawa, ON K1A 0S2, Canada. For information on obtaining material electronically go to http://www.nrc.ca/cisti/irm/unpub_e.shtml. Crystallographic information has also been deposited with the Cambridge Crystallographic Data Centre (CCDC No. 159 012). Copies of the data can be obtained, free of charge, on application to the Director, CCDC, 12 Union Road, Cambridge CB2 1EZ, U.K. (fax: 44-1223-336033 or e-mail: deposit@ccdc.cam.ac.uk).

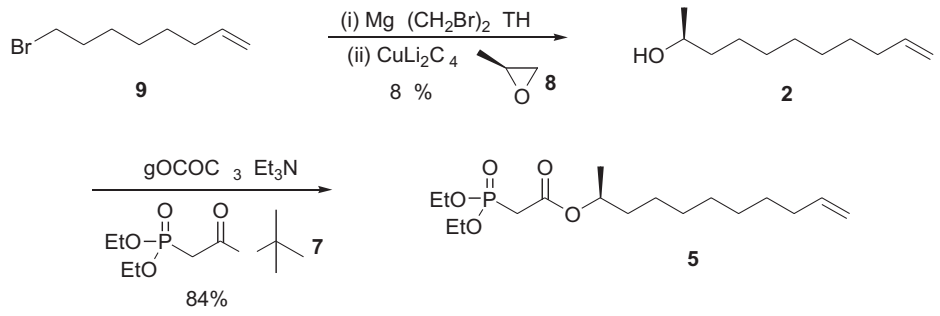
[3] Kindly donated by Professor Hatakeyama.

© 2001 NRC Canada

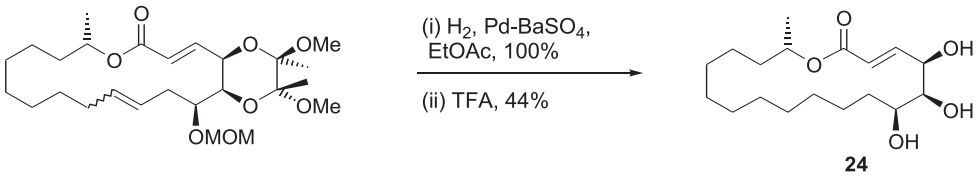
Scheme 5



Scheme 6.



Scheme 7.



tion of dimethyl L-tartrate (100 g, 561 mmol) in MeOH (246 mL) and the reaction was heated to reflux for 7 h. After cooling to room temperature for 1.5 h, $NaHCO_3$ (100 g) was added and the reaction stirred for 2.5 h. The solid was removed by filtration and the filtrate concentrated in vacuo. The residue was taken up in ether (1.6 L) and washed with water (2 × 1.6 L). Each 1.6 L of water was reextracted with ether (0.8 L). The combined organic layers were washed with brine (1.6 L), dried ($MgSO_4$), and concentrated in vacuo. Recrystallization from ether–petrol (650:750 mL) gave white crystals of diester **10** (100.46 g, 61%); mp 109 to 110°C. $[\alpha]_D^{29}$ –148° (*c* 1.00, CH_2Cl_2). R_f = 0.28 (petrol–ether, 1:1). ^{1}H NMR (400 MHz, $CDCl_3$) δ: 4.54 (2H, C*H*CO_2CH_3), 3.77 (s, 6H, CO_2CH_3), 3.33 (s, 6H, OCH_3), 1.36 (s, 6H, CH_3). ^{13}C NMR (100 MHz, $CDCl_3$) δ: 168.4 (*C*O_2CH_3), 99.2 (C-5, C-6), 68.7 (C-2, C-3), 52.5 (CO_2CH_3), 48.4 (OCH_3), 17.3 (CH_3). Anal. calcd. for $C_{12}H_{20}O_8$: C 49.3, H 6.90; found: C 49.3, H 6.87.

(–)-(5*R*,6*R*)-5,6-Dimethoxy-5,6-dimethyl-5,6-dihydro-1,4-dioxin-2,3-dimethyl dicarboxylate (11)

LDA (9.3 mL, 1.0 M in THF) was added via cannula to a stirred solution of diester **10** (1.29 g, 4.43 mmol) in THF

© 2001 NRC Canada

(10 mL) at –78°C. The solution was then stirred at –78°C for 1 h before iodine (1.12 g, 4.43 mmol), as a solution in THF (10 mL), was added via cannula. Saturated aqueous ammonium chloride solution (5 mL) was added to the resultant precipitate and the reaction was warmed to room temperature before being diluted with ether (50 mL) and water (50 mL). The organic layer was separated and the aqueous layer reextracted with ether (10 mL). The combined organic layers were dried ($MgSO_4$) and concentrated in vacuo. The resulting solid was recrystallized from EtOAc–petrol (1:20) to give the diester **11** (732 mg, 57%) as white prisms; mp 83–85°C. $[\alpha]_D^{30}$ –304° (*c* 1.00, $CHCl_3$). R_f = 0.41 (petrol–ether, 1:1). FAB-MS *m*/*z* (%): 291 ($[M + H]^+$, 68), 116 (100) (anal. calcd. (+FAB) for $C_{12}H_{19}O_8$: 291.1080 (MH); found: 291.1081 $[M + H]^+$). ν_{max} (thin film) (cm^{-1}): 1739 (s), 1652 (s). ^{1}H NMR (400 MHz, $CDCl_3$) δ: 3.79 (s, 6H, CO_2CH_3), 3.35 (s, 6H, OCH_3), 1.53 (s, 6H, CH_3). ^{13}C NMR (100 MHz, $CDCl_3$) δ: 167.9 (CO_2CH_3), 130.9 (C-2, C-3), 98.8 (C-5, C-6), 52.5 (CO_2CH_3), 49.4 (OCH_3), 16.7 (CH_3). Anal. calcd. for $C_{12}H_{18}O_8$: C 49.65, H 6.25 found: C 49.67, H 6.28.

(–)-(2*R*,3*S*,5*R*,6*R*)-5,6-Dimethoxy-5,6-dimethyl-1,4-dioxane-2,3-dimethyl dicarboxylate (12)

Rhodium on alumina catalyst (1.00 g, 20 mol%) was added to a solution of unsaturated diester **11** (5.00 g, 17.0 mmol) in MeOH (25 mL). The reaction tube was inserted into a pressure bomb and pressurized with hydrogen to 80 bar (1 bar = 1×10^5 Pa). The reaction was then stirred vigorously for 6 days. After this time the pressure was released and the reaction filtered through celite and washed through with copious MeOH. The solvent was removed in vacuo and the residue was chromatographed (petrol–ether, 1:1) to give diester **12** (4.83 g, 97%) as white prisms; mp 100–102°C. $[\alpha]_D^{30}$ –138° (*c* 1.03, CH_2Cl_2). R_f = 0.26 (petrol–ether, 1:1). FAB-MS *m*/*z* (%): 315 ($[M + Na]^+$, 100), 261 (45), 101 (28) (anal. calcd. (+FAB) for $C_{12}H_{20}O_8Na$: 315.1056 (M + Na); found: 315.1046 ($[M + Na]^+$). ν_{max} (thin film) (cm^{-1}): 2982 (m), 2954 (m), 2901 (m), 2838 (m), 1788 (s), 1741 (s). ^{1}H NMR (400 MHz, $CDCl_3$) δ: 4.69 (d, *J* = 4, 1H, 2-H or 3-H), 4.50 (d, *J* = 4, 1H, 2-H or 3-H), 3.77 (s, 3H, CO_2CH_3), 3.75 (s, 3H, CO_2CH_3), 3.30 (s, 3H, OCH_3), 3.21 (s, 3H, OCH_3), 1.38 (s, 3H, CH_3), 1.33 (s, 3H, CH_3). ^{13}C NMR (100 MHz, $CDCl_3$) δ: 169.7 (CO_2CH_3), 168.8 (CO_2CH_3), 100.5, 99.3 (C-5, C-6), 69.1, 66.1 (C-2, C-3), 52.2 (CO_2CH_3), 52.0 (CO_2CH_3), 50.2 (OCH_3), 48.5 (OCH_3), 17.9 (CH_3), 17.4 (CH_3). Anal. calcd. for $C_{12}H_{20}O_8$: C 49.31, H 6.90; found: C 49.40, H 6.85.

(–)-(2*S*,3*R*,5*R*,6*R*)-2,3-Dimethanol-5,6-dimethoxy-5,6-dimethyl-1,4-dioxane (13)

$LiAlH_4$ (2.05 mL, 1.0 M solution in THF, 2.05 mmol) was added dropwise to a solution of diester **12** (545 mg, 1.86 mmol) in ether (15 mL) at 0°C. Upon completion of the addition the ice bath was removed and the reaction left to warm to room temperature, ca. 30 min. The reaction was then cooled back to 0°C before quenching with EtOAc (1 mL). Sodium sulfate decahydrate (2.0 g) was then added and the reaction stirred at room temperature for 2 h. The solid was filtered off under reduced pressure through a pad of $MgSO_4$ and washed with EtOAc (100 mL). Solvent removal in vacuo left a colorless oil which was chromatographed (ether) to give diol **13** (361 mg, 82%) as a colorless oil which crystallized on standing; mp 69°C. $[\alpha]_D^{29}$ –132° (*c* 1.0, CH_2Cl_2). R_f = 0.17 (ether). FAB-MS *m*/*z* (%): 259 ($[M + Na]^+$, 75), 173 (100) (anal. calcd. (+FAB) for $C_{10}H_{20}O_6Na$: 259.1158 (M + Na); found: 259.1163 ($[M + Na]^+$)). ν_{max} (thin film) (cm^{-1}): 3394 (m), 2950 (m), 2834 (m). ^{1}H NMR (400 MHz, $CDCl_3$) δ: 4.21–4.25 (m, 1H, 2-H), 4.00–4.05 (m, 1H, 1″-H), 3.90–3.92 (m, 1H, OH″), 3.67–3.89 (m, 4H, 3-H, 1′-H), 3.34 (s, 3H, OCH_3), 3.25 (s, 3H, OCH_3), 3.06 (t, *J* = 6, 1H, OH′), 1.33 (s, 3H, CH_3), 1.31 (s, 3H, CH_3). ^{13}C NMR (100 MHz, $CDCl_3$) δ: 99.5, 98.0 (C-5, C-6), 72.7 (C-3), 68.3 (C-2), 63.0 (C–1″), 61.6 (C-1′), 49.2 (OCH_3), 47.9 (OCH_3), 18.2 (CH_3), 17.8 (CH_3). Anal. calcd. for $C_{10}H_{20}O_6$: C 50.84, H 8.53; found: C 50.86, H 8.40.

(–)-(2*S*,3*R*,5*R*,6*R*)-3-*tert*-Butyldimethylsilyloxymethanol-2-methanol-5,6-dimethoxy-5,6-dimethyl-1,4-dioxane (14)

Diol **13** (1.00 g, 4.23 mmol) as a solution in THF (6 + 2 mL washout) was added to a suspension of sodium hydride (186 mg, 60% dispersion in mineral oil, 4.65 mmol) in THF (2 mL). The reaction was then stirred at room temperature for 40 min. TBSCl (638 mg, 4.23 mmol) as a solution in THF (8 mL) was then added to the resultant cream precipitate and the reaction was stirred at room temperature for 2.5 h before being poured into ether (150 mL). Water (150 mL) was added and the layers separated. The aqueous layer was reextracted with ether (100 mL), and the combined organic layers were dried ($MgSO_4$) and concentrated in vacuo. Crude ^{1}H NMR indicated a 6:1 ratio of isomeric products. Purification by flash column chromatography (petrol–ether (2:1) + 1% Et_3N) gave the major isomer of silyl ether separately from some mixed fractions in a combined yield of 98% with the major isomer **14**, a white crystalline solid (1.11 g, 75%); mp 79°C. $[\alpha]_D^{29}$ –119° (*c* 1.05, $CHCl_3$). R_f = 0.63 (petrol–ether, 1:1). EI-MS *m*/*z* (%): 319 ($[M – OMe]^+$, 10), 303 (20), 75 (100) (anal. calcd. (EI) for $C_{15}H_{31}O_5Si$: 319.1941 (M – OMe); found: 319.1939 $[M – OMe]^+$). ν_{max} (thin film) (cm^{-1}): 3491 (br), 2992 (m), 2952 (m), 2930 (m), 2886 (m), 2857 (m), 2833 (m), 1137 (s). ^{1}H NMR (400 MHz, $CDCl_3$) δ: 4.35 (t, *J* = 10, 1H, 1″-H), 4.23–4.28 (m, 1H, 2-H), 3.74 (dt, *J* = 10, 2 Hz, 1H, 3-H), 3.65–3.72 (m, 2H, 1′-H), 3.58 (dd, *J* = 10, 2, 1H, 1″-H), 3.24 (s, 3H, OCH_3), 3.22 (s, 3H, OCH_3), 2.92 (t, *J* = 7, 1H, OH), 1.26 (s, 3H, CH_3), 1.25 (s, 3H, CH_3), 0.88 (s, 9H, $C(CH_3)_3$), 0.082 (s, 3H, $SiCH_3$), 0.081 (s, 3H, $SiCH_3$). ^{13}C NMR (100 MHz, $CDCl_3$) δ: 99.3 (C-6), 98.2 (C-5), 72.8 (C-3), 68.0 (C-2), 62.4 (C-1″), 61.7 (C-1′), 49.3 (OCH_3), 47.9 (OCH_3), 25.8 ($C(CH_3)_3$), 18.1 ($C(CH_3)_3$), 18.1 (CH_3), 17.8 (CH_3), –5.5, –5.6 ($Si(CH_3)_2$). Anal. calcd. for $C_{16}H_{34}O_6Si$: C 54.80, H 9.80; found: C 54.96, H 9.64.

(–)-(2*S*,3*R*,5*R*,6*R*)-2-*tert*-Butyldimethylsilyloxymethanol-3-methanol-5,6-dimethoxy-5,6-dimethyl-1,4-dioxane (15)

Imidazole (22 mg, 0.32 mmol) was added to a stirred solution of diol **13** (50 mg, 0.21 mmol) in THF (1.5 mL) at room temperature and the resulting solution stirred for 5 min. TBSCl (32 mg, 0.21 mmol) was then added as a solid. A white precipitate formed immediately and the reaction was stirred for 90 min. The precipitate was filtered off and washed with ether (10 mL). The organic solution was then washed with water (10 mL), dried ($MgSO_4$), and con-

© 2001 NRC Canada

centrated in vacuo. Crude ^{1}H NMR showed a 17:1 ratio of isomeric silyl ethers **15** and **14**, as well as a small amount of diprotected product which were chromatographed (petrol–ether (2:1) +1% Et_3N) to give separately: colorless oil (54.2 mg, 74%); $[\alpha]_D^{30}$ –74° (*c* 1.35, $CHCl_3$). R_f = 0.42 (petrol–ether, 1:1). EI-MS *m*/*z* (%): 373 ($[M + Na]^+$, 1), 332 (5), 117 (100) (anal. calcd. (EI) for $C_{16}H_{34}O_6SiNa$: 373.2017 (M + Na); found: 373.2028 ($[M + Na]^+$). ν_{max} (thin film) (cm^{-1}): 3480 (br), 2991 (m), 2952 (m), 2930 (m), 2857 (m), 2834 (m), 1132 (s), 1114 (s). ^{1}H NMR (400 MHz, $CDCl_3$) δ: 4.15–4.19 (m, 1H, 3-H), 3.94–3.98 (m, 1H, 1′-H), 3.82–3.86 (m, 3H, 1″-H, 2″-H), 3.71–3.76 (m, 2H, 1′-H, 2-H), 3.34 (s, 3H, OCH_3), 3.25 (s, 3H, OCH_3), 1.32 (s, 3H, CH_3), 1.28 (s, 3H, CH_3), 0.88 (s, 9H, $C(CH_3)_3$), 0.08 (s, 3H, $SiCH_3$), 0.07 (s, 3H, $SiCH_3$). ^{13}C NMR (100 MHz, $CDCl_3$) δ: 99.3 (C-5), 97.9 (C-6), 72.8 (C-2), 68.6 (C-3), 62.8 (C-1′), 62.4 (C-1″), 49.1 (OCH_3), 47.8 (OCH_3), 25.7 ($C(CH_3)_3$), 18.2 (CH_3), 18.1 ($C(CH_3)_3$), 17.8 (CH_3), –5.4, –5.5 ($Si(CH_3)_2$).

(2*S*,3*R*,5*R*,6*R*)-2,3-Di-*tert*-butyldimethylsilyloxymethanol-5,6-dimethoxy-5,6-dimethyl-1,4-dioxane

Colorless oil (4.7 mg, 4.8%). R_f = 0.87 (petrol–ether, 1:1). ESI-MS *m*/*z* (%): 487 ($[M + Na]^+$, 60), 505 (100) (anal. calcd. (ESI) for $C_{22}H_{48}O_6Si_2Na$: 487.2879 (M + Na); found: 487.2887 ($[M + Na]^+$)). ν_{max} (thin film) (cm^{-1}): 2953 (m), 2920 (m), 2857 (m), 1112 (s), 1085 (s). ^{1}H NMR (400 MHz, $CDCl_3$) δ: 4.13–4.20 (m, 2H), 3.70–3.75 (m, 1H,), 3.58–3.65 (m, 3H), 3.29 (s, 3H, OCH_3), 3.24 (s, 3H, OCH_3), 1.28 (s, 3H, CH_3), 1.26 (s, 3H, CH_3), 0.89 (s, 9H, $C(CH_3)_3$), 0.88 (s, 9H, $C(CH_3)_3$), 0.06 (s, 3H, $SiCH_3$), 0.05 (s, 3H, $SiCH_3$), 0.04 (s, 3H, $SiCH_3$), 0.04 (s, 3H, $SiCH_3$). ^{13}C NMR (100 MHz, $CDCl_3$) δ: 99.4, 98.2 (C-5, C-6), 73.1, 70.6 (C-2, C-3), 62.8, 61.9 (C-1′, C-1″), 49.2 (OCH_3), 47.6 (OCH_3), 25.9, 25.8 ($C(CH_3)_3$), 18.3 ($C(CH_3)_3$), 18.2 (CH_3), 18.0 ($C(CH_3)_3$), 17.9 (CH_3), –5.2, –5.4 ($Si(CH_3)_2$).

(–)-(2*R*,3*R*,5*R*,6*R*)-3-*tert*-Butyldimethylsilyloxymethanol-5,6-dimethoxy-5,6-dimethyl-1,4-dioxane-2-carbaldehyde (4)

DMSO (526 μL, 7.42 mmol), as a solution in CH_2Cl_2 (10 mL), was added to a solution of oxalyl chloride (324 μL, 3.71 mmol) in CH_2Cl_2 (10 mL) at –78°C. The reaction was stirred at –78°C for 30 min before alcohol **14** (1.0 g, 2.85 mmol) was added dropwise as a solution in CH_2Cl_2 (20 + 5 mL washout) over 30 min. The reaction was then left stirring at –78°C for 1.5 h before Et_3N (1.4 mL, 9.98 mmol) was added over 15 min. The reaction was then removed from the cooling bath and allowed to warm to room temperature over 1 h. The reaction was then diluted with CH_2Cl_2 (100 mL) and washed with water (2 × 80 mL). The organic layer was dried ($MgSO_4$) and concentrated in vacuo. Purification by flash column chromatography (petrol–ether (1:1) + 1% Et_3N) gave aldehyde **4** as an oily liquid, which solidified on standing to a white crystalline solid (1.00 g, 100%); mp 50°C. $[\alpha]_D^{28}$ –122° (*c* 1.08, $CHCl_3$). R_f = 0.69 (petrol–ether, 1:1). EI-MS *m*/*z* (%): 317 ($[M – OMe]^+$, 10), 291 (30), 259 (50), 245 (50), 101 (100) (anal. calcd. for $C_{15}H_{29}O_5Si$: 317.1784 (M – OMe); found: 317.1788 ($[M – OMe]^+$)). ν_{max} (thin film) (cm^{-1}): 2952 (m), 2359 (m), 2340 (m), 1738 (s). ^{1}H NMR (400 MHz, $CDCl_3$) δ: 9.49 (s, 1H, CHO), 4.49 (d, *J* = 4, 1H, 2-H), 4.30 (ap t, *J* = 10, 1H, 1″-H_A), 4.09 (dt, *J* = 10, 4, 1H, 3-H), 3.62 (dd, *J* = 10, 4, 1H, 1″-H_B), 3.24 (s, 3H, OCH_3), 3.18 (s, 3H, OCH_3), 1.35 (s, 3H, CH_3), 1.26 (s, 3H, CH_3), 0.84 (s, 9H, $C(CH_3)_3$), 0.01 (s, 3H, $SiCH_3$), 0.096 (s, 3H, $SiCH_3$). ^{13}C NMR (100 MHz, $CDCl_3$) δ: 195.8 (C=O), 100.4, 98.6 (C-5, C-6), 74.4 (C-3), 72.0 (C-2), 61.1 (C-1″), 48.6 (OCH_3), 48.2 (OCH_3), 25.7 ($C(CH_3)_3$), 18.4 (CH_3), 18.2 ($C(CH_3)_3$), 17.9 (CH_3), –5.6, –5.6 ($Si(CH_3)_2$). Anal. calcd. for $C_{16}H_{32}O_6Si$: C 55.14, H 9.25; found: C 55.33, H 9.19.

(–)-(2*R*,1′*R*,3*R*,5*R*,6*R*)-3-*tert*-Butyldimethylsilyloxymethanol-2-(1′-hydroxy-but-3′-ene-1′-yl)-5,6-dimethoxy-5,6-dimethyl-1,4-dioxane (16) and (–)-(2*R*,1′*S*,3*R*,5*R*,6*R*)-3-*tert*-butyldimethylsilyloxymethanol-2-(1′-hydroxy-but-3′-ene-1′-yl)-5,6-dimethoxy-5,6-dimethyl-1,4-dioxane (17)

Method 1: zinc(II) chloride mediated allyl addition

$ZnCl_2$ solution (15.5 mL, 0.5 M in THF, 7.75 mmol) was added to a solution of aldehyde **4** (900 mg, 2.58 mmol) in ether (8 mL) at 0°C. The reaction was stirred at 0°C for 20 min before allyltributylstannane (2.4 mL, 7.75 mmol) was added neat. The resulting solution was warmed to room temperature and left stirring overnight. The reaction was diluted with ether (50 mL) and washed with water (2 × 50 mL). The aqueous layer was reextracted with ether (40 mL) and the combined organic layers were washed with brine (40 mL), dried ($MgSO_4$), and concentrated in vacuo. Crude ^{1}H NMR indicated a 9:1 ratio of homoallylic alcohols, which were separated by flash column chromatography (petrol–ether (5:1) + 1% Et_3N) to give **17** (802 mg, 80%) and **16** (96 mg, 9%).

Method 2: ytterbium(III) triflate mediated allyl addition

Ytterbium(III) triflate (534 mg, 0.86 mmol) was added to a solution of aldehyde **4** (100 mg, 0.29 mmol) in ether (2 mL) at 0°C and the reaction stirred for 15 min. Neat allyltributylstannane (267 μL, 0.86 mmol) was then added, the cooling bath removed, and the reaction stirred at room temperature for 14 h. Ether (50 mL) and water (50 mL) were added, the layers separated, and the organic layer dried. After concentration in vacuo the residue (crude ratio of products by ^{1}H NMR 1.4:1) was chromatographed (petrol–ether (4:1) + 1% Et_3N) to give homoallylic alcohols **16** (57 mg, 50%) and **17** (42 mg, 37%).

Method 3: lithium perchlorate mediated allyl addition

Aldehyde **4** (2.0 g, 5.74 mmol) was added to a solution of lithium perchlorate in ether (30 mL, 5 M) and the reaction stirred at 0°C for 15 min. The allyltributylstannane was then added and the reaction warmed to room temperature and stirred for 14 h. Ether (250 mL) and water (250 mL) were added, the layers separated, and the organic layer dried ($MgSO_4$) and concentrated in vacuo. The residue (crude ratio of products by ^{1}H NMR 1:9) was chromatographed (petrol:ether (4:1) + 1% Et_3N) to give the major homoallylic alcohol **16** as a colorless oil (1.56 g, 70%). The minor product co-eluted with some unreacted starting aldehyde.

Method 4: magnesium(II) bromide mediated allyl addition

Magnesium(II) bromide (225 mg, 0.86 mmol) was added to a solution of aldehyde **4** (100 mg, 0.29 mmol) in ether

© 2001 NRC Canada

(2 mL) at 0°C and the reaction stirred for 15 min. The allyltributylstannane (267 μL, 0.86 mmol) was then added, the cooling bath removed, and the reaction stirred at room temperature for 14 h. Ether (50 mL) and water (50 mL) were added, the layers separated, and the organic layer dried ($MgSO_4$). After concentration in vacuo the residue (crude ratio of products by ^1H NMR, 5:13) was chromatographed (petrol–ether (4:1) + 1% Et_3N) to give homoallylic alcohols **17** (23 mg, 20%) and **16** (81 mg, 72%).

Method 5: allyl MgBr addition

Allyl MgBr solution (1.0 M THF, 0.72 mmol, 720 μL) was added to a solution of aldehyde **4** (50 mg, 0.14 mmol) in THF (1 mL) at –78°C and the reaction stirred at –78°C for 6 h. The reaction was then quenched with water and warmed to room temperature. The reaction was diluted with ether and washed with water before the organic layer was dried ($MgSO_4$) and concentrated in vacuo. The crude ^1H NMR showed a 1:2 ratio of **17** to **16**. Purification of the residue by flash column chromatogaphy gave pure homoallylic alcohols (100%).

*(–)-(2*R*,1′*S*,3*R*,5*R*,6*R*)-3-*tert*-Butyldimethylsilyloxymethanol-2-(1′-hydroxy-but-3′-ene-1′-yl)-5,6-dimethoxy-5,6-dimethyl-1,4-dioxane (**17**)*

$[\alpha]_D^{29}$ –126° (*c* 1.23, $CHCl_3$). R_f = 0.49 (petrol–ether, 3:1). ESI-MS *m*/*z* (%): 413 ([M + Na]$^+$, 100), 217 (10) (anal. calcd. (+ESI) for $C_{19}H_{38}O_6SiNa$: 413.2335 (M + Na); found: 413.2361 ([M + Na]$^+$)). ν_{max} (thin film) (cm^{-1}): 3490 (br), 3075 (m), 2953 (m), 2931 (m), 2901 (m), 2858 (m), 2831 (m), 1139 (s), 1115 (s), 1058 (s). ^1H NMR (400 MHz, $CDCl_3$) δ: 5.91–6.01 (m, 1H, 3′-H), 5.13 (d, *J* = 17, 1H, 4′-H_A), 5.07 (d, *J* = 10, 1H, 4′-H_B), 4.43 (ap t, *J* = 10, 1H, C*H*HOTBS), 3.91–3.96 (m, 2H, 2-H, 3-H), 3.70–3.76 (m, 2H, 1′-H, OH), 3.62 (d, *J* = 10, 1H, CH*H*OTBS), 3.25 (s, 3H, OCH_3), 3.24 (s, 3H, OCH_3), 2.59–2.64 (m, 1H, 2′-H_A), 2.16–2.25 (m, 1H, 2′-H_B), 1.27 (s, 3H, CH_3), 1.26 (s, 3H, CH_3), 0.91 (s, 9H, $C(CH_3)_3$), 0.12 (s, 6H, $Si(CH_3)_2$). ^{13}C NMR (100 MHz, $CDCl_3$) δ: 135.3 (C-3′), 116.5 (C-4′), 99.4, 97.94 (C-5, C-6), 72.7 (C-3), 70.5 (C-2), 69.4 (C-1′), 62.9 (*C*H_2OTBS), 49.4 (OCH_3), 48.1 (OCH_3), 37.1 (C-2′), 25.8 ($C(CH_3)_3$), 18.2 ($C(CH_3)_3$), 18.0 (CH_3), 17.9 (CH_3), –5.6 ($Si(CH_3)_2$). Anal. calcd. for $C_{19}H_{38}O_6Si$: C 58.43, H 9.81; found: C 58.61, H 9.89.

*(–)-(2*R*,1′*R*,3*R*,5*R*,6*R*)-3-*tert*-Butyldimethylsilyloxymethanol-2-(1′-hydroxy-but-3′-ene)-5,6-dimethoxy-5,6-dimethyl-1,4-dioxane (**16**)*

$[\alpha]_D^{29}$ –88° (*c* 0.20, $CHCl_3$). R_f = 0.33 (petrol–ether, 3:1). FAB-MS *m*/*z* (%): 413 ([M + Na]$^+$, 10), 327 (40), 101 (100) (anal. calcd. (+FAB) for $C_{19}H_{38}O_6SiNa$: 413.2336 (M + Na); found: 413.2333 ([M + Na]$^+$). ν_{max} (thin film) (cm^{-1}): 3374 (br), 2929 (m), 1113 (s). ^1H NMR (400 MHz, $CDCl_3$) δ: 5.85–5.95 (m, 1H, 3′-H), 5.06–5.13 (m, 2H, 4′-H), 4.31–4.37 (m, 1H, C*H*HOTBS), 3.98–4.01 (m, 1H, 3-H), 3.80–3.85 (m, 1H, 1′-H), 3.65–3.72 (m, 3H, 2-H, CH*H*OTBS, OH), 3.27 (s, 3H, OCH_3), 3.24 (s, 3H, OCH_3), 2.41–2.47 (m, 1H, 2′-H_A), 2.25–2.35 (m, 1H, 2′-H_B), 1.31 (s, 3H, CH_3), 1.26 (s, 3H, CH_3), 0.89 (s, 9H, $C(CH_3)_3$), 0.08 (s, 6H, $Si(CH_3)_2$). ^{13}C NMR (100 MHz, $CDCl_3$) δ: 134.9 (C-3′), 116.9 (C-4′), 100.1, 98.3 (C-5, C-6), 73.5 (C-2), 71.0 (C-3), 68.9 (C-1′), 62.4 (*C*H_2OTBS), 49.3 (OCH_3), 48.0 (OCH_3), 37.0 (C-2′), 25.9 ($C(CH_3)_3$), 18.2 ($C(CH_3)_3$), 18.2 (CH_3), 17.9 (CH_3), –5.37 ($SiCH_3$), –5.43 ($SiCH_3$). Anal. calcd. for $C_{19}H_{38}O_6Si$: C 58.43, H 9.81; found: C 58.90, H 9.78.

(–)-(2*R*,1′*S*,3*R*,5*R*,6*R*)-3-*tert*-Butyldimethylsilyloxymethanol-5,6-dimethoxy-2-(1′-methoxymethylhydroxy-but-3′-ene-1′-yl)-5,6-dimethyl-1,4-dioxane

MOMCl (0.74 mL, 9.79 mmol) was added to a solution of sodium iodide (1.15 g, 7.68 mmol) in DME (15 mL). The reaction was left to stir at room temperature for 1 h before alcohol **17** (750 mg, 1.92 mmol) and DIPEA (1.84 mL, 10.56 mmol) were added as a solution in DME (15 mL). The reaction was then stirred for 1 h at room temperature, warmed to 65°C for 1 h, and then heated to reflux for a further 17 h before finally cooling to room temperature. Saturated sodium carbonate solution (10 mL) was added followed by CH_2Cl_2 (100 mL) then water (50 mL). After separation of the layers, the organic layer was washed again with water (50 mL). The aqueous layer was reextracted with CH_2Cl_2 (50 mL), then the combined organic layers washed with brine (50 mL), dried ($MgSO_4$), and concentrated in vacuo. Purification by flash column chromatography (petrol–ether (5:1) + 1% Et_3N) gave MOM ether as a colorless oil (714.6 mg, 86%). $[\alpha]_D^{28}$ –100° (*c* 0.72, $CHCl_3$). R_f = 0.51 (petrol–ether, 3:1). FAB-MS *m*/*z* (%): 457 ([M + Na]$^+$, 5), 403 (10), 327 (10), 101 (100) (anal. calcd. (+FAB) for $C_{21}H_{42}O_7SiNa$: 457.2598 (M + Na); found: 457.2598 ([M + Na]$^+$)). ν_{max} (thin film) (cm^{-1}): 2955 (m), 2929 (m), 2895 (m), 2856 (m), 2832 (m), 1139 (s), 1109 (s), 1042 (s). ^1H NMR (400 MHz, $CDCl_3$) δ: 5.86–5.96 (m, 1H, 3′-H), 5.12 (d, *J* = 17, 1H, 4′-H_A), 5.06 (d, *J* = 10, 1H, 4′-H_B), 4.73 (d, *J* = 7, 1H, OC*H*HOCH$_3$), 4.60 (d, *J* = 7, 1H, OCH*H*OCH$_3$), 4.17 (dd, *J* = 6, 11, 1H, C*H*HOTBS), 3.94 (dd, *J* = 6, 11, 1H, CH*H*OTBS), 3.74–3.80 (m, 2H, 1′-H, 3-H), 3.36 (s, 3H, OCH_2OCH_3), 3.31 (s, 3H, OCH_3), 3.24 (s, 3H, OCH_3), 2.39–2.56 (m, 2H, 2′-H), 1.27 (s, 3H, CH_3), 1.26 (s, 3H, CH_3), 0.90 (s, 9H, $C(CH_3)_3$), 0.063 (s, 6H, $Si(CH_3)_2$). ^{13}C NMR (100 MHz, $CDCl_3$) δ: 135.1 (C-3′), 116.9 (C-4′), 100.2, 98.41 (C-5, C-6), 96.7 (O*C*H_2OCH$_3$), 76.6 (C-1′), 73.9, 69.3 (C-2, C-3), 62.2 (*C*H_2OTBS), 55.9 (OCH_2OCH_3), 49.5 (OCH_3), 48.1 (OCH_3), 35.6 (C-2′), 26.0 ($C(CH_3)_3$), 18.5 (CH_3), 18.4 ($C(CH_3)_3$), 17.9 (CH_3), –5.2 ($SiCH_3$), –5.3 ($SiCH_3$). Anal. calcd. for $C_{21}H_{42}O_7Si$: C 58.03, H 9.74; found: C 58.25, H 9.73.

(–)-(1′*S*,2*R*,3*R*,5*R*,6*R*)-3-Methanol-5,6-dimethoxy-2-(1′-methoxymethylhydroxy-but-3′-ene-1′-yl)-5,6-dimethyl-1,4-dioxane

TBAF (4.29 mL, 1.0 M solution in THF, 4.29 mmol) was added to a solution of TBS ether (622 mg, 1.43 mmol) in THF (20 mL) at room temperature. The reaction was then stirred at room temperature overnight. After concentration in vacuo the residue was taken up in ether (50 mL) and washed with water (2 × 50 mL). The aqueous layer was reextracted with ether (40 mL) and the combined organic layers were dried ($MgSO_4$) and concentrated in vacuo. Purification by flash column chromatography (ether–petrol (4:1) + 1% Et_3N) gave the alcohol as a colorless oil (458 mg, 100%). $[\alpha]_D^{28}$ –104° (*c* 1.08, $CHCl_3$). R_f = 0.45 (ether). FAB-MS *m*/*z* (%): 434 ([M + Na]$^+$, 25), 257 (60), 101 (100) (anal. calcd.

© 2001 NRC Canada

(+FAB) for $C_{15}H_{28}O_7Na$: 343.17328 (M + Na); found: 434.17259 ($[M + Na]^+$)). ν_{max} (CH_2Cl_2 solution) (cm^{-1}): 3444 (br), 1694 (m), 1644 (m), 1615 (m), 1137 (m), 1111 (m), 1036 (m). ^1H NMR (400 MHz, $CDCl_3$) δ: 5.83–5.93 (m, 1H, 3′-H), 5.07–5.16 (m, 2H, 4′-H_AH_B), 4.74 (ABq, J = 7, 28, 2H, OCH_2OCH_3), 4.02–4.13 (m, 3H, 2-H or 3-H, 1′-H, C*H*HOH), 3.85–3.87 (m, 3H, 2-H or 3-H, OH, C*H*HOH), 3.37 (s, 3H, OCH_2OCH_3), 3.34 (s, 3H, OCH_3), 3.23 (s, 3H, OCH_3), 2.55–2.62 (m, 1H, 2′-H_A), 2.37–2.44 (m, 1H, 2′-H_B), 1.31 (s, 3H, CH_3), 1.27 (s, 3H, CH_3). ^{13}C NMR (100 MHz, $CDCl_3$) δ: 134.2 (C-3′), 117.7 (C-4′), 100.0, 98.0 (C-5, C-6), 96.7 (OCH_2OCH_3), 77.2 (C-1′), 72.7, 69.0 (C-2, C-3), 62.7 (CH_2OH), 56.1 (OCH_2OCH_3), 49.2 (OCH_3), 48.2 (OCH_3), 30.3 (C-2′), 18.3 (CH_3), 17 9 (CH_3). Anal. calcd. for $C_{15}H_{28}O_7$: C 56.23, H 8.81; found: C 55.95, H 8.80.

(2*R*,1′*S*,3*R*,5*R*,6*R*)-5,6-Dimethoxy-2-(1′-methoxymethylhydroxy-but-3′-ene-1′-yl)-5,6-dimethyl-1,4-dioxane-3-carbaldehyde

DMSO (30 μL, 0.42 mmol) as a solution in CH_2Cl_2 (1 mL) was added to a solution of oxalyl chloride (18 μL, 0.20 mmol) in CH_2Cl_2 (1 mL) at –78°C. The reaction was stirred at –78°C for 30 min before alcohol (50 mg, 0.16 mmol) was added dropwise as a solution in CH_2Cl_2 (1 + 0.5 mL washout) over 30 min. The reaction was then left stirring at –78°C for 1.5 h before Et_3N (78 μL, 0.56 mmol) was added over 15 min. The reaction was then removed from the cooling bath and allowed to warm to room temperature over 1 h. The reaction was diluted with CH_2Cl_2 (10 mL) and washed with water (2 × 8 mL). The organic layer was dried ($MgSO_4$) and concentrated in vacuo. R_f = 0.42 (petrol–ether, 1:1). Used crude.

(+)-(*S*)-10-Hydroxy-undec-1-ene (20)

Three drops of 1,2-dibromoethane were added to a stirred suspension of magnesium turnings (837 mg, 34.4 mmol) in THF (10 mL) at room temperature. A solution of 8-bromo-oct-1-ene (**9**) (4.13 mL, 24.6 mmol) in THF (16 mL) was then added as the solution was warmed to 30°C. The reaction was heated to reflux for 6 h, cooled to room temperature, and THF (20 mL) was added. $CuLi_2Cl_4$ (17.2 mL, 0.1 M in THF, 1.72 mmol) was added to (*S*)-propylene oxide **8** (1.0 g, 17.2 mmol) in THF (20 mL) at –78°C. The Grignard solution was further cooled to –78°C, added to the cooled propylene oxide solution, and the reaction stirred for 1 h at –78°C before warming to 0°C over 1 h. The reaction was quenched by addition of saturated aqueous ammonium chloride solution (200 mL) and then EtOAc (200 mL) was added. The layers were separated and the aqueous phase reextracted with EtOAc (150 mL). The combined organic layers were dried ($MgSO_4$) and concentrated in vacuo. The crude product was chromatographed (petrol–EtOAc, 5:1) to give alcohol **20** as a pale yellow liquid (2.53 g, 86%). $[\alpha]_D^{28}$ +6.9° (*c* 1.14, $CHCl_3$). R_f = 0.3 (petrol–EtOAc, 5:1). EI-MS *m*/*z* (%): 170 (M^+, 25), 152 (40), 137 (20), 124 (60), 45 (100) (anal. calcd. for $C_{11}H_{22}O$: 170.1671 (M); found: 170.1670). ν_{max} (CH_2Cl_2 solution) (cm^{-1}): 3073 (s), 2979 (s), 2830 (s), 2856 (s), 1639 (w). ^1H NMR (400 MHz, $CDCl_3$) δ: 5.66–5.77 (m, 1H, 2-H), 4.90 (dd, J = 1, 17, 1H, 1-H_A), 4.83 (dd, J = 1, 10, 1H, 1-H_B), 3.64–3.70 (m, 1H, 10-H), 2.28 (br s, 1H, OH), 1.93–1.98 (m, 2H, 3-H), 1.11–1.42 (m, 12H, $(CH_2)_6$), 1.09 (d, J = 6, 3H, H-11). ^{13}C NMR (100 MHz, $CDCl_3$) δ: 139.0 (C-2), 114.0 (C-1), 67.8 (C-10), 39.2, 33.7, 29.5, 29.4, 29.0, 28.8, 25.7 (C-3–C-9), 23.3 (C-11). Anal. calcd. for $C_{11}H_{22}O$: C 77.59, H 13.02; found: C 77.33, H 13.03.

(+)-(*S*)-10-(Diethylphosphonoacetoxy)-undec-1-ene (5)

Silver trifluoroacetic acid salt (178 mg, 0.80 mmol) was added to a solution of thioester **6** (183 mg, 0.68 mmol), alcohol **20** (126 mg, 0.74 mmol), and Et_3N in THF (2 mL). The reaction was stirred at room temperature for 1 h before the solvent was removed in vacuo. Purification by flash column chromatography (ether) afforded ester **5** as a pale yellow liquid (198 mg, 84%). $[\alpha]_D^{28}$ +2.7° (*c* 1.15, $CHCl_3$). R_f = 0.28 (ether). EI-MS *m*/*z* (%): 371 ($[M + Na]^+$, 100), 349 (30), 305 (10) (anal. calcd. for $C_{17}H_{33}O_5P$: 371.1970 (M + Na); found: 371.1963). ν_{max} (CH_2Cl_2 solution) (cm^{-1}): 3077 (w), 2982 (s), 2931 (s), 2857 (s), 1727 (s), 1281 (s). ^1H NMR (400 MHz, $CDCl_3$) δ: 5.75–5.85 (m, 1H, 2-H), 4.89–5.00 (m, 3H, 1-H_AH_B, 10-H), 4.13–4.20 (m, 4H, OCH_2CH_3 × 2), 2.93 (d, J = 22, 2H, 14-H_AH_B), 2.00–2.05 (m, 2H, 3-H_AH_B), 1.18–1.80 (m, 18H, -$(CH_2)_6$-, OCH_2CH_3 × 2), 1.23 (d, J = 6, 3H, 11-H). ^{13}C NMR (100 MHz, $CDCl_3$) δ: 165.4 (C-13, J = 6), 139.1 (C-2), 114.1 (C-1), 72.6 (C-10), 62.6 (OCH_2CH_3), 62.5 (OCH_2CH_3), 35.8 (CH_2), 34.6 (C-14, J = 134), 29.3, 29.3, 29.0, 28.9, 25.2 (CH_2), 19.8 (C-11), 16.3 (OCH_2CH_3), 16.3 (OCH_2CH_3).

(–)-(*E*)-(2*S*,3*R*,5*R*,6*R*,1′*S*,5″*S*)-5,6-Dimethoxy-2-(1′-methoxymethylhydroxy-but-3′-ene)-5,6-dimethyl-3-(5″-methyltetradec-1″,13″-diene-1″-yl-3″-one)-1,4-dioxane

Aldehyde (0.16 mmol) and DIPEA (28 μL, 0.16 mmol) as a solution in MeCN (1 mL) were added to a stirred suspension of LiCl (8.1 mg, 0.19 mmol) in MeCN (0.5 mL) at room temperature. The phosphonate **5** (61.3 mg, 0.18 mmol), was then added as a solution in MeCN (0.5 mL) and the reaction stirred at room temperature for 24 h. The reaction mixture was diluted with ether (20 mL) and water (20 mL) and the layers separated. The organic phase was washed again with water (15 mL), the aqueous layers reextracted with ether (20 mL), and the combined organic layers dried ($MgSO_4$) and concentrated in vacuo. Purification by flash column chromatography (petrol–ether (2:1) + 1% Et_3N) gave α,β-unsaturated ester as a colorless oil (58.4 mg, 71%). $[\alpha]_D^{29}$ –57° (*c* 0.41, $CHCl_3$). R_f = 0.66 (petrol–ether, 1:1). ν_{max} (CH_2Cl_2 solution) (cm^{-1}): 3890 (w), 3605 (w), 3078 (w), 2931 (m), 2856 (m), 1710 (s), 1143 (s), 1108 (s), 1041 (s). ^1H NMR (400 MHz, $CDCl_3$) δ: 7.46 (dd, J = 10, 16, 1H, 1″-H), 5.75–5.97 (m, 2H, 13″-H, 3′-H), 5.96 (d, J = 16, 1H, 2″-H), 4.91–5.15 (m, 5H, 4′-H, 14″-H, 5″-H), 4.50–4.57 (m, 2H, OCH_2OCH_3), 4.25 (dd, J = 4, 10, 1H, 3-H), 4.15 (dd, J = 4, 9, 1H, 2-H), 3.50–3.55 (m, 1H, 1′-H), 3.31 (s, 3H, OCH_2OCH_3), 3.27 (s, 3H, OCH_3), 3.11 (s, 3H, OCH_3), 2.54–2.62 (m, 1H, 2′-H_A), 2.38–2.45 (m, 1H, 2′-H_B), 2.01–2.06 (m, 2H, 12″-H), 1.21–1.60 (m, 21H, 3 × Me, -$(CH_2)_6$-). ^{13}C NMR (100 MHz, $CDCl_3$) δ: 165.9 (C-3″), 144.2 (C-1′′), 139.1 (C-13″), 134.0 (C-3′), 125.6 (C-2″), 117.5 (C-4′), 114.1 (C-14″), 100.0, 98.4 (C-5, C-6), 96.7 (OCH_2OCH_3), 76.7 (C-1′), 72.2, 71.1 (C-2, C-3), 68.6 (C-5″), 56.1 (OCH_2OCH_3), 48.4 (OCH_3), 48.4 (OCH_3), 36.0, 35.1, 33.7, 29.38, 29.36, 29.0 (C-6″–C-11″), 20.0, 18.2, 17.8

© 2001 NRC Canada

(CH_3 × 3). Anal. calcd. for $C_{28}H_{48}O_8$: C 65.60, H 9.44; found: C 65.43, H 9.39.

(4*E*/*Z*,16*E*)-(1*S*,2*S*,13*S*,18*R*,19a*R*,19b*R*)-19a,19b-Dimethoxy-2-methoxymethylhydroxy-13,19a,19b-trimethyl-14,19,20-trioxa-bicyclo[16.4.0]doicosa-4,16-diene-15-one

Grubb's catalyst (18.4 mg, 0.02 mmol) was added to a stirred solution of triene (107 mg, 0.21 mmol) in CH_2Cl_2 (140 mL). The reaction was stirred at room temperature overnight and concentrated in vacuo. Purification by flash column chromatography (petrol–ether, 4:1) afforded cyclic lactone, a 6:4 inseparable mixture of double bond isomers, as a colorless oil (48 mg, 45%). R_f = 0.66 (petrol–ether, 1:1). ν_{max} (CH_2Cl_2 solution) (cm^{-1}): 2931 (s), 2864 (s), 1712 (s), 1655 (w), 1602 (w), 1377 (m), 1254 (s), 1215 (m), 1183 (m), 1142 (s), 1107 (s), 1038 (s). ^{1}H NMR (400 MHz, $CDCl_3$) δ: 7.48–7.58 (m, $1H_A$ + $1H_B$, 17-H), 6.02 (d, J = 16, $1H_A$, 16-H), 5.97 (d, J = 16, $1H_B$, 16-H), 5.41–5.56 (m, $1H_A$ + $1H_B$, 4-H or 5-H), 5.33–5.40 (m, $1H_A$ + $1H_B$, 4-H or 5-H), 5.14–5.22 (m, $1H_A$ + $1H_B$, 2-H), 4.52–4.65 (m, $2H_A$ + $2H_B$, C*H*$_2$OCH$_3$), 4.32 (dd, $1H_A$, J = 4, 11, 1-H or 18-H), 4.26 (dd, J = 4, 11, $1H_B$, 1-H or 18-H), 4.03–4.08 (m, $1H_A$ + $1H_B$, 1-H or 18-H), 3.37 (s, $3H_A$, CH$_2$OC*H*$_3$), 3.36 (s, $3H_B$, CH$_2$OC*H*$_3$), 3.28 (s, $3H_B$, OCH_3), 3.26 (s, $3H_A$, OCH_3), 3.20 (s, $3H_A$, OCH_3), 3.17 (s, $3H_B$, OCH_3), 2.39–2.53 (m, $1H_A$ + $1H_B$, 3-H), 2.04–2.27 (m, $2H_A$ + $2H_B$, 3-H), 1.85–1.94 (m, $1H_A$ + $1H_B$), 1.39–1.54 (m, $2H_A$ + $2H_B$), 1.15–1.33 (m, $21H_A$ + $21H_B$, 3 × CH_3 and 6 × CH_2).

(16*E*)-(1*S*,2*S*,13*S*,18*R*,19a*R*,19b*R*)-19a,19b-Dimethoxy-2-methoxymethylhydroxy-13,19a,19b-trimethyl-14,19,20-trioxa-bicyclo[16.4.0]doicosa-16-ene-15-one

Pd-$BaSO_4$ (0.5 mg) was added to a solution of diene (5 mg, mmol) in EtOAc (0.5 mL). The reaction was stirred under an atmosphere of hydrogen for 40 min, the catalyst was removed by filtration and the solvent removed in vacuo to leave crude product (5 mg, 100%). $[\alpha]_D^{29}$ –85.6° (*c* 0.45, $CHCl_3$). R_f = 0.66 (petrol–ether, 1:1). EI-MS *m*/*z* (%): 455 ($[M - OMe]^+$, 5), 419 (5), 379 (20), 338 (30), 276 (30), 247 (40), 116 (100). (anal. calcd. (EI) for $C_{24}H_{43}O_7$: 455.3009 (M – OMe); found: 455.2997 ($[M - OMe]^+$). ν_{max} (CH_2Cl_2 solution) (cm^{-1}): 3692 (w), 3605 (w), 2927 (s), 2930 (s), 2857 (s), 1712 (s), 1653 (w), 1607 (w), 1459 (m), 1376 (m), 1264 (s), 1253 (s), 1142 (s), 1109 (s), 1035 (s). ^{1}H NMR (400 MHz, $CDCl_3$) δ: 7.55 (dd, J = 11, 16, 1H, 17-H), 5.97 (d, J = 16, 1H, 16-H), 5.13–5.17 (m, 1H, 13-H), 4.70 (d, J = 7, 1H, C*H*$_2$OCH$_3$), 4.56 (d, J = 7, 1H, C*H*$_2$OCH$_3$), 4.21 (dd, J = 4, 11, 1H, 18-H), 4.13–4.17 (m, 1H, 1-H), 3.41–3.48 (m, 1H, 2-H), 3.38 (s, 3H, OCH_3), 3.26 (s, 3H, OCH_3), 3.17 (s, 3H, OCH_3), 1.15–1.57 (m, 29H, 3 × CH_3, $(CH_2)_{10}$). ^{13}C NMR (100 MHz, $CDCl_3$) δ: 166.1 (C-15), 145.4 (C-16), 124.5 (C-17), 100.1, 98.4 (C-19a, C-19b), 96.6 (*C*H$_2$OCH$_3$), 76.5, 73.0, 70.9, 70.1 (C-1, C-2, C-13, C-18), 55.9 (CH$_2$O*C*H$_3$), 48.3, 47.8 (OCH_3), 36.2, 29.9, 27.9, 27.8, 27.7, 27.5, 26.6, 26.3, 24.8, 24.0 (C-3–C-12), 20.6, 18.2, 17.7 (CH_3).

6-*epi*-Aspicilin (24)

TFA–water (9:1, 500 μL) was added to fully protected 6-*epi*-aspicilin (5 mg, 0.01 mmol) and the reaction was stirred for 30 min. Concentration in vacuo followed by purification by flash column chromatography (ether) gave 6-*epi*-aspicilin as a crystalline white solid (1.4 mg, 44%); mp 116°C. $[\alpha]_D^{29}$ +23.0° (*c* 0.14, $CHCl_3$). R_f = 0.16 (ether). EI-MS *m*/*z* (%): 351 ($[M + Na]^+$, 60), 249 (50) (anal. calcd. for $C_{18}H_{32}O_5Na$: 351.2140 (M + Na); found: 351.2147). ^{1}H NMR (600 MHz, $CDCl_3$) δ: 6.99 (dd, J = 6, 16, 1H, 3-H), 6.10 (dd, J = 1, 16, 1H, 2-H), 5.01–5.09 (m, 1H, 17-H), 4.68 (m, 1H, 4-H), 3.72 (m, 1H, 5-H), 3.60 (m, 1H, 6-H), 2.68 (br s, 1H, OH), 2.49 (br s, 1H, OH), 1.66 (br s, 1H, OH), 1.34–1.55 (m, 20H, $(CH_2)_{10}$), 1.25 (d, J = 6, 3H, CH_3). ^{13}C NMR (100 MHz, $CDCl_3$) δ: 165.5 (C-1), 144.5 (C-3), 123.2 (C-2), 76.7, 72.5, 71.8, 71.0 (C-4, C-5, C-6, C-17), 36.0, 32.2, 27.74, 27.70, 27.5, 27.4, 26.6, 26.4, 24.09, 24.08 (C-7–C-16), 20.4 (CH_3).

(2*R*,1′*R*,3*R*,5*R*,6*R*)-3-*tert*-Butyldimethylsilyloxymethanol-5,6-dimethoxy-2-(1′-methoxymethylhydroxy-but-3′-ene-1′-yl)-5,6-dimethyl-1,4-dioxane (18)

MOMCl (1.55 mL, 20.4 mmol) was added to a solution of sodium iodide (2.39 g, 16.0 mmol) in DME (30 mL) at room temperature and the reaction stirred for 1 h. A solution of alcohol **16** (1.56 g, 4.0 mmol) and DIPEA (3.83 mL, 22.0 mmol) in DME (30 mL) was then added and the reaction stirred for a further hour at room temperature. The reaction was heated to 65°C for 1 h and then to reflux for 13 h. After cooling to room temperature, saturated sodium carbonate solution (20 mL) was added followed by CH_2Cl_2 (200 mL) and water (100 mL). The layers were separated and the organic layer washed again with water (100 mL). The combined aqueous layers were reextracted with CH_2Cl_2 (100 mL), the organic layers washed with brine, dried ($MgSO_4$), and concentrated in vacuo. Purification by flash column chromatography (petrol–ether (4:1) + 1% Et_3N) gave homoallylic ether **18** (1.25 g, 72% (85% brsm)) as a colorless oil. $[\alpha]_D^{30}$ –74.1° (*c* 1.09, $CHCl_3$). R_f = 0.51 (petrol–ether, 3:1). ES-MS *m*/*z* (%): 457 ($[M + Na]^+$, 100) (anal. calcd. (+ES) for $C_{21}H_{42}O_7SiNa$: 457.2597 (M + Na); found: 457.2620 ($[M + Na]^+$)). ν_{max} (neat) (cm^{-1}): 2951 (m), 2930 (m), 2888 (m), 2858 (m), 2833 (m), 1641 (w), 1471 (m), 1373 (m), 1257 (m), 1209 (m), 1134 (s), 1110 (s), 1095 (s). ^{1}H NMR (400 MHz, $CDCl_3$) δ: 5.84–5.94 (m, 1H, H-3′), 5.05–5.11 (m, 2H, H-4′), 4.88 (d, J = 7, 1H, OC*H*HOCH$_3$), 4.70 (d, J = 7, 1H, OCH*H*OCH$_3$), 4.23 (dd, J = 8, 10, 1H, C*H*HOTBS), 4.07 (dd, J = 3, 10, 1H, H-1), 3.68–3.81 (m, 3H, H-2, H-3, CH*H*OTBS), 3.39 (s, 3H, CH$_2$OC*H*$_3$), 3.27 (s, 3H, OCH_3), 3.25 (s, 3H, OCH_3), 2.46–2.53 (m, 1H, H-2′), 2.21–2.29 (m, 1H, H-2′), 1.250 (s, 3H, CH_3), 1.248 (s, 3H, CH_3), 0.90 (s, 9H, C(CH$_3$)$_3$), 0.07 (s, 6H, Si(CH$_3$)$_2$). ^{13}C NMR (100.6 MHz, $CDCl_3$) δ: 134.6 (C-3′), 117.1 (C-4′), 99.8, 98.2 (C-5, C-6), 97.5 (O*C*H$_2$OCH$_3$), 74.9, 73.2 (C-2, C-3), 72.0 (C-1′), 62.3 (*C*H$_2$OTBS), 55.7 (CH$_2$O*C*H$_3$), 49.2 (OCH_3), 47.6 (OCH_3), 36.1 (C-2′), 26.0 (C(*C*H$_3$)$_3$), 18.3 (*C*(CH$_3$)$_3$), 18.26 (CH_3), 17.9 (CH_3), –5.3 (SiCH$_3$), –5.4 (SiCH$_3$).

(2*R*,1′R,3*R*,5*R*,6*R*)-3-Methanol-5,6-dimethoxy-2-(1′-methoxymethylhydroxy-but-3′-ene-1′-yl)-5,6-dimethyl-1,4-dioxane

TBAF (8.21 mL, 1.0 M solution in THF, 8.21 mmol) was added to a solution of TBS ether **18** (1.19 g, 2.74 mmol) in THF (40 mL) and the reaction stirred for 16 h. The solvent was removed in vacuo and the residue chromatographed (petrol–ether (2:1) + 1% Et_3N) to give alcohol as a colorless

© 2001 NRC Canada

oil (0.91 g, 100%). $[\alpha]_D^{30}$ –73.0° (*c* 1.15, $CHCl_3$). R_f = 0.46 (ether). ES-MS *m/z* (%): 343 ($[M + Na]^+$, 100), 257 (15) (anal. calcd. (ES^+) for $C_{15}H_{28}O_7Na$: 343.1733 (M + Na); found 343.1757 ($[M + Na]^+$)). ν_{max} (neat) (cm^{-1}): 3472 (br), 2948 (m), 2833 (m), 1641 (w), 1455 (m), 1374 (m), 1209 (m), 1135 (s), 1115 (s), 1035 (s). ^1H NMR (400 MHz, $CDCl_3$) δ: 5.88 (m, 1H, H-3′), 5.07–5.12 (m, 2H, H-4′), 4.87 (d, *J* = 7, 1H, OC*H*HOCH$_3$), 4.72 (d, *J* = 7, 1H, OCH*H*OCH$_3$), 4.03–4.10 (m, 2H, H-1′, H-2), 3.77–3.90 (m, 2H, C*H*$_2$OH), 3.59–3.66 (m, 2H, OH, H-3), 3.39 (s, 3H, OCH$_3$), 3.37 (s, 3H, OCH$_3$), 3.26 (s, 3H, OCH$_3$), 2.33–2.39 (m, 1H, H-2′), 2.13–2.20 (m, 1H, H-2′), 1.32 (s, 3H, CH$_3$), 1.28 (s, 3H, CH$_3$). ^{13}C NMR (100.6 MHz, $CDCl_3$) δ: 134.0 (C-3′), 117.6 (C-4′), 99.3, 97.8 (C-5, C-6), 97.6 (O*C*H$_2$OCH$_3$), 74.9 (C-1′), 71.9 (C-2), 71.4 (C-3), 63.3 (CH$_2$OH), 55.8 (OCH$_2$O*C*H$_3$), 49.2 (OCH$_3$), 47.8 (OCH$_3$), 36.5 (C-2′), 18.1 (CH$_3$), 17.9 (CH$_3$). Anal. calcd. for $C_{22}H_{37}O_6Si$: C 56.23, H 8.81; found: C 56.18, H 8.78.

(2*R*,1′*R*,3*R*,5*R*,6*R*)-5,6-Dimethoxy-2-(1′-methoxymethylhydroxy-but-3′-ene-1′-yl)-5,6-dimethyl-1,4-dioxane-3-carbaldehyde (19)

DMSO (335 μL, 4.72 mmol) as a solution in CH_2Cl_2 (6 mL) was added to a solution of oxalyl chloride (206 μL, 2.36 mmol) in CH_2Cl_2 (6 mL) at –78°C. The reaction was stirred for 30 min at –78°C before alcohol (581 mg, 1.81 mmol) as a solution in CH_2Cl_2 (6 + 3 mL) was added over 30 min. The reaction was then stirred at –78°C for 1 h before Et_3N (885 μL, 6.35 mmol) was added dropwise over 30 min. The reaction was then allowed to warm to room temperature over 1 h then diluted with CH_2Cl_2 (150 mL). The CH_2Cl_2 solution was washed with water (2 × 150 mL), the combined aqueous layers reextracted with CH_2Cl_2 (100 mL), organics dried ($MgSO_4$), and concentrated in vacuo. The aldehyde (R_f = 0.36 (petrol–ether, 1:1)) was used without further purification in the next reaction.

(*E*)-(2*S*,3*R*,5*R*,6*R*,1′*R*,5″*S*)-5,6-Dimethoxy-2-(1′-methoxymethylhydroxy-but-3′-ene)-5,6-dimethyl-3-(5″-methyltetradec-1″,13″-diene-1″-yl-3″one)-1,4-dioxane (21) and (*Z*)-(2*S*,3*R*,5*R*,6*R*,1′*R*,5″*S*)-5,6-dimethoxy-2-(1′-methoxymethylhydroxy-but-3′-ene)-5,6-dimethyl-3-(5″-methyltetradec-1″,13″-diene-1″-yl-3″one)-1,4-dioxane

Phosphonate **5** (758 mg, 2.18 mmol) as a solution in MeCN (9 mL) was added to a suspension of LiCl (92 mg, 2.18 mmol) in MeCN (3 mL) at room temperature. The aldehyde **19** (1.81 mmol, crude) and DIPEA (316 μL, 1.81 mmol) were then added as a solution in MeCN (6 + 3 mL). The reaction was stirred at room temperature for 16 h before being diluted with ether (100 mL) and washed with water (60 mL). The organic layer was washed again with water (60 mL), the aqueous layers reextracted with ether (100 mL), and the combined organic layers dried ($MgSO_4$) and concentrated in vacuo. Purification by flash column chromatography (petrol–ether (4:1) + 1% Et_3N) gave α,β-unsaturated ester as 2 double bond isomers in a combined yield of 66% from the alcohol.

*(*E*)-(2*S*,3*R*,5*R*,6*R*,1′*R*,5″*S*)-5,6-Dimethoxy-2-(1′-methoxymethylhydroxy-but-3′-ene)-5,6-dimethyl-3-(5″-methyl-tetradec-1″,13″-diene-1″-yl-3″one)-1,4-dioxane (21)*

58% isolated yield; $[\alpha]_D^{29}$ –32.1° (*c* 1.27, $CHCl_3$). R_f = 0.65 (petrol–ether, 1:1). ES-MS *m/z* (%): 535 ($[M + Na]^+$, 100), 522 (5), 439 (8), 404 (5), 341 (15) (anal. calcd. (ES^+) for $C_{28}H_{48}O_8Na$: 535.3247 (M + Na); found: 535.3275 ($[M + Na]^+$)). ν_{max} (neat) (cm^{-1}): 2928 (m), 2856 (m), 1718 (s), 1641 (w), 1454 (m), 1373 (m), 1272 (m), 1248 (m), 1208 (m), 1137 (s), 1115 (s), 1023 (s). ^1H NMR (400 MHz, $CDCl_3$) δ: 7.43 (dd, *J* = 10, 16, 1H, H-1″), 5.96 (d, *J* = 16, 1H, H-2″), 5.75–5.91(m, 2H, H-3′, H-13″), 4.91–5.11 (m, 5H, H-5″, H-4′, H-14″), 4.84 (d, *J* = 7, 1H, OC*H*$_2$OCH$_3$), 4.68 (d, *J* = 7, 1H, OC*H*$_2$OCH$_3$), 4.11 (dd, *J* = 3, 9, 1H, H-2), 4.03 (dd, *J* = 3, 10, 1H, H-3), 3.45–3.54 (m, 1H, H-1′), 3.39 (s, 3H, OCH$_2$OC*H*$_3$), 3.29 (s, 3H, OCH$_3$), 3.10 (s, 3H, OCH$_3$), 2.23–2.29 (m, 1H, H-2′), 2.01–2.07 (m, 3H, H-2′, CH$_2$), 1.21–1.63 (m, 21H). ^{13}C NMR (100.6 MHz, $CDCl_3$) δ: 165.6 (C-3″), 143.3 (C-1″), 139.1 (C-13″), 133.7 (C-3′), 126.0 (C-2″), 117.7 (C-4′), 114.1 (C-14″), 99.6, 98.3 (C-5, C-6), 97.2 (O*C*H$_2$OCH$_3$), 75.2 (C-1′), 71.6, 71.3 (C-2, C-3, C-5″), 55.7 (OCH$_2$O*C*H$_3$), 48.3 (OCH$_3$), 47.8 (OCH$_3$), 36.0, 35.2, 33.7, 29.4, 29.35, 29.0, 28.9, 25.4 (C-6″–C-12″, C-2′), 20.0 (CH$_3$), 18.0 (CH$_3$), 17.7 (CH$_3$ at 5″).

(Z)-(2S,3R,5R,6R,1′R,5″S)-5,6-Dimethoxy-2-(1′-methoxymethylhydroxy-but-3′-ene)-5,6-dimethyl-3-(5″-methyl-tetradec-1″,13″-diene-1″-yl-3″one)-1,4-dioxane

86% isolated yield; $[\alpha]_D^{29}$ –13.0° (*c* 0.80, $CHCl_3$). R_f = 0.71 (petrol–ether, 1:1). ES-MS *m/z* (%): 535 ($[M + Na]^+$, 100), 503 (2), 457 (2), 413 (2), 343 (55) (anal. calcd. (ES^+) for $C_{28}H_{48}O_8Na$: 535.3247 (M + Na); found: 535.3253 ($[M + Na]^+$)). ν_{max} (neat) (cm^{-1}): 2928 (m), 2856 (m), 1716 (s), 1641 (w), 1451 (w), 1416 (m), 1373 (m), 1189 (s), 1113 (s), 1024 (s). ^1H NMR (400 MHz, $CDCl_3$) δ: 6.86 (dd, *J* = 11, 12, 1H, H-1″), 5.92 (d, *J* = 12, 1H, H-2″), 5.75–5.88 (m, 2H, H-3′, H-13″), 5.35 (dd, *J* = 3, 11, 1H, H-3), 4.89–5.12 (m, 5H, H-5″, H-4′, H-14″), 4.86 (d, *J* = 7, 1H, OC*H*$_2$OCH$_3$), 4.68 (d, *J* = 7, 1H, OC*H*$_2$OCH$_3$), 4.12 (dd, *J* = 3, 9, 1H, H-2), 3.49–3.53 (m, 1H, H-1′), 3.39 (s, 3H, OCH$_2$OC*H*$_3$), 3.29 (s, 3H, OCH$_3$), 3.11 (s, 3H, OCH$_3$), 2.24–2.30 (m, 1H, H-2′), 2.00–2.08 (m, 3H, H-2′, CH$_2$), 1.21–1.63 (m, 21H). ^{13}C NMR (100.6 MHz, $CDCl_3$) δ: 165.3 (C-3″), 142.8 (C-1″), 139.1 (C-13″), 133.8 (C-3′), 123.0 (C-2″), 117.7 (C-4′), 114.1 (C-14″), 99.6, 98.1 (C-5, C-6), 97.1 (O*C*H$_2$OCH$_3$), 75.2 (C-1′), 71.8, 71.1, 64.8 (C-2, C-3, C-5″), 55.7 (OCH$_2$O*C*H$_3$), 48.5 (OCH$_3$), 47.7 (OCH$_3$), 35.9, 35.0, 33.7, 29.3, 29.35, 29.0, 28.9, 25.4 (C-6″–C-12″, C-2′), 19.9 (CH$_3$), 18.1 (CH$_3$), 17.7 (CH$_3$ at 5″).

(4*E*/*Z*,16*E*)-(1*S*,2*R*,13*S*,18*R*,19a*R*,19b*R*)-19a,19b-Dimethoxy-2-methoxymethylhydroxy-13,19a,19b-trimethyl-14,19,20-trioxa-bicyclo[16.4.0]doicosa-4,16-diene-15-one (22)

Grubbs' catalyst (34.3 mg, 0.039 mmol) was added to a deoxygenated solution of triene **21** (200 mg, 0.39 mmol) in CH_2Cl_2 (400 mL) and the reaction stirred for 16 h. The solvent was removed in vacuo and the residue chromatographed to yield the desired macrocycle as a 2:1 mixture of double bond isomers **22** (112 mg, 73%) as well as a byproduct, cyclohexene **23** (29 mg, 26%). R_f = 0.29 (petrol–ether, 2:1). ES-MS *m/z* (%): 507 ($[M + Na]^+$, 80), 475 (2), 377 (5) (anal. calcd. (ES^+) for $C_{26}H_{44}O_8Na$: 507.2934 (M + Na); found: 507.2950 ($[M + Na]^+$)). ν_{max} (neat) (cm^{-1}): 2928 (m), 2858 (m), 1720 (s), 1654 (w), 1456 (w), 1373 (m), 1331 (w), 1248 (s), 1209 (m), 1176 (m), 1136 (s), 1110 (s), 1022 (s). ^1H

© 2001 NRC Canada

NMR (400 MHz, $CDCl_3$) δ: 7.53 (dd, *J* = 10, 16, $1H_A$, H-17), 7.52 (dd, *J* = 10, 16, $1H_B$, H-17), 6.05 (d, *J* = 16, $1H_A$, H-16), 5.96 (d, *J* = 16, $1H_B$, H-16), 5.09–5.44 (m, $2H_A$ + $2H_B$, H-4, H-5), 4.91 (d, *J* = 7, $1H_B$, OCH_2OCH_3), 4.87 (d, *J* = 7, $1H_A$, OCH_2OCH_3), 4.73 (d, *J* = 7, $1H_B$, OCH_2OCH_3), 4.71 (d, *J* = 7, $1H_A$, OCH_2OCH_3), 3.99–4.12 (m, $2H_A$ + $2H_B$, H-1, H-18), 3.33–3.50 (m, $2H_A$ + $2H_B$, H-2, H-13), 3.41 (s, $3H_A$, OCH_2OCH_3), 3.38 (s, $3H_B$, OCH_2OCH_3), 3.29 (s, $3H_A$, OCH_3), 3.28 (s, $3H_B$, OCH_3), 3.15 (s, $3H_B$, OCH_3), 3.09 (s, $3H_A$, OCH_3), 1.85–2.19 (m, $3H_A$ + $3H_B$, H-3, CH_2), 1.18–1.40 (m, $20H_A$ + $20H_B$). ^{13}C NMR (100.6 MHz, $CDCl_3$) (major isomer only) δ: 165.6 (C=O), 143.8 (C-17), 132.1, 126.5 (C-4, C-5), 125.4 (C-16), 99.5, 98.2 (19a, 19b), 98.1 (OCH_2OCH_3), 77.1, 72.5, 72.3, 70.8 (CH), 55.9 (OCH_2OCH_3), 48.3 (OCH_3), 47.8 (OCH_3), 36.2, 34.0, 31.3, 27.29, 27.25, 25.2, 23.7 (CH_2), 20.6, 18.0, 17.6 (CH_3). Anal. calcd. for $C_{26}H_{44}O_8$: C 64.44, H 9.15; found: C 64.57, H 9.29.

(4*Z*)-(1*S*,2*R*,6*R*,7a*R*,7b*R*)-7a,7b-Dimethoxy-2-methoxymethylhydroxy-7a,7b-dimethyl-7,8-dioxa-bicyclo[4.4.0]-dec-4-ene (23)

$[\alpha]_D^{29}$ –216.9° (*c* 0.54, $CHCl_3$). R_f = 0.19 (petrol–ether, 2:1). ES-MS *m*/*z* (%): 311 ($[M + Na]^+$, 100), 295 (5), 224 (5), 158 (8) (anal. calcd. (ES^+) for $C_{14}H_{24}O_6Na$: 311.1471 (M + Na); found: 311.1489 ($[M + Na]^+$)). ν_{max} (neat) (cm^{-1}): 2946 (m), 1375 (w), 1137 (s), 1110 (s), 1035 (s). ^1H NMR (400 MHz, $CDCl_3$) δ: 5.80 (d, *J* = 10, 1H, H-5), 5.61 (d, *J* = 10, 1H, H-4), 4.68 (s, 2H, OCH_2OCH_3), 4.31 (br s, 1H, H-6), 4.17 (t, *J* = 4, 1H, H-1), 3.96 (br s, 1H, H-2), 3.36 (s, 3H, OCH_2OCH_3), 3.29 (s, 3H, OCH_3), 3.27 (s, 3H, OCH_3), 2.49 (dt, *J* = 3, 18, 1H, H-3), 2.07 (dd, *J* = 3, 18, 1H, H-3), 1.28 (s, 3H, CH_3), 1.27 (s, 3H, CH_3). ^{13}C NMR (100.6 MHz, $CDCl_3$) δ: 128.3 (C-5), 122.6 (C-4), 99.3, 98.7 (C-7a, C-7b), 95.5 (OCH_2OCH_3), 73.4 (C-2), 66.0 (C-6), 64.4 (C-1), 55.5 (OCH_2OCH_3), 48.8 (OCH_3), 48.0 (OCH_3), 26.6 (C-3), 18.7 (CH_3), 17.9 (CH_3).

(16*E*)-(1*S*,2*R*,13*S*,18*R*,19a*R*,19b*R*)-19a,19b-Dimethoxy-2-methoxymethylhydroxy-13,19a,19b-trimethyl-14,19,20-trioxa-bicyclo[16.4.0]doicosa-16-ene-15-one

Pd-$BaSO_4$ (10 mg) was added to a solution of diene **22** (37.8 mg, 0.08 mmol) in EtOAc (4 mL). The reaction was stirred under an atmosphere of hydrogen for 40 min, the catalyst was removed by filtration and the solvent removed in vacuo to leave crude product. R_f = 0.29 (petrol–ether, 2:1). ES-MS *m*/*z* (%): 509 ($[M + Na]^+$, 100), 435 (5), 413 (3), 365 (2), 313 (10), 292 (8), 224 (5) (anal. calcd. (ES^+) for $C_{26}H_{46}O_8Na$: 509.3091 (M + Na); found: 509.3101 ($[M + Na]^+$)). ν_{max} (neat) (cm^{-1}): 2929 (m), 2857 (m), 1719 (s), 1654 (w), 1460 (m), 1372 (m), 1331 (w), 1247 (s), 1208 (m), 1176 (m), 1135 (s), 1110 (s), 1036 (s). ^1H NMR (400 MHz, $CDCl_3$) δ: 7.52 (dd, *J* = 10, 16, 1H, H-17), 5.96 (d, *J* = 6, 1H, H-16), 5.10–5.16 (m, 1H, H-13), 4.96 (d, *J* = 7, 1H, OCH_2OCH_3), 4.70 (d, *J* = 7, 1H, OCH_2OCH_3), 3.98–4.03 (m, 2H, H-1, H-18), 3.29–3.41 (m, 1H, H-2), 3.39 (s, 3H, OCH_2OCH_3), 3.28 (s, 3H, OCH_3), 3.12 (s, 3H, OCH_3), 1.11–1.59 (m, 29H). ^{13}C NMR (100.6 MHz, $CDCl_3$) (major isomer only) δ: 165.6 (C=O), 144.0 (C-17), 125.3 (C-16), 99.5, 98.2 (19a, 19b), 98.4 (OCH_2OCH_3), 75.5 (C-2), 73.0 (C-18), 72.1 (C-1), 70.5 (C-13), 56.1 (OCH_2OCH_3), 48.3 (OCH_3), 47.8 (OCH_3), 35.3, 30.0, 28.4, 27.5, 27.2, 27.0, 26.6, 25.8, 24.3, 22.8 (CH_2), 20.3, 18.0, 17.6 (CH_3).

(+)-Aspicilin (1)

Ethanedithiol (121 μL, 1.44 mmol) was added to fully protected aspicilin (78 mg, 0.16 mmol) in CH_2Cl_2 (10 mL) and the solution cooled to 0°C. $BF_3{\cdot}OEt_2$ (166 μL, 1.28 mmol) was then added and the solution warmed to room temperature and left stirring for 14 h. The reaction was diluted with EtOAc, washed with saturated $NaHCO_3$ solution, and the organic layer was dried ($MgSO_4$). Concentration in vacuo followed by purification by flash column chromatography (5% MeOH in ether) gave aspicilin as a crystalline white solid (38 mg, 73%); mp 150–155°C. $[\alpha]_D^{29}$ + 35.0° (*c* 0.20, $CHCl_3$). R_f = 0.16 (ether) EI-MS *m*/*z* (%): 351 ($[M + Na]^+$, 100), 292 (50), 224 (28) (anal. calcd. for $C_{18}H_{32}O_5Na$: 351.2148 (M + Na); found: 351.2166). ν_{max} ($CHCl_3$ solution) (cm^{-1}): 3500 (br), 3016 (s), 2931 (s), 2858 (s), 1773 (w), 1709 (s), 1460 (m), 1379 (m), 1360 (w), 1278 (m), 1232 (m), 1180 (s), 1124 (s), 1082 (s), 1040 (s), 1010 (s), 985 (s). ^1H NMR (400 MHz, $CDCl_3$) δ: 6.90 (dd, *J* = 16, 5, 1H, 3-H), 6.12 (dd, *J* = 16, 2, 1H, 2-H), 5.02–5.08 (m, 1H, 4-H), 4.53–4.59 (m, 1H, 5-H), 3.77–3.80 (m, 1H, 6-H), 3.59 (dd, *J* = 3, 7 1H,), 3.10 (d, *J* = 7, 1H, 4-OH), 2.95 (d, *J* = 7, 1H, 5-OH), 2.35 (d, *J* = 3, 1H, 6-OH), 1.08–1.60 (m, 23H, $(CH_2)_{10}$, CH_3CH). ^{13}C NMR (100 MHz, $CDCl_3$) δ: 165.3 (C-1), 144.4 (C-3), 123.1 (C-2), 74.8, 73.2, 71.1, 69.9 (C-4, C-5, C-6, C-17), 35.7, 32.2, 28.3, 27.8, 27.6, 27.3, 27.1, 26.4, 24.3, 23.6 (C7–C16), 20.5 (CH_3).

Acknowledgments

We thank the EPSRC (to D.J.D. and A.C.F), Syngenta (to A.C.F.) and the Novartis Research Fellowship (to S.V.L.) for financial support. Dr. J.E.Davies is kindly thanked for x-ray crystallography and Dr M. Turnbull for helpful discussions.

References

1. E. Schoffers, A. Golebiowski, and C.R. Johnson. Tetrahedron, **52**, 3769 (1996).
2. M.C. Willis. J.Chem. Soc. Perkin Trans. 1, 1765 (1999).
3. H.C. Kolb, M.S. Vannieuwenhze, and K.B. Sharpless. Chem. Rev. **94**, 2483 (1994).
4. P.J. Edwards and S.V. Ley. Synlett, 898 (1995).
5. S.V. Ley and S. Mi. Synlett, 789 (1996).
6. S.V. Ley, S. Mio, and B. Meseguer. Synlett, 791 (1996).
7. D. Laine, M. Fujita, and S.V. Ley. J. Chem. Soc. Perkin Trans. 1, 1639 (1999).
8. S. Huneck, K. Schreiber, and W. Steglich. Tetrahedron, **29**,3697 (1973).
9. O. Hesse. J. Prakt. Chem. **62**,430 (1900).
10. O. Hesse. J. Prakt. Chem. **70**, 449 (1904).
11. G. Quinkert, N. Heim, J.W. Bats, H. Oschkinat, and H. Kessler. Angew. Chem. Int. Ed. Eng. **24**, 987 (1985).
12. D.J. Dixon, A.C. Foster, and S.V. Ley. Org. Lett. **2**, 123 (2000).
13. G. Quinkert, N. Heim, J. Glenneberg, U.M. Billhardt, V. Autze, J.W. Bats, and G. Durner. Angew. Chem. Int. Ed. Engl. **26**, 362 (1987).
14. P.P. Waanders, L. Thijs, and B. Zwanenburg. Tetrahedron Lett. **28**, 2409 (1987).

© 2001 NRC Canada

15. G. Quinkert, N. Heim, J. Glenneberg, U. Doller, M. Eichhorn, U.M. Billhardt, C. Schwarz, G. Zimmermann, J.W. Bats, and G. Durner. Helv. Chim. Acta, **71**, 1719 (1988).
16. G. Quinkert, E. Fernholz, P. Eckes, D. Neumann, and G. Durner. Helv. Chim. Acta, **72**, 1753 (1989).
17. G. Quinkert, U. Doller, M. Eichhorn, F. Kuber, H.P. Nestler, H. Becker, J.W. Bats, G. Zimmermann, and G. Durner. Helv. Chim. Acta, **73**, 1999 (1990).
18. G. Quinkert, H. Becker, and G. Durner. Tetrahedron Lett. **32**, 7397 (1991).
19. S.C. Sinha and E. Keinan. J. Org. Chem. **59**, 949 (1994).
20. D. Enders and O.F. Prokopenko. Liebigs Ann. 1185 (1995).
21. W. Oppolzer, R.N. Radinov, and J. Debrabander. Tetrahedron Lett. **36,** 2607 (1995).
22. R. Chenevert, M. Lavoie, and M. Dasser. Can. J. Chem. **75**, 68 (1997).
23. Y. Kobayashi, M. Nakano, and H. Okui. Tetrahedron Lett. **38**, 8883 (1997).
24. S.C. Sinha and E. Keinan. J. Org. Chem. **62**, 377 (1997).
25. T. Nishioka, Y. Iwabuchi, H. Irie, and S. Hatakeyama. Tetrahedron Lett. **39**, 5597 (1998).
26. M.G. Banwell and K.J. McRae. Org. Lett. **2**, 3583 (2000).
27. N. Maezaki, Y.X. Li, K. Ohkubo, S. Goda, C. Iwata, and T. Tanaka. Tetrahedron, **56**, 4405 (2000).
28. H.J. Liu, P.A. Rose, and D.J. Sasaki. Can. J. Chem. **69**, 934 (1991).
29. D.J. Dixon, A.C. Foster, S.V. Ley, and D.J. Reynolds. J. Chem. Soc. Perkin Trans. 1, 1635 (1999).
30. D.J. Dixon, A.C. Foster, S.V. Ley, and D.J. Reynolds. J. Chem. Soc. Perkin Trans. 1, 1631 (1999).
31. A.J. Mancuso and D. Swern. Synthesis, 165 (1981).
32. J.S. Barlow, D.J. Dixon, A.C. Foster, S.V. Ley, and D.J. Reynolds. J. Chem. Soc. Perkin Trans. 1, 1627 (1999).
33. D. Askin, R.P. Volante, R.A. Reamer, K.M. Ryan, and I. Shinkai. Tetrahedron Lett. **29**, 277 (1988).
34. M.A. Blanchette, W. Choy, J.T. Davis, A.P. Essenfeld, S. Masamune, W.R. Roush, and T. Sakai. Tetrahedron Lett. **25**, 2183 (1984).
35. R.H. Grubbs and S. Chang. Tetrahedron, **54**, 4413 (1998).

© 2001 NRC Canada

Cyclization–cycloaddition cascades for the construction of azapolycyclic ring systems

Albert Padwa, William S. Kissell, and Cheryl K. Eidell

Abstract: Cyclic 2-amidofuranones were obtained from the Rh(II)-catalyzed reaction of α-diazoketo substituted pyrrolidine derivatives. These compounds are derived by a [1,4]-hydrogen transfer from an initially formed carbonyl ylide dipole. Acylation of the amido-substituted furanone with pivalyl chloride provided a fused amidofuran, which underwent bimolecular Diels-Alder cycloaddition with *N*-phenylmaleimide. The Rh(II)-catalyzed decomposition of ethyl 2-diazo-3-oxo-(2-oxo-1-pent-4-enoyl-pyrrolidine-3-yl)propionate was also examined. In this case, the alkenyl group tethered to the amido carbonyl underwent smooth intramolecular [4+2]-cycloaddition with the amidofuran obtained from the acylation reaction. An alternate route for the synthesis of cyclic amidofurans was developed using a Pummerer induced cyclization of the thiophenyl substituted acetal derived from the aldol reaction of methoxyphenylsulfanyl acetaldehyde with α-valerolactam. Treatment of the amido-substituted acetal with dimethyl(methylthio)sulfonium tetrafluoroborate (DMTSF) generated an oxonium ion, which readily cyclized onto the adjacent carbonyl group. The amidofuran that was formed underwent an intramolecular Diels-Alder reaction when heated at 110°C in toluene. Subsequent ring opening of the transient [4+2]-cycloadduct followed by elimination of methanol and tautomerization of the resulting cyclohexadienone gave rise to the observed phenolic lactam in good overall yield.

Key words: intramolecular, cyclization, Diels-Alder, diazo-ketoamide, rhodium(II).

Résumé : On a obtenu des 2-amidofuranones cycliques par la réaction catalysée par du Rh(II) de dérivés α-diazocétopyrrolidines substituées. Ces composés dérivent d'un transfert [1,4] d'hydrogène à partir d'un dipôle ylure de carbonyle formé initialement. L'acylation de l'amidofuranone substituée à l'aide de chlorure de pivaloyle conduit à un amidofurane ponté qui peut donner lieu à une réaction de cycloaddition de Diels-Alder bimoléculaire avec le *N*-phénylmaléimide. On a aussi étudié la réaction de décomposition du 2-diazo-3-oxo-(2-oxo1-pent-4-énoyl-pyrrolidine-3-yl)propionate d'éthyle catalysée par le Rh(II). Dans ce cas, le groupe alcényle attaché au carbonyle de l'amido donne lieu à une réaction facile de cycloaddition [4+2] intramoléculaire avec l'amidofurane obtenu par la réaction d'acylation. On a aussi développé une autre voie de synthèse des amidofuranes cycliques; elle fait appel à une réaction de cyclisation induite à la façon de Pummerer de l'acétal substitué par un thiophényle, dérivé de la réaction aldolique du méthoxyphénylsulfanylacétaldéhyde avec le α-valérolactame. Le traitement de l'acétal substitué par un amido à l'aide de tétrafluoroborate de diméthyl(méthylthio)sulfonium conduit à la formation d'un ion oxonium qui peut se cycliser facilement sur le groupe carbonyle adjacent. Lorsqu'on le chauffe à 110°C dans le toluène, l'amidofurane qui s'est formé subi une réaction de Diels-Alder intramoléculaire. L'ouverture de cycle subséquente du cycloadduit [4+2] transitoire, suivie d'une élimination de méthanol et d'une tautomérisation de la cyclohexadiénone résultante fournit le lactame phénolique observé, avec un bon rendement global.

Mots clés : intramoléculaire, cyclisation, Diels-Alder, diazo-cétoamide, rhodium(II).

[Traduit par la Rédaction]

Introduction

Construction of azapolyheterocycles through metal intervention has been a particularly fruitful area of investigation, and the synthesis of various types of alkaloids by this approach has been carried out by several investigators (1–11). Recent papers from these laboratories have described a route to azapolycyclic ring systems that involved the tandem cyclization–cycloaddition of a transient rhodium carbenoid (Scheme 1) (12). Isomünchnone **2** was easily prepared by the rhodium(II) catalyzed cyclization of a suitable diazoimide precursor **1** (13). The mesoionic oxozolium ylide **2** is the cyclic equivalent of a carbonyl ylide and readily undergoes 1,3-dipolar cycloaddition with suitable dipolarophiles (14). This reaction is an integral part of our program aimed at developing new cascade reactions and achieving the total syntheses of various nitrogen-containing heterocycles (15). Our more recent achievements in this area involve the use of diazo ketoamides

Received April 6, 2001. Published on the NRC Research Press Web site at http://canjchem.nrc.ca on November 12, 2001.

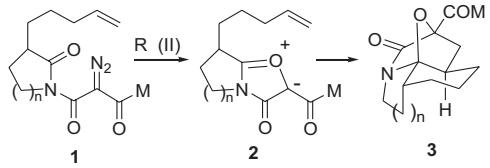
This paper is dedicated to Victor A. Snieckus on the occasion of his 64th birthday and for his many significant contributions to the art of organic synthesis.

A. Padwa,[1] W.S. Kissell, and C.K. Eidell. Department of Chemistry, Emory University, Atlanta, GA 30322, U.S.A.

[1]Corresponding author (telephone: (404) 727-0283; fax: (360) 838-9418; e-mail: chemap@emory.edu).

 DOI: 10.1139/cjc-79-11-1681 © 2001 NRC Canada

Scheme 1.



such as **4** (16). Intramolecular attack of the amido carbonyl oxygen at the rhodium carbenoid center produces a carbonyl ylide (i.e., **5**) (eq. [1]) that is isomeric with the isomünchnone class of dipoles. Several key questions emerged as a result of these investigations (17): (*i*) does the size of the lactam ring influence the efficiency of dipole formation, (*ii*) how would the nature of the substituent groups (R^1–R^3) impact on dipole reactivity, (*iii*) would intramolecular dipolar-cycloaddition of push–pull stabilized ylides such as **5** occur, and (*iv*) if so, what effect would the nature and length of the tether have on the course of the cycloaddition? We, therefore, initiated a study to not only probe these issues but also to use this sequence for the synthesis of various nitrogen heterocycles. In this paper we report results emanating from this investigation.

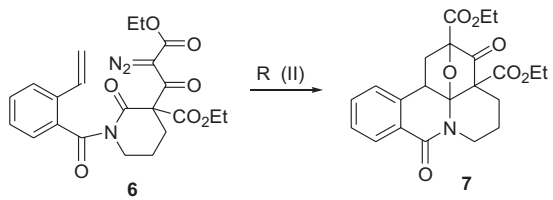
[1]



Results and discussion

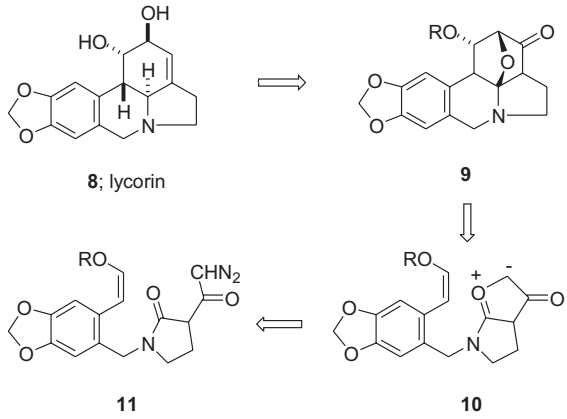
To help address the above questions, the Rh(II)-catalyzed reaction of diazoamido ester **6** was examined. The prerequisite diazo amide necessary for dipole generation was obtained from the reaction of 3-carboethoxy-2-piperidone with ethyl 2-diazomalonyl chloride (18) and this was followed by acylation with *o*-vinyl benzoyl chloride. Formation of the push–pull carbonyl ylide dipole proceeded smoothly upon heating a sample of **6** in benzene in the presence of $Rh_2(OAc)_4$ (eq. [2]). The resultant dipole was trapped by the adjacent vinyl group to afford cycloadduct **7** in 92% yield. The structural assignment was made on the basis of its NMR spectral properties and by comparison with related cycloadducts prepared in other studies in our laboratory (17). Cycloadduct **7** is produced with complete diastereoselectivity and is the result of *endo* cycloaddition with respect to the dipole and *anti* with respect to the carboethoxy group at the ring juncture.

[2]



Prompted by the facility with which **6** underwent cycloaddition to give **7**, we became interested in determining

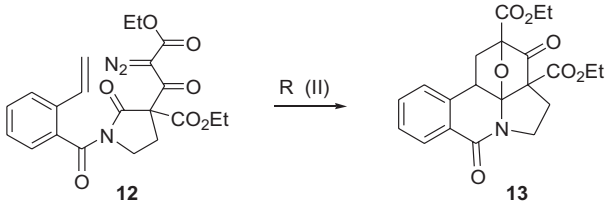
Scheme 2.



whether a related process could be used to assemble the carbon framework of lycorine (**8**). The lycorine alkaloids, a group of compounds isolated from *Amarylidaceae* plants, have attracted the attention of chemists and pharmacologists due to the interesting properties of some of its members (19, 20). Several of these alkaloids possess antineoplastic and antimitotic activities, while others are known to exhibit insect antifeedent activity (19). Lycorine (**8**) was first isolated in 1877 and was shown to be a powerful inhibitor of growth and cell division in higher plants and also to possess antiviral activity (21, 22). Consequently, considerable effort has been directed toward the synthesis of the oxygenated octahydroindole skeleton found in this class of alkaloids (23–29). We envisioned diazoamide **11** functioning as a possible precursor for the generation of dipole **10**. Intramolecular cycloaddition across the neighboring enol ether π-bond followed by reductive ring opening of the transient azabicyclic adduct **9** would provide the lycorine skeleton with the correct stereochemistry (Scheme 2).

As a model system for exploring the cyclization-cycloaddition sequence for an eventual synthesis of lycorine, diazoamide **12** was first examined. In this case, the cascade sequence would lead directly to the proper galanthan skeleton of lycorine. We carried out the Rh(II)-catalyzed reaction under the same conditions employed for the homologous diazoamide **6** and isolated the expected cycloadduct **13**, but only in 40% yield (eq. [3]).

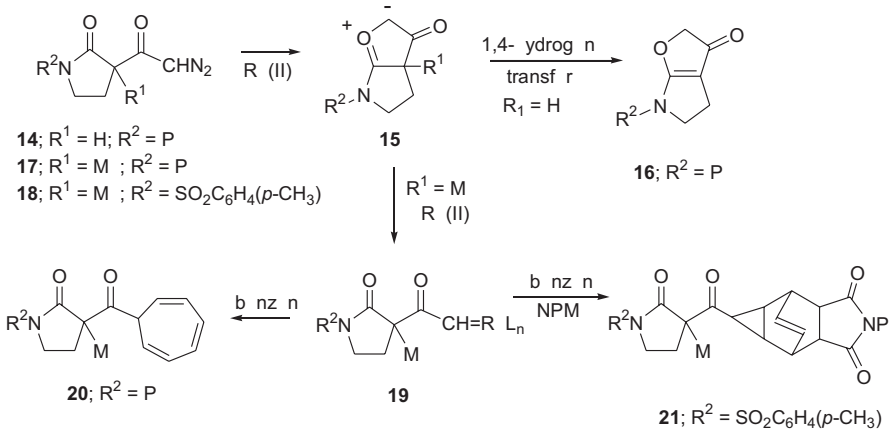
[3]



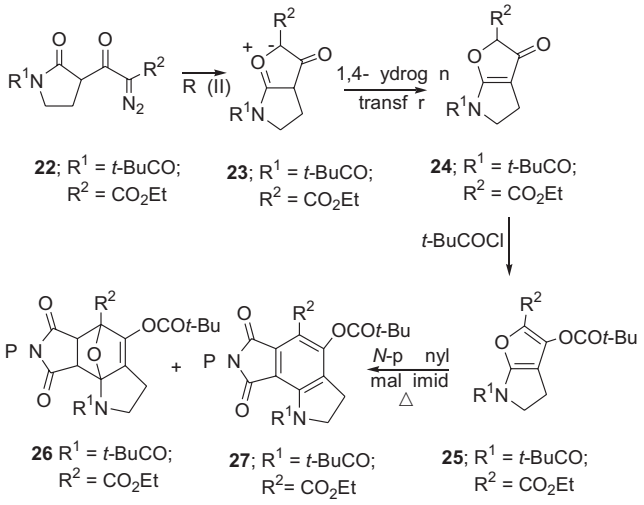
Raising the temperature or extending the reaction time resulted in extensive decomposition, probably as a consequence of the reactivity of the styryl portion of the molecule. We initially thought that a change in the trajectory of attack on the π-bond from the smaller lactam ring may have been responsible for the reduced yield of the cycloaddition. However, reaction of diazoamide **12** with external dipolarophiles provided little or no cycloaddition product. Bimolecular stud-

© 2001 NRC Canada

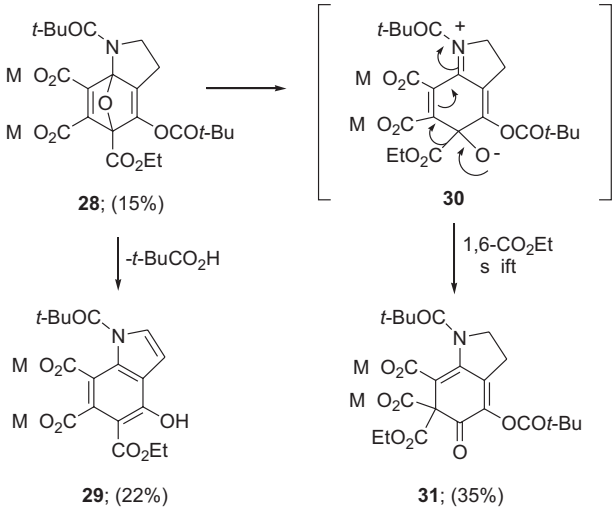
Scheme 3.



Scheme 4.



Scheme 5.



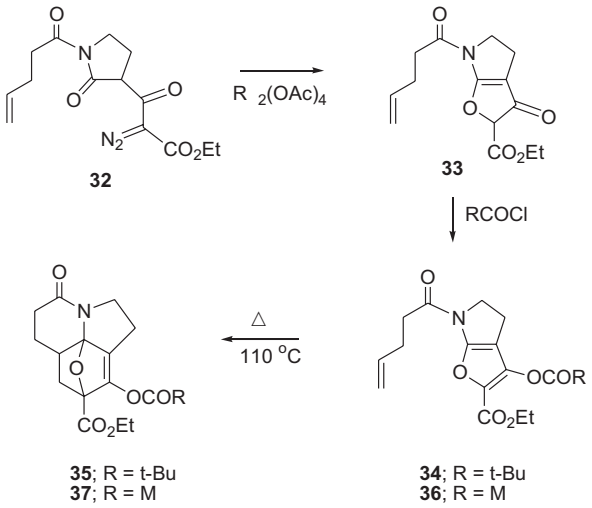
ies with a related diazoamide that did not contain the *o*-vinyl group were also unsatisfactory, clearly indicating that polymerization is not the sole cause of the reduced yields. An extensive study using different rhodium(II) ligands did not lead to an improvement in the yield of cycloadduct **13**. This would tend to imply that the decomposition of the diazoamide either does not lead to significant amounts of the dipole or that the dipole is not long lived enough to react with a dipolarophile in either an inter- or intramolecular fashion. Possibly, this may be due to the strain energy associated with formation of the carbonyl ylide. Presumably, the dipole fused to the five membered pyrrolidine ring would have a larger strain energy associated with it than would the dipole fused to the more flexible piperidine six-membered ring.

We next examined the possibility of using other five-membered push–pull dipoles (e.g., **10**) for further cycloaddition chemistry directed toward alkaloid synthesis. We reasoned that removal of the bulky carboethoxy group at the ring fusion might relieve some of the ring strain and allow the cyclization reaction to proceed with higher efficiency. In addition, the carboethoxy group is not necessary for the alkaloids we had in mind as we would eventually need to remove it in a subsequent step. This analysis led us to study the Rh(II) behavior of diazoamide **14**. Reaction of **14** with $Rh_2(OAc)_4$ led to the expected push–pull dipole **15**. However, even in the presence of an excess of a reactive trapping agent such as DMAD, a rapid [1,4]-hydrogen shift to furanone **16** occurred before bimolecular cycloaddition (Scheme 3). Although the formation of **16** from **14** is somewhat disappointing, it comes as no real surprise since one of the characteristic reactions of carbonyl ylides derived from the reaction of α-diazoalkanes with ketones consists of an intramolecular proton transfer (30). The earliest example of this process was reported by Kharasch and co-workers in 1953 and many related cases have been recorded since that time (30).

Despite our inability to isolate a dipolar cycloadduct from the Rh(II)-catalyzed reaction of diazoamide **14**, we were still interested in determining the efficiency with which cyclization of the pyrrolidinone ring system occurred. To this end, we prepared diazoamides **17** and **18**, which incorporate a methyl substituent in the α-position so as to block the deprotonation step. When submitted to the cyclization–cycloaddition conditions using *N*-phenylmaleimide as the trapping agent, no products resulting from dipolar-cycloaddition could be detected. Rather the product of solvent insertion **20** (or **21**) was isolated in 73 and 68% yield, respectively (Scheme 3). This

© 2001 NRC Canada

Scheme 6.



result suggests that in the presence of the Rh(II)-catalyst, formation of the carbonyl ylide intermediate **15** is reversible and that the bimolecular insertion of **19** into the solvent proceeds at a faster rate than dipolar-cycloaddition of **15** (R^1 = Me) with the added dipolarophile (31).

At this point in time, we decided to use the furanone ring to our advantage for an anticipated Diels-Alder cycloaddition. It was envisioned that acylation of the furanone would provide a fused amidofuran (i.e., **25**) that could be subsequently utilized in a bimolecular cycloaddition reaction (Scheme 4) (32). Exploring this approach required that three key steps be tested. First, the diazoimide must be able to efficiently cyclize to form the furanone ring. Secondly, the furanone would need to readily react with an acylating agent to furnish the fused amidofuran **25**. Finally, the tetrasubstituted furan would need to undergo a facile Diels-Alder reaction with an electron deficient π-bond (33). Diazoimide **22** was synthesized from *N*-pivalyl-pyrrolidinone by deprotonation with $NaN(TMS)_2$ followed by treatment with benzylchloroformate. Hydrogenolysis of the benzyl ester to the carboxylic acid was followed by conversion to the acid chloride and reaction with ethyl diazoacetate. Decomposition of **22** using $Rh_2(OAc)_4$ gave furanone **24** which was transformed into amidofuran **25** by treatment with pivalyl chloride and NEt_3. Heating a sample of **25** with *N*-phenyl maleimide afforded a 1:3-mixture of cycloadduct **26** together with indoline **27**, derived by oxabicyclic ring opening followed by elimination of water, in 95% overall yield (Scheme 4). Indeed, treatment of **26** in the presence of acid afforded **27** in high yield. Interestingly, the reaction of **25** with DMAD afforded a mixture of cycloadduct **28** (15%), indole **29** (22%) and the rearranged cyclohexa-dienone **31** (35%) (Scheme 5). The structure of **31** was unequivocally established by a crystal X-ray analysis, and its formation can be rationalized by a ring opening – rearrangement reaction analogous to that reported in the furo[3,4-*d*]oxazole series (34).

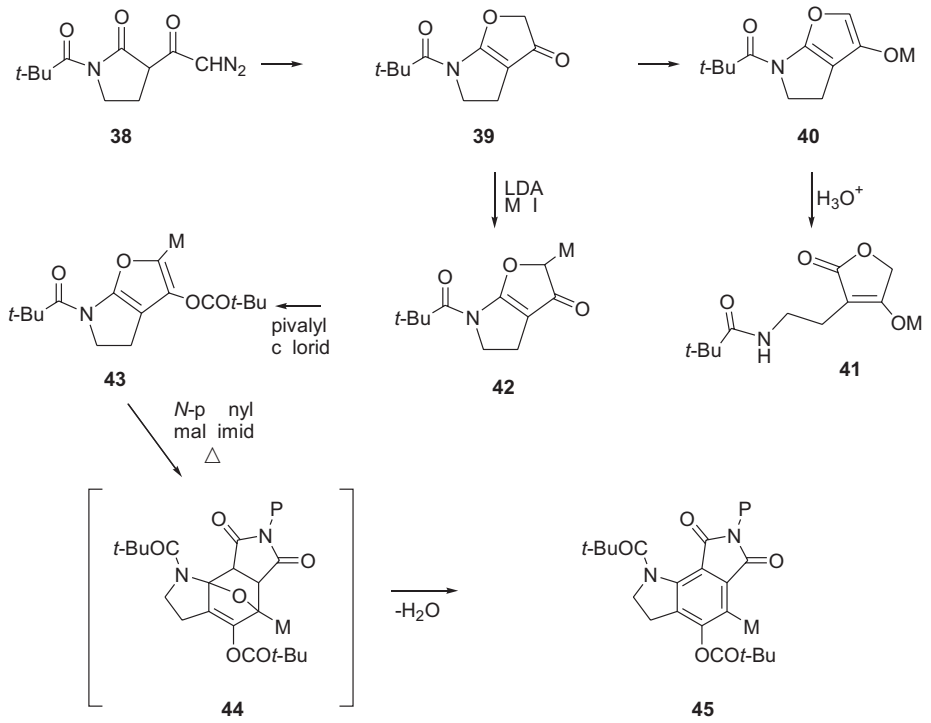
Having established the feasibility of the bimolecular cycloaddition sequence using activated π-bonds, we initiated a study of the intramolecular reaction related to that outlined in Scheme 2. Specifically, we were interested in examining a case where an alkenyl group would be tethered to the imido nitrogen atom. Diazoimide **32** was synthesized in a manner similar to that used to prepare pyrrolidinone **22**. As before, decomposition of the diazoimide using $Rh_2(OAc)_4$ provided the intermediate furanone **33**, which was reacted with pivalyl chloride to furnish amidofuran **34**. Heating a toluene solution of **34** at reflux provided cycloadduct **35** as the only detectable product in high overall yield for the three-step process (70%) (Scheme 6). A similar [4+2]-cycloaddition reaction occurred with the corresponding acetate **36**, but with lower overall yield (25%), perhaps as a consequence of a competitive thermal deacetylation reaction.

We quickly realized that application of this cyclization–cycloaddition sequence to amido furanone **39**, in turn derived from the Rh(II)-catalyzed cyclization of α-diazo keto pyrrolidinone **38**, would represent a new approach to various azapolycyclic ring systems. To further test the generality and scope of the sequence, furanone **39** was treated with trimethyloxonium tetrafluoroborate so as to effect O-methylation. The initially formed methoxyfuran **40** was extremely labile and instead of undergoing [4+2]-cycloaddition with added dienophiles, it readily underwent hydrolysis to give propionamide **41** (Scheme 7). On the other hand, when **39** was treated with LDA followed by reaction with methyl iodide, the *C*-alkylated furanone **42** was formed in 37% yield. Subsequent treatment of **42** with pivalyl chloride in the presence of NEt_3 gave **43** which was immediately allowed to react with *N*-phenylmaleimide. The initially formed Diels-Alder cycloadduct **44** underwent ready dehydration to produce maleimide **45** in 52% overall yield (Scheme 7).

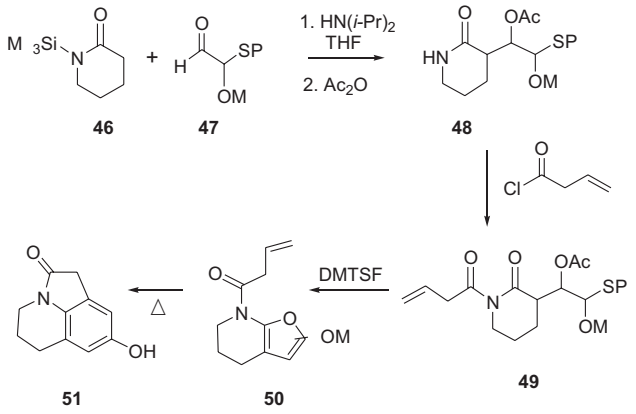
As a consequence of some of the difficulties encountered with the diazo ketoamide cyclizations, we decided to explore an alternate tactic for the preparation of cyclic amidofurans. As detailed in an earlier paper from our laboratory (35), we had employed a Pummerer cyclization of an imido dithioacetal as a method for constructing 2-amido substituted furans. In the current investigation, we found that a similar reaction occurred using the aldol product (i.e., **48**) derived from the reaction of *N*-trimethylsilyl α-valerolactam (**46**) (36) with methoxyphenylsulfanyl acetaldehyde (**47**) (37). Quenching the reaction with acetic anhydride followed by aqueous workup provided the expected acetate **48** in 68% yield as a complex mixture of diastereomers. Cyclic lactam **48** was acylated with 3-butenoyl chloride using powdered 4 Å molecular sieves as a neutral acid scavenger (38) to provide the corresponding imide **49** in 94% yield. It was known from earlier work in the literature that treatment of thioketals with dimethyl(methyl-thio)sulfonium tetrafluoroborate (DMTSF) causes the carbon–sulfur bond to become labile upon methylthiolation (39). The initially formed alkylthiosulfonium ion easily dissociates to produce a thionium ion and methyl sulfide (40). In a similar fashion, treatment of **49** with DMTSF generates an oxonium ion, which cyclizes onto the imido carbonyl group to give amidofuran **50** in 65% yield. Thermolysis of **50** at 110°C for 30 min produced phenol **53** in 58% yield (Scheme 8). The thermal reaction is best rationalized by an initial Diels-Alder reaction of the furan across the tethered π-bond (41) to produce cycloadduct **51** as a transient intermediate. A subsequent ring opening followed by elimination of methanol produces cyclohexadienone **52**, which rapidly tautomerizes to give the observed phenol **53** (Scheme 9).

© 2001 NRC Canada

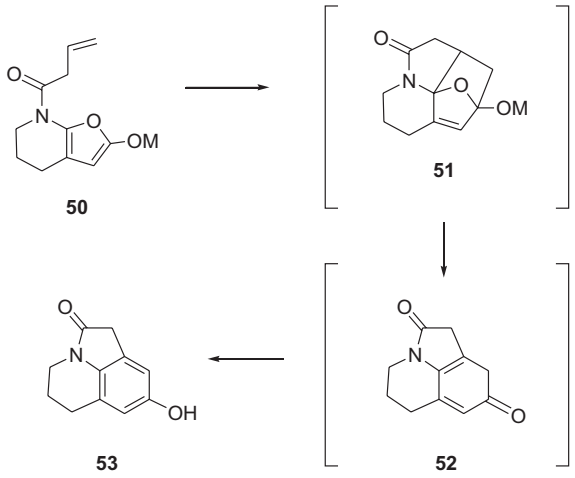
Scheme 7.



Scheme 8.



Scheme 9.



In conclusion, this paper describes several cyclization–cycloaddition cascade sequences that can be used for the construction of various azapolyheterocyclic ring systems. The synthetic procedures described here involve (*i*) the Rh(II)-catalyzed reaction of diazo amidoketones; (*ii*) acylation of an amido substituted furanone followed by a bimolecular Diels-Alder cycloaddition; and (*iii*) the DMTSF induced cyclization–cycloaddition reaction of an imido thiophenylmethoxy substituted acetal. Further studies of the IMDAF cycloaddition of cyclic 2-amidofurans are in progress and will be reported in due course.

Experimental

Melting points are uncorrected. Mass spectra were determined at an ionizing voltage of 70 eV. Unless otherwise noted, all reactions were performed in flame dried glassware under an atmosphere of dry argon. Solutions were evaporated under reduced pressure with a rotary evaporator and the residue was chromatographed on a silica gel column using an ethyl acetate – hexane mixture as the eluent unless specified otherwise. All solids were recrystallized from ethyl acetate – hexane for analytical data.

3-(Diazoethoxycarbonylacetyl)-2-oxo-piperidine-3-carboxylic acid ethyl ester

To a stirred solution of 3-carboethoxy-2-piperidone (0.5 g, 2.9 mmol) in THF (25 mL) at 0°C was added a 2.0 M isopropyl magnesium chloride solution (1.6 mL, 3.2 mmol) over a 20 min period. The reaction mixture was allowed to stir at 0°C for 1 h, and then ethyl 2-diazomalonyl chloride (18) (0.6 g, 3.5 mmol) was added dropwise. After stirring

© 2001 NRC Canada

for 1 h at 0°C, the reaction mixture was quenched with water (50 mL) and extracted with ethyl acetate. The combined extracts were washed with brine, dried over anhydrous $MgSO_4$, filtered, and concentrated under reduced pressure. The residue was subjected to flash chromatography on silica gel to give 0.23 g (25%) of the titled compound as a pale yellow oil. IR (neat) (cm^{-1}): 2139, 1737, 1717, 1677, 1643. ^1H NMR (300 MHz, $CDCl_3$) δ: 1.25–1.31 (m, 6H), 1.71–1.82 (m, 2H), 2.38–2.59 (m, 2H), 3.28–3.45 (m, 2H), 4.21–4.30 (m, 4H), 6.70 (s, 1H). ^{13}C NMR (75 MHz, $CDCl_3$) δ: 13.7, 14.1, 18.7, 27.1, 41.7, 61.5, 62.0, 66.9, 128.1, 160.6, 165.9, 167.3, 186.9. This material was used in the next step without further purification.

3-(Diazoethoxycarbonylacetyl)-2-oxo-1-(2-vinylbenzoyl)-piperidine-3-carboxylic acid ethyl ester (6)

To a sample of *o*-vinyl benzoic acid (42) (0.06 g, 0.39 mmol) in CH_2Cl_2 (10 mL) was added oxalyl chloride (0.12 mL, 1.4 mmol) followed by one drop of DMF. The solution was allowed to stir at rt for 1 h and was concentrated under reduced pressure to remove the excess oxalyl chloride. The residue was dissolved in benzene (8 mL) and this was slowly added to a solution of benzene (5 mL) and the above diazo amide (0.1 g, 0.3 mmol), which contained triethylamine (0.14 mL, 1.0 mmol) at 0°C. The reaction was maintained at 0°C for 30 min and was stirred at rt for 24 h. The solution was quenched with water (50 mL) and extracted with ethyl acetate. The combined extracts were washed with a saturated $NaHCO_3$ solution, brine, dried over anhydrous $MgSO_4$, filtered, and concentrated under reduced pressure. The residue was subjected to flash chromatography on silica gel to give 0.05 g (35%) of **6** as a yellow oil. IR (neat) (cm^{-1}): 2141, 1738, 1712, 1678, 1639. ^1H NMR (300 MHz, $CDCl_3$) δ: 1.21–1.36 (m, 6H), 1.86–2.09 (m, 2H), 2.41 (td, 1H, J = 11.0, 4.2 Hz), 2.64 (m, 1H), 3.90 (td, 1H, J = 11.0, 4.2 Hz), 4.01–4.35 (m, 5H), 5.24 (d, 1H, J = 11.1 Hz), 5.66 (d, 1H, J = 17.3 Hz), 6.79 (dd, 1H, J = 17.3, 11.0 Hz), 7.12–7.34 (m, 3H), 7.54 (d, 1H, J = 7.8 Hz). ^{13}C NMR (75 MHz, $CDCl_3$) δ: 13.9, 14.2, 20.4, 28.4, 44.8, 61.7, 62.8, 69.3, 77.1, 116.1, 125.8, 125.9, 126.8, 129.5, 134.3, 135.3, 136.5, 160.8, 166.2, 167.1, 173.3, 186.4. This material was used in the next step without further purification.

Ethyl 9-aza-13-(ethoxycarbonyl)-16-oxa-8,14-dioxopentacyclo[13.2.1.$0^{2,7}$.$0^{9,17}$-.$0^{13,14}$]octadeca-2(3),4,6-triene-15-carboxylate (7)

To a mixture of diazo amido ester **6** (0.05 g, 0.11 mmol) in benzene (5 mL) was added rhodium(II) acetate (2 mg). The mixture was allowed to stir at 50°C for 6 h. The solvent was removed under reduced pressure, and the residue was subjected to flash chromatography on silica gel to afford 0.05 g (92%) of cycloadduct **7** as a pale yellow solid: mp 176–177°C. IR (neat) (cm^{-1}): 1782, 1736, 1664, 1599. ^1H NMR (300 MHz, $CDCl_3$) δ: 1.19–1.35 (m, 6H), 1.89–1.92 (m, 1H), 2.05–2.13 (m, 2H), 2.29–2.33 (m, 1H), 2.53 (dd, 1H, J = 13.3, 5.0 Hz), 2.94 (dd, 1H, J = 13.3, 9.4 Hz), 3.19–3.21 (m, 1H), 3.97 (dd, 1H, J = 9.4, 5.0 Hz), 4.21–4.32 (m, 4H), 4.66–4.71 (m, 1H), 7.11 (d, 1H, J = 7.7 Hz), 7.34–7.38 (m, 1H), 7.53 (t, 1H, J = 7.5 Hz), 8.17 (d, 1H, J = 7.7 Hz). ^{13}C NMR (75 MHz, $CDCl_3$) δ: 13.9, 14.0, 19.4, 27.1, 36.9, 38.9, 39.4, 58.5, 62.3, 62.4, 85.4, 94.2, 125.3, 126.6, 127.3, 128.7, 133.3, 138.9, 163.7, 164.5, 167.8, 198.2. Anal. calcd. for $C_{22}H_{23}NO_7$: C 63.91, H 5.62, N 3.39; found: C 63.93, H 5.65, N 3.37.

3-(Diazo-ethoxycarbonyl-acetyl)-2-oxo-pyrrolidine-3-carboxylic acid ethyl ester

To a stirred solution of 3-carboethoxy-2-pyrrolidone (43) (1.0 g, 6.4 mmol) in THF (40 mL) at 0°C was added a 2.0 M isopropyl magnesium chloride solution (3.5 mL, 7.0 mmol) dropwise over a 30 min period. The mixture was allowed to stir at 0°C for 1 h and then ethyl 2-diazomalonyl chloride (1.3 g, 7.6 mmol) was added dropwise. After stirring for 1 h at 0°C, the reaction mixture was quenched with water (100 mL) and extracted with ethyl acetate. The combined organic extracts were washed with brine, dried over anhydrous $MgSO_4$, filtered, and concentrated under reduced pressure. The residue was subjected to flash chromatography on silica gel to give 1.1 g (58%) of the titled compound as a colorless oil. IR (neat) (cm^{-1}): 2139, 1743, 1709, 1641. ^1H NMR (300 MHz, $CDCl_3$) δ: 1.18–1.30 (m, 6H), 2.33–2.41 (m, 1H), 3.04–3.11 (m, 1H), 3.19–3.28 (m, 1H), 3.38–3.44 (m, 1H), 4.14–4.29 (m, 4H), 7.54 (br s, 1H). ^{13}C NMR (75 MHz, $CDCl_3$) δ: 13.8, 14.1, 30.2, 39.4, 61.7, 62.1, 66.9, 75.1, 160.8, 167.1, 170.8, 185.8. This material was used in the next step without further purification.

3-(Diazoethoxycarbonylacetyl)-2-oxo-1-(2-vinylbenzoyl)-pyrrolidine-3-carboxylic acid ethyl ester (12)

To a sample of *o*-vinyl benzoic acid (0.3 g, 2.0 mmol) in CH_2Cl_2 (25 mL) was added oxalyl chloride (0.6 mL, 7.3 mmol) and two drops of DMF. The solution was allowed to stir at rt for 1 h and was concentrated under reduced pressure to remove the excess oxalyl chloride. The residue was dissolved in benzene (5 mL) and this solution was added slowly to a solution of benzene (5 mL) and the above diazo amido ester (0.48 g, 1.6 mmol), which contained triethylamine (0.7 mL, 5.0 mmol) at 0°C. The mixture was maintained at 0°C for 30 min and was stirred at rt for 24 h. The solution was quenched with water (50 mL) and extracted with ethyl acetate. The combined organic extracts were washed with a saturated sodium bicarbonate solution, brine, dried over anhydrous $MgSO_4$, filtered, and concentrated under reduced pressure. The residue was subjected to flash chromatography on silica gel to give 0.48 g (72%) of **12** as a colorless oil. IR (neat) (cm^{-1}): 2143, 1766, 1637, 1595. ^1H NMR (300 MHz, $CDCl_3$) δ: 1.20–1.33 (m, 6H), 2.50–2.58 (m, 1H), 3.03–3.13 (m, 1H), 3.70–3.79 (m, 1H), 4.09–4.32 (m, 5H), 5.34 (d, 1H, J = 11.1 Hz), 5.71 (d, 1H, J = 17.4 Hz), 6.30 (dd, 1H, J = 17.4, 11.1 Hz), 7.28–7.45 (m, 3H), 7.58 (d, 1H, J = 7.8 Hz). ^{13}C NMR (75 MHz, $CDCl_3$) δ: 13.6, 14.0, 26.3, 42.2, 60.1, 61.8, 62.3, 69.6, 116.8, 125.4, 126.9, 127.0, 129.9, 133.4, 133.6, 135.3, 160.5, 165.5, 166.6, 169.3, 185.2. This material was used in the next step without further purification.

Ethyl 9-aza-12-(ethoxycarbonyl)-15-oxa-8,13-dioxopentacyclo[12.2.1.$0^{2,7}$.$0^{9,16}$-.$0^{12,16}$]heptadeca-2(3),4,6-triene-14-carboxylate (13)

To a sample of diazo amide **12** (0.35 g, 0.8 mmol) in benzene (10 mL) was added rhodium(II) acetate (2 mg). The reaction mixture was allowed to stir at 50°C for 6 h. The solvent was removed under reduced pressure, and the resi-

© 2001 NRC Canada

due was subjected to flash silica gel chromatography to give 0.06 g (20%) of cycloadduct **13** as a white solid: mp 212–213°C. IR (neat) (cm^{-1}): 1774, 1760, 1734, 1681, 1603, 1238. ^1H NMR (300 MHz, $CDCl_3$) δ: 1.21–1.43 (m, 6H), 2.39–2.52 (m, 1H), 2.63–2.79 (m, 2H), 3.10–3.19 (m, 2H), 3.61–3.74 (m, 2H), 4.01–4.24 (m, 4H), 7.15–8.11 (m, 4H). ^{13}C NMR (75 MHz, $CDCl_3$) δ: 13.9, 15.1, 22.7, 42.7, 63.0, 63.1, 65.4, 92.5, 112.1, 117.0, 125.8, 127.1, 127.2, 130.2, 133.5, 133.6, 135.4, 160.2, 165.9, 169.4, 198.9. Anal. calcd. $C_{21}H_{21}NO_7$: C 63.15, H 5.30, N 3.51; found: C 63.06, H 5.31, N 3.45.

3-Diazoacetyl-2-oxo-1-phenylpyrrolidine (14)

A mixture containing 2-oxo-1-phenylpyrrolidine carboxylic acid (44) (2.0 g, 9.6 mmol), triphosgene (1.0 g, 3.2 mmol), and 1 drop of DMF in *m*-dichlorobenzene (20 mL) was stirred at 60°C for 24 h. The reaction mixture was allowed to cool to rt and was poured into an ethereal solution containing diazomethane (50 mmol). The reaction mixture was stirred overnight and a yellow precipitate formed. The crude product was chromatographed on silica gel to give 1.6 g (75%) of diazo pyrrolidine **14** as a pale yellow solid: mp 127–128°C. MS *m*/*z*: 229 (M^+), 219, 201, 172, 160, 144, 130, 119, 106, 105, 104. IR (neat) (cm^{-1}): 2108, 1690, 1636, 1497, 1304, 1224, 752, 690. ^1H NMR (300 MHz, $CDCl_3$) δ: 2.20–2.31 (m, 1H), 2.68–2.80 (m, 1H), 3.53 (q, 1H, *J* = 3.0 Hz), 3.78–3.98 (m, 2H), 5.92 (s, 1H), 7.16 (t, 1H, *J* = 7.5 Hz), 7.36 (t, 2H, *J* = 7.5 Hz), 7.56 (d, 2H, *J* = 8.4 Hz). ^{13}C NMR (75 MHz, $CDCl_3$) δ: 19.7, 47.2, 54.0, 55.2, 120.0, 125.0, 128.8, 138.7, 169.6, 188.8. Anal. calcd. for $C_{12}H_{11}N_3O_2$: C 62.86, H 4.84, N 18.34; found: C 62.74, H 4.77, N 18.19.

4,5-Dihydro-3-oxo-6-phenyl-2*H*-furo[2,3-*b*]pyrrole (16)

A solution containing diazo pyrrolidine **14** (0.28 g, 1.2 mmol) in CH_2Cl_2 (1 mL) was treated with rhodium(II) acetate (10 mg). The reaction was stirred for 24 h, filtered, and concentrated under reduced pressure to give a quantitative yield of dihydropyrrole **16** as a clear oil. IR ($CHCl_3$) (cm^{-1}): 3066, 2988, 1670, 1584, 1301, 933. ^1H NMR (300 MHz, $CDCl_3$) δ: 2.78 (t, 2H, *J* = 8.1 Hz), 4.32 (t, 2H, *J* = 8.1 Hz), 5.09 (s, 2H), 7.08 (t, 1H, *J* = 7.8 Hz), 7.24 (d, 2H, *J* = 7.8 Hz), 7.32 (t, 2H, *J* = 7.8 Hz). ^{13}C NMR (75 MHz, $CDCl_3$) δ: 18.6, 55.2, 85.4, 95.4, 116.6, 123.6, 129.3, 137.8, 183.5, 184.0. Anal. calcd. for $C_{12}H_{11}NO_2$: C 71.61, H 5.51, N 6.96; found: C 71.53, H 5.44, N 6.85.

3-Diazoacetyl-3-methyl-2-oxo-1-phenylpyrrolidine (17)

To a solution containing diazo pyrrolidine **14** (0.5 g, 2.2 mmol) in dry DMF (5 mL) was added sodium hydride in mineral oil (0.1 g, 60%, 2.5 mmol). The reaction mixture was stirred for 15 min after which time methyl iodide (1.4 g, 10 mmol) was introduced and stirring was continued for an additional 18 h. The reaction was poured into water and extracted with dichloromethane. The solvent was removed under reduced pressure and the crude product was chromatographed on silica gel to give 0.3 g (57%) of **17** as a pale yellow oil. IR (neat) (cm^{-1}): 2110, 1740, 1695, 1600, 1460, 1350, 1050, 770, 700. ^1H NMR (300 MHz, $CDCl_3$) δ: 1.49 (s, 3H), 1.84–1.94 (m, 1H), 2.94–3.02 (m, 1H), 3.65–3.85 (m, 2H), 5.91 (s, 1H), 7.13–7.64 (m, 5H). This material was used in the next step without further purification.

3-(Cyclohepta-2′,4′,6′-trienyl)formyl-3-methyl-2-oxo-1-phenylpyrrolidine (20)

A solution containing rhodium(II) acetate (2 mg) and diazo pyrrolidine **17** (0.2 g, 0.8 mmol) in benzene (20 mL) was heated at 95°C for 1.5 h. The solvent was removed under reduced pressure and the crude mixture was chromatographed on silica gel to give 53% of 3-(cycloheptatrienyl)-pyrrolidinone **20** as a clear oil. HRMS calcd. for $C_{19}H_{19}NO_2$: 293.1416; found: 293.1416. IR (neat) (cm^{-1}): 3036, 1683, 1592, 1492, 1393, 1294, 750, 690. ^1H HMR (300 MHz, $CDCl_3$) δ: 1.53 (s, 3H), 1.93 (dd, 1H, *J* = 12.9, 8.2 Hz), 2.27 (t, 1H, *J* = 5.1 Hz), 2.75–2.85 (m, 1H), 3.70–2.82 (m, 2H), 3.98 (q, 2H, *J* = 2.4 Hz), 6.20–6.38 (m, 4H), 7.13 (t, 1H, *J* = 7.2 Hz), 7.34 (t, 2H, *J* = 8.1 Hz), 7.58 (d, 2H, *J* = 7.8 Hz). ^{13}C NMR (75 MHz, $CDCl_3$) δ: 20.7, 28.9, 36.1, 45.6, 59.3, 119.8, 124.7, 125.9, 126.1, 127.0, 128.8, 139.1, 172.3, 208.0.

3-Methyl-2-oxo-1-(*p*-toluenesulfonyl)pyrrolidine-3-carboxylic acid benzyl ester

To a suspension containing *N*-tosyl-2-pyrrolidinone (45) (7.6 g, 32 mmol) in THF (150 mL) at –78°C was added a 1.0 M solution of $NaN(TMS)_2$ in THF (32 mL). After stirring for 30 min, methyl iodide (2.9 mL, 47 mmol) was added. The mixture was stirred for an additional 1 h while warming to room temperature. The solution was quenched by the addition of a saturated aqueous NH_4Cl solution, extracted with ether, washed with H_2O, and dried over $MgSO_4$. The solvent was removed under reduced pressure, and the residue was purified by flash silica gel chromatography to give 6.9 g (87%) of 3-methyl-1-(*p*-toluenesulfonyl)-pyrrolidinone. Recrystallization from EtOAc–hexane provided a pure sample as white needles: mp 83–85°C. IR (film) (cm^{-1}): 1730, 1353, 1168. ^1H NMR (400 MHz, $CDCl_3$) δ: 1.54 (d, 3H, *J* = 7.0 Hz), 1.70 (m, 1H), 2.56 (m, 1H), 2.43 (s, 3H), 2.47 (m, 1H), 3.68 (td, 1H, *J* = 9.6, 6.9 Hz), 3.59 (m, 1H), 7.33 (d, 2H, *J* = 8.4 Hz), 7.92 (d, 2H, *J* = 8.4 Hz). ^{13}C NMR (100 MHz, $CDCl_3$) δ: 14.9, 21.7, 27.1, 38.2, 45.2, 128.0, 129.6, 135.1, 145.1, 175.8. Anal. calcd. $C_{12}H_{15}NO_3S$: C 56.90, H 5.97, N 5.53; found: C 56.75, H 5.95, N 5.50.

To a solution containing (1.9 g, 7.6 mmol) the above amide in THF (50 mL) was added a 1.0 M solution of $NaN(TMS)_2$ in THF (8 mL). After stirring the solution for 30 min, the mixture was added to a solution containing benzyl chloroformate (1.2 mL, 8.0 mmol) in THF (20 mL). The mixture was quenched by the addition of a saturated NH_4Cl solution, diluted with ether, washed with H_2O, dried over $MgSO_4$, and concentrated under reduced pressure. The residue was purified by flash silica gel chromatography to give 2.3 g (78%) of the titled compound as a colorless oil. HRMS calcd. for $C_{20}H_{21}NO_5S$: 387.1140; found: 387.1149. IR (neat) (cm^{-1}): 1747, 1735, 1166. ^1H NMR (400 MHz, $CDCl_3$) δ: 1.40 (s, 3H), 1.99 (dt, 1H, *J* = 13.1, 8.6 Hz), 2.40 (s, 3H), 2.45 (m, 1H), 3.78 (m, 1H), 3.93 (m, 1H), 4.86 (d, 1H, *J* = 12.4 Hz), 5.05 (d, 1H, *J* = 12.4 Hz), 7.13 (m, 2H), 7.26 (m, 2H), 7.32 (m, 3H), 7.88 (d, 2H, *J* = 8.0 Hz). ^{13}C NMR (100 MHz, $CDCl_3$) δ: 19.6, 21.7, 31.0, 44.6, 52.8,

© 2001 NRC Canada

67.2, 127.6, 128.1, 128.3, 128.5, 129.5, 134.3, 135.0, 145.2, 170.3, 171.5.

3-Methyl-2-oxo-1-(*p*-toluenesulfonyl)pyrrolidine-3-carboxylic acid

A sample of the above benzyl ester (6.7 g, 17 mmol) was dissolved in EtOH (50 mL) and Pd/C (5%, 0.67 g) was added. The reaction mixture was stirred under a hydrogen atmosphere for 24 h. The catalyst was filtered and the solvent was removed under reduced pressure. The residue was taken up in an aqueous solution containing 1 equiv. of Na_2CO_3 and extracted with ether. The solution was acidified to pH 1 by the dropwise addition of concentrated HCl and the aqueous layer was extracted with ether. The combined organic layers were dried over $MgSO_4$ and concentrated under reduced pressure to give 4.1 g (80 %) of the titled compound as a white solid: mp 134 –135°C. IR (film) (cm^{-1}): 3296 (br), 1744, 1737. ^1H NMR (400 MHz, $CDCl_3$) δ: 1.39 (s, 3H), 2.04 (dt, 1H, *J* = 13.4, 7.6 Hz), 2.44 (s, 3H), 2.52 (ddd, 1H, *J* = 13.4, 7.3, 4.7 Hz), 3.80 (br s, 1H), 3.90 (m, 2H), 7.33 (d, 2H, *J* = 8.1 Hz), 7. 90 (d, 2H, *J* = 8.1 Hz). ^{13}C NMR (100 MHz, $CDCl_3$) δ: 19.5, 21.7, 30.6, 44.4, 52.5, 128.1, 129.7, 134.1, 145.6, 171.6, 175.5. Anal. calcd. $C_{13}H_{15}NO_5S$: C 52.51, H 5.08, N 4.71; found: C 52.65, H 4.96, N 4.68.

3-Diazoacetyl-3-methyl-1-(*p*-toluenesulfonyl)pyrrolidinone (18)

To a solution containing the above acid (1.0 g, 3.4 mmol) in ether (20 mL) was added of Et_3N (1.4 mL, 10 mmol) followed by pivalyl chloride (0.5 mL, 4.4 mmol). After stirring for 30 min, the mixed anhydride was filtered into a freshly prepared ether solution of diazomethane (13.4 mmol) at 0°C. The mixture was stirred for 1 h and was concentrated under reduced pressure. Flash chromatographic purification of the residue on silica gel provided 1.0 g (97%) of diazo ketoamide **18** as a yellow oil. IR (neat) (cm^{-1}): 3111, 2108, 1730, 1631. ^1H NMR (400 MHz, $CDCl_3$) δ: 1.36 (s, 3H), 1.82 (dt, 1H, *J* = 13.1, 8.5 Hz), 2.44 (s, 3H), 2.83 (ddd, 1H, *J* = 13.1, 7.3, 3.2 Hz), 3.73 (ddd, 1H, *J* = 9.9, 8.6, 7.2 Hz), 3.85 (ddd, 1H, *J* = 10.1, 8.6, 3.2 Hz), 5.52 (s, 1H), 7.35 (d, 2H, *J* = 8.2 Hz), 7.89 (d, 2H, *J* = 8.2 Hz). This material was used in the next step without further purification.

4-Aza-9-((3-methyl-1-*p*-toluenesulfonyl-2-oxopyrrolidin-3-yl)-carbonyl)-4-phenyl-tetracyclo[5.3.2.$0^{2,6}$.$0^{8,10}$]dodeca-11-ene-3,5-dione (21)

To a solution containing diazo ketoamide **18** (0.22 g, 0.68 mmol) and *N*-phenylmaleimide was added rhodium(II) perfluorobutyrate (4 mg). After stirring overnight, the reaction mixture was concentrated under reduced pressure. Flash chromatography provided adduct **21** as a white solid: mp 219–220°C. IR (film) (cm^{-1}): 1733, 1708, 1171. ^1H NMR (300 MHz, $CDCl_3$) δ: 1.37 (s, 3H), 1.47 (m, 1H), 1.80 (m, 2H), 1.99 (t, 1H, *J* = 2.9 Hz), 2.50 (s, 3H), 2.71 (ddd, 1H, *J* = 12.9, 6.8, 2.9 Hz), 3.03 (dd, 1H, *J* = 8.1, 3.4 Hz), 3.10 (dd, 1H, *J* = 8.1, 3.4 Hz), 3.17 (m, 1H), 3.57 (m, 1H), 3.64 (m, 1H), 3.86 (ddd, 1H, *J* = 10.0, 9.8, 2.9 Hz), 5.89 (m, 2H), 7.15 (d, 2H, *J* = 8.4 Hz), 7.39 (m, 5H), 7.89 (d, 2H, *J* = 8.4 Hz). ^{13}C NMR (100 MHz, $CDCl_3$) δ: 20.1, 21.6, 23.4, 23.7, 24.0, 28.4, 33.0, 33.1, 44.2, 44.4, 59.2, 126.3, 128.0, 128.1, 128.3, 128.6, 129.0, 129.5, 131.5, 134.6, 145.5, 171.8, 176.4, 176.5, 202.5. Anal. calcd. $C_{30}H_{28}N_2O_6S$: C 66.16, H 5.18, N 5.14; found: C 65.90, H 5.09, N 5.03.

1-(2′,2′-Dimethylpropionyl)-2-oxopyrrolidine-3-carboxylic acid

A solution containing $NaN(TMS)_2$ (80 mL, 1.0 M) in THF was cooled to –78°C and 1-(2′,2′-dimethylpropionyl)-pyrrolidin-2-one (46) (6.4 g, 38 mmol) in THF (20 mL) was added. After stirring for 30 min at rt, benzyl chloroformate (5.4 mL, 38 mmol) in THF (20 mL) was added dropwise. After stirring for 30 min at –78°C, the mixture was quenched by the addition of a 10% solution of aqueous HCl. The solution was extracted with ether, and the organic layer was dried over $MgSO_4$. The crude product was used in the next step without further purification.

The crude benzyl ester (10.3 g) was taken up in EtOH (200 mL) and 5% Pd/C was added. The mixture was shaken in a Parr shaker for 30 min under a hydrogen atmosphere at 40 psi. The Pd/C catalyst was filtered, and the solution was concentrated under reduced pressure. The residue was taken up in water containing 2 equiv. of Na_2CO_3 and was washed with ether. The aqueous layer was acidified to pH 1 by the dropwise addition of concentrated HCl, and the precipitate was filtered to provide 5.1 g (62%) of the titled compound as a pale yellow solid: mp 153–154°C. IR (film) (cm^{-1}): 3068 (br), 1752, 1730, 1645. ^1H NMR (400 MHz, $CDCl_3$) δ: 1.34 (s, 9H), 2.41 (m, 2H), 3.67 (t, 1H, *J* = 9.5 Hz), 3.76 (ddd, 1H, *J* = 12.6, 8.8, 8.0 Hz), 3.96 (ddd, 1H, *J* = 12.6, 8.0, 4.4 Hz). Anal. calcd. for $C_{10}H_{15}NO_4$: C 56.33, H 7.09, N 6.57; found: C 56.48, H 7.16, N 6.62.

2-Diazo-3-[1′-(2′′,2′′-dimethylpropionyl)-2′-oxopyrolidin-3′-yl]-3-oxopropionic acid ethyl ester (22)

To a solution containing the above carboxylic acid (1.0 g, 4.7 mmol) and hexachloroacetone (0.6 g, 2.4 mmol) was added dropwise triphenyl phosphine (1.2 g, 4.7 mmol) in THF (20 mL). After stirring for 30 min at rt, the solution was added dropwise to a solution of ethyl diazoacetate (1.1 g, 9.4 mmol) in THF (5 mL). The mixture was heated at 50°C for 2 h. After cooling, the solution was concentrated under reduced pressure, and the residue was purified by flash chromatography to give 1.0 g (70%) of **22** as a yellow oil. IR (neat) (cm^{-1}): 2143, 1716, 1687, 1652. ^1H NMR (400 MHz, $CDCl_3$) δ: 1.31 (s, 9H), 1.34 (t, 3H, *J* = 7.2 Hz), 2.04 (m, 1H), 2.45 (dq, 1H, *J* = 12.8, 9.2 Hz), 3.75 (ddd, 1H, *J* = 11.5, 8.5, 7.6 Hz), 3.94 (ddd, 1H, *J* = 11.5, 8.9, 3.7 Hz), 4.32 (q, 2H, *J* = 7.2 Hz), 4.97 (t, 1H, *J* = 9.2). This material was used in the next step without further purification.

2,2-Dimethylpropionic acid 6-(2′,2′-dimethylpropionyl)-5,6-dihydro-4*H*-furo[2,3-*b*]-pyrrol-3-yl ester (25)

A solution containing diazoketone **22** (0.4 g, 1.3 mmol) and rhodium(II) acetate (3 mg) in benzene (7 mL) was heated at reflux for 30 min. After cooling to rt, Et_3N (0.4 mL, 2.7 mmol) was added followed by pivalyl chloride (0.25 mL, 2.0 mmol). After stirring for 1 h, the reaction mixture was filtered and concentrated under reduced pressure. Flash chromatography on silica gel provided 0.36 g (74%) of furan **25** as a colorless oil. IR (neat) (cm^{-1}): 1766, 1702, 1652, 1616, 1545. ^1H NMR (300 MHz, $CDCl_3$) δ: 1.33 (t, 3H, *J* =

© 2001 NRC Canada

7.3 Hz), 1.36 (s, 9H), 1.37 (s, 9H), 2.88 (m, 2H), 4.30 (q, 2H, *J* = 7.1 Hz), 4.41 (m, 2H). ^{13}C NMR (75 MHz, $CDCl_3$) δ: 14.5, 21.5, 26.5, 27.0, 39.3, 39.7, 55.1, 60.2, 104.7, 130.4, 142.7, 153.0, 157.4, 174.3, 174.4. Anal. calcd. for $C_{19}H_{27}NO_6$: C 62.45, H 7.45, N 3.83; found: C 62.56, H 7.55, N 3.88.

A sample of the highly reactive (2′,2′-dimethylpropionyl)-5,6-dihydro-4*H*-furo[2,3-*b*]pyrrol-3-one (**24**) intermediate was obtained from the column as a minor product and showed the following NMR properties: ^{1}H NMR (400 MHz, $CDCl_3$) δ: 1.34 (t, 3H, *J* = 7.2 Hz), 1.36 (s, 9H) 2.66 (m, 2H), 4.34 (m, 2H), 4.43 (m, 2H), 5.57 (s, 1H).

2,10-Diaza-2-(2,2-dimethyl-propanoyl)-7-(ethoxycarbonyl)-13-oxa-9,11-dioxo-10-phenyltetracyclo[5.5.0^{1,5}.0^{8,12}]-tridec-5(6)-en-6-yl-2,2-dimethyl propanoate (26)

A solution containing amidofuran **25** (0.35 g, 1.0 mmol) and *N*-phenylmaleimide (2.0 g, 1.1 mmol) in toluene (5 mL) was heated at reflux for 2 h. The solution was concentrated under reduced pressure and subjected to flash silica gel chromatography to give 0.5 g (95%) of a 1:3 mixture of compounds **26** and **27**. Chromatographic separation afforded a pure sample of **26** as a clear oil: IR (film) (cm^{-1}): 1769, 1727, 1658, 1623, 1147. ^{1}H NMR (400 MHz, $CDCl_3$) δ: 1.21 (t, 3H, *J* = 7.1 Hz), 1.35 (s, 9H), 1.36 (s, 9H), 2.77 (ddd, 1H, *J* = 15.4, 7.2, 1.1 Hz), 2.97 (m, 1H), 4.08–4.32 (m, 5H), 5.74 (ddd, 1H, *J* = 9.8, 2.9, 0.7 Hz), 7.26 (m, 2H), 7.44 (m, 3H). ^{13}C NMR (75 MHz, $CDCl_3$) δ: 13.7, 26.7, 27.1, 27.4, 39.1, 40.5, 41.1, 46.4, 51.0, 63.5, 82.0, 117.3, 126.4, 128.7, 129.0, 131.6, 154.4, 167.0, 170.6, 173.0, 176.8, 179.8, 182.2. Anal. calcd. for $C_{29}H_{34}N_2O_8$: C 64.67, H 5.20, N 5.38; found: C 64.37, H 6.24, N 5.09.

1-(2,2-Dimethylpropionyl)-4-(2,2-dimethylpropionyloxy)-6,8-dioxo-7-phenyl-1,2,3,6,7,8-hexahydro-1,7-diaza-as-indacene-5-carboxylic acid ethyl ester (27)

The major fraction isolated from the silica gel chromatographic separation was a white solid whose structure was assigned as **27** on the basis of the following spectral data: mp 198–200°C. IR (film) (cm^{-1}): 1765, 1724, 1692, 1284. ^{1}H NMR (400 MHz, $CDCl_3$) δ: 1.36 (s, 9H), 1.38 (t, 3H, *J* = 7.1 Hz), 1.41 (s, 9H), 3.07 (t, 2H, *J* = 7.9 Hz), 4.21 (t, 2H, *J* = 7.9 Hz), 4.41 (q, 2H, *J* = 7.1 Hz), 7.32–7.48 (m, 5H). ^{13}C NMR (75 MHz, $CDCl_3$) δ: 14.0, 27.0, 28.0, 28.0, 39.3, 40.4, 51.0, 62.4, 116.0, 120.7, 126.8, 128.0, 128.9, 130.2, 131.6, 133.9, 143.8, 147.9, 163.4, 163.5, 164.8, 174.7, 178.7. Anal. calcd. for $C_{29}H_{32}N_2O_7$: C 66.91, H 6.20, N 5.38; found: C 66.89, H 6.10, N 5.55.

2-(2,2-Dimethylpropionyl)-6-(2,2-dimethylpropionyloxy)-10-oxa-2-azatricyclo-[5.2.1.0^{1,5}]deca-5,8-diene-7,8,9-tricarboxylic acid 7-ethyl ester 8,9-dimethyl ester (28)

A solution containing amidofuran **25** (1.7 mmol) and dimethyl acetylenedicarboxylate (0.3 mL, 2.6 mmol) in toluene (8 mL) was heated at reflux for 24 h. The solution was concentrated under reduced pressure and subjected to flash silica chromatography to give three major fractions. The minor fraction contained 0.12 g (14%) of **28** as yellow oil. HRMS calcd. for $C_{25}H_{33}NO_{10}$: 507.2104; found: 507.2107. IR (neat) (cm^{-1}): 1759, 1695, 1659, 1211. ^{1}H NMR (400 MHz, $CDCl_3$) δ: 1.23 (s, 9H), 1.26 (t, 3H, *J* = 7.1 Hz), 1.30 (s, 9H), 2.95 (m, 2H), 3.69 (s, 3H), 3.75 (s, 3H), 4.20 (m, 2H), 4.31 (m, 2H). ^{13}C NMR (100 MHz, $CDCl_3$) δ: 13.8, 26.7, 27.4, 38.6, 40.2, 50.4, 52.5, 52.7, 63.3, 81.6, 121.7, 128.2, 139.9, 153.2, 161.5, 163.3, 163.9, 176.2, 180.2, 183.9.

1-(2,2-Dimethylpropionyl)-4-hydroxy-1*H*-indole-5,6,7-tricarboxylic acid 5-ethyl ester 6,7-dimethyl ester (29)

The middle fraction from the silica gel column contained 0.36 g (22%) of indole **29** as a white solid: mp 149–150°C. IR (film) (cm^{-1}): 1745, 1735, 1706, 1660, 1607. ^{1}H NMR (400 MHz, $CDCl_3$) δ: 1.49 (s, 9H), 1.51 (t, 3H, *J* = 7.1 Hz), 3.88 (s, 3H), 3.93 (s, 3H), 4.53 (q, 2H, *J* = 7.1 Hz), 7.10 (d, 1H, *J* = 3.8 Hz), 7.77 (d, 1H, *J* = 3.8 Hz), 11.77 (s, 1H). ^{13}C NMR (100 MHz, $CDCl_3$) δ: 14.2, 28.5, 41.4, 52.7, 52.8, 62.2, 105.1, 108.1, 119.1, 125.8, 126.6, 129.5, 131.7, 156.8, 165.6, 166.5, 170.4, 178.1. Anal. calcd. for $C_{20}H_{23}NO_8$: C 59.25, H 5.72, N 3.45; found: C 59.14, H 5.61, N 3.38.

1-(2,2-Dimethylpropionyl)-4-(2,2-dimethylpropionyloxy)-5-oxo-1,2,3,5-tetrahydro-indole-6,6,7-tricarboxylic acid ethyl ester dimethyl ester (31)

The third fraction contained 0.23 g (35%) of **31** as a pale yellow solid: mp 70–71°C. IR (film) (cm^{-1}): 1766, 1738, 1652, 1289. ^{1}H NMR (400 MHz, $CDCl_3$) δ: 1.27 (t, 3H, *J* = 7.1 Hz), 1.32 (s, 9H), 1.34 (s, 9H), 2.85 (t, 2H, *J* = 6.9 Hz), 3.71 (s, 3H), 3.81 (s, 3H), 4.12 (m, 2H), 4.72 (m, 2H). ^{13}C NMR (100 MHz, $CDCl_3$) δ: 13.6, 25.9, 26.9, 27.6, 39.0, 40.5, 48.8, 51.6, 53.7, 63.1, 70.5, 112.7, 139.3, 139.4, 143.4, 163.9, 164.7, 164.9, 174.6, 177.6, 182.2. Anal. calcd. for $C_{25}H_{33}NO_{10}$: C 59.16, H 6.55, N 2.76; found: C 59.31, H 6.66, N 2.63.

2-Oxo-pyrrolidine-3-carboxylic acid *tert*-butyl ester

A solution containing *N*-trimethylsilylpyrrolidinone (47) (25.0 g, 260 mmol) in THF (150 mL) at –78°C was treated with a 1.0 M solution of $NaN(TMS)_2$ in THF (159 mL). The mixture was stirred for 30 min, and di-*tert*-butyldicarbonate (17.3 g, 80 mmol) in THF (50 mL) was added. The reaction mixture was stirred for 30 min and was quenched by the addition of a saturated NH_4Cl solution, diluted with ether, and dried over magnesium sulfate. The solvent was removed under reduced pressure, and the residue was purified by silica gel chromatography to give 9.1 g (62%) of the title compound as a white solid: mp 79–80°C. IR (film) (cm^{-1}): 3246, 3111, 1730, 1695. ^{1}H NMR (400 MHz, $CDCl_3$) δ: 1.48 (s, 9H), 2.34 (m, 1H), 2.43 (m, 1H), 3.24 (dd, 1H, *J* = 9.3, 6.7 Hz), 3.34 (td, 1H, *J* = 8.8, 6.1 Hz), 3.48 (td, 1H, *J* = 8.9, 5.3 Hz), 6.53 (s, 1H). ^{13}C NMR (100 MHz, $CDCl_3$) δ: 25.1, 27.9, 40.8, 48.8, 81.7, 169.3, 174.4. Anal. calcd. for $C_9H_{15}NO_3$: C 58.36, H 8.16, N 7.56; found: C 58.10, H 8.18, N 7.48.

2-Oxo-1-pent-4-enylpyrrolidine-3-carboxylic acid *tert*-butyl ester

A suspension of the above pyrrolidone (8.9 g, 48 mmol) in THF (250 mL) at –78°C was treated with a 2.5 M solution of *n*-butyllithium in hexane (39 mL, 97 mmol). After stirring at 78°C for 30 min, pentenoyl chloride (5.7 g, 48 mmol) in THF (20 mL) was added dropwise. The reaction mixture was allowed to warm to rt and was quenched by the addition of a saturated NH_4Cl solution. The mixture was diluted with ether, washed with a NH_4Cl solution, and dried

© 2001 NRC Canada

over magnesium sulfate. Purification of the residue by silica gel chromatography afforded 9.8 g (76%) of the title compound as a white solid: mp 51–52°C. IR (film) (cm^{-1}): 1729, 1641, 1359, 1709, 1143. ^1H NMR (400 MHz, $CDCl_3$) δ: 1.50 (s, 9H), 2.26 (m, 1H), 2.33 (m, 1H), 2.40 (m, 2H), 3.01 (td, 2H, *J* = 7.3, 2.4 Hz), 3.51 (dd, 1H, *J* = 9.1, 7.9 Hz), 3.71 (dt, 1H, *J* = 11.4, 7.6 Hz), 3.92 (ddd, 1H, *J* = 11.5, 8.5, 5.1 Hz), 5.00 (dq, 1H, *J* = 10.2, 1.4 Hz), 5.07 (dq, 1H, *J* = 17.1, 1.7 Hz), 5.85 (ddt, 1H, *J* = 17.0, 10.3, 6.6 Hz). ^{13}C NMR (100 MHz, $CDCl_3$) δ: 21.5, 27.9, 28.0, 36.2, 43.8, 51.9, 82.7, 115.4, 136.9, 167.7, 170.8, 173.5. Anal. calcd. for $C_{14}H_{21}NO_4$: C 62.90, H 7.92, N 5.24; found: C 63.02, H 7.84, N 5.19.

2-Oxo-1-pent-4-enyl-pyrrolidinone-3-carboxylic acid

A sample of the above *tert*-butyl ester (4.4 g, 17 mmol) was dissolved in a mixture of trifluoroacetic acid (10 mL) and CH_2Cl_2 (10 mL), and the solution was stirred vigorously at rt for 2 h. The solvent was removed under reduced pressure, and the residue was dissolved in water which contained 2 equiv. of Na_2CO_3. The solution was extracted with ether and acidified to pH 1 by the addition of concentrated HCl. The aqueous solution was extracted with ether, and the combined organic layers were dried over magnesium sulfate. The solvent was removed under reduced pressure to give 3.4 g (96%) of the title compound as a colorless oil. HRMS calcd. for $C_{10}H_{13}NO_4$: 211.0845; found: 211.0842. IR (neat) (cm^{-1}): 3190, 1744, 1701, 1370. ^1H NMR (400 MHz, $CDCl_3$) δ: 2.41 (m, 4H), 3.01 (t, 2H, *J* = 7.4 Hz), 3.68 (t, 1H, *J* = 9.0 Hz), 3.73 (dt, 1H, *J* = 11.8, 7.9 Hz), 3.98 (ddd, 1H, *J* = 11.8, 7.3, 5.7 Hz), 5.00 (dd, 1H, *J* = 10.0, 1.2 Hz), 5.08 (dq, 1H, *J* = 10.0, 1.5 Hz), 5.85 (m, 1H), 6.58 (br s, 1H). ^{13}C NMR (100 MHz, $CDCl_3$) δ: 21.1, 27.8, 36.2, 43.7, 50.4, 115.5, 136.6, 170.5, 172.6, 173.5.

Ethyl 2-diazo-3-oxo-3-(2-oxo-1-pent-4-enoylpyrrolidine-3-yl) propionate (32)

A sample of the above ketoamide (0.6 g, 2.9 mmol) was dissolved in a 2.0 M solution of $(COCl)_2$ in CH_2Cl_2 (2.9 mL, 5.8 mmol) and one drop of DMF was added. The solution was stirred at rt for 2 h, and the solvent was removed under reduced pressure. The residue was dissolved in benzene (5 mL) and this mixture was added to a solution of ethyl diazoacetate in benzene (10 mL). After stirring for 2 h, the solution was concentrated under reduced pressure, and the residue was purified by flash silica gel chromatography to give 0.5 g (55%) of diazo amido ester **32** as a yellow oil. HRMS calcd. for $C_{14}H_{17}N_3O_5$: 307.1168; found: 307.1158. IR (neat) (cm^{-1}): 2143, 1702, 1645, 1367. ^1H NMR (400 MHz, $CDCl_3$) δ: 1.34 (t, 3H, *J* = 7.2 Hz), 2.22 (m, 1H), 2.38 (m, 2H), 2.45 (m, 1H), 2.89 (t, 2H, *J* = 7.4 Hz), 3.70 (dt, 1H, *J* = 11.6, 8.1), 3.95 (ddd, 1H, *J* = 11.6, 9.0, 4.0 Hz), 4.32 (q, 2H, *J* = 5.3 Hz), 5.00 (m, 1H), 5.00 (dq, 1H, *J* = 10.2, 1.7 Hz), 5.06 (dq, 1H, *J* = 17.2, 1.7 Hz), 5.84 (ddt, 1H, *J* = 17.1, 10.4, 6.4 Hz). ^{13}C NMR (100 MHz, $CDCl_3$) δ: 14.2, 20.5, 27.9, 36.1, 43.6, 52.8, 61.8, 115.3, 136.8, 160.7, 170.9, 173.2, 187.4.

6-Aza-1-(ethoxycarbonyl)-12-oxa-7-oxotetracyclo-[8.2.1.0^{3,11}.0^{6,11}]tridec-2-en-2-yl 2,2-dimethyl-propanoate (35)

A solution containing diazo amido ester **32** (0.1 g, 0.3 mmol) in benzene (2 mL) was added dropwise to benzene (2 mL) at reflux that contained rhodium(II) acetate (2 mg). After heating for 30 min, the solution was allowed to cool to room temperature and Et_3N (0.18 mL, 1.3 mmol) was added followed by pivalyl chloride (0.09 mL, 0.75 mmol). After stirring for 1 h, the solution was filtered and the solvent was removed under reduced pressure. The residue was dissolved in toluene (4 mL) and heated at reflux for 20 h. The solvent was removed under reduced pressure and the residue was purified by flash silica gel chromatography to give 0.09 g (70%) of cycloadduct **35** as a white solid: mp 107–109°C. IR (neat) (cm^{-1}): 2975, 1730, 1666, 1617. ^1H NMR (400 MHz, $CDCl_3$) δ: 1.26 (s, 9H), 1.27 (t, 3H, *J* = 7.1 Hz), 1.65 (dq, 1H, *J* = 13.1, 4.6 Hz), 2.10 (m, 1H), 2.22 (dd, 1H, *J* = 12.5, 11.5 Hz), 2.56 (ddd, 1H, *J* = 17.5, 13.2, 5.0 Hz), 2.67 (ddd, 1H, *J* = 17.5, 4.6, 2.1 Hz), 2.82 (m, 2H), 2.88 (dd, 1H, *J* = 12.5, 5.0 Hz), 3.21 (m, 1H), 3.92 (td, 1H, *J* = 11.8, 7.4 Hz), 4.03 (td, 1H, *J* = 11.8, 6.4 Hz), 4.23 (m, 2H). ^{13}C NMR (100 MHz, $CDCl_3$) δ: 13.8, 23.7, 26.0, 26.8, 29.7, 32.1, 37.4, 38.8, 45.8, 62.1. Anal. calcd. for $C_{19}H_{25}NO_6$: C 62.78, H 6.94, N 3.86; found: C 62.91, H 6.87, N 3.84.

6-Aza-1-(ethoxycarbonyl)-12-oxa-7-oxotetracyclo-[8.2.1.0^{3,11}.0^{6,11}]tridec-2-en-2-yl acetate (37)

A solution containing diazoketone **32** (0.1 g, 0.3 mmol) in benzene (2 mL) was added dropwise to benzene (2 mL) at reflux that contained rhodium(II) acetate (2 mg). After heating for 30 min, the solution was allowed to cool to room temperature and Et_3N (0.18 mL, 1.3 mmol) was added followed by acetyl chloride (0.06 mL, 0.65 mmol). After stirring for 1 h, the solution was filtered, and the solvent was removed under reduced pressure. The residue was dissolved in toluene (4 mL) and heated at reflux for 20 h. The solvent was removed under reduced pressure, and the residue was purified by flash silica gel chromatography to give 0.03 g (24%) of cycloadduct **37** as a white solid: mp 171–173°C. IR (neat) (cm^{-1}): 1739, 1725, 1690, 1665, 1606. ^1H NMR (400 MHz, $CDCl_3$) δ: 1.24 (t, 3H, *J* = 7.0 Hz), 1.63 (m, 1H), 2.08 (m, 1H), 2.14 (s, 3H), 2.22 (dd, 1H, *J* = 12.7, 11.5 Hz), 2.56 (ddd, 1H, *J* = 17.5, 13.3, 5.0 Hz), 2.68 (ddd, 1H, *J* = 17.5, 4.7, 2.3 Hz), 2.83 (m, 2H), 2.93 (dd, 1H, *J* = 12.7, 5.2 Hz), 3.23 (m, 1H), 3.91 (td, 1H, *J* = 11.5, 7.8 Hz), 4.03 (m, 1H), 4.23 (m, 2H). ^{13}C NMR (100 MHz, $CDCl_3$) δ: 13.9, 21.0, 23.8, 26.1, 29.8, 32.1, 37.4, 45.8, 62.4, 82.5, 116.0, 160.7, 167.5, 167.7, 169.6, 184.1. Anal. calcd. for $C_{16}H_{19}NO_6$: C 59.79, H 5.96, N 4.36; found: C 59.88, H 5.71, N 4.35.

3-(2-Diazoacetyl)-1-(2,2-dimethylpropionyl)pyrrolidin-2-one (38)

To a solution containing 1-(2′,2′-dimethylpropionyl)-2-oxopyrrolidine-3-carboxylic acid (1.0 g, 4.7 mmol) and hexachloroacetone (0.6 g, 2.4 mmol) was added dropwise triphenyl phosphine (1.2 g, 4.7 mmol) in THF (20 mL) After stirring for 30 min, the solution was allowed to warm to rt and was added dropwise to a solution containing freshly prepared diazomethane (19 mmol) in ether (40 mL). After stirring for 2 h, the solution was concentrated and the residue was purified by flash silica gel chromatography to give 0.5 g (45%) of **38** as a yellow oil. IR (neat) (cm^{-1}): 3103, 2968, 2108, 1738, 1681, 1631. ^1H NMR (400 MHz, $CDCl_3$) δ:

© 2001 NRC Canada

1.30 (s, 9H), 2.10–2.18 (m, 1H), 2.53–2.61 (m, 1H), 3.49–3.54 (m, 1H), 3.72–3.88 (m, 2H), 5.76 (s, 1H). ^{13}C NMR (100 MHz, $CDCl_3$) δ: 19.8, 26.2, 41.8, 46.8, 55.5, 55.9, 169.9, 180.1, 187.9. This material was used in the next step without further purification.

6-(2,2-Dimethylpropionyl)-5,6-dihydro-4*H*-furo[2,3-*b*]-pyrrol-3-one (39)

A solution containing diazoketone **38** (0.5 g, 2.1 mmol) and rhodium(II) acetate (3 mg) in CH_2Cl_2 (10.0 mL) was heated to reflux for 20 min. The solution was concentrated under reduced pressure and the residue was purified by flash silica gel chromato-graphy to give 0.3 g (68%) of **39** as a white solid: mp 110–111°C. IR (film) (cm^{-1}): 3482, 2986, 2939, 1751, 1680, 1582, 1490, 1291. ^{1}H NMR (400 MHz, $CDCl_3$) δ: 1.32 (s, 9H), 2.63–2.67 (m, 2H), 4.38–4.42 (m, 2H), 5.08 (s, 2H). ^{13}C NMR (100 MHz, $CDCl_3$) δ: 17.6, 26.6, 40.4, 56.0, 84.6, 100.7, 175.5, 180.7, 186.7. Anal. calcd. for $C_{11}H_{15}NO_3$: C 63.14, H 7.23, N 6.69; found: C 62.97, H 7.28, N 6.60.

***N*-[2-(4-Methoxy-2-oxo-2,5-dihydrofuran-3-yl)-ethyl]-2,2-dimethyl-propionamide (41)**

To a solution containing furanone **39** (0.2 g, 1.1 mmol) in CH_2Cl_2 (15 mL) was added trimethyloxonium tetrafluoroborate (0.2 g, 1.1 mmol). After stirring at rt for 36 h, the reaction mixture was concentrated under reduced pressure to afford furan **40** as a very labile oil. ^{1}H NMR (400 MHz, $CDCl_3$) δ: 1.34 (s, 9H), 3.19 (t, 2H, *J* = 10.2 Hz), 4.25 (s, 3H), 4.66 (t, 2H, *J* = 10.2 Hz), 5.83 (s, 1H). ^{13}C NMR (100 MHz, $CDCl_3$) δ: 19.0, 26.3, 26.5, 41.7, 58.8, 62.3, 86.4, 107.7, 175.4, 184.2. This material was rapidly converted into **41** when exposed to moisture and this material was obtained as a colorless oil. HRMS calcd. for $C_{12}H_{19}NO_4$: 241.1314; found: 241.1324. IR (neat) (cm^{-1}): 3370, 2963, 2868, 1758, 1663, 1534, 1385, 1047. ^{1}H NMR (400 MHz, $CDCl_3$) δ: 1.14 (s, 9H), 2.47 (t, 2H, *J* = 8.8 Hz), 3.32 (q, 2H, *J* = 16.0, 8.8 Hz), 3.97 (s, 3H), 4.66 (s, 2H), 6.43 (br s, 1H). ^{13}C NMR (100 MHz, $CDCl_3$) δ: 22.0, 27.7, 38.8, 39.3, 58.2, 66.1, 100.9, 173.8, 175.7, 178.9.

6-(2,2-Dimethylpropionyl)-2-methyl-5,6-dihydro-4*H*-furo[2,3-*b*]pyrrol-3-one (42)

To a solution containing diisopropylamine (0.08 mL, 0.6 mmol) in THF (2 mL) was added a solution of *n*-butyllithium in hexane (1.5 M, 0.4 mL, 0.6 mmol) at –78°C. After stirring for 10 min, the reaction was warmed to rt and stirred for 15 min. The temperature was lowered to –78°C and furanone **39** (0.1 g, 0.5 mmol) in THF (7 mL) was added dropwise. The mixture was stirred at this temperature for 30 min and then methyl iodide (0.03 mL, 0.5 mmol) was added. After stirring for 2 h, the reaction was quenched by the addition of a saturated aqueous NH_4Cl solution, extracted with ethyl acetate, and dried over $MgSO_4$. The solvent was removed under reduced pressure, and the residue was purified by flash silica gel chromatography to give 0.04 g (37%) of **42** as a yellow oil. HRMS calcd. for $C_{12}H_{17}NO_3$: 223.1208; found: 223.1213. IR (neat) (cm^{-1}): 3487, 2965, 2863, 1680, 1577, 1490, 1285, 1198. ^{1}H NMR (400 MHz, $CDCl_3$) δ: 1.32 (s, 9H), 1.63 (d, 3H, *J* = 7.2 Hz), 2.61–2.66 (m, 2H), 4.36–4.40 (m, 2H), 5.21 (q, 1H, *J* = 7.2 Hz). ^{13}C NMR (100 MHz, $CDCl_3$) δ: 17.3, 17.9, 26.9, 40.7, 56.0, 94.6, 99.6, 175.8, 179.2, 190.1.

2,2-Dimethylpropionic acid 1-(2,2-dimethylpropionyl)-5-methyl-6,8-dioxo-7-phenyl-1,2,3,6,7,8-hexahydrobenzo-[2,1-*b*:3,4-*c*]dipyrrol-4-yl ester (44)

To a solution containing furanone **42** (0.04 g, 0.2 mmol) in benzene (1.5 mL) was added Et_3N (0.04 mL, 0.3 mmol) followed by pivalyl chloride (0.03 mL, 0.2 mmol). After stirring at rt for 1 h, the reaction mixture was filtered and concentrated under reduced pressure. The residue was dissolved in toluene (10 mL) and heated under reflux for 36 h with *N*-phenylmaleimide (0.03 g, 0.2 mmol). The solution was concentrated under reduced pressure and subjected to flash silica gel chromatography to give 0.04 g (52%) of **44** as a yellow solid: mp 219–221°C. IR (film) (cm^{-1}): 2970, 2929, 1757, 1716, 1685, 1495, 1367, 1101. ^{1}H NMR (400 MHz, $CDCl_3$) δ: 1.40 (s, 9H), 1.42 (s, 9H), 2.51 (s, 3H), 3.01 (t, 2H, *J* = 7.6 Hz), 4.27 (t, 2H, *J* = 7.6 Hz), 7.32–7.48 (m, 5H). ^{13}C NMR (100 MHz, $CDCl_3$) δ: 10.9, 27.4, 28.2, 28.3, 39.7, 40.4, 51.2, 116.9, 127.2, 127.7, 128.0, 129.1, 129.6, 132.1, 133.4, 140.9, 150.7, 164.3, 167.6, 175.5, 178.7. Anal. calcd. for $C_{27}H_{30}N_2O_5$: C 70.11, H 6.54, N 6.06; found: C 70.25, H 6.70, N 5.90.

Acetic acid 2-methoxy-1-(2-oxopiperidin-3-yl)-2-phenylsulfanyl ethyl ester (48)

To a solution containing diisopropylamine (6.5 mL, 46 mmol in THF (150 mL) was added a (1.6 M) solution of *n*-butyllithium in hexanes (29 mL 45 mmol) at –40°C. After stirring for 1 h, the reaction mixture was cooled to –75°C and *N*-trimethylsilyl-2-piperidone (**48**) (36) (7.4 g, 43 mmol) in THF (25 mL) was added. The temperature was raised to –40°C, and the mixture was stirred for 30 min. The temperature was lowered to –75°C and methoxyphenylsulfanyl acetaldehyde (**47**) (37) (8.2 g, 45 mmol) in THF (40 mL) was added over 45 min. Following the addition, the mixture was stirred for an additional 30 min and then acetic anhydride (4.5 mL, 48 mmol) was added. The solution was slowly warmed to rt overnight and was then poured into a saturated aqueous $NaHCO_3$ solution and extracted with CH_2Cl_2. The solvent was removed under reduced pressure and the crude reaction mixture was subjected to flash silica gel chromatography to give 8.1 g (68%) of **48** as a yellow oil, which consisted of a complex mixture of diastereomers. For analytical purposes, the major two diastereomers were separated using HPLC. HRMS calcd. for $C_{16}H_{21}NO_4S$: 323.1191; found: 323.1190. IR (neat) (cm^{-1}): 3303, 3206, 3062, 2945, 1747, 1660, 1491, 1372, 1229. ^{1}H NMR (400 MHz, $CDCl_3$) δ: major diastereomer: 1.64–1.93 (m, 4H), 2.06 (s, 3H), 3.22–3.28 (m, 3H), 3.47 (s, 3H), 5.20 (dd, 1H, *J* = 10.8, 3.6 Hz), 5.54 (d, 1H, *J* = 10.8 Hz), 5.92 (br s, 1H), 7.27–7.33 (m, 3H), 7.46–7.56 (m, 2H); δ minor diastereomer: 1.64–1.93 (m, 4H), 2.08 (s, 3H), 2.93 (ddd, 1H, *J* = 14.7, 7.8, 2.8 Hz), 3.22–3.28 (m, 2H), 3.53 (s, 3H), 5.15–5.19 (m, 1H), 5.43 (d, 1H, *J* = 12.0 Hz), 5.82 (br s, 1H), 7.27–7.33 (m, 3H), 7.46–7.56 (m, 2H). ^{13}C NMR (100 MHz, $CDCl_3$) δ: 21.2, 21.4, 22.2, 22.3, 25.4, 42.0, 42.3, 45.1, 56.9, 74.6, 75.7, 91.1, 91.7, 127.7, 127.9, 128.9, 129.2, 132.9, 133.2, 133.4 133.7, 170.5, 170.8, 171.1, 171.2.

© 2001 NRC Canada

Acetic acid 1-(1-but-3-enoyl-2-oxopiperin-3-yl)-2-methoxy-2-phenylsulfanyl ethyl ester (49)

To a solution containing lactam **22** (0.6 g, 2 mmol) in CH_2Cl_2 (9 mL) was added 3-butenoyl chloride (0.3 g, 3 mmol) (**23**) (48) followed by powdered molecular sieves (1.9 g). After stirring at rt overnight, the suspension was filtered through a pad of silica and washed several times with ether. The filtrate was washed with a saturated aqueous $NaHCO_3$ solution, dried over $MgSO_4$, and concentrated under reduced pressure. The crude reaction mixture was subjected to flash silica gel chromatography to give 0.7 g (94%) of **49** as a yellow oil which consisted of a complex mixture of diastereomers. For analytical purposes, the major two diastereomers were separated using HPLC. FAB-HRMS calcd. for $C_{20}H_{25}NO_5S$: 391.1453; found: 391.1452. IR (neat) (cm^{-1}): 2945, 1747, 1690, 1475, 1291, 1224, 1163. ^1H NMR (400 MHz, $CDCl_3$) δ: major diastereomer: 1.56–1.61 (m, 1H), 1.73–1.80 (m, 1H), 1.84–1.90 (m, 2H), 2.05 (s, 3H), 3.32–3.37 (m, 1H), 3.51 (s, 3H), 3.62–3.65 (m, 2H), 3.67–3.73 (m, 2H), 5.11–5.17 (m, 2H), 5.26 (d, 1H, *J* = 7.2 Hz), 5.32 (dd, 1H, *J* = 7.2, 3.6 Hz), 5.95–6.04 (m, 1H), 7.29–7.34 (m, 3H), 7.50–7.52 (m, 2H); δ minor diastereomer: 1.68–1.79 (m, 2H), 1.87–1.93 (m, 1H), 2.01–2.08 (m, 1H), 2.07 (s, 3H), 3.02–3.07 (m, 1H), 3.47 (s, 3H), 3.62–3.68 (m, 2H), 3.74–3.79 (m, 2H), 4.88 (d, 1H, *J* = 6.8 Hz), 5.09–5.15 (m, 2H), 5.61 (dd, 1H, *J* = 6.8, 3.4 Hz), 5.95–6.04 (m, 1H), 7.28–7.34 (m, 3H), 7.48–7.53 (m, 2H). ^{13}C NMR (100 MHz, $CDCl_3$) δ: major diastereomer: 21.1, 21.7, 24.3, 43.7, 44.2, 45.3, 56.9, 75.0, 91.3, 118.3, 128.2, 129.3, 131.5, 132.8, 133.5, 170.5, 173.1, 174.9; δ minor diastereomer: 21.2, 21.8, 22.1, 43.7, 44.2, 45.6, 56.9, 73.4, 92.3, 118.3, 128.1, 129.3, 131.5, 132.5, 133.3, 133.6, 169.9, 173.6, 175.0.

1-(2-Methoxy-5,6-dihydro-4*H*-furo[2,3-*b*]pyridin-7-yl)-but-3-en-1-one (50)

To a solution containing lactam **49** (0.5 g, 1 mmol) in CH_2Cl_2 (7 mL) was added DMTSF (0.3 g, 1 mmol) in one portion at –40°C. The temperature was allowed to warm slowly to 15°C over 2 h and then Et_3N (1 mL, 7 mmol) was added. The reaction mixture was diluted with ether, poured over a saturated aqueous $NaHCO_3$ solution, extracted with ether, and dried over K_2CO_3. The solvent was removed under reduced pressure and the crude residue was subjected to flash silica gel chromatography to give 0.2 g (65%) of **50** as a yellow oil. HRMS calcd. for $C_{12}H_{15}NO_3$: 221.1052; found: 221.1054. IR (neat) (cm^{-1}): 3073, 2935, 1752, 1670, 1639, 1603, 1434, 1378. ^1H NMR (400 MHz, $CDCl_3$) δ: 1.86–1.94 (m, 2H), 2.43 (t, 2H, *J* = 8.6 Hz), 3.46 (d, 2H, *J* = 8.6 Hz), 3.77–3.82 (m, 2H), 3.83 (s, 3H), 5.08 (s, 1H), 5.13–5.18 (m, 2H), 5.94–6.06 (m, 1H). ^{13}C NMR (100 MHz, $CDCl_3$) δ: 21.0, 23.7, 40.6, 43.2, 58.3, 81.6, 92.3, 118.1, 131.5, 133.6, 157.3, 174.9.

8-Hydroxy-5,6-dihydro-1*H*,4*H*-pyrrolo[3,2,1-*ij*]quinolin-2-one (53)

A solution of furan **50** (0.04 g, 0.2 mmol) in toluene (5 mL) was heated under reflux for 30 min. The solvent was removed under reduced pressure and the residue was subjected to flash silica gel chromatography to give 0.02 g (58%) of **53** as a white solid: mp 200–201°C. HRMS calcd. for $C_{11}H_{11}NO_2$: 189.0780; found: 189.0787. IR (film) (cm^{-1}): 3134, 2975, 2934, 1654, 1629, 1480, 1280. ^1H NMR (400 MHz, $CDCl_3$) δ: 1.92–1.98 (m, 2H), 2.67 (t, 2H, *J* = 6.0 Hz), 3.42 (s, 2H), 3.61–3.64 (m, 2H), 6.48 (br s, 1H), 6.59 (br s, 1H). ^{13}C NMR (100 MHz, $CDCl_3$) δ: 22.7, 25.4, 37.7, 40.2, 111.4, 114.0, 122.7, 125.9, 134.5, 154.8, 176.2.

Acknowledgment

We gratefully acknowledge the National Institutes of Health (Grant GM59384) for their generous support of this work.

References

1. (*a*) F.G. Fang, M. Prato, G. Kim, and S.J. Danishefsky. Tetrahedron Lett. **30**, 3625 (1989); (*b*) F.G. Fang and S.J. Danishefsky. Tetrahedron Lett. **30**, 2747 (1989); (*c*) F.G. Fang, M.E. Maier, and S.J. Danishefsky. J. Org. Chem. **55**, 831 (1990); (*d*) G. Kim, M.Y. Chu-Moyer, and S.J. Danishefsky. J. Am. Chem. Soc. **112**, 2003 (1990).
2. T. Kametani, H. Yukawa, and T. Honda. J. Chem. Soc. Chem. Commun. 651 (1986).
3. (*a*) J.P. Marino, Jr., M.H. Osterhout, and A. Padwa. J. Org. Chem. **60**, 2704 (1995); (*b*) A. Padwa and A.T. Price. J. Org. Chem. **60**, 6258 (1995).
4. (*a*) F.G. West and B.N. Naidu. J. Am. Chem. Soc. **115**, 1177 (1993); (*b*) F.G. West and B.N. Naidu. J. Am. Chem. Soc. **116**, 8420 (1994).
5. C.W. Jefford, Q. Tang, and A. Zaslona. J. Am. Chem. Soc. **113**, 3513 (1991).
6. (*a*) H.M.L. Davies, E. Saikali, and W.B. Young. J. Org. Chem. **56**, 5696 (1991); (*b*) H.M.L. Davies and J.J. Matasi. Tetrahedron Lett. **35**, 5209 (1994); (*c*) H.M.L. Davies, J.J. Matasi, and G. Ahmed. J. Org. Chem. **61**, 2305 (1996).
7. M. Eguchi, Q. Zeng, A. Korda, and I. Ojima. Tetrahedron Lett. **34**, 915 (1993).
8. J.S. Clark and G.A. Whitlock. Tetrahedron Lett. **35**, 6381 (1994).
9. K.J. Doyle and C.J. Moody. Synthesis, 1021 (1994).
10. M.P. Doyle and A.V. Kalinin. Tetrahedron Lett. **37**, 1371 (1996).
11. D.F. Taber and K.K. You. J. Am. Chem. Soc. **117**, 5757 (1995).
12. A. Padwa and M.D. Weingarten. Chem. Rev. **96**, 223 (1996).
13. (*a*) A. Padwa, J.P. Marino, Jr., and M.H. Osterhout. J. Org. Chem. **60**, 2704 (1995); (*b*) A. Padwa, D.L. Hertzog, and W.R. Nadler. J. Org. Chem. **59**, 7072 (1994); (*c*) J.P. Marino, Jr., M.H. Osterhout, A.T. Price, M.A. Semones, and A. Padwa. J. Org. Chem. **59**, 5518 (1994); (*d*) A. Padwa, D.L. Hertzog, W.R. Nadler, M.H. Osterhout, and A.T. Price. J. Org. Chem. **59**, 1418 (1994); (*e*) D.L. Hertzog, D.J. Austin, W.R. Nadler, and A. Padwa. Tetrahedron Lett. **33**, 4731 (1992).
14. M.H. Osterhout, W.R. Nadler, and A. Padwa. Synthesis, 123 (1994).
15. A. Padwa, S.M. Sheehan, and C.S Straub. J. Org. Chem. **64**, 8648 (1999).
16. (*a*) S. Miah, A.M.Z. Slawin, C.J. Moody, I.C. Richards, S.M. Sheehan, J.P. Marino, Jr., M.A. Semones, and A. Padwa. Tetrahedron **52**, 2489 (1996); (*b*) A. Padwa, A.T. Price, and L. Zhi. J. Org. Chem. **61**, 2283 (1996).
17. A. Padwa and A.T. Price. J. Org. Chem. **63**, 556 (1998).
18. A. Padwa, J.P. Marino, Jr., M.H. Osterhout, A.T. Price, and S.M. Sheehan. Tetrahedron Lett. **35**, 849 (1994).
19. (*a*) S.F. Martin. The alkaloids. *Edited by* A. Brossi. Academic Press, New York. 1987; (*b*) J.R. Lewis. Nat. Prod. Rep. **11**, 329 (1994).

© 2001 NRC Canada

20. (*a*) G.R. Pettit, V. Gaddamidi, A. Goswami, and G.M. Gragg. J. Nat. Prod. **47**, 796 (1994); (*b*) S. Ghosal, K.S. Saini, and S. Razdan. Phytochemistry, **24**, 2141 (1985).
21. J.W. Cook and J.D. Loudon. The alkaloids. Vol. 2. *Edited by* R.H.F. Manske and H.L. Holmes. Academic Press, New York. 1952. p. 331.
22. S. Ghosal, K.S. Saini, and S. Razdan. Phytochemistry, **24**, 2141 (1985).
23. A.G. Schultz, M.A. Holoboski, and M.S. Smyth. J. Am. Chem. Soc. **115**, 7904 (1993).
24. A.I. Meyers and R.H. Hutchings. Tetrahedron Lett. **34**, 6185 (1993).
25. D.B. Grotjahn and K.P. Vollhardt. Synthesis, 579 (1993).
26. D. Pérez, G. Burés, E. Guitián, and L. Castedo. J. Org. Chem. **61**, 1650 (1996).
27. M.G. Banwell and A.W. Wu. J. Chem. Soc. Perkin Trans 1, 2671 (1995).
28. C. González, D. Pérez, E. Guitián, and L. Castedo. J. Org. Chem. **60**, 6318 (1995).
29. (*a*) R.K. Hill, J.A. Joule, and L. Loeffler. J. Am. Chem. Soc. **84**, 4951 (1962); (*b*) Y. Tsuda, T. Sano, J. Taga, K. Isobe, J. Toda, H. Irie, H. Tanaka, S. Takagi, S. Yamaki, and M. Murata. J. Chem. Soc. Chem. Commun. 933 (1975); (*c*) G. Stork and D.J. Morgan, Jr., J. Am. Chem. Soc. **101**, 7110 (1979); (*d*) S.F. Martin, C.Y. Tu, M. Kimura, and S.H. Simonsen. J. Org. Chem. **47**, 3634 (1982); (*e*) G. Hwang and P. Magnus. J. Chem. Soc. Chem. Commun. 693 (1983); (*f*) R.K. Boeckman, Jr., J.P. Sabatucci, S.W. Goldstein, D.M. Springer, and P.F. Jackson. J. Org. Chem. **51**, 3740 (1986).
30. (*a*) M.S. Kharasch, T. Ruby, W. Nudenberg, and G. Buchi. J. Org. Chem. **18**, 1030 (1953); (*b*) A. Lottes, J.A. Landgreb, and K. Larsen. Tetrahedron Lett. **30**, 4089 (1989); (*c*) A. Padwa, R.L. Chinn, S.F. Hornbuckle, and Z. Zhang. J. Org. Chem. **56**, 3271 (1991).
31. A. Padwa, J.P. Snyder, E.A. Curtis, S.M. Sheehan, K.J. Worsencroft, and C.O. Kappe. J. Am. Chem. Soc. **122**, 8155 (2000).
32. (*a*) A. Padwa, M. Dimitroff, A.G. Waterson, and T. Wu. J. Org. Chem. **63**, 3986 (1998); (*b*) R.H. Schlessinger and C.P. Bergstrom. J. Org. Chem. **60**, 16 (1995).
33. C.O. Kappe, S.S. Murphree, and A. Padwa. Tetrahedron, **53**, 14179 (1997).
34. (*a*) S. Reck and W. Friedrichson. J. Org. Chem. **63**, 7680 (1998); (*b*) for a related process involving a [1,2]-phenyl shift, see J.E. Cochran and A. Padwa. Tetrahedron Lett. **36**, 3495 (1995).
35. A. Padwa, J.D. Ginn, and M.S. McClure. Org. Lett. **1**, 1559 (1999).
36. D.H. Hua, S.W. Miao, S.N. Bharathi, T. Katsuhira, and A.A. Bravo. J. Org. Chem. **55**, 3682 (1990).
37. V.H. Rawal, M. Akiba, and M.P. Cava. Synth. Commun. **14**, 1129 (1984).
38. L. Weinstock, S. Karady, F. Roberts, A. Hoinowski, G. Brenner, T. Lee, W. Lumma, and M. Sletzinger. Tetrahedron Lett. **16**, 3979 (1975).
39. (*a*) B.M. Trost and E. Murayama. J. Am. Chem. Soc. **103**, 6529 (1981); (*b*) B.M. Trost and T. Sato. J. Am. Chem. Soc. **107**, 719 (1985) (commercially available from Aldrich).
40. (*a*) J.L. Rice and N.A. Favstritsky. J. Am. Chem. Soc. **91**, 1751 (1969); (*b*) S.H. Smallcombe and M.C. Caserio. J. Am. Chem. Soc. **93**, 5826 (1971); (*c*) J. K. Kim, J.K. Pau, and M.C. Caserio. J. Org. Chem. **44**, 1544 (1979).
41. (*a*) D.D. Sternbach, D.M. Rossana, and K.D. Onon. J. Org. Chem. **49**, 3427 (1984); (*b*) M.E. Jung and J. Gervay. J. Am. Chem. Soc. **111**, 5469 (1989).
42. W.J. Dale, L. Starr, and C.W. Strobel. J. Org. Chem. **26**, 2225 (1961).
43. S.L. Crooks and K.J. Lindstrom. Synth. Commun. **20**, 2335 (1990).
44. R.K. Singh and S.J. Danishefsky. Org. Synth. **60**, 66 (1981).
45. T. Luker, H. Hiemstra, and W.N. Speckamp. Tetrahedron Lett. **37**, 8257 (1996).
46. A. Giovannini, D. Savoia, and A. Umani-Ronchi. J. Org. Chem. **54**, 228 (1989).
47. Y. Yamamoto and H. Kiura. Chem. Pharm. Bull. **24**, 1236 (1976).
48. C.M. Marson, U. Grabowska, A. Fallah, T. Walsgrove, D.S. Eggleston, and P.W. Baures. J. Org. Chem. **59**, 291 (1994).

© 2001 NRC Canada

Spectroscopic studies of the electrophilic activation of amides with triflic anhydride and pyridine

André B. Charette and Michel Grenon

Abstract: The reaction of amides with trifluoromethanesulfonic (triflic) anhydride in the presence of pyridine was thoroughly investigated by NMR spectroscopic techniques. Different pyridinium intermediates were generated from secondary amides, tertiary amides with enolizable protons, and tertiary amides lacking enolizable protons. It was found that the actual triflating reagent is *N*-(trifluoromethylsulfonyl)pyridinium triflate **11** which is formed by the initial reaction of triflic anhydride with pyridine. The alcoholysis of these intermediates yields *O*-alkyliminium ethers which can then be easily hydrolyzed under mild acidic conditions to the corresponding esters.

Key Words: amides, triflic anhydride, pyridinium intermediates, NMR study.

Résumé : La réaction entre un amide et l'anhydride trifluorométhanesulfonique (triflique) en présence de pyridine a été examinée minutieusement à l'aide de nombreuses techniques de spectroscopie RMN. Des intermédiaires pyridiniums différents ont été générés à partir d'amides secondaires, d'amides tertiaires avec des protons énolisables et d'amides tertiaires ne possédant pas de protons énolisables. Nous avons aussi démontré que le triflate de *N*-(trifluorométhylsulfonyl)pyridinium **11**, formé lors de la réaction initiale entre l'anhydride triflique et la pyridine, est le véritable agent de triflation. L'alcoolyse de ces intermédiaires donne des éthers *O*-alkyliminiums qui peuvent être facilement hydrolysés dans des conditions légèrement acides aux esters correspondants.

Mots clés : amides, anhydride triflique, intermédiaires pyridiniums, études RMN.

Introduction

In recent years, trifluoromethanesulfonic (triflic) anhydride has proven to be a very useful reagent for the activation of amides and their subsequent transformation into other functional groups (for a recent review on the use of triflic anhydride in synthetic organic chemistry see ref. 1). Our research group has recently extended the use of this reagent to the synthesis of amidines, thiazolines, thioamides, esters as well as cyclic orthoesters from simple amides (2–6) (Scheme 1).

A variety of intermediates have been either isolated or postulated from the reaction of secondary or tertiary amides with triflic anhydride under different conditions (Scheme 2). *O*-Triflyliminium triflates **1** and **2** have been postulated as potential intermediates when secondary and tertiary amides were treated with triflic anhydride either in the presence or absence of a non-nucleophilic base (7–10). In the case of tertiary amides bearing enolizable protons it was found that when the sulfonylation was performed in the presence of a tertiary base, the *O*-sulfonylated derivatives were converted into (*N*,*N*-dialkylamino)alkenyl triflates **3** (11). These can then spontaneously generate keteniminium triflates which are valuable intermediates in [2 + 2] cycloadditions (12–20). Yet another intermediate was observed when tertiary amides were left to react with only 0.5 equiv of triflic anhydride. Stable dicationic ether salts such as **4** were isolated, which presumably arise from the attack of the amide on the initially formed *O*-triflyliminium triflate **2** (21).

Since the nature of the intermediates formed upon exposure of amides to triflic anhydride is dependent upon several variables such as the amide structure, the amount of anhydride used, and the nature of the base (if present), we decided to carry out a careful spectroscopic study to identify the structure of the intermediates generated according to a new reaction protocol developed in our laboratory. This procedure differs from others in that in most cases, we need at least 2 equiv of pyridine to get optimal yields of the desired products. It is noteworthy that pyridine can not only act as a proton scavenger in these reactions but also as a nucleophilic partner. Herein, we disclose the detailed spectroscopic investigation of the reaction of secondary and tertiary amides with triflic anhydride in the presence of pyridine. The emphasis will be on the spectroscopic identification of the reac-

Received March 14, 2001. Published on the NRC Research Press Web site at http://canjchem.nrc.ca on November 12, 2001.

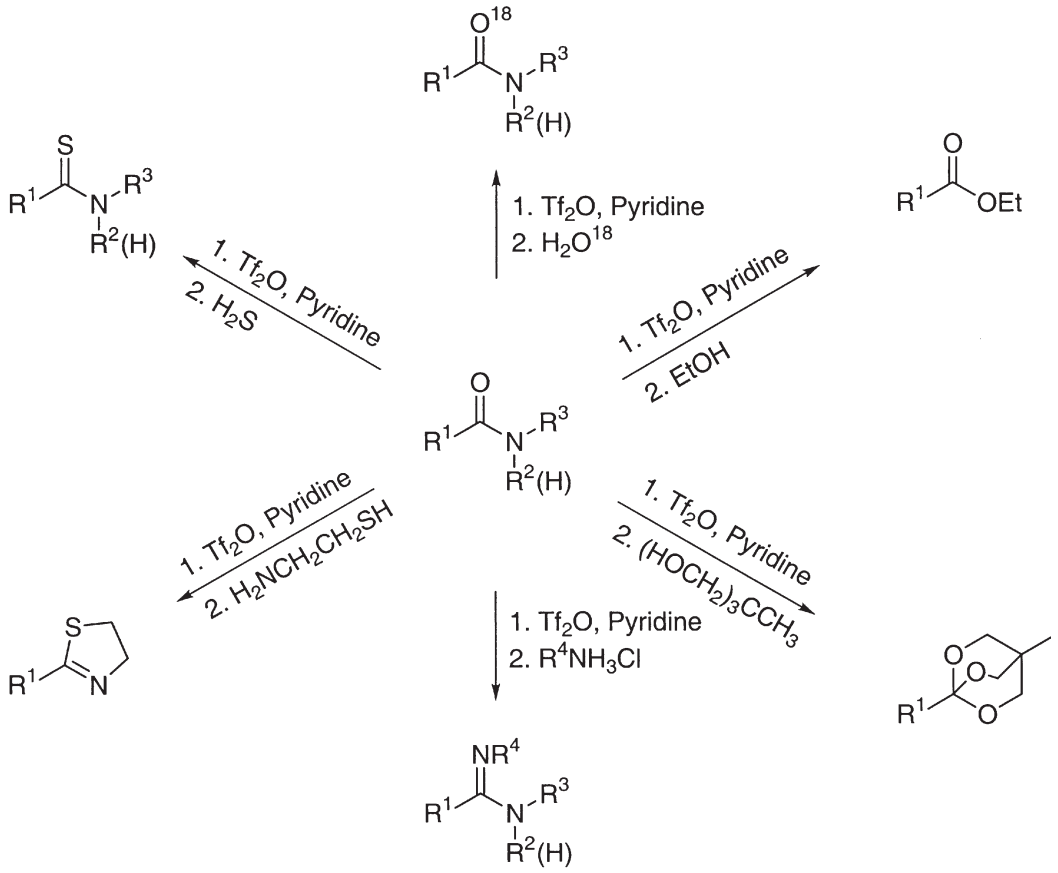
This paper is dedicated to Professor Victor Snieckus in recognition of his many contributions to the science of organic synthesis.

A.B. Charette[1] and M. Grenon. Département de chimie, Université de Montréal, PO Box 6128, Station Downtown, Montréal, QC H3C 3J7, Canada.

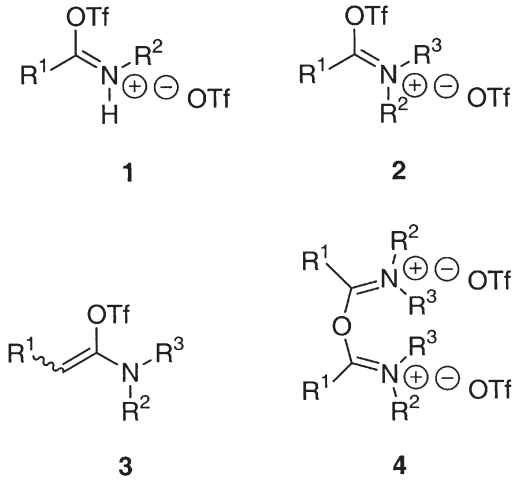
[1]Corresponding author (telephone: (514) 343-2432; fax: (514) 343-5900; e-mail: charetta@chimie.umontreal.ca).

 DOI: 10.1139/cjc-79-11-1694 © 2001 NRC Canada

Scheme 1. Functional group interconversion involving amides as starting materials.



Scheme 2. Postulated intermediates formed in the reaction of amides with triflic anhydride.



1 **2** **3** **4**

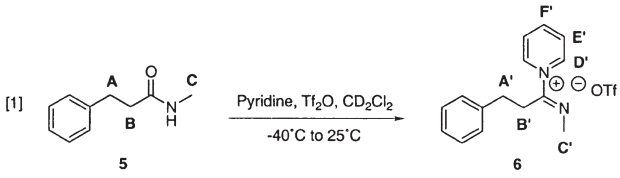
tive intermediates and of the triflating agent, and their subsequent conversion to ethyl esters.

Results and discussion

Reaction of secondary amides with triflic anhydride in the presence of pyridine

In an effort to identify the nature of the intermediates formed in the activation process, we decided to monitor the reactions by NMR spectroscopic techniques. ^{1}H and ^{19}F NMR spectroscopy are particularly suited in view of the inherent ease of analysis and the large amount of structural information it provides.

The first set of experiments involved the slow addition of triflic anhydride to a solution of 1.0 equiv of *N*-methyl-3-phenylpropionamide **5** and 3.0 equiv of pyridine in CD_2Cl_2. After the addition, the solution was warmed to room temperature and the NMR spectra were recorded. NMR analysis indicated that 1-pyridylimidoyl triflate **6** was formed quantitatively in less than 2 h (eq. [1]) (22).

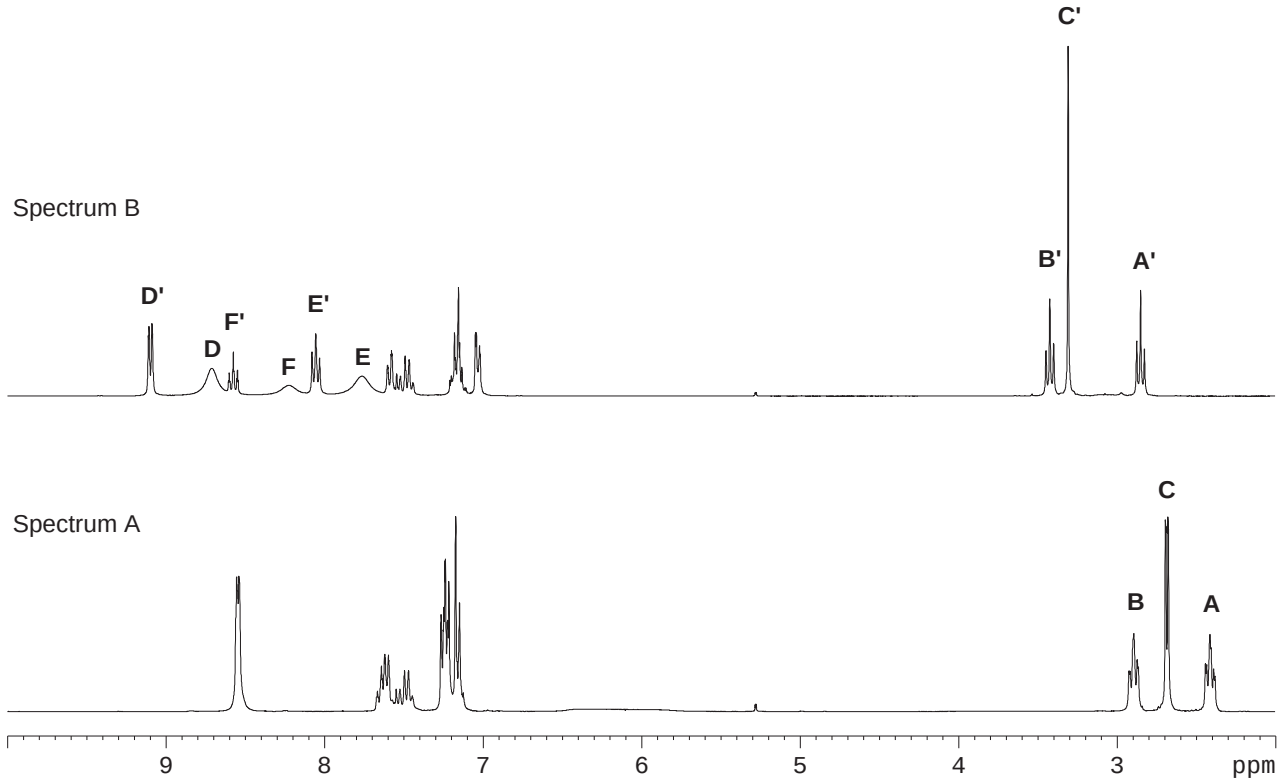


5 **6**

Telltale signs of the existence of this intermediate are found in the ^{1}H NMR spectrum where two distinct sets of signals are found for the pyridine unit. The first set of signals is assigned to pyridinium **6** (see **D′**, **E′**, and **F′**, Spectrum B, Fig. 1). This assignment of the resonances of pyridinium **6** was also confirmed by NOESY. The other set of signals (**D**, **E**, **F**) corresponds to pyridinium hydrotriflate and free pyridine that are involved in a rapid proton exchange process. This was also confirmed by comparing the spectrum with an independent sample prepared by mixing 2 equiv of pyridine and 1 equiv of TfOH. In addition, the doublet (δ = 2.7 ppm) corresponding to the methyl group of the starting amide

© 2001 NRC Canada

Fig. 1. ^{1}H NMR of the reaction of *N*-methyl-3-phenylpropionamide **5** with triflic anhydride in the presence of pyridine. Spectrum A: amide **5** (1.0 equiv) + pyridine (3.0 equiv) + α,α,α-trifluorotoluene (1.0 equiv, used as internal standard) in CD_2Cl_2. Spectrum B: 2 h after the addition of triflic anhydride (1.2 equiv).

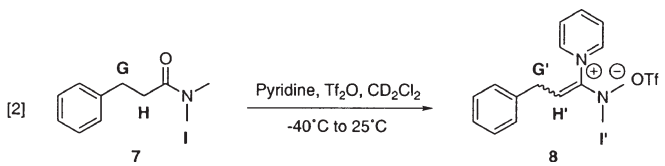


(Spectrum A) is converted into a singlet (δ = 3.3 ppm), which is also consistent with the formation of adduct **6**.

Further evidence is provided by ^{19}F NMR where signals corresponding to the triflate anion (–79.8 ppm) and *N*-(trifluoromethylsulfonyl)pyridinium **11** (–75.9 ppm) are exclusively observed, the latter compound arising from the reaction of the excess triflic anhydride with pyridine (23, 24). Pyridinium **6** proved to be very stable under the reaction conditions, showing no signs of decomposition after 6 days at –3°C under dry atmosphere. It is noteworthy that this behaviour is quite general and has been observed for a vast array of secondary amides. Another striking feature of the activation process is that at no time during the reaction are signals corresponding to the *O*-triflyliminium or *O*-triflylimidate observed, indicating that these intermediates, when formed, react rapidly with pyridine to generate **6**.

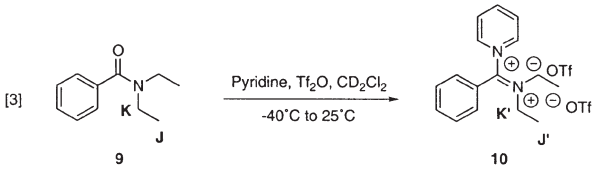
Reaction of tertiary amides with triflic anhydride in the presence of pyridine

Our next spectroscopic study of the activation process was done with tertiary amides with α-enolizable protons. The reaction of *N*,*N*-dimethyl-3-phenylpropionamide **7** with triflic anhydride and pyridine was carried out in a fashion similar to that described above to afford *N*,*N*-(dimethylamino)-alkenylpyridinium triflate **8** as a 5:1 mixture of *Z*:*E* isomers (eq. [2]).



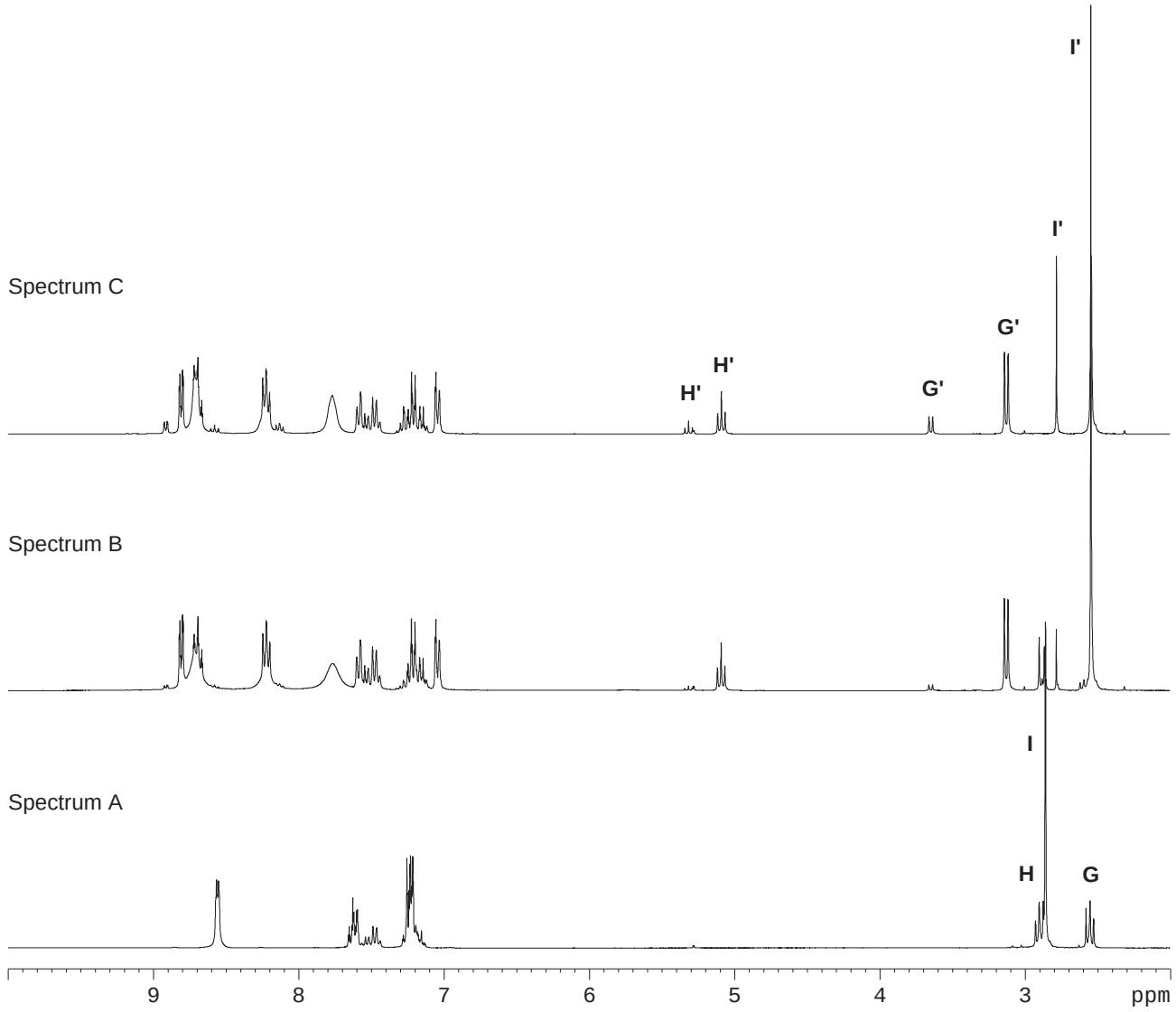
Evidence for the formation of **8** is provided by the ^{1}H NMR spectrum shown in Fig. 2 (Spectrum C). Two triplets corresponding to protons **H′** (δ = 5.3 and 5.1 ppm, *J* = 7.6 Hz), two doublets corresponding to protons **G′** (δ = 3.6 and 3.1 ppm, *J* = 7.6 Hz), and two singlets for protons **I′** (δ = 2.8 and 2.5 ppm) are consistent with the formation of both isomers. Once again, three sets of signals are observed for the pyridine units. Two of them arise from both isomers of **8** and one additional signal arises from the pyridinium hydrotriflate – pyridine equilibrium. Once again, the ^{19}F NMR spectrum shows only signals associated with the triflate anion (–79.8 ppm) and *N*-(trifluoromethylsulfonyl)pyridinium **11** (–75.9 ppm).

Having established the nature of the intermediate formed in the reaction of a tertiary amide with enolizable protons with triflic anhydride in the presence of pyridine, we focused next on the activation of tertiary amides lacking enolizable protons since these substrates can also be activated under these reaction conditions and be converted into esters upon ethanol addition. The reaction of *N*,*N*-diethylbenzamide **9** with triflic anhydride in the presence of pyridine was monitored by NMR spectroscopy and it appears that this amide, quite surprisingly, was also converted into a pyridinium adduct which was assigned as 1-pyridyl-*N*,*N*-diethyliminium ditriflate **10** (eq. [3]).



© 2001 NRC Canada

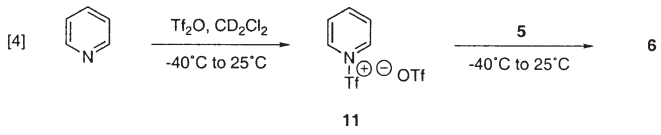
Fig. 2. [1]H NMR of the reaction of *N*,*N*-dimethyl-3-phenylpropionamide **7** with triflic anhydride in the presence of pyridine. Spectrum A: amide **7** (1.0 equiv) + pyridine (3.0 equiv) + α,α,α-trifluorotoluene (1.0 equiv, used as internal standard) in CD_2Cl_2. Spectrum B: 2 h after the addition of triflic anhydride (1.2 equiv). Spectrum C: 3 h after the addition of triflic anhydride.



Longer reaction times were required to get complete consumption of the starting material (Fig. 3). The [1]H NMR spectrum of the reaction mixture shows only 28% conversion of the amide **9** to pyridinium intermediate **10** after 2 h (Spectrum B, Fig. 3). *N*-(trifluoromethylsulfonyl)pyridinium **11** was the major species in the reaction mixture as observed by [19]F NMR (–75.9 ppm). However, after 4 h the [1]H NMR spectrum of the dark blue solution shows complete conversion to pyridinium **10** (Spectrum C, Fig. 3). In contrast with intermediates **6** and **8**, the signals associated with the pyridine unit are much broader and they cover a wider portion of the spectrum. The protons corresponding to the *N*-Et groups (**K′** and **J′**) are well-defined (Spectrum C, Fig. 3). Once again, after 4 h of reaction time, the [19]F NMR spectrum shows only the signals corresponding to triflate anion (OTf^-) and *N*-(trifluoromethylsulfonyl)pyridinium **11**.

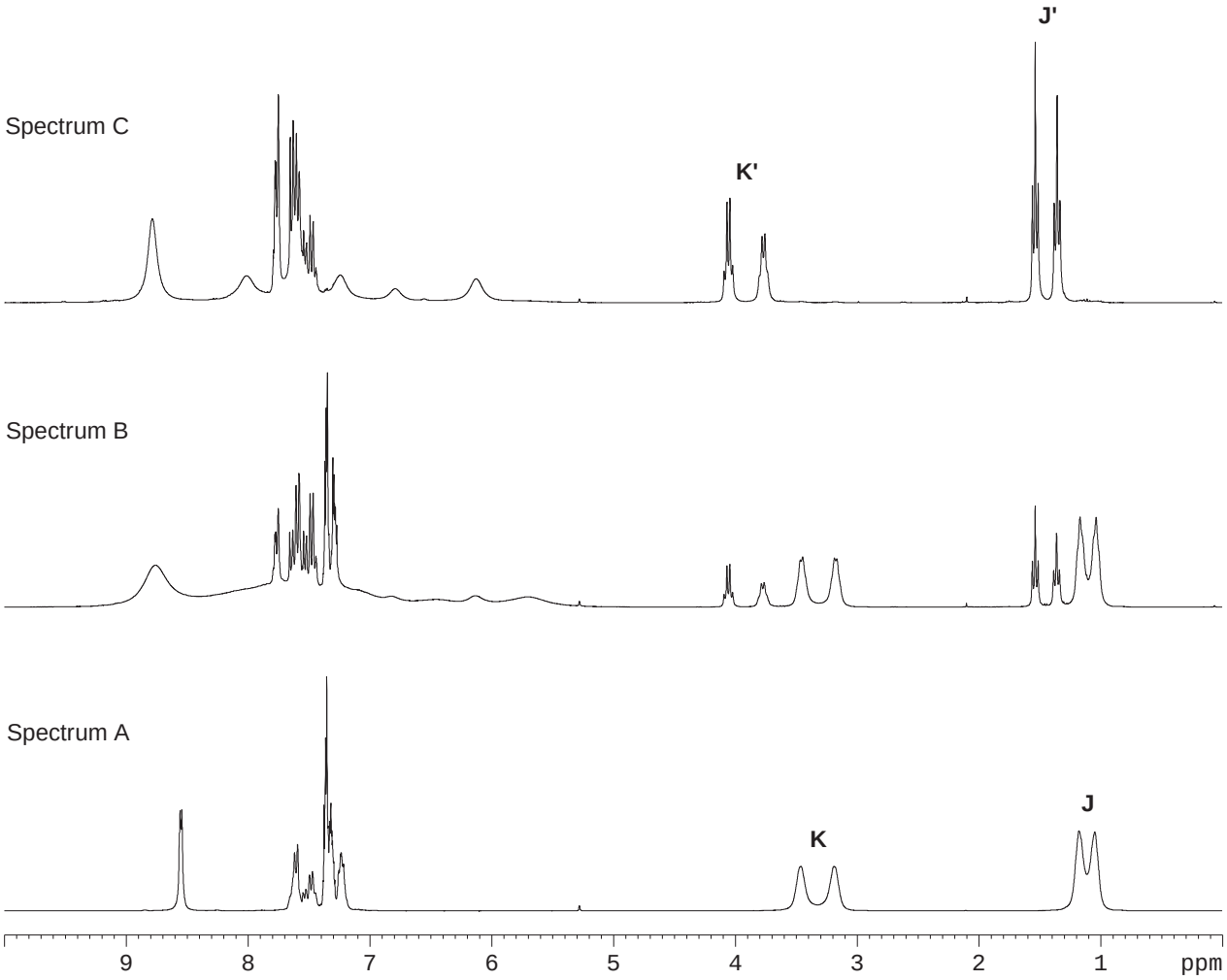
Nature of the triflating agent

An interesting aspect of this amide activation protocol is to further investigate the nature of the triflating reagent. When triflic anhydride is added to a mixture of the amide *and* pyridine in dichloromethane, it can either react with the amide to generate an *O*-triflyliminium intermediate or it can generate *N*-(trifluoromethylsulfonyl)-pyridinium triflate **11**. In principle, both pathways should be competing but what is less clear is whether **11** is sufficiently electrophilic to react with the amide. To clarify this issue, we monitored by NMR the reaction of *N*-methyl-3-phenylpropionamide **5** with *preformed N*-(trifluoromethylsulfonyl)-pyridinium triflate **11** to verify whether this reagent was electrophilic enough to convert amide **5** into the pyridinium intermediate **6** in the presence of pyridine (eq. [4]).



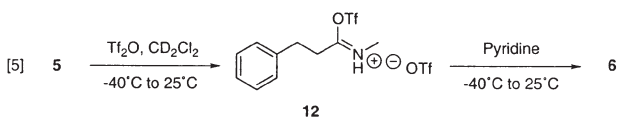
© 2001 NRC Canada

Fig. 3. ^{1}H NMR of the reaction of *N*,*N*-diethylbenzamide **9** with triflic anhydride in the presence of pyridine. Spectrum A: amide **9** (1.0 equiv) + pyridine (3.0 equiv) + α,α,α-trifluorotoluene (1.0 equiv, used as internal standard) in CD_2Cl_2. Spectrum B: 2 h after the addition of triflic anhydride (1.2 equiv). Spectrum C: 4 h after the addition of triflic anhydride.



As expected, the reaction of pyridine with triflic anhydride led to the instantaneous appearance of two signals of equal intensities in the ^{19}F NMR spectrum (Spectrum B, Fig. 4). The triflic anhydride was completely consumed and a precipitate was formed instantly upon its addition. At this point, amide **5** was added at low temperature to *N*-(trifluoromethylsulfonyl)pyridinium triflate **11** and the reaction was allowed to warm to room temperature and monitored by NMR (Fig. 4). After the usual activation period, ^{19}F NMR analysis indicated that the resonance corresponding to the *N*-triflyl group in **11** (–75.9 ppm) significantly decreased in favor of that of triflate anion (–79.8 ppm). In addition, the ^{1}H NMR spectrum obtained after the activation was identical to that observed when our standard activation protocol was used (Spectrum B, Fig. 1). This observation strongly supports the fact that *N*-(trifluoromethylsulfonyl)pyridinium triflate **11** is capable of activating amide **5** by converting it into the pyridinium intermediate **6**.

In a parallel experiment, triflic anhydride was added to amide **5** at –40°C to produce a precipitate that was assigned as the *O*-triflyliminium triflate **12** (eq. [5]). As anticipated, the ^{19}F NMR spectrum showed a signal corresponding to triflate anion (–79.8 ppm) and to the cationic component of adduct **12** (–72.8 ppm). The latter displays a chemical shift very close to that of triflic anhydride (Spectrum B, Fig. 5). Low-temperature addition of pyridine to the reaction mixture followed by the usual activation period resulted in the disappearance of the cationic component of adduct **12** and an increase in the concentration of triflate ion (Spectrum C, Fig. 5). A small amount of *N*-(trifluoromethylsulfonyl)-pyridinium **11** was also observed due to the reaction of the excess triflic anhydride with pyridine. The ^{1}H NMR spectrum of the activated specie is identical to that obtained when the conventional activation protocol was used (Spectrum B, Fig. 1).



Since triflic anhydride and *N*-(trifluoromethylsulfonyl)-pyridinium triflate **11** were both capable of reacting with amides to afford pyridinium intermediates upon exposure to

© 2001 NRC Canada

Fig. 4. ^{19}F NMR of the reaction of *N*-(trifluoromethylsulfonyl)-pyridinium triflate **11** with *N*-methyl-3-phenylpropionamide **5** in the presence of pyridine. Spectrum A: triflic anhydride (1.2 equiv) + α,α,α-trifluorotoluene (1.0 equiv, used as internal standard) in CD_2Cl_2. Spectrum B: after the addition of pyridine (3.0 equiv). Spectrum C: 2 h after the addition of amide **5** (1.0 equiv).

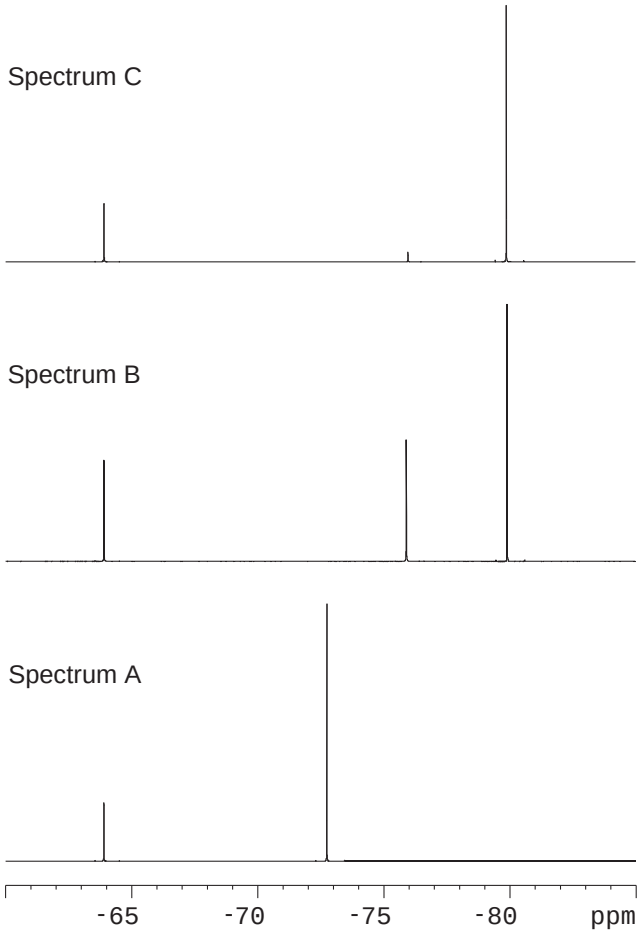
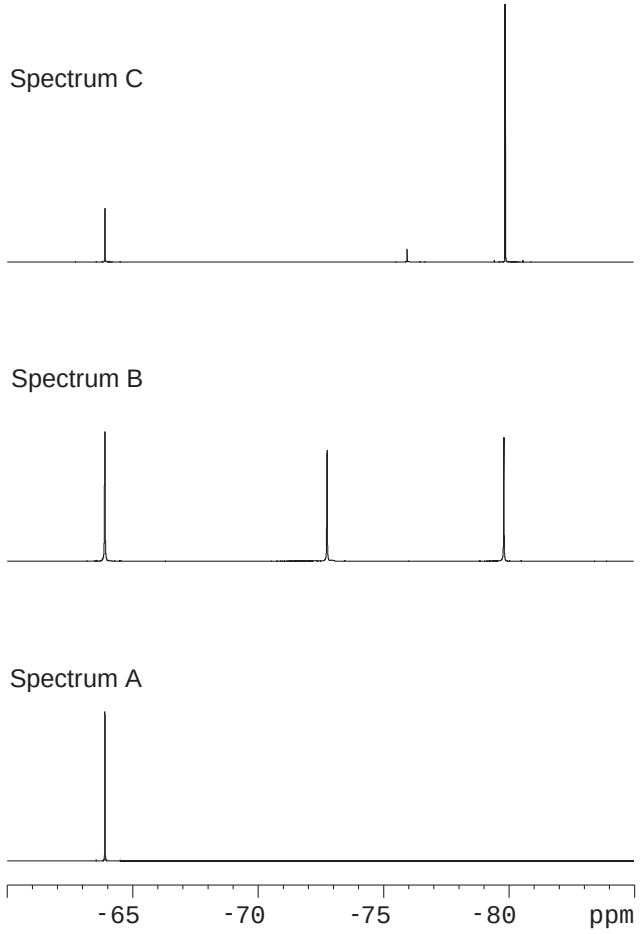


Fig. 5. ^{19}F NMR monitoring of the reaction of *N*-methyl-3-phenylpropionamide **5** with triflic anhydride. Spectrum A: amide **5** (1.0 equiv) + α,α,α-trifluorotoluene (1.0 equiv, used as internal standard) in CD_2Cl_2. Spectrum B: after the addition of triflic anhydride (1.2 equiv). Spectrum C: 2 h after the addition of pyridine (3.0 equiv).



excess pyridine, we carried out low-temperature NMR experiments to establish with which species triflic anhydride reacted first when it was added to a mixture of the amide and pyridine. Accordingly, after adding triflic anhydride to a mixture of the amide **5** and pyridine in CD_2Cl_2 at –40°C, the NMR tube was rapidly transferred to the precooled spectrometer probe at the same temperature. The ^{19}F NMR spectrum of the reaction mixture taken after 16 min showed complete consumption of the triflic anhydride and the exclusive formation of *N*-(trifluoromethylsulfonyl)pyridinium triflate **11**. No detectable amount of adduct **12** was observed. The ^1H NMR spectrum also showed that the amide **5** was left unchanged in the first minutes after the addition. The pyridinium intermediate **6** started to appear only when the reaction mixture was allowed to warm up to higher temperatures. With this experiment in mind, we can conclude that the triflic anhydride reacts initially with pyridine to form *N*-(trifluoromethylsulfonyl)pyridinium triflate **11** which is the actual triflating reagent in these amide activation reactions.

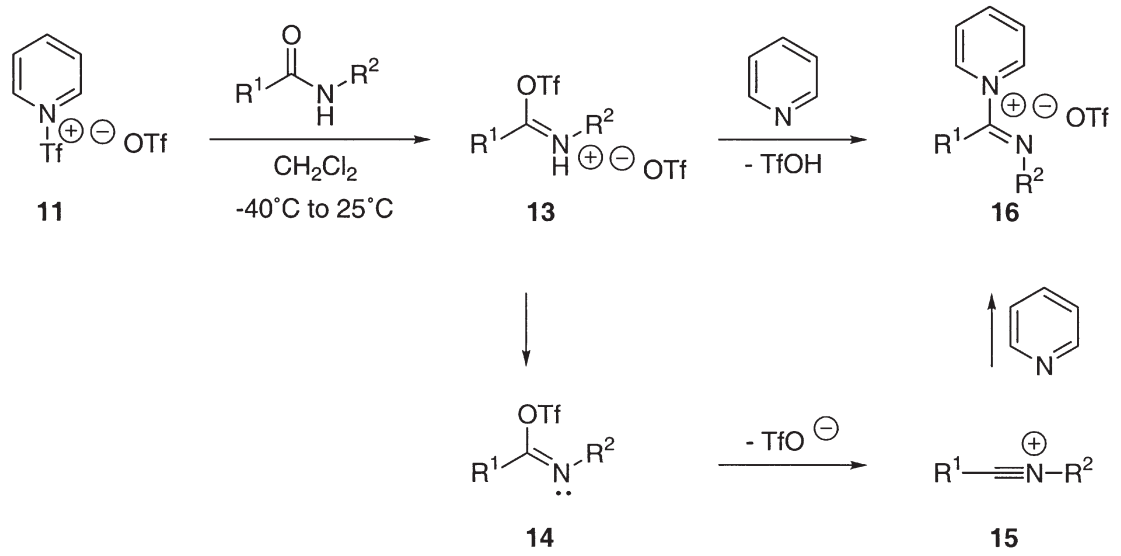
General mechanisms for the amide activation process and conversion of the intermediates into ethyl esters

With these results in hand, we were able to suggest the following mechanistic pathways for the reaction of secondary and tertiary amides with triflic anhydride in the presence of pyridine. Initially, the anhydride reacts with pyridine to form *N*-(trifluoromethylsulfonyl)pyridinium triflate **11**. This is then followed by the reaction of secondary amides with **11** upon warming to yield *O*-triflyliminium triflates **13**, which have not been observed in solution since they reacted immediately with the excess pyridine to yield pyridinium intermediates **16** (Scheme 3). The latter step can proceed through a stepwise addition of pyridine to **13** followed by the expulsion of triflic acid. Alternatively, the elimination of triflate anion from imidoyl triflates **14** can generate nitriliums **15** which then further reacts with pyridine to produce pyridinium intermediates **16**.

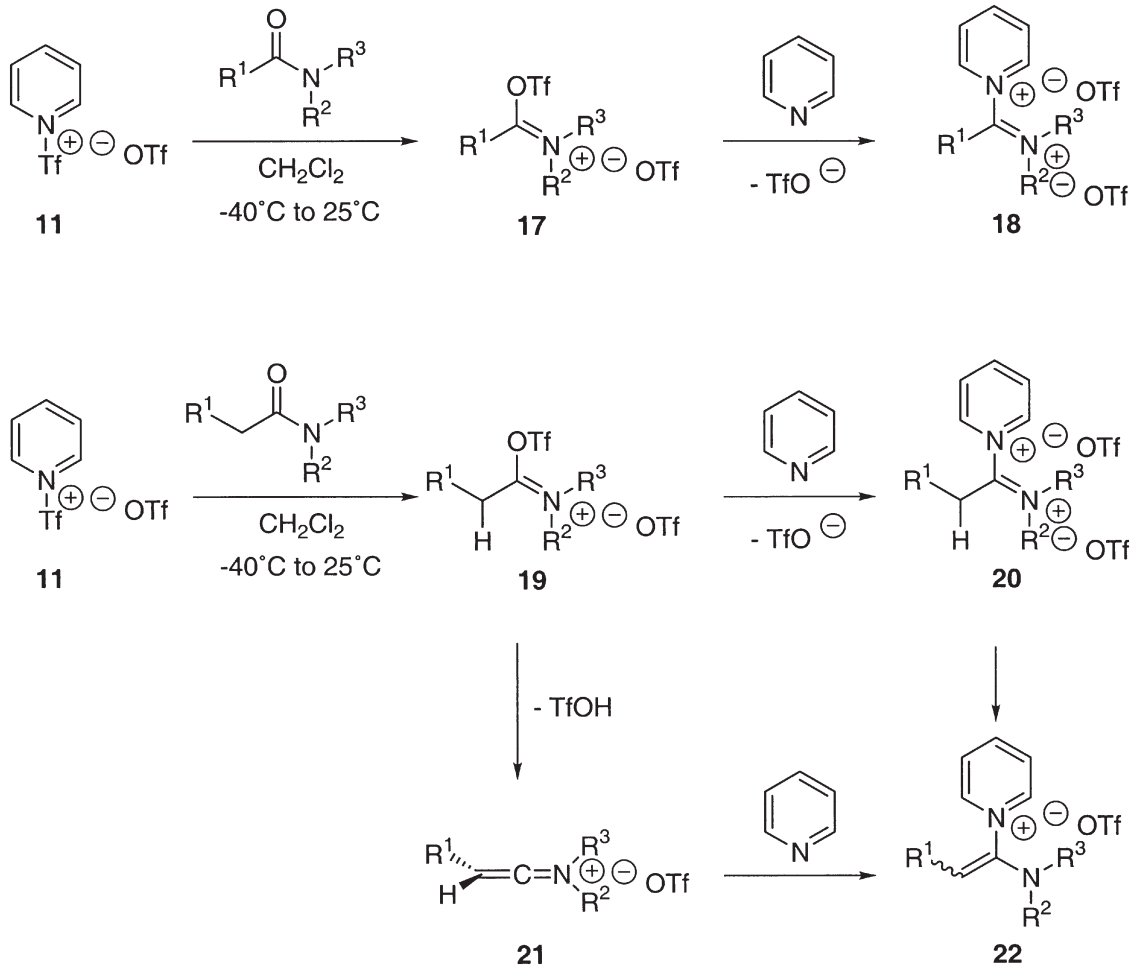
Tertiary amides lacking enolizable protons can also react via a similar reaction pathway (Scheme 4). For these substrates, longer activation times are required to ensure com-

© 2001 NRC Canada

Scheme 3. Proposed mechanistic pathways for the conversion of secondary amides to pyridinium intermediates.



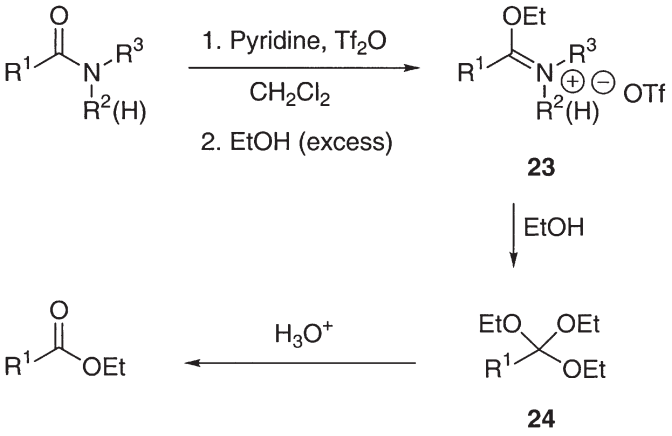
Scheme 4. Proposed mechanistic pathways for the conversion of tertiary amides to pyridinium intermediates.



plete conversion to the pyridinium intermediates **18**. Once again, *O*-triflyliminium triflates **17** are not observed in solution due to their rapid reaction with pyridine. In the case of tertiary amides bearing enolizable protons, two different routes could lead to pyridinium intermediates **22** after the initial formation of adducts **19** (Scheme 4). The first route involves the ejection of triflic acid by deprotonation to yield keteniminium triflates **21** which could then further react

© 2001 NRC Canada

Scheme 5. Alcoholysis of activated amides to form esters.



with excess pyridine. Alternatively, the sequential addition of pyridine and expulsion of triflate anion could afford intermediates **20**. Proton abstraction could then generate pyridiniums **22**.

It is important to point out that all these pyridinium intermediates (**16**, **18**, **22**) are converted into their corresponding ethyl esters upon ethanol addition and work-up. In our original communication on the alcoholysis of amides (5), we postulated that acidic hydrolysis of the acyclic orthoester **24** was the leading pathway to yield the observed esters (Scheme 5). Conversely, there are numerous reported examples of hydrolysis of *O*-alkyliminium ethers such as **23** under acidic (25–31) or basic conditions (32–39). In an effort to identify which of these two intermediates was formed, we decided to monitor the alcoholysis of 1-pyridylimidoyl triflate **6** with ethanol-d_6 by ^{1}H NMR (Fig. 6).

Following the addition of ethanol-d_6, the pyridinium **6** was rapidly converted to the *O*-ethyliminium triflate (Spectrum B, Fig. 6). The latter intermediate persisted in the reaction mixture over an extended period of time, showing only slight decomposition after 9 h at room temperature. No detectable amount of an acyclic orthoester intermediate was observed over the course of the reaction.[2] Interestingly, the alcoholysis of 1-pyridyl-*N*,*N*-diethyliminium ditriflate **10** also occurred rapidly at room temperature requiring less than 1 h, while *N*,*N*-(dimethylamino)alkenylpyridinium triflate **8** required about 6 h. Acidic hydrolysis of these *O*-ethyliminium triflates afforded the expected esters.

Experimental

General

NMR spectra were recorded on a Brucker AV-300 spectrometer, while variable-temperature NMR experiments were performed on a Brucker ARX-400 spectrometer. Pyridine was distilled over CaH_2 prior to use. Triflic anhydride was distilled over a small amount of phosphorus pentoxide before use. Dichloromethane-d_2 was purchased from CDN Isotopes. Ethanol-d_6 was purchased from CIL. Pyridine-d_5, phenyltrimethylsilane. and α,α,α-trifluorotoluene were purchased from Aldrich.

Reaction of N-*methyl-3-phenylpropionamide* ***5*** *with triflic anhydride in the presence of pyridine (eq. [1] and Fig. 1)*

To a dry NMR tube was added *N*-methyl-3-phenylpropionamide **5** (32.6 mg, 0.2 mmol) which was then capped with a rubber septum and purged with nitrogen. Dichloromethane-d_2 (1.0 g) was then added and the NMR tube slightly shaken. Pyridine (48 μL, 0.6 mmol) and α,α,α-trifluorotoluene (24.5 μL, 0.2 mmol) were then added and the NMR tube was shaken again. At this point ^{1}H NMR and ^{19}F NMR reference spectra were taken. The tube was then cooled to −40°C under a nitrogen atmosphere and triflic anhydride (40 μL, 0.24 mmol) was slowly added. The mixture was allowed to slowly warm up to –5°C in the acetone bath over 2 h after which ^{1}H NMR and ^{19}F NMR spectra of the golden solution were taken showing complete consumption of the starting material and formation of 1-pyridylimidoyl triflate **6**.

Reaction of N,N-*dimethyl-3-phenylpropionamide* ***7*** *with triflic anhydride in the presence of pyridine (eq. [2] and Fig. 2)*

To a dry NMR tube was added *N*,*N*-dimethyl-3-phenylpropionamide **7** (35.5 mg, 0.2 mmol) which was then capped with a rubber septum and purged with nitrogen. Dichloromethane-d_2 (1.0 g) was then added and the NMR tube slightly shaken. Pyridine (48 μL, 0.6 mmol) and α,α,α-trifluorotoluene (24.5 μL, 0.2 mmol) were then added and the NMR tube was shaken again. At this point ^{1}H NMR and ^{19}F NMR reference spectra were taken. The tube was then cooled to −40°C under a nitrogen atmosphere and triflic anhydride (40 μL, 0.24 mmol) was slowly added. The mixture was allowed to slowly warm up to –5°C in the acetone bath over 2 h after which ^{1}H NMR and ^{19}F NMR spectra of the reaction mixture were taken. The NMR tube was then kept under nitrogen and left to react for an additional hour at room temperature. ^{1}H NMR and ^{19}F NMR spectra of the deep orange solution showed complete consumption of the starting material and formation of *N*,*N*-(dimethylamino)-alkenylpyridinium triflate intermediates **8** as a 5:1 mixture of isomers.

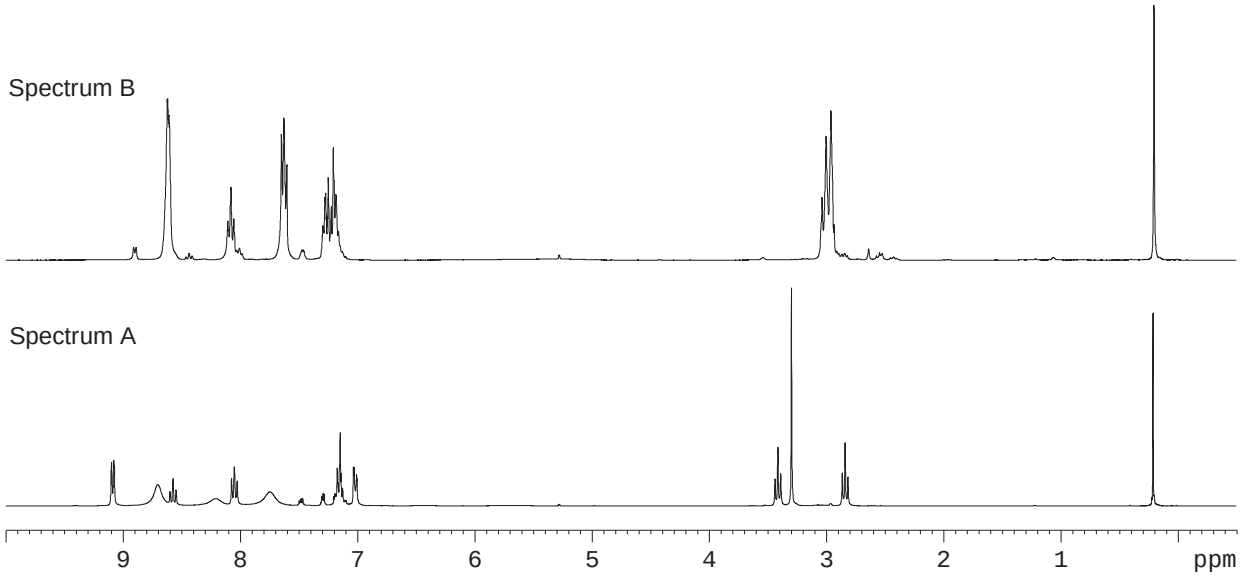
Reaction of N,N-*diethylbenzamide* **9** *with triflic anhydride in the presence of pyridine (eq. [3] and Fig. 3)*

To a dry NMR tube was added *N*,*N*-diethylbenzamide **9** (35.5 mg, 0.2 mmol) which was then capped with a rubber septum and purged with nitrogen. Dichloromethane-d_2 (1.0 g) was then added and the NMR tube slightly shaken. Pyridine (48 μL, 0.6 mmol) and α,α,α-trifluorotoluene (24.5 μL, 0.2 mmol) were then added and the NMR tube was shaken again. At this point ^{1}H NMR and ^{19}F NMR reference spectra were taken. The tube was then cooled to −40°C under a nitrogen atmosphere and triflic anhydride (40 μL, 0.24 mmol) was slowly added. The mixture was allowed to slowly warm up to –5°C in the acetone bath over 2 h after which ^{1}H NMR and ^{19}F NMR spectra of the reaction mixture were taken. The NMR tube was then kept under nitrogen and left to react for two more hours at room temperature. ^{1}H NMR and ^{19}F NMR spectra of the deep blue

[2] It is interesting to note that when 2,2-bis(hydroxymethyl)-1-propanol is used as the nucleophile, we observed the in situ formation of the orthoester. In this case, the formation of the orthoester is probably an entropy driven cyclization.

© 2001 NRC Canada

Fig. 6. ^{1}H NMR monitoring of the reaction of 1-pyridylimidoyl triflate **6** with ethanol-d_6. Spectrum A: reaction mixture containing 1-pyridylimidoyl triflate **6** and phenyltrimethylsilane (used as internal standard). Spectrum B: 1 h after the addition of ethanol-d_6 (33 equiv).



solution showed complete consumption of the starting material and formation of 1-pyridyl-*N*,*N*-diethyliminium ditriflate **10**.

Reaction of N-*methyl-3-phenylpropionamide* ***5*** *with* N-*(trifluoromethylsulfonyl)pyridinium triflate* ***11*** *in the presence of pyridine (eq. [4] and Fig. 4)*

To a dry NMR tube capped with a rubber septum and purged with nitrogen was added dichloromethane-d_2 (1.0 g) and α,α,α-trifluorotoluene (24.5 μL, 0.2 mmol). Triflic anhydride (40 μL, 0.24 mmol) was then added and the NMR tube was slightly shaken. At this point ^{1}H NMR and ^{19}F NMR reference spectra were taken. The NMR tube was then cooled to −40°C under a nitrogen atmosphere and pyridine (48 μL, 0.6 mmol) was slowly added. After 30 min, the NMR tube was warmed up to room temperature at which point ^{1}H NMR and ^{19}F NMR spectra were taken showing the complete consumption of triflic anhydride and formation of *N*-(trifluoromethylsulfonyl)pyridinium triflate **11**. The mixture was then cooled again to −40°C and *N*-methyl-3-phenylpropionamide (32.6 mg, 0.2 mmol) was quickly added. The NMR tube was allowed to slowly warm up to –5°C in the acetone bath over 2 h after which ^{1}H NMR and ^{19}F NMR spectra of the reaction mixture were taken showing complete consumption of the amide and formation of pyridinium intermediate **6**.

Reaction of N-*methyl-3-phenylpropionamide* ***5*** *with triflic anhydride (eq. [5] and Fig. 5)*

To a dry NMR tube was added *N*-methyl-3-phenylpropionamide **5** (32.6 mg, 0.2 mmol) which was then capped with a rubber septum and purged with nitrogen. Dichloromethane-d_2 (1.0 g) was then added and the NMR tube slightly shaken. α,α,α-Trifluorotoluene (24.5 μL, 0.2 mmol) was then added and the NMR tube was shaken again. At this point ^{1}H NMR and ^{19}F NMR reference spectra were taken. The NMR tube was then cooled to −40°C under a nitrogen atmosphere and triflic anhydride (40 μL, 0.24 mmol) was slowly added. After 30 min, the NMR tube was warmed up to room temperature at which point ^{1}H NMR and ^{19}F NMR spectra were taken showing the complete consumption of the amide and formation of *O*-triflyliminium triflate **12**. The mixture was then cooled again to −40°C and pyridine (48 μL, 0.6 mmol) was slowly added. The NMR tube was allowed to slowly warm up to –5°C in the acetone bath over 2 h after which ^{1}H NMR and ^{19}F NMR spectra of the reaction mixture were taken showing complete consumption of *O*-triflyliminium triflate **12** and formation of the pyridinium intermediate **6**.

Alcoholysis of 1-pyridylimidoyl triflate ***6*** *with ethanol-d_6 (Fig. 6)*

To a dry NMR tube was added *N*-methyl-3-phenylpropionamide **5** (32.6 mg, 0.2 mmol) which was then capped with a rubber septum and purged with nitrogen. Dichloromethane-d_2 (1.0 g) was then added and the tube slightly shaken. Pyridine (48 μL, 0.6 mmol) and phenyltrimethylsilane (7.0 μL, 0.04 mmol) were added and the tube was shaken again. The tube was then cooled to −40°C under a nitrogen atmosphere and triflic anhydride (40 μL, 0.24 mmol) was slowly added. The mixture was allowed to slowly warm up to –5°C in the acetone bath over 2 h after which a ^{1}H NMR spectrum was taken. The tube was then kept under nitrogen and ethanol-d_6 (390 μL, 6.6 mmol) was added at room temperature. The tube was shaken and left to react at room temperature. ^{1}H NMR spectra were then recorded at different time intervals.

Conclusion

The reaction of secondary and tertiary amides with triflic anhydride in the presence of pyridine has been investigated by various NMR spectroscopic techniques. Pyridinium intermediates were generated in all cases studied, demonstrating the crucial effect of the base used in the activation processes. We have also demonstrated that *N*-(trifluoromethylsulfonyl)-pyridinium triflate **11**, which is formed by the reaction of

© 2001 NRC Canada

triflic anhydride with the pyridine present during the initial stage of the reaction, was the activating reagent. Alcoholysis of the intermediates affords the expected *O*-alkyliminium triflates which are then converted into esters under the mild acidic work-up conditions.

Acknowledgement

This work was supported by the E.W.R. Steacie Fund, the Natural Science and Engineering Research Council of Canada (NSERC), Merck Frosst Canada, Boehringer Ingelheim, and the Université de Montréal.

References

1. V.G. Nenajdenko, E.S. Balenkova, and I.L. Baraznenok. Tetrahedron, **56**, 3077 (2000).
2. A.B. Charette and M. Grenon. Tetrahedron Lett. **41**, 1677 (2000).
3. A.B. Charette and P. Chua. J. Org. Chem. **63**, 908 (1998).
4. A.B. Charette and P. Chua. Tetrahedron Lett. **39**, 245 (1998).
5. A.B. Charette and P. Chua. Synlett, 163 (1998).
6. A.B. Charette and P. Chua. Tetrahedron Lett. **38**, 8499 (1997).
7. E. Didier, C. Cravallee, and P. Pecquet. Tetrahedron Lett. **39**, 4263 (1998).
8. A. Dossena, S. Sforza, R. Corradini, E. Virgili, and R. Marchelli. Tetrahedron Lett. **39**, 711 (1998).
9. N.J. Sisti, E. Zeller, D.S. Grierson, and F.W. Fowler. J. Org. Chem. **62**, 2093 (1997).
10. A.G. Martínez, R.M. Alvarez, J.O. Barcina, S. Cerero, E.T. Vilar, A.G. Fraile, M. Hannack, and L.R. Subramanian. J. Chem. Soc. Chem. Commun. 1571 (1990).
11. A. Battaglia, G. Barbaro, C. Bruno, P. Giorgianni, and A. Guerrini. J. Org. Chem. **61**, 8480 (1996).
12. L. Ghosez, C. Genicot, and B. Gobeaux. Tetrahedron Lett. **32**, 3827 (1991).
13. L. Ghosez and L. Chen. Tetrahedron: Asymmetry, **2**, 1181 (1991).
14. L. Ghosez and L. Chen. Tetrahedron Lett. **31**, 4467 (1990).
15. L. Ghosez, C. Schmit, J.B. Falmagne, J. Escudero, and H. Vanlierde. Org. Synth. **69**, 199 (1990).
16. L. Ghosez and B. Gobeaux. Heterocycles, **28**, 29 (1989).
17. L. Ghosez, I. Markó, and A.-M. Hesbain-Frisque. Tetrahedron Lett. **27**, 5211 (1986).
18. L. Ghosez, I. Markó, B. Ronsmans, A.-M. Hesbain-Frisque, and S. Dumas. J. Am. Chem. Soc. **107**, 2192 (1985).
19. L. Ghosez, C. Schmit, S. Taleb-Sahraoui, E. Differding, and C.G. Dehasse-De Lombaert. Tetrahedron Lett. **25**, 5043 (1984).
20. L. Ghosez, J.B. Falmagne, J. Escudero, and S. Taleb-Sahraoui. Angew. Chem. Int. Ed. Engl. **20**, 879 (1981).
21. T. Gramstad, S. Husebye, and J. Sæbø. Tetrahedron Lett. **24**, 3919 (1983).
22. V.A. Savëlova, N.A. Taran, and L.P. Drizdh. Russ. J. Org. Chem. **28**, 2031 (1992).
23. E. Anders, M. Haase, and H. Goerls. Synthesis, 195 (1998).
24. R.A. Toscano, M. Hernández-Galindo, R. Rosas, O. García-Mellado, F. Portilla, C. Amábile-Cuevas, and C. Álvarez-Toledano. Chem. Pharm. Bull. **45**, 957 (1997).
25. C.K. McClure and A.J. Kiessling. Synth. Commun. **27**, 923 (1997).
26. R.A. Barcock, D.J. Chadwick, and R.C. Storr. Tetrahedron, **50**, 4149 (1994).
27. R. Menezes and M.B. Smith. Synth. Commun. **18**, 1625 (1988).
28. Y. Kishi, T. Fukuyama, M. Aratani, F. Nakatsubo, T. Goto, S. Inoue, H. Tanino, S. Sugiura, and H. Kakoi. J. Am. Chem. Soc. **94**, 9219 (1972).
29. R.A. Chittenden and G.H. Cooper. J. Chem. Soc. 49 (1970).
30. J.P. Schroeder, D.C. Schroeder, J. Hardin, and J.K. Marshall. J. Org. Chem. **34**, 3332 (1969).
31. W.F. Barthel, J. Leon, and S.A. Hall. J. Org. Chem. **19**, 485 (1954).
32. G.E. Keck, M.D. McLaws, and T.T. Wager. Tetrahedron, **56**, 9875 (2000).
33. J. Aubé and J.E. Forsee. J. Org. Chem. **64**, 4381 (1999).
34. J. Aubé, J.E. Forsee, B.T. Smith, and K.E. Frank. Synlett, 1258 (1998).
35. L.S. Hegedus, A. Kalivretenos, and J.K. Stille. J. Org. Chem. **56**, 2883 (1991).
36. J.S. Baum and H.G. Viehe. J. Org. Chem. **41**, 183 (1976).
37. J.C. Sheehan and M.M. Nafissi-V. J. Org. Chem. **35**, 4246 (1970).
38. H. Muxfeldt, J. Behling, G. Grethe, and W. Rogalski. J. Am. Chem. Soc. **89**, 4991 (1967).
39. S. Hanessian. Tetrahedron Lett. **16**, 1549 (1967).

© 2001 NRC Canada

Catalysis of transesterification reactions by lanthanides — Unprecedented acceleration of methanolysis of aryl and alkyl esters promoted by $La(OTf)_3$ at neutral $^{S}_{S}$pH and ambient temperatures

Alexei. A. Neverov, Todd McDonald, Graham Gibson, and R.S. Brown

Abstract: La^{3+} catalysis of the methanolysis of the esters *p*-nitrophenyl, 2,4-dinitrophenyl, and phenyl acetate (**1**–**3**), phenyl benzoate (**4**), and ethyl, *i*-propyl, cyclohexyl, and *tert*-butyl acetate (**5**, **6a**, **6b**, **7**) was studied at 25°C as a function of $^{S}_{S}$pH and $[La(OTf)_3]$. The active form of the catalyst is attributed to a dimethoxy-bridged dimer of stoichiometry $(La^{3+})_2(^{-}OCH_3)_2$, having maximum activity at $^{S}_{S}$pH 8 to 9. For preparative reactions, the active catalyst can be made in situ simply by adding 0.01 equiv of $La(OTf)_3$, and 0.01 equiv of $NaOCH_3$ to a methanol solution containing the ester (1 M). Strong catalysis of methanolysis of both aryl and alkyl esters was observed, although *tert*-butyl acetate was inert. At $^{S}_{S}$pH 8.5, where the catalyst is maximally active, the transesterification reactions are accelerated by 40 000-fold to 18 000 000-fold in the presence of as little as 5 mM catalyst relative to the background reaction depending on the ester structure. A mechanism for catalysis of transesterification is presented wherein the reactive species is generated by breaking a single La—OCH_3 bond of the dimethoxy-bridged dimer to reveal a nucleophilic metal-bound methoxide – Lewis acid La^{3+} electrophilic pair.

Key words: lanthanides, transesterification, methanolysis, catalysis, kinetics.

Résumé : Opérant à 25°C, on a étudié la catalyse de la méthanolyse d'esters (acétates de *p*-nitrophényle (**1**), de 2,4-dinitrophényle (**2**), de phényle (**3**), benzoate de phényle (**4**) et acétates d'éthyle (**5**), d'*i*-propyle (**6a**), de cyclohexyle (**6b**) et de *tert*-butyle (**7**)) par le La^{3+}, en fonction du $^{S}_{S}$pH et de la $[La(OTf)_3]$. La forme active du catalyseur est attribuée à un dimère avec un pont diméthoxy, de stoechiométrie $(La^{3+})_2(^{-}OCH_3)_2$, dont l'activité maximale se situe à un $^{S}_{S}$pH allant de 8 à 9. Pour des réactions préparatives, on peut préparer le catalyseur actif in situ en ajoutant simplement 0,01 équiv de $La(OTf)_3$ et 0,01 équiv de $NaOCH_3$ à une solution méthanolique d'ester (1 M). On observe une forte catalyse de la méthanolyse des esters des séries tant alkyles qu'aryles, même si l'acétate de *tert*-butyle est inerte. À un $^{S}_{S}$pH de 8,5, alors que le catalyseur est à son activité maximale, la présence de quantités de catalyseur aussi faibles que 5 mM permet d'accélérer les réactions de transestérification par des facteurs allant de 40 000 à 18 000 000 selon la structure de l'ester. On propose un mécanisme de catalyse de la transestérification dans lequel l'espèce réactive est générée par la scission d'une seule liaison La—OCH_3 du dimère avec un pont diméthoxy qui met en présence une paire formée d'un méthylate nucléophile lié à un métal et d'un La^{3+} électrophile qui agit comme acide de Lewis.

Mots clés : lanthanides, transestérification, méthanolyse, catalyse, cinétique.

[Traduit par la Rédaction]

Introduction

Acyl transfer reactions from esters to water or alcohols are important from biological, industrial and academic standpoints (1). Much is known about the mechanism and catalysis of hydrolysis of esters, (2) and considerable attention has been devoted to transesterification reactions, including the acid- (Fischer esterification) and base-promoted pathways (3). Substantial information is available concerning the mechanisms of action of catalysts developed to promote transesterification (4). Examples of metal-catalyzed transesterification have appeared (5), and a recent report has described the related use of lanthanides as recyclable catalysts for the direct acylation of alcohols with acetic acid (6) although, for the most part, the mechanisms of these processes were not reported.

Recently we reported the rapid methanolyses of two *N*-acetylimidazole derivatives (7) and some phosphate diesters (8) catalyzed by $La(OTf)_3$. In the case of *N*-acetylimidazole (7), detailed studies indicated the catalytically active form was $(La^{3+})_2(CH_3O^{-})_2$ and that the mechanism did not involve precoordination of the metal ion to the distal nitrogen of the

Received March 13, 2001. Published on the NRC Research Press Web site at http://canjchem.nrc.ca on November 16, 2001.

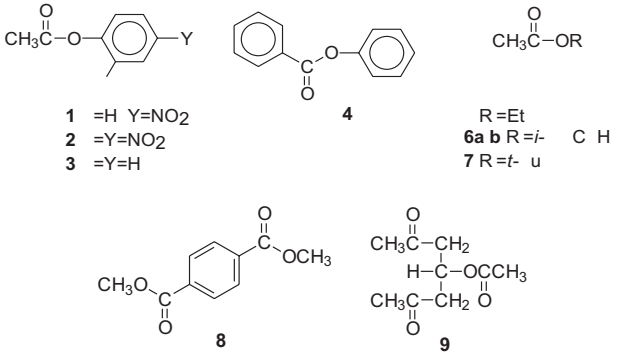
Dedicated to Professor Victor Snieckus for his contributions to Canadian chemistry.

A.A. Neverov, T. McDonald, G. Gibson, and R.S. Brown.[1] Department of Chemistry, Queen's University, Kingston, ON K7L 3N6, Canada.

[1]Corresponding author (telephone: (613) 533-2400; fax: (613) 533-6669; e-mail: rsbrown@chem.queensu.ca).

 DOI: 10.1139/cjc-79-11-1704 © 2001 NRC Canada

substrate, but rather a transient interaction of the La^{3+} dimer with the C=O. It seemed reasonable to expect similar catalysis of acyl transfer from other species including esters **1**–**9**, the preliminary studies of which form the subject of the present report.



Experimental

Materials

$La(OTf)_3$ (Aldrich) was used as received to prepare stock solutions in methanol. $NaOCD_3$ (0.62 M) was prepared in CD_3OD by adding sodium metal to CD_3OD NMR solvent, and was subsequently titrated with standard (0.02 M) HCl in aqueous solution using a combination (glass/calomel) electrode. Ester substrates (**1**–**7**) and dimethyl terephthalate (**8**) and glycerol triacetate (triacetin) (**9**), as well as glycerol and ethylene glycol were all commercial materials and were used as received.

Kinetics

UV kinetics of methanolysis of the aromatic esters were monitored by observing the rate of loss of starting material **1** at 265 nm or **2** at 279 nm or by appearance of *p*-nitrophenol at 311 nm (for **1**), 2,4-dinitrophenol at 325 nm (for **2**), or phenol at 279 nm (for **3** and **4**) under pseudo-first- order conditions of excess metal ([ester] = 4–8 × 10^{-5} M) at 25°C using an OLIS® modified Cary 17 UV–vis spectrophotometer. For these runs, the kinetics were determined under buffered conditions. The methods for determining and controlling the $^{s}_{s}$pH in methanol with buffers are reported in our earlier publications (7, 8) and are based on procedures described by Bosch and co-workers (9). Pseudo-first-order rate constants (k_{obs}) were evaluated by fitting the Abs. vs. time traces (followed for at least three half-times) to a standard exponential model.

Kinetics of transesterification of the other substrates were determined by ^{1}H NMR at 25°C using Bruker AC 200 and Avance 400 NMR machines. The active lanthanum species was generated in situ using 1 × 10^{-2} M $La(OTf)_3$ and 1 equiv (1 × 10^{-2} M) $NaOCH_3$ or $NaOCD_3$ in CD_3OD, after which the substrates, all in 1 M concentrations, were added. For *i*-propyl acetate (**6a**), the kinetics were determined monitoring the change in intensity of each of the $(CH_3)_2$CH-O-C(O)-C*H*$_3$ peaks at δ 1.93, the (C*H*$_3$)$_2$CH-O-C(O)-CH$_3$ peak at δ 1.17, and the $(CH_3)_2$C*H*-O-C(O)-CH$_3$ peak at δ 4.91. For cyclohexyl acetate (**6b**), the ester >C*H*-OC(O)C*H*$_3$ peaks at δ 4.61 and 1.96 were used. For *tert*-butyl acetate (**7**), the (C*H*$_3$)$_3$C-O-C(O)-CH$_3$ peak at δ 1.40 was used. For dimethyl-1,4-terephthalate, a crystalline solid, dissolution in methanol was difficult, so a saturated solution in CD_3OD was prepared, later estimated to be about 0.047 M by an NMR experiment measuring the peak ratio of the aryl ring protons against ethyl acetate as an internal standard. For this substrate, the disappearance of the 1,4-(C*H*$_3$-O-C(O)-)$_2$C$_6$H$_4$ signals at δ 3.92 were used to follow the kinetics. In each case, the pseudo-first-order rate constant (k_{obs}) for transesterification of the substrate was determined by fitting the peak intensity vs. time data to a standard exponential model.

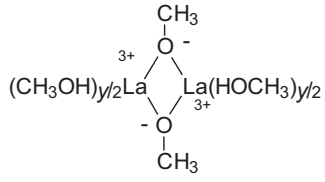
Pseudo-first-order rate constants for transesterification of the above esters in the absence of La^{3+} were determined under conditions of excess [CH_3O^-] (0.01–0.1 M) by UV–vis spectrophotometry or ^{1}H NMR as described above. The second-order rate constants for the methoxide reactions were calculated as k_{obs}/[CH_3O^-]. Given in Table 1 are the second-order rate constants for the methoxide reactions along with those for the La^{3+}-catalyzed reactions.

Electrospray MS

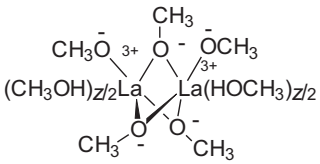
Mass spectra of 0.001 M solutions of $La(OTf)_3$ in methanol were determined using a VG Quattro mass spectrometer equipped with an electospray source operating at cone voltages between 20 and 50 V. Both monomeric and dimeric species' peaks related to $[La(CF_3SO_3)_2]^+$ and $[La_2(CF_3SO_3)_5]^+$can be observed, appearing as clusters having solvating methanol molecules, the number and intensity of which was found to be dependent on cone voltage (Fig. 1). Higher order aggregates are not observed up to mass 2500. The electrospray MS of complexes of La^{3+} with added methoxide anions was undertaken using methanol solutions containing 0.001 M of both $La(OTf)_3$ and Bu_4NOH.

Results and discussion

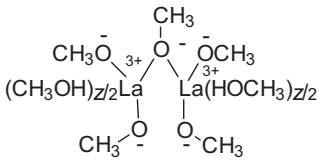
Potentiometric titration of La^{3+} in MeOH at 25°C, undertaken as described in our previous reports (7, 8), indicates sequential consumptions of first, a single CH_3O^-/La^{3+} (apparent $^{s}_{s}pK_a$ 7.55), and then 1.5 CH_3O^-/La^{3+} (apparent $^{s}_{s}pK_a$ 10.2). The methoxy-bridged dimeric structures **10** and **11** suggested previously (7, 8), are consistent with the stoichiometry and with the detailed kinetic data described below for La^{3+}-promoted methanolysis of ester **1**. However, to gain more information about the speciation of La^{3+} in methanol solution, we undertook electrospray MS studies.



10



11a



11b

© 2001 NRC Canada

Table 1. Maximal second-order rate constants for $(La^{3+})_2(CH_3O^-)_2$-catalyzed methanolysis of esters **1**–**7**, and second-order rate constants for methoxide attack on esters **1**–**7** (T = 25°C).

Substrate	${}^{S}_{S}pH_{max}$	k_2^{ester} ($M^{-1}s^{-1}$)[a]	k_{OMe-}^{ester} (M^{-1} s^{-1})[b]	$k_2^{ester}/k_{OMe-}^{ester}$	Acceleration [c]
1	8–9	72	220 ± 100[b]	0.6–0.225	243 000
2	9.8	29 ± 2	410[d]	0.07	42 000
3	8.8	58 ± 3	2.66[e]	21	18 750 000
4	8.7	3.0 ± 0.06	0.338 ± 0.006[f]	8.9	5 300 000[h]
5	8.5[g]	0.143	(5.7 ± 0.2) × 10^{-2}[f]	2.5	2 300 000
6	8.5[g]	0.0083	(7.0 ± 0.1) × 10^{-3}[f]	1.2	1 120 000
7	8.5[g]	<<5.7 × 10^{-6}	(2.0 ± 0.1) × 10^{-4}[f]	<<0.03	

[a]Esters **1**–**4** determined by UV kinetics in CH_3OH; **5**–**7** determined from ^1H NMR in d_4-methanol as described in the text.

[b]At 27.4°C. R.L. Schowen and C.G. Behn. J. Am. Chem. Soc. **90**, 5839 (1968).

[c]Catalytic value at ${}^{S}_{S}pH$ 8.5, in the presence of 5 × 10^{-3} M $(La^{3+})_2(CH_3O^-)_2$. Background rate computed from k_{OMe-}^{ester} assuming the value for the solvent reaction at ${}^{S}_{S}pH$ 8.5 is entirely attributed to CH_3O^- + ester. The autoprotolysis constant of methanol is 1 × $10^{-16.77}$ (9).

[d]V. Machacek, S. Mareckova, and S. Vojeslav. Collect. Czech. Chem. Commun. **44**, 1779 (1979).

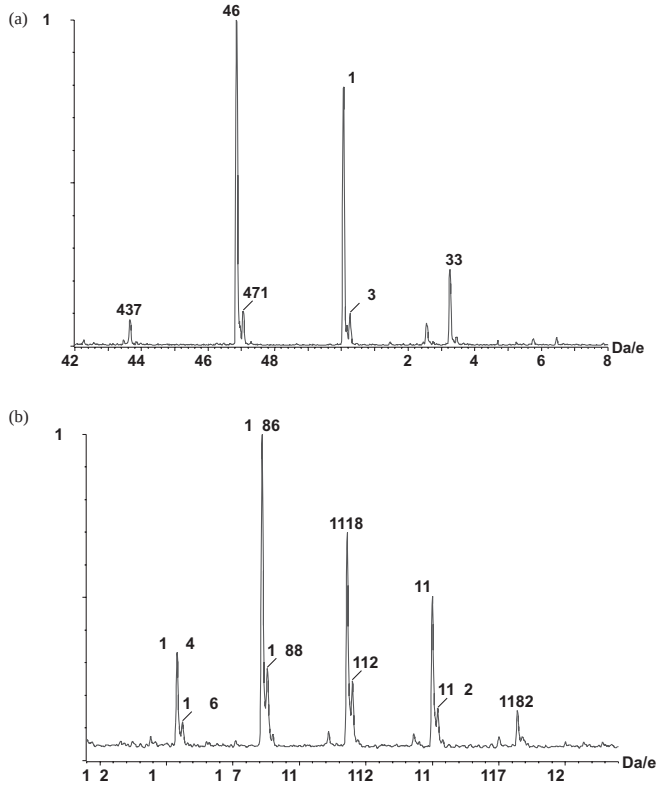
[e]C.G. Milto, M. Gresser, and R.L. Schowen. J. Am. Chem. Soc. **91**, 2047 (1969).

[f]This work.

[g]${}^{S}_{S}pH$ estimated from the titration curve of La^{3+} and set by 1:1 La^{3+}–$^-OCH_3$ stoichiometry.

[h]Acceleration computed at ${}^{S}_{S}pH$ 8.7.

Fig. 1. ES–MS spectra of a 0.001 M solution of $La(OTf)_3$ in methanol, cone voltage 39, showing the presence of monomeric (a) and dimeric (b) La^{3+} forms with associated counter-ions and methanols of solvation.



Shown in Fig. 1 is the electrospray MS of $La^{3+}(OTf^-)_3$ in methanol taken at a cone voltage of 39 V which reveals the presence of a $[La(CF_3SO_3)_2]^+$ monomeric and $[La_2(CF_3SO_3)_5]^+$ dimeric forms with associated methanols of solvation. Stewart and Horlick (10) have reported an extensive study of the ES–MS of Ln^{x+} ions in methanol and acetone and while monomeric Ln^{3+} clusters were observed, their instrument had limited mass range such that the presence of dimers and higher order aggregates could not be ascertained. The number of methanol molecules associated with the cations is dependent on the spectrometer's cone voltage (the potential difference between the sampling plate and skimmer)), with lower voltages promoting higher solvation number. The max solvation number in our case was found to be 4 for $[La(CF_3SO_3)_2(CH_3OH)_4]^+$ (m/z = 565) and 6 for $[La_2(CF_3SO_3)_5(CH_3OH)_6]^+$ (m/z = 1214) (cone voltage 30 V). The increase in cone voltage causes "striping" of solvated methanol molecules due to increasing the energy of collisions between the curtain gas and the analyte ions which results in a decrease of max observed solvation number as well as median solvation number (10).

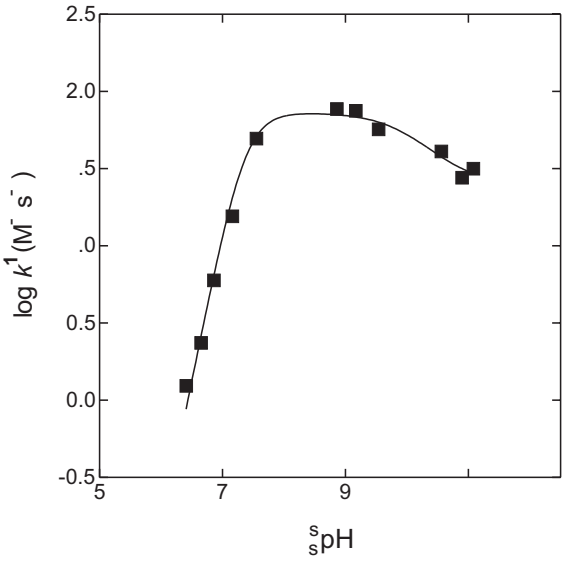
ES–MS analysis of complexes of La^{3+} with methoxide anions was undertaken using a methanol solution of 0.001 M in each of $La(OTf)_3$ and Bu_4NOH. Due to the much higher concentration of methanol compared to the water present in the Bu_4NOH, and their similar ${}^{s}_{s}pK_a$ values, we assumed that most of the hydroxide ions were converted to methoxide, a fact that seems verified by the lack of observation of substantial HO^- based peaks in the ES–MS. The spectrum taken at a cone voltage of 55 V (not shown) reveals the presence of a monomeric species containing one methoxide ($[La(CF_3SO_3^-)(CH_3O^-)]^+$ (m/z = 319)), as well as dimers containing two and three methoxides ($[La_2(CF_3SO_3^-)_3(CH_3O^-)_2]^+$ (m/z = 787) and $[La_2(CF_3SO_3^-)_2(CH_3O^-)_3]^+$ (m/z = 669)). That the above MS spectra clearly indicate the presence of a monomeric La^{3+} species, and not the presence of a dimeric form with charge = 2, can be ascertained from the presence of M^+ + 2 peaks, attributable to the presence of the ^{34}S isotope in the triflate.

(A) Aryl and alkyl ester methanolysis

Determination of the pseudo-first-order rate constants (k_{obs}) for methanolysis of **1** as a function of both $[La^{3+}]_t$ and ${}^{s}_{s}pH$ (9) at 25°C under buffered conditions (7, 8), immediately indicated that the catalytic mechanism involves a greater-than-first-order dependence on both $[La^{3+}]$ and $[CH_3O^-]$. Plots of

© 2001 NRC Canada

Fig. 2. Plot of second-order rate constant (k_2) vs. $^{S}_{S}$pH for $(La^{3+})_2$-dimer-promoted methanolysis of *p*-nitrophenyl acetate (**1**) (T = 25°C). Line through data from NLLSQ fits to eq. [1].



the k_{obs} for transesterification of **1** vs. $[La^{3+}]_t$ at a given $^{s}_{s}$pH (not shown) showed significant upward curvature at low $[La^{3+}]$ ($<10^{-4}$ M), suggesting that the catalytically active species contains two (or more) La^{3+} ions. These plots culminate in straight lines, indicating the complete formation of what we interpret as catalytically active La-dimers at concentrations greater than 3–4 × 10^{-4} M as was observed in our previous work with acetylimidazole (7). Plots of the log second-order rate constant (k_2) for dimeric La^{3+} catalysis (computed from the linear portions of the k_{obs} vs. $[La^{3+}]_t$ plots) vs. $^{s}_{s}$pH (as illustrated for **1** in Fig. 2) show an ascending domain at low $^{s}_{s}$pH having a slope of 2, requiring that two methoxides are present in the catalytically active species, followed by a plateau at $^{s}_{s}$pH 8–9. Further increases in $^{s}_{s}$pH beyond the plateau region gave a decrease in catalytic rate.

Given in Scheme 1 is a mechanism that accounts for the kinetic behavior, including the drop in activity at high $^{s}_{s}$pH which is attributed to the reduced activity of any dimeric La^{3+} species containing more than two CH_3O^-. The latter species are collectively illustrated in Scheme 1 as $(La^{3+})_2(CH_3O^-)_3(CH_3OH)_y$, but also comprise $(La^{3+})_2(CH_3O^-)_4$ and $(La^{3+})_2(CH_3O^-)_5$ with an unspecified number of solvating methanols produced at progressively higher $^{S}_{S}$pH, (subsequent discussion will ignore the presence of solvating methanols). The available data did not allow us to determine whether the reduced activity species $(La^{3+})_2(CH_3O^-)_3$, has residual activity, but this is not important for the subsequent discussion since we focus on the maximally active species (**10**) generated between $^{s}_{s}$pH 8–9. NLLSQ-fitting of the log k_2 vs. $^{s}_{s}$pH data to eq. [1], derived for the process given in Scheme 1,[2] gives the solid line through the data in Fig. 2 and values of 7.35 ± 0.1 for the kinetic $^{S}_{S}pK_a$ for formation of the $La^{3+}{}_2(CH_3O^-)_2$ dimer and 72 M^{-1} s^{-1} for k_2.[2]

$$[1] \qquad k_2 = k_2^{ester}\,{}^{S}_{S}K_a[H^+]/((2({}^{S}_{S}K_a + [H^+]^2)({}^{S}_{S}K'_a + [H^+])) + k'^{ester}_2\,{}^{S}_{S}K'_a/2({}^{S}_{S}K'_a + [H^+])$$

These constants indicate that at a concentration of 5 × 10^{-3} M of La^{3+}-dimer (produced at a $[La^{3+}]_t$ of 1 × 10^{-2} M), $^{s}_{s}$pH 8–9, the half-time for methanolysis of **1** is ~2 s, corresponding to an impressive 243 000-fold acceleration over the spontaneous methanolysis reaction at that $^{s}_{s}$pH.

Since the catalyzed methanolysis of **1** reaches maximal rate constants under conditions where the dimer is fully formed ($[La^{3+}]_t$ > 3–4 × 10^{-4} M) and when it is associated with two methoxides ($^{s}_{s}$pH 8–9), these conditions were utilized to determine the maximal catalytic k_2^{ester} constants exhibited for methanolysis of esters **2**–**4** by $(La^{3+})_2(CH_3O^-)_2$ at 25°C. The data given in Table 1 indicate that there is relatively little dependence of k_2^{ester} on the nature of the aryloxy leaving group, and that there is a 20-fold reduction in activity for phenyl benzoate relative to phenyl acetate, probably due to a steric effect at the acyl portion. Also given in Table 1, for comparison purposes, are the corresponding second-order rate constants for OCH_3^- attack on the esters, the k_{OMe-}^{ester} values for **1**–**3** being available from the literature, while those for **4**–**7** were determined in this work.

To determine both the rate constants of, and the synthetic utility for, methanolysis of alkyl esters, we established a protocol where esters **5**–**7** (1 M) and a catalytic amount of $La(OTf)_3$ (0.01 equiv relative to ester) was placed in d_4-methanol along with 0.01 equiv of $NaOCH_3$. These are conditions where the $(La^{3+})_2(CD_3O^-)_2$ active form of the catalyst is generated in situ. For **5**–**7**, this reaction is conveniently monitored in d_4-methanol at 25°C by ^{1}H NMR as a function of time by integrating the -OC*H*< signals for **5** and **6**, and the -OC(CH_3)$_3$ signals for **7**. Shown in Fig. 3 are kinetic plots from which the pseudo-first-order rate constants (k_{obs}) can be calculated by NLLSQ-fitting to a standard exponential model.[3] Given a concentration of the active dimer of 5 × 10^{-3} M, second-order rate constants of 1.43 × 10^{-1} M^{-1} s^{-1}, 8.3 × 10^{-3} M^{-1} s^{-1}, and 9.36 × 10^{-3} M^{-1} s^{-1} can be computed for k_2^5, k_2^{6a}, and k_2^{6b}, respectively; no reaction of **7** was observed after 28 days, so an upper limit of <5.7 × 10^{-6} M^{-1} s^{-1} is estimated for k_2^7, pointing to a large steric and possibly leaving-group effect for the catalyzed reaction of alkyl esters.

(B) Trigyceride methanolysis model

Triglycerides comprise an important class of biological molecules that store chemical energy as the glycerol esters of long-chain fatty acids to fuel subsequent metabolism by the organism (11). The methanolysis of triglycerides yields

[2] Derivation of the expression given in eq. [1] follows the exact procedure given in ref. 7*b* and considers the equations for the conservation of mass of the La^{3+} species and the various equilibrium and dissociation constants.

[3] Since the transesterification reaction is an equilibrium process, the position of which depends on the relative rate constants for the forward and reverse reactions and the relative concentrations of the reactants, the computed k_{obs} values are the sum of the forward and reverse rate constants. That the actual reaction attains an equilibrium position is readily apparent from the NMR data for **5** and **6**, since at completion, residual starting material is observed. This method could be used to conveniently determine the equilibrium position and the factors affecting this for a variety of esters.

© 2001 NRC Canada

Scheme 1.

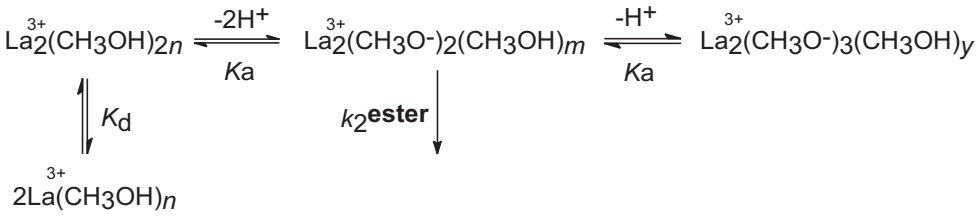
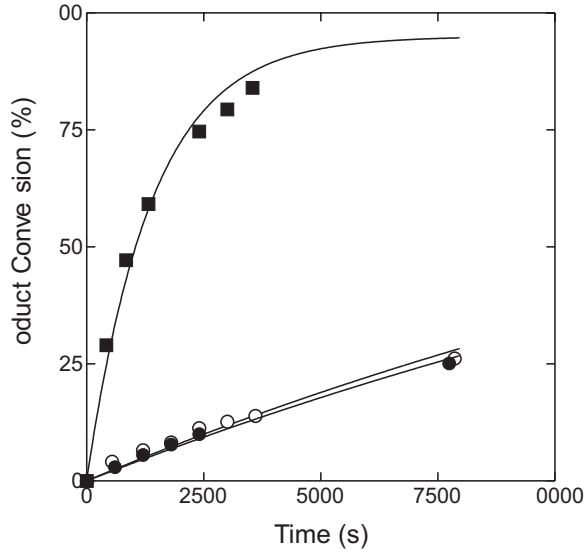
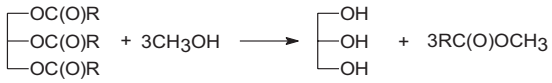


Fig. 3. Plots of % product formed as a function of time as determined by ^{1}H NMR for methanolysis of esters **5**, **6a**, **6b** at ambient temperature: [ester] = 1.0 M, [La(OTf)$_3$] = [$CH_3O^-Na^+$] = 0.01 M, d_4-methanol. ■ (**5**) (k_{obs} = 7.15 × 10^{-4} s^{-1}), ● (**6a**) (k_{obs} = 4.15 × 10^{-5} s^{-1}) ○ (**6b**) (k_{obs} = 4.68 × 10^{-5} s^{-1}).



three methyl esters of fatty acid chains of varying length and saturation, as well as glycerol as in eq. [2]. The combustion properties of long-chain fatty acid methyl esters make for a rich, renewable source of energy known as "biodiesel" (12), the production of which is of current interest as an alternative diesel fuel.

[2] 

Methanolysis of a 1 M solution of the model triglyceride, glycerol triacetate (triacetin, **9**), was studied by ^{1}H NMR in CD_3OD in the presence of 5 × 10^{-3} M dimeric catalyst formed by the addition of 1 × 10^{-2} M La(OTf)$_3$ and 1 × 10^{-2} M Na(OCD_3). Following the reaction by NMR proved difficult both because of the complexity of the multiplets that arise from the glyceryl protons and the complexity of the reaction itself, with the possibility of four distinct intermediates being formed before complete conversion to product. Despite these complications, the disappearance of starting material can be followed by monitoring the rate of change of the AcO-CH_2-C*H*(OAc)-CH_2-OAc signal at δ 5.23 referenced to the sum of all the CH_3 acetate peaks. Under the above conditions, the initial rate of loss of starting material was very fast and ~29% of starting material was converted to one of the intermediates after 9 min. There did not appear to be any great selectivity for methanolysis among the primary and secondary acetates of **9**, a somewhat peculiar observation considering the 17-fold difference noted above for methanolysis of ethyl and *i*-propyl acetates. After the initial rapid methanolysis, further conversion progressed much more slowly, and loss of starting material was observed to be only 36% after 60 min. The kinetic behavior suggests an inhibitory effect either of one of the diol intermediates or the small quantities of the final glycerol product of methanolysis through tight binding to the La^{3+} catalyst. In another experiment when the reaction mixture comprised equimolar amounts of triacetin, $NaOCD_3$ and [La^{3+}] (1 × 10^{-2} M), ~80% conversion was observed in less than 10 min. In this case, the greater conversion can be explained by the smaller product:catalyst ratio consistent with the idea that product inhibition would require more formation of product.

To investigate further the inhibitory effect of polyols on La^{3+} catalysis, the methanolysis of 1 M ethyl acetate was studied (CD_3OD in the presence of 1 × 10^{-2} M each of La(OTf)$_3$ and $NaOCD_3$, and 5 × 10^{-2} M of glycerol). Whereas La^{3+}-catalyzed methanolysis of ethyl acetate at these concentrations normally has a $t_{1/2}$ of about 8 min, (k_{obs}= (7.2 ± 0.4) × 10^{-4} s^{-1}), the added glycerol increases the $t_{1/2}$ to 160 h, (k_{obs} ≅1.2 × 10^{-6} s^{-1}), corresponding to a 600-fold reduction in rate. A similar experiment using 0.1 M ethyl acetate in methanol containing 1 × 10^{-2} M each of La(OTf)$_3$ and $NaOCD_3$ in the presence of 5 × 10^{-2} M ethylene glycol, gave a rate constant for methanolysis of (1.02 ± 0.02) × 10^{-4} s^{-1}, corresponding to a sevenfold rate reduction. These experiments indicate that at the same concentration of 5 × 10^{-2} M, glycerol is about a 100-fold better inhibitor of catalysis than is ethylene glycol.

(C) Complexation of La^{3+} by ethylene glycol and glycerol

The inhibition of catalysis described above suggests strong complexation of the metal ion by polyols to create a bound inactive form. An ^{1}H NMR experiment was performed where the CH_2 signals of an ethylene glycol (0.01 M in CD_3OD) was monitored as a function of varying aliquots of a 0.05 M $La^{3+}(OTf^-)_3$ solution (0, 0.5, 1, 1.5, 2, 3.5, and 5 equiv). The ethylene glycol signal at δ 3.60 asymptotically approaches a value of δ 3.85 for the completely bound form, from which a dissociation constant of 0.006 M can be estimated for the La^{3+}–$(CH_2OH)_2$ complex. This binding constant indicates that at a [La^{3+}] of 1 × 10^{-2} M and [ethylene glycol] of 5 × 10^{-2} M, roughly 85–90% of the metal is bound under these neutral conditions. Such binding can ex-

© 2001 NRC Canada

plain the drop in catalytic activity for methanolysis of ethyl acetate seen in part B above. The existence of complexed forms under neutral conditions could also be confirmed by an ES–MS experiment with a methanol solution of 5×10^{-3} M $La^{3+}(OTf^{-})_3$ containing 5×10^{-2} M $(CH_2OH)_2$ which gives a strong peak at *m*/*z* = 1146, corresponding to $La_2(OTf)_5((CH_2OH)_2)_2$ and *m*/*z* = 499 corresponding to $La(OTf)_2(CH_2OH)_2$. Interestingly, when the ES–MS experiment is done with 5×10^{-3} M $La^{3+}(OTf^{-})_3$ and 5×10^{-3} M $(n\text{-Bu})_4NOH$, conditions similar to the kinetic experiment described in part B above, one sees a very prominent peak at *m*/*z* = 846 corresponding to $La_2(OTf)_3(HOCH_2CH_2O^{-})_2$ with a smaller one at *m*/*z* = 349 corresponding to $La(OTf)(HOCH_2CH_2O^{-})$. The fact that there is no evidence of any methoxide-bound monomer or dimer indicates that the association of the ethylene glycol anion must be very much stronger, and indeed further promotes the formation of a dimeric form.

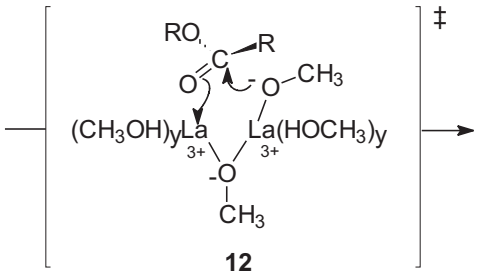
The binding of La^{3+} by glycerol is even stronger than that of ethylene glycol as revealed by ^1H NMR spectra of a 0.01 M solution of glycerol in CD_3OD, recorded in the presence of varying concentrations of $La(OTf)_3$ (0–0.02 M). The addition of 0.5 equiv of $La(OTf)_3$ causes a significant downfield shift of the >C*H*(OH)-signal at δ 3.64–4.04 ppm, while the addition of another 0.5 equiv of $La(OTf)_3$ gives a further downfield shift of the signal to δ 4.20 ppm. Subsequent increases in the $[La(OTf)_3]$ up to 0.02 M (2 equiv) produces almost no change in the signal indicating complete formation of a 1:1 complex at equimolar 0.01 M concentration, which explains the dramatic loss in catalytic activity seen above. ES–MS of a 1:1 0.01 M solution of each (neutral conditions) also reveals the presence of a $La_2(OTf)_5(C_3H_8O_3)_2$ complex (*m*/*z* = 1206) and a monomer peak at *m*/*z* = 529 corresponding to $La(OTf)_2(C_3H_8O_3)$. Under basic conditions, ES–MS of a 1:1:1, 0.01 M solution in each of $La(OTf)_3$, glycerol, and $(n\text{-Bu})_4NOH$, reveals a major peak at *m*/*z* = 906 corresponding to a dimer $((La_2(OTf)_3(C_3H_7O_3^{-})_2)$ and a smaller peak at 379 corresponding to $La(OTf)(C_3H_7O_3)$. As in the case of ethylene glycol under basic conditions, the ES–MS gave no indication of La^{3+} monomers or dimers having associated methoxides, once again pointing to the much stronger complexation by an anionic polyol relative to CH_3O^{-}, probably resulting from polydentate binding. The combined NMR and ES–MS experiments suggest that the origin of the inhibitory effect of polyols results from a decrease in concentration of the catalytically active $(La^{3+})_2(CH_3O^{-})_2$ form due to a displacement of methoxide by the polyols or at higher pH, the polyol anion.

(D) Methanolysis of dimethyl terephthalate

Current industrial protocols for polyester recycling employ methanolysis for digestion into the corresponding methyl esters and dialcohols arising from aliphatic spacer groups (13) or transesterification involving ester–ester interchange catalyzed by various metallic species including dimeric difunctional tetraorganodistannoxanes and titanium tetraalkoxides at elevated temperatures (14). The above studies indicate that La^{3+}-promoted methanolysis of esters is subject to strong inhibition by ethylene glycol, and as such is likely to be the situation with attempted methanolysis of the ethylene glycol – terephthalate polymers. Thus, we preliminarily investigated a simplified model, the methanolysis of dimethyl terephthalate in CD_3OD, by observing the rate of loss of both the CH_3 signals of **9** at δ 3.92. In the presence of 1×10^{-2} M each of $La^{3+}(OTf^{-})_3$ and $NaOCH_3$, the reaction of a 0.047 M solution of **9** (saturated at 25°C), proceeds with an observed pseudo-first-order rate constant of $(5.8 \pm 0.2) \times 10^{-4}$ s^{-1}, corresponding to a $k_2^{\mathbf{9}}$ second-order rate constant of 0.116 M^{-1} s^{-1} which is some 26 times slower than catalyzed methanolysis of phenyl benzoate **4**.

Conclusions

The work herein with esters shows that the La^{+}-catalyzed methanolysis of esters involves an activated complex having one molecule of ester, two La^{3+} ions, and two methoxides; the likely transition structure for transesterification is given in **12**. This is consistent with what we proposed for La^{3+}-catalyzed methanolysis of *N*-acetylimidazole (**7**), wherein one of the methoxy bridges opens to reveal a transient reactive complex with a nucleophilic La^{3+}-$^{-}OCH_3$ portion in close proximity to an electrophilic La^{3+} partner.



12

The La^{3+} catalysis of methanolysis is inhibited by the presence of polyols such as ethylene glycol or glycerol due to strong complex formation with the metal ion which becomes even stronger under conditions where the monodeprotonated polyol exists.

The finding that La^{3+} catalysis of ester methanolysis is optimal at a $[La^{3+}]/[CH_3O^{-}] = 1$ explains the attenuated catalytic propensities reported (5*a*) for $Ln(O\text{-}i\text{-}Pr)_3$ in promoting transesterifications of various esters to primary and secondary alcohols even at high temperatures and prolonged reaction times. This underscores the importance of mechanistic considerations in developing effective catalysts.

The catalyst can be made in situ simply by adding equimolar amounts of CH_3O^{-} and La^{3+} to create an exceptionally active methoxy-bridged dimeric form at neutral $^{s}_{s}$pH which, at concentrations of 5 mM, can accelerate the methanolysis of the esters studied by as much 4×10^4- to 1.8×10^7-fold relative to the background reaction. Interestingly, compared to the OCH_3^{-} reaction, the catalyst is more effective for esters containing poor leaving groups than those having the better NO_2-substituted aryloxy leaving groups. Importantly, the fact that the kinetics are strictly first-order indicates strong turnover of the catalyst with no loss in activity even under conditions where the [ester] > > $[La^{3+}]_t$. These findings suggest that many other active catalysts for involving other lanthanides and alcohols could be developed as will be reported in our subsequent publications.

© 2001 NRC Canada

Acknowledgements

The authors acknowledge the financial assistance of the Natural Sciences and Engineering Research Council of Canada (NSERC) and Queen's University in support of this research.

References

1. J. Otera. Chem. Rev. **93**, 1449 (1993).
2. (*a*) A.J. Kirby. *In* Comprehensive chemical kinetics. Vol. 10. *Edited by* C.H. Bamford and C.F.H. Tipper. Elsevier, Amsterdam. 1972. pp. 57–207; (*b*) A.J. Bennett and R.S. Brown. Physical organic chemistry of acyl transfer reactions. *In* Comprehensive biological catalysis: A mechanistic reference. Vol. 1. *Edited by* M. Sinnott. Academic Press, New York. 1997. pp. 293–326; (*c*) J. March. Advanced organic chemistry: Reactions, mechanisms and structure. 4th ed. John Wiley and Sons, New York. 1992. pp. 378–383; (*d*) E.K. Euranto. *In* The chemistry of carboxylic acids and esters. *Edited by* S. Patai. John Wiley and Sons, New York. 1969. pp. 505–588.
3. (*a*) J. Koskikallio. *In* The chemistry of carboxylic acids and esters. *Edited by* S. Patai. John Wiley and Sons, New York. 1969. pp. 103–136; (*b*) M.A. Ogliaruso and J.A. Wolfe. Synthesis of carboxylic acids, esters and their derivatives. *Edited by* S. Patai and Z. Rappoport. John Wiley and Sons, Chichester. 1991. pp. 465–476.
4. (*a*) J. March. Advanced organic chemistry: Reactions, mechanisms and structure. 4th ed. John Wiley and Sons, New York. 1992 pp. 397–398, and refs. therein; (*b*) M.G. Stanton, C.B. Allen, R.M. Kissling, A.L. Linclon, and M.R. Gagné. J. Am. Chem. Soc. **120**, 5981 (1998), and refs. therein.
5. (*a*) T. Okano, K. Miyamoto, and J. Kiji. Chem. Lett. 246 (1995); (*b*) B.C. Ranu, P. Dutta, and A. Sarkar, J. Org. Chem. **63**, 6027 (1998); (*c*) L. Baldini, C. Bracchini, R. Cacciapaglia, A. Casnati, L. Mandolini, and R. Ungaro. Chem. Eur. J. **6**, 1322 (2000); (*d*) R. Cacciapaglia, S. Di Stephano, E. Kelderman, and L. Mandolini. Angew. Chem. Int. Ed. **38**, 349 (1999); (*e*) W.M. Stevels, M.J.K. Ankoné, P.J. Dijkstra, and J. Feijen. Macromolecules, **29**, 8296 (1996); (*f*) N.J. Hinde and C. Dennis Hall. J. Chem. Soc. Perkin Trans. 2, 1249 (1998), and refs. therein; (*g*) J. Otton, S. Ratton, V.A. Vasnev, G.D. Markova, K.M. Nametov, V.I. Bakhmutov, L.I. Komarova, S.V. Vinogradova, and V.V. Korshak. J. Polym. Sci. Part A: Polym. Chem. **26**, 2199 (1988).
6. A.G.M. Barrett and C. Braddock. J. Chem. Soc. Chem. Commun. 351 (1997).
7. (*a*) A.A. Neverov and R.S. Brown. Can. J. Chem. **78**, 1247 (2000); (*b*) A.A. Neverov, P. Montoya-Pelaez, and R.S. Brown. J. Am. Chem. Soc. **123**, 210 (2001).
8. A.A. Neverov and R.S. Brown. Inorg. Chem. **40**, 3588 (2001).
9. (*a*) E. Bosch, F. Rived, M. Roses, and J. Sales. J. Chem. Soc. Perkin Trans. 2, 1953 (1999); (*b*) F. Rived, M. Rosés, and E. Bosch. Anal. Chim. Acta, **374**, 309 (1998); (*c*) E. Bosch, P. Bou, H. Allemann, and M. Roses. Anal. Chem. **68**, 3651 (1996).
10. I.A. Stewart and G. Horlick. Anal. Chem. **66**, 3983 (1994).
11. D. Voet, J.G. Voet, and C.W. Pratt. Fundamentals of biochemistry. John Wiley and Sons, New York. 1999. pp. 222–223.
12. A. Srivastava and R. Prasad. Renewable Sustainable Energy Rev., **4**, 111 (2000).
13. J. McMurray. Organic chemistry. 3rd ed. Brooks/Cole Publishing Co., Pacific Grove, California. 1992. pp. 1200–1202.
14. I. Pesneau, M. Grégoire, and A. Michel. J. App. Polym. Sci. **79**, 1556 (2001), and refs. therein.

© 2001 NRC Canada

Synthesis of highly functionalized naphthoate precursors to damavaricin D — Observation of kinetically stable benzocyclohexadienones in the bromination reactions of highly functionalized β-naphthol derivatives

William R. Roush, David J. Madar, and D. Scott Coffey

Abstract: Selective syntheses of the highly substituted bromonaphthoates **4a**, **4b**, **19**, and **22** are reported. These compounds were targeted as precursors to the naphthoquinone nucleus of damavaricin D; compound **22** ultimately was used in the successful total synthesis. The synthesis of **22** features the Diels–Alder reaction of the oxygenated diene **5** and 2,6-dibromo-3-methylbenzoquinone **6** to establish the core naphthalenic unit. The quinone was protected throughout this synthesis as a 1,4-bis-methoxymethyl-1,4-dihydroquinone (see **36**). The C-2-carboalkoxy group of **22** was added by carboxylation of the aryllithium intermediate generated from **36**, and protected as a β-trimethylsilylethyl ester. Finally, the C-8-Br substituent was introduced by NBS bromination of **38**. This reaction proceeds by way of bromobenzocyclohexadienone **39**. Related bromobenzo-cyclohexadienones **13** and **29** were observed in the NBS brominations of the highly functionalized β-naphthyl MOM ethers **11** and **28**. The bromobenzocyclohexadienones **29** and **39** undergo facile substitution reactions with chloride ion and reduction with bromide ion at rates competitive with base-promoted aromatization. The surprising kinetic stability of these intermediates is attributed to a combination of steric and stereoelectronic factors.

Key words: damavaricin D, naphthoate precursors, kinetically stable benzocyclohexadienones, aromatic bromination.

Résumé : On a réalisé des synthèses sélectives des bromonaphtoates hautement substitués **4a**, **4b**, **19** et **22**. Ces composés pourraient servir de précurseurs du noyau naphtoquinone de la damavaricine D; dans la synthèse totale, on a finalement utilisé avec succès le composé **22**. La synthèse du composé **22** implique une réaction de Diels–Alder du diène oxygéné **5** et de la 2,6-dibromo-3-méthylbenzoquinone (**6**) pour obtenir l'unité naphtalénique fondamentale. La quinone a été protégée durant toute la synthèse sous la forme d'une 1,4-bis-méthoxyméthyl-1,4-dihydroquinone (voir **36**). Le groupe C-2-carboalkoxy du composé **22** a été ajouté par carboxylation de l'intermédiaire aryllithium généré à partir du composé **36** et il a été protégé sous la forme d'un ester β-triméthylsilyléthyle. Enfin, le substituant C-8-Br a été introduit par une bromation du composé **38** à l'aide de la NBS. Cette réaction se produit par l'intermédiaire de la bromobenzocyclohexadiénone **39**. On a aussi observé la présence des bromobenzocyclohexadiénones **13** et **29** lors des bromations par le NBS des éthers β-naphtylés hautement fonctionnalisés **11** et **28**. Les bromobenzocyclohexadiénones **29** et **39** donnent des réactions faciles de substitutions avec l'ion chlorure et de réduction avec l'ion bromure, avec des vitesses qui sont en compétition avec l'aromatisation catalysée par les bases. On attribue la stabilité cinétique surprenante de ces intermédiaires à une combinaison de facteurs stériques et stéréoélectroniques.

Mots clés : damavaricine D, précurseurs naphtoates, benzocyclohexadiénones cinétiquement stables, bromation aromatique.

[Traduit par la Rédaction]

Introduction

The streptovaricins are a group of biologically active ansamycin antibiotics isolated from *Streptomyces spectablis* (1, 2). The streptovaricins were initially studied for their antibacterial properties, but the toxicity of these agents limited their clinical success (2). The streptovaricins (and congeners such as the damavaricins, vide infra) continue to be of

Received February 5, 2001. Published on the NRC Research Press Web site at http://canjchem.nrc.ca on November 14, 2001.

Dedicated to Professor Victor Snieckus, with deep admiration of his numerous contributions to organic chemistry and the community of organic chemists.

W.R. Roush,[1,2] D.J. Madar, and D.S. Coffey. Department of Chemistry, Indiana University, Bloomington, IN 47405, U.S.A.

[1]Corresponding author (telephone: (734) 647-9278; fax: (734) 647-9279; e-mail: roush@umich.edu).
[2]Present address: Department of Chemistry, University of Michigan, 930 N. University, Ann Arbor, MI 48197, U.S.A.

 DOI: 10.1139/cjc-79-11-1711 © 2001 NRC Canada

interest as potential antiviral agents owing to their ability to inhibit RNA-directed DNA polymerase (i.e., reverse transcriptase) (3–7).

The stereochemistry of streptovaricin C (SvC) was assigned based on the X-ray analysis of a *p*-bromobenzeneboronate derivative (8,[2] 9). The stereochemical assignments for the remaining streptovaricins are based on chemical and biosynthetic interconversions and spectroscopic correlations to SvC (2, 10, 11). Chemical degradations performed on the streptovaricins led to additional interesting products. For example, treatment of streptovaricin D (SvD) with ammonia in methanol provided damavaricin D (DmD) (11). Interestingly, DmD was later found to be a biosynthetic precursor of all of the more highly functionalized members of the streptovaricin family (2, 11). The damavaricins retain many of the important biological properties of the streptovaricin family (4–7).

Several studies on the synthesis of streptovaricins A, D, and G (12–20) streptovaricin U (an early stage biosynthetic precursor) (21, 22), and damavaricin D (23) have been reported. We initiated studies on the synthesis of the streptovaricin D ansa chain in 1988 (24). However, in view of the structural complexity and chemical sensitivity (11) of the quinone methide unit of the streptovaricins, we decided to focus our efforts on the structurally simpler damavaricins in hopes that a late-stage, biomimetic conversion of the damavaricins to the streptovaricins could be developed. While the latter goal has not yet been realized, we have developed a total synthesis of damavaricin D (DmD) (25). Our DmD synthesis is the only synthesis of any member of the streptovaricin or damavaricin family completed to date.

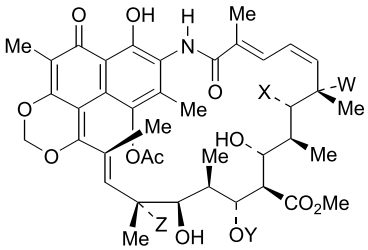
We report herein the details of our synthesis of highly functionalized naphthoate precursors to DmD, including our observations of kinetically stable benzocyclohexadienone intermediates in the bromination of highly functionalized β-naphthol derivatives. Preliminary accounts of this work have been published (25–27). The full details of our synthesis of the fully elaborated ansa chain fragments as well as the successful fragment assembly and deprotection sequence culminating in the total synthesis of DmD will be reported elsewhere.[3]

Results and discussion

Initial synthetic strategy

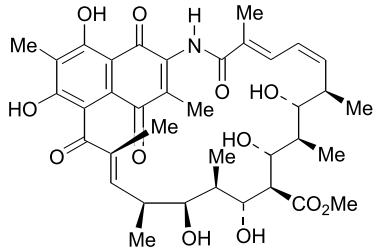
In planning the synthesis of DmD, we hoped to achieve as much convergence as possible by postponing the coupling of the aromatic unit to the ansa chain until late in the synthesis and therefore initially targeted intermediates **1** and **2** (24) for these purposes (Scheme 3). The naphthalenic ring systems of many members of the rifamycin, streptovaricin, and damavaricin families have been assembled by routes involving Diels–Alder reactions (13, 22, 28–32). Indeed, Trost and

Scheme 1.



Streptovaricin	W	X	Y	Z
A	OH	OH	Ac	OH
B	H	OH	Ac	OH
C	H	OH	H	OH
D	H	OH	H	H
E	H	O=	H	OH
G	OH	OH	H	OH
J	H	OAc	H	OH
K	OH	OAc	H	OH

Scheme 2.



Damavaricin D (DmD)

Pearson (13) had reported an extremely brief Diels–Alder based synthesis of naphthyl amine **3** (33), and we hoped that we would be able to adopt their route for preparation of **1**. However, we experienced difficulties in attempts to introduce the aniline unit according to the Trost–Pearson protocol, and the Wisconsin group had also been unable to introduce an ethyl ketone substituent at C-8 on intermediates deriving from **3** (34).[4] Consequently, we decided to target the bromonaphthoate **4a** as a precursor to **1**. We anticipated that the C-8-Br substituent would provide the means to introduce C-8 ethyl ketone, and that the protected aniline unit of **1** would be elaborated by a Curtius degradation of the carbomethoxyl group.

*Synthesis of bromo naphthoate (**4a**)*

The synthesis of bromonaphthoate **4a** commenced with the known (13) Diels–Alder reaction of the oxygenated diene **5** (13) and 2,6-dibromo-3-methylbenzoquinone **6** (35). This provided the crystalline cycloadduct **7** in 70–75% yield (Scheme 4). Although the regiochemistry of the Diels–Alder reactions of highly oxygenated dienes and substituted quinones has been extensively documented by Roberge and Brassard (36), we felt it necessary to confirm the regio-

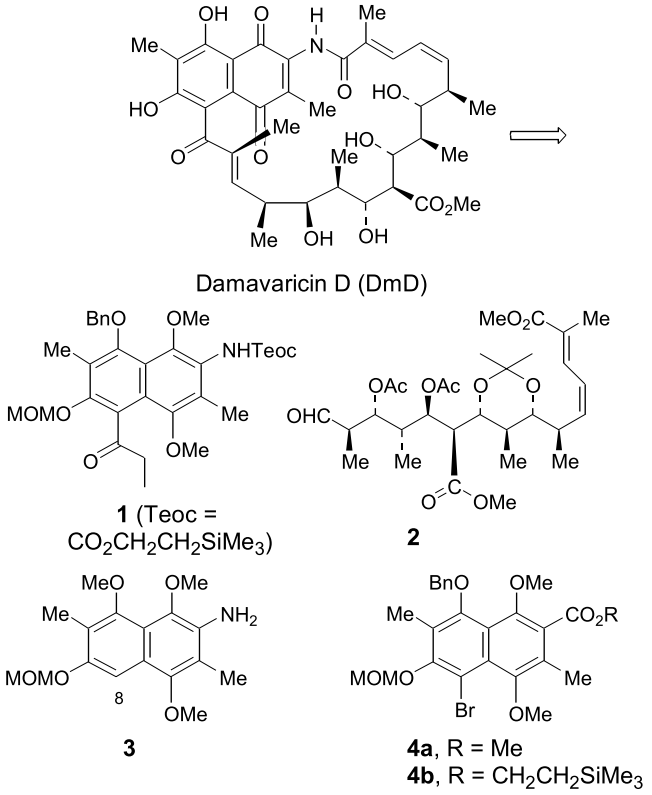
[2] The stereochemistry at C-6 and C-7 of SvC are drawn incorrectly in the two-dimensional structure presented in this paper; the stereoscopic views, however, are correct. The SvC derivative reported in this paper is also in the unnatural atropisomeric configuration (see K.L. Rinehart, Jr., W.M. J. Knöll, K. Kakinuma, F.J. Antosz, I.C. Paul, A.H.-J. Wang, F. Reusser, L.H. Li, and W.C. Krueger. J. Am. Chem. Soc. **97**, 196 (1975)).

[3] W.R. Roush, S.D. Coffey, D.J. Madar, and A.D. Palkowitz. Manuscript in preparation.

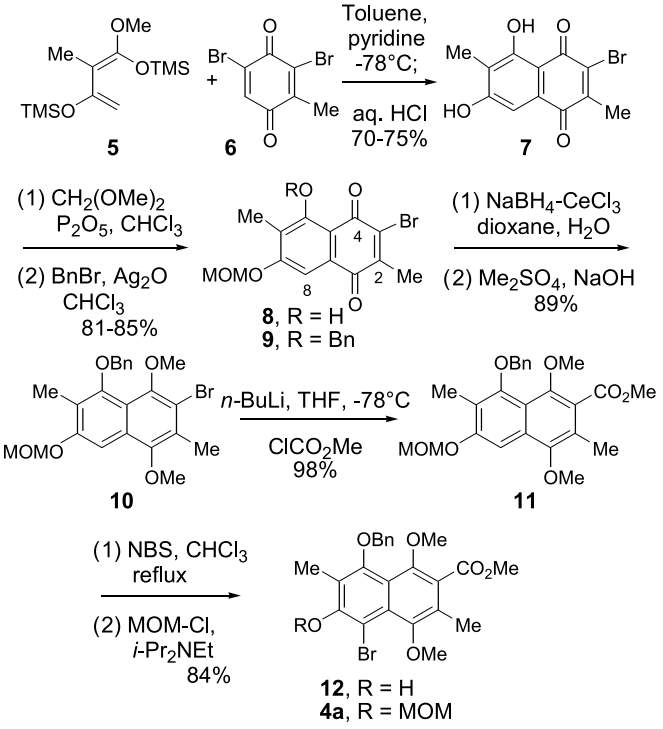
[4] Numerous attempts on our part to introduce the aniline nitrogen directly, without proceeding by way of a carboxylic acid derivative, were unsuccessful.

© 2001 NRC Canada

Scheme 3.



Scheme 4.



chemistry of the reaction leading to **7** before proceeding with the synthesis. Accordingly, we established that the Diels–Alder reaction of **5** and **6** does indeed provide **7** with the correct regioselectivity by performing long-range selective ^{1}H NMR decoupling experiments (37) on the derived MOM ether **8** (which was prepared according to Trost's procedure) (13). The gated decoupled ^{13}C NMR spectrum of **8** displays the C-4 carbonyl carbon as a singlet (δ 181.3) and the C-1 carbonyl carbon as a quintet (δ 181.0, J = 17 Hz). Irradiation of the C-2-Me causes the C-1 carbonyl to collapse to a doublet, while irradiation of the C-8-H caused the C-1 carbonyl to simplify to a quartet.

At this stage, we departed from Trost's sequence, in anticipation that the C-5 methyl ether (see **3**) would not be easy to deprotect deeper into the synthesis. Rather, we decided to protect the C-5-phenol as a benzyl ether, which was accomplished by treatment of **8** with excess benzyl bromide and Ag_2O in $CHCl_3$. Attempted use of other conventional methods for introducing the benzyl ether were unsuccessful. The resulting quinone **9** was reduced by using $NaBH_4$ and $CeCl_3$ (38) in dioxane and the resulting (air sensitive!) 1,4-dihydroquinone was methylated in situ by treatment with Me_2SO_4 and 50% aq NaOH, with careful exclusion of O_2 (13). This one-pot reduction–methylation procedure provided the 1,4-di-*O*-methyldihydroquinone **10** in 89% yield. Next, treatment of **10** with *n*-BuLi in THF at –78°C followed by addition of methyl chloroformate provided naphthoate **11** in 98% yield.

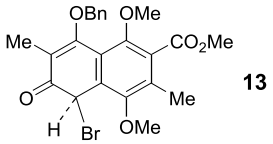
We were now ready to explore the introduction of the C-8 ethyl ketone fragment of **1**. However, attempts to accomplish this reaction by Friedel–Crafts acylation of **11** with propionyl chloride and BF_3 or $AlCl_3$, or by Fries rearrangement of the propionate ester prepared after hydrolysis of the MOM ether, were unproductive. Consequently, we turned to a bromination sequence to introduce a functional group handle at C-8 to facilitate introduction of the targeted ethyl ketone. Accordingly, intermediate **11** was brominated at C-8 by exposure to NBS in $CHCl_3$ at reflux. Chromatographic purification of the crude reaction product afforded the bromophenol **12**, and not the expected bromo MOM ether **4a**. Therefore, the MOM ether was reintroduced by treatment of **12** with MOM-Cl and Hunig's base.

Interestingly, ^{1}H NMR analysis of the crude NBS bromination product mixture (prior to chromatographic purification) revealed that **12** was not present! Rather, the spectrum of the crude product exhibited a sharp, one proton singlet at δ 5.55, and an AB pattern for the benzyl -CH_2 unit, indicating that the molecule possessed a center of asymmetry. These data, plus the observation that treatment of the crude, unchromatographed product with MOM-Cl and Hunig's base provided the phenolic MOM ether **4a** in 84% overall yield, led us to conclude that the initial intermediate observed in the crude reaction mixture was the benzocyclohexadienone **13** (Scheme 5). While it is known that bromocyclohexadienones are intermediates in the bromination of phenols, these compounds are usually transient intermediates and rapidly isomerize to the corresponding bromophenols (39–43). We were not aware of any previous reports of cyclohexadienone intermediates in the bromination reactions of phenolic ethers; additional encounters with intermediates of this type are described subsequently.

The synthesis of the initially targeted napthyl ethyl ketone **1** was completed as follows (see Scheme 6). A –100°C solution of **4a** in THF was treated with *n*-BuLi for 3 min, then

© 2001 NRC Canada

Scheme 5.



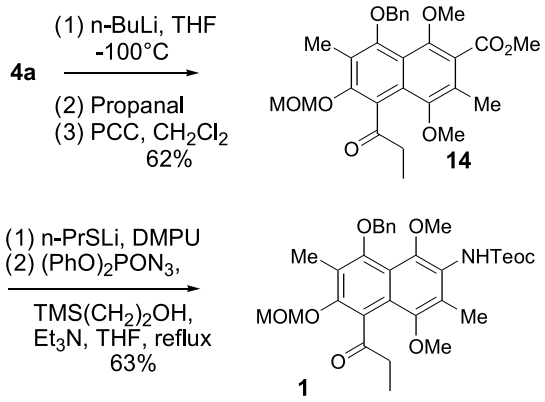
propionaldehyde was added (44). The resulting benzylic alcohol, obtained in 80% yield, was oxidized using PCC to give ethyl ketone **14** in 77% yield. Finally, deprotection of the methoxycarbonyl unit of **14** by treatment with *n*-PrSLi in DMPU (45),[5] followed by Curtius rearrangement of the resulting acid using the Shiori protocol ($(PhO)_2PON_3$, Et_3N, THF, reflux) (46) in the presence of 2-trimethylsilyl ethanol provided the targeted ethyl ketone **1** in 63% yield.

*Synthesis of bromo naphthoate (**4b**)*

We originally planned to perform an aldol reaction between **1** and the damavaricin ansa chain, represented by aldehyde **2**, as part of the late stage fragment assembly sequence. However, preliminary attempts to perform aldol reactions between **1** or **14** and simpler model aldehydes were unpromising. This necessitated that we reconsider our options for coupling of the advanced ansa chain and aromatic segment precursors. Because we had successfully demonstrated that the aryllithium generated from **4a** could be added efficiently to propionaldehyde (en route to **14**), our strategy refocused on use of a fully elaborated α,β-unsaturated ansa chain aldehyde in a coupling reaction with **4a**. However, because deprotection of the methyl ester of **14** was challenging owing to the steric hindrance imposed by the two flanking aromatic substituents, we decided to synthesize bromonaphthoate **4b** that contained a trimethylsilylethyl (TMSE) ester, which we anticipated could be deprotected under much milder conditions than the methyl ester of **4a**.

The synthesis of bromonaphthoate **4b** (Scheme 7) began by carboxylation of the aryllithium intermediate generated from **10**, followed by conversion of the resulting carboxylic acid to the β-trimethylsilyl ethyl ester under Mitsunobu conditions (47). This two-step sequence provided **15** in 77% yield from **10**. Intermediate **15** was brominated by using the conditions described for the synthesis of **11**, and **4b** was obtained in 93% yield after reintroduction of the MOM ether that was lost during the NBS bromination step. To gain confidence that these intermediates might be suitable for eventual coupling with the ansa chain fragment, bromonaphthoate **4b** was metallated by treatment with *n*-BuLi in THF at –100°C, and the resulting aryllithium intermediate was added to the model α,β-unsaturated aldehyde **16**. Oxidation of the resulting mixture of diastereomers with the Dess–Martin periodinane reagent then provided enone **17** in 65% overall yield (48). Finally, deprotection of the β-trimethylsilyl ethyl ester of **17** by treatment with KF-dihydrate in DMSO (23°C, 70 h) and then Curtius degradation (46) of the intermediate carboxylic acid in the presence of β-trimethylsilyl ethanol, then provided **18** in 72% yield. Enones **17** and **18** were obtained as ca. 1:1 mixtures of atropisomers. Variable temperature ^1H NMR studies performed with **17** indicated that the coalescence temperature for the equilibration of the two atropisomers was approximately 125°C, suggesting the barrier to rotation about the aryl—acyl bond is on the order of 20 kcal mol^{-1} (for general reviews of atropisomerism see ref. 49).

Scheme 6.



Revised protecting group scheme

As the synthesis of damavaricin D continued to progress, it became apparent that the benzyl ether used to protect the C-5-phenol could not be removed in the presence of the diene function present in late-stage intermediates. Therefore, an initial, conservative change involved replacing the C-5-benzyl ether with an allyl ether, which we anticipated could be deprotected by using Pd(0)-mediated methods (50). Bromonaphthoate **19** indeed proved useful for the synthesis of 24,27-di-*O*-methyl damavaricin D (**21**), by way of the derived aryllithium intermediate **20** (Scheme 8) (27). However, we were unable to complete a total synthesis of damavaricin D via **21** or its immediate precursors owing to an unexpected oxidative cyclization reaction that occurred during attempts to convert the di-*O*-methyl-1,4-dihydroquinone oxidatively to the quinone nucleus of the natural product. For example, attempted CAN-mediated oxidative deprotection (51) of **24**, an immediate precursor to **21**, provided the interesting but synthetically unproductive (i.e., unstable) heterocycle **25** (Scheme 9) (27). In view of these difficulties, it ultimately proved necessary to use naphthoate **22** with the dihydroquinone protected as the nonconventional bis-MOM ether for completion of the damavaricin D total synthesis (25). We present syntheses for both **19** and **22** here, as kinetically stable benzocyclohexadienone intermediates were observed in each case.

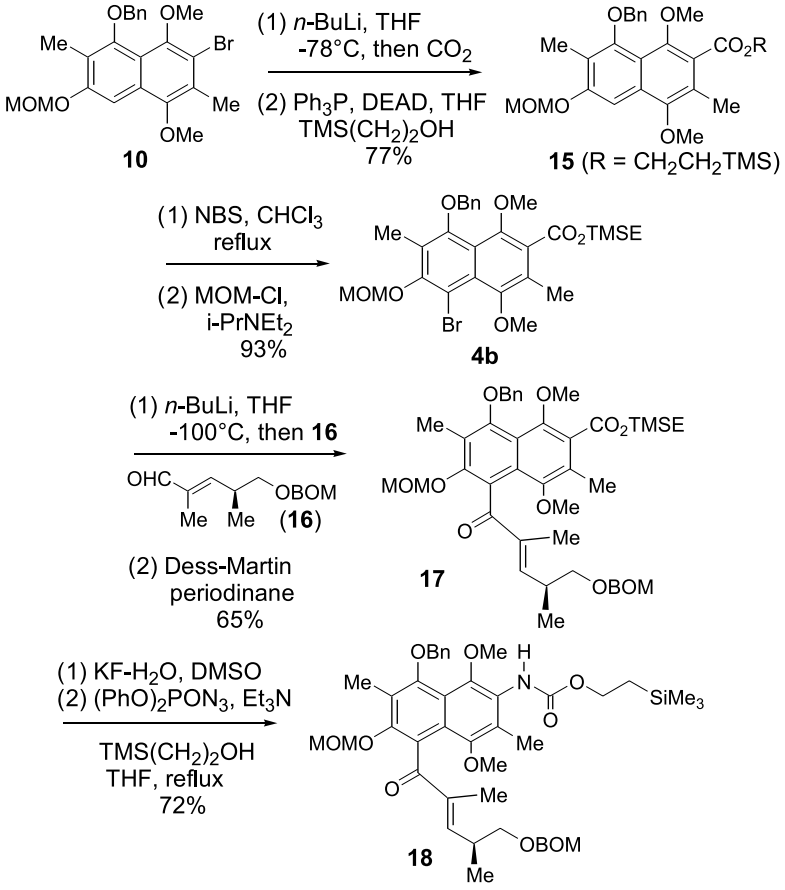
*Synthesis of bromo naphthoate (**19**)*

The synthesis of naphthoate **19** (Scheme 10) originated from the mono-protected bromo naphthoquinone **8** (13). Treatment of **8** with allyl bromide and Ag_2O in $CHCl_3$ provided allyl ether **26** in 86% yield. Reduction of the quinone under Luche conditions (13, 38) followed by in situ methylation of the air-sensitive hydroquinone with Me_2SO_4 and 50% aq NaOH then provided **27** in 84% yield. Metal halogen exchange by treatment of **27** with *n*-BuLi in THF at

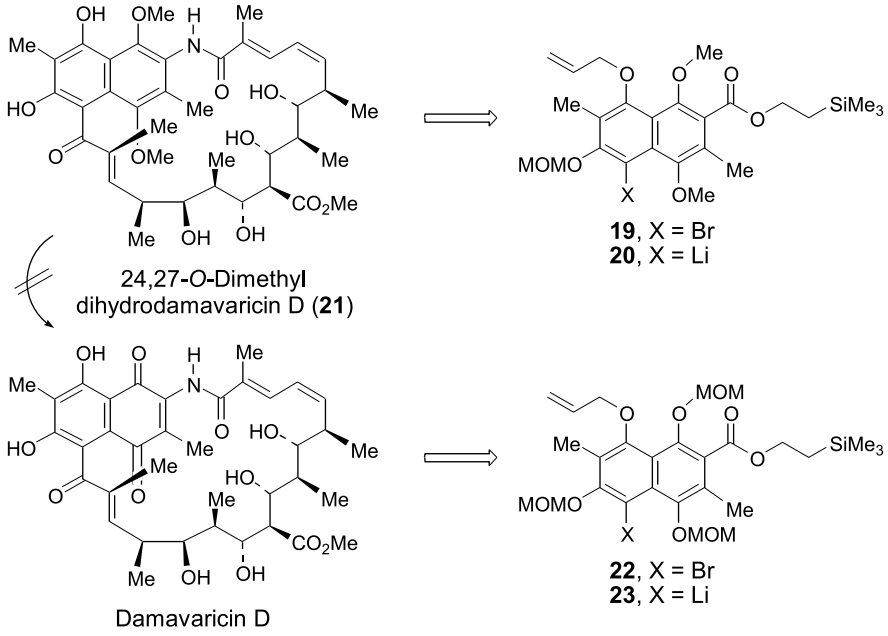
[5] We substituted DMPU for the more hazardous HMPA.

© 2001 NRC Canada

Scheme 7.



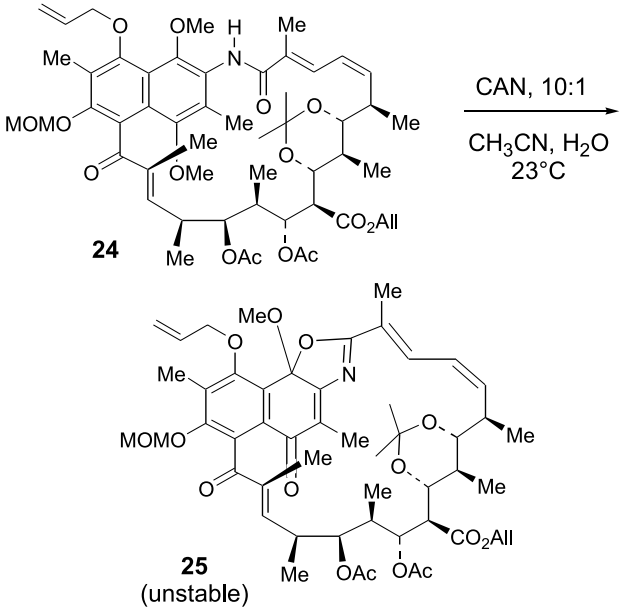
Scheme 8.



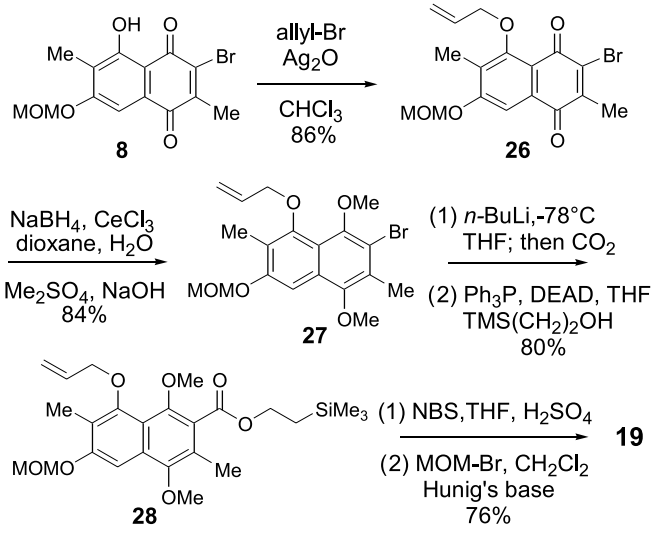
–78°C followed by carboxylation of the aryllithium intermediate with dry CO_2 gave the carboxylic acid. Esterification of this intermediate with β-trimethylsilylethanol by using the Mitsunobu protocol yielded naphthoate **28** in 80% yield (47). Finally, bromination of **28** with NBS in THF containing catalytic H_2SO_4 (52) and reintroduction of the MOM

© 2001 NRC Canada

Scheme 9.



Scheme 10.



group that was lost during the bromination step provided the bromonaphthoate **19** in 76% yield. It proved necessary to use *MOM-Br* and Hunig's base to reintroduce the MOM group, as discussed in the following paragraph.

^{1}H NMR analysis of the crude product obtained from the NBS bromination of **28** (before reintroduction of the MOM ether!) indicated that this material consisted of a ca. 1:1 mixture of the bromobenzocyclohexadienone **29** and bromophenol **30** (Scheme 11). When this mixture was treated with MOM-Cl and Hunig's base, using the protocol followed in the preparation of **4a**, a chromatographically inseparable 1:1 mixture of naphthyl bromide **19** and *naphthyl chloride* **31** was obtained. That chloride **31** was the second product of the bromination–protection sequence became obvious after a 1:1 mixture of **19** and **31** was treated with 1 equiv of *n*-BuLi in THF at –100°C, followed by addition of propionaldehyde at –78°C. This reaction provided benzylic alcohol **32** in 36% yield, along with recovered chloride **31** in 42% yield. When the mixture of **29** and **30** was purified by silica gel chromatography, **29** was not completely converted to **30**; treatment of the chromatographed sample with MOM-Cl and Hunig's base provided **19** with about 90% purity, the remainder being chloride **31**. Consequently, the best method for synthesis of **19** involved treatment of the **29** and **30** mixture with MOM-Br and Hunig's base, so that there was no opportunity for **29** to react with chloride ion to give the corresponding α-chlorobenzocyclohexadienone **33** prior to the aromatization reaction (see Scheme 12). Interestingly, in several instances small amounts of **28** were also recovered from these experiments, even though ^{1}H NMR analysis indicated that **28** and the corresponding phenol **34** were completely absent from the crude bromination product mixture. This indicates that the C—Br bond of bromobenzocyclohexadienone **29** is subject to reduction (40) as well as displacement by halide ions.

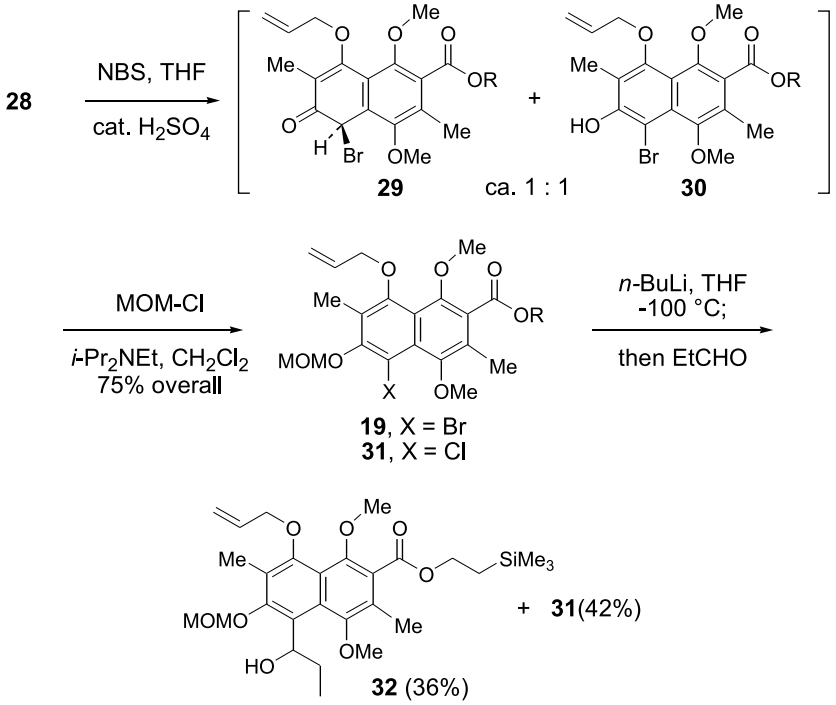
Synthesis of bromo naphthoate (22)

The synthesis of bromonaphthoate **22** (Scheme 13) originated from bromoquinone **26**. It was necessary to replace the MOM ether by a *tert*-butyldiphenylsilyl (TBDPS) ether at the outset, since we found that the bromination reaction leading to **22** was successful only when the C-7-phenol was unprotected. However, attempts to prepare **35** directly from the Diels–Alder adduct **7** were unsuccessful. Therefore, cleavage of the MOM ether of **26** by using *p*-TsOH in MeOH gave the corresponding phenol which was reprotected as a TBDPS ether under standard conditions. Reduction of the quinone and protection of the very sensitive dihydroquinone as a bis-MOM ether proved to be quite challenging, much more so than the reductive protections of intermediates **9** and **26** previously described. Ultimately, we found that the reduction of **35** was best accomplished by using dithionite in an aqueous dichloromethane mixture containing Adogen 464 as a phase transfer agent (53). Addition of aq NaOH and MOM-Cl to the reduction mixture then provided the protected dihydroquinone **36** in 82% overall yield. Elaboration of **36** to the naphthoate **37** proceeded smoothly (77% yield) using the conditions described for the synthesis of **15**. At this stage, the TBDPS protecting group was removed by using $Et_3N{\cdot}HF$ in CH_3CN, giving phenol **38** in 98% yield.

Bromination of phenol **38** was best accomplished by treatment with NBS in $CHCl_3$ at ambient temperature. In this case, the bromobenzocyclohexadienone **39** was the exclusive product obtained following extractive work-up (42). The ^{1}H NMR spectrum of this intermediate contained a sharp, one proton singlet at δ 5.60, assigned to the α-bromo ketone methine, and the two MOM methylene resonances appeared as AB patterns. The ^{13}C NMR spectrum exhibited a resonance at δ 193.4 assigned to the ketone carbonyl (the ester carbonyl resonance appears at δ 166–170 in **38**, **39**, and immediate precursors), and the IR spectrum contained two carbonyl bands (1725 and 1672 cm^{-1}). When **39** was exposed to silica gel, partial aromatization to phenol **40** occurred, with the ratio of **39**:**40** depending on the time of exposure. Under optimal chromatographic conditions (10% EtOAc–hexane), a 1:1 mixture of **39**:**40** was obtained. However, treatment of this mixture with MOM-Br and Hunig's base under the condi-

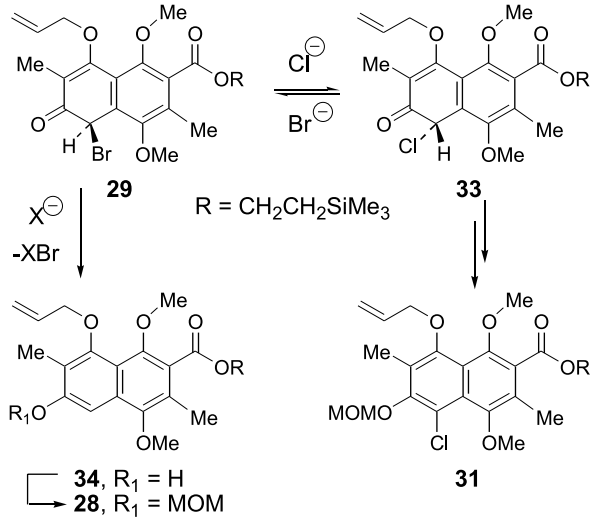
© 2001 NRC Canada

Scheme 11.



tions successfully employed in the preparation of **19** gave **22** in only 40–50% yield, with considerable quantities of the MOM ether of **38** (resulting from reduction of **39**) also being produced. Ultimately, the best method for conversion of **39** to **22** involved treatment of **39** with K_2CO_3 in MeOH, which provided a ca. 8:1 mixture of phenol **40** and the keto tautomer **39**. This mixture was then treated with MOM-Cl and *i*-Pr_2NEt in CH_2Cl_2, which provided a ≥10:1 mixture (inseparable) of the fully protected bromonaphthoate **22** and the corresponding chloronaphthoate **41** in 78% yield overall from **38**. Naphthyl bromide prepared in this way was used for completion of the damavaricin synthesis (25). While production of **41** could be avoided by using MOM-Br in the final protection step, the yield of **22** was considerably lower owing to the reduction of **39** that occurs under these conditions.

Scheme 12.

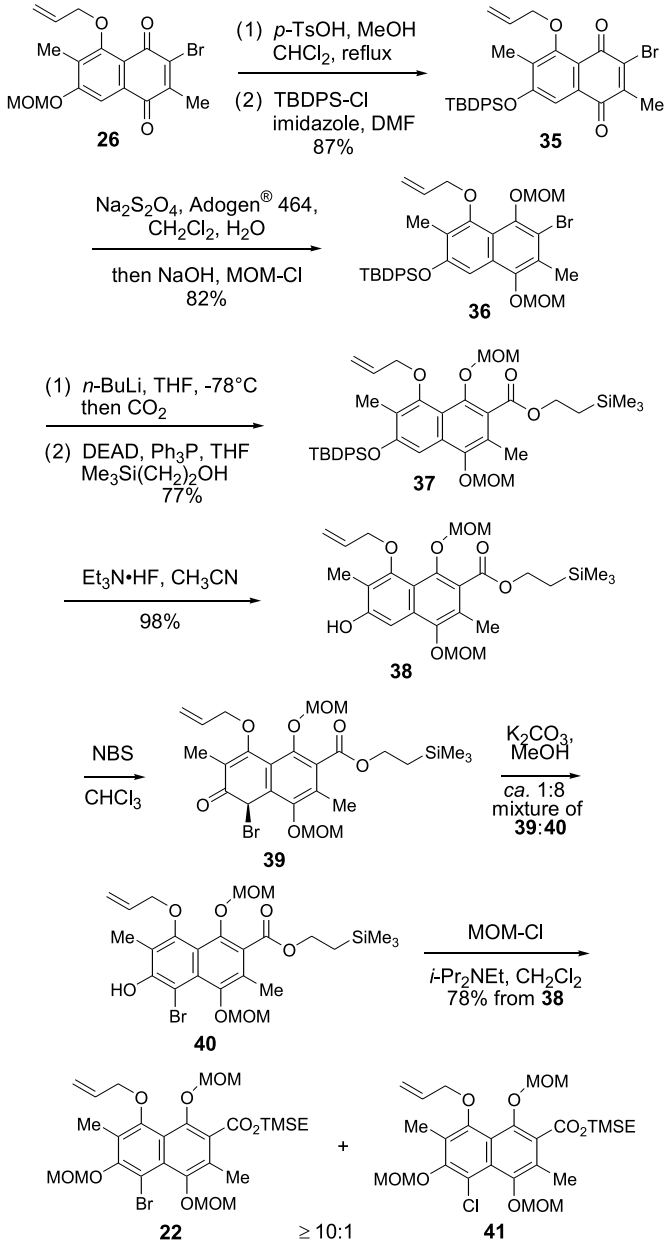


Concerning the kinetic stability of the bromo benzocyclohexadienone intermediates

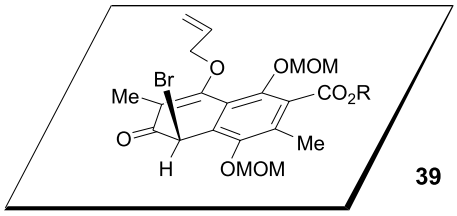
The kinetic stability of the bromo benzocyclohexadienones **13**, **29**, and especially **39** is attributable both to steric effects which slow the rate of enolization to the phenols (39), as well as to stereoelectronic effects. Specifically, allylic strain considerations (54) dictate that the bromine substituent should preferentially adopt a pseudoaxial position on the benzocyclohexadienone ring to avoid 1,3-interactions with the peri-MOM ether unit (43). This imposes an additional kinetic barrier on the enolization process, since the carbonyl α-hydrogen is in the plane of the σ system; for this proton to be removed, it must be aligned with the π system of the carbonyl. This conformational picture also nicely explains the high reactivity of **29** and **39** with chloride ion, as well as the propensity of **29** and **39** to be reduced with bromide ion. While bromobenzocyclohexadienones **13**, **29**, and **39** might be expected to be considerably less stable than their phenolic isomers **12**, **30**, and **40**, the evidence reported here for the **29**/**30** and **39**/**40** pairs suggests that the energy difference between the two tautomers is not particularly great. Presumably, both torsional strain in the phenol tautomer **40**, due to the high density of substituents on the naphthalene nucleus, plus the fact that the β-alkoxy enone unit of the benzocyclohexadienone is resonance stabilized contribute to this situation. To the best of our knowledge, the substitution reactions of **29** and **39** with chloride ion are the first documented examples of reactions of enolizable bromobenzocyclohexadienone intermediates.

© 2001 NRC Canada

Scheme 13.



Scheme 14.



Experimental section

General

All reactions were conducted in oven-dried (125°C) or flame-dried glassware under dry argon or nitrogen. All solvents were purified before use. Ether and THF were distilled from sodium benzophenone ketyl. Dichloromethane (CH_2Cl_2), toluene, and acetonitrile were distilled from CaH_2. Methanol was distilled from magnesium turnings.

^{1}H NMR spectra were measured at 400 MHz on a Varian VNMR 400 instrument or at 500 MHz on a Varian Inova 500 instrument. Chemical shifts are reported in δ units with coupling constants reported in Hz. Residual chloroform (δ 7.26 ppm) was used as internal reference for spectra measured in $CDCl_3$. ^{1}H NMR spectra measured in C_6D_6 were referenced against residual C_6D_5H (δ 7.15). ^{13}C NMR spectra were recorded at 100 MHz. Chemical shifts are reported relative the δ 77.0 ppm resonance of $CDCl_3$ or the δ 128.0 ppm resonance of C_6D_6.

Infrared spectra were recorded using a Mattson Instruments 4020 Galaxy Series FT IR spectrophotometer. High-resolution mass spectra (HRMS) for intermediates with molecular weights ≤900 and low-resolution mass spectra (LRMS) were recorded using a Kratos GC–MS 80 RFA mass spectrometer under electrically or chemically induced ionization at the Indiana University Mass Spectrometry Laboratory. High-resolution mass spectra (HRMS) for intermediates with molecular weights ≥900 were recorded in the Mass Spectrometry Laboratory, School of Chemical Sciences, University of Illinois using a ZAB-SE mass spectrometer, which was purchased in part with grants from the Division of Research Resources, National Institutes of Health (RR 01575), the National Science Foundation (PCM 8121494), and the National Institute of General Medical Sciences (GM 27029). Optical rotations were measured on a Rudolph Autopol III polarimeter using a 1 mL capacity quartz cell with a 10 cm path length. Elemental analyses were performed by Robertson Microlit Laboratories, Inc., Madison, N.J.

Analytical and semipreparative HPLC separations were performed by using an HPLC system composed of two Rainin HXPL pumps (gradient), a Rheodyne 7125 injector, a Dynamax UV-C detector, and a Shimadzu CR601 integrator. Analytical thin layer chromatography (TLC) was performed by using plates coated with a 0.25-mm thickness of silica gel containing PF 254 indicator (Analtech). Compounds were visualized by staining (and charring) of the TLC plates with a solution of ceric sulfate and ammonium molybdate in aqueous sulfuric acid or with a solution of *o*-vanillin in ethanol with acetic and sulfuric acid. Flash chromatography was performed as described by Still et al. (55) using Kieselgel 60 (230–400 mesh) silica gel. Unless otherwise noted, all compounds purified by chromatography are sufficiently pure (>95% by ^{1}H NMR analysis) for use in subsequent reactions.

*5-Benzyloxy-3-bromo-7-methoxymethoxy-2,6-dimethyl-1,4-naphthoquinone (***9***)*

To a 0°C solution of benzyl bromide (3.10 mL, 25.9 mmol) in $CHCl_3$ (80 mL) and silver oxide (7.50 g, 32.3 mmol) was added a solution of phenol **8** (13, 33) (2.20 g, 6.5 mmol) in $CHCl_3$ (40 mL) dropwise via canula. The resulting slurry was stirred for 24 h at 23°C. The reaction mixture was then filtered through a pad of Celite®, which was washed with EtOAc (2 × 100 mL). The filtrate was concentrated in vacuo and the crude benzyl ether was purified by flash chromatography with 15% EtOAc–hexanes

© 2001 NRC Canada

to afford benzyl ether **9** (2.51 g, 90%) as bright yellow crystals, mp 113–115°C. HR MS calcd. for $C_{21}H_{19}BrO_5$ (M^+): 430.0415; found: 430.0390. IR ($CHCl_3$) (cm^{-1}): 3010, 1665, 1610, 1575, 1370, 1310, 1260, 1160, 1120, 1070. ^1H NMR (400 MHz, $CDCl_3$) δ: 7.63–7.34 (m, 6H), 5.35 (s, 3H), 4.94 (s, 3H), 3.49 (s, 3H), 2.34 (s, 3H), 2.18 (s, 3H). ^{13}C NMR (100 MHz, $CDCl_3$) δ: 181.8, 175.4, 160.2, 158.8, 146.1, 141.1, 136.7, 132.4, 129.4, 128.6, 128.5, 128.2, 119.3, 118.2, 108.2, 94.3, 75.7, 56.6, 17.6, 9.7. Anal. calcd. for $C_{21}H_{19}BrO_5$: C 58.64, H 4.42; found: C 58.51, H 4.08.

*5-Benzyloxy-3-bromo-1,4-dimethoxy-7-methoxymethoxy-2,6-dimethoxy naphthalene (**10**)*

To a solution of quinone **9** (2.45 g, 5.7 mmol) in dioxane (50 mL) and H_2O (25 mL) was added $CeCl_3 \cdot 7H_2O$ (3.2 g, 8.5 mmol). The reaction mixture was cooled to 0°C and $NaBH_4$ (395 mg, 10.4 mmol) was added in portions over 15 min. During this time the bright yellow color of the quinone disappeared. After H_2 evolution had ceased, the reaction was warmed to 23°C, 15 mL of Me_2SO_4 was added, and the flask was evacuated and filled with Ar. NaOH (50% aqueous, 3 mL) was added dropwise over 15 min. The reaction mixture was stirred at 23°C for 1 h, cooled to 0°C, and concd NH_4OH (50 mL) and ether (250 mL) were added. The organic layer was washed with 1:1 concd NH_4OH–H_2O (2 × 300 mL), brine (1 × 300 mL), dried over $MgSO_4$, filtered, and concentrated in vacuo. Purification of the residual oil by flash chromatography with 10% ether–hexane afforded dimethyl ether **10** (2.34 g, 89% yield) as a light yellow oil. HRMS calcd. for $C_{23}H_{25}BrO_5$ (M^+): 462.0855; found: 462.0836. IR ($CHCl_3$) (cm^{-1}): 3005, 2920, 1615, 1580, 1560, 1480, 1450, 1410, 1380, 1350, 1320, 1250, 1150, 1120, 1070, 1030. ^1H NMR (300 MHz, $CDCl_3$) δ: 7.71–7.28 (m, 6H), 5.36 (s, 2H), 4.91 (s, 2H), 3.85 (s, 3H), 3.79 (s, 3H), 3.54 (s, 3H), 2.52 (s, 3H), 2.35 (s, 3H). ^{13}C NMR (100 MHz, $CDCl_3$) δ: 155.0, 152.4, 149.8, 148.6, 137.8, 128.7, 128.4, 128.3, 127.8, 127.2, 122.2, 118.4, 117.4, 100.0, 94.6, 76.4, 61.8, 61.0, 56.1, 16.8, 9.7. Anal. calcd. for $C_{23}H_{25}BrO_5$: C 60.13, H 5.43; found: C 59.87, H 5.30.

*5-Benzyloxy-3-carbomethoxy-1,4-dimethoxy-7-methoxymethoxy-2,6-dimethylnaphathalene (**11**)*

To a cold (–78°C) solution of bromide **10** (2.40 g, 5.2 mmol) in THF (50 mL), was added *n*-BuLi (2.5 M, 4.23 mL, 6.8 mmol). The mixture was stirred at –78°C for 15 min. The resulting dark red-yellow anion solution was then treated with methyl chloroformate (0.53 mL, 6.8 mmol) and the resulting mixture was gradually warmed to room temperature over a 4 h period. The reaction mixture was quenched with H_2O (25 mL) and diluted with ether (150 mL). The organic layer was separated, dried with $MgSO_4$, filtered, and concentrated in vacuo to a light yellow oil. Purification of the crude product by flash chromatography with 20% ether–hexane afforded ester **11** (2.28 g, 98% yield) as a clear oil. HRMS calcd. for $C_{25}H_{28}O_7$ (M^+): 440.1835; found: 440.1854. IR ($CHCl_3$) (cm^{-1}): 3020, 2955, 2945, 1725, 1610, 1440, 1340, 1240, 1130, 1070, 1010. ^1H NMR (400 MHz, $CDCl_3$) δ: 7.56–7.35 (m, 6H), 5.37 (s, 2H), 4.89 (s, 2H), 3.89 (s, 3H), 3.84 (s, 3H), 3.54 (s, 3H), 2.34 (s, 3H), 2.32 (s, 3H). Anal. calcd. for $C_{25}H_{28}O_7$: C 68.15, H 6.42; found: C 67.92, H 6.25.

*5-Benzyloxy-8-bromo-3-carbomethoxy-1,4-dimethoxy-7-methoxy-1,4-dimethylnaphthalene (**4a**)*

To a solution of the naphthoate **11** (7.48 g, 17.0 mmol) in $CHCl_3$ (110 mL) was added *N*-bromosuccinimide (3.93 g, 22.0 mmol) in portions over 15 min. The resulting solution was heated at reflux for 6 h at which point the mixture was cooled and diluted with CH_2Cl_2 (150 mL). The organic layer was washed with satd. $NaHSO_3$ (50 mL), dried over $MgSO_4$, filtered, and concentrated in vacuo. The crude oil, consisting primarily of the bromobenzocyclohexadienone **13** (^1H NMR (400 MHz, $CDCl_3$) δ: 7.44–7.34 (m, 5H), 5.55 (s, 1 H), 5.15 and 4.76 (AB, J = 12 Hz), 3.97 (s, 3H), 3.94 (s, 3 H), 3.73 (s, 3H), 2.26 (s, 3H) and 1.80 (s, 3H)) was dissolved in CH_2Cl_2 (150 mL). To the resulting solution was added diisopropylethylamine (4.44 mL, 25.0 mmol) and MOM-Cl (1.68 mL, 22.0 mmol). This mixture was stirred at 23°C for 4 h, then diluted with ether (400 mL). The organic layer was washed with 1 M $NaHSO_4$ (150 mL), satd. $NaHCO_3$ solution (150 mL), and brine (150 mL), then dried over $MgSO_4$, and concentrated in vacuo. The crude residue was purified by flash chromatography with 15% ether–hexane affording bromonaphthoate **4a** (7.40 g, 84% yield) as a thick yellow oil. HRMS calcd. for $C_{25}H_{27}O_7Br$ (M^+): 518.0941; found: 518.0919. IR ($CDCl_3$) (cm^{-1}): 2960, 2640, 1735, 1600, 1450, 1435, 1335, 1315, 1250, 1120, 1060, 1010. ^1H NMR (400 MHz, $CDCl_3$) δ: 7.51–7.35 (m, 5H), 5.19 (s, 2H), 4.85 (s, 2H), 3.99 (s, 3H), 3.76 (s, 3H), 3.71 (s, 3H), 3.69 (s, 3H), 2.42 (s, 3H), 2.37 (s, 3H). ^{13}C NMR (100 MHz, $CDCl_3$) δ: 168.2, 155.1, 152.9, 150.2, 148.1, 137.2, 128.4, 128.1, 127.9, 127.7, 126.0, 125.9, 121.1, 105.9, 100.1, 76.6, 64.1, 61.7, 57.9, 52.3, 13.2, 11.3. Anal. calcd. for $C_{25}H_{27}O_7Br$: C 57.78, H 5.25; found: C 58.09, H 4.96.

If the bromination reaction mixture was purified by silica gel chromatography prior to being treated with MOM-Cl and diisopropylethylamine, phenol **12** was obtained. ^1H NMR (400 MHz, $CDCl_3$) δ: 7.52–7.34 (m, 5H), 6.80 (s, 1 H), 4.84 (s, 2H), 3.99 (s, 3H), 3.76 (s, 3H), 3.70 (s, 3H), 2.36 (s, 6H).

*5-Benzyloxy-3-carbomethoxy-1,4-dimethoxy-7-methoxymethoxy-2,6-dimethyl-(8-propan-1′-one)naphthalene (**14**)*

To a solution of bromide **4a** (572 mg, 1.1 mmol) in THF (8 mL) at –100°C was added *n*-BuLi (2.5 M, 0.55 mL, 1.3 mmol). The resulting deep orange solution was stirred for 3 min at which point propanal (0.11 mL, 1.4 mmol) was added. The reaction mixture was warmed to 0°C, diluted with ether (40 mL) and brine (15 mL). The organic layer was separated, dried with $MgSO_4$, and concentrated in vacuo. The crude alcohol was purified by chromatography on silica gel with 20–50% ether–hexane giving the intermediate benzylic alcohol (428 mg, 80% yield) as light yellow oil. HRMS calcd. for $C_{28}H_{34}O_8$ (M^+): 498.2254; found: 498.2236. IR ($CDCl_3$) (cm^{-1}): 3500 (br), 3020, 3010, 2960, 2940, 1710, 1435, 1415, 1220, 1160, 1110, 1090, 1055, 1010, 910. ^1H NMR (500 MHz, $CDCl_3$) δ: 7.49–7.32 (m, 5H), 5.67–5.62 (m, 1H), 5.20 and 5.11 (AB, J = 5.6 Hz, 2H), 4.87 and 4.82 (AB, J = 10.4 Hz, 2H), 4.34 (d, J = 11.4 Hz, 1H), 3.98 (s, 3H), 3.75 (s, 3H), 3.71 (s, 3H), 3.65 (s, 3H), 2.35 (s, 3H), 2.30 (s, 3H), 2.13–2.01 (m, 1H), 1.89–1.79 (m, 1H), 0.93 (t, J = 7 Hz, 3H). ^{13}C NMR (125 MHz, $CDCl_3$) δ: 168.6, 156.4, 152.7, 151.3, 148.8, 137.5, 128.6, 128.5, 128.4, 128.3, 128.0, 127.7, 127.1, 126.9, 124.5,

© 2001 NRC Canada

124.4, 120.1, 100.7, 76.5, 64.0, 61.6, 57.9, 52.3, 30.8, 13.4, 11.6, 11.3.

To a solution of the benzylic alcohol from the previous experiment (340 mg, 0.7 mmol) in CH_2Cl_2 (5 mL) was added sodium acetate (74 mg, 0.9 mmol) and pyridinium chlorochromate (186 mg, 0.9 mmol). The reaction mixture was stirred at 23°C for 26 h at which point the solution was filtered through a Celite® plug. The Celite® plug was washed with CH_2Cl_2 (3 × 20 mL). Purification of the crude product by flash chromatography with 50% ether–hexane afforded recovered benzyl alcohol (57 mg, 17%) and ethyl ketone **14** (262 mg, 77%, 94% yield based on recovered starting material) as light yellow oils. HRMS calcd. for $C_{28}H_{32}O_8$ (M^+): 496.2098; found: 496.2102. IR ($CDCl_3$) (cm^{-1}): 3005, 2940, 1725, 1695, 1605, 1580, 1560, 1480, 1450, 1440, 1410, 1390, 1350, 1330, 1210, 1160, 110, 1050, 955, 930, 910, 700. ^{1}H NMR (400 MHz, $CDCl_3$) δ: 7.50–7.35 (m, 5H), 5.04 and 5.00 (AB, J = 5.6 Hz, 2H) 4.90 and 4.86 (AB, J = 10.4 Hz, 2H), 3.99 (s, 3H), 3.78 (s, 3H), 3.59 (s, 3H), 3.53 (s, 3H), 2.88 (dt, J = 18 Hz, 7.2 Hz, 1H), 2.56 (dt, J = 18 Hz, 7.2 Hz, 1H), 2.35 (s, 3H), 2.33 (s, 3H), 1.18 (t, J = 7.2 Hz, 3H). ^{13}C NMR (100 MHz, $CDCl_3$) δ: 205.1, 168.3, 153.5, 152.0, 149.4, 148.6, 137.3, 128.4, 128.0, 127.6, 127.0, 125.7, 123.5, 119.5, 101.5, 76.7, 64.2, 61.3, 57.6, 52.4, 38.3, 13.1, 10.6, 7.9.

*5-Benzyloxy-1,4-dimethoxy-7-methoxymethoxy-2,6-dimethyl-8-(propan-1′-one)-3-{*N*-[2″-(trimethylsilyl)ethoxycarbonyl] amino}naphthalene (**1**)*

To a solution of methyl ester **14** (70 mg, 0.01 mmol) in degassed DMPU (1 mL) was added a solution of lithium *n*-propylmercaptide in DMPU (ca. 0.3 M, 2.0 mL, 0.6 mmol). The resulting mixture was stirred at 23°C for 3 h at which point the solution was acidified with 1 M HCl and diluted with ethyl acetate (15 mL). The organic layer was washed with H_2O (3 × 5 mL), dried over $NaSO_4$, filtered, and concentrated in vacuo. Purification of the crude product by flash chromatography using 45% ether:50% hexane:5% acetic acid afforded the intermediate carboxylic acid (59 mg, 87% yield) as a yellow syrup. HRMS calcd. for $C_{27}H_{30}O_8$ (M^+): 482.1974; found: 482.1974. IR ($CDCl_3$) (cm^{-1}): 3500–2700 (br), 3005, 2960, 1700, 1600, 1580, 1560, 1450, 1335, 1160, 1110, 1050, 1010, 950, 910. ^{1}H NMR (500 MHz, $CDCl_3$) δ: 7.52–7.30 (m, 5H), 5.04 and 5.00 (AB, J = 5.6 Hz, 2H), 4.91 and 4.86 (AB, J = 10.4 Hz, 2H), 3.84 (s, 3H), 3.59 (s, 3H), 3.54 (s, 3H), 2.90 (dt, J = 18.2 Hz, 7.2 Hz, 1H), 2.58 (dt, J = 18.2 Hz, 7.2 Hz, 1H), 2.44 (s, 3H), 2.36 (s, 3H), 1.19 (t, J = 7.2 Hz, 3H).

To a solution of the above carboxylic acid (36 mg, 0.07 mmol) was added diphenylphosphoryl azide (20 μL, 0.08 mmol), β-trimethylsilylethanol (70 μL, 0.39 mmol), and triethylamine (15 μL, 0.1 mmol). The resulting solution was heated at reflux for 20 h. The reaction mixture was diluted with EtOAc (15 mL) and the resulting solution was extracted with 1 M HCl (1 × 5 mL) and H_2O (1 × 5 mL). The organic layer was dried with $NaSO_4$, filtered, and concentrated in vacuo. Purification of the crude product by flash chromatography with 5:1 hexane–EtOAc afforded carbamate **1** (32 mg, 73% yield) as a thick yellow oil. HRMS calcd. for $C_{32}H_{43}NO_8Si$ (M^+): 597.2759; found: 597.2746. IR ($CDCl_3$) (cm^{-1}): 3420 N-H, 3050, 2660, 2940, 1730, 1700, 1480, 1340, 1220, 1170, 1090, 1060, 1010, 950, 860, 840. ^{1}H NMR (400 MHz, $CDCl_3$) δ: 7.55–7.35 (m, 5H, Bzl-*H*), 6.60 (br s, 1H, N*H*), 5.02 and 4.98 (AB, J = 5.2 Hz, 2H), 4.93 and 4.77 (AB, J = 10.4 Hz, 2H), 4.27 (t, J = 8.4 Hz, 2H, OCH_2CH_2TMS), 3.67 (s, 3H), 3.59 (s, 3H), 3.57 (s, 3H), 2.93 (dt, J = 18 Hz, 7.2 Hz, 1H), 2.60 (dt, J = 18 Hz, 7.2 Hz, 1H), 2.38 (s, 3H), 2.36 (s, 3H), 1.20 (t, J = 7.2 Hz, 3H), 1.05 (t, J = 8.4 Hz, 2H, CH_2TMS). ^{13}C NMR (100 MHz, $CDCl_3$) δ: 205.4, 155.4, 152.8, 150.7, 149.9, 137.5, 128.4, 128.3, 127.9, 126.9, 126.2, 125.5, 119.1, 101.5, 76.3, 63.9, 62.5, 61.1, 57.7, 38.3, 17.8, 12.6, 10.6, 7.9, –1.4. Anal. calcd. for $C_{32}H_{43}NO_8Si$: C 64.29, H 7.26, N 2.34; found: C 64.07, H 7.02, N 2.16.

*5-Benzyloxy-1,4-dimethoxy-7-methoxymethoxy-2,6- dimethyl-3-[2-(trimethylsilyl)ethoxycarbonyl]naphthalene (**15**)*

To a solution of bromide **10** (840 mg, 1.8 mmol) in THF (8 mL) at –78°C, was added *n*-BuLi (2.5 M, 0.89 mL, 2.2 mmol) dropwise over 5 min. The resulting dark red-brown solution was stirred for 5 min, then CO_2 was bubbled through the reaction mixture for a period of 30 min. The reaction mixture was allowed to warm to 23°C over 3 h at which point 1 M $NaHS0_4$ (20 mL) and EtOAc (40 mL) were added. The organic layer was dried over $MgSO_4$ and concentrated in vacuo. Purification of the crude oil by flash chromatograpy with 2:1 hexane – ethyl acetate:5% acetic acid yields 63 mg of recovered naphthalene **10** and the product carboxylic acid as a white solid (708 mg, 90% yield), mp 140–142°C. HRMS calcd. for $C_{24}H_{26}O_7$ (M^+): 426.1678; found: 426.1680. IR ($CHCl_3$) (cm^{-1}): 3500 (br), 3020, 3000, 2940, 1700, 1640, 1530, 1450, 1430, 1380, 1330, 1250, 1150, 1130, 1090, 1070, 1010, 990, 960, 950. ^{1}H NMR (400 MHz, $CDCl_3$) δ: 7.59–7.36 (m, 6H), 5.39 (s, 3H), 4.92 (s, 3H), 3.89 (s, 3H), 3.88 (s, 3H), 2.51 (s, 3H), 2.35 (s, 3H). ^{13}C NMR (100 MHz, $CDCL_3$) δ: 156.0, 153.2, 149.8, 149.4, 137.5, 130.7, 128.4, 128.4, 127.9, 124.0, 122.3, 117.2, 99.8, 94.4, 76.6, 64.6, 61.0, 56.3, 13.1, 9.6. Anal. calcd. for $C_{24}H_{26}O_7$: C 67.78, H 6.16; found: C 67.58, H 6.19.

To a solution of the carboxylic acid (1.30 g, 3.0 mmol) and triphenylphosphine in THF (15 mL) (1.89 g, 7.2 mmol) was added β-trimethylsilylethanol (0.65 mL, 4.5 mmol). The solution was cooled to 0°C and diethyl azodicarboxylate (1.0 mL, 6.6 mmol) was added dropwise. The reaction was warmed to 23°C and stirred for 4 h. Water (5 mL) and ether (50 mL) were added, the organic layer was washed with 1 M $NaHSO_4$ (1 × 15 mL), satd. $NaHCO_3$ (1 × 15 mL), brine (1 × 15 mL), dried over $MgSO_4$, filtered, and concentrated to a thick oil. Purification of the crude product by flash chromatography with 15% ether–hexanes produced ester **15** (1.35 g, 85% yield) as a clear oil. HRMS calcd. for $C_{29}H_{38}O_7Si$ (M^+): 526.2387; found: 526.2366. IR ($CHCl_3$) (cm^{-1}): 3020, 3010, 2960, 1720, 1620, 1570, 1450, 1400, 1380, 1335, 1250, 1150, 1130, 1070, 1010. ^{1}H NMR (400 MHz, $CDCl_3$) δ: 7.57–7.34 (m, 6H), 5.37 (s, 2H), 4.90 (s, 2H), 4.50 (t, J = 9.0 Hz, 2H), 3.85 (s, 3H), 3.81 (s, 3H), 3.54 (s, 3H), 2.36 (s, 3H), 2.33 (s, 3H), 1.19 (t, J = 9.0 Hz, 2H, 0.09 (s, 9H). ^{13}C NMR (400 MHz, $CDCl_3$) δ: 168.9, 155.5, 153.1, 149.5, 148.5, 137.7, 130.1, 128.5, 128.3, 127.8, 126.3, 122.9, 121.9, 117.5, 99.7, 94.4, 76.5, 64.1, 63.6, 60.9, 56.3, 17.6, 12.8, 9.6, –1.5. Anal. calcd. for $C_{29}H_{38}O_7Si$: C 66.12, H 7.29; found: C 65.89, H 7.43.

© 2001 NRC Canada

*5-Benzyloxy-8-bromo-1,4-dimethoxy-7-methoxymethoxy-2,6-dimethyl-3-[2-(trimethylsilyl)ethoxycarbonyl]naphthalene (**4b**)*

A solution of naphthoate **15** (1.10g, 2.1 mmol) and *N*-bromosuccinimide (480 mg, 2.7 mmol) in chloroform (20 mL) was heated at reflux for 8 h. The reaction was cooled, ether (75 mL) was added, and the mixture was extracted with satd. $NaHCO_3$ (25 mL), brine (25 mL), dried over $MgSO_4$, filtered, and concentrated. The crude reddish-brown oil was dissolved in CH_2Cl_2 (20 mL) and sequentially treated with diisopropylethyl amine (0.8 mL, 4.5 mmol) and MOM-Cl (0.3 mL, 4.0 mmol). This mixture was stirred at 23°C for 1 h then diluted with ether (100 mL), extracted with 1 M $NaHSO_4$ (30 mL), satd. $NaHCO_3$ (30 mL), brine (30 mL), dried over $MgSO_4$, filtered, and concentrated in vacuo. Purification of the crude product by flash chromatography with 15% ether–hexane afforded bromonaphthoate **4b** (1.16 g, 93% yield) as a light yellow oil. HRMS calcd. for $C_{29}H_{38}O_7{}^{81}BrSi$ (M + 1): 607.1836; found: 607.1519. IR ($CHCl_3$) (cm^{-1}): 3010, 2960, 1720, 1600, 1580, 1450, 1330, 1250, 1160, 1120, 1060, 930, 860, 840, 700. ^1H NMR (400 MHz, $CDCl_3$) δ: 7.51–7.35 (m, 5H), 5.19 (s, 2H), 4.85 (s, 2H), 4.50 (t, *J* = 8.5 Hz, 2H), 3.77 (s, 3H), 3.71 (s, 3H), 3.69 (s, 3H), 2.42 (s, 3H), 2.39 (s, 3H), 0.09 (s, 9H). ^{13}C NMR (400 MHz, $CDCl_3$) δ: 167.9, 155.0, 153.0, 150.2, 148.0, 128.7, 128.4, 127.9, 125.9, 121.2, 105.9, 100.2, 76.6, 64.1, 63.8, 61.8, 61.7, 57.9, 17.5, 13.2, 11.4, –1.5. Anal. calcd. for $C_{29}H_{38}O_7BrSi$: C 57.51, H 6.17; found: C 57.77, H 6.20.

*5-Benzyloxy-8-[(4′*S*,2′*E*)-5′-benzyloxymethoxy-2′,4′-dimethyl-pent-2′-en-1′-one]-1,4-dimethoxy-7-methoxymethoxy-2,6-dimethyl- 3-[2″-(trimethylsilyl)ethoxy-carbonyl]naphthalene (**17**)*

To a solution of bromide **4b** (675 mg, 1.1 mmol) in THF (8 mL) at –100°C was added *n*-BuLi (2.5 M, 0.40 mL, 1.0 mmol) The resulting solution was stirred for 5 min at –100°C and enal **16** (189 mg, 0.80 mmol) was added via cannula. The reaction mixture was gradually warmed over 8 h to 0°C, then was quenched wtih brine solution (2 mL), diluted with ether (50 mL), washed with brine (2 × 15 mL). The combined extracts were dried over $MgSO_4$, filtered, and concentrated in vacuo. Purification of the crude product by flash chromatography with 30% ether–hexane to 50% ether–hexane provided recovered enal **16** (23 mg), recovered bromo ester **4b** (58 mg), ester **15** (140 mg (from protonation of the aryllithium intermediate)), and desired allylic alcohol as a 1:1 mixture of diastereomers (470 mg, 75% based on aldehyde). The diastereomers were separable by HPLC using a Whatman M9 column and a flow rate of 4 mL min^{-1} and 25% EtOAc–hexane as eluent. Data for diastereomer A: ^1H NMR (400 MHz, C_6D_6) δ: 7.42–7.07 (m, 10H), 6.72 (d, *J* = 11.6 Hz, 1H), 5.53 (d, *J* = 9.2 Hz, 1H), 5.00 and 4.89 (AB, *J* = 6 Hz, 2H), 4.79 and 4.69 (AB, *J* = 10.4 Hz, 2H), 4.60 (s, 2H), 4.52 (t, *J* = 7.2 Hz, 2H), 4.50 (s, 2H), 3.90 (s, 3H), 3.47–3.35 (m, 2H), 3.40 (s, 3H), 3.29 (s, 3H), 2.84–2.76 (m, 1H), 2.43 (s, 3H), 2.34 (s, 3H), 1.80 (s, 3H), 1.11 (t, *J* = 7.2 Hz, 2 H), 1.01 (d, *J* = 6.4 Hz, 3H), –0.08 (s, 9H). Data for diastereomer B: HRMS calcd. for $C_{44}H_{59}O_{10}Si$ (M + 1): 775.3877; found: 775.3923. IR (CCl_4) (cm^{-1}): 3500 (br), 3020, 2980, 2960, 2940, 2930, 1730, 1590, 1500, 1340, 1250, 1110, 1050. ^1H NMR (400 MHz, C_6D_6) δ: 7.41–7.08 (m, 10H), 6.73 (d, *J* = 10.8 Hz, 1H), 5.54 (d, *J* = 8.8 Hz, 1H), 4.99 and 4.90 (AB, *J* = 6 Hz, 2H), 4.79 and 4.69 (AB, *J* = 10.4 Hz, 2H), 4.57 (s, 2H), 4.53 (t, *J* = 7.2 Hz, 2H), 4.49 (s, 2H), 3.89 (s, 3H), 3.47–3.35 (m, 2H), 3.42 (s, 3H), 3.29 (s, 3H), 2.84–2.76 (m, 1H), 2.44 (s, 3H), 2.34 (m, 3H), 1.78 (s, 3H), 1.11 (t, *J* = 7.2 Hz, 3H), 1.03 (d, *J* = 6.8 Hz, 3H), –0.08 (s, 9H).

To a solution of Dess–Martin periodinane (197 mg, 0.47 mmol) and pyridine (0.1 mL, 0.47 mmol) in CH_2Cl_2 (1.0 mL) at 0°C was added the allylic alcohols from the preceding experiment (239 mg, 0.31 mmol) in CH_2Cl_2 (1 mL) via cannula. The reaction mixture was stirred at 23°C for 5 h, then was diluted with ether (20 mL) and H_2O (10 mL). The organic layer was washed with satd. $NaHCO_3$ (5 mL), 1 M $NaHSO_4$ (2 × 5 mL), dried over $MgSO_4$, filtered, and concentrated in vacuo. Purification of the crude product by flash chromotography with 30% ether–hexanes produced enone **17** (221 mg, 92% yield) as a 1:1 mixture of atropisomers. HRMS calcd. for $C_{42}H_{51}O_9Si$ (M–C_2H_5O): 727.3304; found: 727.3259. IR ($CHCl_3$) (cm^{-1}): 3060, 3000, 2960, 1720, 1650, 1605, 1570, 1560, 1495, 1480, 1450, 1415, 1395, 1375, 1350, 1320, 1265, 1250, 1215, 1160, 1120, 1100, 1050, 955, 930, 860, 840, 695. ^1H NMR (400 MHz, C_6D_6) δ: 7.42–7.07 (m, 20H), 6.06 (dd, *J* = 6.2 Hz, *J* = 1.2 Hz, 1H), 6.03 (dd, *J* = 6.2 Hz, *J* = 1.2 Hz, 1H), 5.24 and 5.14 (AB, *J* = 5.6 Hz, 2H), 5.25 and 5.13 (AB, *J* = 5.6 Hz, 2H), 4.79–4.71 (m, 4 H), 4.51–4.45 (m, 8H), 4.42 and 4.36 (AB, *J* = 6.4 Hz, 2H), 4.38 and 4.31 (AB, *J* = 12 Hz, 2H), 3.89 (s, 3H), 3.88 (s, 3H), 3.388 (s, 3H), 3.387 (s, 3H), 3.35 (s, 3H), 3.33 (s, 3H), 3.22–3.11 (m, 4H), 2.79–2.71 (m, 2H), 2.44 (s, 3H), 2.41 (s, 3H), 2.39 (s, 3H), 2.35 (s, 3H), 2.21 (d, *J* = 1.2 Hz, 3H), 2.19 (d, *J* = 1.2 Hz, 3H), 1.09–1.04 (m, 4H), 0.79 (d, *J* = 6.8 Hz, 3H), 0.69 (d, *J* = 6.8 Hz, 3H), 0.09 (s, 18 H). ^{13}C NMR (100 MHz, C_6D_6, atropisomers) δ: 196.5, 167.8, 154.1, 150.7, 149.0 (2 Cs), 145.1, 145.0, 139.5, 139.4, 138.7, 138.0, 129.6, 129.5 (2 Cs), 128.8. 128.5, 127.5, 127.4, 127.3, 127.0, 126.3 (2 Cs), 125.8 (2 Cs), 124.2, 120.3, 101.9 (2 Cs), 94.6, 94.3, 76.6, 72.1, 71.9, 69.0 (2 Cs), 64.5, 63.5, 61.4, 57.2, 34.4, 17.7, 16.5, 16.3, 13.4, 12.1, 11.0, –1.7. Anal. calcd. for $C_{44}H_{56}O_{10}Si$: C 68.36, H 7.32; found: C 68.59, H 7.44.

*5-Benzyloxy-8-[(4′*S*,2′*E*)-5′-benzyloxymethoxy-2′,4′-dimethypent-2′-en-1′-one]-1,4-dimethoxy-7-methoxymethoxy-2,6-dimethyl-3-{*N*-[2″-(trimethylsilyl)ethoxy-carbonyl]amino}naphthalene (**18**)*

To a solution of **17** (45 mg, 0.06 mmol) in dimethyl sulfoxide (0.8 mL) was added $KF{\cdot}(H_2O)_2$ (56 mg, 0.59 mmol). The resulting solution was stirred for 70 h at 23°C. The reaction mixture was diluted with 10 mL of EtOAc and extracted with 0.5 M HCl (1 × 5 mL), H_2O (1 × 5 mL), dried over $MgSO_4$, and concentrated in vacuo. The crude acid (39 mg, 98% yield) was used without purification in the next step. HRMS calcd. for $C_{39}H_{44}O_{10}$ (M^+): 672.2935; found: 672.2920. IR ($CDCl_3$) (cm^{-1}): 3500 (br), 3010, 2940, 1710, 1650, 1450, 1270, 1230, 1170, 1100, 1060, 950, 860, 840. ^1H NMR (400 MHz, C_6D_6) δ: 7.4–7.1 (m, 20H), 5.63 (dd, *J* = 4.8, 1.2 Hz, 1H), 5.61 (dd, *J* = 4.8, 1.2 Hz, 1H), 4.91–4.75 (m, 8H), 4.56 (s, 4H), 4.40 (s, 3H), 3.73 (s, 3H), 3.70 (s, 3H), 3.41 (s, 3H), 3.400 (s, 3H), 3.399 (s, 3H), 3.37 (s, 3H), 3.42–3.35 (m, 2H), 3.28 and 3.21 (AB,

© 2001 NRC Canada

J = 6.4 Hz, 2H), 2.82–2.74 (m, 2H), 2.29 (s, 3H), 2.25 (s, 3H), 2.24 (s, 3H), 2.20 (s, 3H), 1.901 (s, 3H), 1.899 (s, 3H), 0.87 (d, *J* = 6.4 Hz, 3H), 0.79 (d, *J* = 6.8 Hz, 3H).

A solution of crude carboxylic acid (35 mg, 0.05 mmol), diphenylphosphorylazide (14 μL, 0.07 mmol), β-trimethylsilylethanol (40 μL, 0.26 mmol), and triethylamine (10 μL, 0.07 mmol) in THF (2 mL) was heated at reflux for 24 h. The reaction mixture was diluted with ethyl acetate (15 mL), extracted with 1 M HCl (1 × 5 mL), H_2O (1 × 5 mL), dried over $MgSO_4$, and concentrated in vacuo. Purification of the crude product by flash chromatography with 50% ether–hexane yielded carbamate **18** (29 mg, 72% yield) as a light yellow oil. Data for 1:1 atropisomer mixture: $[\alpha]_D$ –18.7° (c 0.8, $CHCl_3$). HRMS calcd. for $C_{44}H_{57}NO_{10}Si$ (M^+): 787.3751; found: 787.3759. IR ($CHCL_3$) (cm^{-1}): 3420, 3020, 2980, 1710, 1650, 1480, 1360, 1340, 1210, 1190, 1150, 860, 840, 695. ^1H NMR (400 MHz, C_6D_6) δ: 7.5–7.1 (m, 20H), 6.41 (br s, 1H), 6.32 (br s, 1H), 6.09 (d, *J* = 10.2 Hz, 1H), 6.06 (d, *J* = 9.8 Hz, 1H), 5.27 and 5.15 (AB, *J* = 5.2 Hz, 2H), 5.26 and 5.14 (AB, *J* = 5.2 Hz, 2H), 4.87 and 4.74 (AB, *J* = 10.4 Hz, 2H), 4.85 and 4.73 (AB, *J* = 10.4 Hz, 2H), 4.50–4.45 (m, 4H), 4.41 and 4.37 (AB, *J* = 6.4 Hz, 2H), 4.33–4.24 (m, 6H), 3.54 (s, 3H), 3.53 (s, 3H), 3.46 (s, 3H), 3.45 (s, 3H), 3.36 (s, 3H), 3.34 (s, 3H), 3.22–3.12 (m, 4H), 2.80–2.71 (m, 2H), 2.48 (s, 3H), 2.47 (s, 3H), 2.45 (s, 3H), 2.42 (s, 3H), 2.20 (d, *J* = 1.6 Hz, 3H), 2.19 (d, *J* = 1.6 Hz, 3H), 0.98 (t, *J* = 8.8 Hz, 4H), 0.78 (d, *J* = 6.8 Hz, 3H), 0.69 (d, *J* = 6.8 Hz, 3H), –0.09 (s, 18 H). ^{13}C NMR (100.58 MHz, C_6D_6) δ: 196.7, 155.3, 153.3, 153.0, 151.1, 145.8, 145.0, 144.8, 139.6, 139.5, 138.7, 138.3, 129.4, 126.9, 119.7, 101.9, 94.5, 94.3, 76.4, 72.0, 71.9, 69.0, 68.9, 63.7, 62.4, 61.2, 57.2, 34.4, 18.0, 16.5, 12.8, 12.0, 10.9, –1.6. Anal. calcd. for $C_{44}H_{57}NO_{10}Si$: C 67.05, H 7.30, N 1.77; found: C 66.85, H 7.45, N 1.65.

*5-Allyloxy-3-bromo-7-methoxymethoxy-2,6-dimethyl-[1,4]-naphthoquinone (**26**)*

To a solution of silver(I) oxide (27 g, 117 mmol) and allyl bromide (7.6 mL, 88 mmol) in $CHCl_3$ (150 mL) was added a solution of phenol **8** (14,35) (10 g, 29 mmol) in $CHCl_3$ (150 mL). The solution was stirred for 20 h then filtered through a plug of Celite® and concentrated. The crude product was recrystallized from hexanes–EtOAc to give the protected quinone **26** (9.5 g, 86% yield) as a bright yellow solid, mp 109–111°C. FAB–LRMS calcd. for $C_{17}H_{18}O_5Br$ (M^+ + 1) (*m*/*z*): 381; found: 381. IR (KBr) (cm^{-1}): 3078, 2972, 2935, 2650, 1662, 1611, 1570, 1329, 1259, 1140. ^1H NMR (400 MHz, $CDCl_3$) δ: 7.61 (s, 1H), 6.27–6.17 (m, 1H), 5.43 (apparent dq, *J* = 17.1, 1.6 Hz, 1H), 5.35 (s, 2H), 5.30 (apparent dq, *J* = 10.4, 1.6 Hz, 1H), 4.45 (broad d, *J* = 6.0 Hz, 2H), 3.50 (s, 3H), 2.33 (s, 3H), 2.25 (s, 3H). ^{13}C NMR (100 MHz, $CDCl_3$) δ: 181.7, 175.3, 160.1, 158.9, 146.0, 141.0, 133.6, 132.2, 129.2, 118.2, 118.0, 108.0, 94.1, 74.8, 56.5, 17.5, 9.7. Anal. calcd. for $C_{17}H_{17}O_5Br$: C 53.56, H 4.49; found: C 53.27, H 4.47.

*5-Allyloxy-3-bromo-1,4-dimethoxy-7-methoxymethoxy-2,6-dimethylnaphthalene (**27**)*

To a degassed, 0°C solution of quinone **26** (9.0 g, 23.6 mmol) and $CeCl_3 \cdot 7H_2O$ (13.1 g, 35.2 mmol) in dioxane (225 mL) and H_2O (115 mL) was added $NaBH_4$ (1.8 g, 47.2 mmol) over a period of 20 min. The solution was allowed to warm to 23°C, then dimethyl sulfate (Me_2SO_4) (45 mL) was added. The flask was evacuated, filled with Ar then 50% aq NaOH (9 mL) was added. The resulting solution was stirred for 2 h then cooled to 0°C. Concentrated NH_4OH (100 mL) and Et_2O (500 mL) were then added. The phases were separated, and the aqueous phase was extracted with Et_2O (2 × 250 mL). The combined organic extracts were dried over $MgSO_4$, filtered, and concentrated. Purification of the crude product by flash chromatography (5% EtOAc–hexanes) afforded the protected dihydroquinone **27** (8.1 g, 84% yield) as a light yellow oil. HRMS (CI, CH_4) calcd. for $C_{19}H_{24}O_5Br$ (M^+ + 1) (*m*/*z*): 413.0812; found: 413.0788. IR ($CHCl_3$) (cm^{-1}): 3022, 2935, 2861, 1616, 1582, 1484, 1450, 1384, 1350, 1320, 1247. ^1H NMR (400 MHz, $CDCl_3$) δ: 7.41 (s, 1H), 6.26–6.16 (m, 1H), 5.49 (apparent dq, *J* = 17.2, 1.7 Hz, 1H), 5.35 (s, 2H), 5.28 (apparent dq, *J* = 10.4, 1.7 Hz 1H), 4.41 (broad d, *J* = 5.6 Hz, 2H), 3.85 (s, 3H), 3.83 (s, 3H), 3.53 (s, 3H), 2.50 (s, 3H), 2.35 (s, 3H). ^{13}C NMR (75 MHz, $CDCl_3$) δ: 154.9, 152.3, 149.7, 148.3, 134.3, 128.5, 127.2, 122.0, 118.3, 117.3, 117.1, 99.6, 94.4, 75.4, 61.9, 61.1, 56.2, 16.8, 9.6.

*8-Allyloxy-1,4-dimethoxy-6-methoxymethoxy-3,7-dimethylnaphthalene-2-carboxylic acid 2-β-(trimethylsilyl) ethyl ester (**28**)*

To a –78°C solution of bromide **27** (2.1 g, 5.1 mmol) in THF (26 mL) was added *n*-BuLi (2.4 mL, 6.1 mmol, 2.5 M). The solution was stirred for 5 min, then CO_2 was bubbled through the solution for 30 min. The solution was allowed to warm to 23°C then partitioned between 1.0 M $NaHSO_4$ (50 mL) and EtOAc (100 mL). The aqueous phase was extracted with EtOAc (2 × 50 mL). The combined organic extracts were dried $MgSO_4$, filtered, and concentrated to give a yellow oil. Purification of the crude product by flash chromatography (5% HOAc:30% EtOAc:65% hexanes) afforded the carboxylic acid (1.7 g, 89% yield) as a light yellow oil.

To a 0°C solution of the carboxylic acid (1.7 g, 4.5 mmol), PPh_3 (2.8 g, 10.7 mmol) and β-trimethylsilylethanol (0.97 mL, 6.8 mmol) in THF (23 mL) was added diethyl azodicarboxylate (DEAD) (1.6 mL, 9.9 mmol). The resulting solution was warmed to 23°C and stirred for 4 h. The solution was then partitioned between Et_2O (100 mL) and satd. aq $NaHCO_3$ (50 mL). The aqueous phase was extracted with Et_2O (2 × 50 mL). The combined organic extracts were dried over $MgSO_4$, filtered, and concentrated to afford a yellow oil. Purification of the crude product by flash chromatography (10% EtOAc–hexanes) afforded the desired ester **28** (1.9 g, 90% yield) as a clear oil. HRMS (CI, CH_4) calcd. for $C_{25}H_{37}O_7Si$ (M^+ + 1) (*m*/*z*): 477.2309; found: 477.2303. IR ($CHCl_3$) (cm^{-1}): 3044, 2957, 2902, 1717, 1618, 1569, 1451, 1397, 1334, 1251, 1220, 1218, 1066. ^1H NMR (400 MHz, $CDCl_3$) δ: 7.41 (s, 1H), 6.23–6.13 (m, 1H), 5.45 (broad d, *J* = 17.2, 1.4 Hz, 1H), 5.35 (s, 2H), 5.26 (broad d, *J* = 10.3, Hz 1H), 4.48 (t, *J* = 8.8 Hz, 2H), 4.38 (broad d, *J* = 5.6 Hz, 2H), 3.86 (s, 3H), 3.82 (s, 3H), 3.53 (s, 3H), 2.33 (s, 6H), 1.17 (t, *J* = 8.8 Hz, 2H), 0.09 (s, 9H). ^{13}C NMR (75 MHz, $CDCl_3$) δ: 168.7, 155.4, 153.1, 149.4, 148.4, 134.3, 130.1, 126.2, 122.8, 121.7, 117.5, 117.1, 99.6, 94.4, 75.5, 64.2, 63.7, 60.9, 56.3,

© 2001 NRC Canada

17.5, 12.7, 9.6, –1.5. Anal. calcd. for $C_{25}H_{36}O_7Si$: C 63.00, H 7.61; found: C 63.04, H 7.60.

*8-Allyloxy-5-bromo-1,4-dimethoxy-6-methoxymethoxy-3,7-dimethyl-naphthalene-2-carboxylic acid 2-β-(trimethylsilyl)-ethyl ester (**19**)*

Method A: To a solution of naphthoate **28** (140 mg, 0.29 mmol) and H_2SO_4 (1 μL) in THF (1.5 mL) was added *N*-bromosuccinimide (NBS) (68 mg, 0.38 mmol). The resulting solution was stirred for 2.5 h then partitioned between satd. aq $NaHCO_3$ (25 mL) and Et_2O (50 mL). The aqueous phase was extracted with Et_2O (2 × 25 mL). The combined organic extracts were dried over $MgSO_4$, filtered, and concentrated. The crude product (which consisted of a ca. 1:1 mixture of bromobenzocyclohexadienone **29** and the phenol tautomer **30** according to ^1H NMR analysis) was filtered through a plug of silica gel using 10% EtOAc–hexanes to afford a yellow oil. This material was dissolved in CH_2Cl_2 (1.5 mL), then MOM-Cl (110 μL, 1.4 mmol) and Hunig's base (300 μL, 1.7 mmol) were added. The solution was stirred for 1 h then partitioned between satd. aq $NaHCO_3$ (25 mL) and Et_2O (50 mL). The aqueous phase was extracted with Et_2O (2 × 25 mL). The combined organic extracts were dried over $MgSO_4$, filtered, and concentrated. Purification of the crude product by flash chromatography (10% EtOAc–hexanes) afforded an inseparable 1:1 mixture of naphthyl bromide **19** and naphthyl chloride **31** (120 mg, 75% combined yield). Pure choride **31** was obtained by treating the **19**–**31** mixture with *n*-BuLi followed by the addition of propanal. Unreacted chloride **31** was isolated from the reaction mixture. Data for chloride **31**: HRMS (CI, CH_4) calcd. for $C_{25}H_{36}O_7ClSi$ ($M^+ + 1$) (*m*/*z*): 511.1920; found: 511.1928. ^1H NMR (400 MHz, $CDCl_3$) δ: 6.18–6.09 (m, 1H), 5.42 (apparent dq, *J* = 17.2, 1.6 Hz, 1H), 5.26 (broad d, *J* = 10.4 Hz, 1H), 5.19 (s, 2H), 4.48 (t, *J* = 8.8 Hz, 2H), 4.33 (broad d, *J* = 5.6 Hz, 2H), 3.81 (s, 3H), 3.72 (s, 3H), 3.69 (s, 3H), 2.42 (s, 3H), 2.36 (s, 3H), 1.16 (t, *J* = 8.8 Hz, 2H), 0.09 (s, 9H). Data for bromide **19**: HRMS (CI, CH_4) calcd. for $C_{25}H_{36}O_7BrSi$ ($M^+ + 1$) (*m*/*z*): 555.1414; found: 555.1421. IR ($CHCl_3$) (cm^{-1}): 3072, 2960, 2902, 2862, 1721, 1584, 1451, 1395, 1332, 1250, 1160, 1116, 1059. ^1H NMR (400 MHz, $CDCl_3$) δ: 6.18–6.09 (m, 1H), 5.42 (apparent dq, *J* = 17.2, 1.5 Hz, 1H), 5.26 (broad d, *J* = 10.3 Hz, 1H), 5.19 (s, 2H), 4.49 (t, *J* = 8.8 Hz, 2H), 4.34 (broad d, *J* = 5.2 Hz, 2H), 3.81 (s, 3H), 3.70 (s, 3H), 3.68 (s, 3H), 2.44 (s, 3H), 2.36 (s, 3H), 1.16 (t, *J* = 8.8 Hz, 2H), 0.09 (s, 9H). ^{13}C NMR (75 MHz, $CDCl_3$) δ: 168.0, 155.0, 153.0, 150.2, 147.9, 134.0, 128.6, 127.5, 125.8, 121.2, 117.4 (2C), 105.8, 100.2, 75.5, 64.2, 63.9, 61.7, 58.0, 17.5, 13.1, 11.0, –1.5.

Method B: To a solution of **28** (1.8 g, 3.8 mmol) and H_2SO_4 (3 μL) in THF (19 mL) was added *N*-bromosuccinimide (NBS) (2.0 g, 11.4 mmol). The resulting solution was stirred for 9 h, then more NBS (300 mg, 1.7 mmol) and H_2SO_4 (1 μL) were added. The resulting solution was stirred for 1.5 h then partitioned between satd. aq $NaHCO_3$ (30 mL) and Et_2O (50 mL). The aqueous phase was extracted with Et_2O (2 × 50 mL). The combined organic extracts were dried over $MgSO_4$, filtered, concentrated and filtered through a plug of silica gel using 10% EtOAc–hexanes affording a yellow oil. This material was dissolved in CH_2Cl_2 (19 mL) and Hunig's base (2.0 mL, 11.4 mmol) was added. The resulting solution was cooled to 0°C then MOM-Br (620 μL, 7.6 mmol) was added. The solution was stirred overnight then partitioned between satd. aq $NaHCO_3$ (30 mL) and Et_2O (50 mL). The aqueous phase was extracted with Et_2O (2 × 50 mL). The combined organic extracts were dried over $MgSO_4$, filtered, and concentrated. Purification of the crude product by flash chromatography (5% EtOAc–hexanes) afforded bromide **19** (1.6 g, 76% yield) as a yellow oil.

*5-Allyloxy-3-bromo-7-(*tert*-butyldiphenylsilyloxy)-2,6-dimethyl-[1,4]-naphthoquinone (**35**)*

A solution of quinone **26** (5.8 g, 15 mmol) and *p*-TsOH (11.4 g, 60 mmol) in MeOH (75 mL) and CH_2Cl_2 (30 mL) was heated at reflux for 6 h. The solution was partitioned between satd. aq $NaHCO_3$ (200 mL) and EtOAc (200 mL). The aqueous phase was extracted with EtOAc (3 × 200 mL). The combined organic extracts were dried over $MgSO_4$, filtered, and concentrated to give an orange solid. A solution of this solid in DMF (75 mL) was treated with imidazole (2.2 g, 33 mmol) and TBDPS-Cl (7.8 mL, 30 mmol). The resulting mixture was stirred for 14 h then partitioned between H_2O (200 mL) and EtOAc (200 mL). The aqueous phase was extracted with EtOAc (2 × 150 mL). The combined organic extracts were dried over $MgSO_4$, filtered, and concentrated to afford a dark yellow oil. Purification of the crude product by flash chromatography (5% Et_2O–hexanes) afforded the TBDPS-protected quinone **35** (7.4 g, 87% yield) as a yellow solid, mp 136–138°C. HRMS (CI, NH_3) calcd. for $C_{31}H_{31}O_4Br$ (M^+) (*m*/*z*): 574.1175; found: 574.1151. IR ($CHCl_3$) (cm^{-1}): 3073, 2957, 2932, 2859, 1670, 1608, 1577, 1464, 1427, 1360, 1325, 1259, 1134, 1114. ^1H NMR (400 MHz, $CDCl_3$) δ: 7.70–7.67 (m, 4H), 7.48–7.38 (m, 6H), 7.00 (s, 1H), 6.27–6.17 (m, 1H), 5.43 (apparent dq, *J* = 17.2, 1.5 Hz, 1H), 5.30 (broad d, *J* = 9.4 Hz, 1H), 4.45 (broad d, *J* = 5.9 Hz, 2H), 2.39 (s, 3H), 2.17 (s, 3H), 1.14 (s, 9H). ^{13}C NMR (100 MHz, $CDCl_3$) δ: 181.3, 175.4, 159.4, 159.3, 145.9, 141.0, 135.3, 133.6, 131.6, 131.4, 130.9, 130.4, 128.0, 118.2, 117.6, 113.8, 74.8, 26.6, 19.6, 17.4, 10.6.

*5-Allyloxy-3-bromo-7-(*tert*-butyldiphenylsilyloxy)-1,4-bis-methoxymethoxy-2,6-dimethylnaphthalene (**36**)*

To a deoxygenated solution of quinone **35** (6.5 g, 11 mmol) and Adogen 464® (1.6 g, 3.4 mmol) in CH_2Cl_2 (240 mL) and H_2O (240 mL) under Ar was added $Na_2S_2O_4$ (7.8 g, 45 mmol). The solution was stirred for 30 min, then NaOH (38 mL, 113 mmol, 3.0 M) was added. The solution was stirred for 10 min and then cooled to 0°C. MOM-Cl (6.0 mL, 79 mmol) was then added dropwise over a period of 30 min. The resulting solution was allowed to warm to 23°C, stirred for 1 h then partitioned between H_2O (250 mL) and CH_2Cl_2 (200 mL). The aqueous phase was extracted with CH_2Cl_2 (2 × 100 mL). The combined organic extracts were dried over $MgSO_4$, filtered, and concentrated to afford a yellow oil to afford a mixture of mono- and di-MOM-protected hydroquinones. The crude product mixture was dissolved in CH_2Cl_2 (55 mL). To this solution was added MOM-Cl (2.6 mL, 34 mmol) and Hunig's base (7.9 mL, 45 mmol). The resulting solution was stirred for 4 h then partitioned between satd. aq $NaHCO_3$ (150 mL) and Et_2O (150 mL). The aqueous phase was extracted with Et_2O (2 ×

© 2001 NRC Canada

100 mL). The combined organic extracts were dried over $MgSO_4$, filtered, and concentrated. The crude product was purified by flash chromatography (5% Et_2O–hexanes → 10% Et_2O–hexanes) giving the protected hydroquinone **36** (6.0 g, 82% yield) as a light yellow oil. HRMS (CI, NH_3) calcd. for $C_{35}H_{42}O_6BrSi$ ($M^+ + H$) (*m*/*z*): 665.1934; found: 665.1944. IR (thin film) (cm^{-1}): 3071, 3060, 2954, 2931, 2857, 1612, 1582, 1476, 1427, 1319, 1159, 1136. ^1H NMR (400 MHz, $CDCl_3$) δ: 7.74–7.72 (m, 4H), 7.45–7.34 (m, 6H), 6.74 (s, 1H), 6.26–6.12 (m, 1H), 5.44 (apparent dd, *J* = 17.0, 1.5 Hz, 1H), 5.28 (apparent dd, *J* = 10.4, 1.5 Hz, 1H), 5.10 (s, 2H), 4.37 (broad d, *J* = 5.7 Hz, 2H), 4.17 (s, 2H), 3.70 (s, 3H), 3.12 (s, 3H), 2.49 (s, 3H), 2.38 (s, 3H), 1.13 (s, 9H). ^{13}C NMR (100 MHz, $CDCl_3$) δ: 153.3, 152.2, 146.8, 145.3, 135.4, 134.3, 132.3, 130.0, 128.4, 127.9, 127.7, 123.7, 117.5, 117.3, 117.2, 105.6, 101.4, 99.3, 75.3, 58.6, 57.3, 26.5, 19.6, 17.9, 10.7. Anal. calcd. for $C_{35}H_{41}O_6BrSi$: C 63.15, H 6.21; found: C 63.25, H 6.22.

*8-Allyloxy-6-(*tert*-butyldiphenylsilyloxy)-1,4-bis-methoxymethoxy-3,7-dimethylnaphthalene-2-carboxylic acid 2-*β*-trimethylsilyl)ethyl ester (**37**)*

To a –78°C solution of bromide **36** (5.8 g, 8.7 mmol) in THF (43 mL) was added *n*-BuLi (4.2 mL, 2.5 M, 10.4 mmol). The solution was stirred for 10 min, then CO_2 was bubbled through the solution for 20 min. The solution was allowed to warm to 23°C then partitioned between 1.0 M $NaHSO_4$ (150 mL) and Et_2O (150 mL). The aqueous phase was extracted with Et_2O (2 × 100 mL). The combined organic extracts were dried $MgSO_4$, filtered, and concentrated to give a yellow oil. Purification of the crude product by flash chromatography (5% HOAc:30% EtOAc:65% hexanes) afforded the desired carboxylic acid (4.5 g, 82% yield) as a light yellow oil. HRMS (CI, NH_3) calcd. for $C_{36}H_{42}O_8Si$ (M^+) (*m*/z): 630.2649; found: 630.2653. IR ($CHCl_3$) (cm^{-1}): 3018 (br), 2962, 2934, 2860, 1734, 1615, 1427, 1331, 1256, 1158, 1139, 1114, 1073. ^1H NMR (400 MHz, $CDCl_3$) δ: 7.74–7.72 (m, 4H), 7.45–7.35 (m, 6H), 6.78 (s, 1H), 6.20–6.16 (m, 1H), 5.45 (apparent dq, *J* = 17.3, 1.6 Hz, 1H), 5.30 (apparent dq, *J* = 10.4, 1.6 Hz, 1H), 5.15 (s, 2H), 4.34 (broad d, *J* = 5.7 Hz, 2H), 4.19 (s, 2H), 3.42 (s, 3H), 3.13 (s, 3H), 2.49 (s, 3H), 2.32 (s, 3H), 1.14 (s, 9H). ^{13}C NMR (100 MHz, $CDCl_3$) δ: 169.7, 154.5, 153.1, 147.3, 145.5, 235.4, 134.0, 132.2, 130.5, 130.1, 128.0, 124.8, 124.2, 124.0, 117.6, 116.0, 105.8, 101.5, 99.2, 75.3, 57.5, 57.2, 26.5, 19.6, 14.0, 10.6.

To a 0°C solution of carboxylic acid (3.4 g, 5.4 mmol), PPh_3 (3.4 g, 13.4 mmol), and β-trimethylsilylethanol (1.2 mL, 8.1 mmol) in THF (27 mL) was added diethyl azodicarboxylate (1.9 mL, 12.0 mmol). The resulting solution was warmed to 23°C and stirred for 1 h. The solution was then partitioned between Et_2O (150 mL) and satd. aq $NaHCO_3$ (100 mL). The aqueous phase was extracted with Et_2O (2 × 100 mL). The combined organic extracts were dried over $MgSO_4$, filtered, and concentrated to afford a yellow oil. Purification of the crude product by flash chromatography (10% EtOAc–hexanes) afforded the desired ester **37** (3.5 g, 90% yield) as a clear oil. HRMS (CI, NH_3) calcd. for $C_{41}H_{54}O_8Si_2$ (M^+) (*m*/*z*): 730.3357; found: 730.3362. IR (thin film) (cm^{-1}): 3072, 3061, 2954, 2895, 2856, 2827, 1727, 1615, 1426, 1331, 1243, 1159, 1136, 1114. ^1H NMR (400 MHz, $CDCl_3$) δ: 7.74–7.71 (m, 4H), 7.45–7.34 (m, 6H), 6.76 (s, 1H), 6.24–6.14 (m, 1H), 5.43 (apparent dq, *J* = 17.1, 1.6 Hz, 1H), 5.27 (apparent dq, *J* = 10.4, 1.6 Hz, 1H), 5.06 (s, 2H), 4.43–4.39 (m, 4H), 4.17 (s, 2H), 3.49 (s, 3H), 3.11 (s, 3H), 2.48 (s, 3H), 2.21 (s, 3H), 1.14–1.09 (m, 2H), 1.13 (s, 9H), 0.06 (s, 9H). ^{13}C NMR (100 MHz, $CDCl_3$) δ: 168.2, 153.9, 153.2, 146.7, 145.1, 135.4, 134.3, 132.3, 130.0, 130.0, 127.9, 126.2, 123.5, 123.4, 117.2, 117.0, 105.6, 101.7, 99.1, 75.3, 63.4, 57.5, 57.1, 26.5, 19.6, 17.4, 13.7, 10.6, –1.5. Anal. calcd. for $C_{41}H_{54}O_8Si_2$: C 67.36, H 7.45; found: C 67.17, H 7.34.

*8-Allyloxy-6-hydroxy-1,4-bis-methoxymethoxy-3,7-dimethylnaphthalene-2-carboxylic acid 2-*β*-(trimethylsilyl)ethyl ester (**38**)*

To a solution of ester **37** (1.3 g, 1.8 mmol) in CH_3CN (15 mL) was added a solution of $Et_3N{\cdot}HF$ (0.44 g, 3.6 mmol) in CH_3CN (3 mL). The resulting solution was stirred for 10 min then partitioned between Et_2O (500 mL) and H_2O (200 mL). The organic phase was washed with H_2O (2 × 200 mL), dried over $MgSO_4$, filtered, and concentrated to give a yellow oil. The crude product was purified by flash chromatography (25% EtOAc–hexanes) affording the desired phenol **38** (0.87 g, 98% yield) as a clear oil. HRMS (CI, NH_3) calcd. for $C_{25}H_{36}O_8Si$ (M^+) (*m*/*z*): 492.2179; found: 492.2180. IR (thin film) (cm^{-1}): 3072, 3061, 2954, 2895, 2856, 2827, 1727, 1615, 1426, 1331, 1243, 1159, 1136, 1114. ^1H NMR (400 MHz, $CDCl_3$) δ: 7.22 (s, 1H), 6.20–6.11 (m, 1H), 5.42 (apparent dq, *J* = 17.3, 1.6 Hz, 1H), 5.33 (s, 1H), 5.25 (apparent dq, *J* = 10.4, 1.6 Hz, 1H), 5.06 (s, 2H), 5.02 (s, 2H), 4.46 (t, *J* = 8.8 Hz, 2H), 4.37 (broad d, *J* = 5.7 Hz, 2H), 3.65 (s, 3H), 3.50 (s, 3H), 2.36 (s, 3H), 2.31 (s, 3H), 1.16 (t, *J* = 8.8 Hz, 2H), 0.08 (s, 9H). ^{13}C NMR (100 MHz, $CDCl_3$) δ: 168.5, 154.6, 153.3, 146.4, 145.6, 134.2, 130.7, 125.8, 123.4, 120.2, 117.3, 116.7, 101.7, 100.7, 99.7, 75.3, 63.7, 57.9, 57.5, 17.4, 13.8, 9.4, –1.5. Anal. calcd. for $C_{25}H_{36}O_8Si$: C 60.95, H 7.37; found: C 60.89, H 7.23.

*8-Allyloxy-5-bromo-1,4,6-tris-methoxymethoxy-3,7-dimethylnaphthalene-2-carboxylic acid 2-*β*-trimethylsilyl)ethyl ester (**22**)*

To a solution of phenol **38** (0.67 g, 1.4 mmol) in $CHCl_3$ (14 mL) was added *N*-bromosuccinimide (0.27 mg, 1.5 mmol). The resulting solution was stirred for 20 min then partitioned between aq $NaHCO_3$ (40 mL) and Et_2O (100 mL). The organic phase was dried over $MgSO_4$, filtered, and concentrated to give a bright yellow oil. The crude product (consisting of bromobenzocyclohexadienone **39**) was dissolved in MeOH (14 mL), then K_2CO_3 (0.39 g, 2.8 mmol) was added. The resulting solution was stirred for 10 min then partitioned between 1.0 M $NaHSO_4$ (40 mL) and Et_2O (100 mL). The organic phase was dried over $MgSO_4$, filtered, and concentrated to afford a yellow oil. The crude product (a ca. 8:1 mixture of phenol **40** and cyclohexadienone **39**) was dissolved in CH_2Cl_2 (14 mL). To this solution was added MOM-Cl (320 μL, 4.2 mmol) followed by Hunig's base (0.98 mL, 5.6 mmol). The resulting solution was stirred for 1.5 h then partitioned between satd. aq $NaHCO_3$ (40 mL) and Et_2O (100 mL). The aqueous phase was extracted with Et_2O (50 mL). The combined organic ex-

© 2001 NRC Canada

tracts were dried over $MgSO_4$, filtered, and concentrated to afford a yellow oil. Purification of the crude product by flash chromatography (10% EtOAc–hexanes) afforded the desired bromide **22** (0.67 g, 78% yield) (containing ca. 7% of chloride **41**) as a light yellow oil. HRMS (CI, NH_3) calcd. for $C_{27}H_{39}BrO_9Si$ (M^+) (*m*/*z*): 614.1547; found: 614.1564. IR (thin film) (cm^{-1}): 3082, 2953, 2900, 2827, 1729, 1583, 1415, 1330, 1240, 1160, 1066. ^1H NMR (400 MHz, $CDCl_3$) δ: 6.18 (m, 1H), 5.39 (apparent dq, *J* = 17.3, 1.6 Hz, 1H), 5.25 (apparent dq, *J* = 10.4, 1.6 Hz, 1H), 5.16 (s, 2H), 5.01 (s, 2H), 4.94 (s, 2H), 4.46 (t, *J* = 8.8 Hz, 2H), 4.34 (broad d, *J* = 5.6 Hz, 2H), 3.68 (s, 3H), 3.61 (s, 3H), 3.49 (s, 3H), 2.42 (s, 6H), 1.16 (t, *J* = 8.8 Hz, 2H), 0.08 (s, 9H). ^{13}C NMR (100 MHz, $CDCl_3$) δ: 167.6, 155.2, 152.9, 147.3, 144.7, 133.9, 128.8, 127.8, 126.9, 125.7, 121.0, 117.6, 105.7, 101.8, 101.1, 100.2, 75.4, 63.8, 58.1, 58.0, 57.7, 17.4, 14.4, 11.4, –1.5. Anal. calcd. for $C_{27}H_{39}BrO_9Si$: C 52.68, H 6.39; found: C 52.88, H 6.03.

*Data for bromobenzocyclohexadienone **39**:* HRMS (CI, NH_3) calcd. for $C_{25}H_{36}BrO_8Si$ ($M^+ + 1$) (*m*/*z*): 571.1362; found: 571.1385. IR ($CHCl_3$) (cm^{-1}): 2953, 1725, 1672, 1611, 1329, 1302, 1249, 1171, 1045. ^1H NMR (400 MHz, $CDCl_3$) δ: 6.09–5.99 (m, 1H), 5.60 (s, 1H), 5.34 (d, *J* = 17.9 Hz, 1H), 5.26 (d, *J* = 10.4 Hz, 1H), 5.20 and 4.97 (AB quartet, J_{AB} = 5.8 Hz, 2H), 4.99 and 4.84 (AB quartet, J_{AB} = 6.0 Hz, 2H), 4.61 and 4.27 (AB of ABX, J_{AB} = 12.3 Hz, J_{AX} = 5.8 Hz, J_{BX} = 6.4 Hz, 2H), 4.47–4.41 (m, 2H), 3.68 (s, 3H), 3.47 (s, 3H), 2.27 (s, 3H), 1.98 (s, 3H), 1.16–1.11 (m, 2H), 0.08 (s, 9H). ^{13}C NMR (100 MHz, $CDCl_3$) δ: 193.9, 166.8, 160.7, 151.9, 147.0, 134.2, 132.8, 131.3, 130.8, 121.8, 119.5, 119.2, 101.9, 99.8, 73.6, 64.1, 57.8, 57.7, 39.6, 17.4, 14.1, 9.7, –1.6.

*Data for bromophenol **40**:* IR (thin film) (cm^{-1}): 3451, 3080, 2953, 2899, 2828, 1728, 1599, 1419, 1336, 1244, 1160, 1121, 1045. ^1H NMR (400 MHz, $CDCl_3$) δ: 6.71 (s, 1H), 6.18–6.08 (m, 1H), 5.39 (broad d, *J* = 17.3 Hz, 1H), 5.25 (broad d, *J* = 10.4 Hz, 1H), 5.01 (s, 2H), 4.92 (s, 2H), 4.46 (t, *J* = 8.8 Hz, 2H), 4.34 (d, *J* = 6.0 Hz, 2H), 3.62 (s, 3H), 3.49 (s, 3H), 2.41 (s, 3H), 2.36 (s, 3H), 1.16 (t, *J* = 8.8 Hz, 2H), 0.08 (s, 9H). ^{13}C NMR (100 MHz, $CDCl_3$) δ: 167.8, 152.9, 152.0, 145.7, 145.2, 133.9, 127.3, 127.0, 126.9, 120.0, 118.4, 117.6, 101.8, 101.0, 96.4, 75.4, 63.7, 58.1, 57.6, 17.4, 14.4, 10.7, –1.5.

*Data for chloride **41** (recovered from an experiment in which the **22**–**41** mixture was treated with* n-*BuLi):* HRMS (CI, NH_3) calcd. for $C_{27}H_{39}ClO_9Si$ (M^+) (*m*/*z*): 570.2052; found: 570.2044. ^1H NMR (400 MHz, $CDCl_3$) δ: 6.18–6.08 (m, 1H), 5.39 (broad dd, *J* = 17.1, 1.6 Hz, 1H), 5.25 (broad dd, *J* = 10.3 Hz, 1.6 Hz, 1H), 5.16 (s, 2H), 5.01 (s, 2H), 4.96 (s, 2H), 4.46 (t, *J* = 8.8 Hz, 2H), 4.29 (broad d, *J* = 5.7 Hz, 2H), 3.67 (s, 3H), 3.62 (s, 3H), 3.49 (s, 3H), 2.41 (s, 3H), 2.40 (s, 3H), 1.16 (t, *J* = 8.8 Hz, 2H), 0.08 (s, 9H).

Conclusions

We have developed efficient, Diels–Alder based syntheses of several highly functionalized bromonaphthoate derivatives of interest as intermediates in the total synthesis of damavaricin D. Of these, bromonaphthoate **22** played a pivotal role in completion of the total synthesis (25); the full details of this synthesis will be reported elsewhere.[3] Of considerable interest in the work described here is the detection of kinetically stable benzocyclohexadienone intermediates (**13**, **29**, and **39**) from the bromination reactions of β-naphthol derivatives **11**, **28**, and **38**, respectively. It was established that these intermediates undergo displacement with chloride ion at rates competitive with mild base-induced aromatization, and that reduction of the bromobenzocyclohexadienone intermediates also occurs with bromide ion. The surprising stability of the benzocyclohexadienones **13**, **29**, and **39** is presumably due to a combination of steric and stereoelectonic effects that result in the preferential placement of the bromine substituent in an axial position on the benzocyclohexadienone ring system, with the α-C-H placed in the σ-plane of the carbonyl group.

Acknowledgment

Financial support provided by the National Institute of General Medical Sciences (Grant GM 38436 to W.R.R.) and Abbott Laboratories (the Abbott Graduate Fellowship to D.S.C.) is gratefully acknowledged.

References

1. P. Siminoff, R.M. Smith, W.T. Sokolski, and G.M. Savage. Am. Rev. Tuberc. Pulm. Dis. **75**, 576 (1957).
2. K.L. Rinehart and L.S. Shield. Prog. Chem. Org. Nat. Prod. **33**, 231 (1976).
3. K.L. Rinehart, F.J. Antosz, K. Sasaki, P.K. Martin, M.L. Maheshwari, F. Reusser, L.H. Li, D. Moran, and P.F. Wiley. Biochemistry, **13**, 861 (1974).
4. K.L. Rinehart, T.D. Clark, D.M. Moran, L.G. Gray, C.H. Cowie, and L.H. Li. J. Nat. Cancer Inst. **58**, 239 (1977).
5. K. Onodera, S. Ito, and K. Sasaki. Subcell. Biochem. **15**, 69 (1989).
6. S. Ito, N. Yamamoto, K. Nomoto, K. Sasaki, and K. Onodera. J. Antibiot. **42**, 779 (1989).
7. S. Ito, G. Gilljams, B. Wahern, H. Wigzell, N. Yamamoto, K. Sasaki, and K. Onodera. J. Antibiot. **43**, 1045 (1990).
8. A.H.-J. Wang, I.C. Paul, K.L. Rinehart, Jr., and F.J. Antosz. J. Am. Chem. Soc. **93**, 6275 (1971).
9. A.H.-J. Wang and I.C. Paul. J. Am. Chem. Soc. **98**, 4612 (1976).
10. P.V. Deshmukh, K. Kakinuma, J.J. Ameel, K.L. Rinehart, Jr., P.F. Wiley, and L.H. Li. J. Am. Chem. Soc. **98**, 870 (1976).
11. K.L. Rinehart, Jr., F.J. Antosz, P.V. Deshmukh, K. Kakinuma, P.K. Martin, B.I. Milavetz, K. Sasaki, T.R. Witty, L.H. Li, and F. Reusser. J. Antibiot. **29**, 201 (1976).
12. P.A. McCarthy. Tetrahedron Lett. **23**, 4199 (1982).
13. B.M. Trost and W.H. Pearson. Tetrahedron Lett. **24**, 269 (1983).
14. B. Fraser-Reid, L. Magdzinski, B.F. Molino, and D.R. Mootoo. J. Org. Chem. **52**, 4495 (1987).
15. B. Fraser-Reid, B.F. Molino, L. Magdzinski, and D.R. Mootoo. J. Org. Chem. **52**, 4505 (1987).
16. D.R. Mootoo and B. Fraser-Reid. J. Org. Chem. **52**, 4511 (1987).
17. D.R. Mottoo and B. Fraser-Reid. Tetrahedron, **46**, 185 (1990).
18. Z. Wang and S.L. Schreiber. Tetrahedron Lett. **31**, 31 (1990).
19. S.L. Schreiber, Z. Wang, and G. Schulte. Tetrahedron Lett. **29**, 4085 (1988).
20. J.H. Rigby and K.R. Fales. Tetrahedron Lett. **39**, 5717 (1998).

© 2001 NRC Canada

21. M. Miyashita, T. Shiratani, K. Kawamine, S. Hatakeyama, and H. Irie. Chem. Commun. 1027 (1996).
22. M. Miyashita, T. Yamasaki, T. Shiratani, S. Hatakeyama, M. Miyazawa, and H. Irie. Chem. Commun. 1787 (1997).
23. M.P. Hayes. Ph.D. Thesis, Syracuse University, Syracuse, New York. 1998.
24. W.R. Roush and A.D. Palkowitz. J. Org. Chem. **54**, 3009 (1989).
25. W.R. Roush, D.S. Coffey, and D.J. Madar. J. Am. Chem. Soc. **119**, 11331 (1997).
26. W.R. Roush and D.J. Madar. Tetrahedron Lett. **34**, 1553 (1993).
27. W.R. Roush, D.S. Coffey, D.J. Madar, and A.D. Palkowitz. J. Brazil. Chem. Soc. **7**, 327 (1996).
28. H. Nagaoka, G. Schmid, H. Iio, and Y. Kishi. Tetrahedron Lett. **22**, 899 (1981).
29. K.A. Parker and J.J. Petraitis. Tetrahedron Lett. **22**, 397 (1981).
30. M. Nakata, S. Wada, K. Tatsuta, and M. Kinoshita. Bull. Chem. Soc. Jpn. **58**, 1801 (1985).
31. A.P. Kozikowski, K. Sugiyama, and J.P. Springer. Tetrahedron Lett. **21**, 3257 (1980).
32. T.R. Kelly, M. Behforouz, A. Echavarren, and J. Vaya. Tetrahedron Lett. **24**, 2331 (1983).
33. W.H. Pearson. Ph.D. Thesis, University of Wisconsin, Madison, Wisconsin. 1983.
34. D. M. Madar. Ph.D. Thesis, Indiana University, Bloomington, Indiana. 1994.
35. M. Kohn and L. Steiner. Monatsh. Chem. **58**, 92 (1931).
36. G. Roberge and P. Brassard. J. Org. Chem. **46**, 4161 (1981).
37. B.F. Bowden, D.W. Cameron, M.J. Crossley, G.I. Feutrill, P.G. Griffiths, and D.P. Kelly. Aust. J. Chem. **32**, 769 (1979).
38. J.-L. Luche. J. Am. Chem. Soc. **100**, 2226 (1978).
39. H. Hart. Chem. Rev. **79**, 515 (1979).
40. V. Calò, L. Lopez, G. Pesce, F. Ciminale, and P.E. Todesco. J. Chem. Soc. Perkin Trans. 2, 1189 (1974).
41. O.S. Tee and N.R. Iyengar. Can. J. Chem. **65**, 1714 (1987).
42. Y.N. Chow, D.C. Zhao, and C.I. Johansson. Can. J. Chem. **66**, 2556 (1988).
43. M. Koreeda and R. Gopalaswamy. J. Am. Chem. Soc. **117**, 10 595 (1995).
44. W.E. Parham and C.K. Bradsher. Acc. Chem. Res. **15**, 300 (1982).
45. P.A. Bartlett and W.S. Johnson. Tetrahedron Lett. 4459 (1970).
46. K. Ninomiya, T. Shioiri, and S. Yamada. Tetrahedron, **30**, 2151 (1974).
47. D.L. Hughes. Org. React. (N.Y.), **42**, 335 (1992).
48. D.B. Dess and J.C. Martin. J. Org. Chem. **48**, 4155 (1983).
49. (*a*) M. Oki. Top. Stereochem. **14**, 1 (1983); (*b*) H. Kessler. Angew. Chem. Int. Ed. Engl. **9**, 219 (1970).
50. F. Guibe. Tetrahedron, **54**, 2967 (1998).
51. P. Jacob, III, P.S. Callery, A.T. Shulgin, and N. Castagnoli, Jr. J. Org. Chem. **41**, 3627 (1976).
52. R.S. Coleman and E.B. Grant. J. Org. Chem. **56**, 1357 (1991).
53. U. Seitz and J. Daub. Synthesis, 686 (1986).
54. R.W. Hoffmann. Chem. Rev. **89**, 1841 (1989)
55. W.C. Still, M. Kahn, and A. Mitra. J. Org. Chem. **43**, 2923 (1978).

© 2001 NRC Canada

Enantioselective syntheses of (+)- and (–)-nephrosteranic acid employing the Nicholas–Schreiber reaction

Peter A. Jacobi and Prudencio Herradura

Abstract: (+)- and (–)-Nephrosteranic acid (**16**) have been prepared in an enantioselective fashion from alkyne acid **19** (or *ent*-**19**) by a three step sequence involving debenzylation–lactonization, oxidative cleavage, and selective epimerization at C_4. Acids **19** and *ent*-**19** were obtained as single enantiomers employing a Nicholas–Schreiber reaction.

Key words: paraconic acids, nephrosteranic acid, butyrolactones, Nicholas–Schreiber reaction.

Résumé : On a préparé les acides (+)- et (–)-néphrostéraniques (**16**) de façon énantiosélective à partir des alcynes acides **19** (ou *ent*-**19**), par une séquence de trois réactions impliquant une débenzylation–lactonisation, un clivage oxydant et une épimérisation sélective en C_4. Les acides **19** et *ent*-**19** ont été obtenus sous la forme d'énantiomères uniques en faisant appel à la réaction de Nicholas–Schreiber.

Mots clés : acides paraconiques, acide néphrostéranique, butyrolactones, réaction de Nicholas–Schreiber.

[Traduit par la Rédaction]

Introduction

The Nicholas reaction was discovered in 1977 and provides an efficient means for effecting the nucleophilic displacement of propargyl alcohols and related materials (1). This transformation takes advantage of the fact that alkyne cobalt complexes of general structure **2** greatly facilitate the heterolytic cleavage of adjacent alcohols or ethers, which upon acid catalysis afford cobalt stabilized carbocations **3** (Fig. 1). Capture of **3** with nucleophiles such as electron rich aromatics (1*a*), ketone or ester enolates (1*d*, *e*), and enol ethers (1*c*), then affords the products of nucleophilic displacement **4**, which are readily cleaved to the parent alkynes **5** under mild oxidative conditions (1*c*). In 1987 Schreiber et al. (1*h*) reported the first example of a Nicholas reaction employing a homochiral nucleophile. In this work, alkylation of boron enolate **6** with the cobalt complex **7** gave a 12:1 mixture of *syn*-adduct **8** and the corresponding 2,3-*anti*-isomer (not shown). Oxidative decomplexation with CAN then afforded the parent alkyne **9**.

Recently we have extended the Nicholas–Schreiber methodology to prepare a variety of enantiomerically pure alkyne acids **12** (2), which are versatile precursors to natural products as diverse as phytochrome (**13**) (2*a*), thienamycin (**14**) (2*b*), and blastmycinone (**15**) (2*c*, *d*) (Fig. 2). In this paper we describe the application of this methodology to enantioselective syntheses of (+)- and (–)-nephrosteranic acid (**16**) (for isolation and structure of **16**, see refs. 3*a*, *b*; for biological activity of paraconic acids, see refs. 3*c*, *d*), which are members of the paraconic acid family of γ-butyrolactones (**17**). Compounds of this family have attracted considerable recent attention, in part because of their novel biological activity (3*c*, *d*). In addition, the stereochemical relationship between C_3, C_4, and C_5 presents a significant synthetic challenge (3*d*, 4). Nearly all possible combinations are known (e.g., *TT*, *TC*, *CT*, and *CC*), and variants of this type have a pronounced effect on biological properties. Finally it is noteworthy that certain paraconic acids occur naturally in both dextro- and levorotatory forms (3*c*, *d*).

Our strategy for the enantioselective synthesis of (+)-nephrosteranic acid (**16**) is outlined in Scheme 1. Based upon literature precedent (2*b*), we expected that the matched condensation of cobalt complex *R*-**18** with the boron enolate **6** would afford the *syn*-alkyne **19**. Adduct **19** incorporates the desired absolute stereochemistry at C_3 and C_5 in (+)-**16**, and we planned to employ this material as a masked dicarboxylic acid (the common structural feature of the paraconic acids). Next, alkyne **19** would be converted to the lactone **20** by debenzylation followed by cyclization (2*c*, *d*). Finally, oxidative cleavage of the triple bond in **20**, followed by selective epimerization at C_4, would give (+)-**16** in enantiomerically pure form. Beginning with *S*-**18** and *ent*-**6**, we also hoped to prepare (–)-**16** (vide infra).

Each of these transformations was first explored in model studies (Scheme 2). Thus, reaction of boron enolate **6** with cobalt complex **21a** provided a >90% yield of *syn*-adduct

Received April 9, 2001. Published on the NRC Research Press Web site at http://canjchem.nrc.ca on November 14, 2001.

Dedicated to Professor Victor Snieckus, in appreciation of his outstanding contributions to organic chemistry and his dedication and service to the scientific community.

P.A. Jacobi[1] and P. Herradura. Department of Chemistry, Dartmouth College, 6128 Burke Laboratory, Hanover, NH 03755 U.S.A.

[1]Corresponding author (telephone: (603) 646-3495; fax: (603) 646-3946; e-mail: p.jacobi@dartmouth.edu).

 DOI: 10.1139/cjc-79-11-1727 © 2001 NRC Canada

Fig. 1. The Nicholas–Schreiber reaction.

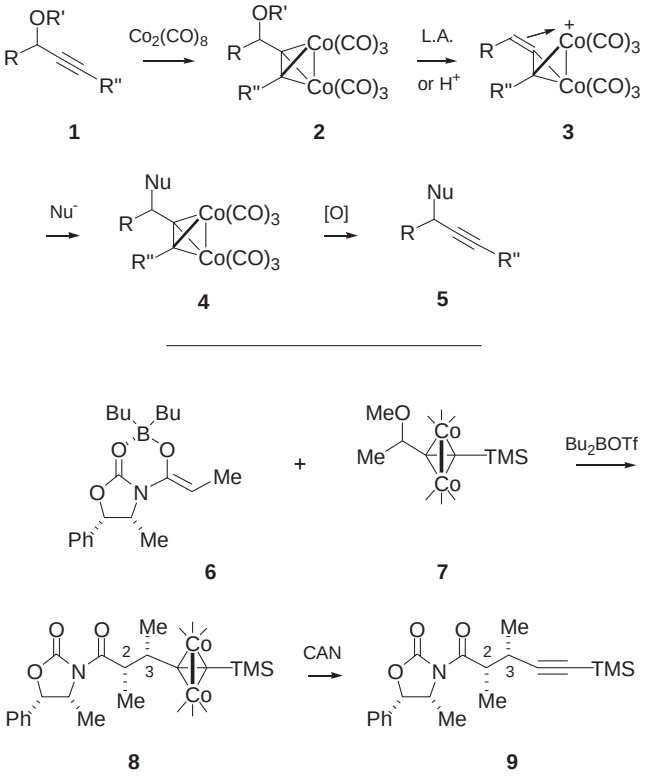
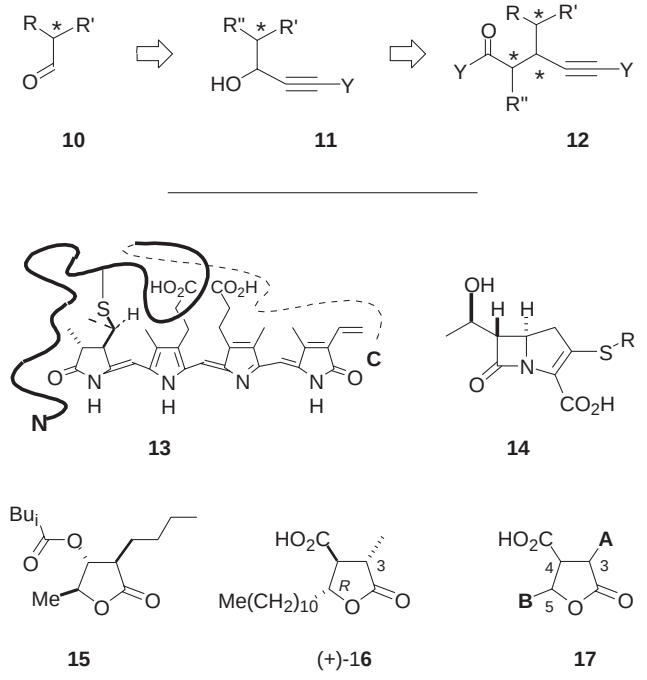
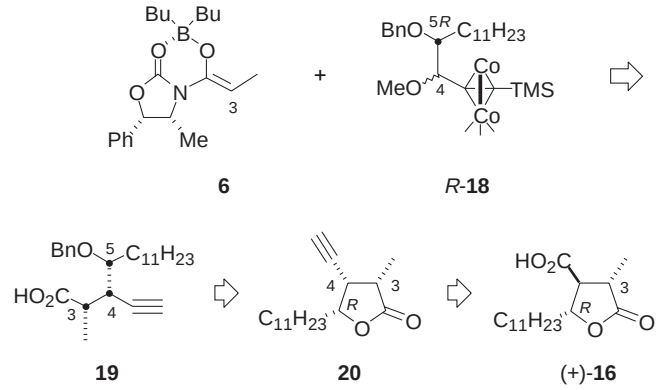


Fig. 2. A general synthesis of alkyne acids **12** — useful substrates in natural product synthesis.

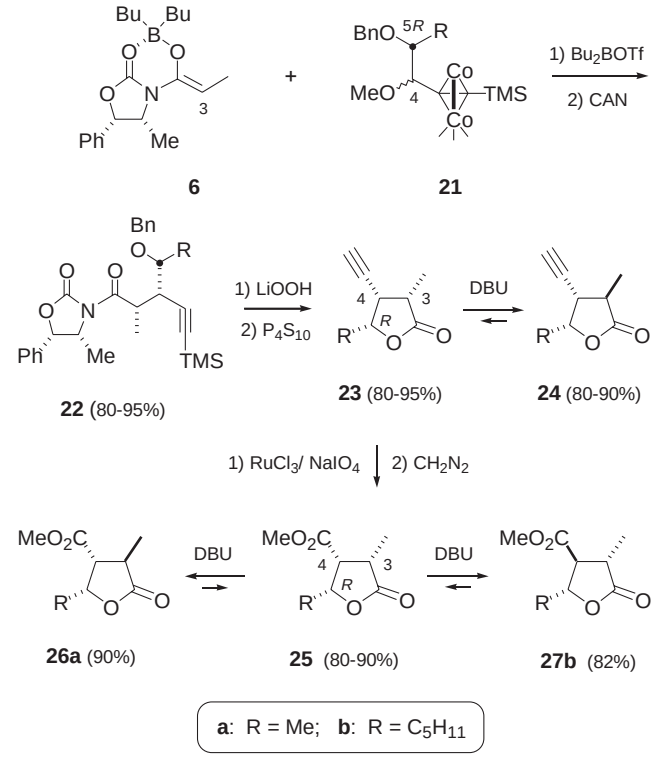


22a (R = Me), which upon hydrolysis and debenzylation gave an 80–90% overall yield of alkyne lactone **23a**. In analogous fashion, but employing cobalt complex **21b**, we obtained excellent overall yields of alkyne lactone **23b** (R = C_5H_{11}). As expected, C_3-epimerization of **23a** and **23b** was

Scheme 1.



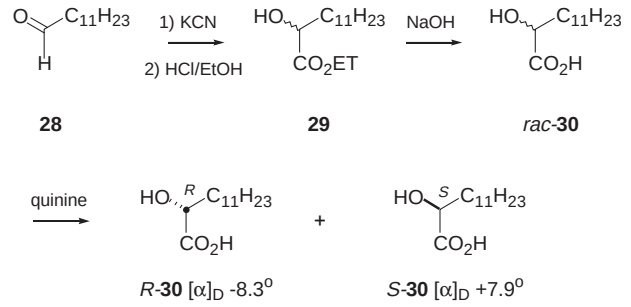
Scheme 2.



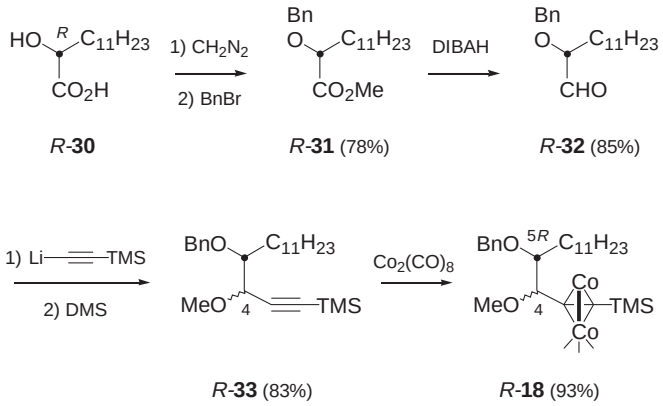
facile (DBU) and afforded an equilibrium mixture of **24** and **23** (**24**:**23**, 85:15; 80–85% yield **24**). The more pertinent study of selective epimerization at C_4 was initially performed with the alkyne lactone **23a** (R = Me). Alkyne **23a** gave a >80% overall yield of methyl ester **25a** upon oxidation with $RuCl_3$–NaIO4 (5), followed by esterification (CH_2N_2). Disappointingly, however, **25a** (R = Me) underwent exclusive epimerization at C_3 to afford the *CT* isomer **26a** (90%; 7% return of **25a**). No trace of the desired all trans (*TT*) isomer **27a** could be detected. In the hope that steric factors would have a positive influence upon thermodynamic equilibration, we repeated the same experiments with the alkyne lactone **23b** (R = C_5H_{11}). In this case we were pleased to find that treatment of methyl ester **25b** with DBU gave predominantly epimerization at C_4, providing the *TT* isomer **27b** in 82% yield (~1–10% return of **25b**; ~1–10%

© 2001 NRC Canada

Scheme 3.



Scheme 4.



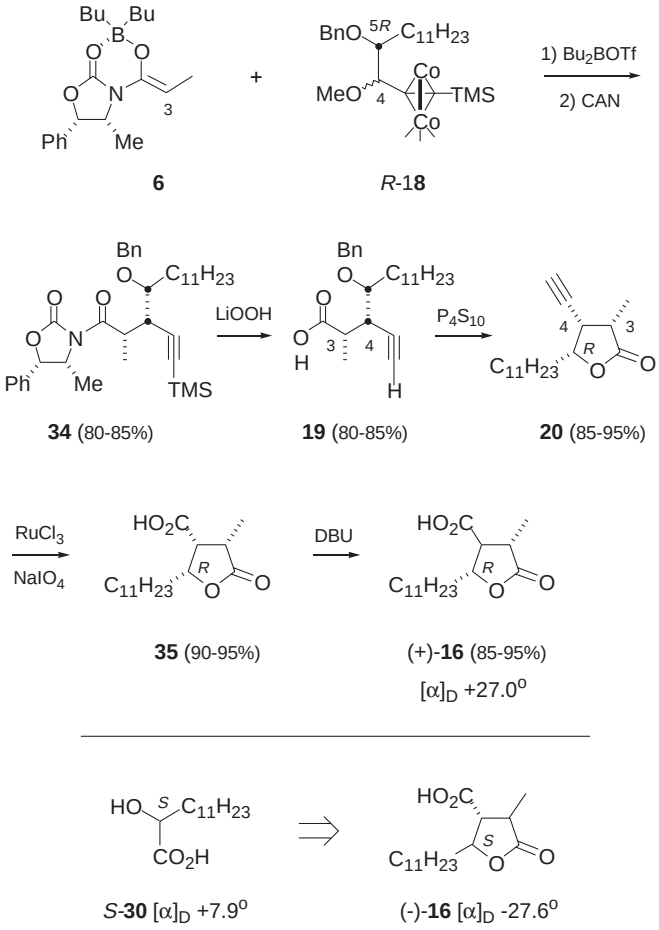
epimerization at C_3). Based upon these results it appears that preferential epimerization at C_4 is a general phenomenon when relatively large R groups occupy C_5. In any event, these model studies were readily extended to the synthesis of nephrosteranic acid (**16**).

Our initial targets for the synthesis of (+)- and (–)-**16** were the homochiral α-hydroxyacids *R*- and *S*-**30** (Scheme 3). Acids of this type are readily accessible by asymmetric reduction of the corresponding trichloromethylketones (6) or by asymmetric hydroxylation (7). In the present case, however, the resolution procedure of Hauser et al. (8) was the most convenient method for providing multigram quantities of starting material. Racemic **30** was easily prepared from dodecylaldehyde (**28**) by initial cyanohydrin formation and ethanolysis to afford **29** (90%), followed by base hydrolysis (99%). Resolution was then accomplished employing quinine for *R*-**30** ($[\alpha]_D$ –8.3) and dehydroabietylamine for *S*-**30** ($[\alpha]_D$ +7.9) (8).

The conversion of *R*-**30** to the requisite cobalt complex *R*-**18** proved to be straightforward (Scheme 4; see also Scheme 1) (2). Thus, *R*-**30** was efficiently transformed to the aldehyde *R*-**32** by a three step sequence involving esterification (CH_2N_2, 96%), alcohol benzylation (BnBr, Ag_2O, 81%), and DIBAH reduction (85%). Condensation of *R*-**32** with lithiotrimethylsilylacetylene, followed by in situ methylation (DMS), then afforded the methyl propargyl ether *R*-**33** in 83% yield (mixture of C_4-epimers). Finally, this last material gave a 93% yield of *R*-**18** upon treatment with $Co_2(CO)_8$.

Once in hand, the condensation of cobalt complex *R*-**18** and boron enolate **6** was carried out in exactly the same

Scheme 5.



manner as described in our model studies (Scheme 5; also see Scheme 2). This reaction gave a 80–85% overall yield of the *syn*-adduct **34** after CAN decomplexation. Upon LiOOH hydrolysis (9), **34** was cleanly converted to the target alkyne acid **19** (80–85%), which was obtained as a single enantiomer. Our plan now called for selective removal of the benzyl protecting group in **19** followed by lactonization. We were pleased to find that this transformation could be accomplished in a single step (85–95%), simply by stirring **19** at rt in CH_2Cl_2 with excess P_4S_{10} (2*c*, *d*). The structure of the alkyne-lactone **20** was readily apparent from its highly characteristic NMR and IR spectra, and also by its eventual conversion to (+)-**16** (vide infra). A possible mechanism for conversions of type **19** → **20** is discussed in ref. 2*c*.

As in our previous studies (Scheme 2), oxidative cleavage of the alkyne bond in **20** was cleanly effected with the reagent system $RuCl_3$–$NaIO_4$ (5), which gave a 90–95% yield of the all-*cis* lactone **35**. Lactone **35** is the C_4-epimer of (+)-nephrosteranic acid (**16**), and we expected to accomplish epimerization by initial conversion of **35** to the corresponding methyl ester (cf. Scheme 2). Surprisingly, however, prior esterification of acid **35** turned out to be unnecessary. Although relatively slow (72 h), **35** was directly epimerized to (+)-**16** upon heating with DBU in toluene (86%). In this case no other isomers of (+)-**16** could be detected (TLC). (+)-Nephrosteranic acid (**16**) thus prepared had closely matching spectral data as that reported in the literature, and was ob-

© 2001 NRC Canada

tained as a single enantiomer [mp 95–97°C (lit. mp 95°C (3*a*), 96–98°C (4*b*)); $[\alpha]_D^{26}$ +27.0 (*c* 1.2, $CHCl_3$) (lit. $[\alpha]_D^{26}$ +27.2 (*c* 1.45, $CHCl_3$))] (4*b*).

In identical fashion but beginning with hydroxyacid *S*-**30** and boron enolate *ent*-**6**, we also prepared (–)-nephrosteranic acid (**16**) (Scheme 5). The material thus obtained had identical spectral and physical properties, and essentially equal but opposite rotation to (+)-**16** [mp 96–98°C; $[\alpha]_D^{26}$ –27.6 (*c* 1.5, $CHCl_3$) (lit. $[\alpha]_D^{26}$ –28.14 (*c* 1.020, $CHCl_3$))] (4*a*). We believe that in some cases the methodology described in this paper will have advantages over more traditional syntheses of these lactones, especially when maximum flexibility is desired in controlling both relative and absolute stereochemistry

Experimental

Melting points were determined in open capillaries and are uncorrected. ^{1}H NMR spectra were recorded at 300, 400, or 500 MHz and are expressed as ppm downfield from tetramethylsilane. All reactions were carried out in oven-dried glassware under an inert atmosphere of nitrogen or argon.

2-Hydroxytridecanoic acid (*rac*-30)

Following the procedure of Hauser et al. (8), a mixture of dodecylaldehyde (**28**) (50 g, 271.3 mmol) in Et_2O (150 mL), potassium cyanide (19.4 g, 298.4 mmol), ice (50 g), and H_2O (100 mL) at 0°C was treated with sodium metabisulfite (31.9 g, 162.8 mmol). The mixture was stirred for 15 min each at 0°C and at rt. The reaction was extracted with Et_2O (3 × 150 mL), and the combined organic extracts were dried over anhydrous $MgSO_4$, filtered, and concentrated under reduced pressure to give a crude cyanohydrin derivative. IR (film) (cm^{-1}): 3350 (OH), 2142 (CN).

The crude cyanohydrin derivative from above in EtOH (350 mL) at 0°C was saturated with hydrogen chloride and was allowed to stand overnight. Excess ethanolic HCl was removed under reduced pressure, and the resulting solid material was treated with ice water (200 mL). The mixture was rapidly extracted with Et_2O (2 × 250 mL) and $CHCl_3$ (2 × 250 mL). The combined organic extracts were dried over anhydrous $MgSO_4$, filtered, and concentrated under reduced pressure to give a solid crude material. The residue was purified by flash chromatography (eluent: 10% EtOAc–hex) to afford 63 g (90%) of the ester derivative **29** as a white solid material. IR (CH_2Cl_2) (cm^{-1}): 3380 (OH), 1731 (CO_2Et).

A mixture of the ester derivative **29** (20 g, 77.4 mmol) in H_2O (100 mL) and dioxane (100 mL) was treated with NaOH (3.7 g, 92.9 mmol) and then the mixture was stirred overnight. The solution was acidified with conc HCl and was extracted with Et_2O (3 × 100 mL). The combined organic extracts were dried over anhydrous $MgSO_4$, filtered, and concentrated under reduced pressure. The residue was purified by flash chromatography (eluent: 20% EtOAc–hex) to afford *rac*-2-hydroxytridecanoic acid (*rac*-**125**) (17.5 g, 98.6%) as a white crystalline solid: mp 70–72°C. IR (CH_2Cl_2) (cm^{-1}): 3410 (OH), 1713 (CO_2H).

2-(*R*)-Hydroxytridecanoic acid (*R*-30)

A solution of anhydrous quinine (14.8 g, 45.6 mmol) and 2-hydroxydodecanoic acid (*rac*-**30**) (10.4 g, 45.2 mmol) in MeOH (200 mL) was heated to boiling. The reaction was treated with hot H_2O (500 mL) and then hot MeOH was added to clarify the solution. The resulting solution was cooled and the salt crystallized from it. The salt was collected and washed with 2:5 MeOH–H_2O followed by drying in vacuo. Recrystallization in 2:5 MeOH–H_2O afforded 10.7 g of crystalline salt.

A solution of crystalline salt (8.1 g, 14.7 mmol) in 2:5 MeOH–H_2O (50 mL) was treated with 20% NaOH solution to pH 8–10. The resulting solution was extracted with Et_2O (3 × 50 mL) to remove quinine. The aqueous portion was acidified to pH 3–4 with conc HCl and was extracted with Et_2O (3 × 150 mL). The combined organic extracts were dried over anhydrous $MgSO_4$, filtered, and concentrated under reduced pressure to afford a crystalline solid. Recrystallization from hexanes gave 3.2 g (42.9%) of optically active 2-(*R*)-hydroxytridecanoic acid (*R*-**30**): mp 71–73°C. $[\alpha]_D^{26}$ –8.3 (*c* 10.4, MeOH). R_f = 0.12 (40% EtOAc–hex + 0.2% AcOH). IR (CH_2Cl_2) (cm^{-1}): 3548, 2951, 2845, 1684, 1476, 1259, 1136, 1101, 1072. ^{1}H NMR (300 MHz, $CDCl_3$) δ: 0.92 (t, *J* = 6.3 Hz, 3H), 1.30–1.50 (m, 16H), 1.73 (m, 2H), 1.88 (m, 2H), 4.23 (m, 1H). ^{13}C NMR (300 MHz, $CDCl_3$) δ: 14.4, 23.0, 25.0, 29.5, 29.6, 29.7, 29.8, 29.9 (2), 32.2, 34.5, 70.5, 180.2. Anal. calcd. for $C_{13}H_{26}O_3$: C 67.79, H 11.38; found: C 67.81, H 11.28.

2-(*S*)-Hydroxytridecanoic acid (*S*-30)

The filtrate from the first crystallization of the quinine salt was treated with conc HCl to pH 3–4, and was extracted with Et_2O (3 × 50 mL). The combined organic extracts were dried over anhydrous $MgSO_4$, filtered, and concentrated under reduced pressure to give a partially resolved 2-(*S*)-hydroxytridecanoic acid.

A solution of dehydroabeitylamine (6.0 g, 19.3 mmol) and the partially resolved acid (4.0 g, 17.5 mmol) in MeOH (100 mL) was heated to boiling. The reaction was treated with hot H_2O (30 mL), and then hot MeOH was added to clarify the solution. The resulting solution was cooled and the salt crystallized from it. The salt was collected and washed with 2:5 MeOH–H_2O followed by drying in vacuo. Recrystallization in 2:5 MeOH–H_2O afforded 8.0 g of the crystalline salt.

A solution of the crystalline salt (7.8 g, 15 mmol) in 2:5 MeOH–H_2O (100 mL) was treated with 20% NaOH solution to pH 8–10. The resulting solution was extracted with Et_2O (3 × 75 mL) to remove dehydroabeitylamine. The aqueous portion was acidified to pH 3–4 with conc HCl, and extracted with Et_2O (3 × 50 mL). The combined organic extracts were dried over anhydrous $MgSO_4$, filtered, and concentrated under reduced pressure to afford a crystalline solid material. Recrystallization from hexanes gave 3.0 g (89%) of optically active 2-(*S*)-hydroxytridecanoic acid (*S*-**30**): mp 73–74°C. $[\alpha]_D^{26}$ +7.9 (*c* 12.3, MeOH). R_f = 0.12 (40% EtOAc–hex + 0.2% AcOH). IR (CH_2Cl_2) (cm^{-1}): 3549, 2951, 2846, 1683, 1468, 1260, 1136, 1101, 1073. ^{1}H NMR (300 MHz, $CDCl_3$) δ: 0.92 (t, *J* = 6.3 Hz, 3H), 1.30–1.51 (m, 16H), 1.71 (m, 2H), 1.87 (m, 2H), 4.33 (m, 1H). ^{13}C NMR (300 MHz, $CDCl_3$) δ: 14.4, 23.0, 25.0, 29.5, 29.6, 29.7, 29.8, 29.9 (2), 32.2, 34.5, 70.5, 180.2. Anal. calcd. for $C_{13}H_{26}O_3$: C 67.79, H 11.38; found: C 67.74, H 11.17.

© 2001 NRC Canada

Methyl 2-(*R*)-hydroxytridecanoate

A solution of 2-(*R*)-hydroxytridecanoic acid (*R*-**30**) (2.7 g, 11.5 mmol) in Et_2O (100 mL) at 0°C was treated with excess CH_2N_2 until the color of the solution turned yellowish. Nitrogen gas was bubbled into the solution to remove excess CH_2N_2 until it became colorless. Et_2O was removed under reduced pressure, and the residue was purified by flash chromatography (eluent: 10% EtOAc–hexanes) to give 2.7 g (96%) of methyl 2-(*R*)-hydroxytridecanoate: mp 33–34°C. $[\alpha]_D^{26}$ –16.9 (*c* 11.7, MeOH). R_f = 0.46 (20% EtOAc–hex). IR (CH_2Cl_2) (cm^{-1}): 3468, 2923, 2853, 1738, 1457, 1216, 1133, 1096. ^1H NMR (300 MHz, $CDCl_3$) δ: 0.91 (t, *J* = 6.9 Hz, 3H), 1.29–1.45 (m, 16H), 1.70 (m, 2H), 1.81 (m, 2H), 2.70 (br s, 1H), 3.82 (s, 3H), 4.23 (m, 1H). Anal. calcd. for $C_{14}H_{28}O_3$: C 68.81, H 11.55; found: C 69.01, H 11.69.

Methyl 2-(*S*)-hydroxytridecanoate

A solution of 2-(*S*)-hydroxytridecanoic acid (*S*-**30**) (2.9 g, 12.5 mmol) in Et_2O (100 mL) at 0°C was treated with excess CH_2N_2 until the color of the solution turned yellowish. Nitrogen gas was bubbled into the solution to remove excess CH_2N_2 until it became colorless. Et_2O was removed under reduced pressure, and the residue was purified by flash chromatography (eluent: 10% EtOAc–hexanes) to give 2.7 g (89%) of methyl 2-(*S*)-hydroxytridecanoate: mp 32–33°C. $[\alpha]_D^{26}$ +18.3 (*c* 8.7, MeOH). R_f = 0.46 (20% EtOAc–hex). IR (CH_2Cl_2) (cm^{-1}): 3473, 2921, 2853, 1733, 1456, 1215, 1133, 1097. ^1H NMR (300 MHz, $CDCl_3$) δ: 0.92 (t, *J* = 6.9 Hz, 3H), 1.29–1.50 (m, 16H), 1.68 (m, 2H), 1.79 (m, 2H), 3.82 (s, 3H), 4.23 (m, 1H). Anal. calcd. for $C_{14}H_{28}O_3$: C 68.81, H 11.55; found: C 69.06, H 11.68.

Methyl 2-(*R*)-benzyloxytridecanoate (*R*-31)

A solution of methyl 2-(*R*)-hydroxytridecanoate (1.4 g, 5.73 mmol) in Et_2O (20 mL) at 0°C under a nitrogen atmosphere was treated with Ag_2O (1.5 g, 6.3 mmol) and then with BnBr (0.75 mL, 6.3 mmol) in Et_2O (5 mL). The resulting suspension was allowed to warm to rt and stirred overnight. Excess Ag_2O was filtered and washed with Et_2O (3 × 10 mL). The combined organic extracts were concentrated under reduced pressure, and the residue was purified by flash chromatography (eluent: 5% EtOAc–hexanes) to give 1.6 g (81%) of methyl 2-(*R*)-benzyloxytridecanoate (*R*-**31**). $[\alpha]_D^{26}$ –30.3 (*c* 12.7, MeOH). R_f = 0.47 (10% EtOAc–hex). CI-HRMS calcd. for $C_{21}H_{34}O_3$ ($[M - H]^+$): 333.2422; found: 333.2422. IR (CH_2Cl_2) (cm^{-1}): 3063, 3030, 2924, 2853, 1752, 1455, 1266, 1201, 1133, 1112, 1027, 735, 697. ^1H NMR (300 MHz, $CDCl_3$) δ: 0.92 (t, *J* = 6.6 Hz, 3H), 1.28–1.44 (m, 18H), 1.80 (m, 2H), 3.80 (s, 3H), 3.98 (t, *J* = 6.3 Hz, 1H), 4.44 (d, *J* = 11.7 Hz, 1H), 4.74 (d, *J* = 11.7 Hz, 1H), 7.36 (m, 5H). ^{13}C NMR (300 MHz, $CDCl_3$) δ: 14.4, 23.0, 25.5, 29.5, 29.6, 29.7, 29.8, 29.9, 32.2, 33.3, 52.1, 72.6, 78.3, 128.1, 128.3, 128.6, 137.8, 173.8.

Methyl 2-(*S*)-benzyloxytridecanoate (*S*-31)

A solution of methyl 2-(*S*)-hydroxytridecanoate (2.1 g, 8.6 mmol) in Et_2O (25 mL) at 0°C under a nitrogen atmosphere was treated with Ag_2O (2.2 g, 9.4 mmol) and BnBr (1.1 mL, 9.4 mmol) in Et_2O (8 mL). The resulting suspension was allowed to warm to rt and stirred overnight. Excess Ag_2O was filtered and washed with Et_2O (3 × 20 mL). The combined organic extract were dried over anhydrous $MgSO_4$, filtered, and concentrated under reduced pressure. The residue was purified by flash chromatography (eluent: 5% EtOAc–hexanes) to afford 2.5 g (86%) of methyl 2-(*S*)-benzyloxytridecanoate (*S*-***31***). $[\alpha]_D^{26}$ +33.1 (*c* 10.1, MeOH). R_f = 0.47 (10% EtOAc–hex). CI-HRMS calcd. for $C_{21}H_{34}O_3$ ($[M - H]^+$): 333.2422; found: 333.2421. IR (CH_2Cl_2) (cm^{-1}): 3063, 3030, 2924, 2854, 1753, 1496, 1455, 1436, 1267, 1201, 1132, 1112, 1026, 734, 697. ^1H NMR (300 MHz, $CDCl_3$) δ: 0.92 (t, *J* = 6.6 Hz, 3H), 1.28–1.45 (m, 18H), 1.78 (m, 2H), 3.79 (s, 3H), 3.98 (t, *J* = 6.6 Hz, 1H), 4.44 (d, *J* = 11.7 Hz, 1H), 4.74 (d, *J* = 11.7 Hz, 1H), 7.35 (m, 5H). ^{13}C NMR (300 MHz, $CDCl_3$) δ: 14.4, 23.0, 25.1, 29.5, 29.6, 29.7, 29.8, 29.9, 32.2, 33.3, 52.1, 72.6, 78.4, 111.6, 128.1, 128.3, 128.7, 137.8, 173.8.

2-(*R*)-Benzyloxytridecanal (*R*-32)

A solution of methyl 2-(*R*)-benzyloxytridecanoate (*R*-**31**) (1.4 g, 4.0 mmol) in CH_2Cl_2 (50 mL) at –78°C under a nitrogen atmosphere was treated with DIBAL-H in toluene (1.0 M, 6 mL, 6.0 mmol. The mixture was stirred for 60 min followed by quenching with MeOH at –78°C. The reaction was allowed to warm to rt and stirred for an additional 5 min, at which time a sodium potassium tartrate solution (1.0 M, 100 mL) was added. The mixture was extracted with CH_2Cl_2 (3 × 200 mL). The combined organic extracts were dried over anhydrous $MgSO_4$, filtered, and concentrated under reduced pressure to afford 1.0 g (85%) of 2-(*R*)-benzyloxytridecanal (*R*-**32**). $[\alpha]_D^{26}$ –24.5 (*c* 16.3, MeOH). R_f = 0.57 (10% EtOAc–hex). CI-HRMS calcd. for $C_{20}H_{32}O_2$ ($[M - H]^+$): 303.2324; found: 303.2308. IR (CH_2Cl_2) (cm^{-1}): 3031, 2924, 2854, 1706, 1456, 1285, 1112, 1080, 969, 735, 697. ^1H NMR (300 MHz, $CDCl_3$) δ: 0.92 (t, *J* = 6.6 Hz, 3H), 1.29–1.43 (m, 18H), 1.73 (m, 2H), 3.79 (td, *J* = 6.3, 2.1 Hz, 1H), 4.57 (d, *J* = 12.0 Hz, 1H), 4.72 (d, *J* = 12.0 Hz, 1H), 7.38 (m, 5H), 9.69 (d, *J* = 2.1 Hz, 1H). ^{13}C NMR (300 MHz, $CDCl_3$) δ: 14.4, 23.0, 25.0, 29.6, 29.7, 29.8, 29.9, 30.3, 32.2, 72.8, 83.8, 128.2, 128.3, 128.8, 137.7, 204.2.

2-(*S*)-Benzyloxytridecanal (*S*-32)

A solution of methyl 2-(*S*)-benzyloxytridecanoate (*S*-**31**) (560 mg, 1.6 mmol) in CH_2Cl_2 (10 mL) at –78°C under a nitrogen atmosphere was treated with DIBAL-H in toluene (1.0 M, 2.4 mL, 2.4 mmol). The resulting mixture was stirred in 60 min followed by quenching with MeOH at –78°C. The reaction was allowed to warm to rt and stirred for an additional 5 min, at which time a sodium potassium tartrate solution (50 mL, 1.0 M) was added. The mixture was extracted with CH_2Cl_2 (3 × 100 mL) and the combined organic extracts were dried over anhydrous $MgSO_4$, filtered, and concentrated under reduced pressure to afford 485 mg (99%) of 2-(*S*)-benzyloxytridecanal (*S*-**32**): $[\alpha]_D^{26}$ +29.2 (*c* 11.5, MeOH). R_f = 0.56 (10% EtOAc–hex). CI-HRMS calcd. for $C_{20}H_{32}O_2$ ($[M - H]^+$): 303.2324; found: 303.2331. IR (CH_2Cl_2) (cm^{-1}): 3031, 2924, 2853, 1707, 1454, 1284, 1111, 1070, 1028, 970, 734, 697. ^1H NMR (300 MHz, $CDCl_3$) δ: 0.92 (t, *J* = 6.9 Hz, 3H), 1.29–1.49 (m, 18H), 1.73 (m, 2H), 3.79 (td, *J* = 6.3, 2.1 Hz, 1H), 4.57 (d, *J* = 12.0 Hz, 1H), 4.72 (d, *J* = 12.0 Hz, 1H), 7.35 (m, 5H), 9.69 (d, *J* = 2.1 Hz,

© 2001 NRC Canada

1H). ^{13}C NMR (300 MHz, $CDCl_3$) δ: 14.4, 23.0, 25.0, 29.6, 29.7, 29.8, 29.9, 30.3, 32.2, 72.8, 83.8, 128.2, 128.3, 128.8, 137.7, 204.2.

Methyl propargyl ether derivative *R*-33

A solution of trimethylsilylacetylene (350 mg, 3.6 mmol) in THF (25 mL) at –78°C under a nitrogen atmosphere was treated with *n*-BuLi in hexanes (1.6 M, 2.4 mL, 3.8 mmol) and was stirred for 20 min. A solution of 2-(*R*)-benzyloxytridecanal (*R*-**32**) (1.0 g, 3.3 mmol) in THF (25 mL) was added to the solution above. The reaction was stirred for an additional 20 min, at which time DMS (0.93 mL, 9.9 mmol) was added. The resulting solution was allowed to warm to rt and stirred for 48 h. The reaction was quenched with saturated NH_4Cl (50 mL) and the mixture was extracted with Et_2O (3 × 20 mL). The combined extracts were dried over anhydrous $MgSO_4$, filtered, and concentrated under reduced pressure. The residue was purified by flash chromatography (eluent: 5% EtOAc–hexanes) to afford 1.1 g (83%) of the corresponding methyl propargyl ether derivative *R*-**33** (diastereomeric mixture): $[\alpha]_D^{26}$ –10.7 (*c* 14.9, MeOH). R_f = 0.63 (5% EtOAc–hex). CI-HRMS calcd. for $C_{26}H_{44}O_2Si$ ($[M - H]^+$): 415.3033; found: 415.2845. IR (CH_2Cl_2) (cm^{-1}): 3030, 2955, 2924, 2853, 2822, 2170, 1724, 1496, 1465, 1454, 1250, 1111, 1028, 844, 760, 734, 697. ^{1}H NMR (300 MHz, $CDCl_3$) δ: 0.18 (s, 9H), 0.92 (t, *J* = 6.3 Hz, 3H), 1.27–1.70 (m, 18H), 1.68 (m, 2H), 3.48 (d, *J* = 4.8 Hz, 3H), 3.54 (m, 2H), 4.07 (m, 1H), 4.60 (m, 1H), 4.62 (d, *J* = 11.7 Hz, 1H), 4.83 (d, *J* = 11.7 Hz, 1H), 7.33 (m, 5H). ^{13}C NMR (300 MHz, $CDCl_3$) δ: 0.2, 14.4, 23.0, 29.7, 29.9, 30.0, 32.2, 57.3 (2), 73.1, 73.7, 74.4, 75.6, 81.0, 81.1, 127.8, 128.0, 128.2, 128.4, 128.5, 128.7, 139.1.

Methyl propargyl ether derivative *S*-33

A solution of trimethylsilylacetylene (142 mg, 1.4 mmol) in THF (12.5 mL) at –78°C under a nitrogen atmosphere was treated with *n*-BuLi in hexanes (1.6 M, 0.9 mL, 1.4 mmol) and was stirred for 20 min. A solution of 2-(*S*)-benzyloxytridecanal (*S*-**32**) (400 mg, 1.3 mmol) in THF (10 mL) was added to the solution above. The reaction was stirred for an additional 20 min, at which time DMS (0.37 mL, 3.94 mmol) was added. The resulting solution was allowed to warm to rt and stirred for 48 h. The reaction was quenched with saturated NH_4Cl (25 mL) and the mixture was extracted with Et_2O (3 × 25 mL). The combined extracts were dried over anhydrous $MgSO_4$, filtered, and concentrated under reduced pressure. The residue was purified by flash chromatography (eluent: 5% EtOAc–hexanes) to afford 495 mg (90%) of the corresponding methyl propargyl ether derivative *S*-**33** (diastereomeric mixture): $[\alpha]_D^{26}$ +14.4 (*c* 9.2, MeOH). R_f = 0.63 (5% EtOAc–hex). CI-HRMS calcd. for $C_{26}H_{44}O_2Si$ ($[M - H]^+$): 415.3033; found: 415.2863. IR (CH_2Cl_2) (cm^{-1}): 3031, 2924, 2854, 2170, 1739, 1496, 1465, 1349, 1250, 1111, 1028, 844, 760, 733. 697. ^{1}H NMR (300 MHz, $CDCl_3$) δ: 0.19 (s, 9H), 0.92 (t, *J* = 6.2 Hz, 3H), 1.29–1.69 (m, 18H), 1.68 (m, 2H), 3.48 (d, *J* = 4.6 Hz, 3H), 3.54 (m, 2H), 4.06 (m, 1H), 4.61 (m, 1H), 4.62 (d, *J* = 11.7 Hz, 1H), 4.83 (d, *J* = 11.7 Hz, 1H), 7.36 (m, 5H). ^{13}C NMR (300 MHz, $CDCl_3$) δ: 0.2, 14.4, 23.0, 29.7, 29.9, 30.1, 32.2, 57.4 (2), 73.1, 73.8, 74.4, 75.6, 81.0, 81.1 (2), 127.8, 128.1, 128.2, 128.4, 128.5, 128.7, 139.2.

Oxazolidinone adduct 34

A solution of *N*-acyloxazolidinone derivative **6** (730 mg, 3.1 mmol) in CH_2Cl_2 (20 mL) at 0°C under a nitrogen atmosphere was treated with *i*-Pr_2NEt (0.54 mL, 3.1 mmol) and then with a solution of Bu_2BOTf in CH_2Cl_2 (1.0 M, 3.1 mL, 3.1 mmol). The solution was stirred for 20 min, after which time additional solution of Bu_2BOTf in CH_2Cl_2 (1.0 M, 1.56 mL, 1.6 mmol) was added. A solution of cobalt complexed derivative *R*-**18** (1.1 g, 1.6 mmol) in CH_2Cl_2 (15 mL) was added to the solution above at –78°C. When addition was complete, the resulting mixture was allowed to warm to 0°C and rt for 20 min, respectively. A pH 7 buffered solution (50 mL) was subsequently added and layers separated. Aqueous layer was further extracted with CH_2Cl_2 (3 × 25 mL). The combined organic extracts were dried over anhydrous $MgSO_4$, filtered, and concentrated under reduced pressure. The residue was passed through a column of silica gel to remove excess *N*-acyloxazolidinone **6** (eluent 5% EtOAc–hexanes) to afford 1.25 g (89%) of the cobalt complex product.

A solution of the above cobalt complex product (1.2 g, 3.3 mmol) in acetone (25 mL) at rt was treated with CAN (1.8 g, 3.3 mmol). Additional CAN (0.9 g, 1.7 mmol) was used and the solvent was removed under reduced pressure. The resulting residue was treated with H_2O (50 mL) and Et_2O (50 mL), and layers were separated. Aqueous layer was further extracted with Et_2O (3 × 30 mL). The combined organic extracts were dried over anhydrous $MgSO_4$, filtered and concentrated under reduced pressure. The residue was purified by preparative chromatography (eluent: 10% EtOAc–hexanes) to afford 660 mg (80%) of **34** as single diastereomer: $[\alpha]_D^{26}$ +60.1 (*c* 7.5, MeOH). R_f = 0.42 (20% EtOAc–hex). CI-HRMS calcd. for $C_{38}H_{55}NO_4Si$ ($[M + H]^+$): 618.3978; found: 618.3985. IR (CH_2Cl_2) (cm^{-1}): 3031, 2924, 2854, 2170, 1786, 1701, 1455, 1367, 1342, 1249, 1195, 1120, 1068, 959, 842, 760, 699. ^{1}H NMR (300 MHz, $CDCl_3$) δ: 0.12 (s, 9H), 0.95 (t, *J* = 7.2 Hz, 3H), 1.18 (d, *J* = 6.9 Hz, 3H), 1.30–1.40 (m, 23H), 3.02 (dd, *J* = 10.5, 3.0 Hz, 1H), 3.61 (td, *J* = 6.6, 2.7 Hz, 1H), 4.42 (m, 1H), 4.62 (d, *J* = 12.0 Hz, 1H), 4.70 (d, *J* = 12.0 Hz, 1H), 4.87 (quint, *J* = 6.6 Hz, 1H), 5.70 (d, *J* = 7.2 Hz, 1H), 7.40 (m, 10 H). ^{13}C NMR (300 MHz, $CDCl_3$) δ: 0.4, 14.4, 15.0, 16.1, 23.0, 26.2, 29.7, 29.8, 29.9 (2), 30.0, 31.4, 32.2, 39.0, 39.4, 55.0, 70.8, 76.9, 78.8, 88.1, 105.6, 125.9 (2), 127.7, 128.1, 128.6, 129.0, 133.8, 139.0, 152.8, 176.3.

Oxazolidinone adduct *ent*-34

A solution of *N*-acyloxazolidinone *ent*-**6** (260 mg, 0.92 mmol) in CH_2Cl_2 (10 mL) at 0°C under a nitrogen atmosphere was treated with *i*-Pr_2NEt (0.32 mL, 1.8 mmol) and then with a solution of Bu_2BOTf in CH_2Cl_2 (1.0 M, 1.85 mL, 1.8 mmol). The solution was stirred for 20 min, after which time additional a solution of Bu_2BOTf in CH_2Cl_2 (1.0 M, 0.92 mL, 0.92 mmol) was added. A solution of cobalt complexed derivative *S*-**18** (650 mg, 0.92 mmol) in CH_2Cl_2 (10 mL) was added to the solution above at –78°C. When addition was complete, the resulting mixture was allowed to warm to rt to 0°C and then at rt for 20 min. A pH 7 buffered solution (30 mL) was subsequently added and layers separated. Aqueous layer was further extracted with CH_2Cl_2 (3 × 40 mL) and the combined organic extracts were

© 2001 NRC Canada

dried over anhydrous $MgSO_4$, filtered, and concentrated under reduced pressure. The residue was passed through a column of silica gel to remove excess *N*-acyloxazolidinone (eluent: 5% EtOAc–hexanes) to afford 675 mg (90%) of the cobalt complex product.

A solution of the above cobalt complex product (670 mg, 0.82 mmol) in acetone (30 mL) at rt was treated with CAN (1.14 g, 2.1 mmol). Additional CAN (570 mg, 1.0 mmol) was used and the solvent was removed under reduced pressure. The resulting residue was treated with H_2O (50 mL) and Et_2O (50 mL), and layers were separated. Aqueous layer was further extracted with Et_2O (3 × 75 mL). The combined organic extracts were dried over anhydrous $MgSO_4$, filtered and concentrated under reduced pressure. The residue was purified by preparative chromatography (eluent: 5% EtOAc–hexanes) to afford 400 mg (93%) of *ent*-**34** as a single diastereomer: $[\alpha]_D^{26}$ –70.3 (*c* 8.6, MeOH). R_f = 0.24 (5% EtOAc–hex). IR (CH_2Cl_2) (cm^{-1}): 3030, 2933, 2860, 2170, 1783, 1703, 1480, 1456, 1385, 1250, 1218, 1107, 1043, 999, 948, 844, 759, 699. ^{1}H NMR (300 MHz, $CDCl_3$) δ: 0.16 (s, 9H), 0.92 (t, *J* = 6.6 Hz, 3H), 1.18 (d, *J* = 6.6 Hz, 3H), 1.29–1.85 (m, 20H), 2.98 (dd, *J* = 3.3, 9.3 Hz, 1H), 3.61 (td, *J* = 3.3, 6.6 Hz, 1H), 4.01 (m, 1H), 4.24 (m, 1H), 4.37 (m, 2H), 4.56 (d, *J* = 11.7 Hz, 1H), 4.72 (d, *J* = 11.7 Hz, 1H), 7.37 (m, 5H).

Alkyne acid derivative 19

A solution of **34** (500 mg, 0.81 mmol) in THF:DMF:H_2O (1.5:1.5:2.0 mL) at 0°C was treated with 30% H_2O_2 (0.83 mL, 8.1 mmol) and then with $LiOH{\cdot}H_2O$ (170 mg, 4.0 mmol). The mixture was allowed to warm to rt and stirred overnight. The mixture was treated with a sodium sulfite solution (20 mL, 1.5 N) at 0°C. The reaction was allowed to warm to rt and stirred for an additional 1 h, and was quenched with 6 mL saturated $NaHCO_3$. THF was removed under reduced pressure. The aqueous residue was washed with CH_2Cl_2 (3 × 20 mL) and acidified to pH 3 with conc HCl followed by 5.0 N HCl solution. The resulting mixture was extracted with EtOAc (6 × 30 mL) and the combined organic extracts were dried over anhydrous $MgSO_4$, filtered, and concentrated under reduced pressure. The resulting residue was purified by flash chromatography (eluent: 20% EtOAc–hexanes + 0.2% AcOH) to give 260 mg (85%) of the corresponding acetylenic acid derivative **137**: $[\alpha]_D^{26}$ +7.3 (*c* 7.8, MeOH). R_f = 0.20 (20% EtOAc–hex + 0.2% AcOH). CI-HRMS calcd. for $C_{25}H_{38}O_3$ ($[M + H]^+$): 387.2899; found: 387.2893. IR (CH_2Cl_2) (cm^{-1}): 3310, 3030, 2924, 2853, 2200, 1711, 1456, 1260, 1072, 733, 697, 643. ^{1}H NMR (300 MHz, $CDCl_3$) δ: 0.92 (t, *J* = 7.2 Hz, 3H), 1.18 (d, *J* = 6.6 Hz, 1H), 1.30–1.44 (m, 18H), 1.81 (m, 2H), 2.22 (d, *J* = 2.4 Hz, 1H), 2.81 (m, 2H), 3.56 (m, 1H), 4.56 (d, *J* = 12.0 Hz, 1H), 4.74 (d, *J* = 12.0 Hz, 1H), 7.35 (m, 5H). ^{13}C NMR (300 MHz, $CDCl_3$) δ: 14.4, 15.8, 23.0, 25.9, 29.6, 29.8, 29.9 (3), 30.0, 31.6, 32.2, 38.9, 41.9, 71.6, 72.5, 76.9, 82.1, 128.0, 128.3, 128.7, 138.4, 181.1.

Alkyne acid derivative *ent*-19

A solution of *ent*-**34** (380 mg, 0.72 mmol) in THF:DMF:H_2O (10:10:3.3 mL) at 0°C was treated with 30% H_2O_2 (0.7 mL, 7.2 mmol) and then with $LiOH{\cdot}H_2O$ (150 mg, 3.6 mmol). The mixture was allowed to warm to rt and stirred for 2 d. The mixture was treated with a sodium sulfite solution (15 mL, 1.5 N) at 0°C. The reaction was allowed to warm to rt and stirred for an additional 1 h, and was quenched with saturated $NaHCO_3$ (5 mL). THF was removed under reduced pressure. The aqueous residue was washed with CH_2Cl_2 (3 × 15 mL) and acidified to pH 3 with conc HCl followed by 5.0 N HCl solution. The resulting mixture was extracted with EtOAc (6 × 30 mL) and the combined organic extracts were dried over anhydrous $MgSO_4$, filtered, and concentrated under reduced pressure. The residue was purified by flash chromatography (eluent: 20% EtOAc–hexanes + 0.2% AcOH) to give 232 mg (82.7%) of the corresponding acetylenic acid derivative *ent*-**19**: $[\alpha]_D^{26}$ –6.2 (*c* 11.8, MeOH). R_f = 0.23 (20% EtOAc–hex + 0.2% AcOH). CI-HRMS calcd. for $C_{25}H_{38}O_3$ ($[M + H]^+$): 387.2899; found: 387.2893. IR (CH_2Cl_2) (cm^{-1}): 3308, 3030, 2922, 2852, 1700, 1652, 1456, 1284, 1069, 733, 696, 668, 641. ^{1}H NMR (300 MHz, $CDCl_3$) δ: 0.92 (t, *J* = 6.6 Hz, 3H), 1.17 (d, *J* = 6.9 Hz, 1H), 1.31–1.45 (m, 18H), 1.82 (m, 2H), 2.21 (d, *J* = 2.4 Hz, 1H), 2.83 (m, 2H), 3.57 (m, 1H), 4.56 (d, *J* = 12.0 Hz, 1H), 4.72 (d, *J* = 12.0 Hz, 1H), 7.38 (m, 5H). ^{13}C NMR (300 MHz, $CDCl_3$) δ: 14.4, 15.8, 23.0, 25.9, 29.7, 29.8, 29.9 (2), 30.0 (2), 32.2, 38.9, 41.9, 71.6, 76.9, 82.1, 128.0, 128.2, 128.3, 128.6, 128.7, 138.4, 181.3.

4-(*S*)-Ethynyl-3-(*S*)-methyl-5-(*R*)-undecyloxolan-2-one (20)

A solution of alkyne acid **19** (210 mg, 0.54 mmol) in CH_2Cl_2 (20 mL) at rt under a nitrogen atmosphere was treated with P_4S_{10} (500 mg, 1.1 mmol) and stirred for 24 h. The mixture was filtered and washed with CH_2Cl_2 (20 mL), and the filtrate was concentrated under reduced pressure. The residue was purified by flash chromatography (eluent: 10% EtOAc–hexanes) to afford 135 mg (90%) of 4-(*S*)-ethynyl-3-(*S*)-methyl-5-(*R*)-undecyloxolan-2-one (**20**): $[\alpha]_D^{26}$ +133.4 (*c* 10.7, MeOH). R_f = 0.66 (30% EtOAc–hex). IR (CH_2Cl_2) (cm^{-1}): 2924, 2854, 2120, 1779, 1456, 1379, 1180, 1128, 998, 962, 854, 641. ^{1}H NMR (300 MHz, $CDCl_3$) δ: 0.92 (t, *J* = 6.9 Hz, 3H), 1.28–1.51 (m, 16H), 1.40 (d, *J* = 6.5 Hz, 3H), 1.82 (m, 2H), 1.99 (m, 2H), 2.34 (d, *J* = 2.7 Hz, 1H), 2.85 (m, 1H), 3.37 (m, 1H), 4.30 (m, 1H). ^{13}C NMR (300 MHz, $CDCl_3$) δ: 11.5, 14.4, 23.0, 25.5, 29.6 (2), 29.7, 29.8, 29.9, 31.7, 32.2, 38.5, 40.1, 76.6, 76.9, 79.7, 111.6, 177.6. Anal. calcd. for $C_{18}H_{30}O_2$: C 77.65, H 10.86; found: C 77.76, H 10.93.

4-(*R*)-Ethynyl-3-(*R*)-methyl-5-(*S*)-undecyloxolan-2-one (*ent*-20)

A solution of acetylenic acid *ent*-**19** (190 mg, 0.49 mmol) in CH_2Cl_2 (25 mL) at rt under a nitrogen atmosphere was treated with P_4S_{10} (550 mg, 1.2 mmol) and stirred for 24 h. The mixture was filtered and washed with CH_2Cl_2 (100 mL), and the filtrate was concentrated under reduced pressure. The residue was purified by flash chromatography (eluent: 10% EtOAc–hexanes) to afford 118 mg (84%) of 4-(*R*)-ethynyl-3-(*R*)-methyl-5-(*S*)-undecyloxolan-2-one (*ent*-**20**): $[\alpha]_D^{26}$ –129.7 (*c* 13.9, MeOH). R_f = 0.66 (30% EtOAc–hex). IR (CH_2Cl_2) (cm^{-1}): 2917, 2848, 2112, 1758, 1463, 1395, 1360, 1327, 1189, 1000, 957, 770, 702, 623. ^{1}H NMR (300 MHz, $CDCl_3$) δ: 0.91 (t, *J* = 6.6 Hz, 3H), 1.28–1.52 (m, 16H), 1.40 (d, *J* = 6.3 Hz, 3H), 1.83 (m, 2H), 1.99 (m, 2H), 2.34 (d, *J* = 2.4 Hz, 1H), 2.85 (m, 1H), 3.38 (m, 1H), 4.32 (m, 1H).

© 2001 NRC Canada

Anal. calcd. for $C_{18}H_{30}O_2$: C 77.65, H 10.86; found: C 77.81, H 10.87.

4-(*S*)-Methyl-5-oxo-2-(*R*)-undecyloxolane-3-(*R*)-carboxylic acid (35)

A solution of 4-(*S*)-ethynyl-3-(*S*)-methyl-5-(*R*)-undecyloxolan-2-one (**20**) (54 mg, 0.19 mmol) in a solvent system of CCl_4:CH_3CN:H_2O (4.3:4.3:6.4 mL) at 0°C was treated with $NaIO_4$ (580 mg, 2.72 mmol). The mixture was treated with $RuCl_3 \cdot H_2O$ (2.4 mg, 0.01 mmol) at 0°C and was allowed to warm to rt for 2 h. H_2O (10 mL) and Et_2O (10 mL) were added, respectively, and layers were separated. The aqueous layer was further extracted with Et_2O (3 × 15 mL). The combined organic extracts were dried over anhydrous $MgSO_4$, filtered, and concentrated under reduced pressure to afford a white solid material. Recrystallization (1:2 Et_2O–hexanes) of the white solid material afforded 53.3 mg (92%) 4-(*S*)-methyl-5-oxo-2-(*R*)-undecyloxolane-3-(*R*)-carboxylic acid (**35**): mp 103–105°C. $[\alpha]_D^{26}$ +80.7 (*c* 8.9, MeOH). R_f = 0.60 (40% EtOAc–hex + 0.4% AcOH). CI-HRMS calcd. for $C_{17}H_{30}O_4$ ($[M + H]^+$): 299.2222; found: 299.2221. IR (CH_2Cl_2) (cm^{-1}): 3375, 3031, 2919, 2869, 1766, 1695, 1456, 1241, 1185, 1002, 966. ^{1}H NMR (300 MHz, $CDCl_3$) δ: 0.92 (t, *J* = 6.9 Hz, 3H), 1.35 (d, *J* = 6.9 Hz, 3H), 1.29–1.65 (m, 16H), 1.70 (m, 2H), 1.90 (m, 2H), 2.99 (quint, *J* = 7.2 Hz, 1H), 3.37 (m, 1H), 4.47 (m, 1H). ^{13}C NMR (300 MHz, $CDCl_3$) δ: 10.6, 14.4, 23.0, 26.2, 29.5, 29.6, 29.7, 29.8, 29.9 (2), 31.2, 32.2, 39.4, 50.5, 79.1, 174.8, 177.1.

4-(*R*)-Methyl-5-oxo-2-(*S*)-undecyloxolane-3-(*S*)-carboxylic acid (*ent*-35)

A solution of 4-(*R*)-ethynyl-3-(*R*)-methyl-5-(*S*)-undecyloxolan-2-one (*ent*-**20**) (60 mg, 0.21 mmol) in a solvent system of CCl_4:CH_3CN:H_2O (5.7:5.7:8.6 mL) at 0°C was treated with $NaIO_4$ (630 mg, 3.0 mmol). The mixture was treated with $RuCl_3 \cdot H_2O$ (2.7 mg, 0.01 mmol) at 0°C and was allowed to warm to rt and stirred for 2 h. H_2O (15 mL) and Et_2O (10 mL) were added, respectively, and layers were separated. The aqueous layer was further extracted with Et_2O (3 × 20 mL). The combined organic extracts were dried over anhydrous $MgSO_4$, filtered, and concentrated under reduced pressure to afford a white solid material. Recrystallization (Et_2O–hexanes, 1:2) of the white solid material afforded 55.3 mg (86%) 4-(*R*)-methyl-5-oxo-2-(*S*)-undecyloxolane-3-(*S*)-carboxylic acid (*ent*-**35**): mp 100–102°C. $[\alpha]_D^{26}$ –75.5 (*c* 7.1, MeOH). R_f = 0.58 (40% EtOAc–hex + 0.4% AcOH). CI-HRMS calcd. for $C_{17}H_{30}O_4$ ($[M + H]^+$): 299.2222; found: 299.2222. IR (CH_2Cl_2) (cm^{-1}): 3300, 3034, 2919, 2850, 1750, 1698, 1456, 1240, 1187, 1002, 966, 909, 872, 781, 733, 668, 596. ^{1}H NMR (300 MHz, $CDCl_3$) δ: 0.92 (t, *J* = 7.2 Hz, 3H), 1.35 (d, *J* = 6.9 Hz, 3H), 1.29–1.64 (m, 16H), 1.69 (m, 2H), 1.87 (m, 2H), 2.97 (m, 1H), 3.30 (m, 1H), 4.38 (m, 1H). ^{13}C NMR (300 MHz, $CDCl_3$) δ: 10.6, 14.4, 23.0, 26.1, 29.5, 29.6, 29.7, 29.8, 29.9, 30.0 (2), 31.2, 32.2, 39.4, 50.5, 79.1, 174.5, 177.1.

(+)-Nephrosteranic acid (16)

A solution of 4-(*S*)-methyl-5-oxo-2-(*R*)-undecyloxolane-3-(*R*)-carboxylic acid (**35**) (30 mg, 0.10 mmol) in toluene (5 mL) under a nitrogen atmosphere at 0°C was treated with DBU (0.16 mL, 1.01 mmol). The solution was heated at reflux for 3 days. Toluene was removed under reduced pressure. The residue was purified by flash chromatography (eluent: 10% EtOAc–hexanes + 0.1% AcOH) to give 25.8 mg (86%) of (+)-nephrosteranic acid (**16**): mp 95–97°C. $[\alpha]_D^{26}$ +27.0 (*c* 1.2, $CHCl_3$). R_f = 0.72 (40% EtOAc–hex + 0.4% AcOH). CI-HRMS calcd. for $C_{17}H_{30}O_4$ ($[M + H]^+$): 299.2222; found: 299.2217. IR (CH_2Cl_2) (cm^{-1}): 3300, 2953, 2917, 2870, 1747, 1717, 1257, 1200, 1172, 697, 673. ^{1}H NMR (300 MHz, $CDCl_3$) δ: 0.92 (t, *J* = 6.8 Hz, 3H), 1.40 (d, *J* = 7.1 Hz, 3H), 1.28–1.92 (m, 20H), 2.74 (m, 1H), 3.02 (m, 1H), 4.51 (m, 1H). ^{13}C NMR (300 MHz, $CDCl_3$) δ: 14.9, 23.4, 26.1, 30.0, 30.1 (2), 30.3, 30.4 (2), 30.5, 32.7, 35.7, 40.6, 54.5, 80.0, 176.2, 177.3.

(–)-Nephrosteranic acid (*ent*-16)

A solution of 4-(*R*)-methyl-5-oxo-2-(*S*)-undecyloxolane-3-(*R*)-carboxylic acid (*ent*-**35**) (28 mg, 0.09 mmol) in toluene (5 mL) under a nitrogen atmosphere at 0°C was added DBU (0.07 mL, 0.47 mmol). The solution was heated at reflux for 3 days. Toluene was removed under reduced pressure. The residue was purified by flash chromatography (eluent: 10% EtOAc–hexanes + 0.1% AcOH) to give 23.8 mg (85%) of (–)-nephrosteranic acid (*ent*-**16**): mp 96–98°C. $[\alpha]_D^{26}$ –27.6 (*c* 1.5, $CHCl_3$). R_f = 0.72 (40% EtOAc–hex + 0.4% AcOH). CI-HRMS calcd. for $C_{17}H_{30}O_4$ ($[M + H]^+$): 299.2222; found: 299.2227. IR (CH_2Cl_2) (cm^{-1}): 3300, 3031, 2953, 2917, 2850, 1747, 1470, 1316, 1257, 1200, 1172, 697. ^{1}H NMR (300 MHz, $CDCl_3$) δ: 0.92 (t, *J* = 6.8 Hz, 3H), 1.41 (d, *J* = 7.2 Hz, 3H), 1.28–1.91 (m, 20H), 2.74 (m, 1H), 3.05 (m, 1H), 4.51 (m, 1H). ^{13}C NMR (300 MHz, $CDCl_3$) δ: 14.8, 23.0, 25.6, 29.5, 29.6, 29.7, 29.8, 29.9, 30.0, 32.2, 40.1, 54.0, 76.9, 79.6, 175.5, 176.8.

Acknowledgment

Financial support of this work by the National Science Foundation, Grant No. CHE-9424476, is gratefully acknowledged.

References

1. (*a*) R.F. Lockwood and K.M. Nicholas. Tetrahedron Lett. **18**, 4163 (1977); (*b*) K.M. Nicholas, M.O. Nestle, and D. Deyferth. Transition metal organometallics. Vol. 2. *Edited by* Halper. Academic Press, New York. 1978. p. 1; (*c*) S.L. Schreiber, T. Sammakia, and W.E. Crowe. J. Am. Chem. Soc. **108**, 3128 (1986); (*d*) K.M. Nicholas, M. Mulvaney, and M. Bayer. J. Am. Chem. Soc. **102**, 2508 (1980); (*e*) H.D. Hodes and K.M. Nicholas. Tetrahedron Lett. **19**, 4349 (1978); (*f*) A.F. Bramwell, L. Crombie, and M.H. Knight. Chem. Ind. (London), 1265 (1965), and refs. cited therein; (*g*) M. Saha, B. Bogby, and K.M. Nicholas. Tetrahedron Lett. **27**, 915 (1986); (*h*) S.L. Schreiber, M.T. Klimas, and T. Sammakia. J. Am. Chem. Soc. **109**, 5749 (1987).
2. (*a*) P.A. Jacobi and D. Pippin. Org. Lett. **3**, 827 (2001), and refs. cited therein; (*b*) P.A. Jacobi, S. Murphree, F. Rupprecht, and W. Zheng. J. Org. Chem. **61**, 2413 (1996); (*c*) P.A. Jacobi and P. Herradura. Tetrahedron Lett. **38**, 6621 (1997); (*d*) P.A. Jacobi and P. Herradura. Tetrahedron Lett. **37**, 8297 (1996).
3. (*a*) S. Huneck, K. Schreiber, G. Holfle, and G. Snatzke. J. Hattori Bot. Lab. **45**, 1 (1979); (*b*) Y. Asahina and M. Yanagita. Ber. Dtsch. Chem. Ges. **70**, 227 (1937); (*c*) B.K. Park, M. Nakagawa, M. Hirota, and M. Nakayama. J. Antibiot.

© 2001 NRC Canada

41, 751 (1988); (*d*) M.M. Murta, M.B.M. de Azevedo, and A.E. Greene. J. Org. Chem. **58**, 7537 (1993).
4. Synthesis of (–)-**16**: (*a*) M. P. Sibi and J. Ji. Angew. Chem., Int. Ed. Engl. **36**, 274 (1997); synthesis of (+)-**16**: (*b*) H. Takahata, Y. Uchida, and T. Momose. J. Org. Chem. **60**, 5628 (1995).
5. Z. Zhang and X. Lu. Tetrahedron: Asymmetry, **7**, 1923 (1996); also see ref. 2*b*.
6. (*a*) E.J. Corey, J.O. Link, and Y. Shao. Tetrahedron Lett. **33**, 3435 (1992); (*b*) E.J. Corey and J.O. Link. Tetrahedron Lett. **33**, 3431 (1992).
7. D.A. Evans, M.M. Morrissey, and R.L. Dorow. J. Am. Chem. Soc. **107**, 4346 (1985).
8. F.M. Hauser, M.L. Coleman, R.C. Huffman, and F.I. Carroll. J. Org. Chem. **39**, 3426 (1974).
9. D.A. Evans, T.C. Britton, and J.A. Ellman. Tetrahedron Lett. **28**, 6141 (1987).

© 2001 NRC Canada

Synthesis of substituted phenols by directed *ortho*-lithiation of in situ *N*-silyl-protected *O*-aryl *N*-monoalkylcarbamates

Matthias Kauch and Dieter Hoppe

Abstract: A simple, high-yield procedure has been developed for the *ortho*-lithiation and subsequent *ortho*-substitution of phenols by a manifold of electrophiles. *N*,*C*-Dilithiation of *O*-aryl *N*-monoalkylcarbamates proved to be impossible due to a cleavage reaction of the monolithiated intermediates. However, in situ *N*-silylation of *O*-aryl *N*-isopropylcarbamates proceeds smoothly with trialkylsilyl triflates – *N*,*N*,*N*′,*N*′-tetramethylethylenediamine (TMEDA). Separation of the formed *O*-aryl *N*-isopropyl-*N*-trialkylsilylcarbamates from the byproduct TMEDA·HOTf, which is insoluble in diethyl ether or toluene, is not required. *ortho*-Lithiation with *n*-butyllithium–TMEDA at –78°C leads to the corresponding aryllithium, which does not undergo anionic *ortho*-Fries rearrangement under the reaction conditions, but is efficiently substituted by electrophilic reagents. During the aqueous work-up, the *N*-silyl group is removed and the corresponding *ortho*-substituted *O*-aryl *N*-isopropylcarbamate is isolated. Among the introduced electrophiles are: Me_3Si, Bu_3Sn, PhS, I, Br, Cl, alkyl, α-hydroxyalkyl. Liberation of the free phenols is performed under mild alkaline conditions.

Key words: directed *ortho*-metalation, *ortho*-lithiated *O*-aryl carbamates, *ortho*-substituted phenols, in situ protection of *N*-monoalkylcarbamates.

Résumé : On a mis au point une méthode simple qui permet d'effectuer avec des rendements élevés l'*ortho*-lithiation et l'*ortho*-substitution subséquente de phénols par un grand nombre d'électrophiles. Les *N*,*C*-dilithiations d'*O*-aryl *N*-monoalkylcarbamates s'avèrent impossibles en raison de la réaction de clivage des intermédiaires monolithiés. Toutefois, la *N*-silylation in situ des *O*-aryl *N*-isopropylcarbamates peut être réalisée facilement avec les couples triflates de trialkylsilyle – *N*,*N*,*N*′,*N*′-tétraméthyléthylènediamine (TMEDA). Il n'est pas nécessaire de séparer les *O*-aryl *N*-isopropyl-*N*-trialkylsilylcarbamates des sous-produits, TMEDA·HOTf qui sont insolubles dans l'éther éthylique ou le toluène. L'*ortho*-lithiation avec du *n*-butyllithium–TMEDA, à –78°C, conduit à la formation de l'aryllithien correspondant, qui ne donne pas lieu à un réarrangement d'*ortho*-Fries anionique dans les conditions de la réaction mais qui donne lieu à des réactions de substitution sous l'influence de réactifs électrophiles. Lors de la procédure d'extraction, le groupe *N*-silyle est éliminé et on peut isoler le *O*-aryl *N*-isopropylcarbamate *ortho*-substitué. Les électrophiles qui ont été introduits sont: Me_3Si, Bu_3Sn, PhS, I, Br, Cl, alkyle, α-hydroxyalkyle. La libération des phénols se fait dans des conditions alcalines douces.

Mots clés : *ortho*-métallation orientée, *O*-aryl carbamates *ortho*-lithiés, phénols *ortho*-substitués, protection in situ de *N*-monoalkylcarbamates.

[Traduit par la Rédaction]

Introduction

Within the last two decades, the directed *ortho*-metalation (DoM) reaction turned out as an important and powerful tool for the construction of polysubstituted aromatics (for reviews see ref. 1*a*–*c*; for a short summary of recent developments in the Snieckus group see ref. 1*d*; for a critical view on DoM and its mechanisms see ref. 2). This strategy supersedes the classical aromatic electrophilic substitution reactions with reference to milder reaction conditions, control of regioselectivity, and the range of functional groups which can be introduced. New applications of DoM chemistry also include the substitution of aromatic ligands of metal complexes leading to planar chiral ferrocenes (3) or arene tricarbonylchromium complexes (for recent work in this field see ref. 4) if chiral bases are employed.

The tertiary carbamoyloxy group has proven to be one of the most powerful directed metalation groups (DMGs). The

Received March 7, 2001. Published on the NRC Research Press Web site at http://canjchem.nrc.ca on November 14, 2001.

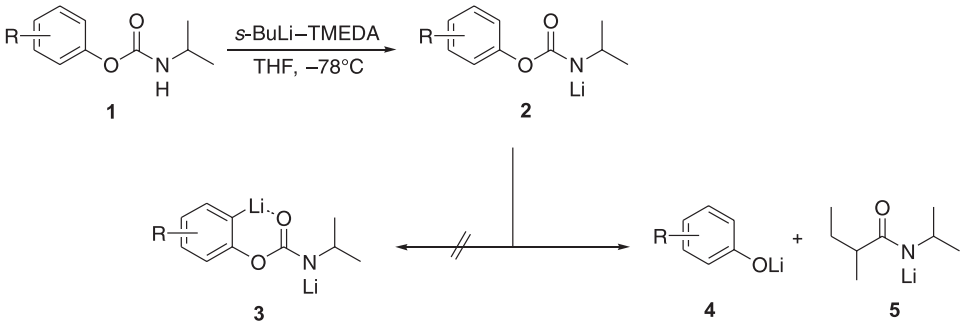
This paper is dedicated with friendship and admiration to Professor Victor Snieckus in recognition of his significant contributions to carbanion chemistry.

M. Kauch and D. Hoppe.[1] Organisch-Chemisches Institut, Westfälische Wilhelms-Universität Münster, Corrensstrasse 40, D-48149 Münster, Germany.

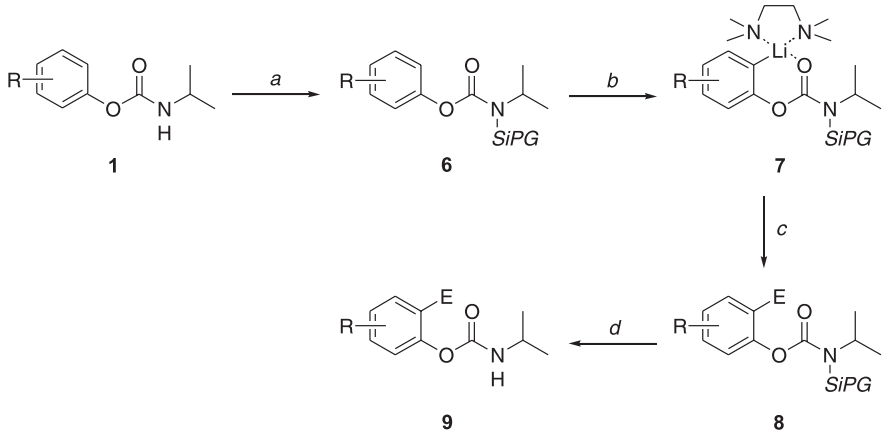
[1]Corresponding author (telephone: +(251)8333211; fax: +(251)8339772; e-mail: dhoppe@uni-muenster.de).

 DOI: 10.1139/cjc-79-11-1736 © 2001 NRC Canada

Scheme 1.



Scheme 2. *SiPG* = TMS, TBDMS, or TIPS. The following standard conditions and reagents are used unless otherwise specified: (*a*) 1.05 to 1.10 equiv of TMSOTf (solution in pentane), TMEDA, Et_2O, 0°C → rt, 0.5 h; (*b*) 2.0 equiv of *n*- or *s*-BuLi – TMEDA, –78°C, 1 h; (*c*) 2.5 to 3.5 equiv of EX, –78°C, 1 to 2 h; (*d*) MeOH, 2 M HCl, –78°C → rt.



N,*N*-diisopropylcarbamoyl and the *N*,*N*-diethylcarbamoyl group were employed for the directed α-lithiation of allylic and benzylic alcohols (for *O*-allyl carbamates see refs. 5*a* and 5*b*; for *O*-benzyl carbamates see ref. 5*c*). The *N*,*N*-diethylcarbamoyloxy group was extensively used by Snieckus for DoM reactions of aromatic compounds (6). A disadvantage of both DMGs is that for deprotection vigorous conditions have to be used. Only reductive methods with lithium aluminium hydride, diisobutylaluminium hydride, or strong basic conditions lead to carbamate ester cleavage, causing problems with sensitive groups. The strength of this group lies in its capability of undergoing anionic *ortho*-Fries rearrangements (1*a*, 6; for recent applications of further O → C carbamoyl transfer reactions in natural product synthesis see ref. 7).

Very recently, the *N*-cumyl-*N*-methylcarbamoyl group, offering hydrolytic lability for a two-step cleavage, was established by Snieckus and co-workers (8). Decumylation with trifluoroacetic acid and subsequent hydrolytic deprotection with bases proceed under mild conditions.

In our group, several carbamoyl residues had been developed for directed lithiation reactions of *O*-alkyl, *O*-allyl, and *O*-benzyl carbamates and their *S*-analogues which are easier to remove than the original *N*,*N*-diisopropylcarbamoyl group (9). *N*-Monoalkylcarbamoyl groups were first used for the generation of *N*,*C*-dilithiated intermediates from *O*-allyl (10) and recently *S*-allyl compounds (11). In our attempt, employing the *N*-isopropylcarbamoyl group for phenol activation, we found that the corresponding *O*-aryl carbamates **1** could not be converted to the dianionic species **3**. The intermediate *N*-lithiated carbamates **2** undergo a cleavage reaction to phenolates **4** and isocyanate, followed by an irreversible addition of the alkyllithium base to the intermediate isocyanate to give the *N*-lithiocarboxamide **5** (Scheme 1).

Herein we report on the simple solution of the problem. *O*-Aryl *N*-monoalkylcarbamates **1** can be in situ transformed into *N*-alkyl *N*-silyl derivatives **6** (12) which are stable substrates for the directed *ortho*-lithiation reaction. The lithiated carbamates **7** react with a broad range of electrophilic reagents to the *ortho*-substituted protected phenols **8** in which the *N*-silyl group is completely removed during aqueous work-up. Subsequently, the carbamoyl residue can easily be removed by mild basic hydrolysis to furnish the free phenols.

Results and discussion

The *O*-aryl *N*-isopropylcarbamates **10a**, **10b**, **10c**, and **15** were easily prepared by addition of the corresponding phenols onto isopropyl isocyanate (THF, DMAP, 60°C) and were isolated as crystalline solids in high yields.

The following standard protocol was employed for directed *ortho*-lithiation reactions (Scheme 2): The *O*-aryl carbamates **1** were *N*-silyl protected by means of trimethylsilyl triflate in the presence of TMEDA. The resulting *N*-silyl intermediates **6** (*SiPG* = TMS) were lithiated with *n*- or *s*-BuLi–TMEDA in diethyl ether at –78°C. The following

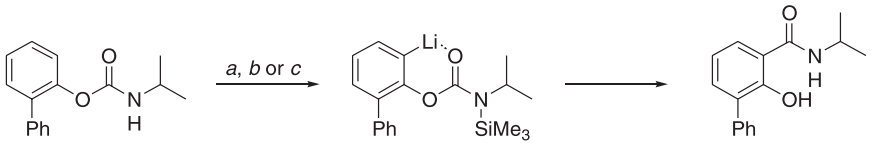
© 2001 NRC Canada

Table 1. Results of *ortho*-trimethylsilylations of *O*-2-biphenylyl carbamate **10a** to form **13aa**.

Entry	Solvent	Protecting reagent	SiPG	Base	Yield (%)[a]
1	Et_2O	TMSOTf	TMS	*s*-BuLi–TMEDA	94
2	Et_2O	TMSOTf	TMS	*n*-BuLi–TMEDA	97
3	Et_2O	TMSOTf	TMS	LDA	0
4	Et_2O	TMSONf	TMS	*n*-BuLi–TMEDA	93
5	Et_2O	TBDMSOTf	TBDMS	*s*-BuLi–TMEDA	93
6	Et_2O	TIPSOTf	TIPS	*n*-BuLi–TMEDA	91
7	Toluene	TMSOTf	TMS	*n*-BuLi–TMEDA	94
8	THF	TMSOTf	TMS	*s*-BuLi–TMEDA	97
9	Et_2O	TMSOTf	TMS	*s*-BuLi–TMEDA[b]	96

[a]No starting material could be recovered, except for the reaction with LDA (entry 3) after which 98% of carbamate **10a** was reisolated.
[b]Reverse addition in the lithiation step: (*i*) 1.5 equiv TMSCl; (*ii*) 1.1 equiv base.

Scheme 3. Conditions and reagents: (*a*) see Scheme 2, *a*; (*b*) 2.2 equiv of *s*-BuLi–TMEDA, –78°C, 1 h, then –78°C → rt, then 2 M HCl; (*c*) 2.5 equiv of LDA, 0°C, 4 h, then 0°C → rt, then 2 M HCl.



10a **11** **12**

reaction with electrophiles and acidic work-up furnished the *ortho*-substituted products **9**.

Voyer and co-workers (12) recently reported on the preparation and characterization, and, as well, deprotonation of *O*-methyl and *O*-*tert*-butyl *N*-silyl-*N*-benzylcarbamates adjacent to the nitrogen atom. In this two-step sequence, the *N*-silyl protected amines were isolated before subjection to metalation. X-ray crystallography of one compound proved the *N*-silyl group (12*c*). Therefore, we strongly suggest that silyl protection of secondary *O*-aryl carbamates occurs, as well, at the carbamoyl nitrogen atom.

To investigate suitable conditions for the protection and deprotonation step, several reagents were used for *ortho*-trimethylsilylation of the 2-biphenylyl carbamate **10a** with TMSCl as electrophile (Table 1). Consecutive lithiation with *n*- or *s*-BuLi in diethyl ether at –78°C, electrophilic quench, and hydrolysis afforded the substitution product **13aa** in excellent yields (entries 1 and 2) whereas deprotonation with LDA (entry 3) did not occur. Several silyl sources can be employed in the *N*-protection step. The use of TMS nonaflate (entry 4), TBDMS triflate, or even the bulkier TIPS triflate (entries 5 and 6) did not affect the yields significantly. Although diethyl ether is employed as standard solvent for the reaction sequence, toluene and THF were used without loss in the yield (entries 7 and 8).

Under our reaction conditions, TMEDA·HOTf separates from the reaction mixture and solidifies on cooling to below –70°C. Although the salt is neutralized only slowly by butyllithium, 2.0 equiv of the alkyllithium were applied for achieving maximum yields.[2]

It is noteable that lithiation and substitution of the *N*,*N*-diethylcarbamoyl-protected phenol require much lower reaction temperatures to avoid the anionic *ortho*-Fries rearrangement (13). No carbamoyl migration product could be detected in reactions under the usual conditions applying *N*-isopropyl-*N*-silylcarbamoyl phenols. Therefore, this DMG may be advantageously used when inter- or intramolecular attack of the carbonyl group must be avoided. Formation of the *ortho*-hydroxy carboxamide **12** was achieved with 63% yield besides 33% of the arylsilane **13aa**, when the solution of the lithiated carbamate **11** was allowed to warm to 0°C (Scheme 3). **12** was also obtained (79%) by stirring the *N*-silyl-protected urethane with 2.5 equiv of lithium diisopropylamide at 0°C to room temperature.

Carbamate **10a** reacted under the above described standard protocol with a variety of electrophilic reagents to give the substituted products **13a** in good to excellent yields (Table 2, Scheme 4). In particular, introduction of heteroatom-based functional groups occurred with high yields (entries 1–6). Only ethylation, allylation (entries 8 and 9) or, in some cases, the reaction with ketones bearing acidic α-hydrogen atoms (entries 14 and 16) gave somewhat lower yields, but these still remained above 60%.

Comparable high yields were achieved with the unsubstituted *O*-phenyl carbamate **10b** and the 2-chloro-functionalized substrate **10c** (Table 2, entries 17–21 and 22–29). In the second case, *n*-BuLi–TMEDA could be advantageously used to give a cleaner lithiation rather than *s*-BuLi–TMEDA (entries 22 and 23). The *O*-1-naphthyl carbamate **15** gave the same results concerning the yields of DoM-substitution sequences (entries 30–34, Scheme 5). In

[2]Using 1.1 equiv of *s*-BuLi after addition of 1.5 equiv TMSC1 (Table 1, entry 9) a yield of 96% of **13aa** was isolated. This result demonstrates that the *C*-deprotonation is much more rapid than deprotonation of the solid ammonium triflate.

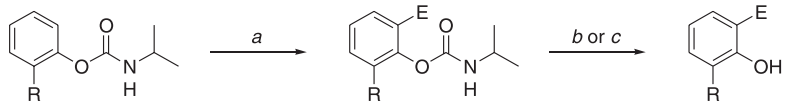
© 2001 NRC Canada

Table 2. Synthesis of *ortho*-substituted carbamates **13** and **16**.

Entry	Substrate	Conditions[a]	R	EX	E	Product	Yield (%)
1	**10a**	B	Ph	TMSCl	TMS	**13aa**	97
2	**10a**	A	Ph	Bu_3SnCl	$SnBu_3$	**13ab**	86
3	**10a**	B	Ph	I_2	I	**13ac**	88
4	**10a**	B	Ph	$BrCH_2CH_2Br$	Br	**13ad**	91
5	**10a**	B	Ph	C_2Cl_6	Cl	**13ae**	93
6	**10a**	B	Ph	$(PhS)_2$	SPh	**13af**	94
7	**10a**	A	Ph	MeI	Me	**13ag**	83
8	**10a**	A	Ph	EtI	Et	**13ah**	68
9	**10a**	A	Ph	$CH_2=CHCH_2Br$	$CH_2CH=CH_2$	**13ai**	63
10	**10a**	A	Ph	BnBr	Bn	**13aj**	74
11	**10a**	A	Ph	PhCHO	CH(OH)Ph	**13ak**	87
12	**10a**	B	Ph	*i*-Pr-CHO	CH(OH)-*i*-Pr	**13al**	85
13	**10a**	B	Ph	Ph_2CO	$C(OH)Ph_2$	**13am**	85
14	**10a**	B	Ph	PhMeCO	C(OH)PhMe	**13an**	70
15	**10a**	B	Ph	Me_2CO	$C(OH)Me_2$	**13ao**	81
16	**10a**	B	Ph	$(CH_2)_5CO$	$C(OH)(CH_2)_5$	**13ap**	64
17	**10b**	B	H	TMSCl	TMS	**13ba**	82
18	**10b**	A	H	Bu_3SnCl	$SnBu_3$	**13bb**	85
19	**10b**	A	H	MeI	Me	**13bc**	83
20	**10b**	A	H	PhCHO	CH(OH)Ph	**13bd**	81
21	**10b**	B	H	Ph_2CO	$C(OH)Ph_2$	**13be**	84
22	**10c**	A	Cl	TMSCl	TMS	**13ca**	82
23	**10c**	B	Cl	TMSCl	TMS	**13ca**	91
24	**10c**	B	Cl	Bu_3SnCl	$SnBu_3$	**13cb**	87
25	**10c**	B	Cl	I_2	I	**13cc**	86
26	**10c**	B	Cl	$(PhS)_2$	SPh	**13cd**	86
27	**10c**	B	Cl	MeI	Me	**13ce**	90
28	**10c**	B	Cl	PhCHO	CH(OH)Ph	**13cf**	84
29	**10c**	B	Cl	Ph_2CO	$C(OH)Ph_2$	**13cg**	82
30	**15**	A	—	TMSCl	TMS	**16a**	91
31	**15**	A	—	Bu_3SnCl	$SnBu_3$	**16b**	85
32	**15**	A	—	MeI	Me	**16c**	86
33	**15**	A	—	PhCHO	CH(OH)Ph	**16d**	83
34	**15**	B	—	Ph_2CO	$C(OH)Ph_2$	**16e**	87

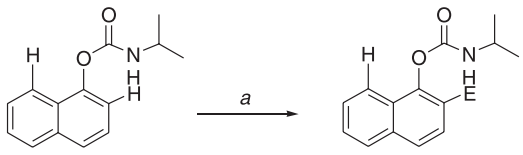
[a]Method A: *s*-BuLi–TMEDA conditions. Method B: *n*-BuLi–TMEDA conditions.

Scheme 4. Conditions and reagents: (*a*) see Scheme 2, *a–d*; (*b*) 4.0 equiv of 2 M NaOH, EtOH, rt, 2 h; or (*c*) 10.0 equiv of K_2CO_3, EtOH, rt, 12 h.



10 **13** **14**

Scheme 5. Conditions and reagents: (*a*) see Scheme 2, *a–d*.



15 **16**

accordance with observations of Snieckus with the *N*,*N*-diethylcarbamate, lithiation of **15** proceeded exclusively at the 2-position (1*a*, 6). No product resulting from lithiation in the *peri*-position could be detected.

Two procedures, using mild bases, have been established for the deprotection of the *ortho*-substituted products (Scheme 4, **13** → **14**). Treatment of several carbamates **13a** and **13c** with 2 M NaOH in ethanol at room temperature afforded phenols **14a** and **14c** in excellent to quantitative yields within 2 h (Table 3). Even substrates **13aa** and **13ca** bearing a base-sensitive TMS group could be deprotected without desilylation (entries 1 and 7). The *o*-iodoaryl carbamates **13ac** and **13cc** reacted smoothly to yield iodophenols **14ab** and **14cb** with complete retention of the iodine substituent as well (entries 3 and 8). The

© 2001 NRC Canada

Table 3. Deblocking the carbamates **13a** and **13c** to form the free phenols **14a** and **14c**.

Entry	Substrate	Conditions[a]	R	E	Product	Yield (%)
1	**13aa**	A	Ph	TMS	**14aa**	99
2	**13aa**	B	Ph	TMS	**14aa**	98
3	**13ac**	A	Ph	I	**14ab**	98
4	**13ad**	A	Ph	Br	**14ac**	99
5	**13af**	A	Ph	SPh	**14ad**	99
6	**13am**	A	Ph	$C(OH)Ph_2$	**14ae**	96
7	**13ca**	A	Cl	TMS	**14ca**	99
8	**13cc**	A	Cl	I	**14cb**	94
9	**13cd**	A	Cl	SPh	**14cc**	91

[a]Method A: 4.0 equiv of 2 M NaOH, EtOH, rt, 2 h. Method B: 10.0 equiv of K_2CO_3, EtOH, rt, 12 h.

carbamoyl group of the *N*-monoalkylcarbamates can also be removed by stirring with a slurry of potassium carbonate in ethanol at room temparature (entry 2).

Experimental section

General information

All reactions were carried out under Ar in flame-dried glassware. All solvents were purified and dried prior to use: Et_2O and toluene were distilled from sodium benzophenone ketyl. THF was distilled from potassium benzophenone ketyl. Pentane was distilled from CaH_2. *N*,*N*,*N*′,*N*′-Tetramethylethylenediamine (TMEDA) was purchased from Merck, refluxed and distilled from CaH_2 before use. *n*-BuLi (1.6 M in hexane) and *s*-BuLi (1.3 M in cyclohexane–hexane = 92:8) were purchased from Acros. The solution of *s*-BuLi was filtered using Celite® and titrated against phenylacetic acid prior to use. Trimethylsilyl trifluoromethanesulfonate was purchased from Acros.

^1H and ^{13}C NMR spectra were recorded on Bruker ARX 300 or AMX 400 spectrometers in $CDCl_3$ solutions using tetramethylsilane as internal standard. IR spectra were recorded on a Nicolet 5DXC spectrometer. Melting points were obtained on Gallenkamp melting point apparatus MFB-595 and are uncorrected. Microanalyses were performed at the Organisch-Chemisches Institut der WWU Münster with Heraeus CHN-O-Rapid or Elementar Analysensysteme VarioEL III analysers. HRMS were recorded on a Finnigan MAT 8200 mass spectrometer (EI, 70 eV).

Products were purified by flash column chromatography on Merck silica gel 60 (0.040–0.063 mm); PE = light petroleum ether, bp 36–46°C.

General procedure for the preparation of O-*aryl* N-*ispropylcarbamates* ***10*** *and* ***16***

To a cooled (0°C) solution of the phenol and DMAP (0.10 equiv) in dry THF (0.5 mL:1 mmol phenol), isopropyl isocyanate (1.10 equiv) was added. The reaction mixture was stirred at 60°C for 24 h, cooled to rt, and treated with 2 M HCl (1.0 mL:1 mmol phenol). After addition of Et_2O, the aqueous layer was separated, extracted with Et_2O, and the combined organic extracts were washed with saturated $NaHCO_3$ solution, dried over $MgSO_4$, filtered, and concentrated in vacuo. The crude product was purified by flash chromatography on silica gel (Et_2O–PE gradient).

O-*2-Biphenylyl* N-*isopropylcarbamate* ***(10a)****:* 2-Hydroxybiphenyl (5.11 g, 30.0 mmol) was stirred with isopropyl isocyanate (3.24 mL, 33.0 mmol) to afford **10a** (7.60 g, 29.8 mmol, 99%) as a white solid, mp 89°C (Et_2O–PE). IR (KBr) ν (cm^{-1}): 3322, 1710, 1539, 769, 742, 696. ^1H NMR (400 MHz) δ: 1.06 (d, ^3J = 6.0 Hz, 6H), 3.74 (m, 1H), 4.69 (s, 1H), 7.18–7.43 (m, 9H). ^{13}C NMR (100 MHz) δ: 22.7, 43.3, 123.2, 125.7, 127.2, 128.1, 128.3, 129.0, 130.7, 135.1, 137.9, 148.0, 153.6. Anal. calcd. for $C_{16}H_{17}NO_2$ (255.32): C 75.27, H 6.71, N 5.49; found: C 75.25, H 6.92, N 5.47.

O-*Phenyl* N-*isopropylcarbamate* ***(10b)*** *(14):* Reaction of phenol (2.82 g, 30.0 mmol) with isopropyl isocyanate (3.24 mL, 33.0 mmol) furnished **10b** (5.03 g, 28.1 mmol, 94%) as a white solid, mp 87°C (Et_2O–PE) (lit. (14) mp 85°C). IR (KBr) ν (cm^{-1}): 3389, 1703, 1545, 788, 703. ^1H NMR (300 MHz) δ: 1.19 (d, ^3J = 6.6 Hz, 6H), 3.87 (m, 1H), 4.98 (s, 1H), 7.10–7.18 (m, 3H), 7.30–7.35 (m, 2H). ^{13}C NMR (75 MHz) δ: 22.7, 43.3, 121.5, 125.0, 129.1, 151.1, 153.6. Anal. calcd. for $C_{10}H_{13}NO_2$ (179.22): C 67.02, H 7.31, N 7.82; found: C 67.21, H 7.41, N 8.00.

O-*2-Chlorophenyl* N-*isopropylcarbamate* ***(10c)****:* 2-Chlorophenol (3.86 g, 30.0 mmol) was stirred with isopropyl isocyanate (3.24 mL, 33.0 mmol) to give **10c** (6.28 g, 29.4 mmol, 98%) as a white solid, mp 65°C (Et_2O–PE). IR (KBr) ν (cm^{-1}): 3309, 1716, 1539, 736. ^1H NMR (400 MHz) δ: 1.22 (d, ^3J = 6.5 Hz, 6H), 3.88 (m, 1H), 5.07 (s, 1H), 7.11–7.15 (m, 1H), 7.19–7.27 (m, 2H), 7.39–7.41 (m, 1H). ^{13}C NMR (100 MHz) δ: 22.7, 43.6, 124.1, 126.4, 127.3, 127.5, 130.1, 147.2, 152.6. Anal. calcd. for $C_{10}H_{12}ClNO_2$ (213.66): C 56.21, H 5.66, N 6.56; found: C 56.09, H 5.65, N 6.55.

O-*1-Naphthyl* N-*isopropylcarbamate* ***(15)*** *(15):* Reaction of 1-naphthol (5.77 g, 40.0 mmol) with isopropyl isocyanate (4.32 mL, 44.0 mmol) yielded **15** (7.97 g, 34.8 mmol, 87%) as a white solid, mp 123°C (Et_2O–PE) (lit. (15) mp 112°C). IR (KBr) ν (cm^{-1}): 3423, 3368, 1716, 1525, 815, 788. ^1H NMR (300 MHz) δ: 1.22 (d, ^3J = 6.7 Hz, 6H), 3.91 (m, 1H), 5.12 (s, 1H), 7.27–7.30 (m, 1H), 7.40–7.51 (m, 3H), 7.67–7.69 (m, 1H), 7.80–7.85 (m, 1H), 7.90–7.96 (m, 1H). ^{13}C NMR (75 MHz) δ: 22.8, 43.5, 118.1, 121.3, 125.4, 125.4, 126.1, 126.2, 127.5, 127.9, 134.6, 146.8, 153.7. Anal. calcd. for $C_{14}H_{15}NO_2$ (229.28): C 73.34, H 6.59, N 6.11; found: C 73.36, H 6.70, N 6.06.

© 2001 NRC Canada

General procedure for the ortho-lithiation of O-*aryl* N-*isopropylcarbamates **10** and **15***

A solution of the carbamate **10** or **15** (1.00 mmol) in dry Et_2O (10 mL) under Ar in a flask, sealed with a rubber septum, was cooled to 0°C. TMEDA (0.128 g, 1.10 mmol, 1.10 equiv) was introduced, and to the solution was added dropwise, via a syringe, TMSOTf (1.05 to 1.10 mmol, 1.05 to 1.10 equiv, 1.25 to 1.35 M solution in pentane). The resulting mixture was stirred for 5 min, allowed to warm to rt over a period of 30 min, and cooled to –78°C. TMEDA (0.232 g, 2.00 mmol, 2.00 equiv) and *n*-BuLi or *s*-BuLi (2.00 mmol, 2.00 equiv) were added consecutively. The reaction mixture was stirred for 1 h and treated with the electrophile (2.50 to 3.50 mmol, 2.50 to 3.50 equiv). After an additional stirring for 1 to 2 h, 0.1 mL of MeOH and 5 mL of 2 M HCl were added and the mixture was allowed to warm to rt. The phases were separated and the aqueous layer was extracted with Et_2O (3 × 20 mL). The combined organic phases were washed with saturated $NaHCO_3$ solution (10 mL), dried over $MgSO_4$, filtered, and concentrated in vacuo to afford the crude product. Flash chromatography on silica gel (Et_2O–PE gradient) gave the *ortho*-substituted carbamate.

O-*3-Trimethylsilyl-2-biphenylyl* N-*isopropylcarbamate (**13aa**):* Reaction of **10a** (0.255 g) with TMSOTf (1.10 mmol), *n*-BuLi, and TMSCl (0.32 mL, 2.5 mmol, 1 h) afforded **13aa** (0.318 g, 0.971 mmol, 97%) as a white solid, mp 161°C (Et_2O–PE). IR (KBr) ν (cm^{-1}): 3329, 1710, 1545, 834, 788, 755, 709. ^1H NMR (300 MHz) δ: 0.30 (s, 9H), 0.94 (d, ^3J = 6.3 Hz, 6H), 3.55 (m, 1H), 4.50 (s, 1H), 7.26–7.47 (m, 8H). ^{13}C NMR (75 MHz) δ: –0.7, 22.6, 43.0, 125.7, 127.0, 128.0, 129.1, 132.1, 133.4, 134.2, 135.6, 138.5, 152.7, 152.9. Anal. calcd. for $C_{19}H_{25}NO_2Si$ (327.50): C 69.68, H 7.69, N 4.28; found: C 69.59, H 7.74, N 4.12.

O-*3-Tributylstannyl-2-biphenylyl* N-*isopropylcarbamate (**13ab**):* Reaction of **10a** (0.255 g) with TMSOTf (1.10 mmol), *s*-BuLi, and Bu_3SnCl (0.68 mL, 2.5 mmol, 1 h) yielded **13ab** (0.467g, 0.858 mmol, 86%) as a white solid, mp 70°C (Et_2O–PE). IR (KBr) ν (cm^{-1}): 3317, 1708, 1528, 782, 754, 701. ^1H NMR (300 MHz) δ: 0.89 (t, ^3J = 7.4 Hz, 9H), 0.95 (d, ^3J = 6.4 Hz, 6H), 1.05–1.13 (m, 6H), 1.25–1.43 (m, 6H), 1.49–1.61 (m, 6H), 3.56 (m, 1H), 4.42 (d, 1H), 7.21–7.44 (m, 8H). ^{13}C NMR (75 MHz) δ: 10.0, 13.6, 22.7, 27.4, 29.1, 43.0, 125.8, 126.9, 128.0, 129.0, 131.1, 135.2, 136.0, 136.2, 139.0, 153.0, 153.2. Anal. calcd. for $C_{28}H_{43}NO_2Sn$ (544.36): C 61.78, H 7.96, N 2.57; found: C 62.18, H 8.06, N 2.66.

O-*3-Iodo-2-biphenylyl* N-*isopropylcarbamate (**13ac**):* Reaction of **10a** (0.255 g) with TMSOTf (1.05 mmol), *n*-BuLi, and I_2 (0.761 g in 3 mL of Et_2O, 3.0 mmol, 1 h) afforded **13ac** (0.366 g, 0.881 mmol, 88%) as a white solid, mp 127°C (Et_2O–PE). IR (KBr) ν (cm^{-1}): 3355, 1719, 1523, 780, 759, 710. ^1H NMR (400 MHz) δ: 1.07 (d, ^3J = 6.4 Hz, 6H), 3.72 (m, 1H), 4.71 (s, 1H), 7.00 (t, 1H), 7.28–7.42 (m, 6H), 7.79 (dd, 1H). ^{13}C NMR (100 MHz) δ: 22.7, 43.4, 92.8, 127.5, 127.6, 128.2, 128.8, 130.9, 137.3, 137.7, 138.4, 148.4, 152.1. Anal. calcd. for $C_{16}H_{16}INO_2$ (381.21): C 50.41, H 4.23, N 3.67; found: C 50.77, H 4.48, N 3.40.

O-*3-Bromo-2-biphenylyl* N-*isopropylcarbamate (**13ad**):* **10a** (0.255 g) reacted with TMSOTf (1.05 mmol), *n*-BuLi, and $BrCH_2CH_2Br$ (0.30 mL, 3.5 mmol, 1 h) to give **13ad** (0.304 g, 0.910 mmol, 91%) as a white solid, mp 123°C (Et_2O–PE). IR (KBr) ν (cm^{-1}): 3362, 1729, 1539, 776, 760, 709. ^1H NMR (300 MHz) δ: 1.08 (d, ^3J = 6.4 Hz, 6H), 3.75 (m, 1H), 4.74 (s, 1H), 7.14 (t, 1H), 7.26–7.43 (m, 6H), 7.57 (dd, 1H). ^{13}C NMR (75 MHz) δ: 22.6, 43.4, 118.4, 126.9, 127.6, 128.2, 128.9, 129.8, 132.3, 137.4, 138.0, 145.6, 152.2. Anal. calcd. for $C_{16}H_{16}BrNO_2$ (334.21): C 57.50, H 4.83, N 4.19; found: C 57.58, H 4.87, N 4.48.

O-*3-Chloro-2-biphenylyl* N-*isopropylcarbamate (**13ae**):* Reaction of **10a** (0.255 g) with TMSOTf (1.10 mmol), *n*-BuLi, and C_2Cl_6 (0.592 g in 3 mL of Et_2O, 2.5 mmol, 1 h) afforded **13ae** (0.270 g, 0.932 mmol, 93%) as a white solid, mp 110°C (Et_2O–PE). IR (KBr) ν (cm^{-1}): 3362, 1723, 1539, 779, 760, 706. ^1H NMR (300 MHz) δ: 1.09 (d, ^3J = 6.4 Hz, 6H), 3.76 (m, 1H), 4.76 (s, 1H), 7.16–7.43 (m, 8H). ^{13}C NMR (75 MHz) δ: 22.6, 43.5, 126.4, 127.6, 128.2, 128.9, 129.1, 129.1, 129.2, 137.2, 137.8, 144.5, 152.4. Anal. calcd. for $C_{16}H_{16}ClNO_2$ (289.76): C 66.32, H 5.57, N 4.83; found: C 66.43, H 5.79, N 4.99.

O-*3-Phenylsulfanyl-2-biphenylyl* N-*isopropylcarbamate (**13af**):* Reaction of **10a** (0.255 g) with TMSOTf (1.05 mmol), *n*-BuLi, and $(PhS)_2$ (0.546 g in 3 mL of Et_2O, 2.5 mmol, 1 h) furnished **13af** (0.341 g, 0.938 mmol, 94%) as a white solid, mp 115°C (Et_2O–PE). IR (KBr) ν (cm^{-1}): 3335, 1703, 1532, 778, 756, 703. ^1H NMR (300 MHz) δ: 1.04 (d, ^3J = 6.4 Hz, 6H), 3.70 (m, 1H), 4.63 (s, 1H), 7.13–7.18 (m, 2H), 7.20–7.46 (m, 11H). ^{13}C NMR (75 MHz) δ: 22.7, 43.3, 125.2, 126.3, 127.4, 128.2, 129.0, 129.2, 129.6, 131.2, 131.5, 131.9, 134.6, 136.8, 137.7, 146.6, 152.7. Anal. calcd. for $C_{22}H_{21}NO_2S$ (363.47): C 72.70, H 5.82, N 3.85; found: C 72.79, H 5.98, N 4.01.

O-*3-Methyl-2-biphenylyl* N-*isopropylcarbamate (**13ag**):* **10a** (0.255 g) reacted with TMSOTf (1.10 mmol), *s*-BuLi, and MeI (0.20 mL, 2.5 mmol, 1 h) to give **13ag** (0.223 g, 0.828 mmol, 83%) as a white solid, mp 109°C (Et_2O–PE). IR (KBr) ν (cm^{-1}): 3326, 1710, 1529, 783, 761, 699. ^1H NMR (300 MHz) δ: 1.05 (d, ^3J = 6.4 Hz, 6H), 2.26 (s, 3H), 3.73 (m, 1H), 4.60 (s, 1H), 7.14–7.22 (m, 3H), 7.27–7.43 (m, 5H). ^{13}C NMR (75 MHz) δ: 16.4, 22.7, 43.2, 125.7, 127.1, 128.1, 128.3, 129.1, 130.2, 131.9, 135.8, 138.4, 146.7, 153.3. Anal. calcd. for $C_{17}H_{19}NO_2$ (269.34): C 75.81, H 7.11, N 5.20; found: C 75.78, H 7.24, N 5.30.

O-*3-Ethyl-2-biphenylyl* N-*isopropylcarbamate (**13ah**):* **10a** (0.255 g) reacted with TMSOTf (1.05 mmol), *s*-BuLi, and EtI (0.20 mL, 2.5 mmol, 2 h) to give **13ah** (0.192 g, 0.678 mmol, 68%) as a white solid, mp 92°C (Et_2O–PE). IR (KBr) ν (cm^{-1}): 3347, 1709, 1528, 786, 759, 704. ^1H NMR (300 MHz) δ: 1.02 (d, ^3J = 6.5 Hz, 6H), 1.02 (t, ^3J = 7.6, 3H), 2.64 (q, 2H), 3.69 (m, 1H), 4.60 (s, 1H), 7.14–7.44 (m, 8H). ^{13}C NMR (100 MHz) δ: 14.1, 22.7, 23.3, 43.2, 125.9, 127.0, 128.0, 128.3, 128.4, 129.1, 135.9, 137.5, 138.5, 146.2, 153.4. Anal. calcd. for $C_{18}H_{21}NO_2$ (283.36): C 76.29, H 7.47, N 4.94; found: C 76.11, H 7.17, N 4.85.

O-*3-Allyl-2-biphenylyl* N-*isopropylcarbamate (**13ai**):* Reaction of **10a** (0.255 g) with TMSOTf (1.10 mmol), *s*-BuLi, and

© 2001 NRC Canada

CH_2CHCH_2Br (0.22 mL, 2.5 mmol, 2 h) furnished **13ai** (0.185g, 0.626 mmol, 63%) as a white solid, mp 112°C (Et_2O–PE). IR (KBr) ν (cm^{-1}): 3344, 1712, 1526, 783, 760, 702. ^1H NMR (300 MHz) δ: 1.02 (d, ^3J = 6.5 Hz, 6H), 3.38 (d, ^3J = 6.7 Hz, 2H), 3.68 (m, 1H), 4.59 (s, 1H), 5.04–5.16 (m, 2H), 5.90–6.05 (m, 1H), 7.19–7.23 (m, 3H), 7.26–7.43 (m, 5H). ^{13}C NMR (75 MHz) δ: 22.7, 34.7, 43.2, 116.1, 125.9, 127.1, 128.0, 128.8, 129.1, 129.2, 133.8, 136.1, 136.2, 138.3, 146.3, 153.2. Anal. calcd. for $C_{19}H_{21}NO_2$ (295.38): C 77.26, H 7.17, N 4.74; found: C 76.96, H 6.92, N 4.69.

O-*3-Benzyl-2-biphenylyl* N-*isopropylcarbamate* ***(13aj)****:* Reaction of **10a** (0.255 g) with TMSOTf (1.05 mmol), *s*-BuLi, and BnBr (0.30 mL, 2.5 mmol, 2 h) gave **13aj** (0.254 g, 0.735 mmol, 74%) as a white solid, mp 109°C (Et_2O–PE). IR (KBr) ν (cm^{-1}): 3322, 1700, 1532, 786, 756, 702. ^1H NMR (300 MHz) δ: 1.00 (d, ^3J = 6.5 Hz, 6H), 3.66 (m, 1H), 3.97 (s, 2H), 4.55 (d, 1H), 7.09 (dd, 1H), 7.13–7.45 (m, 12H). ^{13}C NMR (100 MHz) δ: 22.6, 36.3, 43.2, 125.8, 126.1, 127.1, 128.0, 128.4, 128.9, 129.1, 129.1, 129.8, 134.9, 136.1, 138.3, 140.1, 146.4, 153.1. Anal. calcd. for $C_{23}H_{23}NO_2$ (345.43): C 79.97, H 6.71, N 4.05; found: C 79.82, H 6.93, N 3.86.

O-*3-(Hydroxyphenylmethyl)-2-biphenylyl* N-*isopropylcarbamate* ***(13ak)****:* Reaction of **10a** (0.255 g) with TMSOTf (1.10 mmol), *s*-BuLi, and PhCHO (0.26 mL, 2.5 mmol, 1 h) afforded **13ak** (0.316 g, 0.874 mmol, 87%) as a white solid, mp 111°C (Et_2O–PE). IR (KBr) ν (cm^{-1}): 3397, 3337, 1710, 1538, 789, 759, 703. ^1H NMR (300 MHz) δ: 0.99/1.03 (d, ^3J = 6.5 Hz, 6H), 3.12 (s, 1H), 3.66 (m, 1H), 4.65 (d, 1H), 6.04 (s, 1H), 7.18–7.47 (m, 13H). ^{13}C NMR (75 MHz) δ: 22.5, 43.4, 70.3, 126.3, 126.4, 127.1, 127.3, 128.1, 128.1, 128.3, 129.1, 130.2, 136.0, 137.9, 138.0, 142.6, 145.7, 154.1. Anal. calcd. for $C_{23}H_{23}NO_3$ (361.44): C 76.43, H 6.41, N 3.88; found: C 76.26, H 6.27, N 3.71.

O-*3-(1-Hydroxy-2-methylpropyl)-2-biphenylyl* N-*isopropylcarbamate* ***(13al)****:* Reaction of **10a** (0.255 g) with TMSOTf (1.05 mmol), *n*-BuLi, and *i*-PrCHO (0.32 mL, 3.5 mmol, 2 h) yielded **13al** (0.279 g, 0.853 mmol, 85%) as a white solid, mp 88°C (Et_2O–PE). HRMS calcd. for $C_{20}H_{25}NO_3$ (327.18): 327.1834; found: 327.1831. IR (KBr) ν (cm^{-1}): 3498, 3307, 1720, 1546, 788, 772, 709. ^1H NMR (300 MHz) δ: 0.81/1.08 (d, ^3J = 6.7 Hz, 6H), 0.99/1.05 (d, ^3J = 6.5 Hz, 6H), 2.09 (m, 1H), 2.42 (s, 1H), 3.67 (m, 1H), 4.47 (d, ^3J = 7.9 Hz, 1H), 4.66 (d, 1H), 7.23–7.40 (m, 7H), 7.48 (dd, 1H). ^{13}C NMR (75 MHz) δ: 18.7/19.4, 22.6, 33.5, 43.3, 74.2, 126.1, 127.0, 127.2, 128.1, 129.1, 129.7, 135.8, 137.5, 138.2, 145.6, 153.9. Anal. calcd.: C 76.29, H 7.47, N 4.94; found: C 76.11, H 7.17, N 4.85.

O-*3-(Hydroxydiphenylmethyl)-2-biphenylyl* N-*isopropylcarbamate* ***(13am)****:* Reaction of **10a** (0.255 g) with TMSOTf (1.05 mmol), *n*-BuLi, and Ph_2CO (0.456 g in 3 mL of Et_2O, 2.5 mmol, 1 h) afforded **13am** (0.370 g, 0.846 mmol, 85%) as a white solid, mp 150°C dec (Et_2O–PE). IR (KBr) ν (cm^{-1}): 3589, 3409, 1738, 1513, 780, 752, 699. ^1H NMR (300 MHz) δ: 0.74 (d, ^3J = 6.5 Hz, 6H), 3.24 (m, 1H), 4.10 (d, 1H), 4.54 (s, 1H), 6.77 (dd, 1H), 7.13 (t, 1H), 7.17–7.45 (m, 16H). ^{13}C NMR (75 MHz) δ: 22.2, 43.0, 81.1, 125.2, 126.8, 127.1, 127.4, 127.7, 128.0, 129.0, 129.9, 130.8, 137.6, 138.1, 140.4, 146.1, 146.2, 151.9. Anal. calcd. for $C_{29}H_{27}NO_3$ (437.54): C 79.61, H 6.22, N 3.20; found: C 79.43, H 6.36, N 2.92.

O-*3-(1-Hydroxy-1-phenylethyl)-2-biphenylyl* N-*isopropylcarbamate* ***(13an)****:* Reaction of **10a** (0.255 g), with TMSOTf (1.05 mmol), *n*-BuLi, and PhMeCO (0.41 mL, 3.5 mmol, 2 h) gave **13an** (0.261 g, 0.695 mmol, 70%) as a white solid, mp 127°C (Et_2O–PE). IR (KBr) ν (cm^{-1}): 3253, 1698, 1542, 762, 700. ^1H NMR (300 MHz) δ: 0.78/0.83 (d, ^3J = 6.4 Hz, 6H), 1.90 (s, 1H), 2.57 (s, 1H), 3.29 (m, 1H), 4.12 (d, 1H), 7.12–7.45 (m, 12H), 7.69 (t, 1H). ^{13}C NMR (75 MHz) δ: 22.3, 31.0, 43.0, 75.4, 124.8, 125.7, 126.9, 127.1, 127.8, 128.0, 128.0, 129.1, 130.6, 136.4, 137.6, 138.1, 140.2, 146.1, 152.3. Anal. calcd. for $C_{24}H_{25}NO_3$ (375.47): C 76.77, H 6.71, N 3.73; found: C 76.76, H 6.58, N 3.54.

O-*3-(1-Hydroxy-1-methylethyl)-2-biphenylyl* N-*isopropylcarbamate* ***(13ao)****:* Reaction of **10a** (0.255 g) with TMSOTf (1.05 mmol), *n*-BuLi, and Me_2CO (0.26 mL, 3.5 mmol, 1 h) afforded **13ao** (0.254 g, 0.810 mmol, 81%) as a white solid, mp 154°C (Et_2O–PE). IR (KBr) ν (cm^{-1}): 3568, 3307, 1715, 1531, 767, 703, 671. ^1H NMR (300 MHz) δ: 0.90 (d, ^3J = 6.4 Hz, 6H), 1.64 (s, 6H), 2.60 (s, 1H), 3.52 (m, 1H), 4.07 (d, 1H), 7.21–7.42 (m, 7H), 7.49–7.57 (m, 1H). ^{13}C NMR (75 MHz) δ: 22.5, 30.4, 43.2, 72.3, 125.7, 125.7, 127.1, 128.0, 129.3, 130.0, 137.4, 138.3, 140.9, 145.6, 152.8. Anal. calcd. for $C_{19}H_{23}NO_3$ (313.40): C 72.82, H 7.40, N 4.47; found: C 75.52, H 7.18, N 4.16.

O-*3-(1-Hydroxycyclohexyl)-2-biphenylyl* N-*isopropylcarbamate* ***(13ap)****:* **10a** (0.255 g) reacted with TMSOTf (1.05 mmol), *n*-BuLi, and $(CH_2)_5CO$ (0.37 mL, 3.5 mmol, 2 h) to yield **13ap** (0.225 g, 0.637 mmol, 64%) as a white solid, mp 159°C (Et_2O–PE). HRMS calcd. for $C_{22}H_{27}NO_3$ (353.45): 353.1991; found: 353.1983. IR (KBr) ν (cm^{-1}): 3444, 3308, 1722, 1534, 785, 757, 699. ^1H NMR (300 MHz) δ: 0.90 (d, ^3J = 6.4 Hz, 6H), 1.53–2.08 (m, 10H), 2.38 (s, 1H), 3.52 (m, 1H), 4.65 (d, 1H), 7.21–7.42 (m, 7H), 7.49–7.57 (m, 1H). ^{13}C NMR (75 MHz) δ: 22.1, 22.5, 25.7, 37.2, 43.2, 73.1, 125.8, 126.0, 127.1, 128.0, 129.4, 129.9, 137.5, 138.4, 141.2, 146.0, 153.0.

O-*2-Trimethylsilylphenyl* N-*isopropylcarbamate* ***(13ba)****:* **10b** (0.179 g) was protected with TMSOTf (1.05 mmol) and the lower phase was removed via a syringe. Reaction with *n*-BuLi (1.20 mmol) and TMSCl (0.20 mL, 1.5 mmol, 1 h) afforded **13ba** (0.207 g, 0.823 mmol, 82%) as a white solid, mp 92°C (Et_2O–PE). IR (KBr) ν (cm^{-1}): 3329, 1703, 1532, 841, 736. ^1H NMR (300 MHz) δ: 0.28 (s, 9H), 1.24 (d, ^3J = 6.4 Hz, 6H), 3.91 (m, 1H), 4.77 (s, 1H), 7.09–7.20 (m, 2H), 7.34–7.46 (m, 2H). ^{13}C NMR (75 MHz) δ: –0.9, 22.9, 43.4, 122.2, 124.9, 130.3, 131.6, 134.8, 153.8, 155.7. Anal. calcd. for $C_{13}H_{21}NO_2Si$ (251.40): C 62.11, H 8.42, N 5.57; found: C 62.01, H 8.63, N 5.21.

O-*2-Tributylstannylphenyl* N-*isopropylcarbamate* ***(13bb)****:* Reaction of **10b** (0.179 g) with TMSOTf (1.10 mmol), *s*-BuLi, and Bu_3SnCl (0.68 mL, 2.5 mmol, 1 h) gave **13bb** (0.396 g, 0.846 mmol, 85%) as a colourless oil. IR (film) ν (cm^{-1}): 3335, 1716, 1532, 736. ^1H NMR (300 MHz) δ: 0.88 (t, ^3J = 7.4 Hz, 9H), 1.07 (t, ^3J = 8.2 Hz, 6H), 1.24 (d, ^3J =

© 2001 NRC Canada

6.8, Hz, 6H), 1.26–1.38 (m, 6H), 1.47–1.58 (m, 6H), 3.91 (m, 1H), 4.67 (s, 1H), 7.13–7.18 (m, 2H), 7.28–7.34 (m, 1H), 7.40–7.43 (m, 1H). ^{13}C NMR (75 MHz) δ: 9.8, 13.6, 23.0, 27.3, 29.1, 43.3, 121.4, 125.0, 129.4, 133.6, 136.9, 153.8, 156.1. Anal. calcd. for $C_{22}H_{39}NO_2Sn$ (468.25): C 56.43, H 8.39, N 2.99; found: C 56.62, H 8.55, N 3.07.

O-*2-Methylphenyl* N-*isopropylcarbamate (**13bc**) (16):* **10b** (0.179 g) reacted with TMSOTf (1.10 mmol), *s*-BuLi, and MeI (0.20 mL, 2.5 mmol, 1 h) to give **13bc** (0.160 g, 0.827 mmol, 83%) as a white solid, mp 57°C (Et_2O–PE) (lit. (16) mp 48 to 49°C). IR (KBr) ν (cm^{-1}): 3301, 1705, 1545, 730. ^{1}H NMR (300 MHz) δ: 1.23 (d, ^3J = 6.5 Hz, 6H), 2.21 (s, 3H), 3.89 (m, 1H), 4.86 (s, 1H), 6.99–7.22 (m, 4H). ^{13}C NMR (75 MHz) δ: 16.0, 22.9, 43.4, 122.2, 125.5, 126.7, 130.6, 130.9, 149.6, 153.6. Anal. calcd. for $C_{11}H_{15}NO_2$ (193.25): C 68.37, H 7.82, N 7.25; found: C 68.77, H 7.96, N 7.39.

O-*2-(Hydroxyphenylmethyl)phenyl* N-*isopropylcarbamate (**13bd**):* Reaction of **10b** (0.179 g), with TMSOTf (1.10 mmol), *s*-BuLi, and PhCHO (0.26 mL, 2.5 mmol, 1 h) furnished **13bd** (0.230 g, 0.806 mmol, 81%) as a white solid, mp 100°C (Et_2O–PE). IR (KBr) ν (cm^{-1}): 3423, 3359, 1714, 1519, 756, 744, 705. ^{1}H NMR (300 MHz) δ: 1.19/1.20 (d, ^3J = 6.5 Hz, 6H), 2.91 (s, 1H), 3.82 (m, 1H), 4.81 (s, 1H), 5.99 (s, 1H), 7.09 (dd, 1H), 7.14–7.40 (m, 8H). ^{13}C NMR (75 MHz) δ: 22.7, 43.5, 70.5, 122.6, 126.0, 126.3, 127.2, 128.2, 128.7, 128.7, 136.5, 142.7, 148.3, 154.0. Anal. calcd. for $C_{17}H_{19}NO_3$ (285.34): C 71.56, H 6.71, N 4.91; found: C 71.45, H 6.61, N 4.89.

O-*2-(Hydroxydiphenylmethyl)phenyl* N-*isopropylcarbamate (**13be**):* Reaction of **10b** (0.179 g) with TMSOTf (1.05 mmol), *n*-BuLi, and Ph_2CO (0.456 g in 3 mL of Et_2O, 2.5 mmol, 1 h) afforded **13be** (0.302g, 0.836 mmol, 84%) as a white solid, mp 115°C (Et_2O–PE). IR (KBr) ν (cm^{-1}): 3535, 3349, 1752, 1522, 766, 704. ^{1}H NMR (300 MHz) δ: 0.95 (d, ^3J = 6.4 Hz, 6H), 3.52 (m, 1H), 4.14 (s, 1H), 4.25 (d, 1H), 6.73 (dd, 1H), 6.99–7.08 (m, 1H), 7.18–7.36 (m, 12H). ^{13}C NMR (75 MHz) δ: 22.5, 43.3, 81.0, 124.3, 124.8, 127.0, 127.4, 127.9, 128.8, 130.2, 138.9, 146.1, 149.0, 152.3. Anal. calcd. for $C_{23}H_{23}NO_3$ (361.44): C 76.43, H 6.41, N 3.88; found: C 76.21, H 6.54, N 3.80.

O-*2-Chloro-6-trimethylsilylphenyl* N-*isopropylcarbamate (**13ca**):* Reaction of **10c** (0.214 g) with TMSOTf (1.05 mmol), *n*-BuLi, and TMSCl (0.32 mL, 2.5 mmol, 1 h) gave **13ca** (0.260 g, 0.910 mmol, 91%) as a white solid, mp 102°C (Et_2O–PE). IR (KBr) ν (cm^{-1}): 3310, 1714, 1532, 844, 753. ^{1}H NMR (300 MHz) δ: 0.28 (s, 9H), 1.24 (d, ^3J = 6.7 Hz, 6H), 3.91 (m, 1H), 4.92 (s, 1H), 7.14 (t, 1H), 7.33 (dd, 1H), 7.41 (dd, 1H). ^{13}C NMR (75 MHz) δ: –0.9, 22.9, 43.6, 126.4, 128.0, 131.2, 133.1, 135.4, 151.3, 152.5. Anal. calcd. for $C_{13}H_{20}ClNO_2Si$ (285.84): C 54.62, H 7.05, N 4.90; found: C 54.67, H 7.16, N 5.00.

O-*2-Tributylstannyl-6-chlorophenyl* N-*isopropylcarbamate (**13cb**):* Reaction of **10c** (0.214 g) with TMSOTf (1.05 mmol), *n*-BuLi, and Bu_3SnCl (0.68 mL, 2.5 mmol, 1 h) afforded **13cb** (0.439 g, 0.873 mmol, 87%) as a colourless oil. IR (film) ν (cm^{-1}): 3336, 1723, 1521, 773. ^{1}H NMR (300 MHz) δ: 0.89 (t, 9H), 1.04–1.14 (m, 6H), 1.30 (d, ^3J = 6.6 Hz, 6H), 1.25–1.40 (m, 6H), 1.46–1.59 (m, 6H), 3.90 (m, 1H), 4.83 (d, 1H), 7.11 (t, 1H), 7.30 (dd, 1H), 7.34 (dd, 1H). ^{13}C NMR (75 MHz) δ: 10.0, 13.6, 22.9, 27.3, 29.0, 43.5, 126.6, 127.6, 130.4, 135.1, 137.9, 151.6, 152.6. Anal. calcd. for $C_{22}H_{37}ClNO_2Sn$ (502.70): C 52.27, H 7.62, N 2.79; found: C 52.68, H 7.91, N 2.82.

O-*2-Chloro-6-iodophenyl* N-*isopropylcarbamate (**13cc**):* **10c** (0.214 g) reacted with TMSOTf (1.05 mmol), *n*-BuLi, and I_2 (0.761 g in 3 mL of Et_2O, 3.0 mmol, 1 h) to yield **13cc** (0.291 g, 0.857 mmol, 86%) as a white solid, mp 118°C (Et_2O–PE). IR (KBr) ν (cm^{-1}): 3303, 1726, 1530, 774. ^{1}H NMR (300 MHz) δ: 1.27 (d, ^3J = 6.5 Hz, 6H), 3.92 (m, 1H), 5.02 (s, 1H), 6.88 (t, 1H), 7.39 (dd, 1H), 7.69 (dd, 1H). ^{13}C NMR (75 MHz) δ: 22.8, 43.8, 92.9, 127.9, 130.3, 137.5, 147.8, 151.2, 152.4. Anal. calcd. for $C_{10}H_{11}ClINO_2$ (339.56): C 35.37, H 3.27, N 4.12; found: C 35.51, H 3.49, N 4.01.

O-*2-Chloro-6-(phenylsulfanyl)phenyl* N-*isopropylcarbamate (**13cd**):* Reaction of **10c** (0.214 g) with TMSOTf (1.05 mmol), *n*-BuLi, and $(PhS)_2$ (0.546 g in 3 mL of Et_2O, 2.5 mmol, 1 h) gave **13cd** (0.276 g, 0.858 mmol, 86%) as a white solid, mp 113°C (Et_2O–PE). IR (KBr) ν (cm^{-1}): 3270, 1729, 1537, 786, 751, 689. ^{1}H NMR (300 MHz) δ: 1.24 (d, ^3J = 6.4 Hz, 6H), 3.89 (m, 1H), 4.94 (s, 1H), 6.95–7.06 (m, 2H), 7.20–7.44 (m, 6H). ^{13}C NMR (75 MHz) δ: 22.8, 43.8, 126.7, 127.9, 128.4, 129.0, 129.4, 129.6, 132.6, 133.5, 135.4, 145.4, 151.7. Anal. calcd. for $C_{16}H_{16}ClNO_2S$ (321.83): C 59.71, H 5.01, N 4.35; found: C 59.98, H 5.18, N 4.44.

O-*2-Chloro-6-methylphenyl* N-*isopropylcarbamate (**13ce**):* Reaction of **10c** (0.214 g) with TMSOTf (1.05 mmol), *n*-BuLi, and MeI (0.20 mL, 2.5 mmol, 1 h) afforded **13ce** (0.204 g, 0.895 mmol, 90%) as a white solid, mp 94°C (Et_2O–PE). IR (KBr) ν (cm^{-1}): 3282, 1708, 1535, 771. ^{1}H NMR (300 MHz) δ: 1.24 (d, ^3J = 6.7 Hz, 6H), 2.23 (s, 6H), 3.89 (m, 1H), 4.96 (s, 1H), 6.86–7.09 (m, 3H). ^{13}C NMR (75 MHz) δ: 16.3, 22.7, 43.5, 126.0, 127.5, 128.0, 129.1, 133.5, 145.8, 152.3. Anal. calcd. for $C_{11}H_{14}ClNO_2$ (227.89): C 58.03, H 6.20, N 6.15; found: C 57.98, H 6.29, N 6.00.

O-*2-Chloro-6-(hydroxyphenylmethyl)phenyl* N-*isopropylcarbamate (**13cf**):* Reaction of **10c** (0.214 g) with TMSOTf (1.05 mmol), *n*-BuLi, and PhCHO (0.26 mL, 2.5 mmol, 1 h) afforded **13cf** (0.270 g, 0.844 mmol, 84%) as a white solid, mp 125°C (Et_2O–PE). IR (KBr) ν (cm^{-1}): 3429, 3257, 1731, 1529, 775, 758, 703. ^{1}H NMR (300 MHz) δ: 1.21/1.22 (d, ^3J = 6.4 Hz, 6H), 3.11 (s, 1H), 3.84 (m, 1H), 5.05 (d, 1H), 5.97 (s, 1H), 7.13 (t, 1H), 7.20–7.39 (m, 7H). ^{13}C NMR (75 MHz) δ: 22.7, 43.8, 70.6, 126.4, 126.9, 127.1, 127.4, 128.3, 129.4, 139.6, 142.1, 142.1, 144.8, 152.9. Anal. calcd. for $C_{17}H_{18}ClNO_3$ (319.79): C 63.85, H 5.67, N 4.38; found: C 63.60, H 5.89, N 4.26.

O-*2-Chloro-6-(hydroxydiphenylmethyl)phenyl* N-*isopropylcarbamate (**13cg**):* Reaction of **10c** (0.214 g) with TMSOTf (1.05 mmol), *n*-BuLi, and Ph_2CO (0.456 g in 3 mL of Et_2O, 2.5 mmol, 1 h) provided **13cg** (0.325 g, 0.821 mmol, 82%) as a white solid, mp 82°C (Et_2O–PE). IR (KBr) ν (cm^{-1}): 3425, 3346, 1727, 1523, 774, 735, 700. ^{1}H NMR (300 MHz) δ: 1.03 (d, ^3J = 6.5 Hz, 6H), 3.59 (m, 1H), 4.25 (s, 1H), 4.51

© 2001 NRC Canada

(d, 1H), 6.65–6.73 (m, 1H), 7.00 (t, 1H), 7.17–7.43 (m, 11H). ^{13}C NMR (75 MHz) δ: 22.5, 43.6, 81.0, 125.7, 127.1, 127.4, 127.7, 127.8, 128.1, 129.0, 130.0, 142.2, 145.6, 151.5. Anal. calcd. for $C_{23}H_{22}ClNO_3$ (395.89): C 69.78, H 5.60, N 3.54; found: C 69.65, H 5.77, N 3.23.

O-*2-Trimethylsilyl-1-naphthyl* N-*isopropylcarbamate (**16a**):* Reaction of **15** (0.229 g) with TMSOTf (1.10 mmol), *s*-BuLi, and TMSCl (0.32 mL, 2.5 mmol, 1 h) gave **16a** (0.273 g, 0.906 mmol, 91%) as a white solid, mp 185°C (Et_2O–PE). IR (KBr) ν (cm^{-1}): 3348, 1710, 1532, 848, 762. ^{1}H NMR (300 MHz) δ: 0.36 (s, 9H), 1.27 (d, ^3J = 6.3 Hz, 6H), 3.95 (m, 1H), 5.02 (s, 1H), 7.44–7.59 (m, 3H), 7.68–7.83 (m, 3H). ^{13}C NMR (75 MHz) δ: –0.7, 23.0, 43.5, 121.5, 125.4, 126.3, 126.5, 127.6, 127.8, 128.4, 130.2, 135.5, 152.1, 153.9. Anal. calcd. for $C_{17}H_{23}NO_2Si$ (301.46): C 67.73, H 7.69, N 4.65; found: C 67.40, H 7.58, N 4.62.

O-*2-Tributylstannyl-1-naphthyl* N-*isopropylcarbamate (**16b**):* Reaction of **15** (0.229 g) with TMSOTf (1.10 mmol), *s*-BuLi, and Bu_3SnCl (0.68 mL, 2.5 mmol, 1 h) afforded **16b** (0.438 g, 0.845 mmol, 85%) as a white solid, mp 80°C (Et_2O–PE). IR (KBr) ν (cm^{-1}): 3305, 1703, 1525, 814, 744. ^{1}H NMR (300 MHz) δ: 0.89 (t, ^3J = 7.3 Hz, 9H), 1.11–1.19 (m, 6H), 1.28 (d, ^3J = 6.5, Hz, 6H), 1.27–1.41 (m, 6H), 1.48–1.63 (m, 6H), 3.94 (m, 1H), 4.93 (d, 1H), 7.39–7.52 (m, 3H), 7.63–7.84 (m, 3H). ^{13}C NMR (75 MHz) δ: 9.9, 13.7, 23.1, 27.4, 29.1, 43.5, 121.4, 125.5, 126.0, 126.2, 127.5, 127.9, 131.4, 132.5, 135.2, 152.2, 154.0. Anal. calcd. for $C_{26}H_{41}NO_2Sn$ (518.32): C 60.25, H 7.97, N 2.70; found: C 60.20, H 8.04, N 2.51.

O-*2-Methyl-1-naphthyl* N-*isopropylcarbamate (**16c**):* Reaction of **15** (0.229 g) with TMSOTf (1.10 mmol), *s*-BuLi, and MeI (0.20 mL, 2.5 mmol, 1 h) afforded **16c** (0.209 g, 0.860 mmol, 86%) as a white solid, mp 129°C (Et_2O–PE). IR (KBr) ν (cm^{-1}): 3286, 1705, 1538, 818, 770, 747. ^{1}H NMR (300 MHz) δ: 1.22 (d, ^3J = 6.4 Hz, 6H), 2.36 (s, 3H), 3.91 (m, 1H), 5.09 (s, 1H), 7.30 (d, 1H), 7.36–7.50 (m, 2H), 7.62 (d, 1H), 7.74–7.87 (m, 2H). ^{13}C NMR (75 MHz) δ: 16.2, 22.8, 43.5, 120.9, 125.3, 125.4, 126.3, 127.2, 127.7, 128.1, 128.7, 132.2, 144.3, 153.3. Anal. calcd. for $C_{15}H_{17}NO_2$ (243.13): C 74.05, H 7.04, N 5.76; found: C 73.82, H 7.07, N 5.51.

O-*2-(Hydroxyphenylmethyl)-1-naphthyl* N-*isopropylcarbamate (**16d**):* **15** (0.229 g) reacted with TMSOTf (1.10 mmol), *s*-BuLi, and PhCHO (0.26 mL, 2.5 mmol, 1 h) to give **16d** (0.277 g, 0.826 mmol, 83%) as a white solid, mp 174°C dec (Et_2O–PE). IR (KBr) ν (cm^{-1}): 3564, 3310, 1698, 1533, 757, 727, 700. ^{1}H NMR (300 MHz) δ: 1.29/1.28 (d, ^3J = 6.4 Hz, 6H), 3.16 (s, 1H), 3.93 (m, 1H), 5.18 (d, 1H), 6.20 (s, 1H), 7.20–7.38 (m, 4H), 7.39–7.56 (m, 4H), 7.67 (d, 1H), 7.77–7.84 (m, 1H), 7.87–7.94 (m, 1H). ^{13}C NMR (75 MHz) δ: 22.8, 43.9, 69.8, 121.5, 125.7, 126.3, 126.4, 126.5, 126.7, 127.1, 127.8, 127.9, 128.2, 133.2, 134.2, 142.5, 143.7, 154.4. Anal. calcd. for $C_{21}H_{21}NO_3$ (335.40): C 75.20, H 6.31, N 4.18; found: C 75.10, H 6.01, N 3.88.

O-*2-(Hydroxydiphenylmethyl)-1-naphthyl* N-*isopropylcarbamate (**16e**):* Reaction of **15** (0.229 g) with TMSOTf (1.05 mmol), *n*-BuLi, and Ph_2CO (0.456 g in 3 mL of Et_2O, 2.5 mmol, 1 h) afforded **16e** (0.357 g, 0.868 mmol, 87%) as a white solid, mp 117°C dec (Et_2O–PE). IR (KBr) ν (cm^{-1}): 3411, 3343, 1706, 1525, 765, 746, 711. ^{1}H NMR (300 MHz) δ: 1.05 (d, ^3J = 6.5 Hz, 6H), 3.61 (m, 1H), 4.51 (d, 1H), 4.58 (s, 1H), 6.97 (d, 1H), 7.18–7.33 (m, 6H), 7.40–7.52 (m, 6H), 7.57 (d, 1H), 7.73–7.84 (m, 2H). ^{13}C NMR (75 MHz) δ: 22.6, 43.5, 80.9, 121.9, 125.3, 126.6, 126.6, 126.8, 127.3, 127.7, 127.8, 128.8, 129.8, 134.3, 135.8, 144.5, 146.6, 153.5. Anal. calcd. for $C_{27}H_{25}NO_3$ (411.49): C 78.81, H 6.12, N 3.40; found: C 78.53, H 5.99, N 3.21.

General procedure for deprotection of N-*isopropylcarbamates **13a** and **13c***

To a solution of the *N*-isopropylcarbamate **13** (0.50 mmol) in EtOH (5 mL) under Ar in a flask was added at rt 2 M NaOH (1.0 mL, 2.0 mmol, 4.0 equiv). The resulting reaction mixture was stirred for 2 h. Then, 2 mL of 2 M HCl and 10 mL of Et_2O were added, the phases were separated, and the aqueous layer was extracted with Et_2O (3 × 10 mL). The combined organic phases were washed with saturated NaCl solution (5 mL), dried over $MgSO_4$, and filtered. Evaporation of the solvents provided the crude product. Flash chromatography on silica gel (Et_2O–PE mixtures) afforded the free phenol **14**.

*2-Hydroxy-3-trimethylsilylbiphenyl (**14aa**):* **13aa** (0.164 g) was deprotected to yield **14aa** (0.120 g, 0.495 mmol, 99%) as a colourless oil, which solidifies after a few days to give a white solid, mp 39°C (Et_2O–PE). IR (KBr) ν (cm^{-1}): 3531, 841, 763, 708. ^{1}H NMR (300 MHz) δ: 0.32 (s, 9H), 5.39 (s, 1H), 6.98 (t, 1H), 7.21–7.24 (m, 1H), 7.35–7.52 (m, 6H). ^{13}C NMR (75 MHz) δ: –0.9, 120.4, 125.8, 127.2, 127.9, 129.2, 129.5, 131.3, 134.8, 137.3, 157.0. Anal. calcd. for $C_{15}H_{18}OSi$ (242.39): C 74.33, H 7.48; found: C 74.39, H 7.72.

*2-Hydroxy-3-iodobiphenyl (**14ab**):* **13ac** (0.191 g) was deprotected to give **14ab** (0.145 g, 0.490 mmol, 98%) as a white solid, mp 42°C (Et_2O–PE). IR (KBr) ν (cm^{-1}): 3452, 756, 735, 700. ^{1}H NMR (300 MHz) δ: 5.54 (s, 1H), 6.74 (t, 1H), 7.21–7.25 (m, 1H), 7.34–7.50 (m, 5H), 7.67 (dd, 1H). ^{13}C NMR (75 MHz) δ: 85.8, 122.5, 128.0, 128.8, 129.1, 129.1, 131.0, 137.3, 138.1, 151.6. Anal. calcd. for $C_{12}H_9IO$ (296.10): C 48.68, H 3.06; found: C 48.75, H 3.18.

*3-Bromo-2-hydroxybiphenyl (**14ac**) (17):* **13ad** (0.167 g) was deprotected to yield **14ac** (0.123 g, 0.494 mmol, 99%) as a white solid, mp 59°C (Et_2O–PE) (lit. (17) mp 38 to 39°C). IR (KBr) ν (cm^{-1}): 3498, 759, 733, 701. ^{1}H NMR (300 MHz) δ: 5.65 (s, 1H), 6.87 (t, 1H), 7.22–7.26 (m, 1H), 7.33–7.54 (m, 6H). ^{13}C NMR (75 MHz) δ: 111.0, 121.7, 127.8, 128.5, 129.2, 129.7, 130.1, 131.5, 137.2, 149.3. Anal. calcd. for $C_{12}H_9BrO$ (249.10): C 57.86, H 3.64; found: C 58.08, H 3.46.

*2-Hydroxy-3-phenylsulfanylbiphenyl (**14ad**):* Deprotection of **13af** (0.182 g) gave **14ad** (0.138 g, 0.496 mmol, 99%) as a colourless oil, which solidifies after a few days to give a white solid, mp 71°C (Et_2O–PE). HRMS calcd. for $C_{18}H_{14}OS$ (278.37): 278.0765; found: 278.0759. IR (KBr) ν (cm^{-1}): 3394, 761, 741, 701, 690. ^{1}H NMR (300 MHz) δ: 6.67 (s, 1H), 6.92 (t, 1H), 7.03–7.54 (m, 12H). ^{13}C NMR (75 MHz) δ: 117.7, 121.1, 126.4, 127.4, 127.5, 127.6, 128.2, 128.9, 129.2, 133.0, 135.6, 135.7, 137.6, 154.0.

© 2001 NRC Canada

*2-Hydroxy-3-(hydroxydiphenylmethyl)biphenyl (**14ae**):* **13am** (0.219 g) was deprotected to yield **14ae** (0.169 g, 0.480 mmol, 96%) as a colourless oil, which solidifies after a few days to give a white solid, mp 129°C dec (Et_2O–PE). IR (KBr) ν (cm^{-1}): 3471, 803, 760, 701. ^1H NMR (300 MHz) δ: 4.17 (s, 1H), 6.52 (dd, 1H), 6.80 (t, 1H), 7.22–7.52 (m, 17H). ^{13}C NMR (75 MHz) δ: 83.9, 119.3, 127.4, 127.7, 127.8, 128.1, 128.5, 129.5, 129.7, 129.9, 130.5, 131.4, 137.6, 145.4, 152.1. Anal. calcd. for $C_{25}H_{20}O_2$ (352.43): C 85.20, H 5.72; found: C 84.85, H 5.50.

*2-Chloro-6-trimethylsilylphenol (**14ca**):* Deprotection of **13ca** (0.143 g, 0.500 mmol) furnished **14ca** (0.099 g, 0.493 mmol, 99%) as a colourless liquid. HRMS calcd. for $C_9H_{13}ClOSi$ (200.74): 200.0424; found: 200.0388. IR (film) ν (cm^{-1}): 3539, 842, 759. ^1H NMR (300 MHz) δ: 0.31 (s, 9H), 5.72 (s, 1H), 6.84 (dd, 1H), 7.25 (dd, 1H), 7.30 (dd, 1H). ^{13}C NMR (75 MHz) δ: –1.1, 119.5, 121.1, 127.1, 129.8, 133.7, 155.3. Anal. calcd.: C 53.85, H 6.53; found: C 54.14, H 6.71.

*2-Chloro-6-iodophenol (**14cb**) (18):* **13cc** (0.170 g) was deprotected to yield **14cb** (0.119 g, 0.468 mmol, 94%) as a white solid, mp 59°C (Et_2O–PE) (lit. (18) mp 38 to 39°C). IR (KBr) ν (cm^{-1}): 3433, 760. ^1H NMR (300 MHz) δ: 5.91 (s, 1H), 6.62 (t, 1H), 7.30 (dd, 1H), 7.61 (dd, 1H). ^{13}C NMR (75 MHz) δ: 83.5, 119.3, 122.8, 129.6, 137.8, 150.9. Anal. calcd. for C_6H_4ClI (254.45): C 28.32, H 1.58; found: C 28.31, H 1.82.

*2-Chloro-6-phenylsulfanylphenol (**14cc**):* **13cd** (0.161 g) was deprotected to afford **14cc** (0.108 g, 0.456 mmol, 91%) as a white solid, mp 67°C (Et_2O–PE). HRMS calcd. for $C_{12}H_9ClOS$ (263.72): 236.0063; found: 236.0051. IR (KBr) ν (cm^{-1}): 3408, 774, 739, 690. ^1H NMR (300 MHz) δ: 6.59 (s, 1H), 6.86 (t, 1H), 7.13–7.30 (m, 5H), 7.32–7.40 (m, 2H). ^{13}C NMR (75 MHz) δ: 119.8, 120.8, 121.3, 126.9, 128.5, 129.4, 131.5, 134.1, 134.7, 152.5.

LDA-mediated ortho*-Fries rearrangement of carbamate **10a***

N-*Isopropyl-2-hydroxybiphenyl-3-carboxamide (**12**) (19):* **10a** (0.255 g) was *N*-trimethylsilyl-protected according to the general procedure described above. The resulting mixture was cooled to 0°C and LDA solution (2.50 mmol, 2.50 equiv; prepared by stirring a 1:1 mixture of diisopropylamine (0.253 g) and *n*-BuLi in 2 mL of Et_2O at 0°C for 30 min) was added slowly. The resulting mixture was stirred at 0°C for 4 h and warmed to rt. After an additional stirring for 2 h, 5 mL of 2 M HCl was added, the phases were separated, and the aqueous layer was extracted with Et_2O (3 × 20 mL). The combined organic phases were washed with saturated NaCl solution (10 mL), dried over $MgSO_4$, filtered, and evaporated in vacuo. Purification of the crude product by flash chromatography on silica gel (Et_2O–PE gradient) gave **12** (0.201 g, 0.787 mmol, 79%) as a white solid, along with **13aa** (0.052 g, 0.159 mmol, 16%), mp 119°C (Et_2O–PE) (lit. (19) mp 118 to 119°C). IR (KBr) ν (cm^{-1}): 3399, 1642, 1585, 1540, 766, 752, 700. ^1H NMR (300 MHz) δ: 1.27 (d, ^3J = 6.6 Hz, 6H), 4.29 (m, 1H), 6.17 (s, 1H), 6.87 (t, 1H), 7.29–7.36 (m, 2H), 7.37–7.46 (m, 3H), 7.55–7.61 (m, 2H), 11.35 (s, 1H). ^{13}C NMR (75 MHz) δ: 22.6, 41.8, 114.7, 118.2, 124.5, 127.2, 128.1, 129.3, 131.3, 134.8, 137.5, 158.9, 169.5. Anal. calcd. for $C_{16}H_{17}NO_2$ (255.32): C 75.27, H 6.71, N 5.49; found: C 75.37, H 6.79, N 5.35.

Conclusions

In summary, we found a simple protocol for the electrophilic *ortho*-substitution of phenols. The in situ generated *N*-alkyl-*N*-silylcarbamoyl group serves as a powerful DMG for lithiation reactions. Several silyl sources could be used for in situ silyl protection and complete metalation could be achieved by means of *n*-BuLi–TMEDA at low temperatures. The deprotection of the *N*-monoalkylcarbamates to phenols proceeds quantitatively under mild basic conditions.

Acknowledgements

This work was supported by the Deutsche Forschungsgemeinschaft, the Fonds der Chemischen Industrie, and the Alexander von Humboldt foundation. M.K. gratefully acknowledges a fellowship of the Fonds der Chemischen Industrie. The authors wish to thank Mr. Thomas Vatheuer for his engaged work on the *O*-2-chlorophenyl carbamate series during his "Staatsexamensarbeit für Lehramtskandidaten". M.K. thanks Professor Victor Snieckus and his group for the warm welcome at Queen's University during a collaboration stay.

References

1. (*a*) V. Snieckus. Chem. Rev. **90**, 879 (1990); (*b*) M. Gray, M. Tinkl, and V. Snieckus. *In* Comprehensive organometallic chemistry II. Vol. 11. *Edited by* E.W. Abel, F.G.A. Stone, and G. Wilkinson. Pergamon, New York. 1995. pp. 1–92; (*c*) L. Brandsma. *In* Methoden der organischen Chemie (Houben-Weyl). Vol. E19d. *Edited by* M. Hanack. Thieme, Stuttgart. 1993. pp. 369–447; (*d*) B. Chauder, L. Green, and V. Snieckus. Pure Appl. Chem. **71**, 1521 (1999).
2. S.T. Chadwick, R.A. Rennels, J.L. Rutherford, and D.B. Collum. J. Am. Chem. Soc. **122**, 8640 (2000).
3. (*a*) M. Tsukazaki, M. Tinkl, A. Roglans, B.J. Chapell, N.J. Taylor, and V. Snieckus. J. Am. Chem. Soc. **118**, 685 (1996); (*b*) R.S. Laufer, U. Veith, N.J. Taylor, and V. Snieckus. Org. Lett. **2**, 629 (2000).
4. (*a*) R.A. Ewin, A.M. MacLeod, D.A. Price, N.S. Simpkins, and A.P. Watt. J. Chem. Soc. Perkin Trans. 1, 401 (1997); (*b*) S. Pache, C. Botuha, R. Franz, E.P. Kündig, and J. Einhorn. Helv. Chim. Acta **83**, 2436 (2000), and refs. cited therein.
5. (*a*) D. Hoppe, R. Hanko, and A. Brönneke. Angew. Chem. Int. Ed. Engl. **19**, 625 (1980); (*b*) D. Hoppe, R. Hanko, A. Brönneke, and F. Lichtenberg. Angew. Chem. Int. Ed. Engl. **20**, 1024 (1981); (*c*) D. Hoppe and A. Brönneke. Synthesis, 1045 (1982).
6. M.P. Sibi and V. Snieckus. J. Org. Chem. **48**, 1935 (1983).
7. (*a*) S.-i. Mohri, M. Stefinovic, and V. Snieckus. J. Org. Chem. **62**, 7072 (1997); (*b*) B.A. Chauder, A.V. Kalinin, N.J. Taylor, and V. Snieckus. Angew. Chem. Int. Ed. Engl. **38**, 1435 (1999).
8. C. Metallinos, S. Nerdinger, and V. Snieckus. Org. Lett. **1**, 1183 (1999).
9. D. Hoppe and T. Hense. Angew. Chem. Int. Ed. Engl. **36**, 2282 (1997), and refs. cited therein.
10. R. Hanko and D. Hoppe. Angew. Chem. Int. Ed. Engl. **20**, 100 (1981).
11. F. Marr, R. Fröhlich, and D. Hoppe. Org. Lett. **1**, 2081 (1999).

© 2001 NRC Canada

12. (*a*) C. Barberis and N. Voyer. Synlett, 1106 (1999); (*b*) C. Barberis and N. Voyer. Tetrahedron Lett. **39**, 6807 (1998); (*c*) J. Roby and N. Voyer. Tetrahedron Lett. **38**, 191 (1997).
13. (*a*) A.R. van Doorn, M. Bos, S. Harkema, J. van Eerden, W. Verboom, and D.N. Reinhoudt. J. Org. Chem. **56**, 2371 (1991); (*b*) W. Wang and V. Snieckus. J. Org. Chem. **57**, 424 (1992).
14. T. Mukaiyama, S. Motoki, and Y. Hamada. Bull. Chem. Soc. Jpn. **26**, 49 (1953).
15. J.A. Lambrech. Union Carbide Corp. U.S. Patent 3 084 096, 1955; Chem. Abstr. **59**, 11 381a (1963).
16. K.D. Shvetsova-Shilovskaya, N.N. Melnikov, Z.I. Maksimova, T.S. Zakhaova, and L.P. Bocharova. J. Gen. Chem. **32**, 3176 (1962).
17. E. Schmitz and I. Pagenkopf. J. Prakt. Chem. **327**, 998 (1985).
18. A.W. Baker and A.T. Shulgin. Can. J. Chem. **43**, 650 (1965).
19. L.H. Jules, J.A. Faust, and M. Sahyun. J. Am. Pharm. Assoc. Sci. Ed. **45**, 277 (1956).

© 2001 NRC Canada

Synthesis of trichiliasterones A and B — 16-Ketosteroids isolated from *Trichilia hirta* and *Trichilia americana*

Susanne M. Hantos, Sasmita Tripathy, Najma Alibhai, and Tony Durst

Abstract: The syntheses of trichiliasterone A (3β-hydroxypregnan-2,16-dione) and trichiliasterone B (2-hydroxyandrost-1,4-diene-3,16-dione) have been carried out starting from isoandrosterone and testosterone acetate, respectively. In each synthesis the functionality in the D ring was installed prior to working on ring A. In the case of trichiliasterone A, the D ring chemistry involved a Wittig reaction to generate the 17-methylene group, followed by SeO_2 oxidation to give an α,β-unsaturated ketone. Reaction with lithium dimethyl cuprate gave the required 17-ethyl-16-keto functionality. A 2,3-epoxy enol acetate served as the key intermediate for the generation of the 2-keto-3-hydroxy functions in ring A. The transposition of the keto function from C-16 to C-17 in the synthesis of trichiliasterone B was accomplished via oxymercuration–demercuration of the $\Delta^{16—17}$ double bond followed by oxidation. The hydroxyl group at C-2 and the additional ring A unsaturation were introduced by lead tetra-acetate treatment of the 3-keto-4-enone function and subsequent air oxidation.

Key words: 16-ketosteroids, plant steroids, *Trichilia hirta*, trichiliasterones.

Résumé : On a réalisé les synthèses de la trichiliastérone A (3β-hydroxypregnane-2,16-dione) et de la trichiliastérone B (2-hydroxyandros-1,4-diène-3,16-dione) à partir de l'isoandrostérone et de l'acétate de testostérone respectivement. Dans chacune de ces synthèses, la fonctionnalité dans le cycle D a été installée avant de modifier le cycle A. Dans le cas de la trichiliastérone A, la chimie du cycle D implique une réaction de Wittig pour générer le groupe 17-méthylène, suivie d'une oxydation à l'aide de SeO_2 pour obtenir une cétone α,β-insaturée. La réaction du cuprate de diméthyle et de lithium fournit la fonctionnalité 17-éthyl-16-céto requise. Un acétate énolique 2,3-époxy a servi d'intermédiaire clé dans la génération des fonctions 2-céto-2-hydroxy du cycle A. Dans la synthèse de la trichiliastérone B, la transposition de la fonction céto de la position 16 en position 17 a été réalisée par le biais d'une oxymercuration–démercuration de la double liaison en 16—17, suivie d'une oxydation. Le groupe hydroxyle en C-2 et l'insaturation additionnelle du cycle A ont été introduits par un traitement de la fonction 3-céto-4-énone par du tétraacétate de plomb et une oxydation subséquente à l'air.

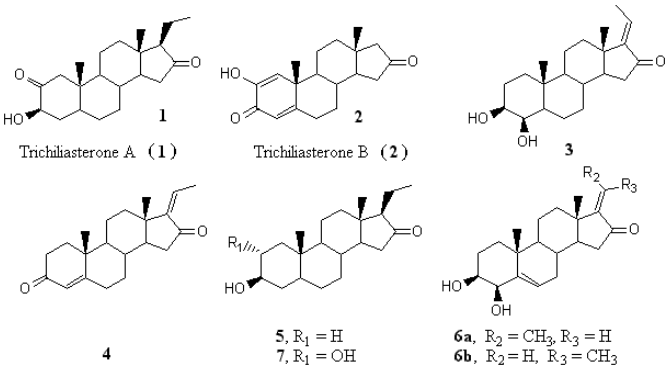
Mots clés : 16-cétostéroïdes, stéroïdes extraits de plantes, *Trichilia hirta*, trichiliastérones.

[Traduit par la Rédaction]

Introduction

Several years ago we reported that the ethanol extracts of the wood and bark of *Trichilia hirta*, a member of the Meliaceae family native to Costa Rica, exhibited significant growth inhibition of larvae of *Ostrinia nubilalis* (European corn borer) and *Peridroma sancia* (variegated cutworm) (1). Partitioning the crude extracts between water and CH_2Cl_2 concentrated the biological activity in the organic layer. Further purification via silica gel chromatography, followed by preparative HPLC afforded two steroids. These were identified as 3β-hydroxypregnan-2,16-dione (**1**) and 2-hydroxyandrost-1,4-diene-3,16-dione (**2**), and given the trivial names, trichiliasterones A and B, respectively. Both possess the relatively rare 16-keto functionality. Additionally, in **1** the ring A substitution pattern is 2-keto-3-hydroxy rather than the more commonly encountered 2-hydroxy-3-keto arrangement.

Relatively few other 16-keto plant steroids have been reported. These include lanisterone E (**3**) isolated from *Lansium anamallayanum* (2), z-guggulsterone (**4**) from *Comminphora mukul* (3), and **5** from *Solanum hainanense*, native to Vietnam (4). Recently, McLaughlin and co-workers (5) reported the isolation of a series of 16-ketosteroids from *Melia volkensii* including E and Z volkendousin (**6a** and **6b**) and meliavosin (**7**). Compounds such as **3** and **5** have been shown to have insecticidal (5), antitumor (5), antiinflammatory (3*a*) and hypocholesteremic (3*a*) activity.



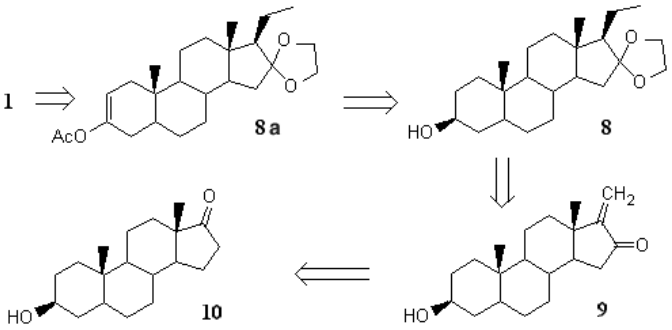
Received August 4, 1999. Published on the NRC Research Press Web site at http://canjchem.nrc.ca on November 22, 2001.

S.M. Hantos, S. Tripathy, N. Alibhai, and T. Durst.[1]
Department of Chemistry, University of Ottawa, ON K1N 6N5, Canada.

[1]Corresponding author (telephone: (613) 562-5800 (ext. 6072); fax: (613) 562-5170; e-mail: tdurst@science.uottawa.ca).

 DOI: 10.1139/cjc-79-11-1747 © 2001 NRC Canada

Scheme 1.



Isolation of **1** and **2** was lengthy and yielded only 0.001% of each component based on dry sawdust. To confirm the structural assignments, based mainly on nanoprobe INADEQUATE NMR technology (1), and to have material available for more complete bioassays, we decided to synthesize both compounds. We also report the synthesis of **5** and the 2-methoxy derivative of **2** which has been isolated from the wood of *Trichilia americana* (Costa Rica).[2]

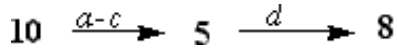
Results and discussion

Trichiliasterone A

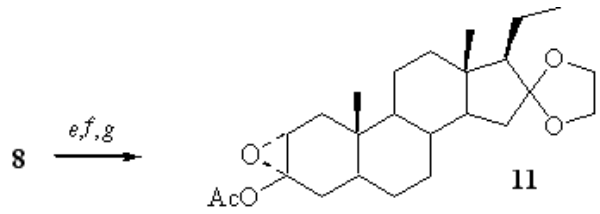
The retrosynthetic analysis for trichiliasterone A (**1**) starting from isoandrosterone (**10**) is shown in Scheme 1. Isoandrosterone was treated with 5 equiv of methylenetriphenylphosphorane affording the corresponding 17-methylene derivative in 88% yield (6). Allylic oxidation with SeO_2-*tert*-butyl hydroperoxide (7) followed by treatment of the crude product mixture, containing both the C-16 allylic alcohol and the enone **9**, with MnO_2 in acetone gave **9** in 48% overall yield. IR (cm^{-1}): 1725 (α,β-unsaturated ketone). ^1H NMR δ: 5.77 and 4.98 (=CH_2).

Reaction of **9** with 2.3 equiv of $(CH_3)_2CuLi$ in diethyl ether at 0°C (8) gave the natural product **5** (4), mp 152 to 153°C (lit. (4) mp 152 to 153°C) in 95% yield. The 16-keto group in **5** was then protected as the ethylene ketal prior to installing the substituents in ring A.

Work on ring A commenced with oxidation of the 3-hydroxy group in **8** with PDC in CH_2Cl_2. The 3-keto derivative (IR (cm^{-1}): 1701 (C=O)), obtained in 96% yield, was converted to the enol acetate **8a** in 84% isolated yield by reaction with excess lithium hexamethyldisilazide followed by acetic anhydride (IR (cm^{-1}): 1602, 1745. ^1H NMR δ: 2.07 (s, 3H), 5.23 (bs, 1H). Subsequent oxidation with MCPBA gave 72% of the epoxy acetate **11** as the major isomer. The structure of **11** (^1H NMR δ: 2.02 (s, 3H), 3.29 (d, J = 5.6 Hz, 1H)) is assumed to be that shown, based on the notion that attack by the oxidizing agent should occur from the less-hindered α-face.

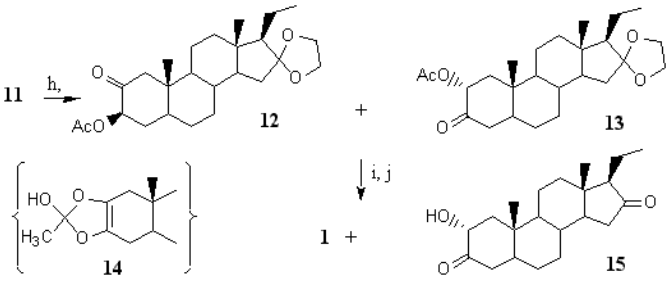


Reagents:
(*a*) $Ph_3{=}CH_2$–DMSO (88%);
(*b*) SeO_2–*t*BuOOH, then MnO_2 – $CHCl_3$ (48%);
(*c*) $(CH)_2CuLi$–ether (95%);
(*d*) $HOCH_2CH_2OH$–H^+ (73%).



Reagents:
(*e*) PDC (96%);
(*f*) $LiN[SiMe_3]_2$–Ac_2O (84%);
(*g*) MCPBA (72%).

The epoxy acetate **11** rearranged upon heating at 160°C and subsequent exposure to basic alumina to a mixture of the acetoxy ketones **12** and **13**. The presumed intermediate in this isomerization is the ortho acetal (partial structure **14** (9)). Since this mixture was difficult to separate, it was subjected to sequential hydrolysis of the ketal and acetate groups. Thus, treatment of the crude mixture of **12** and **13** with PPTS in refluxing aqueous acetone afforded the deprotected C-16 ketones in about 90% crude yield. Further reaction with LiOH in aq THF at 0°C gave 57% of a 1:4 mixture of **1** and **15** that was separated by careful silica gel chromatography. The properties of the sample identified as **1** were identical to those of the natural product trichiliasterone A (1). Trichiliasterone A and the isomeric **15** showed several diagnostic differences in their ^1H NMR spectra which were also noted for **12** and **13** and the sets of partially deprotected intermediates. Most noticeable was that the close spacing of the methyl groups in **1** (δ = 0.67 and 0.76 ppm) vs. a substantial difference for **15** (δ = 0.70 and 1.12 ppm).



Reagents:
(*h*) 160°C, the basic alumina, 24 h;
(*i*) PPTS, acetone, reflux;
(*j*) LiOH–THF, 0°C.

Trichiliasterone B

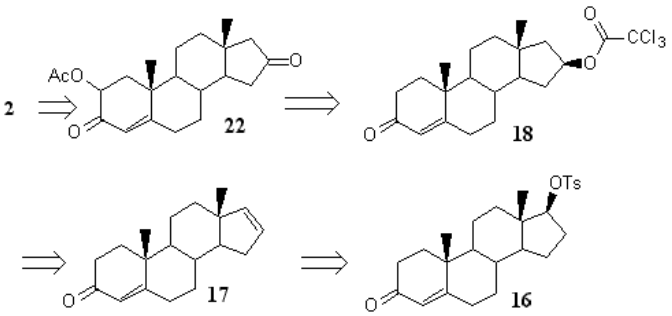
Trichiliasterone B (**2**) was prepared in nine steps starting with testosterone tosylate **16**; the retrosynthetic analysis is outlined in Scheme 2.

Testosterone tosylate was heated with tetrabutylammonium acetate in *N*-methylpyrrolidone at 160°C for 4 h (10). This generated a mixture of the desired alkene **17** (11) and 17-α-acetoxy testosterone, resulting from SN_2 attack by acetate on

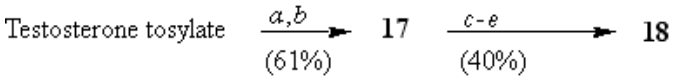
[2] M.B. Isman and D. Wheeler. University of British Columbia. Private communication.

© 2001 NRC Canada

Scheme 2.



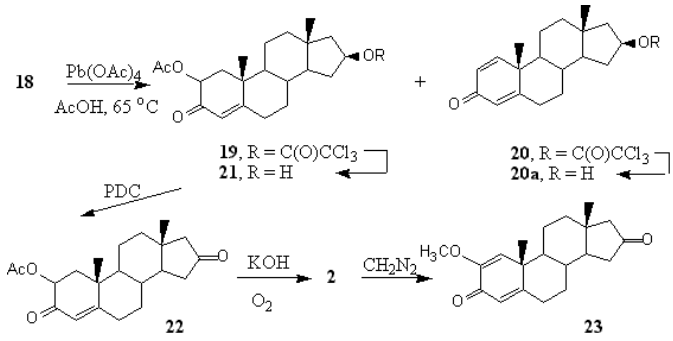
16. Surprisingly, these two reaction products showed almost identical TLC behavior. Therefore, the crude reaction mixture was stirred with KOH in ethanol to generate the more polar 17-α-alcohol that was easily separated from **17**; the yield of **17** was 61%. Other attempts at preparing **17** from **16** either by solvolysis or a DBU-catalyzed elimination reaction were not successful. The former approach resulted in extensive carbocation induced rearrangements while the latter returned only starting material even after 5 h of refluxing in toluene or 24 h refluxing in neat DBU.



Reagents:
(*a*) $Bu_4N^{(+)}AcO^{(-)}$, *N*-methylpyrrolidone, 160°C, 4 h;
(*b*) KOH–methanol;
(*c*) $Hg(OAc)_2$–THF–H_2O;
(*d*) $NaBH_4$–NaOH;
(*e*) $CCl_3C(O)Cl$–DMAP.

Oxymercuration–demercuration of **17** was carried out by stirring with mercuric acetate in a 1:1 mixture of THF–H_2O for 3 days, followed by reduction with sodium borohydride in the presence of NaOH. Surprisingly, no reduction of the A-ring enone system was observed under these conditions and the 16-β alcohol (IR (cm^{-1}): 3624 (OH), 1675, 1618 (enone). ^1H NMR δ: 5.70 (H-4) and 4.4 (H-16)) was obtained in 45% overall yield. Although not crucial, the stereochemistry of the C-16 hydroxyl group was assigned the expected β-stereochemistry based on the presumed attack by $Hg(OAc)_2$ on the less-hindered α-face of the C-16—C-17 double bond. The lack of an observable nOe between H-16 and the C-18 methyl group supports this assignment. In anticipation of the required manipulations in ring A, the C-16 hydroxyl group was protected as the acid-resistant but base-labile trichloroacetate, yielding **18.**

Reaction of **18** with 2 equiv of $Pb(OAc)_4$ in CH_3CO_2H containing a catalytic amount of TsOH for 4 h afforded a 4:1 mixture of the desired 2-acetoxy derivative **19**, as a 1:1 mixture of stereoisomers, and the dienone **20**, based on ^1H NMR analysis of the crude reaction product. Refluxing of this mixture with benzylamine in ethanol for 4 h caused selective removal of the trichloroacetate group yielding the C-16 alcohol **21**. Separation of **21** from the accompanying dienol **20a** was facile. Oxidation of **21** with PDC in CH_2Cl_2 gave 2-acetoxy-androsten-4-ene-3,16-dione **22** (IR (cm^{-1}): 1743 and 1680). Finally, deacetylation of **22** with KOH in methanol under aerobic conditions resulted in the formation of trichiliasterone B (**2**), mp 188 to 189°C, $[\alpha]_D$ = –220° (c = 0.84, CH_2Cl_2), in essentially quantitative yield. The spectroscopic properties of the synthetic product were identical with those of the compound isolated from *T. hirta* (1).



The 2-methyl ether of trichiliasterone B was identified as a component of the CH_2Cl_2 soluble, insecticidally active fraction obtained from the wood of *T. americana*.[2] Reaction of **2** with diazomethane afforded a product whose spectroscopic properties matched those of the natural product thereby confirming its structure assignment as **23**.

Experimental section

General methods

Melting points were determined using a Thomas Hoover capillary melting point apparatus. Mass spectra were determined on a VG 7070E or Kratos concept 2H instrument, using EI unless otherwise specified. ^1H and ^{13}C NMR spectra were obtained as $CDCl_3$ solutions either on a Varian Gemini or Brooker AMX-500 spectrometer. Optical rotations were determined using a PerkinElmer polarimeter (241) set at the sodium D line. Solvents used for reactions or chromatographic separations were distilled prior to use. Usual work-up refers to separating the reaction mixture into aqueous and organic solvent soluble components, drying the organic fraction with $MgSO_4$, and evaporating the solvent.

3-β-Hydroxy-17(20)ene-homoandrostane

n-Butyllithium (8.0 mmol) was added to a suspension of (2.95 g, 8.0 mmol) methyltripenylphosphonium bromide in 45 mL of dry THF at 0°C. The mixture was stirred for 1.5 h and 480 mg (1.65 mmol) of isoandrostane in 30 mL of THF was added. The mixture was stirred overnight at room temperature and then refluxed for 4 h. The cooled mixture was poured into water and extracted twice with 60 mL of ether. Further work-up followed by chromatography (80 g of basic alumina, 9:1 hexane–ethyl acetate) afforded 418 mg (88%) of the title compound, mp 144 to 145°C, (lit. (6) mp 144 to 145°C. IR (CH_2Cl_2) (cm^{-1}): 3313, 1655. ^1H NMR (500 MHz) δ: 4.59–4.57 (m, 2 H) 3.55 (sept. *J* = 4.9 Hz, 1H), 3.44 (bs, 1H), 2.47–2.41 (m, 1H), 2.20–2.17 (m, 1H), 1.78–1.51 (m, 8H), 1.42–1.14 (m, 8H), 1.11–0.87 (m, 2H), 0.79 (s, 3H), 0.73 (s, 3H), 0.74–0.60 (m, 2H). ^{13}C NMR (125 MHz): 161.9, 100.6, 71.2, 54.4, 54.4, 44.9, 38.1, 37.0, 35.7, 35.4, 31.9, 31.4, 29.3, 28.6, 21.1, 18.5, 12.3.

© 2001 NRC Canada

*3β-Hydroxy-16-one-17(20)-ene-homoandrostane (**9**)*

To a mixture of *tert*-butyl hydroperoxide (70%, 0.80 mL, 7.8 mmol) and selenium dioxide (151 mg, 1.34 mmol) in 10 mL of CH_2Cl_2 at room temperature was added 393 mg (1.36 mmol) of 3-β-hydroxy-17(20-ene-homoandrostane in 5 mL of CH_2Cl_2. The reaction mixture was stirred for 48 h. Benzene (10 mL) was added and the solvents were evaporated under reduced pressure. The residue was suspended in CH_2Cl_2 (100 mL) and washed with 10% KOH solution and brine. The organic soluble residue was dissolved in acetic acid (1.5 mL) and stirred with excess dimethyl sulfide (3 mL) for 4 h. Work-up afforded 338 mg of a mixture of **9** and the corresponding allylic alcohol. This mixture was dissolved in 80 mL of $CHCl_3$ and stirred with 1.6 g of activated MnO_2 for 24 h. The mixture was filtered through a Celite pad and the solvent evaporated. Chromatography (18 g silica, 5:1 hexane – ethyl acetate afforded 199 mg (48%) of **9** as a white solid, mp 148–150°C. HRMS calcd. for $C_{20}H_{30}O_2$: 302.2247; found: 302.2238. IR (cm^{-1}): 3393, 1725, 1645. ^{1}H NMR δ: 5.77 (s, 1H), 4.98 (s, 1H), 3.58 (m, 1H), 2.30–1.98 (m, 2H), 1.93–1.90 (m, 1H), 1.83–1.79 (m, 1H), 1.77–1.54 (m, 6H), 1.59–1.21 (m, 8H), 1.17–1.09 (m, 1H), 1.01–0.93 (m, 1H), 0.93 (s, 3H), 0.89–0.76 (m, 1H), 0.84 (s, 3H). ^{13}C NMR δ: 207.0, 156.9, 111.9, 71.2, 54.5, 49.4, 44.5, 42.9, 38.1, 38.0, 36.7, 35.8, 35.4, 34.5, 32.0, 31.4, 28.4, 20.8, 19.2, 12.3.

*3β-Hydroxypregnan-16-one (**5**)*

A 1.4 M solution of CH_3Li in ether (31.4 mL, 43.9 mmol) was added dropwise to a suspension of copper(I) iodide (4.18 g, 0.022 mol) in dry ether (235 mL) at 0°C. After 2 min, an orange solution of the cuprate had formed and a solution of 3β-hydroxy-16-one-17(20)-ene-homoandrostane (**9**) (2.85 g, 9.42 mmol) in dry ether (300 mL) was added dropwise over 30 min. The reaction mixture was warmed to room temperature and allowed to stir for 2 h before quenching with 0.2 M aqueous sulfuric acid (200 mL) and a saturated aqueous solution of ammonium chloride (100 mL). Further work-up and purification by flash chromatography (111 g of silica gel, 9:1 hexanes – ethyl acetate) yielded **5** (2.84 g, 95%) as a white solid, mp 152 to 153°C, (lit. (4) mp 152 to 153°C. IR (cm^{-1}): 3338, 1739. ^{1}H NMR δ: 3.57 (m, 1H), 2.18 (dd, *J* = 18.3, 7.5 Hz, 1H), 1.86 (dd, *J* = 8.6, 2.8 Hz, 1H), 1.84–1.46 (m, 10H), 1.43–1.18 (m, 8H), 1.14–1.08 (m, 1H), 1.00 (t, *J* = 7.5 Hz, 3H), 1.00–0.89 (m, 2H), 0.81 (s, 3H, H-19), 0.81–0.77 (m, 1H), 0.66 (s, 3H). ^{13}C NMR δ: 219.6, 71.1, 65.3, 54.3, 50.5, 44.8, 42.1, 38.5, 38.2, 38.0, 36.7, 35.6, 34.5, 32.2, 31.4, 28.4, 20.7, 17.6, 13.4, 13.4, 12.3.

*3β-Hydroxy-16-ethylenedioxypregnane (**8**)*

A solution of TsOH (5 mg), ethylene glycol (0.46 mL, 8.25 mmol), and **5** (110 mg, 0.344 mmol) was refluxed in dry benzene (12 mL) for 18 h. Water was removed with a Dean–Stark trap. The opaque solution was washed with a saturated aqueous solution of sodium bicarbonate (5 mL) and water (2 × 5 mL). Further work-up, followed by chromatography (11 g of neutral alumina, 9:1 hexanes – ethyl acetate followed by 2:1 hexanes – ethyl acetate) yielded **8** (91 mg, 73%) as a white solid, mp 155–161°C. IR (cm^{-1}): 3412, 1171, 1095, 1022. HRMS calcd. for $C_{23}H_{38}O_3$: 362.2822; found: 362.2830. ^{1}H NMR δ: 3.91–3.85 (m, 2H), 3.84–3.79 (m, 1H), 3.73–3.66 (m, 1H), 3.54 (sept. *J* = 5.0 Hz, 1H), 1.81–1.62 (m, 6H), 1.58–1.19 (m, 13H), 1.16–1.05 (m, 3H), 0.99–0.85 (m, 2H), 0.86 (t, *J* = 7.5 Hz, 3H), 0.77 (s, 3H), 0.68 (s, 3H). ^{13}C NMR δ: 117.5, 71.19, 64.8, 62.9, 60.8, 54.5, 52.1, 44.8, 42.2, 39.9, 38.6, 38.1, 36.8, 35.6, 34.6, 32.0, 31.4, 28.6, 20.8, 17.0, 13.5, 12.9, 12.9.

16-Ethylenedioxypregnan-3-one

Pyridinium dichromate (154 mg, 0.410 mmol) was added to a solution of **8** (59.5 mg, 0.164 mmol) in dry CH_2Cl_2 (1.0 mL) at room temperature. The reaction mixture was stirred for 48 h, diluted with ether (2.0 mL), filtered through anhydrous magnesium sulfate and Celite and rinsed with ether (100 mL). Chromatography of the crude product (7 g of neutral alumina, 4:1 hexanes–acetate) yielded (60 mg, 96%) of the title compound mp 149–151°C. IR (cm^{-1}): 1707, 1172, 1155, 1092 and 1024. HRMS calcd. for $C_{23}H_{36}O_3$: 360.2666; found: 360.2679. ^{1}H NMR δ: 3.92–3.86 (m, 2H), 3.85–3.81 (m, 1H), 3.72–3.67 (m, 1H), 2.38–2.20 (m, 3H), 2.05 (dt, *J* = 15.0, 3.7 Hz, 1H), 1.98 (ddd, *J* = 13.2, 6.4, 2.1 Hz, 1H), 1.81 (dd, *J* = 12.5, 7.0 Hz, 1H), 1.74 (dt, *J* = 12.5, 7.0 Hz, 2H), 1.63–1.22 (m, 11H), 1.18–1.08 (m, 2H), 0.98 (s, 3H), 0.96–0.86 (m, 1H), 0.88 (t, *J* = 7.0 Hz, 3H), 0.78 (dt, *J* = 12.3, 4.0 Hz, 1H), 0.72 (s, 3H). ^{13}C NMR δ: 211.9, 117.4, 64.9, 62.9, 60.8, 53.9, 51.9, 46.6, 44.6, 42.2, 40.0, 38.5, 38.4, 38.2, 35.8, 34.6, 31.7, 28.8, 21.0, 17.0, 13.5, 12.9, 11.5.

*3-Acetoxy-16-ethylenedioxy-2-pregnene (**8a**)*

$LiN(TMS)_2$ (2 equiv) was added to 25 mg (0.069 mmol) of 16-ethylenedioxypregnan-3-one in 5 mL of dry THF at –78°C. The reaction mixture was stirred for 1 h; 3 equiv of acetic anhydride was added and the reaction progress was monitored using TLC (12:1 toluene–acetone). The reaction mixture was quenched after 30 min with water and extracted with EtOAc (3 × 10 mL). Usual work-up provided the title compound in 84% yield as white crystals mp 100–104°C. IR (cm^{-1}): 1745, 1602. HRMS calcd. for $C_{25}H_{38}O_4$: 402.2777; found: 402.2782. ^{1}H NMR δ: 0.71–1.01 (m, 4H), 0.88 (t, 3H, *J* = 7.0 Hz), 0.80 (s, 3H), 0.70 (s, 3H), 1.10–1.61 (m, 11H), 1.81 (ddd, 2H, *J* = 12.8, 7.0 Hz), 1.74 (dt, 1H, *J* = 6.7, 3.7 Hz), 1.91–1.95 (m, 2H), 2.00 (dd, 1H, *J* = 17.0, 3.3 Hz), 2.07 (s, 3H), 3.67–3.72 (m, 1H), 3.81–3.86 (m, 1H), 3.87–3.92 (m, 2H), 5.23 (d, 1H). ^{13}C NMR δ: 169.5, 147.0, 117.5, 112.5, 64.9, 62.9, 60.8, 53.7, 52.0, 42.1, 41.8, 40.0, 38.6, 38.1, 34.7, 31.6, 31.4, 28.3, 21.0, 20.7, 17.0, 13.5, 12.9, 11.7.

*3β-Acetoxy-2α,3α-epoxy-16-ethylenedioxypregnane (**11**)*

To a cooled (0°C) solution of **7** (0.174 g, 0.43 mmol) in dry CH_2Cl_2 (25 mL) was added 2 equiv of MCPBA in one portion. The reaction mixture was warmed to room temperature, stirred for 24 h, and then washed successively with sodium sulfite solution (sat., 2 × 5 mL), sodium bicarbonate (sat., 2 × 5 mL), and water (2 × 10 mL). The resulting oily residue, obtained upon further work-up, was purified by flash column chromatography (9:1 hexane – ethyl acetate) affording 0.13 g, (72%) of **11** as white crystals, mp 95–100°C. IR (cm^{-1}): 1745, 1601. HRMS calcd. for $C_{25}H_{38}O_5$: 418.2720; found: 418.2745. ^{1}H NMR δ: 0.78–0.84 (m, 1H),

© 2001 NRC Canada

0.66–0.69 (m, 1H), 0.68 (s, 3H), 0.87 (t, 3H, *J* = 7.0 Hz), 0.93 (s, 3H), 0.95–1.54 (m, 14H), 1.72 (dt, 1H, *J* = 9.0, 3.0 Hz), 1.79 (dd, 1H, *J* = 12.9, 7.0 Hz), 1.88 (dd, 1H, *J* = 14.0, 11.0 Hz), 1.97–2.07 (m, 2H), 2.02 (s, 3H), 3.29 (d, 1H, *J* = 5.6 Hz), 3.67–3.70 (m, 1H), 3.81–3.86 (m, 1H), 3.87–3.90 (m, 2H). ^{13}C NMR δ: 169.3, 117.4, 83.0, 64.8, 62.9, 60.7, 58.3, 53.5, 51.9, 41.9, 39.9, 38.7, 38.6, 38.4, 34.6, 34.4, 31.5, 30.7, 27.9, 21.1, 20.5, 16.9, 13.4, 12.8, 12.7.

*3β-Hydroxypregnan-2,16-dione (**1**) and 2α-hydroxypregnan-3,16-dione (**15**)*

Compound **11** (220 mg, 0.53 mmol) was heated neat at 160°C for 15 min and then loaded on a basic Al_2O_3 column for 24 h. Elution with solvent ethyl acetate:hexane (3:7) provided a mixture of compound **12** and **13** (132 mg, 60%) as a solid (^{1}H NMR spectrum shows a multiplet at the δ 5.17–5.31 region of the spectrum accounting for the -CH attached to acetate groups). To a solution of the above acetal (**12** and **13**) (132 mg, 0.32 mmol) in aqueous acetone (5 mL) was added pyridinium tosylate (PPTS) (23.0 mg, 0.095 mmol). The resultant solution was refluxed for 3 h. Solvent was removed in vacuo and the residue was extracted into ethyl acetate and was washed with an aqueous solution of sodium bicarbonate and brine. The organic layer was separated and dried and the crude product was used without any further purification. (The ^{1}H NMR spectrum showed the absence of signal due to ethylenedioxy group (δ = 3.8 to 3.9).

To a solution of the above acetates (106 mg, 0.28 mmol) in a THF:H_2O mixture (5 mL, 3:1) at 0°C, was added LiOH (1 M solution, 0.6 mL, 0.56 mmol). The solution was stirred at 0°C for 2 h. The mixture was extracted into ethyl acetate (10 mL) and was washed with water (2 mL). The organic layer was separated, dried, and concentrated. Chromatography (3:7, ethyl acetate: hexane) afforded **1** (12.0 mg, 13%) and **15** (40 mg, 43%).

For compound **1**: mp 144 to 145°C, $[\alpha]_D$ = –78° (c 0.47, MeOH). HRMS calcd. for $C_{21}H_{32}O_3$: 332.2351; found: 332.2336. The spectroscopic properties were identical with the reported data (1). Compound **15**: mp 136 to 137°C. IR (cm^{-1}): 1714, 1734. HRMS calcd. for $C_{21}H_{32}O_3$: 332.2351; found: 332.2359. ^{1}H NMR δ: 4.20 (dd, *J* = 7.1, 12.0 Hz, 1H), 3.50 (bs, 1H, OH), 2.46 (dd, *J* = 7.0, 12.5 Hz, 1H), 2.39 (t, *J* = 13.9 Hz, 1H), 2.27 (dd, *J* = 3.7, 14.1 Hz, 1H), 2.19 (dd, *J* = 7.6, 18.2 Hz, 1H), 1.92 (dt, *J* = 2.9, 12.5 Hz, 1H), 1.78–0.90 (m, 16H), 1.08 (s, 3H), 0.97 (t, *J* = 7.5 Hz, 3H), 0.68 (s, 3H). ^{13}C NMR ($CDCl_3$) δ: 12.8, 13.3, 13.5, 17.5, 21.1, 28.2, 31.8, 33.6, 37.2, 38.0, 38.3, 42.1, 42.2, 48.1, 48.2, 50.1, 53.7, 65.2, 72.6, 210.7, 218.2.

*Androsta-4,16-dien-3-one (**17**)*

Tetrabutylammonium acetate (17.4 g, 57.8 mmol) was added to a clear yellow solution of testosterone tosylate (**16**) (4.15 g) in dry *N*-methylpyrrolidinone (90 mL) at room temperature and warmed to 160°C. The reaction mixture was stirred 4 h, dissolved in ether (200 mL), and washed with water (3 × 50 mL). The aqueous layer was extracted with ether (2 × 100 mL) and the combined extracts were dried (anhydrous magnesium sulfate), filtered through a sintered glass funnel, and concentrated in vacuo. The *N*-methylpyrrolidinone was removed by vacuum distillation (54°C, 5 mmHg (1 mmHg = 133.322 Pa)) and the resulting residue was dissolved in 95% ethanol (60 mL). A 0.54 M aqueous solution of potassium hydroxide (57 mL) was added and the mixture was stirred at room temperature for 48 h. The reaction mixture was diluted with ethyl acetate (120 mL) and neutralized to pH 7.0 with 5% aqueous hydrochloric acid. Further work-up afforded a yellow solid. Column chromatography (200 g of neutral alumina, 2:1 petroleum ether – ether) yielded **17** (1.54 g, 61%) as a pale yellow solid, mp 131–135°C (lit. (11) mp 131–133°C).

16β-Hydroxyandrost-4-en-3-one

Water (10 mL) and mercuric acetate (1.43 g, 4.5 mmol) were added to a solution of androsta-4–16-dien-3-one (**17**) (1.22 g, 4.5 mmol) in THF (10 mL) at room temperature. The reaction mixture was stirred 3 days, 3.0 M aqueous sodium hydroxide (10 mL) was added followed by 0.5 M sodium borohydride in 3.0 M aqueous sodium hydroxide (10 mL), added in 2 mL aliquots. The mixture was stirred for 2 min, stirring was stopped, and mercury was allowed to settle. Salt was added to saturate the aqueous layer followed by THF (6 mL). The mixture was stirred for 30 min, filtered through a cotton plug with suction and the layers were separated. Further usual work-up followed by chromatography (150 g of neutral alumina, 9:1 hexane–ether) afforded the title compound (0.584 g, 45%) as a white solid mp 153.5–155.5°C; 0.22 g, 18% of starting material **17** were reisolated. For 16β-hydroxyandrost-4-en-3-one: IR (5% in CCl_4, solution cell) (cm^{-1}): 3624, 1675, 1618. HRMS calcd. for $C_{19}H_{28}O_2$: 288.2090; found: 288.2087. ^{1}H NMR δ: 5.70 (s, 1H), 4.41–4.36 (m, 1H), 2.43–2.14 (m, 5H), 2.02–1.97 (m, 1H), 1.85–1.80 (m, 1H), 1.76–1.40 (m, 8H), 1.31 (dt, *J* = 13.1, 5.5 Hz, 1H), 1.17 (s, 3H, H-19), 1.17–0.88 (m, 4H), 0.98 (s, 3H). ^{13}C NMR δ: 199.5, 171.2, 123.8, 71.7, 53.8, 53.4, 51.1, 40.0, 38.6, 38.6, 37.0, 35.6, 35.3, 33.9, 32.8, 32.2, 20.6, 18.8, 17.3.

*16β-Trichloroacetoxyandrost-4-en-3-one (**18**)*

Triethylamine (0.69 mL, 0.50 mmol), trichloroacetyl chloride (0.44 mL, 0.40 mmol), and *N*,*N*-dimethylaminopyridine (4.1 mg, 0.040 mmol) were added to a solution of 16β-hydroxyandrost-4-en-3-one (96 mg, 0.33 mmol) in dry methylene chloride (7.5 mL) at 0°C. The reaction mixture was stirred for 30 min at 0°C and 2 h at room temperature, poured into water (10 mL), and worked up in the appropriate manner. Flash chromatography (6 g of silica gel, 9:1 hexanes – ethyl acetate) yielded **18** (120 mg, 83%) as a yellow solid; starting material (20 mg, 11%) was also recovered. For **17**: mp 147–149°C. HRMS calcd. for $C_{21}H_{27}{}^{35}Cl_3O_3$: 432.1028; found: 432.1049. IR (cm^{-1}): 1759, 1669, 1615. ^{1}H NMR δ: 5.69 (s, 1H), 5.29–5.27 (m, 1H), 2.43–2.26 (m, 5H), 2.01–1.98 (m, 1H), 1.99–1.74 (m, 3H), 1.67–1.44 (m, 6H), 1.16 (s, 3H), 1.15–0.99 (m, 4H), 0.95 (s, 3H). ^{13}C NMR δ: 199.2, 170.5, 161.4, 124.0, 80.2 (2 C), 53.7, 53.0, 47.3, 39.9, 38.6, 38.1, 35.6, 35.3, 33.9, 33.8, 32.6, 32.0, 20.6, 17.8, 17.3.

*2β-Acetoxy-16β-trichloroacetoxy-androst-4-en-3-one, 2α-acetoxy-16β-trichloroacetoxy-androst-4-en-3-one (**19**), and 16β-trichloroacetoxyandrosta-1,4-dien-3-one (**20**)*

Lead tetraacetate (719 mg, 1.61 mmol), recrystallized from hot glacial acetic acid, was dissolved in glacial acetic acid (9 mL) at 50°C. The mixture was stirred for 15 min. A

© 2001 NRC Canada

solution of 16β-trichloroacetoxyandrost-4-en-3-one (**18**) (631 mg, 1.50 mmol) and TsOH (approximately 10 mg) in glacial acetic acid (8 mL) was added and the mixture was warmed to 60–70°C for 19 h. The mixture was cooled to room temperature, diluted with ethyl acetate (125 mL), and washed with water (2 × 10 mL) and a saturated aqueous solution of sodium bicarbonate (4 × 10 mL). The crude product (620 mg) was judged to be a mixture of the three title compounds and was used as is.

*2β-Acetoxy-16β-hydroxyandrost-4-en-3-one, 2α-acetoxy-16β-hydroxyandrost-4-en-3-one (**21**) and 16β-hydroxyandrosta-1,4-dien-3-one (**20a**)*

A solution of 2α- and 2β-acetoxy-16β-trichloroacetoxyandrost-4-en-3-one (**19**) and 16β-trichloroacetoxyandrostan-1,4-dien-3-one (**20**) (250 mg) in absolute ethanol (20 mL) was warmed to 30°C and stirred for 1 h. Triethylamine (0.49 mL, 3.5 mmol) and benzylamine (0.41 mL, 3.8 mmol) were added and the mixture was heated at reflux for 4 h. The reaction mixture was diluted with ethyl acetate (100 mL) and washed with 5% aqueous hydrochloric acid (3 × 10 mL) and water (3 × 10 mL). Flash chromatography (32 g of silica gel, 4:1 hexanes – ethyl acetate) yielded a 1:2.4 mixture of **21** (176 mg, 47%) as a yellow solid and **20a** (39 mg, 27%) as a white solid.

For the mixture of 2α- and 2β-acetoxy compounds: IR (cm^{-1}): 3484, 1748, 1686, 1614. ^1H NMR δ (major isomer): 5.71 (d, J = 1.5 Hz, 1H, H-4), 5.41 (dd, J = 14.1, 5.4 Hz, 1H, H-2), 2.13 (s, 3H, H-21, 2-OAc), 1.30 (s, 3H, H-19); (minor isomer): 5.74 (d, J = 1.2 Hz, 1H, H-4), 5.28 (dd, J = 13.2, 4.5 Hz, 1H, H-2), 2.11 (s, 3H, H-21, 2-OAc), 1.17 (s, 3H, H-19); (major + minor): 4.37–4.25 (m, 2H, H-16), 2.51–2.14 (m, 8H), 2.11, 1.95–1.70 (m, 8H), 1.60–1.25 (m, 12H), 1.08–0.85 (m, 8H), 0.96 (s, 6H).

For 16β-hydroxyandrostan-1,4-dien-3-one (**20a**): mp 173–175°C. IR (cm^{-1}): 3407, 1695, 1617. HRMS calcd. for $C_{19}H_{26}O_2$: 286.1934; found: 286.1989. ^1H NMR δ: 7.03 (d, J = 10.2 Hz, 1H), 6.14 (dd, J = 10.2, 1.9 Hz), 6.04 (s, 1H), 4.42–4.32 (m, 1H), 2.49–2.40 (m, 1H), 2.39–2.29 (m, 1H), 2.25–2.11 (m, 2H), 1.98–0.79 (m, 12H), 1.22 (s, 3H), 1.00 (s, 3H). ^{13}C NMR δ: 186.3, 169.1, 153.8, 127.46, 123.8, 71.66, 53.3, 53.1, 51.1, 43.6, 40.3, 38.5, 37.2, 35.3, 33.8, 32.8, 22.6, 19.0, 18.7.

*2α- and 2β-Acetoxyandrost-4-en-3,16-dione (**22**)*

Pyridinium dichromate (89 mg, 0.24 mmol) was added to a solution of 2α- and 2β-acetoxy-16β-hydroxyandrost-4-en-3-one (55 mg, 0.16 mmol) in dry methylene chloride (1 mL) at room temperature. The reaction mixture was stirred for 20 h, diluted with ether (2 mL), filtered through anhydrous magnesium sulfate and Celite in a sintered glass funnel. The product was concentrated in vacuo affording **22** (46 mg, 83%) as a white solid, mp 201 to 202°C. IR (cm^{-1}): 1743, 1650, 1617. ^1H NMR δ (major isomer): 5.75 (d, J = 1.5 Hz, 1H), 5.44 (d, J = 14.1, 8.7 Hz, 1H, H-2), 2.43–2.11 (m, 3H), 2.15 (s, 3H, H-21), 1.98–1.04 (m, 14H), 1.34 (s, 3H, H-19), 0.92 (s, 3H, H-18); (minor isomer): 5.78 (d, J = 1.3 Hz, 1H, H-4), 5.30 (dd, J = 12.5, 5.0 Hz, 1H, H-2), 2.13 (s, 3H, H-21, 2-OAc); all other peaks buried under the major isomer. ^{13}C NMR δ (major isomer): 17.26, 193.4, 170.2, 169.7, 122.1, 71.1, 55.5, 54.0, 50.9, 41.2, 40.6, 39.0, 38.8, 37.6, 35.1, 32.1, 32.0, 22.0, 20.8, 18.1, 17.9.

*2-Hydroxyandrosta-1,4-diene-3,16-dione (**2**)*

A solution of 2α- and 2β-acetoxyandrost-4-ene-3,17-dione (**16**) (118 mg, 0.343 mmol) in 95% ethanol (14 mL) was stirred at room temperature for 30 min. A solution of potassium hydroxide (192 mg, 3.43 mmol) in water (7 mL) was added and the mixture was stirred vigorously for 1 h. Stirring was stopped and the flask was left open to the air for 4 days. The reaction mixture was diluted with ethyl acetate (28 mL), neutralized with 5% aqueous hydrochloric acid, and washed with water (1 × 10 mL) and brine (1 × 10 mL). The aqueous layer was extracted with ethyl acetate (1 × 20 mL) and the combined extracts were dried (anhydrous magnesium sulfate), filtered through a sintered glass funnel, and concentrated in vacuo affording a pale yellow solid. Flash chromatography (10 g of silica gel, 3:1 hexanes – ethyl acetate) yielded **2** (103 mg, 100%) as a white solid, mp 188 to 189 °C. The spectroscopic properties matched those reported (1). Anal. calcd. for $C_{19}H_{24}O_3$: C 75.97, H 8.05; found: C 75.84, H 8.36.

*2-Methoxyandrost-1,4-diene-3,16-dione (**23**)*

A solution of diazomethane in ether (1 mL, approximately 2.8% w/v prepared from nitrosomethylurea) was added to 2-hydroxyandrosta-1,4-diene-3,16-dione (**2**) (21 mg, 0.071 mmol) in methylene chloride (5 mL) at 5°C. The reaction mixture was stirred for 21 h at room temperature and was opened to air to facilitate the evaporation of excess diazomethane and solvent. The pale yellow solid was purified by flash chromatography (2 g of silica gel, 3:1 hexanes – ethyl acetate) yielding **23** (4.2 mg, 19%) as a white solid; (14 mg, 65%) of **2** was recovered. For **23**: HRMS calcd. for $C_{20}H_{26}O_3$: 314.1901; found: 314.1893. ^1H NMR δ: 6.11 (d, J = 1.2 Hz, 1H, H-4), 5.93 (s, 1H, H-1), 3.66 (s, 3H-H-20), 2.51–2.38 (m, 2H), 2.23–2.12 (m, 2H), 2.07–1.71 (m, 5H), 1.53–1.37 (m, 2H), 1.27 (s, 3H), 1.26–1.07 (m, 4H), 0.95 (s, 3H, H-18). These data matched those of the product isolated from *T. americana* (6).

Acknowledgements

We sincerely thank Professor J.B. Orr, Department of Biochemistry, Memorial University of Newfoundland, St. John's, Newfoundland, for a generous donation of testosterone and isoandrostane, the starting materials in our syntheses. The continued support of the Natural Sciences and Engineering Research Council of Canada (NSERC) in the form of an operating grant (TD) is also acknowledged.

References

1. D.C. Chauret, T. Durst, J.T. Arnason, P. Vindas-Sanchez, L. San Ramon, L. Poveda, and P.A. Kiefer. Tetrahedron Lett. **37**, 7875 (1996).
2. K.K. Purushothaman and A. Sarada. Can. J. Chem. **65**, 150 (1987).
3. (*a*) V.D. Patel, R.R. Nayak, and S. Dev. Tetrahedron, **28**, 2341 (1972); (*b*) W.R. Benn and R.M. Dodson. J. Org. Chem. **29**, 1142 (1964).

© 2001 NRC Canada

4. (*a*) G. Adam, H.T. Huong, and N.H. Kho. Phytochemistry, **17**, 1802 (1978); (*b*) G. Adam and K. Schreiber. Ann. Chem. **707**, 191 (1967).
5. L.L. Rogers, L. Zeng, and J.L. McLaughlin. J. Org. Chem. **63**, 3781 (1998).
6. F. Sondheimer and R. Mechoulam. J. Amer. Chem. Soc. **79**, 5029 (1958).
7. M.U. Umbreit and K.B. Sharpless. J. Amer. Chem. Soc. **99**, 5526 (1977).
8. M. Suzuki and R. Noyori. *In* Organocopper reagents. A practical approach. *Edited by* R.J.K. Taylor. Oxford University Press, Oxford. 1994. Chap. 9. p. 195.
9. (*a*) K.L. Williamson and W.S. Johnson. J. Org. Chem. **26**, 4563 (1961); (*b*) L.F. Fieser and R. Stevenson. J. Amer. Chem. Soc. **76**, 1728 (1954); (*c*) A. Bowers, E. Denot, L.C. Ibanez, M.E. Cabezas, and H.J. Ringold. J. Org. Chem. **27**, 1962 (1962).
10. H.B. Henbest and W.R. Jackson. J. Chem. Soc. 954 (1962).
11. G. Ohloff, B. Maurer, B. Winter, and W. Giersch. Helv. Chim. Acta, **66**, 192 (1983).

© 2001 NRC Canada

Ortho-directed metallation of π-deficient heterocycles in connection with palladium-catalyzed biaryl cross-coupling — Synthesis of marine alkaloids of the pyridoacridine series

A. Godard, P. Rocca, F. Guillier, G. Duvey, F. Nivoliers, F. Marsais, and G. Quéguiner.

Abstract: Connection between *ortho*-directed metallation of π-deficient heterocycles and Suzuki cross-coupling reactions provides a very efficient and fruitful strategy to polycyclic molecules of biological interest. The methodology is used to synthesize alkaloids or precursors and analogues of natural compounds of the pyrido[2,3,4-*k*,*l*]acridine series.

Key words: marine alkaloids, pyrido[2,3,4-*k*,*l*]acridines, metallation, cross-coupling.

Résumé : L'association des réactions de métallation et de couplage croisé de type Suzuki est une méthode efficace et fructueuse de synthèse de molécules polycycliques possédant des propriétés biologiques intéressantes. Cette méthode a été utilisée pour synthétiser des composés précurseurs ou analogues de composés naturels de la famille des pyrido[2,3,4-*k*,*l*]acridines.

Mots clès : alcaloïdes marins, pyrido[2,3,4-*k*,*l*]acridines, metallation, couplage croisé.

Introduction

For many years metallation has been an essential tool for the functionalization of aromatics under mild conditions, regioselectively and in good yields. Application of this methodology to π-deficient heterocycles was difficult due to their high electrophilic reactivity, which was overcome in a few laboratories using specific conditions (1). This reaction is now widely used for the synthesis of functionalized pyridines, quinolines, and diazines of biological interest. Moreover, it has been successfully connected to other methodologies, leading to complex molecules via short routes and in good overall yields (2). One of these complementary reactions is the biaryl cross-coupling reaction catalyzed by transition metals. "The connection between the DoM and Suzuki cross-coupling reactions provides an entry into highly functionalized biaryls, *m*-teraryls, and tetraaryls whose generality, and regioselectivity allow anticipation of broad application for the synthesis of polyaryls with interesting properties" wrote Snieckus in 1990 (3). To emphasize this sentence we wish to review herein the main results obtained in the synthesis of a recently discovered series of marine alkaloids.

A wide range of polycyclic alkaloids which contain the common 7*H*-pyrido[2,3,4-*k*,*l*]acridine moiety **1** have been discovered since the isolation of amphimedine **2** in 1983 (4). Ascidiademine **3**, meridine **4**, and cystodytins **5** are a few examples of this family. Most of these natural products exhibit interesting biological properties (Ca-releasing, antiviral, antimicrobial activities, cytotoxicity against L_{1210} cells, topoisomerase inhibitors, etc.) and different syntheses have been published (4).

Our experience in the synthesis of complex polyaromatics prompted us to look for a general route to 4*H*-pyrido[2,3,4-*k*,*l*]acridin-4-ones **6**. As shown on the retrosynthetic pathway depicted on Scheme 1, the intermediate benzo[*c*]-2,7-naphthyridine **7** could be synthesized by a cross-coupling and (or) condensation sequence from 2,3,4-trisubstituted pyridines **8**. We wish to report in the paper the synthesis of polysubstituted pyridines **8** as precursors of pyrido-acridones **6** via the diazaphenanthrenes **7**.

Synthesis of pyridine cross-coupling partners

LDA deprotonation of commercial 4-chloropyridine **9** followed by carboxylation afforded the corresponding 4-chloronicotinic acid **10** which was easily esterified to **11** in 93% overall yield (Scheme 2). Application of LiTMP–TMEDA metallation conditions on the 2-methoxy-nicotinamide **12**, followed by reaction of iodine, furnished

Received March 8, 2001. Published on the NRC Research Press Web site at http://canjchem.nrc.ca on November 15, 2001.

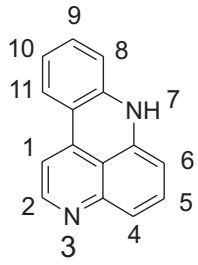
Dedicated to Professor Victor Snieckus for his contributions to Canadian chemistry.

A. Godard,[1] P. Rocca, F. Guillier, G. Duvey, F. Nivoliers, F. Marsais, and G. Quéguiner. UMR 6014 du CNRS – Institut de chimie organique fine – Institut national des sciences appliquées de Rouen – BP08 76131 Mont-Saint-Aignan CEDEX, France.

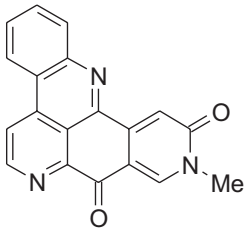
[1]Corresponding author (telephone: (33) 0235528416; fax: (33) 0235528320; e-mail: alain.godard@insa-rouen.fr).

 DOI: 10.1139/cjc-79-11-1754 © 2001 NRC Canada

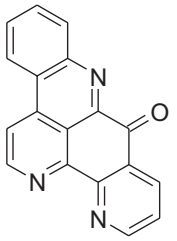
Fig. 1.



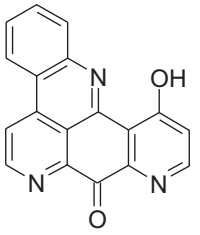
7*H*-Py ido[2,3,4-*k*,*l*]ac idine **(1)**



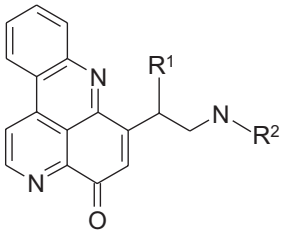
mphimedine **2**



scididemine **3**

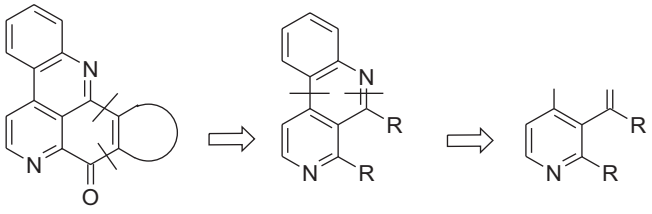


Me idine **4**



Cystodytins **5**

Scheme 1.

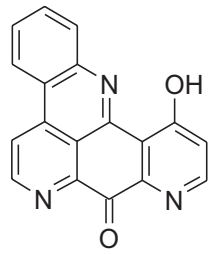


6 **7** **8**

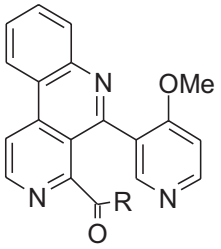
the 4-iodo derivative **13** in modest yield (55%). The same methodology was used for the preparation of the 4-(9-borabicyclononanyl) nicotinamide **14** from **12** (62%) (5) (Scheme 2).

It was established in 1993 by our group (6), that metallation of iodopyridines **15** and **16** by LDA at low temperature was feasible when the pyridine nucleus bears a second halogen (chloro or fluoro). In most cases, lithiation of haloiodopyridines **15** and **16** was regioselectively directed by the iodo group, which subsequently migrates to give the more stabilized 2-substituted 3-lithio-4-iodo-

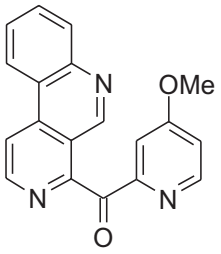
Fig. 2.



(4) Meridine

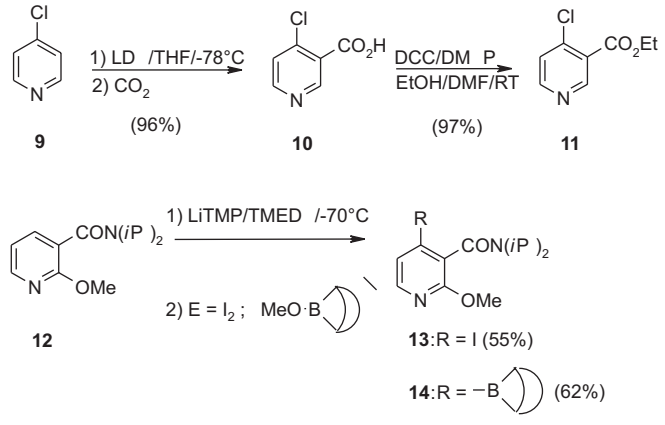


32



33

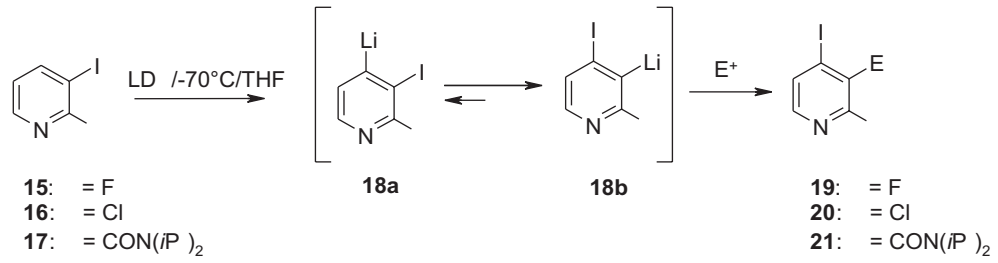
Scheme 2.



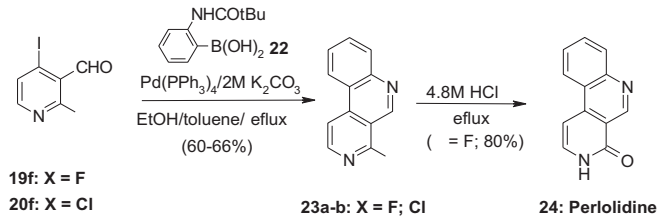
pyridines **18b**. Lithiated products were quenched with an electrophile to provide 4-iodopyridines **19** and **20** (Scheme 3, Table 1). This methodology was later on successfully extended to 2-carboxamido pyridines **17** to give **21** (7).

© 2001 NRC Canada

Scheme 3.



Scheme 4.



Synthesis of alkaloids of pyrido[2,3,4-*k*,*l*]-acridine series and analogues

Some 4-iodopyridines (**19**–**21**) were involved in cross-coupling reactions with 2-pivaloylamino phenyl boronic acid **22** under Suzuki conditions (8) to give 4-phenylpyridines, which were cyclized later on to 4,5-disubstituted benzo[*c*]-2,7-naphthyridines, precursors of polycyclic natural alkaloids or analogues (9).[2]

Synthesis of perlolidine 24

Although perlolidine **24** does not strictly belong to the pyrido-acridine series, its synthesis is representative of the reported methodology (6). Reaction between 2-fluoro- or 2-chloro-4-iodo-3-pyridine carboxaldehyde (**19f** or **20f**) with phenylboronic acid **22** using $Pd(PPh_3)_4$ as catalyst, resulted in hetero cross-coupling and subsequent cyclization to 3,6-diazaphenanthrene **23a**–**b**. Hot acid treatment of the fluoro compound **23a** induces hydrolysis to perlolidine **24**, an alkaloid of New Zealand perennial rye grass *Lolium perenne* L which is effective on plant growth (6) (Scheme 4).

Formal synthesis of amphimedine 2

Amphimedine **2** is the first alkaloid isolated in the pyrido[2,3,4-*k*,*l*]acridine series. This compound possesses interesting cytotoxic properties (10). Compounds **25** (X = OH, Cl) have been described by Prager and co-workers (11) as intermediates in the total synthesis of amphimedine **2**. They could be synthesized from trisubstituted pyridines **13** or **14** as shown on the retrosynthetic pathway depicted on Scheme 5.

The cross-coupling reaction between *N*-pivaloylamino-phenylboronic acid **22** and 4-iodonicotinamide **13** gives the corresponding biaryl compound **27** which, unfortunately, could not be cyclized to the desired tricyclic compound under the conditions used (7) (Scheme 6).

To use milder cyclization conditions, we decided to work on an unprotected amino derivative (5). The corresponding 4-(*ortho*-aminophenyl)pyridine structure was prepared by coupling pyridylborane **14** with *ortho*-iodoaniline under modified Suzuki conditions ($Pd(PPh_3)_4$ – aq NaOH) (12). Biaryl **28** was thus obtained in good yield (Scheme 7). It was subjected to cyclization by treatment with LDA in excess to give a resulting orange substance which was difficult to purify, but its ^{1}H NMR spectrum is consistent with the cyclized structure. Subsequently, it was identified as the benzonaphthyridine triflate **26**, after treatment by triflic anhydride, in an overall yield of 30% from the biaryl **28**.

Compound **26** was then subjected to cross-coupling with 4-(tributylstannyl)pyridine under typical Stille conditions (13). Prager's intermediate **29** was obtained in excellent yield by demethylation of **29** with BBr_3 (Scheme 7). The synthesis of **29** proves the feasibility of the method but the overall yield is low (5% in five steps starting from **12**) (5).

To improve the previous strategy, we decided to introduce the exocyclic pyridine ring before the cross-coupling and cyclization steps (14). Thus, imines **20m** and **21m** (previously obtained from 2-chloro- and *N*,*N*-diisopropyl-2-carboxamido-3-iodopyridines **16** and **17**; Scheme 3, Table 1) were submitted to the cross-coupling reaction with phenylboronic acid **22** following a Suzuki procedure. Spontaneous cyclization of the intermediate phenylpyridines, respectively, led to the expected 4-chloro- and 4-(*N*,*N*-disopropylcarboxamido)-5-(4-pyridyl)benzo[*c*]-2,7-naphthyridines (**30a**–**b**) in high yields (82% and 72%) (Scheme 8). The overall yield is also good (57% for **30a** from **16**, and 53% for **30b** from **17**) (14).

The synthesis of **30a** was carefully studied, and it was found that the overall yield could be improved using a "one-pot" procedure from pyridine **16** (14). Metallation, isomerization, cross-coupling, and cyclisation were performed without isolation of any intermediate (LiOH resulting from hydrolysis of the lithiation mixture acted as a base for the cross-coupling step) (Scheme 9). An excellent overall yield could be then observed: 82% from **16** (14).

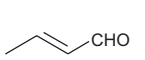
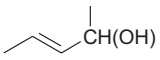
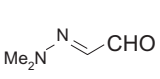
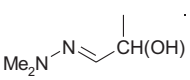
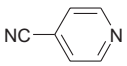
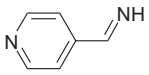
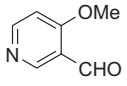
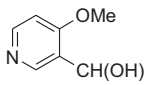
Synthesis of an "open-ring" amphimedine (31)

A rapid and efficient synthesis of an open-ring analogue **31** of amphimedine was achieved (15) by anionic acylation

[2] Gronowitz synthesized some benzo[*c*]-2,7-naphthyridines by cross-coupling between a 4-pyridyl stannane and *ortho*-bromoanilides.

© 2001 NRC Canada

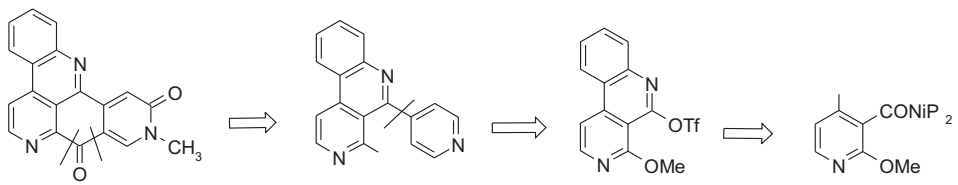
Table 1.

Entry	Electrophile	E	Yield (%) X = F	X = Cl	X = CON(iPr)$_2$	References
1	H_2O	H	96 (**19a**)	73 (**20a**)	95 (**21a**)	(6), (7)
2	D_2O	D	96 (**19b**)	75 (**20b**)	97 (**21b**)	(6), (7)
3	CH_3I	CH_3/CH_3CH_2	93 (**19c**)	69 (**20c**)	90 (**21c**)	(6), (7)[a]
4	PhCHO	PhCH(OH)	61 (**19d**)	64 (**20d**)	89 (**21d**)	(6), (7)
5	TsN_3	NH_2	81 (**19e**)	57 (**20e**)	--	(6)[b]
6	HCO_2Et	CHO	75 (**19f**)	64 (**20f**)	82 (**21f**)	(6), (7)
7	I_2	I	54 (**19g**)	71 (**20g**)	87(**21g**)	(6), (7)
8	CH_3-CHO	CH3-CH(OH)		79 (**20h**)		(20)
9	$(CH_3CO)_2O$	CH_3-CO		46 (**20i**)		(20)
10	NC-CO_2CH_3	CO_2CH_3		70 (**20j**)		(20)
11				69 (**20k**)		(20)
12				60 (**20l**)		(20)
13				70 (**20m**)	73 (**21m**)	(14)
14					80 (**21n**)	(7)

[a] **17** gave the 3-methyl derivative which on further alkylation afforded **21c** (R = Et).

[b] The intermediary crude azide was reduced by treatment by H_2S in MeOH.

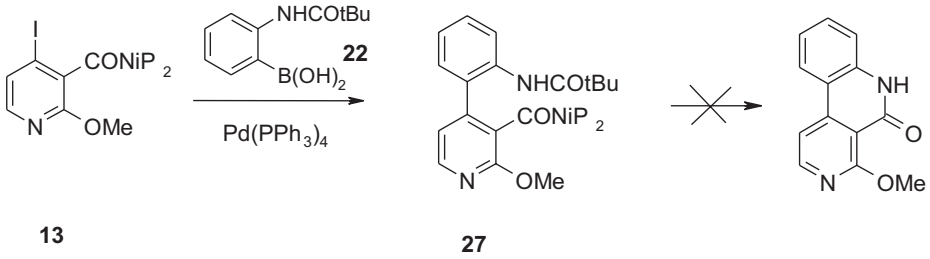
Scheme 5.



of a chloronaphthyridine, following a general strategy described by Miyashita (16) in the pyrimidine series. Thus, 4-chlorobenzonaphthyridine **23b** reacted with N-methyl-2-oxo-5-pyridine carboxaldehyde in the presence of stoichiometric amounts of imidazolium iodide and NaH to give the expected ketone **31** in 55% yield (15) (Scheme 10).

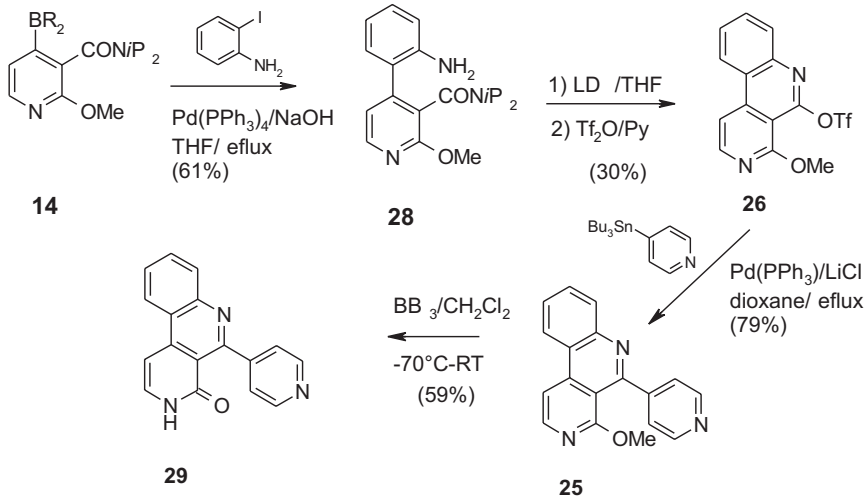
© 2001 NRC Canada

Scheme 6.



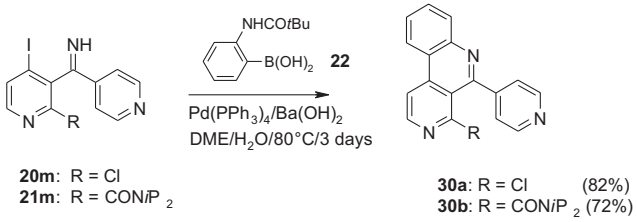
13 27

Scheme 7.



14 28 26 29 25

Scheme 8.



20m: R = Cl
21m: R = CONiP 2

30a: R = Cl (82%)
30b: R = CONiP 2 (72%)

Synthesis of open-ring analogues of meridine 32 and 33

Meridine **4** is a marine alkaloid, isolated by Schmitz et al. (10*c*) in 1991. The natural compound **4** possesses very interesting cytotoxic (10*b*) and antifungal activities (18). Moreover, meridine **4** is a topoisomerase II inhibitor. It was first synthetized by Kubo and co-workers (19) in 1994.

Synthesis of an acyclic analogue (**32**) of meridine (7) was achieved from a 3,3-dipyridylmethanol prepared via a metallation-halogen dance strategy applied on 2-*N*,*N*-diisopropylcarboxamido-3-iodopyridine **17** (Scheme 3, Table 1). Thus, oxidation of alcohol **21n** with manganese dioxide in refluxing toluene led to ketone **34**. Reaction between this ketone and phenyl boronic acid using $Pd(PPh_3)_4$ as the catalyst resulted in hetero ring cross-coupling to the expected 4-phenylketopyridine **35**, which was almost quantitatively cyclized in refluxing formic acid to **32** (Scheme 11). Unfortunately, we were not able to cyclize **32** to meridine, whatever the reaction conditions.

The previously used Miyashita route to seco-amphimedine **31** (16) was successfully applied to the synthesis of a meridine analogue (Scheme 12). Anionic acylation of **23b** with 4-methoxypicolinaldehyde in the presence of imidazolium iodide (1.2 equiv) and sodium hydride afforded **33** in a fairly good yield (65%). Unfortunately, hydrolysis of the methoxy group to seco-meridine could not be cleanly achieved. However, treatment of **33** with hydroiodic acid and sodium iodide gave a mixture from which **36**, an isomer of meridine, could be identified (15).

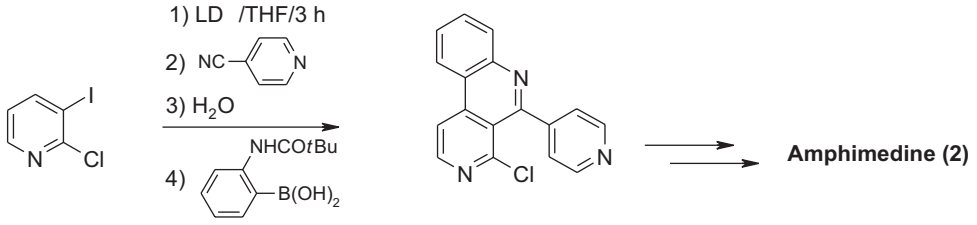
Synthesis of 4*H*-pyrido[2,3,4-*k*,*l*]acridine-4-ones (precursors of cystodytin alkaloids)

Cystodytins belong to a class of more than 10 compounds containing the same 4*H*-pyrido[2,3,4-*k*,*l*]acridine-4-one skeleton (17*a*). Most of them have interesting cytotoxic activity and are topoisomerase inhibitors (17*b*).

When acetylpyridine **20i** was coupled with the ortho-aminophenylboronic acid **22** under modified Suzuki conditions, the corresponding benzonaphthyridine **37** was obtained in good yield (87%) (20). Cross-coupling of the chloro compound **37** with ethoxyvinylstannane almost quantitatively led to 4-(ethoxy-1-vinyl)-5-methylbenzo[*c*]-2,7-naphthyridine (**38**). Treatment of **38** with SeO_2 gave the 4*H*-pyrido[2,3,4-*k*,*l*]acridin-4-one (**39**) in a poor 11% yield, and also a selenylated product with a structure that could be defined

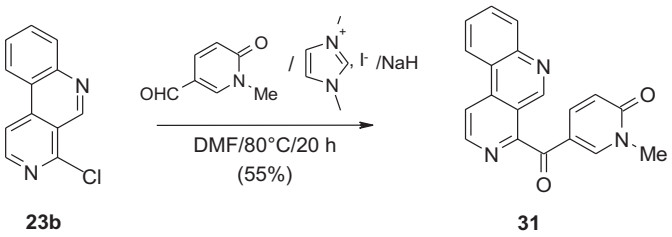
© 2001 NRC Canada

Scheme 9.



16 **30a**

Scheme 10.



23b **31**

as **40** (20) (Scheme 13). Compound **39** is an unsubstituted cystodytin.

The low overall yield of **39** prompted us to look for another route to the pyrido[2,3,4-*k*,*l*]acridin-4-one skeleton; among different opportunities, we decided (21) to prepare benzo[*c*]-2,7-naphthyridines bearing two protected carbonyl groups (acetyl or formyl) at C-4 and C-5, allowing aldol-type construction of the quinone ring of cystodytin under mild conditions.

Synthesis of 5,6-dihydro-4,5-bis(ethoxyvinyl)benzo[*c*]-2,7-naphthyridine (**42**) was first achieved by a preliminary cross-coupling reaction between ethoxyvinylstannane and 4-chlorobenzo[*c*]-2,7-naphthyridine (**23b**) to give **41**. This latter compound was subjected to nucleophilic addition of 1-ethoxyvinyllithium on the 5,6-imine bond (Scheme 14). The resulting bis-protected 4,5-diacetylbenzonaphthyridine derivative **42** was then cyclized to 6-methyl-4*H*-pyrido[2,3,4-*k*,*l*]acridin-4-one (**43**) by treatment with ethanolic hydrogen chloride. Unfortunately, the yield of the last cyclisation step is still very low, and the deacetylated compound **44** was isolated as a side-product (Scheme 14) (21).

Based on the reactivity of diacetyl derivative **42**, the previous strategy could be modified by working on a bis-protected form of 5-formyl-4-acetylbenzo[*c*]-2,7-naphthyridine (22). Thus, oxidation of the activated methyl group of 5-methyl-2-chlorobenzo[c]-2,7-naphthyridine (**37**) by SeO_2, followed by acetalization of the intermediate aldehyde, afforded **45** in a good 71% overall yield (Scheme 15). The latter compound was then subjected to cross-coupling with ethoxyvinyl stannane to give **46**. One-pot cyclization under Mukaiyama conditions (23) and oxidation gave the expected pyridoacridone **47** in good yield (22).

Conclusion

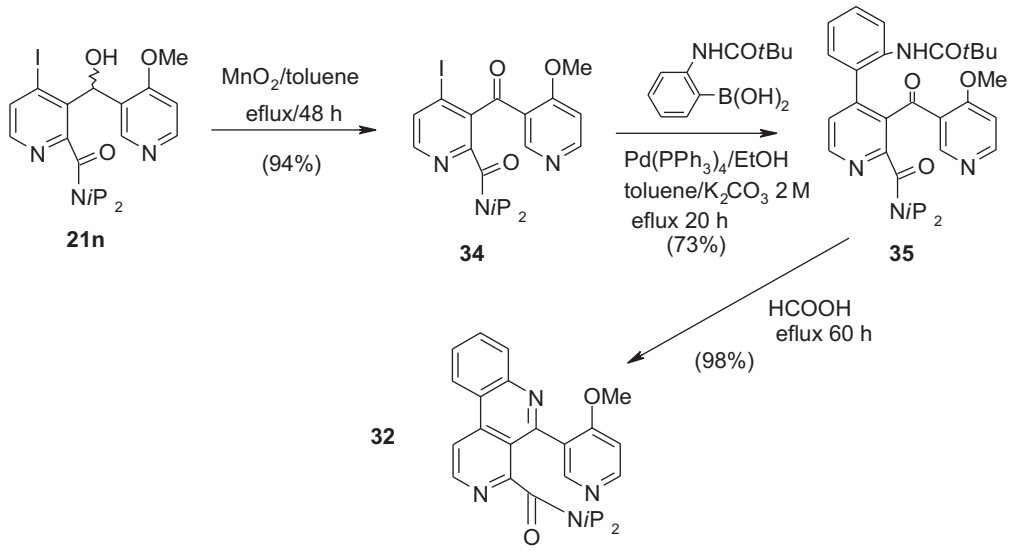
Connection between *ortho*-directed metallation and biaryl cross-coupling provides a very efficient route to polyaromatics of the 7*H*-pyrido[2,3,4-*k*,*l*]acridine series. Analogues or precursors of marine alkaloids such amphimedine, meridine, or cycstodytins have been synthesized with short pathways and in good yields.

References

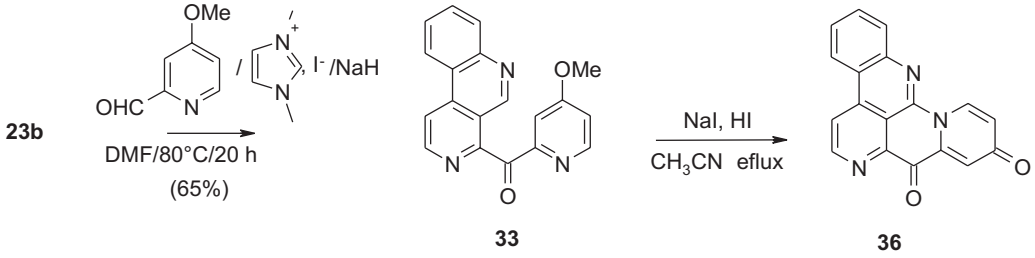
1. G. Quéguiner, F. Marsais, V. Snieckus, and J. Epsztajn. Adv. Heterocycl. Chem. **52**, 187 (1991).
2. A. Godard, F. Marsais, N. Plé, F. Trécourt, and G. Quéguiner. Heterocycles, **40**, 1055 (1995).
3. V. Snieckus. Chem. Rev. **90**, 879 (1990).
4. T.F. Molinski. Chem. Rev. **93**, 1825 (1993).
5. F. Guillier, F. Nivoliers, A. Godard, F. Marsais, G. Quéguiner, M.A. Siddiqui, and V. Snieckus. J. Org. Chem. **60**, 292 (1995).
6. P. Rocca, C. Cochennec, F. Marsais, L. Thomas-dit-Dumont, M. Mallet, A. Godard, and G. Quéguiner. J. Org. Chem. **58**, 7832 (1993).
7. C. Cochennec, P. Rocca, F. Marsais, A. Godard, and G. Quéguiner. Synthesis, 321 (1995).
8. N. Miyaura, T. Yanagi, and A. Suzuki. Synth. Commun. **11**, 513 (1981).
9. J. Malm, P. Björk, S. Gronowitz, and A.-B. Hörnfeldt. Tetrahedron Lett. **35**, 3195 (1994).
10. (*a*) F.J. Schmitz, S.K. Agarwal, S.P. Gunasekera, P.G. Schmidt, F.S. Deguzman, and J.N. Shoolery. J. Am. Chem. Soc. **105**, 4835 (1983); (*b*) F.J. Schmitz, F.S. Deguzman, Y. Choi, M. Bilayet-Hossain, S.K. Rizvi, and D. Van der Helm. Pure Appl. Chem. **62**, 1393 (1990); (*c*) F.J. Schmitz, F.S. Deguzman, M. Bilayet-Hossain, and D. Van der Helm. J. Org. Chem. **56**, 804 (1991).
11. (*a*) R.H. Prager and C. Tsopelas. Heterocycles, **29**, 847 (1989); (*b*) R.H. Prager, C. Tsopelas, and T. Heisler. Austr. J. Chem. **44**, 277 (1991).
12. N. Miyaura, T. Ishiyama, H. Sasaki, M. Ishikawa, M. Satoh, and A. Suzuki. J. Am. Chem. Soc. **111**, 314 (1989).
13. J.K. Stille. Angew. Chem. Int. Ed. Engl. **25**, 508 (1986).
14. F. Guillier, F. Nivoliers, A. Godard, F. Marsais, and G. Quéguiner. Tetrahedron Lett. **35**, 6489 (1994).
15. G. Duvey. Ph.D. Thesis, Université de Rouen, France, 2000.
16. (*a*) A. Miyashita, H. Matsuda, C. Iijima, and T. Higashino. Chem. Pharm. Bull. **38**, 1147 (1990); (*b*) A. Miyashita, H. Matsuda, C. Iijima, and T. Higashino. Chem. Pharm. Bull. **40**, 43 (1992); (*c*) A. Miyashita, H. Matsuda, and T. Higashino. Chem. Pharm. Bull. **40**, 2627 (1992); (*d*) A. Miyashita, H. Matsuda, Y. Suzuki, K. Iwamoto, and T. Higashino. Chem. Pharm. Bull. **42**, 2017 (1994); (*e*) A. Miyashita, H. Matsuda, Y. Suzuki, K. Iwamoto, and T. Higashino. Chem. Pharm. Bull. **42**, 2633 (1994); (*f*) A. Miyashita, Y. Suzuki, M. Kobayashi, N. Kuriyama, and T. Higashino. Heterocycles, **43**, 509 (1996).
17. (*a*) J. Kobayashi, J. Cheng, M.R. Wälchli, H. Nakamura, Y. Hirata, T. Ssaki, and Y. Ohizumi. J. Org. Chem. **53**, 1800

© 2001 NRC Canada

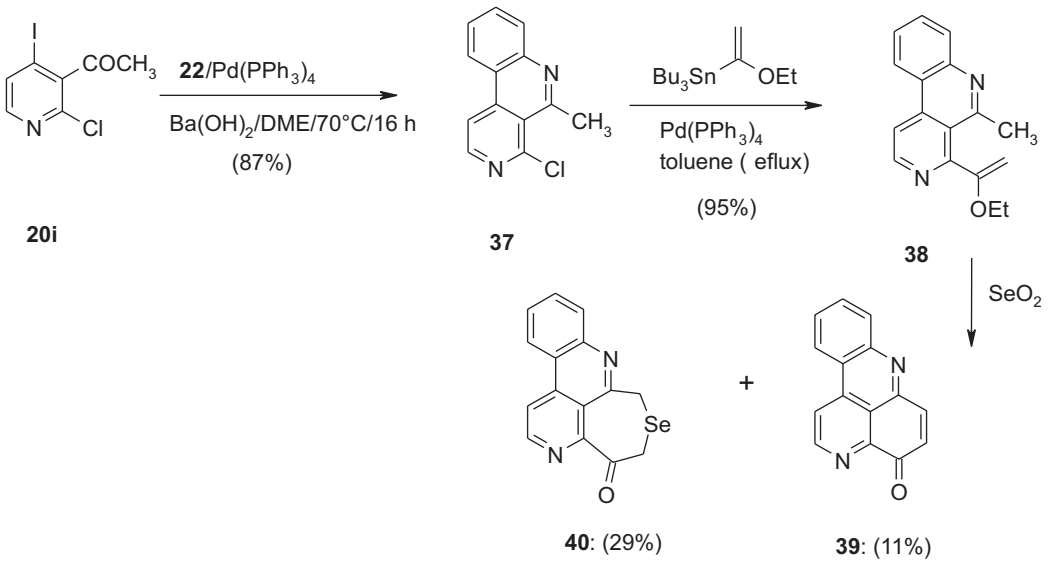
Scheme 11.



Scheme 12.



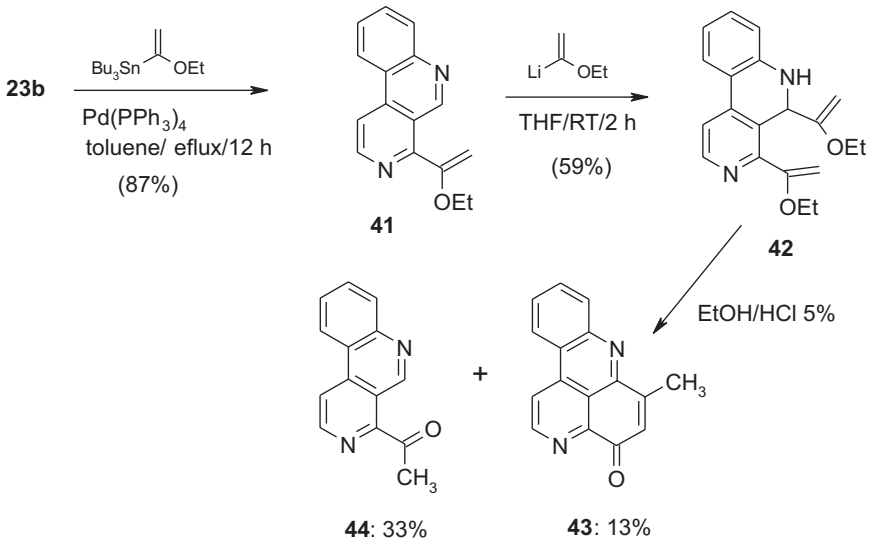
Scheme 13.



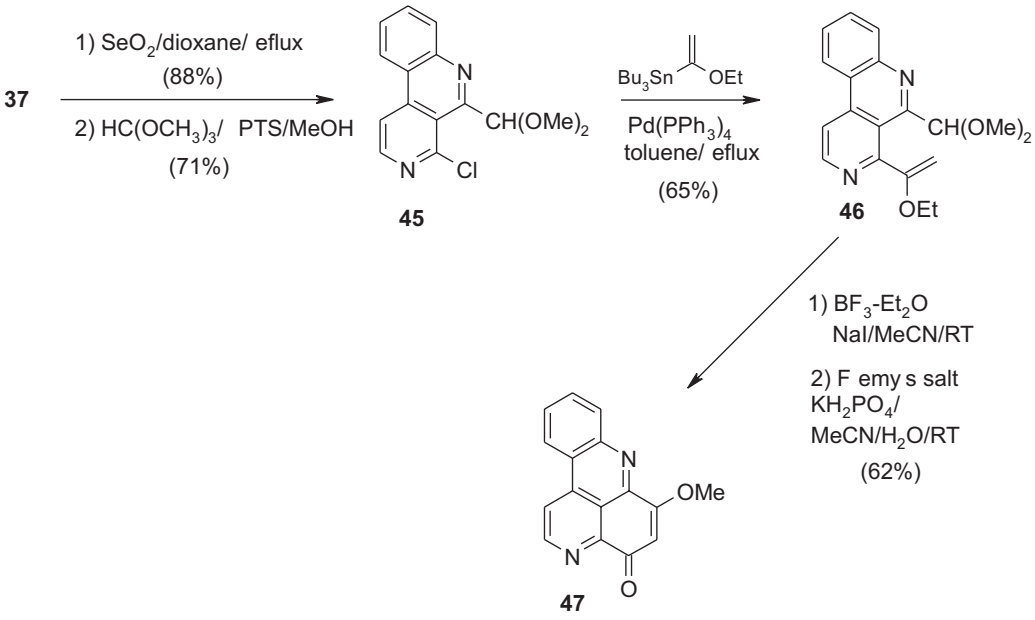
(1988); (*b*) L.A. McDonald, G.S. Elredge, L.R. Barrows, and C.M. Ireland. J. Med. Chem. **37**, 3819 (1994)
18. P.J. Mc Carthy, T.P. Pits, G.P. Gunawardana, M.K. Kelly-Borges, and S.A. Pomponi. J. Nat. Prod. **55**, 1664 (1992).
19. Y. Kitahara, F. Tamura, and A. Kubo. Chem. Pharm. Bull. **42**, 1363 (1994).
20. F. Guillier, F. Nivoliers, C. Cochennec, A. Godard, and G. Quéguiner. Synth. Commun. **26**, 4421 (1996).
21. F. Guillier. MSc. Thesis, Université de Rouen, France, 1996.
22. F. Guillier, F. Nivoliers, A. Godard, F. Marsais, and G. Quéguiner. J. Heterocycl. Chem. **36**, 1157 (1999).
23. T. Mukaiyama. Angew. Chem. Int. Ed. Engl. **16**, 817 (1977).

© 2001 NRC Canada

Scheme 14.



Scheme 15.



© 2001 NRC Canada

Synthesis, characterization, and application in asymmetric catalysis of dendrimers containing chiral ferrocenyl diphosphines

Christoph Köllner and Antonio Togni

Abstract: Starting from the functionalized Josiphos derivatives (*R*)-1-[(*S*)-2-(diphenylphosphino)-1′-(dimethyl-3″-aminopropylsilyl)-ferrocenyl]ethyldicyclohexylphosphine ((*R*)-(*S*)-**3**), (*R*)-1-[(*S*)-2-(diphenylphosphino)-1′-(hydroxymethyl)ferrocenyl]ethyldicyclohexylphosphine ((*R*)-(*S*)-**4**), and (*R*)-1-[(*S*)-2-(diphenylphosphino)-1′-(3″-hydroxypropyl)ferrocenyl]ethyldicyclohexylphosphine ((*R*)-(*S*)-**5**), a series of dendrimers containing up to sixteen ferrocenyl diphosphine units were prepared. Dendrimer cores are based on benzene 1,3,5-tricarboxylic acid and 1,3,5,7-adamantanetetracarboxylic acid, with 5-substituted isophthalic acid derivatives constituting the branching units. The dendrimers have been used in three different asymmetric catalytic reactions: Rh-catalyzed hydrogenation of dimethyl itaconate, Pd-catalyzed allylic substitution, and Rh-catalyzed hydroboration of styrene with catecholborane. In all three reactions the selectivity obtained with the dendrimers was very similar to the one obtained with the parent ligand Josiphos.

Key words: dendrimer, asymmetric catalysis, ferrocenyl ligands, hydrogenation.

Résumé : Utilisant les dérivés fonctionnalisés suivants du josiphos comme produits de départ, (*R*)-1-[(*S*)-2-(diphénylphosphino)-1′-(diméthyl-3″-aminopropylsilyl)ferrocényl]éthyldicyclohexylphosphine ((*R*)-(*S*)-**3**), (*R*)-1-[(*S*)-2-(diphénylphosphino)-1′-(hydroxyméthyl)ferrocényl]éthyldicyclohexylphosphine ((*R*)-(*S*)-**4**) et (*R*)-1-[(*S*)-2-(diphénylphosphino)-1′-(3″-hydroxypropyl)ferrocényl]éthyldicyclohexylphosphine ((*R*)-(*S*)-**5**), on a préparé une série de dendrimères comportant jusqu'à seize unités ferrocényldiphosphine. Les dendrimères fondamentaux ont comme base de l'acide benzène-1,3,5-tricarboxylique et de l'acide adamantane-1,3,5,7-tétracarboxylique alors que les unités de ramification sont formées de dérivés de l'acide isophtalique substitués en position 5. On a utilisé les dendrimères dans trois réactions catalytiques asymétriques différentes: l'hydrogénation catalysée par le Rh de l'itaconate de diméthyle; la substitution allylique catalysée par le Pd et l'hydroboration catalysée par le Rh du styrène par le catécholborane. Dans chacune de ces trois réactions, la sélectivité obtenue avec les dendrimères était très semblable à celle obtenue avec le ligand josiphos parent.

Mots clés : dendrimère, catalyse asymétrique, ligands ferrocényles, hydrogénation.

[Traduit par la Rédaction]

Introduction

The peripheral functionalization of dendrimers (for reviews, see ref. 1) with catalytically active modified transition metal complexes (2), pioneered by van Koten and co-workers (3), has been addressed from the point of view of combining the typical reactivity features of low-molecular-weight homogeneous catalysts with the distinctive physical properties of heterogeneous catalysts. In other words, a major goal being pursued is the incorporation of homogeneous catalysts preserving their selectivity and activity features into dendrimers, but amenable of easy recovery and reuse by virtue of their molecular size (4). Depending on the type of ligands and complexes being incorporated and on the reaction type being catalyzed, the size and structural nature of the dendrimer may have a positive, a neutral, but also a deleterious effect on the catalytic and selectivity properties of the homogeneous catalyst being modified (5). Thus, the first significant cooperative effect in asymmetric catalysis with dendrimers has been reported recently by Breinbauer and Jacobsen (6). In the asymmetric ring opening of epoxides catalyzed by Co(salen) complexes, known to involve bimetallic catalysis, a substantial increase in catalytic activity, attributed to proximity effects between single catalyst units, has been observed upon incorporation into small dendritic structures. Caminade, Majoral, and co-workers (7) also reported a higher activity of dendritic Ru complexes as catalysts for Knoeveagel and Michael-type reaction as compared to the corresponding monomeric species. On the other hand, van Koten and co-workers (8) have nicely demonstrated that

Received March 15, 2001. Published on the NRC Research Press Web site at http://canjchem.nrc.ca on November 19, 2001.

Dedicated to Professor Victor Snieckus for his contributions to Canadian chemistry.

C. Köllner[1] and A. Togni.[2] Laboratory of Inorganic Chemistry, Swiss Federal Institute of Technology, ETH Hönggerberg HCI 239, CH-8093 Zürich, Switzerland.

[1]Current address: Amcis AG, Hauptstrasse 159, CH-4416 Bubendorf, Switzerland.
[2]Corresponding author (telephone: +41 (1) 1 632 2236; fax: +41 (1) 1 632 1310; e-mail: togni@inorg.chem.ethz.ch).

 DOI: 10.1139/cjc-79-11-1762 © 2001 NRC Canada

for Ni complexes, catalytically active in the Kharasch reaction, their fixation at the surface of carbosilane dendrimers may severely affect their catalytic properties. In this case the proximity effect does not lead to improved catalysts.

When the mononuclear nature of a catalyst is known, an initial task with its dendritic forms should be that of clarifying whether the peripheral catalyst units retain their properties, and thus are not altered by the nature of the dendrimer backbone. Functional groups present in the dendrimer and length and conformational rigidity of the branches and spacers, for example, are factors of potential importance when evaluating a dendritic catalyst. This is particularly true for asymmetric catalysts, for which already subtle conformational changes may significantly influence stereoselectivity.

We previously demonstrated that chiral ferrocenyl diphosphines of the Josiphos-type (9), modified with an ω-aminoalkyl side chain, may be incorporated into dendrimers having benzene, adamantane, or phosphazene cores, and aryl amide and (or) ester connecting groups (10). We report here full experimental details on synthesis, spectroscopic characterization, and use in three different asymmetric catalytic reactions of ferrocenyl dendrimers containing up to sixteen Josiphos units.

Results and discussion

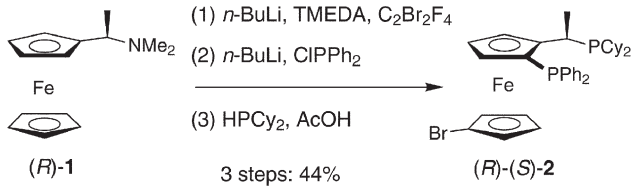
Synthesis and characterization of Josiphos dendrimers

To incorporate ferrocenyl ligands of the Josiphos type into dendritic structures a functionalization and a spacer are required. The choice of the anchoring point and the nature of the spacer on the ferrocenyl ligand molecule is of great importance, and may ultimately influence the catalyst performance by virtue of intramolecular interactions. Intuitively, an anchoring point remote from the two phosphine units should be the best suited because it allows to minimize possible contacts between ligand fragment and dendrimer backbone. This general idea calls for a functionalization of the unsubstituted Cp ring. We previously communicated the synthesis of derivative (*S*)-(*R*)-**2**, a 1′-bromo-Josiphos, which is set up for the introduction of a variety of possible spacers via metallation and reaction with a suited electrophile (10*a*). As shown in Scheme 1, the key intermediate **2** is accessible from the commercially available **1** in three steps and a moderate overall yield of 44%. In the course of this study we prepared derivatives containing three different spacers of different chain length and containing either a primary amine or a primary alcohol as the linking functionalities, as illustrated in Scheme 2.

Thus, after lithiation, (*R*)-(*S*)-**2** reacts with (3-chloropropyl)dimethylchlorosilane almost quantitatively (98%). In a straight forward Gabriel-synthesis (11) with potassium phthalimide and subsequent liberation of the protected amine group with hydrazine hydrate (12), (*R*)-(*S*)-**3** may be easily obtained in gram quantities. Reaction of the lithiated (*R*)-(*S*)-**2** with either paraformaldehyde or trimethylene oxide leads after aqueous work up directly to (*R*)-(*S*)-**4** and (*R*)-(*S*)-**5**, respectively, in moderate yields, both compounds bearing a hydroxyalkyl spacer.

The three Josiphos derivatives **3**–**5** may now be utilized for the reaction with internal dendrimer units bearing acid

Scheme 1.



chloride groups, thus forming amide or ester connecting groups easily and mostly quantitatively.

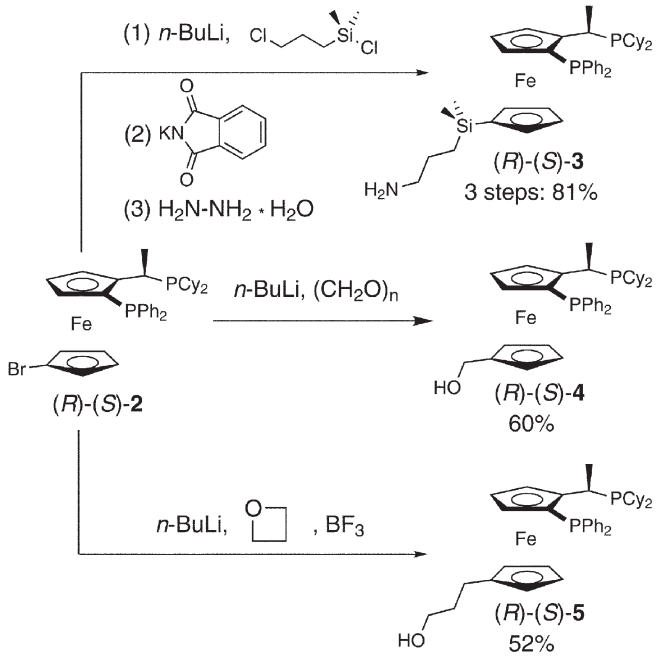
The first simple dendrimer synthesis was realized with (*R*)-(*S*)-**3** and benzene-1,3,5-tricarboxylic acid trichloride (**6**) yielding, in the presence of NEt_3, the zeroth-generation dendrimer **8** (see Scheme 3). The trichloride **6** was used because of its availability and easy handling, which is probably the reason why it is often exploited as core in dendrimer chemistry (13). A slight excess (10%) of the ferrocenyl ligand was used to ensure complete reaction of all three acid chloride functionalities. Purification of (*R*)-(*S*)-**8**, therefore consisting mainly in the separation from the excess (*R*)-(*S*)-**3**, was achieved by simple chromatography on silica gel. Because of its less polar character, as compared to the amine (*R*)-(*S*)-**3**, the zeroth-generation dendrimer was eluted with less polar solvents, and excess (*R*)-(*S*)-**3** could be easily recovered and reused.

1,3,5,7-Adamantanetetracarboxylic acid tetrachloride is a useful core molecule, as the four connecting groups are arranged in a tetrahedral fashion and therefore force the branches to extend in all three dimensions, more so than a planar aromatic core. 1,3,5,7-Adamantanetetracarboxylic acid tetrachloride was prepared in situ from the corresponding tetraacid (14) using thionyl chloride. The dendrimer (*R*)-(*S*)-**9** (Scheme 3) was obtained in a yield of only 73% probably because of an incomplete in situ formation of the tetrachloride from the tetraacid. In fact, as opposed to **6**, which was purified before the reactions by distillation, intermediate **7** was used without isolation and purification. However, possible side products of the synthesis still containing free carboxylic groups can easily be separated chromatographycally from the desired product by virtue of their drastically different polarity. Both hydroxy alkyl ferrocene derivatives (*R*)-(*S*)-**4** and (*R*)-(*S*)-**5** reacted with **6** only in moderate yields to the corresponding dendrimer of the zeroth-generation (*R*)-(*S*)-**10** and (*R*)-(*S*)-**11** (Scheme 4). These two compounds are relevant in terms of a comparison of the possible influence of the spacer length on the catalytic properties (activity, selectivity). As we shall see later, the differences observed for three diverse catalytic reaction types are almost negligible. Therefore, in view of the lower yields obtained in the synthesis of the hydroxy derivatives and their dendrimers, as compared with intermediate **2**, we decided not to pursue the chemistry of these compounds any further.

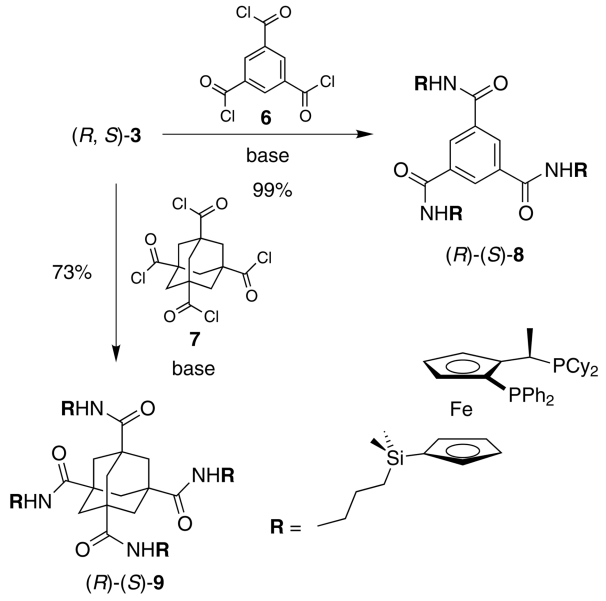
For the convergent synthesis of dendrimers of higher generations based on the modified ligand **3**, the preparation of corresponding dendrons was required. As branching units we adopted isophthalic acid derivatives containing either an amino or a hydroxyl group in position 5. The reasons for this choice were again the type of linkages that would result (amide or ester), the availability and proven utility of these

© 2001 NRC Canada

Scheme 2.



Scheme 3.



groups, as well as the relative conformational rigidity they would confer to the inner core of the small dendrimers. Thus, as illustrated in Scheme 5, reaction of the diacid dichlorides **12** (15) and **15** (16) with (*R*)-(*S*)-**3** in the presence of a base gave high yields of the intermediates **13** and **16**. Whereas the deprotection of the silyl ether **16** under standard conditions (17) afforded the desired dendron **17** almost quantitatively, the reduction of the nitro group of **13** proved unexpectedly problematic. The only method affording the aniline **14** in good yield was the Pd/C-catalyzed reaction with hydrazine hydrate, catalytic hydrogenation procedures under variable hydrogen pressures giving only modest yields (up to 33%).

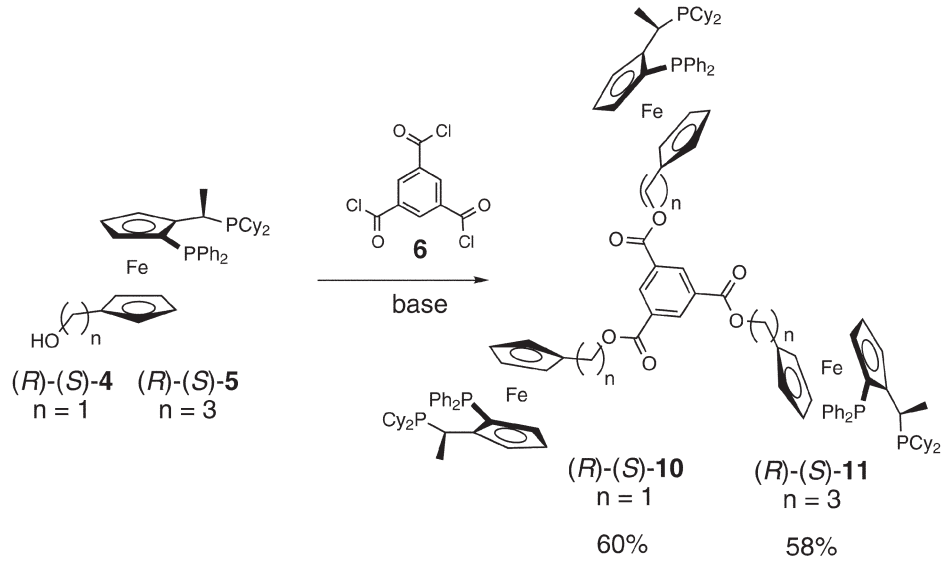
The dendrons **14** and **17** could be coupled to the triacid trichloride **6** or the tetraacid tetrachloride **7** in good to excellent yields, affording the first generation dendrimers **18**–**21** containing six or eight Josiphos units (see Scheme 6). As observed before, the yields tend to be lower when utilizing the adamantane derived core. However, as for the dendrimers of zeroth generation discussed above, the four new compounds **18**–**21** were obtained in analytically pure form after simple chromatographic purification. This allowed the separation of the slight excess of dendron and of any compounds derived from uncomplete core functionalization from the desired products.

The small dendron **14** was then reacted with the diacid **15** and, after deprotection, the doubly branched unit **22** containing four ferrocenyl ligands was obtained in good yield (76%). With this compound in hand, and by following the known procedure, the second generation dendrimers **23** and **24** could be obtained in excellent yield, as shown in Scheme 7. These two macromolecules contain twelve and sixteen Josiphos units at their periphery, respectively. Despite the already relatively high molecular weight of ca. 10 000 and 13 000, respectively, these materials still behave as normal molecules, thus susceptible of standard chromatographic purification. However, in the case of derivative **24**, the isolated material was shown by ^{31}P NMR spectroscopy to contain small amounts of phosphine oxide derivatives, corresponding to an estimated maximum equivalent of one phosphine oxide unit per dendrimer, probably deriving from prolongued exposure to air during the workup and purification operations. The impurities could not be separated from the main product by column chromatography.

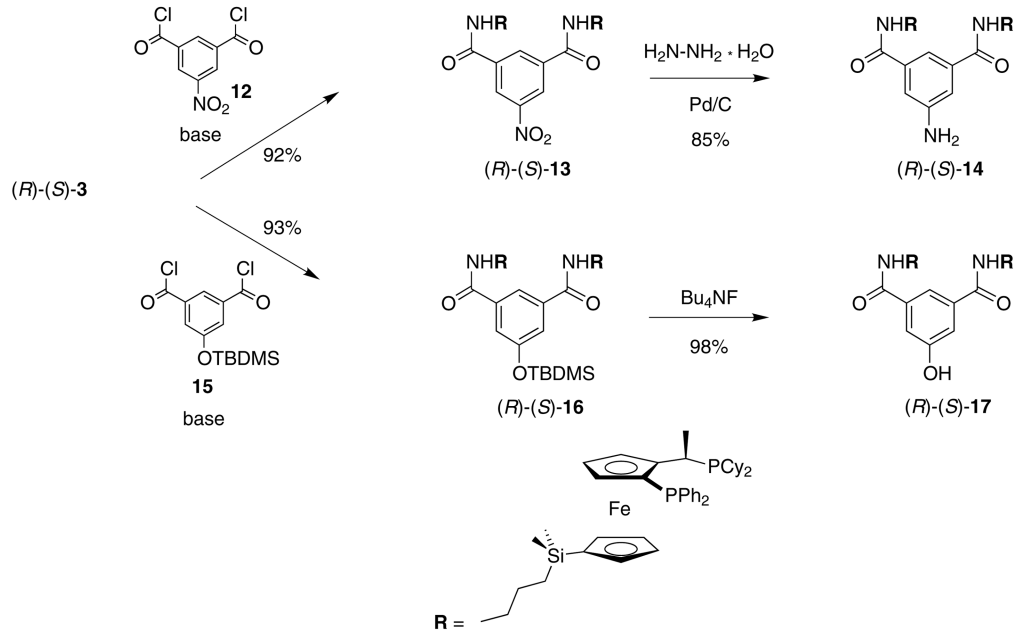
All Josiphos dendrimers prepared during this study are in general, orange solids with melting points above 100°C. They display good to excellent solubility in several common organic solvents including diethyl ether, THF, methylene chloride, chloroform, benzene, and toluene. The ^{31}P NMR spectra of all species show a single AB-spin system, virtually identical to the one of the parent compound Josiphos. We take this observation as an indication of the monodispersity of these compounds. Furthermore, one can assume that the single Josiphos units at the periphery of the dendrimers, because they are not affected in their spectroscopic properties by the linking to the dendrimer, they will also chemically behave as if they were monomeric species. This is reinforced also by the ^{1}H and ^{13}C NMR spectroscopic characteristics, showing one well-defined set of signals for the ligand fragments. However, the larger dendrimers gave relatively broad signals in the aromatic region of the spectra due to the inner part of the molecules, when dissolved in $CDCl_3$ at room temperature. To obviate to this problem and to detect crucial signals of the inner core of the dendrimers, NMR experiments were done with solutions in DMSO-d_6 or DMSO-d_6–$CDCl_3$ mixtures at temperatures up to 100°C, and assignments were done by standard 2D-NMR experiments. Figure 1 shows an example of the phenyl region in both ^{1}H (top) and ^{13}C (bottom) NMR spectra of dendron **22** and dendrimer **23**. Note for comparison that the signals *g* (^{1}H) and *k*, *l*, and *m* (^{13}C) identifying the dendrimer core of **23** are absent in the spectra of dendron **22**. Further diagnostic resonances are those of the inner branching unit. So protons *e* and *f* in **22** are shifted to lower field upon the

© 2001 NRC Canada

Scheme 4.



Scheme 5.

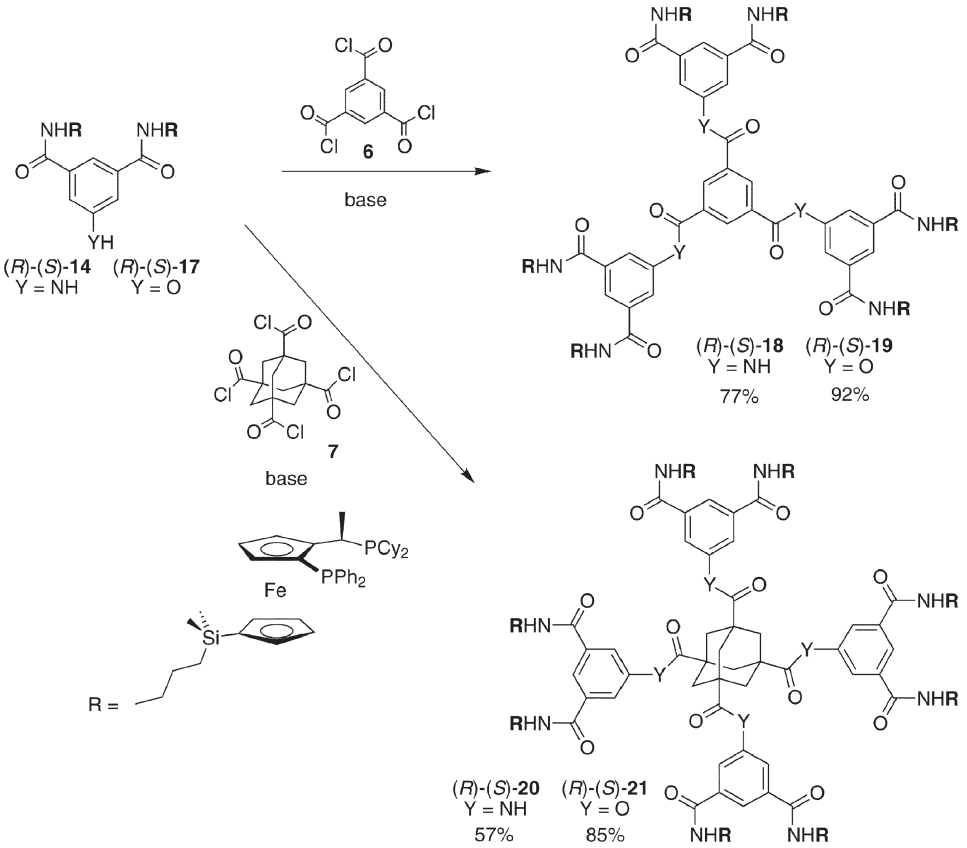


esterification reaction leading to the dendrimer. The dendrimer shows three different signals for the carbonyl groups in the ^{13}C NMR spectrum (*a*, *f*, and *k*), whereas signal *k* is absent in the dendron. Furthermore, carbon nuclei *h*, *i*, and *j* of the phenolic group of **22** are affected by the dendrimer formation, where they reside at the inner branching unit.

For the mass spectroscopic characterization of our dendrimers we used FAB and (or) MALDI-TOF techniques. With the exception of the two largest dendrimers **23** and **24**, signals corresponding to the calculated molecular ion peak could be found. Figure 2 shows an example of a MALDI spectrum of the first generation dendrimer **21**. The highest intensity peak at *m*/*z* 6504.6 is in very good agreement with the calculated molecular weight of 6502.95, and should be assigned to the protonated form of **21**. Interestingly, one observes in the MALDI spectra of these dendrimers in-source fragmentation patterns (18) corresponding to the loss of fragments, as shown by smaller Josiphos derivatives under EI or FAB ionization conditions. Thus, very typically, the loss of PCy_2 groups or of the upper Cp ring of the ligand with its substituents, is characteristic for these type of compounds. Furthermore, peaks revealing the loss of a whole branching unit can be seen in the MALDI spectra of the dendrimers. As mentioned above, for the second generation dendrimers **23** and **24** the molecular ion peak could not be observed. However, in the case of compound **23**, for example, a fairly broad peak at *m*/*z* 10 372 was observed instead. This appears to correspond to the fully oxidized form of the polyphosphine ligand, with a calculated molecular weight of 10 367. This appears to be corroborated by fragmentation patterns indicating the loss of Cp units containing the two

© 2001 NRC Canada

Scheme 6.



oxidized phosphine groups. Why the larger dendrimers suffer this oxidation problem under otherwise identical conditions as applied to their smaller counterparts is not clear at the present time. A more systematic study concerning the MALDI-TOF characterization of this kind of macromolecules would be required to clarify this point, and, at least with our compounds, this technique cannot be applied in a routine fashion yet.

Asymmetric catalytic reactions using Josiphos dendrimers

We have investigated the use of our chiral dendrimers in three different types of well-known catalytic asymmetric reactions, shown in Scheme 8, for which the performance of the parent ligand Josiphos has been reported previously by us (19). This study was carried out in particular with the aim of clarifying the influence of the dendritic backbone on the stereoselectivity and catalytic activity.

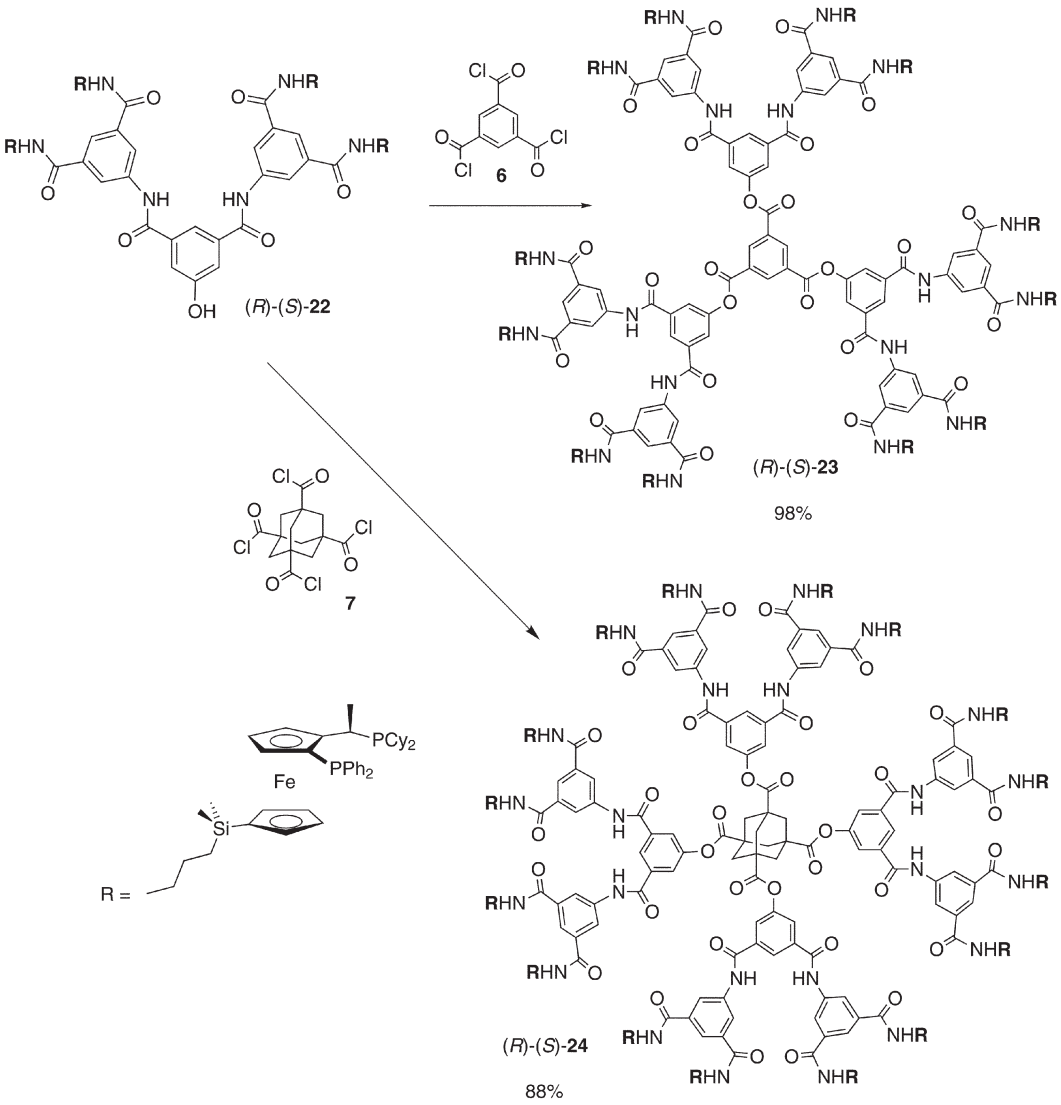
The first standard reaction was the Rh-catalyzed hydrogenation of dimethyl itaconate. The catalyst precursor was generated in situ from the poly(diphosphine) ligand and $[Rh(COD)_2]BF_4$, as it is often done for mononuclear Rh catalysts of this type. The formation of the cationic Rh(I) units [Rh(PP)(COD)] at the periphery of the dendrimers could easily be monitored by ^{31}P NMR spectroscopy in CD_2Cl_2 solution. On mixing one equivalent of a Josiphos dendrimer with as many equivalents of $[Rh(COD)_2]BF_4$ corresponding to the number of ferrocene units in the dendrimer, the clean conversion of all ligand sites into complex sites could be observed. Figure 3 illustrates this experiment for dendrimers **8** and **23**. In both cases the AB-spin system of the equivalent diphosphine sites is converted into an ABX system in which the AB part shows the expected P–Rh coupling (see Fig. 3). Chemical shifts and coupling constants for the new derivatives are virtually identical to those of the corresponding monomeric complex (20).

The hydrogenation reactions were carried out in MeOH. Because most of the dendrimers were only poorly soluble in MeOH, the dendritic catalyst precursors had to be generated in situ in CH_2Cl_2. After evaporation of this solvent, redissolution of the residue in MeOH gave clear solutions ready for the hydrogenation reactions. The results for the reduction of dimethyl itaconate are presented in Table 1. All dendritic catalysts afforded enantioselectivities (ee) only slightly lower than those obtained with the corresponding monomeric Josiphos catalyst (entry 11, 99.0% ee) (19). There was a small, but significant and reproducible difference in the enantioselectivities between the zeroth-generation dendrimers and their first- and second-generation counterparts. Whereas the zeroth-generation catalysts (entry 1–4) reached values close to 99% ee (er $\leq$ 200:1), all other dendrimers (entry 5–10) afforded a decreased enantioselectivity around 98% ee (er 100:1). That the lost of stereoselectivity is relatively minimal and that the dendrimers still give excellent catalysts for this reaction indicates that the modified molecular environment of the single catalyst units due to the incorporation into dendritic structures leads to practically negligible effects.

We also monitored the hydrogen uptake for reaction catalyzed by different dendritic species to compare the different catalysts in simple overall kinetic terms. In Fig. 4 the hydro-

© 2001 NRC Canada

Scheme 7.



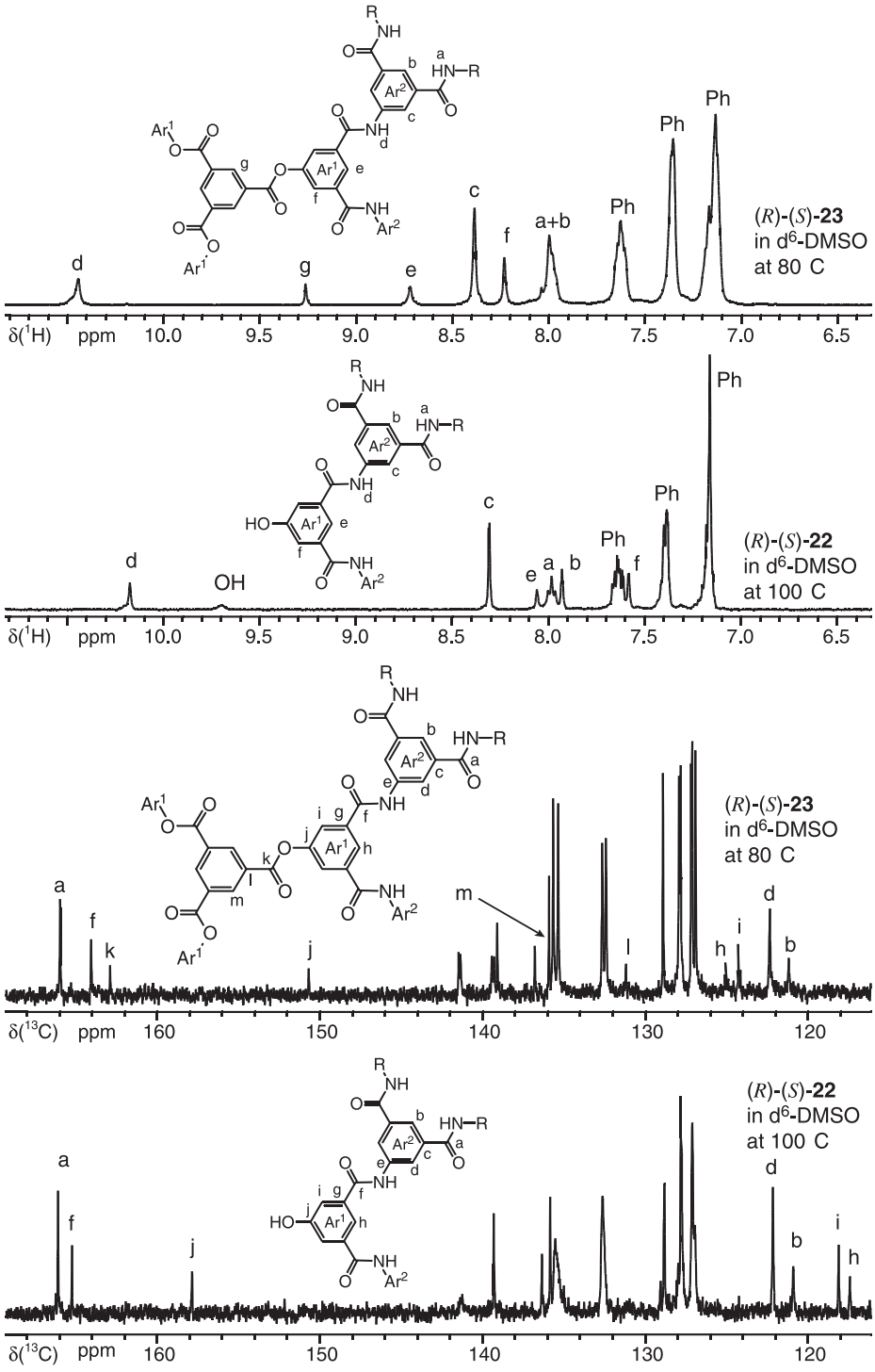
gen uptake vs. time is illustrated for four dendritic ligands and for Josiphos for equal total Rh concentrations. All curves display the same shape and indicate full conversion times similar for all species considered. Full catalytic activity is not present from the beginning, since COD hydrogenation has to take place to generate the actual catalyst, leading to the characteristic increase of the H_2 uptake rate during at least 50% of the reaction time. The curves in Fig. 4 show that the different catalysts display similar but not identical reaction rates. However, no trend dependent on dendrimer size is apparent. Since these reactions have been carried out under 1 atm of hydrogen at room temperature and with magnetic stirring, some uncertainties could derive from the nonideally controlled hydrogen mass transport from the gas phase into solution. It is therefore reasonable and safe to claim that the different dendritic catalysts display very similar reaction rates in the hydrogenation of dimethylitaconate.

The dendritic ligands were also used in the palladium catalyzed substitution of allylic acetate **27** by a soft carbon nucleophile, with the catalyst generated in situ from $Pd(dba)_2$ and a corresponding amount of the dendrimer, such as to ensure a slight excess ligand with respect to Pd. The results are summarized in Table 1. The enantioselectivities afforded by the zeroth- and first-generation dendrimers, with up to eight catalyst units (entry 1–8) were rather constant, i.e., in the narrow range of 89–91% ee, with the exception of (*R*)-(*S*)-**11** which gave only 85% ee. As compared to the parent ligand Josiphos (entry 11, 93% ee) this means a slight loss in selectivity that is comparable, or even less significant, in energetic terms of $\Delta\Delta G^{\ddagger}$, than the one observed for the Rh-catalyzed hydrogenation of dimethyl itaconate described above. For the larger dendrimers (*R*)-(*S*)-**23** and (*R*)-(*S*)-**24** (entry 9, 10), slower catalytic reactions and lower selectivities were observed. However, these results appear to be less reliable than those with other dendrimers, mainly due to the low solubility of the respective catalysts generated in situ. In fact, it was not possible in this case to obtain clear homogeneous solutions of the neutral catalyst precursors.

Rhodium catalyst precursors for the hydroboration of styrene were generated in situ in the same way as for the hydrogenation reactions. Hydroboration reactions were carried out for comparison at room temperature, although the best enantioselectivities were obtained with Josiphos at –78°C (91.5% ee). At this temperature, however, the dendrimers do

© 2001 NRC Canada

Fig. 1. Sections of the ^{1}H and ^{13}C NMR spectra of dendron **22** and dendrimer **23** showing key resonances of the dendrimer backbone.



not display sufficient solubility. The products were analyzed as the resultant alcohols after oxidative workup of the organoboron intermediate. The results are collected in Table 1. There are two possible products, the branched (**30**) and linear (**31**) phenylethanol. The regioselectivity afforded by Josiphos (entry 11) is excellent, with virtually only the branched alcohol being formed. However, the enantioselectivity is with 60–65% ee (depending on the exact reaction condition) only moderate. The stereoselectivity afforded by the dendritic catalysts is in the range 61–68% ee, thus in $\Delta\Delta G^{\ddagger}$ terms virtually identical to that given by the parent catalyst. On the other hand, the regioselectivity dropped slightly. In fact, up to 11% of the undesired linear 2-phenylethanol was formed. The reasons for this drop in regioselectivity are not clear.

Conclusions

We have shown that the functionalization of Josiphos in 1′-position of the ferrocene fragment allows the introduction

© 2001 NRC Canada

Scheme 8.

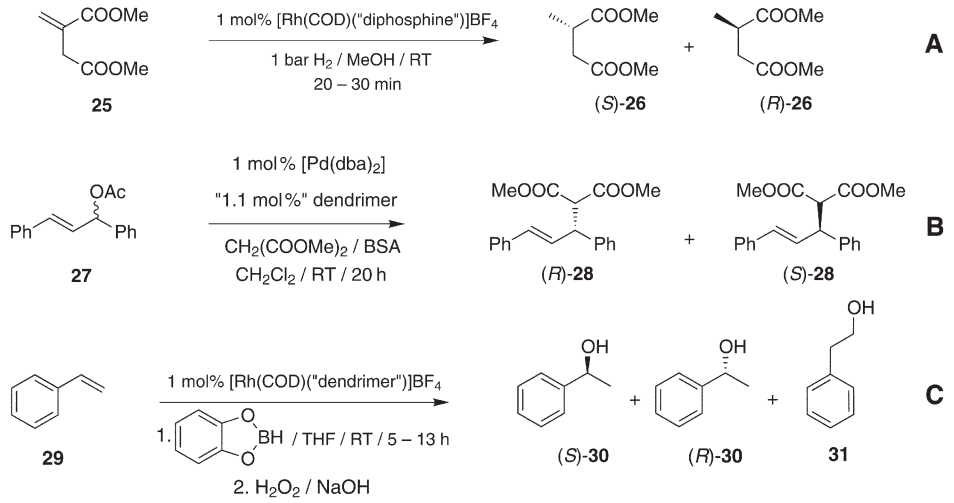


Fig. 2. MALDI-TOF spectrum of the first generation dendrimer **21**; in-source fragmentations typical for this class of compounds.

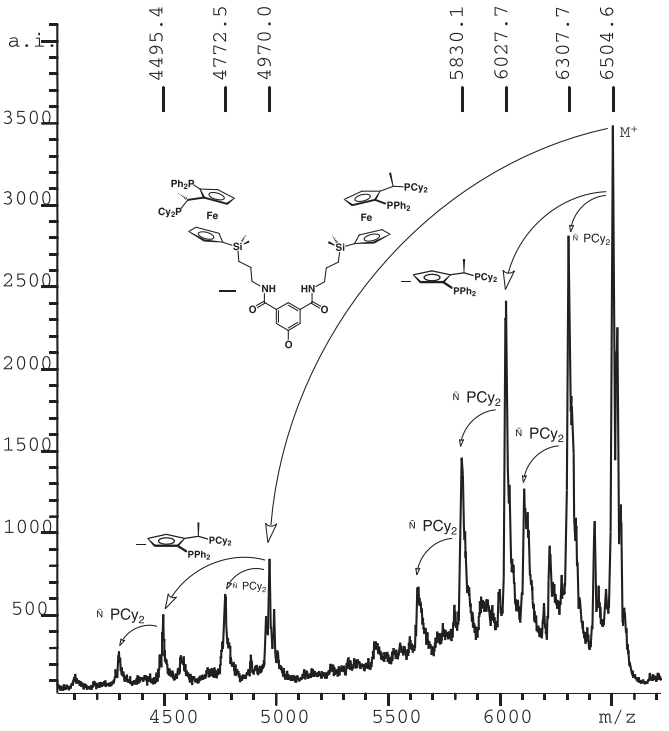
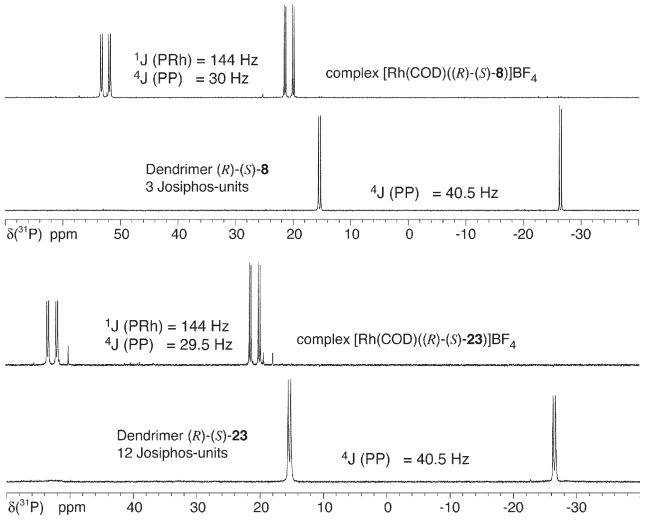


Fig. 3. ^{31}P NMR spectra of dendrimers **8** and **23** and of their corresponding cationic Rh(COD) complexes, generated in situ by the addition of $[Rh(COD)_2]BF_4$.



of a tether by which Josiphos can be attached to the periphery of dendrimers. Corresponding macromolecules containing up to sixteen diphosphine units could be prepared in high yield. Their spectroscopic characterization has shown that these derivatives are monodisperse and that the single ligand units are independent from one another, this being an important prerequisite for the dendritic catalysts to preserve the properties of the parent compound. This was largely confirmed by the catalysis experiments carried out with our dendrimers for three different reaction types, and showing that the stereoselectivities obtained are very similar to, but not significantly better than those afforded by Josiphos. This very point appears to be, in general, the best possible scenario one can expect when working with peripherally functionalized dendrimers, in particular when cooperativity effects between single catalyst units do not play any relevant role. The small but significant loss of stereoselectivity observed, e.g., in the Rh-catalyzed hydrogenation of dimethyl itaconate, could be due to local concentration effects, becoming important in the case of cationic catalyst species, in particular. Similar considerations apply to the observation of lower regioselectivity in the hydroboration reaction. However, it is clear that such minor dendritic effects on selectivity cannot be fully explained based on the available data.

Experimental

Reagents and techniques

Et_2O and THF were purified by distillation from sodium–benzophenone, while CH_2Cl_2 was distilled from CaH_2, EtOH and toluene from sodium, and MeOH from $Mg(OMe)_2$. All solvents were distilled under Ar. All reactions with air sensitive materials were carried out under Ar. (*R*)-*N*,*N*-Dimethyl-1-ferrocenylethylamine ((*R*)-**1**) was a generous gift from

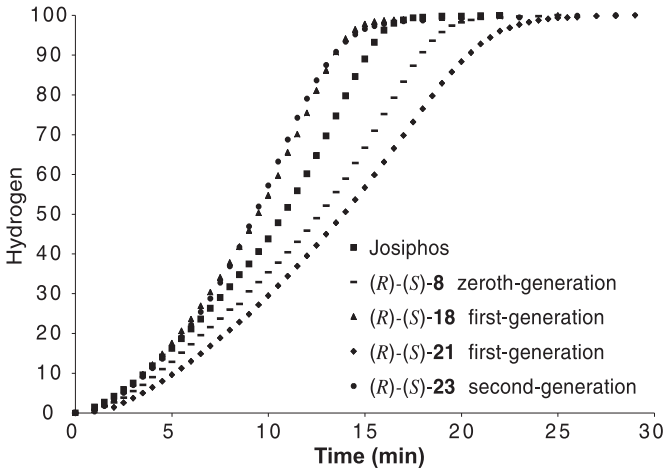
© 2001 NRC Canada

Table 1. Results of the catalytic reactions shown in Scheme 6, carried out with different dendrimers.

Entry	Dendrimer	Generation/ ferrocene units	Hydrogenation		Allylic alkylation		Hydroboration		
			Yield (%)[a]	% ee (*S*)[b]	Yield (%)[c]	% ee (*S*)[b]	Yield (%)[a]	**30**:**31**[b]	% ee (*S*)-**30**[b]
1	(*R*)-(*S*)-**8**	0/3	83	98.6	92	90	77	95:5	64
2	(*R*)-(*S*)-**9**	0/4	74	98.7	96	91	86	98:2	68
3	(*R*)-(*S*)-**10**	0/3	78	98.8	n.d.[d]	91	69	94:6	64
4	(*R*)-(*S*)-**11**	0/3	78	98.7	n.d.[d]	85	87	96:4	68
5	(*R*)-(*S*)-**18**	1/6	86	97.9	92	89	64	90:10	60
6	(*R*)-(*S*)-**19**	1/6	88	98.1	85	90	71	91:9	61
7	(*R*)-(*S*)-**20**	1/8	70	98.0	91	90	71	92:8	61
8	(*R*)-(*S*)-**21**	1/8	78	98.0	96	90	63	95:5	67
9	(*R*)-(*S*)-**23**	2/12	86	98.2	n.d.[d]	(81)[e]	57	97:3	67
10	(*R*)-(*S*)-**24**	2/16	78	98.0	n.d.[d]	(54)[e]	97	89:11	64
11[f]	(*R*)-(*S*)-Josiphos		80–90	99.0	97–99	93	65	99:1	60–65

[a]After Kugelrohr distillation.
[b]Determined by HPLC using a chiral stationary phase (see *Experimental* for details).[c]After column chromatography.
[d]Not determined.
[e]Catalyst not completely dissolved.
[f]Results from ref. 19.

Fig. 4. Hydrogen uptake vs. time for the hydrogenation of dimethyl itaconate using different dendritic catalysts at equal total Rh concentration.



Novartis Ltd. Benzene-1,3,5-tricarboxylicacid trichloride (**6**) (21), 1,3,5,7-adamantanetetracarboxylic acid tetrachloride (**7**) (in situ from 1,3,5,7-adamantanetetracarboxylic acid (14), 5-nitro-isophthaloyl dichloride (14) (**12**), 5-(*tert*-butyldimethylsilyloxy)isophthaloyl dichloride (16) (**15**), $[Rh(COD)_2]BF_4$ (22), $Pd(dba)_2$ (23), as well as substrate **27** (24) were prepared according to literature procedures. The preparation of (*R*)-(*S*)-**2**, (*R*)-(*S*)-**3**, (*R*)-(*S*)-**8**, (*R*)-(*S*)-**9**, (*R*)-(*S*)-**16**, (*R*)-(*S*)-**17**, (*R*)-(*S*)-**19**, and (*R*)-(*S*)-**21** was carried out as previously reported from our laboratory (10*a*). Further chemicals, including substrates **25** and **29** were purchased from Fluka or Aldrich and used as received.

HPLC-analysis were performed with a Hewlett-Packard Series 1050 with UV-detector (wavelength is given); chiral columns: Daicel Chiralcel OD-H (4.6 × 250 mm), Daicel Chiralcel OB-H (4.6 × 250 mm).

General procedure for the reaction of acid chlorides with alcohols or amines

To a solution of the alcohol or amine and a base (NEt_3 and (or) 4-(pyrrolidino)pyridine) in toluene or CH_2Cl_2 was added a solution of the acid chloride in toluene or CH_2Cl_2. After stirring for the given time the solution was filtered through Celite in case of a precipitation and the solvent was removed in vacuo. The products were purified by silica gel flash chromatography.

(*R*)-1-[(*S*)-2-(Diphenylphosphino)-1′-(hydroxymethyl)-ferrocenyl]ethyldicyclohexylphosphine ((*R*)-(*S*)-4)

n-BuLi in hexane (1.60 M, 0.83 mL, 1.34 mmol) was added at –40°C to (*R*)-(*S*)-**2** (719 mg, 1.07 mmol) in Et_2O (10 mL). After 30 min the solution was cooled to –78°C and paraformaldehyde (64 mg, 2.14 mmol) was added. The suspension was warmed slowly to rt and stirred overnight. The resultant solution was quenched with H_2O and extracted several times with Et_2O; the organic extracts were washed with H_2O and dried over anhydrous magnesium sulfate. The product was purified by silica gel flash chromatography (hexane – ethyl acetate (3:1) + 1% NEt_3) to yield (*R*)-(*S*)-**4** as an orange powder: 403 mg (0.65 mmol, 60%); mp 69°C. $[\alpha]_D$ = –312 (*c* = 1.01, $CHCl_3$). EI^+-LRMS *m*/*z* (%): 624 (15), 541 (100), 331 (91). IR (KBr) (cm^{-1}): 2922, 2847. ^1H NMR (250 MHz, $CDCl_3$) δ: 7.65 (m, 2H), 7.39 (m, 3H), 7.18 (m, 5H), 4.36 (s, 1H), 4.30 (m, 1H), 4.10 (m, 2H), 4.05–3.88 (m, 3H), 3.72 (m, 2H), 3.21 (dq, *J* = 7.2, 3.1, 1H), 1.9–0.9 (m, 25H). ^{13}C NMR (62.9 MHz, $CDCl_3$) δ: 141.1–127.1 (PPh_2), 102.4, 74.8, 71.2–68.7 (7Cp-CH, 1Cp-C), 60.3, 32.9–26.1 (PCy_2, *C*HMeP), 17.5. ^{31}P NMR (101.3 MHz, $CDCl_3$) δ: 15.4 (d, *J* = 32.3, PCy_2), –26.6 (d, *J* = 32.3, PPh_2). Anal. calcd. for $C_{37}H_{46}OP_2Fe$: C 71.15, H 7.42; found: C 71.09, H 7.69.

(*R*)-1-[(*S*)-2-(Diphenylphosphino)-1′-(3″-hydroxypropyl)-ferrocenyl]ethyldicyclohexylphosphine ((*R*)-(*S*)-5)

n-BuLi in hexane (1.60 M, 0.77 mL, 1.22 mmol) was added at –40°C to (*R*)-(*S*)-**2** (412 mg, 0.61 mmol) in Et_2O (10 mL). After 30 min the solution was cooled to –78°C, boron trifluoride diethyl etherate (153 μL, 1.22 mmol) and trimethylene oxide (160 μL, 2.45 mmol) were added. The suspension was warmed to rt and stirred for 1h. The resul-

© 2001 NRC Canada

tant solution was quenched with H_2O and extracted several times with Et_2O; the organic extracts were washed with H_2O and dried over anhydrous magnesium sulfate. The product was purified by silica gel flash chromatography (hexane – ethyl acetate (3:1) then hexane – ethyl acetate (1:1) both containing 1% NEt_3) to yield (*R*)-(*S*)-**5** as an orange powder: 207 mg (0.32 mmol, 52%); mp 49–52°C. $[\alpha]_D$ = –297 (*c* = 1.01, $CHCl_3$). EI^+-LRMS *m/z* (%): 652 (2), 569 (100), 454 (26). IR (KBr) (cm^{-1}): 2923, 2848. ^1H NMR (250 MHz, $CDCl_3$) δ: 7.66 (m, 2H), 7.38 (m, 3H), 7.18 (m, 5H), 4.28 (m, 1H), 4.23 (m, 1H), 4.01 (m, 1H), 3.94 (m, 2H), 3.54 (m, 4H) 3.21 (dq, *J* = 7.1, 3.9, 1H), 2.05 (m, 1H), 1.93 (m, 1H), 1.9–0.9 (m, 27H). ^{13}C NMR (62.9 MHz, $CDCl_3$) δ: 141.5–127.0 (PPh_2), 101.7, 88.2, 74.0, 71.9–69.1 (7Cp-CH), 62.4, 34.0, 32.9–25.7 (PCy_2, *C*HMeP), 25.2, 17.8. ^{31}P NMR (101.3 MHz, $CDCl_3$) δ: 15.4 (d, *J* = 30.9, PCy_2), –26.2 (d, *J* = 30.9, PPh_2). Anal. calcd. for $C_{39}H_{50}OP_2Fe$: C 71.78, H 7.72; found: C 71.56, H 7.93.

3-Cascade:benzene[3-1,3,5]:1′-(2-oxa-3-oxo-propyl)-(S_P)-1-diphenylphosphino-2-[1*R*-(dicyclhexylphosphino)-ethyl]ferrocene) ((*R*)-(*S*)-10)

(*R*)-(*S*)-**10** was prepared at –40°C from (*R*)-(*S*)-**4** (177 mg, 283.4 μmol), NEt_3 (79 μL, 0.58 mmol), 4-(pyrrolidino)-pyridine (5 mg, 33.7 μmol) in 5 mL of toluene, and **6** (20.9 mg, 78.7 μmol) in 10 mL of toluene according to the general procedure described above (warmed slowly to rt and stirred overnight) to afford, after silica gel flash chromatography (hexane – ethyl acetate (3:1) + 1% NEt_3), (*R*)-(*S*)-**10** (96 mg, 47.3 μmol, 60%) as an orange powder; mp 113–115°C. $[\alpha]_D$ = –284 (*c* = 1.5, $CHCl_3$). FAB^+-LRMS *m/z* (%): 2030 (49), 1946 (100), 1832 (7). IR (KBr) (cm^{-1}): 2923, 2848, 1729, 1229. ^1H NMR (250 MHz, $CDCl_3$) δ: 8.65 (s, 3H), 7.66 (m, 6H), 7.37 (m, 9H), 7.18 (m, 15H), 4.84 (d, *J* = 11.9, 3H), 4.45 (d, *J* = 11.9, 3H), 4.33 (m, 6H), 4.19 (m, 3H), 4.15 (m, 3H), 4.06 (s, 3H), 3.83 (m, 3H), 3.75 (m, 3H), 3.24 (dq, *J* = 7.0, 3.0, 3H), 1.9–0.9 (m, 75H). ^{13}C NMR (62.9 MHz, $CDCl_3$) δ: 164.5, 141.2–127.0 (PPh_2), 134.5, 131.1, 102.6, 80.6, 75.2, 71.7–69.2 (7Cp-CH), 63.4, 32.9–26.2 (PCy_2, *C*HMeP), 17.4. ^{31}P NMR (101.3 MHz, $CDCl_3$) δ: 15.5 (d, *J* = 33.4, PCy_2), –26.9 (d, *J* = 33.4, PPh_2). Anal. calcd. for $C_{120}H_{140}O_6P_6Fe_3$: C 71.01, H 6.85; found: C 71.22, H 7.00.

3-Cascade:benzene[3-1,3,5]:1′-(4-oxa-5-oxo-pentyl)-(S_P)-1-diphenylphosphino-2-[1*R*-(dicyclohexylphosphino)-ethyl]ferrocene ((*R*)-(*S*)-11)

(*R*)-(*S*)-**11** was prepared at –40°C from (*R*)-(*S*)-**5** (175 mg, 268.1 μmol), NEt_3 (75 μL, 0.54 mmol), 4-(pyrrolidino)-pyridine (5 mg, 33.7 μmol) in 5 mL of toluene, and **6** (19.8 mg, 74.5 μmol) in 10 mL of toluene according to the general procedure described above (warmed slowly to rt and stirred overnight) to afford, after silica gel flash chromatography (hexane – ethyl acetate (3:1) + 1% NEt_3), (*R*)-(*S*)-**11** (91.5 mg, 43.3 μmol, 58%) as an orange powder; mp 78–83°C. $[\alpha]_D$ = –280 (*c* = 1.075, $CHCl_3$). FAB^+-LRMS *m/z* (%): 2110 (11, $[M + 60]^+$), 2194 (18, $[M + 50]^+$), 2178 (51, $[M + 40]^+$), 2162 (39, $[M + 30]^+$), 2146 (11, $[M + 20]^+$), 2130 (5, $[M + 10]^+$), 2114 (2, $[M]^+$), 1948 (16), 1625 (99), 1073 (100). IR (KBr) (cm^{-1}): 2923, 2847, 1729, 1238. ^1H NMR (250 MHz, $CDCl_3$) δ: 8.79 (s, 3H), 7.66 (m, 6H), 7.35 (m, 9H), 7.18 (m, 15H), 4.28 (s, 3H), 4.24 (m, 9H), 4.02 (m, 3H), 3.95 (m, 6H), 3.62 (m, 3H), 3.56 (m, 3H), 3.22 (dq, *J* = 7.0, 3.2, 3H), 2.14 (m, 3H), 1.98 (m, 3H), 1.9–0.9 (m, 81H). ^{13}C NMR (62.9 MHz, $CDCl_3$) δ: 164.9, 141.5–127.0 (PPh_2), 134.4, 131.4, 101.8, 87.6, 74.2, 71.0–69.0 (7Cp-CH), 65.2, 32.9–26.0 (PCy_2, *C*HMeP), 30.0, 25.2, 17.7. ^{31}P NMR (101.3 MHz, $CDCl_3$) δ: 15.4 (d, *J* = 31.7, PCy_2), –26.4 (d, *J* = 31.7, PPh_2). Anal. calcd. for $C_{126}H_{150}O_6P_6Fe_3$: C 71.59, H 7.15; found: C 71.75, H 7.08.

1-Nitro-3,5-bis{6-[(S_P)-1-diphenylphosphino-2-(1*R*-(dicyclohexylphosphino)ethyl)-1′-ferrocenyl]-6-dimethyl-1-oxo-2-aza-6-silahexyl}benzene ((*R*)-(*S*)-13)

(*R*)-(*S*)-**13** was prepared at rt from (*R*)-(*S*)-**3** (2.43 g, 3.42 mmol), NEt_3 (2.27 mL, 16.3 mmol) in 20 mL of CH_2Cl_2, and **12** (404 mg, 1.63 mmol) in 12 mL of CH_2Cl_2 according to the general procedure described above (1 h stirring) to afford, after silica gel flash chromatography (CH_2Cl_2, 5% NEt_3), (*R*)-(*S*)-**13** (2.53 g) as an orange powder. This product contains 1 molecule NEt_3 per molecule product, which means a yield of 2.39 g (1.50 mmol, 92%); mp 116–119°C. $[\alpha]_D$ = –281 (*c* = 0.925, $CHCl_3$). FAB^+-LRMS *m/z* (%): 1594 (13), 1512 (100), 2118 (4), 1198 (5). IR (KBr) (cm^{-1}): 2923, 2849, 1664 (C=O), 1533 ($NO_{2\text{-st,as}}$), 1434, 1348 ($NO_{2\text{-st,sy}}$), 1163, 698. ^1H NMR (250 MHz, $CDCl_3$) δ: 8.64 (s, 2H), 8.46 (s, 1H), 7.64 (m, 4H), 7.37 (m, 6H), 7.18 (m, 10H), 6.45 (t, *J* = 5.5, 2H), 4.34 (m, 4H), 4.25 (m, 2H), 4.03 (m, 4H), 3.77 (m, 2H), 3.36 (m, 4H), 3.25 (m, 4H), 1.9–0.9 (m, 54H), 0.55 (m, 4H), 0.19 (s, 6H), 0.07 (s, 6H). ^{13}C NMR (62.9 MHz, $CDCl_3$) δ: 164.1, 148.2, 141.3–127.0 (PPh_2), 136.7, 131.1, 124.2, 102.0, 74.2, 74.1–69.3 (7Cp-CH), 70.3), 43.3, 33.0–26.1 (PCy_2, *C*HMeP), 24.1, 17.7, 14.3, –2.5. ^{31}P NMR (101.3 MHz, $CDCl_3$) δ: 16.0 (d, *J* = 33.4, PCy_2,), –26.4 (d, *J* = 33.4, PPh_2). Anal. calcd. for $C_{90}H_{115}N_3O_4P_4Si_2Fe_2$ + $1NEt_3$: C 67.99, H 7.73, N 3.30; found: C 67.88, H 7.85, N 3.19.

1-Amino-3,5-bis{6-[(S_P)-1-diphenylphosphino-2-[1*R*-(dicyclohexylphosphino)ethyl]-1′-ferrocenyl]-6-dimethyl-1-oxo-2-aza-6-silahexyl}benzene ((*R*)-(*S*)-14)

To a solution of (*R*)-(*S*)-**13** (1.93 g, 1.21 mmol) in hot EtOH (90 mL) was added palladium on carbon (100 mg, 10% Pd) and during 15 min Ar was bubbled through the suspension. After addition of hydrazine hydrate (1 mL, 20 mmol), the suspension was heated at reflux for 15 min, more palladium on carbon (100 mg, 10% Pd) added, and the reaction mixture was heated at reflux for additional 3 h. After cooling, filtration over celite, and removal of the solvent under vacuo, the product was purified by silica gel flash chromatography (CH_2Cl_2, 4% NEt_3) to yield (*R*)-(*S*)-**14** as an orange powder: 1.61 mg (3.28 mmol, 85%); mp 96–100°C. $[\alpha]_D$ = –281 (*c* = 0.89, $CHCl_3$). MALDI-LRMS *m/z* (%): 1565 ($[M]^+$), 1367 ($[M - HPCy_2]^+$), 1169 ($[M - 2HPCy_2]^+$), 1090 ($[M - C_5H_3(PPh_2)(CH(Me)PCy_2)]^+$). IR (KBr) ($cm^{-1}$): 2923, 2848, 1646 (C=O). ^1H NMR (250 MHz, $CDCl_3$) δ: 7.64 (m, 4H), 7.38 (m, 7H), 7.17 (m, 10H), 7.13 (s, 2H), 6.25 (t, *J* = 5.6, 2H), 4.33 (m, 4H), 4.25 (m, 2H), 4.03 (m, 4H), 3.90 (s, 2H), 3.77 (m, 2H), 3.31 (m, 4H), 3.23 (m, 4H), 1.9–0.9 (m, 54H), 0.53 (m, 4H), 0.16 (s, 6H), 0.06 (s, 6H). ^{13}C NMR (62.9 MHz, $CDCl_3$) δ: 166.7, 147.0, 141.3–127.0 (PPh_2), 136.2, 115.9, 114.5, 101.9, 74.1–69.2

© 2001 NRC Canada

(7Cp-CH), 74.0, 70.5, 43.0, 33.0–25.8 (PCy_2, *C*HMeP), 24.2, 17.6, 14.2, –2.4, –2.5. ^{31}P NMR (101.3 MHz, $CDCl_3$) δ: 16.0 (d, J = 33.5, PCy_2), –26.4 (d, J = 33.5, PPh_2). Anal. calcd. for $C_{90}H_{117}N_3O_2P_4Si_2Fe_2$: C 69.09, H 7.54, N 2.69; found: C 68.83, H 7.72, N 2.89.

6-Cascade:benzene[3-1,3,5]:(5-(1-oxo-2-aza)-1,3-phenylene):1′-(1-dimethyl-6-oxo-5-aza-1-silahexyl)-(S_P)-1-diphenylphosphino-2-[1*R*-(dicyclohexylphosphino)-ethyl]ferrocene ((*R*)-(*S*)-18)

(*R*)-(*S*)-**18** was prepared at 0°C from (*R*)-(*S*)-**14** (751 mg, 480 μmol), NEt_3 (180 μL, 1.30 mmol), 4-(pyrrolidino)-pyridine (5 mg, 33.7 μmol) in 10 mL of toluene, and **6** (35.4 mg, 133 μmol) in 5 mL of toluene according to the general procedure described above (warmed to rt and stirred overnight) to afford, after silica gel flash chromatography (hexane – ethyl acetate (1:1) + 5% NEt_3), (*R*)-(*S*)-**18** (496 mg, 102 μmol, 77%) as an orange powder; mp 125–130°C. $[\alpha]_D$ = –255 (c = 0.94, $CHCl_3$). MALDI-LRMS *m*/*z* (%): 4850 ($[M]^+$), 4653 ($[M - HPCy_2]^+$), 4377 ($[M - C_5H_3(PPh_2)(CH(Me)PCy_2)]^+$). IR (KBr) ($cm^{-1}$): 2923, 2849, 1654 (C=O). ^{1}H NMR (300 MHz, DMSO-d_6, 100°C) δ: 10.50 (s, 3H), 8.79 (s, 3H), 8.36 (d, J = 1.4, 6H), 8.01 (t, J = 5.5, 6H), 7.97 (t, J = 1.4, 3H), 7.63 (m, 12H), 7.38 (m, 18H), 7.18 (m, 30H), 4.37 (m, 6H), 4.33 (m, 6H), 4.30 (m, 6H), 4.08 (m, 12H), 3.77 (m, 6H), 3.34 (m, 6H), 3.24 (m, 18H), 1.9–0.9 (m, 162H), 0.60 (m, 12H), 0.15 (s, 18H), 0.09 (s, 18H). ^{13}C NMR (75.5 MHz, DMSO-d_6, 100°C) δ: 166.0, 164.8, 141.4–127.1 (PPh_2), 139.1, 136.2, 131.4, 129.9, 122.3, 121.2, 101.6, 74.1–69.1 (7Cp-CH), 74.1, 71.2, 42.8, 33.0–26.2 (PCy_2, *C*HMeP), 24.1, 17.1, 14.1, –2.0, –2.1. ^{31}P NMR (121.5 MHz, DMSO-d_6, 100°C) δ: 18.2 (d, J = 35.5, PCy_2), –23.4 (d, J = 35.5, PPh_2). Anal. calcd. for $C_{279}H_{351}N_9O_9P_{12}Si_6Fe_6$: C 69.09, H 7.29, N 2.60; found: C 69.17, H 7.50, N 2.56.

8-Cascade:tricyclo[3.3.1.1^{3,7}]decane[4-1,3,5,7]:(5-(1-oxo-2-aza)-1,3-phenylene):1′-(1-dimethyl-6-oxo-5-aza-1-silahexyl)-(S_P)-1-diphenylphosphino-2-[1*R*-(dicyclohexylphosphino)ethyl]ferrocene ((*R*)-(*S*)-20)

(*R*)-(*S*)-**20** was prepared at rt from (*R*)-(*S*)-**14** (700 mg, 477 μmol), NEt_3 (0.84 mL, 6.0 mmol), 4-(pyrrolidino)-pyridine (5 mg, 33.7 μmol) in 10 mL of toluene, and **7** (93.2 μmol, in situ from 1,3,5,7-adamantanetetracarboxylic acid (29.1 mg)) in 4 mL of toluene according to the general procedure described above (stirred overnight) to afford, after silica gel flash chromatography (hexane – ethyl acetate (1:1) + 1% NEt_3), (*R*)-(*S*)-**20** (348 mg, 53.5 μmol, 57%) as an orange powder; mp 112–117°C. $[\alpha]_D$ = –264 (c = 1.21, $CHCl_3$). MALDI-LRMS *m*/*z*: 6494 ($[M]^+$), 6297 ($[M - HPCy_2]^+$). IR (KBr) (cm^{-1}): 2924, 2849, 1655 (C=O). ^{1}H NMR (300 MHz, DMSO-d_6, 100°C) δ: 9.28 (s, 4H), 8.20 (d, J = 1.4, 8H), 7.95 (t, J = 5.6, 8H), 7.90 (t, J = 1.4, 4H), 7.62 (m, 16H), 7.37 (m, 24H), 7.15 (m, 40H), 4.36 (m, 8H), 4.31 (m, 8H), 4.29 (m, 8H), 4.06 (m, 16H), 3.76 (m, 8H), 3.29 (m, 8H), 3.21 (m, 24H), 2.24 (s, 12H), 1.9–0.9 (m, 216H), 0.58 (m, 16H), 0.14 (s, 24H), 0.07 (s, 24H). ^{13}C NMR (75.5 MHz, DMSO-d_6, 100°C) δ: 174.6, 166.1, 141.4–127.1 (PPh_2), 139.2, 135.9, 122.3, 120.9, 101.6, 74.1–69.1 (7Cp-CH), 74.0, 71.2, 43.6, 42.8, 38.6, 33.0–26.2 (PCy_2, *C*HMeP), 24.0, 17.1, 14.1, –2.0, –2.1. ^{31}P NMR (121.5 MHz, DMSO-d_6, 100°C) δ: 18.2 (d, J = 35.4, PCy_2), –23.3 (d, J = 35.4, PPh_2). Anal. calcd. for $C_{374}H_{476}N_{12}O_{12}P_{16}Si_8Fe_8$: C 69.12, H 7.38, N 2.59; found: C 69.19, H 7.46, N 2.39.

1-(*tert*-Butyldimethylsilyloxy)-3,5-bis{1-oxo-2-aza-2-[3,5-bis{6-[(S_P)-1-diphenylphosphino-2-[1*R*-(dicyclohexyl-phosphino)ethyl]-1′-ferrocenyl]-6-dimethyl-1-oxo-2-aza-6-silahexyl}phenyl]}benzene ((*R*)-(*S*)-22a)

(*R*)-(*S*)-**22a** was prepared at rt from (*R*)-(*S*)-**14** (856 mg, 547 μmol), NEt_3 (280 μL, 2.00 mmol), 4-(pyrrolidino)-pyridine (5 mg, 33.7 μmol) in 20 mL of toluene, and **15** (82.9 mg, 249 μmol) in 5 mL of toluene according to the general procedure described above (5.5 h stirring) to afford, after silica gel flash chromatography (hexane – ethyl acetate (1:1) + 1% NEt_3), (*R*)-(*S*)-**22a** (746 mg, 220 μmol, 88%) as an orange powder; mp 128–133°C. $[\alpha]_D$ = –255 (c = 0.84, $CHCl_3$). MALDI-LRMS *m*/*z*: 3391 ($[M]^+$), 3194 ($[M - HPCy_2]^+$), 2918 ($[M - C_5H_3(PPh_2)(CH(Me)PCy_2)]^+$). IR (KBr) ($cm^{-1}$): 2925, 2849, 1652 (C=O). ^{1}H NMR (300 MHz, DMSO-d_6, 80°C,) δ: 10.35 (s, 2H), 8.33 (d, J = 1.3, 4H), 8.29 (m, 1H), 8.15 (t, J = 5.5, 4H), 7.91 (m, 2H), 7.64 (m, 10H), 7.40 (m, 12H), 7.17 (m, 20H), 4.37 (m, 4H), 4.34 (m, 4H), 4.30 (m, 4H), 4.09 (m, 4H), 4.07 (m, 4H), 3.74 (m, 4H), 3.31 (m, 4H), 3.23 (m, 12H), 1.9–0.9 (m, 108H), 1.05 (s, 9H), 0.58 (m, 8H), 0.31 (s, 6H), 0.15 (s, 12H), 0.08 (s, 12H). ^{13}C NMR (75.5 MHz, DMSO-d_6, 80°C) δ: 166.0, 165.3, 157.8, 141.5–127.1 (PPh_2), 136.5, 122.2, 121.0, 118.0, 117.8, 101.5, 74.2–69.1 (7Cp-CH), 73.8, 70.4, 42.7, 32.8–25.7 (PCy_2, *C*HMeP), 26.2, 24.0, 17.8, 16.9, 14.0, –2.1, –3.1. ^{31}P NMR (101.3 MHz, $CDCl_3$) δ: 15.9 (d, J = 34.4, PCy_2), –26.4 (d, J = 34.4, PPh_2). Anal. calcd. for $C_{194}H_{250}N_6O_7P_8Si_5Fe_4$: C 68.74, H 7.43, N 2.48; found: C 68.46, H 7.56, N 2.46.

1-Hydroxy-3,5-bis{1-oxo-2-aza-2-[3,5-bis{6-[(S_P)-1-diphenylphosphino-2-[1*R*-(dicyclohexylphosphino)ethyl]-1′-ferrocenyl]-6-dimethyl-1-oxo-2-aza-6-silahexyl}-phenyl]}benzene ((*R*)-(*S*)-22)

To a solution of the silylether (*R*)-(*S*)-**22a** (1.05 g, 310 μmol) in 20 mL of THF was added a 1 M solution of tetrabutylammonium fluoride in THF (0.46 mL, 0.46 mmol). After stirring at rt for 20 min the solution was treated with sat. NH_4Cl solution. The aqueous phase was extracted with Et_2O, the organic extracts were washed water (3 times), dried over anhydrous magnesium sulfate, and the solvent was removed in vacuo. The product was purified by silica gel flash chromatography (first hexane – ethyl acetate (3:1) + 5% NEt_3, to elute impurities, then ethyl acetate to elute the product) to yield (*R*)-(*S*)-**22** as an orange powder (890 mg). This product contains 2.5 equivalents of H_2O per molecule of product, which means a yield of 878 mg (268 μmol, 86%); mp 148–154°C. $[\alpha]_D$ = –257 (c = 0.745, $CHCl_3$). MALDI-LRMS *m*/*z*: 3276 ($[M]^+$), 3078 ($[M - HPCy_2]^+$), 2803 ($[M - C_5H_3(PPh_2)(CH(Me)PCy_2)]^+$). IR (KBr) ($cm^{-1}$): 2924, 2848, 1653 (C=O). ^{1}H NMR (300 MHz, DMSO-d_6, 100°C) δ: 10.17 (s, 2H), 9.70 (s, 1H), 8.31 (d, J = 1.4, 4H), 8.06 (m, 1H), 7.98 (t, J = 5.5, 4H), 7.93 (m, 2H), 7.64 (m, 8H), 7.58 (m, 2H), 7.38 (m, 12H), 7.16 (m, 20H), 4.37 (m, 4H), 4.34 (m, 4H), 4.30 (m, 4H), 4.09 (m, 8H), 3.77 (m, 4H), 3.34 (m, 4H), 3.23 (m, 12H), 1.9–0.9 (m, 108H), 0.58 (m, 8H), 0.15 (s, 12H), 0.09 (s, 12H). ^{13}C NMR

© 2001 NRC Canada

(75.5 MHz, $CDCl_3$–DMSO-d_6 (1:1), 100°C) δ: 166.4, 165.5, 158.1, 141.5–127.1 (PPh_2), 139.6, 136.7, 135.4, 122.4, 121.2, 118.4, 117.7, 101.6, 74.1–69.3 (7Cp-CH), 74.2, 71.2, 43.1, 33.1–25.9 (PCy_2, *C*HMeP), 24.3, 17.3, 14.3, –2.2, –2.3. ^{31}P NMR (101.3 MHz, $CDCl_3$) δ: 15.9 (d, J = 34.4, PCy_2), –26.5 (d, J = 34.4, PPh_2). Anal. calcd. for $C_{188}H_{236}N_6O_7P_8Si_4Fe_4$ + 2.5H_2O: C 68.00, H 7.32, N 2.53; found: C 68.03, H 7.46, N 2.56.

12-Cascade:benzene[3-1,3,5]:(5-(1-oxo-2-oxa)-1,3-phenylene):(5-(1-oxo-2-aza)-1,3-phenylene):1′-(1-dimethyl-6-oxo-5-aza-1-silahexyl)-(S_P)-1-diphenylphosphino-2-[1*R*-(dicyclohexylphosphino)-ethyl]ferrocene ((*R*)-(*S*)-23)

(*R*)-(*S*)-**23** was prepared at rt from (*R*)-(*S*)-**22** (542 mg, 165.4 μmol), 4-(pyrrolidino)pyridine (68 mg,460 μmol) in 8 mL of CH_2Cl_2, and **6** (12.2 mg, 46.0 μmol) in 5 mL of CH_2Cl_2 according to the general procedure described above (2 h stirring) to afford, after silica gel flash chromatography (hexane – ethyl acetate (1:1) + 1% NEt_3), (*R*)-(*S*)-**23** (451 mg, 45.2 μmol, 98%) as an orange powder; mp 164–169°C. $[\alpha]_D$ = –268 (c = 1.14, $CHCl_3$). MALDI-LRMS *m/z*: 10372 ($[M + 240]^+$), 9867 ($[10372 – C_5H_3(P(O)Ph_2)-(CH(Me)P(O)Cy_2)]^+$), 9360 ($[10372 – 2C_5H_3(P(O)Ph_2)-(CH(Me)P(O)Cy_2)]^+$). IR (KBr) ($cm^{-1}$): 2923, 2848, 1652 (C=O), 1538, 1444, 1434, 697. ^{1}H NMR (300 MHz, $CDCl_3$–DMSO-d_6 (1:1), 80°C) δ: 10.44 (s, 6H), 9.26 (s, 3H), 8.72 (m, 3H), 8.39 (m, 12H), 8.23 (m, 6H), 8.00 (m, 18H), 7.63 (m, 24H), 7.35 (m, 36H), 7.13 (m, 60H), 4.33 (m, 12H), 4.28 (m, 24H), 4.05 (m, 24H), 3.75 (m, 12H), 3.29 (m, 12H), 3.24 (m, 36H), 2.50 (s, 12H), 1.9–0.9 (m, 324H), 0.54 (m, 24H), 0.15 (s, 36H), 0.08 (s, 36H). ^{13}C NMR (75.5 MHz, $CDCl_3$–DMSO-d_6 (1:1), 80°C) δ: 165.9, 164.0, 162.9, 150.7, 141.4–126.9 (PPh_2), 139.1, 136.8, 135.9, 131.1, 125.0, 124.2, 122.3, 121.2, 101.5, 74.1, 74.0–69.0 (7Cp-CH), 70.9, 42.8, 32.9–26.1 (PCy_2, *C*HMeP), 24.0, 16.9, 14.1, –2.2, –2.3. ^{31}P NMR (121.5 MHz, $CDCl_3$–DMSO-d_6 (1:1), 80°C) δ: 16.7 (d, J = 36.3, PCy_2), –24.9 (d, J = 36.4, PPh_2). Anal. calcd. for $C_{576}H_{708}N_{18}O_{24}P_{24}Si_{12}Fe_{12}$: C 68.94, H 7.15, N 2.53; found: C 68.76, H 7.32, N 2.58.

16-Cascade:tricyclo[3.3.1.1^{3,7}]decane[4-1,3,5,7]:(5-(1-oxo-2-oxa)-1,3-phenylene):(5-(1-oxo-2- aza)-1,3-phenylene):1′-(1-dimethyl-6-oxo-5-aza-1-silahexyl)-(S_P)-1-diphenylphosphino-2-[1*R*-(dicyclohexylphosphino)-ethyl]ferrocene ((*R*)-(*S*)-24)

(*R*)-(*S*)-**24** was prepared at rt from (*R*)-(*S*)-**22** (252 mg, 76.9 μmol), NEt_3 (70 μL, 0.52 mmol), 4-(pyrrolidino)-pyridine (5 mg, 33.7 μmol) in 6 mL of CH_2Cl_2, and **7** (16.0 μmol, in situ from 1,3,5,7-adamantanetetracarboxylic acid (5.0 mg)) in 5 mL of CH_2Cl_2 according to the general procedure described above (stirred overnight) to afford, after silica gel flash chromatography (hexane – ethyl acetate (1:1) + 5% NEt_3), (*R*)-(*S*)-**24** (188 mg, 14.1 μmol, 88%) as an orange powder; mp 164–170°C. $[\alpha]_D$ = –245 (c = 0.755, $CHCl_3$). MALDI-LRMS *m/z*: 3406 ($[OC_6H_3(CONHC_6H_3(CONH$ twice oxidized ferrocene)$_2$)$_2$)]$^+$), 3196 ($[3406 – P(O)Cy_2]^+$), 2901 ($[3406 – C_5H_3(P(O)Ph_2)(CH(Me)P(O)Cy_2)]^+$), 2688 ($[3406 – 2P(O)Cy_2]^+$), 2399 ($[3406 – 2C_5H_3(P(O)Ph_2)(CH-(Me)P(O)Cy_2)]^+$). ^{1}H NMR (300 MHz, $CDCl_3$–DMSO-d_6 (1:1), 80°C) δ: 10.35 (s, 8H), 8.63 (s, 4H), 8.35 (s, 16H), 7.91 (m, 32H), 7.62 (m, 32H), 7.35 (m, 48H), 7.14 (m, 80H), 4.32 (m, 16H), 4.27 (m, 32H), 4.04 (m, 32H), 3.75 (m, 16H), 3.28 (m, 16H), 3.23 (m, 48H), 1.9–0.9 (m, 432H), 0.56 (m, 32H), 0.14 (s, 48H), 0.07 (s, 48H). ^{13}C NMR (75.5 MHz, $CDCl_3$–DMSO-d_6 (1:1), 80°C) δ: 166.1, 166.0, 164.0, 150.8, 141.4–126.9 (PPh_2), 139.1, 136.5, 122.4, 122.2, 121.2, 120.9, 101.5, 74.1, 73.9–69.0 (7Cp-CH), 70.9, 42.8, 42.4, 38.3, 32.9–25.8 (PCy_2, *C*HMeP), 24.0, 16.9, 14.1, –2.2, –2.3. ^{31}P NMR (101.3 MHz, $CDCl_3$) δ: 15.9 (d, J = 34.4, PCy_2), –26.4 (d, J = 34.4, PPh_2). No correct elemental analysis could be obtained.

Dimethyl methylsuccinate (26)

The literature procedure (19) was slightly modified. $[Rh(COD)_2]BF_4$ (19.1 μmol) and the chiral ligand (21.0 μmol divided by the number of ferrocene units in the molecule) were dissolved in 2 mL of CH_2Cl_2 and stirred 15 min at rt. After removing the solvent in vacuo, the residue was dissolved in MeOH. This solution was added to a solution of **25** (302 mg, 1.91 mmol) in 5 mL of MeOH. The inert gas was replaced by hydrogen and a hydrogen filled balloon was connected to the reaction flsk. The solution was stirred vigorously. After 30 min, the solvent was removed in vacuo and the product purified via Kugelrohr distillation (150°C, 10 mbar, 1 bar = 0.1 MPa). Isolated yield: 80–90%. ^{1}H NMR (250 MHz, $CDCl_3$) δ: 3.69 (s, 3H), 3.67 (s, 3H), 2.93 (m, 1H), 2.74 (dd, J = 16.5, 8.1, 1H), 2.40 (dd, J = 16.5, 6.0, 1H), 1.21 (d, J = 7.1, 3H). ee determination by HPLC: OD-H, at 23°C; hexane–*i*-PrOH = 97/3; flow 0.5 mL min^{-1}. Retention times: (*R*) = 13.1 min, (*S*) = 21.5 min (UV: 210 nm).

(1,3-Diphenyl allyl)malonic acid dimethyl ester (28)

The literature procedure (19) was slightly modified. $Pd(dba)_2$ (12.8 μmol) was dissolved in 5 mL of CH_2Cl_2 and the chiral ligand (14.1 μmol divided by the number of ferrocene units in the molecule) was added. This solution was stirred until the color changed from dark red to light orange (up to 16 h). Racemic (*E*)-1,3-diphenyl-2-propenyl-acetate (**27**, 323 mg, 1.28 mmol), dimethyl malonate (338 mg, 2.56 mmol), *N*,*O*-bis(trimethylsilyl)acetamide (BSA) (521 mg, 2.56 mmol), and KOAc (6 mg, 0.06 mmol) were added in this order. After 20 h, the solvent was removed in vacuo and the product was purified by silica gel flash chromatography (hexane – ethyl acetate, 5:1). Isolated yield: 90–99%. ^{1}H NMR (250 MHz, $CDCl_3$) δ: 7.40–7.15 (m, 10H), 6.50 (d, J = 15.8, 1H), 6.33 (dd, J = 15.8, 8.3, 1H), 4.28 (dd, J = 10.9, 8.3, 1H), 3.96 (d, J = 10.9, 1H), 3.71 (s, 3H), 3.52 (s, 3H). ee determination by HPLC: OD-H, at 23°C; hexane–*i*-PrOH = 98/2; flow 0.5 mL min^{-1}. Retention times: (*R*) = 17.7 min, (*S*) = 18.8 min (UV: 254 nm).

1-Phenylethanol (30) and 2-phenylethanol (31)

The literature procedure (19) was slightly modified. $[Rh(COD)_2]BF_4$ (19.1 μmol) and the chiral ligand (21.0 μmol divided by the number of ferrocene units in the molecule) were dissolved in 2 mL of CH_2Cl_2 and stirred for 15 min at rt. After removal of the solvent in vacuo, the residue was dissolved in THF. Styrene (**29**) (199 mg, 1.91 mmol) and 1,3,2-benzodioxaborole (catecholborane) (252 mg, 2.10 mmol) were added in this order. After 5 h, aq.

© 2001 NRC Canada

NaOH solution (4.8 mL, 3 M) and an H_2O_2 solution (0.41 mL, 35% in H_2O) were added and vigorous stirring was continued during 3 h. The mixture was then extracted with Et_2O and the organic extracts were washed twice with 1 M NaOH and once with sat. NH_4Cl solution. After drying over anhydrous magnesium sulfate, the solvent was removed in vacuo and the product purified by Kugelrohr distillation (150°C, 10 mbar). Isolated yield: 60–94%. (**30**): ^{1}H NMR (250 MHz, $CDCl_3$) δ: 6.6–7.4 (m, 5H), 4.89, (q, J = 6.4, 1H), 1.50 (d, J = 6.4, 3H). (**31**): ^{1}H NMR (250 MHz, $CDCl_3$) δ: 6.6–7.4 (m, 5H), 3.87 (t, J = 6.6, 2H), 2.88 (t, J = 6.6, 2H). ee determination by HPLC: OB-H, at 23°C; hexane–*i*-PrOH = 97/3; flow 0.5 mL min^{-1}. Retention times: (*S*)-**30** = 21.5 min, **31** = 24.0 min, (*R*)-**30** = 31.5 min (UV: 214 nm).

Acknowledgments

We are grateful to ETH for financial support and to Walter Amrein (Laboratory of Organic Chemistry, ETH) for measuring MALDI-TOF spectra.

References

1. (*a*) G.R. Newkome, E. He, and C.H. Moorefield. Chem. Rev. **99**, 1689 (1999); (*b*) J.-P. Majoral and A.-M. Caminade. Chem. Rev. **99**, 845 (1999); (*c*) A.W. Bosman, H.M. Janssen, and E.W. Meijer. Chem. Rev. **99**, 1665 (1999); (*d*) A. Archut and F. Vögtle. Chem. Soc. Rev. **27**, 233 (1998); (*e*) M. Fischer and F. Vögtle. Angew. Chem. Int. Ed. **38**, 885 (1999); (*f*) M.A. Hearshaw and J.R. Moss. J. Chem. Soc. Chem. Commun. 1 (1999).
2. G.E. Oosterom, J.N.H. Reek, P.C.J. Cramer, and P.W.N.M. van Leeuwen. Angew. Chem. Int. Ed. **40**, 1828 (2001).
3. J.W.J. Knapen, A.W. van der Made, J.C. de Wilde, P.W.N.M. van Leeuwen, P. Wijkens, D. M. Grove, and G. van Koten. Nature (London), **372**, 659 (1994).
4. (*a*) P.B. Rheiner, H. Sellner, and D. Seebach. Helv. Chim. Acta, **80**, 2027 (1997); (*b*) C. Bolm, N. Derrien and A. Seger. Synlett, 387 (1996); (*c*) H. Brunner. J. Organomet. Chem. **500**, 39 (1995); (*d*) M.T. Reetz, G. Lohmer, and R. Schwickardi. Angew. Chem. Int. Ed. **36**, 1526 (1997); (*e*) G.E. Oosterom, R.J. van Haaren, J.N.H. Reek, P.C.J. Kamer, and P.W.N.M. van Leeuwen. Chem. Commun. 1119 (1999); (*f*) H.P. Dijkstra, P. Steenwinkel, D.M. Grove, M. Lutz, A. L. Spek, and G. van Koten. Angew. Chem. Int. Ed. **38**, 2186 (1999); (*g*) C. Schlenk, A.W. Kleij, H. Frey, and G. van Koten. Angew. Chem. Int. Ed. **39**, 3445 (2000); (*h*) A.W. Kleij, R.J.M. Klein Gebbink, P.A.J. van den Nieuwenhuijzen, H. Kooijman, M. Lutz, A.L. Spek, and G. van Koten. Organometallics, **20**, 634 (2001); (*i*) R.A. Gossage, J.T.B.H. Jastrzebski, J. van Ameijde, S.J.E. Mulders, A.J. Brouwer, R.M.J. Liskamp, and G. van Koten. Tetrahedron, **40**, 1413 (1999); (*j*) T. Mizugaki, O. Masahiko, K. Ebitani, and K. Kaneda. J. Mol. Catal. A, **145**, 329 (1999); (*k*) M. Kimura, A. Sugihara, T. Muto, K. Hanabusa, H. Shirai, and N. Kobayashi. Chem. Eur. J. **5**, 3495 (1999).
5. (*a*) M.T. Reetz, G. Lohmer, and R. Schwickardi. Angew. Chem. Int. Ed. **36**, 1526 (1997); (*b*) T. Suzuki, Y. Hirokawa, K. Ohtake, T. Shibata, and K. Soai. Tetrahedron-Asymmetr. **8**, 4033 (1997); (*c*) I. Sato, T. Shibata, K. Ohtake, R. Kodaka, Y. Hirokawa, N. Shirai, and K. Soai. Tetrahedron Lett. **41**, 3123 (2000).
6. R. Breinbauer and E.N. Jacobsen. Angew. Chem. Int. Ed. **39**, 3604 (2000).
7. V. Maraval, R. Laurent, A.-M. Caminade, and J.-P. Majoral. Organometallics, **19**, 4025 (2000).
8. A.W. Kleij, R.A. Gossage, R.J.M. Klein Gebbink, N. Brinkmann. Ed. J. Reijerse, U. Kragl, M. Lutz, A.L. Spek, and G. van Koten. J. Am. Chem. Soc. **122**, 12112 (2000).
9. (*a*) A. Togni. *In* Metallocenes: synthesis, reactivity, applications. *Edited by* A. Togni and R.L. Halterman. Wiley–VCH, Weinheim, New York. 1998. pp. 685–721, and refs. cited therein; (*b*) A. Togni, N. Bieler, U. Burckhardt, C. Köllner, G. Pioda, R. Schneider, and A. Schnyder. Pure Appl. Chem. **71**, 1531 (1999); (*c*) A. Togni. Angew. Chem. Int. Ed. **35**, 1475 (1996); (*d*) A. Togni. Chimia, **50**, 86 (1996).
10. (*a*) C. Köllner, B. Pugin, and A. Togni. J. Am. Chem. Soc. **120**, 10274 (1998); (*b*) A. Togni, R. Dorta, C. Köllner, and G. Pioda. Pure Appl. Chem. **70**, 1477 (1988); (*c*) R. Schneider, C. Köllner, I. Weber, and A. Togni. Chem. Commun. 2415 (1999).
11. M.S. Gibson and R.W. Bradshaw. Angew. Chem. **80**, 986, (1968).
12. H.R. Ing and R.H.F. Manske. J. Chem. Soc. 2348 (1968).
13. (*a*) H.-T. Chang, C.-T. Chen, T. Kondo, G. Siuzdak, and K.B. Sharpless. Angew. Chem. Int. Ed. **108**, 202 (1996); (*b*) V. Percec, P. Chu, G. Ungar, and J. Zhou. J. Am. Chem. Soc. **711**, 11441 (1995); (*c*) L.J. Twyman, A. Beezer, and J.C. Mitchell. Tetrahedron Lett. **35**, 4423 (1994); (*d*) T.M. Miller and T.X. Neenan. Chem. Mater. **2**, 346 (1990); (*e*) G.J. Marshallsay, T.K. Hansen, A.J. Moore, M.R. Bryce, and J. Becher. Synthesis, 926 (1994); (*f*) G.R. Newkome, X. Lin, and J.K. Young. Synlett, **53** (1992).
14. (*a*) S. Landa and Z. Kamycek. Collect. Czech. Chem. Commun. **28**, 4004 (1959); (*b*) H. Stetter and M. Krause. Liebigs Ann. Chem. **60**, 717 (1968); (*c*) H. Stetter, O.-E. Bänder, and W. Neumann. Ber. Dtsch. Chem. Ges. **89**, 1922 (1956); (*d*) A. Bashir-Hashemi, J. Li, and N. Gelber. Tetrahedron Lett. **36**, 1233 (1995).
15. K.F. Jennings. J. Chem. Soc. 1172 (1957).
16. T.M. Miller, E.W. Kwock, and T.X. Neenan. Macromolecules, **25**, 3143 (1992).
17. (*a*) E.W. Collington, H. Finch, and I.J. Smith. Tetrahedron Lett. **26**, 681 (1985); (*b*) S. Höger. Synthesis, **20** (1997).
18. R.S. Brown, B.L. Carr, and J.J. Lennon. J. Am. Soc. Mass Spectr. **7**, 225 (1995).
19. A. Togni, C. Breutel, A. Schnyder, F. Spindler, H. Landert, and A. Tijani. J. Am. Chem. Soc. **116**, 4062 (1994).
20. A. Togni, C. Breutel, M.C. Soares, N. Zanetti, and F. Spindler. Inorg. Chim. Acta, **222**, 213 (194).
21. W. Ried and F.-J. Königstein. Chem. Ber. **92**, 2532 (1959).
22. M.D. Fryzuk and B. Bosnich. J. Am. Chem. Soc. **99**, 6262 (1977).
23. T. Ukai, H. Kawazura, Y. Ishii, J.J. Bonnet, and J.A. Ibers. J. Organomet. Chem. **65**, 253 (1974).
24. M. Jayamani, N. Pant, S. Ananthan, K. Narayanan, and C.N. Pillai. Tetrahedron, **42**, 4325 (1986).

© 2001 NRC Canada

Attempted enantiotopic group selective cyanohydrin formation from α-alkoxy aldehydes by double stereodifferentiation

Dale E. Ward, Marcelo Sales, and Matthew J. Hrapchak

Abstract: Enantiotopic group selectivity can result from the competition between substrate and reagent double stereodifferentiation. We have examined this approach for enantioselective hydrocyanation of racemic α-alkoxy aldehydes (e.g., 2-(phenylmethoxy)heptanal (**1**)). Reaction of **1** with TMSCN mediated by chiral nonracemic alkoxy Ti(IV) reagents under conditions known to be reasonably enantioface selective in reactions with achiral aldehydes, proceeded with very low enantiotopic group selectivity (<2:1). It was established that TMSCN can react with Ti(IV) reagents to produce "TiCN" adducts that are capable of hydrocyanation but with low substrate-controlled diastereoselectivity in reactions with **1**. The poor enantiotopic group selectivity observed can be rationalized to result from this low diastereoselectivity despite the respectable levels of enantioface selectivity associated with these reagents in hydrocyanation of achiral aldehydes. Highly diastereoselective hydrocyanation of α-alkoxy aldehydes can be achieved with TMSCN in the presence of excess $MgBr_2 \cdot OEt_2$. High diastereoselectivity was also observed using achiral and chiral TiCN adducts in place of TMSCN. Although the putative TiCN adducts obtained from nonracemic alkoxy Ti(IV) reagents are implicated in enantioface selective hydrocyanation, these reagents were not enantiotopic group selective under these conditions and showed no evidence of double stereodifferentiation. The use of nonracemic bisoxazoline ligands for Mg(II) was also ineffective.

Key words: cyanohydrin, 2-alkoxyalkanal, double stereodifferentiation, enantiotopic group selective reaction, kinetic resolution.

Résumé : La sélectivité énantiotopique de groupe peut découler d'une compétition entre la stéréodifférenciation double entre le substrat et le réactif. On a examiné cette approche pour l'hydrocyanuration énantiosélective d'α-alkoxyaldéhydes racémiques (par exemple, le 2-(phénylméthoxy)heptanal (**1**)). Lors de la réaction avec le TMSCN, sous l'influence de réactifs chiraux non racémiques de type alkoxy Ti(IV), dans des conditions reconnues pour être énantiosélectives au cours de réactions avec les faces d'aldéhydes achiraux, la sélectivité énantiotopique de groupe était très faible (< 2:1). Il a été établi que le TMSCN peut réagit avec les réactifs du Ti(IV) pour conduire à la production d'adduits "TiCN" qui, lors de réactions avec le composé **1**, peuvent donner lieu à une hydrocyanuration pour laquelle la diastéréosélectivité contrôlée par le substrat est faible. On peut imaginer que la faible sélectivité énantiotopique de groupe observée résulte de cette faible diastéréosélectivité malgré les niveaux respectables de énantiosélectivité par rapport aux faces qui sont associées à ces réactifs dans l'hydrocyanuration d'aldéhydes achiraux. On peut réaliser des hydrocyanurations hautement diastéréosélectives d'α-alkoxyaldéhydes à l'aide de TMSCN, en présence d'un excès de $MgBr_2 \cdot OEt_2$. On a aussi observé une diastéréosélectivité lorsqu'on a utilisé des adduits TiCN achiraux et chiraux à la place du TMSCN. Les adduits TiCN présumés, obtenus à partir de réactifs non racémiques de type alkoxy Ti(IV), sont impliqués dans des hydrocyanurations énantiosélectives par rapport aux faces; toutefois, dans ces conditions, ces réactifs ne donnent pas lieu à de la sélectivité énantiotopique de groupe et ne présentent pas de signe de double stéréodifférenciation. L'utilisation de ligands bisaxozolines non racémiques pour des composés de type Mg(II) est aussi inefficace.

Mots clés : cyanohydrine, 2-alkoxyalcanal, double stéréodifférenciation, réaction avec sélectivité énantiotopique de groupe, dédoublement cinétique.

[Traduit par la Rédaction]

Received March 22, 2001. Published on the NRC Research Press Web site at http://canjchem.nrc.ca on November 20, 2001.

This paper is dedicated to Professor Victor Snieckus in celebration of his numerous contributions to chemistry and to the chemistry community in Canada.

D.E. Ward,[1] M. Sales, and M.J. Hrapchak. Department of Chemistry, University of Saskatchewan, 110 Science Place, Saskatoon SK S7N 5C9, Canada.

[1]Corresponding author (telephone: (306) 966-4656; fax: (306) 966-4730; e-mail: Dale.Ward@usask.ca).

 DOI: 10.1139/cjc-79-11-1775 © 2001 NRC Canada

Introduction

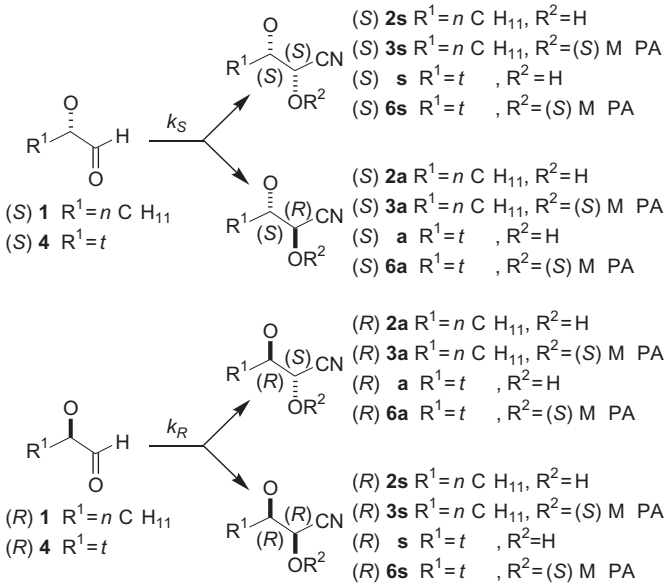
The development of new methods for asymmetric synthesis continues to attract considerable attention (1). Although the majority of known methods involve enantioselective addition to a π-bond of an achiral substrate (i.e., an enantiotopic face selective reaction), the use of enantiotopic group selective reactions for desymmetrization of achiral C_s (or C_i) symmetric substrates has recently emerged as an alternative strategy (2). This approach is particularly effective when the enantiotopic groups can react sequentially thereby coupling an asymmetric synthesis with a kinetic resolution and producing products with high stereoisomeric purity (3). We have previously shown that such processes can yield products with very high stereoisomeric purity from reactions with modest enantioselectivity (4) and even from mixtures of substrate stereoisomers (5). Both the efficiency and efficacy of these processes are improved with recycling, especially if the enantioselectivity is modest (4, 5). Because recycling requires that the product(s) (or byproducts) be efficiently converted back into the starting material(s), enantiotopic group selective reactions that are easily "reversed" are desirable. We have previously targeted enantioselective reduction of chiral aldehydes (reversed by oxidation of the product alcohols) (4) and enantioselective enolization (reversed by protonation of the enolate derivative) (6) as reactions for development. The potential for stereoselective formation of cyanohydrins from aldehydes (vide infra) and the facile loss of HCN from such cyanohydrins prompted us to examine enantiotopic group selective cyanohydrin formation from α-alkoxy aldehydes.

Few design elements are available to guide the development of enantiotopic group selective reactions and many of the successful examples (2) involve application of previously established "reagent-controlled" enantioface selective reactions to chiral[2] or C_s symmetric substrates that impart significant "substrate-controlled" diastereoface selectivity (7).[3] In such cases, enantiotopic group selectivity can be rationalized to result from the matching and mismatching of substrate diastereotopic face selectivity with reagent enantiotopic face selectivity (4, 8, 9). The magnitude of the enantiotopic group selectivity (E) can be estimated from eq. [1] where **r** is the enantiotopic face selectivity associated with the chiral reagent acting on a "model" achiral substrate and **s** is the diastereotopic face selectivity of the chiral substrate with a model achiral reagent (4, 9).[4]

$$[1] \qquad E = \frac{(\mathbf{r})(\mathbf{s}) + 1}{\mathbf{r} + \mathbf{s}}$$

The stereoselective formation of cyanohydrins from aldehydes dates back to the late 19th century when Emil Fischer reported that addition of HCN to L-arabinose gave a 2:1 mixture of cyanohydrins in favor of the *manno* (i.e., 2,3-*anti*) diastereomer (10). Subsequently, this reaction has proven to be quite useful for the chain extension of monosaccharides (11). Cyanohydrins are generally recognized as versatile synthetic intermediates for the preparation of a variety of useful compounds (12, 13). As a consequence, the development of methods for enantioselective formation of cyanohydrins from achiral aldehydes has attracted considerable attention (13) and several highly enantioselective methods using chiral Lewis acid catalysts have been reported recently (14). By contrast, cyanohydrins are often formed with poor diastereoselectivity from chiral aldehydes (15), even in enzyme-mediated processes (16). For example, diastereoselectivities of only 1.5–5:1 in favor of the *syn* isomer have been reported for cyanohydrin formation from α-alkoxy aldehydes using trimethylsilylcyanide (TMSCN) in the presence of various Lewis acids (17). Because the predicted selectivity (*E*) is limited by the lower of **r** and **s** (eq. [1]), the low substrate diastereoselectivity noted above suggested that cyanohydrin formation from α-alkoxy aldehydes would result in poor enantiotopic group selectivity even using methods with excellent enantioface selectivity. We now report several experiments which support this hypothesis and on our efforts to improve on the substrate diastereoselectivity in an attempt to achieve enantiotopic group selective cyanohydrin formation by double stereodifferentiation.

Scheme 1



Results and discussion

We selected the racemic α-alkoxy aldehydes **1** and **4** as substrates to investigate enantiotopic group selective cyanohydrin formation. Under the influence of a chiral nonracemic reagent or catalyst, the individual enantiomers of the aldehyde

[2] Enantiotopic group selective reaction of chiral substrates is equivalent to kinetic resolution. In this case, groups on enantiomeric substrates are enantiotopic by external comparison.

[3] For a discussion and definition of reagent- and substrate-controlled stereoselectivity, see ref. 8.

[4] The face selectivity for one group will be (**r**)(**s**):1 (i.e., "matched"); total reactivity is (**r**)(**s**) + 1. The face selectivity for the enantiotopic group will be (**r**):(**s**) (i.e., "mismatched"); total reactivity is (**r**) + (**s**). The accuracy of this estimation depends on the suitability of the models used for the determination of **r** and **s**. For a detailed discussion of the derivation, assumptions, and sources of error in the above multiplicativity rule, see ref. 8.

© 2001 NRC Canada

Table 1. Enantiotopic group selective hydrocyanation of **1** and **4** with TMSCN–(*i*-Pr-O)$_2$TiCl$_2$–TADDOL at –23°C.[a]

Entry	Aldehyde	Time (h)	(*C*)[b,c]	(*R*)-**2s**[c,d] (%)	(*R*)-**2a**[c,d] (%)	(*S*)-**2s**[c,d] (%)	(*S*)-**2a**[c,d] (%)	k_S/k_R[e]
1	**1**	1	0.31	27	10	42	21	2.0
2	**1**	3	0.68	33	11	39	16	1.5
3	**1**	8	0.87	35	12	37	17	1.6
4	**4**	3	0.71	20[f]	25[f]	43[f]	13[f]	1.5
5	**1**[g]	3	0.20	46	6	23	25	0.91

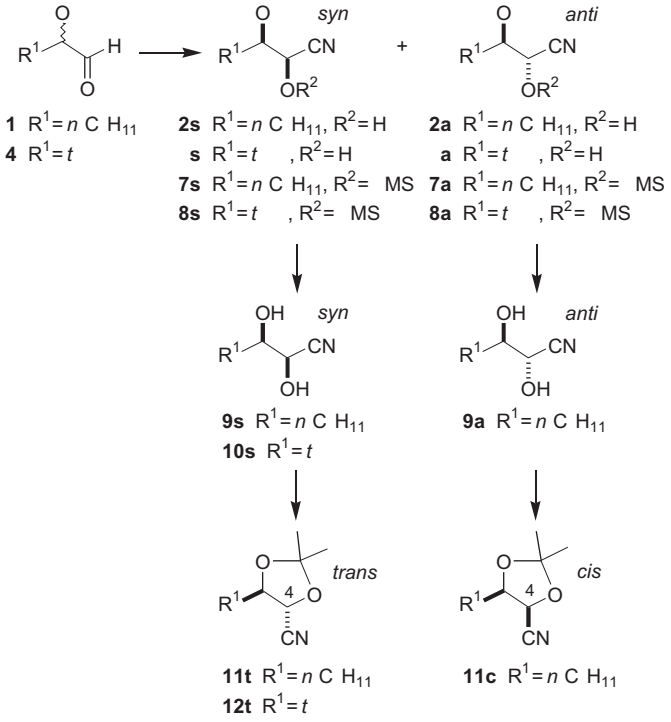
[a]Reagent preparation: TADDOL (1.5 equiv) was added to a toluene solution of (*i*-Pr-O)$_2$TiCl$_2$ (1.5 equiv) at room temperature. After 1 h, MS4A and TMSCN were added.
[b]Determined by ^{1}H NMR of the crude reaction mixture.
[c]Estimated relative error of ±10%.
[d]Determined by ^{1}H NMR of the corresponding Mosher's esters.
[e]Calculated according to footnote 5.
[f]Refers to cyanohydrins **6** (not **2**).
[g](+)-BINOL was used instead of TADDOL.

(e.g., **1**) should form cyanohydrins at different rates (i.e., a kinetic resolution) and with different diastereoselectivities to produce the four possible stereoisomeric products (e.g., (*R*)-**2a**, (*R*)-**2s**, (*S*)-**2a**, and (*S*)-**2s**) (18).

The relative amounts of the product stereoisomers from a reaction of low or known conversion can be used to calculate the relative rates of hydrocyanation of the individual substrate enantiomers (i.e., the enantiotopic group selectivity).[5] Alternatively, the enantiomeric purity of the recovered α-alkoxy aldehyde from a hydrocyanation reaction of known conversion can be used to determine the selectivity.[6] Thus, a method to analyze the composition of the four stereoisomeric cyanohydrins was required.

The relative stereochemical configurations of the cyanohydrins **2** and **5** were determined via NMR analysis of the derived acetonides (17*a*). Reaction of **1** with trimethylsilylcyanide (TMSCN) in the presence of Et_3N (19) gave **7** as a 2:1 mixture of racemic diastereomers in quantitative yield. Hydrolysis of **7** (a 2:1 mixture of diastereomers) with dilute acid gave a 2:1 mixture of cyanohydrins **2.** Alternatively, treatment of **7** with $TiCl_4$ gave the diols **9**, also as a 2:1 mixture of diastereomers, which produced a 2:1 mixture of acetonides **11**. The minor acetonide was assigned as *cis* (i.e., **11c**) on the basis of an 8% nOe observed for HC-5 upon irradiation of HC-4 (nOe was not observed between HC-4 and HC-5 in the major acetonide, **11t**); thus, the major cyanohydrin formed was assigned as the *syn* diastereomer **2s**. Similar processing of **4** gave a separable 3:1 mixture of cyanohydrins **5**; the major diastereomer was assigned as *syn* (i.e., **5s**) on the basis of an 18% nOe observed for HC-4 upon irradiation of the $(H_3C)_3C$ protons in the derived acetonide **12t**. A method for determining the absolute configurations of the four stereoisomers of **2** was established by conversion (20) of a 2.4:1 mixture of racemic **2s** and **2a**, respectively, to a 2.6:2.6:1:1 mixture of diastereoisomeric Mosher's esters (21) **3** in 88% yield from excess (2*S*)-3,3,3-trifluoro-2-methoxy-2-phenylpropanoic acid [(*S*)-MTPA-OH].[7] Assignment of individual signals in the ^{1}H NMR spectrum of the mixture of esters to individual diastereomers was possible on the basis of intensity (i.e., major signals from *syn* diastereomers and minor signals from *anti* diastereomers), homonuclear decoupling experiments (i.e., identifying the pairs of HC-2–HC-3 and H_2CO signals for individual diastereomers), and application of the advanced Mosher's method (22).[8] The same strategy was successfully applied for analysis of the four stereoisomers of **6**.

Scheme 2.



[5] At low conversion, k_S/k_R (= *E*) is closely approximated by ([(*S*)-**2a**] + [(*S*)-**2s**])/([(*R*)-**2a**] + [(*R*)-**2s**]). At higher conversions (*C*) with product stereoisomeric excess (se = ([(*S*)-**2a**] + [(*S*)-**2s**] – [(*R*)-**2a**] – [(*R*)-**2s**])/([(*S*)–**2a**] + [(*S*)-**2s**] + [(*R*)-**2a**] + [(*R*)-**2s**])), *E* = {ln (1 – *C*(1 + se)}/{ln (1 – *C*(1 – se)}. For a discussion, see ref. 18.
[6] If the ee of recovered **1** is ([(*R*)-**1**] – [(*S*)-**1**])/([(*R*)-**1**] + [(*S*)-**1**]) at conversion *C*, then k_S/k_R = *E* = {ln [(1 – *C*)(1 – ee)]}/{ln [(1 – *C*)(1 + ee)]}. For a discussion, see ref. 18.
[7] A control experiment established that acetylation of **2** under these conditions occurred without loss of stereochemical integrity.
[8] This method predicts that for the (*S*)-MTPA esters **3** (and **6**), the HC-2 and H_2CO (and *t*-Bu) signals for the (1*S*) diastereomers will appear downfield relative to the (1*R*) diastereomers.

© 2001 NRC Canada

With an analytical method in place, we chose to examine cyanohydrin formation using TMSCN mediated by the chiral alkoxytitanium generated in situ by mixing (*i*-Pr-O)$_2$TiCl$_2$ and (2*R*,3*R*)-2,3-*O*-(1-phenylethylidene)-1,1,4,4-tetraphenyl-1,2,3,4-butanetetrol (**13**, TADDOL) in the presence of 4 Å molecular sieves (MS4A) as described by Narasaka and co-workers (23). Using this system, 3-phenylpropanal was reported to give the (*R*)-cyanohydrin in high yield and in 74–91% ee depending on the procedure employed. In our hands, the same cyanohydrin was obtained in >80% yield under the reported conditions but in only 60 ± 5% ee despite numerous attempts including using alternative methods (24) for preparing the precatalyst **14a**. Despite this modest result (i.e., 4:1 selectivity for addition of cyanide to the *si* face of the aldehyde), we attempted enantiotopic group selective hydrocyanation of **1** using the Narasaka reagent; the results are presented in Table 1.[9] Although the selectivity (i.e., k_S/k_R) was predictably low,[10] it was surprising that hydrocyanation of **1** occurred without evidence of double stereodifferentiation (8). That is, the cyanohydrins from (*R*)-**1** and (*S*)-**1** were formed with comparable levels of *syn* diastereoselectivity (i.e., 2–3:1; compare (*R*)-**2s**:(*R*)-**2a** with (*S*)-**2s**:(*S*)-**2a** in Table 1, entries 1–3) with the *slower* reacting (*R*)-enantiomer giving slightly higher diastereoselectivity. A 1.5–2:1 enantiotopic group selectivity for hydrocyanation of **1** under these conditions was observed at three different conversions and was confirmed by measuring the ee of the recovered aldehyde.[11]

Formation of cyanohydrins from **4** using the Narasaka reagent also proceeded with low enantiotopic group selectivity (Table 1, entry 4). However in this case, the reaction occurred with the expected double stereodifferentiation (8). Thus, the faster reacting (*S*)-**4** gave cyanohydrins with 3.3:1 *syn* diastereoselectivity (i.e., (*S*)-**4s**/(*S*)-**4a**) whereas the slower reacting (*R*)-**4** was slightly *anti* selective (i.e., (*R*)-**4a**/(R*S*)-**4s** = 1.25); addition of cyanide occurred preferentially to the *si* face of both enantiomers of **4** as expected for this reagent (23) and indicating that the reagent *si* face selectivity was higher than the substrate *syn* diastereoselectivity. We also attempted cyanohydrin formation by replacing TADDOL with (*R*)-(+)-1,1′-bi-2-naphthol (BINOL) in the Narasaka protocol (25).[12] Hydrocyanation of **1** with this modified procedure also showed double stereodifferentiation but very low enantiotopic group selectivity (Table 1, entry 5).

Although the observation of double stereodifferentiation in the hydrocyanation of **1** was encouraging, the very low enantiotopic group selectivity obtained suggested that both the reagent enantioselectivity and the substrate diastereoselectivity required improvement. The low diastereoselectivity observed for cyanohydrin formation from α-alkoxy aldehydes on reaction with TMSCN in the presence of various Lewis acids (17) is in stark contrast to the excellent selectivity often associated with nucleophilic additions to these aldehydes under chelation-controlled conditions (26). For example, Reetz et al. (17*a*) reported that reaction of 2-(phenylmethoxy)propanal with TMSCN mediated by TiCl$_4$ (1 equiv) at –78°C gave a 4:1 mixture of *syn:anti* cyanohydrins in good yield. We obtained the same diastereoselectivity (i.e., a 4:1 mixture of **2s** and **2a**) on hydrocyanation of **1** under these conditions (27). This moderate diastereoselectivity prompted us to investigate this reaction more closely.

Varying amounts of TMSCN were added to a solution of TiCl$_4$ in CDCl$_3$ to determine if these two reagents undergo any reaction. The ^{1}H NMR spectra of the yellow solutions obtained after addition of 1, 2, or 4 equiv of TMSCN showed a single signal (δ 0.43) indistinguishable from chlorotrimethylsilane (TMSCl);[13] addition of 10 equiv of TMSCN gave a 3:2 ratio signals assigned[13] to TMSCN (δ 0.36) and TMSCl, respectively. The propensity of mixtures of TiCl$_4$ and TMSCN to produce cyanohydrins from benzaldehyde and from **1** was assessed (Table 2). Clearly, excess TMSCN was required for high conversions (Table 2, entries 1–3) although the diastereoselectivity was unchanged (Table 2, entries 4–5). Interestingly, the cyanohydrin **2** was produced in similar yield and diastereoselectivity by addition of TMSCN to a solution of **1** and TiCl$_4$ or by addition of **1** to a premixed solution of TiCl$_4$ and TMSCN (cf. entries 5 and 6). To obtain further information on the nature of this reagent, solutions of TMSCN (2, 4, and 6 equiv) and TiCl$_4$ in C$_6$D$_6$ were concentrated in vacuo (0.2 torr 1 torr = 133.322 Pa)) collecting the volatile components in a cold trap. Analysis of the resulting yellow residue by ^{1}H NMR (in C$_6$D$_6$) consistently showed the presence of a single signal at ca. 0.18 indistinguishable from TMSCl.[13] The ^{1}H NMR spectrum (in C$_6$D$_6$) of the volatile components obtained from the 2:1 mixture of TMSCN:TiCl$_4$ indicated the absence of both TMSCl and TMSCN, whereas that from the 4:1 mixture showed the presence of ca. 2 equiv of TMSCl[13] and that from the 6:1 mixture contained ca. 2 equiv each of TMSCl and TMSCN δ (–0.17).[13,14] These ex-

[9] The configurational stability of the cyanohydrins under the reaction conditions was confirmed by control experiments.

[10] Reaction of **1** with TMSCN (2 equiv) in the presence of (*i*-Pr-O)$_2$Cl$_2$Ti(IV) (1 equiv) at 0°C in CH$_2$Cl$_2$ gave a 2.5:1 mixture of *syn:anti* cyanohydrins **2s** and **2a** (cf. 4:1, *syn:anti* diastereoselectivity in TiCl$_4$ mediated reaction of α-alkoxy aldehydes with TMSCN (17*a*)). Assuming a reagent enantioselectivity of 4:1 and a substrate diastereoselectivity of 2.5:1, eq. [1] predicts an enantiotopic group selectivity of 1.5:1.

[11] Aldehyde **1** was recovered (50% yield) from a hydrocyanation reaction proceeding to 35% conversion (^{1}H NMR) and found to have 15% ee in favor of (*R*)-**1** by ^{1}H NMR of the Mosher's ester of the corresponding alcohol (NaBH$_4$, 0°C, MeOH; quantitative). Using the equation in footnote 6, the calculated enantiotopic group selectivity from this data (C = 0.35, ee = 0.15) is 2:1.

[12] Subsequent to our work, Nakai and co-workers (25) reported hydrocyanation of aldehydes with the reagent prepared by mixing (*R*)-BINOL and (*i*-Pr-O)$_4$Ti(IV) (0.2 equiv each, rt, 0.5 h) in CH$_2$Cl$_2$ followed by addition of TMSCN (2.5 equiv, 0°C, 0.5 h) (putative catalyst: (BINOL)(CN)$_2$Ti(IV)). With this reagent, addition of cyanide was *re* face selective giving (*S*) cyanohydrins (10–75% ee) from simple aliphatic aldehydes.

[13] Confirmed by addition of an authentic sample(s).

[14] Experiments were conducted at least in triplicate. Quantification was achieved by addition of internal standards (TMSCN and (or) TMSCl). Varying amounts of TMSOH (δ 0.12) were observed; this signal was counted as being derived from TMSCl which was confirmed (^{1}H NMR) by adding controlled amounts of water to a C$_6$D$_6$ solution of TMSCl and TMSCN. Variation of the calculated stoichiometry among "identical" experiments was ca. ±15%.

© 2001 NRC Canada

Table 2. Hydrocyanation of **1** and benzaldehyde with TiCN reagents.

Entry	Aldehyde	TiCN reagent (equiv)	**15**[a,b] (%)	**2** (**2s**:**2a**)[a,b] (%)
1	PhCHO	$TiCl_4$ (1)/TMSCN (1)[c]	50	
2		$TiCl_4$ (1)/TMSCN (2)[c]	78	
3		$TiCl_4$ (1)/TMSCN (4)[c]	92	
4	**1**	$TiCl_4$ (1)/TMSCN (1)[d]		70 (4:1)
5		$TiCl_4$ (1)/TMSCN (2)[d]		90 (4:1)
6		$TiCl_4$ (1)/TMSCN (2)[d,e]		88 (3.3:1)
7	PhCHO	$TiCl_4CN_2^{2-}(TMS^+)_2$[f] (0.16)[g]	21	
8	**1**	$TiCl_4CN_2^{2-}(TMS^+)_2$[f] (0.5)[g]		63 (2:1)
9	PhCHO	$TiCl_2CN_4^{2-}(TMS^+)_2$[h] (0.16)[g]	50	
10	**1**	$TiCl_2CN_4^{2-}(TMS^+)_2$[h] (0.5)[g]		92 (3:1)
11	**1**	(*i*-Pr-O)$_3$TiCN[i] (1)[g]		75 (1:1.2)

[a]Determined by ^{1}H NMR of the crude reaction mixture; the remainder is aldehyde.
[b]Estimated relative error of ±10%.
[c]Conditions: TMSCN was added to a $CDCl_3$ solution of $TiCl_4$ at room temperature. After 1 h, aldehyde was added; water was added after an additional 1 h.
[d]Aldehyde added at –78°C; reaction at –78 to –25°C over 3 h.
[e]TMSCN added to **1** and $TiCl_4$ at –78°C.
[f]Prepared by concentration of a 2:1 mixture of TMSCN:$TiCl_4$.
[g]Reaction for 30 min at room temperature.
[h]Prepared by concentration of a 4:1 mixture of TMSCN:$TiCl_4$.
[i]Prepared by concentration of a 6:1 mixture of TMSCN:(*i*-Pr-O)$_4$Ti.

Table 3. Hydrocyanation of **1** and with TiCN reagents in the presence of $MgBr_2 \cdot OEt_2$ (5 equiv).[a]

Entry	Reagent (equiv)	**2**[b,c] (%)	(*R*)-**2s**[c,d] (%)	(*R*)-**2a**[c,d] (%)	(*S*)-**2s**[c,d] (%)	(*S*)-**2a**[c,d] (%)	k_S/k_R[e]
1	TMSCN (1.1)[f]	95		**2s**:**2a** = 9:1			
2	Et_4NCN (1.1)[f]	65		**2s**:**2a** = 4:1			
3	$TiCl_2CN_4^{2-}(TMS^+)_2$[g] (1)	60		**2s**:**2a** = 3:1			
4	(*i*-Pr-O)$_3$TiCN[h] (1)	51		**2s**:**2a** = 7.5:1			
5	(*i*-Pr-O)$_4$Ti (1) – Et_4NCN (1)[i]	95		**2s**:**2a** = 8.8:1			
6	**14b** (0.3) – Et_4NCN (0.3)[i]	25	45	6	43	6	0.95
7	**14b** (1) – TMSCN (6)[j]	19	46	4	46	4	1.0
8	**16** (1) – TMSCN (0.33)	30	45	5	44	5	0.98
9	**17** (1) – TMSCN (0.33)	24	31	18	34	17	1.05

[a]Conditions: cyanide reagent added to a suspension of Mg(II) and **1** in CH_2Cl_2 solution, 0°C, 1 h. [b]Determined by ^{1}H NMR of the crude reaction mixture.
[c]Estimated relative error of ±10%.
[d]Determined by ^{1}H NMR of the corresponding Mosher's esters.
[e]Calculated according to footnote 5.
[f]Reference 27.
[g]Prepared by concentration of a 6:1 mixture of TMSCN:$TiCl_4$.
[h]Prepared by concentration of a 6:1 mixture of TMSCN:(*i*-Pr-O)$_4$TiCN.
[i]Addition of Et_4NCN over 30 min
[j]Concentrated prior to use.

periments suggest that reaction of $TiCl_4$ with TMSCN produces an initial 1:2 adduct (e.g., $TiCl_4CN_2^{2-}(TMS^+)_2$) and that additional TMSCN results in the substitution of two Cl ligands with two CN ligands [e.g., $TiCl_2CN_4^{2-}(TMS^+)_2$] with concomitant formation of TMSCl. The capability of the residues obtained after concentration of mixtures of $TiCl_4$ and TMSCN to produce cyanohydrins was confirmed by reactions with benzaldehyde and with **1** (Table 2, entries 7–10). The reagents derived from 6:1 and from 4:1 mixtures of TMSCN:$TiCl_4$ (nominal stoichiometry $TiCl_2CN_4^{2-}(TMS^+)_2$) generated 3 equiv (based on Ti) of mandelonitrile (**15**) from benzaldehyde within 30 min at room temperature. Reaction of excess benzaldehyde with the reagent obtained from a 2:1 mixture of TMSCN:$TiCl_4$ (nominal stoichiometry $TiCl_4CN_2^{2-}(TMS^+)_2$) under similar conditions produced 1.3 equiv of mandelonitrile (**15**); reaction of the same reagent with **1** gave a 2:1 mixture of **2s** and **2a**. We also briefly examined cyanohydrin formation using a reagent prepared by addition of TMSCN (6 equiv) to a solution of (*i*-Pr-O)$_4$Ti in C_6D_6. After 15 min, the pale yellow solution was concentrated in vacuo to produce a residue with a nominal stoichiometry of "(*i*-Pr-O)$_3$TiCN" based on analysis of the volatile components by ^{1}H NMR.[15] Addition of **1** (1 equiv based on Ti) to a CH_2Cl_2 solution of the above residue gave a 1:1.2 mixture of **2s** and **2a** (75%) (Table 2, entry 11).

[15]The amounts of *i*-Pr-OR (*R* = H, TMS, 0.9 to 1.1 equiv), and TMSCN (4.5 to 5.1 equiv) in the "distillate" were quantified using an internal standard.

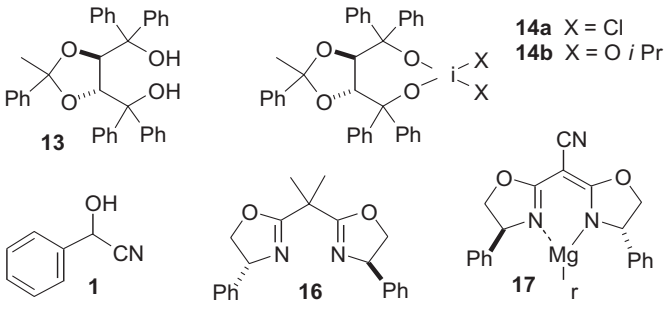
© 2001 NRC Canada

To summarize, TMSCN reacts with $TiCl_4$ and with (*i*-Pr-O)$_4$Ti to give adducts that can generate cyanohydrins from benzaldehyde and from **1**. The low diastereoselectivity observed in reactions with **1** can be rationalized by considering the decreased Lewis acidity of these adducts due to the strongly donating CN ligand(s) which disfavors a "chelation-controlled" pathway. Furthermore, the formation of such adducts suggests that the primary role of the Ti(IV) in these reactions may be to activate the TMSCN rather than the aldehyde. In any event, it seemed apparent that realization of enantiotopic group selective cyanohydrin formation from α-alkoxy aldehydes would require conditions to achieve cyanohydrin formation with much higher diastereoselectivity. We undertook a systematic investigation of cyanohydrin formation from **1** using a variety of cyanide sources (TMSCN, Et_4NCN, $Et_4NAg(CN)_2$), Lewis acids ($BF_3{\cdot}OEt_2$, $TiCl_4$, $SnCl_4$, $ZnBr_2$, $MgBr_2$), and reaction conditions (27). This study revealed Mg(II) as a unique promoter of hydrocyanation as it is capable of chelation of **1** and does not react appreciably with the cyanide source. Under optimized conditions (27), the cyanohydrin **2** was obtained in high yield as a 24:1 mixture of *syn:anti* diastereomers **2s** and **2a**, respectively.[16] Adapting this diastereoselective method to achieve enantiotopic group selectivity would require a chiral nonracemic version of $MgBr_2$ and (or) a chiral nonracemic cyanide source. The latter strategy appeared more promising because optimal diastereoselectivity requires the use of excess solid $MgBr_2{\cdot}OEt_2$ (27) and chiral nonracemic Ti(IV) cyanides are readily available and have been implicated in enantioselective hydrocyanation (14*d*, 23, 25).

Initial experiments evaluated the possibility for diastereoselective cyanohydrin formation from **1** using an achiral "TiCN" reagent in the presence of $MgBr_2{\cdot}OEt_2$ (Table 3). Although the reagent obtained by concentration of a 6:1 mixture of TMSCN and $TiCl_4$ (nominal stoichiometry $TiCl_2CN_4^{2-}(TMS^+)_2$) gave **2** with poor diastereoselectivity (Table 3, entry 3), the reagent prepared from a 6:1 mixture of TMSCN and (*i*-Pr-O)$_4$Ti (nominal stoichiometry (*i*-Pr-O)$_3$TiCN) generated **2** with a diastereoselectivity nearly as high as that obtained with TMSCN (Table 3, cf. entries 1 and 4). The reagent obtained analogously from a 6:1 mixture of TMSCN and **14b** was also very diastereoselective in the presence of $MgBr_2{\cdot}OEt_2$ but produced **2** with very low enantiotopic group selectivity and without evidence for double stereodifferentiation (Table 3, entry 7). We also examined reagents derived from Et_4NCN and Ti(IV) alkoxides in the presence of excess $MgBr_2{\cdot}OEt_2$ for hydrocyanation. The Mg(II) mediated hydrocyanation of **1** with Et_4NCN is a relatively poor method (Table 3, entry 2) (27). However, slow addition of Et_4NCN to a suspension of **1** and $MgBr_2{\cdot}OEt_2$ in the presence of (*i*-Pr-O)$_4$Ti was as effective as TMSCN–$MgBr_2{\cdot}OEt_2$ for stereoselective synthesis of **2s** (Table 3, cf. entries 1 and 5). The successful moderation of the reactivity of Et_4NCN towards $MgBr_2$ (27) by (*i*-Pr-O)$_4$Ti suggests the possible formation of a TiCN reagent under these conditions. Although the chiral titanium alkoxide **14b** was also effective for diastereoselective hydrocyanation of **1** under analogous conditions, the reaction proceeded with very low enantiotopic group selectivity and without double stereodifferentiation.[17]

We briefly examined enantiotopic group selective hydrocyanation using TMSCN in the presence of "chiral versions" of Mg(II). Hydrocyanations of **1** with TMSCN–$MgBr_2{\cdot}OEt_2$ in the presence or absence of the nonracemic bisoxazoline ligand **16** (28) were virtually indistinguishable (cf. Table 3, entries 1 and 8). Finally, the use of the nonracemic Mg(II) reagent **17** (29) in place of $MgBr_2{\cdot}OEt_2$ resulted in low diastereoselectivity (**2s**:**2a** = 2:1), very low enantiotopic group selectivity, and proceeded without double stereodifferentiation (Table 3, entry 9).

In conclusion, attempted hydrocyanations of α-alkoxy aldehydes with TMSCN using chiral nonracemic alkoxy Ti(IV) reagents proceeded with low enantiotopic group selectivity (<2:1). It was established that TMSCN can react with Ti(IV) reagents to produce TiCN adducts that are capable of hydrocyanation but with low substrate-controlled diastereoselectivity in reactions with α-alkoxy aldehydes. The poor enantiotopic group selectivity observed can be rationalized to result from this low diastereoselectivity despite the respectable levels of enantioface selectivity associated with these reagents in hydrocyanation of achiral aldehydes. Highly diastereoselective hydrocyanation of α-alkoxy aldehydes can be achieved with TMSCN in the presence of excess $MgBr_2{\cdot}OEt_2$ (27). High diastereoselectivity was also observed using achiral and chiral TiCN adducts in place of TMSCN. Although the putative TiCN adducts obtained from nonracemic alkoxy Ti(IV) reagents are implicated in enantioface selective hydrocyanation, these reagents were not enantiotopic group selective under these conditions and showed no evidence of double stereodifferentiation. The use of nonracemic bisoxazoline ligands for Mg(II) was also ineffective.



Experimental

General methods

All solvents were distilled prior to use. Et_3N was distilled from CaH_2 and stored over KOH pellets. Anhydrous solvents were distilled under argon as follows: ether and tetrahydrofuran (THF) from benzophenone potassium ketyl; benzene, toluene, and CH_2Cl_2 from P_2O_5 and stored over 3 Å molecular sieves; MeOH from $Mg(OMe)_2$. Unless otherwise

[16]Conditions: $MgBr_2{\cdot}OEt_2$ (5 equiv), $Et_4NAg(CN)_2$ (2 equiv) in CH_2Cl_2, –78 to –20°C, 2 h. This level of diastereoselectivity is five times greater than previously reported for α-alkoxy aldehydes.
[17]Reaction of benzaldehyde under these conditions gave **15** with <10% ee.

© 2001 NRC Canada

noted, reactions were carried out under an atmosphere of argon and reaction temperatures refer to the bath. Concentration refers to removal of volatiles at water aspirator pressure on a rotary evaporator.

Preparative TLC (PTLC) was carried out on glass plates (20 × 20 cm) precoated (0.25 mm) with silica gel 60 F_{254}. Materials were detected by visualization under an ultraviolet lamp (254 nm) and (or) by treating a 1 cm vertical strip removed from the plate with a solution of phosphomolybdic acid (5%) containing a trace of ceric sulfate in aqueous sulfuric acid (5% v/v), followed by charring on a hot plate. Flash column chromatography (FCC) was performed according to Still et al. (30) with Merck silica gel 60 (40–63 μm). Dry FCC was performed according to Harwood (31). All mixed solvent eluents are reported as v/v solutions.

Spectral data

High resolution mass spectra (HRMS) and low resolution mass spectra (LRMS) were obtained on a VG 70E double focussing high resolution spectrometer; only partial data are reported. EI ionization was accomplished at 70 eV and CI at 50 eV with ammonia as the reagent gas; only partial data are reported. IR spectra were recorded on a Fourier transform interferometer using a diffuse reflectance cell (DRIFT); only diagnostic and (or) intense peaks are reported. Unless otherwise noted, NMR spectra were measured in $CDCl_3$ solution at 300 MHz for ^{1}H and 75 MHz for ^{13}C. For ^{1}H NMR, residual $CHCl_3$ in $CDCl_3$ was employed as the internal standard (7.26 δ); for ^{13}C NMR, $CDCl_3$ was employed (77.2 δ). The ^{1}H NMR chemical shifts and coupling constants were determined assuming first-order behavior. Multiplicity is indicated by one or more of the following: s (singlet), d (doublet), t (triplet), q (quartet), m (multiplet), br (broad), ap (apparent); the list of couplings constants (*J*) corresponds to the order of the multiplicity assignment. ^{1}H NMR spectra were normally obtained with a digital resolution of 0.244 Hz/pt (sweep width = 4000 Hz, FID = 32 K data points) and coupling constants are reported to the nearest 0.5 Hz. The ^{1}H NMR assignments were made on the basis of chemical shift and multiplicity and were confirmed, where necessary, by homonuclear decoupling and (or) NOE experiments. The multiplicity of ^{13}C NMR signals refers to the number of attached Hs (i.e., s = C, d = CH, t = CH_2, q = CH_3) and was determined by *J*-modulation (32).

Materials

TMSCN (33), (*i*-Pr-O)$_2$TiCl$_2$ (34), TADDOL (23), (*i*-Pr-O)$_2$Ti(TADDOL) (24), and **18** (29) were prepared according to literature procedures. The aldehydes **1** and **4** were prepared from hexanal and pivaldehyde, respectively, by addition of vinlymagnesium bromide, benzylation, and ozonolyisis according to the procedure of Midland and Koops (35). $TiCl_4$ and (*i*-Pr-O)$_4$Ti were freshly distilled prior to use. All other reagents were commercially available and, unless otherwise noted, were used as received.

General procedure for preparation Mosher's esters

A solution of (*R*)-MTPA-Cl (prepared (20) from (*S*)-MTPA-OH; 1.2 to 1.5 equiv) in CH_2Cl_2 (ca. 0.05 M) was added via syringe to a stirred solution of the alcohol, Et_3N (2.5 equiv), and DMAP (ca. 1 mg) in CH_2C_l (ca. 0.1 M in alcohol) at room temperature. After stirring for 1–3 h, the reaction mixture was concentrated to give the crude Mosher's esters (quantitative conversion was verified by ^{1}H NMR).

General procedure for hydrocyanation with TMSCN–(i-Pr-O)$_2$TiCl$_2$–TADDOL (or BINOL)

A solution of (*i*-Pr-O)$_2$TiCl$_2$ (1.5 equiv) in toluene (ca. 0.5 M) was added via syringe to a stirred solution of TADDOL (1.5 equiv) in toluene (ca. 0.5 M) at room temperature. After 1 h, MS4A (ca. 150 mg/mmol of aldehyde) and then TMSCN (5 equiv) were added and the mixture was cooled to –23°C. A solution of aldehyde (ca. 0.2 mmol) in toluene (ca. 0.1 M) was added to the mixture. After the appropriate time, phosphate buffer (pH 7) was added and the mixture was allowed to warm to room temperature (ca. 25 min) and then was filtered (Celite®) and extracted with EtOAc (×3). The combined organic layers were washed with brine, dried over Na_2SO_4, and concentrated to give the crude cyanohydrin. The conversion was determined by ^{1}H NMR of the crude by integrating signals due to **1** (or **4**) and **2** (or **5**). Fractionation of the crude by PTLC (25% EtOAc in hexane) gave recovered **1** (or **4**) and the cyanohydrins **2** (or **5**) as a mixture of diastereomers; the stereoisomeric composition was determined by ^{1}H NMR of the corresponding Mosher's esters.

General procedure for hydrocyanation with TMSCN–TiCl$_4$ reagents

$TiCl_4$ (11 mg, 0.06 mmol) in $CDCl_3$ (40 μL) was added via syringe to a solution of TMSCN (1, 2, or 4 equiv) in $CDCl_3$ (0.5 mL). After standing at room temperature for 1 h, PhCHO (6 mg, 0.06 mmol) or **1** (13 mg, 0.06 mmol) was added. After standing at room temperature for 1 h, the mixture was poured over H_2O, diluted with CH_2Cl_2, filtered (Celite®), dried over Na_2SO_4, and concentrated giving **15** or **2** as a yellow oil. Analysis and fractionation were performed as described above.

General procedure for hydrocyanation with TiCN reagents

$TiCl_4$ (19 mg, 0.10 mmol) in C_6D_6 (0.2 mL) was added via syringe to a solution of TMSCN (2, 4, or 6 equiv) in C_6D_6 (0.3 mL) in an NMR tube (5 mm). After standing for 15 min, concentrated by freeze drying under high vacuum (0.2 torr (1 torr = 133.322 Pa)) with the volatile components being collected in a liquid nitrogen cooled trap and analyzed by ^{1}H NMR. The yellowish solid residue was dissolved in C_6D_6 (0.5 mL) and PhCHO (63 mg, 0.60 mmol) or **1** (44 mg, 0.20 mmol) was added via syringe. After 30 min, phosphate buffer (pH 7) was added and the mixture was extracted with CH_2Cl_2 (×3). The combined organic extracts were dried over Na_2SO_4 and concentrated to give a mixture of **15** (or **2**) as a yellow oil. Analysis and fractionation as described above. Analogous procedures using (*i*-Pr-O)$_4$Ti or **14b** in place of $TiCl_4$ were employed to prepare and use (*i*-Pr-O)$_3$TiCN or "(TADDOL)(*i*-Pr-O)TiCN", respectively.

General procedure for hydrocyanation with TiCN reagents in the presence of MgBr$_2$·OEt$_2$

A solution of **1** (20 mg, 0.091 mmol) in CH_2Cl_2 (0.5 mL) was added to a stirred suspension of $MgBr_2.OEt_2$ (115 mg,

© 2001 NRC Canada

0.45 mmol) in CH_2Cl_2 (1.5 mL) at room temperature. After stirring for 5 min, the reaction mixture was cooled to 0°C. A solution of the cyanating reagent (TMSCN or Et_4NCN or TiCN) (0.3–1 equiv) was added via syringe. After 1 h at 0°C, phosphate buffer (pH 7, 5 mL) was added and the reaction mixture processed as above to give the crude **2**. For entry 8 of Table 3, **1** was added to a suspension the $MgBr_2 \cdot OEt_2$ containing the ligand **16** (1 equiv). For entry 9 of Table 3, reagent **17** (1 equiv) was used instead of $MgBr_2 \cdot OEt_2$ (5 equiv). Analysis and fractionation were performed as described above.

*2-(Phenylmethoxy)heptanal (**1**):* LRMS (CI, NH_3) *m/z* (relative intensity): 238 ($[M + 18]^+$, 10), 221 ($[M + 1]^+$, 2), 191 (36), 108 (64), 91 (100). HRMS *m/z* calcd. for $C_{14}H_{21}O_2$: 221.1542 (= $[M + H]^+$); found: 221.1542 (CI, NH_3). IR ν_{max} (cm^{-1}): 3088, 2930, 1732, 1454, 1099, 736, 698. ^1H NMR δ: 9.65 (1H, d, *J* = 2 Hz, HC-1), 7.39–7.28 (5H, m, ArH), 4.68 (1H, d, *J* = 12 Hz, HCAr), 4.54 (1H, d, *J* = 12 Hz, HCAr), 3.76 (1H, ddd, *J* = 2, 6.5, 6.5 Hz, HC-2), 1.72–1.62 (2H, m, H_2C-3), 1.51–1.35 (2H, m, H_2C-4), 1.34–1.20 (4H, m, H_2C-5, H_2C-6), 0.92–0.83 (3H, t, *J* = 6.5 Hz, H_3C-7). ^{13}C NMR δ: 203.7 (d, C-1), 137.5 (s, Ph), 128.5 (2d, Ph), 128.3 (d, Ph), 128.0 (2d, C-2), 83.5 (d, C-2), 72.5 (t, CH_2O), 31.6 (t, C-5), 30.0 (t, C-3), 24.4 (t, C-4), 22.4 (t, C-6), 14.0 (q, C-7).

(2R,3R*)-2-Hydroxy-3-(phenylmethoxy)octanenitrile (**2s**) and (2S*,3R*)-2-hydroxy-3-(phenylmethoxy)octanenitrile (**2a**):* LRMS (CI, NH_3) *m/z* (relative intensity): 265 ($[M + 18]^+$, 1), 191 (8), 108 (13), 91 (100). HRMS *m/z* calcd. for $C_{15}H_{21}NO_2$: 265.1916 (= $[M + NH_4]^+$); found: 265.1906 (CI, NH_3). IR ν_{max} (cm^{-1}): 3426, 3031, 2930, 1454, 1073, 744, 698. ^1H NMR δ for **2s**: 7.43–7.32 (5H, m, ArH), 4.75 (1H, d, *J* = 11.5 Hz, HCAr), 4.58 (1H, d, *J* = 11.5 Hz, HCAr), 4.46 (1H, dd, *J* = 4, 9 Hz, HC-2), 3.63 (1H, ddd, *J* = 4, 7, 7 Hz, HC-3), 2.95 (1H, d, *J* = 9 Hz, OH), 1.90–1.76 (1H, m, HC-4), 1.75–1.58 (1H, m, HC-4), 1.47–1.23 (6H, m, H_2C-5, H_2C-6, H_2C-7), 0.97–0.85 (3H, m, H_3C-8); δ for **2a**: 7.43–7.32 (5H, m, ArH), 4.76 (1H, d, *J* = 11.5 Hz, HCAr), 4.71 (1H, d, *J* = 11.5 Hz, HCAr), 4.38 (1H, dd, *J* = 3, 9 Hz, HC-2), 3.68 (1H, dt, *J* = 3, 6.5 Hz, HC-3), 2.95 (1H, d, *J* = 9 Hz, OH), 1.75–1.58 (2H, m, H_2C-4), 1.47–1.23 (6H, m, H_2C-5, H_2C-6, H_2C-7), 0.97–0.85 (3H, m, H_3C-8). ^{13}C NMR δ for **2s**: 137.2 (s, Ph), 128.6 (2d, Ph), 128.2 (d 2, Ph), 128.1 (d, Ph), 119.0 (s, C-1), 79.4 (t, C-2), 73.4 (d, CH_2Ar), 63.2 (d, C-3), 31.6 (t, C-4), 30.4 (t, C-6), 24.8 (t, C-5), 22.4 (t, C-7), 13.9 (q, C-8); δ for **2a**: 137.4 (s, Ph), 128.6 (2d, Ph), 128.2 (2d, Ph), 128.0 (d, Ph), 118.0 (s, C-1), 79.4 (t, C-2), 72.8 (d, CH_2Ar), 64.1 (d, C-3), 31.7 (t, C-4), 30.4 (t, C-6), 24.7 (t, C-5), 22.4 (t, C-7), 13.9 (q, C-8). Elemental anal. calcd. for $C_{15}H_{21}NO_2$: C 72.84, H 8.56, N 5.66; found: C 72.54, H 8.53, N 5.62.

*1-Cyano-2-(phenylmethoxy)heptyl (2S)-3,3,3-trifluoro-2-methoxy-2-phenylpropanoate (**3**):* Fractionation of the crude product from reaction of **2** (a 2.4:1 mixture of racemic **2s** and **2a**; 8 mg, 0.03 mmol) with (*R*)-MTPA-Cl by PTLC (25% EtOAc in hexane) gave a 2.6:2.6:1:1 mixture of (*R*)-**3s**, (*S*)-**3s**, (*R*)-**3a**, and (*R*)-**3a** isomers, respectively, as a colorless oil (13 mg, 88%). LRMS (CI, NH_3), *m/z* (relative intensity): 481 ($[M + 18]^+$, 37), 373 (42), 279 (23), 189 (100), 108 (38), 91 (82). HRMS *m/z* calcd. for $C_{25}H_{28}F_3NO_4$: 463.1970; found: 463.1978 (EI). IR ν_{max} (cm^{-1}): 2953, 1763, 1453, 1172. ^1H NMR δ:[18] 7.51–7.25 (10H, m, ArH), 5.67† (d, *J* = 4 Hz), 5.62‡ (d, *J* = 4.5 Hz), 5.57§ (d, *J* = 6 Hz), and 5.52¶ (d, *J* = 6.5 Hz) (1H, HC-1), 4.69† (d, *J* = 11 Hz), 4.65¶ (d, *J* = 11 Hz), 4.63‡ (d, *J* = 11 Hz), 4.58¶ (d, *J* = 11 Hz), 4.53§ (d, *J* = 11 Hz), 4.51† (d, *J* = 11 Hz), 4.47§ (d, *J* = 11 Hz), and 4.42‡ (d, *J* = 11 Hz) (2H, H_2CAr), 3.81–3.71†¶ (m), and 3.71–3.61‡§ (m) (1H, HC-2), 3.59‡§ (br s), 3.54† (br s), and 3.50¶ (br s) (3H, H_3CO), 1.70–1.14 (8H, m, H_3C-3, H_2C-4, H_2C-5, H_2C-6), 0.90–0.81 (3H, m, H_3C-7).

*3,3-Dimethyl-2-(phenylmethoxy)butanal (**4**):* LRMS (CI, NH_3) *m/z* (relative intensity): 224 ($[M + 18]^+$, 100), 177 (32), 108 (21), 91 (28). HRMS *m/z* calcd. for $C_{13}H_{18}O_2$: 206.1307; found: 206.1298 (EI). IR ν_{max} (cm^{-1}): 2960, 2870, 2714, 1727, 1454, 1110. ^1H NMR δ: 9.73 (1H, d, *J* = 3.5 Hz, HC-1), 7.37–7.29 (5H, m, ArH), 4.65 (1H, d, *J* = 11.5 Hz, HCAr), 4.43 (1H, d, *J* = 11.5 Hz, HCAr), 3.29 (1H, d, *J* = 3.5 Hz, HC-2), 1.01 (9H, s, $(H_3C)_3C$). ^{13}C NMR δ: 204.9 (d, C-1), 137.8 (s, Ph), 128.2 (2d, Ph), 128.1 (3d, Ph), 90.7 (d, C-3), 73.1 (t, CH_2O), 35.6 (s, C-4), 27.0 (3q, $(H_3C)_3C$).

(2R,3R*)-2-Hydroxy-4,4-dimethyl-3-(phenylmethoxy) pentanenitrile (**5s**) and (2S*,3R*)-2-hydroxy-4,4-dimethyl-3-(phenylmethoxy)pentanenitrile (**5a**)*

TMSCN (173 mg, 1.74 mmol) and Et_3N (59 mg, 0.58 mmol) were added to a stirred solution of aldehyde **4** (120 mg, 0.580 mmol) and MS4A (100 mg) in toluene (2.5 mL) at room temperature. After 3 h, the mixture was filtered and concentrated to give **8** (a 3:1 mixture of **8s** and **8a**, respectively, by ^1H NMR; 160 mg, 90%). ^1H NMR δ for **8s**: 7.44–7.22 (5H, m, ArH), 4.89 (1H, d, *J* = 11.5 Hz, HC-Ar), 4.63 (1H, d, *J* = 11.5 Hz, HC-Ar), 4.52 (1H, d, *J* = 5.5 Hz, HC-2), 3.25 (1H, d, *J* = 5.5 Hz, HC-3), 1.04 (9H, s, $(H3C)_3C$), 0.20 (9H, s, $(H_3C)_3Si$); δ for **8a**: 7.44–7.22 (5H, m, ArH), 5.00 (1H, d, *J* = 11.5 Hz, HC-Ar), 4.62 (1H, d, *J* = 4 Hz, HC-2), 4.61 (1H, d, *J* = 11.5 Hz, HC-Ar), 3.25 (1H, d, *J* = 4 Hz, HC-3), 1.00 (9H, s, $(H_3C)_3C$), 0.25 (9H, s, $(H_3C)_3Si$). To a stirred solution of **8** (a 3:1 mixture of **8s** and **8a**, respectively; 160 mg) in Et_2O (10 mL) was added 1 M HCl (10 mL). After 14 h, the mixture was diluted with Et_2O and washed sequentially with H_2O and sat. NaCl, dried over Na_2SO_4, and concentrated to give **5** as a colorless liquid (122 mg, 90%, 3:1 mixture of **5s** and **5a** by ^1H NMR). The residue was fractionated by FCC (10% EtOAc in hexane) giving **5s** as a clear liquid (75 mg, 55%) and **5a** as a clear liquid (10 mg, 8%).

*Spectral data for **5s**:* LRMS (CI, NH_3) *m/z* (relative intensity): 251 ($[M + 18]^+$, 6), 224 (100), 108 (33), 91 (48). HRMS *m/z* calcd. for $C_{14}H_{19}NO_2$: 251.1760 (= $[M + NH_4]^+$); found: 251.1760 (CI). IR ν_{max} (cm^{-1}): 3456, 2959, 2872, 2240 (w), 1395, 1089. ^1H NMR δ: 7.46–7.35 (5H, m, ArH), 5.00 (1H, d, *J* = 10.5 Hz, HCAr), 4.89 (1H, d, *J* = 10.5 Hz, HCAr), 4.58 (1H, dd, *J* = 1.5, 10 Hz, HC-2), 3.47 (1H, d, *J* = 1.5 Hz, HC-3), 3.29 (1H, d, *J* = 10 Hz, OH), 1.00 (9H, s, H_3C). ^{13}C NMR δ: 137.0 (s, Ph), 128.6 (2d, Ph), 128.3 (d, Ph), 128.2 (2d, Ph), 120.6 (s, C-1), 86.4 (d, C-2), 76.0 (t, CH_2O), 59.3 (d, C-3), 35.9 (s, C-4), 26.4 (3q, CH_3). Elemen-

[18]Legend: † = (*R*)-**3a**, ‡ = (*S*)-**3a**, § = (*R*)-**3s**, ¶ = (*S*)-**3s**.

© 2001 NRC Canada

tal anal. calcd. for $C_{14}H_{19}NO_2$: C 72.07, H 8.21l N 6.00; found: C 72.06, H 8.18, N 5.93.

*Spectral data for **5a**:* LRMS (CI, NH_3) *m/z* (relative intensity): 251 ($[M + 18]^+$, 46), 224 (100), 108 (42), 91 (54). HRMS *m/z* calcd. for $C_{14}H_{19}NO_2$: 251.1760 (= $[M + NH_4]^+$); found: 251.1763 (CI, NH_3). IR ν_{max} (cm^{-1}): 3422, 2960, 2872, 2250 (w), 1394, 1105. ^1H NMR δ: 7.44–7.30 (5H, m, ArH), 4.80 (1H, d, *J* = 11.5 Hz, HCAr), 4.76 (1H, d, *J* = 11.5 Hz, HCAr), 4.58 (1H, d, *J* = 3 Hz, HC-2), 3.30 (1H, d, *J* = 3 Hz, HC-3), 2.40 (1H, br s, OH), 1.05 (9H, s, H_3C). ^{13}C NMR δ: 139.0 (s, Ph), 129.7 (2d, Ph), 129.2 (d, Ph), 129.0 (2d, Ph), 118.8 (s, C-1), 93.3 (d, C-2), 76.7 (t, CH_2O), 63.9 (d, C-3), 35.7 (s, C-4), 26.9 (3q, CH_3).

*1-Cyano-3,3-dimethyl-2-(phenylmethoxy)butyl (2S)-3,3,3-trifluoro-2-methoxy-2-phenylpropanoate (**6**):* Fractionation of the crude product from reaction of **5** (a 1.5:1 mixture of **5a** and **5s**, respectively; 10 mg, 0.043 mmol) with (*R*)-MTPA-Cl by PTLC (25% EtOAc in hexane) gave **6** as a 1.5:1.5:1:1 mixture of (*R*)-**6a**, (*S*)-**6a**, (*R*)-**6s**, and (*R*)-**6s** isomers, respectively, as a colorless oil (16 mg, 83%). IR ν_{max} (cm^{-1}): 2959, 1761, 1453, 1227, 1171, 1108, 1021. ^1H NMR δ: [19] 7.57–7.18 (10H, m, ArH), 5.83‡ (d, *J* = 2 Hz), 5.77† (d, *J* = 2 Hz), 5.590§ (d, *J* = 4 Hz), and 5.587¶ (d, *J* = 5.5 Hz) (1H, HC-1), 4.83¶ (d, *J* = 11 Hz), 4.76† (d, *J* = 11 Hz), 4.73§ (d, *J* = 11 Hz), 4.64‡ (d, *J* = 11 Hz), 4.58¶ (d, *J* = 11 Hz), 4.52§ (d, *J* = 11 Hz), 4.38† (d, *J* = 11 Hz), and 4.25‡ (d, *J* = 11 Hz) (2H, H_2CAr), 3.61†¶ (m), 3.52‡ (m), and 3.45§ (m) (3H, H_3CO), 3.53¶ (d, *J* = 5.5 Hz), 3.45§ (d, *J* = 4 Hz), 3.33† (d, *J* = 2 Hz), and 3.18‡ (d, *J* = 2) (1H, HC-2), 1.04¶ (s), 1.03† (s), 0.98‡ (s), and 0.89§ (s), (9H, $(H_3C)_3$). LRMS (EI) *m/z* (relative intensity): 449 ($[M]^+$, 5), 189 (22), 91 (100), 57 (21). HRMS *m/z* calcd. for $C_{24}H_{26}F_3NO_4$: 449.1814; found: 449.1812 (EI). Elemental anal. calcd. for $C_{24}H_{26}F_3NO_4$: C 64.13, H 5.83, N 3.12; found: C 64.42, H 5.82, N 3.13.

*2,3-Dihydroxyoctanenitrile (**9**):* TMSCN (100 mg, 1.01 mmol) and Et_3N (41 μL, 30 mg, 0.30 mmol) was added to a stirred solution of aldehyde (150 mg, 0.68 mmol) in toluene (10 mL) containing powdered MS4A (100 mg). After stirring for 2 h the reaction was filtered and concentrated to give a 2:1 mixture of **7s** and **7a**, respectively, (197 mg, 90%). ^1H NMR δ for the *syn* isomer: 7.33–7.28 (5H, m, ArH), 4.68 (1H, d, *J* = 11.5 Hz, HC-Ar), 4.63 (1H, d, *J* = 11.5 Hz, HC-Ar), 4.38 (1H, d, *J* = 5.5 Hz, HC-2), 3.46 (1H, ddd, *J* = 3, 5.5, 8.5 Hz, HC-3), 1.80–1.20 (8H, m, H_2C-4, H_2C-5, H_2C-6, H_2C-7), 0.90 (3H, m, H_3C-8), 0.19 (9H, s, $(H_3C)_3Si$); δ for the *anti* isomer: 7.33–7.28 (5H, m, ArH), 4.80 (1H, d, *J* = 11.5 Hz, HC-Ar), 4.62 (1H, d, *J* = 11.5 Hz, HC-Ar), 4.33 (1H, d, *J* = 6 Hz, HC-2), 3.59 (1H, ddd, *J* = 5, 6, 7 Hz, HC-3), 1.80–1.20 (8H, m, H_2C-4, H_2C-5, H_2C-6, H_2C-7), 0.90 (3H, m, H_3C-8), 0.22 (9H, s, $(H_3C)_3Si$). Addition of one drop of DCl to the NMR sample resulted in hydrolysis of **7** to give a 2:1 mixture of **2s** and **2a**, respectively. To a stirred solution of **7** (2:1 mixture of **7s**:**7a**; 190 mg, 0.596 mmol) in CH_2Cl_2 (20 mL) was added $TiCl_4$ (71 μL, 123 mg, 0.65 mmol). After 1 h, the reaction was quenched by addition of NH_4Cl (1 M, 20 mL). The mixture was extracted with Et_2O (×3) and the combined organic layers were washed with brine, dried over Na_2SO_4, concentrated, and the residue fractionated by FCC (35% EtOAc in hexane) to give the diol **9** as a 2:1 mixture of **9s** and **9a**, respectively, (54 mg, 58%). LRMS (CI, NH_3) *m/z* (relative intensity): 175 ($[M + 18]^+$, 5), 148 (100), 99 (36), 83 (17). HRMS *m/z* calcd. for $C_8H_{15}NO_2$: 175.1447 (= $[M + NH_4]^+$); found: 175.1447 (CI, NH_3). IR ν_{max} (cm^{-1}): 3421, 2929, 1465, 1077. ^1H NMR δ for **9a**: 4.42 (1H, d, *J* = 3.0 Hz, HC-2), 3.92–3.80 (1H, m, HC-3), 1.72–1.43 (2H, m, H_2C-4), 1.42–1.24 (6H, m, H_2C-5, H_2C-6, H_2C-7), 0.94–0.85 (3H, t, *J* = 6.5 Hz, H_3C-8); for **9s**: 4.33 (1H, d, *J* = 4.5 Hz, HC-2), 3.92–3.80 (1H, m, HC-3), 1.72–1.43 (2H, m, H_2C-4), 1.42–1.24 (6H, m, H_2C-5, H_2C-6, H_2C-7), 0.94–0.85 (3H, t, *J* = 6.5 Hz, H_3C-8). ^{13}C NMR δ for **9a**: 117.9 (s, C-1), 72.6 (d, C-3), 66.0 (d, C-2), 32.6 (t, C-4), 31.5 (t, C-6), 25.0 (t, C-5), 22.4 (t, C-7), 13.9 (q, C-8); δ for **9s**: 118.8 (s, C-1), 72.6 (d, C-3), 64.9 (d, C-2), 32.1 (t, C-4), 31.5 (t, C-6), 25.0 (t, C-5), 22.4 (t, C-7), 13.9 (q, C-8).

(2R,3R*)-2,3-Dihydroxy-4,4-dimethylpentanenitrile (**10s**):* A solution of $TiCl_4$ (0.030 mL, 52 mg, 0.27 mmol) in CH_2Cl_2 (0.2 mL) was added via syringe to a stirred solution of **4s** (32 mg, 0.14 mmol) in CH_2Cl_2 (2.3 mL) at 25°C. After 0.5 h, H_2O was added and the mixture was extracted with CH_2Cl_2 (×3). The combined organic layers were filtered (Celite®), and the filtrate was dried over Na_2SO_4, concentrated, and the residue (29 mg) fractionated by dry FCC (0–50% Et_2O in hexane, gradient elution) to give **10s** as a white solid (10 mg, 51%). LRMS (CI, NH_3) *m/z* (relative intensity): 161 ($[M + 18]^+$, 62), 134 (100). HRMS *m/z* calcd. for $C_7H_{13}NO_2$: 161.1290 (= $[M + NH_4]^+$); found: 161.1284 (CI, NH_3). IR ν_{max} (cm^{-1}): 3416, 3291, 2959, 2873, 2238 (w), 1110, 1020. ^1H NMR δ: 4.61–4.56 (1H, br s, HC-2), 3.59–3.55 (1H, br s, HC-3), 1.00 (9H, br s, *J* = 1 Hz, $(H_3C)_3$). ^{13}C NMR: 120.1 (s, C-1), 78.9 (d, C-2), 61.8 (d, C-3), 35.2 (s, C-4), 26.4 (3q, $(CH_3)_3$). Elemental analysis calcd. for $C_7H_{13}NO_2$: C 58.72, H 9.15, N 9.78; found: C 58.86, H 8.95, N 9.51.

(4R,5R*)-2,2-Dimethyl-5-pentyl-1,3-dioxolane-4-carbonitrile (**11t**) and (4R*,5S*)-2,2-dimethyl-5-pentyl-1,3-dioxolane-4-carbonitrile (**11c**)*

TsOH (24 mg, 0.13 mmol) was added to a stirred solution of **9** (a 2:1 mixture of **9s** and **9a**; 50 mg, 0.32 mmol) in dimethoxypropane (10 mL) at room temperature. After 12 h, the reaction mixture was diluted with CH_2Cl_2 (15 mL), washed sequentially with sat. $NaHCO_3$ (×2) and H_2O, dried over Na_2SO_4, and concentrated giving a colorless oil the crude **11** as 2:1 ratio of *trans*:*cis* diastereomers by ^1H NMR (67 mg). The residue was fractionated by FCC (10% EtOAc in hexane) giving **11t** (25 mg), a 1:1 mixture of **11t** and **11c** (13 mg), and **11c** (12 mg, 80%).

*Spectral data for **11t**:* LRMS (CI, NH_3) *m/z* (relative intensity): 215 ($[M + 18]^+$, 8), 198 ($[M + 1]^+$, 26), 182 (78), 171 (19), 61 (100). HRMS *m/z* calcd. for $C_{11}H_{19}NO_2$: 215.1760 (= $[M + NH_4]^+$); found: 215.1758 (CI). IR ν_{max} (cm^{-1}): 2933, 1460, 1383, 1218, 1067. ^1H NMR δ: 4.36 (1H, ddd, *J* = 6, 6, 6 Hz, HC-5), 4.15 (1H, d, *J* = 6 Hz, HC-4), 1.72–1.63

[19] Legend: † = (*R*)-**6a**, ‡ = (*S*)-**6a**, § = (*R*)-**6s**, ¶ = (*S*)-**6s**.

© 2001 NRC Canada

(2H, m, H_2C-1′), 1.49 (3H, s, H_3CC-2), 1.45 (3H, s, H_3CC-2), 1.40–1.27 (6H, m, H_2C-2′, H_2C-3′, H_2C-4′), 0.93–0.87 (3H, m, H_3C-5′). ^{13}C NMR δ: 117.9 (s, CN), 112.3 (s, C-2), 80.3 (d, C-4), 67.7 (d, C-5), 32.8 (t, C-1′), 31.5 (t, C-3′), 26.8 (t, C-2′), 25.0 (2q, CH_3C-2), 22.4 (t, C-4′), 13.9 (q, C-5′). Elemental anal. calcd. for $C_{11}H_{19}NO_2$: C 66.97, H 9.70, N 7.10; found: C 67.21, H 9.86, N 6.89.

*Spectral data for **11c**:* LRMS (CI, NH_3) *m*/*z* (relative intensity): 215 ($[M + 18]^+$, 8), 198 ($[M + 1]^+$, 26), 182 (78), 171 (19), 61 (100). HRMS *m*/*z* calcd. for $C_{11}H_{19}NO_2$: 215.1760 (= $[M + NH_4]^+$); found: 215.1759 (CI, NH_3). IR ν_{max} (cm^{-1}): 2935, 1467, 1374, 1227, 1064. ^{1}H NMR δ: 4.73 (1H, d, *J* = 5 Hz, HC-4), 4.15 (1H, ddd, *J* = 5, 6, 7 Hz, HC-5), 1.97–1.86 (1H, m, HC-1′), 1.81–1.70 (1H, m, HC-1′), 1.56 (3H, s, H_3CC-2), 1.52–1.44 (1H, m, HC-2′), 1.37 (3H, s, H_3CC-2), 1.39–1.32 (5H, m, HC-2′, H_2C-3′, H_2C-4′), 0.90 (3H, br t, *J* = 7 Hz, H_3C-5′). ^{13}C NMR δ: 116.5 (s, CN), 111.8 (s, C-2), 77.5 (d, C-4), 68.2 (d, C-5), 31.6 (t, C-3′), 30.3 (t, C-1′), 27.2 (t, CH_3C-2), 25.8 (q, C-2′), 25.5 (q, CH_3C-2), 22.4 (t, C-4′), 13.9 (q, C-5′).

*(4*R**,5*R**)-2,2-Dimethyl-5-(1′,1′-dimethylethyl)-1,3-dioxolane-4-carbonitrile (**12t**):*

A solution of **10s** (16 mg, 0.11 mmol) and TsOH (ca. 2 mg) in dimethoxypropane (1.5 mL) was stirred a room temperature for 17 h. The reaction mixture was diluted with CH_2Cl_2, washed sequentially with sat. $NaHCO_3$ (×2) and H_2O, dried over Na_2SO_4, and concentrated to give a yellow oil (19 mg). Bulb-to-bulb distillation (Kugelrohr, 15 torr (1 torr = 133.322 Pa), 90°C) of the residue distillation gave **12t** as a colorless oil (12 mg, 60%). LRMS (CI, NH_3) *m*/*z* (relative intensity): 201 ($[M + 18]^+$, 79), 168 (100), 157 (92). HRMS *m*/*z* calcd. for $C_{10}H_{17}O_2N$: 201.1603 (= $[M + NH_4]^+$); found: 201.1606 (CI, NH_3). IR ν_{max} (cm^{-1}): 2961, 2874, 2250 (w), 1479, 1379, 1214, 1072. ^{1}H NMR δ: 4.56 (1H, d, *J* = 7 Hz, HC-4), 4.13 (1H, d, *J* = 7 Hz, HC-5), 1.50 (3H, s, H_3C-C-2), 1.45 (3H, s, H_3C-C-2), 0.96 (9H, s, $(H_3C)_3C$). ^{13}C NMR δ: 119.2 (s, CN), 112.6 (s, C-2), 88.1 (d, C-4), 64.2 (d, C-5), 33.1 (s, $C(CH_3)_3$), 26.4 (q, CH_3C-2), 25.4 (3q, $(CH_3)_3C$), 24.5 (q, CH_3C-2).

Acknowledgements

Financial support from the Natural Sciences and Engineering Research Council of Canada (NSERC) is gratefully acknowledged.

References

1. G. Helmchen, R.W. Hoffmann, J. Mulzer, and E. Schaumann (*Editors*). Houben-Weyl, stereoselective synthesis. Vols. 1–10. Thieme, Stuttgart. 1996.
2. M.C. Willis. J. Chem. Soc. Perkin Trans. 1, 1765 (1999).
3. (*a*) T. Sugimoto, T. Kobuko, J. Miyazaki, S. Tanimoto, and M. Okano. Bioorg. Chem. **10**, 311 (1981); (*b*) Y.F. Wang, C.S. Chen, G. Girdaukas, and C.J. Sih. J. Am. Chem. Soc. **106**, 3695 (1984); (*c*) Z. Dokuzovoc, N.K. Roberts, J.F. Sawyer, J. Whelan, and B. Bosnich. J. Am. Chem. Soc. **108**, 2034 (1986); (*d*) S.L. Schreiber, T.S. Schreiber, and D.B. Smith. J. Am. Chem. Soc. **109**, 1525 (1987).
4. (*a*) D.E. Ward, Y. Liu, and C.K. Rhee. Can. J. Chem. **72**, 1429 (1994); (*b*) D.E. Ward, Y. Liu, and C.K. Rhee. Synlett, 561 (1993).
5. (*a*) D.E. Ward, D. How, and Y. Liu. J. Am. Chem. Soc. **119**, 1884 (1997); (*b*) D.E. Ward, Y. Liu, and D. How. J. Am. Chem. Soc. **118**, 3025 (1996).
6. D.E. Ward and W.-L. Lu. J. Am. Chem. Soc. **120**, 1098 (1998).
7. A.H. Hoveyda, D.A. Evans, and G.C. Fu. Chem. Rev. **93**, 1307 (1993).
8. (*a*) S. Masamune, W. Choy, J.S. Petersen, and L.R. Sita. Angew. Chem. Int. Ed. Engl. **24**, 1 (1985); (*b*) K. Nakayama. J. Chem. Ed. **67**, 20 (1990); (*c*) W.R. Roush, L.K. Hoong, M.A.J. Palmer, J.A. Straub, and A.D. Palkowitz. J. Org. Chem. **55**, 4117 (1990).
9. C.H. Heathcock, M.C. Pirrung, J. Lampe, C.T. Buse, and S.D Young. J. Org. Chem. **46**, 2290 (1981).
10. E. Fischer. Ber. Dtsch. Chem. Ges. **23**, 2611 (1890).
11. Z. Györgydeá and I. F. Pelyvás. Monosaccharide sugars. Academic Press, San Diego. 1998. Chap. 1. pp. 18–30.
12. (*a*) W.R. Jackson, H.A. Jacobs, G.S. Jayatilake, B.R. Matthews, and K.G. Watson. Aust. J. Chem. **43**, 2045 (1990); (*b*) C.G. Kruze. *In* Chirality in industry. *Edited by* A.N. Collins, G.N. Sheldrake, and J. Crosby. Wiley, New York. 1992. pp. 279–299.
13. (*a*) M. North. Synlett, 807 (1993); (*b*) F. Effenberger. Angew. Chem. Int. Ed. Engl. **33**, 1555 (1994); (*c*) H. Griengl, A. Hickel, D.V. Johnson, C. Kratky, M. Schmidt, and H. Schwab. Chem. Commun. 1933 (1997); (*d*) F. Effenberger. Chimia, **53**, 3 (1999).
14. (*a*) C.-D. Hwang, D.-R. Hwang, and B.-J. Uang. J. Org. Chem. **63**, 6762 (1998); (*b*) Y. Hamashima, D. Sawada, M. Kanai, and M. Shibisaki. J. Am. Chem. Soc. **121**, 2641 (1999); (*c*) Y.N. Belokon', S. Caveda-Cepas, B. Green, N.S. Ikonnikov, V.N. Khrustalev, V.S. Larichev, M.A. Moscalenko, M. North, C. Orizu, V.I. Tararov, M. Tasinazzo, G.I. Timofeeva, and L.V. Yashkina. J. Am. Chem. Soc. **121**, 3968 (1999); (*d*) M. Kanai, Y. Hamashima, and M. Shibasaki. Tetrahedron Lett. **41**, 2405 (2000).
15. (*a*) R. Nishizawa and T. Saino. J. Med. Chem. **20**, 510 (1977); (*b*) D.H. Rich, B.J. Moon, and A.S. Boparai. J. Org. Chem. **45**, 2288 (1980); (*c*) J.R. Luly, C. Hsiao, N. BaMaung, and J.J. Plattner. J. Org. Chem. **53**, 6109 (1988); (*d*) M.T. Reetz, M.W. Drewes, K. Harms, and W. Rief. Tetrahedron Lett. **29**, 3295 (1988); (*e*) R. Herranz, J. Castro-Pichel, and T. Garcia-Lopez. Synthesis, 703 (1989); (*f*) S.D. Rychnovsky, S. Zeller, D.J. Skalitzky, and G. Griesgraber. J. Org. Chem. **55**, 5550 (1990); (*g*) R. Herranz, J. Castro-Pichel, S. Vinuesa, and M.T. Garcia-Lopez. J. Org. Chem. **55**, 2232 (1990); (*h*) R. Herranz, S. Vinuesa, C. Perez, and M.T. Garcia-Lopez. J. Chem. Soc. Perkin Trans. 1, 2749 (1991); (*i*) K. Utimoto, T. Takai, and S. Matsubara. Chem. Lett. 1447 (1991); (*j*) G.A. Molander and J.P. Haar, Jr. J. Am. Chem. Soc. **115**, 40 (1993); (*k*) J.W. Faller and L. Gunderson. Tetrahedron Lett. **34**, 2275 (1993); (*l*) N.A.F. Vogeleisen and D. Uguen. Tetrahedron Lett. **37**, 5893 (1996); (*m*) A.G. Myers, D.W. Kung, B. Zhong, M. Movassaghi, and S. Kwon. J. Am. Chem. Soc. **121**, 8401 (1999).
16. (*a*) G. Roda, S. Riva, and B. Danieli. Tetrahedron: Asymmetry, **10**, 3939 (1999); (*b*) P. Bianchi, G. Roda, S. Riva, B. Danieli, A. Zabelinskaja-Mackova, and H. Griengl. Tetrahedron, **57**, 2213 (2001).
17. (*a*) M.T. Reetz, K. Kesseler, and A. Jung. Angew. Chem. Int. Ed. Engl. **24**, 989 (1985); (*b*) P. Dostert, P. Melloni, A.D. Torre, M. Varasi, L. Merlini, A. Bonsignori, and S. Ricciardi. Eur. J. Med. Chem. **25**, 757 (1990); (*c*) S. Nishimura and N.

© 2001 NRC Canada

Hayashi. Chem. Lett. 1815 (1991); (*d*) F. Effenberger, M. Hopf, T. Ziegler, and J. Hudelmayer. Chem. Ber. **124**, 1651 (1991); (*e*) T. Nakai, J.H. Gu, M. Okamoto, M. Terada, and K. Mikami. Chem. Lett. 1169 (1992); (*f*) M.T. Reetz and D.N.A. Fox. Tetrahedron Lett. **34**, 1119 (1993); (*g*) J. Ipaktschi and A. Heydari. Chem. Ber. **126**, 1905 (1993); (*h*) J. Ipaktschi, A. Heydari, and H.-O. Kalinowski. Chem. Ber. **127**, 905 (1994); (*i*) C. Cativiela, M.D. Díaz-de-Villegas, J.A. Gálvez, and J.I. García. Tetrahedron, **52**, 9563 (1996); (*j*) Y. Yang and D. Wang. Synlett, 1379 (1997).

18. H.B. Kagan and J.C. Fiaud. Top. Stereochem. **18**, 249 (1988).
19. D.A. Evans and R.Y. Wong. J. Org. Chem. **42**, 350 (1977).
20. D.E. Ward and C.K. Rhee. Tetrahedron Lett. **32**, 7165 (1991).
21. J.A. Dale, D.L. Dull, and H.S. Mosher. J. Org. Chem. **34**, 2543 (1969).
22. I. Ohtani, T. Kusumi, Y. Kashman, and H. Kakisawa. J. Am. Chem. Soc. **113**, 4092 (1991).
23. (*a*), H. Minamikawa, S. Hayakawa, T. Yamada, N. Iwasawa, and K. Narasaka. Bull. Chem. Soc. Jpn. **61**, 4379 (1988); (*b*) K. Narasaka, T. Yamada, and H. Minamikawa. Chem. Lett. 2073 (1987).
24. (*a*) E.J. Corey and Y. Matsumura. Tetrahedron Lett. **1991**, *32*, 6289; (*b*) D. Seebach, R. Dahinden, R.E. Marti, A.K. Beck, D.A. Plattner, and F.N.M. Kuhnle. J. Org. Chem. **60**, 1788 (1995).
25. M. Mori, H. Imma, and T. Nakai. Tetrahedron Lett. **38**, 6229 (1997).
26. R.M. Devant and H.-E. Radunz. *In* Houben-Weyl, stereoselective synthesis. Vol. 2. *Edited by* G Helmchen, R.W. Hoffmann, J. Mulzer, and E. Schaumann. Thieme, Stuttgart. 1996. pp. 1196–1216.
27. D.E. Ward, M.J. Hrapchak, and M. Sales. Org. Lett. **2**, 57 (2000).
28. A.K. Ghosh, P. Mathivanan, and J. Cappiello. Tetrahedron: Asymmetry, **9**, 1 (1998).
29. E.J. Corey and Z. Wang. Tetrahedron Lett. **34**, 4001 (1993).
30. W.C. Still, M. Kahn, and A. Mitra. J. Org. Chem. **43**, 2923 (1978).
31. L.M. Harwood. Aldrichimica Acta, **18**, 25 (1985).
32. D.W. Brown, T.T. Nakashima, and D.L. Rabenstein. J. Magn. Reson. **45**, 302 (1981).
33. J.K. Rasmussen and S.M. Heilmann. Synthesis, 523 (1979).
34. K. Mikami, M. Terada, and T. Nakai. J. Am. Chem. Soc. **112**, 3949 (1990).
35. M.M. Midland and R.W. Koops. J. Org. Chem. **55**, 5058 (1990).

© 2001 NRC Canada

Absolute stereochemistry of the spiroxins

Tao Wang, Osamu Shirota, Koji Nakanishi, Nina Berova, Leonard A. McDonald, Laurel R. Barbieri, and Guy T. Carter

Abstract: The absolute configuration of spiroxin A has been determined by exciton-coupled circular dichroism (CD). Namely, the difference CD between spiroxin A – bis-methoxycinnamate, as well as that between spiroxin A – bis-retinoate, both exhibit negative exciton couplings between the acylated phenolic hydroxyl group chromophores. This establishes the absolute configuration as 2*S*,3*R*,4*S*,2′*S*,3′*R*,4′*S*.

Key words: circular dichroism, exciton coupling, spiroxins, antitumor, antifungal.

Résumé : Faisant appel au dichroïsme circulaire (DC) avec couplage d'exciton, on a déterminé la configuration absolue de la spiroxine A. Cette conclusion découle du fait que la différence dans le DC du couple spiroxine A – bis-méthoxycinnamate ainsi que celle du couple spiroxine A – bis-rétinoate présentent toutes les deux des couplages négatifs d'exciton entre les groupes chromophores des hydroxyles phénoliques acétylés. Ces travaux permettent d'établir que la configuration absolue est 2*S*,3*R*,4*S*,2′*S*,3′*R*,4′*S*.

Mots clés : dichroïsme circulaire, couplage d'exciton, spiroxines, antitumoral, antifongique.

[Traduit par la Rédaction]

Introduction

A variety of natural products that contain spiroketal moieties as elements of their molecular framework have been isolated and their structures have been determined. Among them are the preussomerins (1–3), palmarumycins (4–8), diepoxins (9, 10), cladospirone bisepoxides (11, 12), Sch series (13–16), and cladosporol (17). Compounds of this family exhibit significant antitumor and antifungal activities while some demonstrate inhibitory activity against phospholipase D (15).

Recently, a new series of bisnaphthospiroketal compounds, spiroxin A–E (**1**–**5**), have been isolated from a marine fungus (18). These compounds share a common bisnaphthospiroketal skeleton, differing from each other in their levels of oxygenation and halogenation. The absolute configuration of spiroxin A, the relative stereochemistry of which had been determined previously by NMR (18), is described in the following.

Circular dichroic (CD) exciton chirality has been widely used to determine the absolute configuration and (or) conformation of a variety of organic molecules (19). It is based on the through-space chiral interaction between the electric transition moments of two or more chromophores, which preexist in the molecule or, more often, are introduced by derivatization of functional groups (e.g., -OH, $-NH_2$). Herein we wish to report the absolute configuration of the spiroxins as determined by the CD exciton chirality method.

Results and discussions

The absolute configuration of spiroxin A, the major component produced by the fungal strain LL-37H248, has been determined by application of the exciton chirality method after suitable derivatization. The electrophilic activity of the two phenolic hydroxyl groups should distinguish themselves from other functional groups (oxirane, carbonyl, and ketal) in the molecule. Spiroxin A contains several UV–vis absorption bands (in CH_3CN), one at 264 nm (strong, ε = 12 300), and the other at a longer wavelength, 362 nm (weak, ε = 5600) (Fig. 2), which is associated with n-π^* and L_b(π-π^*) transitions of polysubstituted acetophenone chromophores. Therefore, we considered the derivatization of two free phenolic hydroxyl groups with red-shifted chromophores (19, 20). In particular, we selected the *p*-dimethylaminobenzoic group (λ_{max} = 307 nm, ε = 28 200, in CH_3CN), the *p*-methoxycinnamic group (λ_{max} = 306 nm, ε = 23 400, in CH_3CN), the all-*trans* retinoic group (λ_{max} = 356 nm, ε = 39 500, in CH_3CN), and the 5-(4′-carboxylphenyl)-10,15,20-triphenylporphyrin group (TPP) (λ_{max} = 419 nm, ε = 440 000, in CH_2Cl_2). We expected that due to their intense UV–vis absorption above 300 nm, such groups would not interact strongly with the preexisting chromophore(s). On the other hand, the resulting CD exciton coupling between the two new introduced chromophores should be readily distin-

Received April 3, 2001. Published on the NRC Research Press Web site at http://canjchem.nrc.ca on November 20, 2001.

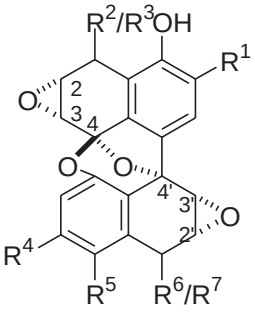
Dedicated to Professor Victor Snieckus for his contributions to Canadian chemistry.

T. Wang, O. Shirota, K. Nakanishi,[1] and N. Berova. Department of Chemistry, Columbia University, New York, NY 10027, U.S.A. **L.A. McDonald, L.R. Barbieri, and G.T. Carter.** Wyeth–Ayerst Research, 401 North Middletown Road, Pearl River, NY 10965, U.S.A.

[1]Corresponding author (telephone: (212) 854-2169; fax: (212) 932-8273; e-mail: kn5@columbia.edu and ndb1@columbia.edu).

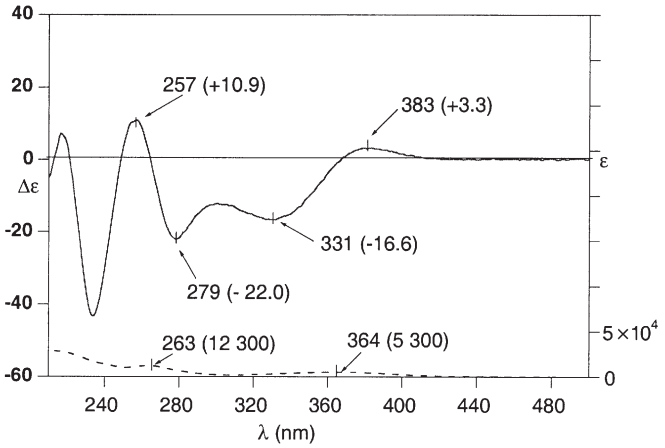
 DOI: 10.1139/cjc-79-11-1786 © 2001 NRC Canada

Fig. 1. Relative configuration of spiroxins.



Spiroxins	R^1	R^2/R^3	R^4	R^5	R^6/R^7
A (1)	Cl	O	H	OH	O
B (2)	Cl	O	Cl	OH	O
C (3)	H	O	H	H	O
D (4)	H	OH/H	H	H	O
E (5)	Cl	O	Cl	OH	OH/H

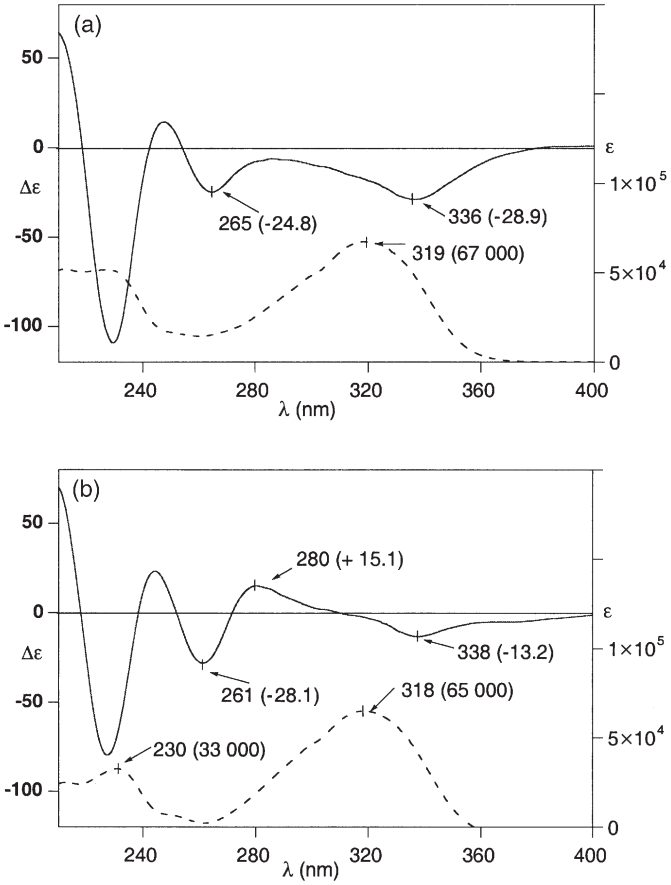
Fig. 2. CD (solid line) and UV (dashed line) spectra of spiroxin A in CH_3CN (2.1×10^{-5} M).



guished either directly or in the difference CD after subtracting the underivatized spiroxin spectrum.

Spiroxin A (1) is highly unstable to acidic treatment. The presence of the oxirane ring also makes it susceptible to nucleophilic reagents. Furthermore, spiroxin A decomposes over prolonged treatment with pyridine, the solvent of choice for esterification of hydroxyl groups, especially in case of chelated hydroxyl functions to break the H-bonding. In addition, since the total amount of compound available was ca. 3.0 mg, derivatization and exploratory experiments with this unstable compound had to be carried out at the microscale level. Incorporation of the tetraphenylporphyrin (TPP) and *p*-dimethylaminobenzoate groups were first attempted. Standard coupling reactions between **1** and 5-(4′-carboxylphenyl)-10,15,20-triphenylporphyrin with

Fig. 3. (*a*) CD (solid line) and UV (dashed line) spectra of spiroxin A – biscinnamate in CH_3CN (1.5×10^{-5} M). (*b*) Difference (biscinnamate–SpA) CD (solid line) and UV (dashed line) spectra of spiroxin–biscinnamate.

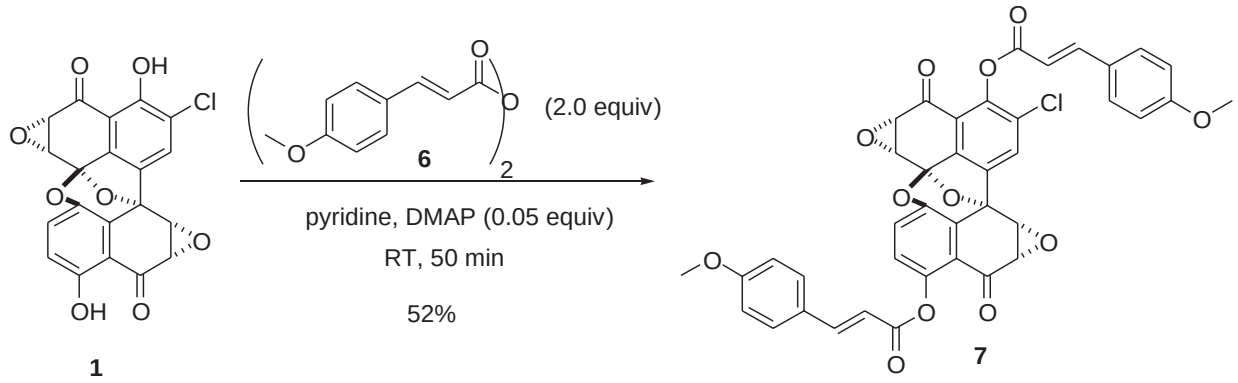


DCC–DMAP led to the decomposition of the starting material. Reactions involving the *p*-dimethylaminobenzoic group (either acid or its anhydride) also led to degradation of the starting material. Treatment of **1** with DBU and *p*-methoxycinnamic anhydride **6**, which had been prepared from the corresponding acid (21), also resulted in decomposition. Base-free acylation of **1** with **6** catalyzed by TMSOTf (22) or $Sc(OTf)_3$ (23) (either catalytic or stoichiometric) did not proceed, leaving the starting material intact. After several unsuccessful trials, it was discovered that the reaction of spiroxin A (1) with anhydride **6** proceeded in pyridine–DMAP at room temperature under argon in 50 min, to give the desired biscinnamate **7** in 52% isolated yield. This reaction had to be monitored very carefully by TLC to check for the decomposition of the product and (or) starting material.

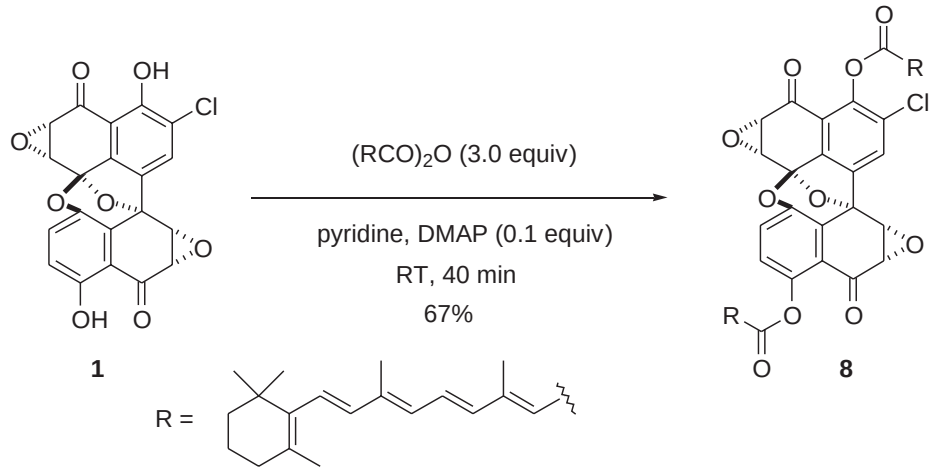
The CD and UV–vis spectra of biscinnamate **7** are shown in Fig. 3*a*. The CD exhibited a negative peak at 336 nm ($\Delta\varepsilon = -28.9$). However, no positive Cotton effect (CE) around the cinnamate absorption could be detected. As Fig. 2 illustrates, the CD spectrum of spiroxin A in CH_3CN exhibits several Cotton effects related to the polysubstituted acetophenone chromophores. The difference CD and difference UV–vis spectra, resulting from subtraction of the respective observed spectra of **1** from those of biscinnamate **7**, are shown in Fig. 3*b*. While the difference

© 2001 NRC Canada

Scheme 1. Synthesis of spiroxin A biscinnamate.



Scheme 2. Synthesis of spiroxin A bisretinoate.



CD in the shorter wavelength region (200–280 nm) mainly shows changes in the intensity of CEs exhibited by spiroxin A itself, at 280 and 338 nm a clear positive ($\Delta\varepsilon$ = +15) – negative ($\Delta\varepsilon$ = –13) couplet is seen. The position of the new bisignate CE centered at 309 nm is very slightly red-shifted when compared with typical data for bis-*p*-methoxycinnamate couplings (287 and 325 nm, centered at 306 nm) (24).

In general, the difference CD spectrum is especially useful when the chiral substrate contains preexisting chromophore(s) and exhibits, before derivatization, an intense and complex CD. Recent examples include strevertenes (25), vinblastine (26), and nemadectines (27). In all three cases, the parent compounds exhibited CD spectra with multiple Cotton effects and only after subtraction of such CD from the CD of the corresponding chromophoric derivative did the net exciton-coupled contribution become clear. In the case of **7**, however, the interaction between *p*-methoxycinnamate with the polysubstituted acetophenone group in the spiroxin A cannot be completely excluded and this is the most likely the reason for the slight deviation in the λ_{max} of the couplet from that of a typical *p*-methoxycinnamate. We, therefore, attempted to incorporate the more red-shifted all-*trans* retinoic group into spiroxin A since the interaction of its chromophore with the innate spiroxin A chromophore would be minimized. The all-*trans* retinoic methyl ester has a λ_{max} at 356 nm (ε = 39 500) with the corresponding electric transition dipole moment (μ) polarized almost parallel to the all-*trans* polyene side chain, as is the case with other known polyene ester systems (19, 20).

Fortunately, the incorporation of all-*trans* retinoic chromophore proceeded smoothly. Treatment of **1** with all-*trans* retinoic anhydride under conditions similar to those described above produced spiroxin A bis-retinoate **8** in 67% yield (Scheme 2). The CD and UV–vis spectra for **8** are shown in Fig. 4*a*. The CD spectrum shows a negative peak at 391 nm ($\Delta\varepsilon$ = –14.6). The difference CD spectrum exhibits a negative peak at 385 nm ($\Delta\varepsilon$ = –17.3) and a positive peak at 331 nm ($\Delta\varepsilon$ = +17.4), *A* = –34.7 (Fig. 4*b*), giving rise to a typical negative bisignate curve with crossover around 359 nm, close to the max of the isolated retinoate chromophore (356 nm).

The difference CD obtained here is in good agreement with the model compound, *trans*-(1*R*,2*R*)-cyclohexanediol derivative **9** prepared earlier (unpublished results). As seen in Fig. 5, the CD spectrum of **9** exhibits a negative peak at 381 nm and a positive peak at 331 nm, *A* = –40.1. Since the parent cyclohexanediol only contains hydroxyl groups absorbing ca. 200 nm, the observed CD represents a typical conservative couplet, i.e., true exciton coupling between two retinoate chromophores. The surprisingly good agreement in position and intensity between the CD spectrum of **9** and the difference CD spectrum shown in Fig. 4*b* exemplifies the ad-

© 2001 NRC Canada

Fig. 4. (*a*) CD (solid line) and UV (dashed line) spectra of spiroxin A – bisretinoate in CH_3CN (2.7×10^{-5} M). (*b*) Difference (bisretinoate–SpA) CD (solid line) and UV (dashed line) spectra of spiroxin–bisretinoate.

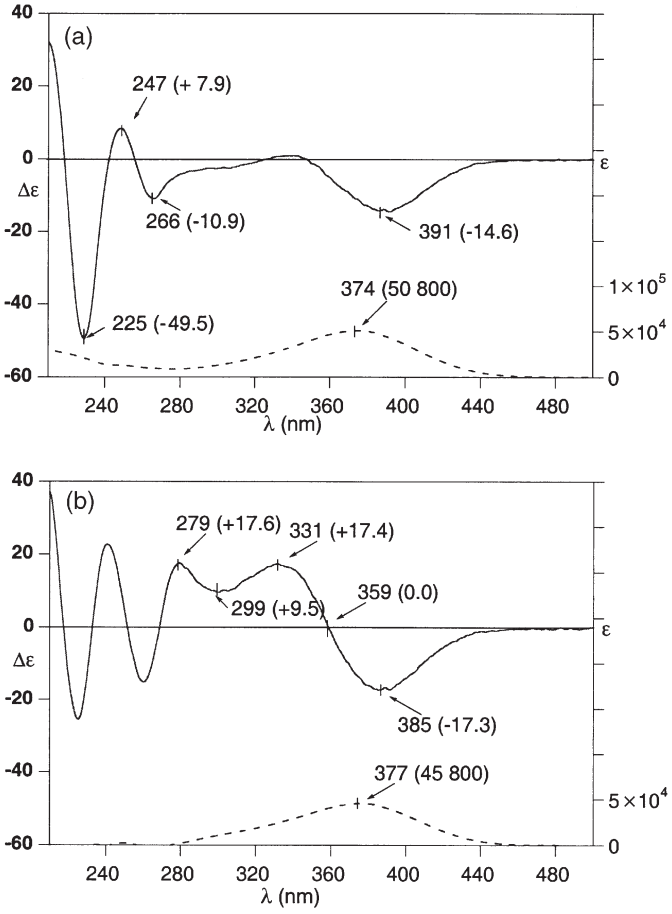


Fig. 5. CD (solid line) and UV (dashed line) spectra of cyclohexyldiolbisretinoate **9** in CH_3CN.

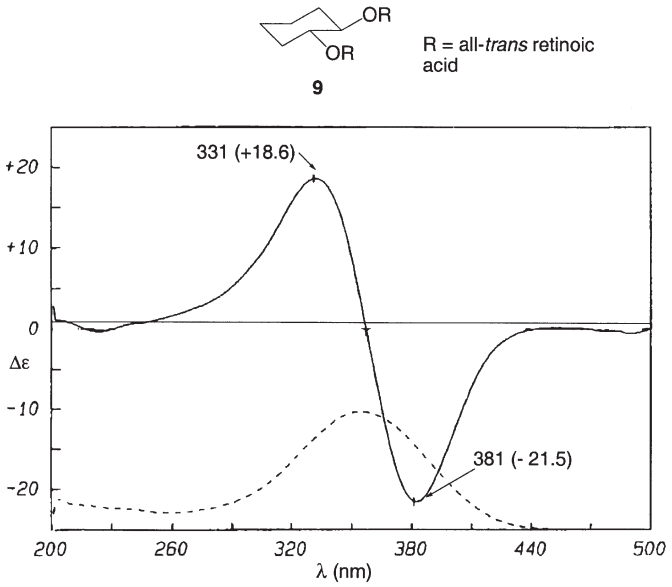
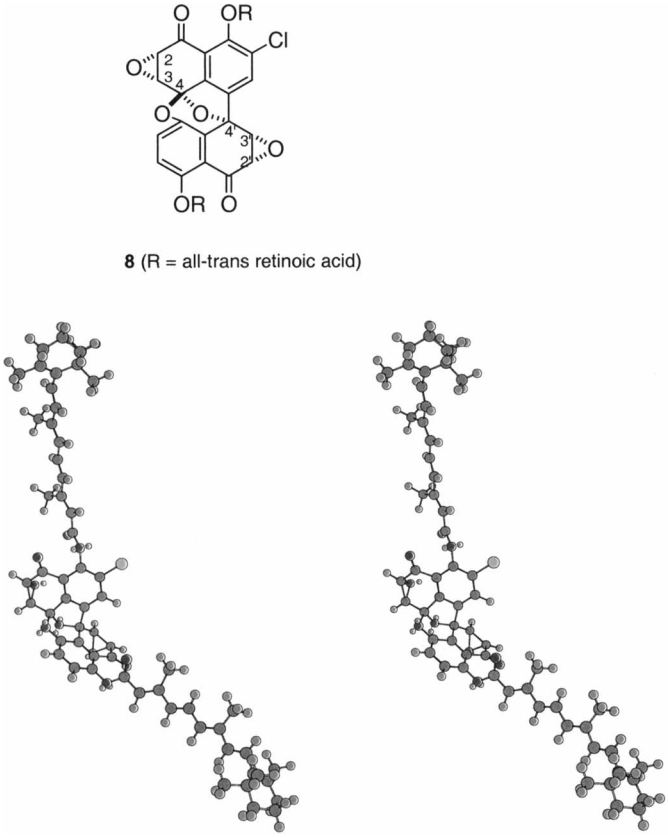


Fig. 6. Lowest energy conformer of **8** (stereo view) from Monte Carlo conformation search (MM2, 1000 structures), and absolute stereochemistry of the six stereogenic centers on compound **8** was determined as 2*S*,3*R*,4*S*,2′*S*,3′*R*,4′*S*.



vantage of using the red-shifted retinoate for the CD analysis of spiroxin A.

Thus, the obtained difference CD couplet at 385 and 331 nm with amplitude $A = -34.7$ represents straightforward evidence for the negative chirality between the two all-*trans* retinoic chromophores, and hence leads to the assignment of the absolute configuration of spiroxin A. For the relative and absolute configuration shown in **8**, the Monte Carlo conformation search (MM2 as force field, 1000 structures) gave the lowest energy conformer shown in Fig. 6, where the two all-*trans* retinoic chromophores form a negative chiral twist. Additionally, all 22 other distinct conformers whose energies fall within a 1 kcal mol^{-1} range of the global min gave negative chirality. Consequently, based on the observed negative couplet in the difference CD, the structure **8** represents the absolute configuration of spiroxin A as 2*S*,3*R*,4*S*,2′*S*,3′*R*,4′*S*.

Conclusion

In summary, based on an exciton-coupled CD study of spiroxin A biscinnamate **7** and spiroxin A bisretinoate **8**, the absolute configurations of the six stereogenic centers of spiroxin A have been determined as 2*S*,3*R*,4*S*,2′*S*,3′*R*,4′*S*. Since NMR studies have shown (18) that all five spiroxins (**A**–**E**) share the same skeletal structure, the absolute

© 2001 NRC Canada

configuration of spiroxin A can be extended to the four other members (**B**–**E**) of the spiroxins.

Experimental

General methods

TLC was performed on a Merck DC-alufolien with Kieselgel 60F-254 and column chromatography was carried out on silica gel 60 (Merck, 230–400 mesh ASTM). ^{1}H and ^{13}C NMR spectra were measured on a Bruker DMX-400 NMR spectrometer in $CDCl_3$ or benzene-d_6. Chemical shifts (δ) were reported in ppm downfield from internal TMS and coupling constants (*J*) in Hz. UV–vis spectra were measured on a PerkinElmer Lambda 6 UV–vis spectrophotometer. CD spectra were measured on a JASCO J-810 spectropolarimeter. The following parameters were employed: band width 1.0 nm, auto slit width, sensitivity 20 mdeg, response 2 s, start wavelength 400 nm or 500 nm, end wavelength 210 nm, scan speed 100 nm min^{-1}, step resolution 0.5 nm, accumulation 8. Mass spectra were measured on a JEOL JMS-DX303 HF mass spectrometer. All molecular mechanics were carried out with MacroModel V6.0 on Silicon Graphics 3D workstation at the Department of Chemistry, Columbia University. The Monte Carlo conformation search was carried out by using MM2 as the force field, and 1000 structures were generated.

Materials

All chemicals were purchased from Aldrich Co. (Milwaukee, Wisconsin) and purified before use by standard methods. Acetonitrile used for UV and CD analysis was of spectrophotometric grade. Dichloromethane was distilled immediately prior to use under nitrogen from calcium hydride.

*Preparation of spiroxin A bis-cinnamate (**7**)*

To a solution of spiroxin A (2.0 mg, 4.85 μmol) and *p*-methoxycinnamic anhydride **6** (3.28 mg, 9.7 μmol) in distilled pyridine (80 μL) under argon at room temperature was added a solution of 4-dimethyaminopyridine in pyridine (0.02 M, 18 μL, 0.36 μmol) and the reaction mixture was stirred for 50 min. The reaction mixture was diluted with ether (20 mL) and the solution was washed with saturated $CuSO_4$ solution and brine. The mixture was dried over anhyd Na_2SO_4 and the solvent was removed in vacuo. Column chromatography on silica gel (hexanes:ethyl acetate = 2:1 to 1:1) gave the desired product **7** (1.8 mg, 52%) as a white solid. APCI MS *m*/*z*: 750.3 $[M + NH_4]^+$. UV–vis λ_{max} (nm) (ε) (CH_3CN): 227.5 (52 000), 320 (67 000). ^{1}H NMR (400 MHz, $CDCl_3$) δ: 3.83 (d, *J* = 3.7 Hz, 1 H), 3.87 (s, 6 H), 3.97 (d, *J* = 4.1 Hz, 1 H), 4.17 (d, *J* = 4.0 Hz, 1 H), 4.24 (d, *J* = 3.7 Hz, 1 H), 6.54 (t, *J* = 15.8 Hz, 2 H), 6.94 (dd, *J* = 8.7, 1.3 Hz, 4 H), 7.08 (d, *J* = 8.9 Hz, 1 H), 7.15 (d, *J* = 8.9 Hz, 1 H), 7.56 (dd, *J* = 8.7, 1.3 Hz, 4 H), 7.86 (t, *J* = 15.8 Hz, 2 H).

*Spiroxin A bisretinoate (**8**)*

FAB–HRMS *m*/*z* calcd. for $C_{60}H_{61}ClO_{10}$: 976.3953; found: 976.3936 (Δ = –1.8 ppm). UV–vis λ_{max} (nm) (ε) (CH_3CN): 374 (50 800). ^{1}H NMR (400 MHz, $CDCl_3$) δ: 1.04 (s, 12 H), 1.25 (m, 4 H), 1.48 (m, 4 H), 1.54 (m, 4 H), 1.73 (s, 6 H), 2.03 (s, 6 H), 2.39 (s, 3 H), 3.80 (d, *J* = 3.7 Hz, 1 H), 3.95 (d, *J* = 4.1 Hz, 1 H), 4.14 (d, *J* = 4.1 Hz, 1 H), 4.23 (d, *J* = 3.7 Hz, 1 H), 6.01 (s, 1 H), 6.07 (s, 1 H), 6.15–6.20 (m, 4 H), 6.30 (d, *J* = 6.0 Hz, 1 H), 6.34 (d, *J* = 6.9 Hz, 1H), 6.37 (d, *J* = 3.9 Hz, 1 H), 6.41 (d, *J* = 3.7 Hz, 1 H), 6.98–7.16 (m, 4 H), 7.47 (s, 1 H).

*trans-(1*R*,2*R*)-Cyclohexanediol bisretinoate (**9**)*

To a solution of *trans*-(1*R*,2*R*)-cyclohexanediol (1.9 mg, 16.6 μmol) and all-*trans* retinoic triazole (18 mg, 57.3 μmol) in distilled CH_2Cl_2 (1 mL) was added five drops of DBU (0.1 M in CH_2Cl_2) and the reaction mixture was stirred for 20 h. The reaction mixture was diluted with ether (20 mL) and the solution was washed with brine. The mixture was dried over anhyd Na_2SO_4 and the solvent was removed in vacuo. Column chromatography on silica gel (hexanes:ethyl acetate = 5:1) gave the desired product **9** (0.9 mg, 8%) as a white solid. FAB–HRMS *m*/*z* calcd. for $C_{46}H_{64}O_4$: 680.9980; found: 680.9568 (Δ = 6.0 ppm). UV–vis λ_{max} (nm) (ε) (CH_3CN): 352 nm (58 000). ^{1}H NMR (300 MHz, $CDCl_3$) δ: 1.07 (s, 12 H), 1.22 (m, 4 H), 1.45 (m, 8 H), 1.55 (m, 6 H), 1.73 (s, 10 H), 2.07 (s, 6 H), 2.40 (m, 4 H), 4.88 (m, 2 H), 5.72 (m, 2 H), 6.10–6.30 (m, 4 H), 6.98–7.05 (m, 4 H), 7.52 (m, 2 H).

Acknowledgment

This work has been supported by a grant from the National Institutes of Health (NIGMS GM34509). We are grateful to Dr. N. Bozhkova for preparation of model compound **9**. We would like to thank also Nathan Fishkin for helpful discussions.

References

1. S.B. Singh, D.L. Zink, J.M. Liesch, R.G. Ball, M.A. Goetz, E.A. Bolessa, R.A. Giacobbe, K.C. Silverman, G.F. Bills, F. Pelaez, C. Cascales, J.B. Gibbs, and R.B. Lingham. J. Org. Chem. **59**, 6296 (1994).
2. H.A. Weber, N.C. Baenziger, and J.B. Gloer. J. Am. Chem. Soc. **112**, 6718 (1990).
3. H.A. Weber and J.B. Gloer. J. Org. Chem. **56**, 4355 (1991).
4. K. Krohn, A. Michel, U. Florke, H.-J. Aust, S. Draeger, and B. Schulz. Liebigs Ann. Chem. 1093 (1994).
5. K. Krohn, A. Michel, U. Florke, H.-J. Aust, S. Draeger, and B. Schulz. Liebigs Ann. Chem. 1099 (1994).
6. K. Krohn, K. Beckmann, H.-J. Aust, S. Draeger, B. Schulz, S. Busemann, and G. Bringmann. Liebigs Ann./Rec. 2531 (1997).
7. K. Krohn, K. Beckmann, U. Florke, H.-J. Aust, S. Draeger, B. Schulz, S. Busemann, and G. Bringmann. Tetrahedron, **53**, 3101 (1997).
8. G. Bringmann, S. Busemann, K. Krohn, and K. Beckmann. Tetrahedron, **53**, 1655 (1997).
9. G. Schlingmann, R.R. West, L. Milne, C.J. Pearce, and G.T. Carter. Tetrahedron Lett. **34**, 7225 (1993).
10. G. Schlingmann, S. Matile, N. Berova, K. Nakanishi, and G.T. Carter. Tetrahedron, **52**, 435 (1996).
11. R. Thiergardt, P. Hug, G. Rihs, and H.H. Peter. Tetrahedron Lett. **35**, 1043 (1994).
12. R. Thiergardt, G. Rihs, P. Hug, and H.H. Peter. Tetrahedron, **51**, 733 (1995).
13. M. Chu, I. Truumees, M.G. Patel, V.P. Gullo, J.-K. Pai, P.R. Das, and M.S. Puar. Bioorg. Med. Chem. Lett. **4**, 1539 (1994).
14. M. Chu, I. Truumees, M.G. Patel, V.P. Gullo, M.S. Puar, and A.T. McPhail. J. Org. Chem. **59**, 1222 (1994).

© 2001 NRC Canada

15. M. Chu, I. Truumees, M.G. Patel, V.P. Gullo, C. Blood, I. King, J.-K. Pai, and M.S. Puar. Tetrahedron Lett. **35**, 1343 (1994).
16. M. Chu, M.G. Patel, J.-K. Pai, P.R. Das, and M.S. Puar. Bioorg. Med. Chem. Lett. **6**, 579 (1996).
17. Y. Sakagami, A. Sano, O. Hara, T. Mikawa, and S. Marumo. Tetrahedron Lett. **36**, 1469 (1995).
18. L.A. McDonald, D.R. Abbanat, L.R. Barbieri, V.S. Bernan, C.M. Discafani, M. Greenstein, K. Janota, J.D. Korshalla, P. Lassota, M. Tischler, and G.T. Carter. Tetrahedron Lett. **40**, 2489 (1999).
19. N. Berova and K. Nakanishi. *In* Circular dichroism: principles and applications. *Edited by* N. Berova, K. Nakanishi, and R.W. Woody. Wiley–VCH, Inc., New York. 2000. pp. 337.
20. G. Cai, N. Bozhkova, J. Odingo, N. Berova, and K. Nakanishi. J. Am. Chem. Soc. **115**, 7192 (1993).
21. R.L. Shriner and H.C. Struck. Org. Syn. Coll. **2**, 560 (1943).
22. P.A. Procopiou, S.P.D. Baugh, S.S. Flack, and G.G.A. Inglis. J. Org. Chem. **63**, 2342 (1998).
23. A.G.M. Barret and D.C. Braddock. Chem. Commun. 351 (1997).
24. W.T. Wiesler, N. Berova, M. Ojika, H.V. Meyers, M. Chang, P. Zhou, L.-C. Lo, M. Niwa, R. Takeda, and K. Nakanishi. Helv. Chim. Acta, **73**, 509 (1990).
25. J. Guo, K. Nakanishi, B. Berova, G. Schlingmann, and G.T. Carter. Chirality, **12**, 43 (2000).
26. C.A. Parish, J. Dong, W. Bornmann, J. Chang, K. Nakanishi, and B. Berova. Tetrahedron, **54**, 15789 (1998).
27. L.-C. Lo, B. Berova, K. Nakanishi, G. Schlingmann, G.T. Carter, and D.B. Border. J. Am. Chem. Soc. **114**, 7371 (1992).

© 2001 NRC Canada

Studies on enolate chemistry of 8-thiabicyclo[3.2.1]-octan-3-one: enantioselective deprotonation and synthesis of sulfur analogs of tropane alkaloids

Marek Majewski, Marc DeCaire, Pawel Nowak, and Fan Wang

Abstract: Enantioselective deprotonation of 8-thiabicyclo[3.2.1]octan-3-one (**1**) with chiral lithium amides, followed by reactions with electrophiles affords sulfur analogs of tropane alkaloids of pyranotropane family. Thus, deprotonation of **1** with (*S*)-*N*-(diphenyl)methyl-1-phenylethylamine (**11d**), followed by the reaction of the resulting nonracemic enolate with benzaldehyde gives the corresponding aldol product as one diastereoisomer (*exo*, threo) and in high enanatiomeric purity (95% ee). Trimethylsilyl chloride, acetic anhydride, and acyl cyanides react readily with the lithium enolate to give the corresponding derivatives of **1**, however common alkylating agents fail to provide *C*-alkylated products. The reaction with acyl cyanides derived from α,β-unsaturated carboxylic acids (e.g., cinnamoyl cyanide) can be utilized in synthesis of thia-analogs of tropane alkaloids physoperuvine and isobellendine (**13**, **15**).

Key words: enantioselective deprotonation, tropane alkaloids.

Résumé : La déprotonation énantiosélective de la 8-thiabicyclo[3.2.1]octan-3-one à l'aide d'amides de lithium chiraux, suivie de réactions avec des électrophiles, conduit à la formation d'analogues sulfurés des alcaloïdes du tropane, de la famille du pyranotropane. Ainsi, la déprotonation du produit **1** avec de la (*S*)-*N*-(diphényl)méthyl-1-phényléthylamine (**11d**), suivie d'une réaction de l'énolate non racémique qui en résulte avec du benzaldéhyde, conduit à la formation du produit aldolique correspondant, sous la forme d'un diastéréoisomère (*exo*, thréo) et avec une pureté énantiotopique éleveée (95% ee). Le chlorure de triméthylsilyle, l'anhydride acétique et les cyanures d'acyles réagissent facilement avec l'énolate de lithium pour conduire à la formation des dérivés correspondants du produit **1**. Toutefois, les agents alkylants habituels ne conduisent pas à la formation de produits *C*-alkylés. On peut toutefois utiliser la réaction avec des cyanures d'acyles dérivés d'acides carboxyliques α,β-insaturés (par exemple, le cyanure de cinnamoyle) pour effectuer la synthèse de la physopéruvine et de l'isobellendine, des analogues sulfurés des alcaloïdes du tropane (**13**, **15**).

Mots clés : déprotonation énantiosélective, alcaloïdes du tropane.

[Traduit par la Rédaction]

Introduction

8-Thiabicyclo[3.2.1]octan-3-one (**1**) is a simple, readily available symmetrical ketone that can be viewed as a potential scaffold for construction of diverse compounds of medium complexity and, perhaps most notably, as a scaffold for construction of sulfur analogs of tropane alkaloids. These alkaloids comprise a group of over 200 natural products of general structure **2** (R groups are typically alkyls or acyls, brackets signify that the group can be at e.g., C-2 or C-4, R and R′ can be connected forming a heterocycle), built around a common 8-azabicyclo[3.2.1]octane skeleton (1). During the last few years we have developed a comprehensive strategy for stereoselective synthesis of tropane alkaloids based on enantioselective deprotonation of tropinone (**3**) with chiral lithium amides (e.g., **4**) as the key reaction. A number of tropane alkaloids were synthesized (2–5), and an elegant synthesis of cocaine utilizing our strategy, which allowed setting up the absolute and relative stereochemistry around all 4 stereogenic centers in 2 steps, has recently been reported by Cha and co-workers (6). Replacement of the nitrogen atom in a biologically active natural product by the sulfur atom is a well known strategy in medicinal chemistry often leading to substantial changes in biological activity of the compound (7, 8). TBON had been used as a replacement for alkaloid intermediates during studies on alkaloid metabolism and on biosynthesis of cocaine (9). We were interested in developing a general synthesis of sulfur analogs of tropane alkaloids and, towards this end, we initiated an investigation of lithiation of **1** with chiral lithium amides and of reactions of the corresponding enolate.

Enantioselective deprotonation of symmetrical ketones (note the enantiotopic protons in structures **1** and **3**) with chiral lithium amides is a relatively new methodology (2,

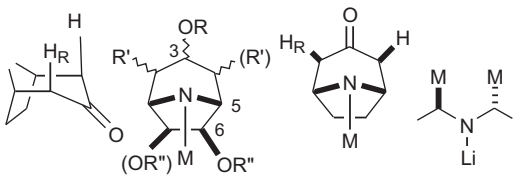
Received April 20, 2001. Published on the NRC Research Press Web site at http://canjchem.nrc.ca on November 19, 2001.

Dedicated to Professor Victor Snieckus, lithiator extraordinarie.

M. Majewski,[1] M. DeCaire, P. Nowak, and F. Wang. Department of Chemistry, University of Saskatchewan, 110 Science Pl., Saskatoon, SK S7N 5C9, Canada.

[1]Corresponding author (telephone: (306) 966-4671; fax: (306) 966-4730; e-mail: majewski@sask.usask.ca).

 DOI: 10.1139/cjc-79-11-1792 © 2001 NRC Canada



1 2 3 4

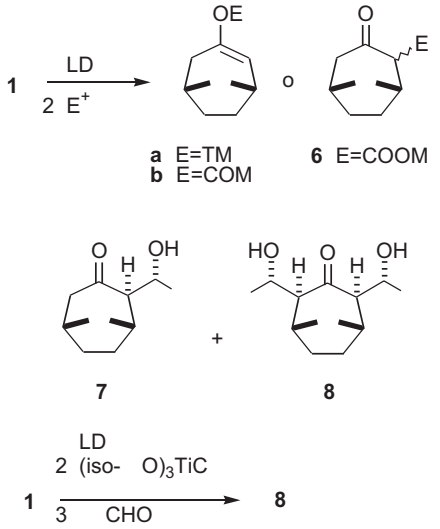
10). A number of diverse ketones have been investigated over the last decade and, even though the mechanism of the reaction is still not fully understood, several trends have emerged: (*i*) certain level of conformational rigidity is necessary for achieving high level of enantioselectivity. Thus, 4-*tert*-butylcyclohexanone could be deprotonated with higher enantioselectivity than the 4-methyl analog (11). (*ii*) Bicyclic, bridged ketones are especially good substrates in reaction with chiral lithium amides (high enantioselectivity) (2, 10). (*iii*) Addition of certain salts, especially LiCl, can be very beneficial from the standpoint of reaction selectivity (12). (*iv*) There is no straightforward correlation between the structure of the ketone, the lithium amide, and selectivity. There is no magic bullet; certain lithium amides can be very selective with some ketones but show poor selectivity in other systems. Thus, every new system must be researched experimentally. It should be noted that a few other heterocyclic compounds containing sulfur have been investigated in the context of enantioselective deprotonation (13, 14). One precedent involving TBON was reported previously by Simpkins and co-workers (15), who also noted a strong effect of the $ZnCl_2$ additive on the selectivity of deprotonation with the chiral base **4**.

On the basis of the foregoing TBON looked like a promising substrate for synthesis using deprotonation with chiral lithium amides as the key step, but it should be emphasized that, as with any new system, the conditions for successful selective deprotonation had to be elaborated from the beginning. Apart from being interesting in the purely theoretical sense TBON could provide a useful starting material for construction of α-substituted cycloheptanones (after desulfurization), and it should be noted that the presence of the sulfur atom in the bridge offers potential for much more diverse chemistry than the corresponding carbon-, oxygen-, or nitrogen-bridged systems due to the ability of dialkylsulfur compounds to exist in three oxidation states (as sulfides, sulfoxides, or sulfones).

Results and discussion

Since little was known about chemical properties of TBON we started by running a series of typical experiments. Lithiation of **1** with LDA proceeded in the usual fashion and the resulting enolate could be efficiently trapped with TMS-Cl, Ac_2O, benzaldehyde, or methyl cyanoformate to afford the corresponding silyl enol ether **5a** (96% isolated yield), enol acetate **5b** (97%), aldol product **7** (92%), or β-ketoester **6** (98%), respectively (Scheme 1). We were, however, unable to effect alkylation of TBON lithium enolate. Most of the attempts with reactive alkylating agents: methyl or ethyl iodide, benzyl bromide, or butyl tosylate gave numerous products that were difficult to purify; in some cases the starting material was recovered. It should be noted that similar failures of the well-known, and all too often taken for granted, alkylation reaction were observed before in cases involving other ketone enolates (16).

Scheme 1.



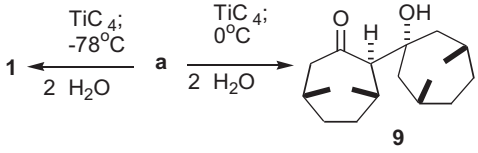
The aldol reaction leading to product **7** proceeded with very high diastereoselectivity and only one isomer out of possible four diastereoisomeric aldols was formed (to the limit of the NMR detection in the crude product). In analogy to tropinone (2) we have assigned the *exo–anti* relative configuration (as drawn) to this compound. The *exo* orientation of the CHOHPh group was also supported by NOE studies. The proton NMR spectrum of the crude aldol product indicated a presence of a minor by-product (ca. 6% by integration). We made no effort to isolate this product from the mixture, but we believe it to be the bis-aldol **8**. Compound **8** was produced in good yield (61%) in a separate experiment involving the titanium enolate of **1** (Scheme 1) and the NMR spectrum of **8** was consistent with the *exo*,*exo*,*anti*,*anti* relative configuration. In the mixture, the bis-aldol **8** could be easily confused with the expected minor product i.e., the *syn* isomer of the aldol **7**, because the benzylic protons of this compounds appear ca. 0.35 ppm downfield of the signal characteristic of the benzylic proton of compound **7**; an accidental juxtaposition of signals resembling a typical mixture of erythro (*syn*) and threo (*anti*) aldols (17). The formation of a bis-aldol as the major product of addition of the titanium enolate of TBON to benzaldehyde is unusual — the expected result would be the *syn* isomer of **7** as the major product (18).

Some oxygen-bridged ketones similar to **1** are known to undergo a ring opening to the corresponding cycloheptenone derivatives upon treatment of their silyl enol ethers with Lewis acids (19). In an attempt to recreate this reaction on TBON, we treated the TMS enolate **5a** with titanium tetrachloride (Scheme 2). There was no evidence of ring opening, however, depending on the reaction temperature, either the self-aldol product **9** was formed in good yield (70% of **9** was isolated when the experiment was done at 0°C) or, at low temperature, the enol ether was presumably cleanly transmetalated and, upon quenching, converted cleanly and quantitatively into the parent ketone **1**.

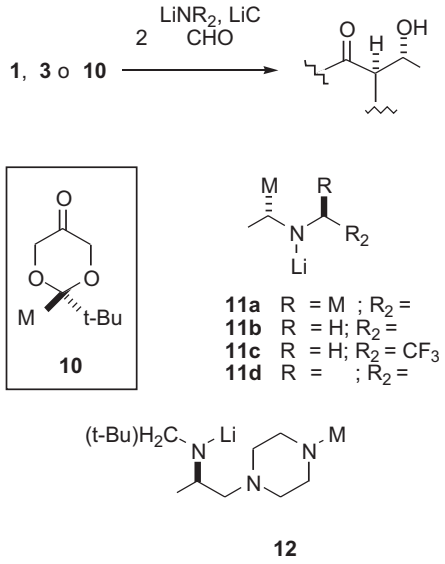
Having achieved reasonable predictability of behavior of the TBON enolate a brief experimental study of enantio-

© 2001 NRC Canada

Scheme 2.

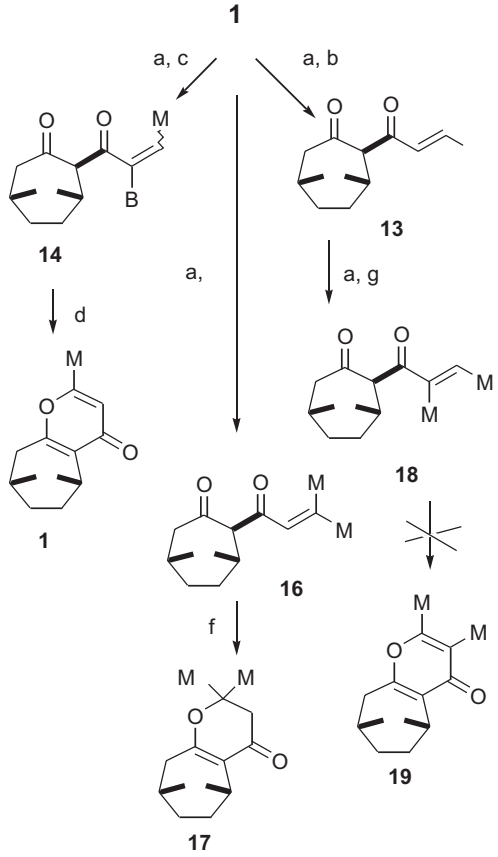


Scheme 3.



selective deprotonation was launched. The chiral lithium amides used in this study are shown in Scheme 3; the aldol addition to benzaldehyde was used as the model reaction because the enantiomeric excess (ee) could be easily measured on the aldol **7** using NMR with a chiral solvating agent [(*S*)-(+)-2,2,2-trifluoro-1-(9-anthryl)ethanol]. The absolute stereochemistry of deprotonation has not been established, but, by analogy to tropinone, we believe that the major, dextrorotatory enantiomer of **7**, which was produced in each case, should be as drawn in Scheme 1. The results are summarized in Table 1, which also includes, for comparison, enantioselectivities attained using the same reagents with other heterocyclic ketones: tropinone **3** and dioxanone **10**. All reactions were done in the presence of LiCl (one mol per one mol of the amide). The reaction with base **4** (i.e., with the enantiomer of **11a**) had been previously reported to proceed with 84% ee (15). Despite numerous attempts the highest ee in our experiments was 70% (as measured by NMR on the crude product; the optical purity of the sample could be easily increased by crystallization). The reaction seemed to be fairly capricious and substantial amounts of the bis-aldol were observed in all experiments involving base **11a** (15–25%). We also noticed that in experiments that yielded more bis-aldol product the optical purity of compound **7** was higher (e.g., 58% ee of **7** at **7**:**8** ratio of 85:15 and 70% ee of **7** at **7**:**8** ratio of 75:25), suggesting that the second aldol reaction had introduced an element of kinetic resolution. In an effort to optimize this reaction we tried a number of conditions and finally we observed that the best selectivity was consistently achieved when the amine hydrochloride was

Scheme 4. Reagents: (*a*) LiCl; (*b*) PhCH=CHCOCN; (*c*) MeCH=CBrCOCN; (*d*) Et_3N; (*e*) Me_2C=CHCOCN; (*f*) Na_2CO_3, EtOH; (*g*) MeCH=CMeCOCN.



used to generate the LiCl–$LiNR_2$ mixture in situ (19) and when the ketone was added slowly (over 90 min) to the solution of the amide (see *Experimental*). All experiments were subsequently run under these conditions. The most selective base turned out to be compound **11d** (Table 1, entry 4). It was interesting to note that bases **11a** and **12**, which provided high selectivity in tropinone deprotonation, were ineffective in both the TBON and the dioxanone systems, and conversely, base **11d** by far the best as far as TBON deprotonation was concerned, performed worse than other bases with substrate **3**, and gave only modest selectivity with compound **10**. Amide **11c**, developed by Aoki and Koga (20) and known to be selective in several systems (2, 21) was not very effective with TBON.

We had previously described stereoselective syntheses of a number of tropane alkaloids via the enantioselective deprotonation strategy (2). Extension of this approach to synthesis of sulfur analogs of tropane alkaloids e.g., chalcostrobamine and darlingine appeared straightforward. Enantioselective deprotonation of TBON with the chiral amide **11d** followed by treatment of the resulting enolate with an acyl cyanide (Scheme 4) proceeded readily to give the corresponding β-diketone (**13**, **14**, **16**, or **18**). The sulfur analog of chalcostrobamine **13** was produced in a modest yield of 61%, even though an analogous reaction with LDA (leading to the racemate of **13**) was very efficient (92% yield). Acylation with 2-bromo-2-butenoyl cyanide gave compound

© 2001 NRC Canada

Table 1. Results of enantioselective deprotonation of TBON (**1**), followed by reaction with benzaldehyde.

		TBON (**1**)			Tropinone	Dioxanone
Entry	Base	ee (%)	**7**:**8**	Yield (%)[a]	**3** ee (%)[b]	**10** ee (%)[c]
1	**11a**	70	75:25	80	90	59
2	**11b**	45	90:10	78	—	39
3	**11c**	70	95:5	72	88	90
4	**11d**	95	98:2	82	87	70
5	**12**	74	90:10	75	94	20

Note: Literature data for analogous reactions on tropinone and dioxanone are provided for comparison.
[a]Combined yield of **7** and **8**.
[b]Refs. 2–4.
[c]Refs. 2, 12, and 21.

14 that, without purification, was converted into a sulfur analog of isobellendine **15** by heating with triethylamine. This sequence of three reactions was quite efficient (48% overall yield, 87% ee). Compound **17**, which is not an analog of a known tropane alkaloid, was produced by a similar reaction sequence (78% yield, 92% ee). We have also attempted a synthesis of a sulfur analog of darlingine, but, even though the acylation proceeded well, we were unable to find an efficient method to introduce the double bond into the pyranone ring. Overall, enantioselective deprotonation of TBON coupled with acylation using acyl cyanides provided an easy entry into sulfur analogs of alkaloids of pyranotropane family.

Experimental

All air sensitive reactions were carried out under nitrogen. Tetrahydrofuran and diethyl ether were distilled under nitrogen from sodium and benzophenone. Dichloromethane and diisopropylamine were distilled from calcium hydride. Lithium chloride was dried at 130–150°C in vacuum overnight and it was used as a solid or as a solution in tetrahydrofuran. *n*-Butyllithium was periodically titrated using 2,5-dimethoxybenzyl alcohol. Flash column chromatography (FCC) and dry flash chromatography (DFC) were carried out using Merck silica gel 60 (230–400 mesh) and Sigma silica gel Type H (10–40 μm), respectively. Thin layer chromatography (TLC) was performed on precoated glass plates (Merck, silica gel 60, F254). The spots were detected using UV light (254 nm) or with a developing solution by charring on a hot plate. The developing solution was prepared by dissolving concentrated sulfuric acid (50 g), cerium(IV) sulfate (10 g), and phosphomolybdic acid hydrate (40 g) in water (1 L). Optical rotations were measured on a Elmer 241 Polarimeter (1 dm, 1 mL cell), all concentrations are given in g per 100 mL. Proton magnetic resonance (^{1}H NMR) and carbon magnetic resonance (^{13}C NMR) spectra were recorded on a Bruker AM-300 (300 MHz) spectrometer in chloroform-*d* solvent unless otherwise noted. Chemical shifts are reported in ppm of δ scale with TMS as the internal standard. Coupling constants (*J*) are reported to the nearest 0.5 Hz.

General procedure A

Diisopropylamine (0.17 mL, 1.20 mmol) was dissolved in THF (10 mL) and the solution was cooled to 0°C. *n*-BuLi (0.44 mL, 2.5 M solution in hexanes, 1.10 mmol) was added dropwise and the solution was stirred for 0.5 h at 0°C was cooled to –78°C, and then **1** (0.142 g, 1.00 mmol) in THF (0.5 mL) was added dropwise over 1 min. The resulting mixture was then stirred for 2 h. Next, the electrophile (1.20 mmol) was added. After 0.5 h, the reaction mixture was quenched with saturated aqueous $NaHCO_3$ solution (5 mL). The reaction mixture was then allowed to warm up to room temperature. Water was added (20 mL) and the mixture was extracted with diethyl ether (3 × 50 mL). The combined organic extracts were washed with saturated aqueous $NaHCO_3$ solution (1 × 20 mL), brine (1 × 20 mL), and dried ($MgSO_4$). The solvent was then removed (rotovap) and the product was purified by dry flash chromatography (hexane → hexane–ethyl acetate, 1:1).

General procedure B

Hydrochloride of the chiral amine **11** (1.10 mmol) was dissolved in THF (10 mL) and cooled to 0°C. *n*-BuLi (0.88 mL, 2.5 M solution in hexanes, 2.20 mmol) was added dropwise and the solution was stirred for 1.5 h. After cooling the amide solution to –78°C, compound **1** (0.142 g, 1.00 mmol) in THF (1.0 mL) was added dropwise over 0.5 h (syringe pump). The resulting mixture was then stirred for 2 h and the electrophile (1–1.2 mmol) in THF (1 mL) was added. After 0.5 h the reaction mixture was quenched with saturated aqueous $NaHCO_3$ solution (5 mL) and was then allowed to warm up to room temperature. Water was added (20 mL) and the mixture was extracted with diethyl ether or with chloroform (3 × 50 mL). The combined organic extracts were washed with saturated aqueous $NaHCO_3$ solution (1 × 20 mL), brine (1 × 20 mL), and dried ($MgSO_4$). The solvent was then removed. The amount of side product (e.g., **8**) and the ee of the main product (e.g., **7**) was next determined by ^{1}H NMR In experiments involving the aldol **7** samples were prepared by dissolving the product (2.5 mg) and the chiral solvating agent (*S*)-(+)-2,2,2-trifluoro-1-(9-anthryl)ethanol (TFAE, 10.0 mg) in C_6D_6 (0.5 mL). The signal at 5.07 ppm showed best splitting and was used to determine ee. The crude product was then purified by dry flash chromatography (hexane → hexane–ethyl acetate, 1:1).

8-Thiabicyclo[3.2.1]octan-3-one (1)

This compound was prepared according to the literature procedure (9*a*). Yield 50%. R_f = 0.3 (hexane–ethyl acetate,

© 2001 NRC Canada

4:1). ^{1}H NMR δ: 3.84–3.79 (m, 2H), 2.78 (dd, *J* = 20.0, 3.0 Hz, 2H), 2.65 (dd, *J* = 16.5, 3.0 Hz, 2H), 2.24–2.07 (m, 2H), 2.07–1.95 (m, 2H). ^{13}C NMR δ: 208.8, 52.8, 45.4, 34.2.

8-Thiabicyclo[3.2.1]oct-2-en-3-yl trimethylsilane (5a)

Diisopropylamine (1.19 mL, 8.40 mmol) was dissolved in THF (50 mL) and cooled to 0°C. *n*-BuLi (3.08 mL, 2.5 M solution in hexanes, 7.70 mmol) was added dropwise and the solution stirred for 0.5 h. After cooling the amide solution to –78°C, trimethylchlorosilane (2.14 mL, 16.80 mmol) was added followed by 8-thiabicyclo[3.2.1]octan-3-one (0.994 g, 7.00 mmol) in THF (5 mL). The resulting mixture was then stirred for 1 h at –78°C and then for 1 h at 0°C. The reaction mixture was then allowed to warm up to room temperature. The solvents and the excess of trimethylsilane were removed and the residue was dissolved in diethyl ether (100 mL). The solution was next washed with saturated aqueous $NaHCO_3$ solution (3 × 25 mL), brine (1 × 25 mL), and dried ($MgSO_4$). The solvent was then removed in vacuum and the product purified by dry flash chromatography (hexane → hexane–ethyl acetate, 4:1). The product was obtained as colorless semisolid (1.435 g, 96%). R_f = 0.59 (hexane–ethyl acetate, 4:1). ^{1}H NMR δ: 5.33 (d, *J* = 7.5 Hz, 1H), 3.89–3.80 (m, 1H), 3.69–3.60 (m, 1H), 2.68–2.56 (m, 1H), 2.38–2.12 (m, 2H), 2.10–1.82 (m, 3H), 0.13 (s, 9H). ^{13}C NMR δ: 150.0, 111.5, 45.6, 43.5, 43.3, 41.6, 34.4, 0.2.

8-Thiabicyclo[3.2.1]oct-2-en-3-ol acetate (5b)

Lithium enolate of 8-thiabicyclo[3.2.1]octan-3-one was generated according to the general procedure A. Acetic anhydride (0.13 mL, 1.25 mmol) was added to the enolate solution. The reaction mixture was stirred at –78°C for 1 h and then at 0°C for another 1 h. The reaction mixture was quenched with saturated aqueous $NaHCO_3$ solution (5 mL). The reaction mixture was then allowed to warm up to room temperature. Water was added (20 mL) and the mixture extracted with diethyl ether (3 × 50 mL). The combined organic extracts were washed with saturated aqueous $NaHCO_3$ solution (1 × 20 mL), brine (1 × 20 mL), and dried ($MgSO_4$). The solvent was then removed in vacuum and the product purified by dry flash chromatography (hexane → ethyl acetate). The product (0.177 g, 97%) was obtained as colorless semisolid. R_f = 0.37 (hexane–ethyl acetate, 4:1). EI-MS *m*/*z* (%): 184 (M^+, 40), 149 (28), 142 (100), 114 (25), 113 (53), 109 (27), 99 (18). HRMS calcd. for $C_9H_{12}O_2S$: 184.0558; found: 184.0559. IR (cm^{-1}): 1755, 1208, 1115. ^{1}H NMR δ: 5.90 (d, *J* = 7.5 Hz, 1H), 3.98–3.90 (m, 1H), 3.78–3.70 (m, 1H), 2.80–2.70 (m, 1H), 2.52–2.41 (m, 1H), 2.33–2.19 (m, 2H), 2.18–2.00 (m, 2H), 2.09 (s, 3H). ^{13}C NMR δ: 169.0, 147.8, 120.9, 45.2, 42.8, 40.9, 40.0, 34.2, 20.8.

2-Methoxycarbonyl-8-thiabicyclo[3.2.1]octan-3-one (6)

This compound was synthesized via lithium enolate of **1** as described in general procedure A. Methyl cyanoformate (0.10 mL, 1.25 mmol) was used as the electrophile. The product (0.180 g, 98%) was obtained as a clear oil, which was comprised of 3 isomers in a ratio of 52:15:33 (established by ^{1}H NMR integration of the OCH_3 signal). Since these compounds could not be separated due to easy equilibration, characterization was done on the acetate derivative. Compound **6** (0.180 g, 0.98 mmol) was dissolved in pyridine (5 mL) and acetic anhydride was added (1 mL). The reaction mixture was stirred at rt for 24 h. Next, water was added (20 mL) and the mixture was extracted with diethyl ether (3 × 50 mL). The combined organic extracts were washed with saturated aqueous $NaHCO_3$ solution (2 × 20 mL), brine (1 × 20 mL), and dried ($MgSO_4$). The solvent was then removed and the product was purified by dry flash chromatography (hexane → hexane–ethyl acetate, 1:1), which yielded a colorless oil (0.221 g, 98%). R_f = 0.23 (hexane–ethyl acetate, 1:1). EI-MS *m*/*z* (%): 242 (M^+, 9), 200 (64), 169 (18), 168 (100), 140 (22), 139 (10). HRMS calcd. for $C_{11}H_{14}O_4S$: 242.0613; found: 242.0607. IR (cm^{-1}): 1765, 1715, 1202, 1163. ^{1}H NMR δ: 4.38 (d, *J* = 5.0 Hz, 1H), 3.89–3.77 (m, 1H), 3.72 (s, 3H), 2.90–2.62 (m, 1H), 2.51–2.40 (m, 1H), 2.30 (dd, *J* = 18.5, 2.5 Hz, 1H), 2.24–2.10 (m, 2H), 2.17 (s, 3H), 2.08–1.97 (m, 1H). ^{13}C NMR δ: 168.4, 164.0, 155.9, 125.7, 51.8, 45.0, 44.0, 42.3, 40.8, 34.6, 20.8.

***exo*-2-(Hydroxybenzyl)-8-thiabicyclo[3.2.1]octan-3-one (7)**

Compound **7** was obtained as described in general procedure A and was further purified by using one of the following methods:

Method 1: The crude aldol product (containing some residual amine and bisaldol **8**) was taken in hexane (40 mL) and brought to reflux. The heating was removed and dichloromethane was added dropwise till the aldol product became soluble. The solution was left in an open flask for 3 h, after which time long needle crystals of **7** (76%) were collected.

Method 2: The crude aldol product was purified by dry flash chromatography (hexane → hexane–ethyl acetate, 1:1) which yielded pure **7** (90%) and **8** (6% when LDA was used as the base): mp 140–142°C. R_f = 0.38 (hexane–ethyl acetate, 1:1). EI-MS *m*/*z* (%): 248 (M^+, 24), 142 (100), 114 (21), 113 (44), 109 (18), 107 (34), 106 (21), 105 (34), 85 (20), 70 (43), 77 (60). HRMS calcd. for $C_{14}H_{16}O_2S$: 248.0871; found: 248.0868. IR (cm^{-1}): 3438, 1706, 1051. ^{1}H NMR ($CDCl_3$) δ: 7.47–7.28 (m, 5H), 5.13 (dd, *J* = 9.0, 2.5 Hz, 1H), 3.40 (s, 1H), 3.16–3.12 (m, 1H), 3.05–2.96 (m, 1H), 2.81 (d, *J* = 2.5 Hz, 1H), 2.75–2.71 (m, 1H), 2.71–2.66 (m, 1H), 2.10–1.82 (m, 4H). ^{1}H NMR (C_6D_6) δ: 7.39–7.30 (m, 2H), 7.28–7.03 (m, 3H), 5.07 (dd, *J* = 9.0, 3.0 Hz, 1H), 3.03–2.90 (m, 2H), 2.84 (d, *J* = 3.0 Hz, 1H), 2.58–2.47 (m, 2H), 2.23 (dd, *J* = 16.5, 3.0 Hz, 1H), 1.57–1.22 (m, 4H). ^{13}C NMR δ: 210.8, 141.0, 128.7, 128.3, 127.0, 75.3, 66.6, 51.6, 48.4, 45.8, 33.8 (2 signals). Note: optically active compound was synthesized using procedure B with chiral Li-amide **11d**. After one recrystallization the compound was enantiomerically pure: $[\alpha]_D^{25}$ +105.7 (*c* 2.04, CH_2Cl_2; c.f., ref. 15).

Compound 8

The lithium enolate of **1** (1.00 mmol) was generated as described in procedure A. Triisopropoxytitanium chloride (0.690 g, 3.00 mmol) was added and the mixture was kept at –78°C for 1 h, warmed up to 0°C and cooled again to –78°C. Benzaldehyde (3.00 mmol, 0.31 mL) was added and the mixture was stirred for another 4 h. The reaction was quenched with water (20 mL), extracted with diethyl ether (3 × 50 mL), dried with anhydrous $MgSO_4$, and

© 2001 NRC Canada

the solvent was evaporated. The ratio of **7**:**8** (18:82) was measured by ^{1}H NMR. The crude mixture was purified by dry flash chromatography (dichloromethane → dichloromethane–ethyl acetate, 1:1), which yielded pure **8** as a white solid (0.217 g, 61%) and pure **7** (0.038 g, 13%).

Properties of **8**: mp 162–164°C. R_f = 0.59 (hexane–ethyl acetate, 1:1). CI-MS (NH_3) *m*/*z* (%): 304 (27), 232 (17), 231 (87), 162 (63), 160 (19), 143 (16), 142 (80), 124 (20), 114 (50), 109 (15), 106 (24), 105 (100), 94 (29), 91 (14), 81 (15), 78 (23), 77 (24), 74 (19), 61 (65). IR (cm^{-1}): 3510, 1701, 1190, 1050. ^{1}H NMR δ: 7.50–7.28 (m, 10H), 5.45 (d, *J* = 9.5 Hz, 2H), 3.20–3.10 (m, 2H), 2.85 (d, *J* = 8.0 Hz, 2H), 2.07–1.80 (m, 6H). ^{13}C NMR δ: 210.5, 141.2, 128.8, 128.5, 127.0, 75.9, 68.0, 48.9, 33.4.

Compound 9

8-Thiabicyclo[3.2.1]oct-2-en-3-yl trimethylsilane (**5a)** (0.320 g, 1.50 mmol) was dissolved in dichloromethane (10 mL), the solution was cooled down to –78°C, and $TiCl_4$ (0.17 mL, 1.50 mmol) was added. The mixture was stirred for 1 h at –78°C and then for 2 h at 0°C. The reaction was then quenched with saturated solution of $NaHCO_3$ (10 mL). Diethyl ether (100 mL) was added, and the organic phase was separated and washed with saturated $NaHCO_3$ (2 × 25 mL), brine (25 mL), and dried with $MgSO_4$. The solvent was evaporated under vacuum and the product was subjected to dry flash chromatography (hexane → hexane–ethyl acetate, 4:1), which yielded two products: **1** (0.037 g, 17%) and **9** (0.150 g, 70%).

Properties of **9**: mp 135–137°C. R_f = 0.19 (hexane–ethyl acetate, 4:1). EI-MS *m*/*z* (%): 284 (M^+, 8), 266 (60), 233 (28), 142 (100), 114 (35), 99 (24), 85 (68), 69 (82). HRMS calcd. for $C_{14}H_{20}O_2S_2$: 284.0905; found: 284.0909. IR (cm^{-1}): 3435, 1696, 1052. ^{1}H NMR δ: 4.18–4.05 (br s, 1H), 3.96–3.87 (m, 1H), 3.83–3.75 (m, 1H), 3.71–3.63 (m, 1H), 3.61–3.52 (m, 1H), 2.88–2.77 (m, 1H), 2.66–1.77 (m, 14H). ^{13}C NMR δ: 208.7, 72.9, 68.7, 53.3, 46.8, 46.5, 46.3, 45.9, 45.8, 45.5, 33.8, 33.4, 33.0, 32.9.

(–)-2-Cinnamoyl-8-thiabicyclo[3.2.1]octan-3-one (13)

Lithium enolate of **1** (0.5 mmol) was prepared as described in procedure B (base **11d**). After stirring at –78°C for 3 h, cinnamoyl cyanide (100 mg, 0.60 mmol) in THF (1 mL) was added to the enolate, and the resulting mixture was stirred at –78°C for 30 min, followed by quenching with 40% K_2CO_3 (2 mL). After warming up to rt, the reaction mixture was extracted with $CHCl_3$ (3 × 10 mL). The combined extracts were dried over $MgSO_4$ and the solvent was removed under vacuum. Column chromatography (SiO_2, hexane–ethyl acetate, 4:1) afforded the pure product **13** as a yellow oil (83 mg, 61%). This product had 87% ee as determined by NMR with (*S*)-(+)-TFAE. $[\alpha]_D^{25}$ –330 (*c* 0.99, MeOH). R_f = 0.40 (hexane–ethyl acetate, 4:1). HRMS calcd. for $C_{16}H_{16}O_2S$: 272.0871; found: 272.0866. IR (cm^{-1}): 1626, 1576, 1558, 1540. ^{1}H NMR δ: 7.67 (d, *J* = 15.5 Hz, 1H), 7.60–7.54 (m, 2H), 7.43–7.33 (m, 3H), 7.01 (d, *J* = 15.5 Hz, 1H), 4.56–4.49 (m, 1H), 3.92–3.78 (m, 1H), 3.00 (dd, *J* = 19.0, 6.0 Hz, 1H), 2.58 (dd, *J* = 19.0, 2.0 Hz, 1H), 2.40–2.20 (m, 4H), 2.10–1.93 (m, 1H). ^{13}C NMR δ: 199.3, 169.8, 140.9, 135.3, 129.9, 128.8, 127.9, 117.6, 116.5, 48.8, 44.4, 44.0, 40.0, 34.5.

5,5-Dimethyl-6-oxa-12-thia-tricyclo[7.2.1.0^{2,7}]dodec-2(7)-en-3-one (17)

Lithium enolate of **1** (0.5 mmol) was prepared according to procedure B (base **11d**). Senecioyl cyanide (0.055 mL, 0.72 mmol) in THF (1 mL) was added, and the resulting mixture was stirred at –78°C for 30 min, followed by quenching with 40% K_2CO_3 (2 mL). After warming up to rt the reaction mixture was extracted with ether (3 × 10 mL). The combined extracts were dried over $MgSO_4$ and the solvent was removed under vacuum to give the crude product **16**. Compound **16** was subjected to cyclization without purification: the entire sample was dissolved in EtOH (7 mL), anhydrous Na_2CO_3 (0.14 g) was added, and the mixture was heat at reflux for 1 h. The solvent was then removed under vacuum, the residue was taken in ether and the carbonate was filtered off. Column chromatography (hexane–EtOAc, 4:1) afforded the product **17** as a white solid (91 mg, 81%). This sample had 92% ee as determined by HPLC using a ChiraDex 250–4 column (Merck), an UV detector (at 254 nm) in 50% MeOH – phosphate buffer (pH = 6.8, *c* = 0.025 M), flow: 0.4 mL min^{-1}. mp 90–92°C (note: racemate mp 75–77°C). $[\alpha]_D^{25}$ –94.1 (*c* 1.03, MeOH). R_f = 0.20 (hexane–EtOAc, 4:1). EI-MS *m*/*z* (%): 224 (100), 209 (76), 168 (26), 155 (13), 140 (44), 135 (11), 97 (12), 85 (10), 83 (10), 79 (17), 71 (23). IR (cm^{-1}): 1652, 1603. ^{1}H NMR δ: 1.35 (s, 3H), 1.37 (s, 3H), 1.80–1.88 (m, 1H), 2.10–2.31 (m, 4H), 2.42 (d, *J* = 16.6 Hz, 1H), 2.49 (d, *J* = 16.6 Hz, 1H), 2.79 (dq, *J* = 18.6, 2.1 Hz, 1H), 3.87(m, 1H), 4.55 (m,1H). ^{13}C NMR δ: 25.8, 27.2, 34.4, 40.1, 40.6, 42.3, 45.0, 47.3, 80.5, 119.5, 168.4, 188.3. Anal. calcd. for $C_{12}H_{16}O_2S$: C 64.26, H 7.19; found: C 64.47, H 7.17.

5-Methyl-6-oxa -12-thia-tricyclo[7.2.1.0^{2,7}]dodeca-2(7)-4-dien-3-one (15)

Lithium enolate of **1** (0.5 mmol) was generated according to procedure B (base **11d**). 2-Bromo-2-butenoyl cyanide (95 mg, 97%, 0.53 mmol) in THF (1 mL) was then added and the resulting mixture was stirred at –78°C for 30 min. followed by quenching with 40% K_2CO_3 (2 mL). After warming up to rt the reaction mixture was extracted with ether (3 × 10 mL). The combined extracts were dried over $MgSO_4$ and the solvent was removed under vacuum to give the crude product **14** that was refluxed over 3 h in triethylamine (5 mL). The solvent (Et_3N) was then removed under vacuum. The residues were basified with 40% K_2CO_3 (10 mL) and extracted with ether (3 × 10 mL). The extracts were dried over $MgSO_4$. After removal of the solvent, column chromatography afforded the product as oil (53 mg, 51%). This sample had 87% ee as determined by ^{1}H NMR with (*S*)-(+)-TFAE. R_f = 0.50 (CH_2Cl_2–MeOH, 9:1). EI-MS *m*/*z* (%): 208 (100), 180 (65), 179 (34), 175 (55), 161 (13), 91 (9),77 (5). HRMS calcd. for $C_{11}H_{12}O_2S$: 208.0557 (M^+); found: 208.0558. IR (cm^{-1}): 1659, 1611, 1596. ^{1}H NMR δ: 1.82–1.93 (m, 1H), 2.16 (s, 3H), 2.10–2.40 (m, 3H), 2.52 (dd, *J* = 18.1, 2.3 Hz, 1H), 3.08 (dq, *J* = 18.1, 2.1 Hz, 1H), 3.95 (m, 1H), 4.67 (d, *J* = 4.9 Hz, 1H), 6.03 (s, 1H). ^{13}C NMR δ: 20.0, 34.6, 39.8, 40.4, 40.5, 44.9, 113.5, 129.6, 162.3, 165.1, 176.1. Note:

© 2001 NRC Canada

racemic **15** produced via an analogous synthesis using LDA (mp 89–91°C).

Acknowledgments

The authors thank Natural Sciences and Engineering Research Council of Canada (NSERC) and the University of Saskatchewan for financial support of this project (for a preliminary communication, see ref. 22).

References

1. M. Lounasmaa. The Alkaloids, **44**, 1 (1993).
2. M. Majewski. *In* Advances in asymmetric synthesis. Vol. 3. *Edited by* A. Hassner. JAI Press, London. 1998. p. 39–76.
3. M. Majewski and R. Lazny. J. Org. Chem. **60**, 5825 (1995).
4. M. Majewski, R. Lazny, and A. Ulaczyk. Can. J. Chem. **75**, 754 (1997).
5. M. Majewski and R. Lazny. Synlett, 785 (1996).
6. J.C. Lee, K. Lee, and J.K. Cha. J. Org. Chem. **65**, 4773 (2000).
7. (*a*) D.P. Williams, P. Munir, D.J. Naisbitt, J.P. Uetrecht, and B.K. Park. Mol. Pharmacol. **58**, 207 (2000); (*b*) C.R. Schmidt, J.P. Sluka, K.M. Duke, and A.W. Glasebrook. Bioorg. Med. Chem. Lett. **9**, 523 (1999); (*c*) T. Morie, S. Kato, H. Harada, N. Yoshida, I. Fujiwara, and J. Matsumoto. Chem. Pharm. Bull. **43**, 1137 (1995).
8. (*a*) Z.Q. Wang, Y.H. Kuo, D. Schnurr, J.P. Bowen, S.Y. Liu, F.S. Han, J.Y. Chang, Y.C. Cheng, and K.H. Lee. J. Med. Chem. **33**, 2660 (1990); (*b*) J.R. Luly, N. Yi, J. Soderquist, H. Stein, J. Cohen, T.J. Perun, and J.J. Plattner. J. Med. Chem. **30**, 1609 (1987); (*c*) K.S. Atwal, J.L. Bergey, A. Hedberg, and S. Moreland. J. Med. Chem. **30**, 635 (1987); (*d*) M. Kolb, C. Danzin, J. Barth, and N. Claverie. J. Med. Chem. **25**, 550 (1982).
9. (*a*) A.J. Parr, N.J. Walton, S. Bensalem, P.H. McCabe, and W. Routledge. Phytochemistry, **30**, 2607 (1991); (*b*) E. Leete, J.A. Bjorklund, M.M. Couladis, and S.H. Kim. J. Am. Chem. Soc. **113**, 9286 (1991); (*c*) T. Hashimoto, K. Nakajima, G. Ongena, and Y. Yamada. Plant. Physiol. **100**, 836 (1992).
10. (*a*) P.J. O'Brien. J. Chem. Soc. Perkin Trans. 1, 1439 (1998); (*b*) K. Koga. Pure Appl. Chem. **66**, 1487, 1994; (*c*) P.J. Cox and N.S. Simpkins. Tetrahedron: Asymmetry, **2**, 1 (1991).
11. (*a*) R. Shirai, M. Tanaka, and K. Koga J. Am. Chem. Soc. **108**, 543 (1986); (*b*) M. Majewski and J. MacKinnon. Can. J. Chem. **72**, 1699 (1994).
12. M. Majewski, R. Lazny, and P. Nowak. Tetrahedron Lett. **36**, 5465 (1995).
13. (*a*) P.J. Cox, A. Persad, and N.S. Simpkins. Synlett, 194 (1992); (*b*) R. Armer, M.J. Begley, P. Cox, A. Persad, and N.S. Simpkins. J. Chem. Soc. Perkin Trans. 1, **19**, 3105 (1993).
14. M. Lautens, E. Fillion, and M. Sampat. J. Org. Chem. **62**, 7080 (1997).
15. P. Coggins, S. Gaur, and N.S. Simpkins. Tetrahedron Lett. **36**, 1545 (1995).
16. M. Murakata, M. Nakajima, and K. Koga. J. Chem. Soc. Chem. Commun. 1657 (1990).
17. C.H. Heathcock. *In* Asymmetric synthesis. Vol. 3. *Edited by* J.D. Morrison. Academic Press, Toronto. 1984. Chap. 2. p. 111.
18. I. Paterson. *In* Comprehensive organic synthesis. Vol. 2. *Edited by* C.H. Heathcock. Pergamon, Oxford. 1991. Chap. 1.9. p. 305.
19. (*a*) M.M.M. Rubinger and J. Mann. J. Chem. Res. Synop. **7**, 454, 1999; (*b*) L.C.A. Barbosa, M.M.M. Rubinger, J. Mann, and H.L. Mansell. Tetrahedron, **52**, 11297 (1996); (*c*) I. Stohrer, H. Hoffman, and R. Martin. Tetrahedron, **48**, 6021 (1992).
20. K. Aoki and K. Koga. Tetrahedron Lett. **38**, 2505 (1997) and refs. therein.
21. (*a*) M. Majewski and P. Nowak. Synlett, 1447 (1999); (*b*) M. Majewski and P. Nowak. J. Org. Chem. **65**, 5152 (2000).
22. M. Majewski, M. DeCaire, P. Nowak, and F. Wang. Synlett, 1321 (2000).

© 2001 NRC Canada

The use of palladium chloride as a precatalyst for the amination of aryl bromides

Xiao-Xiang Zhang, Michele C. Harris, Joseph P. Sadighi, and Stephen L. Buchwald

Abstract: The use of palladium chloride as a precatalyst for the amination of aryl bromides is reported. To overcome the poor solubility of palladium chloride in commonly used solvents, a procedure was developed in which $PdCl_2$ was preheated with neat amine in the presence of a phosphine ligand before the addition of the other reaction components. This protocol is effective for a broad range of substrate combinations using several types of phosphine ligands.

Key words: palladium chloride, amination, aryl bromide, phosphine ligand.

Résumé : On démontre l'utilité du chlorure de palladium comme précatalyseur pour l'amination de bromures d'aryle. Pour surmonter la piètre solubilité du chlorure de palladium dans les solvants normalement utilisés, on a mis au point une procédure dans laquelle le $PdCl_2$ est préchauffé avec de l'amine pure, en présence d'un ligand phosphine, avant l'addition des autres réactifs. Ce protocole est efficace pour un large spectre de combinaisons de substrats faisant appel à plusieurs types de ligands phosphines.

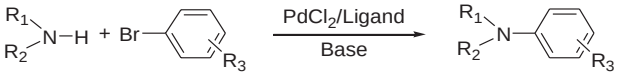
Mots clés : chlorure de palladium, amination, bromure d'aryle, ligand phosphine.

[Traduit par la Rédaction]

Introduction

The palladium-catalyzed amination of aryl halides and triflates has proven to be a useful method for the formation of carbon–nitrogen bonds and has found numerous applications (1), including the synthesis of natural products (2), biologically and pharmaceutically important compounds (3), and new ligands and materials (4). A variety of amines can be coupled with aryl halides and aryl triflates when a palladium precatalyst is combined with an appropriate phosphine ligand (5–9, and for the use of other electron-rich bulky phosphine ligands for amination reactions, see ref. 10).

We have commonly employed $Pd_2(dba)_3$ and $Pd(OAc)_2$ as precatalysts in our C–N bond-forming protocol. Although $PdCl_2$ is readily available and cheaper than $Pd(OAc)_2$ and $Pd_2(dba)_3$, it hasn't found wide application in Pd-catalyzed cross-coupling methodology, due to its insolubility in commonly used solvents. We have found that when $PdCl_2$ and a suitable ligand are preheated in the neat amine prior to the addition of other reaction components until a homogeneous solution was obtained, the coupling reactions proceed smoothly (for a recent report that described the use of $PdCl_2$ for amination, see ref. 11). Using this new protocol, we have demonstrated that $PdCl_2$ is an efficient palladium source for the arylation of primary anilines and other amines with aryl bromides (eq. [1]); the results are summarized in Tables 1 and 2.

[1] 

The chelating ligand bis[2-(diphenylphosphino)phenyl] ether (DPEphos) has been recently demonstrated to be an effective ligand for the palladium-catalyzed aryl amination reaction (6, 12). Most of the reactions with $PdCl_2$ were carried out using DPEphos as the supporting ligand. Typically, reactions were performed in toluene at 80 or 100°C using 0.5 mol% $PdCl_2$ (L/Pd = 1.5) in the presence of 1.4 equiv. of base, NaO-*t*-Bu. The $PdCl_2$ and DPEphos were first heated with the arylamine under an inert atmosphere to generate a clear solution, followed by sequential addition of aryl bromide and the base. Using this procedure, most reactions proceed to completion in ≤18 h. The results (Table 1) indicate that the combination of $PdCl_2$ and DPEphos is as active as $Pd(OAc)_2$–DPEphos (6) or $Pd(OAc)_2$–BINAP (5) for the amination of the examples listed.

Both *para*- and *otho*-substituted anilines can been efficiently coupled with electron-neutral or electron-rich bromides (Table 1, entries 1–4). As was the case for the $Pd(OAc)_2$–DPEphos system (6), the combination of $PdCl_2$ and a chelating phosphine can be used to effect couplings of highly steric substrates. For example, the sterically demanding 2,6-diisopropylaniline can be coupled with 2-methylbromobenzene in 96% yield (Table 1, entry 10). When 4-bromochlorobenzene was used (Table 1, entry 9), 2,6-diisopropylaniline was chemoselectively coupled with

Received April 2, 2001. Published on the NRC Research Press Web site at http://canjchem.nrc.ca on November 19, 2001.

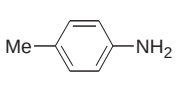
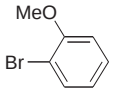
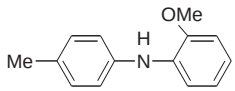
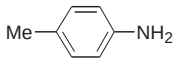
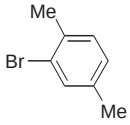
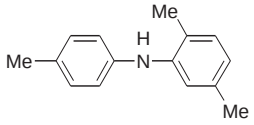
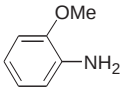
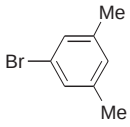
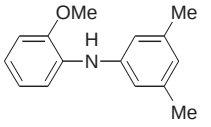
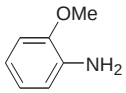
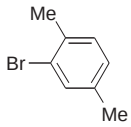
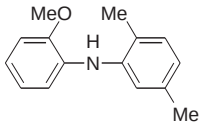
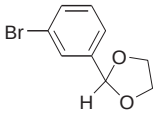
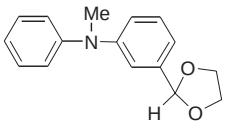
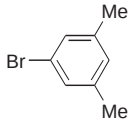
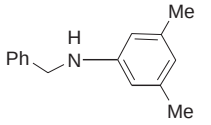
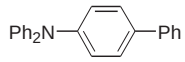
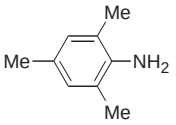
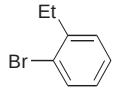
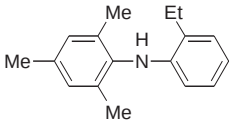
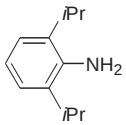
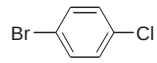
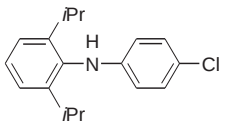
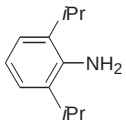
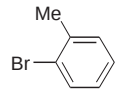
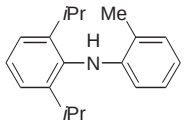
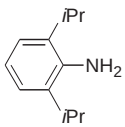
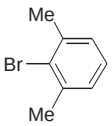
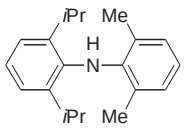
Dedicated with respect and affection to Professor Victor Snieckus; a great chemist and worthy role model.

X.-X. Zhang, M.C. Harris, J.P. Sadighi, and S.L. Buchwald.[1] Department of Chemistry, Massachusetts Institute of Technology, Cambridge, MA 02139, U.S.A.

[1]Corresponding author (telephone: (617) 253-1885; fax: (617) 253-3297; e-mail: sbuchwal@mit.edu).

 DOI: 10.1139/cjc-79-11-1799 © 2001 NRC Canada

Table 1. Catalytic amination of aryl bromides using $PdCl_2$ and bisphosphine ligands.

Entry	Amine	Bromide	Product	mol % $PdCl_2$	Ligand (L/Pd)	Time[a] (h)	Yield[b] (%)
1				0.5	DPEphos (1.5)	3	97
2				0.5	DPEphos (1.5)	17	98
3				0.5	DPEphos (1.5)	17	97
4				0.5	DPEphos (1.5)	4	93
5				0.5	Xantphos (1.5)	4	92
6				0.5	BINAP (1.5)	3	87
7				1.0	DPEphos (1.5)	18	85[c]
8				0.5	DPEphos (1.5)	18	97
9				0.5	DPEphos (1.5)	18	98[c]
10				0.5	DPEphos (1.5)	18	96[c]
11				5.0	DPEphos (1.5)	18	91[c]

Note: Reactions were run at 80°C with ArBr (1.0 equiv.), $Ar'NH_2$ (1.2 equiv.), NaO-*t*-Bu (1.4 equiv.), cat. $PdCl_2$, and cat. ligand. Concentration: 2 mL toluene per mmol ArBr.

[a]Reaction times have not been optimized.

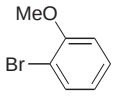
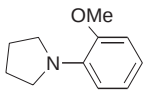
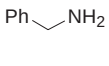
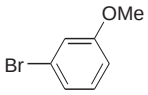
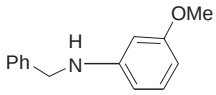
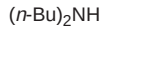
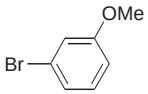
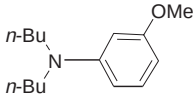
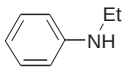
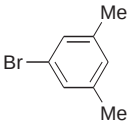
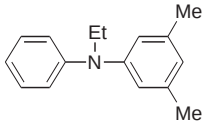
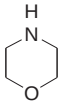
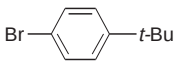
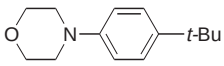
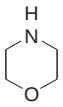
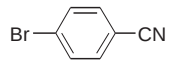
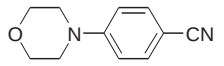
[b]Yields represent isolated yields (average of two runs) of compounds estimated to be >95% pure by ^1H NMR, GC, and for new compounds, combustion analysis.

the bromide. With a higher catalyst loading (5 mol%), a very hindered diarylamine was prepared in 91% yield from the coupling of 2,6-diisopropylaniline with 2-bromo-*m*-xylene (Table 1, entry 11). Secondary anilines (Table 1, entries 5 and 7) and benzyl amine (entry 6) are also suitable coupling partners under similar reaction conditions.

In addition to DPEphos, $PdCl_2$ can also be used with a number of other commonly employed phosphine ligands for

© 2001 NRC Canada

Table 2. Catalytic amination of aryl bromides using $PdCl_2$ and monophosphine ligands.

Entry	Amine	Bromide	Product	mol % $PdCl_2$	Ligand[a] (L/Pd)	Time[b] (h)	Yield[c] (%)
1				1.0	**1** (1.5)	43	65
2				1.0	**1** (1.5)	23	93
3				1.0	**1** (1.5)	21	83
4				0.5	**1** (1.5)	28	72
5				1.0	**1** (1.5)	21	93
6				3.0	**2** (1.5)	28	74[d]

Note: Reactions were run at 80°C with ArBr (1.0 equiv.), Ar′NH_2 (1.2 equiv.), NaO-*t*-Bu (1.4 equiv.), cat. $PdCl_2$, and cat. ligand. Concentration: 2 mL toluene per mmol ArBr.

[a]**1**: 2-(di-*tert*-butylphosphino)biphenyl; **2**: 2-(dicyclohexylphosphino)biphenyl.

[b]Reaction times have not been optimized.

[c]Yields represent isolated yields (average of two runs) of compounds estimated to be >95% pure by ^{1}H NMR, GC, and for new compounds, combustion analysis.

[d]The reaction was conducted at 100°C using K_3PO_4 as the base and DME as the solvent.

catalyzing C–N bond forming reactions, as is shown for the bisphosphine ligands Xantphos (Table 1, entry 5) and BINAP (entry 6) as well as for biphenyl-based electron-rich bulky monophosphine ligands (Fig. 1) (9) 2-(di-*tert*-butylphosphino)biphenyl (**1**) and 2-(dicyclohexylphosphino)-biphenyl (**2**) (Table 2). By applying the combination of $PdCl_2$ and **1** or **2**, secondary cyclic amines such as pyrrolidine and morpholine can be effectively coupled with electron-rich (Table 2, entry 1), -neutral (entry 5), and -poor (entry 6) aryl bromides to afford the corresponding desired products in good to excellent yields. Acyclic primary (Table 2, entry 2) and secondary (entry 3) amines as well as *N*-ethylaniline (entry 4) are also suitable for coupling with aryl bromides. When the weak base K_3PO_4 was used instead of NaO-*t*-Bu, 4-bromobenzonitrile was successfully coupled with morpholine to give *N*-(4-cyanophenyl)-morpholine in good yield in DME at 100°C using a combination of $PdCl_2$ (3.0 mol%) and **2** (Table 2, entry 6).

In conclusion, we have demonstrated a procedure to use $PdCl_2$ in the amination of aryl bromides. This protocol was successfully applied with several different phosphine ligands and substrate combinations. In general, the effectiveness of the use of $PdCl_2$ as a precatalyst in the amination of aryl bromides is comparable with $Pd(OAc)_2$ and $Pd_2(dba)_3$ when the common bisphosphine ligands are applied. However, at present, it is less effective when the biphenyl-based electron-rich bulky monophosphine ligands are employed. This causes it to be ineffective for the amination of aryl chlorides, as indicated by our preliminary results. The reason for these limitations will be the subject of future research in our laboratory.

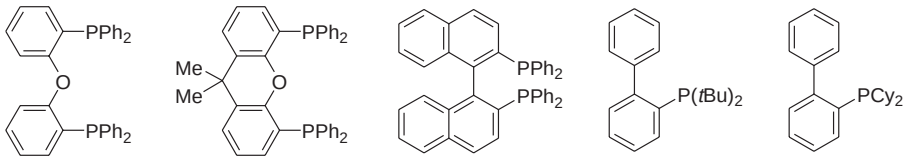
Experimental

General

All reactions were carried out under an argon atmosphere in oven-dried glassware. Elemental analyses were performed by Atlantic Microlabs Inc., Norcross, GA. Toluene was distilled under nitrogen from molten sodium. Aryl halides were purchased from commercial sources and were used without further purification. Amines were purchased from commercial sources and were passed through alumina before use. DPEphos and Xantphos were prepared as previously described (6, 7). Palladium chloride, *rac*-BINAP, **1**, and **2** were purchased from Strem Chemical company. Sodium *tert*-

© 2001 NRC Canada

Fig. 1. Structures of chelating ligands and biphenyl-based electron-rich bulky monophosphine ligands.



butoxide was purchased from Aldrich; the bulk of this material was stored under nitrogen in a Vacuum Atmospheres glovebox, small portions (1–2 g) were removed from the glovebox in glass vials, stored in the air in desiccators filled with anhydrous calcium sulfate, and weighed in the air. Proton and carbon nuclear magnetic resonance spectra (^{1}H and ^{13}C NMR) were recorded on a Varian Mercury 300 spectrometer and referenced with respect to TMS internal standard. Infrared spectra were obtained using a PerkinElmer 1600 Series FT-IR spectrometer. Samples were prepared as films on NaCl plate by evaporating $CHCl_3$ solutions. High-resolution mass spectroscopy (HRMS) was performed by the MIT Department of Chemistry Instrumentation Facility on a Finnigan MAT system 8200 double-focusing sector mass spectrometer using electron impact (EI) ionization technique. Yields in Tables 1 refer to isolated yields (average of two runs) of compounds estimated to be >95% pure as determined by ^{1}H NMR and GC analysis or combustion analysis.

General procedure

Arylamine (2.40 mmol), $PdCl_2$ (1.8 mg, 0.010 mmol, 0.5 mol%), and bisphosphine (0.015 mmol, 0.75 mol%) were placed in a dried, resealable Schlenk tube, which was fitted with a Teflon screwcap, evacuated, and backfilled with argon. The tube was sealed, and its contents were heated at 80°C until a clear solution formed (ca. 30 min). The tube was then cooled to room temperature, and the Teflon screwcap was replaced with a rubber septum. Toluene (2 mL) was added via syringe, followed by aryl bromide (2.00 mmol). The resulting solution was stirred for a few seconds, then the septum was removed. Sodium *tert*-butoxide was added, then the septum was replaced. An additional portion of toluene (2 mL) was added to wash into the reaction any base adhering to the side of the tube. The tube was purged with argon for 3 min, then the septum was replaced with the Teflon screwcap. The tube was sealed, and its contents were heated at 80°C with stirring until the starting aryl bromide was completely consumed as judged by GC analysis. The reaction mixture was then cooled to room temperature, taken up in diethyl ether (50 mL), and washed with brine (30 mL). The resulting solution was dried over anhydrous potassium carbonate, filtered, and concentrated in vacuo. The crude product was purified by flash column chromatography on silica gel.

N-(*p*-Tolyl)-*o*-anisidine (Table 1, entry 1) (13)

The general procedure was used for coupling *p*-toluidine with 2-bromoanisole, using DPEphos as the supporting ligand and a reaction time of 3 h. The title compound was isolated as a colorless oil (413 mg, 97%). EI-HRMS calcd. for $C_{14}H_{15}NO$: 213.1154; found: 213.1158 (M^+). IR (film, cm^{-1}): 3411, 3022, 2937, 2862, 2834, 1600, 1519, 1243, 740. ^{1}H NMR (300 MHz, $CDCl_3$) δ: 7.21–7.18 (m, 1H), 7.09–7.02 (m, 4H), 6.86–6.75 (m, 3H), 6.05 (s, 1H), 3.85 (s, 3H), 2.29 (s, 3H). ^{13}C NMR (75 MHz, $CDCl_3$) δ: 147.9, 139.9, 133.9, 131.1, 129.9, 120.9, 119.7, 119.3, 113.8, 110.4, 55.7, 21.0.

N-(*p*-Tolyl)-2,5-dimethylaniline (Table 1, entry 2) (13)

The general procedure was used for the coupling of *p*-toluidine with 2-bromo-*p*-xylene, using DPEphos as the supporting ligand and a reaction time of 17 h. The title compound was obtained as an orange solid (414 mg, 98%): mp 49–50°C. EI-HRMS calcd. for $C_{15}H_{17}N$: 211.1361; found: 211.1356 (M^+). IR (film, cm^{-1}): 3414, 3020, 2917, 2862, 1610, 1577, 1526, 1511, 814, 800. ^{1}H NMR (300 MHz, $CDCl_3$) δ: 7.06 (d, J = 8.1 Hz, 2H), 7.02 (d, J = 7.5 Hz, 1H), 6.98 (s, 1H), 6.89 (d, J = 8.1 Hz, 2H), 6.68 (d, J = 7.5 Hz, 1H), 5.23 (s, 1H), 2.29 (s, 3H), 2.24 (s, 3H), 2.19 (s, 3H). ^{13}C NMR (75 MHz, $CDCl_3$) δ: 141.9, 141.2, 136.5, 130.7, 130.4, 129.9, 124.0, 121.9, 118.8, 118.0, 21.5, 21.0, 17.7.

N-(2-Methoxyphenyl)-3,5-dimethylaniline (Table 1, entry 3) (6)

The general procedure was used for the coupling of *o*-anisidine with 5-bromo-*m*-xylene, using DPEphos as the supporting ligand and a reaction time of 17 h. The title compound was obtained as a pale yellow oil (443 mg, 97%). EI-HRMS calcd. for $C_{15}H_{17}NO$: 227.1310; found: 227.1304 (M^+). IR (film, cm^{-1}): 3411, 3024, 3001, 2939, 2916, 2855, 2833, 1590, 1520, 1494, 1463, 829, 742. ^{1}H NMR (300 MHz, $CDCl_3$) δ: 7.30–7.27 (m, 1H), 6.87–6.82 (m, 3H), 6.77 (s, 2H), 6.58 (s, 1H), 6.06 (s, 1H), 3.84 (s, 3H), 2.27 (s, 3H), 2.26 (s, 3H). ^{13}C NMR (75 MHz, $CDCl_3$) δ: 148.2, 142.7, 139.0, 133.2, 123.1, 120.9, 119.7, 116.4, 114.9, 110.5, 55.8, 21.7.

N-(2-Methoxyphenyl)-2,5-dimethylaniline (Table 1, entry 4) (6, 9*c*)

The general procedure was used for the coupling of *o*-anisidine with 2-bromo-*p*-xylene, using DPEphos as the supporting ligand and a reaction time of 4 h. The title compound was isolated as a white solid (424 mg, 93%): mp 88.5–90.5°C. EI-HRMS calcd. for $C_{15}H_{17}NO$: 227.1310; found: 227.1306 (M^+). IR (film, cm^{-1}): 3409, 3061, 3042, 3003, 2962, 2930, 2833, 1560, 1573, 740. ^{1}H NMR (300 MHz, $CDCl_3$) δ: 7.12 (s, 1H), 7.07 (d, J = 7.6 Hz, 1H), 7.01 (dd, J = 6.9, 2.4 Hz, 1H), 6.88–6.77 (m, 3H), 6.75 (d, J = 7.6 Hz, 1H), 5.82 (s, 1H), 3.87 (s, 3H), 2.27 (s, 3H), 2.21 (s, 3H). ^{13}C NMR (75 MHz, $CDCl_3$) δ: 148.0, 140.6,

© 2001 NRC Canada

136.4, 134.0, 130.8, 126.3, 123.1, 120.9, 120.3, 119.2, 114.5, 110.4, 55.8, 21.5, 17.7.

2-[3-(*N*-Methylanilino)phenyl]-1,3-dioxolane (Table 1, entry 5)

The general procedure was used for the coupling of *N*-methylaniline with 2-(3-bromophenyl)-1,3-dioxolane, using Xantphos as the supporting ligand and a reaction time of 4 h. The title compound was isolated as a colorless oil (470 mg, 92%). EI-HRMS calcd. for $C_{16}H_{17}NO_2$: 255.1259; found: 255.1264 (M^+). IR (film, cm^{-1}): 3058, 3035, 2950, 2884, 2815, 1609, 1595, 1585, 1496, 696. ^{1}H NMR (300 MHz, $CDCl_3$) δ: 7.29–7.21 (m, 3H), 7.12 (m, 1H), 7.06–6.92 (m, 5H), 5.73 (s, 1H), 4.12–3.96 (m, 4H), 3.31 (s, 3H). ^{13}C NMR (75 MHz, $CDCl_3$) δ: 149.1, 148.9, 139.0, 129.3, 129.2, 121.7, 121.0, 120.9, 119.1, 117.8, 103.9, 65.4, 40.5. Anal. calcd. for $C_{16}H_{17}NO_2$: C 75.27, H 6.71; found: C 75.36, H 6.75.

***N*-(3,5-Dimethylphenyl)-benzylamine (Table 1, entry 6) (14)**

The general procedure was used for the coupling of benzylamine with 5-bromo-*m*-xylene, using *rac*-BINAP as the supporting ligand and a reaction time of 3 h. The title compound was isolated as a colorless oil (368 mg, 87%). EI-HRMS calcd. for $C_{15}H_{17}N$: 211.1361; found: 211.1354 (M^+). IR (film, cm^{-1}): 3409, 3027, 2915, 2856, 1603, 1512, 1494, 1473, 1452, 1337, 1182, 821. ^{1}H NMR (300 MHz, $CDCl_3$) δ: 7.35–7.21 (m, 5H), 6.36 (s, 1H), 6.25 (s, 2H), 4.26 (s, 2H), 3.84 (br s, 1H), 2.21 (s, 6H). ^{13}C NMR (75 MHz, $CDCl_3$) δ: 148.4, 139.7, 139.0, 128.7, 127.6, 127.2, 119.7, 110.8, 48.5, 21.8.

4-(Diphenylamino)biphenyl (Table 1, entry 7) (15)

The general procedure was used for the coupling of diphenylamine with 4-bromobiphenyl, using DPEphos as the supporting ligand and a reaction time of 18 h. The reaction was conducted at 100°C with 1.0 mol% $PdCl_2$ and 1.5 mol% DPEphos. The title compound was isolated as white crystals (553 mg, 86%): mp 111–112°C. EI-HRMS calcd. for $C_{24}H_{19}N$: 321.1518; found: 321.1509 (M^+). IR (film, cm^{-1}): 3058, 3030, 1589, 1519, 1485, 1280, 747, 693. ^{1}H NMR (300 MHz, $CDCl_3$) δ: 7.58–7.52 (m, 2H), 7.48–7.36 (m, 4H), 7.31–7.20 (m, 5H), 7.12 (d, J = 7.5 Hz, 6H), 7.01 (t, J = 7.2 Hz, 2H). ^{13}C NMR (75 MHz, $CDCl_3$) δ: 147.7, 147.2, 140.7, 135.2, 129.4, 128.8, 127.9, 126.9, 126.8, 124.5, 124.0, 123.0.

2,4,6-Trimethyl-2′-ethyldiphenylamine (Table 1, entry 8) (6)

The general procedure was used for the coupling of 2,4,6-trimethylaniline with 2-ethylbromobenzene, using DPEphos as the supporting ligand and a reaction time of 18 h. The title compound was isolated as a tan solid (465 mg, 97%): mp 74–75°C. EI-HRMS calcd. for $C_{17}H_{21}N$: 239.1674; found: 239.1678 (M^+). IR (film, cm^{-1}): 3384, 2965, 2912, 1601, 1582, 1505, 1496, 1454, 1252, 744. ^{1}H NMR (300 MHz, $CDCl_3$) δ: 7.12 (dd, J = 7.2, 1.5 Hz, 1H), 6.94 (td, J = 7.5, 1.2 Hz, 1H), 6.93 (s, 2H), 6.71 (td, J = 7.5, 1.2 Hz, 1H), 6.13 (dd, J = 7.2, 1.5 Hz, 1H), 4.96 (s, 1H), 2.67 (q, J = 7.8 Hz, 2H), 2.30 (s, 3H), 2.13 (s, 6H), 1.35 (t, J = 7.8 Hz, 3H). ^{13}C NMR (75 MHz, $CDCl_3$) δ: 143.9, 136.0, 135.7, 135.2, 129.3, 128.3, 127.9, 126.9, 118.0, 111.8, 24.5, 21.2, 18.5, 13.5.

2,6-Diisopropyl-4′-chlorodiphenylamine (Table 1, entry 9) (6)

The general procedure was used for the coupling of 2,6-diisopropylaniline with 4-bromochlorobenzene, using DPEphos as the supporting ligand and a reaction time of 18 h. The reaction was conducted at 100°C. The title compound was isolated as a red-orange oil (564 mg, 98%). EI-HRMS calcd. for $C_{18}H_{22}ClN$: 287.1441; found: 287.1447 (M^+). IR (film, cm^{-1}): 3412, 2962, 2928, 2867, 1600, 1587, 1493, 1466, 1304, 817. ^{1}H NMR (300 MHz, $CDCl_3$) δ: 7.31–7.19 (m, 3H), 7.06 (d, J = 9.0 Hz, 2H), 6.38 (d, J = 9.0 Hz, 2H), 5.11 (s, 1H), 3.14 (sept, J = 6.8 Hz, 2H), 1.13 (d, J = 6.8 Hz, 12H). ^{13}C NMR (75 MHz, $CDCl_3$) δ: 147.6, 146.9, 134.8, 129.2, 127.7, 124.1, 122.3, 114.1, 28.5, 24.1.

2,6-Diisopropyl-2′-methyldiphenylamine (Table 1, entry 10) (6)

The general procedure was used for the coupling of 2,6-diisopropylaniline with 2-methylbromobenzene, using DPEphos as the supporting ligand and a reaction time of 18 h. The reaction was conducted at 100°C. The title compound was isolated as a light-orange oil (511 mg, 96%). EI-HRMS calcd. for $C_{19}H_{25}N$: 267.1987; found: 267.1982 (M^+). IR (film, cm^{-1}): 3425, 2961, 2926, 2867, 1606, 1585, 1500, 1464, 1442, 746. ^{1}H NMR (300 MHz, $CDCl_3$) δ: 7.31–7.19 (m, 3H), 7.11 (dd, J = 7.5, 1.2 Hz, 1H), 6.93 (td, J = 7.5, 1.2 Hz, 1H), 6.65 (td, J = 7.5, 1.2 Hz, 1H), 6.11 (dd, J = 7.5, 1.2 Hz, 1H), 4.89 (s, 1H), 3.10 (sept, J = 6.9 Hz, 2H), 2.33 (s, 3H), 1.16 (d, J = 6.9 Hz, 6H), 1.11 (d, J = 6.9 Hz, 6H). ^{13}C NMR (75 MHz, $CDCl_3$) δ: 147.3, 146.1, 135.8, 130.2, 127.2, 127.1, 123.9, 121.4, 117.6, 111.5, 28.5, 25.0, 23.3, 17.9.

2,6-Diisopropyl-2′,6′-dimethyldiphenylamine (Table 1, entry 11) (6, 9*c*)

The general procedure was used for the coupling of 2,6-diisopropylaniline with 2-bromo-*m*-xylene, except that the reaction was carried out at 100°C, using 5 mol% $PdCl_2$ and 7.5 mol% DPEphos. The title compound was isolated as a red-brown oil (514 mg, 91%). EI-HRMS calcd. for $C_{20}H_{27}N$: 281.2144; found: 281.2150 (M^+). IR (film, cm^{-1}): 3433, 2961, 2927, 2867, 1596, 1472, 1446, 1333, 795. ^{1}H NMR (300 MHz, $CDCl_3$) δ: 7.15–7.07 (m, 3H), 6.92 (d, J = 7.5 Hz, 2H), 6.70 (t, J = 7.5 Hz, 1H), 4.78 (s, 1H), 3.14 (sept, J = 6.9 Hz, 2H), 1.97 (s, 6H), 1.11 (d, J = 6.9 Hz, 12H). ^{13}C NMR (75 MHz, $CDCl_3$) δ: 144.2, 143.2, 138.9, 129.6, 125.7, 124.9, 123.4, 119.7, 28.3, 23.8, 19.7.

***N*-(2-Methoxyphenyl)pyrrolidine (Table 2, entry 1)**

The general procedure was used for the coupling of pyrrolidine with 2-bromoanisole, using **1** as the supporting ligand and a reaction time of 43 h. The title compound was isolated as a colorless liquid (0.216 g, 61%). IR (film, cm^{-1}): 3060, 2960, 2830, 1504, 1232, 730. ^{1}H NMR (300 MHz, $CDCl_3$) δ: 6.90–6.85 (m, 3H), 6.82–6.78 (m, 1H), 3.84 (s, 3H), 3.30–3.26 (m, 4H), 1.95–1.91 (m, 4H). ^{13}C (75 MHz, $CDCl_3$) δ: 150.6, 140.0, 121.3, 119.8, 115.6, 111.7, 55.7,

© 2001 NRC Canada

50.6, 24.8. Anal. calcd. for $C_{11}H_{15}NO$: C 74.54, H 8.53; found: C 74.30, H 8.52.

***N*-(3-Methoxyphenyl)-benzylamine (Table 2, entry 2)**

The general procedure was used for the coupling of benzylamine with 3-bromoanisole, using **1** as the supporting ligand and a reaction time of 23 h. The title compound was isolated as a yellow liquid (0.397 g, 93%). IR (film, cm^{-1}): 2970, 2917, 1590, 1495, 692. ^1H NMR (300 MHz, $CDCl_3$) δ: 7.40–7.27 (m, 5H), 7.08 (t, J = 8.1 Hz, 1H), 6.31–6.25 (m, 2H), 6.21–6.19 (m, 1H), 4.32 (s, 2H), 4.10 (br s, 1H), 3.75 (s, 3H). ^{13}C (75 MHz, $CDCl_3$) δ: 160.9, 149.7, 139.4, 130.1, 128.7, 127.6, 127.4, 106.1, 102.7, 98.9, 55.2, 48.4. Anal. calcd. for $C_{14}H_{15}NO$: C 78.84, H 7.09; found: C 78.76, H 7.01.

***N*-(3-Methoxyphenyl)-di-*n*-butylamine (Table 2, entry 3)**

The general procedure was used for the coupling of di-*n*-butylamine with 3-bromoanisole, using **1** as the supporting ligand and a reaction time of 21 h. The title compound was isolated as a yellow liquid (0.415 g, 88%). IR (film, cm^{-1}): 2956, 2871, 1609, 1500, 1204, 746. ^1H NMR (300 MHz, $CDCl_3$) δ: 7.10 (t, J = 8.1 Hz, 1H), 6.29–6.25 (m, 1H), 6.21–6.18 (m, 2H), 3.78 (s, 3H), 3.24 (t, J = 7.8 Hz, 4H), 1.61–1.51 (m, 4H), 1.40–1.28 (m, 4H), 0.95 (t, J = 6.9 Hz, 6H). ^{13}C (75 MHz, $CDCl_3$) δ: 161.0, 149.7, 129.9, 105.1, 99.7, 98.4, 55.2, 51.0, 29.6, 20.5, 14.2. Anal. calcd. for $C_{15}H_{25}NO$: C 76.55, H 10.71; found: C 76.40, H 10.59.

***N*-(3,5-Dimethylphenyl)-*N*-ethylaniline (Table 2, entry 4)**

The general procedure was used for the coupling of *N*-ethylaniline with 5-bromo-*m*-xylene, using **1** as the supporting ligand and a reaction time of 28 h. The title compound was isolated as a yellow liquid (0.308 g, 68%). IR (film, cm^{-1}): 3415, 3027, 2834, 1614, 1162. ^1H NMR (300 MHz, $CDCl_3$) δ: 7.27–7.21 (m, 2H), 6.96–6.90 (m, 3H), 6.64–6.63 (m, 3H), 3.75 (q, J = 7.2 Hz, 2H), 2.26 (s, 6H), 1.21 (t, J = 7.2 Hz, 3H). ^{13}C (75 MHz, $CDCl_3$) δ: 148.0, 147.7, 139.0, 129.3, 123.6, 120.5, 120.3, 119.5, 46.6, 21.6, 12.9. Anal. calcd. for $C_{16}H_{19}N$: C 85.29, H 8.50; found: C 85.39, H 8.49.

***N*-(4-*tert*-Butylphenyl)morpholine (Table 2, entry 5)**

The general procedure was used for the coupling of morpholine with 1-bromo-4-*tert*-benzene, using **1** as the supporting ligand and a reaction time of 21 h. The title compound was isolated as a yellow solid (0.403 g, 92%): mp 53–55°C. IR (film, cm^{-1}): 2958, 2853, 1612, 1118. ^1H NMR (300 MHz, $CDCl_3$) δ: 7.31 (d, J = 8.7 Hz, 2H), 6.86 (d, J = 9.0 Hz, 2H), 3.87–3.84 (m, 4H), 3.15–3.12 (m, 4H), 1.30 (s, 9H). ^{13}C (75 MHz, $CDCl_3$) δ: 149.0, 142.9, 126.1, 115.5, 67.1, 49.7, 34.1, 31.6. Anal. calcd. for $C_{14}H_{21}NO$: C 76.67, H 9.65; found: C 76.56, H 9.57.

***N*-(4-Cyanophenyl)morpholine (Table 2, entry 6)**

The general procedure was used for the coupling of morpholine with 4-bromobenzonitrile, using **2** as the supporting ligand, K_3PO_4 as the base, DME as the solvent, and a reaction time of 28 h. The reaction was conducted at 100°C. The title compound was isolated as a yellow solid (0.287 g, 76%): mp 73–75°C. IR (film, cm^{-1}): 2980, 2831, 2217, 1606, 1116. ^1H NMR (300 MHz, $CDCl_3$) δ: 7.53 (d, J = 8.7 Hz, 2H), 6.87 (d, J = 9.0 Hz, 2H), 3.88–3.85 (m, 4H), 3.31–3.27 (m, 4H). ^{13}C (75 MHz, $CDCl_3$) δ: 153.6, 133.6, 120.0, 114.2, 101.1, 66.6, 47.4. Anal. calcd. for $C_{11}H_{12}N_2O$: C 70.19, H 6.43; found: C 69.93, H 6.27.

Acknowledgments

This work was supported in part by grants from the Office of Naval Research and the National Institutes of Health (GM58160). M.C.H. is grateful to the National Cancer Institute for support under training grant NCI CI (T32C A09 112).

References

1. (*a*) J.P. Wolfe, S. Wagaw, J.-F. Marcoux, and S.L. Buchwald. Acc. Chem. Res. **31**, 805 (1998); (*b*) J.F. Hartwig. Angew. Chem. Int. Ed. **37**, 2046 (1998); (*c*) B.Y. Yang and S.L. Buchwald. J. Organomet. Chem. **576**, 125 (1999).
2. (*a*) F. He, B.M. Foxman, and B.B. Snider. J. Am. Chem. Soc. **120**, 6417 (1998); (*b*) G.J. Tanoury, C.H. Senanayake, R. Hett, A.M. Kuhn, D.W. Kessler, and S.A. Wald. Tetrahedron Lett. **39**, 6845 (1998).
3. (*a*) E.A. Harwood, S.T. Sigurdsson, N.B.F. Edfeldt, B.R. Reid, and P.B. Hopkins. J. Am. Chem. Soc. **121**, 5081 (1999); (*b*) M.K. Lakshman, J.C. Keeler, J.H. Hilmer, and J.Q. Martin. J. Am. Chem. Soc. **121**, 6090 (1999); (*c*) S. Wagaw, B.H. Yang, and S.L. Buchwald. J. Am. Chem. Soc. **121**, 10251 (1999); (*d*) O.J. Plante, S.L. Buchwald, and P.H. Seeberger. J. Am. Chem. Soc. **122**, 7148 (2000).
4. (*a*) L.-C. Liang, R.R. Schrock, W.M. Davis, and D.H. McConville. J. Am. Chem. Soc. **121**, 5797 (1999); (*b*) R.A. Singer, J.P. Sadighi, and S.L. Buchwald. J. Am. Chem. Soc. **120**, 213 (1998); (*c*) J.P. Sadighi, R.A. Singer, and S.L. Buchwald. J. Am. Chem. Soc. **120**, 4960 (1998); (*d*) X.-X. Zhang, J.P. Sadighi, T.W. Mackewitz, and S.L. Buchwald. J. Am. Chem. Soc. **122**, 7606 (2000); (*e*) X.-X. Zhang and S.L. Buchwald. J. Org. Chem. **65**, 8027 (2000).
5. J.P. Wolfe and S.L. Buchwald. J. Org. Chem. **65**, 1144 (2000).
6. J.P. Sadighi, M.C. Harris, and S.L. Buchwald. Tetrahedron Lett. **39**, 5327 (1998).
7. Y. Guari, D.S. van Es, J.N.H. Reek, P.C.J. Kamer, and P.W.N.M. van Leeuwen. Tetrahedron Lett. **40**, 3789 (1999).
8. M.S. Driver and J.F. Hartwig. J. Am. Chem. Soc. **118**, 7217 (1996).
9. (*a*) D.W. Old, J.P. Wolfe, and S.L. Buchwald. J. Am. Chem. Soc. **120**, 9722 (1988); (*b*) J.P. Wolfe and S.L. Buchwald. Angew. Chem. Int. Ed. **38**, 2413 (1999); (*c*) J.P. Wolfe, H. Tomori, J.P. Sadighi, J. Yin, and S.L. Buchwald. J. Org. Chem. **65**, 1158 (2000); (*d*) J.P. Wolfe, R.A. Singer, B.H. Yang, and S.L. Buchwald. J. Am. Chem. Soc. **121**, 9550 (1999); (*e*) J.M. Fox, X. Huang, A. Chieffi, and S.L. Buchwald. J. Am. Chem. Soc. **122**, 1360 (2000); (*f*) A. Aranyos, D.W. Old, A. Kiyomori, J.P. Wolfe, J.P. Sadighi, and S.L. Buchwald. J. Am. Chem. Soc. **121**, 4369 (1999).
10. (*a*) M. Nishiyama, T. Yamamoto, and Y. Koie. Tetrahedron Lett. **39**, 617 (1998); (*b*) T. Yamamoto, M. Nishiyama, and Y. Koie. Tetrahedron Lett. **39**, 2367 (1998); (*c*) B.C. Hamann and J.F. Hartwig. J. Am. Chem. Soc. **120**, 7369 (1998); (*d*) J.F. Hartwig, M. Kawatsura, S.I. Hauck, K.H. Shaughnessy, and L.M. Alcazar-Roman. J. Org. Chem. **64**, 5575 (1999).
11. V. Bavetsias and E.A. Henderson. J. Chem. Res.-S, 418 (2000).

© 2001 NRC Canada

12. B.C. Hamann and J.F. Hartwig. J. Am. Chem. Soc. **120**, 3694 (1998).
13. R.J. Sundberg and K.B. Sloan. J. Org. Chem. **38**, 2052 (1973).
14. J.P. Wolfe, S. Wagaw, and S.L. Buchwald. J. Am. Chem. Soc. **118**, 7215 (1996).
15. J. Piccard and F. de Montmollin. Helv. Chim. Acta, **6**, 1011 (1923).

© 2001 NRC Canada

Diastereotopic group recognition in the solid state — A unique intramolecular β-cyclodextrin inclusion complex

Manfred T. Reetz, Joachim Rudolph, and Richard Goddard

Abstract: The phenomenon of diastereotopic group recognition has been structurally documented for the first time. A diphenylphosphine-modified β-cyclodextrin having two diastereotopic phenyl groups in close vicinity to the inner cavity of this host was prepared. The crystal structure analysis reveals selective intramolecular complexation of one of the two diastereotopic phenyl groups.

Key words: supramolecular chemistry, stereotopic group recognition, cyclodextrins, intramolecular complexation.

Résumé : Le phénomène de reconnaissance de groupement diastéréotopique a été structurellement demontré pour la première fois. Une β-cyclodextrine fonctionnalisée avec un groupement diphénylphosphine a été synthétisée. Les deux groupements phényle sont situés à proximité de la cavité de la cyclodextrine et la structure déterminée par rayons X fait apparaître une complexation sélective et intramoléculaire d'un des deux groupement phényle.

Mots clés : chimie supramoléculaire, reconnaissance de groupement stéréotopique, cyclodextrines, complexation intramoléculaire.

Introduction

Although enantio- or diastereo-differentiation of prochiral groups is the crucial step in desymmetrization reactions, little is known about what occurs during the actual molecular recognition process. The desymmetrization of a prochiral or a *meso*-compound is usually achieved by enzymes, chiral chemical reagents, or by synthetic catalysts (1–6).

The actual chemical conversion of prochiral compounds bearing enantiotopic groups is believed to be preceded by selective recognition of one of these groups. However, in spite of the large body of experimental results in the area of reagent controlled or catalytic desymmetrization, the actual recognition process itself has only recently become the subject of investigation. We reported the first direct evidence for enantiotopic group recognition in solution, the system being based on a chiral crown ether as the host and *meso*-diammonium compounds as guest molecules (7, 8). The chiral crown ether binds selectively to one of the two enantiotopic ammonium groups as demonstrated by NMR spectroscopy. Subsequently, we described a case in which enantiotopic group recognition can be observed both in solution and solid state (9, 10). In this example, selective group recognition was induced by reversible formation of a chiral borate complex. In addition, we were able to show that in a subsequent chemical reaction step, a chiral product is obtained with an enantiomeric purity corresponding to the diastereoselectivity occurring in the preceding enantiotopic group recognition event (9, 10).

Although the general phenomenon of enantiotopic group recognition (Scheme 1) in this case was successfully elucidated by means of NMR spectroscopy and X-ray crystallography (9, 10), until now we have not come across direct evidence of the second variant of stereotopic group recognition, i.e., the case of *dia*stereotopic group recognition. This occurs when selective recognition of heterotopic groups occurs within *the same* molecule (Scheme 2). Here we report what we believe to be the first example of such a case.

Results and discussion

Some time ago we described the preparation of a water-soluble, phosphine-modified β-cyclodextrin **3** (Scheme 3) and its corresponding rhodium complex (11–13). Our intention was to test the catalytic activity of such a potential supramolecular catalyst in a two-phase (org.–H_2O) system. The idea was to combine possible host–guest effects with transition-metal catalysis and phase-transfer catalysis. The choice of β-cyclodextrin as the host was based on extensive previous work concerning its supramolecular chemistry (14–17).

Received March 12, 2001. Published on the NRC Research Press Web site at http://canjchem.nrc.ca on November 20, 2001.

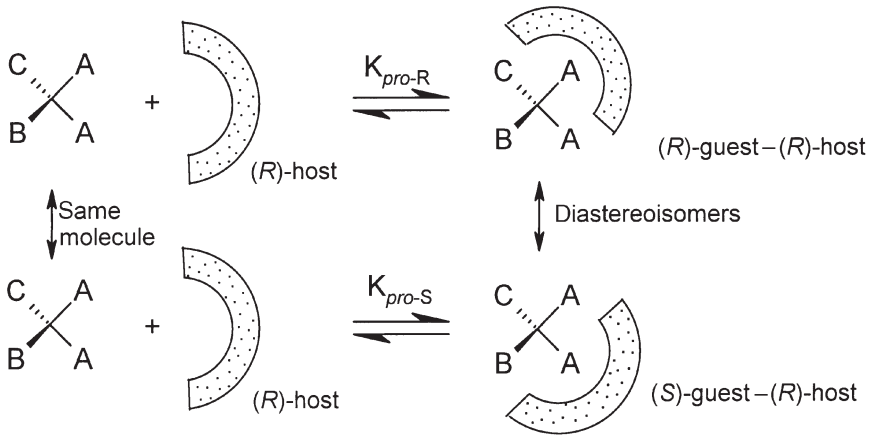
Dedicated to Professor Victor Snieckus, a pioneer in organometallic chemistry.

M.T. Reetz,[1] J. Rudolph,[2] and R. Goddard. Max-Planck-Institut für Kohlenforschung, Kaiser-Wilhelm-Platz 1, 45470 Mülheim/Ruhr, Germany.

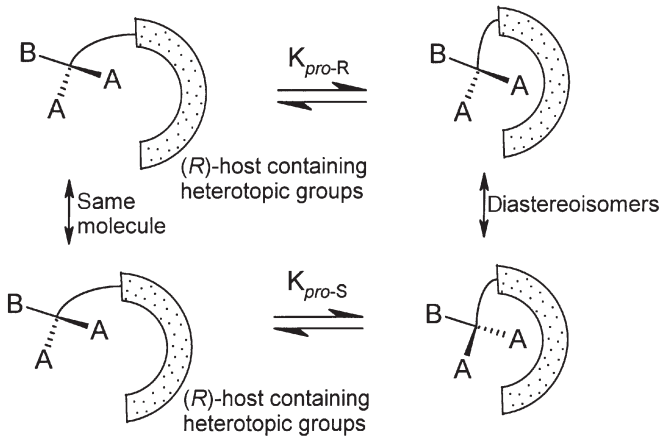
[1]Corresponding author (telephone: (208) 306-2000; fax: (208) 306-2985; e-mail: reetz@mpi-muelheim.mpg.de).
[2]New address: Bayer AG, Central Research, 51368 Leverkusen, Germany.

 DOI: 10.1139/cjc-79-11-1806 © 2001 NRC Canada

Scheme 1. Enantiotopic group recognition by a chiral host.



Scheme 2. Diastereotopic group recognition by a chiral host.



Furthermore, since β-cyclodextrin is chiral, it has also been used as an auxiliary for asymmetric transformations (14–17). However, the Rh-complex of **3** was not an effective catalyst, in contrast to diphosphine analogs (18, 19). As a result the chemistry of ligand **3** remained largely unexplored.

β-Cyclodextrin has a hydrophobic inner cavity capable of hosting organic molecules, especially aromatic compounds (14–17). Indeed, intramolecular complexation in the form of self-inclusion compounds are known (20–22). It is therefore conceivable that intramolecular complexation of the phenyl groups of the phosphine moiety in compound **3** can occur. If this were to be the case, then the phenomenon of diastereotopic group recognition could arise. Two different diastereomeric complexes are possible, depending upon which of the two diastereotopic phenyl groups enters the cavity of the chiral β-cyclodextrin host. To see whether this is the case, we prepared crystals of **3** and performed an X-ray structure analysis. The results of the investigation are summarized in Fig. 1, which shows the structure of the molecule. The atom numbering system is given in Scheme 4.

The compound crystallizes as the undecahydrate and the water molecules are omitted from the figure for clarity. The structure analysis reveals that the β-cyclodextrin annulus adopts an almost ideally symmetrical structure in which only one of the diastereotopic phenyl rings of the diphenyl phosphinyl groups is included into the hydrophobic β-cyclodextrin cavity. The centroid of the phenyl ring lies in the mean plane of the C-5 atoms of the glucose subunits of the β-cyclodextrin ring (±0.1 Å). P and S lie, respectively, 3.1(1) and 2.8(1) Å above this plane. The β-cyclodextrin ring has approximate seven-fold symmetry and is largely undistorted by the inclusion of the phenyl group. The P atom lies almost on the mean rotation axis of the β-cyclodextrin ring. Important is the fact that the same diastereotopic phenyl group is intramolecularly incorporated in all molecules of the crystal. To stipulate which phenyl group it is, the CIP nomenclature (23) needs to be extended. We propose that of the two relevant diastereotopic groups the supramolecularly complexed phenyl entity has the higher priority. Consequently, phosphorus adopts the *S*-configuration (Fig. 1). To determine whether the incorporation of the pro-S phenyl group into the β-cyclodextrin cavity was fortuitous, we recrystallized the sample, took another crystal and also determined its structure. In this crystal we also found that the pro-S phenyl group is intramolecularly encapsulated in the β-cyclodextrin annulus. Attempts to determine whether the crystalline sample was uniform by means of powder diffraction were unsuccessful since the mortared sample was amorphous, presumably as a result of loss of water from the crystals during preparation of the powder.

Why does the β-cyclodextrin appear to preferentially select the pro-S phenyl group? Two alternative explanations are examined. The first possibility is that of diastereotopic group selectivity, i.e., the pro-S configuration is energetically more stable than the corresponding pro-R arrangement (Scheme 2). It may, however, be that the chiral conformation of the diphenylphosphine moiety is limited to the crystalline state, and that the observed configuration is a result of preferential precipitation of one of the two diastereomeric complexes, either because its crystals are formed more quickly (kinetic control) or because the crystals are inherently more stable (thermodynamic control). In the following, we confine ourselves to a discussion of whether intramolecular interactions alone or a combination of intramolecular and intermolecular interactions may predominate.

To establish whether incorporation of the pro-S phenyl group into the β-cyclodextrin cavity is the energetically favoured conformation, we undertook force field calculations

© 2001 NRC Canada

Scheme 3. Preparation of the phosphine-modified β-cyclodextin **3**.

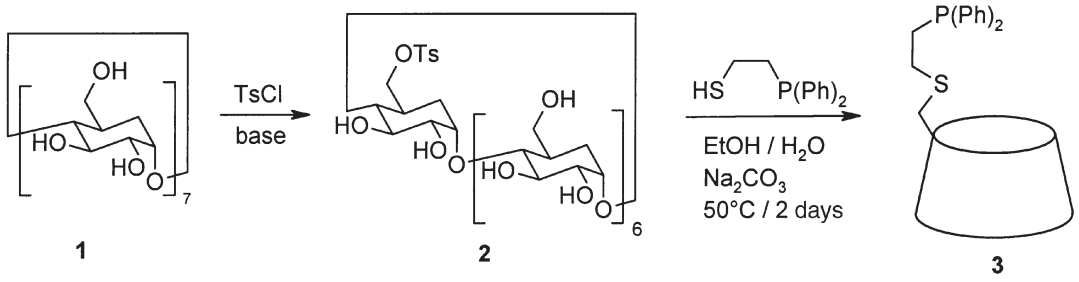
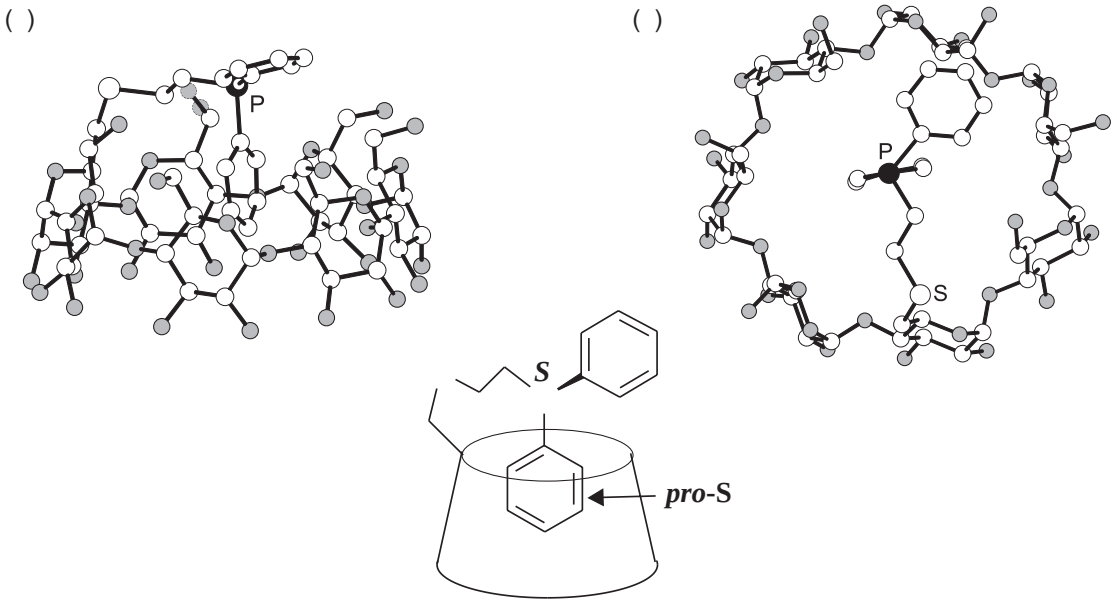


Fig. 1. Molecular structure of 6-deoxy-6-(diphenylphosphino-ethylenethio)-β-cyclodextrin (**3**) in the solid. (*a*) Side view; (*b*) top view.



Scheme 4. Schematic representation of the atom numbering system used in the crystal structure determination of **3**·11H_2O (atoms in the amylose groups G2–G7 were numbered according to the convention: Axy, where x defines the location of the atom A in the group y.

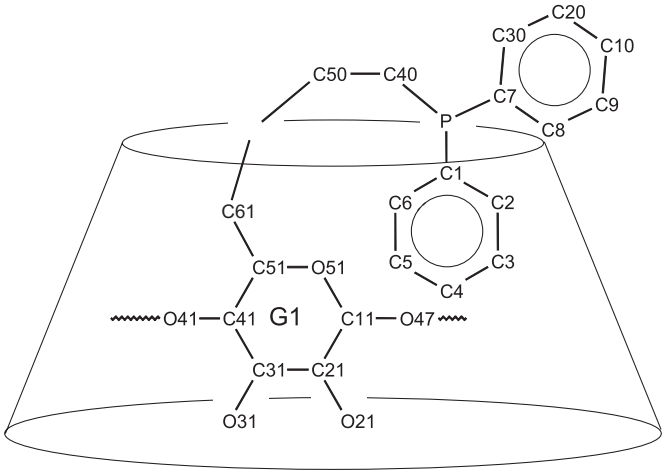


Table 1. Torsion angles in the diphenylphosphinothioethylene side chain in the *S*-configured structure in the crystal and the modeled *R*-configuration.[a]

Torsion angle	*S*-Configuration (°)[b]	*R*-Configuration (°)[c]
O51-C51-C61-S	69	70
C51-C61-S-C50	83	86
C61-S-C50-C40	–157	–152
S-C50-C40-P	180	178
C50-C40-P-C1	–61	–50
C50-C40-P-C7	–169	83
C40-P-C1-C2	111	83
C40-P-C7-C8	–159	–68

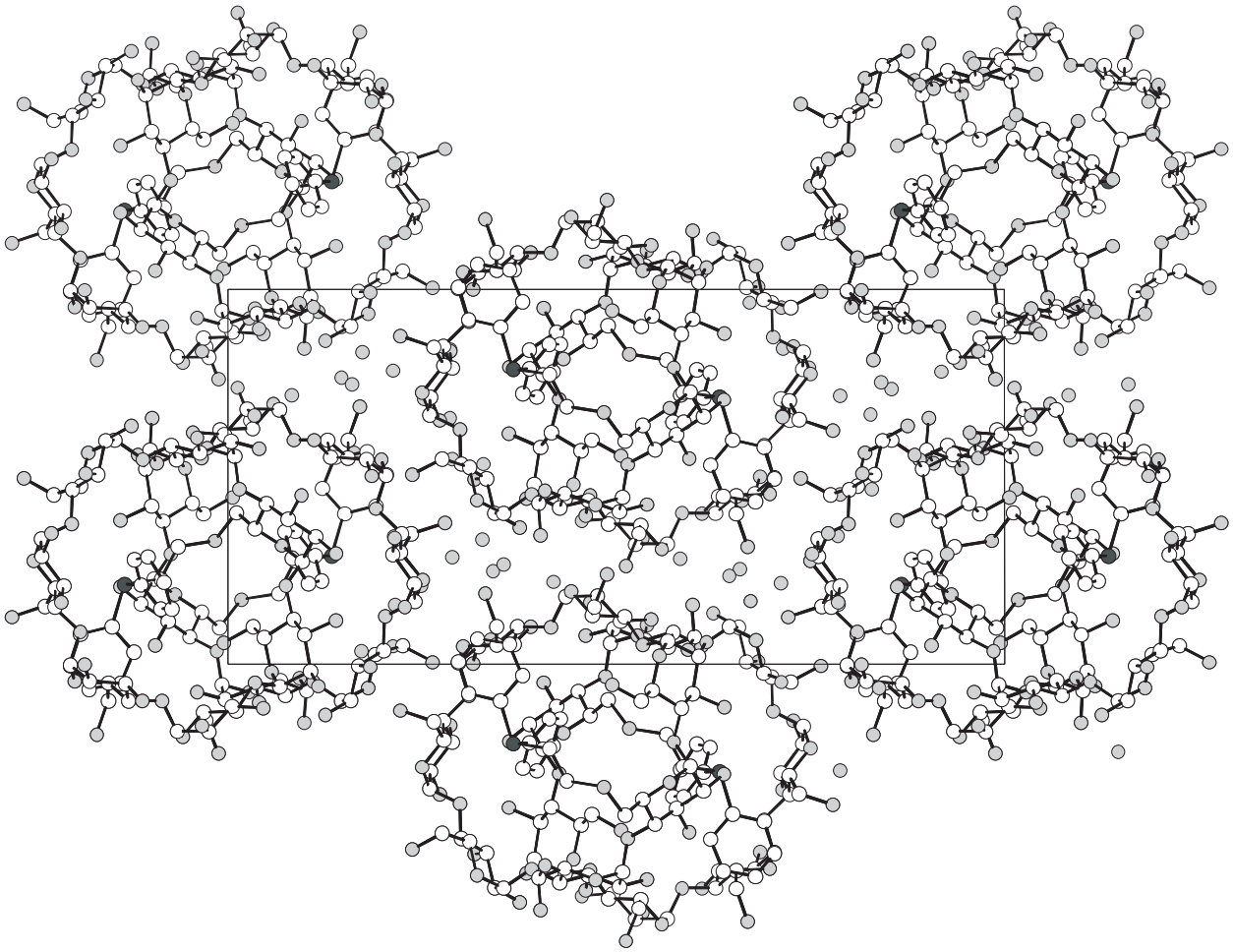
[a]See Scheme 4 for a designation of the side chain.
[b]Experimental structure.
[c]Modeled structure (24).

on both diastereomers in the free state (24).[3] First, we simulated the *R*-configuration by rotating the diphenyl phosphine group of the X-ray structure around the P—C-40 bond until the pro-R phenyl group was situated in the cavity at the position previously occupied by pro-S phenyl group. As the

[3] Force field: Tripos version 5.2; minimization algorithm: BFGS; convergence criterion: RMS gradient < 0.001 kcal mol^{-1} $Å^{-1}$, nonbonded cutoff 8 Å.

© 2001 NRC Canada

Fig. 2. The unit cell of **3**·11H_2O viewed down the column axis (**a**), showing the close-packing of the substituted β-cyclodextrin molecules.



starting point for the structure containing the pro-S phenyl group, we used the geometry observed in the crystal. The energies of both diastereomers were then minimized under equivalent conditions and compared (same force-field parameters, absence of solvent) (24).[3] There was no appreciable energy difference between the two minimized structures (<2.1 kcal mol^{-1}). Apart from the location of the phenyl groups, the largest difference in the conformation of the two structures was found in the chain linking the phosphine to the β-cyclodextrin annulus. Table 1 gives the torsion angles along this chain. Although the differences are small, the torsion angles most affected involve the S atom. This appears to be a result of the fixed arrangement of the C-51—C-61 bond relative to the β-cyclodextrin group, which has a built-in handedness and is necessarily directed to one side of the ring.

Since force field calculations suggest that energy difference between both diastereomers is relatively small, we turn our attention to the results of the X-ray analysis for a possible explanation of the observed diastereomer. The crystal structure contains much information about the intramolecular and intermolecular interactions that may affect the stabilization of the *S*-configuration. Figure 2 shows the packing of the substituted β-cyclodextrin and water molecules in the unit cell. Inspection of the figure and examination of the shortest intermolecular distances (Table 2) reveal that the β-cyclodextrin rings stack in a head-to-tail fashion in columns, as has been observed previously for unsubstituted cyclodextrin molecules (25). The columns are essentially separated by solvate water molecules, which are located in channels between the β-cyclodextrin molecules and extend contiguously throughout the structure. Particularly worthy of note is the number of water molecules in the crystal. The compound crystallizes with no less than 11 solute water molecules for each substituted β-cyclodextrin annulus. Consequently, most of the intermolecular interactions are between the substituted β-cyclodextrin and water molecules and between the water molecules themselves. Indeed, there are only four short intermolecular interactions (<3.1 Å) between the substituted β-cyclodextrin molecules and three of them involve hydrogen bonds between primary hydroxyl groups on one ring and secondary hydroxyl groups on the β-cyclodextrin annulus above it (Table 2). This suggests that the water molecules make an important contribution to the packing of the molecules in the crystal. Interestingly, the region of space which we would expect to be occupied by pro-R phenyl group in the other diastereomer is completely occupied by solute water molecules and hence strongly hydrophilic. Moreover, one water molecule appears to be strongly bound to the P atom since its O atom lies 3.43(3) Å from P along the axis of the expected position of the P lone pair. Unfortunately, we have thus far not been able to obtain crystals of the

© 2001 NRC Canada

Table 2. Short intermolecular distances between non-H atoms in solid **3**·11H_2O.

Atom 1	Atom 2	Distance (Å)	Symmetry operation
Between the substituted β-cyclodextrin molecules			
O66	O52	2.91(1)	*x*, *y* – 1, *z*
O66	O26	2.69(1)	*x* – 0.5, 2.5 – *y*, –*z*
O62b	O36	2.68(2)	*x* – 0.5, 1.5 – *y*, –*z*
O67	O32	3.09(1)	*x* – 0.5, 1.5 – *y*, –*z*
Between the substituted β-cyclodextrin molecules and solute water			
P	O110	3.34(3)	*x*, *y*, *z*
O62a[a]	O108	2.88(3)	–*x*, *y* – 0.5, 0.5 – *z*
O62b[a]	O111	2.92(5)	*x*, *y*, *z*
O63[a]	O106	2.63(2)	*x*, *y*, *z*
O63[a]	O101	2.71(1)	–1.0 – *x*, *y* – 0.5, 0.5 – *z*
O64[a]	O107	2.68(2)	x, *y*, *z*
O64[a]	O104	2.80(2)	–0.5 – *x*, 1.0 – *y*, 0.5 + *z*
O65[a]	O105	2.84(2)	–1.0 – *x*, 0.5 + *y*, 0.5 – *z*
O65[a]	O109	2.85(3)	*x*, *y*, *z*
O21[b]	O106	2.77(2)	–0.5 – *x*, 1.0 – *y*, *z* – 0.5
O22[b]	O102	2.65(1)	*x*, *y*, *z*
O23[b]	O103	2.70(2)	*x* – 0.5, 1.5 – *y*, –*z*
O24[b]	O105	2.73(2)	*x*, *y*, *z*
O25[b]	O101	2.72(1)	*x*, *y*, *z*
O31[b]	O101	2.83(1)	0.5 + *x*, 1.5 – *y*, –*z*
O35[b]	O103	2.91(1)	*x* – 0.5, 2.5 – *y*, –*z*
O36[b]	O102	2.80(1)	*x*, 1.0 + *y*, *z*
O37[b]	O107	2.68(2)	–0.5 – *x*, 2.0 – *y*, *z* – 0.5

[a]Primary hydroxyl groups.
[b]Secondary hydroxyl groups.

diastereomer. It seems, however, that if crystal packing forces are the reason for the preferred configuration then the observed diastereomer must be a result of a subtle interplay between the requirement for close packing of the substituted β-cyclodextrin molecules and strong cooperative intermolecular interactions between the solvate water molecules (26).

To establish whether selective intramolecular complexation occurs in solution, NMR experiments were performed. ^1H and ^{13}C NMR measurements of a solution of the compound showed the presence of two, but not four, magnetically nonequivalent phenyl groups. This shows that either neither of the two phenyl rings is incorporated in the cavity or that the two phenyl groups of the two possible diastereomers equilibrate rapidly on the NMR timescale. The latter would mean that the process of entering and leaving the cavity by the phenyl groups is fast. Unfortunately, upon cooling the sample to –78°C the compound precipitated. Thus, it was not possible to detect the two diastereomeric complexes nor to determine their ratio, which would be a measure of diastereotopic group recognition in solution. We observed the same phenomenon upon treating β-cyclodextrin itself with such prochiral compounds as diphenylsufoxide or benzhydryl alcohol (13). In both cases 1:1 host–guest complexes were detected by NMR spectroscopy, two different phenyl groups being observed. This is in line with a single diastereomer and 100% enantiotopic group recognition, or two rapidly equilibrating diastereomers. It was impossible to resolve this because at lower temperatures the material precipitated.

Experimental

General

Melting points were obtained on a Gallenkamp melting point apparatus and are uncorrected. Elemental analyses were performed at the Microanalytisches Labor Kolbe, Mülheim/Ruhr. Optical rotations were measured on a JASCO digital polarimeter (model DIP 360). ^1H NMR spectra were recorded on a Bruker WH 400 spectrometer in DMF-d_7 or pyridine-d_5 using the solvent signals as internal references; in the case of pyridine, the β-H at δ = 7.38 and the β-C at δ = 123.6 were taken as references. The chemical shifts are reported in δ (ppm) relative to TMS and in the case of ^{31}P NMR spectra, relative to 85% aqueous phosphoric acid (0.0 ppm). The coupling constants (*J*) are given in Hertz (Hz). FAB mass spectrometry was performed on a Finnigan-MAT 95 mass spectrometer using diethanolamine as matrix.

*Mono[6-deoxy-6-(2′-diphenylphosphinoethyl)thio]-β-cyclodextrin (**3**)*

In an inert atmosphere, the known (27) 6-mono-6-*p*-toluenesulfonyl-β-cyclodextrin (**2**) (2.0 g, 1.55 mmol) was dissolved in a mixture of 100 mL water and 25 mL ethanol. Na_2CO_3 was added to give a pH of 12. Then 2-(diphenylphosphino)ethane thiol (2.0 g, 8.1 mmol) was added under argon and the mixture was vigorously stirred for 2 days at 50°C. After cooling, oxygen-free 1 N aq HCl solution was added until a pH of 6 to 7 was reached. The excess thiol was removed in a micro perforator using ether as extractant for 3 days. The product together with inorganic salts remained in the aqueous phase while the thiol accumulated in the ether phase. After recrystallization from water–ethanol (95:5) and drying in vacuo, product **3** (1.4 g, 1.03 mmol, 66%) was obtained as a white powder, mp 302–310°C (dec.). $[\alpha]^{22}_{D}$ = +12.0 (*c* 2.5, DMF). FAB-MS (pos.) $[M + H]^+$: 1363. ^1H NMR (400 MHz, pyridine-d_5) δ: 2.76 (m, 2H, CH_2-P), 3.19 (m, 2H, CH_2-S), 3.55 (dd, 1H, *J* = 14 Hz, 6 Hz, H-6a′), 3.80 (d, 1H, *J* = 13 Hz, H-6b′), 4.29–4.36 (m, 7H, H-2), 4.29–4.41 (m, 7H, H-4), 4.54–4.68 (m, 16H, H-5,6, H_2O), 4.80–4.91 (m, 7H, H-3), 5.72–5.94 (m, 7H, H-1), 7.44–7.52, 7.71–7.75 (m, 10H, arom. H). ^{13}C NMR (100.6 MHz, pyridine-d_5) δ: 28.9 (d, $J_{P,C}$ = 15.3 Hz, CH_2-P), 30.1 (d, $J_{P,C}$ = 20.9 Hz, CH_2-S), 34.0 (C-6′), 61.4–61.6 (C-6), 73.0 (C-5′), 73.7–74.6 (C-2, 3, 5), 83.1–83.4 (C-4), 85.9 (C-4′), 103.5–103.8 (C-1), 128.7, 133.0, 138.8 (m, dd, d, arom. C). ^{31}P NMR (161.3 MHz, DMF-d_7) δ: –17.2. Anal. calcd. for $C_{56}H_{83}O_{34}PS$: C 49.33, H 6.14, S 6.14, P 2.35; found: C 49.32, H 6.16, S 6.16, P 2.39.

*X-ray crystallographic structure determination of **3***

Needle-shaped crystals suitable for an X-ray analysis were grown from water–ethanol (95:5) by slowly cooling from 50°C to room temperature. Crystal data: $C_{56}H_{83}O_{34}PS·11(H_2O)$, M_w = 1561.43; colorless prism 0.21 × 0.49 × 0.53 mm; orthorhombic $P2_12_12_1$ (no. 19); *a* = 14.968(1), *b* = 15.331(1), *c* = 31.808(2) Å; *U* = 7299.1(8) Å^3; *T* = 293 K; D_x = 1.421 g cm^{-3}; λ = 1.54178 Å; μ = 1.514 cm^{-1}; Enraf–Nonius CAD-4 diffractometer, 1.39 < θ < 74.95°; 8220 independent measured reflections, 5209 with $I > 2\sigma(I)$. Structure solved by direct methods (28) and refined by least-squares

© 2001 NRC Canada

(29) using Chebyshev weights on F_o^2 to R_1 = 0.090 [$I > 2\sigma(I)$], wR_2 = 0.286, 831 parameters, one hydroxyl group is disordered over two positions (50:50), these atoms, together with the C atoms of the two phenyl groups and the 11 O atoms of the solvent water of crystallization, were refined with isotropic adps; H atoms, except on the disordered hydroxyl group and solvent water molecules, were calculated and allowed to ride, S = 1.014, residual electron density +0.552/–0.371 e Å^{-3}. Depository material may be purchased from the Depository of Unpublished Data, Document Delivery, CISTI, National Research Council Canada, Ottawa, ON K1A 0S2, Canada (http://www.nrc.ca/cisti/irm/unpub_e.shtml for information on ordering electronically). Crystallographic data (excluding structure factors) for the structure have been deposited with the Cambridge Crystallographic Data Centre (CCDC 159 058). Copies of the data can be obtained, free of charge, on application to the Director, CCDC, 12 Union Road, Cambridge CB2 1EZ, U.K. (Fax: 44-1223-336033 or e-mail: deposit@ccdc.cam.ac.uk).

Conclusion

The crystal structure of the phosphine-modified β-cyclodextrin **3** shows selective intramolecular complexation of one of the diastereotopic phenyl groups. This unique process induces chirality at phosphorus. To specify which phenyl group participates, an extension of the CIP nomenclature to include supramolecular interactions is required. Neither molecular modeling calculations nor inspection of the crystal packing gives an unequivocal explanation for the observed *S*-configuration in the crystal, and until we have further examples of this interesting phenomenon for comparison we are not in a position to say what the determining factor is in this case.

References

1. M.C. Willis. J. Chem. Soc. Perkin Trans. 1, 1765 (1999).
2. J.B. Jones. Aldrichimica Acta, **26**, 105 (1993).
3. K. Faber. Biotransformations in organic chemistry. 3rd ed. Springer, Berlin. 1997.
4. E. Schoffers, A. Golebiowski, and C.R. Johnson. Tetrahedron, **52**, 3769 (1996).
5. R.S. Ward. Chem. Soc. Rev. **19**, 1 (1990).
6. C. Bolm, I. Schiffers, C.L. Dinter, and A. Gerlach. J. Org. Chem. **65**, 6984 (2000).
7. M.T. Reetz, J. Rudolph, and R. Mynott. J. Am. Chem. Soc. **118**, 4494 (1996).
8. M.T. Reetz. Pure Appl. Chem. **68**, 1279 (1996).
9. J. Huskens, R. Goddard, and M.T. Reetz. J. Am. Chem. Soc. **120**, 6617 (1998).
10. J. Huskens and M.T. Reetz. Eur. J. Org. Chem. 1775 (1999).
11. J. Rudolph. Diploma Thesis, Universität Bonn, Germany, 1993.
12. M.T. Reetz and J. Rudolph. Tetrahedron: Asymmetry, **4**, 2405 (1993).
13. J. Rudolph. Ph.D. Dissertation, Universität Bochum, Germany, 1995.
14. G. Wenz. Angew. Chem. **106**, 851 (1994); Angew. Chem. Int. Ed. Engl. **33**, 803 (1994).
15. J.L. Atwood, J.E.D. Davies, and F. Vögtle (*Editors*). Cyclodextrins. *In* Comprehensive supramolecular chemistry. Vol. 3. Pergamon, Oxford. 1996.
16. J. Szejtli. Chem. Rev. **98**, 1743 (1998); and reviews which follow this article.
17. C.J. Easton and S.F. Lincoln. Modified cyclodextrins: scaffolds and templates for supramolecular chemistry. Imperial College Press, London. 1999.
18. M.T. Reetz and S.R. Waldvogel. Angew. Chem. **109**, 870 (1997); Angew. Chem. Int. Ed. Engl. **36**, 865 (1997).
19. M.T. Reetz. Catal. Today, **42**, 399 (1998).
20. Z. Chen, J.S. Bradshaw, G. Yi, D. Pyo, D.R. Black, S.S. Zimmerman, M.L. Lee, W. Tong, and V.T. D'Souza. J. Org. Chem. **61**, 8949 (1996).
21. M.J. Field, B.L. May, P. Clements, J. Tsanaktsidis, C.J. Easton, and S.F. Lincoln. J. Chem. Soc. Perkin Trans. 1, 1251 (2000).
22. Y. Liu, C.-C. You, T. Wada, and Y. Inoue. J. Org. Chem. **64**, 3630 (1999).
23. E.L. Eliel, S.H. Wilen, and N.N. Mander. Stereochemistry of organic compounds. Wiley, New York. 1994.
24. Program SYBYL 6.7. Tripos, Inc., St. Louis, Missouri, U.S.A. 2001.
25. W. Saenger. Structural aspects of inclusion compounds formed by organic host lattices. *In* Inclusion compounds. Vol. 2. *Edited by* J.L. Atwood, J.E.D. Davies, and D.D. MacNicol. Academic Press, New York. 1984. pp. 231–259.
26. G.A. Jeffrey and W. Saenger. Hydrogen bonding in biological structures. Springer, Berlin. 1991. p. 35 ff.
27. Y. Matsui and A. Okimoto. Bull. Chem. Soc. Jpn. **51**, 3030 (1978).
28. G.M. Sheldrick. Acta Crystallogr. Sect. A: Fundam. Crystallogr. **46**, 467 (1990).
29. G.M. Sheldrick. SHELXL-97. Program for crystal structure refinement. Universität Göttingen, Germany. 1997.

© 2001 NRC Canada

Total synthesis of polyoximic acid

Stephen Hanessian and Jian-min Fu

Abstract: The structure and stereochemistry of polyoximic acid, a degradation product of polyoxins, was originally designated as *trans*-3-ethylidene-L-azetidine-2-carboxylic acid. However, total synthesis revealed that the correct structure was in fact *cis*-3-ethylidene-L-azetidine-2-carboxylic acid, which was confirmed by X-ray crystallography. The synthesis of the *trans*-isomer was also done and its identity was confirmed by X-ray analysis as well. The key step for constructing the four-membered ring was a rhodium catalyzed carbenoid insertion into the N—H bond of a β-amino acid derivative. The stereoselectivity of the *exo*-double bond was controlled by conducting a Horner-Emmons-Wadsworth or a Wittig reaction to generate the *trans*- and *cis*-isomers, respectively. Weinreb's amide was used as a latent methyl group for the separation of *trans* and *cis* mixtures. The double bond stereochemistry of polyoximic acid in the parent polyoxin was also confirmed to be *cis* by extensive 2D NMR studies.

Key words: diazoinsertion, azetidine, olefination.

Résumé : La structure et la stéréochimie originalement attribuées à l'acide polyoximique, un produit de dégradation des polyoxines, étaient celles de l'acide *trans*-3-éthylidène-L-azétidine-2-carboxylique. Une synthèse totale a toutefois permis de démontrer qu'il s'agit plutôt de son isomère, l'acide *cis*-3-éthylidène-L-azétidine-2-carboxylique, ce qui a été confirmé par diffraction des rayons X. On a aussi réalisé la synthèse de l'isomère *trans* et son identité a aussi été confirmée par diffraction des rayons X. L'étape clé dans la construction du cycle à quatre chaînons est une insertion de carbénoïde dans la liaison N—H d'un dérivé d'acide β-aminé, catalysée par le rhodium. La stéréosélectivité de la double liaison *exo* est contrôlée en procédant à une réaction d'Horner-Emmons-Wadsworth ou d'une réaction de Wittig qui conduisent respectivement aux isomères *trans* et *cis*. L'amide de Weinreb a été utilisé comme groupe méthyle latent pour la séparation des mélanges *trans* et *cis*. En se basant sur des études approfondies de RMN 2D, on a aussi confirmé que la stéréochimie de la double liaison de l'acide polyoximique de la polyoxine de base est aussi *cis*.

Mots clés : diazoinsertion, azétidine, oléfination.

[Traduit par la Rédaction]

Introduction

In the 1960's, Isono and co-workers (1*a*, *c*–*j*) first isolated and characterized a series of nucleoside antibiotics designated as the polyoxins from culture broths of *Streptomyces cacacoi var asoensis*. Since then, new members were added to this family that constitute the fifteen known polyoxins A–O (2). These compounds are potent inhibitors of chitin synthetase and could be used as fungicides for treating plant diseases (3) and other applications (for other biological uses of polyoxins, see ref. 4). Consequently a great deal of effort has been devoted to the structural elucidation (5), biosynthesis (6), structural–activity relationships (7), and total synthesis (8) of this small family of antibiotics. The structures and configurations of the polyoxins, represented by polyoxin A and its degradation product polyoximic acid (**1**), were proposed as depicted in Fig. 1.

The structural elucidation was based on the analysis of the degradation products (5). For example, treatment of polyoxin A (Scheme 1) with acid or base led to the generation of 5-hydroxymethyl uracil (**3**), polyoxin C (**4**), polyoxamic acid (**5**), and polyoximic acid (**1**). The latter is a unique amino acid that is a component of polyoxins A, F, H, and K. Total syntheses of polyoxin C (9), polyoxins B and D (10), polyoxins J and L (11), and polyoxamic acid (12) have been reported. Only two reports in the literature address the total synthesis of polyoximic acid (13, 14). Baumann and Duthaler (13) described an approach using a Claisen rearrangement or cycloaddtion reaction for the synthesis of key intermediates. Emmer (14) reported a total synthesis of racemic *trans*-polyoximic acid using a rhodium catalyzed intramolecular carbenoid insertion reaction.

Initially, racemic polyoximic acid (*rac*-**1**) was obtained from polyoxin A by either basic or acidic hydrolysis (Scheme 2) (5). Upon ozonolysis, the characterizable product **6** was produced, thus establishing the atomic composition of the molecule. The stereochemistry of the exocyclic double bond was established as *trans* based on an NOE study using a 60 MHz NMR instrument. Additionally, hydrogenolysis of the parent polyoxin A produced the saturated intermediate

Received May 10, 2001. Published on the NRC Research Press Web site at http://canjchem.nrc.ca on November 21, 2001.

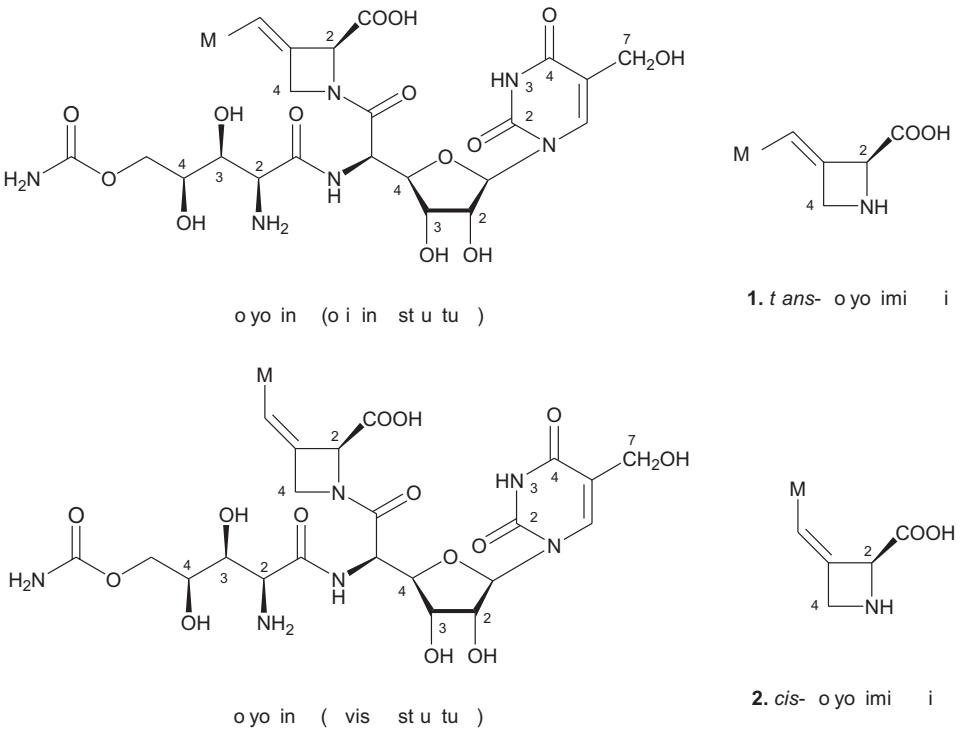
Dedicated to Professor Victor Snieckus: a friend, scholar, and chemist extraordinaire.

S. Hanessian.[1] Department of Chemistry, Université de Montréal, Montréal, QC H3C 3J7 Canada.
J.-m. Fu. Pharmacia Corp. 7255-209-706, Structural, Analytical and Medicinal Chemistry, 301 Henrietta St., Kalamazoo, MI 49007, U.S.A.

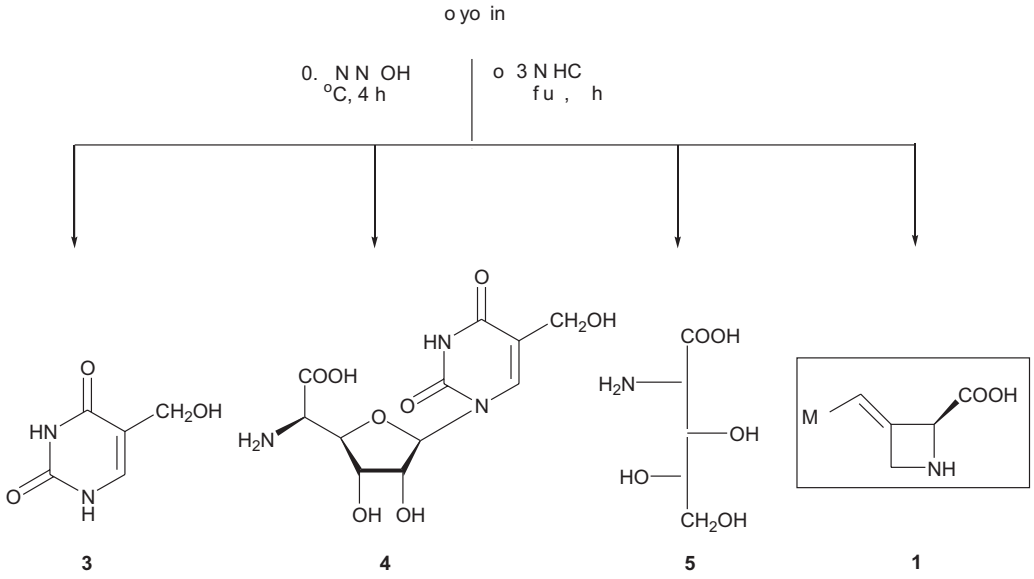
[1]Corresponding author (telephone: (514) 343-6738; fax: (514) 343-5728; e-mail: stephen.hanessian@umontreal.ca).

 DOI: 10.1139/cjc-79-11-1812 © 2001 NRC Canada

Fig 1.



Scheme 1.



dihydropolyoxin A **7**, and subsequent basic hydrolysis generated the dihydro polyoximic acid **8**, which was converted to its *N*-dithiocarbethoxy derivative whose positive Cotton effect was compared to that of the known analogous derivative prepared from L-azetidine-2-carboxylic acid. Thus, the absolute configuration of the amino acid was established as (*S*) (5).

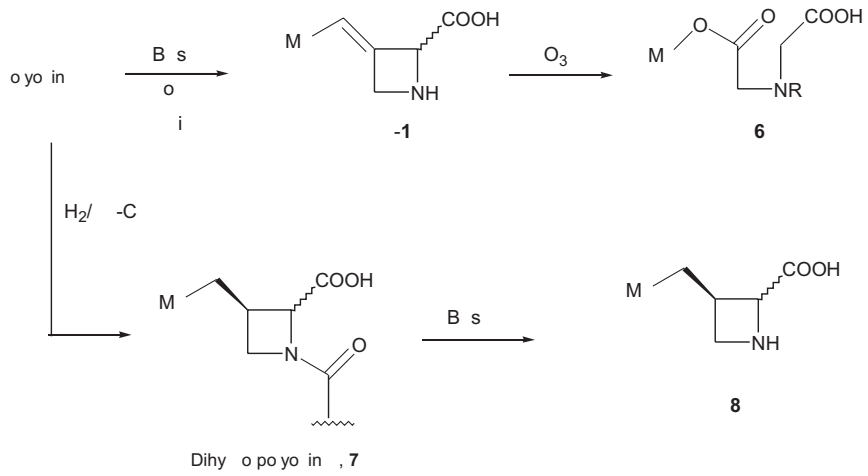
In the course of our studies (15*a*) directed at the total synthesis of polyoximic acid, we discovered that the structure was originally assigned incorrectly as the *trans*-isomer (15*b*). Here we wish to report in detail the total synthesis of this four-membered amino acid as the *cis*-isomer, as well as a synthesis of the *trans*-isomer.

Results and discussion

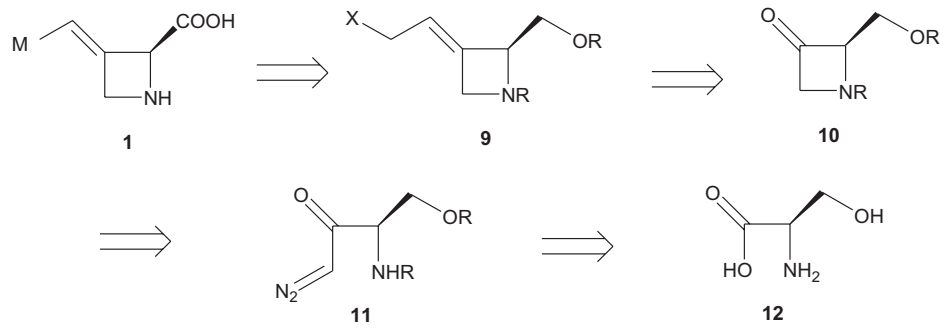
We envisioned that the total synthesis of polyoximic acid could be accomplished from D-serine, as illustrated by the disconnections shown in Scheme 3. The carboxylic acid could be derived from a latent functional group like an alcohol **9**, and the *exo*-double bond would originate from a Wittig reaction on the azetidinone **10**. The four-membered ring of **10**

© 2001 NRC Canada

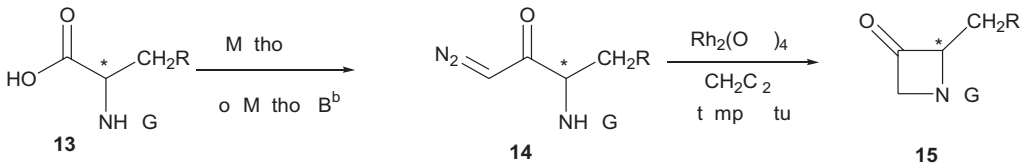
Scheme 2.



Scheme 3.



Scheme 4.



would be constructed by an intramolecular rhodium catalyzed carbene insertion into the N—H bond of the diazoketone, which in turn could be generated from the amino acid D-serine (**12**). This approach to the synthesis does not require us to build any new stereogenic centers on an sp^3 carbon, and relies on the general design principles embodied in the "Chiron" approach (16).

Thus, the formation of azetidinone **10**, from the rhodium catalyzed intramolecular carbenoid insertion reaction, would be the pivotal step of the total synthesis. Although rhodium catalyzed carbene insertions to C—H and O—H bonds have been extensively studied (17), to our knowledge, there was no precedence in the literature of using rhodium catalysis to promote an intramolecular carbene insertion into an N—H bond to form a four-membered ring from enantiopure α-amino acids (18). Hence, a methodological study was carried out first on simple amino acid templates such as phenylalanine and alanine (Scheme 4, Table 1) to explore the appropriate conditions. The diazoketones **14a–f** were prepared from different amino acids by reacting with diazomethane via either a mixed anhydride (method A) or an acyl chloride (method B). Subjection of the phenylalanine diazoketone **14a** to catalysis by rhodium(III) at different temperatures (rt, –20, –40, –78°C) revealed that –40°C was the optimal temperature giving a 70% yield of the expected 3-azetidinone. This temperature (–40°C) appeared to work well for the alanine system (Table 1, entries 6 and 7) with Cbz and Ts as the amino protecting groups. In contrast, when the amino protecting group was changed to Boc, the reaction led to the formation of unidentified materials (Table 1, entries 5 and 9) and no product could be isolated. Normally, carbene insertion reactions are carried out at rt or higher (17).

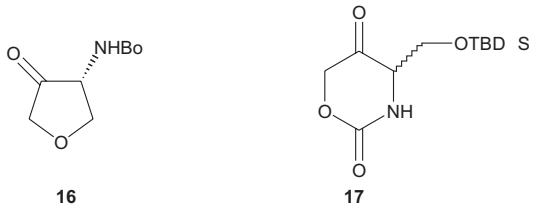
These low temperature conditions were then applied to the synthesis of polyoximic acid, starting with D-serine (**12**). In sharp contrast to the phenylalanine and alanine systems, the Boc group emerged as a better amino protecting group than Cbz (Scheme 4, Table 1, entries 10 and 11). In addition, the TBDPS (19) hydroxyl protecting group was found better than TBDMS (20). From the rhodium catalyzed reaction of diazoketone **14h**, two side products **16** and **17** were isolated in addition to the desired product **15h**. Compound **16** was formed by insertion of the carbene into the oxygen—silicon

© 2001 NRC Canada

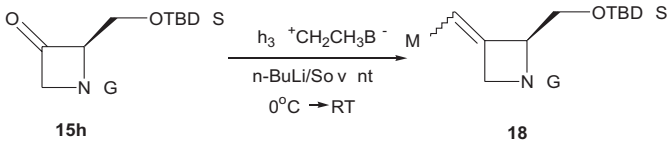
Table 1.

Entry	R	PG	Configuration	Method[a]	Product **14** (yield, %)	Temp. (°C)	Product **15** (yield, %)
1	Ph	Cbz	*R*	A	**14a** (74)	rt	**15a** (0)
2	Ph	Cbz	*R*	A		–20 → rt	**15a** (61)
3	Ph	Cbz	*R*	A		–40 → rt	**15a** (70)
4	Ph	Cbz	*R*	A		–78 → rt	**15a** (46)
5	Ph	Boc	*R*	A	**14b** (71)	–40 → rt	**15b** (0)
6	H	Cbz	*R*	A	**14c** (69)	–40 → rt	**15c** (71)
7	H	Cbz	*S*	A	**14d** (75)	–40 → rt	**15d** (68)
8	H	Ts	*R*	B	**14e** (77)	–40 → rt	**15e** (75)
9	H	Boc	*rac*	A	**14f** (95)	–78 → rt	**15f** (0)
10	OTBDMS	Cbz	*R*	A	**14g** (35)	–40 → rt	**15g** (19)
11	OTBDPS	Boc	*R*	A	**14h** (97)	–40 → rt	**15h** (50)
12	OTBDPS	Boc	*R*	A		–78 → rt	**15h** (57)
13	OTBDPS	Boc	*R*	A		–95 → rt	**15h** (67)

[a]Method A: *t*-BuOCOCl, *N*-methylmorpholine, $CH_2N_2 \cdot Et_2O$, CH_2Cl_2, –10 to 0°C ; Method B: (*i*) PCl_5, Et_2O, (*ii*) $CH_2N_2 \cdot Et_2O$, 0°C.



Scheme 5.



bond, and **17** was derived from the ylide, which was formed by reaction of the carbene with the Boc carbonyl. Since the four-membered ring product **15h** was the kinetic product, lower temperature was presumed to be beneficial. When the reaction was carried out at –78°C, the yield increased to 57% (Table 1, entry 12). A further decrease of the reaction temperature to –95°C furnished **15h** in 67% yield. A temperature lower than –95°C was not pursued since the reaction mixture starts to freeze at –95°C in CH_2Cl_2. The highest yield (75%) was observed in the case of the N-Ts analog **15e**. However, the synthesis was continued with the N-Boc derivative **15h** for ease of deprotection.

Having secured a method to construct the four-membered ring skeleton, the next stage of the synthesis was to introduce the ethylidene group by conducting the Wittig reaction. Under normal Wittig conditions (Scheme 5 and Table 2, entry 1), a 1:2 mixture of *E*:*Z* olefins **18** was produced in favor of the *Z* isomer, which were not separable by normal chromatography methods. The stereoselectivity of the double bond formation was not improved by solvent variations (toluene, HMPA, Table 2, entries 2 and 3), or by using salt free conditions (entry 4). In addition, Schlosser's conditions (21) (entry 5) reversed the stereoselectivity in favor of the *E* isomer (*E*:*Z*, 2:1).

Table 2.

Entry	Solvent	Yield (%)	*E*:*Z*
1	THF	54	33:67
2	Toluene	50	37:63
3	HMPA	19	37:63
4	THF[a]	55	37:63
5	THF[b]	24	61:39

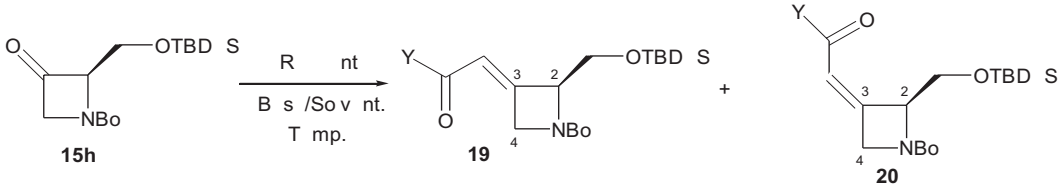
[a]Salt free conditions: NaHMDS, 0°C.
[b]Wittig–Schlosser conditions (ref. 21).

To better control the stereochemistry of the double bond, we changed the Wittig ylide from an unstabilized one to a stabilized one with either an aldehyde or ester (Scheme 6), since stabilized ylides normally favor *E*-isomer formation (22). Moreover, the aldehyde or ester could be considered as a latent methyl group as required in polyoximic acid. The results (Table 3, entries 1–6) showed that the stereoselectivity was not improved, and the *E*:*Z* mixture of olefins was still inseparable for both the aldehyde and the ester cases. Alternatively, an Horner-Emmons-Wadsworth reaction was considered. Indeed, *E*-isomer formation was favored, and the ratio was improved as expected (Table 3, entries 7–10). We then turned our attention to the cyano group (Table 3, entries 11–17), and found that the *E*:*Z* mixture of cyano olefins could be separated by iterative preparative TLC. It appeared that the phosphine oxide was the best choice with respect to obtaining a higher *E*:*Z* ratio (Table 3, entries 16 and 17). With both isomers in hand, we could determine the double bond geometry by an NOE study (Fig. 2). Although the enhancement was not significant, the *E*- and *Z*-isomers were differentiated by comparing the corresponding enhancements of the two isomers. Retrospectively, this evidence was used to confirm the stereochemical outcome of the Wittig and Horner-Emmons-Wadsworth reactions for the inseparable *E*- and *Z*-product mixtures (Schemes 5 and 6) by comparing their ^{1}H NMR spectra.

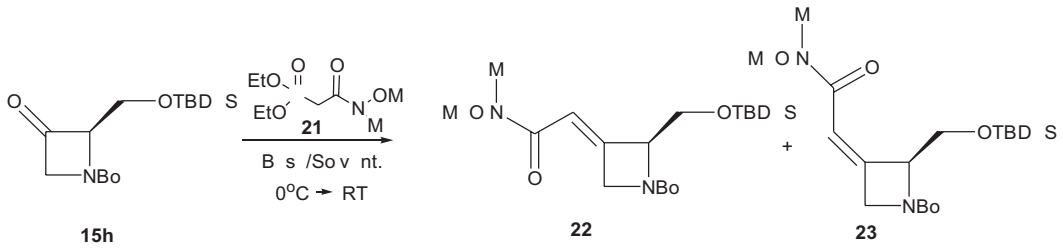
After separation of the cyano olefins **19** and **20**, the *E*-isomer was subjected to reduction to obtain the corresponding aldehyde. Unfortunately, using DIBAL-H (1–5 equiv.) in

© 2001 NRC Canada

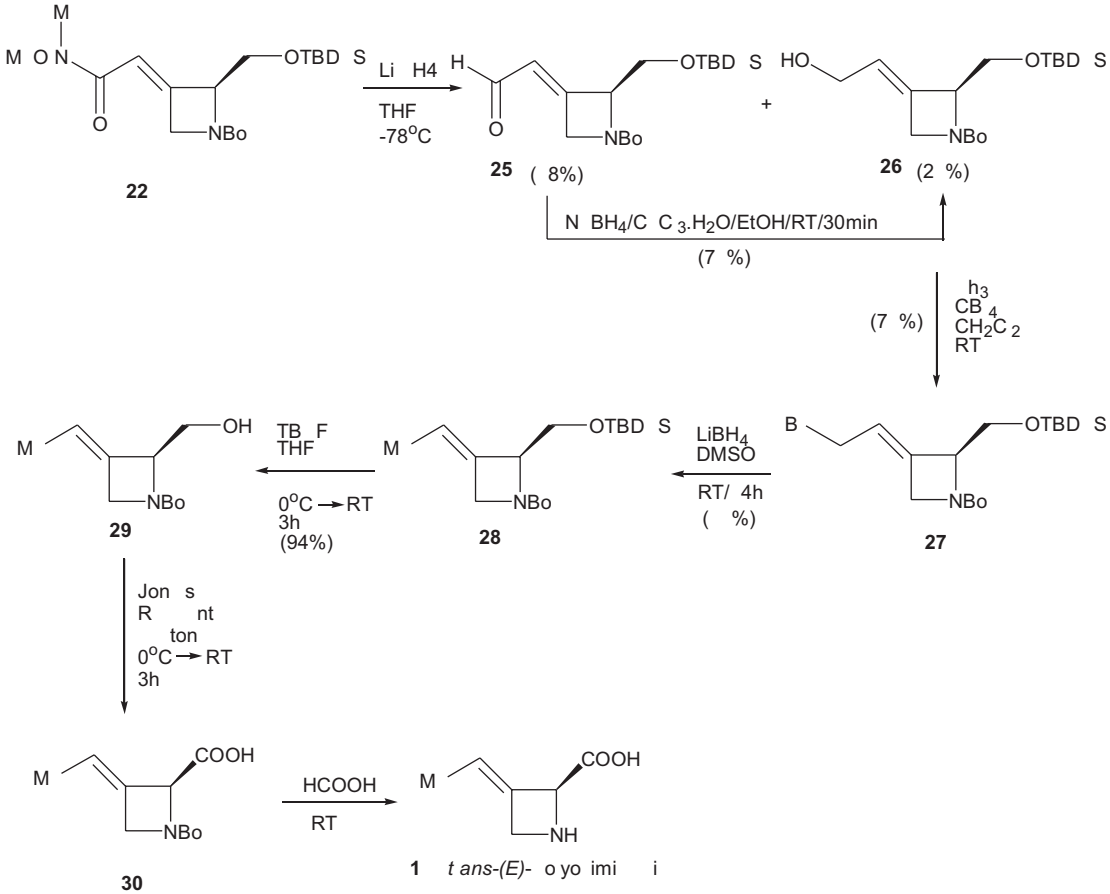
Scheme 6.



Scheme 7.



Scheme 8.



Et_2O or toluene at 0, –40, or –78°C gave at best 30% yield of the expected aldehyde. Either products of decomposition or starting material was recovered from the reduction. Therefore this route using the cyano group as the latent methyl group in the natural product was not pursued further.

Nevertheless, we discovered that the phosphonate amide by Nahm and Weinreb (23) provided a solution for this problem since it could be reduced more easily than the cyano group. Different conditions for the Horner-Emmons-Wadsworth reaction (Scheme 7) of compound **15h** with reagent **21** were explored. A mixture of *E*- (**22**) and *Z*- (**23**) isomers was obtained and separated by column chromatography. Sodium hydride in THF (Table 4, entry 5) was found to give the best result with a 94:6 ratio in favor of the *E*-iso-

© 2001 NRC Canada

Table 3.

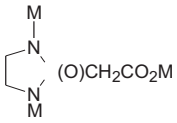
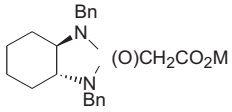
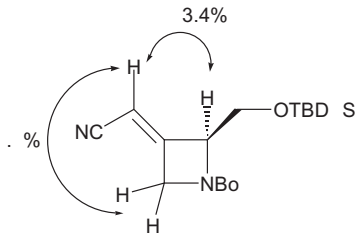
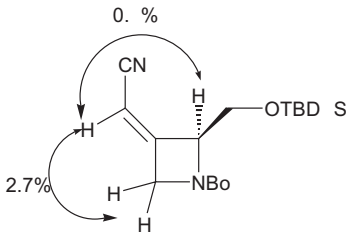
Entry	Reagent	Base	Solvent	Temp. (°C)	Y	Yield (%)	*E*:*Z*
1	$Ph_3P{=}CHCO_2Et$	—	CH_3CN	Reflux	EtO	77	26:74
2	$Ph_3P{=}CHCO_2Et$	—	MeOH	0 → rt	EtO	78	17:83
3	$Ph_3P{=}CHCO_2Et$	—	MeOH	–78 → rt	EtO	84	14:86
4	$Ph_3P{=}CHCO_2Et$	—	DMF	0 → rt	EtO	93	25:75
5	$Ph_3P{=}CHCO_2Et$	—	CF_3CH_2OH	0 → rt	EtO	84	61:39
6	$Ph_3P{=}CHCHO$	—	CH_3CN	Reflux	H	35	50:50
7	$(i\text{-}PrO)_2P(O)CH_2CO_2Et$	*n*-BuLi	DME	rt	EtO	82	80:20
8	$(EtO)_2P(O)CH_2CO_2$-*t*-Bu	*n*-BuLi	DME	rt	*t*-BuO	52	87:13
9		NaH	THF	0 → rt	MeO	71	80:20
10		NaH	THF	0 → rt	MeO	32	91:9
11	$(EtO)_2P(O)CH_2CN$	*n*-BuLi	DME	rt	CN	78	73:27
12	$(EtO)_2P(O)CH_2CN$	NaH	DME	rt	CN	61	83:17
13	$(EtO)_2P(O)CH_2CN$	KH	DME	rt	CN	77	79:21
14	$Ph_3P{=}CHCN$	KH	CH_3CN	Reflux	CN	78	55:45
15	$Ph_3P{=}CHCN$	KH	PhH	Reflux	CN	78	64:36
16	$Ph_2P(O)CH_2CN$	KH	DME	rt	CN	53	89:11
17	$Ph_2P(O)CH_2CN$	KH	THF	rt	CN	51	77:23

Fig 2.



19 *t ans, (E-)*



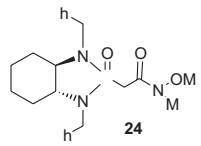
20 *cis, (Z-)*

mer. The chiral non-racemic phosphonamide reagent **24**, developed in our laboratories (24), was also attempted and gave an *E*:*Z* ratio of 88:12.

Our efforts toward the synthesis of the *trans*-(*E*)-isomer of polyoximic acid is shown in Scheme 8. Reduction of the amide **22** with LAH gave a mixture of the α,β-unsaturated aldehyde **25** and the alcohol **26**. The aldehyde was reduced under

Table 4.

Entry	Base	Solvent	Yield (%)	**22**:**23**
1	*n*-BuLi	DME	65	88:12
2	NaH	DME	61	87:13
3	KH	DME	66	85:15
4	*n*-BuLi	THF	56	86:14
5	NaH	THF	7	94:6
6[a]	NaH	THF	83	88:12

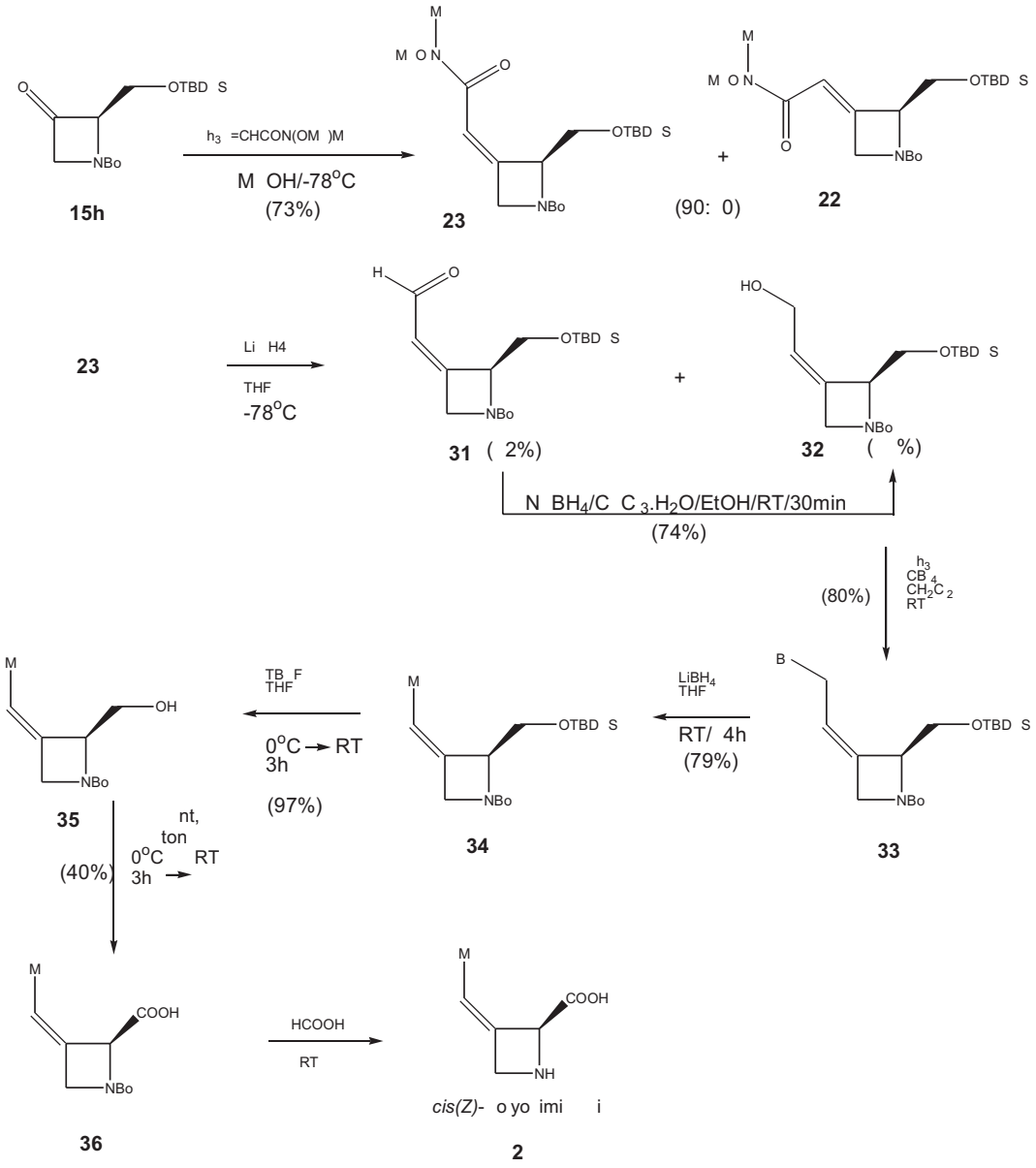
[a] 

24

Luche conditions (25) to the alcohol **26** in good yield. The latter was converted to the bromide **27**, which was further reduced to the methyl compound **28**. Removal of the TBDPS group of **28** and attempts to oxidize the alcohol group in **29** to the carboxylic acid **30** proved problematic. The corresponding aldehyde, obtained from Swern or Dess-Martin oxidations was unstable. Eventually, the classic Jones oxidation emerged as the best method to yield **30** in 40% yield. Finally, the *N*-Boc protecting group was removed by stirring compound **30** with formic acid to produce the *trans*-(*E*)-polyoximic acid **1**, as a crystalline solid, whose structure was definitively confirmed by X-ray analysis. After completing the synthesis of *trans*-(*E*) **1**, and being unaware of the incorrect stereochemistry of the natural product, we compared the ^{1}H NMR spectrum of the synthetic sample with an

© 2001 NRC Canada

Scheme 9.



authentic one kindly provided by Professor Isono. The spectra were in fact different, and we had synthesized the incorrect isomer.

Faced with this dilemma, we were fortunate that the sample of racemic polyoximic acid received from Professor Isuno was in excellent physical state and amenable to X-ray analysis. The result shown in Fig. 3 confirms unambiguously that the geometry of the exocyclic double bond of the natural product is indeed *cis*-(*Z*), contrary to the original assignment (5).

With this important stereochemical revision, we turned our attention to the synthesis of the natural *cis*-(*Z*)-polyoximic acid **2**. The ready availability of the 3-azetidinone **15h** (Scheme 6), urged us to develop methodology directed at enriching the desired *Z*-isomer. Our studies on olefin formation had shown that the Wittig reaction favors the *Z*-product particularly in a protic solvent (Table 3, compare with Table 4). Therefore the Weinreb ester of the Wittig reagent became a logical choice as a (*Z*)-olefinating reagent in methanol (Scheme 9). Under these conditions, the *E*:*Z*-mixture of olefins was obtained in 73% yield and in a ratio of 10:90. In acetonitrile or THF, the ratios were 64:36 and 61:39, respectively, as determined by ^{1}H NMR spectroscopy. With a satisfactory method to obtain the (*Z*)-isomer **23**, the synthesis was carried out in a manner similar to that of the (*E*)-isomer, affording crystalline *cis*-(*Z*)-polyoximic acid **2** (Scheme 9).

Comparison of the spectroscopic and physical data of the synthetic material **2** with that of the natural product, confirmed the proposed structure, and the geometry of the double bond. The spectra in CD_3OD for the *cis*-(*Z*)- and *trans*-(*E*)-synthetic products, as well as that of the racemic natural product are shown in Fig. 4. It is interesting that the vinylic proton and the methyl protons in the *trans*-isomer **1** are shifted downfield and upfield, respectively, compared to the signals of the *cis*-isomer **2**. This pattern was also found in

© 2001 NRC Canada

Scheme 10.

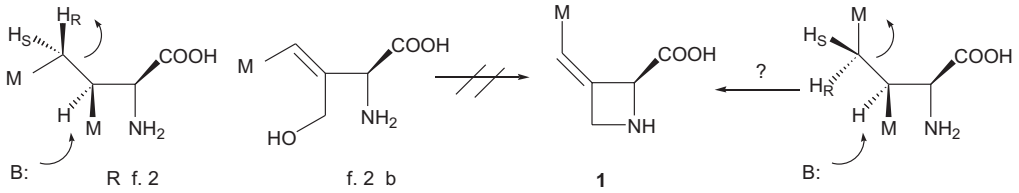
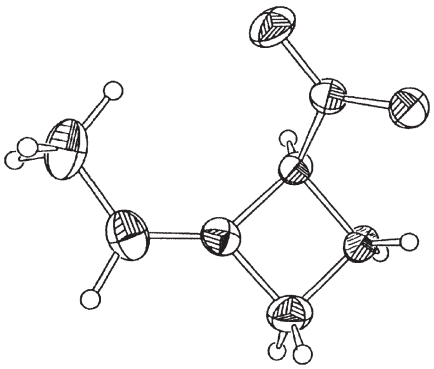


Fig. 3. Ortep drawing and structure of racemic *cis*-polyoximic acid.



D_2O and DMSO-d_6. The amino acid **2** was partially racemized in methanol containing a drop of Et_3N (~50% within 20 h at rt).

The geometry of the exocyclic double in the 3-azetidinone **15h**, could be controlled by conducting either the Horner-Emmons-Wadworth reaction or the Wittig reaction to generate a (*E*)- or (*Z*)-olefin preponderantly. Apparently, the Horner-Emmons-Wadsworth reaction gives the thermodynamic product as a major isomer at 0°C, and the Wittig reaction gives the kinetic product. To what extent, the nature of the Weinreb amide influences the respective transition states compared to normal esters is a matter of speculation (Tables 3 and 4). Dipolar and stereoelectronic effects could be playing important roles in both reactions. In addition, the nature of the solvent and cation is important in the phosphonate case, while the protic medium may promote a faster collapse of the more congested (*Z*)-betaine via the corresponding oxaphosphetane.

Since polyoximic acid was the degradation product of polyoxin, we had to be assured that no isomerization of the double bond had occurrred during the hydrolysis process or subsequent isolation. The 1D ^1H NMR spectrum of polyoxin A provided by Professor Isono is shown in Fig. 5, where the 6″-methyl, 5″-vinylic, and 2″-α-carboxyamide protons are clearly distinguishable. These correspond in pattern and in chemical shift differences to the *cis*- rather than the *trans*-polyoximic acid moiety.

Proton connectivities by the J-correlated spectroscopy (COSY) technique located the "intact" polyoximic acid moiety. Next, we carried out a 2D NOE correlated spectroscopy experiment (NOESY) to secure the *cis* orientation of the ethylenic group vis-à-vis the carboxamide group. Positive enhancements were observed between the ethylene methyl group and the α-carboxamide hydrogen, which is consistent with a *cis*-type geometry. These were independently corroborated by NOE studies on the *cis*- and *trans*-polyoximic acids in D_2O and DMSO-d_6.

With the establishment of the *cis* stereochemistry for polyoximic acid, the proposal of an elimination of the pro-*R* hydrogen at C-4 of L-isoleucine (26*a*), and the possible intermediacy of a hypothetical precursor, L-2-amino-3-hydroxymethyl-3-pentenoic acid (26*b*), must be reassessed (Scheme 10). If the double bond is indeed introduced by an enzymatic process, it most likely involves a synperiplanar elimination.

Finally, it is of interest to point out that the structures of polyoximic acids **1** and **2**, and related structures resulting from the methodology developed in this work represent constrained analogs of amino acids (27) such as L-isoleucine, L-vinyl glycine (28), and their congeners. As such, they are interesting structures for exploitation as β-turn mimetics (for selected reviews, see ref. 29) in a variety of peptide-like motifs.

In summary, after more than 30 years since the isolation and structure determination of polyoxin (5), the diminutive yet intriguing amino acid polyoximic acid was synthesized in enantiopure form, and the geometry of the double bond was reassigned as *cis* rather than *trans* through NMR spectroscopy and X-ray crystallography.

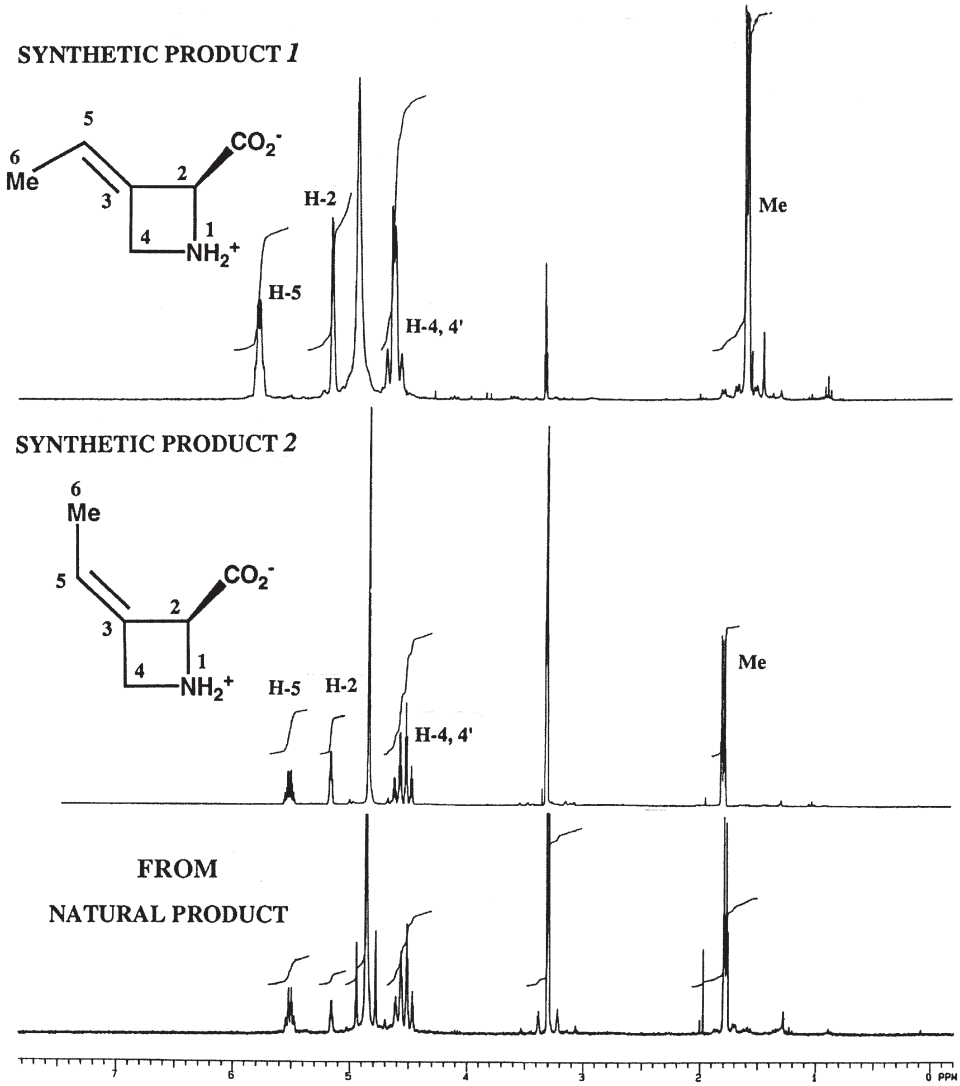
Experimental

General procedure

Flash chromatography was carried out using 230–400 mesh silica gel. Mixtures of ethyl acetate–hexanes were used as the eluents unless otherwise specified. Analytical thin layer chromatography (TLC) was performed on glass plates coated with 0.02 mm layer of silica gel 60 F-254. Melting points were uncorrected. IR spectra were recorded as films. ^1H NMR and ^{13}C NMR spectra were recorded at 300 and 75 MHz, respectively, and the chemical shifts are reported in parts per million on the δ scale with $CDCl_3$ as reference unless otherwise specified. MS and HRMS spectra were recorded using electron ionization (EI) or by the FAB technique. Elemental analyses were performed by Guelph Laboratories, Guelph, Ontario. Optical rotations were measured in $CHCl_3$ at 23°C. All reactions were carried out under nitrogen or argon atmosphere unless otherwise specified. The –78°C temperature is approximate as achieved by a dry ice – acetone bath. The –95°C temperature is approximate as achieved by a liquid nitrogen – methanol bath. The term "normal workup" means the addition of saturated aqueous NH_4Cl solution to the reaction mixture, followed extraction with ethyl acetate, drying over Na_2SO_4, filtration, and evaporation of the filtrate in vacuo to afford the crude product.

© 2001 NRC Canada

Fig. 4. 300 MHz ^{1}H NMR (CD_3OD) spectra of synthetic *trans* **1**, synthetic *cis*-**2** obtained by acid hydrolysis (ref. 5).



General procedure for the preparation of diazoketones (method A)

To a solution of the protected amino acid (1.00 mmol) in dichloromethane at –10°C was added simultaneously isobutyl chloroformate (1.07 mmol) and 4-methylmorpholine (1.07 mmol). After stirring for 45 min at –10°C, a solution of freshly prepared diazomethane in ether (18.75 mL, 6.68 mmol) was added, and stirring continued for 7 h at rt, followed by concentration in vacuo to dryness. The residue was subjected to column chromatography to afford the desired product.

*(3*R*)-1-Diazo-3-(*N*-benzyloxycarbonylamino)-4-phenyl-2-butanone (**14a**)*

According to method A, the title compound was prepared in 74% yield: mp 82–83°C (hexanes–CH_2Cl_2); $[\alpha]_D$ –13 (*c* 1.2, $CHCl_3$). FAB-MS (NBA) *m/z* (rel intensity): 324 ($[M + 1]^+$, 3), 307 (13), 289 (16), 154 (100), 136 (91), 106 (58). HRMS calcd. for $C_{18}H_{18}N_3O_3$ + H: 324.1349; found: 324.1329. IR (KBr) υ_{max} (cm^{-1}): 3335, 3082, 2118, 1700, 1626. ^{1}H NMR δ: 3.04 (d, *J* = 6.6 Hz, 2H), 4.46–4.55 (m, 1H), 5.08 (s, 2H), 5.20 (s, 1H), 5.38–5.40 (m, 1H), 7.15–7.38 (m, 10H). ^{13}C NMR δ: 54.6, 58.7, 67.0, 127.0, 128.0, 128.1, 128.4, 128.5, 128.6, 129.1, 129.2, 135.8, 136.0, 155.6, 192.6.

*(3*R*)-1-Diazo-3-(*N*-tert-Butyloxycarbonylamino)-4-phenyl-2-butanone (**14b**)*

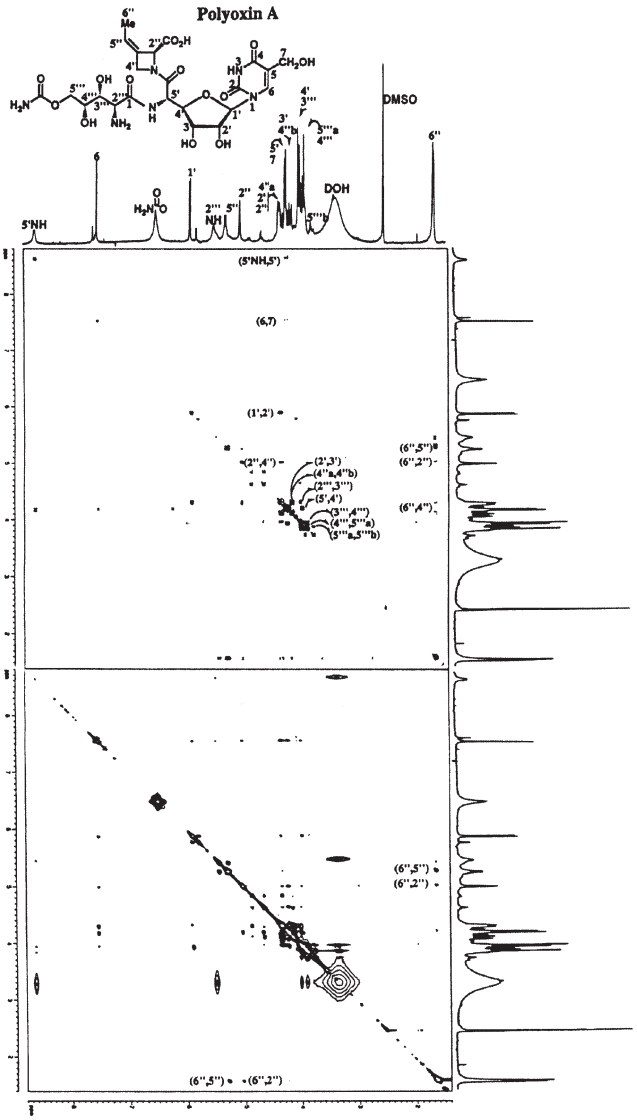
According to method A, the title compound was prepared in 71% yield: mp 87–89°C (hexanes–CH_2Cl_2); $[\alpha]_D$ –8.1 (*c* 1.02, $CHCl_3$). FAB-MS (NBA) *m/z* (rel intensity): 290 ($[M + 1]^+$, 18), 206 (100), 164 (31), 154 (70), 136 (52), 120 (84). HRMS calcd. for $C_{15}H_{20}N_3O_3$: 290.1506; found: 290.1472. IR (KBr) υ_{max} (cm^{-1}): 3340, 2102, 1690, 1640. ^{1}H NMR δ: 1.39 (s, 9H), 2.98–3.09 (m, 2H), 4.35–4.48 (br s, 1H), 5.14 (d, *J* = 7.7 Hz, 1H), 5.23 (s, 1H). ^{13}C NMR ($CDCl_3$) δ: 28.1, 38.4, 54.2, 58.3, 79.9, 126.8, 128.5, 129.2, 136.2, 155.0, 193.2.

*(3*R*)-1-Diazo-3-(*N*-benzyloxycarbonylamino)-2-butanone (**14c**)*

According to method A, the title compound was prepared in 69% yield: mp 92–94°C (hexanes–CH_2Cl_2); $[\alpha]_D$ +4.1 (*c* 1.0, $CHCl_3$). FAB-MS (NBA) *m/z* (rel intensity): 268 ($[M + 1]^+$, 16), 240 (38), 197 (62), 154 (100), 139 (20). HRMS calcd. for $C_{12}H_{14}N_3O_3$ + H: 248.1036; found: 248.1037. IR ($CHCl_3$) υ_{max} (cm^{-1}): 3326, 2124, 1730, 1650. ^{1}H NMR δ:

© 2001 NRC Canada

Fig. 5. 2D COSY NMR spectrum of natural polyoxin A in DMSO-d_6 at 400 MHz (top); 2D NOESY NMR spectrum in DMSO-d_6 at 400 MHz (bottom).



1.35 (d, *J* = 7.1 Hz, 3H), 4.20–4.37 (m, 1H), 5.11 (s, 2H), 5.40 (s, 1H), 5.47 (br, 1H), 7.31–7.37 (m, 5H). ^{13}C NMR ($CDCl_3$) δ: 18.5, 53.4, 53.5, 66.9, 128.0, 128.1, 128.4, 136.0, 155.5, 193.6.

rac-*1-Diazo-3-(*N-tert-*butyloxycarbonylamino)-2-butanone (**14f**)*

According to method A, the title compound was prepared in 95% yield: mp 87–89°C (hexanes–CH_2Cl_2). FAB-MS (NBA) *m*/*z* (rel intensity): 214 ([M + 1]$^+$, 35), 158 (50), 154 (80), 144 (26), 136 (71), 130 (100). ^{1}H NMR δ: 1.31 (d, *J* = 7.1, 3H), 1.43 (s, 9H), 4.14–4.29 (br s, 1H), 5.09–5.21 (br s, 1H), 5.44 (s, 1H). ^{13}C NMR ($CDCl_3$) δ: 18.3, 28.2, 53.0, 53.2, 79.9, 155.0, 194.3.

*(3*R*)-1-Diazo-3-(*N-tert-*butyloxycarbonyl)amino-4-*tert-*butyl-diphenyl-silyloxy-2-butanone (**14h**)*

According to method A, the title compound was prepared in 97% yield: mp 89–90°C (hexanes). [α]$_D$ –0.67 (*c* 1.05, $CHCl_3$). FAB-MS (NEA) *m*/*z* (rel intensity): 468 ([M + H]$^+$, 49), 410 (16), 199 (64), 135 (100). HRMS calcd. for $C_{25}H_{34}N_3O_4Si$ (M + H): 468.2320; found: 468.2266. IR ($CHCl_3$) υ$_{max}$ (cm^{-1}): 2103, 1711, 1641. ^{1}H NMR δ: 1.06 (s, 9H), 1.46 (s, 9H), 3.79–3.84 (dd, *J* = 10.2, 4.8 Hz, 1H), 3.96–4.01 (dd, *J* = 10.2, 3.9 Hz, 1H), 4.20–4.38 (br s, 1H), 5.35–5.38 (d, *J* = 7.8 Hz, 1H), 5.49 (s, 1H), 7.40–7.45 (m, 6H), 7.61–7.64 (m, 4H). ^{13}C NMR δ: 19.1, 26.4, 28.2, 54.1, 59.0, 64.0, 80.0, 127.7, 129.8, 132.6, 135.4, 155.2, 192.8.

(3*R*)-(+)-1-Diazo-3-(*N*-4-toluenesulphonylamino)-2-butanone (14e) (method B)

To a solution of *N*-4-toluenesulphonyl-D-alanine (5.73 g, 23.6 mmol) in ether (55.0 mL) was added pentachlorophosphorus (10.1 g, 48.3 mmol). After vigorous stirring at rt for 1 h, the reaction mixture was filtered. To the filtrate was added hexane (200 mL). The generated solid was filtered and collected to give 5.00 g (82%) of the chloride compound. The chloride was dissolved in ether (50.0 mL). To this solution was added diazomethane-etherate solution (140 mL) at 0°C. After 1 h, the reaction mixture was filtered through a pad of silica gel. The filtrate was concentrated in vacuo to dryness. The residue was subjected to column chromatography (EtOAc–hexane, 1:2) to afford 3.94 g (77%) of the desired product: oil. [α]$_D$ +116.2 (*c* 2.36, $CHCl_3$). FAB-MS *m*/*z* (rel intensity): 268 ([M + 1]$^+$, 16), 240 (35), 197 (61), 154 (100). HRMS calcd. for $C_{11}H_{14}N_3O_3S$: 268.0757; found: 268.0788. IR (neat) υ$_{max}$ (cm^{-1}): 3260, 2105, 1735, 1641, 1366. ^{1}H NMR δ: 1.24 (d, *J* = 7.1 Hz, 3H), 2.40 (s, 3H), 3.76–3.89 (m, 1H), 5.45 (s, 1H), 5.51 (d, *J* = 7.5 Hz, 1H), 7.28 (d, *J* = 8.0 Hz, 2H), 7.69–7.73 (m, 2H). ^{13}C NMR ($CDCl_3$) δ: 19.4, 21.4, 53.9, 55.2, 127.0, 129.7, 136.6, 143.7, 192.7.

General procedure for the preparation of azetidinone 15 (method C)

To a solution of the diazo compound **14** (1.00 mmol) in dichloromethane (10.0 mL) at the reaction temperature indicated was added rhodium acetate dimer (0.009 g, 0.020 mmol). The resulting reaction mixture was stirred that reaction temperature for 1 h and allowed to warm to rt for 14 h. The solvent was removed and the residue was subjected to column chromatography.

*(2*R*)-1-Benzyloxycarbonyl-2-benzyl-3-azetidinone (**15a**)*

The reaction was carried out at –40°C to give 70% of product **15a**: mp 85–87°C (hexanes–CH_2Cl_2). [α]$_D$ –124.6 (*c* 1.0, $CHCl_3$). EI-MS *m*/*z* (rel intensity): 295 (M$^+$, 3), 267 (18), 204 (38), 132 (30), 88 (100). HRMS calcd. for $C_{18}H_{17}NO_3$: 295.1209; found: 295.1238. IR (neat) υ$_{max}$ (cm^{-1}): 1819, 1691. ^{1}H NMR δ: 3.14 (dd, *J* = 14.3, 4.0 Hz, 1H), 3.24 (dd, *J* = 14.3, 6.3 Hz, 1H), 4.08 (dd, *J* = 16.5, 4.4 Hz, 1H), 4.59 (d, *J* = 16.5 Hz, 1H), 5.20 (s, 2H), 5.21–5.25 (m, 1H), 7.12–7.15 (m, 2H), 7.23–7.29 (m, 2H), 7.35–7.41 (m, 6H). ^{13}C NMR ($CDCl_3$) δ: 35.4, 67.3, 69.2, 83.5, 126.9, 128.1, 128.2, 128.4, 128.5, 129.7, 134.9, 136.0, 155.8, 198.7.

*(2*R*)-1-Benzyloxycarbonyl-2-methyl-3-azetidinone (**15c**)*

The reaction was carried out at –40°C to give 71% of product **15c**: mp 80–81°C (hexane–CH_2Cl_2). [α]$_D$ –39.7

© 2001 NRC Canada

(*c* 0.99, $CHCl_3$). EI-MS *m*/*z* (rel intensity): 219 (M^+, 1), 191 (4), 91 (100). HRMS calcd. for $C_{12}H_{13}NO_3$: 219.0896; found: 219.0935. IR ($CHCl_3$) υ_{max} (cm^{-1}): 1816, 1694. ^1H NMR δ: 1.49 (d, *J* = 7.0 Hz, 3H), 4.67 (dd, *J* = 16.5, 4.2 Hz, 1H), 4.97–5.07 (m, 1H), 5.17 (s, 2H), 7.27–7.39 (m, 2H).

*(2*R*)-1-*p-*Toluenesulphonyl-2-methyl-3-azetidinone (**15e**)*

According to method C, the reaction was carried out at –40°C to give 75% of product **15e**: mp 76–78°C (hexane–CH_2Cl_2). $[\alpha]_D$ –65.1 (*c* 1.09, $CHCl_3$). EI-MS *m*/*z* (rel intensity): 240 (M^+, 8), 211 (16), 155 (20), 105 (17), 91 (100). HRMS calcd. for $C_{11}H_{14}NO_3S$: 239.0617; found: 239.0605. IR (KBr) υ_{max} (cm^{-1}): 1831, 1599, 1345. ^1H NMR δ: 1.46 (d, *J* = 7.0 Hz, 3H), 2.47 (s, 3H), 4.43–4.60 (m, 2H), 4.76–4.80 (m, 1H), 7.38–7.41 (d, *J* = 8.3 Hz, 2H), 7.78–7.82 (m, 2H). ^{13}C NMR ($CDCl_3$) δ: 15.6, 21.5, 69.5, 80.9, 128.3, 130.0, 131.8, 144.9, 196.7.

*(2*R*)-1-*tert-*Butyloxycarbonyl-2-*tert-*butyldiphenylsilyloxymethylene-3-azetidinone (**15h**)*

The reaction was carried out at –95°C to give 67% of product **15h** as a colorless oil. $[\alpha]_D$ –41.9 (*c* 1.50, $CHCl_3$). FAB-MS (NBA) *m*/*z* (rel intensity): 440 ($[M + H]^+$, 4), 384 (10), 326 (57), 306 (63), 198 (78), 197 (77), 135 (100). HRMS calcd. for $C_{25}H_{34}NO_4Si$ (M + H): 440.2258; found: 440.2294. IR (film) υ_{max} (cm^{-1}): 1831, 1705. ^1H NMR δ: 1.03 (s, 9H), 1.46 (s, 9H), 3.90–3.94 (dd, *J* = 11.4, 1.7 Hz, 1H), 4.00–4.20 (br s, 1H,), 4.68–4.70 (m, 2H), 4.88 (br s, 1H), 7.37–7.47 (m, 6H), 7.62–7.73 (m, 4H). ^{13}C NMR δ: 19.1, 26.5, 28.2, 60.3, 70.0, 80.6, 84.0, 127.7, 129.8, 132.6, 135.4, 155.1, 198.9.

(2*R*)-2-(*tert*-Butyloxycarbonylamino)-4-oxacyclopentanone (16)

Compound **16** was isolated as a side product when preparing compound **15h** (12%): oil. IR (neat) υ_{max} (cm^{-1}): 3431, 1770, 1711. ^1H NMR δ: 1.45 (s, 9H), 3.78 (dd, *J* = 10.4, 9.0 Hz, 1H), 3.93 (d, *J* = 17.2 Hz, 1H), 4.09–4.21 (br s, 1H), 4.20 (d, *J* = 17.2 Hz, 1H), 4.64–4.72 (m, 1H), 4.91–5.01 (br s, 1H).

***rac*-2-(*tert*-Butyldiphenylsilyloxymethyl)-3-aza-5-oxa-1,4-cyclohexanedione (17)**

Compound **17** was isolated as a side product when preparing compound **15h** (8%): mp 137–139°C. EI-MS *m*/*z* (rel intensity): 327 ($[M + 1]^+$, 38), 326 (M^+, 57), 296 (62), 282 (46), 248 (48), 199 (100). HRMS calcd. for $C_{17}H_{16}NO_4Si$: 326.0849; found: 326.0872. IR (KBr) υ_{max} (cm^{-1}): 3270, 1736, 1720. ^1H NMR δ: 1.04 (s, 9H), 3.80 (dd, *J* = 10.3, 2.8 Hz, 1H), 3.91–3.94 (br s, 1H), 4.56 (d, *J* = 17.0 Hz, 1H), 4.65 (d, *J* = 17.0 Hz, 1H), 6.49 (s, 1H), 7.37–7.46 (m, 6H), 7.58–7.67 (m, 4H). ^{13}C NMR ($CDCl_3$) δ: 19.0, 26.5, 61.1, 64.6, 71.8, 127.9, 130.1, 132.0, 135.5, 154.3, 200.9.

(2*S*,*E*/*Z*)-1-*tert*-Butyloxycarbonyl-2-*tert*-butyldiphenylsilyloxymethyl-3-ethylidene azetidine (18)

To a solution of (ethyl)triphenylphosphonium bromide (1.94 g, 5.23 mmol) in THF (30.0 mL) at rt was added *n*-butyllithium (2.12 mL, 2.19 M in hexanes, 4.65 mmol). The resulting orange red solution was stirred for 30 min and cooled down to 0°C. A solution of compound **15h** (0.511 g, 1.16 mmol) in THF (10.0 mL) was added. After stirring at rt for 14 h, water (30.0 mL) was added, THF was removed in vacuo and the aqueous solution was extracted with EtOAc (3 × 30 mL). The extracts were dried (Na_2SO_4) and filtered. Column chromatography (EtOAc–hexanes, 1:8) afforded 0.281 g (54%) of product **18** as a colorless oil. IR (film) υ_{max} (cm^{-1}): 1705. ^1H NMR δ: 1.05 (s, 9H), 1.40 (s, 9H), 1.58–1.60 (m, 3H), 3.79–3.86 (m, 1H), 3.90–4.10 (br s, 1H), 4.29–4.41 (m, 2H), 4.67 (br s, 1H), 4.80 (br s, 1H), 7.34–7.46 (m, 6H), 7.65–7.74 (m, 4H).

(2*S*,*E*)-1-*tert*-Butyloxycarbonyl-2-*tert*-butyldiphenylsilyloxymethyl-3-cyanocarbonyl methylidene-azetidine (19) and (2*S*,*Z*)-1-*tert*-butoxycarbonyl-2-*tert*-butyldiphenysilyloxymethyl-3-cyanocarbonyl-methylidene-azetidine (20)

To a solution of diethyl cyanomethylphosphonate (62.0 mg, 0.250 mmol) in DME (1.50 mL) at 0°C was added *n*-butyllithium (0.14 mL, 2.30 M in hexanes, 0.32 mmol). The resulting light yellow solution was stirred at 0°C for 20 min and rt for 20 min. The solution of compound **15h** (0.128 g. 0.29 mmol) in DMF (1.50 mL) was added. After stirring at rt for 2 h, the reaction was quenched with saturated NH_4Cl solution (1.00 mL). The aqueous solution was extracted with EtOAc (3 × 5.00 mL) and the combined EtOAc solutions were dried (Na_2SO_4) and filtered. The filtrate was concentrated in vacuo to dryness. Column chromatography (EtOAc–hexanes, 1:3) afforded 77.0 mg (57%) of product **19** and 22.0 mg (16%) of product **20**, both as colorless oils. For **19**: $[\alpha]_D$ –24.0 (*c* 1.22, $CHCl_3$). FAB-MS *m*/*z* (rel intensity): 463 ($[M + H]^+$, 47), 407 (66), 349 (46), 329 (52), 198 (52), 154 (70), 137 (71). 106 (59), 57 (100). HRMS calcd. for $C_{27}H_{34}N_2O_3Si$ (M+ H): 463.2419; found: 463.2435. IR (film) υ_{max} (cm^{-1}): 2221, 1710. ^1H NMR δ: 1.07 (s, 9H), 1.42 (s, 9H), 3.85–3.90 (dd, *J* = 10.6, 3.3 Hz, 1H), 3.97–4.08 (br s, 1H), 4.63–4.65 (dd, *J* = 2.9, 2.9 Hz, 2H), 4.84 (m, 1H), 5.38 (m, 1H). 7.37–7.48 (m, 6H), 7.62–7.67 (m, 4H). ^{13}C NMR δ: 19.1, 26.6, 28.1, 56.7, 62.8, 70.5, 80.5, 93.1, 114.3, 127.7, 129.8, 132.5, 135.4, 155.4. 160.7.

For **20**: $[\alpha]_D$ +61.3 (*c* 1–22, $CHCl_3$). FAB-MS *m*/*z* (rel intensity): 463 ($[M + H]^+$, 66), 407 (71), 349 (49), 329 (52), 307 (42), 137 (37), 106 (68), 57 (100). HRMS calcd for $C_{27}H_{34}N_2O_3Si$ (M + H): 463.2419; found: 463.2397. IR (film) υ_{max} (cm^{-1}): 2219, 1706. ^1H NMR δ: 1.06 (s, 9H), 1.42 (s, 9H), 4.08–4.25 (br s, 2H), 4.51–4.58 (ddd, *J* = 15.4, 2.0, 1.9 Hz, 1H), 4.61–4.68 (ddd, *J* = 15.4, 4.2, 2.3 Hz, 1H), 4.95–4.97 (m, 1H), 5.45–5.47 (m, 1H). 7.36–7.47 (m, 6H), 7.63–7.73 (m, 4H). ^{13}C NMR δ: 19.3. 26.7. 28.3. 57.2, 61.2. 72.3, 80.4, 92.9, 114.2, 127.7. 129.8, 132.9, 135.5, 155.2, 160.4.

(2*S*,*E*)-1-*tert*-Butyloxycarbonyl-2-*tert*-butyldiphenylsilyloxymethyl-3-(*N*-methoxy-*N*-methylcarbamoyl)methylidene-azetidine (22)

To a suspension of NaH (1.76 g, 60% in oil, 44.0 mmol, washed three times with ether) in THF (500 mL) at 0°C was added the solution of diethyl (*N*-methoxy-*N*-methylcarbamoylmethyl)phosphonate **21** (11.0 g, 46.0 mmol) in THF (50.0 mL). The resulting reaction mixture was stirred at 0°C for 10 min and at rt for 20 min, a solution of compound **15h** (17.9 g, 42.0 mmol) in THF (50.0 mL) was added. After stirring at rt for 14 h, water (30.0 mL) was added, THF was evaporated, and the aqueous solution was extracted with

© 2001 NRC Canada

EtOAc (3 × 30.0 mL). The combined EtOAc solution was dried (Na_2SO_4) and filtered. Column chromatography (CH_2Cl_2–C_6H_6–EtOAc, 4:2:1) afforded 16.0 g (73%) of product **22** as a colorless oil and 1.0 g (4.6%) of product **23** as a colorless solid. For **22**: $[\alpha]_D$ +3.2 (*c* 1.7 1, $CHCl_3$). FAB-MS *m*/*z* (rel intensity): 525 ($[M + H]^+$, 52), 469 (73), 451 (18), 411 (47), 213 (21), 197 (72), 154 (76), 136 (100). HRMS calcd. for $C_{29}H_{40}N_2O_5Si$ (M + H): 525.2786; found: 525.2723. IR (film) υ_{max} (cm^{-1}): 1718, 1644. ^1H NMR δ: 1.06 (s, 9H), 1.40 (s, 9H), 3.23 (s, 3H), 3.65 (s, 3H), 3.93–4.01 (br s, 2H), 4.83–4.91 (m, 3H), 6.52–6.55 (br s, 1H), 7.34–7.46 (m, 6H), 7.65–7.69 (m, 4H). ^1H NMR (C_6D_6) δ: 1.13 (s, 9H), 1.39 (s, 9H), 2.87 (s, 3H), 3.10 (s, 3H), 3.86–4.30 (br s, 2H), 4.72–4.79 (br s, 1H), 5.12–5.27 (m, 2H), 6.60–6.70 (br s, 1H), 7.21–7.26 (m, 6H), 7.73–7.80 (m, 4H). ^{13}C NMR δ: 19.1, 26.6, 28.2, 31.8, 59.3, 61.6, 63.3, 70.2, 79.6, 110.3, 127.6, 129.6, 129.7, 132.9, 135.4, 154.4, 165.9. ^{13}C NMR (C_6D_6) δ: 19.5, 26.9, 28.4, 31.8, 60.2, 61.1, 63.7, 70.7, 79.2, 110.9, 128.1, 128.6, 130.0. 133.6, 136.0, 154.8, 166.0.

(2*S*,*Z*)-1-*tert*-Butyloxycarbonyl-2-*tert*-butyldiphenylsilyloxymethyl-3-(*N*-methoxy-*N*-methylcarbamoyl)methylidene-azetidine (23)

A mixture of compound **15h** (0.647g, 1.47 mmol) and *N*-methoxy-*N*-methyl-2-(triphenylphosphoranylidene)acetamide (0.642 g, 1.77 mmol) in MeOH (15.0 mL) was stirred at –78°C for 1 h and at rt for 24 h. After concentration to dryness, column chromatography (CH_2Cl_2–C_6H_6–EtOAc, 4:2:1) afforded 0.515 g (67%) of product **23** and 0.059 g (7.7%) of product **22**. For **23**: mp 119–121°C (CH_2Cl_2–hexanes). $[\alpha]_D$ +15.9 (*c* 0.79, $CHCl_3$). FAB-MS *m*/*z* (rel intensity): 525 ($[M + H]^+$, 44), 469 (27), 451 (16), 411 (40), 212 (54), 197 (66), 154 (82), 136 (100). HRMS calcd. for $C_{29}H_{40}N_2O_5Si$ (M + H): 525.2786; found: 525.2836. IR (film) υ_{max} (cm^{-1}): 1711, 1645. ^1H NMR δ: 1.03 (s, 9H), 1.40 (s, 9H), 3.18 (s, 3H), 3.70 (s, 3H), 4.05–4.15 (br s, 1H), 4.34–4.39 (m, 1H), 4.44–4.53 (m, 1H), 4.64–4.73 (m, 1H), 5.18–5.20 (br s, 1H), 6.34–6.41 (br s, 1H), 7.29–7.41 (m, 6H), 7.59–7.68 (m, 4H). ^1H NMR (C_6D_6) δ: 1.16 (s, 9H), 1.40 (s, 9H), 2.86 (s, 3H), 3.06 (s, 3H), 4.22–4.40 (br s, 2H), 4.66–4.76 (m, 2H), 5.37–5.38 (br s, 1H), 6.17 (br s, 1H), 7.21–7.29 (m, 6H), 7.76–7.84 (m, 4H). ^{13}C NMR δ: 18.9, 26.4, 28.0, 31.6, 56.9, 61.0, 61.3, 73.4, 79.2, 110.7, 126.8, 129.0, 133.1, 133.4, 135.1, 153.2, 165.1. ^{13}C NMR (C_6D_6) δ: 19.6, 27.1, 28.5, 31.8, 57.4, 61.1, 61.8, 74.1, 79.1, 111.6, 128.6, 129.8, 134.0, 134.3, 136.1, 153.8, 165.9. Anal. calcd for $C_{29}H_{40}N_2O_5Si$: C 66.38, H 7.68, N 5.34; found: C 66.38, H 7.62, N 5.25.

(2*S*,*E*)-1-*tert*-Butyloxycarbonyl-2-*tert*-butyldiphenylsilyloxymethyl-3-(formyl)methylidene-azetidine (25)

To a solution of **22** (8.70 g, 16.6 mmol) in THF (170 mL) at –78°C was added lithium aluminum hydride (3.15 g, 82.9 mmol). The resulting reaction mixture was stirred at –78°C for 1 h and quenched with H_2O (3.15 mL) at –78°C. After warming to rt, a 15% NaOH solution (3.15 mL) was added and the slurry was stirred for 15 min at rt followed by addition of H_2O (6.30 mL). The reaction mixture was filtered and the filtrate was concentrated in vacuo to dryness. Column chromatography (EtOAc–hexanes, 1:3) afforded 5.23 g (68%) of product **25** as a colorless oil and 1.65 g (21%) of product **26** as a colorless oil. For **25**: $[\alpha]_D$ –16.0 (*c* 2.01, $CHCl_3$). FAB-MS (NEA) *m*/*z* (rel intensity): 466 ($[M + H]^+$, 5), 427 (9), 352 (12), 197 (74), 154 (64), 135 (100). HRMS calcd. for $C_{27}H_{36}N_3O_4Si$ (M + H): 466.2415; found: 466.2390. IR ($CHCl_3$) υ_{max} (cm^{-1}): 2739, 1703, 1696. ^1H NMR δ: 1.05 (s, 9H), 1.43 (s, 9H), 3.87–3.91 (dd, *J* = 10.6, 2.7 Hz, 1H), 4.00–4.17 (br s, 1H), 4.86–4.88 (m, 2H), 4.93 (br s, 1H), 6.07–6.10 (m, 1H), 7.35–7.47 (m, 6H), 7.61–7.67 (m, 4H), 9.62–9.65 (d, *J* = 6.8 Hz, 1H). ^{13}C NMR δ: 19.4, 26.9, 28.4, 60.0, 62.2, 63.4, 71.6, 79.6, 122.4, 128.6, 130.1, 133.9, 135.9, 155.4, 159.2, 187.8.

(2*S*,*E*)-1-*tert*-Butyloxycarbonyl-2-*tert*-butyldiphenyisilyloxymethyl-3-(hydroxymethyl)methylidene-azetidine (26)

To a solution of **25** (5.11 g, 11.0 mmol) in ethanol (300 mL) at rt was added sodium borohydride (0.415 g, 11.0 mmol) and cerium trichloride heptahydrate (4.10 g, 11.0 mmol) simultaneously. The resulting reaction mixture was stirred at rt for 30 min and quenched with H_2O (300 mL). The aqueous solution was extracted with ethyl acetate (3 × 500 mL) and the combined ethyl acetate solution was dried (Na_2SO_4) and filtered. The filtrate was concentrated in vacuo to dryness. Column chromatography (CH_2Cl_2–hexanes–EtOAc, 2:1:1) afforded 4.54 g (89%) of product **26** as a colorless oil: $[\alpha]_D$ –13.3 (*c* 1.56, $CHCl_3$). FAB-MS (NBA) *m*/*z* (rel intensity): 468 ($[M + H]^+$, 20), 429 (18), 354 (44), 334 (43), 307 (40), 198 (63), 154 (90), 136 (100). HRMS calcd. for $C_{27}H_{38}NO_4Si$ (M + H): 468.2571; found: 468.2618. IR ($CHCl_3$) υ_{max} (cm^{-1}): 3420, 1700, 1676. ^1H NMR δ: 1.06 (s, 9H), 1.41 (s, 9H), 3.83–3.87 (dd, *J* = 10.4, 3.0 Hz, 1H), 3.95–4.09 (br s, 1H), 4.10–4.12 (d, *J* = 5.7 Hz, 2H), 4.51 (br s, 2H), 4.73 (br s, 1H), 5.61 (m, 1H), 7.35–7.43 (m, 6H), 7.65–7.70 (m, 4H). ^{13}C NMR δ: 19.2, 26.7, 28.3, 55.8, 60.0, 63.5, 70.1, 79.5, 120.8, 127.6, 129.6, 133.3, 133.4, 135.5, 155.8.

(2*S*,*E*)-1-*tert*-Butyloxycarbonyl-2-*tert*-butyldiphenylsilyloxymethyl-3-(bromomethyl)methylidene-azetidine (27)

To a solution of **26** (1.98 g, 4.23 mmol) in dichloromethane (85.0 mL) at rt was added triphenylphosphine (1.67 g, 6.35 mmol) and carbon tetrabromide (2.11 g, 6.35 mmol). The resulting reaction mixture was stirred at rt for 14 h and concentrated in vacuo to dryness. Column chromatography (EtOAc–hexanes, 1:6) afforded 1.67 g (75%) of product **27** as a colorless oil: $[\alpha]_D$ –10.9 (*c* 2.27, $CHCl_3$). FAB-MS (NBA) *m*/*z* (rel intensity): 532 ($[M + H]^+$, 3), 530 ($[M + H]^+$, 1), 418 (14), 416 (12), 199 (55), 197 (52), 135 (100). HRMS calcd. for $C_{27}H_{37}BrNO_3Si$ (M + H): 530.1727; found: 530.1783. IR ($CHCl_3$) υ_{max} (cm^{-1}): 1702. ^1H NMR δ: 1.06 (s, 9H), 1.41 (s, 9H), 3.84–3.88 (m, 3H), 3.90–4.10 (br s, 1H), 4.51 (br s, 2H), 4.76 (br s, 1H), 5.77 (m, 1H), 7.36–7.46 (m, 6H), 7.66–7.73 (m, 4H). ^{13}C NMR δ: 19.1, 26.6, 27.3, 28.2, 54.3, 63.1, 69.9, 79.7, 118.4, 127.6, 129.6, 133.1, 135.5, 138.3, 155.6.

(2*S*,*E*)-1-*tert*-Butyloxycarbonyl-2-*tert*-butyldiphenylsilyloxymethyl-3-ethylidene-azetidine (28)

To a solution of **27** (2.85 g, 5.36 mmol) in dimethyl sulphoxide (110 mL) at rt was added lithium borohydride (5.36 mL, 2.0 M solution in THF, 10.7 mmol). The resulting reaction mixture was stirred at rt for 14 h. Water (110 mL) was added followed by extraction with ethyl acetate (3 ×

© 2001 NRC Canada

200 mL). The combined ethyl acetate solution was dried (Na_2SO_4) and filtered. The filtrate was concentrated in vacuo to dryness. Column chromatography (EtOAc–hexanes, 1:8) afforded 1.60 g (66%) of product **28** as a colorless oil: $[\alpha]_D$ –10.7 (*c* 1.34, $CHCl_3$). FAB-MS (NBA) *m*/*z* (rel intensity): 452 ($[M + H]^+$, 9), 396 (7), 338 (100), 318 (84), 199 (83), 154 (42), 135 (100). HRMS calcd. for $C_{27}H_{37}NO_3Si$ (M + H): 452.2685; found: 452.2667. IR ($CHCl_3$) υ_{max} (cm^{-1}): 1701. ^1H NMR δ: 1.05 (s, 9H), 1.40 (s, 9H), 1.58–1.60 (m, 3H), 3.79–3.83 (dd, *J* = 10.3, 2.9 Hz, 1H), 3.90–4.10 (br s, 1H), 4.41 (br s, 2H), 4.67 (br s, 1H), 5.39–5.50 (m, 1H), 7.34–7.46 (m, 6H), 7.65–7.72 (m, 4H). ^{13}C NMR δ: 13.5, 19.5, 26.6, 28.3, 55.1, 63.6, 69.9, 79.2, 116.8, 127.5, 129.5, 131.5, 133.4, 135.5, 155.9.

(2*S*,*E*)-1-*tert*-Butyloxycarbonyl-2-hydroxymethyl-3-ethylidene-azetidine (29)

To a solution of compound **28** (0.589 g, 1.30 mmol) in THF (40.0 mL) at 0°C was added tetrabutylammonium fluoride (1.96 mL, 1.0 M solution in THF, 1.96 mmol). The resulted reaction mixture was stirred towards rt for 3 h. The reaction mixture was concentrated in vacuo to dryness. Column chromatography (EtOAc–hexanes, 1:3) afforded 0.261 g (94%) of product **29** as a colorless oil: $[\alpha]_D$ –8.9 (*c* 1.56, $CHCl_3$). FAB-MS (NBA) *m*/*z* (rel intensity): 214 ($[M + H]^+$, 78), 182 (54), 158 (100), 136 (98), 126 (81), 107 (96), 97 (74). HRMS calcd. for $C_{11}H_{20}NO_3$ (M + H): 214.1444; found: 214.1422. IR ($CHCl_3$) υ_{max} (cm^{-1}): 3425, 1701, 1658. ^1H NMR δ: 1.43 (s, 9H), 1.50–1.53 (m, 3H), 3.66–3.78 (m, 2H), 4.31–4.42 (m, 2H), 4.81 (br s, 1H), 5.30–5.40 (m, 1H). ^{13}C NMR δ: 13.3, 28.1, 55.1, 65.6, 71.3, 80.3, 117.7, 128.7, 156.9.

(2*S*,*E*)-1-*tert*-Butyloxycarbonyl-carboxylic acid 3-ethylidene-2-azetidine (30)

To a solution of **29** (64.6 mg, 0.30 mmol) in acetone (3.00 mL) at 0°C was added chromic acid (1.16 mL, 2.6 M solution, 3.03 mmol). The resulting reaction mixture was stirred towards rt for 3 h. Isopropanol was added to destroy the residual chromic acid followed by the addition of water (5.00 mL). The mixture was extracted with ether (3 × 10.0 mL) and the combined ether solution was dried (Na_2SO_4), filtered, and the filtrate was concentrated in vacuo to dryness. Column chromatography (EtOAc–hexanes, 1:2, with 1% of AcOH) afforded 26.5 mg (39%) of product **30**: mp 138–140°C (CH_2Cl_2–hexane). $[\alpha]_D$ –63.5 (*c* 1.28, $CHCl_3$). FAB-MS (NBA) *m*/*z* (rel intensity): 228 ($[M + H]^+$, 8), 220 (45), 172 (25), 154 (100), 136 (98), 107 (89). HRMS calcd. for $C_{11}H_{18}NO_4$ (M + H): 228.1236; found: 228.1244. IR ($CHCl_3$) υ_{max} (cm^{-1}): 3700–2500, 1729, 1707, 1687. ^1H NMR δ: 1.45 (s, 9H), 1.57–1.61 (m, 3H), 4.39–4.57 (m, 2H), 5.19 (br s, 1H), 5.78 (br s, 1H). ^{13}C NMR δ: 13.5, 28.2, 55.5, 67.9, 81.7, 120.7, 124.9, 156.6, 171.7. Anal. calcd for $C_{11}H_{17}NO_4$: C 58.14, H 7.54, N 6.16; found: C 57.99, H 7.57, N 6.12.

(2*S*,*E*)-3-Ethylidene-azetidine-2-carboxylic acid (1)

A solution of compound **30** (0.104 g, 0.459 mmol) in formic acid (5.00 mL) was stirred at rt for 5 h. After filtration through a fine sintered glass funnel, the filtrate was concentrated in vacuo on an oil pump to dryness to give 0.058 g (100%) of product **1**: mp 147–149°C (triturated with methanol and isopropanol). $[\alpha]_D$ +17.3 (*c* 2.10, MeOH). CI-MS *m*/*z* (rel intensity): 129 ($[M + H]^+$, 98), 84 (100). HRMS calcd. for $C_6H_{10}NO_2$ (M + H): 128.0794; found: 128.0722. IR (neat) υ_{max} (cm^{-1}): 3700–2000, 1614, 1379, 1291, 759, 690. ^1H NMR (CD_3OD) δ: 1.56–1.58 (m, 3H), 4.50–4.70 (m, 2H), 5.09 (br s, 1H), 5.70–5.83 (m, 1 H). ^1H NMR (D_2O) δ: 1.53–1.56 (m, 3H), 4.60–4.73 (m, 2H), 5.24 (br s, 1H), 5.66–5.77 (m, 1H). ^{13}C NMR (CD_3OD) δ: 13.1, 53.3, 70.7, 121.3, 128.4, 170.6.

(2*S*,*Z*)-1-*tert*-Butyloxycarbonyl-2-*tert*-butyldiphenylsilyl-oxymethyl-3-(formyl)methylidene-azetidine (31)

Compound **23** (0.505 g, 0.962 mmol) was reduced with lithium aluminum hydride (0.192 g, 95%, 4.81 mmol) at –78°C for 2 h to afford 0.274 g (61%) of **31** and 0.109 g (24%) of **32** both as colorless oils. For **31** : $[\alpha]_D$ +35.9 (*c* 1.79, $CHCl_3$). FAB-MS (NBA) *m*/*z* (rel intensity): 466 ($[M + H]^+$, 31), 427 (17), 352 (12), 198 (72), 154 (76), 135 (100). HRMS calcd. for $C_{27}H_{36}NO_4Si$ (M + H): 466.2415; found: 466.2371. IR ($CHCl_3$) υ_{max} (cm^{-1}): 2739, 1701, 1685. ^1H NMR δ: 1.06 (s, 9H), 1.44 (s, 9H), 3.87–3.91 (d, *J* = 9.3 Hz, 1H), 4.55–4.61 (m, 1H), 4.62–4.69 (m, 2H), 5.20 (br s, 1H), 6.09–6.13 (m, 1H), 7.35–7.47 (m, 6H), 7.61–7.76 (m, 4H), 9.68–9.71 (d, *J* = 7.3 Hz, 1H). ^{13}C NMR δ: 19.1, 26.6, 28.2, 56.9, 62.7, 63.1, 71.7, 80.2, 123.8, 127.6, 129.7, 129.8, 132.6, 155.1, 159.3, 189.0.

(2*S*,*Z*)-1-*tert*-Butyloxycarbonyl-2-*tert*-butyldiphenylsilyl-oxymethyl-3-(hydroxymethyl)methylidene-azetidine (32)

Compound **31** (1.40 g, 3.01 mmol) was reduced with sodium borohydride (0.125 g, 3.31 mmol) in the presence of cerium trichloride heptahydrate (1.24 g, 3.31 mmol) to afford 1.16 g (82%) of **32** as a colorless oil: $[\alpha]_D$ –0.2 (*c* 1.53, $CHC1_3$). FAB-MS (NBA) *m*/*z* (rel intensity): 468 ($[M + H]^+$, 21), 412 (14), 354 (52), 334 (46), 198 (71), 154 (85), 136 (100). HRMS calcd. for $C_{27}H_{38}NO_4Si$ (M + H): 468.2571, found 468.2598. IR (neat) υ_{max} (cm^{-1}): 3420, 1700, 1676. ^1H NMR δ: 1.08 (s, 9H), 1.34 (s, 9H), 3.89–3.92 (dd, *J* = 10.3, 2.8 Hz, 1H), 3.95–4.21 (br s, 3H), 4.37–4.49 (m, 2H), 4.96 (br s, 1H), 5.63 (m, 1H), 7.36–7.45 (m, 6H), 7.66–7.70 (m, 4H). ^{13}C NMR δ: 19.1, 26.7, 28.2, 56.0. 59.7, 64.0, 70.0, 79.5, 122.3, 127.7, 129.7, 132.8, 133.3, 135.4, 155.6.

(2*S*,*Z*)-1-*tert*-Butyloxycarbonyl-2-*tert*-butyldiphenylsilyl-oxymethyl-3-(bromomethyl)methylidene-azetidine (33)

Compound **32** (0.315 g, 0.672 mmol) was reacted with triphenylphosphine (0.265 g, 1.01 mmol) and carbon tetrabromide (0.335 g, 1.01 mmol) to afford 0.285 g (80%) of **33** as a colorless oil: $[\alpha]_D$ +60.3 (*c* 1.19, $CHCl_3$). FAB-MS (NBA) *m*/*z* (rel intensity): 532 ($[M + H]^+$, 3), 530 ($[M + H]^+$, 2), 417 (11), 415 (10), 198 (37), 195 (34), 135 (100). HRMS calcd. for $C_{27}H_{37}BrNO_3Si$ (M + H): 530.1727; found: 530.1754. IR (neat) υ_{max} (cm^{-1}): 1701. ^1H NMR δ: 1.09 (s, 9H), 1.39 (s, 9H), 3.81–3.96 (m, 2H), 3.96–4.15 (br s, 2H), 4.39–4.53 (m, 2H), 4.93 (br s, 1H), 5.73 (m, 1H), 7.37–7.47 (m, 6H), 7.69–7.72 (m, 4H). ^{13}C NMR δ: 19.1, 26.7, 27.5, 28.2, 55.7, 63.2, 69.9, 79.6, 119.4, 127.6, 129.6, 132.9, 135.4, 137.4, 155.4.

(2*S*,*E*)-1-*tert*-Butyloxycarbonyl-2-*tert*-butyldiphenylsilyl-oxymethyl-3-ethylidene-azetidine (34)

Compound **33** (0.285 g, 0.537 mmol) was reacted with

© 2001 NRC Canada

lithium borohydride (0.54 mL, 2.0 M solution in THF, 1.08 mmol) to afford 0.181 g (79%) of **34** as a colorless oil: $[\alpha]_D$ +4.4 (*c* 1.38, $CHCl_3$). FAB-MS (NBA) *m/z* (rel intensity): 452 ($[M + H]^+$, 20), 396 (19), 352 (18), 338 (54), 318 (51), 225 (52), 199 (61), 154 (82), 136 (100). HRMS calcd. for $C_{27}H_{38}NO_3Si$ (M + H): 452.2685; found: 452.2598. IR (neat) υ_{max} (cm^{-1}): 1700. ^1H NMR δ: 1.08 (s, 9H), 1.43 (s, 9H), 1.59–1.61 (m, 3H), 3.85–3.89 (dd, *J* = 10.7, 2.1 Hz, 1H), 4.00–4.25 (br s, 1H), 4.30–4.52 (m, 2H), 4.82 (br s, 1H), 5.39–5.50 (m, 1H), 7.35–7.47 (m, 6H), 7.67–7.75 (m, 4H). ^{13}C NMR δ: 13.6, 19.2, 26.8, 28.3, 56.1, 62.5, 70.2, 79.1, 117.3, 127.5, 129.5, 130.8, 133.3, 135.5, 155.6.

(2*S*,*Z*)-1-*tert*-Butyloxycarbonyl-2-hydroxymethyl-3-ethylidene-azetidine (35)

Compound **34** (0.912 g, 2.02 mmol) was reacted with tetrabutylammonium fluoride (3.03 mL, 1.0 M solution in THF, 3.03 mmol) to afford 0.418 g (97%) of **35** as a colorless oil: $[\alpha]_D$ –12.3 (*c* 1.98, $CHCl_3$). FAB-MS (NBA) *m/z* (rel intensity): 214 ($[M + H]^+$, 20), 158 (55), 136 (100), 107 (92). HRMS calcd. for $C_{11}H_{20}NO_3$ (M + H): 214.1444; found: 214.1460. IR (neat) υ_{max} (cm^{-1}): 3423, 1701, 1658. ^1H NMR δ: 1.45 (s, 9H), 1.57–1.61 (m, 3H), 3.78–3.85 (dd, *J* = 11.6, 7.6 Hz, 1H), 3.90–3.95 (dd, *J* = 11.6, 7.6 Hz, 1H) 4.32–4.34 (m, 2H), 4.96 (br s, 1H), 5.31–5.42 (m, 1H). ^{13}C NMR δ: 13.6, 28.2, 55.9, 64.5, 71.3, 80.4, 119.0, 128.1, 154.6.

(2*S*,*Z*)-1-*tert*-Butyloxycarbonyl-3-ethylidene-azetidine-2-carboxylic acid (36)

Compound **35** (0.178 g, 0.840 mmol) was oxidized with chromic acid (3.22 mL, 2.6 M solution, 8.36 mmol) to afford 76.0 mg (40%) of **36**: mp 83–84°C (CH_2Cl_2–hexane). $[\alpha]_D$ –15.3 (*c* 2.10, $CHCl_3$). EI-MS *m/z* (rel intensity): ($[M + H]^+$, 21), 182 (52), 172 (58), 154 (33), 142 (58), 126 (74), 76 (100). HRMS calcd. for $C_{11}H_{18}NO_4$ (M + H): 228.1236; found: 228.1214. IR (neat) υ_{max} (cm^{-1}): 3700–2500, 1731, 1702, 1690. ^1H NMR δ: 1.45 (s, 9H), 1.69–1.72 (m, 3H), 4.36–4.42 (m, 1H), 4.50–4.58 (m, 1H), 5.21 (m, 1H), 5.48–5.59 (m, 1H). ^{13}C NMR δ: 13.5, 28.2, 56.8, 68.0, 81.0, 121.3, 125.1, 155.8, 172.4. Anal. calcd for $C_{11}H_{17}NO_4$: C 58.14, H 7.54, N 6.16; found: C 57.81, H 7.42, N 6.06.

(2*S*,*Z*)-3-Ethylidene-azetidine-2-carboxylic acid (2)

A solution of **36** (0.107 g, 0.472 mmol) in formic acid (5.00 mL) was stirred at rt for 5 h. After filtration through a fine sintered glass funnel, the filtrate was concentrated in vacuo on an oil pump to dryness to afford 0.060 g (100%) of **2**: mp 153–155°C (triturated with methanol and EtOAc). $[\alpha]_D$ +41.3 (*c* 0.55, MeOH). CI-MS *m/z* (rel intensity): 128 ($[M + H]^+$, 20), 84 (43), 82 (100), 68 (48). HRMS calcd. for $C_6H_{10}NO_2$ (M + H): 128.0794; found: 128.0722. IR (neat) υ_{max} (cm^{-1}): 3700–2000, 1640, 1383, 1290, 851, 690. ^1H NMR (CD_3OD) δ: 1.76–1.80 (m, 3H), 4.45–4.63 (m, 2H), 5.14–5.16 (br s, 1H), 5.46–5.56 (m, 1H). ^1H NMR (D_2O) δ: 1.63–1.68 (m, 3H), 4.49–4.68 (m, 2H), 5.29 (m, 1H), 5.50–5.60 (m, 1H). ^{13}C NMR (CD_3OD) δ: 13.6, 54.7, 71.2, 122.8, 127.7, 170.1.

Acknowledgments

We are grateful to NSERC for financial support of this work. We thank Drs. J.-L. Chiara and R. DiFabio for initial studies in carbenoid insertions, and Dr. Y. Tu for NMR experiments. We are grateful to Professor K. Isono for an authentic samples of polyoximic acid and polyoxin A and to Dr. Michel Simard for X-ray analyses.

References

1. (*a*) K. Isono. Biotechnol. Ser. **28**, 597 (1995); (*b*) K.Y.I. El-Shahed. Egypt. J. Microbio. **29**, 315 (1995); (*c*) M. Uramoto, M. Matsuoka, J.G. Liehr, J.A. McCloskey, and K. Isono. Agr. Biol. Chem. (Tokyo) **45**, 1901 (1981); (*d*) S. Suzuki, K. Isono, M. Uramoto, H. Okamoto, and M. Matsuoka. Japan patent, No. 5 2020 555 (1977); (*e*) K. Isono and S. Suzuki. Tetrahedron, **24**, 1133 (1968); (*f*) K. Isono, K. Kobinata, and S. Suzuki. Agr. Biol. Chem. (Tokyo) **32**, 1193 (1968); (*g*) K. Isono and S. Suzuki. Agr. Biol. Chem. (Tokyo) **32**, 792 (1968); (*h*) S. Suzuki, K. Isono, J. Nagatsu, Y. Kawashima, K. Yamagata, K. Sasaki, and K. Hashimoto. Agr. Biol. Chem. (Tokyo) **30**, 817 (1966); (*i*) S. Suzuki, K. Isono, J. Nagatsu, T. Mizutani, K. Kawashina, and T. Mizuno. J. Antibiotic **A18**, 131 (1965); (*j*) K. Isono, J. Nagatsu, Y. Kawashima, and S. Suzuki. Agr. Biol. Chem. (Tokyo) **29**, 848 (1965).
2. S. Suzuki. Hakko To Taisha, **31**, 16 (1975); Chem. Abstr. **83**, 193 595 (1975).
3. (*a*) K. Isono. *In* Shokubutsu byogai no kagaku. *Edited by* A. Ichihara and T. Ueno. Gakkai Shuppan Senta, Tokyo. 1997. p. 263; Chem. Abstr. **130**, 263 433 or 85 598 (1999); (*b*) I.K.O. Cann, Y. Kobayashi, A. Onoda, M. Wakita, and S. Hoshino. J.Appl. Bacteriol. **74**, 127 (1993).
4. (*a*) M. Reuveni, H. Cohen, T. Zahavi, and A. Venezian. Crop Prot. **19**, 393 (2000); (*b*) Y. Jiang. Int. J. Food Sci. Technol. **32**, 535 (1997); (*c*) Y. Elad, B. Kirshner, and Y. Gotlib. Crop Prot. **12**, 69 (1993); (*d*) E. Krainer, J.M. Becker, and F.J. Naider. Med. Chem. **34**, 174 (1991).
5. K. Isono, K. Asabi, and S. Suzuki. J. Am. Chem. Soc. **91**, 7490 (1969) and refs. cited therein.
6. (*a*) T. Sato, K. Hirasawa, J. Uzawa, T. Inaba, and K. Isono. Tetrahedron Lett. **36**, 3441 (1979); (*b*) K. Isono, T. Sato, K. Hirasawa, S. Funayama, and S. Suzuki. J. Am. Chem. Soc. **100**, 3937 (1978); (*c*) K. Isono and R. Suhadolnik. J. Arch. Biochem. Biophys. **173**, 141 (1976); (*d*) K. Isono, K. Funayama, and R. Suhadolnik. Biochemistry, **14**, 2992 (1975).
7. H. Sakurai, T. Akashiba, and S. Suzuki. Noyaku Seisan Gijutsu, **21**, 13 (1970); Chem. Abstr. **74**, 52 425 (1971).
8. D. Zhang and M.J. Miller. Curr. Pharm. Des. **5**, 73 (1999) and refs. cited there in.
9. (*a*) O. Tamura, K. Gotanda, J. Yoshino, Y. Morita, R. Terashima, M. Kikuchi, T. Miyawaki, N. Mita, M. Yamashita, H. Ishibashi, and M. Sakamoto. J. Org. Chem. **65**, 8544 (2000); (*b*) P. Merino, S. Franco, F. Merchan, and T. Tejero. J. Org. Chem. **65**, 5575 (2000); (*c*) A. Chen, E. J. Thomas, and P.D. Wilson. J. Chem. Soc., Perkin Trans. 1, 3305 (1999); (*d*) K. Kato, C.Y. Chen, and H. Akita. Synthesis, 1527 (1998); (*e*) A.K. Ghosh and Y. Wang. J. Org. Chem. **63**, 6735 (1998); (*f*) P. Merino, S. Franco, F.L. Merchan, and T. Tejero. Tetrahedron Lett. **39**, 6411 (1998); (*g*) J.-Q. Wang, C. Archer, J. Li, S.G. Bott, and P.G. Wang. J. Org. Chem. **63**, 4850 (1998); (*h*) H. Akita, K. Uchida, C.Y. Chen, and K. Kato. Chem. Pharm. Bull. **46**, 1034 (1998); (*i*) H. Akita, K. Uchida, and C.Y. Chen. Heterocycles, **46**, 87 (1997); (*j*) C. Dehoux, E. Fontaine, J.-M. Escudier, M. Baltas, and L. Gorrichon. Adv. Chitin Sci. **2**, 279 (1997); (*k*) D. Zhang and M.J. Miller. J. Org. Chem. **63**, 755 (1998); (*l*) D.M. Gethin and N.S. Simpkins. Tetrahedron, **53**, 14417 (1997); (*m*) V.K. Aggarwal and N.J. Monteiro. Chem. Soc. Perkin

© 2001 NRC Canada

Trans. 1, 2531 (1997); (*n*) C.M. Evina and G. Guillerm. Tetrahedron Lett. **37**, 163 (1996); (*o*) A. Dondoni, F. Junquera, F. Merchan, P. Merino, and T. Tejero. Tetrahedron Lett. **35**, 9439 (1994); (*p*) A. Chen, I. Savage, E.J. Thomas, and P.D. Wilson. Tetrahedron Lett. **34**, 6769 (1993); (*q*) Y. Auberson and P. Vogel. Tetrahedron, **46**, 7019 (1990); (*r*) A.G.M. Barrett and S.A. Lebold. J. Org. Chem. **55**, 3853 (1990); (*s*) P. Garner and J.M. Park. J. Org. Chem. **55**, 3772 (1990); (*t*) G. Emmer, N.S. Ryder, and M.A. Grassberger. J. Med. Chem. **28**, 278 (1985).

10. K. Uchida, K. Kato, K. Yamaguchi, and H. Akita. Heterocycles **53**, 2253 (2000).
11. (*a*) K. Uchida, K. Kato, and H. Akita. Synthesis, 1678 (1999); (*b*) K.M.K. Kutterer and G. Just. Heterocycles, **51**, 1409 (1999); (*c*) A.K. Ghosh and Y.J. Wang. Org. Chem. **64**, 2789 (1999); (*d*) H. Akita, K. Uchida, and K. Kato. Heterocycles, **47**, 157 (1998); (*e*) A. Dondoni, S. Franco, F. Junquera, F.L. Merchan, P. Merino, and T. Tejero. J. Org. Chem. **62**, 5497 (1997); (*f*) A. Dondoni, F. Junquera, F.L. Merchan, P. Merino, and T.J. Tejero. Chem. Soc. Chem. Commun. 2127 (1995); (*g*) N. Chida, K. Koizumi, Y. Kitada, C. Yokoyama, and S. Ogawa. J. Chem. Soc. Chem. Commun. 111 (1994).
12. (*a*) I. Savage and E.J. Thomas. J. Chem. Soc. Chem. Commun. 717 (1989); (*b*) P. Garner and J.M. Park. J. Org. Chem. **53**, 2979 (1988); (*c*) H. Kuzuhara, M. Kimura, and S. Emoto. Carbohydr. Res. **45**, 245 (1975).
13. H. Baumann and R.O. Duthaler. Helv. Chim. Acta, **71**, 1025, 1035 (1988).
14. G. Emmer. Tetrahedron, **48**, 7165 (1992).
15. (*a*) S. Hanessian, J.-M. Fu, J.L. Chiara, and R. DiFabio. Tetrahedron Lett. **34**, 4157 (1993); (*b*) S. Hanessian, J.-M. Fu, Y. Tu, and K. Isono. Tetrahedron Lett. **34**, 4153 (1993).
16. S. Hanessian. *In* Total synthesis of natural compounds: The "Chiron" approach. Vol. 3. *Edited by* J.E. Baldwin. Organic Chemistry Series, Pergamon Press, Oxford. 1983.
17. (*a*) M.P. Doyle, M.A. McKervey, and T. Ye. *In* Modern catalytic methods for organic synthesis with diazo compounds: From cyclopropanes to ylides. Wiley, New York. 1998; (*b*) M. Doyle, M.A. McKervey, and T. Ye. *In* Reaction synthesis with α-diazocarbonyl compounds. Wiley, New York. 1997; (*c*) T. Ye and M.A. McKervey. Chem. Rev. **94**, 1091 (1994); (*d*) H. Brunner. Angew. Chem. Int. Ed. Engl. **31**, 1183 (1992); (*e*) A. Padwa and K.E. Krumpe. Tetrahedron, **48**, 5385 (1992); (*f*) D.F. Taber. *In* Comprehensive organic synthesis. Vol. 3. *Edited by* B.M. Trost, I. Fleming, and G. Pattenden. Pergamon Press, New York. 1991. p. 1045; (*g*) J. Adams and D.M. Spero. Tetrahedron, **47**, 1765 (1991); (*h*) A. Padwa and S.F. Hombuckle. Chem. Rev. **91**, 263 (1991) and refs. cited therein.
18. (*a*) G. Lawton, C.J. Moody, and C.J. Pearson. J. Chem. Soc. Perkin Trans. 1, 899 (1987); (*b*) M.P. Moyer, P.L. Feldman, and H. Rapoport. J. Org. Chem. **50**, 5223 (1985).
19. S. Hanessian and P. Lavallee. Can. J. Chem. **53**, 2975 (1975).
20. E.J. Corey and A. Venkateswarlu. J. Am. Chem. Soc. **94**, 6190 (1972).
21. M. Schlosser, K.-F. Christmann, and A. Piskala. Chem. Ber. **103**, 2814 (1970).
22. B.E. Maryanoff and A.B. Reitz. Chem. Rev. **89**, 863 (1989).
23. S. Nahm and S. Weinreb. Tetrahedron Lett. **22**, 3815 (1981).
24. S. Hanessian and Y.L. Bennani. Chem. Rev. **97**, 3161 (1997); S. Hanessian, Y. Bennani, and Y. Leblanc. Heterocycles, **35**, 1411 (1993).
25. J.-L. Luche. J. Am. Chem. Soc. **103**, 5454 (1981).
26. (*a*) R.K. Hill, S.W. Rhee, K. Isono, D.H.G. Crout, and R.J. Suhadolnik. Biochemistry, **20**, 7040 (1981); (*b*) R. Doyle and B. Levenberg. Biochemistry, **7**, 2457 (1968).
27. S. Hanessian, N. Bernstein, R.-Y. Yang, and R. Maguire. Bioorg. Med. Chem. Lett. **9**, 1437 (1999).
28. (*a*) W.J. Krol, S. Mao, D.L. Steele, and C.A. Townsend. J. Org. Chem. **56**, 728 (1991); (*b*) S. Mzengeza and R.A. Whitney. J. Org. Chem. **53**, 4024 (1989); (*c*) D.H.R. Barton, D. Crich, Y. Herve, P. Potier, and J. Thierry. Tetrahedron, **41**, 4347 (1985); (*d*) S. Hanessian and S.P. Sahoo. Tetrahedron Lett. **25**, 1425 (1984); (*e*) A. Afzali-Ardakin and H.J. Rapoport. J. Org. Chem. **45**, 4817 (1980).
29. (*a*) S. Hanessian, C. McNaugton-Smith, H.-G. Lombart, and W.D. Lubell. Tetrahedron, **53**, 12789 (1997); (*b*) J. Rizo and L.M. Giersach. Ann. Rev. Biochem. **61**, 387 (1992); (*c*) G. Holzmann. Kontakte, 3 (1991); (*d*) J.B. Ball and P.F. Alewood. J. Mol. Recogn. **3**, 55 (1990); (*e*) M. Kahn, S. Wilke, B. Chen, K. Fujita, Y.-H. Lee, and M.E. Johnson. J. Mol. Recogn. **1**, 75 (1988).

© 2001 NRC Canada

Studies of palladium-catalyzed coupling reactions for preparation of hindered 3-arylpyrroles relevant to (–)-rhazinilam and its analogues

Léon Ghosez, Cécile Franc, Frédéric Denonne, Claire Cuisinier, and Roland Touillaux

Abstract: Suzuki cross-coupling reactions of 3-pyrroleboronic acid derivatives with haloaromatics and the reverse process i.e., the coupling of 3-iodo(bromo)pyrroles with arylboronic acids have been investigated as a potential key step in the synthesis of (–)-rhazinilam and analogues. It was found that 3-iodo-2-formyl-1-tosylpyrroles efficiently coupled with a variety of arylboronic acids in the presence of $PdCl_2$(dppf) as catalyst. This catalytic system is compatible with a broad spectrum of arylboronic acids — electron-rich, electron-poor, hindered, heterocyclic — which easily coupled with the pyrrole substrate.

Key words: 2-substituted-3-arylpyrroles, biaryls, coupling reactions, arylboronic acids, palladium coupling, catalysis.

Résumé : Nous avons étudié les réactions de couplage de Suzuki entre les acides 3-pyrroleboroniques et divers aromatiques halogénés ainsi que les réactions inverses de couplage entre les 3-iodo(bromo)- pyrroles avec des acides boroniques aromatiques. Cette réaction de couplage pourrait être une étape clé dans la synthèse du (–)-rhazinilame. Nous avons découvert que les 3-bromo- et 3-iodo-2-formyl-1-tosylpyrroles pouvaient être couplés efficacement avec un grand nombre d'acides boroniques en utilisant $PdCl_2$(dppf) comme catalyseur. Ce catalyseur permet d'introduire facilement une grande diversité d'acides arylboroniques (riches ou pauvres en électrons, encombrés ou hétérocycliques) en position 3 du pyrrole.

Mots clés : pyrroles 2-substitués-3-halogénés, biaryles, réactions de couplage, acides arylboroniques, couplage au palladium, catalyse.

Introduction

The pyrrole ring is common to many compounds which have found applications in the pharmaceutical field (1) and also in material sciences (see for example ref. 2). Not surprisingly, they have represented a continuous challenge for synthetic chemists (1, 3). In the context of a total synthesis of the alkaloid (–)-rhazinilam **1**, an inhibitor of microtubules disassembly (4) (Scheme 1), we became interested in the development of a convenient synthetic route towards 1,2-disubstituted-3-aryl pyrroles. Our goal was to develop a method applicable to the synthesis of the natural product and a large variety of simpler analogues **2**.

A literature survey indicated that efficient methods of synthesis of 1,2,3-trisubstituted pyrroles are not numerous (5). Most of them give rather low yields or lack generality. On the other hand, coupling reactions of aromatic compounds in the presence of Pd^0 or Ni^0 catalysts are nowadays part of the armamentarium of synthetic chemists (for a recent review see ref. 6). The palladium-catalyzed cross-coupling of arylboronic acids with aryl bromides or iodides was first described by Suzuki and co-workers (for recent reviews, see ref. 7). It has been shown to be applicable to the coupling of pyrrole derivatives with other aromatic compounds (8, 9). We selected a Suzuki coupling reaction of **3** with **4** as an attractive approach towards **2** since: (*i*) it is highly convergent; (*ii*) aryl- and heteroaryl halides as well as boron derivatives are easily available and readily undergo the cross-coupling reaction (see for example refs. 10, 11); (*iii*) the presence of a carbonyl or a carboxyl group at C-2 of the pyrrole should allow numerous transformations; (*iv*) a tosyl group on nitrogen should be a good model for a polymer-bound arylsulfonic group. An account of our first results was published in 1999 (12). Two more recent papers also report the

Received April 20, 2001. Published on the NRC Research Press Web site at http://canjchem.nrc.ca on November 22, 2001.

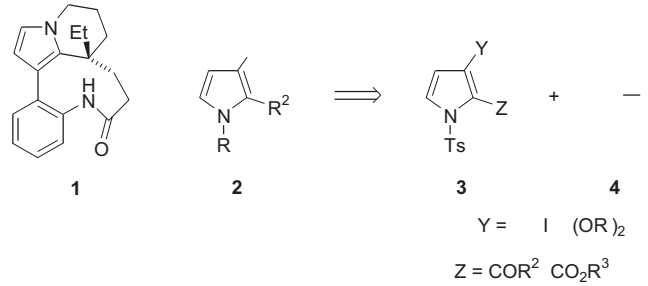
This paper is dedicated to Professor Victor Snieckus in recognition of his important contribution to the development of organic synthesis.

L. Ghosez,[1,2] C. Franc, F. Denonne,[1] C. Cuisinier, and R. Touillaux. Département de chimie, Université Catholique de Louvain, place Louis Pasteur, 1, B-1348 Louvain-la-Neuve, Belgique.

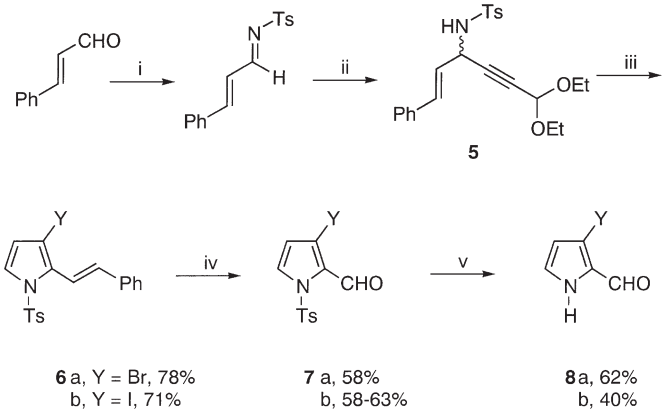
[1]Institut Européen de Chimie et Biologie, ENSCPB, 16, Avenue Pey Berland, 33607 Pessac CEDEX, France.
[2]Corresponding author (fax: 32 10 47 27 88; e-mail: ghosez@chim.ucl.ac.be or l.ghosez@iecb-polytechnique.u-bordeaux.fr).

 DOI: 10.1139/cjc-79-11-1827 © 2001 NRC Canada

Scheme 1.



Scheme 2. Reagents and conditions: (*i*) $TsNH_2$, $BF_3{\cdot}OEt_2$, toluene, Δ; (*ii*) $HCCCH(OEt)_2$, *n*-BuLi, ether, –78°C then $ZnCl_2$ in ether, –78°C; (*iii*) 8.8 M HBr(aq) (9.5 equiv), 15 min, 80°C or 57% HI(aq) (7 equiv), 1 h, –10°C; (*iv*) $KMnO_4$ (3 equiv), H_2O–dioxane, 1 h, rt; (*v*) same as (*iv*) but at 90°C, yield from **5**.



use of a cross-coupling reaction involving substituted 3-iodopyrroles for the synthesis of analogues of (–)-rhazinilam (13). We now report the full details of our studies.

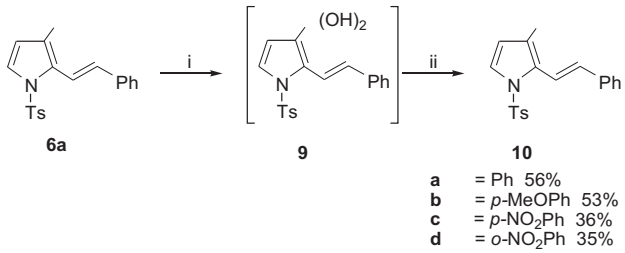
Synthesis of 1,2-disubstituted 3-halopyrroles

Our strategy required an easy access to 3-halopyrroles **3** (Y = Br, I) and the corresponding boronic acid (Y = $B(OH)_2$). We selected the efficient method described by Masquelin and Obrecht (3) using aldimines and acetylenic acetals or ketones as starting materials. Compound **5** was obtained in excellent yields as described (Scheme 2).

However, very low yields (<3%) of **6a** were obtained from the treatment of **5** with 2.4 M aq HBr as described by the authors. The use of a more concentrated HBr solution at 80°C for 15 min gave **6a** in 78% yield. Similarly, treatment of **5** with 57% aq HI gave a 71% yield of **6b** if the temperature was kept at –10°C to avoid degradation of the product under these strongly acidic conditions. This practical sequence has been applied to the preparation of up to 23 g of **6a** and 43 g of **6b**.

Pyrroles are extremely sensitive to oxidizing agents (1). However, the selective oxidation of the olefinic double bond of a 3-vinylpyrrole bearing an electron-withdrawing benzenesulfonyl group on nitrogen has been successfully performed with $NaIO_4$–OsO_4 cat (14). However, under these conditions, the oxidation of the styryl double bond of **6a**, **6b** took approximately 5 days. The oxidative cleavage with aq $KMnO_4$ was much faster. At room temperature, the products were the expected aldehydes **7a**, **7b**. At 90°C, hydrolytic cleavage of the tosyl group simultaneously occurred to yield **8a**, **8b**.

Scheme 3. Reagents and conditions: (*i*) *t*-BuLi in hexane, THF, –78°C then $B(OMe)_3$, –78°C then H_2O–MeOH, work-up; (*ii*) compound **9** (1.5 equiv), ArX (1 equiv), benzene–water–methanol (5:1.5:1), $Ba(OH)_2$ (1.5 equiv), $Pd(PPh_3)_4$ (5%), reflux.



Coupling reactions with 1-tosyl-2-styrylpyrrole boronic acid (9)

We first studied the synthesis of pyrroleboronic acid **9** and its coupling reaction with aryl iodides. Compound **9** was obtained from **6a** by a metal-bromide exchange with *t*-BuLi followed by treatment with trimethylborate and hydrolysis (Scheme 3).

Compound **9** was used without purification. The coupling reactions were performed under the conditions described by Muchowski (8*a*) for related cases. Yields were moderate with phenyl iodide and *o*-iodoanisole. However the presence of an electron-withdrawing nitro group in *para* or *ortho* position of the iodide considerably lowered the yields. The coupling of **9** with *o*-iodonitrobenzene was of special interest in the context of the rhazinilam problem. Next to the expected coupling product **10d**, we found a reduction product **11** (30%) and, more surprisingly, a compound **12** (25%) resulting from a coupling at position 5 of pyrrole **9** (Scheme 4).

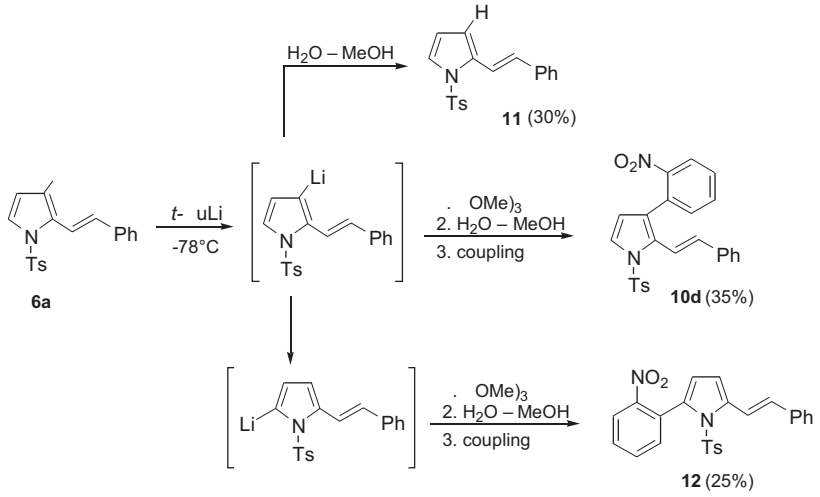
We were able to show that the reduction product was formed as a result of the incomplete conversion of the organolithium intermediate into the corresponding boronic acid. Product **12** could be the result of an isomerization of the 3-lithio compound to the thermodynamically more stable 5-lithio isomer. There was little hope to improve the yields of **10d** by bringing the temperature further down; this would probably slow down the isomerization of the organolithium compound but also increase the amount of reduction product. We thus decided to study the Suzuki coupling reactions between 3-bromo- or 3-iodo-pyrrole derivatives **6a**, **6b** and **7a**, **7b** with various arylboronic acids.

Study of the coupling conditions of 1,2-disubstituted-3-halopyrroles with arylboronic acids

We first examined the reaction of **6b** with the commercially available phenylboronic acid **13a**. We used $Ba(OH)_2$ (15) as base (Scheme 5, Table 1). In the presence of $Pd(PPh_3)_4$ as catalyst, no coupling product **10a** was obtained in solvent mixtures (entries 1 and 2) which had been successfully used in similar coupling reactions (6, 7).

© 2001 NRC Canada

Scheme 4.



Scheme 5.

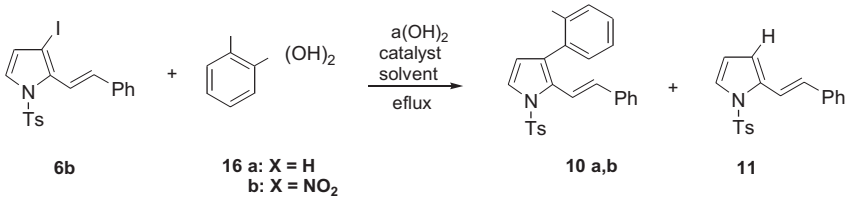


Table 1. Conditions for the cross-coupling of **6b** with phenyl- and *o*-nitrophenylboronic acids.

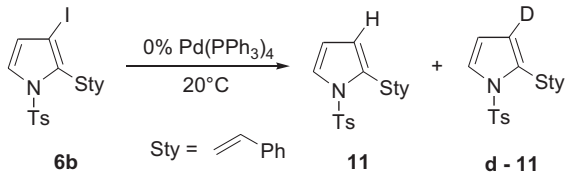
Entry	X	Catalyst	Solvent	*T* (°C)	Yield of **10** (%)	Yield of **11** (%)
1	H	5% $Pd(PPh_3)_4$	MeOH–C_6H_6–H_2O (1:3:2)	80	0	—
2	H	5% $Pd(PPh_3)_4$	DME–H_2O (2:1)	80	0	—
3	H	5% $Pd(PPh_3)_4$	DMF–H_2O (4:1)	80	86[a]	—
4	NO_2	10% $Pd(PPh_3)_4$	DMF–H_2O (4:1)	120	36[b]	64[b]
5	NO_2	10% $PdCl_2(PPh_3)_2$	DMF–H_2O (4:1)	120	50[b]	50[b]
6	NO_2	10% $PdCl_2$dppe	DMF–H_2O (4:1)	120	42[b]	58[b]
7	NO_2	10% $PdCl_2$dppf	DMF–H_2O (4:1)	120	80[a]	—
8	NO_2	10% $PdCl_2$dppf	DMF–H_2O (4:1)	120	73[a]	—

[a]Isolated pure coupling products.
[b]NMR yields.

Table 2. Hydrodeiodination of **6b**.

Entry	Base	Solvent	Product
1	None	DMF–H_2O (1:1)	**6b**
2	$Ba(OH)_2$	$MeCONMe_2$–H_2O (1:1)	**6b**
3	$Ba(OH)_2$	DMF–D_2O (1:1)	**11**
4	$Ba(OH)_2$	$DCONMe_2$–H_2O (1:1)	**11**
5	$Ba(OH)_2$	$DCON(CD_3)_2$–H_2O (1:1)	**d-1**

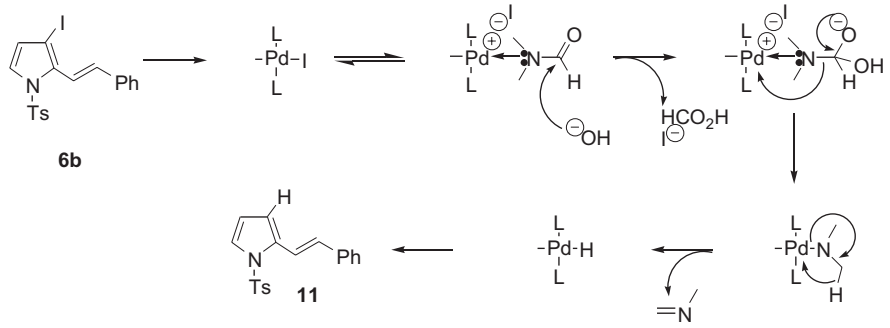
Scheme 6.



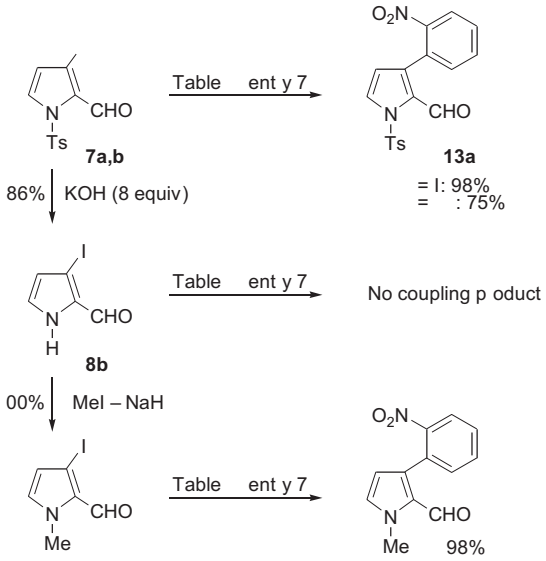
Running the coupling reaction in a more polar solvent (entry 3) led to a high yield of **10a**. The accelerating effect of a polar solvent such as DMF had been used before to effect Suzuki coupling reactions (15*b*, 15*e*) of bromo- and iodo-pyrroles (9*a*). However, when we applied these conditions to the coupling of **6b** with the electron-deficient and hindered *o*-nitrophenylboronic acid, we observed a dramatic decrease of the yield of coupling product **10b**, even at higher temperatures (entry 4). The presence of chloride ion (16) or the use of a bidentate phosphine (17) such as dppe (18) (entries 5 and 6) did not much improve the yield of coupling product **10b**. The major product **11** of the reaction resulted

© 2001 NRC Canada

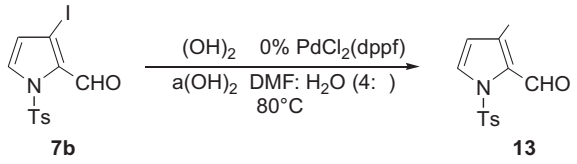
Scheme 7.



Scheme 8.



Scheme 9.



from the reductive cleavage of the carbon—iodine bond. We also observed variable amounts of nitrobenzene resulting from a base-catalyzed hydrolysis of *o*-nitrophenylboronic acid (19).

The use of 1,1′-bis(diphenylphosphino)ferrocene (dppf) bidentate ligand (20*a*, 20*b*; for a more recent example see ref. 20*c*) on palladium led to a significant increase of rate and yield (entries 7 and 8); the reaction was over in a few minutes even at 80°C and yields of coupling product **10b** were up to 80%. After completion of our work, Buchwald, Hermann, Fu and co-workers (21) reported new efficient catalysts for Suzuki cross-coupling reactions. However, no cross-coupling reactions involving a pyrrole derivative was described and we have not examined these new catalysts.

The palladium-catalyzed dehalogenation of aromatic compounds has been abundantly documented (review see ref. 22). Hydrodehalogenation products have sometimes been observed as by-products of Pd-catalyzed cross-coupling reactions (23). In these cases, water or tertiary amines have been assigned the role of hydride donors. In Table 2, we describe a study of the hydrodeiodination reaction of **6b** (Scheme 6).

It shows that: (*i*) no hydrodeiodination was observed in the absence of base or when DMF was replaced by *N*,*N*-dimethylacetamide (entries 1 and 2); (*ii*) no incorporation of deuterium was observed in the presence of D_2O or $Me_2NC(O)D$ (entries 3 and 4); (*iii*) incorporation of deuterium at C-3 of **11** occurred when the reaction was run in $(D_3C)_2NC(O)D$ (entry 5). These observations were rationalized by the mechanism outlined in Scheme 7.

We have successfully applied the conditions of Table 1, entry 7 to the coupling of 2-formyl-3-halo-1-tosylpyrroles **7a**, **7b** with *o*-nitrophenylboronic acid (Scheme 8). Under these conditions, $Ba(OH)_2$ did not add to the aldehyde function of **7a**, **7b** (NMR control) and was thus available for the coupling reaction.

As expected, the reaction of iodopyrrole was much faster than that of the corresponding bromide and gave a higher yield of **13a**. The coupling reaction could also be effected in very high yield on the *N*-methylated pyrrole but did not occur when nitrogen was unsubstituted.

Generalization of the coupling reaction

With these optimized conditions in hand, we carried out the cross-coupling reaction of **7b** with a wide variety of aryl and heteroarylboronic acids (Scheme 9, Table 3).

High yields of cross-coupled 1,2-disubstituted-3-arylpyrroles have been obtained. The reaction tolerates both electron-rich and electron-poor arylboronic acids. It could also be applied successfully to the coupling of **7b** with the sterically hindered mesitylboronic acid.

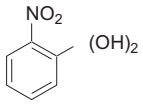
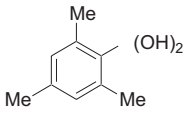
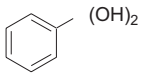
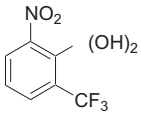
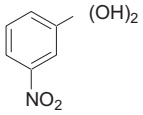
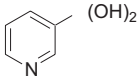
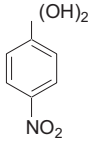
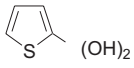
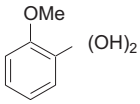
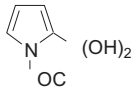
The electron-poor 2-nitro-6-(trifluoromethyl)phenylboronic acid **14** was prepared by nitration of 2-(trifluoromethyl)-phenylboronic acid (Scheme 10). The conditions described for the nitration of boric acid (28), gave no reaction and sulfuric acid had to be used to obtain **14** in a 42% yield, together with its isomer **15** (12%). However, 2-nitro-6-(trifluoromethyl)phenylboronic acid **14** gave no coupling product. Interestingly, the corresponding aniline **16** gave 3-tosyl-9-(trifluoromethyl)-3*H*-pyrrolo[2,3-*c*]-quinoline **17** in 26% yield (Scheme 10).

This illustrates a further application of this coupling reaction for the synthesis of pyrroles fused to other heterocycles. However, at this stage, we did not try to optimize the reaction.

In conclusion, we have fulfilled our goal and developed a practical synthetic route towards 1,2-disubstituted-3-aryl-(heteroaryl)pyrroles. The method should offer the possibility of

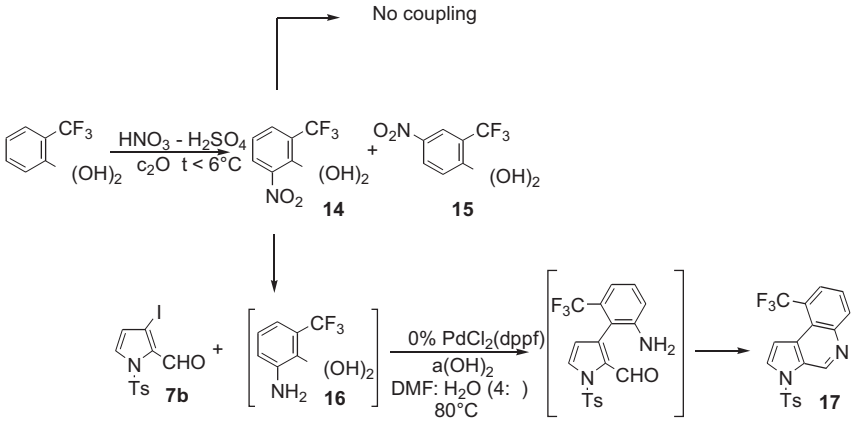
© 2001 NRC Canada

Table 3. Cross-coupling reactions of iodopyrrole **7b** with aryl- and heteroarylboronic acids.

$ArB(OH)_2$	Ref.	Yield[a]	$ArB(OH)_2$	Ref.	Yield[a]
	(24)	98		(25)	61
	[b]	92			-
	[b]	88		[b]	66
	(24)	84		(26)	85
	[b]	88		(27)	77

[a]Yield of isolated pure products.
[b]Commercially available.

Scheme 10.



building libraries of a wide variety of 2-substituted-3-arylpyrroles or polycyclic heteroaromatics derived therefrom using a polystyrene-bound 2-formyl-3-iodo-1-sulfonylpyrrole. Further applications of these findings to the total synthesis of (–)-rhazinilam and analogues will be reported in due course.

Experimental

General

Melting points were taken on Buchi Melting Point B-545 or on a Microthermal 8103 apparatus. NMR experiments

© 2001 NRC Canada

were performed on GEMINI-200, GEMINI-300, and Brucker AM-500 spectrometers. Internal standards were TMS (^{1}H NMR) and $CDCl_3$ (77.23 ppm, ^{13}C NMR). IR spectra were recorded on PerkinElmer 681 and Bio-Rad FTS 135 spectrometers (polystyrene ref. 1601 cm^{-1}). Mass spectra were recorded on Varian MAT-44 or FINNIGAN-MAT TSQ-70 spectrometers (electronic impact 70 eV or chemical ionization 100 eV with 2 μbar isobutane as the ionizing gas).

Tetrakis(triphenylphosphine)palladium (29) and dichloro-(diphenylphosphinoferrocene)palladium (30), *o*-nitrophenylboronic and *p*-nitrophenylboronic acids were prepared as described in the literature (28). Unless otherwise noted, the other boronic acids used were purchased from commercial sources. THF and toluene were distilled from sodium-benzophenone. Organic phases were dried over magnesium sulphate. Solvents were degassed by bubbling argon for at least 15 min. Chromatographic separations were performed with silica gel purchased from Merck (thickness 40–63 μm)

*3-Bromo-2-styryl-1-tosylpyrrole (**6a**) (RN: 168030-84-0)*

To a solution of *(E)-N*-(4,4′-diethoxy-1-styrylbut-2-ynyl)-4-toluenesulfonamide (3) (18 g, 45 mmol) in toluene (100 mL) was added bromohydric acid (48% aqueous, 48 mL, 425 mmol). The reaction mixture was stirred for 10 min at 80°C and then allowed to cool to room temperature. It was poured into ice and ether, sodium hydroxide (14.4 g, 360 mmol) was then added, and the pH adjusted to 7 with 1 N aqueous sodium hydroxide. The aqueous phase was extracted with ether, the organic layers were washed with brine, dried and concentrated in vacuo. Purification by flash chromatography on silica gel (10% diethyl ether in petroleum ether) Yield of **4**: 14.1 g, 78%, pale yellow solid (mp 97°C). R_f = 0.38 (30% diethyl ether in petroleum ether). MS (EI) *m*/*z* (IE, 70 eV): 403 (100, $[M + 2]^{\bullet+}$), 401 (80, $M^{\bullet+}$), 249 (18, $[M + 2\text{-Tos} + H]^{\bullet+}$), 247 (20, $[M\text{-Tos} + H]^{\bullet+}$), 168 (48), 167 (97, (249 and 247 -Br)$^{\bullet+}$), 166 (14), 139 (14). IR: 3149–3025, 1596, 1469, 1371, 1145–1089, 1028, 965. ^{1}H NMR ($CDCl_3$, 500 MHz) δ: 7.67 (d, ^3J = 8.5 Hz, 2H, $NSO_2C(CHCH)_2CCH_3$), 7.49 (d, ^3J = 8.3 Hz, 2H, $CHC(CHCH)_2CH$), 7.38 (t, ^3J = 8.3 Hz, 2H, $CHC(CHCH)_2CH$), 7.36 (d, ^3J = 16.5 Hz, 1H, $CHCHC(CHCH)_2CH$), 7.33 (d, ^3J = 3.4 Hz, 1H, $NCHCH$), 7.35–7.22 (m, 1H, $CHC(CHCH)_2CH$), 7.23 (d, ^3J = 8.5 Hz, 2H, $NSO_2C(CHCH)_2CCH_3$), 7.20 (d, ^3J = 16.5 Hz, 1H, $CHCHC(CHCH)_2CH$), 6.35 (d, ^3J = 3.4 Hz, 1H, $NCHCH$), 2.36 (s, 3H, CH_3). ^{13}C NMR ($CDCl_3$, 125 MHz) δ: 145.33 ($NSO_2C(CHCH)_2CCH_3$), 136.81 ($CHC(CHCH)_2CH$), 135.27 ($NSO_2C(CHCH)_2CCH_3$), 133.81 ($CHC(CHCH)_2CH$), 129.19 (NCC), 129.85 ($NSO_2C(CHCH)_2CCH_3$), 128.65 ($CHCHC(CHCH)_2CH$), 128.05 ($CHCHC(CHCH)_2CH$), 127.13 ($NSO_2C(CHCH)_2CCH_3$), 126.47 ($CHCHC(CHCH)_2CH$), 122.32 ($NCHCH$), 116.15 ($NCHCH$), 115.18 ($CHCHC(CHCH)_2CH$), 102.13 (NCC), 21.48 (CH_3).

*3-Iodo-2-styryl-1-tosylpyrrole (**6b**) (RN: 233770-17-7)*

To a solution of *(E)-N*-(4,4′-diethoxy-1-styrylbut-2-ynyl)-4-toluenesulfonamide **5** (3) (25 g, 61 mmol) in toluene (200 mL) at –10°C was added iodohydric acid (57% aqueous, 57 mL, 424 mmol). The mixture was stirred for 1 h at room temperature then poured into ice and ether. Sodium hydroxide (13.3 g, 333 mmol) was then added and the pH adjusted to 7 with 1 N aqueous sodium hydroxide. The aqueous phase was extracted with ether, the combined organic layers washed with brine, dried and concentrated in vacuo. Purification by flash chromatography on silica gel (10% diethyl ether in petroleum ether) Yield of **4**: 19 g, 71%, pale solid (mp 119°C). R_f = 0.7 (30% diethyl ether in petroleum ether). MS (EI) *m*/*z*: 449 (100, $M^{\bullet+}$), 335 (18), 279 (18), 167 (33). HRMS calcd. for $C_{19}H_{16}INO_2S$: 448.9946; found: 448.9950. IR: 1369, 1175, 670. ^{1}H NMR ($CDCl_3$, 500 MHz) δ: 7.65 (d, ^3J = 8.5 Hz, 2H, $NSO_2C(CHCH)_2CCH_3$), 7.49 (d, ^3J = 8.3 Hz, 2H, $CHC(CHCH)_2CH$), 7.39 (t, ^3J = 8.3 Hz, 2H, $CHC(CHCH)_2CH$), 7.34 (d, ^3J = 3.4 Hz, 1H, $NCHCH$), 7.31 (m, 1H, $CHC(CHCH)_2CH$), 7.29 (d, ^3J = 16.5 Hz, 1H, $CHCHC(CHCH)_2CH$), 7.21 (d, ^3J = 8.5 Hz, 2H, $NSO_2C(CHCH)_2CCH_3$), 7.12 (d, ^3J = 16.5 Hz, 1H, $CHCHC(CHCH)_2CH$), 6.43 (d, ^3J = 3.4 Hz, 1H, $NCHCH$), 2.37 (s, 3H, CH_3). ^{13}C NMR ($CDCl_3$, 500 MHz) δ: 145.30 ($NSO_2C(CHCH)_2CCH_3$), 136.53 ($CHC(CHCH)_2CH$), 135.21 ($NSO_2C(CHCH)_2CCH_3$), 134.74 ($CHC(CHCH)_2CH$), 132.11 (NCC), 129.80 ($NSO_2C(CHCH)_2CCH_3$), 128.67 ($CHCHC(CHCH)_2CH$), 128.15 ($CHCHC(CHCH)_2CH$), 127.21 ($NSO_2C(CHCH)_2CCH_3$), 126.50 ($CHCHC(CHCH)_2CH$), 123.71 ($NCHCH$), 120.64 ($NCHCH$), 116.24 ($CHCHC(CHCH)_2CH$), 69.16 (NCC), 21.51 (CH_3).

*2-Formyl-3-bromo-1-tosylpyrrole (**7a**)*

To a solution of **6a** (0.1 g, 0.25 mmol) in dioxane (3 mL) was added potassium permanganate (0.2 g, 0.75 mmol) and water (1 mL). The mixture was stirred at room temperature for 1 h then treated with saturated aqueous sodium thiosulfate (1 mL), then with 1 N HCl until the mixture was discoloured. The aqueous phase was extracted with ethyl acetate, the combined organic layers were washed with brine, dried and concentrated in vacuo. Purification by flash chromatography on silica gel (20% diethyl ether in petroleum ether). Yield of **7a**: 52 mg, 58%, pale yellow solid (mp 70°C). R_f = 0.54 (40% diethyl ether in petroleum ether). MS (EI) *m*/*z*: 329 (15, $[M + 2]^{\bullet+}$), 327 (16, $M^{\bullet+}$), 265 (26, $[M + 2\text{-}SO_2]^+$), 263 (26, $[M - SO_2]^+$), 174 (24, $[M + 2\text{-}C_7H_7SO_2]^+$), 172 (23, $[M - C_7H_7SO_2]^+$), 155 (84, $[C_7H_7SO_2]^+$), 91 (100, $[C_7H_7]^+$). IR: 1677, 1373, 1175. ^{1}H NMR ($CDCl_3$, 300 MHz) δ: 9.84 (s, 1H, CHO), 7.87 (d, ^3J = 8.4 Hz, 2H, $NSO_2C(CHCH)_2CCH_3$), 7.70 (d, ^3J = 3.3 Hz, 1H, $NCHCH$), 7.33 (d, ^3J = 8.4 Hz, 2H, $NSO_2C(CHCH)_2CCH_3$), 6.48 (d, ^3J = 3.3 Hz, 1H, $NCHCH$), 2.43 (s, 3H, CH_3). ^{13}C NMR ($CDCl_3$, 75 MHz) δ: 176.89 (CHO), 145.46 ($NSO_2C(CHCH)_2CCH_3$), 133.79 ($NSO_2C(CHCH)_2CCH_3$), 129.24 ($NSO_2C(CHCH)_2CCH_3$), 128.52 (NCH), 127.53 ($NSO_2C(CHCH)_2CCH_3$), 127.33 ($NCCHO$), 115.11 (CBr), 114.84 ($NCHCH$), 20.97 (CH_3). Anal. calcd. for $C_{12}H_{10}BrNO_3S$: C 43.92, H 3.07, N 4.27; found: C 43.80, H 2.78, N 4.15.

*2-Formyl-3-iodo-1-tosylpyrrole (**7b**) (RN: 233770-15-5)*

To a solution of **6b** (17 g, 37.8 mmol) in dioxane (300 mL) was added potassium permanganate (17.9 g, 113.4 mmol) and water (150 mL). The mixture was stirred at room temperature for 1 h, then treated with a saturated aqueous sodium thiosulfate (100 mL) and with 1 N HCl until the mixture was discoloured. The mixture was stirred overnight. The pale yellow precipitate was filtered, dissolved in ethyl acetate, washed with brine, dried and concentrated in vacuo.

© 2001 NRC Canada

Purification by recrystallization from cyclohexane and ether. Yield of **7b**: 8.3 g, 58%, pale yellow solid (mp 104°C). R_f = 0.50 (30% diethyl ether in petroleum ether). MS (EI) *m/z* (70eV): 375 (46, M^+), 311 (44), 220 (34), 155 (72), 91 (100). IR: 3140, 1682, 1429, 1317, 1175, 668. ^{1}H NMR ($CDCl_3$, 300 MHz) δ: 9.79 (s, 1H, C*H*O), 7.84 (d, ^3J = 8.3 Hz, 2H, $NSO_2C(CHCH)_2CCH_3$), 7.66 (d, ^3J = 3.3 Hz, 1H, NC*H*CH), 7.33 (d, ^3J = 8.3 Hz, 2H, $NSO_2C(CHCH)_2CCH_3$), 6.60 (d, ^3J = 3.3 Hz, 1H, NCHC*H*), 2.42 (s, 3H, CH_3). ^{13}C NMR ($CDCl_3$, 75 MHz) δ: 178.7 (*C*HO), 145.89 ($NSO_2C(CHCH)_2CCH_3$), 134.45 ($NSO_2C(CHCH)_2CCH_3$), 130.00 (N*C*H), 129.76 ($NSO_2C(CHCH)_2CCH_3$), 129.38 (N*C*CHO), 127.84 ($NSO_2C(CHCH)_2CCH_3$), 120.58 (NCH*C*H), 82.17 (*C*I), 21.51 (CH_3). Anal. calcd. for $C_{12}H_{10}INO_3S$: C 38.42, H 2.69, N 3.73; found: C 38.32, H 2.49, N 3.62.

*3-Bromo-2-formylpyrrole (**8a**)*

To a solution of **6a** (0.50 g, 1.24 mmol) in dioxane (10 mL) was added potassium permanganate (0.59 g, 3.73 mmol) and water (3 mL). The mixture was refluxed overnight then allowed to cool to room temperature and filtered on a Celite® pad. The organic layer was washed with sodium thiosulfate, brine, dried and concentrated in vacuo. Purification by flash chromatography on silica gel (30% diethyl ether in petroleum ether). Yield of **8a**: 134 mg, 62%, white solid (mp 118°C). R_f = 0.40 (40% diethyl ether in petroleum ether). MS (EI) *m/z* (70 eV): 175 (94, $[M + 2]^{\bullet+}$), 173 (100, $M^{\bullet+}$), 146 (20, $[M + 2\text{-}COH]^+$), 144 (20, $[M - COH]^+$). IR: 3238, 1635. ^{1}H NMR ($CDCl_3$, 500 MHz) δ: 9.82 (br s, 1H, N*H*), 9.59 (s, 1H, C*H*O), 7.07 (ddd, ^3J = 3.2 Hz, ^3J = 2.6 Hz, ^5J = 1.1 Hz, 1H, NC*H*CH), 6.39 (dd, ^3J = 2.6 Hz, ^4J = 2.4 Hz, 1H, NCHC*H*). ^{13}C NMR ($CDCl_3$, 125 MHz) δ: 178.47 (*C*HO), 129.0 (N*C*CHO), 125.77 (N*C*H), 114.24 (NCH*C*H), 109.34 (*C*Br). Anal. calcd. for C_5H_4BrNO: C 34.51, H 2.32, N 8.05; found: C 34.79, H 2.04, N 7.78.

*3-Iodo-2-formylpyrrole (**8b**) (RN: 40566-07-2)*

To a solution of **6a** (0.1g, 0.22 mmol) in dioxane (2 mL) was added potassium permanganate (0.1g, 0.66 mmol) and water (0.6 mL). The mixture was refluxed overnight then allowed to cool to room temperature and filtered on a Celite® pad. The organic layer was then washed with sodium thiosulfate, brine, dried and concentrated in vacuo. Purification by flash chromatography on silica gel (30% diethyl ether in petroleum ether). Yield of **8b**: 20 mg, 40%, white solid (decomposed at 128°C). R_f = 0.57 (50% diethyl ether in petroleum ether). MS (EI) *m/z* (70 eV): 221 (100, $M^{\bullet+}$), 220 (100, $[M - H]^+$), 192 (16, $[M - COH]^+$). IR: 3255, 1635, 1340, 758, 737. ^{1}H NMR ($CDCl_3$, 200 MHz) δ: 9.90 (br s, 1H, N*H*), 9.45 (s, 1H, C*H*O), 7.12–7.05 (m, 1H, NC*H*CH), 6.53 (t, ^3J = ^4J = 2.55 Hz, 1H, NCHC*H*). ^{13}C NMR ($CDCl_3$, 50 MHz) δ: 180.00 (*C*HO), 130.78 (*C*CHO), 126.98 (N*C*H), 119.21 (NCH*C*H), 77.23 (*C*I).

*2-Styryl-1-tosylpyrrole boronic acid (**9**)*

To a solution of 3-bromo-2-styryl-1-tosylpyrrole **6a** in dry THF (12 mL) at –78°C was added *t*-BuLi (1.7 M in pentane, 3.3 mL, 5.3 mmol). The mixture was stirred for 25 min and turned brown. A solution of trimethyl borate (2.8 mL, 25 mmol) in THF (50 mL) at –78°C was then added via cannula. The reaction mixture turned orange. After 45 min, the reaction was quenched by adding 0.5 mL of methanol and 0.5 mL of water. The solution was poured into water (20 mL), the aqueous phase extracted with diethyl ether. The combined organic phases were washed with brine, dried and concentrated in vacuo. The crude product was used in the coupling reaction without further purification.

Coupling reactions

Method A refers to the coupling reaction of 2-styryl-1-tosylpyrrole boronic acid **9** with iodoaryls: A mixture of aryliodide (1 equiv), crude boronic acid **9** (1.5 equiv, 0.16 M), barium hydroxide octahydrate (1.5 equiv), and tetrakis(triphenylphosphine)palladium (0.05 equiv) in a degassed mixture of water, methanol, and benzene (3:2:10) was refluxed for 16 h. It was then concentrated and the crude material was dissolved in ethyl acetate and filtered on a Celite® pad to remove metallic palladium. The filtrate was then dried and concentrated in vacuo. The crude product was purified by flash chromatography on silica gel.

Method B refers to the coupling reaction of 3-iodo-2-styryl-1-tosylpyrrole **6b** with an arylboronic acid: A mixture of 3-iodo-2-styryl-1-tosylpyrrole **6b** (1 equiv, 0.044 M), boronic acid (1.5 equiv), barium hydroxide octahydrate (1.5 equiv), and catalyst (0.05 or 0.1 equiv) in a degassed mixture of DMF and water (4:1) was placed in a bath which had been preheated to 120°C. After 20 min, it was cooled to room temperature and diluted with ethyl acetate and water. After filtration on a Celite® pad, the solution was washed with water, brine, dried and concentrated in vacuo. The crude product was purified by flash chromatography on silica gel.

Method C refers to the coupling reaction of 2-formyl-3-iodo-1-tosylpyrrole **7b** with an arylboronic acid: A mixture of 2-formyl-3-iodopyrrole (1 equiv, 0.044 M), aryl boronic acid (1.5 equiv), barium hydroxide octahydrate (1.5 equiv) and dichloro(diphenylphosphinoferrocene)palladium(II) (0.1 equiv) in a degassed mixture of DMF and water (4:1) was placed in a bath which had been preheated to 80°C. After 5 min, it was cooled to room temperature and diluted with ethyl acetate and water. After filtration on a Celite® pad, the solution was washed with water, brine, dried and concentrated in vacuo. The crude product was purified by flash chromatography on silica gel.

*3-Phenyl-2-styryl-1-tosylpyrrole (**10a**)*

Method A: 1.36 g (3.71 mmol) of the crude boronic acid **9**, 0.5 g (2.47 mmol) of iodobenzene, 1.17 g (3.71 mmol) of barium hydroxide octahydrate, 57 mg (0.05 mmol) of tetrakis(triphenylphosphine)palladium. Eluent: 10% of diethyl ether in petroleum ether. Yield of **10a**: (560 mg, 56%).

Method B: 0.3 mg (0.7 mmol) of the 3-iodo-2-styryl-1-tosylpyrrole **6b**, 0.5 mg (1 mmol) of phenylboronic acid, 0.17 mg (1 mmol) of barium hydroxide octahydrate, and 38 mg (0.03 mmol) of tetrakis(triphenylphosphine)palladium. Eluent: 10% diethyl ether in petroleum ether. Yield of **10a**: 240 mg, 90%, white solid (mp 140°C). R_f = 0.74 (30% diethyl ether in petroleum ether). MS (CI) *m/z*: 400 (100, $[M + 1]^+$), 247 (46, $[400 - SO_2C_6H_4CH_3]^{\bullet+}$), 157 (16, $[SO_2C_6H_5CH_3 + 2H]^+$). HRMS calcd. for $C_{25}H_{22}NO_2S$: 400.1371; found: 400.1351. IR: 3148–2869, 1369, 1175, 1136. ^{1}H NMR ($CDCl_3$, 500 MHz) δ: 7.68 (d, ^3J = 8.4 Hz, 2H,

© 2001 NRC Canada

$NSO_2C(CHCH)_2CCH_3$), 7.41 (d, ^3J = 3.4 Hz, 1H, NC*H*CH), 7.41–7.38 (m, 2H), 7.38 (d, ^3J = 16.5 Hz, 1H, C*H*CHC(CHCH)$_2$CH), 7.32–7.28 (m, 4H), 7.25–7.19 (m, 4H), 7.20 (d, ^3J = 8.4 Hz, 2H, $NSO_2C(CHCH)_2CCH_3$), 6.38 (d, ^3J = 16.5 Hz, 1H, CHC*H*C(CHCH)$_2$CH), 6.36 (d, ^3J = 3.4 Hz, 1H, NCHC*H*), 2.35 (s, 3H, CH_3). ^{13}C NMR ($CDCl_3$, 125 MHz) δ: 144.86 ($NSO_2C(CHCH)_2CCH_3$), 137.03 (CHC(CHCH)$_2$CH), 135.88 ($NSO_2C(CHCH)_2CCH_3$), 135.35 (CC(CHCH)$_2$CH), 133.99 (CHC(CHCH)$_2$CH), 129.68 ($NSO_2C(CHCH)_2CCH_3$), 128.58 (CC(CHCH)$_2$CH), 128.54 (CHC(CHCH)$_2$CH), 128.47 (NCC), 128.41 (CC(CHCH)$_2$CH), 127.68 (CHC(CHCH)$_2$CH), 127.20 ($NSO_2C(CHCH)_2CCH_3$), 127.17 (NCC), 126.76 (CC(CHCH)$_2$CH), 126.18 (CHCHC(CHCH)$_2$CH), 122.57 (NCHCH), 116.35 (CHCHC(CHCH)$_2$CH), 113.45 (NCHCH), 21.48 (CH_3).

*3-(*o*-Methoxyphenyl)-2-styryl-1-tosylpyrrole (**10b**)*

Method A: 1.36 g (3.71 mmol) of the crude boronic acid **9**, 0.58 g (2.47 mmol) of *o*-iodomethoxybenzene, 1.17 g (3.71 mmol) of barium hydroxide octahydrate, 57 mg (0.05 mmol) of tetrakis(triphenylphosphine)palladium. Eluent: 10% diethyl ether in petroleum ether. Yield of **10c**: 0.56 g, 53%, yellow solid (mp 147°C). R_f = 0.56 (30% diethyl ether in petroleum ether). MS (CI) *m*/*z*: 430 (57, $[M + 1]^+$), 275 (100, $[M + 1\text{-}C_7H_7SO_2]^{\bullet+}$). HRMS calcd. for $C_{26}H_{24}NO_3S$: 430.1476; found: 430.1459. IR: 1594, 1496, 1369, 1178, 1137, 671. ^{1}H NMR ($CDCl_3$, 500 MHz) δ: 7.71 (d, ^3J = 8.2 Hz, 2H, $NSO_2C(CHCH)_2CCH_3$), 7.47 (d, ^3J = 16.5 Hz, 1H, CHCHC(CHCH)$_2$CH), 7.41 (d, ^3J = 3.4 Hz, 1H, NCHCH), 7.30–7.20 (m, 7H, CHC(CHCH)$_2$CH and $NSO_2C(CHCH)_2CCH_3$), 6.91 (dt, ^3J = 8.2 Hz, ^4J = 1.2 Hz, 1H, $CH_3OCCCHCH$), 6.90 (d, ^3J = 8.2 Hz, 1H, CH_3OCCH), 6.85 (m, 2H, $CH_3OCCHCHCH$), 6.37 (d, ^3J = 3.4 Hz, 1H, NCHCH), 6.25 (d, ^3J = 16.5 Hz, 1H, CHCHC(CHCH)$_2$CH), 3.02 (s, 3H, CH_3), 2.35 (s, 3H, CH_3). ^{13}C NMR ($CDCl_3$, 125 MHz) δ: 156.60 (CH_3OC), 144.69 ($NSO_2C(CHCH)_2C$), 137.37 (CHCHC(CHCH)$_2$C), 136.05 (NSO_2C), 131.97 (CHCHC(CHCH)$_2$CH), 131.29 (CH_3OCCCH), 129.65 ($NSO_2C(CHCH)_2C$), 129.33 (NCC), 128.57 (CHCHC-(CHCH)$_2$CH), 128.42 (CHCHC(CHCH)$_2$CH), 127.35 ($CH_3OCCHCH$), 127.06 ($NSO_2C(CHCH)_2C$), 126.05 (CHCHC(CHCH)$_2$CH), 124.67 (NCC), 124.30 (CH_3OCC), 122.04 (NCHCH), 120.54 ($CH_3OCCCHCH$), 116.92 (CHCHC(CHCH)$_2$CH), 115.40 (NCHCH), 111.17 (CH_3OCCH), 55.38 (CH_3O), 21.45 (CH_3).

*3-(*p*-Nitrophenyl)-2-styryl-1-tosylpyrrole (**10c**)*

Method A: 1.36 g (3.71 mmol) of crude boronic acid **9**, 0.62 g (2.47 mmol) of *p*-iodonitrobenzene, 1.17 g (3.71 mmol) of barium hydroxide octahydrate, 57 mg (0.05 mmol) of tetrakis(triphenylphosphine)palladium. Eluent: 20% diethyl ether in petroleum ether. Yield of **10c**: 400 mg, 36%, yellow solid (mp 141°C). R_f = 0.36 (30% diethyl ether in petroleum ether). MS (EI) *m*/*z*: 444 (100, $M^{\bullet+}$), 289 (69, $[M - C_7H_7SO_2]^+$), 243 (85, $[289 - NO_2]^{\bullet+}$), 241 (62). IR: 3052–2850, 1598, 1516, 1374, 1342, 1178, 1139, 670. ^{1}H NMR ($CDCl_3$, 300 MHz) δ: 8.14 (d, ^3J = 9.0 Hz, 2H, $NO_2CCHCHC$), 7.65 (d, ^3J = 8.5 Hz, 2H, $NSO_2C(CHCH)_2CCH_3$), 7.58 (d, ^3J = 8.9 Hz, 2H, $NO_2CCHCHC$), 7.46 (d, ^3J = 3.4 Hz, 1H, NCHCH), 7.39 (d, ^3J = 16.5 Hz, 1H, CHCHC(CHCH)$_2$CH), 7.34–7.22 (m, 7H, CHC(CHCH)$_2$CH and $NSO_2C(CHCH)_2CCH_3$), 6.40 (d, ^3J = 3.4 Hz, 1H, NCHCH), 6.30 (d, ^3J = 16.5 Hz, 1H, CHCHC(CHCH)$_2$CH), 2.36 (s, 3H, CH_3). ^{13}C NMR ($CDCl_3$, 125 MHz) δ: 146.02 (CNO_2), 144.96 ($NSO_2C(CHCH)_2C$), 142.12 ($NO_2CCHCHC$), 135.98 (NSO_2C), 135.73 (CHCHC(CHCH)$_2$CH), 135.23 (CHCHC-(CHCH)$_2$C), 129.47 ($NO_2C(CHCH)_2C$), 128.77 (NSO_2C-(CHCH)$_2$C), 128.41 (CHCHC(CHCH)$_2$CH), 128.40 (NO_2C-(CHCH)$_2$C), 128.05 (CHCHC(CHCH)$_2$CH), 127.97 (NCC), 127.07 ($NSO_2C(CHCH)_2C$), 126.00 (CHCHC-(CHCH)$_2$CH), 125.99 ($NO_2C(CHCH)_2C$), 125.31 (NCC), 123.45 (NCHCH), 115.46 (CHCHC(CHCH)$_2$CH), 113.04 (NCHCH). Anal. calcd. for $C_{25}H_{20}N_2O_4S$: C 67.55, H 4.54, N 6.30; found: C 67.82, H 4.40, N 6.09.

Reaction of 2-styryl-1-tosylpyrrole boronic acid and o-*iodonitrobenzene (method A)*

1.36 g (3.71 mmol) of crude boronic acid **9**, 0.62 g (2.47 mmol) of *o*-iodonitrobenzene, 1.17 g (3.71 mmol) of barium hydroxide octahydrate, 57 mg (0.05 mmol) of tetrakis(triphenylphosphine)palladium. Eluent: 10–30% diethyl ether in petroleum ether. Yield of **11** : 359 mg, 30%; **10d**: 385 mg, 35%; and **12**: 275 mg, 25%. R_f = 0.26 (30% diethyl ether in petroleum ether). MS (EI) *m*/*z*: 444 (100, M^+), 240 (48), 230 (42). HRMS calcd. for $C_{25}H_{20}N_2O_4S$: 444.1143; found: 444.1149. IR: 3160–2853, 1528, 1370–1348, 1172. ^{1}H NMR ($CDCl_3$, 500 MHz) δ: 8.09 (dd, ^3J = 7.9 Hz, ^4J = 1.4 Hz, 1H, $NO_2CCHCHCH$), 7.67 (d, 2H, ^3J = 7.2 Hz, CHC(CHCH)$_2$CH), 7.60 (dt, ^3J = 7.9 Hz, ^4J = 1.4 Hz, 1H, $NO_2CCHCHCH$), 7.55 (dt, ^3J = 7.7 Hz, ^4J = 1.4 Hz, 1H, $NO_2CCHCHCH$), 7.50 (d, ^3J = 16.5 Hz, 1H, CHCHC(CHCH)$_2$CH), 7.39 (d, ^3J = 8.0 Hz, 2H, NSO_2C-(CHCH)$_2$CCH$_3$), 7.42–7.37 (m, 2H, CHC(CHCH)$_2$CH), 7.35 (dd, ^3J = 7.7 Hz, ^4J = 1.4 Hz, 1H, NO_2CCCH), 7.30–7.26 (m, 1H, CHC(CHCH)$_2$CH), 7.14 (d, ^3J = 8.0 Hz, 2H, $NSO_2C(CHCH)_2CCH_3$), 6.57 (d, ^3J = 3.4 Hz, 1H, NCCH), 6.52 (d, ^3J = 16.5 Hz, 1H, CHCHC(CHCH)$_2$CH), 6.24 (d, ^3J = 3.4 Hz, 1H, NC(CHCHPh)CH), 2.33 (s, 3H, CH_3). ^{13}C NMR ($CDCl_3$, 125 MHz) δ: 149.06 (CNO_2), 144.86 ($NSO_2C(CHCH)_2CCH_3$), 137.47 (CHC(CHCH)$_2$CH), 136.94 ($NCCCNO_2$), 135.83 ($NSO_2C(CHCH)_2CCH_3$), 133.22 ($CHCCNO_2$), 132.58 (NCCHCHPh), 131.79 ($CHCHCCNO_2$), 130.42 (CHC(CHCH)$_2$CH), 129.51 ($CCNO_2$), 129.42 ($NSO_2C(CHCH)_2CCH_3$), 129.08 (NO_2CCHCH), 128.67 (CHCHC(CHCH)$_2$CH), 127.82 (CHCHC(CHCH)$_2$CH), 126.94 ($NSO_2C(CHCH)_2CCH_3$), 126.55 (CHCHC(CHCH)$_2$CH), 124.16 (NO_2CCH), 118.49 (CHCHC(CHCH)$_2$CH), 116.64 (NC(CHCHPh)CH), 111.99 (NCCH), 21.60 (CH_3).

*3-(*o*-Nitrophenyl)-2-styryl-1-tosylpyrrole (**10d**)*

Method B: 90 mg (0.2 mmol) of the 3-iodo-2-styryl-1-tosylpyrrole **6b**, 50 mg (0.3 mmol) of *o*-nitrophenylboronic acid, 95 mg (0.3 mmol) of barium hydroxide octahydrate, and 15 mg (0.02 mmol) of dichloro(diphenylphosphinoferrocene)palladium(II). Eluent: 20% diethyl ether in petroleum ether. Yield of **10d**: 71 mg, 80%, yellow solid (mp 104°C). R_f = 0.33 (30% diethyl ether in petroleum ether). MS (EI) *m*/*z*: 444 (100, M^+), 289 (16, $[M - C_7H_7SO_2]^{\bullet+}$), 255 (18), 242 (19). HRMS calcd. for $C_{25}H_{20}N_2O_4S$: 444.1143; found: 444.1131. IR: 3162–2859, 1526, 1370, 1190–1089. ^{1}H NMR

© 2001 NRC Canada

($CDCl_3$, 500 MHz) δ: 7.87 (dd, ^3J = 8.0 Hz, ^4J = 1.3 Hz, 1H, $NO_2CCHCHCH$), 7.63 (d, ^3J = 8.0 Hz, 2H, $NSO_2C(CHCH)_2CCH_3$), 7.50 (dt, ^3J = 7.7 Hz, ^4J = 1.4 Hz, 1H, $NO_2CHCHCH$), 7.41 (dt, ^3J = 7.7 Hz, ^4J = 1.4 Hz, 1H, $NO_2CHCHCH$), 7.41 (d, ^3J = 3.4 Hz, 1H, NCHCH), 7.37 (dd, ^3J = 7.9 Hz, ^4J = 1.3 Hz, 1H, NO_2CCCH), 7.30 (d, ^3J = 16.5 Hz, 1H, $CHCHC(CHCH)_2CH$), 7.28–7.20 (m, 3H, $CHC(CHCH)_2CH$), 7.22 (d, ^3J = 8.0 Hz, 2H, $NSO_2C(CHCH)_2CCH_3$), 7.16–7.14 (m, 2H, $CHC(CHCH)_2CH$), 6.24 (d, ^3J = 3.4 Hz, 1H, NCHCH), 6.02 (d, ^3J = 16.5 Hz, 1H, $CHCHC(CHCH)_2CH$), 2.35 (s, 3H, CH_3). ^{13}C NMR ($CDCl_3$, 125 MHz) δ: 149.48 (CNO_2), 145.07 ($NSO_2C(CHCH)_2CCH_3$), 136.62 ($CHC(CHCH)_2CH$), 135.77 ($NSO_2C(CHCH)_2CCH_3$), 134.00 ($CHC(CHCH)_2CH$), 132.64 ($CHCCNO_2$), 132.60 ($CHCHCHCCNO_2$), 130.36 ($CCNO_2$), 129.80 ($NSO_2C(CHCH)_2CCH_3$), 129.75 (NCC), 128.47 ($CHCHC(CHCH)_2CH$), 128.17 (NO_2CCHCH), 127.90 ($CHCHC(CHCH)_2CH$), 126.87 ($NSO_2C(CHCH)_2CCH_3$), 126.23 ($CHCHC(CHCH)_2CH$), 124.2 (NO_2CCCH), 123.30 (NCC), 122.93 (NCHCH), 115.85 ($CHCHC(CHCH)_2CH$), 113.82 (NCHCH), 21.60 (CH_3).

*2-Styryl-1-tosylpyrrole (**11**) and 3-[^{2}H]-2-styryl-1-tosylpyrrole (**d-11**)*

To 3-iodo-2-styryl-1-tosylpyrrole **6b** (100 mg, 0.22 mmol), barium hydroxide octahydrate (1.5 equiv), and catalyst (0.05 or 0.1 equiv), a degassed mixture of DMF (8 mL) and water (2 mL) was added. The mixture was then placed in a bath preheated to 120°C. After 20 min, it was cooled to room temperature and diluted with ethyl acetate and water. After filtration on a Celite® pad (washed with ethyl acetate), the solution was washed with water, brine, and dried. Purification by flash chromatography on silica gel (20% diethyl ether in petroleum ether). Yield of **11**: 57 mg, 79%, colourless oil. R_f = 0.38 (30% diethyl ether in petroleum ether). MS (EI) *m*/*z*: 323 (100, M^+), 168 (54, $[M - C_7H_7SO_2]^+$). HRMS calcd. for $C_{19}H_{17}NO_2S$: 323.0980; found: 323.0979. ^{1}H NMR ($CDCl_3$, 500 MHz) δ: 7.68 (d, ^3J = 8.5 Hz, 2H, $(NSO_2C(CHCH)_2CCH_3$), 7.55 (d, ^3J = 15.5 Hz, 1H, $CHCHC(CHCH)_2CH$), 7.45 (d, ^3J = 8.3 Hz, 2H, $CHC(CHCH)_2CH$), 7.35 (dd (t), ^3J = 8.3 Hz, 2H, $CHC(CHCH)_2CH$), 7.33 (dd, ^3J = 3.4 Hz, ^4J = 1.6 Hz, 1H, NCHCH), 7.30–7.26 (m, 1H, $CHC(CHCH)_2CH$), 7.23 (d, ^3J = 8.5 Hz, 2H, $NSO_2C(CHCH)_2CCH_3$), 6.78 (d, ^3J = 15.5 Hz, 1H, $CHCHC(CHCH)_2CH$), 6.52 (dd, ^3J = 3.4 Hz, ^4J = 1.6 Hz, 1H, NCCH), 6.27 (t, ^3J = 3.4 Hz, 1H, NCHCH), 2.35 (s, 3H, CH_3). ^{13}C NMR ($CDCl_3$, 125 MHz) δ: 144.85 ($NSO_2C(CHCH)_2CCH_3$), 136.94 ($CHC(CHCH)_2CH$), 135.93 ($NSO_2C(CHCH)_2CCH_3$), 129.80 ($NSO_2C(CHCH)_2CCH_3$), 129.56 ($CHC(CHCH)_2CH$), 128.60 ($CHCHC(CHCH)_2CH$), 128.20 (NCCH), 127.63 ($CHCHC(CHCH)_2CH$), 126.77 ($NSO_2C(CHCH)_2CCH_3$), 126.33 ($CHCHC(CHCH)_2CH$), 123.23 (NCHCH), 116.79 ($CHCHC(CHCH)_2CH$), 112.46 (NCHCH), 111.56 (NCCH), 21.47 (CH_3).

When using deuterated DMF-d_7, **d-11** was obtained. R_f = 0.38 (30% diethyl ether in petroleum ether). MS (EI) *m*/*z*: 324 (38, M^+), 169 (100, $[M - C_7H_7SO_2]^{\bullet+}$), 168 (58, [M-D + H-$C_7H_7SO_2]^+$), 91 (24, $[C_7H_7]^+$), 44 (64). HRMS calcd. for $C_{19}H_{16}DNO_2S$: 324.1042; found: 324.1048. ^{1}H NMR ($CDCl_3$, 500 MHz) δ: 7.68 (d, ^3J = 8.5 Hz, 2H, $(NSO_2C(CHCH)_2CCH_3$), 7.55 (d, ^3J = 15.5 Hz, 1H, $CHCHC(CHCH)_2CH$), 7.45 (d, ^3J = 8.3 Hz, 2H, $CHC(CHCH)_2CH$), 7.35 (t, ^3J = 8.3 Hz, 2H, $CHC(CHCH)_2CH$), 7.33 (d, ^3J = 3.4 Hz, 1H, NCHCH), 7.27–7.25 (m, 1H, $CHC(CHCH)_2CH$), 7.23 (d, ^3J = 8.5 Hz, 2H, $NSO_2C(CHCH)_2CCH_3$), 6.78 (d, ^3J = 15.5 Hz, 1H, $CHCHC(CHCH)_2CH$), 6.27 (d, ^3J = 3.4 Hz, 1H, NCHCH), 2.35 (s, 3H, CH_3). ^{13}C NMR ($CDCl_3$, 125 MHz) δ: 144.85 ($NSO_2C(CHCH)_2CCH_3$), 136.94 ($CHC(CHCH)_2CH$), 135.93 ($NSO_2C(CHCH)_2CCH_3$), 133.84 (NCCH), 127.63 ($CHCHC(CHCH)_2CH$), 129.80 ($NSO_2C(CHCH)_2CCH_3$), 129.56 ($CHC(CHCH)_2CH$), 128.60 ($CHCHC(CHCH)_2CH$), 126.77 ($NSO_2C(CHCH)_2CCH_3$), 126.33 ($CHCHC(CHCH)_2CH$), 123.23 (NCHCH), 116.79 ($CHCHC(CHCH)_2CH$), 112.38 (NCHCH), 111.34 (t, NCCD), 21.47 (CH_3).

*2-Formyl-3-(*o*-nitrophenyl)-1-tosylpyrrole (**13a**) (RN: 233770-18-8)*

Method C: 120 mg (0.32 mmol) of the 3-iodo-2-formyl-1-tosylpyrrole **7b**, 80 mg (0.48 mmol) of *o*-nitrophenylboronic acid, 150 mg (0.48 mmol) of barium hydroxide octahydrate, 23 mg (0.032 mmol) of dichloro(diphenylphosphinoferrocene)palladium(II). Eluent: 30% diethyl ether in petroleum ether. Yield of **13a**: 120 mg, 98%, pale yellow solid (mp 143°C). R_f = 0.29 (40% diethyl ether in petroleum ether). MS (EI) *m*/*z*: 369 (8, M^+), 341 (42, $[M - CO]^+$), 324 (38, $[M - NO_2]^+$), 215 (100, $[M - C_7H_7SO_2]^+$), 187 (50, $[215 - CO]^+$), 155 (47, $[C_7H_7SO_2]^+$), 91 (88, $[C_7H_7]^+$). IR: 3074, 1678, 1536, 1269, 740. ^{1}H NMR ($CDCl_3$, 500 MHz) δ: 9.88 (s, 1H, CHO), 8.04 (dd, ^3J = 8.1 Hz, ^4J = 1.5 Hz, 1H, $CHCNO_2$), 7.79 (d, ^3J = 8.1 Hz, 2H, $NSO_2C(CHCH)_2CCH_3$), 7.67 (d, ^3J = 3.3 Hz, 1H, NCHCH), 7.59 (td, ^3J = 7.7 Hz, ^4J = 1.4 Hz, 1H, $NO_2CCHCHCH$), 7.52 (td, ^3J = 7.7 Hz, ^4J = 1.4 Hz, 1H, NO_2CCHCH), 7.35 (d, ^3J = 8.1 Hz, 2H, $NSO_2C(CHCH)_2CCH_3$), 7.33 (dd, ^3J = 7.7 Hz, ^4J = 1.4 Hz, 1H, NO_2CCCH), 6.39 (d, ^3J = 3.3 Hz, 1H, NCHCH), 2.43 (s, 3H, CH_3). ^{13}C NMR ($CDCl_3$, 125 MHz) δ: 178.9 (CHO), 148.98 (CNO_2), 145.98 ($NSO_2C(CHCH)_2CCH_3$), 135.42 ($NSO_2C(CHCH)_2CCH_3$), 135.26 (NCCHO), 132.44 ($NO_2CCHCHCH$), 132.25 (NO_2CCCH), 130.15 ($NSO_2C(CHCH)_2CCH_3$), 129.2 (NO_2CCHCH), 128.48 (NO_2CC), 128.34 (NCC), 128.34 (NCH), 127.24 ($NSO_2C(CHCH)_2CCH_3$), 124.39 ($CHCNO_2$), 113.85 (NCHCH), 21.59 (CH_3). Anal. calcd. for $C_{18}H_{14}N_2O_5S$: C 58.37, H 3.81, N 7.56; found: C 58.23, H 3.56, N 7.37.

*2-Formyl-3-phenyl-1-tosylpyrrole (**13b**)*

Method C: 150 mg (0.4 mmol) of the 3-iodo-2-formyl-1-tosylpyrrole **7b**, 73 mg (0.6 mmol) of phenylboronic acid, 189 mg (0.6 mmol) of barium hydroxide octahydrate, 30 mg (0.04 mmol) of dichloro(diphenylphosphinoferrocene)palladium(II). Eluent: 30% diethyl ether in petroleum ether. Yield of **13b**: 120 mg, 92%, white solid (mp 175°C). R_f = 0.37 (40% diethyl ether in petroleum ether). MS (EI) *m*/*z*: 325 (78, $M^{\bullet+}$), 260 (45, $[M - SO_2]^+$), 170 (100, $[M - C_7H_7SO_2]^+$), 169 (75), 155 (38, $[C_7H_7SO_2]^+$), 115 (41), 91 (53, $[C_7H_7]^+$). HRMS calcd. for $C_{18}H_{15}NO_3S$: 325.0772; found: 325.0765. IR: 1675, 1374, 1174. ^{1}H NMR ($CDCl_3$, 500 MHz) δ: 9.62 (s, 1H, CO*H*), 7.94 (d, ^3J = 8.8 Hz, 2H, $(NSO_2C(CHCH)_2CCH_3$), 7.84 (d, ^3J = 3.4 Hz, 1H, NCHCH), 7.40 (s, 5H), 7.34 (d, ^3J = 8.8 Hz, 2H, $NSO_2C(CHCH)_2CCH_3$),

© 2001 NRC Canada

6.49 (d, ^3J = 3.4 Hz, 1H, NCHC*H*), 2.43 (s, 3H, CH_3). ^{13}C NMR ($CDCl_3$, 125 MHz) δ: 178.22 (*C*HO), 145.36 (NSO_2C-$(CHCH)_2CCH_3$), 143.46 (N*C*CHO), 135.11 (NSO_2C-$(CHCH)_2CCH_3$), 132.27 (NCC*C*$(CHCH)_2CH$), 129.54 ($NSO_2C(CHCH)_2CCH_3$), 129.54 (N*C*HCH), 129.47 (NCCC-$(CHCH)_2C$), 128.63 (NCCC$(CHCH)_2CH$), 128.44 (NCCC-$(CHCH)_2CH$), 128.34 ($NSO_2C(CHCH)_2CCH_3$), 127.98 (NC*C*C$(CHCH)_2CH$), 112.80 (NCH*C*H), 21.61 (*C*H_3).

*2-Formyl-3-(*m-*nitrophenyl)-1-tosylpyrrole (**13c**) (RN: 233770-24-6)*

Method C: 150 mg (0.4 mmol) of the 3-iodo-2-formyl-1-tosylpyrrole **7b**, 102 mg (0.6 mmol) of *m*-nitrophenylboronic acid, 189 mg (0.6 mmol) of octahydrate barium hydroxide, 30 mg (0.04 mmol) of dichloro(diphenylphosphinoferrocene)palladium(II). Eluent: 30% diethyl ether in petroleum ether. Yield of **13c**:130 mg, 88%, pale yellow solid (mp 142°C). R_f = 036 (40% diethyl ether in petroleum ether). MS (EI) *m*/*z*: 370 (51, $M^{\bullet+}$), 306 (67, $[215 + 91]^{\bullet+}$), 215 (63, $[M - C_7H_7SO_2]^+$), 214 (61, $[215 - H]^{\bullet+}$), 155 (100, $[C_7H_7SO_2]^+$), 91 (92, $[C_7H_7]^+$). IR: 1676, 1526, 1348, 1175, 669. ^{1}H NMR ($CDCl_3$, 500 MHz) δ: 9.87 (s, 1H, C*H*O), 8.25 (dd, ^4J = 2.3 Hz, ^4J = 1.7 Hz, 1H, CC*H*CNO$_2$), 8.20 (dd, ^3J = 8.3 Hz, ^4J = 2.3 Hz, 1H, CCHCNO$_2$C*H*), 7.87 (d, ^3J = 8.8 Hz, 2H, $NSO_2C(CHCH)_2CCH_3$), 7.77 (d, ^3J = 3.4 Hz, 1H, NC*H*CH), 7.74 (ddd, ^3J = 7.7 Hz, ^4J = 1.7 Hz, ^4J = 1.1 Hz, 1H, C*H*CCHCNO$_2$), 7.55 (t, ^3J = 7.7 Hz, 2H, C*H*CHCCHCNO$_2$), 7.34 (d, ^3J = 8.8 Hz, 2H, $NSO_2C(CHCH)_2CCH_3$), 6.50 (d, ^3J = 3.3 Hz, 1H, NCHC*H*), 2.42 (s, 3H, CH_3). ^{13}C NMR ($CDCl_3$, 125 MHz) δ: 178.33 (*C*HO), 147.98 (*C*NO$_2$), 146.01 ($NSO_2C(CHCH)_2CCH_3$), 138.42 (N*C*CHO), 135.33 (*C*HCCHCNO$_2$), 135.01 (*C*CHNO$_2$), 134.76 (NSO_2C-$(CHCH)_2CCH_3$), 129.97 ($NSO_2C(CHCH)_2CCH_3$), 129.15 (N*C*H), 129.05 (C*H*CHCCHNO$_2$), 127.97 (NC*C*), 127.83 ($NSO_2C(CHCH)_2CCH_3$), 124.16 (CCHNO$_2$), 123.17 (CCHCNO$_2$*C*H), 113.24 (NCH*C*H), 21.58 (*C*H_3). Anal. calcd. for $C_{18}H_{14}N_2O_5S$: C 58.37, H 3.81, N 7.56; found: C 58.46, H 3.72, N 7.33.

*2-Formyl-3-(*p-*nitrophenyl)-1-tosylpyrrole (**13d**) (RN: 233770-26-8)*

Method C: 150 mg (0.4 mmol) of the 3-iodo-2-formyl-1-tosylpyrrole **7b**, 102 mg (0.6 mmol) of *p*-nitrophenylboronic acid, 189 mg (0.6 mmol) of barium hydroxide octahydrate, 30 mg (0.04 mmol) of dichloro(diphenylphosphinoferrocene)palladium(II). Eluent: 30% diethyl ether in petroleum ether. Yield of **13d**: 124 mg, 84%, pale yellow solid (mp 167°C). R_f = 0.38 (40% diethyl ether in petroleum ether). MS (EI) *m*/*z*: 370 (56, $M^{\bullet+}$), 306 (67, $[215 + 91]^{\bullet+}$), 294 (49), 226 (57), 215 (49, $[M - C_7H_7SO_2]^+$), 214 (43, $[215 - H]^{\bullet+}$), 155 (88, $[C_7H_7SO_2]^+$), 91 (86, $[C_7H_7]^+$), 44 (100). IR: 1677, 1517, 1345, 1137, 669. ^{1}H NMR ($CDCl_3$, 500 MHz) δ: 9.88 (s, 1H, C*H*O), 8.25 (d, ^3J = 8.8 Hz, 2H, NO$_2$CC*H*), 7.90 (d, ^3J = 8.8 Hz, 2H, $NSO_2C(CHCH)_2CCH_3$), 7.80 (d, ^3J = 3.3 Hz, 1H, NC*H*CH), 7.59 (d, ^3J = 8.8 Hz, 2H, NO$_2$CCHC*H*), 7.37 (d, ^3J = 8.8 Hz, 2H, NSO_2C-$(CHCH)_2CCH_3$), 6.51 (d, ^3J = 3.3 Hz, 1H,NCHC*H*), 2.45 (s, 3H, CH_3). ^{13}C NMR ($CDCl_3$, 125 MHz) δ: 178.36 (*C*HO), 147.67 (*C*NO$_2$), 146.07 ($NSO_2C(CHCH)_2CCH_3$), 139.16 (N*C*CHO), 138.69 (NO$_2$CCHCH*C*), 134.81 (NSO_2C-$(CHCH)_2CCH_3$), 130.29 (NO$_2$CCH*C*H), 129.96 (NSO_2C-$(CHCH)_2CCH_3$), 129.14 (N*C*H), 128.08 (NC*C*), 128.01 ($NSO_2C(CHCH)_2CCH_3$), 123.46 (NO$_2$C*C*H), 113.14 (NCH*C*H), 21.65 (*C*H_3). Anal. calcd. for $C_{18}H_{14}N_2O_5S$: C 58.37, H 3.81, N 7.56; found: C 58.30, H 3.66, N 7.48.

*2-Formyl-3-(*o-*methoxyphenyl)-1-tosylpyrrole (**13e**) (RN: 233770-28-0)*

Method C: 250 mg (0.7 mmol) of the 3-iodo-2-formyl-1-tosylpyrrole **7b**, 151 mg (1 mmol) of o-methoxyphenylboronic acid, 315 mg (1 mmol) of barium hydroxide octahydrate, 48 mg (0.07 mmol) of dichloro(diphenylphosphinoferrocene)palladium(II). Eluent: 30% diethyl ether in petroleum ether. Yield of **13e**: 210 mg, 89%, white solid (mp 131°C). R_f = 0.31 (40% diethyl ether in petroleum ether). MS (EI) *m*/*z*: 355 (30, $M^{\bullet+}$), 324 (100, $[355 - OMe-H]^+$), 201 (44, $[M - C_7H_7SO_2]^+$), 185 (45), 170 (57, $[201 - OMe]^+$), 152 (49), 134 (30), 91 (45, $[C_7H_7]^+$). IR: 1676, 1174, 672. ^{1}H NMR ($CDCl_3$, 500 MHz) δ: 9.48 (s, 1H, C*H*O), 7.96 (d, ^3J = 8.8 Hz, 2H, $NSO_2C(CHCH)_2CCH_3$), 7.82 (d, ^3J = 3.3 Hz, 1H, NC*H*), 7.36–7.33 (m, 3H, CH$_3$OCCHC*H* and NSO_2C-$(CHCH)_2CCH_3$), 7.21 (d, ^3J = 8.2 Hz, 1H, CH$_3$OCCC*H*), 6.97–6.95 (m, 2H,CH$_3$OCC*H*CHC*H*), 6.49 (d, ^3J = 3.3 Hz, 1H, NCHC*H*), 3.23 (s, 3H, OCH_3), 2.41 (s, 3H, CH_3). ^{13}C NMR ($CDCl_3$, 125 MHz) δ: 178.32 (*C*HO), 156.62 (CH$_3$O*C*), 145.08 ($NSO_2C(CHCH)_2CCH_3$), 139.37 (N*C*CHO), 136.02 (NSO_2C), 131.75 (CH$_3$OCC*C*H), 130.08 (CH$_3$OCCH*C*H), 129.37 ($NSO_2C(CHCH)_2CCH_3$), 128.98 (N*C*H), 128.43 (NC*C*), 128.28 ($NSO_2C(CHCH)_2CCH_3$), 120.32 (CH$_3$OCCCH*C*H), 113.89 (NCH*C*H), 110.93 (CH$_3$OC*C*H), 55.36 (*C*H$_3$O), 21.50 (*C*H_3). Anal. calcd. for $C_{19}H_{17}NO_4S$: C 64.21, H 4.82, N 3.94; found: C 63.91, H 4.69, N 3.97.

*2-Formyl-3-mesityl-1-tosylpyrrole (**13f**) (RN: 233770-32-6)*

Method C: 150 mg (0.4 mmol) of the 3-iodo-2-formyl-1-tosylpyrrole **7b**, 98 mg (0.6 mmol) of mesitylboronic acid (26), 189 mg (0.6 mmol) of barium hydroxide octahydrate, 30 mg (0.04 mmol) of dichloro(diphenylphosphinoferrocene)palladium(II). Eluent: 20% diethyl ether in petroleum ether. Yield of **13f**: 90 mg, 61%, white solid (mp 141°C). R_f = 0.57 (40% diethyl ether in petroleum ether). MS (EI) *m*/*z*: 367 (83, M^+), 212 (43, $[M - C_7H_7SO_2]^+$), 184 (100 $[212 - CO]^+$), 168 (32, $[184 - CH_3\text{-}H]^+$), 155 (32, $[C_7H_7SO_2]^+$), 91 (33, $[C_7H_7]^+$). IR: 1679, 1370, 1175. ^{1}H NMR ($CDCl_3$, 500 MHz) δ: 9.32 (s, 1H, C*H*O), 7.87 (d, ^3J = 8.8 Hz, 2H, $NSO_2C(CHCH)_2CCH_3$), 7.85 (d, ^3J = 3.3 Hz, 1H, NC*H*), 7.33 (d, ^3J = 8.8 Hz, 2H, $NSO_2C(CHCH)_2CCH_3$), 6.89 (s, 2H, CH$_3$C(C*H*CCH$_3$)$_2$C), 6.26 (d, ^3J = 3.3 Hz, 1H, NCHC*H*), 2.43 (s, 3H, CH_3), 1.94 (s, 9H, CH_3). ^{13}C NMR ($CDCl_3$, 125 MHz) δ: 177.87 (*C*HO), 145.34 (NSO_2C-$(CHCH)_2CCH_3$), 142.1 (N*C*CHO), 137.84 (CH$_3$*C*-(CHCCH$_3$)$_2$C), 136.41 (CH$_3$C(CH*C*CH$_3$)$_2$C), 135.19 ($NSO_2C(CHCH)_2CCH_3$), 129.97 (N*C*H), 129.57 (NSO_2C-$(CHCH)_2CCH_3$), 128.74 (CH$_3$C(CHCCH$_3$)$_2$*C*), 128.40 (NC*C*), 128.03 (CH$_3$C(*C*HCCH$_3$)$_2$C), 127.80 (NSO_2C-$(CHCH)_2CCH_3$), 113.81 (NCH*C*H), 21.58 (*C*H$_3$), 20.38 (CH$_3$). Anal. calcd. for $C_{21}H_{21}NO_3S$: C 68.64, H 5.76, N 3.81; found: C 68.52, H 5.79, N 3.76.

© 2001 NRC Canada

*2-Formyl-3-(3-pyridyl)-1-tosylpyrrole (**13g**)*

Method C: 150 mg (0.4 mmol) of the 3-iodo-2-formyl-1-tosylpyrrole **7b**, crude 3-pyridylboronic acid (28) from diethyl-3-pyridylborane (588 mg, 4 mmol), 189 mg (0.6 mmol) of barium hydroxide octahydrate, 30 mg (0.04 mmol) of dichloro(diphenylphosphinoferrocene)palladium(II). Eluent: 30% ethyl acetate in dichloromethane. Yield of **13g**: 128 mg, 77%, pale yellow oil. R_f = 0.49 (50% ethyl acetate in dichloromethane). MS (EI) *m/z*: 326 (100, $M^{\bullet+}$), 262 (27), 261 (28), 171 (35, $[M - SO_2C_7H_7)^+]$, 170 (29), 155 (44, $[SO_2C_7H_7]^+$), 91 (66, C_7H_7). HRMS calcd. for $C_{17}H_{14}N_2O_3S$: 326.0725; found: 326.0711. IR: 1675, 1377, 1175. ^{1}H NMR ($CDCl_3$, 300 MHz) δ: 9.82 (s, 1H, CO*H*), 8.66 (s, 1H, CC*H*N), 8.62 (d, ^3J = 4.8 Hz, 1H, (NC*H*CHCH), 7.91 (d, ^3J = 8.2 Hz, 2H, ($NSO_2C(CHCH)_2CCH_3$), 7.82 (d, ^3J = 3.1 Hz, 1H, NC*H*CH), 7.79 (d, ^3J = 3.1 Hz, 1H, (NCHCHC*H*), 7.39–7.26 (m, 3H, NCHC*H*CH and $NSO_2C(CHCH)_2CCH_3$), 6.51 (d, ^3J = 3.2 Hz, 1H, NCHC*H*), 2.44 (s, 3H, CH_3). ^{13}C NMR ($CDCl_3$, 50 MHz) δ: 177.80 (*C*HO), 149.30 (C*C*HN), 149.1 (N*C*HCHCH), 145.48 ($NSO_2C(CHCH)_2CCH_3$), 137.57 ($NSO_2C(CHCH)_2CCH_3$), 136.37 (*C*HCCHN), 134.59 (N*C*CHO), 129.51 (NSO_2C-$(CHCH)_2CCH_3$), 128.92 (N*C*HCH), 128.21 (*C*CHN), 127.87 (NC*C*), 127.64 ($NSO_2C(CHCH)_2CCH_3$), 122.64 (*C*HCHN), 112.75 (NCH*C*H), 21.26 (CH_3).

*2-Formyl-3-thiophenyl-1-tosylpyrrole (**13h**) (RN: 233770-30-4)*

Method C: 150 mg (0.4 mmol) of the 3-iodo-2-formyl-1-tosylpyrrole **7b**, 77 mg (0.6 mmol) of 2-thiophenylboronic acid, 189 mg (0.6 mmol) of octahydrate barium hydroxide, 30 mg (0.04 mmol) of dichloro(diphenylphosphinoferrocene)palladium(II). Eluent: 30% diethyl ether in petroleum ether. Yield of **13h**: 113 mg, 85%, white solid (mp 146°C). R_f = 0.34 (40% diethyl ether in petroleum ether). MS (EI) *m/z*: 331 (72, M^+), 176 (100, $[M - C_7H_7SO_2]^+$). IR: 1670, 1374, 1174. ^{1}H NMR ($CDCl_3$, 500 MHz) δ: 9.99 (s, 1H, CO*H*), 7.87 (d, ^3J = 8.8 Hz, 2H, $NSO_2C(CHCH)_2CCH_3$), 7.75 (d, ^3J = 3.4 Hz, 1H, NC*H*CH), 7.44 (dd, ^3J = 3.6 Hz, ^4J = 1.1 Hz, 1H, SCC*H*), 7.39 (dd, ^3J = 5.1 Hz, ^4J = 1.1 Hz, 1H, SC*H*CH), 7.33 (d, ^3J = 8.8 Hz, 2H, $NSO_2C(CHCH)_2CCH_3$), 7.08 (dd, ^3J = 5.1 Hz, ^4J = 3.6 Hz, 1H, SCHC*H*), 6.58 (d, ^3J = 3.4 Hz, 1H, NCHC*H*), 2.42 (s, 3H, CH_3). ^{13}C NMR ($CDCl_3$, 125 MHz) δ: 178.37 (*C*HO), 145.61 ($NSO_2C(CHCH)_2$-CCH_3), 135.01($NSO_2C(CHCH)_2CCH_3$), 134.42 (N*C*CHO), 133.61 (S*C*CH), 129.77 ($NSO_2C(CHCH)_2CCH_3$), 129.38 (N*C*HCH), 129.04 (SC*C*H), 127.94 ($NSO_2C(CHCH)_2CCH_3$), 127.67 (S*C*HCH), 127.48 (NC*C*), 112.92 (NCH*C*H), 21.61 (CH_3). Anal. calcd. for $C_{16}H_{13}NO_3S_2$: C, 57.98, H 3.95, N 4.23; found: C 58.09, H 4.07, N 4.13.

*2-Formyl-3-(1-*tert*-butoxycarbonyl)-pyrrole-1-tosylpyrrole (**13i**)*

Method C: 150 mg (0.4 mmol) of the 3-iodo-2-formyl-1-tosylpyrrole **7b**, 127 mg (0.6 mmol) of 1-*tert*-butoxycarbonylpyrrol-2-ylboronic acid (31), 189 mg (0.6 mmol) of barium hydroxide octahydrate, 30 mg (0.04 mmol) of dichloro(diphenylphosphinoferrocene)palladium(II). Eluent: 20% diethyl ether in petroleum ether. Yield of **13i**: 128 mg, 77%, pale yellow oil. R_f = 0.59 (40% diethyl ether in petroleum ether). MS (EI) *m/z*: 414 (71, M^+), 314 (100), 159 (96). HRMS calcd. for $C_{21}H_{22}N_2O_5S$: 414.1249; found: 414.1241. IR: 1700, 1700, 1371, 1316, 1174. ^{1}H NMR ($CDCl_3$, 300 MHz) δ: 9.64 (s, 1H, CO*H*), 7.91 (d, ^3J = 8.4 Hz, 2H, $NSO_2C(CHCH)_2CCH_3$), 7.71 (d, ^3J = 3.4 Hz, 1H, NC*H*CH), 7.38 (dd, ^3J = 3.3 Hz, ^4J = 1.8 Hz, 1H, NCHC*H*CH), 7.33 (d, ^3J = 8.4 Hz, 2H, $NSO_2C(CHCH)_2CCH_3$), 6.40 (d, ^3J = 3.4 Hz, 1H, NCHC*H*), 6.22–6.18 (m, 2H, NCC*H* and NCHC*H*), 2.42 (s, 3H, CH_3), 1.37 (s, 9H, CH_3). ^{13}C NMR ($CDCl_3$, 75 MHz) δ: 178.13 (*C*HO), 148.55 (O*C*ON), 145.41 ($NSO_2C(CHCH)_2CCH_3$), 135.14 ($NSO_2C(CHCH)_2CCH_3$), 134.18 (N*C*CHO), 129.58 ($NSO_2C(CHCH)_2CCH_3$), 129.35 (N*C*CH), 128.17 ($NSO_2C(CHCH)_2CCH_3$), 128.08 (N*C*HCH), 124.11 (NC*C*), 123.53 (*C*HNC), 117.68 (NC*C*H), 114.25 (NCH*C*H), 110.55 (NCH*C*HCH), 84 ($C(CH_3)_3$), 27.49 ($C(CH_3)_3$), 21.57 (CH_3).

*2-Nitro-6-trifluoromethylboronic acid (**14**) and 4-nitro-6-trifluoromethylboronic acid (**15**)*

To a solution of nitric acid (90% aqueous, 2.25 mL, 48 mmol) and sulfuric acid (6.8 mL, 128 mmol) and a few urea crystals at 0°C, a solution of 2-(trifluoromethyl)phenylboronic acid (3.2 g, 16 mmol) in acetic anhydride (42 mL) was slowly added through an addition funnel. During the addition, the temperature was kept under 5°C. After the addition, the mixture was stirred for 4 h at 0°C and overnight at room temperature. It was then poured onto ice (500 mL) and sodium hydroxide was added until the pH reached a value between 3 and 5. The aqueous phase was then extracted with diethyl ether. The organic layer was washed with brine, dried and concentrated in vacuo. The purification by reverse-phase MPLC yielded 2-nitro-6-trifluoromethylboronic acid (**14**) (1.6 g, 42%) as a white solid (mp 154°C) and 4-nitro-2-trifluoromethylboronic acid (**15**) (0.46 g, 12%) as a white solid (mp 141°C).

***(14)**:* r.t. = 11.9 min (col. MATREX 4 RP 18 15 μ; eluent: CH_3CN–H_2O, 35:65; flow 0.5 mL min^{-1}; UV detector 254 nm, 25°C). MS (EI) *m/z*: 235 (3, $M^{\bullet+}$), 191 (100, $[M - B(OH)_2 + H]^{\bullet+}$), 171 (88, $[M - NO_2\text{-}F]^+$). HRMS calcd. for $C_7H_5BF_3NO_4$: 235.0263; found: 235.0266. IR: 3591 and 3385, 1543, 1387–1292 (B—OH), 1134. ^{1}H NMR (DMSO-d_6, 500 MHz) δ: 8.46 (d, ^3J = 7.6 Hz, 1H, C*H*CNO_2), 8.28 (s, 2H, $B(OH)_2$), 8.14 (d, ^3J = 7.6 Hz, 1H, C*H*CF_3), 7.81 (t, ^3J = 7.6 Hz, 1H, CHC*H*CH). ^{13}C NMR (DMSO-d_6, 75 MHz) δ: 150.47 (*C*NO_2), 133.5–132 (m, C-B), 131.77 (CH*C*HCH), 130.02 (*C*HCCF_3), 125.32 (*C*CF_3), 126.56 (*C*HCNO_2), 120.92 (*C*F_3).

***(15)**:* r.t. = 19.2 min (col. MATREX 4 RP 18 15 μ; eluent: CH_3CN–H_2O 35:65; flow 0.5 mL min^{-1}; UV detector 254 nm, 25°C). MS (EI) *m/z*: 235 (100, $M^{\bullet+}$), 189 (24, $[M - NO_2]^+$), 171 (55, $[189 - F]^+$), 125 (39, $[189 - B(OH)_2\text{-}F]^+$), 75 (25, $[M - CF_3\text{-}NO_2\text{-}B(OH)_2]^{\bullet+}$). HRMS calcd. for $C_7H_5BF_3NO_4$: 235.0263; found: 235.0257. IR: 3470–3359, 1530, 1409–1321 (B—OH), 1287, 1128. ^{1}H NMR (DMSO-d_6, 75 MHz) δ: 8.71 (s, 2H, $B(OH)_2$), 8.42 (d, ^3J = 9.2 Hz, 1H, C*H*CNO_2), 8.14 (s, 1H, NO_2C*H*CF_3), 7.83 (d, ^3J = 9.2 Hz, 1H, C*H*$CB(OH)_2$). ^{13}C NMR (DMSO-d_6, 50 MHz) δ: 146.80 (NO_2C), 134.11 (NO_2CCHCH), 132.5–130.85 (m, *C*-B), 126.28 (*C*CF_3), 125.94 (NO_2CCH*C*H), 121.35 (*C*F_3), 119.85 (NO_2C*C*HCF_3).

© 2001 NRC Canada

*2-Amino-6-trifluoromethylboronic acid (**16**)*

Palladium (10% on activated carbon, 38 mg) was added to a solution of *o*-nitro-*o*′-trifluoromethylboronic acid (**14**) in ethanol (10 mL). The resulting suspension was then stirred under hydrogen (2 bar) overnight, filtered on a Celite® pad and concentrated in vacuo. Owing to its unstability, the product was used in the coupling reaction without further purification.

*3-Tosyl-9-(trifluoromethyl)-3*H*-pyrrolo[2,3-*c*]-quinoline (**17**)*

Method C: 150 mg (0.4 mmol) of the 3-iodo-2-formyl-1-tosylpyrrole **7b**, 120 mg (0.6 mmol) of the crude *o*-amino-*o*′-trifluoromethylboronic acid (**16**), 189 mg (0.6 mmol) of barium hydroxide octahydrate, 30 mg (0.04 mmol) of dichloro(diphenylphosphinoferrocene)palladium(II). Eluent: 30% ethyl acetate in petroleum ether. Yield of **17**: 40 mg, 26%, pale yellow solid (mp 163°C). R_f = 0.5 (70% diethyl ether in petroleum ether). MS (EI) *m*/*z*: 390 (100, $M^{\bullet+}$), 235 (15, $[M - C_7H_7SO_2]^+$), 155 (29, $[C_7H_7SO_2]^+$), 91 (21, $[C_7H_7]^+$) HRMS calcd. for $C_{19}H_{13}F_3N_2O_2S$: 390.0649; found: 390.0654. IR: no carbonyl signal. ^{1}H NMR ($CDCl_3$, 500 MHz) δ: 9.70 (s, 1H, C*H*N), 8.40 (d, ^3J = 8.0 Hz, 1H, C*H*CCCF$_3$), 8.02 (d, ^3J = 8.0 Hz, 1H, C*H*CCF$_3$), 7.86 (d, ^3J = 3.7 Hz, 1H, NC*H*CH), 7.85 (d, ^3J = 8.5 Hz, 1H, $NSO_2C(CHCH)_2CCH_3$), 7.69 (t, ^3J = 8.0 Hz, 1H, CHCHCCF$_3$), 7.45–7.43 (m, 1H, NCHC*H*), 7.26 (d, ^3J = 8.6 Hz, 2H, $NSO_2C(CHCH)_2CCH_3$), 2.34 (s, 3H, CH_3). ^{13}C NMR ($CDCl_3$, 125 MHz) δ: 145.94 ($NSO_2C(CHCH)_2CCH_3$), 144.74 (*C*NCH), 138.73 (CN*C*H), 135.26 (*C*HCNCCCF$_3$), 134.72 ($NSO_2C(CHCH)_2CCH_3$), 130.22 ($NSO_2C(CHCH)_2CCH_3$), 128.90 (N*C*C), 128.03 (N*C*H), 126.96 ($NSO_2C(CHCH)_2CCH_3$), 126.03 (*C*HCCF$_3$), 125.83 (NCCH*C*HCHCCF$_3$), 21.51 (*C*H$_3$).

Acknowledgements

This work was supported by fellowships from the European Community (C.F.), the Fonds National de la Recherche Scientifique, and the European Institute for Chemistry and Biology (F.D.). We thank the Ministère de l'Education et de la Recherche Scientifique de la Communauté Française de Belgique (Action concertée 96/01–197) for a generous grant. We also thank L. Delhaye and V. Gevears for technical help.

References

1. R.J. Sundberg. Pyrroles and their benzo derivatives. *In* Comprehensive heterocyclic chemistry. Vol. 4. *Edited by* A.R. Katritzky and C.W. Rees. Pergamon Press, Oxford. 1984. Part 3. pp. 246–254.
2. R.E. Niziurski-Mann and M.P. Cava. Heterocycles, **34**, 2003 (1992).
3. T. Masquelin and D. Obrecht. Synthesis, 276 (1995), and refs. cited therein.
4. (*a*) A. Banerji, P.L. Pajumder, and A. Chaterjee. Phytochemistry, **9**, 1491 (1970); (*b*) D.J. Abraham, R.D. Rosenstein, R.L. Lyon, and H.H.S. Fong. Tetrahedron Lett. **10**, 909 (1972); (*c*) K.T. De Silva, A.H. Ratcliffe, G.F. Smith, and G.N. Smith. Tetrahedron Lett. **10**, 913 (1972); (*d*) B. David, T. Sévenet, M. Morgat, D. Guénard, A. Moisand, Y. Tollon, and M. Wright. Cell Motil. Cytoskeleton, **28**, 317 (1994); (*e*) B. David, T. Sévenet, O. Thoison, K. Awong, M. Païs, M. Wright, and D. Guénard. Bioorg. Med. Chem. Lett. **7**, 2155 (1997); (*f*) C. Pascal, J. Dubois, D. Guénard, L. Tchertanov, S. Thoret, and F. Guéritte. Tetrahedron, **54**, 14737 (1998).
5. (*a*) K. Tanaka, K. Karigone, and S. Umio. Chem. Pharm. Bull. **17**, 611 (1969); (*b*) G.C. Spence, E.C. Taylor, and O. Büchardt. Chem. Rev. **70**, 231 (1970); (*c*) A.H. Ratcliffe, G.F. Smith, and G.N. Smith. Tetrahedron Lett. **52**, 5179 (1973); (*d*) F. Bellamy, P. Martz, and J. Streith. Heterocycles, **3**, 395 (1975); (*e*) H. Horikawa, T. Iwasaki, K. Matsumoto, and M. Miyoshi. J. Org. Chem. **43**, 335 (1978); (*f*) D.J. Arnold, L. Burgess-Dean, J.Hubbard, and M.A. Rahman. Aust. J. Chem. **47**, 969 (1994); (*g*) J.T. Gupton, S.A. Petrich, L.L. Smith, M.A. Bruce, P. Vu, K.X. Du, and E.E. Dueno. Tetrahedron, **52**, 6879 (1996).
6. S.P. Stanforth. Tetrahedron, **54**, 263 (1998).
7. N. Miyaura and A. Suzuki. Chem. Rev. **95**, 2457 (1995); A. Suzuki. J. Organomet. Chem. **576**, 147 (1999).
8. (*a*) J.M. Muchowski. J. Org. Chem. **57**, 1653 (1992); (*b*) G.G Grieb and D.M. Ketcha. Synth. Commun. **25**, 2195 (1995); (*c*) R. D'Alessio and A. Rossi. Synlett, 513 (1996); (*d*) D. Bolton, I. Boyfield, M.C. Coldwell, M.S. Hadley, A. Johns, C.N. Johnson, R.E. Markwell, D.J. Nash, G.I. Riley, E.E. Scott, S.A. Smith, G. Stemp, H.J. Wadsworth, and E.A. Watts. Bioorg. Med. Chem. Lett. **7**, 327 (1997); (*e*) C.N. Johnson, G. Stemp, N. Arnaud, S.C. Stephen, and T. Gallagher. Synlett, 1025 (1998); (*f*) T. Murashima, D. Shiya, K. Nishi, H. Uno, and N. Quo. J. Chem. Soc. Perkin Trans. 1, **16**, 2671 (2000).
9. (*a*) C.K. Chang, and N. Bag. J. Org. Chem. **60**, 7030 (1995); (*b*) J. Cossy and D. Belotti. J. Org. Chem. **62**, 7900 (1997); (*c*) M.G. Banwell, B.L. Flynn, E. Harmel, and D.C.R. Hockless. J. Chem. Soc. Chem. Commun. 207 (1997); (*d*) H.W. Chan, P.C. Chan, J.H. Lin, and H.N.C. Wong. J. Chem. Soc. Chem. Commun. 1515 (1997); (*e*) A. Fürstner, J. Grabowski, and C.W. Lehmann. J. Org. Chem. **64**, 8275 (1999); (*f*) T. Murashima, D. Shiya, K. Nishi, H. Uno, and N. Ono. J. Chem. Soc. Perkin Trans. 1, **16**, 2671 (2000); (*g*) J.H. Liu, Q.-C. Yang, T.C.W. Mak, and H.N.C. Wong. J. Org. Chem. **65**, 3587 (2000).
10. (*a*) F.R. Bean and J.R. Johnson. J. Am. Chem. Soc. **54**, 4415 (1932); (*b*) H.L. Mutreities. *In* The chemistry of boron and its compounds. Wiley, New York. 1967; (*b*) S. Murahashi, M. Yamamura, K. Yanagisawa, N. Mita, and K. Kondo. J. Org. Chem. **44**, 2408 (1979); (*c*) M.J. Sharp and V. Snieckus. Tetrahedron Lett. **26**, 5997 (1985); (*d*) N. Miyaura, T. Ishiyama, H. Sazaki, M. Ishikawa, M. Satoh, and A. Suzuki. J. Am. Chem. Soc. **111**, 314 (1989); (*e*) M.P. Groziak, A.D. Ganguly, and P.D. Robinson. J. Am. Chem. Soc. **116**, 7597 (1994).
11. V. Snieckus. Chem. Rev. **90**, 879 (1990).
12. C. Franc, F. Denonne, C. Cuisinier, and L. Ghosez. Tetrahedron Lett. **40**, 4555 (1999).
13. (*a*) M. Banwell, A. Edwards, J. Smith, E. Hamel, and P. Verdier-Pinard. J. Chem. Soc. Perkin Trans. 1, 1497 (2000); (*b*) C. Dupond, D. Guénard, C. Thal, S. Thoret, and F. Guéritte. Tetrahedron Lett. **41**, 5853 (2000).
14. D. Xiao and D.M. Ketcha. Org. Prep. Proced. Int. **4**, 503 (1995).
15. (*a*) T. Watanabe, N. Miyaura, and A. Suzuki. Synlett, 207 (1992); (*b*) A. Suzuki. Pure Appl. Chem. **66**, 213 (1994); (*c*) J.M. Fu, M.J. Sharp, and V. Snieckus. Can. J. Chem. **72**, 227 (1994); (*d*) A. James and V. Snieckus. Tetrahedron Lett. **38**, 8142 (1997); (*e*) J.C. Anderson, H. Namli, and C.A. Roberts. Tetrahedron, **53**, 15123 (1997).
16. C. Amatore, A. Tatand, and A. Suarez. J. Am. Chem. Soc. **115**, 9531 (1993).

© 2001 NRC Canada

17. G.W. Parshall and S.D. Ittel. Homogeneous catalysis. Wiley, New York. 1992.
18. J. Chatt, F.A. Hart, and H.R. Watson. J. Chem. Soc. 2537 (1962).
19. S. Gronowitz, A.B. Hörnfeldt, and Y. Yang. Chem. Scr. **28**, 281 (1988).
20. (*a*) T. Oh-e, N. Miyaura, and A. Suzuki. J. Org. Chem. **58**, 2201 (1993); (*b*) N.A. Bumaym, A.F. Nikitina, and I.P. Beletskaya. Russ. J. Org. Chem. **30**, 1619 (1994); (*c*) S. Mohri, M. Stefnovic, and V. Snieckus. J. Org. Chem. **62**, 7072 (1997).
21. (*a*) J.P. Wolfe, R.A. Singer, B.H. Yang, and S.L. Buchwald. J. Am. Chem. Soc. **121**, 9550 (1999); (*b*) V.P.W. Böhm, T. Weskamp, C.W.K. Gstöttmayr, and W.A. Hermann. Angew. Chem. Int. Ed. **39**, 1602 (2000); (*c*) A.F. Littke, C. Dai, and G.C. Fu. J. Am. Chem. Soc. **122**, 4020 (2000).
22. J. Tsuji. Palladium reagents and catalysis. John Wiley and Sons, New York. 1995. p. 249.
23. (*a*) F.R.S. Clark, R.O.C. Norman, and B.C. Thomas J. Chem. Soc. Perkin Trans. 1, 121 (1975); (*b*) W. Cabri and S. Penco. J. Org. Chem. **56**, 5796 (1991); (*c*) N.M. Ali, A. McKillop, M.B. Mitchell, R.A. Rebelo, and P.J. Wallbank. Tetrahedron, **48**, 8117 (1992); (*d*) S. Wiegand and H.J. Schäfer. Tetrahedron, **18**, 5341 (1995); (*e*) J.S. Mahenty, D. Mahnya, and N.G. Kundu. J. Chem. Soc. Perkin Trans. 1, 2577 (1997).
24. M.P. Groziak, A.D. Ganguly, and P.D. Robinson. J. Am. Chem. Soc. **116**, 7597 (1994). The separation of the *o*- (r.t. = 3.56 min) and *p*- (r.t. = 6.71 min) isomers was performed by HPLC (col. KROMASIL 10 μ, 4.6 × 250 mm, eluent: CH_3CN–H_2O 50:50, flow 0.5 ml min^{-1}. UV detector 254 mm, 25°C).
25. M.F. Hawthorne. J. Org. Chem. **23**, 1579 (1958).
26. M. Terashima, H. Kakim, M. Isihikura, and K. Kamata. Chem. Pharm. Bull. **31**, 4573 (1983).
27. S. Martina, V. Enkelmann, G. Wegner, and A.D. Schlater. Synthesis, 613 (1991).
28. W. Seaman and J.R. Johnson. J. Am. Chem. Soc. **53**, 71 (1931)
29. D.R. Coulson. Inorg. Synth. **13**, 121 (1972).
30. T. Hayashi, M. Konishi, and M. Kumada. Tetrahedron Lett. **20**, 1871 (1979).
31. L. Grehn and U. Ragnarsson. Angew. Chem. Int. Ed. Engl. **23**, 296 (1984).

© 2001 NRC Canada

Canadian Journal of Chemistry

Author Index
Volume 79, 2001

Revue canadienne de chimie

Index des auteurs
Volume 79, 2001

Abdur-Rashid, K., 964
Abraham, M.H., 1466
Acree, Jr., W.E., 1466
Adams, H., 731, 760
Agustinho, S.C.M., 760
Akhmedov, N.G., 1655
Akim, L.G., 201
Albinati, A., 693
Albrecht, M., 709
Alexiou, C., 992
Alguindigue, S.S., 809
Alibhai, N., 1747
Alper, H., 587
Amoroso, D., 958
Anderson, C., 1477
Anderson, O.P., 1562
Angelici, R.J., 578
Aragoni, M.C., 1483
Arakawa, H., 1415
Arca, M., 1483
Aresta, M., 570
Argyropoulos, D.S., 201, 1394
Armstrong, D.A., 405
Asadi, M., 70, 1360
Asao, N., 1624
Ashby, M.T., 809
Askalany, A.H., 42
Atwood, J.D., 1036
Aylward, W.M., 1
Baboulène, M., 1153
Bachmann, P., 519
Baerlocher, F.J., 1115
Baerlocher, M.O., 1115
Bailey, A.J., 792
Baines, K.M., 461
Baird, M.C., 1012
Baker, P.K., 263
Bakhmutov, V.I., 479
Bakhmutova, E.V., 479
Bakos, J., 725, 1040
Balakrishnan, V.K., 157
Balch, A.L., 922
Balci, M., 35
Ball, J.M., 304
Barba, V., 1229
Barbieri, L.R., 1786
Barrett, A.G.M., 1562
Barthazy, P., 904
Bartosh, K., 1026
Bartosz-Bechowski, H., 752
Basickes, L., 854
Batchelor, R.J., 938, 1272
Batista, A.A., 1030
Battaglia, L., 621
Beagley, P., 731
Beckmann, O., 1593
Belchior, J.C., 211
Belkova, N.V., 479
Bennett, M.A., 655
Benson, G.C., 388
Bényei, A.C., 635
Bergens, S.H., 1019
Berges, J., 405
Bergman, R.G., 525
Berners-Price, S.J., 1030
Berova, N., 1786
Bertotti, M., 679
Besenyei, G., 649, 688
Bhattacharyya, S., 938
Bianchini, C., 479
Blanco, C.A., 448
Blaser, H.-U., 566
Boch, R., 1068
Bolm, C., 1593
Bond, A.M., 613
Bonilla, R.J., 719
Bottomley, F., 1321
Boubaker, T., 1617
Boule, P., 1179
Bourgeois, M.-J., 257
Bowden, A.A., 1036
Boyd, S.E., 1030
Braga, J.P., 211
Braig, V., 1528
Brechbiel, M.W., 1105
Breed, P.G., 1049
Broggini, D., 904
Brouillard, R., 1173
Brown, J.M., 1049
Brown, M.A., 463
Brown, R.S., 1704
Bruce, D.W., 472
Buchanan, G.W., 195, 1505
Buchwald, S.L., 1799
Buckley, A.V., 1284
Buckley, R.W., 1030
Buncel, E., 157, 1617
Bunn, A.G., 854
Burford, N., 342
Butkus, E., 1598
Butler, D.C.D., 472
Cadoret, J., 626
Cai, Z.-S., 29
Calderazzo, F., 495
Cameron, T.S., 342
Campagnole, M., 257
Cantin, A.M., 377
Cao, D., 455
Cao, S., 272
Carmona, J., 1447
Carpenter, B.E., 291, 857
Carter, G.T., 1786
Casagrande, B., 566
Casey, C.P., 1002
Castellano, E.E., 1030
Catellani, M., 742
Centoducatte, R., 121
Chan, C., 1659
Chan, T.H., 1536
Chapados, C., 13
Charette, A.B., 1694
Chen, L., 29
Chen, Y.-T., 221, 455
Chim, J.L.C., 607
Choi, H.Y., 337
Chomka, K., 760
Chow, A., 437
Chung, M.-K., 949
Ciunik, Z., 752, 868
Claver, C., 560
Cobos, J.C., 1447
Coffey, D.S., 1711
Cole-Hamilton, D.J., 472
Colodette, J.L., 201
Cooper, L., 490
Cordes, A.W., 1352
Coulter, K.R., 930
Cowan, J.J., 792
Cromer, M., 370
Crowe, D.A.J., 1145
Cserépi-Szűcs, S., 725

© 2001 NRC Canada

Cuahutle, D., 1229
Cugini, F., 742
Cuisinier, C., 1827
Das, P.K., 809
Dave, V., 461
Davies, P., 731
Davies, S.C., 490
Dawid, M., 110, 1294
de Almeida Santos, R.H., 679
Dean, P.A.W., 1293, 1330
de Blois, S., 13
DeCaire, M., 1792
de Castro, E.V.R., 121
Decken, A., 1115, 1321
Delamere, C., 1492
Delaude, L., 529
Delmarre, D., 1068
del Rio, I., 560
Demchenko, A.P., 358
Demonceau, A., 529
Denisenko, S.N., 1655
Denmark, S.E., 1606
Denonne, F., 1827
den Reijer, C.J., 693
Devillanova, F.A., 1483
de Vries, J.G., 1086
Dibenedetto, A., 570
Dileo, C., 570
Dilworth, J.R., 490
Dixon, D.J., 1668
Dobó, A., 1040
Dolphin, D., 1068
dos Santos Silva, H.A., 679
Dotta, P., 693
Drake, J.E., 983
Drew, M.G.B., 263
Drouin, M., 1439
Durran, S.E., 780
Durst, T., 1747
Duś, D., 868
Dust, J.M., 157, 1617
Duval, P.B., 536
Duvey, G., 1754
Dworschak, R.G., 437
Dyson, P.J., 705
Ebadi, M., 992
Edmunds, J.J., 1562
Eidell, C.K., 1681
Einstein, F.W.B., 938, 1272
Ellena, J., 1030
Ellis, D.J., 705
Elzner, S., 593
Emmett, M.R., 546
Enders, D., 1528
Englert, U., 495
Ens, W., 437
Epstein, L.M., 479
Escher, E., 377
Evans, D.S., 263
Fabbri, D., 670
Fackler, J.P., Jr., 896
Fang, Q., 174
Farcas, S.I., 983
Farfán, N., 1229
Faria, R.B., 1135
Feng, J.-K., 1366
Ferguson, G., 949
Ferraro, J.R., 1483
Fish, R.H., 888
Fitzpatrick, S.J., 1101
Fleischer, M.A., 75
Fogg, D.E., 958
Fornika, R., 642
Foster, A.C., 1668
Fougerousse, A., 1173
Franc, C., 1827
Franco, D.W., 679
Fraser, H.L., 1515
Fryzuk, M.D., 536, 1194
Fu, J.-m., 1812
Fu, W., 1366
Funahashi, S., 1344
Gagnon, J., 1439
Gaisberger, B., 394
Gałęzowski, W., 1128
Gao, H., 578
Gao, Y., 915
Garcia de la Fuente, I., 1447
Gay, I.D., 1272
Gelbrich, T., 780
Geletti, Y.V., 792
Gevorgyan, V., 1624
Ghiviriga, I., 1659
Ghosez, L., 1827
Gibson, G., 1704
Gill, M.A., 1101
Gillis, H.A., 80
Ghandi, M., 1505
Gladiali, S., 670
Godard, A., 1754
Goddard, R., 1806
Gömöry, Á., 725
Gonzalez, E., 1173
Gonzalez, J.A., 1447
Görls, H., 642
Graziano, G., 105, 1310
Greaney, M., 546
Grenon, M., 1694
Gribble, G.W., 1515
Griffith, W.P., 598
Grundwald-Wyspiańska, M., 775
Grześkowiak, I., 1128
Guagnano, V., 1606
Guillier, F., 1754
Guliński, J., 775
Gulyás, H., 1040
Gupta, R.N., 418
Hachiya, S.-I., 1562
Haines, R.I., 54
Hanessian, S., 1812
Hantos, S.M., 1747
Hark, R.R., 1632
Harris, M.C., 1799
Harrod, J.F., 1075
Hartman, J.S., 426
Harvey, P.D., 552, 1439
Hassan, A.A., 42
Haunert, F., 1511
Hauze, D.B., 1632
He, D., 1213
He, S., 510
He, W., 127
Healy, P.C., 1030
Hegedüs, C., 725
Hemscheidt, T., 418
Hendrickson, C.L., 546
Hendrix, J.A., 1562
Henry, B.R., 279
Herradura, P., 1727
Herraiz-Sierra, I., 448
Hidai, M., 632
Hill, C.L., 792
Hill, J.M., 817
Hioka, N., 1068
Hiyama, T., 593, 1522
Hnatiw, J.B., 304
Holly, S., 649
Hook, J.M., 1330
Hoppe, D., 1736
Horikawa, Y., 388
Horita, K., 1562
Hou, Z., 29
Hrapchak, M.J., 1775
Hsieh, Y.-H., 1272
Hu, T.Q., 1201
Huang, Y., 719
Hudlicky, T., 1659
Hughes, D.L., 490
Hursthouse, M.B., 780, 983
Hutchings, D.R., 54
Ibrahim, M.S., 1431
Imamura, K.-i., 1624
Isaia, F., 1483
Iwatsuki, S., 1344
Jablonski, C., 463
Jacobi, P.A., 1727
Jafarpour, L., 626
Jakins, C., 1492

© 2001 NRC Canada

James, B.R., 1201
James, S.L., 709
Jamshid, K.A., 70
Jan, D., 529
Janda, K.D., 1556
Jarczewski, A., 1128
Jenkins, H.A., 1293, 1330
Jennings, M., 1330
Jennings, M.C., 915
Jensen, C.M., 823
Jessop, P.G., 719
Jezierski, A., 570
Jiang, M.H., 174
Jiang, X., 127
Johnson, M.D., 1546
Joó, F., 635
Jorge, F.E., 121
Joullié, M.M., 1632
Jurasek, L., 1394
Kaneno, D., 1598
Kashiwabara, K., 1344
Katritzky, A.R., 1655
Kauch, M., 1736
Keay, B.A., 1541
Kenawy, I., 42
Kessler, M., 642
Khan, M.A., 830
Khomutov, O.G., 183
Kim, C.-K., 1238
Kinal, A., 35
King, J.F., 461
Kirby, C.W., 296
Kissell, W.S., 1681
Kleinke, H., 1338
Kliegel, W., 226
Klymchenko, A.S., 358
Knoblauch, S., 977
Koch, H.F., 977
Kodess, M.I., 183
Köllner, C., 1762
Konkol, M., 490
Koshino, N., 1344
Koteva, K.P., 377
Kovács, J., 635
Krisdhasima, V., 848
Krištofová, L., 1394
Krüger, C., 642
Kumamaru, K., 1422
Kurokawa, G.S., 1058
Lam, K.C., 342
Langner, R., 1376
Lau, M.-K., 607
Lau, S.Y.W., 1541
Laurenczy, G., 635
Le, N., 238
LeBlanc, D.J., 342
Lee, D.W., 823
Lee, J., 830
Lee, K.J., 1556
Lee-Ruff, E., 114
Legzdins, P., 502
Leitner, W., 642
Lelj, F., 1483
Lemes, N.H.T., 211
Lemieux, R.U., 238
Leung, W.-H., 607
Lever, A.B.P., 992
Lewandowski, M., 775
Lewars, E., 1492
Ley, S.V., 1668
Leznoff, C.C., 878
Li, H.L., 328
Li, L.-H., 1536
Li, W., 1366
Li, Y.-N., 29
Light, M.E., 780, 983
Lightfoot, P., 472
Lin, H.-K., 221, 455
Ling, C.-C., 238
Lippolis, V., 1483
Liu, S., 1058
Long, G.S., 1026
Loop, I., 183
López, M.C., 1460
López-de-Luzuriaga, J.M., 896
Lord, G., 337
Lork, E., 183
Lough, A.J., 964
Lu, A.Z., 1201
Lu, B.C.-Y., 388
Lu, J., 127
Lu, X., 319, 364
Lubell, W.D., 94
Lubkowitz, G., 226
Lucas, R.J., 54
Luo, H., 1105
Ma, M., 1213
Macdonald, C.L.B., 342
Machado, S.P., 1135
Machuca-Herrera, J.O., 1135
MacRae, A.I., 1101
Madar, D.J., 1711
Magnuson, K., 823
Mahajan, D., 848
Mahiuddin, S., 1207
Mainar, A.M., 1460
Majewski, M., 1792
Malecha, J.W., 1562
Małecka, E., 775
Małgorzata, D., 1294
Malinauskienė, J., 1598
Malonga, H., 1415
Mamer, O., 1381
Mann, B.E., 760
March, R.E., 124
Marciniec, B., 775
Markó, L., 725
Marsais, F., 1754
Marshall, A.G., 546
Martin, M., 519
Martinez, H.E., 50
Martinsson, A., 938
Masi, D., 479
Max, J.-J., 13
McAuley, A., 930
McComb, M.E., 437
McDonald, L.A., 1786
McDonald, R., 291
McDonald, T., 1704
McGarvey, B.R., 679
McGlinchey, M.J., 1295
Medici, S., 670
Meilleur, D., 552
Mele, G., 587
Menzek, A., 35
Merkley, N., 312
Meunier, L., 1179
Mezzetti, A., 904
Middel, O., 1525
Miller, D., 54
Miller, J.M., 1220, 1224
Mingie, J.R., 1352
Mitchell, T.R.B., 655
Mizobe, Y., 632
Moghimi, A., 1505
Moineau, C., 587
Montaudon, E., 257
Morales-Morales, D., 823
Mori, A., 1522
Mori, V., 679
Morlay, C., 370
Morris, R.H., 964
Mouginot, Y., 370
Moulik, S.P., 1
Murray, M.C., 1012
Nâdasdi, L., 635
Nakanishi, K., 1786
Narracci, M., 570
Natansohn, A., 1093
Neault, J.F., 1415
Neil, M.A., 1321
Neszmélyi, A., 649
Netherton, M.R., 461
Neugebauer, W.A., 377
Neverov, A.A., 1704
Ng, F.T.T., 817
Niesyty, K., 752
Nikolcheva, L.G., 1115

© 2001 NRC Canada

Nishihara, Y., 1522
Nivoliers, F., 1754
Noels, A.F., 529
Nolan, S.P., 626
Noll, B.C., 922
Norman, D.W., 1115
North, M.R., 75
Nowak, P., 1792
Nozaki, K., 593
Oakley, R.T., 1352
Obeyama, K., 1344
Okajima, T., 22
Oleschuk, R.D., 437
Olmstead, M.M., 922
Opolski, A., 868
Orvig, C., 1058
Osmond, D.A., 1201
Ott, C., 1511
Ozturk, T., 358
Padwa, A., 1681
Palazzi, C., 1593
Palepu, R., 1
Pampaloni, G., 495
Pan, P., 131
Panosyan, F.B., 1110
Papp, G., 635
Pardo, J.I., 1460
Park, D.K., 337
Park, Y.S., 337
Párkányi, L., 649
Parkinson, C.J., 1562
Parvez, M., 857
Pashkevich, K.I., 183
Passarelli, V., 495
Patrick, B.O., 1194, 1201
Pawliszyn, J., 1403
Perez-Encabo, A., 448
Perreault, H., 437
Perumal, S., 1655
Peruzzini, M., 479
Petrovskaia, O., 1632
Petryk, M.W.P., 279
Phillips, A.D., 342
Phillips, S., 922
Piers, W.E., 291, 857
Pilichowski, J.-F., 1179
Pincock, J.A., 63
Pinna, F., 621
Pirri, G., 670
Pivovarenko, V.G., 358
Pokriefke, J.O., 226
Polydore, C., 977
Pope, M.T., 802
Pouet, M.-J., 1617
Povar, I., 1166
Powell, D.R., 830, 1002
Power, W.P., 296
Pregosin, P.S., 693
Preston, K.R., 437
Pruchnik, F.P., 868
Puddephatt, R.J., 915
Pulacchini, S., 670
Punniyamurthy, T., 1546
Purcell, M., 1415
Qian, K., 546
Qian, X., 272
Qian, Y., 127
Quéguiner, G., 1754
Queiroz, S.L., 1030
Quickenden, T.I., 80
Raabe, G., 1528
Rabion, A., 888
Rajalingam, U., 1293, 1330
Ramnauth, J., 114
Ramos, J.F., 50
Ramsden, J.A., 1049
Rastegar, M.F., 195, 1505
Rauk, A., 405
Redón, R., 823
Reed, R.W., 1352
Reetz, M.T., 1806
Reid, D.L., 319
Reinhoudt, D.N., 1525
Rettig, S.J., 226, 502, 536, 857, 930
Rheingold, A.L., 342
Richards, R.L., 490
Richardt, P.J.S., 613
Richter-Addo, G.B., 830
Riesco, N., 1447
Rifai, S., 63
Riggio, R., 50
Rinner, U., 1659
Ro, S., 1238, 1259
Robertson, V., 949
Rocca, P., 1754
Rocha, R.C., 145
Rochon, P., 1093
Rodgers, R.P., 546
Roehri-Stoeckel, C., 1173
Rogers, R.D., 1105
Rojas, A., 448
Röschenthaler, G.-V., 183
Rösler, R., 983
Rotar, A., 983
Roundhill, D.M., 977
Roush, W.R., 1711
Rudolph, J., 1806
Sadighi, J.P., 1799
Sales, M., 1775
Samonte, J.L., 802
Samuel, E., 1075
Sánchez, M.A., 1460
Sanders, J.R., 490
Santillan, R., 1229
Santos, C.M.P., 1135
Saraçoglu, N., 35
Sarvestani, A.H., 1360
Sauriol, F., 1381
Sayer, B.G., 418
Scheffer, J.R., 349
Schilling, S., 1659
Schlaf, M., 949
Seino, H., 632
Sen, A., 1026
Serni, G., 495
Sevenard, D.V., 183
Seward, C., 1187
Shehetta, I., 42
Shehatta, I.S., 1431
Sheldon, R.A., 688
Shi, Y.-L., 328
Shi, Z., 1238, 1259, 1278
Shibahara, F., 593
Shirota, O., 1786
Shoemaker, J.A.W., 426
Shu, R., 1075
Shubina, E.S., 479
Sibi, M.P., 1546
Siebenhaar, B., 566
Silvestru, A., 983
Silvestru, C., 983
Simal, F., 529
Simándi, L.I., 649
Singer, S.W., 1002
Six, C., 642
Slawin, A.M.Z., 780
Smith, D.C., Jr., 626
Smith, K.M., 502
Smith, M.B., 780
Smith, P.J., 1145
Smith, S., 760
Snedeker, B., 1026
Sobota, P., 490
Solar, S., 394
Somogyi, L., 1159
Song, B., 1058
Song, G., 272
Song, H., 29
Song, J.H., 337
Souirti, S., 1153
Spek, A.L., 709
Spenser, I.D., 418
Spey, S., 760
Spinney, H.A., 1115
Spirlet, M.R., 529
Spohr, U., 238
Sproull, R.D., 848
Squires, C., 760

© 2001 NRC Canada

Standing, K.G., 437
Staples, R.J., 896
Stark, L., 342
Starosta, R., 868
Stefanova, R., 63
Sternberg, E., 1068
Stevens, E.D., 626
Stevens, M.R., 655
Still, I.W.J., 1110
Stojanovic, N., 1101
Stončius, A., 1598
Strukul, G., 621
Studer, M., 566
Stynes, D.V., 795
Su, X.-C., 221, 455
Suchozak, B., 878
Sudo, T.,1624
Sun, D.-A., 1381
Sun, H.-W., 221
Sun, Y., 1394
Suriaatmaja, M., 598
Suzuki, T., 1344
Swaddle, T.W., 75, 841
Symons, M.C.R., 124
Szöllősy, Á., 725
Tajmir-Riahi, H.A., 1415
Takagi, F., 632
Takagi, H.D., 1344
Takahisa, E., 1522
Tellers, D.M., 525
Terrier, F., 1617
Thomas, C.A., 719
Tiefenthaler, D., 742
Tietze, L.F., 1511
Togni, A., 1762
Toma, H.E., 145
Tommasi, I., 570
Tomoda, S., 1598
Touillaux, R., 1827
Tracey, A.S., 938
Tregloan, P.A., 613
Tripathy, S., 1747
Trotter, J., 226
Trzeciak, A.M., 752
Tsuzuki, H., 1422
Urieta, J.S., 1460
van Koten, G., 709
van Leeuwen, P.W.N.M., 560
vanLoon, G.W., 157
VanSickle, A., 1562
van Zyl, W.E., 896
Vaugeois, J.,1606
Veilleux, A., 13
Veldman, N., 709
Venneri, P.C., 110, 312, 1294
Verani, G., 1483
Verboom, W., 1525
Verspui, G., 688
Vézina, M., 1439
Vialemaringe, M., 257
Vichard, D., 1617
Vincent, J.-M., 888
Vittori, O., 370
Vogels, C.M., 1115
Vorontsov, E.V., 479
Wagner, B.D., 1101
Wahab, A., 1207
Walsh, D., 342
Wang, C., 174
Wang, F., 1792
Wang, H., 1213
Wang, R., 495
Wang, S., 1187
Wang, T., 1786
Wang, X.M., 174
Wang, Z., 328, 388, 823
Ward, D.E., 1775
Warkentin, J., 110, 312, 319, 364, 1294
Wayland, B.B., 854
Wedd, A.G., 613
Wei, L., 94
Wei, Q.-L., 29
Weinberg, N., 1284
Weinstock, I.A., 792
Welton, T., 705
Werner, H., 519
Werner, M.L., 1026
Westaway, K.C., 1145
Westcott, S.A., 1115
White, C., 731
White, J.M., 613
Wietrzyk, J., 868
Wiles, J.A., 1019
Williams, I.D., 607
Willis, A.C., 655
Withers, S.G., 510
Wojdat, E., 868
Wolfe, S., 1238, 1259, 1272, 1278, 1284
Wong, A.W., 510
Wong, W.-T., 607
Woo, H.-G., 1075
Wu, B.-X., 29
Xie, Y., 127
Yachandra, V.K., 888
Yamamoto, Y., 1624
Yamato, T., 1422
Yan, P., 127
Yap, G.P.A., 195, 857, 958, 1505
Yi, G.-B., 830
Yoshikawa, E., 1624
Young, V.G., Jr., 1019
Yu, P., 1194
Yu, W.T., 174
Yung, C., 823
Zahir, K.O., 1124
Zamir, L.O., 1381
Zanobini, F., 479
Zhang, H., 1352
Zhang, H.-X., 1366
Zhang, X.X., 1799
Zhao, G.-H., 221
Zhao, R., 131
Zhao, X., 174
Zhao, X.-Z., 29
Zhou, J., 841
Zhou, P., 1213
Zhou, Y.F., 174
Zhou, Z.-F., 221, 455
Zhu, S.-R., 221, 455
Zhuang, Q., 1220, 1224
Ziolkowski, J., 570
Ziólkowski, J.J., 752
Znamirowski, M., 437
Zobi, F., 795
Zundel, G., 1376

© 2001 NRC Canada

PREVIEW / APERÇU

Forthcoming special issues / Numéros spécials à paraître

June 2002	In honour of Professor J. Bryan Jones
August 2002	In honour of Professor Ray Lemieux
November 2002	In honour of Professor Tris Chivers
June 2003	In honour of Professor Don Arnold

Forthcoming articles / Articles à paraître

2001 E.W.R. Steacie Award Lecture — The imido ligand in main group element chemistry	T. Chivers
Effect of the molecular weight on the lower critical solution temperature of poly(*N*,*N*-diethylacrylamide) in aqueous solutions	D.G. Lessard, M. Ousalem, and X.X. Zhu
Kinetics and mechanistic study of the ruthenium(III) catalyzed oxidative deamination and decarboxylation of L-valine by alkaline permanganate	D.C. Bilehal, R.M. Kulkarni, and S.T. Nandibewoor
Kinetic stabilizing effect of the 4-*N*-methylacetamido substituent on the phenylnitrenium ion	P.H. Ruane and R.A. McClelland
Microwave-assisted Diels-Alder synthesis	G. LeClair, C.K. Jankowski, J.M. Bélanger, J.J.R. Paré, and M.-R.VanCalsteren
Molar excess volumes of ternary mixtures containing ether	V.K. Sharma and Romi
MONOREG — an expert system for structural elucidation on monoterpenes	M.J.P. Ferreira, G.V. Rodirgues, and V.P. Emerenciano
Penicillamine as a ligand in the catalytic asymmetric reduction of ketones	S. Hanessian, E. Jnoff, and A.M. Griffin
Quasiclassical trajectory studies on the gas-phase BrO self-reaction	D.K. Papayannis and A.M. Kosmas
Reaction of arylnitrenium ions with guanine derivatives: N^1-methylguanosine and N^2,N^2-dimethylguanosine	B. Cheng and R.A. McClelland
Rhodium-catalyzed hydroborations of allylamine and allylimines	C.M. Vogels, P.E. O'Connor, T.E. Phillips, K.J. Watson, M.P. Shaver, P.G. Hayes, and S.A. Westcott
The nature of the transition state in diarylmethyl cation–nucleophile combination reactions as probed by secondary alpha-deuterium isotope effects	T.V. Pham and R.A. McClelland
Volumes of activation for electrode processes of various charge-type in nonaqueous solvents	M. Matsumoto, D. Lamprecht, M.R. North, and T.W. Swaddle

© 2001 NRC Canada

This issue is dedicated to

Professor Victor Snieckus

for his outstanding contributions to the field of synthetic organic chemistry

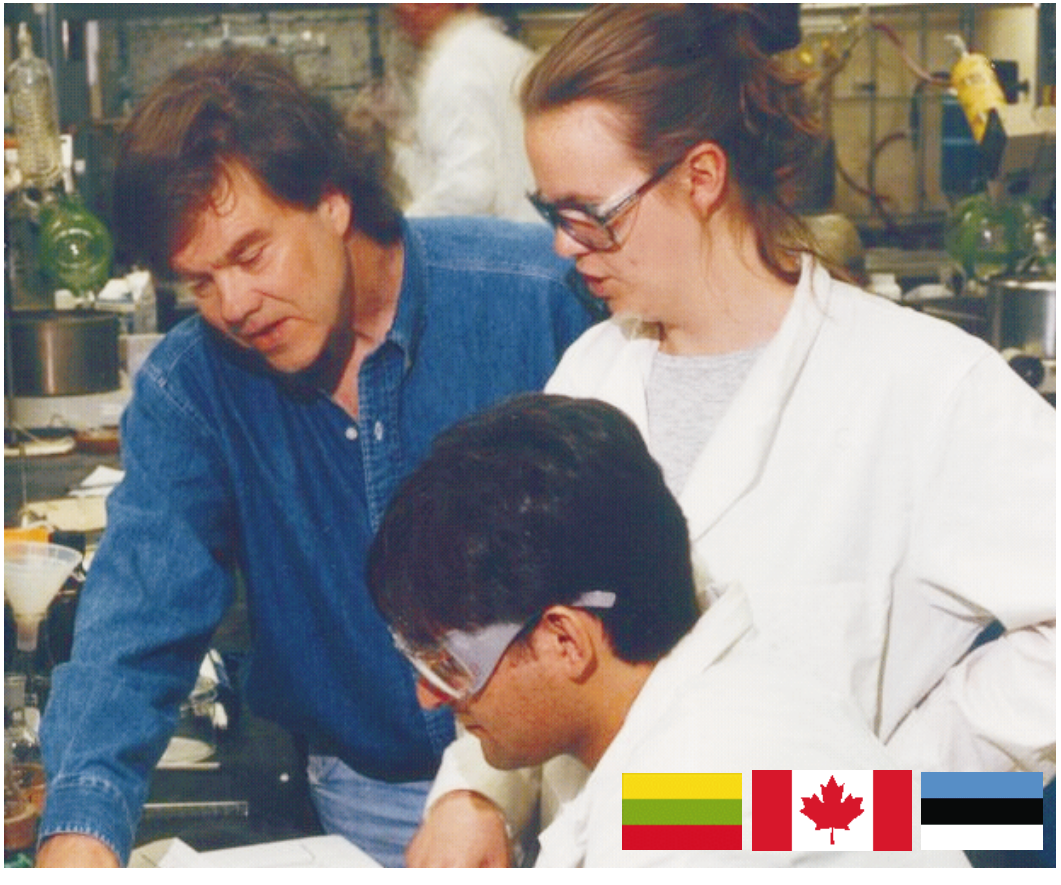
Associate Editors: R. Green and R. Kazlauskas

Le présent numéro est dédié au

Professeur Victor Snieckus

pour ses precieuses contributions au domaine de la chimie organique de synthèse

Directeurs scientifiques associés : R. Green et R. Kazlauskas



Professor Victor Snieckus

This Special Issue of The Canadian Journal of Chemistry honours the scientific accomplishments of Victor Snieckus. The contributions to this issue are indicative of the many researchers influenced by his chemistry and the number of areas on which he has had impact.

Victor was born in Kaunas, Lithuania, on Aug. 1, 1937 to an Estonian mother and a Lithuanian father. His early years were influenced by the onset of World War II; his family spent the war years in Germany, and immigrated to Canada in 1948, arriving in Foremost, AB, and ultimately settling in Calgary. Victor completed his B.Sc. (Honours) at the University of Alberta (1959), acquired an M.Sc. degree with D.S. Noyce at the University California, Berkeley (1961), and completed his Ph.D. degree with Virgil Boekelheide at the University of Oregon (1965). Following postdoctoral work with Ted Edwards at the NRC (1965–66), Victor then joined the University of Waterloo as an Assistant Professor, becoming an Associate Professor in 1971, and a Full Professor in 1979. From 1992–98, Victor held an NSERC–Monsanto Industrial Research Chair in Chemical Synthesis and Biomolecular Design. In 1998, he moved to Queen's University, where he was appointed to the inaugural Bader Chair in Organic Chemistry.

His early research career at Waterloo was focused on heterocyclic chemistry, particularly on the chemistry of the new 1,2-diazepine system. The realization of the practical synthetic potential of directed *ortho* lithiation of tertiary benzamides altered his direction permanently, beginning in 1978–79. Since this time, Victor has advanced the directed metalation (DoM) process to a point where it is commonly employed tactic in organic synthesis in both academic and industrial settings. He and his group have developed a number of directed metalation groups, particularly the *O*-aryl carbamate. En route, his group has discovered the anionic *ortho* Fries rearrangement, directed benzylic and remote metalation (DreM) and advanced new carbanionic chemistry of aliphatic amides and carbamates. As the DoM reaction matured, he linked the tactic to other processes such as cross-coupling reactions of several different types, radical cyclizations, and ring-closing metathesis. Throughout, his work has been characterized by a thoroughness of investigation and by the application of new methodological results to practical synthetic questions. In industrial labs, "let's do it by Snieckus chemistry" is an immediately understood phrase.

Victor has trained 61 graduate students, including 30 Ph.D.s, and has supervised over 70 postdoctoral fellows.[1] Group members will remember his endlessly positive style of motivation, his attention to detail and the literature, and a genuine interest in their progress after they leave the VS group. He is also known for his availability, patience, and willingness to talk to absolutely anyone on any subject, but especially to share and understand chemical ideas. As someone who interacts regularly and willingly with his students, Victor is renowned for group Christmas parties that invariably turn into road-hockey games, and for a suspiciously consistent inability to remember his wallet on trips to the Graduate Club.

Professeur Victor Snieckus

Ce numéro spécial du Journal canadien de chimie est publié pour rendre hommage aux réalisations scientifiques de Victor Snieckus. Les contributions contenues dans ce numéro mettent en relief l'importance du nombre des chercheurs qui ont été influencés par sa chimie et de la diversité des domaines sur lesquels il a eu un impact.

Victor est né à in Kaunas, en Lituanie, le premier août 1937, d'une mère estonienne et d'un père lithuanien. Ses jeunes années ont été marquées par la deuxième guerre mondiale pendant laquelle ses parents ont vécu en Allemagne avant d'immigrer au Canada en 1948, alors qu'ils sont arrivés à Foremost, AB, avant de s'établir à Calgary. Victor a obtenu un B.Sc. (Honours) à l'Université d'Alberta (1959), un M.Sc. à l'Université de la Californie, Berkeley (1961) pour des travaux effectués sous la direction de D. S. Noyce , et un Ph.D. de l'Université de l'Orégon (1965), pour des travaux réalisés sous la direction de Virgil Boekelheide. Après avoir effectué des travaux postdoctoraux au Conseil National de Recherches sous la direction de Ted Edwards (1965–66), Victor a été engagé comme Assistant professeur à l'Université de Waterloo où il est devenu professeur agrégé en 1971 et professeur titulaire en 1979. De 1992–98, Victor a été le titulaire d'une chaire de recherches industrielles CRSNG/Monsanto en synthèse chimique et en modélisation biomoléculaire. In 1998, il s'est déplacé vers l'Université Queens où il a été le premier titulaire de la nouvelle chaire Bader en chimie organique.

Ses travaux de recherches à l'Université de Waterloo étaient orientés vers la chimie hétérocyclique, principalement vers la chimie du nouveau système des 1,2-diazépines. À partir de 1978–79, la réalisation du potentiel pratique en synthèse des réactions de lithiation de benzamides tertiaires orientées en *ortho* l'a amené à modifier ces orientations d'une façon permanente. Depuis lors, Victor a tellement bien développé les réactions de métalations orientées («DoM») qu'elles sont maintenant utilisées d'une façon tactique, en synthèses organiques, tant dans les milieux académiques qu'industriels. Avec son groupe, il a mis au point un certain nombre de groupes permettant de réaliser des métalations orientés, en particulier le carbamate de *O*-aryle. En route, son groupe a découvert le réarrangement d'*ortho* Fries anionique, la métallation à distance et orienté par un groupe benzylique («DreM») et une nouvelle chimie carbanionique avancée des amides et des carbamates aliphatiques. Une fois la réaction «DoM» bien établie, il a lié cette tactique à d'autres processus, tels que les réactions de couplage croisé de plusieurs types différents, aux réactions de cyclisations radicalaires, et aux réactions de fermeture de cycle de métathèse. Tous ses travaux ont été caractérisés par des investigations minutieuses et par l'application de nouveaux résultats méthodologiques à des questions synthétiques pratiques. Dans les laboratoires industriels, la phrase "Faisons cela par la chimie de Snieckus" est immédiatement comprise.

Victor a dirigé les travaux de 61 étudiants gradués, y compris 30 au Ph.D. et il a supervisé les travaux de plus de 70 postdoctorants. Les membres de son groupe de recherche se souviennent de son style de motivation qui était toujours positif, de son attention aux détails et à la littérature ainsi qu'à son intérêt manifeste pour l'évolution de leur carrière une fois après avoir quitté le groupe VS. Il est aussi connu pour sa dis-

© 2001 NRC Canada

With the increased acceptance of the DoM strategy and its synthetic connections has come recognition in the form of awards which include the Alfred Bader Award (1993), Fellow, Royal Society of Canada (1993), Humbolddt-Forschungspreis (1996), R.U. Lemieux Award (1997), Fellow, Lithuanian Academy of Sciences (1999), Killam Fellowship (2000–01), ISHC Award in Heterocyclic Chemistry (2001), and the Cope Scholar Award (2001). He is the Organic Editor for the Canadian Journal of Chemistry, Editor for the American Continents for Synlett, and Topical Editor for Polycyclic Aromatic Compounds. In addition, he has contributed to the organic chemistry community as a member of the Editorial Board for Organic Process Research & Development, the Editorial Advisory Board of Advanced Synthesis and Catalysis, and as a past member of Editorial Advisory Board for the Journal of Organic Chemistry and Progress in Heterocyclic Chemistry. He was Chair of the International Conference in Heterocyclic Chemistry (1985) and Balticum Organicum Syntheticum (BOS 2000). Victor served as President of the International Society of Heterocyclic Chemistry (1985) and Chairman of the ACS Organic Division (1989–90). For over a decade, he has actively promoted closer interaction between the Canadian Society for Chemistry and the American Chemical Society. Most recently, he has been tireless in his efforts to assist in the exposure of the organic chemistry community of the Baltic States to Western chemists.

A long time before metalating (1966), Victor married Anne and they have two children, Darius and Naomi. He readily acknowledges his family's encouragement and support of his dedication to chemistry and particularly Anne, whose sustenance of VS groups over the years are cherished by all.

The article authors and the editors are pleased to offer this Special Issue. We anticipate continuing contributions of importance from his research group. Victor has every intention of exploring new directions of research, and mentoring many more young scientists (7 students are graduating as of this writing).

James R. Green

ponibilité et sa patience alors qu'il est toujours prêt à parler à quiconque de n'importe quel sujet, mais particulièrement pour échanger et comprendre des idées chimiques. Comme il s'agit d'une personne qui interagit d'une façon régulière et empressée, Victor est réputé pour les parties de Noël de son groupe qui se terminent toujours par des parties de hockey dans la rue ainsi que par son inhabilité proverbiale à oublier son portefeuille chaque fois qu'il se rend au Graduate Club.

Avec l'augmentation de l'acceptation de la stratégie «DoM» et de ses implications synthétiques, la valeur de ses travaux a été reconnue par des prix et des distinctions honorifiques: Alfred Bader Award (1993), Fellow, Royal Society of Canada (1993), Humbolddt-Forschungspreis (1996), R. U. Lemieux Award (1997), Fellow, Lithuanian Academy of Sciences (1999), Killam Fellowship (2000–01), ISHC Award in Heterocyclic Chemistry (2001) et la Cope Scholar Award (2001). Il est aussi éditeur pour le Journal Canadien de Chimie (organique), éditeur pour les continents américains pour Synlett, et Topical Editor pour Polycyclic Aromatic Compounds. De plus, il a contribué à la communauté de la chimie organique en agissant comme membre de l'Editorial Board de Organic Process Research & Development, d'Advanced Synthesis and Catalysis, and comme ancien membre de l'Editorial Advisory Board du Journal of Organic Chemistry et de Progress in Heterocyclic Chemistry. Il a été le président de la Conférence international de chimie hétérocyclique (1985) et du Balticum Organicum Syntheticum (BOS 2000). Victor a aussi agit comme Président de l'International Society of Heterocyclic Chemistry (1985) et comme président de la division organique de l'ACS (1989–90). Pendant plus de dix ans, il a travaillé activement à la promotion de meilleures interactions entre la Société canadienne de chimie et l'American Chemical Society. Plus récemment, il n'a pas ménagé ses efforts pour faire la promotion de la communauté de chimie organique des pays de la Baltique auprès des chimistes de l'Ouest.

Longtemps avant de procéder à des métalations (1966), Victor s'est marié à Anne et ils ont deux enfants, Darius et Naomi. Il est toujours fier de reconnaître tout le support et l'encouragement qui lui a été apporté par sa famille dans son attachement à la chimie, particulièrement celui d'Anne qui a si bien soutenu les groupes VS au cours des années, un support qui a été apprécié de tous.

Les auteurs des articles et les éditeurs sont heureux de lui offrir ce numéro spécial. Nous espérons que son groupe continuera à produire des contributions importantes. Victor compte bien explorer de nouvelles voies de recherche et de superviser plusieurs autres jeunes scientifiques (Au moment d'écrire cette introduction, il est encore entouré de sept étudiants gradués).

James R. Green

Ph.D. Theses/*Thèses doctorat*: Gordon Kan (1970), Kuldip Bhandari (1970), Johan Eenkhoorn (1971), Heinz Bernhard (1971), S. Osmund de Silva (1973), Ijaz Ahmad (1976), David Harris (1976), Fred Widmer (1977), George Mpango (1980), Marek Majewski (1982), Robert Mills (1985), J. Norman Reed (1985), M.A. Jalil Miah (1985), Mohammad Mumtaz (1986), James Green (1987), Edward Doadt (1988), M. Arshad Siddiqui (1990), Jian-min Fu (1990), Xin Wang (1992), Bao-ping Zhao (1994), Francis Beaulieu (1994), Masao Tsukazaki (1995), Mike Campbell (1996), Claude Quesnelle (1996), Clint James (1998), Sylvie Chamoin (2000), Brian Chapell (2001).

M.Sc. Theses/*Thèses à la maîtries*: Elizabeth Watson (1970), Anthony Wu (1975), Irene Tse (1976), Roman Wojtyk (1977), John Oakleaf (1977), Bulent Mutus (1977), J. Norman Reed (1979), Roland Billedeau (1983), Nesrin Altintas (1985), Matthew Sharp (1986), Chuck Sloan (1987), Kevin Cullen (1988), Helene Perrier (1989), Cathleen Unrau (1991), Wei Wang (1991), Jalaj Arora (1995), Lisbeth Benesch (1995), Ileana Ionica (1995), Aaron Kinsman (1997), Karen Puumala (1997), Radoslaw Laufer (1998), Bing Miao (1998), Steve MacNeil (1999), Robert Milburn (1999), Christopher Kendall (1999).

© 2001 NRC Canada

Postdoctoral Fellows, Visiting Scientists, Trainees/Associés du postdoctoral, scientifiques en visite, stagiaires: Babajide Alo, Tania Alves, Michael Annis, Thierry Aubert, Radu Balint, Lucia Bertelli, Cornelius Bessler, Ilaria Bientinesi, Laura Biggs, Eva Boehringer, Sylvester Bonnet, Justin Bower, Marcos Brandao, Paul Brough, Sabine Bruestle, Paul Bury, Subhagata Chattopadhyay, William Cheng, Sultan Chowdhury, Andre Chieffi, Rosie Chong, Antonio Coehlo, Magnus Conradi, Jeanne Constante, Marlyse Coquoz, Paul Cox, Carlos Cuevas, John Dankwardt, Alcides da Silva, Volker Derdau, Charles Dexter, Gary Dmitrienko, Borje Egestad, Neville Emslie, Jan Epsztajn, Jurg Faessler, Jakob Felding, Wole Familoni, Thilo Focken, Jesus Garcia, Milind Gharpure, Jorg Glaenzer, Matt Gray, Zoltan Greff, Carlos Gregorio, Ed Griffen, Denis Guillaneux, Nadine Henaff, Stephen Houldsworth, Lise Hubbard, Thomas Hundsdorf, Teruyuki Iihama, Masatomo Iwao, Wouter Iwema-Bakker, Chet Jablonski, Yanying Jia, Zhong-En Jin, Matt Johnson, Babu Joseph, Alexei Kalinine, Ali Kandil, Kimio Katsuura, Matthias Kauch, Taro Kimachi, Bart Koning, Leif Laakso, Charlotte Lane, Magda Leite, Mei-Sie Lin, Magali Maillet, Kumar Mahalanabis, Robert Marchhart, Bryan McKibben, Guobin Miao, Oskar Middel, Ichiro Mohri, Kunihiko Mohri, Tsukasa Moriya, Pascale Moreau, Sarah Mountford, Sven Nerdinger, Tam Nguyen, Thai Nguyen, Nobu Nomura, Shahla O'Brien, Don Orr, James Padfield, Andrew Parsons, Prakash Patil, Olaf Prien, Dayananda Rajapaksa, Hector Ramirez, Peter Riebel, Denise Rodrigues, David Roe, Mark Rogers-Evans, Anna Roglans, Jean Claude Schwaller, Saumitra Sengupta, Kothandaraman Shankaran, Mukund Sibi, Neusa Somera, Tibor Soos, Nuria Sotomayor, Marian Stefinovic, Andre Stoller, Stefano Superchi, Hauke Szillat, Thomas M. Thomas, Ryan Thomas, Michael Tinkl, Mike Tjepkema, Gino Troisi, Theo Tschamber, Takashi Tsuchiya, Ulrich Veith, Mitsuaki Watanabe, Markus Wicki, Charles Wiesner, Kerstin Williams, Poh Lee Wong, R. Venkateswarlu, Karen-Anne Xavier, Carlos Zani.

Current Group/Groupe courant: Manlio Alessi, Glaucia Alves , Eric Anctil , Xiongwei Cai , Brian Chauder, Laine Green, Andrew Larkin, Adam McCubbin, Stevie MacNeil, Costa Metallinos, Claire Milburn, Rob Milburn, Roseanne Quinn, Brian Wilson, Chunfeng Yin, Zhongdong Zhao; *PDF's*: Jerome Blanchet, Anja Fecher, Hideya Mizufune, Mark Reed, Zhiming Zhou.

© 2001 NRC Canada

National Research Council Canada
Ottawa, Canada K1A 0R6

Conseil national de recherches Canada
Ottawa, Canada K1A 0R6

Postage paid at Ottawa
Publications mail
Registration No. 1240447

Port payé à Ottawa
Poste-publication
Enregistrement n° 1240447

Canadian Journal of Chemistry

Revue canadienne de chimie

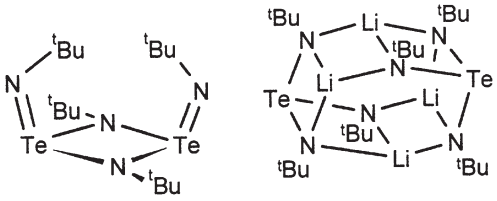
Volume 79, Number 12, December 2001

Volume 79, numéro 12, décembre 2001

2001 E.W.R. Steacie Award Lecture
The imido ligand in main group element chemistry

Tristram Chivers

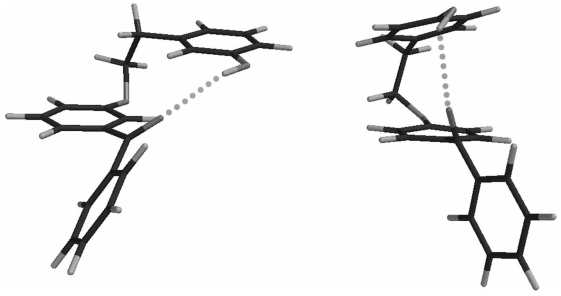
1841–1850



Geometric and solvent effects on intramolecular phenolic hydrogen abstraction by carbonyl *n*,π* and π,π* triplets

Edward C. Lathioor and William J. Leigh

1851–1863



Volumes of activation for electrode processes of various charge-types in nonaqueous solvents

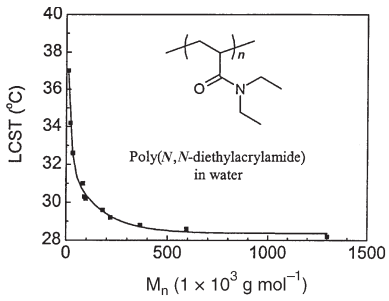
Mitsuru Matsumoto, Delanie Lamprecht, Michael R. North, and Thomas W. Swaddle

1864–1869

Effect of the molecular weight on the lower critical solution temperature of poly(*N*,*N*-diethylacrylamide) in aqueous solutions

D.G. Lessard, M. Ousalem, and X.X. Zhu

1870–1874



Continued on inside back cover / Suite au verso

Canada

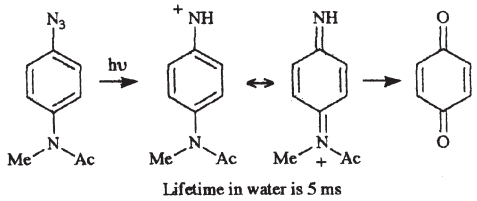
Printed in Canada by / Imprimé au Canada par
University of Toronto Press Inc.
Typesetting by / Typographie par
NRC Research Press / Presses scientifiques du CNRC

000 -4042 200112 79 12 1-E

Kinetic stabilizing effect of the 4-*N*-methylacetamido substituent on the phenylnitrenium ion

Patrick H. Ruane and Robert A. McClelland

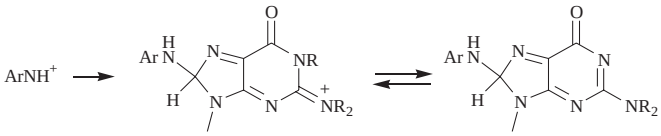
1875–1880



Reaction of arylnitrenium ions with guanine derivatives: N^1-methylguanosine and N^2, N^2-dimethylguanosine

Bernice Cheng and Robert A. McClelland

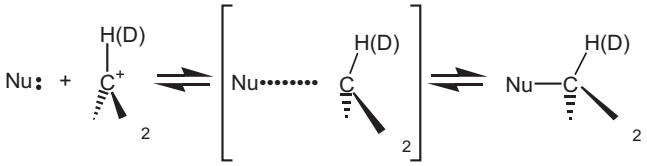
1881–1886



The nature of the transition state in diarylmethyl cation – nucleophile combination reactions as probed by secondary α-deuterium isotope effects

Thuy Van Pham and Robert A. McClelland

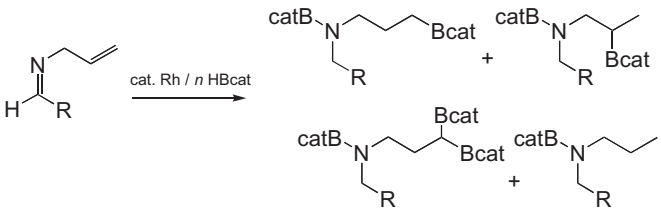
1887–1897



Rhodium-catalyzed hydroborations of allylamine and allylimines

Christopher M. Vogels, Paul E. O'Connor, Trevor E. Phillips, Keith J. Watson, Michael P. Shaver, Paul G. Hayes, and Stephen A. Westcott

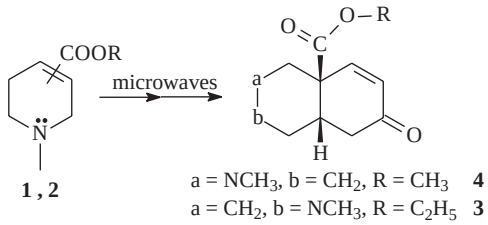
1898–1905



Microwave-assisted Diels-Alder synthesis

Christopher K. Jankowski, Gaëtan LeClair, Jacqueline M.R. Bélanger, Jocelyn R.J. Paré, and Marie-Rose VanCalsteren

1906–1909



Molar excess volumes of ternary mixtures containing ether

V.K. Sharma and Romi

1910–1914

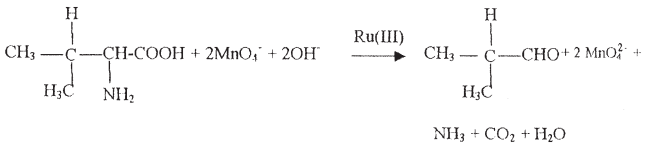
Concluded on facing page / Suite et fin à la page précédente

MONOREG – an expert system for structural elucidation of monoterpenes

Marcelo J.P. Ferreira, Gilberto V. Rodrigues, and Vicente P. Emerenciano

1915–1925

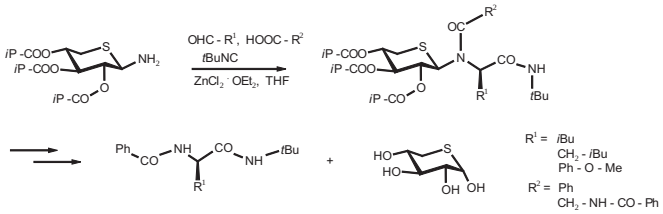
Kinetics and mechanistic study of the ruthenium(III) catalyzed oxidative deamination and decarboxylation of L-valine by alkaline permanganate



Dinesh C. Bilehal, Raviraj M. Kulkarni, and Sharanappa T. Nandibewoor

1926–1933

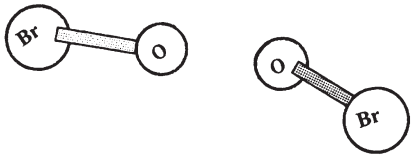
Stereoselective syntheses of α-amino acid and peptide derivatives by the U-4CR of 5-desoxy-5-thio-D-xylopyranosylamine



Günther Ross and Ivar Ugi

1934–1939

Quasiclassical trajectory studies on the gas-phase BrO self-reaction



Demetrios K. Papayannis and Agnie M. Kosmas

1940–1945

Note of appreciation	**iii**	**Note de reconnaissance**	**iii**
Author Index	**AI-1**	**Index des auteurs**	**AI-1**
Contents for volume 79	**C-1**	**Sommaire pour volume 79**	**C-1**

The Canadian Journal of Chemistry is affiliated with the Canadian Society for Chemistry and publishes papers in all areas of chemistry.

La Revue canadienne de chimie est affiliée à la Société canadienne de chimie et publie des articles dans tous les domaines de la chemie.

2001 E.W.R. Steacie Award Lecture The imido ligand in main group element chemistry[1]

Tristram Chivers

Abstract: The imido group (NR) is a versatile ligand in main group chemistry. The high reactivity of multiply bonded (terminal) imido derivatives of *p*-block elements is used, for example, in the aza-Wittig reaction, allylic aminations, and in peptide synthesis. As a bridging ligand, the imido group provides a cornerstone for a wide variety of binary cluster structures. This review is primarily concerned with the synthesis, structures, reactions, and ligand behaviour of imido derivatives of the heavy chalcogens (selenium and tellurium) as exemplified by the tellurium diimide dimer *t*-BuNTe(μ-N-*t*-Bu)$_2$TeN-*t*-Bu and the homoleptic trisimido-tellurite dianion $[Te(N\text{-}t\text{-}Bu)_3]^{2-}$. The synthesis and cluster structures of alkali metal and alkaline earth metal derivatives of heteroleptic imido-oxo anions of sulfur, e.g., $[O_xS(NR)_{3-x}]^{2-}$ (x = 1, 2) and $[O_2S(\mu\text{-}NPh)SO_2]^{2-}$, are also discussed.

Key words: main group chemistry, imido ligand, chalcogens.

Résumé : Le groupe imido est un ligand versatile dans la chimie du groupe principale. On utilise, par exemple, la grande réactivité des dérivés imido à liaisons multiples (terminaux) des éléments du bloc-p dans la réaction aza-Wittig, les aminations allyliques et en synthèse peptidique. Comme ligand formant un pont, le groupe imido est la pierre angulaire d'une grande variété de structures binaires d'agrégats. Cette revue est orientée principalement vers la synthèse, les structures, les réactions et le comportement comme ligand de dérivés imido de chalcogènes lourds (sélénium et tellure) tels que représentés par le dimère du diimide de tellure, *t*-BuNTe(μ-N-*t*-Bu)$_2$TeN-*t*-Bu, et le dianion trisimido-tellurite homoleptique, $[Te(N\text{-}t\text{-}Bu)_3]^{2-}$. On discute aussi de la synthèse et des structures des agrégats des dérivés des métaux alcalins et alcalino-terreux des anions imido-oxo hétéroleptiques du soufre, par exemple $[O_xS(NR)_{3-x}]^{2-}$ (x = 1, 2) et $[O_2S(\mu\text{-}NPh)SO_2]^{2-}$.

Mots clés : chimie du groupe principal, ligand imido, chalcogènes.

[Traduit par la Rédaction]

Introduction

The work described in this account began with the discovery of the first tellurium diimides about 7 years ago (1–3). Investigations of the reactivity of these multiply bonded species led to the generation of some of the first examples of homoleptic polyimido anions of the *p*-block elements in the form of chalcogen-centered anions that are isoelectronic with common oxo anions such as tellurite, selenite, or sulfite (4–6). As a natural extension, we have also studied the related imido-oxo systems (7–8).

The emphasis in this work initially was on the structures of the multiply bonded systems and the clusters that are formed by alkali metal derivatives of the homoleptic and heteroleptic anions with the long-term goal of being able to control the formation of extended structures with specific cavity sizes (9). In addition to their structural interest, these cluster systems are noteworthy as precursors of intensely coloured, long-lived radicals and the anions themselves, especially in the case of tellurium, have an extensive coordination chemistry involving metal complexes that are potential single-source precursors to semiconducting metal chalcogenides.

By way of introduction, let us begin by considering the properties and applications of multiply bonded imido derivatives of *p*-block elements. Monomeric iminoboranes RB=NR′ are metastable at room temperature and convert to cyclic oligomers in a few days even when the organic groups attached to boron and nitrogen are bulky (10). Very recently, monomeric imides of the heavier group 13 elements aluminum and gallium have been stabilized by the use of extremely bulky groups on nitrogen and the metal (11). Certain carbodiimides, e.g., CyN=C=NCy, are commercially available reagents that are widely used as coupling reagents in peptide synthesis. Such reagents are familiar to organometallic chemists as a source of amidinate ligands by reaction with organolithium reagents (12, 13). Iminophosphoranes (R_3P=NR′) are useful

Received July 30, 2001. Published on the NRC Research Press Web site at http://canjchem.nrc.ca on December 3, 2001.

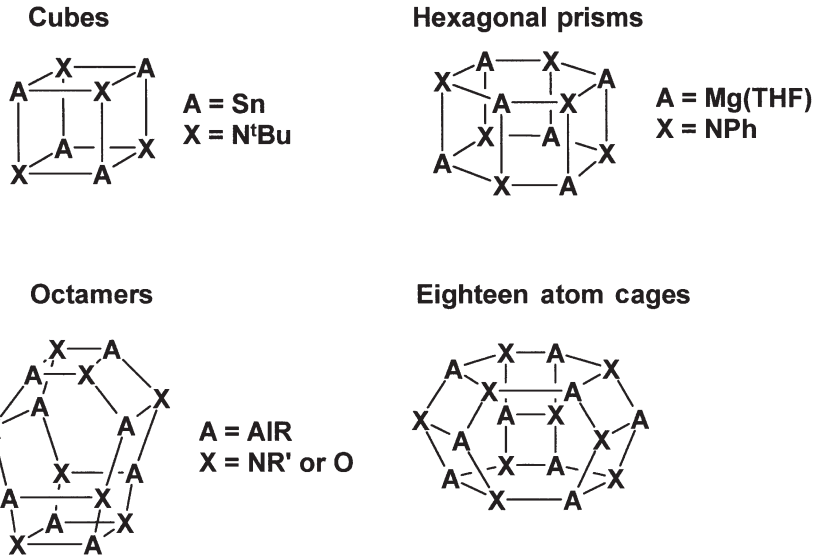
T. Chivers.[2] Department of Chemistry, University of Calgary, Calgary, AB T2N 1N4, Canada.

[1]This is an invited review article based on the 2001 E.W.R. Steacie Award Lecture presented at the 84th Annual Conference of the Canadian Society for Chemistry, Montreal, Quebec, May 26–30, 2001.

[2]Corresponding author (telephone: (403) 220-5741; fax: (403) 289-9488; e-mail: chivers@ucalgary.ca).

 DOI: 10.1139/cjc-79-12-1841 © 2001 NRC Canada

Fig. 1. The imido ligand (NR) as a cornerstone in cluster structures.



for the conversion of carbonyl to imido functionalities in the so-called aza-Wittig reaction (14). Sulfur diimides (RN=S=NR) are versatile ligands that adopt several different bonding modes towards transition metals (15) and the selenium analogues have been utilized for allylic aminations (16).

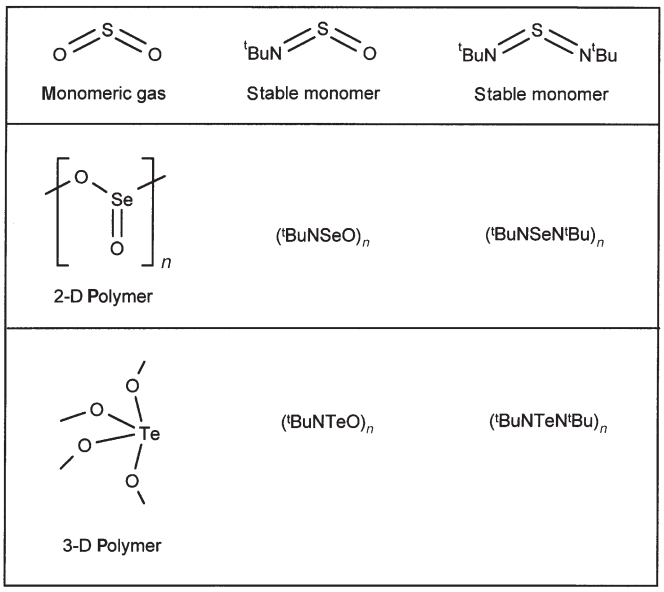
The imido ligand may also participate in a variety of cluster structures as illustrated by the selected examples of binary systems shown in Fig. 1. A cubic arrangement is characteristic of the group 14 imides as exemplified by the *tert*-butylimidotin tetramer (17). Magnesium anilide adopts a hexameric structure in the form of a hexagonal prism (or cyclic ladder) (18). The imidoalanes form an especially rich series of clusters compounds depending on the size of the substituent attached to aluminum or nitrogen (19), e.g., an octamer that can be viewed as a face-to-face dimer of a cube and an 18-atom cage, which is related to a hexagonal prism via insertion of three monomer units between the hexagonal faces.

Selenium and tellurium diimides

Chalcogen diimides are isoelectronic with the well-known chalcogen dioxides, which exhibit structural trends that reflect the preference of the heavier chalcogens for the formation of single bonds (Scheme 1). Sulfur dioxide is a monomer whereas the heavier chalcogen congeners adopt either two- or three-dimensional polymeric structures. Sulfur diimides invariably form monomers with formal S=N double bonds. At the beginning of our work, selenium diimides RN=Se=NR (*R* = *t*-Bu, *t*-Oct) (20) and the hybrid imido-oxo system *t*-BuNSeO (21) had been obtained as thermally unstable yellow oils, but they had not been structurally characterized in the solid state. Tellurium diimides of the type $(RN{=}Te{=}NR)_n$ (R = alkyl, aryl) were unknown.

The first tellurium diimide **1** was discovered accidentally when Dr. Gao was investigating the reactions of a hybrid PN–TeN ring system. As illustrated in Scheme 2, an attempt to replace the Cl substituent on tellurium with a *tert*-butylimido group resulted in the formation of a tellurium diimide dimer as the *trans*-isomer (1). It is reasonable to assume that the first step in this transformation involves nucleophilic displacement

Scheme 1.

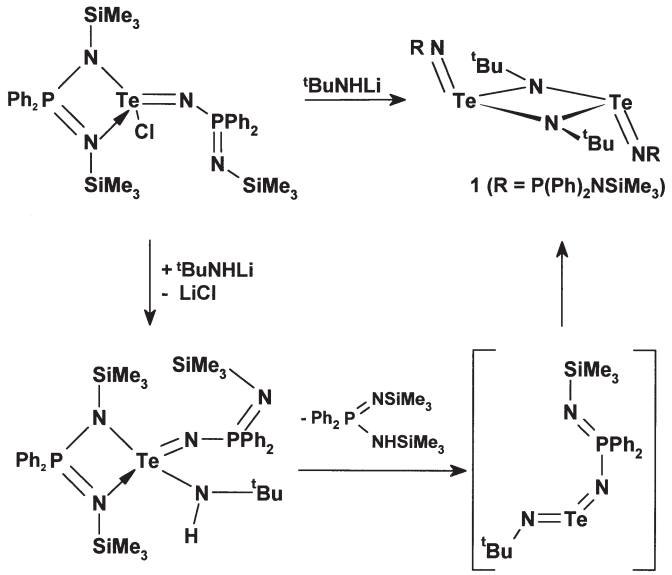


of chloride by the *t*-BuNH group. Subsequent elimination of the imido–amido phosphorane $Ph_2P(NSiMe_3)(NHSiMe_3)$, which was identified by ^{31}P NMR, yields the putative tellurium diimide monomer, which spontaneously associates to give the observed dimer **1**. Interestingly, the *trans* isomer isomerizes to the *cis*-isomer in solution over a period of 1 day (3).

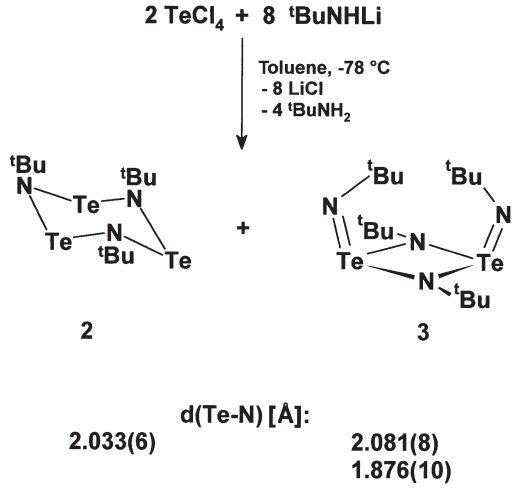
Following this discovery, Dr. Gao was able to show that a symmetrical tellurium diimide, with *tert*-butyl groups attached to both nitrogen atoms, could be obtained by the reaction of tellurium tetrachloride with *tert*-butylamidolithium in the appropriate stochiometry (Scheme 3). When this reaction is carried out in toluene some reduction of tellurium(IV) to tellurium(II) occurs to give the cyclic tellurium imide $(TeN\text{-}t\text{-}Bu)_3$ **2** (2). This minor product is a six-membered ring in the chair conformation with Te—N bond lengths in the range expected for single bonds. Interestingly, the tellurium diimide dimer **3** is obtained as the *cis*-isomer with terminal

© 2001 NRC Canada

Scheme 2.



Scheme 3.



tert-butyl groups in the *endo,endo* conformation. The TeN bond lengths are consistent with double bonds for the terminal imido groups and single bonds for the bridging imido groups. This orange compound exhibits remarkable thermal stability for a tellurium–nitrogen compound. It can be sublimed without decomposition at 95°C. When THF is used as the solvent for this reaction, the yield of **3** is ca. 80% and the cyclic tellurium(II) imide **2** is not formed (22).

To gain some insight into the different structures of chalcogen diimides, Nicole Sandblom carried out Density Functional Theory calculations on the dimerization of model systems with methyl groups attached to the nitrogen atoms, i.e., MeN=E=NMe (E = S, Se, Te) (23). The dimerization process can be viewed in two steps (Scheme 4). The first involves distortion of two monomeric systems and the stretching of one of the Te=N double bonds in each monomer. The second step includes both a steric and an electronic component. The calculations show that formation of a tellurium diimide dimer is strongly exothermic (ΔE = –82.9 kJ mol^{-1}) whereas

Scheme 4.

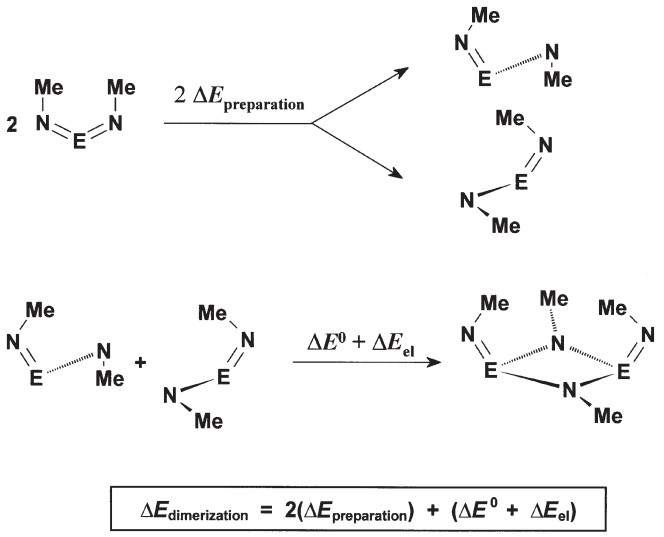
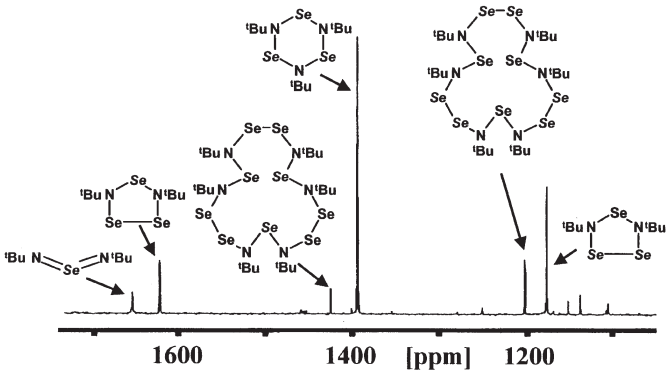


Fig. 2. ^{77}Se NMR spectrum of *t*-BuNSeN-*t*-Bu in toluene at 20°C after 2 days. Peak assignments are designated by *Se* atoms in italics.

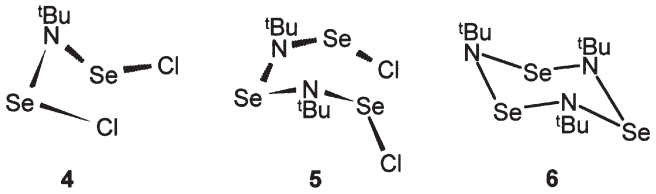


the dimerization energy for the sulfur analogue is endothermic (ΔE = +34.9 kJ mol^{-1}), consistent with experimental observations. Interestingly, the calculated dimerization energy for the corresponding selenium diimide is approximately thermoneutral (ΔE = –2.8 kJ mol^{-1}), so it was not clear from the calculations whether a monomeric or a dimeric structure will be preferred.

In the light of this uncertainty, it is appropriate to turn now to a consideration of selenium imides. In addition to $SeCl_4$, we have the advantage in selenium chemistry of the availability of pure $SeCl_2$, which Arto Maaninen has shown to be stable in THF solution (24). Tellurium dichloride is not available as a stable reagent in the absence of donor ligands such as thioureas. The reaction of selenium dichloride with *tert*-butylamine is noteworthy for two reasons. Firstly, it gives rise to the imidoselenium dihalides **4** and **5**, which represent the first two members of a new class of compounds in chalcogen–nitrogen chemistry (25). Secondly, an increase in the amount of *tert*-butylamine leads to the formation of the six-membered ring (SeN-*t*-Bu)$_3$ (**6**), which has a chair structure like the tellurium analogue **2** and exhibits a characteristic ^{77}Se NMR resonance at ca. 1400 ppm. The characterization

© 2001 NRC Canada

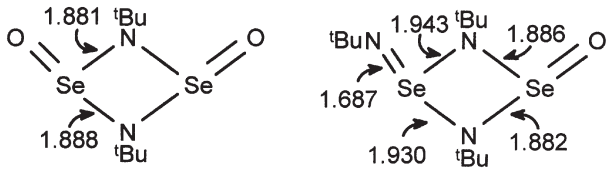
of **2** enabled us to identify the products of decomposition of the corresponding selenium(IV) diimide.



4 **5** **6**

Tiina Maaninen monitored the decomposition of the selenium diimide *t*-BuN=Se=N-*t*-Bu by ^{77}Se NMR and the spectrum of the mixture of products that is obtained after 2 days at 20°C is shown in Fig. 2 (26). The resonance for the selenium diimide had almost disappeared after this time. The major product is the six-membered ring **6**, which is readily evident from the central resonance at ca. 1400 ppm. It can be isolated from the reaction mixture by fractional crystallization. The other two major products are ring systems containing both diselenido and monoselenido bridges between imido groups. The 15-membered ring is a known compound, previously reported by Roesky et al. (27). The second, more abundant, oligomer is a new compound that we have tentatively identified as a five-membered (or, less likely, a 10-membered) ring (26).

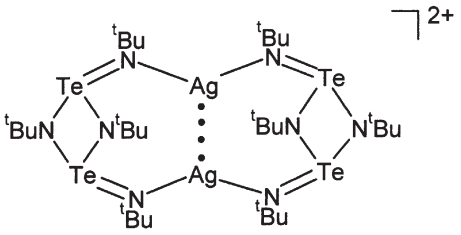
Although we know what happens when *t*-BuNSeN-*t*-Bu decomposes, the solid-state structure of this low-melting chalcogen diimide has not yet been determined. Our Finnish collaborators have, however, been able to show that the symmetrical and asymmetrical imido-oxo systems **7**[3] (1) and **8** (26), respectively, both exhibit dimeric structures with long, presumably weak, bridging selenium–nitrogen bonds. Although the values of 1.88 to 1.89 Å in the symmetrical system **7** are only slightly longer than the expected single bond value of 1.85 Å (28), the bridging SeN bonds adjacent to the terminal *tert*-butylimido group in the unsymmetrical system **8** are elongated to 1.93 to 1.94 Å. These recent findings lead to the suggestion that the corresponding selenium diimide (*t*-BuNSeN-*t*-Bu) may be a weakly associated dimer in the solid state.



7 **8**

Let us return now to the tellurium diimide dimers. We have seen that these potentially interesting ligands can form *trans*- or *cis*-isomers in the solid state. In the two examples that have been structurally characterized (**1** and **3**), the terminal R groups adopt an *endo,endo* arrangement (1–3). Other isomers in which one or both of the terminal imido groups adopt an *exo* orientation can be envisaged (Fig. 3). This versatility leads to the prediction that these imido systems could behave as either bridging or chelating ligands towards metal centres. The complexes of the tellurium diimide dimer **3** with coinage metals provide a nice illustration of this versatility (29).

Dr. Schatte has shown that the reaction of the *cis*-dimer **3** with silver triflate produces complex **9** in which the ligand retains the *cis* geometry, but the terminal *tert*-butyl groups flip to the *exo* positions. The two Ag^+ ions bridge the terminal N-*t*-Bu groups of two ligands. Alternatively, this complex can be viewed as involving chelation of both ligands to an Ag^{2+} unit. Indeed, the structural parameters indicate some sort of attractive force between the two Ag^+ ions in this complex; in particular, the bond angle ∠ N-Ag-N is distinctly nonlinear (163°) (for a discussion of d^{10}–d^{10} metallophilic interactions see ref. 30). A different type of behaviour is observed for the reaction of **3** with copper triflate. In this case, the product **10** contains two Cu^+ ions bridging three dimeric tellurium diimide ligands. Most significantly, the central ligand adopts the *trans (exo,exo)* conformation, while the two terminal ligands retain the *cis* geometry, but with *exo,endo* terminal substituents. Thus, it appears that Cu^+ ions promote the *cis* → *trans* isomerization of **3**. Complex **10** can be viewed as a small section of a polymeric chain in which Cu^+ ions bridge alternating *cis* and *trans*-isomers of **3**. Interestingly, hydrolysis of this copper complex results in the replacement of one terminal *tert*-butylimido group in the tellurium diimide dimer by an oxo ligand to give [*t*-BuNTe(μ-N-*t*-Bu)$_2$Te(μ-O)]$_2$ (**11**) complexed via terminal N-*t*-Bu groups to two Cu^+ ions. Unlike the selenium analogue **7**, **11** forms a dimer with a central, unsymmetrical Te_2O_2 ring (31).



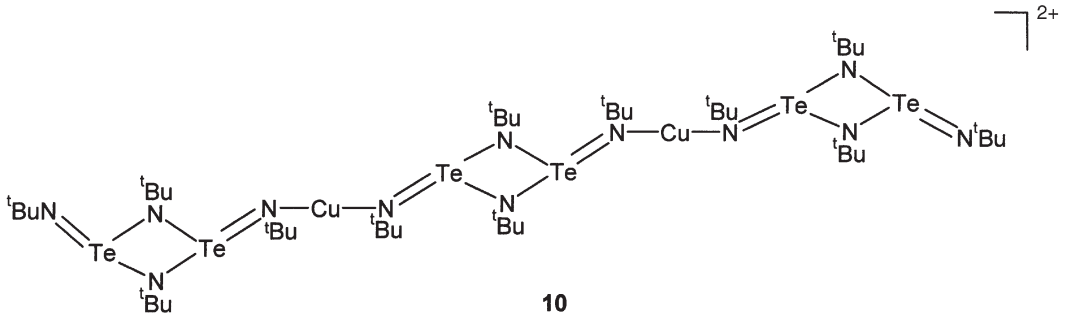
9

Another interesting feature of the chemistry of tellurium diimide dimer **3** involves the reactions with heteroallenes as illustrated by the example of *tert*-butyl isocyanate (Scheme 5). With equimolar amounts of **3** and *t*-BuNCO, Dr. Schatte showed that a ureato ligand is generated in a manner reminiscent of the behaviour of certain transition-metal imides (32). The product (**12**) of this reaction can be viewed as the result of a [2 + 2] cycloaddition of a tellurium diimide monomer and the isocyanate. In the presence of an excess of *tert*-butyl isocyanate, the ureato telluroxide **13** is formed, formally by the replacement of a terminal imido group in **12** by an oxo ligand. This transformation brings to mind the behaviour of iminophosphoranes in the aza-Wittig reaction (14). The telluroxide **13** has a dimeric structure in which the ureato ligands adopt a *cis* arrangement with respect to the central Te_2O_2 ring. In the solid state **13** forms an extended helical network via weak ›C=O···Te interactions (Te···O = 3.020(2) Å) (33).

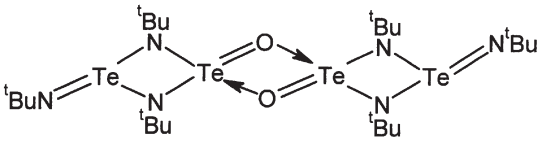
The tellurium diimide dimer **3** also readily undergoes redistribution with tellurium tetrahalides in THF to give *tert*-butylimidotellurium dihalides (22). Nicole Sandblom

[3] T. Maaninen, R. Laitinen, M. Nissinen, T. Chivers, and G. Schatte. Unpublished results. 2001.

© 2001 NRC Canada

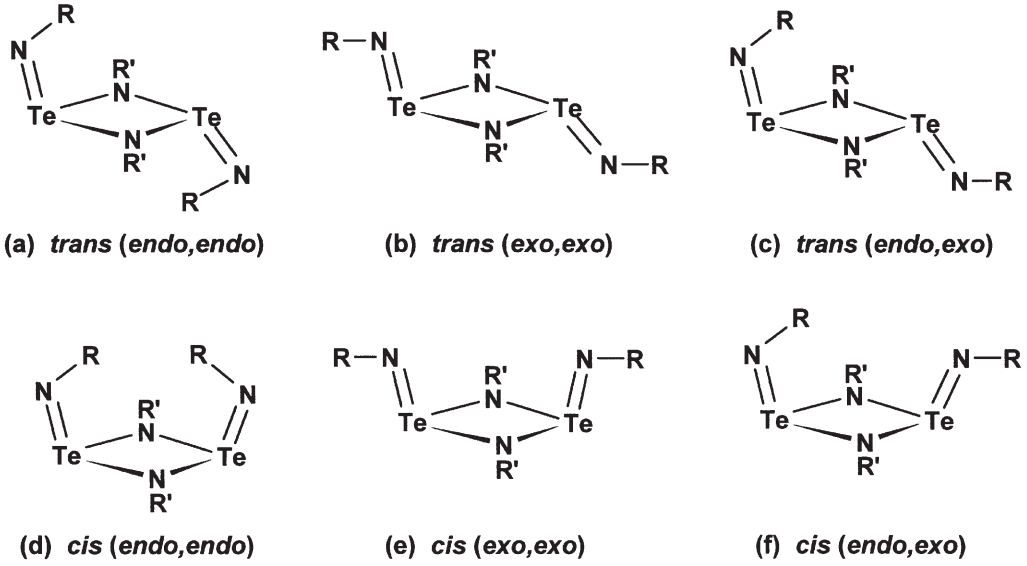


10



11

Fig. 3. Isomers of tellurium diimide dimers.



(a) *trans* (*endo,endo*) (b) *trans* (*exo,exo*) (c) *trans* (*endo,exo*)

(d) *cis* (*endo,endo*) (e) *cis* (*exo,exo*) (f) *cis* (*endo,exo*)

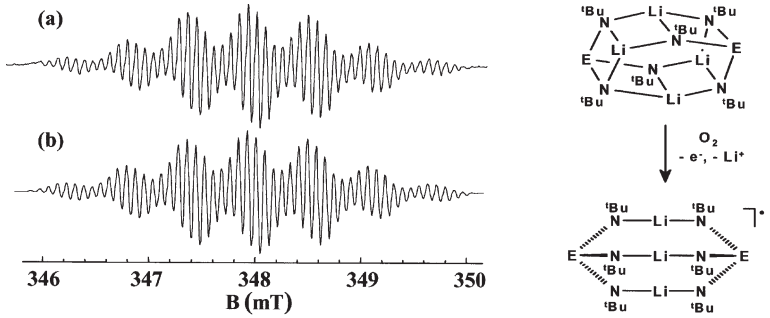
has shown that the dichloride **14** is obtained in essentially quantitative yield as mica-like golden crystals by this reaction (Scheme 5). In the solid state, **14** exists as a hexamer in which three dimeric units are connected by chloride bridges (22). More importantly, this new class of compound is a potentially useful reagent for extending tellurium–nitrogen chemistry via nucleophilic replacement of the chloride ligands. For example, the reaction of the dichloride with 2 equiv of potassium *tert*-butoxide produces the corresponding bis(*tert*-butoxy) derivative **15**, which is a weakly associated dimer in the solid state (22). The geometry at tellurium in **15** is that of a distorted trigonal bipyramid with the lone pair in one of the equatorial positions. Most significantly, there is a large difference, ca. 0.27 Å, between the axial and equatorial Te—N bond lengths. In particular, the value of 1.94 Å for the equatorial TeN bonds suggests that the monomeric units retain substantial double bond character in the dimer as depicted by the schematic drawing of **15** in Scheme 5. Accordingly, the generation of a monomeric tellurium imide by the attachment of even more bulky alkoxy or aryloxy groups to tellurium seems feasible.

Trisimidochalcogenite anions

The tellurium diimide dimer **3** is, as expected, readily susceptible to nucleophilic attack at the tellurium centre. Thus, the reaction of **3** with potassium *tert*-butoxide generates the pyramidal *tert*-butoxybis(*tert*-butylimido)tellurite anion $[Te(N\text{-}t\text{-}Bu)_2(O\text{-}t\text{-}Bu)]^-$ (34). In the solid state, as its potassium salt, this anion adopts the dimeric arm-chair structure **16** with five-coordinate K^+ ions (Scheme 6). A similar type of behaviour is observed in the reaction of **3** with lithium *tert*-butylamide. In this case, however, the final product is the tris(*tert*-butylimido)tellurite dianion, isoelectronic with

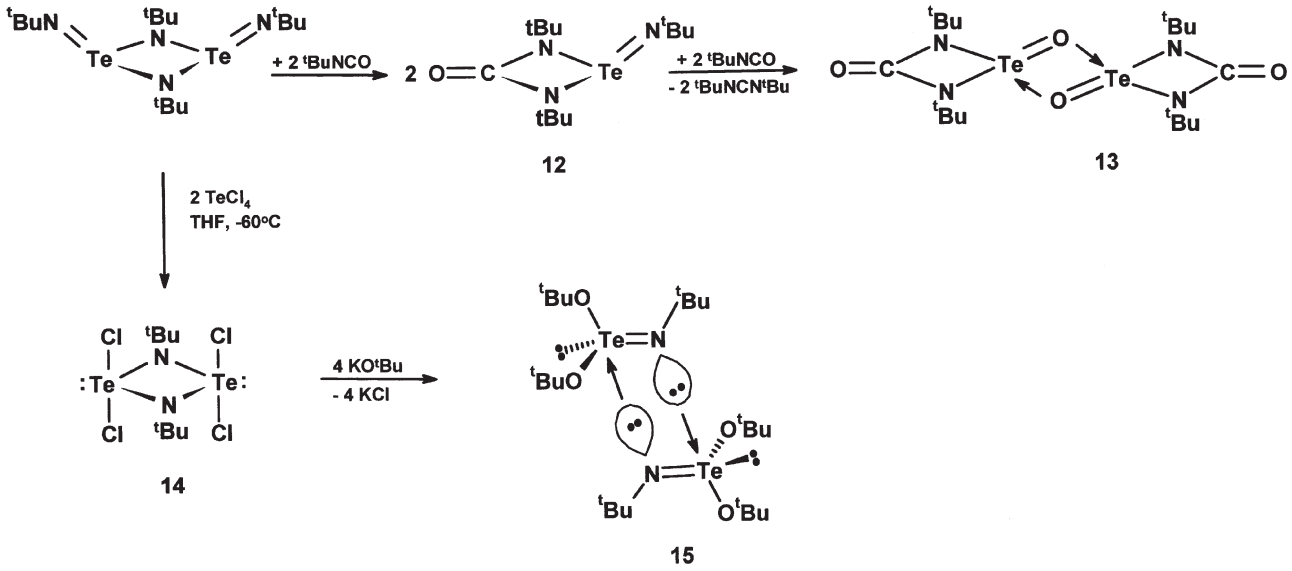
© 2001 NRC Canada

Fig. 4. EPR spectra of $Li_3[S(N\text{-}t\text{-}Bu)_3]_2^{\cdot}$. (*a*) Experimental; and (*b*) simulated (taken from ref. 8).



E	g	a(^{14}N)	a(^{7}Li)	a(^{77}Se)
S	2.0039	5.69	0.82	–
Se	2.0065	5.41	0.79	4.3

Scheme 5.



Scheme 6.



the tellurite ion TeO_3^{2-} (4). As its dilithium derivative, this dianion forms the dimer **17** with a hexagonal prismatic (or cyclic ladder) structure (Scheme 6). By analogy with the reaction with potassium *tert*-butoxide, the formation of this cluster likely involves the initial formation of the monoanion $[Te(N\text{-}t\text{-}Bu)_2(NH\text{-}t\text{-}Bu)]^-$, which is subsequently deprotonated by lithium *tert*-butylamide to give the pyramidal tris(*tert*-butylimido) tellurite dianion.

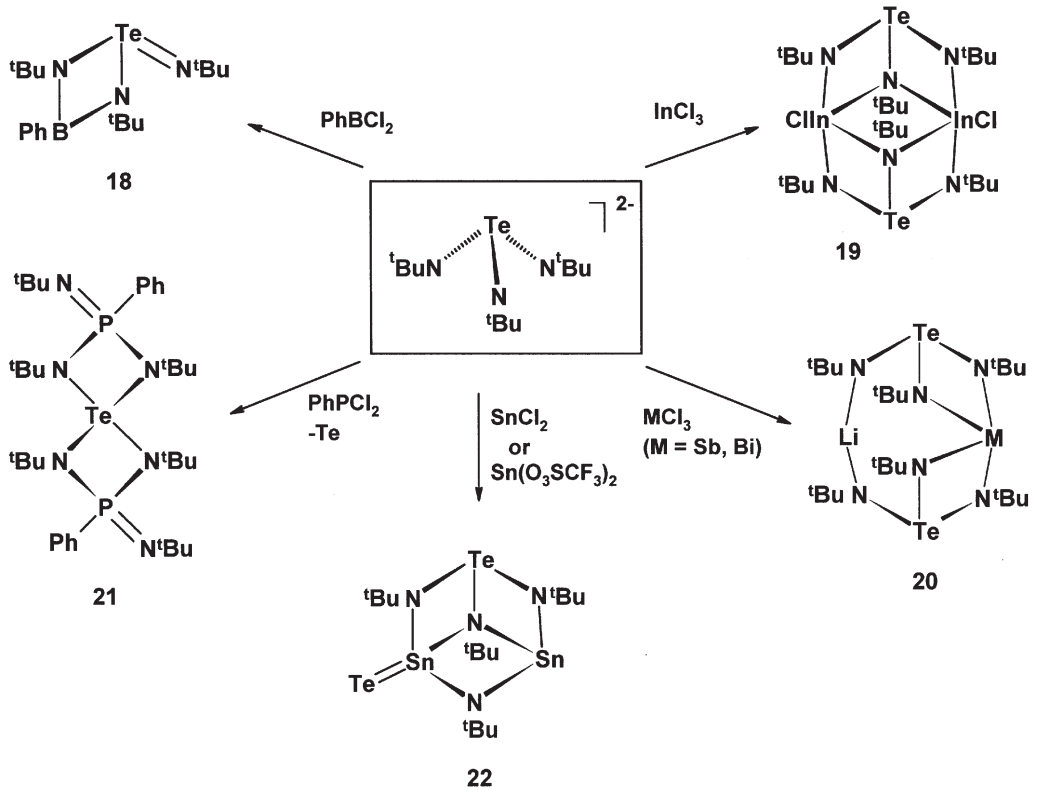
A similar approach can be used to prepare the sulfur and selenium analogues of the tris(*tert*-butylimido)tellurite dianion (5, 6). The dilithium derivatives of these dianions are made by the reaction of the chalcogen diimide with the appropriate amount of lithium *tert*-butylamide in a hydrocarbon solvent (eq. [1]). These ternary cluster systems also adopt hexagonal prismatic structures, which are more distorted than that of the tellurium analogue as a result of the shorter chalcogen—nitrogen distances. Stalke and co-workers (6) reported the characterization of the sulfur analogue while we described the selenium system (5).

$$[1] \qquad 2t\text{-BuN=E=N-}t\text{-Bu} + 4\text{LiNH-}t\text{-Bu} \xrightarrow[-78°C]{\text{toluene}} [Li_2E(N\text{-}t\text{-}Bu_3)_3]_2 + 2t\text{-BuNH}_2 \quad (E = S, Se)$$

A fascinating feature of these cluster systems is the formation of intensely coloured solutions upon exposure of hydrocarbon solutions to oxygen. For example, a deep blue colour is immediately apparent if a solution of $[Li_2S(N\text{-}t\text{-}Bu)_3]_2$ is allowed to come in contact with a trace of air (6, 8, 35). The EPR spectra of these coloured solutions show essentially the same pattern for both the sulfur and selenium systems (8, 35) (Fig. 4). The spectra consist of a septet of decets and the simulated spectra show a good fit for coupling of the unpaired

© 2001 NRC Canada

Scheme 7.



Scheme 8.

$$\text{Te(+IV)} \xrightarrow{+6\ e^-} \text{Te(-II)}$$

$$\text{Sn(+II)} \xrightarrow{-2\ e^-} \text{Sn(+IV)}$$

$$2\ {}^t\text{BuN}^{2-} \xrightarrow{-4\ e^-} {}^t\text{BuN=N}{}^t\text{Bu}$$

electron with three equivalent ^{14}N nuclei (I = 1), which gives rise to a 1:2:3:4:3:2:1 septet, and three equivalent ^{7}Li nuclei (I = 3/2), which generates the decet. On the basis of these EPR data, it has been suggested that the one-electron oxidation of these clusters is accompanied by the removal of one Li^+ ion from the hexagonal prism to give a neutral radical that consists of a radical anion and a dianion bridged by the remaining three Li^+ ions (8, 35) (Fig. 4).

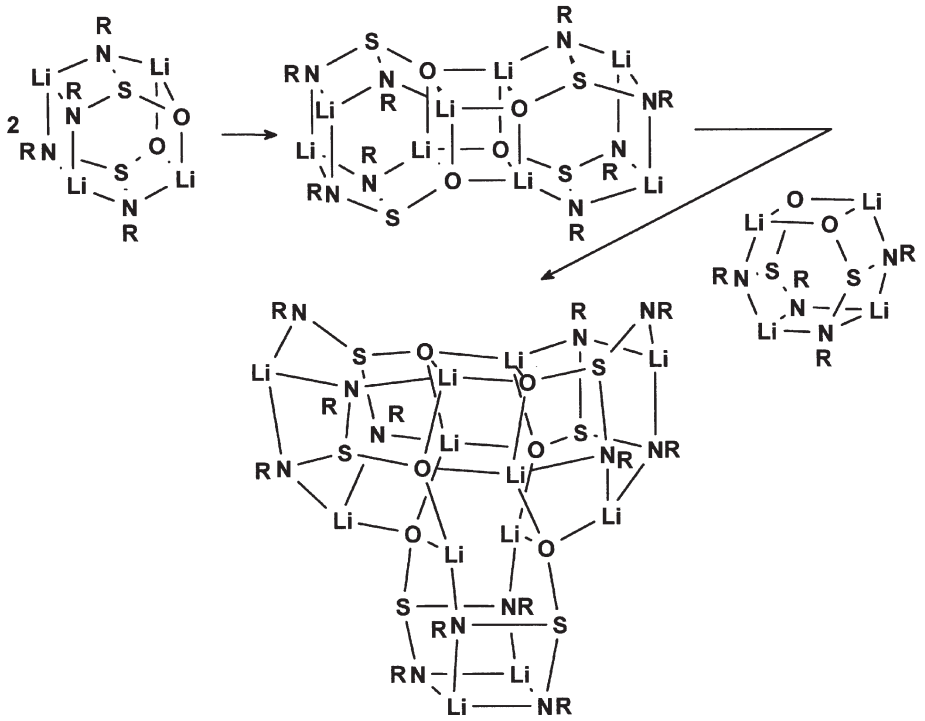
In view of the facile oxidation of the tris(*tert*-butylimido) sulfite dianion it is not surprising that Fleischer and Stalke (36) have found that attempts to coordinate this tripodal ligand to metal centres frequently result in redox behaviour. On the other hand, our results show that the tris(*tert*-butylimido)tellurite dianion has a rich coordination chemistry as illustrated in Scheme 7, although redox processes are sometimes observed. For example, this pyramidal dianion reacts with $PhBCl_2$ to give the *N*,*N*′-chelated complex **18** (4), which is an unique example of a monomeric tellurium imide apparently stabilized by the dianionic boramidinato ligand $[PhB(N\text{-}t\text{-}Bu)_2]^{2-}$ (37). The dimeric cluster **19**, obtained from the reaction with $InCl_3$, involves a second chelation of the tris(*tert*-butylimido)tellurite ligand to the other monomeric unit to give five-coordinate indium centres in an arm-chair structure.[4] The tris(*tert*-butylimido)tellurite ligand also chelates to heavier group 15 centres in the complexes **20** (M = Sb, Bi) in which the terminal N-*t*-Bu groups are bridged by the Li^+ counter-ion (38). By contrast, redox behaviour is observed in the reaction of $[Te(N\text{-}t\text{-}Bu)_3]^{2-}$ with phenyldichlorophosphine (4). In this reaction, half of the tellurium is reduced to tellurium metal while the two phosphorus atoms are oxidized from the +3 to the +5 oxidation state to give **21**, a spirocyclic complex of tellurium(IV) chelated by two tris(*tert*-butylimido)phenylphosphonate ligands ($[PhP(N\text{-}t\text{-}Bu)_3]^{2-}$). To our knowledge, this is the first example of a complex of this dianion, which is isoelectronic with the well-known phenylphosphonate ligand $[PhPO_3]^{2-}$.

An especially intriguing outcome of a redox process results from the reaction of the tris(*tert*-butylimido)tellurite dianion with tin(II) chloride or triflate (39). The pyramidal ligand can be readily discerned in the complex **22** (Scheme 7) bridging two tin atoms in different oxidation states, one of which is attached to a terminal telluride. This is the first stannatellurone that involves four-coordinate tin; the only previous example of this particular type of "heavy ketone" has a five-coordinate tin centre (40). The overall redox process for the formation of **22** involves the six-electron reduction of one tellurium(IV) centre to tellurium (-II) (telluride), accompanied by oxidation of one tin atom from +2 to +4 and the formation of *tert*-butyldiazene from the oxidation of two *tert*-butylimido ligands (Scheme 8). The SnTe bond length of 2.59 Å is, as expected, a little shorter than the value of 2.62 Å reported by Leung et al. (40) for the related

[4] T. Chivers and G. Schatte. Unpublished results. 2001.

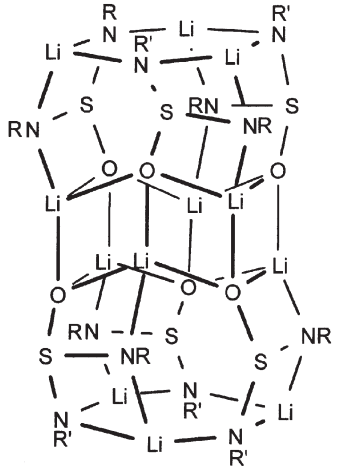
© 2001 NRC Canada

Fig. 5. Self-assembly of the 36-atom cluster $\{Li_2[OS(N\text{-}t\text{-}Bu)_2]\}_6$ (**23**) by the aggregation of three hexagonal prisms.



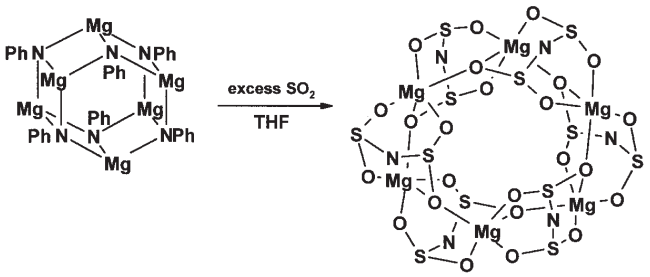
23 (R = ^{t}Bu)

Fig. 6. Structure of $\{Li_2[OS(N\text{-}t\text{-}Bu)(NSiMe_3)]\}_6$ (**24**).



24 (R = ^{t}Bu, R' = $SiMe_3$)

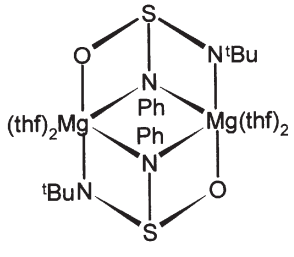
Scheme 9.



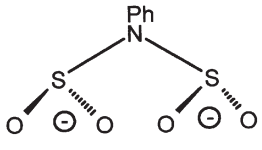
26

(Ph groups on N and THF ligands attached to Mg^{2+} are omitted)

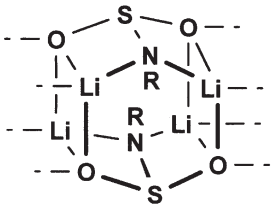
Scheme 10.

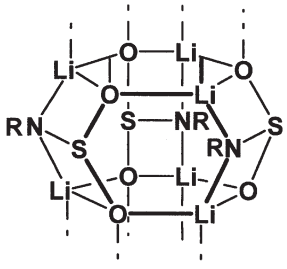


25



27





© 2001 NRC Canada

complex with five-coordinate tin. It is also predictably somewhat longer than the value of 2.54 Å calculated for the prototypical three-coordinate stannatellurone ($H_2Sn{=}Te$), derivatives of which are not known (41).

Heteroleptic imido-oxo anions of chalcogens

A logical sequel to investigations of homoleptic polyimido anions of chalcogens is the study of heteroleptic systems in which both imido groups and oxo ligands are attached to the central *p*-block element, e.g., sulfur. The synthetic methodology used to prepare bisimidosulfites is similar to that used for trisimidochalcogenites. Justin Brask has shown that the dithium derivatives are obtained in excellent yields by the reaction of a sulfinylamine with two equivalents of the lithium derivative of a primary amine (eq. [2]) (7). This is a versatile route that can be applied to a variety of R and R′ groups. Our initial interest was in the structures of the clusters formed by dilithium derivatives of bisimidosulfites. In particular, what is the effect of replacing one of the bulky N-*t*-Bu groups in $[Li_2E(N\text{-}t\text{-}Bu)_3]_2$ (E = S, Se, Te) by an oxo ligand? Does changing the R group have an additional structural effect? Preliminary answers to those questions have been obtained from the structural characterization of two derivatives (7).

[2] $$RNSO + 2LiNHR' \xrightarrow[-78°C]{\text{toluene}} \{Li_2[OS(NR)(NR')]\}_n + R'NH_2$$

The heteroleptic system containing two N-*t*-Bu groups and one oxygen atom attached to sulfur forms a hexameric 36-atom cluster $\{Li_2[OS(N\text{-}t\text{-}Bu)_2]\}_6$ (**23**, R = *t*-Bu) (Fig. 5). Perusal of the structure of **23** reveals that aggregation has occurred through the lithium—oxygen bonds, all of which are in the centre of the molecule while the lipophilic N-*t*-Bu groups occupy the peripheral positions. A closer look suggests that this self-assembly process involves the trimerization of hexagonal prisms as depicted in Fig. 5. The observed structure can be derived from three hexagonal prisms in which the lithium—oxygen bonds, i.e., the most polar bonds, are juxtaposed to give a four-membered Li_2O_2 face in each unit. Aggregation of two of these fundamental building blocks by their Li_2O_2 faces formally generates a dimer. The interposition of the Li_2O_2 face of a third hexagonal prism gives rise to the 36-atom cluster **23** with a central Li_6O_6 scaffold.

Interestingly, the subtle change of replacing one of the *t*-Bu groups in the bis(*tert*-butylimido)sulfite dianion by a trimethylsilyl group has a remarkable effect on the cluster structure. Like **23**, the cluster $\{Li_2[OS(N\text{-}t\text{-}Bu)(NSiMe_3)\}_6$ (**24**) is hexameric and involves 36 atoms. In this case, however, the fundamental building block is an 18-atom cluster reminiscent of the nonameric alumoxane system shown in Fig. 1 (42). The cluster **24** can be viewed to result from the face-to-face dimerization of two of these building blocks via their Li_3O_3 faces. Thus, the common feature of the cluster structures **23** and **24** is self-assembly via highly polar, sterically unencumbered lithium–oxygen faces of smaller building blocks.

Unsymmetrical bisimidosulfites containing an arylimido group can be generated by using magnesium anilide as the source of the arylimido group. For example, the reaction of $[Mg(NPh)]_6$ with *t*-BuNSO generates the dimer **25** (43). More interesting, however, is the reaction of the hexameric magnesium anilide with an excess of sulfur dioxide which produces the 48-atom cluster **26** (Scheme 9) (43). The insertion of a single SO_2 molecule into a metal-amide bond is a known process, e.g., for Me_3SnNMe_2 (44). The cluster **26** is formally derived from six double insertions of SO_2 molecules into the magnesium-nitrogen bonds of the hexamer $[Mg(NPh)]_6$, which generates the novel imidodisulfite dianion $[O_2S(\mu\text{-}NPh)SO_2]^-$ (**27**). Each of these dianions bridges two Mg^{2+} cations in the observed hexameric cluster **26**.

The next phase of this work is to determine whether extended structures can be generated from building blocks which contain two Li_2O_2 or Li_3O_3 faces as depicted in Scheme 10. These structural units can be anticipated for lithium derivatives of monoalkylimidosulfites, which are readily prepared by reaction of SO_2 with 2 equiv of the lithium derivative of a primary amine (8). The products of these reactions have not yet been structurally characterized primarily because of their tendency to form gels in organic solvents, an observation that may indicate the formation of extended structures with the incorporation of solvent molecules. This intriguing prospect and the synthesis of alkylimido analogues of aluminophosphates, for which it may be able to control cavity size by suitable variations in the R group attached to nitrogen, is currently being pursued.

Acknowledgements

I wish to thank all members of my research group for their dedicated work, especially Dr. X. Gao, Dr. G. Schatte, Justin Brask, Arto Maaninen, Tiina Maaninen, and Nicole Sandblom for their contributions to the experimental studies described in this account. Collaboration with Professor Risto Laitinen (selenium chemistry) has been especially fruitful. The expertise of Professors R.T. Boeré and B. McGarvey (EPR spectroscopy), Professor T. Ziegler (DFT calculations), and the invaluable assistance of X-ray crystallographers Drs. M. Parvez and G. Schatte (University of Calgary), Dr. R. MacDonald (University of Alberta), Dr. G.P.A. Yap (University of Ottawa), and Dr. G. Enright (NRC, Ottawa) have been pivotal in our work on chalcogen imide chemistry. The continued financial support of the Natural Sciences and Engineering Research Council of Canada (NSERC) is gratefully acknowledged.

References

1. T. Chivers, X. Gao, and M. Parvez. J. Chem. Soc. Chem. Commun. 2149 (1994).
2. T. Chivers, X. Gao, and M. Parvez. J. Am. Chem. Soc. **117**, 2359 (1995).
3. T. Chivers, X. Gao, and M. Parvez. Inorg. Chem. **35**, 9 (1996).
4. T. Chivers, X. Gao, and M. Parvez. Angew. Chem. Int. Ed. Engl. **34**, 2549 (1995).
5. T. Chivers, M. Parvez, and G. Schatte. Inorg. Chem. **35**, 4094 (1996).

© 2001 NRC Canada

6. R. Fleischer, S. Freitag, F. Pauer, and D. Stalke. Angew. Chem. Int. Ed. Engl. **35**, 204 (1996).
7. J.K. Brask, T. Chivers, M. Parvez, and G. Schatte. Angew. Chem. Int. Ed. Engl. **36**, 1986 (1997).
8. J.K. Brask, T. Chivers, G. Schatte, B. McGarvey, R. Sung, and R.T. Boeré. Inorg. Chem. **37**, 4633 (1998).
9. J.K. Brask and T. Chivers. Angew. Chem. Int. Ed. **40**, 3960 (2001).
10. P. Paetzold. Phosphorus Sulfur Silicon Relat. Elem. **93**–**94**, 39 (1994).
11. N.J. Hardman, C. Cui, H.W. Roesky, W.H. Fink, and P.P. Power. Angew. Chem. Int. Ed. **40**, 2172 (2001).
12. F.T. Edelmann. Coord. Chem. Rev. **137**, 403 (1994).
13. J. Barker and M. Kilner. Coord. Chem. Rev. **133**, 219 (1994).
14. A.W. Johnson. Ylides and imides of phosphorus. John Wiley and Sons Ltd., London, U.K. 1993. pp. 429–430.
15. A.F. Hill. Adv. Organomet. Chem. **36**, 159 (1994).
16. M. Bruncko, T.-A.V. Khuong, and K.B. Sharpless. Angew. Chem. Int. Ed. Engl. **35**, 454 (1996), and refs. cited therein.
17. M. Veith and O. Recktenwald. Z. Naturforsch. B: Anorg. Chem. Org. Chem. **38b**, 1054 (1983).
18. T. Hascall, K. Ruhlandt-Senge, and P. Power. Angew. Chem. Int. Ed. Engl. **33**, 356 (1994).
19. C.E. Housecroft. Cluster molecules of the *p*-block elements. Oxford University Press, Oxford, U.K. 1994. p. 24.
20. B. Wrackmeyer, B. Distler, S. Gerstmann, and M. Herberhold. Z. Naturforsch. B: Chem. Sci. **48b**, 1307 (1993).
21. M. Herberhold and W. Jellen. Z. Naturforsch. B: Anorg. Chem. Org. Chem. **41b**, 144 (1986).
22. T. Chivers, G.D. Enright, N. Sandblom, G. Schatte, and M. Parvez. Inorg. Chem. **38**, 5431 (1999).
23. N. Sandblom, T. Ziegler, and T. Chivers. Inorg. Chem. **37**, 354 (1998).
24. A. Maaninen, T. Chivers, M. Parvez, J. Pietikäinen, and R.S. Laitinen. Inorg. Chem. **38**, 4093 (1999).
25. T. Maaninen, T. Chivers, R. Laitinen, and E. Wegelius. Chem. Commun. 759 (2000).
26. T. Maaninen, T. Chivers, R. Laitinen, and M. Nissinen. Inorg. Chem. **39**, 5341 (2000).
27. H.W. Roesky, K.-L. Weber, and J.W. Bats. Chem. Ber. **117**, 2686 (1984).
28. M. Björgvinsson and H.W. Roesky. Polyhedron, **10**, 2353 (1991).
29. T. Chivers, M. Parvez, and G. Schatte. Angew. Chem. Int. Ed. **38**, 2217 (1999).
30. P. Pykkö. Chem. Rev. **97**, 597 (1997).
31. T. Chivers, M. Parvez, and G. Schatte. Inorg. Chem. **38**, 5171 (1999).
32. W.-H. Leung, G. Wilkinson, B. Hussain-Bates, and M.B. Hursthouse. J. Chem. Soc. Dalton Trans. 2791 (1991).
33. G. Schatte, T. Chivers, C. Jaska, and N. Sandblom. Chem. Commun. 1657 (2000).
34. T. Chivers, X. Gao, and M. Parvez. Inorg. Chem. **35**, 4633 (1996).
35. R. Fleischer, S. Freitag, and D. Stalke. J. Chem. Soc. Dalton Trans. 193 (1998).
36. R. Fleischer and D. Stalke. Organometallics, **17**, 832 (1998).
37. J.K. Brask, T. Chivers, and G. Schatte. Chem. Commun. 1805 (2000).
38. T. Chivers, M. Parvez, G. Schatte, and G.P.A. Yap. Inorg. Chem. **38**, 1380 (1999).
39. T. Chivers and G. Schatte. Chem. Commun. 2264 (2001).
40. W.-P. Leung, W.-H. Kwok, L.T.C. Law, Z.-Y. Zhou, and T.C.W. Mak. Chem. Commun. 505 (1996).
41. R. Okazaki and N. Tokitoh. Acc. Chem. Res. **33**, 625 (2000).
42. M.R. Mason, J.M. Smith, S.G. Bott, and A.R. Barron. J. Am. Chem. Soc. **115**, 4971 (1993).
43. J.K. Brask, T. Chivers, and M. Parvez. Angew. Chem. Int. Ed. **39**, 958 (2000).
44. T.A. George, K. Jones, and M.F. Lappert. J. Chem. Soc. 2157 (1965).

© 2001 NRC Canada

Geometric and solvent effects on intramolecular phenolic hydrogen abstraction by carbonyl *n*,π* and π,π* triplets

Edward C. Lathioor and William J. Leigh

Abstract: The photochemistry of a series of alkoxyacetophenone, -benzophenone, and -indanone derivatives, which contain a remote phenolic group linked to the ketone by a *para*,*para*′- or *meta*,*meta*′-oxyethyl spacer, has been studied in acetonitrile and dichloromethane solutions using laser flash photolysis techniques. The corresponding methoxy-substituted compounds and, in the case of the alkoxyindanones, derivatives bearing just a remote phenyl substituent, have also been examined. The triplet lifetimes of the phenolic compounds are determined by the rates of intramolecular abstraction of the remote phenolic hydrogen, and depend on the solvent, the geometry of attachment and the configuration of the lowest triplet state. In contrast to the large (>500-fold) difference in lifetime of the *para*,*para*′- and *meta*,*meta*′-alkoxyacetophenone derivatives, both of which have lowest π,π* triplet states, smaller differences are observed for the alkoxyindanone (lowest charge transfer triplet, ~twofold difference) and alkoxybenzophenone (lowest *n*,π* triplet, ~18-fold difference) derivatives in acetonitrile solution. The triplet lifetimes of the acetophenone and benzophenone are significantly shorter in dichloromethane than in acetonitrile, consistent with the intermediacy of a hydrogen-bonded triplet exciplex in the reaction. This is not the case with the *para*,*para*′-indanone derivative, sugesting that hydrogen abstraction in this compound is dominated by a mechanism involving initial charge transfer rather than hydrogen bonding. This is most likely due to orientational constraints that prevent the remote phenolic -O-H group from adopting a coplanar arrangement with the *n*-orbitals of the carbonyl group.

Key words: photochemistry, aromatic ketone, phenol, triplet, intramolecular, quenching, hydrogen abstraction, phenoxyl radical, kinetics, kinetic isotope effect, laser flash photolysis.

Résumé : Faisant appel à des techniques de photolyse éclair au laser et opérant dans des solutions d'acétonitrile et de dichlorométhane, on a étudié la photochimie d'une série de dérivés alkoxyacétophénones, -benzophénones et -indanones comportant un groupe phénolique dans une position éloignée, mais liée à la cétone par un espaceur oxyéthyle en *para*,*para*′- ou *méta*,*méta*′-. On a aussi étudié les composés correspondants portant des substituants méthoxy ainsi que, dans le cas des alkoxyindanones, des dérivés ne portant qu'un substituant phényle en position éloignée. On a déterminé les temps de vie du triplet des composés phénoliques à partir des vitesses d'enlèvement intramoléculaire de l'hydrogène phénolique éloigné; ils dépendent du solvant, de la géométrie de fixation et de la configuration de l'état triplet le plus bas. Par opposition à la grande différence (>500 fois) dans les temps de vie des dérivés *para*,*para*′- et *méta*,*méta*′-alkoxyacétophénones qui ont tous les deux des états triplets π,π* plus faibles, on observe des différences plus faibles pour les dérivés alkoxyindanones (triplet de transfert de charge le plus faible; différence du simple au double) et alkoxybenzophénones (triplet *n*,π* le plus faible; différence correspondant à une réaction environ 18 fois plus rapide) dans une solution d'acétonitrile. Les temps de vie des dérivés de l'acétophénone et de la benzophénone sont beaucoup plus courts en solution dans le dichlorométhane que dans l'acétonitrile; ce résultat ets en accord avec une réaction se produisant par l'intermédiaire d'un exciplex triplet avec liaison hydrogène. Ce n'est pas le cas pour le dérivé *para*,*para*′-indanone et ce résultat suggère l'enlèvement de l'hydrogène dans ce composé est dominé par un mécanisme impliquant dans un premier temps un transfert de charge plutôt que la formation d'une liaison hydrogène. Cette différence résulte vraisemblablement de contraintes qui font que le groupe -O-H phénolique éloigné ne peut s'orienter dans un arrangement coplanaire avec les orbitales *n* du groupe carbonyle.

Mots clés : photochimie, cétone aromatique, phénol, triplet, intramoléculaire, piégeage, enlèvement d'hydrogène, radical phénoxyle, cinétique, effet isotopique cinétique, photolyse éclair au laser.

[Traduit par la Rédaction]

Received June 18, 2001. Published on the NRC Research Press Web site at http://canjchem.nrc.ca on December 10, 2001.

E.C. Lathioor and W.J. Leigh.[1] Department of Chemistry, McMaster University, 1280 Main Street West, Hamilton, ON L8S 4M1, Canada.

[1]Corresponding author (fax: (905) 522-2509; e-mail: leigh@mcmaster.ca).

Introduction

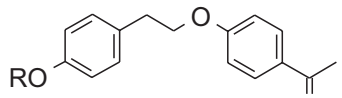
Hydrogen abstraction from phenols by the excited triplet states of most aromatic ketones occurs at rates in excess of 1×10^9 M^{-1} s^{-1} in solution, resulting in the formation of the corresponding phenoxyl and hemipinacol radicals in close to unit quantum yields (1–6). Unlike hydrogen abstraction from alkanes, alcohols, or substituted toluenes (7), however, the

 DOI: 10.1139/cjc-79-12-1851 © 2001 NRC Canada

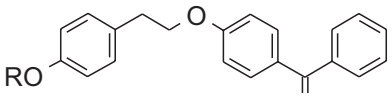
normal dependence of the rate constant for reaction on the configuration of the lowest triplet state is not observed, and ketones with lowest π,π* triplet states tend to exhibit greater reactivity than those with lowest *n*,π* triplets. This characteristic is suggestive of an electron-transfer mechanism, where the hydrogen atom is transferred as a proton after initial electron transfer to yield the corresponding $PhOH^{\cdot+}/Ar_2CO^{\cdot-}$ radical ion pair. While recent work suggests that this is indeed the mechanism followed by benzophenone and other aromatic ketones in pure water (8, 9), electron transfer is more endergonic in nonaqueous solvents, where the reduction potentials of ketones are higher than in hydroxylic media (10). To be sure, previous kinetic studies indicate that the situation in nonaqueous solvents is generally more complicated than a simple electron transfer mechanism can accommodate (3, 11).

We have recently proposed that in acetonitrile solution, quenching of π,π* aromatic ketone triplets proceeds via electron and (or) proton transfer within a hydrogen-bonded triplet exciplex, in which the hydrogen bond serves mainly to facilitate electron transfer from the phenol to the ketone by lowering the oxidation and reduction potentials of the redox pair (11). Phenolic quenching of ketones with lowest *n*,π* triplet states was suggested to proceed by two mechanisms, depending on the triplet state reduction potential and the proximity of the higher lying π,π* triplet state, on the basis of the observation of a V-shaped Hammett plot for the quenching of a series of substituted benzophenone triplets by *para*-cresol. Electron-acceptor-substituted benzophenone derivatives were proposed to be quenched by the charge-transfer exciplex mechanism common to abstraction from substituted toluenes (12–15), which presumably transforms into the "simple" electron transfer mechanism when the reduction potential of the ketone is low enough. Quenching of electron-donor-substituted derivatives, on the other hand, was proposed to proceed via the hydrogen-bonded exciplex mechanism and involve the higher lying, relatively basic π,π* triplet state.

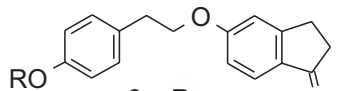
Phenolic quenching of aromatic ketone triplets also occurs *intra*molecularly, as has been demonstrated in a study of the photochemistry of the oxyethyl-linked phenolic ketones **1a**–**3a** (11, 16, 17). The triplet lifetimes of these compounds in acetonitrile solution at room temperature are in the 10–30 ns range, orders of magnitude shorter than the corresponding methoxy-substituted analogues (**1b**–**3b**), and they vary throughout the series in a similar way as do the rate constants for bimolecular quenching of the corresponding (methoxy-substituted) model compounds by *para*-cresol under the same conditions (11). Surprisingly, this correlation fails for the *meta,meta′*-analogue of the phenolic acetophenone derivative **1a**, 3-[2-(3′-hydroxyphenyl)ethoxy]acetophenone (**4a**) (18). The triplet lifetime of this compound exceeds 10 μs in acetonitrile solution at 23°C and is similar to that of the methoxy analogue **4b**, indicating that intramolecular abstraction of the remote phenolic hydrogen is over 500 times slower in this compound than in **1a**. The rate constant for the analogous bimolecular reaction is quite fast, so the very low reactivity of the triplet state of **4a** must be due to specific geometrical factors that are not present in the *para,para′*-derivative **1a**. Molecular mechanics calculations indicate that **4a** can adopt several conformations in which the phenolic hydrogen is within abstracting distance (less than ca. 2.65 Å) of the carbonyl oxygen, but in which there is little or no overlap between the aryl rings. We have proposed that the much longer lifetime of **4a** is due to the preferred formation of one or more of these exciplex conformers, in which quenching is presumably relatively slow, as well as orbital symmetry restrictions to electron and (or) proton transfer in the (higher energy) sandwich-like conformer similar to the one that must be involved in intramolecular hydrogen abstraction in **1a**.



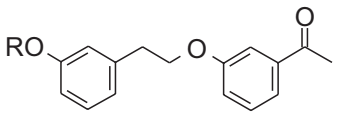
1a R =
1b R = Me



2a R =
2b R = Me



3a R =
3b R = Me

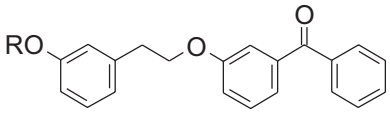


4a R =
4b R = Me

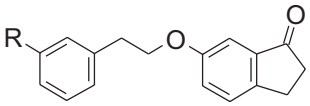
In the present paper, we report the results of further studies of the role of geometrical factors in intramolecular phenolic hydrogen abstraction by aromatic ketone triplets, and the effects of solvent polarity on the rate constants. We have thus prepared two new phenolic ketones (**5a** and **6a**), which feature the same *meta,meta′*-linkage as is present in **4a**, and have examined their photochemistry under similar conditions as the *para,para′*-analogues **2a** and **3a**. As with **1a**–**3a**, the main difference between the three *meta,meta′*-substituted compounds (**4a**–**6a**) is the configuration of the lowest triplet state (π,π* in **4a** and **6a**; *n*,π* in **5a**). Further, **4a** and **6a** differ in the degree of charge-transfer character associated with their lowest π,π* triplet states, an effect which is due to the differing abilities of the carbonyl group to twist out of the plane of its attached aromatic ring in the two molecules. As before, the role of intramolecular hydrogen abstraction in controlling the triplet lifetimes of the two compounds is assessed through a comparison to the triplet state behavior of the corresponding methoxy-analogues (**5b** and **6b**, respectively), and in the case of the indanone derivatives, to the phenyl-substituted analogues **6c** and **7** as well. Finally, the triplet state behavior of the entire series of compounds (**1**–**7**), as well as rate constants for bimolecular phenolic hydro-

© 2001 NRC Canada

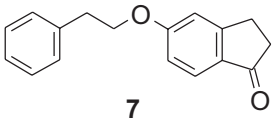
gen abstraction in appropriate model compounds, have been determined in dichloromethane solution. Comparison of these data to those in acetonitrile solution allows an assessment of the effects of (aprotic) solvent polarity on the rates of both inter- and intramolecular versions of the reaction.



5a: R =
5b: R = Me



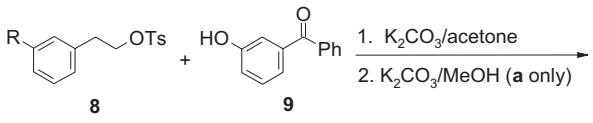
6a: R = O
6b: R = OMe
6c: R =



7

Results

Compounds **5a** and **6a** were prepared by reaction of the ditosylate ester of 3-hydroxy-β-phenethyl alcohol (**8a**) with 3-hydroxybenzophenone (**9**) and 6-hydroxy-1-indanone (**10**), respectively, in acetone solution, followed by alkaline hydrolysis in methanol (eqs. [1] and [2]). The others (**5b**, **6b**, **6c**, and **7**) were prepared in similar fashion, by reaction of the tosylate esters of 3-methoxy-β-phenethyl alcohol (**8b**) or β-phenethyl alcohol (**8c**) with **9**, **10**, or 5-hydroxy-1-indanone (**11**). The structures of **5**–**7** were assigned on the basis of their ^{1}H and ^{13}C NMR, IR and mass spectra, and combustion analyses.

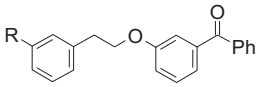
[1] 

8

a. R = OTs
b. R = OMe

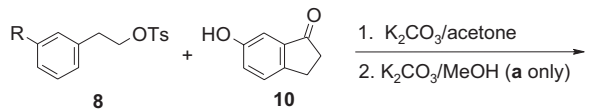
9

1. K_2CO_3/acetone
2. K_2CO_3/MeOH (**a** only)



a. R = OH
b. R = OMe

5

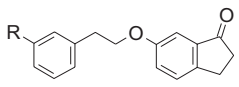
[2] 

8

a. R = OTs
b. R = OMe
c. R = H

10

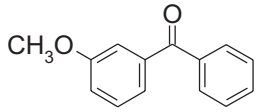
1. K_2CO_3/acetone
2. K_2CO_3/MeOH (**a** only)



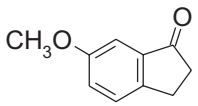
a. R = OH
b. R = OMe
c. R = H

6

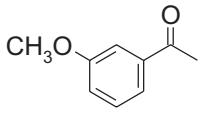
As was found previously for **1**–**4** (11, 18), ultraviolet absorption spectra of **5** and **6** in acetonitrile were in each case indistinguishable from those of the corresponding model compounds **12** and **13**, indicating that no ground-state interactions exist between the carbonyl group and the remote aryl group in these molecules. The same conclusion was derived from comparison of the UV absorption spectra of **1**–**7** with those of the corresponding model compounds (**12**–**17**) in dichloromethane solution.



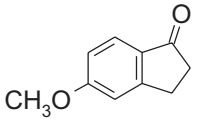
12



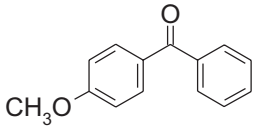
13



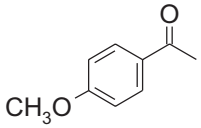
14



15



16



17

Phosphorescence emission spectra of **5a** and **6a** were recorded in 4:1 ethanol:methanol glasses at 77 K, with similar measurements made on the model compounds for comparison. The spectra of **5a**, **5b**, and **12** were similar, as were those of **6a**, **6b**, and **13**. Triplet energies were estimated from the short wavelength onset of the 0–0 emission bands in the spectra; these are 68.3 ± 0.3 kcal mol^{-1} for **5a**, **b** and 71.4 ± 0.1 kcal mol^{-1} for **6a**, **b**. The appearance of the spectra are consistent with an n,π^* assignment for the lowest triplet states of **5a**, **b**, and a π,π^* assignment for **6a**, **b**.

Steady state photolyses (300 nm) were carried out on deoxygenated 0.0025 M acetonitrile solutions of **5a** and **6a**, with periodic monitoring of the solutions by gas chromatography. As observed previously for **1a**–**3a** (11, 18), no photoproducts of similar or lower molecular weight to the starting ketones could be detected in any case. Exhaustive irradiation of the solutions produced small amounts of high molecular weight materials. Quantum yields for substrate photolysis were estimated to be in the 0.001–0.01 range using the disappearance of **1a** (Φ = 0.006) (16) as actinometer. Compounds **5b** and **6b** were found to be similarly unreactive.

Nanosecond laser flash photolysis (NLFP) experiments employed a pulsed excimer laser filled with N_2–He (337 nm, 4 mJ, 6 ns), Xe–HCl–He (308 nm, 55 mJ, 15 ns), or Kr–F_2–N (248 nm, 100 mJ, 25 ns) for excitation, and a microcomputer-controlled detection system (19). Sample concentrations were such that the absorbance at the excitation wavelength (3- or 7-mm path length) was 0.2–0.9 and each sample was deoxygenated with argon or dry nitrogen until constant transient lifetimes were obtained.

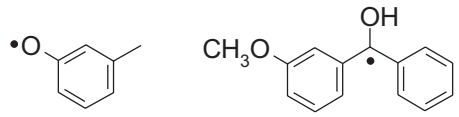
© 2001 NRC Canada

Absolute rate constants for bimolecular quenching of the triplet states of **12**–**17** by *para*- or *meta*-cresol were determined in acetonitrile and (or) dichloromethane solution at 23–25°C using the 337 nm laser for excitation. In each case, the pseudo-first-order triplet decay rate constant (k_{decay}) was determined at or near the triplet–triplet absorption maximum (380 nm for the acetophenone and indanone derivatives; 525 or 600 nm for the benzophenone derivatives) as a function of concentration of added phenol. Addition of the phenols resulted in an increase in triplet decay rate and the formation of new, long-lived absorptions assignable to *para*- or *meta*-cresyloxyl radicals and the corresponding hemipinacol radicals. While these absorptions overlap with those due to the ketone triplets at 380 nm, they were sufficiently long-lived that triplet decay rate constants could generally be determined with reasonable accuracy by simply taking the absorption due to the radical products as the infinity level in the least-squares analyses of the ΔOD vs. time data. At low phenol concentrations where the triplet lifetime was only ≤5 times shorter than those of the radicals, the triplet decay rates were determined by two-exponential least-squares fitting of the data. Bimolecular quenching rate constants (k_q) were determined from plots of the ketone triplet decay rate (k_{decay}) vs. cresol concentration ([Q]) according to eq. [3], where k_o is the pseudo-first-order rate constant for triplet decay in the absence of quencher. The results of these experiments are collected in Table 1.

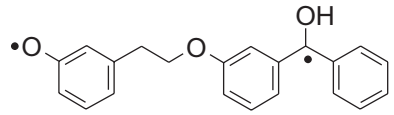
$$[3] \qquad k_{decay} = k_o + k_q[Q]$$

Laser flash photolysis of solutions of the non-phenolic ketones **5b**, **6b**, **c**, and **7** in deoxygenated, dry acetonitrile solution led to the formation of strongly absorbing transients which decayed with clean pseudo-first-order kinetics (at low laser intensities) and exhibited lifetimes in the 1–10 μs range. These were assigned to the corresponding triplet states on the basis of their absorption spectra, which were indistinguishable from those of the corresponding model compounds (**12** in the case of **5b**, **13** in the case of **6b** and **6c**, and **15** in the case of **7**), and the fact that they are quenched rapidly by 1,3-cyclohexadiene (CHD, k_q = 6–9 × 10^9 M^{-1} s^{-1}) and oxygen ($k_q > 1 \times 10^9$ M^{-1} s^{-1}). The triplet–triplet absorption spectra of **5b** and **6b** in acetonitrile are shown in Fig. 1, while the inserts show typical decay profiles recorded at 600 and 385 nm, respectively. The spectra shown were recorded over ca. 200 ns time windows, starting just after the peak in the transient decay profiles.

The transient absorption spectra from flash photolysis of the phenolic ketones **5a** and **6a** are significantly different from those of the corresponding methoxy analogues. For example, Fig. 2*a* shows the spectra obtained from a 2.2×10^{-4} M solution of **5a** in acetonitrile (λ_{exc} = 248 nm), at the point corresponding to the peak in the transient decay profile and over the 0.5–1.0 μs time window after the peak. For comparison, spectra recorded of an acetonitrile solution containing **12** (0.0076 M) and *meta*-cresol (0.0058 M) over similar time windows, using the 337 nm laser for excitation, are shown in Fig. 2*b*. The early spectrum of Fig. 2*b* is a superposition of spectra due to the triplet state of **12** (λ_{max} = 330 nm, plus a broad absorption centered at λ ~ 530 nm) and the monoradicals **18** (λ_{max} = 405 nm) and **19** (λ_{max} = 330, 545 nm), while that recorded at later times is due to **18** and **19** alone. The spectra of Fig. 2*a* can thus be assigned to mixtures of the triplet state of **5a** and biradical **20**, with the later spectrum consisting of a correspondingly greater proportion of biradical relative to triplet. The decays followed clean pseudo-first-order kinetics at all wavelengths between 300 and 700 nm, but exhibited different lifetimes and quenching behavior depending on the monitoring wavelength. Decays recorded above 600 nm exhibited a lifetime of ~280 ns and were quenched cleanly by CHD ($k_q = 7.5 \times 10^9$ M^{-1} s^{-1}), indicating them to be due to the triplet state of the ketone exclusively. Those recorded at 520 or 300 nm exhibited lifetimes of ~850 ns; the lifetime did not change upon addition of the diene, although the intensities of the absorptions appeared to decrease as the diene concentration was increased. This behavior suggests that the transient absorptions in the 300–550 nm region of the spectrum are mainly due to the biradical (**20**), which is formed by intramolecular hydrogen abstraction in the triplet state of the ketone. Oxygen quenched the lifetime of the transient absorptions throughout the complete range of the spectrum, with a rate constant $k_{O2} \sim 1 \times 10^9$ M^{-1} s^{-1}.



18 **19**



20

As expected, the triplet lifetime of **5a** (measured at 600 nm) varies with the concentration of the ketone. Figure 3 shows a plot of the triplet decay rate constant (τ_T^{-1}) vs. [**5a**] in deoxygenated acetonitrile solution at 25.0°C. The intercept of the plot affords the infinite dilution triplet lifetime (τ_T = 362 ± 16 ns) while the slope is the bimolecular rate constant for self-quenching of the triplet state of **5a** by the ground state ketone (k_{sq} = (2.2 ± 0.4) × 10^9 M^{-1} s^{-1}). The latter agrees quite well with the bimolecular rate constant for quenching of the triplet state of 3-methoxybenzophenone (**12**) by *meta*-cresol under similar conditions (Table 1).

The transient absorption spectrum obtained from 248 nm laser flash photolysis of **6a** under similar conditions is shown in Fig. 4. In this case, however, the spectrum changes imperceptibly (other than in intensity) with time, and there is no variation in lifetime (τ ~ 630 ns) throughout the wavelength range monitored. The lifetime of the absorption is shortened upon addition of oxygen ($k_{O2} \sim 1 \times 10^9$ M^{-1} s^{-1}), but addition of CHD resulted only in reductions in the initial transient absorbance (ΔOD_{max}) at each wavelength, to an extent that depends on the concentration of CHD added. This behavior indicates that the species is a product of the triplet state of the ketone, and we hence assign it to biradical **21**. As expected, the spectrum is similar to that of a mixture of the analogous monoradicals **18** and **22**, generated by 308 nm flash photolysis of **13** (0.001 M) and *meta*-cresol (0.0011 M) in acetonitrile (not shown).

© 2001 NRC Canada

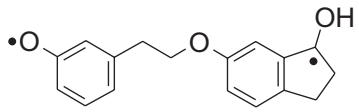
Table 1. Absolute rate constants for quenching of ketone triplets by *para*- and *meta*-cresol in acetonitrile (MeCN) and dichloromethane (DCM) at 23–25°C, in units of 1×10^9 M^{-1} s^{-1}.[a]

	k_q (MeCN)		k_q (DCM)	
Ketone	*para*-Cresol	*meta*-Cresol	*para*-Cresol	*meta*-Cresol
4-Methoxy acetophenone (**17**)	1.14 ± 0.09	0.71 ± 0.02[b]	5.51 ± 0.10	—
3-Methoxy acetophenone (**14**)	1.32 ± 0.04[b]	1.06 ± 0.05[b]	—	5.4 ± 0.3
4-Methoxy benzophenone (**16**)	1.17 ± 0.06[c,d]	0.96 ± 0.05[e]	6.5 ± 0.3	—
3-Methoxy benzophenone (**12**)	2.01 ± 0.15	1.66 ± 0.09	—	5.4 ± 0.2
5-Methoxy-1-indanone (**15**)	1.74 ± 0.13[c]	0.88 ± 0.09	7.1 ± 0.2	—
6-Methoxy-1-indanone (**13**)	2.18 ± 0.11	1.69 ± 0.05	—	5.3 ± 0.2

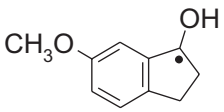
[a]Measured by 337 nm laser flash photolysis of 0.01–0.03 M solutions of the ketones in deoxygenated acetonitrile. In units of 1×10^9 M^{-1} s^{-1}.
[b]From ref. 18.
[c]From ref. 11.
[d]Measured at 27°C.
[e]Measured at 29°C.

Figure 5 shows a Stern–Volmer plot of the maximum signal intensities at 385 nm (ΔOD_{max}) obtained by flash photolysis of **6a** in the presence of CHD at various concentrations. The data were analyzed according to eq. [4], where $(\Delta OD_{max})_0$ is the value in the absence of diene, $(\Delta OD_{max})_{[Q]}$ is the value in the presence of diene at concentration [Q], k_q is the rate constant for quenching of the triplet state of the ketone by the diene, and τ_T is the ketone triplet lifetime. A triplet lifetime of $\tau_T = 53 \pm 5$ ns was obtained from the slope of the plot ($k_q\tau_T = 564 \pm 42$ M^{-1}), using a value of $k_q = 1.05 \times 10^{10}$ M^{-1} s^{-1}, the rate constant for bimolecular quenching of the triplet state of **13** by CHD in acetonitrile at 23°C.

[4] $$(\Delta OD_{max})_0/(OD_{max})_{[Q]} = 1 + k_q\tau_T[Q]$$



21



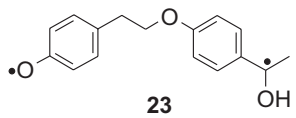
22

Addition of 0.028 M H_2O or D_2O to the acetonitrile solutions of **5a** and **6a** resulted in small changes in triplet lifetime (determined in the same fashion as described above) compared to those obtained in the dry solvent, but the lifetimes were slightly greater in D_2O–MeCN than in H_2O–MeCN. Table 2 lists the triplet lifetimes determined for **5**–**7** under the three sets of conditions, k_H/k_D values calculated from the lifetimes in wet acetonitrile, and the analogous data for **1**–**4** (11) for purposes of comparison.

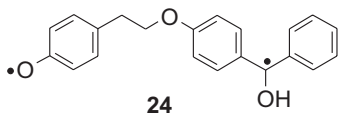
Laser flash photolysis of **1**–**7** in deoxygenated dichloromethane solution afforded similar results to those obtained in acetonitrile (see above and ref. 11), and triplet lifetimes were measured in analogous fashion in each case. Those of the non-phenolic ketones (**1b**–**6b**, **6c**, and **7**) and the phenolic compounds **4a** and **5a** were long enough that they could be measured directly, and so they were determined using the 248 nm laser and solutions containing ~2×10^{-4} M ketone. Doubling the concentration of ketone had no discernible effect on the lifetime of **5a** but did in the case of **4a**, so the infinite dilution lifetime was estimated from a plot of τ_T^{-1} vs. [**4a**], constructed from solutions of various concentrations up to ~0.002 M and using the 308 or 337 nm lasers for solutions of higher concentrations. The data afforded a value of $k_{sq} = (4.6 \pm 0.8) \times 10^9$ M^{-1} s^{-1} for the self-quenching rate constant and an infinite dilution triplet lifetime of $\tau_T = 1.6 \pm 0.3$ μs at 23°C.

Only biradical absorptions could be detected in the cases of **1a**–**3a** and **6a** in dichloromethane, as shown by the response of the signals to added oxygen and CHD. Thus, triplet lifetimes were determined either by Stern–Volmer quenching with CHD (**3a** and **6a**) or the 1-methylnaphthalene (MN) probe technique (20) (**1a** and **2a**) (21), with solutions containing ~0.01 M ketone and using the 337 nm laser for excitation. For example, Fig. 6 shows plots of ΔOD_{max} at 425 nm (the maximum in the triplet–triplet absorption spectrum of MN) vs. [MN] for **1a** and **3a**. The solid lines in the plots represent the best fit of the data to the expression of eq. [5], where *C* is a constant proportional to the pathlength, the extinction coefficient of the MN triplet–triplet absorption at 425 nm, the light intensity, and the intersystem crossing yield of the ketone triplet. Triplet lifetimes were calculated from the Stern–Volmer constants ($k_q\tau_T$) using a value of $k_q = (7.5 \pm 0.4) \times 10^9$ M^{-1} s^{-1} for the rate constant for ketone triplet quenching by MN, determined for ketones **16** and **17** under similar conditions. The dichloromethane data for **1**–**7** are listed in Table 2 along with those for acetonitrile solution. Table 3 lists the lifetimes of the phenoxyl-hemipinacol biradicals **20**, **21**, and **23**–**25** in the two solvents.

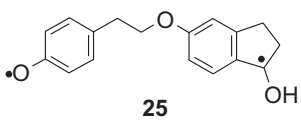
[5] $$\Delta OD_{max} = Ck_q\tau_T[MN]/(1 + k_q\tau_T[MN])$$



23



24



25

Discussion

From the transient spectra, isotope effects on the triplet lifetimes, and a comparison of the triplet lifetimes of the phenolic compounds **5a** and **6a** with those of their methoxy analogues **5b** and **6b**, it is clear that triplet state deactivation

© 2001 NRC Canada

Fig. 1. Transient absorption spectra from laser flash photolysis of deoxygenated ~1 × 10^{-4} M acetonitrile solutions of **5b** (*a*) and **6b** (*b*) at 25.0 ± 0.2°C. The inserts show decay traces monitored at 600 nm (**5b**) and 385 nm (**6b**).

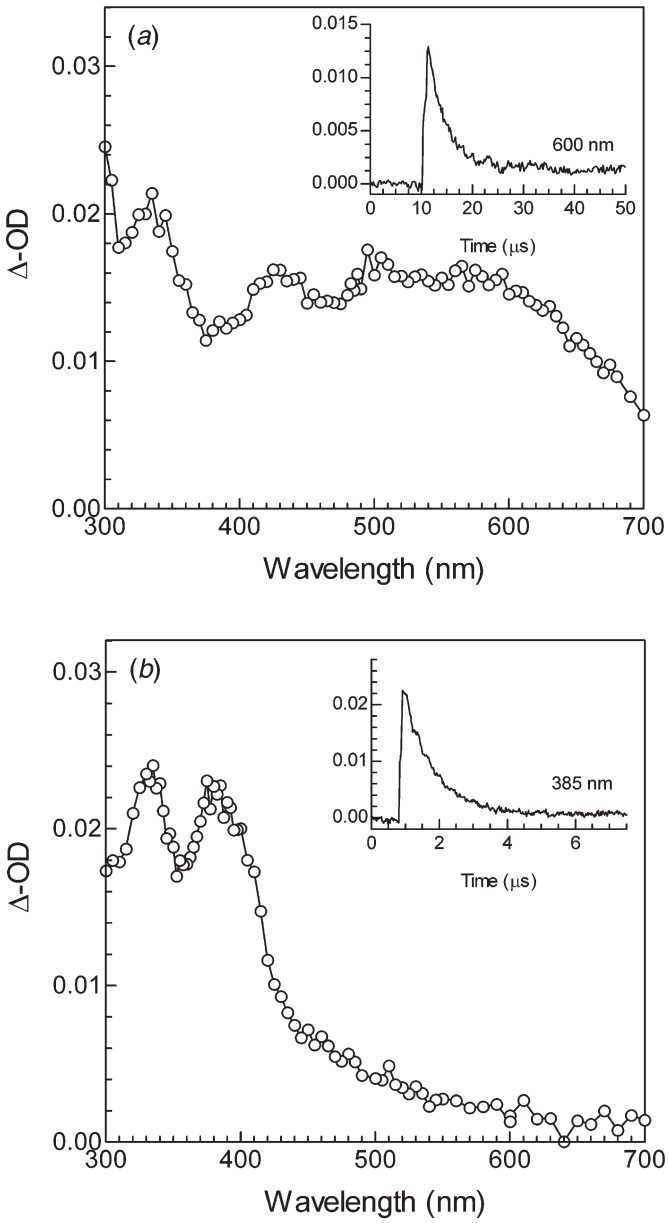
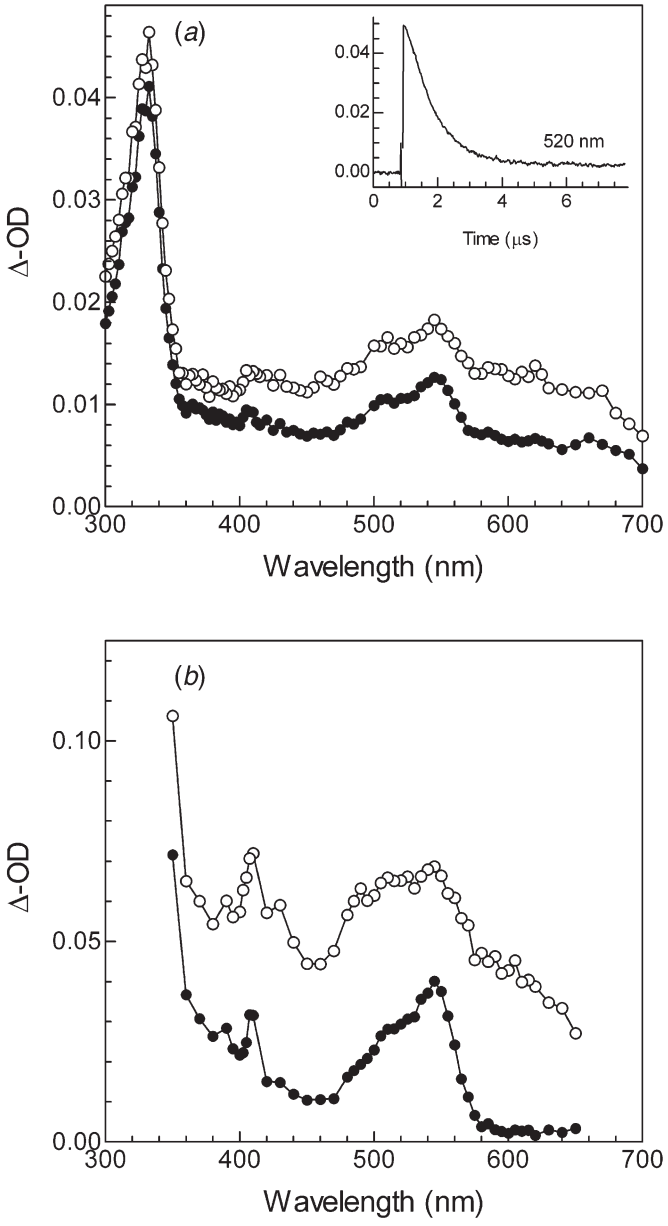


Fig. 2. (*a*) Transient absorption spectra from 248 nm laser flash photolysis of a deoxygenated 2 × 10^{-4} M solution of the phenolic ketone **5a** in dry acetonitrile solution at 25.0 ± 0.2°C, at the peak of the decay profile (○) and 0.5 to 1.0 μs later (●). The insert shows a typical decay trace, recorded at a monitoring wavelength of 520 nm. (*b*) Transient absorption spectra from 337 nm laser flash photolysis of an acetonitrile solution containing *meta*-methoxybenzophenone (**12**, 0.0076 M) and *meta*-cresol (0.0058 M) at 23.0 ± 0.2°C, 75–85 ns (○) and 4.0 to 4.3 μs (●) after the pulse.



in the two phenolic ketones is dominated by remote phenolic hydrogen atom abstraction, as we found previously for **1a**–**3a** (11). Both ketones exhibit significantly longer triplet lifetimes than their *para*,*para*′-positional isomers (**2a** and **3a**, respectively) in dry acetonitrile, but in contrast to the situation with the acetophenone derivatives **1a** and **4a** ($\tau_T^{4a}/\tau_T^{1a} \geq 500$) (18), the geometric dependence of the rates is much smaller in the benzophenone ($\tau_T^{5a}/\tau_T^{2a} \sim 18$) and indanone ($\tau_T^{6a}/\tau_T^{3a} \sim 2.5$) derivatives. As the data in Table 1 show, these differences are well beyond what might be expected on the basis of the (small) differences in the rate constants for the corresponding bimolecular hydrogen abstraction processes. The individual triplet lifetimes of the acetophenone and benzophenone derivatives are consistently shorter in dichloromethane than in acetonitrile solution, but the differences between *para*,*para*′- and *meta*,*meta*′-positional isomers follow the same trends in the two solvents; in dichloromethane at 23°C, the lifetime ratios are a $\tau_T^{4a}/\tau_T^{1a} \sim 800$, $\tau_T^{5a}/\tau_T^{2a} \sim 25$ for the acetophenone and benzophenone derivatives, respectively. In contrast, the corresponding lifetime ratio for for the indanone derivatives is inverted in dichloromethane relative to acetonitrile.

© 2001 NRC Canada

Fig. 3. Plot of k_{decay} vs. ketone concentration for the triplet state of **5a** in dry acetonitrile at 25°C, monitored at 600 nm.

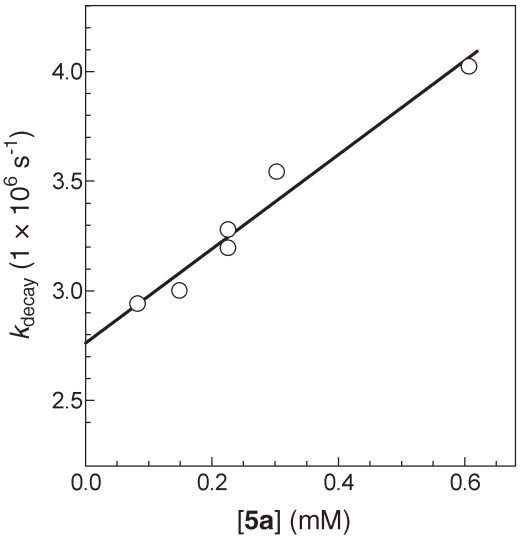
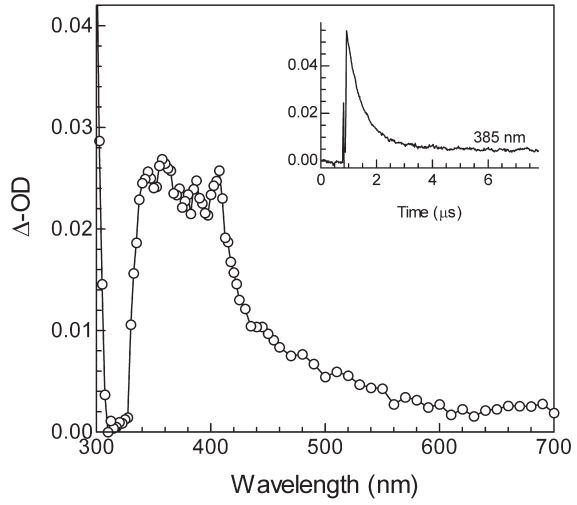
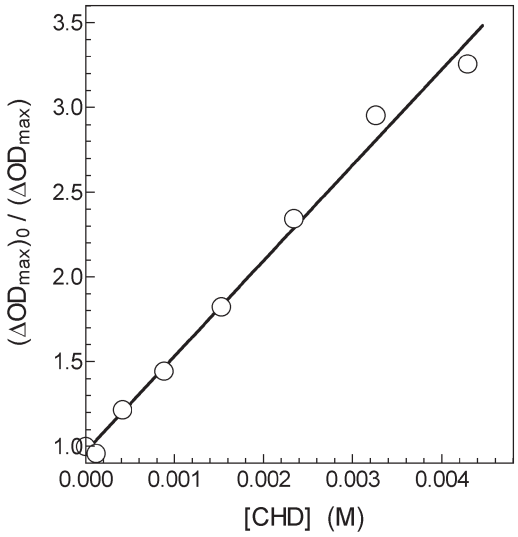


Fig. 4. Transient absorption spectrum from 248 nm laser flash photolysis of a deoxygenated 2 × 10^{-4} M solution of the phenolic ketone **6a** in dry acetonitrile solution at 23.0 ± 0.2°C, corresponding to the peak of the decay profile (ΔOD_{max}). The insert shows a typical decay trace recorded at a monitoring wavelength of 385 nm.



In principle, hydrogen abstraction from phenols might be expected to proceed by at least three distinct mechanisms depending on the configuration and electronic structure of the lowest triplet state of the ketone, and the redox potentials of the ketone and the phenol in the particular solvent of interest. Two of these are analogous to those proposed for the photoreduction of benzophenone and acetophenone derivatives by substituted toluenes (13): (*i*) sequential electron and (or) proton-transfer ("ET–PT") when electron transfer is sufficiently exergonic; (*ii*) when it is not, charge transfer assisted hydrogen abstraction (without prior hydrogen bonding), via an "*n*-type" exciplex for lowest *n*,π* triplet ketones ("*n*X–HT") or a "π-type" exciplex for lowest π,π* triplets. In the latter cases, charge transfer from the phenol to the triplet ketone should increase the acidity of the phenolic

Fig. 5. Stern–Volmer quenching of the initial yield (ΔOD_{max}) of the transient from 337 nm laser flash photolysis of ketone **6a** (0.0015 M) in dry acetonitrile in the presence of various concentrations of 1,3-cyclohexadiene (CHD), monitored at 385 nm (see eq. [4]).



hydrogen and the basicity of the carbonyl oxygen, effectively enhancing the rate of hydrogen transfer above what might be expected on the basis of a "pure" hydrogen abstraction model. The third possibility (*iii*) involves the intermediacy of a hydrogen-bonded, "π-type" triplet exciplex that collapses to radicals by coupled electron- and proton-transfer ("HBX–EPT"). Reaction by this mechanism should be favored in ketones with particularly basic lowest triplet states, and hence should be fastest in ketones with lowest charge-transfer π,π* triplet states. Reaction of *n*,π* ketone triplets by this mechanism presumably requires the involvement of the higher lying π,π* state, so will be fastest in those cases where the *n*,π*–π,π* triplet energy gap is small and the upper state is relatively basic. The three mechanistic possibilities are shown in Scheme 1.

The rate of reaction by any of these three mechanisms is expected to be sensitive to solvent polarity. It is well-known that reaction by the ET–PT (22, 23) and charge-transfer assisted (12, 13) mechanisms proceeds with enhanced rates as solvent polarity increases. In contrast, reaction by the HBX–EPT mechanism can be expected to be faster in solvents of low polarity, because hydrogen bonding is favored in nonpolar solvents. This leads to the conclusion that for the acetophenone and benzophenone chromophores, the triplet states of both isomers react via the HBX–EPT mechanism. This may also be true of the *meta*,*meta′*-phenolic indanone (**6a**), but the results for the *para*,*para′*-derivative (**3a**) are more consistent with a mechanism in which the phenolic hydrogen is activated toward abstraction by π-type charge transfer interactions between the aryl rings rather than by hydrogen-bonding.

The very slow rate of intramolecular hydrogen abstraction in **4a** compared to that in its *para*,*para′*-positional isomer **1a** has been proposed to result from a combination of conformational and orbital symmetry effects on the rate of electron/proton transfer within the hydrogen-bonded triplet

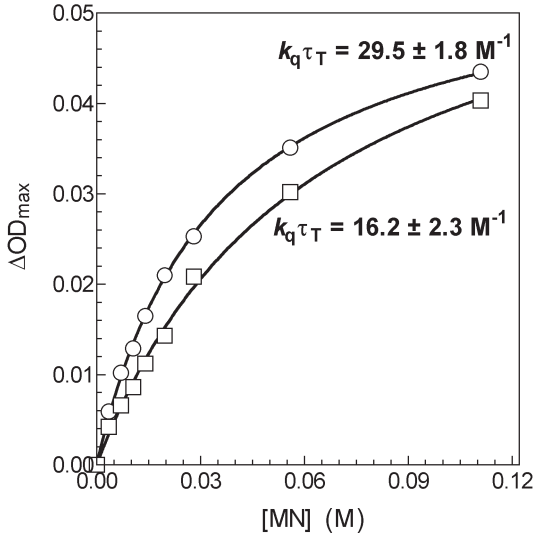
© 2001 NRC Canada

Table 2. Lifetimes (in ns) of carbonyl triplets in dry acetonitrile ([H_2O] ~ 1×10^{-4} M), in acetonitrile containing 0.028 M H_2O and 0.028 M D_2O, and in dichloromethane at 23–25°C.[a]

Compound	R	MeCN	Wet MeCN[b]	k_H/k_D[c]	CH_2Cl_2
1	H (a)	12 ± 2[d]	14 ± 2[d]	1.3 ± 0.2[d]	2.2 ± 0.3[e]
	Me (b)	3500 ± 200[d]	—	—	3110 ± 40
4	H (a)	11 500 ± 1800[f,g]	7900 ± 2300 [f,g]	1.2 ± 0.2[f]	1600 ± 300[g]
	Me (b)	8500 ± 800[f]	—	—	7040 ± 180
2	H (a)	19 ± 2[d]	14 ± 2[d]	1.4 ± 0.3[f]	3.9 ± 0.3[e]
	Me (b)	5000 ± 200[d]	—	—	6400 ± 110
5	H (a)	362 ± 17[g]	315 ± 8[g]	1.2 ± 0.2[f]	100 ± 3
	Me (b)	9800 ± 300	—	—	10 500 ± 400
3	H (a)	22 ± 2[d]	11 ± 1[d]	1.2 ± 0.2[f]	76 ± 16[h]
	Me (b)	281 ± 4[d]	—	—	445 ± 8
6	H (a)	53 ± 5[h]	56 ± 5[h]	1.4 ± 0.2[f]	38 ± 8[h]
	Me (b)	970 ± 20	—	—	1630 ± 30
7	—	1370 ± 20	—	—	1160 ± 20
6c	—	3190 ± 40	—	—	3660 ± 60

[a]Measured directly by 248 nm NLFP, using rigorously deoxygenated, 0.8–1.2 × 10^{-4} M solutions.
[b]0.028 M H_2O in MeCN.
[c]Ratio of lifetimes in acetonitrile containing 0.028 M D_2O and 0.028 M H_2O.
[d]Data from ref. 11.
[e]Determined using the 1-methylnaphthalene probe method (see Fig. 6).
[f]Data from ref. 18.
[g]At infinite dilution.
[h]Estimated from the $k_q\tau_T$ value for 1,3-cyclohexadiene quenching of biradical formation, obtained by 308 or 337 nm LFP of rigorously deoxygenate solutions, and using k_q values determined from quenching of model ketones (**12**–**17**) by 1,3-cyclohexadiene.

Fig. 6. Plot of transient ΔOD_{max} vs. 1-methylnaphthalene concentration for **1a** (□) and **3a** (○) in deoxygenated dichloromethane at 25.0 ± 0.2°C. The solid lines represent the least-squares fits to eq. [5].



exciplex (18). Intramolecular hydrogen bonding in the lowest triplet state of **1a** can only take place in a conformer in which the two aryl rings are arranged in a sandwich-like structure; this obviously represents a "good" quenching geometry because the triplet lifetime of the molecule is so short. On the other hand, there are a number of conformers accessible to the *meta*,*meta′*-isomer (**4a**) which would allow hydrogen bonding between the phenolic hydrogen and the carbonyl oxygen, but in which there is little or no overlap between the π-systems of the two aryl rings. These are calculated to be of considerably lower energy than the sandwich-like conformer analogous to that of **1a**, and hence should dominate the conformational equilibrium. This will lead to a much longer triplet lifetime if electron/proton transfer within these conformers is slow. Secondly, orbital overlap between the two phenyl rings in the (relatively high energy) sandwich-like exciplex conformer akin to **1a** is unfavorable, as a result of the nodal properties of the HOMO-1 and HOMO of the acceptor and donor, respectively. This can be expected to lead to a modest retardation of the rate of intramolecular electron transfer within the sandwich-like exciplex, relative to that in **1a** (24–30). At any rate, we consider the almost three-orders-of-magnitude difference between the triplet lifetimes of **4a** and **1a** to be a characteristic of intramolecular phenolic hydrogen abstraction by ketones tethered via *meta*,*meta′*- vs. *para*,*para′*-oxyethyl linkages, when the lowest triplet states are of the π,π* configuration and possess moderate charge transfer character.

Table 3. Lifetimes (in ns) of the phenoxyl-hemipinacol biradicals **20**, **21**, and **23**–**25** in dry acetonitrile ([H_2O] ~ 1×10^{-4} M) and in dichloromethane at 23–25°C.[a]

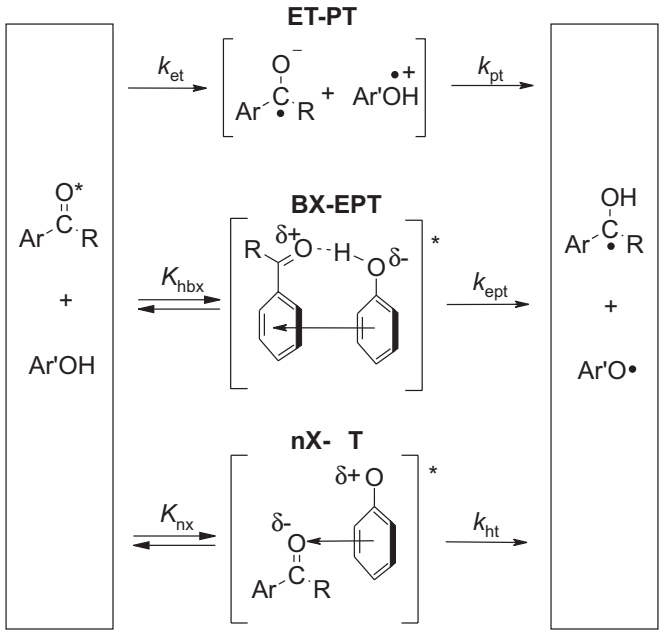
Biradical	MeCN	CH_2Cl_2
23	170 ± 20[b]	120 ± 15
24	285 ± 35[b]	360 ± 40
20	830 ± 90	450 ± 50
25	90 ± 10[b]	120 ± 20
21	630 ± 70	590 ± 60

[a]Measured directly by 248 nm NLFP, using rigorously deoxygenated, 0.8–1.2 × 10^{-4} M solutions.
[b]Data from ref. 11.

The triplet decay rates of the *para*,*para′*-phenolic benzophenone derivative (**2a**) and its acetophenone counterpart

© 2001 NRC Canada

Scheme 1.



(**1a**) correlate with the relative rates of bimolecular hydrogen abstraction from *para*-cresol by the corresponding model compounds, *para*-methoxybenzophenone (**16**) and *para*-methoxyacetophenone (**17**), respectively. The slower rates of inter- and intramolecular reaction of the 4-alkoxybenzophenone derivatives compared to the 4-alkoxyacetophenones are suggested to be due to the fact that the former have lowest n,π^* triplet states, and are intrinsically less reactive than lowest π,π^* triplets of comparable reduction potential. As mentioned above, it is thought that they react as fast as they do because the lowest triplet state has some π,π^* character, the amount of which increases as the energy separation between the zero-order n,π^* and π,π^* states decreases. If this is true, then on the basis of the relative reactivities of **1a** and **4a**, one would expect the rate of intramolecular hydrogen abstraction in the *meta*,*meta′*-phenolic benzophenone **5a** to be significantly slower than in the *para*,*para′*-isomer **2a**, in agreement with the observed results.

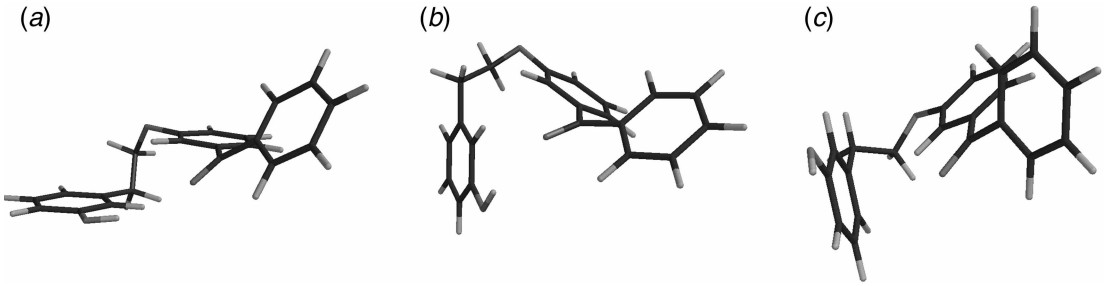
The rate deceleration caused by the *meta*,*meta′*-linkage in **5a** is at least an order of magnitude less pronounced than in the acetophenone series (**1a** and **4a**), however. The reason for this may be related to the fact that unlike the case with the acetophenone and indanone compounds, the bimolecular reactivity of the *meta*,*meta′*-pair (as defined by the rate of quenching of **12** by *meta*-cresol, see Table 1) is significantly *higher* than that of the *para*,*para′*-pair (i.e., **16** + *para*-cresol). This may be the result of the net electron-withdrawing character of the *meta*-alkoxy substituent, which places **12** (and **5a**) within the group of n,π^* benzophenone triplets in which the *n*X–HT mechanism is thought to be the predominant quenching pathway (11). In fact, molecular models indicate that the *meta*,*meta′*-linkage allows the facile formation of conformers in which the *n*-orbital of the carbonyl oxygen is directed into the π-system of the remote phenolic group. This is illustrated in Fig. 7, which shows three of the possible quenching conformers available to **5a**: a displaced face-to-face conformer (*a*); a face-to-face conformer (*b*); and an *n*-type exciplex conformer (*c*). While the solvent effect on τ_T (Table 2) suggests that the *main* quenching mechanism in **5a** is the same as in the *para*,*para′*-analogue **2a** (i.e., the HBX–EPT pathway), it is possible that quenching via the *n*X–HT mechanism competes to a small extent, resulting in somewhat higher reactivity than would be expected on the basis of the behavior of the *meta*,*meta′*-acetophenone derivative **4a**. Quenching via the *n*X–HT mechanism is geometrically impossible in the *para*,*para′*-analogue.

Even smaller differences in reactivity are observed for the *para*,*para′*- and *meta*,*meta′*-indanone derivatives (**3a** and **6a**), in spite of the fact that like **1a** and **4a**, both possess lowest π,π^* triplet states. The reason for this most likely originates in the coplanar arrangement of the carbonyl group and its associated aryl ring that is enforced by the benzannelated C-5 ring in these compounds. This results in a greater degree of charge-transfer in the π,π^* triplet state, which should have the effect of increasing its basicity. Thus, in the absence of geometric constraints, the rate of phenolic hydrogen abstraction should be higher than in the corresponding acetophenone derivatives if the quenching proceeds via the hydrogen-bonded exciplex mechanism. Indeed, the rate constants for bimolecular phenolic hydrogen abstraction by the model compounds **13** and **15** are significantly higher than those for the analogous acetophenone derivatives **14** and **17**, respectively, (see Table 1). In spite of this, intramolecular abstraction in the *para*,*para′*-derivative **3a** is significantly slower than in the acetophenone **1a**, a result which has been attributed to the less than optimal geometry for intramolecular hydrogen bonding that is enforced at the carbonyl group by the benzannelated C-5 ring. The fact that the triplet lifetime of **3a** is increased in dichloromethane relative to acetonitrile suggests that this explanation is correct, and hydrogen bonding is indeed not involved in the dominant quenching mechanism for this compound. This problem should be much less severe in **6a**, because the *meta*,*meta′*-linkage allows hydrogen bonding between the carbonyl and the remote phenolic group to occur with much greater facility than in the *para*,*para′*-derivatives.

Also relevant to this discussion are the unusually short triplet lifetimes of the anisyl derivatives of these two ketones, which indicates that they possess a route for nonproductive intramolecular triplet deactivation that is not present to the same extent in the corresponding acetophenone and benzophenone derivatives. For example, the triplet lifetimes of **3b** (τ_T = 280 ns) and **6b** (τ_T = 970 ns) in deoxygenated acetonitrile are more than an order of magnitude shorter than those of **15** and **13** under the same conditions (τ_T > 10 μs), while those of the phenyl-derivatives **7** (τ_T = 1.4 μs) and **6c** (τ_T = 3.2 μs) are intermediate between these extremes. These effects appear to be strictly confined to the intramolecular systems, since the bimolecular rate constants for 1,4-dimethoxybenzene quenching of the triplet states of **15** ($k_q = (4.8 \pm 0.8) \times 10^7$ M^{-1} s^{-1}) and **13** ($k_q = (1.8 \pm 0.4) \times 10^7$ M^{-1} s^{-1}) in acetonitrile are nearly identical to the corresponding values for the acetophenone homologues **17** ($k_q = (4.4 \pm 0.4) \times 10^7$ M^{-1} s^{-1}) and

© 2001 NRC Canada

Fig. 7. Potential quenching geometries for **5a**: (*a*) lowest energy H-bonded conformer; (*b*) sandwich-like H-bonded conformer; (*c*) *n*-type exciplex conformer.



14 (k_q = (2.2 ± 0.2) × 10^7 M^{-1} s^{-1}), respectively, under the same conditions.[2] A charge transfer quenching mechanism, presumably via the π-type triplet exciplex pathway first suggested by Singer and co-workers (31), is suggested by the fact that the triplet lifetimes of the four compounds are longer in the less polar solvent dichloromethane. Certainly, (endothermic) triplet energy transfer can most likely be ruled out as a possibility. We suspect that the reason for the enhanced intramolecular charge transfer quenching in the indanone series compared to the acetophenones may be related to exciplex structure; the results suggest that the optimum exciplex geometry for charge transfer between the aroyl and the donor aryl rings is somewhat different in the indanones than in the acetophenones, with that in the former being more compatible with the orientational constraints placed on the molecules by the oxyethyl tether in the intramolecular systems. In any event, the solvent effects on the triplet lifetimes of **3a** and **6a** suggest that this mechanism dominates over the hydrogen-bonded exciplex mechanism in **3a** (in which geometric factors prevent in-plane bonding between the carbonyl oxygen and the phenolic hydrogen); but only competes with it in **6a**, where these constraints are relaxed.

Summary and conclusions

The intriguing geometry dependence on the rate constants for remote phenolic hydrogen abstraction in the π,π* triplet states of the *para*,*para′*- and *meta*,*meta′*-oxyethyl linked phenolic ketones **1a** and **4a** has been investigated in the corresponding benzophenone (*n*,π* lowest triplet) and indanone (CT–π,π* lowest triplet) homologues. Solvent effects on the triplet lifetimes suggest that all ketones in the series but one react mainly via a hydrogen-bonded triplet exciplex, which collapses to the corresponding biradical by coupled electron and (or) proton transfer.

The new compounds exhibit similar structural dependences on intramolecular reactivity as observed for the acetophenone derivatives **1a** and **4a**, but the differences between *meta*,*meta′*- and *para*,*para′*-positional isomers are an order of magnitude smaller for the benzophenone derivatives (**2a** and **5a**), and two orders of magnitude smaller for the indanones (**3a** and **6a**). In the benzophenone case, the higher than expected reactivity of the *meta*,*meta′*-isomer may be due to competing reaction via the *n*-type exciplex (*n*X–HT) mechanism analogous to that involved in the quenching of benzophenone *n*,π* triplets by substituted toluenes. The even higher relative reactivity of the *meta*,*meta′*-indanone derivative is proposed to be due to more facile charge transfer between the two aryl rings in the hydrogen-bonded exciplex associated with this compound. In the *para*,*para′*-isomer, on the other hand, a relatively poor geometry for intramolecular hydrogen bonding is enforced by the benzannelated C-5 ring, which prevents the remote O—H bond from adopting a coplanar arrangement with the carbonyl group. As a result, hydrogen abstraction is initiated by a simple charge transfer interaction between the electron-rich phenolic ring and the indanone moiety, which increases the acidity of the phenolic hydrogen and activates its transfer. Supporting evidence for this conclusion is derived from the behavior of analogues bearing remote anisyl groups, which exhibit significantly shorter triplet lifetimes than do the corresponding anisyl-substituted acetophenone derivatives.

Future work in this area will further address the factors responsible for the substantial structural dependence on the rates of intramolecular phenolic hydrogen abstraction in acetophenone derivatives, and explore the mechanisms of the bimolecular process in aromatic ketones of various structure.

Experimental

^{1}H and ^{13}C NMR spectra were recorded on Bruker AC200 (200 MHz) or AC300 (300 MHz) spectrometers in deuterated solvents, and are reported in ppm downfield from tetramethylsilane. Ultraviolet absorption spectra were recorded on Cary 50 or Cary 300 UV–vis spectrophotometers. Mass spectra and exact masses were recorded on a VG Analytical ZABE mass spectrometer employing a mass of 12.000000 for carbon. Infrared spectra were recorded on a Biorad FTS-40 FT IR spectrometer. Melting points were determined on a polarizing microscope fitted with a Mettler hot stage and Mettler FP80 processor, and are not corrected. Gas chromatographic analyses employed a Hewlett-Packard 5890 Series 2 gas chromatograph equipped with a flame ionization detector, a Hewlett-Packard 3396A recording integrator, and a 15 m × 0.53 mm DB-17A or 5 m × 0.53 mm HP-1 column (Chromatographic Specialties, Inc.). Radial chromatography was carried out using a Chromatotron® (Harrison Research) with 4 mm silica gel 60 (EM Science) thick-layer plates. Elemental analyses were carried out by Guelph Chemical Laboratories, Inc.

Acetone (Caledon Reagent) was dried over anhydrous potassium carbonate and freshly distilled before use, hexanes

[2] E.C. Lathioor, and W.J. Leigh. Unpublished results.

© 2001 NRC Canada

(Caledon Reagent) were distilled, acetonitrile (Caledon reagent) was distilled from calcium hydride and passed repeatedly through activated Brockmann alumina (Aldrich), and pyridine (Fisher Reagent) was distilled from barium oxide. All other solvents were reagent grade and were used as received from the suppliers (Caledon or Fisher).

meta-Cresol (Caledon) and 3-hydroxybenzophenone (Aldrich) were used as received, while 1,3-cyclohexadiene (Aldrich) was bulb-to-bulb distilled and stored at –20°C under argon. 6-Hydroxy-1-indanone was prepared by demethylating 6-methoxy-1-indanone (Aldrich) with $AlCl_3$ as described by Miyake et al. (32), followed by recrystallization from water. 3-Methoxybenzophenone was prepared by Friedel–Crafts acylation of benzene with *meta*-anisoyl chloride, and purified by silica gel chromatography. 1-Bromo-2-(3-methoxyphenyl)ethane and 1-tosyloxy-2-(3-tosyloxyphenyl)ethane were prepared as previously described (18).

3-[2-(3-Hydroxyphenyl)ethoxy]benzophenone (5a)

To a 100 mL round-bottom flask attached to a reflux condenser and equipped with a magnetic stir bar was added anhydrous acetone (50 mL), 3-hydroxybenzophenone (1 g, 0.005 mol), 1-tosyloxy-2-(3-tosyloxyphenyl)ethane (4.50 g, 0.011 mol), and anhydrous potassium carbonate (0.87 g, 0.006 mol). The mixture was refluxed for 72 h, after which it was stripped of solvent on the rotary evaporator, acidified with dilute HCl until gas evolution ceased, and then taken up in ethyl acetate (50 mL). The orange-colored organic phase was then washed with water (2 × 50 mL) and saturated brine (50 mL), dried with anhydrous magnesium sulfate, filtered, and concentrated under reduced pressure. The crude tosylate ester was hydrolyzed by dissolving in methanol (100 mL) containing potassium carbonate (10 g, 0.07 mol) and refluxing for 80 h. Work-up as before yielded 2.54 g of a light brown oil consisting of a mixture of the desired product with minor amounts of 3-hydroxystyrene. Purification by radial chromatography (30% ethyl acetate in hexanes as eluant), followed by column chromatography (3% ether in dichloromethane with 10 drops acetic acid/100 mL as eluant) yielded a colorless oil (1.2 g, 0.0040 mol, 80%) which was identified as **5a** on the basis of the following data. MS (*m*/*e*) (I): 318 (10), 199 (3), 121 (100), 105 (23), 91 (16), 77 (45), 65 (8), 51(8). HRMS calcd. for $C_{21}H_{18}O_3$: 318.12564; found: 318.125592. UV λ_{max} (MeCN) (nm): 220 (ε 27 600 M^{-1} cm^{-1}), sh. 253, 307. IR (KBr, cm^{-1}): 3413 (br m), 3064 (w), 2934 (w), 2875 (w), 1716 (s), 1661 (s), 1594 (s), 1489 (w), 1451 (m), 1363 (m), 1287 (s), 1224 (s), 1161 (w), 1039 (w), 876 (w), 787 (w), 728 (m), 708 (m), 535 (w). ^{1}H NMR ($CDCl_3$) δ: 3.00 (t, *J* = 7 Hz, 2H), 4.14 (t, *J* = 7 Hz, 2H), 6.2 (s, 1H), 6.7–6.85 (m, 3H), 7.1–7.2 (m, 2H), 7.3–7.6 (m, 6H), 7.79 (d, *J* = 8 Hz, 2H). ^{13}C NMR ($CDCl_3$) δ: 35.4, 68.6, 113.6, 115.0, 116.0, 119.6, 121.1, 123.0, 128.3, 129.2, 129.6, 130.1, 132.6, 137.3, 138.6, 139.7, 155.9, 158.7, 197.2. Anal. calcd. for $C_{21}H_{18}O_3$: C 79.22, H 5.70; found: C 79.52, H 5.85.

6-[2-(3-Hydroxyphenyl)ethoxy]-1-indanone (6a)

To a 100 mL round-bottom flask attached to a reflux condenser and equipped with a magnetic stir bar was added anhydrous acetone (50 mL), 6-hydroxy-1-indanone (0.68 g, 0.00459 mol), anhydrous potassium carbonate (1.42 g, 0.0103 mol), and 1-tosyloxy-2-(3-tosyloxyphenyl)ethane (2.24 g, 0.00510 mol). The mixture was refluxed with stirring for 10 h, additional quantities of potassium carbonate (0.71 g, 0.005 mol) and the ditosylate (1.02 g, 0.0023 mol) were added, and the reflux continued for a further 60 h. The reaction mixture was stripped of solvent on the rotary evaporator and then acidified with dilute HCl until gas evolution ceased. The aqueous mixture was extracted with ethyl acetate (50 mL), which caused the formation of an emulsion that was clarified with the addition of brine (25 mL). The orange-colored organic phase was washed with water (2 × 80 mL) and saturated brine (100 mL), dried with anhydrous magnesium sulfate, filtered, and concentrated under reduced pressure. The mixture was then taken up in methanol (25 mL), potassium carbonate (5.0 g, 0.04 mol) was added, and the resulting solution was refluxed for 48 h. Work-up as above yielded a deep brown oil (1.76 g). Column chromatography on silica gel with chloroform as eluant yielded compound **6a** (0.34 g, 0.0013 mol, 30%) as light yellow crystals, which were recrystallized from chloroform–cyclohexane with 1% methanol (mp 135.5 to 136.0°C) and identified on the basis of the following data. MS (*m*/*e*) (I): 268 (25), 121 (100), 103 (31), 91 (39), 77 (44), 65 (12). HRMS calcd. for $C_{17}H_{16}O_3$: 268.1072; found: 268.1099. UV λ_{max} (MeCN) (nm): 219 (ε 32 650 M^{-1} cm^{-1}) 244 (sh), 275, 280, 317. IR (KBr, cm^{-1}): 3417 (br m), 3278 (w), 3051 (w), 3009 (w), 2938 (w), 1716 (s), 1690 (m), 1623 (w), 1590 (w), 1493 (w0, 1364 (m), 1287 (m), 1224 (m), 1161 (w), 1090 (w), 1040 (w), 951 (w), 838 (w), 703 (w), 527 (w). ^{1}H NMR (CD_3CN) δ: 2.60–2.64 (m, 3H), 2.97–3.06 (m, 4H), 4.22 (t, *J* = 7 Hz, 2H), 6.65–6.70 (m, 1H), 6.8 (m, 2H), 7.08–7.2 (m, 2H), 7.41 (d, *J* = 8 Hz, 1H), 7.74 (d, *J* = 3 Hz, 1H). ^{13}C NMR (CD_3CN) δ: 25.4, 35.9, 37.3, 69.6, 95.0 106.5, 114.0, 116.6, 121.0, 124.2, 128.4, 130.1, 139.0, 140.9, 148.7, 158.0, 159.3. Anal. calcd. for $C_{17}H_{16}O_3$: C 76.10, H 6.01; found: C 75.50, H 6.07.

3-[2-(3-Methoxyphenyl)ethoxy]benzophenone (5b)

A mixture of 3-hydroxybenzophenone (2.50 g, 0.0126 mol), 1-bromo-2-(3-methoxyphenyl)ethane (4.79 g, 0.0223 mol), and anhydrous potassium carbonate (1.74 g, 0.013 mol) were combined in acetone (20 mL), and stirred under reflux for 16 h. A second portion of potassium carbonate (0.50 g, 0.0036 mol) was added, and the mixture was refluxed for a further 4 days. The reaction was still not complete, so additional potassium carbonate (0.025 g, 0.0018 mol) and bromide (2.02 g, 0.009 mol) were added and reflux was continued for another 5 days. The ^{1}H NMR spectrum of a portion of the reaction mixture (after work-up as described below) indicated only 80% consumption of the 3-hydroxybenzophenone starting material, so an additional portion of bromide (1.09 g, 0.005 mol) was added and the mixture was refluxed for a further 3 days. The reaction mixture was cooled, and then taken up in a mixture of 1:1 ether:ethyl acetate (50 mL) and water (50 mL). The layers were separated, the aqueous portion was acidified with 3 M HCl, and extracted with ether (50 mL) and ethyl acetate (2 × 25 mL). The combined organic layers were washed with water (200 mL), 5% aq sodium bicarbonate (100 mL) and brine (100 mL), dried over anhydrous magnesium sulfate, and fil-

© 2001 NRC Canada

tered. Removal of the organic solvents on the rotary evaporator yielded an orange-brown oil, which was purified by silica gel column chromatography using 1:1 hexane:dichloromethane as eluant to yield a yellow oil (2.73 g, 0.008 mol, 65%). The compound was identified as **5b** on the basis of the following data. MS (*m*/*e*) (I): 332(10), 135(100), 120(7), 105(56), 91(28), 77(68), 65(12), 51(16). HRMS calcd. for $C_{22}H_{20}O_3$: 332.1413; found: 332.1413. UV λ_{max} (MeCN) (nm): 220 nm) (ε 28 300 M^{-1} cm^{-1}), sh. 252, 305. IR (KBr, cm^{-1}): 3060 (w), 2939 (w), 2835 (w), 1658 (m), 1596 (m), 1488 (m), 1438 (m), 1281 (s), 1164 (m), 1043 (s), 971 (w), 872 (w), 781 (s), 724 (s). ^{1}H NMR ($CDCl_3$) δ: 3.07 (t, 2H, *J* = 7 Hz), 3.77 (s, 3H), 4.20 (t, 2H, *J* = 7 Hz), 6.75–6.86 (m, 3H), 7.08–7.12 (m, 1H), 7.20 (d, 1H, *J* = 8 Hz), 7.31–7.35 (m, 3H), 7.42–7.47 (m, 2H), 7.53–7.58 (m, 1H), 7.76–7.79 (m, 2H). ^{13}C NMR ($CDCl_3$) δ: 35.6, 55.0, 68.6, 111.7, 114.7, 115.0, 119.2, 121.2, 122.7, 128.1, 129.1, 129.4, 129.9, 132.3, 137.7, 138.7, 139.5, 158.6, 159.6, 196.3. Anal. calcd. for $C_{20}H_{22}O_3$: C 79.50, H 6.06; found: C 79.90, H 5.93.

6-[2-(3-Methoxyphenyl)ethoxy]-1-indanone (6b)

To a 25 mL round-bottom flask fitted with a condenser, nitrogen inlet, and magnetic stirrer was added anhydrous potassium carbonate (0.47 g, 0.0034 mol), acetone (10 mL), 6-hydroxy-1-indanone (0.46 g, 0.0034 mol), and 1-bromo-2-(3-methoxyphenyl)ethane (1.51 g, 0.007 mol). The mixture was refluxed under a nitrogen atmosphere for 10 days, with periodic monitoring by TLC. Additional quantities of acetone (10 mL) and potassium carbonate (0.50 g) were added, and the mixture was then refluxed for a further 5 days. The mixture was filtered and the solvent was removed on the rotary evaporator to yield a red oil, which was taken up in ether (50 mL) and 2% aq HCl (50 mL). The layers were separated, and the aqueous fraction was extracted with ether (2 × 50 mL). The organic fractions were combined, washed with water (100 mL) and brine (100 mL), dried with anhydrous magnesium sulfate, and filtered. Removal of the ether under reduced pressure yielded an orange oil (1.4 g), which was purified by column chromatography using 10% ethyl acetate in hexanes as eluant, followed immediately by column chromatography using chloroform as an eluant. The product was obtained as a yellow oil (0.47 g, 0.0016 mol, 53%), which was identified as **6b** on the basis of the following data. ^{1}H NMR ($CDCl_3$) δ 2.61 (m, 2H), 3.00 (m, 4H), 3.71 (s, 3H), 4.12 (t, *J* = 7 Hz, 2H), 6.65–6.72 (m, 1H), 6.8 (m, 2H), 7.08–7.2 (m, 3H), 7.22 (d, *J* = 8 Hz, 1H), 7.74 (d, *J* = 3 Hz, 1H). ^{13}C NMR ($CDCl_3$) δ: 25.1, 35.6, 37.0, 68.9, 105.9, 111.9, 114.8, 121.3, 124.3, 127.4, 128.3, 129.5, 138.2, 139.6, 148.0, 158.6, 159.8, 206.9. UV λ_{max} (MeCN) (nm): 218 (ε 29 250 M^{-1} cm^{-1}), sh. 243, 272, 279, 315. IR (KBr, cm^{-1}): 3005 (w), 2925 (w), 2837 (w), 1711 (s), 1613 (w), 1492 (m), 1446 (w), 1296 (m), 1275 (m), 1222 (m), 1168 (w), 1155 (w), 1040 (m), 837 (w), 785 (w), 697 (w), 558 (w), 530 (w). MS (*m*/*e*) (I): 282 (18), 135 (100), 120 (8), 105 (25), 91 (30), 67 (27), 65 (22), 51 (12), 43 (33). HRMS calcd. for $C_{18}H_{18}O_3$: 282.1256; found: 282.1256. Anal. calcd. for $C_{18}H_{18}O_3$: C 76.57, H 6.43; found: C 76.74, H 6.61.

6-[2-(Phenyl)ethoxy]-1-indanone (6c)

To an oven-dried 100-mL round-bottom flask equipped with magnetic stirrer, reflux condenser, and nitrogen inlet was added freshly distilled acetone (50 mL), 1-tosyloxy-2-phenylethane (0.50 g, 0.0018 mol), anhydrous potassium carbonate (0.28 g, 0.002 mol), and 6-hydroxy-1-indanone (0.24 g, 0.0016 mol). The mixture was then refluxed under nitrogen for 48 h. The dark brown mixture was stripped of solvent to leave a grey-brown residue, which was acidified by the addition of 0.4 M H_2SO_4 (20 mL) and concd HCl (1 mL), and then extracted with a mixture of ether (50 mL) and benzene (5 mL). The resulting bright yellow organic phase was washed with 10% aq NaOH (30 mL), water (30 mL), and brine (30 mL), and then dried with anhydrous magnesium sulfate. The solvent was removed under reduced pressure to yield an orange semisolid (0.44 g), which was recrystallized from methanol to yield yellow needles (mp 69.0–71°C; 0.26 g, 0.001 mol, 64%). The compound was identified as **6c** on the basis of the following data. MS (*m*/*e*) (I): 252 (10), 105 (100), 91 (13), 79 (20), 77 (23), 65 (7), 51 (10). HRMS calcd. for $C_{17}H_{16}O_2$: 252.115028; found: 252.115080. UV λ_{max} (MeCN): 205 (ε 24 555 M^{-1} cm^{-1}), 213 (ε 24 691 M^{-1} cm^{-1}), 244 (ε 8200 M^{-1} cm^{-1}), 316 (ε 3600 M^{-1} cm^{-1}). IR (KBr, cm^{-1}): 3061 (vw), 2948 (w), 2918 (w), 1705 (vs), 1620 (w), 1491, 1447, 1297, 1254, 1226, 1196 (w), 1170 (w), 1018, 918 (vw), 835, 720, 696. ^{1}H NMR ($CDCl_3$) δ: 2.65 (t, 2H, *J* = 6 Hz), 2.98–3.09 (m, 5H), 4.15 (t, 2H, *J* = 7 Hz), 7.09–7.32 (m, 8H). ^{13}C NMR ($CDCl_3$) δ : 25.3, 35.7, 37.1, 69.2, 106.1, 124.5, 126.7, 127.5, 128.7, 129.1, 138.2, 138.4, 148.1, 158.7, 207.0. Anal. calcd. for $C_{17}H_{16}O_2$: C 80.93, H 6.39; found: C 80.64, H 6.59.

5-[2-(Phenyl)ethoxy]-1-indanone (7)

This compound was prepared in analogous fashion to **6c**, from 1-tosyloxy-2-phenylethane (1.16 g, 0.0042 mol), 5-hydroxy-1-indanone (0.61 g, 0.0041 mol), and anhydrous potassium carbonate (0.70 g, 0.005 mol) in dry acetone (50 mL). After refluxing under nitrogen for 5 days, the reaction mixture was worked up as above to yield an orange solid (1.09 g), which was recrystallized from methanol to yield a pale yellow powder (mp 79 to 79.5°C; 0.48 g, 0.0019 mol, 46%). The compound was identified as **7** on the basis of the following data. ^{1}H NMR ($CDCl_3$) δ: 2.59 (t, 2H, *J* = 6 Hz), 2.99 (t, 2H, *J* = 6 Hz), 3.06 (t, 2H, *J* = 7 Hz), 4.18 (t, 2H, *J* = 7 Hz), 6.83 (d, 2H, *J* = 6 Hz), 7.18–7.27 (m, 5H), 7.61 (d, 1H, *J* = 9 Hz). ^{13}C NMR ($CDCl_3$) δ: 26.0, 35.7, 36.5, 69.2, 110.6, 115.7, 125.5, 126.8, 128.7, 129.1, 130.6, 137.9, 158.1, 164.6, 205.2. UV λ_{max} (MeCN): 200 (ε 24 500 M^{-1} cm^{-1}), 220 (ε 17 000 M^{-1} cm^{-1}), 264 (ε 17 800 M^{-1} cm^{-1}), 287 (ε 10 000 M^{-1} cm^{-1}), 295 (ε 10 000 M^{-1} cm^{-1}). IR (KBr, cm^{-1}): 3060 (vw), 3039 (vw), 2938 (w), 2908(w), 1702 (vs), 1593 (s), 1489, 1460, 1440, 1303, 1255 (vs), 1140, 1089, 1013, 855, 835, 806, 760, 708, 643 (w), 588, 535 (vw). MS (*m*/*e*) (I): 252 (17), 105 (100), 91 (15), 79 (25), 77 (33), 65 (11), 51 (13). HRMS calcd. for $C_{17}H_{16}O_2$: 252.115028; found: 252.110220. Anal. calcd. for $C_{17}H_{16}O_2$: C 80.93, H 6.39; found: C 81.09, H 6.52.

Nanosecond laser flash photolysis experiments employed the pulses from a Lumonics TE-861M excimer laser filled

© 2001 NRC Canada

with Xe–HCl–H_2He (308 nm, 15 ns, ca. 40 mJ) or N_2–He (337 nm, 6 ns, ca. 4 mJ), a Lumonics 510 excimer laser filled with Kr–F_2–He (248 nm, 20 ns, ca. 60 mJ), or a Lambda Physik Compex 120 filled with Kr–F_2–Ne (248 nm, 25 ns, 100–140 mJ), and a computer-controlled detection system which has been described elsewhere (17, 19). All samples were contained in 3 × 7 mm or 7 × 7 mm Suprasil quartz cells which were sealed with rubber septa. Substrate concentrations were adjusted to yield an absorbance between 0.2 and 0.9 at the excitation wavelength. Each solution was deoxygenated with dry nitrogen or argon until constant lifetimes were achieved. Quenchers were added as aliquots of standard solutions.

Phosphorescence emission spectra were determined with either a PerkinElmer LS-5 or Photon Technologies LS-100 spectrofluorimeter. Sample concentrations were ~1 mg mL^{-1} and were contained in 2-mm i.d. Suprasil quartz tubes that were sealed with rubber septa and deoxygenated with dry nitrogen.

Steady-state irradiations were performed in a Rayonet Reactor (New England Ultraviolet Co.) using RPR-300 lamps and a merry-go-round apparatus. Samples were contained in 3-mm i.d. quartz tubes sealed with rubber septa, and were deoxygenated with nitrogen. Progress of the photolyses was monitored periodically by GC using the disappearance of **1a** as an actinometer. Hexadecane was employed as an internal standard.

Semiempirical (AM1) calculations were carried out using Spartan™ 5.0.3 (Wavefunction, Inc.) on a dual-processor Silicon Graphics Octane workstation. The (ground state) hydrogen-bonded conformers of Figs. 7*a*, 7*b* (ΔH_f = –39.61 and –40.19 kcal mol^{-1}, respectively) were minimized with the OH—OC distance constrained at 2.60 Å, while the *n*-type exciplex conformer of Fig. 7*c* (ΔH_f = – 36.50 kcal mol^{-1}) was minimized with a constrained distance of 3.60 Å between the carbonyl oxygen and the *ortho*- (with respect to the linker group) carbons of the remote phenolic ring.

Acknowledgements

We thank the Natural Sciences and Engineering Research Council of Canada (NSERC) for financial support of this work.

References

1. N.J. Turro and R. Engel. J. Am. Chem. Soc. **91**, 7113 (1969).
2. N.J. Turro and T.J. Lee. Mol. Photochem. **2**, 185 (1970).
3. P.K. Das, M.V. Encinas, and J.C. Scaiano. J. Am. Chem. Soc. **103**, 4154 (1981).
4. R. Das, R. Bhatnagar, and B. Venkataraman. Proc. Indian Acad. Sci. Chem. Sci. **106**, 1681 (1994).
5. L. Biczok, T. Berces, and H. Linschitz. J. Am. Chem. Soc. **119**, 11 071 (1997).
6. S.V. Jovanovic, D.G. Morris, C.N. Pliva, and J.C. Scaiano. J. Photochem. Photobiol. A, **107**, 153 (1997).
7. P.J. Wagner and B.-S. Park. Org. Photochem. **11**, 227 (1991).
8. S. Canonica, U. Jans, K. Stemmler, and J. Hoigne. Environ. Sci. Technol. **29**, 1822 (1995).
9. S. Canonica, B. Hellrung, and J. Wirz. J. Phys. Chem. A. **104**, 1226 (2000).
10. P.H. Given, M.E. Poever, and J. Schoen. J. Chem. Soc. 2674 (1958).
11. W.J. Leigh, E.C. Lathioor, and M.J. St. Pierre. J. Am. Chem. Soc. **118**, 12 339 (1996).
12. P.J. Wagner and R.A. Leavitt. J. Am. Chem. Soc. **95**, 3669 (1973).
13. P.J. Wagner, R.J. Truman, A.E. Puchalski, and R. Wake. J. Am. Chem. Soc. **108**, 7727 (1986).
14. P. Jacques, X. Allonas, M. von Raumer, P. Suppan, and E. Haselbach. J. Photochem. Photobiol. A. **111**, 41 (1997).
15. P. Jacques. J. Photochem. Photobiol. A. **56**, 159 (1991).
16. J.C. Scaiano, W.G. McGimpsey, W.J. Leigh, and S. Jakobs. J. Org. Chem. **52**, 4540 (1987).
17. W.J. Leigh, M.S. Workentin, and D. Andrew. J. Photochem. Photobiol. A. **57**, 97 (1991).
18. E.C. Lathioor, W.J. Leigh, and M.J. St. Pierre. J. Am. Chem. Soc. **121**, 11 984 (1999).
19. C.J. Bradaric and W.J. Leigh. Can. J. Chem. **75**, 1393 (1997).
20. G. Beck, G. Dobrowolski, J. Kiwi, and W. Schnabel. Macromolecules, **8**, 9 (1975).
21. J.P. Bays, M.V. Encinas, and J.C. Scaiano. Macromolecules, **13**, 815 (1980).
22. S. Inbar, H. Linschitz, and S.G. Cohen. J. Am. Chem. Soc. **103**, 1048 (1981).
23. S. Inbar, H. Linschitz, and S.G. Cohen. J. Am. Chem. Soc. **104**, 1679 (1982).
24. R.L.J. Zsom, L.G. Schroff, C.J. Bakker, J.W. Verhoeven, Th. J. De Boer, J.D. Wright, and H. Kuroda. Tetrahedron, **34**, 3225 (1978).
25. H.A. Staab and W. Rebafka. Chem. Ber. **110**, 3333 (1977).
26. H.A. Staab, C.P. Herz, C. Krieger, and M. Rentea. Chem. Ber. **110**, 3351 (1977).
27. H.A. Staab, C.P. Herz, C. Krieger, and M. Rentea. Chem. Ber. **116**, 3813 (1983).
28. Y. Sakata, H. Tsue, Y. Goto, S. Misumi, T. Asahi, S. Nishikawa, T. Okada, and N. Mataga. Chem. Lett. 1307 (1991).
29. N. Helsen, L. Viaene, M. Van der Auweraer, and F.C. De Schryver. J. Phys. Chem. **98**, 1532 (1994).
30. T. Fiebig, W. Kuhnle, and H. Staerk. Chem. Phys. Lett. **282**, 7 (1998).
31. M.W. Wolf, R.E. Brown, and L.A. Singer. J. Am. Chem. Soc. **99**, 526 (1977).
32. A. Miyake, K. Itoh, N. Tada, M. Tanabe, M. Hirata, and Y. Oka. Chem. Pharm. Bull. **31**, 2329 (1983).

© 2001 NRC Canada

Volumes of activation for electrode processes of various charge-types in nonaqueous solvents

Mitsuru Matsumoto, Delanie Lamprecht, Michael R. North, and Thomas W. Swaddle

Abstract: Volumes of activation ($\Delta V^{\ddagger}_{el}$) are reported for electron transfer at a Pt electrode of Mn(CN-*cyclo*-C_6H_{11})$_6^{2+/+}$ in acetonitrile, acetone, methanol, and propylene carbonate, and of Fe(phen)$_3^{3+/2+}$ in acetonitrile. In all cases, $\Delta V^{\ddagger}_{el}$ is markedly positive, whereas for the homogeneous self-exchange reactions of these couples in the same solvents the corresponding parameter is known to be strongly negative. The rate constants for the electrode reactions correlate loosely with the mean reactant diffusion coefficients (i.e., with solvent fluidity) and the $\Delta V^{\ddagger}_{el}$ values with the volumes of activation for diffusion (i.e., for viscous flow), consistent with solvent dynamical control of the electrode reaction rate in organic solvents. A detailed analysis of $\Delta V^{\ddagger}_{el}$ values of the kind presented for a couple with an uncharged member (Zhou and Swaddle, Can. J. Chem. **79**, 841 (2001)) fails, however, either because of ion-pairing effects with these more highly charged couples or because of breakdown of transition-state theory in predicting the contribution of the activational barrier. Attempts to measure $\Delta V^{\ddagger}_{el}$ for the oxidation of the uncharged molecule ferrocene at various electrodes in acetonitrile were unsuccessful, although $\Delta V^{\ddagger}_{el}$ was again seen to be clearly positive.

Key words: electrode kinetics, volumes of activation, nonaqueous electron transfer, solvent dynamics.

Résumé : On a mesuré les volumes d'activation, $\Delta V^{\ddagger}_{él}$, pour le transfert d'électron d'une électrode de platine de Mn(CN-*cyclo*-C_6H_{11})$_6^{2+/+}$, dans l'acétonitrile, l'acétone, le méthanol et le carbonate de propylène ainsi que de Fe(phen)$_3^{3+/2+}$ dans l'acétonitrile. Dans tous les cas, le $\Delta V^{\ddagger}_{él}$ est très positif alors que, pour les réactions d'auto-échange homogènes de ces couples, dans les mêmes solvants, on sait que le paramètre correspondant est fortement négatif. Il existe une légère corrélation entre les constantes de vitesse pour les réactions à l'électrode et les coefficients de diffusion moyens des réactifs (c'est-à-dire avec la fluidité du solvant) ainsi que pour les valeurs de $\Delta V^{\ddagger}_{él}$ avec les volumes d'activation de la diffusion (c'est-à-dire avec l'écoulement visqueux); ces corrélations sont en accord avec le contrôle dynamique par le solvant de la vitesse de réaction à l'électrode dans les solvants organiques. Toutefois, on ne peut faire d'analyse détaillée des valeurs de $\Delta V^{\ddagger}_{él}$, du type présenté pour un couple avec un membre ne portant pas de charge (Zhou et Swaddle, Can. J. Chem. **79**, 841 (2001)); cet échec résulte de la formation de paires d'ions avec les couples portant des charges plus grandes ou du fait que la théorie de l'état de transition ne permet pas de prédire la contribution de la barrière d'activation. Il a été impossible de mesurer la valeur du $\Delta V^{\ddagger}_{él}$ pour l'oxydation de la molécule de ferrocène non chargée, à diverses électrodes, dans l'acétonitrile; il apparaissait toutefois que le $\Delta V^{\ddagger}_{él}$, est clairement positif.

Mots clés : cinétique à l'électrode, volumes d'activation, transfert d'électron en milieu non aqueux, dynamique de solvant.

[Traduit par la Rédaction]

Introduction

For outer-sphere electron transfer in cationic transition-metal couples $ML_x^{z+/(z-1)+}$ in *aqueous* solution at 25°C, the volumes of activation $\Delta V^{\ddagger}_{ex}$ and $\Delta V^{\ddagger}_{el}$ ($\Delta V^{\ddagger} = -RT(\partial \ln k/\partial P)_T$, where k is the corresponding rate constant) for the homogeneous self-exchange reaction and the equivalent electrode process respectively have invariably been found to be negative (1–5). Furthermore, for aqueous systems, $\Delta V^{\ddagger}_{el}$ is found (1–5) to be one-half of $\Delta V^{\ddagger}_{ex}$:

[1] $$\Delta V^{\ddagger}_{el} = (0.50 \pm 0.02)\Delta V^{\ddagger}_{ex}$$

which is consistent with the corresponding relationship proposed theoretically by Marcus (6) for the free energies of activation

[2] $$\Delta G^{\ddagger}_{el} = \Delta G^{\ddagger}_{ex}/2$$

As an "exception that proves the rule," $\Delta V^{\ddagger}_{ex}$ and $\Delta V^{\ddagger}_{el}$ for electron transfer in water can be positive where the reaction is *not* of the simple, bimolecular, outer-sphere type — for example, the self-exchange pathway for anionic cyanometalate couples that is mediated by alkali-metal cations (7, 8) — but even in such cases eq. [1] still holds with remarkable accuracy. We, therefore, refer to eq. [1] for convenience as the "50% rule." Since $\Delta V^{\ddagger}_{ex}$ for the uncatalyzed outer-sphere reactions can be accounted for in terms of an extension (9) of the Marcus and Sutin model (10) based on transi-

Received 12 06 2001. Published on the NRC Research Press Web site at http://canjchem.nrc.ca on December 5, 2001.

M. Matsumoto,[1] D. Lamprecht, M.R. North, and T.W. Swaddle. Department of Chemistry, University of Calgary, Calgary, AB T2N 1N4, Canada.

[1]Corresponding author (telephone: (403) 220-5358; fax: (403) 284-1372; e-mail: swaddle@ucalgary.ca).

 DOI: 10.1139/cjc-79-12-1864 © 2001 NRC Canada

tion-state theory, $\Delta V^{\ddagger}_{el}$ for aqueous electrode reactions can be said to be understood on this same basis.

For *nonaqueous* electron transfer reactions, however, the high-pressure experimental information obtained to date has revealed a sharp dichotomy between homogeneous self-exchange reactions, for which $\Delta V^{\ddagger}_{ex}$ is negative (and, for polar solvents such as acetonitrile, quantitatively consistent with theory (9, 11, 12)), and the corresponding electrode processes, for which $\Delta V^{\ddagger}_{el}$ turns out to be quite strongly *positive*. In other words, eq. [1] as such seems not to apply to nonaqueous systems. On the other hand, $\Delta V^{\ddagger}_{el}$ for the nonaqueous systems does correlate loosely with the volume of activation $\Delta V^{\ddagger}_{diff}$ for diffusion of the reactants in the particular solvent, and $\Delta V^{\ddagger}_{diff}$ can be identified, through the Stokes–Einstein relation

$$[3] \qquad D = k_B T/6\pi r_{eff}\eta$$

(in which D is the diffusion coefficient of a solute molecule of effective radius r_{eff} in a solvent of viscosity η), with the volume of activation $\Delta V^{\ddagger}_{visc}$ for viscous flow of the solvent. The implication is that the electrode reactions in nonaqueous media are either diffusion-controlled (which is highly unlikely, as the rates are generally too low and dependent on the particular system) or controlled by solvent dynamics (solvent "friction"). The latter possibility has been put forward in the context of electrode reactions of transition-metal complexes by several research groups (13–21), and depends on the notion (19, 22–25) that η is at least approximately proportional to the longitudinal solvent relaxation time τ_L. In the event that solvent dynamical effects control the reaction rate, the preexponential factor of the Eyring equation is expected to be proportional to τ_L^{-1} (26–34) and, therefore, the rate constant to η^{-1}. As far as pressure effects on rate coefficients are concerned, this means that the observed volume of activation $\Delta V^{\ddagger}_{obsd}$ for a reaction subject to solvent dynamics comprises a (normally negative) term $\Delta V^{\ddagger}_{TST}$ representing the pressure dependence of the free-energy activation barrier $\Delta G^{\ddagger}_{SD}$ and a solvent-dynamical term $\Delta V^{\ddagger}_{SD}$ representing that of the frequency factor. The term $\Delta V^{\ddagger}_{SD}$ ($\approx RT(\partial \ln \tau_L/\partial P)_T$) can be replaced by the volume of activation for viscous flow of the solvent $\Delta V^{\ddagger}_{visc}$ ($= RT(\partial \ln \eta/\partial P)_T$) which, in high-pressure electrochemical experiments, is conveniently obtained from the pressure dependence of the mean diffusion coefficient D of the reactants:

$$[4] \qquad \Delta V^{\ddagger}_{obsd} = \Delta V^{\ddagger}_{TST} + \Delta V^{\ddagger}_{SD}$$

$$[5] \qquad \Delta V^{\ddagger}_{SD} \approx \Delta V^{\ddagger}_{visc} = \Delta V^{\ddagger}_{diff} = RT(\partial \ln D/\partial P)_T$$

Equations [4] and [5] have a counterpart in Zusman's proposal (22) that the apparent activation energy for an electrode reaction subject to solvent friction will be higher than that predicted by Marcus by an amount representing the activation energy for viscous flow of the solvent. Because $\Delta V^{\ddagger}_{diff}$ is strongly positive for solvents *other than water* (for which it is fortuitously negligible at near-ambient temperatures and the usual experimental pressure range of 0–200 MPa (5, 20)), we have a first-order explanation in terms of solvent dynamics for the fact that $\Delta V^{\ddagger}_{obsd}$ for electrode reactions (i.e., $\Delta V^{\ddagger}_{el}$) is typically negative for aqueous systems, representing $\Delta V^{\ddagger}_{TST}$ regardless of any solvent-dynamical control, but markedly positive for nonaqueous solvents, in which $\Delta V^{\ddagger}_{SD}$ overwhelms $\Delta V^{\ddagger}_{TST}$. For the corresponding bimolecular self-exchange reactions for nonaqueous as well as aqueous couples, however, $\Delta V^{\ddagger}_{obsd}$ (i.e., $\Delta V^{\ddagger}_{ex}$) is generally negative and consistent with expectations based on TST (9, 12), implying independence of solvent dynamics. Consequently, for a given couple for which the electrode reaction is subject to solvent friction in a nonaqueous solvent, one can, *in the absence of complicating effects such as ion-pairing*, equate $\Delta V^{\ddagger}_{TST}$ for the electrode process with $\Delta V^{\ddagger}_{ex}/2$ and relate $\Delta V^{\ddagger}_{el}$ to $\Delta V^{\ddagger}_{diff}$ through eqs. [4] and [5].

A refined form of eqs. [4] and [5] is given elsewhere (5, 20, 21), but the refinements tend to cancel, and eqs. [4] and [5] have proved adequate in accounting for the positive values of $\Delta V^{\ddagger}_{obsd}$ found for the electrode reaction in four polar nonaqueous solvents of the couple $Ru(hfac)_3^{3+/2+}$,[2] for which interpretation is simplified because, for such a one-electron transfer involving a neutral species, the coulombic work terms, medium effects of the Debye–Hückel type, and the effects of ion-pairing should all be negligible (21). Such is not the case, however, for couples in which both reactants are charged. For example, for the $Co(bpy)_3^{3+/2+}$ system, reported by Murray and co-workers (13–15) to display viscosity effects indicative of solvent dynamics, $\Delta V^{\ddagger}_{el}$ in acetonitrile, acetone and PC[2] is strongly positive and runs close to $\Delta V^{\ddagger}_{diff}$, suggesting that $\Delta V^{\ddagger}_{TST}$ is close to zero, yet $\Delta V^{\ddagger}_{el}$ for the same couple in water is strongly negative, indicating just the opposite (20). Thus, eqs. [4] and [5] are not quantitatively applicable to the $Co(bpy)_3^{3+/2+}$ couple, and the most likely explanation is that these highly charged ions are sufficiently ion-paired with the counter-ion in organic solvents to invalidate these relationships while leaving $\Delta V^{\ddagger}_{SD}$ as the dominating component of $\Delta V^{\ddagger}_{el}$.

The object of the present study was to extend the very limited database on $\Delta V^{\ddagger}_{el}$ in nonaqueous solvents and to examine the validity of eqs. [4] and [5] for a range of couples of various charge-types. Because, for an electrode reaction, $\Delta V^{\ddagger}_{TST}$ in eq. [4] can be expected to equal 50% of $\Delta V^{\ddagger}_{ex}$ for the corresponding self-exchange reaction (5, 20, 21), attention was focused upon couples for which $\Delta V^{\ddagger}_{ex}$ data are available. The selected couples were, therefore, ferricenium/ferrocene ($FeCp_2^{+/0}$) (35), $Mn(CNchx)_6^{2+/+}$ (36, 37), and $Fe(phen)_3^{3+/2+}$ (38). The last couple is advantageous in that $\Delta V^{\ddagger}_{ex}$ is available for both water and a nonaqueous solvent (38), and that electron transfer is of the low-spin – low-spin type (in contrast to the previously studied $Co(bpy)_3^{3+/2+}$ (13, 14, 20), in which electron transfer entails a spin-state change with attendant interpretational challenges (9)).

Experimental

Materials

$[Mn(CNchx)_6](BF_4)$ and $FeCp_2$ were made and purified by published methods (39, 40). $[Fe(phen)_3](ClO_4)_2$ was made by precipitation from an aqueous solution of the sul-

[2] Abbreviations: ($hfac^-$) 1,1,1,5,5,5-hexafluoroacetylacetonate, (bpy) 2,2′-bipyridine, (PC) propylene carbonate, (chx) cyclohexyl, (phen) 1,10-phenanthroline, (Cp) cyclopentadienyl, (TBAP) tetrabutylammonium perchlorate, (TBAHFP) tetrabutylammonium hexafluorophosphate, (CV) cyclic voltammogram and (or) voltammetry, (ACV) alternating current voltammogram and (or) voltammetry.

© 2001 NRC Canada

fate salt (38) with aq $NaClO_4$. TBAP and TBAHFP[2] (Fluka, puriss.) were used as received. Acetone (BDH, ACS Assured) was refluxed with $KMnO_4$ until the purple color persisted, then shaken with Na_2CO_3 to remove acidic impurities and distilled twice, the second time from anhyd $CaSO_4$. Acetonitrile (BDH, ACS Assured) was distilled from P_2O_5 under N_2 and stored over activated 4 A molecular sieves. Methanol was dried by refluxing it over iodine-activated Mg turnings and distilling it twice. PC[2] (Aldrich, anhydrous, 99.7%) was used as received.

Electrochemical measurements

CVs and ACVs[2] were obtained as functions of pressure (0.1–200 MPa) as described previously (1–4, 20, 21), except that a PARC Model 273 potentiostat was generally used in place of the Model 173/175 combination and the O-rings in the electrochemical cell were of silicone rubber rather than viton or neoprene which were attacked by acetonitrile and some other solvents. The working and counter electrodes were of Pt wire. Before each experiment, the working electrode was gently polished with 0.05 μm Al_2O_3 powder and then sonicated, first in aq HNO_3 (6 mol L^{-1}) and then water, for 10 s each. The potential cycling procedure used in earlier work (1–4) to clean electrodes in situ during high pressure runs on aqueous solutions proved to be impracticable with the present nonaqueous systems. The reference electrode was a silver rod in contact with $AgNO_3$ solution (0.01 mol L^{-1}) in acetonitrile. Solutions contained 1.0–2.5 mmol L^{-1} of the complex salt, and 0.1 to 0.5 mol L^{-1} of the supporting electrolyte. As $Mn(CNchx)_6^{2+}$ was only generated transiently, the need to work at low temperatures to avoid its decomposition, as advocated by Wherland and co-workers (36), was obviated.

Results

For each sample at every pressure, electrode reaction rate constants k_{el} were derived from corrected phase angles f obtained from ACVs for three frequencies f (25–45 Hz for $Mn(CNchx)_6^{2++}$, 25–85 or 45–150 Hz for $Fe(phen)_3^{3+/2+}$, and 25–85 Hz for $FeCp_2$) in conjunction with determinations of the uncompensated resistance R_u at 10 kHz at a potential 250 mV away from the ACV peak potential E_{max}, in the manner previously described (2, 20, 21). Only those pressure cycles for which the initial and final (lowest-pressure) measurements agreed within the experimental uncertainty were accepted.

$$[6] \qquad \cot \phi = 1 + (2D\omega)^{1/2}/\alpha^{-\alpha}(1-\alpha)^{-(1-\alpha)}k_{el}$$

In eq. [6], ω is the AC angular frequency (= $2\pi f$) and D is the mean diffusion coefficient of the redox-active species (concentration c), determined from the peak currents I_p of CVs taken over a range of scan rates v:

$$[7] \qquad I_p = 2.686 \times 10^5 AD^{1/2}v^{1/2}c$$

where the effective electrode area A was determined from an I_p vs. $v^{1/2}$ plot for a solution of $FeCp_2$ in acetonitrile (c = 2.4 mmol L^{-1}, $D = 2.4 \times 10^{-5}$ cm^2 s^{-1} (41)) at 0.1 MPa and 25°C. It was acceptable to use a mean value of D for both the oxidized and reduced species, since the oxidation and reduction peak currents of the CVs were essentially the same. The transfer coefficients α were obtained from the relation

$$[8] \qquad E_{dc} = \Delta E_{cell} + (RT/F) \ln [\alpha/(1-\alpha)]$$

where E_{dc} is the potential corresponding to the max current in ACV and ΔE_{cell} is the half-wave potential found in CV. In all cases, $0.50 \le \alpha \le 0.60$. In this frequency range, k_{el} was independent of f. Because R_u was fairly large (100–200 Ω in acetone, acetonitrile, and methanol and 450 Ω in PC, at 0.1 MPa) and increased with increasing pressure, it is important to note that R_u was carefully measured and corrected for in calculating k_{el}. Thus, the k_{el} data reported here are not artifacts arising from R_u. The authenticity of k_{el} was confirmed by its reproducibility and its independence of f and the metal-complex concentration.

From ΔE_{cell} and the mean diffusion coefficients D, obtained from CVs at variable pressure relative to the reported atmospheric pressure value for $FeCp_2^+$ (41), the volume of reaction ΔV_{cell} for the cell (i.e., for the particular couple relative to the $Ag/AgNO_3$–CH_3CN electrode) and the volume of activation for diffusion $\Delta V_{diff}^{\ddagger}$ were calculated:

$$[9] \qquad \Delta V_{cell} = -F(\partial \Delta E_{cell}/\partial P)_T$$

$$[10] \qquad \Delta V_{diff}^{\ddagger} = -RT(\partial \ln D/\partial P)_T$$

Substitution of E_{max} (from ACVs) for ΔE_{cell} in eq. [9] gave the same ΔV_{cell} values, within the experimental uncertainty, regardless of the value of α. A set of typical pressure dependences of $E_{1/2}$, ln D, and k_{el} is shown in Fig. 1, and similar representative diagrams for the other four systems for which reproducible data were obtained are available as material on deposit (Figs. S1–S4). The numerical results are summarized in Table 1. The value of $E_{1/2}$ for $Mn(CNchx)_6^{2+/+}$ relative to that for $FeCp_2^{+/0}$ agreed well with the reported value (0.057 V (42)). Values of ΔV_{cell} for $FeCp_2^{+/0}$ and $Fe(phen)_3^{3+/2+}$ in acetonitrile are in acceptable agreement with those of Tregloan and co-workers (43), given the differences in the nature and concentrations of the supporting electrolytes.

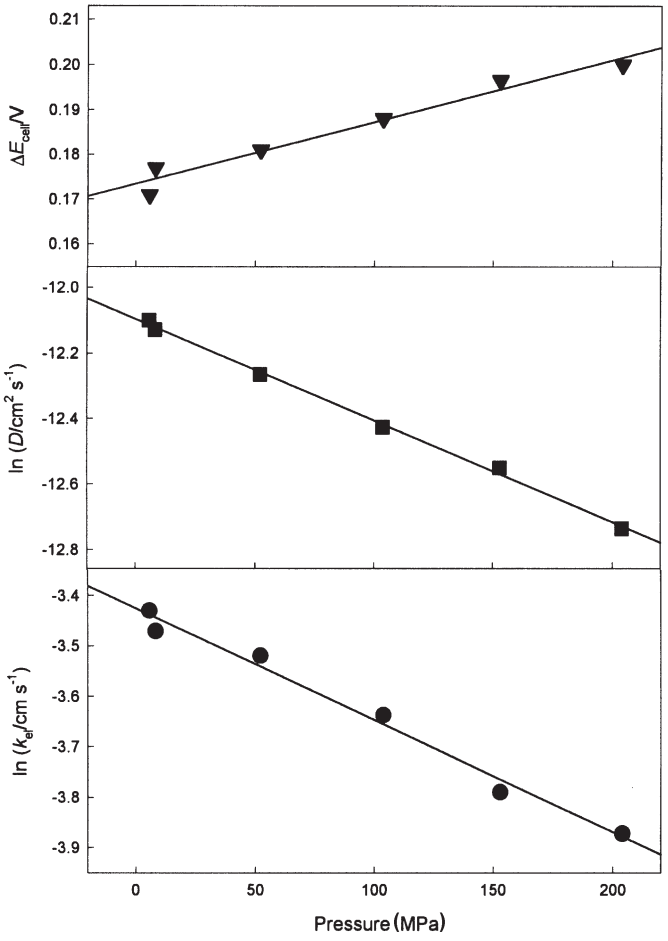
Discussion

For the $Mn(CNchx)_6^{2+/+}$ system, the ΔV_{cell} values of Table 1 are remarkably consistent between the various media except for methanol, which is the only solvent listed for which hydrogen bonding is operative. For the Fe and Mn complexes taken together, the lack of any obvious correlation of ΔV_{cell} with charge type of the sort found by Tregloan and co-workers (44) for a series of related Fe(III/II) couples in water is not surprising, as the couples of Table 1 differ from each other chemically.

The mean diffusion coefficients D given in Table 1 for the $Mn(CNchx)_6^{2+/+}$ couple with TBAP (0.5 mol L^{-1}) suggest an effective radius r_{eff} of 710 ± 15 pm for these complex ions in acetonitrile, methanol, and PC, according to the Stokes–Einstein relation (eq. [3]) in which η is taken to be the viscosity of the pure solvent. A larger value of r_{eff} (910 pm) obtained for the same couple in acetone presumably reflects the expected influence of ion pairing due to the lower dielectric constant of this solvent.

© 2001 NRC Canada

Fig. 1. Pressure dependence of electrode reaction properties of the $Mn(CNchx)_6^{2+/+}$ couple ($[Mn(CNchx)_6(BF_4)]$ = 1.06 mmol L^{-1}) at 25.0°C in methanol containing TBAP (0.5 mol L^{-1}). Duplicate low-pressure data are initial and final measurements in the pressure cycle. Top frame: reaction volume relative to Ag/0.01 mol L^{-1} $AgNO_3$–CH_3CN (from CV). Middle frame: Logarithm of mean reactant diffusion coefficient (from CV). Bottom frame: Logarithm of standard electrode reaction rate constant (from current maxima in ACV).



The k_{el} values for $Mn(CNchx)_6^{2+/+}$ in Table 1 correlate roughly with D, with $k_{el} \sim 4.7 \times 10^3 D$ for acetonitrile and acetone (0.5 mol L^{-1} TBAP) and some 30% faster than this for the non-Debye solvents methanol and PC (Fig. S5, material on deposit). As noted previously (21), proportionality between the preexponential factor of the Eyring equation and η^{-1} (and hence the validity of eqs. [4] and [5]) is expected only for Debye solvents, i.e., those which can be represented in terms of quasispherical molecules rotating freely in a continuous dielectric, whereas methanol is subject to hydrogen-bonding complications and PC has an irregular shape and a high dipole moment. Nevertheless, the rough proportionality between k_{el} and D strongly suggests solvent dynamical control of the electrode reaction rate.

The salient feature of the $\Delta V_{el}^{\ddagger}$ data of Table 1 is that they are all quite strongly positive, whereas the corresponding parameters $\Delta V_{ex}^{\ddagger}$ for the homogeneous self-exchange reactions are all markedly negative. An approximate dependence of $\Delta V_{el}^{\ddagger}$ on $\Delta V_{diff}^{\ddagger}$ is also evident (Table 1) — for the Mn couple (Fig. S6, material on deposit), the slope is about 1.5, but this is strongly influenced by the one point for PC as solvent. In the event that the activational barrier contribution $\Delta V_{TST}^{\ddagger}$ (eq. [4]) were negligible, the slope of this correlation would be 1.0. If, however, $\Delta V_{TST}^{\ddagger}$ can be identified even roughly with 0.5 $\Delta V_{ex}^{\ddagger}$, then it is clear that eqs. [4] and [5] fail for the 2+/+ and 3+/2+ couples considered here, despite their applicability to the reduction of the uncharged $Ru^{III}(hfac)_3$ complex (21). Furthermore, the discrepancy is most evident for the most highly charged couple, $Fe(phen)_3^{3+/2+}$, for which $\Delta V_{el}^{\ddagger}$ is actually much larger than $\Delta V_{diff}^{\ddagger}$ in CH_3CN despite an anticipated $\Delta V_{TST}^{\ddagger}$ contribution of about –3 cm^3 mol^{-1} based on $\Delta V_{ex}^{\ddagger}$. It was also noted previously (20) that the $\Delta V_{TST}^{\ddagger}$ contribution is not clearly evident for the $Co(bpy)_3^{3+/2+}$ electrode reaction in nonaqueous solvents.

In gross terms, then, the very sharp contrast between $\Delta V_{el}^{\ddagger}$ and $\Delta V_{ex}^{\ddagger}$ (and the general parallelism between k_{el} and D) in organic solvents for all couples studied to date implies solvent dynamical control of the electrode, but not the homogeneous, electron transfer reactions. On the other hand, the present work makes it clear that a more detailed analysis of $\Delta V_{el}^{\ddagger}$ along the lines of eqs. [4] and [5] is not possible for couples in which both reactants are charged (particularly highly charged). This is not surprising, as extensive ion pairing is expected for complexes of charge 2+ or more in organic solvents, but it is not clear at this time what influence (if any) ion pairing should have on k_{el} or $\Delta V_{el}^{\ddagger}$. For self-exchange electron transfer reactions in aqueous systems, counter-ion effects are strong only for anion–anion electron transfer reactions (7). It is not clear how counter-ion effects would affect electrode reaction kinetics in nonaqueous solvents. Table 1 shows that changing the anion of the supporting electrolyte from perchlorate to hexafluorophosphate reduces k_{el} significantly but has only a small effect on $\Delta V_{el}^{\ddagger}$. Fawcett and co-workers (19) found that ion pairing did not affect the rate of the $Ru(phen)_3^{3+/2+}$ electrode reaction appreciably in aprotic solvents, and Pyati and Murray (13) considered the possibility of ion-pairing effects on the kinetics of the $Co(bpy)_3^{3+/2+}$ electrode reaction in nonaqueous media but decided that they were not a major factor (both groups, however, concluded that the reaction rates were controlled by solvent dynamics). An alternative qualitative interpretation is that transition-state theory breaks down completely for charged couples in nonaqueous electrode reactions, leaving $\Delta V_{SD}^{\ddagger}$ (represented at least approximately by $\Delta V_{diff}^{\ddagger}$) to determine $\Delta V_{el}^{\ddagger}$.

It is unfortunate that we were unable to measure $\Delta V_{el}^{\ddagger}$ for the much-studied $FeCp_2^{+/0}$ couple accurately at Pt, Au, or glassy carbon electrodes, as this could have confirmed or denied the applicability of eqs. [4] and [5] to couples with an uncharged member. Qualitatively, we found that the apparent k_{el} decreased substantially with increasing pressure even after an approximate correction for its drift to smaller values in the time frame of a high pressure experiment had been applied. Thus, $\Delta V_{el}^{\ddagger}$ was again unequivocally positive, in contrast with the negative $\Delta V_{ex}^{\ddagger}$ value reported for $FeCp_2^{+/0}$ in CH_3CN (35) and consistent with the picture of solvent dynamical control of the rates of electrode reactions, but not of the corresponding homogeneous reactions, in organic solvents.

© 2001 NRC Canada

Table 1. Parameters describing pressure effects on reactions of the hexa(cyclohexylisocyano)manganese(II/I) and tri(1,10-phenanthroline)iron(III/II) couples at a Pt electrode in selected organic solvents.

Couple/solvent/electrolyte[a] (N)[b]	$E_{1/2}$[c,d] (V)	α[d]	ΔV_{cell}[c] ($cm^3\ mol^{-1}$)	k_{el}[d] (10^{-2} cm s^{-1})	D[d] ($10^{-6}\ cm^2\ s^{-1}$)	$\Delta V^{\ddagger}_{el}$ ($cm^3\ mol^{-1}$)	$\Delta V^{\ddagger}_{diff}$ ($cm^3\ mol^{-1}$)	$\Delta V^{\ddagger}_{ex}$ ($cm^3\ mol^{-1}$)
$Mn(CNchx)_6^{2+/+}/CH_3CN$/TBAP[e] (2)	0.15	0.58	–17.3 ± 0.5	5.1 ± 0.2	11.7 ± 0.1	6.7 ± 0.8	7.3 ± 0.2	
$Mn(CNchx)_6^{2+/+}/CH_3CN$/TBAP (5)	0.17	0.54	–17.5 ± 0.6	4.3 ± 0.1	9.3 ± 0.3	8.0 ± 0.5	9.3 ± 0.4	–20[f,g], –17[f,h]
$Mn(CNchx)_6^{2+/+}/CH_3CN$/TBAHFP (1)	0.14	0.55	–18.7 ± 0.6	1.32 ± 0.15	8.4 ± 0.1	6.4 ± 0.7	8.9 ± 0.2	
$Mn(CNchx)_6^{2+/+}/(CH_3)_2CO$/TBAP (2)	0.17	0.56	–18.6 ± 1.0	3.9 ± 0.1	8.2 ± 0.3	11.4 ± 0.6	9.9 ± 0.3	–20[h,i]
$Mn(CNchx)_6^{2+/+}/CH_3OH$//TBAP (2)	0.17	0.57	–13.4 ± 0.6	3.3 ± 0.1	5.5 ± 0.1	5.8 ± 0.3	7.5 ± 0.2	–16[h,i]
$Mn(CNchx)_6^{2+/+}$/PC/TBAP (3)	0.12	0.53	–19.3 ± 0.4	0.74 ± 0.02	1.22 ± 0.01	20.3 ± 0.6	17.3 ± 0.1	
$Fe(phen)_3^{3+/2+}/CH_3CN$/TBAP (3)	0.78	0.50	2.5 ± 0.6	5.9 ± 0.6	5.4 ± 0.5	14.3 ± 1.3	8.0 ± 0.1	–5.9[j]
$Fe(phen)_3^{3+/2+}/CH_3CN$/TBAP[k] (1)	0.80	0.50	5.6 ± 1.6	4.5 ± 0.3	6.7 ± 0.1	16.0 ± 1.2	6.7 ± 0.2	
$FeCp_2^{+/0}/CH_3CN$/TBAHFP (2)	0.08	0.50	–7.7 ± 0.8	15 ± 1[l,m]	30 ± 2[l,m]	—[m]	—[m]	–7[n]

[a] 25°C, [complex] = 2 mmol L^{-1}, [TBA salt] = 0.5 mol L^{-1}, except as stated.
[b] Data averaged over N independent runs.
[c] Relative to $Ag/AgNO_3$ (0.01 mol L^{-1})/CH_3CN.
[d] At 0.1 MPa.
[e] 0.2 mol L^{-1}.
[f] Reference 36; anion BF_4^-.
[g] 12°C.
[h] 2°C.
[i] Reference 37; anion BF_4^-.
[j] Reference 38; 0–10°C.
[k] 0.1 mol L^{-1}.
[l] Initial value.
[m] k_{el} and D decreased over the time-span of a pressure cycle.
[n] Reference 35; no supporting electrolyte.

The $Fe(phen)_3^{3+/2+}$ couple is of particular interest in that it is the only couple for which we now have $\Delta V^{\ddagger}_{el}$ and $\Delta V^{\ddagger}_{ex}$ data for both aqueous and nonaqueous systems (2, 38). For the aqueous electron transfer reaction, both $\Delta V^{\ddagger}_{el}$ and $\Delta V^{\ddagger}_{ex}$ are small negative numbers (–1.6 and –2.2 $cm^3\ mol^{-1}$, respectively) and, given their numerical smallness, are consistent with the 50% rule as well as with theoretical predictions (9). In acetonitrile, $\Delta V^{\ddagger}_{ex}$ is again negative (Table 1) and in close accord with theoretical predictions, but $\Delta V^{\ddagger}_{el}$ is strongly positive and substantially exceeds $\Delta V^{\ddagger}_{diff}$. Thus, the special character of the nonaqueous electrode reaction is highlighted, as is the inadequacy of eqs. [4] and [5] in the case of this highly charged couple. Either there are strong electrostatic effects (presumably ion-pairing) that invalidate eqs. [4] and [5], or else the assumption that $\Delta V^{\ddagger}_{ex}$ can serve as even an approximate measure of $\Delta V^{\ddagger}_{TST}$ in nonaqueous solvents is unjustified.

In closing, we reiterate that the pressure criterion of the incursion of solvent dynamics is inapplicable in aqueous systems at near-ambient temperatures because the pressure dependence of the viscosity of water is fortuitously negligible over the usual experimental pressure range (0–200 MPa). Accordingly, it could be that solvent dynamics control the rates of aqueous as well as nonaqueous electrode reactions. However, the $\Delta V^{\ddagger}_{el}$ data for the aqueous and nonaqueous electrode reactions of both $Co(bpy)_3^{3+/2+}$ and $Fe(phen)_3^{3+/2+}$ stand in such sharp contrast as to imply that electrode dynamics in water need to be treated differently from those in organic solvents.

Acknowledgements

We thank the Natural Sciences and Engineering Research Council of Canada (NSERC) for financial support, and the Alexander von Humboldt Stiftung for a Research Award (to TWS).

Material on Deposit

Copies of material on deposit may be purchased from the Depository of Unpublished Data, Document Delivery, CISTI, National Research Council Canada, Ottawa, ON K1A 0S2, Canada (http://www.nrc.ca/cisti/irm/unpub_e.shmtl for information on ordering electronically).

References

1. Y. Fu and T.W. Swaddle. Chem. Commun. 1171 (1996).
2. Y. Fu and T.W. Swaddle. J. Am. Chem. Soc. **119**, 7137 (1997).
3. Y. Fu and T.W. Swaddle. Inorg. Chem. **38,** 876 (1999).
4. P.D. Metelski, Y. Fu, K. Khan, and T.W. Swaddle. Inorg. Chem. **38**, 3103 (1999).
5. T.W. Swaddle. *In* High pressure chemistry. *Edited by* R. van Eldik and F.-G. Klärner. Wiley–VCH, Weinheim. In press.
6. R.A. Marcus. Electrochim. Acta, **13**, 995 (1968), and refs. therein.
7. P.D. Metelski and T.W. Swaddle. Inorg. Chem. **38**, 301 (1999).
8. Y. Fu and T.W. Swaddle. Inorg. Chem. **38**, 876 (1999)
9. T.W. Swaddle. Can. J. Chem. **74**, 631 (1996), and refs. cited therein.
10. R.A. Marcus and N. Sutin. Biochim. Biophys. Acta, **811**, 265 (1985).
11. H. Doine and T.W. Swaddle. Inorg. Chem. **27**, 665 (1988).
12. H. Takagi and T.W. Swaddle. Chem. Phys. Lett. **248**, 207 (1996).
13. R. Pyati and R.W. Murray. J. Am. Chem. Soc. **118**, 1743 (1996).
14. M.E. Williams, J.C. Crooker, R. Pyati, L.J. Lyons, and R.W. Murray. J. Am. Chem. Soc. **119**, 10 249 (1997).
15. J.C. Crooker and R.W. Murray. Anal. Chem. **72**, 3245 (2000).

© 2001 NRC Canada

16. X. Zhang, J. Leddy, and A.J. Bard. J. Am. Chem. Soc. **107**, 3719 (1985).
17. X. Zhang, H. Yang, and A.J. Bard. J. Am. Chem. Soc. **109**, 1916 (1987).
18. D.E. Khoshtariya, T.D. Dolidze, D. Krulic, N. Fatouros, and D. Devilliers. J. Phys. Chem. B, **102**, 7800 (1998).
19. K. Winkler, N. McKnight, and W.R. Fawcett. J. Phys. Chem. B, **104**, 3575 (2000).
20. Y. Fu, A.S. Cole, and T.W. Swaddle. J. Am. Chem. Soc. **121**, 10 410 (1999).
21. J. Zhou and T.W. Swaddle. Can. J. Chem. **79**, 841 (2001).
22. L.D. Zusman. Chem. Phys. **112**, 53 (1987).
23. Z. Galus. Advan. Electrochem. Sci. Eng. **4**, 217 (1995).
24. T. Asano. Pure Appl. Chem. **71**, 1691 (1999).
25. M.J. Weaver. Chem. Rev. **92**, 463 (1992).
26. M.J. Weaver. J. Mol. Liq. **60**, 57 (1994).
27. H. Heitele. Angew. Chem. Intl. Ed. Engl. **32**, 359 (1993).
28. J.T. Hynes. J. Phys. Chem. **90**, 3701 (1986).
29. W.R. Fawcett and M. Opallo. Angew. Chem. Int. Ed. Engl. **33**, 2131 (1994).
30. W.R. Fawcett and C.A. Foss, Jr. J. Electroanal. Chem. **270**, 103 (1989).
31. T. Gennett, D.F. Milner, and M.J. Weaver. J. Phys. Chem. **89**, 2787 (1985).
32. G.E. McManis, M.N. Golovin, and M.J. Weaver. J. Phys. Chem. **90**, 6563 (1986).
33. G. Grampp, W. Harrer, and W. Jaenicke. J. Chem. Soc. Faraday Trans. 1, **83**, 161 (1987).
34. K. Hara. *In* High pressure liquids and solutions. *Edited by* Y. Taniguchi, M. Senoo, and H. Hara. Elsevier, Amsterdam. 1994. p. 67.
35. K. Kirchner, S.-Q. Dang, M. Stebler, H.W. Dodgen, S. Wherland, and J.P. Hunt. Inorg. Chem. **28**, 3604 (1989).
36. R.M. Nielson, J.P. Hunt, H.W. Dodgen, and S. Wherland. Inorg. Chem. **25**, 1964 (1986).
37. M. Stebler, R.M. Nielson, W.F. Siems, J.P. Hunt, H.W. Dodgen, and S. Wherland. Inorg. Chem. **27**, 2893 (1988).
38. H. Doine and T.W. Swaddle. Can. J. Chem. **66**, 2763 (1988).
39. R.M. Nielson and S. Wherland. J. Am. Chem. Soc. **107**, 1505 (1985).
40. W.L. Jolly. Inorg. Synth. **11**, 120 (1968).
41. T. Kuwana, D.E. Bublitz, and G. Hoh. J. Am. Chem. Soc. **82**, 5811 (1960).
42. R.M. Nielson and S. Wherland. Inorg. Chem. **24**, 1803 (1985).
43. J.I. Sachinidis, R.D. Shalders and P.A. Tregloan. Inorg. Chem. **35**, 2497 (1996).
44. J.I. Sachinidis, R.D. Shalders and P.A. Tregloan. Inorg. Chem. **33**, 6180 (1994).

© 2001 NRC Canada

Effect of the molecular weight on the lower critical solution temperature of poly(*N*,*N*-diethylacrylamide) in aqueous solutions[1]

D.G. Lessard, M. Ousalem, and X.X. Zhu

Abstract: The molecular weight dependence of the lower critical solution temperature of poly(*N*,*N*-diethylacrylamide) was studied with 11 samples of the polymer with a number-average molecular weight (M_n) ranging from 9.6×10^3 to 1.3×10^6 g mol^{-1} and relatively narrow polydispersity indices from 1.19 and 2.60. These samples were obtained by fractional precipitation of the polymer. LCST values of polymers were measured by turbidimetry and microcalorimetry. An inverse dependence of LCST on the molar mass was found and the LCST of the samples remained more or less a constant above a critical molecular weight of ca. 2×10^5 g mol^{-1}. The enthalpy and the entropy changes as well as the LCST of the polymer depend strongly on the molar mass of the polymer, especially in low molecular weight range.

Key words: poly(*N*,*N*-diethylacrylamide), LCST, thermosensitive, phase diagram, effect of molecular weight.

Résumé : L'effet de la masse molaire sur la température critique de dissolution inférieure (LCST) du poly(*N*,*N*-diéthylacrylamide) a été étudié sur 11 fractions de masses molaires moyennes en nombre (M_n) variant entre 9.6×10^3 à 1.3×10^6 g mol^{-1} et ayant un indice de polydispersité situé entre 1.19 et 2.60. Ces échantillons ont été obtenus par précipitation fractionée. La LCST des solutions aqueuses du polymère a été mesurée par turbidimétrie et par microcalorimétrie. Il a été constaté que la LCST diminue avec la masse molaire de l'échantillon. Les valeurs de la LCST demeurent cependant relativement constantes pour des masses molaires supérieures à 2×10^5 g mol^{-1}. L'enthalpie et l'entropie associées aux changements de phases diminuent de la même façon avec l'augmentation de la masse molaire.

Mots clés : poly(*N*,*N*-diéthylacrylamide), température critique de dissolution inférieure, thermosensible, diagramme de phase, effet de la masse molaire.

Introduction

Thermosensitive polymers are known to undergo changes in their physical properties when the temperature is varied. Many *N*-substituted polyacrylamides in water exhibit reversible-phase separation upon heating. The temperature at which precipitation of the polymer occurs is called the lower critical solution temperature (LCST). Materials which show this behavior in water are of a great interest for medical (1) and industrial (2) applications. The most extensively studied polymer in this family is probably poly(*N*-isopropylacrylamide) (PNIPAM). Our research focuses on the effect of the molar mass on the LCST of aqueous solutions of poly(*N*,*N*-diethylacrylmide) (PDEA), which behaves similarly as PNIPAM.

Different researchers have explained the LCST phenomenon of polymers in water. It was ascribed to the greater entropy in the two-phase system than in a homogeneous solution (3, 4), the formation of hydrogen bonds between the polymer and water (3, 5), the hydrophobic interactions between the polymer side chain groups (3, 6), and the disruption of specific hydrogen-bonded cyclic structure in alkyl amide units and hydroxyl functions of water (7).

Only a few studies were conducted on PDEA even though this polymer behaves similarly as PNIPAM without the ability to form hydrogen bridges with a proton on the amide group and the solvent. This polymer may be synthesized by anionic polymerization (8, 9), group transfer polymerization (8, 10), or free radical polymerization (7, 8, 10–14). It was observed that for PDEA of low molar masses ($M_n < 5000$ g mol^{-1}) the transition temperature is 10°C higher for isotactic polymers than for their syndiotactic homologues. Different initiators were used for these tactic samples and the difference in the end-group was attributed as the origin of the discrepancy in their LCST values (8).

The aqueous solutions of PDEA can undergo precipitation between 25 and 36°C as determined by means of turbidimetry (8, 11, 15–17), differential scanning calorimetry (7, 8, 11, 17, 18), small angle neutron scattering (20), dynamic and static light scattering (10), IR spectroscopy (7), and rheology (10, 14). Early research focused on the parameters such as the addition of salts (11, 15, 17) and surfactant (11), co-monomer content (13, 14, 17, 19), and concentration of the polymer (8, 11, 16). The self-diffusion coefficients of small molecules in PDEA aqueous solutions and gels were also determined by the use of pulsed-gradient spin-echo

Received August 14, 2001. Published on the NRC Research Press Web site at http://canjchem.nrc.ca on December 6, 2001.

D.G. Lessard, M. Ousalem, and X.X. Zhu.[2] Département de chimie, Université de Montréal, C.P. 6128, Succ. Centre-ville, Montréal, QC H3C 3J7, Canada.

[1]This paper is dedicated to Professor G.R. Brown, who passed away on June 19, 2001.

[2]Corresponding author (telephone: (514) 343-6733; fax: (514) 343-7586; e-mail: julian.zhu@umontreal.ca).

 DOI: 10.1139/cjc-79-12-1870 © 2001 NRC Canada

NMR techniques (12). Most of these studies dealt with polydisperse PDEA samples, and none of them addressed clearly the question of the molecular weight effect on the LCST of the polymers.

In the present work, using fractional precipitation, we prepared 11 PDEA fractions with molar masses ranging from 9.6×10^3 to 1.3×10^6 g mol^{-1}. Turbidimetry, also called cloud point technique, and microcalorimetry were used to study the effect of molecular weight on the LCST of these fractions in aqueous solutions.

A number of parameters have been reported to influence the LCST of thermosensitive polymers. It was shown that the presence of salts in the solution generally decrease the LCST of the solution (5, 20) and added surfactants improve the solubility of the polymer, thereby raising the LCST (20–22). Also, phase separations were studied as functions of the amount of cosolvent (23), polymer concentration (24), and pressure (25). Investigations of molecular weight influence on the LCST, however, showed a large discrepancy in the results obtained. Some authors reported an inverse dependence of the LCST on the molar mass (5, 24), while others claimed the opposite (26). Several studies also reported that the molecular weight had no influence on the LCST (6, 27). It is worthwhile to mention that the fractionation of this kind of polymers is quite difficult due to the amphiphilicity of the macromolecule.

Experimental section

All chemicals were purchased from Sigma (St. Louis, Missouri, U.S.A.) and Aldrich (Milwaukee, Wisconsin, U.S.A.) and were used as received. Ammonium persulfate was recrystallized before use.

Polymer synthesis

N,*N*-Diethylacrylamide (DEA) was prepared, as reported previously (11), by reacting acryloyl chloride (97%) with an excess of diethylamine (98%) in methylene chloride at 0°C. The salt was filtered off and the solvent was evaporated. Distillation of the liquid under 0.5 mmHg (1 mmHg = 133.322 Pa) vacuum at 40–50°C in the presence of hydroquinone yielded a clear liquid, which was kept in a freezer until use.

PDEA was obtained by radical solution polymerization of DEA using ammonium persulfate as the initiator and *N*,*N*,*N*′,*N*′-tetramethylethylenediamine as the accelerator. Purified water was degassed with nitrogen and was used as the solvent. The reaction was carried out at room temperature for 4 h. The solvent was then evaporated and PDEA, after dissolution into a small amount of acetone, was purified twice by precipitation in petroleum ether, resulting in a white solid.

Fractionation and characterization

PDEA fractions were obtained by fractional precipitation using acetone as the solvent and hexane as the nonsolvent. To ensure good results, the concentration of the PDEA solution was kept low (less than 0.1 wt%) and the temperature was maintained constant at 25°C. Hexane was added until the solution turned cloudy. Then the temperature was raised by 1 or 2°C to dissolve the precipitated polymer and then allowed to cool down to the precipitation temperature. The system was kept without stirring for at least 1 day before the precipitated fraction was recovered. The remaining solution underwent further precipitation in the same way as described above. This process was repeated to obtain further fractions. In total, 11 fractions were obtained.

The molecular weight and its distribution of the polymer samples were determined by size exclusion chromatography (SEC) on a Waters system equipped with an online Waters 410 differential refractometer and a set of three Ultrastyragel columns. Tetrahydrofuran was used as the mobile phase, and polystyrene samples as the standards in the calibration of the molar masses.

Determination of LCST

The cloud point of PDEA in water was set as the temperature at the inflexion point of the curve obtained by turbidimetry. A CARY 1 BIO UV–vis spectrophotometer coupled to a temperature controller was used in the absorbance mode at a wavelength of 500 nm. A 1-cm sample cell containing ca. 80 μL of solution was used for the measurement against deionized Milli-Q water as the reference. The cloud point of sample with higher concentration was impossible to determine with enough precision due to the saturation of the signal on the spectrophotometer.

Microcalorimetry was also used to determine the LCST of PDEA aqueous solutions. The endothermic signal at its maximum (corresponding to the LCST) was recorded for each sample on a DSC VP-microcalorimeter from Microcal Inc. A cell filled with deionized Milli-Q water was used as the reference. Heating rates of 0.1 and 1.0°C min^{-1} were used, with both methods, to see their effect on the LCST.

The LCST values of aqueous PDEA solutions with different molecular weight were determined by means of turbidimetry and microcalorimetry at a concentration of 1 wt% to ensure an exact value of the cloud point and the LCST.

Results and discussion

The fractionated samples of PDEA have a wide range of molar masses, from 9.6×10^3 to 1.3×10^6 g mol^{-1}. The polydispersity of the fractions were lower than that of the bulk sample ($M_w/M_n = 3.59$) as shown in Table 1.

The LCST of a solute dissolved in a solvent can be obtained from the phase diagram of the system. The phase diagrams of two polymer samples F2 and F9 are shown in Fig. 1, where the cloud point is plotted as a function of concentrations ranging from 0.0001 to 10 wt%. The LCST is given by the lower temperature at which the phase transition occurs. It appears that the most accurate value of the LCST can be obtained for concentrations ranging from 1 to 5 wt% for low and high molecular weight samples, and no significant differences on the LCST are observed within this interval of polymer concentrations.

As shown in Fig. 2*a*, the transmittance of the 1 wt% PDEA solution decreases sharply at a certain temperature owing to the turbidity of the solutions when precipitation occurred. The exact values of the cloud point (LCST), ΔH, and ΔS are listed in Table 1. The general trend observed for this series of samples is that the LCST is lower for the higher molecular weight polymers.

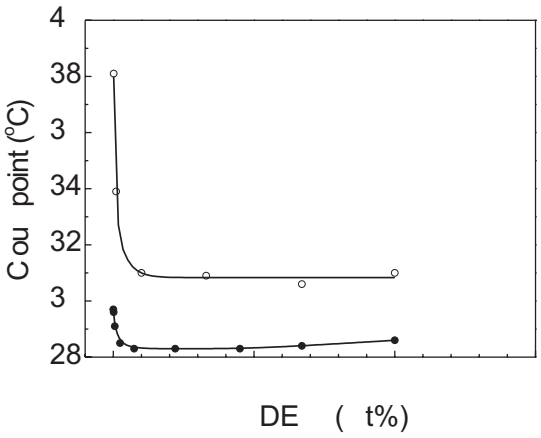
© 2001 NRC Canada

Table 1. Molecular weight and LCST of the PDEA fractions.

Samples	M_n (g mol^{-1})	M_w (g mol^{-1})	M_w/M_n	ΔH (J g^{-1})	ΔS (J g^{-1} K^{-1})	LCST (°C)[a]	
						Turbidimetry	Microcalorimetry
F1	9 600	13 300	1.39	16.9	0.036	32.9	37.0
F2	19 200	40 300	2.10	26.0	0.069	31.0	34.2
F3	32 500	58 500	1.80	16.6	0.039	30.9	32.6
F4	81 600	165 700	2.03	20.1	0.016	30.1	31.0
F5	90 400	132 000	1.46	26.0	0.085	29.7	30.3
F6	96 900	252 000	2.60	22.2	0.059	29.5	30.2
F7	180 900	376 300	2.08	5.3	0.010	29.3	29.6
F8	218 000	311 700	1.43	5.7	0.018	29.1	29.2
F9	363 600	709 000	1.95	8.1	0.003	28.4	28.8
F10	593 600	890 400	1.50	2.0	0.003	28.6	28.6
F11	1 300 000	1 547 000	1.19	1.2	0.006	28.6	28.2

[a]Heating rate at 0.1°C min^{-1}.

Fig 1. Phase diagram of the aqueous solution of PDEA of a low molar mass fraction F2 (open circles) and high molar mass fraction F9 (closed circles).



Microcalorimetric studies confirmed the general tendency of the behavior of the PDEA fractions. The endothermic phase transition occurs at lower temperatures for higher molecular weight samples as illustrated in Fig. 2*b*.

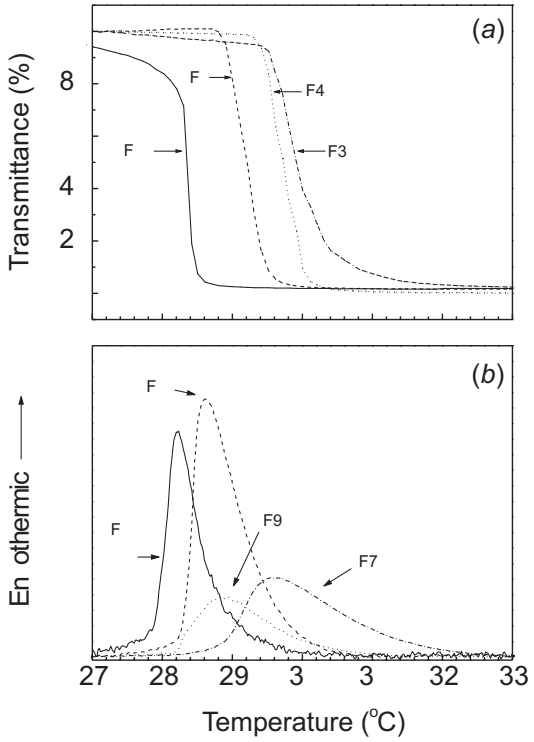
The inverse dependence on molar mass of the LCST was recently observed on PNIPAM (24). This phenomenon is attributed to the difference in the free volumes caused by the polymer chains and the solvent molecules. This difference is much more significant for the longer polymer chains, since they should precipitate at lower temperatures (28, 29). It was demonstrated by Patterson (28) that the LCST is proportional to the critical value of the Flory–Huggins interaction parameter (χ_c) and that the LCST decreases with the ratio of the molar volume of the polymer to that of the solvent (r):

$$[1] \qquad \chi_c = 1/2(1 + r^{-1/2})^2$$

In eq. [1], if the molar volume of the polymer increases with the length of the chain, it is clear that the LCST of the polymer must decrease with the molecular weight of the polymer.

The shape of the curves presented in Fig. 3 suggests a more pronounced effect for lower molecular weight fractions. The slope is steep for values of M_n lower than 2×10^5 g mol^{-1} and becomes more gradual for higher values of M_n. This may explain the broadening of the transmittance curves (Fig. 2*a*) and of the endothermic peaks as M_n decreases (Fig. 2*b*). This implies a minor role of the polydispersity on the width of transition for heavier fractions. A critical value of M_n seems to lie at ca. 2×10^5 g mol^{-1}, after which the LCST values of the samples in water remained nearly constant.

Fig. 2. LCST of 1 wt% aqueous solutions of selected PDEA fractions (see Table 1) obtained at a heating rate of 0.1°C min^{-1} by: (*a*) turbidimetry; and (*b*) microcalorimetry.



The effect of the heating rate (1.0 and 0.1°C min^{-1}) was also investigated. At higher heating rates, the transition temperature is expected to be overestimated because of the poor heat transfer. When working with the 1.0 wt% PDEA fractions, the cloud point technique was found to be more sensitive to the heating rate as shown in Fig. 3*a*, where the LCST

© 2001 NRC Canada

Fig. 3. Effect of the molecular weight on the LCST of the PDEA fractions measured by: (*a*) spectrophotmetry (circles); and (*b*) microcalorimetry (squares) for different heating rates. Open symbols, heating at 1.0°C min^{-1}; closed symbols, 0.1°C min^{-1}.

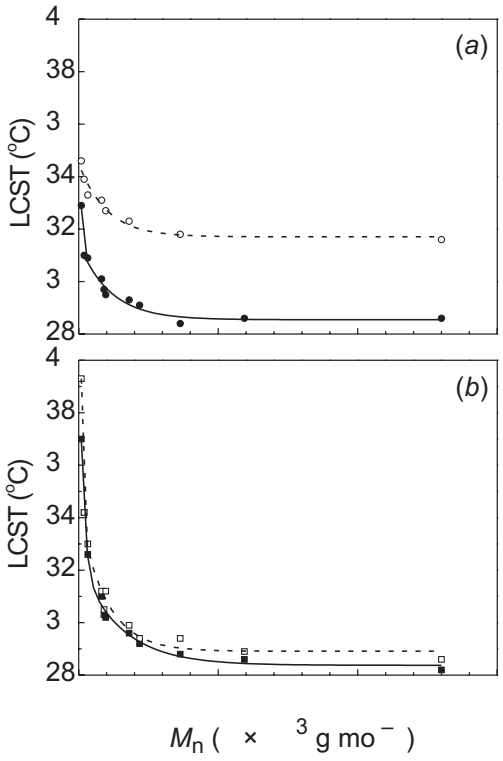
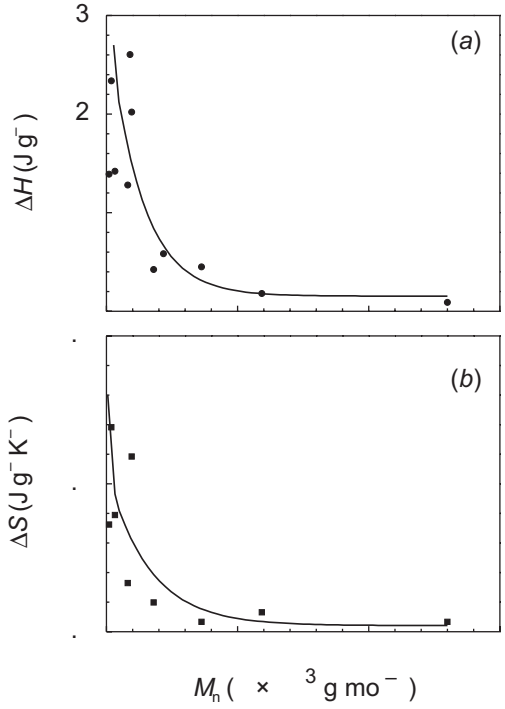


Fig. 4. Effect of the molecular weight on: (*a*) ΔH; and (*b*) ΔS for the PDEA fractions obtained by microcalorimetry at a heating rate of 0.1°C min^{-1}.



obtained at 0.1°C min^{-1} were 3°C lower than those measured at 1.0°C min^{-1}. Such a dependence of the LCST on the heating rate was already reported for a polydisperse sample (11). This was attributed to the poor heat transfer inherent to the method where the recorded temperature is higher than the effective temperature of the sample. Microcalorimetry has a much better heat transfer and, therefore, this effect is less pronounced as shown in Fig. 3*b*.

As seen in Fig. 4, microcalorimetry can be used also to determine the enthalpy (ΔH) and the entropy (ΔS) at the transition. These quantities seem to be strongly dependent on the molecular weight. ΔH and ΔS follow the same trend as the LCST for the samples, i.e., a hyperbolic decrease from 21.0 J g^{-1} and 0.070 J g^{-1} K^{-1} for ΔH and ΔS to limit values of 0.6 J g^{-1} and 0.003 J g^{-1} K^{-1}, respectively. In each case, the final plateau corresponds to a sample with a molar mass of 2×10^5 g mol^{-1}. The value obtained here for ΔH is consistent with that reported by Idziak et al. (11) for a PDEA sample (ΔH = 22.9 J g^{-1} for $M_n = 2.0 \times 10^4$ g mol^{-1}).

It is understandable that the entropy change is smaller for the longer polymer chains. The ΔS values decrease as a function of the average molar mass of the polymer and remain constant after a critical point at $M_n = 2 \times 10^5$ g mol^{-1}. When a hydrophobic solute such as PDEA is dissolved in water, the surrounding molecules tend to organize themselves in an ice-like structure (3). The order created decreases the entropy of the solution. The LCST phenomenon for polymer in aqueous media is possible only if the dissolution is exothermic and the entropy of the mixture is negative (28). A low molar mass polymer at a given weight concentration needs to interact with more water molecules to be solvated, creating more order in the system. This increased order decreases the overall entropy of the solution. The ΔS of the transition is therefore greater.

It can also be demonstrated mathematically that lower molecular weight polymers correspond to higher the ΔH values. It is known that χ_c decrease with the molecular weight of the polymer (28) because the lower molar volume of the polymer gives a lower value of the ratio (r) in eq. [1]. Since χ_c is proportional to the energy required to break the contact between the polymer and the solvent (28), the energy needed to induce the phase separation (ΔH) will be greater for shorter polymer chains.

Conclusion

PDEA fractions were prepared by fractional precipitation despite the amphiphilicity of the polymer. The phase diagrams showed that the changes of the LCSTs of the PDEA aqueous solutions are not significant in the concentration range from 1 to 5 wt%. Low heating rates provide more reliable results with turbidimetry, but this effect is negligible for microcalorimetric measurements. Turbidimetric and microcalorimetric measurements have shown a sharp decrease in their LCST, ΔH, and ΔS values as a function of the molar mass of PDEA. The values become constant after a critical molar mass at ca. $M_n = 2 \times 10^5$ g mol^{-1}. Polydispersity of the polymer seems to plays a minor role for the heavier PDEA fractions.

© 2001 NRC Canada

Acknowledgements

The financial support from Natural Sciences and Engineering Research Council of Canada (NSERC) and Fonds FCAR of Quebec is gratefully acknowledged.

References

1. R. Yoshida, K. Sakai, T. Okano, Y. Sakurai, Y.H. Bae, and S.W. Kim. J. Biomater. Sci. Polym. Ed. **3**, 155 (1991).
2. K.S. Kazanskii and S.A. Dubrovskii. Adv. Polym. Sci. **104**, 97 (1992).
3. H.G. Schild. Prog. Polym. Sci. **17**, 163 (1992).
4. M. Heskins and J.E. Guillet. J. Macromol. Sci.-Chem. Part A, **8**, 1441 (1968).
5. H.G. Schild and D.A. Tirrell. J. Phys. Chem. **94**, 4352 (1990).
6. S. Fujishige, K. Kubota, and I. Ando. J. Phys. Chem. **93**, 3311 (1989).
7. N.A. Platé, T.L. Lebedeva, and L. Valuev. Polym. J. (Tokyo), **31**, 21 (1999).
8. R. Freitag, T. Baltes, and M. Eggert. J. Polym. Sci. Part A: Polym. Chem. **32**, 3019 (1994).
9. M. Kobayashi, T. Ishizone, and S. Nakahama. Macromolecules, **33**, 4411 (2000).
10. M. Itakura, K. Inomata, and T. Nose. Polymer, **41**, 8681 (2000).
11. I. Idziak, D. Avoce, D. Lessard, D. Gravel, and X.X. Zhu. Macromolecules, **32**, 1260 (1999).
12. L. Masaro, M. Ousalem, W.E. Baille, D. Lessard, and X.X. Zhu. Macromolecules, **32**, 4375 (1999).
13. L. Bromberg and G. Levin. J. Polym. Sci. Part A: Polym. Chem. **34**, 2595 (1996).
14. J. Hrouz and M. Ilavsky. Polym. Bull. **22**, 271 (1989).
15. R. Freitag, T. Baltes, M. Eggert, K. Schügerl, and U. Bahr. Bioseparation, **4**, 353 (1994).
16. M. Eggert and R. Freitag. J. Polym. Sci. Part A: Polym. Chem. **32**, 803 (1994).
17. A. Percot, M. Lafleur, and X.X. Zhu. Polymer, **41**, 7231 (2000).
18. L.D. Taylor and L.D. Cerankosky. J. Polym. Sci. **13**, 2551 (1975).
19. J. Plestil, Y.M. Ostanevich, S. Borbely, J. Stejskal, and M. Ilavsky. Polym. Bull. **17**, 465 (1987).
20. J. Eliassaf. J. Appl. Polym. Sci. **22**, 873 (1978).
21. L.T. Lee and B. Cabane. Macromolecules, **30**, 6559 (1997).
22. G. Staikos. Macromol. Rapid Commun. **16**, 913 (1995).
23. H.G. Schild, M. Muthukumar, and D.A.Tirrell. Macromolecules, **24**, 948 (1991).
24. Z. Tong, F. Zeng, and X. Zheng. Macromolecules, **32**, 4488 (1999).
25. K. Otake, R. Karaki, T. Ebina, C. Yokoyama, and S. Takahashi. Macromolecules, **26**, 2194 (1993).
26. X. Zheng, Z. Tong, X. Xie, and F. Zeng. Polym. J. (Tokyo), **30**, 284 (1998).
27. E.I. Tiktopoulo, V.N. Uversky, V.B. Lushchik, S.I. Klenin, V.E. Bychkova, and O.B. Ptitsyn. Macromolecules, **28**, 7519 (1995).
28. D. Patterson. Macromolecules, **2**, 672 (1969).
29. F. Wang, S. Saeki, and T. Yamaguchi. Polymer, **40**, 2779 (1999).

© 2001 NRC Canada

Kinetic stabilizing effect of the 4-*N*-methylacetamido substituent on the phenylnitrenium ion

Patrick H. Ruane and Robert A. McClelland

Abstract: Photolysis of 4-(*N*-methylacetamido)phenyl azide in aqueous solution results in quantitative formation of the 4-(*N*-methylacetamido)phenylnitrenium ion, this cation arising from solvent protonation of an initially formed singlet arylnitrene. The cation is observed by flash photolysis, and is identified through characteristic quenching by azide ion and by 2′-deoxyguanosine, both excellent nucleophiles for arylnitrenium ions in water. The nitrenium ion is protonated in acidic solutions to form the 4-(*N*-methylacetamido)aniline dication, whose pK_a is determined to be 1.5 based on the rate–pH profile. This means that the nitrenium ion is relatively basic, which suggests that there is significant positive charge on the *N*-methylacetamido group. Further evidence for this is seen in the remarkably long lifetime (5 ms) of the nitrenium ion in water. In fact, the 4-(*N*-methylacetamido)phenylnitrenium ion is 5000-fold longer-lived than the 4-methoxy-substituted analog. A 4-methoxy substituent on a phenyl ring is more electron donating according to σ^+ values (–0.78 for MeO vs. –0.60 for NMeAc). The dramatic reversal in the arylnitrenium ions is another example of the failure of these to follow the carbocation scale.

Key words: nitrenium ion, flash photolysis, amide substituent.

Résumé : La photolyse de l'azoture de 4-(*N*-méthylacétamido)phényle, en solution aqueuse, conduit à la formation quantitative de l'ion 4-(*N*-méthylacétamido)phénylnitrénium qui découle de la protonation par le solvant de l'arylnitrène singulet qui se forme originalement. On observe ce cation par photolyse éclair et on l'a identifié par un piégeage caractéristique à l'aide de l'ion azoture ou de la 2′-désoxyguanosine qui sont deux excellents nucléophiles pour les ions arylnitrénium dans l'eau. L'ion nitrénium se protone en solutions acides pour former le dication 4-(*N*-méthylacétamido)aniline qui, sur la base d'un profil vitesse–pH, aurait un pK_a de 1,5. Ce résultat indique que l'ion nitrénium est relativement basique et ceci suggère que le groupe *N*-méthylacétamido porte une charge positive importante. Cette suggestion est confirmée par le temps de vie relativement long (5 ms) de l'ion nitrénium dans l'eau. En fait, le temps de vie de l'ion 4-(*N*-méthylacétamido)phénylnitrénium est 5000 fois plus long que celui de son analogue portant un substituant 4-méthoxy. Un substituant 4-méthoxy sur un noyau phényle est plus électrorépulsif selon les valeurs de σ^+ (–0,78 pour MeO vs. –0,60 pour NMeAc). Cette inversion dramatique dans les ions arylnitrénium est un autre exemple du fait que ces entités ne suivent pas l'échelle des carbocations.

Mots clés : ion nitrénium, photolyse éclair, substituant amide.

[Traduit par la Rédaction]

The carcinogenicity observed with many aromatic amines is now recognized to be the result of metabolic activation (1–3). This bioactivation involves oxidation to a hydroxylamine derivative **2** followed by *O*-esterification, with either an acetyl or a sulfate transferase. Heterolysis of the N—O bond of the acetate or sulfate ester **3** yields a nitrenium ion **4**, which reacts with DNA, principally at the C-8 position of guanine. Adducts such as the C-8 adduct **5** have been characterized in both biological and model systems (Scheme 1) (4–6).

Arylnitrenium ions have not been spectroscopically characterized in super acids (7–9), although there have been reports of their observation in electrochemical experiments (10–12). Our group (13–23), as well as others (24–27), have recently reported their observation using laser flash photolysis (LFP) with aryl azides serving as the photochemical precursors. Nitrenium ions have also been observed with LFP by the Falvey group (28–31) using other photochemical methods. As shown in Scheme 1, the nitrenium ion from the aryl azide arises through protonation of a singlet nitrene **7**. The latter is the initial product of photolysis, being formed by loss of nitrogen from the azide. Singlet nitrenes are highly reactive species (32), but they are also remarkably basic (14). The singlet 4-biphenylylnitrene **7** (R = Ph), for example, is protonated by a solvent water molecule on the ps time scale in 20% acetonitrile:80% water (14).

Included amongst the intermediates that we have studied were a series of 4-alkoxyphenylnitrenium ions (15, 19). The

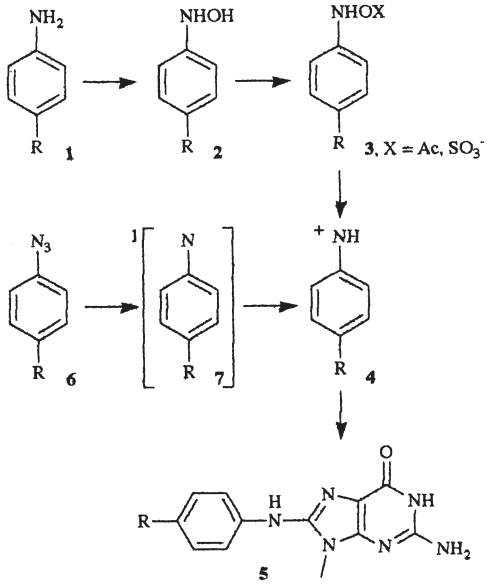
Received July 12, 2001. Published on the NRC Research Press Web site at http://canjchem.nrc.ca on December 10, 2001.

P.H. Ruane and R.A. McClelland.[1] Department of Chemistry, University of Toronto, Toronto, ON M5S 3H6, Canada.

[1]Corresponding author (telephone: (416) 978-3592; fax: (416) 978-3592; e-mail: rmcclell@alchemy.chem.utoronto.ca).

 DOI: 10.1139/cjc-79-12-1875 © 2001 NRC Canada

Scheme 1.



4-ethoxyphenylnitrenium ion would be derived from the carcinogen phenacetin, an analgesic long removed from the market. These cations were obtained essentially quantitatively upon irradiation of the appropriate azide in aqueous solutions; they had lifetimes in water of the order of 1 ms.

In this paper, we report a study of the *N*-(methylacetamido) phenylnitrenium ion, generated from the appropriate azide. This represents the first spectroscopic detection of an arylnitrenium ion bearing a 4-acetamido substituent. A para amido substituent, on the σ^+ scale, is substantially electron donating ($\sigma^+ = -0.60$) but it is not as good as *p*-methoxy ($\sigma^+ = -0.78$). One of the objectives of our work was to see if the σ^+ order was also observed when these substituents were present on nitrenium ions.

Experimental section

4-Acetamidophenyl azide (6, R = $NHCOCH_3$)

4′-Aminoacetanilide (0.1 mol) was dissolved in 95% ethanol (100 mL) and, with cooling in an ice bath, 5.0 mL of concentrated sulfuric acid was added. After 10 min, amyl nitrite (6.0 mL) was added in small portions. The reaction temperature was raised to 35–40°C for 20 min, and after cooling, the aryldiazonium salt was precipitated by the addition of ether (200 mL). The resultant precipitate was washed repeatedly with ether until the ethereal washings gave no coloration. The semiwet precipitate with ether was treated at 0°C with a solution of sodium azide (5.0 g) and sodium acetate (10 g) in 50 mL of water. After stirring for 1 h, the product was extracted into ether, which was washed with dilute sulfuric acid, water, 10% sodium carbonate, and water. The ethereal extract was dried over magnesium sulfate and the solvent was evaporated under reduced pressure. 4-Acetamidophenyl azide was obtained as a solid with mp 114–118°C which was judged sufficiently pure to proceed to the next reaction stage. ^{1}H NMR (200 MHz, DMSO-d_6) δ: 10.02 (s, 1H, disappeared in D_2O), 7.63 (d, J = 8.8 Hz, 2H), 7.04 (d, J = 8.5 Hz, 2H), 2.04 (s, 3H).

4-(*N*-Methylacetamido)phenyl azide (6, R = $N(CH_3)COCH_3$)

The 4-acetamidophenyl azide (2.5 mmol) and methyl iodide (3.0 mmol) were dissolved in anhydrous dimethyl sulfoxide (50 mL) and sodium hydride hydride (95%, 3.0 mmol) was added under argon. After stirring for 1 h at room temperature, the reaction mixture was diluted with ether (150 mL) and the organic layer was washed with water, dried over magnesium sulfate, and the solvent evaporated under reduced pressure to give an oily residue which solidified on standing. The crude product was purified by column chromatography on silica gel eluting with 50:50 ethyl acetate:hexanes. 4-(*N*-Methylacetamido)phenyl azide decomposed on heating above 100°C. HRMS *m*/*z* 190.0859; $C_9H_{10}N_4O$ requires 190.0855. IR (cm^{-1}): 2219. ^{1}H NMR (300 MHz, $CDCl_3$) δ: 7.62 (d, J = 8.5 Hz, 2H), 7.10 (d, J = 8.5 Hz, 2H), 3.26 (s, 3H), 1.94 (s, 3H). HPLC (see below) showed only a single peak.

Laser flash photolysis experiments involved ca. 20 ns pulses at 248 nm (60–120 mJ per pulse) from a Lumonics excimer laser. A pulsed Xenon lamp providing monitoring light. The sample was placed in a 4 × 1 × 1 cm cuvette, irradiated with the laser on the 4 × 1 face, and monitored perpendicular so that the path length was 4 cm. The cuvette was replaced with a fresh solution after each irradiation. After passing through a monochromator, the signal from the photomultiplier tube was digitized and sent to a computer for analysis.

Conventional flash photolysis experiments were performed using an apparatus previously described (33) with the sample being irradiated with a broad band flash lamp of ca. 100 μs duration.

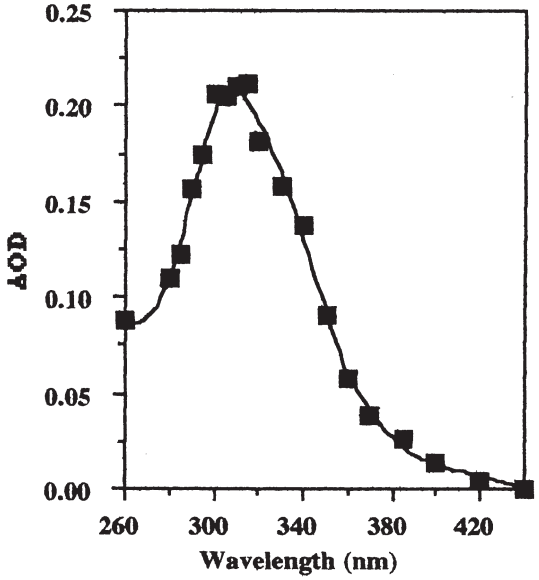
Product analyses were performed with a Waters HPLC system using a C^{18} column with 2 mL per minute flow rate and the UV–vis detector set at 260 nm. Elution was carried out with isocratic 60:40 acetonitrile:water. The 4-(*N*-methylacetamido)phenyl azide was dissolved in water and dilute aqueous buffers to give solutions of concentration 5×10^{-4} M. Injection of these solutions before irradiation gave only one peak in the chromatogram. As discussed in the *Results section*, irradiation of this aqueous solution at 254 nm in a Rayonet reactor resulted in clean conversion to a peak for an unstable species, which thermally converted over time to a third peak with a retention time identical to that of *p*-benzoquinone. That this peak did correspond to benzoquinone was verified from a scaled-up reaction where the product was isolated and its ^{1}H NMR spectrum recorded. The conversions of the azide to the benzoquinone were quantitatively analyzed by determining the response factors for the two, and using these to correct peak areas of the irradiated solutions.

Results and discussion

As shown in Fig. 1, 248 nm laser irradiation of an aqueous solution of 4-(*N*-methylacetamido)phenyl azide resulted in a strong absorbance with a λ_{max} at 310 nm. This absorbance was quite stable, showing only a small decay at the longest times available with our laser apparatus (1 ms). Addition of small concentrations of sodium azide accelerated the decay, resulting in excellent first-order plots proceeding to the baseline above 290 nm. A plot of the decay

© 2001 NRC Canada

Fig. 1. Transient spectrum obtained on 248 nm laser irradiation of a solution of 4-(*N*-methylacetamido)phenyl azide (2×10^{-4} M) in water. (Note that this is a difference spectrum, i.e., the optical density after the laser pulse – the optical density before the pulse).

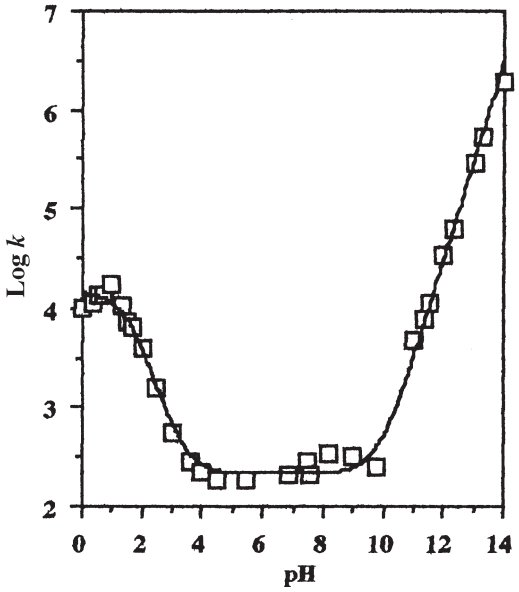


rate constants *k* (obs) vs. the concentration of azide was linear, with a slope of 3.9×10^9 M^{-1} s^{-1}.

Highly efficient quenching by azide ion is a characteristic of carbocations and arylnitrenium ions (34). More compelling evidence for the 4-(*N*-methylacetamido)phenylnitrenium ion comes in the analysis of the products of irradiation in aqueous solutions. Protonation of a singlet arylnitrene is obvious in the products (14), since the nucleophilic adducts derived from the further reactions of a nitrenium ion are very different in nature from the products associated with other reactions of singlet arylnitrenes, such as intersystem crossing to a triplet or ring expansion to a didehydroazepine. In the case of the nitrenium ion in question in this study, we anticipated that the reaction with water would follow the course outlined in Scheme 2. The solvent should react at the position para to the formal nitrenium center, the normal fate of simple arylnitrenium ions in water (14, 35–37). This would give an intermediate **8** which would eliminate *N*-methylacetamide to give the monoimine of benzoquinone **9**. This species is unstable in aqueous solutions, undergoing hydrolysis of the imine to give *p*-benzoquinone **10** (38).

Indeed irradiation of 4-(*N*-methylacetamido)phenyl azide at 254 nm in aqueous solutions for times up to 75% conversion resulted in the formation of benzoquinone as the only stable product that could be observed by HPLC. The yield of this product, based upon quantitative HPLC analysis, was 100% (95 ± 5%). A second peak could be seen at early times. This peak disappeared and was replaced by the peak for the benzoquinone. The material responsible for this early peak can be identified as the quinoneimine **9**. This assignment is based upon an identical UV spectrum and, in particular, kinetic behavior for this material with that previously published for an authentic sample of the quinoneimine (38). This same imine was also observed in our earlier studies with the *p*-alkoxyphenyl azides (19). The nitrenium ions derived from these azides react in an analogous manner, with

Fig. 2. Log rate vs. pH for the 4-(*N*-methylacetamido)phenylnitrenium ion. Points are experimental and have been extrapolated to zero buffer concentration where measurements were performed in buffers. The line through the experimental points has been drawn according to the equation $k_{OH}[OH^-] + (k_w^+{}^2[H^+] + k_w^+K_a)$: $([H^+] + K_a)$ using the values for the parameters given in the text. It can be noted that the plateau in acid decreases slightly. This may be related to a specific salt effect, as was observed in a previous study (14).



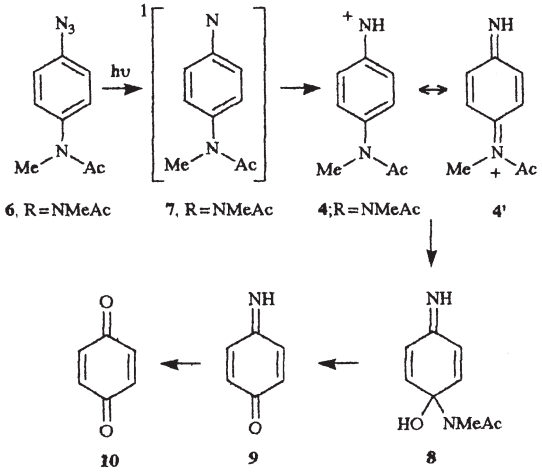
water reacting at the para position to give an adduct that eliminates an alcohol to give the same imine **9**.

It can be noted that there is an alternative mechanism for the formation of **9** from the *N*-methylacetamidophenyl nitrenium ion. This involves hydrolytic deacylation of the nitrenium ion, rather than water addition at the para position. This route can be ruled out on two grounds. The first is that this reaction results in an intermediate bis-imine, 1-imino–4-methyliminobenzoquinone. According to data for the analog without the methyl group (38) this should be long-lived, particularly at higher pH. The second is that the bis-imine is likely to hydrolyze both imino groups at comparable rates, so that there would be two different monoimine intermediates, **9** and the *N*-methyl analog of **9**. Thus, this route predicts that there could be three intermediates observable by HPLC. In fact, there is only one such intermediate.

While the decay of the nitrenium ion in water alone was too slow for the apparatus, it could be observed by irradiating an aqueous solution of 4-(*N*-methylacetamido)phenyl azide with a lamp flash photolysis apparatus. This showed an excellent first-order decay occurring on the ms time scale with a rate constant of 2×10^2 s^{-1}. The rate constant for quenching by azide ion is interesting in this regard, since the value, 3.9×10^9 M^{-1} s^{-1}, is still quite close to the maximum value of 9 to 10×10^9 $M^{-1}s^{-1}$ found for more reactive nitrenium ions (16). This maximum is associated with the azide–nitrenium combination becoming diffusion controlled, i.e., the rate-limiting step is encounter (16, 34). Combinations of azide and short-lived benzylic-type carbocations are also diffusion-controlled (34, 39). What is interesting is that

© 2001 NRC Canada

Scheme 2.



6, R=NMeAc 7, R=NMeAc 4;R=NMeAc 4' 10 9 8

the break to rate-limiting bond formation as the carbocation becomes less reactive occurs at a much earlier point then it does with a nitrenium ion. For example, a triphenylmethyl cation that reacted with water with a rate constant of 2×10^2 s^{-1} would react with azide ion with a rate constant around 1×10^8 M^{-1} s^{-1}, well below the diffusion limit (39).

Figure 2 provides further kinetic information about the behavior of the nitrenium ion in the form of the dependence of its rate constant for decay as a function of pH. This figure was constructed through a combination of experiments with laser and lamp flash photolysis, the latter being used for the solutions with pH 2–10, and the former for the faster reactions in the acidic and basic solutions. It can be seen that there is a pH-independent region from pH 4–10. This represents the reaction of the cation with water. In more basic solutions, this breaks to a linear dependence on hydroxide ion, with the slope $k_{OH} = 3 \times 10^6$ M^{-1} s^{-1}. This is clearly explained by reaction with hydroxide ion. The acceleration in acid is a feature of nitrenium ions that we have observed previously (14, 19). It is explained by the mechanism of Scheme 3, whereby under acidic conditions, reaction occurs via the dication **11**, the conjugate acid of the nitrenium ion.

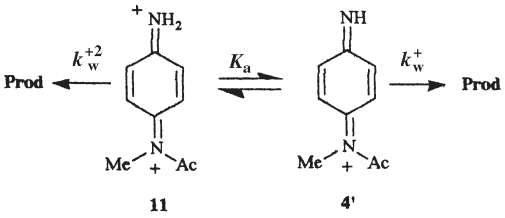
The levelling below pH 2 indicates that the protonation equilibrium actually shifts to the dication. The experimental data can be fit to eq. [1],

$$[1] \qquad k_{obs} = \frac{F(k_w^{+2}[H^+] + k_w^+ K_a}{[H^+] + K_a}$$

where k_w^{+2} and k_w^+ are the rate constants for the reaction of water with the dication and monocation, respectively, and K_a is the acidity constant of the dication. Parameters obtained from this fit are provided in Table 1, where they are also compared with values obtained from other systems.

The basicity of the NH group of an arylnitrenium ion is one indicator that the structure Ar-N^+H is only a very minor resonance contributor. There must, in fact, be little positive charge at this nitrogen, i.e., that the cation is better written as a cyclohexadienyl cation with an imine substituent, as in the resonance structure **4′** in Scheme 3. Recent time-resolved IR (30, 31) and resonance Raman (27) spectra have provided excellent evidence for this. The data in Table 1 show that the

Scheme 3.



11 4'

nitrenium ion of this study is one of the more basic examples, although it is not nearly as basic as the nitrenium ion derived from benzidine (23). This suggests that the *N*-methylacetamido group in the cation bears a considerable fraction of the positive charge. This is clearly also evident in the kinetic stability of this cation.

The 4-(*N*-methylacetamido)phenylnitrenium ion was also generated from the azide in the presence of 2′-deoxyguanosine. The nucleoside did quench the cation, with a rate constant k_{dG} of 9.0×10^6 M^{-1} s^{-1}. Efficient quenching by guanine derivatives is also a characteristic of arylnitrenium ions. We have previously determined k_{dG} values for a series of biphenylylnitrenium ions (17). The reactive derivatives in this series combined at the diffusion limit with a constant k_{dG} of 2×10^9 M^{-1} s^{-1}. The less reactive derivatives react more slowly, and showed a constant k_{dG}:k_w selectivity of 2 to 3×10^4 M^{-1}. The value of k_{dG}:k_w for the cation of this study is 4.5×10^4 M^{-1}. Thus, this cation is behaving in a similar manner as the biphenylyl derivatives.

One of the remarkable features of the 4-(*N*-methylacetamido)phenylnitrenium ion is its long lifetime in water. This is dramatically illustrated in Fig. 3 in terms of a Hammett plot of the rate constants for water addition vs. σ^+. As originally noted by Novak et al. (35) this correlation is scattered. What is particularly notable is that the lifetime of the 4-NMeAc derivative is 5000-fold longer than that of the 4-methoxy-substituted cation, despite the fact that 4-MeO is more electron donating according to its σ^+ value (–0.78 for MeO vs. –0.60 for NMeAc (40)). As noted above, there is now excellent evidence that arylnitrenium ions have substantial cyclohexadienyl cation character. With heteroatom substituents such as oxygen and nitrogen, the positive charge will be further significantly delocalized onto the heteroatom. Thus, the 4-methoxyphenylnitrenium ion is probably best described as an oxocarbocation (C=O$^+$Me), and the cation of this study as a acyliminium ion (C=N$^+$MeAc). Since σ^+ calibrates the effect of a substituent on the transition state for a developing positive charge on a benzylic carbon, it is therefore not surprising that the arylnitrenium correlation is poor. There is in fact some evidence that intrinsic barriers for addition to oxocarbocations are low, i.e., that the cations are inherently reactive (41). No such data exists for acetylated iminium ions. The present study suggests that this class of cation is inherently less reactive.

In conclusion, this paper further describes the remarkable basicity of singlet nitrenes, especially those bearing an electron-donating group in the 4- position. The results provide further confirmation that arylnitrenium ions are better described as imino cyclohexadienyl cations. The 4-*N*-methylacetamidophenylnitrenium ion is in fact remarkably long lived in aqueous solution especially when compared to

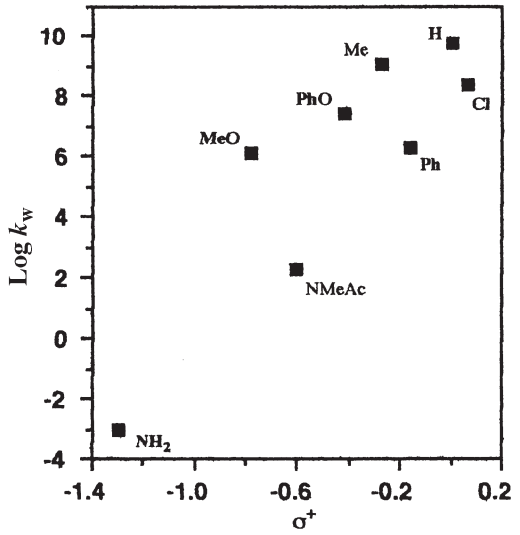
© 2001 NRC Canada

Table 1. Acidity constants for aniline dications, and rate constants for reaction of the dications and their nitrenium conjugate bases with water.

Constant	A	B	C	D	E
pK_a $(ArNH_2)^{+2}$	5.0	1.5	0.6	0.1	<–0.3
k_w^{+2} $(ArNH_2)^{+2}$ (s^{-1})	8×10^{-5}	1.4×10^{4}	1.9×10^{6}	6.0×10^{7}	$>4 \times 10^{8}$
k_w^{+} $(ArNH)^{+}$ (s^{-1})	1×10^{-2}	2.2×10^{2}	1.3×10^{4}	1.1×10^{6}	1.1×10^{6}

Note: A: Ar = 4′-aminobiphenylyl (23); **B**: Ar = 4-(*N*-methylacetamido)phenyl (this work); **C**: Ar = 2-fluorenyl (14); **D**: Ar = 4-biphenylyl (14); **E**: Ar = 4-methoxyphenyl (19).

Fig. 3. Hammett plot for the hydration of arylnitrenium ions 4-$XC_6H_4NH^+$. Data for H (37), 4-Me (36), and 4-Cl (36) are based on a clock method. Other rate constants are directly measured: 4-Ph (14), 4-MeO (19), 4-PhO (19), 4-NH_2 (monoprotonated benzoquinone bis-imine) (38).



other aryl nitrenium ion bearing electron-donating groups in the para position such as alkoxy. Their long lifetimes in water make them viable intermediates in mechanistic models that explain biological effects associated with monoamides of *p*-benzenediamines.

Acknowledgement

Financial support from the Natural Sciences and Engineering Research Council of Canada (NSERC) is gratefully acknowledged.

References

1. R.H. Heflich and R.E. Neft. Mutat. Res. **318**, 73, (1994).
2. A. Parkinson. *In* Casarett and Doull's toxicology: The basic science of poisons. 5th ed. *Edited by* C.D. Klassen. McGraw Hill, New York. 1996. pp. 113–186.
3. H.C. Pitot, III, and Y.P. Dragon. *In* Casarett and Doull's toxicology: The basic science of poisons. 5th ed. *Edited by* C.D. Klassen. McGraw Hill, New York. 1996. pp. 201–267.
4. S.A. Kennedy, M. Novak, and B.A. Kolb. J. Am. Chem. Soc. **119,** 7654 (1997).
5. R.A. McClelland, A.R. Ahmad, A.P. Dicks, and V.E. Licence. J. Am. Chem. Soc. **121**, 3303 (1999).
6. A. Dipple. Carcinogenesis, **16**, 437 (1995).
7. G.A. Olah and D.J. Donovan. J. Org. Chem. **43**, 1743 (1978).
8. G.A. Olah, G.K.S. Prakash, and M. Arvanaghi. J. Am. Chem. Soc. **102**, 6640 (1980).
9. G.A. Olah, M. Arvanaghi, and G.K.S. Prakash. J. Am. Chem. Soc. **104**, 1628 (1982).
10. U. Svanholm and V.D. Parker. J. Am. Chem. Soc. **96**, 1234 (1974).
11. D. Serve. J. Am. Chem. Soc. **97**, 432 (1975).
12. A. Riecker and B. Reiser. Tetrahedron Lett. **31**, 5013 (1990).
13. R.A. McClelland, P.A. Davidse, and G. Hadzialic. J. Am. Chem. Soc. **117**, 4173 (1995).
14. R.A. McClelland, M.J. Kahley, P.A. Davidse, and G. Hadzialic. J. Am. Chem. Soc. **118**, 4794 (1996).
15. P. Sukhai and R.A. McClelland. J. Chem. Soc. Perkin Trans. 2, 1529 (1996).
16. D. Ren and R.S. McClelland. Can. J. Chem. **76**, 78 (1998).
17. R.A. McClelland, T.A. Gadosy, and D. Ren. Can. J. Chem. **76**, 1327 (1998).
18. A.P. Dicks, A. Ahmad, and R.A. McClelland. J. Chem. Soc. Perkin Trans. 2, 1 (1999).
19. P. Ramlall and R.A. McClelland. J. Chem. Soc. Perkin Trans. 2, 225 (1999).
20. T.A. Gadosy and R.A. McClelland. J. Am. Chem. Soc. **121**, 1459 (1999).
21. R. Bose, A.R. Ahmad, A.P. Dicks, M. Novak, K.J. Kayser, and R.A. McClelland. J. Chem. Soc. Perkin Trans. 2, 1591 (1999).
22. P. Ramlall, Y. Li, and R.A. McClelland. J. Chem. Soc. Perkin Trans. 2, 1601 (1999).
23. R.A. McClelland, D. Ren, R. D'Sa, and A.R. Ahmed. Can. J. Chem. **78**, 1178 (2000).
24. J. Michalak, H.B. Zhai, and M. Platz. J. Phys. Chem. **100**, 14 028 (1996).
25. R. Born, C. Burda, P. Senn, and J. Wirz. J. Am. Chem. Soc. **119**, 5061 (1997).
26. N.P. Gritsan, T. Yuzawa, and M.S. Platz. J. Am. Chem. Soc. **119**, 5059 (1997).
27. P. Zhu, S.Y. Ong, P.Y. Chan, K.H. Leung, and D.L. Phillips. J. Am. Chem. Soc. **123**, 2645 (2001).
28. G.B. Anderson and D.E. Falvey. J. Am. Chem. Soc. **115**, 9870 (1993).
29. R.J. Robbins, L.L.-N. Yang, G.B. Anderson, and D.E. Falvey. J. Am. Chem. Soc. **117**, 6544 (1995).
30. S. Srivastava, J.P. Toscano, R.J. Moran, and D.E. Falvey. J. Am. Chem. Soc. **119**, 11 552 (1997).
31. S. Srivastava, P.H. Ruane, J.P. Toscano, M.B. Sullivan, C.J. Cramer, D. Chiapperino, E.C. Reed, and D.E. Falvey. J. Am. Chem. Soc. **122**, 8271 (2000).
32. G.B. Schuster and M.S. Platz. Adv. Photochem. **17**, 143 (1992).
33. A.A. Allen, A.J. Kresge, N.P. Schepp, and T.T. Tidwell. Can. J. Chem. **65**, 1719 (1987).
34. R.A. McClelland. Tetrahedron, **52**, 6823 (1996).
35. M. Novak, M.J. Kahley, J. Lin, S.A. Kennedy, and L.A. Swanegan. J. Am. Chem. Soc. **116**, 11 626 (1994).

© 2001 NRC Canada

36. M. Novak, M.J. Kahley, J. Lin, S.A. Kennedy, and T.G. James. J. Org. Chem. **60**, 8294 (1995).
37. J.C. Fishbein and R.A. McClelland. Can. J. Chem. **74**, 1321 (1996).
38. J.F. Corbett. J. Chem. Soc. B, 213 (1969).
39. R.A. McClelland, V.M. Kanagasabapathy, N. Banait, and S. Steenken. J. Am. Chem. Soc. **113**, 1009 (1991).
40. V.M. Csizmadia, K.M. Koshy, K.C.M. Lau, R.A. McClelland, V.J. Nowland, and T.T. Tidwell. J. Am. Chem. Soc. **101**, 974 (1979).
41. V. Jagannadham, T.L. Amyes, and J.P. Richard. J. Am. Chem. Soc. **115**, 8465 (1993).

© 2001 NRC Canada

Reaction of arylnitrenium ions with guanine derivatives: N^1-methylguanosine and N^2,N^2-dimethylguanosine

Bernice Cheng and Robert A. McClelland

Abstract: A prior flash photolysis study of the direct reaction of arylnitrenium ions with 2′-deoxyguanosine identified a second intermediate that grew in as the transient nitrenium ion reacted with the nucleoside. This intermediate was identified as the the product of the addition of the nitrenium ion to the C-8 position of guanine prior to loss of the C-8 proton — the C-8 intermediate. A feature of the C-8 intermediate is that it exists in acid–base forms. This behavior was evident in both a spectroscopic analysis as well as in the rate–pH profile, which showed a break around pH 4 from a pH-independent reaction to a reaction that was first-order in H^+. The present study was designed to identify the structure of the conjugate base form. This involved a kinetic study of the decay of the C-8 intermediate derived from the reaction of the 2-fluorenylnitrenium ion with N^1-methylguanosine and N^2,N^2-dimethylguanosine. The rationale was that the former is unable to lose the N-1 proton, while the latter cannot deprotonate at the NH_2 group. The rate–pH profiles clearly show that it is the N-1 proton that is acidic. The rate constants for the C-8 intermediate of N^2,N^2-dimethylguanosine show the same downward break observed with 2′-deoxyguanosine and guanosine associated with conversion to the conjugate base form. In contrast, the rate constants for the N^1-methylguanosine intermediate are independent of pH. Rate constants for the reaction forming the C-8 intermediate are also reported. These show that the reaction of nitrenium ions with the N^2,N^2-dimethylguanine derivative is significantly faster (except where the reactions are diffusion controlled). This is consistent with the initial step of the reaction of an arylnitrenium ion and guanine occurring by direct addition at C-8. The developing positive charge in such a reaction can be delocalized to the C-2 position where π donors such as NH_2 and NMe_2 can exert a stabilizing effect.

Key words: nitrenium, arylnitrenium, guanosine, DNA adduct.

Résumé : Une étude antérieure par photolyse éclair de la réaction directe des ions arylnitrénium avec la 2′-désoxyguanosine a identifié une deuxième intermédiaire dont la concentration croissait alors que l'ion nitrénium réagissait avec le nucléoside. L'intermédiaire avait été identifié comme le produit d'addition de l'ion nitrénium sur la position C-8 de la guanine, avant la perte du proton C-8 — l'intermédiaire C-8. Une caractéristique de l'intermédiaire C-8 est sa possibilité d'exister sous les formes acide et base. Ce comportement était évident tant dans une analyse spectroscopique que dans le profil vitesse–pH qui mettait bien en évidence un bris autour du pH 4 d'une réaction indépendante du pH à une réaction du premier ordre en ions H^+. L'étude présente a été réalisée afin d'identifier la structure de la forme de la base conjuguée. Elle implique une étude cinétique de la décroissance de l'intermédiaire C-8 obtenu par réaction de l'ion 2-fluorénylnitrénium avec les N^1-méthyl- et N^2,N^2-diméthylguanosines. La base de ce choix réside dans le fait que le premier intermédiaire ne peut perdre de proton en N-1 alors que le deuxième ne peut pas se déprotoner au niveau du groupe NH_2. Les profils de vitesse–pH montrent clairement que le proton acide est en N-1. Les constantes de vitesse de l'intermédiaire de la N^2,N^2-diméthylguanosine présentent la même diminution que celles observées avec la 2′-désoxyguanosine et la guanosine associées avec la conversion en forme conjuguée basique. Par ailleurs, les constantes de vitesse pour l'intermédiaire de la N^1-méthylguanosine sont indépendantes du pH. On a aussi déterminé les constantes de vitesse pour la formation de l'intermédiaire C-8. Celles-ci démontrent que la réaction des ions nitrénium avec le dérivé N^2,N^2-diméthylguanidine est beaucoup plus rapide (à l'exception des cas où les réactions sont sous le contrôle de la diffusion). Ce résultat est en accord avec une étape initiale de la réaction d'un ion arylnitrénium avec la guanidine qui se produirait par une addition directe en C-8. La charge positive qui se développerait dans une telle réaction peut être délocalisée vers la position C-2 dans laquelle des donneurs π tels que NH_2 et NMe_2 peuvent exercer un effet stabilisant.

Mots clés : nitrénium, arylnitrénium, adduit avec l'ADN, guanosine.

[Traduit par la Rédaction]

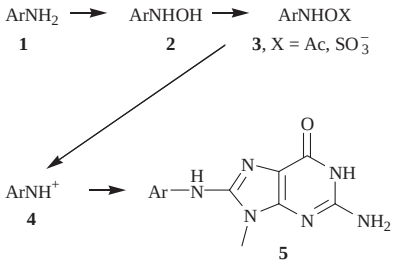
Received July 19, 2001. Published on the NRC Research Press Web site at http://canjchem.nrc.ca on December 10, 2001.

B. Cheng and R.A. McClelland.[1] Department of Chemistry, University of Toronto, Toronto, ON M5S 3H6, Canada.

[1]Corresponding author (telephone: (416) 978-3592; fax: (416) 978-3592; e-mail: rmcclell@alchemy.chem.utoronto.ca).

 DOI: 10.1139/cjc-79-12-1881 © 2001 NRC Canada

Scheme 1.



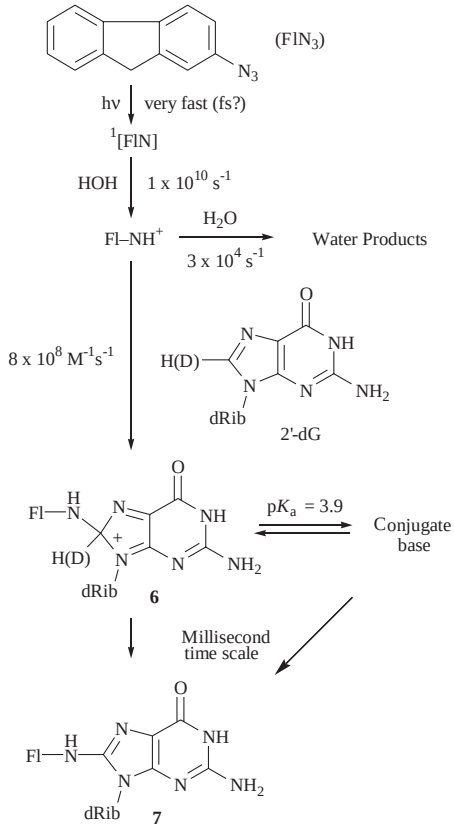
A common product formed in vivo with arylamine carcinogens **1** is a covalent DNA adduct **5** derived from arylamination at the C-8 position of guanine residues (1). The reactive intermediate responsible for this product is an arylnitrenium ion **4** (2–5). This electrophile is obtained after metabolic activation of the arylamine (6–8) – P450-mediated oxidation to a hydroxylamine **2**, followed by acetylation or sulphation to a reactive ester **3** whose S_N1-type ionization produces the nitrenium ion (Scheme 1).

While there can be no doubt these days that the C-8 adduct is obtained from the reaction of the nitrenium ion and guanine (2–5), there has been debate over the reaction mechanism. Based upon experiments with C-8-methylated guanine derivatives, both Humphreys et al. (9) and Kennedy et al. (3) have suggested that the nitrenium ion reacts initially at the N-7 position, followed by migration to C-8. This same suggestion has been advanced in a recent paper, also from the Guengerich group (10). Our group, however, has suggested that the mechanism is essentially a straightforward electrophilic aromatic substitution, with initial reaction directly at the C-8 carbon, followed by loss of the C-8 proton (5).

Our evidence was based on experiments employing flash photolysis where arylnitrenium ions were observed as transient intermediates, and their reactions with guanine derivatives directly monitored (5). The important aspects of this work are summarized in Scheme 2 with the 2-fluorenylnitrenium ion ($Fl–NH^+$).

The cation is obtained in the flash photolysis experiments by irradiation of 2-azidofluorene (FlN_3). Photolysis of this azide results in extremely rapid (probably fs time scale (11)) loss of nitrogen to give a singlet nitrene ^{1}[FlN]. In aqueous solutions, this is protonated by the solvent on the ps time scale (12) to give the conjugate acid, the nitrenium ion. This cation is observed on the ns time scale in laser flash photolysis experiments as an intensely absorbing transient intermediate with λ_{max} at 450–460 nm. Assignment of this transient as the ground state 2-fluorenylnitrenium ion was based on a number of arguments (12); this assignment has recently been confirmed by time-resolved resonance Raman spectroscopy (13). The nitrenium ion decays with a lifetime of 30 μs in water alone, and at the completion of the decay there is little absorbance above 310 nm. Guanine derivatives are excellent nucleophiles for arylnitrenium ions, and compete very effectively even with the aqueous solvent (2–4). Thus, with 2′-deoxyguanosine (dG) present, the decay is significantly accelerated. Moreover, as the cation decays, there is a significant growth in absorbance in the region 310–400 nm. This new absorbance turns out to be associated with a second intermediate, whose reaction to give the stable C-8 adduct **7** can be observed with lamp flash photolysis on the ms time scale. Several pieces of evidence identify this intermediate as being derived from addition of the nitrenium ion to the C-8 carbon prior to loss of the C-8 proton and the formation of the final C-8 adduct. We will term this species the "C-8 intermediate" to distinguish it from the stable final product derived from loss of the C-8 proton — "the C-8 adduct". As expected, there is a large primary kinetic isotope effect for the decay of the C-8 intermediate when dG is substituted with deuterium at the 8-position. A small inverse kinetic isotope effect observed for the initial reaction forming the C-8 intermediate indicates that the nitrenium ion adds directly to the C-8 position, i.e., that the mechanism is an addition–elimination at the C-8 carbon as shown in Scheme 2. The latter isotope effect eliminates mechanisms where the C-8 intermediate is formed after initial addition at N-7; the latter possibility can also be ruled out on the basis of kinetic arguments (5).

Scheme 2.



One of the features of the second intermediate is that it exists in conjugate acid–base forms. This was seen both in the rate–pH profile for its subsequent reaction to the stable C-8 adduct and in the change in its spectra as a function of pH. Acidity constants were obtained with both methods, and were in agreement, at $pK_a = 3.9$. While the conjugate acid of this intermediate must be the cation **6**, there was uncertainty in the structure of the base form. In this paper this question has been addressed by generating this second intermediate from N^1-methylguanosine, where loss of the N^1-H proton cannot occur, and from N^2,N^2-dimethylguanosine, where loss of an NH_2 proton has been eliminated. Derivatives of

© 2001 NRC Canada

guanosine, rather than 2′-deoxyguanosine, were employed for economical reasons. A further aspect of the present study involves the measurement of the kinetics of the initial reaction of the two methylated guanine derivatives with nitrenium ions. These show some interesting effects that are also consistent with the initial reaction occurring at the C-8 position.

Experimental section

2-Fluorenyl azide (12), 4-biphenylyl azide (12), 4′-methyl-4-biphenylyl azide (14), and 4′-methoxy-4-biphenylyl azide (14) were from previous studies. N^1-Methylguanosine was prepared by the reaction of guanosine and *N*,*N*-dimethylacetamide dimethyl acetal in methanol (15). N^2,N^2-Dimethylguanosine was prepared in a multistep procedure: (*i*) guanosine was converted to 2′,3′,5′-tri-*O*-acetylguanosine by the reaction with acetic acid anhydride in the presence of 4-dimethylpyridine and triethylamine (16); (*ii*) 2′,3′,5′-tri-*O*-acetylguanosine was reacted with phosphorus oxychloride in acetonitrile containing tetraethylammonium chloride and *N*,*N*-dimethylaniline to give 2-amino-6-chloro-9-(2, 3, 5-tri-*O*-acetyl-β-D-ribofuranosyl)purine (17); (*iii*) this was converted to 2-amino-6-chloro-9-β-D-ribofuranosylpurine by treatment with saturated methanolic ammonia (18); (*iv*) the 2-amino-6-chloro-9-β-D-ribofuranosylpurine was reacted with sodium benzyloxide in benzyl alcohol to give 2-amino-6-benzyloxy-9-β-D-ribofuranosylpurine (91); (*v*) diazotization with sodium nitrite in 48% aqueous fluoroboric acid afforded 2-fluoro-6-benzyloxy-9-β-D-ribofuranosylpurine (19); (*vi*) the fluoride was substituted in 20% methanolic dimethylamine to give 2-dimethylamino-6-benzyloxy-9-β-D-ribofuranosylpurine (19); (*vii*) hydrogenolysis with palladium on carbon gave the desired product N^2,N^2-dimethylguanosine (19). Full experimental details of our preparations of N^1-methylguanosine and N^2,N^2-dimethylguanosine are available as supplementary material.[2]

Laser flash photolysis experiments involved ca. 20 ns pulses at 308 nm (60–120 mJ per pulse) from a Lumonics excimer laser. A pulsed Xenon lamp provided the monitoring light. After passing through a monochromator, the signal from the photomultiplier tube was digitized and sent to a computer for analysis. Stock solutions of the nucleosides — guanosine (0.001 M), N^1-methylguanosine (0.001 M), and N^2,N^2-dimethylguanosine (0.0004 M) — were prepared in 20% acetonitrile containing 0.002 M NaH_2PO_4:0.002 M Na_2HPO_4. For each nucleoside, a series of solutions of 100 mL volume were prepared by adding volumes of the stock solutions — 100, 80, 60, 40, 20, 0 mL — to a 100 mL volumetric flask, and filling to the mark with the 20% acetonitrile solution containing the phosphate buffer. These 100 mL solutions were divided into four 25 mL volumetric flasks. A concentrated acetonitrile solution of the four azides — 2-fluorenyl, 4-biphenylyl, 4′-methyl-4-biphenylyl, and 4′-methoxy-4-biphenylyl azide — was added to each of these flasks immediately before irradiation to give a solution of final concentration ~10 μM. This solution was transferred to a 4 × 1 × 1 cm cuvette, and irradiated at 308 nm, with the decay of the transient nitrenium ion being monitored at its λ_{max} (14) — 2-fluorenyl (450 nm), 4-biphenylyl (455 nm), 4′-methyl-4-biphenylyl (475 nm), and 4′-methoxy-4-biphenylyl (500 nm). First-order rate constants were obtained by fitting the decay traces to the equation for a single exponential process. Solutions were flashed once and replaced with 4 to 5 kinetic runs being performed with each solution.

Lamp flash photolysis experiments were performed using an apparatus previously described (20). Aqueous solutions were prepared containing 2×10^{-4} M of the nucleoside. The pH was maintained by HCl, acetate buffer, or cacodylate buffer. In the case of the buffers, serial buffer dilutions were employed so that rate constants could be extrapolated to zero buffer concentrations. Shortly before irradiation, a concentrated acetonitrile solution of 2-fluorenyl azide was added to give a final azide concentration of 8 μM. The solution was irradiated with a broad band flash lamp of ca. 100 μs duration. The absorbance decay at 365 nm was monitored and fit to the exponential equation. For a given solution, 4 to 5 kinetic traces were obtained and the rate constants for these averaged. After irradiation, the pH of the solution was measured.

Results

Laser flash photolysis — Reaction of arylnitrenium ions and nucleosides

In these experiments, four nitrenium ions were generated and their decay studied in the presence of the three nucleosides guanosine, N^1-methylguanosine, and N^2,N^2-dimethylguanosine. The nucleosides significantly accelerated the decay of the nitrenium ion. Plots of the observed first-order rate constant for the decay were linear in the concentration of the nucleosides. The slopes of these plots are the second-order rate constants for the reaction of the nitrenium ion and the nucleoside. These rate constants are provided in Table 1, along with pertinent values that had been previously obtained.

Lamp flash photolysis — Decay of intermediate

These experiments were conducted with the intermediate formed by the reaction of the 2-fluorenylnitrenium ion and the three nucleosides guanosine, N^1-methylguanosine, and N^2,N^2-dimethylguanosine. Concentrations of the nucleosides were kept constant at 200 μM, a concentration where greater than 90% of the nitrenium ion reacts with the added nucleoside. As observed in the previous experiments with 2′-deoxyguanosine, a second intermediate is observed following the initial reaction of the nitrenium ion and the nucleoside. We monitored the decay of this intermediate at 365 nm, a wavelength where there is a significant difference between the absorbance of the intermediate and the absorbance of the final product. Rate constants were obtained in a series of HCl solutions and in acetate and cacodylate buffers. In the case of the buffers, serial buffer dilutions were performed. The buffer does accelerate the rate of decay (5). This aspect of the kinetics was not investigated in detail in this study, since our interest was in the rate constant extrapolated to zero buffer concentration. These rate

[2] Copies of material on deposit may be purchased from the Depository of Unpublished Data, Document Delivery, CISTI, National Research Council Canada, Ottawa, ON K1A 0S2, Canada (http://www.nrc.ca/cisti/irm/unpub_e.shtml for information on ordering electronically).

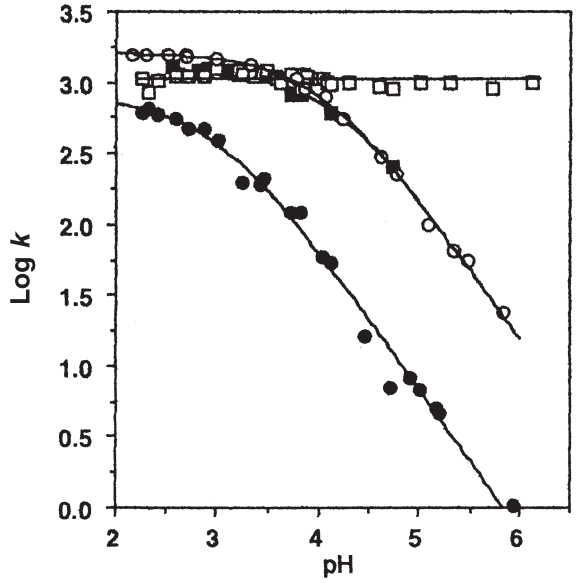
© 2001 NRC Canada

Table 1. Second-order rate constants (M^{-1} s^{-1}) for the trapping of nitrenium ions by nucleosides.

	Arylnitrenium ion			
Nucleophile	BiPh[a]	4′-MeBiPh[a]	2-Fluorenyl	4′-MeOBiPh[a]
2′-Deoxyguanosine[b]	2.0×10^9	1.5×10^9	7.6×10^8	3.6×10^7
Guanosine	1.7×10^9	1.3×10^9	7.1×10^8 (7.2×10^8)[b]	3.9×10^7
N^1-Methylguanosine	2.2×10^9	1.4×10^9	8.3×10^8	2.3×10^7
N^2,N^2-Dimethylguanosine	1.8×10^9	1.8×10^9	2.0×10^9	3.1×10^8
2′-Deoxyinosine[b]			$\sim 9 \times 10^5$	
Water (units are s^{-1})[c]	2.7×10^6	2.7×10^5	3.0×10^4	1.6×10^3

Note: Conditions: 20°C, 20% acetonitrile, pH 7 phosphate buffer.
[a]BiPh = 4-biphenylyl.
[b]Reference 4.
[c]Reference 14.

Fig. 1. Effect of pH on the rate constants at 20°C for the decay of the intermediate formed by the reaction of the 2-fluorenylnitrenium ion and nucleosides: guanosine (closed squares), N^1-methylguanosine (open squares), N^2,N^2-dimethylguanosine (closed circles), and 2′-deoxyguanosine (open circles) (data from ref. 5). Rate constants have been measured in HCl solutions (pH < 3.5) and in acetate and phosphate buffers; for the latter the values plotted are based on extrapolation to zero buffer concentration. The points are experimental; the lines have been based on eq. [1].



constants, alongside data previously obtained with 2′-deoxyguanosine (5), are depicted in the form of a rate–pH profile in Fig. 1.

Discussion

Structure of the conjugate base of C-8 intermediate

Using flash photolysis, two short-lived intermediates can be observed for the reaction that produces the C-8 adduct found as a product of the interaction of arylamine carcinogens and guanine — the arylnitrenium ion and the subsequent intermediate that we have identified as the C-8 intermediate. This second intermediate is relatively long-lived. Its deprotonation to give the final product, the stable C-8 adduct, occurs on the ms time scale.

The open circles in Fig. 1 show the acidic portion of the rate–pH profile previously obtained for the decay of the C-8 intermediate derived from the reaction of 2′-deoxyguanosine with the 2-fluorenylnitrenium ion (5). The present study shows that a C-8 intermediate is also observed in the reaction of this nitrenium ion with guanosine as well as with N^1-methylguanosine and with N^2,N^2-dimethylguanosine. The rate constants for the breakdown of the guanosine C-8 intermediate, shown in Fig. 1 as closed squares, are not surprisingly very similar to those of the deoxy derivative. These two profiles show a region in acidic solutions where the rate constant is essentially unchanged with changing pH, with a break around pH 4 to a reaction which is first-order in H^+. It was this downward break that indicated the presence of acid–base forms of the C-8 intermediate; this was verified by obtaining spectra as a function of pH (5).

While other mechanisms operate at higher pH (5), the rate–pH profile in acid is explained by the mechanism of Scheme 3. This involves a rapid and reversible equilibration of the cationic form of the C-8 intermediate **6** with a conjugate base. The cation is the reactive species, with the C-8 proton being transferred to a water molecule.

The rate equation for this mechanism is given in eq. [1],

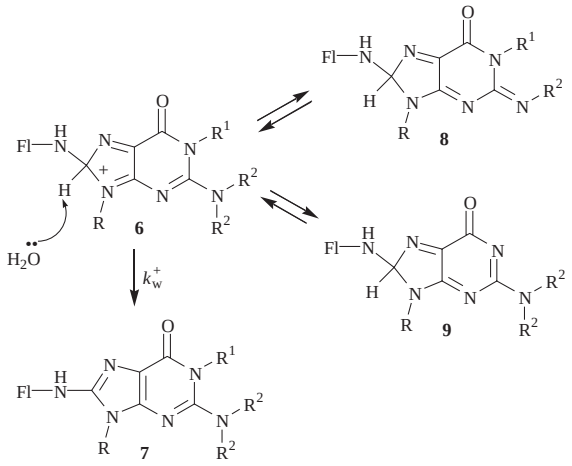
$$[1] \qquad k = \frac{k_w^+[H^+]}{[H^+] + K_a}$$

where k_w^+ is the first-order rate constant for the removal of the C-8 proton in the cation by the solvent and K_a is the acidity constant for conversion to the conjugate base form. There are two candidates for the conjugate base form, structure **8** that is derived from loss of one of the NH_2 protons and structure **9** that is derived from loss of the N-1 proton. These are tautomers of one another, and also tautomers of the stable C-8 adduct. The tautomer **8** or **9** is derived from loss of proton from a heteroatom, a process that is very fast. Thus, this conjugate base will form as a kinetic product in solutions that have a pH higher than the pK_a. The slower loss of the C-8 proton results in the thermodynamic product.

To determine the structure of the conjugate base form, rate–pH profiles were obtained for the C-8 intermediates derived from N^1-methylguanosine and N^2,N^2-dimethylguanosine. The former is obviously unable to lose the N-1 proton, while the

© 2001 NRC Canada

Scheme 3.



latter cannot deprotonate at the NH_2 group. The results in Fig. 1 show that it is the intermediate from N^1-methylguanosine that lacks the break associated with the deprotonation. Rate constants for this species are the same within experimental error from pH 2 to pH 6. The N^2,N^2-dimethyl derivative, on the other hand, shows qualitatively the same behavior as the non-methylated analogs. Thus, it is the N-1 proton that is being lost when the C-8 intermediate undergoes ionization, and the conjugate base is **9**.

Table 2 provides values of the rate constants k_w^+ and the acidity constants (as pK_a values) obtained by fitting the experimental data to eq. [1] (with only k_w^+ obviously available for N^1-methylguanosine). The values of k_w^+ are within a factor of two of one another. The one significant difference is the pK_a of the C-8 intermediate from the dimethylguanosine that shows that this species is one log unit more acidic than the intermediates from guanosine and 2′-deoxyguanosine. There is no obvious reason for this difference. The N-1 proton in guanosine is acidic (pK_a = 9.2). This acidity can be explained by delocalization of the negative charge onto the adjacent oxygen. Thus, one possibility to explain the behavior in the C-8 intermediates is that these have significant contributions from zwitterionic resonance contributors such as structures **10** and **11** of Scheme 4. According to their σ^+ values (21), the *N*,*N*-dimethylamino group is better than NH_2 at providing resonance stabilization to positive charge. Thus, the contribution from the zwitterionic resonance contributor **11** would be more important with the dimethylamino group as opposed to the simple amino group. This resonance contributor has the closer proximity of the positive and negative charge, so that this effect would be overall stabilizing to the compound.

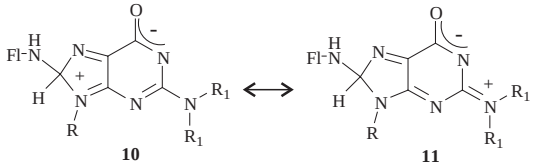
Effect of substituents on reactions of nitrenium ions with guanosine derivatives

The greater stabilizing effect of NMe_2 over NH_2 can also be seen in the rate constants for the reaction where the C-8 intermediate forms from the arylnitrenium ion and the guanosine derivative. As shown in Table 1, we investigated four nitrenium ions with lifetimes in water varying by three orders of magnitude. The rate constants for the most reactive, the 4-biphenylyl derivative, are, within experimental error, the same, with values around 2×10^9 M^{-1} s^{-1}. We have argued that this rate constant corresponds to a cation–nucleoside combination that is diffusion controlled (or very close to diffusion controlled). Thus, there is no discrimination between the four guanine derivatives. This is also the case for the next most reactive member of the series, the 4′-methylbiphenylyl derivative, although the rate constants are somewhat smaller than the value associated with diffusion control. Selectivity starts appearing with the 2-fluorenylnitrenium ion. With this cation, guanosine, the 2′-deoxy derivative and the N^1-methyl derivative, have very similar reactivities, with rate constants below the diffusion limit. The dimethyl analog in contrast is over twofold more reactive, and its rate constant is at the diffusion limit. This difference with the dimethylamino derivative also applies to the least reactive member of the series, the 4′-methoxy-4-biphenylyl cation. Here, however, the effect is quite substantial, with an order of magnitude difference between the dimethylguanosine and the other three.

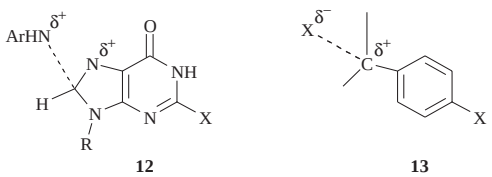
Table 2. Rate constants k_w^+ and acidity constants pK_a for the C-8 intermediates derived from the reaction of the 2-fluorenylnitrenium ion with guanine derivatives.

Nucleoside	k_w^+ (s^{-1})	pK_a
2′-Deoxyguanosine (5)	1.6×10^3	3.9
Guanosine	1.3×10^3	4.1
N^2,N^2-Dimethylguanosine	7.8×10^2	2.9
N^1-Methylguanosine	1.0×10^3	—

Scheme 4.



When an electrophile such as a nitrenium ions adds at the C-8 carbon of a purine ring, there is a formal build-up of positive charge at N-7, as shown in the transition-state structure **12**. Conjugative electron donating substituents at C-2 of the purine, such as the NH_2 group of a guanine derivative, are located in a position para to this developing positive charge. The interaction with this charge should therefore occur in exactly the same fashion as that of a para substituent in an S_N1 solvolysis of a benzyl derivative, i.e., as in the transition-state structure **13**. The effects of such substituents in the latter solvolysis are measured on the σ^+ scale. Relevant values (21) are σ^+ = 0.00 (H), –1.3 (NH_2). and –1.7 (NMe_2).



© 2001 NRC Canada

With this analogy to S_N1 solvolysis, it is not surprising that a 6-oxopurine derivative with a hydrogen at C-2 (2′-deoxyinosine) does not react efficiently with nitrenium ions in comparison to a guanine derivative, where there is an NH_2 group. Replacing the NH_2 group with NMe_2 adds further stabilization, with a further increase in reactivity. The order of reactivity — H << NH_2 < NMe_2 — is a further indication that the reactions of arylnitrenium ions and guanine derivatives are occurring via direct addition at the C-8 carbon, as shown in Scheme 2 in the introduction. Substituents at the 2-position of a purine are unlikely to show the same large effects for a reaction where the rate-limiting step involves bonding to the N-7 nitrogen. Although there is positive charge developing at N-7 in the transition state for such a reaction, this charge cannot be delocalized to a π-donor at C-2.

Acknowledgement

Financial support from the Natural Sciences and Engineering Research Council of Canada (NSERC) is gratefully acknowledged.

References

1. A. Dipple. Carcinogenesis, **16**, 437 (1995).
2. M. Novak and S.A. Kennedy. J. Am. Chem. Soc. **117**, 574 (1995).
3. S.A. Kennedy, M. Novak, and B.A. Kolb. J. Am. Chem. Soc. **119**, 7654 (1997).
4. R.A. McClelland, T.A. Gadosy, and D. Ren. Can. J. Chem. **76**, 1327 (1998).
5. R.A. McClelland, A.R. Ahmad, A.P. Dicks, and V.E. Licence. J. Am. Chem. Soc. **121**, 3303 (1999).
6. R.H. Heflich and R.E. Neft. Mutat. Res. **318**, 73, (1994).
7. A. Parkinson. *In* Casarett and Doull's toxicology: The basic science of poisons. 5th ed. *Edited by* C.D. Klassen. McGraw Hill, New York. 1996. pp 113–186.
8. H.C. Pitot, III and Y.P. Dragon. *In* Casarett and Doull's toxicology: The basic science of poisons. 5th ed. *Edited by* C. D. Klassen. McGraw Hill, New York. 1996. pp. 201–267.
9. W.G. Humphreys, F.F. Kadlubar, and F.P. Guengerich. Proc. Natl. Acad. Sci. U.S.A. **89**, 8278 (1992).
10. F.P. Guengerich, R.G. Mundkowski, M. Voehler, and F.F. Kadlubar. Chem. Res. Toxicol. **12**, 906 (1999).
11. R. Born, C. Burda, P. Senn, and J. Wirz. J. Am. Chem. Soc. **119**, 5061 (1997).
12. R.A. McClelland, M.J. Kahley, P.A. Davidse, and G. Hadzialic. J. Am. Chem. Soc. **118**, 4794 (1996).
13. P. Zhu, S.Y. Ong, P.Y. Chan, K.H. Leung, and D.L. Phillips. J. Am. Chem. Soc. **123**, 2645 (2001).
14. D. Ren and R.S. McClelland. Can. J. Chem. **76**, 78 (1998).
15. L.J. McBride, R. Kierzek, S.L. Beaucage, and M.H. Caruthers. J. Am. Chem. Soc. **108**, 2040 (1986).
16. A. Matsuda, M. Shinozaki, K. Watanabe, and T. Miyasaka. Synth. Commun. 385 (1986).
17. I.M. Buck, A. Eleuteri, and C.B. Reese. Tetrahedron, **50**, 9195 (1994).
18. J.F. Robins, J.W. Jones, and R.K. Robins. J. Org. Chem. **28**, 945 (1963).
19. J.F. Gerster and R.K. Robins. J. Am. Chem. Soc. **87**, 3752 (1965).
20. A.A. Allen, A.J. Kresge, N.P. Schepp, and T.T. Tidwell. Can. J. Chem. **65**, 1719 (1987).
21. E.M. Kosower. *In* An introduction to physical organic chemistry. John Wiley and Sons, New York. 1968. p. 49.

© 2001 NRC Canada

The nature of the transition state in diarylmethyl cation – nucleophile combination reactions as probed by secondary α-deuterium isotope effects

Thuy Van Pham and Robert A. McClelland

Abstract: Transition-state structures for the carbocation–nucleophile combination reactions of (4-substituted-4′-methoxydiphenyl)methyl cations with water, chloride, and bromide ions in acetonitrile–water mixtures have been investigated by measuring the secondary α-deuterium kinetic and equilibrium isotope effects. Rate constants in the combination direction were measured with laser flash photolysis. Equilibrium constants were measured for the water reaction by a comparison method in moderately concentrated sulfuric acid solutions, for the bromide reaction via the observation of reversible combination, and for the chloride reaction from the ratio of the combination rate constant and the rate constant for the ionization of the diarylmethyl chloride product. The fraction of bond making in the transition state has been calculated as the ratio log (kinetic isotope effect):log (equilibrium isotope effect). For the water reaction, there is 50–65% bond making in the transition state; this is also true for cations that are many orders of magnitude less reactive. The same conclusions, 50–65% bond formation in the transition state independent of reactivity, have previously been made in correlations of log k_w vs. log K_R. Thus, two quite different measures of transition structure provide the same result. The k^H:k^D values for the halide combinations in 100% acetonitrile are within experimental error of unity. This is consistent with suggestions that these reactions are occurring with diffusional encounter as the rate-limiting step. Addition of water has a dramatic retarding effect on the halide reactions, with rate constants decreasing steadily with increased water content. Small inverse kinetic isotope effects are observed (in 20% acetonitrile:80% water) indicating that carbon—halogen bond formation is rate-limiting. Comparison of the kinetic and equilibrium isotope effects shows ~25 and ~40% bond formation in the transition states for the reactions with bromide and chloride, respectively.

Key words: carbocation, isotope effect, transition state, halide.

Résumé : On a étudié les structures des états de transition pour les réactions carbocation–nucléophile de cations (4-X-4′-méthoxydiphényl)méthyles avec l'eau et les ions chlorure et bromure, en solution dans des mélanges acétonitrile–eau, en se basant sur des mesures d'effets isotopiques d'équilibre et cinétiques secondaires de deutérium en α. Les constantes de réaction dans la direction de la combinaison ont été déterminées en faisant appel à la photolyse éclair au laser. Les constantes d'équilibre ont été mesurées: pour la réaction de l'eau, par une méthode de comparaison dans des solutions relativement concentrées d'acide sulfurique; pour la réaction de l'ion bromure, par le biais de l'observation de la combinaison réversible; et pour la réaction de l'ion chlorure, à partir du rapport de la constante de constante de vitesse de la combinaison et la constante de vitesse pour l'ionisation du produit, le chlorure de diarylméthyle. On considère que la fraction de formation de liaison dans l'état de transition est égale au rapport log (effet isotopique cinétique) : log (effet isotopique d'équilibre). Dans le cas de l'eau, le pourcentage de formation de liaison dans l'état de transition est de 50 à 65 %; ceci est aussi vrai pour des cations qui sont plusieurs ordres de grandeur moins réactifs. Dans des corrélations faites antérieurement entre le log k_w en fonction de log K_R, des conclusions similaires ont été obtenues: valeurs de 50 à 65 % pour le pourcentage de formation dans l'état de transition. Deux méthodes fort différentes de mesure de l'état de transition conduisent donc au même résultat. Les valeurs de k^H : k^D pour les combinaisons des halogénures dans l'acétonitrile à 100 % sont égales à l'unité, dans les limites des erreurs expérimentales. Ce résultat en accord les suggestions à l'effet que ces réactions se produisent par une étape dont la vitesse est limitée par la diffusion. L'addition d'eau diminue de façon dramatique les vitesses de réaction des ions halogénures; cet effet augmente avec une augmentation de la quantité d'eau ajoutée. On observe de faibles effets isotopiques cinétiques inverses (dans un mélange 20 % acétonitrile : 80 % eau); ceci indique que l'état cinétiquement limitante est la formation de la liaison carbone—halogène. Une comparaison des effets isotopiques cinétiques et d'équilibre montre que, pour les réactions des ions bromure et chlorure, les pourcentages de formation de liaison dans les états de transition sont respectivement d'environ 25 et 40 %.

Mots clés : carbocation, effet isotopique, état de transition, halogénure.

[Traduit par la Rédaction]

Received July 13, 2001. Published on the NRC Research Press Web site at http://canjchem.nrc.ca on December 12, 2001.

T. Van Pham and R.A. McClelland.[1] Department of Chemistry, University of Toronto, Toronto, ON M5S 3H6, Canada.

[1]Corresponding author (telephone: (416) 978-3592; fax: (416) 978-3592; e-mail: rmcclell@alchemy.chem.utoronto.ca).

 DOI: 10.1139/cjc-79-12-1887 © 2001 NRC Canada

Introduction

Several methods have now been described for the direct study of diarylmethyl cations using the technique of laser flash photolysis (LFP) (1). One of the principle ones is photosolvolysis, in which a diarylmethyl-leaving group bond is formally cleaved upon excitation. This reaction occurs with a variety of leaving groups. These include acetate (2, 3), 4-cyanophenoxide (2, 3), chloride (4), bromide (4), and triphenylphosphine (5). The initial photochemical event is very fast, and results in ion pairs (6, 7), possibly via electron transfer in initially formed radical pairs (8, 9). On the timescale of a ns LFP experiment where observation occurs after a 10–20 ns laser pulse, the intermediate is a free ground state cation (1, 6, 7). The time-resolved measurements that can be performed with LFP then provide direct kinetic data for the capture of the cation. Included here are the reactions with alcohol and aqueous solvents, as well as the combinations with added nucleophiles present in these solvents. The parent diphenylmethyl cation (Ph_2CH^+) turns out to be very short-lived in water, ethanol, and methanol, with a lifetime of less than 1 ns (10). This means that this particular cation is too reactive to be observed by ns LFP in these solvents, although it can be observed with this technique in solvents of lower nucleophilicity such as 2,2,2-trifluoroethanol (2). Diarylmethyl cations with at least one of the phenyl rings bearing a 4-methoxy substituent are longer-lived. Such cations have lifetimes of 100 ns to 10 ms in water (2, 3), and thus, can be studied in this solvent with ns LFP.

In this paper, we describe the measurement of secondary α-hydrogen and (or) deuterium kinetic isotope effects and equilibrium isotope effects for reactions of diarylmethyl cations with water, bromide ion, and chloride ion. The experiments were carried out in acetonitrile:water mixtures and in 100% acetonitrile. Because of the constraints imposed by lifetimes referred to in the last paragraph, at least one of the phenyl rings bore a 4-methoxy substituent. The objective of this study was to obtain information about the nature of the transition state for these cation–nucleophile combination reactions, and in particular to see how this is affected by changing the substituents on the cation, the nucleophile and the solvent.

Secondary α-kinetic isotope effects have been extensively employed to probe the mechanism and transition state of solvolysis reactions (11). For an S_N1 reaction, a normal k_H/k_D is observed. This is mainly caused by a change of the frequency of the C_a–H out-of-plane bending vibration in proceeding from reactant to transition state. Based upon a change in the out-of-plane bending vibration from 1350 cm^{-1} to 800 cm^{-1}, Streitweiser et al. (12) initially concluded that the maximum k^H/k^D would be 1.41. Bartell (13), however, pointed out that steric crowding at the α-carbon can alter these frequencies. Experimental studies, performed mainly by the Shiner group (14–18) found k^H/k^D values ranging from 1.10–1.25. The general conclusions for S_N1 solvolytic displacements is that the α-kinetic isotope effects are not very dependent upon the solvent or upon the substituent for a particular structure type. There is, however, a predictable (16, 18, 19) variation with the nature of the leaving group.

In contrast to the situation with S_N1 solvolysis, there is very limited data concerning α-kinetic isotope effects for cation–nucleophile combinations. Mayr et al. (20) have examined the reaction of a diarylmethyl cation with three alkenes. Values of k^H/k^D of 0.79 to 0.80 were obtained. Inverse isotope effects are, of course, expected since in such reactions, the carbon bearing the isotope is being converted from sp^2 to sp^3 hybridization. The relatively large inverse values were interpreted in terms of a tight, product-like, transition state. In an earlier study, Bunton et al. (21) examined reactions of two ferrocenyl-substituted cations. With water as the nucleophile, both the kinetic and equilibrium isotope effects were obtained. These results will be discussed later in a comparison with data obtained in the present study.

Experimental section

Compounds — diarylmethyl chlorides

Deuterated and undeuterated chlorides were prepared by modification of the method of Schneider and Mayr (22). A typical preparation is as follows:

Previously prepared (4-methoxydiphenyl)methanol, 0.45 g (2.1 mmol) was dissolved in 30 mL of dry CH_2Cl_2 and stirred with 2 g of finely ground anhyd $CaCl_2$. After cooling to –78°C, a stream of HCl gas was bubbled through the mixture for 3 min. After warming to room temperature, the mixture was gravity filtered and the solvent removed with a rotary evaporator. Distillation at 10 torr (1 torr = 13.322 Pa) and 170–175°C gave (4-methoxydiphenyl)methyl chloride (0.31 g), mp 61 to 62°C (lit. (23) mp 61 to 62°C, lit. (24) mp 62 to 63°C). ^{1}H NMR (200 MHz, $CDCl_3$) δ: 3.82 (s, 3H), 6.18 (s, 1H), 6.91 (d, 2H), 7.37 (m, 5H), 7.48 (d, 2H). ^{13}C NMR (200 MHz, $CDCl_3$) δ: 55.25, 64.19, 113.83, 127.59, 127.84, 128.37, 129.02, 133.30, 141.15, 159.24.

Similarly prepared from the corresponding alcohols were:

*(4-Methoxydiphenyl)methyl-α-*d *chloride*

^{1}H NMR (200 MHz, $CDCl_3$) δ: 3.82 (s, 3H), 6.91 (d, 2H), 7.37 (m, 5H), 7.48 (d, 2H). At high magnification, a peak at 6.18 ppm due to C*H*Cl was observed. Based upon the integration of the peaks at 6.18 ppm and 3.78 ppm, the compound was 98% deuterated at the α-carbon.

(4-Methyl-4′-methoxydiphenyl)methyl chloride

^{1}H NMR (200 MHz, $CDCl_3$) δ: 2.45 (s, 3H), 3.86 (s, 3H), 6.23 (s, 1H),6.98 (d, 2H), 7.26 (d, 2H), 7.46 (two overlapping doublets, 4H). ^{13}C NMR (200 MHz, $CDCl_3$) δ: 21.00, 55.12, 64.15, 113.68, 127.45, 128.88, 128.97, 133.35, 137.53, 138.24, 159.08.

*(4-Methyl-4′-methoxydiphenyl)methyl-α-*d *chloride*

^{1}H NMR was identical to that of undeuterated compound, except that deuterated compound had only a very small peak at 6.23 ppm seen at higher magnification. Integrating at 6.23 ppm vs. 2.45 ppm shows 98% deuteration.

(4-Trifluoromethyl-4′-methoxydiphenyl)methyl chloride

^{1}H NMR (200 MHz, $CDCl_3$) δ: 3.82 (s, 3H), 6.18 (s, 1H), 6.92 (s, 2H), 7.32 (d, 2H), 7.5–7.6 (overlapping doublets, 4H). ^{13}C NMR (200 MHz, $CDCl_3$) δ: 55.29, 63.19, 114.07, 125.36, 127.98, 129.00, 130.0 (quartet, CF_3), 132.43, 138.74, 145.04, 159.55.

© 2001 NRC Canada

(4-Trifluoromethyl-4′-methoxydiphenyl)methyl-α-d chloride

^{1}H NMR was identical to that of undeuterated compound except for the peak at 6.18 ppm; the α-position was 98% deuterated based upon integration at 6.18 and 6.92 ppm.

Diarylmethanols

(4,4′-Dimethoxydiphenyl)methanol was prepared by adding 2.0 g (8.0 mmol) of 4,4′-dimethoxybenzophenone dissolved in 50 mL of dry tetrahydrofuran (THF) to a stirred suspension of 0.75 g (19.8 mmol) of lithium aluminum hydride in 50 mL of anhydrous diethyl ether. After refluxing for 1 h, the mixture was cooled to –78°C and quenched with ethyl acetate followed by 5% aq H_2SO_4. Standard work-up of the organic portion, drying over $MgSO_4$, filtration and removal of the solvents with a rotary evaporator gave a white solid that was recrystallized from diethyl ether:hexanes. Yield: 1.50 g, mp 66.5 to 67.5°C (lit. (23) 67.5 to 68.5°C). ^{1}H NMR (200 MHz, $CDCl_3$) δ: 3.40 (s, 1H, OH), 3.89 (s, 6H), 5.80 (s, 1H), 6.86 (d, 4H), 7.38 (d, 4H). ^{13}C NMR (200 MHz, $CDCl_3$) δ: 55.0, 74.9, 113.5, 127.6, 136.3, 158.5.

(4,4′-Dimethoxydiphenyl)methanol-α-*d* was prepared in a similar manner using $LiAlD_4$ (Aldrich, 98% D). This sample had an identical NMR to the undeuterated sample except for the α-CH peak at 5.80 ppm. Integration of the small peak at 5.80 ppm and the peak at 3.89 ppm indicated 98% deuteration.

(4-Methoxydiphenyl)methanol and (4-methoxydiphenyl) methanol α-D were prepared in a similar manner through the reduction of 4-methoxybenzophenone with $LiAlH_4$ and $LiAlD_4$ respectively. The undeuterated compound had mp 64.5 to 66°C (lit. (24) 65 to 66°C). ^{1}H NMR (400 MHz, $CDCl_3$) δ: 2.65 (d, 1H, OH), 3.77 (s, 3H), 5.74 (d, 1H), 6.84 (d, 2H), 7.30–7.35 (m, 5H), 7.37 (d, 2H). ^{13}C NMR (400 MHz, $CDCl_3$) δ: 55.15, 75.58, 113.68, 126.26, 127.20, 127.76, 128.24, 136.06, 145.89, 158.75. The deuterated compound had a mp of 64.5 to 65.5°C, with the same NMR except for the doublet at 5.74 ppm. Integration of the small peak at 5.74 ppm vs. the peak at 3.75 ppm indicated 98% deuteration.

(4-Methyl-4′-methoxydiphenyl)methanol and (4-trifluoromethyl-4′-methoxy-diphenyl)methanol were prepared by adding 4-tolualdehyde and α,α,α-trifluoro-4-tolualdehyde (dissolved in dry ether) to a slight excess of 4-methoxyphenyl magnesium bromide in dry ether. After quenching and work-up procedures standard for Grignard–aldehyde reactions, the alcohols were purified by silica gel column chromatography using 15% by volume ethyl acetate in hexane. The alcohols were recrystallized from diethyl ether:hexanes. The 4-methyl derivative had a mp of 60.5 to 62°C (lit. (25) 60 to 61°C). ^{1}H NMR (200 MHz, $CDCl_3$) δ: 2.28 (d, 1H, OH), 2.33 (s, 3H), 3.78 (s, 3H), 5.75 (d, 1H), 6.84 (d, 2H), 7.14 (d, 2H), 7.27 (overlapping doublets, 4H). ^{13}C NMR (400 MHz, $CDCl_3$) δ: 21.11, 55.24, 75.57, 113.73, 126.28, 127.70, 129.01, 136.24, 136.97, 141.07, 158.80. The trifluoromethyl derivative had a mp of 75 to 76°C (lit. (26) 76 to77°C). ^{1}H NMR (400 MHz, $CDCl_3$) δ: 2.25 (d, 1H, OH), 3.78 (s, 3H), 5.82 (d, 1H), 6.86 (d, 2H), 7.30 (d, 2H), 7.40 (d, 2H), 7.54 (d, 2H). ^{13}C NMR (400 MHz, $CDCl_3$) δ: 55.31, 75.29, 114.07, 124.05 (q, $^1J_{C–F}$ = 272.4 Hz), 125.27 (q, $^3J_{C–F}$ = 3.7 Hz), 126.46, 127.97, 129.10 (q, $^2J_{C–F}$ = 32.2 Hz), 135.40, 147.67, 159.30.

4-Methyl-4′-methoxybenzophenone and 4-trifluoromethyl-4′-methoxybenzophenone were prepared by chromic acid oxidation of the above diarylmethanols following literature procedures (27–29). The 4-methyl derivative had a mp of 89 to 90.5°C (lit. (30) 90–92°C). ^{1}H NMR (200 MHz, $CDCl_3$) δ: 2.44 (s, 3H), 3.89 (s, 3H), 6.96 (d, 2H), 7.28 (d, 2H), 7.68 (d, 2H), 7.82 (d, 2H). ^{13}C NMR (200 MHz, $CDCl_3$) δ: 21.51, 55.37, 113.40, 128.78, 129.89, 130.39, 132.31, 135.44, 142.49, 162.95, 195.18. The trifluoromethyl derivative had a mp of 120 to 120.5°C (lit. (31) 119–121°C). ^{1}H NMR (200 MHz, $CDCl_3$) δ: 3.90 (s, 3H), 6.96 (d, 2H), 7.7–7.8 (three overlapping doublets, 6H). ^{13}C NMR (200 MHz, $CDCl_3$) δ (ppm): 55.51, 113.79, 123.72 (q, $^1J_{C–F}$ = 272.6 Hz), 125.22 (q, $^3J_{C–F}$ = 3.8 Hz), 129.34, 129.75, 132.58, 133.21, (q, $^2J_{C–F}$ = 32.7 Hz), 141.51, 163.71, 194.18.

(4-Methyl-4′-methoxydiphenyl)methanol-α-D and (4-trifluoromethyl-4′-methoxydiphenyl)methanol-α-D were prepared by reducing the appropriate benzophenones with $LiAlD_4$ as described previously. The 4-methyl derivative had a mp of 60–62°C, and the 4-trifluoromethyl derivative had a mp of 75 to 75.5°C. The ^{1}H NMR (400 MHz, $CDCl_3$) of both alcohols indicated 98% deuteration.

Diarylmethyl 4-cyanophenyl ethers were prepared by treating freshly prepared diarylmethyl chloride (typically 15 mmol) with excess sodium 4-cyanophenoxide (25 mmol) in dry THF (200 mL). The cyanophenoxide was prepared by treating 4-cyanophenol (11.8 g) in anhydrous methanol (100 mL) with slightly less than 1 equiv of 1 M sodium methoxide in ethanol. After removal of the methanol with a rotary evaporator, the salt was washed several times with dry ether. The mixtures of the sodium cyanophenoxide and the diarylmethyl chloride were refluxed in dry THF, typically for 3 days. The reaction mixture was poured into 200 mL of water, the organic phase separated and washed with dilute aqueous sodium hydroxide to remove residual 4-cyanophenol. After drying (Na_2SO_4) and filtration, the solvent was removed and the product purified by silica gel column chromatography using ethyl acetate:hexanes (5.95 to 20:80).

(4-Methyl-4′-methoxydiphenyl)methyl 4-cyanophenyl ether had a mp of 78.5–81°C. ^{1}H NMR (400 MHz, $CDCl_3$) δ: 2.37 (s, 3H), 3.82 (s, 3H), 6.25 (s, 1H), 6.9–7.5 (m, 12H). ^{13}C NMR (400 MHz, $CDCl_3$) δ: 21.10, 55.21, 81.59, 103.88, 114.06, 116.62, 119.14, 126.56, 128.12, 129.39, 132.23, 133.78, 137.17, 137.80, 159.30, 161.32.

(4-Methoxydiphenyl)methyl 4-cyanophenyl ether had a mp of 74.5–77°C. ^{1}H NMR (400 MHz, $CDCl_3$) δ: 3.77 (s, 3H), 6.23 (s, 1H), 6.9–7.5 (m, 12H). ^{13}C NMR (400 MHz, $CDCl_3$) δ: 55.19, 81.65, 103.99, 114.08, 116.59, 119.08, 126.54, 127.97, 128.17, 128.69, 132.01, 133.78, 140.12, 159.34, 161.21.

(4-Trifluoromethyl-4′-methoxydiphenyl)methyl 4-cyanophenyl ether had a mp of 93.5–95.5°C. ^{1}H NMR (400 MHz, $CDCl_3$) δ: 3.78 (s, 3H), 6.29 (s, 1H), 6.9–7.7 (m, 12H). ^{13}C NMR (400 MHz, $CDCl_3$) δ: 55.18, 80.95, 104.44, 114.29, 116.57, 118.92, 123.85 (q, $^1J_{C–F}$ = 272.4 Hz), 125.65 (q, $^3J_{C–F}$ = 3.6 Hz), 126.75, 128.14, 130.08 (q, $^2J_{C–F}$ = 21.7 Hz), 131.16, 133.85, 144.27, 159.62, 160.77.

The α-deuterated versions of these three ethers were also prepared: (4-methyl-4′-methoxydiphenyl)methyl-α-D 4-cyanophenyl ether, mp 77–79°C; (4-methoxydiphenyl) methyl-α-D 4-cyanophenyl ether, mp 78.85–81°C; (4-trifluoromethyl-4′-

© 2001 NRC Canada

methoxydiphenyl)methyl-α-D 4-cyanophenyl ether, mp 83–90°C. In each case, a small peak corresponding to an α-CH proton could be observed in the ^{1}H NMR at high magnification. Integration relative to the OCH_3 peak indicated 98% deuteration.

Diarylmethylmethyl acetates were prepared by refluxing for 14 h a mixture of the diarylmethanol (typically 1 g), pyridine (2 mL), and acetic anhydride (10 mL). After quenching with 100 mL of water, the product was extracted with three portions of 50 mL of diethyl ether. The combined ether reactions were washed with aq 0.1 N NaOH, 5% aq H_2SO_4, and then twice with water. After drying ($MgSO_4$) and filtration, the solvent was removed on a rotary evaporator.

(4-Methoxydiphenyl)methyl acetate was a viscous oil that was distilled at 170–175°C and 10 torr (1 torr = 133.322 Pa). ^{1}H NMR (200 MHz, $CDCl_3$) δ: 2.12 (s, 3H), 3.75 (s, 3H), 6.87 (d, 2H), 6.90 (s, 1H), 7.31 (m, 5H), 7.37 (d, 2H). ^{13}C NMR (200 MHz, $CDCl_3$) δ: 21.20, 55.10, 76.43, 113.76, 126.73, 127.64, 128.35, 128.59, 132.31, 140.32, 159.21, 169.95.

(4-Methyl-4′-methoxydiphenyl)methyl acetate recrystallized slowly in hexane to white needles, mp 80–82°C. ^{1}H NMR (200 MHz, $CDCl_3$) δ: 2.18 (s, 3H), 2.37 (s, 3H), 3.80 (s, 3H), 6.88 (d, 2H), 6.90 (s, 1H), 7.15 (d, 2H), 7.36–7.40 (overlapping doublets, 2H). ^{13}C NMR (200 MHz, $CDCl_3$) δ: 20.95, 21.13, 25.05, 76.36, 113.71, 126.76, 128.42, 128.99, 132.49, 137.31, 137.43, 159.11, 169.87.

(4-Trifluoromethyl-4′-methoxydiphenyl)methyl acetate was a viscous oil after purification by silica gel column chromatography. ^{1}H NMR (200 MHz, $CDCl_3$) δ: 2.17, (s, 3H), 3.80 (s, 3H), 6.84 (d, 2H), 6.87 (s, 3H), 7.26 (d, 2H), 7.47 (d, 2H), 7.60 (d, 2H). ^{13}C NMR (200 MHz, $CDCl_3$) δ: 20.99, 55.10, 75.88, 114.01, 123.92 (q, $^1J_{C-F}$ = 272 Hz), 125.35 (q, $^3J_{C-F}$ = 3.87 Hz), 126.97, 128.72, 129.13 (q, $^2J_{C-F}$ = 32.62 Hz), 131.53, 144.45, 159.56, 169.74. The three α-deuterated acetates were also prepared in the same manner, the 4-methyl compound as a solid with mp 76–79°C, and the other two as viscous oils.

Measurements of kinetic isotope effects for reaction with water

(1) Three 25 mL volumetric flasks each containing exactly 25 mL of a particular water:acetonitrile mixture were prepared. Into one flask, the blank, was injected 20 μL of pure acetonitrile, into one flask was injected 20 μL of an 0.05 M solution of an undeuterated diarylmethyl acetate or 4-cyanophenyl ether, and into the third flask was injected 20 μL of an 0.05 M solution of the corresponding α-deuterated substrate. These three solutions were thermostated at 25 ± 0.1°C in a water bath.

(2) After temperature equilibration, kinetic measurements were performed by transferring 4 mL of the blank solution to a 1 × 1 × 4 cm UV cuvette.

(3*a*) This cell was placed in a sample holder which was thermostated at 25°C, and the remaining solution returned to the water bath. After temperature equilibration, a 20 ns 248 nm laser pulse was applied perpendicular to the cuvette onto one of the 1 × 4 faces. The absorbance changes in the cuvette were followed by passing a UV–vis beam through the long axis into a detection system set at the λ_{max} of the cation: 482 nm for 4-Me, 4′-MeO, 464 nm for 4-H, 4′-MeO, and 436 nm for 4-CF_3, 4′-MeO. The voltage output from the detector was digitized with a Tektronix SCD-1000 transient digitizer, and then passed to a DX-386 computer where the signal was converted to optical density based upon the base line output from the photomultiplier tube just before the laser pulse.

(3*b*) The solution was removed from the UV cuvette, the cuvette cleaned and dried, and 4 mL of the 25 mL stock solution of the undeuterated substrate was added. This cuvette was placed in the sample holder, and after temperature equilibrium, the solution was irradiated under identical conditions to those employed in step 3*a*. Procedures 3*a* and 3*b* were then repeated two to four times, alternating blank and undeuterated substrate.

(4) The procedures described in steps (3*a*) and (3*b*) were then repeated with the deuterated substrate.

(5) Each digitized signal was converted into a Microsoft Excel file of 512 data points. A solvent corrected trace was then obtained for each transient decay by subtracting the blank data from the data obtained immediately afterwards with substrate present. The computer program Grafit was then used with the corrected data to obtain first-order rate constants (k_{obs}), by fitting to the exponential equation, $A_{time} = (A_0 - A)\exp(-k_{obs}t) + A$, where A_0 is the initial absorbance and A the final absorbance (normally near zero). Average values of k_w^H and k_w^D were then obtained from the three to five k_{obs} obtained with the undeuterated and deuterated substrate, respectively; k_w^H:k_w^D was then calculated from these values. For each substrate, this whole procedure was repeated five times on five different days. The five k_w^H:k_w^D values so obtained were then averaged.

Measurements of kinetic isotope effects for reactions with bromide and chloride

A similar procedure was employed for the combinations with the halide ions, except that now seven solutions of varying concentrations of the halide (supplied as the tetra-*n*-butylammonium salt) were employed. These concentrations were incremental and were chosen after preliminary experiments such that each incremental increase in concentration caused an approximately 50% increase in k_{obs} over the value obtained with no halide present. Second-order rate constants were then obtained from the least-squares slopes of plots of k_{obs} vs. halide concentration. Excellent linear correlations were observed, with correlation coefficients of at least 0.997. On a given day, the set of experiments were performed with both the undeuterated and deuterated substrate; this generated two lines, and one value of k_X^H:k_X^D calculated from the two slopes. As above, the entire set of experiments was repeated three to five times with a given cation in a given solvent, and an average value of k_X^H:k_X^D obtained.

Measurement of equilibrium isotope effects for reactions of diarylmethyl cations with water

Before measuring the equilibrium isotope effect, a "titration curve" was constructed applying method C of Deno et al. (32). This curve plots the optical density vs. sulfuric acid concentration at the λ_{max} of the cation for a series of solutions containing the same concentration of added diarylmethanol. This optical density ranges from zero in dilute

© 2001 NRC Canada

acids where there is no cation present in the diarylmethanol–diarylmethyl cation equilibrium to some constant value in concentrated acids where the equilibrium has completely shifted to the cation side.

From the titration curve for each diarylmethanol, one H_2SO_4 concentration corresponding to max cation formation was chosen, along with three to four concentrations near the midpoint, i.e., where there are significant amounts of both cation and alcohol in equilibrium. Three 25 mL volumetric flasks were then prepared each containing sulfuric acid solution near the midpoint, one for a blank, one for the undeuterated alcohol, and one for the deuterated alcohol. Seven 25 mL flasks were prepared for the concentration corresponding to 100% cation solution; one for a blank, three for undeuterated, and three for deuterated alcohols. The volumetric flasks were equilibrated at 25°C, and measurements started by rapidly injecting 50 μL of an acetic acid solution containing 5.0×10^{-3} M of undeuterated or deuterated diarylmethanol (or just 50 μL of acetic acid for the blank). A digital clock was started as the solution was prepared. The reaction flask was shaken for 10 s, placed back in the thermostating bath until bubbles had cleared, transferred to a UV cuvette, and the absorbance recorded at the λ_{max} of the cation for 3–5 min. The absorbance reading was then extrapolated to zero time using the computer programs Microsoft Excel and Grafit. This extrapolation was necessary since the diarylmethyl cations were unstable at the intermediate acidities (32), with approximately a 10% decrease in absorbance over 10 min. The equilibrium isotope effects were calculated from the extrapolated absorbances, as will be discussed in the *Results* section.

Measurement of kinetic isotope effects for solvolysis reactions of diarylmethyl chlorides in 2:98 water:acetonitrile

A solution containing 50 mL of an 0.001 M hydroxide solution was prepared by slowly mixing 1 mL of 0.05 M aqueous tetramethylammonium hydroxide with acetonitrile in a 50 mL volumetric flask and filling to the mark. This solution was thermostated at 25.0 ± 0.1°C, and 3 mL aliquots transferred to a UV cuvette which was further thermostated at 25.0 ± 0.1°C in a Cary 2200 spectrophotometer. Kinetic runs were initiated by injecting 3 μL of a stock solution of the diarylmethyl chloride (0.05 M) into the cuvette. An absorbance decrease at 249 nm was monitored, with the absorbance–time data being directly digitized. Observed first-rate constants were obtained by converting to Grafit files and fitting to the exponential equation as above. Four kinetic runs were performed for the deuterated and undeuterated substrates; the data for each were averaged to provide individual k^H or k^D values, and k^H:k^D ratio calculated. This procedure was repeated on several different days, and the k^H:k^D values averaged.

Results

As has been previously described (3), the diarylmethyl cations were generated in LFP experiments from acetate and 4-cyanophenoxide precursor. In most cases, the latter was employed because of its strong absorbance at the exciting wavelength of 248 nm. Following the laser pulse, the decay in absorbance at the λ_{max} of the cation was monitored. Because of a small absorbance drift (especially at times longer than 5 ms), the signal was corrected by subtracting a base line signal obtained without the substrate. With the exception of some of the experiments with bromide ion as nucleophile, the experimental data fit well to a single exponential equation.

Reactions with water

A typical set of experimental data is shown in Table 1. To ensure good precision, rate constants were measured on different days. The individual rate constants did vary slightly from day to day, probably due to small fluctuations in temperature. The values however did not vary as much. When calculated as the average over several days, the errors were less than 2%.

Table 2 summarizes the k_w^H:k_w^D values for three diarylmethyl cations, each in two solvents, 80:20 and 10:90 water:acetonitrile. Within the experimental uncertainty, all these kinetic isotope effects are identical, with k_w^H:$k_w^D \sim 0.89$. This is true even upon inclusion of the literature data (21) for the considerably more stabilized ferrocenyl-substituted cations.

Reactions with bromide and chloride ions

Second-order rate constants for reactions with the two halide ions were obtained as the slopes of the plots of k_{obs} vs. halide concentration. Six to seven different concentrations of tetra-*n*-butylammonium bromide or chloride were employed, with the undeuterated and deuterated compounds been studied in parallel in the same set of solutions. The correlation coefficients of the least-squares fits were at least 0.999. A given set of data generated one k_X^H:k_X^D value. As with the water reaction, a given experiment was repeated three to five times to generate an average. Table 3 summarizes the results. The kinetic isotope effects in 100% acetonitrile are all, within experimental error, equal to unity, while there is a small but statistically significant inverse kinetic isotope effect in 80:20 water:acetonitrile.

As shown by the data in Table 4, and as depicted graphically in Fig. 1, solvent composition has a dramatic effect on the actual rate constants for the reactions of the diarylmethyl cations with bromide and chloride ions. Both halides react in 100% acetonitrile with similar rate constants in the range 2 to 3×10^{10} M^{-1} s^{-1} and there is little or no effect of aromatic substituent. The rate constants decrease in a continuous fashion as water is added, reminiscent of behavior previously seen with diarylmethyl cations and primary amines (34). As soon as there is water present in the solvent, bromide ion is always more reactive than chloride ion for a given cation in a given solvent. In addition, for a particular nucleophile in a given solvent, there is a normal substituent effect, the trifluoromethyl substituted cation being the most reactive and the methyl derivative the least.

Equilibrium with water

The pseudo acid:base reaction of eq. [1] is the equilibrium of interest. Equilibrium constants are defined as K_R and have been measured in the past using the acidity function method (32).

[1] $ArC^+H(D) + H_2O \rightleftharpoons ArCH(D)\text{-}OH + H^+$

© 2001 NRC Canada

Table 1. Rate constants k_w^H and k_w^D and kinetic isotope effects $k_w^H:k_w^D$ for reactions of water with undeuterated and α-deuterated (4-methoxydiphenyl)methyl cations in 80:20 water:acetonitrile at 25°C.

Experiment	k_w^H (1×10^6 s^{-1})	k_w^D (1×10^6 s^{-1})	$k_w^H:k_w^D$
1	1.851	2.137	
	1.856	2.132	0.877 ± 0.016[a]
	1.917	2.173	
	1.906	2.169	
Average	1.890 ± 0.029[b]	2.154 ± 0.021[b]	
2	2.003	2.235	
	2.046	2.290	0.904 ± 0.024[a]
	2.060	2.188	
	1.976	2.230	
Average	2.021 ± 0.039[b]	2.236 ± 0.042[b]	
3	1.886	2.131	
	1.893	2.162	0.885 ± 0.010[a]
	1.906	2.126	
	1.914	2.168	
Average	1.900 ± 0.013[b]	2.147 ± 0.021[b]	
4	1.900	2.209	
	1.977	2.165	0.880 ± 0.017[a]
	1.928	2.196	
	1.919	2.208	
Average	1.931 ± 0.033[b]	2.195 ± 0.020[b]	
5	1.905	2.173	
	1.908	2.140	0.886 ± 0.006[a]
	1.915	2.149	
	1.906	2.155	
Average	1.908 ± 0.005[b]	2.154 ± 0.014[b]	
			Average 0.886 ± 0.011[a]

Note: 4-Cyanophenyl ether was employed as precursor in LFP experiments.
[a] $1/k^D[(\Delta k^H)^2 + (k^H/k^D)^2 + (\Delta k^D)^2]^{1/2}$ where Δk^H and Δk^D are standard deviations of k^H and k^D (equation from ref. 33).
[b] Standard deviation of mean.

Table 2. Rate constants and secondary α-kinetic and equilibrium isotope effects for reactions of undeuterated and deuterated diarylmethyl cations with water.[a]

$Ar_1C^+H(D)Ar_2$						log ($k_w^H:k_w^D$)/ log ($K_R^H:K_R^D$)
Ar_1	Ar_2	Solvent[b]	k_w^H (s^{-1})[c]	$k_w^H:k_w^D$	$K_R^H:K_R^D$[d]	
4-$MeOC_6H_4$	4-$CF_3C_6H_4$	80:20	4.0×10^6	0.890 ± 0.012		
		10:90	4.1×10^6	0.899 ± 0.011		0.58[e]
4-$MeOC_6H_4$	C_6H_5	80:20	1.9×10^6	0.886 ± 0.011		
		10:90	1.5×10^6	0.892 ± 0.011		
		100:0	1.9×10^6		0.831 ± 0.009	0.64[f]
4-$MeOC_6H_4$	4-MeC_6H_4	80:20	8.3×10^5	0.898 ± 0.011		
		10:90	6.5×10^5	0.898 ± 0.011		
		100:0	7.8×10^5		0.820 ± 0.011	0.54
4-$MeOC_6H_4$	4-$MeOC_6H_4$	100:0	1.0×10^5		0.831 ± 0.010	0.63[g]
Ferrocenyl	4-$MeOC_6H_4$[h]	100:0	4.3×10^1	0.874 ± 0.016	0.760 ± 0.049	0.49
Ferrocenyl	Ferrocenyl[h]	44:56	2.7×10^{-2}	0.915 ± 0.024	0.847 ± 0.027	0.53

[a] All data at 25°C.
[b] Water:acetonitrile (v/v).
[c] First-order rate constant for decay in solvent for non-deuterated compounds.
[d] K_R refers to the equilibrium $Ar_2C^+H(D) + H_2O \rightleftharpoons Ar_2CH(D)\text{-}OH + H^+$.
[e] Uses $k_w^H:k_w^D = 0.895$ and $K_R^H:K_R^D = 0.826$.
[f] With $k_w^H:k_w^D = 0.889$.
[g] With $k_w^H:k_w^D = 0.89$.
[h] Data from ref. 21.

© 2001 NRC Canada

Table 3. Rate constants and values of $k_X^H:k_X^D$ for the reactions of bromide and chloride ions with (4-*R*-4′-methoxydiphenyl)methyl cations (25°C).

		Acetonitrile:water (20:80)		Acetonitrile (100%)	
R	X^-	k_X^H (1×10^8 M^{-1} s^{-1})	$k_X^H:k_X^D$	k_X^H (1×10^{10} M^{-1} s^{-1})	$k_X^H:k_X^D$
CF_3	Br^-	9.90 ± 0.14	0.963 ± 0.013	2.83 ± 0.05	1.013 ± 0.021
H	Br^-	3.78 ± 0.12	0.966 ± 0.007	2.73 ± 0.03	1.007 ± 0.007
Me	Br^-	1.59 ± 0 10	0.947 ± 0.024[a]	2.59 ± 0.32	0.997 ± 0.004
CF_3	Cl^-	1.30 ± 0.08	0.936 ± 0.012	2.43 ± 0.14	0.994 ± 0.014
H	Cl^-	0.54 ± 0.03	0.940 ± 0.003	2.20 ± 0.15	1.005 ± 0.006
H	Cl^-			1.68 ± 0.16[b]	0.999 ± 0.021[b]

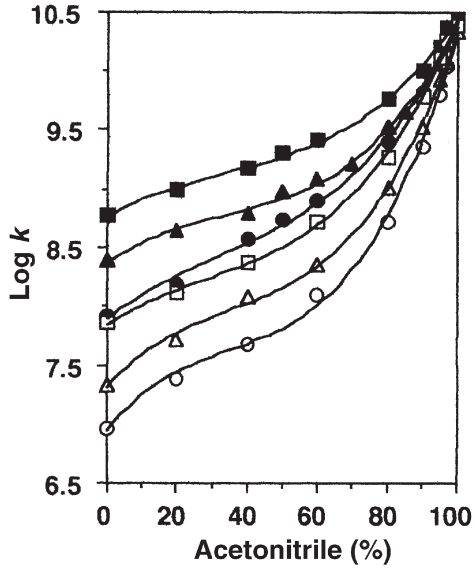
[a]Based upon analysis of double exponential decays.
[b]Measured in acetonitrile:water (98:2).

Table 4. Second-order rate constants for the reactions of (4-*R*-4′-methoxydiphenyl)methyl cations with bromide and chloride ions in water:acetonitrile at 25°C.

	R = CH_3		R = H		R = CF_3	
CH_3CN (%)	k_{Br}^H	k_{Cl}^H	k_{Br}^H	k_{Cl}^H	k_{Br}^H	k_{Cl}^H
100	25.9	24.4	27.3	22.0	28.3	24.3
97	16.6	11.1	18.4	12.1	23.8	17.9
95	11.6	6.36	13.3	8.38	16.2	13.1
90	6.58	2.26	7.02	3.33	10.3	6.06
85	—	—	4.50	—	—	—
80	2.52	0.529	3.40	1.02	5.72	1.90
70	—	—	1.65	—	—	—
60	0.811	0.127	1.21	0.226	2.60	0.522
50	0.537	—	0.929	—	2.05	—
40	0.372	0.0482	0.615	0.118	1.48	0.240
20	0.153	0.0241	0.437	0.0522	0.990	0.130
0	0.0824	0.00924	0.241	0.0216	0.600	0.0709

Note: Rate constants in the table are 1×10^9 M^{-1} s^{-1}.

Fig. 1. Variation in rate constants (plotted as log *k*) for the combination of bromide ion (closed symbols) and chloride ion (open symbols) with diarylmethyl cations in acetonitrile:water mixtures. (4-Trifluoromethyl-4′-methoxydiphenyl)methyl cation (squares), (4-methoxydiphenyl)methyl cation (triangles), (4-trifluoromethyl-4′-methoxy-diphenyl)methyl cation (circles).



Thus, for a given sulfuric acid solution, eq. [2] applies,

$$[2] \qquad K_R = ([ROH]/[R^+]) \times (f_{ROH}/f_R^+) \times (a_{H_2O}/a_H^+)$$

where f_{ROH} and f_R^+ are activity coefficients for the alcohol and cation and a_{H_2O} and a_H^+ are the activities of water and the proton. When the equilibria involving the undeuterated and α-deuterated systems are compared in the same acid solution, eq. [3] can be derived from eq. [2]. The common terms in a_{H_2O} and a_H^+ cancel, as do the terms in the activity coefficients, since these should not be affected significantly by isotopic variation.

$$[3] \qquad K_R^H/K_R^D = ([ROH]/[R^+])_H/([ROH]/[R^+])_D$$

Thus measurement of the ratios $[ROH]:[R^+]$ for the undeuterated and deuterated systems in the same acid solution furnishes the required equilibrium isotope effect (without even measuring K_R).

For experiments in which the same amount of alcohol is added to solutions of varying acid concentrations, the desired ratio is calculated by eq. [4],

$$[4] \qquad [ROH]/[R^+] = (A_{Acid} - A/A - A_{dil})$$

where the *A*s are optical densities measured at the λ_{max} of the cation; *A* being the value in the solution of interest, A_{acid} being the value at high acid concentration where there is only cation present, and A_{dil} being the value in dilute acid

© 2001 NRC Canada

where there is only alcohol present. The last value is in fact zero, since the alcohol does not absorb at the cation λ_{max}. To obtain the equilibrium isotope effect, absorbances were measured at several acid concentrations along with one in concentrated acid. This was done in the same solutions for both the undeuterated and deuterated systems, and eq. [5] was then employed to calculate the isotope effect.

$$[5] \qquad K_R^H/K_R^D = (A_{Acid} - A/A)_H/(A_{Acid} - A/A)_D$$

Data were obtained with three to four different acid concentrations on a given day, providing K_R^H:K_R^D values with a standard deviation of 2 to 3%. This error was reduced by repeating the procedure several times. The average values so obtained are given in Table 2. The trifluoromethyl cation could not be studied since the decomposition of this system in moderately dilute acids was too rapid to permit accurate extrapolation to zero time. To provide a third equilibrium isotope effect, we examined the bis-4-methoxyphenyl compound. As can be seen in Table 2, the three diarylmethyl cations examined in this work have the same equilibrium isotope effects within experimental error. Mocek and Stewart (35) previously obtained an equilibrium isotope effect of 0.847 for the bis-*p*-methoxyphenyl cation, in good agreement with the value obtained in the present work for the same system.

Equilibration with bromide ion

The equilibrium isotope effect for the (4-methyl-4′-methoxydiphenyl)methyl cation reacting with bromide ion in 20:80 acetonitrile could be measured directly in the LFP experiments. The approach took advantage of the fact that this reaction proved to be reversible in this solvent. Such reversibility had previously been observed for the combination of the triphenyl methyl cation and bromide in 1:2 acetonitrile:water (36). The kinetic system that applies in the present case is shown in eqs. [6] and [7].

$$[6] \qquad Ar_2C^+H(D) + Br^- \rightleftharpoons ArCH(D)\text{-}Br$$

$$[7] \qquad Ar_2C^+H(D) + H_2O \rightarrow ArCH(D)\text{-}OH$$

Bromide ion combines with the cation with a pseudo first-order rate constant equal to $k_{Br}[Br^-]$ (since bromide is in excess). On the same time scale, the diarylmethyl bromide that is the product of this combination is undergoing ionization back to the cation with a first-order rate constant of k_{ion}. The cation is reacting with water with a first-order rate constant k_w; the alcohol is ultimately the predominant product because of the reversibility of the bromide addition.

Evidence for this behavior was the appearance of decay traces that no longer fit to a single exponential equation, but which were satisfied by a double exponential (Absorbance = $A_1\exp(-k_1t) + A_2\exp(-k_2t)$. Solution of the differential equations applicable to this kinetic system (37) provides the two exponential coefficients, k_1 and k_2, as shown in eq. [8].

$$[8] \qquad k_1,\ k_2 = 1/2\{(k_{ion} + k_{Br}[Br^-] + k_w) \pm \sqrt{(k_{ion} + k_{Br}[Br^-] + k_w)^2 - 4k_{ion}k_w)}\}$$

The sum of the two is a simple expression: $k_1 + k_2 = (k_{ion} + k_w) + k_{Br}[Br^-]$. Thus, for a series of experiments at different concentrations of bromide, a plot of the sum of the two exponential coefficients ($k_1 + k_2$) vs. [Br^-] is predicted to be linear with a slope equal to k_{Br} and an intercept equal to the sum ($k_{ion} + k_w$).

Experiments were therefore performed in which the undeuterated and deuterated cations were generated by LFP and reacted in the presence of five to six different concentrations of bromide. Three to five traces were obtained at each bromide concentration. Each trace was fit to a double exponential, and plots of ($k_1 + k_2$) vs. bromide constructed, one for the undeuterated and one for the deuterated cation. Excellent linear correlations were obtained with least-squares correlation coefficients of at least 0.995. The rate constant k_{Br} comes directly from the slope. The intercept provides ($k_{ion} + k_w$). To obtain k_{ion}, k_w was measured at the same time from the single exponential decay in a solution with no bromide present. The ratio k_{Br}:k_{ion} then provides the equilibrium constant written in the direction $Ar_2CH^+ + Br^- \rightleftharpoons Ar_2CHBr$.

This set of experiments was performed five times on five different days; the average values of the rate constants, equilibrium constants, and kinetic and equilibrium isotope effects are provided as the entry for reaction A in Table 5. It can be seen that while k_{Br}^H:k_{Br}^D is obtained with good precision, there are larger errors in k_{ion}^H:k_{ion}^D and the equilibrium isotope effect. This arises since k_{ion} is obtained as an intercept of a linear plot, after subtraction of a the rate constant k_w which has a similar magnitude. It can be noted that the value of the equilibrium isotope effect when written in the ionization direction $Ar_2CHBr\ A \rightleftharpoons Ar_2CH^+ + Br^-$ is 1.18 ± 0.03. This is within the range of the max value of 1.15 for k^H:k^D suggested by other workers (18) for an S_N1 solvolysis of a secondary alkyl bromide.

Equilibration with chloride ion

The equilibrium isotope effect for a chloride combination, was obtained by measuring the rate constants and kinetic isotope effects for the reactions in both the forward and reverse directions. The appropriate ratios then provides the equilibrium constants and equilibrium isotope effects. The isotope effect in the cation:anion combination direction (k_{Cl}^H:k_{Cl}^D) was obtained using LFP in the normal manner (see the last entry in Table 3). The isotope effect in the ionization direction (k_{ion}^H:k_{ion}^D) was obtained through a kinetic study of the solvolysis of undeuterated and deuterated (4-methoxydiphenyl)methyl chlorides in 2:98 water:acetonitrile containing 0.001 M tetramethylammonium hydroxide. This particular solvent combination was chosen so that the solvolysis occurred with a reasonable rate when studied in a conventional spectrometer. The hydroxide ion was added so as to quench the cation as it formed, i.e., so that the ionization was rate-limiting. Experiments with the undeuterated substrate verified that the rate constant for the solvolysis was not affected by either varying the concentration of hydroxide ion or by changing to 0.001 M azide ion as the trapping nucleophile. Although the chloride–cation combination in this solvent combination occurs with a rate constant of ~2×10^{10} M^{-1} s^{-1} (Table 3), this is also true for hydroxide ion[2]

[2] R.A. McClelland. Unpublished result.

© 2001 NRC Canada

Table 5. Rate constants, equilibrium constants, kinetic and equilibrium isotope effects for reaction A ((4-methyl-4′-methoxydiphenyl)methyl cation plus bromide ion in 80:20 W:AN) and reaction B ((4-methoxydiphenyl)methyl cation and chloride ion in 2:98 W:AN).

Constant	Reaction A	Reaction B
k_{ion}^{H} (s^{-1})	(3.8 ± 0.4) × 10^{5}	(3.50 ± 0.01) × 10^{-2}
k_{X}^{H} (M^{-1} s^{-1})	(1.53 ± 0.07) × 10^{8}	(1.68 ± 0.016) × 10^{10}
$K_{eq}^{H} = k_{X}^{H}:k_{ion}^{H}$ (M^{-1})	(4.0 ± 0.5) × 10^{3}	(4.80 ± 0.05) × 10^{11}
$k_{ion}^{H}:k_{ion}^{D}$	1.13 ± 0.03	(1.154 ± 0.009)
$k_{X}^{H}:k_{X}^{D}$	0.950 ± 0.005	(0.999 ± 0.021)
$K_{eq}^{H}:K_{eq}^{D}$	0.840 ± 0.023	0.860 ± 0.019

and for azide ion (38). Since the concentration of chloride ion is always much lower than that of either hydroxide or azide, the cation, when formed in an ionization, is trapped by the added nucleophile so that cation formation is rate-limiting.

To minimize experimental error, the kinetic isotope effect for the solvolysis was measured by performing four kinetic runs with each substrate on a given day; this procedure was repeated for a total of 7 days The data are provided as the entry under reaction B in Table 5. Because of the high acetonitrile content of the solvent employed in this study (see *Discussion*), the kinetic isotope effect for the cation–anion combination reaction is unity, so that the equilibrium isotope effect is determined by the kinetic isotope effect for the ionization. This value is 1.155, when written in the ionization reaction $Ar_2CH(D)\text{-}Cl \rightarrow Ar_2C^{+}H(D) + Cl^{-}$. This is in good agreement with the max $k^{H}:k^{D}$ predicted for S_N1 solvolysis with chloride as the leaving group (18).

Discussion

Bond formation in the transition state for the water reaction

Kinetic isotope effects can change because of a different size of the nucleophile or because of different extents of bond formation in the transition state. To eliminate the former so that the latter can be evaluated, it is necessary to compare the kinetic isotope effect with the equilibrium isotope effect for the same reaction. As discussed by Schowen (39), the fraction of bond formation in the transition state can be calculated by dividing the logarithm of the kinetic isotope effect by the logarithm of the equilibrium isotope effect for the reaction in the same direction. The final column of Table 2 shows the results of such a calculation for the reactions of diarylmethyl cations with water. Included in this table are the literature data (21) for the considerably more stabilized ferrocenyl derivatives. The values range from 0.49 to 0.64. Since the uncertainties are of the order of 0.05 to 0.1, these are not distinguishable. In other words, within experimental error, there is 50–65% C_α—OH_2 bond formation in the transition state for the reaction of these diarylmethyl cations with water. What is particularly interesting is that this is true in spite of a 1 × 10^{8}-fold change in the rate constant k_w and a 1 × 10^{15}-fold change in the equilibrium constant. Thus, the position of the transition state does not change even though there is a large variation in the reactivity of the cations.

These same conclusions, 50–65% bond formation in the transition state independent of reactivity, are also made with rate-equilibrium correlations (40, 41) where log k_w is plotted against log K_R for cations with changing substituents in the aryl rings attached to the C^+ center. A series of such plots is shown in Fig. 3 of ref. 1. While the data separate into families dependent on the type of cation, there is a good linear correlation within each family. Slopes range from 0.54 to 0.68; the diarylmethyl cation family has a slope of 0.54, the triarylmethyl cation family, a slope of 0.60. The data extend over very wide ranges of reactivity, with changes in k_w and K_R of 1 × 10^{15} and 1 × 10^{25}, respectively. Within experimental error, there is little sign of curvature. Thus, despite the change in reactivity, the position of the transition state is relatively unchanged.

The slope of the plot of log k_w – log K_R can be taken as a measure of the change in charge at the C^+ center in the transition state (41). Thus, there has been approximately 60% charge neutralization at the transition state. The log $(k_w^H:k_w^D)$:log $(K_R^H:K_R^D)$ values can be taken as a measure of the extent of geometry change and bond formation. Thus, there is approximately 60% bond formation at the transition state. The two approaches provide different measures of the nature of the transition state, with different assumptions inherent in each. That each leads to the same conclusion, a transition state that is about 60% developed, provides confidence that this is a true picture.

Transition states for halide reactions

In 100% acetonitrile, there is no kinetic isotope effect in the reaction of the diarylmethyl cations with either bromide or chloride ion (Table 3). Moreover the rate constants lie within the range 2 to 3 × 10^{10} M^{-1} s^{-1}, regardless of both the substituents present in the diarylmethyl cation and the anionic nucleophile. The latter two observations have previously been made and include other anionic nucleophiles (3, 38). This has led to the conclusion that diarylmethylcation–anion combinations in 100% acetonitrile are diffusion controlled; i.e., the rate-limiting step is the encounter of the cation and the anion. The kinetic isotope effects are clearly consistent with this interpretation. Rate-limiting encounter means that there is no bond formation in the transition state. Thus, no isotope effect is expected.

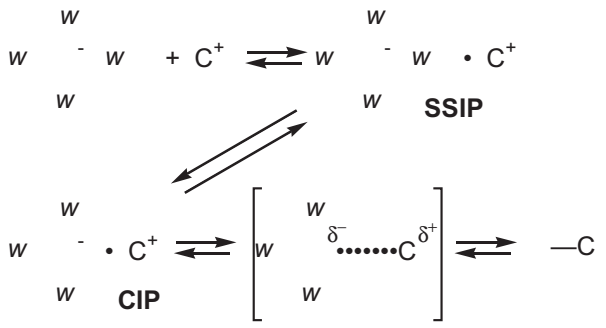
In 20% acetonitrile, 80% water on the other hand, small inverse kinetic isotope effects are observed. This shows that bond formation has become rate-limiting, with some C_α—halide bond making in the transition state. This, in fact, must be true for the reactions in virtually all of the acetonitrile:

© 2001 NRC Canada

water mixtures. This conclusion can be made on the basis of the observation that once water is present, the rate constants become dependent on the nature of the substituent in the diarylmethyl cation, with the expected order $CH_3 < H < CF_3$. In 100% acetonitrile, the halide ion is poorly solvated. Once there is some water present to solvate the anion, the reaction switches from rate-limiting encounter to rate-limiting bond formation. One also sees the effect of rate constants decreasing with increased water content, presumably associated with the halide ions becoming more strongly hydrated and consequently less reactive. The greater reactivity of bromide over chloride is likely associated with the greater hydration of the latter.

The extent of bond formation in the transition states in 20% acetonitrile can be determined as discussed above, by calculating the ratios log (k_X^H:k_X^D):log (K_{eq}^H:K_{eq}^D). Such a calculation shows that the reactions have ~25% bond formation

Scheme 1.



with bromide as the nucleophile and ~40% with chloride. Thus, the transition states become more reactant-like as one moves from water to chloride to bromide, i.e., as the reactivity of the nucleophile increases.

Scheme 1 provides the mechanism of a cation–halide combination in an aqueous solutions, based on the classic ion pair mechanism for solvolysis written in reverse. The hydrated halide ion ("*w*" = waters of hydration) diffuses to the cation to form a solvent-separated ion pair **SSIP**, which then eliminates a water (or waters) of hydration to form the contact ion pair **CIP**. The rate-limiting step in the present case is the halide—carbon bond formation within this ion pair. As noted in the previous paragraph the transition state (in 20% acetonitrile) is reached at about 25 and 40% bond formation with bromide and chloride, respectively. As seen in Fig. 1, increasing the amount of water in an acetonitrile:water mixture has a dramatic retarding effect on the rate for this reaction. There are two factors that could contribute to this. In the cation–anion combination direction, the contact ion pair is in equilibrium with the solvent-separated ion pair as well as the free ions. Adding water will shift the equilibrium away for the contact ion pair, thus lowering its concentration in the solution, and slowing the rate. In addition, the contact ion pair will still be associated with waters of hydration which will modify its reactivity. Increasing the water content in the solution could well increase the binding of these additional waters, thus decreasing the reactivity of the ion pair.

Acknowledgements

The continued financial support of the Natural Sciences and Engineering Research Council of Canada (NSERC) is gratefully acknowledged.

References

1. R.A. McClelland. Tetrahedron, **52**, 6823 (1996).
2. R.A. McClelland, V.M. Kanagasabapathy, and S. Steenken. J. Am. Chem. Soc. **110**, 6913 (1988).
3. R.A. McClelland, V.M. Kanagasabapathy, N. Banait, and S. Steenken. J. Am. Chem. Soc. **111**, 3966 (1989).
4. J. Bartl, S. Steenken, H. Mayr, and R.A. McClelland. J. Am. Chem. Soc. **112**, 6918 (1990).
5. E.O. Alonso, L.J. Johnston, J.C. Scaiano, and V.G. Toscano. J. Am. Chem. Soc. **112**, 1270 (1990).
6. K.D. Peters and B. Li. J. Phys. Chem. **98**, 401 (1994).
7. M. Lipson, A.A. Deniz, and K.S. Peters. J. Am. Chem. Soc. **118**, 2992 (1996).
8. J.W. Hilborn and J.A. Pincock. J. Am. Chem. Soc. **113**, 2683 (1991).
9. J.A. Pincock and P.J. Wedge. J. Org. Chem. **59**, 5587 (1994).
10. J. Chateauneuf. J. Chem. Soc. Chem. Commun. 1437 (1991).
11. C.J. Collins and N.S. Bowman. Isotope effects in chemical reactions. ACS Monograph 167. Van Rostrand Reinhold Co., New York. 1970.
12. A. Streitweiser, Jr., R.H. Jagow, R.C. Fahey. and S. Suzuki. J. Am. Chem. Soc. **80**, 2326 (1958).
13. L.S. Bartell. J. Am. Chem. Soc. **83**, 3567 (1961).
14. V.J. Shines, Jr., R.D. Fisher, and W. Dowd. J. Am. Chem. Soc. **91**, 7748 (1969).
15. V.J. Shines, Jr. and R.D. Fisher. J. Am. Chem. Soc. **93**, 2553 (1971).
16. V.J. Shines, Jr. and W. Dowd. J. Am. Chem. Soc. **93**, 1029 (1971).
17. V.J. Shiner, Jr., W.E. Buddenbaum, B.L. Murr, and G. Lamaty. J. Am. Chem. Soc. **90**, 418 (1968).
18. V.J. Shiner, Jr. and M.W. Rapp. J. Am. Chem. Soc. **90**, 7171 (1968).
19. K.C. Westaway and S.F. Ali. Can. J. Chem. **57**, 1354 (1979).
20. H. Mayr, R. Schneider, C. Schade, J. Bartl, and R. Bederke. J. Am. Chem. Soc. **112**, 4446 (1990).
21. C.A. Bunton, W.E. Watts, N. Carrasco, and F. Davoudazadeh. J. Chem. Soc. Perkin Trans. 2, 1520 (1980).
22. R. Schneider and H. Mayr. Ber. Bunsen–Ges. **91**, 1369 (1987).
23. T. Ohwada and K. Shudo. J. Am. Chem. Soc. **110**, 1862 (1988).
24. Z. Wang, W.D. Chandler, and D.G. Lee. Can. J. Chem. **76**, 919 (1998).
25. M.P. Balfe. J. Chem. Soc. 797 (1946).
26. D.P. Kelly and J.M. Jenkins. J. Org. Chem. **49**, 409 (1984).
27. F. Uehara, M. Sato, C. Kaneko, and H. Kurihara. J. Org. Chem. **64**, 1436 (1999).
28. P.D. Bartlett and R.W. Nebel. J. Am. Chem. Soc. **62**, 1345 (1940).
29. A. Bowers, T.G. Halsall, E.R.H. Jones, and A.J. Lemin. J. Chem. Soc. 2548 (1953).
30. B.P. Bandgar and V.S. Sadavarte. Synth. Commun. **29**, 2587 (1999).
31. W.J. Middleton and C. Ford. U.S. Patent 3 732 307, 1970.
32. N.C. Deno, J.J. Jaruzelski, and A. Schriesheim. J. Am. Chem. Soc. **77**, 4044 (1955).
33. K.C. Westaway and G. Lai. Can. J. Chem. **67**, 345 (1989).

© 2001 NRC Canada

34. R.A. McClelland, V.M. Kanagasabapathy, N.S. Banait, and S. Steenken. J. Am. Chem. Soc. **114**, 1816 (1992).
35. M.M. Mocek and R. Stewart. Can. J. Chem. **41**, 1641 (1963).
36. R.A. McClelland, N. Banait, and S. Steenken. J. Am. Chem. Soc. **108**, 7023 (1986).
37. C.D. Ritchie. *In* Physical organic chemistry, the fundamental concepts. Marcel Dekker, Onc., New York. 1975. pp. 6–30.
38. R.A. McClelland, V.M. Kanagasabapathy, N. Banait, and S. Steenken. J. Am. Chem. Soc. **113**, 1009 (1991).
39. R.L. Schowen. J. Am. Chem. Soc. **102**, 7530 (1980).
40. J.E. Leffler and E. Grunwald. *In* Rates and equilibria of organic reactions. Wiley, New York. 1963. pp. 156–161.
41. A. Williams. Acc. Chem. Res. **17**, 425 (1984).

© 2001 NRC Canada

Rhodium-catalyzed hydroborations of allylamine and allylimines[1]

Christopher M. Vogels, Paul E. O'Connor, Trevor E. Phillips, Keith J. Watson, Michael P. Shaver, Paul G. Hayes, and Stephen A. Westcott

Abstract: The in situ rhodium-catalyzed addition of catecholborane (HBcat, cat = 1,2-$O_2C_6H_4$) and pinacolborane (HBpin, pin = 1,2-$O_2C_2Me_4$) to allylamine, allylimine, 2- and 4-vinylpyridines, and a thienyl imine has been examined using multinuclear NMR spectroscopy. Although reactions of allylamine ($H_2NCH_2CH{=}CH_2$) and HBcat gave complex product distributions arising from competing dehydrogenative borylation pathways, addition of HBpin to allylamine using a rhodium catalyst afforded only products arising from hydroboration (RN(Bpin)$CH_2CH_2CH_2$Bpin, where R = H, Bpin) and hydrogenation (RN(Bpin)$CH_2CH_2CH_3$). Hydroboration of allylimines (RHC=N$CH_2CH{=}CH_2$, R = Ar) with HBcat occurs initially at the more reactive imine functionality to give unsaturated borylamines (RCH_2N(Bcat)$CH_2CH{=}CH_2$). Further reaction with HBcat gives varying amounts of hydroboration products RCH_2N(Bcat)$CH_2CH_2CH_2$Bcat and RCH_2N(Bcat)CH_2CH(Bcat)CH_3 as well as the diboration product RCH_2N(Bcat)CH_2CH_2CH(Bcat)$_2$, depending on the choice of catalyst. Reactions with related unsaturated pyridine derivatives are complicated by extensive degradation, which can be avoided by coordination of the pyridine nitrogen to a Lewis acid. The first examples of metal-catalyzed hydroboration of imines using HBpin are also reported.

Key words: catalysis, hydroboration, boronate esters, dehydrogenative borylation, allylimines.

Résumé : Faisant appel à la spectroscopie RMN multinucléaire, on a étudié la réaction in situ, catalysée par le rhodium, du catécholborane (HBcat, cat= 1,2-$O_2C_6H_4$) et du pinacolborane (HBpin, pin = 1,2-$O_2C_2Me_4$) avec l'allylamine, l'allylimine, les 2- et 4-vinylpyridines et une thiénylimine. Même si les réactions de l'allylamine ($H_2NCH_2CH{=}CH_2$) avec le HBcat conduisent à des distributions complexes de produits provenant de voies de borylation déshydrogénante en compétition, l'addition du HBpin à l'allylamine en présence d'un catalyseur de rhodium ne conduit qu'aux produits provenant d'une hydroboration (RN(Bpin)$CH_2CH_2CH_2$Bpin dans lequel R = H ou Bpin) ou d'une hydrogénation (RN(Bpin)$CH_2CH_2CH_3$). L'hydroboration des allylimines (RHC=N$CH_2CH{=}CH_2$, R = Ar) à l'aide de HBcat se produit initialement au niveau de la fonctionnalité imine qui est la plus réactive pour conduire à la formation de borylamines (RCH_2N(Bcat)$CH_2CH{=}CH_2$). Une réaction subséquente avec du HBcat conduit à des quantités variables de produits d'hydroboration, RCH_2N(Bcat)$CH_2CH_2CH_2$Bcat et RCH_2N(Bcat)CH_2CH(Bcat)CH_3 ainsi qu'au produit de diboration, RCH_2N(Bcat)CH_2CH_2CH(Bcat)$_2$, suivant le catalyseur choisi. Les réactions avec les dérivés insaturés de la pyridine apparentés sont compliquées par d'importantes réactions de dégradation que l'on peut éviter en procédant à une coordination de l'azote de la pyridine à l'aide d'un acide de Lewis. On rapporte aussi les premiers exemples de réactions d'hydroboration, catalysées par des métaux, d'imines à l'aide de HBpin.

Mots clés : catalyse, hydroboration, esters de l'acide boronique, borylation déshydrogénante, allylimines.

[Traduit par la Rédaction]

Introduction

The hydroboration of alkenes and alkynes, which constitutes the formal addition of a B—H bond across a carbon—carbon multiple bond, is an extremely important reaction in organic synthesis (1). Although simple boron hydride reagents such as borane ($H_3B{\cdot}X$, where X is a Lewis base) and 9-borabicyclo[3.3.1]nonane react readily with alkenes at room temperature, hydroborations with catecholborane (HBcat, cat = 1,2-$O_2C_6H_4$) generally require elevated temperatures. The discovery that transition metals can be used to catalyze the addition of HBcat to organic substrates has become an important and well-established technique in organic synthesis (for an excellent review on hydroborations catalyzed by transition-metal complexes, see ref. 2) (3, 4). These reactions can have regio-, chemo-, or stereoselectivities, complementary, or more remarkably, opposite to those from products obtained via the uncatalyzed variant. Indeed, hydroborations of 5-hexene-2-one with HBcat proceed readily at room temperature to give exclusive formation of a borate product where the borane has added to the more reactive carbonyl double bond (4). However, when the reaction is carried out at 0°C in the pres-

Received 24 May 2001. Published on the NRC Research Press Web site at http://canjchem.nrc.ca on December 10, 2001.

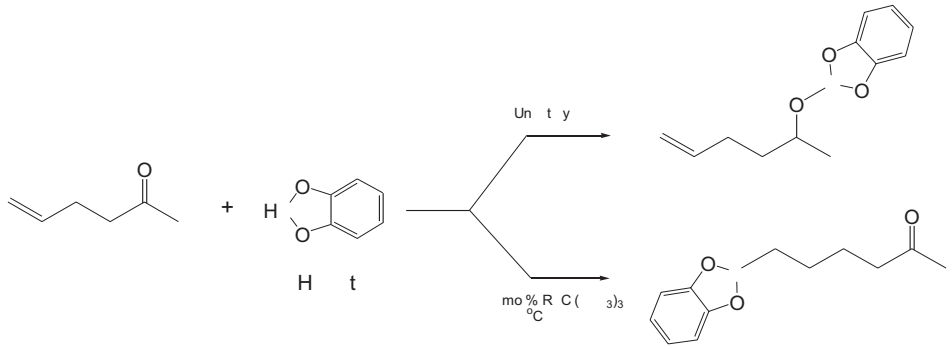
C.M. Vogels, P.E. O'Connor, T.E. Phillips, K.J. Watson, M.P. Shaver, P.G. Hayes, and S.A. Westcott.[2] Department of Chemistry, Mount Allison University, Sackville, NB E4L 1G8, Canada.

[1]Dedicated to the memory of Dr. Slayton A. Evans, Jr.

[2]Corresponding author (telephone: (506) 364-2351; fax: (506) 364-2313; e-mail: swestcott@mta.ca).

 DOI: 10.1139/cjc-79-12-1898 © 2001 NRC Canada

Scheme 1.



ence of a catalytic amount of Wilkinson's catalyst ($RhCl(PPh_3)_3$), addition of the B—H bond occurs primarily at the less reactive alkene moiety to give an organoboronate ester product (Scheme 1).

Organoboronate esters ($RB(OR')_2$) and boronic acids ($RB(OH)_2$) belong to a remarkable class of compounds that have been used extensively in organic (5–9), organometallic (10, 11), and solid-phase synthesis (12, 13), as well as in macrocyclic chemistry (14), molecular recognition (15), transporting molecules across biological membranes (16), redox switching (17), and as glucose sensors (18, 19). Interest in these compounds also arises from their unique biological activities (20). For instance, peptide boronic acids are among the most potent, known inhibitors of serine proteases (21). As a result, the synthesis of boron-containing amino acid derivatives has become an area of considerable interest (22, 23).

Hydroborations of tertiary allylic amines ($R_2NCH_2CH{=}CH_2$, R = alkyl, aryl) with borane ($H_3B{\cdot}X$, X = SMe_2, THF) are known to give initial formation of the expected *anti*-Markovnikov products, $R_2NCH_2CH_2CH_2BH_2$ (6, 24–26). Analogous reactions with primary and secondary amines, however, are complicated by direct interaction with the N—H bond to give a number of *N*-boryl products (27, 28). Protection of the N—H bond is usually required in these reactions to ensure chemoselective addition of the borane at the allyl group (29, 30). Unfortunately, deprotection methodologies frequently compromise the integrity of the B—C bond (31). We, therefore, decided to investigate the in situ reactions of allylamine ($H_2NCH_2CH{=}CH_2$, **1**) and related allylimine derivatives with catecholborane (HBcat, cat = 1,2-$O_2C_6H_4$) and pinacolborane (HBpin, pin = 1,2-$O_2C_2Me_4$) to see if we could generate novel aminoboron compounds without using a protecting group.

Experimental

All reagents and solvents used were obtained from Aldrich Chemicals. Complexes $RhCl(PPh_3)_3$ (32), $[RhCl(coe)_2]_2$ (coe = *cis*-cyclooctene, (33)), and $[RhCl(cod)]_2$ (cod = *cis*-cyclooctadiene, (34)) were prepared as described elsewhere. Imines were prepared by well-established procedures (35–38). NMR spectra were recorded on a JEOL JNM-GSX270 FT NMR spectrometer. ^{1}H NMR chemical shifts are reported in ppm and referenced to residual protons in deuterated solvent at 270.1 MHz. ^{11}B NMR chemical shifts are referenced to external $F_3B{\cdot}OEt_2$ at 86.6 MHz. ^{13}C NMR chemical shifts are referenced to solvent carbon resonances as internal standards at 67.8 MHz. Multiplicities are reported as (s) singlet, (d) doublet, (t) triplet, (q) quartet, (m) multiplet, (br) broad, and (ov) overlapping. Infrared spectra were obtained using a Mattson Genesis II FT IR spectrometer and are reported in cm^{-1}. Microanalyses for C, H, and N were carried out at Desert Analytics (Tucson, Arizona).

Preparation of $Rh(acac)(coe)_2$

$Rh(acac)(coe)_2$ was prepared by modification of an established procedure (39). Tl(acac) (0.42 g, 1.40 mmol) was dissolved in 10 mL of THF and added dropwise to a solution of $[RhCl(coe)_2]_2$ (0.50 g, 0.70 mmol) in 10 mL of THF. The reaction was allowed to stir for 18 h then stored for 48 h at –25°C. A greenish precipitate was filtered whereupon subsequent removal of the THF under vacuum afforded an orange solid. IR (Nujol): 2904, 1581, 1520, 1464, 1377, 1317, 1269, 1020, 897, 766, 735, 604, 550, 519. ^{1}H NMR (in C_6D_6) δ: 5.03 (s, 1H), 2.51 (br, 4H), 2.41 (br, 8H), 1.68 (br s, 12H), 1.55 (br, 4H), 1.40 (br, 6H). ^{13}C NMR δ: 185.0, 98.8 (CH), 78.0 (d, $J_{C\text{-}Rh}$ = 12 Hz, -CH=CH-), 30.3 (CH_2), 27.9 (CH_2), 27.0 (CH_2), 26.8 (CH_3).

Addition of catecholborane (HBcat) to allylamine (1)

In a typical reaction, 2 equiv of HBcat in 0.5 mL of C_6D_6 were added dropwise to a 0.5 mL C_6D_6 solution of allylamine. The mixture was allowed to stir for 1 h and then analyzed by multinuclear NMR spectroscopy. Attempts to control the selectivity of these reactions always gave minor amounts of **2**, which precipitated out of solution after ca. 1 h. **2**: IR (Nujol): 3200, 2940, 2868, 2443, 1600, 1464, 1377, 1350, 1232, 1099, 1057, 1083, 912, 808, 739, 700. ^{1}H NMR (in d_6-acetone) δ: 8.00 (br, cat), 7.09 (br ov m, cat), 6.48 (br, cat), 6.05 (br ov m, 1H, $CH{=}CH_2$), 5.40 (br ov m, 2H, $CH{=}CH_2$), 3.88 (br, 2H, -CH_2CH=CH_2). ^{11}B NMR δ: 23 (br, NBcat), 13 (s, N → HBcat). **3**: ^{1}H NMR (in C_6D_6) δ: 7.01 (d of d, *J* = 6, 3 Hz, 4H, cat), 6.73 (d of d, *J* = 6, 3 Hz, 4H, cat), 5.82 (ov d of d of t, *J* = 17, 10, 7 Hz, 1H, -C*H*=CH_2), 5.16 (d of d, *J* = 17, 2 Hz, 1H, -CH=C*H*H), 4.94 (d of d, *J* = 10, 2 Hz, 1H, -CH=CH*H*), 3.92 (d, *J* = 7 Hz, 2H, -CH_2CH=CH_2). ^{11}B NMR δ: 26 (br, NBcat). ^{13}C NMR δ: 148.6, 136.3, 122.3, 115.1, 112.1, 46.3.

Catalyzed hydroborations of allylamine (1) with HBcat

In a typical reaction, 5 equiv of HBcat in 0.5 mL of C_6D_6 were added to a 0.5 mL C_6D_6 solution of allylamine and 1 mol% $RhCl(PPh_3)_3$. The mixture was allowed to stir for 1 h and then analyzed by multinuclear NMR spectroscopy. **4**: IR

© 2001 NRC Canada

(Nujol): 3060, 2962, 2935, 2873, 1610, 1511, 1467, 1344, 1232, 1182, 1130, 1083, 1007, 941, 866, 806, 733, 680, 498. ^{1}H NMR (in d_6-acetone) δ: 7.60 (br ov m, min), 7.23 (br s, cat), 7.13 (br s, cat), 6.57 (br s, cat), 4.1–3.9 (ov m, min), 3.80 (t, J = 8 Hz, -NCH_2-), 3.58 (t, J = 8 Hz, -NCH_2-), 2.09 (ov m, -CH_2CH_2CH_2-), 1.72 (ov t of t, J = 8 Hz, -CH_2CH_2CH_2-), 1.34 (t, J = 8 Hz, -CH_2B), 0.88 (t, J = 8 Hz, -CH_2B). ^{11}B NMR δ: 35 (br, CBcat), 22 (br, NBcat), 13 (s, N → HBcat). **5**: ^{1}H NMR (in C_6D_6) δ: 7.06–6.68 (ov m, 12H, cat), 3.46 (t, J = 8 Hz, 2H, -NCH_2-), 1.90 (ov t of t, J = 8 Hz, 2H, -CH_2CH_2CH_2-), 1.07 (t, J = 8 Hz, 2H, -CH_2B). ^{11}B NMR δ: 34 (br, CBcat), 26 (br, NBcat). **6**: ^{1}H NMR δ: 7.06–6.68 (ov m, 12H, cat), 3.76 (2nd order d of d, J = 14, 8 Hz, 1H, -NCH*H*-), 3.64 (2nd order d of d, J = 14, 8 Hz, 1H, -NC*H*H-), 1.87 (ov t of q, J = 8 Hz, 1H, -C*H*(Bcat)CH_3), 1.15 (d, J = 8 Hz, 3H, -CH_3. ^{11}B NMR δ: 34 (br, CBcat), 26 (br, NBcat). **8**: ^{1}H NMR δ: 7.06–6.68 (ov m, 16H, cat), 3.62 (t, J = 8 Hz, 2H, -NCH_2-), 2.48 (ov d of t, J = 8 Hz, 2H, -CH_2CH_2CH-), 1.70 (t, J = 8 Hz, 1H, -C*H*(Bcat)$_2$). ^{11}B NMR δ: 34 (br, CBcat), 26 (br, NBcat). **9**: ^{1}H NMR δ: 7.17–6.64 (ov m, 8H, cat), 3.34 (t, J = 8 Hz, 2H, -NCH_2-), 1.57 (ov t of q, J = 8 Hz, 2H, -CH_2C$H_2$$CH_3$), 0.81 (t, J = 8 Hz, 3H, -CH_3).

Catalyzed hydroborations of $H_2NCH_2CH{\equiv}CH$ with HBcat

In a typical reaction, 5 equiv of HBcat in 0.5 mL of C_6D_6 were added to a 0.5 mL C_6D_6 solution of propargyl amine and 1 mol% $RhCl(PPh_3)_3$. The mixture was allowed to stir for 1 h and then analyzed by multinuclear NMR spectroscopy. Products were similar to those observed for reactions with **1**.

Addition of pinacolborane (HBpin) to allylamine (1)

In a typical reaction, 2 equiv of HBpin in 0.5 mL of C_6D_6 were added dropwise to a 0.5 mL C_6D_6 solution of allylamine. The mixture was allowed to stir for 1 h and then analyzed by multinuclear NMR spectroscopy. **10**: ^{1}H NMR (in C_6D_6) δ: 5.73 (ov d of d of t, J = 16, 8, 8 Hz, 1H, -CH_2C*H*=CH_2), 5.10 (d of d, J = 16, 1 Hz, 1H, -CH_2CH=C*H*H), 4.92 (d of d, J = 8, 1 Hz, 1H, -CH_2CH=CH*H*), 3.53–3.50 (br d, J = 8 Hz, 2H, -CH_2CH=CH_2), 2.21 (br s, 1H, N*H*), 1.10 (s, 12H, pin). ^{13}C NMR δ: 139.4, 112.7, 81.7, 43.7, 24.5. ^{11}B NMR δ: 24 (br, NBpin).

Catalyzed hydroborations of allylamine (1) with HBpin

In a typical reaction, 3 equiv of HBpin in 0.5 mL of C_6D_6 were added to a 0.5 mL C_6D_6 solution of allylamine and $RhCl(PPh_3)_3$ (1 mol%). The reaction mixture was allowed to stir for 12 h and then analyzed by multinuclear NMR spectroscopy. **11**: ^{1}H NMR (in C_6D_6) δ: 6.50 (ov d of d of t, J = 18, 10, 8 Hz, 1H, -CH_2C*H*=CH_2), 4.50 (d of d, J = 18, 2 Hz, 1H, -CH_2CH=C*H*H), 4.37 (d of d, J = 10, 2 Hz, 1H, -CH_2CH=C*H*H), 3.90 (d, J = 8 Hz, 2H, -CH_2CH=CH_2), 1.10 (s, 24H, pin). ^{11}B NMR δ: 26 (br, NBcat). **12**: ^{1}H NMR (in C_6D_6) δ: 3.00 (ov d of t, J = 8 Hz, 2H, -NCH_2-), 2.27 (br, 1H, N*H*), 1.60 (ov t of t, J = 8 Hz, 2H, -CH_2CH_2CH_2-), 1.07–0.99 (ov m, 26H, -CH_2B and pin). ^{11}B NMR δ: 33 (br, CBpin), 25 (br, NBpin). **13**: ^{1}H NMR δ: 3.50 (t, J = 8 Hz, 2H, -NCH_2-), 2.04 (ov t of t, J = 8 Hz, 2H, -CH_2CH_2CH_2-), 1.26–1.03 (ov m, 38H, -CH_2B and pin). ^{11}B NMR δ: 33 (br, CBpin), 25 (br, NBpin). **14**: ^{1}H NMR δ: 2.84 (ov d of t, J = 8 Hz, 2H, -NCH_2-), 2.18 (br, 1H, N*H*), 1.26 (ov t of q, J = 8 Hz, 2H, -CH_2C$H_2$$CH_3$), 1.11 (s, 12H, pin), 0.75 (t, J = 8 Hz, 3H, -CH_3). ^{11}B NMR δ: 25 (br, NBpin). **15**: ^{1}H NMR δ: 3.39 (t, J = 8 Hz, 2H, -NCH_2-), 1.74 (ov t of q, J = 8 Hz, 2H, -CH_2C$H_2$$CH_3$), 1.05 (s, 24H, pin), 0.93 (t, J = 8 Hz, 3H, -CH_3). ^{11}B NMR δ: 25 (br, NBpin).

Catalyzed hydroborations of allylimines (16a–16d) with HBcat

In a typical reaction, 3 equiv of catecholborane in 0.5 mL of C_6D_6 were added to a 0.5 mL C_6D_6 solution of allylimine **16c** in the presence of 1 mol% $RhCl(PPh_3)_3$. The mixture was allowed to stir for 1 h and then analyzed by multinuclear NMR spectroscopy. **17c**: ^{1}H NMR (in C_6D_6) δ: 7.01–6.65 (ov m, 11H, cat and Ar), 4.30 (s, 2H, -NCH_2Ar), 3.09 (t, J = 8 Hz, 2H, -NCH_2-), 1.69 (ov t of t, J = 8 Hz, 2H, -CH_2CH_2CH_2-), 0.99 (t, J = 8 Hz, 2H, -CH_2B). ^{11}B NMR δ: 35 (br, CBcat), 26 (br, NBcat). **18c**: ^{1}H NMR δ: 7.01–6.65 (ov m, 11H, cat and Ar), 4.31 (s, 2H, -NCH_2Ar), 3.46 (2nd order d of d, J = 14, 8 Hz, 1H, -NCH*H*-), 3.31 (2nd order d of d, J = 14, 8 Hz, 1H, -NC*H*H-), 1.68 (ov t of q, J = 8 Hz, 1H, -C*H*(Bcat)CH_3), 1.07 (d, J = 8 Hz, 3H, -CH_3). ^{11}B NMR δ: 35 (br, CBcat), 26 (br, NBcat). **19c**: ^{1}H NMR δ: 7.01–6.65 (ov m, 15H, cat and Ar), 4.30 (s, 2H, -NCH_2Ar), 3.25 (t, J = 8 Hz, 2H, -NCH_2-), 2.18 (ov d of t, J = 8 Hz, 2H, -CH_2CH_2CH-), 1.63 (t, J = 8 Hz, 1H, -C*H*(Bcat)$_2$). ^{11}B NMR δ: 35 (br, CBcat), 26 (br, NBcat). **20c**: ^{1}H NMR δ: 7.01–6.65 (ov m, 7H, cat and Ar), 4.30 (s, 2H, -NCH_2Ar), 3.00 (t, J = 8 Hz, 2H, -NCH_2-), 1.38 (ov t of q, J = 8 Hz, 2H, -CH_2C$H_2$$CH_3$), 0.71 (t, J = 8Hz, 3H, -CH_3). ^{11}B NMR δ: 26 (br, NBcat).

Catalyzed hydroborations of vinylpyridines-BF_3 with HBcat

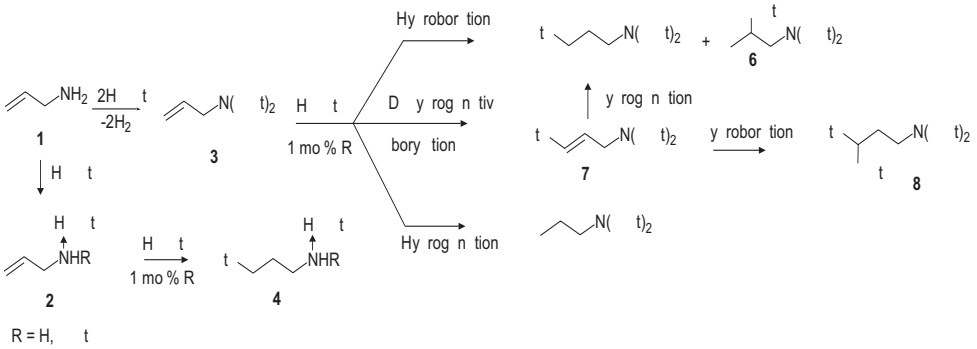
In a typical reaction, 1.1 equiv of $BF_3{\cdot}OMe_2$ were added to a 0.5 mL solution of the vinylpyridine in C_6D_6. The resulting solution was allowed to stir for 2 h whereupon 1 mol% of $Rh(acac)(coe)_2$/dppb (dppb = 1,4-bis(diphenylphosphino)butane) in 0.25 mL of C_6D_6 was added to the mixture, followed by the addition of a 0.25 mL C_6D_6 solution of 1.2 equiv of HBcat. The mixture was allowed to stir for 1 h and then analyzed by multinuclear NMR spectroscopy. **22**: ^{1}H (in C_6D_6) δ: 8.55 (d, J = 5 Hz, 1H), 7.04–6.78 (ov m, 6H), 6.50 (app t, J = 5 Hz, 1H), 4.34 (q, J = 8 Hz, 1H, -C*H*(Bcat)-), 1.36 (d, J = 8 Hz, 3H, -CH_3). ^{11}B NMR δ: 34 (br, CBcat), 1 (s, NBF_3). ^{13}C NMR δ: 162.2, 148.5, 143.7, 142.5, 125.4, 123.0, 122.4, 112.7, 23.8 (br, CB), 14.9. **24**: ^{1}H NMR δ: 8.28 (d, J = 5 Hz, 2H), 7.07 (d of d, J = 3, 1 Hz, 2H), 6.88 (d of d, J = 3, 1 Hz, 2H), 6.66 (d, J = 5 Hz, 2H), 2.39 (q, J = 8 Hz, 1H, -C*H*(Bcat)-), 1.14 (d, J = 8Hz, 3H, -CH_3). ^{11}B NMR δ: 34 (br, CBcat), 1 (s, NBF_3). ^{13}C NMR δ: 161.2, 148.8, 143.3, 125.5, 124.1, 113.2, 25.6 (br, CB), 15.0.

Catalyzed hydroborations of vinylpyridines-BF_3 with HBpin

In a typical reaction, 1.1 equiv of $BF_3{\cdot}OMe_2$ were added to a 0.5 mL solution of the vinylpyridine in C_6D_6. The resulting solution was allowed to stir for 2 h whereupon $RhCl(PPh)_3$ (1 mol%) in 0.25 mL of C_6D_6 was added to the mixture, followed by the addition of a 0.25 mL C_6D_6 solution of 1.2 equiv of HBpin. The mixture was allowed to stir for 12 h and then analyzed by multinuclear NMR spectroscopy. Selected spectroscopic data for reactions with **21**: ^{1}H NMR (in C_6D_6)

© 2001 NRC Canada

Scheme 2.



δ: 3.90 (br q, *J* = 8 Hz, 1H, -C*H*(Bpin)-), 3.07 (q, *J* = 8 Hz, 2H, -CH_2CH$_3$), 1.28 (d, *J* = 8 Hz, 3H, -CH(Bpin)CH_3), 1.00 (s, Bpin), 0.94 (t, *J* = 8 Hz, 3H, -CH$_2$CH_3). ^{11}B NMR δ: 33 (br, CBpin), 23, 21, 1 (s, NBF$_3$). Selected spectroscopic data for reactions with **23**: ^{1}H NMR δ: 2.72 (d, *J* = 8 Hz), 2.30 (t, *J* = 8 Hz, -CH_2CH$_2$B), 2.14 (q, *J* = 8 Hz, 1H, C*H*(Bpin)-), 1.95 (q, *J* = 8 Hz, 2H, -CH_2CH$_3$), 1.17 (br s), 1.06 (d, *J* = 8 Hz, 3H, -CH(Bpin)CH_3), 0.98 (s, Bpin), 0.66 (t, *J* = 8 Hz, 3H, -CH$_2$CH_3). ^{11}B NMR δ: 33 (br, CBpin), 21, 1 (s, NBF$_3$).

Catalyzed hydroborations of aldimine 25 with pinacolborane (HBpin)

To a 0.5 mL C_6D_6 solution of **25** and 1 mol% RhCl(PPh$_3$)$_3$ was added 1.2 equiv of HBpin in 0.5 mL of C_6D_6. The reaction was heated at reflux for 2 h and then analyzed by multinuclear NMR spectroscopy. **26**: ^{1}H NMR (in C_6D_6) δ: 6.88–6.73 (ov m, 3H, Ar), 4.33 (s, 2H, -NCH_2Ar), 3.01 (t, *J* = 8 Hz, 2H, -NCH_2-), 1.42 (ov t of q, *J* = 8 Hz, 2H, -CH$_2$CH_2CH$_3$), 1.15 (s, 12H, pin), 0.78 (t, *J* = 8 Hz, 3H, -CH_3). ^{13}C NMR δ: 145.8, 126.4, 124.8, 124.1, 82.2, 46.8, 44.4, 24.5, 22.0, 11.1. ^{11}B NMR δ: 24 (br, NBpin).

Results and discussion

As with reactions using borane, we have found that the in situ addition of HBcat to allylamine (**1**) resulted in the initial formation of a mixture of products. Although minor amounts of Lewis acid–base adducts HBcat·HNRCH$_2$CH=CH$_2$ (**2**, R = H, Bcat) are formed (40), a competing reaction gave N(Bcat)$_2$CH$_2$CH=CH$_2$ (**3**) as the major boron-containing product in solution. No adduct formation is observed with **3**, however, as coordination of two electron-withdrawing boryl groups has either significantly reduced the nucleophilic nature of the amine or increased the steric hindrance around the nitrogen atom. Although HBcat eventually adds to the activated allyl group in these aminoboryl species, reactions take several days. However, we have found that certain rhodium complexes can be used to catalyze this addition. Rhodium-catalyzed hydroborations are believed to arise via oxidative addition of the B—H bond of the boronate ester at the metal centre, followed by coordination and subsequent insertion of the alkene into the Rh—H or Rh—B bond (41). Reductive elimination affords the desired organoboronate ester product.

Addition of excess HBcat is required in all of these catalyzed reactions to ensure 100% conversion of the starting alkene. While hydroboration of intermediate **2** gave minor amounts of HBcat·HNRCH$_2$CH$_2$CH$_2$Bcat (**4**, R = H, Bcat), reactions with **3** gave surprisingly complex product distributions, regardless of the catalyst system used to affect this transformation (Scheme 2). Although significant amounts of the hydroboration products **5** and **6** were formed in these reactions, products (such as **8**) derived from a competing dehydrogenative borylation pathway were also observed (by NMR spectroscopy). We propose that these unique products originate from the transient alkenylboronate ester **7**, which presumably results from insertion of the activated alkene into the Rh—B bond (3, 41). Subsequent β-hydride elimination would afford the alkenylboronate ester with concomitant formation of dihydrogen (2, 41). It is possible that "hydroboration product" **5** also arises from hydrogenation of alkenylboronate ester **7**. Hydride elimination appears to be specific as products arising from abstraction of a methylene hydrogen α to the activated amine group are not observed. Alkenylboronate ester **7** can also add another equiv of HBcat to give **8**. Interestingly, we have found that compound **8** can also be generated as the major product in analogous hydroborations of H$_2$NCH$_2$C≡CH. As with most catalyzed hydroboration reactions, a small amount of hydrogenation product (**9**) is almost always observed.

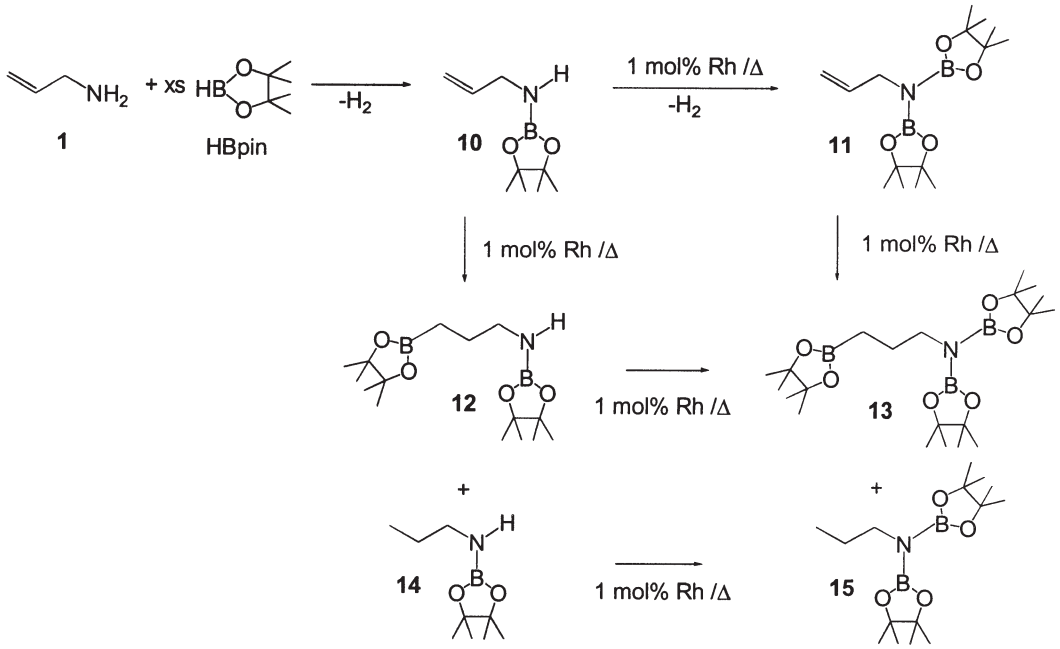
The formation of these products is somewhat unusual as catalyzed hydroborations of simple alkenes, such as 1-octene, proceed smoothly to give predominant formation of the expected organoboronate ester product (2, 4). In this study, replacement of the two N—H bonds with N-Bcat groups in **3** appears to be ineffective in deactivating the amine group and catalyzed reactions proceed to give complex product distributions. The formation of multiple boronated compounds has recently been an area of considerable interest (42–44).

Metal-catalyzed hydroborations of unsaturated C—C bonds using HBpin have been reported previously (45–47).[3] In a further attempt to control selectivity we decided to examine hydroborations using HBpin (Scheme 3). Unlike reactions with HBcat, which is a stronger Lewis acid, no adduct formation was observed. Addition of excess HBpin gave the monoboryl amine HN(Bpin)CH$_2$CH$_2$=CH$_2$ (**10**), where a second equiv of the boronate ester failed to add to the amine N—H bond even at elevated temperatures. Remarkably, we have found

[3] C.M. Crudden and A. Chen. Unpublished results.

© 2001 NRC Canada

Scheme 3.



that a rhodium catalyst could be used to facilitate the addition of another equiv of HBpin to give $N(Bpin)_2CH_2CH_2{=}CH_2$ (**11**). This observation provides the first example of a metal-catalyzed hydroboration of N—H bonds.

Compound **11** was observed in only minor amounts (<5% by ^{1}H NMR spectroscopy) as a competing hydroboration reaction occurred at the alkene moiety to afford a mixture of $HN(Bpin)CH_2CH_2CH_2Bpin$ (**12**) and $N(Bpin)_2CH_2CH_2CH_2Bpin$ (**13**). Not surprisingly, significant amounts of hydrogenation products $RN(Bpin)CH_2CH_2CH_3$ (where R = H or Bpin, **14** and **15**, respectively) were also observed in these reactions. The ^{1}H NMR data for the propyl group in **13** is similar to that observed for **12**, except that chemical shifts are moved to a lower field due to addition of another electron-withdrawing Bpin group. For instance, the middle CH_2 resonance in **12** is observed as an overlapping triplet of triplets at 1.60 ppm, yet for **13** this peak is found at 2.04 ppm. The ^{11}B NMR of $RN(Bpin)CH_2CH_2CH_2Bpin$ (where R = H or Bpin) shows a peak at 25 ppm corresponding to the B—N bond and a resonance at 33 ppm for the new B—C bond. No appreciable intramolecular interactions are observed in these molecules as the boron atoms appear to be three-coordinate (40, 48). This result is consistent with previous NMR data on related $NH_2CH_2CH_2CH_2B(OH)_2{\cdot}HCl$ which shows a peak in the ^{11}B NMR at 32.6 ppm (49). Interestingly, the analogous neutral compound ($NH_2CH_2CH_2CH_2B(OH)_2$) displays a resonance at 8 ppm suggesting intramolecular adduct formation between the nitrogen and the boron atom (50).

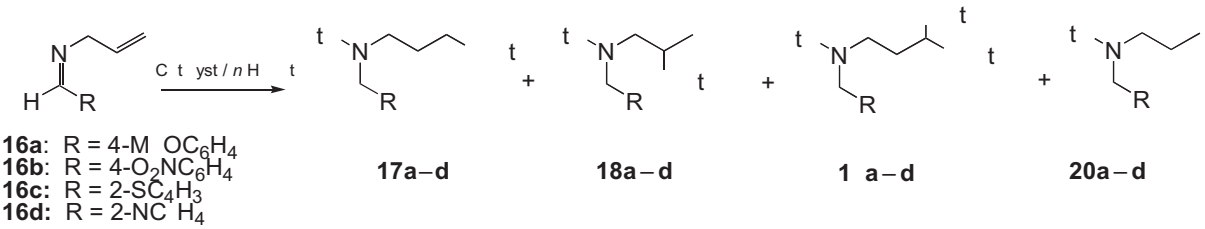
To avoid complications arising from addition of the boronate esters at the amine N—H bond, we decided to investigate hydroborations of allylimine derivatives **16a**–**d**. Addition of 1 equiv of catecholborane to allylimines **16a**–**c** proceeds cleanly to give the corresponding borylamines, where the electron-deficient boron group has added to the nitrogen atom of the imine double bond (51). A rhodium catalyst can once again be used to facilitate the addition of a second equiv of HBcat to the alkene moiety. While selectivity to 3-aminopropylboronate esters has been increased in these reactions, products arising from competing Markovnikov hydroboration, dehydrogenative borylation, and hydrogenation are all still observed to some extent (Table 1).

Reactions with **16c** were carried out with 3 equiv of HBcat to ensure complete conversion of the allyl group. Although $RhCl(PPh_3)_3$ (entry 1) gave 71% of the *anti*-Markovnikov product **17c**, use of $[RhCl(coe)_2]_2/4PPh_3$ (coe = *cis*-cyclooctene, entry 7) as a catalyst precursor gave 88% of this desired product (using ^{1}H NMR spectroscopy). Significant amounts (23%) of the hydroboration product **18c** were observed in reactions using $[RhCl(coe)_2]_2$ as a catalyst precursor (entry 6). This product arises from a Markovnikov addition of the borane to the allyl moiety. Remarkably, the diboronated ester **19c** was a major product (38%) in reactions using $Rh(acac)(coe)_2$/dppm (dppm = 1,1-bis(diphenylphosphino)methane) (entry 10). Catalyst precursors of this type are known to generate the active zwitterionic catalyst Rh(dppm)(η^6-catBcat) (52, 53). It is interesting to note that no significant change in product distributions is observed when reactions were conducted using an excess of HBcat (entry 12) or when hydroborations were carried out in $CDCl_3$ (entry 11). Although only minor differences in product distributions were observed when **16a** was used as the substrate (cf. entries 1 and 13), reactions with **16b** gave significant amounts of hydrogenation product **20b** (entry 14). Hydrogenation products are also observed in other reactions where extensive borane and (or) catalyst decomposition occurs (entries 6 and 8; (29)).

Hydroborations of the pyridine derivative **16d** gave rise to a number of different boron-containing products, also arising from the degradation of HBcat (2). Since no degradation was observed with the thiophene imine **16c** using HBcat, it is plausible that the harder nitrogen atom in the pyridine ring is responsible for this unwanted degradation pathway. To test this hypothesis, we decided to investigate the analogous hydroborations with 2- and 4-vinylpyridine (**21** and **23**, respectively). Catalyzed hydroborations of styrene proceed

© 2001 NRC Canada

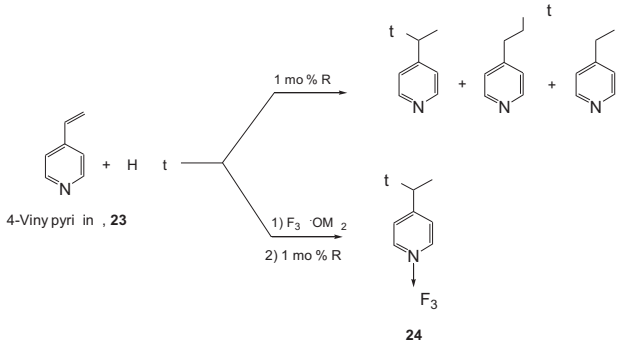
Table 1. Hydroboration of allylimines with HBcat.



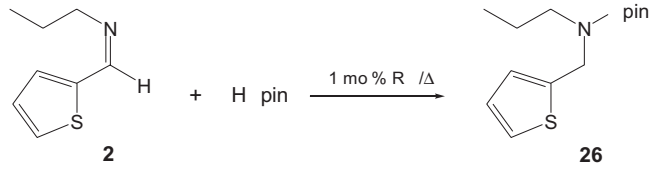
Entry	Allylimine	Catalyst system	Solvent	HBcat (*n*)	**17a–17d**	**18a–18d**	**19a–19d**	**20a–20d**
1	**16c**	$RhCl(PPh_3)_3$	C_6D_6	3	71	7	20	2
2	**16c**	$RhCl(PPh_3)_3/10PPh_3$	C_6D_6	3	78	8	13	1
3	**16c**	$[Rh(cod)Cl]_2$/dppb/$AgBF_4$	C_6D_6	3	86	5	6	3
4	**16c**	$Rh(H)(CO)(PPh_3)_3$	C_6D_6	3	80	7	10	3
5	**16c**	$Rh(H)(PPh_3)_4$	C_6D_6	3	77	14	5	4
6	**16c**	$[RhCl(coe)_2]_2$	C_6D_6	3	63	23	2	12
7	**16c**	$[RhCl(coe)_2]_2/4PPh_3$	C_6D_6	3	88	2	8	2
8	**16c**	$Rh(acac)(coe)_2$	C_6D_6	3	51	16	12	21
9	**16c**	$Rh(acac)(coe)_2/2PPh_3$	C_6D_6	3	79	18	2	1
10	**16c**	$Rh(acac)(coe)_2$/dppm	C_6D_6	3	37	20	38	5
11	**16c**	$Rh(acac)(coe)_2$/dppm	$CDCl_3$	3	59	9	15	17
12	**16c**	$RhCl(PPh_3)_3$	C_6D_6	6	75	5	19	1
13	**16a**	$RhCl(PPh_3)_3$	C_6D_6	3	88	6	5	1
14	**16b**	$RhCl(PPh_3)_3$	C_6D_6	3	51	11	1	37

Note: All reactions were conducted with 1 mol% catalyst at room temperature. Yields were calculated using ^{1}H NMR data.

Scheme 4.



Scheme 5.



smoothly to give selective formation of either the Markovnikov or *anti*-Markovnikov product, depending upon the metal catalyst employed (2). Not surprisingly, we have found that catalyzed reactions of the vinylpyridines with HBcat gave a mixture of hydroboration products, along with a significant amount of ethylpyridine. Although a number of metal complexes were examined as catalysts for this reaction, all gave mixtures of products. Oxidation of the resulting hydroborated mixtures with NaOH–H_2O_2 gave 4-ethylpyridine as the only isolable organic product (54). Similar results are also seen in reactions with HBpin. Coordination of a strong Lewis acid, such as BF_3 (55–57), to the vinylpyridines effectively eliminated these degradation pathways and the Marknovnikov hydroboration products (**22** and **24**, respectively) could be obtained in high yields (>95% by NMR spectroscopy) using $Rh(acac)(coe)_2$/dppb (dppb = 1,4-bis(diphenylphosphino)butane) as a catalyst precursor (Scheme 4) and HBcat. Reactions with HBpin gave a mixture of hydroboration products along with a significant amount of hydrogenation. Unfortunately, attempts to protect the nitrogen group with BF_3 in the hydroboration of allylamines **1** and **16d** led to polymerization of the activated alkene moiety.

We then decided to examine the rhodium-catalyzed hydroboration of allylimine **16c** using HBpin. Although no reaction was observed at room temperature, complex product distributions arising from addition at the allyl group and the imine functionality were observed when reactions were carried out at elevated temperatures (60°C). Reduction of the imine was observed by disappearance of the aldimine hydrogen at 7.89 ppm with concomitant appearance of a benzylic hydrogen at 4.36 ppm. A peak at 24 ppm in the ^{11}B NMR spectrum arises from the newly formed N—Bpin bond. This result is somewhat surprising as previous attempts to hydroborate imines using HBpin proved unsuccessful (58). To confirm that the imine was being reduced in these reactions, we decided to investigate hydroborations with saturated aldimine **25** (Scheme 5). Indeed, these reactions proceeded

© 2001 NRC Canada

to give selective formation of the desired *N*-boryl product **26** and represent the first examples of a metal-catalyzed hydroboration of an imine using HBpin (45–47).[3] Although the synthesis of chiral amines is of utmost importance in organic and medicinal chemistry, the enantioselective reduction of simple ketimine derivatives is often a synthetically challenging problem (59). As a result, future work in this area will focus on the asymmetric reduction of related ketimines using HBpin.

Conclusion

We have found that the in situ addition of HBcat to allylamine using a number of rhodium catalysts gave products derived from competing hydroboration and dehydrogenative borylation pathways.[4] The use of HBpin effectively eliminated the dehydrogenative borylation reaction and a novel rhodium-catalyzed hydroboration of N—H bonds was observed to give $N(Bpin)_2CH_2CH_2CH_2Bpin$ along with various amounts of hydrogenation product. Hydroboration of allylimines with HBcat occurs initially at the more reactive imine functionality to give unsaturated borylamines. Further reaction gives the corresponding *anti*-Markovnikov and Markovnikov hydroboration products. Reactions with related unsaturated pyridine derivatives are complicated by extensive degradation, which can be avoided by coordination of the pyridine nitrogen to a Lewis acid. We have also shown that catalyzed hydroborations of aldimines can be accomplished using HBpin. Further work will examine other catalyst systems to fine-tune product selectivities in these reactions.

Acknowledgements

Thanks are gratefully extended to the Natural Sciences and Engineering Research Council of Canada (NSERC) and Mount Allison University for financial support and Johnson Matthey Ltd. for the generous gift of rhodium chloride. We also wish to thank Dan Durant (MAU), Roger Smith (MAU), and John Marcone (DuPont Co.) for their expert technical assistance, Dr. R. Tom Baker (Los Alamos) and Dr. Cathleen Crudden (UNB) for very valuable discussions, and anonymous reviewers for helpful comments.

References

1. H.C. Brown, G.W. Kramer, A.B. Levy, and M.M. Midland. Organic syntheses via boranes. Wiley–Interscience, New York. 1975.
2. I. Beletskaya and A. Pelter. Tetrahedron, **53**, 4957 (1997).
3. D.E. Kadlecek, P.J. Carroll, and L.G. Sneddon. J. Am. Chem. Soc. **122**, 10 868 (2000), and refs. therein.
4. D. Männig and H. Nöth. Angew. Chem. Int. Ed. Engl. **24**, 878 (1985).
5. N. Miyaura and A. Suzuki. Chem. Rev. **95**, 2457 (1995).
6. D.S. Matteson. Tetrahedron, **45**, 1859 (1989).
7. N.A. Petasis and I.A. Zavialov. J. Am. Chem. Soc. **120**, 11 798 (1998).
8. M. Murata, T. Oyama, S. Watanabe, and Y. Masuda. J. Org. Chem. **65**, 164 (2000).
9. A.F. Littke, C. Dai, and G.C. Fu. J. Am. Chem. Soc. **122**, 4020 (2000).
10. F. Minutolo and J.A. Katzenellenbogen. Organometallics, **18**, 2519 (1999).
11. Y. Kobayashi, K. Watatani, and Y. Tokoro. Tetrahedron Lett. **39**, 7533 (1998).
12. D.G. Hall, J. Tailor, and M. Gravel. Angew. Chem. Int. Ed. Engl. **38**, 3064 (1999).
13. B. Carboni, C. Pourbaix, F. Carreaux, H. Deleuze, and B. Maillard. Tetrahedron Lett. **40**, 7979 (1999).
14. N. Farfan, H. Hopfl, V. Barba, M.E. Ochoa, R. Santillan, E. Gomez, and A. Gutierrez. J. Organomet. Chem. **581**, 70 (1999).
15. H. Kitano, M. Kuwayama, N. Kanayama, and K. Ohno. Langmuir, **14**, 165 (1998).
16. P.R. Westmark and B.D. Smith. J. Am. Chem. Soc. **116**, 9343 (1994).
17. A.N.J. Moore and D.D.M. Wayner. Can. J. Chem. **77**, 681 (1999).
18. M. Takeuchi, S. Yoda, Y. Chin, and S. Shinkai. Tetrahedron Lett. **40**, 3745 (1999).
19. H. Eggert, J. Frederiksen, C. Morin, and J. Chr. Norrild. J. Org. Chem. **64**, 3846 (1999).
20. C. Morin. Tetrahedron, **50**, 12521 (1994).
21. Z.-Q. Tian, B.B. Brown, D.P. Mack, C.A. Hutton, and P.A. Bartlett. J. Org. Chem. **62**, 514 (1997).
22. S.Y. Chen, B.S. Burnham, B.F. Spielvogel, A. Sood, S.D. Wyrick, and I.H. Hall. Appl. Organomet. Chem. **10**, 279 (1996).
23. M.C. Miller, III, A. Sood, B.F. Spielvogel, and I.H. Hall. Arch. Pharm. (Weinheim, Ger.), **331**, 153 (1998).
24. M. Ferles, J. Hauer, J. Kolar, Z. Polivka, and P. Stern. Coll. Czech. Chem. Commun. **37**, 2464 (1972).
25. M. Baboulène, J.L. Torregrosa, V. Speziale, and A. Lattes. Bull. Soc. Chim. Fr. 565 (1980).
26. J.-B. Le Toumelin and M. Baboulène. New. J. Chem. **23**, 111 (1999).
27. (*a*) A. Dicko, M. Montury, and M. Baboulène. Tetrahedron Lett. **28**, 6041 (1987); (*b*) S. Colin, L. Vaysee-Ludot, J.-P. Lecouvé, and J. Maddaluno. J. Chem. Soc. Perkin Trans. 1, 4505 (2000).
28. R. Köster. Organobor-Verbindungen II. *In* Methoden der Organischen Chemie (Houben–Weyl). Vol. XIII/3b. Thieme, Stuttgart. 1983, and refs. therein.
29. K. Burgess and M.J. Ohlmeyer. Chem. Rev. **91**, 1179 (1991).
30. M.P. Sibi and B. Li. Tetrahedron Lett. **33**, 4115 (1999).
31. K. Burgess and M.J. Ohlmeyer. J. Org. Chem. **56**, 1027 (1991).
32. J.A. Osborn and G. Wilkinson. Inorg. Synth. **28**, 77 (1990).
33. G. Giordano and R.H. Crabtree. Inorg. Synth. **28**, 88 (1990).
34. J. Chatt and L.M. Venanzi. J. Chem. Soc. 4753 (1957).
35. A.G.M. Barrett, M.A. Seefeld, A.J.P. White, and D.J. Williams. J. Org. Chem. **61**, 2677 (1996).
36. G. Wolf and E.-U. Würthwein. Chem. Ber. **124**, 655 (1991).
37. E.J. Roskamp and S.F. Pedersen. J. Am. Chem. Soc. **109**, 6551 (1987).
38. C.K. Govindan and G. Taylor. J. Org. Chem. **48**, 5348 (1983).
39. P.J. Fennis, P.H.M. Budzelaar, J.H.G. Frijns, and A.G. Orpen. J. Organomet. Chem. **393**, 287 (1990).
40. J.S. Hartman, Z. Yuan, A. Fox, and A. Nguyen. Can. J. Chem. **74**, 2131 (1996), and refs. therein.
41. C. Widauer, H. Grützmacher, and T. Ziegler. Organometallics, **19**, 2097 (2000).
42. T.B. Marder and N.C. Norman. Top. Catal. **5**, 63 (1998).

[4] Supplementary material (NMR data) may be purchased from the Depository of Unpublished Data, Document Delivery, CISTI, National Research Council Canada, Ottawa, ON K1A 0S2, Canada (http://www.nrc.ca/cisti/irm/unpub_e.shtml for information on ordering electronically).

© 2001 NRC Canada

43. F.-Y. Yang and C.-H. Cheng. J. Am. Chem. Soc. **123**, 761 (2001), and refs. therein.
44. R.T. Baker, T.M. Cameron, and S.A. Westcott. Chem. Commun. 2395 (1998).
45. S. Pereira and M. Srebnik. Tetrahedron Lett. **37**, 3283 (1996).
46. T. Ohmura, Y. Yamamoto, and N. Miyaura. J. Am. Chem. Soc. **122**, 4990 (2000), and refs. therein.
47. C.M. Vogels, P.G. Hayes, M.P. Shaver, and S.A. Westcott. Chem. Commun. 51 (2000).
48. H. Nöth and B. Wrackmeyer. *In* Nuclear magnetic resonance spectroscopy of boron compounds. Springer–Verlag, Berlin. 1978.
49. J.M. Jego, B. Carboni, and M. Vaultier. J. Organomet. Chem. **435**, 1 (1992).
50. A. Dicko, M. Montury, and M. Baboulène. Synth. Commun. **18b**, 459 (1988).
51. R.T. Baker, J.C. Calabrese, and S.A. Westcott. J. Organomet. Chem. **498**, 109 (1995).
52. C. Dai, E.G. Robins, A.J. Scott, W. Clegg, D.S. Yufit, J.A.K. Howard, and T.B. Marder. Chem. Commun. 1983 (1998).
53. S.A. Westcott, H.P. Blom, T.B. Marder, and R.T. Baker. J. Am. Chem. Soc. **114**, 8863 (1992).
54. T. Hayashi, Y. Matsumoto, and Y. Ito. Tetrahedron: Asymmetry, **111**, 601 (1991).
55. J.M. Grevy, Z. García-Hernández, A. Ramos-Organillo, and R. Contreras. *In* Contemporary boron chemistry. RSC, Cambridge. 2000. p. 422.
56. L. Weber, M. Schnieder, R. Boese, and D. Bläser. J. Chem. Soc. Dalton Trans. 378 (2001).
57. H. Höpfl. J. Organomet. Chem. **581**, 129 (1999).
58. C.M. Vogels, L.G. Nikoltcheva, H.A. Spinney, D.W. Norman, M.O. Baerlocher, F.J. Baerlocher, and S.A. Westcott. Can. J. Chem. **79**, 1115 (2001).
59. C. Bolm. Angew. Chem. Int. Ed. Engl. **32**, 232 (1993).

© 2001 NRC Canada

Microwave-assisted Diels-Alder synthesis

Christopher K. Jankowski, Gaëtan LeClair, Jacqueline M.R. Bélanger, Jocelyn R.J. Paré, and Marie-Rose VanCalsteren

Abstract: The synthesis of isoquinolinone carboxylates was performed using arecoline or its isomer *N*-methyl tetrahydro pyridine carboxylate with Danishefsky's diene via thermal or microwave assisted Diels-Alder reaction. The comparison of both condensation modes showed that the microwave method not only afforded higher yields of the adducts, but also lead to the formation of a new α,β-unsaturated pyridyl ketone. All structures were identified with the help of high resolution 2D NMR.

Key words: Diels-Alder microwave assisted reaction, microwave synthesis, Michael, diene, isoquinoline carboxylate synthesis, Danishefsky diene synthesis, MAP Diels-Alder[2].

Résumé : On a réalisé des synthèses d'isoquinoléinone carboxylates à partir de l'arécoline ou de son isomère (des *N*-méthyl tétrahydropyridine carboxylates) et du diène de Danishefsky, par le biais d'une réaction de Diels-Alder thermique ou assistée par microondes. Une comparaison des deux modes de condensation a montré que la méthode aux microondes conduit à des rendements supérieurs d'adduits avec la formation d'une nouvelle pyridylcétone α,β-insaturée. Toutes les structures ont été identifiées à l'aide de la RMN bidimensionnelle à haute résolution.

Mots clés : réaction de Diels-Alder assistée par microondes, Michael, diène, synthèse d'isoquinoléine carboxylate, synthèse à l'aide du diène de Danishefsky, « MAP » Diels-Alder.

[Traduit par la Rédaction]

Introduction

The Diels-Alder reaction remains one of the most fascinating and useful condensation reactions leading to functionalized heterocyclic or carboxylic unsaturated compounds. The diene and dienophile react without particular restriction, producing adducts under several thermal, photochemical, or catalytical (e.g., acid or Lewis acid) conditions displaying important stereo- and regioselectivities. Two variations, thermal and photochemical, are also well studied because of strict rules governing the stereochemistry of adduct formation (Woodward-Hoffmann). Despite this, the yield of some adducts coming from less activated substrates, e.g., because of the poor electronic compatibility of the diene–dienophile couple, is low. Also, some of the reactions are still taking a considerable amount of time, and the diene, in particular, can undergo the polymerization.

Here, we report on the Diels-Alder cycloaddition between some heterocyclic vinylic α,β-unsaturated esters and active (hot) diene, such as Danishefsky's diene family, leading to the *N*-methyloctahydro isoquinoline adducts, important by-products, e.g., for the design and synthesis of pharmaceuticals.

The thermal condensation of the arecoline (**1**) (methyl *N*-methyl-1,2,5,6-tetrahydropyridine-3-carboxylate) or its isomer **2** (ethyl *N*-methyl-1,2,3,6-tetrahydropyridine-4-carboxylate) with Danishefsky's diene (1-methoxy-3-trimethylsilyloxy-1,3-butadiene) under thermal conditions (160°C in toluene for 5 days) gave 30% of the methyl *cis*-*N*-methyl isoquinolidin-8-en-7-one-10-carboxlyate (**3**) adduct for arecoline and 50% for the isomeric dienophile — ethyl *cis*-*N*-methylisoquinolidin-6-en-7-one-5-carboxylate (**4**) (Fig. 1, Scheme 1). Both adducts were fully characterized by spectroscopic methods (see *Experimental*).

Under thermal reaction conditions, however, a significant level of diene decomposition and polymerization as well as the presence of dienophile dimers was observed. For the Lewis acid ($AlCl_3$, BF_3) catalysis of these reactions, the adduct yield remains low.

The spontaneous formation of the α,β-unsaturated ketone in the newly formed ring is observed accordingly to the usual behaviour of these dienes (1–6). The vinylic esters, which are not considered particularly active dienophiles, do not react more readily at this time; however, the carboalkoxy group of the adducts is suitably situated in the *cis* fused bicyclic compound for further transformations, such as the synthesis of HIV protease inhibitor isoquinoline carboxylate pharmaceuticals (7).

When the same two reactions were carried out using the microwave-assisted processes (MAP™) (8–11) in sealed

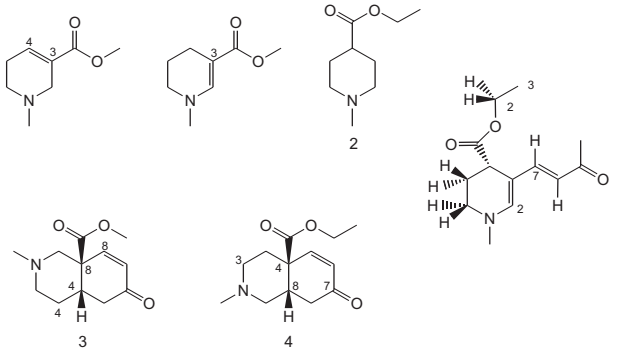
Received June 1, 2001. Published on the NRC Research Press Web site at http://canjchem.nrc.ca on December 12, 2001.

C.K. Jankowski,[1] G. LeClair, and M.-R. VanCalsteren. Département de chimie et biochimie, Université de Moncton, Moncton, NB E1A 3E9 Canada.
J.M.R. Bélanger and J.R.J. Paré. ETC, Environnement Canada, Ottawa, ON K1A 0H3 Canada.

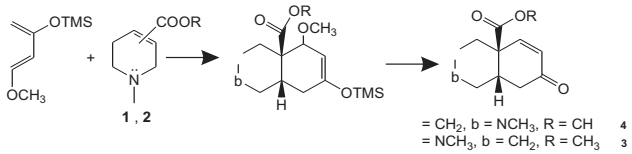
[1]Corresponding author (telephone: (506) 858-4331; fax (506) 858-4086; e-mail: jankowc@umoncton.ca).
[2]MAP is a trademark of Her Majesty the Queen of Right of Canada as represented by the Minister of the Environment.

 DOI: 10.1139/cjc-79-12-1906 © 2001 NRC Canada

Fig. 1. Structures of compounds **1**–**5**.



Scheme 1.



tubes as a toluene solution for 5 min the same adducts, of the identical stereochemistry, were obtained in both series. It is to be noted that this process involves the irradiation of the reaction vessel with a focalized beam of microwaves and not the scattered microwaves from a conventional oven. This focalized beam gives the user control over the amount of energy given to the vessel, and hence, thermal loss is kept to a minimum. The yield of these two adducts improved significantly, for both **3** (73%) as well as **4** (63%) (Table 1), and the dimerization of the dienophiles, as identified from GC–MS experiments, was lower. In addition, the remaining diene could be recovered.

The dimerization of vinylic dienophiles in Diels-Alder reactions are not surprising. Studied under electron impact mass spectrometry conditions using direct inlet introduction of both dienophiles arecoline (**1**) and its isomer **2** displayed, after 48 h, an important dimerization level: up to 40% for **2** and 18% for **1**, which were liberated from its hydrobromide. However, using freshly purified arecoline (distilled on a cold finger) reduced the dimer concentration. Also, once treated with microwave both dienophiles displayed an important reduction of the dimers (at *m*/*z* 310 and 338 for **1** and **2**, respectively) within 2–3% range only. One of the possible explanations for better yield of the Diels-Alder condensation under microwave conditions, could then be that this treatment maintains the dienophile in its monomeric form.

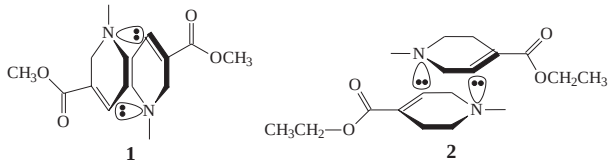
Searching for an explanation of dienophile dimer formation, molecular modelling was performed. The absence of spectral evidences on the presence of the cyclobutane structures for these dimers led to a hypothesis of strongly bound electrostatic dimers between the N-CH_3 lone pair of the first molecule and the positive pole of the α,β-unsaturated ester of the other molecule. Molecular mechanics modelling of two resulting structures showed that the arecoline **1** dimer is more stable by 1.5 kcal mol^{-1} than the similar dimer of **2** (Fig. 2).

The reaction of dienophile **2** with Danishefsky's diene under microwaves also produced an unexpected product (~50%),

Table 1. Yield (%) of Diels-Alder adducts.

Adduct	Thermal reaction	Microwave reaction
3	30	73
4	50	63

Fig. 2. Dimer structures from tetrahydropyridine carboxylates **1** and **2**.



identified as ethyl *N*-methyl-3-(oxo-3′-buten-1′-yl)-1,4,5,6-tetrahydropyridine carboxylate (**5**). The formation of this product can be explained by the isomerization of the double bond of dienophile **2** from the conjugated position 3 to position 2, which then subsequently reacts with the diene to afford compound **5**.

The absence of a similar compound for the arecoline (**1**) can be rationalized by the fact that under microwave conditions the β-aminovinyl ester is analogously isomerized to the fairly stable enamine-vinyle **1a** (difference of 1 kcal mol^{-1}) ester, which does not react with Danishefsky's diene.

Although the microwave assisted Diels-Alder condensations (as well as the retro Diels-Alder reactions) have been tried for several compounds (12–22), to our knowledge the MAP Diels-Alder condensation reported here is the first condensation of less reactive enol ester and cyclic amines. This method is an important practical improvement of the condensation conditions. The mechanism of these reaction under microwave treatment remains unknown. The analogy to thermal reaction is confirmed from our study and the adduct stereochemistry for both dienophiles is the same as in thermal condensation. The reaction time, however, was reduced and the reaction was carried out in much simpler and cleaner ways. The additional product formation observed for the dienophile **2**, the enamine formation and suggestions prior to condensation, is an interesting feature of the microwave Diels-Alder reaction.

Experimental

The diene and dienophiles were purchased from Aldrich and Coger-Acros Chemicals. The arecoline hydrobromide was freed from its hydrobromide by potassium bicarbonate 10% solution treatment under ethyl ether extraction with the quantitative yield, prior to the condensation. Thermal condensation of Danishefsky's diene with dienophile **1** or **2** was performed in toluene in sealed tube, the post-reaction work-up was done according to our previous methodology (1, 5, 21, 22). The mixture was treated as follows: the solvent was evaporated in vacuo and resulting oil was purified using flash chromatography (12–15 cm column) over silica gel using acetone–benzene elution system. After the separation of dienophiles in the first fraction (10% acetone) the adducts were isolated (25% acetone). Under these conditions both the desilylation of adducts and their demethanolysis took

© 2001 NRC Canada

place. The diene was used in slight excess (1.1 mol). MAP Diels-Alder reactions were carried out on a Soxwave-10 (Prolabo prototype) atmospheric pressure focused microwave-assisted extraction system (Prolabo, Fontenay-Sous-Bois, France). The Soxwave-10 is made up of one command box and one microwave cavity able to accommodate 20 mL type headspace vials. The system used operated with an emission frequency of 2450 MHz and a continuously variable power output of 10–200 watts. A sealed tube containing the reaction mixture (1 mmol of dienophile, 1.1 mmol of diene, 10 mL of toluene) was introduced into the microwave cavity. The sample tube bulb was warm when taken out of microwave cavity. The power was set at 20% (40 watts) and the sample mixture was irradiated for 5 min. The sample was then taken out of the cavity and allowed to cool before proceeding with the next steps.

The NMR spectra were recorded on Bruker 200 MHz (UdeM), 300 MHz (St. Hyacinthe), or 500 MHz (Instituto de Quimica) apparatus. The samples were dissolved in $CDCl_3$ and TMS was used as an internal standard. The typical NMR high-resolution experiments were run according to the procedure described in our previous paper (23).

The chemical shifts (^{13}C or ^{1}H) are expressed in δ (ppm) and the coupling constants (*J*) in Hz. The complete set of 1D high resolution and different 2D experiments for compounds **1**–**5** are available on request from CKJ.

The positive ion (PI) mass spectra were determined on Nermag Riber R-1010 (CEA) apparatus in either EI or DCI (NH_3) mode using EI–CI source. The ion chromatograms were used to follow-up the progress of purification of adducts **3**–**5** from their characteristic protonated pseudo-molecular ion sweeping and retention time values.

The molecular mechanics calculations were done with the help of HyperChem Mm^+ program for PC at the Université de Moncton.

Results

*Dienophile **1***

EI-MS (*m*/*z*) (%): 310 ($[2M]^+$), 155 ($[M]^+$), 140 (100), 124, 112, 108, 71, 43, 42. ^1H NMR (500 MHz) δ: 2.37 (dtt, $^3J_{5,6}$ = 6, $^3J_{4,5}$ = 4, $^5J_{2,5}$ = 3, H5), 2.41 (s, NCH_3), 2.50 (t, $^3J_{5,6}$ = 6, H6), 3.15 (dt, $^4J_{2,4}$ = –1.5, $^5J_{2,5}$ = 3, H2), 3.74 (s, OCH_3), 7.00 (tt, $^3J_{4,5}$ = 4, $^4J_{2,4}$ = 1.5, H4). ^{13}C NMR (125 MHz) δ: 26.5 (C5), 45.6 (NCH_3), 50.7 (C6), 51.4 (OCH_3), 53.2 (C6), 128.9 (C3), 137.5 (C4), 166.9 (C=O).

*Dienophile **2***

EI-MS (*m*/*z*) (%): 338 ($[2M]^+$), 169 ($[M]^+$), 140, 124, 96 (100), 81, 42. CI-MS (NH_3) (*m*/*z*) (%): 339 ($[2M + 1]^+$), 170 ($[M + 1]^+$), 141, 125, 97 (100), 82, 44, 43. ^1H NMR (200 MHz) δ: 1.28 (t, ^3J = 8, CH_2CH_3), 2.37 (s, NCH_3), 2.44 (dtt, $^3J_{5,6}$ = 6, $^4J_{3,5}$ = –1.5, $^5J_{2,5}$ = 3, H5), 2.55 (t, $^3J_{5,6}$ = 6, H6), 3.09 (dt, $^3J_{2,3}$ = 2, $^5J_{2,5}$ = 3, H2), 4.21 (q, ^3J = 8, CH_2CH_3), 6.89 (tt, $^3J_{2,3}$ = 2, $^4J_{3,5}$ = 1.5, H3). ^{13}C NMR (50 MHz) δ: 15.0 (CH_2CH_3), 26.2 (C3), 31.3 (NCH_3), 52.3 (C2), 55.3 (C6), 61.3 (CH_2CH_3), 129.4 (C4), 137.3 (C5), 167.7 (C=O).

*Adduct **3***

EI-MS (*m*/*z*) (%): 223 ($[M]^+$), 164, 152, 138, 122, 91, 71, 58, 43 (100), 31. ^1H NMR (300 MHz) δ: 1.62 (H4), 1.74 (H4′), 2.05 (H3), 2.28 (NCH_3), 2.32 (H5), 2.39 (d, $^2J_{1,1'}$ = –10.9, H1), 2.63 (d, $^4J_{8,4a}$ = 1.6, H4a), 2.67 (H3′), 2.71 (H5′), 2.91 (d, $^2J_{1,1'}$ = –10.9, H1′), 3.75 (OCH_3), 6.05 (d, $^3J_{7,8}$ = 10.1, H7), 6.75 (d, $^3J_{7,8}$ = 10.1, H8). ^{13}C NMR (75 MHz) δ: 27.5 (C4), 34.5 (C4a), 40.8 (C5), 46.4 (NCH_3), 49.1 (C8a), 52.7 (OCH_3), 54.2 (C3), 62.4 (C1), 129.9 (C7), 149.4 (C8), 172.5 (COO), 198.2 (C=O).

*Adduct **4***

EI-MS (*m*/*z*) (%): 237 ($[M]^+$), 208, 194, 164 (100), 149, 136, 121, 120, 108, 84, 65, 51, 43. ^1H NMR (200 MHz) δ: 1.28 (t, ^3J = 7.2, CH_2CH_3), 1.84 (H1), 1.96 (H1′), 2.01 (H3), 2.09 (H4), 2.23 (NCH_3), 2.32 (H8), 2.59 (H4′), 2.63 (H8a), 2.67 (H3′), 2.71 (H8′), 4.15 (CH_2CH_3), 6.05 (d, $^3J_{5,6}$ = 10.3, H6), 6.64 (d, $^3J_{5,6}$ = 10.3, H5). ^{13}C NMR (50 MHz) δ: 14.7 (CH_2CH_3), 31.4 (C4), 34.5 (C8a), 40.8 (C8), 46.4 (NCH_3), 49.1 (C4a), 57.2 (C3), 60.2 (C1), 61.2 (CH_2CH_3), 129.8 (C6), 149.6 (C5), 173.6 (COO), 197.9 (C=O).

*Ketone **5***

EI-MS (*m*/*z*) (%): 237 ($[M]^+$), 208, 194, 164 (100), 149, 136, 121, 120, 108, 84, 65, 51, 43. ^1H NMR (300 MHz) δ: 1.25 (dd, $^3J_{12,13}$ = 7.1, $^3J_{12',13}$ = 7.1, H13), 1.90 (dddd, $^2J_{5,5'}$ = –13.6, $^3J_{5',6}$ = 13, $^3J_{4,5'}$ = 5.5, $^3J_{5',6'}$ = 5.1, H5′), 2.15 (dddd, $^2J_{5,5'}$ = –13.6, $^3J_{5,6}$ = 3.7, $^3J_{5,6'}$ = 2.1, $^3J_{4,5}$ = 1.8, H5), 2.18 (s, H10), 3.0 (s, NCH_3), 3.1 (dddd, $^2J_{6,6'}$ = –12.8, $^3J_{5',6'}$ = 5.1, $^3J_{5,6'}$ = 2.1, $^4J_{4,6'}$ = –1.5, H6′), 3.37 (ddd, $^3J_{4,5'}$ = 5.5, $^3J_{4,5}$ = 1.8, $^4J_{4,6'}$ = 1.5, H4), 3.43 (ddd, $^3J_{5',6}$ = 13.0, $^2J_{6,6'}$ = –12.8, $^3J_{5,6}$ = 3.7, H6), 4.13 (dq, $^2J_{12,12'}$ = –10.9, $^3J_{12',13}$ = 7.1, H12′), 4.16 (dq, $^2J_{12,12'}$ = –10.9, $^3J_{12',13}$ = 7.1, H12), 5.81 (d, $^3J_{7,8}$ = 15.2, H8), 6.69 (s, H2), 7.18 (d, $^3J_{7,8}$ = 15.2., H7). ^{13}C NMR (75 MHz) δ: 14.1 (CH_2CH_3), 23.6 (C5), 26.9 (C10), 35.7 (C4), 42.8 (NCH_3), 44.6 (C6), 60.7 (CH_2CH_3), 101.6 (C3), 114.1 (C8), 146.5 (C7), 147.7 (C2), 174.0 (COO), 196.9 (C=O).

Acknowledgments

We would like to thank H. Virelizier (CEA, Saclay, France) for his help with several mass spectrometric determinations as well as Dr. E. Diaz (UNAM, Mexico) for NMR analysis on 500 MHz spectrometer. This work was supported by FESR-Université de Moncton grant to one of us (CKJ).

References

1. J. Belanger, N.L. Landry, J.R.J. Paré, and C.K. Jankowski. J. Org. Chem. **47**, 3649 (1982).
2. S. Danishefsky and T. Kitahara. J. Am. Chem. Soc. **96**, 7807 (1974).
3. S. Danishefsky, R.K. Singh, and R.B. Gammill. J. Org. Chem. **43**, 379 (1978).
4. S. Danishefsky, T. Kitahara, C.F. Yan, and J. Morris. J. Am. Chem. Soc. **101**, 7863 (1979).
5. H. Melanson, D. Labrecque, and C.K. Jankowski. Revista, **20**, 21 (1989).
6. S. Rafel, G. Cabarrocas, M. Ventura, and T. Parella. J. Chem. Soc. Perkin 1, 3837 (1998).
7. Hoffman LaRoche. Extracarbon AIDS drugs saqvianausinh. Ref. Birstol-Myers BMS-182 193.
8. J.R.J. Paré, M. Sigouin, and J. Lapointe. U.S. Patent, No. 5 002 784. 1991.

© 2001 NRC Canada

9. (*a*) J.R.J. Paré, J.M.R. Bélanger, and S.S. Stafford. TrAC, Trends Anal. Chem. (Pers. Ed.) **13**, 176 (1994); (*b*) M.M. Punt. U.S. Patent No. 6 061 426. 2001.
10. J.R.J. Paré and J.M.R. Bélanger. Instrumental methods in food analysis. Techniques and instrumentation in analytical chemistry. Vol. 18. *Edited by* J.R.J. Paré and J.M.R. Bélanger. Elsevier, Amsterdam. 1997. Chap. 10.
11. V.A. Yaylayan, G. Matni, J.R.J. Paré, and J.M.R. Bélanger. J. Agric. Food Chem. **45**, 149 (1997).
12. S. Deshayes, M. Liagre, A. Loupy, J.-L. Luche, and A. Petit. Tetrahedron, **55**, 10851 (1999).
13. Kiangjun Liao. Microwave-enhanced Diels-Alder reaction. Environment Canada, Reports. Ottawa, ON. 1999.
14. F. Cado, P. Jacquault, M.-J. Dozias, J.P. Bazureau, and J. Hamelin. J. Chem. Res. Synop. **5**, 176 (1997).
15. (*a*) A. Diaz-Ortiz, J.R. Carrillo, M.J. Gomez-Escalonilla, A. de la Hoz, A. Moreno, and P. Prieto. Synlett, **10**, 1069 (1998); (*b*) A. Diaz-Ortiz, E. Diez-Barra, A. de la Hoz, P. Prieto, A. Moreno, F. Langa, T. Prange, and A. Neuman. J. Org. Chem. **60**, 4160 (1995).
16. (*a*) M. Bortolussi, R. Bloch, and A. Loupy. J. Chem. Res. Synop. **1**, 34 (1998); (*b*) P. Garrigues and B. Garrigues. C.R. Acad. Sci. Ser. IIc: Chim. **1**, 545 (1998).
17. R.N. Gedye and J.B. Wei. Can. J. Chem. **76**, 525 (1998).
18. A. de la Hoz, A. Diaz-Ortis, A. Moreno, and F. Langa. Eur. J. Org. Chem. **365**, 9 (2000).
19. R.J. Giguere, T.I. Bray, and S.M. Duncan. Tetrahedron Lett. **27**, 4945 (1986).
20. C.R. Strauss and R.W. Trainor. Austr. J. Chem. **48**, 1665 (1995).
21. R. Vienneau and C.K. Jankowski. Revista, **20**, 148 (1989).
22. C.K. Jankowski and D.W. Lu. Spectroscopy, **11**, 59 (1993).
23. C.K. Jankowski, M. Jimenez-E. R. Chilpa-R, A. Aumelas, and M.-R. VanCalsteren. Can. J. Chem. **78**, 248 (2000).

© 2001 NRC Canada

Molar excess volumes of ternary mixtures containing ether

V.K. Sharma and Romi

Abstract: Molar excess volumes (V^E_{ijk}) of 1,3-dioxolane (*i*) + benzene (*j*) + cyclohexane (*k*); 1,3-dioxolane (*i*) + benzene (*j*) + *n*-hexane (*k*); and 1,3-dioxolane (*i*) + benzene (*j*) + *n*-heptane (*k*) ternary mixtures have been measured dilatometrically as a function of composition at 298.15 K. The observed data have been analysed in terms of (*i*) Graph theoretical approach; (*ii*) Flory's theory; and (*iii*) Lacombe and Sanchez's theory of liquid mixtures. It has been observed that V^E_{ijk} values predicted by graph theoretical approach compare better with the corresponding experimental values than with the V^E_{ijk} data predicted by other approaches.

Key words: molar excess volumes, molar volume interaction parameters, connectivity parameter of third degree $^3\xi$.

Résumé : Faisant appel à la dilatométrie et opérant à 298,15 K, on a mesuré les volumes molaires en excès (V^E_{ijk}), de mélanges ternaires 1,3-dioxolane (*i*) + benzène (*j*) + cyclohexane (*k*); 1,3-dioxolane (*i*) + benzène (*j*) + hexane (*k*); et 1,3-dioxolane (*i*) + benzène (*j*) + heptane (*k*). On a analysé les données obtenues en termes de (*i*) l'approche théorique graphique; (*ii*) la théorie de Flory; et (*iii*) la théorie des mélanges liquides de Lacombe et Sanchez. On a observé que les valeurs de V^E_{ijk} prédites par l'approche théorique graphique se rapprochent plus des valeurs expérimentales que celles prédites par les autres méthodes.

Mots clés: volumes molaires en excès, paramètres molaires d'interaction volumique, paramètres de connectivité du troisième degré $^3\xi$.

[Traduit par la Rédaction]

Introduction

Recent studies (1–4) have shown that thermodynamic properties of ternary mixtures can be determined from the thermodynamic properties of the respective binary mixtures. In continuation of our earlier work (5, 6) on molar excess volumes and molar excess enthalpies of 1,3-dioxolane (*i*) + benzene, toluene, or -xylenes (*j*) or + cyclohexane, *n*-hexane, or *n*-heptane (*j*) binary mixtures, we report here molar excess volumes data (V^E_{ijk}) for 1,3-dioxolane (*i*) + benzene (*j*) + cyclohexane (*k*); 1,3-dioxolane (*i*) + benzene (*j*) + *n*-hexane (*k*); and 1,3-dioxolane (*i*) + benzene (*j*) + *n*-heptane (*k*) ternary mixtures as a function of composition at 298.15 K. It would be of interest to see how various theories of liquid mixtures explain the V^E_{ijk} data of the studied mixtures.

Experimental

1,3-Dioxolane (D) (Fluka), benzene, cyclohexane, *n*-hexane, and *n*-heptane (AR Grade) were purified by standard methods (7). The purities of the purified liquids were checked by measuring their densities at 298 ± 0.01 K and 293 ± 0.01 K (for 1,3-dioxolane) and these agreed to within $\pm 5 \times 10^{-5}$ gm cm^{-3} with the values reported in literature (7).

Received April 12, 2001. Published on the NRC Research Press Web site at http://canjchem.nrc.ca on December 14, 2001.

V.K. Sharma[1] and Romi. Department of Chemistry, Maharshi Dayanand University, Rohtak-124001, India.

[1]Corresponding author (e-mail: vksharma17@redifmail.com).

Molar excess volumes (V^E_{ijk}) for the various ($i + j + k$) ternary mixtures were measured in a three limbed dilatometer in the manner as described elsewhere (8). The change in liquid level of the dilatometer capillary was measured with a cathetometer that could read to ±0.001 cm and the uncertainties in our measured values are of the order of 0.5%.

Results

The measured V^E_{ijk} for *D* (*i*) + benzene (*j*) + cyclohexane, *n*-hexane, or *n*-heptane (*k*) ternary mixtures as a function of composition at 298.15 K (recorded in Table 1 and plotted in Figs. (1–3)) were fitted to eq. [1].

$$[1]\quad V^E_{ijk} = x_i x_j \left[\sum_{n=0}^{2} V^{(n)}_{ij}\,(x_i - x_j)^n\right] + x_j x_k \left[\sum_{n=0}^{2} V^{(n)}_{jk}(x_j - x_k)^n\right] + x_k x_i \left[\sum_{n=0}^{2} V^{(n)}_{ik}\,(x_k - x_i)^n x_i^{\,n}\right] + x_i x_j x_k \left[\sum_{n=0}^{2} V^{(n)}_{ijk}\,(x_j - x_k)^n x_i^{\,n}\right]$$

$V^{(n)}_{ij}$ (n = 0–2) are parameters characteristics of ($i + j$), ($j + k$), and ($k + i$) binary mixtures and have been taken from literature (5–11), whereas $V^{(n)}_{ijk}$ (n = 0–2) are parameters charac-

 DOI: 10.1139/cjc-79-12-1910 © 2001 NRC Canada

Table 1. Comparison of measured V^E_{ijk} values for the various (i + j + k) ternary mixtures at 298.15 K with the corresonding values evaluated from Graph, Flory, and Sanchez theories.

		V^E (cm^3 mol^{-1})			
x_i	x_j	Expt. l	Graph	Flory	Sanchez
1,3-Dioxolane (*i*) + benzene (*j*) + cyclohexane (*k*)[a]					
0.0399	0.8405	0.254	0.080	0.334	0.574
0.0710	0.7662	0.317	0.193	0.455	0.588
0.1244	0.5829	0.481	0.283	0.750	0.472
0.1621	0.2853	0.613	0.365	1.028	0.308
0.1905	0.6802	0.104	0.353	0.451	0.521
0.2601	0.4398	0.490	0.486	0.902	0.457
0.3072	0.2007	0.429	0.433	1.234	0.360
0.3897	0.3928	0.309	0.590	0.816	0.490
0.6028	0.1554	0.428	0.420	1.025	0.543
0.6714	0.1308	0.400	0.381	0.908	0.598
0.7174	0.0712	0.399	0.235	0.978	0.671
0.7811	0.0519	0.390	0.183	0.824	0.824
0.8157	0.0817	0.275	0.264	0.548	0.919
0.8501	0.0398	0.309	0.139	0.317	0.968
1,3-Dioxolane (*i*) + benzene (*j*) + *n*-hexane (*k*)[b]					
0.0977	0.7949	0.092	0.029	0.267	0.166
0.1108	0.7391	0.129	0.049	0.365	0.145
0.1511	0.6782	0.122	0.062	0.439	0.113
0.1958	0.6170	0.108	0.077	0.511	0.115
0.2603	0.5174	0.116	0.108	0.648	0.121
0.2849	0.4527	0.153	0.131	0.768	0.165
0.3120	0.4701	0.101	0.123	0.682	0.133
0.3601	0.3524	0.163	0.152	0.911	0.143
0.4059	0.2575	0.147	0.095	0.230	0.146
0.4525	0.3005	0.134	0.144	0.884	0.161
0.4912	0.2411	0.127	0.126	0.984	0.232
0.5825	0.1639	0.098	0.143	1.014	0.266
0.6478	0.1511	0.093	0.128	0.860	0.294
0.7427	0.1170	0.070	0.111	0.653	0.445
0.8833	0.0491	0.033	0.052	0.343	0.672
1,3-Dioxolane (*i*) + benzene (*j*) + *n*-heptane (*k*)[c]					
0.589	0.8472	0.150	0.101	0.252	0.530
0.0971	0.7597	0.203	0.148	0.390	0.459
0.1035	0.8023	0.124	0.063	0.279	0.486
0.1476	0.7159	0.160	0.101	0.409	0.466
0.1919	0.5836	0.251	0.222	0.650	0.348
0.2567	0.4901	0.257	0.247	0.776	0.325
0.3092	0.4521	0.221	0.217	0.728	0.286
0.3609	0.4026	0.211	0.212	0.825	0.279
0.4269	0.3048	0.272	0.272	0.971	0.276
0.4781	0.2734	0.250	0.251	0.955	0.368
0.5055	0.2909	0.178	0.178	0.828	0.393
0.5527	0.2012	0.273	0.267	1.003	0.362
0.6413	0.1844	0.178	0.173	0.791	0.516
0.7132	0.1029	0.231	0.216	0.858	0.574
0.7513	0.1035	0.177	0.166	0.707	0.682
0.7974	0.0911	0.134	0.123	0.567	0.716
0.8219	0.0722	0.135	0.124	0.543	0.773
0.8511	0.0415	0.049	0.124	0.551	0.806

Note: Included below are the various $V^{(n)}_{ijk}$ (n = 0–2) parameters, along with the standard deviation $\sigma(V^E_{ijk})$ of V^E_{ijk}, the interaction parameters (χ'_{ii} χ'_{ij}, ect.), and ${}^3\xi_i$, etc. $V^{(n)}_{ijk}$ (n = 0–2), $\sigma(V^E_{ijk})$, and χ''_{ii}, etc. are in cm^3 mol^{-1} and χ^{**}_{ij} χ^{**}_{ij} etc. are in J mol^{-1}.

[a] $V^{(0)}_{ijk}$ = –4.131, $V^{(1)}_{ijk}$ = 40.550, $V^{(2)}_{ijk}$ = –971.316; $\sigma(V^E_{ijk})$ = 0.003; ${}^3\xi_i$ = 0.530, ${}^3\xi_j$ = 0.666, ${}^3\xi_k$ = 1.50; χ''_{ij} = 4.544, χ''_{ik} = –3.062, χ''_{ik} = 0.072; χ^{*}_{ij} = 4.544, χ^{*}_{jk} = 41.650, χ^{*}_{ik} = 100.530; θ_j = 0.544, θ_k = 0.531, θ_i = 0.575; χ^{**}_{ij} = –3.999, χ^{**}_{jk} = 8.131, χ^{**}_{ik} = 8.069.

[b] $V^{(0)}_{ijk}$ = –3.614, $V^{(1)}_{ijk}$ = 29.431, $V^{(2)}_{ijk}$ = –360.635; $\sigma(V^E_{ijk})$ = 0.001; ${}^3\xi_i$ = 0.530, ${}^3\xi_j$ = 0.666, ${}^3\xi_k$ = 0.957; χ''_{ij}= 0.683, χ''_{jk}= –1.148, χ''_{ik} = 0.453; χ^{*}_{ij} = 4.544, χ^{*}_{jk} = 44.522, χ^{*}_{ik} = 115.569; θ_j = 0.544, θ_k = 0.556, θ_i = 0.599; χ^{**}_{ij} = –3.999, χ^{**}_{jk} = 7.557, χ^{**}_{ik} = 8.556.

[c] $V^{(0)}_{ijk}$ = –2.155, $V^{(1)}_{ijk}$ = –19.330, $V^{(2)}_{ijk}$ = 28.827; $\sigma(V^E_{ijk})$ = 0.001; ${}^3\xi_i$ = 0.530, ${}^3\xi_j$ = 0.666, ${}^3\xi_k$ = 1.207; χ''_{ij}= –1.277, χ''_{jk}= –0.366, χ''_{ik} = 2.534; χ^{*}_{ij} = 4.544, χ^{*}_{jk} = 43.945, χ^{*}_{ik} = 109.572; θ_j = 0.544, θ_k = 0.578, θ_i = 0.620; χ^{**}_{ij} = –3.999, χ^{**}_{jk} = 7.612, χ^{**}_{ik} = 7.985.

© 2001 NRC Canada

Fig. 1. Molar excess volume (V^E_{ijk}) of 1,3-dioxolane (i) + benzene (j) + cyclohexane (k) at 298.15 K.

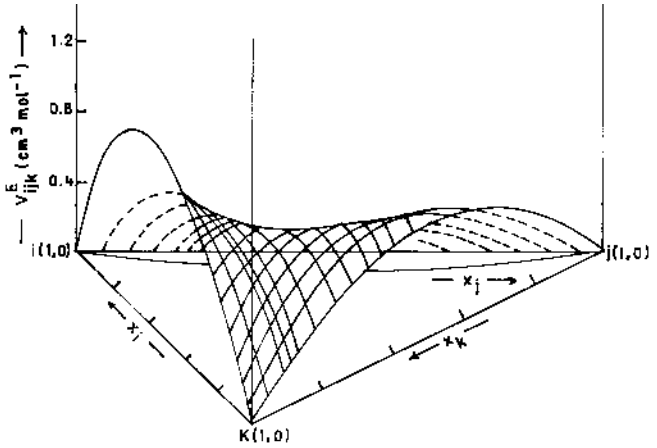
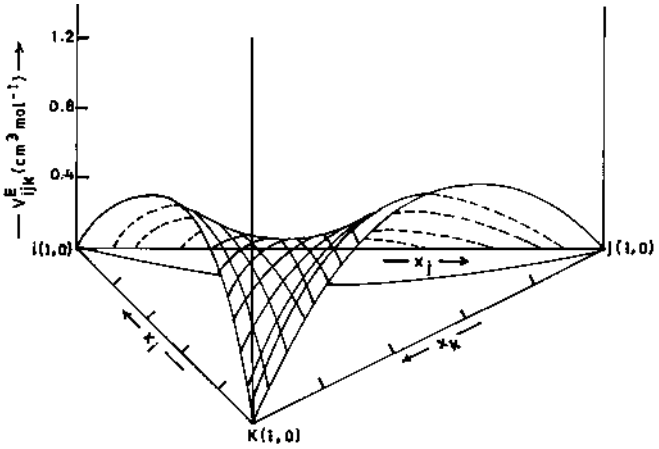


Fig 2. Molar excess volume (V^E_{ijk}) of 1,3-dioxolane (i) + benzene (j) + n-hexane (k) at 298.15 K.



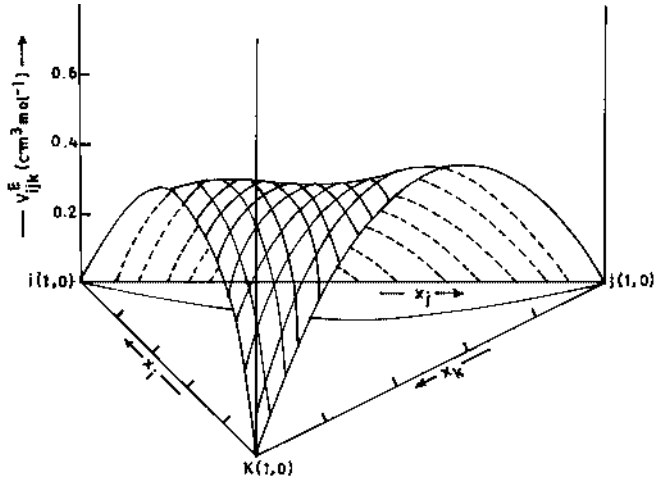
teristic of ($i + j + k$) ternary mixtures and were calculated by fitting experimental V^E_{ijk} to the following expression:

$$[2]\quad \left(\begin{array}{l} V^E_{ijk} \quad - x_i x_j\left[\sum_{n=0}^{2} V^{(n)}_{ij}(x_i - x_j)^n\right] \\ \qquad - x_j x_k\left[\sum_{n=0}^{2} V^{(n)}_{jk}(x_j - x_k)^n\right] \\ \qquad - x_k x_i\left[\sum_{n=0}^{2} V^{(n)}_{ik}(x_k - x_i)^n\right] \end{array}\right) \times [x_i x_j x_k]^{-1} = V^{(0)}_{ijk} + V^{(1)}_{ijk}(x_j - x_k)x_i + V^{(2)}_{ijk}(x_j - x_k)^2 x_i^2$$

by the least square method. Such parameters along with the standard deviation, $\sigma(V^E_{ijk})$ expressed by the following relation:

$$[3]\quad \sigma(V^E_{ijk}) = \left[\sum \{V^E_{ijk\,(\text{exptl})} - V^E_{ijk\,(\text{cald})}\}\right]^2/[(m-n)]^{0.5}$$

Fig. 3. Molar excess volume (V^E_{ijk}) of 1,3-dioxolane (i) + benzene (j) + n-heptane (k) at 298.15 K.



where m is the number of data points and n is the number of adjustable parameters of eq. [1] are recorded in Table 1.

Discussion

We are unaware of any V^E_{ijk} data of the present mixtures with which to compare our results.

Conceptual aspect of the Graph approach and results

Recent studies (5) have revealed that D (i) + benzene, toluene, or -xylene (j) binary mixtures are characterized by (i) specific interactions between delocalized π-electrons of benzene of aromatic hydrocarbons and π-electrons of the oxygen atoms in D (i). Consequently, change in molar property X^E($X = V$ or H) due to these interactions were expressed (5) by eq. [4]

$$[4]\quad X^E_{(X = V \text{ or } H)} = [x_i x_j V_j/\Sigma\, x_i V_i]\,[\chi_{ij} + x_j \chi_{12}]$$

where χ_{ij} and χ_{12} are molar volumes interaction parameters due to unlikely contact i–j formation and specific interaction between the i and j components, respectively. Furthermore, in D (i) + cyclohexane, n-hexane, or n-heptane (j) binary mixtures, if D (i) and cyclohexane, n-hexane, or n-heptane undergo weak specific interactions, then $X^E_{(X = V \text{or } H)}$ data of these mixtures would be expressible (6) by the following relation:

$$[5]\quad X^E = [x_i x_k (V_i)/\Sigma\, x_i V_i]\,\chi_{ik}$$

The basic arguments in deriving eqs. [4] and [5] were justified (5, 6) as X^E data of these binary mixtures were reproduced by employing χ_{ij}, χ_{12}, and χ_{ik} parameters (evaluated from X^E data at $x_i = 0.4$ and 0.5).

If a hydrocarbon such as cyclohexane, n-hexane, or h-heptane (k) is added to D (i) + benzene (j) mixture, then ternary ($i + j + k$) mixture formation would involve the establishment of i–j (a), j–k (b), and i–k (c) contacts (process 1) between i, j, and k components of ($i + j + k$) mixture, with specific interaction between i and j component to yield i–j molecular entity (process 2). Consequently if χ'_{ij}, χ'_{jk}, χ'_{ik} are the molar volume interaction parameter of unlike contacts,

© 2001 NRC Canada

then change in molar properties (12–14), due to process 1 (*a*, *b*, and *c*) are given by the following expression:

$$[6] \quad \Delta X_1 = x_i \chi'_{ij} S_j + x_j \chi'_{jk} S_k + x_k \chi'_{ij} S_i$$

where S_i etc. are defined by $S_i = x_i V_i / \Sigma x_i V_i$.

$$\Delta X_1 = [x_i x_j V_j / \Sigma x_i V_i]\chi'_{ij} + [x_j x_k V_k / \Sigma x_k V_i]\chi'_{jk} + [x_k x_i V_i / \Sigma x_k V_k]\chi'_{ik}$$

Furthermore, if χ_{12} is the molar interaction parameter due to specific interactions (leading to formation of *i*–*j* molecular entity), then change in molar property (14) due to process 2, can be expressed by eq. [7].

$$[7] \quad \Delta X_2 = x_i x_j^2 \chi_{12} / \sum x_i V_i$$

The overall change in thermodynamic property due to processes 1 (*a*, *b*, *c*) and 2 is given by

$$[8] \quad V^E_{ijk} = [x_i x_j V_j / xIV_i + xjV_j]\,[\chi'_{ij} + x_j \chi_{12}] + [x_j x_k V_k / x_j V_j + x_k V_k]\chi'_{jk} + [x_i x_k V_i / x_i V_k + x_k V_k]\chi'_{ik}$$

Since $V_i/V_j = {}^3\xi_j/{}^3\xi_i$, where ${}^3\xi_i$ etc., are the connectivity parameters of third degree of *i*th etc. component of the mixture, are defined by (15)

$$[9] \quad {}^3\xi_i = \sum_{m<n<o<p} \delta^v_m \delta^v_n \delta^v_o \delta^v_p$$

where δ^v_m reflects explicitly the valence of *m*th vertex in molecular graph, and is related to maximum valency (Z_m) and number of hydrogen atoms attached to mth vertex by $\delta^v_m = Z_m - h_m$. Equation [8] then reduces to:

$$[10] \quad V^E_{ijk} = [x_i x_j({}^3\xi_i/{}^3\xi_j)/x_i + x_j({}^3\xi_i/{}^3\xi_j)][\chi'_{ij} + x_j\chi_{12}] + [x_j x_k({}^3\xi_j/{}^3\xi_k)/x_j + x_i({}^3\xi_j/{}^3\xi_k)]\chi'_{ij} + [x_i + x_k({}^3\xi_i/{}^3\xi_k)/x_i + x_k({}^3\xi_i/{}^3\xi_k)]\chi'_{ik}$$

Furthermore, if it be assumed that $\chi_{ij} \simeq \chi_{12} = \chi''_{ij}$, then eq. [10] reduces to eq. [11] expressed by

$$[11] \quad V^E_{ijk} = [x_i x_j({}^3\xi_i/{}^3\xi_j)]/[x_i + x_j({}^3\xi_i/{}^3\xi_j)][(1 + x_j)\chi''_{ij}] + [x_j x_k({}^3\xi_j/{}^3\xi_k)]/[x_j + x_k({}^3\xi_j/{}^3\xi_k)]\chi'_{jk} + [x_k x_i({}^3\xi_k/{}^3\xi_{i2})]/[x_i + x_{i2}({}^3\xi_i/{}^3\xi_i)]\chi'_{ik}$$

Equation [11] contains three unknown parameters χ''_{ij}, χ'_{ij}, and χ'_{ik}. These parameters were calculated employing experimental V^E_{ijk} data of these ternary mixtures at three compositions and were subsequently utilized to predict V^E_{ijk} values at other values of x_i. Such predicted V^E_{ijk} values along with various parameters are recorded in Table 1.

Examination of Table 1 reveals that V^E_{ijk} values evaluated from the Graph approach compare well with the corresponding experimental values (for $x_i \leq 0.2$, the calculated V^E_{ijk} values are of the correct magnitude, but quantitative agreement is not good) and thus lends support to the assumptions made in deriving eq. [11].

V^E_{ijk} values were next analyzed in terms of Lacombe and Sanchez theory (16, 17). According to this theory, V^E_{ijk}, for a ternary mixture is given by

$$[12] \quad V^E_{ijk} = r_{\text{mix}} v^*_{\text{mix}} \left[\bar{v}_{\text{mix}} - \sum \phi_i \bar{v}_i\right]$$

where

$$[13] \quad \phi_i = m_i(\rho^*_i)^{-1}\left[\sum (m_i \rho^*_i)^{-1}\right]$$

$$[14] \quad m_i = x_i M_i \left[\sum (x_i M_i)^{-1}\right]$$

$$[15] \quad r_{\text{mix}} = \sum_{l=i}^{k} x_i r_i$$

$$[16] \quad r_i = r_i^0 [v^*_i (v^*_{\text{mix}})^{-1}]$$

$$[17] \quad v^*_{\text{mix}} = \sum \phi^*_i v^*_i$$

$$[18] \quad \bar{v}_{\text{mix}} = 1 / \bar{\rho}_{\text{mix}}$$

$$[19] \quad \phi^0_i = m_i(\rho^*_i v^*_i)^{-1}\left[\sum (m_i/\rho_i v^*_i)^{-1}\right]$$

and all the terms have the same significance as described elsewhere (16, 17).

Evaluation of V^E_{ijk} according to this theory requires a knowledge of reduced density of ternary mixture ($\bar{\rho}_{ijk}$) and can be determined from the equation of state of the mixture

$$[20] \quad (\bar{\rho}_{ijk})^2 + \bar{P} + [RT/\epsilon^*_{\text{mix}}][\ln[1 - \bar{\rho}_{ijk}] + [1 - [r_{\text{mix}}]^{-1}]\bar{\rho}_{ijk}] = 0$$

where

$$\epsilon^*_{\text{mix}} = \left[\phi_i^2 \epsilon_{ii} + \phi_j^2 \epsilon_{jj} + \phi_k^2 \epsilon_{kk}\right] - \left[\sum \phi_i \phi_j \chi^*_{ij}\right]$$

χ^*_{ij} etc. are the parameters characteristics for the ($i + j$), ($j + k$), and ($i + k$) binary mixture and have been evaluated from the experimental H^E data (18–20) ($x_i = 0.5$) by means of eq. [21].

$$[21] \quad H^E_{ij} = 2\phi_i \phi_j \chi_{ij} \bar{\rho}_{ij}(\epsilon^*_{ii} + \epsilon^*_{jj} - 2\epsilon^*_{ij}) + RT\, r_{\text{mix}}\left[\sum (\phi^0_i \bar{\rho}_i - \bar{\rho}_{ij}\phi_i)(\bar{T}_i)^{-1}\right]$$

As ($i + j$) and ($j + k$) are ($i + k$) binary mixtures of the studied ($i + j + k$) mixtures that satisfy eq. [22].

$$[22] \quad (\bar{\rho}_{ij})^2 + \bar{P} + RT/\epsilon^*_{ij}\,[\ln[1 - \bar{\rho}_{ij}) + [1 - r_{\text{mix}}{}^{-1}]\rho_{ij}] = 0.008 - 0.029$$

It suggests that ($i + j + k$) mixture would not satisfy eq. [20]. In view of the fact, that present mixtures satisfy equation of state like (20), it is considered that the extent to which ternary mixture deviates from eq. [20] would be nearly one third of the sum to which sub-binary mixtures deviated from eq. [22]. Consequently, eq. [20] reduces to

$$[23] \quad (\bar{\rho}_{ijk})^2 + \bar{P} + [RT/\epsilon^*_{\text{mix}}][\ln(1 - \bar{\rho}_{ijk}) + (1 - r_{\text{mix}}{}^{-1})\bar{\rho}_{ijk}] = (1/3)\left[\sum \text{R.H.S of eq. [11] for } (i + j), (j + k), \text{ and } (i + k) \text{ mixtures}\right]$$

and the V^E_{ijk} values were then predicted using established equation of state (23). Such V^E_{ijk} values along with χ^*_{ij}, χ^*_{jk}

© 2001 NRC Canada

and χ_{ik}^{*} parameters are recorded in Table 1 and are also compared with their experimental values.

According to Flory's theory (18, 19), V_{ijk}^{E} for a ternary mixture is given by

$$[24] \quad V_{ijk}^{E} = \overline{V}_{\text{cal}}^{E}[\bar{x}_i v_i^{*} + x_j v_j^{*} + x_k v_k^{*}]$$

where

$$[25] \quad \bar{v}_i^{-1} = [\{\alpha_i T/(3\alpha_i T + 3) + 1\}]^3$$

$$[26] \quad v_i^{*} = v_i[\bar{v}_i]^{-1}$$

$$[27] \quad T_i^{*} = T_i \bar{v}_i^{4/3}[\bar{v}_i^{1/3} - 1]^{-1}$$

$$[28] \quad P^{*} = \sum \phi_i^{*} P_i^{*} - \sum \phi_i^{*} \theta_j \chi_{ij}^{**}$$

$$[29] \quad \overline{T}_0 = [\bar{v}_0^{1/3} - 1] / \bar{v}_0^{4/3}$$

$$[30] \quad \overline{V}_{\text{cal}}^{E} = \bar{v}_0^{7/3}[\overline{T} - \overline{T}_0] / (4/3) - \bar{v}_0]$$

all the terms have the same significance as described by Flory (18, 19).

Evaluation of V_{ijk}^{E} by Flory's theory requires a knowledge of adjustable parameter $\theta_j \chi_{ij}^{**}$ etc. characteristic of $(i + j)$, $(j + k)$, and $(i + k)$ binary mixture of $(i + j + k)$ ternary mixture. These parameters were determined by fitting H^E experimental data (18–20) at $x_i = 0.5$ to eq. [31].

$$[31] \quad H_{ij}^{E} = \sum x_i \rho_i^{*} V_i^{*} (\overline{V}_i^{-1} - \overline{V}_{\text{cal}}^{-1}) + x_i V_i^{*} \theta_j \chi_{ij}^{**} \overline{V}_{\text{cal}}^{-1}$$

The parameters of pure component were determined using isothermal compressibility values (k_T) reported in the literature (20). k_T values of 1,3-dioxolane was calculated using ΔH_V values (7) in manner as suggested by Hildebrand (21). Such V_{ijk}^{E} values alongwith $\theta_j \chi_{ij}^{**}$ etc. parameters are recorded in Table 1 and are also compared with their corresponding experimental values.

Examination of data in Table 1 reveals that V_{ijk}^{E} values evaluated by Lacombe and Sanchez approach are of the right of order of magnitude, but the quantitative argument is not impressive. This may be attributed to the failure of the assumption that χ_{ij} etc. values are constant over the entire values of x_i, x_j, or x_k. However, V_{ijk}^{E} values predicted by Flory's theory make only qualitative agreement.

Acknowledgments

The authors are grateful to the Head, Chemistry Department and authorities of M.D. University, Rohtak, for providing research facilities.

References

1. P.P. Singh and V.K. Sharma. Can. J. Chem. **61**, 2321 (1983).
2. P.P. Singh, R. Malik, S. Maken, W.E. Acree, Jr., and A. Sheryl. Thermochim. Acta, **162**, 291 (1990).
3. V.K. Sharma, K.C. Kalra, and A. Katoch. Indian J. Chem. **38A**, 330 (1990).
4. P.P. Singh, S. Maken, and R. Malik. Indian J. Chem. **36A**, 46 (1997).
5. V.K. Sharma and Romi. Indian J. Chem. (in press).
6. V.K. Sharma and Romi. Indian J. Chem. (in press).
7. J.A. Riddick, W.B. Bunger, and T.K. Sakano. Organic solvent, physical properties, and methods of purification. Wiley, New York. 1986.
8. P.P. Singh and S.P. Sharma. J. Chem. Eng. Data, **30**, 477 (1985).
9. K.N. Marsh. Int. DATA Ser. (Sel. Data Mixtures, Ser. A) **23** (1973).
10. M.K. Kumaran and G.C. Benson. J. Chem. Thermodyn. **16**, 599 (1984).
11. K.R. Harris and P.J. Dunlop. J. Chem. Thermodyn. **2**, 813 (1970).
12. M.L. Huggins. J. Phys. Chem. **34**, 371 (1970).
13. M.L. Huggins. Polymer, **12**, 389 (1971).
14. P.P. Singh and M. Bhatia. J. Chem. Soc. Faraday Trans. 1, **86**, 3807 (1990).
15. L.B. Kier. *In* Physico-chemical properties of drugs. *Edited by* S.H. Yalokowski, A.A. Sinkula, and S.C. Vakani. Marcel Dekker, New York. 1980. p. 295.
16. R.H. Lacombe and I.C. Sanchez. J. Phys. Chem. **80**, 2352 (1976).
17. R.H. Lacombe and I.C. Sanchez. J. Phys. Chem. **80**, 2568 (1976).
18. P.J. Flory. J. Am. Chem. Soc. **87**, 1833 (1965).
19. P.J. Flory and A. Abe. J. Am. Chem. Soc. **87**, 1838 (1965).
20. R.C. Weast (*Editor*). Handbook of chemistry and physics. 68th ed. CRC Press, Boca Raton Florida. 1987.
21. J.H. Hildebrand, J.M. Prausnitz, and R.L. Scott. Regular and related solutions. Van-Nostrand – Reinhold Company, New York. 1970.

© 2001 NRC Canada

MONOREG – an expert system for structural elucidation of monoterpenes

Marcelo J.P. Ferreira, Gilberto V. Rodrigues, and Vicente P. Emerenciano

Abstract: This paper describes a new expert system denominated MONOREG for structural determination of monoterpenes. This system is composed of five programs capable of performing ^{13}C NMR spectra data analyses and analyses of systematic data from living organisms. At the end of this procedure, it shows the likely skeletons of the compound in question as well as the substructures compatible with the ^{13}C NMR data. The system was tested on the skeleton elucidation of 40 monoterpenes from a wide variety of structure types and exhibited excellent results in the skeleton prediction process.

Key words: monoterpenes, ^{13}C NMR, structure elucidation, computer-aided analyses, expert system.

Résumé : Cet article décrit un nouveau système expert, dénommé MONOREG, utilisé pour la détermination structurale des monoterpènes. Ce système se compose de cinq programmes qui réalisent l'analyse RMN du ^{13}C d'un composé et utilize aussi des données de systématiques d'organismes vivants. Les squelettes probables sont déterminés ainsi que les sous-structures compatibles avec les données spectrales. Le système a été testé pour l'élucidation de 40 monoterpènes qui appartiennent à divers types de squelettes, et montre d'excellents résultats.

Mots clés : monoterpènes, RMN du ^{13}C, élucidation structurale, analyse assisteé par ordinateur, système expert.

Introduction

The quick development of computers in the last decades has allowed researchers of a wide variety of knowledge fields to develop computational methods capable of aiding them in solutions of complex problems in their work (1).

The programs that use computational techniques that try to simulate human reasoning to solve complex problems are called expert systems (2). They act in the problem solutions of restricted domains, using an individual method based on a computational model of the specialist's logic.

Several types of problems are solved through expert systems, especially in scientific and technologic areas. Various examples of expert system for chemistry in the structural determination area may be cited,such as DENDRAL (3), ACCESS (4), DARC/EPIOS (5–9), SpecInfo (10), and more recently, the Assemble 2.0 systems (11, 12).

In the last couple of years, our research group has developed the SISTEMAT expert system (13, 14), whose objective is to aid natural product researchers in the structural determination process of organic substances. For that, the SISTEMAT system utilizes, principally, ^{13}C NMR, mass spectrometry (MS), and systematic information (family, genus, and species) data. Thus, some natural product classes have been studied by us, for example, sesquiterpenes, sesquiterpene lactones, diterpenes, and triterpenes (15–19), by using the programs of the SISTEMAT, to construct, at the end of the work, a system for elucidation of any terpenoid structure.

The aim of this paper is to present an expert system, denoted MONOREG, capable of structural determination of monoterpenes,.

Methodology

For the database, elaborations were collected from the literature (1960–95) of monoterpenes showing ^{13}C NMR or systematic data. The obtained monoterpenes were automatically encoded by our DATASIS program (20, 21). The database we built for this work contains 2328 monoterpenes distributed in 158 different skeletons, 1369 ^{13}C NMR spectra data, and 13 067 occurrences in 124 families of plants, marine organisms, and fungi.

The MONOREG system

MONOREG is a system that performs data analyses of monoterpenes. The idea for this name comes from the Portuguese words monoterpenos (Engl., monoterpenes) and regras (Engl. rules). Basically, this system is composed of five programs: MACRONO, SISCONST, C13MACH, SISOCBOT,

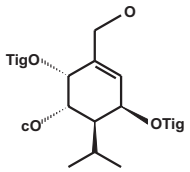
Received March 30, 2001. Published on the NRC Research Press Web site at http://canjchem.nrc.ca on December 14, 2001.

M.J.P. Ferreira and V.P. Emerenciano.[1] Instituto de Química, Universidade de São Paulo, Caixa Postal 26077, 05513-970, São Paulo, Brazil.
G.V. Rodrigues. Departamento de Química, ICEx, Universidade Federal de Minas Gerais, 30161000, Belo Horizonte, Minas Gerais, Brazil.

[1]Corresponding author (telephone: +55-11-3818-2056; fax: +55-11-3815-5579; e-mail: vdpemere@quim.iq.usp.br).

 DOI: 10.1139/cjc-79-12-1915 © 2001 NRC Canada

Fig. 1. Monoterpene used to exemplify the MONOREG system.



Data from ^{13}C NMR spectra: (CDCl $_3$) 139.7(s), 124.6(d), 69.2(d), 40.2(d), 68.9(d), 65.9(d), 63.0(t), 26.7(d), 20.1(q), 20.0(q); Tig: 167.0(s), 128.3(s), 138.2(d), 11.9(q), 14.5(q); Ac: 170.4(s), 21.3(q)

Fig. 2. Substructures with signal attribution exhibited by the SISCONST program.

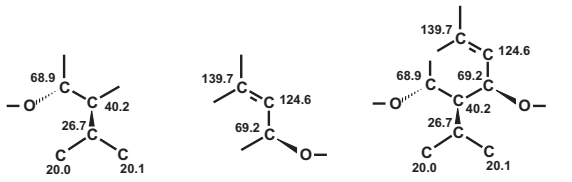


Fig. 3. Compounds with higher similarity index shown by the C13MACH program.

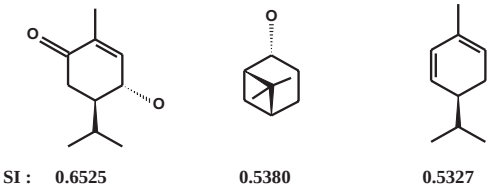


Fig. 4. Flowchart of the MONOREG system.

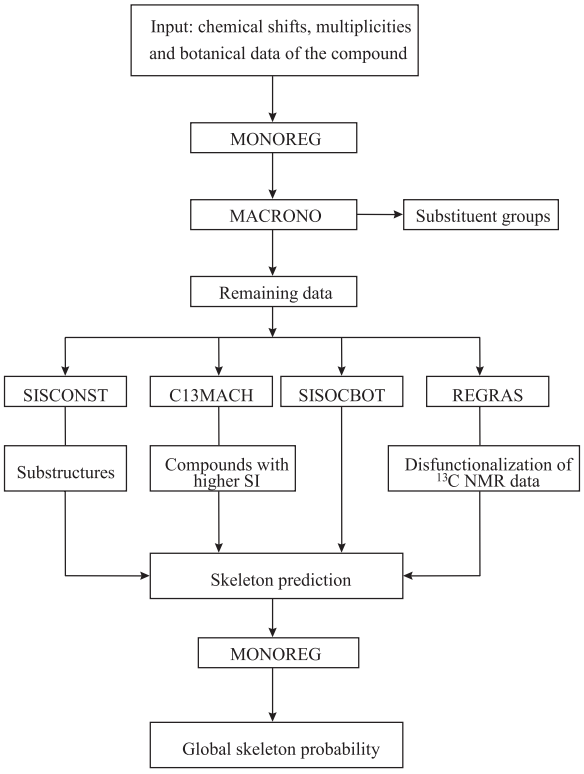


Table 1. Substituent groups proposed by the MACRONO program.

Proposed substituents	Assigned chemical shifts	Error range
Tigloyl	167.0, 138.2, 128.3, 14.5, 11.9	0.410
Acetyl	170.4, 21.3	0.700
Tigloyl	167.0, 138.2, 128.3, 14.5, 11.9	0.895

Table 2. Skeleton probability exhibited by the SISCONST program.

Skeleton	Probability
Menthane	98.5
7-Normenthane	1.5

Table 3. Skeleton probability presented by the C13MACH program.

Skeleton	Probability
Menthane	60.5
Myrcane	10.0
7-Norpinane	10.0
Pinane	9.9
Thujane	9.6

Table 4. Skeleton probability shown by the SISOCBOT program.

Skeleton	Probability
Menthane	91.5
Pinane	6.4
Myrcane	2.1

and REGRAS, which propose, at the end of analysis, a probable skeleton compatible with the entered data. This system is also capable of carrying out analyses of data from MS, however, these data were not inserted in the system. Therefore, they were not evaluated. The programs mentioned above are described below.

The MACRONO program

The MACRONO program (22, 23) identifies the common substituent groups present in the natural products, such as acetate, angelate, tiglate. From the ^{13}C NMR chemical shifts and respective multiplicities of the substance in question, the program searches the database for the most probable substituent groups present in this substance and shows to the user the selected substituent groups together with their average error range of chemical shifts. The average error range is the average deviation calculated from the chemical shifts of the sample in question and then matched with the chemical shifts values stored in the database. Therefore, the smaller the range, the more reliable the result be will.

The database especially elaborated for this program contains 161 substituent groups that are frequently encountered in terpenoid compounds. It is essential that the MACRONO program is the first program to be used in the MONOREG

© 2001 NRC Canada

Table 5. Summary of the skeleton probability displayed by the MONOREG system.

Skeleton	SISCONST	C13MACH	SISOCBOT	REGRAS	GLOBAL
Menthane	98.5	60.5	91.5	100.0	89.3
Pinane	—	9.9	6.4	—	3.3
Myrcane	—	10.0	2.1	—	2.5
7-Norpinane	—	10.0	—	—	2.3
Thujane	—	9.6	—	—	2.2
7-Normenthane	1.5	—	—	—	0.4

system. This procedure is done because the MACRONO program removes all the ^{13}C NMR signals corresponding to the substituent groups. Thus, the other programs of the MONOREG system, which carry out analysis and prediction of skeletons from ^{13}C NMR data, can in fact work with a better performance, showing a greater hit probability, once the chemical shift signals pertaining to the substituent groups are removed from and thereby do not interfere with the skeleton analysis.

To exemplify the use of the MACRONO program, a monoterpene pertaining to menthane skeleton, which was isolated from *Sphaeranthus suaveolens* — Compositae (24) (Fig. 1), was selected. After the ^{13}C NMR experimental data are inserted in the system, the MACRONO program accomplishes the analysis by matching these data with the ^{13}C NMR data of the database. This analysis is performed with an error range previously chosen by the user. In this specific case, we have chosen δ 1.0 as the error range. From this process, the program selects the most probable substituent groups for a data set. The proposed substituent groups for the monoterpene in Fig. 1 are displayed in Table 1. We can verify, from the MACRONO program analysis, that the substituent groups proposed by the program (tigloyl and acetyl) are present in the monoterpene structure. It is necessary to point out here that, after removing the ^{13}C NMR signals of these substituent groups, the remaining chemical shifts, which belong to the rest of the structure, will be utilized by other programs of the MONOREG system.

The SISCONST program

The name of this program originates from the words SISTEMAT, which is our system's name, and the English word for constraint, and it is used as a constraint generator. The SISCONST program (25) performs ^{13}C NMR data analysis. From the chemical shifts and multiplicities of a given sample, the program predicts its' probable skeleton. After that, the program identifies the substructures (parts of a structure) with their suitable attributed signals compatible with the experimental ^{13}C NMR data and then shows them to the user.

The SISCONST program only selects substructures that have a minimum number of carbon atoms and their respective interlinked chemical shifts. This minimum number is chosen by the user, to whom it is suggested to select about half the total number of carbons of the chemical class in question. Hence, the minimum number for monoterpenes is always five carbon atoms.

The SISCONST program works by matching the signals of the experimental spectrum with those of all spectra stored in the database. If a spectrum signal and its respective multiplicity are present in a determined carbon atom, the signals of the interlinked carbons are matched with those from the experimental data. This searching process is repeated to obtain the largest substructures. All selected substructures will show a minimum number of the carbon atoms as requested by the user as well as the chemical shifts compatible with the experimental ^{13}C NMR data. The skeleton probability of the substance is computed from the compounds that have a substructure containing at least half of the total carbon number. So, from each chosen compound and for its skeleton, the program calculates the skeleton probability as previously described (25).

The ^{13}C NMR data that remained after the MACRONO program analysis were submitted to SISCONST program. The program exhibited the skeleton probability (Table 2) and the two substructures with signal attributions (Fig. 2). The substructures, when overlapped as in the DARC system (5–9), give a larger substructure compatible with the correct structure.

The C13MACH program

The C13MACH program executes ^{13}C NMR data analysis too. From the chemical shifts and multiplicities this program selects *x*-compounds (*x* may change from 1 to 50) that display higher similarity index (SI) with the experimental data according to the system of Bremser and co-workers (26). From the listed compounds, the program computes the skeleton probability. In this program, the chemical shifts do not need to be necessarily interlinked like those in the SISCONST program.

For the monoterpene shown in Fig. 1, the C13MACH program calculates the skeleton probability (Table 3), and Fig. 3 shows the three compounds with a high similarity index in relation to the monoterpene tested.

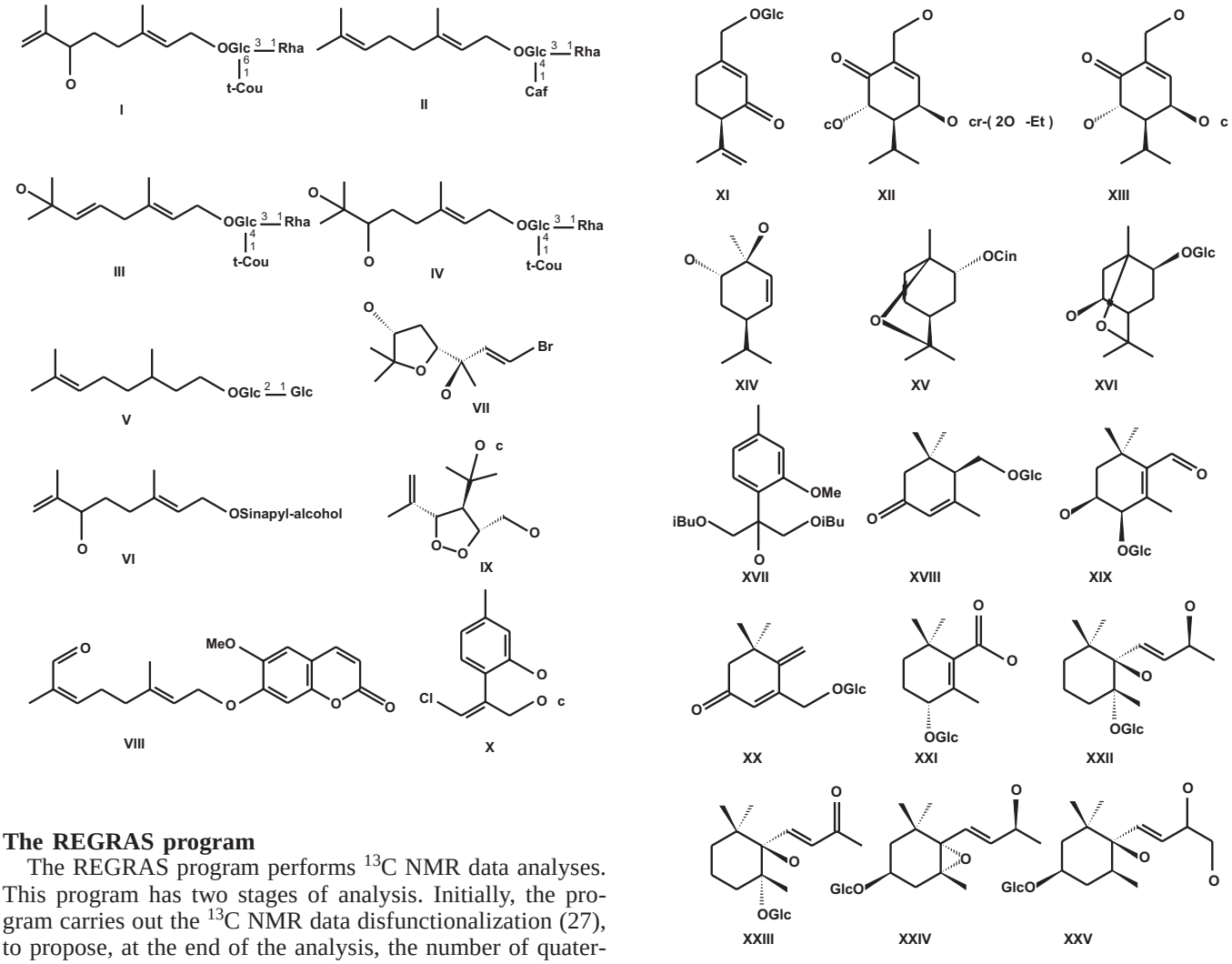
The SISOCBOT program

The SISOCBOT program (23) was developed mostly to analyze botanical data. By this reason, it was given this name originating from the Portuguese words SISTEMAT, ocorrência (Engl. occurrence), and botânica (Engl. botanical). The program carries out the analysis of the information originated from the systematic classification of any organism. From the family and genus names of plants, marine organisms, fungi, etc., the program searches in the database for the number of skeleton occurrences present in the family and genus of the species in question. And then it estimates and supplies to the user the probability of finding any carbonic skeleton in the determined organism.

For the monoterpene displayed in Fig. 1, the skeleton probability calculated by the SISOCBOT program is shown in Table 4.

© 2001 NRC Canada

Fig. 5. Monoterpenes used to test the MONOREG system.



The REGRAS program

The REGRAS program performs ^{13}C NMR data analyses. This program has two stages of analysis. Initially, the program carries out the ^{13}C NMR data disfunctionalization (27), to propose, at the end of the analysis, the number of quaternary, methine, methylene, and methyl carbons on the skeleton of the substance in question. After obtaining these data, the program matches the types of carbon atoms found with a database containing this information for all the skeletons of a determined chemical class, thus getting all the likely skeletons of the substance. Secondly, from the proposed skeletons at the first step, the program accomplishes a search for possible skeletons through the characteristic chemical shift ranges. For each monoterpene skeleton, a set of chemical shift ranges was selected that characterize it toward other skeleton types (28).

Summarizing, the REGRAS program exhibits two analysis steps: the first is a rough search, which is fundamental, by means of ^{13}C NMR data disfunctionalization. Skeletons that show a determined set of carbon atoms are selected. At the second analysis step, the program, from these previously selected skeletons, performs a fine search through the characteristic chemical shift ranges of each skeleton or subskeleton.

To test the REGRAS program, the ^{13}C NMR data of the monoterpene (Fig. 1) were analyzed. After the data disfunctionalization and search through the characteristic chemical shift ranges, the REGRAS program showed the following skeleton probability: menthane skeleton, 100.0%.

The global probability

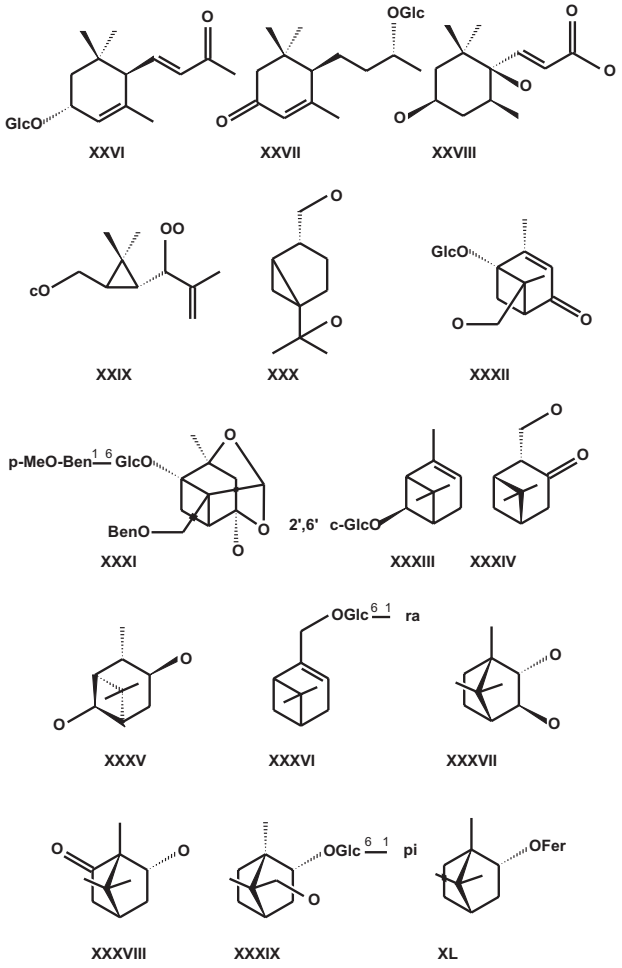
At the end of all analyses, the results obtained from each program are combined, thereby generating a global probability. The global probability is computed from the weighed mean of the results of each program. Thus, the following weights 0.9, 0.7, 0.5, and 1.0 were assigned to programs SISCONST, C13MACH, SISOCBOT, and REGRAS, respectively. The weights assigned to each program varied from 0 to 1 and the vaules were obtained by testing 20 substances to assess the hit percental of each program. The global probability calculated for the monoterpene (Fig. 1) is shown in Table 5 together with the skeleton probabilities displayed by each program. Figure 4 shows the work flow chart of the PASCAL language written MONOREG system.

Results and discussion

To test the performance and efficiency of the MONOREG system, our option was to randomly collect the data of 40 new monoterpenes (Fig. 5) from recently published literature (29–55). These data, which are not yet inserted in our database, were then submitted to analyses in the programs. Ini-

© 2001 NRC Canada

Fig. 5 (*concluded*).

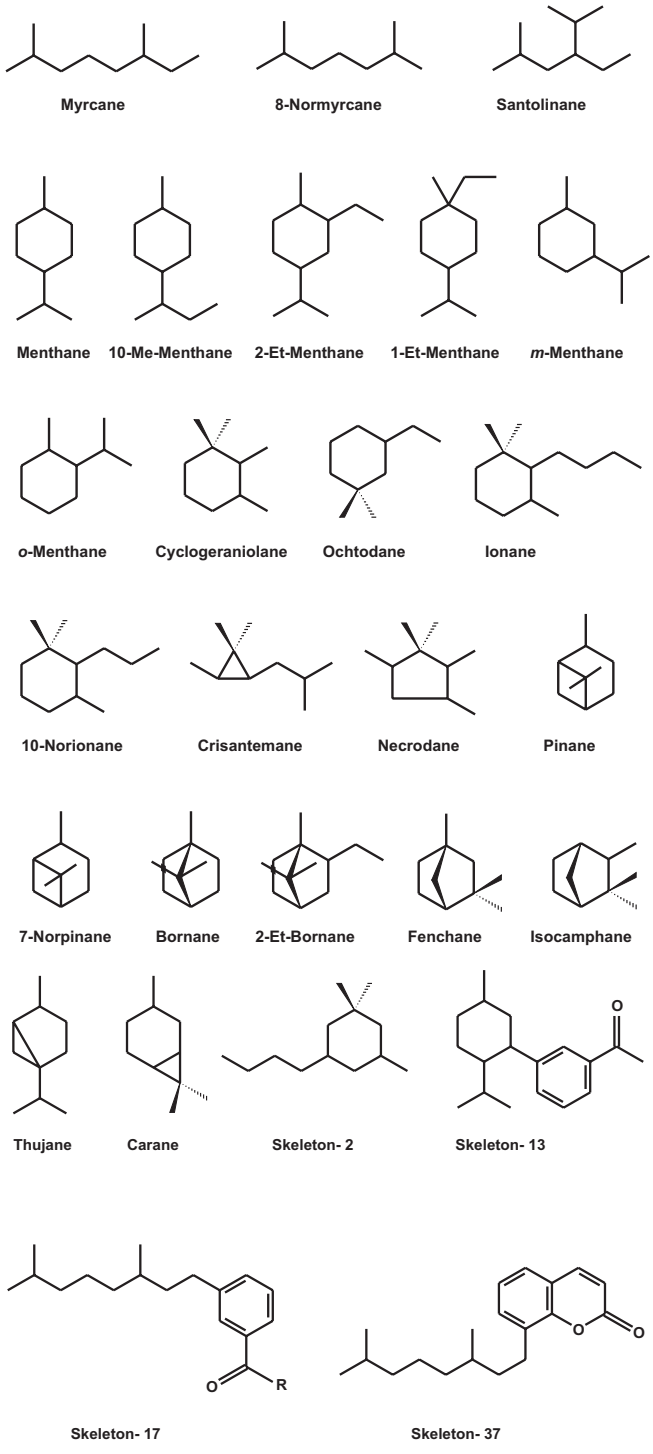


tially, the MACRONO program removed all the ^{13}C NMR chemical shifts signals attributed to the substituent groups. The remaining signals pertaining to the rest of the molecular skeletons were then tested in the other programs of the MONOREG system. The results obtained with the SISCONST, C13MACH, SISOCBOT, and REGRAS programs are shown in Table 6. This table also exhibits the first three monoterpene skeletons suggested by the system (see Fig. 6), the global skeleton probability, their ^{13}C NMR data, and respective references.

From the results obtained and exhibited in Table 6 one can verify that the MONOREG system showed the correct skeleton for the compounds in 97.5% of the cases. Only in test XXVIII did the system not supply the correct skeleton of the substance because the 10-norionane skeleton is a new skeleton whose data were not present in our database. The most probable skeleton proposed by the system is, however, the biogenetic precursor. If we consider the tests of the substances whose skeletons are present in the database, the skeleton prediction percental hit of the MONOREG system was 100.0%.

Analyzing each program separately, the SISCONST program showed the correct skeleton in 85.0% of the studied cases, with the remaining cases distributed among incorrect skeletons (tests XVIII, XXVIII, and XXX) and tests where

Fig. 6. Skeletons proposed by the MONOREG system.



the program did not display skeleton prediction (tests III, XX, and XXIX).

In general it has been observed that the SISCONST program, even with having an 85.0% hit in skeleton prediction, can show wrong results in the following cases: (*i*) the number of the substances referring to such a skeleton is very small or nonexistent (tests XXVIII, XXIX, and XXX); (*ii*) the compound shows a rare functionalization for such a skeleton (tests III and XX); or (*iii*) the ^{13}C NMR spectra

© 2001 NRC Canada

Table 6. Results obtained by the MONOREG system.

Compound	Botanical and ^{13}C NMR data (C_1–C_{10})[a]	Skeletons[b]	SISCONST	C13MACH	SISOCBOT	REGRAS	Global result	Ref.
I	111.5 (t), 148.7 (s), 76.1 (d), 34.2 (t), 36.6 (t), 142.1 (s), 121.4 (d), 66.3 (t), 29.9 (q), 16.6 (q)	*Myrcane*	92.5	53.0	100.0	100.0	87.2	29
	Oleaceae — *Ligustrum robustum*	Menthane	2.5	18.5	—	—	4.9	
		Skeleton-17	—	10.6	—	—	2.4	
II	25.9 (q), 132.5 (s), 125.0 (d), 27.4 (t), 40.6 (t), 142.0 (s), 121.4 (d), 66.5 (t), 17.8 (q), 16.5 (q)	*Myrcane*	96.4	79.8	100.0	100.0	94.4	29
	Oleaceae — *Ligustrum robustum*	Skeleton-37	—	10.1	—	—	2.3	
		Skeleton-13	—	10.1	—	—	2.3	
III	24.9 (q), 82.4 (s), 128.7 (d), 137.6 (d), 43.4 (t), 140.8 (s), 122.2 (d), 66.6 (t), 24.9 (q), 16.6 (q)	*Myrcane*	—	39.4	100.0	100.0	80.7	29
	Oleaceae — *Ligustrum robustum*	Ionane	—	19.2	—	—	6.1	
		Skeleton-17	—	12.5	—	—	4.0	
IV	25.7 (q), 73.8 (s), 78.9 (d), 30.4 (t), 37.7 (t), 142.3 (s), 121.6 (d), 66.6 (t), 25.0 (q), 16.6 (q)	*Myrcane*	96.6	70.0	100.0	100.0	92.2	29
	Oleaceae — *Ligustrum robustum*	Ionane	—	30.0	—	—	6.8	
		Menthane	2.3	—	—	—	0.7	
V	27.7 (q), 134.0 (s), 128.1 (d), 27.8 (t), 39.2 (t), 31.5 (d), 38.6 (t), 72.0 (t), 19.8 (q), 21.6 (q)	*Myrcane*	95.4	20.5	75.0	100.0	76.7	30
	Rosaceae – *Rosa damascena*	Menthane	2.3	30.0	15.0	—	9.9	
		Skeleton-37	—	19.3	—	—	4.4	
VI	111.0 (t), 147.2 (s), 75.2 (d), 32.5 (t), 35.4 (t), 141.0 (s), 120.6 (d), 69.2 (t), 17.4 (q), 16.1 (q)	*Myrcane*	92.1	79.6	75.0	100.0	89.1	31
	Compositae — *Ligularia duciformis*	Menthane	3.2	—	25.0	—	5.0	
		8-Normyrcane	3.2	9.5	—	—	3.1	
VII	25.5 (q), 85.4 (s), 76.6 (d), 35.4 (t), 80.7 (d), 75.8 (s), 140.6 (d), 107.3 (d), 22.3 (q), 26.0 (q)	*Myrcane*	84.8	40.3	—	100.0	78.7	32
	Delesseraceae — *Pantoneura plocamiodes*	Menthane	12.1	10.0	—	—	6.9	
		Ionane	3.0	9.9	—	—	3.7	
VIII	195.0 (d), 139.8 (s), 153.1 (d), 26.9 (t), 37.8 (t), 140.4 (s), 119.8 (d), 66.0 (t), 9.2 (q), 16.8 (q)	*Myrcane*	96.4	100.0	15.2	100.0	85.3	33
	Compositae — *Artemisia keiskeana*	Menthane	2.4	—	24.0	—	4.6	
		Pinane	—	—	13.3	—	2.1	
IX	118.1 (t), 139.8 (s), 86.6 (d), 60.4 (d), 84.2 (d), 63.4 (t), 81.6 (s), 24.1 (q), 24.0 (q), 17.3 (q)	*Santolinane*	60.0	9.6	8.8	100.0	53.3	34
	Compositae — *Artemisia fragrans*	Myrcane	20.0	61.4	15.2	—	22.1	
		Menthane	20.0	9.8	24.0	—	11.9	
X	140.4 (s), 116.8 (d), 153.4 (s), 121.0 (s), 130.0 (d), 121.3 (d), 21.2 (q), 135.3 (s), 121.6 (d), 62.7 (t)	*Menthane*	86.6	22.4	85.7	100.0	76.3	35
	Compositae — *Arnica sachalinensis*	Myrcane	—	37.4	—	—	8.5	
		10Me-menthane	11.3	12.3	—	—	6.0	
XI	164.2 (s), 125.0 (d), 202.2 (s), 55.8 (d), 28.8 (t), 26.7 (t), 71.2 (t), 144.8 (s), 20.9 (q), 114.1 (t)	*Menthane*	89.7	31.7	63.5	100.0	75.7	36

© 2001 NRC Canada

Table 6 (*continued*).

Compound	Botanical and ^{13}C NMR data (C_1–C_{10})[a]	Skeletons[b]	SISCONST	C13MACH	SISOCBOT	REGRAS	Global result	Ref.
	Labiatae — *Mentha piperita*	Myrcane	3.5	29.2	15.9	—	10.2	
		2Et-menthane	—	10.1	—	—	2.3	
XII	139.6 (s), 138.6 (d), 67.4 (d), 46.8 (d), 73.8 (d), 195.0 (s), 60.5 (t), 27.8 (d), 19.7 (q), 19.6 (q)	*Menthane*	96.8	53.7	91.5	100.0	87.2	24
	Compositae — *Sphaeranthus suaveolens*	Myrcane	—	18.3	2.1	—	4.5	
		Pinane	—	9.2	6.4	—	3.1	
XIII	138.1 (s), 139.4 (d), 71.7 (d), 48.8 (d), 67.4 (d), 201.6 (s), 60.3 (t), 27.8 (q), 19.7 (q), 19.7 (q)	*Menthane*	83.7	59.0	91.5	100.0	84.0	24
	Compositae — *Sphaeranthus suaveolens*	Myrcane	—	21.0	2.1	—	5.6	
		Thujane	—	19.1	—	—	4.8	
XIV	71.2 (s), 132.0 (d), 132.1 (d), 38.6 (d), 28.8 (t), 73.5 (d), 23.5 (q), 32.0 (d), 20.0 (q), 19.9 (q)	*Menthane*	97.7	72.1	—	100.0	76.9	37
	Zingiberaceae — *Alpinia densibracteata*	Isocamphane	—	—	100.0	—	16.1	
		Thujane	—	18.3	—	—	4.1	
XV	71.0 (s), 72.9 (d), 32.8 (t), 33.9 (d), 22.0 (t), 26.1 (t), 23.1 (q), 73.8 (s), 28.9 (q), 28.1 (q)	*Menthane*	98.0	100.0	75.0	100.0	95.4	37
	Zingiberaceae — *Alpinia densibracteata*	Isocamphane	—	—	25.0	—	4.0	
		Myrcane	2.0	—	—	—	0.6	
XVI	72.6 (s), 74.2 (d), 30.2 (t), 42.1 (d), 69.0 (d), 42.4 (t), 23.6 (q), 73.9 (s), 31.6 (q), 30.5 (q)	*Menthane*	96.9	61.6	38.1	100.0	80.4	38
	Umbelliferae — *Foeniculum vulgare*	Myrcane	2.6	9.1	9.5	—	4.3	
		Ionane	—	18.9	—	—	4.3	
XVII	124.4 (s), 112.0 (d), 156.4 (s), 139.4 (s), 121.4 (d), 127.6 (d), 21.3 (q), 75.6 (s), 67.1 (t), 67.1 (t)	*Menthane*	100.0	100.0	—	33.3	74.3	39
	Compositae — *Carpesium lipskyi*	*o*-Menthane	—	—	—	33.3	12.8	
		m-Menthane	—	—	—	33.3	12.8	
XVIII	36.3 (s), 49.5 (t), 203.2 (s), 127.6 (d), 165.5 (s), 52.8 (d), 69.3 (t), 27.3 (q), 29.4 (q), 24.2 (q)	*Ciclogeraniolane*	—	10.1	40.0	100.0	41.0	40
	Rubiaceae — *Gardenia jasminoides*	Ionane	100.0	49.0	—	—	40.1	
		Bornane	—	—	40.0	—	6.5	
XIX	36.7 (s), 44.0 (t), 67.0 (d), 84.2 (d), 151.2 (s), 142.6 (s), 194.9 (d), 29.2 (q), 27.3 (q), 17.4 (q)	*Ciclogeraniolane*	56.3	—	40.0	100.0	55.0	40
	Rubiaceae — *Gardenia jasminoides*	Myrcane	—	20.1	20.0	—	7.8	
		Ochtodane	25.0	—	—	—	7.3	
XX	39.8 (s), 52.9 (t), 201.9 (s), 125.1 (d), 154.9 (s), 150.1 (s), 114.6 (t), 28.6 (q), 28.6 (q), 68.5 (t)	*Ciclogeraniolane*	—	10.2	40.0	100.0	57.8	40
	Rubiaceae — *Gardenia jasminoides*	Menthane	—	49.9	—	—	15.9	
		Bornane	—	—	40.0	—	9.1	
XXI	32.7 (s), 33.7 (t), 24.0 (t), 73.1 (d), 129.8 (s), 140.5 (s), 171.7 (s), 26.9 (q), 27.9 (q), 17.9 (q)	*Ciclogeraniolane*	61.0	29.9	30.8	100.0	61.7	41
	Scrophulariaceae — *Rehmannia glutinosa*	Ionane	36.4	17.9	69.2	—	25.8	
		Pinane	—	17.5	—	—	4.0	

© 2001 NRC Canada

Table 6 (*continued*).

Compound	Botanical and ^{13}C NMR data (C_1–C_{10})[a]	Skeletons[b]	SISCONST	C13MACH	SISOCBOT	REGRAS	Global result	Ref.
XXII	38.9 (s), 36.9 (t),18.3 (t), 32.0 (t), 82.9 (s), 79.4 (s), 135 (d), 130.8 (d), 68.1 (d), 24.8 (q), 25.6 (q), 27.8 (q), 22.8 (q)	*Ionane*	100.0	61.2	69.2	100.0	86.3	41
	Scrophulariaceae — *Rehmannia glutinosa*	Ciclogeraniolane	—	—	30.8	—	5.0	
		Myrcane	—	15.3	—	—	3.5	
XXIII	39.4 (s), 36.6 (t), 18.2 (t), 32.0 (t), 82.6 (s), 79.7 (s), 152 (d), 131.9 (d), 198.3 (s), 25.8 (q), 27.0 (q), 27.6 (q), 22.8 (q)	*Ionane*	100.0	92.1	69.2	100.0	93.3	41
	Scrophulariaceae — *Rehmannia glutinosa*	Ciclogeraniolane	—	—	30.8	—	5.0	
		Menthane	—	7.9	—	—	1.8	
XXIV	35.9 (s), 45.7 (t), 73.0 (d), 38.5 (t), 67.7 (s), 71.3 (s), 126 (d), 139.1 (d), 68.7 (d), 23.8 (q), 20.2 (q), 25.2 (q), 29.8 (q)	*Ionane*	49.3	28.9	—	100.0	63.3	42
	Tiliaceae — *Corchorus olitorius*	Myrcane	6.7	51.2	—	—	16.1	
		Ciclogeraniolane	34.3	—	—	—	11.9	
XXV	40.7 (s), 42.9 (t), 75.8 (d), 38.5 (t), 35.5 (d), 78.8 (s), 137 (d), 131.2 (d), 75.4 (d), 68.0 (t), 26.5 (q), 26.2 (q), 16.8 (q)	*Ionane*	94.9	56.1	100.0	100.0	88.6	43
	Celastraceae — *Maytenus ilicifolia*	Myrcane	—	16.4	—	—	3.7	
		Skeleton-02	—	10.2	—	—	2.3	
XXVI	34.6 (s), 40.7 (t), 73.9 (d), 125.9 (d), 136.7 (s), 55.7 (d), 149.7 (d), 134.4 (d), 201 (s), 27.1 (q), 29.6 (q), 25.4 (q)	*Ionane*	76.7	39.8	—	100.0	63.5	44
	Labiatae — *Stachys byzantina*	Ochtodane	18.0	20.7	—	—	9.9	
		Menthane	—	—	50.0	—	8.1	
XXVII	37.2 (s), 48.0 (t), 202.3 (s), 125.3 (d), 170.0 (s), 52.3 (d), 26.7 (t), 37.7 (t), 75 (d), 19.8 (q), 27.5 (q), 29.0 (q), 25 (q)	*Ionane*	93.6	39.7	—	100.0	68.4	44
	Labiatae — *Stachys byzantina*	Menthane	—	9.9	50.0	—	10.3	
		Myrcane	—	29.6	21.4	—	10.1	
XXVIII[c]	40.9 (s), 45.7 (t), 67.3 (d), 39.6 (t), 35.3 (d), 78.9 (s), 154.3 (d), 123.3 (d), 170.3 (s), 25.2 (q), 25.9 (q), 16.4	Ionane	100.0	83.6	—	—	47.9	45
	Rutaceae — *Glycosmis arborea*	1Et-menthane	—	—	—	100.0	32.3	
		Myrcane	—	8.1	100.0	—	18.0	
XXIX	64.7 (t), 27.9 (d), 30.8 (d), 89.8 (d), 143.7 (s), 113.6 (t), 17.6 (q), 21.8 (s), 21.5 (q), 21.9 (q)	*Crisantemane*	—	10.1	1.1	100.0	48.9	46
	Compositae — *Achillea nobilis*	Menthane	—	50.8	35.9	—	24.3	
		Myrcane	—	9.4	12.1	—	5.7	
XXX	42.5 (d), 23.4 (d), 11.0 (t), 37.6 (d), 25.1 (t), 27.3 (t), 67.4 (t), 71.3 (s), 28.1 (q), 27.4 (q)	*Thujane*	—	—	—	100.0	38.5	47
	Fungi — *Glomerella cingulata*	Pinane	41.8	29.9	—	—	22.5	
		Menthane	35.8	33.0	—	—	21.3	
XXXI	85.8 (s), 88.7 (s), 22.7 (t), 43.6 (d), 105.7 (s), 44.5 (t), 19.6 (q), 71.3 (s), 61.2 (t), 101.5 (d)	*Pinane*	69.4	39.9	50.0	—	37.2	48
	Paeoniaceae — *Paeonia suffruticosa*	Menthane	30.6	18.5	43.8	25.0	28.2	
		o-Menthane	—	—	—	25.0	8.1	
XXXII	173.4 (s), 84.4 (s), 43.4 (t), 48.1 (d), 201.1 (s), 121.3 (d), 19.9 (q), 63.6 (s), 66.3 (t), 16.1 (q)	*Pinane*	53.7	—	50.0	100.0	55.9	48

© 2001 NRC Canada

Table 6 (*concluded*).

Compound	Botanical and ^{13}C NMR data (C_1–C_{10})[a]	Skeletons[b]	SISCONST	C13MACH	SISOCBOT	REGRAS	Global result	Ref.
	Paeoniaceae — *Paeonia suffruticosa*	Menthane	19.5	28.7	43.8	—	19.2	
		Myrcane	—	41.0	—	—	9.3	
XXXIII	141.9 (s), 45.0 (d), 83.4 (d), 50.6 (d), 31.9 (t), 118.2 (d), 22.6 (q), 37.4 (s), 26.5 (q), 22.7 (q)	*Pinane*	85.2	46.5	6.1	100.0	68.5	49
	Compositae — *Erigeron linifolius*	Myrcane	—	25.9	39.4	—	12.2	
		Menthane	—	9.8	33.3	—	7.6	
XXXIV	53.7 (d), 40.5 (d), 29.7 (t), 38.2 (d), 44.6 (t), 216.3 (s), 63.3 (t), 39.8 (s), 19.9 (q), 26.1 (q)	*Pinane*	51.8	22.5	—	100.0	62.4	47
	Fungi — *Glomerella cingulata*	7-Norpinane	14.0	29.4	—	—	12.8	
		Isocamphane	7.0	10.6	—	—	5.3	
XXXV	40.7 (d), 2.3 (d), 69.6 (d), 46.7 (d), 33.4 (t), 67.3 (d), 19.9 (q), 32.1 (s), 27.2 (q), 19.9 (q)	*Pinane*	39.3	39.3	—	100.0	62.7	50
	Fungi — *Glomerella cingulata*	Isocamphane	36.0	—	—	—	12.4	
		Necrodane	—	20.0	—	—	5.5	
XXXVI	146.3 (s), 44.6 (d), 32.6 (t), 42.2 (d), 32.3 (t), 121.0 (d), 72.9 (t), 39.0 (s), 21.6 (q), 26.7 (q)	*Pinane*	69.2	39.3	100.0	100.0	77.4	51
	Crassulaceae — *Rhodiola sacra*	7-Norpinane	9.4	20.0	—	—	7.2	
		Ionane	—	19.5	—	—	4.4	
XXXVII	47.2 (s), 86.1 (d), 84.6 (d), 52.5 (d), 25.1 (t), 25.4 (t), 12.9 (q), 50.3 (s), 21.0 (q), 19.3 (q)	*Bornane*	91.9	90.4	—	100.0	94.6	52
	—	Fenchane	5.9	9.6	—	—	4.6	
		Other	2.1	—	—	—	0.7	
XXXVIII	63.8 (s), 216.7 (s), 43.5 (t), 41.5 (d), 37.7 (t), 75.9 (d), 7.3 (q), 48.7 (s), 20.7 (q), 19.8 (q)	*Bornane*	60.2	10.9	7.1	100.0	53.3	53
	Compositae — *Artemisia lucentica*	Fenchane	37.2	9.7	—	—	13.0	
		Myrcane	—	19.7	15.2	—	6.9	
XXXIX	54.5 (s), 28.0 (t), 28.7 (t), 42.3 (d), 36.5 (t), 84.2 (d), 14.8 (q), 50.0 (s), 15.2 (q), 64.5 (t)	*Bornane*	92.3	72.3	—	100.0	89.9	54
	Umbelliferae — *Glehnia littoralis*	Carane	—	19.0	—	—	5.1	
		Menthane	—	8.8	—	—	2.4	
XL	48.9 (s), 79.8 (d), 36.8 (t), 44.9 (d), 28.0 (t), 27.2 (t), 13.5 (q), 47.8 (s), 19.7 (q), 18.8 (q)	*Bornane*	82.3	91.7	100.0	100.0	93.0	55
	Compositae — *Coreopsis mutica*	Fenchane	7.7	8.3	—	—	4.1	
		2-Ethylbornane	4.3	—	—	—	1.2	

[a]Solvents: CD_3OD: I–IV, XI, XVIII–XX, XXIV–XXVIII, XXXVI; D_2O: V, VI; $CDCl_3$: VII, VIII–X, XII–XVI, XV, XVII, XXIX, XXX, XXXIII–XXXV, XXXVII, XXXVIII, XL; C_5D_5N: XVI, XXI, XXIX, XXII, XXIII, XXXI, XXXII, XXIX.

[b]The skeletons in italics represent the correct skeleton of the substance.

[c]The correct skeleton is 10-norionane

© 2001 NRC Canada

data of the substance in question are very similar to those of other substance belonging to another skeleton (test XVIII).

If one analyzes the SISCONST's results through the skeleton series, itcan be seen that the cyclogeraniolane series (XVIII–XXI) is the most atypical, as the results are not uniform. Regarding test XVIII, the incorrect skeleton proposed by the SISCONST program was that of ionane. However, this mistake can occur and be easily explained, since there are in the database data of several substances bearing the ionane skeleton, which present the structural nucleus of the substance XVIII. Concerning the tests XIX and XXI, the program furnished the correct skeleton of the substance, but, on the other hand, there was variation in percental hits observed. This occurred because the program considers the carbon numbers of the substructure selected in the analysis as well as the skeleton type which these substructures belong to. In test XX, the program did not provide skeleton prediction, because the substance shows an unusual functionalization for its corresponding skeleton as previously commented.

By comparing the results obtained by the C13MACH program, which showed the correct skeleton in 67.5% of the studied cases, with those of the SISCONST program, the SISCONST program is shown to be more efficient because it selects only monoterpenes that contain a minimum number of carbon atoms interlinked for skeleton prediction, whereas the C13MACH program does not have this restriction.

The REGRAS program predicted the correct skeleton of the compounds in 95.0% of the cases. Two errors were detected: (*i*) in test XXVIII, the program recongnized the correct disfunctionalization of the ^{13}C NMR data, however, during the search only the 1-ethylmenthane skeleton was found, as the 10-norionane skeleton is a new compound whose data was not registered in our database; and (*ii*) in test XXXI, the REGRAS program rendered incorrect disfunctionalization of the ^{13}C NMR data. This fact occurred with the chemical shift at 71.3 (s) ppm, which is related to C_8. This chemical shift should not be disfunctionalized because it refers to a quaternary carbon. However, as this chemical shift is found in the C-OR range, established in the program (27), it was disfunctionalized to a methine carbon.

In relation to the 40 tests here shown, the MACRONO program was used for 32 of them. In all 32 tests, the program correctly identified the substituent groups present in the respective substances.

The SISOCBOT program showed the correct skeleton of the substance in 68.75% of the cases. When the analyzed substance belongs to a genus that is absent in the database, the search may be accomplished at family level, however, as the result is less reliable, the search was only conducted at genera level present in the database. When we compared the results of the SISOCBOT program with those of the C13MACH program, we found that the former displayed a slightly higher percentual hit, thereby demonstrating the validity and importance of the systematic data for skeleton prediction of substances from natural sources.

Conclusions

The results of the analyses of monoterpenes in this work show an excellent performance of the programs comprised of the MONOREG system for the identification and skeleton prediction with 97.5% hits. From the obtained results, we can conclude that this system may be introduced as a valuable tool for the process of monoterpene skeleton determination, thereby increasing the spectral interpretation capacity of the researchers, once the characterization of the skeleton type of new natural products is at the crucial point in structural elucidation of these compounds.

The information obtained from the programs of the MONOREG system, such as skeleton types, substructures, probable substituent groups bonded to structures, might be utilized as a restriction module for the structure generator that is being developed for the expert SISTEMAT system, i.e., instead of the generator working with all the skeletons of a class of substance to start the process of generation of likely structures, it will only have to initiate the process utilizing just three or four first skeletons proposed by the MONOREG system. The immediate consequence of the utilization of this system on the structure generator will be the reduction of computational time and of the number of displayed structural proposals, hence avoiding the combinatorial explosion problem observed in other expert systems developed up to now (9, 11, 12, 56, 57).

Acknowledgments

This work was supported by grants from the Fundação de Amparo à Pesquisa do Estado de São Paulo (FAPESP) and by the Conselho Nacional de Desenvolvimento Científico e Tecnológico (CNPq). The authors thank Antônio J.C. Brant for helpful discussion during the preparation of the manuscript.

References

1. E. Rich. Inteligência artificial. McGraw-Hill, São Paulo. 1988.
2. S.M. Weiss and C.A. Kulikowski. Guia prático para projetar sistemas especialistas. Livros Técnicos e Científicos, Rio de Janeiro. 1988.
3. R.K. Lindsay, B.G. Buchanan, E.A. Feigenbaum and J. Lederberg. Applications of artificial intelligence for organic chemistry: the DENDRAL project. McGraw-Hill, New York. 1980.
4. W. Bremser and W. Fachinger. Magn. Res. Chem. **23**, 1056 (1985).
5. M. Carabedian, J. Dagane, and J.E. Dubois. Anal. Chem. **60**, 2186 (1988).
6. J.E. Dubois and M. Carabedian. J. Chem. Inf. Comp. Sci. **31**, 557 (1991).
7. M. Carabedian and J.E. Dubois. J. Chem. Inf. Comp. Sci. **31**, 564 (1991).
8. M. Carabedian and J.E. Dubois. J. Chem. Inf. Comp. Sci. **34**, 701 (1994).
9. M. Carabedian and J.E. Dubois. J. Chem. Inf. Comp. Sci. **38**, 100 (1998).
10. M. Will, W. Fachinger, and J.R. Richert. J. Chem. Inf. Comp. Sci. **36**, 221 (1996).
11. M.E. Munk. J. Chem. Inf. Comp. Sci. **38**, 997 (1998).
12. M. Badertscher, A. Korytko, K.P. Schulz, M. Madison, M.E. Munk, P. Portmann, M. Junghans, P. Fontana, and E. Pretsch. Chemometr. Intell. Lab. **51**, 73 (2000).

© 2001 NRC Canada

13. J.P. Gastmans, M. Furlan, M.N. Lopes, J.H.G. Borges, and V.P. Emerenciano. Quím. Nova, **13**, 10 (1990).
14. V.P. Emerenciano, G.V. Rodrigues, P.A.T. Macari, S.A. Vestri, J.H.G. Borges, J.P. Gastmans, and D.L.G. Fromanteau. Spectroscopy, **12**, 91 (1994).
15. V.P. Emerenciano, A.C. Bussolini, G.V. Rodrigues, M. Furlan, and D.L.G. Fromanteau. Spectroscopy, **11**, 95 (1993).
16. F.C. Oliveira, M.J.P. Ferreira, C.V. Nuñez, G.V. Rodrigues, and V.P. Emerenciano. Prog. Nucl. Magn. Reson. Spectrosc. **35**, 1 (2000).
17. G.V. Rodrigues. Criação de um sistema especialista em determinação estrutural de sesquiterpenos lactonizados – Um enfoque multiespectral aliado a requisitos botânicos. Ph.D. thesis. Institute of Chemistry, University of São Paulo. 1996.
18. S.A.V. Alvarenga, J.P. Gastmans, G.V. Rodrigues, and V.P. Emerenciano. Spectroscopy, **13**, 227 (1997).
19. P.A.T. Macari, J.P. Gastmans, G.V. Rodrigues, and V.P. Emerenciano. Spectroscopy, **12**, 139 (1994).
20. V.P. Emerenciano, G.V. Rodrigues, and J.P. Gastmans. Quím. Nova, **16**, 431 (1993).
21. M.J.P. Ferreira, V.P. Emerenciano, G.A.R. Linia, P. Romoff, P.A.T. Macari, and G.V. Rodrigues. Prog. Nucl. Magn. Reson. Spectrosc. **33**, 153 (1998).
22. G.V. Rodrigues, I.P.A. Campos, and V.P. Emerenciano. Spectroscopy, **13**, 191 (1997).
23. M.J.P. Ferreira. Um sistema especialista em determinação estrutural de monoterpenos e iridóides. M.Sc. thesis. Institute of Chemistry, University of São Paulo. 1998.
24. A.A. Ahmed and A.A. Mahmoud. Phytochemistry, **45**, 533 (1997).
25. D.L.G. Fromanteau, J.P. Gastmans, S.A. Vestri, V.P. Emerenciano, and J.H.G. Borges. Comp. & Chem. **17**, 369 (1993).
26. W. Bremser, M. Klier, and E. Meyer. Org. Magn. Resonace, **7**, 97 (1975).
27. M.J.P. Ferreira, A.J.C. Brant, G.V. Rodrigues, and V.P. Emerenciano. Anal. Chim. Acta, **429**, 151 (2001).
28. M.J.P. Ferreira, G.V. Rodrigues, A.J.C. Brant, and V.P. Emerenciano. Spectroscopy, **15**, 65 (2001).
29. J. Tian, H. Zhang, H. Sun, L. Pan, P. Yao, and D. Chen. Phytochemistry, **48**, 1013 (1998).
30. N. Oka, A. Ikegami, M. Ohki, K. Sakata, A. Yagi, and N. Watanabe. Phytochemistry, **47**, 1527 (1998).
31. K. Gao, W. Wang, and Z. Jia. Phytochemistry, **47**, 269 (1998).
32. M. Cueto and J. Darias. Tetrahedron, **52**, 5899 (1996).
33. J.H. Kwak, W.Y. Jang, O.P. Zee, and K.R. Lee. Planta Med. **63**, 474 (1997).
34. J.A. Marco, J.F. Sanz-Cervera, F.J. Ropero, N. Battle, M. Guara, and J. Vallès-Xirau. Phytochemistry, **47**, 1417 (1998).
35. C.M. Passreiter, U. Matthiesen, and G. Willuhn. Phytochemistry, **49**, 777 (1998).
36. S. Park, K. Kim, Y. Suzuki, and S. Kim. Phytochemistry, **44**, 623 (1997).
37. L. Sy and G.D. Brown. Phytochemistry, **45**, 537 (1997).
38. M. Ono, Y. Ito, T. Ishikawa, J. Kitajima, Y. Tanaka, Y. Niiho, and T. Nohara. Chem. Pharm. Bull. **44**, 337 (1996).
39. Y. Shi, W. Guo, C. Yang, and Z. Jia. Planta Med. **64**, 671 (1998).
40. K. Machida, R. Onodera, K. Furuta, and M. Kikuchi. Chem. Pharm. Bull. **46**, 1295 (1998).
41. M. Yoshikawa, Y. Fukuda, T. Taniyama, and I. Kitagawa. Chem. Pharm. Bull. **44**, 41 (1996).
42. M. Yoshikawa, H. Shimada, M. Saka, S. Yoshizumi, J. Yamahara, and H. Matsuda. Chem. Pharm. Bull. **45**, 464 (1997).
43. N. Zhu, N. Sharapin, and J. Zhang. Phytochemistry, **47**, 265 (1998).
44. Y. Takeda, H. Zhang, T. Masuda, G. Honda, H. Otsuka, E. Sezik, E. Yesilada, and H. Sun. Phytochemistry, **44**, 1335 (1997).
45. A.K. Chakravarty, B. Das, K. Masuda, and H. Ageta. Chem. Pharm. Bull. **44**, 1421 (1996).
46. U. Kastner, J. Breuer, S. Glasl, A. Baumann, W. Robien, J. Jurenitsch, G. Rüker, and W. Kubelka. Planta Med. **61**, 83 (1995).
47. M. Miyazawa, Y. Suzuki, and H. Kameoka. Phytochemistry, **45**, 935 (1997).
48. H. Lin, H. Ding, T. Wu, and P. Wu. Phytochemistry, **41**, 237 (1996).
49. C.Y. Ragasa, J.A. Rideout, J.O. Sy, D. Alcachupas, V.M.L. Inte, and J.C. Coll. Phytochemistry, **46**, 151 (1997).
50. M. Miyazawa, Y. Suzuki, and H. Kameoka. Phytochemistry, **45**, 945 (1997).
51. M. Yoshikawa, H. Shimada, S. Horikawa, T. Murakami, H. Shimoda, J. Yamahara, and H. Matsuda. Chem. Pharm. Bull. **45**, 1498 (1997).
52. M. Miyazawa, M. Nobata, M. Hyakumachi, and H. Kameoka. Phytochemistry, **44**, 79 (1997).
53. J.A. Marco, J.F. Sanz-Cervera, V. García-Lliso, and N. Batlle. Phytochemistry, **45**, 775 (1997).
54. J. Kitajima, C. Okamura, T. Ishikawa, and Y. Tanaka. Chem. Pharm. Bull. **46**, 1595 (1998).
55. E. Maldonado, M.T.R. Apan, and A.L. Pérez-Castorena. Planta Med. **64**, 660 (1998).
56. R.E. Carhart, D.H. Smith, N.A.B. Gray, J.G. Nourse, and C. Djerassi. J. Org. Chem. **46**, 1708 (1981).
57. M. Jaspars. Nat. Prod. Rep. **16**, 241 (1999).

© 2001 NRC Canada

Kinetics and mechanistic study of the ruthenium(III) catalyzed oxidative deamination and decarboxylation of L-valine by alkaline permanganate

Dinesh C. Bilehal, Raviraj M. Kulkarni, and Sharanappa T. Nandibewoor

Abstract: The kinetics of ruthenium(III) catalyzed oxidation of L-valine by permanganate in alkaline medium at a constant ionic strength has been studied spectrophotometrically. The reaction between permanganate and L-valine in alkaline medium exhibits 2:1 stoichiometry ($KMnO_4$:L-valine). The reaction shows first-order dependence on the concentration of permanganate and ruthenium(III) and less than unit-order dependence on the concentrations of L-valine and alkali. The reaction rate increases both with an increase in ionic strength and a decrease in solvent polarity of the medium. Initial addition of reaction products did not significantly affect the rate. A mechanism involving the formation of a complex between catalyst and substrate has been proposed. The activation parameters were computed with respect to the slowest step of the mechanism.

Key words: oxidation, L-valine, catalysis, ruthenium(III), kinetics.

Résumé : Faisant appel à des méthodes spectrophotométriques, on a étudié la cinétique de l'oxydation de la L-valine par le permanganate, catalysée par le ruthénium(III), en milieu alcalin et à force ionique constante. En milieu alcalin, la réaction entre le permanganate et la L-valine présente une stoechiométrie de 2:1 ($KMnO_4$:L-valine). La réaction présente une dépendance du premier ordre avec les concentrations de permanganate et de ruthénium(III) et cette dépendance est inférieure à l'unité pour les concentrations de L-valine et de base. La vitesse de réaction augmente avec une augmentation de la force ionique et avec une diminution dans la polarité du solvant. L'addition initiale de produits réactionnels n'affecte pas la vitesse de façon significative. On propose un mécanisme impliquant la formation initiale d'un complexe entre le catalyseur et le substrat. On a calculé les paramètres d'activation par rapport à l'étape la plus lente du mécanisme.

Mots clés : oxydation, L-valine, catalyse, ruthénium(III), cinétique.

[Traduit par la Rédaction]

Introduction

Potassium permanganate is widely used as an oxidizing agent in synthetic as well as in analytical chemistry and also as a disinfectant. The reactions with permanganate are governed by pH of the medium. Among the six oxidation states of manganese from 2+ to 7+, permanganate Mn(VII) is the most potent oxidation state in both acid and alkaline medium.

The manganese chemistry involved in these multistep redox reactions is an important source of information as the manganese intermediates are relatively easy to identify when they have sufficiently long life times and the oxidation states of the intermediates permit useful conclusions as to the possible reaction mechanism including the nature of intermediates.

Received February 2001. Published on the NRC Research Press Web site at http://canjchem.nrc.ca on December 14, 2001.

D.C. Bilehal, R.M. Kulkarni, and S.T. Nandibewoor.[1] P.G. Department of Studies in Chemistry, Karnatak University, Dharwad 580 003, India.

[1]Corresponding author (fax: 0836-747-884; e-mail: karuni@bgl.vsnl.net.in).

The oxidation by permanganate ion finds extensive applications in organic syntheses (1–7), especially since the advent of phase transfer catalysis (3, 4, 6), which permits the use of solvents such as methylene chloride and benzene. Kinetic studies are important sources of mechanistic information on the reactions, as demonstrated by the results referring to unsaturated acids in both aqueous (1, 3, 7) and nonaqueous media (8).

During the oxidation by permanganate, it is evident that permanganate is reduced to various oxidation states in acidic, alkaline, and neutral media. Furthermore, the mechanism by which the multivalent oxidant oxidizes a substrate depends not only on the substrate but also on the medium (9) used for the study. In strongly alkaline medium, the stable reduction product (10, 11) of permanganate ion is manganate ion, MnO_4^{2-}. No mechanistic information is available to distinguish between a direct one-electron reduction to Mn(VI) (Scheme 1) and a mechanism in which a hypomanganate is formed in a two-electron reduction followed by a rapid oxidation of the hypomanganate ion (12) (Scheme 2).

L-valine is one of the essential basic amino acids, which is essential in the nutrition of mammals. Its role is crucial in

 DOI: 10.1139/cjc-79-12-1926 © 2001 NRC Canada

Scheme 1.

$$\mathrm{Mn(VII)} + \mathrm{S} \xrightarrow{k_1'} \mathrm{Mn(VI)} + \mathrm{S}^{\cdot}$$

$$\mathrm{Mn(VII)} + \mathrm{S}^{\cdot} \xrightarrow{k_2'} \mathrm{Mn(VI)} + \mathrm{Products}$$

Where, S = substrate; $k_2' >> k_1'$

Scheme 2.

$$\mathrm{Mn(VII)} + \mathrm{S} \xrightarrow{k_3'} \mathrm{Mn(V)} + \mathrm{Products}$$

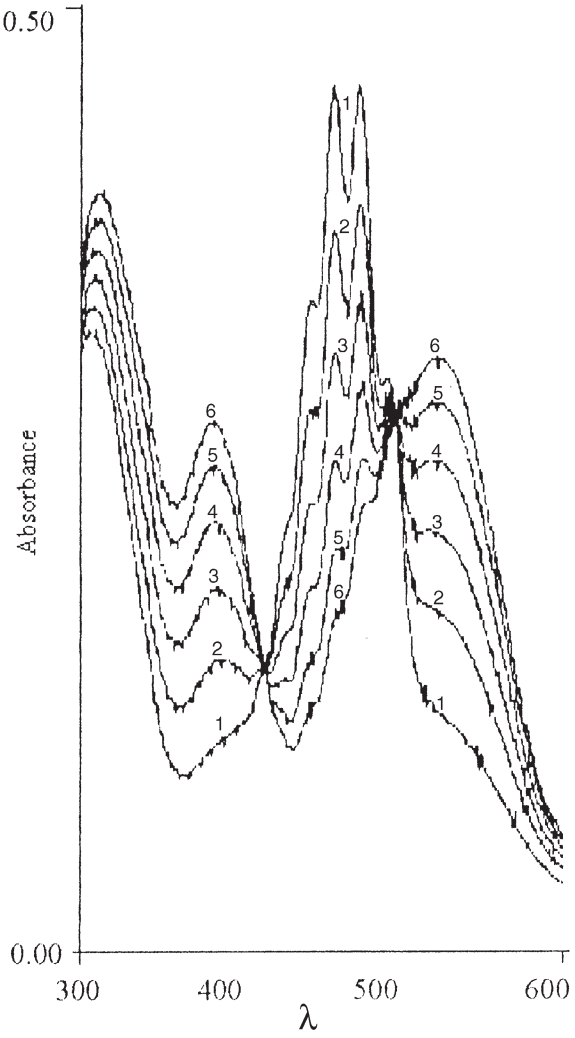
$$\mathrm{Mn(VII)} + \mathrm{Mn(V)} \xrightarrow{k_4'} 2\ \mathrm{Mn(VI)}$$

Where, S = substrate; $k_4' >> k_3'$

the development of organs, especially in children. It also finds applications in medicine and pharmaceuticals. Amino acids have been oxidized by a variety of oxidizing agents (13). Although several types of organic (14) and inorganic (10, 11) substrates are oxidized by permanganate in aqueous alkaline medium, there are only a few reports on the oxidation of amino acids by aqueous alkaline permanganate. The kinetic investigation of the oxidation of amino acids has been carried out under different experimental conditions (15). In many cases it was reported that amino acids undergo oxidative decarboxylation. Jayaprakash Rao et al. (16) suggested that the oxidation of amino acids by two-electron oxidants such as diperiodatoargentate(III) in alkaline medium involves a two-electron transfer, which produces an imino acid intermediate in the rate determining step. This intermediate subsequently undergoes hydrolysis to yield the keto acids. One electron oxidants such as ceric sulphate (17), peroxomonosulphate (18), and hexacyanoferrate(III) (19) also oxidize amino acids to keto acids. But other studies with amino acids report the oxidation products as the corresponding aldehydes (20). Thus, the study of amino acids becomes important because of their biological significance and their selectivity towards the oxidants.

Ruthenium(III) is known to be an efficient catalyst in several redox reactions particularly in alkaline medium (21). The mechanism of catalysis can be quite complicated due to the formation of different intermediate complexes, free radicals, and different oxidation states of ruthenium. The kinetics of fast reactions between ruthenate(VII), RuO_4^-, and manganate(VI), i.e., MnO_4^{2-}, have been studied (22) and the reaction is presumed to proceed via an outer-sphere mechanism. The rapid exchange between MnO_4^{2-} and MnO_4^- has been studied in detail by a variety of techniques (23). The uncatalyzed reaction between L-valine and permanganate in alkaline medium has been studied previously (24). A micro amount of ruthenium(III) is sufficient to catalyze the reaction in alkaline medium and a variety of mechanisms are possible. Thus, to explore the mechanism of oxidation by permanganate ion in strongly aqueous alkaline medium and to check the selectivity of L-valine towards permanganate in catalyzed system, we have selected ruthenium(III) as a catalyst. The present study deals with the title reaction to investigate the redox chemistry of permanganate and L-valine in presence of a catalysis.

Fig. 1. Spectral changes during the ruthenium (III) catalyzed oxidation of L-valine by alkaline permanganate (scanning time interval = 1 min). $[MnO_4^-] = 2.0 \times 10^{-4}$, [L-valine] = 2.0×10^{-3}, [Ru(III)] = 7.5×10^{-8}, $[OH^-] = 0.30$, $I = 0.50$ mol dm^{-3}.

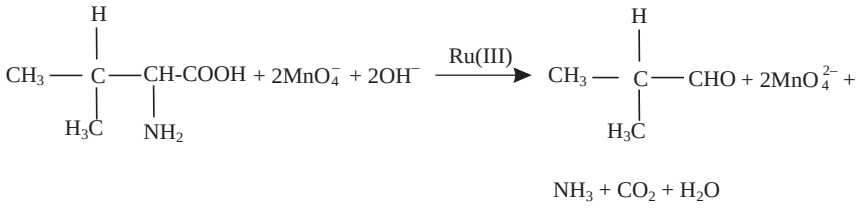


Experimental

Materials and methods

Stock solution of L-valine (Sisco Research Labs, India) was prepared by dissolving the appropriate amount of sample in doubly distilled water. The solution of potassium permanganate (BDH) was prepared and standardized against oxalic acid (25). Potassium manganate solution was prepared as described by Carrington and Symons (26).The solution was standardized by measuring the absorbance on a Hitachi 150-20 spectrophotometer with a 1 cm quartz cell at 608 nm (ε = 1530 ± 20 dm^3 mol^{-1} cm^{-1}). The ruthenium(III) solution was prepared by dissolving a known weight of $RuCl_3$ (S.D. Fine Chemicals) in 0.20 mol dm^{-3} HCl. Mercury was added to the ruthenium(III) solution to reduce any Ru(IV) formed during the preparation of ruthenium(III) stock solution and kept for a

© 2001 NRC Canada

[1] 

day. The ruthenium(III) concentration was assayed (27) by EDTA titration.

All other reagents were of analytical grade and their solutions were prepared by dissolving the requisite amounts of the samples in doubly distilled water. NaOH and $NaClO_4$ were used to provide the required alkalinity and to maintain the ionic strength, respectively.

Kinetic procedure

All kinetic measurements were performed under pseudo-first-order conditions with [L-valine]:[MnO_4^-] ≥ 10:1 at a constant ionic strength of 0.50 mol dm^{-3}. The reaction was initiated by mixing previously thermostated solutions of MnO_4^-, and L-valine, which also contained the necessary quantities of Ru(III), NaOH, and $NaClO_4$ to maintain the required alkalinity and ionic strength, respectively. The temperature was uniformly maintained at 26 ± 0.1°C. The course of reaction was followed by monitoring the decrease in the absorbance of MnO_4^- in a 1 cm quartz cell of a Hitachi model 150-20 spectrophotometer at its absorption maximum of 526 nm as a function of time. The application of Beer's law to permanganate at 526 nm had been verified, giving ε = 2083 ± 50 dm^3 mol^{-1} cm^{-1} (lit. (10) ε = 2200 dm^3 mol^{-1} cm^{-1}). The first-order rate constants (k_{obs}) were evaluated by plots of log [MnO_4^-] vs. time. The first-order plots in almost all cases were linear to 80% completion of the reaction and k_{obs} were reproducible within ±5%.

During the course of measurements, the solution changed from violet to blue and then to green. The spectrum of the green solution was identical to that of MnO_4^{2-}. It is probable that the blue colour originated from the violet of permanganate and the green from the manganate, excluding the accumulation of hypomanganate. It is also evident from the Fig. 1 that the absorbance of permanganate decreases at 526 nm, whereas the absorbance of manganate increases at 608 nm.

The effect of dissolved oxygen on the rate of reaction was checked by preparing the reaction mixture and following the reaction in an atmosphere of nitrogen. No significant difference between the results obtained under the nitrogen and in the presence of air was observed. In view of the ubiquitous contamination of basic solutions by carbonate, the effect of carbonate on the reaction was also studied. Added carbonate had no effect on the reaction rate. However, fresh solutions were used when conducting the experiments.

Results

Stoichiometry and product analysis

The reaction mixtures containing an excess permanganate concentration over L-valine and constant concentration of Ru(III) (0.30 mol dm^{-3}), NaOH, and an adjusted ionic strength of 0.50 mol dm^{-3} was allowed to react for 2 h at 26 ± 0.1°C. After completion of the reaction, solid KI was added followed by acidification by 10% H_2SO_4. The remaining MnO_4^- was then titrated against standard sodium thiosulphate (28). The results indicated that two mol of MnO_4^- are consumed by one mol of L-valine as given by eq. [1]. The main reaction products were identified as aldehyde by spot test (29), ammonia by Nessler's reagent (30), and manganate by its visible spectrum. CO_2 was qualitatively detected by bubbling N_2 gas through the acidified reaction mixture and passing the liberated gas through a tube containing lime water (31). The quantitative estimation of aldehyde by 2,4-DNP derivative (32), yielded nearly 74%. The nature of the aldehyde, was confirmed by its IR spectrum (33), which showed a carbonyl stretching at 1729 cm^{-1} and a band at 2928 cm^{-1} due to aldehydic C—H stretching, thus confirming the presence of isobutylaldehyde. It was further observed that the aldehyde does not undergo further oxidation under the present kinetic conditions. The test for corresponding acid was negative.

Reaction orders

The reaction orders were determined from the slopes of log k_{obs} vs. log (concentration) plots by varying the concentration of reductant, catalyst, and alkali in each, while keeping others constant. The oxidant, potassium permanagate, concentration was varied in the range of 5.0×10^{-5} to 5.0×10^{-4} mol dm^{-3}, and the fairly constant k_{obs} values indicate that the order with respect to [MnO_4^-] was one. This was also confirmed by varying the concentration of MnO_4^-, which did not show any change in pseudo-first-order constants (k_{obs}) values as shown in Table 1. The substrate L-valine was varied in the range of 5.0×10^{-4} to 5.0×10^{-3} mol dm^{-3} at 26°C; the order with respect to [L-valine] was found to be less than unity. The catalyst Ru(III) was varied in the range of 1.0×10^{-8} to 1.0×10^{-7} mol dm^{-3} at 26°C; the order with respect to [Ru(III)] was found to be unity. The effect of alkali on the reaction was studied at constant concentrations of L-valine, Ru(III), and potassium permanganate and at a constant ionic strength of 0.50 mol dm^{-3} at 26°C. The rate constant increased with the increase in the concentration of alkali, indicating an apparent less than unit order dependence on [alkali] as given in Table 1.

Effect of initially added products

The externally added products such as manganate, ammonium hydroxide, and aldehyde did not show any significant effect on the rate of the reaction.

Effect of ionic strength and dielectric constant

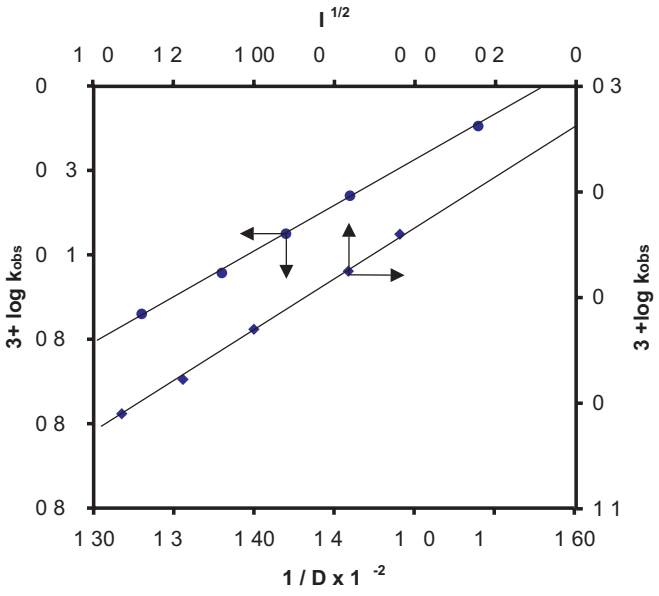
The effect of ionic strength was studied by varying the sodium perchlorate concentration from 0.3 to 2.0 mol dm^{-3} at constant concentrations of permanganate, L-valine, and

© 2001 NRC Canada

Table 1. Effects of [L-valine], [MnO_4^-], [Ru(III)], and [OH^-] on ruthenium(III) catalyzed oxidation of L-valine by $KMnO_4$ at 26°C; I = 0.50 mol dm^{-3} and error ±4%.

				$k_{obs} \times 10^3$ (s^{-1})	
$[MnO_4^-] \times 10^4$ (mol dm^{-3})	[L-valine] $\times 10^3$ (mol dm^{-3})	$[OH^-]$ (mol dm^{-3})	[Ru(III)] $\times 10^8$ (mol dm^{-3})	Expt.	Calcd.
0.5	2.0	0.3	7.5	3.60	3.67
1.0	2.0	0.3	7.5	3.70	3.67
2.0	2.0	0.3	7.5	3.75	3.67
3.0	2.0	0.3	7.5	3.70	3.67
5.0	2.0	0.3	7.5	3.60	3.67
2.0	0.5	0.3	7.5	2.45	2.38
2.0	1.0	0.3	7.5	3.03	3.11
2.0	2.0	0.3	7.5	3.75	3.67
2.0	3.0	0.3	7.5	4.07	3.91
2.0	5.0	0.3	7.5	4.16	4.12
2.0	2.0	0.05	7.5	1.05	1.03
2.0	2.0	0.1	7.5	1.76	1.81
2.0	2.0	0.2	7.5	2.80	2.92
2.0	2.0	0.3	7.5	3.75	3.47
2.0	2.0	0.5	7.5	4.68	4.61
2.0	2.0	0.3	1.0	0.51	0.49
2.0	2.0	0.3	2.5	1.31	1.22
2.0	2.0	0.3	5.0	2.60	2.45
2.0	2.0	0.3	7.5	3.75	3.67
2.0	2.0	0.3	10.0	5.06	4.90

Fig. 2. Plot of log k_{obs} vs. $I^{1/2}$ and log k_{obs} vs. 1/D.



alkali. It was found that the rate constant increased with increase in concentration of $NaClO_4$ and the plot of log k_{obs} vs. $I^{1/2}$ was linear (Fig. 2).

The effect of dielectric constant (D) was studied by varying the *tert*-butanol–water content in the reaction mixture with all other conditions being constant. Attempts to measure the relative permittivities were not successful. However, they were computed from the values of pure liquids (34). The solvent did not react with the oxidant under the experimental conditions. The rate constants (k_{obs}) increased with a decrease in the dielectric constant of the medium. The plot of log k_{obs} vs. 1/D was linear with positive slope as shown in Fig. 2.

Table 2. Thermodynamic activation parameters for the ruthenium(III) catalyzed oxidation of L-valine by aqueous alkaline permanganate with respect to slow step of Scheme 3.

Activation parameters	Values
Ea (kJ mol^{-1})	72 (±4)
$\Delta H^{\ddagger}$ (kJ mol^{-1})	69 (±4)
$\Delta S^{\ddagger}$ (J K^{-1} mol^{-1})	75 (±4)
$\Delta G^{\ddagger}$ (kJ mol^{-1})	46 (±3)

Test for free radicals

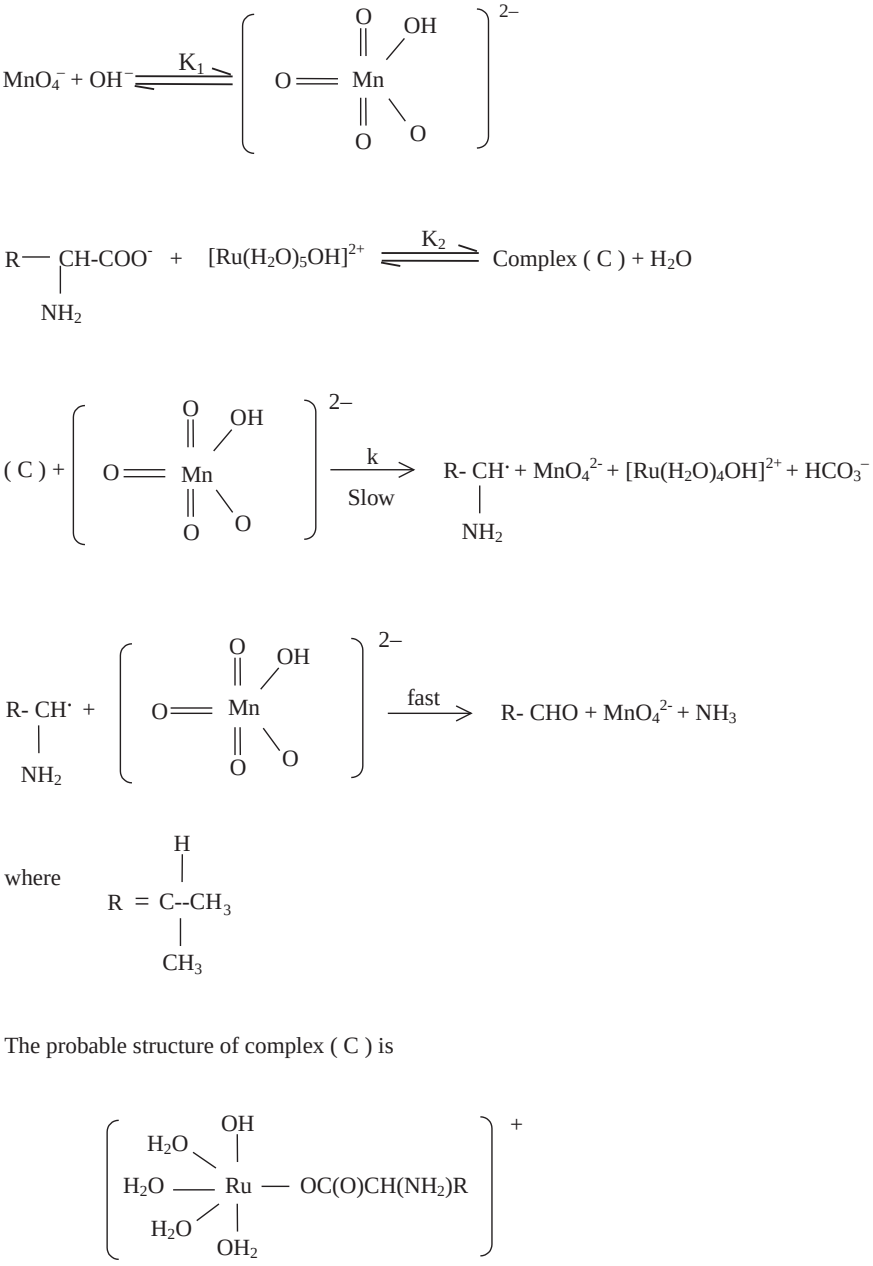
The reaction mixture was mixed with acrylonitrile monomer and kept for 2 h in an inert atmosphere. On diluting with methanol a white precipitate was formed, indicating the intervention of free radicals in the reaction.

Effect of temperature

The rate of the reaction was measured at four different temperatures with varying the concentration of OH^-, keeping other conditions constant. The rate was found to increase with increase in temperature. The rate constant (k) of the slow step of Scheme 3 were obtained from the intercept of the plots of [Ru(III)]/k_{obs} vs. 1/[OH^-] for different temperatures. The energy of activation corresponding to these constants were evaluated from the plot of log k vs. 1/T and other activation parameters for reaction were calculated and are given in Table 2.

© 2001 NRC Canada

Scheme 3.



Discussion

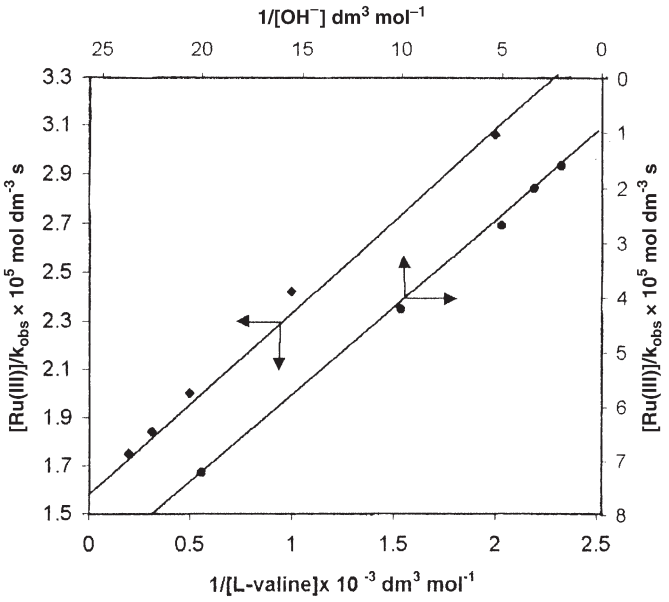
Permanganate ion (MnO_4^-) is a powerful oxidant in an aqueous alkaline medium, and because it exhibits many oxidation states, the stoichiometric results and pH of the reaction media play an important role. Under the prevailing experimental conditions at pH > 12, the reduction product of Mn(VII) is stable and further reduction of Mn(VI) might be stopped (10, 11). Diode Array Rapid Scan Spectrophotometric (DARSS) studies have shown that at pH > 12, the product of Mn(VII) is Mn(VI) and no further reduction was observed as reported by Simandi et al. (10). However, on prolonged standing, the green Mn(VI) is reduced to Mn(IV) under our experimental conditions.

The permanganate in alkaline medium exhibits various oxidation states, such as Mn(VII), Mn(V), and Mn(VI). The colour of the solution changed from violet to blue and further to green excluding the accumulation of hypomanganate. The violet colour originates from pink of permanganate and blue from hypomanganate is observed during the course of the reaction. The colour change of $KMnO_4$ solution from the violet Mn(VII) ion to the dark green Mn(VI) ion through the blue Mn(IV) ion has been observed.

It is interesting to identify the probable species of ruthenium(III) chloride in alkaline medium. Electronic spectral studies (21) have confirmed that ruthenium(III) chloride exists in hydrated form as $[Ru(H_2O)_6]^{3+}$. In the present study it is quite probable that the species $[Ru(H_2O)_5OH]^{2+}$ might assume the general form $[Ru(III)(OH)_x]^{3-x}$. The value of x would always be less than six because there are no definite reports of any hexahydroxy species of ruthenium. The remainder of the coordination sphere will be filled by water mol-

© 2001 NRC Canada

Fig. 3. Plot of [Ru(III)]/ k_{obs} vs. 1/[L-valine] and [Ru(III)]/k_{obs} vs. 1/[OH^-] (conditions as in Table 1).



ecules. Hence under the experimental conditions [OH^-] >> [Ru^{III}], Ru^{III} is mostly present as the hydroxylated species $[Ru(H_2O)_5OH]^{2+}$.

The reaction between permanganate and L-valine in alkaline medium has a stoichiometry of 1:2 with a first-order dependence on the concentration of MnO_4^- and Ru(III) and less than unit order dependence on both theconcentration of alkali and L-valine. No effect of added products such as aldehyde and ammonia was observed. It is known that L-valine exists as deprotonated form in basic medium (24). The results suggest that first alkali combines with permanganate to form an alkali–permanganate species $[MnO_4 \cdot OH]^{2-}$ in a pre-equilibrium step (35). L-valine in the deprotonated form reacts with ruthenium(III) species to form a complex (*C*). Complex *C* reacts with the alkali–permanganate species in a slow step to form a free radical derived from L-valine, which further reacts with another permanganate species in a fast step to yield the products. The experimental results can be accommodated as seen in Scheme 3.

Spectroscopic evidence for complex formation was not successful, since there is no change in the λ_{max} (except some hyperchromicity is observed) for the mixture of L-valine and ruthenium(III) compared with that of L-valine or ruthenium(III) itself. This might be due to the involvement of weak interactions. However, the evidence for complex formation is obtained by kinetic studies (i.e., from the Michaelis–Menten plot). The plot of [Ru(III)]/k_{obs} vs. 1/[L-valine] is linear with an intercept supporting the Ru(III)–L-valine complex. Such type of substrate–catalyst complex formation has been reported previously (36). The observed modest enthalpy of activation, relatively low value of the entropy of activation and higher rate constant for the slow step of the mechanism, indicates that oxidation presumably occurs by an inner-sphere mechanism. This conclusion is supported by earlier work (37). Since Scheme 3 is in accordance with generally well-accepted principle of non-complementary oxidations taking place in a sequence of one-electron steps, the reaction would involve a radical intermediate. Since permanganate is a one-electron oxidant in alkaline medium, the reaction between substrate and oxidant would give rise to a radical intermediate. A free radical scavenging experiment revealed such a possibility. This type of radical intervention in the oxidation of amino acids has also been observed earlier (20).

The thermodynamic quantities for the first equilibrium step in Scheme 3 and activation parameters for the limiting step in Scheme 3 can be evaluated as follows: the hydroxyl ion concentration as in Table 1 was varied at four different temperatures and the K_1 value was determined at each temperature. The values of K_1 (dm^3 mol^{-1}) were obtained as 3.2, 5.0, 6.8, and 8.1 at 26, 30, 35, and 40°C, respectively. A Vant Hoff's plot was made for the variation of K_1 with temperature (i.e., log K_1 vs. 1/*T*) and the values of the enthalpy of the reaction (ΔH), entropy of the reaction (ΔS), and free energy of reaction (ΔG), were calculated as 47.9 kJ mol^{-1}, –74.3 J K^{-1} mol^{-1}, and 70.6 kJ mol^{-1}, respectively. Similarly the L-valine concentration as in Table 1 was varied at four different temperatures and the K_2 value was determined at each temperature. The values of K_2 (dm^3 mol^{-1}) were obtained as 2.2×10^3, 3.5×10^3, 4.7×10^3, and 6.4×10^3 at 26, 30, 35, and 40°C, respectively. A plot was made for the variation of K_2 with temperature (i.e., log K_2 vs. 1/*T*) and the values of ΔH, ΔS, and ΔG, were calculated as 51.9 kJ mol^{-1}, –6.1 J K^{-1} mol^{-1}, and 53.8 kJ mol^{-1}, respectively. A comparison of the latter values with those obtained for the slow step of the reaction shows that these values mainly refer to the rate limiting step, supporting the fact that the reaction before the rate determining step are fairly rapid and involves only little activation energy.

Scheme 3 leads to the following rate law, and can be derived as follows:

$$[2] \qquad \frac{\text{Rate}}{[MnO_4^-]} = k_{obs} = \frac{kK_1K_2[\text{L-val}][\text{Ru(III)}][OH^-]}{1 + K_1[OH^-] + K_2[\text{L-val}] + K_1K_2[OH^-][\text{L-val}]}$$

The terms $(1 + K_1K_2[OH^-][Ru(III)][MnO_4^-])$, $(1 + K_1[MnO_4^-])$, and $(1 + K_2[Ru(III)])$ also should be in the denominator of eq. [2], but in view of low concentration of MnO_4^- and ruthenium(III) used, they approximate to unity. Thus the above eq. [2] can be rearranged to the following form, which is used for the verification of the rate law.

$$[3] \qquad \frac{[\text{Ru(III)}]}{k_{obs}} = \frac{1}{kK_1K_2[\text{L-val}][OH^-]} + \frac{1}{kK_2[\text{L-val}]} + \frac{1}{kK_1[OH^-]} + \frac{1}{k}$$

According to eq. [3], the plots of [Ru(III)]/k_{obs} vs. 1/[L-val] and [Ru(III)]/k_{obs} vs. 1/[OH^-] should be linear, which is verified in Fig. 3. The slopes and intercepts of such plots lead to the values of *k*, K_1, and K_2 at 26°C of 12.2 (±0.6) × 10^4 dm^3 mol^{-1} s^{-1}, 3.2 (±0.1) dm^3 mol^{-1}, and 2.2 (±0.1) × 10^3 dm^3 mol^{-1}, respectively. Using these values, the rate constants under different experimental conditions were calculated by eq. [2] and compared with experimental data. There is a good agreement between them, which supports the

© 2001 NRC Canada

Scheme 3. The value of K_1 is in good agreement with earlier work (38).

The effect of ionic strength on the rate can be understood essentially on the basis of ionic species as in Scheme 3. The effect of solvent on the reaction kinetics has been described detail in the literature (39). In the present study the rate determining step involves the reaction between two ions and so eq. [4] is applicable:

$$[4] \qquad \ln k = \ln k_\infty - Z_A Z_B e^2/k_B T r_{AB} D$$

where k_∞ is the rate constant in a medium of infinite dielectric constant, r_{AB} is the sum of the ionic radii, Z_A and Z_B are the charges on the two ions, and D is the dielectric constant of the medium. The observed linear plot of log k_{obs} vs. $1/D$ with positive slope (Fig. 2) is in accordance with eq. [4] as Z_A and Z_B have opposite charges (Scheme 3). The values of $\Delta H^\ddagger$ and $\Delta S^\ddagger$ were both favourable for electron transfer process. The value of $\Delta S^\ddagger$, within the range for radical reaction, has been ascribed to the nature of electron pairing and unpairing processes and to the loss of degree of freedom formerly available to the reactants upon the formation of a rigid transition state (40).

Conclusions

It is interesting that the oxidant species [MnO_4^-] requires a pH > 12, below which the system becomes disturbed and the reaction will proceed further to give a reduced product of the oxidant as Mn(IV), which slowly develops yellow turbidity. Hence, it becomes apparent that in carrying out this reaction the role of pH in a reaction medium is crucial. It is also noteworthy that under the conditions studied the reaction occurs in two successive one-electron reductions (Scheme 3) rather than two-electron in a single step (Scheme 2). A micro amount of Ru(III) is sufficient to catalyze the title reaction. It is interesting to note that uncatalyzed reaction follows a two path mechanism, while catalyzed reaction follows a single path. The description of the mechanism is consistent with all the experimental evidence including both kinetic and product studies.

References

1. R. Stewart. *In* Oxidation in organic chemistry. Part A. *Edited by* K.B. Wiberg. Academic Press, New York. 1965. Chap. 1.
2. F. Freeman. Rev. React. Species Chem. React. **1**, 179 (1976).
3. D.G. Lee. *In* Oxidation of organic compounds by permanganate ion and hexavalent chromium. Open Court Pub. Co., La Salle, IL. 1980.
4. D.G. Lee. *In* Oxidation in organic chemistry. Part D. *Edited by* W.S. Trahanovsky. Academic Press. New York. 1982. p. 147.
5. L.I. Simandi. *In* The Chemistry of functional groups. Suppl. C. *Edited by* S. Patai and Z. Rappoport. Wiley, Chichester. 1983. Chap. 13.
6. D.G. Lee, E.J. Lee, and K.C. Brown. Phase transfer catalysis, new chemistry, catalysts and applications. ACS symposium series No. 326. American Chemical Society, Washington DC. 1987. p. 82.
7. A.J. Fatiadi. Synthesis, 85 (1987).
8. J.F. Perez-Benito and D.G. Lee. J. Org. Chem. **52**, 3239 (1987).
9. K.A. Gardner, L.L. Kuehnert, and J.M. Mayer. Inorg. Chem. **36**, 2069 (1997), and ref. 1.
10. L.I. Simandi, M. Jaky, C.R. Savage, and Z.A. Schelly. J. Am. Chem. Soc. **107**, 4220 (1985).
11. P.L. Timmanagoudar, G.A. Hiremath, and S.T. Nandibewoor. Transition Met. Chem. **22**, 193 (1997); P.L. Timmanagoudar, G.A. Hiremath, and S.T. Nandibewoor. Polish J. Chem. **70**, 1459 (1996); S. Nadimpalli, R. Rallabandi, and L.S.A. Dikshitulu. Transition Met. Chem. **18**, 510 (1993).
12. R.G. Panari, R.B. Chougale, and S.T. Nandibewoor. Polish J. Chem. **72**, 99 (1998).
13. D.S. Mahadevappa, K.S. Rangappa, N.N.M. Gowda, and B. Thimmegouda. Int. J. Chem. Kinet. **60**, 589 (1986); K. Bal Reddy, B. Sethuram, and T. Navaneeth Rao. Indian J. Chem. **20A**, 395 (1981).
14. J. Szammer, M. Jaky, and O.V. Germasimov. Int. J. Chem. Kinet. **20A**, 395 (1981).
15. D.S. Mahadevappa, S. Ananda, A.S.A. Murthy, and K.S. Rangappa. Indian J. Chem. **23A**, 17 (1984); B.T. Gouda and R. Vijayalakshmi. Oxid. Commun. **11**, 45 (1988); B.T. Gouda and R. Vijayalakshmi. J. Indian Chem. Soc. **64**, 403 (1987).
16. P. Jayaprakash Rao, B. Sethuram, and T. Navneeth Rao. React. Kinet. Catal. Lett. **29**, 289 (1985).
17. M. Adinarayana, B. Sethuram, and T. Navneeth Rao. J. Indian Chem. Soc. **53**, 877 (1976).
18. R.M. Shanmugan and T.V. Subburamiyar. J. Chem. Soc. Perkin Trans. 2, 1341 (1988).
19. M.K. Mohanti and D. Laloo. J. Chem. Soc. Dalton. Trans. 311 (1996).
20. M.P. Hogle and P.K. Pawar. Acta Ciencia Indica. Chem. **12A**, 228 (1986); R.B. Chougale, G.A. Hiremath, and S.T. Nandibewoor. Polish J. Chem. **71**, 1471 (1997); R.G. Panari, R.B. Chougale, and S.T. Nandibewoor. Oxid. Commun. **21**, 503 (1998).
21. A.M. Balado, B.C. Galon, and F.J.P. Marton. Anal. Quim. **88**, 170 (1992); H.S. Singh, R.K. Singh, S.M. Singh, and A.K. Sisodia. J. Phys. Chem. **81**, 1044 (1977); G.A. Hiremath, P.L. Timmanagoudar, and S.T. Nandibewoor. React. Kinet. Catal. Lett. **63**, 403 (1998); S.T. Nandibewoor, G.A. Hiremath, and P.L. Timmanagoudar. Transition Met. Chem. **25**, 394 (2000).
22. Comprehensive inorganic chemistry. Vol. 3. *Edited by* J.C. Bailar, H.J. Emeleus, Sir Donald Nyholm, and A.F. Trotman-Dickenson. Pergamon Press, Oxford. 1975. p. 810.
23. A.G. Sykes. Advances in inorganic and radiochemistry. Vol. 10. *Edited by* H. Gemeleus and A.G. Sharpe. Academic Press, New York. 1967. p. 153.
24. A.L. Harihar, M.R. Kembhavi, and S.T. Nandibewoor. Monatsh. Chem. **131**, 739 (2000).
25. G.H. Jeffery, J. Bassett, J. Mendham, and R.C. Denney. A.I. Vogel's A text book of quantitative chemical analysis. 5th ed. ELBS. Longman, Essex, U.K. 1991. p. 371.
26. A. Carrington and M.C.R. Symons. J. Chem. Soc. 3373 (1956).
27. C.S. Reddy and T. Vijaykumar. Indian J. Chem. **34A**, 615 (1995).
28. M. Jaky, I.V. Kozhevnikov, and V. Hoft. Int. J. Chem. Kinet. **24**, 1055 (1992); R.G. Panari, A.L. Harihar, and S.T. Nandibewoor. J. Phy. Org. Chem. **12**, 340 (1999).
29. F. Feigl. Spot tests in organic analysis. Elsevier, New York. 1975. p. 195.
30. A.I. Vogel. A text book of practical organic chemistry including qualitative organic analysis. 3rd ed. Longman, London. 1973. p. 679.
31. A.K. Das and M. Das. J. Chem. Soc. Dalton Trans. 483 (1995).
32. Ref. 30, p. 332.
33. L.J. Bellamy. *In* The IR spectra of complex organic molecules. 2nd ed. Methuen and Co., London. 1958. p. 425.

© 2001 NRC Canada

34. G.H. Hugar and S.T. Nandibewoor. Transition Met. Chem. **19**, 215 (1994).
35. N.N. Halligudi, S.M. Desai, and S.T. Nandibewoor. Transition Met. Chem. **26**, 28 (1999); S. Vivekanandan, K.Venkatarao, M. Santappa, and S.P. Shanmuganathan. Indian J. Chem. **22A**, 244 (1983).
36. S.V. Rao and V. Jagannadhan. React. Kinet. Catal. Lett. **27**, 239 (1985); V.A. Morab and S.T. Nandibewoor. React. Kinet. Catal. Lett. **53**, 25 (1994).
37. N.N. Halligudi, S.M. Desai, and S.T. Nandibewoor. Int. J. Chem. Kinet. **31**, 789 (1999); F.M. Moore and K.W. Hicks. J. Inorg. Nucl. Chem. **14**, 413 (1975); K.W. Hicks. J. Inorg. Nucl. Chem. **38**, 1381 (1976).
38. R.G. Panari, R.B. Chougale and S.T. Nandibewoor. J. Phys. Org. Chem. **11**, 448 (1998).
39. K.J. Laidler. *In* Reaction kinetics. Pergamon Press, New York. 1963; S.G. Entelis and R.P. Tiger. *In* Reaction kinetics in the liquid. Wiley, New York. 1976; E.S. Amis. *In* Solvent effects on reaction rates and mechanisms. Academic Press, New York. 1966.
40. C. Walling. *In* Free radicals in solution. Academic Press, New York. 1957.

© 2001 NRC Canada

Stereoselective syntheses of α-amino acid and peptide derivatives by the U-4CR of 5-desoxy-5-thio-D-xylopyranosylamine

Günther Ross and Ivar Ugi

Abstract: Since 1961, the synthesis of α-amino acids derivatives by the four-component reaction of isocyanides (U-4CR) as a one-pot reaction has been developed. Only recently it was found that a variety of these α-amino acids compounds can be formed stereoselectively by the U-4CR using 1-amino-5-deoxy-5-thio-2,3,4-tri-*O*-isobutanoyl-β-D-xylopyranose as the amine component. The stereoselectivity inducing auxiliary 5-desoxy-5-thio-D-xylopyranosyl group of the so-formed products can be replaced selectively by hydrogen.

Key words: stereoselective U-4CR, chiral amine component, amino carbohydrate, α-amino acid derivatives.

Résumé : La synthèse de dérivés d'acides α-aminés par le biais de la réaction monotope d'isocyanures à quatre composants (U-4CR) a été développée depuis 1961. Ce n'est que récemment qu'il a été observé qu'une variété de ces dérivés d'acides α-aminés peuvent se former de façon stéréosélective par la réaction U-4CR en utilisant le 1-amino-5-désoxy-5-thio-2,3,4-tri-*O*-isobutanoyl-β-D-xylopyranose comme composant aminé. Le groupe auxiliaire 5-désoxy-D-xylopyranosyle qui induit la stéréosélectivité peut être remplacé sélectivement par de l'hydrogène à partir des produits qui se forment ainsi.

Mots clés : U-4CR stéréosélective, composant aminé chiral, hydrate de carbone aminé, dérivés d'acides α-aminés.

[Traduit par la Rédaction]

The four decades of developing the U-4CR

In 1959, the four-component one-pot reaction of the isocyanides (1–5) was introduced, and shortly later the term Ugi reaction (U-4CR) (4*a*, 5) was increasingly often used by colleagues. Due to the variability of the educts and products of the U-4CR, more chemical compounds have thus been prepared than by other reactions (5).

In 1961, it was also realized that derivatives of chiral α-amino acids and peptides **6** can be prepared by the stereoselective U-4CR of suitable chiral primary amines **1**, aldehydes **2**, carboxylic acids **3**, and isocyanides **4** (2, 3, 6). The products **6** must be cleavable into **7** and **8**, and it would be advantageous to resynthesize the initial chiral educt **1** from **8** by converting the group X, like an OH-group, into an amino group.

In 1966, Bodanszky and Ondetti (7) mentioned the potentially great preparative advantages of peptide syntheses by the one-pot U-4CR, compared to the usual multistep procedures, particularly if the α-amino acids and their derivatives are not readily available as natural compounds.

Received August 1, 2001. Published on the NRC Research Press Web site at http://canjchem.nrc.ca on December 14, 2001.

Dedicated to Professor Victor Snieckus.

G. Ross and I. Ugi.[1] Tech. University of Munich, Dep. of Organic Chemistry, Chair I, Lichtenbergstr. 4, D-85747 Garching, Germany.

[1]Corresponding author (telephone: +49-89-289-13229; fax +49-89-289-13249; e-mail: ivar.ugi@ch.tum.de).

It took almost four decades until the peptide derivatives **7** could be sufficiently well prepared by stereoselective U-4CRs and the subsequent selective cleavage of the chiral auxiliary group.

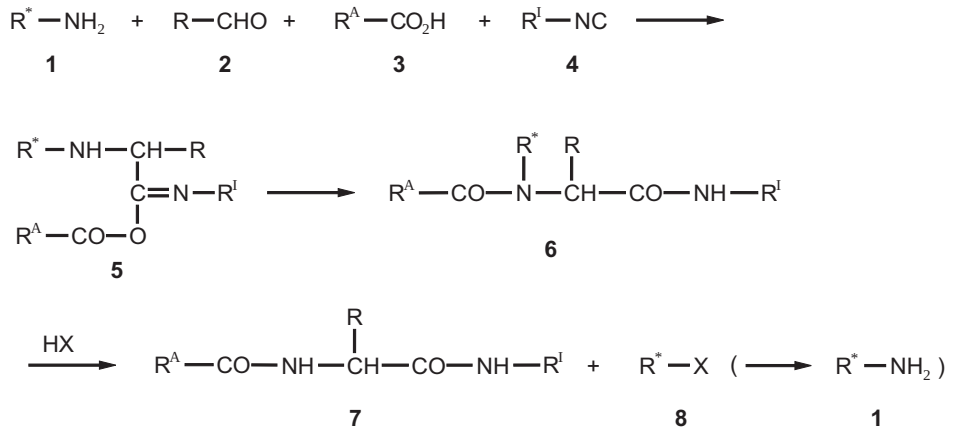
The first achiral peptide derivatives were prepared by U-4CR in 1961 (8), and shortly thereafter, stereoselective syntheses of diastereoisomeric products could be formed by the U-4CR of chiral primary amines (2, 9) with a stereoselectivity of up to 80:20. The reaction mechanism of an U-4CR in methanol at 0°C was investigated from 1964–1967 (3, 10). During that time, the equilibrium between isobutyraldehyde-(*S*)-α-phenylethylimine and benzoic acid with their cations and anions was determined. In a second series of experiments, the stereoselectivities of the U-4CR with *tert*-butylisocyanide was investigated. It was then found that four different reaction mechanisms compete. Depending on the reaction conditions, one or the other chiral product can be formed preferentially.

It was also realized early on that the preparation of peptides from chiral primary amines requires the removability of the corresponding *N*-alkyl group of the amine component. The prestudies of the cleavage of the corresponding group began in 1964 when alkyl- and alkenyl-groups were used as models (11).

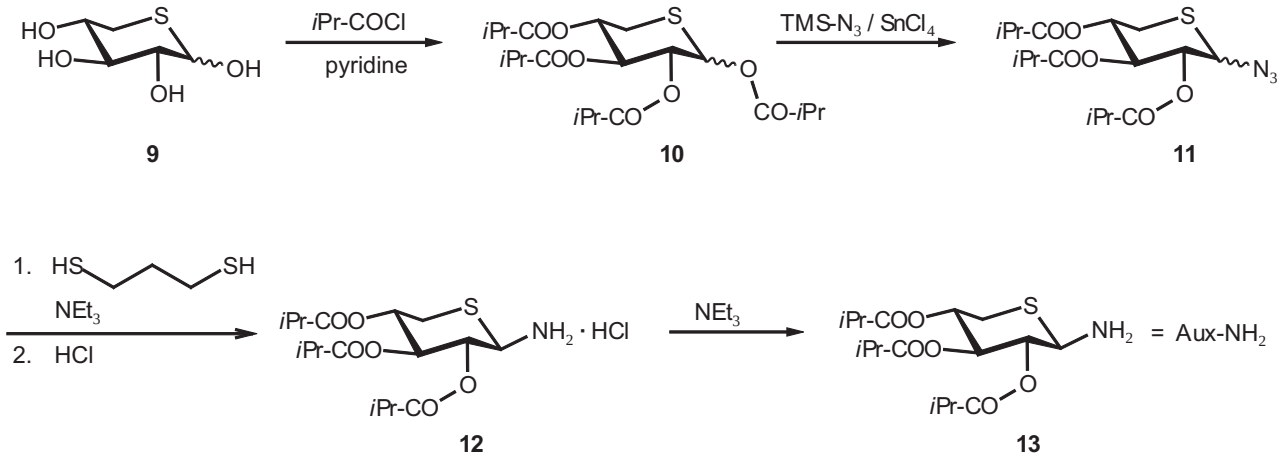
In 1969, the first peptide syntheses were accomplished by stereoselective U-4CRs with suitable chiral α-ferrocenylalkylamines (3, 6, 12). The necessary ferrocene derivatives were not readily available at that time, and therefore, the necessary chemistry was developed (6, 13, 14). The U-4CR products of suitable chiral ferrocene derivatives can be cleaved in a way that chiral ferrocenyl alkyl cations result,

 DOI: 10.1139/cjc-79-12-1934 © 2001 NRC Canada

Scheme 1.



Scheme 2.



which subsequently react with ammonia and allow, in that way, the regeneration of the initial chiral α-ferrocenyl-alkylamine (6). This chemistry was intensely investigated for more than two decades (6, 14), but it was ultimately realized that peptide syntheses by the U-4CR with α-ferrocenylalkylamine had too many preparative disadvantages, and therefore, this methodology was given up.

Likhosherstov et al. (15, 16) realized that 1-amino-carbohydrates can be directly prepared from carbohydrates and ammonia. The chiral 1-amino-carbohydrates of xylose, glucose and 2-acetylamino-glucose were thus prepared, however, the stereoisomeric desirable U-4CR products of these amines were hardly separable from the by-products.[2]

In 1988, Kunz et al. (17–20) introduced the highly stereoselective formation of α-amino acid derivatives by U-4CRs with *O*-pivaloyl amino-carbohydrates in the presence of zinc chloride etherates. Thus, products could be achieved in often excellent yields (85–95%) and with a stereoselectivity of up to 92:8. However, the disadvantage is that no peptide derivatives can be formed since only formic acid can be used as the acid component in these reactions. Furthermore, these U-4CR products could only be converted into α-amino acids or their amides by hydrolyzing them in hot one-to-one mixtures of concentrated hydrochloric acid and methanol. Kunz and co-workers (21) have recently also prepared α-amino acid derivatives by stereoselective solid-phase U-4CRs with *O*-acetylated galactosylamine.

In 1990, Goebel and Ugi (22) formed peptide derivatives by the U-4CR with tetra-*O*-alkyl-1-glucopyranosylamines. These reactions had the advantage that any carboxylic acid could participate in such U-4CRs. However, the auxiliary groups of those products could not be easily removed under sufficiently mild conditions either.

Lehnhoff et al. (23) used 1-amino-2-deoxy-2-*N*-acetyl-3,4,6-tri-*O*-acetyl-β-D-glucopyranose as the amine component of the U-4CR. A large collection of the corresponding peptide derivatives could be prepared stereoselectively in excellent yields (24), but also their auxiliary group could not easily be removed under sufficiently mild conditions.

Zychlinski (25) prepared by a synthesis of 11 steps the 1-amino-2-deoxy-2-acetamido-3,4,6-tri-*O*-acetyl-β-D-glucopyranose. This amine component forms peptide derivatives very well by the U-4CRs. However, the products are quite unstable since they are already in neutral media partly cleaved. Therefore, this amine component does not yet have all the desirable properties. It is conceivable that more stable U-4CR products can be formed from 1-amino-2-acylamino-carbohydrates with other *N*-acyl groups.

[2] J. Drabik, J. Achatz, and I. Ugi. In preparation.

© 2001 NRC Canada

1-Amino-5-deoxy-5-thio-2,3,4-tri-*O*-isobutyryl-β-D-xylopyranose as a particularly suitable chiral amine component of stereoselective U-4CRs

1-Amino-5-deoxy-5-thio-2,3,4-tri-*O*-isobutanoyl-β-D-xylopyranose hydrochloride **12** can be prepared from xylose via the 5-desoxy-5-thio-D-xylopyranose **9** (26–28).

5-Desoxy-5-thio-D-xylopyranose **9** is acylated by isobutanoic acid chloride in the presence of pyridine (29), and the product **10** is reacted with trimethylsilylazide and tin tetrachloride to yield **11** (30, 31). The azide **11** is reduced by 1,3-propanedithiol (32) to give the preferentially storable 1-amino-5-deoxy-5-thio-2,3,4-tri-*O*-isobutanoic-β-D-xylopyranose hydrochloride **12**. The hydrochloride **12** can easily be converted into the free amine **13** (33).

The U-4CR of the amine component **13** with isovaleraldehyde, benzoic acid, and *tert*-butylisocyanide in the presence of zinc(II) chloride forms stereoselectively the *R*-leucine derivative **16A**, whose absolute configuration was confirmed by an X-ray structure analysis of its deacylated product **17** (34).[3] Therefore, we assume the U-4CR runs via a mechanism involving a chelate complex **15** of the precondensed imine **14** with the zinc(II) chloride (Scheme 3). This could explain the high degree of stereoselectivity (92% de at −40°C) and the high yield (91.8%) of this U-4CR. The complexation causes a strong activation of the imine and enhances the rigidity of the system. Thus, for the α-addition of the isocyanide and the carboxylic acid the *si*-attack is strongly preferred.

After the U-4CR, the chiral template can be easily removed in a two-step process. First, the thiosugar rest is deacylated by aminolysis with methylamine, then the thioxylopyranosyl group of **17** is cleaved by treatment with dilute trifluoroacetic acid and mercury(II) acetate for 3 h at room temperature.

The variability of 1-amino-5-deoxy-5-thio-2,3,4-tri-*O*-isobutanoyl-β-D-xylopyranose **13** as a chiral amino component in the U-4CR is illustrated by its use in the synthesis of a phenylglycine derivative **16B** (57% de at 20°C, yield 91.2%) and a dipeptide **16C** (61% de at 20°C, yield 69.6%). Of course, in these cases higher diastereomeric excesses would have been reached at lower reaction temperatures. According to the proofed configuration of **16A**/**17**, we assume that the *R*-configuration of the newly synthesized amino acid unit is preferred.

The relatively bulky *O*-isobutanoyl groups of **13** allow the U-4CRs to proceed in a stereoselective way. Even at room temperature, de values of about 60% are obtained; if the reaction temperature is reduced to −40°C, U-4CR products in a purity of more than 90% de are formed. On the other hand, the *O*-isobutanoyl groups of **13** cause less hindrance than the *O*-pivaloyl group and allow reaction rates of more than 90% within days (17–20).[2]

A particular advantage of the amine component **13** from xylose is, that, besides the D-isomer, the other diastereomeric amine can be prepared, using the well available L-xylose.

Experimental

1,2,3,4-Tetra-*O*-isobutanoyl-5-desoxy-5-thio-D-xylopyranose (10)

At 0°C, 6.30 g (38 mmol) of 5-desoxy-5-thio-D-xylopyranose in 20 mL pyridine **9** was reacted with 20.24 g (190 mmol) of isobutanoic acid chloride until the precipitate dissolved. This mixture was allowed to further react at 20°C for 1 h. Then 100 mL of 1 N hydrochloric acid and 100 mL methylene chloride were added. The organic solution of the product was washed by an aqueous sodium bicarbonate solution, dried with magnesium sulphate, and evaporated. 16.12 g (95%) of **10** was obtained as an anomeric mixture. ^{1}H NMR ($CDCl_3$): α-anomer: 6.11 (d, 1H, ^3J = 2.75), 5.52 (dd, 1H, ^3J = 10.08), 5.24 (dd, 1H), 5.14 (m, 1H), 2.99 (dd, 1H, ^3J = 10.97, ^2J = 12.2), 2.78 (dd, 1H, $^3J_{4,5eq}$= 3.65), 2.6 (m, 4H), 1.15 (m, 24H). β-anomer (only characteristic signals): 5.9 (d, 1H, ^3J = 9.15), 5.39 (dd, 1H, ^3J = 9.15). ^{13}C NMR ($CDCl_3$): α-anomer: 175.14, 174.96, 174.8, 172.76, 73.7, 72.44, 70.84, 69.83, 34.02, 33.87, 33.86, 33.84, 26.50, 19.33, 19.15, 19.13, 19.10, 19.06, 19.04, 18.99, 18.94. β-anomer (only characteristic signals): 72.94, 72.02, 71.85, 71.63, 27.93.

2,3,4-Tri-*O*-isobutanoic-5-desoxy-5-thio-D-xylopyranosyl-azide (11)

In 50 mL methylene chloride, 4.30 g (9.60 mmol) of 1,2,3,4-tetra-*O*-isobutanoic-5-desoxy-5-thio-D-xylopyranose **10** and 1.30 g (11.04 mmol, 1.11 equiv) trimethylsilylazide were dissolved. At 0°C, 2.10 g (8.16 mmol, 0.85 equiv) tin tetrachloride was added, and this mixture was kept for 2 h at 20°C. After adding 50 mL of ice water, the organic layer was separated and filtred through Celite®, washed twice with sodium bicarbonate solution, dried with magnesium sulphate, and the solvent evaporated. The product was obtained in a yield of 90% as the anomeric mixture of α/β = 0.43:1. ^{1}H NMR ($CDCl_3$): β-anomer: 5.39 (t, 1H, ^3J = 9.78), 5.05 (m, 2H), 4.46 (d, 1H, ^3J = 9.15), 2.97 (dd, 1H, ^2J = 13.1), 2.7 (dd, 1H, ^3J = 3.67), 2.45 (m, 3H), 1.1 (m, 18H). α-anomer (only characteristic signals): 4.46 (d, 1H, ^3J = 2.63). ^{13}C NMR ($CDCl_3$): β-anomer: 175.49, 175.28, 175.13, 73.64, 73.33, 72.08, 63.24, 33,75, 33.73, 28.46, 18.74, 18.71, 18.64, 18.60, 18.56. α-anomer (only characteristic signals): 62.57, 25.73.

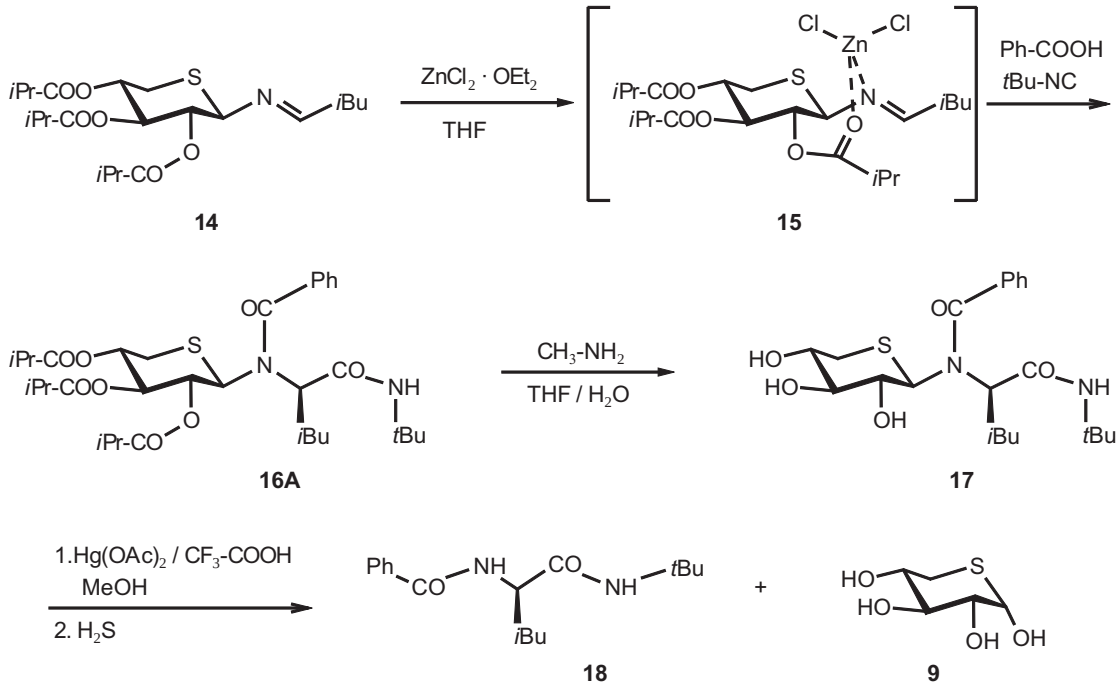
2,3,4-Tri-*O*-isobutanoic-5-desoxy-5-thio-D-xylopyranosyl-amine hydrochloride (12)

2,3,4-Tri-*O*-isobutanoic-5-desoxy-5-thio-D-xylopyranosyl-azide (**11**) (5.82 g, 14.5 mmol) was dissolved in 50 mL of methylene chloride. Subsequently, 50 mL methanol, 3.30 g (29 mmol, 2.0 equiv) 1,3-propanedithiol, and 3.0 g (29 mmol, 2.0 equiv) triethylamine were added. This mixture was stirred at 20°C for 2 to 3 h until no further nitrogen was formed. All volatile compounds were evaporated in vacuo and the residue was dissolved in 50 mL diethyl ether. Insoluble compounds were removed by filtration. Concentrated hydrochloric acid (2 mL) was stirred with this solution and the β-anomer **12** crystallized. The remaining volatile res-

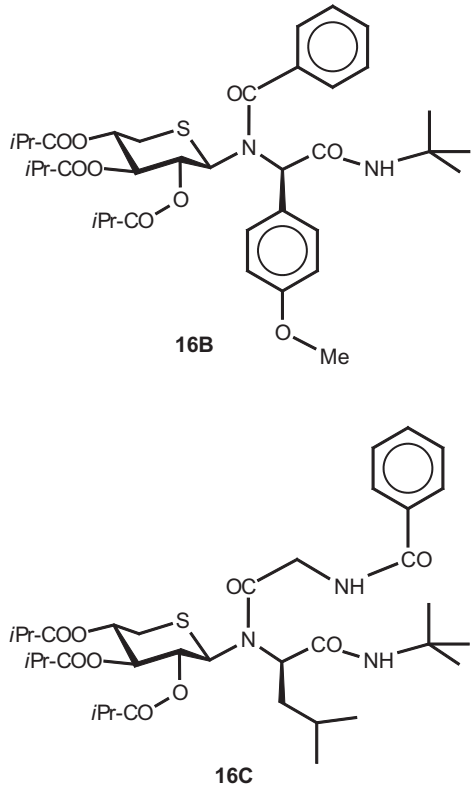
[3] G. Ross, I. Ugi, and E. Herdtweck. Tetrahedron, submitted.

© 2001 NRC Canada

Scheme 3.



Scheme 4.



idues were removed in vacuo. Thus, **12** was obtained as an anomeric mixture in a yield of 35%. ^{1}H NMR (DMSO-d_6, D_2O): 5.26 (t, 1H, ^3J = 9.15), 5.17 (dd, 1H, ^3J = 9.46), 4.96 (ddd, 1H, ^3J = 10.68, ^3J = 4.76), 4.75 (d, 1H, ^3J = 9.46), 3.09 (dd, 1H, ^2J = 13.43), 2.95 (dd, 1H), 2.7–2.4 (m, 3H), 1.05 (m, 18H). ^{13}C NMR (DMSO-d_6, D_2O): 175.36, 175.28, 174.98, 72.41, 71.95, 71.46, 50.54, 33.17, 33.02, 27.24, 18.67, 18.51, 18.34, 18.31, 18.12, 17.73.

2,3,4-Tri-*O*-isobutanoyl-5-desoxy-5-thio-D-xylopyranosylamine (13)

The amine hydrochloride **12** can be converted into the corresponding free amine **13** by treatment with triethylamine in ether. ^{1}H NMR ($CDCl_3$): 5.15–5.03 (m, 3H), 4.04 (d, 1H, ^3J = 9.25), 2.77 (dd, 1H, ^3J = 4.86, ^2J = 13.72), 2.68 (dd, 1H, ^3J = 10.19), 2.58–2.43 (m, 3H), 1.17–1.09 (m, 18H). ^{13}C NMR ($CDCl_3$): 176.54, 175.84, 175.57, 75.53, 72.67, 72.63, 57.76, 34.02, 33.95, 33.93, 29.29, 19.01, 18.87, 18.83, 18.8.

2,3,4-Tri-*O*-isobutanoyl-5-desoxy-5-thio-D-xylopyranosylimines (14)

General procedure

In 20 mL diethyl ether, 0.752 g (2 mmol) of **12**, 2.4 mmol (1.25 equiv) of an aldehyde, and 2.4 mmol (1.25 equiv) triethylamine were combined. Magnesium sulphate (2.0 g) was added. After 12 h, the solid materials were removed and the solvent was evaporated.

The formation of U-4CR products 16 from 14, carboxylic acids, and isocyanides

General procedure

In 10 mL THF at 20 to –40°C, 2.00 mmol of 2,3,4-tri-*O*-isobutanoic-5-desoxy-5-thio-D-xylopyranosylimine (**14**) and 2.2 mmol (1.1 equiv) of $ZnCl_2 \cdot OEt_2$ were mixed and 15 min later, 2.2 mmol (1.1 equiv) of the isocyanide and 2.2 mmol (1.1 equiv) of the carboxylic acid were added. When the reaction was finished, according to the DC-control (ethylacetate–hexane, 1:2), the solvent was evaporated. The

© 2001 NRC Canada

residue was dissolved in 50 mL of diethyl ether, washed with 0.5 N hydrochloric acid and with aqueous sodium bicarbonate. This solution was dried over magnesium sulphate and then evaporated in vacuo. Solid products in 70–95% yields were isolated.

_N_-Benzoyl-_N_-(2,3,4-tri-_O_-isobutanoyl-5-desoxy-5-thio-β-D-xylopyranosyl)-leucin-_tert_-butylamide (16A)

Imine **14** was formed from **12**, triethylamine, and 0.207 g (2.4 mmol) isovaleraldehyde.

To the precondensed imine **14** in THF were added (at −40°C): $ZnCl_2 \cdot OEt_2$, 0.182 g (2.2 mmol) *tert*-butylisocyanide, and 0.269 g (2.2mmol) benzoic acid. After stirring for 72 h at −40°C, 1.19 g (91.8%) of product **16A** with 92% de (according to HPLC–MS) was obtained. ^{1}H NMR ($CDCl_3$): 7.95 (s, 1H), 7.60–7.45 (m, 5H), 5.31 (d, 1H, ^3J = 10.2), 5.18 (t, 1H, ^3J = 9.29), 5.08 (t, 1H), 4.97 (dt, 1H, ^3J = 4.18, ^3J= 10.31), 4.01 (dd, 1H, ^3J = 4.86, ^3J = 9.72), 2.83 (dd, 1H, ^2J= 13.28), 2.53–2.32 (m, 6H), 1.72 (m, 1H), 1.34 (s, 9H), 1.19–0.99 (m, 24H). ^{13}C NMR ($CDCl_3$): 175.71, 175.61, 175.60, 173.93, 169.49, 135.28, 131.12, 128.73, 126.65, 74.01, 72.94, 72.02, 64.00, 63.10, 50.87, 40.51, 33.96, 33.90, 33.79, 28.68, 28.31, 25.67, 23.55, 22.22, 18.93–18.53.

_N_-Benzoyl-_N_-(2,3,4-tri-_O_-isobutanoyl-5-desoxy-5-thio-β-D-xylopyranosyl)-_p_-methoxy-phenylglycin-_tert_-butylamide (16B)

Imine **14** was formed from **12**, triethylamine, and 0.300 g (2.4 mmol) *p*-methoxybenzaldehyde.

To the precondensed imine **14** in THF were added (at 20°C): $ZnCl_2 \cdot OEt_2$, 0.182 g (2.2 mmol) *tert*-butylisocyanide, and 0.269 g (2.2mmol) benzoic acid. After stirring for 48 h at 20°C, 1.27 g (91.2%) of product **16B** with 57% de (according to HPLC–S) was obtained. ^{1}H NMR ($CDCl_3$): 7.64–7.43 (m, 7H), 6.91 (m, 2H), 5.18–4.70 (m, 5H), 3.89 (s, 1H), 2.91–2.07 (m, 3H), 1.22 (s, 9H), 1.08–0.82 (m, 6H). ^{13}C NMR ($CDCl_3$): 175.75, 175.55, 175.40, 172.97, 167.85, 159.75, 135.57, 131.99, 130.95, 128.73, 128.59, 126.83, 114.30, 74.06, 72.62, 71.76, 70.27, 63.90, 63.00, 55.28, 51.17, 34.15, 33.86, 33.46, 29.57, 28.49, 19.08–18.12.

Bz-_N_-Gly-_N_-(2,3,4-tri-_O_-isobutanoyl-5-desoxy-5-thio-β-D-xylopyranosyl)-leucine-_tert_-butyl-amide (16C)

Imine **14** was formed from **12**, triethylamine, and 0.207 g (2.4 mmol) isovaleraldehyde.

To the precondensed imine **14** in THF were added (at 20°C): $ZnCl_2 \cdot OEt_2$, 0.182 g (2.2 mmol) *tert*-butylisocyanide, and 0.394 g (2.2 mmol) *N*-benzoylglycine. After stirring for 48 h at 20°C, 0.98 g (69.6%) of product **16C** with 61% de (according to HPLC–MS) was isolated. ^{1}H NMR ($CDCl_3$): 7.98 (d, 2H, ^3J = 8.34), 7.86 (bs, 2H), 7.57 (t, 1H, ^3J = 7.06), 7.49 (t, 2H), 5.5–5.0 (m, 6H), 3.89 (dd, 1H, ^3J = 9.72, ^3J = 3.53), 3.03 (t, 1H, $^3J_{4,5\ ax} = {}^2J_{5ax,5eq}$ = 12.38), 2.9–2.4 (m, 6H), 1.83 (m, 1H), 1.36 (s, 9H), 1.16–1.09 (m, 18H), 0.96–0.89 (m, 6H). ^{13}C NMR ($CDCl_3$): 176.01, 176.92, 175.73, 173.63, 168.01, 163.40, 132.80, 128.83, 128.58, 127.81, 74.30, 73.14, 72.89, 61.64, 59.17, 51.45, 43.30, 42.88, 33.97, 33.88, 33.84, 28.63, 24.16, 23.75, 22.01, 21.80, 18.89–18.56.

The _O_-deacylation of 16A to yield 17

In 100 mL THF, 3.00 g (4.60 mmol) *N*-benzoyl-*N*-(2,3,4-tri-*O*-isobutanoyl-5-desoxy-5-thio-β-xylopyranosyl)-leucine-*tert*-butylamide **16A** and 60 mL of 40% aqueous methylamine were reacted at 20°C for 24 h. The volatile compounds was removed in vacuo, and the *N*-methylisobutyramide was removed by its solubility in diethyl ether. Thus, 1.94 g (96%) *N*-benzoyl-*N*-(5-deoxy-5-thio-β-xylopyranosyl)-leucine-*tert*-butylamide (**17**) was obtained. The X-ray structure of product **17** was recently confirmed (31). ^{1}H NMR ($CDCl_3$): 7.79 (d, 2H, ^3J = 7.3), 7.51 (t, 1H, ^3J = 7.2), 7.43 (t, 2H), 6.77 (bd, 1H, ^3J= 8.2), 6.00 (bs, 1H), 4.54 (dt, 1H, ^3J = 8.2, ^3J = 5.8), 1.76–1.60 (m, 3H), 1.35 (s, 9H), 0.97 (2 × d, 6H). ^{13}C NMR ($CDCl_3$): 171.75, 167.06, 133.86, 131.21, 128.15, 127.12, 52.67, 51.02, 41.22, 28.48, 24.76, 22.84, 22.10.

Cleavage of chiral auxiliaries of 17 to form 9 and 18

At 20°C, 0.50 g (1.14 mmol) of the U-4CR product **17** and 0.36 g (1.14 mmol) of mercury(II) acetate in 20 mL methanol and 10 mL of trifluoroacetic acid were reacted for 3 h. Subsequently, 150 mL of saturated aqueous sodium bicarbonate and 50 mL of diethyl ether were added, and then solid sodium bicarbonate was added until a neutral solution resulted. The divalent mercury was precipitated by hydrogen sulfide. The product solution filtered through Celite®, and the solvent was evaporated in vacuo. NMR (MeOH-d_4) and HPLC–MS spectroscopic data indicated that there was a mixture of equal amounts of **9** and **18**. This mixture was extracted with chloroform. The solvent was evaporated in vacuo, and 200 mg (60%) of the solid product **18** resulted. ^{1}H NMR ($CDCl_3$): 7.79 (d, 2H, ^3J = 7.3), 7.51 (t, 1H, ^3J = 7.2), 7.43 (t, 2H), 6.77 (bd, 1H, ^3J= 8.2), 6.00 (bs, 1H), 4.54 (dt, 1H, ^3J = 8.2, ^3J = 5.8), 1.76–1.60 (m, 3H), 1.35 (s, 9H), 0.97 (2 × d, 6H). ^{13}C NMR ($CDCl_3$): 171.75, 167.06, 133.86, 131.21, 128.15, 127.12, 52.67, 51.02, 41.22, 28.48, 24.76, 22.84, 22.10.

Acknowledgement

The authors thank Mrs. Gertrut Weidner, Dr. Birgit Werner, and Dr. Thomas Lindhorst for their help in producing this manuscript.

References

1. I. Ugi, R. Meyr, U. Fetzer, and C. Steinbrückner. Angew. Chem. **71**, 386 (1959).
2. I. Ugi. Angew. Chem. **74**, 9 (1962); Angew. Chem. Int. Ed. Engl. **1**, 8 (1962).
3. I. Ugi. Isonitrile chemistry. Academic Press, New York. 1971.
4. (*a*) I. Ugi, S. Lohberger, and R. Karl. Comprehensive organic synthesis: Selectivity for synthetic efficiency. Vol. 2. *Edited by* B.M. Trost and C.H. Heathcock. Pergamon, Oxford. 1991. chap. 4.6. p. 1083; (*b*) I. Ugi, S. Lohberger, and R. Karl. Comprehensive organic synthesis: Selectivity for synthetic efficiency. Vol. 2. *Edited by* B.M. Trost and C.H. Heathcock. Pergamon, Oxford. 1991. chap. 4.6. p. 1090.
5. A. Dömling and I. Ugi. Angew. Chem. **112**, 3300 (2000); Angew. Chem. Int. Ed. Engl. **39**, 3168 (2000).

© 2001 NRC Canada

6. I. Ugi, D. Marquarding, and R. Urban. Chemistry and biochemistry of amino acids, peptides, and proteins. Vol. 6. *Edited by* B. Weinstein. Marcel Dekker, New York. 1982. p. 245.
7. M. Bodanszky and M.A. Ondetti. Peptide synthesis. *Edited by* G.A. Olah. J. Wiley and Sons, New York. 1966. p. 129.
8. I. Ugi and C. Steinbrückner. Chem. Ber. **94**, 2802 (1961).
9. I. Ugi and K. Offermann. Angew. Chem. **75**, 917 (1963); Angew. Chem. Int. Ed. Engl. **2**, 624 (1963).
10. I. Ugi and G. Kaufhold. Liebigs Ann. Chem. **709**, 11 (1967).
11. I. Ugi and K. Offermann. Chem. Ber. **97**, 2996 (1964).
12. I. Ugi. Rec. Chem. Prog. **30**, 289 (1969).
13. G. Wagner and R. Herrmann. Ferrocenes. *Edited by* A. Togni and T. Hayashi. VCH, Weinheim, Germany. 1995.
14. A. Demharter and I. Ugi. J. Prakt. Chem. (Weinheim, Ger.), **335**, 244 (1993).
15. L.K. Likhosherstov, O.S. Novikova, V.A. Derivitkava, and N.K. Kochetkov. Carbohydr. Res. C1 (1986).
16. L.K. Likhosherstov, O.S. Novikova, V.N. Shbaev, and N.K. Kochetkov. Russ. Chem. Bull. **45**, 1760 (1996).
17. (*a*) H. Kunz and W. Pfrengle. J. Am. Chem. Soc. **110**, 651 (1988); (*b*) H. Kunz and W. Pfrengle. Tetrahedron, **44**, 5487 (1988).
18. H. Kunz, W. Pfrengle, and W. Sager. Tetrahedron Lett. **30**, 4109 (1989).
19. H. Kunz, W. Pfrengle, K. Rück, and W. Sager. Synthesis, 1039 (1991).
20. H. Kunz and K. Rück. Angew. Chem. **105**, 355 (1993); Angew. Chem. Int. Ed. Engl. **32**, 336 (1993).
21. K. Oertel, G. Zech, and H. Kunz. Angew. Chem. **112**, 1489 (2000); Angew. Chem. Int. Ed. Engl. **39**, 1431 (2000).
22. M. Goebel and I. Ugi. Tetrahedron Lett. **36**, 6043 (1995).
23. S. Lehnhoff, M. Goebel, R.M. Karl, R. Klösel, and I. Ugi. Angew. Chem. **107,** 1208 (1995); Angew. Chem. Int. Ed. Engl. **34,** 1104 (1995).
24. S. Lehnhoff. Ph.D Thesis, Technical University of Munich, Munich, Germany, 1994.
25. A.v. Zychlinski. Multicomponent reactions & combinatorial chemistry. *Edited by* Z. Hippe and I. Ugi. p. 31. German-Polish Workshop, Rzeszów, 28–30. Sept. 1, 1998, University of Technology, Rzeszów / Technical University, Munich.
26. D.L. Ingles and R.L. Whistler. J. Org. Chem. **27**, 3896 (1962).
27. H. Paulsen and K. Todt. Adv. Carbohydr. Chem. **23**, 115 (1968).
28. D. Horton and J.D. Wander. The carbohydrates. Vol. IB. *Edited by* W. Pigman, D. Horton, and J.D. Wander. Academic Press, New York. 1980. p. 799.
29. R. Behrend and R. Roth. Liebigs Ann. Chem. **331**, 359 (1904).
30. L. Birkofer and A. Ritter. Angew. Chem. **77**, 414 (1965); Angew. Chem. Int. Ed. Engl. **4**, 417 (1965).
31. H. Paulsen, Z. Gyorgydeak, and M. Friedmann. Chem. Ber. **107**, 1568 (1974); Chem. Ber. **107**, 1590 (1974).
32. H. Bayley, D.N. Standring, and J.R. Knowles. Tetrahedron Lett. 3633 (1978).
33. I. Ugi, G. Ross, and C. Burdack. Publication at the 1st International Symposium on Macro- and Supermolecular Architectures and Materials (MAM-01): Biological and Synthetic Systems, on April 11–14, 2001 at Kwangju, South Korea.
34. G. Ross. Ph.D Thesis, Technical University of Munich, Munich, Germany, 2001.

© 2001 NRC Canada

Quasiclassical trajectory studies on the gas-phase BrO self-reaction

Demetrios K. Papayannis and Agnie M. Kosmas

Abstract: The effect of initial vibrational energy and the mode of disposal of available energy into products for the disproportionation reaction between BrO radicals are studied using the quasiclassical trajectory (QCT) technique. The calculations are performed on an analytical potential enegy surface based on ab initio results reported for the three isomeric forms of $(BrO)_2$ system. The results indicate a mild dependence on reactant vibrational energy, which is discussed in terms of the mechanistic aspects of the reaction. The study of the distribution of total accessible energy among products indicates a different mode of energy disposal in each path and hence important differences on the mechanism by which each channel takes place.

Key words: quasiclassical trajectories, internal energy, disposal of total energy.

Résumé : La méthode des trajectoires quasi-classiques est employée a l'étude de l'éfet de l'énergie vibrationale à la réactivité de la réaction entre des radicals de BrO et la distribution de l'énergie totale entre des produits. Les calculations sont executées sur une surface potentielle analytique, fondée aux résultats quantomechaniques pour les isomers du système de $(BrO)_2$. Les résultas indiquent une dépendence faible de l'énergie vibrationale à la réactivité de la réaction. Enfin la distribution de l'énergie totale entre des produits manifeste des différences importantes au méchanisme pour chaque canal de la réaction.

Mots clés : trajectoires quasi-classiques, énergie intérieure, la distribution de l'énergie totale.

Introduction

The disproportionation reactions between halogen monoxide radicals have received considerable attention over the last years, due to their important role in the stratospheric ozone depletion cycles (1–8). Numerous experimental studies have been devoted to this subject (9–24), and in addition, several quantum mechanical electronic structure calculations (25–32) have investigated the geometry and the stability of the various intermediate complexes and their role in the mechanism of these reactions.

The reaction between BrO radicals is an interesting such system that has been found to proceed through two main channels:

$$(a)\ BrO(^2\Pi) + BrO(^2\Pi) \rightarrow BrOO + Br \rightarrow 2Br + O_2(^3\Sigma_g^-) \qquad \Delta H^\circ_{298} = -6.6 \text{ kcal mol}^{-1}$$

$$(b)\quad BrO(^2\Pi) + BrO(^2\Pi) \rightarrow Br_2(^1\Sigma_g^+) + O_2(^3\Sigma_g^-) \qquad \Delta H^\circ_{298} = -52.6 \text{ kcal mol}^{-1}$$

Received June 4, 2001. Published on the NRC Research Press Web site at http://canjchem.nrc.ca on December 15, 2001.

D.K. Papayannis and A.M. Kosmas.[1] Physical Chemistry Laboratory, Department of Chemistry, University of Ioannina, Ioannina, Greece 45110.

[1]Corresponding author (e-mail: amylona@cc.uoi.gr).

Channel (*a*) is the major pathway at 298 K and produces atomic bromine and BrOO, which instantly decomposes into Br and O_2 as a result of the very low Br—O bond energy of about 1 kcal mol^{-1} (17). The molecular elimination channel (*b*), although the most exothermic, is the secondary channel. However, it gains in significance at lower temperatures as the branching ratio for channel (*a*) drops from 0.84 at 298 K to 0.68 at 220 K (20), where this decrease benefits the second pathway. Several measurements of the total rate coefficient (*k*) have been reported in the literature(14–24) and the most recent values range from (2.98 ± 0.42) to (2.59 ± 0.28) × 10^{-12} cm^3 $molecule^{-1}$ s^{-1} (22–24).

In a recent theoretical study (31), we examined the effect of initial translational energy (E_T) on the rate coefficient to investigate the increasing importance of the second channel as the temperature lowers. Employing a simple, six-dimensional analytical potential energy surface we carried out quasiclassical trajectory calculations for a series of values of the initial kinetic energy (E_T) between 0.5 and 5.0 kcal mol^{-1}. These calculations produced reactive cross sections, rate coefficients, and branching ratios in fair consistency with the experimental values, indicating a reasonable description of the reaction by the constructed surface.

The reactant vibration is another significant factor that has been shown to affect the dynamics of several gas-phase elementary reactions (33). Also, the mode of disposal of available energy in large exothermicity pathways is of interest. In the present work we extend the previous studies and employ the constructed surface to examine the effect of initial vibrational excitation on the reactivity of BrO self-reaction. Reactive cross sections are calculated for a series of vibrational quantum numbers and the results are discussed. The mode of

 DOI: 10.1139/cjc-79-12-1940 © 2001 NRC Canada

disposal of total available energy into products is also investigated and the results are analyzed in terms of the mechanism of the reaction.

PES and trajectory calculations

A short outline of the potential energy surface (PES) will be presented here since the detailed description has been given elsewhere (31). The lowest singlet PES was constructed based on the LEPS-type functional form including a three-body polynomial Sorbie–Murrell-type term to describe the BrOO triatomic in channel (*a*). Despite their simplicity, LEPS surfaces have been widely used for the kinetic and dynamic investigation of many triatomic systems with good success and have served with suitable modifications as the starting point for the description of more complex polyatomic systems. In a recent study, Espinosa-Garcia (34) reviewed the applicability of LEPS-type functional forms for collinear reactions and examined their possibilities to adequately describe the kinetics and dynamics of systems with non-collinear reaction paths.

The six-dimensional analytical PES employed to describe the BrO + BrO reaction has been given the following form:

$$[1]\qquad V(r_{ij}) = V_{\mathrm{LEPS}}(r_{ij}) + V_{\mathrm{M}}(r_{\mathrm{OO'}}, r_{\mathrm{OBr}}, r_{\mathrm{O'Br}}) + V_{\mathrm{M}}(r_{\mathrm{OO'}}, r_{\mathrm{OBr'}}, r_{\mathrm{O'Br'}})$$

where $V_{\mathrm{LEPS}}(r_{ij})$ represents an extended four-atom LEPS-type function (35, 36)

$$[2]\qquad V_{\mathrm{LEPS}}(r_{ij}) = W_{\mathrm{BrO}} + W_{\mathrm{OO'}} + W_{\mathrm{OBr'}} + W_{\mathrm{BrO}} + W_{\mathrm{BrBr'}} + W_{\mathrm{O'Br'}} - (1/4)[(J_{\mathrm{BrO}} - J_{\mathrm{OO'}})^2 + (J_{\mathrm{OO'}} - J_{\mathrm{O'Br'}})^2 + (J_{\mathrm{O'Br'}} - J_{\mathrm{Br'Br}})^2 + (J_{\mathrm{Br'Br}} - J_{\mathrm{Br'O}})^2 + (J_{\mathrm{Br'O}} - J_{\mathrm{O'Br}})^2 + (J_{\mathrm{O'Br}} - J_{\mathrm{BrO}})^2]^{1/2}$$

with

$$[3]\qquad W_{ij} = [D^e_{ij}/4(1 + S_{ij})]\{(3 + S_{ij})\exp[-2\beta_{ij}(r_{ij} - r^e_{ij})] - 2(1 + 3S_{ij})\exp[-\beta_{ij}(r_{ij} - r^e_{ij})]\}$$

$$[4]\qquad J_{ij} = [D^e_{ij}/4(1 + S_{ij})]\{(1 + 3S_{ij})\exp[-2\beta_{ij}(r_{ij} - r^e_{ij})] - 2(3 + S_{ij})\exp[-\beta_{ij}(r_{ij} - r^e_{ij})]\}$$

and $V_{\mathrm{M}}(s_i)$ is the three-atom Sorbie–Murrell-type term (37).

$$[5]\qquad V_{\mathrm{M}}(s_i) = D^{\mathrm{o}}_{\mathrm{BrOO}}\,P(s_1, s_2, s_3)Q(s_1, s_2, s_3) = [1 + c_1s_1 + c_2(s_2 + s_3) + c_{11}s^2 + c_{22}(s_2^2 + s_3^2) + c_{12}s_1(s_2 + s_3) + c_{23}s_2s_3][1 - \tanh(0.5\gamma_1s_1)] \times [1 - \tanh(0.5\gamma_2s_2)][1 - \tanh(0.5\gamma_2s_3)]$$

The extended four-atom LEPS function has been employed to describe the four-body interaction and the two corrective Sorbie–Murrell-type, three-body polynomial terms, V_{M} were added to help reproduce as close as possible the BrOO′Br′ well and the BrOO′ + Br or Br′OO′ + Br exit channels.

Great care has been taken in the calibration of the PES to reproduce the three energy minima corresponding to the three isomeric structures of Br_2O_2 system, i.e., BrOOBr, $BrBrO_2$, and BrOBrO, possibly formed in the course of the reaction. These structures have been identified in extended ab initio calculations at the B3LYP/6–311++G(3*df*, 3*dp*) (27), MP2/AREP-TZ(2*df*) (29), and MP2(full)/6–311++G(2*d*) (31) levels of theory. Also, the *cis*- and *trans*-conformations of the skewed BrOOBr isomer were incorporated, which have been fully characterized by frequency analysis and have been shown to be saddle points in the internal rotational motion of BrOOBr (38). Based on these results and reported ab initio values for the related triatomic and diatomic fragments of Br_2O_2 system, the systematic optimization of the adjustable parameters of the PES have been carried out. The adjustable parameters include the Sato parameters and the Sorbie–Murrell polynomial coefficients. Due to the symmetry of the system there are only three Sato parameters (S_{ij}) for the diatomic pairs O–O, Br–Br, and O–Br that have to be varied for surface optimization. The most critical one is the O–Br parameter, which appears in four out of the six diatomic interactions and severely affects the magnitude of the energy minima. The displacement coordinates (s_i) in eq. [5] are given by $r_i - r_i^{\mathrm{o}}$, where the r_i^{o} distances represent the equilibrium reference frame distances for BrOO′ or Br′OO′ triatomics and have been approximated by the equilibrium values reported in the ab initio studies of these triatomics by Pacios and Gomez (39). A final point that has been taken into account in the calibration of the PES is the experimental evidence (40) for a low energy barrier (E_b) of about 1 kcal mol^{-1} at the entrance valley of the reaction. Thus, the constructed surface was optimized to present such an energy barrier as the two BrO radicals approach in a near-linear geometry. In summary, the three Sato parameters (S_{OO}, S_{BrBr}, S_{OBr}) and the Sorbie–Murrell parameters D^{o}, c_i, c_{ij}, and γ_i were optimized to yield a PES function that reproduces the three ab initio determined bound intermediates in the correct energy order BrOOBr < $BrBrO_2$ < BrOBrO, the *cis*- and *trans*-BrOOBr conformers, the two exit channels Br + BrOO and Br_2 + O_2, and the low energy barrier of about 1 kcal mol^{-1} at the entrance of the reaction.

The resulting reaction path involves the formation of the non-planar BrOOBr isomer as a reaction intermediate, which either decomposes into BrOO + Br or leads to the bimolecular elimination channel Br_2 + O_2. Figure 1 presents a schematic energy diagram of the various species possibly involved in the BrO + BrO reaction, and Fig. 2 depicts the potential energy profile for the approach of the oxygen ends of two colliding BrO radicals with and without the additional Sorbie–Murrell terms and for both BrO bond dstances fixed at the equilibrium value. The ambiguous point that arises here and in general, in the PES describing the XO + YO (X, Y = H, halogen atom) systems in which the XOOY intermediate formation is considered, is the concern about the spin conservation rules. The second pathway, channel (*b*), produces ground state oxygen molecules, yet if a singlet state intermediate formation intervenes, spin conservation requires that singlet state oxygen ($^1\Delta$)O_2 is the product. The problem then is the probability of a singlet–triplet crossing mechanism. The subject has been discussed several times and various workers adopt different views. In recent theoretical studies of OH + ClO reaction (41, 42) the spin conservation rule was followed and the calculations adopted HCl +

© 2001 NRC Canada

Fig. 1. Schematic energy diagram of various species involved in $(BrO)_2$ system.

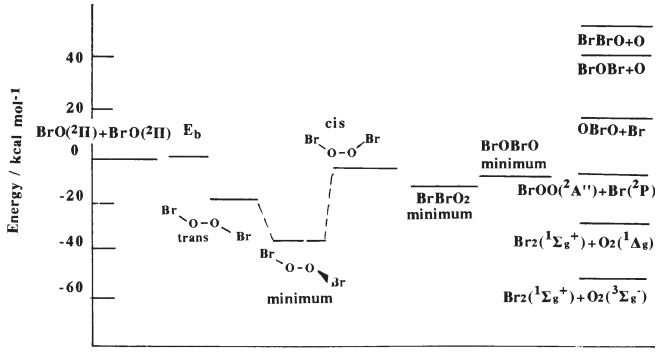
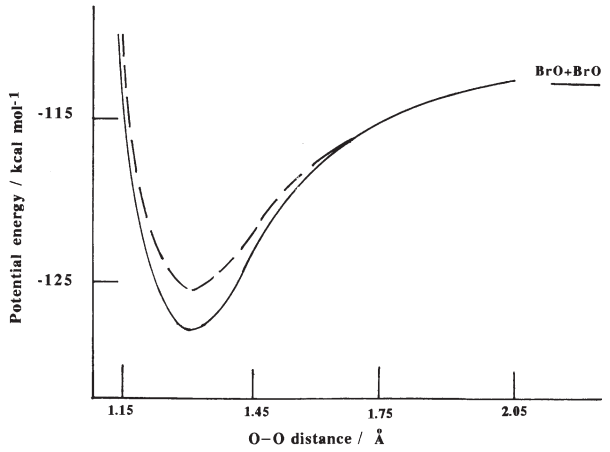


Fig. 2. Potential energy profile for the approach of the O ends of two colliding BrO radicals with both BrO bond distances held constant at the equilibrium values. The dashed line represents the LEPS function solely and the solid line incorporates the Sorbie–Murrell term.



$(^1\Delta_g)O_2$ as the products of the molecular elimination channel. However, in other occasions as in the experimental study of OH + BrO reaction (43) the singlet–triplet crossing has been assumed as the mechanism leading to ground-state molecular oxygen produced in the second channel. We adopt such a mechanism in our heavy system here too, i.e., we assume that spin-orbit induced quenching to ground state triplet O_2 may operate somewhere in the exit channel or alternatively a removal of spin conservation restriction between singlet and triplet states may occur by the heavy Br atom (44).

The kinetics and dynamics of the reaction on the constructed energy surface were followed by three-dimensional quasiclassical trajectory calculations performed using an appropriate version of Hase's Mercury program (45) modified to incorporate the optimized surface. The accuracy of the numerical integration was checked by the total energy and angular momentum conservation criteria; the time interval was set to 2.5×10^{-16} s and the initial reactant separation to 5.0 Å. Values of b_{max} in the range 3.9–4.0 Å were used. Two values of the initial collision energy E_T (0.65 and 0.89 kcal mol^{-1}) were studied, which, assuming Boltzmann thermal energy distribution, correspond to 220 and 298 K, respectively, temperatures at which the reaction has been studied experimentally.

Fig. 3. Effect of reagent vibrational excitation on the reactive cross section for channel (*a*). Solid line represents the best line drawn through the calculated points.

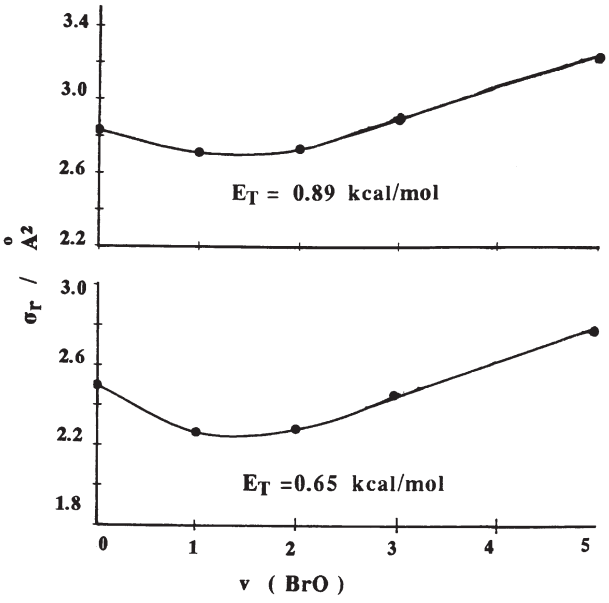
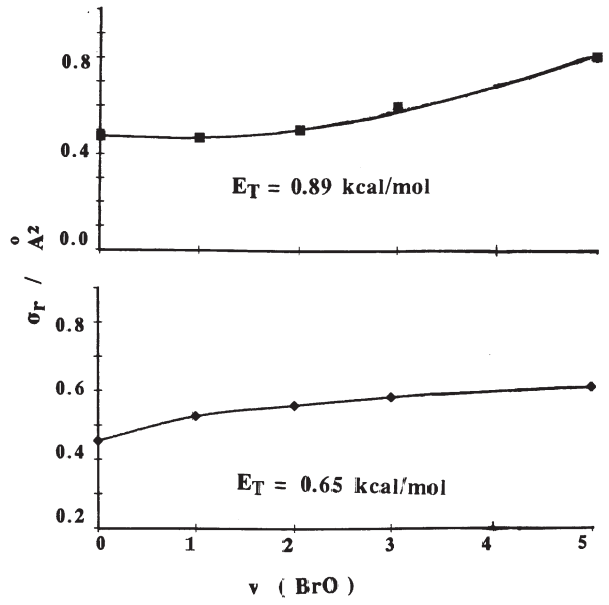


Fig. 4. Effect of reagent vibrational excitation on the reactive cross section for channel (*b*). Solid line represents the best line drawn through the calculated points.



The effect of the initial vibration was examined using a series of vibrational quantum numbers in the initial conditions for both BrO partners while keeping fixed the initial rotational energy at the most probable *J* values at 220 and 298 K of 13 and 15, respectively. Although the range of vibrational energies is higher and not directly related to the range of temperatures in stratospheric conditions, it is worthwhile to study the effect of reactant vibration since the present system is also an interesting diatom–diatom reaction.

At each collision energy and for each initial vibrational number 20 000 trajectories were run. The large number of

© 2001 NRC Canada

Fig. 5. Product translational energy distributions.

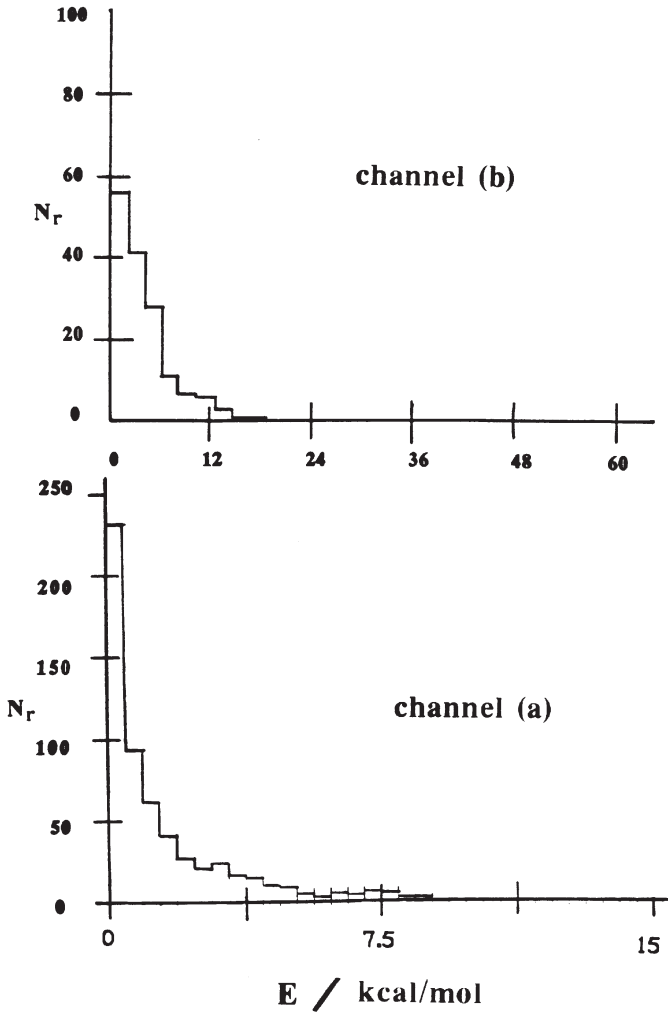
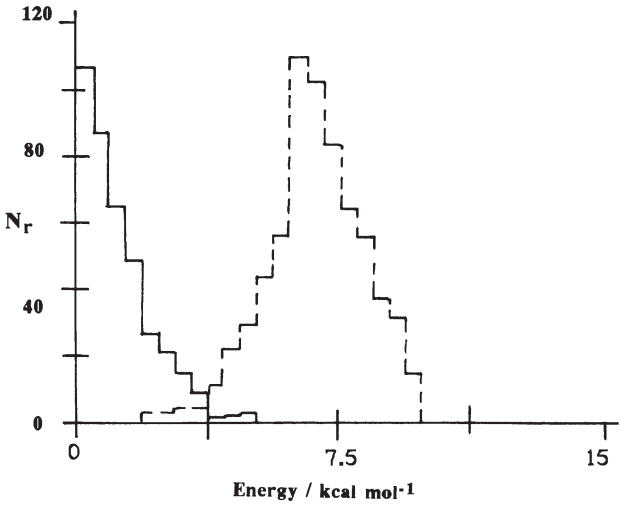
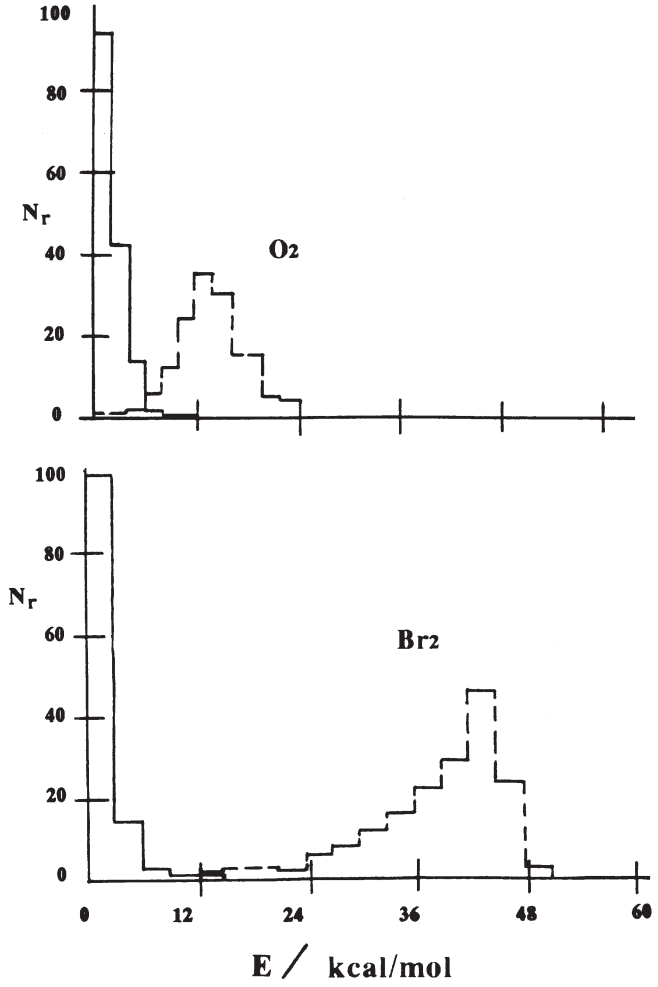


Fig. 6. Product rotational (solid line) and vibrational (dashed line) distribution, channel (*a*).



trajectories was necessary to obtain a satisfactory statistics for each run especially for the low yield second channel. The outcome of the trajectories into the various reactive

Fig. 7. Product rotational (solid line) and vibrational (dashed line) distribution, channel (*b*), for O_2 (top) and Br_2 (bottom).



events has been classified according to the following reactive paths:

path 1 BrO + BrO

path 2 BrOO + Br

path 3 BrBr + OO

The distribution of total available energy into products was examined for both E_T = 0.65 and 0.89 kcal mol^{-1} and for the corresponding most probable rotational levels, J = 13 and 15 with zero-point reactant vibrational energy. However, since the distributions obtained for each initial collision energy are quite similar, results are presented only for E_T = 0.89 kcal mol^{-1}. The total energy (E_{tot}) accessible in a collision between BrO radicals results from three contributions: the difference in binding energies between reactants and products (ΔD_e), the thermal collision kinetic energy (E_T), and the internal energy of reactants (rotational and zero-point energies of BrO radicals)

$$[6] \qquad E_{tot} = \Delta D_e + E_T + E_{int} = E'_T + E'_{int}$$

where the prime quantities refer to products. This energy is distributed among translational and internal energies of the products and the mode of disposal can reveal interesting fea-

© 2001 NRC Canada

tures of the mechanism of the reaction. In particular, the second channel is very exothermic and there is a considerable amount of total available energy of about 53 kcal mol^{-1} to be disposed between oxygen and bromine molecules. Hence the mode of disposal is significant. A smaller amount of energy of about 7 kcal mol^{-1} is to be disposed in the first channel.

Results and discussion

Figures 3 and 4 present the effect of initial reactant vibration for channels (*a*) and (*b*), respectively, displaying the corresponding reactive cross sections from

$$[7] \qquad \sigma_r(v, J, E_T) = \pi b_{max}(E_T)[N_r(v, J, E_T)/N_{tot}]$$

for the various initial conditions studied. It is seen that the initial vibrational excitation leads to a modest overall effect on the reactive cross sections and shows a rather weak influence on the reactivity of the system. The BrO ($v = 1$) results are about the same as the BrO ($v = 0$) for both channels within the statistical uncertainty. Furthermore, vibrational excitation in the first channel causes a slight decrease in the cross section as a result of the effect of the small energy barrier present at the entrance valley of the PES. When the number of vibrational quanta increases further a gradual increase in the reactivity is observed resulting from the increased total available initial energy. In the second channel a definite increase in reactivity is obtained as the initial vibrational excitation increases, manifested stronger at the lower kinetic energy studied, $E_T = 0.65$ kcal mol^{-1}, where the importance of the second pathway is increased. Such an increase in reactivity with reactant vibration is consistent with the assumption of the existence of another energy barrier located late in the exit valey of the PES (33). Consequently, we suggest that the reaction path for channel (*b*) involves the passage of the non-planar BrOOBr intermediate through a four-center, planar saddle point configuration that subsequently leads to the elimination products $Br_2 + O_2$. Such a saddle point geometry is the cis-planar conformer of bromine peroxide where the two Br atoms approach and eventually produce Br_2.

At first glance the above results are in contrast with other diatom–diatom systems where reagent vibrational excitation, especially that of the breaking bond is known to produce a severe enhancement in reactivity. Examples include the H_2 ($v = 1$) + OH, CN, BO cross sections, which have been found considerably larger than in H_2 ($v = 0$) + OH, CN, BO cross sections (46–49) and the same effect has been observed in the study of NH + NO and OH + Cl_2 reactions (50–52). However, a much milder influence of reagent vibrational excitation is expected in cases where a bound intermediate is formed like the OH + CO reaction at the low energy region. In the quasiclassical trajectory study of OH + CO → H + CO_2 reaction by Schatz and co-workers (53), reagent vibrational excitation was found to lead to only modest increases in the reactive cross sections. They found that the mild influence of reagent vibration is consistent with the assumption of a bound complex formation mechanism, which is dominant at low energies for the OH + CO system. With the same arguments the present results support and enhance the assumption that the disproportionation reaction of BrO radicals proceeds through the intervening formation of the bound indermediate. This is the skewed BrOOBr isomer, which contains the reactant initial energy and thus, it is formed in an energy rich state, BrOOBr*. This intermediate either dissociates directly producing mainly BrOO + Br in channel (*a*) or a significant percentage of it proceeds to the molecular elimination channel (*b*) through the *cis*-conformational barrier of this complex.

The distribution of total energy into products at $E_T = 0.89$ kcal mol^{-1} of the initial collision energy for both reaction pathways is presented in Figs. 5–7, where $< f_v' >$, $< f_R' >$, and $< f_T' >$ represent the average fractions of total available energy directed into products. We see that the larger part of the available energy, i.e., of the exothermicity of each channel is released into product vibration ($< f_v' > = 85$–90%) with negligible parts going into translation and rotation ($< f_R' > + < f_T' > = 15$–10%), as expected of a reaction proceeding through a bound complex formation. However, an interesting selectivity is observed in the partitioning of product vibrational energy among oxygen and bromine molecules produced in the second pathway. Although the large energy release in the second channel covers several quanta of possible O_2 vibrational excitation, the major part of it is directed preferably into bromine vibration. This is probably the result of the high tension associated with the close approach of the two Br atoms in the cyclic *cis*-conformation of BrOOBr isomer to form the Br_2 molecule.

We conclude that the internal energy effect and the mode of disposal of total energy are consistent with the hypothesis of an intermediate energy-rich complex formation, BrOOBr*. In channel (*a*) the two colliding radicals after passing through this energized form of BrOOBr peroxide dissociate directly into products. In the second pathway however, the intermediate formed, better stabilized as the temperature drops, proceeds through a *cis*-saddle point configuration, which facilitates the production of highly excited vibrationally molecular bromine.

Summary

The reagent vibrational excitation effect and the mode of disposal of the total available energy into products for the self-reaction of BrO radicals are studied, using the quasiclassical trajectory technique. The results indicate a only weak influence of initial vibration on reactivity, which is consistent with the assumption of a bound intermediate formation. In both channels the major part of the total available energy is converted into product vibration. In particular, the strong tension that accompanies the four-center intermediate geometry involved in the second channel to bring the two Br atoms close and produce molecular bromine, leads the greater part of the large exothermicity of the second channel into Br_2 vibration.

Acknowledgment

Computer services provided by the the Computer Center of the University of Ioannina, are gratefully acknowledged.

© 2001 NRC Canada

References

1. G. Brasseur and S. Solomon. *In* Aeronomy of the middle atmosphere: chemistry and physics of the stratosphere and mesosphere. D. Reidel Pub. Co., Dordrecht. 1986.
2. R.P. Wayne. Chemistry of atmospheres. Clarendon Press, Oxford. 1991.
3. M.J. Molina and F.S. Rowland. Nature (London), **249**, 810 (1974).
4. L.T. Molina and M.J. Molina. J. Phys. Chem. **91**, 433 (1987).
5. M.B. McElroy, R.J. Salawitch, S.C. Wofsy, and J.A. Logan. Nature (London), **321**, 759 (1986).
6. K.K. Tung, M.K.W. Ko, J.M. Rodriguez, and N.D. Sze. Nature (London), **322**, 811 (1986).
7. S. Solomon. Nature (London), **347**, 347 (1990).
8. K. Yagi, J. Williams, N.Y. Wang, and R.J. Cicerone. Science (Washsington, D.C.), **267**, 1979 (1995).
9. S.L. Nickolaisen, R.R. Friedl, and S.P. Sander. J. Phys. Chem. **98**, 155 (1994).
10. A. Horowitz, J.N. Crowley, and G.K. Moortgat. J. Phys. Chem. **98**, 11924 (1994).
11. R.R. Friedl and S.P. Sander. J. Phys. Chem. **93**, 4756 (1989).
12. S.P. Sander and R.R. Friedl. J. Phys. Chem. **93**, 4764 (1989).
13. A.A. Turnipseed, J.W. Birks, and J.G. Calvert. J. Phys. Chem. **95**, 4356 (1991).
14. M.A.A. Clyne and R.T. Watson. J. Chem. Soc. Faraday Trans. 1, **71**, 336 (1975).
15. M.A.A. Clyne and R.T. Watson. J. Chem. Soc. Faraday Trans. 1, **73**, 1169 (1977).
16. S. Jaffe and W.K. Mainquist. J. Phys. Chem. **84**, 3277 (1980).
17. S.P. Sander and R.T. Watson. J. Phys. Chem. **85**, 4000 (1981).
18. A.A. Turnipseed and J.W. Birks. J. Phys. Chem. **94**, 7477 (1990)
19. I.T. Lancar, G. Laverdet, G. Le Bras, and G. Poulet. Int. J. Chem. Kin. **23**, 37 (1991).
20. R.L. Mauldin, A. Wahner, and A.R. Ravishankara. J. Phys. Chem. **97**, 7585 (1993).
21. I. Bridier, B. Veyret, and R. Lesclaux. Chem. Phys. Lett. **201**, 563 (1993).
22. D.M. Rowley, M.H. Harwood, R.A. Freshwater, and R.L. Jones. J. Phys. Chem. **100**, 3020 (1996).
23. M.H. Harwood, D.M. Rowley, R.A. Cox, and R.L. Jones. J. Phys. Chem. A, **102**, 1790 (1998).
24. M.K. Gilles, A.A. Turnipseed, J.B. Burkholder, A.R. Ravishankara, and S. Salomon. J. Phys. Chem. A, **101**, 5526 (1997).
25. T.J. Lee, C.M. Rohfling, and J.E. Rice. J. Chem. Phys. **97**, 6593 (1992).
26. W.K. Li and C.Y. Ng. J. Phys. Chem. A, **101**, 113 (1997).
27. S. Guha and J. Francisco. J. Phys. Chem. A, **101**, 5347 (1997).
28. J.T. Gleghorn. Chem. Phys. Lett. **271**, 296 (1997).
29. P.C. Gomez and L.F. Pacios. J. Phys. Chem. A, **103**, 739 (1999).
30. A. Beltran, J. Andres, S. Noury, and B. Silvi. J. Phys. Chem. A, **103**, 3078 (1999).
31. D. Papayannis, A.M. Kosmas, and V.S. Melissas. Chem. Phys. **243**, 249 (1999).
32. Z. Li and G. Jeong. Chem. Phys. Lett. **340**, 194 (2001).
33. R.D. Levine and R.B. Bernstein. Molecular reaction dynamics and chemical reactivity. Oxford University Press, New York. 1987.
34. J. Espinosa-Garcia. J. Phys. Chem. A, **105**, 134 (2001).
35. M.H. Mok and J.C. Polanyi. J. Chem. Phys. **53**, 4588 (1970).
36. M.T. Rayez, J.C. Rayez, B. Duguay, and P. Halvick. Chem. Phys. **134**, 55 (1989).
37. J.N. Murrell, S. Carter, S.C. Farantos, P. Huxley, and A.C.J. Varandas. Molecular potential energy functions. Wiley, New York. 1984.
38. D.K. Papayannis, V.S. Melissas, and A.M. Kosmas. J. Phys. Chem. A, **105**, 2209 (2001).
39. L.F. Pacios and P.C. Gomez. J. Phys. Chem. A, **101**, 1767 (1997).
40. J. Brown and G. Burns. Can. J. Chem. **48**, 3487 (1979).
41. M.K. Dubey, M.P. McGraph, G.P. Smith, and F.S. Rowland. J. Phys. Chem. A, **102**, 3127 (1998).
42. J.B. Lipson, T.W. Beiderhase, L.T. Molina, M.J. Molina, and M. Olzmann. J. Phys. Chem. A, **103**, 6540 (1999).
43. D.J. Bogan, R.P. Thorn, F.L. Nesbitt, and L.J. Stief. J. Phys. Chem. **100**, 14383 (1996).
44. S.W. Benson. Thermochemical kinetics. 2nd ed. Wiley, New York. 1976.
45. W.L. Hase. QCPE Bull. 453 (1983).
46. D.C. Clary. J. Chem. Phys. **96**, 3656 (1992).
47. D. Wang and J.M. Bowman. J. Chem. Phys. **96**, 8906 (1992).
48. W. Zhu, J.Z.H. Zhang, Y.C. Zhang, Y.B. Zhang, L.X. Zhan, S.L. Zhang, and D.H. Zhang. J. Chem. Phys. **108**, 3509 (1997).
49. J. Sogas, M.Alberti, X. Gimenez, R. Sayos, and A. Aguilar. J. Phys. Chem. A, **101**, 8877 (1997).
50. K.S. Bradley, P. McCabe, G.C. Schatz, and S.P. Walch. J. Chem. Phys. **102**, 6696 (1995).
51. H. Szichman and M. Baer. J. Chem. Phys. **105**, 10380 (1996).
52. V.S. Melissas, E. Drougas, E.G. Bakalbassis, and A.M. Kosmas. J. Phys. Chem. A, **104**, 626 (2000).
53. K.K. Kudla, G.C. Schatz, and A.F. Wagner. J. Chem. Phys. **95**, 1635 (1991).

© 2001 NRC Canada

Canadian Journal of Chemistry

Author Index
Volume 79, 2001

Revue canadienne de chimie

Index des auteurs
Volume 79, 2001

Abdur-Rashid, K., 964
Abraham, M.H., 1466
Acree, Jr., W.E., 1466
Adams, H., 731, 760
Agustinho, S.C.M., 760
Akhmedov, N.G., 1655
Akim, L.G., 201
Albinati, A., 693
Albrecht, M., 709
Alexiou, C., 992
Alguindigue, S.S., 809
Alibhai, N., 1747
Alper, H., 587
Amoroso, D., 958
Anderson, C., 1477
Anderson, O.P., 1562
Angelici, R.J., 578
Aragoni, M.C., 1483
Arakawa, H., 1415
Arca, M., 1483
Aresta, M., 570
Argyropoulos, D.S., 201, 1394
Armstrong, D.A., 405
Asadi, M., 70, 1360
Asao, N., 1624
Ashby, M.T., 809
Askalany, A.H., 42
Atwood, J.D., 1036
Aylward, W.M., 1
Baboulène, M., 1153
Bachmann, P., 519
Baerlocher, F.J., 1115
Baerlocher, M.O., 1115
Bailey, A.J., 792
Baines, K.M., 461
Baird, M.C., 1012
Baker, P.K., 263
Bakhmutov, V.I., 479
Bakhmutova, E.V., 479
Bakos, J., 725, 1040
Balakrishnan, V.K., 157
Balch, A.L., 922
Balci, M., 35
Ball, J.M., 304
Barba, V., 1229
Barbieri, L.R., 1786
Barrett, A.G.M., 1562
Barthazy, P., 904
Bartosh, K., 1026
Bartosz-Bechowski, H., 752
Basickes, L., 854
Batchelor, R.J., 938, 1272
Batista, A.A., 1030
Battaglia, L., 621
Beagley, P., 731
Beckmann, O., 1593
Bélanger, J.M.R., 1906
Belchior, J.C., 211
Belkova, N.V., 479
Bennett, M.A., 655
Benson, G.C., 388
Bényei, A.C., 635
Bergens, S.H., 1019
Berges, J., 405
Bergman, R.G., 525
Berners-Price, S.J., 1030
Berova, N., 1786
Bertotti, M., 679
Besenyei, G., 649, 688
Bhattacharyya, S., 938
Bianchini, C., 479
Bilehal, D.C., 1926
Blanco, C.A., 448
Blaser, H.-U., 566
Boch, R., 1068
Bolm, C., 1593
Bond, A.M., 613
Bonilla, R.J., 719
Bottomley, F., 1321
Boubaker, T., 1617
Boule, P., 1179
Bourgeois, M.-J., 257
Bowden, A.A., 1036
Boyd, S.E., 1030
Braga, J.P., 211
Braig, V., 1528
Brechbiel, M.W., 1105
Breed, P.G., 1049
Broggini, D., 904
Brouillard, R., 1173
Brown, J.M., 1049
Brown, M.A., 463
Brown, R.S., 1704
Bruce, D.W., 472
Buchanan, G.W., 195, 1505
Buchwald, S.L., 1799
Buckley, A.V., 1284
Buckley, R.W., 1030
Buncel, E., 157, 1617
Bunn, A.G., 854
Burford, N., 342
Butkus, E., 1598
Butler, D.C.D., 472
Cadoret, J., 626
Cai, Z.-S., 29
Calderazzo, F., 495
Cameron, T.S., 342
Campagnole, M., 257
Cantin, A.M., 377
Cao, D., 455
Cao, S., 272
Carmona, J., 1447
Carpenter, B.E., 291, 857
Carter, G.T., 1786
Casagrande, B., 566
Casey, C.P., 1002
Castellano, E.E., 1030
Catellani, M., 742
Centoducatte, R., 121
Chan, C., 1659
Chan, T.H., 1536
Chapados, C., 13
Charette, A.B., 1694
Chen, L., 29
Chen, Y.-T., 221, 455
Cheng, B., 1881
Chim, J.L.C., 607
Chivers, T., 1841
Choi, H.Y., 337
Chomka, K., 760
Chow, A., 437
Chung, M.-K., 949
Ciunik, Z., 752, 868
Claver, C., 560
Cobos, J.C., 1447
Coffey, D.S., 1711
Cole-Hamilton, D.J., 472
Colodette, J.L., 201
Cooper, L., 490
Cordes, A.W., 1352
Coulter, K.R., 930
Cowan, J.J., 792
Cromer, M., 370
Crowe, D.A.J., 1145

© 2001 NRC Canada

Cserépi-Szűcs, S., 725
Cuahutle, D., 1229
Cugini, F., 742
Cuisinier, C., 1827
Das, P.K., 809
Dave, V., 461
Davies, P., 731
Davies, S.C., 490
Dawid, M., 110, 1294
de Almeida Santos, R.H., 679
Dean, P.A.W., 1293, 1330
de Blois, S., 13
DeCaire, M., 1792
de Castro, E.V.R., 121
Decken, A., 1115, 1321
Delamere, C., 1492
Delaude, L., 529
Delmarre, D., 1068
del Rio, I., 560
Demchenko, A.P., 358
Demonceau, A., 529
Denisenko, S.N., 1655
Denmark, S.E., 1606
Denonne, F., 1827
den Reijer, C.J., 693
Devillanova, F.A., 1483
de Vries, J.G., 1086
Dibenedetto, A., 570
Dileo, C., 570
Dilworth, J.R., 490
Dixon, D.J., 1668
Dobó, A., 1040
Dolphin, D., 1068
dos Santos Silva, H.A., 679
Dotta, P., 693
Drake, J.E., 983
Drew, M.G.B., 263
Drouin, M., 1439
Durran, S.E., 780
Durst, T., 1747
Duś, D., 868
Dust, J.M., 157, 1617
Duval, P.B., 536
Duvey, G., 1754
Dworschak, R.G., 437
Dyson, P.J., 705
Ebadi, M., 992
Edmunds, J.J., 1562
Eidell, C.K., 1681
Einstein, F.W.B., 938, 1272
Ellena, J., 1030
Ellis, D.J., 705
Elzner, S., 593
Emerenciano, V.P., 1915
Emmett, M.R., 546
Enders, D., 1528
Englert, U., 495
Ens, W., 437
Epstein, L.M., 479
Escher, E., 377
Evans, D.S., 263
Fabbri, D., 670
Fackler, J.P., Jr., 896
Fang, Q., 174
Farcas, S.I., 983
Farfán, N., 1229
Faria, R.B., 1135
Feng, J.-K., 1366
Ferguson, G., 949
Ferraro, J.R., 1483
Ferreira, M.J.P., 1915
Fish, R.H., 888
Fitzpatrick, S.J., 1101
Fleischer, M.A., 75
Fogg, D.E., 958
Fornika, R., 642
Foster, A.C., 1668
Fougerousse, A., 1173
Franc, C., 1827
Franco, D.W., 679
Fraser, H.L., 1515
Fryzuk, M.D., 536, 1194
Fu, J.-m., 1812
Fu, W., 1366
Funahashi, S., 1344
Gagnon, J., 1439
Gaisberger, B., 394
Gałęzowski, W., 1128
Gao, H., 578
Gao, Y., 915
Garcia de la Fuente, I., 1447
Gay, I.D., 1272
Gelbrich, T., 780
Geletti, Y.V., 792
Gevorgyan, V., 1624
Ghiviriga, I., 1659
Ghosez, L., 1827
Gibson, G., 1704
Gill, M.A., 1101
Gillis, H.A., 80
Ghandi, M., 1505
Gladiali, S., 670
Godard, A., 1754
Goddard, R., 1806
Gömöry, Á., 725
Gonzalez, E., 1173
Gonzalez, J.A., 1447
Görls, H., 642
Graziano, G., 105, 1310
Greaney, M., 546
Grenon, M., 1694
Gribble, G.W., 1515
Griffith, W.P., 598
Grundwald-Wyspiańska, M., 775
Grześkowiak, I., 1128
Guagnano, V., 1606
Guillier, F., 1754
Guliński, J., 775
Gulyás, H., 1040
Gupta, R.N., 418
Hachiya, S.-I., 1562
Haines, R.I., 54
Hanessian, S., 1812
Hantos, S.M., 1747
Hark, R.R., 1632
Harris, M.C., 1799
Harrod, J.F., 1075
Hartman, J.S., 426
Harvey, P.D., 552, 1439
Hassan, A.A., 42
Haunert, F., 1511
Hauze, D.B., 1632
Hayes, P.G., 1898
He, D., 1213
He, S., 510
He, W., 127
Healy, P.C., 1030
Hegedüs, C., 725
Hemscheidt, T., 418
Hendrickson, C.L., 546
Hendrix, J.A., 1562
Henry, B.R., 279
Herradura, P., 1727
Herraiz-Sierra, I., 448
Hidai, M., 632
Hill, C.L., 792
Hill, J.M., 817
Hioka, N., 1068
Hiyama, T., 593, 1522
Hnatiw, J.B., 304
Holly, S., 649
Hook, J.M., 1330
Hoppe, D., 1736
Horikawa, Y., 388
Horita, K., 1562
Hou, Z., 29
Hrapchak, M.J., 1775
Hsieh, Y.-H., 1272
Hu, T.Q., 1201
Huang, Y., 719
Hudlicky, T., 1659
Hughes, D.L., 490
Hursthouse, M.B., 780, 983
Hutchings, D.R., 54
Ibrahim, M.S., 1431
Imamura, K.-i., 1624
Isaia, F., 1483
Iwatsuki, S., 1344

© 2001 NRC Canada

Jablonski, C., 463
Jacobi, P.A., 1727
Jafarpour, L., 626
Jakins, C., 1492
James, B.R., 1201
James, S.L., 709
Jamshid, K.A., 70
Jan, D., 529
Janda, K.D., 1556
Jankowski, C.K., 1906
Jarczewski, A., 1128
Jenkins, H.A., 1293, 1330
Jennings, M., 1330
Jennings, M.C., 915
Jensen, C.M., 823
Jessop, P.G., 719
Jezierski, A., 570
Jiang, M.H., 174
Jiang, X., 127
Johnson, M.D., 1546
Joó, F., 635
Jorge, F.E., 121
Joullié, M.M., 1632
Jurasek, L., 1394
Kaneno, D., 1598
Kashiwabara, K., 1344
Katritzky, A.R., 1655
Kauch, M., 1736
Keay, B.A., 1541
Kenawy, I., 42
Kessler, M., 642
Khan, M.A., 830
Khomutov, O.G., 183
Kim, C.-K., 1238
Kinal, A., 35
King, J.F., 461
Kirby, C.W., 296
Kissell, W.S., 1681
Kleinke, H., 1338
Kliegel, W., 226
Klymchenko, A.S., 358
Knoblauch, S., 977
Koch, H.F., 977
Kodess, M.I., 183
Köllner, C., 1762
Konkol, M., 490
Koshino, N., 1344
Kosmas, A.M., 1940
Koteva, K.P., 377
Kovács, J., 635
Krisdhasima, V., 848
Krištofová, L., 1394
Krüger, C., 642
Kulkarni, R.M., 1926
Kumamaru, K., 1422
Kurokawa, G.S., 1058
Lam, K.C., 342
Lamprecht, D., 1864
Langner, R., 1376
Lathioor, E.C., 1851
Lau, M.-K., 607
Lau, S.Y.W., 1541
Laurenczy, G., 635
Le, N., 238
LeBlanc, D.J., 342
LeClair, G., 1906
Lee, D.W., 823
Lee, J., 830
Lee, K.J., 1556
Lee-Ruff, E., 114
Legzdins, P., 502
Leigh, W.J., 1851
Leitner, W., 642
Lelj, F., 1483
Lemes, N.H.T., 211
Lemieux, R.U., 238
Lessard, D.G., 1870
Leung, W.-H., 607
Lever, A.B.P., 992
Lewandowski, M., 775
Lewars, E., 1492
Ley, S.V., 1668
Leznoff, C.C., 878
Li, H.L., 328
Li, L.-H., 1536
Li, W., 1366
Li, Y.-N., 29
Light, M.E., 780, 983
Lightfoot, P., 472
Lin, H.-K., 221, 455
Ling, C.-C., 238
Lippolis, V., 1483
Liu, S., 1058
Long, G.S., 1026
Loop, I., 183
López, M.C., 1460
López-de-Luzuriaga, J.M., 896
Lord, G., 337
Lork, E., 183
Lough, A.J., 964
Lu, A.Z., 1201
Lu, B.C.-Y., 388
Lu, J., 127
Lu, X., 319, 364
Lubell, W.D., 94
Lubkowitz, G., 226
Lucas, R.J., 54
Luo, H., 1105
Ma, M., 1213
Macdonald, C.L.B., 342
Machado, S.P., 1135
Machuca-Herrera, J.O., 1135
MacRae, A.I., 1101
Madar, D.J., 1711
Magnuson, K., 823
Mahajan, D., 848
Mahiuddin, S., 1207
Mainar, A.M., 1460
Majewski, M., 1792
Malecha, J.W., 1562
Małecka, E., 775
Małgorzata, D., 1294
Malinauskienė, J., 1598
Malonga, H., 1415
Mamer, O., 1381
Mann, B.E., 760
March, R.E., 124
Marciniec, B., 775
Markó, L., 725
Marsais, F., 1754
Marshall, A.G., 546
Martin, M., 519
Martinez, H.E., 50
Martinsson, A., 938
Masi, D., 479
Matsumoto, M., 1864
Max, J.-J., 13
McAuley, A., 930
McClelland, R.A., 1875, 1881, 1887
McComb, M.E., 437
McDonald, L.A., 1786
McDonald, R., 291
McDonald, T., 1704
McGarvey, B.R., 679
McGlinchey, M.J., 1295
Medici, S., 670
Meilleur, D., 552
Mele, G., 587
Menzek, A., 35
Merkley, N., 312
Meunier, L., 1179
Mezzetti, A., 904
Middel, O., 1525
Miller, D., 54
Miller, J.M., 1220, 1224
Mingie, J.R., 1352
Mitchell, T.R.B., 655
Mizobe, Y., 632
Moghimi, A., 1505
Moineau, C., 587
Montaudon, E., 257
Morales-Morales, D., 823
Mori, A., 1522
Mori, V., 679
Morlay, C., 370
Morris, R.H., 964
Mouginot, Y., 370
Moulik, S.P., 1

© 2001 NRC Canada

Murray, M.C., 1012
Nâdasdi, L., 635
Nakanishi, K., 1786
Nandibewoor, S.T., 1926
Narracci, M., 570
Natansohn, A., 1093
Neault, J.F., 1415
Neil, M.A., 1321
Neszmélyi, A., 649
Netherton, M.R., 461
Neugebauer, W.A., 377
Neverov, A.A., 1704
Ng, F.T.T., 817
Niesyty, K., 752
Nikolcheva, L.G., 1115
Nishihara, Y., 1522
Nivoliers, F., 1754
Noels, A.F., 529
Nolan, S.P., 626
Noll, B.C., 922
Norman, D.W., 1115
North, M.R., 75, 1864
Nowak, P., 1792
Nozaki, K., 593
Oakley, R.T., 1352
Obeyama, K., 1344
O'Connor, P.E., 1898
Okajima, T., 22
Oleschuk, R.D., 437
Olmstead, M.M., 922
Opolski, A., 868
Orvig, C., 1058
Osmond, D.A., 1201
Ott, C., 1511
Ousalem, M., 1870
Ozturk, T., 358
Padwa, A., 1681
Palazzi, C., 1593
Palepu, R., 1
Pampaloni, G., 495
Pan, P., 131
Panosyan, F.B., 1110
Papayannis, D.K., 1940
Papp, G., 635
Pardo, J.I., 1460
Paré, J.R.J., 1906
Park, D.K., 337
Park, Y.S., 337
Párkányi, L., 649
Parkinson, C.J., 1562
Parvez, M., 857
Pashkevich, K.I., 183
Passarelli, V., 495
Patrick, B.O., 1194, 1201
Pawliszyn, J., 1403
Perez-Encabo, A., 448
Perreault, H., 437
Perumal, S., 1655
Peruzzini, M., 479
Petrovskaia, O., 1632
Petryk, M.W.P., 279
Phillips, A.D., 342
Phillips, S., 922
Phillips, T.E., 1898
Piers, W.E., 291, 857
Pilichowski, J.-F., 1179
Pincock, J.A., 63
Pinna, F., 621
Pirri, G., 670
Pivovarenko, V.G., 358
Pokriefke, J.O., 226
Polydore, C., 977
Pope, M.T., 802
Pouet, M.-J., 1617
Povar, I., 1166
Powell, D.R., 830, 1002
Power, W.P., 296
Pregosin, P.S., 693
Preston, K.R., 437
Pruchnik, F.P., 868
Puddephatt, R.J., 915
Pulacchini, S., 670
Punniyamurthy, T., 1546
Purcell, M., 1415
Qian, K., 546
Qian, X., 272
Qian, Y., 127
Quéguiner, G., 1754
Queiroz, S.L., 1030
Quickenden, T.I., 80
Raabe, G., 1528
Rabion, A., 888
Rajalingam, U., 1293, 1330
Ramnauth, J., 114
Ramos, J.F., 50
Ramsden, J.A., 1049
Rastegar, M.F., 195, 1505
Rauk, A., 405
Redón, R., 823
Reed, R.W., 1352
Reetz, M.T., 1806
Reid, D.L., 319
Reinhoudt, D.N., 1525
Rettig, S.J., 226, 502, 536, 857, 930
Rheingold, A.L., 342
Richards, R.L., 490
Richardt, P.J.S., 613
Richter-Addo, G.B., 830
Riesco, N., 1447
Rifai, S., 63
Riggio, R., 50
Rinner, U., 1659
Ro, S., 1238, 1259
Robertson, V., 949
Rocca, P., 1754
Rocha, R.C., 145
Rochon, P., 1093
Rodgers, R.P., 546
Rodrigues, G.V., 1915
Roehri-Stoeckel, C., 1173
Rogers, R.D., 1105
Rojas, A., 448
Romi, 1910
Röschenthaler, G.-V., 183
Rösler, R., 983
Ross G., 1934
Rotar, A., 983
Roundhill, D.M., 977
Roush, W.R., 1711
Ruane P.H., 1875
Rudolph, J., 1806
Sadighi, J.P., 1799
Sales, M., 1775
Samonte, J.L., 802
Samuel, E., 1075
Sánchez, M.A., 1460
Sanders, J.R., 490
Santillan, R., 1229
Santos, C.M.P., 1135
Saraçoglu, N., 35
Sarvestani, A.H., 1360
Sauriol, F., 1381
Sayer, B.G., 418
Scheffer, J.R., 349
Schilling, S., 1659
Schlaf, M., 949
Seino, H., 632
Sen, A., 1026
Serni, G., 495
Sevenard, D.V., 183
Seward, C., 1187
Sharma V.K., 1910
Shaver, M.P., 1898
Shehetta, I., 42
Shehatta, I.S., 1431
Sheldon, R.A., 688
Shi, Y.-L., 328
Shi, Z., 1238, 1259, 1278
Shibahara, F., 593
Shirota, O., 1786
Shoemaker, J.A.W., 426
Shu, R., 1075
Shubina, E.S., 479
Sibi, M.P., 1546
Siebenhaar, B., 566
Silvestru, A., 983
Silvestru, C., 983
Simal, F., 529

© 2001 NRC Canada

Simándi, L.I., 649
Singer, S.W., 1002
Six, C., 642
Slawin, A.M.Z., 780
Smith, D.C., Jr., 626
Smith, K.M., 502
Smith, M.B., 780
Smith, P.J., 1145
Smith, S., 760
Snedeker, B., 1026
Sobota, P., 490
Solar, S., 394
Somogyi, L., 1159
Song, B., 1058
Song, G., 272
Song, H., 29
Song, J.H., 337
Souirti, S., 1153
Spek, A.L., 709
Spenser, I.D., 418
Spey, S., 760
Spinney, H.A., 1115
Spirlet, M.R., 529
Spohr, U., 238
Sproull, R.D., 848
Squires, C., 760
Standing, K.G., 437
Staples, R.J., 896
Stark, L., 342
Starosta, R., 868
Stefanova, R., 63
Sternberg, E., 1068
Stevens, E.D., 626
Stevens, M.R., 655
Still, I.W.J., 1110
Stojanovic, N., 1101
Stončius, A., 1598
Strukul, G., 621
Studer, M., 566
Stynes, D.V., 795
Su, X.-C., 221, 455
Suchozak, B., 878
Sudo, T.,1624
Sun, D.-A., 1381
Sun, H.-W., 221
Sun, Y., 1394
Suriaatmaja, M., 598
Suzuki, T., 1344
Swaddle, T.W., 75, 841, 1864
Symons, M.C.R., 124
Szöllősy, Á., 725
Tajmir-Riahi, H.A., 1415
Takagi, F., 632
Takagi, H.D., 1344
Takahisa, E., 1522
Tellers, D.M., 525
Terrier, F., 1617
Thomas, C.A., 719
Tiefenthaler, D., 742
Tietze, L.F., 1511
Togni, A., 1762
Toma, H.E., 145
Tommasi, I., 570
Tomoda, S., 1598
Touillaux, R., 1827
Tracey, A.S., 938
Tregloan, P.A., 613
Tripathy, S., 1747
Trotter, J., 226
Trzeciak, A.M., 752
Tsuzuki, H., 1422
Ugi, I., 1934
Urieta, J.S., 1460
VanCalsteren, M., 1906
van Koten, G., 709
van Leeuwen, P.W.N.M., 560
vanLoon, G.W., 157
Van Pham, T., 1887
VanSickle, A., 1562
van Zyl, W.E., 896
Vaugeois, J.,1606
Veilleux, A., 13
Veldman, N., 709
Venneri, P.C., 110, 312, 1294
Verani, G., 1483
Verboom, W., 1525
Verspui, G., 688
Vézina, M., 1439
Vialemaringe, M., 257
Vichard, D., 1617
Vincent, J.-M., 888
Vittori, O., 370
Vogels, C.M., 1115, 1898
Vorontsov, E.V., 479
Wagner, B.D., 1101
Wahab, A., 1207
Walsh, D., 342
Wang, C., 174
Wang, F., 1792
Wang, H., 1213
Wang, R., 495
Wang, S., 1187
Wang, T., 1786
Wang, X.M., 174
Wang, Z., 328, 388, 823
Ward, D.E., 1775
Warkentin, J., 110, 312, 319, 364, 1294
Watson, K.J., 1898
Wayland, B.B., 854
Wedd, A.G., 613
Wei, L., 94
Wei, Q.-L., 29
Weinberg, N., 1284
Weinstock, I.A., 792
Welton, T., 705
Werner, H., 519
Werner, M.L., 1026
Westaway, K.C., 1145
Westcott, S.A., 1115, 1898
White, C., 731
White, J.M., 613
Wietrzyk, J., 868
Wiles, J.A., 1019
Williams, I.D., 607
Willis, A.C., 655
Withers, S.G., 510
Wojdat, E., 868
Wolfe, S., 1238, 1259, 1272, 1278, 1284
Wong, A.W., 510
Wong, W.-T., 607
Woo, H.-G., 1075
Wu, B.-X., 29
Xie, Y., 127
Yachandra, V.K., 888
Yamamoto, Y., 1624
Yamato, T., 1422
Yan, P., 127
Yap, G.P.A., 195, 857, 958, 1505
Yi, G.-B., 830
Yoshikawa, E., 1624
Young, V.G., Jr., 1019
Yu, P., 1194
Yu, W.T., 174
Yung, C., 823
Zahir, K.O., 1124
Zamir, L.O., 1381
Zanobini, F., 479
Zhang, H., 1352
Zhang, H.-X., 1366
Zhang, X.X., 1799
Zhao, G.-H., 221
Zhao, R., 131
Zhao, X., 174
Zhao, X.-Z., 29
Zhou, J., 841
Zhou, P., 1213
Zhou, Y.F., 174
Zhou, Z.-F., 221, 455
Zhu, S.-R., 221, 455
Zhu, X.X., 1870
Zhuang, Q., 1220, 1224
Ziolkowski, J., 570
Ziólkowski, J.J., 752
Znamirowski, M., 437
Zobi, F., 795
Zundel, G., 1376

© 2001 NRC Canada

Canadian Journal of Chemistry

Revue canadienne de chimie

Contents
Volume 79, 2001

Sommaire
Volume 79, 2001

January / janvier

ARTICLES

S.P. Moulik, Wanda M. Aylward, and R. Palepu Phase behaviours and conductivity study of water/CPC/alkan-1-ol (C_4 and C_5)/1-hexane water/oil microemulsions with reference to their structure and related thermodynamics **1**

Jean-Joseph Max, Serge de Blois, Alain Veilleux, and Camille Chapados IR Spectroscopy of aqueous alkali halides. Factor analysis **13**

Toshiya Okajima Theoretical study on the influence of H_2O for the 1,2-hydrogen shift from hydrogen peroxide (H_2O_2) to water oxide (O-OH_2) **22**

Yan-Ni Li, Hao Song, Zun-Sheng Cai, Lan Chen, Zhe Hou, Qing-Li Wei, Ben-Xiang Wu, and Xue-Zhuang Zhao New chaotic behavior and its effective control in Belousov–Zhabotinsky reaction **29**

Nurullah Saraçoğlu, Abdullah Menzek, Armağan Kınal, and Metin Balci Synthesis of new substituted dihydroheptalene derivatives: SiO_2- and base-catalyzed rearrangement of dimethyl *trans*-3,8-dihydroheptalene-3,8-dicarboxylate **35**

I. Shehatta, I. Kenawy, A.H. Askalany, and Ayman A. Hassan Thermodynamic of metal complexation of the macrocyclic antibiotic rifampicin **42**

Roque Riggio, Juan F. Ramos, and Hector E. Martinez Excess properties for acetophenone + butanols at 298.15 K **50**

Robert Ivor Haines, Dean Reginald Hutchings, Rhonda Jane Lucas, and David Miller Structure and redox kinetics of nickel(II) tetraazamacrocycles containing pendant carboxylate groups **54**

J.A. Pincock, S. Rifai, and R. Stefanova The photochemistry of the 4-cyanobenzoic acid esters of *trans*- and *cis*-2-phenylcyclohexanol **63**

Mozaffar Asadi and Khosrow Aein Jamshid Thermodynamics of triaryltin chloride adduct complexes **70**

Michael R. North, M. Alejandra Fleischer, and Thomas W. Swaddle Precipitation from alkaline aqueous aluminosilicate solutions **75**

Hugh A. Gillis and Terence I. Quickenden Excess electrons in aqueous glasses and crystalline ice **80**

Lan Wei and William D. Lubell Scope and limitations in the use of *N*-(PhF)serine-derived cyclic sulfamidates for amino acid synthesis **94**

Instructions to Authors / Recommendations aux auteurs **I-1**

Notes for authors of papers presenting the results of X-ray crystal structure analyses / Recommandations aux auteurs d'articles décrivant la détermination de structures par diffraction des rayons X **I-5**

February / février

ARTICLES

Giuseppe Graziano Solvation of a water molecule in cyclohexane and water **105**

Małgorzata Dawid, Paul C. Venneri, and John Warkentin Epoxide of a ketene acetal. The first 2,2-dialkoxyoxirane to be isolated **110**

Jailall Ramnauth and Edward Lee-Ruff Photochemical preparation of cyclopropanes from cyclobutanones **114**

R. Centoducatte, E.V.R. de Castro, and F.E. Jorge Gaussian basis sets for the atoms from K through Xe **121**

Martyn C.R. Symons and Raymond E. March Possible structures for H-Cu-CH_3 molecules **124**

© 2001 NRC Canada

Jun Lu, Yi Xie, Xuchuan Jiang, Wei He, Ping Yan, and Yitai Qian Potassium borohydride reducing route to phase-pure nanocrystalline InSb at low temperature **127**

Renhai Zhao and Pujing Pan A spectrophotometric study of Fe(II)-chloride complexes in aqueous solutions from 10 to 100°C **131**

Reginaldo C. Rocha and Henrique E. Toma Intervalence transfer in a new benzotriazolate bridged ruthenium-iron complex **145**

Vimal K. Balakrishnan, Julian M. Dust, Gary W. vanLoon, and Erwin Buncel Catalytic pathways in the ethanolysis of fenitrothion, an organophosphorothioate pesticide. A dichotomy in the behaviour of crown/cryptand cation complexing agents **157**

XiaoMei Wang, Chun Wang, WenTao Yu, YuFang Zhou, Xian Zhao, Qi Fang, and MinHua Jiang Two-photon absorption of styryl-quinolinium, -pyridinium, and -barbituric acid derivatives, and intramolecular charge transfer **174**

D.V. Sevenard, O.G. Khomutov, M.I. Kodess, K.I. Pashkevich, I. Loop, E. Lork, and G.-V. Röschenthaler Novel polyfluoroalkylated pyrazoles from 2-polyfluoroacylcycloalkanones and hydrazines: syntheses and unequivocal molecular structure assignment **183**

Gerald W. Buchanan, Majid F. Rastegar, and Glenn P.A. Yap Synthesis, X-ray crystal structure, and solid-state ^{13}C NMR study of tris(9-crown-3)triphenylene **195**

Leonid G. Akim, Jorge Luiz Colodette, and Dimitris S. Argyropoulos Factors limiting oxygen delignification of kraft pulp **201**

J.C. Belchior, J.P. Braga, and N.H.T. Lemes Classical analysis of intermolecular potentials for Ar–CO_2 rotational collisions **211**

Xun-Cheng Su, Zhi-Fen Zhou, Hua-Kuan Lin, Shou-Rong Zhu, Hong-Wei Sun, Guang-Hua Zhao, and Yun-Ti Chen Studies on the synthesis and properties of bischelating dioxotetraamine macrocycle, its metal complexes and thermodynamic stability in aqueous solution **221**

Wolfgang Kliegel, Gottfried Lubkowitz, Jens O. Pokriefke, Steven J. Rettig, and James Trotter Formation of heterocyclic arylboronates by thermally induced 1,4-aryl migration in diarylboron chelates of *C*-(1-hydroxyalkyl)nitrones. Crystal and molecular structures of some of the rearrangement products and of one of the educts **226**

Ulrike Spohr, Nghia Le, Chang-Chun Ling, and Raymond U. Lemieux The syntheses of 6-*C*-alkyl derivatives of methyl α-isomaltoside for a study of the mechanism of hydrolysis by amyloglucosidase **238**

Author Index / Index des auteurs **AI-1**

March / mars

ARTICLES

Marie-Josèphe Bourgeois, Marianne Vialemaringe, Monique Campagnole et Evelyne Montaudon Réaction compétitive de la substitution homolytique intramoléculaire : décomposition de peroxydes allyliques dans le thioglycolate de méthyle **257**

Paul K. Baker, Michael G.B. Drew, and Deborah S. Evans Bis(1-phenyl-1-propyne) complexes of tungsten(II): crystal structures of $[WI_2(CO)(NCR)(\eta^2\text{-}MeC_2Ph)_2]$ (R = Me, Et, or Ph) **263**

S. Cao, X. Qian, and G. Song *N′-tert*-Butyl-*N′*-aroyl-*N*-(alkoxycarbonylmethyl)-*N*-aroylhydrazines, a novel nonsteroidal ecdysone agonist: syntheses, insecticidal activity, conformational, and crystal structure analysis **272**

Michael W. P. Petryk and Bryan R. Henry Overtone intensities in neopentane and tetramethylsilane **279**

Bryon E. Carpenter, Warren E. Piers, and Robert McDonald Synthesis of the diborylated ferrocene 1,1′-bis-(bis-pentafluorophenylboryl)ferrocene and the X-ray structure of its trimethylphosphine adduct **291**

Christopher W. Kirby and William P. Power Cobalt-59 chemical shift and quadrupolar tensors of simple octahedral cobalt(III) complexes **296**

J.M. Ball and J.B. Hnatiw The reduction of I_2 by H_2O_2 in aqueous solution **304**

Nadine Merkley, Paul C. Venneri, and John Warkentin Cyclopropanation of benzylidenemalononitrile with dialkoxycarbenes and free radical rearrangement of the cyclopropanes **312**

Xiaosong Lu, Darren L. Reid, and John Warkentin Diaryloxycarbenes from oxadiazolines **319**

© 2001 NRC Canada

Zhen Wang, Yan-Li Shi, and Hu-Lin Li Investigation of two-component mixed self-assembled monolayers on gold **328**

Hong Yeob Choi, Jin Hyang Song, Yong Sung Park, Gabriel Lord, and Dong Ki Park Flow injection-chemiluminescent assay for the determination of superoxide dismutase activity **337**

Neil Burford, T. Stanley Cameron, Kim-Chung Lam, Daren J. LeBlanc, Charles L.B. Macdonald, Andrew D. Phillips, Arnold L. Rheingold, Laura Stark, and Denise Walsh Synthesis and characterization of an homologous series of bis(amido)diazadipnictetidines (Pnict = P, As, Sb, Bi) **342**

Author Index / Index des auteurs **AI-1**

April / avril

ARTICLES

John R. Scheffer 2000 ALFRED BADER AWARD LECTURE In the footsteps of Pasteur: asymmetric induction in the photochemistry of crystalline ammonium carboxylate salts **349**

Andrey S. Klymchenko, Turan Ozturk, Vasyl G. Pivovarenko, and Alexander P. Demchenko Synthesis and spectroscopic properties of benzo- and naphthofuryl-3-hydroxychromones **358**

Xiaosong Lu and John Warkentin Mechanism of ipso aromatic substitution by reaction of aryloxy(methoxy)carbenes and diaryloxycarbenes with DMAD **364**

Catherine Morlay, Yolande Mouginot, Monique Cromer, and Olivier Vittori Determination of the complexation properties of a crosslinked poly(acrylic acid) gel with copper(II), nickel(II), and lead(II) in dilute aqueous solution **370**

K.P. Koteva, André M. Cantin, W.A. Neugebauer, and E. Escher Synthesis and evaluation of novel β-lactam inhibitors of human leukocyte elastase **377**

Zhaohui Wang, Yoshiteru Horikawa, George C. Benson, and Benjamin C.-Y. Lu Excess enthalpies of the ternary mixtures: ethyl *tert*-butylether + *n*-heptane + (*n*-decane or *n*-dodecane) at 298.15 K **388**

Birgit Gaisberger and Sonja Solar Demethoxylation and hydroxylation of methoxy- and hydroxybenzoic acids by OH-radicals. Processes of potential importance for food irradiation **394**

A. Rauk, D.A. Armstrong, and J. Berges Glutathione radical: Intramolecular H abstraction by the thiyl radical **405**

Ram Nath Gupta, Thomas Hemscheidt, Brian G. Sayer, and Ian D. Spenser Incorporation of ^{13}C glucose into nicotinamide in *E. coli* and in *S. cerevisiae* **418**

J. Stephen Hartman and James A.W. Shoemaker Chelated fluoroboron cations. III. Spectroscopic evidence for ring size and steric limitations to chelate formation by amine chelating donors **426**

Mark E. McComb, Richard D. Oleschuk, Art Chow, Hélène Perreault, Ragnar G. Dworschak, Marek Znamirowski, Werner Ens, Kenneth G. Standing, and Ken R. Preston Application of nonporous polyurethane (PU) membranes and porous PU thin films as sample supports for MALDI-MS of wheat proteins **437**

Antonio Rojas, Alfonso Perez-Encabo, Ignacio Herraiz-Sierra, and Carlos A. Blanco Tautomerization tendencies of 2-acetylcycloalkanones, 2-acetyl-1,3-cycloalkanediones, and cyclic β-keto esters of five- and six-membered rings **448**

Dengke Cao, Huakuan Lin, Zhifen Zhou, Shourong Zhu, Xuncheng Su, and Yun-Ti Chen Potentiometric titration study of two novel polydenate ligands and investigations of their complexes **455**

James F. King, Kim M. Baines, Matthew R. Netherton, and Vinod Dave Bis(trimethylsilyl)methanesulfonyl and tris(trimethylsilyl)methanesulfonyl chlorides and their reactions by way of sulfenes: Addendum **461**

Author Index / Index des auteurs **AI-1**

May-June / mai-juin

This issue is dedicated to Professor Brian R. James
Ce tirage est dédié au Professeur Brian R. James

Dedication / Dédicace **iii**

ARTICLES

Martyn Brown and Chet Jablonski Synthesis, characterization, and C—N bond cleavage of tungsten(VI)arylimido-calix[4]arene complexes **463**

© 2001 NRC Canada

David C.D. Butler, Duncan W. Bruce, Philip Lightfoot, and David J. Cole-Hamilton On the reduction of rhodium trichloride in the presence of triisopropylphosphine **472**

Vladimir I. Bakhmutov, Ekaterina V. Bakhmutova, Natalia V. Belkova, Claudio Bianchini, Lina M. Epstein, Dante Masi, Maurizio Peruzzini, Elena S. Shubina, Evgenii V. Vorontsov, and Fabrizio Zanobini In-depth NMR and IR study of the proton transfer equilibrium between [{(MeC(CH_2PPh_2)$_3$}Ru(CO)H_2] and hexafluoroisopropanol **479**

Lyndsey Cooper, Sian C. Davies, Jonathan R. Dilworth, David L. Hughes, Marcin Konkol, Raymond L. Richards, J. Roger Sanders, and Piotr Sobota Iron complexes of the $N(CH_2CH_2S)_3^{3-}$ (NS_3) ligand with isocyanide co-ligands **490**

Fausto Calderazzo, Ulli Englert, Guido Pampaloni, Vincenzo Passarelli, Giovanna Serni, and Ruimin Wang Synthesis, characterization, and reactivity of manganese(II) and iron(II) trifluoroacetates. Crystal and molecular structure of two linkage isomers of polynuclear $[Mn(CF_3COO)_2(THF)_2]_n$ **495**

Peter Legzdins, Kevin M. Smith, and Steven J. Rettig Synthesis, characterization, and properties of some cyclopentadienyl molybdenum nitrosyl benzyl complexes **502**

Alexander W. Wong, Shouming He, and Stephen G. Withers Synthesis of 5-fluoro-β-D-glucopyranosyluronic acid fluoride and its evaluation as a mechanistic probe of *Escherichia coli* β-glucuronidase **510**

Helmut Werner, Petra Bachmann, and Marta Martin Homobinuclear Ru–Ru and heterobinuclear Ru–Rh complexes with alkynyl and vinylidene ligands as molecular units **519**

David M. Tellers and Robert G. Bergman Mechanistic study of ligand substitution processes in TpIr(III) complexes **525**

François Simal, Dominique Jan, Lionel Delaude, Albert Demonceau, Marie-Rose Spirlet, and Alfred F. Noels Evaluation of ruthenium-based complexes for the controlled radical polymerization of vinyl monomers **529**

Michael D. Fryzuk, Paul B. Duval, and Steven J. Rettig Formation and reactivity of the zirconium ethylene complexes [η^5-C_5H_3-1,3-($SiMe_2CH_2PR_2$)$_2$]Zr(η^2-CH_2=CH_2)(X) (R = Me, Pr^i; X = Br, C_5H_5) **536**

Ryan P. Rodgers, Christopher L. Hendrickson, Mark R. Emmett, Alan G. Marshall, Mark Greaney, and Kuangnan Qian Molecular characterization of petroporphyrins in crude oil by electrospray ionization Fourier transform ion cyclotron resonance mass spectrometry **546**

Daniel Meilleur and Pierre D. Harvey Structural, electronic and spectroscopic features of the dihydride $Pd_4(dppm)_4(H)_2^{2+}$ cluster catalyst **552**

Inmaculada del Río, Piet W.N.M. van Leeuwen, and Carmen Claver Study of the hydroformylation of 2,5-dihydrofuran catalyzed by rhodium diphosphine complexes **560**

Bernd Siebenhaar, Bruno Casagrande, Martin Studer, and Hans-Ulrich Blaser An easy-to-use heterogeneous catalyst for the Knoevenagel condensation **566**

M. Aresta, I. Tommasi, C. Dileo, A. Dibenedetto, M. Narracci, J. Ziolkowski, and A. Jezierski Synthesis and spectroscopic (^{1}H NMR, ESR) characterization of new aryloxy–Mn(II) complexes: steric control over *O*– vs. phenyl–π-coordination of ArO^- ligands (ArO^- = $C_6H_5O^-$, 4-methyl-$C_6H_4O^-$, 3,5-dimethyl-$C_6H_3O^-$, 2,6-di-*tert*-butyl-$C_6H_3O^-$, 2,6-dimethyl-$C_6H_3O^-$) to the "Mn(II)Cp" moiety, and their reactivity with carbon dioxide **570**

Hanrong Gao and Robert J. Angelici $Rh_2Cl_2(CO)_4$ adsorbed and tethered on gold powder: IR spectroscopic characterization and olefin hydrogenation activity **578**

Christophe Moineau, Giuseppe Mele, and Howard Alper Palladium-catalyzed alternating copolymerization of carbon monoxide with olefins bearing carbamate and amide functionalities **587**

Kyoko Nozaki, Fumitoshi Shibahara, Stephan Elzner, and Tamejiro Hiyama Alternating copolymerization of ω-perfluoroalkyl-1-alkenes with carbon monoxide catalyzed by homogeneous and polymer-supported Pd-complexes **593**

William P. Griffith and Maria Suriaatmaja Studies on transition-metal nitrido and oxo complexes. Part 20. Oxoruthenates and oxo-osmates in oxidation catalysis; *cis*-$[Os(OH)_2O_4]^{2-}$ as a catalytic oxidant for primary amines and for alcohols **598**

Man-Kit Lau, Joyce L.C. Chim, Wing-Tak Wong, Ian D. Williams, and Wa-Hung Leung Synthesis and molecular structures of monooxo aryl complexes of osmium(VI) **607**

Peter J.S. Richardt, Jonathon M. White, Peter A. Tregloan, Alan M. Bond, and Anthony G. Wedd One-electron reduction of the γ*-isomer of $[S_2W_{18}O_{62}]^{4-}$ leads to isolation of the α-isomer **613**

© 2001 NRC Canada

Lorenzo Battaglia, Francesco Pinna, and Giorgio Strukul Thioacetalization of aldehydes and ketones in the presence of hydroxo complexes of platinum(II): An example of Lewis acid catalytic activity **621**

Dale C. Smith, Jr., Jérémie Cadoret, Laleh Jafarpour, Edwin D. Stevens, and Steven P. Nolan Synthetic and solution calorimetric investigations of chelating phosphine ligands in $Ru(allyl)_2(PP)$ complexes (PP = diphosphine) **626**

Fusao Takagi, Hidetake Seino, Yasushi Mizobe, and Masanobu Hidai Addition of bridging-hydrosulfido ligands in diiridium complex to acrylonitrile. Synthesis of diiridium cyanoethylthiolato complexes and $RuIr_2$ sulfido-cyanoethylthiolato cluster **632**

Gábor Papp, József Kovács, Attila Cs. Bényei, Gábor Laurenczy, Levente Nádasdi, and Ferenc Joó (*para*-Diphenylphosphino)benzenesulfonic acid and its ruthenium(II) complexes: an old water soluble phosphine ligand in a new perspective **635**

Roland Fornika, Christian Six, Helmar Görls, Magnus Kessler, Carl Krüger, and Walter Leitner Synthesis and structural features of complexes $[(P^{\frown}P)_2Rh][hfacac]$ containing hexafluoroacetyl-acetonate as a noncoordinating anion **642**

Gábor Besenyei, András Neszmélyi, Sándor Holly, László I. Simándi, and László Párkányi A relationship between the catalytic carbonylation of (*N*-arenesulfonyl)imides and iodonium ylides **649**

Martin A. Bennett, Thomas R.B. Mitchell, Mark R. Stevens, and Anthony C. Willis Mono- and bis-(acetylacetonato) complexes of arene–ruthenium(II) and arene–osmium(II): variation of the binding mode of η^1-acetylacetonate with the nature of the arene **655**

Serafino Gladiali, Serenella Medici, Giovanna Pirri, Sonia Pulacchini, and Davide Fabbri BINAPS — An axially chiral *P*,*S*-heterodonor ligand for asymmetric catalysis based on binaphthalene backbone **670**

Hildo Antonio dos Santos Silva, Bruce R. McGarvey, Regina Helena de Almeida Santos, Mauro Bertotti, Vânia Mori, and Douglas Wagner Franco Sulfate as a ligand in ruthenium(II) and (III) ammines **679**

Göran Verspui, Gábor Besenyei, and Roger A. Sheldon Amide directed hydrocarboxylation of *N*-allylacetamide catalyzed by the aqueous Pd – tppts – Brønsted acid system (tppts = $P(C_6H_4\text{-}m\text{-}SO_3Na)_3$)[1] **688**

Carolien J. den Reijer, Pascal Dotta, Paul S. Pregosin, and Alberto Albinati Binap and MeO-Biphep complexes of Ru(II). Dicationic ligands as 6e donors. Unexpected cyclometallation in connection with P—C bond breaking **693**

Paul J. Dyson, David J. Ellis, and Thomas Welton A temperature-controlled reversible ionic liquid – water two phase – single phase protocol for hydrogenation catalysis **705**

Martin Albrecht, Stuart L. James, Nora Veldman, Anthony L. Spek, and Gerard van Koten Transmetalation reactions with nitrogen-containing "pincer"-class ligands on platinum(II) centers **709**

Colin A. Thomas, R. Jason Bonilla, Yong Huang, and Philip G. Jessop Hydrogenation of carbon dioxide catalyzed by ruthenium trimethylphosphine complexes — Effect of gas pressure and additives on rate in the liquid phase **719**

J. Bakos, S. Cserépi-Szűcs, Á. Gömöry, C. Hegedüs, L. Markó, and Á. Szöllősy Asymmetric hydroformylation of styrene catalyzed by platinum complexes of chiral diphosphites with atropisomeric terminal moieties **725**

Paul Beagley, Philip Davies, Harry Adams, and Colin White Chiral metallocenes: the synthesis and X-ray crystal structures of $TiCl_2(\eta^5\text{:}\eta^5\text{-}C_5Me_4SiMe_2C_5H_3R^*)$ (R^* = menthyl or neomenthyl) and related compounds **731**

Marta Catellani, Federica Cugini, and Domenico Tiefenthaler New pathways of site selective aromatic alkylation of palladium complexes: fragmentation to arenes vs. ring closure to hexahydromethano-fluorenes or -phenanthrenes **742**

Anna M. Trzeciak, Hubert Bartosz-Bechowski, Zbigniew Ciunik, Katarzyna Niesyty, and Józef J. Ziółkowski Structural studies of $PdCl_2L_2$ complexes with fluorinated phosphines, phosphites, and phosphinites as precursors of benzyl bromide carbonylation catalysts, and X-ray crystal structure of *cis*-$PdCl_2[PPh_2(OEt)]_2$ **752**

Harry Adams, Sylvana C.M. Agustinho, Krystyna Chomka, Brian E. Mann, Stephen Smith, Clare Squires, and Sharon E. Spey The fluxionality and crystal structures of $[Fe_3(CO)_{10}L_2]$ (L_2 = dppm, $(Ph_2P)_2NH$, $\{(EtO)_2P\}_2O$) and $[Fe_3(CO)_9(dppm)\{P(OMe)_3\}]$ **760**

Bogdan Marciniec, Ewa Małecka, Jacek Guliński, Monika Grundwald-Wyspiańska, and Mariusz Lewandowski Functionalization vs. degradation of 1,4-polybutadiene by ruthenium complex catalyzed reaction with vinylsilanes **775**

Sean E. Durran, Martin B. Smith, Alexandra M.Z. Slawin, Thomas Gelbrich, Michael B. Hursthouse, and Mark E. Light Synthesis and coordination studies of new aminoalcohol functionalized tertiary phosphines **780**

© 2001 NRC Canada

Yurii V. Geletii, Alan J. Bailey, Jennifer J. Cowan, Ira A. Weinstock, and Craig L. Hill Highly efficient and stable catalyst for peroxynitrite decomposition **792**

Fabio Zobi and Dennis V. Stynes Hetero trinuclear oxo-bridged complexes of ruthenium porphyrin and iron phthalocyanine **795**

Joseph L. Samonte and Michael T. Pope Derivatization of polyoxotungstates in aqueous solution. Exploration of the kinetic stability of cobalt(II)- and cobalt(III) derivatives of lacunary anions with pyridine and pyridine-type ligands **802**

P.K. Das, Susan Stanislav Alguindigue, and Michael T. Ashby A DFT study of Zr–S rotational barriers of $(\eta^5\text{-}C_5H_5)_2Zr(Cl)(SR)$; the origin of an inverse steric effect **809**

Josephine Mary Hill and Flora T.T. Ng Adsorption of etioporphyrin and Ni-etioporphyrin on a fractal silica **817**

David Morales-Morales, Rocío Redón, Zhaohui Wang, Do W. Lee, Cathleen Yung, Kevin Magnuson, and Craig M. Jensen Selective dehydrogenation of alcohols and diols catalyzed by a dihydrido iridium PCP pincer complex **823**

Jonghyuk Lee, Geun-Bae Yi, Douglas R. Powell, Masood A. Khan, and George B. Richter-Addo Synthesis, characterization, and protonation of octaethylporphyrin osmium nitrosyl complexes containing axial thiolate ligands — X-ray structures of an alkyl thionitrite (RSNO) and its (OEP)Os(NO)(SR) addition product **830**

Jinkui Zhou and Thomas W. Swaddle Pressure effects and solvent dynamics in the electrochemical kinetics of the tris(hexafluoroacetylacetonato)ruthenium(III)/(II) couple in nonaqueous solvents **841**

Devinder Mahajan, Viwat Krisdhasima, and Robert D. Sproull Kinetic modeling of homogeneous methanol synthesis catalyzed by base-promoted nickel complexes **848**

Leah Basickes, Andrew G. Bunn, and Bradford B. Wayland Equilibrium thermodynamic studies for the formation of 1:1 complexes of CO and ethene with a rhodium(II) porphyrin metallo-radical **854**

Bryon E. Carpenter, Warren E. Piers, Masood Parvez, Glenn P.A. Yap, and Steven J. Rettig Synthesis, characterization and chemistry of bis-(pentafluorophenyl)boryl ferrocene **857**

Florian P. Pruchnik, Radosław Starosta, Zbigniew Ciunik, Adam Opolski, Joanna Wietrzyk, Elżbieta Wojdat, and Danuta Duś Tetraacetatodirhodium(II) complexes with tris(methoxyphenyl)phosphines, their reactivity, structure, and antitumor activity **868**

Clifford C. Leznoff and Bohdan Suchozak Octaarylethynyl and octaarylbutadiynyl phthalocyanines **878**

Jean-Marc Vincent, Alain Rabion, Vittal K. Yachandra, and Richard H. Fish Fluorous biphasic catalysis. 2. Synthesis of fluoroponytailed amine ligands along with fluoroponytailed carboxylate synthons, $[M(C_8F_{17}(CH_2)_2CO_2)_2]$ (M = Mn^{2+} or Co^{2+}): Demonstration of a perfluoroheptane soluble precatalyst for alkane and alkene functionalization in the presence of *tert*-butyl hydroperoxide and oxygen gas **888**

Werner E. van Zyl, José M. López-de-Luzuriaga, John P. Fackler, Jr., and Richard J. Staples Dithiophosphinates of gold (I); oxidative addition of Cl_2 to a neutral, dinuclear gold(I) dithiophosphinate complex, and X-ray crystal structures of $[AuS_2P(C_2H_5)_2]_2$, $[AuS_2PPh_2]_2$, $Au_2(CH_2)_2PMe_2(S_2PPh_2)$, and $Au_2Cl_2[(CH_2)_2PMe_2][S_2PPh_2]$ **896**

Peter Barthazy, Diego Broggini, and Antonio Mezzetti Making a 16-electron bromo (or iodo) complex of ruthenium(II) and a C—F bond in one pot **904**

Yuan Gao, Michael C. Jennings, and Richard J. Puddephatt Hydrogen transfer from formic acid to alkynes catalyzed by a diruthenium complex **915**

Shane Phillips, Bruce C. Noll, Marilyn M. Olmstead, and Alan L. Balch Oxidation of copper(II) hydroxyporphyrin (oxophlorin); oxidative ring opening and formation of an ester-linked, dinuclear copper complex **922**

Kevin R. Coulter, Alexander McAuley, and Steven Rettig Synthesis and characterization of the pentadentate macrobicyclic ligand, 14-thia-1,4,8,11-tetraazabicyclo[9.5.3]nonadecane (L1) and its nickel(II) complexes. X-ray crystal structure of $[Ni(L1)(ClO_4)](ClO_4)\cdot 2[Ni(L1)(OH_2)](ClO_4)_2\cdot 6H_2O$ **930**

Sudeep Bhattacharyya, Anette Martinsson, Raymond J. Batchelor, F.W.B. Einstein, and Alan S. Tracey *N*,*N*-dimethylhydroxamidovanadium(V). Interactions with sulfhydryl-containing ligands: V(V) equilibria and the structure of a V(IV) dithiothreitolato complex **938**

Mee-Kyung Chung, George Ferguson, Valerie Robertson, and Marcel Schlaf Nature of the active silane alcoholysis catalyst in the $Ru_wCl_x(CO)_y(PMe_3)_z$ (*w*, *x*, *y*, *z* = 1 or 2) system; $Ru_2(\mu\text{-}Cl)_2Cl_2(CO)_4(PMe_3)_2$ as a new catalyst for silane alcoholysis in a polar solvent **949**

© 2001 NRC Canada

Dino Amoroso, Glenn P.A. Yap, and Deryn E. Fogg The life, death, and ROMP activity of ruthenium complexes containing the basic, chelating diphosphine bis(dicyclohexyl)-1,4-phosphinobutane **958**

Kamaluddin Abdur-Rashid, Alan J. Lough, and Robert H. Morris Intra- and inter-ion-pair protonic—hydridic bonding in polyhydridobis(phosphine)rhenates **964**

Stephan Knoblauch, H. Fred Koch, Catherine Polydore, and D. Max Roundhill A computational approach to seeking methylmercury(II) thiolate calix[4]arene hosts for both octasulfur and organosulfur compounds as guests **977**

Anca Silvestru, Adina Rotar, John E. Drake, Michael B. Hursthouse, Mark E. Light, Sorin I. Farcas, Roland Rösler, and Cristian Silvestru Synthesis, spectroscopic characterization, and structural studies of new Cu(I) and Cu(II) complexes containing organophosphorus ligands, and crystal structures of $(Ph_3P)_2Cu[S_2PMe_2]$, $(Ph_3P)_2Cu[(OPPh_2)_2N]$, $Cu[(OPPh_2)_2N]_2$, and $Cu[(OPPh_2)(SPPh_2)N]_2$ **983**

Mehrdad Ebadi, Christos Alexiou, and A.B.P. Lever The reduction of oxygen and hydrogen peroxide on dinuclear ruthenium phthalocyanine electrocatalytic surfaces **992**

Charles P. Casey, Steven W. Singer, and Douglas R. Powell The role of a hydroxycyclopentadienyl ruthenium dicarbonyl formate in formic acid reductions of carbonyl compounds catalyzed by Shvo's diruthenium catalyst **1002**

Michael C. Murray and Michael C. Baird Polymerization of 1-hexene catalyzed by Cp^*TiMe_3-$B(C_6F_5)_3$; a mechanistic and structural study **1012**

Jason A. Wiles, Steven H. Bergens, and Victor G. Young, Jr. Stereochemistry at carbon upon protonolysis of a late transition metal-alkyl bond: a reaction of relevance to catalytic enantioselective hydrogenation of olefins **1019**

Gregory S. Long, Benjamin Snedeker, Kyle Bartosh, Michelle L. Werner, and Ayusman Sen Transition metal phthalocyanine and porphyrin complexes as catalysts for the polymerization of alkenes **1026**

Alzir A. Batista, Salete L. Queiroz, Peter C. Healy, Robbie W. Buckley, Sue E. Boyd, Susan J. Berners-Price, Eduardo E. Castellano, and Javier Ellena A novel coordination mode for a pyridylphosphine ligand. X-ray structures of $[RuCl_2(NO)L]$ (I) and $[RuCl_2(NO)L]\cdot DMSO$ (II) ($L = [(2\text{-py})_2PC_2H_4POO(2\text{-py})_2]^-$) **1030**

Allen A. Bowden and Jim D. Atwood Reactions of SO_2 with *trans*-$Ir(CO)(Cl)(TPPTS)_2$ in water **1036**

H. Gulyás, A. Dobó, and J. Bakos Synthesis of sulfated mono- and ditertiary phosphines, complex chemistry and catalysis **1040**

Peter G. Breed, James A. Ramsden, and John M. Brown Scope and limitations of ruthenium-catalyzed metathesis of simple polymer-bound alkenes **1049**

Bin Song, Glen S. Kurokawa, Shuang Liu, and Chris Orvig Proton- and lanthanide-coordinating properties of the tetraaza macrocycle $(EDDA–KA)_2$ in aqueous solution **1058**

David Delmarre, Noboru Hioka, Ron Boch, Ethan Sternberg, and David Dolphin Aggregation studies of benzoporphyrin derivative **1068**

John F. Harrod, Ronghua Shu, Hee-Gweon Woo, and Edmond Samuel Titanocene(III) catalyzed homogeneous hydrosilation–hydrogenation of pyridines **1075**

Johannes G. de Vries The Heck reaction in the production of fine chemicals **1086**

Author Index / Index des auteurs **AI-1**

July / juillet

ARTICLES

Almeria Natansohn and Paul Rochon 2000 MACROMOLECULAR SCIENCE AND ENGINEERING AWARD LECTURE
The versatility of azobenzene polymers **1093**

Brian D. Wagner, Shannon J. Fitzpatrick, Monica A. Gill, Andrew I. MacRae, and Natasa Stojanovic A fluorescent host–guest complex of cucurbituril in solution: a molecular Jack O'Lantern **1101**

Hongyan Luo, Robin D. Rogers, and Martin W. Brechbiel A convenient and selective route to a *trans*-difunctionalized macrocyclic hexadentate N_4O_2 ligand **1105**

Francis B. Panosyan and Ian W.J. Still An efficient route to 5-iodo-1-methylimidazole: synthesis of xestomanzamine A **1110**

© 2001 NRC Canada

Christopher M. Vogels, Liliya G. Nikolcheva, David W. Norman, Heather A. Spinney, Andreas Decken, Mark O. Baerlocher, Felix J. Baerlocher, and Stephen A. Westcott Synthesis and antifungal properties of benzylamines containing boronate esters **1115**

K. Omar Zahir Reduction of hexaammineruthenium(III) ions by a series of tris(polypyridyl)chromium(II) ions — Revisiting the $Cr(NN)_3^{3+/2+}$ self-exchange rate **1124**

Iwona Grześkowiak, Włodzimierz Gałęzowski, and Arnold Jarczewski Kinetic study of the proton transfer reaction between 1-nitro-1-(4-nitrophenyl)alkanes and TBD and MTBD bases in acetonitrile solvent **1128**

Cristina Maria P. Santos, Roberto B. Faria, Juan O. Machuca-Herrera, and Sérgio de P. Machado Equilibrium geometry, vibrational frequencies, and heat of formation of HOBr, $HBrO_2$, and $HBrO_3$ isomers **1135**

Peter James Smith, David A.J. Crowe, and Kenneth Charles Westaway Using secondary alpha deuterium kinetic isotope effects to determine the stereochemistry of an E2 reaction; the stereochemistry of the E2 reaction of 1-chloro-2-phenylethane with potassium *tert*-butoxide in *tert*-butyl alcohol **1145**

Souad Souirti and Michel Baboulène Original disymmetric bolaforms bearing at least one sulfobetaine head; synthesis and surface properties **1153**

László Somogyi Elimination, ring-contraction, and fragmentation reactions of 1-thioflavanone 1-oxides **1159**

Igor Povar Détermination de la stabilité du complexonate peu soluble à partir des données pH-métriques **1166**

Christine Roehri-Stoeckel, Emmanuel Gonzalez, André Fougerousse, and Raymond Brouillard Synthetic dyes: simple and original ways to 4-substituted flavylium salts and their corresponding vitisin derivatives **1173**

Laurence Meunier, Jean-François Pilichowski, and Pierre Boule Photochemical behaviour of 1,4-dichlorobenzene in aqueous solution **1179**

Corey Seward and Suning Wang Dimeric and polymeric $[Eu(tta)_3L]$ complexes (tta = thenoyltrifluoroacetonato, L = 4,4′-bipyridine, *trans*-1,2-bis(4-pyridyl)ethylene, 4,4′-bipyridine-*N*,*N*′-dioxide) **1187**

Michael D. Fryzuk, Peihua Yu, and Brian O. Patrick Synthesis, structure, and reactivity of diamidophosphine complexes of yttrium and the lanthanides **1194**

Author Index / Index des auteurs **AI-1**

August / août

ARTICLES

Andy Z. Lu, Thomas Q. Hu, David A. Osmond, Brian O. Patrick, and Brian R. James Tetrazole ethers from lignin model phenols: synthesis, crystal structures, and photostability **1201**

Abdul Wahab and Sekh Mahiuddin Electrical conductivity, speeds of sound, and viscosity of aqueous ammonium nitrate solutions **1207**

Dingsheng He, Ming Ma, Hui Wang, and Pandeng Zhou Effect of kinetic synergist on transport of copper(II) through a liquid membrane containing P_{507} in kerosene **1213**

Quan Zhuang and Jack M. Miller One-pot sol-gel synthesis of sulfated ZrO_2–SiO_2 catalysts for alcohol dehydration **1220**

Quan Zhuang and Jack M. Miller Sol-gel synthesis of ternary phosphate–ZrO_2–SiO_2 catalysts for alcohol dehydration **1224**

Victor Barba, Damian Cuahutle, Rosa Santillan, and Norberto Farfán Stereoselective addition of acetone to the C=N bond of [4.3.0] boron heterobicycles **1229**

Saul Wolfe, Stephen Ro, Chan-Kyung Kim, and Zheng Shi Synthesis and decarboxylation of Δ^2-cephem-4,4-dicarboxylic acids **1238**

Saul Wolfe, Stephen Ro, and Zheng Shi Generation, electrocyclic ring opening, and unprecedented conversion of a 3-acylaminoazetinone into *cis*-3,4-disubstituted azetidinones **1259**

Saul Wolfe, Yih-Huang Hsieh, Raymond J. Batchelor, Frederick W.B. Einstein, and Ian D. Gay A topochemical rearrangement with multiple inversions of configuration **1272**

Saul Wolfe and Zheng Shi The ozonolysis of *ortho*-xylene and its relevance to the history of the benzene problem **1278**

© 2001 NRC Canada

Saul Wolfe, Anthony V. Buckley, and Noham Weinberg A comprehensive computational examination of transannular Diels–Alder reactions of unsubstituted C14 trienes — Barriers, template effects, and the Curtin–Hammett principle **1284**

ADDITIONS AND CORRECTIONS / AJOUTS ET CORRECTIONS

Umarani Rajalingam, Philip A.W. Dean, and Hilary A. Jenkins Solution multinuclear (^{31}P,^{111}Cd,^{77}Se) magnetic resonance studies of cadmium complexes of heterocyclic aromatic thiones and the structure of [tetrakis(2(1*H*)-pyridinethione)cadmium] nitrate, $[Cd(C_5H_5NS)_4](NO_3)_2$ **1293**

ADDITIONS AND CORRECTIONS / AJOUTS ET CORRECTIONS

Małgorzata Dawid, Paul C. Venneri, and John Warkentin Expoxide of a ketene acetal. The first 2,2-dialkoxyoxirane to be isolated **1294**

Author Index / Index des auteurs **AI-1**

September / septembre

ARTICLES

Michael J. McGlinchey 2000 ALCAN AWARD LECTURE Adventures in organometallic NMR: steric restraints, slowed rotations, and skeletal rearrangements **1295**

Giuseppe Graziano An analysis of the hydration thermodynamics of the CONH group **1310**

Andreas Decken, Melanie A. Neil, and Frank Bottomley Synthesis and characterization of manganese complexes of the dibenzophospholyl ligand **1321**

Umarani Rajalingam, Philip A.W. Dean, Hilary A. Jenkins, Michael Jennings, and James M. Hook Cadmium complexes of thiones. Part II.[1] A synthetic, solution, and solid-state MAS $^{111/113}Cd$ NMR study of cadmium complexes of 1,3-thiazolidine-2-thione, and the structures of [tetrakis(1,3-thiazolidine-2-thione)cadmium] trifluoromethanesulfonate ($[Cd(C_3H_5NS_2)_4](CF_3SO_3)_2$) and [tetrakis(1,3-thiazolidine-2-thione)cadmium][tetrakis(nitrato-*O*,*O*′)cadmate] ($[Cd(C_3H_5NS_2)_4][Cd(O_2NO)_4]$) **1330**

Holger Kleinke $Ti_5Si_{1.3}Sb_{1.7}$ — The first titanium silicide antimonide, forming a crystal structure not found in either binary system **1338**

Satoshi Iwatsuki, Kenji Obeyama, Nobuyoshi Koshino, Shigenobu Funahashi, Kazuo Kashiwabara, Takayoshi Suzuki, and Hideo D. Takagi New low-spin Co(II) complexes with novel tripodal 1,1,1-tris(dimethylphosphinomethyl)ethane ligand: electron transfer kinetics and spectroscopic characterization of $Co(II)P_6$ and $Co(II)P_3S_3$ ions in aqueous solution **1344**

A. Wallace Cordes, James R. Mingie, Richard T. Oakley, Robert W. Reed, and Hongzhou Zhang Quinoxaline-1,2,3-dithiazolyls — Synthesis, EPR characterization, and redox chemistry **1352**

Mozaffar Asadi and Ali Hossein Sarvestani Synthesis, characterization, and thermodynamics of tertiary phosphine cobalt(III) Schiff-base complexes **1360**

Wei Fu, Hong-Xing Zhang, Ji-Kang Feng, and Wei Li Calculations on the electronic structure and non-linear second-order susceptibilities of fulleropyrrolidine–tetrathiafulvalene(C_{60}PY–TTF) based on donor–bridge–acceptor dyads **1366**

Roland Langner and Georg Zundel ^1H NMR studies of proton transfer equilibria in hydrogen bonds — the role of the entropy **1376**

Di-An Sun, Françoise Sauriol, Orval Mamer, and Lolita O. Zamir Reanalysis of the biotransformation of 4(20),11(12)-taxadiene derivatives **1381**

Lubo Jurasek, Lívia Krištofová, Yujun Sun, and Dimitris S. Argyropoulos Alkaline oxidative degradation of diphenylmethane structures — Activation energy and computational analysis of the reaction mechanism **1394**

Author Index / Index des auteurs **AI-1**

October / octobre

ARTICLES

Janusz Pawliszyn 2000 MAXXAM AWARD LECTURE Unified theory of extraction **1403**

© 2001 NRC Canada

M. Purcell, J.F. Neault, H. Malonga, H. Arakawa, and H.A. Tajmir-Riahi Interaction of human serum albumin with oxovanadium ions studied by FT-IR spectroscopy and gel and capillary electrophoresis **1415**

Takehiko Yamato, Kenji Kumamaru, and Hirohisa Tsuzuki The metal template effect on *O*-alkylation of tetrahydroxy[3.1.3.1]metacyclophane with 4-(chloromethyl)pyridine to afford tetrakis-[(4-pyridylmethyl)oxy]-[3.1.3.1]metacyclophanes and their conformational studies **1422**

I.S. Shehatta and M.S. Ibrahim Binding of anti-inflammatory drug indomethacin with cyclodextrin and DNA: solubility, spectroscopic, and voltammetric studies **1431**

Jonathan Gagnon, Martin Vézina, Marc Drouin, and Pierre D. Harvey Regioselective upper-rim functionalizations of calix[4]arene by diphenylphosphino groups **1439**

Juan Antonio Gonzalez, Javier Carmona, Nicolas Riesco, Isaias Garcia de la Fuente, and Jose Carlos Cobos DISQUAC predictions on thermodynamic properties of ternary and higher multicomponent mixtures. II. Results for H^E of ternary mixtures containing nonpolar components, or one polar compound, two polar compounds, or one alcohol and hydrocarbons, or CCl_4 **1447**

Miguel Angel Sánchez, Ana María Mainar, Juan Ignacio Pardo, María Carmen López, and José Santiago Urieta Solubility of nonpolar gases in 2,2,2-trifluoroethanol and 1,1,1,3,3,3-hexafluoropropan-2-ol at several temperatures and 101.33 kPa partial pressure of gas **1460**

William E. Acree, Jr. and Michael H. Abraham Solubility predictions for crystalline nonelectrolyte solutes dissolved in organic solvents based upon the Abraham general solvation model **1466**

Craig Anderson Synthesis of chloro(2-methylimidazole)ruthenium(III) complexes and their aqueous solution chemistry, and the crystal structure of $[2\text{-MeImH}]_2[RuCl_5\text{2-MeIm}]$ **1477**

M. Carla Aragoni, Massimiliano Arca, Francesco A. Devillanova, John R. Ferraro, Francesco Isaia, Francesco Lelj, Vito Lippolis, and Gaetano Verani An experimental and theoretical approach to phosphonodithioato complexes: molecular orbital analysis by hybrid-DFT and EHT calculations on *trans*-bis[*O*-alkyl-phenyl-phosphonodithioato]Ni^{II}, and vibrational assignments **1483**

C. Delamere, C. Jakins, and E. Lewars Tests for aromaticity applied to the pentalenoquinones — A computational study **1492**

G.W. Buchanan, M.F. Rastegar, G.P.A. Yap, A. Moghimi, and M. Ghandi Oxidative coupling of naphtho-9-crown-3 ether: X-ray crystal structure and solution and solid-state NMR analysis of the dimer **1505**

Author Index / Index des auteurs **AI-1**

November / novembre

This issue is dedicated to Professor V. Snieckus
Ce tirage est dédié au Professeur V. Snieckus

Dedication / Dédicace **iii**

ARTICLES

Lutz F. Tietze, Christian Ott, and Frank Haunert Efficient and regioselective synthesis of bridged ring systems by domino Knoevenagel – hetero-Diels–Alder reaction **1511**

Heidi L. Fraser and Gordon W. Gribble A synthesis of 6,11-disubstituted benzo[*b*]carbazoles **1515**

Atsunori Mori, Eisuke Takahisa, Yasushi Nishihara, and Tamejiro Hiyama Isomerization of (*Z*)-alkenylsilanes to (*E*)-isomers with hydrosilane and $RhI(PPh_3)_3$ **1522**

Oskar Middel, Willem Verboom, and David N. Reinhoudt Fourfold homologous anionic *ortho*-Fries rearrangement on a partially bridged resorc[4]arene **1525**

Dieter Enders, Volker Braig, and Gerhard Raabe Asymmetric synthesis of 3-aryl-substituted 2,3-dihydro-1*H*-isoindol-1-ones **1528**

Lian-Hai Li and Tak Hang Chan Organometallic reactions in aqueous media — Antimony-mediated allylation of carbonyl compounds and the nature of allylstibine intermediates **1536**

Stephen Y.W. Lau and Brian A. Keay A highly efficient strategy for the synthesis of 3-substituted salicylic acids by either directed *ortho*-lithiation or halogen–metal exchange of substituted MOM protected phenols followed by carboxylation **1541**

© 2001 NRC Canada

Mukund P. Sibi, Michael D. Johnson, and T. Punniyamurthy Enantioselective synthesis of peperomins A, C, D, and analogs — Examination of diastereoselective cuprate conjugate additions to *N*-enoyl-4-diphenylmethyl-2-oxazolidinones **1546**

Kyung Joo Lee and Kim D. Janda Traceless solid-phase synthesis of 5-benzoylbenzimidazoles **1556**

Oren P. Anderson, Anthony G.M. Barrett, Jeremy J. Edmunds, Shun-Ichiro Hachiya, James A. Hendrix, Kiyoshi Horita, James W. Malecha, Christopher J. Parkinson, and Andrew VanSickle Applications of crotyldiisopinocampheylboranes in synthesis: a formal total synthesis of (+)-calyculin A **1562**

Carsten Bolm, Oliver Beckmann, and Chiara Palazzi Chiral aluminum complexes as catalysts in asymmetric Baeyer-Villiger reactions of cyclobutanones **1593**

Eugenius Butkus, Arvydas Stončius, Julė Malinauskienė, Shuji Tomoda, and Daisuke Kaneno Stereoelectronic and conformational effects on the stereochemical course of reduction of bicyclo[3.3.1]nonane 1,3-diketones **1598**

Scott E. Denmark, Vito Guagnano, and Jean Vaugeois Studies on the reduction and hydrolysis of nitroso acetals **1606**

Dominique Vichard, Taoufik Boubaker, François Terrier, Marie-José Pouet, Julian M. Dust, and Erwin Buncel The versatile reactivity of 2-aryl-4,6-dinitrobenzotriazole 1-oxides in Diels–Alder type condensations and in σ-complexation — A relationship between superelectrophilicity and pericyclic reactivity **1617**

Ken-ichiro Imamura, Eiji Yoshikawa, Vladimir Gevorgyan, Tomoko Sudo, Naoki Asao, and Yoshinori Yamamoto Lewis acid-mediated intramolecular addition of silyl enol ethers to internal unactivated alkynes **1624**

Richard R. Hark, Diane B. Hauze, Olga Petrovskaia, and Madeleine M. Joullié Synthetic studies of novel ninhydrin analogs **1632**

Alan R. Katritzky, Novruz G. Akhmedov, Sergey N. Denisenko, and Subbu Perumal An ^{1}H and ^{13}C NMR conformational study of 2-(benzotriazol-1-yl)-substituted tetrahydropyrans **1655**

Stefan Schilling, Uwe Rinner, Collin Chan, Ion Ghiviriga, and Tomas Hudlicky Structure assignment of aminoconduritols by ^{15}N NMR correlation spectroscopy; synthesis of a positional isomer of 7-deoxypancratistatin **1659**

Darren J. Dixon, Alison C. Foster, and Steven V. Ley The total synthesis of (+)-aspicilin using 2,3-butane diacetal protected butane tetrols via a chiral memory protocol **1668**

Albert Padwa, William S. Kissell, and Cheryl K. Eidell Cyclization–cycloaddition cascades for the construction of azapolycyclic ring systems **1681**

André B. Charette and Michel Grenon Spectroscopic studies of the electrophilic activation of amides with triflic anhydride and pyridine **1694**

Alexei. A. Neverov, Todd McDonald, Graham Gibson, and R.S. Brown Catalysis of transesterification reactions by lanthanides — Unprecedented acceleration of methanolysis of aryl and alkyl esters promoted by $La(OTf)_3$ at neutral $\overset{S}{S}$pH and ambient temperatures **1704**

William R. Roush, David J. Madar, and D. Scott Coffey Synthesis of highly functionalized naphthoate precursors to damavaricin D — Observation of kinetically stable benzocyclohexadienones in the bromination reactions of highly functionalized β-naphthol derivatives **1711**

Peter A. Jacobi and Prudencio Herradura Enantioselective syntheses of (+)- and (–)-nephro-steranic acid employing the Nicholas–Schreiber reaction **1727**

Matthias Kauch and Dieter Hoppe Synthesis of substituted phenols by directed *ortho*-lithiation of in situ *N*-silyl-protected *O*-aryl *N*-monoalkylcarbamates **1736**

Susanne M. Hantos, Sasmita Tripathy, Najma Alibhai, and Tony Durst Synthesis of trichiliasterones A and B — 16-Ketosteroids isolated from *Trichilia hirta* and *Trichilia americana* **1747**

A. Godard, P. Rocca, F. Guillier, G. Duvey, F. Nivoliers, F. Marsais, and G. Quéguiner *Ortho*-directed metallation of π-deficient heterocycles in connection with palladium-catalyzed biaryl cross-coupling — Synthesis of marine alkaloids of the pyridoacridine series **1754**

Christoph Köllner and Antonio Togni Synthesis, characterization, and application in asymmetric catalysis of dendrimers containing chiral ferrocenyl diphosphines **1762**

Dale E. Ward, Marcelo Sales, and Matthew J. Hrapchak Attempted enantiotopic group selective cyanohydrin formation from α-alkoxy aldehydes by double stereodifferentiation **1775**

Tao Wang, Osamu Shirota, Koji Nakanishi, Nina Berova, Leonard A. McDonald, Laurel R. Barbieri, and Guy T. Carter Absolute stereochemistry of the spiroxins **1786**

© 2001 NRC Canada

Marek Majewski, Marc DeCaire, Pawel Nowak, and Fan Wang Studies on enolate chemistry of 8-thiabicyclo-[3.2.1]-octan-3-one: enantioselective deprotonation and synthesis of sulfur analogs of tropane alkaloids **1792**

Xiao-Xiang Zhang, Michele C. Harris, Joseph P. Sadighi, and Stephen L. Buchwald The use of palladium chloride as a precatalyst for the amination of aryl bromides **1799**

Manfred T. Reetz, Joachim Rudolph, and Richard Goddard Diastereotopic group recognition in the solid state — A unique intramolecular β-cyclodextrin inclusion complex **1806**

Stephen Hanessian and Jian-min Fu Total synthesis of polyoximic acid **1812**

Léon Ghosez, Cécile Franc, Frédéric Denonne, Claire Cuisinier, and Roland Touillaux Studies of palladium-catalyzed coupling reactions for preparation of hindered 3-arylpyrroles relevant to (–)-rhazinilam and its analogues **1827**

Author Index / Index des auteurs **AI-1**

December / décembre

Note of appreciation / Note de reconnaissance **iii**

ARTICLES

Tristram Chivers 2001 E.W.R. STEACIE AWARD LECTURE The imido ligand in main group element chemistry **1841**

Edward C. Lathioor and William J. Leigh Geometric and solvent effects on intramolecular phenolic hydrogen abstraction by carbonyl n,π^* and π,π^* triplets **1851**

Mitsuru Matsumoto, Delanie Lamprecht, Michael R. North, and Thomas W. Swaddle Volumes of activation for electrode processes of various charge-types in nonaqueous solvents **1864**

D.G. Lessard, M. Ousalem, and X.X. Zhu Effect of the molecular weight on the lower critical solution temperature of poly(*N*,*N*-diethylacrylamide) in aqueous solutions **1870**

Patrick H. Ruane and Robert A. McClelland Kinetic stabilizing effect of the 4-*N*-methylacetamido substituent on the phenylnitrenium ion **1875**

Bernice Cheng and Robert A. McClelland Reaction of arylnitrenium ions with guanine derivatives: N^1-methylguanosine and N^2,N^2-dimethylguanosine **1881**

Thuy Van Pham and Robert A. McClelland The nature of the transition state in diarylmethyl cation – nucleophile combination reactions as probed by secondary α-deuterium isotope effects **1887**

Christopher M. Vogels, Paul E. O'Connor, Trevor E. Phillips, Keith J. Watson, Michael P. Shaver, Paul G. Hayes, and Stephen A. Westcott Rhodium-catalyzed hydroborations of allylamine and allylimines **1898**

Christopher K. Jankowski, Gaëtan LeClair, Jacqueline M.R. Bélanger, Jocelyn R.J. Paré, and Marie-Rose VanCalsteren Microwave-assisted Diels-Alder synthesis **1906**

V.K. Sharma and Romi Molar excess volumes of ternary mixtures containing ether **1910**

Marcelo J.P. Ferreira, Gilberto V. Rodrigues, and Vicente P. Emerenciano MONOREG – an expert system for structural elucidation of monoterpenes **1915**

Dinesh C. Bilehal, Raviraj M. Kulkarni, and Sharanappa T. Nandibewoor Kinetics and mechanistic study of the ruthenium(III) catalyzed oxidative deamination and decarboxylation of L-valine by alkaline permanganate **1926**

Günther Ross and Ivar Ugi Stereoselective syntheses of α-amino acid and peptide derivatives by the U-4CR of 5-desoxy-5-thio-D-xylopyranosylamine **1934**

Demetrios K. Papayannis and Agnie M. Kosmas Quasiclassical trajectory studies on the gas-phase BrO self-reaction **1940**

Author Index / Index des auteurs **AI-1**

Contents for volume 79 / Sommaire pour volume 79 **C-1**

© 2001 NRC Canada

Note of appreciation / Note de reconnaissance

The quality of the papers in this journal depends a great deal on the efforts of those who agree to act as critical readers of manuscripts. The editors gratefully acknowledge the following, who helped us between November 1, 2000 and October 31, 2001:

Abrams, M.
Acree, W.E.
Adam, W.
Adamowicz, L.
Alexakis, A.
Allin, S.M.
Alper, H.
Alyea, E.C.
Andrews, L.
Antonelli, D.
Appleton, T.
Armstrong, D.A.
Arnold, D.R.
Arnold, J.
Ashbaugh, H.S.
Atake, T.
Atwood, D.A.
Aubke, F.
Back, T.G.
Badiali, J.-P.
Bailey, W.F.
Bain, A.D.
Baird, M.C.
Baker, W.E.
Balaban, A.T.
Baldwin, J.E.
Baldwin, R.L.
Bally, T.
Bana, M.
Bancroft, G.M.
Baranski, A.S.
Bard, A.J.
Barra, M.
Barrett, A.G.M.
Barriault, L.
Bayly, S.
Becke, A.
Belanger, D.
Bennet, A.J.
Benson, G.C.
Berg, D.J.
Berghuis, A.M.
Bernasconi, C.F.
Berry, D.
Bestmann, H.
Bin, S.
Blandamer, M.J.
Boeré, R.T.
Bohne, C.
Boivin. P.
Bolm, C.
Borden, W.T.
Boukouvalas, J.
Boulton, J.
Bowden, K.
Box, V.G.S.
Boyd, R.J.
Brinker, U.
Brisard, G.M.
Brossard, L.
Brown, R.S.
Brown, I.D.
Brunger, M.
Brzezinski, B.
Buhro, W.E.
Bunce, N.J.
Buncel, E.
Bunzli, J.-C.
Burford, N.
Burgess, K.
Burnell, D.J.
Bursten, B.
Calhoun, L.A.
Cane, D.
Capretta, A.
Cerny, M.S.
Chan, T.H.
Charette, A.B.
Charlton, J.L.
Chenevert, R.
Chin, J.
Chong, D.P.
Chow, A.
Christe, O.
Clarke, D.B.
Coates, G.W.
Cocivera, M.
Cole, B.
Comins, D.
Cook, J.
Corbett, J.
Corey, E.J.
Corrie, J.E.
Corrigan, J.F.
Cossy, J.
Costas, C.
Couture, A.
Cox, R.A.
Crabtree, R.H.
Creary, X.
Crich, D.
Crudden, C.
Crutchley, R.J.
Csizmadia, I.G.
Cullen, W.R.
Cunningham, A.
Daggett, V.
Daily, W.P.
Damha, M.J.
Danheiser, R.I.
Dannenberg, J.J.
Darensbourg, D.
Davis, F.A.
de Meijere, A.
Deleuze, M.S.
Delfourne, E.
Della, E.
Denk, M.
Denny, W.A.
Deslongchamps, P.
Desnoyers, J.
DiCosimo, R.
Dicks, A.
Dill, K.A.
Dini, A.
Dirk, C.W.
Dodelet, J.P.
Dolphin, D.
Dory, Y.
Drake, J.E.
Dubois, J.-E.
Duhamel, J.
Dunbar, K.
Dunitz, J.D.
Durst, T.
Dutasta, J.P.
Dyadin, Y.A.
Easteal, A.J.
Edwards, P.G.
Einspahr, H.
Eisenberg, A.
Elzanowska, H.
Enders, D.
Endicott, J.
Erker, G.
Espinosa-García, J.
Evans, D.H.
Evans, C.H.
Faber, K.
Fabian, W.M.F.
Fallis, A.G.
Falvey, D.E.
Fenske, D.
Field, R.J.
Fillion, F.
Forniés, J.
Fournier, R.
Francisco, J.S.
Franzen, H.F.
Fraser-Reid, B.
Fryzuk, M.D.
Fyles, T.M.
Gambarotta, S.
Ganem, B.
Garegg, P.J.
Gattrell, M.
Gauld, J.
Gauthier, M.
Georges, M.
Georghiou, P.E.
Gervay-Hague, J.
Gevorgyan, V.
Ghosez, L.
Gilchrist, T.
Glaser, R.
Goddard, J.D.
Goldberg, K.
Gossage, R.A.
Gotor, V.
Grabner, G.
Green, J.R.
Greenstock, C.L.
Grev, R.S.

La qualité des articles publié dans notre revue dépend beaucoup de ceux qui acceptent de faire une lecture critique des manuscripts. Les directeurs scientifique expriment leur reconnaissance aux personnes suivantes qui nous ont aidé, du 1er novembre 2000 au 31 octobre 2001 :

© 2001 NRC Canada

Grigg, R.
Grindley, T.B.
Grolier, J.P.
Grundy, K.R.
Grushin, V.
Guay, D.
Gudat, D.
Guthrie, J.P.
Gutsche, C.D.
Guy, R.D.
Hadad, C.M.
Haim, A.
Hakin, A.W.
Halkier, B.A.
Hamilton, A.D.
Hammond, G.B.
Hanack, M.
Hanessian, S.
Harata, K.
Harvey, P.D.
Hauptman, E.
Hay, M.
Hegarty, A.F.
Hilinski, E.F.
Hindsgaul, O.
Hirsch, A.
Hiyama, T.
Hodgson, D.M.
Hoffmann, H.M.R.
Hogarth, G.
Holland, H.L.
Holzwarth, J.
Honek, J.F.
Hopf, H.
Hoppe, D.
Houk, K.N.
Hudlicky, T.
Huffman, J.W.
Hutlin, P.
Huttner, G.
Höpfl, H.
Jackson, J.E.
James, B.R.
James, T.L.
Jarvis, B.B.
Jerkiewicz, G.
Jessop, P.G.
Johnston, L.J.
Jones, M.
Jordan, R.B.
Joule, J.
Juaristi, E.
Just, G.
Kadla, J.F.
Kallin, C.
Kaneda, K.
Kaszynski, P.
Katritzky, A.R.
Katzenellenbogen, J.A.
Kayser, M.M.
Keay, B.A.
Kenney, M.E.
Kerr, M.A.
Kimizuka, N.
King, J.F.
Kirk, M.
Kirk, A.D.
Kliegel, W.
Koch, S.A.
Koga, Y.
Kolis, J.
Koreeda, M.
Kotovych, G.
Kovak, P.
Kraatz, H.-B.
Kresge, A.J.
Krull, U.J.
Kündig, E.P.
Kutney, J.
Kwak, J.C.T.
LaRock, R.
Langa, F.
Langer, P.
Laporterie, A.
Lappin, A.G.
Lautens, M.
Leach, G.
Leaist, D.
Leary, G.
Lebel, H.
Lee, D.G.
Lee-Ruff, E.
Leigh, W.J.
Lemieux, R.P.
Lessard, J.
Letcher, T.M.
Lever, A.B.P.
Lewars, E.
Ley, S.V.
Leznoff, C.C.
Leznoff, D.B.
Lipkowski, J.
Lippert, B.
Liu, Z.
Liu, L.
Long, E.C.
Love, B.
Lowary, T.
Lown, W.J.
Lubell, W.D.
Lucy, C.
MacDougall, P.
Macartney, D.H.
Madison, S.A.
Magee, D.I.
Maier, G.
Majewski, M.
Manderville, R.E.
Mandolini, L.
Mar, A.
Marat, K.
Marsan, B.
Martire, D.O.
Mateescu, A.
Mather, A.
Mathey, F.
Matt, D.
Mattar, S.M.S.
Mattey, J.
Mauk, G.
McAuley, A.
McClelland, R.A.
McDonald, R.S.
McKillop, A.
McKinnon, D.
McLachlan, M.
Meegan, M.J.
Mellon, C.
Menard, H.
Menger, F.
Meth-Cahn, O.
Meyers, A.I.
Mihichuk, L.M.
Mikkelsen, S.
Miller, M.
Miller, S.J.
Mitchell, R.
Molina, P.
Molinski, T.F.
Montgomery, C.D.
Moody, C.
Morin, M.
Moss, R.A.
Muchowski, J.M.
Münck, E.
Nagarajan, R.
Nathansohn, A.
Nelson, J.H.
Newcombe, G.
Normant, J.
Oakley, R.T.
O'Brien, P.
Olah, G.A.
Oldfield, E.
Organ, M.G.
Oro, L.
Orvig, C.
Osawa, E.
Otter, A.
Pacey, P.D.
Packdel, H.
Padwa, A.
Palepu, R.
Parnis, J.M.
Parsons, P.
Parvez, M.
Passmore, J.
Pattenden, G.
Paulson, S.
Peltonen, K.
Penner, G.H.
Perrin, C.L.
Perron, G.
Petersen, N.O.
Pfleiderer, W.
Picard, C.
Piers, W.E.
Piers, E.
Pietro, W.J.
Pilli, R.
Pincock, J.A.
Pinto, B.M.
Poirier, R.A.
Posner, G.
Prakash, G.K.S.
Prausnitz, J.M.
Pregosin, P.S.
Price, W.S.
Pryor, W.A.
Pye, C.C.
Quail, J.W.
Radom, L.
Ragauskas, A.
Rainier, J.
Rapoport, H.
Ratner, M.A.
Rauk, A.
Reedijk, J.
Reid, D.
Reinhoudt, D.N.
Richon, D.
Richter-Addo, G.B.
Rigby, J.H.
Roberge, P.R.
Robins, M.J.
Robins, C.
Rochon, F.D.
Rodrigo, R.
Rollin, P.
Rorabacher, D.B.
Roscoe, S.G.
Rotello, V.M.

© 2001 NRC Canada

Roush, W.R.
Rowley, D.M.
Ruelle, P.
Rüterjans, H,
Sadler, P.J.
Sandall, J.P.B.
Sarma, R.H.
Saunders, W.H.
Schaefer, T.
Schäfer, L.
Schepp, N.P.
Schmidt, R.
Schultz, T.P.
Schwan, A.
Schwarz, H.A.
Scott, A.P.
Secrist, J.A.
Seebach, D.
Serpone, N.
Sessler, J.
Sharp, K.A.
Shaw, C.F.
Sherman, J.C.
Sherry, A.D.
Shimizu, S.
Shinkai, S.
Showalter, K.
Sibi, M.P.
Silverman, R.B.
Smith, G.P.
Smith, D.
Soliman, A.A.
Sorensen, T.S.
Spanget-Larsen, J.
Spino, C.
St-Amant, A.
Stanforth, S.P.
Storer, R.
Storr, A.
Stradiotto, M.
Strukul, G.
Stuchebrukhov, A.A.
Stynes, D.V.
Sung, K.
Swaddle, T.W.
Szarek, W.
Takacs, J.M.
Takasaki, B.
Takats, J.
Tanaka, H.
Tanner, M.E.
Taylor, P.G.
Tee, O.S.
Tennant, B.
Terrier, F.
Thompson, A.
Tidwell, T.T.
Tillyer, R.
Tius, M.A.
Togni, A.
Tomasini, C.
Toscano, J.P.
Townsend, L.B.
Tremaine, P.R.
Tremaine, P.
Trotter, J.
Trusler, J.P.M.
Tsantrizos, Y.S.
Turner, N.J.
Tykwinski, R.
Udagawa, Y.
Urieta, J.S.
van Koten, G.
Vanysek, P.
Vederas, J.C.
Verboom, W.
Verrall, R.E.
Vijayan, M.
Wagner, P.J.
Wan, P.
Wang, H.
Ward, D.E.
Ward, M.D.
Warkentin, J.
Wasserman, H.H.
Wasylishen, R.E.
Wayland, B.B.
Waymouth, R.M.
Wayner, D.D.M.
Weil, J.A.
Weinberg, N.
Wentzell, P.D.
Werstiuk, N.H.
West, R.
Westcott, S.A.
Wherland, S.E.
Whitcombe, T.
Winnik, M.A.
Withers, S.G.
Wolf, M.
Wong, C.-H.
Wood, J.
Woody, R.W.
Woolley, E.M.
Workentin, M.S.
Wuts, P.
Yamaguchi, S.
Yamamoto, Y.
Zargarian, D.
Zhao, X.-Z.
Ziegler, T.

© 2001 NRC Canada

PREVIEW / APERÇU

Forthcoming special issues / Numéros spécials à paraître

June 2002	In honour of Professor J. Bryan Jones
August 2002	In honour of Professor Ray Lemieux
November 2002	In honour of Professor Tris Chivers
June 2003	In honour of Professor Don Arnold

Forthcoming articles / Articles à paraître

Electron-spin conservation and methyl-substitution effects on bonds in closed- and open-shell systems — A G3 ab initio study of small boron-containing molecules and radicals	C. Poon and P.M. Mayer
Inhibition de la corrosion de l'alliage d'aluminium 6063 au moyen de composes inorganiques dans une solution de chlorure de sodium à 3%	L. Bazzi, R. Salghi, E. Zine, S. El Issami, S. Kertit, and P. Hammouti
Cationic thiolate and selenolate complexes of platinum(IV)	M.C. Janzen, M.C. Jennings, and R.J. Puddephatt
Synthesis and reactivity of novel Schiff bases containing boronate esters	D.W. Norman, J.P. Edwards, C.M. Vogels, A. Decken, and S.A. Westcott
Iron complexes of the dibenzophospholyl ligand — A synthetic and crystallographic study	A. Decken, M.A. Neil, C.A. Dyker, and F. Bottomley
Environmental photodegradation of pyrimidine fungicides — Kinetics of the visible-light-promoted interactions between riboflavin and 2-amino-4-hydroxy-6-methylpyrimidine	E. Haggi, S. Bertolotti, S. Miskoski, F. Amat-Guerri, and N.A. García
Synthesis of a hexasaccharide fragment of the capsular polysaccharide of *Streptococcus pneumoniae* type 3	D.J. Lefeber, E.A. Arévalo, J.P. Kamerling, and J.F.G. Vliegenthart
Kinetics and mechanism of hydrolysis of 3-diazobenzofuran-2-one and its hydrolysis product (3-hydroxybenzofuran-2-one)	Y. Chiang, A.J. Kresge, and Q. Meng
Monte-Carlo calculation of the primary yields of the primary yields of H_2O_2 in the $^{1}H^{+}$, $^{2}H^{+}$, $^{4}He^{2+}$, $^{7}Li^{3+}$, and $^{12}C^{6+}$ radiolysis of liquid water at 25 and 300°C	J. Meesungnoen, J.-P. Jay-Gerin, A. Filali-Mouhim, and S. Mankhetkorn
On the generation of oxirene and dimethyloxirene by retro Diels–Alder reactions, and reactions of dimethyloxirene — A computational study	C. Delamere, C. Jakins, and E. Lewars
Mechanistic studies of photohydration of *m*-hydroxy-1,1-diaryl alkenes	J.G. Cole and P. Wan
The endothermic nature of the binding of anionic bile salts to a cationic adsorbent	C.K. Williams, W.C. Galley, and G.R. Brown
1-Propanol hydrate by IR spectroscopy	J.-J. Max, S. Daneault, and C. Chapados
Mother Nature and the molecular Big Bang	R.J.D. Miller

© 2001 NRC Canada